Pathology & Oncology Research

Pathology and Oncology Research (POR) | 2023-2024 Retrospective

Issue Editors

József Tímár
Semmelweis University, Hungary

László Kopper
Semmelweis University, Hungary

Andrea Ladányi
National Institute of Oncology, Hungary

Anna Sebestyén
Semmelweis University, Hungary

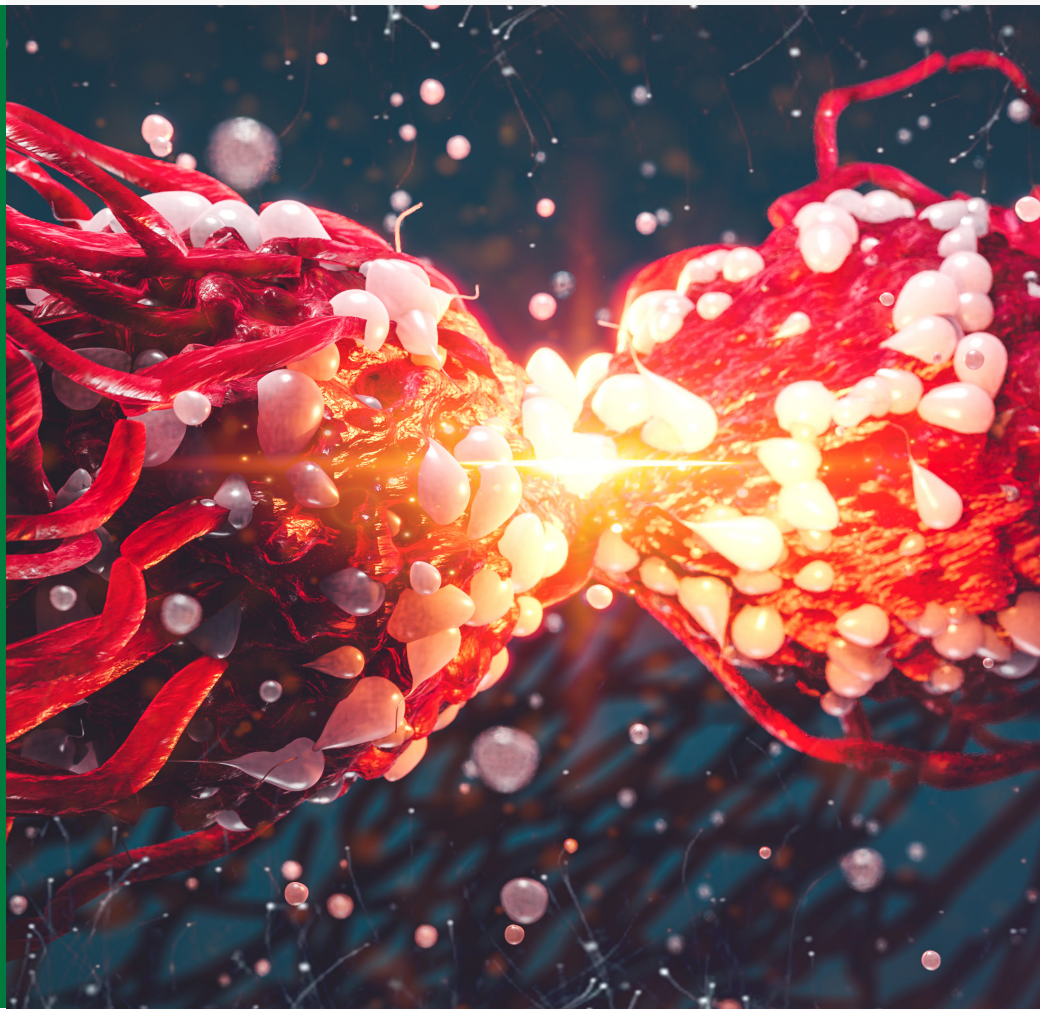

frontiers | Publishing Partnerships

Pathology &
Oncology Research

Pathology and Oncology Research (POR) | 2023-2024 Retrospective

Pathology and Oncology Research (POR) is a typical multidisciplinary journal which attempts to support translational medical research. Pathological diagnostics is clearly strongly represented involving not only tumor pathology but non-cancer fields as well. On the other hand, oncology covers not only clinical oncology but cancer research as well. More recently, other diagnostic disciplines such as radiology or laboratory medicine started to appear in the journal further promoting the translational aspects of research. In 2024, POR ranked in Q2 (in the upper range) on the Oncology and the Pathology and Forensic Medicine categories of the SCImago Journal Rank (SJR), indicating that the papers published in the last two years are recognized by a wide audience. It is also evident from this collection that POR supports the Central-European research community thanks to the continuous support of the Arányi Lajos Foundation.

József Tímár
László Kopper
Andrea Ladányi
Anna Sebestyén

Editors-in-Chief



Pathology & Oncology Research
eBook Copyright Statement

The copyright in the text of individual articles in this eBook is the property of their respective authors or their respective institutions or funders. The copyright in graphics and images within each article may be subject to copyright of other parties. In both cases this is subject to a license granted to Frontiers, the publisher of Pathology & Oncology Research.
Each article within this eBook, and the eBook itself, are published under the most recent version of the Creative Commons CC-BY licence. The version current at the date of publication of this eBook is CC-BY 4.0. If the CC-BY licence is updated, the licence granted by Frontiers is automatically updated to the new version.
When exercising any right under the CC-BY licence, Frontiers must be attributed as the original publisher of the article or eBook, as applicable.
Authors have the responsibility of ensuring that any graphics or other materials which are the property of others may be included in the CC-BY licence, but this should be checked before relying on the CC-BY licence to reproduce those materials. Any copyright notices relating to those materials must be complied with.
Copyright and source acknowledgement notices may not be removed and must be displayed in any copy, derivative work or partial copy which includes the elements in question.
All copyright, and all rights therein, are protected by national and international copyright laws. The above represents a summary only. For further information please read Frontiers' Conditions for Website Use and Copyright Statement, and the applicable CC-BY licence.

ISSN 1532-2807
ISBN 978-2-8325-6612-1
DOI 10.3389/978-2-8325-6612-1

Generative AI statement
Any alternative text (Alt text) provided alongside figures in the articles in this ebook has been generated by Frontiers with the support of artificial intelligence and reasonable efforts have been made to ensure accuracy, including review by the authors wherever possible. If you identify any issues, please contact us.

Pathology & Oncology Research

Table of contents

Breast Cancer

20 Association between pathological characteristics and recurrence score by OncotypeDX in resected T1-3 and N0-1 breast cancer: a real-life experience of a North Hungarian regional center
DOI: 10.3389/pore.2024.1611735
Dániel Deme, Bálint Ferenc Tamaskovics, Nizar Jammoul, Sándor Kovács, Emmanuel Oladunjoye Kayode, James W. Grice and András Telekes

47 Invasive micropapillary carcinoma of the breast and invasive breast carcinoma of no special type: a comparison of claudin proteins' expression and its impact on survival
DOI: 10.3389/pore.2024.1611987
Zsófia Kramer, András Budai, Adrián Pesti, Janina Kulka and Anna-Mária Tőkés

59 A new perspective on the proper timing of radiotherapy during CDK4/6 inhibitor therapy in patients with "bone-only" metastatic breast cancer
DOI: 10.3389/pore.2023.1611369
Ilona Tornyi, Peter Árkosy, Ildikó Horváth and Andrea Furka

67 NAD+ biosynthesis metabolism predicts prognosis and indicates immune microenvironment for breast cancer
DOI: 10.3389/pore.2023.1610956
Yuting Yang, Ze Wang, Mengqi He, Lihong Diao, Biyue Yu and Dong Li

Cancer Immunity and Immunotherapy

79 Potential predictors of immunotherapy in small cell lung cancer
DOI: 10.3389/pore.2023.1611086
Valeria Skopelidou, Jan Strakoš, Jozef Škarda, Milan Raška and Leona Kafková-Rašková

91 Cytokine-induced killer cell treatment is superior to chemotherapy alone in esophageal cancer
DOI: 10.3389/pore.2023.1610710
Jiayang Sun, Yushu Sun, Miniderima and Xiumei Wang

101 The role of immunotherapy in early-stage and metastatic NSCLC
DOI: 10.3389/pore.2024.1611713
Attila Lieber, Attila Makai, Zsuzsanna Orosz, Tamás Kardos, Susil Joe Isaac, Ilona Tornyi and Nóra Bittner

118 Tumor PD-L1 expression and molecular profiling are not associated with immune checkpoint inhibitor-induced thyroid dysfunction in advanced NSCLC patients
DOI: 10.3389/pore.2023.1610951
Adi Horesh, Rena Pollack, Hovav Nechushtan, Rivka Dresner-Pollak and Tzahi Neuman

126 PD-1 and PD-L1 expression in rare lung tumors
DOI: 10.3389/pore.2023.1611164
Marton Gyulai, Zsolt Megyesfalvi, Lilla Reiniger, Tunde Harko, Bence Ferencz, Luca Karsko, Laszlo Agocs, Janos Fillinger, Balazs Dome, Zoltan Szallasi and Judit Moldvay

135 Characterization of the input material quality for the production of tisagenlecleucel by multiparameter flow cytometry and its relation to the clinical outcome
DOI: 10.3389/pore.2023.1610914
Martin Štach, Robert Pytlík, Kristýna Šmilauerová, Jana Rychlá, Martin Mucha, Jan Musil, Abhishek Koladiya, Matěj Nemec, Martina Petráčková, Iva Kaštánková, Pavla Pecherková, Lucie Šrámková, Kamila Polgárová, Marek Trněný, Petr Lesný, Jan Vydra and Pavel Otáhal

147 Higher Nodal expression is often associated with poorer survival in patients diagnosed with melanoma and treated with anti-PD1 therapy
DOI: 10.3389/pore.2024.1611889
Philippe D. Gascard, Xianhong Wang, Mehdi Nosrati, Kevin B. Kim, Mohammed Kashani-Sabet, Thea D. Tlsty, Stanley P. Leong and Mary J. C. Hendrix

155 The efficacy outcomes in non-small cell lung cancer patients treated with PD axis inhibitor agents - a population-based study of the Vojvodina region
DOI: 10.3389/pore.2024.1611717
Nensi Lalić, Marko Bojović, Daliborka Bursać, Darijo Bokan, Vesna Čeriman Krstić, Ivan Kuhajda, Biljana Parapid, Sanja Tomić and Aleksandar Šipka

167 Predicting prognosis and clinical efficacy of immune checkpoint blockade therapy *via* interferon-alpha response in muscle-invasive bladder cancer
DOI: 10.3389/pore.2023.1611117
Bohan Fan, Xin Zheng, Yicun Wang and Xiaopeng Hu

178 Expression of the immune targets in tumor-infiltrating immunocytes of gestational trophoblastic neoplasia
DOI: 10.3389/pore.2023.1610918
Hongyan Cheng, Liju Zong, Shuangni Yu, Jie Chen, Xirun Wan, Yang Xiang and Junjun Yang

Cancer Molecular Targets and Therapeutics

186 Combination of farnesyl-transferase inhibition with KRAS G12D targeting breaks down therapeutic resistance in pancreatic cancer

DOI: 10.3389/pore.2024.1611948

Eszter Molnár, Marcell Baranyi, Krisztina Szigeti, Luca Hegedűs, Fanni Bordás, Zsófia Gábriel, Gréta Petényi, József Tóvári, Balázs Hegedűs and József Tímár

198 CircRNA: A new class of targets for gastric cancer drug resistance therapy

DOI: 10.3389/pore.2023.1611033

Ying Zheng, Zhe Li, Yao Wang, Wanjiao Chen, Yifan Lin, Junming Guo and Guoliang Ye

208 Recent advances and future directions in etiopathogenesis and mechanisms of reactive oxygen species in cancer treatment

DOI: 10.3389/pore.2023.1611415

Priyanka Verma, Bhavika Rishi, Noreen Grace George, Neetu Kushwaha, Himanshu Dhandha, Manpreet Kaur, Ankur Jain, Aditi Jain, Sumita Chaudhry, Amitabh Singh, Fouzia Siraj and Aroonima Misra

220 FACILITATE: A real-world, multicenter, prospective study investigating the utility of a rapid, fully automated real-time PCR assay versus local reference methods for detecting epidermal growth factor receptor variants in NSCLC

DOI: 10.3389/pore.2023.1610707

Anke Behnke, Anne Cayre, Giovanna De Maglio, Giuseppe Giannini, Lionel Habran, Marina Tarsitano, Massimiliano Chetta, David Cappellen, Alexandra Lespagnol, Cecile Le Naoures, Gabriella Massazza, Annarita Destro, Irina Bonzheim, Achim Rau, Achim Battmann, Bettina Kah, Emmanuel Watkin and Michael Hummel

235 Can long-read sequencing tackle the barriers, which the next-generation could not? A review

DOI: 10.3389/pore.2024.1611676

Nikolett Szakállas, Barbara K. Barták, Gábor Valcz, Zsófia B. Nagy, István Takács and Béla Molnár

247 mTOR hyperactivity and *RICTOR* amplification as targets for personalized treatments in malignancies

DOI: 10.3389/pore.2024.1611643

Dániel Sztankovics, Dorottya Moldvai, Gábor Petővári, Titanilla Dankó, Fatime Szalai, Risa Miyaura, Viktória Varga, Noémi Nagy, Gergő Papp, Judit Pápay, Ildikó Krencz and Anna Sebestyén

Diagnostics

266 Novel diagnostic processes and challenges in bronchoscopy
DOI: 10.3389/pore.2024.1611774
Zsolt Pápai-Székely, Gábor Grmela and Veronika Sárosi

275 Crystal induced arthropathies—a comparative study of 40 patients with apatite rheumatism, chondrocalcinosis and primary synovial chondromatosis
DOI: 10.3389/pore.2024.1611454
Miklós Bély and Ágnes Apáthy

290 HUNCHEST projects—advancing low-dose CT lung cancer screening in Hungary
DOI: 10.3389/pore.2024.1611635
Anna Kerpel-Fronius and Krisztina Bogos

298 Wide-field optical coherence tomography for microstructural analysis of key tissue types: a proof-of-concept evaluation
DOI: 10.3389/pore.2023.1611167
Beryl Rabindran and Adriana D. Corben

308 Molecular genetic investigation of hereditary breast and ovarian cancer patients in the Southern Transdanubian region: widening the mutation spectrum and searching for new pathogenic variants using next-generation methods
DOI: 10.3389/pore.2024.1611813
László Baráti, Anita Maász, Alexandra Mikó, Éva Bércesi, Sultan Al Kalbani, Judit Bene, Sebestyén Kovács, László Mangel and Kinga Hadzsiev

320 Correlations between the histopathological alterations in minor salivary glands and the clinically suspected Sjögren's syndrome
DOI: 10.3389/pore.2023.1610905
Mária Janka and Attila Zalatnai

327 Evaluating complete response prediction rates in locally advanced rectal cancer with different radiomics segmentation approaches
DOI: 10.3389/pore.2024.1611744
Gizem Kaval, Merve Gulbiz Dagoglu Kartal, Sena Azamat, Eda Cingoz, Gokhan Ertas, Sule Karaman, Basak Kurtuldu, Metin Keskin, Neslihan Berker, Senem Karabulut, Ethem Nezih Oral and Nergiz Dagoglu Sakin

336 Three-dimensional analysis of perineural invasion in extrahepatic cholangiocarcinoma using tissue clearing
DOI: 10.3389/pore.2023.1611284
Hirokazu Ogasawara, Tadashi Yoshizawa, Kiyoko Oshima, Kenta Ogasawara, Shunsuke Kubota, Shintaro Goto, Satoko Morohashi, Taiichi Wakiya, Norihisa Kimura, Keinosuke Ishido, Hiroshi Kijima and Kenichi Hakamada

343 Association between radiomics features of DCE-MRI and CD8+ and CD4+ TILs in advanced gastric cancer
DOI: 10.3389/pore.2023.1611001
Huizhen Huang, Zhiheng Li, Yue Xia, Zhenhua Zhao, Dandan Wang, Hongyan Jin, Fang Liu, Ye Yang, Liyijing Shen and Zengxin Lu

354 Artificial intelligence-based automated determination in breast and colon cancer and distinction between atypical and typical mitosis using a cloud-based platform
DOI: 10.3389/pore.2024.1611815
Nilay Bakoglu, Emine Cesmecioglu, Hirotsugu Sakamoto, Masao Yoshida, Takashi Ohnishi, Seung-Yi Lee, Lindsey Smith and Yukako Yagi

369 Genetic characterization of intramuscular myxomas
DOI: 10.3389/pore.2024.1611553
William John Hatchett, Marta Brunetti, Kristin Andersen, Maren Randi Tandsæther, Ingvild Lobmaier, Marius Lund-Iversen, Thomas Lien-Dahl, Francesca Micci and Ioannis Panagopoulos

379 Development, testing and validation of a targeted NGS-panel for the detection of actionable mutations in lung cancer (NSCLC) using anchored multiplex PCR technology in a multicentric setting
DOI: 10.3389/pore.2024.1611590
Jörg Kumbrink, Melanie-Christin Demes, Jan Jeroch, Andreas Bräuninger, Kristin Hartung, Uwe Gerstenmaier, Ralf Marienfeld, Axel Hillmer, Nadine Bohn, Christina Lehning, Ferdinand Ferch, Peter Wild, Stefan Gattenlöhner, Peter Möller, Frederick Klauschen and Andreas Jung

394 Diagnostic challenges in complicated case of glioblastoma
DOI: 10.3389/pore.2024.1611875
Tatiana Aghova, Halka Lhotska, Libuse Lizcova, Karla Svobodova, Lucie Hodanova, Karolina Janeckova, Kim Vucinic, Martin Gregor, Dora Konecna, Filip Kramar, Jiri Soukup, David Netuka and Zuzana Zemanova

404 Diagnostic performance of intracystic carcinoembryonic antigen (CEA) versus glucose in differentiation of mucinous and non-mucinous pancreatic cysts
DOI: 10.3389/pore.2024.1611881
György Gyimesi, Bánk Keczer, Péter Rein, Miklós Horváth, Ákos Szűcs, Tamás Marjai, Attila Szijártó and István Hritz

411 Semi-automated analysis of HER2 immunohistochemistry in invasive breast carcinoma using whole slide images: utility for interpretation in clinical practice
DOI: 10.3389/pore.2024.1611826
Chiu-Hsiang Connie Liao, Nilay Bakoglu, Emine Cesmecioglu, Matthew Hanna, Fresia Pareja, Hannah Y. Wen, Timothy M. D'Alfonso, Edi Brogi, Yukako Yagi and Dara S. Ross

Gastrointestinal Cancers - Colorectal

421 Feasibility of indocyanine green (ICG) fluorescence in *ex vivo* pathological dissection of colorectal lymph nodes—a pilot study
DOI: 10.3389/pore.2024.1611853
Lorand Lakatos, Ildiko Illyes, Andras Budai, Viktoria Bencze, Attila Szijarto, Andras Kiss and Balazs Banky

428 Fibroblast activation protein-α expression in fibroblasts is common in the tumor microenvironment of colorectal cancer and may serve as a therapeutic target
DOI: 10.3389/pore.2023.1611163
K. Greimelmaier, N. Klopp, E. Mairinger, M. Wessolly, S. Borchert, J. Steinborn, K. W. Schmid, J. Wohlschlaeger and F. D. Mairinger

437 Development and validation of a prognostic nomogram for rectal cancer patients who underwent surgical resection
DOI: 10.3389/pore.2023.1611014
Bochao Zhao, Jingchao Wang, Zhicheng Ma, Haikun Ye, Tao Yang and Kewei Meng

447 An epithelial–mesenchymal transition-related mRNA signature associated with the prognosis, immune infiltration and therapeutic response of colon adenocarcinoma
DOI: 10.3389/pore.2023.1611016
Yu Zhang, Yan Li, Zan Zuo, Ting Li, Ying An and Wenjing Zhang

461 Diagnostic and prognostic significance of keloid-like collagen remodeling patterns in the extracellular matrix of colorectal cancer
DOI: 10.3389/pore.2024.1611789
Nauryzbay M. Imanbayev, Yerbolat M. Iztleuov, Yevgeniy K. Kamyshanskiy and Aigul V. Zhumasheva

471 New staging systems for left-sided colon cancer based on the number of retrieved and metastatic lymph nodes provide a more accurate prognosis
DOI: 10.3389/pore.2023.1610874
Guiru Jia, Purun Lei, Yanru Zhang, Zongheng Zheng, Jiafeng Fang, Xiaofeng Yang, Hongbo Wei and Tufeng Chen

483 Potential predictors for CDX2 expression loss and mismatch repair deficiency in colorectal cancer
DOI: 10.3389/pore.2023.1610908
Ivan Vlahović, Jasmina Rajc, Ivan Švagelj, Krešimir Šolić and Dražen Švagelj

494 Expression of aquaporin 1, 3 and 5 in colorectal carcinoma: correlation with clinicopathological characteristics and prognosis
DOI: 10.3389/pore.2023.1611179
Guangwen Zhang, Yongfei Hao, Ling Chen, Zengshan Li, Langlang Gao, Jian Tian, Qing Qiao and Jinsong Zhang

504 Increased Kremen2 predicts worse prognosis in colon cancer
DOI: 10.3389/pore.2023.1611082
Junxian Long, Fengyun Cong, Yousheng Wei, Jungang Liu and Weizhong Tang

515 Conjoint analysis of clinical, imaging, and pathological features of schistosomiasis and colorectal cancer
DOI: 10.3389/pore.2023.1611396
Fang Zhang, XiaoShuang Wang, YuanTing Zhu and Peng Xia

Gastrointestinal Cancers - Gastric/Esophageal

523 Expression significance of Emi1, UBCH10 and CyclinB1 in esophageal squamous cell carcinoma
DOI: 10.3389/pore.2023.1611081
Hui Li, Chenbo Yang, Kuisheng Chen and Miaomiao Sun

535 High expression of TMEM200A is associated with a poor prognosis and immune infiltration in gastric cancer
DOI: 10.3389/pore.2023.1610893
Hongyang Deng, Tengfei Li, Fengxian Wei, Wei Han, Xiaodong Xu and Youcheng Zhang

553 Clinicopathologic features of gastric glomus tumor: A report of 15 cases and literature review
DOI: 10.3389/pore.2022.1610824
Minying Deng, Rongkui Luo, Jie Huang, Yuanlong Luo, Qi Song, Huaiyu Liang, Chen Xu, Wei Yuan and Yingyong Hou

568 Intraoperative pyloric drainage is unnecessary during esophagectomies: a meta-analysis and systematic review of randomized controlled trials
DOI: 10.3389/pore.2024.1611823
Armand Csontos, Dávid Németh, Lajos Szakó, Gergő Berke, Dóra Lili Sindler, Dávid Berki, Csenge Papp, Péter Hegyi, András Vereczkei and András Papp

579 Prognostic role of lymph node regression in patients with esophageal cancer undergoing neoadjuvant therapy
DOI: 10.3389/pore.2024.1611844
Pingrun Chen, Maojia Chen, Yijie Bu, Guowei Che, Chao Cheng and Yan Wang

590 Integrated oxidative stress score for predicting prognosis in stage III gastric cancer undergoing surgery
DOI: 10.3389/pore.2023.1610897
Yu-hang Liu, Rui Meng, Bing Zhu, Qi-qi Zhan, Xin Yang, Guan-yi Ding, Chun-liang Jia, Qian-yu Liu and Wei-guo Xu

603 Gastric epithelial neoplasm of fundic-gland mucosa lineage: representative of the low atypia differentiated gastric tumor and Ki67 may help in their identification
DOI: 10.3389/pore.2024.1611734
Houqiang Li, Lanqing Zheng, Guodong Zhong, Xunbin Yu, Xia Zhang, Linying Chen and Xin Chen

613 A combined approach for individualized lymphadenectomy in gastric cancer patients
DOI: 10.3389/pore.2023.1611270
Zsolt Varga, Adrienn Bíró, Miklós Török and Dezső Tóth

623 Prognostic value of pretreatment Controlling Nutritional Status score in esophageal cancer: a meta-analysis
DOI: 10.3389/pore.2023.1611221
Jing Lv, Peirui Chen, Jianqiang Wu and Caihong Hu

633 Comprehensive landscape and future perspectives of non-coding RNAs in esophageal squamous cell carcinoma, a bibliometric analysis from 2008 to 2023
DOI: 10.3389/pore.2024.1611595
Jiaxin Wu, Yuanying Wang, Yi Cheng, Li Cheng and Lushun Zhang

645 Cohort size required for prognostic genes analysis of stage II/III esophageal squamous cell carcinoma
DOI: 10.3389/pore.2023.1610909
Linghong Kong, Ming Yang, Zhiyi Wan and Lining Wang

649 Efficacy of the low dose apatinib plus deep hyperthermia as third-line or later treatment in HER-2 negative advanced gastric cancer
DOI: 10.3389/pore.2023.1611114
Guohu Han, Changchun Sun, Lihua Cui, Yufeng Huang, Lijiang Yu, Shenzha Liu and Min Tao

657 Prognostic role of pretreatment skeletal muscle index in gastric cancer patients: A meta-analysis
DOI: 10.3389/pore.2023.1611055
Xiaohong He, Sicheng Zhou, Hongjun Li, Yue Gou and Dan Jia

667 APOC1 predicts a worse prognosis for esophageal squamous cell carcinoma and is associated with tumor immune infiltration during tumorigenesis
DOI: 10.3389/pore.2023.1610976
Xiying Cao, Bingqun Wu, Shaoming Guo, Weixiang Zhong, Shenyu Zhu, Zuxiong Zhang, Liang Gu and Hui Li

682 Emerging roles of the HECT E3 ubiquitin ligases in gastric cancer
DOI: 10.3389/pore.2023.1610931
Aiqin Sun, Xianyan Tian, Yifei Chen, Wannian Yang and Qiong Lin

Gastrointestinal Cancers - Hepato/Pancreatic/Biliary

690 Pancreatic SABR using peritumoral fiducials, triggered imaging and breath-hold

DOI: 10.3389/pore.2023.1611456
Katalin Kisivan, Andrea Farkas, Peter Kovacs, Csaba Glavak, Gabor Lukacs, Karoly Mahr, Zsolt Szabo, Melinda Petone Csima, Akos Gulyban, Zoltan Toth, Zsolt Kaposztas and Ferenc Lakosi

702 Prognostic value of albumin-bilirubin score in pancreatic cancer patients after pancreatoduodenectomy with liver metastasis following radiofrequency ablation

DOI: 10.3389/pore.2023.1611175
Lei Zhang, Xuefei Zhang, Bolin Wu, Xue Han, Cunli Guo, Bo Li, Hui Jing and Wen Cheng

716 Tumor budding as a predictor of disease-free survival in patients with cholangiocarcinoma

DOI: 10.3389/pore.2023.1611216
Kyung Bin Kim, Ji Hyun Ahn, Soon Wook Kwon, Su Ji Lee, Yury Lee, Seo Young Park, Ahrong Kim, Kyung Un Choi, Chang Hun Lee and Gi Yeong Huh

726 Development and validation of a nomogram prediction model based on albumin-to-alkaline phosphatase ratio for predicting the prognosis of gallbladder carcinoma

DOI: 10.3389/pore.2022.1610818
Zizheng Fan, Bing Liu and Peizhong Shang

Genitourinary Cancer

739 Correlation between fibroblast growth factor receptor mutation, programmed death ligand-1 expression and survival in urinary bladder cancer based on real-world data

DOI: 10.3389/pore.2023.1611077
Janos Revesz, Boglarka Posfai, Laszlo Pajor, Timea Papdan, Linda Varga, Viktor R. Paczona, Zoltan Varga, Farkas Sukosd and Aniko Maraz

751 Grade Group accuracy is improved by extensive prostate biopsy sampling, but unrelated to prostatectomy specimen sampling or use of immunohistochemistry

DOI: 10.3389/pore.2023.1611157
Kristóf Levente Korpás, Lívia Beke, Dániel Varga, László Bidiga, Gábor Méhes and Sarolta Molnár

761 Low-grade oncocytic tumour (LOT) of the kidney is characterised by GATA3 positivity, FOXI1 negativity and mTOR pathway mutations

DOI: 10.3389/pore.2023.1610852
Tongbing Chen, Yan Peng, Ting Lei, Chao Wu, Hui Wang and Yongqiang Shi

768 Angiomyolipoma of the kidney—Clinicopathological analysis of 52 cases
DOI: 10.3389/pore.2022.1610831
Zsuzsanna Fejes, Fanni Sánta, Alex Jenei, István Előd Király, Linda Varga and Levente Kuthi

Gynecological Cancer

779 Comparative analysis of EZH2, p16 and p53 expression in uterine carcinosarcomas
DOI: 10.3389/pore.2023.1611547
Evelin Makk, Noémi Bohonyi, Angéla Oszter, Klára Éles, Tamás Tornóczky, Arnold Tóth, Endre Kálmán and Krisztina Kovács

790 Modified clock mapping biopsy sec. Della Corte-Bifulco in the preoperative assessment of excisional surgery for vulvar Paget's disease
DOI: 10.3389/pore.2024.1611803
Luigi Della Corte, Mario Ascione and Giuseppe Bifulco

794 Long non-coding RNA MYU promotes ovarian cancer cell proliferation by sponging miR-6827-5p and upregulating HMGA1
DOI: 10.3389/pore.2023.1610870
Shaoyu Wang, Qiaomei Zheng, Jinhua Wang, Shaozhan Chen and Lihong Chen

Head and Neck Cancer

805 *RET* rearrangements are relevant to histopathologic subtypes and clinicopathological features in Thai papillary thyroid carcinoma patients
DOI: 10.3389/pore.2023.1611138
Thitima Khonrak, Sasithorn Watcharadetwittaya, Yaovalux Chamgramol, Piyapharom Intarawichian and Raksawan Deenonpoe

818 Patient delay and its clinical significance among head and neck cancer patients in Hungary
DOI: 10.3389/pore.2023.1611206
Kornél Dános, Angéla Horváth, Judit Halász, László Tamás and Gábor Polony

828 Positive correlation between persistence of medical nutrition therapy and overall survival in patients with head and neck cancer
DOI: 10.3389/pore.2024.1611664
Andrea Molnár, Erzsébet Pálfi, Barbara Belák, Célia Blasszauer, Dániel Reibl and József Lövey

838 Screening of core genes and prediction of ceRNA regulation mechanism of circRNAs in nasopharyngeal carcinoma by bioinformatics analysis
DOI: 10.3389/pore.2023.1610960
HongMin Chen, XiaoXiao Shi, Li Ren, YuMing Wan, HongYu Zhuo, Li Zeng, WangMu SangDan and Feng Wang

850 The characteristics of head and neck squamous cell cancer in young adults: A retrospective single-center study
DOI: 10.3389/pore.2023.1611123
Mónika Révész, Ferenc Oberna, András Slezák, Örs Ferenczi, István Kenessey and Zoltán Takácsi-Nagy

Hematologic Malignancies

858 Effective venetoclax-based treatment in relapsed/refractory multiple myeloma patients with translocation t(6;14)
DOI: 10.3389/pore.2023.1611375
Andrea Ceglédi, Zoltán Csukly, Mónika Fekete, András Kozma, Zsuzsanna Szemlaky, Hajnalka Andrikovics and Gábor Mikala

865 Obesity as a risk factor for multiple myeloma: insight on the role of adipokines
DOI: 10.3389/pore.2023.1611338
Wenting Tie, Tao Ma, Zhigang Yi, Jia Liu, Yanhong Li, Jun Bai, Lijuan Li and Liansheng Zhang

875 Spectrum of BCR-ABL mutations in Azerbaijanian imatinib-resistant patients with chronic myeloid leukemia
DOI: 10.3389/pore.2023.1611518
Aypara Hasanova, Chingiz Asadov, Nigar Karimova, Aytan Shirinova, Gunay Aliyeva and Zohra Alimirzoyeva

886 High prevalence of Wilms tumor 1 expression in multiple myeloma and plasmacytoma: A cohort of 142 Asian patients' samples
DOI: 10.3389/pore.2023.1610844
Ployploen Phikulsod, Sanya Sukpanichnant, Chutima Kunacheewa, Thaweesak Chieochansin, Mutita Junking and Pa-Thai Yenchitsomanus

894 The efficacy and safety of second salvage autologous transplantation in myeloma patients
DOI: 10.3389/pore.2024.1611851
Reka Rahel Bicsko, Renata Nyilas, Robert Szasz, Laszlo Varoczy, Attila Kiss, Miklos Udvardy, Arpad Illes and Lajos Gergely

901 Flow cytometry in the differential diagnosis of myelodysplastic neoplasm with low blasts and cytopenia of other causes
DOI: 10.3389/pore.2024.1611811
Márk Plander, Mária Kányási, Tamás Szendrei, Judit Skrapits and Botond Timár

909 A prognostic 15-gene model based on differentially expressed genes among metabolic subtypes in diffuse large B-cell lymphoma
DOI: 10.3389/pore.2023.1610819
Jun Hou, Peng Guo, Yujiao Lu, Xiaokang Jin, Ke Liang, Na Zhao, Shunxu Xue, Chengmin Zhou, Guoqiang Wang, Xin Zhu, Huangming Hong, Yungchang Chen, Huafei Lu, Wenxian Wang, Chunwei Xu, Yusheng Han, Shangli Cai and Yang Liu

922 The roles of phosphorylation of signaling proteins in the prognosis of acute myeloid leukemia
DOI: 10.3389/pore.2024.1611747
Adrienn Márton, Katalin Beáta Veres, Ferenc Erdődi, Miklós Udvardy, Árpád Illés and László Rejtő

941 Investigating the effect of immunomagnetic separation on the immunophenotype and viability of plasma cells in plasma cell disorders
DOI: 10.3389/pore.2024.1611882
Ágnes Czeti, Soma Sashalmi, Ferenc Takács, Gábor Szalóki, Csilla Kriston, Gergely Varga, Péter Farkas, Aryan Hamed, Ágnes Márk and Gábor Barna

951 Soluble B-cell maturation antigen as a monitoring marker for multiple myeloma
DOI: 10.3389/pore.2023.1611171
Ádám Wiedemann, Virág Réka Szita, Róbert Horváth, Attila Szederjesi, Attila Sebő, András Dávid Tóth, Tamás Masszi and Gergely Varga

959 Diagnostic challenges in patients with Castleman disease, a single center experience from Hungary
DOI: 10.3389/pore.2024.1611785
Boglárka Brúgós, Zsófia Simon, Gábor Méhes, Árpád Illés and György Pfliegler

969 Long term follow-up of refractory/relapsed hairy cell leukaemia patients treated with low-dose vemurafenib between 2013 and 2022 at the Department of Internal Medicine and Oncology, Semmelweis University
DOI: 10.3389/pore.2023.1611378
Kata Ferenczi, Zsófia Flóra Nagy, Ildikó Istenes, Hanna Eid, Csaba Bödör, Botond Timár and Judit Demeter

977 Comorbidities and outcomes of patients with chronic myeloid leukemia treated with tyrosine kinase inhibitors: a real-world, nationwide, retrospective study from Hungary
DOI: 10.3389/pore.2024.1611497
Peter Batar, Hussain Alizadeh, Gyorgy Rokszin, Zsolt Abonyi-Toth and Judit Demeter

In Vitro and In Vivo Tumor Models

988 3D bioprinting and the revolution in experimental cancer model systems—A review of developing new models and experiences with *in vitro* 3D bioprinted breast cancer tissue-mimetic structures
DOI: 10.3389/pore.2023.1610996
Dániel Sztankovics, Dorottya Moldvai, Gábor Petővári, Rebeka Gelencsér, Ildikó Krencz, Regina Raffay, Titanilla Dankó and Anna Sebestyén

1010 Spatial distribution of tumor-associated macrophages in an orthotopic prostate cancer mouse model
DOI: 10.3389/pore.2024.1611586
Korie A. Grayson, Joshua D. Greenlee, Lauren E. Himmel, Lauren A. Hapach, Cynthia A. Reinhart-King and Michael R. King

1023 Cancer apelin receptor suppresses vascular mimicry in malignant melanoma
DOI: 10.3389/pore.2023.1610867
Koichi Inukai, Kazuyoshi Kise, Yumiko Hayashi, Weizhen Jia, Fumitaka Muramatsu, Naoki Okamoto, Hirotaka Konishi, Keigo Akuta, Hiroyasu Kidoya and Nobuyuki Takakura

1034 CVM-1118 (foslinanib), a 2-phenyl-4-quinolone derivative, promotes apoptosis and inhibits vasculogenic mimicry via targeting TRAP1
DOI: 10.3389/pore.2023.1611038
Lifen Shen, Yen-Ling Chen, Chu-Chun Huang, Yu-Chiau Shyu, Richard E. B. Seftor, Elisabeth A. Seftor, Mary J. C. Hendrix, Du-Shieng Chien and Yi-Wen Chu

Molecular Pathology and Biomarkers

1051 Clinical significance of integrin αV and β superfamily members and focal adhesion kinase activity in oral squamous cell carcinoma: a retrospective observational study
DOI: 10.3389/pore.2024.1611571
Shigeru Sakurai, Yasutaka Ishida, Tomoaki Shintani, Sachiko Yamasaki, Kensaku Matsui, Tomoaki Hamana, Tadayoshi Nobumoto, Souichi Yanamoto and Yasutaka Hayashido

1062 The roles of NOP56 in cancer and SCA36
DOI: 10.3389/pore.2023.1610884
Shimin Zhao, Dongdong Zhang, Sicheng Liu and Jun Huang

1071 Analysis of HIF-1α expression and genetic polymorphisms in human clear cell renal cell carcinoma
DOI: 10.3389/pore.2023.1611444
Daniela Vargova, Zuzana Kolková, Jan Dargaj, Lukas Bris, Jan Luptak, Zuzana Dankova, Sona Franova, Jan Svihra, Pavol Slávik and Martina Sutovska

1081 Predictive role of neostromal CD10 expression in breast cancer patients treated with neoadjuvant chemotherapy
DOI: 10.3389/pore.2022.1610598
Orsolya Olah, Edit Majlat, Renata Koszo, Zoltan Vereb and Andras Voros

1089 Tumor subtypes and signature model construction based on chromatin regulators for better prediction of prognosis in uveal melanoma
DOI: 10.3389/pore.2023.1610980
Yue Li, Chao Xiong, Li Li Wu, Bo Yuan Zhang, Sha Wu, Yu Fen Chen, Qi Hua Xu and Hong Fei Liao

1106 Microsatellite instability and mismatch repair protein deficiency: equal predictive markers?
DOI: 10.3389/pore.2024.1611719
Maja L. Nádorvári, Gábor Lotz, Janina Kulka, András Kiss and József Tímár

1118 G protein-coupled estrogen receptor 1 and collagen XVII endodomain expression in human cutaneous melanomas: can they serve as prognostic factors?
DOI: 10.3389/pore.2024.1611809
Uğur Çakır, Petra Balogh, Anikó Ferenczik, Valentin Brodszky, Tibor Krenács, Sarolta Kárpáti, Miklós Sárdy, Péter Holló and Melinda Fábián

1130 Microenvironment, systemic inflammatory response and tumor markers considering consensus molecular subtypes of colorectal cancer
DOI: 10.3389/pore.2024.1611574
Anna Jakab, Árpád V. Patai, Mónika Darvas, Karolina Tormássi-Bély and Tamás Micsik

1150 The prognostic value of stem cell markers in triple-negative breast cancer
DOI: 10.3389/pore.2023.1611365
Szintia Almási, Ágnes Nagy, Tibor Krenács, Tamás Lantos, Tamás Zombori and Gábor Cserni

1163 Prognostic value of long non-coding RNA *MALAT1* in hepatocellular carcinoma: A study based on multi-omics analysis and RT-PCR validation
DOI: 10.3389/pore.2022.1610808
Xiaoli Liao, Junming Chen, DongCheng Luo, Baohua Luo, Wenfeng Huang and Weimin Xie

1189 Molecular classification of endometrial cancer: preliminary experience from a single Portuguese academic center
DOI: 10.3389/pore.2024.1611835
João Casanova, Ana G. da Costa, Ana Pestana Lopes, Ana Catarino, Mónica Nave, Ana Carla Sousa and Jorge Lima

1197 Immunohistochemistry-based molecular subtyping of triple-negative breast cancer and its prognostic significance

DOI: 10.3389/pore.2023.1611162
Marisa Leeha, Kanyanatt Kanokwiroon, Suphawat Laohawiriyakamol and Paramee Thongsuksai

1207 Correlation analysis of circulating tumor cells and Claudin-4 in breast cancer

DOI: 10.3389/pore.2023.1611224
Jie Chai, Xiangli Liu, Xinju Hu and Chunfang Wang

Neuro-Oncology

1216 Extracellular vesicles as modulators of glioblastoma progression and tumor microenvironment

DOI: 10.3389/pore.2024.1611549
Jie Dai, Yong Jiang, Haoyue Hu, Shuang Zhang and Yue Chen

1230 Concordance analysis of cerebrospinal fluid with the tumor tissue for integrated diagnosis in gliomas based on next-generation sequencing

DOI: 10.3389/pore.2023.1611391
Qiang Wang, Qiujin Liang, Wuting Wei, Wenhao Niu, Chong Liang, Xiaoliang Wang, Xiaoxuan Wang and Hao Pan

Thoracic Cancer

1241 Advances in combined neuroendocrine carcinoma of lung cancer

DOI: 10.3389/pore.2024.1611693
Zesen Han, Fujun Yang, Fang Wang, Huayu Zheng, Xiujian Chen, Hongyu Meng and Fenglei Li

1247 Applied models and molecular characteristics of small cell lung cancer

DOI: 10.3389/pore.2024.1611743
Gabriella Mihalekné Fűr, Kolos Nemes, Éva Magó, Alexandra Á. Benő, Petronella Topolcsányi, Judit Moldvay and Lőrinc S. Pongor

1260 Targeted therapeutic options in early and metastatic NSCLC-overview

DOI: 10.3389/pore.2024.1611715
Gabriella Gálffy, Éva Morócz, Réka Korompay, Réka Hécz, Réka Bujdosó, Rita Puskás, Tímea Lovas, Eszter Gáspár, Kamel Yahya, Péter Király and Zoltán Lohinai

1281 The role of chemoradiotherapy and immunotherapy in stage III NSCLC

DOI: 10.3389/pore.2024.1611716
Zsuzsanna Orosz and Árpád Kovács

1287 Prognostic value of lung immune prognostic index in non-small cell lung cancer patients receiving immune checkpoint inhibitors: a meta-analysis
DOI: 10.3389/pore.2024.1611773
Yi Wang, Yu Lei, Delai Zheng, Yanhui Yang, Lei Luo, Ji Li and Xiaoyang Xie

1300 Decreasing incidence and mortality of lung cancer in Hungary between 2011 and 2021 revealed by robust estimates reconciling multiple data sources
DOI: 10.3389/pore.2024.1611754
Gabriella Gálffy, Géza Tamás Szabó, Lilla Tamási, Veronika Müller, Judit Moldvay, Veronika Sárosi, Anna Kerpel-Fronius, Tamás Kardos, Edit Csada, Zsolt Pápai-Székely, Zoltán Szász, Zsolt Király, Gábor Hódi, Zsuzsanna Kovács, Éva Balogh, Krisztina Andrea Kovács, Miklós Darida, Viktória Buga, György Rokszin, Zsolt Abonyi-Tóth, Zoltán Kiss, Zoltán Vokó and Krisztina Bogos

1311 Claudin expression in pulmonary adenoid cystic carcinoma and mucoepidermoid carcinoma
DOI: 10.3389/pore.2023.1611328
Marton Gyulai, Tunde Harko, Katalin Fabian, Luca Karsko, Laszlo Agocs, Balazs Szigeti, Janos Fillinger, Zoltan Szallasi, Orsolya Pipek and Judit Moldvay

1321 KRASG12C mutant lung adenocarcinoma: unique biology, novel therapies and new challenges
DOI: 10.3389/pore.2023.1611580
Judit Moldvay and József Tímár

1330 Identification and validation of molecular subtype and prognostic signature for lung adenocarcinoma based on neutrophil extracellular traps
DOI: 10.3389/pore.2023.1610899
Yanhua Zuo, Guangyi Leng and Ping Leng

1344 The rapidly changing field of predictive biomarkers of non-small cell lung cancer
DOI: 10.3389/pore.2024.1611733
László József Tóth, Attila Mokánszki and Gábor Méhes

1371 Stereotactic body radiotherapy in lung cancer: a contemporary review
DOI: 10.3389/pore.2024.1611709
Emese Csiki, Mihály Simon, Judit Papp, Márton Barabás, Johanna Mikáczó, Kristóf Gál, David Sipos and Árpád Kovács

1384 Quantitative analysis of endobronchial elastography combined with serum tumour markers of lung cancer in the diagnosis of benign and malignant mediastinal and hilar lymph nodes
DOI: 10.3389/pore.2023.1611377
Zhen Wang, Peng Li, Jiayu Bai, Yujia Liu and Guangyu Jiao

1397 *RICTOR* amplification is associated with Rictor membrane staining and does not correlate with PD-L1 expression in lung squamous cell carcinoma
DOI: 10.3389/pore.2024.1611593
Ildikó Krencz, Dániel Sztankovics, Anna Sebestyén, Judit Pápay, Titanilla Dankó, Dorottya Moldvai, Elmar Lutz and Andras Khoor

1407 LINAC-based SBRT in treating early-stage NSCLC patients—single institution experience and survival data analysis
DOI: 10.3389/pore.2024.1611589
Árpád Kovács, Krisztina Trási, Márton Barabás, Kristóf Gál, Emese Csiki, Dávid Sipos, Judit Papp and Mihály Simon

1413 Advancing neoadjuvant therapies in resectable non-small cell lung cancer: implications for novel treatment strategies and biomarker discovery
DOI: 10.3389/pore.2024.1611817
Hyein Jeon, Rajvi Gor, Angelica D'Aiello, Brendon Stiles, Peter B. Illei and Balazs Halmos

Others/Miscellaneous

1427 Active cancer as the main predictor of mortality for COVID-19 in oncology patients in a specialized center
DOI: 10.3389/pore.2023.1611236
Freddy Villanueva-Cotrina, Juan Velarde, Ricardo Rodriguez, Alejandra Bonilla, Marco Laura, Tania Saavedra, Diana Portillo-Alvarez, Yovel Bustamante, Cesar Fernandez and Marco Galvez-Nino

1439 Influence of the microbiota on the effectiveness and toxicity of oncological therapies, with a focus on chemotherapy
DOI: 10.3389/pore.2023.1611300
Massimiliano Cazzaniga, Giordano Bruno Zonzini, Francesco Di Pierro, Chiara Maria Palazzi, Marco Cardinali and Alexander Bertuccioli

1448 Geroscience and pathology: a new frontier in understanding age-related diseases
DOI: 10.3389/pore.2024.1611623
Monika Fekete, David Major, Agnes Feher, Vince Fazekas-Pongor and Andrea Lehoczki

1462 Percutaneous tracheostomy: Comparison of three different methods with respect to tracheal cartilage injury in cadavers—Randomized controlled study
DOI: 10.3389/pore.2023.1610934
Fruzsina Bódis, Gábor Orosz, József T. Tóth, Marcell Szabó, László Gergely Élő, János Gál and Gábor Élő

1470 Impact of limb ischemic preconditioning on the incidence of vein thrombosis in patients with peripherally inserted central catheter

DOI: 10.3389/pore.2024.1611596

Han Zhao, Changhua Kou, Hao Zhao, Qing Liu, Maosheng He, Cong Wang, Saisai Zhu, Li Ma and Yun Wang

1479 Delayed spontaneous remission of acquired factor V inhibitor refractory to immunosuppressive therapy with pregnancy-associated improvement

DOI: 10.3389/pore.2023.1611250

Andrea Ceglédi, János Dolgos, Mónika Fekete, László Gopcsa, Andrea Várkonyi, Beáta Vilimi, Gábor Mikala and Imre Bodó

Pathology & Oncology Research | frontiers

TYPE Original Research
PUBLISHED 16 April 2024
DOI 10.3389/pore.2024.1611735

Check for updates

OPEN ACCESS

EDITED BY
Anna Sebestyén,
Semmelweis University, Hungary

*CORRESPONDENCE
Dániel Deme,
danieldeme_md@ymail.com

RECEIVED 19 February 2024
ACCEPTED 21 March 2024
PUBLISHED 16 April 2024

CITATION
Deme D, Tamaskovics BF, Jammoul N, Kovács S, Kayode EO, Grice JW and Telekes A (2024), Association between pathological characteristics and recurrence score by OncotypeDX in resected T1-3 and N0-1 breast cancer: a real-life experience of a North Hungarian regional center.
Pathol. Oncol. Res. 30:1611735.
doi: 10.3389/pore.2024.1611735

COPYRIGHT
© 2024 Deme, Tamaskovics, Jammoul, Kovács, Kayode, Grice and Telekes. This is an open-access article distributed under the terms of the Creative Commons Attribution License (CC BY). The use, distribution or reproduction in other forums is permitted, provided the original author(s) and the copyright owner(s) are credited and that the original publication in this journal is cited, in accordance with accepted academic practice. No use, distribution or reproduction is permitted which does not comply with these terms.

Association between pathological characteristics and recurrence score by OncotypeDX in resected T1-3 and N0-1 breast cancer: a real-life experience of a North Hungarian regional center

Dániel Deme[1]*, Bálint Ferenc Tamaskovics[1,2,3], Nizar Jammoul[4], Sándor Kovács[5], Emmanuel Oladunjoye Kayode[1], James W. Grice[6] and András Telekes[1]

[1]Department of Clinical Oncology, Center of Radiotherapy and Oncology, Nógrád Vármegyei Szent Lázár Hospital, Salgótarján, Hungary, [2]Department of Radiation Oncology, Medical Faculty and University Hospital Düsseldorf, Henrich Heine University, Düsseldorf, Germany, [3]Center of Integrated Oncology Aachen Bonn Cologne Düsseldorf (CIO ABCD), Aachen, Germany, [4]Department of Pathology, Center of Radiotherapy and Oncology, Nógrád Vármegyei Szent Lázár Hospital, Salgótarján, Hungary, [5]Department of Economical and Financial Mathematics, University of Debrecen, Debrecen, Hungary, [6]Department of Psychology, Oklahoma State University, Stillwater, OK, United States

Introduction: The 21-gene analysis (OncotypeDX) is validated test for pT1-3, pN0-1 with hormone receptor (HR) positive and normal expression of human epidermal growth factor receptor-2 (HER2) breast cancer (BC) to determine the aggressiveness of the disease based on the calculation of Recurrence Score (RS).

Methods: In this retrospective study the authors correlated pathological characteristics and Recurrence Score (RS) by traditional statistical methods and Observed Oriented Modeling (OOM) in a realistic cohort of BC patients.

Results: OncotypeDX tests were performed in 94 tumour specimens of 90 BC patients. >83% of node-negative (pN0) and >72% of node-positive (pN1) cases could avoid chemotherapy. For pN0 cases, non-parametric correlation and tests demonstrated significant association in eight types of characteristics [progesterone receptor (PR) expression, Ki-67 value, Ki-67 group, PR group, grade, estrogen receptor (ER) expression, Nottingham Prognostic Index (NPI) and Clinical Risk]. For pN1 cases, parametric correlation and tests showed significant association in six characteristic types (number of positive nodes, ER and PR expression, PR group, Ki-67 group and NPI). Based on OOM for pN0 cases, significant associations were established in three characteristics (Ki-67 group, grade and NPI group). For pN1 cases OOM found significant associations in seven characteristics (PR group, PNI, LVI, Ki-67 group, grade, NPI group and number of positive nodes).

Conclusion: First in oncology, OOM was applied, which found some other significant characteristics associated with RS than traditional statistical methods. There were few patients, where no clinical associations were found between characteristics and RS contrary to statistically significant differences. Therefore, the results of these statistical analyses can be neither applied for individual cases nor able to provide the bases for screening patients, i.e., whether they need for OncotypeDX testing or not. OncotypeDX still provides a personalised approach in BC.

KEYWORDS

breast cancer, pathological characteristics, OncotypeDX, recurrence score, observation oriented modeling

Introduction

In 2020 breast cancer (BC) was the third most common cancer in Hungary, accounting for 11.3% of all new cancer cases according to the GLOBOCAN database [1]. Based on the reported cases in the Hungarian National Cancer Registry 7,335 new BCs were registered, including 144 cases in Nógrád County of North Hungary [2]. Hungary is ranked eighteenth for incidence and ninth for mortality of BC among the European countries [3]. The age-standardised rate of BC mortality per 100,000 women is above the European average [4]. Overall survival has improved for BC significantly in the period between 2011–2015 compared to the period of 2001–2005 [5], which is attributed to the national BC screening program started in 2001 (2002 in Nógrád County), and consequently to the treatment initiated for earlier stage BC.

About 80% of all BC cases are estrogen positive. Endocrine therapy has already significantly improved the outcome of these patients [6]. In 1997, adjuvant chemotherapy became the new standard for estrogen positive BC based on the results of the National Surgical Adjuvant Breast and Bowel Project (NSABP) B20 trial irrespective of age, tumour stage, and nodal burden [7].

To identify patients with a high risk of recurrence, who benefit from adjuvant chemotherapy, and to avoid overtreating patients with a low risk of recurrence, several prospective and retrospective studies were conducted in hormone receptor (HR) positive, and normal expression of human epidermal growth factor receptor-2 (HER2) BC. Milestones emerged with the demonstration of the results of the prospective Trial Assigning Individualized Options for Treatment (TAILORx) in 2018 [8] and the Clinical Trial RX for Positive Node, Endocrine Responsive Breast Cancer (RxPONDER) in 2021 [9] using 21-gene analysis (OncotypeDX, Exact Sciences Corporation, CA, United States). OncotypeDX generates a recurrence score (RS), which predicts the benefit of chemotherapy, i.e., the reduction in the 10-year risk of recurrence of BC. Based on these data, OncotypeDX is recommended for HR positive and HER2 normal BC [pT1b, pN0 grade 2-3 or with lymphovascular invasion (LVI); pT1c-3, pN0; pT1-3, and pN1] according to the National Comprehensive Cancer Network (NCCN) BC Guideline Version 1.2024 [10]. OncotypeDX supports clinicians to optimise the treatment of these patients: either omit or administer adjuvant chemotherapy [10].

For the first time in Hungary, the authors summarise their experience with OncotypeDX in 90 BC cases. They demonstrate the statistical associations between the RS and the pathological characteristics with both the traditional procedures and a method called observation oriented modeling (OOM).

Materials and methods

Patients

Data was collected from patients at the institution of the authors in North Hungary (Nógrád Vármegyei Szent Lázár Hospital, Salgótarján) retrospectively. OncotypeDX analysis was offered to patients operated for HR positive and HER2 normal T1-3 N0-1 BC based on the pathology report and discussed with the patient per the NCCN BC Guideline Version 1.2018, 3.2018, 3.2019, 5.2020, 8.2021, 4.2022, and 4.2023 [11]. Patients with available OncotypeDX results were included in this analysis. Adjuvant chemoterapy was omitted in node-negative (pN0) disease, if RS < 26 in patients >50 years, and if RS < 16 in patients ≤50 years. Postmenopausal patients with node-positive (pN1) disease and RS < 26 were also considered to gain no benefit from adding chemotherapy to endocrine treatment. However, premenopausal patients with nodal micrometastasis (pN1mi) or pN1 disease and RS < 26 had two options: either chemotherapy followed by endocrine therapy, or ovarian suppression and endocrine treatment.

Methods

Surgical specimens (formalin fixed paraffin embedded representative blocks) obtained by breast-conserving surgery or mastectomy of BC were routinely evaluated. Based on the NCCN BC Guideline [11], HR-positive and HER2 normal BC

TABLE 1 Characteristics of patients.

(a) pN0																		
Patient no.	Age at surgery(yrs)	TBSH (days)	TBHO (days)	Breast surgery	Axillary surgery	Histology	TNM	Stage	Tumour (cm)	Grade	ER (%)	PR (%)	Ki67 (%)	PNI	LVI	Clinical risk	NPI	NPI risk group	RS
1	72.2	0	25	Breast conservation	SLNB	IDC (NST)	pT1c,pN0	IA	1.5	1	90	90	5	Yes	No	Low	2.30	Excellent	14
2	62.2	20	13	Breast conservation	SLNB	IDC (NST)	pT1c,pN0	IA	1.1	1	90	90	2	No	No	Low	2.22	Excellent	9
3	63.9	20	14	Mastectomy	SLNB	IDC (NST)	pT1c,pN0	IA	1.5	2	90	2	10	Yes	No	Low	3.30	Good	27
7	64.4	2	17	Breast conservation	SLNB	IDC (NST)	pT1c,pN0	IA	1.7	2	90	90	20	Yes	No	Low	3.34	Good	15
9	54.4	12	30	Breast conservation	SLNB	IDC (NST)	pT1c,pN0	IA	1.2	1	90	90	1	No	No	Low	2.24	Excellent	12
10	76.1	8	30	Mastectomy	SLNB	Lobular cc	pT1c,pN0	IA	1.3	2	90	90	15	No	No	Low	3.26	Good	9
11	51	18	29	Breast conservation	SLNB	IDC (NST)	pT1c,pN0	IA	1.6	1	90	40	1	No	No	Low	2.32	Excellent	17
12	58.7	12	28	Breast conservation	SLNB	IDC (NST)	pT2c,pN0	IIA	3	2	90	70	15	Yes	No	Low	3.60	Moderate I	21
13	51.9	21	27	Breast conservation	SLNB	IDC (NST)	pT2c,pN0	IIA	2.3	2	100	100	5	No	Yes	High	3.46	Moderate I	11
18*	75.9	15	23	Bilateral mastectomy	Left SLNB	IDC (NST)	pT2c,pN0	IIA	3	2	100	90	10	No	No	High	3.60	Moderate I	12
19	56	16	28	Breast conservation	SLNB	IDC (NST)	pT1c,pN0	IA	1.3	1	100	80	1	No	No	Low	2.26	Excellent	9
20	50.2	15	22	Breast conservation	SLNB	IDC (NST)	pT1c,pN0	IA	1.2	1	80	50	1	No	No	Low	2.24	Excellent	18
21	65.7	8	26	Breast conservation	SLNB	IDC (NST)	pT2c,pN0	IIA	2.8	1	90	50	2	Yes	No	Low	2.56	Good	9
23	56.5	15	21	Breast conservation	Partial ABD	IDC (NST)	pT1c,pN0	IA	1.8	2	90	0	15	No	No	Low	3.36	Good	32
25	56.9	14	19	Mastectomy	SLNB	IDC (NST)	pT1c,pN0	IA	1.9	1	100	100	5	No	No	Low	2.38	Excellent	7
26	68.9	20	24	Breast conservation	SLNB	IDC (NST)	pT1c,pN0	IA	1.8	1	100	90	3	Yes	No	Low	2.36	Excellent	9
27	65.4	24	26	Breast conservation	SLNB	Lobular cc	pT1c,pN0	IA	1.9	1	90	70	2	No	No	Low	2.38	Excellent	10
28	68.4	26	22	Mastectomy	SLNB	IDC (NST)	pT1c,pN0	IA	1.8	1	100	100	5	No	No	Low	2.36	Excellent	8
29	63.7	16	20	Breast conservation	SLNB	IDC (NST)	pT1c,pN0	IA	1.2	2	100	70	15	No	No	Low	3.24	Good	36
30	70.5	15	22	Mastectomy	SLNB	IDC(NST)	pT1c,pN0	IA	1.3	3	90	85	35	No	No	High	4.26	Moderate I	21
33	64.6	18	24	Breast conservation	SLNB	IDC (NST)	pT1c,pN0	IA	1.7	2	100	90	15	No	No	Low	3.34	Good	15
35	75.2	14	25	Mastectomy	SLNB	IDC (NST)	pT1c,pN0	IA	1.9	1	80	0	5	Yes	No	Low	2.38	Excellent	28

(Continued on following page)

10.3389/pore.2024.1611735

TABLE 1 (*Continued*) Characteristics of patients.

(a) pN0																			
Patient no.	Age at surgery(yrs)	TBSH (days)	TBHO (days)	Breast surgery	Axillary surgery	Histology	TNM	Stage	Tumour (cm)	Grade	ER (%)	PR (%)	Ki67 (%)	PNI	LVI	Clinical risk	NPI	NPI risk group	RS
36	69.9	9	28	Mastectomy	SLNB	Lobular cc	pT2c,pN0	IIA	2.7	1	90	30	3	No	No	Low	2.54	Good	15
37	74.1	19	51	Mastectomy	SLNB	Lobular cc	pT2c,pN0	IIA	2.3	2	100	20	1	No	No	High	3.46	Moderate I	14
38	63.9	8	25	Mastectomy	SLNB	IDC (NST)	pT1c,pN0	IA	1.9	1	90	30	5	Yes	No	Low	2.38	Excellent	21
40	59.6	16	26	Breast conservation	SLNB	IDC (NST)	pT1c,pN0	IA	1.3	1	100	0	3	No	No	Low	2,26	Excellent	26
41	61	10	31	Breast conservation	SLNB	IDC (NST)	pT1c,pN0	IA	1.1	1	100	5	1	No	No	Low	2.22	Excellent	16
42	59.4	20	21	Breast conservation	SLNB	Lobular cc	pT2c,pN0	IIA	2.2	1	90	90	3	No	No	Low	2.44	Excellent	15
43	64.9	21	30	Breast conservation	SLNB	IDC (NST)	pT1c,pN0	IA	1.6	1	80	70	1	No	No	Low	2.32	Excellent	14
44	57.8	13	33	Breast conservation	SLNB	IDC (NST)	pT2c,pN0	IIA	2.1	1	90	40	3	Yes	No	Low	2.42	Excellent	16
47	60.8	10	28	Breast conservation	SLNB	Lobular cc	pT2c,pN0	IIA	2.3	1	100	100	15	No	No	Low	2.46	Good	13
48	68.4	16	28	Breast conservation	SLNB	IDC (NST)	pT1c,pN0	IA	1.3	1	100	40	5	No	No	Low	2.26	Excellent	15
50	63.3	14	23	Breast conservation	SLNB	Lobular cc	pT2c,pN0	IIA	2.2	1	100	70	1	No	No	Low	2.44	Excellent	4
51	52.9	15	28	Breast conservation	SLNB	IDC (NST)	pT2c,pN0	IIA	2.3	1	100	50	5	No	No	Low	2.46	Good	12
55	60.8	15	42	Breast conservation	SLNB	IDC (NST)	pT1c,pN0	IA	1.5	2	90	90	15	No	No	Low	3.30	Good	23
56	63	17	47	Mastectomy	SLNB	IDC (NST)	pT1c,pN0	IA	1.8	1	90	60	15	Yes	No	Low	2.36	Excellent	24
57	80.1	26	44	Mastectomy	SLNB	IDC (NST)	pT2c,pN0	IIA	3.5	2	90	90	10	No	No	High	3.70	Moderate I	24
60	77.9	24	24	Breast conservation	SLNB	IDC (NST)	pT1c,pN0	IA	1.6	2	100	100	15	No	No	Low	3.32	Good	0
61	61.5	23	33	Mastectomy	SLNB	IDC (NST)	pT2c,pN0	IIA	3.7	2	80	15	40	No	No	High	3.74	Moderate I	19
62	68.2	22	34	Breast conservation	SLNB	IDC (NST)	pT1c,pN0	IA	1.3	1	100	70	15	No	No	Low	2.26	Excellent	13
63	68.5	14	45	Mastectomy	ABD	IDC (NST)	pT2c,pN0	IIA	3.2	2	100	65	25	No	No	High	3.64	Moderate I	29
66#	64.4	35	29	Breast conservation	SLNB	IDC (NST)	pT1c,pN0	IA	1.2	1	100	80	30	No	No	Low	2.24	Excellent	22
66#	64.4	35	29	Breast conservation	SLNB	IDC (NST)	pT1c,pN0	IA	1.3	1	90	100	15	No	No	Low	2.26	Excellent	17
67	55.4	15	28	Breast conservation	SLNB	IDC (NST)	pT1c,pN0	IA	1.3	1	100	0	1	No	No	Low	2.26	Excellent	15

(Continued on following page)

10.3389/pore.2024.1611735

TABLE 1 (*Continued*) Characteristics of patients.

(a) pN0

Patient no.	Age at surgery(yrs)	TBSH (days)	TBHO (days)	Breast surgery	Axillary surgery	Histology	TNM	Stage	Tumour (cm)	Grade	ER (%)	PR (%)	Ki67 (%)	PNI	LVI	Clinical risk	NPI	NPI risk group	RS
72	68.6	10	20	Mastectomy	SLNB	IDC (NST)	pT2c,pN0	IIA	2.3	1	100	60	10	No	No	Low	2.46	Good	8
73	46.2	10	24	Breast conservation	SLNB	IDC (NST)	pT1c,pN0	IA	1.1	1	80	80	1	No	No	Low	2.22	Excellent	12
74	68	9	35	Breast conservation	SLNB	IDC (NST)	pT1c,pN0	IA	1.8	1	100	90	1	No	No	Low	2.36	Excellent	8
75	61.6	14	24	Breast conservation	SLNB	IDC (NST)	pT1c,pN0	IA	1.9	2	100	90	5	No	No	Low	3.38	Good	12
76	47.9	15	30	Breast conservation	SLNB	IDC (NST)	pT1c,pN0	IA	1.9	1	100	100	5	No	No	Low	2.38	Excellent	11
79	61.9	20	37	Breast conservation	SLNB	IDC (NST)	pT2c,pN0	IIA	2.6	3	100	6	15	Yes	No	High	4.52	Moderate II	26
81	84.3	23	20	Mastectomy	SLNB	IDC (NST)	pT1c,pN0	IA	1.8	3	100	20	30	No	No	High	4.38	Moderate I	32
82	47.1	28	20	Breast conservation	ABD	IDC (NST)	pT2,pNx (no lymphoid tissue found)	IIA	2.5	1	90	70	40	No	No	Low	2.50	Good	33
83	59.8	9	26	Breast conservation	SLNB	IDC (NST)	pT1c,pN0	IA	1.4	2	100	40	5	No	No	Low	3.28	Good	23
84	65.5	14	24	Breast conservation	ABD	IDC (NST)	pT1c,pN0	IA	1.5	1	100	20	1	No	No	Low	2.30	Excellent	12
85	65.4	14	27	Breast conservation	SLNB	IDC (NST)	pT1c,pN0	IA	1.5	1	100	90	3	No	No	Low	2.30	Excellent	1
89	53.9	16	56	Breast conservation	SLNB	IDC (NST)	pT1c,pN0	IA	1.4	2	90	90	10	No	No	Low	3.28	Good	16

(b) pN1

Patient No.	Age at surgery (yrs)	TBSH (days)	TBHO(days)	Breast Surgery	Axillary surgery	Histology	TNM	Stage	Tumour (cm)	Node(s)	Grade	ER (%)	PR (%)	Ki67(%)	PNI	LVI	NPI	NPI Risk group	RS
4	67	3	14	Mastectomy	ABD	Lobular cc	pT1c,pN1mi	IB	1.1	2	2	90	90	3	Yes	Yes	4.22	Moderate I	3
5#	46.1	33	28	Mastectomy	SLNB	IDC (NST)	pT1c,pN1	IIA	1.2	3	3	95	70	15	No	Yes	5.24	Moderate II	18
5#	46.1	33	28	Mastectomy	SLNB	IDC (NST)	pT1c,pN1mi	IB	1.1	3	3	95	70	15	No	Yes	5.22	Moderate II	23
6	55.6	16	24	Mastectomy	ABD	IDC (NST)	pT3,pN1	IIIA	5	3	2	90	0	25	Yes	Yes	5.00	Moderate II	35

(Continued on following page)

10.3389/pore.2024.1611735

TABLE 1 (*Continued*) Characteristics of patients.

(b) pN1																			
Patient No.	Age at surgery (yrs)	TBSH (days)	TBHO (days)	Breast Surgery	Axillary surgery	Histology	TNM	Stage	Tumour (cm)	Node(s)	Grade	ER (%)	PR (%)	Ki67(%)	PNI	LVI	NPI	NPI Risk group	RS
8	51.9	14	26	Breast conservation	ABD	IDC (NST)	pT2,pN1	IIB	3	1	2	90	90	15	No	Yes	4.60	Moderate II	9
14	54.2	15	25	Breast conservation	ABD	IDC (NST)	pT2,pN1	IIB	2.3	2	1	90	60	1	No	No	3.46	Moderate I	8
15	64.8	15	29	Mastectomy	SLNB	Lobular cc	pT3,pN1mi	IIIA	6	1	2	100	1	1	No	Yes	5.20	Moderate II	17
16	62.2	22	22	Breast conservation	ABD	IDC (NST), Lobular cc	pT2,pN1	IIB	2.3	1	2	100	90	5	No	No	4.46	Moderate II	8
17	51.4	11	39	Mastectomy	ABD	IDC (NST)	pT1c,pN1	IIA	1.8	1	1	90	90	5	No	No	3.36	Good	9
18*	75.9	15	23	Bilateral mastectomy	Right ABD	IDC (NST)	pT2,pN1	IIB	2.4	1	1	95	0	5	No	Yes	3.48	Moderate I	0
22	75.5	8	77	Mastectomy	SLNB	IDC (NST)	pT1c,pN1mi	IB	1.9	1	2	100	100	2	Yes	No	4.38	Moderate II	5
24	65.4	15	25	Breast conservation	SLNB	IDC (NST)	pT2,pN1	IIB	2.3	1	2	90	40	20	Yes	Yes	4.46	Moderate II	18
31	64.5	16	28	Mastectomy	SLNB	IDC (NST)	pT2,pN1	IIB	3.5	2	2	100	15	5	No	Yes	4.70	Moderate II	12
32#	62.8	21	26	Mastectomy	SLNB	IDC (NST)	pT2,pN1	IIB	4	1	2	100	30	20	Yes	Yes	4.80	Moderate II	14
32#	62.8	21	26	Mastectomy	SLNB	IDC (NST)	pT2,pN1	IIB	2.5	1	1	40	10	5	Yes	Yes	3.50	Moderate I	26
34	74.9	16	25	Mastectomy	SLNB	IDC (NST)	pT3,pN1	IIIA	6	2	2	100	70	3	No	No	5.20	Moderate II	0
39	71.5	22	34	Mastectomy	ABD	IDC (NST), Lobular cc	pT2,pN1	IIB	2.1	1	3	10	5	25	Yes	Yes	5.42	Poor	34
45	48.9	20	27	Breast conservation	SLNB	Lobular cc	pT2,pN1	IIB	3	2	2	100	90	10	Yes	Yes	4.60	Moderate II	16
46	54	14	53	Breast conservation	SLNB	IDC (NST)	pT2,pN1	IIB	2.1	1	2	100	100	1	Yes	Yes	4.42	Moderate II	18
49	72.7	29	27	Breast conservation	SLNB	IDC (NST)	pT1c,pN1	IIA	1.4	1	1	100	90	5	No	No	3.28	Good	8
52	72	14	36	Breast conservation	ABD	IDC (NST)	pT1c,pN1	IIA	1.8	3	1	100	80	15	No	Yes	3.36	Good	12
53	71.3	19	23	Mastectomy	ABD	Lobular cc	pT2,pN1	IIB	3.5	3	2	100	10	1	Yes	Yes	4.70	Moderate II	27
54	72.1	27	30	Breast conservation	SLNB	IDC (NST)	pT1c,pN1	IIA	1.1	1	1	90	95	15	No	No	3.22	Good	9
58	43	17	32	Mastectomy	ABD	IDC (NST)	pT2,pN1	IIB	2.6	3	1	90	90	1	Yes	Yes	3.52	Moderate I	25
59	50	14	27	Breast conservation	ABD	IDC (NST)	pT1b,pN1	IB	0.8	1	1	100	60	3	No	No	3.16	Good	11

(Continued on following page)

10.3389/pore.2024.1611735

TABLE 1 (*Continued*) Characteristics of patients.

(b) pN1																			
Patient No.	Age at surgery (yrs)	TBSH (days)	TBHO(days)	Breast Surgery	Axillary surgery	Histology	TNM	Stage	Tumour (cm)	Node(s)	Grade	ER (%)	PR (%)	Ki67(%)	PNI	LVI	NPI	NPI Risk group	RS
64	70.1	39	27	Breast conservation	ABD	IDC (NST)	pT2,pN1	IIB	2.5	1	1	90	90	5	No	Yes	3.50	Moderate I	16
65	56.9	19	44	Breast conservation	ABD	Lobular cc	pT2,pN1	IIB	2.3	1	2	90	90	60	No	Yes	4.46	Moderate II	17
68	51.3	12	40	Mastectomy	SLNB	IDC (NST)	pT2,pN1 (1+1mi)	IIB	3	2	2	80	90	30	No	No	4.60	Moderate II	12
69	60.3	27	29	Breast conservation	SLNB	Lobular cc	pT2,pN1	IIB	4.9	1	2	80	0	3	No	Yes	4.98	Moderate II	17
70	67.2	15	28	Mastectomy	ABD	Lobular cc	pT2,pN1	IIB	3.3	3	2	100	20	5	No	No	4.66	Moderate II	26
71	71.3	20	23	Mastectomy	ABD	IDC (NST)	pT2,pN1	IIB	2.5	1	1	90	80	5	No	No	3.50	Moderate I	2
77	47.2	14	36	Breast conservation	SLNB	IDC (NST)	pT1c,pN1	IIA	1.8	3	1	90	90	25	No	No	3.36	Good	29
78	67.9	19	25	Breast conservation	ABD	Lobular cc	pT2,pN1	IIB	3.5	2	2	100	70	20	No	No	4.70	Moderate II	31
80	38.1	21	37	Breast conservation	ABD	IDC (NST)	pT2,pN1	IIB	2.5	2	1	90	80	3	No	Yes	3.50	Moderate I	13
86	62.9	24	24	Mastectomy	ABD	IDC (NST)	pT2,pN1	IIB	3.5	3	2	100	0	25	Yes	Yes	4.70	Moderate II	31
87§	51.5	28	51	Mastectomy	ABD	IDC (NST), Lobular cc	pT2,pN1	IIB	4.8	1	2	0	100	2	No	No	4.96	Moderate II	32
88	82	49	36	Mastectomy	ABD	IDC (NST)	pT2,pN1	IIB	2.5	1	1	100	5	5	No	Yes	3.50	Moderate I	28
90	72.8	14	34	Mastectomy	SLNB	IDC (NST)	pT1c,pN1	IIA	1.9	1	2	100	40	10	Yes	Yes	4.38	Moderate I	24

Total No. of patients* = 55 Total No. of tumours# = 56.

* = Patient No. 18. had two primaries: in the left breast (pT2pN0, PR neg., lumB1, RS = 12) and in the right breast (pT2pN1, lumA, RS = 0). Therefore the data of this patient is registered in the table of node-negative and node-positive cases.

= Patient No. 66. had two primaries in the same breast.

ABD, axillary block dissection; Clinical Risk: Low (Grade 1 and Tumour ≤3 cm, Grade 2 and Tumour ≤2 cm, Grade 3 and Tumour ≤1 cm), High (all other cases); IDC, invasive ductal carcinoma; LVI, lymphovascular invasion; NPI, nottingham prognostic index; NPI, Risk Groups: Excellent (NPI ≤ 2.4), Good (NPI = 2.41–3.4), Moderate I (NPI = 3.41–4.4), Moderate II (NPI = 4.41–5.4), Poor (NPI ≥ 5.41); NST, non-specified type; PNI, perineural invasion; RS, recurrence score; SLNB, sentinel lymph node biopsy; TNM, tumour, Node, Metastasis; TBSH, time between surgery and histology; TBHO, time between surgery and OncotypeDX, result.

Total No. of patients* = 36 Total No. of tumours# = 38.

*Patient No. 18. had two primaries: in the left breast (pT2pN0, PR, neg., lumB1, RS = 12) and in the right breast (pT2pN1, lumA, RS = 0). Therefore the data of this patient is registered in the table of node-negative and node-positive cases.

#Patient No. 5. and 32. had two primaries in the same breast.

§specimen of the patient No. 87 was examined by Exact Sciences for ER, score (9.2—ER, positive) based on quantitative ESR1 expression and PR, score (8.0—PR, positive) based on quantitative PGR, expression. Thus this case is both ER, and PR, positive, although immunohistocemically ER, was negative.

ABD, axillary block dissection; IDC, invasive ductal carcinoma; LVI, lymphovascular invasion; NPI, nottingham prognostic index; NPI, Risk Groups: Excellent (NPI≤2.4), Good (NPI = 2.41–3.4), Moderate I (NPI = 3.41–4.4), Moderate II (NPI = 4.41–5.4), Poor (NPI≥5.41); NST, non-specified type; PNI, perineural invasion; RS, recurrence score; SLNB, sentinel lymph node biopsy; TNM, tumour, Node, Metastasis; TBSH, time between surgery and histology; TBHO, time between surgery and OncotypeDX, result.

10.3389/pore.2024.1611735

cases (pT1b, pN0 grade 2-3 or with LVI; pT1c-3, pN0; pT1-3, and pN1) were appointed for OncotypeDX analysis, therefore the blocks were sent to the central laboratory of Exact Sciences Corporation (formerly Genomic Health Inc. in Redwood City, California, United States). Collection and performing the transport of the blocks, and providing the results of the analyses were organised by MED GEN-SOL Ltd., Hungary.

Statistical analysis

The authors evaluated the data of pN0 and pN1 cohorts separately with non-parametric, parametric analyses and OOM [12, 13] regarding pathological characteristics such as pathological and anatomical stage (tumour size, number of positive nodes), grade (based on tubule formation, nuclear polymorphism and mitotic counts) [14], perineural invasion (PNI), LVI, estrogen receptor (ER) and progesterone receptor (PR) expression, proliferation rate (Ki-67 value, which was calculated as proposed by the International Ki67 in Breast Cancer Working Group) [15, 16] and Nottingham Prognostic Index (NPI) [17]. Based on ER expression three categories were distinguished: negative (0%); low (≤10%) and high (>10%). Regarding PR expression, three groups were formed [18]: negative (0%); low (<20%) and high (≥20%). The authors stratified the Ki-67 values to three categories [16]: low (≤5%); intermediate (6%–29%) and high (≥30%). p53 values were classified into two groups [19]: negative (<10%) and positive (≥10%). NPI was calculated from tumour size, nodal status and grade with the equitation [20]: NPI = 0.2 x tumour size (cm) + nodal involvement (1 for pN0, 2 for pN1) + grade (1-3 for grades 1–3). Based on the NPI scores, five risk groups are distinguished [21]: excellent (≤2.4); good (2.41–3.4); moderate I (3.41–4.4); moderate II (4.41–5.4); poor (>5.4). Only for pN0 disease the clinical risk was calculated by tumour size and grade as in the TAILORx and formerly in the MINDACT (Microarray in Node Negative Disease May Avoid Chemotherapy) trial. The definition of low clinical risk was low histologic grade (i.e., grade 1) and tumour size ≤3 cm, intermediate histologic grade (i.e., grade 2) and tumour size ≤2 cm, or high histologic grade (i.e., grade 3) and tumour size ≤1 cm. The high clinical risk group included all other cases [22].

Normality was checked with the Kolmogorov-Smirnov test and the equality of variances was checked by using the Levene test. For the not normal distribution of RS the authors have used non-parametric analyses, such as the Mann-Whitney test to compare mean differences of the RS within two groups formed by the pathological characteristics. To test mean differences between more than two groups, the authors used the Kruskal-Wallis test statistic. To measure the strength of correlation between the RS and the pathological characteristics measured on an interval scale, the non-parametric Spearman rank correlation coefficient was calculated. For normal distribution of RS, the authors used parametric methods like the analysis of variance (ANOVA) for more than two groups and the *t*-test in the comparison of two groups. The parametric Pearson's correlation coefficient was used to measure the strength of correlation between the RS and interval scale variables. The level of significance was 5%.

OOM arranges data into "deep structures" which are matrices of ones and zeros (rows correspond to observations/patients, columns correspond to categories of a given variable) similar to, but distinct from, effect and dummy coding. Binary Procrustes rotation is then performed on these matrices. During this process, the grouping variable's structure (in the form of a conforming matrix) is transformed into the target variable's structure (target matrix). The main feature of OOM is to provide a simple statistic after the rotation, namely the percent of correct classifications (PCC) and with it a common platform to compare and rank influential factors. The other advantage of using this methodology is that it is also focused on actual replicability of given data. Using randomisation, OOM provides a so-called chance value (c-value) instead of *p*-values. During the randomisation test the conforming and target observations are paired randomly, say 1,000 times as determined by the researcher, and the PCC values are calculated. The proportion of PCC values that are greater than or equal to the observed PCC index is called the chance value (c-value). If the c-value is lower than 0.10 (10%) then the observed pattern can be judged as having arisen from factors not plausibly attributable to physcial chance [23]. In other words, a low c-value lends plausibility to a causal interpretation of the observed pattern. C-values of ≤0.10 with corresponding PCCs of 60% or higher were regarded as meaningful for interpretation. The binary Procrustes rotation function (Build/Test Model option) was used in the OOM software to create multigrams, and when the pattern of observations in the multigram provided meaningful classification of values ("eye test") then *ordinal analyses* were followed and PCC and c-values were calculated. These ordinal analyses compared every person in one group to every person in another group and tallied the number of instances (reported as a PCC index) in which the ordinal pattern of scores matched expectation (e.g. ordinal patterns were tested on RS in both pN0 and pN1 subsets for Grade 1 > Grade 2 > Grade 3; Ki-67 group low > intermediate > high; PR group high > low > negative; NPI Risk Group excellent > good > moderate; Stage 1 > 2 > 3 and in only pN1 subset for Node 1 > 2 > 3). The aggregation of the PCCs of ordinal analyses result in "omnibus" PCC values. In addition to "omnibus" PCCs for these ordinal patterns with three groups, "pairwise" PCCs were computed as well to provide greater detail regarding the pattern of results. For example, the following ordinal patterns were tested for RS scores: Grade 1 > Grade 2, Grade 1 > Grade 3, and Grade 2 > Grade 3. When the RS scores matched the ordinal pattern, then the case was regarded as a "complete classification." Reporting results for complete and pairwise analyses is similar

to the practice of reporting both the omnibus and pairwise F-value in an ANOVA. When only two groups were compared (two stages, PNI, LVI, Clinical Risk), the pairs and complete PCCs were equal. For continuous variables (tumour size, ER/PR expression, Ki-67 values, NPI values) the RS was dichotomised (low RS < 26 and high RS ≥ 26), therefore two groups were compared. In cases for which the multigram was not interpretable, then PCC values were judged as not meaningful, and no further analyses were conducted. Therefore, the so-called "eye test" was prioritised first, then the PCC, and finally the c-value, thus the order of significant variables was established. The association of RS was investigated by supervised classification with OOM in joint pN0 and pN1 cohorts.

Results

Patient characteristics

Between July 2018 and June 2023, 90 BC patients (pT1-3, pN0-1) were tested by Exact Sciences for OncotypeDX and a total of 94 analyses were performed. A patient (No. 21.) had synchronous bilateral BC (one pN0 and on the other side pN1, therefore this case was included in both cohorts), and three other patients (No. 5, 32 and 66) had two foci of BC in their ipsilateral breasts. Summarised data is available in Supplementary Material S1. Average age of the patients was 62.6 (46.2–84.3) years at the diagnosis. The average time elapsed from surgery to final pathological report, and pathological report to OncotypeDX result were 17.3 (0–49) days and 29.3 (12–56) days, respectively. Thus, a therapeutic decision based on RS was possible in about 6 weeks after operation. Chemotherapy was recommended for 16.3% (9/55) of pN0, and for 27.7% (10/36) of pN1 (included No. 21.) patients (for Stage IA: 6/39; for Stage IIA: 3/24; for Stage IIB: 8/24; for Stage IIIA: 1/3). There was no Stage IIB case in the pN0 cohort, and all 4 cases in Stage IB of the pN1 cohort had low RS. In 87.5% (7/8) of premenopausal pN1 patients with RS < 26, the preference of all patients was the combination of ovarian suppression with endocrine treatment. For 67.9% (19/28) of postmenopausal patients with RS < 26 chemotherapy was not recommended. Only 27.8% (10/36) of pN1 cases received chemotherapy. A postmenopausal patient (No. 46) developed bone metastases 28 months after the diagnosis (pT2,pN1, Grade 2, ER/PR 100%, Ki-67 1%, PNI, LVI and RS = 18). Data of patient characteristics are described in Table 1. Data of description statistics are summarised in Table 2. Significant results of parametric and non-parametric tests and OOM are described in Tables 3–6. All results are presented in Supplementary Tables S1–S12 in Supplementary Material S2, and a detailed description of the association of pathological characteristics with RS is also found in Supplementary Material S2. A summary of characteristics in significant association with RS by OOM is included in Supplementary Material S3. The data of patients that had the highest and lowest recurrence scores with diverse characteristics are depicted in Supplementary Material S4.

Significant association between pathological characteristics and RS

In the pN0 cohort, the distribution of RS was not normal, therefore non-parametric correlation and test were applied. With the traditional statistical methods, eight characteristics were significantly associated with RS (Figures 1A, 2; Table 3A). The significance of association was the strongest for PR (%) followed by Ki-67 (%), Ki-67 group, PR group, grade, ER (%), NPI, and clinical risk. In the subgroup of >50 years and RS < 26 cases, the following characteristics were significant in order: ER (%), Ki-67 (%), Ki-67 group and PR (%) (Table 3B).

In the pN1 cohort, parametric correlation and test were used due to the normal distribution of RS. Six characteristics of pN1 cases were significantly associated with RS (Figures 1B, 2; Table 4A). The strongest association was observed for the number of positive nodes followed by ER (%), PR (%), PR group, Ki-67 group and NPI. In the subgroup of postmenopausal cases with RS < 26, the only significant characteristic was LVI (Table 4B). In the subgroup of postmenopausal cases with RS ≥ 26, two significant characteristics were found in order: Ki-67 group and Ki-67 (%) (Table 4C). In the subgroup of premenopausal cases with RS < 26, only the number of positive nodes was associated significantly with RS (Table 4D).

OOM was applied independent of the normality of the distribution and case numbers in both pN0 and pN1 cohorts. Based on multigrams, PCC and c-values for the pN0 cohort three characteristics were found, where the association was significant with RS in order (Supplementary Material S3): Ki-67 group, grade and NPI risk group (Table 5A). In the subgroup of >50years cases, four characteristics were significant in order: PR (%), Ki-67 group, grade, and NPI risk group (Figure 3; Table 5B).

For the pN1 cohort, OOM found seven significant characteristics in order (Supplementary Material S3): PR group, PNI, LVI, Ki-67 group, grade, NPI risk group, and the number of positive lymph nodes (Figure 3; Table 6A). In the subgroup of postmenopausal cases, eight characteristics were significant in order: PR (%), grade, PR group, NPI, LVI, NPI risk group, stage and Ki-67 group (Figure 3; Table 6B).

Results of supervised classification of joint pN0 and pN1 cohorts by OOM

On analysis of joint pN0 and pN1 cohorts by OOM significant associations were found between pathological

TABLE 2 Description statistics of patients.

(a) pN0				
	Age ≤50		Age >50	
	RS < 16	RS ≥ 16	RS < 26	RS ≥ 26
	Endocrine therapy	Chemotherapy, endocrine therapy	Endocrine therapy	Chemotherapy, endocrine therapy
Total No. Of Patients*	2	1	44	8
Median age (range)—yr	47.1 (46.2–47.9)	NA—47.1	64.1 (50.2–80.1)	63.8 (56.4–84.3)
Age category—no. (%)				
<40 years	0 (0)	0 (0)	NA	NA
40–49 years	2 (100)	1 (100)	NA	NA
50–59 years	0 (0)	0 (0)	13 (29.5)	2 (25.0)
60–69 years	NA	NA	24 (54.5)	4 (50.0)
≥70 years	NA	NA	7 (15.9)	2 (25.0)
Primary surgery—no. (%)				
Mastectomy	0 (0)	0 (0)	12 (27.3)	4 (50.0)
Breast conservation	2 (100)	1 (100)	32 (72.7)	4 (50.0)
Axillary surgery—no. (%)				
Axillary lymph-node dissection, with or without sentinel-node mapping	0 (0)	1 (100)	1 (2.3)	2 (25.0)
Sentinel-node biopsy without axillary lymph-node dissection	2 (100)	0 (0)	43 (97.7)	6 (75.0)
Total No. Of Tumours Tested#	2	1	45	8
Tumour size in the largest dimension—cm				
Median (IQR)	1.5 (NA)	NA—2.5	1.7 (0.95)	1.8 (0.85)
Mean (range)	1.5 (1.8–2.6)	NA—2.5	1.8 (1.1–3.7)	1.9 (1.2–3.2)
Histologic grade of tumour—no./total no. (%)				
Low	2 (100)	1 (100)	30 (66.7)	2 (25.0)
Intermediate	0 (0)	0 (0)	14 (31.1)	4 (50.0)
High	0 (0)	0 (0)	1 (2.2)	2 (25.0)

(Continued on following page)

Published by Frontiers

10.3389/pore.2024.1611735

TABLE 2 (*Continued*) Description statistics of patients.

(a) pN0				
	Age ≤50		Age >50	
	RS < 16	RS ≥ 16	RS < 26	RS ≥ 26
	Endocrine therapy	Chemotherapy, endocrine therapy	Endocrine therapy	Chemotherapy, endocrine therapy
Perineural invasion—no./total no. (%)				
No	2 (100)	1 (100)	37 (82.2)	5 (62.5)
Yes	0 (0)	0 (0)	8 (17.7)	3 (37.5)
Lymphovascular invasion—no./total no. (%)				
No	2 (100)	1 (100)	44 (97.7)	8 (100)
Yes	0 (0)	0 (0)	1 (2.2)	0 (0)
Estrogen-receptor expression—no. (%)				
Negative	0 (0)	0 (0)	0 (0)	0 (0)
Low (≤10%)	0 (0)	0 (0)	0 (0)	0 (0)
High (>10%)	2 (100)	1 (100)	45 (100)	8 (100)
Progesteron-receptor expression—no./total no. (%)				
Negative	0 (0)	0 (0)	1 (2.2)	3 (37.5)
Low (<20%)	0 (0)	0 (0)	3 (6.6)	2 (25.0)
High (≥20%)	2 (100)	1 (100)	41 (91.1)	3 (37.5)
Mean Ki67 (range)	3 (1–5)	NA—40	8.4 (1–40)	14.8 (3–30)
Ki67—no./total no. (%)				
Low (≤5%)	2 (100)	0 (0)	28 (62.2)	2 (25.0)
Intermediate (6%–29%)	0 (0)	0 (0)	14 (31.1)	5 (62.5)
High (≥30%)	0 (0)	1 (100)	3 (6.7)	1 (12.5)
Stage—no./total no. (%)				
IA	2 (100)	0 (0)	31 (68.9)	6 (75.0)
IIA	0 (0)	1 (100)	14 (31.1)	2 (25.0)

(Continued on following page)

Published by Frontiers

10.3389/pore.2024.1611735

TABLE 2 (*Continued*) Description statistics of patients.

(a) pN0				
	Age ≤50		Age >50	
	RS < 16	RS ≥ 16	RS < 26	RS ≥ 26
	Endocrine therapy	Chemotherapy, endocrine therapy	Endocrine therapy	Chemotherapy, endocrine therapy
IIB	0 (0)	0 (0)	0 (0)	0 (0)
Clinical Risk—no./total no. (%)				
Low	2 (100)	1 (100)	38 (84.4)	5 (62.5)
High	0 (0)	0 (0)	7 (15.6)	3 (37.5)
Mean NPI (range)	2.3 (2.2–2.4)	NA—2.5	2.73 (2.2–4.3)	3.38 (2.3–4.5)
NPI risk group—no./total no. (%)				
Excellent (NPI≤2.4)	2 (100)	0 (0)	25 (55.6)	2 (25.0)
Good (NPI = 2.41–3.4)	0 (0)	1 (100)	13 (28.8)	3 (37.5)
Moderate I (NPI = 3.41–4.4)	0 (0)	0 (0)	7 (15.6)	2 (25.0)
Moderate II (NPI = 4.41–5.4)	0 (0)	0 (0)	0 (0)	1 (12.5)
Poor (NPI>5.4)	0 (0)	0 (0)	0 (0)	0 (0)
Mean Recurrence Score (range)	11.5 (11–12)	NA—33	13.7 (0–24)	29.5 (26–36)
Recommendation for chemotherapy - no./total no. (%)				
No	2 (100)	0 (0)	44 (100)	0 (0)
Yes	0 (0)	1 (100)	0 (0)	8 (100)
(b) pN1				
	Premenopausal§		Postmenopausal	
	RS < 26	RS ≥ 26	RS < 26	RS ≥ 26
	Endocrine Therapy	Chemotherapy, Endocrine Therapy	Endocrine Therapy	Chemotherapy, Endocrine Therapy
Total No. Of Patients*	7	1	19	9
Median age (range)—yr	48.9 (38.3–52.1)	47.3 (NA)	67.1 (54.2–75.9)	67.3 (51.7–82.2)

(Continued on following page)

10.3389/pore.2024.1611735

TABLE 2 (*Continued*) Description statistics of patients.

(b) pN1				
	Premenopausal§		Postmenopausal	
	RS < 26	RS ≥ 26	RS < 26	RS ≥ 26
	Endocrine Therapy	Chemotherapy, Endocrine Therapy	Endocrine Therapy	Chemotherapy, Endocrine Therapy
Age category—no. (%)				
<40 years	1 (14.2)	0 (0)	NA	NA
40–49 years	3 (42.9)	1 (100)	NA	NA
50–59 years	3 (42.9)	0 (0)	4 (21.1)	2 (22.2)
60–69 years	NA	NA	6 (31.6)	4 (44.4)
≥70 years	NA	NA	9 (47.3)	3 (33.3)
Primary surgery—no. (%)				
Mastectomy	4 (50.0)	0 (0)	9 (45.0)	8 (88.9)
Breast conservation	4 (50.0)	1 (100)	11 (55.0)	1 (11.1)
Axillary surgery—no. (%)				
Axillary lymph-node dissection, with or without sentinel-node mapping	5 (71.4)	0 (0)	8 (42.1)	8 (88.9)
Sentinel-node biopsy without axillary lymph-node dissection	2 (28.6)	1 (100)	12 (57.9)	1 (11.1)
Positive nodes—no. (%)				
1 node	3 (42.8)	0 (0)	13 (68.4)	4 (44.4)
2 nodes	2 (28.6)	0 (0)	5 (26.3)	1 (11.1)
3 nodes	2 (28.6)	1 (100)	1 (5.3)	4 (44.4)
Total No. Of Tumours Tested#	8	1	20	9
Tumour size in the largest dimension—cm				
Median (IQR)	2.2 (1.7)	NA—1.8	2.3 (1.4)	3.5 (1.7)
Mean (range)	2 (0.8–3)	NA—1.8	2.8 (1.1–6.0)	3.4 (2.1–5)
Histologic grade of tumour—no./total no. (%)				

(Continued on following page)

10.3389/pore.2024.1611735

TABLE 2 (*Continued*) Description statistics of patients.

(b) pN1				
	Premenopausal§		Postmenopausal	
	RS < 26	RS ≥ 26	RS < 26	RS ≥ 26
	Endocrine Therapy	Chemotherapy, Endocrine Therapy	Endocrine Therapy	Chemotherapy, Endocrine Therapy
Low	4 (50.0)	1 (100)	7 (35.0)	2 (22.2)
Intermediate	2 (25.0)	0 (0)	13 (65.0)	6 (66.7)
High	2 (25.0)	0 (0)	0 (0)	1 (11.1)
Perineural invasion—no./total no. (%)				
No	6 (75.0)	1 (100)	14 (70.0)	4 (44.4)
Yes	2 (25.0)	0 (0)	6 (30.0)	5 (55.6)
Lymphovascular invasion—no./total no. (%)				
No	2 (25.0)	1 (100)	8 (40.0)	3 (33.3)
Yes	6 (75.0)	0 (0)	12 (60.0)	6 (66.7)
Estrogen-receptor expression—no. (%)				
Negative	0 (0)	0 (0)	0 (0)	1 (11.1)
Low (≤10%)	0 (0)	0 (0)	0 (0)	1 (11.1)
High (>10%)	8 (100)	1 (100)	20 (100)	7 (77.8)
Progesteron-receptor expression—no./total no. (%)				
Negative	0 (0)	0 (0)	2 (10.0)	2 (22.2)
Low (<20%)	0 (0)	0 (0)	2 (10.0)	4 (44.4)
High (≥20%)	8 (100)	1 (100)	16 (80.0)	3 (33.3)
Mean Ki67 (range)	8.4 (1–15)	NA—25	10.7 (1–60)	12.5 (1–25)
Ki67—no./total no. (%)				
Low (≤5%)	4 (50.0)	0 (0)	13 (65.0)	5 (55.6)
Intermediate (6%–29%)	4 (50.0)	1 (100)	5 (25.0)	4 (44.4)

(Continued on following page)

10.3389/pore.2024.1611735

TABLE 2 (*Continued*) Description statistics of patients.

(b) pN1				
	Premenopausal§		Postmenopausal	
	RS < 26	RS ≥ 26	RS < 26	RS ≥ 26
	Endocrine Therapy	Chemotherapy, Endocrine Therapy	Endocrine Therapy	Chemotherapy, Endocrine Therapy
High (≥30%)	0 (0)	0 (0)	2 (10.0)	0 (0)
Stage—no./total no. (%)				
IB	2 (25.0)	0 (0)	2 (10.0)	0 (0)
IIA	2 (25.0)	1 (100)	4 (20.0)	0 (0)
IIB	4 (50.0)	0 (0)	12 (60.0)	8 (88.9)
IIIA	0 (0)	0 (0)	2 (10.0)	1 (11.1)
Mean NPI (range)	4.15 (3.16–5.24)	NA—3.36	4.20 (3.28–5.20)	4.57 (3.50–5.42)
NPI risk group—no./total no. (%)				
Excellent (NPI≤2.4)	0 (0)	0 (0)	0 (0)	0 (0)
Good (NPI = 2.41–3.4)	2 (25.0)	1 (100)	3 (15.0)	0 (0)
Moderate I (NPI = 3.41–4.4)	2 (25.0)	0 (0)	6 (30.0)	2 (22.2)
Moderate II (NPI = 4.41–5.4)	3 (50.0)	0 (0)	11 (55.0)	6 (66.7)
Poor (NPI>5.4)	0 (0)	0 (0)	0 (0)	1 (11.1)
Mean Recurrence Score (range)	15.1 (6–25)	NA—29	11 (0–24)	30 (26–35)
Recommendation for chemotherapy - no./total no. (%)				
No	7 (100)§	0 (0)	19 (100)	0 (0)
Yes	0 (0)	1 (100)	0 (0)	9 (100)

*Patient No. 18. had two primaries: in the left breast (pT2pN0, PR, neg., lumB1, RS = 12) and in the right breast (pT2pN1, lumA, RS = 0). Therefore the data of this patient is registered in the table of node-negative and node-positive cases.
#Patient No. 66. had two primaries in the same breast.
Clinical Risk: Low (Grade 1 and Tumour ≤3 cm, Grade 2 and Tumour ≤2 cm, Grade 3 and Tumour ≤1 cm), High (all other cases); IQR, interquartile range; NA, not applicable; NPI, Nottingham Prognostic Index.
*Patient No. 18. had two primaries: in the left breast (pT2pN0, PR, neg., lumB1, RS = 12) and in the right breast (pT2pN1, lumA, RS = 0). Therefore the data of this patient is registered in the table of node-negative and node-positive cases.
#Patient No. 5. and 32. had two primaries in the same breast.
§Premenopausal patients with RS < 26 had two options for treatment: either chemotherapy or endocrine therapy with ovarian suppression. All seven patients chose the latter option.
IQR, interquartile range; NA, not applicable; NPI, Nottingham Prognostic Index.
Bold values represent the Age, RS, Premenopausal and Postmenopausal.

10.3389/pore.2024.1611735

TABLE 3 Significant results of non-parametric analyses.

(A) In all pN0 cases							
Variable	Scale	Analysis*	Average RS (n =) in			Statistics	p-value
			0. Group	1. Group	2. Group		
Grade	0 = I	Kruskal-Wallis	14.09 (35)	18.78 (18)	26.33 (3)	H = 8.523	0.014
	1 = II						
	2 = III						
ER (%)	-	Spearman	-	-	-	ρ = −0.297	0.026
PR (%)	-	Spearman	-	-	-	ρ = −0.524	<0.001
PR group	0 = negative	Kruskal-Wallis	25.25 (4)	22 (4)	15.02 (48)	H = 8.795	0.012
	1 = low						
	2 = high						
Ki-67 (%)	-	Spearman	-	-	-	ρ = 0.466	<0.001
Ki-67 group	0 = low	Kruskal-Wallis	13.22 (32)	18.95 (19)	25.40 (5)	H = 12.784	0.002
	1 = intermediate						
	2 = high						
Clinical Risk	0 = low	Mann-Whitney	15.24 (46)	20.90 (10)	-	Z = −2.03	0.043
	1 = high						
NPI	-	Spearman	-	-	-	ρ = 0.286	0.033
(B) in pN0 cases >50years and RS < 26							
Variable	Scale	Analysis*	Average RS (n =) in			Statistics	p =
			0. Group	1. Group	2. Group		
ER (%)	-	Spearman	-	-	-	ρ = −0.425	0.004
PR (%)	-	Spearman	-	-	-	ρ = −0.296	0.048
Ki-67 (%)	-	Spearman	-	-	-	ρ = 0.382	0.010
Ki-67 group	0 = low	Kruskal-Wallis	12.36 (28)	15.00 (14)	20.67 (3)	H = 7.126	0.028
	1 = intermediate						
	2 = high						

*Spearman parametric rank correlation coefficient: very weak <=0.19; weak 0.20- <=0.39; moderate 0.40- <=0.59; strong 0.60- <=0.79; very strong 0.80- <=1.00; level of significance was 5%.
ER = estrogen receptor; PR = progesteron receptor.

characteristics and RS in order: PR group (PCC = 75.00%; c = 0.001), Ki-67 group (PCC = 69.51%; c < 0.001), and PNI (PCC = 66.19%; c = 0.01). In 39.00% (c < 0.01) of the cases no, low, and high PR groups were correlated with lower and higher RS. In 30.41% (c = 0.01) of the cases low, intermediate, and high Ki-67 groups were correlated with lower and higher RS (Table 7).

Discussion

In this retrospective analysis, the authors evaluated the association of pathological characteristics and RS in the dataset of 90 patients (operated on BC, and accomplished OncotypeDX tests) of a North Hungarian single institution (Nógrád Vármegyei Szent Lázár Hospital, Salgótarján, Hungary) (Tables 1, 2).

TABLE 4 Significant results of parametric analyses.

(A) In all pN1 cases								
Variable	Scale	Analysis*	Average RS (n =) in group				Statistics	p =
			0	1	2	3		
Node	0 = 1 node	ANOVA	15.33 (21)	11.88 (8)	25.11 (9)	-	F = 5.446	0.009
	1 = 2 nodes							
	2 = 3 nodes							
ER (%)	-	Pearson	-	-	-	-	r = −0.384	0.017
PR (%)	-	Pearson	-	-	-	-	r = −0.381	0.018
PR group	0 = negative	*t*-test	20.75 (4)	24 (6)	14.86 (28)	-	t = 2.350	0.025
	1 = low							
	2 = high							
Ki-67 group	0 = low	*t*-test	14.14 (22)	21.64 (14)	14.50 (2)	-	t = −2.293	0.028
	1 = intermediate							
	2 = high							
NPI	-	Pearson	-	-	-	-	r = 0.322	0.049
(B) in pN1 postmenopausal cases with RS < 26								
Variable	Scale	Analysis	Average RS (n =) in				Statistics	p =
			0. group	1. group	2. group	3. group		
LVI	0 = no	*t*-test	6.50 (8)	14.00 (12)	-	-	t = −2.856	0.011
	1 = yes							
(C) in pN1 postmenopausal cases with RS ≥ 26								
Variable	Scale	Analysis	Average RS (n =) in				Statistics	p =
			0. Group	1. Group	2. Group			
Ki-67 (%)	-	Pearson	-	-	-		r = 0.753	0.019
Ki-67 group	0 = low	ANOVA	27.80 (5)	32.75 (4)	-		F = 10.150	0.015
	1 = intermediate							
	2 = high							
NPI	-	Pearson	-	-	-		r = 0.692	0.039
(D) in pN1 premenopausal cases with RS < 26								
Variable	Scale	Analysis	Average RS (n =) in				Statistics	p =
			0. Group	1. Group	2. Group			
Node	0 = 1 node	ANOVA	9.67 (3)	14.50 (2)	22.00 (3)		F = 17.399	0.006
	1 = 2 nodes							
	2 = 3 nodes							

*Pearson correlation coefficient: very weak <=0.19; weak 0.20- <=0.39; moderate 0.40- <=0.59; strong 0.60- <=0.79; very strong 0.80- <=1.00; level of significance was 5%.
ANOVA, analysis of variance; ER, estrogen receptor; LVI, lymphovascular invasion; NPI, nottingham prognostic index; PR, progesteron receptor.

TABLE 5 Significant results of randomisation (omnibus; complete*) and pairwise ordinal analysis by OOM (multigrams, PCC and c-values).

(A) In all pN0 cases						
Variable	Scale	Average RS (n =) in group			PCC (%)	c-value§
		0	1	2		
Grade	0 = I	14.09 (35)	18.78 (18)	26.33 (3)	69.07; 40.58*	0.002; 0.01
	1 = II				0 vs. 1 = 65.08	0.03
	2 = III				0 vs. 2 = 90.48	0.01
					1 vs. 2 = 74.07	0.11
Ki-67 group	0 = low	13.22 (32)	18.95 (19)	25.40 (5)	73.35; 39.47*	<0.001; <0.01
	1 = intermediate				0 vs. 1 = 68.75	0.01
	2 = high				0 vs. 2 = 93.13	<0.01
					1 vs. 2 = 69.47	0.07
NPI Risk group**	0 = excellent	13.89 (29)	17.53 (17)	20.90 (10)	62.75; 22.86*	0.02; 0.09
	1 = good				0 vs. 1 = 56.80	0.18
	2 = moderate				0 vs. 2 = 74.48	0.01
					1 vs. 2 = 60.00	0.18
(B) in pN0 cases >50 years						
Variable	Scale	Average RS (n =) in			PCC (%)	c-value§
		0. Group	1. Group	2. Group		
Grade	0 = I	12.77 (30)	15.28 (14)	21 (1)	70.25	0.001
	1 = II				0 vs. 1 66.15	0.02
	2 = III				0 vs. 2 92.71	<0.01
					1 vs. 2 74.07	0.08
PR (%)	-	-	-	-	86.67	<0.001
Ki-67 group	0 = low	12.36 (28)	15.00 (14)	20.67 (3)	71.02	0.001
	1 = intermediate				0 vs. 1 67.89	0.01
	2 = high				0 vs. 2 90.83	<0.01
					1 vs. 2 63.16	0.21
NPI Risk group**	0 = excellent	13.04 (25)	13.08 (13)	17.43 (7)	61.48	0.03
	1 = good				0 vs. 1 53.01	0.29
	2 = moderate				0 vs. 2 73.70	0.01
					1 vs. 2 63.75	0.09

*Omnibus PCC, aggregates the PCCs, of ordinal analysis for all pN0 and pN0 >50years subgroup. Complete PCC, values were calculated only for the pN0 cohort with corresponding c-values. This refers to the ideal situation, when the RS, scores matched the ordinal pattern of the categorised variable, and the case was regarded as "Complete Classification."

**There was one case in the moderate II, group, therefore this case was classified to the moderate I group.

§c-values are regarded significant <10% along with PCC>60%.

c-value, chance value; ER, estrogen receptor; NPI, nottingham prognostic index; OOM, observation oriented modeling; PCC, percent of correct classification; PR, progesteron receptor.

TABLE 6 Significant results of randomisation (omnibus; complete*) and pairwise ordinal analysis by OOM (multigrams, PCC and c-values).

(A) in all pN1 cases							
Variable	Scale	Average RS (n =) in group				PCC (%)	c-value§
		0	1	2	3		
Node	0 = 1 node	15.33 (21)	11.88 (8)	25.11 (9)	-	63.17; 23.81*	0.04; 0.10
	1 = 2 nodes					0 vs. 1 36.31	0.83
	2 = 3 nodes					0 vs. 2 79.37	0.01
						1 vs. 2 83.33	0.01
Grade	0 = I	14.00 (14)	17.71 (21)	25.00 (3)	-	65.41; 37.53*	0.03; 0.03
	1 = II					0 vs. 1 = 61.56	0.10
	2 = III					0 vs. 2 = 80.95	0.06
						1 vs. 2 = 73.02	0.12
PR group	0 = negative	20.75 (4)	24 (6)	14.68 (28)	-	70.07; 36.16*	0.02; 0.02
	1 = low					0 vs. 1 = 50.00	0.49
	2 = high					0 vs. 2 = 63.39	0.18
						1 vs. 2 = 77.38	0.02
Ki-67 (%)	-	-	-	-	-	71.05##	<0.01
Ki-67 group	0 = low	14.14 (22)	21.64 (14)	14.50 (2)	-	65.53#	0.03
	1 = intermediate					0 vs. 1 = 71.10	<0.01
	2 = high					0 vs. 2 = 52.27	0.43
						1 vs. 2 = 25.00	0.85
PNI	0 = no	14.68 (25)	21.23 (13)	-	-	68.92###	0.03
	1 = yes						
LVI	0 = no	13.57 (14)	18.88 (24)	-	-	67.86###	0.03
	1 = yes						
NPI Risk group	0 = good	13.89 (6)	17.53 (10)	20.90 (21)	20.90 (1)	63.35#	0.03
	1 = moderate I					0 vs. 1 = 50.00	0.50
	2 = moderate II					0 vs. 2 = 71.21	0.04
	3 = poor**					1 vs. 2 = 62.27	0.11
(B) in pN1 postmenopausal cases							
Variable	Scale	Average RS (n =) in group				PCC (%)	c-value§
		0	1	2	3		
Stage	0 = IB	4.00 (2)	13.25 (4)	11.83 (12)	8.50 (2)	66.50	0.04
	1 = IIA					0 vs.1 = 100.00	0.07
	2 = IIB					0 vs. 2 = 90.00	0.03

(Continued on following page)

TABLE 6 (*Continued*) Significant results of randomisation (omnibus; complete*) and pairwise ordinal analysis by OOM (multigrams, PCC and c-values).

(B) in pN1 postmenopausal cases							
Variable	Scale	Average RS (n =) in group				PCC (%)	c-value§
		0	1	2	3		
	3 = IIIA					0 vs. 3 = 66.67	0.39
						1 vs. 2 = 67.50	0.12
						1 vs. 3 = 58.33	0.40
						2 vs. 3 = 46.67	0.56
Grade	0 = I	7.86 (7)	12.69 (13)	-	-	71.36	0.01
	1 = II					0 vs. 1 = 67.25	0.05
	2 = III					0 vs.2 = 100.00	0.08
						1 vs. 2 = 94.74	0.10
PR (%)	-	-	-	-	-	72.78	0.02
PR group	0 = negative	8.50 (2)	14.50 (2)	10.88 (16)	-	69.63	0.03
	1 = low					0 vs. 1 = 50.00	0.49
	2 = high					0 vs. 2 = 78.07	0.02
Ki-67 group	0 = low	8.76 (13)	15.40 (5)	14.50 (2)	-	65.74	0.06
	1 = intermediate					0 vs. 1 = 74.07	0.02
	2 = high					0 vs. 2 = 50.00	0.52
						1 vs. 2 = 22.22	0.87
LVI	0 = no	6.50 (8)	14.00 (12)	-	-	69.19	0.03
	1 = yes						
NPI	-	-	-	-	-	69.44	0.04
NPI Risk group	0 = good	9.67 (3)	8.83 (6)	12.54 (11)	-	68.02	0.03
	1 = moderate I					0 vs. 1 = 50.00	0.49
	2 = moderate II					0 vs. 2 = 79.63	0.04
						1 vs. 2 = 66.67	0.08

*Omnibus PCC, aggregates the PCCs of ordinal analysis for pN1 and pN1 postmenopausal subgroup. Complete PCC values were calculated only for the pN1 cohort with corresponding c-values. This refers to the ideal situation, when the RS scores matched the ordinal pattern of the categorised variable, and the case was regarded as "Complete Classification."
#For Ki-67 group and NPI, Risk Group in the pN1 cohort, the complete PCCs were not significant (included in Supplementary Material S2).
##For Ki-67 (%) the omnibus and complete PCCs, are the same, because two groups were compared (RS < 26 and RS ≥ 26).
###For PNI, and LVI, the omnibus and complete PCCs, are the same, because two groups were compared.
**In NPI-poor group only one case was present, therefore this case was not included in the analysis.
§c-values are regarded significant <10% along with PCC>60%.
c-value, chance value; ER, estrogen receptor; LVI, lymphovascular invasion; NPI, nottingham prognostic index; OOM, observation oriented modeling; PCC, percent of correct classification; PNI, perineural invasion; PR, progesteron receptor.

In 2004 the results of the validation study of OncotypeDX were published, which predicted the likelihood of distant recurrence in tamoxifen-treated ER-positive, HER2 normal and pN0 early BC [24]. This 21-gene analysis investigates 16 cancer-related genes, and 5 reference genes in the specimen after complete resection of the primary BC [25]. Cancer-related genes are classified into five groups coupled with: 1. Estrogen receptor pathway (ER, PR, Bcl2 and SCUBE2); 2. Proliferation (Ki-67, STK15, Survivin, Cyclin B1 and MYBL2); 3. HER2 receptor pathway (GRB7, HER2); 4. Invasion (Stromelysin 3, Cathepsin L2); and 5. Other processes i.e., progression (CD68), protection against oxidative stress

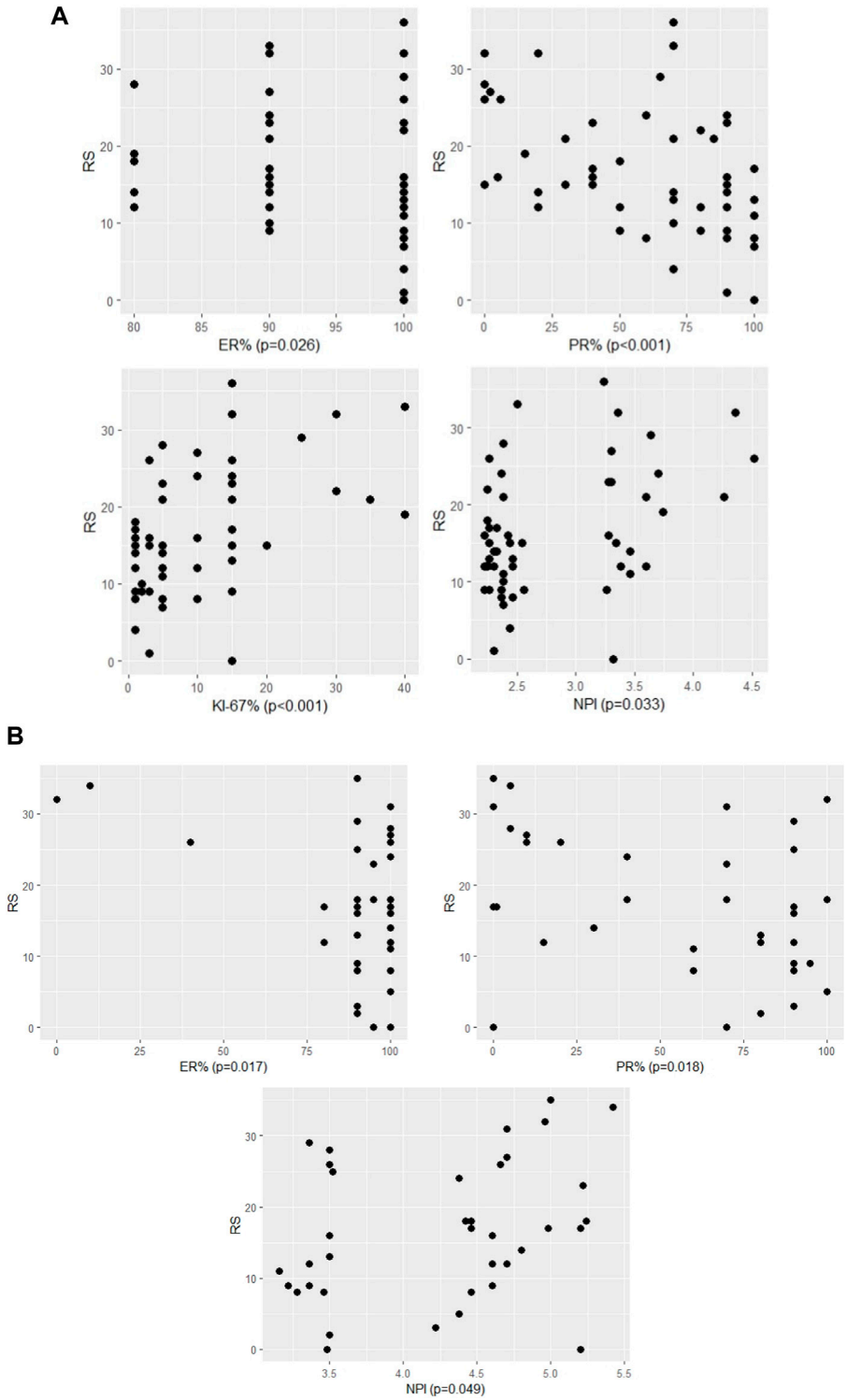

FIGURE 1
The significant association between RS and continous variables of characteristics **(A)** in pN0 cases: four characteristics (*p*-values of Spearman correlation) **(B)** in pN1 cases: three characteristics (*p*-values of Pearson correlation).

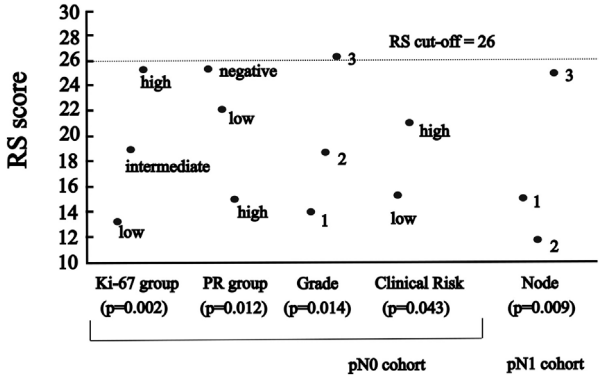

FIGURE 2
The significant association between RS and categorised variables of characteristics **(A)** in pN0 cases: four characteristics (*p*-values for Ki-67 group, PR group and grade of Kruskal-Wallis; for clinical risk of Mann-Whitney) **(B)** in pN1 cases: one characteristic (*p*-value for number of nodes of ANOVA).

(GSTM1), and pathogenesis or progression (BAG1). Reference genes used in this assay play a role in cellular function (Beta-actin), energy metabolism (GAPDH), deoxyribonucleic acid repair (RPLP0), glycosyl hydrolysis (GUS) and iron transport (TFRC). Based on OncotypeDX analysis, the RS is generated with the value between 0 and 100.

In 2006 and 2009 the results of the analysis of the prospective-retrospective NSABP-B20 trial were published [26], which predicted the benefit of addition of chemotherapy to tamoxifen in pN0, ER positive BC in case of high RS (≥31).

In 2010 the results of the prospective-retrospective Southwest Oncology Group (SWOG) 8,814 trial demonstrated [27], that in pN1 and ER-positive patients with high RS (≥31) had the benefit of chemotherapy.

In 2017 the results of the prospective phase III PlanB trial were published, which compared the prognostic value of histological grade, ER, PR, and Ki-67 with that of a genomic-signature, confirming their prognostic value in univariate analysis. However, RS eliminated them in the multivariate analysis [28].

In 2018 the results of the prospective TAILORx study (n = 10,273) revealed [8], that in patients >50 years with RS < 26, and in patients <50 years with RS < 16 chemotherapy did not decrease the risk of recurrence significantly compared to endocrine therapy in pT1b, pN0 with grade 3, or pT1c-3, pN0 (grade 1–3) disease. Chemotherapy was not necessary in approximately 85% of patients. To determine clinical risk, the same criteria were used in the TAILORx as in the MINDACT randomised phase 3 trial (n = 6,693) based on tumour size and histological grade. The results were published in 2016, where the investigators described, that based on the 70-gene signature about 46% of 1,550 patients with high clinical risk might not require chemotherapy [18]. In TAILORx, four cohorts of patients were analysed: high RS (≥26) received chemoendocrine therapy; one of two cohorts of RS with 11–25 was treated with chemoendocrine treatment, and the other with endocrine therapy alone; for low RS (≤10) cases endocrine therapy was administered. Proportions of patients with high Clinical Risk were determined of these cohorts in the following order: 57%, 27%, 26%, and 22%, respectively [8].

In 2021 the results of the prospective RxPONDER trial (n = 5,083) were presented [9], which showed, that pT1-3, pN1

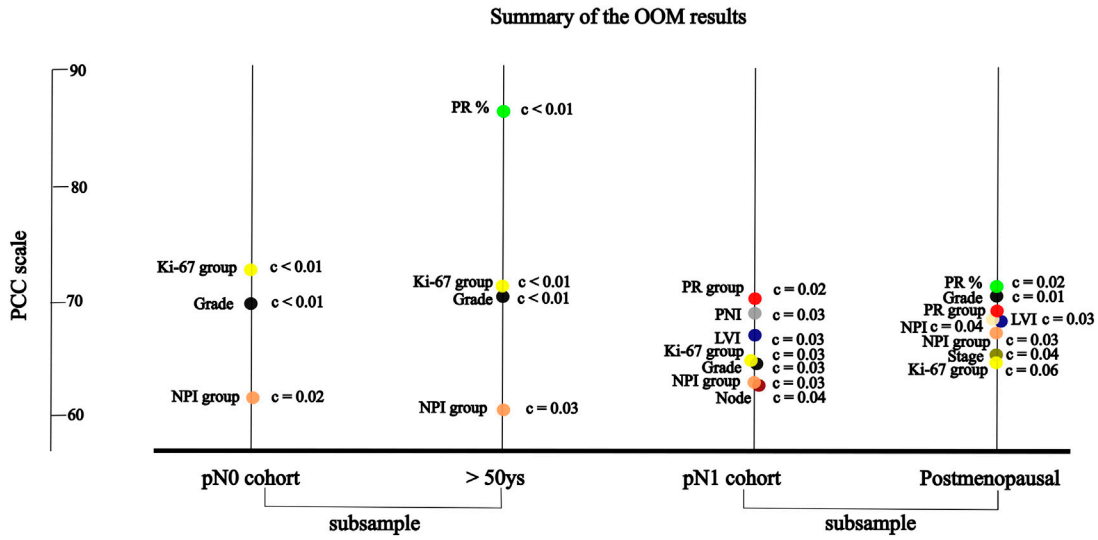

FIGURE 3
The significant association between RS and variables of characteristics by randomisation results of OOM **(A)** in pN0 cases: three characteristics; four characteristics in >50 years cohort **(B)** in pN1 cases: seven characteristics; eight characteristic in postmenopausal cohort.

TABLE 7 Significant results of randomisation (omnibus; complete*) and pairwise ordinal analysis by OOM on joint pN0 and pN1 cohorts (multigrams, PCC and c-values).

Variable	Scale	PCC (%)	c-value§
PR group	0 = negative	75.00; 39.00*	0.001; <0.01
	1 = low	0 vs. 1 = 53.75	0.35
	2 = high	0 vs. 2 = 73.36	0.01
		1 vs. 2 = 78.55	<0.01
Ki-67 group	0 = low	69.51; 30.41*	<0.001; 0.01
	1 = intermediate	0 vs. 1 = 69.08	<0.001
	2 = high	0 vs. 2 = 79.63	0.01
		1 vs. 2 = 56.28	0.26
PNI	0 = no	66.19**	0.01
	1 = yes		

*Omnibus PCC aggregates the PCCs of ordinal analysis. Complete PCC, values were calculated with corresponding c-values. This refers to the ideal situation, when the RS scores matched the ordinal pattern of the categorised variable, and the case was regarded as, "Complete Classification."
**For PNI the omnibus and complete PCCs are the same, because two groups were compared.
§c-values are regarded significant <10% along with PCC>60%.
c-value, chance value; OOM, observation oriented modeling; PCC, percent of correct classification; PNI, perineural invasion; PR, progesteron receptor.

(pN1mi excluded) postmenopausal patients with RS < 26 had no benefit of adding chemotherapy to endocrine treatment (in about 67%), while premenopausal patients with RS < 26 did have decreased risk of distant recurrence with the administration of chemotherapy (relative increase of 40% in invasive disease-free survival and 42% in distant relapse-free survival). A prospective randomised controlled trial is necessary to clarify, whether the benefit seen in premenopausal patients is attributed only to the ovarian suppression by the chemotherapy.

The authors analysed their data using both the traditional statistical methods (non-parametric as well as parametric) and the OOM methodology first in onclogy. During the analysis, the conforming variables were the pathological characteristics [for pN0 cases Tumour size, grade, PNI, LVI, ER (%), PR (%), PR group, Ki-67 (%), Ki-67 group, stage, clinical risk, NPI, NPI risk group; for the pN1 cohort all characteristics of the pN0 cohort were analysed except clinical risk, and the number of positive nodes] and the target variable was the RS.

In 2011 OOM was introduced as a relatively new methodology [12], mainly applied to ordered or categorical data, and is very similar to the traditional non-parametric methods as it can be performed without assuming normality and equal subsample variances or homoscedasticity. OOM focuses on patterns of variations observed [13]. Moreover, non-parametric methods are very popular and can also tackle with the above-mentioned challenges. Traditional hypothesis testing has many pitfalls, which has been criticised for focusing on the selection of the appropriate test statistic and finding lower *p*-values [29]. OOM provides a simple statistic, the PCC, making it possible to compare and rank influential factors across the analyses. The other advantage of OOM is that it also focuses on actual replicability of the given data by relying on randomisation tests and the chance value (c-value) rather than *p*-values. These feature might be very useful when dealing with relatively small samples. For the application of pairwise ordinal analysis of OOM, researchers are required to hypothesise an expected pattern of results and then determine how many individuals or entities match that predicted pattern [30]. OOM has been used for numerous investigations so far, i.e., social reinforcement delays, timing, taste aversion learning, and is also recommended in comparative psychology of neuroscience research [30]. For the analyses relying on multigrams, prior predications are not necessary. The analysis classifies the observations based on their patterns of frequencies, and then the researcher interprets the meaning (if there is one) of the pattern in the multigram.

Similar to the results of the present analyses, in a retrospective study (n = 461) there was no correlation between Ki-67 values and RS in the overall population. High Ki-67 values were associated with high RS, however, 68% of patients with high Ki-67 values had low RS. 6% of patients with low Ki-67 values had high RS. In conclusion, the Ki-67 value has limited utility in identifying patients with high or low RS [31]. The prognostic role of PR and Ki-67 levels have been retrospectively (n = 687) confirmed recently [32].

On retrospective analysis of TAILORx data [33], the distant recurrence-free survival of patients (n = 2,246) with Anne Arundel Medical Center (AAMC) low risk (i.e., with grade 1, PR>3% and ER>20%) tumours did not differ for those, who received adjuvant

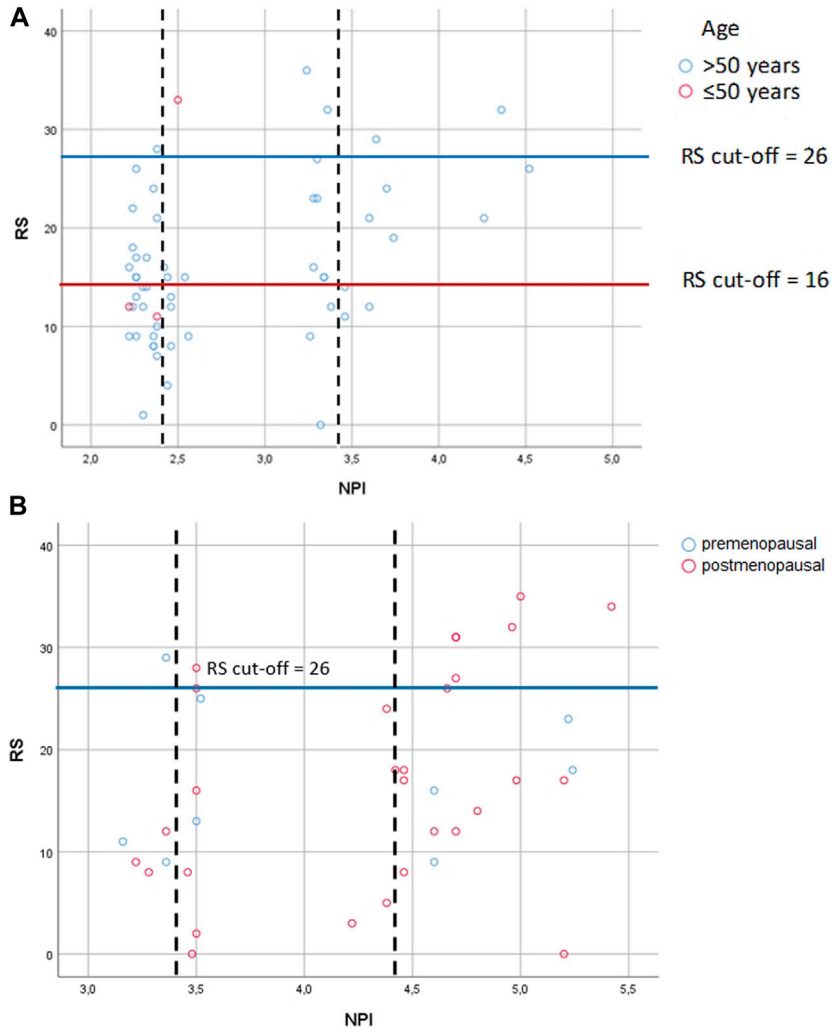

FIGURE 4
Correlation between RS and NPI risk groups **(A)** in pN0 cases: Spearman ρ = 0.286 (p = 0.033); dashed lines: thresholds for NPI between the excellent (≤2.4) and the good (>2.4 and ≤3.4); the good (>2.4 and ≤3.4) and the moderate (>3.4) groups; correlation between NPI score and RS for patients with the excellent group [Spearman ρ = −0.151 (p = 0.435)]; correlation between NPI score and RS with the good group [Spearman ρ = 0.159 (p = 0.541)]; correlation between NPI score and RS with the moderate groups [Spearman ρ = 0.719 (p = 0.019)] **(B)** in pN1 cases: Pearson correlation r = 0.322 (p = 0.049); dashed lines: thresholds for NPI between the good (>2.4 and ≤3.4) and the moderate I (>3.4 and ≤4.4); the moderate I (>3.4 and ≤4.4) and the moderate II (>4.4) groups; correlation between NPI score and RS for patients with the good group [Pearson r = 0.399 (p = 0.434)]; correlation between NPI score and RS for patients with the moderate I group [Pearson r = 0.025 (p = 0.945)]; correlation between NPI score and RS for patients with the moderate II group [Pearson r = 0.294 (p = 0.185)] RS = recurrence score generated through OncotypeDX testing; RS cut-off: for pN0 >50years high RS ≥ 26, and ≤50 years high RS ≥ 16, for pN1 pre- and postmenopausal high RS ≥ 26; NPI = Nottingham Prognostic Index.

chemotherapy versus those who did not (98% vs. 96%, p = 0.46). Thus, in conclusion, OncotypeDX testing does not benefit in this population. Here, if the authors applied AAMC criteria for the pN0 cohort, 57% (32/56) of cases would be classified as low risk, however, one patient had high RS (=33), who would have not been tested by OncotypeDX based on AAMC criteria.

In 1982 NPI was described by multiple-regression analysis of 387 BC patients [17]. NPI generates 5 and 10-year survival score and is most commonly used to guide adjuvant chemotherapy in early BC. However, it is demonstrated, that NPI significantly underestimates 10-year overall survival in both young and old patients [34]. Although OncotypeDX has advantage compared to NPI, there is an effort to select those patients, which probably most benefit from OncotypeDX, and at the same time to exclude those, who may have low RS based on predicting tools. For instance, the National Institute of Health and Care Excellence (NICE) recommends OncotypeDX for moderate risk NPI (>3.4) [35]. By the NICE recommendation, a retrospective study in the United Kingdom with pN0 patients (n = 46) demonstrated, that low risk NPI (excellent and good NPI risk groups) strongly correlates with RS, therefore OncotypeDX

may be unnecessary for low risk NPI saving significant costs [36]. An other retrospective analysis in Ireland with pN0 patients (n = 1,382) found, that 329 patients underwent OncotypeDX testing, but neither NPI nor RS were predictors of survival. While for the entire study population NPI predicted both disease free survival and overall survival independently, thus the authors concluded, that NPI outperformed RS as providing accurate prognostication in BC [37]. These results here (Figures 4A, B), did not confirm the strong association found between RS and NPI in the excellent/good NPI groups of the previous study [35]. If the authors applied the NICE recommendation for the pN0 and pN1 cases, they would acknowledge, that 18% (10/56) of the pN0 cohort and 81% (31/38) of the pN1 cohort would have only been tested (NPI>3.4). However, there was also a high RS observed in 13% (6/46) of pN0 cases with excellent and good prognosis. Regarding pN1 cases, 83.3% (5/6) of pN1 cases with good prognosis had a high RS. In 22.86% of pN0 cases excellent, good, and moderate groups were correlated with lower and higher RS. Similarly in 20.83% of pN1 cases good, moderate I, II and poor groups were non-significantly correlated with lower and higher RS [38].

Although the significant association between PNI or LVI and RS has been demonstrated in this present study, a retrospective analysis (n = 445) did not find significant impact of the presence of PNI, LVI or ER intensity on concordance between OncotypeDX and PREDICT. Patients with PREDICT very low risk (grade 1, tumour ≤1 cm, PR positive, Ki-67 < 10%) may be treated based on clinical risk assessment without performing OncotypeDX [37]. Since 2011 PREDICT as an online tool [39], has estimated the absolute benefit of adjuvant treatment on overall survival by using large cancer registries without delay in decision-making and additional costs. Based on a recent retrospective analysis (n = 191), PNI was proven as an independent unfavorable prognostic factor for distant metastasis-free survival and disease specific survival, thereofore the researchers concluded, that PNI could be useful in predicting aggressive phenotypes in BC [40].

The results of this retrospective analysis demonstrate the same pattern as PlanB trial. In comparison with the results of TAILORx, here chemotherapy was spared in 83.6% (46/55) of the cases with pN0 (vs. 85% in TAILORx).

This analysis has some limitations. First, the total number of patients is relatively small. Second, only the association between the pathological characteristics and RS was analysed, and no survival analysis was performed due to the short follow-up time (only 5 years were elapsed from the first OncotypeDX test). Third, the results of the statistical analyses cannot be applied for individual cases. There were a few patients, where no clinical associations were established between characteristics and RS, contrary to the statistically significant differences.

Conclusion

The authors have found that chemotherapy could be spared for >83% of pN0 and >72% of pN1 cases using OncotypeDX. They analysed the association between pathological characteristics and recurrence score with traditional statistical methods and OOM first in oncology. Some characteristics were found significant by OOM compared to the traditional statistical methods, providing a meaningful insight into the studied phenomenon. Furthermore, the order of significant characteristics was also established by OOM. While significant associations were found between particular pathological characteristics and RS, these results are not able to provide the bases for screening patients, to determine, if they require OncotypeDX testing or not. It is also worth mentioning that some patients in these cohorts had a low RS with unfavorable characteristics, while other patients had unexpectedly high RS with tumor characteristics usually recognised as favorable (Supplementary Material S4). Thus, implementing the 21-gene assay in the clinical routine appears favorable for these patients, providing a better risk estimation, and aiding treatment decisions. Based on the data of the literature it seems, that very low risk patients (e.g., according PREDICT) may have no benefit of OncotypeDX testing, since very low risk strongly associates with RS. It also should be emphasised, that if only one patient can be identified with a high risk of recurrence by OncotypeDX among the very low risk population determined by e.g. PREDICT, or the opposite, i.e., low risk of recurrence by OncotypeDX in high-risk population, the goal of personalised approach would be fulfilled.

Data availability statement

The original contributions presented in the study are included in the article/Supplementary Material, further inquiries can be directed to the corresponding author.

Ethics statement

The studies involving human participants were reviewed and approved by Hungarian Medical Research Council (No. BM/14679-1/2023). The patients did not provide written informed consent to participate in this study in view of the retrospective nature of the study.

Author contributions

DD had the idea, collected the data, summarised them in a datasheet, created the tables of statistical results, and wrote the manuscript. BT has reviewed the manuscript, contributed in

the interpretation of the results and created the Box-plots. NJ created the institutional pathology reports, and summarised the pathological characteristics in a data sheet. SK has performed all statistical tests, and drawn the statistical figures. EK created the tables of the patient characteristics. JG supported the statistical analysis, and contributed to the methods and the discussion section. AT supported the study and critically reviewed the manuscript. All authors contributed to the article and approved the submitted version.

Funding

The author(s) declare that financial support was received for the research, authorship, and/or publication of this article. The authors declare that the publication fee of this study is covered by MED GEN-SOL Ltd., Hungary. The funder was not involved in the study design, collection, analysis, interpretation of data, the writing of this article or the decision to submit it for publication.

Conflict of interest

The authors declare that the research was conducted in the absence of any commercial or financial relationships that could be construed as a potential conflict of interest.

Acknowledgments

Hereby the authors of this work thank the detailed evaluations and the valuable suggestions of Med. Habil. Andrea Furka, Oncology Clinic of the Clinical Center at the Debrecen University, Debrecen, Hungary.

Supplementary material

The Supplementary Material for this article can be found online at: https://www.por-journal.com/articles/10.3389/pore.2024.1611735/full#supplementary-material

References

1. WHO. *International agency for research on cancer*. Hungary: World Health Organization (2023). Available from: https://gco.iarc.fr/today/data/factsheets/populations/348-hungary-fact-sheets.pdf (Accessed June 01, 2023).

2. Hungarian National Cancer Registry. *Hungarian national cancer Registry* (2023). Available from: https://stat.nrr.hu/nrrstat/regi/0 (Accessed June 01, 2023).

3. Dyba T, Randi G, Bray F, Martos C, Giusti F, Nicholson N, et al. The European cancer burden in 2020: incidence and mortality estimates for 40 countries and 25 major cancers. *Eur J Cancer* (2021) 157:308–47. doi:10.1016/j.ejca.2021.07.039

4. ECIS. *European cancer information system (ECIS)* (2020). Available from: https://stat.link/p4cg6v (Accessed June 01, 2023).

5. Kenessey I, Szőke G, Dobozi M, Szatmári I, Wéber A, Fogarassy G, et al. Comparison of cancer survival trends in Hungary in the periods 2001-2005 and 2011-2015 according to a population-based cancer Registry. *Pathol Oncol Res* (2022) 28:1610668. doi:10.3389/pore.2022.1610668

6. Fisher B, Dignam J, Bryant J, Wolmark N. Five versus more than five years of tamoxifen for lymph node-negative breast cancer: updated findings from the National Surgical Adjuvant Breast and Bowel Project B-14 randomized trial. *J Natl Cancer Inst* (2001) 93:684–90. doi:10.1093/jnci/93.9.684

7. Fisher B, Dignam J, Wolmark N, DeCillis A, Emir B, Wickerham DL, et al. Tamoxifen and chemotherapy for lymph node-negative, estrogen receptor-positive breast cancer. *J Natl Cancer Inst* (1997) 89:1673–82. doi:10.1093/jnci/89.22.1673

8. Sparano JA, Gray RJ, Makower DF, Pritchard KI, Albain KS, Hayes DF, et al. Adjuvant chemotherapy guided by a 21-gene expression assay in breast cancer. *N Engl J Med* (2018) 379:111–21. doi:10.1056/NEJMoa1804710

9. Kalinsky K, Barlow WE, Gralow JR, Meric-Bernstam F, Albain KS, Hayes DF, et al. 21-Gene assay to inform chemotherapy benefit in node-positive breast cancer. *N Engl J Med* (2021) 385:2336–47. doi:10.1056/NEJMoa2108873

10. Breast Cancer. *National comprehensive cancer Network (NCCN) clinical practice guidelines in oncology, version 1* (2024). Available from: https://www.nccn.org/professionals/physician_gls/pdf/breast.pdf (Accessed January 31, 2024).

11. National Comprehensive Cancer Network. *Clinical practice guidelines in oncology, breast cancer version 1.2018 (may 20), 3.2018 (october 25), 3.2019 (september 6), 5.2020 (july 15), 8.2021 (september 13), 4.2022 (June 21) and 4.2023 (march 23)* (2023). Available from: https://www.nccn.org/ (Accessed July 19, 2018 for 1.2018; November 23, 2018 for 3.2018; November 11, 2019 for 3.2019; September 4, 2020 for 5.2020; October 7, 2021 for 8.2021; July 4, 2022 for 4.2022; June 12, 2023 for 4.2023).

12. Grice JW. *Observation oriented modeling: analysis of cause in the behavioral Sciences*. Academic Press, Elsevier (2011).

13. Grice JW, Cota LD, Barrett PT, Wuensch KL, Potetat GM. A simple and transparent alternative to logistic regression. *Adv Soc Sci Res J* (2016) 3:147–65. doi:10.14738/assrj.37.2125

14. Elston CW, Ellis O. Pathological prognostic factors in breast cancer. I. The value of histological grade in breast cancer: experience from a large study with long-term follow-up. *Histopathology* (1991) 19:403–10. doi:10.1111/j.1365-2559.1991.tb00229.x

15. Dowsett M, Nielsen TO, A'Hern R, Bartlett J, Coombes RC, Cuzick J, et al. Assessment of Ki67 in breast cancer: recommendations from the international Ki67 in breast cancer working group. *J Natl Cancer Inst* (2011) 103:1656–64. doi:10.1093/jnci/djr393

16. Nielsen TO, Leung SCY, Rimm DL, Dodson A, Acs B, Badve S, et al. Assessment of Ki67 in breast cancer: updated recommendations from the international Ki67 in breast cancer working group. *J Natl Cancer Inst* (2021) 113:808–19. doi:10.1093/jnci/djaa201

17. Haybittle JL, Blamey RW, Elston CW, Johnson J, Doyle PJ, Campbell FC, et al. A prognostic index in primary breast cancer. *Br J Cancer* (1982) 45:361–6. doi:10.1038/bjc.1982.62

18. Allison KH, Hammond ME, Dowsett M, McKernin SE, Carey LA, Fitzgibbons PL, et al. Estrogen and progesterone receptor testing in breast cancer: American Society of Clinical Oncology/College of American Pathologists guideline update. *Arch Pathol Lab Med* (2020) 144:545–63. doi:10.5858/arpa.2019-0904-SA

19. Dash SS, Sahu A, Toppo A. p53 expression in breast carcinoma and its association with tumor aggressiveness. *J Datta Meghe Inst Med Sci Univ* (2021) 16:266–72. doi:10.4103/jdmimsu.jdmimsu_10_21

20. Galea MH, Blamey RW, Elston CE, Ellis IO. The Nottingham prognostic index in primary breast cancer. *Breast Cancer Res Treat* (1992) 22:207–19. doi:10.1007/BF01840834

21. Blamey RW, Ellis IO, Pinder SE, Lee AH, Macmillan RD, Morgan DA, et al. Survival of invasive breast cancer according to the Nottingham Prognostic Index in cases diagnosed in 1990-1999. *Eur J Cancer* (2007) 43:1548–55. doi:10.1016/j.ejca.2007.01.016

22. Cardoso F, van't Veer LJ, Bogaerts J, Slaets L, Viale G, Delaloge S, et al. 70-Gene signature as an aid to treatment decisions in early-stage breast cancer. *N Engl J Med* (2016) 375:717–29. doi:10.1056/NEJMoa1602253

23. Grice JW. Drawing inferences from randomization tests. *Personal Individual Differences* (2021) 179:110931. doi:10.1016/j.paid.2021.110931

24. Paik S, Shak S, Tang G, Kim C, Baker J, Cronin M, et al. A multigene assay to predict recurrence of tamoxifen-treated, node-negative breast cancer. *N Engl J Med* (2004) 351:2817–26. doi:10.1056/NEJMoa041588

25. Paik S, Tang G, Shak S, Kim C, Baker J, Kim W, et al. Gene expression and benefit of chemotherapy in women with node-negative, estrogen receptor-positive breast cancer. *J Clin Oncol* (2006) 24:3726–34. doi:10.1200/JCO.2005.04.7985

26. Simon RM, Paik S, Hayes DF. Use of archived specimens in evaluation of prognostic and predictive biomarkers. *J Natl Cancer Inst* (2009) 101:1446–52. doi:10.1093/jnci/djp335

27. Albain KS, Barlow WE, Shak S, Hortobagyi GN, Livingston RB, Yeh IT, et al. Prognostic and predictive value of the 21-gene recurrence score assay in postmenopausal women with node-positive, oestrogen-receptor-positive breast cancer on chemotherapy: a retrospective analysis of a randomised trial. *Lancet Oncol* (2010) 11:55–65. doi:10.1016/S1470-2045(09)70314-6

28. Nitz U, Gluz O, Christgen M, Kates RE, Clemens M, Malter W, et al. Reducing chemotherapy use in clinically high-risk, genomically low-risk pN0 and pN1 early breast cancer patients: five-year data from the prospective, randomised phase 3 West German Study Group (WSG) PlanB trial. *Breast Cancer Res Treat* (2017) 165:573–83. doi:10.1007/s10549-017-4358-6

29. Valentine KD, Buchanan EM. JAM-boree: an application of observation oriented modeling to judgements of associative memory. *J Cogn Psychol* (2013) 25:400–22. doi:10.1080/20445911.2013.775120

30. Abramson CI. Why the study of comparative psychology is important to neuroscientists. *Front Behav Neurosci* (2023) 16:1095033. doi:10.3389/fnbeh.2022.1095033

31. Patel R, Hovstadius M, Kier MW, Moshier E, Zimmerman BS, Cascetta KP, et al. *Correlation of Ki67 working group prognostic risk categories with oncotype DX recurrence score (RS) in early breast cancer (EBC)*. Wiley Online Library (2022). Available at: https://onlinelibrary.wiley.com/. downloaded from ascopubs.org on June 15, 2023.

32. Diana A, Carlino F, Buono G, Antoniol G, Famiglietti V, De Angelis C, et al. Prognostic relevance of progesterone receptor levels in early luminal-like HER2 negative breast cancer subtypes: a retrospective analysis. *Front Oncol* (2022) 12:813462. doi:10.3389/fonc.2022.813462

33. Sibia US, Mylander C, Martin T, Rosman M, Sanders TJ, Lee Y, et al. OncotypeDX testing does not benefit patients with estrogen and progesterone receptor positive grade 1 breast cancers: a TAILORx validated study. *Hematol Oncol Stem Cel Ther* (2023) 16:412–9. doi:10.56875/2589-0646.1089

34. Lambertini M, Pinto AC, Ameye L, Jongen L, Del Mastro L, Puglisi F, et al. The prognostic performance of Adjuvant! Online and Nottingham Prognostic Index in young breast cancer patients. *Br J Cancer* (2016) 115:1471–8. doi:10.1038/bjc.2016.359

35. NICE Guidance. *NICE Guidance [DG34]: tumour profiling tests to guide adjuvant chemotherapy decisions in early breast cancer* (2018). Available from: https://www.nice.org.uk/guidance/dg34 (Accessed June 01, 2023).

36. Hillyar C, Rizki H, Abbassi O, Miles-Dua S, Clayton G, Gandamihardja T, et al. Correlation between oncotype DX, PREDICT and the Nottingham prognostic index: implications for the management of early breast cancer. *Cureus* (2020) 12:e7552. doi:10.7759/cureus.7552

37. Kerin EP, Davey MG, McLaughlin RP, Sweeney KJ, Barry MK, Malone CM, et al. Comparison of the Nottingham Prognostic Index and OncotypeDX© recurrence score in predicting outcome in estrogen receptor positive breast cancer. *Breast* (2022) 66:227–35. doi:10.1016/j.breast.2022.11.001

38. Goldstein DA, Mayer C, Shochat T, Reinhorn D, Moore A, Sarfaty M, et al. The concordance of treatment decision guided by OncotypeDX and the PREDICT tool in real-world early-stage breast cancer. *Cancer Med* (2020) 9:4603–12. doi:10.1002/cam4.3088

39. Predict breast cancer. *What is Predict?* (2023). Available from: https://breast.predict.nhs.uk/predi%E2%80%8Bct_v2.1/tool (Accessed August 10, 2023).

40. Hosoya K, Wakahara M, Ikeda K, Umekita Y. Perineural invasion predicts unfavorable prognosis in patients with invasive breast cancer. *Cancer Diagn Progn* (2023) 3:208–14. doi:10.21873/cdp.10203

Pathology & Oncology Research | frontiers

TYPE Original Research
PUBLISHED 02 December 2024
DOI 10.3389/pore.2024.1611987

Check for updates

OPEN ACCESS

EDITED BY
Anna Sebestyén,
Semmelweis University, Hungary

*CORRESPONDENCE
Zsófia Kramer,
kramer.zsofia@semmelweis.hu

RECEIVED 02 October 2024
ACCEPTED 20 November 2024
PUBLISHED 02 December 2024

CITATION
Kramer Z, Budai A, Pesti A, Kulka J and Tőkés A-M (2024) Invasive micropapillary carcinoma of the breast and invasive breast carcinoma of no special type: a comparison of claudin proteins' expression and its impact on survival.
Pathol. Oncol. Res. 30:1611987.
doi: 10.3389/pore.2024.1611987

COPYRIGHT
© 2024 Kramer, Budai, Pesti, Kulka and Tőkés. This is an open-access article distributed under the terms of the Creative Commons Attribution License (CC BY). The use, distribution or reproduction in other forums is permitted, provided the original author(s) and the copyright owner(s) are credited and that the original publication in this journal is cited, in accordance with accepted academic practice. No use, distribution or reproduction is permitted which does not comply with these terms.

Invasive micropapillary carcinoma of the breast and invasive breast carcinoma of no special type: a comparison of claudin proteins' expression and its impact on survival

Zsófia Kramer *, András Budai, Adrián Pesti, Janina Kulka and Anna-Mária Tőkés

Department of Pathology, Forensic and Insurance Medicine, Semmelweis University, Budapest, Hungary

Invasive micropapillary carcinoma of the breast is characterized by clusters of cells presenting with inverted polarity. Although the apico–basal polarity is a fundamental property of the epithelium, the biological alterations leading to the inside-out pattern observed in invasive micropapillary carcinoma (IMPC) remain mostly unknown. The regulation of tight junctions in polarity formation and maintenance is acknowledged. By using immunohistochemistry, we have analysed claudin-1, -3, -4, and -7 tight junction proteins expression and their prognostic value on IMPCs and compared them to invasive breast carcinomas of no special type (IBC-NST) tumors. Our cohort consisted of 37 IMPCs, 36 IBC-NST and 9 mixed IMPC/IBC-NST tumors. Two scoring systems were used to quantify protein expression: a 4-tier scoring system and the H-score method. Distant metastasis free survival (DMFS) intervals and overal survival (OS) data were used for prognosis evaluation. The analysed samples were characterized mainly by low or no claudin-1 expression whereas claudins-3, -4 and -7 showed variable positivity. We have found no significant differences in claudin-3 and -4 protein expression between IMPC and IBC-NST groups with either scoring methods, however high claudin-7 expression was found in significantly more IMPCs than IBC-NST tumors according to the H-score system (p = 0.02). The 4-tier scoring method revealed association of claudin-7 expression with molecular tumor subtypes (p = 0.001). IMPC and IBC-NST tumors did not show difference in DMFS (p = 0.70). In the analysis of pure IMPC and IBC-NST tumors, positive/high claudin-4 protein expression was

Abbreviations: IMPC, Invasive micropapillary carcinoma; IBC-NST, Invasive breast carcinoma of no special type; DMFS, Distant metastasis free survival; OS, Overall survival; HR, Hazard ratio value; EMA, Epithelial membrane antigen; JAM-A, junctional adhesion molecule A; ZO-1, ZO-2, ZO-3, Zonula occludens-1, -2 and -3; DCIS, Ductal carcinoma *in situ*; *CLDN1, -3, -4, -7*, claudin-1, -3, -4 and -7 genes; LUM-A, Luminal-A; LUM-B1, Luminal B-HER2 negative; LUM-B2, Luminal B-HER2 positive; TNBC, Triple negative breast carcinoma; HR+, Hormone receptor positive; HR-, Hormone receptor negative; FFPE, Formalin fixed paraffin embedded; TJ, Tight junction; TGF-ß, Transforming growth factor-ß; ER, Estrogen receptor.

significantly associated with shorter DMFS (p = 0.02/p = 0.008, respectively according to the two scoring methods). Claudin-3 and claudin-7 expression showed no association with DMFS or OS. Changes in epithelial polarity seem not to be related to claudin-1, -3, and -4 expression. Increased claudin-4 expression may have a role in breast cancer progression.

KEYWORDS

invasive micropapillary carcinoma of the breast, invasive breast carcinoma of no special type, claudin expression, tight junction, prognosis

Introduction

Invasive micropapillary carcinoma of the breast, is a special carcinoma phenotype composed of small, hollow, or morula-like clusters of malignant cells, surrounded by clear spaces and presenting an inside-out growth pattern with epithelial membrane antigen (EMA). In pure invasive micropapillary carcinoma (IMPC), >90% of the tumour consists of hollow or morula-like aggregates of cuboidal to columnar neoplastic cells. IMPC has been described in tumors of several tissues, such as breast, urinary bladder, stomach, colon, pancreas and lung [1–4]. Although this histological subtype is well defined, the underlying mechanisms leading to its unique appearance are not fully understood. IMPCs comprise 1%–8.4% of all breast carcinomas [5, 6] and were previously thought to have poor prognosis, however, recent studies, as well as our previous study have shown no difference in outcome compared to invasive breast carcinomas of no special type (IBC-NST) [7–10].

Several research groups have studied the genetic alterations present in pure IMPCs and have found that these tumors comprise a heterogenous group with genetic alterations different from that of IBC-NST tumors [11, 12].

Cell polarity alterations and changes in the expression of cell adhesion and tight junction molecules have been widely studied in carcinogenesis and cancer progression, however their implication in the inside-out pattern observed in IMPCs is scarcely known. The majority of the studies focus on the eventual higher metastatic potential of IMPCs [13–15]. There are several open questions about the role of abnormal polarity in the direction of secretion and the interaction of these cells with tumor microenvironment.

Tight junctions, which form stable selective paracellular barriers between epithelial cells, are mostly located in the apical end of the lateral membrane of the cells, maintaining cell polarity and cell adhesion. Claudins, first described by Furuse et al. [16], are main components of the tight junctions and compose continuous strands in the apical region, but are also found along the lateral membrane as free strand ends. The turnover of claudins is continuous along the lateral membrane [17], providing stability to the tight junctions.

Claudins, together with other tight junction molecules play an important role in cell adhesion and cell polarity maintenance [18]. Zonula occludens-1, -2 and -3 (ZO-1, ZO-2, ZO-3) proteins independently, while junctional adhesion molecule A (JAM-A) together with claudins are required for epithelial polarity [19], among several other structures. The role of claudins in cancer progression have been in the focus of several studies. Altered expression of claudins in different cancer types plays role in tumor progression in a tissue-specific manner [20].

Of the 27 human claudins known to date the most intensively studied claudins in breast carcinomas are claudin-1, -3, -4 and -7. Several tumor features are associated with different claudins expression in breast carcinomas. Decreased or loss of claudin-1 expression has been shown to be associated with higher recurrence rate and metastatic potential and with poor prognosis [21]. On the other hand, high claudin-1 and -4 expression was found in a majority of "basal-like," triple negative breast carcinomas [22–24]. Some studies have shown correlation between claudin-3 and -4 expression and tumor grade [22, 25, 26], while other studies have found that certain breast cancer subtypes are associated with different claudin expression levels with different prognostic significance [21–32]. High level of cytoplasmic claudin-3 expression in triple negative breast carcinomas has been associated with poor survival [28].

Increased claudin-4 expression has been associated with higher tumor grade and with basal like phenotype [24, 32]. Decreased/loss of claudin-7 expression has been shown to correlate with histological grade in DCIS lesions as well as in invasive carcinomas [29, 31].

A subset of breast carcinomas show claudin "low" expression profile (as defined by decreased gene-expression of claudins-1, -3, -4, -7, and -8 [23], or by decreased expression of claudin-3, -4, -7, E-cadherin and calcium-dependent cell-cell adhesion glycoprotein [27, 30]). Histologically these tumors are mostly triple negative, high-grade tumors, commonly showing metaplastic or medullary features [23, 27, 30].

In our previous study we have compared claudin expression profiles of IMPCs and IBC-NST tumors on RNA level. We have found higher expression levels of *CLDN*s 3, 4, and 7, and lower *CLDN1* levels in IMPCs. We have also shown that high *CLDN3* expression level is associated with grade 3 tumors and with worse distant metastasis free survival (DMFS) [10].

The aim of our current study was to examine claudin expression on protein level in a mostly similar cohort, to analyse whether their expression is associated with prognosis and to compare RNA and protein expression levels of claudins.

To date – to the best of our knowledge - claudin protein expression has not been examined in IMPCs. Claudins, as part of the tight junction proteins might play role in the special histological appearance of IMPCs. Understanding their role may open new possibilities for targeted therapy of this special tumor subtype.

Materials and methods

Eighty-two breast carcinoma cases [37 IMPC, 36 age- and stage-matched IBC-NST (for statistical comparison) and 9 mixed IMPC/IBC-NST cases] were selected from the archive of the Department of Pathology, Forensic and Insurance Medicine - Semmelweis University, Budapest from the period of 2000–2021, with the ethical permission of Semmelweis University Research Ethics Committee (permission number: 240/2016). All cases were reviewed by expert pathologists and classified based on the World Health Organisation criteria [33]. Additionally, IMPC cases were confirmed by the typical inside-out staining pattern of EMA immunohistochemistry [34] (performed with automated Ventana BenchMark ULTRA system using Cell Marque Mouse Monoclonal antibody, 1:200). Breast cancer surrogate molecular subtypes were defined according to the St. Gallen International Expert Consensus – 2013 [35]. Tumor characteristics and patient data as well as clinical follow up information were obtained from the Semmelweis University Health Care Database and the National Cancer Registry.

Immunohistochemical analysis of claudin-1, -3, -4, and -7

Formalin fixed paraffin embedded tissues were used to perform immunohistochemical studies. 3–5 μm thick sections were cut, and immunohistochemical reactions were performed on Ventana BenchMark Ultra system according to the Universal UltraView DAB manufacturer's protocol. The following primary antibodies were used: claudin-1 (Cell Marque, Rabbit polyclonal antibody, 1: 100), claudin-3 (Invitrogen, Rabbit polyclonal antibody, 1:100), claudin-4 (Invitrogen, Rabbit polyclonal antibody, 1:100), claudin-7 (Invitrogen, Rabbit polyclonal antibody, 1:100). All primary antibodies were incubated for 32 min on 42°C. Counterstaining with haematoxylin was used after antibody visualisation. All immunohistochemical reactions were performed using external positive control tissue.

Quantification of claudin expression

Slides were scanned with 3D HISTECH Pannoramic® 1000 digital slide scanner. All immunohistochemical slides were analysed by one expert histopathologist (ZK) on digitized slides. Twenty percent of the cases were analysed by a second expert (AT), the two results were concordant. In cases of mixed IMPC/IBC-NST tumors the two components were separately evaluated. Accordingly 91 samples, 46 IMPC and 45 IBC-NST were analysed.

No standardized methods are available for the quantification of claudin proteins expression [25, 36, 37].

Two methods were used to quantify the IHC results:

a. A 4-tier immunohistochemical score system was applied on the cohort. No evidence of membranous or cytoplasmic staining was evaluated as score 0, increasing staining intensities were scored from 1+ to 3+. Samples showing score 0 were declared as negative, score 1+, 2+ and 3+ were grouped as positive samples for protein expression.
b. H-score was determined by adding the results of multiplication of the percentage of cells with staining intensity ordinal value (scored from 0 for "no signal" to 3 for "strong signal") with values between 0 and 300. Low and high expression was determined by calculating median values. H-score values above the median were considered as high expression and those below the median were considered low expression.

Statistical analysis

Clinical data and histology score values were processed using JupyterLab with R language (v 4.2.0). Homogeneity test of data was performed by Kolmogorov-Smirnov test. Categorical data were compared using Chi-square test. Cox proportional hazard model calculation was performed to evaluate predictive and hazard value of variables, both regarding DMFS and OS. The results of this calculation were indicated as hazard ratio (HR) and confidence intervals (CI). *P*-values presented in the tables are representative to population wise measurements (compared to the reference variable or between positive and negative expression) and are not subgroup (IBC-NST, IMPC or Mixed IMPC/IBC-NST) related due to statistical adequacy. Mixed IMPC/IBC-NST cases were excluded from survival analysis due to the low patient number. Plotting was performed using ggpubr and survminer package. *P*-values <0.05 were considered statistically significant. Survival curves calculated by Cox proportional hazard model were created with ggsurvplot function of ggplot2 R package.

Results

Patient characteristics

Tumors of 82 breast cancer patients were included in our study, 36 IBC-NST, 37 IMPC and 9 mixed IMPC/IBC-NST

TABLE 1 Patient characteristics.

	IBC-NST	IMPC	Mixed IMPC/IBC-NST	*p*-value*
Total patient number	36	37	9	
Number of samples examined	45	46		
Median years of age (range)	63 (34–83)	63 (33–85)	61 (34–69)	
Median of Ki67 LI (range)	15 (1–100)	15 (1–90)	16 (5–90)	0.22[a]
Grade I II III	 3 (8.3%) 20 (55.5%) 13 (35.2%)	 3 (8.1%) 23 (62.2%) 11 (29.7%)	 1 (11.1%) 4 (44.45%) 4 (44.45%)	0.90[b]
T 1 2 3 4	 14 (38.9%) 11 (30.6%) 8 (22.2%) 3 (8.3%)	 18 (48.6%) 8 (21.6%) 8 (21.6%) 3 (8.1%)	 3 (33.3%) 4 (44.5%) 1 (11.1%) 1 (11.1%)	0.85[b]
N 0 1 2 3	 17 (47.2%) 8 (22.2%) 6 (16.7%) 5 (13.9%)	 20 (54.1%) 8 (21.6%) 3 (8.1%) 6 (16.2%)	 3 (33.3%) 4 (44.5%) 1 (11.1%) 1 (11.1%)	0.73[b]
ER + -	 27 (75%) 9 (25%)	 35 (94.6%) 2 (5.4%)	 8 (88.9%) 1 (11.1%)	0.05[b]
PR + –	 17 (47.2%) 19 (52.8%)	 29 (78.4%) 8 (21.6%)	 8 (88.9%) 1 (11.1%)	0.005[b]
HER2 + –	 5 (13.9%) 31 (86.1%)	 8 (21.6%) 29 (78.4%)	 1 (11.1%) 8 (88.9%)	0.59[b]
Distant metastasis Absent Present	 22 (61.1%) 14 (38.9%)	 29 (78.4%) 8 (21.6%)	 6 (66.7%) 3 (33.3%)	0.27[b]
Surrogate molecular subtypes LUM-A LUM-B1 LUM-B2 HER2 positive TNBC	 10 (27.8%) 14 (38.9%) 3 (8.3%) 2 (5.6%) 7 (19.4%)	 20 (54.1%) 7 (18.9%) 8 (21.6%) 0 2 (5.4%)	 4 (44.5%) 3 (33.3%) 1 (11.1%) 0 1 (11.1%)	0.93[b]

[a]Kruskal-Wallis test.
[b]Chi-square test.
IMPC, invasive micropapillary carcinoma; IBC-NST, Invasive breast carcinoma - no special type; ER, estrogen receptor; PR, progesterone receptor; LI, labeling index (%); LUM-A, Luminal-A type breast carcinoma; LUM-B1, Luminal B-HER2 negative type breast carcinoma; LUM-B2, Luminal B-HER2 positive type breast carcinoma; TNBC, triple negative breast cancer.

tumors were examined. Mixed tumor components were analysed separately for protein expression and were included to the IMPC (46 samples) and IBC-NST (45 samples) groups respectively (totally 91 samples). Median age of the patients was 63 years in the IBC-NST group, 63 years in the IMPC and 61 in the mixed IMPC/IBC-NST group. About half of the patients presented with lymph node metastasis (42/82), and most of the tumors were grade 2, stage pT1-2. Median follow up time was 49 months (range: 0–198 months). Distant metastasis occurred in 25 out of 82 cases (14/36 in IBC-NST, 8/37 in IMPC and 3/9 in mixed IMPC/IBC-NST cases).

Patients' and tumors' characteristics are shown in Table 1. All three patient groups showed similar distribution regarding age and prognostic factors.

Localization and expression of the analysed proteins

Protein expression of claudin-1 was mainly weak membranous and/or cytoplasmic or negative by immunohistochemical staining. Claudins-3, -4 and -7 showed

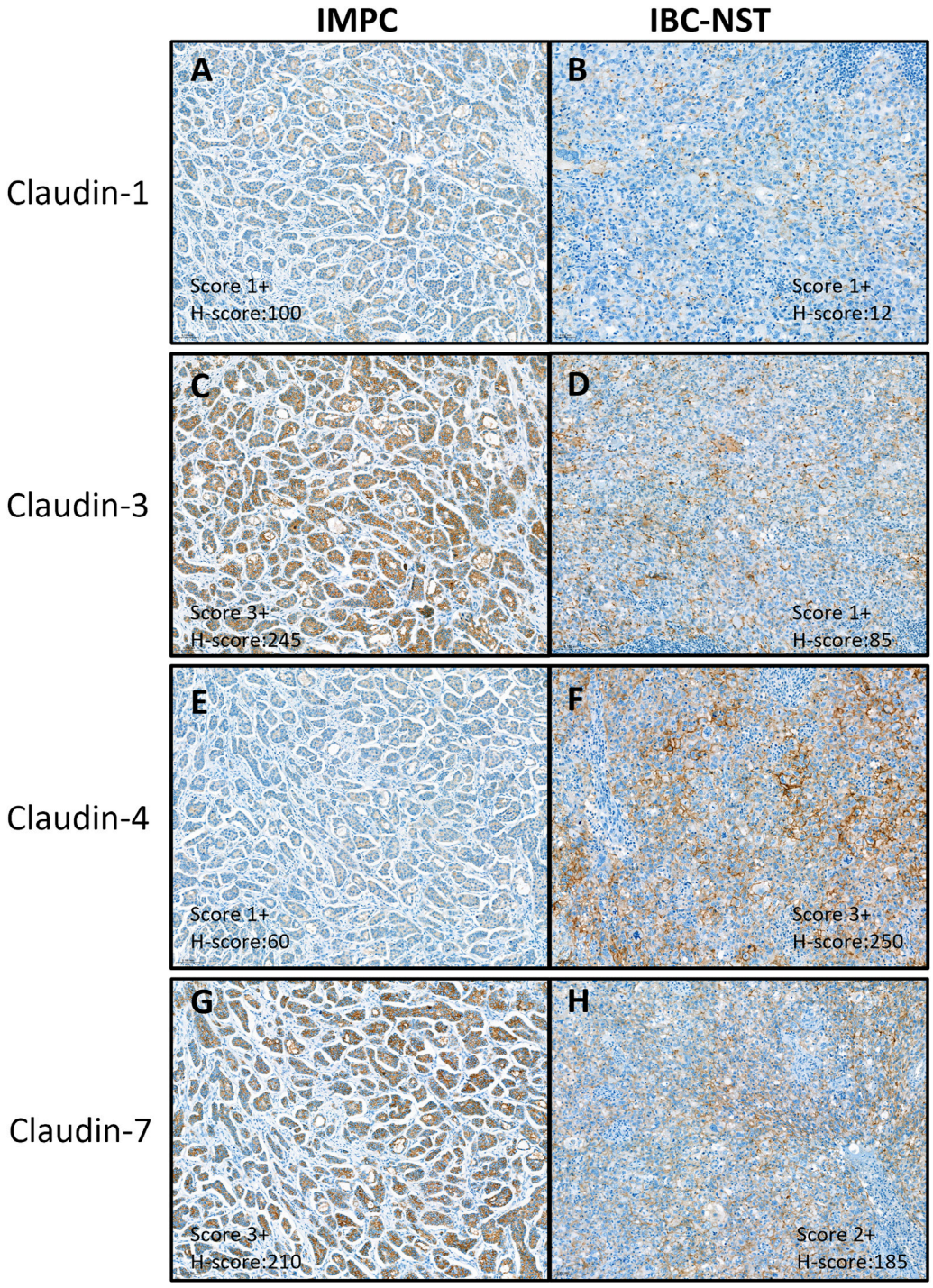

FIGURE 1
Immunohistochemical expression of claudin proteins. Immunohistochemical analysis showed mainly weak or no cytoplasmic and/or membrane staining of claudin-1 **(A, B)** and variable staining intensity of claudin-3 **(C, D)**, –4 **(E, F)**, and –7 **(G, H)**. **(A, C, E, G)** is a sample of IMPC, grade 2, LUM-A tumor. **(B, D, F, H)** is a sample of IBC-NST, grade 3, TNBC tumor. IMPC, Invasive micropapillary carcinoma; IBC-NST, Invasive breast carcinoma - no special type; LUM-A, Luminal-A type breast carcinoma; TNBC, Triple negative breast cancer.

variable intensity, mostly circumferential or partial membrane positivity (Figure 1).

Semiquantitative scoring method results

After scoring our cohort according to the traditional 0, 1+, 2+, 3+ system, we have found no significant difference between claudin-1, -3, -4, and -7 protein expression levels between the IMPC and IBC-NST groups (p = 0.17, 0.31, 0.34, 0.22, respectively).

None of the samples (0/91) showed high claudin-1 expression (score 3+) whereas high claudin-3 expression (score 3+) was detected in 5/91 samples (2 IBC-NST, 3 IMPC), high claudin-4 in 1/91 sample (IBC-NST) and high claudin-7 expression was seen in 13/91 samples (5 IBC-NST and 8 IMPC).

8/91 samples (6 IBC-NST, 2 IMPC) were negative for claudin-3, -4 and -7 whereas 36/91 samples (15 IBC-NST, 21 IMPC) presented with positivity for all of the above three claudins.

Cytoplasmic positivity was also seen in a minority of samples (8.8%, 32/364) in both IMPC and IBC-NST groups (11 and 21, respectively) as follows: 9.9% (9/91) of claudin-1, 8.8% (8/91) of claudin-3, 12% (11/91) of claudin-4, and 4.4% (4/91) of claudin-7.

H-score analysis

To compare the proteins expression with mRNA analysed in our earlier study [10] the results of H-score evaluation was applied. Variable staining intensity of claudins-1, -3, -4 and -7 was observed. Median H-score values of claudin-3 and claudin-7 expression were 115 and 150, respectively. Most of our samples showed no staining with claudin-1 (median value 0.5). Claudin-1 H-score above 100 occurred in 5 samples, showing no correlation with tumor subtype, grade, or receptor status. Claudin-4 expression was below 50 to no expression in 60/91 of the samples, with a median value of 10. Expression values between 50 and 100 of claudin-4 was found in 14 samples. Claudin-4 values above 100 were found in 17 samples, with no connection to tumor characteristics.

Comparison of protein and RNA expression

In our previous study [10] we have examined mRNA expression on a largely identical cohort to this present study by using NanoString nCounter Analysis system. Median values of mRNA expression levels were used as threshold for determining low and high expression for each of the examined 43 genes. We have shown, that *CLDN3*, *CLDN4* and *CLDN7* mRNA expression is significantly higher in IMPC tumors compared to the IBC-NST group, while *CLDN1* showed significantly lower mRNA expression in the IMPC group. Examining protein expression of claudin-1, -3, and -4 did not show differences in the two histological groups. We have compared mRNA expression levels of our previous study and H-score values of the current study. Median values were very low for both *CLDN1* mRNA (184.74) and claudin-1 protein expression (0.5). Interestingly median value of claudin-4 protein expression was low [10], compared to the high median value of *CLDN4* mRNA expression (3683.8). High mRNA expression correlated with high protein expression in about 2/3 of samples (claudin-3: 68%, claudin-4: 61% and claudin-7: 70%), while samples showing low mRNA expression have also shown low protein expression in 36% (claudin-3), 49% (claudin-4) and 34% (claudin-7) of the samples. In case of claudin-1, the correlation was 52% (high expression) and 47% (low expression).

Breast cancer subtype distribution

Of the analysed cases 94.6% of the IMPCs and 75% of IBC-NST samples were hormone receptor positive (HR+). Analysing separately the HR+ and HR- samples we have found that the distribution of the different claudins in the HR+ samples was the following: 56.71% were claudin-3 positive, 46.1% claudin-4 positive and 89% claudin-7 positive. In the HR- samples this ratio was 69%, 53% and 53%, respectively.

The distribution of the different claudins in each molecular and histological subtype is presented in Table 2 (after evaluation according to the 4-tier method) and Table 3 (after evaluation according to the H-score). The most representative subtype in our cohort was the LUM-A subtype (38/91, 41.7%) characterized by claudin-3 and claudin-7 positivity and claudin-4 negativity in 76%, 92% and 58% of the samples, respectively. The 4-tier evaluation showed that claudin-7 expression is associated with molecular subtype distribution (p = 0.001). Evaluation of the samples with the H-score method showed a mostly similar distribution of histological and molecular subtypes in cases of claudin-3 and claudin-4 expression. According to the histological subtype, high claudin-7 expression occurred in significantly more IMPC cases compared to IBC-NST tumors (p = 0.02).

In our cohort 8 samples were considered as negative for claudin-3, -4, and -7 with immunohistochemistry (IHC) (claudin all low group). Four samples were LUM-A, 2 samples LUM-B1 and 2 samples TNBC subtype. Due to the relatively low number of samples, further statistical analysis was not performed on the claudin all low group. Of the 45 IBC-NST samples, 6 were negative for claudin-3, -4, and -7 whereas of the 46 IMPC samples 2 were negative for claudin-3, -4, and -7.

Analysing the prognostic value of claudin-3, -4, and -7 expression

Statistical analysis was performed with both scoring methods. Based on H-score evaluation claudin-1 staining

TABLE 2 Claudin expression distribution between molecular subtypes in the 91 samples using the 4-tier method.

	Claudin-1 neg.	Claudin-1 pos.	*p*-value	Claudin-3 neg.	Claudin-3 pos.	*p*-value	Claudin-4 neg.	Claudin-4 pos.	*p*-value	Claudin-7 neg.	Claudin-7 pos.	*p*-value
All	76	15		26	65		48	43		14	77	
IBC-NST	40	5	0.17[a]	15	30	0.31[a]	26	19	0.34[a]	9	36	0.22[a]
IMPC	36	10		11	35		22	24		5	41	
LUM-A	29	9	0.76[a]	9	29	0.59[a]	22	16	0.67[a]	3	35	0.001[a]
LUM-B1	27	0		10	17		12	15		4	23	
LUM-B2	9	4		3	10		8	5		1	12	
HER2	2	0		0	2		0	2		0	2	
TNBC	9	2		4	7		6	5		6	5	

[a]Chi square test.

IMPC, invasive micropapillary carcinoma; IBC-NST, Invasive breast carcinoma - no special type; LUM-A, Luminal-A type breast carcinoma; LUM-B1, Luminal B-HER2 negative type breast carcinoma; LUM-B2, Luminal B-HER2 positive type breast carcinoma; TNBC: triple negative breast cancer.

10.3389/pore.2024.1611987

TABLE 3 Claudin expression distribution between molecular subtypes in the 91 samples using the H-score method.

	Claudin-3 low	Claudin-3 high	*p*-value	Claudin-4 low	Claudin-4 high	*p*-value	Claudin-7 low	Claudin-7 high	*p*-value
All	44	47		41	50		44	47	
IBC-NST	24	21	0.34[a]	20	25	0.90[a]	27	18	0.02[a]
IMPC	20	26		21	25		17	29	
LUM-A	22	16	0.47[a]	19	19	0.69[a]	18	20	0.76[a]
LUM-B1	13	14		10	17		11	16	
LUM-B2	5	8		7	6		7	6	
HER2	0	2		0	2		1	1	
TNBC	4	7		5	6		7	4	

[a]Chi square test.

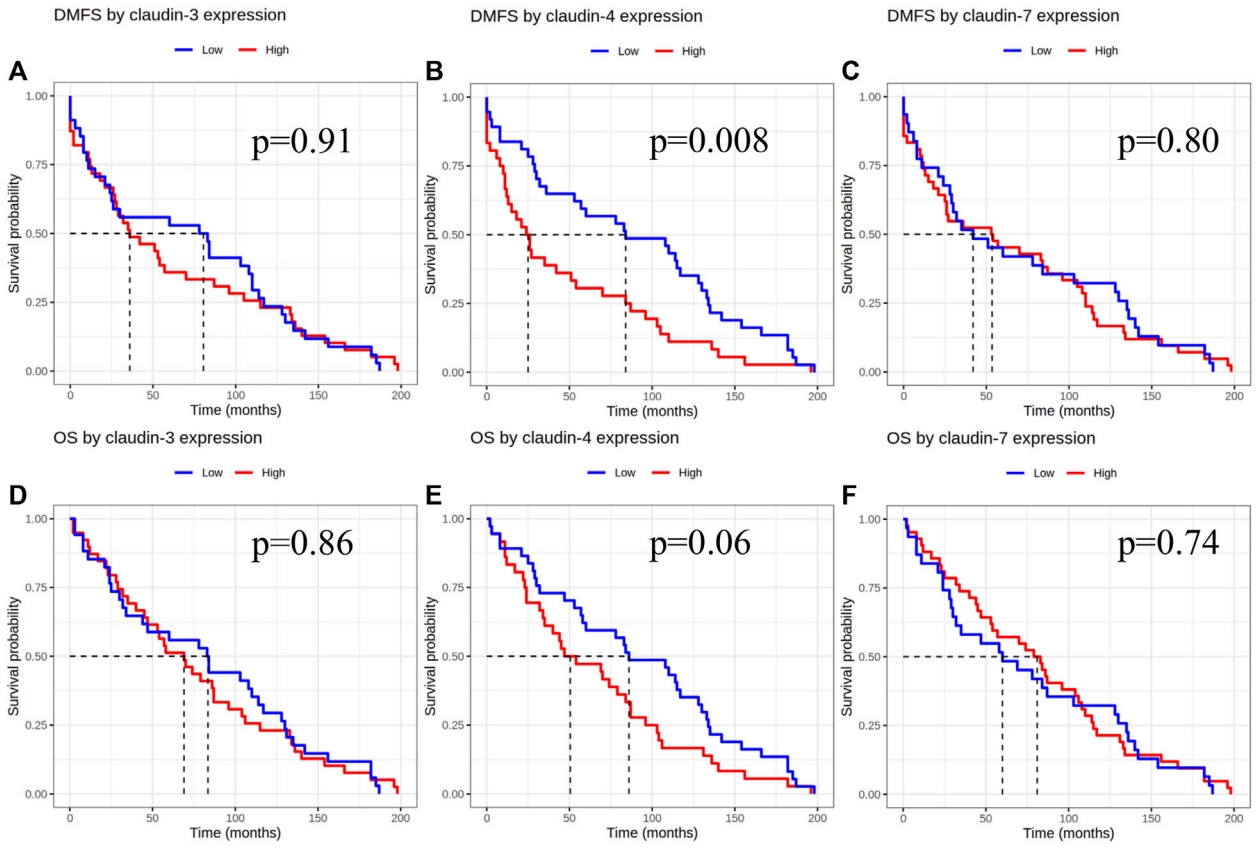

FIGURE 2
Claudin expression effect on DMFS and OS after evaluation of immunoexpression according to the H-score. DMFS by claudin-3, -4 and -7 expression **(A–C)**, OS by claudin-3, -4 and -7 expression **(D–F)**. DMFS, Distant metastasis free survival; OS, Overall survival.

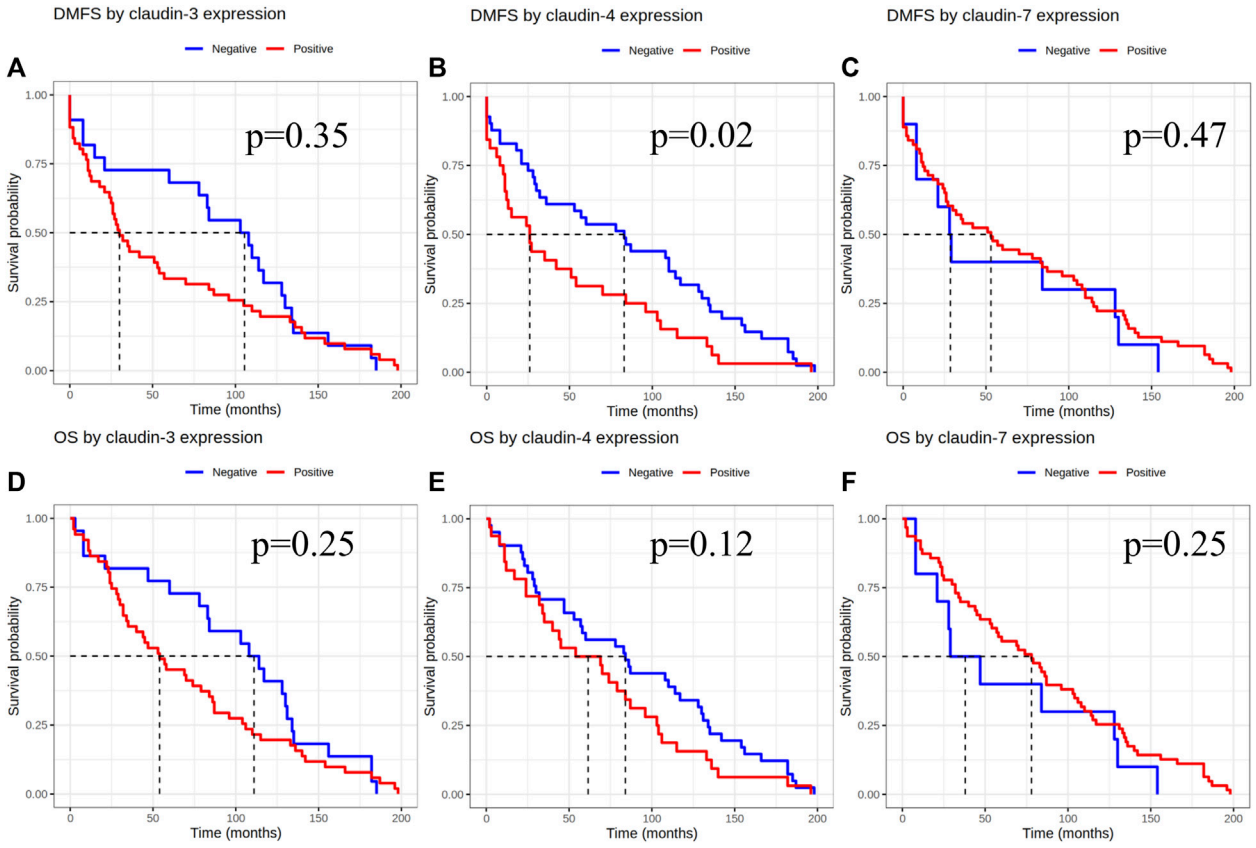

FIGURE 3
Claudin expression effect on DMFS and OS after evaluation of immunoexpression using the 4-tier system. DMFS by claudin-3, -4 and -7 expression **(A–C)**, OS by claudin-3, -4 and -7 expression **(D–F)**. DMFS, Distant metastasis free survival; OS, Overall survival.

showed low to no reaction, with low median values (0.5), low claudin-4 expression was detected in 45% of the samples, and the median value of claudin-4 expression was low (H-score 10). Due to the extremely low median value of claudin-1, we did not perform further statistical analysis on claudin-1 expression. Low claudin-4 expression was associated with significantly longer DMFS [p = 0.008 (HR-CI): 0.529 (0.329–0.848)] when examining the pure IMPC and IBC-NST cases. Claudin-3 and claudin-7 expression did not show any correlation with DMFS [p-values 0.91 (HR-CI): 0.976 (0.611–1.557) and 0.80 (HR-CI): 0.943 (0.588–1.510), respectively]. Claudin expression did not show correlation with overall survival (Figure 2).

Based on the results of the 4-tier and examining pure IMPC and IBC-NST cases, samples considered as claudin-4 negative by IHC were also associated with significantly longer DMFS [p = 0.02, HR-CI: 1.744 (1.084–2.804)], but no difference was seen in overall survival [p = 0.12, HR-CI: 1.446 (0.903–2.315)]. Claudin-3 and -7 expression did not show any effect on overall survival or DMFS (Figure 3).

Discussion

In the present study, 45 IBC-NST and 46 IMPC samples (36 IBC-NST, 37 IMPCs and 9 mixed IMPC/IBC-NST cases with 91 tumor samples) were evaluated for claudin-1, -3, -4, and -7 immunohistochemical expression in search for the possible role of these markers in the formation of inverted polarity, in differentiating between IBC-NST and IMPC subtypes and as potential prognostic indicators. To date no standardized methods are available for the quantification of claudin proteins expression. Some study groups use a semiquantitative scale from 0 to 3, others the H-score, while there are studies presenting the results of a unique scoring system by combining staining intensity and percentage of positive cells. Not just the methods differ between study groups, but also the cut-off values to distinguish positive and negative cases are different [25, 36–42].

In one of our earlier studies by analysing fresh and FFPE breast tissues we demonstrated that claudin-1 protein is absent, or its expression is markedly decreased in the majority of

different types of invasive breast carcinomas as compared with normal ducts and *CLDN1* mRNA expression investigated by real-time PCR confirmed this finding. Related to claudin-4 our earlier study showed downregulated claudin-4 protein expression in grade 1 IDC-NSTs [32]. In this current cohort claudin-4 downregulation was not correlated with tumor grade, however positive claudin-4 expression was associated with a shorter DMFS.

IMPC tumors have a distinct histological appearance. As we have shown in our previous study, this subtype shows higher mRNA expression levels of *CLDN*s 3, 4, and 7, and lower *CLDN1* levels, when compared with IBC-NST tumors, which might contribute to the unique histological features [10]. In our current, mostly similar cohort, we could not show differences between the two groups on the protein expression level. Correlation between gene and protein expression of claudins has been studied by Li et al. [43]. They have shown that the expression levels do not necessarily correlate with each other, which can occur due to epigenetic alterations, transcription factors, RNA alternative- or mis-splicing, posttranslational modifications, or signalling pathway effects. In our study we have also seen only partial correlation between RNA and protein expression levels.

Polarity formation and maintenance require the regulation of tight junctions and accordingly the involvement of the actin and microtubule cytoskeleton. Although several proteins participate in maintaining apicobasal polarity, three major polarity complexes are mentioned as the core proteins. These are the apical Crumbs and Par complexes and the basolateral Scribble complex [44–46].

It is known that tight junction proteins modulate various signalling cascades which have effect on cellular differentiation, growth, proliferation and cell migration. Polarity switching has been described as a critical step in metastasis formation. Tumor cell clusters may switch from apical-in to apical-out polarity in the course of vascular invasion. Integrins are key molecules in the interaction between the cells and the extracellular matrix. Intracellular activation of cytoskeletal and regulatory proteins by integrin signalling has been described to be activated in cancer [47]. Several signalling pathways have been linked to tight junction proteins, including TGF-ß-dependent pathway signalling, Ras-Raf-MEK-ERK and PI3K/Akt signalling, Wnt/ß-catenin signalling, STAT signalling, the Hedgehog and the Notch pathways [48].

Based on our results changes in epithelial polarity in IMPCs seems not to be related to claudin-1, -3, and -4 expression as the distribution of the mentioned proteins was mostly similar in IMPC and IBC-NST tumors. However high claudin-7 expression occurred in significantly more IMPC cases compared to IBC-NST tumors.

Tetsuhisa et al. tested the role of TJs in epithelial polarity by systematically knocking out TJ components and they have found that epithelial polarity was disorganized in ZO-1/ZO-2–deficient cells, but not in claudin-deficient cells. They concluded that claudins and JAM-A co-ordinately regulate TJ formation and epithelial polarity [19].

The prognostic role of different claudins have been analysed in several studies. Changes in claudin expression have different effects in different cancer types. In breast cancer claudin-4 overexpression has been associated with progression, migration and worst prognosis, which is in concordance with our findings [25, 26, 41, 49]. In triple negative breast carcinomas (TNBC) high cytoplasmic but not membranous claudin-3 and claudin-7 expression is predictive of poor outcome according to a study group [28], while another group has shown that membranous claudin-3 overexpression is associated with poor survival in TNBCs [26]. Claudin-7 expression was shown to be lower in high grade breast carcinomas and decreased expression was found in ER- tumors [29, 50].

Claudin low phenotype of breast carcinoma is defined by low expression of cell adhesion genes, high expression of epithelial-mesenchymal transition genes, and stem cell-like expression pattern [30]. These tumors show marked immune and stromal cell infiltration, low level of genomic instability and lower proliferation rates. Fougner et al. have re-evaluated the characteristics of claudin low breast cancer subtype tumors and have found that these tumors are not a distinct, sixth subtype of breast carcinomas. Claudin low tumors are found in all breast cancer subtypes, showing characteristics closer to their intrinsic subtype rather than to claudin low tumors [51]. Claudin low tumors show low gene expression levels of claudins-3-, -4, and -7.

It would be interesting to analyse whether the loss of several claudins is associated with inversed cell polarity. In our cohort only a low number of samples were considered as negative by IHC for all three claudins (6 IBC-NST and 2 IMPC) so, further analysis was not performed on this group. A recent study has described that the decrease or loss of claudin expression is accompanied by cell-cell adhesion- and polarity damage [52].

Molecular therapies that target claudin-4 are being developed continuously. As seen in many studies [25, 26, 41, 49, 53], including our cohort, high claudin-4 expression is associated with worse prognosis. Luo Yi et al. showed that anti-claudin-4 extracellular domain antibody, 4D3 enhances the chemotherapeutic antitumor effect of paclitaxel in two human breast cancer cell lines [53]. Patients with breast carcinomas showing high claudin-4 protein expression may benefit from anti-claudin-4 antibody treatment as part of the treatment protocol. Hence, the specific antibody connection enhancing the chemotherapeutic effect in these potentially high-risk tumors may increase patient survival.

Conclusion

Changes in epithelial polarity seems not to be related to claudin-1, -3, and -4 expression as IMPC and IBC-NST tumors showed mostly similar expression of these proteins in our cohort. Differences were observed in claudin-7 protein expression between the two histological subtypes. No statistically

significant differences were detected in DMFS between the two groups. Based on the survival data of the pure IMPC and IBC-NST cases claudin-4 positive tumors were associated with significantly shorter DMFS, suggesting a role of claudin-4 in cancer progression. If inverted polarity is a feature seen only in cancer cells, then better understanding of its development may provide crucial targets for therapy.

Further research will be necessary to understand the significance of the dysregulated polarity in IMPC cells and of the clustered tumor cells situated within empty stromal spaces.

Data availability statement

The original contributions presented in the study are included in the article/supplementary material, further inquiries can be directed to the corresponding author.

Ethics statement

The studies involving humans were approved by Semmelweis University Research Ethics Committee 240/2016. The studies were conducted in accordance with the local legislation and institutional requirements. Written informed consent for participation was not required from the participants or the participants' legal guardians/next of kin in accordance with the national legislation and institutional requirements.

Author contributions

ZK evaluated the immunohistochemical stains, wrote the manuscript. AB performed the statistical analysis. AP scanned the immunohistochemical slides. A-MT participated in the evaluation of the immunohistochemical stains, and in writing the manuscript. JK initiated the study and helped writing the manuscript. All authors contributed to the article and approved the submitted version.

Funding

The author(s) declare that no financial support was received for the research, authorship, and/or publication of this article.

Conflict of interest

The authors declare that the research was conducted in the absence of any commercial or financial relationships that could be construed as a potential conflict of interest.

Generative AI statement

The author(s) declare that no Generative AI was used in the creation of this manuscript.

References

1. Cakir E, Yilmaz A, Demirag F, Oguztuzun S, Sahin S, Yazici UE, et al. Prognostic significance of micropapillary pattern in lung adenocarcinoma and expression of apoptosis-related markers: caspase-3, bcl-2, and p53. *APMIS* (2011) 119(9):574–80. doi:10.1111/j.1600-0463.2011.02778.x

2. Comperat E, Roupret M, Yaxley J, Reynolds J, Varinot J, Ouzaid I, et al. Micropapillary urothelial carcinoma of the urinary bladder: a clinicopathological analysis of 72 cases. *Pathology* (2010) 42(7):650–4. doi:10.3109/00313025.2010.522173

3. Fisher ER, Palekar AS, Redmond C, Barton B, Fisher B. Pathologic findings from the national surgical adjuvant breast project (protocol no. 4). VI. Invasive papillary cancer. *Am J Clin Pathol* (1980) 73(3):313–22. doi:10.1093/ajcp/73.3.313

4. Guzinska-Ustymowicz K, Niewiarowska K, Pryczynicz A. Invasive micropapillary carcinoma: a distinct type of adenocarcinomas in the gastrointestinal tract. *World J Gastroenterol* (2014) 20(16):4597–606. doi:10.3748/wjg.v20.i16.4597

5. Chen H, Wu K, Wang M, Wang F, Zhang M, Zhang P. Invasive micropapillary carcinoma of the breast has a better long-term survival than invasive ductal carcinoma of the breast in spite of its aggressive clinical presentations: a comparison based on large population database and case-control analysis. *Cancer Med* (2017) 6(12):2775–86. doi:10.1002/cam4.1227

6. Wu SG, Zhang WW, Sun JY, Li FY, Chen YX, He ZY. Postoperative radiotherapy for invasive micropapillary carcinoma of the breast: an analysis of Surveillance, Epidemiology, and End Results database. *Cancer Manag Res* (2017) 9:453–9. doi:10.2147/CMAR.S141338

7. Hao S, Zhao YY, Peng JJ, Ren F, Yang WT, Yu KD, et al. Invasive micropapillary carcinoma of the breast had no difference in prognosis compared with invasive ductal carcinoma: a propensity-matched analysis. *Sci Rep* (2019) 9(1):286. doi:10.1038/s41598-018-36362-8

8. Li G, Yang S, Yao J, Wang Z, Yao G, Liu M, et al. Invasive micropapillary carcinoma of the breast had poor clinical characteristics but showed no difference in prognosis compared with invasive ductal carcinoma. *World J Surg Oncol* (2016) 14(1):207. doi:10.1186/s12957-016-0960-z

9. Ye F, Yu P, Li N, Yang A, Xie X, Tang H, et al. Prognosis of invasive micropapillary carcinoma compared with invasive ductal carcinoma in breast: a meta-analysis of PSM studies. *Breast* (2020) 51:11–20. doi:10.1016/j.breast.2020.01.041

10. Kramer Z, Kenessey I, Gango A, Lendvai G, Kulka J, Tokes AM. Cell polarity and cell adhesion associated gene expression differences between invasive micropapillary and no special type breast carcinomas and their prognostic significance. *Sci Rep* (2021) 11(1):18484. doi:10.1038/s41598-021-97347-8

11. Gruel N, Benhamo V, Bhalshankar J, Popova T, Freneaux P, Arnould L, et al. Polarity gene alterations in pure invasive micropapillary carcinomas of the breast. *Breast Cancer Res* (2014) 16(3):R46. doi:10.1186/bcr3653

12. Marchio C, Iravani M, Natrajan R, Lambros MB, Savage K, Tamber N, et al. Genomic and immunophenotypical characterization of pure micropapillary carcinomas of the breast. *J Pathol* (2008) 215(4):398–410. doi:10.1002/path.2368

13. Yu JI, Choi DH, Huh SJ, Cho EY, Kim K, Chie EK, et al. Differences in prognostic factors and failure patterns between invasive micropapillary carcinoma and carcinoma with micropapillary component versus invasive ductal carcinoma of the breast: retrospective multicenter case-control study (KROG 13-06). *Clin Breast Cancer* (2015) 15(5):353–61.e612. e1-2. doi:10.1016/j.clbc.2015.01.008

14. Shi Q, Shao K, Jia H, Cao B, Li W, Dong S, et al. Genomic alterations and evolution of cell clusters in metastatic invasive micropapillary carcinoma of the breast. *Nat Commun* (2022) 13(1):111. doi:10.1038/s41467-021-27794-4

15. Badyal RK, Bal A, Das A, Singh G. Invasive micropapillary carcinoma of the breast: immunophenotypic analysis and role of cell adhesion molecules (CD44 and E-cadherin) in nodal metastasis. *Appl Immunohistochem Mol Morphol* (2016) 24(3):151–8. doi:10.1097/PAI.0000000000000167

16. Furuse M, Fujita K, Hiiragi T, Fujimoto K, Tsukita S. claudin-1 and -2: novel integral membrane proteins localizing at tight junctions with no sequence similarity to occludin. *J Cel Biol* (1998) 141(7):1539–50. doi:10.1083/jcb.141.7.1539

17. Van Itallie CM, Lidman KF, Tietgens AJ, Anderson JM. Newly synthesized claudins but not occludin are added to the basal side of the tight junction. *Mol Biol Cel* (2019) 30(12):1406–24. doi:10.1091/mbc.E19-01-0008

18. Lal-Nag M, Morin PJ. The claudins. *Genome Biol* (2009) 10(8):235. doi:10.1186/gb-2009-10-8-235

19. Otani T, Nguyen TP, Tokuda S, Sugihara K, Sugawara T, Furuse K, et al. Claudins and JAM-A coordinately regulate tight junction formation and epithelial polarity. *J Cel Biol* (2019) 218(10):3372–96. doi:10.1083/jcb.201812157

20. Singh AB, Sharma A, Dhawan P. Claudin family of proteins and cancer: an overview. *J Oncol* (2010) 2010:541957. doi:10.1155/2010/541957

21. Morohashi S, Kusumi T, Sato F, Odagiri H, Chiba H, Yoshihara S, et al. Decreased expression of claudin-1 correlates with recurrence status in breast cancer. *Int J Mol Med* (2007) 20(2):139–43. doi:10.3892/ijmm.20.2.139

22. Blanchard AA, Skliris GP, Watson PH, Murphy LC, Penner C, Tomes L, et al. Claudins 1, 3, and 4 protein expression in ER negative breast cancer correlates with markers of the basal phenotype. *Virchows Arch* (2009) 454(6):647–56. doi:10.1007/s00428-009-0770-6

23. Lu S, Singh K, Mangray S, Tavares R, Noble L, Resnick MB, et al. Claudin expression in high-grade invasive ductal carcinoma of the breast: correlation with the molecular subtype. *Mod Pathol* (2013) 26(4):485–95. doi:10.1038/modpathol.2012.187

24. Kulka J, Szasz AM, Nemeth Z, Madaras L, Schaff Z, Molnar IA, et al. Expression of tight junction protein claudin-4 in basal-like breast carcinomas. *Pathol Oncol Res* (2009) 15(1):59–64. doi:10.1007/s12253-008-9089-x

25. Lanigan F, McKiernan E, Brennan DJ, Hegarty S, Millikan RC, McBryan J, et al. Increased claudin-4 expression is associated with poor prognosis and high tumour grade in breast cancer. *Int J Cancer* (2009) 124(9):2088–97. doi:10.1002/ijc.24159

26. Kolokytha P, Yiannou P, Keramopoulos D, Kolokythas A, Nonni A, Patsouris E, et al. claudin-3 and claudin-4: distinct prognostic significance in triple-negative and luminal breast cancer. *Appl Immunohistochem Mol Morphol* (2014) 22(2):125–31. doi:10.1097/PAI.0b013e31828d9d62

27. Dias K, Dvorkin-Gheva A, Hallett RM, Wu Y, Hassell J, Pond GR, et al. Claudin-low breast cancer; clinical and pathological characteristics. *PLoS One* (2017) 12(1):e0168669. doi:10.1371/journal.pone.0168669

28. Jaaskelainen A, Soini Y, Jukkola-Vuorinen A, Auvinen P, Haapasaari KM, Karihtala P. High-level cytoplasmic claudin 3 expression is an independent predictor of poor survival in triple-negative breast cancer. *BMC Cancer* (2018) 18(1):223. doi:10.1186/s12885-018-4141-z

29. Kominsky SL, Argani P, Korz D, Evron E, Raman V, Garrett E, et al. Loss of the tight junction protein claudin-7 correlates with histological grade in both ductal carcinoma *in situ* and invasive ductal carcinoma of the breast. *Oncogene* (2003) 22(13):2021–33. doi:10.1038/sj.onc.1206199

30. Prat A, Parker JS, Karginova O, Fan C, Livasy C, Herschkowitz JI, et al. Phenotypic and molecular characterization of the claudin-low intrinsic subtype of breast cancer. *Breast Cancer Res* (2010) 12(5):R68. doi:10.1186/bcr2635

31. Sauer T, Pedersen MK, Ebeltoft K, Naess O. Reduced expression of claudin-7 in fine needle aspirates from breast carcinomas correlate with grading and metastatic disease. *Cytopathology* (2005) 16(4):193–8. doi:10.1111/j.1365-2303.2005.00257.x

32. Tokes AM, Kulka J, Paku S, Szik A, Paska C, Novak PK, et al. claudin-1, -3 and -4 proteins and mRNA expression in benign and malignant breast lesions: a research study. *Breast Cancer Res* (2005) 7(2):R296–305. doi:10.1186/bcr983

33. Lakhani IafRoC SR. *WHO classification of breast tumours*. 5th ed. (2019).

34. Luna-More S, Gonzalez B, Acedo C, Rodrigo I, Luna C. Invasive micropapillary carcinoma of the breast. A new special type of invasive mammary carcinoma. *Pathol Res Pract* (1994) 190(7):668–74. doi:10.1016/S0344-0338(11)80745-4

35. Goldhirsch A, Winer EP, Coates AS, Gelber RD, Piccart-Gebhart M, Thurlimann B, et al. Personalizing the treatment of women with early breast cancer: highlights of the St Gallen international expert Consensus on the primary therapy of early breast cancer 2013. *Ann Oncol* (2013) 24(9):2206–23. doi:10.1093/annonc/mdt303

36. Nakazawa T, Hasegawa A, Nagasaka T, Yoshida K, Guo F, Wu D, et al. Differential expression of claudin 1 and 4 in basal cell carcinoma of the skin. *Dermatol Res Pract* (2023) 2023:9936551. doi:10.1155/2023/9936551

37. Naimi A, Zare N, Amjadi E, Soltan M. High claudin-4 antigen expression in triple-negative breast cancer by the immunohistochemistry method. *J Res Med Sci* (2022) 27:20. doi:10.4103/jrms.jrms_1389_20

38. Gyulai M, Harko T, Fabian K, Karsko L, Agocs L, Szigeti B, et al. Claudin expression in pulmonary adenoid cystic carcinoma and mucoepidermoid carcinoma. *Pathol Oncol Res* (2023) 29:1611328. doi:10.3389/pore.2023.1611328

39. Dottermusch M, Kruger S, Behrens HM, Halske C, Rocken C. Expression of the potential therapeutic target claudin-18.2 is frequently decreased in gastric cancer: results from a large Caucasian cohort study. *Virchows Arch* (2019) 475(5):563–71. doi:10.1007/s00428-019-02624-7

40. Szade J, Kunc M, Pieczynska-Uzieblo B, Swierblewski M, Biernat W, Jassem J, et al. Comparison of claudin-3 and claudin-4 expression in bilateral and unilateral breast cancer. *Neoplasma* (2021) 68(2):283–9. doi:10.4149/neo_2020_200816N867

41. Murakami-Nishimagi Y, Sugimoto K, Kobayashi M, Tachibana K, Kojima M, Okano M, et al. Claudin-4-adhesion signaling drives breast cancer metabolism and progression via liver X receptor β. *Breast Cancer Res* (2023) 25(1):41. doi:10.1186/s13058-023-01646-z

42. Graudenz MS, Cadore E, Ferreira BP, Schulz R, Borba C, Uchoa D, et al. Claudins 1, 3, 4, 7 and 10-year survival in triple-negative breast tumors. *Mastology* (2019) 29(2):71–8. doi:10.29289/2594539420190000419

43. Li J. Dysregulated expression of claudins in cancer. *Oncol Lett* (2021) 22(3):641. doi:10.3892/ol.2021.12902

44. Goehring NW. PAR polarity: from complexity to design principles. *Exp Cel Res* (2014) 328(2):258–66. doi:10.1016/j.yexcr.2014.08.009

45. Bonello TT, Peifer M. Scribble: a master scaffold in polarity, adhesion, synaptogenesis, and proliferation. *J Cel Biol* (2019) 218(3):742–56. doi:10.1083/jcb.201810103

46. Tan B, Yatim S, Peng S, Gunaratne J, Hunziker W, Ludwig A. The mammalian Crumbs complex defines a distinct polarity domain apical of epithelial tight junctions. *Curr Biol* (2020) 30(14):2791–804.e6. doi:10.1016/j.cub.2020.05.032

47. Onuma K, Inoue M. Abnormality of apico-basal polarity in adenocarcinoma. *Cancer Sci* (2022) 113(11):3657–63. doi:10.1111/cas.15549

48. Nehme Z, Roehlen N, Dhawan P, Baumert TF. Tight junction protein signaling and cancer biology. *Cells* (2023) 12(2):243. doi:10.3390/cells12020243

49. Ma X, Miao H, Jing B, Pan Q, Zhang H, Chen Y, et al. claudin-4 controls the proliferation, apoptosis, migration and *in vivo* growth of MCF-7 breast cancer cells. *Oncol Rep* (2015) 34(2):681–90. doi:10.3892/or.2015.4037

50. Park D, Karesen R, Axcrona U, Noren T, Sauer T. Expression pattern of adhesion molecules (E-cadherin, alpha-beta-gamma-catenin and claudin-7), their influence on survival in primary breast carcinoma, and their corresponding axillary lymph node metastasis. *APMIS* (2007) 115(1):52–65. doi:10.1111/j.1600-0463.2007.apm_524.x

51. Fougner C, Bergholtz H, Norum JH, Sorlie T. Re-definition of claudin-low as a breast cancer phenotype. *Nat Commun* (2020) 11(1):1787. doi:10.1038/s41467-020-15574-5

52. Pan C, Xu A, Ma X, Yao Y, Zhao Y, Wang C, et al. Research progress of claudin-low breast cancer. *Front Oncol* (2023) 13:1226118. doi:10.3389/fonc.2023.1226118

53. Luo Y, Kishi S, Sasaki T, Ohmori H, Fujiwara-Tani R, Mori S, et al. Targeting claudin-4 enhances chemosensitivity in breast cancer. *Cancer Sci* (2020) 111(5):1840–50. doi:10.1111/cas.14361

Pathology & Oncology Research | frontiers

TYPE Review
PUBLISHED 11 October 2023
DOI 10.3389/pore.2023.1611369

Check for updates

OPEN ACCESS

EDITED BY
József Tímár,
Semmelweis University, Hungary

*CORRESPONDENCE
Ildikó Horváth,
horvath.ildiko@med.unideb.hu,
ildiko.horvath@koranyi.hu

RECEIVED 23 June 2023
ACCEPTED 25 September 2023
PUBLISHED 11 October 2023

CITATION
Tornyi I, Árkosy P, Horváth I and Furka A (2023), A new perspective on the proper timing of radiotherapy during CDK4/6 inhibitor therapy in patients with "bone-only" metastatic breast cancer. *Pathol. Oncol. Res.* 29:1611369. doi: 10.3389/pore.2023.1611369

COPYRIGHT
© 2023 Tornyi, Árkosy, Horváth and Furka. This is an open-access article distributed under the terms of the Creative Commons Attribution License (CC BY). The use, distribution or reproduction in other forums is permitted, provided the original author(s) and the copyright owner(s) are credited and that the original publication in this journal is cited, in accordance with accepted academic practice. No use, distribution or reproduction is permitted which does not comply with these terms.

A new perspective on the proper timing of radiotherapy during CDK4/6 inhibitor therapy in patients with "bone-only" metastatic breast cancer

Ilona Tornyi[1], Peter Árkosy[2], Ildikó Horváth[1]* and Andrea Furka[2,3]

[1]Department of Pulmonology, Faculty of Medicine, University of Debrecen, Debrecen, Hungary, [2]Department of Oncology, Faculty of Medicine, University of Debrecen, Debrecen, Hungary, [3]Department of Clinical Radiology, Faculty of Health Care, Institute of Practical Methodology and Diagnostics, University of Miskolc, Miskolc, Hungary

The vast majority of hormone positive and HER2 negative advanced breast cancers can be controlled well by endocrine therapy combined with the groundbreaking use of CDK4/6 inhibitors in the metastatic first-line setting. Approximately 50%–60% of these patients have "bone-only" metastatic disease. In oligometastatic cases or if a certain number of uncontrolled lesions develop during the aforementioned therapy, ablative radiotherapy can be delivered or, in symptomatic cases, urgent irradiation is needed with palliative intent. To achieve the most effective results, parallel with good quality of life, the timing of radiotherapy must be determined precisely, taking into account that different cell cycles are involved during different treatment modalities; therefore, optimization of treatment schedules ensures longer and safer post-progression overall survival. The key question is whether the two treatment modalities are safe concurrently or whether they should be administered separately, and if so, what is the optimal sequence and why? This manuscript aims to answer this important question, with a focus on quality of life. Existing publications focus on safety and toxicity profiles, and efficacy is detailed only tangentially and minimally.

KEYWORDS

breast cancer, radiotherapy, radiosensitivity, CDK4/6 inhibitors, treatment timing

Introduction

Breast cancer is the most frequently diagnosed malignancy and the leading cause of cancer-related mortality in women, worldwide [1]. The vast majority, approximately 75% of breast cancer patients, belongs to hormone-positive subtypes, with a relatively good prognosis [2]; thus, endocrine therapy is a highly effective treatment for these patients. Approximately 30% of women with an early-stage breast cancer diagnosis develop metastasis [3]. The metastatic site depends on the pathological subtype of the

primary tumor, but in breast cancer, 30%–60% have metastases in the bone, 21%–32% in the lung, 15%–32% in the liver, and 4%–10% in the brain based on the SEER database [4]. Only 13% of primary breast cancer patients who developed metastasis in the bone survived >5 years in a Danish population-based cohort study [5].

New targeted drugs had to be developed to treat such cases. In cases of hormone receptor (HR)-positive and human epidermal growth factor receptor 2 (HER2)-negative breast cancer, based on risk factors, selective cyclin-dependent kinase 4/6 (CDK4/6) inhibitors are widely used to postpone the need for chemotherapy. Up until now, three CDK4/6 inhibitors have been approved for the treatment of HR-positive advanced or metastatic breast cancer [6]. Palbociclib was the first authorized by the European Medicine Agency in November 2016 based on PALOMA studies [7], followed by ribociclib in August 2017 based on MONALEESA studies [8] and abemaciclib in September 2018 based on MONARCH studies [9]. These drugs are generally used in combination with hormone replacement therapies, considering current menopausal status, although abemaciclib was also approved as monotherapy. The latter was also approved for node-positive, high recurrence risk, Ki67 score ≥20% HR+ luminal B type breast cancer patients in adjuvant settings in October 2021 based on a monarchE study [10]. Beyond these, there are further drugs on the horizon. Dalpiciclib, which has good penetration of the blood-brain barrier, based on a DAWNA-1 randomized phase 3 trial [11], was conducted only in Chinese subjects, so its performance in other populations is still an open question. GLR2007 is also a promising new CDK4/6 inhibitor [12] that is effective in smaller concentrations compared with abemaciclib, which also has proper blood-brain barrier permeation. This suggests fewer adverse events and more effective treatment in cases of central nervous system metastasis. Lerociclib accumulates better in xenografts in preclinical studies; thus, fewer hematological and gastrointestinal side effects are presumed to be observed. Trilaciclib is also a promising new drug, which differs from all the above-mentioned drugs due to its intravenous administration route [13].

Approximately 50%–60% of hormone-positive and HER2-negative advanced breast cancer patients have “bone-only” disease [14]. Depending on the number, site, and size of metastasis, radiotherapy is often suggested as a local treatment modality to dominate symptoms or block tumor growth. Radiation can be delivered with palliative intent, e.g., pain relief, or even with local ablative intent to destroy certain small-size metastasis, mainly in oligometastatic settings. The main question is whether the two treatment modalities are safe concurrently or should be administered separately, and if so, what is the optimal sequence and why? This study investigates this pressing question from a molecular biology point of view and how we can implement the results, based on preclinical studies [15–17], into daily clinical practice.

Molecular biology aspects of certain breast cancer treatments

Radiotherapy

More than 100 years passed between the first breast radical mastectomy being performed and the development of targeted therapies in breast cancer treatment [18]. As we understand more about the biology of cancer, more sophisticated treatment methodologies will become available. Since there are still gaps in our knowledge, we are only able to achieve partial success with our commonly available (surgery, radiotherapy, chemotherapy) and more frequently used (hormone, immunotherapy, targeted therapy) tools.

Radiotherapy (RT) is widely used in cancer treatment. The first utilization of RT was in the early 20th century. RT treatment modalities—from superficial X-ray to ultra-high dose rate FLASH radiotherapy—have changed substantially [19], yet the main radiobiology concept remains the same. Ionizing radiation has direct and indirect effects by producing water radicals on DNA chains. Both causes mainly double-strand break and single-strand lesions, respectively [20, 21]. When DNA suffers irreparable damage, a damage signal cascade starts involving ATM, Chk2, and p53 proteins and stops cell cycles at the G1/S phase [22]. When DNA suffers single-strand break DNA damage, another pathway starts involving ATR, and Chk1, and this stops the cell cycle at the G2/M checkpoint [23]. Cancer cells often lose normal p53 function and cannot stop at the G1/S checkpoint. In this case, cells can only use G2/M checkpoints, while normal cells can stop and repair DNA at the G1/S phase.

Cells have a different sensitivity to ionization exposure that leads to different radiation-induced cell death [24]. The most sensitive phase of radiotherapy is mitosis.

Radiotherapy is not target selective, it acts on rapidly growing cancer and normal cells, too, but we can modulate its fraction, energy, and direction. Novel technological advances, such as intensity-modulated and image-guided radiotherapy were improved to deliver therapeutic doses and boost the gross tumor volume (GTV), thus increasing the difference between tumor control probability and normal tissue complications. Other advances, such as stereotactic body radiotherapy (SBRT), have enhanced dose conformity to substantially limit treatment margins, so a critical ablative dose of irradiation can be delivered to the tumor in one (radiosurgery) or in several fractions [25].

CDK4/6 inhibitors

Cell cycle is a highly ordered system, driven by cyclin-dependent kinases (CDKs). Cyclin-dependent kinase inhibitors target overactive CDKs. CDK4 and CDK6 have two key

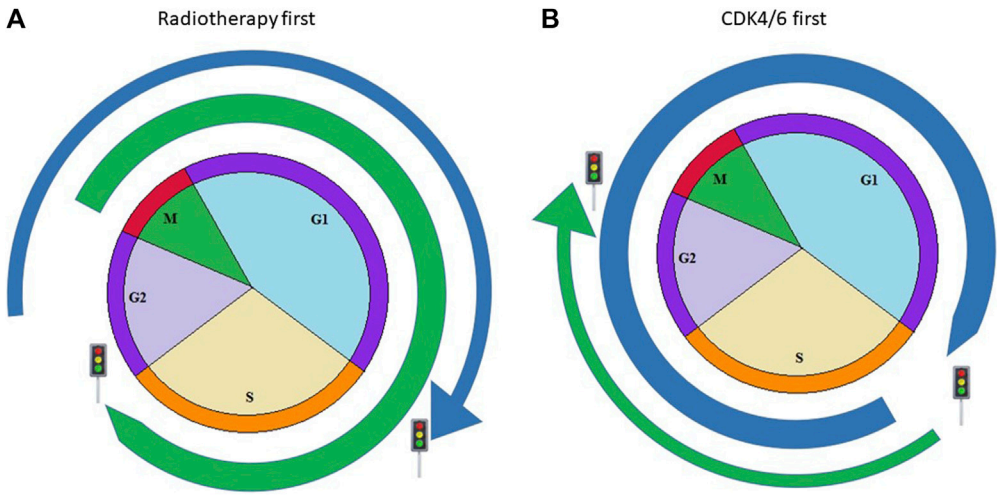

FIGURE 1
Possible combination of CDK4/6 inhibitors with radiotherapy. Blue arrow simulates the effect of CDK4/6 inhibitors according to cell cycles, green arrow shows the acting point of radiotherapy in cell cycle. **(A)** Figure shows the case when radiotherapy is delivered before CKD4/6 inhibitors and acts in the M phase, resulting in more cancer cell deaths **(B)** Figure shows the case when CDK4/6 inhibitors block cancerous cells in an earlier phase; therefore, tumorous cells cannot reach the M phase, which is the most sensitive phase to radiotherapy.

functions. In a complex with cyclin-D, CDKs phosphorylate retinoblastoma (Rb) protein, a tumor suppressor protein that activates E2F transcription factor, and sequestering cell cycle inhibitors p21Cip1 and p27Kip1 proteins, which leads to activation of cyclin-E dependent CDK2 containing complexes [26]. Cyclin-D has three isoforms: cyclin-D1, cyclin-D2, and cyclin-D3. Isoforms have different lengths; cyclin-D1 is 295 (UniProt:P24385), cyclin-D2 is 289 (UniProt:P30281), and cyclin-D3 is 292 (UniProt:P30279) amino acids long. The phosphorylation site for ubiquitination is also different in cyclin-D1 at Thr-286, in cyclin-D2 at Thr-280, and in cyclin-D3 at Thr-283 position. These isoforms form a heterodimer complex with CDK4/6 and in this complex can phosphorylate and, thus, inactivate Rb.

CDK4/6 inhibitors bind to the ATP domain of CDK4/6 but have different cyclin-D targets. Palbociclib inhibits D1-CDK4, D2-CDK6, and D3-CDK4. Ribociclib attacks D1-CDK4 and D3-CDK6. Abemaciclib targets D1-CDK4 and D1-CDK6 [17].

Mechanistically, pharmacological CDK4/6 inhibition prevents the phosphorylation of downstream cell cycle proteins, such as Rb, that control cell cycle progression through the G1/S checkpoint [27]. Inhibition of CDK4 and CDK6 induces cell cycle arrest at the G1/S checkpoint.

In breast cancer, active cyclin-D in a complex with CDK4/6 is considered to play a high-impact role in estrogen-driven cell proliferation [28, 29]. In clinical practice, novel FDA-approved CDK4/6 inhibitors are used in breast cancer treatment [30].

A combination of common and new treatments is recommended in clinical guidelines. However, the ideal treatment combination and timing to reach their synergistic effect are not yet clear. CDK4/6 inhibitors and other DNA-damaging therapies, like certain chemotherapies or radiotherapy, need proper therapeutic order as they target different cell cycle phases. If CDK4/6 inhibitors arrest the cycle in the G1/S or G0/G1 phase, it prevents the cells from entering the subsequent phase. An antagonistic effect occurs as cell cycles do not enter into their next phases, so radiotherapy cannot develop its complete effect [13]. If irradiation is required and CDK4/6 inhibitors should be suspended, the elimination time of different drugs must be taken into account (Figure 1).

Pharmacokinetics of CDK4/6 inhibitors are slightly different. Their metabolism is through CYP3A4 enzyme, and palbociclib also interacts with SULT2A1. Their half-life times are also different: 24–34 h of palbociclib, 30–55 h of ribociclib, and 17–38 h of abemaciclib. Within 3 days, they half, suggesting a 1 week drug-free period before irradiation [12].

CDK4/6 and radiotherapy *in vitro*/*in vivo* studies

Pesch et al. tested the effect of CDKi alone and in combination with RT on ER+ breast cancer cell lines and in mouse xenografts. They conclude that in radiosensitized cell lines, CDKi suppresses cell cycle signaling and changes the DNA repair response. In mouse xenograft models, concurrent administration of CDKi and RT suppressed the tumor growth and prolonged tumor doubling time compared to controls that received monotherapies [31]. In a recent study, Klapp et al. tested a sequenced RT and CDKi treatment and measured its

TABLE 1 Ongoing clinical trials of CDK4/6 inhibitors in combination with radiotherapy in metastatic breast cancer.

Trial number/ name	Phase	Enrollment criteria	Fractionation	Drug	Association RT/ CDK4/6inhibitors	Treatment sequence	Recruitment status	Planned enrollment	Actual enrollment
NCT03691493 ASPIRE	Phase 2	*de novo* bone metastasis	Conventionally	Palbociclib	Concurrent	-	Active, not recruiting	42	38
NCT05334459 ISTMET	Phase 1	*de novo* oligometastatic	Conventionally	CDK 4/6i	Sequential	N.A.	Recruiting	40	N.A.
NCT03870919 PALATINE	N.A.	*de novo* bone-only	Conventionally	Palbociclib	Sequential	RT after 6 cycles systemic treatment	Recruiting	200	N.A.
NCT03750396 CLEAR	Phase 2	*de novo* metastatic	Mainly SBRT	CDK 4/6i or mTORi	N.A.	N.A.	Recruiting	110	N.A.
ACTRN12620001212943 AVATAR	Phase 2	*de novo* oligometastatic	SBRT	CDK4/6i	Sequential	Radiotherapy in CDK4/6 pause	Recruiting	32	N.A.

optimal schedule through cellular senescence. They demonstrated that the RT-first approach induced an increased level of cellular senescence in cell lines and a mouse model, respectively [32].

The bone-only metastatic breast cancer treatment cannot be modeled in preclinical cell culture or in animal experiments as it is special circumstance.

CDK4/6 and radiotherapy clinical trials

The main difference between the two modalities is that radiotherapy stimulates cells toward certain cell death, while CDK4/6 inhibitors block cell cycle progression at the G1/S checkpoint. Pretreated cells by CDK4/6 inhibitors theoretically are less sensitive to radiotherapy as they are blocked at G1/S.

Few trials have investigated the effects of CDK4/6 inhibitors alone or in combination with radiotherapy according to ClinicalTrials.gov. There are only five ongoing or recruiting clinical trials investigating CDK4/6 inhibitors with radiation therapy in breast cancer with bone metastases (Table 1).

In an NCT03691493 phase 2 trial, CDK4/6 inhibitor (palbociclib) in combination with a nonsteroidal aromatase inhibitor and radiation therapy was used; in an NCT03870919 trial, only a locoregional treatment with palbociclib was used; and in NCT04923542 phase 1 & 2 trials, abemaciclib in combination with endocrine therapy and stereotactic radiosurgery was used. According to the currently recruiting AVATAR phase 2 study protocol, CDK4/6 inhibitors must be stopped at least 3 days prior to SRT and allowed to continue 3 days following STR completion. The authors also declare that a week off after CDK4/6 inhibitor treatment is optimal if feasible [33].

Besides breast cancer, there are trials investigating the effects of CDK4/6 inhibitors in prostate cancer, head and neck cancer, and gliomas.

Toxicity of radiotherapy and CDK 4/6 inhibitor therapies

Meattini et al. reported preliminary experience with five metastatic breast cancer patients who received concomitant ribliciclib and palliative RT. Two of five patients had G3-4 adverse events (neutropenia, vomiting, and diarrhea) [34]. David et al. reported five cases with G2-5 adverse events (pneumonitis, dermatitis, oesophagitis) during palbociclib and RT concurrent or separate treatment [35]. A safety and feasibility study conducted on 288 ER+ advanced breast cancer patients used RT and CDKi sequentially and concurrently. This retrospective study mainly focused on severe adverse events. They found that neutropenia was more frequent in a concurrent treatment arm [36]. Based

on these studies, concurrent treatment has the potential to result in more adverse events.

The concurrent use of CDK4/6 inhibitors and radiotherapy may indeed lead to an increased risk of side effects. Both CDK4/6 inhibitors and radiotherapy can individually cause side effects, and their combination can potentially amplify these. However, it is important to note that the specific side effects and their severity can vary depending on the individual patient, specific drugs, and radiation protocols used. When CDK4/6 inhibitors and radiotherapy are used concurrently, there can be overlapping or additive effects on the body, potentially leading to increased side effects.

Translational implications/clinical applications

The optimal timing of radiotherapy and CDK4/6 inhibitor plus endocrine partner therapy administration is translational implication; therefore, it could be a major benefit from the view of clinical application [16].

In drug registration clinical trials [37–40], irradiation was allowed during CDK4/6 inhibitor therapy. In a PALOMA trial, only 1.9% of the randomized subjects received radiotherapy [7, 41, 42] and it was highlighted that in cases of central nervous system metastasis treated with irradiation, CDK4/6 inhibitors were prohibited.

The more metastatic treatment lines we indicate, the shorter the progression-free survival time. Therefore, it is very important to maintain effective treatment albeit it could not dominate a certain number (less than three) lesions. Thus, with the implementation of impressive local ablative treatment, there is no need for drug switching. This is a paradigm shift in oncology: we understand that malignancies have heterologous clone populations and just those can skip from treatment control whose have acquired resistance. Therefore, except for these lines, properly chosen therapy can block sensitive clones and can be continued safely and undisturbed. Uncontrolled lines can be treated by local ablative treatment methods. If the required result appears on re-staging, i.e., the blockade or destruction of the so-far uncontrolled tumor lesions, the post-progression overall survival time can be prolonged. Significant benefits and overall survival improvement are expected. In such a case, there is no need to modify further therapeutic lines; therefore, good quality of life can be maintained by postponing new drug introduction. Patients can gain time, with a considerably improved and extended lifespan.

Moreover, the latest studies have revealed that CDK4/6 inhibitors may stimulate the immune system, namely, CD8 T-cell immune memory cells, interact with the tumor microenvironment, and have antitumor immunity effects [15, 43].

Radiotherapy is also an immunogenic treatment modality as it causes stress-driven regulated cell death; nowadays, so-called immunogenic cell death is an adaptive immune response [15, 21, 44]. It sensitizes the microenvironment before immune therapies [45], so the primary given radiotherapy may not just be synergistic but may even be a supra-additive effective treatment, taking into account that CDK4/6 inhibitors also affect the immune response.

Discussion

The toxicity profile of concomitant CDK4/6 inhibitor therapy with irradiation is still unclear, though there are few preclinical studies [30, 45, 46] targeting this question. There are a few that conclude the radiosensitization effects of CDK4/6 inhibitors, although not in every tumor type, mainly in HPV-positive, high-mitotic activity, and head and neck squamous cell cancer, whose biological features are different from relatively slow-growing hormone receptor-positive breast cancers. These studies speculate that the CDK4/6 inhibitor probably blocks cell cycle progression into the radioresistant S phase, but these conclusions have not been substantiated in daily clinical practice [47].

Following exhaustive publication searches, few case series and reports were found to be available, involving few subjects and without control groups, focusing mainly on toxicity profiles with controversial results. Furthermore, the efficacy results of concomitant CDK4/6 inhibitor therapy with irradiation are not detailed. A recently published clinical investigation within a multi-institutional safety and toxicity study reported higher toxicity rates when these two modalities were administered concurrently. According to this clinical investigation, safety and toxicity results appear to be clear. Therefore, the question remains as to which administration schedule is more favorable.

The sequence and timing of different therapies are crucial to reach optimal antitumor effects [16]. The main difference between radiotherapy and CDK4/6 inhibitors is their cancer control: radiotherapy drives cells to certain cell death, while CDK4/6 inhibitors block the cell cycle at the G1/S checkpoint. Pre-treated cells by CDK4/6 inhibitors are theoretically less sensitive to radiotherapy as they block at G1/S. In case of proper order palliative effect is more favorable; therefore, a longer progression-free survival and a better quality of life can be achieved.

The authors suggest the following order in those cases when the delivery of radiotherapy and CDK4/6 inhibitor treatment are both indicated.

If *de novo* diagnosed metastatic breast cancer requires CDK4/6 inhibitor therapy, start with irradiation and then administer CDK4/6 inhibitors and endocrine replacement therapy [48].

When a patient is under treatment with CDK4/6 inhibitor, there are two options depending on the aim and intent of high-energy radiotherapy. In the first case, if palliative ultra-hypofractionated radiation is planned due to severe pain

relief, or if there is a risk of fracture or compression caused by bone metastasis that cannot be treated with local ablative dose, 8Gy in a single fraction can be scheduled. Radiotherapy can be given at the end of the drug therapeutic gap (21/7 days schema) in the case of palbociclib and ribociclib. Nota bene, the abemaciclib schedule is continuous; therefore, it can be suspended and radiotherapy can be implemented a week later.

In the second case, in oligometastatic disease or in certain non-responder foci or few (less than three) newer lesions, where treatment with a curative dose is planned, even with stereotactic body radiation or intensity-modulated radiotherapy (IMRT) or volumetric modulated arc therapy (VMAT) with simultaneous integrated boost (SIB), the radiation can be initiated a week after the last pastille intake of CDK4/6 inhibitor. Following the suspension of CDK4/6 inhibitors and completion of radiotherapy, it can be re-administered safely and allowed to continue if restaging radio-biological images show no progression. The re-evaluation of radiological images has to be conducted using the same method used for diagnosis and must be scheduled 6–8 weeks following the completion of radiotherapy. In the case of metabolic information that can be measured on PET/CT, the maximum standardized uptake value (SUVmax) can show the activity changes (hopefully decay) of the tumor.

Conclusion

After publications and clinical trials were investigated, from molecular biology and clinical aspects, all these findings suggest a new treatment perspective is necessary.

We can conclude that CDK4/6 inhibitor therapy combined with radiotherapy is safe and the authors recommend this therapy for better and more effective outcomes appropriate sequence, which is not written in the official summary of product characteristics. Radiotherapy should be the initial treatment, followed by CDK4/6 inhibitors in *de novo* discovered cases; otherwise, a short suspension of the drug is advised to eliminate the CDK4/6 inhibitor from plasma and let the radiotherapy destroy cancerous cells arriving in the G2/M phase.

The adequate local ablative treatment in oligo-progression could be sufficient and, following this, we can maintain the otherwise effective systemic therapy. Therefore, we can extend and prolong the time interval of the metastatic first-line treatment with CDK4/6 inhibitor, even changing the endocrine partner (letrozole to fulvestrant). This is why it is important to ensure an effective local ablative treatment with radiotherapy in bone-only oligo-metastatic cases. If necessary, bone modifying agent can be shifted (bisphosphonate to denosumab) in another step. In the case of infectivity of these treatment changes, the main component of the first-line treatment (CDK4/6 inhibitor) should be relied on in the second-line treatment. With this soft change, patients can gain time and a good quality of life as we know that further line treatments are usually associated with more adverse events and lead to shorter progression-free intervals. In our daily practice, we deliver SBRT (stereotactic body radiation therapy) for two main reasons: stereotactic radiotherapy doses are potentially more lethal to metastases and may dominate the disease; meanwhile, SBRT requires a shorter treatment time.

Further questions can be addressed by scientists, such as "What about particle radiotherapy combined with targeted agents?" Preliminary data suggest that high LET radiation, such as heavy ion radiation like C ion irradiation may be a favorable partner to CDK4/6 inhibitor application [49]. Probably, this is the future hope when high-energy heavy ion radiation would be the essential part of cancer treatment and wide spread would be available [50].

All oncological treatment must be discussed in a multidisciplinary team and individualized options must be calculated, taking into account further possibilities and as far as possible, maintaining an effective, highly tolerable therapy for as long as we can with the hope of prolonging the good quality of post-limited-progression life.

Author contributions

Conceptualization, IT, PA, and AF; methodology, AF and PA; data curation, IT and AF; writing—original draft preparation, AF and IT; writing—review and editing, AF, IT, IH, and PA; visualization, IT; supervision, AF, PA, and IH. All authors have read and agreed to the published version of the manuscript.

Conflict of interest

The authors declare that the research was conducted in the absence of any commercial or financial relationships that could be construed as a potential conflict of interest.

References

1. Sung H, Ferlay J, Siegel RL, Laversanne M, Soerjomataram I, Jemal A, et al. Global cancer statistics 2020: GLOBOCAN estimates of incidence and mortality worldwide for 36 cancers in 185 countries. *Ca: Cancer J Clin* (2021) 71(3):209–49. doi:10.3322/caac.21660

2. Howlader N, Altekruse SF, Li CI, Chen VW, Clarke CA, Ries LA, et al. US incidence of breast cancer subtypes defined by joint hormone receptor and HER2 status. *Jnci: J Natl Cancer Inst* (2014) 106(5):dju055–8. doi:10.1093/jnci/dju055

3. Bosacki C, Bouleftour W, Sotton S, Vallard A, Daguenet E, Ouaz H, et al. CDK 4/6 inhibitors combined with radiotherapy: a review of literature. *Clin Transl Radiat Oncol* (2021) 26:79–85. doi:10.1016/j.ctro.2020.11.010

4. Feng Y, Spezia M, Huang S, Yuan C, Zeng Z, Zhang L, et al. Breast cancer development and progression: risk factors, cancer stem cells, signaling pathways, genomics, and molecular pathogenesis. *Genes Dis* (2018) 5:77–106. doi:10.1016/j.gendis.2018.05.001

5. Wu Q, Li J, Zhu S, Wu J, Chen C, Liu Q, et al. Breast cancer subtypes predict the preferential site of distant metastases: a SEER based study. *Oncotarget* (2017) 8:27990–6. doi:10.18632/oncotarget.15856

6. Svensson E, Christiansen CF, Ulrichsen SP, RørthSørensen MRHT, Sørensen HT. Survival after bone metastasis by primary cancer type: a Danish population-based cohort study. *BMJ open* (2017) 7:e016022–7. doi:10.1136/bmjopen-2017-016022

7. Cristofanilli M, Turner NC, Bondarenko I, Ro J, Im SA, Masuda N, et al. Fulvestrant plus palbociclib versus fulvestrant plus placebo for treatment of hormone-receptor-positive, HER2-negative metastatic breast cancer that progressed on previous endocrine therapy (PALOMA-3): final analysis of the multicentre, double-blind, phase 3 randomised controlled trial. *Lancet Oncol* (2016) 17:425–39. doi:10.1016/S1470-2045(15)00613-0

8. Tripathy D, Im SA, Colleoni M, Franke F, Bardia A, Harbeck N, et al. Ribociclib plus endocrine therapy for premenopausal women with hormone-receptor-positive, advanced breast cancer (MONALEESA-7): a randomised phase 3 trial. *Lancet Oncol* (2018) 19:904–15. doi:10.1016/S1470-2045(18)30292-4

9. Johnston S, Martin M, Di Leo A, Im SA, Awada A, Forrester T, et al. MONARCH 3 final PFS: a randomized study of abemaciclib as initial therapy for advanced breast cancer. *NPJ Breast Cancer* (2019) 5:5–8. doi:10.1038/s41523-018-0097-z

10. Johnston SR, Harbeck N, Hegg R, Toi M, Martin M, Shao ZM, et al. Abemaciclib combined with endocrine therapy for the adjuvant treatment of HR+, HER2–, node-positive, high-risk, early breast cancer (monarchE). *J Clin Oncol* (2020) 38:3987–98. doi:10.1200/JCO.20.02514

11. Xu B, Zhang Q, Zhang P, Hu X, Li W, Tong Z, et al. Dalpiciclib or placebo plus fulvestrant in hormone receptor-positive and HER2-negative advanced breast cancer: a randomized, phase 3 trial. *Nat Med* (2021) 27:1904–9. doi:10.1038/s41591-021-01562-9

12. Yin L, Yao Z, Wang Y, Huang YH, Mazuranic M, Yin A. 4MO Preclinical evaluation of novel CDK4/6 inhibitor GLR2007 in breast and lung cancer models. *Ann Oncol* (2021) 32:S362–362. doi:10.1016/j.annonc.2021.08.282

13. Braal CL, Jongbloed EM, Wilting SM, Mathijssen RH, Koolen SL, Jager A. Inhibiting CDK4/6 in breast cancer with palbociclib, ribociclib, and abemaciclib: similarities and differences. *Drugs* (2021) 81:317–31. doi:10.1007/s40265-020-01461-2

14. Parkes A, Clifton K, Al-Awadhi A, Oke O, Warneke CL, Litton JK, et al. Characterization of bone only metastasis patients with respect to tumor subtypes. *NPJ Breast Cancer* (2018) 4:2–7. doi:10.1038/s41523-018-0054-x

15. Petroni G, Galluzzi L. Impact of treatment schedule on the efficacy of cytostatic and immunostimulatory agents. *Oncoimmunology* (2021) 10:1889101–4. doi:10.1080/2162402X.2021.1889101

16. Petroni G, Buqué A, Yamazaki T, Bloy N, Liberto MD, Chen-Kiang S, et al. Radiotherapy delivered before CDK4/6 inhibitors mediates superior therapeutic effects in ER^+ breast cancer. *Clin Cancer Res* (2021) 27:1855–63. doi:10.1158/1078-0432.CCR-20-3871

17. Yang Y, Luo J, Chen X, Yang Z, Mei X, Ma J, et al. CDK4/6 inhibitors: a novel strategy for tumor radiosensitization. *J Exp Clin Cancer Res* (2020) 39:188–11. doi:10.1186/s13046-020-01693-w

18. Ades F, Tryfonidis K, Zardavas D. The past and future of breast cancer treatment—from the papyrus to individualised treatment approaches. *Ecancermedicalscience* (2017) 11:746–11. doi:10.3332/ecancer.2017.746

19. Vozenin MC, Baumann M, Coppes RP, Bourhis J. FLASH radiotherapy international workshop. *Radiother Oncol* (2019) 139:1–3. doi:10.1016/j.radonc.2019.07.020

20. Yokoya A, Shikazono N, Fujii K, Urushibara A, Akamatsu K, Watanabe R. DNA damage induced by the direct effect of radiation. *Radiat Phys Chem* (2008) 77:1280–5. doi:10.1016/j.radphyschem.2008.05.021

21. O'neill P, Fielden EM. Primary free radical processes in DNA. *Adv Radiat Biol* (1993) 17:53–120. doi:10.1016/B978-0-12-035417-7.50005-2

22. Abraham RT. Checkpoint signalling: focusing on 53BP1. *Nat Cel Biol* (2002) 4:E277–9. doi:10.1038/ncb1202-e277

23. Lin Y, Raj J, Li J, Ha A, Hossain MA, Richardson C, et al. APE1 senses DNA single-strand breaks for repair and signaling. *Nucleic Acids Res* (2020) 48:1925–40. doi:10.1093/nar/gkz1175

24. Galluzzi L, Vitale I, Aaronson SA, Abrams JM, Adam D, Agostinis P, et al. Molecular mechanisms of cell death: recommendations of the nomenclature committee on cell death 2018. *Cell Death Differ* (2018) 25:486–541. doi:10.1038/s41418-017-0012-4

25. Kumari S, Mukherjee S, Sinha D, Abdisalaam S, Krishnan S, Asaithamby A. Immunomodulatory effects of radiotherapy. *Int J Mol Sci* (2020) 21:8151–29. doi:10.3390/ijms21218151

26. Lim S, Kaldis P. Cdks, cyclins and CKIs: roles beyond cell cycle regulation. *Development* (2013) 140:3079–93. doi:10.1242/dev.091744

27. Pesch AM, Hirsh NH, Michmerhuizen AR, Jungles KM, Wilder-Romans K, Chandler BC, et al. RB expression confers sensitivity to CDK4/6 inhibitor–mediated radiosensitization across breast cancer subtypes. *JCI Insight* (2022) 7:e154402–18. doi:10.1172/jci.insight.154402

28. Filmus J, Robles AI, Shi W, Wong MJ, Colombo LL, Conti CJ. Induction of cyclin D1 overexpression by activated ras. *Oncogene* (1994) 9:3627–33.

29. Tanyi J, Tory K, Bánkfalvi A, Shröder W, Rath W, Füzesi L. Analysis of p53 mutation and cyclin D1 expression in breast tumors. *Pathol Oncol Res* (1999) 5(2):90–4. doi:10.1053/paor.1999.0201

30. Asghar U, Witkiewicz AK, Turner NC, Knudsen ES. The history and future of targeting cyclin-dependent kinases in cancer therapy. *Nat Rev Drug Discov* (2015) 14:130–46. doi:10.1038/nrd4504

31. Pesch AM, Hirsh NH, Chandler BC, Michmerhuizen AR, Ritter CL, Androsiglio MP, et al. Short-term CDK4/6 inhibition radiosensitizes estrogen receptor-positive breast cancers. *Clin Cancer Res* (2020) 26:6568–80. doi:10.1158/1078-0432.CCR-20-2269

32. Klapp V, Buqué A, Bloy N, Sato A, Yamazaki T, Zhou XK, et al. Cellular senescence in the response of HR+ breast cancer to radiotherapy and CDK4/6 inhibitors. *J Transl Med* (2023) 21:110–0. doi:10.1186/s12967-023-03964-4

33. Alomran R, White M, Bruce M, Bressel M, Roache S, Karroum L, et al. Stereotactic radiotherapy for oligoprogressive ER-positive breast cancer (AVATAR). *BMC Cancer* (2021) 21:303–9. doi:10.1186/s12885-021-08042-w

34. Meattini I, Desideri I, Scotti V, Simontacchi G, Livi L. Ribociclib plus letrozole and concomitant palliative radiotherapy for metastatic breast cancer. *Breast* (2018) 42:1–2. doi:10.1016/j.breast.2018.08.096

35. David S, Ho G, Day D, Harris M, Tan J, Goel S, et al. Enhanced toxicity with CDK 4/6 inhibitors and palliative radiotherapy: non-consecutive case series and review of the literature. *Transl Oncol* (2021) 14:100939–7. doi:10.1016/j.tranon.2020.100939

36. Kubeczko M, Gabryś D, Gawkowska M, Polakiewicz-Gilowska A, Cortez AJ, Krzywon A, et al. Safety and feasibility of radiation therapy combined with CDK 4/6 inhibitors in the management of advanced breast cancer. *Cancers* (2023) 15:690–17. doi:10.3390/cancers15030690

37. Harbeck N, Franke F, Villanueva-Vazquez R, Lu YS, Tripathy D, Chow L, et al. Health-related quality of life in premenopausal women with hormone-receptor-positive, HER2-negative advanced breast cancer treated with ribociclib plus endocrine therapy: results from a phase III randomized clinical trial (MONALEESA-7). *Ther Adv Med Oncol* (2020) 12:1758835920943065–8. doi:10.1177/1758835920943065

38. Dickler MN, Tolaney SM, Rugo HS, Cortés J, Diéras V, Patt D, et al. MONARCH 1, A phase II study of abemaciclib, a CDK4 and CDK6 inhibitor, as a single agent, in patients with refractory hr+/HER2- metastatic breast cancer. *Clin Cancer Res* (2017) 23:5218–24. doi:10.1158/1078-0432.CCR-17-0754

39. Sledge GW, Jr, Toi M, Neven P, Sohn J, Inoue K, Pivot X, et al. Monarch 2: abemaciclib in combination with fulvestrant in women with HR+/HER2– advanced breast cancer who had progressed while receiving endocrine therapy. *J Clin Oncol* (2017) 35:2875–84. doi:10.1200/JCO.2017.73.7585

40. Goetz MP, Toi M, Campone M, Sohn J, Paluch-Shimon S, Huober J, et al. Monarch 3: abemaciclib as initial therapy for advanced breast cancer. *J Clin Oncol* (2017) 35:3638–46. doi:10.1200/JCO.2017.75.6155

41. Finn RS, Crown JP, Lang I, Boer K, Bondarenko IM, Kulyk SO, et al. The cyclin-dependent kinase 4/6 inhibitor palbociclib in combination with letrozole versus letrozole alone as first-line treatment of oestrogen receptor-positive, HER2-negative, advanced breast cancer (PALOMA-1/TRIO-18): a randomised phase 2 study. *Lancet Oncol* (2015) 16:25–35. doi:10.1016/S1470-2045(14)71159-3

42. Finn RS, Martin M, Rugo HS, Jones S, Im SA, Gelmon K, et al. Palbociclib and letrozole in advanced breast cancer. *N Engl J Med* (2016) 375:1925–36. doi:10.1056/NEJMoa1607303

43. Lelliott EJ, Kong IY, Zethoven M, Ramsbottom KM, Martelotto LG, Meyran D, et al. CDK4/6 inhibition promotes antitumor immunity through the induction of T-cell memory. *Cancer Discov* (2021) 11:2582–601. doi:10.1158/2159-8290.CD-20-1554

44. Galluzzi L, Vitale I, Warren S, Adjemian S, Agostinis P, Martinez AB, et al. Consensus guidelines for the definition, detection and interpretation of

immunogenic cell death. *J Immunother Cancer* (2020) 8:e000337–21. doi:10.1136/jitc-2019-000337

45. Göttgens EL, Bussink J, Leszczynska KB, Peters H, Span PN, Hammond EM. Inhibition of CDK4/CDK6 enhances radiosensitivity of HPV negative head and neck squamous cell carcinomas. *Int J Radiat Oncol Biol Phys* (2019) 105:548–58. doi:10.1016/j.ijrobp.2019.06.2531

46. Xie X, Zheng W, Chen T, Lin W, Liao Z, Liu J, et al. CDK4/6 inhibitor palbociclib amplifies the radiosensitivity to nasopharyngeal carcinoma cells via mediating apoptosis and suppressing DNA damage repair. *Onco Targets Ther* (2019) 12:11107–17. doi:10.2147/OTT.S234221

47. Al-Rashdan A, Quirk S, Roumeliotis M, Abedin T, Amaro CP, Barbera L, et al. Radiation therapy with cyclin-dependent kinase 4/6 inhibitors: a multi-institutional safety and toxicity study. *Int J Radiat Oncol Biol Phys* (2022) 114:399–408. doi:10.1016/j.ijrobp.2022.07.005

48. Rubovszky G, Kocsis J, Boér K, Chilingirova N, Dank M, Kahán Z, et al. Systemic treatment of breast cancer. 1st central-eastern European professional consensus statement on breast cancer. *Pathol Oncol Res* (2022) 28:1–26. doi:10.3389/pore.2022.1610383

49. Helm A, Fournier C, Durante M. Particle radiotherapy and molecular therapies: mechanisms and strategies towards clinical applications. *Expert Rev Mol Med* (2022) 24:e8–11. doi:10.1017/erm.2022.2

50. Nikitaki Z, Velalopoulou A, Zanni V, Tremi I, Havaki S, Kokkoris M, et al. Key biological mechanisms involved in high-LET radiation therapies with a focus on DNA damage and repair. *Expert Rev Mol Med* (2022) 24:e15–15. doi:10.1017/erm.2022.6

Pathology & Oncology Research | frontiers

TYPE Hypothesis & Theory
PUBLISHED 17 March 2023
DOI 10.3389/pore.2023.1610956

Check for updates

OPEN ACCESS

EDITED BY
Andrea Ladányi,
National Institute of Oncology (NIO), Hungary

*CORRESPONDENCE
Dong Li,
lidong.bprc@foxmail.com

†These authors have contributed equally to this work

RECEIVED 18 November 2022
ACCEPTED 28 February 2023
PUBLISHED 17 March 2023

CITATION
Yang Y, Wang Z, He M, Diao L, Yu B and Li D (2023), NAD+ biosynthesis metabolism predicts prognosis and indicates immune microenvironment for breast cancer.
Pathol. Oncol. Res. 29:1610956.
doi: 10.3389/pore.2023.1610956

COPYRIGHT
© 2023 Yang, Wang, He, Diao, Yu and Li. This is an open-access article distributed under the terms of the Creative Commons Attribution License (CC BY). The use, distribution or reproduction in other forums is permitted, provided the original author(s) and the copyright owner(s) are credited and that the original publication in this journal is cited, in accordance with accepted academic practice. No use, distribution or reproduction is permitted which does not comply with these terms.

NAD+ biosynthesis metabolism predicts prognosis and indicates immune microenvironment for breast cancer

Yuting Yang[1†], Ze Wang[2†], Mengqi He[2†], Lihong Diao[3], Biyue Yu[4] and Dong Li[1,2*]

[1]Department of Immunology, Medical College of Qingdao University, Qingdao, Shandong, China, [2]State Key Laboratory of Proteomics, Beijing Proteome Research Center, National Center for Protein Sciences, Beijing Institute of Lifeomics, Beijing, China, [3]School of Traditional Chinese Medicine, Beijing University of Chinese Medicine, Beijing, China, [4]School of Life Sciences, Hebei University, Baoding, Hebei, China

The growing evidence implies that tumor cells need to increase NAD+ levels by upregulating NAD+ biosynthesis to satisfy their growth demand. NAD+ biosynthesis metabolism is implicated in tumor progression. Breast cancer (BC) is the most common malignant malignancy in the world. Nevertheless, the prognostic significance of NAD+ biosynthesis and its relationship with the tumor immune microenvironment in breast cancer still need further investigation. In this study, we obtained the mRNA expression data and clinical information of BC samples from public databases and calculated the level of NAD+ biosynthesis activity by single-sample gene set enrichment analysis (ssGSEA). We then explored the relationship between the NAD+ biosynthesis score, infiltrating immune cells, prognosis significance, immunogenicity and immune checkpoint molecules. The results demonstrated that patients with high NAD+ biosynthetic score displayed poor prognosis, high immune infiltration, high immunogenicity, elevated PD-L1 expression, and might more benefit from immunotherapy. Taken together, our studies not only deepened the understanding of NAD+ biosynthesis metabolism of breast cancer but also provided new insights into personalized treatment strategies and immunological therapies to improve the outcomes of breast cancer patients.

KEYWORDS

immunotherapy, breast cancer, prognosis, immune microenvironment, NAD+ biosynthesis

Introduction

Breast cancer (BC) is the most common malignancy in the world and the fifth leading cause of cancer death worldwide (1). With advance in the diagnosis and treatment of breast cancer, the survival rate of breast cancer patients has significantly improved (2). However, as a malignancy with high heterogeneity at the molecular level, BC patients with similar clinical

features may have different prognosis (3). Therefore, it is essential to consider other important factors in guiding clinical practice.

The tumor microenvironment (TME) is a highly complex cellular network, including tumor cells, stromal cells, fibroblasts, immune cells, soluble factors, signaling molecules and extracellular matrix components (4). Recent studies suggest that the immune components in the TME are closely associated with tumor development, recurrence, and metastasis. These components are called the tumor immune microenvironment (TIME) (5). Immune cells or immune-related genes in TIME can predict the prognosis and treatment efficacy of cancer patients (6–8). For instance, tumor-infiltrating lymphocytes (TILs) have been shown to have a strong prognostic effect in patients with early stage TNBC and HER2-positive breast cancer (9, 10). Exploring TIME in BC would conductive to guide and optimize immunotherapy and improve the prognosis of BC patients.

NAD+ (nicotinamide adenine dinucleotide) is a coenzyme for redox reactions and a substrate for different signaling enzymes that can directly or indirectly affect many important cellular functions, such as metabolic pathways, DNA repair, and immune cell function (11, 12). Many of these processes are associated with cancer development. Given that NAD+ -dependent signaling responses involve the degradation of molecules, sustained NAD+ production *via* different biosynthetic pathways is a hallmark of many types of tumor (13, 14). Enzymes involved in NAD+ biosynthesis have been reported to be aberrantly expressed or dysregulated in many cancer types, including breast cancer. NAMPT, one of the rate-limiting enzymes of NAD+ biosynthesis, has been shown to be overexpressed in breast cancer and associated with breast cancer proliferation and invasiveness (15, 16). However, the relationship between NAD+ biosynthesis and the immune microenvironment of breast cancer has not been systematically investigated.

In the current study, a series of bioinformatic methods were used to analyze the features of NAD+ biosynthesis in BC based on transcriptional profiling data from public databases. BC patients were classified into the high and low NAD+ biosynthetic subtypes based on the NAD+ biosynthesis score and survival analysis was performed. We further explored the hallmark pathways and TME immune cell infiltration characteristics of the two subtypes. Moreover, we analyzed the relationship between the NAD+ biosynthesis score and several immunotherapy biomarkers. These findings may provide a new perspective for exploring the metabolic mechanism and treatment of breast cancer.

Materials and methods

Retrieval of NAD+ biosynthesis-related genes

NAD+ biosynthesis-related genes were obtained from the Kyoto Encyclopedia of Genes and Genomes (KEGG) pathway database (Pathway: hsa00760) and Reactome database (R-HSA-196807) (17). We also reviewed the literature and added the previously reported genes (11). After selecting genes associated with NAD+ biosynthesis from all gene sets, a total of 19 genes were retrieved (Supplementary Table S1).

Datasets and data preprocessing

The mRNA sequencing, gene somatic mutations, and clinical data of breast invasive carcinoma (BRCA) patients were downloaded from The Cancer Genome Atlas (TCGA) database and included data form 99 normal samples and 1069 tumor samples. RNA-sequencing data (FPKM values) were transformed into transcripts per million (TPM) values and normalized into log2 (TPM +1) for the following analysis. Datasets of GSE20711, GSE48390 and GSE88770 from the Gene Expression Omnibus (GEO) were selected to validate the results of TCGA data analysis. The GSE20711 dataset was used by Dedeurwaerder et al. to study epigenetic variation (methylation) related to gene expression in breast cancer (18). GSE20711 consists of 88 breast cancer and 2 normal breast tissue samples, with only the gene expression profiles of 88 breast cancer patients retained for subsequent analysis. The GSE48390 dataset was used by Huang et al. to identify genes with coherent patterns of both copy number variation (CNV) and differential gene expression, and to use these genes to derive signatures related to clinical ER and HER2 status and disease-free survival (19). GSE48390 consists of 81 breast cancer samples. The GSE88770 dataset was used by Metzger-Filho et al. to analyze the prognostic value of histological grading (HG) in breast cancer (20). GSE88770 contains 117 breast cancer samples. The three datasets were based on GPL570 platforms (Affymetrix Human Genome U133 Plus 2.0 Array). We downloaded the original expression profile and used the robust multi-array average (RMA) algorithm to perform background correction and quantile normalization (21). We merged GEO datasets and used the combat algorithm to eliminate the batch effects by R package “sva” (22).

Evaluation of tumor NAD+ biosynthesis score

We applied the single-sample gene-set enrichment analysis (ssGSEA) for the NAD+ biosynthesis gene set to quantify the NAD+ biosynthesis activity (NAD+ biosynthesis score) (23). The optimal cutoff threshold for classifying breast cancer (BC) patients into high and low NAD+ biosynthetic subtypes was determined using the “surv_cutpoint” function from the R package “survminer”.

Differential gene expression analysis and enrichment analysis

We identified differentially expressed genes (DEGs) between the high and low NAD+ biosynthetic subtypes using the R

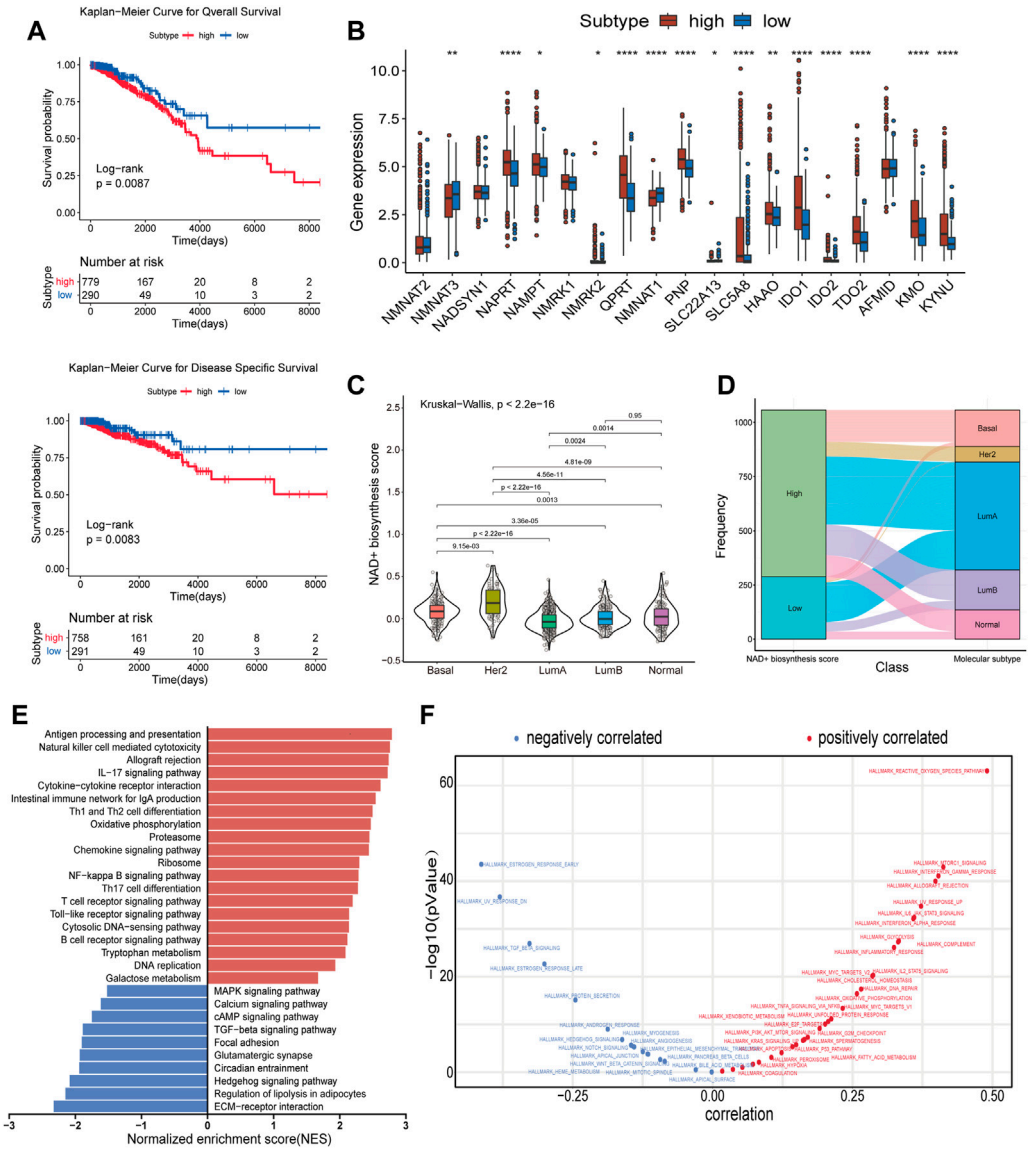

FIGURE 1
Subtypes of NAD+ biosynthesis and biological characteristics in BRCA. **(A)** Survival analysis of the high and low NAD+ biosynthetic subtypes in TCGA cohort. **(B)** Differential expression of NAD+ biosynthesis-related genes between the high and low NAD+ biosynthetic subtypes in TCGA cohort. **(C)** Violin plots showed the correlation between the NAD+ biosynthesis score and molecular subtypes in TCGA cohort. **(D)** Alluvial plot for the NAD+ biosynthetic subtypes versus different molecular subtypes in TCGA cohort. **(E)** Differential pathway activities scored by GSEA between the high and low biosynthetic subtypes in TCGA cohort. The red bars indicated the upregulated pathways, while the blue bars indicated the downregulated pathways. **(F)** Correlation between the NAD+ biosynthesis score and ssGSEA enrichment scores of cancer hallmark pathways in TCGA cohort. *$p < 0.05$; **$p < 0.01$; ***$p < 0.001$, and ****$p < 0.0001$.

package "limma," with a significance threshold of adjusted p-value <0.05 and |log2FoldChange| > 1. To assess the differences in biological signaling pathway between the high and low NAD+ biosynthetic subtypes, GSEA analysis was performed using the gseKEGG function of the R package "clusterProfiler," with $p < 0.05$ considered statistically significant (24).

Immune infiltration analysis

Immune cell gene signatures and immune-related signatures were collected from previously published works (25, 26), and ssGSEA was used to calculate the enrichment scores of infiltrating immune cells and immune functions. In addition, the "ESTIMATE" package was used to assess the

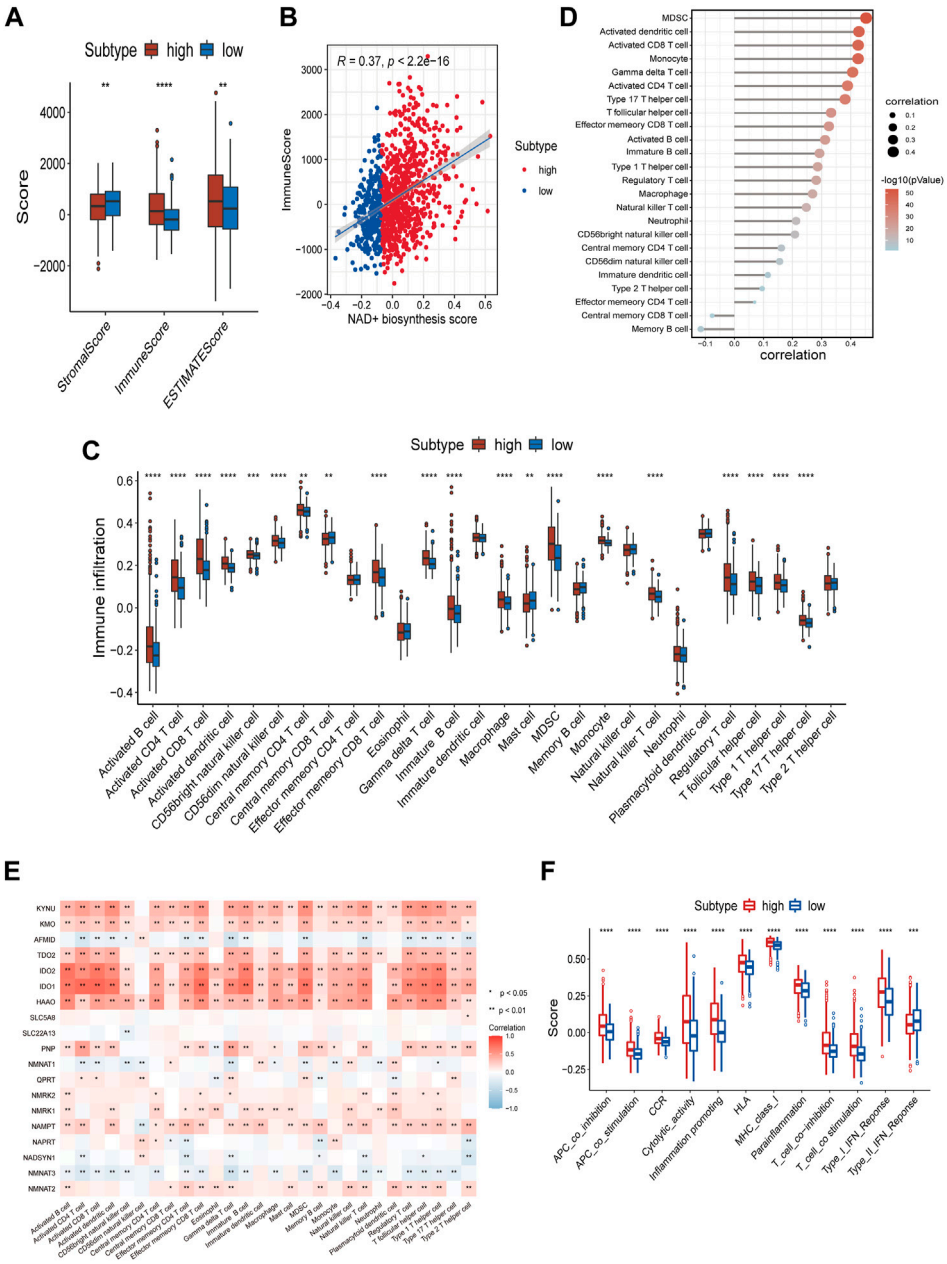

FIGURE 2
Correlation of the NAD+ biosynthesis score with the immune landscape of patients with breast cancer. **(A)** Comparison of the stromal score, immune score, and ESTIMATE score between the high and low NAD+ biosynthetic subtypes. **(B)** The correlation between the NAD+ biosynthesis score and immune score. **(C)** Relative infiltration of 28 types of immune cells in the high and low NAD+ biosynthetic subtypes. **(D)** The correlation between the NAD+ biosynthesis score and the ssGSEA enrichment scores of immune cells. **(E)** The heatmap showed the associations between the 19 NAD+ biosynthesis-related genes and immune cells. Red indicated positive correlations, and blue indicated negative correlations. Asterisks denoted *p*-value. Blank cells represented no statistical significance of the correlation. **(F)** Relative enrichment score of 12 immune-related signatures in the high and low NAD+ biosynthetic subtypes. **p* < 0.05; ***p* < 0.01; ****p* < 0.001, and *****p* < 0.0001.

composition of the immune stroma in the tumor microenvironment of breast cancer patients, and the immune score, stromal score, and estimated score (ESTIMATE Score) were calculated (27).

Construction of TF-IRG networks

We extracted differentially expressed immune-related genes (DEIRGs) and transcription factors (DETFs) from DEGs based

on the lists obtained from ImmPort and Cistrome Cancer database (Supplementary Tables S2, S3). We then calculated the correlation between DETFs and DEIRGs. Correlation coefficients >0.5 (or less than −0.5) and adjusted *p*-value <0.01 were considered to be significantly correlated (Supplementary Table S4).

Mutation and evaluation of the therapeutic efficacy

The R package "maftools" was used to estimate the tumour mutation burden (TMB) for each patient between the two subtypes (28). Additionally, the neoantigen load and homologous recombination deficiency (HRD) in BRCA patients were collected from published studies (29, 30). For the immunotherapy sensitivity prediction analysis, the immunophenoscore (IPS) of breast cancer patients was downloaded from the TCIA database (25). For drug sensitivity prediction analysis, the "pRRophetic" R package was used to calculate the IC50 of common chemotherapeutic agents (31). The difference in the IC50 of agents between the high and low NAD+ biosynthetic subtypes was evaluated with the Wilcoxon test, and *p*-value <0.05 was considered significant.

Statistical and computational analysis

All statistical analyses were done in R (version 4.1). The significance of differences in continuous variables between the two subtypes was calculated using the Wilcoxon test. The Kruskal-Wallis test and Dunn's *post hoc* multiple comparison test were used for more than two subtypes. The optimal cutoff values for each cohort were evaluated using the "surv_cutpoint" function in the "survminer" package. For prognostic analysis, the survival curves were constructed using the Kaplan-Meier method and log-rank test was used to judge differences between the subtypes. Spearman correlation analysis was carried out to determine the correlation coefficient. Statistical significance was considered as *p*-value <0.05.

Results

Identification of NAD+ biosynthetic subtypes and their correlation with biological functions in BRCA

NAD+ is essential for the proper function and metabolism of all living cells, including cancer cells. We used ssGSEA to calculate the NAD+ biosynthesis score of patients from TCGA database and found that NAD+ biosynthesis score of breast cancer tissue was significantly higher than that of normal breast tissue, which is consistent with previous findings (Supplementary Figure S1). To better understand the effect of NAD+ biosynthesis on breast cancer prognosis, the BC patients were divided into the high and low NAD+ biosynthetic subtypes based on the optimal cut-off value (−0.0743) in TCGA cohort, and subjected to survival comparison. Figure 1A showed that patients in the low NAD+ biosynthetic subtype had significantly better overall survival and disease specific survival than patients in the high NAD+ biosynthetic subtype. The prognostic significance of the NAD+ biosynthesis score was validated in GEO cohort (Supplementary Figure S2A). Compared to low NAD+ biosynthetic subtype, twelve NAD+ biosynthesis-related genes were significantly upregulated in the high NAD+ biosynthetic subtype, which indicated that NAD+ biosynthesis score may reflect the activity of NAD+ biosynthesis to some extent (Figure 1B). Next, we analyzed the clinical features differences between the two subtypes, including pathological stage, molecular subtypes and TNM stage (Supplementary Figure S3). We found that only molecular subtypes and NAD+ biosynthesis score exhibited statistical significance (Figures 1C, D). In detail, the HER2-enriched subtype had significantly higher NAD+ biosynthesis score than other four molecular subtypes, whereas the LumA subtype had the lowest NAD+ biosynthesis score.

GSEA was used to investigate the biological differences between the two subtypes. As shown in Figure 1E, the results showed that many immune-related pathways were significantly upregulated in the high NAD+ biosynthetic subtype, including antigen processing and presentation, IL-17 signaling pathway and chemokine signaling pathway. The low NAD+ biosynthetic subtype was enriched in pathways related to ECM-receptor interaction and regulation of lipolysis in adipocytes. Besides, to explore the potential pathways which NAD+ biosynthesis was involved in, the correlation between the NAD+ biosynthesis score and cancer hallmarks was analyzed. We found a significant positive association between the NAD+ biosynthesis score and some hallmark pathways, including reactive oxygen species, glycolysis, and DNA repair, which may explain the inconsistent clinical outcome between the two subtypes. We also found that the NAD+ biosynthesis score was positively correlated with immune-related pathways such as allograft rejection, IFN-γsignaling, inflammatory response. While pathways such as estrogen response, TGF-beta and hedgehog signaling were negatively correlated with the NAD+ biosynthesis score (Figure 1F). Similar biological differences between the two subtypes were observed in GEO cohort (Supplementary Figures S2C, D). Collectively, these findings suggested that NAD+ biosynthesis metabolism may play an important role not only in the development of breast cancer, but also in tumor immune environment.

Immune landscape of NAD+ biosynthetic subtypes

The state of TIME determines the fate of cancer cells. As indicated by the above results, NAD+ biosynthesis had a certain

connection with immune response. As such, we assessed the differences in the immune microenvironment of patients in the two subtypes. The immune score, stromal score, and ESTIMATE score for the two subtypes were calculated using the ESTIMATE algorithm. The findings suggested that high NAD+ biosynthetic subtype had a higher ESTIMATE score, immune score, but a lower stromal score compared to the low NAD+ biosynthetic subtype (Figure 2A). We also found a significant positive correlation between the NAD+ biosynthesis score and immune score in breast cancer (Figure 2B), indicating that increased NAD+ biosynthesis was associated with immune activation and high immune infiltration in breast cancer. By comparing the ssGSEA score of 28 types of immune cells using the Wilcoxon test, we found that most immune cells, such as activated B cells, activated $CD8^+$ T cells, activated dendritic cells, myeloid-derived suppressor cells (MDSCs) and regulatory T cells, were significantly enriched in the high NAD+ biosynthetic subtype, while few immune cells, such as central memory CD8 T cells and mast cells, were significantly enriched in the low NAD+ biosynthetic subtype (Figure 2C). The NAD+ biosynthesis score was observed closely associated with various categories of infiltrating immune cell, especially MDSCs (Figure 2D). The findings were similar in GEO cohort (Supplementary Figure S4). MDSCs are important components of TIME and can suppress the anti-tumor functions of T cells and natural killer cells (32). We believed that this immunosuppressive cell type may play an important role in the adverse clinical outcome of patients with high NAD+ biosynthesis score. The correlation analysis showed that most NAD+ biosynthesis-related genes, including NMRK1, PNP, IDO1 and NAMPT, were positively correlated with most immune cells, while negative correlations were demonstrated in molecules such as NMNAT2 and AFMID (Figure 2E). Moreover, the scores of most immune-related pathways were significantly higher in the high NAD+ biosynthetic subtype, including major histocompatibility complex (MHC) class I, and interferon response (Figure 2F). These results suggested that patients with high NAD+ biosynthetic activity tend to present a high immune infiltration and suppressive immune microenvironment.

Potential TF-IRG regulatory network

To further explore the potential regulatory mechanism of NAD+ biosynthesis affecting TIME, we identified 59 differentially expressed immune-related genes (DEIRGs), including 45 upregulated DEIRGs and 14 downregulated DEIRGs, which may play a major role in regulating TIME. DEIRGs are strongly associated with chemokine-mediated signaling (Figure 3A). Enhanced expression levels of T-cells recruiting chemokines such as CXCL9, CXCL10, and CXCL11 were found in the high NAD+ biosynthetic subtype, consistent with their abundant T cells infiltration. Additionally, the overexpression of CXCL13 (which can recruit MDSC) and other tumor suppressive chemokines (e.g., CCL18, CCL8 and CCL20) was also observed in the high NAD+ biosynthetic subtype (Supplementary Table S2). Transcriptional factors (TFs) can control the expression of critical genes and thus play an important role in the regulation of tumor inflammation and immunity (33, 34). To explore the potential upstream regulatory mechanism of DEIRGs, 11 differentially expressed TFs (DETFs) were also found from DEGs (Supplementary Table S3). A TF-IRG network was constructed based on the correlation of gene expression between DETFs and DEIRGs. Only gene pairs with correlation coefficients >0.5 (or less than −0.5) and adjusted p-value <0.01 were incorporated into the network (Supplementary Table S4). The TF-IRG network was visualized in Cytoscape (Figure 3B). We found that two TF genes, BATF2 and SPIB were significantly elevated in the high NAD+ biosynthetic subtype. Notably, SPIB was significantly associated with PDCD1 and CTLA4 (Figures 3C, D). The relationships between SPIB, PDCD1 and CTLA4 were also verified in GEO cohort (Supplementary Figure S5B). SPIB has been reported to play a negative role in immune cell regulation (35). Therefore, the SPIB-centered regulatory network may play an important role in immune infiltration and immune escape in the high NAD+ biosynthetic subtypes. We further confirmed that the expression level of SPIB was significantly higher in tumor tissues than in adjacent normal tissues (Figure 3E).

Mutation and immunotherapy sensitivity prediction of NAD+ biosynthetic subtypes

Immunotherapy has become an emerging clinical strategy for treating cancer (36). Considering that enhanced tumor immunogenicity predicts long-term clinical benefits for patients from immune checkpoint inhibitors (ICIs), we wanted to explore the relationship between NAD+ biosynthesis scores and tumor immunogenicity. Therefore, we took the perspective of the tumor mutational burden (TMB), neoantigen load and homologous recombination deficiency (HRD). Results showed that patients in the high NAD+ biosynthetic subtype had higher TMB, neoantigen and HRD (Figures 4A–C). The subsequent correlation analysis showed that TMB, neoantigen load and HRD were positively correlated with the NAD+ biosynthesis score (Supplementary Figure S6). These results suggested that patients in the high NAD+ biosynthetic subtype had relatively high immunogenicity. Somatic mutation analysis revealed higher TP53 mutation rates in the high NAD+ biosynthetic subtype and higher PIK3CA mutation rates in the low NAD+ biosynthetic subtype. (Figures 4D, E). Additionally, the expression of immune checkpoint molecules such as PD-L1, LAG3, PD-1, and CTLA-4 was higher in the high NAD+

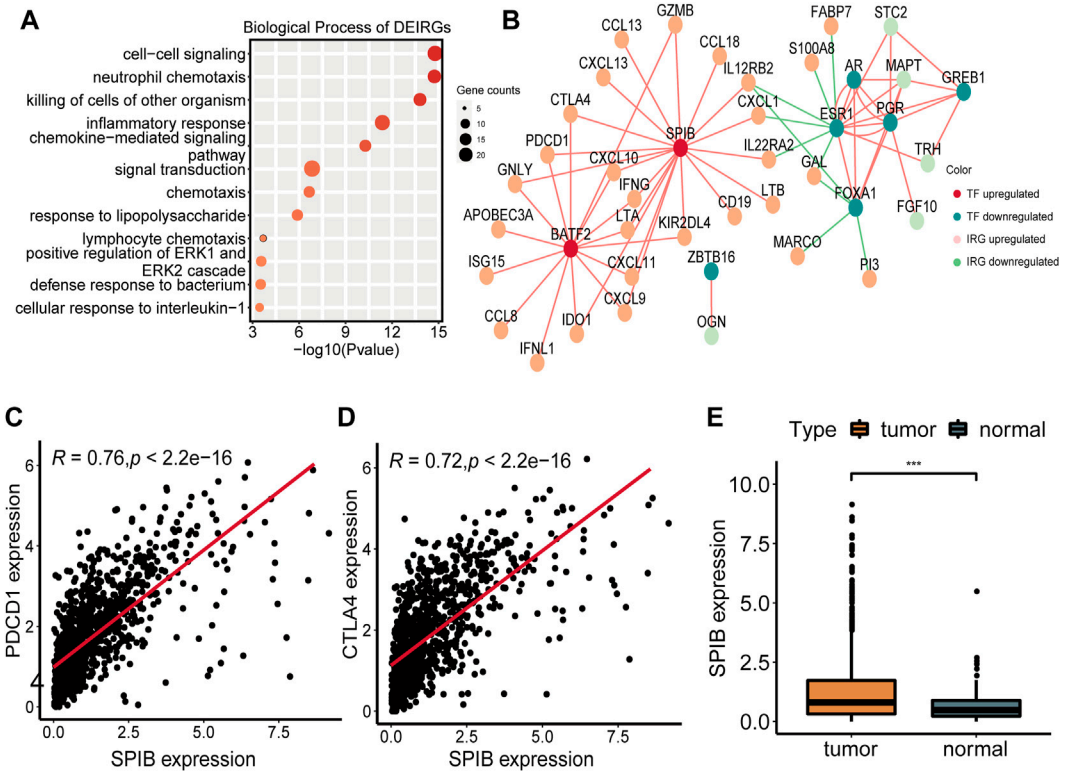

FIGURE 3
Construction of the TF-IRG network in BRCA. **(A)** GO enrichment analysis of 59 differentially expressed immune-related genes (DEIRGs). **(B)** A TF-IRG network in TCGA cohort. The pink line is the positive correlation between differentially expressed transcription factors (DETFs) and differentially expressed immune-related genes (DEIRGs). The green line is the negative correlation between DETFs and DEIRGs. **(C)** The correlation between the expression of SPIB and PDCD1 in TCGA cohort. **(D)** The correlation between the expression of SPIB and CTLA4 in TCGA cohort. **(E)** Differential expression of SPIB between breast normal and tumor tissues.

biosynthetic subtype (Figure 4F) We also assessed the association between IPS and NAD+ biosynthesis score. The results illustrated that the IPS for PD1/PD-L1/PD-L2 blocker, CTLA-4 blocker and PD1/PD-L1/PD-L2 plus CTLA-4 blocker in high NAD+ biosynthetic subtype were significantly higher than those in low NAD+ biosynthetic subtype (Figure 4G). These findings suggested that patients with high NAD+ biosynthetic score may be appropriate candidates for immunotherapy.

Drug sensitivity prediction

Considering that drug chemosensitivity can influence the clinical outcomes of breast cancer treatment, we predicted the IC50 of usual chemotherapeutic drugs and compared them between the two subtypes. Results showed that the estimated IC50 for doxorubicin was lower in the low NAD+ biosynthetic subtype, while the estimated IC50s for docetaxel, paclitaxel and gefitinib were lower in the high NAD+ biosynthetic subtype. However, there was no significant difference in the estimated IC50s for cisplatin and etoposide (Figures 5A–F). These results suggested that the NAD+ biosynthesis score may differentiate more patients for appropriate therapy.

Discussion

The role of NAD+ in cellular metabolism and signal transduction is crucial as it cannot be obtained directly from food, making NAD+ biosynthesis essential (12). Previous works have shown that NAD+ is critical for the development and progression of breast cancer. For example, QPRT, one of the rate-limiting enzymes of NAD+ biosynthesis, was shown to potentially enhance breast cancer invasiveness through purinergic signaling (37). However, little work has explored the relationship between NAD+ biosynthesis metabolism and TIME in breast cancer. Thus, in this study, we quantified NAD+ biosynthesis metabolism based on ssGSEA and demonstrated that the NAD+ biosynthesis score was significantly associated with the overall survival. Further bioinformatics analyses revealed that the NAD+ biosynthesis score was significantly related to different tumor-infiltrating immune cells and other

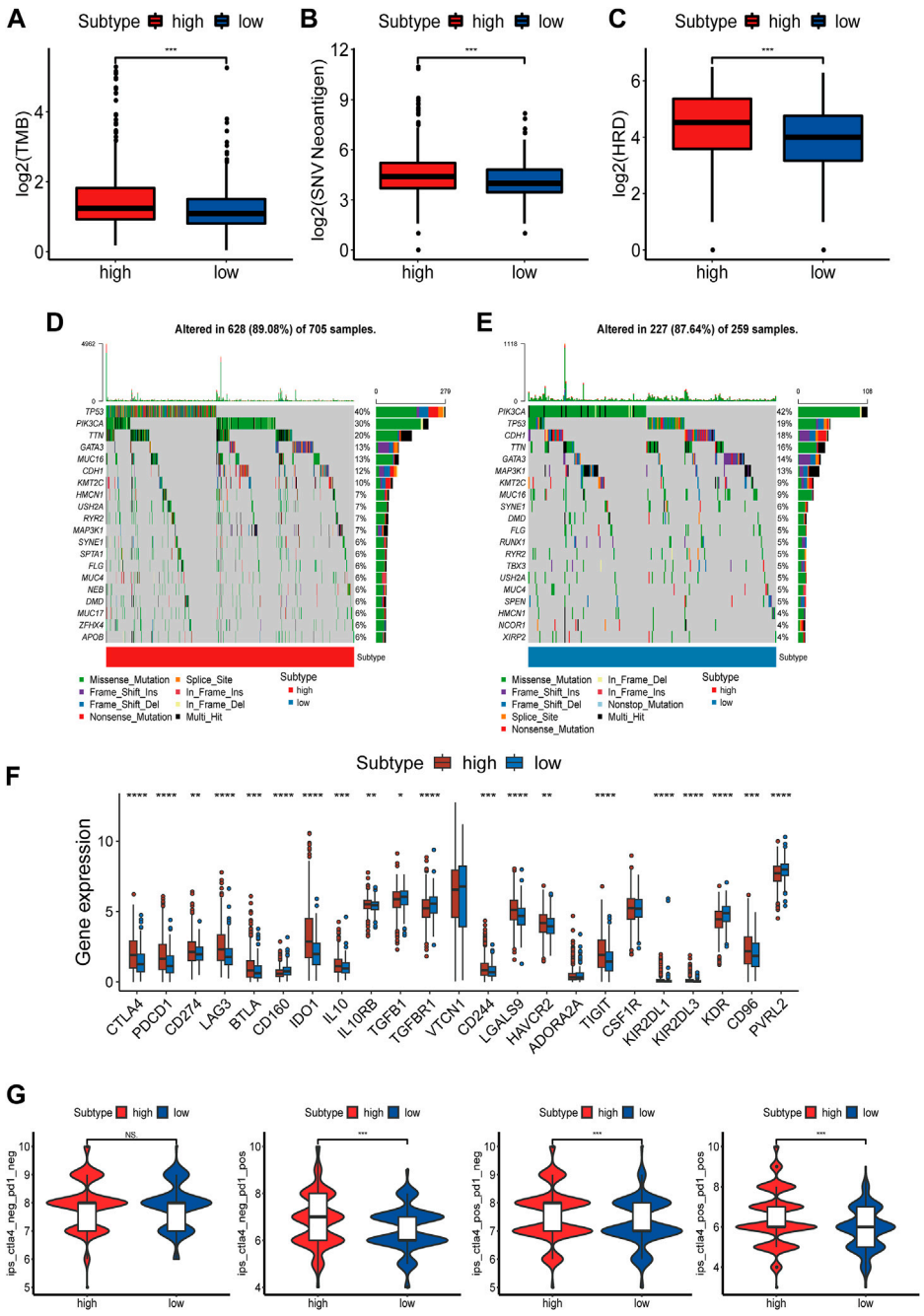

FIGURE 4
Mutation and Immunotherapy Sensitivity Prediction of the NAD+ biosynthesis signature. **(A–C)** TMB, Neoantigen and HRD between the high and low NAD+ biosynthetic subtypes. **(D,E)** Waterfall plot of tumor somatic mutation in the high and low NAD+ biosynthetic subtypes. **(F)** Comparison of immune checkpoints expression levels between the high and low NAD+ biosynthetic subtypes. **(G)** Comparison of the immunophenoscore (IPS) between the high and low NAD+ biosynthetic subtypes. *$p < 0.05$; **$p < 0.01$; ***$p < 0.001$, and ****$p < 0.0001$.

immune-related signatures. Interestingly, we also found that the NAD+ biosynthesis score was positively associated with several immunotherapy biomarkers. This indicates that patients in the high NAD+ biosynthesis subtype may be more suitable for immunotherapy. As far as we know, this study is the first study to systematically explore the relationship between NAD+ biosynthesis metabolism and TIME in breast cancer.

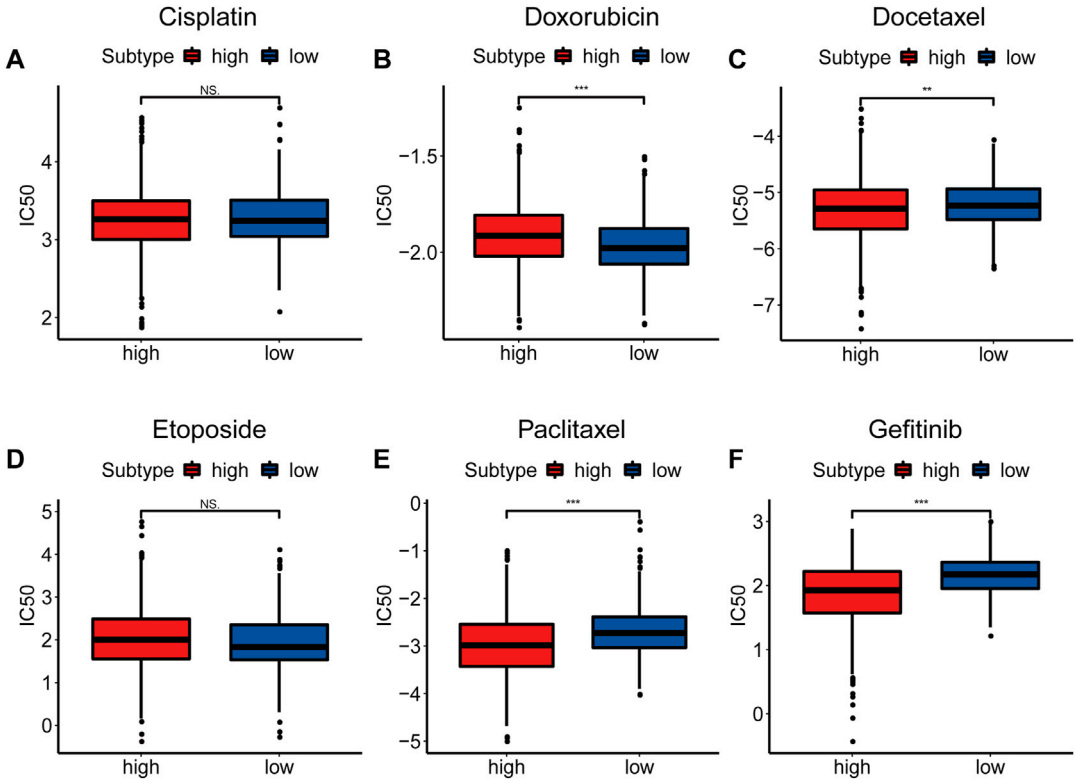

FIGURE 5
Drug Sensitivity Prediction. **(A–F)** Box plots of the estimated IC50 for Cisplatin (A), Doxorubicin (B), Docetaxel (C), Etoposide(D), Paclitaxel (E) and Gefitinib (F). *$p < 0.05$; **$p < 0.01$; ***$p < 0.001$.

In this study, we divided patients with breast cancer into the high and low biosynthetic subtypes based on the NAD+ biosynthesis score. We found that high NAD+ biosynthetic subtype was associated with poor prognosis. This correlation was validated in GEO cohort. GSEA analysis revealed that the NAD+ biosynthesis score was positively correlated with immune-related biological processes and pathways, suggesting that the difference in survival between the two subtypes may be due to immune heterogeneity. Then, analysis of the immune microenvironment showed that high NAD+ biosynthetic subtype was characterized by immune activation and accompanied with immune suppression. The ssGSEA scores of most immune cells in high NAD+ biosynthetic subtypes were higher than those in low NAD+ biosynthetic subtypes, which indicated that the immune microenvironment in BC with high biosynthesis score tended to be "hot." Our results also showed that HER2-enriched and Basal subtypes had higher NAD+ biosynthesis score, which were consistent with higher TILs infiltration in the two molecular subtypes (38). However, high NAD+ biosynthetic subtype did not display a corresponding survival advantage and we found MDSC might play a key role. MDSC could promote immune evasion, tumor angiogenesis and metastasis (39). Besides, there is a positive association between IFN-γ signaling and NAD+ biosynthesis score. IFN-γ has a dual role. On the one hand, IFN-γ can enhance anticancer activity by increasing MHC class I and cytotoxic proteins associated with the CTL response. On the other hand, it also promotes the expression of PD-L1, CTLA-4, IDO1, CXCL12 and other molecules to promote tumor immune escape(40, 41). In fact, it has been reported that NAD+ could enhance IFN-γ-induced PD-L1 expression and promote tumor immune evasion (42). Therefore, we believe that IFN-γ signaling and MDSC could contribute to the immunosuppressive microenvironment in NAD+ biosynthesis-activated breast cancer.

Besides, the TF-IRG regulatory network implied that two transcription factors, BATF2 and SPIB, may play an active role in transcriptional events associated with the infiltration of immune cells in the high NAD+ biosynthetic subtype. BATF2, a member of the basic leucine zipper transcription factor family, can be involved in the gene regulation of IFN-γ-activated classical macrophages and induce pro-inflammatory responses (43, 44). SPIB, belongs to the ETS family, plays an important role in the differentiation of B cells and plasmacytoid dendritic cells (45, 46). SPIB has been shown to promote tumor aerobic glycolysis (47)

and participate in the recruitment of tumor-associated macrophages (TAMs) (35), which promotes cancer progression. In conclusion, the construction of the TF-IRG network provided some insights into the interaction between NAD+ biosynthesis and TIME in breast cancer.

Immunotherapy, represented by immune checkpoint inhibitors (ICIs), is changing the treatment of cancer. The higher immunogenicity in the high NAD+ biosynthetic subtype may lead to a better prognosis after receiving immunotherapy (48). TMB is a more reliable biomarker for predicting immunotherapy efficacy. Patients with high TMB will achieve higher objective response rates to immunotherapy (49, 50). The positive association between HRD and TMB has been reported in BC (51). The underlying mechanism for this correlation is that HRD may drive tumorigenesis, increasing the number of tumor mutations and the neoantigen rate in BC (52, 53). Neoantigens can promote $CD8^+$ T cell infiltration and cytolytic activity, which are closely associated with response to immunogenicity. Mutation analysis showed high NAD+ biosynthesis was associated with high TP53 mutation rate. One study reported that patients with mutant TP53 showed stronger tumor antigenicity and tumor antigen presentation and were more likely to benefit from immunotherapy (54), which was consistent with our findings. Moreover, we also found that patients with different NAD+ biosynthesis scores might exhibit distinct sensitivity to doxorubicin, docetaxel, paclitaxel, and gefitinib. These results suggested that NAD+ biosynthesis score can assess the efficacy of immunotherapy and chemotherapy, facilitating personalized treatment for breast cancer.

This study has some limitations. Firstly, in our study, the clinical cohorts were derived from public databases and need further validated by prospective studies. Secondly, the association between NAD+ biosynthesis and TIME requires additional experimental validation.

In conclusion, our study suggests that NAD+ biosynthetic activity was correlated with the prognosis of breast cancer and the immune microenvironment. NAD+ biosynthetic activity may also serve as a potential prognostic biomarker for ICI immunotherapy, which may help to screen patients eligible for immunotherapy and guide future individualized precision therapy.

Data availability statement

The public datasets to support the results of this research can be gained from TCGA (https://portal.gdc.cancer.gov/) and GEO (https://www.ncbi.nlm.nih.gov/geo/).

Author contributions

YY, ZW and MH drafted the manuscript. YY, LD and BY contributed to the data collection and analysis. DL designed and supervised this study. All authors contributed to the article and approved the submitted version.

Funding

This study was supported by National key Research and Development Program of China (2020YFE0202200, 2021YFA1301603), National Natural Science Foundation of China (32088101, 32271518).

Conflict of interest

The authors declare that the research was conducted in the absence of any commercial or financial relationships that could be construed as a potential conflict of interest.

Acknowledgments

The authors express sincere gratitude for the availability of data by public databases such as ImmPort, GEO and TCGA.

Supplementary material

The Supplementary Material for this article can be found online at: https://www.por-journal.com/articles/10.3389/pore.2023.1610956/full#supplementary-material

References

1. Sung H, Ferlay J, Siegel RL, Laversanne M, Soerjomataram I, Jemal A, et al. Global cancer statistics 2020: GLOBOCAN estimates of incidence and mortality worldwide for 36 cancers in 185 countries. *CA Cancer J Clin* (2021) 71:209–49. doi:10.3322/caac.21660

2. McDonald ES, Clark AS, Tchou J, Zhang P, Freedman GM. Clinical diagnosis and management of breast cancer. *J Nucl Med Off Publ Soc Nucl Med* (2016) 57(1): 9S–16S. doi:10.2967/jnumed.115.157834

3. Januškevičienė I, Petrikaitė V. Heterogeneity of breast cancer: The importance of interaction between different tumor cell populations. *Life Sci* (2019) 239:117009. doi:10.1016/j.lfs.2019.117009

4. Catalano V, Turdo A, Di Franco S, Dieli F, Todaro M, Stassi G. Tumor and its microenvironment: A synergistic interplay. *Semin Cancer Biol* (2013) 23:522–32. doi:10.1016/j.semcancer.2013.08.007

5. Fu T, Dai L-J, Wu S-Y, Xiao Y, Ma D, Jiang YZ, et al. Spatial architecture of the immune microenvironment orchestrates tumor immunity and therapeutic response. *J Hematol Oncolj Hematol Oncol* (2021) 14:98. doi:10.1186/s13045-021-01103-4

6. Wang S, Zhang Q, Yu C, Cao Y, Zuo Y, Yang L. Immune cell infiltration-based signature for prognosis and immunogenomic analysis in breast cancer. *Brief Bioinform* (2021) 22:2020–31. doi:10.1093/bib/bbaa026

7. Oshi M, Asaoka M, Tokumaru Y, Yan L, Matsuyama R, Ishikawa T, et al. CD8 T cell score as a prognostic biomarker for triple negative breast cancer. *Int J Mol Sci* (2020) 21:E6968. doi:10.3390/ijms21186968

8. Gao W, Wen H, Liang L, Dong X, Du R, Zhou W, et al. IL20RA signaling enhances stemness and promotes the formation of an immunosuppressive microenvironment in breast cancer. *Theranostics* (2021) 11:2564–80. doi:10.7150/thno.45280

9. Savas P, Salgado R, Denkert C, Sotiriou C, Darcy PK, Smyth MJ, et al. Clinical relevance of host immunity in breast cancer: From TILs to the clinic. *Nat Rev Clin Oncol* (2016) 13:228–41. doi:10.1038/nrclinonc.2015.215

10. Dieci MV, Miglietta F, Guarneri V. Immune infiltrates in breast cancer: Recent updates and clinical implications. *Cells* (2021) 10:223. doi:10.3390/cells10020223

11. Covarrubias AJ, Perrone R, Grozio A, Verdin E. NAD+ metabolism and its roles in cellular processes during ageing. *Nat Rev Mol Cel Biol* (2021) 22:119–41. doi:10.1038/s41580-020-00313-x

12. Navas LE, Carnero A. NAD+ metabolism, stemness, the immune response, and cancer. *Signal Transduct Target Ther* (2021) 6:2. doi:10.1038/s41392-020-00354-w

13. Chiarugi A, Dölle C, Felici R, Ziegler M. The NAD metabolome--a key determinant of cancer cell biology. *Nat Rev Cancer* (2012) 12:741–52. doi:10.1038/nrc3340

14. Ghanem MS, Monacelli F, Nencioni A. Advances in NAD-lowering agents for cancer treatment. *Nutrients* (2021) 13:1665. doi:10.3390/nu13051665

15. Zhang H, Zhang N, Liu Y, Su P, Liang Y, Li Y, et al. Epigenetic regulation of NAMPT by NAMPT-AS drives metastatic progression in triple-negative breast cancer. *Cancer Res* (2019) 79:3347–59. doi:10.1158/0008-5472.CAN-18-3418

16. Gholinejad Z, Kheiripour N, Nourbakhsh M, Ilbeigi D, Behroozfar K, Hesari Z, et al. Extracellular NAMPT/Visfatin induces proliferation through ERK1/2 and AKT and inhibits apoptosis in breast cancer cells. *Peptides* (2017) 92:9–15. doi:10.1016/j.peptides.2017.04.007

17. Li C, Zhu Y, Chen W, Li M, Yang M, Shen Z, et al. Circulating NAD+ metabolism-derived genes unveils prognostic and peripheral immune infiltration in amyotrophic lateral sclerosis. *Front Cel Dev Biol* (2022) 10:831273. doi:10.3389/fcell.2022.831273

18. Dedeurwaerder S, Desmedt C, Calonne E, Singhal SK, Haibe-Kains B, Defrance M, et al. DNA methylation profiling reveals a predominant immune component in breast cancers. *EMBO Mol Med* (2011) 3:726–41. doi:10.1002/emmm.201100801

19. Huang C-C, Tu S-H, Lien H-H, Jeng JY, Huang CS, Huang CJ, et al. Concurrent gene signatures for han Chinese breast cancers. *PLoS One* (2013) 8:e76421. doi:10.1371/journal.pone.0076421

20. Metzger-Filho O, Michiels S, Bertucci F, CatteAu A, Salgado R, Galant C, et al. Genomic grade adds prognostic value in invasive lobular carcinoma. *Ann Oncol Off J Eur Soc Med Oncol* (2013) 24:377–84. doi:10.1093/annonc/mds280

21. Gautier L, Cope L, Bolstad BM, Irizarry RA. affy--analysis of Affymetrix GeneChip data at the probe level. *Bioinforma Oxf Engl* (2004) 20:307–15. doi:10.1093/bioinformatics/btg405

22. Johnson WE, Li C, Rabinovic A. Adjusting batch effects in microarray expression data using empirical Bayes methods. *Biostat Oxf Engl* (2007) 8:118–27. doi:10.1093/biostatistics/kxj037

23. Hänzelmann S, Castelo R, Guinney J. Gsva: Gene set variation analysis for microarray and RNA-seq data. *BMC Bioinformatics* (2013) 14:7. doi:10.1186/1471-2105-14-7

24. Yu G, Wang L-G, Han Y, He Q-Y. clusterProfiler: an R Package for comparing biological themes among gene clusters. *OMICS J Integr Biol* (2012) 16:284–7. doi:10.1089/omi.2011.0118

25. Charoentong P, Finotello F, Angelova M, Mayer C, Efremova M, Rieder D, et al. Pan-cancer immunogenomic analyses reveal genotype-immunophenotype relationships and predictors of response to checkpoint blockade. *Cell Rep* (2017) 18:248–62. doi:10.1016/j.celrep.2016.12.019

26. Bindea G, Mlecnik B, Tosolini M, Kirilovsky A, Waldner M, Obenauf AC, et al. Spatiotemporal dynamics of intratumoral immune cells reveal the immune landscape in human cancer. *Immunity* (2013) 39:782–95. doi:10.1016/j.immuni.2013.10.003

27. Yoshihara K, Shahmoradgoli M, Martínez E, Vegesna R, Kim H, Torres-Garcia W, et al. Inferring tumour purity and stromal and immune cell admixture from expression data. *Nat Commun* (2013) 4:2612. doi:10.1038/ncomms3612

28. Mayakonda A, Lin D-C, Assenov Y, Plass C, Koeffler HP. Maftools: Efficient and comprehensive analysis of somatic variants in cancer. *Genome Res* (2018) 28:1747–56. doi:10.1101/gr.239244.118

29. Shi Z, Shen J, Qiu J, Zhao Q, Hua K, Wang H. CXCL10 potentiates immune checkpoint blockade therapy in homologous recombination-deficient tumors. *Theranostics* (2021) 11:7175–87. doi:10.7150/thno.59056

30. Thorsson V, Gibbs DL, Brown SD, Wolf D, Bortone DS, Ou Yang TH, et al. The immune landscape of cancer. *Immunity* (2018) 48:812–30.e14. doi:10.1016/j.immuni.2018.03.023

31. Geeleher P, Cox N, Huang RS. pRRophetic: an R package for prediction of clinical chemotherapeutic response from tumor gene expression levels. *PLoS One* (2014) 9:e107468. doi:10.1371/journal.pone.0107468

32. Hinshaw DC, Shevde LA. The tumor microenvironment innately modulates cancer progression. *Cancer Res* (2019) 79:4557–66. doi:10.1158/0008-5472.CAN-18-3962

33. Yu H, Pardoll D, Jove R. STATs in cancer inflammation and immunity: A leading role for STAT3. *Nat Rev Cancer* (2009) 9:798–809. doi:10.1038/nrc2734

34. Marigo I, Bosio E, Solito S, Mesa C, Fernandez A, Dolcetti L, et al. Tumor-induced tolerance and immune suppression depend on the C/EBPbeta transcription factor. *Immunity* (2010) 32:790–802. doi:10.1016/j.immuni.2010.05.010

35. Huang Q, Liu J, Wu S, Zhang X, Xiao Z, Liu Z, et al. Spi-B promotes the recruitment of tumor-associated macrophages via enhancing CCL4 expression in lung cancer. *Front Oncol* (2021) 11:659131. doi:10.3389/fonc.2021.659131

36. Zhao Z, Zheng L, Chen W, Weng W, Song J, Ji J. Delivery strategies of cancer immunotherapy: Recent advances and future perspectives. *J Hematol Oncolj Hematol Oncol* (2019) 12:126. doi:10.1186/s13045-019-0817-3

37. Liu C-L, Cheng S-P, Chen M-J, Lin CH, Chen SN, Kuo YH, et al. Quinolinate phosphoribosyltransferase promotes invasiveness of breast cancer through myosin light chain phosphorylation. *Front Endocrinol* (2020) 11:621944. doi:10.3389/fendo.2020.621944

38. Hammerl D, Smid M, Timmermans AM, Sleijfer S, Martens JWM, Debets R. Breast cancer genomics and immuno-oncological markers to guide immune therapies. *Semin Cancer Biol* (2018) 52:178–88. doi:10.1016/j.semcancer.2017.11.003

39. Gabrilovich DI. Myeloid-derived suppressor cells. *Cancer Immunol Res* (2017) 5:3–8. doi:10.1158/2326-6066.CIR-16-0297

40. Lin C-F, Lin C-M, Lee K-Y, Wu SY, Feng PH, Chen KY, et al. Escape from IFN-γ-dependent immunosurveillance in tumorigenesis. *J Biomed Sci* (2017) 24:10. doi:10.1186/s12929-017-0317-0

41. Mojic M, Takeda K, Hayakawa Y. The dark side of IFN-γ: Its role in promoting cancer immunoevasion. *Int J Mol Sci* (2017) 19:89. doi:10.3390/ijms19010089

42. Lv H, Lv G, Chen C, Zong Q, Jiang G, Ye D, et al. NAD+ metabolism maintains inducible PD-L1 expression to drive tumor immune evasion. *Cell Metab* (2021) 33:110–27.e5. doi:10.1016/j.cmet.2020.10.021

43. Guler R, Mpotje T, Ozturk M, Nono JK, Parihar SP, Chia JE, et al. Batf2 differentially regulates tissue immunopathology in Type 1 and Type 2 diseases. *Mucosal Immunol* (2019) 12:390–402. doi:10.1038/s41385-018-0108-2

44. Roy S, Guler R, Parihar SP, Schmeier S, Kaczkowski B, Nishimura H, et al. Batf2/Irf1 induces inflammatory responses in classically activated macrophages, lipopolysaccharides, and mycobacterial infection. *J Immunol Baltim* (2015) 194:6035–44. doi:10.4049/jimmunol.1402521

45. Garrett-Sinha LA, Su GH, Rao S, Kabak S, Hao Z, Clark MR, et al. PU.1 and Spi-B are required for normal B cell receptor-mediated signal transduction. *Immunity* (1999) 10:399–408. doi:10.1016/s1074-7613(00)80040-0

46. Schotte R, Nagasawa M, Weijer K, Spits H, Blom B. The ETS transcription factor Spi-B is required for human plasmacytoid dendritic cell development. *J Exp Med* (2004) 200:1503–9. doi:10.1084/jem.20041231

47. Wang J, Wang X, Guo Y, Ye L, Li D, Hu A, et al. Therapeutic targeting of SPIB/SPI1-facilitated interplay of cancer cells and neutrophils inhibits aerobic glycolysis and cancer progression. *Clin Transl Med* (2021) 11:e588. doi:10.1002/ctm2.588

48. Wang S, He Z, Wang X, Li H, Liu XS. Antigen presentation and tumor immunogenicity in cancer immunotherapy response prediction. *eLife* (2019) 8: e49020. doi:10.7554/eLife.49020

49. Chan TA, Yarchoan M, Jaffee E, Swanton C, Quezada SA, Stenzinger A, et al. Development of tumor mutation burden as an immunotherapy biomarker: Utility for the oncology clinic. *Ann Oncol Off J Eur Soc Med Oncol* (2019) 30:44–56. doi:10.1093/annonc/mdy495

50. Barroso-Sousa R, Jain E, Cohen O, Kim D, Buendia-Buendia J, WinEr E, et al. Prevalence and mutational determinants of high tumor mutation burden in breast cancer. *Ann Oncol Off J Eur Soc Med Oncol* (2020) 31:387–94. doi:10.1016/j.annonc.2019.11.010

51. Budczies J, Kluck K, Beck S, Ourailidis I, Allgauer M, Menzel M, et al. Homologous recombination deficiency is inversely correlated with microsatellite instability and identifies immunologically cold tumors in most cancer types. *J Pathol Clin Res* (2022) 8:371–82. doi:10.1002/cjp2.271

52. Pellegrino B, Musolino A, Llop-Guevara A, Serra V, De Silva P, Hlavata Z, et al. Homologous recombination repair deficiency and the immune response in breast cancer: A literature review. *Transl Oncol* (2020) 13:410–22. doi:10.1016/j.tranon.2019.10.010

53. Solinas C, Marcoux D, Garaud S, Vitoria JR, Van den Eynden G, de Wind A, et al. BRCA gene mutations do not shape the extent and organization of tumor infiltrating lymphocytes in triple negative breast cancer. *Cancer Lett* (2019) 450: 88–97. doi:10.1016/j.canlet.2019.02.027

54. Madel M-B, Ibáñez L, Wakkach A, de Vries TJ, Teti A, Apparailly F, et al. Immune function and diversity of osteoclasts in normal and pathological conditions. *Front Immunol* (2019) 10:1408. doi:10.3389/fimmu.2019.01408

Pathology & Oncology Research | frontiers

TYPE Review
PUBLISHED 03 May 2023
DOI 10.3389/pore.2023.1611086

Check for updates

OPEN ACCESS

EDITED BY
Anna Sebestyén,
Semmelweis University, Hungary

*CORRESPONDENCE
Valeria Skopelidou,
val.skop@outlook.com

RECEIVED 29 January 2023
ACCEPTED 18 April 2023
PUBLISHED 03 May 2023

CITATION
Skopelidou V, Strakoš J, Škarda J, Raška M and Kafková-Rašková L (2023), Potential predictors of immunotherapy in small cell lung cancer.
Pathol. Oncol. Res. 29:1611086.
doi: 10.3389/pore.2023.1611086

COPYRIGHT
© 2023 Skopelidou, Strakoš, Škarda, Raška and Kafková-Rašková. This is an open-access article distributed under the terms of the Creative Commons Attribution License (CC BY). The use, distribution or reproduction in other forums is permitted, provided the original author(s) and the copyright owner(s) are credited and that the original publication in this journal is cited, in accordance with accepted academic practice. No use, distribution or reproduction is permitted which does not comply with these terms.

Potential predictors of immunotherapy in small cell lung cancer

Valeria Skopelidou[1,2]*, Jan Strakoš[1,2], Jozef Škarda[1,2,3], Milan Raška[4,5] and Leona Kafková-Rašková[4,5]

[1]Institute of Molecular and Clinical Pathology and Medical Genetics, University Hospital Ostrava, Ostrava, Czechia, [2]Institute of Molecular and Clinical Pathology and Medical Genetics, Faculty of Medicine, University of Ostrava, Ostrava, Czechia, [3]Department of Clinical and Molecular Pathology, Faculty of Medicine and Dentistry, Palacký University Olomouc, Olomouc, Czechia, [4]Department of Immunology, Faculty of Medicine and Dentistry, Palacký University Olomouc, Olomouc, Czechia, [5]Department of Immunology, University Hospital Olomouc, Olomouc, Czechia

Lung cancer is one of the leading causes of cancer-related deaths worldwide, with small cell lung cancer (SCLC) having the worst prognosis. SCLC is diagnosed late in the disease's progression, limiting treatment options. The most common treatment for SCLC is chemotherapy. As the disease progresses, immunotherapy, most commonly checkpoint inhibitor medication, becomes more important. Efforts should be made in the development of immunotherapy to map specific biomarkers, which play a role in properly assigning a type of immunotherapy to the right cohort of patients, where the benefits outweigh any risks or adverse effects. The objective of this review was to provide a thorough assessment of current knowledge about the nature of the tumor process and treatment options for small cell lung cancer, with a focus on predictive biomarkers. According to the information obtained, the greatest potential, which has already been directly demonstrated in some studies, has characteristics such as tumor microenvironment composition, tumor mutation burden, and molecular subtyping of SCLC. Several other aspects appear to be promising, but more research, particularly prospective studies on a larger number of probands, is required. However, it is clear that this field of study will continue to expand, as developing a reliable method to predict immunotherapy response is a very appealing goal of current medicine and research in the field of targeted cancer therapy.

KEYWORDS

tumor microenvironment, PD-L1 expression, small cell lung cancer, mutational burden, molecular subtyping

Introduction

Lung cancer is one of the most common causes of cancer-related deaths not only in the Czech Republic, but also worldwide. With more than half of patients having an advanced stage of cancer at the time of diagnosis, where aggressive surgical treatment is no longer an option, there are over 2 million new cases, and 1.76 million fatalities reported

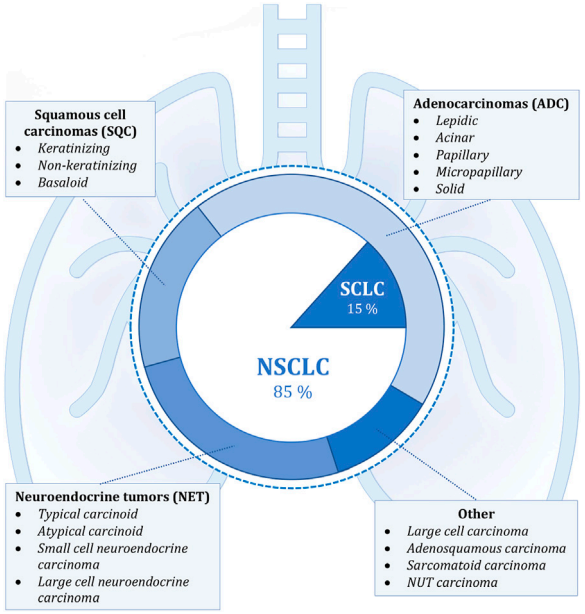

FIGURE 1
Shows the classification of lung cancer according to histopathological morphology. The internal simpler division corresponds to the basic categorization into non-small cell (NSCLC) and small cell lung cancer (SCLC). The external, more detailed classification into individual groups corresponds to the new classification according to the WHO, which was implemented in 2021. The most frequently occurring malignant lesions are listed in the individual categories (4, 6–8).

each year. Among the significant etiological factors are active smoking, passive smoking, inhalation of radon or asbestos and exposure to ionizing radiation (1–5).

Lung carcinomas represent a heterogeneous group of malignant epithelial tumors with a wide spectrum of clinicopathological features (Figure 1). These cancerous tumors can develop from the parenchyma of the lung or the bronchial tissue. It is not always feasible to accurately identify the origin of tumor cells, and it is also not necessary for future diagnosis or treatment. The key role in the diagnostic process is played by the identification of the histological type of tumor cells, which is done through the evaluation of cytological (including cytoblocks) or histological samples. Histopathological evaluation to determine the exact diagnosis can be based on several types of samples—the most common is bronchoscopic, needle (namely CT-guided transthoracic or transbronchial needle aspiration—depending on the location of the lesion) or surgical biopsy (surgical resection specimens), which also includes thoracoscopy, excisional wedge biopsy, lobectomy, or pneumonectomy. The simpler classification involves dividing lung tumors into two subgroups, namely non-small cell (NSCLC; approximately 85% of all tumors) and small cell (SCLC; the remaining 15%) lung cancers. This basic division roughly expresses the biological nature of the cancer tissue (higher growth rate and early metastasis in SCLC) and was previously sufficient for therapeutic purposes, since the same treatment procedures were used in clinical practice for all non-small cell carcinomas regardless of further histopathological subtyping. However, it's diametrically opposed from the therapeutic strategy for small cell carcinomas (these are mainly non-surgical procedures). More emphasis is currently being placed on improving morphological classification as new and more specialized anti-tumor therapies, particularly immunotherapy or biological treatment, develop. Molecular genetic subtyping methods are also becoming more significant (2, 3, 6, 9–13).

Small cell lung carcinoma (SCLC) is defined as a malignant epithelial tumor consisting of small round, oval, or spindle-shaped cells with a faint rim of cytoplasm, weakly defined cell border, finely granular nuclear chromatin, and indistinct or absent nucleoli (Figure 2). Typical SCLC involves only small cells (90% of cases), other types are classified as combined disease where the tumor also contains large cell components. It is considered to be one of the most aggressive malignant tumors ever. This form of lung cancer, which mainly affects heavy smokers, is frequently discovered in its advanced stages, which is linked to a greater early mortality rate than in NSCLC. The five-year survival rate for patients diagnosed with SCLC ranges between 2.2% and 3.7%, which is significantly lower than the 10.8%–14% range for non-small cell carcinoma. Although the suspicion of small cell carcinoma already arises from the results of imaging methods or the patient's symptoms, a pathological or cytological examination is required to confirm the diagnosis. Samples from the primary tumor, lymph nodes or metastatic locations should be taken by bronchoscopic biopsy or fine needle aspiration. Immunohistochemical methods must be used to confirm equivocal and complicated cases, with testing of neuroendocrine markers such as chromogranin, synaptophysin, and CD56 being among the most useful. Less than 10% of all small cell carcinomas are negative for all of the aforementioned markers. SCLCs are also positive for TTF-1 in up to 90% of cases. Testing the expression of epithelial markers such as cytokeratins is also appropriate, as they are observed in many small cell carcinomas and help distinguish them from lymphomas or other small round cell tumors. The proliferative Ki-67 index ranges between 80 and 100 percent, which also serves to differentiate SCLC from carcinoids. Approximately 90% of all small cell carcinomas are located centrally. With the gradual expansion of the tumor, the surrounding bronchi are frequently compressed. Two additional pathways for tumour spread are the lymphangitic network in the lungs and regional lymph nodes (14–17).

Several treatment options are currently available for small cell lung cancer. While it is critical to act in the patient's best interest, it is also necessary to carefully weigh the risks and benefits of any therapy in order to obtain an effective therapeutic

10.3389/pore.2023.1611086

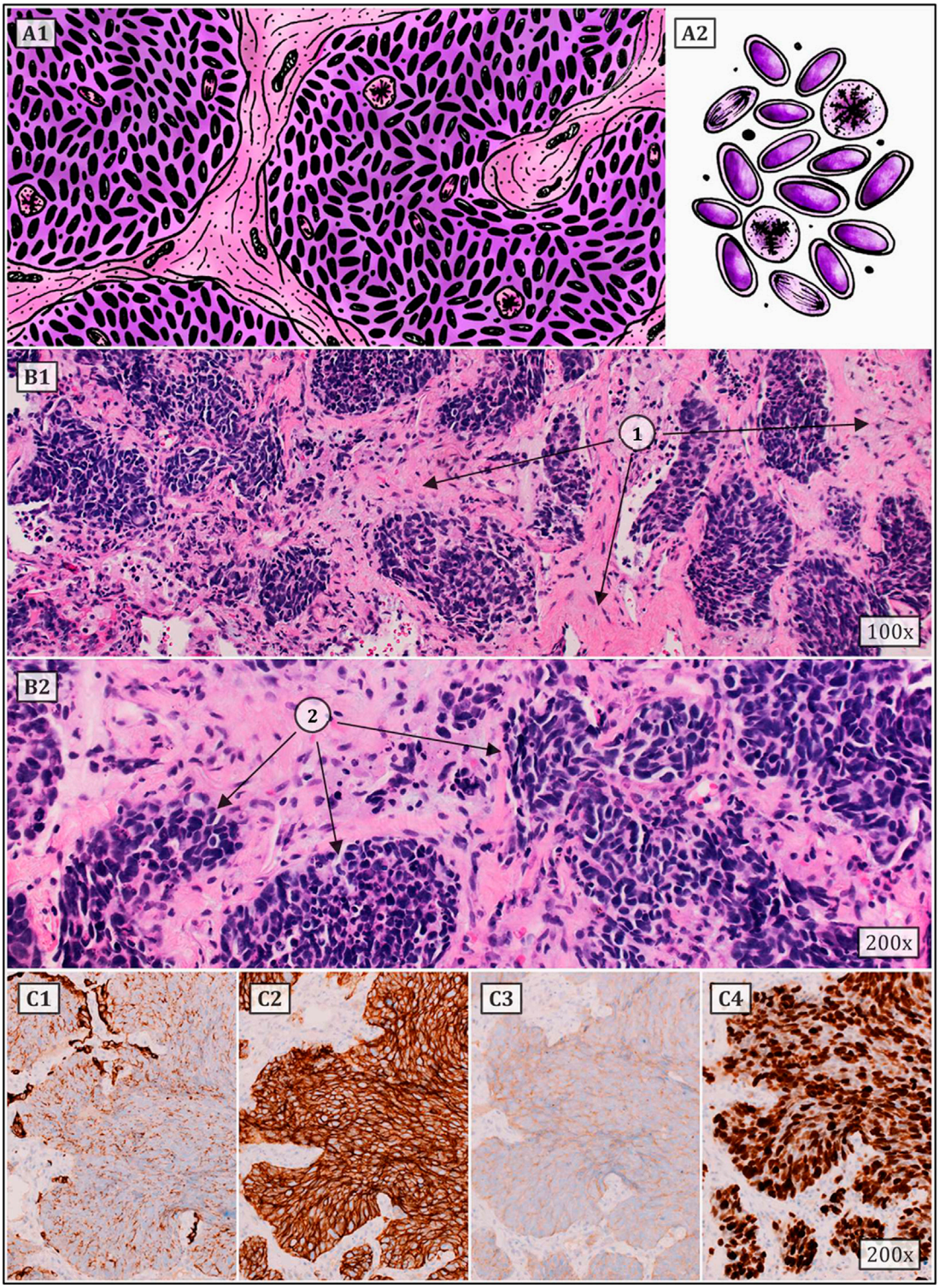

FIGURE 2
Typical SCLC consists of small cells (they can be round, oval or spindle-shaped) with a faint rim of cytoplasm, weakly defined cell border, finely granular nuclear chromatin, and indistinct or absent nucleoli. Numerous mitoses (also atypical) are common. Architectural patterns include nesting, trabeculae, peripheral palisading, and rosette formation. **(A1,2)** show a schematic drawing of SCLC. **(B1,2)** represent classic HE staining (1 – tumor stroma, 2 – tumor cell population). **(C1–4)** correspond to immunohistochemistry staining, i.e., **(C1)** – cytokeratin 7, **(C2)** – CD56, **(C3)** – synaptophysin and **(C4)** – proliferative Ki67 index (approx. 80%) (6, 12, 14–17).

10.3389/pore.2023.1611086

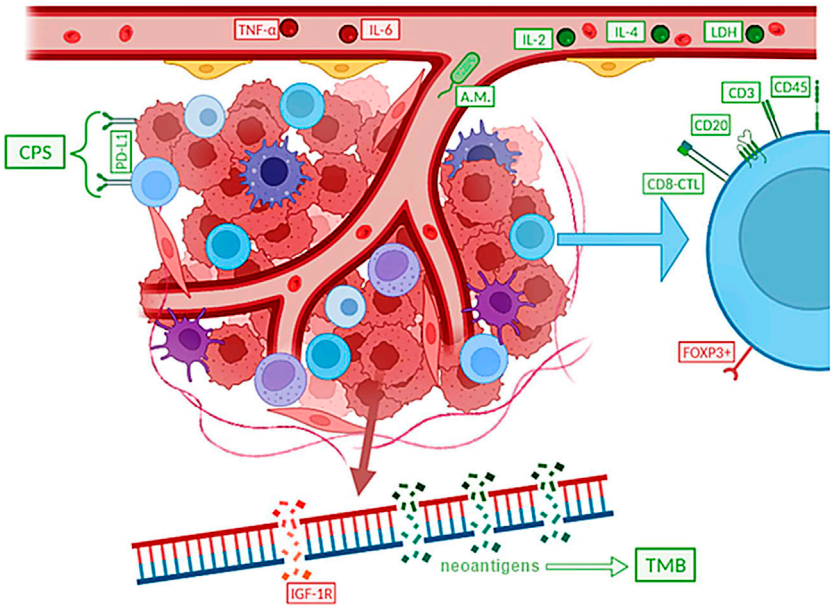

FIGURE 3
Provides a flowchart that was approved by the FDA in 2021. Figure depicts the only approved indication for immunotherapy so far, in the treatment of advanced stage SCLC. An important differentiating factor is PS, the so-called performance status, which corresponds to the patient's overall condition (according to WHO: 1 – full health, 5 – dead) (18–23).

effect. Chemotherapy is the most common treatment for SCLC, at least in the present. This is regarded as basic therapy by the American Cancer Society (ACS) recommendations as of 2021. However, the administration of chemotherapeutic drugs is associated with several side effects that can significantly limit the patient's recovery, with the most common being hair loss, oral ulcers, weight changes, nausea or vomiting, and constipation or diarrhoea dominating gastrointestinal problems. The negative effect is also observed in the bone marrow, due to which symptoms of fatigue (anaemia), bleeding (thrombocytopenia) and infection (leukopenia) appear, all of which often improve once the treatment is stopped. SCLC is a type of tumor that frequently has numerous metastatic foci at the time of its diagnosis, and thus curative surgery is considered in less than 1 in 20 patients in whom the oncological disease was detected at the stage of a solitary operable centre without metastases. The indication of appropriate treatment is also influenced by the cancer's overall stage. If the SCLC is limited, then concurrent chemoradiation is considered. However, if the stage of the tumor is advanced, radiation therapy is abandoned, and this is where, in addition to chemotherapy, immunotherapy also comes into play (Figure 3). Small cell lung carcinoma's treatment choices are rather restricted, as can be observed, thus efforts to enhance and streamline therapeutic approaches are necessary. The focus should be on immunotherapy techniques, which are now only used for advanced stages of the illness (18, 24–26).

Potential predictors of immunotherapy in small cell lung cancer

An effort is being made to identify specific biomarkers, which are molecules, cellular, or gene components that can be found in bodily fluids, on the surface of cells, or elsewhere, in order to develop more precise methods of immunotherapy. Disease biomarkers can generally be divided into three categories. Diagnostic biomarkers are substances with the highest sensitivity and specificity for identifying a properly defined nosological unit. Molecules whose levels are directly or indirectly connected to the typical course and severity of the disease are referred to be prognostic biomarkers. These indicators are frequently used to estimate overall survival (OS). The final category includes predictive biomarkers (27–29). Particularly in the treatment of small cell lung cancer, where therapeutic options are sometimes relatively constrained from the start, the identification of reliable predictors is crucial (Figure 4). Predictive markers are primarily useful for correctly assigning a certain immunotherapy type to the right patient cohort, in which the treatment will be most effective, and the benefit will outweigh any potential dangers or side effects. The search for suitable biomarkers among the dozens to hundreds of available choices is ongoing at the moment, but it is yet not possible to identify molecules that are unmistakably appropriate (19, 30, 31).

10.3389/pore.2023.1611086

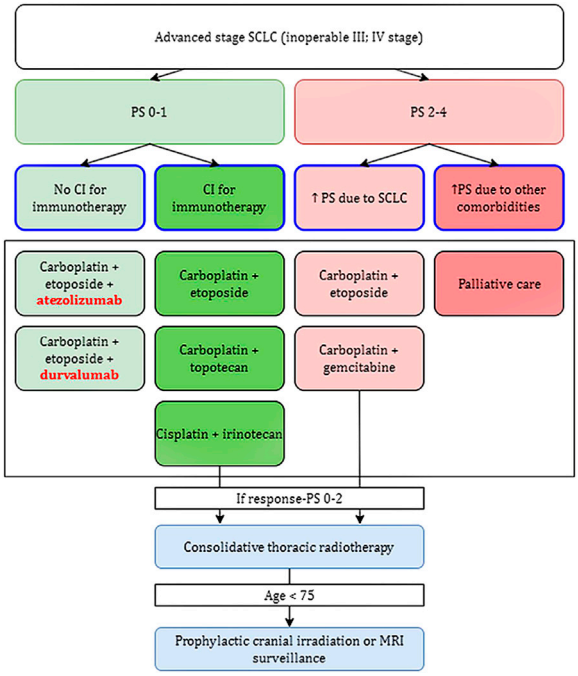

FIGURE 4
Simply summarizes potential predictive biomarkers of immunotherapy in SCLC, with negative predictive factors marked in red and positive predictive factors in green. It appears that a worse response to immunotherapy is associated with higher levels of TNF-α and IL-6, a higher proportion of Treg (FOXP3+), or other factors such as IGF-1R mutations. Other signs, on the other hand, indicate to the potential effectiveness of the immunotherapy treatment.

Composition of the tumor microenvironment and TIL as potential immunotherapy predictors

Until recently, the main focus of cancer research aimed at the malignant cells themselves, while the importance of other structures in the tumor itself and its immediate surroundings was relatively neglected. Currently, it is already known that many different characteristics, including, for example, standardly assessed aspects such as tumor histopathological morphology, tumor stroma, innervation, or vascularization, have a great influence on the resulting nature of the tumor, its behaviour, response to therapy, and therefore the final prognosis of the malignant disease. Tumor tissue is also known to have antigenic properties and can elicit an immune response, due to the production of altered proteins that can be recognized as dangerous by the host immune system. For this and other reasons, inflammatory cellularization in tumorous, peritumorous and surrounding healthy tissue has been increasingly investigated recently. Over the past 20 years, the general idea of so-called "cancer immunosurveillance" has been further developed, leading to the hypothesis of "tumor immunoediting," which places more focus on interactions between tumors and the immune system (Figure 5). The original theory that malignant tumors are autonomous cellular diseases with only six biological capabilities (the so-called "hallmarks of cancer") is gradually being disproved, and research is now focused on the hypothesis that it is a controlled disease involving immune components of the tumor microenvironment itself (and knowledge about the biological capabilities of tumors was also expanded and supplemented). Immune cells have been reported to be able to affect the fate of the tumor according to the three "E" phases—elimination, equilibrium, and escape, by activating innate and adaptive immunity through interactions with tumor cells. One of the most significant and promising areas of research is the ability of human cancers to resist immune destruction. This is related to the increasing focus on the research of so-called tumor-infiltrating lymphocytes (TILs), whose potential is being revealed in terms of prognostic significance as well as a key predictive positive (and in some cases negative) response factor during therapy, especially with immune checkpoint inhibitors (ICIs) (40–43).

The key influence of the composition of the tumor microenvironment and especially the representation of individual TIL components has been debated for a long time, but there is still a lack of conclusive evidence that would permit the introduction of the evaluation of TIL components as a definitive predictive biomarker (Figure 6). Several studies agree that a greater number of tumor-infiltrating and tumor-tissue-related lymphocytes is associated with a more favourable prognosis and higher overall survival, regardless of clinical variables such as TNM staging or operability (51–54). It is assumed that the distribution of CD markers, which reflects the profiles of immune cellularization in the tumor microenvironment, can be a potential predictive biomarker of the effectiveness of immunotherapy in SCLC since the primary mechanism of immunotherapy is precisely the activation of the immune response against tumorous tissue. It is believed that higher levels of the TIL surface biomarkers CD3, CD20, and CD45 are associated with more favourable prognoses and higher survival rates (51–53, 55–57). On the other hand, FOXP3+ TIL (Treg) components are typically viewed as suppressive cells that affect autotolerance and immunological homeostasis, ultimately promoting the growth of the tumorous tissue. Therefore, the interaction between tumor cells and Tregs, which regulate the activity of other T-lymphocytes, particularly cytotoxic T-lymphocytes (CTLs), may have an impact on the effectiveness of immunotherapy in SCLC. A worse prognosis has been documented for SCLC patients with tumor infiltrates that contain larger proportion of FOXP3+ cells. Certain SCLC tumor cell lines induce *de novo* differentiation of functional FOXP3+ Tregs in healthy blood lymphocytes. These are the mechanisms through which SCLC cells suppress

10.3389/pore.2023.1611086

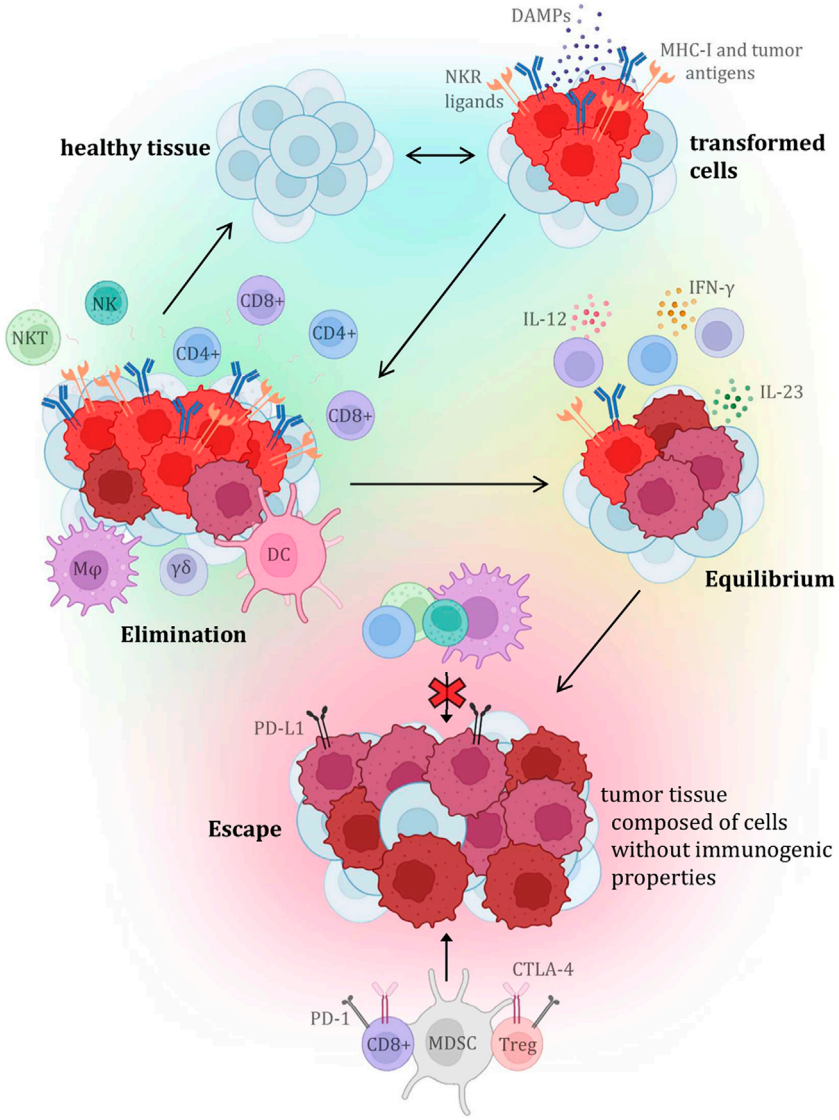

FIGURE 5
Presents the individual steps of the tumor immunoediting process, which consists of three phases (or three "E"), which are elimination, equilibrium, and escape. Each stage is characterized by specific interactions with variable immune cellularization (primarily with TIL components), and the molecules produced by them (32–39).

immunological responses, which has an impact on immunotherapy efficacy as well as patient survival. However, it is important to note that FOXP3+ TILs are a heterogeneous group that includes not only suppressive elements, but also a non-suppressive population with significant antitumor activity, which necessitates further investigation of the given issue and the definition of a clear opinion on the influence of Treg on tumor progression and treatment with immunotherapeutic methods (51, 52, 57–62). Additionally, it was discovered that patients with a better prognosis had a greater percentage of CD45RO+ memory T-lymphocytes in TIL population. In addition, high numbers of effector T-lymphocytes (especially CTL) were more often found in LD-SCLC (limited-stage disease) compared to ED-SCLC (extensive-stage), and a higher ratio of effector and regulatory T-lymphocytes was also associated with a better outcome. There is a growing list of immune cell markers and specific expression patterns of immunoactive proteins (stimulatory and inhibitory immune checkpoints and cytokines) that need to be researched in the hopes of enhancing the efficacy of immunotherapy since the tumor microenvironment contains not only TILs but also a

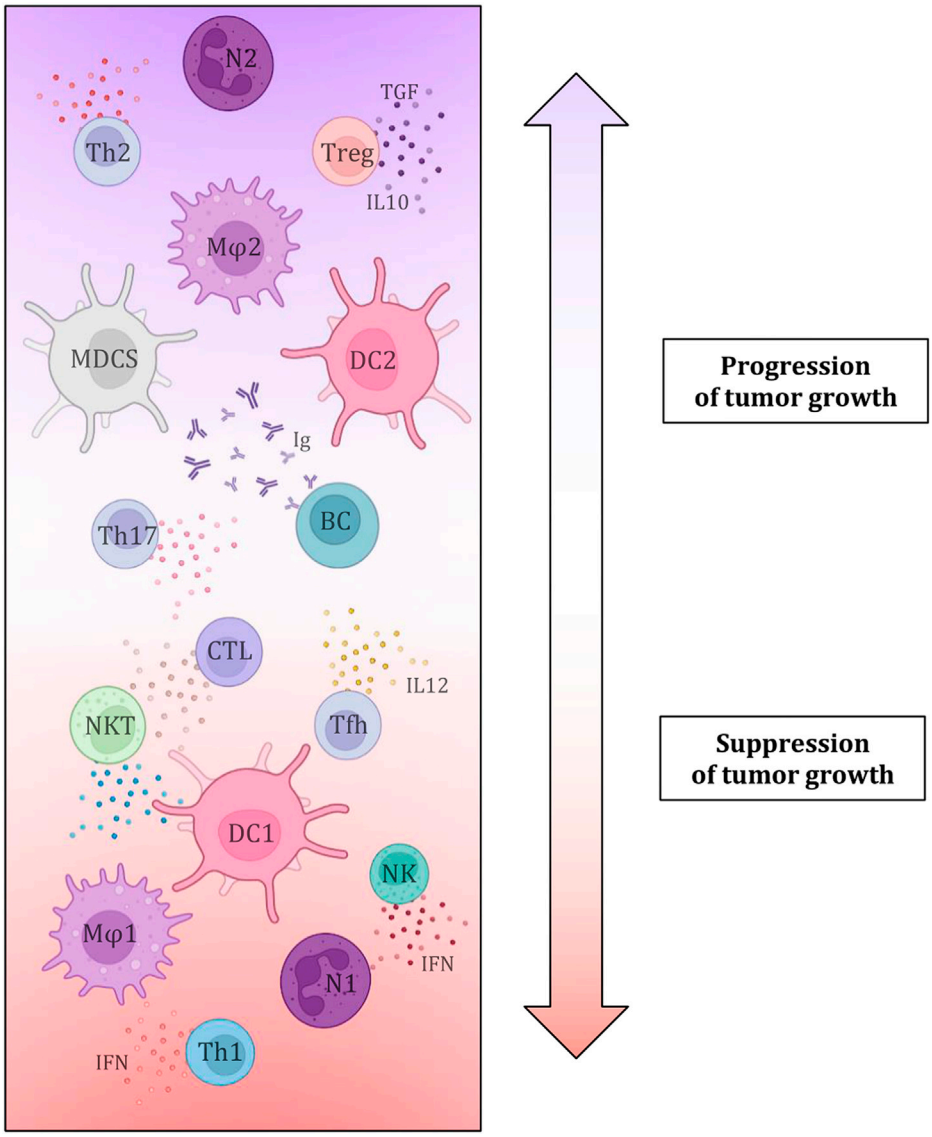

FIGURE 6
Simply depicts the effect of individual tumor microenvironment components, namely immune cell elements and the substances produced by them, on tumor growth characteristics. This demonstrates conclusively that immune cellularization plays a crucial part in the development of cancer and can, in general, have a favourable impact on the disease (by eliminating tumorous tissue) or, contrary, a negative one (growth potential) (41, 42, 44–50).

plethora of other immune cells (dendritic cells, suppressor myeloid cells, macrophages, or neutrophils) along with tumor cellularization and tumor stromal cells (52–56, 60, 63, 64).

Mutational burden of tumor tissue

Tumor mutation burden (TMB) is defined as the total number of non-synonymous mutations in the tumor genome. Small cell lung cancer is characterized by one of the highest numbers of somatic mutations across malignant tumors, including alterations in DNA repair mechanisms. It is thought to be triggered by long-term smoking, a chronic inflammatory process associated with it, and gene changes brought on by chemicals in cigarette smoke. In general, tumors with higher mutational loads are more likely to produce specific neoantigens that can activate the adaptive immune system's response. The formation of microsatellite instability (MSI), which results from a lack in DNA mismatch repair genes, is the primary reason for the correlation between

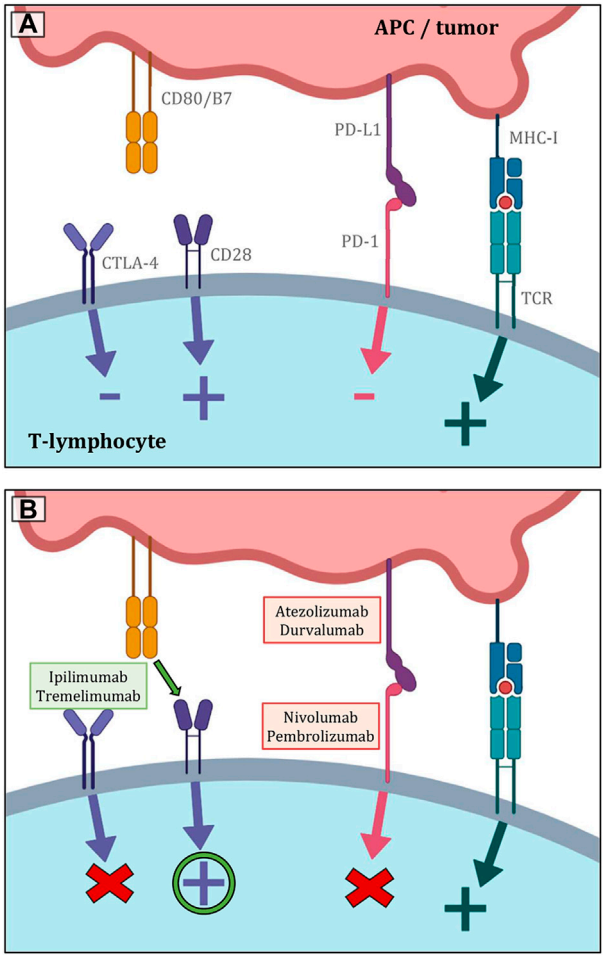

FIGURE 7
(A) Shows the most significant immunological pathways that are crucial for both inducing and inhibiting T-lymphocyte function. The basic stimulatory signal is mediated by the MHC complex during antigen presentation to the TCR receptor. The second signal is co-stimulation by the binding of CD80/B7 to CD28. The primary inhibitory route, in contrast, is represented by the contact between PD-L1 and PD-1. The CTLA-4 receptor then competes with CD28 for CD80/B7 affinity, and the result of its activity is also the inhibition of lymphocyte function. **(B)** Indicates the essential sites of action of the most used immunotherapeutics in the treatment of lung malignancies. Inhibitors of PD-L1 and PD-1 both lessen lymphocytes' physiological inhibition, which eventually improves anticancer activity. Similar principles govern the blockage of CTLA-4 receptors. As a result, there are more CD80/B7 molecules available to CD28 on the surface of T lymphocytes, stimulating the cell (19–23).

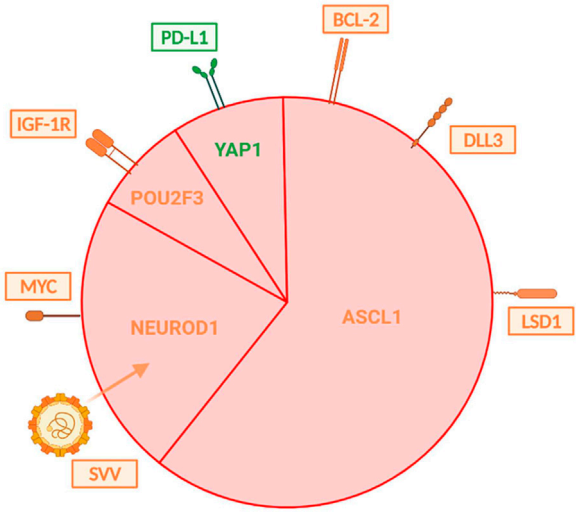

FIGURE 8
Illustrates the distribution of individual types of SCLC that are distinguished by differences in gene expression. The subtypes vary in their expression of surface molecules, which may play a role in one's response to appropriate treatment. Immunotherapy targets are shown in green, whereas those for chemotherapy are shown in orange (57, 67).

a higher number of mutations and the formation of neoepitopes and a stronger response to immunotherapy. Therefore, MSI is a favourable predictive factor of response to ICI therapy, particularly PD-1 blockers. TMB has been shown to be beneficial as an immunotherapy predictor primarily in melanoma and NSCLC, but this suggests that it may also be beneficial for SCLC (51, 52, 65–69). The results of the studies show that TMB is a promising predictive biomarker for checkpoint inhibitor therapy, especially in metastatic SCLC, and the first reliable tissue biomarker for immune checkpoint blockade. Furthermore, patients with high TMB (which represent approximately ¼ of all SCLC cases) have been found to benefit long-term from nivolumab therapy (with or without combination with ipilimumab) (30, 53, 54, 70, 71).

Despite the generally encouraging research findings, standardizing the assessment of cancer tissue mutational load as a specific immunotherapy prognostic factor is currently not entirely feasible in routine clinical practice. The primary issue is that patients with SCLC are given cytological or small biopsy samples, of which quality assessment is quite challenging (which is an obstacle not only for the TMB, but also for the other biomarkers). The increased amount of SCLC-specific necrosis complicates the assessment even more. Therefore, in order to provide reliable standard TMB testing, sufficient tumor tissue must be obtained, ideally through a core cut biopsy, which is not always attainable in all patients (51, 52, 65). In addition, it is advisable to place greater emphasis on the quality rather than just the quantity of the mutations under investigation, as certain mutations are more immunogenic than the others. For instance, indel mutations have a stronger therapeutic response than mismatch mutations. Contrarily, individuals who have mutations in the genes for the IFN-γ signalling pathway receptors (JAK1, JAK2, and APLNR) have a significant treatment resistance (72–76).

PD-L1 expression

As it is known, the interaction between PD-1 and PD-L1 represents a key mechanism for the escape of tumor cells from immunological elimination, especially by cytotoxic T-lymphocytes (Figure 7). This mechanism basically works in opposition to the increased immunogenicity that comes from a more prominent TMB. In many solid tumors, including NSCLC, the assessment of PD-L1 expression on the surface of tumor cells is recognized to be a highly significant predictive factor for the effectiveness of immunotherapy with PD-1 inhibitors. The primary challenges include the lower prevalence, the fluctuating dynamics of expression, the lack of diagnostic kits and specific antibodies, the heterogeneity of this biomarker's expression in the context of SCLC, difficulty of obtaining suitable samples, as well as the lack of clear evidence of a correlation between PD-L1 expression and a greater effect of immunotherapeutic procedures. The so-called combined proportion score (CPS), which has a better correlation with treatment outcomes, is also being studied. It is calculated by dividing the total number of viable tumor cells by the number of PD-L1-positive cells, including both tumorous and TIL cells, and multiplying the result by 100. It was also discovered that in SCLC (despite the low prevalence of PD-L1 expression on tumor cells), stromal expression may be more frequent and appears to be a predictive biomarker of therapeutic benefit of pembrolizumab. In contrast, the general hypothesis in the case of nivolumab is that PD-L1 expression cannot be considered a unique criterion for predicting and determining the appropriate patient population that will have a good response to anti-PD-L1 antibody treatment, as the clinical benefit of immunotherapeutic agents has also been observed in patients with PD-L1 negative SCLC (30, 31, 51–53, 65, 71, 77–79). As the heterogeneity of PD-L1 expression is not fully captured by the small sample of tumor tissue collected, circulating tumor cells were examined. However, this type of examination also faces technical problems, such as difficult isolation and subsequent validation. To summarize the data regarding PD-L1 expression in SCLC, this biomarker does not appear to be suitable for patients treated with chemotherapy plus ICI. Furthermore, considering the heterogeneity and plasticity of SCLC, future studies should evaluate other biomarkers than PD-L1 or CPS expression (73, 79–84).

Molecular subtyping of small cell lung cancer

In contrast to the more personalized approach to NSCLC, SCLCs are still considered a single malignant entity in routine clinical practice. However, gene expression profiling techniques have shown that SCLC displays clinical and molecular heterogeneity, pointing to the existence of four genetically different subtypes of this cancer (Figure 8). They are distinguished based on the relative expression of three or four key transcriptional regulators—ASCL1, NEUROD1, POU2F3, and YAP1 – with ASCL1 and NEUROD1 playing a crucial role in healthy neuroendocrine development. The most significant seems to be the SCLC-I subtype, which is characterized by low expression of ASCL1, NEUROD1 and POU2F3 (and conversely higher expression of YAP1) and also an inflammatory gene profile. This subtype has a higher proportion of cytotoxic $CD8^+$ T-lymphocytes in TIL, as well as NK-cells, macrophages, and B-lymphocytes. The expression of HLA, other antigen presentation mechanisms and important molecules such as PD-L1, PD1, CTLA-4, IDO-1, LAG-3 and TIGIT is also more significant. Patients with SCLC-I subtype are thought to have a better therapeutic response to checkpoint inhibitor immunotherapy. Increased expression of BCL-2, DLL3 or LSD1 proteins is described in ASCL1 type, so this could also become a potential therapeutic target. On the other hand, NEUROD1 type is correlated with MYC amplification, suggesting that c-MYC inhibitor therapy may be an option. The enhanced susceptibility of cells to the oncolytic SVV (Seneca Valley virus), which assaults and destroys neuroendocrine tumor cells by cell lysis, is another intriguing characteristic of the NEUROD1 group. For POU2F3, overall therapy could be enhanced by exposure of the tumor to IGF-1R inhibitors, given the higher occurrence of these markers on the cell surface. Regarding the last YAP1 type, a higher expression of PD-L1 was detected compared to the other three mentioned groups, and based on this finding, it is believed that this cohort could show the greatest therapeutic effect in immunotherapy compared to the others. Furthermore, small cell carcinomas are divided into high and low neuroendocrine (NE) groups according to the expression of various neuroendocrine biomarkers (chromogranin, synaptophysin, nerve cell adhesion molecules or gastrin-releasing peptide). Low NE SCLC is characterized by an increased infiltration of immune cells, whereas high NE is characterized by a reduced infiltration, which also indicates different responses to immunotherapy (especially ICI) (19, 52, 57, 85–89).

The role of the gut microbiome

More research has recently been done on the impact of the gut microbiota on the efficacy of different types of treatment, including immunotherapy. It is a complex ecosystem, the composition of which has a significant impact not only on the development of intestinal tumors but also on the way extraintestinal malignancies respond to chemo- and immunotherapy. In instance, it has been demonstrated that sensitivity to ICI or chemoimmunotherapy in patients with advanced solid tumors, such as melanoma, ovarian, or lung cancer, correlates with the prevalence of particular bacterial species or evidence of an immune response targeting them. One of the microorganisms that can be used as a positive predictor for

immunotherapy is *Akkermansia muciniphila*. It is possible that microbial antigens could improve antigen presentation capability and amplify the reactivity of TIL components, even though the underlying mechanisms are yet not fully understood. Additionally, it is hypothesized that gut microorganisms can enter the tumor microenvironment and create chemotactic substances that can promote immune cell migration to tumor locations. This feature of the antitumor immune response demands additional research in light of the considerable preclinical and clinical discoveries of recent years (62, 74, 76, 90, 91).

Other potential predictors

Other biomarkers that are actively being investigated in an attempt to discover a suitable predictive marker include, for example, the pulmonary immune prognostic index (LIPI; calculated from the serum LDH level and lymphocyte-to-neutrophil ratio), inflammatory biomarkers such as NLR (the neutrophil to lymphocyte ratio) and PLR (the platelet to lymphocyte ratio), galectin-9 expression on TIL or circulating tumor cells. Since it has been established in the past that elevated (or rising) levels of LDH or CRP have a detrimental impact on the disease's natural course, they are regarded as unfavourable prognostic indicators. In contrast, positive prognostic factors include tumor-expressed organic anion transport polypeptides (OATPs). Further, the density of TCR receptors on the surface of T-lymphocytes or the cfDNA methylation status both show significant promise as prognostic biomarkers. Despite all efforts and the number of potential biomarkers, the possibilities of predicting the response to immunotherapy in SCLC are incredibly dismal and further research with larger cohorts of patients is necessary (52, 53, 73, 92).

Conclusion

In order to compile an overview of the current state of knowledge about the nature of the tumor process and potential therapeutic options for small cell lung cancer, a literature review was conducted. The significance of potential predictive biomarkers that would allow the appropriate assignment of a certain immunotherapeutic treatment to a suitable cohort of patients was assessed in this context. Although more explored predictive biomarkers are promising, particularly the composition of the tumor microenvironment or the tumor mutation burden, further prospective studies involving more probands are required to confirm their reliability. However, it is clear that this field of study will continue to expand, as developing a reliable method to predict immunotherapy response is a very appealing goal of current medicine and research in the field of targeted cancer therapy.

Author contributions

VS—literature research, conceptualization, investigation, writing—original draft, writing—review and editing, visualization (Figures 1, 2, 5, 6); JS—literature research, writing—review and editing, visualization (Figures 3, 4, 7, 8); JŠ—conceptualization, validation, supervision, critical revision; MR and LK-R—critical revision. All authors contributed to manuscript revision, read, and approved the submitted version.

Funding

This work was supported by the Ministry of Health of the Czech Republic (NU21-03-00372).

Conflict of interest

The authors declare that the research was conducted in the absence of any commercial or financial relationships that could be construed as a potential conflict of interest.

References

1. Petruželka L, Votruba J. *Karcinom plic*. Prague: Farmakon Press (2019). 192.

2. Skřičková J, Babičková L, Špedlová J. Postavení chemoterapie v léčbě karcinomu plic. In: *Onkologie. Olomouc: Print* (2009). 285–91.

3. Skřičková J. *Nádory plic a průdušek: Jak léčit nádory plic a průdušek?* Olomouc: Solen (2013). 28.

4. Thai AA, Solomon BJ, Sequist LV, Gainor JF, Heist RS. Lung cancer. *Lancet* (2021) 398(10299):535–54. doi:10.1016/s0140-6736(21)00312-3

5. Travis WD. Pathology of lung cancer. *Clin Chest Med* (2011) 32(4):669–92. doi:10.1016/j.ccm.2011.08.005

6. Zheng M. Classification and pathology of lung cancer. *Surg Oncol Clin N Am* (2016) 25(3):447–68. doi:10.1016/j.soc.2016.02.003

7. Nicholson AG, Tsao MS, Beasley MB, Borczuk AC, Brambilla E, Cooper WA, et al. The 2021 WHO classification of lung tumors: Impact of advances since 2015. *J Thorac Oncol* (2022) 17(3):362–87. doi:10.1016/j.jtho.2021.11.003

8. Šutić M, Vukić A, Baranašić J, Försti A, Džubur F, Samaržija M, et al. Diagnostic, predictive, and prognostic biomarkers in non-small cell lung cancer (NSCLC) management. *J Pers Med* (2021) 11(11):1102. doi:10.3390/jpm11111102

9. Latimer KM, Mott TF. Lung cancer: Diagnosis, treatment principles, and screening. *Am Fam Physician* (2015) 91(4):250–6.

10. Rodriguez-Canales J, Parra-Cuentas E, Wistuba, II. Diagnosis and molecular classification of lung cancer. *Cancer Treat Res* (2016) 170:25–46. doi:10.1007/978-3-319-40389-2_2

11. Ryška A. Doporučený postup pro histologické vyšetření karcinomu plic. In: *Lékařské listy*. Prague: Ambit Media (2013). 4–6.

12. Travis WD. Classification of lung cancer. *Semin Roentgenol* (2011) 46(3): 178–86. doi:10.1053/j.ro.2011.02.003

13. Petersen I. The morphological and molecular diagnosis of lung cancer. *Dtsch Arztebl Int* (2011) 108(31–32):525–31. doi:10.3238/arztebl.2011.0525

14. Pešek M, Mužík J. Malobuněčný karcinom plic: Epidemiologie, diagnostika a léčba. In: *Vnitřní lékařství*. Prague: Solen (2018). 876–83.

15. van Meerbeeck JP, Fennell DA, De Ruysscher DKM. Small-cell lung cancer. *Lancet* (2011) 378(9804):1741–55. doi:10.1016/s0140-6736(11)60165-7

16. Carter BW, Glisson BS, Truong MT, Erasmus JJ. Small cell lung carcinoma: Staging, imaging, and treatment considerations. *Radiographics* (2014) 34(6): 1707–21. doi:10.1148/rg.346140178

17. Rudin CM, Brambilla E, Faivre-Finn C, Sage J. Small-cell lung cancer. *Nat Rev Dis Primers* (2021) 7(1):3. doi:10.1038/s41572-020-00235-0

18. Dingemans A-MC, Früh M, Ardizzoni A, Besse B, Faivre-Finn C, Hendriks LE, et al. Small-cell lung cancer: ESMO clinical practice guidelines for diagnosis, treatment and follow-up☆. *Ann Oncol* (2021) 32(7):839–53. doi:10.1016/j.annonc.2021.03.207

19. Poirier JT, George J, Owonikoko TK, Berns A, Brambilla E, Byers LA, et al. New approaches to SCLC therapy: From the laboratory to the clinic. *J Thorac Oncol* (2020) 15(4):520–40. doi:10.1016/j.jtho.2020.01.016

20. Hořejší V, Bartůňková J, Brdička T, Špíšek R. *Základy imunologie*. Prague: Triton (2017). 304.

21. Zatloukalová P. Úloha PD-1/PD-L1 signalizace v protinádorové imunitní odpovědi. In: *Klinická onkologie*. Brno: ApS BRNO (2016). 72–7.

22. Solomon BL, Garrido-Laguna I. Tigit: A novel immunotherapy target moving from bench to bedside. *Cancer Immunol Immunother* (2018) 67(11):1659–67. doi:10.1007/s00262-018-2246-5

23. Chauvin J-M, Zarour HM. TIGIT in cancer immunotherapy. *J Immunother Cancer* (2020) 8(2):e000957. doi:10.1136/jitc-2020-000957

24. Hirsch FR, Scagliotti GV, Mulshine JL, Kwon R, Curran WJ, Jr, Wu Y-L, et al. Lung cancer: Current therapies and new targeted treatments. *Lancet* (2017) 389(10066):299–311. doi:10.1016/S0140-6736(16)30958-8

25. Martínková J. *Farmakologie pro studenty zdravotnických oborů*. Prague: Grada Publishing (2018). 520.

26. American Cancer Society. Treating small cell lung cancer (2021). Available from: https://www.cancer.org/cancer/lung-cancer/treating-small-cell.html (Accessed July 06, 2022).

27. Ku GY, Yuan J, Page DB, Schroeder SEA, Panageas KS, Carvajal RD, et al. Single-institution experience with ipilimumab in advanced melanoma patients in the compassionate use setting: Lymphocyte count after 2 doses correlates with survival. *Cancer* (2010) 116(7):1767–75. doi:10.1002/cncr.24951

28. Mahoney KM, Atkins MB. Prognostic and predictive markers for the new immunotherapies. In: *Oncology*. Williston Park: CMP Media (2014). 39–48.

29. Bianconi F, Fravolini ML, Bello-Cerezo R, Minestrini M, Scialpi M, Palumbo B. Evaluation of shape and textural features from CT as prognostic biomarkers in non-small cell lung cancer. *Anticancer Res* (2018) 38(4):2155–60. doi:10.21873/anticanres.12456

30. Taniguchi H, Sen T, Rudin CM. Targeted therapies and biomarkers in small cell lung cancer. *Front Oncol* (2020) 10:741. doi:10.3389/fonc.2020.00741

31. Guo H, Li L, Cui J. Advances and challenges in immunotherapy of small cell lung cancer. *Chin J Cancer Res* (2020) 32(1):115–28. doi:10.21147/j.issn.1000-9604.2020.01.13

32. O'Donnell JS, Teng MWL, Smyth MJ. Cancer immunoediting and resistance to T cell-based immunotherapy. *Nat Rev Clin Oncol* (2019) 16(3):151–67. doi:10.1038/s41571-018-0142-8

33. Kalbasi A, June CH, Haas N, Vapiwala N. Radiation and immunotherapy: A synergistic combination. *J Clin Invest* (2013) 123(7):2756–63. doi:10.1172/JCI69219

34. von Locquenghien M, Rozalén C, Celià-Terrassa T. Interferons in cancer immunoediting: Sculpting metastasis and immunotherapy response. *J Clin Invest* (2021) 131(1):e143296. doi:10.1172/JCI143296

35. Schreiber RD, Old LJ, Smyth MJ. Cancer immunoediting: Integrating immunity's roles in cancer suppression and promotion. *Science* (2011) 331(6024):1565–70. doi:10.1126/science.1203486

36. Swann JB, Smyth MJ. Immune surveillance of tumors. *J Clin Invest* (2007) 117(5):1137–46. doi:10.1172/JCI31405

37. Tavakoli F, Sartakhti JS, Manshaei MH, Basanta D. Cancer immunoediting: A game theoretical approach. *Silico Biol* (2021) 14(1–2):1–12. doi:10.3233/ISB-200475

38. Kim R, Emi M, Tanabe K. Cancer immunoediting from immune surveillance to immune escape. *Immunology* (2007) 121(1):1–14. doi:10.1111/j.1365-2567.2007.02587.x

39. Wagner M, Koyasu S. Cancer immunoediting by innate lymphoid cells. *Trends Immunol* (2019) 40(5):415–30. doi:10.1016/j.it.2019.03.004

40. Bremnes RM, Busund L-T, Kilvær TL, Andersen S, Richardsen E, Paulsen EE, et al. The role of tumor-infiltrating lymphocytes in development, progression, and prognosis of non-small cell lung cancer. *J Thorac Oncol* (2016) 11(6):789–800. doi:10.1016/j.jtho.2016.01.015

41. Hanahan D, Weinberg RA. Hallmarks of cancer: The next generation. *Cell* (2011) 144(5):646–74. doi:10.1016/j.cell.2011.02.013

42. Hendry S, Salgado R, Gevaert T, Russell PA, John T, Thapa B, et al. Assessing tumor-infiltrating lymphocytes in solid tumors: A practical review for pathologists and proposal for a standardized method from the international immunooncology biomarkers working group: Part 1: Assessing the host immune response, TILs in invasive breast carcinoma and ductal carcinoma *in situ*, metastatic tumor deposits and areas for further research. *Adv Anat Pathol* (2017) 24(5):235–51. doi:10.1097/PAP.0000000000000162

43. Dundr P, Němejcová K, Bártů M, Matěj R, Rohan Z, Tichá I. Evaluation of inflammatory cells (tumor infiltrating lymphocytes) in solid tumors. *Klin Onkol* (2017) 30:10–21. doi:10.14735/amko20173S10

44. Hanahan D, Coussens LM. Accessories to the crime: Functions of cells recruited to the tumor microenvironment. *Cancer Cell* (2012) 21(3):309–22. doi:10.1016/j.ccr.2012.02.022

45. Galli F, Aguilera JV, Palermo B, Markovic SN, Nisticò P, Signore A. Relevance of immune cell and tumor microenvironment imaging in the new era of immunotherapy. *J Exp Clin Cancer Res* (2020) 39(1):89. doi:10.1186/s13046-020-01586-y

46. Bhardwaj N. Harnessing the immune system to treat cancer. *J Clin Invest* (2007) 117(5):1130–6. doi:10.1172/JCI32136

47. Zhang Q, Lou Y, Bai X-L, Liang T-B. Immunometabolism: A novel perspective of liver cancer microenvironment and its influence on tumor progression. *World J Gastroenterol* (2018) 24(31):3500–12. doi:10.3748/wjg.v24.i31.3500

48. Goubran HA, Kotb RR, Stakiw J, Emara ME, Burnouf T. Regulation of tumor growth and metastasis: The role of tumor microenvironment. *Cancer Growth Metastasis* (2014) 7:9–18. doi:10.4137/CGM.S11285

49. Regan D, Dow S. Manipulation of innate immunity for cancer therapy in dogs. *Vet Sci* (2015) 2(4):423–39. doi:10.3390/vetsci2040423

50. Le Q-V, Yang G, Wu Y, Jang HW, Shokouhimehr M, Oh Y-K. Nanomaterials for modulating innate immune cells in cancer immunotherapy. *Asian J Pharm Sci* (2019) 14(1):16–29. doi:10.1016/j.ajps.2018.07.003

51. Lim JU, Kang HS. A narrative review of current and potential prognostic biomarkers for immunotherapy in small-cell lung cancer. *Ann Transl Med* (2021) 9(9):809. doi:10.21037/atm-21-68

52. Longo V, Catino A, Montrone M, Pizzutilo P, Annese T, Pesola F, et al. What are the biomarkers for immunotherapy in SCLC? *Int J Mol Sci* (2021) 22(20):11123. doi:10.3390/ijms222011123

53. Gibney GT, Weiner LM, Atkins MB. Predictive biomarkers for checkpoint inhibitor-based immunotherapy. *Lancet Oncol* (2016) 17(12):e542–51. doi:10.1016/s1470-2045(16)30406-5

54. Uruga H, Mino-Kenudson M. Predictive biomarkers for response to immune checkpoint inhibitors in lung cancer: PD-L1 and beyond. *Virchows Arch* (2021) 478(1):31–44. doi:10.1007/s00428-021-03030-8

55. Zhao X, Kallakury B, Chahine JJ, Hartmann D, Zhang Y, Chen Y, et al. Surgical resection of SCLC: Prognostic factors and the tumor microenvironment. *J Thorac Oncol* (2019) 14(5):914–23. doi:10.1016/j.jtho.2019.01.019

56. Muppa P, Parrilha Terra SBS, Sharma A, Mansfield AS, Aubry M-C, Bhinge K, et al. Immune cell infiltration may be a key determinant of long-term survival in small cell lung cancer. *J Thorac Oncol* (2019) 14(7):1286–95. doi:10.1016/j.jtho.2019.03.028

57. Pavan A, Attili I, Pasello G, Guarneri V, Conte PF, Bonanno L. Immunotherapy in small-cell lung cancer: From molecular promises to clinical challenges. *J Immunother Cancer* (2019) 7(1):205. doi:10.1186/s40425-019-0690-1

58. Wang W, Hodkinson P, McLaren F, MacKinnon A, Wallace W, Howie S, et al. Small cell lung cancer tumour cells induce regulatory T lymphocytes, and patient survival correlates negatively with FOXP3+ cells in tumour infiltrate. *Int J Cancer* (2012) 131(6):E928–37. doi:10.1002/ijc.27613

59. Miyara M, Yoshioka Y, Kitoh A, Shima T, Wing K, Niwa A, et al. Functional delineation and differentiation dynamics of human CD4+ T cells expressing the

FoxP3 transcription factor. *Immunity* (2009) 30(6):899–911. doi:10.1016/j.immuni.2009.03.019

60. Spigel DR, Socinski MA. Rationale for chemotherapy, immunotherapy, and checkpoint blockade in SCLC: Beyond traditional treatment approaches. *J Thorac Oncol* (2013) 8(5):587–98. doi:10.1097/JTO.0b013e318286cf88

61. Sakaguchi S, Miyara M, Costantino CM, Hafler DA. FOXP3+ regulatory T cells in the human immune system. *Nat Rev Immunol* (2010) 10(7):490–500. doi:10.1038/nri2785

62. Bonanno L, Pavan A, Dieci MV, Di Liso E, Schiavon M, Comacchio G, et al. The role of immune microenvironment in small-cell lung cancer: Distribution of PD-L1 expression and prognostic role of FOXP3-positive tumour infiltrating lymphocytes. *Eur J Cancer* (2018) 101:191–200. doi:10.1016/j.ejca.2018.06.023

63. Hendriks LEL, Menis J, Reck M. Prospects of targeted and immune therapies in SCLC. *Expert Rev Anticancer Ther* (2019) 19(2):151–67. doi:10.1080/14737140.2019.1559057

64. Wang W, Hodkinson P, McLaren F, Mackean MJ, Williams L, Howie SEM, et al. Histologic assessment of tumor-associated CD45(+) cell numbers is an independent predictor of prognosis in small cell lung cancer. *Chest* (2013) 143(1):146–51. doi:10.1378/chest.12-0681

65. Gelsomino F, Lamberti G, Parisi C, Casolari L, Melotti B, Sperandi F, et al. The evolving landscape of immunotherapy in small-cell lung cancer: A focus on predictive biomarkers. *Cancer Treat Rev* (2019) 79(101887):101887. doi:10.1016/j.ctrv.2019.08.003

66. Calles A, Aguado G, Sandoval C, Álvarez R. The role of immunotherapy in small cell lung cancer. *Clin Transl Oncol* (2019) 21(8):961–76. doi:10.1007/s12094-018-02011-9

67. Boumber Y. Tumor mutational burden (TMB) as a biomarker of response to immunotherapy in small cell lung cancer. *J Thorac Dis* (2018) 10(8):4689–93. doi:10.21037/jtd.2018.07.120

68. Sen T, Gay CM, Byers LA. Targeting DNA damage repair in small cell lung cancer and the biomarker landscape. *Transl Lung Cancer Res* (2018) 7(1):50–68. doi:10.21037/tlcr.2018.02.03

69. Fumet J-D, Truntzer C, Yarchoan M, Ghiringhelli F. Tumour mutational burden as a biomarker for immunotherapy: Current data and emerging concepts. *Eur J Cancer* (2020) 131:40–50. doi:10.1016/j.ejca.2020.02.038

70. Hellmann MD, Callahan MK, Awad MM, Calvo E, Ascierto PA, Atmaca A, et al. Tumor mutational burden and efficacy of nivolumab monotherapy and in combination with ipilimumab in small-cell lung cancer. *Cancer Cell* (2018) 33(5):853–61. doi:10.1016/j.ccell.2018.04.001

71. Tay RY, Heigener D, Reck M, Califano R. Immune checkpoint blockade in small cell lung cancer. *Lung Cancer* (2019) 137:31–7. doi:10.1016/j.lungcan.2019.08.024

72. Ott PA, Bang Y-J, Piha-Paul SA, Razak ARA, Bennouna J, Soria J-C, et al. T-cell-inflamed gene-expression profile, programmed death ligand 1 expression, and tumor mutational burden predict efficacy in patients treated with pembrolizumab across 20 cancers: KEYNOTE-028. *J Clin Oncol* (2019) 37(4):318–27. doi:10.1200/JCO.2018.78.2276

73. Iams WT, Porter J, Horn L. Immunotherapeutic approaches for small-cell lung cancer. *Nat Rev Clin Oncol* (2020) 17(5):300–12. doi:10.1038/s41571-019-0316-z

74. Galluzzi L, Chan TA, Kroemer G, Wolchok JD, López-Soto A. The hallmarks of successful anticancer immunotherapy. *Sci Transl Med* (2018) 10(459):eaat7807. doi:10.1126/scitranslmed.aat7807

75. Sadeghi Rad H, Bazaz SR, Monkman J, Ebrahimi Warkiani M, Rezaei N, O'Byrne K, et al. The evolving landscape of predictive biomarkers in immuno-oncology with a focus on spatial technologies. *Clin Transl Immunol* (2020) 9(11):e1215. doi:10.1002/cti2.1215

76. Lei Y, Li X, Huang Q, Zheng X, Liu M. Progress and challenges of predictive biomarkers for immune checkpoint blockade. *Front Oncol* (2021) 11:617335. doi:10.3389/fonc.2021.617335

77. Ragavan M, Das M. Systemic therapy of extensive stage small cell lung cancer in the era of immunotherapy. *Curr Treat Options Oncol* (2020) 21(8):64. doi:10.1007/s11864-020-00762-8

78. Ott PA, Elez E, Hiret S, Kim D-W, Morosky A, Saraf S, et al. Pembrolizumab in patients with extensive-stage small-cell lung cancer: Results from the phase Ib KEYNOTE-028 study. *J Clin Oncol* (2017) 35(34):3823–9. doi:10.1200/jco.2017.72.5069

79. Esposito G, Palumbo G, Carillio G, Manzo A, Montanino A, Sforza V, et al. Immunotherapy in small cell lung cancer. *Cancers (Basel)* (2020) 12(9):2522. doi:10.3390/cancers12092522

80. Ulrich BC, Guibert N. Non-invasive assessment of tumor PD-L1 status with circulating tumor cells. *Ann Transl Med* (2018) 6:S48. doi:10.21037/atm.2018.10.09

81. Reck M, Heigener D, Reinmuth N. Immunotherapy for small-cell lung cancer: Emerging evidence. *Future Oncol* (2016) 12(7):931–43. doi:10.2217/fon-2015-0012

82. Chae YK, Pan A, Davis AA, Mohindra N, Matsangou M, Villaflor V, et al. Recent advances and future strategies for immune-checkpoint inhibition in small-cell lung cancer. *Clin Lung Cancer* (2017) 18(2):132–40. doi:10.1016/j.cllc.2016.07.004

83. Horn L, Reck M, Spigel DR. The future of immunotherapy in the treatment of small cell lung cancer. *Oncologist* (2016) 21(8):910–21. doi:10.1634/theoncologist.2015-0523

84. Schwendenwein A, Megyesfalvi Z, Barany N, Valko Z, Bugyik E, Lang C, et al. Molecular profiles of small cell lung cancer subtypes: Therapeutic implications. *Mol Ther Oncolytics* (2021) 20:470–83. doi:10.1016/j.omto.2021.02.004

85. Zhang B, Birer SR, Dvorkin M, Shruti J, Byers L. New therapies and biomarkers: Are we ready for personalized treatment in small cell lung cancer? *Am Soc Clin Oncol Educ Book* (2021) 41:1–10. doi:10.1200/EDBK_320673

86. Gazdar AF, Bunn PA, Minna JD. Small-cell lung cancer: What we know, what we need to know and the path forward. *Nat Rev Cancer* (2017) 17(12):725–37. doi:10.1038/nrc.2017.87

87. Rudin CM, Poirier JT, Byers LA, Dive C, Dowlati A, George J, et al. Molecular subtypes of small cell lung cancer: A synthesis of human and mouse model data. *Nat Rev Cancer* (2019) 19(5):289–97. doi:10.1038/s41568-019-0133-9

88. Gay CM, Stewart CA, Park EM, Diao L, Groves SM, Heeke S, et al. Patterns of transcription factor programs and immune pathway activation define four major subtypes of SCLC with distinct therapeutic vulnerabilities. *Cancer Cell* (2021) 39(3):346–60.e7. doi:10.1016/j.ccell.2020.12.014

89. Ruan J. Tumor cell plasticity and intrinsic immunogenicity: Implications for immunotherapy resistance in small-cell lung cancer. *Thorac Cancer* (2021) 12(19):2523–5. doi:10.1111/1759-7714.14117

90. Shigematsu Y, Inamura K. Gut microbiome: A key player in cancer immunotherapy. *Hepatobiliary Surg Nutr* (2018) 7(6):479–80. doi:10.21037/hbsn.2018.10.02

91. Zitvogel L, Ma Y, Raoult D, Kroemer G, Gajewski TF. The microbiome in cancer immunotherapy: Diagnostic tools and therapeutic strategies. *Science* (2018) 359(6382):1366–70. doi:10.1126/science.aar6918

92. Krajsová I. Importance of the immune system and immunotherapeutic options in malignant melanoma. *Klin Onkol* (2015) 28:4S56–63. doi:10.14735/amko20154s56

Pathology & Oncology Research | frontiers

TYPE Systematic Review
PUBLISHED 05 June 2023
DOI 10.3389/pore.2023.1610710

Check for updates

OPEN ACCESS

EDITED BY
József Tímár,
Semmelweis University, Hungary

*CORRESPONDENCE
Xiumei Wang,
wangxiumei75@163.com

†These authors share second authorship

RECEIVED 15 July 2022
ACCEPTED 18 May 2023
PUBLISHED 05 June 2023

CITATION
Sun J, Sun Y, Miniderima and Wang X (2023), Cytokine-induced killer cell treatment is superior to chemotherapy alone in esophageal cancer.
Pathol. Oncol. Res. 29:1610710.
doi: 10.3389/pore.2023.1610710

COPYRIGHT
© 2023 Sun, Sun, Miniderima and Wang. This is an open-access article distributed under the terms of the Creative Commons Attribution License (CC BY). The use, distribution or reproduction in other forums is permitted, provided the original author(s) and the copyright owner(s) are credited and that the original publication in this journal is cited, in accordance with accepted academic practice. No use, distribution or reproduction is permitted which does not comply with these terms.

Cytokine-induced killer cell treatment is superior to chemotherapy alone in esophageal cancer

Jiayang Sun[1], Yushu Sun[2†], Miniderima[2†] and Xiumei Wang[2*]

[1]Department of Thoracic Surgery, Affiliated Hospital of Inner Mongolia Medical University, Hohhot, Inner Mongolia, China, [2]Department of Oncology, Inner Mongolia Cancer Hospital and Affiliated People's Hospital of Inner Mongolia Medical University, Hohhot, Inner Mongolia, China

Background: The therapeutic efficacy of cytokine-induced killer (CIK) cells versus dendritic cells (DC) co-cultured with CIK cells (DC-CIK) in treating esophageal cancer (EC) remains unclear due to the absence of a direct comparison of these two regimens. This study evaluated the comparative efficacy and safety of CIK cells versus DC-CIK using network meta-analysis in treating EC.

Material and methods: We identified eligible studies from previous meta-analyses, then conducted an updated search to retrieve additional trials between February 2020 and July 2021. The primary outcomes included overall survival (OS), objective response rate (ORR), and disease control rate (DCR), and the secondary outcomes included quality of life improved rate (QLIR) and adverse events (AEs). A network meta-analysis of 12 studies was conducted using ADDIS software.

Results: Twelve studies were identified, including six comparing CIK or DC-CIK plus chemotherapy (CT) with CT alone. Immunotherapy plus CT significantly improved overall survival (OS) (odds ratio [OR] 4.10, 95% confidence interval [CI] 1.23–13.69), objective response rate (ORR) (OR 2.72, 95% CI 1.79–4.11), disease control rate (DCR) (OR 3.45, 95% CI 2.32–5.14), and quality of life improvement rate (QLIR) (OR 3.54, 95% CI 2.31–5.41). DC-CIK+CT decreased the risk of leukopenia compared with CT alone. However, no statistical difference was detected between CIK-CT and DC-CIK+CT.

Conclusion: Based on the available evidence, we concluded that CIK cell treatment is superior to CT alone, but CIK-CT and DC-CIK+CT may be comparable in treating EC. However, comparing CIK-CT and DC-CIK+CT is only based on indirect evidence, so it is undoubtedly necessary to conduct studies to compare CIK-CT with DC-CIK+CT in EC patients directly.

KEYWORDS

esophageal cancer, immunotherapy, cytokine-induced killer cells, dendritic cells, network meta-analysis

Introduction

Esophageal cancer (EC) is one of the most common digestive malignant tumors. It has been reported that approximately 604,100 new EC cases and 544,076 deaths resulted from EC in 2020 [1]. Incidence and mortality of EC in China remain challenging, which is more than global statistics [2]. Surgery, radiation therapy (RT), and chemotherapy (CT) have been most extensively applied to treat EC patients [3]; however, the application of these therapeutic regimens was greatly limited due to the failure to thoroughly eliminate tumor cells, drug resistance, and other adverse reactions [4, 5]. Therefore, developing newer effective, safer therapeutic strategies for EC is imperative.

Studies suggest that immunodeficiency plays a crucial role in the relapse and metastasis of EC [6]; thus, immunotherapy attracts extensive attention and has been widely investigated worldwide. More importantly, immunotherapy has been regarded as the fourth most powerful treatment strategy following surgery, RT, and CT [5]. Among currently available immunotherapy regimens, adoptive cellular immunotherapy protocols, such as natural killer cells (NK) [7], tumor-infiltrating lymphocytes (TILs) [8], cytotoxic T lymphocytes (CTLs) [9], dendritic cells (DC) [10], and cytokine-induced killer (CIK) cells [11] have been flourishing in at-cancer treatment [12]. Compared with other immune cells, CIK cells can be easily obtained from peripheral and umbilical cord blood mononuclear cells. More importantly, it maintains a higher proliferation capacity *in vitro* and has a stronger antitumor activity and a broader spectrum [13].

CIK cells have been extensively applied in at-cancer treatment owing to the following two reasons, including a) the cytotoxicity of CIK cells could not be affected by immune inhibitors [14], and b) CIK cell-mediated cytotoxicity is independent of the major histocompatibility complex (MHC) [15]. Moreover, as the most potent antigen-presenting cells and the essential element for CIK activation, proliferation, phenotype expression, and cytokine secretion [4, 16], the addition of DCs to CIK cells (DC-CIK) further improved the therapeutic efficacy of CIK cells in treating cancer [17]. Several clinical trials have confirmed the therapeutic values of immunotherapy, including CIK or DC-CIK, in treating EC patients [18–20].

It is noted that immunotherapy based on CIK or DC-CIK has been demonstrated to be superior to CT alone for treating EC patients. However, the comparative therapeutic efficacy and safety of CIK versus DC-CIK remain unclear because the study directly comparing these two regimes is absent, significantly limiting the appropriate selection of therapeutic strategies for treating EC patients. It is exciting that network meta-analysis, as an expansion of conventional pairwise meta-analysis, provides a possible strategy for evaluating the difference between the two interventions that were never directly compared. Therefore, we performed this network meta-analysis to assess whether immunotherapy based on CIK+CT significantly differed from immunotherapy based on DC-CIK+CT in therapeutic efficacy and safety for the treatment of EC.

Materials and methods

This network meta-analysis was conducted according to the recommendations proposed by the Cochrane Collaboration (CC) [21], and all results were reported according to the preferred reporting items for systematic reviews and meta-analyses (PRISMA) for network meta-analysis (PRISMA-NMA) checklist [22, 23]. This study did not require ethical approval and patients' informed consent because data analysis was performed based on published studies.

Search strategy

We designed a two-step search strategy to identify eligible studies. Firstly, we identified previously published meta-analyses from PubMed and China National Infrastructure Knowledgement (CNKI) and retrieved eligible studies. In the second phase, two reviewers independently searched PubMed and CNKI to retrieve additional relevant studies published between February 2020 and July 2021. Subject heading terms and complimentary words were used to construct the search strategy. We summarized the search strategy of PubMed in Supplementary Table S1. Any conflicts about the identification of eligible studies were resolved by consulting a third reviewer.

Study selection

We selected studies using EndNote software according to the following three steps: a) we first removed repeat records by matching the title, author, and journal of each record, b) we initially excluded ineligible records by screening titles and abstracts of remaining unique records, and c) we excluded ineligible studies by checking eligibility based on full texts. We recorded the number of excluded studies and the reasons for excluding each study.

Selection criteria

According to the previous meta-analyses, we developed the following inclusion criteria: a) patients were confirmed as EC based on histopathology and cytological diagnostic criteria; b) randomized controlled trials (RCTs) contained at least a CT arm and either a CIK+CT arm or a DC-CIK+CT arm; c) studies reported at least one of the six outcome measures of interest, including overall survival (OS), objective response rate (ORR),

disease control rate (DCR), quality of life improvement rate (QLIR), adverse events (AEs), including gastrointestinal adverse reaction (GIAR) or leukopenia. Studies were excluded if they met the following criteria: a) abstract without sufficient data; b) Did not report sufficient data; c) repeat studies with insufficient information and poor quality; and d) other treatments such as radiotherapy, target therapy, and Chinese herbal medicine were incorporated into regimes.

Outcomes

The primary outcomes included overall survival (OS) and treatment efficacy involving objective response rate (ORR) and disease control rate (DCR). The secondary outcomes included quality of life improved rate and adverse events, including gastrointestinal adverse reactions and leukopenia. OS was described as the time from initiating treatment to death from any cause [24]. ORR and DCR were calculated based on some specific indicators, including complete response (CR), partial response (PR), stable disease (SD), or progressive disease (PD). CR plus PR equals ORR, and ORR plus SD equals CDR [20].

Data extraction

Two independent reviewers used a standard information extraction table designed by our team based on Microsoft Word to extract the essential information: name of the first author, publication year, details of regimes, including culture conditions, cell dose (once), cycles of CIK treatments, timing relative to CT, sample size, age, outcomes of interest, and details of methodological quality. We invited a third reviewer to assist us in resolving any disagreement.

Assessment of risk of bias

Studies were reviewed for risk of bias by using the Cochrane Collaboration's risk of bias tool [25] from the following seven items, including random sequence generation, allocation concealment, blinding of participants and personnel, detection bias blinding of outcome assessor, incomplete data, selective reporting, and other bias. In this network meta-analysis, we regarded it as experiencing a high risk if the sample size assigned in each arm of the individual study was less than 30. We invited a third reviewer to assist us in resolving any disagreement.

Statistical analysis

We first conducted a pairwise meta-analysis built on the random-effects model using RevMan 5.3 (The Nordic Cochrane Centre, the Cochrane Collaboration, Copenhagen, 2014) to establish the role of immunotherapy plus CT for EC. All outcomes in this network meta-analysis were dichotomous variables, and therefore, we used the odds ratio (OR) with a 95% confidence interval (CI) to calculate the pooled results. Heterogeneity was examined using the Chi-square test [26] and I^2 statistic [27]. Moreover, we investigated the comparative efficacy and safety of CIK+CT or DC-CIK+CT versus CT alone through subgroup analysis.

Following pairwise meta-analysis, we utilized the aggregate data drug information system (ADDIS) software (Groningen, the Netherlands, www.drugis.org) to conduct a network meta-analysis built on Markov Chain Monte Carlo (MCMC) simulation. We set up the following parameters to calculate network meta-analysis: 4 chains, 20,000 tuning iterations, 50,000 simulation iterations, the thinning interval of 10, 10,000 inference samples, and a variance scaling factor of 2.5 [28]. This network meta-analysis was star-shaped, and no loop was constructed; thus, it's impossible to perform a test for inconsistency [29, 30]. Pooled results in network meta-analysis were presented in OR with a 95% creditable interval (CrI). We utilized the Brooks Gelman-Rubin statistical method to evaluate the convergence, and a potential proportional

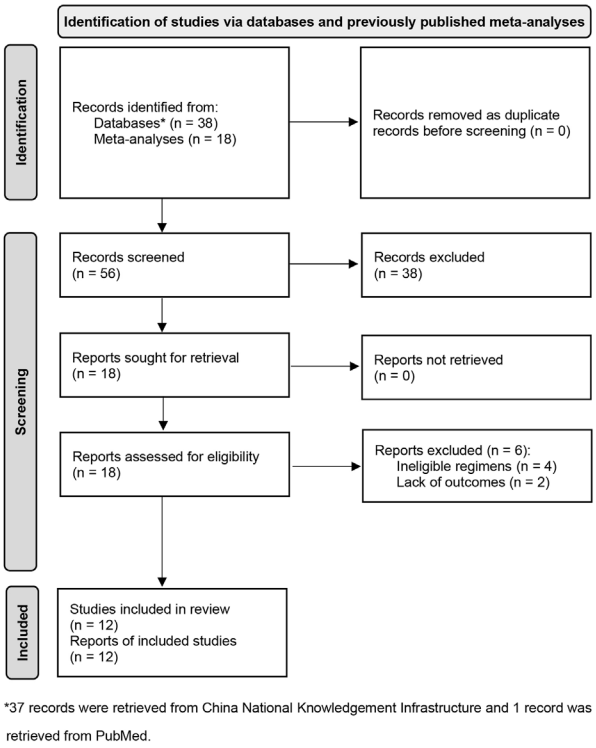

FIGURE 1
Flow diagram of identification and selection of eligible studies. CNKI, China National Knowledgement Infrastructure; DC, dendritic cells; CIK, cytokine induced killer cells.

TABLE 1 Characteristics of 12 eligible studies.

Study	KPS	Tumor stage	Sample size	Age (mean or median)	Exp regime	Timing relative to CT	Culture conditions	Cell dose (once), cycles	Infusion model	Source	Outcomes
Chang 2013	>70	III–IV	33 vs. 33	66.0 vs. 66.0▲	CIK+CT	2 days	IFN-γ, IL-2, OKT-3	1.0 × 10^9, 2 cycles	ivgtt.	APB	ORR, DCR, QLIR, GIAR, LP
Gu 2013	>60	n.r.	15 vs. 15	62.0 vs. 64.0▲	CIK+CT	7 days	IFN-γ, IL-2, OKT-3	n.r.	ivgtt.	APB	ORR, DCR, QLIR
Liu 2011	>70	III–IV	20 vs. 20	62.0 vs. 62.0▲	CIK+CT	2 days	IFN-γ, IL-2, OKT-3	>(1.0–2.0) × 10^9, 3 cycles	ivgtt.	APB	OS, ORR, DCR, QLIR, GIAR, LP
Qu 2015	n.r.	IV	100 vs. 100	56.3 vs. 56.3▼	CIK+CT	14 days	IFN-γ, OKT-3	5.0 × 10^9, 4 cycels	ivgtt.	APB	ORR, DCR
Zhu 2014	>60	III–IV	38 vs. 38	59.6 vs. 59.8▼	CIK+CT	14 days	n.r.	n.r., 4 cycles	ivgtt.	APB	ORR, DCR
Xu 2010	n.r.	III–IV	28 vs. 28	45.0 vs. 42.0▲	CIK+CT	12–14 days	IFN-γ, IL-1α, IL-2, OKT-3	(1.0–10.0) × 10^9, 4 cycles	ivgtt.	APB	ORR, DCR
Xi 2015	≥60	II–IIIb	26 vs. 26	60.0 vs. 62.0▲	DC-CIK+CT	7 days	IFN-γ, IL-1, IL-2, OKT-3 (CIK); GM-CSF, IL-4, TNF-α, IL-1 (DC)	(6.0–8.0) × 10^9, 2 cycles	ivgtt.	APB	QLIR
Yang 2015	n.r.	n.r.	100 vs. 100	70.2 vs. 72.3▼	DC-CIK + CT	14 days	n.r.	n.r., 2 cycles	ivgtt.	APB	OS, ORR, DCR, QLIR
Yang 2016	n.r.	n.r.	35 vs. 35	64.9 vs. 65.3▼	DC-CIK+CT	14 days	IFN-γ, IL-1, IL-2, OKT-3 (CIK); GM-CSF, IL-4, TNF-α, IL-1 (DC)	5.0 × 10^9, 2 cycles	ivgtt.	APB	OS, ORR, QLIR
Zhang 2016	≥60	IV	32 vs. 28	56.9 vs. 56.0▼	DC-CIK+CT	7 days	n.r.	≥6.0 × 10^9, 2 cycles	ivgtt.	APB	ORR, DCR, QLIR
Zhang 2017	≥60	II–IIIb	30 vs. 30	64.0 vs. 64.2▼	DC-CIK+CT	7 days	IFN-γ, IL-1, IL-2, OKT-3 (CIK); GM-CSF, IL-4, TNF-α, IL-1 (DC)	(6.0–8.0) × 10^9, 2 cycles	ivgtt.	APB	ORR, DCR, QLIR
Zhao 2015	>70	IIIb–IV	50 vs. 50	55.9 vs. 56.5▼	DC-CIK+CT	7 days	n.r.	n.r., 4 cycles	ivgtt.	APB	ORR, DCR, GIAR, LP

Abbreviations: KPS, Karnofsky performance score; n. r., not reported; CT, chemotherapy; Exp, experimental; CIK, cytokine-induced killer cell; DC, dendritic cell; ivgtt., intravenously guttae; APB, autolougs peripheral blood; OS, overall survival; ORR, objective response rate; DCR, disease control rate; QLIR, quality-of-life improved rate; GIAR, gastrointestinal adverse reaction; LP, leukopenia. Regular (▲) and inverted (▼) triangle median and mean age, respectively.

reduction factor (PRF) of close to 1 indicates achieving a satisfactory convergence [31, 32]. Finally, we also estimated the surface under the cumulative ranking curve to rank all regimes [33]. We did not examine publication bias and small study effects because the number of eligible studies for individual comparison was not more than 10 [34].

Results

Identification and selection of study

We captured three eligible meta-analyses during the initial search phase. Then, a total of 18 potentially eligible studies were identified from them. An updated search in PubMed and CNKI did not identify any additional study. According to our selection criteria, we excluded six for the following reasons: ineligible regimes (n = 4) and lack of outcome (n = 2). Eventually, 12 eligible studies [35–46] met our inclusion criteria. We used Figure 1 to display the process of identifying and selecting studies.

Basic characteristics of eligible studies

Among 12 eligible studies included in this network meta-analysis, six studies [35–38, 40, 46] compared CIK+CT with CT, and six studies [39, 41–45] compared DC-CIK+CT with CT. All studies were published between 2010 and 2017 in China. The sample size of individual studies varied from 30 to 100, with an

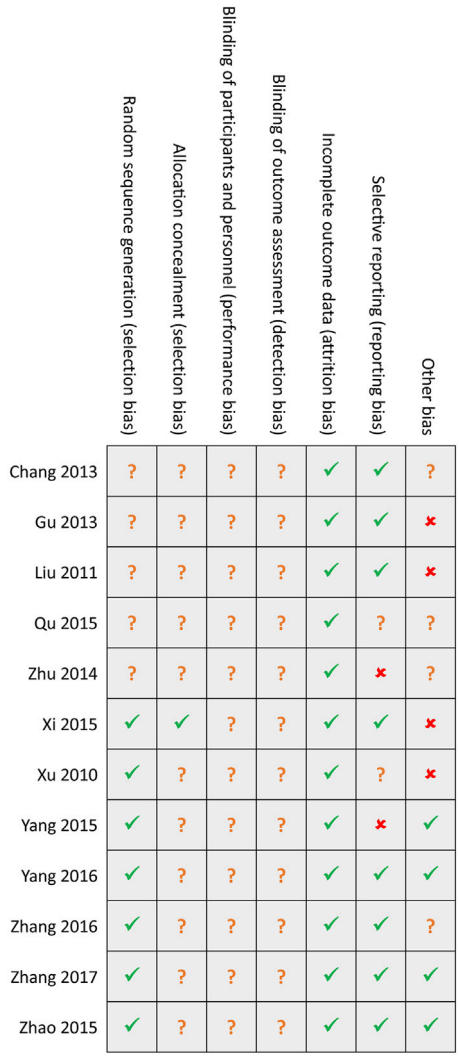

FIGURE 2
Risk of bias summary. Green hook, yellow question mark, and red cross indicates low, unclear, and high risk, respectively.

accumulated sample of 1,010. Among these 12 studies, four studies [36, 42, 45, 46] did not report details of cell dose, three studies [36, 41, 42] did not report tumor stage of patients, and four studies [38, 40–42] did not report KPS. Details of all included studies are shown in Table 1.

Methodological quality

Among included 12 studies, seven studies [39–45] generated random sequences using an appropriate method, such as a random number table, but only one study [39] reported the details of concealed random sequences. Not eligible studies reported the details of avoiding performance and detection biases. Attrition bias was assessed as the low risk among all eligible studies. Two studies [42, 46] did not report all anticipated outcomes, and four studies [36, 37, 39, 40] were assessed as high risk due to insufficient sample size. Generally, the overall methodological quality of all included studies was moderate level. Details of the risk of bias in each study are summarized in Figure 2.

Meta-analysis of OS

Three eligible studies [37, 41, 42] reported OS when comparing immunotherapy plus CT with CT alone, and a meta-analysis suggested that immunotherapy plus CT improved OS among patients with EC (OR 4.10, 95% CI 1.23–13.69, $p = 0.02$, Supplementary Figure S1). Subgroup analysis revealed that CIK+CT (1 RCT, OR 27.00, 95% CI 4.57–159.66, $p < 0.001$) or DC-CIK+CT (2 RCTs, OR 2.10, 95% CI 1.26–3.48, $p = 0.004$) was also better than CT alone for OS (Supplementary Figure S1).

Network meta-analysis supported that CIK+CT was superior to CT alone (OR 0.03, 95% CrI 0.00–0.98); however, no statistical difference was detected between DC-CIK+CT and CIK+CT (OR 0.07, 95% CrI 0.00–4.62) or CT alone (OR 0.05, 95% CrI 0.05–3.91) for OS (Figure 3A). Ranking results suggested that CIK+CT was the optimal option, followed by DC-CIK+CT and CT alone (Figure 3A).

Meta-analysis of ORR

A total of 11 studies [35–38, 40–46] reported ORR, and meta-analysis suggested that immunotherapy plus CT (OR 2.72, 95% CI 1.79–4.11, $p < 0.001$) was better than CT alone for ORR. Subgroup analysis revealed that CIK+CT (6 RCTs, OR 2.79, 95% CI 1.47–5.30, $p = 0.002$) or DC-CIK+CT (5 RCTs, OR 2.60, 95% CI 1.45–4.67, $p = 0.001$) was also better than CT alone for OS (Supplementary Figure S2).

Network meta-analysis supported that CIK+CT (OR 0.40, 95% CrI 0.22–0.83) or DC-CIK+CT (OR 0.36, 95% CrI 0.18–0.71) was superior to CT alone; however, no statistical difference was detected between DC-CIK+CT and CIK+CT (OR 1.12, 95% CrI 0.45–3.24) (Figure 3B). Ranking results suggested that DC-CIK+CT was the optimal option, followed by CIK+CT and CT alone (Figure 3B).

Meta-analysis of DCR

The meta-analysis of 10 studies [35–38, 40, 42–46] suggested that immunotherapy plus CT (OR 3.45, 95% CI 2.32–5.14, $p < 0.001$) was better than CT alone for DCR (Supplementary Figure S3). Subgroup analysis revealed that CIK+CT (6 RCTs, OR 3.59,

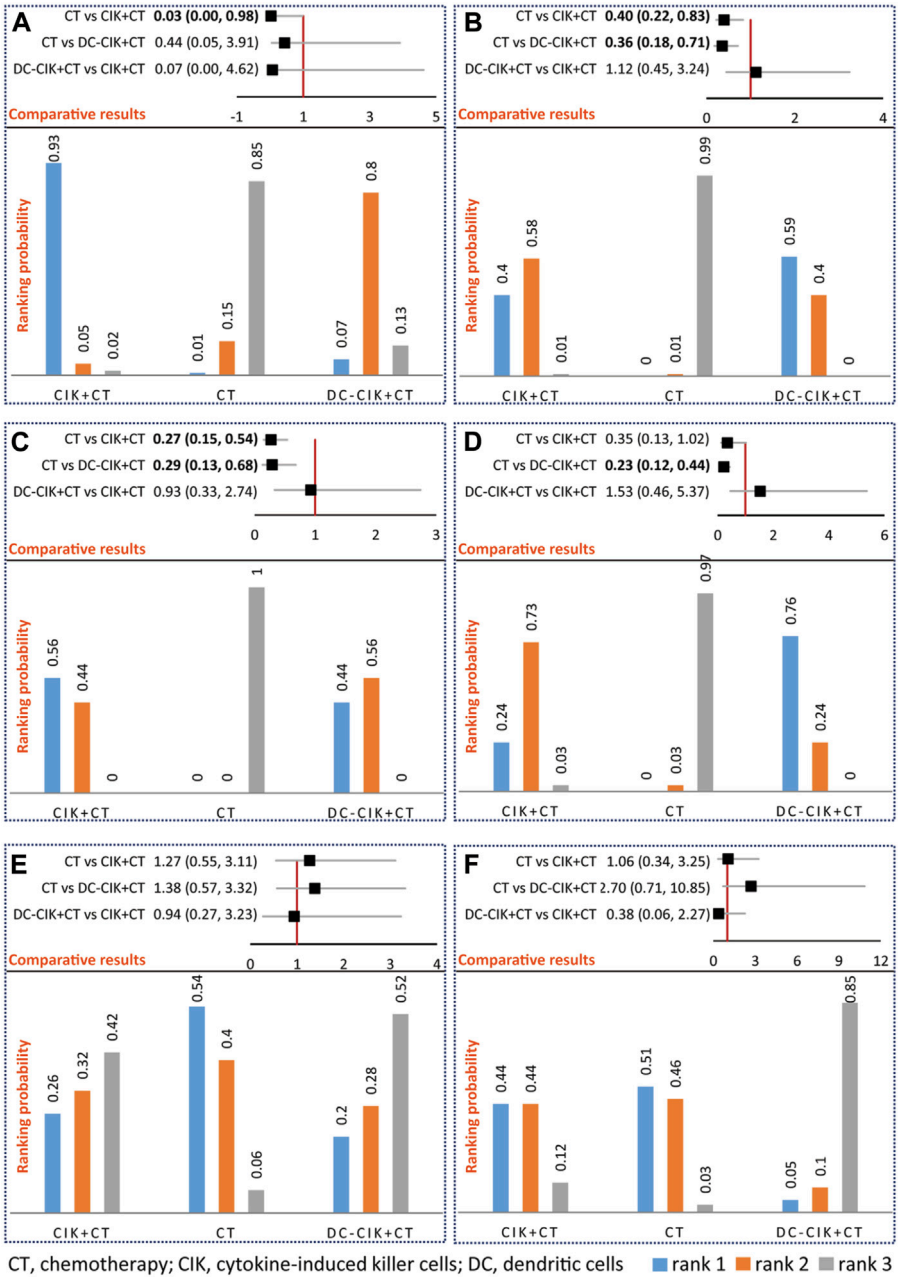

FIGURE 3
Network meta-analysis of OS **(A)**, ORR **(B)**, DCR **(C)**, QLIR **(D)**, GIAR **(E)**, and leukopenia **(F)**. The upper section represents pooled result of network meta-analysis and the lower section represents ranking probability in an individual figure. For positive outcomes including OS, ORR, DCR, and QLIR, rank 1 indicates the optimal option, rank 2 indicates relatively better option, and rank 3 indicates the worst option. For negative outcomes, including GIAR and leukopenia, rank 1 indicates the worst option, rank 2 indicates a worse option, and rank 3 indicates the optimal option.

95% CI 2.16–5.98, $p < 0.001$) or DC-CIK+CT (4 RCTs, OR 3.24, 95% CI 1.71–6.15, $p < 0.001$) was also better than CT alone (Supplementary Figure S3).

Network meta-analysis supported that CIK+CT (OR 0.27, 95% CrI 0.15–0.54) or DC-CIK+CT (OR 0.29, 95% CrI 0.13–0.68) was superior to CT alone for DCR; however, no statistical difference was detected between DC-CIK+CT and CIK+CT (OR 0.93, 95% CrI 0.33–2.74) (Figure 3C). Ranking results suggested that CIK+CT was the optimal option, followed by DC-CIK+CT and CT alone (Figure 3C).

10.3389/pore.2023.1610710

Meta-analysis of QLIR

Meta-analysis of 8 studies [35–37, 39, 41–44] suggested a better QLIR among patients treated by immunotherapy plus CT (OR 3.54, 95% CI 2.31–5.41, $p < 0.001$) compared with CT alone (Supplementary Figure S4). Subgroup analysis revealed that CIK+CT (3 RCTs, OR 2.42, 95% CI 1.09–5.40, $p = 0.03$) or DC-CIK+CT (5 RCTs, OR 4.10, 95% CI 2.48–6.76, $p < 0.001$) was also better than CT alone (Supplementary Figure S4).

Network meta-analysis supported that DC-CIK+CT (OR 0.23, 95% CrI 0.12–0.44) was superior to CT alone for QLIR; however, no statistical difference was detected between CIK+CT and DC-CIK+CT (OR 1.53, 95% CrI 0.46–5.37) or CT alone (OR 0.35, 95% CrI 0.13–1.02) (Figure 3D). Ranking results suggested that DC-CIK+CT was the optimal option, followed by CIK+CT and CT alone (Figure 3D).

Meta-analysis of AEs

Among 12 included studies, only 3 studies [35, 37, 45] reported AEs, including GIAR and QLIR. The meta-analysis did not detect a significant difference in any comparisons (Supplementary Figure S5), supported by network meta-analysis (Figures 3E, F). Meanwhile, network meta-analysis did not detect a statistical difference between CIK+CT and DC-CIK+CT for any AEs (Figures 3E, F). Ranking results suggested that DC-CIK+CT was the optimal option, followed by CIK+CT and CT alone regarding AEs (Figures 3E, F).

Discussion

EC remains one of the most common digestive malignant tumors worldwide [1]. Although surgery, radiotherapy, and chemotherapy are most widely used for EC, their application is limited by failing to thoroughly eliminate tumor cells, drug resistance, and other adverse effects [4, 5]. Immunotherapy has rapidly developed [3] since immunodeficiency is often considered a decisive factor in the recurrence and metastasis of EC patients [6]. Among numerous immunotherapy regimes, CIK and the combination of DC and CIK were more frequently applied in clinical practice due to advantages such as easy access [5] and cytotoxicity is neutral on MHC [14]. Multiple RCTs and meta-analyses have established the treatment efficacy and safety of immunotherapy built on CIK or DC-CIK plus CT for the treatment of patients with EC; however, it's unclear whether the presence of a difference between CIK and DC-CIK because of a trial directly comparing these two regimes is unlikely to occur. In this network meta-analysis, we further established the role of immunotherapy based on CIK or DC-CIK in treating EC patients, although no difference is detected in

TABLE 2 Comparison of the present network meta-analysis and previous meta-analyses.

Study	IT+CT vs. CT alone						CIK+CT vs. CT alone						DC-CIK+CT vs. CT alone						CIK+CT vs. DC-CIK+CT					
	OS	ORR	DCR	QLIR	GIAR	LP	OS	ORR	DCR	QLIR	GIAR	LP	OS	ORR	DCR	QLIR	GIAR	LP	OS	ORR	DCR	QLIR	GIAR	LP
Liu 2017	✓	✓	✓	✓	?	?	n.a.						n.a.						n.a.					
Ling 2021	✓	✓	✓	✓	?	?	n.a.						n.a.						n.a.					
Yuan 2021	✓	✓	✓	✓	?	?	n.a.						n.a.						n.a.					
The present study	✓	✓	✓	✓	?	?	✓	✓	✓	?	?	?	?	✓	✓	✓	?	?	?	?	?	?	?	?

Notes: n.a., not available. "✓" indicates benefiting to the combination regime of immunotherapy and CT; and "?" indicates no difference between two regimes.

terms of AEs. We also establish the beneficial therapeutic value of CIK or DC-CIK for the treatment of EC patients compared with CT alone. It's noted that CIK and DC-CIK are comparable in treatment efficacy and safety among patients with EC.

Currently, three meta-analyses [18–20] have been identified to compare immunotherapy built on CIK or DC-CIK with CT alone for treating patients with EC. Liu et al. conducted a meta-analysis of 11 RCTs to investigate the role of CIK/DCs-CIK immunotherapy in treating Chinese EC patients and suggested that the combination of CIK/DC-CIK immunotherapy and CT is safe and markedly prolongs survival time, enhances immune function, and improves the treatment efficacy for EC [19]. In 2021, Ling et al. conducted a meta-analysis of 13 RCTs to determine the efficacy and safety of CIK of adoptive immunotherapy combined with CT for the treatment of EC. They indicated that CIK cells of adoptive immunotherapy combined with CT could improve the clinical efficacy of EC patients, improve their quality of life and enhance their immune response [18]. In the same year, another meta-analysis of 17 RCTS revealed that the combination therapy of CIK/DC-CIK immunotherapy and CT enhances the immune function and improves the therapeutic efficacy of patients with EC [20]. In this network meta-analysis, we only focused on clinical outcomes, including treatment efficacy and AEs, and conventional pairwise meta-analysis obtained consistent results with previous meta-analyses. The comparison of the present network meta-analysis and previous meta-analyses is summarized in Table 2. It's noted that we only considered studies that compared CIK/DC-CIK plus CT with CT alone to be eligible, and thus heterogeneity resulting from regimes could be reduced. As a result, more reliable and robust results are generated from our study.

Additionally, we investigated the potential treatment value of CIK or DC-CIK for treating patients with EC based on subgroup analysis, which does not occur in previous meta-analyses. In the pairwise meta-analysis, the treatment efficacy of CIK or DC-CIK in treating EC is suggested. However, a significant difference between DC-CIK+CT and CT alone for OS and a significant difference between CIK+CT and CT alone for ORR is not retained in network meta-analysis, which may result from the limited number of included studies for individual comparison. More importantly, to date, no study has been conducted to directly compare CIK with DC-CIK for the treatment of EC patients, and thus it's unclear whether there is a difference between these two regimes. This network meta-analysis first investigates the comparative efficacy and safety between CIK+CT and DC-CIK+CT in EC patients. Interestingly, our network meta-analysis does not detect the difference between CIK+CT and DC-CIK+CT for all outcomes among EC patients.

Although this network meta-analysis generates more reliable and robust findings for decision-making, several limitations must be further interpreted. First, 12 eligible studies with a limited sample size were included in the final analysis, which greatly impaired the reliability of pooled results. Second, we did not conduct a publication bias test and small study effects due to a limited number of eligible studies for individual comparison. And thus, we must consider the possible impact of publication bias on the pooled results when interpreting pooled results. Third, a closed-loop cannot be available for any outcomes, and thus we could not evaluate inconsistency between direct and indirect comparisons with star-shaped network geometry. Forth, we cannot design subgroup analysis to investigate treatment efficacy and safety due to the limited number of eligible studies, although variations are detected in cell dose, KPS, and tumor stage. Fifth, all eligible studies are conducted in China; thus, these findings should be cautiously implemented in other cultural settings. Sixth, we also must acknowledge that variations in the sources of CIK and DC cells were not further investigated due to insufficient eligible studies, which might negatively affect the reliability of the pooled results.

Conclusion

Our network meta-analysis further demonstrated that immunotherapy plus CT is better than CT alone for treating EC patients. Meanwhile, CIK+CT or DC-CIK+CT is superior to CT alone for OS and treatment efficacy. However, CIK+CT and DC-CIK+CT may be statistically comparable for EC patients. Therefore, we concluded that CIK cell treatment is superior to CT alone in treating patients with EC. However, our findings of comparing CIK-CT and DC-CIK+CT are only obtained from indirect evidence, and therefore, it is undoubtedly necessary to conduct studies to directly compare CIK-CT with DC-CIK+CT in EC patients in the future.

Data availability statement

The original contributions presented in the study are included in the article/Supplementary Material, further inquiries can be directed to the corresponding author.

Author contributions

Conceptualization: JS. Data curation: JS and XW. Formal analysis: JS and Miniderima. Funding acquisition: JS and XW. Investigation: JS and XW. Methodology: YS. Project

administration: XW. Resources: XW. Software: JS and YS. Supervision: XW. Validation: XW. Visualization: Miniderima. Writing-original draft: JS and XW. Writing-review and editing: Miniderima. All authors contributed to the article and approved the submitted version.

Conflict of interest

The authors declare that the research was conducted in the absence of any commercial or financial relationships that could be construed as a potential conflict of interest.

Acknowledgments

We would like to deeply appreciate all authors who performed all eligible studies which have been included in the present network meta-analysis.

Supplementary material

The Supplementary Material for this article can be found online at: https://www.por-journal.com/articles/10.3389/pore.2023.1610710/full#supplementary-material

References

1. Sung H, Ferlay J, Siegel RL, Laversanne M, Soerjomataram I, Jemal A, et al. Global cancer statistics 2020: GLOBOCAN estimates of incidence and mortality worldwide for 36 cancers in 185 countries. *CA Cancer J Clin* (2021) 71(3):209–49. doi:10.3322/caac.21660

2. Zhang S, Sun K, Zheng R, Zeng H, Wang S, Chen R, et al. Cancer incidence and mortality in China, 2015. *J Natl Cancer Cent* (2021) 1(1):2–11. doi:10.1016/j.jncc.2020.12.001

3. Goode EF, Smyth EC. Immunotherapy for gastroesophageal cancer. *J Clin Med* (2016) 5(10):84. doi:10.3390/jcm5100084

4. Mu Y, Zhou CH, Chen SF, Ding J, Zhang YX, Yang YP, et al. Effectiveness and safety of chemotherapy combined with cytokine-induced killer cell/dendritic cell-cytokine-induced killer cell therapy for treatment of gastric cancer in China: A systematic review and meta-analysis. *Cytotherapy* (2016) 18(9):1162–77. doi:10.1016/j.jcyt.2016.05.015

5. Zhou C, Liu D, Li J, Sun H, Zheng X, Wang S, et al. Chemotherapy plus dendritic cells co-cultured with cytokine-induced killer cells versus chemotherapy alone to treat advanced non-small-cell lung cancer: A meta-analysis. *Oncotarget* (2016) 7(52):86500–10. doi:10.18632/oncotarget.13394

6. Shi L, Zhou Q, Wu J, Ji M, Li G, Jiang J, et al. Efficacy of adjuvant immunotherapy with cytokine-induced killer cells in patients with locally advanced gastric cancer. *Cancer Immunol Immunother* (2012) 61(12):2251–9. doi:10.1007/s00262-012-1289-2

7. Zhao Z, Liao H, Ju Y. Effect of compound Kushen injection on T-cell subgroups and natural killer cells in patients with locally advanced non-small-cell lung cancer treated with concomitant radiochemotherapy. *J Tradit Chin Med* (2016) 36(1):14–8. doi:10.1016/s0254-6272(16)30002-4

8. Dudley ME, Gross CA, Somerville RP, Hong Y, Schaub NP, Rosati SF, et al. Randomized selection design trial evaluating CD8+-enriched versus unselected tumor-infiltrating lymphocytes for adoptive cell therapy for patients with melanoma. *J Clin Oncol* (2013) 31(17):2152–9. doi:10.1200/JCO.2012.46.6441

9. Chia WK, Teo M, Wang WW, Lee B, Ang SF, Tai WM, et al. Adoptive T-cell transfer and chemotherapy in the first-line treatment of metastatic and/or locally recurrent nasopharyngeal carcinoma. *Mol Ther* (2014) 22(1):132–9. doi:10.1038/mt.2013.242

10. Peoples GE, Gurney JM, Hueman MT, Woll MM, Ryan GB, Storrer CE, et al. Clinical trial results of a HER2/neu (E75) vaccine to prevent recurrence in high-risk breast cancer patients. *J Clin Oncol* (2005) 23(30):7536–45. doi:10.1200/JCO.2005.03.047

11. Jäkel CE, Vogt A, Gonzalez-Carmona MA, Schmidt-Wolf IG. Clinical studies applying cytokine-induced killer cells for the treatment of gastrointestinal tumors. *J Immunol Res* (2014) 2014:897214. doi:10.1155/2014/897214

12. Mesiano G, Todorovic M, Gammaitoni L, Leuci V, Giraudo Diego L, Carnevale-Schianca F, et al. Cytokine-induced killer (CIK) cells as feasible and effective adoptive immunotherapy for the treatment of solid tumors. *Expert Opin Biol Ther* (2012) 12(6):673–84. doi:10.1517/14712598.2012.675323

13. Schmidt-Wolf IG, Negrin RS, Kiem HP, Blume KG, Weissman IL. Use of a SCID mouse/human lymphoma model to evaluate cytokine-induced killer cells with potent antitumor cell activity. *J Exp Med* (1991) 174(1):139–49. doi:10.1084/jem.174.1.139

14. Mehta BA, Schmidt-Wolf IG, Weissman IL, Negrin RS. Two pathways of exocytosis of cytoplasmic granule contents and target cell killing by cytokine-induced CD3+ CD56+ killer cells. *Blood* (1995) 86(9):3493–9. doi:10.1182/blood.v86.9.3493.bloodjournal8693493

15. Zhu Y, Zhang H, Li Y, Bai J, Liu L, Liu Y, et al. Efficacy of postoperative adjuvant transfusion of cytokine-induced killer cells combined with chemotherapy in patients with colorectal cancer. *Cancer Immunol Immunother* (2013) 62(10):1629–35. doi:10.1007/s00262-013-1465-z

16. Wei XC, Yang DD, Han XR, Zhao YA, Li YC, Zhang LJ, et al. Bioactivity of umbilical cord blood dendritic cells and anti-leukemia effect. *Int J Clin Exp Med* (2015) 8(10):19725–30.

17. Zhang Y, Ellinger J, Ritter M, Schmidt-Wolf IGH. Clinical studies applying cytokine-induced killer cells for the treatment of renal cell carcinoma. *Cancers (Basel)* (2020) 12(9):2471. doi:10.3390/cancers12092471

18. Ling JY, Wang QL, Fan JC, Han T, Yang ZQ. Cytokine-induced killers of adoptive immunotherapy combined with chemotherapy for the treatment of esophageal cancer: A meta-analysis [in Chinese]. *J Mod Oncol* (2021) 29(9):1524–30.

19. Liu Y, Mu Y, Zhang A, Ren S, Wang W, Xie J, et al. Cytokine-induced killer cells/dendritic cells and cytokine-induced killer cells immunotherapy for the treatment of esophageal cancer in China: A meta-analysis. *Onco Targets Ther* (2017) 10:1897–908. doi:10.2147/OTT.S132507

20. Yuan X, Zhang AZ, Ren YL, Wang XL, Jiang CH, Yang L, et al. Cytokine-induced killer cells/dendritic cells and cytokine-induced killer cells immunotherapy for the treatment of esophageal cancer: A meta-analysis. *Medicine* (2021) 100(13):e24519. doi:10.1097/MD.0000000000024519

21. Higgins JPT, Green S. *Cochrane handbook for systematic reviews of interventions*. Version 5.1.0. London, United Kingdom: The Cochrane Collaboration (2011). Available from www.handbookcochrane.org (updated March, 2011).

22. Page MJ, Moher D, Bossuyt PM, Boutron I, Hoffmann TC, Mulrow CD, et al. PRISMA 2020 explanation and elaboration: Updated guidance and exemplars for reporting systematic reviews. *BMJ (Clin Res ed)* (2021) 372:n160. doi:10.1136/bmj.n160

23. Hutton B, Salanti G, Caldwell DM, Chaimani A, Schmid CH, Cameron C, et al. The PRISMA extension statement for reporting of systematic reviews incorporating network meta-analyses of health care interventions: Checklist and explanations. *Ann Intern Med* (2015) 162(11):777–84. doi:10.7326/M14-2385

24. Han RX, Liu X, Pan P, Jia YJ, Yu JC. Effectiveness and safety of chemotherapy combined with dendritic cells co-cultured with cytokine-induced killer cells in the treatment of advanced non-small-cell lung cancer: A systematic review and meta-analysis. *PloS one* (2014) 9(9):e108958. doi:10.1371/journal.pone.0108958

25. Higgins JP, Altman DG, Gotzsche PC, Juni P, Moher D, Oxman AD, et al. The Cochrane Collaboration's tool for assessing risk of bias in randomised trials. *BMJ* (2011) 343:d5928. doi:10.1136/bmj.d5928

26. Bowden J, Tierney JF, Copas AJ, Burdett S. Quantifying, displaying and accounting for heterogeneity in the meta-analysis of RCTs using standard and generalised Q statistics. *BMC Med Res Methodol* (2011) 11:41. doi:10.1186/1471-2288-11-41

27. Higgins JP, Thompson SG. Quantifying heterogeneity in a meta-analysis. *Stat Med* (2002) 21(11):1539–58. doi:10.1002/sim.1186

28. Cipriani A, Higgins JPT, Geddes JR, Salanti G. Conceptual and technical challenges in network meta-analysis. *Ann Intern Med* (2013) 159(2):130–7. doi:10.7326/0003-4819-159-2-201307160-00008

29. Dias S, Welton NJ, Caldwell DM, Ades AE. Checking consistency in mixed treatment comparison meta-analysis. *Stat Med* (2010) 29(7-8):932–44. doi:10.1002/sim.3767

30. Albert I, Makowski D. Ranking crop species using mixed treatment comparisons. *Res Synth Methods* (2019) 10(3):343–59. doi:10.1002/jrsm.1328

31. Brooks S, Gelman A. General methods for monitoring convergence of iterative simulations. *J Comput Graphi Stat* (1998) 7:434–55. doi:10.1080/10618600.1998.10474787

32. Burger DA, Schall R. A bayesian nonlinear mixed-effects regression model for the characterization of early bactericidal activity of tuberculosis drugs. *J Biopharm Stat* (2015) 25(6):1247–71. doi:10.1080/10543406.2014.971170

33. Salanti G, Ades AE, Ioannidis JP. Graphical methods and numerical summaries for presenting results from multiple-treatment meta-analysis: An overview and tutorial. *J Clin Epidemiol* (2011) 64(2):163–71. doi:10.1016/j.jclinepi.2010.03.016

34. Palma Perez S, Delgado Rodriguez M. Practical considerations on detection of publication bias. *Gac Sanit* (2006) 20(3):10–6. doi:10.1157/13101085

35. Chang ZG, Xu QX, Ma L, He LM. Clinical observation on the treatment of advanced esophageal cancer with cytokine induced killer cell infusion combined with chemotherapy [in Chinese]. *Shandong Med J* (2013) 53(23):53–4.

36. Gu MW, Sun ZY, Wang MF. Application of DIK combined with chemotherapy in the treatment of advanced esophagus cancer [in Chinese]. *J Hunan Univ Chin Med* (2013) 33(12):8.

37. Liu GJ, Mei JZ, Xiao P, Li RJ, Li M. Efficacy of chemotherapy combined with cytokine-induced killer cells in treatment of advanced esophageal carcinoma [in Chinese]. *J Zhengzhou Univ (Med Sci)* (2011) 46(2):169–73.

38. Qu WF, Zhang WM, Ding XY. IL-12 induced CIK cells combined with chemotherapy improve immune function and efficacy in patients with esophageal carcinoma- 12 induced CIK cells combined with chemotherapy on esophageal cancer and immune function [in Chinese]. *World Chin J Digestol* (2015) 23(28):4553–7. doi:10.11569/wcjd.v23.i28.4553

39. Xi XX, Lyu BH, Ye T, Chen R, Xu X. Effect of DC-CIK cells' biotherapy in comprehensive therapy of esophagus cancer: Arandomized controlled trial [in Chinese]. *Chin J Clin Thorac Cardiovasc Surg* (2015) 22(8):765–9.

40. Xu Y, Huang Y. Effect of endoscopic chemo-seed implantation combined with DC-ClK therapy on tumor malignancy in patients with obstructive esophageal cancer [in Chinese]. *J Hainan Med Univ* (2018) 24(9):967–70.

41. Yang B, Chen YM, Wang LH, Tian ZY. Treatment of esophageal cancer in the elderly by gastroscopic implantation of chemotherapy particles combined with DC-CIK immune cell infusion [in Chinese]. *Chin J Clin Res* (2016) 29(3):331–3.

42. Yang B, Li W, Su XA, Chen YM. The clinical efficacy of endoscopic implantation with chemotherapeutic slow-release combined with DC-CIK immune cells infusion for patients with obstructive esophageal cancers [in Chinese]. *China J Endosc* (2015) 21(5):483–6.

43. Zhang NB, He MW. Clinical research of DCIK cell combined chemotherapy in treatment of patients with advanced esophageal squamous carcinoma [in Chinese]. *Chin J Prim Med Pharm* (2016) 23(6):859–62.

44. Zhang ZS, Yao TY, Zhang M, Wang GH. Efficacy of dendritic cells and cytokine-induced killercells for esophageal cancer [in Chinese]. *Chin J Clin Oncol Rehabil* (2017) 24(7):828–30.

45. Zhao Y, Ning S, Yang G, Zhang SG. Evaluation on clinical efficacy of DC-CIK combined with hemotherapy in treating moderate and advanced esophageal carcinoma [in Chinese]. *Lab Med Clin* (2015) 12(19):2823–6.

46. Zhu HP, Zhang QA. Analysis of the effect of injection in treatment of advanced esophageal cancer paclitaxel cisplatin regimen combined with autologous CIK cells [inn Chinese]. *Chin J Clin Oncol Rehabil* (2014) 21(7):837–9.

Pathology & Oncology Research | frontiers

TYPE Review
PUBLISHED 04 July 2024
DOI 10.3389/pore.2024.1611713

Check for updates

OPEN ACCESS

EDITED BY
Maximilian Hochmair,
Klinik Floridsdorf, Austria

*CORRESPONDENCE
Attila Lieber,
lieber.attila@med.unideb.hu

RECEIVED 31 January 2024
ACCEPTED 05 June 2024
PUBLISHED 04 July 2024

CITATION
Lieber A, Makai A, Orosz Z, Kardos T, Isaac SJ, Tornyi I and Bittner N (2024), The role of immunotherapy in early-stage and metastatic NSCLC. *Pathol. Oncol. Res.* 30:1611713. doi: 10.3389/pore.2024.1611713

COPYRIGHT
© 2024 Lieber, Makai, Orosz, Kardos, Isaac, Tornyi and Bittner. This is an open-access article distributed under the terms of the Creative Commons Attribution License (CC BY). The use, distribution or reproduction in other forums is permitted, provided the original author(s) and the copyright owner(s) are credited and that the original publication in this journal is cited, in accordance with accepted academic practice. No use, distribution or reproduction is permitted which does not comply with these terms.

The role of immunotherapy in early-stage and metastatic NSCLC

Attila Lieber[1]*, Attila Makai[1], Zsuzsanna Orosz[1], Tamás Kardos[1], Susil Joe Isaac[1], Ilona Tornyi[1] and Nóra Bittner[2]

[1]Department of Pulmonology, University of Debrecen, Debrecen, Hungary, [2]National Koranyi Institute of Pulmonology, Budapest, Hungary

In the past decade we have seen new advances and thus remarkable progress in the therapeutic options for non-small cell lung cancer (NSCLC). Among cytostatic therapies with new approaches in molecularly targeted therapies, we see new developments in a wide range of applications for immunotherapies. In this review we discuss the new potential modalities for the use of immune checkpoint inhibitors (ICIs) in the frontlines, including in early-stage (perioperative) and metastatic settings. The perioperative use of ICIs in both neoadjuvant and adjuvant settings may show benefits for patients. In early-stage NSCLC (from stage IIB and above) a multimodality approach is recommended as the gold standard for the treatment. After surgical resection platinum-based adjuvant chemotherapy has been the standard of care for many years. Based on the benefit of disease-free survival, the approval of adjuvant atezolizumab and adjuvant pembrolizumab was a significant breakthrough. In the metastatic setting, the use of immune checkpoint inhibitors with chemotherapy, regardless of PD-L1 expression or ICI alone (PD-L1 expression equal to or greater than 50%) also improves overall survival and progression-free survival.

KEYWORDS

NSCLC, PD-(L)1, ICI, perioperative, metastatic

Introduction

Non-small cell lung cancer (NSCLC) is the leading cause of cancer death worldwide, with more than 40% of patients diagnosed at stage IV [1]. The management approach for NSCLC primarily relies on the stage of the disease. However, advances in molecular pathology diagnostics, targeted therapy, and immunotherapy are expanding the range of treatment options and enhancing the prospects for improved survival rates. Immunotherapy has altered the treatment approach for several malignancies over the past 6–8 years, with NSCLC being among the most impacted. Tumor cells frequently reduce the expression of immune surveillance-related proteins, shielding them from the host's protective immune response [2]. Numerous approaches have been developed to boost the body's immune system in its fight against cancer cells by targeting pathways that suppress immune responses. In typical circumstances, activated T cells carry a receptor

called the programmed cell death-1 (PD-1) protein. PD-1 helps regulate immune responses to prevent them from becoming overly aggressive. Its counterpart, PD-L1, is found in both immune and tumor cells. The interplay between the PD-1/PD-L1 pathways plays a critical role in allowing tumors to evade the immune system. However, when this interaction is blocked, it reactivates T cell-mediated antitumor immunity, offering a survival advantage in various advanced and treatment-resistant cancers [3]. In total, seven immune checkpoint inhibitors (ICIs) have been approved in the United States (US) and Europe (EU) for the initial treatment of advanced or metastatic NSCLC. These ICIs include pembrolizumab, atezolizumab, cemiplimab, nivolumab + ipilimumab, and durvalumab + tremelimumab. Available treatment options include ICI monotherapy, combined ICI therapy, and ICI in conjunction with chemotherapy [4–16].

Perioperative treatment

Immunotherapy has become a very important part of the perioperative treatment of NSCLC. As shown in the following studies, the addition of ICI to perioperative chemotherapy treatment is very promising. Some studies tried the ICI + ICI combination, but because of its higher toxicity, this study was canceled [17]. Immunotherapy has become an increasingly important component of the perioperative treatment of NSCLC. The *National Comprehensive Cancer Network* (NCCN) has made its recommendations regarding the treatment with atezolizumab or pembrolizumab in the adjuvant setting, and nivolumab + chemotherapy or pembrolizumab + cisplatin doublet therapy and postoperative therapy in the neoadjuvant-adjuvant setting for specific patient populations with NSCLC [18].

Biomarkers

PD-L1 overexpression means a worse prognosis for the patients, namely, decreased disease-free survival (DFS) and overall survival (OS), which is clearly true in the cases of resected NSCLC tumors, so higher levels of PD-L1 indicate worse survival data. In the case of tumor mutation burden (TMB), the results are controversial as to whether they have a prognostic value for resected stage I-II NSCLC. Perioperative ctDNA analysis appears to be very useful in predicting event-free survival (EFS). Low preoperative and undetectable postoperative ctDNA levels mean better EFS [19]. From the perspective of response to therapy, in the IMpower010 trial in patients whose NSCLC tumor expressed PD-L1 more than 1%, better tumor regression was seen, but after deeper statistical analysis, it seems the high PD-L1 expressing (≥50%) group benefits the most in DFS. In contrast to the Keynote-091 study this benefit could not be demonstrated. A relatively new approach in the determination of minimal residual disease (MRD) is to use ctDNA analysis as another biomarker of perioperative ICI. After publications such as the results of the Mermaid studies we will see the place of this approach. Other potential future biomarkers such as blood TMB level, the ratio of lymphocytes that are infiltrating the tumor, and, e.g., KEAP1, STK11, and TP53 gene mutations may predict the benefit of ICI therapy [20].

Neoadjuvant treatment

Some trials have examined the efficacy of neoadjuvant cisplatin-based chemotherapy, showing an increase in overall survival (HR 0.84) [21]. Objectivizing the efficacy of neoadjuvant therapy is easier compared to adjuvant treatment because the pathologic response can be seen directly in the surgical specimen. A complete pathologic response (pCR) which means that no living tumor cells can be seen in the surgical specimen was found to be more beneficial for survival [22]. Major pathologic response (MPR) is an important parameter, which is defined as 10% or less of living tumor cells compared to necrosis and stromal cells in resected tissue [23]. This definition of MPR has been set to predict OS in prospective treatment [24]. In cases where neoadjuvant therapy was chosen, the proposed risk of delay or cancellation of surgery due to treatment-induced adverse events (AE) or disease progression was also considered. A few trials of neoadjuvant immunotherapy treatment are presented that may provide clarity in some of these situations (Table 1).

In the **Checkmate 816** trial the examined patients had stage IB-IIIA NSCLC (TNM 7th edition), no previous anticancer therapy, PD-L1 expression determined, ECOG 0-1, while EGFR and ALK alterations were excluded. In the experimental arm they received nivolumab + chemoterapy (3 cycles every 3 weeks) or chemotherapy alone in the control arm, equally distributed. In total, 83.2% of the experimental arm and 77.8% of the control group had R0 resection. Surgery was canceled only in 1.1% and 0.6% of patients due to adverse events. The follow-up period was not less than 21 months in this study. The median EFS was 31.6 months (statistically not reached) in the experimental arm and 20.8 months in the control arm. HR for recurrence, death or progression was 0.63. The greatest benefit in EFS was observed in stage IIIA, with PD-L1 expression of more than 1%, a non-squamous histological type and a carboplatin component in the treatment. PCR was 24% in the experimental arm and 2.2% in the control arm. The MPR was 36.9% in the experimental arm and 8.9% in the control arm. The statistically calculated median OS was not reached in either group (HR 0.57). After exploratory analysis, it became obvious that in patients with a complete pathologic response, the median EFS was significantly better in the experimental arm (26.6 vs. 18.4 months). The ctDNA clearance was higher in the experimental arm (56%) than in the control arm (35%), which correlated with the differences in

TABLE 1 Clinical trials of perioperative immunotherapy for NSCLC.

Trial	ICI agent	Stage	pCR (ICI arm)	MPR (ICI arm) (%)	G3 or higher TRAE (ICI arm) (%)	Rate of surgery (ICI arm)
Checkmate 816	nivolumab	IB-IIIA (TNM 7)	24%	36.9	33.5	83.2%
NADIM	nivolumab	IIIA	63.4%	82.9	13.5	90.2%
NADIM II	nivolumab	IIIA and IIIB	37%	54	19	93%
Checkmate77T	nivolumab	II-IIIB	25.3%	35.4	78	32%
Impower030	atezolizumab	II, IIIA, or select IIIB (T3N2)	only the study design was available			
Neotorch	toripalimab	II-III	24.8%	48.5	64.3	not known
Keynote-671	pembrolizumab	II, IIIA or IIIB (N2)	18.1%	30.2	44.9	81.2%
AEGEAN	durvalumab	IIA-IIIB (N2)	only the study design was available			

TRAE: treatment-related adverse event, ICI: immune checkpoint inhibitor, pCR: pathologic complete response, MPR: major pathologic response.

EFS between the two groups. The investigators also found a positive correlation between pCR and ctDNA clearance. Grade 3 or higher side effects were almost equal in the two groups (33.5% and 36.9%) [25, 26].

Neoadjuvant + adjuvant treatment

NADIM is a single-arm study that is now in phase II. Its aim was to measure the role of the ctDNA level in prognosis. The researchers enrolled stage IIIA NSCLC patients who were likely to have the potential for surgical removal of the tumor. The treatment was carboplatin doublet with paclitaxel plus nivolumab in the neoadjuvant setting, followed after surgery by nivolumab for 1 year (at a known dose). In total, 90.2% of the planned population underwent surgery. OS was 81.9% in the overall treated group and 91% in the nivolumab group at 36 months follow-up. A total of 63.4% of patients had pCR, including 82.9% of patients with MPR. The researchers found that neither TMB nor PD-L1 were independent predictors of long-term survival. Before treatment, low ctDNA levels were associated with longer progression-free survival (PFS) and OS (HR: 0.20) and zero ctDNA levels after the adjuvant treatment were associated with improved PFS and OS (HR: 0.26). Treatment-related adverse events (TRAEs) of grade 3 or higher were observed in 13.5% of patients [27].

NADIM II is a phase II trial that enrolled stage IIIA and IIIB NSCLC patients. They were randomly assigned in a 2:1 ratio to receive 3 cycles of nivolumab with paclitaxel + carboplatin (experimental arm), and after surgery (R0 resections) mono nivolumab 4 weekly for 6 months. The chemotherapy alone (3 cycles of paclitaxel + carboplatin) control group, before and after surgery received paclitaxel and carboplatin. PCR was 37% in the ICI arm and 7% without ICI treatment (this benefit was observed more in patients whose tumor expressed more than one percent PD-L1). The MPR was 57% vs. 14%. At 24 months PFS was 67.2% in the ICI arm and 40.9% in the only chemotherapy arm (HR 0.47). At the same follow-up time, OS was 85.0% in the ICI arm and 63.6% in the non-ICI arm (HR 0.43). In total, 93% of patients in the ICI arm and 69% of patients in the non-ICI group underwent surgery. One surgery was canceled because of ICI-related adverse events. Grade 3 or higher grade side effects were noted in 19% of patients. CtDNA analysis was also regularly performed in 66% of patients before and after neoadjuvant treatment. Pretreatment ctDNA levels were correlated with tumor size. After neoadjuvant treatment, ctDNA was negative in 67% of patients in the ICI arm and in 44% of patients in the non-ICI arm [28].

Checkmate 77T is a phase III trial that is currently in its interim analysis phase. The investigators are evaluating nivolumab with platinum-doublet chemotherapy (4 cycles) followed by surgery and nivolumab (1 year), or placebo with platinum-doublet chemotherapy (4 cycles) followed by surgery and placebo (1 year) in R0 resected stage II-IIIB, NSCLC, ECOG 0-1, EGFR/ALK wild-type, PD-L1 any expression patients. In this study, the follow-up time was no less than 15.7 months. At this time point, the median EFS in the ICI + chemotherapy + adjuvant group was observed. In the ICI arm, the median EFS is 28.9 months, compared to 18.4 months in the chemotherapy + placebo arm (HR: 0.58). PCR rates were improved as well (25.3% vs 4.7%), and MPR rates were higher in the ICI group (35.4% vs 12.1%). In total, 78% and 77% of patients in the two groups underwent definitive surgery and R0 resection was achieved in nearly 90% of cases. Grade 3 or higher adverse events were 32% and 25%, respectively [29].

Impower030 is a phase III trial in which the study population was potentially resectable stage II, IIIA, or select IIIB (T3N2) NSCLC patients with ECOG 0-1 performance status, EGFR wild-type, and without ALK translocation, but PD-L1 expression was not measured. The subjects received neoadjuvant atezolizumab

or placebo plus chemotherapy (platinum-doublet). After surgery patients in the experimental arm received atezolizumab treatment for 16 cycles or until recurrence or unacceptable toxicity, and patients in the control arm received the best supportive care and follow-up. The results of this study are not yet available [30].

Neotorch (phase III) enrolled patients with stage II/III, NSCLC, without EGFR or ALK alterations. Patients received 3 cycles of toripalimab or placebo with chemotherapy, and 13 cycles of toripalimab or placebo treatment after resection Q3W. While the trial is ongoing and EFS has not yet been reached in the ICI arm, it is 15.1 months in the control group (HR 0.40); the outcome is quite promising after 18 months of follow-up. The PCR was higher in the ICI group (24.8% vs. 1%), and MPR was also better in the toripalimab group (48.5%) versus 8.4% in the control group. AEs (grade 3 or higher) were almost equal, with 63.4% in the ICI group and 54.0% in the control group [31].

Keynote-671 is a phase III study in which only interim analysis is available at the moment. The trial enrolled patients eligible for R0 resection of stage II, IIIA or IIIB (N2) NSCLC. Patients received a total of 4 cycles of neoadjuvant pembrolizumab or placebo + cisplatin doublet therapy every 3 weeks and pembrolizumab or placebo (13 cycles) after surgery. With a median follow-up of 25.2 months EFS at 24 months was 62.4% in the ICI arm and 40.6% in the placebo group (HR 0.58). The calculated 24-month OS was 80.9% in the ICI arm and 77.6% in the control arm (not statistically significant). The PCR was 18.1% in the ICI arm and 4.0% in the control arm. MPR was 30.2% in the ICI arm and 11.0% in the control arm. In total, 81.2% of participants in the ICI arm and 79.4% of participants in the control arm underwent surgery. Grade 3 or higher toxicity was 44.9% in the ICI group and 37.3% in the control group. Toxicity that led to cancellation occurred in 12.6% of the patients in the ICI arm and 5.3% of the patients in the control group. Subgroup analysis showed that patients who are smokers, stage III have more benefit in EFS and in contrast to other trials nonsquamous phenotypes have benefitted in terms of EFS compared to squamous phenotypes. Every PD-L1 expression subgroup has benefitted in terms of EFS, but the biggest benefits were observed in the high (TPS>50%) expression group (HR: 0.42) [32].

AEGEAN will be a phase III trial, but only the study design has been published. Eligible patients are: no prior oncotherapy, candidates for complete resection, stage IIA to select (N2) IIIB NSCLC (according to TNM 8), without EGFR mutations or ALK rearrangement, with measured PD-L1 expression. Eligible participants will receive durvalumab or placebo on platinum doublet treatment and durvalumab or placebo after resection for 12 cycles. The primary endpoints are pCR and EFS [33].

The combination of IO + IO in the neoadjuvant setting is an exciting area of inquiry. It has greater immune activation and increased T-cell infiltration into the tumor tissue with ipilimumab + nivolumab therapy but surgical outcomes are not better. A study evaluating the effect of the neoadjuvant ipilimumab and nivolumab combination was stopped early (only 9 participants were selected) because of high rates of toxicity and progression, which canceled resection [17]. Despite a better response, the addition of ipilimumab seems to have a greater risk of serious adverse events leading to the cancellation of a potential complete resection of the tumor [34].

In the neoadjuvant setting there is a two-step approach, the only preoperative treatment as Checkmate816 and after neoadjuvant treatment and surgical resection with "adjuvant" immunotherapy treatment in various cycles. Assessing the efficacy of this treatment is straightforward since the pathological response can be objectively observed in surgical samples. The PCR rate is unexpectedly high after neoadjuvant chemo + ICI therapies (e.g., 18%, 24%, and 37%), and MPR (including pCR as well) is also very promising (37%, 57%, and even 82% were observed) compared to the chemotherapy-only group, where rates are around 2.2% and 4%. It is too early to draw conclusions from the survival data because of the short follow-up time, but the results that have already been presented are very promising. Another question is: were many surgeries canceled because of the high toxicity of this combination of neoadjuvant treatments? The answer is no. The Checkmate816 trial served as the prototype for the neoadjuvant ICI + chemo combination, in this trial, 1%–2% of patients were not operated on because of adverse events, and in NADIM II there are no patients in the same conditions. While in the majority of the trials stage IB-IIIA patients were enrolled, the greatest DFS survival benefit from ICI therapy was seen in stage IIIA patients with more than 1% PD-L1 expression, nonsquamous histology and those who received carboplatin treatment. Surprisingly, this same finding was not found in Keynote-671 in the nonsquamous histology type. The follow of the ctDNA level happened in the trials and they found positive correlation between complete ctDNA clearance and pCR. This approach is very promising and new in both the adjuvant and neoadjuvant settings as well.

Adjuvant therapy

Why is adjuvant immunotherapy useful?

Many trials have compared resection alone with surgery and adjuvant cisplatin-based doublet therapy. In a meta-analysis of adjuvant cisplatin-based doublet therapy, the addition of chemotherapy improved OS (HR 0.89) with a 5.4% risk of disease recurrence [35].

Despite the limited benefit of adjuvant therapy in overall survival (OS), it is administered when indicated. In such cases, the goal of adjuvant therapy is to eradicate potential micrometastases and prevent recurrence of lung cancer [20]. Given the very good results from ICI therapy in metastatic

NSCLC, the question arose as to whether we could achieve similarly good results with ICI therapy in the adjuvant setting. First, the background of the potential effectiveness and the possible targets of adjuvant ICI therapy were examined. It is known that cancer-related immune dysfunction can occur after surgical resection and may be a theoretical target of ICI, since the immune system reacts to surgery with various inflammatory responses and metabolic events [36, 37]. The surgical procedure itself, which includes trauma, blood loss, and hypothermia, may result in immunosuppression. More specifically, Th2 immunity increases in the postoperative period causing the release of growth factors and stress hormones [38]. These changes also lead to the expansion of myeloid-derived suppressor cells, M2 macrophages and T regulatory cells [36], which in turn will lead to suppression of the cellular immune system, resulting in higher expression of PD-L1 and CTLA-4. The altered PD-L1 and CTLA-4 expression appear to make adjuvant ICI treatment highly beneficial and effective in this setting [39]. The synergistic effect of combined ICI and chemotherapy is more effective in the destruction of MRD after surgical resection [40].

Clinical trials

Various immune checkpoint inhibitors have been and are still under examination to prove their effectiveness in the adjuvant setting. Some of these trials are presented below.

BR31/IFCT1401 is a phase III, double-blind trial. The investigators enrolled patients with completely removed stage IB-IIIA NSCLC (according to TNM 7th edition). This trial started in 2014 and is planned to finish in 2024 [41]. It is planned to enroll 1,415 patients and EGFR or ALK alterations are not part of the exclusion criteria. After R0 resection and completion of adjuvant chemotherapy, patients received durvalumab or placebo for 1 year. The primary endpoint was DFS for NSCLC participants with PD-L1 expression (greater than 25%) and without EGFR mutations or ALK rearrangements [20].

In **Impower010** 1,280 patients were enrolled in this phase III trial. Eligible patients for the study included those who had undergone R0 resection, and were in stage IB-IIIA according to the TNM 7 stage and ECOG 0-1. Participants were administered either 16 cycles of adjuvant atezolizumab or received best supportive care following cisplatin doublet chemotherapy (consisting of pemetrexed, docetaxel, vinorelbine, or gemcitabine) for 1-4 cycles. The median follow-up period was 32.8 months. Data processing focused on stage II-IIIA patients, where the primary endpoint was based on PD-L1 expression. Specifically, it looked at the difference in DFS between patients with PD-L1 expression greater than 1%. The analysis revealed a stratified HR for DFS of 0.66 when comparing the ICI group to the control group. In the overall study population (regardless of PD-L1 expression), the difference between the intent-to-treat group and the control group was observed with an HR of 0.79 for DFS. In the stage II–IIIA population with PD-L1 expression ≥1%, the 3-year DFS rates were 60% in the ICI group and 48% in the control group. In the overall population of stage II–IIIA participants, the 3-year DFS rates were 56% in the ICI group and 49% in the control group. The 5-year DFS rates could not be measured because this was an interim analysis. For the secondary endpoint of DFS in patients whose tumors had high PD-L1 expression (>50%), the unstratified HR was 0.43. In further exploratory analyses in stage II–IIIA participants whose tumors expressed 1%–49%, PD-L1 the unstratified HR was 0.87, and in patients with PD-L1<1%, the unstratified HR was 0.97. Unfortunately, OS data were immature in this analysis. Grade 3 or higher grade toxicity occurred in 22% of participants who received ICI and 12% in the control group. Looking at the risk of disease recurrence, new primary tumor appearance or death, it was reduced by 34% with ICI compared to the best supportive care in the PD-L1>1% expressing group and by 21% in the overall patient population. The DFS benefit with atezolizumab was of course highest in patients with tumors expressing PD-L1 >50%, but surprisingly a high DFS benefit could not be seen in the 1%–49% PD-L1 expression subgroup. As EGFR or ALK alterations were not exclusion criteria, it is an interesting question whether there is a difference in the DFS data in these patients. The data indicate that patients with driver mutations did not show a difference in DFS compared to patients without driver mutations. However, these findings should be interpreted with caution due to the low number of participants [42].

PEARLS/Keynote-091 is a triple-blind trial and has now reached its interim analysis. In total, 1,177 participants were enrolled with R0 resected NSCLC, stage IB-IIIA (according to TNM 7), ECOG 0-1 performance status, any verified PD-L1 expression level, and known EGFR and ALK alterations was not a requirement for inclusion. Patients who received adjuvant chemotherapy received ICI treatment within 3–12 weeks after the last dose of chemotherapy. The trial did not exclude patients who did not receive adjuvant chemotherapy previously; therefore, their ICI treatment began within 12 weeks after surgery. Eligible participants received pembrolizumab or placebo every 3 weeks until disease recurrence or intolerable adverse events (up to a maximum of 18 cycles). Crossover was not possible in this trial. Median DFS was 53.6 months in the ICI arm and 42.0 months in the control arm (HR 0.76). When examining the high PD-L1 expressing population, the median DFS was not statistically met in either the ICI arm or the control arm (HR 0.82). It was surprising that the benefit of DFS for ICI was not detected in the PD-L1 > 50% group which is likely due to the relative benefit of ICI treatment increasing with increasing PD-L1 expression in the setting of locally advanced or metastatic NSCLC. Despite this, median DFS in the ICI arm was numerically higher in the PD-L1 >50% population compared with the lower (1%–49% or <1%) PD-L1 expressed populations. What we did not expect was that median DFS in the control arm was also numerically improved in the PD-L1> 50% population compared with the lower (1%–49% and <1%) expressing

group. These statistical imbalances probably occurred due to the short follow-up period. As this was an interim analysis, the median OS data are immature (HR 0.87). Grade 3 or higher side effects occurred in 34% of patients in the ICI arm and 26% of patients in the placebo group [43].

ANVIL is an ongoing trial that started in May 2016 and is planned to be completed in July 2024. Unfortunately, only the study design is accessible. In total, 903 patients were enrolled with operated NSCLC (stage IB-IIIA, according to TNM7). Tumors with an EGFR mutation or ALK rearrangement were excluded. Adjuvant chemotherapy and radiotherapy were not mandatory. Randomized patients received adjuvant nivolumab or were observed for 1 year. The primary endpoints are DFS and OS. The secondary endpoint is the incidence of AEs and their severity [44].

Alchemist is a National Cancer Institute clinical trial platform for biomarker analysis of high-risk resected NSCLC that supports different randomized trials of new adjuvant therapies within the National Clinical Trials Network (NCTN). It includes a screening trial that enrolled participants with stage IB-IIIA (according to TNM7) who underwent R0 surgical resection, and had tissue and blood samples collected for analysis of EGFR and ALK alterations and PD-L1 expression. After the results patients were enrolled to receive adjuvant erlotinib, adjuvant crizotinib or adjuvant nivolumab after adjuvant chemotherapy [45].

ACCIO is a new three-arm trial in the Alchemist portfolio that started in June 2020. The study design is very interesting as it contains 3 arms (Arm A: 4 cycles of platinum doublet and observation, Arm B: 4 cycles of platinum doublet treatment + sequential pembrolizumab therapy for 16 cycles and Arm C: 4 cycles of platinum doublet chemotherapy + pembrolizumab with maintenance pembrolizumab of maximum 12 cycles) with or without postoperative radiotherapy (when needed). Stratification factors were NSCLC histologic type, any stratified PD-L1 expression, smoking habits and stage IB and II vs. IIIA. The primary endpoints are DFS and OS and this study design allowed for the secondary objective of comparing the primary DFS and OS endpoints between arms B and C in the overall population [46].

MERMAID-1 is an interesting phase III parallel-arm, placebo-controlled, double-blind, multicenter trial that was initiated in July 2020. Its estimated completion date is September 2026. Patient enrollment criteria are no EGFR or ALK alterations, stage II-III (according to TNM 8), R0 resection, ECOG 0-1, NSCLC histology, and stratified PD-L1 status. Minimal residual disease (MRD) status was determined by ctDNA analysis of blood samples collected 3–4 weeks after resection. Patients will be randomized 1:1 to get durvalumab or placebo, plus chemotherapy, for 12 weeks. Treatment continues with durvalumab or placebo, until week 48 or disease recurrence. It is very exciting that the primary endpoint (DFS), is determined by the measurement of MRD. Secondary endpoints will be: DFS, DFS in the minimal residual disease positive analysis set; and FAS (blinded independent central review) and OS in the MRD+ analysis set and FAS [47].

MERMAID-2 was launched in November 2020 and is planned to finish in October 2027. Enrolled patients were selected according to the MERMAID-1 requirements (R0 resected, stage II-III (TNM 8), no EGFR or ALK alterations). MRD is monitored by ctDNA levels from plasma samples and patients without visible recurrence but MRD+ with ctDNA levels are selected in this trial, so subjects with definitive therapy (R0 resection + optional neoadjuvant and/or adjuvant therapy) are elected in a 96- week follow-up phase, which means that patients will be examined regularly for MRD with ctDNA level measurement of blood samples. MRD-positive participants are evaluated with negative imaging (no visible tumor) and measured PD-L1 expression to determine eligibility for the trial. Eligible subjects receive durvalumab or placebo for up to 2 years or until disease recurrence. The primary endpoint is DFS in participants whose tumor expresses PD–L1 ≥1%. Secondary endpoints are DFS in the full analysis set, PFS, OS, quality of life questionnaires and rate of side effects [48].

Adjuvant-designed NADIM is an open-label trial that started in January 2021. Enrolled patients receive four cycles of chemotherapy + nivolumab and after 6 cycles of nivolumab or chemotherapy alone 4 cycles. The primary endpoint is DFS. Similar studies have been launched with toripalimab and canakinumab (interleukin-1β blocker) [20].

In the adjuvant setting, many trials are still ongoing; some have only reached the study design and interim analysis phase. The enrollment criteria are similar in many ways, but there are also some differences. In all trials patients were enrolled with completely resected NSCLC with stage II-IIIA (TNM 7 or 8). Impower010 and Keynote-091 did not exclude EGFR and ALK alterations. In Impower010 adjuvant cisplatin base doublet chemotherapy was mandatory while in Keynote-091 it was not, but previous radiotherapy or chemotherapy was prohibited [42, 43]. Despite the relatively immature data, each trial showed a significant EFS benefit compared to adjuvant chemotherapy. In Impower010 the greatest DFS benefit could be seen in the PD-L1 expression ≥50% group, but interestingly in Keynote-091 the PD-L1 ≥50% group did not show this benefit despite the results with pembrolizumab in metastatic disease [42, 43]. There were two interesting study designs that are very promising and may become the basis for future treatments. In ACCIO, the three-arm study design allows a head-to-head comparison of adjuvant chemotherapy versus adjuvant chemotherapy combined with ICI in both sequential and synchronous settings [46]. In Mermaid I and II the use of ctDNA measurement to determine the MRD before adjuvant treatment is quite exciting, but the results of the study are still ongoing [47, 48].

Advanced and metastatic stages

First line

In stage IV lung cancer, the advanced stage itself may be diagnosed primarily at metastatic sites. In practice, we are

TABLE 2 Clinical trials of first line immunotherapy in advanced and metastatic NSCLC.

Trial	ITT treatment regimen vs. cht	N (patients)	mOS (months)	mPFS (months)
Keynote 024	pembrolizumab	305	30 vs. 14.2 HR 0.63	10.3 vs. 6.0 HR: 0.50
EMPOWER-Lung 1	cemiplimab	712	26.1 vs. 13.3 HR 0.57	8.1 vs. 5.3 HR 0.51
IMpower 110	atezolizumab	572	20.2 vs. 13.1 HR 0,59	8.1 vs. 5.0 HR 0.63
Keynote-189 (nonsquamous)	pembrolizumab/pemetrexed/platinum	616	22.0 vs. 10.6 HR 0.49 (at 5 years)	8.8 vs. 4.9 HR 0.52
Keynote-407 (squamous)	pembroliumab/(nab)-paclitaxel/carboplatin	559	15.9 vs. 11.3 HR 0.64	6.4 vs. 4.8 HR0.56
EMPOWER-Lung-3 (squam + nonsqu.)	cemiplimab + cht	466	21.9 vs. 13.0 HR 0.71	8.2/5.5 HR 0.56
IMpower130	atezolizumab + nab-paclitaxel + carboplatin	723	18.6 vs. 13.9 HR 0.79	7.0/5.5 HR 0.64
IMpower150 (nonsquamous)	atezolizumab + carboplatin + paclitaxel + bevacizumab	1,202	19.2 vs. 14.7 HR 0.78	8.4 vs. 6.8 HR 0.57
CheckMate227	nivolumab + ipilimumab	1739	17.1 vs. 13.9 HR 0.79	7.2 vs. 5.5 HR 0.58
CheMate 9LA	nivolumab + ipilimumab + cht (2 cycles)	719	15.6 vs. 10.9 HR 0.66	6.8 vs. 5.0 HR 0.70

generally dealing with small samples. All patients diagnosed with stage IV NSCLC (nonsquamous, squamous) should be tested for driver mutations and for PD-L1 expression. When deciding on the treatment plan for a patient without an oncogene driver, several factors need to be considered. These factors include the histology, the tumor genotype, the level of PD-L1 expression, patient performance status (PS), any existing medical conditions (comorbidities), and the patient's own preferences [49]. ICIs that focus on either PD-1 or PD-L1 have been incorporated into the standard clinical strategy for the treatment of NSCLC. Key phase III studies (Table 2) evaluating various anti-PD-(L)-1 drugs, either alone or in combination with chemotherapy, have established ICI as the primary first-line therapy for metastatic NSCLC without targetable genetic mutations. Despite the progress made, there are unresolved challenges that include determining the best treatment regimen for individual patients. To date, there has been no direct comparison of different ICI-containing therapies in the first-line setting [49, 50].

Checkpoint inhibitor monotherapy

The standard of care for patients with squamous- and nonsquamous NSCLC, who also have a high PD-L1 expression, now involves the use of single-agent ICI. This is now the first-line therapy for patients with PD-L1 ≥50% with no contraindications for ICI. The significance of tumor mutational burden (in both blood and tissue samples) as a predictive indicator of response to cancer immunotherapy in metastatic NSCLC patients is still unclear. While the predictive utility of tumor mutational burden appears to be somewhat limited when it comes to patients receiving a combination of cancer immunotherapy and chemotherapy, recent data indicate that it may have a more meaningful predictive role in the context of immunotherapy alone, without the addition of chemotherapy [51]. If the choice is to use a single checkpoint inhibitor as a standalone treatment, either pembrolizumab, atezolizumab, or cemiplimab can be considered suitable options. The first evidence of enhanced survival outcomes emerged from investigations of NSCLC patients who had already experienced disease progression following platinum-based chemotherapy. This benefit was later extended to the frontline treatment of metastatic disease, whether used as a standalone therapy or in conjunction with chemotherapy. Additionally, this was also observed to be beneficial for patients with locally advanced unresectable disease [52]. A randomized trial has not directly compared the combination of a checkpoint inhibitor and chemotherapy with the use of a checkpoint inhibitor alone in individuals with high PD-L1 levels in NSCLC. Pembrolizumab, cemiplimab and nivolumab are anti-PD1 monoclonal antibodies, while atezolizumab and durvalumab are anti-PD-L1 monoclonal antibodies [18, 53]. To utilize pembrolizumab or cemiplimab as monotherapies in the initial treatment stage, it is necessary to have PD-L1 expression of more than 50%, which means that at least 50% of a minimum of 100 tumor cells (TCs) should show membrane expression of PD-L1. On the other hand, for nivolumab plus ipilimumab in the first line (although not approved by the European Medicines Agency), or pembrolizumab in the second line, a minimum of 1% PD-L1 expression on TCs is required [49].

Pembrolizumab

The KEYNOTE-024 trial demonstrated that pembrolizumab, compared to platinum-based chemotherapy, significantly

extended median PFS in previously untreated NSCLC patients with a PD-L1 tumor proportion score of at least 50% and no EGFR or ALK genetic alterations (10.3 vs. 6.0 HR 0.50). Importantly, the pembrolizumab group displayed an undefined median duration of response, suggesting the potential for long-lasting benefit. Additionally, the incidence of grade 3–5 TRAEs was less frequent in the pembrolizumab-treated patients. This study confirms the efficacy of pembrolizumab in the treatment of advanced NSCLC with high PD-L1 expression, highlighting its potential to provide better outcomes and improved tolerability compared to conventional chemotherapy [4]. Based on the 5-year median OS for pembrolizumab compared to chemotherapy (26.3 months vs. 13.4 months) and its 5-year OS rate (31.9% vs. 16.3%) the US Food and Drug Administration (FDA) approved the utilization of pembrolizumab as an initial treatment option in patients with advanced NSCLC [54, 55]. The KEYNOTE-598 study concludes that incorporating ipilimumab with pembrolizumab does not enhance efficacy and is linked to higher levels of adverse effects compared to using pembrolizumab alone in this group of patients (Grade 3 or higher TRAEs: 62.4% in pembrolizumab-ipilimumab recipients versus 50.2% in pembrolizumab-placebo recipients). Therefore, the findings do not support the use of the pembrolizumab-ipilimumab combination over the use of pembrolizumab alone in this context [56].

Cemiplimab

Cemiplimab demonstrated enhanced OS and PFS in comparison to chemotherapy. The EMPOWER-Lung 1 trial compared the use of cemiplimab alone to the choice of chemotherapy made by the investigators in patients who were newly diagnosed with advanced NSCLC and tumor PD-L1 expression of at least 50%, along with no EGFR mutations or ALK or ROS1 fusions. This study involved 712 participants, 85% of whom were men. The cemiplimab group showed significantly longer median OS (26.1 months vs. 13.3 months) and PFS (8.1 months vs. 5.3 months) compared to the chemotherapy group (HR 0.57 and HR 0.51, respectively). Regarding adverse events, grade 3 or higher TRAEs were less prevalent in the cemiplimab group (18%) in comparison to the chemotherapy group (40%). In conclusion, this study supports the use of cemiplimab as a first-line monotherapy in patients with advanced NSCLC who have a high level of PD-L1 expression. Interestingly, combining chemotherapy with cemiplimab at disease progression showed significant clinical benefit, suggesting a potential novel treatment approach for these patients [11, 57].

Atezolizumab

When considering atezolizumab as a first-line monotherapy treatment, criteria include PD-L1 expression of at least 50% on TCs or at least 10% on tumor-infiltrating immune cells [49]. The FDA approval of atezolizumab was based primarily on the outcomes of the IMpower 110 study. This research aimed to assess the efficacy and safety of atezolizumab compared to platinum-based chemotherapy. It was conducted as an initial treatment for patients with mNSCLC who exhibit PD-L1 expression. During the study 572 treatment-naïve patients were enrolled with metastatic nonsquamous or squamous NSCLC. In the high PD-L1 expression subgroup (205 patients), atezolizumab demonstrated a 7.1-month longer median overall survival (20.2 months vs. 13.1 months; HR for death 0.59) and an 8.1-month longer median PFS compared to chemotherapy (HR 0.63). Notably, grade 3 or higher TRAEs occurred in approximately 30% of atezolizumab patients and 53% of chemotherapy patients. These findings suggest that atezolizumab may be a more effective treatment option compared to traditional chemotherapy for these patients with NSCLC, regardless of histologic type [8]. The outcomes in terms of overall survival based on the degree of PD-L1 expression were consistent with those observed in the KEYNOTE-042 study comparing pembrolizumab to chemotherapy [5]. The main goal of the research was to evaluate the impact of OS on various population subgroups categorized by their PD-L1 expression levels. The study found varying degrees of OS benefit in these subgroups: those with PD-L1 >50%, PD-L1 >20%, and PD-L1 >1%. Notably, no significant PFS improvement was observed in patients with PD-L1 expression between 1% and 49% (HR: 0.92), leading to the approval of pembrolizumab monotherapy for subjects with PD-L1 expression above 50%. In both trials, individuals with high PD-L1 expression experienced the greatest benefit in terms of survival [5].

Nivolumab, durvalumab

Unfortunately, in addition to the remarkable results described above, we also find studies that did not show promising results. The CheckMate026 study conducted a comparison between nivolumab and platinum-based chemotherapy in patients diagnosed with stage IV NSCLC who had PD-L1 expression levels greater than 5% in their tumor cells and did not have EGFR- or ALK-activating mutations. The results in this instance were unfavorable. Nivolumab had a shorter median PFS (4.2 months vs. 5.9 months for CT, HR: 1.15), similar OS (14.4 months vs. 13.2 months for CT, HR: 1.02), but significantly fewer severe adverse effects (17.6% vs. 50.6% for CT) [58]. Another negative result was seen in the MYSTIC trial which sought to evaluate the efficacy of durvalumab (anti- PD-L1), either alone or in combination with tremelimumab, compared to chemotherapy as the initial treatment in treatment-naive metastatic patients. The MYSTIC study did not meet its primary objective of showing

a significant improvement in OS with durvalumab over chemotherapy, although durvalumab patients had a median OS of 16.3 months compared to 12.9 months for chemotherapy. Additionally, there was no statistically significant difference observed in PFS, which was a secondary endpoint of the study [59].

Checkpoint inhibitors + chemotherapy

In accordance with international treatment recommendations for lung cancer, the standard approach for patients with PD-L1 expression levels below 50% involves using a combination of chemotherapy and immunotherapy. This combination has been established as the preferred treatment based on the positive outcomes observed in phase III clinical trials, specifically in terms of improved survival rates, response rates, and the duration of the response [60]. The common approach for the treatment of newly diagnosed stage IV NSCLC is to combine platinum-based chemotherapy with PD-(L)1 inhibition, irrespective of tumor PD-L1 status and in the absence of any contraindication to ICI [49]. Each combination presents its own balance of efficacy and safety, offering valuable options for first-line treatment in this patient population.

Pembrolizumab + chemotherapy

In the KEYNOTE-189 trial involving newly diagnosed metastatic nonsquamous NSCLC patients without EGFR/ALK mutations, chemoimmunotherapy with pembrolizumab, pemetrexed, and platinum-based chemotherapy resulted in a lower risk of death (HR: 0.60), improved 5-year survival (19.4% vs. 11.3%), and better disease control (HR: 0.50, 5-year PFS: 7.5% vs. 0.6%) compared to the placebo group. Interestingly, these benefits remained consistent across various levels of PD-L1 expression in tumor cells. In conclusion, the 5-year results from the KEYNOTE-189 study strongly support the use of pembrolizumab in conjunction with pemetrexed and platinum-based chemotherapy as the standard therapy in previously untreated nonsquamous mNSCLC patients, providing substantial and long-lasting enhancements in overall and progression-free survival [6, 61]. In the KEYNOTE-407 study on untreated metastatic squamous NSCLC patients, 559 participants were randomly divided into two groups. One group received pembrolizumab with chemotherapy (paclitaxel/nab-paclitaxel + carboplatin), while the other received a placebo with chemotherapy. After 56.9 months, the pembrolizumab group showed significant improvements in both OS and PFS. Notably, the 5-year OS rate was 18.4% with pembrolizumab, nearly double that of the placebo group at 9.7%. The study reported manageable toxicity levels with a 3-year OS rate of 69.5%. Pembrolizumab with chemotherapy is now the standard first-line treatment for untreated metastatic squamous NSCLC, regardless of PD-L1 expression, showcasing significant survival benefits and becoming the preferred first-line option [7, 62].

Cemiplimab + chemotherapy

Cemiplimab, an anti PD-1 inhibitor, was studied in the EMPOWER-Lung 3 trial in patients with advanced mNSCLC without EGFR, ALK, or ROS1 abnormalities. A total of 466 patients were randomly assigned (2:1 ratio) to receive cemiplimab with specific platinum-doublet chemotherapy or a placebo with chemotherapy. After 28.4 months, the cemiplimab group had a median OS of 21.1 months, compared to 12.9 months in the chemotherapy-only group (HR 0.65), with a median PFS of 8.2 months for cemiplimab vs. 5.5 months for chemotherapy alone (HR 0.55). Overall, the combination of cemiplimab with chemotherapy improved OS, PFS, and overall response rate (ORR) in patients with advanced NSCLC, irrespective of histological subtype and PD-L1 expression levels, but with a higher incidence of TRAEs [63]. In the KEYNOTE-407 study, the median OS in patients with mNSCLC treated with pembrolizumab plus chemotherapy was 17.2 months. These data were derived from a median follow-up period of 40.1 and 56.9 months [64]. In the 2-year analysis of the EMPOWER-Lung 3 studies [63], the HR for overall survival OS in patients with squamous NSCLC was 0.61, while in the final analysis of KEYNOTE-407, the HR for OS in patients with metastatic squamous NSCLC was 0.71 [65]. Cemiplimab stands out as the second PD-(L)1 inhibitor that has demonstrated efficacy in advanced NSCLC, either on its own or in combination with chemotherapy, regardless of whether the cancer is of squamous or nonsquamous histology [12].

Atezolizumab plus chemotherapy ± bevacizumab

In addition to pembrolizumab and cemiplimab, there are other approved treatment options available. One such alternative is the combination of atezolizumab with carboplatin and nab-paclitaxel chemotherapy for mNSCLC lung cancer. This approach was studied in the IMpower130 trial, which aimed to assess the efficacy and safety of this combination compared to chemotherapy alone as a first-line treatment. The study involved 724 patients. The co-primary goals focused on assessing PFS and OS in the intention-to-treat population that lacked EGFR or ALK mutations. The trial ran from 2015 to February 13, 2017. The results showed significant improvements in both OS (18.6 vs. 13.9 months; HR 0.79) and PFS (7.0 vs. 5.5 months; HR 0.64) with atezolizumab plus chemotherapy compared to chemotherapy alone. The most common grade 3 or higher

TRAEs were myelosuppression-related events. These findings suggest that the combination of atezolizumab with carboplatin and nab-paclitaxel chemotherapy may be a valuable first-line treatment option for patients with mNSCLC lung cancer, and it was generally well tolerated [9]. The IMpower150 trial assessed the combination of atezolizumab with bevacizumab and chemotherapy as a first-line treatment for mNSCLC patients, including those with varying levels of PD-L1 expression and previous EGFR or ALK alterations. After 1,202 patients were enrolled, they were divided into three groups: ACP (atezolizumab-carboplatin-paclitaxel), ABCP (atezolizumab-bevacizumab-carboplatin-paclitaxel), and BCP (bevacizumab-carboplatin-paclitaxel). Results revealed a median OS of 19.0 months for ACP vs. 14.7 months for BCP (HR 0.84), with ABCP also showing a longer OS (19.5 months) compared to BCP (HR 0.80). Exploratory analyses suggested a longer OS with ACP and ABCP in PD-L1–high and PD-L1–positive subgroups, while PD-L1–negative subgroups had similar OS. The safety profile remained consistent. While ACP showed a numerical OS improvement over BCP, it was not statistically significant. However, with additional follow-up data, further OS improvement was observed with ABCP. This study supports the combination of immunotherapy, chemotherapy, and angiogenesis inhibitors like bevacizumab as an effective treatment for certain lung cancers, with FDA approval as an alternative option for advanced nonsquamous NSCLC patients without driver mutations [66]. In addition to FDA approval this first-line treatment option is also approved by the EMA [48]. The advantage of ABCP over BCP in terms of PFS was evident even in patients who had liver metastases at the beginning of the study. In the KEYNOTE-189 trial, patients with liver metastases had positive outcomes with pembrolizumab and chemotherapy, suggesting that this combination may also be a viable treatment option for this subset [67, 68].

Dual ICI

Anti-PD1 + anti-CTLA-4

Among the use of a combination chemotherapy and immunotherapy, researchers have investigated the efficacy of using anti-PD-1 and anti-CTLA-4 in different situations related to NSCLC [69]. First, researchers examined anti-PD-1/PD-L1 and anti-CTLA-4 combinations in metastatic melanoma, and found that these combinations generated enduring positive responses, irrespective of PD-L1 expression levels [70]. Researchers in the CheckMate227 trial observed a significant improvement in OS across all levels of PD-L1 expression, including patients with less than 1% expression. This study was a groundbreaking phase III trial evaluating the efficacy of combining nivolumab (anti-PD1) and ipilimumab (anti-CTLA-4) in the treatment of advanced NSCLC. The trial included a total of 1739 patients regardless of their PD-L1 expression. In patients with PD-L1 expression ≥1%, nivolumab plus ipilimumab resulted in a median OS of 17.1 months, a higher objective response rate of 35.9%, and a significantly longer duration of response (median 23.2 months) compared to chemotherapy (OS: 14.9 months, response rate: 30.0%, duration: 6.2 months). In terms of TRAEs, 32.8% of patients experienced grade 3 or 4 events with nivolumab plus ipilimumab, while 36.0% of patients had these events with chemotherapy. Discontinuation due to TRAEs was more common with dual immunotherapy (18%) compared to chemotherapy (9%). The most common immun-related adverse effects observed in individuals receiving nivolumab plus ipilimumab were skin-related issues (occurring in 34% of cases) and endocrine events (experienced by 24% of patients). This study supports the use of dual immunotherapy as a highly effective first-line treatment for advanced NSCLC, offering a substantial improvement in OS and response duration compared to traditional chemotherapy, irrespective of the patient's PD-L1 expression level [12]. In the CheckMate-227 study, the 5-year overall survival rate for patients with advanced NSCLC with PD-L1 ≥1% was 24% when treated with the nivolumab-ipilimumab combination, as opposed to 14% for those receiving chemotherapy alone. The use of dual ICI demonstrated enhanced OS in both histologic subcategories, with a greater advantage in squamous compared to nonsquamous. Moreover, within the squamous subtype, the benefit was more pronounced in patients with PD-L1 expression less than 1% than for those with PD-L1 expression greater than or equal to 1% in lung cancer [71].

Dual ICI + Cht

Anti-PD-(L)1 + anti-CTLA-4 + chemotherapy

Building on the findings of CheckMate227, researchers in the CheckMate-9LA trial found that adding a short course of two cycles of platinum-doublet chemotherapy to the combination of nivolumab and ipilimumab had a significant impact on overall survival compared to using chemotherapy alone. This combination also showed a favorable risk-benefit profile. Results showed a median OS of 15.6 months with nivolumab/ipilimumab/chemotherapy, compared to 10.9 months in the control group, representing a significant OS improvement (HR 0.66 in favor of the experimental group). Moreover, there were improvements in PFS (6.8 months vs. 5.0 months in the control group, HR 0.70) and a higher overall response rate (38% vs. 25% in the control group) in the experimental group. It is worth noting that the most common grade 3–4 TRAEs included neutropenia (7% vs. 9%) and anemia (6% vs. 14%) [14]. At three-year follow-up, the combination of nivolumab, ipilimumab, and two cycles of chemotherapy maintained significant OS benefit (mOS 15.8 months vs. 11.0 months, HR 0.7) compared to chemotherapy alone in the intent-to-treat population.

Additionally, the three-year overall survival rate (3-year OS) was notably higher in the nivolumab-ipilimumab group (27% vs. 19%). In patients with baseline brain metastases, nivolumab-ipilimumab showed impressive efficacy, including a median OS of 19.3 months (HR 0.45), significantly improved systemic PFS (9.7 vs. 4.1 months, HR 0.44), and substantial intracranial PFS benefit (11.4 vs. 4.6 months, HR 0.42). These results indicate the efficacy of combination therapy in patients with pretreated baseline brain metastases [72]. The POSEIDON trial investigated the combination of tremelimumab (anti-CTLA-4) with durvalumab (anti-PD-L1) and chemotherapy (T + D + CT) and durvalumab with chemotherapy (D + CT) versus chemotherapy alone (CT) as the initial treatment for mNSCLC in patients with EGFR/ALK wild-type tumors. Results showed that D + CT significantly improved PFS over CT alone (HR 0.74; median PFS 5.5 vs. 4.8 months), while T + D + CT significantly enhanced both PFS (HR 0.72; median PFS 6.2 vs. 4.8 months) and OS (HR 0.77; median OS 14.0 vs. 11.7 months) compared to CT alone. However, the improvement in OS for D + CT versus CT did not reach statistical significance (HR 0.86; median OS 13.3 vs. 11.7 months). The 24-month OS rates were also significantly higher with T + D + CT (32.9% vs. 22.1%). TRAEs of maximum grade 3-4 were observed in 51.8% for T + D + CT, 44.6% for D + CT, and 44.4% for CT.

In summary, the combination of durvalumab with chemotherapy enhanced PFS compared to chemotherapy alone, and the addition of a short course of tremelimumab to durvalumab and chemotherapy resulted in significant improvements in both OS and PFS compared to chemotherapy, without a significant increase in tolerability issues [15]. This suggests that it may be a promising new option for the first-line treatment of mNSCLC. It is important to mention that regulatory approval has been granted for the combined use of tremelimumab and durvalumab alongside platinum-based chemotherapy in patients with metastatic NSCLC with no EGFR or ALK genetic alterations. In the Checkmate-227 study, when patients had to stop treatment due to TRAEs, the median OS was 41.5 months, and the 5-year OS rate was 39% [72]. Similarly, in the CheckMate-9LA trial, 48% of patients experienced grade 3–4 TRAEs, and 18% of them had to discontinue treatment. The median OS in this group was 27.5 months, with a 4-year OS rate of 41% [73]. Comparable findings were observed in the POSEIDON trial, where 58% of patients experienced grade 3 TRAEs, and 9.4% had to discontinue treatment [15]. Thus, the safety profile should not be an obstacle to the widespread application of dual ICI, whether with or without chemotherapy, in routine clinical practice.

In the IMpower 131 and POSEIDON trials, the combination of atezolizumab and durvalumab with chemotherapy led to median OS times of 14.2 and 14.0 months, respectively, but no survival benefit over chemotherapy was observed in either trial [15, 74]. Cemiplimab in combination with platinum-based doublet chemotherapy (EMPOWER-Lung 3), the combination of durvalumab, tremelimumab, and platinum-based doublet chemotherapy (POSEIDON), and the combination of nivolumab with ipilimumab (CheckMate 227, specifically for PD-L1≥1% tumors) have obtained FDA approval but are awaiting approval by the EMA [49].

Among the previously mentioned studies with predominantly favorable results, there are a few exceptions where the outcomes were not favorable. In MYSTIC, durvalumab plus tremelimumab did not improve OS or PFS in patients with ≥25% PD-L1 expression. Similarly, in the NEPTUNE trial (which included metastatic NSCLC patients with a blood tumor mutational burden of ≥20 mutations per megabase), durvalumab and tremelimumab did not enhance overall survival compared to chemotherapy [59, 75].

Role of immunotherapy in NSCLC with driver mutation

Mutations such as EGFR, ALK, KRAS, and other genetic changes (including MET, RET, BRAF, and ROS1) have brought about a significant shift in the way this type of NSCLC is treated. In the era of immuno-oncology, there is growing evidence suggesting that prominent oncogenes have different impacts on the immune microenvironment within tumors, which in turn affects the clinical advantages of using ICIs as a treatment approach.

EGFR

EGFR-activating mutations, which are common in NSCLC, are treatable with targeted therapies and more prevalent in non-smokers, light smokers, young, Asian, and female patients. ICIs have limited efficacy in EGFR-mutant NSCLC based on data from studies like CA209-012 and Keynote 001, where response rates were lower than in wild-type patients. The ATLANTIC and PACIFIC studies also found that EGFR- or ALK-positive patients had worse outcomes with durvalumab treatment compared to wild-type patients. The IMpower 150 trial showed improved OS in EGFR-mutant patients treated with ABCP compared to BCP, but overall, ICIs alone or with chemotherapy have limited efficacy in EGFR-mutant NSCLC [10, 76, 77].

ALK

Studies like ATLANTIC and IMMUNOTARGET did not find immunotherapy to be effective. These findings were further supported by retrospective analyses conducted in Massachusetts and a multicenter study in France. In the IMpower150 trial, the combination of chemotherapy with atezolizumab and

bevacizumab did not show a significant difference in PFS in ALK-positive patients compared to bevacizumab/chemotherapy (8.3 vs. 5.9 months; HR 0.65; not significant), consistent with the results of IMpower130. In ALK-rearranged NSCLC, ICIs alone do not appear to be promising; chemotherapy remains the standard after ALK tyrosine kinase inhibitors (TKIs) lose efficacy [10, 78].

KRAS

In advanced NSCLC, KRAS mutations stand out as the most common molecular abnormalities. These KRAS mutations exhibit considerable diversity and involve substitutions at codons 12, 13, or 61. The most frequent of these substitutions which is present in 41% of KRAS-mutant NSCLC cases is KRAS p.G12C. Studies have shown that immunotherapy consistently demonstrates clinical activity that is at least equivalent to that seen in patients who have wild-type KRAS. In a meta-analysis, it was observed that KRAS-mutant patients responded more favorably to ICI treatment when compared to receiving docetaxel monotherapy [79–81].

BRAF

BRAF mutations, present in approximately 2% of NSCLC cases, with p.V600E being the most common type, have shown clinical efficacy with ICIs in two retrospective cohorts of 39 and 38 patients, including those with p.V600E variants. PFS ranged from 3.0 to 4.1 months, and OS was 13.1 months in the second cohort. Smoking-related factors, such as higher mutational burden and PD-L1 expression, may contribute to increased ICI sensitivity in BRAF mutant NSCLC, similar to KRAS mutations [82, 83].

ROS1

ROS1 rearrangements occur in approximately 2.5% of lung adenocarcinoma patients, with various fusion partners. Tyrosine kinase inhibitors like crizotinib, entrectinib and lorlatinib are approved for treatment, but the efficacy of ICIs remains uncertain. The IMMUNOTARGET registry, which included six patients, reported a low response rate (17%) and a median OS of 18.4 months in ROS1 fusion-positive NSCLC. Negrao et al suggested in their study that PD-L1 may not be an independent predictor of immunotherapy response [81, 84, 85].

MET

MET, a receptor tyrosine kinase, is crucial in cell processes and is implicated in NSCLC, with MET exon 14 skipping mutations in 3%–5% of cases and amplifications in 1%–5% of NSCLC patients, effectively treated with drugs like crizotinib, capmatinib, savolitinib, and tepotinib. In the IMMUNOTARGET registry it was observed that the efficacy of ICIs was not influenced by either high PD-L1 expression or a high TMB. If targeted therapy for MET is available, it is advisable to consider its use as a first-line treatment [81, 84, 86–88].

Her2

HER2 mutations and amplifications are found in 2%–4% of lung adenocarcinomas, often in non-smokers, and are effectively treated with drugs like ado-trastuzumab emtansine (T-DM1) and TKIs. Lung tumors with Her2 amplification have high TMB and low PD-L1, which may explain the reduced efficacy of immunotherapy. In the IMMUNOTARGET study, Her2-mutant patients showed lower ORR, median PFS, and OS, suggesting that chemo-immunotherapy should not be the initial treatment option [81, 89].

TP53

TP53, a well-studied gene, is vital for cell cycle regulation, DNA repair, and apoptosis. TP53 mutations, when co-occurring with KMT2C, may lead to a better ICI response in patients with advanced NSCLC, while mutations in STK11 and KEAP1 do not notably affect ICI response in this genetic context [90, 91].

RET

RET rearrangements are found in approximately 1%–2% of patients with NSCLC. Patients with RET fusions are generally never smokers with lung adenocarcinoma and early development of intracranial metastases. The FDA and EMA have granted approval for the use of highly selective RET inhibitors, such as selpercatinib and pralcetinib, specifically for NSCLC cases with RET fusion. While there is a lack of prospective data, existing evidence indicates that NSCLC with RET rearrangements characterized as biologically “cold” tumors do not respond well to ICIs. Therefore, it is advisable to prioritize targeted therapies when they are available for these RET-rearranged NSCLC patients [84, 92].

NTRK

NTRK gene fusions occur in approximately 0.2% of cases without a clear correlation to sex, age, or smoking history. Larotrectinib and entrectinib are approved for the treatment of these tumors. In NSCLC, NTRK gene fusions exhibit higher

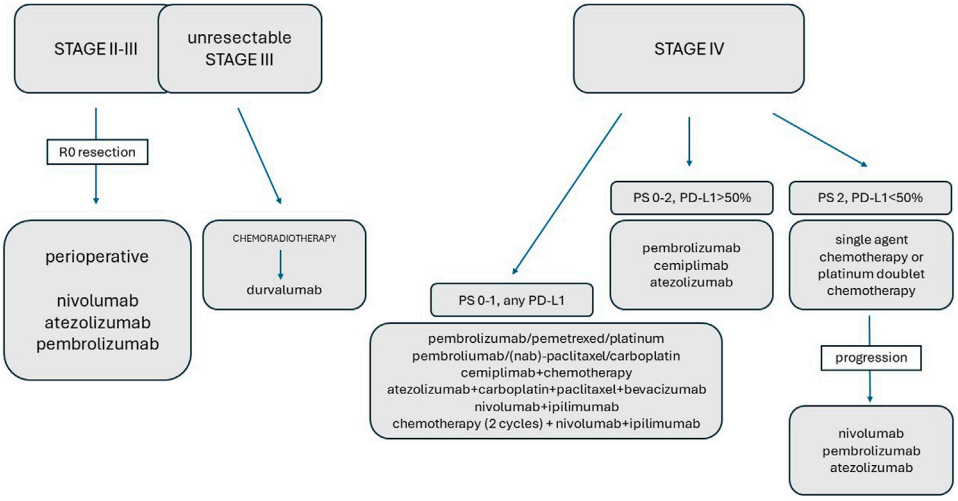

FIGURE 1
The role of immunotherapy in the treatment of NSCLC.

TMB and PD-L1 expression than EGFR, ALK, and ROS1 alterations, suggesting a combination of chemotherapy and immunotherapy for comprehensive treatment [93, 94].

Beyond the first line, rechallenge

When patients cannot receive first-line immunotherapy for any reason or show progression after platinum doublet treatment, and they become eligible for ICI therapy, anti-PD-(L)1 monotherapy is the preferred choice. The FDA and EMA subsequently approved the anti-PD-1 antibody nivolumab and the anti PD-L1 antibody atezolizumab irrespective of PD-L1 status and the anti PD-1 antibody pembrolizumab only in patients with PD-L1 expression. Nivolumab was the first approved agent to show efficacy in patients with advanced and metastatic NSCLC in the second-line and beyond setting. These results are based on two trials, CheckMate-017 and -057. CheckMate-017 evaluated nivolumab at a dose of 3 mg/kg Q2W compared versus docetaxel 75 mg/m^2 Q3W in 272 patients with advanced or metastatic squamous cell lung carcinoma. Both OS (9.2 vs. 6 months; HR: 0.59) and PFS (3.5 vs. 2.8 months; HR: 0.62) showed a significant improvement for the nivolumab arm independent of PD-L1 status [95]. The CheckMate-057 trial also demonstrated an OS benefit (12.2 vs. 9.4 months; HR: 0.73) of nivolumab (3 mg/kg Q2W) over docetaxel (75 mg/m^2 Q3W) showed inferiority in terms of PFS (2.3 vs. 4.2 months), but it was superior at 1 year (19% vs. 8%; HR: 0.92). The higher the PD-L1 expression the greater the survival benefit [96]. Based on these data the drug received approval from both medical agencies in both histologic subtypes. Another optional anti-PD-1 agent for second-line treatment is pembrolizumab which was found to be superior to docetaxel. In the KeyNote-010 trial the effects of pembrolizumab at 2 or 10 mg/kg Q3W were compared to docetaxel (75 mg/m^2 Q3W) in patients with advanced or metastatic NSCLC with PD-L1 expression (≥1%). Both doses of pembrolizumab demonstrated an OS benefit (10.4 months for pembrolizumab 2 mg/kg (HR: 0.71), 12.7 months for pembrolizumab 10 mg/kg (HR: 0.61), and 8.5 months for docetaxel) but no PFS benefit. In a subgroup of patients with higher PD-L1 expression (TPS ≥50%), the PFS was also significantly better (HR: 0.59) [97]. Based on the above data pembrolizumab was also approved by the FDA and EMA for second-line use in PD-L1 positive (≥1%) patients. The third agent which is an anti PD-L1 antibody and therefore slightly different from the other two agents was atezolizumab. The OS (13.8 vs. 9.6 months; HR: 0.73) superiority and PFS non-inferiority over docetaxel was demonstrated in the OAK trial [98]. Based on these results, atezolizumab was also approved by the european (EMA) and american (FDA) medical agencies. In selected patients rechallenge with ICI (especially with pembrolizumab) may be an option if the reason for previous discontinuation was not disease progression or toxicity and clinical benefit was achieved during ICI administration [54, 99].

Discussion

The future landscape of NSCLC immunotherapy is promising and continually evolving, revolutionizing the treatment paradigm for this aggressive disease. Immunotherapy has emerged as a game-changer, offering new hope and improved outcomes for these patients. ICIs targeting PD-1/PD-L1 have become a cornerstone of this treatment. They have shown significant improvements in OS,

PFS, and durable responses compared to conventional chemotherapy. Initially limited to patients with high PD-L1 expression, ICIs are now being considered for a broader patient population, including those with low or no PD-L1 expression. The future lies in combining immunotherapeutic agents with other immunotherapies, chemotherapy, targeted therapies, or even radiation. These combinations aim to enhance the immune response and address tumor heterogeneity and resistance mechanisms. Research into novel biomarkers beyond PD-L1 and TMB is ongoing. Identifying more precise predictors of response to immunotherapy will enable better patient selection and personalized treatment strategies. Research is underway to develop and validate new checkpoint inhibitors targeting different immune checkpoints other than PD-1/PD-L1 and CTLA-4. These could potentially offer improved responses and reduced resistance. The role of immunotherapy is expanding beyond advanced stages. The neoadjuvant approach with an adjuvant ICI combination may be the best option for patients who have no contraindication to immunotherapy, but another ICI + chemotherapy combination may be better than standard-of-care chemotherapy alone even in the adjuvant setting. It is anticipated that ICI will become a mandatory part of the perioperative treatment of resectable NSCLC and ctDNA level measurement may become critical in deciding whether or not patients require adjuvant therapy or not (with or without prior neoadjuvant treatment). This is being explored in the adjuvant setting after surgery or in combination with chemoradiotherapy for locally advanced disease, potentially preventing recurrence. These therapeutic possibilities are summarized in Figure 1. Resistance mechanisms limit the efficacy of immunotherapy. Strategies to overcome this hurdle include combination therapies, the development of novel drugs, and a better understanding of the tumor microenvironment. The landscape is shifting to a more patient-centered approach that emphasizes quality of life, management of treatment-related toxicities, and addressing the unique needs of each patient. Patients with BRAF or KRAS/TP53 mutations benefit most from ICIs, while those with EGFR or ALK/ROS1 rearrangements show lower PD-L1 and mutational burden, leading to ICI resistance. Understanding the genomics of NSCLC will help select ICI candidates. Targeting immunosuppressive mechanisms alongside oncogene signaling may sensitize NSCLC to ICIs. Tumors with driver mutations are diverse, therefore they require precision medicine. Frontline TKIs are preferred to ICIs, with chemo-immunotherapy as an alternative. Combinations of targeted therapy and ICIs are being studied. Broader oncogenic factors should be considered in future NSCLC ICI studies. Ongoing clinical trials are exploring new treatment modalities, innovative drug combinations, and novel therapeutic targets. These trials are crucial for advancing the field and bringing new therapies to the clinic. Despite advancements, the high cost of immunotherapies poses a challenge to accessibility. Efforts to balance innovation and affordability through biosimilars and health policy interventions remain critical. The future of NSCLC immunotherapy is bright, driven by a deep understanding of tumor biology, rapid advancements in technology, and collaborative efforts across the scientific community. As research continues, the goal remains to further improve outcomes, extend survival, and ultimately transform NSCLC into a manageable, chronic condition for more patients.

Author contributions

Conceptualization: AL, NB; writing—original draft preparation: AL, AM, TK, ZO; writing—review and editing: AL, SI, IT; supervision, AL, NB. All authors contributed to the article and approved the submitted version.

Funding

The author(s) declare that no financial support was received for the research, authorship, and/or publication of this article.

Conflict of interest

The authors declare that the research was conducted in the absence of any commercial or financial relationships that could be construed as a potential conflict of interest.

References

1. Siegel RL, Miller KD, Wagle NS. Cancer statistics, 2023. *Ca Cancer J Clin* (2023) 73:17–48. doi:10.3322/caac.21763

2. Yang H, Shen K, Zhu C, Li Q, Zhao Y, Ma X. Safety and efficacy of durvalumab (MEDI4736) in various solid tumors. *Drug Des Devel Ther* (2018) 12:2085–96. doi:10.2147/DDDT.S162214

3. Naidoo J, Page DB, Wolchok JD. Immune checkpoint blockade. *Hematol Oncol Clin North Am* (2014) 28:585–600. doi:10.1016/j.hoc.2014.02.002

4. Reck M, Rodríguez-Abreu D, Robinson AG, Hui R, Csőszi T, Fülöp A, et al. Pembrolizumab versus chemotherapy for PD-L1-positive non-small-cell lung cancer. *N Engl J Med* (2016) 375:1823–33. doi:10.1056/NEJMoa1606774

5. Mok TS, Wu YL, Kudaba I, Kowalski DM, Cho BC, Turna HZ, et al. Pembrolizumab versus chemotherapy for previously untreated, PD-L1-expressing, locally advanced or metastatic non-small-cell lung cancer (KEYNOTE-042): a randomised, open-label, controlled, phase 3 trial. *Lancet* (2019) 393:1819–30. doi:10.1016/S0140-6736(18)32409-7

6. Gandhi L, Rodríguez-Abreu D, Gadgeel S, Esteban E, Felip E, De Angelis F, et al. Pembrolizumab plus chemotherapy in metastatic non-small-cell lung cancer. *N Engl J Med* (2018) 378:2078–92. doi:10.1056/NEJMoa1801005

7. Paz-Ares L, Luft A, Vicente D, Tafreshi A, Gümüş M, Mazières J, et al. Pembrolizumab plus chemotherapy for squamous non-small-cell lung cancer. *N Engl J Med* (2018) 379:2040–51. doi:10.1056/NEJMoa1810865

8. Herbst RS, Giaccone G, de Marinis F, Reinmuth N, Vergnenegre A, Barrios CH, et al. Atezolizumab for first-line treatment of PD-L1-selected patients with NSCLC. *N Engl J Med* (2020) 383:1328–39. doi:10.1056/NEJMoa1917346

9. West H, McCleod M, Hussein M, Morabito A, Rittmeyer A, Conter HJ, et al. Atezolizumab in combination with carboplatin plus nab-paclitaxel chemotherapy compared with chemotherapy alone as first-line treatment for metastatic non-squamous non-small-cell lung cancer (IMpower130): a multicentre, randomised, open-label, phase 3 trial. *Lancet Oncol* (2019) 20:924–37. doi:10.1016/S1470-2045(19)30167-6

10. Socinski MA, Jotte RM, Cappuzzo F, Orlandi F, Stroyakovskiy D, Nogami N, et al. Atezolizumab for first-line treatment of metastatic nonsquamous NSCLC. *N Engl J Med* (2018) 378:2288–301. doi:10.1056/NEJMoa1716948

11. Sezer A, Kilickap S, Gümüş M, Bondarenko I, Özgüroğlu M, Gogishvili M, et al. Cemiplimab monotherapy for first-line treatment of advanced non-small-cell lung cancer with PD-L1 of at least 50%: a multicentre, open-label, global, phase 3, randomised, controlled trial. *Lancet* (2021) 397:592–604. doi:10.1016/S0140-6736(21)00228-2

12. Gogishvili M, Melkadze T, Makharadze T, Giorgadze D, Dvorkin M, Penkov K, et al. Cemiplimab plus chemotherapy versus chemotherapy alone in non-small cell lung cancer: a randomized, controlled, double-blind phase 3 trial. *Nat Med* (2022) 28:2374–80. doi:10.1038/s41591-022-01977-y

13. Hellmann MD, Paz-Ares L, Bernabe Caro R, Zurawski B, Kim SW, Carcereny Costa E, et al. Nivolumab plus ipilimumab in advanced non-small-cell lung cancer. *N Engl J Med* (2019) 381:2020–31. doi:10.1056/NEJMoa1910231

14. Paz-Ares L, Ciuleanu TE, Cobo M, Schenker M, Zurawski B, Menezes J, et al. First-line nivolumab plus ipilimumab combined with two cycles of chemotherapy in patients with non-small-cell lung cancer (CheckMate 9LA): an international, randomised, open-label, phase 3 trial. *Lancet Oncol* (2021) 22:198–211. doi:10.1016/S1470-2045(20)30641-0

15. Johnson ML, Cho BC, Luft A, Alatorre-Alexander J, Geater SL, Laktionov K, et al. Durvalumab with or without tremelimumab in combination with chemotherapy as first-line therapy for metastatic non-small-cell lung cancer: the phase III POSEIDON study. *J Clin Oncol* (2023) 41:1213–27. doi:10.1200/JCO.22.00975

16. Akinboro O, Larkins E, Pai-Scherf LH, Mathieu LN, Ren Y, Cheng J, et al. FDA approval summary: pembrolizumab, atezolizumab, and cemiplimab-rwlc as single agents for first-line treatment of advanced/metastatic PD-L1-high NSCLC. *Clin Cancer Res* (2022) 28:2221–8. doi:10.1158/1078-0432.CCR-21-3844

17. Reuss JE, Anagnostou V, Cottrell TR, Smith KN, Verde F, Zahurak M, et al. Neoadjuvant nivolumab plus ipilimumab in resectable non-small cell lung cancer. *J Immunother Cancer* (2020) 8:e001282. doi:10.1136/jitc-2020-001282

18. National Comprehensive Cancer Network. NCCN clinical practice guideline in oncology: non small cell lung cancer, version 1 (2024). Available from: https://www.nccn.org/guidelines/guidelines-detail?category=1&id=1450 (Accessed December 21, 2023).

19. Cao W, Tang Q, Zeng J, Jin X, Zu L, Xu S. A review of biomarkers and their clinical impact in resected early-stage non-small-cell lung cancer. *Cancers* (2023) 15:4561. doi:10.3390/cancers15184561

20. Tang WF, Ye HY, Tang X, Su JW, Xu KM, Zhong WZM, et al. Adjuvant immunotherapy in early-stage resectable non–small cell lung cancer: a new milestone. *Front Oncol* (2023) 13:1063183. doi:10.3389/fonc.2023.1063183

21. Song WA, Zhou NK, Wang W, Chu XY, Liang CY, Tian XD, et al. Survival benefit of neoadjuvant chemotherapy in nonsmall cell lung cancer: an updated meta-analysis of 13 randomized control trials. *J Thorac Oncol* (2010) 5:510–6. doi:10.1097/JTO.0b013e3181cd3345

22. Pisters KM, Kris MG, Gralla RJ, Zaman MB, Heelan RT, Martini N. Pathologic complete response in advanced non-small-cell lung cancer following preoperative chemotherapy: implications for the design of future non-small-cell lung cancer combined modality trials. *J Clin Oncol* (1993) 11:1757–62. doi:10.1200/JCO.1993.11.9.1757

23. Travis WD, Dacic S, Wistuba I, Sholl L, Adusumilli P, Bubendor L, et al. IASLC multidisciplinary recommendations for pathologic assessment of lung cancer resection specimens after neoadjuvant therapy. *J Thorac Oncol* (2020) 15:709–40. doi:10.1016/j.jtho.2020.01.005

24. Pataer A, Kalhor N, Correa AM, Raso MG, Erasmus JJ, Kim ES, et al. Histopathologic response criteria predict survival of patients with resected lung cancer after neoadjuvant chemotherapy. *J Thorac Oncol* (2012) 7:825–32. doi:10.1097/JTO.0b013e318247504a

25. Forde PM, Spicer J, Lu S, Provencio M, Mitsudomi T, Awad MM, et al. Neoadjuvant nivolumab plus chemotherapy in resectable lung cancer. *N Engl J Med* (2022) 386:1973–85. doi:10.1056/NEJMoa2202170

26. Passaro A, Attili I, de Marinis F. Neoadjuvant chemotherapy plus immunotherapy in early-stage resectable non–small-cell lung cancer. *J Clin Oncol* (2022) 40:2871–7. doi:10.1200/JCO.22.00873

27. Provencio M, Serna-Blasco R, Nadal E, Insa A, García-Campelo MR, Casal Rubio J, et al. Overall survival and biomarker analysis of neoadjuvant nivolumab plus chemotherapy in operable stage IIIA non–small-cell lung cancer (NADIM phase II trial). *J Clin Oncol* (2022) 40:2924–33. doi:10.1200/JCO.21.02660

28. Provencio Pulla M, Nadal E, González Larriba JL, Martínez Martí A, Bernabé R, Bosch Barrera J, et al. Perioperative nivolumab and chemotherapy in stage III non–small-cell lung cancer. *N Engl J Med* (2023) 389:504–13. doi:10.1056/NEJMoa2215530

29. Cascone T, Awad MM, Spicer JD, He J, Lu S, Sepesi B, et al. LBA1 CheckMate 77T: phase III study comparing neoadjuvant nivolumab (NIVO) plus chemotherapy (chemo) vs neoadjuvant placebo plus chemo followed by surgery and adjuvant NIVO or placebo for previously untreated, resectable stage II–IIIb NSCLC. *Ann Oncol* (2023) 34:S1295. doi:10.1016/j.annonc.2023.10.050

30. Peters S, Kim AW, Solomon B, Gandara DR, Dziadziuszko R, Brunelli A, et al. IMpower030: phase III study evaluating neoadjuvant treatment of resectable stage II-IIIB non-small cell lung cancer (NSCLC) with atezolizumab (atezo) + chemotherapy. *Ann Oncol* (2019) 30:ii30. doi:10.1093/annonc/mdz064.014

31. Lu S, Wu L, Zhang W, Zhang P, Wang W, Fang W, et al. Perioperative toripalimab+ platinum-doublet chemotherapy vs chemotherapy in resectable stage II/III non-small cell lung cancer (NSCLC): interim event-free survival (EFS) analysis of the phase III Neotorch study. *J Clin Oncol* (2023) 41:425126. doi:10.1200/JCO.2023.41.36_suppl.425126

32. Wakelee H, Liberman M, Kato T, Tsuboi M, Lee SH, Gao S, et al. Perioperative pembrolizumab for early-stage non–small-cell lung cancer. *N Engl J Med* (2023) 389:491–503. doi:10.1056/NEJMoa2302983

33. Heymach JV, Mitsudomi T, Harpole D, Aperghis M, Jones S, Mann H, et al. Design and rationale for a phase III, double-blind, placebo-controlled study of neoadjuvant durvalumab + chemotherapy followed by adjuvant durvalumab for the treatment of patients with resectable stages II and III non-small-cell lung cancer: the AEGEAN trial. *Clin Lung Cancer* (2022) 23:e247–e251. doi:10.1016/j.cllc.2021.09.010

34. Isaacs J, Stinchcombe TE. Neoadjuvant and adjuvant systemic therapy for early-stage non-small-cell lung cancer. *Drugs* (2022) 82:855–63. doi:10.1007/s40265-022-01721-3

35. Pignon JP, Tribodet H, Scagliotti GV, Douillard JY, Shepherd FA, Stephens RJ, et al. Lung adjuvant cisplatin evaluation: a pooled analysis by the LACE Collaborative Group. *J Clin Oncol* (2008) 26:3552–9. doi:10.1200/JCO.2007.13.9030

36. Bakos O, Lawson C, Rouleau S, Tai LH. Combining surgery and immunotherapy: turning an immunosuppressive effect into a therapeutic opportunity. *J Immunother Cancer* (2018) 6:86–11. doi:10.1186/s40425-018-0398-7

37. Stoecklein VM, Osuka A, Lederer JA. Trauma equals danger–damage control by the immune system. *J Leukocyte Biol* (2012) 92:539–51. doi:10.1189/jlb.0212072

38. Ogawa K, Hirai M, Katsube T, Murayama M, Hamaguchi K, Shimakawa T, et al. Suppression of cellular immunity by surgical stress. *Surgery* (2000) 127:329–36. doi:10.1067/msy.2000.103498

39. Xu P, Zhang P, Sun Z, Wang Y, Chen J, Miao C. Surgical trauma induces postoperative T-cell dysfunction in lung cancer patients through the programmed death-1 pathway. *Cancer Immunol Immunother CII* (2015) 64:1383–92. doi:10.1007/s00262-015-1740-2

40. Vansteenkiste J, Wauters E, Reymen B, Ackermann CJ, Peters S, De Ruysscher D. Current status of immune checkpoint inhibition in early-stage NSCLC. *Ann Oncol* (2019) 30:1244–53. doi:10.1093/annonc/mdz175

41. Kuchuk M, Kuchuk I, Sabri E, Hutton B, Clemons M, Wheatley-Price P. The incidence and clinical impact of bone metastases in non-small cell lung cancer. *Lung Cancer* (2015) 89:197–202. doi:10.1016/j.lungcan.2015.04.007

42. Felip E, Altorki N, Zhou C, Csőszi T, Vynnychenko I, Goloborodko O, et al. Adjuvant atezolizumab after adjuvant chemotherapy in resected stage IB–IIIA non-small-cell lung cancer (IMpower010): a randomised, multicentre, open-label, phase 3 trial. *Lancet* (2021) 398:1344–57. doi:10.1016/S0140-6736(21)02098-5

43. O'Brien M, Paz-Ares L, Marreaud S, Dafni U, Oselin K, Havel L, et al. Pembrolizumab versus placebo as adjuvant therapy for completely resected stage IB–IIIA non-small-cell lung cancer (PEARLS/KEYNOTE-091): an interim analysis of a randomised, triple-blind, phase 3 trial. *Lancet Oncol* (2022) 23:1274–86. doi:10.1016/S1470-2045(22)00518-6

44. Chaft JE, Dahlberg SE, Khullar OV, Edelman MJ, Simone CB, Heymach J, et al. EA5142 adjuvant nivolumab in resected lung cancers (ANVIL). *J Clin Oncol* (2018) 36:TPS8581. doi:10.1200/jco.2018.36.15_suppl.tps8581

45. Sands J, Mandrekar SJ, Oxnard GR, Kozono DE, Hillman SL, Dahlberg SE, et al. ALCHEMIST: adjuvant targeted therapy or immunotherapy for high-risk resected NSCLC. *J Clin Oncol* (2020) 38:TPS9077. doi:10.1200/JCO.2020.38.15_suppl.TPS9077

46. Sands JM, Mandrekar SJ, Kozono D, Oxnard GR, Hillman SL, Wigle DA, et al. Integration of immunotherapy into adjuvant therapy for resected non-small-cell

lung cancer: ALCHEMIST chemo-IO (ACCIO). *Immunotherapy* (2021) 13:727–34. doi:10.2217/imt-2021-0019

47. Peters S, Spigel D, Ahn M, Tsuboi M, Chaft J, Harpole D, et al. P03.03 MERMAID- 1: a phase III study of adjuvant durvalumab plus chemotherapy in resected NSCLC patients with MRD+ post-surgery. *J Thorac Oncol* (2021) 16:S258–9. doi:10.1016/j.jtho.2021.01.376

48. Spigel DR, Peters S, Ahn MJ, Tsuboi M, Chaft J, Harpole D, et al. 93TiP MERMAID-2: phase III study of durvalumab in patients with resected, stage II-III NSCLC who become MRD+ after curative-intent therapy. *J Thorac Oncol* (2021) 16: S745–6. doi:10.1016/S1556-0864(21)01935-3

49. Hendriks LE, Kerr KM, Menis J, Mok TS, Nestle U, Passaro A, et al. Non-oncogene-addicted metastatic non-small-cell lung cancer: ESMO clinical practice guideline for diagnosis, treatment and follow-up. *Ann Oncol* (2023) 34:358–76. doi:10.1016/j.annonc.2022.12.013

50. Singh N, Temin S, Baker S, Blanchard E, Brahmer JR, Celano P, et al. Therapy for stage IV non–small-cell lung cancer without driver alterations: ASCO living guideline. *J Clin Oncol* (2022) 40:3323–43. doi:10.1200/JCO.22.00825

51. Garassino M, Rodriguez-Abreu D, Gadgeel S, Esteban E, Felip E, Speranza G, et al. Evaluation of TMB in KEYNOTE-189: pembrolizumab plus chemotherapy vs placebo plus chemotherapy for nonsquamous NSCLC. *J Thorac Oncol* (2019) 14: S216–7. doi:10.1016/j.jtho.2019.08.427

52. Mantia CM, Buchbinder EI. Immunotherapy toxicity. *Hematol Oncol Clin North Am* (2019) 33:275–90. doi:10.1016/j.hoc.2018.12.008

53. Hanna NH, Schneider BJ, Temin S, Baker S, Jr, Brahmer J, Ellis PM, et al. Therapy for stage IV non-small-cell lung cancer without driver alterations: ASCO and OH (CCO) joint guideline update. *J Clin Oncol* (2020) 38:1608–32. doi:10.1200/JCO.19.03022

54. Reck M, Rodríguez-Abreu D, Robinson AG, Hui R, Csőszi T, Fülöp A, et al. Five-year outcomes with pembrolizumab versus chemotherapy for metastatic non-small-cell lung cancer with PD-L1 tumor proportion score ≥ 50. *J Clin Oncol* (2021) 39:2339–49. doi:10.1200/JCO.21.00174

55. US National Library of Medicine. Pembrolizumab injection. United States prescribing information (2024). Available from: https://www.accessdata.fda.gov/drugsatfda_docs/label/2020/125514s059s064s076s083lbl.pdf (Accessed on January 29, 2024).

56. Boyer M, Şendur MA, Rodríguez-Abreu D, Park K, Lee DH, Çiçin I, et al. Pembrolizumab plus ipilimumab or placebo for metastatic non-small-cell lung cancer with PD-L1 tumor proportion score ≥ 50%: randomized, double-blind phase III KEYNOTE-598 study. *J Clin Oncol* (2021) 39:2327–38. doi:10.1200/JCO.20.03579

57. Özgüroğlu M, Kilickap S, Sezer A, Gümüş M, Bondarenko I, Gogishvili M, et al. First-line cemiplimab monotherapy and continued cemiplimab beyond progression plus chemotherapy for advanced non-small-cell lung cancer with PD-L1 50% or more (EMPOWER-Lung 1): 35-month follow-up from a mutlicentre, open-label, randomised, phase 3 trial. *Lancet Oncol.* (2023) 24: 989–1001. doi:10.1016/S1470-2045(23)00329-7

58. Carbone DP, Reck M, Paz-Ares L, Creelan B, Horn L, Steins M, et al. First-line nivolumab in stage IV or recurrent non-small-cell lung cancer. *N Engl J Med* (2017) 376:2415–26. doi:10.1056/NEJMoa1613493

59. Rizvi NA, Cho BC, Reinmuth N, Lee KH, Luft A, Ahn MJ, et al. Durvalumab with or without tremelimumab vs standard chemotherapy in first-line treatment of metastatic non-small cell lung cancer: the MYSTIC phase 3 randomized clinical trial. *JAMA Oncol* (2020) 6:661–74. doi:10.1001/jamaoncol.2020.0237

60. Planchard D, Popat S, Kerr K, Novello S, Smit EF, Faivre-Finn C, et al. Metastatic non-small cell lung cancer: ESMO clinical practice guidelines for diagnosis, treatment and follow-up. *Ann Oncol* (2018) 29:v192–237. doi:10.1093/annonc/mdy275

61. Garassino MC, Gadgeel S, Speranza G, Felip E, Esteban E, Dómine M, et al. Pembrolizumab plus pemetrexed and platinum in nonsquamous non-small-cell lung cancer: 5-year outcomes from the phase 3 KEYNOTE-189 study. *J Clin Oncol* (2023) 41:1992–8. doi:10.1200/JCO.22.01989

62. Novello S, Kowalski DM, Luft A, Gümüş M, Vicente D, Mazières J, et al. Pembrolizumab plus chemotherapy in squamous non-small-cell lung cancer: 5-year update of the phase III KEYNOTE-407 study. *J Clin Oncol* (2023) 41:1999–2006. doi:10.1200/JCO.22.01990

63. Makharadze T, Gogishvili M, Melkadze T, Baramidze A, Giorgadze D, Penkov K, et al. Cemiplimab plus chemotherapy versus chemotherapy alone in advanced NSCLC: 2-year follow-up from the phase 3 EMPOWER-lung 3 part 2 trial. *J Thorac Oncol* (2023) 18:755–68. doi:10.1016/j.jtho.2023.03.008

64. Robinson AG, Vicente D, Tafreshi A, Parra HS, Mazieres J, Cicin I, et al. 97O First-line pembrolizumab plus chemotherapy for patients with advanced squamous NSCLC: 3-year follow-up from KEYNOTE-407. *J Thorac Oncol* (2021) 16:S748–9. doi:10.1016/S1556-0864(21)01939-0

65. Paz-Ares L, Vicente D, Tafreshi A, Robinson A, Parra HS, Mazières J, et al. A randomized, placebo-controlled trial of pembrolizumab plus chemotherapy in patients with metastatic squamous NSCLC: protocol-specified final analysis of KEYNOTE-407. *J Thorac Oncol* (2020) 15:1657–69. doi:10.1016/j.jtho.2020.06.015

66. Socinski MA, Nishio M, Jotte RM, Cappuzzo F, Orlandi F, Stroyakovskiy D, et al. IMpower150 final overall survival analyses for atezolizumab plus bevacizumab and chemotherapy in first-line metastatic nonsquamous NSCLC. *J Thorac Oncol* (2021) 16:1909–24. doi:10.1016/j.jtho.2021.07.009

67. Reck M, Mok TS, Nishio M, Jotte RM, Cappuzzo F, Orlandi F, et al. Atezolizumab plus bevacizumab and chemotherapy in non-small-cell lung cancer (IMpower150): key subgroup analyses of patients with EGFR mutations or baseline liver metastases in a randomised, open-label phase 3 trial. *Lancet Respir Med* (2019) 7:387–401. doi:10.1016/S2213-2600(19)30084-0

68. Reck M, Wehler T, Orlandi F, Nogami N, Barone C, Moro-Sibilot D, et al. Safety and patient-reported outcomes of atezolizumab plus chemotherapy with or without bevacizumab versus bevacizumab plus chemotherapy in non-small-cell lung cancer. *J Clin Oncol* (2020) 38:2530–42. doi:10.1200/JCO.19.03158

69. Kvistborg P, Philips D, Kelderman S, Hageman L, Ottensmeier C, Joseph-Pietras D, et al. Anti-CTLA-4 therapy broadens the melanoma-reactive CD8+ T cell response. *Sci transl Med* (2014) 6:254ra128. doi:10.1126/scitranslmed.3008918

70. Larkin J, Chiarion-Sileni V, Gonzalez R, Grob JJ, Cowey CL, Lao CD, et al. Combined nivolumab and ipilimumab or monotherapy in untreated melanoma. *N Engl J Med* (2015) 373:23–34. doi:10.1056/NEJMoa1504030

71. Brahmer JR, Lee JS, Ciuleanu TE, Caro RB, Nishio M, Urban L, et al. Five-year survival outcomes with nivolumab plus ipilimumab versus chemotherapy as first-line treatment for metastatic non-small-cell lung cancer in CheckMate 227. *J Clin Oncol* (2023) 41:1200–12. doi:10.1200/JCO.22.01503

72. Paz-Ares LG, Ciuleanu TE, Cobo M, Bennouna J, Schenker M, Cheng Y, et al. First-line nivolumab plus ipilimumab with chemotherapy versus chemotherapy alone for metastatic NSCLC in CheckMate 9LA: 3-year clinical update and outcomes in patients with brain metastases or select somatic mutations. *J Thorac Oncol* (2023) 18:204–22. doi:10.1016/j.jtho.2022.10.014

73. Carbone DP, Ciuleanu TE, Schenker M, Cobo-Dols M, Bordenave S, Juan-Vidal O, et al. First-line (1L) nivolumab (N) + ipilimumab (I) + chemotherapy (C) vs C alone in patients (pts) with metastatic NSCLC (mNSCLC) from CheckMate 9LA: 4-y clinical update and outcomes by tumor histologic subtype (THS). *J Clin Oncol* (2023) 41:LBA9023. doi:10.1200/JCO.2023.41.17_suppl.LBA9023

74. Jotte R, Cappuzzo F, Vynnychenko I, Stroyakovskiy D, Rodríguez-Abreu D, Hussein M, et al. Atezolizumab in combination with carboplatin and nab-paclitaxel in advanced squamous NSCLC (IMpower131): results from a randomized phase III trial. *J Thorac Oncol* (2020) 15:1351–60. doi:10.1016/j.jtho.2020.03.028

75. de Castro G, Jr, Rizvi NA, Schmid P, Syrigos K, Martin C, Yamamoto N, et al. NEPTUNE: phase 3 study of first-line durvalumab plus tremelimumab in patients with metastatic NSCLC. *J Thorac Oncol* (2023) 18:106–19. doi:10.1016/j.jtho.2022.09.223

76. Addeo A, Passaro A, Malapelle U, Banna GL, Subbiah V, Friedlaender A. Immunotherapy in non-small cell lung cancer harbouring driver mutations. *Cancer Treat Rev* (2021) 96:102179. doi:10.1016/j.ctrv.2021.102179

77. Attili I, Passaro A, Corvaja C, Aliaga PT, Del Signore E, Spitaleri G, et al. Immune checkpoint inhibitors in EGFR-mutant non-small cell lung cancer: a systematic review. *Cancer Treat Rev* (2023) 119:102602. doi:10.1016/j.ctrv.2023.102602

78. Addeo A, Tabbò F, Robinson T, Buffoni L, Novello S. Precision medicine in ALK rearranged NSCLC: a rapidly evolving scenario. *Crit Rev Oncol Hemat* (2018) 122:150–6. doi:10.1016/j.critrevonc.2017.12.015

79. Hong DS, Fakih MG, Strickler JH, Desai J, Durm GA, Shapiro GI, et al. KRASG12C inhibition with sotorasib in advanced solid tumors. *N Engl J Med* (2020) 383:1207–17. doi:10.1056/NEJMoa1917239

80. Torralvo J, Friedlaender A, Achard V, Addeo A. The activity of immune checkpoint inhibition in KRAS mutated non-small cell lung cancer: a single centre experience. *Cancer Genom Proteom* (2019) 16:577–82. doi:10.21873/cgp.20160

81. Mazieres J, Drilon A, Lusque A, Mhanna L, Cortot AB, Mezquita L, et al. Immune checkpoint inhibitors for patients with advanced lung cancer and oncogenic driver alterations: results from the IMMUNOTARGET registry. *Ann Oncol* (2019) 30:1321–8. doi:10.1093/annonc/mdz167

82. Frisone D, Friedlaender A, Malapelle U, Banna G, Addeo A. A BRAF new world. *Crit Rev Oncol Hemat* (2020) 152:103008. doi:10.1016/j.critrevonc.2020.103008

83. Dudnik E, Peled N, Nechushtan H, Wollne,r M, Onn A, Agbarya A, et al. BRAF mutant lung cancer: programmed death ligand 1 expression, tumor mutational burden, microsatellite instability status, and response to immune check-point inhibitors. *J Thoracic Oncol* (2018) 13:1128–37. doi:10.1016/j.jtho.2018.04.024

84. Negrao MV, Skoulidis F, Montesion M, Schulze K, Bara I, Shen V, et al. Oncogene-specific differences in tumor mutational burden, PD-L1 expression, and outcomes from immunotherapy in non-small cell lung cancer. *J Immunother Cancer* (2021) 9:e002891. doi:10.1136/jitc-2021-002891

85. Cai R, Zhu H, Liu Y, Sha H, Peng W, Yin R, et al. To be, or not to be: the dilemma of immunotherapy for non-small cell lung cancer harboring various driver mutations. *J Cancer Res Clin Oncol* (2023) 149:10027–40. doi:10.1007/s00432-023-04919-4

86. Sabari JK, Leonardi GC, Shu CA, Umeton R, Montecalvo J, Ni A, et al. PD-L1 expression, tumor mutational burden, and response to immunotherapy in patients with MET exon 14 altered lung cancers. *Ann Oncol* (2018) 29:2085–91. doi:10.1093/annonc/mdy334

87. Guisier F, Dubos-Arvis C, Viñas F, Doubre H, Ricordel C, Ropert S, et al. Efficacy and safety of anti–PD-1 immunotherapy in patients with advanced NSCLC with BRAF, HER2, or MET mutations or RET translocation: GFPC 01-2018. *J Thorac Oncol* (2020) 15:628–36. doi:10.1016/j.jtho.2019.12.129

88. Drilon A, Clark JW, Weis J, Ou SH, Camidge DR, Solomon BJ, et al. Antitumor activity of crizotinib in lung cancers harboring a MET exon 14 alteration. *Nat Med* (2020) 26:47–51. doi:10.1038/s41591-019-0716-8

89. Lai WC, Feldman DL, Buonocore DJ, Brzostowski EB, Rizvi H, Plodkowski AJ, et al. PD-L1 expression, tumor mutation burden and response to immune checkpoint blockade in patients with HER2-mutant lung cancers. *J Clin Oncol* (2018) 36:9060. doi:10.1200/JCO.2018.36.15_suppl.9060

90. Assoun S, Theou-Anton N, Nguenang M, Cazes A, Danel C, Abbar B, et al. Association of TP53 mutations with response and longer survival under immune checkpoint inhibitors in advanced non-small-cell lung cancer. *Lung Cancer* (2019) 132:65–71. doi:10.1016/j.lungcan.2019.04.005

91. Wang S, Jiang M, Yang Z, Huang X, Li N. The role of distinct co-mutation patterns with TP53 mutation in immunotherapy for NSCLC. *Genes Dis* (2020) 9:245–51. doi:10.1016/j.gendis.2020.04.001

92. Kohno T, Ichikawa H, Totoki Y, Yasuda K, Hiramoto M, Nammo T, et al. KIF5B-RET fusions in lung adenocarcinoma. *Nat Med* (2012) 18:375–7. doi:10.1038/nm.2644

93. Krzyżanowska N, Krawczyk P, Wojas-Krawczyk K, Kucharczyk T, Milanowski J. Immunotherapy in non-small-cell lung cancer patients with driver alterations: a new strategy? *Cells* (2022) 11:3280. doi:10.3390/cells11203280

94. Meira DD, de Castro E, Caetano MC, Casotti MC, Zetum ASS, Gonçalves AFM, et al. Prognostic factors and markers in non-small cell lung cancer: recent progress and future challenges. *Genes (Basel)* (2023) 14:1906. doi:10.3390/genes14101906

95. Brahmer J, Reckamp KL, Baas P, Crinò L, Eberhardt WE, Poddubskaya E, et al. Nivolumab versus docetaxel in advanced squamous-cell non-small-cell lung cancer. *N Engl J Med* (2015) 373:123–35. doi:10.1056/NEJMoa1504627

96. Borghaei H, Paz-Ares L, Horn L, Spigel DR, Steins M, Ready NE, et al. Nivolumab versus docetaxel in advanced nonsquamous non-small-cell lung cancer. *N Engl J Med* (2015) 373:1627–39. doi:10.1056/NEJMoa1507643

97. Herbst RS, Baas P, Kim DW, Felip E, Pérez-Gracia LJ, Han JY, et al. Pembrolizumab versus docetaxel for previously treated, PD-L1-positive, advanced NonSmall-cell lung cancer (KEYNOTE-010): a randomised controlled trial. *Lancet* (2016) 387:1540–50. doi:10.1016/S0140-6736(15)01281-7

98. Rittmeyer A, Barlesi F, Waterkamp D, Park K, Ciardiello F, von Pawel J, et al. Atezolizumab versus docetaxel in patients with previously treated non-small-cell lung cancer (OAK): a phase 3, open-label, multicentre randomised controlled trial. *Lancet* (2017) 389:255–65. doi:10.1016/S0140-6736(16)32517-X

99. Herbst RS, Garon EB, Kim DW, Cho BC, Gervais R, Perez-Gracia JL, et al. Five year survival update from KEYNOTE-010: pembrolizumab versus docetaxel for previously treated, programmed death-ligand 1-positive advanced NSCLC. *J Thorac Oncol* (2021) 16:1718–32. doi:10.1016/j.jtho.2021.05.001

Pathology & Oncology Research | frontiers

TYPE Original Research
PUBLISHED 17 April 2023
DOI 10.3389/pore.2023.1610951

Check for updates

OPEN ACCESS

EDITED BY
József Tímár,
Semmelweis University, Hungary

*CORRESPONDENCE
Tzahi Neuman,
tneuman@hadassah.org.il

†These authors have contributed equally to this work

RECEIVED 16 November 2022
ACCEPTED 27 March 2023
PUBLISHED 17 April 2023

CITATION
Horesh A, Pollack R, Nechushtan H, Dresner-Pollak R and Neuman T (2023), Tumor PD-L1 expression and molecular profiling are not associated with immune checkpoint inhibitor-induced thyroid dysfunction in advanced NSCLC patients.
Pathol. Oncol. Res. 29:1610951.
doi: 10.3389/pore.2023.1610951

COPYRIGHT
© 2023 Horesh, Pollack, Nechushtan, Dresner-Pollak and Neuman. This is an open-access article distributed under the terms of the Creative Commons Attribution License (CC BY). The use, distribution or reproduction in other forums is permitted, provided the original author(s) and the copyright owner(s) are credited and that the original publication in this journal is cited, in accordance with accepted academic practice. No use, distribution or reproduction is permitted which does not comply with these terms.

Tumor PD-L1 expression and molecular profiling are not associated with immune checkpoint inhibitor-induced thyroid dysfunction in advanced NSCLC patients

Adi Horesh[1†], Rena Pollack[1,2†], Hovav Nechushtan[1,3], Rivka Dresner-Pollak[1,2] and Tzahi Neuman[1,4*]

[1]The Faculty of Medicine, Hebrew University of Jerusalem, Jerusalem, Israel, [2]Department of Endocrinology and Metabolism, Hadassah-Hebrew University Medical Center, Jerusalem, Israel, [3]Department of Oncology, Hadassah-Hebrew University Medical Center, Jerusalem, Israel, [4]Department of Pathology, Hadassah-Hebrew University Medical Center, Jerusalem, Israel

Background: Immune-checkpoint inhibitors (ICIs) have revolutionized the treatment of advanced non-small cell lung cancer (NSCLC), however are frequently associated with thyroid immune-related adverse events (IRAEs). We investigated the association between patient characteristics, tumor PD-L1 expression and molecular profile with the development of thyroid IRAEs in NSCLC patients.

Methods: Single center, retrospective study including 107 NSCLC patients treated with PD-1/PD-L1 inhibitors from April 2016 to July 2020. All patients were euthyroid at baseline with at least two TSH measurements post-treatment initiation. The primary outcome was the difference in tumor PD-L1 expression in patients who developed any thyroid IRAEs versus those who remained euthyroid. Additional outcomes included development of overt thyroid dysfunction, the association of specific molecular alterations with thyroid IRAEs, and onset of thyroid IRAEs as a function of tumor PD-L1 expression.

Results: Overall, 37 (34.6%) patients developed any thyroid dysfunction and 18 (16.8%) developed overt thyroid dysfunction. Tumor PD-L1 staining intensity was not associated with thyroid IRAEs. TP53 mutation was less likely to be associated with any thyroid dysfunction ($p < 0.05$) and no association was found between EGFR, ROS, ALK or KRAS mutations. There was no association between PD-L1 expression and time to develop thyroid IRAEs.

Conclusion: PD-L1 expression is not associated with the development of thyroid dysfunction in advanced NSCLC patients treated with ICIs, suggesting that thyroid IRAEs are unrelated to tumor PD-L1 expression.

Abbreviations: NSCLC, Non-small cell lung cancer; PD-1, programmed cell death 1; PD-L1, programmed cell death ligand 1.

KEYWORDS
PD-L1, NSCLC, immune checkpoint inhibitors, immune-related adverse events, thyroid

Introduction

Immune checkpoint inhibitors (ICIs) have revolutionized the management of advanced non-small cell lung cancer (NSCLC). Specifically, programmed cell death 1 (PD-1) and programmed cell death ligand 1 (PD-L1) inhibitors as monotherapy or in combination with chemotherapy are associated with improved response rates and overall survival compared with conventional chemotherapy (1). Thus, ICIs are now widely used as first line monotherapy in patients with advanced stage NSCLC and >50% membranous PD-L1 positive tumor cells and in combination with chemotherapy irrespective of PD-L1 expression (2). In the setting of specific oncogenic driver mutations such as anaplastic lymphoma kinase (ALK), v-Raf murine sarcoma viral oncogene homolog B1 (BRAF), epithelial growth factor receptor (EGFR), c-ros oncogene 1 (ROS1) and neurotrophic tyrosine receptor kinase (NTRK) targeted therapies are recommended.

While the use of ICIs has provided significant benefit with an improved side effect profile, their use has been associated with the development of immune-related adverse events (irAEs). These irAEs have been known to affect all organ systems, however frequently result in thyroid dysfunction with a reported incidence of 9%–42% in patients treated with PD-1 or PD-L1 inhibitor therapy (3–7). Importantly, the development of irAEs has been associated with improved clinical outcomes (7–10).

The mechanism of thyroid irAEs has yet been understood and the underlying causes for the thyroid gland to frequently become affected remain elusive. Several studies have suggested that the thyroid dysfunction seen with ICI use is a manifestation of destructive thyroiditis due to unleashing cytotoxic T cells against thyroid antigens. This leads to humoral immune response which produces anti-thyroid antibodies (11). Another hypothesis is that ICI-induced thyroid dysfunction may be due to unmasking of latent autoimmunity in those with a predisposition to develop autoimmune disease (12–14). Interestingly, a recently published study suggests that patients without thyroid autoantibodies are also at increased risk of developing thyroid irAE after treatment with a combination of PD-1/CTLA-4-Ab compared to PD-1 Ab-alone, and this risk is similar to the risk of thyroid irAE in patients with ATA at baseline after PD-1 Ab therapy (15).

Several predictors of thyroid irAE development have been proposed including the presence of thyroid autoantibodies at baseline, higher TSH at baseline, increased BMI, and duration of treatment (13, 16–19). Data regarding the relationship between tumor characteristics and risk of irAEs are limited. In the present study, we aimed to explore the association between patient factors, tumor PD-L1 expression and molecular profile and the development of thyroid irAEs in NSCLC patients treated with PD-1 or PD-L1 inhibitors.

Materials and methods

We conducted a non-interventional retrospective study utilizing deidentified data from the Hadassah Hebrew-University Medical Center clinical and pathologic database. Complete demographic, clinical and pathologic data are recorded in the Hadassah Hebrew-University Medical Center electronic medical records (EMR), including medical diagnoses, laboratory tests, pathology data, prescribed medications, and information on all patient medical interactions including outpatient visits, acute medical services, and hospitalizations. Approval was obtained from the Hadassah Medical Center Institutional Review Board and Ethics Committee for the purpose of accessing and analyzing the data. Individual patient informed consent was not required because of the anonymized nature of the patient records and the non-interventional study.

Study population

The present study included patients aged 18 years or above with biopsy proven advanced NSCLC and PD-L1 tumor expression data from 1 April 2016 to 30 July 2020. Patients meeting inclusion criteria were ≥18 years old with biopsy-proven NSCLC and PD-L1 tumor immunohistochemistry (IHC) staining results, who initiated treatment with single agent PD-1 inhibitor (nivolumab, pembrolizumab) or PD-L1 inhibitor (durvalumab, atezolizumab) according to standard protocols. Thyroid function tests (TFTs) within 3 months prior to treatment initiation and at least 2 measurements thereafter were required. Subjects were excluded if they had known history of thyroid dysfunction, including prior diagnosis of thyroid disease, past treatment with antithyroid drugs or levothyroxine, or evidence of abnormal thyroid function tests at baseline. Patients were censored at the date of last contact or date of death.

Assessment of outcome

The relationship between PD-L1 tumor staining and each of the clinical outcomes was assessed. The primary outcome

was defined as the association of tumor PD-L1 expression in patients developing any thyroid dysfunction versus remaining euthyroid. Additional outcomes included: 1) the association of PD-L1 expression with the development of overt thyroid dysfunction versus remaining euthyroid 2) the association of specific molecular alterations (EGFR, ALK, ROS, tumor protein 53 (TP53) and Kirsten rat sarcoma (KRAS) with the development of any thyroid dysfunction versus remaining euthyroid, and 3) time to development of thyroid dysfunction as a function of tumor PD-L1 expression.

Variables, definitions, derivations, and measurements

Clinical data collected included age, sex, smoking status, type and stage of malignancy, previous chemotherapy or radiation, type of ICI agent, line of treatment, thyroid function tests at baseline and all available measurements post ICI treatment. Pathologic data including the biopsy method, pathologic diagnosis, tumor PD-L1 expression and molecular profiling was also collected.

Each tissue sample was evaluated morphologically and with immunostaining when required for diagnostic purposes. Following the common guidelines, only two immunostains were performed (TTF1 and P40) to preserve tissue for additional evaluation (20). If the specific diagnosis was not definitive, the case was concluded as "NSCLC." Once the pathologic diagnosis was determined, each advanced-stage sample was followed routinely by IHC for PD-L1 and molecular profiling.

Immunohistochemistry staining

PD-L1 IHC staining was performed with 22C2 PharmDx, Dako, concentrated antibody, 1:33 dilution), using the automated staining platform (Ventana BenchMark Ultra), according to the Israeli harmonization protocol (21). The tissue blocks were cut at 5-μm thick sections. On each slide, a section of benign tonsillar tissue was used as a positive external control to evaluate the proper dynamic range of staining. In addition, positive histocytes involved within the tissue in each section was used as a positive internal control. Pathologists experienced in PD-L1 interpretation evaluated all the stained material. The samples were divided into 3 categories of staining intensity: negative (<1% membranous PD-L1 positive cells), weakly positive (1%–49% membranous PD-L1 positive cells), and strongly positive (≥50% membranous PD-L1 positive tumor cells) following the established protocol in the Keynote 024 clinical trial (1).

Molecular profile

Molecular profiling from 2016 to 2017 included EGFR alterations status (Cobas® EGFR mutation kit; Cobas® z 480 analyzer), ALK (D5F3 antibody; Ventana BenchMark XT) and ROS (D4D6 antibody; ULTRA) immunostains. In 2018, the Cobas® system was replaced by a 24-gene panel, including EGFR, BRAF, KRAS and TP53 (Ion Torrent System; Oncomine™ Solid Tumor DNA Kit). As of 2020, comprehensive genomic profiling is performed using a next-generation sequencing assay including more than 500 relevant genes for tumorigenesis (Ion Torrent system; Oncomine™ Comprehensive Assay Plus Kit; sequencing performed using Ion S5™ System).

Thyroid outcomes were defined as follows:

(1) Any thyroid dysfunction was defined as a TSH value above or below the laboratory-specific reference range, irrespective of FT4 and FT3 levels during follow-up.
(2) Overt thyroid dysfunction was defined as either overt hypothyroidism, overt thyrotoxicosis, or central hypothyroidism. Overt hypothyroidism was defined as either elevated TSH with decreased FT4 and/or FT3 or TSH ≥10 mU/L. Overt thyrotoxicosis was defined as a suppressed TSH with elevated FT4 and/or FT3 levels. Central hypothyroidism was defined as a TSH value below the laboratory-specific reference range with a low FT4 and/or FT3 or a normal TSH value with a low FT4.
(3) Thyroiditis was defined as subclinical or overt thyrotoxicosis followed by progression to overt hypothyroidism.

Statistical analysis

The association between two categorical variables was tested by applying either the Chi-square test or the Fisher's exact test. Comparing quantitative variables between two independent groups was carried out using the t-test or the non-parametric Mann-Whitney test. The non-parametric test was used for data which was not normally distributed. A p-value of 0.05 or less was considered statistically significant. Analyses were performed using the IBM SPSS statistics software, version 25.

Results

Study cohort

We identified 1,234 patients diagnosed with biopsy proven non-small cell lung cancer (NSCLC) from 1 April 2016 to 30 July 2020 in the Hadassah-Hebrew University pathology database. Of these, 470 patients had demographic, clinical and pathologic data available in the Hadassah-Hebrew University Medical Center EMR. A total of 143 patients received treatment with a PD-1 or

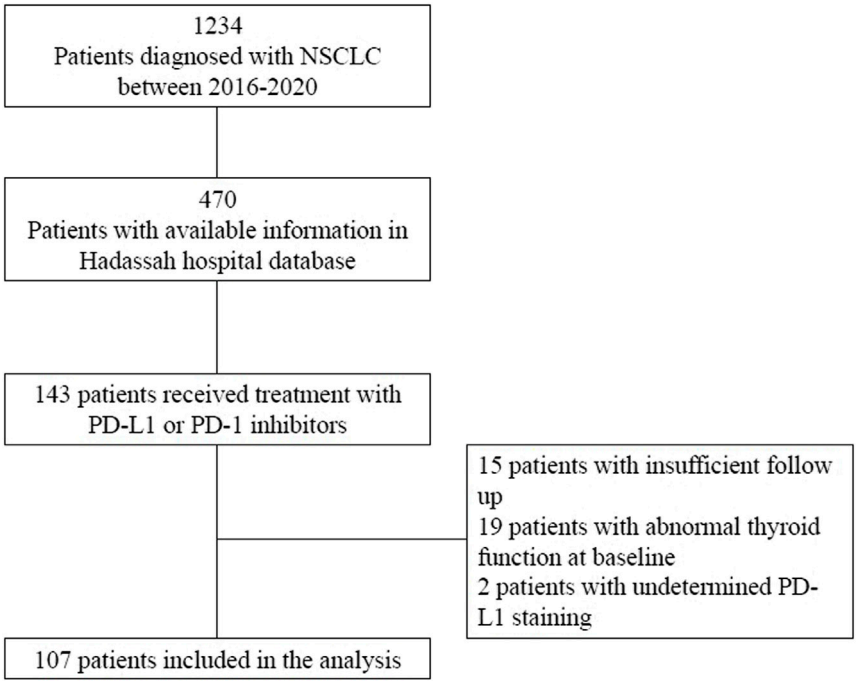

FIGURE 1
Consort Diagram. Abbreviations: NSCLC, Non-small cell lung cancer; PD-1, programmed cell death 1; PD-L1, programmed cell death ligand 1.

PD-L1 inhibitor. After applying all inclusion and exclusion criteria, 107 patients were included in the study and followed for a median 371 (IQR 169.8–620.0) days (Figure 1).

Baseline characteristics of the overall cohort are presented in Table 1.

The study population consisted of 72.9% men, 82.2% smokers, with mean age 66.1 ± 9.6 years. Overall, 78.5% were diagnosed at stage IV and 58.9% had adenocarcinoma of the lung. Mean baseline TSH was 1.6 ± 0.9 mU/L.

Biopsies were performed using transthoracic needle biopsy in 46 (42.9%) patients, transbronchial biopsy in 24 (22.4%) patients, endobronchial ultrasound-guided biopsy in 14 (13.1%) patients, and 10 patients (9.4%) underwent open biopsy.

Outcomes

Any thyroid dysfunction

A total of 37 (34.6%) patients developed any thyroid dysfunction. Patients developing any thyroid dysfunction were of similar age, gender, and smoking status compared to those who remained euthyroid. Furthermore, baseline TSH was similar between the two groups (Table 2).

Of those that developed any thyroid dysfunction, 13 (35.1%) had negative PD-L1 IHC staining, 9 (24.3%) were weakly positive and 15 (40.5%) were strongly positive. No difference was noted in PD-L1 IHC staining intensity between those that developed any thyroid dysfunction vs. remained euthyroid (Table 3).

Overt thyroid dysfunction

Eighteen (16.8%) patients developed overt thyroid dysfunction, including 5 (4.7%) overt hypothyroidism, 7 (6.5%) overt thyrotoxicosis and 6 (5.6%) thyrotoxicosis with progression to overt hypothyroidism consistent with thyroiditis. No significant difference in baseline characteristics were noted between the two groups (Supplementary Table S1). Of those that developed overt thyroid dysfunction, no significant difference identified regarding the age, gender, specific diagnosis, tumoral stage, prior treatment (chemotherapy or radiation) or the specific ICI treatment. Regarding PD-L1 expression, 8 (44.4%) had negative PD-L1 IHC staining, 3 (16.7%) were weakly positive and 7 (38.9%) were strongly positive. PD-L1 IHC staining intensity was similar between patients that developed overt thyroid dysfunction vs. remained euthyroid (Supplementary Table S2).

Molecular markers

We further analyzed the relationship between any thyroid dysfunction and the presence of EGFR, ALK, ROS, TP53 and KRAS mutations. Overall, 10/98 (10.2%) patients tested positive for an EGFR mutation, 1/46 (2.2%) was positive for a ROS rearrangement, 46/92 (50.0%) had a TP53 mutation, and 27/90 (25.2%) patients were positive for a KRAS mutation. No patients

TABLE 1 Baseline characteristics of the overall cohort.

Variable	N = 107
Age, y ± SD	66.1 ± 9.6
Sex	
Male	78 (72.9)
Female	29 (27.1)
Smoking	88 (82.8)
BMI, kg/m^2 ± SD	24.5 ± 3.7
Lung Malignancy	
SCC	27 (25.2)
Adenocarcinoma	63 (58.9)
NSCLC	17 (15.9)
Tumor Stage	
II/III	23 (21.5)
IV	86 (78.5)
ICI type	
PD-1	98 (91.6)
PD-L1	9 (8.4)
Line of treatment	
1	49 (45.8)
2	49 (45.8)
≥3	9 (8.4)
Prior chemotherapy	79 (73.8)
Prior of radiation	64 (59.8)
Baseline TSH, mU/L± SD	1.6 ± 0.9

Continuous parameters are shown as mean ± SD. Categorical variables are shown as n (%) of the overall population. Abbreviations: BMI, Body Mass Index; SCC, Squamous Cell Carcinoma; NSCLC, Non-small cell lung cancer; ICI, Immune-checkpoint inhibitor; PD-1, programmed cell death 1; PD-L1, programmed cell death ligand 1; TSH, Thyroid-Stimulating Hormone.

were found to have an ALK rearrangement. There was no association found between the development of any thyroid dysfunction and EGFR, ROS, ALK or KRAS mutations, however patients with TP53 mutation were less likely to be associated with the development of any thyroid dysfunction ($p < 0.05$; Table 3). No association was noted between overt thyroid dysfunction and the presence of these mutations (Supplementary Table S2).

Time to development of any thyroid dysfunction

The median time to the development of any thyroid dysfunction among the entire cohort was 45.0 (IQR 29.5–91.0) days. There was no association between PD-L1 expression and time to develop thyroid dysfunction.

Discussion

This single center, retrospective study assessed the association between clinical parameters, tumor PD-L1 expression, molecular profiling and the development of thyroid irAEs in NSCLC patients treated with PD-1 or PD-L1 inhibitors. Overall, 34.6% of patients developed thyroid dysfunction, including 16.8% of patients with overt thyroid dysfunction, consistent with previously reported studies (3–7). We did not find an association between baseline clinical parameters or tumor PD-L1 expression and the development of thyroid irAEs. TP53 mutation was associated with a decreased tendency to develop any thyroid dysfunction. The time to develop thyroid dysfunction was similar among the patients, regardless of PD-L1 expression.

Several studies have demonstrated a relationship between treatment response and the development of irAEs in NSCLC patients treated with immunotherapy (7, 9, 10). Specifically, thyroid dysfunction was associated with improved treatment response in NSCLC. In a subgroup analysis of patients with NSCLC treated with pembrolizumab in the KEYNOTE-001 trial, overall survival was significantly longer in subjects who developed ICI-induced thyroid dysfunction (14). Similarly, a study including patients with NSCLC, renal cell carcinoma and metastatic melanoma treated with anti PD-1 immunotherapy demonstrated improved progression-free survival (PFS) and overall survival (OS) in patients who developed thyroid dysfunction compared to patients without (22). It has therefore been proposed that irAEs, and specifically, thyroid dysfunction may serve as a surrogate marker for treatment response in patients treated with ICIs.

Considering the mechanism of ICI therapy, it seems reasonable that irAEs may be more likely to occur in patients with high tumor PD-L1 expression. The relationship between PD-L1 expression and irAEs has been examined, with discrepant results noted among studies. Sugisaka et. al performed a retrospective analysis of 44 patients with advanced NSCLC treated with PD-1 monotherapy (23). Overall, 70% of patients developed irAEs of any grade. Patients who developed irAEs demonstrated improved objective response rate (ORR), disease control rate and PFS. High PD-L1 expression (≥50%) was identified as an independent predictor of irAE development. In a recent real-world study including 877 patients with NSCLC and PD-L1 expression ≥50% treated with PD-1 monotherapy, endocrine irAEs were noted in 27% of patients (9). Patients who developed endocrine irAEs had improved ORR, PFS and OS in multivariate analyses. In contrast, a significant relationship between PD-L1 expression and irAE development was not found in a subgroup of patients treated with PD-1 inhibitor monotherapy in the KEYNOTE-001 trial (24). While 40% of patients developed irAEs associated with improved ORR, PFS, OS, no association with PD-L1 status or a targetable mutation (EGFR or ALK) was noted. Similarly, in the BIRCH trial which studied PD-L1 inhibitor treatment in NSCLC, a significant association between treatment response and PD-L1 expression was noted, however there was no association between PD-L1 expression and irAEs (25). In the current study, we did not demonstrate an association between PD-L1 expression and the

TABLE 2 Demographic and clinical characteristics associated with the development of any thyroid dysfunction.

	Euthyroid (N = 70)	Any thyroid dysfunction (N = 37)	*p*-Value
Age, y± SD	65.5 ± 10.3	67.1 ± 8.2	0.41
Male (*n* = 78)	49 (62.8)	29 (37.2)	0.35
Lung Malignancy			0.59
SCC (*n* = 27)	19 (70.4)	8 (29.6)	
Adenocarcinoma (*n* = 63)	41 (65.1)	22 (34.9)	
NSCLC (*n* = 17)	10 (62.5)	7 (37.5)	
Tumor Stage			
II/III (*n* = 23)	15 (65.2)	8 (34.8)	0.98
IV (*n* = 86)	55 (65.5)	29 (34.5)	
ICI type			
PD-1 (*n* = 98)	66 (67.3)	32 (32.7)	0.27
PD-L1 (*n* = 9)	4 (44.4)	5 (55.6)	
Prior chemotherapy (*n* = 79)	49 (62.0)	30 (38.0)	0.22
Prior radiation (*n* = 64)	42 (65.6)	22 (34.4)	0.96
Baseline TSH, mU/L	1.6 ± 0.8	1.6 ± 1.1	0.82

Continuous parameters are shown as mean ± SD. Categorical variables are shown as n (%) of the overall population of each row. SCC, Squamous Cell Carcinoma; NSCLC, Non-small cell lung cancer; ICI, Immune-checkpoint inhibitor; PD-1, programmed cell death 1; PD-L1, programmed cell death ligand 1; TSH, Thyroid-Stimulating Hormone. *p*-value is shown for comparison of euthyroid patients (*n* = 70) versus all patients with any thyroid dysfunction (*n* = 37). Chi square test and Fisher's exact test were applied in the comparison of categorical variables; T-test or Mann-Whitney test were used to compare quantitative variables.

TABLE 3 Pathologic characteristics associated with the development of any thyroid dysfunction.

	Overall	Euthyroid (N = 70)	Any thyroid dysfunction (N = 37)	*p*-value
PD-L1 (N = 107)				
Negative	33 (30.8)	20 (60.6)	13 (39.4)	0.22
Weakly positive	19 (17.8)	10 (52.6)	9 (47.4)	
Strongly positive	55 (51.4)	40 (72.7)	15 (27.3)	
EGFR mutated (N = 98)	10 (10.2)	9 (90.0)	1 (10.0)	1.00
ALK mutated (N = 52)	0 (0.0)	0 (0.0)	0 (0.0)	1.00
ROS mutated (N = 46)	1 (2.2)	1 (100.0)	0 (0.0)	0.66
TP53 mutated (N = 92)	46 (50.0)	36 (78.3)	10 (21.7)	0.01
KRAS mutated (N = 90)	27 (30.0)	18 (66.7)	9 (33.3)	1.00

Variables are shown as n (%) of the overall population in each row. *p*-value is shown for comparison of euthyroid patients (*n* = 70) versus all patients with any thyroid dysfunction (*n* = 37). Chi square test and Fisher's exact test were applied in the comparison of categorical variables.

thyroid irAEs suggesting that the development of thyroid irAEs is unrelated to PD-L1 expression in the tumor.

Even though no statistically significant correlation was shown for the classic molecular alterations, TP53 mutation was associated with a decreased tendency to develop any thyroid dysfunction following PD-1/L1 therapy. This phenomenon is interesting, with the understanding that not only does TP53 loss or mutation predispose to cancer, but hyperactive TP53 also drives various pathologies, including developmental phenotypes, premature aging, neurodegeneration, and side effects of cancer therapies (26). It has been previously shown that TP53 activation in response to genotoxic cancer therapies can promote side effects associated with DNA-damaging therapies (27). In our study, we demonstrate a decreased predisposition to endocrine side effects in patients treated with immunotherapy alone or with combined chemotherapy and a TP53 alteration. There was no association between PD-L1 expression and TP53 mutation in this cohort.

A biological rationale for this positive effect can be through the role of TP53 in regulating signaling within the tumor microenvironment, a function of great significance for antitumor immune responses, including both innate and adaptive immune responses (28). Thus, the subgroup of tumors with TP53 alteration might react differently with less

of an immunomodulatory effect on the thyroid. However, additional data is required for further validation of this finding.

The strength of our study lies in our assessment of a large cohort of NSCLC patients with PD-L1 expression data, and for whom we have computerized access to all clinical, laboratory, and pathology data. Several limitations of our study are noted. First, it was retrospective, performed at a single institution which may introduce bias in the analysis. Furthermore, the number of patients with NSCLC treated with a PD-1 or PD-L1 inhibitor was limited and further examination in a larger population is warranted. In addition, not all patients had comprehensive molecular profiling, as it was not yet standard of care in the initial study period. Lastly, the relationship between PD-L1 tumor expression, thyroid irAEs and clinical response was not evaluated in this study.

In conclusion, our study does not demonstrate an association between high PD-L1 expression and thyroid irAEs in advanced NSCLC patients treated with immunotherapy. Further studies in a larger patient population are indicated to further understand the complex relationship between irAEs, tumor characteristics and treatment response.

Data availability statement

The original contributions presented in the study are included in the article/Supplementary Material, further inquiries can be directed to the corresponding author.

Ethics statement

Approval was obtained from the Hadassah Medical Center Institutional Review Board and Ethics Committee for the purpose of accessing and analyzing the data. Individual patient informed consent was not required because of the anonymized nature of the patient records and the non-interventional study.

Author contributions

All authors contributed to the study conception and design. Material preparation, data collection and analysis were performed by RP, AH, and TN. The first draft of the manuscript was written by RP, AH, and TN and all authors commented on previous versions of the manuscript. All authors read and approved the final manuscript.

Conflict of interest

The authors declare that the research was conducted in the absence of any commercial or financial relationships that could be construed as a potential conflict of interest.

Acknowledgments

Special thanks to Tali Bedolach-Avram for her help in performing the statistical analyses. This research was conducted as part of AH's MD thesis.

Supplementary material

The Supplementary Material for this article can be found online at: https://www.por-journal.com/articles/10.3389/pore.2023.1610951/full#supplementary-material

References

1. Reck M, Rodríguez-Abreu D, Robinson AG, Hui R, Csőszi T, Fulop A, et al. Pembrolizumab versus Chemotherapy for PD-L1–Positive Non–small-cell Lung Cancer. *N Engl J Med* (2016) 375:1823–33. doi:10.1056/nejmoa1606774

2. Gandhi L, Rodríguez-Abreu D, Gadgeel S, Esteban E, Felip E, De Angelis F, et al. Pembrolizumab Plus Chemotherapy in Metastatic Non–small-cell Lung Cancer. *N Engl J Med* (2018) 378:2078–92. doi:10.1056/nejmoa1801005

3. Scott ES, Long GV, Guminski A, Clifton-Bligh RJ, Menzies AM, Tsang VH. The Spectrum, Incidence, Kinetics and Management of Endocrinopathies with Immune Checkpoint Inhibitors for Metastatic Melanoma. *Eur J Endocrinol* (2018) 178: 173–80. doi:10.1530/EJE-17-0810

4. Morganstein DL, Lai Z, Spain L, Diem S, Levine D, Mace C, et al. Thyroid Abnormalities Following the Use of Cytotoxic T-Lymphocyte Antigen-4 and Programmed Death Receptor Protein-1 Inhibitors in the Treatment of Melanoma. *Clin Endocrinol (Oxf)* (2017) 86:614–20. doi:10.1111/cen.13297

5. D'aiello A, Lin J, Gucalp R, Tabatabaie V, Cheng H, Bloomgarden NA, et al. Thyroid Dysfunction in Lung Cancer Patients Treated with Immune Checkpoint Inhibitors (Icis): Outcomes in a Multiethnic Urban Cohort. *Cancers (Basel)* (2021) 13:1464. doi:10.3390/cancers13061464

6. Brody HM, Macherla S, Bulumulle A, Namireddy P, Cherry CR. The Real-World Incidence of Immunotherapy-Related Thyroid Dysfunction: A Retrospective Analysis of a Single center's Experience over Five Years. *J Clin Oncol* (2020) 38:98. doi:10.1200/jco.2020.38.5_suppl.98

7. Hosoya K, Fujimoto D, Morimoto T, Kumagai T, Tamiya A, Taniguchi Y, et al. Association between Early Immune-Related Adverse Events and Clinical Outcomes in Patients with Non–small Cell Lung Cancer Treated with Immune Checkpoint Inhibitors. *Clin Lung Cancer* (2020) 21:e315–28. doi:10.1016/j.cllc.2020.01.003

8. Freeman-Keller M, Kim Y, Cronin H, Richards A, Gibney G, Weber JS. Nivolumab in Resected and Unresectable Metastatic Melanoma: Characteristics of Immune-Related Adverse Events and Association with Outcomes. *Clin Cancer Res* (2016) 22:886–94. doi:10.1158/1078-0432.CCR-15-1136

9. Cortellini A, Friedlaender A, Banna GL, Porzio G, Bersanelli M, Cappuzzo F, et al. Immune-related Adverse Events of Pembrolizumab in a Large Real-World Cohort of Patients with NSCLC with a PD-L1 Expression ≥ 50% and Their Relationship with Clinical Outcomes. *Clin Lung Cancer* (2020) 21:498–508.e2. doi:10.1016/j.cllc.2020.06.010

10. Baldini E, Lunghi A, Cortesi E, Turci D, Signorelli D, Stati V, et al. Immune-related Adverse Events Correlate with Clinical Outcomes in NSCLC Patients Treated with Nivolumab: The Italian NSCLC Expanded Access Program. *Lung Cancer* (2020) 140:59–64. doi:10.1016/j.lungcan.2019.12.014

11. Narita T, Oiso N, Taketomo Y, Okahashi K, Yamauchi K, Sato M, et al. Serological Aggravation of Autoimmune Thyroid Disease in Two Cases Receiving Nivolumab. *J Dermatol* (2016) 43:210–4. doi:10.1111/1346-8138.13028

12. Hollowell JG, Staehling NW, Dana Flanders W, Hannon WH, Gunter EW, Spencer CA, et al. Serum TSH, T4, and Thyroid Antibodies in the United States Population (1988 to 1994): National Health and Nutrition Examination Survey (NHANES III). *J Clin Endocrinol Metab* (2002) 87:489–99. doi:10.1210/jcem.87.2.8182

13. Kobayashi T, Iwama S, Yasuda Y, Okada N, Tsunekawa T, Onoue T, et al. Patients with Antithyroid Antibodies Are Prone to Develop Destructive Thyroiditis by Nivolumab: A Prospective Study. *J Endocr Soc* (2018) 2:241–51. doi:10.1210/JS.2017-00432

14. Osorio JC, Ni A, Chaft JE, Pollina R, Kasler MK, Stephens D, et al. Antibody-mediated Thyroid Dysfunction during T-Cell Checkpoint Blockade in Patients with Non-small-cell Lung Cancer. *Ann Oncol* (2017) 28:583–9. doi:10.1093/annonc/mdw640

15. Iwama S, Kobayashi T, Yasuda Y, Okuji T, Ito M, Ando M, et al. Increased Risk of Thyroid Dysfunction by PD-1 and CTLA-4 Blockade in Patients without Thyroid Autoantibodies at Baseline. J Clin Endocrinol Metab *Published Online First* (2021) 107:e1620–e1630. doi:10.1210/CLINEM/DGAB829

16. Wang Z, Aguilar EG, Luna JI, Dunai C, Khuat LT, Le CT, et al. Paradoxical Effects of Obesity on T Cell Function during Tumor Progression and PD-1 Checkpoint Blockade. *Nat Med* (2019) 25:141–51. doi:10.1038/s41591-018-0221-5

17. Pollack RM, Kagan M, Lotem M, Dresner-Pollak R. Baseline TSH Level Is Associated with Risk of Anti–PD-1–induced Thyroid Dysfunction. *Endocr Pract* (2019) 25:824–9. doi:10.4158/EP-2018-0472

18. Fuchs CS, Doi T, Jang RW, Muro K, Satoh T, Machado M, et al. Safety and Efficacy of Pembrolizumab Monotherapy in Patients with Previously Treated Advanced Gastric and Gastroesophageal junction Cancer: Phase 2 Clinical KEYNOTE-059 Trial. *JAMA Oncol* (2018) 4:e180013. doi:10.1001/jamaoncol.2018.0013

19. Pollack R, Ashash A, Cahn A, Rottenberg Y, Stern H, Dresner-Pollak R. Immune Checkpoint Inhibitor-Induced Thyroid Dysfunction Is Associated with Higher Body Mass Index. *J Clin Endocrinol Metab* (2020) 105:dgaa458–8. doi:10.1210/CLINEM/DGAA458

20. Ettinger DS, Wood DE, Chair V. *Continue NCCN Guidelines Panel Disclosures NCCN Guidelines Version 7.2021 Non-small Cell Lung Cancer* (2021).

21. Neuman T, London M, Kania-Almog J, Litvin A, Zohar Y, Fridel L, et al. A Harmonization Study for the Use of 22C3 PD-L1 Immunohistochemical Staining on Ventana's Platform. *J Thorac Oncol* (2016) 11:1863–8. doi:10.1016/J.JTHO.2016.08.146

22. Basak EA, Van Der Meer JWM, Hurkmans DP, Schreurs MWJ, Oomen-de Hoop E, van der Veldt AAM, et al. Overt Thyroid Dysfunction and Anti-thyroid Antibodies Predict Response to Anti-PD-1 Immunotherapy in Cancer Patients. *Thyroid* (2020) 30:966–73. doi:10.1089/THY.2019.0726

23. Sugisaka J, Yukihoro T, Taguri M, Kawashima Y, Aiba T, Kawana S, et al. Relationship between Programmed Cell Death Protein Ligand 1 Expression and Immune-Related Adverse Events in Non-small-cell Lung Cancer Patients Treated with Pembrolizumab. *JMA J* (2019) 3:58–66. doi:10.31662/jmaj.2019-0005

24. Lisberg A, Andrew Tucker D, Goldman JW, Wolf B, Carroll J, Hardy A, et al. Treatment-related Adverse Events Predict Improved Clinical Outcome in Nsclc Patients on KEYNOTE-001 at a Single center. *Cancer Immunol Res* (2018) 6:288–94. doi:10.1158/2326-6066.CIR-17-0063

25. Peters S, Gettinger S, Johnson ML, Janne PA, Garassino MC, Christoph D, et al. Phase II Trial of Atezolizumab as First-Line or Subsequent Therapy for Patients with Programmed Death-Ligand 1-Selected Advanced Non-small-cell Lung Cancer (BIRCH). *J Clin Oncol* (2017) 35:2781–9. doi:10.1200/JCO.2016.71.9476

26. Wang M, Attardi LD. A Balancing Act: P53 Activity from Tumor Suppression to Pathology and Therapeutic Implications. *Review* (2021) 17. doi:10.1146/ANNUREV-PATHOL-042320-025840

27. Gudkov AV, Komarova EA. The Role of P53 in Determining Sensitivity to Radiotherapy. *Nat Rev Cancer* (2003) 3:117–29. doi:10.1038/nrc992

28. Blagih J, Zani F, Chakravarty P, Hennequart M, Pilley S, Hobor S, et al. Cancer-Specific Loss of P53 Leads to a Modulation of Myeloid and T Cell Responses. *Cell Rep* (2020) 30:481–96.e6. doi:10.1016/J.CELREP.2019.12.028

Pathology & Oncology Research | frontiers

TYPE Original Research
PUBLISHED 18 May 2023
DOI 10.3389/pore.2023.1611164

Check for updates

OPEN ACCESS

EDITED BY
Anna Sebestyén,
Semmelweis University, Hungary

*CORRESPONDENCE
Judit Moldvay,
drmoldvay@hotmail.com

RECEIVED 06 March 2023
ACCEPTED 08 May 2023
PUBLISHED 18 May 2023

CITATION
Gyulai M, Megyesfalvi Z, Reiniger L, Harko T, Ferencz B, Karsko L, Agocs L, Fillinger J, Dome B, Szallasi Z and Moldvay J (2023), PD-1 and PD-L1 expression in rare lung tumors. *Pathol. Oncol. Res.* 29:1611164. doi: 10.3389/pore.2023.1611164

COPYRIGHT
© 2023 Gyulai, Megyesfalvi, Reiniger, Harko, Ferencz, Karsko, Agocs, Fillinger, Dome, Szallasi and Moldvay. This is an open-access article distributed under the terms of the Creative Commons Attribution License (CC BY). The use, distribution or reproduction in other forums is permitted, provided the original author(s) and the copyright owner(s) are credited and that the original publication in this journal is cited, in accordance with accepted academic practice. No use, distribution or reproduction is permitted which does not comply with these terms.

PD-1 and PD-L1 expression in rare lung tumors

Marton Gyulai[1,2], Zsolt Megyesfalvi[3,4,5], Lilla Reiniger[6], Tunde Harko[3], Bence Ferencz[3,4], Luca Karsko[3], Laszlo Agocs[3,4], Janos Fillinger[3], Balazs Dome[3,4,5], Zoltan Szallasi[3,7,8] and Judit Moldvay[3]*

[1]County Institute of Pulmonology, Torokbalint, Hungary, [2]Károly Rácz Doctoral School of Clinical Medicine, Semmelweis University, Budapest, Hungary, [3]National Koranyi Institute of Pulmonology, Budapest, Hungary, [4]Department of Thoracic Surgery, National Institute of Oncology, Semmelweis University, Budapest, Hungary, [5]Department of Thoracic Surgery, Comprehensive Cancer Center, Medical University of Vienna, Vienna, Austria, [6]Institute of Pathology and Experimental Cancer Research, Semmelweis University, Budapest, Hungary, [7]Department of Bioinformatics, Semmelweis University, Budapest, Hungary, [8]Computational Health Informatics Program, Boston Children's Hospital and Harvard Medical School, Boston, MA, United States

Background: Our knowledge is still limited about the characteristics and treatment of rare lung tumors. The aim of our study was to determine programmed cell death ligand-1 (PD-L1) and programmed cell death-1 (PD-1) expression in rare pulmonary tumors to assess the potential role of immunotherapy.

Methods: 66 pathologically confirmed rare lung tumors including 26 mucoepidermoid carcinomas (MECs), 27 adenoid cystic carcinomas (ACCs), and 13 tracheobronchial papillomas (TBPs) were collected retrospectively. Immunohistochemical (IHC) staining was performed on formalin fixed paraffin embedded (FFPE) tumor tissues, and PD-L1 expression on tumor cells (TCs) and immune cells (ICs), and PD-1 expression on ICs were determined. The cut off value for positive immunostaining was set at 1% for all markers.

Results: PD-L1 expression on TCs was observed in two cases of MEC (7.7%), one case of ACC (3.7%), and was absent in TBP samples. PD-L1 expression on ICs could be demonstrated in nine cases of MEC (34.6%), four cases of ACC (14.8%), and was absent in TBPs. All PD-L1 TC positive tumors were also PD-L1 IC positive. Higher expression level than 5% of PD-L1 TC and/or IC was observed only in one ACC and in two MEC patients. Among them, strong PD-L1 immunopositivity of >50% on TCs and of >10% on ICs could be demonstrated in one MEC sample. PD-L1 expression of ≥1% on ICs was significantly more common in MEC, than in TBP ($p < 0.001$). In MEC ≥1% PD-L1 TC or IC expressions were significantly more common in patients aged 55 or older, than in younger patients ($p = 0.046$, and $p = 0.01$, respectively).

Abbreviations: ACC, adenoid cystic carcinoma; ADC, adenocarcinoma; IC, immune cell; IHC, immunohistochemistry; MEC, mucoepidermoid carcinoma; NSCLC, non-small cell lung cancer; PD-1, programmed cell death-1; PD-L1, programmed cell death ligand-1; SCC, squamous cell carcinoma; TBP, tracheobronchial papilloma; TC, tumor cell.

PD-1 expression on ICs was found in five cases of MEC (19.2%), four cases of ACC (14.8%), and in two cases of TBP (15.4%). Only one MEC case showed a higher than 5% expression level of PD-1 on ICs.

Conclusion: This retrospective study comprehensively demonstrated the rare expression of PD-L1 and PD-1 in pulmonary MEC, ACC, and TBP. However, we found very strong PD-L1 immunopositivity on both TCs and ICs in one MEC sample, which warrants further investigations in a larger cohort.

KEYWORDS

adenoid cystic carcinoma, mucoepidermoid carcinoma, programmed cell death ligand-1 (PD-L1), programmed cell death-1 (PD-1), rare lung tumors

Introduction

Lung cancer is the leading cause of cancer death worldwide with a still very low 5-year survival rate of around 20% [1]. During the last decade immunotherapy has revolutionized lung cancer management especially in non-small cell lung cancer (NSCLC). By applying anti PD-1 (programmed cell death-1) and PD-L1 (programmed cell death ligand-1) immune checkpoint inhibitor treatment, unprecedented long survival could be achieved in both adenocarcinoma (ADC) and squamous cell carcinoma (SCC) subtypes of NSCLC [2, 3]. Patient selection for immunotherapy still represents challenges. Although PD-L1 immunohistochemistry (IHC) is not a perfect marker to predict the efficacy of immunotherapy, it is still the most widely used predictive marker in clinical practice [4]. PD-L1 status can be assessed with various primary antibodies and methods with different sensitivity, which limits the comparability of results from different investigations [5].

Rare lung cancer is a very heterogenous group of malignant tumors, which includes adenosquamous lung cancer, pulmonary sarcomatoid carcinoma, primary salivary gland-type lung tumor, and NUT (nuclear protein in testis) carcinoma. Mucoepidermoid carcinoma (MEC) and adenoid cystic carcinoma (ACC) derive from the salivary glands of the tracheobronchial tree and represent 0.1%–0.2% of all lung cancer cases [6]. These tumors are often located endobronchially, therefore, bronchoscopic excision can provide sufficient tissue sample for pathologic diagnosis. In well-localized, early-stage cases mechanical tumor extraction with or without LASER treatment using rigid bronchoscope under general anesthesia is an important part of patient management. In metastatic cases, therapeutic options are often limited and the combination of radiotherapy and chemotherapy yields only modest survival gains [7].

Tracheobronchial papilloma (TBP) is a rare benign lung tumor and in small size cases complete bronchoscopic removal may be a therapeutic solution. However, it has a high recurrence rate, and multiple recurrences may lead to malignant transformation into SCC.

The optimal treatment for MEC and ACC has not yet been determined, especially in metastatic cases. Radiotherapy and chemotherapy are used as systemic treatments, albeit with a very low cure rate [8]. The role of immunotherapy in the management of MEC and ACC is not clear, and PD-L1 expression levels have only been assessed using immunohistochemistry (IHC) in a few ACC cases and have not yet been investigated in MEC and TBP [9].

The aim of our present work was to comprehensively determine PD-L1/PD-1 expression in rare pulmonary tumors to study the potential applicability of immunotherapy.

Patients and methods

Ethics statement

The present study was conducted in accordance with the guidelines of the Helsinki Declaration of the World Medical Association. The study was approved by the national ethics committees (Hungarian Scientific and Research Ethics Committee of the Medical Research Council, ETT TUKEB 7214-1/2016/EKU [0109/16], ÁNTSZ IF-77-3/2016, SE IKEB 241/2016). The need for individual informed consent for this retrospective study was waived. After the collection of clinical information, patient identifiers were removed, and subsequently, patients could not be directly or indirectly identified.

Patients

Our retrospective study included 66 pathologically confirmed rare lung tumors including 26 mucoepidermoid carcinomas (MECs), 27 adenoid cystic carcinomas (ACCs), and 13 tracheobronchial papillomas (TBPs). Patients were diagnosed and treated in the National Koranyi Institute of Pulmonology in Budapest between 1987 and 2019, therefore, all tumor samples were re-examined. The ACC and MEC diagnoses were confirmed with the following IHC markers: pancytokeratin, actin, S100, and p63.

TABLE 1 Major characteristics of 66 patients diagnosed with and treated for mucoepidermoid carcinoma, adenoid cystic carcinoma, and tracheobronchial papilloma between 1987 and 2019.

Variables		MEC	ACC	TBP
Number of cases		26	27	13
Gender	Male	16 (62%)	9 (33%)	11 (85%)
	Female	10 (38%)	18 (67%)	2 (15%)
Mean age, range (years)		43.4 (24–67)	54.4 (32–83)	54.2 (21–80)
Smoking history, never/ex/current/nd		14/1/6/5	11/6/5/5	3/1/4/5
Bronchoscopic excision/Surgical material		7/19	18/9	12/1
Stage	IA/IB	9/8	0/7	
	IIA/IIB	0/3	0/1	
	IIIA/IIIB	2/0	16/0	
	IV/nd	1/3	0/3	

MEC, mucoepidermoid carcinoma; ACC, adenoid cystic carcinoma; TBP, tracheobronchial papilloma; nd, no data.

The clinicopathological characteristics of patients including age, gender, smoking history, histology, stage and the type of biopsy material are summarized in Table 1.

Immunohistochemistry

In the case of surgical specimens immunohistochemical IHC staining was performed on tissue microarrays (TMAs) (5 × 6; diameter, 2 mm) with double or triple cores per patient, prepared from selected areas of formalin fixed paraffin embedded (FFPE) tissue samples (TMA Master; 3DHistech, Budapest, Hungary). In the case of bronchoscopic excisions 3-μm-thick sections were prepared for IHC without TMA construction.

Ventana SP142 was first used as a primary antibody for PD-L1 (clone SP142, dilution 1:100; Spring Bioscience, Ventana; Oro Valley, AZ). However, we did not detect any immunoreaction either on tumor cells (TC) or on immune cells (IC), therefore, we subsequently applied PharmDx 22C3 antibody. For PD-1 staining Abcam 52587 antibody was used. The mouse monoclonal PD-L1 and PD-1 antibodies (PharmDx, clone 22C3, ready to use, and Abcam, clone NAT105, dilution 1:50, respectively) were used for IHC in line with standardized protocols. After deparaffinization and rehydration, the sections were incubated in a 3% H_2O_2 solution for 10 min in order to reduce the nonspecific background staining. It was heated afterwards for 40 min in a 10 mM citrate buffer (pH 6.0) at 98°C. Slides were then incubated for 5 min at room temperature with Ultra V Block (UltraVision LP detection system, Lab Vision Corporation, Thermo Fisher Scientific Inc., Pittsburgh, MA, United States), followed by PD-L1 and PD-1 antibody incubation for overnight at 4°C. Immunoreaction was detected using the UltraVision LP Detection System following the manufacturer's recommendations (Lab Vision Corporation). The antibody visualization was performed with 3–3′-diaminobenzidine (DAB) and counterstained with hematoxylin. As a positive control, placental tissue was used.

All sections were examined and evaluated by an experienced pathologist at ×400 magnification. The amount of positive TC and IC was determined by a semi-quantitative method as the percentage of positive cells. For TC 1%, 5%, and 50%, while for IC 1%, 5%, and 10% cut off levels were recorded, which are the most commonly used thresholds and wich we also used in our previous studies [10–15].

Statistical analysis

All statistical analyses were performed using SPSS Statistics 25.0 package (SPSS Inc., Chicago, IL, United States). Dichotomization concerning age was performed by using one of the widely used threshold values in cancer studies (55 years) [16]. Due to the low number of cases, categorical parameters, such as age (≤55 years vs. >55 years), gender (male vs. female) and smoking history (never smoker vs. ex-smoker vs. smoker) were analyzed by Fisher's exact test. Different PD-L1/PD-1 subgroups (<1% vs. ≥1%) were also compared using Fisher's exact test. All reported p values were two-sided, and a level of 0.05 or lower was considered statistically significant.

Results

PD-L1 expression

Since the first immunostaining for PD-L1 with Ventana SP142 antibody did not yield positive immunoreaction on any of the slides, we also used PharmDx 22C3 antibody.

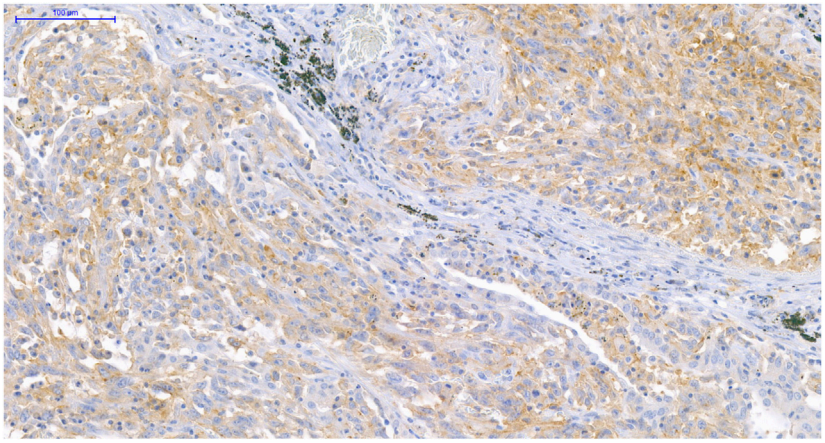

FIGURE 1
PD-L1 immunohistochemistry (IHC) of MEC. IHC shows >50% PD-L1 positive TCs and >10% PD-L1 positive ICs in MEC (×200).

PD-L1 expression on TCs was observed in two cases of MEC (7.7%), one case of ACC (3.7%), and was absent in TBP samples, while PD-L1 expression on ICs could be demonstrated in nine cases of MEC (34.6%), four cases of ACC (14.8%), and was absent in TBPs. Although these ratios indicate a higher positivity rate in MEC compared to ACC, the difference was not significant ($p = 0.119$). All PD-L1 TC positive tumors were also PD-L1 IC positive. Expression level higher than 5% of PD-L1 TC and IC was observed only in one ACC and in two MEC patients. Among them only one female smoker patient with MEC presented with strong PD-L1 expression both on TCs (≥50%) and ICs (≥10%) (Figure 1); a male patient with MEC had 5%–49% PD-L1 TC level, and another male patient with ACC had 5%–9% PD-L1 IC level.

PD-1 expression

PD-1 expression on ICs was observed in five cases of MEC (19.2%), four cases of ACC (14.8%), and two cases of TBP (15.4%). A higher than 5% expression level of PD-1 on ICs was observed only in one MEC case.

Since we only found very few samples with higher than 5% PD-L1/PD-1 expression on TCs and ICs, we used dichotomized categories (i.e., positive [≥1%] vs. negative [<1%]) for statistical analysis.

Correlation between PD-1/PD-L1 expression and clinicopathological findings

We examined the potential correlation between clinicopathological findings and the different PD-1/PD-L1 expression profiles of the tumors. In MEC cases, PD-L1 expression levels of ≥1% on TCs and ICs were significantly more common in patients aged 55 years or older, than in younger patients ($p = 0.046$, and $p = 0.01$, respectively). Apart from these observations, no other significant correlation was found between PD-L1/PD-1 expression levels and patient characteristics, such as age, gender or smoking history. These results are summarized in Tables 2–4.

The association between tumor histology and PD-L1 expression on TCs and ICs, and PD-1 expression on ICs was also examined. A PD-L1 expression level of ≥1% on ICs were significantly more common in MEC, than in TBP ($p < 0.001$) (Table 5). No other significant correlations were observed.

Since the age of FFPE blocks can influence the IHC reactions, we compared older and newer tissue materials, however, we found no statistically significant difference in IHC positivity rates between pre- and post-2006 samples.

Discussion

The role of immunotherapy in the treatment of MEC and ACC has not been extensively studied, and the majority of available publications focus on head and neck salivary gland tumors. In a recent case report successful treatment with low-dose radiotherapy combined with immunotherapy was described in a patient with metastatic submandibular salivary gland ACC, however, no such data have been reported in lung ACC so far [17]. Farhat et al. reported a case of advanced high-grade MEC of the parotid salivary gland after pembrolizumab treatment as a first line therapy [18]. The tumor was downstaged as a result of the immunotherapy, allowing for

TABLE 2 Association between PD-L1 expression on TCs and clinicopathological factors.

Clinicopathological characteristics		MEC (n = 26)			ACC (n = 27)			TBP (n = 13)		
		PD-L1 TC <1%	PD-L1 TC ≥ 1%	p-value[a]	PD-L1 TC <1%	PD-L1 TC ≥ 1%	p-value[a]	PD-L1 TC <1%	PD-L1 TC ≥ 1%	p-value[a]
Age (years)	≤55	20	0	**0.046**[b]	11	1	0.444[b]	7	0	0.999[b]
	>55	4	2		15	0		6	0	
Gender	Male	15	1	0.999[b]	8	1	0.333[b]	11	0	0.999[b]
	Female	9	1		18	0		2	0	
Smoking history	Never smoker	13	1	0.604[b]	10	1	0.681[b]	3	0	0.999[b]
	Ex-smoker	1	0		6	0		1	0	
	Smoker	5	1		5	0		4	0	
	nd	5	0		5	0		5	0	

[a]p values refer to PD-L1 negative versus PD-L1 positive subgroups.
[b]Fisher's exact test was used between categorical variables; MEC, mucoepidermoid carcinoma; ACC, adenoid cystic carcinoma; TBP, tracheobronchial papilloma; nd, no data; TC, tumor cell; PD-L1, programmed death ligand-1.
Bold represents statistically significant p value.

surgical excision. Recently, two cases of metastatic high-grade MECs presented as left neck mass with prolonged response to pembrolizumab have been published [19]. In 2022, a comprehensive overview summarized novel therapeutic approaches including targeted therapy and immunotherapy in different subtypes of salivary gland cancer [20]. However, this publication only focused on head and neck tumors. In a very recent publication, Hu et al. provided a thorough overview of the main diagnostic and therapeutic implications of pulmonary MEC including targeted therapy, chemotherapy, and immunotherapy [21]. They confirm that the immunotherapy approach for this type of tumor is limited so far and needs to be explored in-depth. They reported only one publication dealing with PD-L1/PD-1 expression in lung MEC, however, this article was published in Fujian Medical Journal, and is not available on PubMed [22].

The potential predictive value of PD-L1/PD-1 expression for the efficacy of immunotherapy in salivary gland tumors is not yet understood, and the majority of publications related to ACC focus on PD-L1 and PD-1 expression in head and neck tumors [23]. Zheng et al. compared the PD-L1 expression in tracheobronchial ACC and SCC, and found no expression in the studied 16 ACC samples, whereas 80% of SCCs were PD-L1 positive [9]. Their methodology was similar to our current study in terms of the applied clone (PD-L1 22C3 clone) and the threshold for PD-L1 positivity (expression ≥1%). In our present work PD-L1 was positive in 1/27 ACC tumors on TCs, and in 4/27 tumors on ICs. In one of our MEC samples, a strong PD-L1 immunopositivity of >50% could be observed on TCs.

Witte et al. investigated PD-L1 expression on ICs in 94 head and neck salivary gland carcinomas including 41 ACCs, 21 MECs, 16 acinic cell carcinomas, 12 adenocarcinomas not otherwise specified, 2 epithelial-myoepithelial carcinomas, one salivary duct carcinoma, and one carcinoma ex pleomorphic adenoma. Using SP263 clone for PD-L1 IHC, they identified significantly elevated IC scores in adenocarcinomas not otherwise specified compared to ACC and MEC [24]. In our study, PD-L1 positivity on ICs was more common in MEC than in ACC (34.6% vs. 14.8%), although the difference was not statistically significant. Higher than 5% expression levels were observed in three MEC samples, and in one case it was even >10%.

In salivary gland tumors, data regarding PD-1 expression are even more scarce, than on PD-L1 expression. In our study, PD-1 expression on ICs was found in 19.2% of MEC, 14.8% of ACC, and 15.4% of TBP samples. This is lower than what Xu et al. observed in salivary duct carcinoma, where PD-1 positivity on ICs was noted in 66% of cases, but higher than in the study by Mosconi et al. which found scarce PD-1 positivity in 36 salivary gland ACCs [25, 26].

TBPs are often treated with bronchoscopic excision, and radical removal of the tumor usually results in complete recovery.

TABLE 3 Association between PD-L1 expression on ICs and clinicopathological factors.

Clinicopathological characteristics		MEC (n = 26)			ACC (n = 27)			TBP (n = 13)		
		PD-L1 IC <1%	PD-L1 IC ≥ 1%	p-value[a]	PD-L1 IC <1%	PD-L1 IC ≥ 1%	p-value[a]	PD-L1 IC <1%	PD-L1 IC ≥ 1%	p-value[a]
Age (years)	≤55	16	4	**0.01**[b]	11	1	0.999[b]	7	0	0.999[b]
	>55	1	5		12	3		6	0	
Gender	Male	12	4	0.667[b]	7	2	0.581[b]	11	0	0.999[b]
	Female	5	5		16	2		2	0	
Smoking history	Never smoker	9	5	0.613[b]	9	2	0.582[b]	3	0	0.999[b]
	Ex-smoker	1	0		5	1		1	0	
	Smoker	3	3		4	1		4	0	
	nd	4	1		5	0		5	0	

[a]p values refer to PD-L1 negative versus PD-L1 positive subgroups.
[b]Fisher's exact test was used between categorical variables; MEC, mucoepidermoid carcinoma; ACC, adenoid cystic carcinoma; TBP, tracheobronchial papilloma; IC, immune cell; nd, no data; PD-L1, programmed death ligand-1.
Bold represents statistically significant p value.

TABLE 4 Association between PD-1 expression on ICs and clinicopathological factors.

Clinicopathological characteristics		MEC (n = 26)			ACC (n = 27)			TBP (n = 13)		
		PD-1 IC <1%	PD-1 IC ≥ 1%	p-value[a]	PD-1 IC <1%	PD-1 IC ≥ 1%	p-value[a]	PD-1 IC <1%	PD-1 IC ≥ 1%	p-value[a]
Age (years)	≤55	17	3	0.558[b]	11	1	0.999[b]	6	1	0.999[b]
	>55	4	2		12	3		5	1	
Gender	Male	13	3	0.999[b]	7	2	0.582[b]	9	2	0.999[b]
	Female	8	2		16	2		2	0	
Smoking history	Never smoker	11	3	0.613[b]	9	2	0.582[b]	3	0	0.218[b]
	Ex-smoker	1	0		5	1		1	0	
	Smoker	4	2		4	1		4	0	
	nd	5	0		5	0		3	2	

[a]p values refer to PD-1 negative versus PD-1 positive subgroups.
[b]Fisher's exact test was used between categorical variables; MEC, mucoepidermoid carcinoma; ACC, adenoid cystic carcinoma; TBP, tracheobronchial papilloma; IC, immune cell; nd, no data; PD-1, programmed death-1.

TABLE 5 Association between the tumor histology and PD-L1 expression on TCs/ICs and PD-1 expression on ICs.

PD-L1 TC	MEC (%)	ACC (%)	TBP (%)	p-value[a]	PD-L1 IC	MEC (%)	ACC (%)	TBP (%)	p-value[a]	PD-1 IC	MEC (%)	ACC (%)	TBP (%)	p-value[a]
<1%	24 (92.3%)	26 (96.3%)	13 (100%)	0.192[b]	<1%	17 (65.4%)	23 (85.2%)	13 (100%)	**<0.001**[b,c]	<1%	21 (80.8%)	23 (85.2%)	11 (84.6%)	0.082[b]
≥1%	2 (7.7%)	1 (3.7%)	0 (0%)		≥1%	9 (34.6%)	4 (14.8%)	0 (0%)		≥1%	5 (19.2%)	4 (14.8%)	2 (15.4%)	

[a]p values refer to PD-L1/PD-1 negative versus PD-L1/PD-1 positive subgroups.
[b]Fisher's exact test was used between categorical variables.
[c]A PD-L1 expression level of ≥1% on ICs were significantly more common in MEC, than in TBP; MEC, mucoepidermoid carcinoma; ACC, adenoid cystic carcinoma; TBP, tracheobronchial papilloma; TC, tumor cell; IC, immune cell; nd, no data; PD-1, programmed death-1; PD-L1, programmed death ligand-1.
Bold represents statistically significant p value.

In recurrent cases and/or in tracheobronchial papillomatosis, there is a risk of malignant transformation to SCC, and bronchoscopic tumor resection is no longer feasible in extensive disease. Therefore, it is important to determine the potential role of immunotherapy in irresectable cases. Currently, PD-L1 expression on TCs and ICs is the most widely used predictive biomarker for immunotherapy in head and neck SCC. Nevertheless, patients with PD-L1 negative tumors may still respond to treatment. In our present study, we found no PD-L1 expression on TC-s or ICs in TBP tumor samples, and only 2 TBP cases (15.4%) showed weak PD-1 positivity on ICs.

Several antibodies are used to examine PD-L1 protein expression. At the beginning of the 2010s, SP142 proved to be the most suitable antibody. A few years later a comparative study was carried out, in which the goal was to analyze four commercially available antibodies that had already appeared in clinical practice. During this, it was determined that in lung cancer, Ventana's SP142 antibody is less sensitive than the other three antibodies (Ventana SP263, Dako 22C3, Dako 28–8) [27]. The results of our present study also confirm this observation, as no IHC positive samples were found when SP142 antibody was used initially, and highlight the importance of using anti-PD-L1 antibody with proper sensitivity in order to avoid false negative IHC results.

In lung cancer, indications for immunotherapy are constantly expanding. Previously, it was mainly used in advanced-stage NSCLC as second- or third line treatment, however, nowadays the range of indications extends to the first line treatment, usually combined with chemotherapy [2]. Furthermore, the role of immunotherapy in the neoadjuvant and adjuvant settings is also being investigated [28]. It has been clearly demonstrated that the most favorable therapeutic response can be expected in case of >50% PD-L1 expression, however, patients with PD-L1 negative tumors may also respond to immunotherapy [29–31]. Furthermore, many clinical trials use the PD-L1 cut-off value of 1% as an inclusion criterion. In our work 34.6% of MEC and 14.8% of ACC cases belonged to the ≥1% PD-L1 IC group, and higher than 5% expression levels on TC and/or IC were detected in one ACC and two MEC samples.

Lung cancer subtypes previously considered homogeneous are increasingly being recognized as heterogeneous, which has important therapeutic implications. In lung adenocarcinoma, the determination of the molecular subtype and PD-L1 expression level is now essential for treatment decision-making. Although certain molecular subtypes comprise only few patients, such as Her2 (3%), MET (3%), RET (1%), and ROS1 (1%), targeted therapy may offer significant benefits for them [32]. Similarly, small cell lung cancer is no longer considered a homogenous group, since four molecular subgroups have been discovered, which also have major therapeutic implications [33, 34]. The different PD-L1 and PD-1 expression levels in MEC and ACC tumors found in our study raise the possibility of heterogeneity in these groups, too, which seems to be supported by recent molecular genetic studies in salivary gland ACC [35].

Notwithstanding, our results might suffer from the limitations of having a relatively small number of cases. Undoubtedly, a significantly larger cohort would give more reliable insights into the expression of the described biomarkers in MEC, ACC and TBP, however, in rare tumors, usually it takes many years to collect the number of cases suitable for such examinations. Other limitation might be the age of FFPE tissue samples, which may affect IHC reactions. In order to investigate this, we compared the IHC results of early and late tissue samples and found no significant difference.

Based on PubMed publications, our study is the first to report comprehensive data on PD-L1/PD-1 expressions in primary pulmonary MEC and TBP, and confirms the results of the very few published studies in lung ACC. In these rare pulmonary tumors, there is unmet need to develop more efficient therapeutic modalities, especially for patients with advanced-stage disease. Our results demonstrate that primary lung salivary gland tumors are heterogeneous not only in terms of the MEC/ACC subgroups, but also within these histologic subtypes. A more comprehensive exploration of this observation in a larger cohort may contribute to personalized therapy in rare lung cancers. If ≥50% PD-L1 TC in MEC is confirmed even if only in a low proportion of patients, MEC with high PD-L1 expression might be regarded as a separate subgroup with distinct treatment option, such as immune checkpoint inhibition therapy.

Data availability statement

The original contributions presented in the study are included in the article/supplementary material, further inquiries can be directed to the corresponding author.

Ethics statement

The present study was conducted in accordance with the guidelines of the Helsinki Declaration of the World Medical Association. The study was approved by the national ethics committees (Hungarian Scientific and Research Ethics Committee of the Medical Research Council, ETT TUKEB 7214-1/2016/EKU [0109/16], ÁNTSZ IF-77-3/2016, SE IKEB 241/2016). The need for individual informed consent for this retrospective study was waived. After the collection of clinical information, patient identifiers were removed, and subsequently, patients could not be directly or indirectly identified.

Author contributions

MG: conceptualization, methodology, bronchoscopic sampling, investigation, and writing—original draft. ZM: statistical analysis and writing—review editing. LR: immunohistochemical investigations. TH: TMA construction and investigation. BF: statistical analysis and writing—original draft. LK: development of clinical database. LA: providing surgical materials. JF: methodology and supervision. BD: supervision and validation. ZS: supervision and writing—review editing. JM: conceptualization, validation, supervision, writing—original draft. All authors contributed to the article and approved the submitted version.

Funding

ZM was supported by the UNKP-20-3 and UNKP-21-3 New National Excellence Program of the Ministry for Innovation and Technology of Hungary and by the Hungarian Respiratory Society (MPA #2020). ZM is also the recipient of the IASLC/ILCF Young Investigator Grant. BF is a recipient of Semmelweis 250+ Excellence PhD Scholarship (EFOP-3.6.3-VEKOP-16-2017-00009) by Semmelweis University. BD acknowledge funding from the Hungarian National Research, Development and Innovation Office (KH130356, K129065, and KNN121510) and the Austrian Science Fund (FWF I3977 and I4677). ZS was supported by the Breast Cancer Research Foundation and the Novo Nordisk Foundation Interdisciplinary Synergy Programme Grant (NNF15OC0016584). JM was supported by the Hungarian National Research, Development and Innovation Office (K129065) and by the Hungarian Brain research Program (grant 2017-1.2.1-NKP-2017-00002).

Conflict of interest

The authors declare that the research was conducted in the absence of any commercial or financial relationships that could be construed as a potential conflict of interest.

References

1. Sung H, Ferlay J, Siegel RL, Laversanne M, Soerjomataram I, Jemal A, et al. Global cancer Statistics 2020: GLOBOCAN estimates of incidence and mortality worldwide for 36 cancers in 185 countries. *CA: A Cancer J Clin* (2021) 71(3):209–49. doi:10.3322/caac.21660

2. Shao T, Zhao M, Liang L, Tang W. A systematic review and network meta-analysis of first-line immune checkpoint inhibitor combination therapies in patients with advanced non-squamous non-small cell lung cancer. *Front Immunol* (2022) 13:948597. doi:10.3389/fimmu.2022.948597

3. O'Byrne K, Popoff E, Badin F, Lee A, Yuan Y, Lozano-Ortega G, et al. Long-term comparative efficacy and safety of nivolumab plus ipilimumab relative to other first-line therapies for advanced non-small-cell lung cancer: A systematic literature review and network meta-analysis. *Lung Cancer* (2023) 177:11–20. doi:10.1016/j.lungcan.2023.01.006

4. Ancevski Hunter K, Socinski MA, Villaruz LC. PD-L1 testing in guiding patient selection for PD-1/PD-L1 inhibitor therapy in lung cancer. *Mol Diagn Ther* (2018) 22(1):1–10. doi:10.1007/s40291-017-0308-6

5. Maule JG, Clinton LK, Graf RP, Xiao J, Oxnard GR, Ross JS, et al. Comparison of PD-L1 tumor cell expression with 22C3, 28-8, and SP142 IHC assays across multiple tumor types. *J Immunother Cancer* (2022) 10(10):e005573. doi:10.1136/jitc-2022-005573

6. Pisano C, Witel G, De Filippis M, Listì A, Napoli F, Righi L, et al. Moving through rare lung cancer histologies: A narrative review on diagnosis and treatment of selected infrequent entities. *Precis Cancer Med* (2022) 5:27. doi:10.21037/pcm-22-4

7. Lee RH, Wai KC, Chan JW, Ha PK, Kang H. Approaches to the management of metastatic adenoid cystic carcinoma. *Cancers (Basel)* (2022) 14(22):5698. doi:10.3390/cancers14225698

8. Garg PK, Sharma G, Rai S, Jakhetiya A. Primary salivary gland-type tumors of the lung: A systematic review and pooled analysis. *Lung India* (2019) 36(2):118–22. doi:10.4103/lungindia.lungindia_284_18

9. Zheng KF, Liu YJ, Ma N, Xiong YL, Tang XY, Zhang Q, et al. PD-L1 expression and immune cells infiltration in primary tracheobronchial neoplasm. *Transl Lung Cancer Res* (2021) 10(12):4617–30. doi:10.21037/tlcr-21-958

10. Festino L, Botti G, Lorigan P, Masucci GV, Hipp JD, Horak CE, et al. Cancer treatment with anti-PD-1/PD-L1 agents: Is PD-L1 expression a biomarker for patient selection? *Drugs* (2016) 76(9):925–45. doi:10.1007/s40265-016-0588-x

11. Yang CY, Lin MW, Chang YL, Wu CT, Yang PC. Programmed cell death-ligand 1 expression is associated with a favourable immune microenvironment and better overall survival in stage I pulmonary squamous cell carcinoma. *Eur J Cancer* (2016) 57:91–103. doi:10.1016/j.ejca.2015.12.033

12. Téglási V, Pipek O, Lózsa R, Berta K, Szüts D, Harkó T, et al. PD-L1 expression of lung cancer cells, unlike infiltrating immune cells, is stable and unaffected by therapy during brain metastasis. *Clin Lung Cancer* (2019) 20(5):363–9. doi:10.1016/j.cllc.2019.05.008

13. Reiniger L, Téglási V, Pipek O, Rojkó L, Glasz T, Vágvölgyi A, et al. Tumor necrosis correlates with PD-L1 and PD-1 expression in lung adenocarcinoma. *Acta Oncol* (2019) 58(8):1087–94. doi:10.1080/0284186X.2019.1598575

14. Rojkó L, Reiniger L, Téglási V, Fábián K, Pipek O, Vágvölgyi A, et al. Chemotherapy treatment is associated with altered PD-L1 expression in lung cancer patients. *J Cancer Res Clin Oncol* (2018) 144(7):1219–26. doi:10.1007/s00432-018-2642-4

15. Téglási V, Reiniger L, Fábián K, Pipek O, Csala I, Bagó AG, et al. Evaluating the significance of density, localization, and PD-1/PD-L1 immunopositivity of mononuclear cells in the clinical course of lung adenocarcinoma patients with brain metastasis. *Neuro Oncol* (2017) 19(8):1058–67. doi:10.1093/neuonc/now309

16. Guan R, Lyu Q, Lin A, Liang J, Ding W, Cao M, et al. Influence of different age cutoff points on the prediction of prognosis of cancer patients receiving ICIs and potential mechanistic exploration. *Front Oncol* (2021) 11:670927. doi:10.3389/fonc.2021.670927

17. Li D, Pang X, Zhu X, Shanzhou Q, Wen G, Ma D. Low-dose radiotherapy combined with immunotherapy for suboral adenoid cystic carcinoma with bilateral lung metastasis: A case report and literature review. *Oncol Lett* (2022) 24(2):279. doi:10.3892/ol.2022.13399

18. Farhat R, Asna N, Avraham Y, Khater A, Asakla M, Safia A, et al. Pembrolizumab as a first line therapy in a patient with extensive mucoepidermoid salivary gland carcinoma. A complete clinical, radiological and pathological response. A very specific case. *Discov Oncol* (2022) 13(1):37. doi:10.1007/s12672-022-00502-4

19. Pharaon RR, Gernon T, Chang S, Vora N, Villaflor VM, Bell D, et al. Prolonged response to checkpoint inhibitor therapy in two metastatic mucoepidermoid salivary gland carcinoma cases: A research report. *Cold Spring Harb Mol Case Stud* (2022) 8(3):a006189. doi:10.1101/mcs.a006189

20. Mueller SK, Haderlein M, Lettmaier S, Agaimy A, Haller F, Hecht M, et al. Targeted therapy, chemotherapy, immunotherapy and novel treatment options for different subtypes of salivary gland cancer. *J Clin Med* (2022) 11(3):720. doi:10.3390/jcm11030720

21. Hu S, Gong J, Zhu X, Lu H. Pulmonary salivary gland tumor, mucoepidermoid carcinoma: A literature review. *J Oncol* (2022) 2022:9742091. doi:10.1155/2022/9742091

22. Liu J, Wu L, Lin Q. Expression of programmed death receptor 1 and its ligand in primary lung mucoepidermoid carcinoma and its clinical significance. *Fujian Med J* (2018) 40(6):16–9.

23. Gerdabi S, Asadian F, Kiani R, Khademi B, Haghshenas MR, Erfani N. Simultaneous expression of PD-1 and PD-L1 in peripheral and central immune cells and tumor cells in the benign and malignant salivary gland tumors microenvironment. *Head Neck Pathol* (2022) 17(1):178–92. doi:10.1007/s12105-022-01486-x

24. Witte HM, Gebauer N, Lappöhn D, Umathum VG, Riecke A, Arndt A, et al. Prognostic impact of PD-L1 expression in malignant salivary gland tumors as assessed by established scoring criteria: Tumor proportion score (TPS), combined positivity score (CPS), and immune cell (IC) infiltrate. *Cancers* (2020) 12(4):873. doi:10.3390/cancers12040873

25. Xu B, Jungbluth AA, Frosina D, Alzumaili B, Aleynick N, Slodkowska E, et al. The immune microenvironment and expression of PD-L1, PD-1, PRAME and MHC I in salivary duct carcinoma. *Histopathology* (2019) 75(5):672–82. doi:10.1111/his.13944

26. Mosconi C, de Arruda JAA, de Farias ACR, Oliveira GAQ, de Paula HM, Fonseca FP, et al. Immune microenvironment and evasion mechanisms in adenoid cystic carcinomas of salivary glands. *Oral Oncol* (2019) 88:95–101. doi:10.1016/j.oraloncology.2018.11.028

27. Hendry S, Byrne DJ, Wright GM, Young RJ, Sturrock S, Cooper WA, et al. Comparison of four PD-L1 immunohistochemical assays in lung cancer. *J Thorac Oncol* (2018) 13(3):367–76. doi:10.1016/j.jtho.2017.11.112

28. Peng Y, Li Z, Fu Y, Pan Y, Zeng Y, Liu J, et al. Progress and perspectives of perioperative immunotherapy in non-small cell lung cancer. *Front Oncol* (2023) 13:1011810. doi:10.3389/fonc.2023.1011810

29. Shah M, Marmarelis ME, Mamtani R, Hennessy S. Association between survival and very high versus high PD-L1 expression in patients receiving pembrolizumab as first-line treatment for advanced non-small cell lung cancer. *Clin Lung Cancer* (2022) 23(8):731–6. doi:10.1016/j.cllc.2022.07.003

30. Stinchcombe TE. Narrative review: Blood and tumor biomarker testing in non-small cell lung cancer without an oncogenic driver. *Transl Lung Cancer Res* (2023) 12(1):158–67. doi:10.21037/tlcr-22-530

31. Wankhede D, Hofman P, Grover S. PD-1/PD-L1 inhibitors in treatment-naïve, advanced non-small cell lung cancer patients with < 1% PD-L1 expression: A meta-analysis of randomized controlled trials. *J Cancer Res Clin Oncol* (2022) 149:2179–89. doi:10.1007/s00432-022-04286-6

32. Chevallier M, Borgeaud M, Addeo A, Friedlaender A. Oncogenic driver mutations in non-small cell lung cancer: Past, present and future. *World J Clin Oncol* (2021) 12(4):217–37. doi:10.5306/wjco.v12.i4.217

33. Lang C, Lantos A, Megyesfalvi Z, Egger F, Hoda MA, Mosleh B, et al. Clinical and prognostic implications of CD47 and PD-L1 expression in surgically resected small-cell lung cancer. *ESMO Open* (2022) 7(6):100631. doi:10.1016/j.esmoop.2022.100631

34. Qi J, Zhang J, Liu N, Zhao L, Xu B. Prognostic implications of molecular subtypes in primary small cell lung cancer and Their correlation with cancer immunity. *Front Oncol* (2022) 12:779276. doi:10.3389/fonc.2022.779276

35. de Sousa LG, Jovanovic K, Ferrarotto R. Metastatic adenoid cystic carcinoma: Genomic landscape and emerging treatments. *Curr Treat Options Oncol* (2022) 23(8):1135–50. doi:10.1007/s11864-022-01001-y

Pathology & Oncology Research | frontiers

TYPE Original Research
PUBLISHED 20 April 2023
DOI 10.3389/pore.2023.1610914

Check for updates

OPEN ACCESS

EDITED BY
Anna Sebestyén,
Semmelweis University, Hungary

*CORRESPONDENCE
Pavel Otáhal,
pavel.otahal@uhkt.cz

RECEIVED 31 October 2022
ACCEPTED 28 March 2023
PUBLISHED 20 April 2023

CITATION
Štach M, Pytlík R, Šmilauerová K, Rychlá J, Mucha M, Musil J, Koladiya A, Nemec M, Petráčková M, Kaštánková I, Pecherková P, Šrámková L, Polgárová K, Trněný M, Lesný P, Vydra J and Otáhal P (2023), Characterization of the input material quality for the production of tisagenlecleucel by multiparameter flow cytometry and its relation to the clinical outcome.
Pathol. Oncol. Res. 29:1610914.
doi: 10.3389/pore.2023.1610914

COPYRIGHT
© 2023 Štach, Pytlík, Šmilauerová, Rychlá, Mucha, Musil, Koladiya, Nemec, Petráčková, Kaštánková, Pecherková, Šrámková, Polgárová, Trněný, Lesný, Vydra and Otáhal. This is an open-access article distributed under the terms of the Creative Commons Attribution License (CC BY). The use, distribution or reproduction in other forums is permitted, provided the original author(s) and the copyright owner(s) are credited and that the original publication in this journal is cited, in accordance with accepted academic practice. No use, distribution or reproduction is permitted which does not comply with these terms.

Characterization of the input material quality for the production of tisagenlecleucel by multiparameter flow cytometry and its relation to the clinical outcome

Martin Štach[1,2], Robert Pytlík[1,3], Kristýna Šmilauerová[1,2], Jana Rychlá[1], Martin Mucha[1,2], Jan Musil[1], Abhishek Koladiya[1], Matěj Nemec[1], Martina Petráčková[1], Iva Kaštánková[1], Pavla Pecherková[1], Lucie Šrámková[4], Kamila Polgárová[3,5], Marek Trněný[3,5], Petr Lesný[1], Jan Vydra[1] and Pavel Otáhal[1,3]*

[1]Institute of Hematology and Blood Transfusion, Praha, Czechia, [2]Faculty of Science, Charles University, Praha, Czechia, [3]First Faculty of Medicine, Charles University, Praha, Czechia, [4]Second Faculty of Medicine (2. LF UK), University Hospital in Motol, Praha, Czechia, [5]General University Hospital in Prague, Praha, Czechia

Tisagenlecleucel (tisa-cel) is a CD19$^-$specific CAR-T cell product approved for the treatment of relapsed/refractory (r/r) DLBCL or B-ALL. We have followed a group of patients diagnosed with childhood B-ALL (n = 5), adult B-ALL (n = 2), and DLBCL (n = 25) who were treated with tisa-cel under non-clinical trial conditions. The goal was to determine how the intensive pretreatment of patients affects the produced CAR-T cells, their *in vivo* expansion, and the outcome of the therapy. Multiparametric flow cytometry was used to analyze the material used for manufacturing CAR-T cells (apheresis), the CAR-T cell product itself, and blood samples obtained at three timepoints after administration. We present the analysis of memory phenotype of CD4/CD8 CAR-T lymphocytes (CD45RA, CD62L, CD27, CD28) and the expression of inhibitory receptors (PD-1, TIGIT). In addition, we show its relation to the patients' clinical characteristics, such as tumor burden and sensitivity to prior therapies. Patients who responded to therapy had a higher percentage of CD8$^+$CD45RA$^+$CD27$^+$ T cells in the apheresis, although not in the produced CAR-Ts. Patients with primary refractory aggressive B-cell lymphomas had the poorest outcomes which was characterized by undetectable CAR-T cell expansion *in vivo*. No clear correlation of the outcome with the immunophenotypes of CAR-Ts was observed. Our results suggest that an important parameter predicting therapy efficacy is CAR-Ts' level of expansion *in vivo* but not the immunophenotype. After CAR-T cells' administration, measurements at several timepoints accurately detect their proliferation intensity *in vivo*. The outcome of CAR-T cell therapy largely depends on biological characteristics of the tumors rather than on the immunophenotype of produced CAR-Ts.

10.3389/pore.2023.1610914

KEYWORDS

immunotherapy, CAR-T cells, tisagenlecleucel, B-cell lymphoma and leukemia, Kymriah

Introduction

Tisagenlecleucel (tisa-cel, Kymriah®) is CD19$^-$specific CAR-T-cell product approved for the treatment of relapsed/refractory (r/r) DLBCL or B-ALL. First, an input material is obtained *via* apheresis from individual patients to produce CAR-T cells. Collected peripheral blood mononuclear cells (PBMCs) are then cryopreserved and supplied to the manufacturer. Followingly, PBMCs are transduced with lentiviral vector, expanded *in vitro*, and cryopreserved. The generated CAR-T cells are usually within a month supplied back to the hospital site. However, such a highly complex process utilizes materials obtained from patients who received multiple lines of intensive chemotherapeutic regimens and have active disease. Additionally, the variability within differentiation/memory subsets of T cells in the apheresis might affect the quality of produced CAR-T cells and subsequently limit the efficacy of the treatment (1, 2).

Treatment of DLBCL with CD19$^-$specific CAR-T cells such as tisa-cel is slightly less effective than identical approach to patients with B-ALL (2–6). Generally, two types of treatment failure are encountered. The first type is non-responsiveness—the patients do not achieve even a partial remission (PR) within 2–3 months post-treatment. The second type is late relapse after achievement of good clinical response following CAR-T cell treatment (7). Detailed analysis of the input material and the produced CAR-T cells could help identify factors responsible for these types of treatment failures (8–10).

The first goal of our study was to perform a detailed FACS analysis of the apheretic material used for CAR-T cells' production to determine present leukocyte subsets and the immunophenotype of T cells. Secondly, the manufactured product was analyzed to determine the percentage of CAR$^+$ cells and their memory phenotype. Thirdly, CAR-T cells' expansion kinetics and their differentiation status were measured in samples of peripheral blood after treatment. Collected measurements were compared with the treatment efficiency and patients' survival.

In summary, this study describes the analysis of apheresis, manufactured CAR-T cells and samples of patients treated with tisa-cel. Based on obtained measurements and clinical data, our results suggest that a specific phenotype of starting material (i.e., apheresis) influences possible success of the therapy. The results also show that undetectable CAR-T cell expansion at D+14 is linked to early treatment failure ($p < 0.05$) which might provide a chance to effectively indicate the patient enrollment into clinical trials.

Results

Detection of CAR-T cells and gating strategy for their phenotyping

To identify CAR-T cells, we used recombinant PE-conjugated CD19 protein for the first eight patients due to the unavailability of anti-FMC63 antibody, which was then used for the remaining patients. Example of staining is presented in Supplementary Figure S1. CAR-T cells were further stained with a multicolor antibody panel to determine their differentiation immunophenotype using antibodies against antigens CD3, CD4, CD8, CD14, CD45RA, CD62L, CD27, CD28, PD-1, and TIGIT (11). Additionally, samples were analyzed with a second antibody panel to determine the composition of all significant leukocyte subsets using antibodies against antigens CD3, CD4, CD8, CD14, CD16, CD19, CD45, CD56, and TCRgd. Figure 1 shows an example of typical CAR detection. Gating strategy of CAR-T memory subsets is similarly presented in Figure 2. Pre-gating on CD3$^+$ cells is shown in Supplementary Figure S2. Controls for CAR staining (healthy donor) and immunophenotype staining (FMOs, healthy donor) are presented in Supplementary Figures S3, S4, respectively. Threshold for the detection of CAR$^+$ cells was set at 0.1% out of CD3 T cells, and the percentage of CAR-T cells was further converted to the absolute counts per microliter using the total white blood cell count values obtained from hematology analyzer. The antibody panels are presented in Supplementary Table S1.

Analysis of apheresis and CAR-T cell products

The first goal was to characterize patients' apheresis and to determine whether differences in their T cell memory subsets are associated with stronger *in vivo* expansion of CAR-T cells and improved clinical outcome. For each patient, the apheretic product samples were cryopreserved, as well as from five healthy donors functioning as control samples. Prior to flow cytometry analysis, the cells were thawed and let to rest in media overnight. We have found out that 27 out of 32 subjects had undetectable B-cells in apheresis due to preceding treatment by rituximab (Figure 3A, Supplementary Figure S2). To characterize the T cells, we determined their immunophenotype with the differentiation antibody panel (omitting the anti-FMC63 antibody). The patients' T cells were characterized by highly variable numbers of Tem/Tcm/Temra CD8$^+$ and CD4$^+$ memory subsets, similarly to what was detected in healthy donors

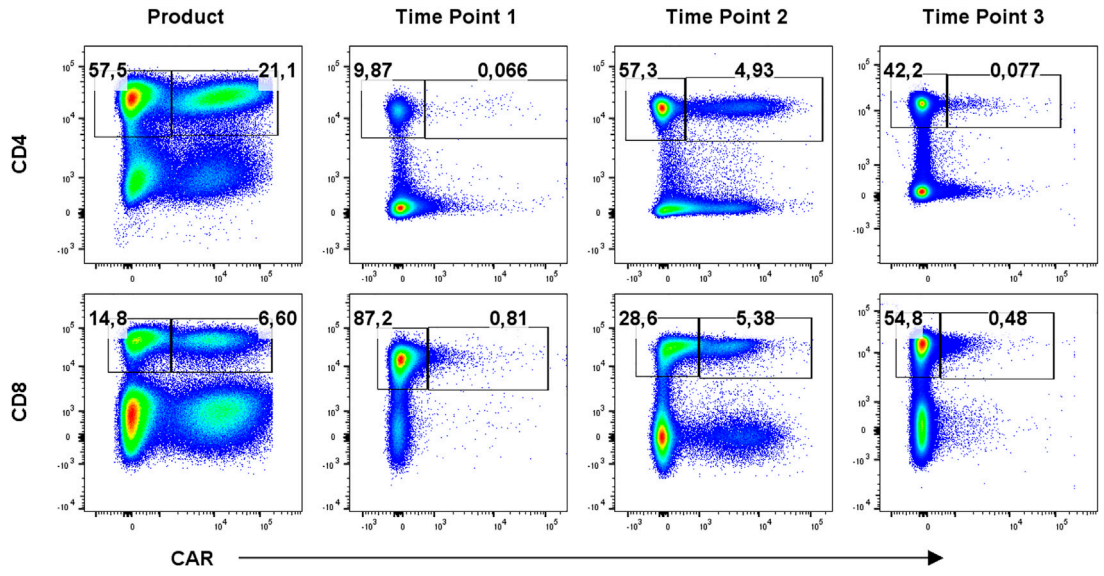

FIGURE 1
Detection of CAR-T cells in the product and in blood at three timepoints: T1 early after infusion (day 2–4), T2 at the expected peak of expansion (days 10–14), and T3 at the predicted contraction phase (days 30–60). Percentages of CAR$^-$ (left gate) and CAR$^+$ (right gate) cells of CD3$^+$ cells are shown for one representative patient. Gates were set based on measurements of healthy donor control.

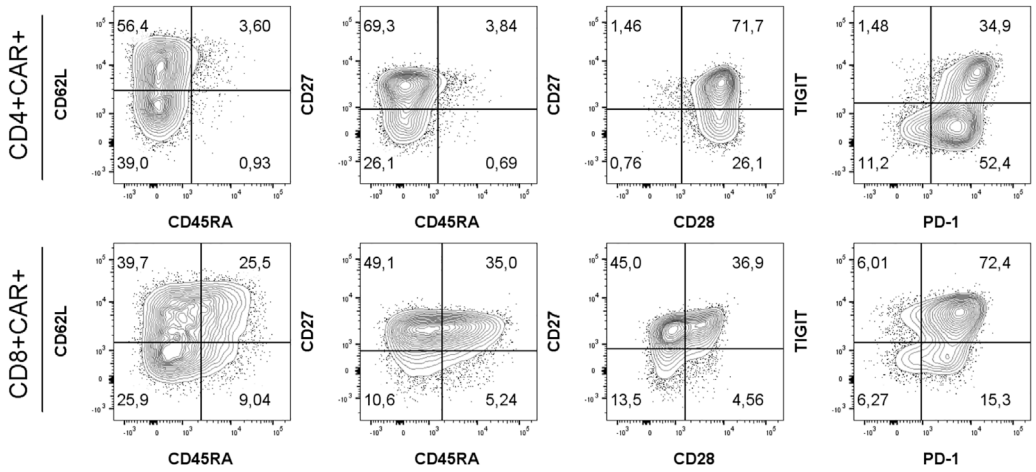

FIGURE 2
Gating strategy for immunophenotyping of CD4$^+$/CD8$^+$ CAR-T cells using antibodies against antigens CD45RA, CD62L, CD27, CD28, PD-1 and TIGIT. Memory subsets were defined as: SCM, stem cell memory (CD45RA$^+$CD62L$^+$); CM, central memory (CD45RA$^-$CD62L$^+$); EM, effector memory (CD45RA$^-$CD62L$^-$); EMRA, terminally differentiated effector memory (CD45RA$^+$CD62L$^-$). One representative patient is shown. Percentages of populations of CD4$^+$CAR$^+$ or CD8$^+$CAR$^+$ shown in respective quadrants. Gates were set based on measurements of healthy donor control and FMO controls.

(Figure 3B, Supplementary Figure S6). Nevertheless, the patients' T cells contained more exhausted T cells expressing PD-1 receptor compared to healthy donors—50% vs. 12% CD4$^+$ (p = <0.001) and 35% vs. 14% CD8$^+$ (p = 0.046). In addition, the non-responders were characterized by significantly reduced numbers of CD8$^+$ CD45RA$^+$ CD27$^+$ T cells (Figure 3C) in the apheresis, in agreement with report by Fraietta et al. (12).

Subsequently, the manufactured CAR-T cells were analyzed using aforementioned antibody panel with added anti-FMC63 antibody. The samples for measurements were obtained from

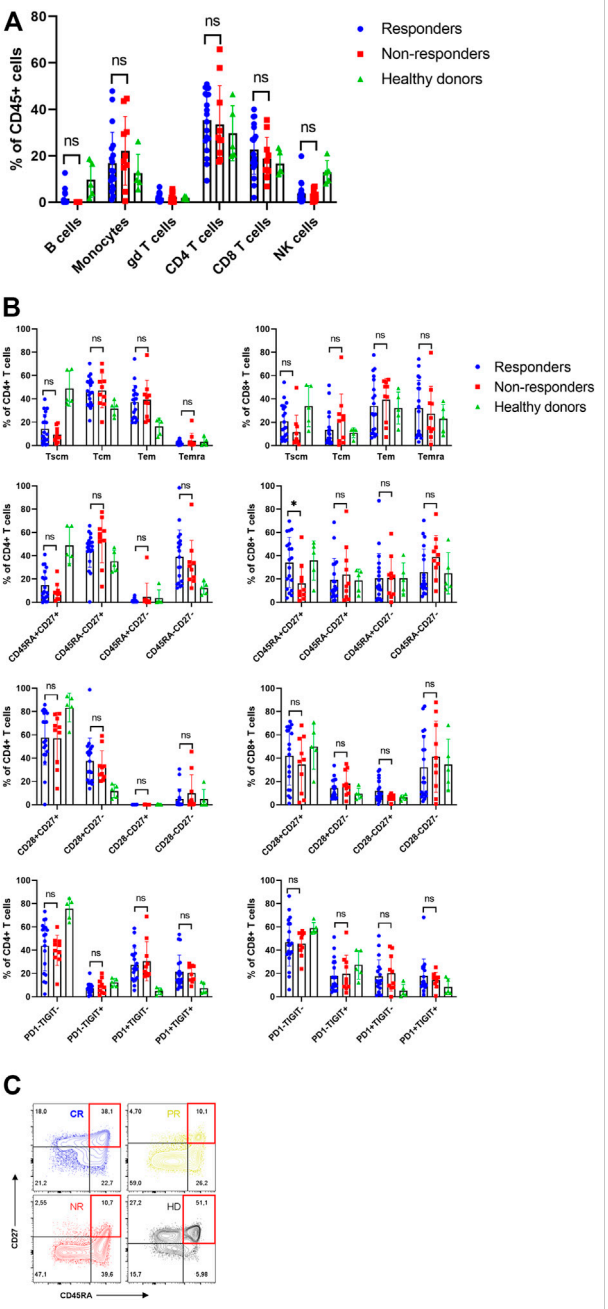

FIGURE 3
Analysis of apheresis. **(A)** Composition of individual leukocyte subsets in the apheresis. **(B)** Immunophenotype of CD4$^+$ and CD8$^+$ T cells in apheresis of responders, non-responders and healthy donors. SCM, stem cell memory; CM, central memory; EM, effector memory; EMRA, terminally differentiated effector memory. **(C)** Representative immunophenotypes of T cells (CD8$^+$CD27$^+$DC45RA$^+$) as percentages of CD8$^+$ cells in four subjects: CR, complete response; PR, partial response; NR, non-responder; HD, healthy donor. Unpaired *t*-test *$p < 0.05$, ns-not significant.

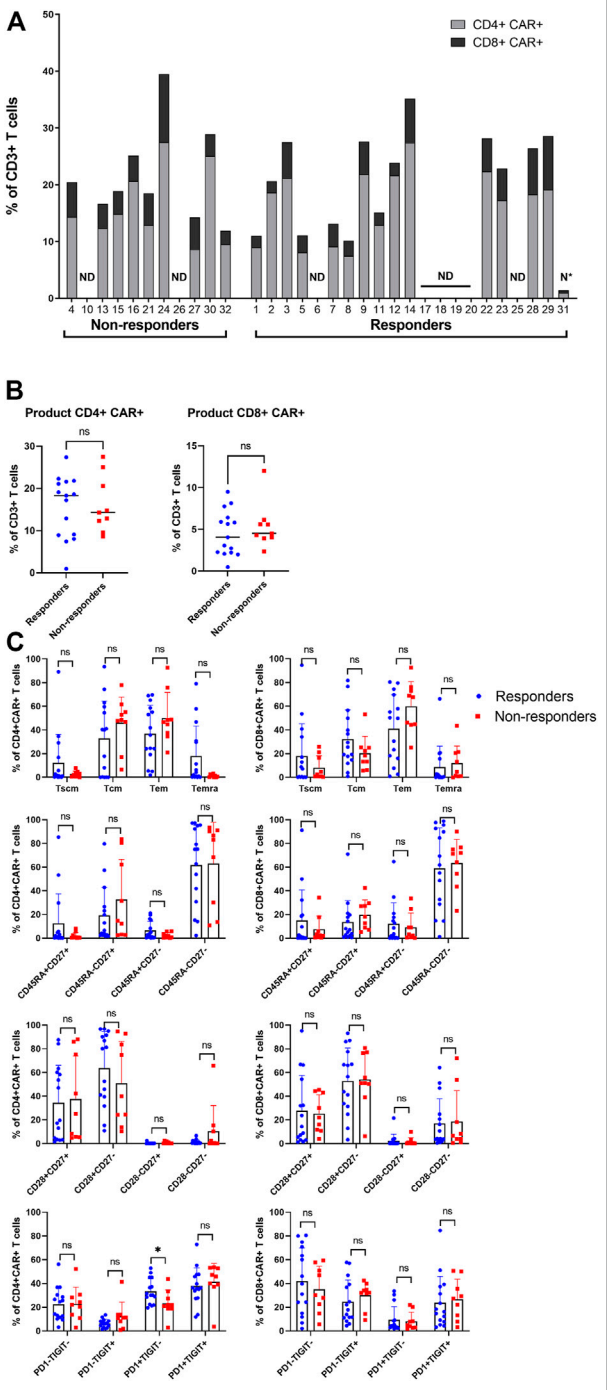

FIGURE 4
Analysis of the product. **(A)** Manufactured products cells were analyzed to determine the percentage of CAR$^+$ in CD4$^+$ and CD8$^+$ T cells out of all CD3$^+$ T cells. ND, not done; N*, product not meeting specifications. **(B)** Statistical analysis of the percentages of CD4$^+$CAR$^+$ (left) and CD8$^+$CAR$^+$ (right) in product of responders and non-responders. **(C)** Immunophenotypes of CD4$^+$CAR$^+$ and CD8$^+$CAR$^+$ cells in product of responders and non-responders. SCM, stem cell memory; CM, central memory; EM, effector memory; EMRA, terminally differentiated effector memory. Unpaired *t*-test; ns, not significant, *$p < 0.05$.

10.3389/pore.2023.1610914

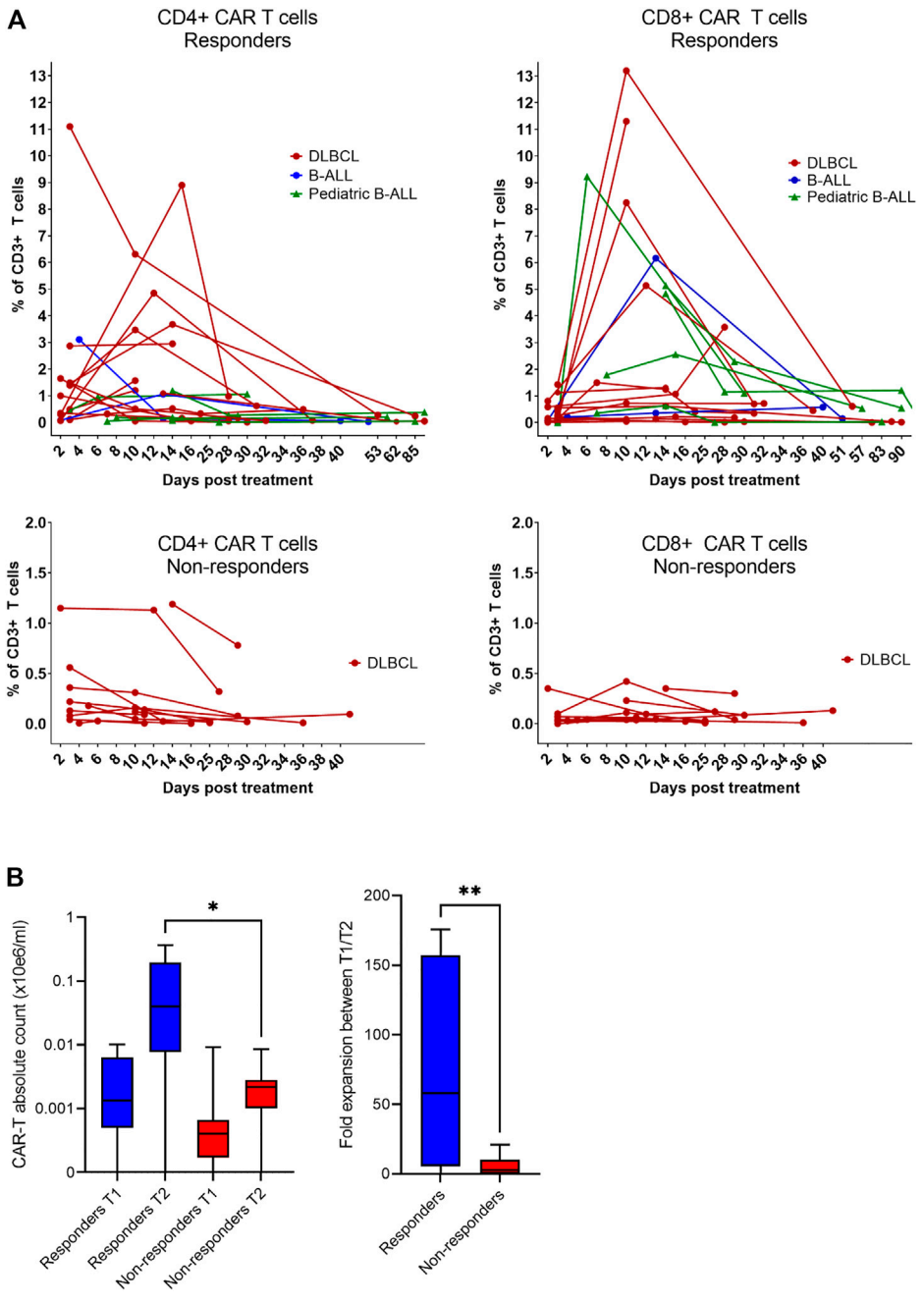

FIGURE 5
Expansion of CAR-T cells *in vivo*. **(A)** The level of expansion of CAR-T cells was determined in peripheral blood samples at three timepoints after administration: early after infusion (day 2–4), at the expected peak of expansion (days 10–14), and at the predicted contraction phase (days 30–60). The left panels show the expansion kinetics of $CD4^+CAR^+$ cells and right panels shows $CD8^+CAR^+$ cells as a percentage of $CD3^+$ T cells. **(B)** Statistical analysis of the level of expansion in responders (n = 13) vs. non-responders (n = 10) at indicated timepoints shown as a total number of CAR-T cells in the blood and as a fold expansion of absolute CAR-T cell counts in the blood between timepoint 1 (T1) and timepoint 2 (T2). Unpaired t-test $^*p < 0.05$, $^{**}p < 0.005$.

discarded infusion bags after administration to the patients. The infusion bags and their filters were thoroughly washed with PBS to acquire the remaining cells. In some cases, we were unable to measure administered products for technical reasons. We observed that the products contained a highly variable percentage of CAR^+ cells (range 1%–40%) and that the majority of CAR-T cells were CD4 positive (Figure 4A). There was no significant difference of percentage of $CD4^+$ or $CD8^+$

TABLE 1 Patients' characteristics.

Patient ID	Age	Dg	Primary refractory dissease	Sensitivity to bridge treatment before CAR-T	Clinical stage before CAR-T	Response to CAR-T at 3 m/6 m	Lymphodepletion regimen	Number of lines of treatment before CAR-T	T1 % $CD4^+CAR^+$	T2% CD4	T1 % CD8	T2 % CD8	CAR-T expansion
1	25	ALL	No	Yes	CR	CR/CR	Flu/Cy	3+alloSCT	0	1.06	0	6.17	Yes
2	27	ALL	No	Yes	CR	CR/relapse	Flu/Cy	5+alloSCT	3.11	0.15	0.21	0.36	Yes
3	69	DLBCL	No	Yes	CR	CR/CR	Flu/Cy	4+ASCT	0	4.85	0.81	5.14	Yes
4	67	DLBCL	No	Yes	2	progression	None	4+ASCT	1.15	1.13	0.35	0	No
5	43	DLBCL	No	Yes	1	CR/CR	Flu/Cy	4	1.39	3.47	0.4	8.25	Yes
6	53	DLBCL	Yes	No	4	PR/CR	bendamustine	4	0.35	0.16	0	0.22	Yes
7	74	DLBCL	No	Yes	1	CR/CR	Flu/Cy	5+ASCT	2.87	2.95	1.13	1.32	Yes
8	77	DLBCL	No	Yes	4	CR/CR	Flu/Cy	3	1.46	3.68	0.55	0.62	Yes
9	34	DLBCL	No	No	4	PR/progression	Flu/Cy	3+ASCT	0.3	8.9	0.59	1.07	Yes
10	61	DLBCL	Yes	No	4 (bulky)	progression	Flu/Cy	4	ND	1.19	ND	0.35	Yes
11	72	DLBCL	No	Yes	CR	CR/CR	bendamustine	3+ASCT	ND	1.1	ND	0.14	Yes
12	39	DLBCL	No	Yes	2	CR/CR	Flu/Cy	3+ASCT	1	0	0.16	0	No
13	57	DLBCL	Yes	No	4	progression	bendamustine	4	0	0	0	0	No
14	41	FL/DLBCL	No	Yes	4	CR/CR	bendamustine	3+ASCT	1.65	0	0	0	No
15	54	DLBCL	No	No	3	progression	bendamustine	3+ASCT	0.56	0	0	0	No
16	49	DLBCL	No	Yes	4	progression	bendamustine	2	0.18	0	0	0.11	No
17	10	ALL	No	Yes	4	CR/CR	Flu/Cy	1	ND	1.19	ND	4.84	Yes
18	15	ALL	No	Yes	2	CR/CR	Flu/Cy	1	0.18	0.14	1.79	2.56	Yes
19	5	ALL	No	Yes	1	CR/CR	Flu/Cy	1	0	0.18	0.36	0.64	Yes
20	3	ALL	No	Yes	2	CR/CR	Flu/Cy	1	ND	0	ND	5.14	Yes
21	74	DLBCL	Yes	No	4	progression	Flu/Cy	3	0.10	0.12	0	0.23	Yes
22	72	DLBCL	No	No	2	CR/CR	bendamustine	3	11.10	6.31	1.43	13.20	Yes
23	71	FL/DLBCL	No	Yes	1	CR/CR	bendamustine	4	1.49	0.51	0.27	0.73	Yes
24	70	DLBCL	Yes	Yes	2	progression	bendamustine	2	0.22	0.14	0	0	No
25	10	ALL	No	Yes	PR	CR/CR	Flu/Cy	1	0.45	0.95	0	9.23	Yes
26	44	DLBCL	Yes	No	4	progression	None	2	0	0	0	0	No
27	76	DLBCL	No	No	4	progression	bendamustine	2	0.36	0.31	0.10	0.42	Yes
28	23	DLBCL	No	Yes	4	PR/---	pixantron+ benda	5	0.12	1.57	0	11.30	Yes
29	49	DLBCL	No	Yes	4	CR/CR	Flu/Cy	4+ASCT	0.49	1.20	0.22	0.12	Yes
30	64	DLBCL	Yes	No	4 (bulky)	progression	Flu/Cy	3	0.13	0	0	0	No
31	56	DLBCL	No	Yes	4 (bulky)	PR/progression	Flu/Cy	3	0.10	0.32	0.14	1.50	Yes
32	70	FL/DLBCL	No	Yes	3	progression	Flu/Cy	3	0	0.16	0	0	No

10.3389/pore.2023.1610914

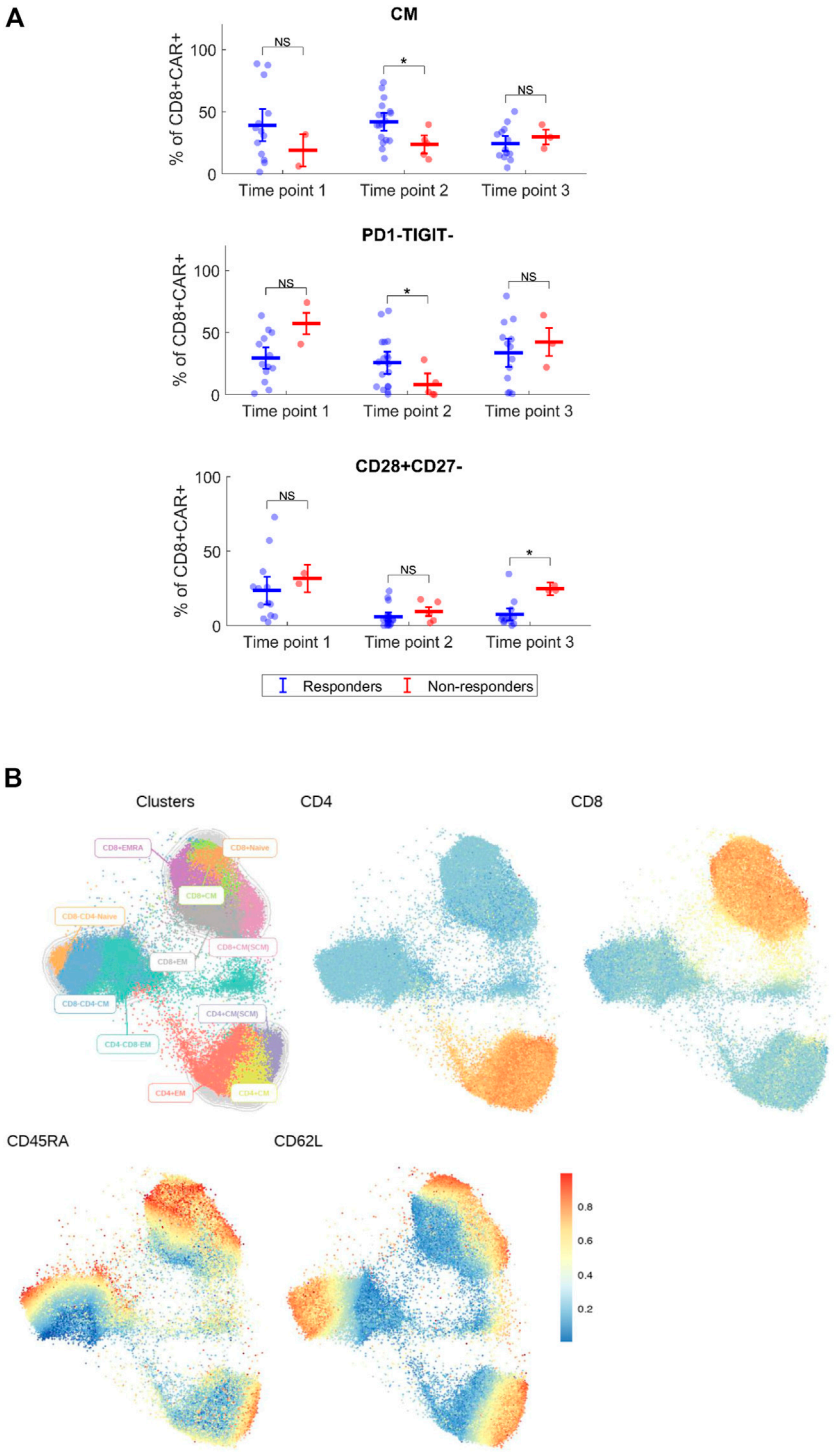

FIGURE 6
Immunophenotype of CAR-T cells *in vivo*. **(A)** Expanded CD4$^+$ and CD8$^+$ CAR$^+$ T cells were analyzed for each patient by multiparameter flow cytometry to determine the expression of major surface antigens reflecting their differentiation status. Phenotypes with significant difference between responders and non-responders are shown. Percentages of phenotype subsets are of CD8$^+$ CAR$^+$ T cells. CM, central memory (CD45RA$^-$CD62L$^+$). Mann-Whitney test; ns, not significant, *$p < 0.05$. **(B)** Cluster analysis of detected CAR$^+$ T cells at the first timepoint for indicated antigens, all identified CAR-T cells from all responders and non-responders at the first timepoint were analyzed together. EmbedSOM algorithm was used. The scale indicates relative intensity of detected antigens.

TABLE 2 Characteristics of DLBCL patients.

	Expansion of CAR-T	Primary refractory disease	Response to bridge treatment before CAR-T	Median clinical stage before CAR-T
Responders	87.5% (12/14)	7.1% (1/14)	78.5% (11/14)	3
Non-responders	27.3% (3/11)	54.5% (6/11)	36.4% (4/11)	4

CAR-T cells in product between responders and non-responders (Figure 4B). The immunophenotype of CAR-T cells was likewise highly variable between individual patients in regards to the proportion of Tscm/Tcm/Tem/Temra, and CD27/CD28/PD-1/TIGIT positive cells (Figure 4C, Supplementary Figure S7). There was a slightly higher PD1+TIGIT− percentage of $CD4^+CAR^+$ T cells in responders ($p = 0.039$, Figure 4C). CAR^+ T cells in the product had almost identical immunophenotype as the CAR^- population (data not shown), suggesting that their differentiation during manufacturing was driven more by polyclonal anti-CD3/CD28 activation than by CAR signaling. One product (P31) did not meet the entry specifications since it contained only 1% of CAR-T cells. Despite such a low percentage of CAR-T cells, this patient responded to the therapy and achieved PR by PET/CT (nonetheless relapsed later). Conversely to apheresis, we did not detect a significant difference in the numbers of $CD8^+$ $CD45RA^+$ $CD27^+$ T cells in the product (Figure 4C).

Fate of CAR-T cells *in vivo*

Expansion and immunophenotype of CAR-T cells were determined in the patients' blood samples after administration at three timepoints—between days 2–4 (T1), days 10–14 (T2), and days 30–60 (T3). Since the study was performed in a non-clinical trial setting, the samples could be obtained only during regular medical examinations including signing of the informed consent form by the patient. To determine the kinetics of CAR-T cells' expansion, we measured percentage of $CD4^+$/$CD8^+$ CAR-T out of $CD3^+$ T cells and calculated their absolute counts in blood. The CAR-T cell percentages were compared between T1 and T2 to assess CAR-T cells' expansion kinetics. If the percentage of either $CD4^+$ or $CD8^+$ CAR^+ at T2 was higher than their percentage at T1, the patient was categorized as showing a detectable expansion. Figure 5A shows the kinetics of CAR-T cell expansion for each patient. In addition, we calculated the absolute number of CAR-T cells per μl of blood in the responders and the non-responders at T1 and T2 (Figure 5B). Table 1 shows the measured values of CAR-T cells in blood for each patient and demonstrates that only 27% (3/11) of non-responders had a detectable expansion of CAR-T cells and that 90% (19/21) of responders had detectable expansion (Table 2). Out of 25 patients with DLBCL, 10 subjects had no expansion of CAR-T cells (all patients with B-ALL were responders with detectable CAR-T cell expansion). 80% of these "non-expanders" were also non-responders, but only 40% of them had primary refractory disease. Following this, we determined the immunophenotype of detected CAR-T cells in the blood similarly as was done for the product (Supplementary Figure S8). Threshold for the detection of CAR-T cells was set at 0.1% of $CD3^+$ T cells, samples with CAR^+ percentage below this value were not analyzed. Significant differences between responders and non-responders are presented in Figure 6A. At time point 2, responders had higher numbers of $CD8^+CAR^+$ Tcm ($p = 0.030$) and PD1−TIGIT− than non-responders ($p = 0.048$). At time point 3, $CD28^+CD27^-$ percentage was higher in non-responders ($p = 0.025$), although only 3 samples were used for the analysis. Clustering by EmbedSOM algorithm (13) shows relative distribution of memory subsets of CAR-T cells for time point 1 (Figure 6B).

Non-blood samples and second dose administration

In addition to blood samples, we analyzed samples obtained from bone marrow and in three subjects with lung infiltration also from the malignant pleural effusion. Figure 7A shows percentages of CAR-T cells detected at a single time point in blood with corresponding bone marrow or pleural effusion (lung) sample. Interestingly, we observed effective migration of CAR-T cells into the tumor sites, demonstrated by high CAR-T percentage in the pleural effusion. We also detected long-term persisting CAR-T cells in the bone marrow of several subjects.

Immunophenotype of CAR-T cells in bone marrow was compared to paired blood samples (Figure 7B). $CD8^+$ CAR-T cells in blood had elevated Tcm ($p = 0.038$), Temra ($p = 0.046$), and $CD45RA^+CD27^-$ ($p = 0.032$) phenotypes compared to bone marrow. $CD8^+$ CAR-T cells in bone marrow had slightly higher percentage of PD1+TIGIT+ ($p = 0.003$), PD1+TIGIT− ($p = 0.028$) populations, and lower PD1−TIGIT+ ($p = 0.004$) percentage. Phenotype of CAR-T cells in pleural effusion was not statistically analyzed due to insufficient number of paired blood samples with detectable CAR-T cells (Supplementary Figure S9).

Four patients from the selected study group were administered a second dose of CAR-T cells after they relapsed; the source of the

10.3389/pore.2023.1610914

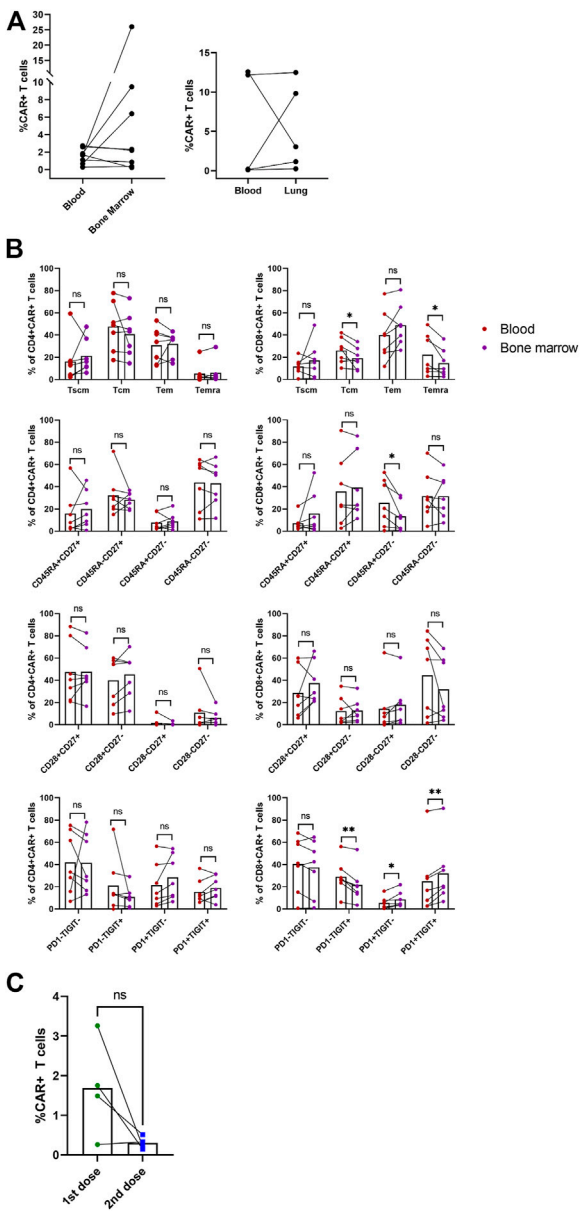

FIGURE 7
Non-blood samples and second dose administration. The indicated samples were analyzed by multiparametric flow cytometry to determine the percentage and immunophenotype of CAR-T cells. **(A)** Paired percentages of $CD3^+CAR^+$ cells in blood/bone marrow or blood/fluidothorax (lung). **(B)** Comparison of phenotypes of CAR^+ cells in blood and bone marrow. SCM, stem cell memory; CM, central memory; EM, effector memory; EMRA, terminally differentiated effector memory. Paired *t*-test; ns, not significant, $*p < 0.05$, $**p < 0.005$. **(C)** Percentages of CAR-T cells in blood for the first and second dose at T2—D+14. Paired *t*-test; ns, not significant.

CAR-T cells was a remaining cryopreserved bag of the original product. Subject P09 received the second dose simultaneously with anti-PD-1 antibody pembrolizumab. Subject P16 received the second dose concurrently with lenalidomide treatment. Subjects P18 and P19 were pediatric B-ALL patients in clinical remission, although B-cell presence in the peripheral blood was established, suggesting the therapy's failure. Therefore, the second CAR-T cells' dose was used successfully as a bridging therapy before allo-HSCT. Furthermore, we observed that the subjects P16, P18, and P19 had a non-detectable expansion of the second CAR-T cells' dose. In contrast, in the subject P09, we observed high levels of CAR-T cells in the pleural effusion even though they were almost undetectable in the blood sample. Figure 7C shows percentage of CAR-T cells at D+14 for first and second administration. The immunophenotype of these CAR-T cells was very similar to the immunophenotype of CAR-T cells detected in the patient's blood sample following the administration of the first dose. Unfortunately, despite such a very efficient expansion of CAR-T cells, subject P09 did not achieve complete remission (CR) and the disease continually progressed.

Discussion

In this report, we analyzed a group of 32 patients diagnosed with either B-ALL or DLBCL and treated in a real-world setting with tisa-cel, $CD19^-$specific CAR-T cell product. The high costs of commercial CAR-T cell therapy and extended production time emphasize the need to search for clinical and laboratory parameters that will enable selection of patients with the highest chances to respond to therapy and determine what prior therapies might adversely affect the efficiency of the production of CAR-T cells. Thus, the main goals of our study were to correlate the efficacy of the therapy with the immunophenotype of input material used for the production of CAR-T cells (i.e., the apheresis) and with the immunophenotype of the produced CAR-T cells. Additionally, we observed CAR-T cell expansion kinetics after administration in the blood and measured their immunophenotype. The analysis presents a comprehensive data set from 32 subjects, including detailed clinical parameters such as prior treatments and complications associated with CAR-T cell therapy.

We observed a similar efficiency of the treatment in comparison to reported results of other real-world experiences (13). A noticeable subset of patients were non-responders who were characterized by continuously progressing disease after CAR-T cell therapy without achieving even a PR at 3-month restaging by PET/CT or by flow cytometry. In all cases, these patients were diagnosed with DLBCL and have shown no detectable expansion of CAR-T cells. Unfortunately, several patients with promising CR relapsed at later time points. The highly variable numbers and ratios of $CD4^+$ and $CD8^+$ T cells and the depletion of central memory (Tcm)/stem cell memory T cell (Tscm) subsets due to prior chemotherapies is a challenging issue for cellular therapy approaches. These subsets are essential for durable anti-tumor responses in adoptive cell therapy (14). For example, B-cell lymphoma patients have an increased percentage of terminal effector memory $CD8^+$ T cells (15).

Comparably to published reports (12), we found that an increased number of stem-cell-like memory $CD45RA^+CD27^+$ $CD8^+$ T cells in the apheresis correlated with enhanced efficacy of CAR-T therapy, suggesting that the quality of the input material influences outcome of the treatment. However, the responders did not have a significantly higher number of $CD45RA^+CD27^+$ CAR-T cells in the product in comparison to the non-responders.

Next, the product analysis showed an interesting, highly variable CD4/CD8 ratio of CAR-T cells between products. Moreover, the percentage of CAR^+ T cells in the product did not correlate with the response to the treatment suggesting that out-of-specification products might be equally efficient and worth administering (Figure 4B). For example, patient 32 had a bulky tumor and achieved near CR despite the administered product containing only 2% of CAR^+ cells. These findings indicate that an efficient response probably requires a relatively small number of CAR^+ cells with stem-cell memory phenotype, which can be reliably achieved in most patients despite significant differences in the T cell subsets between products.

Immunophenotypic analysis of expanded CAR-T cells *in vivo* revealed higher numbers of central memory and PD1−TIGIT− $CD8^+CAR^+$ cells in responders at time point 2 (Figure 6A). This might contribute to the hypothesis that early memory phenotypes are persisting longer, and thus leading to a better response. However, more data is needed to further support these findings.

Performed studies analyzing factors associated with responsiveness to CAR-T cell therapy among patients with DLBCL showed that one of the most significant negative factors is tumor mass volume (5, 7). We similarly observed the lowest efficacy of the treatment among patients with primary refractory DLBCL who frequently were at clinical stage IV with a large tumor burden. Furthermore, these patients continuously undergo intensive chemotherapy, negatively impacting CAR-T cells' quality. Thus, a combination of these factors might severely impair the treatment outcome among patients with primary refractory DLBCL. Any solution to these problems would be complicated – for example, such patients could be considered for clinical trials with enhanced next-generation CAR-T cell products, which can be rapidly manufactured from the original apheresis for commercial CAR-T cell products (16). Hence, patients with primary refractory DLBCL without detectable CAR-T cell expansion would be such candidates. Therapeutic options for relapsed patients after CAR-T cell therapy are purely experimental; a frequently used option is the second dose of CAR-T cell infusion (17). We have analyzed four of these subjects. However, we observed, similarly to already reported data, a significantly reduced expansion of CAR-T cells compared to the first treatment except for subject P09 (who also received an anti-PD1 antibody). Analysis of non-blood samples such as bone marrow and malignant pleural effusion showed efficient infiltration of CAR-T cells into these compartments without apparent differences in their immunophenotype. This data suggests that undetectable or very low expansion of CAR-T cells in the blood might falsely indicate a treatment failure as the majority of expanding CAR-Ts *in vivo* might be localized in tumor or other tissues. In summary, our results suggest that the outcome of CAR-T cell therapy largely depends on the biological characteristics of the tumors rather than on the immunophenotype of produced CAR-T cells.

Methods

Patient samples

Samples were acquired from patients diagnosed with DLBCL and B-ALL who were treated with tisagenlecleucel at the Institute of Hematology and Blood Transfusion, General University Hospital in Prague, and University Hospital in Motol. All patients (or their parents/guardians) signed informed consent form. Following samples were collected from each patient: 1) apheresis used for CAR-T cell manufacturing, 2) CAR-T-cell product from infusion bag, 3) whole blood sample from patients following CAR-T infusion at three time points—first early after administration (days 2–4), second at the time of expected maximal CAR-T-cell expansion (days 10–14), and third after the retraction of the immune response (days 30–60). The control samples were obtained from age-matched healthy volunteers. In addition to FACS analysis, a total blood cell count was determined as part of a regular medical examination. Peripheral blood mononuclear cells (PBMCs) were isolated from whole blood samples by gradient centrifugation using Ficoll-Paque premium (GE Healthcare). After isolation, PBMCs were resuspended in PBS and were either stained immediately or frozen in CryoStor CS10 (StemCell Technologies) for further processing. For unfreezing, cells were thawed and cultivated in cell culture media overnight. For all experiments, CellGro media (CellGenix, Germany) supplemented with 10% heat-inactivated fetal calf serum (Gibco, United States) was used with addition of antibiotics penicillin and streptomycin (Gibco, United States).

Patients' characteristics

The study group includes patients with pediatric B-ALL (n = 5, age 3–10), adult B-ALL (n = 2, age 25–27), or with DLBCL (n = 25, age 34–77) who were eligible for treatment with tisa-cel (Table 1). In total, 32 patients received the treatment under non-clinical trial settings according to recommended clinical practice. All patients with B-ALL were in complete remission before infusion of CAR-T cells. In contrast, 24 out of 25 (96%) of the remaining patients with DLBCL had active disease with a significant tumor burden. After administration of CAR-T cells,

the patients were monitored, and when necessary, treated for CRS/neurotoxicity symptoms with corticosteroids or tocilizumab according to recommended CAR-T cells' medication protocols. A grade 2 CRS was observed in 5 patients, which required hemodynamic support. However, no patient required mechanical ventilation, all rapidly recovered from CRS symptoms. The effects of CAR-T cell therapy were determined at three and six-months' time points *via* PET/CT (18) and by flow cytometry. Those patients who either progressed or failed to achieve at least a PR at 3 months were classified as non-responders. The remaining individuals were classified as responders and were further followed. All relevant pretreatment and post-treatment parameters are presented in Table 1. Patient P28 had a significant CAR-T expansion, so we included them as a responder; however, this patient died within a month due to complications connected with primary disease. In summary, the patients' responses to CAR-T cell treatment and associated complications were similar to the currently known clinical experience with tisa-cel (19).

Antibody panels and staining

Approximately five million freshly isolated PBMCs per sample were used for staining. For the first eight patients, we used PE-Labeled Human CD19 (20–291) Protein (Acro Biosystems). Later, anti-FMC63-FITC antibody by Acro Biosystems was used. Comparison of staining with protein CD19 and anti-FMC63 antibody is shown in Supplementary Figure S1. Besides detection of CAR-T cells the samples were stained with antibodies against antigens CD3, CD4, CD8, CD45RA, CD62L, CD27, CD28, CD57, PD-1, TIM-3, and TIGIT. A second detection panel against antigens CD3, CD4, CD8, CD14, CD16, CD19, CD45, CD56, and TCRgd was used to determine significant leukocyte subsets in the samples. Antibody panels used in this study were used previously (20) and can be found in Supplementary Tables S1, S2. All antibodies were titrated before use, and fluorescence-minus-one controls for selected antibodies were measured. Firstly, PBMCs were stained using a fixable blue dead cell stain kit (Thermo Fisher Scientific, United States), washed with FACS buffer, and then stained with antibody mix in Brilliant Stain Buffer (BD) at room temperature for 30 min. The samples were washed with FACS buffer prior to measurement.

Flow cytometry

Sample data were acquired on a five-laser BD LSRFortessa instrument (BD Biosciences). All measurements were standardized using 8-peak Rainbow beads (Spherotech, Lake Forest, IL). BD CompBeads (BD, anti-rat #552844, and anti-mouse #552843) were used for compensation.

Data analysis

Manual analysis of cytometry data was performed using FlowJo software (TreeStar).

Statistical analysis was carried out using GraphPad Prism version 9 (GraphPad Software) and MATLAB (R2022b, The MathWorks Inc.).

Key Clinical Message

Non-responders to therapy with CD19-specific CAR-T cells (tisagenlecleucel) are characterized by undetectable expansion of CAR-T cells and in the majority of cases are diagnosed with primary refractory aggressive B-cell lymphomas..

Data availability statement

The raw data supporting the conclusion of this article will be made available by the authors, without undue reservation.

Ethics statement

Ethical review and approval was not required for the study on human participants in accordance with the local legislation and institutional requirements. Written informed consent to participate in this study was provided by the participants' legal guardian/next of kin. Written informed consent was obtained from the patients to publish this report in accordance with the journal's patient consent policy.

Author contributions

MŠ and AK: data analysis, sample measurements, and manuscript writing. RP, LŠ, PL, and JV: clinical data analysis and management. MP, JR, and IK: sample processing and data administration. KŠ and MM: data analysis and sample measurements. JM: flow-cytometry analysis and assay development. PO: manuscript writing and data analysis. PP: statistical analysis.

Funding

This work was supported by the Czech health research council NU22-05-00374 and by grant OPVVV CZ.02.1.01/0.0/0.0/16_025/0007428.

Conflict of interest

The authors declare that the research was conducted in the absence of any commercial or financial relationships that could be construed as a potential conflict of interest.

Supplementary material

The Supplementary Material for this article can be found online at: https://www.por-journal.com/articles/10.3389/pore.2023.1610914/full#supplementary-material

References

1. Siddiqi T, Abramson JS, Li D, Brown W, Devries T, Dave K, et al. Patient characteristics and pre-infusion biomarkers of inflammation correlate with clinical outcomes after treatment with the defined composition, CD19-targeted CAR T cell product, JCAR017. *Blood* (2017) 130:193. doi:10.1182/blood.V130.Suppl_1.193.193

2. Zhang X, Yang JF, Li JJ, Li WQ, Song D, Lu XA, et al. Factors associated with treatment response to CD19 CAR-T therapy among a large cohort of B cell acute lymphoblastic leukemia. *Cancer Immunol Immunother* (2022) 71(3):689–703. doi:10.1007/s00262-021-03009-z

3. Martino M, Alati C, Canale FA, Musuraca G, Martinelli G, Cerchione C. A Review of clinical outcomes of CAR T-Cell therapies for B-Acute lymphoblastic leukemia. *Int J Mol Sci* (2021) 22:2150. doi:10.3390/ijms22042150

4. Schuster SJ, Bishop MR, Tam CS, Waller EK, Borchmann P, McGuirk JP, et al. Tisagenlecleucel in adult relapsed or refractory diffuse large B-cell lymphoma. *N Engl J Med* (2019) 380:45–56. doi:10.1056/NEJMoa1804980

5. Vercellino L, Di Blasi R, Kanoun S, Tessoulin B, Rossi C, D'Aveni-Piney M, et al. Predictive factors of early progression after CAR T-cell therapy in relapsed/refractory diffuse large B-cell lymphoma. *Blood Adv* (2020) 4(22):5607–15. doi:10.1182/bloodadvances.2020003001

6. Riedell PA, Walling C, Nastoupil LJ, Pennisi M, Maziarz RT, McGuirk JP, et al. A multicenter retrospective analysis of clinical outcomes, toxicities, and patterns of use in institutions utilizing commercial axicabtagene ciloleucel and tisagenlecleucel for relapsed/refractory aggressive B-cell lymphomas. *Blood* (2019) 134:1599. doi:10.1182/blood-2019-127490

7. Dean EA, Mhaskar RS, Lu H, Mousa MS, Krivenko GS, Lazaryan A, et al. High metabolic tumor volume is associated with decreased efficacy of axicabtagene ciloleucel in large B-cell lymphoma. *Blood Adv* (2020) 4(14):3268–76. doi:10.1182/bloodadvances.2020001900

8. Monfrini C, Stella F, Aragona V, Magni M, Ljevar S, Vella C, et al. Phenotypic composition of commercial anti-CD19 CAR-T cells affects *in vivo* expansion and disease response in large B-cell lymphoma patients. *Clin Cancer Res* (2022) 28:3378–86. doi:10.1158/1078-0432.ccr-22-0164

9. Cuffel A, Allain V, Faivre L, Di Blasi R, Morin F, Vercellino L, et al. Real-world characteristics of T-cell apheresis and clinical response to tisagenlecleucel in B-cell lymphoma. *Blood Adv* (2022) 6:4657–60. doi:10.1182/bloodadvances.2022007057

10. Byrne M, Oluwole OO, Savani B, Majhail NS, Hill BT, Locke FL. Understanding and managing large B cell lymphoma relapses after chimeric antigen receptor T cell therapy. *Biol Blood Marrow Transplant* (2019) 25:e344–e351. doi:10.1016/j.bbmt.2019.06.036

11. Blache U, Weiss R, Boldt A, Kapinsky M, Blaudszun AR, Quaiser A, et al. Advanced flow cytometry assays for immune monitoring of CAR-T cell applications. *Front Immunol* (2021) 12:658314. doi:10.3389/fimmu.2021.658314

12. Fraietta JA, Lacey SF, Orlando EJ, Pruteanu-Malinici I, Gohil M, Lundh S, et al. Determinants of response and resistance to CD19 chimeric antigen receptor (CAR) T cell therapy of chronic lymphocytic leukemia. *Nat Med* (2018) 24(5):563–71. doi:10.1038/s41591-018-0010-1

13. Schuster SJ, Svoboda J, Chong EA, Nasta SD, Mato AR, Anak O, et al. Chimeric antigen receptor T cells in refractory B-cell lymphomas. *N Engl J Med* (2017) 377:2545–54. doi:10.1056/NEJMoa1708566

14. Gattinoni L, Klebanoff CA, Palmer DC, Wrzesinski C, Kerstann K, Yu Z, et al. Acquisition of full effector function *in vitro* paradoxically impairs the *in vivo* antitumor efficacy of adoptively transferred CD8+ T cells. *J Clin Invest* (2005) 115(6):1616–26. doi:10.1172/JCI24480

15. Sommermeyer D, Hudecek M, Kosasih PL, Gogishvili T, Maloney DG, Turtle CJ, et al. Chimeric antigen receptor-modified T cells derived from defined CD8+ and CD4+ subsets confer superior antitumor reactivity *in vivo*. *Leukemia* (2016) 30(2):492–500. doi:10.1038/leu.2015.247

16. An L, Lin Y, Deng B, Yin Z, Zhao D, Ling Z, et al. Humanized CD19 CAR-T cells in relapsed/refractory B-ALL patients who relapsed after or failed murine CD19 CAR-T therapy. *BMC Cancer* (2022) 22(1):393. doi:10.1186/s12885-022-09489-1

17. Park JH, Riviere I, Gonen M, Wang X, Senechal B, Curran KJ, et al. Long-term follow-up of CD19 CAR therapy in acute lymphoblastic leukemia. *N Engl J Med* (2018) 378(5):449–59. doi:10.1056/NEJMoa1709919

18. Štach M, Ptáčková P, Mucha M, Musil J, Klener P, Otahal P. Inducible secretion of IL-21 augments anti-tumor activity of piggyBac-manufactured chimeric antigen receptor T cells. *Cytotherapy* (2020) 22(12):744–54. doi:10.1016/j.jcyt.2020.08.005

19. Cheson BD, Fisher RI, Barrington SF, Cavalli F, Schwartz LH, Zucca E, et al. Recommendations for initial evaluation, staging, and response assessment of hodgkin and non-hodgkin lymphoma: The lugano classification. *J Clin Oncol* (2014) 32(27):3059–68. doi:10.1200/JCO.2013.54.8800

20. Kratochvíl M, Koladiya A, Vondrášek J. Generalized EmbedSOM on quadtree-structured self-organizing maps. *F1000Res* (2020) 8:2120, doi:10.12688/f1000research.21642.2

Pathology & Oncology Research | frontiers

TYPE Brief Research Report
PUBLISHED 23 September 2024
DOI 10.3389/pore.2024.1611889

Check for updates

OPEN ACCESS

EDITED BY
József Tímár,
Semmelweis University, Hungary

*CORRESPONDENCE
Mary J. C. Hendrix,
mhendrix@shepherd.edu
Stanley P. Leong,
stanley.leong@sutterhealth.org

RECEIVED 21 June 2024
ACCEPTED 12 September 2024
PUBLISHED 23 September 2024

CITATION
Gascard PD, Wang X, Nosrati M, Kim KB, Kashani-Sabet M, Tlsty TD, Leong SP and Hendrix MJC (2024) Higher Nodal expression is often associated with poorer survival in patients diagnosed with melanoma and treated with anti-PD1 therapy.
Pathol. Oncol. Res. 30:1611889.
doi: 10.3389/pore.2024.1611889

COPYRIGHT
© 2024 Gascard, Wang, Nosrati, Kim, Kashani-Sabet, Tlsty, Leong and Hendrix. This is an open-access article distributed under the terms of the Creative Commons Attribution License (CC BY). The use, distribution or reproduction in other forums is permitted, provided the original author(s) and the copyright owner(s) are credited and that the original publication in this journal is cited, in accordance with accepted academic practice. No use, distribution or reproduction is permitted which does not comply with these terms.

Higher Nodal expression is often associated with poorer survival in patients diagnosed with melanoma and treated with anti-PD1 therapy

Philippe D. Gascard[1], Xianhong Wang[1], Mehdi Nosrati[2], Kevin B. Kim[2], Mohammed Kashani-Sabet[2], Thea D. Tlsty[1], Stanley P. Leong[2]* and Mary J. C. Hendrix[3]*

[1]Department of Pathology, University of California San Francisco, San Francisco, CA, United States, [2]California Pacific Medical Center, Center for Melanoma Research and Treatment, Sutter Health, San Francisco, CA, United States, [3]Department of Biology, Shepherd University, Shepherdstown, WV, United States

Advanced melanoma is considered the most aggressive and deadly form of skin cancer whose incidence has been rising over the past three decades. In the absence of treatment, the median overall survival for advanced-stage metastatic disease is less than 6 months. Although most melanomas detected at an early stage can be cured with surgery, a subset of these eventually metastasize. Therefore, a critical need exists to identify unique molecular features that would be predictive of long-term outcome and response to specific therapies. Recent promising therapeutic regimens have included the use of immune checkpoint inhibitors, such as anti-PD1 antibodies. However, the ability to identify responders and non-responders to this therapy remains elusive. To address this challenge at the molecular level, previously our laboratory identified the emergence of a stem cell phenotype associated with advanced melanoma and other aggressive forms of cancer. Underlying this phenotype is the aberrant re-expression of the embryonic morphogen "Nodal". Particularly noteworthy, we have observed Nodal to remain in advanced tumors of non-responders to standard-of-care therapies (i.e., BRAFi). This pilot study is the first proof-of-principle attempt to predict treatment response survival outcome in a small cohort of melanoma patients receiving anti-PD1 immune checkpoint inhibitor therapy – based on their Nodal expression profile. Using advanced multiplex immunohistochemistry-based digital

Abbreviations: BRAF, B-Raf Proto-Oncogene, Serine/Threonine Kinase; BRAFi, B-Raf Proto-Oncogene, Serine/Threonine Kinase inhibitor; BSA, Bovine Serum Albumin; CTLA4, Cytotoxic T-Lymphocyte Associated Protein 4; Cy3, Cyanine 3; Cy5, Cyanine 5; DAPI, 4′,6-diamidino-2-phenylindole; EMT, Epithelial Mesenchymal Transition; FFPE, Formalin Fixed Paraffin Embedded; FITC, Fluorescein Isothiocyanate; HRP, Horseradish Peroxidase; LAG3, Lymphocyte Activation Gene 3; LNM, lymph node metastasis; mIHC, multiplex immunohistochemistry; NaOH, sodium hydroxide; PD1, Programmed Cell Death Protein 1; PFS, Progression-Free Survival; RT, Room Temperature; SQ, subcutaneous; TSA, Tyramide Signal Amplification.

pathology, the major finding of this preliminary study indicates that higher Nodal expression is often associated with poorer overall survival after anti-PD1 therapy, reaching nearly statistical relevance.

KEYWORDS

melanoma, nodal, anti-PD1 therapy, immune checkpoint inhibitors, multiplex immunohistochemistry

Introduction

Melanoma is an aggressive type of cancer whose rates have been rising rapidly over the past three decades worldwide. It is estimated that about 97,610 new melanomas will be diagnosed in the United States and that about 7,990 people will die of this disease [1]. However, melanoma mortality rates have declined significantly - by about 5% per year in adults younger than 50% and 3% per year in those 50 and older - since 2011, as a result of diagnostic and treatment advances. Although most melanomas detected at an early stage can be cured with surgery, a small portion of these cancers eventually metastasize. In a continuing effort to advance the field, multiple research teams have concentrated their efforts on identifying unique molecular characteristics associated with primary tumor or sentinel lymph node features that would be predictive of long-term outcome [2–5]. Especially relevant is the recent validation of a 31-gene expression signature [4], which has been developed as a clinical test known as "DecisionDx-Melanoma." This test allows one to predict the risk of recurrence and metastasis, classifying patients as Class 1A (lowest risk), 1B/2A (increased risk), or 2B (highest risk), and thus inform patient management decisions, resulting in the recommendation of a sentinel lymph node biopsy, additional treatment, or close follow-up after treatment to monitor signs of recurrence.

In recent years, therapeutic regimens relying on the use of immune checkpoint inhibitors (anti- CTLA4, anti-PD1, and anti-LAG3 antibodies) have shown promising results and have therefore become mainstream treatment for advanced melanomas. However, even the success of these latest therapies has been hampered by recurrence and death associated with resistance [6]. Therefore, an urgent clinical need remains to gain new insights into the molecular features underlying the most advanced melanomas to better inform therapeutic strategies and to overcome treatment resistance-associated deaths.

The molecular signature of such aggressive melanomas has come to light in recent years and is associated with the emergence of a plastic, stem cell phenotype [7, 8]. Confirming findings in other highly aggressive cancers, including the re-emergence of embryonic developmental programs and gain in activity of fetal oncogenes – demonstrate that extensive cell plasticity and loss of differentiation and tissue identity are characteristic of such highly lethal cancers. One of the hallmarks of this cancer stem cell phenotype is the pathological re-expression of the TGF-beta superfamily member "Nodal" – occurring in the absence of its embryonic regulator "Lefty" [9], which underlies the progression to advanced disease in melanoma [10, 11]. Also noteworthy is the re-expression of Nodal in other advanced forms of cancer, including aggressive breast cancer [12, 13], prostate, pancreatic, ovarian and colon cancer, in addition to glioblastoma and neuroblastoma [14].

Nodal not only underlies unregulated growth and metastasis, but it is also associated with tumor heterogeneity and resistance to therapy. One example of this was observed in melanoma patients with unresectable stage lll and IV disease -- treated with BRAF inhibitor (BRAFi) therapy. The results showed that BRAFi treatment failed to significantly affect Nodal levels in melanoma tissues from these patients, all of which eventually succumbed to their disease [15].

The management of high-risk cancer patients with heterogeneous tumors is benefiting from an array of increasingly sophisticated assessment technologies. One of these diagnostic tools relies on multiplex immunohistochemistry-based digital pathology, an approach that has gained momentum over the last 10 years [16]. This success has stemmed from a combination of technological advancements, such as: 1) the use of the Tyramide Signal Amplification (TSA) technology that allows greatly increased sensitivity [17]; and 2) the generation of automated staining platforms and imaging and analysis software that mitigates concerns related to procedure inconsistencies and diagnostic discordance.

Given the therapeutic challenges we face with targeting the stem cell phenotype of aggressive tumors described above, we have hypothesized that continued Nodal expression would be detrimental to patient outcome. This pilot study is the first proof-of-principle attempt to predict treatment response and/or survival outcome among melanoma patients -- based on their Nodal expression profile relevant to anti-PD1 immune checkpoint inhibitor therapy. To this end, we first optimized a biomarker panel consisting of Nodal together with a melanoma antigen cocktail used to identify melanoma cancer cells. We found that widespread expression of Nodal (i.e., expression in >45% of melanoma antigen-expressing cells) is associated (with nearly statistical significance) with shorter survival after treatment. Our comparative assessment of patient outcome for specimens presenting with either homogeneous or heterogeneous Nodal spatial expression did not identify patterns associated with either better or worse overall survival outcome with anti-PD1 therapy, likely due to small sample size.

Methods

Clinical melanoma samples and patient demographics

The melanoma database at California Pacific Medical Center Research Institute was queried for melanoma patients with sufficient clinical data to assess immunotherapy response. The criteria for inclusion for this analysis were: 1) follow up duration of at least 18 months from the start time of checkpoint inhibitor therapy; and 2) unequivocal response status, either clinical response or early progression to anti-PD1 antibody-based immunotherapy. We identified 25 patients who met these criteria and were included in this analysis. The cohort consisted of 16 males and 9 females all reporting as White/Caucasian and ranging in age from 22.4 to 84.0 years old at the time of diagnosis (median age: 59.0 ± 16.4 years old). Patients were treated with immune checkpoint inhibitors (range: 51–8,616 days post-diagnosis, mean ± SD: 2009 ± 2,199 days) and followed up for treatment response. A responder was defined as a patient whose disease responded to the anti-PD1-containing checkpoint inhibitor therapy with disease control duration of at least 12 months after initializing the treatment. A non-responder (progressor) was defined as a patient whose disease progressed to anti-PD1-containing checkpoint inhibitor therapy within less than 6 months after initializing the treatment. Patients whose disease progressed during 1 year of adjuvant anti-PD1 therapy period were also considered progressors. Patient characteristics, including age at the start of treatment, are summarized in Supplementary File S1. Among the 10 responders, 3 specimens were from regional lymph node metastases, 3 from regional skin/subcutaneous metastases, 1 from distant lymph node metastasis, 2 from distant metastatic organs and 1 from a primary skin site. Among the 15 progressors, 8 specimens were from regional lymph node metastases, 1 from distant lymph node metastasis, 3 from distant metastatic organs and 3 from primary skin sites (Supplementary File S1). For each patient, five-micron thick tissue sections cut from Formalin Fixed Paraffin Embedded (FFPE) melanoma tumor blocks were laid on positively charged Superfrost Plus microscopy slides and processed for Hematoxylin & Eosin staining or multiplex immunohistochemistry (mIHC). Detailed specimen information is provided in Supplementary Files S1, S2.

Hematoxylin and eosin (H&E) staining

Five-micron thick tissue sections were deparaffinized in two baths of xylene(s) (10 min each), then rehydrated in two baths of 100% ethanol (5 min each), two baths of 95% ethanol (2 min each), and one bath of 70% ethanol (2 min). After a brief wash in distilled water, slides were stained in Mayer's hematoxylin solution for 8 min. Slides were washed under running warm tap water for 10 min, rinsed in distilled water and then in a bath of 95% ethanol (10 brief dips). Slides were stained in 0.25% eosin Y solution (250 mL 1% Eosin Y solution (Sigma Aldrich Inc.), 750 mL 80% ethanol, and 5 mL concentrated glacial acetic acid) for 1 min. Slides were dehydrated in two baths of 95% ethanol followed by two baths of 100% ethanol (3 min each). Slides were finally cleared in two baths of xylene(s), 5 min each, and then mounted with resin-based mounting medium (Richard-Allan Scientific).

Multiplex immunohistochemistry (mIHC)

Slides with five-micron thick tissue sections were baked at 60°C overnight, deparaffinized in two baths of xylene(s) (10 min each) and rehydrated in graded ethanols: 100%, 100%, 95%, 85%, 70% (5 min each), and finally in distilled H_2O. Heat-induced antigen retrieval was carried out in citrate buffer, pH 6.0 (Sigma-Aldrich) at 95°C for 10 min. Endogenous peroxidase and autofluorescence quenching was achieved by incubating slides in PBS containing 4.5% H_2O_2 and 10 mM NaOH under a bright light for 45 min. Non-specific antibody binding was blocked using Background Sniper (Biocare Medical). Tissue sections were incubated for 1 h at room temperature (RT) with the Nodal primary antibody in 1% BSA and 30 min in pre-diluted MACH 2 Horseradish peroxidase (HRP) labeled goat anti-mouse micro-polymer secondary antibody (Biocare Medical). The slides were washed in TNT buffer (0.1 M Tris-HCl pH 7.5, 0.15M NaCl, and 0.05% Tween-20), and the FITC signal was developed using Tyramide Signal Amplification (TSA) solution (Akoya Biosciences) for 2 min. Removal of the Nodal antibody complex was achieved by heating in 95°C citrate buffer pH 6.0 for 5 min. Tissue sections were blocked with Background Sniper, incubated for 1h at RT with the melanoma antigen cocktail primary antibody in 1% BSA then for 30 min in pre-diluted MACH 2 conjugated anti-rabbit secondary antibody (Biocare Medical). After washes in TNT buffer, the Cy5 signal was developed using Tyramide Signal Amplification (TSA) solution (Akoya Biosciences) for 7 min. After washes in TNT buffer, nuclei were counterstained with 3 μM DAPI in PBS for 5°min, washed in distilled H_2O, and mounted with Vectashield HardSet Mounting Medium (Vector Laboratories). Detailed antibody information is provided in Supplementary File S2.

Imaging

H&E-stained slides were imaged at a ×20 magnification using an Aperio AT2 whole slide scanner (Leica). Analysis was performed using Qupath software (v0.2.0-m3) [18]. Positive pixel count was performed using a threshold for FITC or Cy5 signals based on primary antibody omitted controls (Supplementary Figure S1). Slides stained with the Nodal/melanoma antigen cocktail mIHC module were imaged using a BZ-X800 fluorescence microscope (Keyence). Each multiplex-

stained specimen was first scanned at low resolution using ×4 magnification, and then imaged at high resolution at a ×20 magnification - at least three independent ×20 fields were imaged and analyzed to determine positive pixel count. Stitching of overlapping ×20 fields was performed using the BZ-X800 analyzer. Images were prepared as 8-bit merged image files and then as tiff merged image files for quantitative analysis using Image J/Fiji (version 2.1.0/1.53c). Detailed imaging information is provided in Supplementary File S2.

Quantitative analysis

Images prepared with ImageJ were then analyzed in QuPath as follows: fields were first subjected to single cell detection based upon DAPI nuclear staining using the built-in watershed-based cell segmentation algorithm. Fields were then subjected to segmentation in order to distinguish "epithelium" versus "stroma." Lastly, positive pixel counting for each dye (classifier) was then performed using fluorescence intensity thresholds defined after analysis of control specimens for which primary antibody had been omitted. Individual classifiers were trained for each marker and combined to create a composite classifier script for automated scoring cells within the annotated regions of interest.

Statistical analysis

Kaplan-Meier survival analyses were conducted to extract overall survival outcome timelines (calculated from the time of treatment initiation until death or a last follow up) by computing median survival with its 95% confidence interval. Comparative assessments used Fisher's exact test (GraphPad Prism v10.1.1). Log rank (Mantel-Cox) or Gehan-Breslow-Wilcoxon tests (Chi-square, *p*-value) and corresponding hazard ratios for each comparison are shown in Supplementary File S3. Level of significance used was * < 0.05. Staining, imaging, and scoring of the melanoma tissue specimens were carried out in a blinded manner to ensure generation of unbiased results. Two types of predicted "events" were analyzed: response (or lack of response) to therapy and survival (or death).

Results

Design and optimization of a multiplexed immunohistochemistry (mIHC)-based tool to assess Nodal expression in patients diagnosed with melanoma prior to anti-PD1 therapy

As a first step, we designed and optimized a multiplex immunohistochemistry (mIHC)-based assay to assess expression levels of Nodal in tissue specimens collected from a training set of 3 patients diagnosed with melanoma prior to treatment with anti-PD1 immune checkpoint inhibitors (Methods section; Figure 1). The optimized protocol was then used to stain and analyze specimens available for 25 of the 28 enrolled patients. The analysis allowed us to monitor the number of melanoma antigen-positive cells expressing Nodal or not. Representative mIHC images and downstream imaging and quantitative analysis for two patients -- with either predicted poor or good overall survival outcome -- are detailed in Supplementary Figures S2, S3. The expression profiles for these Melanoma antigen+Nodal+ and Melanoma antigen+Nodal- cell populations are illustrated for the 25 patients in Figure 2. Results were plotted ranking patients according to decreasing Nodal positivity. Results were then contrasted with two endpoints, i. e., subsequent treatment response (responder vs. non-responder) and overall survival outcome (alive vs. deceased).

Higher Nodal expression is often associated with poorer overall survival outcome with anti-PD1 therapy

We then investigated the potential predictive value of biomarker expression on overall survival outcome in patients who were treated with anti-PD1 immunotherapy. We first assessed the impact of Nodal positivity by assessing the percentage of melanoma antigen-positive tumor cells expressing Nodal or not. The expression patterns across the 25 patients ranked according to NODAL expression identified a group of 16 patients with high NODAL positivity and a group of 9 patients with low NODAL positivity (with ≥45% and <45% of melanoma antigen-expressing tumor cells being positive for Nodal) based upon distinct alive/deceased and treatment response status (Figure 2A). Indeed, the "high NODAL positivity" group showed lower survival, but a similar treatment response compared to the "low NODAL positivity" group [survival: 31.25% (5/16) vs. 77.78% (7/9); treatment response: 37.5% (6/16) vs. 44.44% (4/9), respectively]. A survival analysis showed a nearly statistically significant association ($p = 0.0503$) between NODAL positivity and overall survival outcome (Figure 2B; Supplementary File S3, sheet#5), patients with high NODAL positivity presenting with subsequent shorter overall survival with anti-PD1 therapy.

Lesion heterogeneity does not predict overall survival outcome with anti-PD1 therapy

Aggressive tumors are often characterized by a high degree of histological and molecular heterogeneity that reflect an extensive loss of tissue differentiation. We therefore conducted a comparative assessment of overall survival outcome for patients with specimens presenting with either homogeneous or heterogeneous Nodal spatial expression (Supplementary File S3, sheet#6). Indeed,

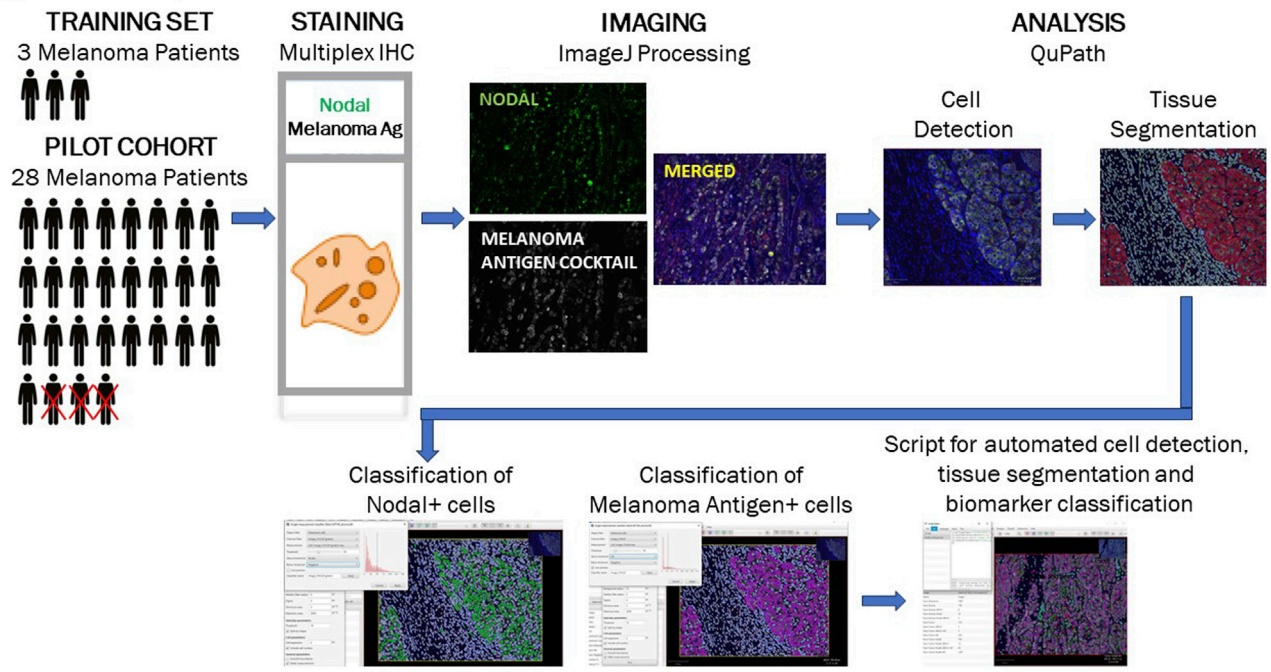

FIGURE 1
Study workflow for optimization of multiplex immunohistochemistry-based detection of a Nodal/melanoma antigen biomarker module. A training set of specimens collected from 3 melanoma patients was used to design and optimized a mIHC-based detection tool for assessment of Nodal expression in melanoma antigen-positive epithelial cells. The optimized tool was subsequently used to analyze specimens collected from a pilot cohort of 25 patients diagnosed with melanoma prior to treatment with anti-PD1 therapy. The successive steps depicted (immunostaining, imaging and quantitative analysis) are described in detail in the *Methods* section.

we quantified lesion homogeneity/heterogeneity by expressing standard deviation (SD) across the images taken for each specimen. Based on means for NODAL+ positivity (51.99%) for the cohort, we defined heterogeneous specimens as specimens with an SD greater than a 1/3 of the mean, i.e., specimens with NODAL+ SD ≥ 17.33%. Homogeneous specimens were defined as specimens with NODAL+ SD < 17.33%. This allowed us to define two NODAL+ positivity groups with either high (SD range: 18.14%–32.22%; n = 11) or low (SD range: 4.25%–16.65%; n = 14) intra-specimen heterogeneity. Survival analyses showed that lesions with highly heterogeneous NODAL expression were not more likely to be associated with shorter overall survival with the treatment compared to lesions with lower heterogeneous NODAL expression (Supplementary File S3, sheet#6).

Timeline of treatment post-diagnosis, patient gender or age do not correlate with overall survival outcome with anti-PD1 therapy

Finally, we assessed whether patient profiles would correlate with overall survival outcome post-treatment. As expected, patients not responding to treatment showed a very significant decrease in overall survival outcome, HR = 5.866; *p*-value = 0.0082 (Supplementary File S3, sheet#1). However, since there was a very wide range of time elapsed between diagnosis and implementation of treatment (13–8,616 days), we then compared overall survival outcome for the 12 patients treated early (<1,020 days) post-diagnosis (range: 13–1,017 days; mean ± SD: 350 ± 367 days) versus the 13 patients treated late (>1,020 days) post-diagnosis (range: 1,483–8,616 days; mean ± SD: 3,540 ± 2064 days). A survival analysis did not identify a significant difference in overall survival between these two groups (HR = 0.4349; *p*-value = 0.09), suggesting that patient outcome was not influenced by the time elapsed between diagnosis and implementation of treatment (Supplementary File S3, sheet#2). Survival analyses did not identify any statistically significant association between overall survival outcome post-treatment, including patient gender -- although female patients showed a trend towards improved overall survival (Supplementary File S3, sheet#3), and age at time of diagnosis (Supplementary File S3, sheet#4).

Discussion

There is a continuing critical need for early detection of patients at high risk for developing cancer as well as early

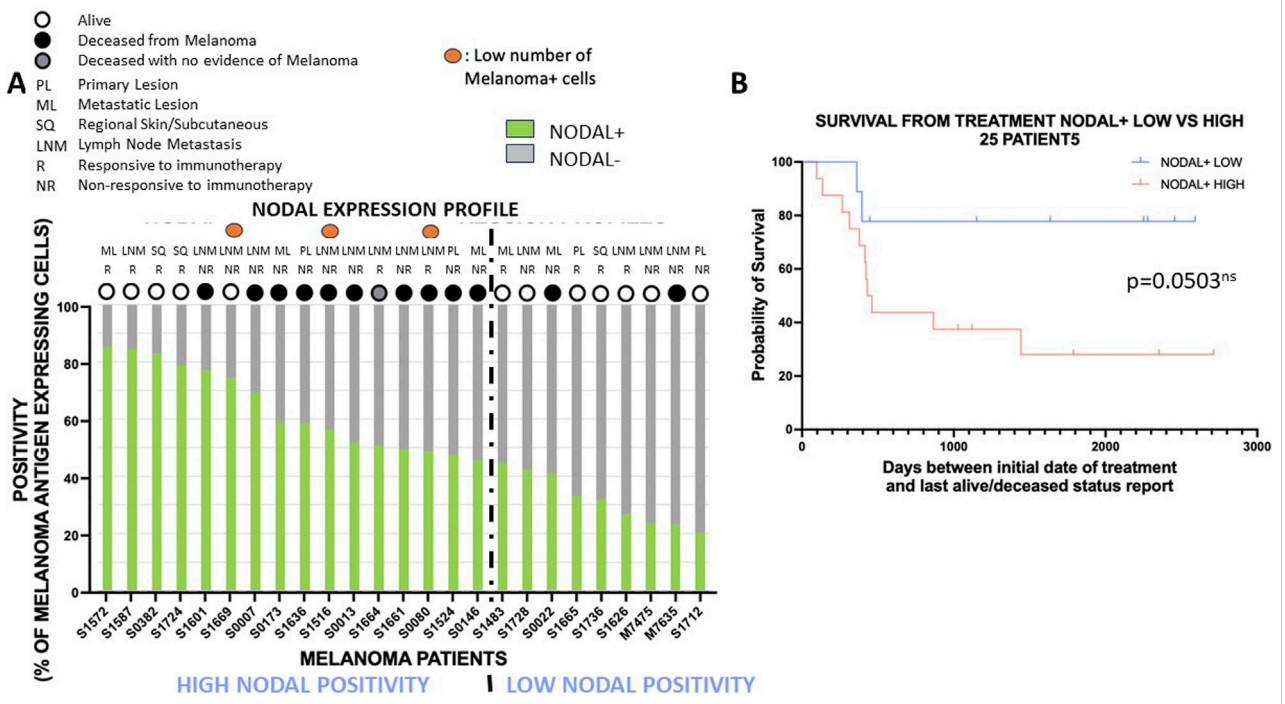

FIGURE 2
High Nodal positivity is often associated with poor overall survival outcome with anti-PD1 therapy. **(A)**: Expression profiles with percentages of melanoma antigen-positive tumor cells expressing NODAL (green) or not (grey) are shown for each patient. Patients are ranked from the ones with the highest NODAL positivity (left) to the lowest NODAL positivity (right). The dotted line partitions the cohort in two groups: group with the highest NODAL positivity and with the lowest NODAL positivity. Specimen type (PL, primary lesion; ML, metastatic lesion; SQ, Regional Skin/Subcutaneous; LNM, lymph node metastasis), response to therapy (NR, non-responsive; R, responsive), and survival outcome (alive: white circle, deceased: black or grey circles) are mentioned for each patient. **(B)**: Survival analysis for patients with low and high NODAL positivity defined in **(A)**. The high NODAL positivity group had an almost statistically significant shorter overall survival with anti-PD1 therapy than the low NODAL positivity group.

prediction of response to therapy and survival outcome for these patients. This is of particular importance for identifying the most advanced cancers at the earliest stages of development. Cancer progression has been shown to be associated with clinical, but also molecular features, that contribute to the design of customized detection, prevention, and intervention tools. Among the most prominent molecular features in advanced cancers are poor differentiation, i.e., an extensive loss of tissue identity, concomitant with the acquisition of a plastic phenotype. This loss of tissue identity coincides with the re-emergence of embryonic developmental programs underlying a stem cell signature. For example, Nodal is a powerful embryonic morphogen whose expression is quintessential for normal development; however, its aberrant re-expression observed in highly lethal cancers portends unregulated growth and disease progression. Also noteworthy is that Nodal re-expression has been documented with the expression of genes conferring resistance to therapy [12, 13, 19].

In this pilot study, we conducted an assessment on a limited number of clinical samples available to us -- to evaluate the feasibility of using a multiplex immunohistochemistry-based tool to ultimately predict response to therapy and overall survival outcome in patients diagnosed with melanoma and subsequently treated with anti-PD1 immune checkpoint inhibitors -- based upon their Nodal expression profile. This immunotherapy-based regimen has gained momentum in the past decade as it has undoubtedly improved survival outcome in many patients diagnosed with melanoma. However, there remains a notable lack of response to this class of agents and subsequent recurrence in a significant number of patients [6]. Identifying and stratifying patients who will benefit or not from such treatments or who may require combination therapies is therefore of high clinical relevance.

Previously, we observed that higher expression of Nodal correlated with advanced stage disease and resistance to therapy -- in the context of BRAFi therapy in melanoma patients [15] and independently in breast cancer patients receiving standard-of-care therapy [13]. The current study allowed us to extend the BRAFi observations to anti-PD1 therapy in melanoma patients. Since clinical samples were taken before therapy began, our evaluation of the Nodal biomarker -- on a small cohort available to us, was assessed

for its predictive value. The clinically relevant observation is that Nodal positivity is associated (with nearly statistical significance) with subsequent poorer overall survival with anti-PD1 therapy. We did not observe any effect of patient gender or age at diagnosis -- on overall survival outcome with the treatment. These observations are in accordance with the results of a large meta-analysis across 801 cancer patients -- representative of nine types of cancer, and 372 respective healthy controls [20]. This analysis concluded that Nodal was frequently expressed in tumors (56.7%) and that higher Nodal expression correlated with tumor size, differentiation degree, and disease progression, but not with patient gender, age or lymphatic metastasis status.

The encouraging preliminary findings that emerged from this proof-of-concept study will require further validation in larger and independent cohorts. With full transparency, we recognize the following limitations of the current investigation: 1) this pilot cohort is small; 2) it includes specimens consisting of regional skin/subcutaneous lesions or lesions isolated from distant organs or lymph nodes; and 3) the timeline between diagnosis and treatment implementation varies widely (13–8,616 days); and 4) anti-PD1 antibody therapies were administered in two different settings: some patients received them in the adjuvant setting, while others were treated in the metastatic setting. In our study, we included adjuvant PD-1 therapies only for early progressors – those whose melanoma progressed during 1 year of the adjuvant immunotherapy, indicating *de novo* resistance to the treatment. Although the responder patients were treated with various agents (nivolumab, pembrolizumab or nivolumab/ipilimumab), these agents have shown the same clinical efficacy (response rates, PFS, 5-year survival rates) in patients with melanoma [21–24]. However, despite all these considerations, the strength of this pilot study includes the demonstrated potential value of using multiplex IHC to assess the expression of specific biomarkers, such as Nodal, for prediction of patient outcome to current therapies. Beyond the scientific and technical advances presented in this study, the data should also provide valuable new tools for clinicians as they determine the most effective treatment for their patients based on molecular biomarkers.

Data availability statement

The raw data supporting the conclusions of this article will be made available by the authors, without undue reservation.

Ethics statement

The studies involving humans were approved by California Pacific Medical Center IRB#349056-35. The studies were conducted in accordance with the local legislation and institutional requirements. The participants provided their written informed consent to participate in this study. Written informed consent was obtained from the individual(s) for the publication of any potentially identifiable images or data included in this article.

Author contributions

PG, TT, and XW: Writing, experimental design and execution, data analyses, figure and table composition. SL, MN, KK, and MK-S: Clinical sample acquisition, data analyses, figure and table composition, manuscript review. MH: Topic concept, writing, data analyses. All authors contributed to the article and approved the submitted version.

Funding

The authors declare that no financial support was received for the research, authorship, and/or publication of this article.

Acknowledgments

The authors wish to thank Dr. Frank Shen for his review and thoughtful suggestions for this manuscript.

Conflict of interest

MH holds patents related to targeting Nodal as a therapy to inhibit aggressive cancers.

The remaining authors declare that the research was conducted in the absence of any commercial or financial relationships that could be construed as a potential conflict of interest.

Supplementary material

The Supplementary Material for this article can be found online at: https://www.por-journal.com/articles/10.3389/pore.2024.1611889/full#supplementary-material

SUPPLEMENTARY FILE S1
Detailed patient cohort information. This table provides information related to alive/deceased status, cause of death, gender, race, age at diagnosis, number of days from initial diagnosis to date dead/alive status assessed, number of days from initial date of treatment to date dead/alive status assessed, subtype (pathology) of primary and metastasis diagnosis, treatment and anatomical location/ tissue type of immunostained tissue specimens. For each group (responders vs. non-responders) information includes median age at the start of treatment, gender, stage, serum LDH level, average time from initial diagnosis to immunotherapy initiation (months), average time from immunotherapy initiation to death report/last follow up (months) and type of anti-PD1 immune checkpoint treatment.

SUPPLEMENTARY FILE S2
Antibody and specimen imaging specifications. **Sheet 1**: Description of antibodies used in multiplex immunohistochemistry, including antigen, vendor, catalog number, antibody clonality, animal species in which antibody was raised, working dilution, incubation conditions (time and temperature) and fluorescent dye used for detection. **Sheet 2**: Patient study codes, number of ×20 fields imaged, exposure times for each fluorescent dye (exposure times are identical for all images for a given patient), summary for all ×20 fields combined showing numbers of cells (and percentages in parentheses) including: total number of melanoma antigen-positive tumor epithelial cells and total number of melanoma antigen-positive tumor epithelial cells expressing Nodal.

SUPPLEMENTARY FILE S3
Survival analyses. **Sheet 1**: Comparison of survival between responders and non-responders used as a "quality control" comparison. As expected, there is a highly significant difference between survival for responders (longer survival) and non-responders (shorter survival); HR: 4.443; 95% CI: 1.489-13.26. **Sheet 2**: Impact of timeline between diagnosis and treatment implementation on overall survival outcome with anti-PD1 therapy: no significant difference. **Sheet 3**: Impact of gender on overall survival outcome with anti-PD1 therapy: no significant difference. Note: female patients show longer survival at earlier time points. **Sheet 4**: Impact of age at diagnosis on overall survival outcome with anti-PD1 therapy: no significant difference. A 59-year-old cut off was used as the dividing time point between "young" and "old" since the median age at diagnosis for the 25-patient pilot cohort is 59.0 years old. **Sheet 5**: Impact of NODAL positivity on overall survival outcome with anti-PD1 therapy: close to significant difference. **Sheet 6**: Impact of homogeneity/heterogeneity of NODAL positivity on overall survival outcome with anti-PD1 therapy: no significant difference.

References

1. American Cancer Society. *Key statistics for melanoma skin cancer* (2023).

2. Garg M, Couturier DL, Nsengimana J, Fonseca NA, Wongchenko M, Yan Y, et al. Tumour gene expression signature in primary melanoma predicts long-term outcomes. *Nat Commun* (2021) 12(1):1137. doi:10.1038/s41467-021-21207-2

3. Netanely D, Leibou S, Parikh R, Stern N, Vaknine H, Brenner R, et al. Classification of node-positive melanomas into prognostic subgroups using keratin, immune, and melanogenesis expression patterns. *Oncogene* (2021) 40(10):1792–805. doi:10.1038/s41388-021-01665-0

4. Whitman ED, Koshenkov VP, Gastman BR, Lewis D, Hsueh EC, Pak H, et al. Integrating 31-gene expression profiling with clinicopathologic features to optimize cutaneous melanoma sentinel lymph node metastasis prediction. *JCO Precis Oncol* (2021) 5:1466–79. doi:10.1200/PO.21.00162

5. Karapetyan L, Gooding W, Li A, Yang X, Knight A, Abushukair HM, et al. Sentinel lymph node gene expression signature predicts recurrence-free survival in cutaneous melanoma. *Cancers (Basel)* (2022) 14(20):4973. doi:10.3390/cancers14204973

6. Shui IM, Scherrer E, Frederickson A, Li JW, Mynzhassarova A, Druyts E, et al. Resistance to anti-PD1 therapies in patients with advanced melanoma: systematic literature review and application of the Society for Immunotherapy of Cancer Immunotherapy Resistance Taskforce anti-PD1 resistance definitions. *Melanoma Res* (2022) 32(6):393–404. doi:10.1097/CMR.0000000000000850

7. Bittner M, Meltzer P, Chen Y, Jiang Y, Seftor E, Hendrix M, et al. Molecular classification of cutaneous malignant melanoma by gene expression profiling. *Nature* (2000) 406(6795):536–40. doi:10.1038/35020115

8. Topczewska JM, Postovit LM, Margaryan NV, Sam A, Hess AR, Wheaton WW, et al. Embryonic and tumorigenic pathways converge via Nodal signaling: role in melanoma aggressiveness. *Nat Med* (2006) 12(8):925–32. doi:10.1038/nm1448

9. Postovit LM, Margaryan NV, Seftor EA, Hendrix MJ. Role of nodal signaling and the microenvironment underlying melanoma plasticity. *Pigment Cel Melanoma Res* (2008) 21(3):348–57. doi:10.1111/j.1755-148X.2008.00463.x

10. Strizzi L, Postovit LM, Margaryan NV, Lipavsky A, Gadiot J, Blank C, et al. Nodal as a biomarker for melanoma progression and a new therapeutic target for clinical intervention. *Expert Rev Dermatol* (2009) 4(1):67–78. doi:10.1586/17469872.4.1.67

11. Yu L, Harms PW, Pouryazdanparast P, Kim DS, Ma L, Fullen DR. Expression of the embryonic morphogen Nodal in cutaneous melanocytic lesions. *Mod Pathol* (2010) 23(9):1209–14. doi:10.1038/modpathol.2010.101

12. Hendrix MJC, Seftor EA, Margaryan NV, Seftor REB. *Heterogeneity and plasticity of melanoma: challenges of current therapies. Cutaneous melanoma: etiology and therapy*. Brisbane, Australia: Codon Publications (2017).

13. Margaryan NV, Hazard-Jenkins H, Salkeni MA, Smolkin MB, Coad JA, Wen S, et al. The stem cell phenotype of aggressive breast cancer cells. *Cancers (Basel)* (2019) 11(3):340. doi:10.3390/cancers11030340

14. Strizzi L, Sandomenico A, Margaryan NV, Foca A, Sanguigno L, Bodenstine TM, et al. Effects of a novel Nodal-targeting monoclonal antibody in melanoma. *Oncotarget* (2015) 6(33):34071–86. doi:10.18632/oncotarget.6049

15. Hendrix MJ, Kandela I, Mazar AP, Seftor EA, Seftor RE, Margaryan NV, et al. Targeting melanoma with front-line therapy does not abrogate Nodal-expressing tumor cells. *Lab Invest* (2017) 97(2):176–86. doi:10.1038/labinvest.2016.107

16. Harms PW, Frankel TL, Moutafi M, Rao A, Rimm DL, Taube JM, et al. Multiplex immunohistochemistry and immunofluorescence: a practical update for pathologists. *Mod Pathol* (2023) 36(7):100197. doi:10.1016/j.modpat.2023.100197

17. Stack EC, Wang C, Roman KA, Hoyt CC. Multiplexed immunohistochemistry, imaging, and quantitation: a review, with an assessment of Tyramide signal amplification, multispectral imaging and multiplex analysis. *Methods* (2014) 70(1):46–58. doi:10.1016/j.ymeth.2014.08.016

18. Bankhead P, Loughrey MB, Fernandez JA, Dombrowski Y, McArt DG, Dunne PD, et al. QuPath: open source software for digital pathology image analysis. *Sci Rep* (2017) 7(1):16878. doi:10.1038/s41598-017-17204-5

19. Strizzi L, Hardy KM, Kirschmann DA, Ahrlund-Richter L, Hendrix MJ. Nodal expression and detection in cancer: experience and challenges. *Cancer Res* (2012) 72(8):1915–20. doi:10.1158/0008-5472.CAN-11-3419

20. Ning F, Wang HF, Guo Q, Liu ZC, Li ZQ, Du J. Expression and significance of Nodal in human cancers: a meta-analysis. *Int J Clin Exp Med* (2015) 8(11):20227–35.

21. Hamid O, Robert C, Daud A, Hodi FS, Hwu WJ, Kefford R, et al. Five-year survival outcomes for patients with advanced melanoma treated with pembrolizumab in KEYNOTE-001. *Ann Oncol* (2019) 30(4):582–8. doi:10.1093/annonc/mdz011

22. Larkin J, Chiarion-Sileni V, Gonzalez R, Grob JJ, Rutkowski P, Lao CD, et al. Five-year survival with combined nivolumab and ipilimumab in advanced melanoma. *N Engl J Med* (2019) 381(16):1535–46. doi:10.1056/NEJMoa1910836

23. Robert C, Ribas A, Schachter J, Arance A, Grob JJ, Mortier L, et al. Pembrolizumab versus ipilimumab in advanced melanoma (KEYNOTE-006): post-hoc 5-year results from an open-label, multicentre, randomised, controlled, phase 3 study. *Lancet Oncol* (2019) 20(9):1239–51. doi:10.1016/S1470-2045(19)30388-2

24. Wolchok JD, Chiarion-Sileni V, Gonzalez R, Grob JJ, Rutkowski P, Lao CD, et al. Long-term outcomes with nivolumab Plus ipilimumab or nivolumab alone versus ipilimumab in patients with advanced melanoma. *J Clin Oncol* (2022) 40(2):127–37. doi:10.1200/JCO.21.02229

Pathology & Oncology Research | frontiers

TYPE Original Research
PUBLISHED 12 July 2024
DOI 10.3389/pore.2024.1611717

Check for updates

OPEN ACCESS

EDITED BY
Jelena Stojsic,
University of Belgrade, Serbia

*CORRESPONDENCE
Marko Bojović,
marko.bojovic@mf.uns.ac.rs

RECEIVED 01 February 2024
ACCEPTED 24 June 2024
PUBLISHED 12 July 2024

CITATION
Lalić N, Bojović M, Bursać D, Bokan D, Čeriman Krstić V, Kuhajda I, Parapid B, Tomić S and Šipka A (2024), The efficacy outcomes in non-small cell lung cancer patients treated with PD axis inhibitor agents - a population-based study of the Vojvodina region.
Pathol. Oncol. Res. 30:1611717.
doi: 10.3389/pore.2024.1611717

COPYRIGHT
© 2024 Lalić, Bojović, Bursać, Bokan, Čeriman Krstić, Kuhajda, Parapid, Tomić and Šipka. This is an open-access article distributed under the terms of the Creative Commons Attribution License (CC BY). The use, distribution or reproduction in other forums is permitted, provided the original author(s) and the copyright owner(s) are credited and that the original publication in this journal is cited, in accordance with accepted academic practice. No use, distribution or reproduction is permitted which does not comply with these terms.

The efficacy outcomes in non-small cell lung cancer patients treated with PD axis inhibitor agents - a population-based study of the Vojvodina region

Nensi Lalić[1,2], Marko Bojović[1,3]*, Daliborka Bursać[1,2], Darijo Bokan[1,2], Vesna Čeriman Krstić[4,5], Ivan Kuhajda[1,2], Biljana Parapid[4,5], Sanja Tomić[1] and Aleksandar Šipka[1,3]

[1]Faculty of Medicine, University of Novi Sad, Novi Sad, Serbia, [2]Institute for Pulmonary Diseases of Vojvodina, Sremska Kamenica, Serbia, [3]Oncology Institute of Vojvodina, Sremska Kamenica, Serbia, [4]Faculty of Medicine, University of Belgrade, Belgrade, Serbia, [5]University Clinical Center of Serbia, Belgrade, Serbia

Background: By 2021, the FDA approved the use of the drugs pembrolizumab and atezolizumab in the first-line treatment of patients with high positivity of programmed death ligand-1 (PD-L1) in locally advanced and metastatic non-small-cell-lung cancer (NSCLC). This approval was the result of statistically significant evidence from international, multicentric clinical studies that all reported increasing progression-free survival (PFS) and overall survival (OS) in these patients.

Methods: In our study, we reported the demographic and clinical characteristics of 79 patients diagnosed with NSCLC with expression of PD-L1 ≥50% from January 2019 to December 2022 at the Institute for Pulmonary Diseases of Vojvodina, who received pembrolizumab therapy as the first-line treatment. Patients were divided according to the histological type of lung cancer as adenocarcinoma (ADC) or squamous cell carcinoma (SCC) of the lung. In 52 of the 79 patients, PFS and in 32 of them overall survival (censored OS) was shown according to the histological type of tumor, the tumor proportion score (TPS) of PDL-1 expression, and the metastatic status within the Tumor Nodes Metastasis (TNM) disease classification. Independent factors of death outcome were shown by multivariable proportional hazard regression analysis.

Results: The study included 79 patients diagnosed with NSCLC with an expression of PD-L1 ≥50%, 50 (63.3%) patients with ADC, and 29 (36.7%) patients with SCC, whose 55 (69.6%) PDL-1 expression was obtained from broncho biopsy (BB). The majority of patients, 49 (62%), had a TPS PD-L1 score of 51%–79%. Median, PFS for adenocarcinoma was 22 months and censored OS

was 27 months, while for squamous cell carcinoma, median PFS was 12 months, and censored OS was 21 months. M1b disease stage, which was the most common in patients, had a PFS of 16 months and a censored OS of 18 months.

Conclusion: Pembrolizumab monotherapy in patients with NSCLC in the fourth stage of the disease and with the positivity of the immune checkpoint protein TPS PD-L1 above 50% represents a safe therapy that allows a satisfactory period without disease progression and overall survival with acceptable treatment complications.

KEYWORDS

lung carcinoma, immune checkpoint inhibitors, immunotherapy, PD-L1 receptor, pembrolizumab

Introduction

The survival of patients with lung cancer in the last decade has had an increasing trend if data from all over the world is compared. In particular, NSCLC accounts for about 85% of all malignant lung tumors, with ADC (40%) taking the lead to SCC and other pathological types of lung cancer [1]. Targeted molecular therapy has significantly improved the treatment of advanced and metastatic NSCLC when compared to standard chemotherapy. Among the new treatments for advanced lung cancer now available, immunotherapy is the newest and most promising [2]. Malignant tumor cells have characteristics that allow them to spread and maintain their neoplastic state, evade the immune system, and inhibit the immune response, by preventing the activation of immune T cells increasing the expression of immune checkpoint proteins on T cells [3]. The basis of new therapeutic procedures was the inhibition of those pathways that led to the evasion of the immune system through immune checkpoints, which changed the paradigm of cancer treatment. The drugs of this group are called immune checkpoint inhibitors (ICIs). The suppression of signaling pathways involving programmed cell death ligand-1 (PD-L1) and programmed cell death-1 (PD1) increases the functionality and the response strength of $CD8^+$ T (cluster of differentiation 8 thymus) cells. By suppressing the signaling that PD-1 receives from its ligand, it is possible to restore the activity of T lymphocytes and increase their antitumor activity with a further increase in PD-L1 expression in the tumor microenvironment (TME) [4]. Immunotherapy in oncology began with the approval of antibody therapy against cytotoxic T lymphocyte antigen-4 (CTLA-4) in 2011 for the treatment of metastatic melanoma. This was followed by the approval of seven additional immune checkpoint inhibitors (ICIs) focusing on suppressing the PD-1 pathway: ipilimumab, pembrolizumab, nivolumab, atezolizumab, avelumab, durvalumab, and cemiplimab, which are currently used to treat 18 different types of cancer [5]. There is evidence that PD-L1 is found in a higher percentage in NSCLC and it is expressed in the majority of tumor-infiltrating lymphocytes, which has been the reason for to introduce PD-L1 or PD-1 inhibitors into the treatment of NSCLC. The level of PD-L1 expression in the tumor shows a better response and longer survival rate (proportional score >50% of tumor cells for first-line immunotherapy and >1 for second-line immunotherapy) compared to conventional chemotherapy. Based on these results, the FDA approved the drug pembrolizumab in the first-line therapy of advanced NSCLC for ≥50% PD-L1 expression without the presence of epidermal growth factor receptor (EGFR) mutation and anaplastic lymphoma kinase gene (ALK) rearrangement [6]. The KEYNOTE 024 study investigated the role of pembrolizumab in first-line therapy in patients with high PD-L1 expression (≥50%). Updated analyses showed that pembrolizumab as monotherapy improved overall survival (OS) compared with platinum-based chemotherapy, with a median overall survival (median OS) of 30.0 vs. 14.2 months [7]. It was also proven that there was a synergistic effect of the drug pembrolizumab with chemotherapy, that both agents reduced the activity of T regulatory cells and increased the presentation of tumor antigen cells [8]. The third phase KEYNOTE 189 study primarily studied and confirmed improvements in PFS and OS in the group of patients with combined therapy of pembrolizumab and chemotherapy [9]. The KEYNOTE 407 study related to combined immunochemotherapy in squamous metastatic NSCLC showed an improvement in PFS and OS but also the effect on PD-L1 expression [10, 11]. This trial changed the indication for receiving immunotherapy for patients with advanced squamous NSCLC, which until recently was treated with cytotoxic chemotherapy due to the absence of targetable aberrations in this pathohistological type of tumor [12]. The purpose of this paper is to elaborate on the demographic and clinical characteristics of metastatic NSCLC patients diagnosed as PD-L1 positive (with over 50% positivity) who underwent first-line therapy with pembrolizumab and to show disparities between squamous and non-squamous NSCLC, segmented by the number (1, 2, 3, or more) and location of metastases (liver, bone, and brain, and other sites).

Materials and methods

Methodology

The retrospective study involved 79 patients with metastatic ADC and SCC lung cancer who were treated with pembrolizumab as the first line of treatment from January 2019 to December 2022 at the Institute for Pulmonary Diseases of Vojvodina. Out of these 79 patients, 52 who started the treatment by the end of 2021 were grouped together in a subgroup of the study so that the PFS and censored OS outcomes could be observed over a 2-year period. Inclusion criteria: patients above 18 years old, pato-histological confirmed NSCLC, metastatic disease, previously not treated with chemo or radiotherapy. Exclusion criteria: low ECOG performance status, another synchronic malignancy, heavy comorbidities. The minimum follow-up period was 24 months.

Immunohistochemical analysis

After sectioning Formalin-Fixed-Paraffin-Embedded (FFPE) on 4–5 μm of tumor tissue be mounted on Fisherbrand Superfrost Plus slides and stained using the PD-L1 clone 22C3 pharmDx kit and Dako Automated Link 48 platform (Agilent Technologies/Dako, Carpinteria, CA, United States).

The Tumor Proportion Score (TPS) was calculated as the percentage of at least 100 viable tumor cells. Based on partial or complete staining of the membrane all samples were divided into one of three groups: with <1% (no expression), 1%–49% (low expression), or ≥50% (high expression) positive tumor cells.

Statistical analysis

Attribute descriptors were presented of frequency and percentage. The difference in frequency of attribute descriptors was tested using the Chi-Square test. The normality of data distribution was assessed using the Shapiro-Wilk test. The values of PFS and censored OS were depicted using the median, Kaplan-Meier curves, and Cox regression analysis.

A statistical significance level of $p < 0.05$ was employed. Results were displayed both in tabular format and using Kaplan-Meier curves. Tables were created using Microsoft Word v 2021. IBM SPSS Statistics v26 and JASP v0.11.3 were utilized for statistical data analysis.

Ethical statement

This study was approved by the Institutional Ethical Committee (Ethical Committee of the Institution for Pulmonary Diseases of Vojvodina No. A203/2). The identities of all the patients from our study was removed and the study was conducted according to the Helsinki Declaration of the World seventh revision.

TABLE 1 Demographic and clinical characteristics of the patients treated with pembrolizumab from January 2019 to December 2022.

		N = 79
Age (years)		64.9 (±6.71)
Gender	Males	48 (60.8%)
	Females	31 (39.2%)
Smoking status	Never-smoker	7 (8.9%)
	Former smoker	61 (77.2%)
	Current-smoker	11 (13.9%)
Comorbidities	COPD	10 (12.7%)
	Cardiovascular diseases	23 (29.1%)
	Renal diseases	2 (2.5%)
	Diabetes Mellitus	1 (1.3%)
	Rheumatoid arthritis	1 (1.3%)
	Autoimmune diseases	1 (1.3%)
	Other pulmonary diseases	2 (2.5%)
	Other diseases	3 (3.8%)

TABLE 2 Tumor characteristic; sample types; sampling method.

Hystological type	Adenocarcinoma	50 (63.3%)
	Squamous	29 (36.7%)
Type of samples	Histology	77 (97.5%)
	Cytology (Cytoblock)	2 (2.5%)
Type of sampling	Bronchoscopy	55 (69.6%)
	Surgery	13 (16.5%)
	Tru-cut	2 (2.5%)
	Biopsy of metastasis	5 (6.3%)
	Cytoblock from bronchoscopy	2 (2.5%)
	Cytoblock from pleural effusion	2 (2.5%)

Results

We presented 79 patients with metastatic NSCLC who received monotherapy with the drug pembrolizumab. Demographic and clinical characteristics of the patients

TABLE 3 Metastasis characteristics.

TNM M status	M1a	29 (36.7%)
	M1b	41 (51.9%)
	M1c	9 (11.4%)
Localization of metastasis	Lung	28 (36.7%)
	Brain	7 (8.9%)
	Liver	6 (7.6%)
	Bone	11 (13.9%)
	Adrenal node	9 (11.4%)
	Pleura	1 (1.3%)
	Multi	9 (11.4%)
	Other	8 (10.1%)

according to age, gender, smoking status, and comorbidities are shown in Table 1.

For all 79 patients in the study who received pembrolizumab in the first line of treatment, ADC or SCC lung cancer in the metastatic stage of the disease was previously confirmed histologically or from a cellblock. The majority, i.e., 50 of them (64.1%), had lung ADC. The tumor tissue sample most often obtained for the PD-L1 test was a biopsy from bronchoscopy, among 55 (69.6%) patients. The number of CT-guided core biopsies is low in our study, we rarely performed that procedure. These results are shown in Table 2.

Given that among our patients, immunotherapy was applied only to patients in the metastatic stage of the disease, we were interested in the representation of tumor metastases according to the number and localization in each patient (Table 3). Most of the patients were in the M1b stage of the disease, and the most common localization of metastases was pulmonary metastasis, in 28 (36.7%) patients.

PD-L1 protein expression in tumor cells and tumor-infiltrating immune cells (ICs) were assessed by immunohistochemistry. The tumor proportion score (TPS) as the percentage of viable tumor cells determined the PD-L1 protein expression in the tumor. All samples from the patients in the study had TPS as ≥50% (high expression) positive tumor cells of the PD-L1 test. The patients were divided into three subgroups: PD-L1 with 50% positivity, PD-L1 with 51%–79% positivity, and PD-L1 over 80% positivity evaluation. The positivity of the test was also compared according to the histological type of the tumor and according to the metastatic status of the tumor. PD-L1 positivity of 51%–79% was most common in both histological types of tumors and within M1b metastatic tumor status. There was no statistically significant difference in the strength of PD-L1 expression for either of the mentioned tumor characteristics (Table 4).

In this paper, we monitored the first follow-up response (FUP1) according to the modified Response Evaluation Criteria in Solid Tumors (RECIST version 1.1) used in malignant tumors immunotherapy trials, so-called iRECIT, for all 79 patients who received pembrolizumab therapy for at least 3 months until the end of 2022. Therapeutic response was presented as partial regression (PR), stable disease (SD), progressive disease (PD), and pseudoprogression disease (psPD). There was no statistically significant difference at FUP1 according to the histological tumor type, i.e., at FUP1 most patients of both histology types of tumors had stable disease (SD). The same applied to M status, that is, patients of M1a, M1b, and M1c status most often had SD at FUP1 (Table 5).

We also investigated the type of disease progression according to the histological type of tumor and according to the metastatic stage of the disease, whereby the disease progression causes were marked as locoregional disease progression or distant (appearance of new metastatic lesions). The most common type of progression was the occurrence of distant progression in both ADC and SCC lung cancer, as well as in previous (before therapy) existing M1b disease stage. According to different histology or different M statuses, there was no statistically significant difference in the type of disease progression (Table 6).

TABLE 4 TPS PD-L1 by histology type and by M status.

		PD L1 status			*p*-value
		50%	51%–79%	80% and more	
Histological type	ADC	2 (4.0%)	28 (56.0%)	20 (40.0%)	0.127[a]
	SCC	2 (7.1%)	21 (75.0%)	5 (17.9%)	
Characteristics of metastasis	M1a	2 (6.9%)	17 (58.6%)	10 (34.5%)	0.509[a]
	M1b	2 (4.9%)	28 (68.3%)	11 (26.8%)	
	M1c	0 (0%)	4 (44.4%)	5 (55.6%)	

ADC, Adenocarcinoma; SCC, Squamous cell carcinoma; PD L1, Programmed cell death receptor ligand 1.
[a]Chi-Square test.

TABLE 5 Response (FUP1) by histological type of tumor and by M status.

		Response				*p*-value
		PR	SD	PD	psPD	
Histological type	ADC	16 (32.0%)	28 (56.0%)	2 (4.0%)	3 (6.0%)	0.136[a]
	SCC	5 (17.9%)	17 (60.7%)	3 (10.7%)	0 (0%)	
Characteristics of metastasis	M1a	9 (31.0%)	16 (55.2%)	0 (0%)	2 (6.9)	0.363[a]
	M1b	10 (24.4%)	26 (63.4%)	4 (9.8%)	0 (0%)	
	M1c	2 (22.2%)	4 (44.4%)	1 (11.1)	1 (11.1%)	

ADC, Adenocarcinoma; SCC, Squamous cell carcinoma; PR, Partial Response; SD, Stable Disease; PD, Progressive Disease; psPD, Pseudoprogression Disease.
[a]Chi-Square test.

TABLE 6 Progression causes by histology type and by M status.

		Progression			*p*-value
		Locoregional	Distant	Without progression	
Histological type	ADC	5 (10.2%)	11 (22.4%)	33 (67.3%)	0.953[a]
	SCC	3 (12.0%)	5 (20.0%)	17 (68.9%)	
Characteristics of metastasis	M1a	2 (7.4%)	5 (18.5%)	20 (74.1%)	0.608[a]
	M1b	4 (10.0%)	10 (25.0%)	26 (65.0%)	
	M1c	2 (25.0%)	1 (12.5%)	5 (62.5%)	

ADC, Adenocarcinoma; SCC, Squamous cell carcinoma.
[a]Chi Square test.

TABLE 7 Therapy discontinuation caused by histology type and by M status.

		Response					*p*-value
		Progression	Complications	ECOG	Death	Without disrupt	
Histological type	ADC	13 (30.6%)	6 (12.0%)	2 (4.0%)	6 (12.0%)	23 (46.0%)	0.363[a]
	SCC	6 (26.9%)	2 (7.7%)	3 (11.5%)	5 (19.2%)	10 (38.5%)	
Characteristics of metastasis	M1a	6 (22.2%)	2 (7.4%)	2 (7.4%)	2 (7.4%)	15 (55.6%)	0.666[a]
	M1b	12 (29.3%)	4 (9.8%)	2 (4.9%)	7 (17.1%)	16 (39.0%)	
	M1c	1 (11.1%)	2 (22.2%)	1 (11.1%)	2 (22.2%)	3 (33.3%)	

ADC, Adenocarcinoma; SCC, Squamous cell carcinoma; ECOG, Eastern Cooperative Oncology Group.
[a]Chi Square test.

We also examined the reasons for discontinuation of pembrolizumab therapy (disease progression, treatment complications occurrence, worsening of the patient's ECOG performance status, death). There was no statistically significant difference in the reasons for discontinuation of therapy according to histology type of tumor or M status of the disease (Table 7).

Therapy postponement (up to 30 days, over 30 days, without delay) as well as the cycle in which the therapy was delayed are shown in Table 8.

After the discontinuation of pembrolizumab therapy, we examined the continuation of other types of therapy according to the histology type of the tumor and according to the M status of the disease. The most common type of continued

TABLE 8 Postponed therapy distribution.

		N = 79
Postpone	Up to 30 days	12 (15.2%)
	30 days and more	3 (3.8%)
	Without postponement	64 (81.0%)

TABLE 9 Pembrolizumab therapy complications.

			N = 79
Complications	Yes	Hypothyroidism	11 (13.9%)
		Pneumonitis	5 (6.3%)
		Kidney disease	4 (5.1%)
		Infections	4 (5.1%)
		Pneumonia	3 (3.8%)
		Skin toxicities	3 (3.8%)
		Hepatic failure	3 (3.8%)
		Hematological toxicity	3 (3.8%)
		Pulmonary thromboembolism	2 (2.5%)
	No		41 (51.9%)

therapy for all observed subgroups of patients was supportive therapy, followed by chemotherapy (five patients with ADC, three patients with SCC, four patients with M1a, and four patients with M1b status), radiotherapy was received by one patient with ADC and one patient with M1b disease status, while one patient with SCC and one patient with ADC received chemoradiotherapy.

The most common adverse event (AD) in all subjects was the occurrence of hypothyroidism, which did not lead to discontinuation, but only to therapy postponement up to 30 days. A specialist endocrinologist was involved in the treatment and monitoring of hypothyroidism. Therapy complications are shown in Table 9.

A group of patients who underwent surgical treatment of lung tumors before the appearance of metastatic disease was specially monitored. There was a total of 8 patients, of which before pembrolizumab therapy 3 had radiotherapy, chemotherapy 4 of them, and chemo and radiotherapy one of them. These patients, i.e., the therapeutic outcome with pembrolizumab, was not compared to patients who did not have surgery. Also, one patient had palliative radiotherapy for some metastases or palliative radiotherapy for superior vena cava syndrome (SVCS) before or during the administration of pembrolizumab. The treatment outcome among these patients compared to patients who did not have palliative radiotherapy while receiving the drug pembrolizumab was not separately compared.

PFS and censored OS

79 patients in our study started therapy with the drug pembrolizumab from December 2019 to January 2022. For a 2-year PFS and censored OS presentation, we singled out 52 patients whose pembrolizumab therapy was scheduled to start by the end of 2021. Accordingly, some of the 52 patients were alive by the end of 2022, the OS value was lower than the PFS and was calculated and shown in our study as censored OS. PFS and censored OS were observed according to the histology type of the tumor, with a longer 2-year disease progression and overall survival among patients with ADC (Figures 1, 2). Median PFS (censored) for ADC was 22 months, and for SCC was 12 months (half of the observed patients with ADC have been progressed in 22 months).

Median OS (censured) for ADC was 27 months and for SCC 21 months (half of observed patients were dead in 27 months and 21 months).

According to the percentage of PD-L1 positivity (PD-L1 50%, PD-L1 51%–79%, and PD-L1 over 80%) there was no statistically significant difference in 2-year PFS and censored OS (Figures 3, 4).

According to M disease status (M1a, M1b, and M1c) there was no statistically significant difference in 2-year PFS and censored OS (Figures 5, 6).

Discussion

Among various malignancies, NSCLC is a type of solid tumor that showed an extremely good therapeutic response to the introduction of immunotherapy in the last decade. For the prevention and regulation of malignant tumors, immunosurveillance is essential [13]. The activity of the immune system T-cells as the main active component of the immune response is regulated by stimulatory as well as inhibitory signals called checkpoints. The main checkpoint that regulates the immune response is the interaction between the PD-1 receptor and its programmed cell death ligand-1 (PD-L1). Monoclonal antibody therapy can effectively inhibit these proteins and thus modulate tumor growth and development [14]. Pembrolizumab (Keytruda®), formerly lambrolizumab, is a humanized IgG4 kappa monoclonal antibody that inhibits PD-1 receptor activity. The drug was originally approved by the Food Drug Administration (FDA) in 2014, and by the European Commission in 2015 for the treatment of unresectable and metastatic melanoma that progressed after ipilimumab therapy [15]. So far, there have been several trials where lung cancer patients have been treated with pembrolizumab. In KEYNOTE-010, pembrolizumab in the second line of treatment showed long-term benefits compared to chemotherapy (docetaxel), while the patients were previously treated with chemotherapy. According to PD-L1 status, patients were divided into subgroups of PD-L1 TPS (tumor proportion score) ≥50%

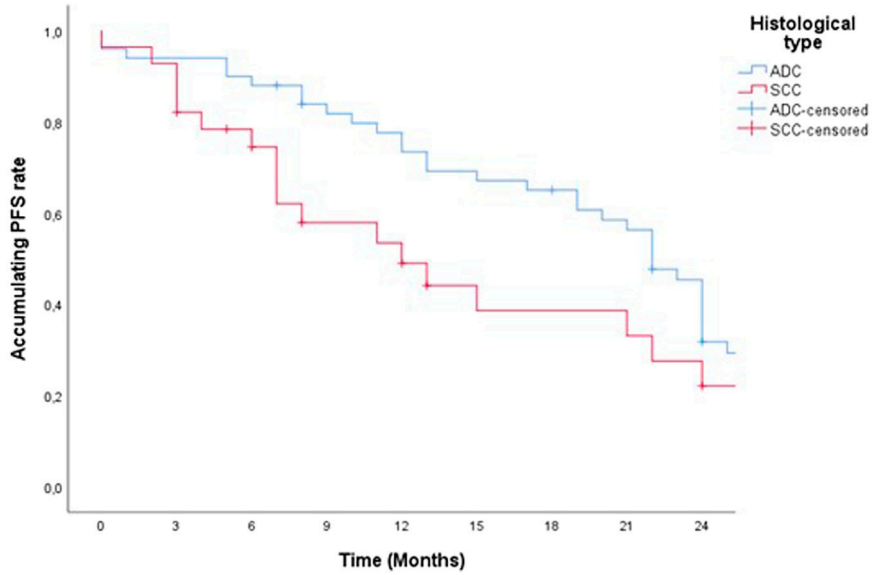

FIGURE 1
Two-year PFS of patients treated with pemrolizumab according to histological tumor type.

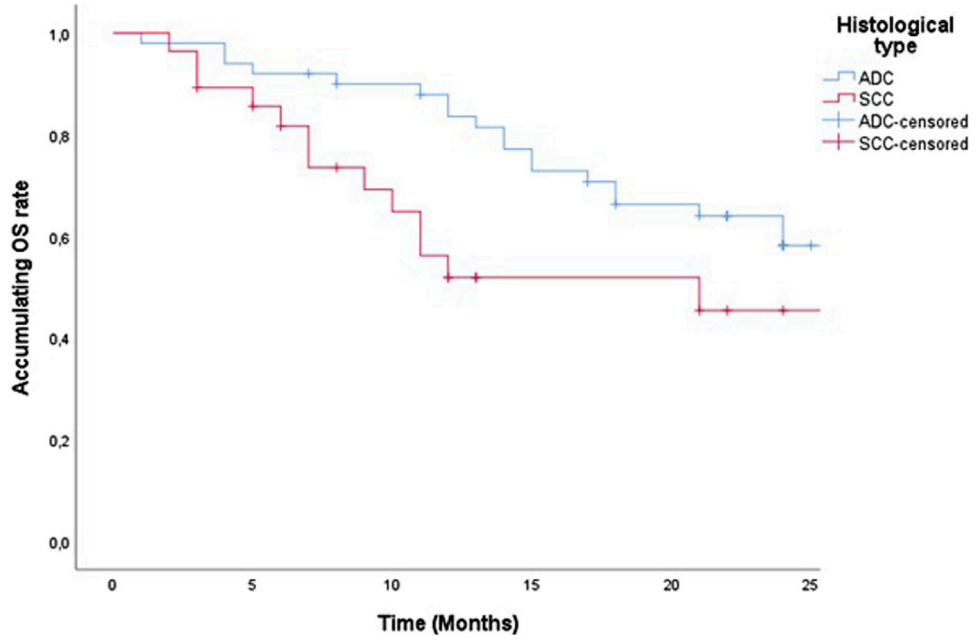

FIGURE 2
Two-year censored OS of patients treated with pemrolizumab according to histological tumor type.

and ≥1% [16]. A randomized, phase 2 KEYNOTE-021 study showed a significantly better therapeutic response among the patients treated with pembrolizumab and chemotherapy compared to chemotherapy alone. In this study, pembrolizumab was given as a first-line treatment in combination with chemotherapy to patients with advanced or metastatic NSCLC [17]. KEYNOTE-024 as a randomized phase 3 multicenter study investigated the therapeutic response of the first-line pembrolizumab as monotherapy versus first-line platinum-based chemotherapy among patients with NSCLC.

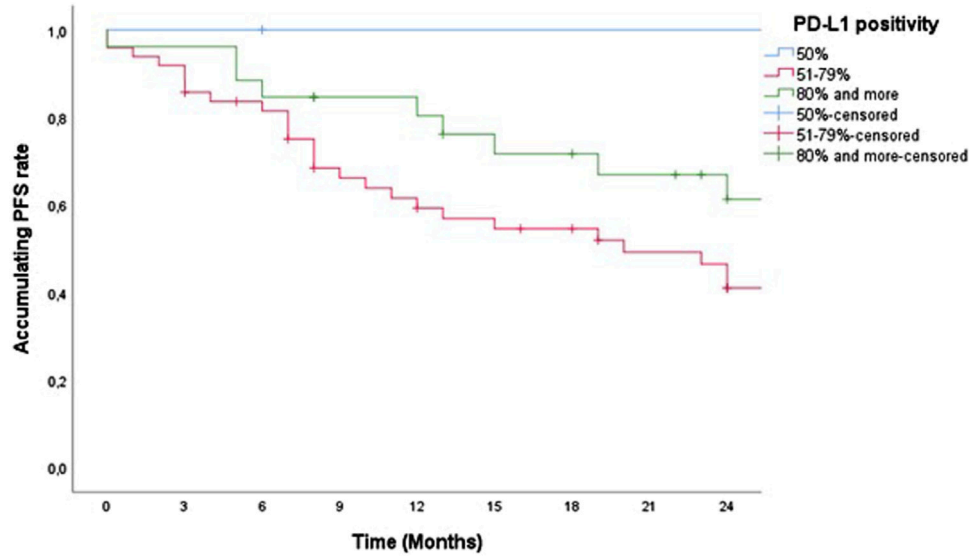

FIGURE 3
Two-year PFS of patients treated with pemrolizumab according to PD-L1 positivity.

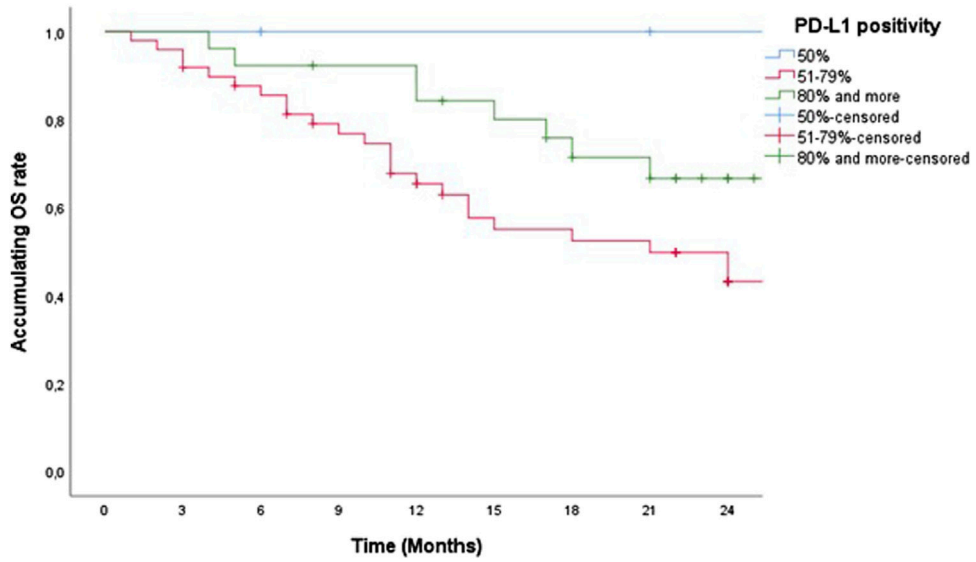

FIGURE 4
Two-year censored OS of patients treated with pemrolizumab according to PD-L1 positivity.

All patients in the study with advanced or metastatic LC had PD-L1 TPS ≥50% [18]. KEYNOTE-042 is a multicenter phase 3 study similarly designed as KEYNOTE-024, which enrolled treatment-naïve patients whose tumors showed strong (PD-L1 TPS ≥50%) versus weak (PD-L1 TPS 1%–49%) PD-L1 positivity [19]. Both studies showed a better therapeutic response in patients treated with immunotherapy. In our study, we showed the effect of pembrolizumab treatment as monotherapy in the first-line treatment of advanced or metastatic NSCL with PD-L1 TPS ≥50%, where the primary objective of the study was to illustrate disparities and therapeutic response between metastatic squamous and non-squamous NSCLC, according to the number and location of metastases and according to PD-L1 TPS positivity.

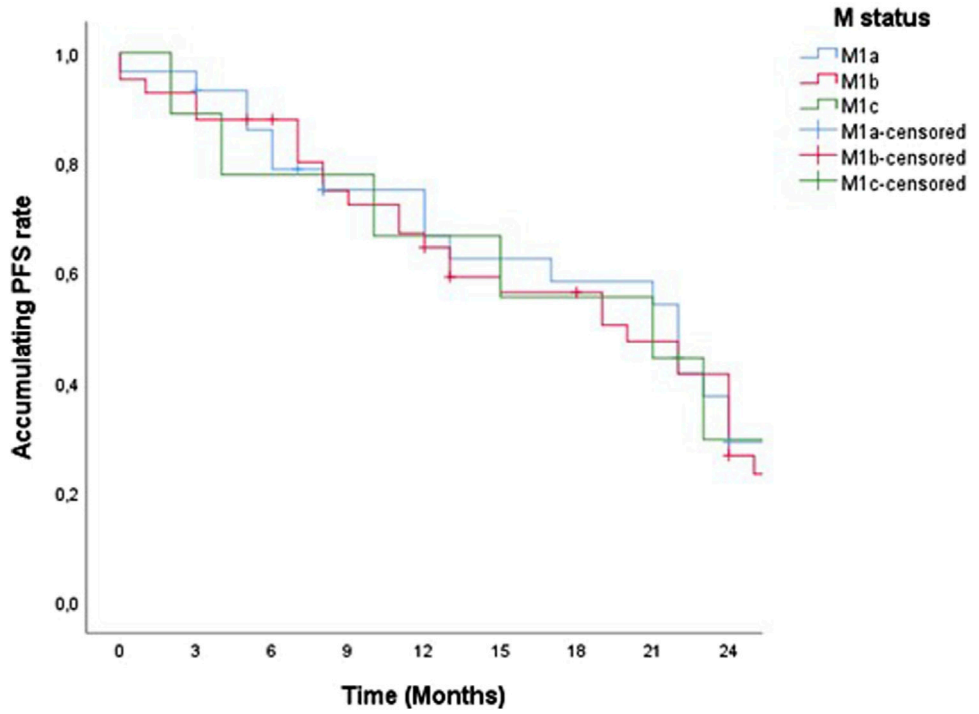

FIGURE 5
Two-year PFS of patients treated with pemrolizumab according to M status.

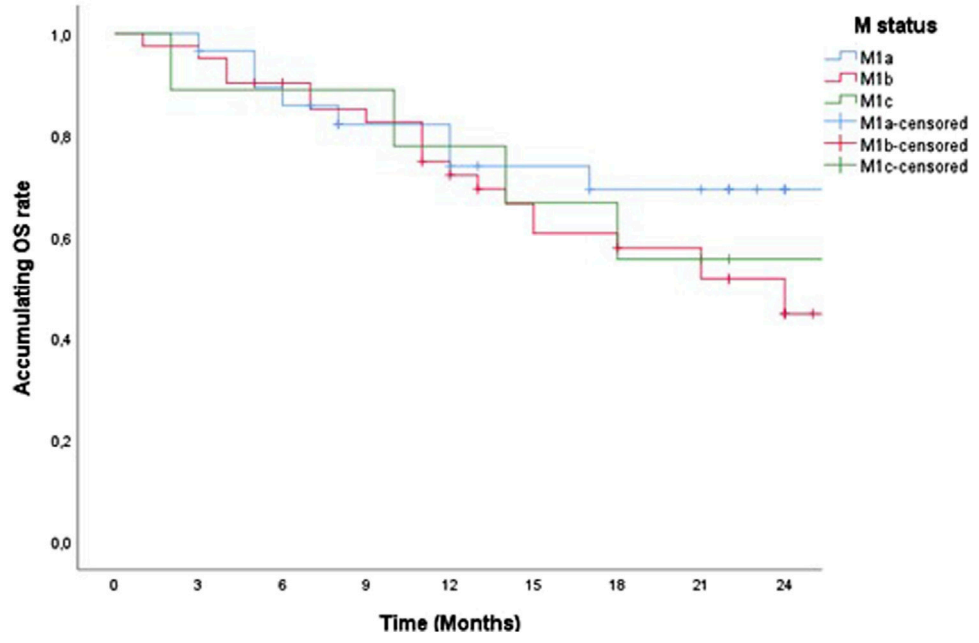

FIGURE 6
Two-year censored OS of patients treated with pemrolizumab according to M status.

Testing for PD-L1 expression is performed using a diagnostic immunohistochemical test. PD-L1 expression requires histological samples, as the sample formalin fixation should be done with at least 100 tumor cells [20]. Tissue sampling for PD-L1 testing in this study was most often from biopsies obtained by bronchoscopy, which corresponded to the patients included in the study, who all had metastatic disease. Only a small number of patients had a tissue sample resected during surgery, and these were the patients who after a certain time progressed to stage IV of the disease, and a tissue sample was taken from the initial phase of the disease. One of the studies evaluated the concordance of PD-L1 expression between bronchoscopic small biopsies and surgical resections. PD-L1 expression was investigated in 79 patients for whom bronchoscopic biopsy specimens and surgical resection specimens were available. The concordance of PD-L1 expression between small biopsies and surgical resections was 92.4% [21]. In our study, two samples for PD-L1 testing were from the cytoblock obtained from the endobronchial ultrasound transbronchial needle aspiration (EBUS-TBNA) bronchoscopy. In on other study the concordance rate between EBUS-TBNA versus surgical specimens was 87% for PD-L1 ≥1% and 82% for PD-L1 ≥50%. However, the sensitivity of EBUS-TBNA samples dropped from 72% to only 47% at a PD-L1 expression cutoff of ≥50% (vs. ≥1%), raising concerns about false-negative PD-L1 results on EBUS-TBNA samples [22].

In our study, patients were treated with pembrolizumab monotherapy at a dose of 200 mg of body weight every 21 days, where all patients had metastatic disease, PD-L1 TPS ≥50%, ECOG (European Cooperative Oncology Group) status 0 or 1. The smallest number of drug cycles received was 3, and the largest was 56. After 2 years of this type of therapeutic regimen, 6 patients switched to the regimen of administering the drug dose of 400 mg every 6 weeks. Currently, the definition of permanent response among immunotherapy patients has been controversial. Permanent response is defined as the patient's progression-free survival (PFS) exceeding three times the median PFS of the same cohort [23]. Permanent responses to administered ICIs can last for months or years, with some patients even having improved responses to ICIs over time according to iRECIST criteria and thus even longer censored OS [24]. The National Comprehensive Cancer Network (NCCN) guidelines recommend that patients with NSCLC should receive maintenance ICIs for 2 years if they have received first-line immunotherapy. Maintenance therapy is administered for 2 years in patients who received first-line immunotherapy and until disease progression in patients who received second-line immunotherapy [25, 26]. In tumors, there may be a transient increase in the volume or number of lesions (temporary progression) after ICI treatment, but after that period partial regression (PR) or stable disease (SD) may occur, which is defined as pseudoprogression [27]. Pseudoprogression, as an unusual but useful pattern of treatment with ICIs, should be emphasized and carefully recognized. The increased tumor volume is likely to be the result of the recruitment of activated T cells to the tumor site during ICI treatment. Before these cells achieve their antitumor functions, they lead to inflammation and tumor volume enlargement, as well as immune infiltration, edema, and necrosis. The incidence of pseudoprogression varies among tumor types but is rarely >10% [28–31]. Pseudoprogression often occurs after initial treatment with ICIs [29]. In our study, at the first follow-up visit (FUP1), a total of six patients had psPD (pseudoprogression disease) response, and during the entire study, a total of 7 patients had psPD, as in the above-mentioned studies, at the beginning of treatment. All patients continued therapy, with PFS and censored OS being significantly longer compared to pseudoprogression-free patients if we observe a 2-year overall survival.

A total of 38 out of 79 (48%) patients had complications of pembrolizumab administration in our study, which is a good result compared to other studies where the frequency of complications in monotherapy with ICIs ranged from 15% to 90% [19, 32]. In a systematic review of 50 studies, the incidence of grade 3/4 adverse events (AEs) was 21% (range 0%–66%) [33]. Comparing our results with studies where immunotherapy was given as monotherapy for NSCLC, the most frequent AE was hypothyroidism CTCAE grade 1, classified according to Common Terminology Criteria for Adverse Events (CTCAE), found in 11 (13%) patients, compared to other complications that were individually represented by no more than 1 (1%). The postponement of therapy until the stabilization of the hormone concentration by medication did not amount to more than 30 days, and there was no interruption of therapy for that reason. In a retrospective cohort study of 1,246 patients treated with ICIs, immune-related AEs (IRAEs) occurred in 518 (42%) patients. Subclinical thyrotoxicosis (n = 234) was the most common thyroid IRAE, followed by overt thyrotoxicosis (n = 154), subclinical hypothyroidism (n = 61), and overt hypothyroidism (n = 39) (89). Thyroid dysfunction is the most common endocrine IRAE in NSCLC [34].

In this paper, we were able to show 2-year overall survival (censored OS) and progression-free survival (PFS) according to certain clinical and pathological tumor characteristics for 52 patients out of the total of 79 patients who received pembrolizumab therapy by the end of 2021. The studies which included pembrolizumab as monotherapy showed the following results: KEYNOTE-010 study showed better OS over docetaxel for both groups of PD-L1 TPS ≥50% and ≥1% positivity, (hazard ratio [HR] 0.53; 95% CI and HR, 0.69; 95% CI, $p < 0.00001$, respectively) [16]. In the KEYNOTE-021 Cohort G study, PFS for pembrolizumab in combination therapy (n = 60) versus chemotherapy (n = 63) was (median: 24.5 versus 9.9 months; hazard ratio: 0.54; 95% confidence interval: 0.35–0.83). Median overall survival was 34.5 versus 21.1 months (hazard ratio: 0.71; 95% confidence interval: 0.45–1.12) [35].

In our study, 59 (64.1%) patients had ADC, and 20 (35.9%) of them had squamous cell carcinoma (SCC). According to the histological type of lung cancer, patients with ADC had a longer censored PFS and censored OS compared to SCC, which amounted to (PFS HR 0.626 95% CI 0.358–1.09, $p = 0.101$ and censored OS HR, 0.550; 95% CI 0.280–1.08, $p = 0.08$). A multicentric study published in 2022 reported potential differences in the efficacy of ICIs in the treatment of squamous NSCLC and non-squamous NSCLC. ICI monotherapy improves OS in SCC and ADC (OS HR 0.71, 0.80), and overall all of the studies showed a greater OS for SCC (OS HR 0.89, 95% CI 0.80–0.99). For PFS ICI monotherapy also showed a reduction in the risk of disease progression and even more so for SCC compared to ADC (35% for SCC vs. 10% for ADC) [36].

We observed both PFS and censored OS in our study according to the degree of PD-L1 positivity, whereby we divided patients into three groups (PD-L1 TPS = 50%, 51%–79%, and over 80%). There was no statistically significant difference in PFS and censored OS according to the degree of high positivity of PD-L1 TPS (PFS, $p = 0.587$ and censored OS, $p = 0.583$) because all the groups that were observed for this characteristic are essentially groups with high expression of PD-L1. The correlation analysis between PD-L1 expression levels and clinicopathological parameters was shown in 1,008 SCC or ADC, it was concluded that PD-L1 expression is higher in men, smokers, squamous cell carcinoma tumors with a maximum diameter >3 cm, patients with poor differentiation and/or high TNM disease stage. Among patients with well to moderately differentiated ADC, clinical stages I-II, without a history of smoking, lymph node metastases, or distant metastases, no PD-L1 testing was recommended. However, a strong recommendation for testing has been established for patients with SCC who have lymph node metastases or poorly differentiated NSCLC with N3 disease, especially smokers with N3 disease [37, 38].

According to the localization of metastases and their number and taking into account the TNM classification for the M stage of the disease patients in our study were divided into M1a, M1b, and M1C stages. The M1c rate was so low in the study maybe because we did not perform PET/CT on all the patients, only to some of them. In addition, there was no difference in PFS and censored OS between these three groups of patients with NSCLC treated with pembrolizumab (PFS, $p = 0.473$ and censored OS $p = 0.09$). So far, comparative studies that would monitor PFS and censored OS according to this characteristic have not been done, but in one of the multicentric studies that included 16 randomized clinical trials (RCTs) and 14 observational trials, a survival improvement for ICIs (ICI monotherapy, ICI + chemotherapy, dual ICI therapy and dual ICI + Chemotherapy) versus standard therapies was reported among NSCLC patients with liver metastases: (PFS HR, 0.77; 95% CI, 0.61–0.97; censored OS HR, 0.78; 95% CI, 0.68–0.90). In data analysis from multiple studies, liver metastases could be used as an independent prognostic risk factor, increasing the risk of death by 21% in lung cancer patients receiving ICI treatment compared with those without liver metastases (censored OS HR, 1.21; 95% CI, 1.17–1.27; $p < 0.0001$) [39].

Data availability statement

The raw data supporting the conclusions of this article will be made available by the authors, without undue reservation.

Ethics statement

This study was approved by the Institutional Ethical Committee (Ethical Committee of the Institution for Pulmonary Diseases of Vojvodina No. A203/2). The identities of all the patients from our study were removed and the study was conducted to the Helsinki Declaration of the World seventh revision.

Author contributions

Conceptualization, NL and MB; methodology, NL and MB; software, AŠ; validation, DB, IK, DB, ST, BP, and VČ; formal analysis, NL, and MB; investigation, NL; resources, NL; data curation, NL, DB, and IK; writing—original draft preparation, NL, ST, AŠ, and BP; all authors participated in writing—review and editing. All authors contributed to the article and approved the submitted version.

Funding

The authors declare that no financial support was received for the research, authorship, and/or publication of this article.

Conflict of interest

The authors declare that the research was conducted in the absence of any commercial or financial relationships that could be construed as a potential conflict of interest.

References

1. Sung H, Ferlay J, Siegel RL, Laversanne M, Soerjomataram I, Jemal A, et al. Global cancer Statistics 2020: GLOBOCAN estimates of incidence and mortality worldwide for 36 cancers in 185 countries. *CA Cancer J Clin* (2021) 71(3):209–49. doi:10.3322/caac.21660

2. Lee JB, Kim HR, Ha SJ. Immune checkpoint inhibitors in 10 Years: contribution of basic research and clinical application in cancer immunotherapy. *Immune Netw* (2022) 22(1):e2. doi:10.4110/in.2022.22.e2

3. Vinay DS, Ryan EP, Pawelec G, Talib WH, Stagg J, Elkord E, et al. Immune evasion in cancer: mechanistic basis and therapeutic strategies. *Semin Cancer Biol* (2015) 35:S185–98. doi:10.1016/j.semcancer.2015.03.004

4. Vaddepally RK, Kharel P, Pandey R, Garje R, Chandra AB. Review of indications of FDA-approved immune checkpoint inhibitors per NCCN guidelines with the level of evidence. *Cancers (Basel)* (2020) 12(3):738. doi:10.3390/cancers12030738

5. Zam W, Ali L. Immune checkpoint inhibitors in the treatment of cancer. *Curr Rev Clin Exp Pharmacol* (2022) 17(2):103–13. doi:10.2174/1574884716666210325095022

6. Chen J, Jiang CC, Jin L, Zhang XD. Regulation of PD-L1: a novel role of pro-survival signaling in cancer. *Ann Oncol* (2016) 27(3):409–16. doi:10.1093/annonc/mdv615

7. Reck M, Rodríguez-Abreu D, Robinson AG, Hui R, Csőszi T, Fülöp A, et al. Pembrolizumab versus chemotherapy for PD-L1-positive non-small-cell lung cancer. *N Engl J Med* (2016) 375(19):1823–33. doi:10.1056/NEJMoa1606774

8. Apetoh L, Ladoire S, Coukos G, Ghiringhelli F. Combining immunotherapy and anticancer agents: the right path to achieve cancer cure? *Ann Oncol* (2015) 26(9):1813–23. doi:10.1093/annonc/mdv209

9. Rodríguez-Abreu D, Powell SF, Hochmair MJ, Gadgeel S, Esteban E, Felip E, et al. Pemetrexed plus platinum with or without pembrolizumab in patients with previously untreated metastatic nonsquamous NSCLC: protocol-specified final analysis from KEYNOTE-189. *Ann Oncol* (2021) 32(7):881–95. doi:10.1016/j.annonc.2021.04.008

10. Paz-Ares L, Luft A, Vicente D, Tafreshi A, Gümüş M, Mazières J, et al. Pembrolizumab plus chemotherapy for squamous non-small-cell lung cancer. *N Engl J Med* (2018) 379(21):2040–51. doi:10.1056/NEJMoa1810865

11. Paz-Ares L, Vicente D, Tafreshi A, Robinson A, Soto Parra H, Mazières J, et al. A randomized, placebo-controlled trial of pembrolizumab plus chemotherapy in patients with metastatic squamous NSCLC: protocol-specified final analysis of KEYNOTE-407. *J Thorac Oncol* (2020) 15(10):1657–69. doi:10.1016/j.jtho.2020.06.015

12. Soldera SV, Leighl NB. Update on the treatment of metastatic squamous non-small cell lung cancer in new era of personalized medicine. *Front Oncol* (2017) 7:50. doi:10.3389/fonc.2017.00050

13. Schreiber RD, Old LJ, Smyth MJ. Cancer immunoediting: integrating immunity's roles in cancer suppression and promotion. *Science* (2011) 331(6024):1565–70. doi:10.1126/science.1203486

14. Pardoll DM. The blockade of immune checkpoints in cancer immunotherapy. *Nat Rev Cancer* (2012) 12(4):252–64. doi:10.1038/nrc3239

15. Hamid O, Puzanov I, Dummer R, Schachter J, Daud A, Schadendorf D, et al. Final analysis of a randomised trial comparing pembrolizumab versus investigator-choice chemotherapy for ipilimumab-refractory advanced melanoma. *Eur J Cancer* (2017) 86:37–45. doi:10.1016/j.ejca.2017.07.022

16. Herbst RS, Garon EB, Kim DW, Cho BC, Perez-Gracia JL, Han JY, et al. Long-term outcomes and retreatment among patients with previously treated, programmed death-ligand 1–positive, advanced non–small-cell lung cancer in the KEYNOTE-010 study. *J Clin Oncol* (2020) 38(14):1580–90. doi:10.1200/JCO.19.02446

17. Gadgeel S, Rodríguez-Abreu D, Speranza G, Esteban E, Felip E, Dómine M, et al. Updated analysis from KEYNOTE-189: pembrolizumab or placebo plus pemetrexed and platinum for previously untreated metastatic nonsquamous non-small-cell lung cancer. *J Clin Oncol* (2020) 38(14):1505–17. doi:10.1200/JCO.19.03136

18. Reck M, Rodríguez-Abreu D, Robinson AG, Hui R, Csőszi T, Fülöp A, et al. Five-year outcomes with pembrolizumab versus chemotherapy for metastatic non–small–cell lung cancer with PD-L1 tumor proportion score ≥ 50. *J Clin Oncol* (2021) 39(21):2339–49. doi:10.1200/JCO.21.00174

19. de Castro G, Kudaba I, Wu YL, Lopes G, Kowalski DM, Turna HZ, et al. Five-year outcomes with pembrolizumab versus chemotherapy as first-line therapy in patients with non-small-cell lung cancer and programmed death ligand-1 tumor proportion score ≥ 1% in the KEYNOTE-042 study. *J Clin Oncol* (2023) 41(11):1986–91. doi:10.1200/JCO.21.02885

20. Skov BG, Skov T. Paired comparison of PD-L1 expression on cytologic and histologic specimens from malignancies in the lung assessed with PD-L1 IHC 28-8pharmDx and PD-L1 IHC 22C3pharmDx. *Appl Immunohistochem Mol Morphol* (2017) 25(7):453–9. doi:10.1097/PAI.0000000000000540

21. Kitazono S, Fujiwara Y, Tsuta K, Utsumi H, Kanda S, Horinouchi H, et al. Reliability of small biopsy samples compared with resected specimens for the determination of programmed death-ligand 1 expression in non-small-cell lung cancer. *Clin Lung Cancer* (2015) 16(5):385–90. doi:10.1016/j.cllc.2015.03.008

22. Sakata KK, Midthun DE, Mullon JJ, Kern RM, Nelson DR, Edell ES, et al. Comparison of programmed death ligand-1 immunohistochemical staining between endobronchial ultrasound transbronchial needle aspiration and resected lung cancer specimens. *Chest* (2018) 154(4):827–37. doi:10.1016/j.chest.2018.07.017

23. Pons-Tostivint E, Latouche A, Vaflard P, Ricci F, Loirat D, Hescot S, et al. Comparative analysis of durable responses on immune checkpoint inhibitors versus other systemic therapies: a pooled analysis of phase III trials. *JCO Precis Oncol* (2019) 3(3):1–10. doi:10.1200/PO.18.00114

24. Frelaut M, du Rusquec P, de Moura A, Le Tourneau C, Borcoman E. Pseudoprogression and hyperprogression as new forms of response to immunotherapy. *BioDrugs* (2020) 34(4):463–76. doi:10.1007/s40259-020-00425-y

25. Ettinger DS, Wood DE, Aisner DL, Akerley W, Bauman JR, Bharat A, et al. Non–small cell lung cancer, version 3.2022, NCCN clinical practice guidelines in oncology. *J Natl Compr Cancer Netw* (2022) 20(5):497–530. doi:10.6004/jnccn.2022.0025

26. Ettinger DS, Wood DE, Aisner DL, Akerley W, Bauman JR, Bharat A, et al. NCCN Guidelines® insights: non-small cell lung cancer, version 2.2023. *J Natl Compr Canc Netw* (2023) 21(4):340–50. doi:10.6004/jnccn.2023.0020

27. Chiou VL, Burotto M. Pseudoprogression and immune-related response in solid tumors. *J Clin Oncol* (2015) 33(31):3541–3. doi:10.1200/JCO.2015.61.6870

28. Manitz J, D'Angelo SP, Apolo AB, Eggleton SP, Bajars M, Bohnsack O, et al. Comparison of tumor assessments using RECIST 1.1 and irRECIST, and association with overall survival. *J Immunother Cancer* (2022) 10(2):e003302. doi:10.1136/jitc-2021-003302

29. Wang Q, Gao J, Wu X. Pseudoprogression and hyperprogression after checkpoint blockade. *Int Immunopharmacol* (2018) 58:125–35. doi:10.1016/j.intimp.2018.03.018

30. Borcoman E, Nandikolla A, Long G, Goel S, Le Tourneau C. Patterns of response and progression to immunotherapy. *Am Soc Clin Oncol Educ B* (2018) 38(38):169–78. doi:10.1200/EDBK_200643

31. Tanizaki J, Hayashi H, Kimura M, Tanaka K, Takeda M, Shimizu S, et al. Report of two cases of pseudoprogression in patients with non–small cell lung cancer treated with nivolumab—including histological analysis of one case after tumor regression. *Lung Cancer* (2016) 102:44–8. doi:10.1016/j.lungcan.2016.10.014

32. Thompson JA, Schneider BJ, Brahmer J, Andrews S, Armand P, Bhatia S, et al. NCCN guidelines insights: management of immunotherapy-related toxicities, version 1.2020. *J Natl Compr Cancer Netw* (2020) 18(3):230–41. doi:10.6004/jnccn.2020.0012

33. Chen TW, Razak AR, Bedard PL, Siu LL, Hansen AR. A systematic review of immune-related adverse event reporting in clinical trials of immune checkpoint inhibitors. *Ann Oncol* (2015) 26(9):1824–9. doi:10.1093/annonc/mdv182

34. Zhou N, Velez MA, Bachrach B, Gukasyan J, Fares CM, Cummings AL, et al. Immune checkpoint inhibitor-induced thyroid dysfunction is a frequent event post-treatment in NSCLC. *Lung Cancer* (2021) 161:34–41. doi:10.1016/j.lungcan.2021.08.009

35. Awad MM, Gadgeel SM, Borghaei H, Patnaik A, Yang JCH, Powell SF, et al. Long-term overall survival from KEYNOTE-021 cohort G: pemetrexed and carboplatin with or without pembrolizumab as first-line therapy for advanced nonsquamous NSCLC. *J Thorac Oncol* (2021) 16(1):162–8. doi:10.1016/j.jtho.2020.09.015

36. Li F, Zhai S, Lv Z, Yuan L, Wang S, Jin D, et al. Effect of histology on the efficacy of immune checkpoint inhibitors in advanced non-small cell lung cancer: a systematic review and meta-analysis. *Front Oncol* (2022) 12:968517. doi:10.3389/fonc.2022.968517

37. Reck M, Rodríguez–Abreu D, Robinson AG, Hui R, Csőszi T, Fülöp A, et al. Updated analysis of KEYNOTE-024: pembrolizumab versus platinum-based chemotherapy for advanced non-–non-small-cell lung cancer with PD-L1 tumor proportion score of 50% or greater. *J Clin Oncol* (2019) 37(7):537–46. doi:10.1200/JCO.18.00149

38. Liu LU, Xie B, Zhu W, He Q, Zhou J, Liu S, et al. High expression of PD-L1 mainly occurs in non-small cell lung cancer patients with squamous cell carcinoma or poor differentiation. *Oncol Res* (2023) 31(3):275–86. doi:10.32604/or.2023.028227

39. Xia H, Zhang W, Zhang Y, Shang X, Liu Y, Wang X. Liver metastases and the efficacy of immune checkpoint inhibitors in advanced lung cancer: a systematic review and meta-analysis. *Front Oncol* (2022) 12:978069. doi:10.3389/fonc.2022.978069

Pathology & Oncology Research | frontiers

TYPE Hypothesis & Theory
PUBLISHED 04 April 2023
DOI 10.3389/pore.2023.1611117

Check for updates

OPEN ACCESS

EDITED BY
Anna Sebestyén,
Semmelweis University, Hungary

*CORRESPONDENCE
Xiaopeng Hu,
xiaopeng_hu@sina.com

RECEIVED 14 February 2023
ACCEPTED 24 March 2023
PUBLISHED 04 April 2023

CITATION
Fan B, Zheng X, Wang Y and Hu X (2023), Predicting prognosis and clinical efficacy of immune checkpoint blockade therapy *via* interferon-alpha response in muscle-invasive bladder cancer.
Pathol. Oncol. Res. 29:1611117.
doi: 10.3389/pore.2023.1611117

COPYRIGHT
© 2023 Fan, Zheng, Wang and Hu. This is an open-access article distributed under the terms of the Creative Commons Attribution License (CC BY). The use, distribution or reproduction in other forums is permitted, provided the original author(s) and the copyright owner(s) are credited and that the original publication in this journal is cited, in accordance with accepted academic practice. No use, distribution or reproduction is permitted which does not comply with these terms.

Predicting prognosis and clinical efficacy of immune checkpoint blockade therapy *via* interferon-alpha response in muscle-invasive bladder cancer

Bohan Fan[1,2], Xin Zheng[3,4,5], Yicun Wang[1,2] and Xiaopeng Hu[1,2]*

[1]Department of Urology, Beijing Chao-Yang Hospital, Capital Medical University, Beijing, China, [2]Institute of Urology, Capital Medical University, Beijing, China, [3]Comprehensive Transplant Center, Northwestern University Feinberg School of Medicine, Chicago, IL, United States, [4]Department of Surgery, Northwestern University Feinberg School of Medicine, Chicago, IL, United States, [5]Department of Urology, Beijing Youan Hospital, Capital Medical University, Beijing, China

Background: Immune checkpoint blockade (ICB) can prompt durable and robust responses in multiple cancers, involving muscle-invasive bladder cancer (MIBC). However, only a limited fraction of patients received clinical benefit. Clarifying the determinants of response and exploring corresponding predictive biomarkers is key to improving outcomes.

Methods: Four independent formerly published cohorts consisting of 641 MIBC patients were enrolled in this study. We first analyzed the associations between various cancer hallmarks and ICB therapy response in two immunotherapeutic cohorts to identify the leading prognostic hallmark in MIBC. Furthermore, advanced machine learning methods were performed to select robust and promising predictors from genes functioning in the above leading pathway. The predictive ability of selected genes was also validated in multiple MIBC cohorts.

Results: We identified and verified IFNα response as the leading cancer hallmark indicating better treatment responses, favorable overall survival, and an inflamed tumor microenvironment with higher infiltration of immune effector cells in MIBC patients treated with ICB therapy. Subsequently, two commonly selected genes, *CXCL10* and *LAMP3*, implied better therapy response and the $CXCL10^{high}LAMP3^{high}$ patients would benefit more from ICB therapy, which was comprehensively validated from the perspective of gene expression, clinical response, patient survival and immune features.

Conclusion: Higher IFNα response primarily predicted better ICB therapeutic responses and reflected an inflamed microenvironment in MIBC. A composite of *CXCL10* and *LAMP3* expression could serve as promising predictive biomarkers for ICB therapeutic responses and be beneficial for clinical decision-making in MIBC.

KEYWORDS

muscle-invasive bladder cancer, immune checkpoint blockade therapy, interferon-alpha response, tumor microenvironment, prognostic biomarkers

Introduction

As one of the most lethal urinary malignancies worldwide, bladder cancer occurs with a high risk of treatment failure rate, recurrence and morbidity (1, 2). About 25% of patients would be initially diagnosed as muscle-invasive bladder cancer (MIBC) with a 5-year survival rate of less than 15% who did not receive intervention (3). Radical cystectomy complemented by cisplatin-based perioperative chemotherapy remains the mainstay of MIBC management. However, the treatment outcome and patient prognosis were still unsatisfying (4). Studies have recently shown that tumor immunotherapy, like immune checkpoint blockade (ICB), especially programmed cell death-1 (PD-1)/programmed cell death ligand-1 (PD-L1), could be used for PD-L1 immune positive and platinum ineligible patients, as well as newly for those who are responding to platinum as maintenance therapy, it could also invigorate antitumor immune response and prolong survival of advanced MIBC patients resistant to chemotherapy, which revolutionized the therapeutic landscape (5, 6). Nevertheless, as only a small subset of patients would benefit from ICB therapy, effective biomarkers were urgently required to predict patient responsiveness to ICB therapy (7).

Multiple biomarkers have been introduced to predict immunotherapeutic response, including PD-L1 expression level, tumor-specific neoantigens such as tumor mutational burden (TMB), and immune-infiltration indicative markers like gene-expression profile associated with T cell effector (3, 8). However, it was controversial to merely use PD-L1 as a biomarker considering its dynamic expression regulation (9). Besides, it has been well recognized that PD-L1 expression suggested a sustained immunosuppressive-factor-regulated immune response in the tumor microenvironment (10). Moreover, each of PD-L1, TMB and T cell-inflamed gene-expression profile could predict immunotherapy efficacy with only moderate correlation in previous studies (3, 11). Considering the economic burden, difficulties in detection and unsatisfying clinical needs, we attempt to correlate molecular mechanisms with clinical data to identify robust genes as potential biomarkers for therapy response prediction.

Interferon-α (IFNα), a cytokine belonging to type I IFN family can elicit robust immune responses and exert various antiviral and antitumor effects (12). IFNα enhances immune recognition by increasing class I and II MHC molecules expressions surfaced on tumor cells and it is regarded as a potential treatment strategy by directly blocking cell-cycle progression and promoting apoptosis, thus suppressing tumor extension through stimulating the expression of antitumor IFN-stimulated gene products and tumor suppressor proteins (13, 14). Moreover, IFNα plus PD-1 blockade was recently identified as a promising treatment strategy in melanoma and hepatocellular carcinoma (15–17). Despite such results, there was little understanding of the effects of IFNα response in ICB therapy of MIBC patients. In this research, IFNα response was first evaluated as the primary factor for the better prognosis of ICB therapy, then we employed advanced machine learning algorithms to further select eligible genes, which was validated in multiple immunotherapeutic MIBC cohorts.

Materials and methods

Data collection and preprocessing

Three independent cohorts consisting of MIBC patients treated with ICB therapy and the Cancer Genome Atlas (TCGA) cohort were included for analysis. The detailed patient characteristics can be seen in Table 1. Normalization and $\log_2$-transformation were conducted in all RNA-seq and microarray data.

The training cohort enrolled 168 MIBC patients three times weekly treated with 1,200 mg atezolizumab from IMvigor210 trial, patients with other cancer types or unconfirmed overall responses were excluded, corresponding data were downloaded by the IMvigor210CoreBiologies R package (18). A total of 76 MIBC patients treated with at least one dose of anti-PD-1 or anti-PD-L1 immunotherapy with response and survival information were recruited as validation I cohort (19). A small series of expression profiles taken from 11 MIBC patients treated with pembrolizumab was considered as validation II cohort used for expression validation. The last validation III cohort contained 386 MIBC patients from TCGA database. Full transcriptome data and characteristics of the patients were assessed from http://www.cbioportal.org/ in July 2022. Patients achieving complete response (CR) or partial response (PR) were regarded as responders, while patients with progressive disease (PD) or stable disease (SD) were defined as non-responders in the training and validation I cohort. Responses of immunotherapy in TCGA cohort were conducted using the Tumor immune dysfunction and exclusion (TIDE) analysis, responders were patients with TIDE score <0, otherwise, non-responders (20).

TABLE 1 Clinical characteristics of MIBC patients in four independent cohorts.

Characteristics	IMvigor210	GSE176307	GSE111636	TCGA	Overall
Total	168	76	11	386	641
Application	Training	Validation I	Validation II	Validation III	
ICB Therapy (%)					
Atezolizumab	168 (100)	30 (39.5)			198 (77.6)
Pembrolizumab		40 (52.6)	11 (100)		51 (20.0)
Nivolumab		4 (5.3)			4 (1.6)
Avelumab		1 (1.3)			1 (0.4)
Durvalumab		1 (1.3)			1 (0.4)
Therapy response (%)					
CR	15 (8.9)	7 (9.2)	6 (54.5)	145 (37.6, *TIDE*)	207 (32.3)
PR	27 (16.1)	7 (9.2)			
SD	35 (20.8)	4 (5.3)	5 (45.5)	241 (62.4, *TIDE*)	434 (67.7)
PD	91 (54.2)	58 (76.3)			
Overall survival (%)					
Alive	61 (36.3)	28 (36.8)			89 (36.5)
Deceased	107 (63.7)	48 (63.2)			155 (63.5)
Follow-up time (Months, mean ± SD)	11.72 ± 7.48	7.97 ± 7.24			10.55 ± 7.59

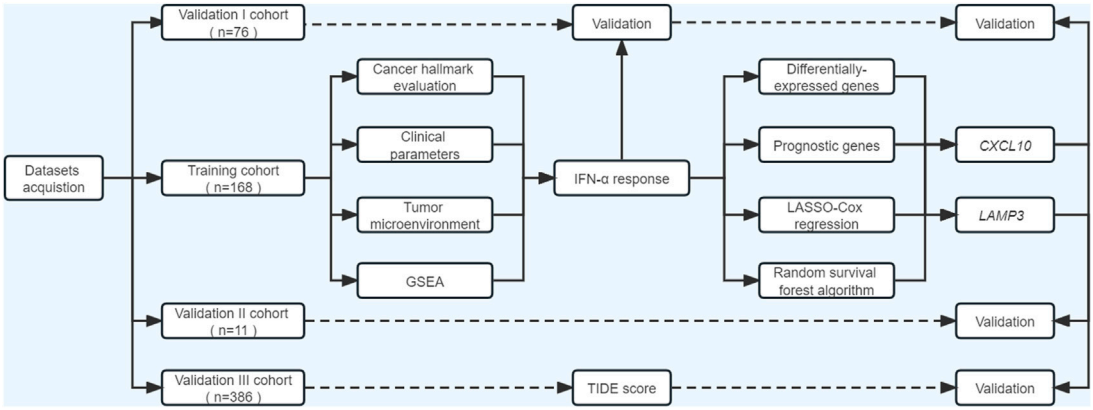

FIGURE 1
Flowchart of the current study. ssGSEA, single-sample gene set enrichment analysis; GSEA, gene set enrichment analysis; TIDE, Tumor immune dysfunction and exclusion.

Study design

As illustrated in Figure 1, our study included three phases. In the discovery phase, we measured the performances of 50 cancer hallmarks, identified and validated IFNα response as the leading factor for the favorable prognosis of ICB therapy from the survival, functional and tumor microenvironment perspectives. Secondly, differentially expressed prognostic genes mapping on IFNα response pathways were included for machine learning algorithms to select robust genes with better performance in therapy response prediction. Moreover, the expression levels and predictive abilities of the above candidate genes were verified in external validation cohorts.

Cancer hallmark assessment

In the training cohort, we quantified levels of cancer hallmarks based on transcriptional profiles and hallmark gene sets acquired from the Molecular Signatures Database (MsigDB) through ssGSEA algorithms (21). Subsequently, the prognostic significance of cancer hallmarks was evaluated by univariate Cox

analysis in MIBC patients after ICB therapy. We also applied gene set enrichment analysis (GSEA) to compare the enriched pathways between responders and non-responders referring to the hallmark gene sets (22). As a result, IFN-α response (IFNAR) was found with the lowest hazard ratio (HR) value. Subsequently, according to the IFNAR-related score, we divided patients into high-, middle- and low-score groups, the survival differences, responder proportion, PD-L1 protein expression levels on immune cells (IC) and immune phenotype were compared among groups.

Tumor microenvironment evaluation

The overall infiltration of immune cells, stromal cells and tumor cell purity were inferred by ESTIMATE algorithm (23). Moreover, we evaluated the infiltration of 22 immune cell subpopulations in MIBC biopsies through CIBERSORT (Cell-type Identification by Estimating Relative Subsets of RNA Transcripts), a deconvolution algorithm to characterize immune cell composition using gene expression profiles (24). Immune cell abundance variations in the high- and low- IFNAR-related score groups were detected, correlations between immune cell infiltration and IFNAR were also calculated.

Machine learning methods

Ninety-five genes that participated in the process of IFNAR were derived from MSigDB. We then screened differentially expressed genes (DEGs) between responders and non-responders through "limma" package when false discovery rate (FDR) was less than 0.05 (25). Meanwhile, prognostic genes were identified by univariate Cox analysis with a threshold of $p < 0.05$. Prognostic DEGs were selected for further analysis. Subsequently, two machine learning algorithms, least absolute shrinkage and selection operator (LASSO) Cox regression and random survival forest (RSF) analysis were commonly applied to perform gene selection. LASSO used 10-fold cross-validation to estimate the penalty parameters by "glmnet" package to avoid over-fitting. RSF adapts random forests to survival analysis based on ensemble trees. Variable importance (VIMP) evaluates the predictive ability alterations of RSF model when genes are randomly permuted, higher VIMP indicates greater significance, while the average depth of genes among all survival trees was implied by minimal depth, smaller values suggest increased importance (26). They measure the impact of genes from different points of view, eligible genes identically selected by LASSO, VIMP and minimal depth were obtained for further validation.

Tumor immune dysfunction and exclusion analysis

To predict the therapeutic response to ICB therapy of MIBC patients in TCGA cohort, we applied TIDE algorithm to evaluate diverse mechanisms in tumor immune evasion, comprising of immunosuppressive factors induced cytotoxic T lymphocytes (CTLs) exclusion and dysfunction. Before analysis in TCGA cohort, we conducted TIDE in the training and validation I cohort to test its predictive ability in ICB therapy response. The infiltration of immunosuppressive myeloid suppressor cells (MDSC), cancer-associated fibroblasts (CAFs) and M2 subtypes of tumor-associated macrophages (TAM.M2) were also evaluated (20). Lower TIDE scores imply better clinical efficacy of immune checkpoint inhibitors.

Statistical analysis

We performed all statistical analyses with R software. The D'Agostino and Pearson omnibus normality tests were initially carried out to assess whether the data fit a normal distribution. When parameters were normally distributed, a two-tailed unpaired t-test, one-way ANOVA with Tukey's correction and the Pearson correlation would be conducted. Once data did not achieve the assumptions of parametric tests, the Mann–Whitney U test, one-way ANOVA using Kruskal–Wallis with Dunn's correction and Spearman correlation would be employed. Results met the level of 5% ($p < 0.05$) were considered statistically significant.

Results

Identification and validation of IFNα response as the leading favorable factor for the prognosis of ICB therapy

In the training cohort, we quantified the performance of 50 cancer hallmarks, then each HR value was calculated and ranked through univariate Cox analysis (Supplementary Table S1; Supplementary Figure S1). Among hallmarks, IFNAR ranked first with the lowest HR value (Figure 2A, HR = 0.667, $p = 0.008$), and high IFNAR-related score indicated favorable overall survival (OS) (Figure 2B, $p = 0.002$). Moreover, GSEA also revealed that IFNAR was significantly higher enriched in patients with responses to ICB therapy (Figure 2C; Supplementary Table S2). Based on the IFNAR-related score, we equally divided patients into three groups, the fraction of patients achieving CR or PR were 37.5%, 21.4%, and 16.1% in the high-, middle- and low-score group, respectively (Figure 2D, $p = 0.024$). Besides, the IFNAR-related score was higher in the group of patients achieving CR, patients with the higher protein expression level of PD-L1 on IC and patients with inflamed immune phenotype than other groups (Figures 2E–G). Likewise,

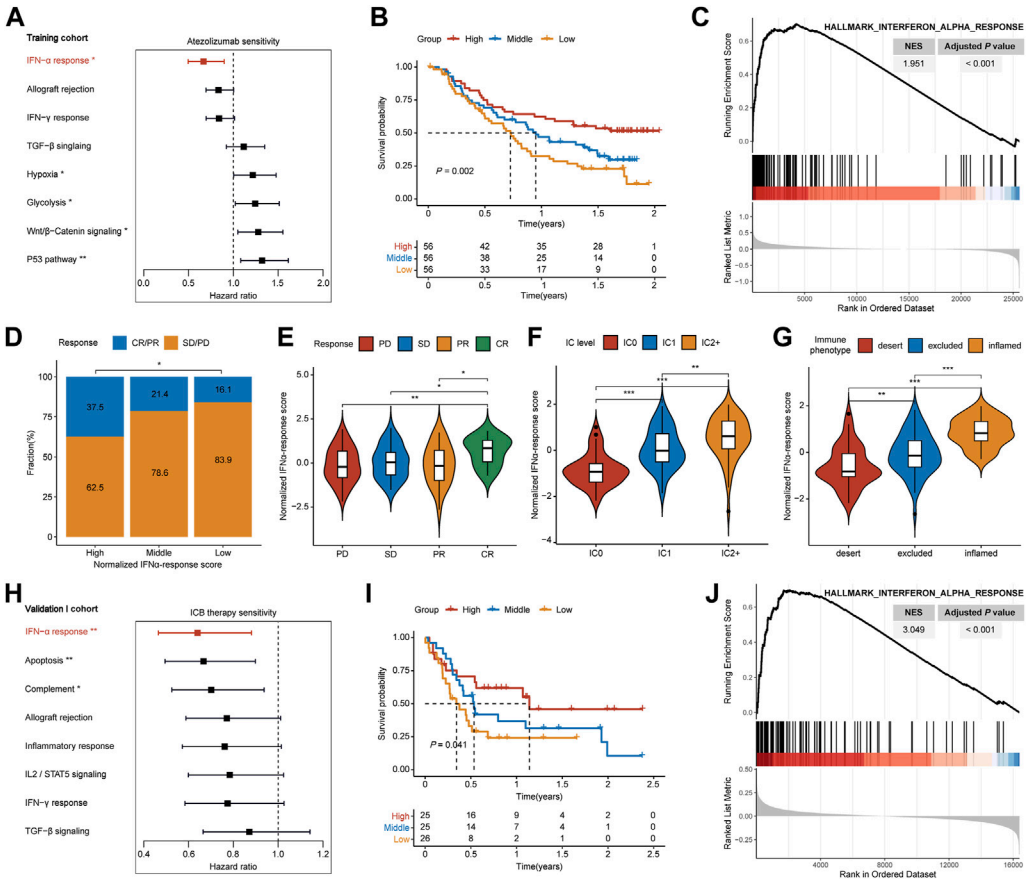

FIGURE 2
Detection of IFNα response as the leading favorable factor for therapeutic response and prognosis of ICB therapy in MIBC. In the training cohort, **(A)** forest plot shows that IFNα response has the lowest hazard ratio with statistical significance among various cancer hallmarks, **(B)** Kaplan–Meier survival curves depict that higher IFNAR-related score was associated with better overall survival, **(C)** GSEA plot illustrates that IFNα response is significantly enriched in responders than non-responders, **(D)** higher IFNAR-related score present significantly higher percentages of responses (CR/PR) and lower percentages of non-responses (SD/PD), **(E–G)** violin plot show that the IFNAR-related score was higher in patients with CR, the higher protein expression level of PD-L1 on IC, and inflamed immune phenotype. In the validation I cohort, **(H,I)** IFNα response was similarly regarded as a positive indicator for patient prognosis, **(J)** and it was significantly higher enriched in responders. NES, normalized enrichment score; CR, complete response; PR, partial response; SD, stable disease; PD, progressive disease; IC, immune cells. $*p < 0.05$, $**p < 0.01$, $***p < 0.001$.

in the validation I cohort, IFNAR was ordered first among cancer hallmarks (Figure 2H, HR = 0.640, $p = 0.006$) (Supplementary Table S3), high IFNAR-related score was linked to better OS (Figure 2I, $p = 0.041$), IFNAR was significantly upregulated in responders (Figure 2J; Supplementary Table S4). Together, our study suggested that the IFNAR pathway was a leading favorable factor with promising predictive value for the prognosis of ICB therapy in MIBC patients.

IFNα response ignites inflamed tumor microenvironment in MIBC

It has been well established that the tumor microenvironment influences clinical efficacy of immunotherapy. Therefore, we utilized ESTIMATE and CIBEROSRT to calculate the immune cell infiltration in tumor tissues. Both for training and validation I cohorts, the high-IFNAR-related-score subgroup exhibited higher immune and stromal scores, lower tumor purity than the low-score subgroup did (Figure 3A). In particular, immune effector cells, including $CD8^+$ T cells, $CD4^+$ memory-activated T cells and type 1 proinflammatory macrophage (M1) were increasingly infiltrated, while $CD4^+$ memory-resting T cells were decreasingly infiltrated in the high-IFNAR-related-score subgroup in both cohorts (Figure 3B). Furthermore, the IFNAR-related score was positively correlated with above mentioned immune effector cells and negatively associated with $CD4^+$ memory-resting T cells (Figure 3C). Collectively, these results illustrated high levels of IFNAR were

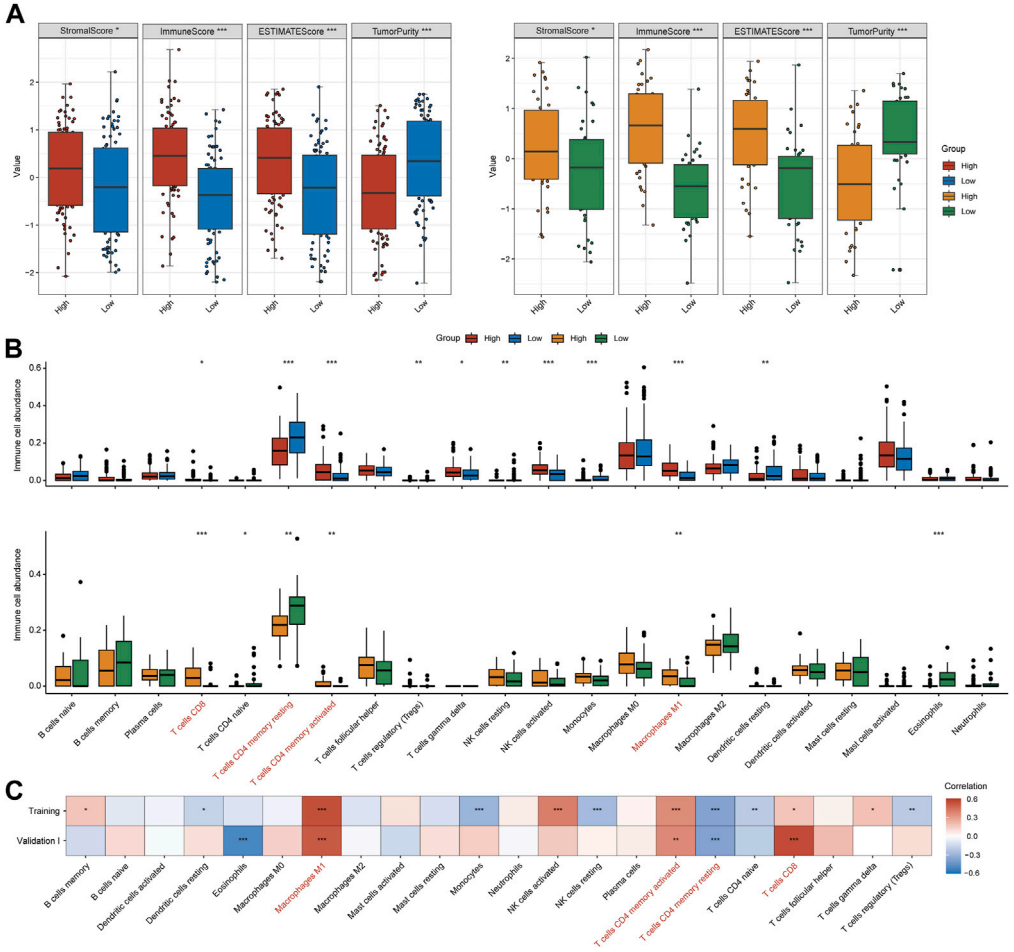

FIGURE 3
IFNα response represents an inflamed immune context in MIBC. In the training and validation I cohort, **(A)** box plots display that higher immune score, stromal score and lower tumor purity were seen in the high-IFNAR-related-score subgroup, **(B)** several types of immune effector cells including $CD4^+$ memory-activated T cells, $CD8^+$ cells and macrophage M1 were higher infiltrated, while $CD4^+$ memory-resting T cells were lower infiltrated in the tumor microenvironment of MIBC patients with high IFNAR-related score. **(C)** The correlation heatmap shows the association between IFNAR-related score and immune cell infiltration. The blanks are filled in proportion to Spearman's coefficient values, positive and negative correlations are colored in red and blue, respectively. $*p < 0.05$, $**p < 0.01$, $***p < 0.001$.

accompanied by an immune-active tumor microenvironment in MIBC.

Detection of *CXCL10* and *LAMP3* for the prediction of ICB therapy response

We acquired IFNAR-related genes ($n = 95$) for subsequent analyses. With the threshold of FDR <0.05, twenty-four upregulated DEGs and 5 downregulated DEGs in tumor tissues of responders compared to non-responders were identified (Figure 4A). Meanwhile, seventeen prognostic genes with $p < 0.05$ were also discovered (Figure 4B). Ten intersected prognostic DEGs were then applied to machine learning algorithms (Figure 4C). Then four genes (*CXCL10*, *LAMP3*, *TAP1*, *TRIM5*) were selected by LASSO Cox regression analysis (Figure 4D), three genes (*CXCL10*, *LAMP3*, *IRF1*) were acquired based on VIMP and minimal depth through RSF (Figure 4E). Among them, *CXCL10* and *LAMP3* were co-selected as promising predictive biomarkers for the responses of ICB therapy.

CXCL10 and *LAMP3* show robust predictive ability in the clinical benefits of ICB therapy

In the training cohort, *CXCL10* and *LAMP3* were significantly higher expressed in responders (Figure 5A, $p = 0.006$, $p = 0.019$, respectively). The same trend was also observed in another two validation cohorts (Figures 5B, C). Besides, both *CXCL10* and

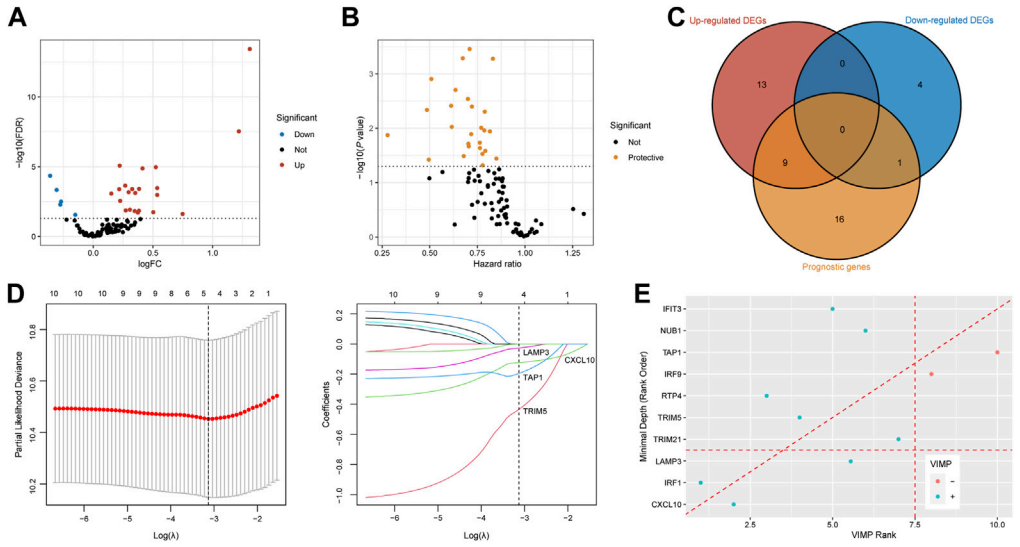

FIGURE 4
Recognition of *CXCL10* and *LAMP3* for immunotherapeutic response prediction by machine learning methods. **(A,B)** Volcano plots show DEGs between responders and non-responders and prognostic genes calculated by the univariable Cox regression. Red dots are upregulated genes, blue dots present downregulated genes, protective genes are dotted in yellow. **(C)** Venn diagram shows 10 intersected genes between DEGs and prognostic genes. **(D)** Tenfold cross-validation was utilized to calculate optimal lambda which leads to minimum mean cross-validation error by LASSO Cox regression analysis. Four genes were finally selected under the optimal lambda. **(E)** Variable importance plot of the random survival forest analysis comparing rankings with VIMP and minimal depth. The VIMP rank is reported on the x-axis and minimal depth (rank order) is on the y-axis. The horizontal line indicates the minimal depth threshold, important variables are below the line. The vertical line divides variables with positive VIMP (left) from those with negative VIMP (right, unimportant). *CXCL10* and *LAMP3* were commonly selected by LASSO, VIMP and minimal depth. FDR, false discovery rate; FC, fold change; DEGs, differentially expressed genes; VIMP, variable importance.

LAMP3 expression in the tumor tissues indicated favorable OS in the training cohort (Figure 5D, $p = 0.006$, $p = 0.001$, respectively) and validation I cohort (Figure 5E, $p = 0.029$, $p = 0.005$, respectively). Moreover, we noted the patients who achieved CR or PR were more frequent in $CXCL10^{high}LAMP3^{high}$ subgroups, and the combination of *CXCL10* and *LAMP3* expression significantly indicated improved OS in both cohorts (Figures 5F, G). Moreover, the expression levels of *CXCL10* and *LAMP3* were higher in patients with inflamed immune phenotype and higher PD-L1 protein expression levels on IC than in other groups (Supplementary Figure S2). Together, our study suggested that *CXCL10* plus *LAMP3* could serve as an ideal and stable predictive biomarker for patient response to ICB therapy in clinical settings.

Higher IFNα response, expression levels of *CXCL10* and *LAMP3* indicate better ICB therapy response in TCGA cohort

In the training and validation I cohort, lower TIDE scores were seen in patients with CR/PR, and patients in the high-TIDE-score group showed worse overall survival (Supplementary Figure S3), which proved the predictive ability of TIDE in ICB therapy response. To further evaluate the universal applicability of *CXCL10* and *LAMP3* in predicting the responsiveness to ICB therapy, we evaluated therapy responses of MIBC patients through TIDE algorithm in TCGA cohort. The TIDE score was significantly higher in the low-IFNAR-related-score subgroup, which indicates lower therapeutic sensitivity (Figure 6A, $p < 0.001$). Furthermore, a strong correlation was found between IFNAR-related scores and TIDE scores ($R = -0.32$, $p = 1.7e\text{-}10$), the IFNAR-related score was also negatively associated with exclusion ($R = -0.14$, $p = 0.006$) and dysfunction ($R = -0.41$, $p = 2.2e{-}16$) (Figure 6B). As for the combination of *CXCL10* and *LAMP3*, the TIDE score was lower and the responder frequency was higher in the $CXCL10^{high}LAMP3^{high}$ subgroup (Figures 6C, D). Intriguingly, the scores of three reported immunosuppressive cells that suppress tumor T-cell infiltration, consisting of CAFs, MDSCs and TAM.M2 were higher in the $CXCL10^{low}LAMP3^{low}$ subgroup (Figure 6E). The above results implied that high expression levels of *CXCL10* and *LAMP3* may predict a tumor microenvironment that favors immunotherapeutic response and indicate better ICB therapy response.

Discussion

ICB therapy has revolutionized cancer management in the last few years, and it could improve the prognosis of platinum-refractory advanced MIBC patients (6, 27). Despite considerable

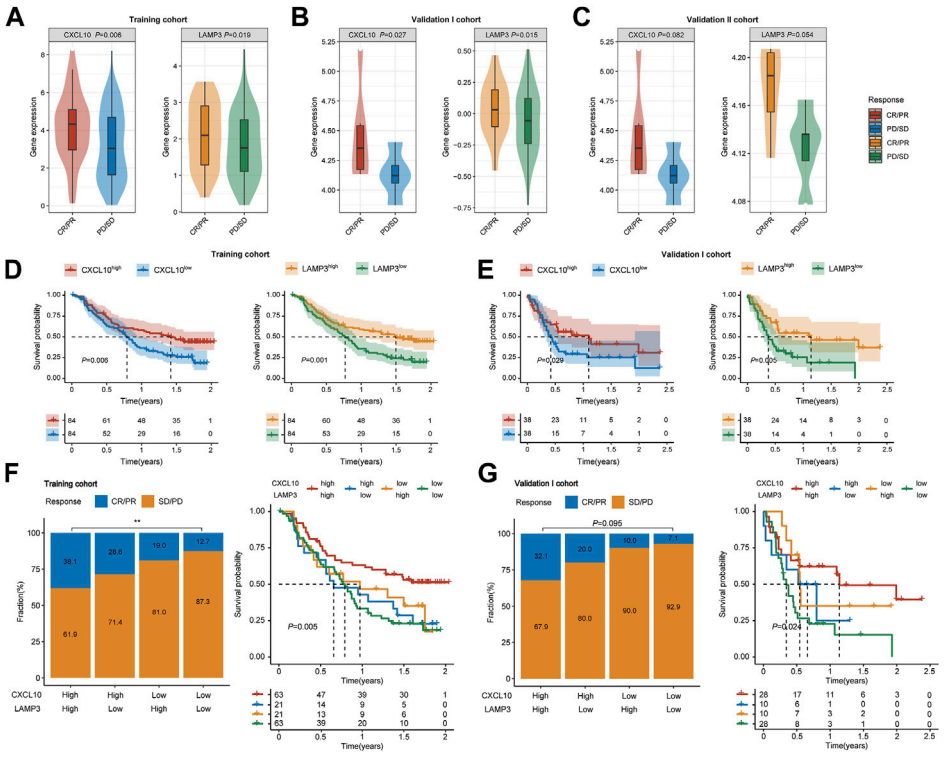

FIGURE 5
Expression and predictive ability validation of *CXCL10* and *LAMP3* in multiple cohorts. **(A–C)** Variations of *CXCL10* and *LAMP3* mRNA expression between the responder and non-responder group in the training and validation I and II cohorts. **(D,E)** Kaplan-Meier analyses of overall survival in patients in the training and validation I cohort, stratified according to the median values of *CXCL10* and *LAMP3* mRNA expression. Data were analyzed by log-rank test. **(F,G)** Clinical response to ICB therapy and Kaplan-Meier analyses of overall survival stratified according to the combination of *CXCL10* and *LAMP3* in the training and validation I cohort. $^{**}p < 0.01$.

progress, immune checkpoint inhibitors could benefit only a subset of patients, with the incidence of adverse events up to 16% (28). Elucidation of the underlying characteristics will better identify patients who will be more benefited from ICB therapy.

IFNα, collectively known as type I IFNs, functions as a dynamic immune mediator that orchestrates both innate and adaptive antitumor immune responses (29). Although IFNα is not individually used for cancer treatment anymore due to its systematic side effects, its large impacts on the immune system hold immense potential for IFNα to elicit a cytotoxic immune response thus serving as a promising adjuvant agent with PD-1/PD-L1 inhibitors (16, 30). Recent clinical trials and preclinical models proposed that IFNα plus an anti-PD-1 antibody was an efficient treatment strategy in cancer, emphasizing the great potential of IFNα-based combination ICB (15, 31, 32). In this research, we first identified and validated IFNα response as a dominant favorable factor for the therapy response and prognosis of ICB therapy in two independent cohorts. Patients with higher IFNAR-related scores were associated with better therapeutic response and ignites inflamed immune context in MIBC, our results further demonstrated its great potential in improving and predicting ICB therapy response. In the previous IMvigor210 study, TGFβ signaling was found to attenuate tumor response to PD-L1 blockade. However, no clear difference was seen in the overall survival of patients with different TGFβ signaling scores in our study, possibly because of the inclusion of only bladder cancer patients, while the IMvigor210 study included other cancer types.

Due to powerful immunostimulatory properties, $CD4^+$ T cells have been recognized to play essential roles in augmenting endogenous immune response (33). A recent study demonstrated that the predominance and persistence of $CD4^+$ T cells could induce decade-long leukemia remission (34). Therefore, stimulating $CD4^+$ T cells is crucial to achieving long-term antitumor immune memory in cancer immunotherapy (35). In this research, $CD4^+$ memory T cells take up high contents in the tumor environment. Besides, the IFNAR-related score was positively corrected with $CD4^+$ memory-activated T cells and negatively associated with $CD4^+$ memory-resting T cells. It has also been reported that an increased amount of $CD4^+$ effector memory T cells was found in IFNα treated chronic myeloid leukemia patients (36). Apart from this, the repolarization of macrophages from a pro-tumor phenotype (M2) to cytotoxic anti-tumor effectors (M1) is expected to refine the tumor environment and promote anti-tumor response (37). Similarly, higher infiltration of macrophage M1 was

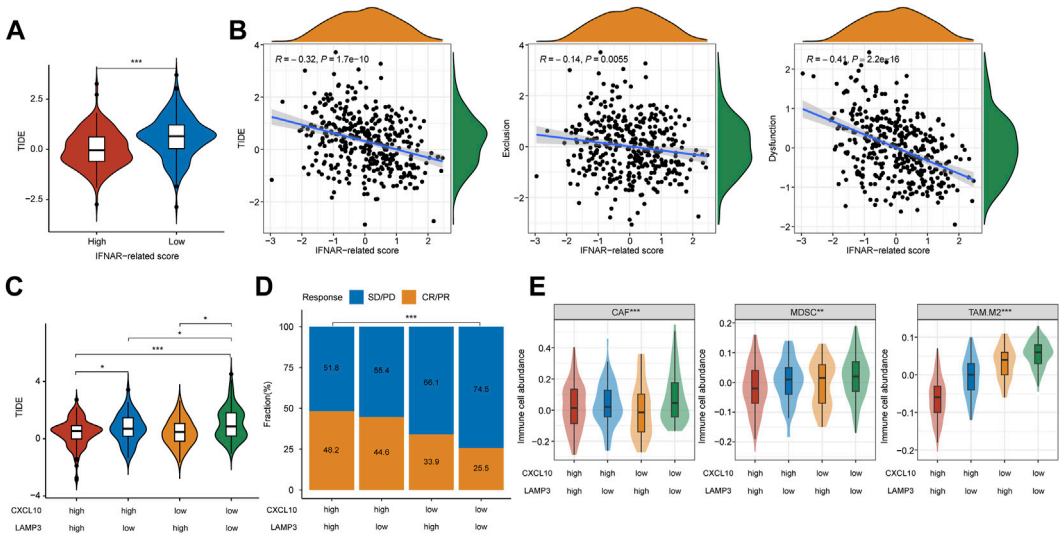

FIGURE 6
CXCL10 and *LAMP3* expression indicate estimated ICB therapy benefit in TCGA cohort. **(A)** TIDE score was lower in the high-IFNAR-related-score subgroup, indicating better ICB therapy response. **(B)** Correlation analysis between IFNAR-related score and TIDE, tumor immune exclusion and dysfunction scores. **(C)** TIDE score was higher in the $CXCL10^{low}LAMP3^{low}$ subgroup, indicating worse ICB therapy response. **(D,E)** Differences in clinical response and three types of immunosuppressive cell infiltration including tumor-associated fibroblast (CAF), myeloid-derived suppressor cell (MDSCs) and M2 subtype of tumor-associated macrophage (TAM.M2) among groups. $*p < 0.05$, $**p < 0.01$, $***p < 0.001$.

also seen in the high IFNAR-related score group. Collectively, our results illustrated that high IFNα response represents an inflamed immune microenvironment and further confirmed its promising role in predicting the therapeutic responses of ICB therapy in MIBC.

Migration and trafficking of $CD8^+$ effector T cells into the tumor microenvironment along with sensing of chemokine gradients are essential to immunotherapy efficacy (38, 39), which is consistent with our results that more $CD8^+$ T cells were infiltrated in the high-IFNAR-related-score subgroup. Preclinical studies have illustrated that chemokines C-X-C motif chemokine ligand 9 (CXCL9) and CXCL10 predominantly drive the recruitment of activated $CD8^+$ T cells into tumor sites by engaging the corresponding chemokine receptor CXCR3 expressed on immune cells, with CXCL10 being more abundantly expressed (38, 40, 41). Therefore, strategies *via* induction of CXCL10 to support effector T cell recruitment have been considered as a mechanism-based intervention to enhance immunotherapy efficacy (10). Furthermore, CXCL10 expression in tumor tissues has been reported to be strongly associated with responses to ICB therapy (38, 42), which is consistent with our results. LAMP3 (lysosome-associated membrane protein 3), a dendritic cell (DC)—specific glycoprotein induced upon DC maturation after inflammatory stimulation that leads to primary T-cell responses (43). In patients with IIIA non-small cell lung cancer after neoadjuvant pembrolizumab and chemotherapy, LAMP3+ DCs involved in the process of lymphocytes recruitment and regulation, its increased levels were found to be associated with positive clinical outcomes by single-cell profiling (44). Besides, LAMP3 was also reported to be in the immunotherapy-response-associated signature of tertiary lymphoid structures in melanoma (45). As a consequence, the predictive ability of *CXCL10* and *LAMP3* expression was sensible, illustrating the interplay between immunity and cancer, which could better reflect the therapeutic responsiveness in MIBC patients.

Several limitations existed in this study. We included an ICB untreated TCGA dataset as the validation III cohort, and the TIDE score was applied as the surrogate endpoint, which may not align with actual therapy responses. Moreover, the training cohort included only atezolizumab-treated patients while the validation cohorts were either mixed or included only pembrolizumab-treated patients, which may be confounding factors. This study was a retrospective analysis including four independent cohorts to assess the ability of IFNα response, the combined *CXCL10* and *LAMP3* expression in predicting the clinical efficiency of ICB therapy, which needs to be verified in a larger and prospective trial in the future. Due to the lack of complete clinicopathological information, we should also correlate our results with clinical characteristics in further study. Besides, immune cell abundance and functional enrichment analysis were estimated by bioinformatic approaches in this study, lacking direct evidence and requiring further experimental verification.

Conclusion

In summary, we identified IFNα response as the primary indicator associated with better ICB therapeutic response and an immune-inflamed microenvironment, and the combination of *CXCL10* and *LAMP3* expression could serve as effective predictive biomarkers for ICB treatment response and would be beneficial for patient-tailored treatment decisions in MIBC.

Data availability statement

Corresponding author may be contacted for article data if there is a valid reason.

Author contributions

BF and XH designed this work. BF, XZ, and YW performed data collection and analysis. BF wrote the manuscript. BF, XZ, YW, and XH revised the manuscript. All authors read and approved the final manuscript.

Conflict of interest

The authors declare that the research was conducted in the absence of any commercial or financial relationships that could be construed as a potential conflict of interest.

Acknowledgments

We would like to express our sincere thanks to all the editors, reviewers and other staff who participated in reviewing and producing this paper.

Supplementary material

The Supplementary Material for this article can be found online at: https://www.por-journal.com/articles/10.3389/pore.2023.1611117/full#supplementary-material

SUPPLEMENTARY FIGURE S1
Higher TGFβ-signaling-score showed no survival differences in both training and validation I cohorts, but indicated worse overall survival in the IMvigor210 whole cohort.

SUPPLEMENTARY FIGURE S2
Patients with higher IC levels or inflamed immune phenotype had higher expression levels of *CXCL10* and *LAMP3*..

SUPPLEMENTARY FIGURE S3
Higher TIDE score was associated with better ICB therapy responses and overall survival in both training and validation I cohort.

SUPPLEMENTARY TABLE S1
Univariate Cox analysis of cancer hallmarks in the training cohort.

SUPPLEMENTARY TABLE S2
Gene set enrichment analysis in the training cohort.

SUPPLEMENTARY TABLE S3
Univariate Cox analysis of cancer hallmarks in the validation I cohort.

SUPPLEMENTARY TABLE S4
Gene set enrichment analysis in the validation I cohort.

References

1. Sung H, Ferlay J, Siegel RL, Laversanne M, Soerjomataram I, Jemal A, et al. Global cancer statistics 2020: Globocan estimates of incidence and mortality worldwide for 36 cancers in 185 countries. *CA Cancer J Clin* (2021) 71(3): 209–49. doi:10.3322/caac.21660

2. Antoni S, Ferlay J, Soerjomataram I, Znaor A, Jemal A, Bray F. Bladder cancer incidence and mortality: A global overview and recent trends. *Eur Urol* (2017) 71(1):96–108. doi:10.1016/j.eururo.2016.06.010

3. Liu C, Liu Z, Jin K, Zeng H, Shao F, Chang Y, et al. Integrative tumour mutation burden with Cd39 and Pd-L1 for the prediction of response to Pd-L1 blockade and adjuvant chemotherapy in muscle-invasive bladder cancer patients. *Br J Cancer* (2022) 127(9):1718–25. doi:10.1038/s41416-022-01943-y

4. Witjes JA, Bruins HM, Cathomas R, Compérat EM, Cowan NC, Gakis G, et al. European association of urology guidelines on muscle-invasive and metastatic bladder cancer: Summary of the 2020 guidelines. *Eur Urol* (2021) 79(1):82–104. doi:10.1016/j.eururo.2020.03.055

5. Rijnders M, de Wit R, Boormans JL, Lolkema MPJ, van der Veldt AAM. Systematic review of immune checkpoint inhibition in urological cancers. *Eur Urol* (2017) 72(3):411–23. doi:10.1016/j.eururo.2017.06.012

6. Balar AV, Galsky MD, Rosenberg JE, Powles T, Petrylak DP, Bellmunt J, et al. Atezolizumab as first-line treatment in cisplatin-ineligible patients with locally advanced and metastatic urothelial carcinoma: A single-arm, multicentre, phase 2 trial. *Lancet* (2017) 389(10064):67–76. doi:10.1016/S0140-6736(16)32455-2

7. Chen X, Xu R, He D, Zhang Y, Chen H, Zhu Y, et al. $CD8^+$ T effector and immune checkpoint signatures predict prognosis and responsiveness to immunotherapy in bladder cancer. *Oncogene* (2021) 40(43):6223–34. doi:10.1038/s41388-021-02019-6

8. Litchfield K, Reading JL, Puttick C, Thakkar K, Abbosh C, Bentham R, et al. Meta-analysis of tumor- and T cell-intrinsic mechanisms of sensitization to checkpoint inhibition. *Cell* (2021) 184(3):596–614.e14. doi:10.1016/j.cell.2021.01.002

9. Davis AA, Patel VG. The role of Pd-L1 expression as a predictive biomarker: An analysis of all us food and drug administration (fda) approvals of immune checkpoint inhibitors. *J Immunother Cancer* (2019) 7(1):278. doi:10.1186/s40425-019-0768-9

10. Shen X, Zhao B. Efficacy of Pd-1 or Pd-L1 inhibitors and Pd-L1 expression status in cancer: Meta-analysis. *BMJ* (2018) 362:k3529. doi:10.1136/bmj.k3529

11. Ott PA, Bang Y-J, Piha-Paul SA, Razak ARA, Bennouna J, Soria J-C, et al. T-Cell-Inflamed gene-expression profile, programmed death ligand 1 expression, and tumor mutational burden predict efficacy in patients treated with pembrolizumab across 20 cancers: Keynote-028. *J Clin Oncol* (2019) 37(4): 318–27. doi:10.1200/JCO.2018.78.2276

12. Ivashkiv LB, Donlin LT. Regulation of type I interferon responses. *Nat Rev Immunol* (2014) 14(1):36–49. doi:10.1038/nri3581

13. Herzer K, Hofmann TG, Teufel A, Schimanski CC, Moehler M, Kanzler S, et al. Ifn-alpha-induced apoptosis in hepatocellular carcinoma involves promyelocytic leukemia protein and trail independently of P53. *Cancer Res* (2009) 69(3):855–62. doi:10.1158/0008-5472.CAN-08-2831

14. Cheon H, Borden EC, Stark GR. Interferons and their stimulated genes in the tumor microenvironment. *Semin Oncol* (2014) 41(2):156–73. doi:10.1053/j.seminoncol.2014.02.002

15. Davar D, Wang H, Chauvin J-M, Pagliano O, Fourcade JJ, Ka M, et al. Phase ib/ii study of pembrolizumab and pegylated-interferon alfa-2b in advanced melanoma. *J Clin Oncol* (2018) 36(35):JCO1800632. doi:10.1200/JCO.18.00632

16. Zhu Y, Chen M, Xu D, Li T-E, Zhang Z, Li J-H, et al. The combination of Pd-1 blockade with interferon-A has a synergistic effect on hepatocellular carcinoma. *Cell Mol Immunol* (2022) 19(6):726–37. doi:10.1038/s41423-022-00848-3

17. Hu B, Yu M, Ma X, Sun J, Liu C, Wang C, et al. Ifnα potentiates anti-Pd-1 efficacy by remodeling glucose metabolism in the hepatocellular carcinoma microenvironment. *Cancer Discov* (2022) 12(7):1718–41. doi:10.1158/2159-8290.CD-21-1022

18. Mariathasan S, Turley SJ, Nickles D, Castiglioni A, Yuen K, Wang Y, et al. Tgfβ attenuates tumour response to Pd-L1 blockade by contributing to exclusion of T cells. *Nature* (2018) 554(7693):544–8. doi:10.1038/nature25501

19. Rose TL, Weir WH, Mayhew GM, Shibata Y, Eulitt P, Uronis JM, et al. Fibroblast growth factor receptor 3 alterations and response to immune checkpoint inhibition in metastatic urothelial cancer: A real world experience. *Br J Cancer* (2021) 125(9):1251–60. doi:10.1038/s41416-021-01488-6

20. Jiang P, Gu S, Pan D, Fu J, Sahu A, Hu X, et al. Signatures of T Cell dysfunction and exclusion predict cancer immunotherapy response. *Nat Med* (2018) 24(10): 1550–8. doi:10.1038/s41591-018-0136-1

21. Liberzon A, Birger C, Thorvaldsdóttir H, Ghandi M, Mesirov JP, Tamayo P. The molecular signatures Database (msigdb) hallmark gene set collection. *Cell Syst* (2015) 1(6):417–25. doi:10.1016/j.cels.2015.12.004

22. Subramanian A, Tamayo P, Mootha VK, Mukherjee S, Ebert BL, Gillette MA, et al. Gene set enrichment analysis: A knowledge-based approach for interpreting genome-wide expression profiles. *Proc Natl Acad Sci U S A* (2005) 102(43): 15545–50. doi:10.1073/pnas.0506580102

23. Yoshihara K, Shahmoradgoli M, Martínez E, Vegesna R, Kim H, Torres-Garcia W, et al. Inferring tumour purity and stromal and immune cell admixture from expression data. *Nat Commun* (2013) 4:2612. doi:10.1038/ncomms3612

24. Newman AM, Liu CL, Green MR, Gentles AJ, Feng W, Xu Y, et al. Robust enumeration of cell subsets from tissue expression profiles. *Nat Methods* (2015) 12(5):453–7. doi:10.1038/nmeth.3337

25. Ritchie ME, Phipson B, Wu D, Hu Y, Law CW, Shi W, et al. Limma powers differential expression analyses for rna-sequencing and microarray studies. *Nucleic Acids Res* (2015) 43(7):e47. doi:10.1093/nar/gkv007

26. Taylor JMG. Random survival forests. *J Thorac Oncol* (2011) 6(12):1974–5. doi:10.1097/JTO.0b013e318233d835

27. Murciano-Goroff YR, Warner AB, Wolchok JD. The future of cancer immunotherapy: Microenvironment-targeting combinations. *Cell Res* (2020) 30(6):507–19. doi:10.1038/s41422-020-0337-2

28. Marin-Acevedo JA, Chirila RM, Dronca RS. Immune checkpoint inhibitor toxicities. *Mayo Clin Proc* (2019) 94(7):1321–9. doi:10.1016/j.mayocp.2019.03.012

29. Liu S, Galat V, Galat Y, Lee YKA, Wainwright D, Wu J. Nk cell-based cancer immunotherapy: From basic biology to clinical development. *J Hematol Oncol* (2021) 14(1):7. doi:10.1186/s13045-020-01014-w

30. Rahimi Kalateh Shah Mohammad G, Ghahremanloo A, Soltani A, Fathi E, Hashemy SI. Cytokines as potential combination agents with Pd-1/Pd-L1 blockade for cancer treatment. *J Cel Physiol* (2020) 235(7-8):5449–60. doi:10.1002/jcp.29491

31. Terawaki S, Chikuma S, Shibayama S, Hayashi T, Yoshida T, Okazaki T, et al. Ifn-A directly promotes programmed cell death-1 transcription and limits the duration of T cell-mediated immunity. *J Immunol* (2011) 186(5):2772–9. doi:10.4049/jimmunol.1003208

32. Liang Y, Tang H, Guo J, Qiu X, Yang Z, Ren Z, et al. Targeting ifnα to tumor by anti-Pd-L1 creates feedforward antitumor responses to overcome checkpoint blockade resistance. *Nat Commun* (2018) 9(1):4586. doi:10.1038/s41467-018-06890-y

33. Adusumilli PS, Cherkassky L, Villena-Vargas J, Colovos C, Servais E, Plotkin J, et al. Regional delivery of mesothelin-targeted car T cell therapy generates potent and long-lasting Cd4-dependent tumor immunity. *Sci Transl Med* (2014) 6(261): 261ra151. doi:10.1126/scitranslmed.3010162

34. Melenhorst JJ, Chen GM, Wang M, Porter DL, Chen C, Collins MA, et al. Decade-long leukaemia remissions with persistence of $CD4^+$ CAR T cells. *Nature* (2022) 602(7897):503–9. doi:10.1038/s41586-021-04390-6

35. Peng P, Lou Y, Wang S, Wang J, Zhang Z, Du P, et al. Activated nk cells reprogram mdscs via nkg2d-nkg2dl and ifn-Γ to modulate antitumor T-cell response after cryo-thermal therapy. *J Immunother Cancer* (2022) 10(12): e005769. doi:10.1136/jitc-2022-005769

36. Ilander M, Kreutzman A, Mustjoki S. Ifnα induces prolonged remissions modeling curative immunologic responses in chronic myeloid leukemia. *Oncoimmunology* (2014) 3:e28781. doi:10.4161/onci.28781

37. Zhao H, Wu L, Yan G, Chen Y, Zhou M, Wu Y, et al. Inflammation and tumor progression: Signaling pathways and targeted intervention. *Signal Transduct Target Ther* (2021) 6(1):263. doi:10.1038/s41392-021-00658-5

38. Reschke R, Yu J, Flood B, Higgs EF, Hatogai K, Gajewski TF. Immune cell and tumor cell-derived Cxcl10 is indicative of immunotherapy response in metastatic melanoma. *J Immunother Cancer* (2021) 9(9):e003521. doi:10.1136/jitc-2021-003521

39. Chen P-L, Roh W, Reuben A, Cooper ZA, Spencer CN, Prieto PA, et al. Analysis of immune signatures in longitudinal tumor samples yields insight into biomarkers of response and mechanisms of resistance to immune checkpoint blockade. *Cancer Discov* (2016) 6(8):827–37. doi:10.1158/2159-8290.CD-15-1545

40. Harlin H, Meng Y, Peterson AC, Zha Y, Tretiakova M, Slingluff C, et al. Chemokine expression in melanoma metastases associated with Cd8+ T-cell recruitment. *Cancer Res* (2009) 69(7):3077–85. doi:10.1158/0008-5472.CAN-08-2281

41. Spranger S, Dai D, Horton B, Gajewski TF. Tumor-residing Batf3 dendritic cells are required for effector T cell trafficking and adoptive T cell therapy. *Cancer Cell* (2017) 31(5):711–23.e4. doi:10.1016/j.ccell.2017.04.003

42. Chow MT, Ozga AJ, Servis RL, Frederick DT, Lo JA, Fisher DE, et al. Intratumoral activity of the Cxcr3 chemokine system is required for the efficacy of anti-Pd-1 therapy. *Immunity* (2019) 50(6):1498–512.e5. doi:10.1016/j.immuni.2019.04.010

43. Saviano A, Henderson NC, Baumert TF. Single-cell genomics and spatial transcriptomics: Discovery of novel cell states and cellular interactions in liver physiology and disease biology. *J Hepatol* (2020) 73(5):1219–30. doi:10.1016/j.jhep.2020.06.004

44. Hui Z, Zhang J, Ren Y, Li X, Yan C, Yu W, et al. Single-cell profiling of immune cells after neoadjuvant pembrolizumab and chemotherapy in iiia non-small cell lung cancer (nsclc). *Cell Death Dis* (2022) 13(7):607. doi:10.1038/s41419-022-05057-4

45. Hoffmann C, Noel F, Grandclaudon M, Massenet-Regad L, Michea P, Sirven P, et al. Pd-L1 and icosl discriminate human secretory and helper dendritic cells in cancer, allergy and autoimmunity. *Nat Commun* (2022) 13(1):1983. doi:10.1038/s41467-022-29516-w

Pathology & Oncology Research | frontiers

TYPE Original Research
PUBLISHED 16 February 2023
DOI 10.3389/pore.2023.1610918

Check for updates

OPEN ACCESS

EDITED BY
Andrea Ladányi,
National Institute of Oncology (NIO), Hungary

*CORRESPONDENCE
Yang Xiang,
xiangy@pumch.cn
Junjun Yang,
yangjunjun@pumch.cn

†These authors have contributed equally to this work

RECEIVED 02 November 2022
ACCEPTED 07 February 2023
PUBLISHED 16 February 2023

CITATION
Cheng H, Zong L, Yu S, Chen J, Wan X, Xiang Y and Yang J (2023), Expression of the immune targets in tumor-infiltrating immunocytes of gestational trophoblastic neoplasia.
Pathol. Oncol. Res. 29:1610918.
doi: 10.3389/pore.2023.1610918

COPYRIGHT
© 2023 Cheng, Zong, Yu, Chen, Wan, Xiang and Yang. This is an open-access article distributed under the terms of the Creative Commons Attribution License (CC BY). The use, distribution or reproduction in other forums is permitted, provided the original author(s) and the copyright owner(s) are credited and that the original publication in this journal is cited, in accordance with accepted academic practice. No use, distribution or reproduction is permitted which does not comply with these terms.

Expression of the immune targets in tumor-infiltrating immunocytes of gestational trophoblastic neoplasia

Hongyan Cheng[1†], Liju Zong[1,2†], Shuangni Yu[2], Jie Chen[2], Xirun Wan[1], Yang Xiang[1*] and Junjun Yang[1*]

[1]Department of Obstetrics and Gynecology, National Clinical Research Centre for Obstetric and Gynecologic Diseases, Peking Union Medical College Hospital, Chinese Academy of Medical Sciences and Peking Union Medical College, Beijing, China, [2]Department of Pathology, Peking Union Medical College Hospital, Chinese Academy of Medical Sciences and Peking Union Medical College, Beijing, China

Objectives: To evaluate the expression of emerging immune targets in the tumor-infiltrating immunocytes (TIIs) of human gestational trophoblastic neoplasia (GTN) specimens, and to analyze the correlation between the expression patterns and prognosis of GTN patients.

Methods: Between January 2008 and December 2017, patients who were diagnosed histologically with GTN were included in this study. The expression densities of LAG-3, TIM-3, GAL-9, PD-1, CD68, CD8, and FOXP3 in the TIIs were assessed independently by two pathologists blinded to clinical outcomes. The expression patterns and correlation with patient outcomes were analyzed to identify prognostic factors.

Results: We identified 108 patients with GTN, including 67 with choriocarcinoma, 32 with placental site trophoblastic tumor (PSTT), and 9 with epithelioid trophoblastic tumor (ETT). Almost all GTN patients showed expression of GAL-9, TIM-3, and PD-1 in TIIs (100%, 92.6%, and 90.7%, respectively); LAG-3 was expressed in 77.8% of the samples. The expression densities of CD68 and GAL-9 were significantly higher in choriocarcinoma than that in PSTT and ETT. The TIM-3 expression density in choriocarcinoma was higher than that in PSTT. In addition, the expression density of LAG-3 in the TIIs of choriocarcinoma and PSTT was higher than that in ETT. There was no statistical difference in the expression pattern of PD-1 among different pathological subtypes. The positive expression of LAG-3 in tumor TIIs was a prognostic factor for disease recurrence, and patients with positive expression of LAG-3 in the TIIs had poorer disease-free survival (p = 0.026).

Conclusion: Our study evaluated the expression of immune targets PD-1, TIM-3, LAG-3, and GAL-9 in the TIIs of GTN patients and found that they were widely expressed but not associated with patients' prognoses, excepting the positive expression of LAG-3 was a prognostic factor for disease recurrence.

KEYWORDS

gestational trophoblastic neoplasia, tumor-infiltrating immunocyte, PD-1, TIM-3, GAL-9, LAG-3

Introduction

Gestational trophoblastic neoplasia (GTN) is a group of malignant diseases arising from the abnormal proliferation of placental trophoblastic cells, which includes invasive mole, choriocarcinoma, placental site trophoblastic tumor (PSTT), and epithelioid trophoblastic tumor (ETT) (1). The specific marker beta-human chorionic gonadotropin (β-HCG) is secreted by tumor cells and can be used as a monitoring index for treatment. Although almost all low-risk patients can be cured with standardized chemotherapy, the five-year survival rate is less than 70% for patients with drug-resistant and recurrent disease (2, 3). Recently, emerging immunotherapies such as programmed cell death 1 (PD-1) inhibitors have shown excellent efficacy in the treatment of drug-resistant and recurrent GTN (4).

The fetus and fetus-derived trophoblast cells are part of the semi-allogeneic conceptus; however, the fetus and placenta are not rejected by the maternal immune system because the fetus and its affiliated tissues express paternal antigens that establish immune tolerance at the maternal–fetal interface (5). Previous studies have shown that programmed cell death ligand (PD-L1) is expressed in human placentas and GTN specimens (6,7,8). The B7 family and their receptors are major immune checkpoints that regulate the activation and function of T cells. In addition to PD-L1, other immunoregulatory molecules of the B7 family show high expression in GTN, including B7-H3 and the V-type immunoglobulin domain–containing suppressor of T cell activation (8).

In addition to T cells, tumor-infiltrating immunocytes (TIIs) also include macrophages, natural killer (NK) cells, and dendritic cells (DC). Many studies have investigated the expression of immune checkpoints in tumor cells, but there is no study on these in TIIs of GTN. In this study, we investigated the expression of PD-1, lymphocyte activation gene-3 (LAG-3), T cell immunoglobulin-3 (TIM-3), and galectin-9 (GAL-9) in the TIIs of human GTN specimens and analyzed the correlation between expression difference and prognosis of GTN patients to explore potential new targets for immunotherapy of drug-resistant and recurrent GTN.

Materials and Methods

Patients and samples

This study included patients diagnosed histologically with choriocarcinoma, PSTT, or ETT and who had enough tumor samples for immunohistochemistry at Peking Union Medical College Hospital (Beijing, China) between January 2008 and December 2017. The clinicopathological data were obtained from patients' admission and discharge files. The treatment and follow-up methods have been described as our previous studies (3, 8, 9). This study was approved by the Institutional Review Board (SK-995); informed consent was not required due to its retrospective nature.

Immunohistochemistry and assessment

Immunohistochemistry was performed using our laboratory protocol described previously (8,9). Briefly, 4-μm serial sections were deparaffinized and subjected to heat-induced epitope retrieval using 10 mM sodium citrate (pH 6.0) at 95°C for 20 min. The endogenous peroxidase activity was quenched using a 0.3% hydrogen peroxide solution. Sections were

TABLE 1 Clinicopathologic characteristics of patients with gestational trophoblastic neoplasia (n = 108).

Characteristics	N (%)
Pathological type	
Choriocarcinoma	67 (62.1)
PSTT	32 (29.6)
ETT	9 (8.3)
Disease type	
Chemo-naive	34 (31.5)
Relapsed	57 (52.8)
Chemo-refractory	17 (15.7)
Age	
<40	91 (84.3)
≥40	17 (15.7)
FIGO stage	
I	29 (26.8)
II	3 (2.8)
III	64 (59.3)
IV	12 (11.1)
FIGO score	
1–3	27 (25.0)
4–6	11 (10.2)
7–12	62 (57.4)
12	8 (7.4)
Specimen type	
Uterus	47 (43.5)
Pulmonary metastasis	57 (52.8)
Brain metastasis	2 (1.9)
Recto-uterine pouch	1 (0.9)
Intestinal metastasis	1 (0.9)

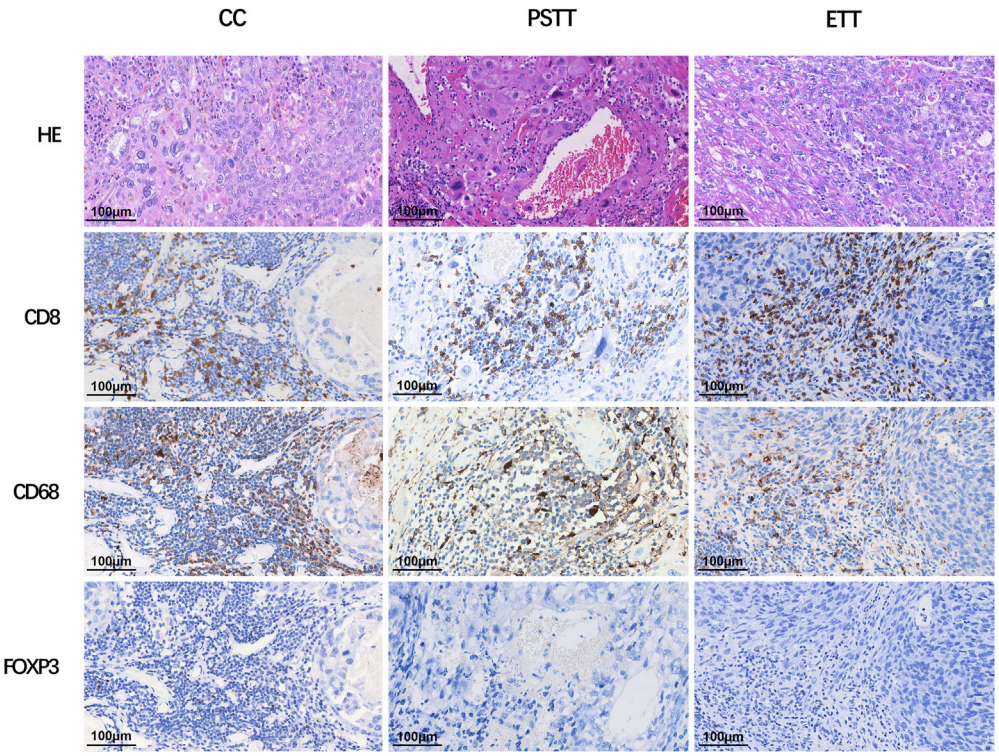

FIGURE 1
Expression of CD8, CD68, and FOXP3 in different types of gestational trophoblastic neoplasia. CC: choriocarcinoma; PSTT: placental site trophoblastic tumor; ETT: epithelioid trophoblastic tumor; HE: hematoxylin and eosin staining.

incubated with primary antibodies against LAG-3 (Clone D4G40, 1:100), TIM-3 (Clone D5D5R, 1:200), GAL-9 (Clone D9G40, 1:200), PD-1 (Clone D4W2J, 1:200), CD68 (Clone D4B9C, 1:500), CD8 (Clone D8A8Y, 1:200), and FOXP3 (Clone D2W8E, 1:200). All antibodies were obtained from Cell Signaling Technology (Boston, United states). All slides were stained using an automatic immunohistochemistry staining instrument (Bond Max, Leica Biosystems; Buffalo Grove, IL, United states) according to the manufacturer's protocol. Human tonsil tissues stained using the primary antibodies were used as positive controls; the same tissues with isotypematched immunoglobulins comprised the negative controls.

The tumors were distinguished from the stroma and TIIs using hematoxylin and eosin staining. The expression of LAG-3, TIM-3, GAL-9, PD-1, CD68, CD8, and FOXP3 in the TIIs was assessed independently by two pathologists (LJ. Z and SN. Y), who were blinded to clinical outcomes. Five representative fields were selected for each slide at ×40 magnification. The percentages of cells that stained positive for each marker were quantified in 5% increments of the overall tumor section. The density of the positive immune cells in the TIIs was classified using a semi-quantitative score as 0 (negative, <5%), 1 (sporadic, 5%–25%), 2 (moderate, 25%–50%), or 3 (strong positive, >50%).

Statistical analysis

The χ^2 test or Fisher's exact test was used to evaluate the association between categorical variables. The Kruskal–Wallis (H) test and Dunn *post hoc* test were performed to evaluate expression differences among the different pathological types of GTN. Disease-free survival (DFS) was defined as the period between surgery and the detection of the first local, regional, or distant relapse. Overall survival (OS) was defined as the period between surgery and death from any cause. The Kaplan-Meier survival analysis and log-rank test were performed to describe recurrence and OS. All statistical analyses were performed using SPSS software version 19 (IBM Company, Armonk, NY, United states). A two-sided p-value < 0.05 (or a Bonferroni-corrected significance threshold) was considered statistically significant.

Results

Clinical characteristics

A total of 108 patients had adequate tumor samples for immunohistochemistry; 67 were diagnosed with choriocarcinoma, 32 had PSTT, and 9 had ETT. The median

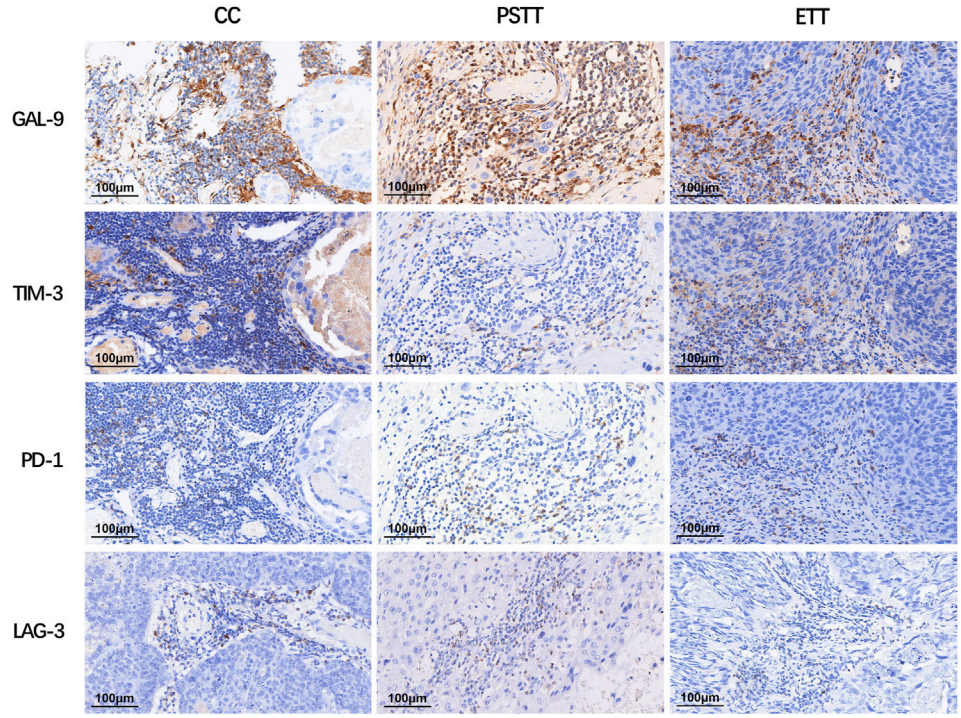

FIGURE 2
Expression of immune targets in tumor-infiltrating immunocytes of gestational trophoblastic neoplasia. LAG-3: lymphocyte activation gene-3; TIM-3: T cell immunoglobulin-3; GAL-9: galectin-9; PD-1: programmed cell death 1.

TABLE 2 Expression of immunomarkers of tumor-infiltrating immunocytes in gestational trophoblastic neoplasia (n = 108).

	LAG-3	TIM-3	GAL-9	PD-1	CD68	CD8	FOXP3
Density of positive TIIs							
0	24	8	0	10	2	0	100
1	79	55	6	42	34	25	8
2	4	35	27	50	42	64	0
3	1	10	75	6	30	19	0

age at surgery was 32 (range: 21–53) years. The prognostic score according the 2000 International Federation of Gynecology Obstetrics (FIGO) scoring system, had a median of 8 (range: 1–15 scores) (10). Of the 67 choriocarcinoma specimens, 7 were from hysterectomies or diagnostic curettages, 57 from pulmonary metastases, 2 from brain metastasis, and 1 from intestinal metastasis. Among the 108 samples, 34 were from chemo-naive patients, and 74 were obtained from patients after chemotherapy (57 relapsed and 17 chemo-refractory). All PSTT and ETT specimens were acquired *via* hysterectomy, except in one ETT case (recto-uterine pouch), as reported previously (11). The detailed clinicopathological characteristics of the patients are shown in Table 1.

Expression of immune targets

As shown in Figure 1, $CD8^+$ T cells and $CD68^+$ macrophages were widely infiltrated in all GTN stromal cells (100% and 98.1%, respectively). $FOXP3^+$ regulatory T cells (Tregs) were detected in 8 choriocarcinoma samples but were not detected in PSTT and ETT. The expression of PD-1 in the TIIs was positive in 98 (90.7%) patients, and moderate-to-strong density was detected in 56 patients (51.9%) (Figure 2). TIM-3 and GAL-9 were expressed in the TIIs of almost all GTN patients (92.6% and 100%, respectively). A sporadic density for TIM-3 was noted in 55 patients (50.9%), and moderate -to-strong density was found in 45 patients (41.7%). In contrast to TIM-3, 102 patients

TABLE 3 Expression of immunomarkers of tumor-infiltrating immunocytes in different pathological subtypes of gestational trophoblastic neoplasia.

Targets	Density	Choriocarcinoma	PSTT	ETT	*p*
LAG-3	0	7	9	8	<0.001*
	1	57	21	1	
	2	3	1	0	
	3	0	1	0	
TIM-3	0	1	6	1	<0.001*
	1	28	22	5	
	2	28	4	3	
	3	10	0	0	
GAL-9	0	0	0	0	<0.001*
	1	0	5	1	
	2	7	17	3	
	3	60	10	5	
PD-1	0	2	6	2	0.581
	1	29	10	3	
	2	34	12	4	
	3	2	4	0	
CD68	0	0	2	0	<0.001*
	1	9	20	5	
	2	30	8	4	
	3	28	2	0	
CD8	0	0	0	0	0.145
	1	13	8	4	
	2	41	18	5	
	3	13	6	0	
FOXP3	0	59	32	9	0.073
	1	8	0	0	
	2	0	0	0	
	3	0	0	0	

(94.4%) were found to have a moderate-to-strong density of GAL-9 expression. LAG-3 showed positive expression in 84 patients (77.8%), 79 of which had sporadic expression, 4 had moderate expression, and one was strongly positive. The expression of each immune target in GTN is shown in Table 2.

Expression patterns and correlations among pathological subtypes of gestational trophoblastic neoplasia

The expression differences of LAG-3, TIM-3, GAL-9, PD-1, CD68, and CD8 in TIIs among three pathological subtypes are shown in Table 3 and Figure 3. The Kruskal–Wallis test results showed that the expression density of CD68 and GAL-9 in choriocarcinoma TIIs was significantly higher than that in PSTT and ETT. The expression density of TIM-3 in choriocarcinoma TIIs was higher than that in PSTT. Moreover, the expression of LAG-3 in the TIIs of choriocarcinoma and PSTT was higher than that in ETT. There was no statistical difference in the expression pattern of PD-1 across pathological subtypes. As shown in Supplementary Tables S1, S2, statistical testing showed that LAG-3 expression was associated with the expression of TIM-3, PD-1, CD68, and FOXP3, and PD-1 expression was found associated with TIM-3 and CD68. The association between the expression patterns of these targets suggests a positive correlation and co-expression.

Survival outcome

At the last follow-up, 12 patients had died from GTN, 7 were alive with GTN, and 89 had achieved complete remission. The follow-up duration among the 96 patients alive at their last follow-up had a median of 60 months (range: 27–172 months). The positive expression of LAG-3 in tumor TIIs was a prognostic factor for disease recurrence in patients, and patients with positive expression of LAG-3 in TIIs had a poorer DFS (p = 0.026). Patients with negative expression of LAG-3 had higher OS, but there was no statistical difference (3-year OS: 100% vs 81.4%, 5-year OS: 100% vs 77.7%) (Figure 4). There was no association between patients' outcomes and the expression of other immune targets in the TIIs.

Discussion

In the present study, we found that the immune targets PD-1, TIM-3, LAG-3, and GAL-9 were widely expressed in the TIIs of GTN patients but not associated with the patients' prognoses, excepting that the positive expression of LAG-3 was a prognostic factor for disease recurrence. The co-expressions among these immune targets may support treatments using immune checkpoint inhibitor combinatorial approaches. The co-expression of multiple immune molecules was not prognostic, consistent with previous reports in ovarian cancer and lung cancer (12, 13).

The correlation between the origins of GTN tumors and immune tolerance suggests that immunotherapy may be a promising salvage treatment for drug-resistant and recurrent GTN. Research focused on PD-L1 expression in GTN tumor cells showed that inhibitors targeting PD-1 in GTN were therapeutically efficacious in several cases (4,6,7,8). Although our study showed that PD-1^+ TIIs were present in 90.7% of GTN patients, its expression does not affect a patient's outcome. It has been reported that PD-1^+ $CD4^+$ tumor infiltrating lymphocytes (TILs) and $CD8^+$ TILs had less proliferative capacity comparing to the PD-1^- $CD8^+$ or $CD4^+$ TILs, suggesting that both $CD8^+$ and $CD4^+$ TILs are functionally anergic through activation of the PD-1/PD-

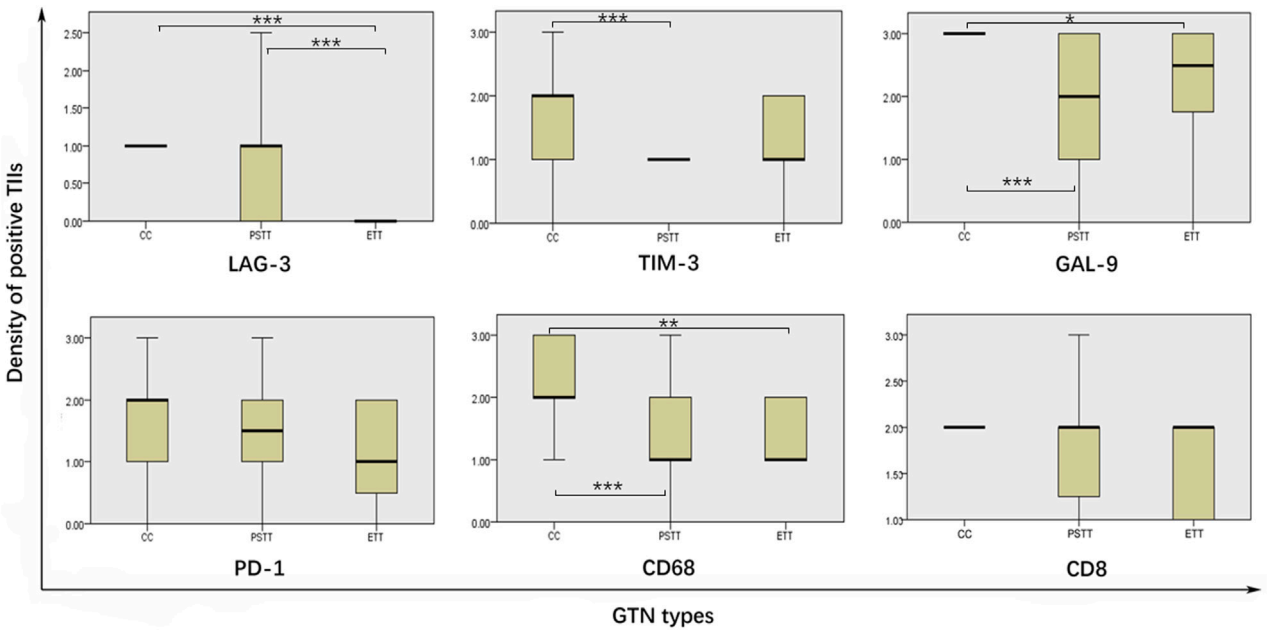

FIGURE 3
Comparison of immune targets expression level in different pathological gestational trophoblastic neoplasia types. TIIs: tumor-infiltrating immunocytes; GTN: gestational trophoblastic neoplasia; * = $p < 0.01$, ** = $p < 0.01$, *** = $p < 0.001$.

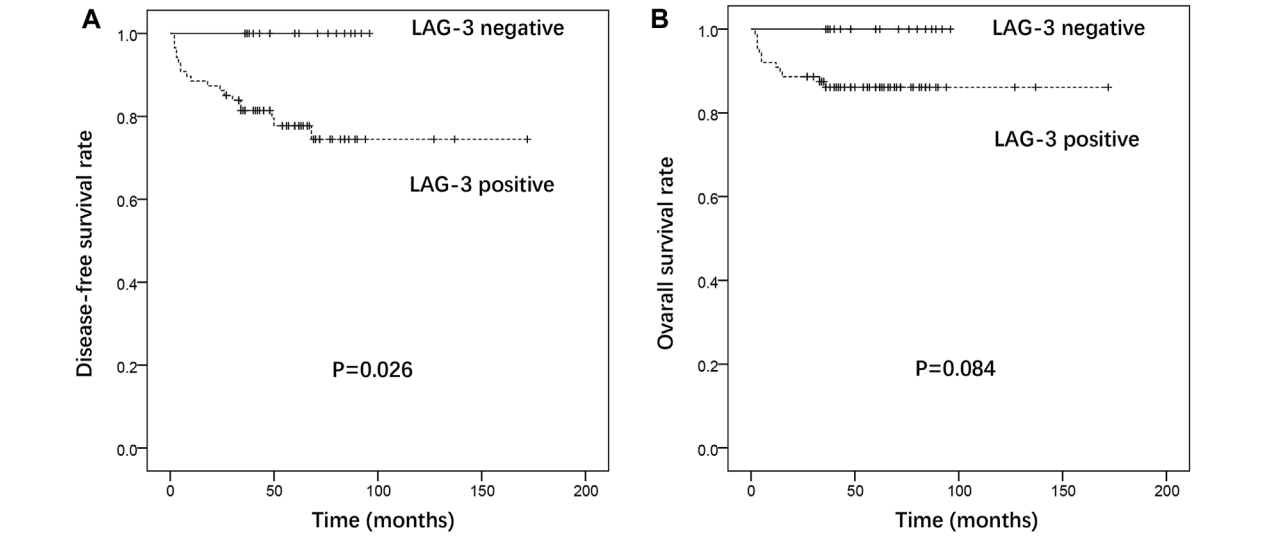

FIGURE 4
Association of LAG-3 expression with disease-free survival **(A)** and overall survival **(B)** in gestational trophoblastic neoplasia.

L1 pathway (14). Notably, multiple clinical trials are currently investigating the efficacy of PD-1/PD-L1 inhibitors in GTN patients (NCT: 03135769 and 04047017).

LAG-3 structurally resembles the CD4 co-receptor and is expressed mainly on activated T cells, DCs, and NK cells (15). LAG-3 binds the class II major histocompatibility complex (MHC II) with a high affinity. Studies indicated that the blockade of LAG-3 improves cytotoxic T lymphocyte proliferation and effector function (16, 17). The frequency of antigenic sharing for the human leukocyte antigen (HLA) DR

locus in GTN couples is significantly higher than that in normal fertile couples, indicating that the states of an MHC-linked gene (HLA-DR) influence the development of GTN (18). LAG-3 may play an important role in the development of ovarian and cervical cancer (19, 20). Dual blockade of LAG-3 and PD-1 efficiently augments proliferation and cytokine production by $CD8^+$ T cells (21). This study is the first to identify that LAG-3 is expressed in the majority of GTN patients. In addition, the positive expression of LAG-3 in tumor TIIs was a prognostic factor for disease recurrence and poorer DFS in patients with GTN. Patients with negative expression of LAG-3 had a higher OS rate; however, it was not statistically different. Since the expression pattern in different pathological types was not significant, these results suggest that the expression of LAG-3 in tumor TIIs may be a prognostic factor and therapeutic target in GTN.

TIM-3 is a type I transmembrane protein expressed mainly on $CD8^+$ and $CD4^+$ T cells, DCs, monocytes, NK cells, and Tregs (22). GAL-9 is a ligand of TIM-3. The binding of TIM-3 with GAL-9 promotes calcium influx, cell aggregation, and apoptosis, further inhibiting the activation and proliferation of T cells and ultimately inducing peripheral immune tolerance (23, 24). In this study, TIM-3 and GAL-9 were expressed in the TIIs of almost all GTN patients. Moderate -to-strong densities of TIM-3 and GAL-9 were found in 41.7% and 94.4% of patients, respectively. Although studies have shown that high expression of GAL-9 in solid tumors is associated with a poor prognosis (25), our data did not show a correlation between GAL-9 expression in TIIs and patient outcomes. Additionally, the effects of the TIM-3/GAL-9 pathway on innate immunity are different from those of adaptive immunity. In the study of Lv et al. (26), overexpression of GAL-9 was associated with M2 macrophages, whereas its downregulation promoted macrophage polarization into M1macrophages. A previous study had indicated that M1 macrophages greatly enhance cytotoxicity and reduce tumor growth, whereas M2 macrophages increase cell invasion and survival (27).

Our results showed that macrophages were detected constitutively in almost all GTNs; their density in choriocarcinoma was significantly higher than those in PSTT and ETT but unrelated to patient outcomes. Macrophages are traditionally considered as typical antitumor cell in innate immunity, and tumor-associated macrophages can directly kill cancer cells and stimulate the antitumor activity of T cells. However, clinical and basic studies have shown that tumor-associated macrophages can promote the malignant progression of tumors in some cases (28-30). Moreover, studies have suggested that there is a strong association between poor survival and increased macrophage density in solid tumors (28, 29). . The tumor-promoting functions of macrophages include tumor angiogenesis, cell invasion, migration, and intravasation, as well as the inhibition of antitumor immune responses (28, 30). In addition to GAL-9 inducing polarization of macrophages from the M1 to M2 type, as mentioned above, tumor-associated macrophages can also inhibit T cell function through the PD-1/PD-L1 axis (31). In summary, therapies targeting tumor-associated macrophages may complement the immunosuppressive effects of the PD-1/PD-L1 pathway.

This study had some limitations. First, selection bias may have occurred due to the retrospective nature of the study. Second, atypical necrosis of tumor tissue after chemotherapy adds difficulty to the interpretation of pathological findings. Third, the heterogenous set of samples from different subtypes may have led to the lack of distinction in immune marker expression. In addition, immunohistochemical methods cannot distinguish the expression of targets among immunocyte subtypes.

Conclusion

Evaluation of the expression of immune targetsPD-1, TIM-3, LAG-3, and GAL-9 in GTN TIIs showed that they were widely expressed in TIIs but not associated with patients' prognoses, excepting the positive expression of LAG-3 was a prognostic factor for disease recurrence. These findings suggest that LAG-3 may provide the basis for the study of pathogenesis and be a novel therapeutic target in GTN treatment.

Data availability statement

The raw data supporting the conclusion of this article will be made available by the authors, without undue reservation.

Ethics statement

This study was approved by the Institutional Review Board (SK-995) of Peking Union Medical College Hospital. Written informed consent was waived due to its retrospective nature.

Author contributions

Conceptualization and design: YX and JY. Data curation, software, formal analysis, and writing-original draft: HC and LZ. Investigation and methodology: HC, LZ, SY, JC, and XW. Funding acquisition and project administration: JC, XW, YX, and JY. Supervision, validation, writing—review, and editing: YX and JY.

Funding

This study was supported by National Natural Science Foundation of China (Nos. 81971475, and 81972451).

Conflict of interest

The authors declare that the research was conducted in the absence of any commercial or financial relationships that could be construed as a potential conflict of interest.

Supplementary material

The Supplementary Material for this article can be found online at: https://www.por-journal.com/articles/10.3389/pore.2023.1610918/full#supplementary-material

References

1. Ngan HYS, Seckl MJ, Berkowitz RS, Xiang Y, Golfier F, Sekharan PK, et al. Update on the diagnosis and management of gestational trophoblastic disease. *Int J Gynaecol Obstet* (2018) 143(2):79–85. doi:10.1002/ijgo.12615

2. Zong L, Yang J, Wang X, Kong Y, Ren T, Zhao J, et al. Management and prognosis of patients with liver metastases from gestational trophoblastic neoplasia: A retrospective cohort study. *Cancer Manag Res* (2018) 10:557. doi:10.2147/CMAR.S160606

3. Kong Y, Yang J, Jiang F, Zhao J, Ren T, Li J, et al. Clinical characteristics and prognosis of ultra high-risk gestational trophoblastic neoplasia patients: A retrospective cohort study. *Gynecol Oncol* (2017) 146:81–6. doi:10.1016/j.ygyno.2017.04.010

4. Ghorani E, Kaur B, Fisher RA, Short D, Joneborg U, Carlson JW, et al. Pembrolizumab is effective for drug-resistant gestational trophoblastic neoplasia. *Lancet* (2017) 390:2343–5. doi:10.1016/S0140-6736(17)32894-5

5. Nakashima A, Shima T, Aoki A, Kawaguchi M, Yasuda I, Tsuda S, et al. Molecular and immunological developments in placentas. *Hum Immunol* (2021) 82:317–24. doi:10.1016/j.humimm.2021.01.012

6. Veras E, Kurman RJ, Wang TL, Shih IM. PD-L1 expression in human placentas and gestational trophoblastic diseases. *Int J Gynecol Pathol* (2017) 36:146–53. doi:10.1097/pgp.0000000000000305

7. Bolze PA, Patrier S, Massardier J, Hajri T, Abbas F, Schott AM, et al. PD-L1 expression in premalignant and malignant trophoblasts from gestational trophoblastic diseases is ubiquitous and independent of clinical outcomes. *Int J Gynrcol Cancer* (2017) 27:554–61. doi:10.1097/IGC.0000000000000892

8. Zong L, Zhang M, Wang W, Wan X, Yang J, Xiang Y. PD-L1, B7-H3 and VISTA are highly expressed in gestational trophoblastic neoplasia. *Histopathology* (2019) 75:421–30. doi:10.1111/his.13882

9. Yang J, Zong L, Wang J, Wan X, Feng F, Xiang Y. Epithelioid trophoblastic tumors: Treatments, outcomes, and potential therapeutic targets. *J Cancer* (2019) 10:11–9. doi:10.7150/jca.28134

10. Kohorn EI. The new FIGO 2000 staging and risk factor scoring system for gestational trophoblastic disease: Description and critical assessment. *Int J Gynrcol Cancer* (2010) 11:73–7. doi:10.1046/j.1525-1438.2001.011001073.x

11. Jiang F, Xiang Y, Guo LN. Laparoscopic diagnosis and treatment of an isolated epithelioid trophoblastic tumor in recto-uterine pouch. *J Obstet Gynaecol Res* (2018) 44:960–5. doi:10.1111/jog.13593

12. Blanc-Durand F, Genestie C, Galende EY, Gouy S, Morice P, Pautier P, et al. Distribution of novel immune-checkpoint targets in ovarian cancer tumor microenvironment: A dynamic landscape. *Gynecol Oncol* (2021) 160:279–84. doi:10.1016/j.ygyno.2020.09.045

13. Carvajal-Hausdorf D, Altan M, Velcheti V, Gettinger SN, Herbst RS, Rimm DL, et al. Expression and clinical significance of PD-L1, B7-H3, B7-H4 and TILs in human small cell lung Cancer (SCLC). *J Immunother Cancer* (2019) 7:65. doi:10.1186/s40425-019-0540-1

14. Mattox AK, Lee J, Westra WH, Pierce RH, Ghossein R, Faquin WC, et al. PD-1 expression in head and neck squamous cell carcinomas derives primarily from functionally anergic CD4(+) TILs in the presence of PD-L1(+) TAMs. *Cancer Res* (2017) 77:6365–74. doi:10.1158/0008-5472.can-16-3453

15. Gagliani N, Magnani CF, Huber S, Gianolini ME, Pala M, Licona-Limon P, et al. Coexpression of CD49b and LAG-3 identifies human and mouse T regulatory type 1 cells. *Nat Med* (2013) 19:739–46. doi:10.1038/nm.3179

16. Grosso JF, Kelleher CC, Harris TJ, Maris CH, Hipkiss EL, Angelo DM, et al. LAG-3 regulates CD8+ T cell accumulation and effector function in murine self- and tumor-tolerance systems. *J Clin Invest* (2007) 117:3383–92. doi:10.1172/JCI31184

17. Lui Y, Davis SJ. LAG-3: A very singular immune checkpoint. *Nat Immunol* (2018) 19:1278–9. doi:10.1038/s41590-018-0257-1

18. Sbracia M, Scarpellini F, Mastrone M, Grasso JA. HLA antigen sharing in Italian couples in which women were affected by gestational trophoblastic tumors. *Am J Reprod Immunol* (1996) 35:252–5. doi:10.1111/j.1600-0897.1996.tb00039.x

19. Tu L, Yang H, Zhou Y, Guan R. Assessment of the expression of the immune checkpoint molecules PD-1, CTLA4, TIM-3 and LAG-3 across different cancers in relation to treatment response, tumor-infiltrating immune cells and survival. *Int J Cancer* (2019) 147:423–39. doi:10.1002/ijc.32785

20. Heeren AM, Rotman J, Stam AGM, Pocorni N, Gassama AA, Samuels S, et al. Efficacy of PD-1 blockade in cervical cancer is related to a CD8+FoxP3+CD25+ T-cell subset with operational effector functions despite high immune checkpoint levels. *J ImmunoTherapy Cancer* (2019) 7:43. doi:10.1186/s40425-019-0526-z

21. Matsuzaki J, Gnjatic S, Mhawechfauceglia P, Beck A, Miller A, Tsuji T, et al. Tumor-infiltrating NY-ESO-1-specific CD8+ T cells are negatively regulated by LAG-3 and PD-1 in human ovarian cancer. *Proc Natl Acad Sci U S A* (2010) 107:7875–80. doi:10.1073/pnas.1003345107

22. Cheng H, Zong L, Kong Y, Gu Y, Yang J, Xiang Y. Emerging targets of immunotherapy in gynecologic cancer. *Emerging Targets Immunother Gynecol Cancer* (2020) 13:11869–82. doi:10.2147/ott.s282530

23. Kuchroo VK. The Tim-3 ligand galectin-9 negatively regulates T helper type 1 immunity. *Nat Immunol* (2005) 6:1245–52. doi:10.1038/ni1271

24. Sabatos CA, Chakravarti S, Cha E, Schubart A, Sánchez-Fueyo A, Zheng XX, et al. Interaction of Tim-3 and Tim-3 ligand regulates T helper type 1 responses and induction of peripheral tolerance. *Nat Immunol* (2003) 4:1102–10. doi:10.1038/ni988

25. Wang K, Chen Z, Wu R, Yin J, Fan M, Xu X. Prognostic role of high gal-9 expression in solid tumours: A meta-analysis. *Cell Physiol Biochem* (2018) 45:993–1002. doi:10.1159/000487294

26. Lv R, Bao Q, Li Y. Regulation of M1-type and M2-type macrophage polarization in RAW264.7 cells by Galectin-9. *Mol Med Rep* (2017) 16:9111–9. doi:10.3892/mmr.2017.7719

27. Dumas G, Dufresne M, Asselin E, Girouard J, Carrier C, Reyes-Moreno C. CD40 pathway activation reveals dual function for macrophages in human endometrial cancer cell survival and invasion. *Cancer Immunol Immunother* (2013) 62:273–83. doi:10.1007/s00262-012-1333-2

28. Qian BZ, Pollard JW. Macrophage diversity enhances tumor progression and metastasis. *Cell* (2010) 141:39–51. doi:10.1016/j.cell.2010.03.014

29. Bingle L, Brown NJ, Lewis CE. The role of tumour-associated macrophages in tumour progression: Implications for new anticancer therapies. *J Pathol* (2002) 196:254–65. doi:10.1002/path.1027

30. Condeelis J, Pollard JW. Macrophages: Obligate partners for tumor cell migration, invasion, and metastasis. *Cell* (2006) 124:263–6. doi:10.1016/j.cell.2006.01.007

31. Duraiswamy J, Freeman GJ, Coukos G. Therapeutic PD-1 pathway blockade augments with other modalities of immunotherapy T-cell function to prevent immune decline in ovarian cancer. *Cancer Res* (2013) 73:6900–12. doi:10.1158/0008-5472.can-13-1550

Pathology & Oncology Research | frontiers

TYPE Original Research
PUBLISHED 02 December 2024
DOI 10.3389/pore.2024.1611948

Check for updates

OPEN ACCESS

EDITED BY
Andrea Ladányi,
National Institute of Oncology (NIO), Hungary

*CORRESPONDENCE
Marcell Baranyi,
baranyi2marci@gmail.com

†These authors have contributed equally to this work

RECEIVED 29 August 2024
ACCEPTED 18 November 2024
PUBLISHED 02 December 2024

CITATION
Molnár E, Baranyi M, Szigeti K, Hegedűs L, Bordás F, Gábriel Z, Petényi G, Tóvári J, Hegedűs B and Tímár J (2024) Combination of farnesyl-transferase inhibition with KRAS G12D targeting breaks down therapeutic resistance in pancreatic cancer. *Pathol. Oncol. Res.* 30:1611948. doi: 10.3389/pore.2024.1611948

COPYRIGHT
© 2024 Molnár, Baranyi, Szigeti, Hegedűs, Bordás, Gábriel, Petényi, Tóvári, Hegedűs and Tímár. This is an open-access article distributed under the terms of the Creative Commons Attribution License (CC BY). The use, distribution or reproduction in other forums is permitted, provided the original author(s) and the copyright owner(s) are credited and that the original publication in this journal is cited, in accordance with accepted academic practice. No use, distribution or reproduction is permitted which does not comply with these terms.

Combination of farnesyl-transferase inhibition with KRAS G12D targeting breaks down therapeutic resistance in pancreatic cancer

Eszter Molnár[1†], Marcell Baranyi[1,2*†], Krisztina Szigeti[1], Luca Hegedűs[3], Fanni Bordás[1], Zsófia Gábriel[1], Gréta Petényi[1], József Tóvári[4], Balázs Hegedűs[1,3] and József Tímár[1]

[1]Department of Pathology, Forensic and Insurance Medicine, Semmelweis University, Budapest, Hungary, [2]KINETO Lab Ltd., Budapest, Hungary, [3]Department of Thoracic Surgery, University Medicine Essen - Ruhrlandklinik, University Duisburg-Essen, Essen, Germany, [4]Department of Experimental Pharmacology and the National Tumor Biology Laboratory, National Institute of Oncology, Budapest, Hungary

Pancreatic adenocarcinoma is one of the deadliest forms of cancer with no effective therapeutic options. A KRAS mutation can be found in up to 90% of all pancreatic tumors, making it a promising therapeutic target. The introduction of new KRAS inhibitors has been a milestone in the history of KRAS mutant tumors; however, therapeutic resistance limits their efficacy. Thus, new therapeutic options, including combination therapies, are urgently needed. Recently, we have shown that KRAS G12C inhibitors in combination with farnesyl-transferase inhibitors exert synergistic antitumor effects. Here, we provide evidence for the feasibility of this combinational approach to break down resistance in KRAS G12D mutant pancreatic cancer. Although we have shown that the 3D environment dramatically sensitizes cells to MRTX1133 treatment, the synergistic effect of this drug combination is present in both 2D and 3D in the PANC1 pancreatic adenocarcinoma model, which showed high resistance to MRTX1133 in 2D. The effects of the combination treatment show an association with the inhibition of farnesylated regulatory proteins, including HRAS and RHEB, along with the expression level of KRAS. Our study warrants further investigation for the potential applicability of KRAS G12D inhibitors in combination with farnesyl-transferase inhibitors for the treatment of KRAS mutant pancreatic adenocarcinoma.

KEYWORDS

PDAC, G12D mutant KRAS, KRAS inhibitor resistance, FTI, combination therapy

Introduction

Pancreatic adenocarcinoma (PDAC) is one of the deadliest cancer types, with a 5-year survival rate of only 10% [1]. Due to the lack of specific early symptoms, the majority of the patients are diagnosed at an advanced disease stage with already established metastasis. Moreover, mostly due to the lack of targetable molecular alterations, surgical removal and conventional chemotherapy are the only available treatment options for PDAC patients [1].

Although a number of driver mutations have been identified in PDAC tumors in addition to several tumor suppressors [CDKN2A (cyclin-dependent kinase inhibitor 2A), TP53 (tumor protein p53)] and the predominant KRAS (Kirsten Rat Sarcoma) mutations, the percentage of patients with therapeutically targetable mutations is low [2]. One exception is the relatively rare BRCA1/2 (Breast Cancer type 1/2 susceptibility protein) mutation which renders tumor cells sensitive to PARP [Poly (ADP-ribose) polymerase] inhibitors [3]. Furthermore, PDACs are generally stroma-rich, "cold" tumors with low immunogenicity, in which immunotherapeutic modalities provide no clinical benefit [4] with the exception of the rare occurrence of MMR deficiency which results in sensitivity to immunotherapy [5].

Approximately 90% of PDAC tumors harbor an activating mutation in the KRAS proto-oncogene [6], among which the most frequently present is the G12D mutation at ~50%, G12V at ~30% and G12R at 10% while other mutations do not reach the frequency of 5% [7]. In PDAC, G12D mutant KRAS is considered to be a major driver in contrast to lung or colorectal cancer [8]. Mutant KRAS has long been considered "undruggable" due to its compact structure and specific molecular properties, but the recent introduction of allele-specific inhibitors has challenged this label [9]. Covalent inhibitors of the G12C mutant KRAS have already been approved for clinical application [10]. Nevertheless, the vast majority of G12C mutations are mainly linked to lung adenocarcinoma [7]. Clinically available therapeutic options for tumors with other forms of KRAS mutations are yet to be developed. Notably, there are several established KRAS G12D inhibitors available, and even the first reports on the possibility of covalent targeting of KRAS G12D have been published [11]. Among the new KRAS G12D inhibitors, MRTX1133 is the first-in-class specific, non-covalent inhibitor of the KRAS G12D oncoprotein [12]. This small-molecule inhibitor shows high selectivity for the G12D form of KRAS over the wild-type protein, preventing effector protein binding and blocking subsequent cell signaling activation [13]. MRTX1133 can inhibit the viability of KRAS G12D mutation harboring cell lines at nanomolar concentrations and it also shows potent *in vivo* activity [13].

The treatment of KRAS-mutant tumors has been dramatically shifted with recent advances in targeted therapies. However, evidence of acquired or *de novo* resistance to covalent G12C inhibitors has already been demonstrated, with only approximately 40% of patients showing partial response to KRAS-targeting monotherapies in lung adenocarcinoma and less than 20% in colorectal cancer [14]. Several resistance mechanisms have been already described, ranging from new mutations in the KRAS gene to the rewiring of the tumor cells' signalization network [14, 15]. The latter is most evident in the feedback reactivation of RAS signaling by wild-type RAS proteins (HRAS, NRAS, or the wild-type KRAS allele in the case of heterozygous KRAS mutations) [15]. Additionally, resistance mechanisms revealed in KRAS G12C mutant tumors have been observed following MRTX1133 treatment in G12D mutant cancer models. Upstream activation of ERBB (erythroblastic leukemia viral oncogene homolog) receptors after MRTX1133 exposure has also been shown in colorectal and pancreatic cancers, leading to sustained wild-type RAS signaling [16–18]. Upregulation of mammalian target of rapamycin (mTOR) signaling, epithelial-to-mesenchymal transitions, or specific gene amplifications have also been observed [19].

Thus, several combination approaches have been proposed, most of which focus on the concomitant targeting of mutant KRAS and reactivation of wild-type RAS signaling. These include the combination of KRAS G12C inhibitors with therapeutic modalities targeting upstream elements of the RAS pathway like EGFR (epidermal growth factor receptor) -blocking antibodies or SOS1 (son of sevenless 1) inhibitors in addition to targeting SHP2 (Src homology 2-containing protein tyrosine phosphatase 2), which is also a positive modulator of RAS signaling [20]. The application of immunomodulatory therapies, cell cycle inhibitors, or horizontal targeting of the PI3K-AKT pathway in combination with KRAS G12C inhibitors is also being investigated [20]. As the more effective, covalent targeting of G12D is much harder than in the case of the G12C mutant KRAS, and the first-in-class drug MRTX1133 is also a non-covalent drug, the application of combinational therapy seems to be rational.

Our group has previously shown that the combination of KRAS G12C inhibitors with farnesyl-transferase inhibitors exerts synergistic anti-tumoral effects in several KRAS G12C tumor models, including pancreatic tumor cells [21]. As farnesylation is a key post-translational modification of multiple important regulatory proteins, the addition of farnesyl-transferase inhibitors appears to integrate the advantages of agents used in various KRAS combination therapies. These include inhibition of feedback reactivation of HRAS, horizontal targeting of the PI3K-AKT pathway by RHEB (ras homolog enriched in brain), and cell cycle arrest by inducing defects in the nuclear lamina and CENPE/F (centromere associated protein E/F) proteins [21].

Here, we describe that this combination strategy facilitates the anti-tumoral activity of KRAS G12D inhibition and successfully breaks down therapeutic resistance in pancreatic adenocarcinoma.

Materials and methods

Cell culture conditions

PANC1, ASPC1, and SW1990 human pancreatic adenocarcinoma cell lines were obtained from ATCC (The American Type Culture Collection). Cells were cultured in normal tissue culture flasks in DMEM (Dulbecco's Modified Eagle's Medium) (Capricorn Scientific, Germany, Ebsdorfergrund) supplemented with 10% FBS (fetal bovine serum) (Euroclone, Italy, Pero) and 1% Penicillin-Streptomycin cocktail (Biosera, France, Cholet) in atmospheric O_2 and 5% CO_2 level at 37°C in a cell culture incubator in a humidified atmosphere.

SRB assay

On the first day of the experiment, cells at 80%–90% confluence were trypsinized (Capricorn Scientific, Germany, Ebsdorfergrund) and counted using a Luna II Automated Cell Counter (Logos Biosystems, South Korea, Anyang). Cells were seeded at a density of 2,500–5,000 cells/well in 300 µL on a 48-well plate depending on the growth rate of each cell line. The next day, an additional 100 µL of medium containing four times the final concentration of MRTX1133 (Medchemexpress, Sweden, Sollentuna) was added to the wells. After a 6-day treatment, the wells were washed with DPBS (Dulbecco's Phosphate Buffered Saline Solution) (Capricorn Scientific, Germany, Ebsdorfergrund) and the cells were fixed with 10% trichloroacetic acid (TCA) (Reanal, Hungary, Budapest) for 1 h at 4°C. After fixation, TCA was removed, and the wells were serially washed with tap water followed by 15 min of incubation with 0.04% SRB (Sulforhodamine B) dye (Merck, Germany, Darmstadt) dissolved in 1% acetic acid. After staining the cells with SRB, the excess dye was removed, and the cells were washed with 1% acetic acid. Cell-bound SRB was then dissolved in 10 mM Tris buffer and was measured using a Biotek EL800 spectrophotometer (Agilent, United States, Santa Clara) at a wavelength of 570 nm. Measurement data were averaged and normalized using control values and graphed using GraphPad Prism 5 software (GraphPad Software, United States, Boston). Each treatment group contained 3 technical replicates, and the experiments were carried out in 3 independent biological replicates.

2D combination tests

For 2D combination tests, PANC1 cells were trypsinized, counted, and seeded onto 48-well plates at a density of 2,500 cells/well. The next day, following the attachment of cells, the wells were treated with fresh medium containing MRTX1133 (Medchemexpress, Sweden, Sollentuna) and tipifarnib (Medchemexpress, Sweden, Sollentuna) at various concentrations and their combinations for 6 days. At the end of the treatment, cells were fixed and quantified as described in the SRB assay section. The experiments were carried out in 3 independent biological replicates.

3D combination tests

3D combination tests were performed as previously described [21]. Briefly, PANC1 cells were seeded at 1,000 cells/well on the inner 60 wells of a polyHEMA-coated [Poly (2-hydroxyethyl methacrylate)] (Merck, Germany, Darmstadt) round bottom 96-plate, and left for spheroid formation for a week. Following the formation of regular, compact spheroids 150 µL of fresh medium was added to the cells containing MRTX1133 and tipifarnib alone or in combination at various concentrations for 6 days. On the last day of the experiment, 10 µL of CCK8 reagent (Cell counting kit 8) reagents (Merck, Germany, Darmstadt) were added to each well containing the spheroids and to blank wells. After 24 h of incubation, the optical density was measured using a Biotek EL800 spectrophotometer (Agilent, United States, Santa Clara) at a wavelength of 450 nm. Values for blank wells were extracted from each data set, which were later normalized to control wells and plotted using GraphPad Prism 5 software (GraphPad Software, United States, Boston). Each treatment group contained 3 technical replicates, and the experiments were carried out in 3 independent biological replicates.

Western blot analyses

Activation of proteins in the PI3K/Akt pathway or the RAF/MEK/ERK cascade along with expression of regulatory proteins and apoptosis/proliferation markers were investigated by Western blot analysis. Briefly, cells were seeded at a density of 300,000 cells/well in 6-well plates and were treated on the next day with 100 nM MRTX1133 (Medchemexpress, Sweden, Sollentuna) and/or 500 nM tipifarnib (Medchemexpress, Sweden, Sollentuna) for 48 h. Following treatment, wells were washed with DPBS (Capricorn Scientific, Germany, Ebsdorfergrund), and cells were fixed with 6% TCA (Reanal, Hungary, Budapest) for 1 h at 4°C. Following fixation, cells were mechanically harvested and centrifuged at 10,000 RCF (relative centrifugal force) for 10 min. The supernatant was then discarded and the centrifuged protein was dissolved in a modified Läemmli-type sample buffer containing 0.02% bromophenol blue (Merck, Germany, Darmstadt), 10% glycerol (Merck, Germany, Darmstadt), 2% SDS (sodium-dodecyl-sulfate) (Merck, Germany, Darmstadt), 100 mM dithiothreitol (DTT) (Merck, Germany, Darmstadt), 5 mM EDT (Merck, Germany, Darmstadt) A, 125 mg/mL urea (Merck, Germany, Darmstadt), 90 mM Tris-HCl, pH 7.9. For the determination of protein concentration, a Qubit 4 fluorometer (Thermo Fisher Scientific,

United States, Massachusetts, Waltham) was used according to the manufacturer's recommendations. For electrophoretic separation, equal amounts of protein (25 μg/lane) were loaded onto 10% polyacrylamide gels (Bio-Rad Laboratories, United States, California, Hercules). The separated proteins were transferred to PVDF (polyvinylidene fluoride) membranes (Thermo Fisher Scientific, United States, Waltham).

Analyses of protein expression/activation were performed using the following antibodies: p-AKT (4058) (Cell Signaling Technology, United States, Massachusetts, Danvers), AKT (9272) (Cell Signaling Technology, United States, Massachusetts, Danvers), p-S6 (2215) (Cell Signaling Technology, United States, Massachusetts, Danvers), S6 (2217) (Cell Signaling Technology, United States, Massachusetts, Danvers), p-ERK1/2 (9101) (Cell Signaling Technology, United States, Massachusetts, Danvers), ERK1/2 (9102) (Cell Signaling Technology, United States, Massachusetts, Danvers), RHEB (13879S) (Cell Signaling Technology, United States, Massachusetts, Danvers), PARP (9542) (Cell Signaling Technology, United States, Massachusetts, Danvers),p-Histone H3 (9701) (Cell Signaling Technology, United States, Massachusetts, Danvers), (Cell Signaling Technology, United States, Danvers) KRAS4B (WH0003845M1) (Merck, Germany, Darmstadt), and HRAS (18295-1-ap) (Proteintech, United Kingdom, Manchester). All antibodies were dissolved according to the manufacturer's instructions in 5% BSA or dried milk in 1x TTBS (tris-buffered saline supplemented with 1% Tween80) buffer. Membranes were blocked in Everyblot buffer (Bio-Rad Laboratories, United States, California, Hercules) for 5 min at room temperature. Following blocking, the membranes were incubated in primary antibodies overnight at 4°C. Horseradish peroxidase (HSP) conjugated rabbit or mouse secondary antibodies (Cell Signaling Technology, United States, Massachusetts, Danvers) (1:5,000, 1 h, room temperature), and WesternBright ECL (Advansta, United States, California, San Jose) were used for visualization with light-sensitive films. For total proteins, membranes were stripped by boiling in distilled water. Ponceau staining was used for normalization. Quantification was performed using ImageLab software (Bio-Rad Laboratories, United States, California, Hercules). Each cell line was analyzed in 3 biological replicates.

Cell cycle investigation

Determination of DNA content in each cell was used to evaluate the number of cells in each cell cycle phase as previously described [21]. Briefly, 500 nM tipifarnib (Medchemexpress, Sweden, Sollentuna), 100 nM MRTX1133 (Medchemexpress, Sweden, Sollentuna), or their combination were used for a 96-hour-long treatment. Cells were trypsinized, fixed with ice-cold 70% ethanol and lysed, followed by DAPI (4′,6-diamidino-2-phenylindole) (Chemometec, Denmark, Allerod) staining for 5 min at 37°C. A stabilization buffer was then added, and 10 μL of each sample was loaded onto an 8-well NC slide (Chemometec, Denmark, Allerod). NucleoCounter NC-3000™ system (Chemometec, Denmark, Allerod) was used for quantification of cellular fluorescence (Figure 1).

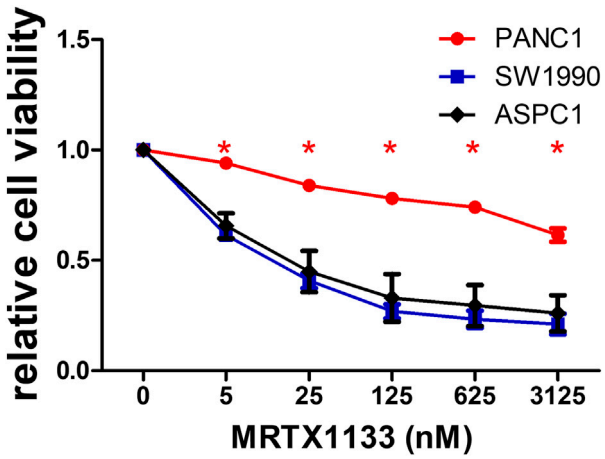

FIGURE 1
2D cell viability data of pancreatic adenocarcinoma cell lines. Cells were treated with various concentrations of MRTX1133 for 6 days. Control-normalized data show the resistant PANC1 cell line and the sensitive SW1990 and ASPC1 cells. Data were derived from three independent experiments and graphed using GraphPad Prism 5 (n = 3, average ± SEM). Asterisks mark significant differences ($p < 0.05$) measured by two-way ANOVA with Bonferroni post-test, comparing viability data of SW1990 and ASPC1 to PANC1.

Results

Sensitivity of pancreatic adenocarcinoma cells to MRTX1133 treatment

Three KRAS G12D mutant human pancreatic adenocarcinoma cell lines were tested in conventional 2D cultures for sensitivity to MRTX1133, a specific non-covalent inhibitor of the KRAS G12D protein. While two of them (SW1990 and ASPC1, both harboring a homozygous KRAS G12D mutation) showed high sensitivity to MRTX1133 (IC50 values are 11 and 21 nM, respectively), heterozygous PANC1 was found to be highly resistant (IC50 > 3,125 nM).

Changes in KRAS-related signaling after MRTX1133 treatment

Next, we examined changes in KRAS-related signaling following 48 h of treatment with 100 nM MRTX1133. Strong

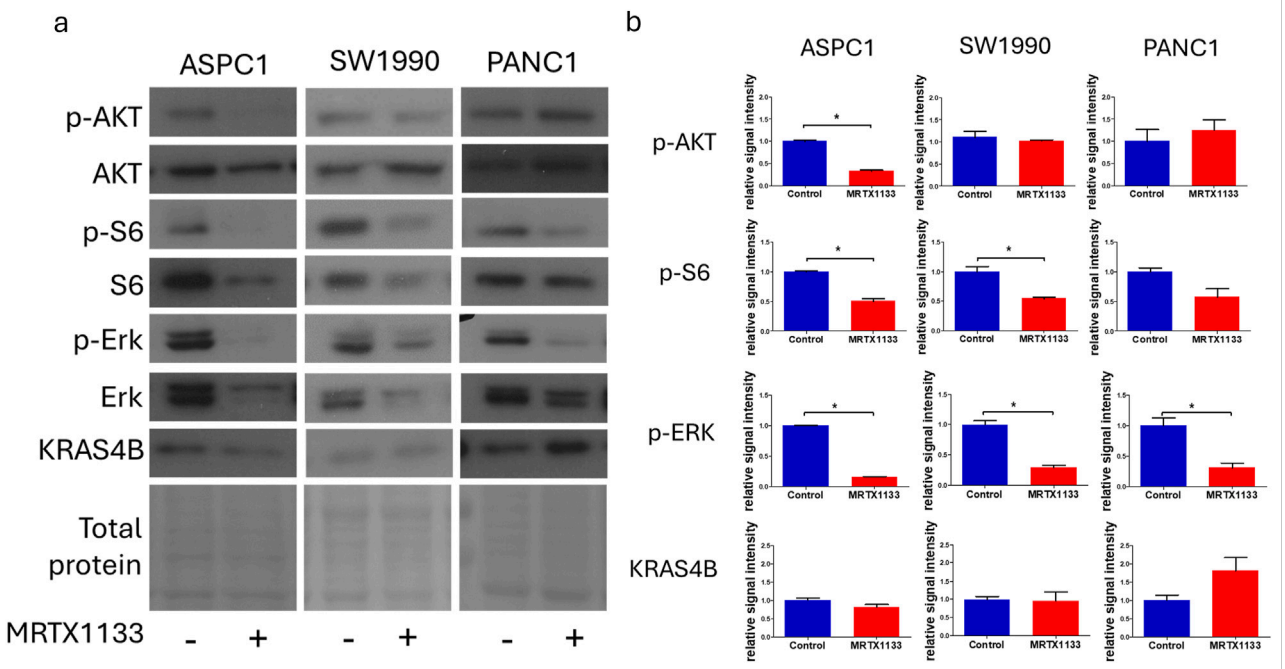

FIGURE 2
Changes in cell signaling after MRTX1133 treatment. Cells were treated with 100 nM MRTX1133 for 48 h. RAS-related cell signaling was determined by Western blotting. **(A)** Representative bands of the proteins investigated. Activated, phosphorylated proteins are marked with the "p-" prefix. **(B)** Densitometric evaluation of the activation or expression of the represented proteins. Data were normalized to total protein level and expressed relative to control using GraphPad Prism 5 software (±SEM). Data are derived from three independent experiments. Asterisks mark significant differences ($p < 0.05$) as determined by an unpaired t-test.

inhibition of ERK activation could be observed in all cell lines, independently of cell sensitivity data, and a more modest, but still pronounced reduction in S6 phosphorylation in all cell lines tested, although the reduction in the PANC1 cell was not statistically significant ($p = 0.11$) (Figure 2). Interestingly, activation of AKT, an upstream member of the PI3K-AKT-mTOR signaling pathway of which S6 is a downstream element, was significantly reduced in the ASPC-1 cell line after MRTX1133 treatment. Importantly, the expression level of KRAS4B was elevated in the MRTX1133-resistant PANC1 cell line following treatment, although this increase was not statistically significant ($p = 0.17$).

A combination of farnesyl-transferase inhibitors with MRTX1133 shows synergistic anti-tumoral effects in the resistant cell line

We also focused on the PANC1 cell line, which showed high resistance to KRAS targeting. Previously, we had demonstrated the synergistic effects of farnesyl-transferase inhibitors with KRAS G12C inhibitors, so we investigated whether they could potentiate the effect of MRTX1133 to break down resistance. Notably, the combination of tipifarnib with MRTX1133 resulted in strong synergistic anti-tumor effects with a Loewe synergy score of 12 based on the website[1] (Figure 3) [22]. Synergy scores greater than 10 are considered to have synergistic effects. Notably, the synergy map revealed that the highest synergy occurred when low-dose tipifarnib and high-dose MRTX1133 were applied. Additionally, combining an alternative farnesyl-transferase inhibitor, lonafarnib, with MRTX1133 also resulted in an average Loewe synergy score of 6.182. Of note, the combination of MRTX1133 with high-dose lonafarnib showed strong synergistic interactions as visualized in the synergy map in Supplementary Figure S1.

PANC1 cells showed enhanced sensitivity to single agent MRTX1133 in 3D spheroid model

Next, we intended to examine the effects of single and combination treatment in a more complex, spheroid-based

1 https://synergyfinder.org

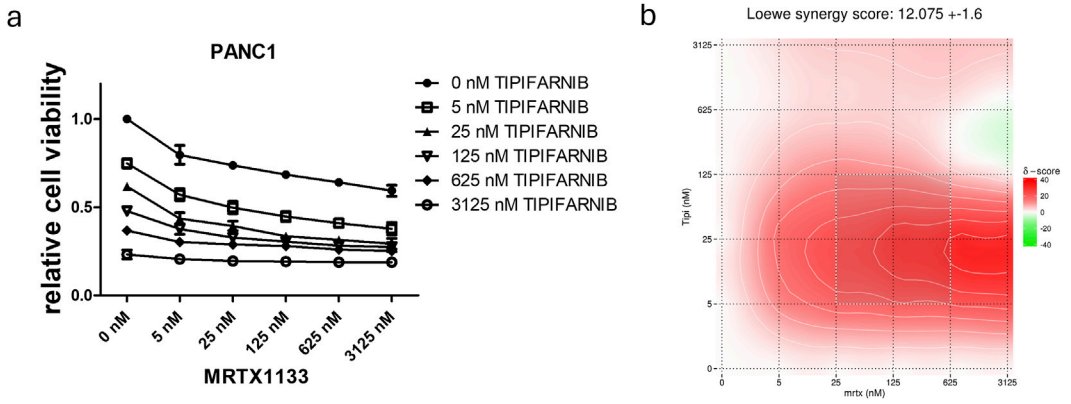

FIGURE 3
Combination of farnesyl-transferase inhibition with KRAS G12D targeting in MRTX1133 resistant PANC1. 6-day combination therapy of tipifarnib and MRTX1133 was applied to 2D cultures of PANC1 cells. **(A)** Control-normalized viability values. Data are derived from three independent experiments and are expressed relative to control (n = 3, ±SEM) **(B)** Synergy map calculated from viability results using synergyfinder.org. In general, a synergy score greater than 10 is considered to have synergistic effects. Note that the most synergistic area is at low dose tipifarnib and high dose MRTX1133.

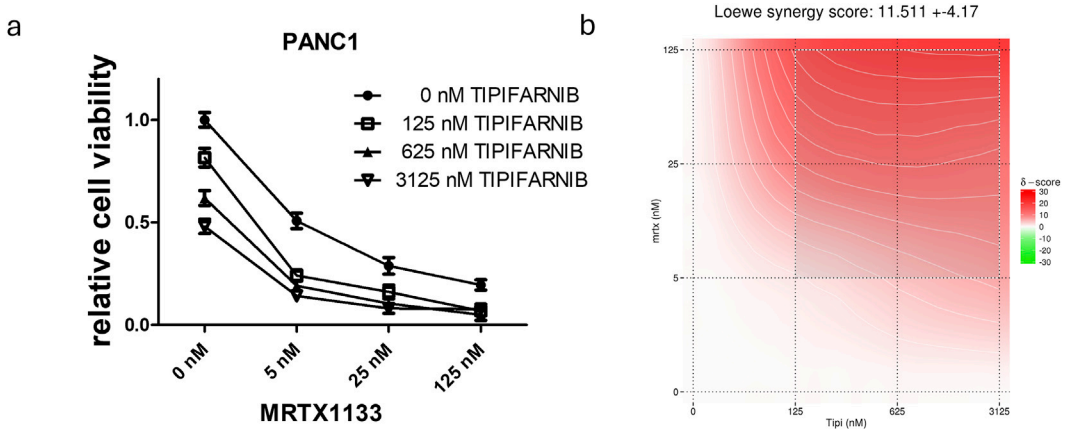

FIGURE 4
Combination of farnesyl-transferase inhibition with KRAS G12D targeting in PANC1 spheroids. A 6-day-long combination therapy of tipifarnib and MRTX1133 was applied to spheroid cultures of PANC1 cells. **(A)** Control-normalized viability values. Data are derived from three independent experiments and are expressed relative to control (n = 9, ±SEM) **(B)** Synergy map calculated from viability results using synergyfinder.org. Generally, a synergy score greater than 10 is considered to have synergistic effects. Note that the most synergistic area is at high dose tipifarnib and high dose MRTX1133.

model in a 3D environment. Notably, we observed that sensitivity to MRTX1133 already as a single agent was greatly enhanced (Figure 4). Changes in MRTX1133 sensitivity could not be tested in the SW1990 and ASPC1 cell lines, as these cells did not show growth in 3D conditions in our settings (data not shown). The combination of MRTX1133 with tipifarnib resulted in synergistic drug interactions in 3D conditions with a Loewe synergy score of 11.5.

Changes in RAS-related cell signaling in PANC1 cells after combination therapy

We also investigated the effects of combination therapy on RAS signaling (Figure 5). As described above, MRTX1133 single-agent treatment strongly reduced the activation of S6 and ERK but evoked no change in the phosphorylation of AKT. Interestingly, both tipifarnib alone and in combination with

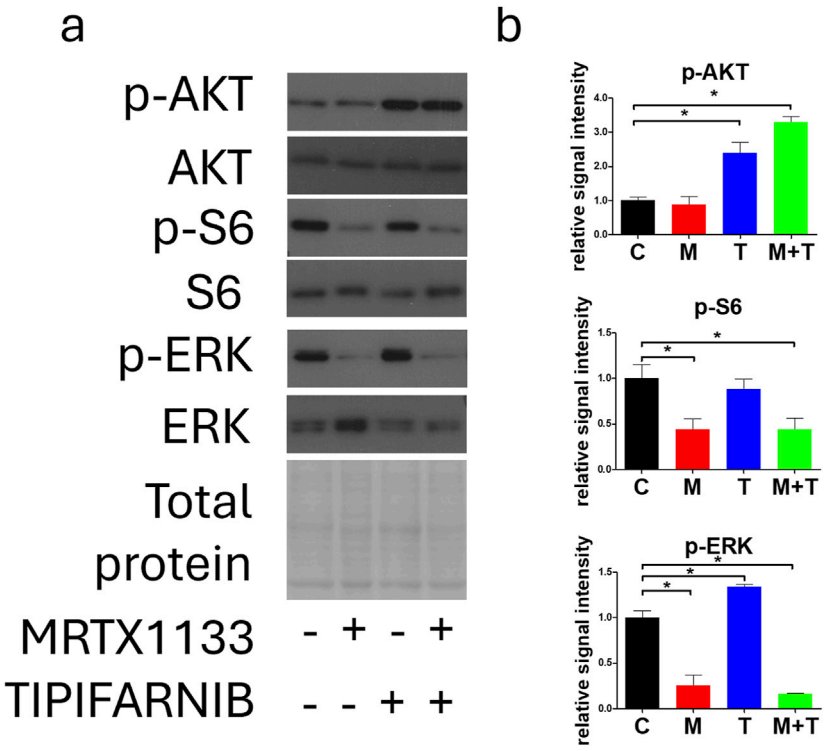

FIGURE 5
Changes in cell signaling after MRTX1133 (M), tipifarnib (T), or combination treatment (M+T). PANC1 cells were treated with 100 nM MRTX1133 and 500 nM tipifarnib alone or in combination for 48 h. RAS-related cell signaling was determined by Western blotting. **(A)** Representative bands of the proteins investigated. Activated, phosphorylated proteins are marked with the "p-"prefix. **(B)** Densitometric evaluation of the activation of the represented proteins. Data were normalized to total protein and expressed relative to the control and graphed with GraphPad Prism 5 software ("C", ±SEM). Data are derived from three independent experiments. Asterisks mark significant differences ($p < 0.05$) tested with one-way ANOVA followed by Bonferroni's Multiple Comparison test comparing treatment groups to control samples.

MRTX1133 strongly increased AKT phosphorylation in PANC1 cells. Tipifarnib alone significantly increased ERK phosphorylation but it did not alter S6 activation. Combination treatment substantially reduced both S6 and ERK activation.

Effects of combination therapy on apoptosis, proliferation, and farnesylation in PANC1 cells

Next, we examined the effect of MRTX1133, tipifarnib, and combination therapy on apoptosis induction, proliferation, and changes in farnesylation of RAS family members in the PANC1 cell line. Notably, no apoptosis could be detected based on the complete absence of cleaved PARP in all the treatments (Figure 6). We found that the expression of p-Histone H3, a known marker of M-phase cells, was drastically reduced with MRTX1133 treatment. Combination treatment also reduced p-Histone H3 expression, although this change was not statistically significant. Interestingly, tipifarnib treatment caused a visible (but not statistically significant) increase in the levels of p-Histone H3. Notably, tipifarnib and the combination induced an upward shift in HRAS and RHEB proteins, which is a well-known sign of farnesylation inhibition. KRAS farnesylation was not affected by any of the treatments as expected. However, clear trends, although not statistically significant could be observed in changes in KRAS expression, where combination therapy reduced the mean level of total KRAS, in contrast to the slight increase seen with MRTX1133 monotherapy.

Effects of combination therapy on cell cycle distribution of PANC1 cells

Next, we examined the effects of combination therapy on cell cycle distribution after a 96-hour treatment. We observed significantly reduced cell numbers after MRTX1133 and combination treatment, consistent with the results of the 2D and 3D combination tests (Figure 7A). However, only numerical, statistically insignificant changes could be observed in the

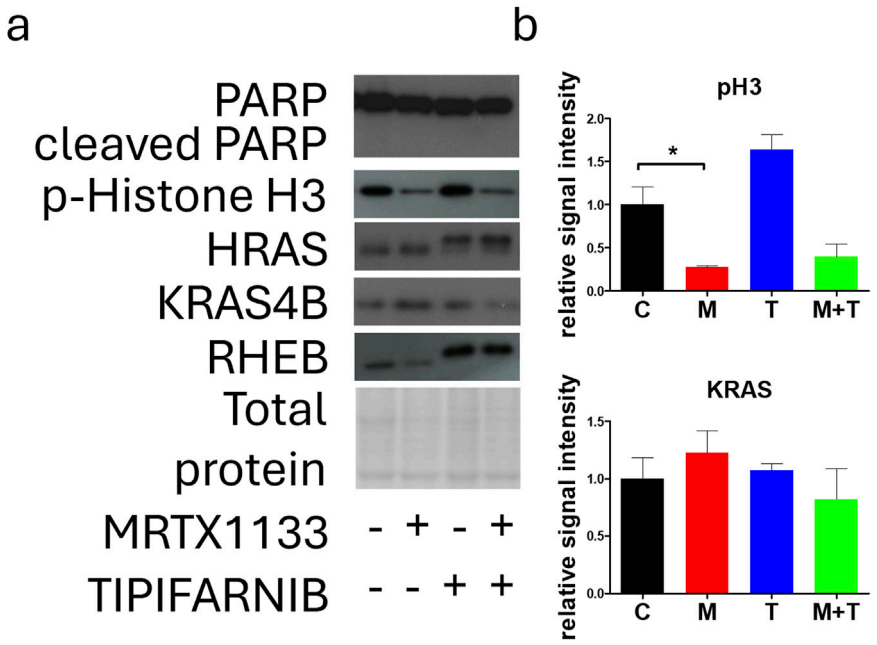

FIGURE 6
Effects of MRTX1133 (M), tipifarnib (T), or combination(M+T) treatment on apoptosis, proliferation, and farnesylation. PANC1 cells were treated with 100 nM MRTX1133, 500 nM tipifarnib, or their combination for 48 h. RAS-related cell signaling was determined by Western blotting. **(A)** Representative bands of the proteins investigated. **(B)** Densitometric evaluation of the activation or expression of the represented proteins. Data were normalized to total protein and expressed relative to the control (C) and graphed with GraphPad Prism 5 software (n = 3, ±SEM). Data are derived from three independent experiments. Asterisks mark significant differences ($p < 0.05$) tested with one-way ANOVA followed by Bonferroni's Multiple Comparison test comparing treatment groups to control samples.

distribution of cells within distinct cell cycle phases. MRTX1133 monotreatment and combination treatment slightly, but not statistically significantly reduced the ratio of S-phase cells and increased the ratio of subG1 cells. Tipifarnib treatment induced no change in cell cycle distribution (Figure 7B). Interestingly, when we investigated the morphology of the DAPI-stained nuclei, we observed a mixed population of PANC1 cells in the control group exhibiting mainly smaller nuclei, in addition to a population of larger, presumably tetra-or polyploid cells. MRTX1133 treatment almost completely eliminated the latter fraction and induced a doughnut-like nuclear morphology that was previously linked with mitotic defects [23]. Notably, tipifarnib and combination treatment resulted in aberrant, lobed, and segmented nuclear morphology (Figure 7C).

Discussion

In the past few years, intensive work by the research community has led to breakthroughs in the treatment of KRAS-mutant cancers, especially in the G12C mutant form [20]. KRAS was considered undruggable due to its compact form, picomolar affinity for GTP (Guanosine-5′-triphosphate), and high homology between the different RAS genes [20]. Therefore, an activating mutation in this proto-oncogene simply served as an exclusion criterion for any targeted therapy, like EGFR-targeting agents [7]. Thus, the development of allele-specific inhibitors of KRAS represents a major step forward, especially considering the positive responses to these agents observed in the clinic. Although these clinically observed anti-tumoral activities are unprecedented in treating KRAS mutant tumors, the majority of patients still show intrinsic resistance to KRAS inhibitors [14]. For this reason, combination settings are urgently needed to break down resistance and to increase the number of patients that show response. Accordingly, various combination therapies are being tested, including the combination of KRAS G12C inhibitors with EGFR, SOS1, SHP2, and cell cycle inhibitors or horizontal targeting of the AKT-mTOR pathway, the majority of which are currently being investigated in clinical trials [20].

Recently, we have shown that the combination of farnesyl-transferase inhibition with KRAS G12C inhibitors results in synergistic antitumoral effects, independent of the tissue of origin in 2D, 3D, and *in vivo* models [21]. We have demonstrated that the addition of farnesyl-transferase inhibitors to KRAS targeting interferes with multiple signaling mechanisms, like feedback reactivation of RAS signaling through

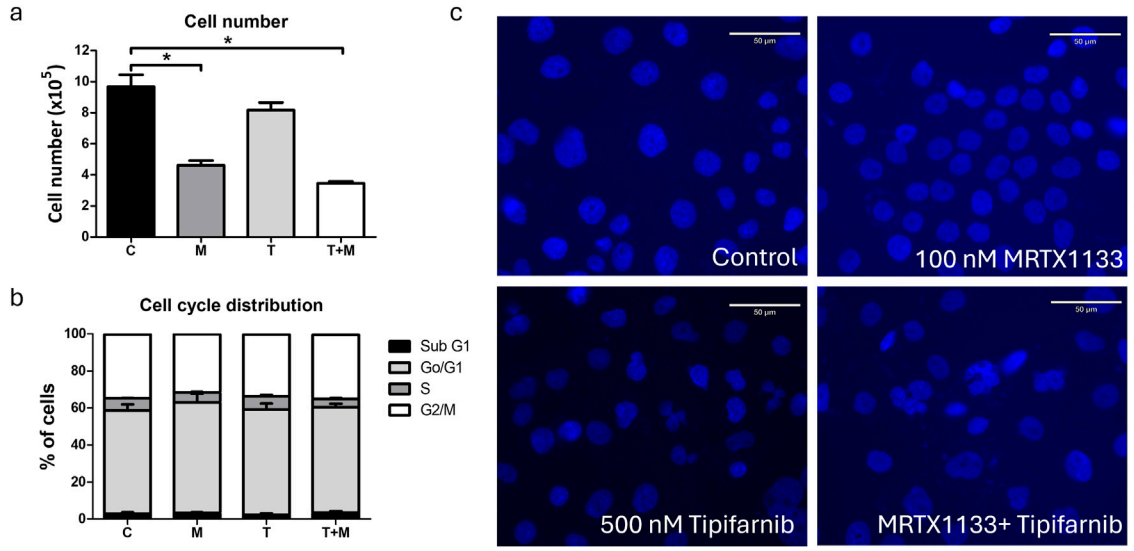

FIGURE 7
Effects of MRTX1133 (M), tipifarnib (T), or combination (M+T) treatment on cell cycle distribution. Cells were treated with 100 nM MRTX1133, 500 nM tipifarnib, or their combination for 96 h **(A)** Changes in total cell number following treatment. **(B)** Cell cycle distribution of cells following treatment. MRTX1133 and combination therapy reduced the ratio of cells in the S-phase, although these changes are not statistically significant. **(C)** Morphology of cell nucleus following 96 h of treatment. Note the aberrant nuclear morphology after tipifarnib or combination treatment. Scale bar = 50 µm. Data shown in the graphs are derived from three independent experiments and are expressed as mean ± SEM. Asterisks mark significant differences ($p < 0.05$) tested by one-way ANOVA followed by Bonferroni's Multiple Comparison test comparing treatment groups to control samples.

wild-type HRAS proteins, AKT-mTOR signaling by blockade of farnesylated RHEB, or blocking cell cycle progression by interfering with the laminar network and farnesylation of CENPE/F [21]. Notably, most of these mechanisms overlap with the currently investigated combinational approaches targeting oncogenic and wild-type RAS signaling in parallel (KRAS G12C inhibitors plus EGFR, SOS1, or SHP2 targeting) or with inhibitors of the cell cycle or the AKT-mTOR pathway [15, 20].

Here, we have demonstrated that the application of tipifarnib, one of the most potent farnesyl-transferase inhibitors results in synergistic anticancer effects in combination with KRAS G12D targeting pancreatic adenocarcinoma cells that have been shown to be therapy-resistant under 2D conditions.

In our panel of pancreatic adenocarcinoma cell lines, PANC1, a well-known model of human PDAC, showed resistance to MRTX1133 single agent treatment (IC50 > 3,000 nM) in contrast with ASPC1 (IC50 = 21.9 nM) and SW1990 (IC50 = 11.6 nM). In assessing changes in RAS-related signaling after MRTX1133 treatment, we observed strong inhibition of ERK and S6 activation, key members of the two most-studied RAS-regulated pathways. The most unique - although not statistically significant - change in the therapy-resistant cell line was the elevation in KRAS expression after the MRTX1133 application. As this phenomenon could not be observed in the other cell lines, it may reflect a compensatory resistance mechanism.

Next, we sought to examine whether combining tipifarnib with MRTX1133 could overcome the resistance of the PANC1 cell line *in vitro*. Notably, the combination therapy in the 2D model resulted in synergistic anti-cancer effects with a Loewe score of 12. The strongest effect could be seen when the highest MRTX1133 dose was combined with a lower tipifarnib concentration. Additionally, the combination of MRTX1133 with lonafarnib, an alternative farnesyl-transferase inhibitor, also showed synergistic drug interactions, especially at higher FTi concentrations.

We also evaluated the efficacy of combination therapy in PANC1 tumor spheroids. In line with previous findings by others [24], we observed a dramatic change in sensitivity to KRAS targeting when we compared 2D to 3D conditions, more specifically, from IC50 > 3,000 nM in 2D conditions to IC50 = 4.8 nM in the 3D environment. Differential effects of 3D compared to 2D culture conditions are a well-known phenomenon in preclinical cancer research and 3D culture is considered to be more representative of the *in vivo* situation [25, 26]. Notably, it has been shown that culturing cells in spheroids enhances the effects of chemotherapeutic agents [27], or sensitizes towards KRAS targeting [24, 28]. We also have demonstrated in our previous work that KRAS G12C mutant models are more prone to direct KRAS targeting in 3D or *in vivo*

compared to 2D monoculture [21]. Unfortunately, the other 2 cell lines were not able to grow into spheroids in our settings, therefore the sensitivity of PANC1 to MRTX1133 could not be directly compared to them in 3D.

Still, the addition of tipifarnib resulted in synergism with a Loewe score of 11.5, although the most synergistic area in the synergy map visualizing synergy scores has shifted to higher tipifarnib concentrations combined with higher MRTX1133 doses.

Examination of RAS signaling revealed that tipifarnib and combination therapy elevated the level of activated AKT while reducing the phosphorylation of S6, which is a downstream target of AKT. This phenomenon can be partly explained by inhibition of RHEB farnesylation as well as crosstalk between the RAS/MEK/ERK pathway and the PI3K-AKT-mTOR signaling [29]. Indeed, we demonstrated that tipifarnib and combination therapy successfully blocked RHEB farnesylation, leading to the accumulation of its non-farnesylated, non-functional form. ERK activation was also significantly increased after tipifarnib treatment; however, combination therapy reduced ERK phosphorylation similar to MRTX1133 monotherapy.

Investigation of HRAS revealed that tipifarnib and combination therapy depleted functional, farnesylated HRAS by interfering with its farnesylation. Previously, we have shown that KRAS targeting results in compensatory reactivation of wild-type RAS proteins, more specifically, overactivation of HRAS induced by KRAS G12C inhibitors [21]. Thus, successful inhibition of its farnesylation can also abrogate this resistance mechanism in KRAS G12D targeting.

We also assessed changes in KRAS expression, although this protein is not sensitive to farnesylation inhibition due to alternative geranyl-geranylation [30]. In line with this, no upward shift could be observed after farnesyl-transferase inhibitor treatment. Interestingly, although not statistically significant, visible trends in changes in KRAS expression could be observed, with the combination treatment reducing KRAS levels not only compared to MRTX1133 monotherapy, which increased them, but also compared to the control. Although the mechanism behind this phenomenon is not known, it may contribute to the observed synergy between the two drugs.

No apoptosis could be detected in any of the treatments based on the level of cleaved PARP. This could be explained by the fact that PANC1 has homozygous mutations in TP53 (p.Arg273His), a key regulator of apoptosis. Interestingly, the expression of p-Histone H3, a known marker of M-phase cells was decreased by MRTX1133 and combination therapy (the latter change was not statistically significant), whereas tipifarnib monotherapy slightly increased its expression. This finding is in line with our previous observation, where we showed that farnesyl-transferase inhibition leads to defects in cell division, leading to the accumulation of M-phase cells [21]. Interestingly, when we analyzed the cell cycle distribution after a longer, 96-hour treatment, we observed a decrease in the S-phase cell ratio after MRTX1133 and combination therapy, with a more pronounced effect of the latter. In line with our previous findings, we found that tipifarnib and combination therapy led to an accumulation of cells with aberrant, segmented nuclear morphology, indicating defects in the mitotic process [21].

In summary, we have demonstrated that MRTX1133 sensitivity shows high variability in KRAS G12D mutant pancreatic adenocarcinoma models in 2D culture. Further investigation of the resistant cell model revealed that the addition of a farnesyl-transferase inhibitor to MRTX1133 can abrogate this resistance, leading to synergistic antitumoral effects. Interestingly, culturing cells in spheroid culture dramatically sensitized resistant cells to MRTX1133 treatment. Nevertheless the synergistic effects of combination treatment are also maintained in the 3D environment.

Regarding the mechanisms behind the synergistic effects, we identified elevated KRAS expression after MRTX1133 treatment, which was ultimately decreased by combination therapy. Additionally, similar to our previous observations, we found that inhibition of farnesylation of RHEB and HRAS may contribute to synergistic effects.

Our findings warrant further investigation of the applicability of KRAS G12D targeting in combination with farnesyl-transferase inhibitors in KRAS G12D mutant pancreatic adenocarcinoma.

Data availability statement

The raw data supporting the conclusions of this article will be made available by the authors, without undue reservation.

Ethics statement

Ethical approval was not required for the studies on humans in accordance with the local legislation and institutional requirements because only commercially available established cell lines were used.

Author contributions

EM, MB, KSz, BH, and JTí conceived, designed and supervised the study. EM, MB, KSz, BH, JTó, and JTí analyzed and interpreted the data and wrote the manuscript. EM, MB, KSz, ZG, GP, and FB performed the 2D and 3D viability experiments and immunoblot studies. LH and BH performed the cell cycle experiments. Statistical analyses were carried out by MB, EM, KSz, and BH. The corresponding author had full access to all the data used in the study and had final responsibility for

the decision to submit the article for publication. All authors contributed to the article and approved the submitted version.

Funding

The author(s) declare that financial support was received for the research, authorship, and/or publication of this article. This study was supported by the Hungarian National Research, Development and Innovation Office (NVKP-16-1-2016-0020, 2020-1.1.6-JÖVŐ-2021-00004 and K147400).

Acknowledgments

The authors acknowledge financial support from the National Laboratories Excellence program [under the National Tumor Biology Laboratory Project (NLP-17, 2022-2.1.1-NL-2022-00010) and the Hungarian Thematic Excellence Program (project: TKP2021-EGA-44). The funders of the study had no role in the study design; the data collection, analysis, or interpretation; or the writing or submission of the report.

Conflict of interest

Author MB was employed by the company Kineto Lab Ltd.

The remaining authors declare that the research was conducted in the absence of any commercial or financial relationships that could be construed as a potential conflict of interest.

Supplementary material

The Supplementary Material for this article can be found online at: https://www.por-journal.com/articles/10.3389/pore.2024.1611948/full#supplementary-material

References

1. Wood LD, Canto MI, Jaffee EM, Simeone DM. Pancreatic cancer: pathogenesis, screening, diagnosis, and treatment. *Gastroenterology* (2022) 163(2):386–402 e1. doi:10.1053/j.gastro.2022.03.056

2. Hu HF, Ye Z, Qin Y, Xu XW, Yu XJ, Zhuo QF, et al. Mutations in key driver genes of pancreatic cancer: molecularly targeted therapies and other clinical implications. *Acta Pharmacol Sin* (2021) 42(11):1725–41. doi:10.1038/s41401-020-00584-2

3. Golan T, Hammel P. Management of BRCA mutation carriers with pancreatic adenocarcinoma. *J Natl Compr Canc Netw* (2021) 19(4):469–73. doi:10.6004/jnccn.2021.7031

4. Tran LC, Ozdemir BC, Berger MD. The role of immune checkpoint inhibitors in metastatic pancreatic cancer: current state and outlook. *Pharmaceuticals (Basel)* (2023) 16(10):1411. doi:10.3390/ph16101411

5. Wong W, Alouani E, Wei A, Ryu YK, Chabot JA, Manji GA. Future of immunotherapy in pancreas cancer and the trials, tribulations and successes thus far. *Semin Oncol* (2021) 48(1):57–68. doi:10.1053/j.seminoncol.2021.02.007

6. Kleeff J, Korc M, Apte M, La Vecchia C, Johnson CD, Biankin AV, et al. Pancreatic cancer. *Nat Rev Dis Primers* (2016) 2:16022. doi:10.1038/nrdp.2016.22

7. Timar J, Kashofer K. Molecular epidemiology and diagnostics of KRAS mutations in human cancer. *Cancer Metastasis Rev* (2020) 39(4):1029–38. doi:10.1007/s10555-020-09915-5

8. Temko D, Tomlinson IPM, Severini S, Schuster-Bockler B, Graham TA. The effects of mutational processes and selection on driver mutations across cancer types. *Nat Commun* (2018) 9(1):1857. doi:10.1038/s41467-018-04208-6

9. Liu P, Wang Y, Li X. Targeting the untargetable KRAS in cancer therapy. *Acta Pharm Sin B* (2019) 9(5):871–9. doi:10.1016/j.apsb.2019.03.002

10. Rathod LS, Dabhade PS, Mokale SN. Recent progress in targeting KRAS mutant cancers with covalent G12C-specific inhibitors. *Drug Discov Today* (2023) 28(5):103557. doi:10.1016/j.drudis.2023.103557

11. Zheng Q, Zhang Z, Guiley KZ, Shokat KM. Strain-release alkylation of Asp12 enables mutant selective targeting of K-Ras-G12D. *Nat Chem Biol* (2024) 20:1114–22. doi:10.1038/s41589-024-01565-w

12. Wei D, Wang L, Zuo X, Maitra A, Bresalier RS. A small molecule with big impact: MRTX1133 targets the KRASG12D mutation in pancreatic cancer. *Clin Cancer Res* (2024) 30(4):655–62. doi:10.1158/1078-0432.CCR-23-2098

13. Hallin J, Bowcut V, Calinisan A, Briere DM, Hargis L, Engstrom LD, et al. Anti-tumor efficacy of a potent and selective non-covalent KRAS(G12D) inhibitor. *Nat Med* (2022) 28(10):2171–82. doi:10.1038/s41591-022-02007-7

14. Ye W, Lu X, Qiao Y, Ou WB. Activity and resistance to KRAS(G12C) inhibitors in non-small cell lung cancer and colorectal cancer. *Biochim Biophys Acta Rev Cancer* (2024) 1879(3):189108. doi:10.1016/j.bbcan.2024.189108

15. Ryan MB, Coker O, Sorokin A, Fella K, Barnes H, Wong E, et al. KRAS(G12C)-independent feedback activation of wild-type RAS constrains KRAS(G12C) inhibitor efficacy. *Cell Rep* (2022) 39(12):110993. doi:10.1016/j.celrep.2022.110993

16. Gulay KCM, Zhang X, Pantazopoulou V, Patel J, Esparza E, Pran Babu DS, et al. Dual inhibition of KRASG12D and pan-ERBB is synergistic in pancreatic ductal adenocarcinoma. *Cancer Res* (2023) 83(18):3001–12. doi:10.1158/0008-5472.CAN-23-1313

17. Kataoka M, Kitazawa M, Nakamura S, Koyama M, Yamamoto Y, Miyazaki S, et al. Cetuximab enhances the efficacy of MRTX1133, a novel KRAS(G12D) inhibitor, in colorectal cancer treatment. *Anticancer Res* (2023) 43(10):4341–8. doi:10.21873/anticanres.16629

18. Feng J, Hu Z, Xia X, Liu X, Lian Z, Wang H, et al. Feedback activation of EGFR/wild-type RAS signaling axis limits KRAS(G12D) inhibitor efficacy in KRAS(G12D)-mutated colorectal cancer. *Oncogene* (2023) 42(20):1620–33. doi:10.1038/s41388-023-02676-9

19. Dilly J, Hoffman MT, Abbassi L, Li Z, Paradiso F, Parent BD, et al. Mechanisms of resistance to oncogenic KRAS inhibition in pancreatic cancer. *Cancer Discov* (2024) 14:2135–61. doi:10.1158/2159-8290.CD-24-0177

20. Punekar SR, Velcheti V, Neel BG, Wong KK. The current state of the art and future trends in RAS-targeted cancer therapies. *Nat Rev Clin Oncol* (2022) 19(10):637–55. doi:10.1038/s41571-022-00671-9

21. Baranyi M, Molnar E, Hegedus L, Gabriel Z, Petenyi FG, Bordas F, et al. Farnesyl-transferase inhibitors show synergistic anticancer effects in combination with novel KRAS-G12C inhibitors. *Br J Cancer* (2024) 130(6):1059–72. doi:10.1038/s41416-024-02586-x

22. Zheng S, Wang W, Aldahdooh J, Malyutina A, Shadbahr T, Tanoli Z, et al. SynergyFinder plus: toward better interpretation and annotation of drug combination screening datasets. *Genomics Proteomics Bioinformatics* (2022) 20(3):587–96. doi:10.1016/j.gpb.2022.01.004

23. Almacellas E, Pelletier J, Day C, Ambrosio S, Tauler A, Mauvezin C. Lysosomal degradation ensures accurate chromosomal segregation to prevent chromosomal instability. *Autophagy* (2021) 17(3):796–813. doi:10.1080/15548627.2020.1764727

24. Janes MR, Zhang J, Li LS, Hansen R, Peters U, Guo X, et al. Targeting KRAS mutant cancers with a covalent G12C-specific inhibitor. *Cell* (2018) 172(3):578–89.e17. doi:10.1016/j.cell.2018.01.006

25. Brancato V, Oliveira JM, Correlo VM, Reis RL, Kundu SC. Could 3D models of cancer enhance drug screening? *Biomaterials* (2020) 232:119744. doi:10.1016/j.biomaterials.2019.119744

26. Han K, Pierce SE, Li A, Spees K, Anderson GR, Seoane JA, et al. CRISPR screens in cancer spheroids identify 3D growth-specific vulnerabilities. *Nature* (2020) 580(7801):136–41. doi:10.1038/s41586-020-2099-x

27. Tidwell TR, Rosland G, Tronstad KJ, Soreide K, Hagland HR. Comparing *in vitro* cytotoxic drug sensitivity in colon and pancreatic cancer using 2D and 3D cell models: contrasting viability and growth inhibition in clinically relevant dose and repeated drug cycles. *Cancer Med* (2024) 13(11):e7318. doi:10.1002/cam4.7318

28. Kumarasamy V, Wang J, Frangou C, Wan Y, Dynka A, Rosenheck H, et al. The extracellular niche and tumor microenvironment enhance KRAS inhibitor efficacy in pancreatic cancer. *Cancer Res* (2024) 84(7):1115–32. doi:10.1158/0008-5472.CAN-23-2504

29. Cao Z, Liao Q, Su M, Huang K, Jin J, Cao D. AKT and ERK dual inhibitors: the way forward? *Cancer Lett* (2019) 459:30–40. doi:10.1016/j.canlet.2019.05.025

30. Baranyi M, Buday L, Hegedus B. K-Ras prenylation as a potential anticancer target. *Cancer Metastasis Rev* (2020) 39(4):1127–41. doi:10.1007/s10555-020-09902-w

Pathology & Oncology Research | frontiers

TYPE Review
PUBLISHED 30 March 2023
DOI 10.3389/pore.2023.1611033

Check for updates

OPEN ACCESS

EDITED BY
Jozsef Dudas,
Innsbruck Medical University, Austria

*CORRESPONDENCE
Junming Guo,
guojunming@nbu.edu.cn
Guoliang Ye,
ndfyygl@126.com

RECEIVED 24 December 2022
ACCEPTED 22 March 2023
PUBLISHED 30 March 2023

CITATION
Zheng Y, Li Z, Wang Y, Chen W, Lin Y, Guo J and Ye G (2023), CircRNA: A new class of targets for gastric cancer drug resistance therapy.
Pathol. Oncol. Res. 29:1611033.
doi: 10.3389/pore.2023.1611033

COPYRIGHT
© 2023 Zheng, Li, Wang, Chen, Lin, Guo and Ye. This is an open-access article distributed under the terms of the Creative Commons Attribution License (CC BY). The use, distribution or reproduction in other forums is permitted, provided the original author(s) and the copyright owner(s) are credited and that the original publication in this journal is cited, in accordance with accepted academic practice. No use, distribution or reproduction is permitted which does not comply with these terms.

CircRNA: A new class of targets for gastric cancer drug resistance therapy

Ying Zheng[1,2,3], Zhe Li[2,3], Yao Wang[1,2,3], Wanjiao Chen[2], Yifan Lin[2,3], Junming Guo[1,2,3]* and Guoliang Ye[2,3]*

[1]Department of Biochemistry and Molecular Biology, Zhejiang Key Laboratory of Pathophysiology, Medical School of Ningbo University, Ningbo, China, [2]Department of Gastroenterology, The First Affiliated Hospital of Ningbo University, Ningbo, China, [3]Institute of Digestive Diseases of Ningbo University, Ningbo, China

Gastric cancer (GC) is one of the most common malignancies worldwide. Patients with advanced GC need palliative care to ensure survival. This includes the use of chemotherapy agents, such as cisplatin, 5-fluorouracil, oxaliplatin, paclitaxel, and pemetrexed, as well as targeted agents. However, the emergence of drug resistance evidence in poor patient outcomes and poor prognosis is a motivation to determine the specific mechanism of drug resistance. Interestingly, circular RNAs (circRNAs) play an important part in the carcinogenesis and progression of GC and are involved in GC drug resistance. This review systematically summarizes the functions and mechanisms of circRNAs underlying GC drug resistance, especially chemoresistance. It also emphasizes that circRNAs can serve as promising targets for improving drug resistance and therapeutic efficacy.

KEYWORDS

gastric cancer, drug resistance, circular RNA, therapeutic target, biogenesis

Introduction

Cancer is one of the primary causes of death. Gastric cancer (GC) is a type of gastrointestinal tumor with an incidence that ranks it among the top five cancers and mortality rates that place it among the top four (1). The main reason for the high GC mortality rate is likely due to its diagnosis in the advanced or metastatic stage (2). At that time, radical surgery is no longer a feasible option and palliative therapy is necessary to improve the survival rate of patients (3). Chemotherapy, targeted therapy, and immunotherapy are novel methods that can be used as an adjunct combined with surgery or as the main treatment for advanced cancer (4). For example, research in gastroesophageal cancer patients who have underwent postoperative adjuvant chemotherapy has shown that the overall survival at 1, 3, and 5 years in the adjuvant chemotherapy group was 5% higher than that in the resection alone group (5). However, one small study has shown that when patients with advanced GC were divided into three groups based on their sensitivity to chemotherapy drugs, the one-year survival rate in the sensitive group was

significantly higher than that in the resistant group, whereas the time to progression in the sensitive group was significantly longer than that in the resistant group (6). Based on this, chemoresistance has become a barrier to existing treatments, which has a significant impact on the follow-up treatment effect and patient survival rates. In another trial, researchers have classified advanced GC after clinical sequencing based on biomarkers (7). Among them, the GC therapeutic drug capivasertib is a selective pan-AKT serine/threonine kinase (*AKT*) inhibitor with the ability to inhibit kinase activity of three *AKT* subtypes. The sequencing results have shown that GC can be divided into microsatellite instability-high (MSI-H) GC, microsatellite-stable (MSS) tumor, genomically stable, or mesenchymal subtype groups based on phosphatidylinositol-4,5-bisphosphate 3-kinase catalytic subunit alpha (*PIK3CA*) hot spot mutations (E542K, E545K, and H1047R) (7). Researchers have observed that different GC subtypes have different sensitivity to the capivasertib treatment. Among the eight patients with E542K mutation, four had a persistent response to the combination of capitaserib/paclitaxel (PTX), and none of the four patients with H1047R *PIK3CA* mutations responded to capivasertib. Thus, identifying specific targets can improve GC sensitivity to specific drugs (7). In general, a variety of new treatment modalities have been used alone or as a supplement in addition to surgery for cancer treatment. It is very important to improve and refine the above methods, including reducing the rate of chemotherapy resistance.

Circular RNAs have potential as drug resistance targets

Circular RNAs (circRNAs) are formed by alternative splicing of the 5′ and 3′ ends of RNA molecules. They are significantly more stable than the associated linear RNAs and demonstrate resistance to RNase R digestion (8). Therefore, circRNAs have a unique covalently closed circular structure that gives them stability and the potential as a target for a variety of therapies. For example, circAKT3 is significantly overexpressed in cisplatin (CDDP)-resistant GC tissues and cells and eliminates the inhibition of miR-198 to activate the *PI3K/AKT* signaling pathway in GC cells, leading to CDDP-based DNA-damaging chemotherapy resistance (9) (Figure 1; Supplementary Table S1). However, the molecular mechanisms by which circRNAs regulate the therapeutic effects of drugs in GC remain unclear. Further research is needed to study the drug resistance mediated by circRNAs in GC. The present review summarizes the roles of circRNAs in drug resistance during several GC treatments and discusses their potential mechanisms. Clinical application of circRNAs as a therapeutic target needs to be discussed further.

Biogenesis and functions of circular RNAs

CircRNAs are stable covalently closed ncRNAs that were first identified in plant viruses in the 1970s (10). They were deemed to be miscleavage byproducts during precursor messenger RNA (pre-mRNA) processing (11). With the development of biomolecular techniques, circRNAs have been found to have potential biological functions that play vital roles in cancers (8). In addition, circRNAs can be divided into exon-derived circRNAs (ecRNAs) (8), exon-intron circRNAs (EIciRNAs) (12), and intron-derived circRNAs (ciRNAs) based on their composition (13). The ecRNAs can be formed *via* intron- or lariat-driven circularization (Figures 2A, C). The mechanism for intron-driven circularization is mediated by base pairing between introns located on the exon flanks (Alu repeats or non-repeating elements with a length of about 300 nt) or dimerization of RNA-binding proteins (RBPs), which leads to the tight binding of the upstream 3′ splice site to the 5′ splice site that forms a circular structure after the introns are removed. The mechanism for lariat-driven circularization relies on exon skipping in pre-mRNA during post-transcription and can decrease the distance between non-adjacent exons. Furthermore, ecRNAs can be formed by removing introns. EIciRNAs are formed by intron-driven circularization (Figure 2B). They are generated when the introns between the acceptor and the donor are not removed. In addition, ciRNAs that originate from tRNA intronic circular RNAs or pre-mRNAs are produced by forming a 2′-5′end linkage. This linkage is a branchpoint between the 5′ splice site after the release of the 3′ exon and terminal 2′-OH intron group (Figures 2B, C) (14).

With the advent of the sequencing technology age, more and more circRNA have been discovered to be widely expressed in eukaryotes and participating in various human pathological and physiological processes (15). The circRNAs affect numerous cancer hallmarks by sponging microRNA (miRNA), mutual effecting with and translating into proteins, regulating gene transcription, and competing with mRNA linear splicing. Among them, miRNA sponging is the most iconic circRNA feature (Figure 2D). For example, circVAPA is upregulated in CDDP-resistant GC cell lines (16). It has been reported that constitutive activation of signal transducer and activator of transcription 3 (STAT3) contributes to the chemotherapy resistance of GC cells (16). Researchers have found that circVAPA as a sponge for miR-125b-5p can act on STAT3 in GC *via* the miR-125b-5p/STAT3 axis to promote chemotherapy resistance of GC (17) (Figure 1; Supplementary Table S1). RBPs regulate at the post-RNA transcriptional level (Figure 2E) (18). For instance, heterogeneous nuclear ribonucleoprotein U-like 1 (HNRNPUL1) belongs to the family of RBPs and is involved in

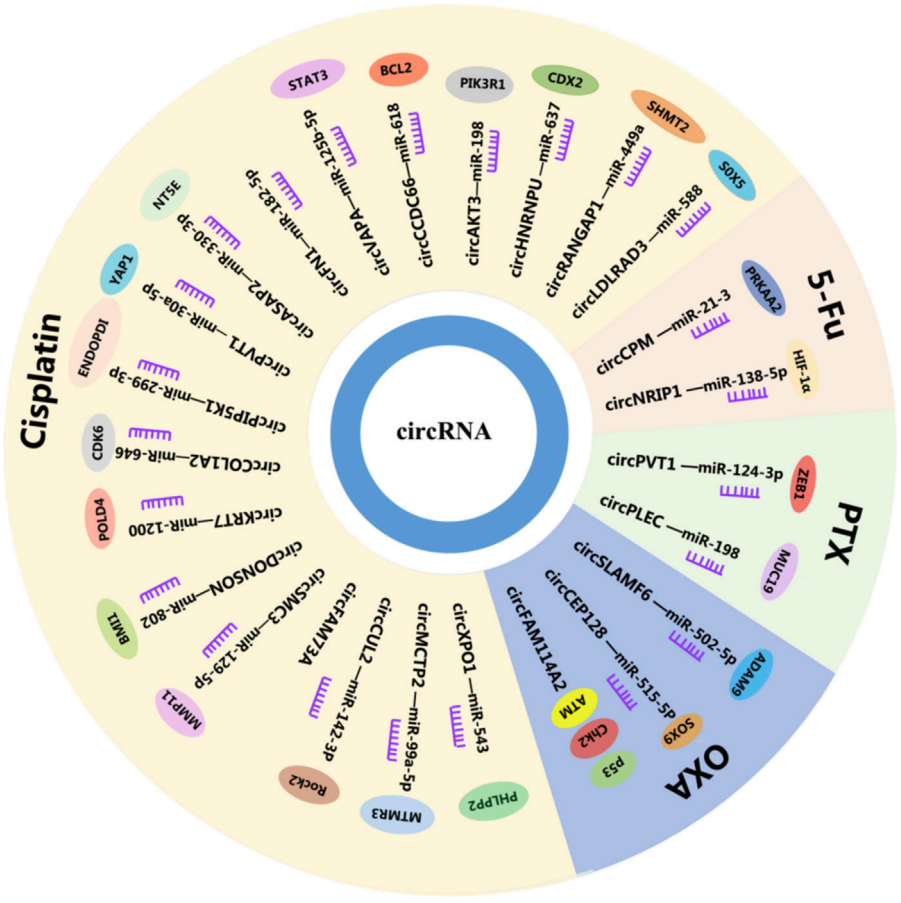

FIGURE 1
CircRNAs in GC. CircRNAs play a vital role in drug resistance by interacting with miRNAs and mRNAs, circRNAs, circular RNAs; miRNAs, microRNAs; mRNAs, and messenger RNAs.

DNA damage repair. Through regulation of CDDP sensitivity-inhibited circMAN1A2 formation, HNRNPUL1 can inhibit CDDP sensitivity of esophageal cancer (19). In addition to interacting with RBPs, circRNAs also function as protein scaffolds, decoys, and recruiters (16, 20–22). The translation of circRNAs requires an internal ribosome entry site sequence (IRES) located in RNA to initiate cap-independent translation (23). IRES initiates the open reading frame for translation (24). In addition, m6A-induced ribosomal binding sites may be another mechanism that is independent of cap translation (Figure 2F) (25). ASK1-272a.a is a novel protein encoded by circASK1 that mediates the chemosensitivity-inducing effect of epidermal growth factor receptor (*EGFR*)-mutant lung adenocarcinoma (26). Furthermore, ASK1-272a.a has a function of competing with ASK1 for Akt1 binding, which competes with Akt1-induced ASK1 phosphorylation and inactivation, resulting in the activation of ASK1-induced apoptosis and alleviating gefitinib resistance (26). EIciRNAs and intron-derived RNAs are located in the nucleus, where they perform transcriptional regulation and other functions (27, 28). Studies have shown that EIciRNAs form the EIciRNA-U1 snRNP complex by binding with U1 snRNP, which ultimately enhances gene expression after interacting with Pol II at the gene promoter (28). Similarly, intron-derived RNAs can adjust the transcription of their parental genes by facilitating the elongation activity of Pol II (Figure 2G) (13). Flanking intron sequences are the main factor determining the efficiency of exon circularization. Moreover, circRNAs containing cyclization-promoting sequences can result in reduced efficiency of the flanking exon linear splicing, thereby competing with linear splicing of mRNAs (29).

In conclusion, circRNAs play important roles in cancer through their various functions. Multiple pathways dominated by circRNAs regulate the expression of the downstream genes. Therefore, an in-depth study of specific circRNA mechanisms in cancer drug resistance is crucial, which will contribute to the rapid development of cancer treatment.

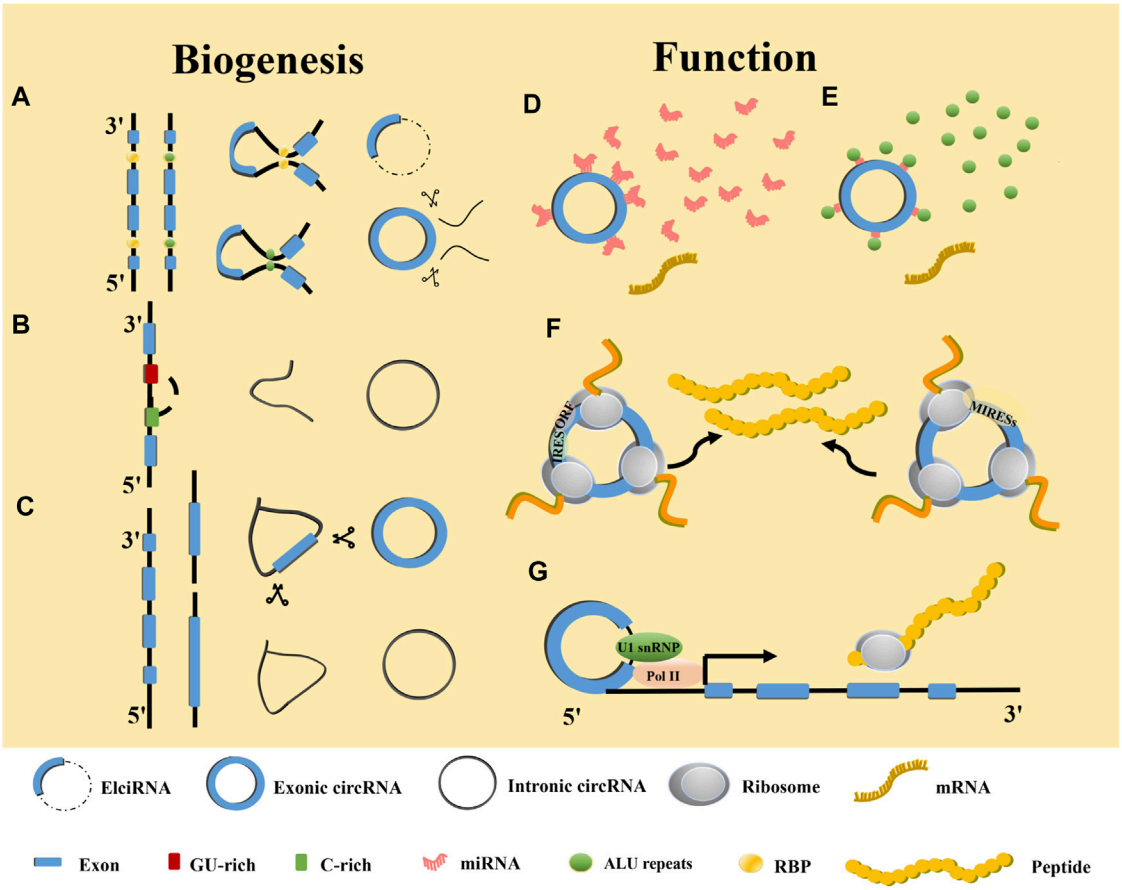

FIGURE 2
Biogenesis and functions of circRNAs. **(A)** RBP and ALU-mediated circRNA generation. **(B)** Mechanism of intronic circRNA generation. **(C)** Lariat-driven mediated circRNA generation. **(D)** Function as miRNA sponge. **(E)** Interaction with RBPs. **(F)** Translation into proteins or polypeptides. **(G)** Enhancer of gene expression.

The circular RNAs and gastric cancer drug resistance

The circular RNAs and chemoresistance

Chemotherapy has shown good efficacy as the main treatment for advanced cancer, but the occurrence of chemotherapy resistance hinders the integrity of the course of treatment and is a mainspring for chemotherapy failure in improving patients (30). Diverse mechanisms are involved in drug resistance, including DNA damage repair, operation of cell death-related pathways, regulation of cell viability and proliferation, modification of drug efflux, and metabolism (31), in which circRNAs play a crucial part. Moreover, circFAM114A2 is downregulated in GC and sponged miR-421 to upregulate the expression level of *ATM* (ATM serine). At the same time, circFAM114A2 inhibits the chemoresistance of L-OPH (Oxaliplatin) through the activation of the *ATM/Chk2* (checkpoint kinase 2)/*p53*-dependent pathway. *ATM* is a master gene regulator in the DNA damage response. Its activation leads to the execution of DNA repair or initiation of apoptosis (32). Furthermore, circHECTD1 expression is significantly upregulated in GC and facilitates GC cell glutaminolysis, growth, and invasiveness (33). In addition, circHECTD1 has been found to target miR-1256 to regulate ubiquitin-specific peptidase 5 expression levels and modulate the downstream β-catenin/*c-Myc* signaling pathway (33). Therefore, circHECTD may serve as a latent chemotherapy drug target for GC treatment (Figure 1; Supplementary Table S1).

Cisplatin resistance of circRNAs in gastric cancer

CDDP is the first-line chemotherapy drug for GC that blocks transcription and DNA replication by forming intra-strand DNA cross-links, resulting in apoptosis (34). However, tumor cells can develop resistance to CDDP by interfering with CDDP-induced

apoptosis *via* unique mechanisms, which ultimately limits the overall medical efficacy of the treatment (35).

The mechanisms of resistance to CDDP are varied, in which circRNAs play an important part. In particular, circCUL2 inhibits the proliferation, migration, invasion, and drug resistance of GC cells (36). Studies have shown that abnormally activated autophagy induced by chemotherapeutic drugs can offer energy to cancer cells (36). Interestingly, circCUL2 inhibits autophagy in CDDP-resistant GC cells through miR-142-3p/*ROCK2* (Rho-associated coiled-coil containing protein kinase 2), thus affecting the CDDP sensitivity of GC cells (36). Researchers have found that circCCDC66 was significantly overexpressed in CDDP-resistant GC cells (37). In addition, circCCDC66 induces CDDP resistance in GC cells *via* miR-618, significantly inhibiting the mRNA and protein levels of *BCL2* (BCL2 apoptosis regulator), which is a key regulator of the apoptosis signaling pathway (37). Sun et al. have found that circMCTP2 upregulation suppressed the proliferation of CDDP-resistant GC cells and induced CDDP-resistant GC cell apoptosis (38). It also reduced autophagy in CDDP-resistant GC, which has been demonstrated to promote resistance to tumor chemotherapy. In addition, as a sponge of miR-99a-5p, circMCTP2 inhibits the resistance of GC to CDDP by upregulating myotubularin-related protein 3 (*MTMR3*). Therefore, circMCTP2 might be a new therapeutic strategy for interference with CDDP resistance in GC (38). Furthermore, circFN1 is a novel circRNA that reinforces CDDP resistance in GC by sponging miR-182-5p, which has the capacity of activating apoptosis *via* the caspase-3 signaling pathway (39). Moreover, circFN1 functions as a ceRNA, abolishing the ability of miRNA to activate apoptosis and enhancing CDDP resistance (39). In addition, circASAP2 is upregulated in CDDP-resistant GC tissues and cells. Knockdown of circASAP2 promotes CDDP sensitivity and inhibited malignant behaviors of CDDP-resistant GC cells by targeting the miR-330-3p/*NT5E* (5′-nucleotidase ecto) axis (40). Zhang et al. have found that enhancing the expression of circXPO1 promoted the apoptosis of CDDP-resistant GC cells and inhibited their growth and metastasis. In other words, circXPO1 has the ability to sensitize the GC patients to CDDP therapy (41). Knockdown of miR-543 can promote tumor-suppressor factor leucine-rich repeat protein phosphatase 2 (*PHLPP2*), which can impact CDDP-resistant cell behaviors and chemotherapy sensitivity. Thus, circXPO1 can act as a sponge for miR-543 and be a latent therapeutic agent against CDDP-resistant GC (41). Prior research has shown that circDONSON can promote the resistance of GC cells to CDDP (42). In addition, miR-802 was determined to be a tumor suppressor in many human cancers. Targeting circDONSON can promote CDDP resistance in GC cells. Furthermore, BMI1 proto-oncogene (*BMI1*) is an oncogene that was found to be an miR-802 target that was overexpressed in CDDP-resistant GC tissues and cells (42). Therefore, these findings demonstrated that circDONSON regulated the sensitivity of CDDP resistance in GC *via* the miR-802/*BMI1* axis (42). Exosomes are endocytosis extracellular lipid bilayer vesicles that can transport specific proteins or nucleic acids to the corresponding recipient cells through intercellular communication mechanisms (43, 44). They are stable in a variety of extracellular fluids, including blood and urine (45). It is important that circRNAs are enriched and stable in exosomes, and that exosomal circRNAs can regulate the occurrence and development of GC by acting as a sponge of miRNAs (46). Exosomal circPVT1 might be a prospective indicator for GC in CDDP therapy (47). CircPVT1 knockdown suppressed CDDP resistance in CDDP-resistant GC cells by promoting apoptosis and inhibiting invasion or autophagy by negatively targeting miR-30a-5p. Yes1-associated transcriptional regulator (*YAP1*) is a direct target of miR-30a-5p, and reduction of its level by miR-30a-5p can promote CDDP resistance (47). In addition, circPIP5K1A knockdown enhances CDDP sensitivity of GC *via* the miR-299-3p/*ENDOPDI* (thioredoxin domain containing 5) axis (48). CircCOL1A2 induces GC CDDP resistance by effecting the miR-646/*CDK6* (cyclin dependent kinase 6) pathway (49). CircKRT7 heightens CDDP resistance in GC *via* the miR-1200/P*OLD4* (DNA polymerase delta 4) pathway (50). CircSMC is an miR-129-5p sponge that can promote the CDDP resistance of GC by upregulating matrix metallopeptidase 11 (*MMP11*) (51). In addition, circFAM73A has the ability to facilitate *in vitro* CDDP resistance in GC (52). CircHNRNPU facilitates cisplatin resistant of GC through miR-637/caudal type homeobox 2 (*CDX2*) (53). Exosomal circRANGAP1 promotes GC resistance to CDDP by regulating the miR-449a/serine hydroxymethyltransferase 2(*SHMT2*) axis (54). circLDLRAD3 knockdown can reduce CDDP resistance by regulating miR-588/SRY-box transcription factor 5 (*SOX5*) pathway and block the malignant development of CDDP resistant GC (55) (Figure 1; Supplementary Table S1).

The 5-fluorouracil resistance of circRNAs in gastric cancer

The 5-fluorouracil (5-FU) was first synthesized in 1957 and quickly became a routine anticancer drug that remains essential in many chemotherapy regimens today (56). The 5-FU cytotoxicity occurs due to the mistaken entrance of fluoronucleotides into RNA and DNA as well as nucleotide synthetic enzyme thymidylate synthase (TS) inhibition (57). Furthermore, circRNAs may participate in these mechanisms to regulate the sensitivity of 5-FU in GC. Research has shown that autophagy dysregulation may be one of the main reasons for drug resistance in cancer, in which circCPM participates (31). CircCPM was overexpressed in 5-FU resistant GC cell lines

and tissues. It improves the expression level of protein kinase AMP-activated catalytic subunit alpha 2 (*PRKAA2*) by directly binding to miR-21-3p and leading to the activation of autophagy and chemoresistance (31). In addition, silencing circCPM can improve chemosensitivity of 5-FU in GC (31). Emerging proof has shown that glycolysis plays an important role in hypoxia-induced chemoresistance. HIF-1α is one of the major regulators in the metabolic process. Downregulation of circNRIP1 can sensitize GC cells to 5-FU under hypoxic conditions (58). The miR-138-5p is a circNRIP1 sponge that can inhibit the effect of hypoxia-induced 5-FU resistance *via* circNRIP1 through HIF-1α (58) (Figure 1; Supplementary Table S1).

Oxaliplatin resistance of circRNAs in gastric cancer

Oxaliplatin (OXA) is an alkylating agent that inhibits DNA replication by forming adducts between two adjacent guanine or guanine and adenine molecules and is the third-generation derivative of platinum complex anticancer drugs. At present, the resistance mechanism for GC to OXA is very complex, involving microenvironmental, cell mitochondrial, cell membrane, cell protein, signal transduction, and other factors related to tumor growth. Morevoer, circRNAs are a novel landmark in OXA resistance in GC (59). The Gao et al. study has led to the identification of circSLAMF that promoted GC oxaliplatin resistance by regulating the miR-502-5p/*ADAM9* (ADAM metallopeptidase domain 9) axis (60). CircSLAMF is overexpressed in OXA-resistant tissues and cells. In addition, miR-502-5p efficiently inhibited OXA resistance in OXA-resistant GC cells, reversing the promoting effect of circSLAMF (60). Finally, *ADAM9* upregulation may act as an oncogene aggravating OXA resistance to GC treatment (60). CircCEP128 is highly expressed in OXA-resistant GC cells and its exosomes. It has the ability to boost OXA resistance of GC cells partly *via* the miR-515-5p/*SOX9* (SRY-box transcription factor 9) pathway, which is a promising therapeutic target (61) (Figure 1; Supplementary Table S1).

Paclitaxel resistance of circRNAs in gastric cancer

Paclitaxel (PTX) is a stable tubulin cytotoxic agent that has become the first-line treatment for various cancers, including GC (62). It can induce cellular processes by disrupting normal microtubule dynamics required for cell division and interphase processes and by inducing tumor necrosis factor-alpha gene expression, leading to apoptosis or programmed cell death (63). PTX resistance in tumors has been reported to be associated with increased drug efflux, alteration of intercellular signaling, tubulin mutation, and overexpression of β-tubulin isotype composition (64). In addition, circRNAs have been found to be associated with the mechanisms of PTX resistance. For example, circPVT1 downregulation can result in a noteworthy decrease in P-gp and GST-π, which can reduce cytotoxicity by reducing the concentration of antineoplastic drugs (65). As the target of circPVT1, miR-124-3p promotes sh-circ-PVT1-caused PTX sensitivity in PTX-resistant GC cells and the expression of zinc finger E-box binding homeobox 1 (*ZEB1*). Overexpression can promote PTX resistance of GC cells (65). Thus, circPLEC can interact with miR-198 in GC cells and through miR-198 to regulate the downstream gene mucin 19 and oligomeric (*MUC19*). MUC19 downregulation weakened GC resistance to PTX and improved the apoptosis of PTX-resistant GC cells (66). Therefore, circPLEC can promote PTX resistance through the miR-198/*MUC19* axis, which has the potential to be a therapeutic target (66) (Figure 1; Supplementary Table S1).

Pemetrexed resistance of circRNAs in gastric cancer

Pemetrexed is an antifolate analog that inhibits enzyme thymidylate synthase (TS) and is also active on dihydrofolate reductase and glycine ribonucleotide folate-dependent enzymes, which forms an effective combination with OXA for locally advanced or metastatic disease treatment (67). Drug resistance is common in cancer. Thus, determining the mechanism of pemetrexed resistance is vital for improving treatment. Prior research has shown that cell drug resistance increased significantly in the circMTHFD2 overexpression group (68). In addition, miR-124 is a target of circMTHFD2 that can increase the protein expression of TS and ATP-binding cassette subfamily C member 11 (*ABCC11*) and decrease the protein expression of RCF1 (respiratory supercomplex factor 1, mitochondrial). There are also reports that *ABCC11* is a drug efflux pump used for drug metabolism. Thus, circMTHFD2 has the ability of enhancing the pemetrexed resistance in GC (68) (Figure 1; Supplementary Table S1).

CircRNAs and gastric cancer targeted drug resistance

Trastuzumab

Human epidermal growth factor receptor 2 (*HER2*) pertains to the epidermal growth factor receptor (*EGFR*), which is related to proliferation, apoptosis, and tumor cell migration (69). In addition, *HER2* is overexpressed or amplified in approximately 10%–20% of advanced GC cases (70). Therefore, trastuzumab is a new targeted drug that can be used in a combination of drugs to

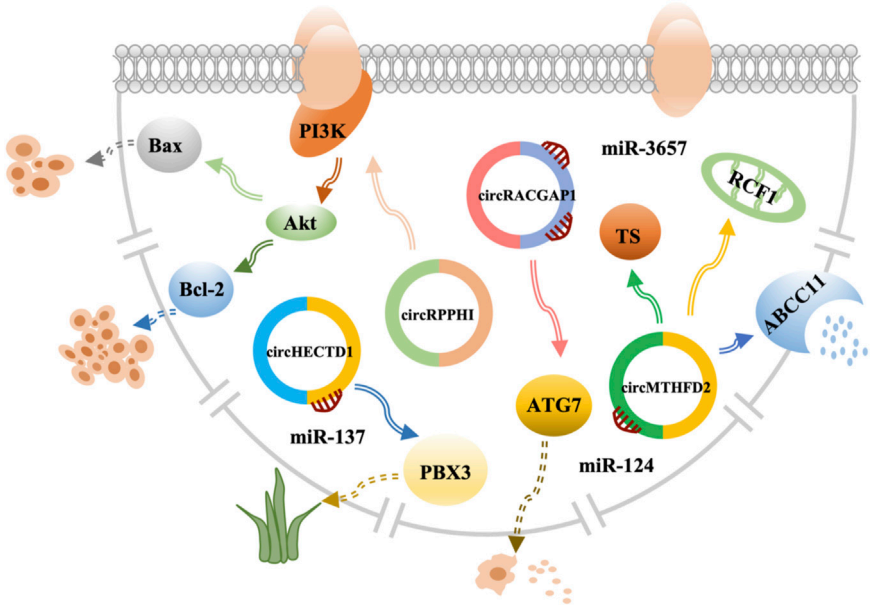

FIGURE 3
CircRNAs mediate the mechanism of drug resistance in GC.

improve the treatment of advanced GC and has an important relationship with circRNAs. However, patients are prone to trastuzumab resistance. Therefore, research on the specific mechanism for the treatment of trastuzumab resistance has shown that circRPPH1 level was much lower upon trastuzumab treatment and had a low expression in cancer (71). Further research by Lv et al. has demonstrated that circRPPH1 had the ability to restrain proliferation and promote apoptosis in GC, indicating that it reduced trastuzumab resistance in GC cells (71). The study has also shown that cell viability of GC cells treated with signaling pathway activator insulin-like growth factor 1 (*IGF-1*) was significantly increased with a decrease in apoptosis (71). BCL2-associated X is an apoptosis gene that downregulates the expression, while anti-apoptosis gene BCL2 apoptosis regulator (*Bcl-2*) upregulates the expression (71). In conclusion, circRPPH1 can reduce trastuzumab resistance by inhibiting the phosphatidylinositol 3-kinase-threonine kinase 1 (*PI3K*)-*AKT* in GC. Thus, it could be a new target for GC treatment (71) (Figure 3; Supplementary Table S1).

Apatinib

Apatinib is known as a highly selective inhibitor of vascular endothelial growth factor receptor-2 tyrosine kinase, which can induce apoptosis and inhibit proliferation and metastasis to participate in anti-angiogenesis and anticancer activities. It has been approved for treatment of metastatic GC (72). Increasing the efficacy of apatinib in GC has become a critical issue. Ling et al. have confirmed that apatinib promoted GC autophagy activation and downregulated the expression of autophagy-related gene 7 (*ATG7*) to sensitize apatinib in GC cells (73). Researchers have then selected circRACGAP1, which was differentially expressed in the apatinib and control groups, as the binding site for miR-3657 (73). Apatinib can increase *ATG7* expression *via* selective miR-3657 knockout. Using a co-transfecting plasmid and incubation with apatinib, the levels of autophagosomes and autolysosomes were reduced in circRACGAP1 loss GC cells and rescued *via* transfection with miR-3657 inhibitors (73). Therefore, the data indicated that circRACGAP1 regulated apatinib-induced autophagy by targeting miR-3657 and *ATG7*. Thus, circRACGAP1 can be used as a therapeutic target to regulate the role of apatinib in GC (73) (Figure 3; Supplementary Table S1).

Diosbulbin-bulbifera

Dioscorea bulbifera (DB) is a traditional Chinese medicine that is considered to be related to cancer treatment (74). Lu et al. have discovered that circHECTD1 is overexpressed in GC tissues and cells and serves as a sponge for miR-137 (75). Moreover, PBX homeobox 3 (*PBX3*) is a key cofactor that plays an important role in the carcinogenesis, development, and progression of GC (76), which is as downstream miR-137 gene target that is DB-resistant (75). These findings indicate that circHECTD1 prevents

sensitivity *via* the miR-137/*PBX3* axis in GC (Figure 3; Supplementary Table S1).

Conclusion and future perspective

Chemotherapy, targeted therapy, and immunotherapy are needed in advanced GC as they are able to provide some therapeutic effects (77). However, they inevitably result in drug resistance in the course of treatment, which will lead to a significant decline in treatment efficacy. Drug resistance has become one of the major obstacles to the therapeutic efficacy for GC. Therefore, it is crucial to explore all of the related mechanisms. As a new biomarker, circRNAs have been widely utilized in early screening of GC as they can be used as an miRNA sponge to regulate the downstream processes (78). Moreover, circRNAs play important roles in drug resistance through different mechanisms. In addition, circRNAs take part in the drug resistance process of target therapeutic drugs and even traditional Chinese medicines. Therefore, circRNAs have the potential to become new biomarkers of drug resistance in GC. However, their clinical application remains a challenge, as a large number of GC patient samples are necessary for detection and analysis. The method of measuring drug resistance of patients to GC by quantifying the expression of circRNAs also needs to be considered. At the same time, there are circRNAs that are abnormally expressed in multi-drug resistance, which makes identifying specific drugs a problem to be resolved. Therefore, a very important aspect of future research is to determine the specific molecular pathogenic pathways, which will provide more information about cancer and additional potential targets.

Author contributions

YZ collected references and wrote the manuscript. ZL and YW provided ideas. WC and YL participated in drawing. JG and GY revised and edited the manuscript. All authors read and approved the final manuscript.

Funding

This work was supported by the Zhejiang Province Public Welfare Technology Application Research Project (no. LGF22H160039), the Ningbo Key Technology Research and Development Special Project (no. 2021Z133), the Medical Health Science and Technology Project of Zhejiang Provincial Health Commission (no. 2019ZH007), and the Medical and Health Research Project of Zhejiang Province (no. 2023RC262).

Conflict of interest

The authors declare that the research was conducted in the absence of any commercial or financial relationships that could be construed as a potential conflict of interest.

Supplementary material

The Supplementary Material for this article can be found online at: https://www.por-journal.com/articles/10.3389/pore.2023.1611033/full#supplementary-material

References

1. Sung H, Ferlay J, Siegel RL, Laversanne M, Soerjomataram I, Jemal A, et al. Global cancer statistics 2020: GLOBOCAN estimates of incidence and mortality worldwide for 36 cancers in 185 countries. *CA Cancer J Clin* (2021) 71:209–49. doi:10.3322/caac.21660

2. Lu T, Sun L, Zhu X. Yes-associated protein enhances proliferation and attenuates sensitivity to cisplatin in human gastric cancer cells. *Biomed Pharmacother* (2018) 105:1269–75. doi:10.1016/j.biopha.2018.06.031

3. McDonald J, Swami N, Hannon B, Lo C, Pope A, Oza A, et al. Impact of early palliative care on caregivers of patients with advanced cancer: Cluster randomised trial. *Ann Oncol* (2017) 28:163–8. doi:10.1093/annonc/mdw438

4. Japanese Gastric Cancer Treatment Guidelines 2021. Japanese gastric cancer treatment guidelines 2021 (6th edition). *Gastric Cancer* (2023) 26:1–25. doi:10.1007/s10120-022-01331-8

5. Mokdad AA, Yopp AC, Polanco PM, Mansour JC, Reznik SI, Heitjan DF, et al. Adjuvant chemotherapy vs postoperative observation following preoperative chemoradiotherapy and resection in gastroesophageal cancer: A propensity score-matched analysis. *JAMA Oncol* (2018) 4:31–8. doi:10.1001/jamaoncol.2017.2805

6. Naitoh H, Yamamoto H, Murata S, Kobayashi H, Inoue K, Tani T. Stratified phase II trial to establish the usefulness of the collagen gel droplet embedded culture-drug sensitivity test (CD-DST) for advanced gastric cancer. *Gastric Cancer* (2014) 17:630–7. doi:10.1007/s10120-013-0320-4

7. Lee J, Kim ST, Kim K, Lee H, Kozarewa I, Mortimer PGS, et al. Tumor genomic profiling guides patients with metastatic gastric cancer to targeted treatment: The VIKTORY umbrella trial.*Cancer Discov* (2019) 9:1388–405. doi:10.1158/2159-8290.CD-19-0442

8. Jeck WR, Sorrentino JA, Wang K, Slevin MK, Burd CE, Liu J, et al. Circular RNAs are abundant, conserved, and associated with ALU repeats. *RNA* (2013) 19:141–57. doi:10.1261/rna.035667.112

9. Huang X, Li Z, Zhang Q, Wang W, Li B, Wang L, et al. Circular RNA AKT3 upregulates PIK3R1 to enhance cisplatin resistance in gastric cancer via miR-198 suppression. *Mol Cancer* (2019) 18:71. doi:10.1186/s12943-019-0969-3

10. Sanger HL, Klotz G, Riesner D, Gross HJ, Kleinschmidt AK. Viroids are single-stranded covalently closed circular RNA molecules existing as highly base-paired rod-like structures. *Proc Natl Acad Sci U S A* (1976) 73:3852–6. doi:10.1073/pnas.73.11.3852

11. Cocquerelle C, Mascrez B, Hétuin D, Bailleul B. Mis-splicing yields circular RNA molecules. *Faseb j* (1993) 7:155–60. doi:10.1096/fasebj.7.1.7678559

12. Zheng W, Su H, Lv X, Xin S, Xu T. Exon-intron circular RNA circRNF217 promotes innate immunity and antibacterial activity in teleost fish by reducing miR-130-3p function. *J Immunol* (2022) 208:1099–114. doi:10.4049/jimmunol.2100890

13. Zhang Y, Zhang XO, Chen T, Xiang JF, Yin QF, Xing YH, et al. Circular intronic long noncoding RNAs. *Mol Cel* (2013) 51:792–806. doi:10.1016/j.molcel.2013.08.017

14. Kristensen LS, Andersen MS, Stagsted LVW, Ebbesen KK, Hansen TB, Kjems J. The biogenesis, biology and characterization of circular RNAs. *Nat Rev Genet* (2019) 20:675–91. doi:10.1038/s41576-019-0158-7

15. Misir S, Wu N, Yang BB. Specific expression and functions of circular RNAs. *Cell Death Differ* (2022) 29:481–91. doi:10.1038/s41418-022-00948-7

16. Conn SJ, Pillman KA, Toubia J, Conn VM, Salmanidis M, Phillips CA, et al. The RNA binding protein quaking regulates formation of circRNAs. *Cell* (2015) 160:1125–34. doi:10.1016/j.cell.2015.02.014

17. Deng P, Sun M, Zhao WY, Hou B, Li K, Zhang T, et al. Circular RNA circVAPA promotes chemotherapy drug resistance in gastric cancer progression by regulating miR-125b-5p/STAT3 axis. *World J Gastroenterol* (2021) 27:487–500. doi:10.3748/wjg.v27.i6.487

18. Yu CY, Li TC, Wu YY, Yeh CH, Chiang W, Chuang CY, et al. The circular RNA circBIRC6 participates in the molecular circuitry controlling human pluripotency. *Nat Commun* (2017) 8:1149. doi:10.1038/s41467-017-01216-w

19. Li J, Sang M, Zheng Y, Meng L, Gu Z, Li Z, et al. HNRNPUL1 inhibits cisplatin sensitivity of esophageal squamous cell carcinoma through regulating the formation of circMAN1A2. *Exp Cel Res* (2021) 409:112891. doi:10.1016/j.yexcr.2021.112891

20. Li X, Yang L, Chen LL. The biogenesis, functions, and challenges of circular RNAs. *Mol Cel* (2018) 71:428–42. doi:10.1016/j.molcel.2018.06.034

21. Zhang W, Chen S, Du Q, Bian P, Chen Y, Liu Z, et al. CircVPS13C promotes pituitary adenoma growth by decreasing the stability of IFITM1 mRNA via interacting with RRBP1. *Oncogene* (2022) 41:1550–62. doi:10.1038/s41388-022-02186-0

22. Wu N, Yuan Z, Du KY, Fang L, Lyu J, Zhang C, et al. Translation of yes-associated protein (YAP) was antagonized by its circular RNA via suppressing the assembly of the translation initiation machinery. *Cel Death Differ* (2019) 26: 2758–73. doi:10.1038/s41418-019-0337-2

23. Chen CK, Cheng R, Demeter J, Chen J, Weingarten-Gabbay S, Jiang L, et al. Structured elements drive extensive circular RNA translation. *Mol Cel* (2021) 81: 4300–18.e13. doi:10.1016/j.molcel.2021.07.042

24. Legnini I, Di Timoteo G, Rossi F, Morlando M, Briganti F, Sthandier O, et al. Circ-ZNF609 is a circular RNA that can Be translated and functions in myogenesis. *Mol Cel* (2017) 66:22–37.e9. doi:10.1016/j.molcel.2017.02.017

25. Meyer KD, Patil DP, Zhou J, Zinoviev A, Skabkin MA, Elemento O, et al. 5' UTR m(6)A promotes cap-independent translation. *Cell* (2015) 163:999–1010. doi:10.1016/j.cell.2015.10.012

26. Wang T, Liu Z, She Y, Deng J, Zhong Y, Zhao M, et al. A novel protein encoded by circASK1 ameliorates gefitinib resistance in lung adenocarcinoma by competitively activating ASK1-dependent apoptosis. *J].Cancer Lett* (2021) 520: 321–31. doi:10.1016/j.canlet.2021.08.007

27. Li J, Sun D, Pu W, Wang J, Peng Y. Circular RNAs in cancer: Biogenesis, function, and clinical significance. *Trends Cancer* (2020) 6:319–36. doi:10.1016/j.trecan.2020.01.012

28. Li Z, Huang C, Bao C, Chen L, Lin M, Wang X, et al. Exon-intron circular RNAs regulate transcription in the nucleus. *Nat Struct Mol Biol* (2015) 22:256–64. doi:10.1038/nsmb.2959

29. Ashwal-Fluss R, Meyer M, Pamudurti NR, Ivanov A, Bartok O, Hanan M, et al. circRNA biogenesis competes with pre-mRNA splicing. *Mol Cel* (2014) 56: 55–66. doi:10.1016/j.molcel.2014.08.019

30. Brabec V, Kasparkova J. Modifications of DNA by platinum complexes. Relation to resistance of tumors to platinum antitumor drugs. *Drug Resist Updat* (2005) 8:131–46. doi:10.1016/j.drup.2005.04.006

31. Fang L, Lv J, Xuan Z, Li B, Li Z, He Z, et al. Circular CPM promotes chemoresistance of gastric cancer via activating PRKAA2-mediated autophagy. *Clin Transl Med* (2022) 12:e708. doi:10.1002/ctm2.708

32. Wu Q, Wang H, Liu L, Zhu K, Yu W, Guo J. Hsa_circ_0001546 acts as a miRNA-421 sponge to inhibit the chemoresistance of gastric cancer cells via ATM/Chk2/p53-dependent pathway. *Biochem Biophys Res Commun* (2020) 521:303–9. doi:10.1016/j.bbrc.2019.10.117

33. Cai J, Chen Z, Wang J, Wang J, Chen X, Liang L, et al. circHECTD1 facilitates glutaminolysis to promote gastric cancer progression by targeting miR-1256 and activating β-catenin/c-Myc signaling. *Cell Death Dis* (2019) 10:576. doi:10.1038/s41419-019-1814-8

34. Dong X, Wang Y, Zhou Y, Wen J, Wang S, Shen L. Aquaporin 3 facilitates chemoresistance in gastric cancer cells to cisplatin *via* autophagy. *Cell Death Discov* (2016) 2:16087. doi:10.1038/cddiscovery.2016.87

35. Lin XM, Li S, Zhou C, Li RZ, Wang H, Luo W, et al. Cisplatin induces chemoresistance through the PTGS2-mediated anti-apoptosis in gastric cancer. *Int J Biochem Cel Biol* (2019) 116:105610. doi:10.1016/j.biocel.2019.105610

36. Peng L, Sang H, Wei S, Li Y, Jin D, Zhu X, et al. circCUL2 regulates gastric cancer malignant transformation and cisplatin resistance by modulating autophagy activation via miR-142-3p/ROCK2. *Mol Cancer* (2020) 19:156. doi:10.1186/s12943-020-01270-x

37. Zhang Q, Miao Y, Fu Q, Hu H, Chen H, Zeng A, et al. CircRNACCDC66 regulates cisplatin resistance in gastric cancer via the miR-618/BCL2 axis. *Biochem Biophys Res Commun* (2020) 526:713–20. doi:10.1016/j.bbrc.2020.03.156

38. Sun G, Li Z, He Z, Wang W, Wang S, Zhang X, et al. Circular RNA MCTP2 inhibits cisplatin resistance in gastric cancer by miR-99a-5p-mediated induction of MTMR3 expression. *J Exp Clin Cancer Res* (2020) 39:246. doi:10.1186/s13046-020-01758-w

39. Huang XX, Zhang Q, Hu H, Jin Y, Zeng AL, Xia YB, et al. A novel circular RNA circFN1 enhances cisplatin resistance in gastric cancer via sponging miR-182-5p. *J Cel Biochem* (2020) 122:1009–20. doi:10.1002/jcb.29641

40. Sun Y, Ma J, Lin J, Sun D, Song P, Shi L, et al. Circular RNA circ_ASAP2 regulates drug sensitivity and functional behaviors of cisplatin-resistant gastric cancer cells by the miR-330-3p/NT5E axis. *Anticancer Drugs* (2021) 32: 950–61. doi:10.1097/CAD.0000000000001087

41. Zhang J, Zha W, Qian C, Ding A, Mao Z. Circular RNA circ_0001017 sensitizes cisplatin-resistant gastric cancer cells to chemotherapy by the miR-543/PHLPP2 Axis. *Biochem Genet* (2022) 60:558–75. doi:10.1007/s10528-021-10110-6

42. Liu Y, Xu J, Jiang M, Ni L, Ling Y. CircRNA DONSON contributes to cisplatin resistance in gastric cancer cells by regulating miR-802/BMI1 axis. *Cancer Cel Int* (2020) 20:261. doi:10.1186/s12935-020-01358-w

43. Lugea A, Waldron RT. Exosome-mediated intercellular communication between stellate cells and cancer cells in pancreatic ductal adenocarcinoma. *Pancreas* (2017) 46:1–4. doi:10.1097/MPA.0000000000000686

44. Ashrafizaveh S, Ashrafizadeh M, Zarrabi A, Husmandi K, Zabolian A, Shahinozzaman M, et al. Long non-coding RNAs in the doxorubicin resistance of cancer cells. *Cancer Lett* (2021) 508:104–14. doi:10.1016/j.canlet.2021.03.018

45. Lässer C, Alikhani VS, Ekström K, Eldh M, Paredes PT, Bossios A, et al. Human saliva, plasma and breast milk exosomes contain RNA: Uptake by macrophages. *J Transl Med* (2011) 9:9. doi:10.1186/1479-5876-9-9

46. Wang H, Zeng X, Zheng Y, Wang Y, Zhou Y. Exosomal circRNA in digestive system tumors: The main player or coadjuvants?[J]. *Front Oncol* (2021) 11:614462. doi:10.3389/fonc.2021.614462

47. Yao W, Guo P, Mu Q, Wang Y. Exosome-derived circ-PVT1 contributes to cisplatin resistance by regulating autophagy, invasion, and apoptosis via miR-30a-5p/YAP1 Axis in gastric cancer cells. *Cancer Biother Radiopharm* (2021) 36:347–59. doi:10.1089/cbr.2020.3578

48. Yang X, Zhang Q, Guan B. Circ_0110805 knockdown enhances cisplatin sensitivity and inhibits gastric cancer progression by miR-299-3p/ENDOPDI Axis. *Onco Targets Ther* (2020) 13:11445–57. doi:10.2147/OTT.S279563

49. Xue M, Li G, Fang X, Wang L, Jin Y, Zhou Q. hsa_circ_0081143 promotes cisplatin resistance in gastric cancer by targeting miR-646/CDK6 pathway. *Cancer Cel Int* (2019) 19:25. doi:10.1186/s12935-019-0737-x

50. Zhang Z, Yu X, Zhou B, Zhang J, Chang J. Circular RNA circ_0026359 enhances cisplatin resistance in gastric cancer via targeting miR-1200/POLD4 pathway. *Biomed Res Int* (2020) 2020:5103272. doi:10.1155/2020/5103272

51. Liu S, Wu M, Peng M. Circ_0000260 regulates the development and deterioration of gastric adenocarcinoma with cisplatin resistance by upregulating MMP11 via targeting MiR-129-5p. *Cancer Manag Res* (2020) 12:10505–19. doi:10.2147/CMAR.S272324

52. Xia Y, Lv J, Jiang T, Li B, Li Y, He Z, et al. CircFAM73A promotes the cancer stem cell-like properties of gastric cancer through the miR-490-3p/HMGA2 positive feedback loop and HNRNPK-mediated β-catenin stabilization. *J Exp Clin Cancer Res* (2021) 40:103. doi:10.1186/s13046-021-01896-9

53. Xu B, Guo J, Chen M. Circ_0017274 acts on miR-637/CDX2 axis to facilitate cisplatin resistance in gastric cancer. *Clin Exp Pharmacol Physiol* (2022) 49: 1105–15. doi:10.1111/1440-1681.13692

54. Yang G, Tan J, Guo J, Wu Z, Zhan Q. Exosome-mediated transfer of circ_0063526 enhances cisplatin resistance in gastric cancer cells via regulating miR-449a/SHMT2 axis. *Anticancer Drugs* (2022) 33:1047–57. doi:10.1097/CAD.0000000000001386

55. Liang Q, Chu F, Zhang L, Jiang Y, Li L, Wu H. circ-LDLRAD3 knockdown reduces cisplatin chemoresistance and inhibits the development of gastric cancer with cisplatin resistance through miR-588 enrichment-mediated SOX5 inhibition. *Gut Liver* (2022) [Epub ahead of print]. doi:10.5009/gnl210195

56. Christensen S, Van der Roest B, Besselink N, Janssen R, Boymans S, Martens JWM, et al. 5-Fluorouracil treatment induces characteristic T>G mutations in human cancer. *Nat Commun* (2019) 10:4571. doi:10.1038/s41467-019-12594-8

57. Longley DB, Harkin DP, Johnston PG. 5-fluorouracil: Mechanisms of action and clinical strategies. *Nat Rev Cancer* (2003) 3:330–8. doi:10.1038/nrc1074

58. Xu G, Li M, Wu J, Qin C, Tao Y, He H. Circular RNA circNRIP1 sponges microRNA-138-5p to maintain hypoxia-induced resistance to 5-fluorouracil through HIF-1α-Dependent glucose metabolism in gastric carcinoma. *Cancer Manag Res* (2020) 12:2789–802. doi:10.2147/CMAR.S246272

59. Yang F, Yan Z, Nie W, Cheng X, Liu Z, Wang W, et al. LACTB induced apoptosis of oxaliplatin-resistant gastric cancer through regulating autophagy-mediated mitochondrial apoptosis pathway. *Am J Transl Res* (2021) 13:601–16.

60. Gao H, Xu J, Qiao F, Xue L. Depletion of hsa_circ_0000144 suppresses oxaliplatin resistance of gastric cancer cells by regulating miR-502-5p/ADAM9 Axis. *Onco Targets Ther* (2021) 14:2773–87. doi:10.2147/OTT.S281238

61. Zhong Y, Wang D, Ding Y, Tian G, Jiang B. Circular RNA circ_0032821 contributes to oxaliplatin (OXA) resistance of gastric cancer cells by regulating SOX9 via miR-515-5p. *Biotechnol Lett* (2021) 43:339–51. doi:10.1007/s10529-020-03036-3

62. Yin S, Zeng C, Hari M, Cabral F. Paclitaxel resistance by random mutagenesis of α-tubulin. *Cytoskeleton (Hoboken)* (2013) 70:849–62. doi:10.1002/cm.21154

63. Sakamoto J, Matsui T, Kodera Y. Paclitaxel chemotherapy for the treatment of gastric cancer. *Gastric Cancer* (2009) 12:69–78. doi:10.1007/s10120-009-0505-z

64. Wang M, Qiu R, Yu S, Xu X, Li G, Gu R, et al. Paclitaxel-resistant gastric cancer MGC-803 cells promote epithelial-to-mesenchymal transition and chemoresistance in paclitaxel-sensitive cells via exosomal delivery of miR-155-5p. *Int J Oncol* (2019) 54:326–38. doi:10.3892/ijo.2018.4601

65. Liu YY, Zhang LY, Du WZ. Circular RNA circ-PVT1 contributes to paclitaxel resistance of gastric cancer cells through the regulation of ZEB1 expression by sponging miR-124-3p. *Biosci Rep* (2019) 39(12):BSR20193045. doi:10.1042/BSR20193045

66. Zhou N, Wang W, Xu C, Yu W. Circular RNA PLEC acts as a sponge of microRNA-198 to promote gastric carcinoma cell resistance to paclitaxel and tumorigenesis. *Pathol Res Pract* (2021) 224:153487. doi:10.1016/j.prp.2021.153487

67. Celio L, Sternberg CN, Labianca R, La Torre I, Amoroso V, Barone C, et al. Pemetrexed in combination with oxaliplatin as a first-line therapy for advanced gastric cancer: A multi-institutional phase II study. *Ann Oncol* (2009) 20:1062–7. doi:10.1093/annonc/mdn766

68. Xu QY, Xie MJ, Huang J, Wang ZW. Effect of circ MTHFD2 on resistance to pemetrexed in gastric cancer through regulating expression of miR-124. *Eur Rev Med Pharmacol Sci* (2019) 23:10290–9. doi:10.26355/eurrev_201912_19667

69. Aoki M, Iwasa S, Boku N. Trastuzumab deruxtecan for the treatment of HER2-positive advanced gastric cancer: A clinical perspective. *Gastric Cancer* (2021) 24:567–76. doi:10.1007/s10120-021-01164-x

70. Gravalos C, Jimeno A. HER2 in gastric cancer: A new prognostic factor and a novel therapeutic target. *Ann Oncol* (2008) 19:1523–9. doi:10.1093/annonc/mdn169

71. Lv X, Li P, Wang J, Gao H, Hei Y, Zhang J, et al. hsa_circ_0000520 influences herceptin resistance in gastric cancer cells through PI3K-Akt signaling pathway. *J Clin Lab Anal* (2020) 34:e23449. doi:10.1002/jcla.23449

72. Zhao L, Peng Y, He S, Li R, Wang Z, Huang J, et al. Apatinib induced ferroptosis by lipid peroxidation in gastric cancer. *Gastric Cancer* (2021) 24:642–54. doi:10.1007/s10120-021-01159-8

73. Ma L, Wang Z, Xie M, Quan Y, Zhu W, Yang F, et al. Silencing of circRACGAP1 sensitizes gastric cancer cells to apatinib via modulating autophagy by targeting miR-3657 and ATG7. *Cel Death Dis* (2020) 11:169. doi:10.1038/s41419-020-2352-0

74. Wang JM, Ji LL, Branford-White CJ, Wang ZY, Shen KK, Liu H, et al. Antitumor activity of Dioscorea bulbifera L. rhizome *in vivo*. *Fitoterapia* (2012) 83:388–94. doi:10.1016/j.fitote.2011.12.001

75. Lu Y, Li L, Li L, Wu G, Liu G. Circular RNA circHECTD1 prevents Diosbulbin-B-sensitivity via miR-137/PBX3 axis in gastric cancer. *Cancer Cel Int* (2021) 21:264. doi:10.1186/s12935-021-01957-1

76. Ma YY, Zhang Y, Mou XZ, Liu ZC, Ru GQ, Li E. High level of homeobox A9 and PBX homeobox 3 expression in gastric cancer correlates with poor prognosis. *Oncol Lett* (2017) 14:5883–9. doi:10.3892/ol.2017.6937

77. Cann C, Ciombor KK. Systemic therapy for gastric cancer: Perioperative strategies and beyond. *J Surg Oncol* (2022) 125:1151–60. doi:10.1002/jso.26834

78. Beilerli A, Gareev I, Beylerli O, Yang G, Pavlov V, Aliev G, et al. Circular RNAs as biomarkers and therapeutic targets in cancer. *Semin Cancer Biol* (2022) 83:242–52. doi:10.1016/j.semcancer.2020.12.026

Pathology & Oncology Research | frontiers

TYPE Review
PUBLISHED 18 October 2023
DOI 10.3389/pore.2023.1611415

Check for updates

OPEN ACCESS

EDITED BY
Jozsef Dudas,
Innsbruck Medical University, Austria

*CORRESPONDENCE
Fouzia Siraj,
fouziasiraj2009@gmail.com
Aroonima Misra,
dr.aroo.2402@gmail.com

†These authors have contributed equally to this work and share first authorship

RECEIVED 21 July 2023
ACCEPTED 03 October 2023
PUBLISHED 18 October 2023

CITATION
Verma P, Rishi B, George NG, Kushwaha N, Dhandha H, Kaur M, Jain A, Jain A, Chaudhry S, Singh A, Siraj F and Misra A (2023), Recent advances and future directions in etiopathogenesis and mechanisms of reactive oxygen species in cancer treatment. *Pathol. Oncol. Res.* 29:1611415. doi: 10.3389/pore.2023.1611415

COPYRIGHT
© 2023 Verma, Rishi, George, Kushwaha, Dhandha, Kaur, Jain, Jain, Chaudhry, Singh, Siraj and Misra. This is an open-access article distributed under the terms of the Creative Commons Attribution License (CC BY). The use, distribution or reproduction in other forums is permitted, provided the original author(s) and the copyright owner(s) are credited and that the original publication in this journal is cited, in accordance with accepted academic practice. No use, distribution or reproduction is permitted which does not comply with these terms.

Recent advances and future directions in etiopathogenesis and mechanisms of reactive oxygen species in cancer treatment

Priyanka Verma[1†], Bhavika Rishi[1†], Noreen Grace George[1], Neetu Kushwaha[1], Himanshu Dhandha[1], Manpreet Kaur[1], Ankur Jain[2], Aditi Jain[2], Sumita Chaudhry[2], Amitabh Singh[2], Fouzia Siraj[1*] and Aroonima Misra[1*]

[1]Department of Health Research, Indian Council of Medical Research-National Institute of Pathology, New Delhi, India, [2]Vardhman Mahavir Medical College and Safdarjung Hospital, New Delhi, India

A class of exceptionally bioactive molecules known as reactive oxygen species (ROS) have been widely studied in the context of cancer. They play a significant role in the etiopathogenesis for cancer. Implication of ROS in cancer biology is an evolving area, considering the recent advances; insights into their generation, role of genomic and epigenetic regulators for ROS, earlier thought to be a chemical process, with interrelations with cell death pathways- Apoptosis, ferroptosis, necroptosis and autophagy has been explored for newer targets that shift the balance of ROS towards cancer cell death. ROS are signal transducers that induce angiogenesis, invasion, cell migration, and proliferation at low to moderate concentrations and are considered normal by-products of a range of biological activities. Although ROS is known to exist in the oncology domain since time immemorial, its excessive quantities are known to damage organelles, membranes, lipids, proteins, and nucleic acids, resulting in cell death. In the last two decades, numerous studies have demonstrated immunotherapies and other anticancer treatments that modulate ROS levels have promising *in vitro* and *in vivo* effects. This review also explores recent targets for therapeutic interventions in cancer that are based on ROS generation or inhibition to disrupt the cell oxidative stress balance. Examples include-metabolic targets, targeted therapy with biomarkers, natural extracts and nutraceuticals and targets developed in the area of nano medicine. In this review, we present the molecular pathways which can be used to create therapy plans that target cancer by regulating ROS levels, particularly current developments and potential prospects for the effective implementation of ROS-mediated therapies in clinical settings. The recent advances in complex interaction with apoptosis especially ferroptosis and its role in epigenomics and modifications are a new paradigm, to just mechanical action of ROS, as highlighted in this review. Their inhibition by nutraceuticals

and natural extracts has been a scientific challenging avenue that is explored. Also, the inhibition of generation of ROS by inhibitors, immune modulators and inhibitors of apoptosis and ferroptosis is explored in this review.

KEYWORDS

reactive oxygen species (ROS), recent advances, future directions, cancer therapy, ferroptosis

Introduction

Cancer remains a significant global health burden, affecting both developed and developing nations, despite advancements in cancer diagnosis, treatment, and prevention. Annually, approximately 10 million individuals lose their lives to cancer, while 19–20 million new cancer cases are diagnosed worldwide [1]. ROS are closely linked to a number of malignancies, including cancers of lung, breast, colorectal, cervical, and hepatocellular carcinoma, which are among the most common cancers in terms of incidence cases globally. The etiopathogenesis of cancer is multifaceted [2]. An extensive understanding of the role of ROS in the causes and progression of cancer, along with their function in the progression of the disease, can greatly enhance targeted therapies. The latest advances in understanding the generation of ROS, including role of ferroptosis, epigenetic changes associated with ROS and its etiopathogenesis in cancer and its role in cancer progression is continuously being explored.

"ROS" is an umbrella term attributing to unstable, reactive, partially reduced oxygen derivatives generated by oxidation-reduction (redox) or electronic excitation processes [3] (Figure 1A). They are made up of free radicals such as hydroxyl (HO*)and superoxide (O_2*), in addition to non-radical molecules such as hydrogen peroxide (H_2O_2), which are generally less reactive than most ROS but can enter any cellular compartment before they're broken down into oxygen and water by peroxiredoxins and GPXs (glutathione peroxidases) [3].

H_2O_2 contributes to redox signalling by acting as a second messenger in a variety of pathways that influence gene expression and the transmission of external signals [3]. ROS are by-products of several biological activities, including oxygen consumption, playing a crucial role in various biological processes within both healthy and malignant cells [3]. Increasingly evident research indicates that ROS behave in cancer cells in a " double-edged " way [4]. At low to moderate concentrations, reactive oxygen species (ROS) act as signal transducers, stimulating cancer cell motility, drug resistance, angiogenesis, and invasion. On the other hand, high quantities of ROS injure cancer cells and ultimately cause cell death (Figure 1B). Therefore, tight synchronization of ROS levels is essential for cellular life [4]. Thus, antioxidants are important in Redox biology (Figure 1A). Superoxide dismutases (SODs) found in the cytoplasm, mitochondria, and extracellular matrix (ECM), along with glutathione reductase (GR), GPX, thioredoxin, peroxiredoxin and catalase, each function collectively in eukaryotic cells to recycle antioxidants in the reduced state and reduce O_2* anions into water [5]. In this article, we examine existing cancer therapy approaches that employ ROS pathways and offer insights into their potential as therapies in the future.

Generation of ROS and redox homeostasis

ROS are produced by various exogenous and endogenous sources. The electron transport chain (ETC) and the trans-membrane NADPH oxidases (NOXs) on the inner mitochondrial membrane are the most important endogenous enzymatic producers of O_2* and HO* free radicals [3, 6]. In addition, oxidants can be produced by peroxisomes and endoplasmic reticulum (ER) and enzymes, including xanthine oxidase, cyclooxygenases, nitric oxide synthase, cytochrome P450 enzymes, and lipoxygenases [2] (Figure 2A). NOXs have many cellular localizations, which contribute to the local generation of ROS and allow H_2O_2 compartmentalization for cell signalling via cell surface receptors. The two vital areas for generation of ROS are complexes I and III where the leakage of electrons leads to the generation of O_2* [4]. While complex III releases its products into the cristae lumen and the intermembrane gap, complex I releases its products into the mitochondrial ETC in the direction of the mitochondrial matrix [6]. Along with complex I and III of mitochondrial ETC as major sources of ROS, downregulation of Complex IV of cytochrome c-oxidase also contributes to the generation of increased levels of mitochondrial and cellular ROS and enhanced glycolysis, as revealed by Agnireddy et al. The Fenton reaction involving Fe^{2+} can also give rise to ROS non-enzymatically. Fe [2] reacts H_2O_2 with to yield HO* radicals, which can cause destruction to genome and other biomolecules [6]. Beside intracellular sources, multiple external factors, known as the "exposome," induce exogenous ROS as a result of accumulative environmental exposure, including molecular components such as nutrients, drugs, pollutants, and toxicants, along with physical stressors such as UV, X-ray, and other ionising radiations, and lifestyle [3, 7]. Therefore, multiple intracellular and external stimuli work together to promote the generation of ROS in tumour cells (Figure 2B).

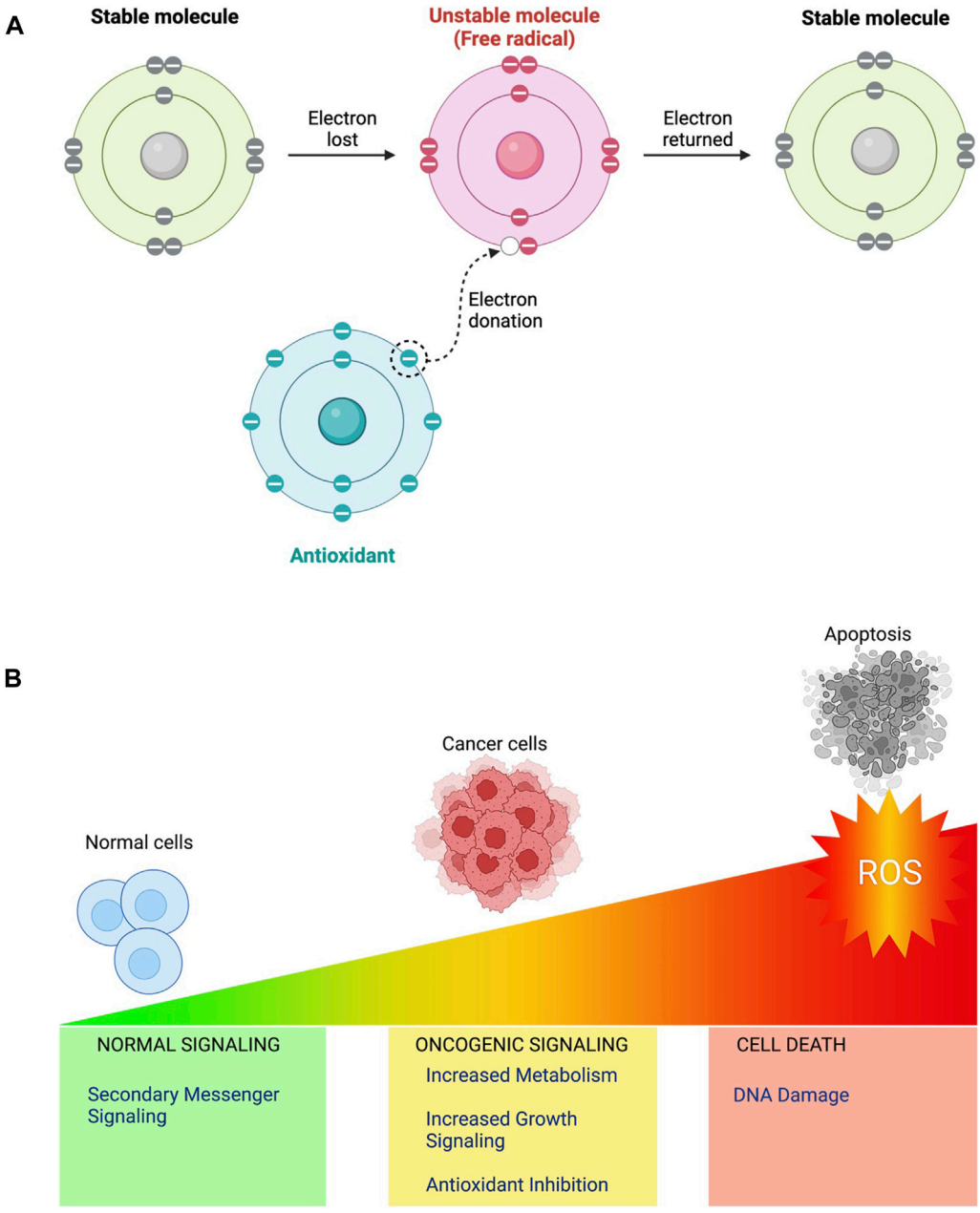

FIGURE 1
(A) When electrons are lost from stable compounds in biological systems, free radicals or ROS are frequently produced. This generated unstable, highly reactive molecules with unpaired electrons are especially reactive because they want to couple their unpaired electrons. Antioxidants are stable compounds which can donate an electron or a hydrogen atom to stabilise a free radical. **(B)** ROS function as intracellular second messengers at low doses and take part in cell communication and control a variety of physiological functions. Moderate ROS levels can inhibit antioxidant activity, limiting the cell's capacity to combat ROS and contributing to cancer cell survival. Excess ROS can cause oxidative stress, which can damage biological components, including DNA and can activate apoptotic pathways, resulting in programmed cell death (apoptosis).

Apoptosis and cell-cycle arrest are brought on by excessive ROS concentrations. In response to oxidative stress, cancer cells increase the production of antioxidant enzymes as a protective measure against excessive intracellular reactive oxygen species (ROS). The NRF2-KEAP1 complex is an example of a physiological sensor-effector apparatus based on thiols that responds to an oxidant challenge and plays a part in eukaryotic redox homeostasis [4]. It is a key detector for electrophilic and oxidative stressors, and KEAP1 that serves as an NRF2 inhibitor contains many cysteine residues which are vulnerable to oxidation. The oxidation process plays a crucial role in the formation of Cys-disulfide within the KEAP1 dimer. This

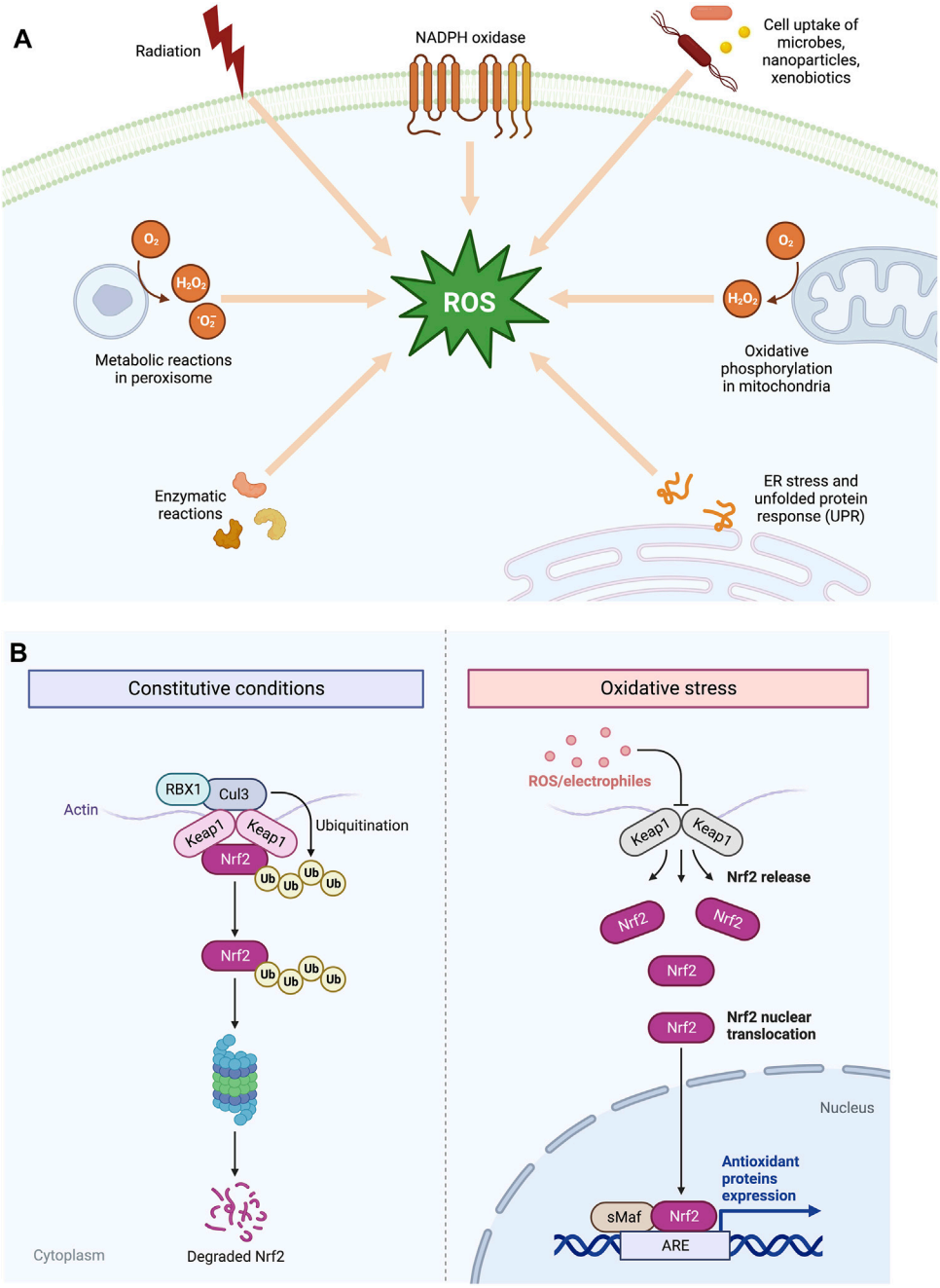

FIGURE 2
(A) Endogenous and exogenous sources of Reactive Oxygen Species (ROS). **(B)** The pathway between KEAP1 and NRF2 is shown schematically. Under normal physiological circumstances, NRF2 is found next to KEAP1 in the cytoplasm to activate Cul3-dependent ubiquitination and its degradation via the proteasome. Under oxidative stress, NRF2 separates from KEAP1 and moves into the nucleus and activates several cytoprotective genes.

oxidation induces a conformational change in KEAP1, enhancing its stability and facilitating the transportation of NRF2 to the nucleus. In the nucleus, NRF2 acts as a transcription factor (TF), regulating the expression of various antioxidant defences proteins [4] (Figure 2B).

ROS interactions with lipids, proteins, genome and epigenome

In ROS synthesis with an increase or decrease in the amount of ROS scavenged, cells experience oxidative stress. Further,

elevated intracellular ROS levels may affect proteins lipids, and DNA, and this capacity of ROS has been used in a number of anti-tumor approaches, as mentioned below. ROS have the ability to oxidize intracellular lipids, proteins, and DNA, resulting in the accumulation of damaged biological elements.

ROS and lipids

One important area of research in ROS is lipid-derived ROS, which is generated when polyunsaturated fatty acids are oxidised and result in lipid H_2O_2 and related radicals like peroxyl and alkoxyl [3]. ROS can produce oxidative stress by their interactions with lipids via a feedback loop initiated by fatty acid peroxidation, which changes lipid bilayer of cellular membranes [5]. Such oxidised lipids have an important function in redox signalling, especially in immunological signalling. Examples of enzymes that create reactive oxidants are lipoxygenases and prostaglandin synthases (cyclooxygenases), which operate as mediators in the mechanisms that start and control inflammatory responses. The breakdown of ETC complexes I and III and mitochondrial phospholipids peroxidation, which may potentially affect the integrity of PTPs (permeability transition pores) and enhance electron transport is potentially harmful to the cells [5].

ROS and proteins

Protein function is affected by redox signalling, which results in alterations in signalling outputs, activity of enzymes, DNA transcription, and membrane and chromosomal integrity [5, 6]. The biological effects of ROS are exerted in redox regulation mostly through thiol-based protein modification. Cysteines are particularly susceptible to oxidation in many proteins, including cytoskeletal components, scaffold proteins like 14-3-3, and, HSPs (heat shock proteins), and various ribonucleoproteins (RNPs), raising the prospect of functional protein networks controlled by redox [3]. Since the by-product of protein folding is H_2O_2, ROS are crucial to ER stress and protein folding [3]. ROS by interacting with proteins impacts signaling pathways implicated in the regulated cell expansion and apoptosis control. They tend to inhibit phosphatases whereas kinases can either be activated or inhibited. The Src family of nonreceptor protein kinases, small G proteins like Ras, growth factor tyrosine kinase receptors, and elements of the c-Jun p38 kinase (p38MAPK) and c-Jun N-terminal kinase (JNK) pathways that trigger apoptosis are all particularly activated by ROS [5, 8]. Small rise in ROS are predicted to preferentially trigger the PI3-K/Akt pathway, whereas larger levels are predicted to cause p38MAPK-dependent apoptosis [8]. Additionally, ROS affect calcium channel function. They cause the release of calcium from cellular reserves, which in turn activates kinases like protein kinase C, and is a key factor in the growth of cancer cells [5].

ROS interactions with genome

Single-strand and double-strand breaks, base modifications, deoxyribose alterations, and DNA cross-linking are all examples of DNA damage brought on by ROS. Finally, ROS has a direct impact on TFs' capacity to bind DNA [2]. For instance, ROS boost the nucleus localization of the Fos/Jun DNA-binding protein redox factor-1 (Ref-1), and the ataxia-telangiectasia mutated (ATM) serine/threonine kinase, which is responsible for DNA damage repair [5].

To avoid excessive ROS production, cancer cells activate the transcription of antioxidant enzymes, demonstrating usefulness of a comprehensive understanding of these networks in unravelling the treatments responsible for lowering ROS levels. When ROS levels rise, JNK activates the forkhead box O (FOXO) family of TFs, which stimulates the synthesis of SODs and catalase. Despite the fact that the H_2O_2 produced by SODs from O* serves as a substrate for catalase, activation of SODs by a FOXO4 TF appears to counteract their antioxidant effect [5]. The expression of the antioxidant gene is significantly regulated by p53, another significant TF is inhibited by moderately raised ROS levels, but its expression is encouraged by greater ROS levels [5]. Further, ROS can activate or impede NFκB role depending on the context. By oxidizing and activating the inhibitor of NFκB (IκB) kinases, which inhibit IκB stability, cytosolic H_2O_2 can activate the NFκB pathway. Since the DNA binding domain of NFκB contains oxidizable cysteines, H_2O_2 can also directly influence its activity. During this situation, increasing nuclear H_2O_2 production hampered NFκB DNA binding and decreased transcriptional activity, but increasing nuclear levels of the H_2O_2 scavenger peroxiredoxin 1 boosted transcriptional activity [3].

When ROS levels are moderate, they activate HIF1 (Hypoxia Inducing Factor) which results in the activation of numerous genes crucial for the growth of cancer, including VEGF and VEGF receptors [3].

ROS interactions with epigenome

ROS impact the functioning of epigenetic modifiers such as DNA methyltransferases (DNMTs) and histone deacetylases (HDACs) with repercussions for target gene expression and can result in both hypomethylation and hypermethylation of DNA [9]. They oxidise DNA as well, particularly guanine and adenine (8-oxo-G and 8-oxo-A). It has been discovered among every 100,000 guanines in regular cells, a portion undergoes oxidation, and this proportion rises by 35%–50% in cancer cells

[3]. Unrepaired 8-oxo-G is highly mutagenic, particularly when it interacts with A, leading to G to T transversions. Due to these characteristics, it holds significant potential as an indicator of mutagenesis and cancer triggered by reactive oxygen species (ROS). Furthermore, 8-oxo-Gs build up at telomeres, inhibiting telomerase and reduce telomeric protein binding, altering telomere length and impeding chromosomal-end capping maintenance [3, 10]. Other sorts of oxidative damage can cause DNA demethylation like ROS hydroxylate methylcytosine to produce 5-hydroxymethylcytosine (5hmC) [6]. A feedback loop potentially resulting from alterations in mitochondrial DNA caused by ROS, results in mutations in genes producing ETC complexes that may significantly impair electron transport efficiency.

Heterogenous function of ROS in cancer

The world's second-leading cause of death is Cancer, and it is distinguished by a number of hallmarks, which includes cell transformation, DNA instability, angiogenesis, hyper growth, epithelial-mesenchymal transition (EMT), immortalization, and metastasis, all of these are regulated in a variety of manners by intracellular ROS. To develop more effective cancer therapies, the mechanism of ROS in carcinogenesis must be investigated. When ROS levels surpass normal levels, they can trigger carcinogenesis and accelerate tumour growth. Excessive ROS production can lead to genetic mutations, which stimulate oncogenes and block tumour suppressor genes including KRAS oncogene and p53, resulting in cancer development [2]. Raised ROS additionally boosts tumour formation by lowering the activity of NK cells and T cells and increasing macrophage engagement and M2 polarization. Furthermore, high levels of ROS encouraged tumour invasion and metastasis mediated EMT [2]. As discussed in Section *ROS interactions with epigenome*, the buildup of 8-oxodG in cellular genomes causes cancer. It is noteworthy that iron-mediated oxidative stress is a predictor underlying emergence of several malignancies. Cancer-associated fibroblasts (CAFs), which are especially abundant in tumour microenvironment (TME), contribute actively to the control of tumour homeostasis, encouraging tumour growth and cancer cell migration [2].

ROS inhibit the proliferation of cancer cells, hence preventing their expansion. ROS directly reduce EGF and EGFR expression leading to blockage of downstream signaling molecules responsible for proliferation including ERK and PI3K/Akt. H_2O_2 injection can inhibit ERK1/2 phosphorylation in breast cancer cells, slowing the growth of cancer cells dependent on its dosage [11]. Additionally, high ROS prevent androgen-independent prostate cancer cell growth by preventing EGF-triggered EGFR-mediated PI3K/Akt signaling. Additionally, ROS interfere with the PI3K/Akt/NFκB signaling network, preventing the growth of A549 human lung cancer cell [2]. ROS buildup in multiple myeloma cells decreases phosphorylation of Src and Janus kinases (JAK1, JAK2), obstructing STAT3/STAT5 phosphorylation and reducing the transcription of cyclins (B1, D1 and E) and cyclin dependent kinases (CDK2,CDK4) ultimately resulting in arresting of cell cycle and slowing cancer growth [2]. Moreover, the buildup of ROS regulates molecules that govern the cell cycle, including the CDC25 (cell division cycle) and CDK inhibitors. CDC25B is rendered inactive by LGH00031, which then dephosphorylates CDK1's tyrosine to stimulate the CDK1/cyclin B complex, causing the cell cycle to be arrested and the proliferation of cancer cells to be inhibited [12]. Highly mitotic cells require an adequate supply of nucleotides and ATP. As a result of the buildup of ROS, cancer cells may be unable to produce enough ATP and nucleotides to support cell growth [2].

ROS induced programmed cell death

ROS and apoptosis

Higher concentrations of ROS either intrinsically or extrinsically control the "apoptosis" process and H_2O_2 is one of the most significant ROS in terms of its ability to directly and powerfully cause apoptosis. ROS interacts with mitochondrial ETC, causing cytochrome c release by rupturing the mitochondrial membrane and opening PTP. Cytochrome-c, in collaboration with Apaf-1 (apoptotic peptidase activating factor 1) and procaspase-9, generates "apoptosomes" in the cytosol that activate caspase-9, which in turn triggers effector caspases such as caspase-3 or 7, culminating in protein breakdown and apoptotic cell death [5] (Figure 3A). The extrinsic route is activated by death-inducing ligands binding to cognate receptors, such as Fas ligands and TNF-related apoptosis-inducing ligands (TRAIL-R1/2) which in turn attract pro-caspases and adaptor proteins. As a result, the death-inducing signalling complex (DISC) forms, effector caspases are activated, and apoptosis is triggered [4]. Additionally, Caspase-8 and Caspase-10 cleave Bid to create truncated Bid (tBid), which translocates to mitochondria, inhibits BcL-2 and BcL-xL's anti-apoptotic activity and activates Bax and Bak [4] (Figure 3A). Additionally, the generation of oxidative stress in mitochondria is necessary for the activation of the p53-induced intrinsic apoptosis signalling pathway [13]. The elevated ROS level influences p53's translational modification and stabilisation, which activates p21-mediated cell cycle arrest [13].

Chemotherapy and radiation generate intracellular ROS, which can employ intrinsic or extrinsic routes to trigger apoptosis. Procarbazine generates oxidative damage of DNA that is not mended by the BER/NER system in brain tumours and Hodgkin's lymphoma. ROS production during doxorubicin-relied cytotoxicity is successfully utilised to treat, breast cancer,

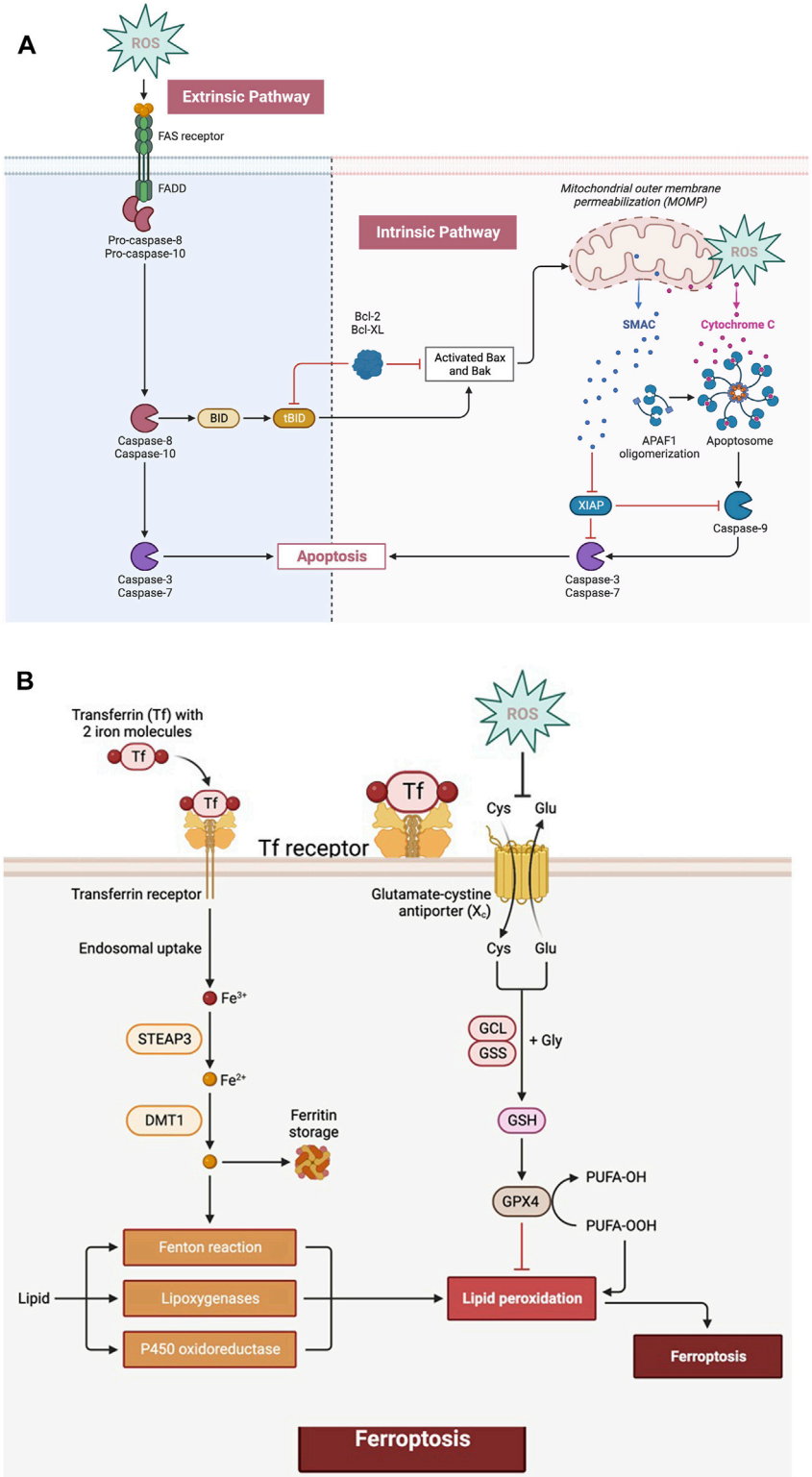

FIGURE 3
(A) ROS can increase death receptor clustering and aggregation on the cell membrane, boosting their signalling potential and extrinsic pathway. The activation of initiator caspases subsequently activate downstream effector caspases, leading to apoptosis. Intracellular stress signals activate the intrinsic route, also known as the mitochondrial pathway. Permeabilization of the mitochondrial membrane allows for the release of cytochrome c from the mitochondria, which, together with other components, forms the apoptosome, which activates the caspases leading to apoptosis. **(B)**
(*Continued*)

FIGURE 3 (Continued)
The absorption of extracellular iron by particular transporters, such as transferrin receptor 1 (TfR1), initiates ferroptosis. The free iron in the cytoplasm can participate in Fenton reactions, which produce highly reactive OH* radicals. Furthermore, lipid metabolism in cells generates lipid peroxides (LOOH) which react with polyunsaturated fatty acids (PUFAs), causing lipid peroxidation. During ferroptosis, there is a significant depletion of GSH due to a decrease in cystine absorption, and the activity of antioxidant enzymes such as GPX4 is reduced, resulting in increased oxidative stress.

Kaposi's sarcoma and acute lymphocytic leukaemia (ALL) [5, 14]. Apoptosis has been demonstrated to be triggered by a course of therapy that includes the DNA replication-impairing agent arabinocytosine, followed by the ROS-increasing agent anthracyclines, and has been proven to be advantageous for AML patients [15]. Furthermore, the administration of platinum-based medications together with poly ADP-ribose polymerase (PARP) inhibitors, a protein indulged in maintaining DNA integrity, has demonstrated in BRCA-deficient models as well to stop the development of breast cancer cells, raising ROS levels that stimulate apoptosis [16]. Increased ROS on sphingomyelinase, creates ceramide from sphingomyelin and leads to binding to death receptors on cancer cell membranes, may also be an apoptosis mediator [5, 13]. Likewise employing medications that impact mitochondria, which create more than half of all ROS, is an efficient strategy to induce oxidative stress and death in cancer cells [5]. Several medications have been developed to escalate ER stress in cancer cells by inducing oxidative stress. These include celecoxib, an anti-inflammatory drug, which exacerbates ER stress and promotes apoptosis by changing ratio of Bax/BcL-2 and elevating ROS in prostate cancer cells, and bortezomib, a proteasome inhibitor, which leads to ER stress via ROS in squamous carcinoma cells of the head and neck [5].

ROS and autophagy

"Self-eating" or autophagy is a tightly regulated process that eliminates dysregulated or harmed intracellular proteins. Recently, ROS-induced autophagy has been introduced as a significant therapeutic strategy to eradicate cancer cells. In particular, it has been reported that LC3-associated autophagosomes are increased by H_2O_2-dependent inactivation of the autophagy-related gene-4 (ATG4) and that the critical autophagy inhibitor mTORC1 is downregulated by ATM-mediated oxidation of AMPK (AMP-activated protein kinase) [13]. It has been shown that polycyclic ammonium ion sanguinarine therapy, that boosts electron leakage from mitochondria and produces NOXs, causes H_2O_2 to cause autophagy in glioma cells [17]. When rapamycin and HSP90 inhibitors are used together, they produce mitochondrial damage, oxidative stress, and autophagy, which slows the development of RAS-dependent tumours [17]. ROS can also regulate autophagy via the stimulation of TF such as NFκB which modulates the transcription of autophagy inducing genes like BECLIN1/ATG6 or SQSTM1/p62 in tumour cells [7].

ROS and necroptosis

Necroptosis is regulated necrosis mediated by death receptors. It exhibits morphological features of both apoptosis and necrosis and requires protein RIPK3 (receptor-interacting protein kinase 1) and its substrate MLKL, the crucial players of this pathway [7]. ROS can also induce necrosis. According to certain studies, ROS produced following ceramide production or after a rise in energy metabolism both by NOXs or in the mitochondrial ETC have been shown to promote necroptosis [7].

ROS and ferroptosis

One of the most crucial ways to prevent cancer is through ROS-induced ferroptosis. A very fascinating ROS-associated mechanism of p53's tumour regression has newly come to light that causes ferroptosis (dependent on the existence of intracellular iron) by increasing ROS levels [18]. In the investigation by Yang et al., several ferroptosis-inducing substances (FINs) were used, and it was discovered that every FIN inhibited GPX4 either directly or indirectly by depleting GSH [19, 20]. They concluded that the main regulator of ferroptosis is GPX4. Phospholipid hydroperoxides (PLOOH) are reduced into their corresponding phospholipid alcohols by the catalytic action of GPX4. For GPX4 to operate normally physiologically, GSH is required. Glutamate-cysteine ligase catalyses the formation of intracellular GSH. Thus, cysteine is a rate-limiting amino acid for GSH synthesis, and it is absorbed as cystine via the cystine/glutamate antiporter (Xc) system. Due to build-up of PLOOH caused by the inactivation of GPX4, cell membrane damage and ferroptotic death may result. It was also shown in Yang et al.'s work that genetically inhibiting GPX4 can cause tumour cell ferroptosis and stop tumour development *in vivo* [20]. Ferroptosis, an iron-dependent kind of cell death, is characterised by an increase in the labile iron pool (LIP), a tiny pool of Fe2+ [21]. The main mechanisms by which cellular iron absorption is mediated is through the binding of transferrin to its receptor, was discovered in 1997. Alternatively, elevated intracellular LIP can contribute to the phospholipids peroxidation to form PLOOH and can produce free radicals via the Fenton reaction. Alternatively, iron catalyses the majority of ROS production in cells.

The production of ROS starts lipid peroxidation, which ultimately results in ferroptosis. It has been demonstrated that cancer cells require more iron to survive than healthy ones. Rapidly reproducing cancer cells have increased iron intake and intracellular iron levels, raising the possibility that ferroptosis induction might be used as a therapeutic target for cancer [18]. According to research by Alvarez et al., raising intracellular LIP in lung cancer cells by inhibiting NFS1 makes them more susceptible to ferroptosis and slows the development *in vivo*. Lipoxygenases and cytochrome P450 oxidoreductase (POR) can also be involved in the synthesis of PLOOH during enzymatic lipid peroxidation. The deoxygenation of free and esterified PUFAs by lipooxygenases, nonheme iron-containing enzymes, results in PLOOH [19]. The classical GPX4-controlled route, the lipid metabolism pathway, and the iron metabolism pathway are the three primary avenues to reverse chemotherapy resistance, according to the principles driving ferroptosis [19]. Erastin is a synthetic medication that causes tumour cells with mutant RAS to undergo ferroptosis and by changing the outer mitochondrial membrane's permeability and raising intracellular ROS levels [18]. According to studies, synthetic medicines like artesunate, sorafenib, and erastin suppress the production of glutathione (GSH), inactivating GPX, which causes oxidative stress in cancer cells and eventually results in ferroptosis [18] (Figure 3B). Through genome-wide, CRISPR-Cas9-mediated suppressor screens, Zou et al. investigated POR as a requirement for ferroptotic cell death in cancer cells [22]. High hopes have been placed on ferroptosis as a novel, promising means of eliminating cancer cells because of ferroptosis inducers.

ROS in cancer prevention and therapy

Role of ROS in tumor immunity

In the TME, controlling ROS levels have been demonstrated to have anti-tumour effects. Their response promote cancer cell apoptosis, impede angiogenesis, prevent immune escape, alter tumour metabolic reorganisation, and improve drug resistance. T regulatory (Treg) cells are attracted and act as potent immunosuppressors in TME [23]. It is known in general that the TME, which is constructed of a vast range of cell types, including cancer cells, fibroblasts linked with cancer, and immune cells, produces a region with significant concentration of ROS with high ROS level as the main components responsible for TME's resistance to immunotherapies, particularly immune checkpoint blockades [23]. Due to the increased ROS concentration present in the TME, tumour-infiltrating Treg cells die. It is noteworthy that tumour-infiltrating apoptotic Treg cells inhibit programmed death-ligand 1-blockade-mediated anti-tumour T cell immunity by switching ATP to adenosine, despite their poor NRF2-associated antioxidant system making them particularly susceptible to ROS [5]. Based on this scenario, the ROS reduction in TME can enhance the effectiveness of cancer immunotherapies. Precisely, by removing ROS, a novel nano-scavenger anchoring on the ECM alleviated suppressive immunogenic cell death [5, 23].

In addition to Treg cells, ROS are important metabolic regulators of cytotoxic T cells and Dendritic cell (DC) mediated anti-tumour immunity [5]. In general, the link between ROS and cancer immunity remains a mystery, which emphasises the ongoing need to research this to increase the effectiveness of immunotherapies.

Antioxidant nutraceuticals in cancer prevention

Antioxidant nutraceuticals are a grouping of nutraceuticals (a combination of nutrition and medicines) that have antioxidant properties. Numerous antioxidant substances and enzymes in our body control the amount of ROS. In addition to vitamins and minerals like zinc and selenium, it also contains enzymes like GPXs and catalases, whose primary goal is to scavenge ROS. The consumption of naturally occurring antioxidant-rich foods has been suggested as one of the best strategies to ward off cancer. It has been discovered that many nutrients, including vitamins A, C, D, and E, choline (the richest dietary sources of choline are meat, fish, dairy, and eggs) and theanine, have potent antioxidant properties that inhibit the growth of cancer stem cells and tumorigenesis in a variety of tumour types, including breast, lung, brain, and others [24]. Vitamin A can mix with peroxyl radicals and function as a chain-breaking antioxidant before the peroxyl radicals can interact with lipids and produce hydroperoxides, avoiding cellular damage [22]. Supplemental 25-hydroxyvitamin D (Vitamin D) has been shown to lower breast and colorectal cancer death rates while having the reverse impact on prostate cancer [24, 25]. Additionally, it has been shown that enhanced absorption of DHA, an oxidised version of vitamin C, showed preferential death of colorectal cancer cells with KRAS or BRAF mutations through the glucose transporter 1 (GLUT1) pathway [26]. Thyroid cancer cell growth is suppressed by vitamin C, which has been shown to increase the formation of ROS and limit the ERK phosphorylation by reducing EGF release and phosphorylation of its receptor [27]. The class of fat-soluble antioxidant compounds known as vitamin E includes tocopherols and tocotrienols that lower ROS, inhibits the growth of tumours and carcinogenesis, and encourage the death of cancer cells [28]. The few therapies currently available for treating pancreatic cancer by increasing intracellular ROS levels to promote apoptosis are gemcitabine, BITC (Benzyl isothiocyanate) and capsaicin [7]. Aminoflavone (AF), a synthetic substance related to flavonoids, has shown antiproliferative action against many cell lines from the kidney, breast, and ovary. MCF7 and MDA-MB231 cells are killed by AF, whereas normal, non-malignant breast cells are unaffected [7, 27]. An increase in intracellular ROS is seen following AF therapy, coinciding with a rise in the activation of Caspase

3 following apoptosis [29]. Similar to AF, many substances, including IOA, pancratistatin, and Triphala, cause the death of breast cancer cells by raising intracellular ROS concentration through the dissipation of the membrane potential of mitochondria [7].

Phytochemicals and natural extracts with anticancer properties

Plant-derived chemicals including polyphenols and flavonoids have been demonstrated to be particularly beneficial in the treatment of cancer, with their effect being mediated through scavenging ROS [30]. Strong metal ion chelators and tea polyphenols limit the liberation of ROS from the auto-oxidation of numerous substances. EGCG is the tea catechin that reacts with the majority of ROS most effectively [31]. In HepG2 (hepatic cancer), PC-3 (prostate cancer), and MCF-7 (breast cancer) cells, it has been found that the natural polyphenol resveratrol induces apoptosis through regulating antioxidant enzymes [32]. Further, lower quantities of curcumin (isolated from the dried root of rhizome Curcuma Longa) have been linked to decreased ROS generation, but greater concentrations of curcumin have been linked to increased ROS levels in solid tumours and leukaemia [23]. In the transgenic prostate cancer model, nimbolide was found to create oxidative stress, which delayed tumour development via STAT3 signalling [33, 34]. By preventing ROS from activating MAPKs, β-caryophyllene oxide has been proven to inhibit tumour development and promote apoptosis [30]. The main bioactive component of cayenne peppers is capsaicin, a homovanillic acid derivative [35] causes redox imbalance and ferroptosis in glioblastoma cells via ACSL4/GPx4 signalling pathways [36]. Piperine administration lowered mitochondrial lipid peroxidation caused by oxidative stress in mice with lung cancer and improved the activity of both the enzymatic (catalase, SOD, and GPX) and non-enzymatic (reduced GSH, vitamin C and vitamin E) anti-oxidant defence system [37]. Koumine, a common alkaloid monomer in *Gelsemium* plants, has a strong antioxidant impact which prevents ERK from being phosphorylated and, as a result, slows the growth of HCCs [38]. Genistein, a particular class of isoflavone occurs naturally in soy and soy products [39] acts as an inhibitor of radiation- and carcinogen-induced tumours of the liver and mammary glands due to its antioxidant and antiproliferative properties. The scavenging of ROS, the prevention of oxidative and photodynamic DNA damage, and the inhibition of tyrosine protein kinase are some of the potential mechanisms behind genistein's anticarcinogenic effects [39, 40]. In addition, the phenol thymol causes human glioblastoma cells to undergo both apoptosis and necrosis. Thymol stimulates the ROS formation, which causes DNA damage and cell membrane rupturing in addition to having lethal actions on many malignant cells [34]. The monoterpene compound thymoquinone, the primary essential oil component of *N. sativa* seeds [34], inhibits the PI3K/Akt signalling network in bladder and breast malignancies while activating ROS production to phosphorylate p38 [40].

The anticancer efficacy of plant extracts against various cancer cell lines that have been examined *in vitro* and *in vivo*. Some plant metabolites that have been identified and extracted have distinctive bioactivities that improve therapeutic efficacy through ROS-mediated mechanisms [30]. SW480 (human colorectal cancer cells) underwent cell growth arrest and apoptosis when treated *with M. alba* root bark extract. In this investigation, the extract showed that cyclin D1 was degraded by the proteasome and that ATF3 was activated by ROS and GSK3-dependent signalling. Additionally, the growth of the Calu-6 (pulmonary), HCT-116 (colon) and MCF-7 (breast) cancer cell lines was suppressed by a methanolic extract of *M. alba* leaves [30]. The pharmacological effects of platycodin D, a significant triterpenoid saponin isolated from *P. grandiflorus* roots, including its anti-tumour, anti-inflammatory, anti-obesity, and antiallergy properties, have also been thoroughly researched. Platypodin D activated the Egr-1 gene in human leukemic U937 cells, resulting in eventual generation of ROS that induced apoptosis and cell death [30].

Role of ROS in nanomaterial-mediated targeted cancer therapy

With the exceptional qualities of nanoparticles, like strong biocompatibility, favourable pharmacological parameters, inherent targeting capabilities, and perfect physical and chemical attributes, nanotechnology has spurred significant advances in medicine during the last decades [41]. Nanomaterials' physicochemical features, such as size and charge, make them highly penetrating, allowing them to be targeted at the tumor location. By targeting ROS metabolic routes, ROS-based nanoparticulate enhance ROS production intracellularly, eventually triggering cancer cell death. ROS-producing nanoparticles can be triggered in several ways, involving sonodynamic therapy, photodynamic treatment, chemodynamic therapy, and chemically administered ROS inducers [42]. Chemodynamic treatment is activated by the Fenton reaction, which uses endogenous H_2O_2 and metal ions like iron and copper. Photodynamic therapy is caused by an internalized photosensitizer agent that is activated by light, whereas sonodynamic treatment is caused by very penetrating acoustic waves that induce a family of sound-responsive sonosensitizers [42]. These therapy techniques can cause electron transport to the surrounding environment and the generation of ROS. Metal-based NPs such as iron, gold, copper, cerium or titanium, and organic nanoparticles employed as PSs or sonosensitizers, nanoscale DDSs (drug delivery systems), with small molecules carrying chemically encapsulated medicines are examples of ROS-based nanomaterials [42]. So far, protein-based nanomedicine for anticancer therapy has a large family of members, even though the proteins employed in nanomedicine

construction frequently vary in their operative activities [43]. Since mitochondria play an important function in tumor formation and development, mitochondria-targeting nanotechnology may be a potential technique for next-generation cancer treatment. The principal generator of ROS is mitochondrion. Huang et al. described the use of mitochondria-targeted hybrid nanozymes as superoxide scavengers to safeguard mitochondria from oxidative damage [44]. They developed a biomimetic nanozyme using ferritin-heavy-chain protein and a metal nanoparticle core. Animal investigations showed that the synthesized nanonzyme has superoxide dismutase and catalase-like capabilities and targets mitochondria by curbing numerous biological barriers, providing an alternative route for regenerative medicine to alleviate oxidative damage. As a result, it was plausible to assume that mitochondrial ROS modulation may be an excellent therapeutic method for cancer treatment [45].

Conclusion and future perspectives

Given the importance of ROS in tumour cell adaptability, it has been suggested that administration of antioxidants like vitamin E or C could be an approach to avoid malignant conversion. Ferroptosis is expected to play a significant role in modern anticancer medicines, and targeting the apoptotic process is a frequent strategy in cancer therapy. The primary barriers to treating cancer are intrinsic and acquired resistance. According to certain reports, tumour cells may dramatically strengthen their ability to protect against oxidative stress by adversely regulating ferroptosis, which results in resistant survival. Nanomaterials that produce deadly ROS selectively in tumour cells have been developed as a result of breakthroughs in nanotechnology used in cancer therapeutic applications. The advantages of ROS scavenging techniques for cancer avoidance, on the other hand, remain contradictory. Many cancers enhance the activity of antioxidant systems, implying that a delicate balance of antioxidants and oxidants is required for cancer. Cancer cells' high antioxidant capacity is intermittently associated to chemotherapy resistance, as a number of anticancer medications currently in use are recognized for inducing cytotoxicity to varying degrees by producing oxidants. Plant extracts include numerous active substances such as alkaloids, terpenes, flavonoids, steroids, saponins, and glycosides; the mechanisms and therapeutic effects are the integrated impact of their separate activities that are synergistic, antagonistic, or neutralised. Therefore, to determine and identify the minimum effective dosage and maximum acceptable dose of a specific sample, toxicity studies are necessary. Predominantly for effective anticancer therapy, the use of oxidant generating chemotherapeutics to activate antioxidants or oxidative stress to disrupt the redox balance required for tumour development should be customized to the specific condition, taking into account the degree and type of cancer, oxidant levels in the tumour environment, and the tumour's internal antioxidant competence. Considering the most recent established methods for analysing specific oxidants, an important way ahead for future investigations to comprehend the complexities of oxidant contributions to physiology is to limit the study of "ROS," which does not represent one molecule after all, *in lieu* of examining unique molecular drivers like H_2O_2* or O_2*, which have completely distinct characteristics, mechanisms, and impact on physiology and may necessitate entirely distinct methodologies. Furthermore, it is important to better characterise the context-dependent boundary between oxidative distress and oxidative eustress in various physiological contexts. Therefore, it is necessary to characterise redox balance in various circumstances to effectively apply redox regulation as a therapeutic strategy. Access to comprehending such global consequences will be made possible by genomics and imaging technology. We believe that these developments will help the developing area of redox medicine reach its full potential.

Author contributions

Conceptualization: FS and AM contributed to the conception and initial idea of the review article. Literature Review: HD, MK, NG, and NK conducted an extensive literature review, analyzing relevant peer-reviewed articles, and conference proceedings. They summarized the current state of knowledge in ROS cancer therapy, Ferroptosis including its history, mechanisms of action, and emerging trends. Writing: The initial draft of the review article was primarily written by PV and BR. They organized the information gathered from the literature review and composed the main sections of the manuscript, ensuring clarity and coherence, Figures: MK, NG, and NK were responsible for creating the figures used in the article. Critical Revision and Editing: PV, BR, FS and AM participated in the critical revision and editing of the manuscript. They reviewed the draft offering valuable feedback and suggestions to improve the article's quality and scientific rigor. Clinical Perspectives: Adj, AJ, SC, and AS, being clinicians with expertise in oncology, provided valuable insights into the practical aspects of the discussed therapies. They shared the practical implications and potential challenges faced in clinical settings. Final Approvals: PV, BR, FS, and AM reviewed, and approved the final version of the manuscript before its submission.

Conflict of interest

The authors declare that the research was conducted in the absence of any commercial or financial relationships that could be construed as a potential conflict of interest.

Acknowledgments

Figures of the manuscript were created using BioRender.com.

References

1. Chhikara Bhupender S, Keykavous P. Global cancer statistics 2022: the trends projection analysis. *Chem Biol Lett* (2022) 1:451.

2. Huang R, Chen H, Liang J, Li Y, Yang J, Luo C, et al. Dual role of reactive oxygen species and their application in cancer therapy. *J Cancer* (2021) 12(18): 5543–61. doi:10.7150/jca.54699

3. Sies H, Jones DP. Reactive oxygen species (ROS) as pleiotropic physiological signalling agents. *Nat Rev Mol Cel Biol* (2020) 21(7):363–83. doi:10.1038/s41580-020-0230-3

4. Article R, Takada K. Reactive oxygen species in cancer: current findings and future directions. *Cancer Sci* (2021) 2(10):3945–52. doi:10.1111/cas.15068

5. Perillo B, Di Donato M, Pezone A, Di Zazzo E, Giovannelli P, Galasso G, et al. ROS in cancer therapy: the bright side of the moon. *Exp Mol Med* (2020) 52: 192–203. doi:10.1038/s12276-020-0384-2

6. Sullivan LB, Chandel NS. Mitochondrial reactive oxygen species and cancer. *Cancer Metab* (2014) 2:17. doi:10.1186/2049-3002-2-17

7. Kirtonia A, Sethi G, Garg M, Artesunate ART. The multifaceted role of reactive oxygen species in tumorigenesis. *Cell Mol Life Sci* (2020) 77:4459–83. doi:10.1007/s00018-020-03536-5

8. Redza-dutordoir M, Averill-bates DAB Activation of apoptosis signalling pathways by reactive oxygen species. *Biochim Biophys Acta* (2016) 1863(12): 2977–92. doi:10.1016/j.bbamcr.2016.09.012

9. Wu Q, Ni X. ROS-mediated DNA methylation pattern alterations in carcinogenesis. *Curre Drug Targets* (2015) 16(1):13–9. doi:10.2174/1389450116666150113121054

10. Angireddy R, Kazmi HR, Srinivasan S, Sun L, Iqbal J, Fuchs SY, et al. Cytochrome c oxidase dysfunction enhances phagocytic function and osteoclast formation in macrophages. *FASEB J* (2019) 10:9167–81. doi:10.1096/fj.201900010RR

11. Reczek CR, Chandel NS. The two faces of reactive oxygen species in cancer. *Annu Rev Cancer Biol* (2017) 1:79–98. doi:10.1146/annurev-cancerbio-041916-065808

12. Zhou Y, Feng X, Wang L, Du J, Yu H LGH00031, a novel ortho-quinonoid inhibitor of cell division cycle 25B, inhibits human cancer cells via ROS generation. *Acta Pharmacol Sin* (2009) 30(9):1359–68. doi:10.1038/aps.2009.131

13. Ramalingam V, Rajaram R. A paradoxical role of reactive oxygen species in cancer signaling pathway: physiology and pathology. *Process Biochem* (2021) 100: 69–81. doi:10.1016/j.procbio.2020.09.032

14. Renschler MF. The emerging role of reactive oxygen species in cancer therapy. *Eur J Cancer* (2004) 40(13):1934–40. doi:10.1016/j.ejca.2004.02.031

15. Prieto-Bermejo R, Romo-González M, Pérez-Fernández A, Ijurko C, Hernández-Hernández Á. Reactive oxygen species in haematopoiesis: leukaemic cells take a walk on the wild side. *J Exp Clin Cancer Res* (2018) 37:125. doi:10.1186/s13046-018-0797-0

16. Oliveira MDS, Barbosa MIF, de Souza TB, Moreira DRM, Martins FT, Villarreal W, et al. A novel platinum complex containing a piplartine derivative exhibits enhanced cytotoxicity, causes oxidative stress and triggers apoptotic cell death by ERK/p38 pathway in human acute promyelocytic leukemia HL-60 cells. *Redox Biol* (2019) 20:182–94. doi:10.1016/j.redox.2018.10.006

17. Hasan A, Rizvi SF, Parveen S, Pathak N, Nazir A, Mir SS. Crosstalk between ROS and autophagy in tumorigenesis: understanding the multifaceted paradox. *Front Oncol* (2022) 12:852424. doi:10.3389/fonc.2022.852424

18. Li J, Cao F, Yin HL, Huang ZJ, Lin ZT, Mao N, et al. Ferroptosis: past, present and future. *Cell Death Dis* (2020) 11:88. doi:10.1038/s41419-020-2298-2

19. Zhang C, Liu X, Jin S, Chen Y, Guo R. Ferroptosis in cancer therapy: a novel approach to reversing drug resistance. *Mol Cancer* (2022) 21:47–12. doi:10.1186/s12943-022-01530-y

20. Yang WS, SriRamaratnam R, Welsch ME, Shimada K, Skouta R, Viswanathan VS, et al. Regulation of ferroptotic cancer cell death by GPX4. *Cell* (2015) 156: 317–31. doi:10.1016/j.cell.2013.12.010

21. Galaris D, Skiada V, Barbouti A. Redox signaling and cancer: the role of labile iron. *Cancer Lett* (2008) 266:21–9. doi:10.1016/j.canlet.2008.02.038

22. Zou Y, Graham ET, Deik AA, Eaton JK, Wang W Cytochrome P450 oxidoreductase contributes to phospholipid peroxidation in ferroptosis. *Nat Chem Biol* (2020) 16(3):302–9. doi:10.1038/s41589-020-0472-6

23. Liang WEI, He X, Bi J, Hu T, Sun Y. Role of reactive oxygen species in tumors based on the ' seed and soil ' theory: a complex interaction (Review). *Oncol Rep* (2021) 46(3):208. doi:10.3892/or.2021.8159

24. Didier AJ, Fang L, Watkins D, Dworkin LD, Creeden JF. Antioxidant and anti-tumor effects of dietary vitamins A, C, and E. *Antioxidants (Basel)* (2023) 12(3):632. doi:10.3390/antiox12030632

25. Grant WB. Review of recent advances in understanding the role of vitamin D in reducing cancer risk: breast, colorectal, prostate, and overall cancer. *Anticancer Res* (2020) 40(1):491–9. doi:10.21873/anticanres.13977

26. Yun J, Mullarky E, Lu C, Bosch KN, Kavalier A, Rivera K, et al. Vitamin C selectively kills KRAS and BRAF mutant colorectal cancer cells by targeting GAPDH. *Science* (2016) 350:1391–6. doi:10.1126/science.aaa5004

27. Liou G, Storz P. Reactive oxygen species in cancer. *Free Radic Res* (2010) 44: 479–96. doi:10.3109/10715761003667554

28. Xin J, Jiang X, Ben S, Yuan Q, Su L, Zhang Z, et al. Association between circulating vitamin E and ten common cancers: evidence from large - scale Mendelian randomization analysis and a longitudinal cohort study. *BMC Med* (2022) 20:168. doi:10.1186/s12916-022-02366-5

29. Mclean L, Soto U, Agama K, Francis J, Jimenez R, Pommier Y, et al. Aminoflavone induces oxidative DNA damage and reactive oxidative species-mediated apoptosis in breast cancer cells. *Int J Cancer* (2008) 122(7):1665–74. doi:10.1002/ijc.23244

30. Das K, Roychoudhury A, Bhattacharjee H, Deka A, Yambem D, Tahiliani PS, et al. Parasitic diseases of zoonotic importance in humans of northeast India, with special reference to ocular involvement. *Front Environ Sci* (2014) 2:1–8. doi:10.2147/EB.S64404

31. Khan N, Mukhtar H. Cancer and metastasis: prevention and treatment by green tea. *Cancer Metastasis Rev* (2010) 2010:435–45. doi:10.1007/s10555-010-9236-1

32. Khan A, Chen HC, Wan XX, Tania M, Xu AH, Chen FZ, et al. Regulatory effects of resveratrol on antioxidant enzymes: a mechanism of growth inhibition and apoptosis induction in cancer cells. *Mol Cell* (2013) 35:219–25. doi:10.1007/s10059-013-2259-z

33. Elumalai P, Ezhilarasan D, Raghunandhakumar S. Molecular targets of nimbolide for anti-cancer therapy: an updated review. *J Environ Pathol Toxicol Oncol* (2022) 41:69–88. doi:10.1615/JEnvironPatholToxicolOncol.2021040263

34. Gupta SC, Hevia D, Patchva S, Park B, Koh W, Aggarwal BB. Upsides and downsides of reactive oxygen species for cancer: the roles of reactive oxygen species in tumorigenesis, prevention, and therapy. *Antioxid Redox Signal* (2012) 16(11): 1295–322. doi:10.1089/ars.2011.44.14

35. Kashyap D, Tuli HS, Varol A, Thakral F, Yerer MB, Sak K, et al. Role of reactive oxygen species in cancer progression: molecular mechanisms and recent advancements. *Biomolecules* (2019) 9:735. doi:10.3390/biom9110735

36. Hacioglu C, Kar F. Capsaicin induces redox imbalance and ferroptosis through ACSL4/GPx4 signaling pathways in U87-MG and U251 glioblastoma cells. *Metab Brain Dis* (2023) 38:393–408. doi:10.1007/s11011-022-00983-w

37. Rather RA, Bhagat M. Cancer chemoprevention and piperine: molecular mechanisms and therapeutic opportunities. *Front Cel Dev Biol* (2018) 6:10. doi:10.3389/fcell.2018.00010

38. Yuan Z, Liang Z, Chen X, Li R, Wu Y Protective effect of koumine, an alkaloid from Gelsemium sempervirens, on injury induced by H-O-in IPEC-J2 cells. *Int J Mol Sci* (2019) 20(3):754. doi:10.3390/ijms20030754

39. Rahman A, Hongsprabhas P. Genistein as antioxidant and antibrowning agents in *in vivo* and *in vitro*: a review. *Biomed Pharmacother* (2016) 82:379–92. doi:10.1016/j.biopha.2016.05.023

40. Osman Y, Subramaniam B, Nyamathulla S, Shamsuddin N, Arshad NM, Mun KS, et al. Natural products for cancer therapy: a review of their mechanism of actions and toxicity in the past decade. *J Trop Med* (2022) 2022:5794350. doi:10.1155/2022/5794350

41. Zhang C, Wang X, Du J, Gu Z, Zhao Y. Reactive oxygen species-regulating strategies based on nanomaterials for disease treatment. *Adv Sci* (2020) 8(3): 2002797. doi:10.1002/advs.202002797

42. Li Y, Yang J, Sun X. Reactive oxygen species-based nanomaterials for cancer therapy. *Front Chem* (2021) 9:1–12. doi:10.3389/fchem.2021.650587

43. Zhang Q, Zhang J, Song J, Liu Y, Ren X, Zhao Y. Protein-based nanomedicine for therapeutic bene fi ts of cancer. *ACS Nano* (2021) 5:8001–38. doi:10.1021/acsnano.1c00476

44. Zhang Y, Khalique A, Du X, Gao Z, Wu J, Zhang X, et al. Biomimetic design of mitochondria-targeted hybrid nanozymes as superoxide scavengers. *Adv Mater* (2021) 33(9):2006570. doi:10.1002/adma.202006570

45. Qin J, Gong N, Liao Z, Zhang S, Timashev P, Huo S, et al. Recent progress in mitochondria-targeting-based nanotechnology for cancer treatment. *Nanoscale* (2021) 13:7108–18. doi:10.1039/d1nr01068a

Pathology & Oncology Research | frontiers

TYPE Original Research
PUBLISHED 31 January 2023
DOI 10.3389/pore.2023.1610707

Check for updates

OPEN ACCESS

EDITED BY
József Tímár,
Semmelweis University, Hungary

*CORRESPONDENCE
Michael Hummel,
michael.hummel@charite.de

RECEIVED 14 July 2022
ACCEPTED 11 January 2023
PUBLISHED 31 January 2023

CITATION
Behnke A, Cayre A, De Maglio G, Giannini G, Habran L, Tarsitano M, Chetta M, Cappellen D, Lespagnol A, Le Naoures C, Massazza G, Destro A, Bonzheim I, Rau A, Battmann A, Kah B, Watkin E and Hummel M (2023), FACILITATE: A real-world, multicenter, prospective study investigating the utility of a rapid, fully automated real-time PCR assay versus local reference methods for detecting epidermal growth factor receptor variants in NSCLC.
Pathol. Oncol. Res. 29:1610707.
doi: 10.3389/pore.2023.1610707

COPYRIGHT
© 2023 Behnke, Cayre, De Maglio, Giannini, Habran, Tarsitano, Chetta, Cappellen, Lespagnol, Le Naoures, Massazza, Destro, Bonzheim, Rau, Battmann, Kah, Watkin and Hummel. This is an open-access article distributed under the terms of the Creative Commons Attribution License (CC BY). The use, distribution or reproduction in other forums is permitted, provided the original author(s) and the copyright owner(s) are credited and that the original publication in this journal is cited, in accordance with accepted academic practice. No use, distribution or reproduction is permitted which does not comply with these terms.

FACILITATE: A real-world, multicenter, prospective study investigating the utility of a rapid, fully automated real-time PCR assay versus local reference methods for detecting epidermal growth factor receptor variants in NSCLC

Anke Behnke[1], Anne Cayre[2], Giovanna De Maglio[3], Giuseppe Giannini[4], Lionel Habran[5], Marina Tarsitano[6], Massimiliano Chetta[6], David Cappellen[7], Alexandra Lespagnol[8], Cecile Le Naoures[9], Gabriella Massazza[10], Annarita Destro[11], Irina Bonzheim[12], Achim Rau[12], Achim Battmann[13], Bettina Kah[14], Emmanuel Watkin[15] and Michael Hummel[1]*

[1]Charité-Universitätsmedizin Berlin, Institute of Pathology and Berlin Institute of Health, Corporate Member of Freie Universität Berlin and Humboldt-Universität zu Berlin, Berlin, Germany, [2]Département de Pathologie, Centre Jean-Perrin, Clermont-Ferrand, France, [3]Azienda Sanitaria Universitaria Friuli Centrale, Pathology Department, Santa Maria della Misericordia Hospital, Udine, Italy, [4]Department Molecular Medicine, Università di Roma La Sapienza, Rome, Italy, [5]Anatomopathology Department, CHU Liège, Liège, Belgium, [6]Di Laboratorio, A.O.R.N. Cardarelli, Medical Genetics Laboratory, and Ospedale Antonio Cardarelli, U.O.C. di Genetica Medica, Naples, Italy, [7]Service de Biologie des Tumeurs, Centre Hospitalier Universitaire de Bordeaux, Hôpital du Haut Lévêque, Pessac, France, [8]CHU de Rennes, Laboratoire de Génétique Somatique des Cancers, Rennes, France, [9]CHU de Rennes, Service d'Anatomie et Cytologie Pathologiques, Rennes, France, [10]Dipartimento Medicina di Laboratorio Anatomia Patologica, ASST Papa Giovanni XXIII, Bergamo, BG, Italy, [11]Pathology Department, Humanitas Clinical and Research Center—IRCCS, Milan, Italy, [12]Institute of Pathology and Neuropathology, Eberhard Karls University of Tübingen and Comprehensive Cancer Center, University Hospital Tübingen, Tübingen, Germany, [13]Institut für Pathologie und Zytodiagnostik am Krankenhaus Nordwest, Frankfurt, Germany, [14]Institut für Hämatopathologie Hamburg, Hamburg, Germany, [15]CYPATH, Villeurbanne, France

Accurate testing for epidermal growth factor receptor (*EGFR*) variants is essential for informing treatment decisions in non-small cell lung cancer (NSCLC). Automated diagnostic workflows may allow more streamlined

Abbreviations: AF, allele frequency; aTAT, analytical turnaround time; CI, confidence interval; CNS, central nervous system; Cq, quantitation cycle; EGFR, epidermal growth factor receptor; ddPCR, digital droplet polymerase chain reaction; ESMO, European Society for Medical Oncology; Ex19del, exon 19 deletions; Ex20ins, exon 20 insertions; FFPE, formalin-fixed and paraffin-embedded; HC, hybrid capture; ND, no data; NGS, next-generation sequencing; NPA, negative percentage diagnostic agreement; NSCLC, non-small cell lung cancer; OPA, overall percentage diagnostic agreement; PCR, polymerase chain reaction; PPA, positive percentage diagnostic agreement; Q, quartile; RT-PCR, real-time polymerase chain reaction; SD, standard deviation; TKI, tyrosine kinase inhibitor.

initiation of targeted treatments, where appropriate, while comprehensive variant analysis is ongoing. FACILITATE, a real-world, prospective, multicenter, European study, evaluated performance and analytical turnaround time of the Idylla™ EGFR Mutation Test compared with local reference methods. Sixteen sites obtained formalin-fixed paraffin-embedded biopsy samples with ≥ 10% neoplastic cells from patients with NSCLC. Consecutive 5 µm sections from patient samples were tested for clinically relevant NSCLC-associated *EGFR* variants using the Idylla™ EGFR Mutation Test and local reference methods; performance (concordance) and analytical turnaround time were compared. Between January 2019 and November 2020, 1,474 parallel analyses were conducted. Overall percentage agreement was 97.7% [*n* = 1,418; 95% confidence interval (CI): 96.8–98.3], positive agreement, 87.4% (*n* = 182; 95% CI: 81.8–91.4) and negative agreement, 99.2% (*n* = 1,236; 95% CI: 98.5–99.6). There were 38 (2.6%) discordant cases. Ninety percent of results were returned with an analytical turnaround time of within 1 week using the Idylla™ EGFR Mutation Test versus ~22 days using reference methods. The Idylla™ EGFR Mutation Test performed well versus local methods and had shorter analytical turnaround time. The Idylla™ EGFR Mutation Test can thus support application of personalized medicine in NSCLC.

KEYWORDS

non-small cell lung cancer, epidermal growth factor receptor, DNA mutational analysis, clinical decision-making, turnaround time

Introduction

Molecular profiling in non-small cell lung cancer (NSCLC) is of key importance in identifying presence of oncogenic drivers, allowing implementation of targeted treatment approaches where applicable [1]. The epidermal growth factor receptor (*EGFR*) is an established oncogenic target in NSCLC [2–4]. A meta-analysis of 456 studies showed that *EGFR* variants have a prevalence of 17.4% [95% confidence interval (CI): 15.8–18.9] and 38.8% (95% CI: 36.8–40.8) in Caucasian and Asian patients with NSCLC, respectively [5]. The 25 currently described exon 19 deletion variants, which are referred to as exon 19 deletions (Ex19del) and the c.2573T>G [p.Leu858Arg (commonly referred to as L858R)] variant are the most common and represent approximately 90% of all *EGFR* pathogenic variants [6].

EGFR tyrosine kinase inhibitors (TKIs) are used in the treatment of NSCLC harboring EGFR-TKI sensitizing pathogenic variants such as Ex19del and p.Leu858Arg [7–10]. Resistance to EGFR-TKIs can be acquired, which depending on the specific EGFR-TKI used, can involve other *EGFR* pathogenic variants such as c.2369C>T [p.Thr790Met (commonly referred to as T790M)] and c.2389T>A [p.Cys797Ser (commonly referred to as C797S)] [11]. It should be noted that tumor cells in which the p.Cys797Ser and p.Thr790Met variants occur together in the cis-configuration (on the same allele) were shown to be insensitive to currently approved EGFR-TKIs, including third-generation EGFR-TKIs [12]. Cases in which the *EGFR* p.Cys797Ser and p.Thr790Met variants occur together in the trans-configuration (on separate alleles) may be sensitive to first- and third-generation EGFR-TKI-combination treatment [12]. Currently, the preferred first-line treatment in patients with EGFR-TKI-sensitizing variant-positive (e.g., Ex19del, p.Leu858Arg) advanced NSCLC is osimertinib [4, 13]. Osimertinib is a third-generation, irreversible, oral EGFR-TKI that potently and selectively inhibits EGFR-TKI-sensitizing and *EGFR* p.Thr790Met variants with demonstrated efficacy in *EGFR* variant-positive NSCLC, including in patients with central nervous system (CNS) metastases [10,14–18].

Guidelines, endorsements and recommendations concerning advanced NSCLC from the European Society for Medical Oncology (ESMO) and American Society of Clinical Oncology, among other societies, suggest that patients should be tested for oncogenic drivers at the time of diagnosis due to the benefits of targeted treatment [4,19–21]. Per ESMO guidelines, *EGFR* profiling must cover Ex19del variants and p.Leu858Arg variants in exon 21; however, complete coverage of genomic alterations across exons 18–21 is recommended [4]. While the *EGFR* p.Thr790Met exon 20 substitution variant is rarely found in patients with treatment-naïve *EGFR* mutated NSCLC, germline p.Thr790Met has been reported [4, 22]. Implications of this variant in patients with previously untreated disease are unclear, but with the availability of osimertinib, p.Thr790Met testing on relapse with earlier-generation EGFR-TKIs is mandatory [4].

Clinical testing for *EGFR* variants may involve single variant-genotyping technologies, but multiplex gene-sequencing technologies such as next-generation sequencing (NGS) have been adopted as the standard approach in many instances [4, 23].

These latter technologies are used with targeted gene panels and can screen several genes simultaneously [24–26].

Guidelines specify that molecular testing results for recommended predictive biomarkers should be available 10 days after tissue acquisition [27]. Despite this, lengthy analytical turnaround times (aTAT) remain an important potential barrier to provision of genomic data ahead of treatment initiation. In the UK for example, the National Cancer Audit found that irrespective of the test performed, the median turnaround time was 18 days [27]. Based on clinical experience regarding test type, comprehensive testing such as with NGS (currently the most common approach) is generally associated with longer turnaround times compared with simpler techniques based on polymerase chain reaction (PCR); 5–14 days (or more) versus 1–7 days, respectively [28, 29]. Moreover, while many large academic hospitals have inhouse testing facilities suitable for performing comprehensive variant screening, others must send samples to external laboratories; this can risk additional delays [30].

Lengthy turnaround times can result in patients and clinicians feeling it is necessary to choose between waiting for variant test results and starting treatment plans based on incomplete information, potentially resulting in initiation of sub-optimal therapies [28, 31]. This is significant in frail patients, patients with high symptom burden, and those with advanced NSCLC (e.g., stage IV) who can deteriorate rapidly while waiting for test results, as flagged in several reports [28, 32, 33]. Prompt molecular test turnaround times are also important in the stage I–III resectable NSCLC setting. Unlike in the advanced setting, few targeted treatment strategies are available (which require prior molecular testing) in resectable NSCLC. *EGFR* is one such target in this setting that is appliable for targeted treatment. This follows the approval of adjuvant osimertinib based on results of the ADAURA study [34]. In line with this, variant testing in resectable tissue is now recommended per the ESMO guidelines [35].

Limited availability of tissue samples of sufficient size and sub-optimal workflows can pose additional barriers to pre-treatment *EGFR* variant testing. This can put restrictions on clinical laboratories regarding number and types of tests possible [31, 36, 37]. Methods and streamlined workflows that permit accurate *EGFR* variant testing, shorten turnaround time and make best use of samples are imperative to improve care in NSCLC [38]. This is important in relation to the availability of treatment strategies such as EGFR-TKIs, which can target various *EGFR* variants.

The Idylla™ EGFR Mutation Test performed on the Biocartis Idylla™ System (Biocartis, Belgium), is a fully automated real-time PCR (RT-PCR)-based test designed specifically to detect common clinically relevant NSCLC-associated EGFR variants. It can be used directly on formalin-fixed and paraffin-embedded (FFPE) tissue sections with neoplastic cell content of at least 10%. This *EGFR* specific test has been evaluated for clinical utility in lung cancer workflows. Previous studies demonstrated its benefits in facilitating rapid and accurate testing [39]. For instance, it has been examined regarding *EGFR* variant screening [40] and reflex testing [29]. In these studies, turnaround times ranged from 1 to 3 days [29, 40] and concordance with NGS was approximately 98.5% [40]. Recently, a single center-experience study described use of the Idylla™ EGFR Mutation Test, with NGS in a sequential multi-test approach, and reported an average turnaround time of 2 days and 96.4% concordance with NGS [41]. In addition, the Idylla™ EGFR Mutation Test requires modest input samples quantities, making efficient use of samples [42].

To help improve *EGFR* variant clinical testing and examine use of rapid variant testing methods in NSCLC, the FACILITATE (fast, accurate, Idylla™-based investigation of turnaround time in *EGFR* testing) study was performed. FACILITATE was a real-world, multicenter prospective European study evaluating performance and turnaround time of the Idylla™ EGFR Mutation Test compared with reference methods in real-life NSCLC settings.

Materials and methods

Patient criteria

For inclusion in this study, samples must have been obtained as part of routine clinical practice from patients with confirmed NSCLC (any stage); and sample *EGFR* variant status must have been unknown prior to *EGFR* variant analysis with the Idylla™ EGFR Mutation Test. No further inclusion and exclusion criteria were included in the study design as one of the aims was to conduct the study under real-life conditions, including the diversity of incoming NSCLC samples, in order to be representative of everyday clinical practice.

Study design

FACILITATE was a real-world, multicenter, prospective study across 16 clinical sites in Belgium, France, Germany and Italy. Samples were obtained prospectively from patients and prepared as 5 µm FFPE human tumor samples. Consecutive sections were tested for *EGFR* variants in parallel at each site using the Idylla™ EGFR Mutation Test and a local reference method (Figure 1). Sample sections used in the Idylla™ EGFR Mutation Test were required to have a neoplastic cell content of at least 10%; if sections had less than 10% neoplastic cell content, macro-dissection was performed. Sample sections used in each of the local reference methods must have fulfilled the sample requirements as noted in respective manufacturer's instructions for use. Time points for the following were

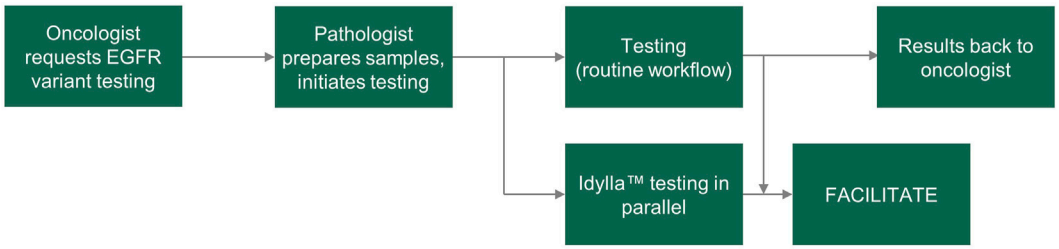

FIGURE 1
FACILITATE study workflow. *EGFR*, epidermal growth factor receptor.

recorded in each case: sample receipt by laboratory and results ready to be sent to the clinician.

Ethics statement

Use of patient samples in this study was approved by the respective local ethics committees and was in accordance with the Declaration of Helsinki.

Objectives

The main objectives were to assess utility of the Idylla™ EGFR Mutation Test in the European clinical setting using real-life patient NSCLC samples and to assess its impact on aTAT in accurate reporting of *EGFR* results. aTAT was defined as time between laboratory receipt of sample and when the molecular diagnostic test result was ready for the clinician. Performance was also assessed across centers and described by the level of concordance between the Idylla™ EGFR Mutation Test and the local reference method.

Idylla™ EGFR mutation test

The Idylla™ EGFR Mutation Test performed on the Biocartis Idylla™ System (Biocartis, Belgium) is an *in vitro* sample-to-result diagnostic test with a rapid technical run time (approximately 150 min) for the qualitative detection of 51 common NSCLC-associated *EGFR* variants across exons 18–21 [43]. The limit of detection in terms of allele frequency (AF) is 5%. All 51 *EGFR* variants detectable with the Idylla™ EGFR Mutation Test are presented in Supplementary Table S1 [43].

During testing, disposable Idylla™ EGFR Mutation Test cartridges were loaded with FFPE human NSCLC tissue sections without prior manual deparaffinization or FFPE pre-processing. Cartridges were inserted into the Idylla™ instrument, per the manufacturer's instructions. The Idylla™ console and instruments were Conformité Européene marked. Inside the Idylla™ cartridge, deoxyribonucleic acid (DNA) was liberated from FFPE material using a combination of reagents, enzymes, heat and high intensity-focused ultrasound. Within the cartridge, allele-specific multiplex PCR was performed for the amplification of specific mutated *EGFR* gene sequences. Conserved regions of the *EGFR* genes served as sample processing controls and as a measure of the amplifiable DNA in each sample, which is represented in each case by the quantitation cycle (Cq) value. The conserved regions were amplified in parallel with mutated *EGFR* gene sequences, where present. All required consumables were provided in the cartridge. The official *in vitro* diagnostic-certified Idylla™ console report was used as the final Idylla™ result.

The Idylla™ Explore tool was used to facilitate discordance analysis and invalid or non-processable result identification and investigation. The Idylla™ Explore tool is available to registered users *via* a web browser and allowed users to view the raw amplification data in more detail. This Idylla™ Explore tool serves as data visualization aid for research purposes only.

Reference methods

Local reference methods used in parallel with the Idylla™ EGFR Mutation Test across sites in FACILITATE, included amplicon- or hybrid capture-based NGS, cobas® EGFR Test, Sanger sequencing, Therascreen® EGFR Rotor-Gene Q (RGQ) PCR, MassARRAY® and Entrogen RT-PCR (see Supplementary Table S2 for more details).

Discordance analyses

After the results of the in-parallel run Idylla™ EGFR Mutation Test and reference methods were available for a sample, additional steps were taken, and where relevant, third method analysis was conducted. The third method selected was

dependent on local availability; it could not be the Idylla™ EGFR Mutation Test or the reference method used at the respective site. To identify, verify, and if possible, understand or resolve instances of discordance or invalid or non-processable results, in-depth curve investigation was performed by the Idylla™ EGFR Mutation Test manufacturer. If needed, digital droplet PCR (ddPCR) was performed on DNA retrieved from the Idylla™ EGFR Mutation Test cartridge or relevant reference method equipment. Additionally, or alternatively, appropriate FFPE tissue sections and/or DNA retrieved from the Idylla™ cartridge were analyzed using a BioRad (Hercules, CA) QX100 system per the manufacturer's instructions.

Cases in which the Idylla™ EGFR Mutation Test detected an *EGFR* variant but the reference method did not, were defined as "discordant positive"; cases in which the contrary occurred were defined as "discordant negative." Cases in which samples were concordant for the primary variant but discordant for a secondary variant were also identified. Cases in which *EGFR* variants were detected by the reference method but not by the Idylla™ EGFR Mutation Test because the specific variant sequences were not part of the Idylla™ 51-member panel, were defined as "discordant by design."

Statistical methods

Agreement between the Idylla™ EGFR Mutation Test and the comparator method was evaluated based on point estimates for overall, positive and negative percentage diagnostic agreement (OPA, PPA and NPA, respectively) together with 95% two-sided Wilson score CIs. Per 2 × 2 concordance table agreement calculations with 95% CIs including lower and upper limits, it was determined that a minimum of approximately 700 parallel analyses would be required to obtain a lower limit ≥ 90% (assuming a prevalence of 15% and a concordance of 95%). However, to account for invalid or non-processable samples or dropouts, we aimed to conduct 1,500 analyses. aTAT is reported as median [Q1–Q3 (Quartile 1–Quartile 3)] days from time of laboratory receipt of sample to availability of molecular diagnostic test result to the clinician.

Results

Patient demographics and samples

Between January 2019 and November 2020, 1,474 patients with NSCLC (any stage) were included in 16 sites across France (five sites), Germany (five sites), Italy (five sites) and Belgium (one site), with each site processing approximately 100 paired samples for prospective *EGFR* variant analysis. Detailed patient demographics were not collected for analysis.

Using these samples, a total of 1,474 parallel analyses (Idylla™ EGFR Mutation Test vs. the local reference methods) were conducted to determine *EGFR* variant status (Table 1). The following local reference methods [*n* samples analyzed (% of total analyses) over *n* sites at which the respective method was employed] were used: Amplicon-based NGS [*n* = 865 (58.7%) over 10 sites], hybrid capture NGS and cobas® [*n* = 83 (5.6%) and *n* = 20 (1.4%), respectively, both performed at one site], Sanger sequencing [*n* = 100 (6.8%) in one site], Therascreen® EGFR RGQ PCR [*n* = 101 (6.9%) in one site], MassARRAY® [*n* = 200 (13.6%) over two sites] and Entrogen RT-PCR [*n* = 105 (7.1%) in one site]. An overview of the sample flow is provided in Figure 2. Results of pre-analytical investigations, including sample neoplastic cell content are also provided in Table 1.

Mutational analysis

Overview

Across the study, 170 (11.5%) and 186 (12.6%) samples tested positive for *EGFR* variants in the Idylla™ EGFR Mutation Test and local reference methods, respectively. The median (range) percentage of analyses in which *EGFR* variants were detected (Table 1) and the OPA (Table 2) across sites were 12.0% (5.0–18.0) and 98.0% (93.5–100.0), respectively. *EGFR* control Cq values were consistent across all 16 sites (Table 1). A summary of the Idylla™ EGFR Mutation Test results versus reference methods results is provided in Table 3.

OPA and concordance

As summarized in Table 3, OPA for *EGFR* variant detection comparing the Idylla™ EGFR Mutation Test and the reference methods was 97.7% (*n* = 1,418; 95% CI: 96.8–98.3), with a PPA of 87.4% (*n* = 182; 95% CI: 81.8–91.4) and an NPA of 99.2% (*n* = 1,236; 95% CI: 98.5–99.6). When excluding cases in which *EGFR* variants were detected by the reference method but not by the Idylla™ EGFR Mutation Test because the specific sequences were not part of the Idylla™ 51-member panel (discordant-by-design cases), OPA was 98.6% (*n* = 1,405; 95% CI: 97.8–99.1), with a PPA of 94.1% (*n* = 169; 95% CI: 89.5–95.7) and an NPA of 99.2% (*n* = 1,236; 95% CI: 98.5–99.6). The negative agreement value remained the same as only the positive agreement value is affected by exclusion of discordance-by-design cases. There was no difference in the OPA for all reference methods compared with OPA for NGS method alone, irrespective of inclusion of cases in which there was discordance by design. The 56 cases of "No results" (defined as invalid results, error results or no results because the sample was not tested) analyses were not included in the OPA analysis. The mean [± standard deviation (SD)] quantification Cq for total analyses (*n* = 1,453; invalid or non-processable results cases are not included), concordant analyses (*n* = 1,380) and discordant (+p.Thr790Met) analyses (*n* = 38), were 22.6 (±2.7), 22.6 (±2.7) and 23.6 (±3.0), respectively.

TABLE 1 Frequency of *EGFR* variants detected, pre-analytical and analytical details per site.

Site	Reference method used	No. of analyses	Frequency of sections with *EGFR* variants (%)	Testing site	Neoplastic cells (mean %, ±SD)	*EGFR* control Cq values per site (mean cycles, ±SD)
1	NGS[a]	100	10	Comprehensive cancer center	63 ± 23	23.0 ± 3.10
2	NGS[b]	110	14	Private lab	ND	21.3 ± 2.09
3	NGS[a]	101	16	Academic public hospital	ND	22.6 ± 2.88
4	NGS[a]	14	ND	Community public hospital	ND	21.6 ± 3.01
5	HC or cobas®[a]	103	12	Private lab	49 ± 23	23.2 ± 2.52
6	NGS[a]	109	6	Academic public hospital	58 ± 22	22.4 ± 2.39
7	NGS[a]	31	ND	Community public hospital	62 ± 19	23.9 ± 2.14
8	MassARRAY®[a]	102	18	Academic public hospital	68 ± 20	23.9 ± 2.59
9	Entrogen RT-PCR[a]	105	12	Community public hospital	68 ± 22	22.2 ± 2.56
10	Therascreen® EGFR RGQ PCR[a]	101	10	Community public hospital	52 ± 22	21.6 ± 2.43
11	MassARRAY®[a]	98	16	Community public hospital	ND	24.0 ± 1.20
12	Sanger sequencing[a]	100	13	Community public hospital	56 ± 27	22.5 ± 2.50
13	NGS[b]	197	5	Academic public hospital	45 ± 26	22.4 ± 2.97
14	NGS[a]	99	15	Academic public hospital	ND	23.7 ± 2.79
15	NGS[a]	54	9	Academic public hospital	65 ± 24	22.1 ± 2.34
16	NGS[a]	50	12	Academic public hospital	45 ± 17	21.2 ± 2.28

[a]In-house testing.
[b]External testing.
Data for each reference method (HC-NGS and cobas®) at Site 5 were assessed as one data set due low sample numbers for each method if analyzed individually. Cq, quantification cycle; EGFR, epidermal growth factor receptor; HC, hybrid capture; ND, no data; NGS, next-generation sequencing; RGQ, rotor gene Q; RT-PCR, real-time polymerase chain reaction; SD, standard deviation.

Discordance

Overall, 38 (2.6%) cases were discordant across the study. Of these, 10 (26.3%) were discordant positive, 10 (26.3%) were discordant negative, five (13.2%) were discordant for secondary p.Thr790Met but concordant for primary variant and 13 (34.2%) were discordant by design (Figure 2; Supplementary Table S3).

Discordant-positive cases

The 10 cases of discordant positive analyses (Idylla™ EGFR Mutation Test, positive; local reference method, negative) included detection of four Ex19del, two exon 20 insertions (Ex20ins), two p.Leu858Arg variants, one p.Ser768Ile variant and one p.Thr790Met variant (Figure 2; Supplementary Table S3). In nine of these 10 cases, third method analysis (i.e., using another available testing method, independent of the Idylla™ EGFR Mutation Test and the respective routine reference method) was performed to investigate the result (Supplementary Table S3). The Idylla™ EGFR Mutation Test result (variant detected) or reference method (variant not detected) result was confirmed in three out of nine and five out of the nine cases, respectively. In one case, in which third method analysis was performed, left-over material in the cartridge was tested with ddPCR, but the results were inconclusive. In the remaining one case, in which third method analysis was not appliable, left-over material in the cartridge could not be tested. The 10 discordant positive cases had a mean total *EGFR* Cq value of 24.2 ± 1.6 cycles.

Discordant-negative cases

The 10 cases of discordant-negative analyses (Idylla™ EGFR Mutation Test negative; local reference method positive) included detection of three p.Leu858Arg variants, three p.Leu861Gln variants, one p.Gly719Ala variant, one Ex19del

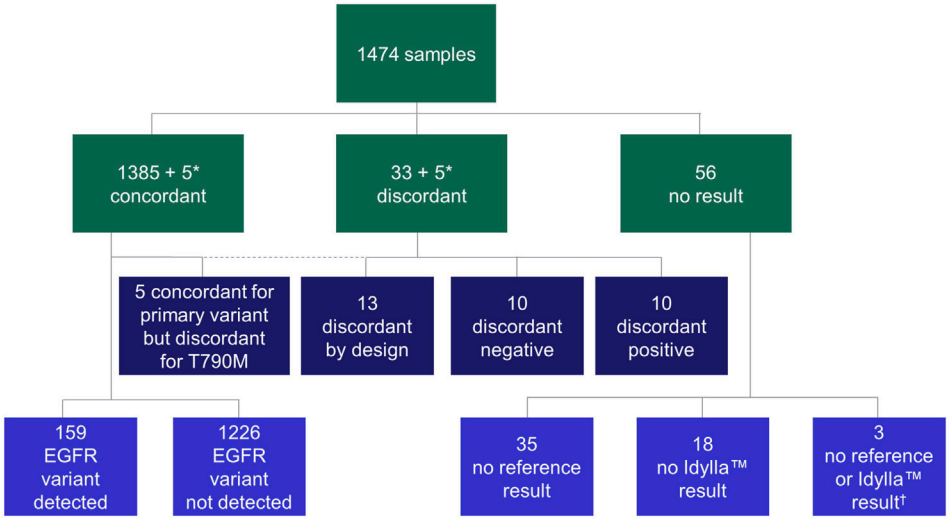

FIGURE 2
Flow chart of samples. In all cases, concordance was calculated on primary variant level (variant vs. variant). Discordant positive: variant by Idylla™ EGFR Mutation Test, no variant by reference method; discordant negative: variant by reference method, no variant by Idylla™ EGFR Mutation Test; discordant by design: rare *EGFR* variant not in panel of Idylla™ EGFR Mutation Test. *A total of five samples were concordant for the primary variant but discordant for secondary variant; therefore, the same five samples appear in both the concordant and discordant categories. †No results were available from the respective reference tests or the Idylla™ EGFR Mutation Test for these three samples. *EGFR*, epidermal growth factor receptor.

(p.Ser752_Ile759del) variant, one Ex20ins (p.Asp770_Asn771insGly) variant and one case of concurrent p.Gly719X and p.Thr790Met variants (Figure 2; Supplementary Table S3). The p.Gly719X alteration was reported using colloquially used nomenclature that currently identifies three different variants: (i) c.2156G>C (p.Gly719Ala), (ii) c.2155G>A (p.Gly719Ser) and (iii) c.2155G>T (p.Gly719Cys).

In one of the three cases in which the p.Leu858Arg variant was detected, a hematoxylin and eosin-stained FFPE tissue section was used in the Idylla™ cartridge. In the two other cases, NGS reference methods detected p.Leu858Arg and p.Leu861Gln variants, however, the AF was 3% and 4%, respectively. *EGFR* total Cq values in these two cases were 27.3 and 24.6 cycles, respectively.

Third method analysis using ddPCR was performed in two of the overall 10 discordant-negative cases; left-over material in the cartridges was used for third method analyses in both cases. In one of these two cases, ddPCR [screening for p.Gly719Ala, p.Gly719Cys, p.Gly719Cys(2), p.Gly719Ser and p.Thr790Met variants] confirmed that p.Gly719X and p.Thr790Met variations were not present in the sample tested with Idylla™ EGFR Mutation Test. In the other, ddPCR confirmed that p.Leu861Gln was present in the sample tested with the Idylla™ EGFR Mutation Test but with an AF of 0.4%.

For the remaining five discordant-negative cases, no third method analysis was conducted, however, in-depth curve investigations were completed by the Idylla™ EGFR Mutation Test manufacturer. In two of these five cases (one in which p.Leu861Gln was detected and one in which p.Leu858Arg was detected), an amplification curve was observed but the curve was not valid and had Cq values of 25.0 and 26.6 cycles, respectively. In the third case, in which a p.Gly719Ala variant was detected, an amplification curve was observed but variants were not formally identified because the amount of amplifiable DNA present in the cartridge (*EGFR* total Cq was 25.7 cycles) was low. In this third case, the sample-in comprised 5% neoplastic cells, which was also below the study testing requirements (i.e., at least 10% neoplastic cells).

In the remaining two cases, which included one Ex19del (deletion 24) and one Ex20ins (InsG), no amplification curve was observed with the Idylla™ EGFR Mutation Test; total Cq values (27.6 and 25.7 cycles, respectively) confirmed that low amounts of amplifiable DNA were present in the cartridges. The deletion 24 had a COSMIC database prevalence of 0.02%. Overall, the 10 discordant negative cases had a mean *EGFR* total Cq value of 24.0 ± 3.9.

Primary concordant but secondary discordant cases

The five cases that were primary concordant but secondary discordant included detection of three Ex19del and two p.Leu858Arg primary variants (Figure 2; Supplementary Table S3). In terms of sample types, three were progression samples and

TABLE 2 Performance of the Idylla™ EGFR Mutation Test compared with reference methods across sites.

Site	Reference method	*N* OPA	OPA (%)	*N* aTAT (Δ)[c]	aTAT using references method (days; median Q1–Q3)	aTAT using Idylla™ EGFR mutation test (days; median Q1–Q3)	ΔaTAT (days; median ± Q1-Q3)
1	NGS[a]	99	99.4	98	11.0 (8.0–13.0)	2.0 (1.0–4.0)	8.0 (6.0–11.0)
2	NGS[b]	105	100.0	110	12.5 (9.0–21.0)	1.0 (0.0–2.0)	11.0 (7.0–19.0)
3	NGS[a]	91	97.8	ND	ND	ND	ND
4	NGS[a]	13	100.0	ND	ND	ND	ND
5	HC or cobas®[a]	97	100.0	97	13.0 (12.0–15.0)	2.0 (1.0–4.0)	11.0 (8.0–13.0)
6	NGS[a]	108	99.1	109	6.0 (5.0–8.0)	4.0 (2.0–5.0)	2.0 (1.0–4.0)
7	NGS[a]	31	93.5	ND	ND	ND	ND
8	MassARRAY®[a]	99	100.0	95	4.0 (2.0–5.0)	2.0 (1.0–5.0)	1.0 (0.0–2.0)
9	Entrogen RT-PCR[a]	104	94.2	ND	ND	ND	ND
10	Therascreen® EGFR RGQ PCR[a]	96	100.0	ND	ND	ND	ND
11	MassARRAY®[a]	97	100.0	ND	ND	ND	ND
12	Sanger sequencing[a]	95	95.8	93	6.0 (6.0–7.0)	2.0 (1.0–3.0)	4.0 (4.0–5.0)
13	NGS[b]	170	99.4	164	21.0 (18.8–26.0)	6.0 (3.0–10.5)	14.0 (13.0–16.0)
14	NGS[b]	94	98.9	ND	ND	ND	ND
15	NGS[a]	53	96.2	49	10.0 (7.0–11.0)	1.0 (1.0–2.0)	7.0 (6.0–10.0)
16	NGS[a]	50	100.0	50	6.0 (4.0–8.0)	1.0 (0.0–1.0)	5.0 (2.0–7.0)

[a]In-house testing.
[b]External testing.
[c]Seven sites with no aTAT data for the Idylla™ EGFR Mutation Test had not completed aTAT analyses at the time of data collection or did not record any aTAT data.
ΔaTAT, aTAT for reference method—aTAT for Idylla™ EGFR mutation test.
aTAT, analytical turnaround time; EGFR, epidermal growth factor receptor; HC, hybrid capture; NGS, next-generation sequencing; N aTAT(Δ), number of samples that had an aTAT result using both methods; ND, not determined; N OPA, number of samples that had a valid result using both tests for concordance analysis, excluding discordant-by-design cases; OPA (%), overall percentage diagnostic agreement (excluding discordant by design); RGQ, rotor gene Q; RT-PCR, real-time polymerase chain reaction; Q1, Quartile 1 (25%); Q3, Quartile 3 (75%).

one was a baseline sample; for the remaining sample, this information was unknown.

AF in three of the five cases were unknown. Regarding these three cases, curve investigation of the Idylla™ EGFR Mutation Test runs indicated it was likely that the amount of amplifiable DNA present in the cartridge was too low for detection of p.Thr790Met. One sample had an AF of 4% and one sample had an estimated AF of 10%. Concerning the latter, third method analysis with ddPCR, using a residual DNA extract, was invalid due to the low amount of genomic DNA. The Cq total determined using the Idylla™ EGFR Mutation Test was relatively high (26.1 cycles) and may have been due to low quantities and/or poor quality of DNA. The five primary concordant but secondary discordant cases had a mean total *EGFR* Cq value of 23.0 ± 2.3 cycles.

Discordant-by-design cases

Thirteen cases of discordance by design occurred across seven different sites; 10 used amplicon-based NGS as the reference method, two used Sanger sequencing and one used hybrid capture NGS (Figure 2; Supplementary Table S3). Five of 13 variants were described in the COSMIC database and occurred as the following base changes (variant; prevalence in NSCLC, %): c.2127_2129del (p.Glu709_Thr710delinsAsp; 0.35%), c.2125G>A (p.Glu709Lys; 0.12%), c.2311_2319dup (p.Asn771_His773dup; 0.24%), c.2224G>A (p.Val742Ile; 0.03%) and c.2239_2240delinsCC (p.Leu747Pro; 0.29%). All 13 cases had a 'no variant' result with the Idylla™ EGFR Mutation Test with a mean (±SD) *EGFR* total Cq value of 23.2 ± 3.5 cycles.

Analytical turnaround time

At the time of data collection, seven sites had not completed aTAT analyses or did not record any aTAT data for the Idylla™ EGFR Mutation Test. Therefore, aTAT data were available for nine of 16 sites. With the Idylla™ EGFR Mutation Test, 90% (n = 810) of a total of 900 samples with recorded aTAT data were tested within 7 days. Whereas with the reference methods, samples with recorded aTAT data (n = 865) were tested within approximately 22 days (Figure 3; cumulative percentage of test results obtained plotted against aTAT). One site had a median aTAT of results with external NGS reference methods of 21.0 days (Site 13), which was much longer than the median aTAT of results for other sites. When excluding this site, the longest median aTAT of results using reference methods was 13.0 days (Site 5), which is in-line with previous reports [44]. The

TABLE 3 Contingency table for Idylla™ EGFR Mutation Test and reference methods.

		Reference method			
	All samples				
Idylla™ EGFR mutation test		*EGFR* variant	No *EGFR* variant	No result[a]	Total
	EGFR variant	159	10	1	170
	No *EGFR* variant	23	1,226	34	1,283
	No result[a]	4	14	3	21
	Total	186	1,250	38	1,474
	Summary				
	OPA[b]: 97.7% (*n* = 1,418; 95% CI: 96.8–98.3)				
	Positive agreement: 87.4% (*n* = 182; 95% CI: 81.8–91.4)				
	Negative agreement: 99.2% (*n* = 1,236; 95% CI: 98.5–99.6)				
	Excluding 13 discordant-by-design samples				
	EGFR variant	159	10	1	170
	No *EGFR* variant	10	1,226	34	1,270
	No result[a]	4	14	3	21
	Total	173	1,250	38	1,461
	Summary				
	OPA[b]: 98.6% (*n* = 1,405; 95% CI: 97.8–99.1)				
	Positive agreement: 94.1% (*n* = 169; 95% CI: 89.5–95.7)				
	Negative agreement: 99.2% (*n* = 1,236; 95% CI: 98.5–99.6)				

[a]"No result" includes invalid results, error results or not tested results.
[b]Cases of "no results" were not included.
CI, confidence interval; EGFR, epidermal growth factor receptor; OPA, overall percentage diagnostic agreement.

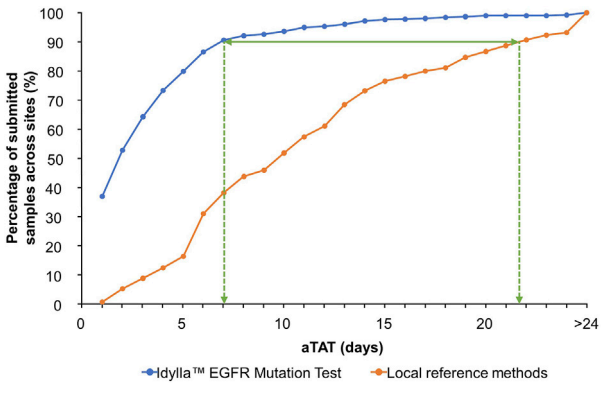

FIGURE 3
Overall cumulative percentage of tested sample results returned to the submitting clinician per aTAT: Idylla™ EGFR Mutation Test versus local reference methods. Percentage of submitted samples for which clinically actionable results were available per increasing aTAT when analyzed using the Idylla™ EGFR Mutation Test or reference methods across sites. aTAT, analytical turnaround time; *EGFR*, epidermal growth factor receptor.

differences between aTAT values were calculated as single points (*n* = 865 for the Idylla™ EGFR Mutation Test aTAT and reference methods aTAT, and *n* = 580 for the Idylla™ EGFR Mutation Test aTAT and NGS reference methods only aTAT), to determine overall reduction in median aTAT with the Idylla™ EGFR Mutation Test and reference methods. Across the nine of 16 sites with available aTAT data, the Idylla™ EGFR Mutation Test reduced the overall median (Q1–Q3) aTAT of results by 7.0 days (4.0–13.0 days) compared with the aTAT of results from reference methods (*n* = 862), and by a median of 9.6 days (5.0–14.0 days) compared with the aTAT of results from NGS reference methods only (*n* = 580).

The median (Q1–Q3) aTAT for Idylla™ EGFR Mutation Test results ranged from 1.0 day (0.0–1.0 day) to 6.0 days (3.0–10.5 days) across sites. The median (Q1–Q3) aTAT for reference methods results ranged from 4.0 days (2.0–5.0; MassARRAY®) to 21.0 days (18.8–26.0; outsourced NGS) across sites (Figure 4). Median (Q1–Q3) difference in aTAT between reference method and Idylla™ EGFR Mutation Test results varied across sites and, therefore, by the specific reference method used, ranging from 1.0 day (0.0–2.0; MassARRAY®) to

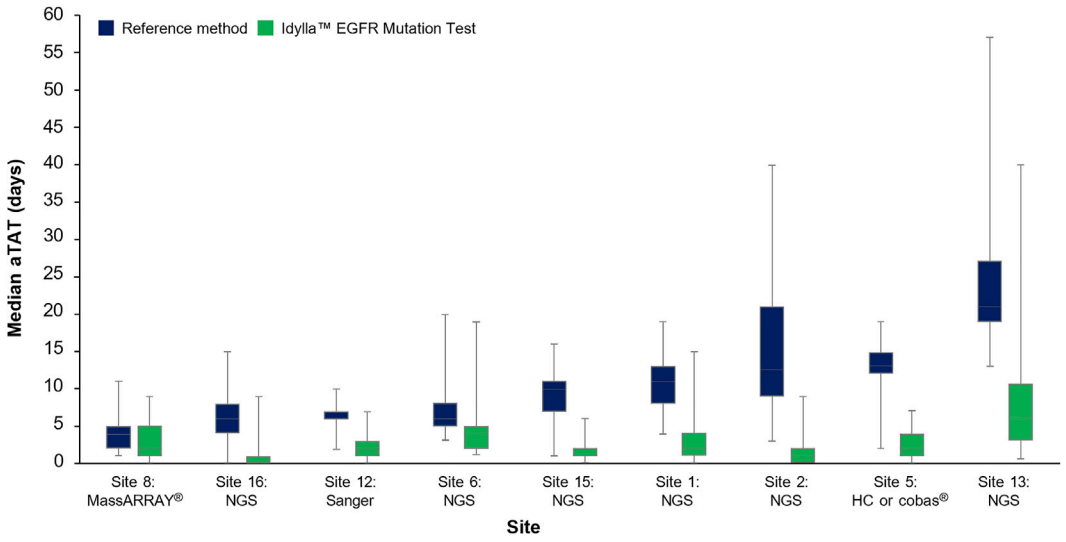

FIGURE 4
Median aTAT determined for Idylla™ and reference methods across sites where data were available. Data for each reference method (HC-NGS and cobas®) at Site 5 were assessed as one data set (involving a total of *n* = 97 samples) due to low sample numbers for each method if analyzed individually. Error bars represent minimum and maximum values; box plot represents Q1, median, and Q3. aTAT, analytical turnaround time; *EGFR*, epidermal growth factor receptor; HC, hybrid capture; NGS, next-generation sequencing.

14.0 days (13.0–16.0; outsourced NGS; Table 2). In depth country-specific differences were not analyzed.

Discussion

Clinical guidelines in NSCLC generally require that *EGFR* variant status is analyzed before a treatment plan is initiated to identify patients who are suitable for targeted treatments. *EGFR* variant testing should be conducted for common EGFR TKI-sensitizing variants (e.g., Ex19del or p.Leu858Arg in exon 21) in eligible patients with metastatic NSCLC and for patients with resectable stages IB to IIIA NSCLC [4,13,19,20,21,38]. It should also be used for identifying resistance variants in patients who relapse while receiving first or second-generation EGFR-TKIs [4]. Additionally, *EGFR* testing is recommended for rarer *EGFR* variants (e.g., *EGFR* Ex20ins variants; *EGFR* p.Ser768Ile, p.Leu861Gln and/or p.Gly719X) in eligible patients with metastatic NSCLC [13].

Various methods are used in routine *EGFR* variant testing; however, most require specialized testing facilities, or external access to such facilities, with trained staff to perform analyses and interpret results [30]. These methods, particularly when outsourced, are often used to batch test patient samples [30]. The frequent requirement for batch testing, multiple preparatory procedures and results interpretation as well as potential transport delays, if testing is outsourced, can result in lengthy aTATs. The automated Idylla™ EGFR Mutation Test avoids need for specialized testing facilities, does not require trained staff, and can be operated rapidly, with a run time of approximately 150 min, on a targeted (non-batch-related) patient-by-patient basis [43, 45]. Performance of the assay has been reported in previous studies [39–41,46]. Incorporation of this *EGFR* variant test into existing clinical workflows is expected to help reduce aTAT and, in turn, reduce time to treatment initiation, especially where samples test positive for targetable *EGFR* variants. These rapid and accessible test types may be of high value in streamlining clinical workflows, both in every-day clinical practice and during national health crises, such as the COVID-19 pandemic. In fact, a recent study demonstrated that preference for PCR-based methodologies over highly multiplexing assay approaches was one of several local strategies implemented to help overcome COVID-19 pandemic-related delays and other related challenges in lung cancer clinical practice [47]. It should be noted that the FACILITATE study was not impacted by the COVID-19 pandemic due to timing of the study.

FACILITATE was a real-world, prospective, multicenter European study that evaluated performance and aTAT of the Idylla™ EGFR Mutation Test compared with local reference methods in real-life NSCLC settings. Across FACILITATE, there was a high level of concordance between the Idylla™ EGFR Mutation Test and local reference methods. No difference in OPA was observed for the Idylla™ EGFR Mutation Test versus all reference methods, or Idylla™ EGFR Mutation Test versus NGS reference methods only. The high

level of concordance illustrates robustness and accuracy of the Idylla™ EGFR Mutation Test in a real-world setting. Concordance was higher when discordance-by-design cases were excluded. Cases classified as discordant by design involved specific *EGFR* variants that were detected by the reference method but not by the Idylla™ EGFR Mutation Test because those specific variants were not part of the Idylla™ 51-member panel.

Regarding discordant cases, these represented less than 2% of all analyses across the study when excluding for discordance-by-design cases. Most of these non-design-related discordances were resolved on third-method analysis; the main causes of discordance were insufficient material, low quality sample input and/or low AF. This can be explained because the Idylla™ EGFR Mutation Test does not allow for in-process quality control of extracted DNA, therefore, selection based on DNA quality was not possible. As a result, samples with low analyzable DNA content (indicated by high mean *EGFR* control Cq values) [48] or low numbers of mutated cells may have led to an increased risk of false-negative results. Furthermore, it is important to consider the effects of tumor heterogeneity on the discordance observed in this study. Single samples collected for tissue testing cannot truly encompass the diverse profile of the tumor due to inter-metastatic and even intra-tumor heterogeneity. The latter of which can also contribute to false results [49–51].

Five cases (three confirmed progression samples; one confirmed baseline sample; one was unknown as to if it was a progression or baseline sample) were concordant for a primary variant but discordant for *EGFR* p.Thr790Met. The relatively high frequency at which *EGFR* p.Thr790Met discordances occurred was expected, because the Idylla™ EGFR Mutation Test versus reference methods has lower inherent technical performance in detecting *EGFR* p.Thr790Met resistance variants compared with primary variants. The sensitivity of the Idylla™ EGFR Mutation Test for p.Thr790Met is design-limited to an allelic frequency of ≥ 5%; this design limitation is in place to avoid risk of false-positive results caused by deamination-related issues that can affect p.Thr790Met [45]. It should be noted that the one confirmed baseline sample in which the p.Thr790Met variant was detectable with the local reference method but not with the Idylla™ EGFR Mutation Test, was positive for primary variants with both methods. In view of this and because osimertinib is currently the preferred first-line treatment in EGFR-TKI-sensitizing variant-positive (eg, Ex19del, p.Leu858Arg) advanced NSCLC [4, 13, 19], cases of primary variant concordance but p.Thr790Met variant discordance are of less clinical importance at diagnosis. This is because osimertinib targets p.Thr790Met variants irrespective of whether they are primary or acquired [14]. However, in cases of NSCLC progression on first- or second-generation EGFR-TKIs, reliable and accurate p.Thr790Met variant testing remains essential [4].

In terms of discordant-by-design cases, the Idylla™ EGFR Mutation test is designed to test primarily for commonly occurring NSCLC-associated *EGFR* primary variants, including the group of Ex19del variants and the p.Leu858Arg variant in exon 21 [6], with rapid aTAT of results. Although, the 51 *EGFR* variants included in the Idylla™ EGFR Mutation test panel [43] does account for several rarer ("uncommon") clinically relevant variants [such as p.Gly719Ala, p.Gly719Ser and p.Gly719Cys in exon 18, p.Ser768Ile in exon 20, five Ex20ins (p.Asp770_Asn771insGly, p.Val769_Asp770insAlaSerVal, p.Val769_Asp770insAlaSerVal, p.Asp770_Asn771insSerValAsp and p.His773_Val774insHis), and p.Leu861Gln in exon 21] [43], other uncommon *EGFR* variants are not included in the Idylla™ EGFR Mutation test panel, and therefore are undetectable (by design) with the Idylla™ EGFR Mutation test. More comprehensive techniques can be used to detect whether these variants are present. In FACILITATE, less than 1% of samples were designated discordant by design. Although rare, these *EGFR* variants should be accounted for in clinical practice, highlighting the recommendation for complementary testing of negative samples (by the Idylla™ EGFR Mutation Test) by NGS. This integrated workflow could ensure that any uncommon *EGFR* variants undetectable by the Idylla™ EGFR Mutation Test are captured by NGS [52, 53]. However, while it would be preferable for the Idylla™ EGFR Mutation Test panel to include all these variants, there are likely to be few implications of these remaining undetected, considering approved treatments are lacking for most of these missing, uncommon variants [54].

Preliminary clinical data suggest that some uncommon variants are sensitive to EGFR-TKI treatment, as noted in a recent review [55]; however, clinical data interpretation may be confounded by the concomitant presence of complex variants. Moreover, reports regarding uncommon variants in NSCLC can be limited by small patient populations and the often-retrospective nature of these studies, which makes these data hard to interpret. As such, more clinical studies in patients with uncommon, rare, and complex *EGFR* variants are needed. It should be noted that increasing numbers of new treatments are being developed for targeting rare variants including those related to exon 20 [56] and, therefore, the amount of published clinical data regarding such rare variants is expected to increase.

The total percentage of discordant results reported in FACILITATE may be lower than expected in clinical practice. This is because there was an unanticipated bias by clinicians in the study to submit suitably or generously sized patient samples with sufficient neoplastic cells and exclude smaller, more challenging samples (i.e., patient samples with suboptimal quantities of material available for genetic testing using both the Idylla™ EGFR Mutation Test and the respective local reference method). This is likely due to the risk and clinical consequences of obtaining no or invalid results for patients for whom sample quantities were limited. The result of this understandable bias may mean that sample quantity-related issues related to the Idylla™ EGFR Mutation Test and the reference methods are underrepresented to some extent.

In our study, the Idylla™ EGFR Mutation Test reduced overall aTAT of results by a median of 1 week versus local reference methods results. Moreover, per cumulative analysis of samples processed per aTAT, results were available for 90% of samples within 1 week versus approximately 3 weeks using the Idylla™ EGFR Mutation Test versus local reference methods, respectively. The overall results indicate that incorporation of the Idylla™ EGFR Mutation Test into clinical workflows may be advantageous. The assay detects the most common clinically relevant *EGFR* variants and, therefore, may serve as a rapid and targeted sample-to-result screening technology conducted in parallel with more comprehensive variant testing (associated with longer aTAT of results). A recent report on data from 1,157 patients with advanced NSCLC in the UK indicated that approximately 25% of patients in whom targetable *EGFR* variants were reported did not receive targeted therapy initially [27]; one potential explanation noted was lengthy *EGFR* variant test turnaround times [27]. Incorporation of the Idylla™ EGFR Mutation Test into NSCLC clinical work flows thus may help mitigate clinician and patient delay-related motivations to initiate potentially suboptimal treatments while awaiting molecular testing results regarding *EGFR* variants [28, 31]. This may be particularly important in frail patients, patients with significant comorbidities or high symptom burden or patients with advanced disease including those with CNS metastases, all of whom are vulnerable to potentially rapid deterioration [28, 32, 33].

Most academic sites in our study used targeted NGS as their reference testing method that was conducted onsite; in community and private sites, specific testing methods varied and were sometimes outsourced. aTAT of results varied between sites and was typically shorter in academic sites than in community and private sites. This was expected as outsourcing is usually more common in smaller less equipped centers [57]. No country-specific differences could be deduced from the results as the study was not designed for this purpose. However, it can be concluded that in this study, aTAT of results was influenced predominantly by the methodology used at each site (Idylla™ EGFR Mutation Test vs. reference methods) rather than the country in which testing was performed. However, it should be noted that in standard clinical practice, country-specific reimbursement regulations may affect a center's diagnostic testing strategy and, therefore, influence aTAT of results. Rapid single-gene testing (screening) completed in parallel with, or immediately followed by, comprehensive NGS testing is often the clinician's preferred strategy, but this is not always feasible due to reimbursement restrictions.

In academic sites with comprehensive onsite specialized testing facilities, incorporation of the Idylla™ EGFR Mutation test may be importantly useful for designing fast-track workflows for triaging and quickly identifying patients eligible for EGFR-TKI treatment. In community or private sites where testing is often conducted offsite, aside from also helping with effective workflow design, the Idylla™ EGFR Mutation Test could importantly permit rapid onsite single-gene profiling. This may be critical given the risk of offsite batch testing- and sample transport-related delays, and the associated clinical implications for patients who are later found to be positive for common and actionable *EGFR* variants. However, it should be kept in mind that per ESMO precision working group recommendations, multiparametric NGS approaches should be favored from the outset and conducted as soon as possible to test for the presence of actionable variants [23]. In this way, patients who are found to be negative for common clinically relevant *EGFR* variants with the more rapid Idylla™ EGFR Mutation Test, will not experience added delays in obtaining comprehensive gene profiling results.

Irrespective of site-type and location, if the results using the Idylla™ EGFR Mutation Test are positive, appropriate targeted treatments could be started sooner, while comprehensive testing continues in the background. Currently, osimertinib is an applicable adjuvant targeted therapy in patients with resectable NSCLC, provided the patient's disease has an appropriate molecular profile [23]. Therefore, an accurate, rapid, and *EGFR*-specific variant test such as the Idylla™ EGFR Mutation Test could be a beneficial and cost-effective approach in facilitating treatment decisions in patients with resectable early-stage NSCLC. It should be re-emphasized that rare or co-occurring variants will not be detected with this test. As such, in any patient with NSCLC, when results are negative with the Idylla™ EGFR Mutation Test (i.e., no common and clinically relevant *EGFR* variants identified) more comprehensive molecular testing results are required as soon as possible. Therefore, as noted previously, comprehensive testing should be conducted from the outset in parallel with this more rapid *EGFR*-specific approach, if used [23]. This is particularly important in advanced NSCLC because targeted treatments are available for several molecular targets (not limited to EGFR). Related to this and in all scenarios, clinicians should ensure that sufficient tissue sample quantity is always available for comprehensive molecular testing. If there is limited tissue available, use of tissue samples for comprehensive molecular testing should be prioritized.

Limitations of this study include an unanticipated clinician-driven sample-size selection bias that may have meant that the rate of discordances and invalid or non-processable results were underrepresented compared with that expected in clinical practice. Also, although the overall data were analyzable, data were not sufficient to permit site-specific aTAT determination at some sites or an analysis of the results by patient demographics. This was expected as FACILITATE was conducted in a real-world setting, in which incomplete record keeping and missing data are common [58]. Some clinicians may not have had the opportunity to record the exact time at which they submitted samples and/or received results. This was made more difficult by the high sample numbers analyzed at each site, each of which had only one Idylla™ console available for *EGFR* analysis, meaning that test results were not always returned at convenient hours when the submitting clinician was practicing, and therefore, other clinicians may have received the results on their behalf. In these instances, record keeping may have been less detailed. Lastly, the FACILITATE study did not analyze data on the impact of turnaround time on date of targeted therapy

initiation where indicated. However, a recent bicentric prospective study [54] showed that aTAT of results (defined in that study as time from tumor sampling to initiation of EGFR-TKIs) was reduced by 12.5 calendar days when using the Idylla™ EGFR Mutation Test versus NGS with a reported OPA of 96.4%. The results of that bicentric prospective study [54], therefore, support the results of FACILITATE (a comparatively larger and multicentric study) concerning overall median aTAT reduction (7.0 days; from time of sample receipt by laboratory to when results were ready to be sent to the clinician) when using the Idylla™ EGFR Mutation Test versus local reference methods (NGS and several other methods).

Conclusion and outlook

We demonstrate in a real-world multicenter setting, using samples with equal to or more than 10% neoplastic cell content, that the Idylla™ EGFR Mutation Test performed very well (~98% OPA) compared with routinely used *EGFR* variant reference tests. Using an analysis of cumulative percentage of tested sample results returned by aTAT, we also show that the Idylla™ EGFR Mutation Test was able to deliver actionable and clinically relevant results typically in less time compared with local reference methods. The Idylla™ EGFR Mutation Test may serve as an enabling technology to detect common clinically relevant *EGFR* variants in NSCLC, either to complement existing workflows permitting a fast-track route, or to establish in-house *EGFR*-specific initial testing in sites without in-house testing facilities. However, in all cases, the feasibility of comprehensive molecular testing should be considered especially in cases where limited quantities of tissue sample are available; this is important given the possibility that common clinically relevant *EGFR* variants are not present. Considering the availability of targeted treatments such as EGFR-TKIs, the Idylla™ EGFR Mutation Test is a feasible and convenient means to help facilitate the application of personalized medicine in NSCLC.

Data availability statement

The raw data supporting the conclusion of this article will be made available by the authors, without undue reservation.

Ethics statement

Use of patient samples in this study was approved by the respective local ethics committees at each site, and was in accordance with the Declaration of Helsinki. Written informed consent from the participants' legal guardian/next of kin was not required to participate in this study in accordance with the national legislation and the institutional requirements.

Author contributions

MH was responsible for the study conception and the study design; ABe, AC, GDM, GG, LH, MT, MC, DC, AL, CLN, GM, AD, IB, AR, ABa, BK, EW, and MH were responsible for the data acquisition; ABe, AC, GDM, GG, LH, MT, MC, DC, AL, CLN, AD, IB, AR, ABa, BK, EW, and MH performed the data analysis; ABe, AC, GDM, GG, MT, MC, DC, AL, CLN, GM, AD, IB, AR, ABa, BK, EW, and MH performed the data interpretation. MH is the guarantor of this work, had full access to all the data in the study and takes responsibility for the integrity of the data and the accuracy of the data analysis. All authors reviewed drafts of the manuscript and provided their approval to submit the manuscript.

Conflict of interest

IB declares receipt of honoraria from Novartis, Bayer, Pfizer, Takeda, AstraZeneca and BMS. EW declares the receipt of honoraria from AstraZeneca and MSD. MH declares membership in advisory councils or committees for AstraZeneca, Roche, Novartis, Pierre Fabre GDM, Sanofi, MSD and BMS; and receipt of grants or funds from AstraZeneca. Author EW was employed by the company CYPATH.

The remaining authors declare that the research was conducted in the absence of any commercial or financial relationships that could be construed as a potential conflict of interest.

The authors declare that this study received funding from AstraZeneca, Cambridge, UK and Biocartis, Mechelen, Belgium. Biocartis were involved in study design, and analysis and interpretation of data. AstraZeneca were not involved in study design or analysis and interpretation of data. The funders were not involved in collection of data. The funders reviewed the manuscript before submission.

Acknowledgments

Thanks to all the patients and their families. The authors would like to acknowledge Leon Newman, PhD, of Ashfield MedComms, an Ashfield Health Company for medical writing support that was funded by AstraZeneca, Cambridge, United Kingdom, in accordance with Good Publications Practice (GPP) guidelines (https://www.ismpp.org/gpp-2022).

Supplementary material

The Supplementary Material for this article can be found online at: https://www.por-journal.com/articles/10.3389/pore.2023.1610707/full#supplementary-material

References

1. Brown NA, Aisner DL, Oxnard GR. Precision medicine in non–small cell lung cancer: Current standards in Pathology and biomarker interpretation. *Am Soc Clin Oncol Educ Book* (2018) 38:708–15. doi:10.1200/EDBK_209089

2. Lynch TJ, Bell DW, Sordella R, Gurubhagavatula S, Okimoto RA, Brannigan BW, et al. Activating mutations in the epidermal growth factor receptor underlying responsiveness of non-small-cell lung cancer to gefitinib. *N Engl J Med* (2004) 350(21):2129–39. doi:10.1056/NEJMoa040938

3. Paez JG, Janne PA, Lee JC, Tracy S, Greulich H, Gabriel S, et al. EGFR mutations in lung cancer: Correlation with clinical response to gefitinib therapy. *Science* (2004) 304(5676):1497–500. doi:10.1126/science.1099314

4. Planchard D, Popat S, Kerr K, Novello S, Smit EF, Faivre-Finn C, et al. *Metastatic non-small cell lung cancer: ESMO clinical practice guidelines for diagnosis, treatment and follow-up. Updated version published 15 september 2020 by the ESMO guidelines committee [online]. (2020)* (2020). Available: https://www.esmo.org/guidelines/lung-and-chest-tumours/clinical-practice-living-guidelines-metastatic-non-small-cell-lung-cancer (Accessed September 25, 2020).

5. Zhang YL, Yuan JQ, Wang KF, Fu XH, Han XR, Threapleton D, et al. The prevalence of EGFR mutation in patients with non-small cell lung cancer: A systematic review and meta-analysis. *Oncotarget* (2016) 7(48):78985–93. doi:10.18632/oncotarget.12587

6. Murray S, Dahabreh IJ, Linardou H, Manoloukos M, Bafaloukos D, Kosmidis P. Somatic mutations of the tyrosine kinase domain of epidermal growth factor receptor and tyrosine kinase inhibitor response to TKIs in non-small cell lung cancer: An analytical database. *J Thorac Oncol Official Publ Int Assoc Study Lung Cancer* (2008) 3(8):832–9. doi:10.1097/JTO.0b013e31818071f3

7. Rosell R, Carcereny E, Gervais R, Vergnenegre A, Massuti B, Felip E, et al. Erlotinib versus standard chemotherapy as first-line treatment for European patients with advanced EGFR mutation-positive non-small-cell lung cancer (eurtac): A multicentre, open-label, randomised phase 3 trial. *Lancet Oncol* (2012) 13(3):239–46. doi:10.1016/S1470-2045(11)70393-X

8. Mok TS, Wu YL, Thongprasert S, Yang CH, Chu DT, Saijo N, et al. Gefitinib or carboplatin-paclitaxel in pulmonary adenocarcinoma. *N Engl J Med* (2009) 361(10): 947–57. doi:10.1056/NEJMoa0810699

9. Wu YL, Zhou C, Liam CK, Wu G, Liu X, Zhong Z, et al. First-line erlotinib versus gemcitabine/cisplatin in patients with advanced EGFR mutation-positive non-small-cell lung cancer: Analyses from the phase III, randomized, open-label, ENSURE study. *Ann Oncol* (2015) 26(9):1883–9. doi:10.1093/annonc/mdv270

10. Soria JC, Ohe Y, Vansteenkiste J, Reungwetwattana T, Chewaskulyong B, Lee KH, et al. Osimertinib in untreated EGFR-mutated advanced non-small-cell lung cancer. *N Engl J Med* (2018) 378(2):113–25. doi:10.1056/NEJMoa1713137

11. Leonetti A, Sharma S, Minari R, Perego P, Giovannetti E, Tiseo M. Resistance mechanisms to osimertinib in EGFR-mutated non-small cell lung cancer. *Br J Cancer* (2019) 121(9):725–37. doi:10.1038/s41416-019-0573-8

12. Niederst MJ, Hu H, Mulvey HE, Lockerman EL, Garcia AR, Piotrowska Z, et al. The allelic context of the C797S mutation acquired upon treatment with third-generation EGFR inhibitors impacts sensitivity to subsequent treatment strategies. *Clin Cancer Res* (2015) 21(17):3924–33. doi:10.1158/1078-0432.Ccr-15-0560

13. NCCN Clinical Practice Guidelines. *Referenced with permission from the NCCN Clinical Practice Guidelines in Oncology (NCCN Guidelines®) for Non-Small Cell Lung Cancer V.3.2022. © National Comprehensive Cancer Network, Inc. 2022. All rights reserved. Accessed March 17, 2022. To view the most recent and complete version of the guideline, go online to NCCN.org. NCCN makes no warranties of any kind whatsoever regarding their content, use or application and disclaims any responsibility for their application or use in any way* (2022).

14. Cross DA, Ashton SE, Ghiorghiu S, Eberlein C, Nebhan CA, Spitzler PJ, et al. AZD9291, an irreversible EGFR TKI, overcomes t790m-mediated resistance to EGFR inhibitors in lung cancer. *Cancer Discov* (2014) 4(9):1046–61. doi:10.1158/2159-8290.CD-14-0337

15. Reungwetwattana T, Nakagawa K, Cho BC, Cobo M, Cho EK, Bertolini A, et al. CNS response to osimertinib versus standard epidermal growth factor receptor tyrosine kinase inhibitors in patients with untreated EGFR-mutated advanced non–small-cell lung cancer. *J Clin Oncol* (2018) 36(33):3290–7. doi:10.1200/jco.2018.78.3118

16. Ramalingam SS, Vansteenkiste J, Planchard D, Cho BC, Gray JE, Ohe Y, et al. Overall survival with osimertinib in untreated, EGFR-mutated advanced NSCLC. *N Engl J Med* (2020) 382(1):41–50. doi:10.1056/NEJMoa1913662

17. Wu YL, Ahn MJ, Garassino MC, Han JY, Katakami N, Kim HR, et al. CNS efficacy of osimertinib in patients with t790m-positive advanced non-small-cell lung cancer: Data from a randomized phase III trial (AURA3). *J Clin Oncol* (2018) 36(26):2702–9. doi:10.1200/jco.2018.77.9363

18. Mok TS, Wu YL, Ahn MJ, Garassino MC, Kim HR, Ramalingam SS, et al. Osimertinib or platinum-pemetrexed in EGFR t790m-positive lung cancer. *N Engl J Med* (2017) 376(7):629–40. doi:10.1056/NEJMoa1612674

19. Hanna NH, Robinson AG, Temin S, Baker S, Brahmer JR, Ellis PM, et al. Therapy for stage IV non–small-cell lung cancer with driver alterations: ASCO and OH (CCO) joint guideline update. *J Clin Oncol* (2021) 20:1040–91. doi:10.1200/JCO.20.03570

20. Leighl NB, Rekhtman N, Biermann WA, Huang J, Mino-Kenudson M, Ramalingam SS, et al. Molecular testing for selection of patients with lung cancer for epidermal growth factor receptor and anaplastic lymphoma kinase tyrosine kinase inhibitors: American society of clinical Oncology endorsement of the college of American pathologists/international association for the study of lung cancer/association for molecular Pathology guideline. *J Clin Oncol* (2014) 32(32):3673–9. doi:10.1200/JCO.2014.57.3055

21. Lindeman NI, Cagle PT, Aisner DL, Arcila ME, Beasley MB, Bernicker E, et al. Updated molecular testing guideline for the selection of lung cancer patients for treatment with targeted tyrosine kinase inhibitors: Guideline from the college of American pathologists, the international association for the study of lung cancer, and the association for molecular Pathology. *Arch Pathol Lab Med* (2018) 142(3): 321–46. doi:10.5858/arpa.2017-0388-CP

22. Oxnard GR, Miller VA, Robson ME, Azzoli CG, Pao W, Ladanyi M, et al. Screening for germline EGFR T790M mutations through lung cancer genotyping. *J Thorac Oncol* (2012) 7(6):1049–52. doi:10.1097/JTO.0b013e318250ed9d

23. Mosele F, Remon J, Mateo J, Westphalen CB, Barlesi F, Lolkema MP, et al. Recommendations for the use of next-generation sequencing (NGS) for patients with metastatic cancers: A report from the ESMO precision medicine working group. *Ann Oncol* (2020) 31(11):1491–505. doi:10.1016/j.annonc.2020.07.014

24. Mardis ER. DNA sequencing technologies: 2006–2016. *Nat Protoc* (2017) 12(2):213–8. doi:10.1038/nprot.2016.182

25. Grossmann V, Kohlmann A, Klein HU, Schindela S, Schnittger S, Dicker F, et al. Targeted next-generation sequencing detects point mutations, insertions, deletions and balanced chromosomal rearrangements as well as identifies novel leukemia-specific fusion genes in a single procedure. *Leukemia* (2011) 25(4): 671–80. doi:10.1038/leu.2010.309

26. Takeda M, Sakai K, Terashima M, Kaneda H, Hayashi H, Tanaka K, et al. Clinical application of amplicon-based next-generation sequencing to therapeutic decision making in lung cancer. *Ann Oncol* (2015) 26(12):2477–82. doi:10.1093/annonc/mdv475

27. Royal College of Physicians. *Spotlight report on molecular testing in advanced lung cancer* (2020). Available: https://www.hqip.org.uk/wp-content/uploads/2020/01/REF100_NLCA_Spotlight-Molec-Test_FINAL-TYPESET_web_20200108.pdf (Accessed July 14, 2021).

28. Gregg JP, Li T, Yoneda KY. Molecular testing strategies in non-small cell lung cancer: Optimizing the diagnostic journey. *Transl Lung Cancer Res* (2019) 8(3): 286–301. doi:10.21037/tlcr.2019.04.14

29. Lassalle S, Hofman V, Heeke S, Benzaquen J, Long E, Poudenx M, et al. Targeted assessment of the EGFR status as reflex testing in treatment-naive non-squamous cell lung carcinoma patients: A single laboratory experience (LPCE, Nice, France). *Cancers* (2020) 12(4):955. doi:10.3390/cancers12040955

30. Kerr KM, Bibeau F, Thunnissen E, Botling J, Ryška A, Wolf J, et al. The evolving landscape of biomarker testing for non-small cell lung cancer in europe. *Lung Cancer* (2021) 154:161–75. doi:10.1016/j.lungcan.2021.02.026

31. Lim C, Tsao MS, Le LW, Shepherd FA, Feld R, Burkes RL, et al. Biomarker testing and time to treatment decision in patients with advanced non-small-cell lung cancer. *Ann Oncol* (2015) 26(7):1415–21. doi:10.1093/annonc/mdv208

32. Rangachari D, Drake L, Huberman MS, McDonald DC, VanderLaan PA, Folch E, et al. Rapidly fatal advanced EGFR-mutated lung cancers and the need for rapid tumor genotyping in clinical practice. *Cancer Treat Commun* (2016) 9:41–3. doi:10.1016/j.ctarc.2016.07.001

33. Gutierrez ME, Choi K, Lanman RB, Licitra EJ, Skrzypczak SM, Pe Benito R, et al. Genomic profiling of advanced non-small cell lung cancer in community settings: Gaps and opportunities. *Clin Lung Cancer* (2017) 18(6):651–9. doi:10.1016/j.cllc.2017.04.004

34. Wu Y-L, Tsuboi M, He J, John T, Grohe C, Majem M, et al. Osimertinib in resected EGFR-mutated non–small-cell lung cancer. *N Engl J Med* (2020) 383(18): 1711–23. doi:10.1056/NEJMoa2027071

35. Remon J, Soria JC, Peters S, clinicalguidelines@esmo.org EGCEa. Early and locally advanced non-small-cell lung cancer: An update of the ESMO clinical practice guidelines focusing on diagnosis, staging, systemic and local therapy. *Ann Oncol* (2021) 32(12):1637–42. doi:10.1016/j.annonc.2021.08.1994

36. Liam C-K, Mallawathantri S, Fong KM. Is tissue still the issue in detecting molecular alterations in lung cancer? *Respirology* (2020) 25(9):933–43. doi:10.1111/resp.13823

37. Kris MG, Johnson BE, Berry LD, Kwiatkowski DJ, Iafrate AJ, Wistuba B, et al. Using multiplexed assays of oncogenic drivers in lung cancers to select targeted drugs. *JAMA* (2014) 311(19):1998–2006. doi:10.1001/jama.2014.3741

38. Cheema PK, Gomes M, Banerji S, Joubert P, Leighl NB, Melosky B, et al. Consensus recommendations for optimizing biomarker testing to identify and treat advanced EGFR-mutated non-small-cell lung cancer. *Curr Oncol* (2020) 27(6):321–9. doi:10.3747/co.27.7297

39. Delgado-García M, Weynand B, Gómez-Izquierdo L, Hernández MJ, Blanco ÁM, Varela M, et al. Clinical performance evaluation of the Idylla™ EGFR mutation test on formalin-fixed paraffin-embedded tissue of non-small cell lung cancer. *BMC cancer* (2020) 20(1):275. doi:10.1186/s12885-020-6697-7

40. Momeni-Boroujeni A, Salazar P, Zheng T, Mensah N, Rijo I, Dogan S, et al. Rapid EGFR mutation detection using the Idylla platform: Single-institution experience of 1200 cases analyzed by an in-house developed pipeline and comparison with concurrent next-generation sequencing results. *J Mol Diagn* (2021) 23(3):310–22. doi:10.1016/j.jmoldx.2020.11.009

41. Arcila ME, Yang S-R, Momeni A, Mata DA, Salazar P, Chan R, et al. Ultrarapid EGFR mutation screening followed by comprehensive next-generation sequencing: A feasible, informative approach for lung carcinoma cytology specimens with a high success rate. *JTO Clin Res Rep* (2020) 1(3):100077. doi:10.1016/j.jtocrr.2020.100077

42. De Luca C, Rappa AG, Gragnano G, Malapelle U, Troncone G, Barberis M. Idylla assay and next generation sequencing: An integrated EGFR mutational testing algorithm. *J Clin Pathol* (2018) 71(8):745–50. doi:10.1136/jclinpath-2018-205197

43. Biocartis. *Technical sheet Idylla™ ctEGFR mutation assay* (2019). Available: https://www.biocartis.com/sites/default/files/2021-03/Idylla_ctEGFR-RUO_Tech-Sheet.pdf (Accessed May 31, 2022).

44. Lee Y, Clark EW, Milan MSD, Champagne C, Michael KS, Awad MM, et al. Turnaround time of plasma next-generation sequencing in thoracic oncology patients: A quality improvement analysis. *JCO Precis Oncol* (2020) 4:1098–108. doi:10.1200/PO.20.00121

45. Evrard SM, Taranchon-Clermont E, Rouquette I, Murray S, Dintner S, Nam-Apostolopoulos YC, et al. Multicenter evaluation of the fully automated PCR-based Idylla EGFR mutation assay on formalin-fixed, paraffin-embedded tissue of human lung cancer. *J Mol Diagn* (2019) 21(6):1010–24. doi:10.1016/j.jmoldx.2019.06.010

46. Ilie M, Butori C, Lassalle S, Heeke S, Piton N, Sabourin J-C, et al. Optimization of EGFR mutation detection by the fully-automated qPCR-based Idylla system on tumor tissue from patients with non-small cell lung cancer. *Oncotarget* (2017) 8(61):103055–62. doi:10.18632/oncotarget.21476

47. Malapelle U, Pisapia P, Iaccarino A, Barberis M, Bellevicine C, Brunnström H, et al. Predictive molecular Pathology in the time of coronavirus disease (COVID-19) in Europe. *J Clin Pathol* (2020) 74:391–5. doi:10.1136/jclinpath-2020-206957

48. Grant J, Stanley A, Balbi K, Gerrard G, Bennett P. Performance evaluation of the Biocartis Idylla EGFR mutation test using pre-extracted DNA from a cohort of highly characterised mutation positive samples. *J Clin Pathol* (2021) 75:241–9. doi:10.1136/jclinpath–2020–20733810.1136/jclinpath-2020-207338

49. Park S, Holmes-Tisch AJ, Cho EY, Shim YM, Kim J, Kim HS, et al. Discordance of molecular biomarkers associated with epidermal growth factor receptor pathway between primary tumors and lymph node metastasis in non-small cell lung cancer. *J Thorac Oncol* (2009) 4(7):809–15. doi:10.1097/JTO.0b013e3181a94af4

50. Chang S, Shim HS, Kim TJ, Choi YL, Kim WS, Shin DH, et al. Molecular biomarker testing for non-small cell lung cancer: Consensus statement of the Korean cardiopulmonary pathology study group. *J Pathol Transl Med* (2021) 55(3):181–91. doi:10.4132/jptm.2021.03.23

51. Bordi P, Del Re M, Danesi R, Tiseo M. Circulating DNA in diagnosis and monitoring EGFR gene mutations in advanced non-small cell lung cancer. *Transl Lung Cancer Res* (2015) 4(5):584–97. doi:10.3978/j.issn.2218-6751.2015.08.09

52. Nkosi D, Casler VL, Syposs CR, Oltvai ZN. Utility of select gene mutation detection in tumors by the Idylla rapid multiplex PCR platform in comparison to next-generation sequencing. *Genes (Basel)* (2022) 13(5):799. doi:10.3390/genes13050799

53. Gilson P, Saurel C, Salleron J, Husson M, Demange J, Merlin JL, et al. Evaluation of the Idylla ctEGFR mutation assay to detect EGFR mutations in plasma from patients with non-small cell lung cancers. *Sci Rep* (2021) 11(1):10470. doi:10.1038/s41598-021-90091-z

54. Petiteau C, Robinet-Zimmermann G, Riot A, Dorbeau M, Richard N, Blanc-Fournier C, et al. Contribution of the IdyllaTM system to improving the therapeutic care of patients with NSCLC through early screening of EGFR mutations. *Curr Oncol* (2021) 28(6):4432–45. doi:10.3390/curroncol28060376

55. Harrison PT, Vyse S, Huang PH. Rare epidermal growth factor receptor (EGFR) mutations in non-small cell lung cancer. *Semin Cancer Biol* (2020) 61:167–79. doi:10.1016/j.semcancer.2019.09.015

56. Friedlaender A, Subbiah V, Russo A, Banna GL, Malapelle U, Rolfo C, et al. EGFR and HER2 exon 20 insertions in solid tumours: From biology to treatment. *Nat Rev Clin Oncol* (2022) 19(1):51–69. doi:10.1038/s41571-021-00558-1

57. Vigliar E, Malapelle U, Bellevicine C, de Luca C, Troncone G. Outsourcing cytological samples to a referral laboratory for EGFR testing in non-small cell lung cancer: Does theory meet practice? *Cytopathology* (2015) 26(5):312–7. doi:10.1111/cyt.12221

58. Yang DX, Khera R, Miccio JA, Jairam V, Chang E, Yu JB, et al. Prevalence of missing data in the National Cancer Database and association with overall survival. *JAMA Netw Open* (2021) 4(3):e211793. doi:10.1001/jamanetworkopen.2021.1793

Pathology & Oncology Research | frontiers

TYPE Review
PUBLISHED 16 May 2024
DOI 10.3389/pore.2024.1611676

Check for updates

OPEN ACCESS

EDITED BY
Attila Patocs,
Semmelweis University, Hungary

*CORRESPONDENCE
Nikolett Szakállas,
szakallasn3@gmail.com

RECEIVED 10 January 2024
ACCEPTED 30 April 2024
PUBLISHED 16 May 2024

CITATION
Szakállas N, Barták BK, Valcz G, Nagy ZB, Takács I and Molnár B (2024), Can long-read sequencing tackle the barriers, which the next-generation could not? A review.
Pathol. Oncol. Res. 30:1611676.
doi: 10.3389/pore.2024.1611676

COPYRIGHT
© 2024 Szakállas, Barták, Valcz, Nagy, Takács and Molnár. This is an open-access article distributed under the terms of the Creative Commons Attribution License (CC BY). The use, distribution or reproduction in other forums is permitted, provided the original author(s) and the copyright owner(s) are credited and that the original publication in this journal is cited, in accordance with accepted academic practice. No use, distribution or reproduction is permitted which does not comply with these terms.

Can long-read sequencing tackle the barriers, which the next-generation could not? A review

Nikolett Szakállas[1]*, Barbara K. Barták[2], Gábor Valcz[2,3], Zsófia B. Nagy[2], István Takács[2] and Béla Molnár[2]

[1]Department of Biological Physics, Faculty of Science, Eötvös Loránd University, Budapest, Hungary, [2]Department of Internal Medicine and Oncology, Faculty of Medicine, Semmelweis University, Budapest, Hungary, [3]HUN-REN-SU Translational Extracellular Vesicle Research Group, Budapest, Hungary

The large-scale heterogeneity of genetic diseases necessitated the deeper examination of nucleotide sequence alterations enhancing the discovery of new targeted drug attack points. The appearance of new sequencing techniques was essential to get more interpretable genomic data. In contrast to the previous short-reads, longer lengths can provide a better insight into the potential health threatening genetic abnormalities. Long-reads offer more accurate variant identification and genome assembly methods, indicating advances in nucleotide deflect-related studies. In this review, we introduce the historical background of sequencing technologies and show their benefits and limits, as well. Furthermore, we highlight the differences between short- and long-read approaches, including their unique advances and difficulties in methodologies and evaluation. Additionally, we provide a detailed description of the corresponding bioinformatics and the current applications.

KEYWORDS

sequencing, short-read, long-read, bioinformatics, DNA

Introduction

The complete genetic information of the organisms is stored and transferred in single- and double-stranded ribonucleic (RNA) and deoxyribonucleic (DNA) acids [1]. The mystery behind rare genetic conditions, like chromosomal irregularities or unique sequence variation and mutation profiles in cancer, induced the need of molecular examination at deeper levels. For many years, only a deficient tool set was available to get a better insight into the genetic attributes of genomes. This encouraged the development of novel technologies, such as RNA and DNA sequencing methods. Provoked by the technical and computational progress of the past 50 years, the features of sequence determination changed and evolved. In the early periods, only a few hundred bases were reachable in length; however, the emergence of long-read technologies allowed the reading of longer genomic sequences even with thousands of kilo bases.

The timeline of the sequencing techniques' evolution can be divided into three main parts: first-generation (FGS), next-generation (NGS), and third-generation (TGS) sequencing. Before short-read NGS approaches became available, FGS techniques were the only tools capable of describing the nucleic acid sequence of different organisms. Thus, their main advantage is that they emphasized the need to use and develop novel sequencing methods to get a deeper knowledge regarding DNA and RNA sequences with repetitive regions, alternative bases, splicing variants and telomeric regions. Later in time, the NGS and mainly TGS methods were capable of opening closed doors for the detection of the listed alteration types, thereby exploring many reasons (and also the curing solution) for diseases. In our review, we strived to show FGS techniques from this point of view, without explaining their applications and attributes in more detail. In this scope, FGS were the pioneers of sequencing around the 1980s, including Sanger's chromatography and Maxam-Gilbert's chemical modification-based assays. In the early times, these technologies allowed focusing on relatively small genomes with a few hundred base pairs (bp) in length [2]. Sanger's idea was to sequence the DNA strand by chain termination. Consequently, in this case, the DNA fragments were converted into chains by DNA polymerases and by the incorporation of nucleotides [3]. Maxam and Gilbert provided a process, during which the sequences of DNA fragments were determined using the combination of radiolabeling, chemical cleaving, and gel electrophoresis of nucleotides, and autoradiography served as the detection method [4].

The second generation, namely, NGS, includes pyrosequencing [5] and sequencing-by-synthesis [6] approaches. They have a feature in common, which is that DNA polymerase moves along the template DNA and sequencing is performed by catalyzing the incorporation of deoxynucleotide triphosphates (dNTPs) in a new complementary DNA strand [7]. Pyrosequencing is a sequence-based form, where a pyrophosphate is released, when dNTPs are sequentially added to the end of a nascent DNA fragment [8]. Sequencing-by-synthesis is the construction of a nucleic acid chain from the emission spectra of fluorescently labeled nucleotides [6].

Although NGS provides more acceptable error rates and more sophisticated sequencing results than FGS, they have several weaknesses that should be mentioned. Read lengths are shorter than demanded, that is why they are referred to as short read techniques nowadays. Consequently, their shortness limits the study of full-length transcript variants, centromere and telomere genomic regions, and gene fusions [9]. Additionally, they are unable to resolve repetitive regions of the genome, making genetic variations challenging to identify, including repeat expansion disorders and structural variants [10]. Extreme guanine-cytosine (GC) content or sequences with multiple homologous elements in the genome and the epigenetically modified bases of DNA and RNA, like N6-methyladenosine (6mA), 5-methylcytosine (5mC), and 5-hydroxymethylcytosine (5hmC) are challenging to characterize with NGS [11]. PCR amplification is essential, which results in higher costs and longer times in the overall sequencing and evaluation process, involves the usage of large equipment and laborious experimental procedures, and expands the bioinformatics analysis with a data preprocessing step. To overcome the limitations, further sequencing techniques have been developed, the representatives of the TGS family, often referred to as long-read sequencing methods [12, 13].

Many scientific papers describing the methodology, evaluation and use of different sequencing assays become available yearly. Currently, long-read TGS and short-read NGS methods are used problem-specifically, either interchangeably or in combination. Although both methods have their own advantages and disadvantages, reviews setting against the methods cannot be found among the currently available publications. Encouraged by this, our goal is to provide a general comparison of long- and short-read techniques. In the present paper, we aimed to review the development of sequencing assays, presenting a brief characteristics of FGS, NGS and TGS, with special emphasis on the possibilities offered by the TGS methods. We also detail the bioinformatics approaches along with the aspects considered during evaluation, as well as related clinical and biological applications.

Long-read sequencing

TGS provides more precise mapping of reads for reference genomes, promotes different variant detection methods, and offers new solutions for characterizing the epigenetic diversity [14]. In contrast to NGS systems, the generated data is analyzed in real-time and generally, PCR amplification steps are not required before sequencing due to natural isolated nucleic acid strands can be read as well. The longer sequenced reads are the consequences of the improved sequencing chemistries [15, 16]. The increased sequencing speed and accuracy during experiments and the higher quality bioinformatics results also mark the effectiveness of the newly emerged technologies and the inherent chemical kits [17].

TGS technologies conceal the opportunity to emerge as long-term applicable tools in the future. As they provide the long-read sequencing of whole genomes, their usage in the field of genomics entails the chance of more and more accurate description of both human and non-human genetic diversities. Furthermore, improvements aimed to decrease costs and analysis time could invoke their application in routine diagnostics.

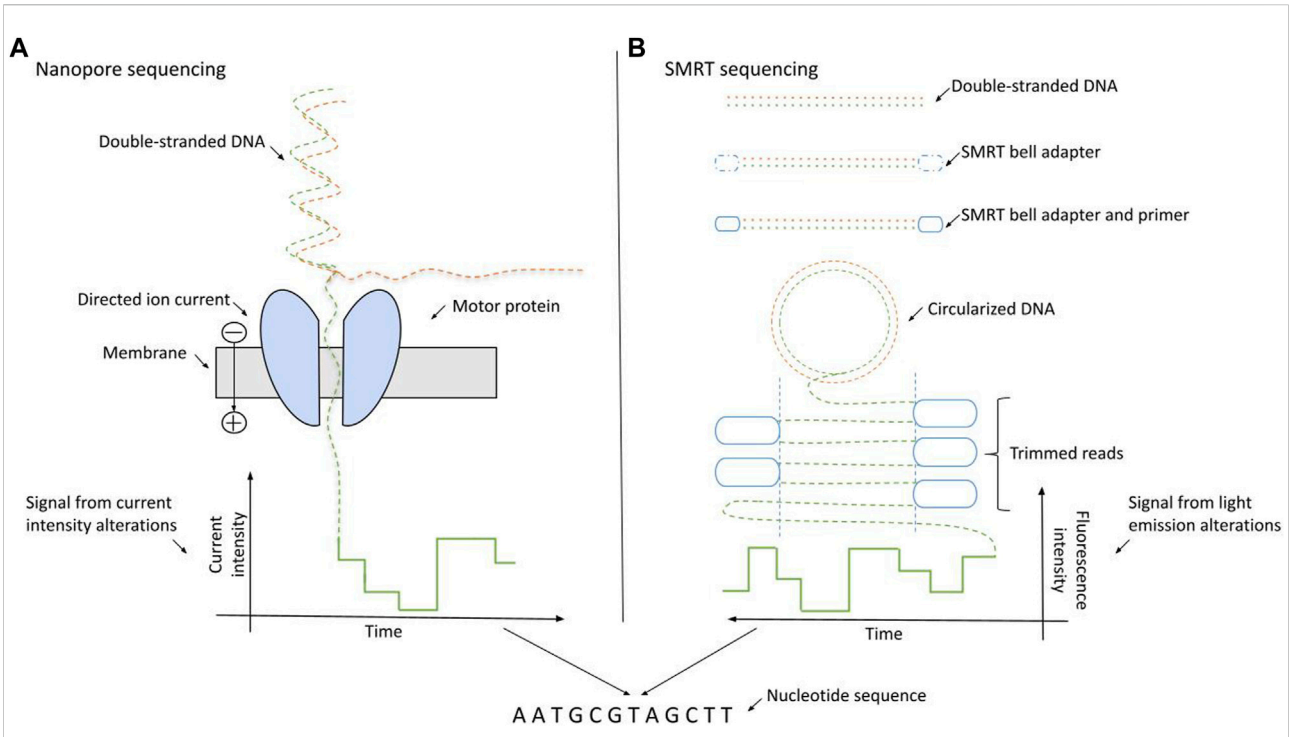

FIGURE 1
Schematics of long-read sequencing approaches: nanopore sequencing (Oxford Nanopore Technologies) and SMRT sequencing (Pacific BioSciences). **(A)** NS relies on the passage of the ssDNA through the membrane driven by the motor protein. The nucleotide bases are identified using the directed ionic current intensities arising from the motion of particles through the membrane. **(B)** During SMRT sequencing, dsDNAs are circularized into a SMRT bell. The SMRT bell contains the four fluorescently labeled nucleotides with unique emission spectra. The bases are distinguished by the alterations in the light emission spectra.

Nanopore sequencing

The nanopore sequencing (NS) method, distributed by Oxford Nanopore Technologies (ONT), is based on the detection of the electric current changes provoked by the disorganization of nanopore proteins [16–19]. The alterations in the real-time produced electric current can be measured directly. During NS, dsDNA molecules are denatured, and the motor protein directs ssDNAs through the nanochannels (pores) one after the other. The passage of ssDNA molecules leads to disturbances in the electric current, which is detected by specific reader sensor proteins. The deflections are distinct for all nucleotides resulting in unique signatures for each base. The entire process happens inside a device-specific flow cell [20], which contains thousands of nanopore channels. The schematics of NS sequencing is presented on Figure 1A.

Since the release of the first ONT sequencing device—named MinION—in the mid-2010s, the continuous improvement of the key factors, like accuracy, read length, and sequencing throughput is present. The throughput is determined by the number of active pores on the flow cells and by the DNA/RNA translocation speed. To provide the maximal amount of available active pores on the flow cells, their periodical revision is secured [16, 21]. The read length and the accuracy are highly dependent on the released version and quality of the sequencing chemistry—which in this case includes the traits of nanopores and motor proteins,—however, by introducing special adapters during penetration, an increase in accuracy measure can also be reached with higher ~420 bps per sec sequencing speeds compared to the previous ~70 bps per sec rate [22].

NS reads are characterized by longer lengths of 10 kb up to 100 kb, which means more sequenced bases, more generated data and increased informatics resource needs compared to NGS. The large amount of data means longer bioinformatics analysis time and more expensive informatics hardware park. However, due to the increased information amount, a more accurate identification of alterations becomes available. As the most important disadvantage of the increased generated data, higher error rate and read misclassification can be experienced on the ONT platforms compared to NGS [23, 24].

SMRT sequencing

Pacific BioSciences provided the first nanosensor-based technology in the early 2010s relying on the single molecule

real-time (SMRT) sequencing model [25]. The key factor in this method is the detection of alterations in light emission when the DNA polymerase incorporates a nucleotide [26]. In more detail, SMRT sequencing is done by the immobilization of the DNA polymerase in each well of a special silicone chip (SMRTcell) using DNA as the mobile molecule. DNA templates are presented as closed, single-stranded DNA (ssDNA) molecules, named SMRTbells, which are created by ligating hairpin adaptors to both ends of a target double-stranded DNA (dsDNA). The SMRTcells contain four fluorescently labeled nucleotides with unique emission spectra. Zero mode waveguides (ZMW) are optical waveguides developed for rapid light sensing and provide the interface for the detection of light emitted by the incorporation of phosphate-labeled dNTPs of SMRTcells [27, 28]. The process of SMRT sequencing is illustrated on Figure 1B.

Compared to NGS, the precision of SMRT sequencing is lower, as an example, due to the many inaccuracies during base identification. Although, in contrast to the experienced higher error rates and costs-per-base, the technology grants several orders of magnitude increase in read lengths (few Mbps in contrast to the previous few hundred bps) and faster sequencing runs. As a possibility, the arising conflict regarding the advantages and disadvantages of NGS and SMRT sequencing suggests the consideration of hybrid-sequencing solutions in the future. Hybrid units are the combinations of different sequencing methods and can be promising to overcome the deficiencies [29].

Technical advances and difficulties of long reads

Following a brief histological and methodological overview of long-read approaches, we detail the technical background and give comprehensive knowledge regarding sequencing challenges and advances. Compared to NGS approaches, the main difficulties of TGS are the overall lower per read accuracy and poorer read quality [30]. In contrast to short reads, long reads are much noisier. Prolonged lengths induce an increase in the number of bases and in reading time. Both contribute to a higher probability of collecting false information, promoting more noise and uncertainty [31]. The continuous change of the sequencing reads in length during a single run also indicates the higher chance of inaccuracies. Due to the above-listed reasons, the proper handling of deflections cannot be emphasized enough and the problem-concentrated improvements are published continuously [32]. Although in the early times base identifying accuracy was around 85% (indicating the error rate to be nearly 15%), nowadays almost 99% (SMRT) and 95% (NS) can be reached [31, 33]. Error correction methods [34, 35] provide a solution to resolve the inaccuracies and are divided into two groups: hybrid and non-hybrid approaches [36]. Hybrid methods take the advantage of the high accuracy of short reads for correcting errors in the long threads, while non-hybrid methods perform self-correction with long reads using overlap information. The effectiveness of error correction methods is highly dependent on the sequencing coverage [36], thus shows a dependence on the percentage of all sequenced base pairs or loci of the genome.

In SMRT devices, the read quality is proportional to the number of DNA fragment transitions. For example, the reading accuracy is around 85%–87% in a 10 kb long sequence if it is passing only once [37]; however, with multiple reading, it can be further improved reaching 99%. In contrast, the quality of NS reads is independent of the reading repetition times and the length of nucleic acid sequences. It only depends on the ratchet rate per base through the nanopores. Fragments traverse only once, the median sign-pass accuracy is around 95% [38], and read length depends only on the amount and the quality of the high-molecular weight input DNA. To reach the maximal sequencing precision, companies focusing on long-reads tend to release chemistry, software, and hardware updates regularly [16, 39].

Reference genomes are integral parts of sequencing assays as they provide the organism-specific support during base order construction [40]. The progression of sequencing methods derived the breakthroughs regarding the imprecision of reference genomes [41], variant identification, genomic assemblies, and other specialized data analyses in the field of genetics. The Genome Reference Consortium (GRC) released the current form of human reference genome (GRCh38. p13) in 2013 with an origin tracing to the Human Genome Project [42, 43]. In contrast to the continuous improvement of the GRCh38.p13 genome, over the last years, due to the technical limitations of NGS short reads, many problems remained unsolved. The underrepresentation of repetitive sequences, the unsolved assembly gaps due to structural polymorphisms and the unfinished polymorphic regions resulted in the need of further investigation. The 151 mega-base (Mbp) pair long unknown sequence data distributed throughout the GRCh38. p13 genome turned out to be fundamental and included centromere and telomere regions, segmental duplications, amplicon gene arrays and ribosomal DNA (rDNA) arrays, all highly affecting cellular processes [44]. Long-read sequencing proved to be the problem-solver, indicating the birth of the Telomere-to-Telomere (T2T) Consortium to construct a new and almost complete human reference genome, the T2T-CHM13 assembly [44]. In this cooperation, the advances of long-read techniques, including the multi-kilobase single-molecule reads of SMRT and the ultra-long reads of NS were combined, providing evidence to the beneficial applications of hybrid sequencing methods. The T2T-CHM13 assembly resulted in a 3 billion-base pair long complete human haplotype, contributing to the recognition of almost 4,000 new genes, with high rates of protein coding nature. In addition, T2T-CHM13 includes the gapless telomere-to-telomere assemblies for all 22 human autosomes and chromosome X, contains the corrected version of the 151 Mbp

TABLE 1 Summary of the most recent and common-used long-read bioinformatics tools.

Long-read bioinformatics tools				
	Data analysis step	**Tool name**	**Background and performance**	**References**
Complex user – friendly interfaces capable of perform the whole analysis process exept error correction : PacBio : SMRT link (BioSciences) Nanopore : EPI2ME Labs (Nanopore)	QC metrics	FastQC, MultiQC, LongQC, NanoPack, MinIONQC, NanoR, RNASeQC	The listed items are quality control (QC) tools suitable for sequencing approaches, including long- and short-reads. Their aim is to provide QC checks on raw sequence data (FastQC) or dataset (MultiQC) and give detailed feedback regarding the occurring problems. For RNA-seq data, an unique algorithm (RNA-SeQC) was developed	[47–54]
	Base calling	SMRT analysis tools, Dorado, Guppy	Neural network and statistical method based base calling methods; SMRT reads require specific analysis tools. Dorado and Guppy were developed for NS reads	[55–57]
	Variant calling	Clair3, Sniffles	Sniffles perform structural variant calling on noisy long-read data. Clair3 is a deep neural network based variant caller even capable of haplotype-sensitive variant detecion performing variant detection from sequencing data containing modified bases	[58–60]
		wf-human-variation, wf-somatic-variation	Complex command line compatible workflows for NS variant detection. On demand, the separate or combined usage of tumor and normal data is insured with the production of well-detailed analysis reports	[61]
	Modified base calling	Modbamtools, Guppy, Mekada, DeepSignal, DeepMod	Set of tools to manipulate and visualize DNA/RNA base modification and methylation data that are stored in.bam format. Some of them is suitable for all long-read techniques. The detectable modified bases are 5mC, 5hmC and 6 mA	[33, 57–59, 62, 63]
	Genome assembly	Flye, Canu, HiCanu, BLASR, FALCON	Some of them are graph construction-based method (Flye) or using hierarchical genome assembly process with clustering (BLASR) and overlap-based error correction, also carry out phasing (FALCON) during the accomplishment of *de novo* genome assembly on high-noise single-molecule sequencing data	[64–68]
	Visualization	NanoPack, R packages: maftools, ggplot2, Python packages: matplotlib (pyVolcano)	Packages offering universal and problem-specific solutions for long-read data visualization	[50, 69–72]
	Error correction	Pilon, Racon, DeepConsensus, Medaka	Neural network- and transformer-based methods, which are intended as standalone modules to correct raw contigs generated by rapid assembly methods which include or do not include a consensus step. An advantage of the application of transformer-based error correction methods is that they leverage a unique alignment loss to correct sequencing errors	[33, 35, 71]

Additional packages are listed on webpage https://long-read-tools.org and can be found on bioinformatics-related pages.

10.3389/pore.2024.1611676

long unknown genomic sequence data, and has the chance to arise as the mainly applied reference genome in human genomics-related fields. The successful application of the combination of NS and SMRT reads as a hybrid solution in the T2T Consortium projects that the further development of sequencing methods can be still expected, and the seeking to eliminate their limitations is continuous.

Bioinformatics of long reads

After exploring the scientific literature in detail, it clarified that sequencing techniques cannot address questions in genomics without bioinformatics. With the rise of new sequencing approaches, a new generation of bioinformatics tools emerged, being compatible with the unique features of long reads and trying to overcome their biases. As long reads, their analysis also presented many opportunities and challenges. Increased read lengths particularly affects how aligners, assemblers, variant callers store and analyze the data. Many software tools specialized for long-read sequencing data are provided by ONT and PacBio with continuous monitorization [45, 46]. Additional sources and packages are also presented, as it is demonstrated in Table 1.

As a summary of bioinformatics steps, the following section will provide a brief general discussion regarding base calling, detection of base modifications, variant calling, genome assembly, and a bit of specialized evaluation possibilities including both long-read and NGS techniques, emphasizing their unique prominences.

Base calling

The first main step in bioinformatics analysis is always a process named base calling during which the specific electric signals are translated into known nucleotides. The phrase of translation in this case means the conversion process from electric signals to nucleic acid sequences [73]. Raw current and light pulse data and read information are stored in specific format files. In the NGS system, the primary analysis of sequencing data is a critical step before base calling. These sequencing platforms have their own chemical- or sensor-origin biases which should be eliminated before or during base calling [74]. As a result of the pre-sequencing PCR amplification, many redundant PCR duplicates are present among aligned reads, which are marked and excluded in later analysis stages [75]. Considering the two long-read techniques, base calling means the conversion of fluorescent light pulses in SMRT devices, while during NS, the translation of current intensities into k-mers of bases. The alignment of sequencing reads to a reference sequence is a compulsory step after base calling in NGS bioinformatics, however many TGS base callers [55–57] execute the alignment in parallel with base identification [55, 56]. As a side note, we would like to emphasize the importance of quality check of sequencing reads [47–54, 76, 77] preferably before and after every principal step, paying special attention to base calling and variant calling.

Epigenetic modifications: modified base calling

In addition to traditional bases, like adenine (A), thymine (T), uracil (U), guanine (G) and cytosine (C), DNA and RNA molecules can contain modified bases that alter from their original mates in nature and frequency and have different functional roles. In nucleic acids, the most frequently occurring modified bases are 6mA, 5mC, and 5hmC. Considering the location of 5mC and 5hmC in DNA, they are mostly observed on CpG dinucleotide sites. RNA modifications, including 6mA, are frequent in non-coding RNA like ribosomal RNA (rRNA), transfer RNA (tRNA), and also in coding mRNA. Modified DNA and RNA nucleotides play a key role in many biological processes including development, aging, and cancer [78–80]. Their identification secures the analysis of open chromatin regions, the detection of DNA replication and the measurement of RNA metabolism using base analogs [81–83].

The methylation signature is not preserved in PCR amplification—which is essential before NGS assays -, thus approaches have been developed to conserve the epigenetic information. These pretreatments rely on methylation-dependent enzymatic restriction, methyl-DNA enrichment, and direct bisulfite conversion [84]. In NGS base modification analysis bisulfite-treated DNAs require specialized alignment to account for the C to T conversion. Encouraged by this, short read alignment algorithms were implemented that can be configured for bisulfite-converted DNA alignment [85].

However, the available NGS methods provided some sort of identification of modified bases in nucleic acid sequences as well, but the real landscape demonstration became fulfilled with TGS assays. The detection of modified bases in SMRT is based on the delay between fluorescence pulses [86]. NS relies on the recognition of the signal shifts resulting from the different current flow through nanopores [19, 87]. Most TGS computational tools are capable of modified base detection from reference-aligned reads [34, 57–59, 62, 63, 88], and are based on machine learning training models and statistical tests. Algorithms using neural networks show the highest performance, although statistics-based approaches are the best suited for the identification of *de novo* modifications [34, 89]. Because of software developmental progress, long-read base callers became capable of calling modified bases directly [55, 56]. The key is the application of specific base calling configuration models indicating in their labels the name of the modified bases of interest [56].

Variant calling

Sequence variations can be grouped based on their somatic or germline nature. Germline variants are presented in all cells of the body, including the germ cells, while somatic mutations arise during lifetime. The standard pipeline of somatic mutation calling is the paired tumor-normal sequencing strategy [90]. It can provide the true somatic mutations by filtering out the germlines of the normal from the tumor mutation data according to some known tissue-specific non-tumorous variant profiles. Germline and somatic groups also involve subtypes like structural variants, single nucleotide variations, short insertions/deletions, and copy number variations.

The shortest variations are single nucleotide polymorphisms, which are germline substitutions of single nucleotides at specific genomic positions. Copy number variation (CNV) is an alteration type describing the uniqueness among individual genomes, meaning a few and thousands of base-scale variations in the copy numbers of specific DNA segments. SVs are large genomic alterations, like insertions, deletions, inversions, and translocations. They are typically longer than 50 bp, describing different combinations of DNA losses, gains, or rearrangements [91]. Structures shorter than 50 bp and longer than few bases are usually referred to as indels.

The key aspect of variant calling is the choice of a robust variant caller concerning NGS and TGS assays as well. To achieve the optimal performance, a prior fine-tuning considering the features of the input is needed. This optimal performance is reached by training and pre-testing the variant callers using the characteristics of the datasets. The exclusion of redundant and duplicate reads from binary alignment mapping (.bam) files, the quality control of .bams, and the identification and the reduction of false-positive variant calls caused by alignment artifacts are crucial steps in input preparation. The accuracy of variant calling can be validated by benchmarking datasets, which are publicly available. The quality of the collected variants is dependent on the precision (and version) of the reference genome, and on the error rate and accuracy of the base and variant identification method. Sequencing coverage affects the sensitivity in a hidden manner, since the appropriateness of the variant caller input is highly dependent on the coverage [92]. We must consider the variant representation differences when searching valid variations from the reference by excluding the low coverage b(i)ases. The appropriate post-filtering of the output data is often required; it prevents us from artificial and false-positive calls [75].

TGS variant callers [58–61, 88] are built upon *de novo* assembly, short-read alignment, or long-read mapping approaches. *De novo*-assembled sequences cover the alignment of the current assembly to another, or to a reference sequence, and the alterations can be identified by a pointwise positional comparison. During short-read alignment, the presence of SVs induces the appearance of abnormally oriented and spaced reads replacing the organized paired-end form. Long-read mapping approaches can span repetitive and other problematic regions simply, showing an overall better performance [93].

In nowadays-used techniques, long-read sequencing is the most suitable and the most accurate variant calling approach, but especially for the detection of structural variants (SVs) [94]. The special role of genetic variations, especially SVs, has been highlighted primarily in medicine and molecular biology, e.g., in neurological diseases [95, 96], or during the detection of oncogene-specific variations in breast, prostate, or primary gastric tumors [97]. Although their importance is unquestionable, they have been understudied in the past. The origin of this issue arises from the fact that they can overlap or be nested giving rise to complex patterns, which are hard to identify with short-read approaches [93].

Genome assembly

Probably the most important benefit of long-read computational biology can be experienced in the fields of genomic *de novo* assemblies [64–68]. The phrase assembly in this case means the comparison and coupling of the read sequences to each other. Assembly construction is crucial to understand the impact of genomic diversity on health and disease [98]. In the last few years, the process has been simplified and the results are more accurate due to the improvements in the bioinformatics routines [99]. Besides the sequence construction, another important application of genomic assemblies is the reassembling and fixing of the errors of former reference genomes (of fungal, plant, animal, and human) [44]. Unfortunately, repetitive sequences with unresolved repeats are still problematic, enhancing confusion while joining assembled sequences. Linked sequences contain many gaps. To get rid of these, the scaffolding of sequences is a crucial aspect. The term scaffolding means the proper ordering and orientation of assembled sequences using genetic markers, optical maps, or linked reads [100]. Assemblies of the short and long reads are both presented taking their advantages in different issues. Besides the success of their combination in T2T Consortium, many other hybrid applications have been published recently [29, 101], invoking that for accurate genomic assemblies we need error-free short and long sequences.

Applications of long-read sequencing

Although the topic of long-read sequencing is quite recent, its successful application in several fields is highly presented in the scientific literature including cancer genomics, laboratory medicine, methylation studies and rare genetic conditions, as well.

In laboratory medicine, the currently applied diagnostic strategies involve the use of targeted NGS gene panels, exome

sequencing, and genome sequencing. Targeted gene panels are somatic and hereditary disease-specific with the ability to maximize coverage, sensitivity, and specificity of characteristic genes. They offer higher diagnostic yield thanks to lower costs and faster diagnostic times, than exome or genome sequencing [102]. The combination of whole-genome and long-read targeted sequencing has already been applied in hematology. Hematologic disorders, like hemophilia A, often involve the appearance of gene fusions and other pathologic events, thus the characterization of fusion transcripts is often done by the combination of NGS and TGS assay-based methods [103]. Another example of laboratory medicine related application of long reads is the characterization of the human leukocyte antigen (HLA) system. The HLA system contains the genes that encode key components of the adaptive immune system, and accounts for the major genetic differences among ethnic populations [104]. HLA-genotyping information is often yielded from targeted exome and non-targeted genome sequence data [105].

For diploid genomes, chromosomal DNA has two haplotypes. These are combinations of alleles from multiple genetic loci on the same chromosome including complex structural variants, one inherited from each parent. Distinguishing the maternal and paternal haplotypes allows the recognition of homozygous and heterozygous mutations in the human genome. Haplotypes within a diploid chromosome are determined by finding a partitioning of reads to two sets, one for each haplotype, such that the reads within subsets have a minimal number of errors compared to a consensus [106]. Their presence helps to discover the nested structural variations, inversions, and other complex rearrangements and studies the interactions between variants in regulatory elements, aneuploidy, evolutionary processes, and drug resistance in viral infections. The key concept to derive haplotypes using sequencing reads is the phasing of heterozygous variants. The advancements in sequencing associated computational tools like reference-based phasing, *de novo* assembly, or strain-resolved metagenome assembly [107] entail the potential for the near-complete human haplotype structure reconstruction.

The investigation of genomes containing segments with small allele fraction variants and observed rearrangements in regions of associated genes is still challenging even for current long-read methods [108]. The appearance of sequencing techniques with higher-depths and longer-lengths is expected. Regardless, many successful applications can be discussed already. The characterization of tumor genomes and transcriptomes with the analysis of mRNA expression, mutation detection, gene fusions, or chromosomal copy number alterations can highlight new markers of malignancy. With better depiction of the genome-wide landscape and the extent of mutational processes, whole-genome long-read sequencing yields better treatment options in advanced thyroid [109] and other cancers [110]. Improvements in sequencing technologies allowed the recognition and the description of long non-coding RNAs (lncRNAs). They are non-protein coding nucleic acids with lengths greater than 200 nucleotides and characterized by high cell type specificity [111]. LncRNAs are found to be key players in tumorigenesis and immune responses, and evidence supports their unique cellular functions in the tumor immune microenvironment [112]. Most studies related to lncRNAs relied on bulk RNA-sequencing; however, the potentials of scRNAseq can open new possibilities to understand the cell type-specific functions of lncRNA genes [112].

The examination of abnormal RNA expressions helps to understand the molecular mechanisms behind human cancer initiation, development, progression, and metastasis. RNA techniques include the classic bulk RNA (RNAseq), the single-cell RNA (scRNAseq), the spatial RNA (spRNAseq) [113] and the direct RNA (DRS) [114] sequencing methods. Bulk RNAseq means the sequencing of mRNA-only or whole transcriptome libraries with single-end short or paired-end longer approaches. scRNAseq procedures always include single-cell isolation and capture, cell lysis, reverse transcription, cDNA amplification, and library preparation [115]. spRNAseq combines the transcriptional analysis of bulk RNAseq and *in situ* hybridization providing whole transcriptome data with spatial information [113]. As a novelty, NS terminology offers the direct sequencing of individual polyadenylated RNAs without the need of any amplification step [114].

Circulating cell-free DNA (cfDNA) in the blood of cancer patients can be the signal of worsening tumor progression. Sequencing analyses revealed that tumor-derived cfDNA accounts for only a fraction of the total amount of cfDNAs and this fraction varies according to the tumor burden [116]. Due to the low level and high fragmentation of cfDNAs, their analysis is challenging. In the past few years, NGS techniques were suitable tools for this assay [117], however, the long-reads will possibly promote the provision of deeper cfDNA characteristics providing higher clinical sensitivity for the detection of cancers [117].

The clinical diagnosis of rare genetic disorders often requires the identification of CNVs or repeat variants. Long-read genome sequencing provides an improved opportunity for CNV detection and broadens the possibilities of gene and variant level annotation [118]. As an interesting example, primary mitochondrial diseases (PMD) comprise a group of rare genetic conditions characterized by impaired mitochondrial oxidative phosphorylation. The presence of mixed populations of mitochondria, named heteroplasmy, and the fact that those mitochondria contain its own genome consisting of mitochondrial DNA (mtDNA) poses a challenge in identifying PMD. Long-read sequencing enables the entire mitochondrial genome to be sequenced in one read, ensuring the overcome of the obstacles mentioned-above [119].

Using epigenetic alterations as biomarkers presents a unique opportunity for early cancer detection, monitoring, and prognosis. Methylation is the most widely studied epigenetic

modification of nucleic acids and its landscape in cancer tissues is evidently complex and highly variable. DNA methylation plays an important role in the regulation of gene expression. The methylation-associated transcriptional inactivation of genes involved in cell cycle control and damage repair suggest that aberrant nucleotide methylations are hallmarks of carcinogenesis [120, 121]. NS provides the most precise detection and description of methylation landscapes [122]. Studies showed that the methylation of both 5mC and 5hmC has a role in the pathogenesis of pediatric cancer [123], while the presence of 6mA in pancreatic tumors is highly upregulated and has a lower occurrence compared to 5mC [124]. Thus, the idea to use methylation as a biomarker for cancer detection is not far to seek. Due to its prognostic property, DNA methylation was already applied as a prognostic marker in several cancer types, including prostate, bladder, colorectal, non-small-cell lung, breast, ovarian, cervical cancer, and liver malignancies [125, 126].

Although we presented the potentials of TGS long-read sequencing, their utilization in routine diagnostics has not widespread yet. NGS whole exome and targeted sequencing techniques offer well applicable results in routine diagnostics including inborn discrepancy detection, cancer research and diagnostics, hematology, and neurological disorders [72, 127–130]. Their instrumentation, the corresponding chemicals, and flow cells are more affordable, and the generated data are more targeted [131]. On the other hand, as long-read techniques offer a wider genomic picture, thus providing a deeper insight into nucleic acid traits, their introduction into routine examinations has started [132–136] and their spreading is expected in the near future.

Conclusion

In this review, we discussed the milestones of sequencing techniques, their progression, current applications, and future opportunities. We also provided a general comparison between short- and long-read assays highlighting their strengths and drawbacks from various aspects including methodology, data analysis, and applications. As we introduced in the last chapter, the spread of long-read techniques has led to a rapid progress in genomics-related areas. By expanding and refining sequencing routines, it becomes possible to explore the genetic complexity of biological systems in greater depths facilitating a radical future advance in the field of sequence variances.

Author contributions

NS, BK, and BM: conceptualization and revision; NS: literature research and drafting; BK, GV, BM, ZN, and IT: critical revision of the manuscript. All authors contributed to the article and approved the submitted version.

Funding

The authors declare that financial support was received for the research, authorship, and/or publication of this article. This project was financed from the Hungarian Scientific Research Fund (NKFI-143002), from the NRDI Fund FK0201NEPE/TKPNKTA-47 and from the Fund National Cardiovascular Laboratory RRF-2.3.1-21-2022-00003. This project has been implemented with the support provided by the Ministry of Culture and Innovation of Hungary and from the National Research, Development, and Innovation Fund, financed under the KDP-2023/C2270480.

Conflict of interest

The authors declare that the research was conducted in the absence of any commercial or financial relationships that could be construed as a potential conflict of interest.

References

1. Alberts B. 4th chapter: DNA, chromosomes and genomes. In: *Molecular biology of the cell*. 6th ed. W.W. Norton & Company (2015).

2. Adewale BA. Will long-read sequencing technologies replace short-read sequencing technologies in the next 10 years? *Afr J Lab Med* (2020) 9(1):1340. doi:10.4102/ajlm.v9i1.1340

3. Sanger F, Nicklen S, Coulson AR. DNA sequencing with chain-terminating inhibitors. *Proc Natl Acad Sci USA* (1977) 74(12):5463–7. doi:10.1073/pnas.74.12.5463

4. Maxam AM, Gilbert W. A new method for sequencing DNA. *Proc Natl Acad Sci USA* (1977) 74(2):560–4. doi:10.1073/pnas.74.2.560

5. Marulies M, Egholm M, Altman WE, Attiya S, Bader JS, Bemben LA, et al. Genome sequencing in microfabricated high-density picolitre reactors. *Nature* (2005) 437:376–80. doi:10.1038/nature03959

6. Guo J, Yu L, Turro NJ, Ju J. An integrated system for DNA sequencing by synthesis using novel nucleotide analogues. *Acc Chem Res* (2010) 43(4):551–63. doi:10.1021/ar900255c

7. Liu L, Li Y, Li S, Hu N, He Y, Pong R, et al. Comparison of next-generation sequencing systems. *J Biomed Biotechnol* (2012) 2012:251364. doi:10.1155/2012/251364

8. Harrington CT, Lin EI, Olson MT, Eshleman JR. Fundamentals of pyrosequencing. *Arch Pathol Lab Med* (2013) 137(9):1296–303. doi:10.5858/arpa.2012-0463-RA

9. Grigorev K, Foox J, Bezdan D, Butler D, Luxton JJ, Reed J, et al. Haplotype diversity and sequence heterogeneity of human telomeres. *Genome Res* (2021) 31(7):1269–79. doi:10.1101/gr.274639.120

10. Kumar KR, Cowley MJ, Davis RL. Next-generation sequencing and emerging technologies. *Semin Thromb Hemost* (2019) 45(7):661–73. doi:10.1055/s-0039-1688446

11. Chen X, Xu H, Shu X, Song CX. Mapping epigenetic modifications by sequencing technologies. *Cell Death Differ* (2023). doi:10.1038/s41418-023-01213-1

12. Xiao T, Zhou W. The third generation sequencing: the advanced approach to genetic diseases. *Transl Pediatr* (2020) 9(2):163–73. doi:10.21037/tp.2020.03.06

13. Athanasopoulou K, Boti MA, Adamopoulos PG, Skourou PC, Scorilas A. Third-generation sequencing: the spearhead towards the radical transformation of modern genomics. *Life (Basel)* (2021) 12(1):30. doi:10.3390/life12010030

14. Kaplun L, Krautz-Peterson G, Neerman N, Stanley C, Hussey S, Folwick M, et al. ONT long-read WGS for variant discovery and orthogonal confirmation of short read WGS derived genetic variants in clinical genetic testing. *Front Genet* (2023) 14:1145285. doi:10.3389/fgene.2023.1145285

15. Roberts RJ, Carneiro MO, Schatz MC. The advantages of SMRT sequencing. *Genome Biol* (2013) 14(7):405. doi:10.1186/gb-2013-14-6-405

16. ONT Nanopore Technologies. *Continuous development and improvement* (2023). Available from: https://nanoporetech.com/about-us/continuous-development-and-improvement (Accessed 2024).

17. Pollard MO, Gurdasani D, Mentzer AJ, Porter T, Sandhu MS. Long reads: their purpose and place. *Hum Mol Genet* (2018) 27(R2):R234–R241. doi:10.1093/hmg/ddy177

18. Quick J, Loman NJ. *Nanopore sequencing: an introduction*. World Scientific Press (2019).

19. Deamer D, Akeson M, Branton D. Three decades of nanopore sequencing. *Nat Biotechnol* (2016) 34:518–24. doi:10.1038/nbt.3423

20. ONT Nanopore Technologies. *Flow cells* (2023). Available from: https://nanoporetech.com/how-it-works/flow-cells-and-nanopores (Accessed 2023).

21. Nicholls SM, Quick JC, Tang S, Loman NJ. Ultra-deep, long-read nanopore sequencing of mock microbial community standards. *GigaScience* (2019) 8(5):giz043. doi:10.1093/gigascience/giz043

22. Ni Y, Liu X, Simeneh ZM, Yang M, Li R. Benchmarking of Nanopore R10.4 and R9.4.1 flow cells in single-cell whole-genome amplification and whole-genome shotgun sequencing. *Comput Struct Biotechnol J* (2023) 21:2352–64. doi:10.1016/j.csbj.2023.03.038

23. Jennings W. *Illumina sequencing* (2016). doi:10.1201/9781315181431-7

24. Stefan CP, Hall AT, Graham AS, Minogue TD. Comparison of illumina and Oxford nanopore sequencing technologies for pathogen detection from clinical matrices using molecular inversion probes. *J Mol Diagn* (2022) 24(4):395–405. doi:10.1016/j.jmoldx.2021.12.005

25. Harris TD, Buzby PR, Babcock H, Beer E, Bowers J, Braslavsky I, et al. Single-molecule DNA sequencing of a viral genome. *Science* (2008) 320(5872):106–9. doi:10.1126/science.1150427

26. Eid J, Fehr A, Gray J, Luong K, Lyle J, Otto G, et al. Real-time DNA sequencing from single polymerase molecules. *Science* (2009) 323(5910):133–8. doi:10.1126/science.1162986

27. Levene MJ, Korlach J, Turner SW, Foquet M, Craighead HG, Webb WW. Zero-mode waveguides for single-molecule analysis at high concentrations. *Science* (2003) 299(5607):682–6. doi:10.1126/science.1079700

28. Garrido-Cardenas JA, Garcia-Maroto F, Alvarez-Bermejo JA, Manzano-Agugliaro F. DNA sequencing sensors: an overview. *Sensors (Basel)* (2017) 17(3):588. doi:10.3390/s17030588

29. Vasudevan K, Devanga Ragupathi NK, Jacob JJ, Veeraraghavan B. Highly accurate-single chromosomal complete genomes using IonTorrent and MinION sequencing of clinical pathogens. *Genomics* (2020) 112(1):545–51. doi:10.1016/j.ygeno.2019.04.006

30. Warburton PE, Sebra RP. Long-read DNA sequencing: recent advances and remaining challenges. *Annu Rev Genomics Hum Genet* (2023) 24:109–32. doi:10.1146/annurev-genom-101722-103045

31. Ebler J, Haukness M, Pesout T, Marschall T, Paten B. Haplotype-aware diplotyping from noisy long reads. *Genome Biol* (2019) 20:116. doi:10.1186/s13059-019-1709-0

32. Delahaye C, Nicolas J. Sequencing DNA with nanopores: troubles and biases. *PLoS One* (2021) 16(10):e0257521. doi:10.1371/journal.pone.0257521

33. Amarasinghe SL, Su S, Dong X, Zappia L, Ritchie ME, Gouil Q. Opportunities and challenges in long-read sequencing data analysis. *Genome Biol* (2020) 21:30. doi:10.1186/s13059-020-1935-5

34. Liu Q, Fang L, Yu G, Wang D, Xiao CL, Wang K. Detection of DNA base modifications by deep recurrent neural network on Oxford Nanopore sequencing data. *Nat Commun* (2019) 10(1):2449. doi:10.1038/s41467-019-10168-2

35. Baid G, Cook DE, Shafin K, Yun T, Llinares-López F, Berthet Q, et al. DeepConsensus: gap-aware sequence transformers for sequence correction. *Nat Biotechnol* (2023) 41(2):232–8. doi:10.1038/s41587-022-01435-7

36. Zhang H, Jain C, Aluru S. A comprehensive evaluation of long read error correction methods. *BMC Genomics* (2020) 21(6):889. doi:10.1186/s12864-020-07227-0

37. Ardui S, Ameur A, Vermeesch JR, Hestand MS. Single molecule real-time (SMRT) sequencing comes of age: applications and utilities for medical diagnostics. *Nucleic Acids Res* (2018) 46(5):2159–68. doi:10.1093/nar/gky066

38. ONT Nanopore Technologies. *Clive Brown's keynote at nanopore community meeting* (2018). Available from: https://nanoporetech.com/resource-centre/clive-brown-ncm-2018 (Accessed 2018).

39. Pacific BioSciences *HiFi sequencing* (2023). Available from: https://www.pacb.com/technology/hifi-sequencing/ (Accessed 2024).

40. Completing Human Genomes. Completing human genomes. *Nat Methods* (2022) 19:629. doi:10.1038/s41592-022-01537-9

41. Goodwin S, Gurtowski J, Ethe-Sayers S, Deshpande P, Schatz MC, McCombie WR. Oxford Nanopore sequencing, hybrid error correction, and *de novo* assembly of a eukaryotic genome. *Genome Res* (2015) 25(11):1750–6. doi:10.1101/gr.191395.115

42. Hood L, Rowen L. The Human Genome Project: big science transforms biology and medicine. *Genome Med* (2013) 5:79. doi:10.1186/gm483

43. Lander ES, Linton LM, Birren B, Nusbaum C, Zody MC, Baldwin J, et al. Initial sequencing and analysis of the human genome. *Nature* (2001) 409:860–921. doi:10.1038/35057062

44. Nurk S, Koren S, Rhie A, Rautiainen M, Bzikadze AV, Mikheenko A, et al. The complete sequence of a human genome. *Science* (2022) 376:44–53. doi:10.1126/science.abj6987

45. Suzuki Y. Informatics for PacBio long-reads. Single molecule and single cell sequencing. In: Suzuki Y, editor. *Advances in experimental medicine and biology*. Springer (2019).

46. Oxford Nanopore Technologies. *Oxford nanopore community* (2023). Available from: https://nanoporetech.com/community (Accessed 2024).

47. Bioinformatics. *Babraham bioinformatics* (2023). Available from: https://www.bioinformatics.babraham.ac.uk/projects/fastqc/ (Accessed 2023).

48. Ewels P, Magnusson M, Lundin S, Käller M. MultiQC: summarize analysis results for multiple tools and samples in a single report. *Bioinformatics* (2016) 32(19):3047–8. doi:10.1093/bioinformatics/btw354

49. Fukasawa Y, Ermini L, Wang H, Carty K, Cheung MS. LongQC: a quality control tool for third generation sequencing long read data. *G3 Genes, Genomes, Genet* (2020) 10(4):1193–6. doi:10.1534/g3.119.400864

50. Coster WD, D'Hert S, Schultz DT, Cruts M, Van Broeckhoven C. NanoPack: visualizing and processing long-read sequencing data. *Bioinformatics* (2018) 34(15):2666–9. doi:10.1093/bioinformatics/bty149

51. Lanfear R, Schalamun M, Kainer D, Wang W, Schwessinger B. MinIONQC: fast and simple quality control for MinION sequencing data. *Bioinformatics* (2019) 35(3):523–5. doi:10.1093/bioinformatics/bty654

52. Bolognini D, Bartalucci N, Mingrino A, Vannucchi AM, Magi A. NanoR: a user-friendly R package to analyze and compare nanopore sequencing data. *PLoS One* (2019) 14(5):e0216471. doi:10.1371/journal.pone.0216471

53. Graubert A, Aguet F, Ravi A, Ardlie KG, Getz G. RNA-SeQC 2: efficient RNA-seq quality control and quantification for large cohorts. *Bioinformatics* (2021) 37(18):3048–50. doi:10.1093/bioinformatics/btab135

54. PacBio *SMRT®. Tools reference guide (v11.0)* (2022). Available from: https://www.pacb.com/wp-content/uploads/SMRT_Tools_Reference_Guide_v11.0.pdf (Accessed 2022).

55. Oxford Nanopore Technologies. *Oxford nanopore technologies* (2023). Available from: https://github.com/nanoporetech/dorado (Accessed 2023).

56. Oxford Nanopore Technologies. *Oxford nanopore technologies* (2024). Available from: https://community.nanoporetech.com/docs/prepare/library_prep_protocols/Guppy-protocol/v/gpb_2003_v1_revax_14dec2018/guppy-software-overview (Accessed 2024).

57. Zheng Z, Li S, Su J, Leung AWS, Lam TW, Luo R. Symphonizing pileup and full-alignment for deep learning-based long-read variant calling. *Nat Comput Sci* (2022) 2(12):797–803. doi:10.1038/s43588-022-00387-x

58. Sedlazeck FJ, Rescheneder P, Smolka M, Fang H, Nattestad M, von Haeseler A, et al. Accurate detection of complex structural variations using single-molecule sequencing. *Nat Methods* (2018) 15:461–8. doi:10.1038/s41592-018-0001-7

59. Romagnoli S, Bartalucci N, Vannucchi AM. Resolving complex structural variants via nanopore sequencing. *Front Genet* (2023) 14:1213917. doi:10.3389/fgene.2023.1213917

60. Oxford Nanopore Technologies. *Oxford nanopore technologies* (2018). Available from: https://github.com/nanoporetech/medaka (Accessed 2018).

61. Ni P, Huang N, Zhang Z, Wang DP, Liang F, Miao Y, et al. DeepSignal: detecting DNA methylation state from Nanopore sequencing reads using deep-learning. *Bioinformatics* (2019) 35(22):4586–95. doi:10.1093/bioinformatics/btz276

62. Kolmogorov M, Yuan J, Lin Y, Pevzner P. Assembly of long error-prone reads using repeat graphs. *Nat Biotechnol* (2019) 37(5):540–6. doi:10.1038/s41587-019-0072-8

63. Koren S, Walenz BP, Berlin K, Miller JR, Bergman NH, Phillippy AM. Canu: scalable and accurate long-read assembly via adaptive k-mer weighting and repeat separation. *Genome Res* (2017) 27(5):722–36. doi:10.1101/gr.215087.116

64. Nurk S, Walenz BP, Rhie A, Vollger MR, Logsdon GA, Grothe R, et al. HiCanu: accurate assembly of segmental duplications, satellites, and allelic variants from high-fidelity long reads. *Genome Res* (2020) 30(9):1291–305. doi:10.1101/gr.263566.120

65. Chaisson MJ, Tesler G. Mapping single molecule sequencing reads using basic local alignment with successive refinement (BLASR): application and theory. *BMC Bioinformatics* (2012) 13:238. doi:10.1186/1471-2105-13-238

66. Chin CS, Peluso P, Sedlazeck FJ, Nattestad M, Concepcion GT, Clum A, et al. Phased diploid genome assembly with single-molecule real-time sequencing. *Nat Methods* (2016) 13(12):1050–4. doi:10.1038/nmeth.4035

67. Mayakonda A, Lin DC, Assenov Y, Plass C, Koeffler HP. Maftools: efficient and comprehensive analysis of somatic variants in cancer. *Genome Res* (2018) 28(11):1747–56. doi:10.1101/gr.239244.118

68. Wickham H *ggplot2: elegant graphics for data analysis*. New York: Springer-Verlag (2016). Available from: https://ggplot2.tidyverse.org (Accessed 2009).

69. Hunter JD. Matplotlib: a 2D graphics environment. *Comput Sci Eng* (2007) 9(3):90–5. doi:10.1109/MCSE.2007.55

70. Bruce J, Abeel T, Shea T, Priest M, Abouelliel A, Sakthikumar S, et al. Pilon: an integrated tool for comprehensive microbial variant detection and genome assembly improvement. *PLoS ONE* (2014) 9(11):e112963. doi:10.1371/journal.pone.0112963

71. Vaser R, Sović I, Nagarajan N, Šikić M. Fast and accurate *de novo* genome assembly from long uncorrected reads. *Genome Res* (2017) 27(5):737–46. doi:10.1101/gr.214270.116

72. Yépez VA, Gusic M, Kopajtich R, Mertes C, Smith NH, Alston CL, et al. Clinical implementation of RNA sequencing for Mendelian disease diagnostics. *Genome Med* (2022) 14(1):38. doi:10.1186/s13073-022-01019-9

73. Perešíni P, Boža V, Brejová B, Vinař T. Nanopore base calling on the edge. *Bioinformatics* (2021) 37(24):4661–7. doi:10.1093/bioinformatics/btab528

74. Ledergerber C, Dessimoz C. Base-calling for next-generation sequencing platforms. *Brief Bioinform* (2011) 12(5):489–97. doi:10.1093/bib/bbq077

75. Koboldt DC. Best practices for variant calling in clinical sequencing. *Genome Med* (2020) 12(91):91. doi:10.1186/s13073-020-00791-w

76. Schmieder R, Edwards R. Quality control and preprocessing of metagenomic datasets. *Bioinformatics* (2011) 27(6):863–4. doi:10.1093/bioinformatics/btr026

77. Bolognini D, Semeraro R, Magi A. Versatile quality control methods for nanopore sequencing. *Evol Bioinform Online* (2019) 15:1176934319863068. doi:10.1177/1176934319863068

78. Frye M, Harada BT, Behm M, He C. RNA modifications modulate gene expression during development. *Science* (2018) 361(6409):1346–9. doi:10.1126/science.aau1646

79. Field AE, Robertson NA, Wang T, Havas A, Ideker T, Adams PD. DNA methylation clocks in aging: categories, causes, and consequences. *Mol Cel* (2018) 71(6):882–95. doi:10.1016/j.molcel.2018.08.008

80. Esteller M. Cancer epigenomics: DNA methylomes and histone-modification maps. *Nat Rev Genet* (2007) 8:286–98. doi:10.1038/nrg2005

81. Kumar S, Chinnusamy V, Mohapatra T. Epigenetics of modified DNA bases: 5-methylcytosine and beyond. *Front Genet* (2018) 9(18):640. doi:10.3389/fgene.2018.00640

82. Duffy K, Arangundy-Franklin S, Holliger P. Modified nucleic acids: replication, evolution, and next-generation therapeutics. *BMC Biol* (2020) 18(112):112. doi:10.1186/s12915-020-00803-6

83. Kumar S, Mohapatra T. Deciphering epitranscriptome: modification of mRNA bases provides a new perspective for post-transcriptional regulation of gene expression. *Front Cel Dev. Biol.* (2021) 9(16):628415. doi:10.3389/fcell.2021.628415

84. Soto J, Rodriguez-Antolin C, Vallespín E, de Castro Carpeño J, Ibanez de Caceres I. The impact of next-generation sequencing on the DNA methylation–based translational cancer research. *Translational Res* (2016) 169:1–18. doi:10.1016/j.trsl.2015.11.003

85. Hirst M, Marra MA. Next generation sequencing based approaches to epigenomics. *Brief Funct Genomics* (2010) 9(5-6):455–65. doi:10.1093/bfgp/elq035

86. Flusberg BA, Webster DR, Lee JH, Travers KJ, Olivares EC, Clark TA, et al. Direct detection of DNA methylation during single-molecule, real-time sequencing. *Nat Methods* (2010) 7:461–5. doi:10.1038/nmeth.1459

87. Xu L, Seki M. Recent advances in the detection of base modifications using the Nanopore sequencer. *J Hum Genet* (2020) 65:25–33. doi:10.1038/s10038-019-0679-0

88. Smolka M, Paulin LF, Grochowski CM, Horner DW, Mahmoud M, Behera S, et al. Detection of mosaic and population-level structural variants with Sniffles2. *Nat Biotechnol* (2024). doi:10.1038/s41587-023-02024-y

89. Stoiber M, Quick J, Egan R, Lee JE, Celniker S, Neely RK, et al. *De novo identification of DNA modifications enabled by genome-guided nanopore signal processing*. bioRxiv 094672 (2017). doi:10.1101/094672

90. Mandelker D, Ceyhan-Birsoy O. Evolving significance of tumor-normal sequencing in cancer care. *Trends Cancer* (2020) 6(1):31–9. doi:10.1016/j.trecan.2019.11.006

91. Alkan C, Coe B, Eichler E. Genome structural variation discovery and genotyping. *Nat Rev Genet* (2011) 12:363–76. doi:10.1038/nrg2958

92. Zverinova S, Guryev V. Variant calling: considerations, practices, and developments. *Hum Mutat* (2022) 43(8):976–85. doi:10.1002/humu.24311

93. Mahmoud M, Gobet N, Cruz-Dávalos DI, Mounier N, Dessimoz C, Sedlazeck FJ. Structural variant calling: the long and the short of it. *Genome Biol* (2019) 20(246):246. doi:10.1186/s13059-019-1828-7

94. Mitsuhashi S, Matsumoto N. Long-read sequencing for rare human genetic diseases. *J Hum Genet* (2020) 65:11–9. doi:10.1038/s10038-019-0671-8

95. Schüle B, McFarland KN, Lee K, Tsai YC, Nguyen KD, Sun C, et al. Parkinson's disease associated with pure ATXN10 repeat expansion. *Parkinson's Dis* (2017) 3(27):27. doi:10.1038/s41531-017-0029-x

96. McColgan P, Tabrizi SJ. Huntington's disease: a clinical review. *Eur J Neurol* (2018) 25(1):24–34. doi:10.1111/ene.13413

97. Sakamoto Y, Zaha S, Suzuki Y, Seki M, Suzuki A. Application of long-read sequencing to the detection of structural variants in human cancer genomes. *Comput Struct Biotechnol J* (2021) 19:4207–16. doi:10.1016/j.csbj.2021.07.030

98. Phillippy A. New advances in sequence assembly. *Genome Res* (2017) 27(5):xi–xiii. doi:10.1101/gr.223057.117

99. van Dijk EL, Jaszczyszyn Y, Naquin D, Thermes C. The third revolution in sequencing technology. *Trends Genet* (2018) 34(9):666–81. doi:10.1016/j.tig.2018.05.008

100. Nagarajan N, Pop M. Sequence assembly demystified. *Nat Rev Genet* (2013) 14:157–67. doi:10.1038/nrg3367

101. Chen Z, Erickson DL, Meng J. Benchmarking hybrid assembly approaches for genomic analyses of bacterial pathogens using Illumina and Oxford Nanopore sequencing. *BMC Genomics* (2020) 21:631. doi:10.1186/s12864-020-07041-8

102. Zhong Y, Xu F, Wu J, Schubert J, Li MM. Application of next generation sequencing in laboratory medicine. *Ann Lab Med* (2021) 41(1):25–43. doi:10.3343/alm.2021.41.1.25

103. Bartalucci N, Romagnoli S, Vannucchi AM. A blood drop through the pore: nanopore sequencing in hematology. *Trends Genet* (2022) 38(6):572–86. doi:10.1016/j.tig.2021.11.003

104. Erlich RL, Jia X, Anderson S, Banks E, Gao X, Carrington M, et al. Next-generation sequencing for HLA typing of class I loci. *BMC Genomics* (2011) 12:42. doi:10.1186/1471-2164-12-42

105. Klasberg S, Surendranath V, Lange V, Schöfl G. Bioinformatics strategies, challenges, and opportunities for next generation sequencing-based HLA genotyping. *Transfus Med Hemother* (2019) 46(5):312–25. doi:10.1159/000502487

106. Garg S. Computational methods for chromosome-scale haplotype reconstruction. *Genome Biol* (2021) 22(1):101. doi:10.1186/s13059-021-02328-9

107. Cilibrasi R, van Iersel L, Kelk S, Tromp J. The complexity of the single individual SNP haplotyping problem. *Algorithmica* (2007) 49:13–36. doi:10.1007/s00453-007-0029-z

108. Sakamoto Y, Sereewattanawoot S, Suzuki A. A new era of long-read sequencing for cancer genomics. *J Hum Genet* (2020) 65:3–10. doi:10.1038/s10038-019-0658-5

109. Tarabichi M, Demetter P, Craciun L, Maenhaut C, Detours V. Thyroid cancer under the scope of emerging technologies. *Mol Cel Endocrinol* (2022) 541:111491. doi:10.1016/j.mce.2021.111491

110. Muñoz-Barrera A, Rubio-Rodríguez LA, Díaz-de Usera A, Jáspez D, Lorenzo-Salazar JM, González-Montelongo R, et al. From samples to germline and somatic sequence variation: a focus on next-generation sequencing in melanoma research. *Life (Basel)* (2022) 12(11):1939. doi:10.3390/life12111939

111. Vollmers AC. Long noncoding RNA. Introduction and overview. In: Crusio WE, Dong H, Radeke HH, Rezaei N, Steinlein O, Xiao J, editors. *Advances in experimental medicine and biology*. Springer (2022).

112. Park EG, Pyo SJ, Cui Y, Yoon SH, Nam JW. Tumor immune microenvironment lncRNAs. *Brief Bioinform* (2022) 23(1):bbab504. doi:10.1093/bib/bbab504

113. Li X, Wang C-Y. From bulk, single-cell to spatial RNA sequencing. *Int J Oral Sci* (2021) 13(36):36. doi:10.1038/s41368-021-00146-0

114. Depledge DP, Srinivas KP, Sadaoka T, Bready D, Mori Y, Placantonakis DG, et al. Direct RNA sequencing on nanopore arrays redefines the transcriptional complexity of a viral pathogen. *Nat Commun* (2019) 10:754. doi:10.1038/s41467-019-08734-9

115. Jovic D, Liang X, Zeng H, Lin L, Xu F, Luo Y. Single-cell RNA sequencing technologies and applications: a brief overview. *Clin Trans Med* (2022) 12(3):e694. doi:10.1002/ctm2.694

116. Razavi P, Li BT, Brown DN, Jung B, Hubbell E, Shen R, et al. High-intensity sequencing reveals the sources of plasma circulating cell-free DNA variants. *Nat Med* (2019) 25:1928–37. doi:10.1038/s41591-019-0652-7

117. Song P, Wu LR, Yan YH, Zhang JX, Chu T, Kwong LN, et al. Limitations and opportunities of technologies for the analysis of cell-free DNA in cancer diagnostics. *Nat Biomed Eng* (2022) 6(3):232–45. doi:10.1038/s41551-021-00837-3

118. Shieh JTC. Genomic technologies to improve variation identification in undiagnosed diseases. *Ped Neonatal* (2023) 64(S1):S18–S21. doi:10.1016/J.pedneo.2022.10.002

119. Macken WL, Vandrovcova J, Hanna MG, Pitceathly RDS. Applying genomic and transcriptomic advances to mitochondrial medicine. *Nat Rev Neurol* (2021) 17:215–30. doi:10.1038/s41582-021-00455-2

120. Esteller M. Epigenetic gene silencing in cancer: the DNA hypermethylome. *Hum Mol Genet* (2007) 16(Spec No 1):R50–9. doi:10.1093/hmg/ddm018

121. Lakshminarasimhan R, Liang G. The role of DNA methylation in cancer. *Adv Exp Med Biol* (2016) 945:151–72. doi:10.1007/978-3-319-43624-1_7

122. Abante J, Kambhampati S, Feinberg AP, Goutsias J. Estimating DNA methylation potential energy landscapes from nanopore sequencing data. *Sci Rep* (2021) 11(1):21619. doi:10.1038/s41598-021-00781-x

123. Jhanwar S, Deogade A. 5-Methylcytosine and 5-hydroxymethylcytosine signatures underlying pediatric cancers. *Epigenomes* (2019) 3(2):9. doi:10.3390/epigenomes3020009

124. Zhou D, Guo S, Wang Y, Zhao J, Liu H, Zhou F, et al. Functional characteristics of DNA N6-methyladenine modification based on long-read sequencing in pancreatic cancer. *Brief Funct Genomics* (2023) 23:150–62. doi:10.1093/bfgp/elad021

125. Brockley LJ, Souza VGP, Forder A, Pewarchuk ME, Erkan M, Telkar N, et al. Sequence-based platforms for discovering biomarkers in liquid biopsy of non-small-cell lung cancer. *Cancers (Basel)* (2023) 15(8):2275. doi:10.3390/cancers15082275

126. Ibrahim J, Peeters M, Van Camp G, Op de Beeck K. Methylation biomarkers for early cancer detection and diagnosis: current and future perspectives. *Eur J Cancer* (2023) 178:91–113. doi:10.1016/j.ejca.2022.10.015

127. Sahm F, Schrimpf D, Jones DTW, Meyer J, Kratz A, Reuss D, et al. Next-generation sequencing in routine brain tumor diagnostics enables an integrated diagnosis and identifies actionable targets. *Acta Neuropathol* (2016) 131(6):903–10. doi:10.1007/s00401-015-1519-8

128. Arts P, Simons A, AlZahrani MS, Yilmaz E, AlIdrissi E, van Aerde KJ, et al. Exome sequencing in routine diagnostics: a generic test for 254 patients with primary immunodeficiencies. *Genome Med* (2019) 11:38. doi:10.1186/s13073-019-0649-3

129. Breinholt MF, Nielsen K, Schejbel L, Fassi DE, Schöllkopf C, Novotny GW, et al. The value of next-generation sequencing in routine diagnostics and management of patients with cytopenia. *Int J Lab Hematol* (2022) 44(3):531–7. doi:10.1111/ijlh.13802

130. Fogel BL, Lee H, Strom SP, Deignan JL, Nelson SF. Clinical exome sequencing in neurogenetic and neuropsychiatric disorders. *Ann N Y Acad Sci* (2016) 1366(1):49–60. doi:10.1111/nyas.12850

131. Schmidt J, Blessing F, Fimpler L, Wenzel F. Nanopore sequencing in a clinical routine laboratory: challenges and opportunities. *Clin Lab* (2020) 66(6). doi:10.7754/Clin.Lab.2019.191114

132. Olivucci G, Iovino E, Innella G, Turchetti D, Pippucci T, Magini P. Long read sequencing on its way to the routine diagnostics of genetic diseases. *Front Genet* (2024) 15:1374860. doi:10.3389/fgene.2024.1374860

133. Eagle SHC, Robertson J, Bastedo DP, Liu K, Nash JHE. Evaluation of five commercial DNA extraction kits using Salmonella as a model for implementation of rapid Nanopore sequencing in routine diagnostic laboratories. *Access Microbiol* (2023) 5(2):000468v3. doi:10.1099/acmi.0.000468.v3

134. Erdmann H, Schöberl F, Giurgiu M, Leal Silva RM, Scholz V, Scharf F, et al. Parallel in-depth analysis of repeat expansions in ataxia patients by long-read sequencing. *Brain* (2023) 146(5):1831–43. doi:10.1093/brain/awac377

135. Matern BM, Olieslagers TI, Groeneweg M, Duygu B, Wieten L, Tilanus MGJ, et al. Long-read nanopore sequencing validated for human leukocyte antigen class I typing in routine diagnostics. *J Mol Diagn* (2020) 22(7):912–9. doi:10.1016/j.jmoldx.2020.04.001

136. Buenestado-Serrano S, Herranz M, Otero-Sobrino Á, Molero-Salinas A, Rodríguez-Grande C, Sanz-Pérez A, et al. Accelerating SARS-CoV-2 genomic surveillance in a routine clinical setting with nanopore sequencing. *Int J Med Microbiol* (2024) 314:151599. doi:10.1016/j.ijmm.2024.151599

Pathology & Oncology Research | frontiers

TYPE Review
PUBLISHED 07 March 2024
DOI 10.3389/pore.2024.1611643

Check for updates

OPEN ACCESS

EDITED BY
Jozsef Dudas,
Innsbruck Medical University, Austria

*CORRESPONDENCE
Anna Sebestyén,
hsebanna@gmail.com,
sebestyen.anna@semmelweis.hu

†These authors have contributed equally to this work

RECEIVED 15 December 2023
ACCEPTED 27 February 2024
PUBLISHED 07 March 2024

CITATION
Sztankovics D, Moldvai D, Petővári G, Dankó T, Szalai F, Miyaura R, Varga V, Nagy N, Papp G, Pápay J, Krencz I and Sebestyén A (2024), mTOR hyperactivity and *RICTOR* amplification as targets for personalized treatments in malignancies.
Pathol. Oncol. Res. 30:1611643.
doi: 10.3389/pore.2024.1611643

COPYRIGHT
© 2024 Sztankovics, Moldvai, Petővári, Dankó, Szalai, Miyaura, Varga, Nagy, Papp, Pápay, Krencz and Sebestyén. This is an open-access article distributed under the terms of the Creative Commons Attribution License (CC BY). The use, distribution or reproduction in other forums is permitted, provided the original author(s) and the copyright owner(s) are credited and that the original publication in this journal is cited, in accordance with accepted academic practice. No use, distribution or reproduction is permitted which does not comply with these terms.

mTOR hyperactivity and *RICTOR* amplification as targets for personalized treatments in malignancies

Dániel Sztankovics, Dorottya Moldvai, Gábor Petővári, Titanilla Dankó, Fatime Szalai, Risa Miyaura, Viktória Varga, Noémi Nagy, Gergő Papp, Judit Pápay, Ildikó Krencz† and Anna Sebestyén*†

Department of Pathology and Experimental Cancer Research, Semmelweis University, Budapest, Hungary

The increasing knowledge of molecular alterations in malignancies, including mutations and regulatory failures in the mTOR (mechanistic target of rapamycin) signaling pathway, highlights the importance of mTOR hyperactivity as a validated target in common and rare malignancies. This review summarises recent findings on the characterization and prognostic role of mTOR kinase complexes (mTORC1 and mTORC2) activity regarding differences in their function, structure, regulatory mechanisms, and inhibitor sensitivity. We have recently identified new tumor types with *RICTOR* (rapamycin-insensitive companion of mTOR) amplification and associated mTORC2 hyperactivity as useful potential targets for developing targeted therapies in lung cancer and other newly described malignancies. The activity of mTOR complexes is recommended to be assessed and considered in cancers before mTOR inhibitor therapy, as current first-generation mTOR inhibitors (rapamycin and analogs) can be ineffective in the presence of mTORC2 hyperactivity. We have introduced and proposed a marker panel to determine tissue characteristics of mTOR activity in biopsy specimens, patient materials, and cell lines. Ongoing phase trials of new inhibitors and combination therapies are promising in advanced-stage patients selected by genetic alterations, molecular markers, and/or protein expression changes in the mTOR signaling pathway. Hopefully, the summarized results, our findings, and the suggested characterization of mTOR activity will support therapeutic decisions.

KEYWORDS

mTOR, mTORC2 hyperactivity, *RICTOR* amplification, Rictor overexpression, malignancies

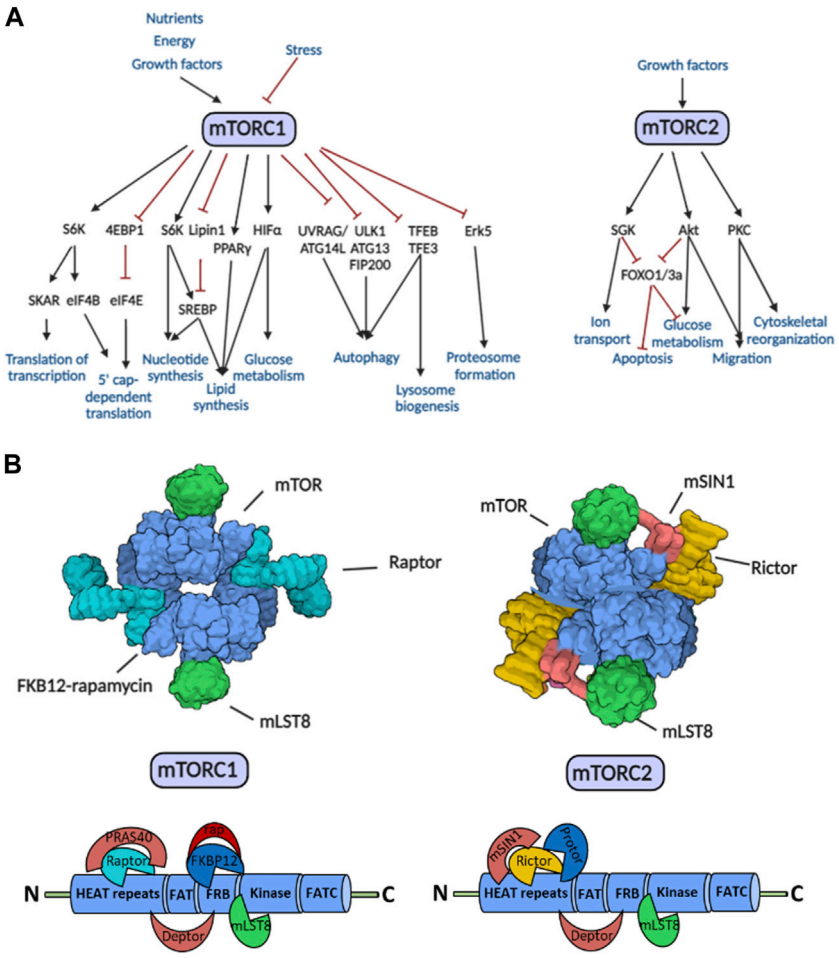

FIGURE 1
The regulatory roles, target proteins, and structure of the mTORC1 and mTORC2. **(A)** Effector mechanisms and functions of the mTORC1 and mTORC2. The schematic diagram shows the activating (black lines with arrows) and inhibitory (red lines with inhibition signs) effects. **(B)** Structural elements mTORC1 and mTORC2. The X-ray crystallographic field structure of mTOR complexes and the binding sites of specific partner molecules on the mTOR kinase domain are shown in the figure. Abbreviations: Deptor, DEP domain containing mTOR-interacting protein; HEAT repeats, Huntingtin, elongation factor 3 (EF3), protein phosphatase 2A (PP2A), TOR1; FAT domain, FRAP, ATM, TRRAP; FRB domain, FKBP12-rapamycin binding; FATC domain, C-terminal FAT domain; mLST8, mammalian lethal with sec-13 protein 8; mSin1, mammalian stress-activated map kinase-interacting protein 1; PRAS40, proline-rich Akt substrate of 40 kDa; Protor, protein observed with Rictor; rap, rapamycin; Raptor, regulatory-associated protein of mTOR; Rictor, rapamycin-insensitive companion of mTOR; other explanations in text.

Regulatory role of mTOR and its hyperactivity in cancer

The mechanistic (formerly mammalian) target of rapamycin (mTOR) influences various cellular processes (proliferation, motility, migration, metabolism, protein synthesis, transcription, etc.,) by integrating signals from the tissue environment. mTOR promotes cell growth and survival, depending on the actual state of the cell. In addition, a decrease in mTOR activity in the absence of growth factors, nutrients, or other energy sources (e.g., oxygen) inhibits cell growth and triggers survival-promoting cellular processes such as autophagy. As a central signaling pathway hub, mTOR kinase plays an essential role in metabolic regulation to maintain the balance between anabolic and catabolic processes, including metabolic adaptation in stress responses and tumor cell survival (Figure 1A). Dysfunction (hyper- or underactivation) of the mTOR kinase may contribute to regulatory failures and subsequently to the development and progression of diseases (e.g., metabolic, neurodegenerative, and cardiovascular diseases, accelerated aging, tumors) [1, 2].

mTOR is a serine-threonine kinase that forms two complexes (mTOR complex 1—mTORC1; mTOR complex 2—mTORC2) organized from different, functionally distinct proteins (Figure 1B). The identical subunits in the two complexes are mTOR kinase, mLST8 (mammalian lethal with sec-13 protein 8),

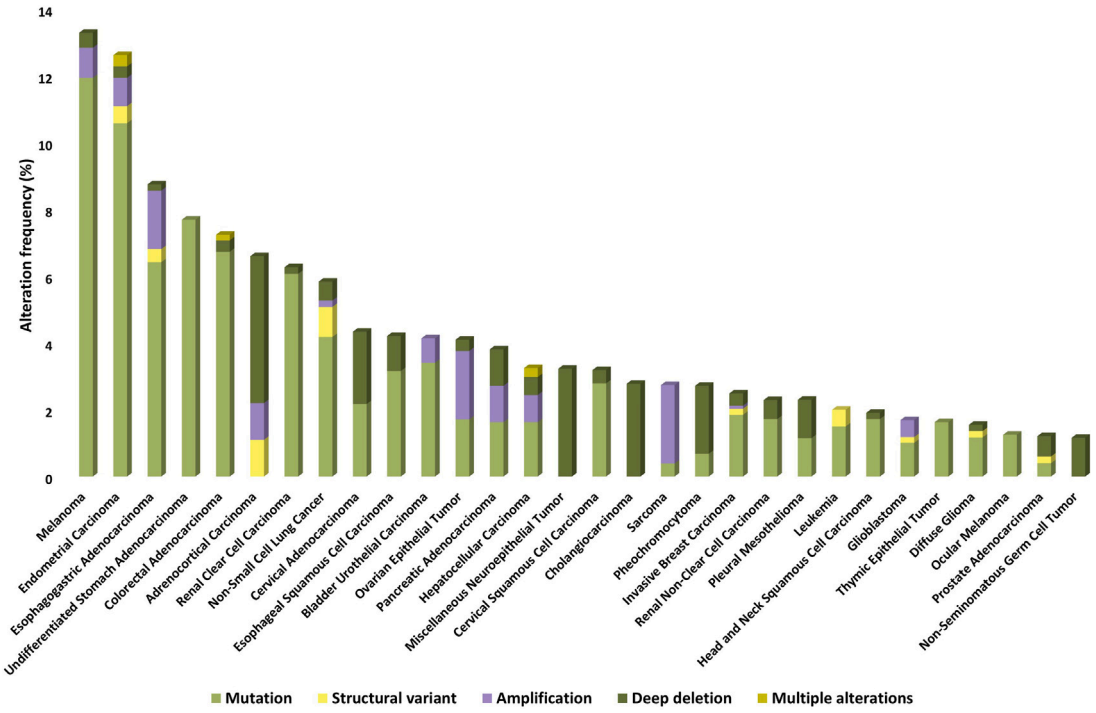

FIGURE 2
Prevalence of *MTOR* gene mutations, amplifications, deletions, and other structural gene defects in human tumors (based on TCGA PanCancer Atlas Studies databases).

and Deptor (DEP domain containing mTOR-interacting protein). PRAS40 (proline-rich Akt substrate of 40 kDa) and the scaffolding protein Raptor (regulatory-associated protein of mTOR) are involved in the assembly of mTORC1. mSin1 (mammalian stress-activated map kinase-interacting protein 1), Protor 1/2 (protein observed with Rictor 1 and 2), and the scaffolding protein Rictor (rapamycin-insensitive companion of mTOR) instead of Raptor are in mTORC2 [3].

mTORC1 plays a role in several cellular processes (e.g., protein, lipid and nucleotide synthesis, ribosome biogenesis), whereas mTORC2 has a significant role in the modulation of cell survival, differentiation, growth, and migration and the maintenance of the actin cytoskeleton, mainly through the phosphorylation of Akt (Ser473), PKCα, and SGK1 [4].

mTOR complexes and their dysfunction—mainly hyperactivity—have been associated with the development and progression of malignancies. Hyperactivity of mTOR complexes can occur in several ways; including gene mutations affecting mTOR kinase, mutations in proteins that directly regulate the mTOR complex activity, or other changes in the signaling network (e.g., mutations in oncogenic or tumor suppressor genes).

Nearly 5% of solid tumors may carry an activating mutation of mTOR kinase, which may be more common (>5%) in melanoma, endometrial, gastrointestinal, kidney, breast, and lung cancers [5]. On the basis of publicly available databases, the frequencies of genetic alterations associated with/related to mTOR kinase in different malignancies are summarized in Figure 2.

The enzymatic activity and oncogenic role of mTOR kinase are generally increased by somatic mutations affecting six different kinase regions. The most common activating mutations are E1799K, T1977R, V2006F, S2215Y, and R2505P, which are responsible for amino acid substitutions (Figure 3). Activating mutations do not affect the assembly of the mTOR complex but can reduce the binding of Deptor—an inhibitor of mTOR kinase—and increase the phosphorylation of target molecules (e.g., P70S6K, 4EBP1) [6, 7]. Some mutations alter the structure of the complex, leading to resistance to allosteric mTOR inhibitors (e.g., rapamycin) by preventing drug binding. For instance, F2108L point mutation occurs in the FKBP-binding (FRB) domain of mTOR, where the FKB12-rapamycin binding site is located [8].

Most commonly, other mutations can cause pathway hyperactivity or loss of negative regulators in the signaling network (e.g., *PI3KCA*, *PTEN*, *TSC1/2*, *STK11*, and *AKT1*). *PI3KCA* mutations occur in more than 20% of breast and gynecological cancers and are also common in colorectal tumors. *PTEN* mutations are found in 10% of central nervous system and endometrial tumors, *TSC1* mutations in 5%–6% of

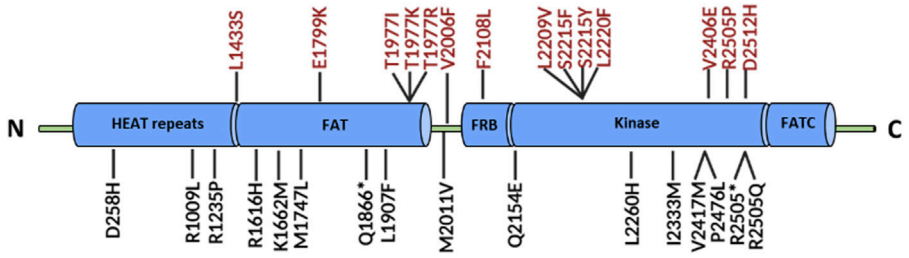

FIGURE 3
The structure of the mTOR kinase domain and some common mutations. The most common mutations responsible for changes in the structure of mTOR kinase are highlighted in red. Abbreviations: HEAT repeats, Huntingtin, elongation factor 3 (EF3), protein phosphatase 2A (PP2A), TOR1; FAT domain, FRAP, ATM, TRRAP; FRB domain, FKBP12-rapamycin binding; FATC domain, C-terminal FAT domain; other explanations in text.

urinary tract and endometrial tumors, and *TSC2* mutations in 4%–7% of gynecological, liver, and lung tumors. *STK11* mutations occur in 10%–15% of the cervical, small bowel, and lung tumors, while *AKT1* mutations are the least frequent of the signaling mutations (3%–5%). In many cases, mutations in receptor tyrosine kinases and growth factor receptors (EGFR and HER2) underline mTOR hyperactivity [9].

In addition to direct mutations in the mTOR kinase and the above-mentioned mutations affecting mTOR signaling, other gene mutations can occur in different subunits of the mTOR complex. One of the most common alterations is *RICTOR* amplification, which—in addition to increased expression of the Rictor protein—can increase the activity of the mTORC2 complex. In this context, it can affect/activate the target protein Akt kinase, which plays an essential role in the growth and survival of tumor cells (see below).

In situ studies of mTOR activity

The discovery of mTOR complexes and the potential therapeutic relevance of the mTOR kinase inhibitor rapamycin focused attention on the need to characterize mTOR activity. First-generation allosteric mTOR inhibitors are effective in the case of mTORC1 hyperactivity, although these may be ineffective in specific known FRB domain mutations or the presence of high mTORC2 activity. Therefore, the development of a new generation of mTOR kinase inhibitors that inhibit both mTORC1 and mTORC2 and additional inhibitors such as dual inhibitors has been initiated. Based on many published data, it is necessary to characterize mTOR activity *in situ* before starting mTOR-targeted therapies, as the efficacy of drug treatment may also depend on the ratio of the complexes.

In our studies, we have developed marker panels that can be used in a wide range of tumor types to quantify and morphologically characterize not only mTORC1 but also mTORC2 complex activity in tumor cells or tissues.

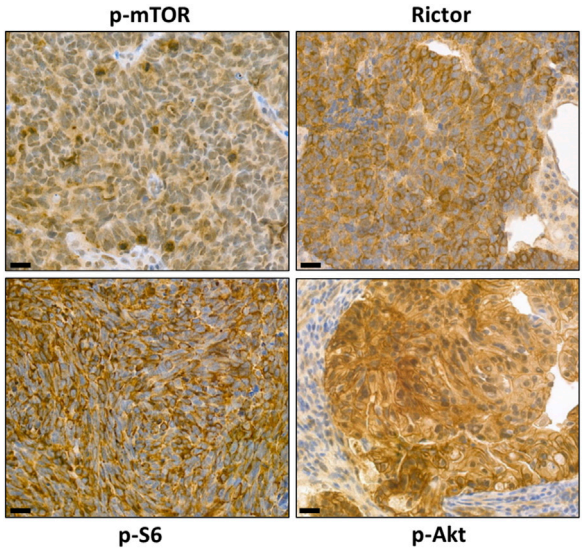

FIGURE 4
Representative images of characterizing mTORC1 and mTORC2 activity with our marker panel using immunohistochemistry. Detection of high levels of p-mTOR, p-S6, and Rictor *in situ* in brain metastases of small cell lung carcinoma and detection of p-Akt on paraffin sections of colorectal adenocarcinoma specimens. The magnifications are indicated, with 50 μm for IHC.

Characterization of mTOR activity in different cell lines and patient material can be performed by staining/measuring the active, phosphorylated form of mTOR kinase (p-mTOR) and its phosphorylated targets (e.g., p-4EBP1, p-p70S6K, p-S6) using immunohistochemistry (IHC)/immunocytochemistry and/or Western blot/Wes™ Simple. One of the target proteins of the mTORC2 complex is the Akt kinase, where the amino acid serine 473 can only be phosphorylated by active mTORC2. On the basis of publicly available results, quantitative and *in situ* analysis of p-Akt (Ser473) is the most appropriate way to monitor the mTORC2 activity.

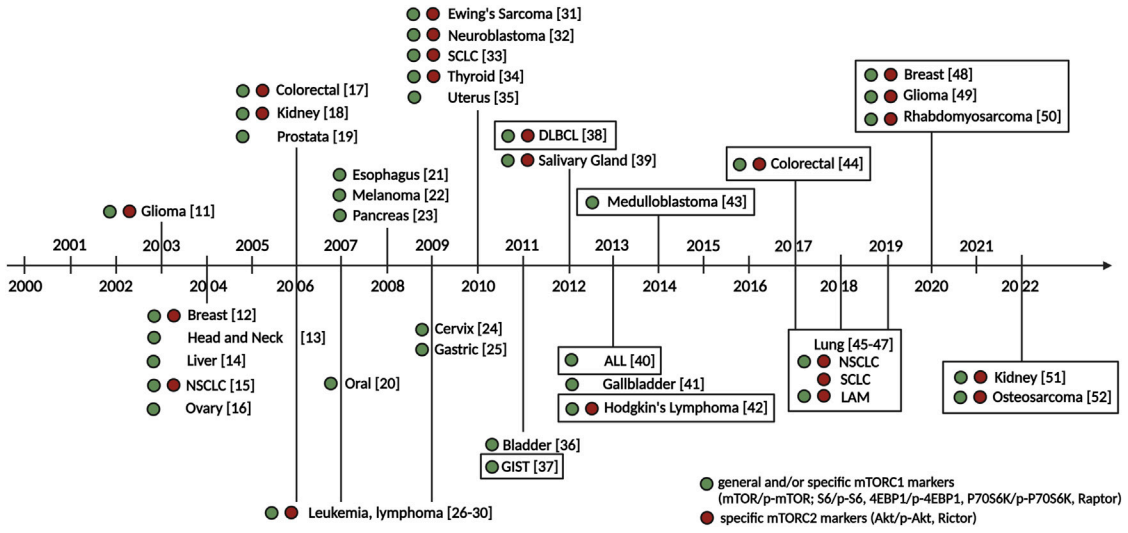

FIGURE 5
Milestones in the early characterization of mTOR hyperactivity in tumors. The first immunohistochemical characterizations of mTOR activity in the most common and later less common tumor types in the early 2000 s and our domestic characterizations (our work highlighted in a frame) are shown in the figure. Green and red circles indicate histopathological studies that detected general and/or specific mTORC1 complex markers (mTOR/p-mTOR; S6/p-S6, 4EBP1/p-4EBP1, P70S6K/p-P70S6K, Raptor) and specific mTORC2 complex markers (Akt/p-Akt, Rictor). Numbers indicate references. Abbreviations: ALL, acute lymphoblastic leukemia; DLBCL, diffuse large B-cell lymphoma; GIST, gastrointestinal stromal tumor; LAM, lymphangioleiomyomatosis; NSCLC, non-small cell lung cancer; SCLC, small cell lung cancer [11–52].

A quantitative comparison of the two mTOR complexes can also be determined from the ratio of specific scaffold proteins (Raptor for mTORC1 and Rictor for mTORC2). The optimal *in situ* marker panel is either a combination of p-mTOR, Raptor, and Rictor or a combination of mTORC1 target proteins (e.g., p-S6, p-70S6K, p-4EBP1) and a specific mTORC2 target protein [p-Akt (Ser473)] (Figure 4).

mTOR and mTORC1 hyperactivity in malignant tumors

The first clinical anti-tumor observation of the mTOR inhibitor, the immunosuppressive drug rapamycin, was detected in the treatment of post-transplant kidney cancer [10]. Following the discovery of mTOR complexes, the mTOR hyperactivity and/or sensitivity of tumor cells against mTOR inhibitors, quantitative changes in the mTOR signaling pathway elements, target proteins, and their active forms have been described and partially characterized in various tumor types by the end of the last century and early 2000 s (detailed in Figure 5).

Our studies have contributed to the characterization of mTORC1 activity in hematological malignancies and even to the investigation of both mTOR complexes in leukemias and lymphomas. Summarizing these studies, acute lymphoblastic leukemia (ALL) cells and several lymphoma model cell lines (Hodgkin's lymphoma, diffuse large B-cell lymphoma (DLBCL), anaplastic large cell lymphoma, mantle cell lymphoma, lymphoplasmacytic lymphoma, Burkitt's lymphoma) show high mTORC1 activity. In addition to the generally high mTOR activity, the poorest survival outcomes were observed with the co-occurrence of high mTOR activity and increased Rictor expression. These findings highlight the unfavorable prognostic role of increased mTORC2 activity in the majority of lymphoid malignancies studied [38, 40, 42].

In addition to *in vitro* lymphoma models, mTOR hyperactivity has been characterized in the most common solid tumors and several human malignant tissues. In gastrointestinal tumors (colon tumors, gastrointestinal stromal tumors—GIST), we first characterized the activity of mTOR complexes, based on the amount of mTORC1 and mTORC2 scaffold proteins, and classified Hungarian colon tumor cases into three main groups (low Raptor and high Rictor expression—high mTORC2 activity; high Raptor and low Rictor expression—high mTORC1 activity; similar levels of Raptor and Rictor expression—balanced mTORC1 and mTORC2 activity). We compared our results with the clinical characteristics of the patients and found the best treatment and survival outcomes in cases with low mTORC1 activity, whereas the worst survival outcomes were observed in cases with high mTOR activity and high Rictor expression. Our results also showed that Rictor expression was associated with poor prognosis independently of mTOR activity [37, 44]. In our human breast cancer studies over the past few years, we have detected mTORC1 hyperactivity in 50% of our cases, supporting the use of previously introduced mTOR inhibitor

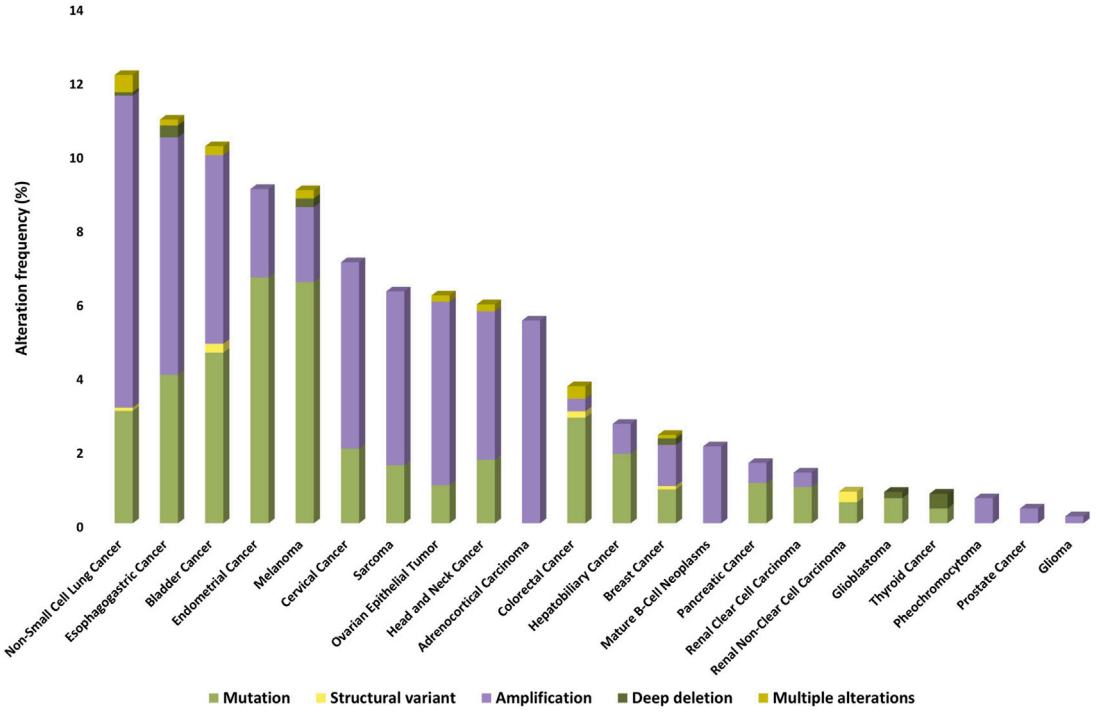

FIGURE 6
Prevalence of *RICTOR* gene mutations, amplifications, deletions, and other structural gene defects in human tumors (based on TCGA PanCancer Atlas Studies databases).

therapy. In addition, we observed high Rictor expression—the increased presence of the mTORC2 complex—in more than 40% of the cases studied, which may explain the ineffectiveness of conventional rapalogue (rapamycin and its derivatives) treatments [48]. We also characterized mTOR activity in renal tumors. In our comparative studies, we could detect higher expression of p-mTOR and p-S6 markers in clear cell renal cell carcinoma compared to papillary renal cell carcinoma and normal tubular epithelial cells. Moreover, papillary renal cell carcinoma was characterized by high Rictor expression and potential mTORC2 activity, also highlighting the role of mTORC2 activity in this tumor type [51]. There has been an emerging need to characterize mTOR activity in rare solid tumors. Our studies also aimed to investigate the mTOR activity in rare tumor types, such as central nervous system tumors, childhood rhabdomyosarcoma, osteosarcoma, medulloblastoma, and fibrosarcoma [43, 49, 50, 52, 53].

Overexpression of the Rictor protein and the associated increase in the amount and activity of mTORC2

Rictor is a characteristic actin coordinating scaffold protein of the mTORC2 complex, and its primary function is to ensure the formation and structure of the mTORC2 complex. Rictor contributes to the formation of a spatially structured mTORC2 complex in which the FKBP-rapamycin binding region of the mTOR kinase is located inside the molecule, blocking access to the best-known and most widely used inhibitor of rapamycin and its first-generation derivatives (rapalogs) [1]. Consequently, these inhibitors do not directly affect the mTORC2 target proteins (e.g., Akt). Increased Rictor expression is generally associated with transcriptional and translational changes. One of the best-known oncogenic mutations affecting the mTOR kinase pathway is the amplification of the *RICTOR* gene. *RICTOR* amplification can lead to increased expression of the Rictor protein and, in most cases, an increase in mTORC2 complex activity and a shift in the ratio of mTORC1 to mTORC2 complexes. *RICTOR* amplification has been described to play an essential role in the progression of certain tumors and metastasis via the regulation of signaling pathways (e.g., MAPK/ERK, Wnt/β-catenin pathways) [54].

Among the genetic defects of *RICTOR*, the most frequently observed change is its amplification, but other alterations have also been described [55]. The genetic alteration frequency of *RICTOR* in different malignancies is summarized in Figure 6 (based on public databases).

Additionally, higher Rictor expression has been described in several tumor types, including lung [56], esophageal [57], breast

TABLE 1 Prevalence, prognostic, and therapeutic implications of Rictor expression and/or *RICTOR* amplification in various tumor types.

Tumor types		Data on Rictor expression and/or *RICTOR* amplification	Prognostic and therapeutic implications	Relevant publications
Breast Tumors	HER2+, Luminal A/B, and Triple-Negative Breast Cancer	37%–50% expression (IHC)	Increased mTORC2 activity is associated with an increased risk of metastasis and poorer prognosis	[48, 62–64]
	Metastatic Breast Cancer (lymph node)	—		[65]
Central Nervous System Tumors	Glioma, Glioblastoma	—	mTORC2 can be a potential therapeutic target.	[49, 66–69]
Digestive System Tumors	Colorectal Cancer	58% expression (IHC)	Increased Rictor expression is associated with therapy resistance, poorer prognosis, and shorter overall survival. Treatment with mTOR inhibitors may be beneficial in combination with other therapies (e.g., EGFR inhibitors, platinum-based chemotherapy)	[44, 70–73]
	Esophageal Squamous Cell Carcinoma	70% expression (IHC)		[57]
	Gastric Cancer	46%–78% expression (IHC), 38% amplification (FISH)		[73–75]
	Hepatocellular Carcinoma, Cholangiocarcinoma	40%–43% expression (IHC)		[73, 76, 77]
	Pancreatic Cancer	—		[59, 78]
Female Genital Tumors	Endometrial Cancer	44% expression (IHC)	Increased Rictor expression correlates with stage, metastasis, and poorer prognosis	[79]
Head and Neck Tumors	—	70% expression (IHC)	—	[80–82]
	HPV-associated Oral Squamous Cell Carcinoma	—	Increased Rictor expression is associated with a poorer prognosis	[83]
Other tumors	Pheochromocytoma	80% expression (IHC)	—	[84]
Skin Tumors	Melanoma	—	The presence of liver metastasis correlates with increased Rictor expression, and inhibition of mTORC2 may reduce metastasis formation	[61, 85]
Soft Tissue and Bone Tumors	—	28% expression (IHC), 20% expression (Western blot)	High mTORC2 activity is associated with a poorer prognosis	[73, 86]
	Myxofibrosarcoma	—		[87]
	Osteosarcoma	25% expression (IHC)		[52]
	Rhabdomyosarcoma	82% expression (IHC)		[50]
Thoracic Tumors	Lymphangioleiomyomatosis	55% expression (IHC)	—	[47]
	Metastatic Lung Cancer	66% expression (IHC)	—	[45]
	Non-Small Cell Lung Cancer	37% expression (IHC)	—	[45, 73]
	Small Cell Lung Cancer	14% expression (IHC), 6%–15% amplification (sequencing)	—	[46, 88–90]
Tumors of Haematopoietic and Lymphoid Tissues	Leukemia and Lymphoma (Acute Myeloid Leukemia, Acute Lymphoid Leukemia, Chronic Lymphocytic Leukemia, Chronic Myeloid Leukemia, Diffuse Large B-cell Lymphoma)	43%–63% expression (IHC)	High mTORC2 activity is associated with a poorer prognosis; inhibition of mTORC2 may be effective	[38, 42, 91–94]
Urinary and Male Genital Tumors	Bladder Cancer	—	Increased mTORC2 activity may affect the invasiveness of bladder cancer cells	[95]
	Kidney Cancer	47% expression (IHC)	Resistance to rapalogs is associated with increased mTORC2 activity	[51, 73, 96]

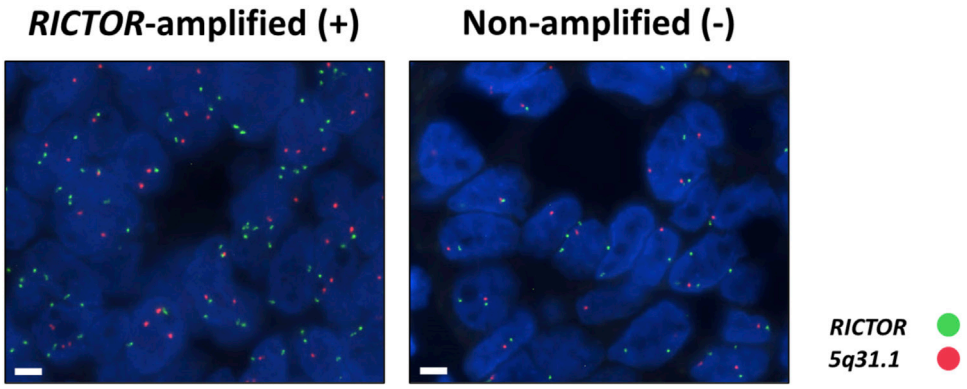

FIGURE 7
Representative images of the *RICTOR* FISH assay in *RICTOR*-amplified (+) and non-amplified (–) human tumor cases (*RICTOR* FISH was performed on the patient population of reference #97). The *RICTOR* (green) was used alongside the assay designed for the long arm (*5q31.1*) of chromosome 5 (orange) as a control (ZytoLight SPEC *RICTOR/5q31.1* Dual Color Probe—ZytoVision GmbH; Bremerhaven, Germany). The magnifications are indicated, with 5 µm for FISH.

[58], pancreatic [59], liver [60], and melanoma [61], where high Rictor expression was associated with poorer prognosis and shorter survival [55]. Table 1 summarizes mTORC2 hyperactivity and/or *RICTOR* amplification in different tumor types.

Methods to study *RICTOR* amplification, Rictor expression, and mTORC2 activity

RICTOR amplification may indicate high mTORC2 activity and may be a predictive marker of effective inhibition of the PI3K/mTOR/Akt axis. Fluorescence *in situ* hybridization (FISH) is considered the gold standard validation diagnostic method for identifying *RICTOR* amplification (Figure 7). In addition, potential changes in copy number can be detected by sequencing (e.g., next-generation sequencing) or Droplet Digital PCR (ddPCR). The Rictor protein expression can be detected by immunohistochemistry or immunocytochemistry. As mentioned above, the mTORC2 complex is exclusively responsible for the phosphorylation of serine 373 in the Akt protein. Increased p-Akt (Ser473) protein expression is a clear sign and an excellent marker of increased mTORC2 complex activity [46, 50]. It is important to note that tissue sample preparation and fixation require special attention when testing for p-Akt (Ser473) expression. Failures in the process and the timing of tissue sample fixation may reduce the detectability of phosphorylated proteins.

In our latest study, the diagnostic next-generation sequencing presumed *RICTOR* amplification was further analyzed in different human tumor tissues. *RICTOR* amplification was tested by ddPCR and validated using the "gold standard" FISH. In addition, Rictor and p-Akt (Ser473) protein expression was also examined by immunohistochemistry. The 10 novel and 4 previously described various tumor types with FISH-validated *RICTOR* amplification demonstrate the significance of *RICTOR* amplification in a wide range of malignancies (detailed in Figure 8). The newly described entities with *RICTOR* amplification may initiate further studies with larger cohorts to analyze the prevalence of *RICTOR* amplification also in rare diseases [97].

mTOR hyperactivity and *RICTOR* amplification in lung tumors

Dysregulation of the PI3K/Akt/mTOR signaling pathway plays an important role in the development and progression of the majority of lung cancers [98]. mTOR activity can be affected by failures in other signaling pathways related to the mTOR pathway and the known alterations in mTOR pathway activity (see above). In this context, the combined inhibition of mTOR and other kinases may provide additional therapeutic options for treating lung tumors [56].

Among non-small cell lung cancers (NSCLC), 90% of adenocarcinomas, 40% of squamous cell carcinomas, and 60% of large cell carcinomas are characterized by increased activity of PI3K/Akt/mTOR axis [99]. Elevated levels of phosphorylated mTORC1 targets (e.g., p-4EBP1, p-S6) have been observed in adenocarcinoma and squamous cell carcinoma. In these studies, tumor invasiveness, metastasis, and poorer prognosis are associated with increased activity of mTOR [100]. Activating mutations in *PIK3CA* have been detected in 4%–7% of NSCLCs, amplification in more than 30% of squamous cell carcinomas,

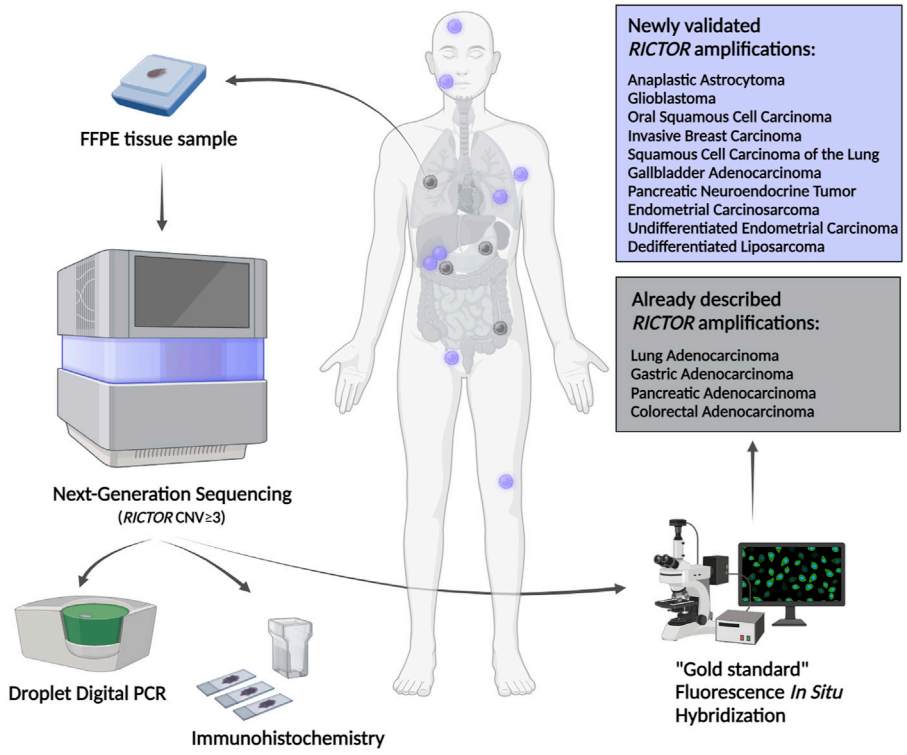

FIGURE 8
Newly described tumor types with FISH-validated *RICTOR* amplification. Abbreviations: FFPE, formalin-fixed, paraffin-embedded; CNV, copy number variation.

and about 1% of adenocarcinomas. *RICTOR* amplification has been described in 10% of NSCLCs, and mutations in the tumor suppressor genes *PTEN* and *STK11*, which are negative regulators of mTOR signaling, have also been observed in squamous cell and adenocarcinomas [101–103]. Moreover, mTOR activation correlates with mutations in both *KRAS* and epidermal growth factor receptor (EGFR) and may serve as a resistance mechanism to treatment with EGFR inhibitors [104].

In our studies, we examined the p-mTOR, p-S6, and Rictor proteins *in situ* in primary lung adenocarcinomas and brain metastases. Increased p-mTOR, p-S6, and Rictor protein expressions were observed in more than 30% of primary adenocarcinomas and around 70% of brain metastases. Additionally, all studied markers (p-mTOR, p-S6, and Rictor) showed a stronger positivity in the majority of the brain metastases studied. In some cases, high p-mTOR levels were associated with low p-S6 and high Rictor expression, which characterized about 20% of primary lung adenocarcinomas and more than 50% of brain metastases. Further associations were found between higher stage and Rictor expression in primary adenocarcinomas and high Rictor and low p-S6 expression in solitary brain metastases. Comparing primary tumor and brain metastases samples from the same patient, we observed increased mTORC1 activity in metastases; in 60% of the cases, p-mTOR and p-S6 expression was increased in brain metastases, whereas in 40% of cases, Rictor expression was increased in brain metastases. These data highlight the presence and prognostic role of mTORC2 activity in this tumor type [45].

Among lung tumors of neuroendocrine origin, small cell lung carcinoma (SCLC) is the most common, accounting for 15%–20% of all lung tumors [105]. In addition to mutations in the *TP53* and *RB1* genes and *MYC* amplification, genetic alterations affecting elements of the PI3K/Akt/mTOR pathway (e.g., *PIK3CA*, *PTEN*, *AKT2*, *AKT3*, *MTOR*, and *RICTOR*) are common in SCLC. *RICTOR* amplification is the most common targetable genetic alteration in SCLC (6%–14%) [106]. Activation of the mTOR pathway in SCLC has been detected by immunohistochemistry for p-mTOR and p-S6 proteins [33], although less data are available on the activity, background, and significance of mTORC2.

Our *RICTOR* amplification studies were initiated in collaboration with the Mayo Clinic, and within the framework of this collaboration, we analyzed 100 samples from 92 SCLC patients. The presence of *RICTOR* amplification was confirmed by FISH. We detected *RICTOR* amplification in 15% of cases, 3% of our cases were equivocal, and 82% were negative. In these samples, we characterized Rictor and p-Akt levels by immunohistochemistry. Of the cases, 14% showed high, 23%

TABLE 2 Classification, highest clinical phase, status, and application of PI3K/Akt/mTOR inhibitors in various tumor types based on the GlobalData database.

Target	Drug Name	Tumor types	Highest phase and ID number of the clinical trial	Status
PI3K inhibitors				
Non-subunit-specific PI3K inhibitor	AZD8186	Solid Tumor	Phase II—NCT04001569	Active
	buparlisib (NVP-BKM120)	Head and Neck Cancer	Phase III—NCT04338399	Active
	copanlisib	Lymphoma	—	Marketed
	duvelisib	Leukemia, Lymphoma	—	Marketed
	MEN1611 (CH5132799)	Colorectal Cancer	Phase II—NCT04495621	Active
	tenalisib (RP6530)	Breast Cancer	Phase II—NCT05021900	Active
	TQB-3525	Breast Cancer, Endometrial Cancer, Leukemia, Lymphoma, Ovarian Cancer	Phase II—NCT04324879, NCT04355520, NCT04398953, NCT04610970, NCT04615468, NCT04808570, NCT04836663	Active
PI3Kα inhibitor	alpelisib	Breast Cancer	—	Marketed
	CYH-33 (HHCYH-33)	Solid Tumor	Phase I—NCT04586335, NCT04856371	Active
	inavolisib (GDC-0077)	Breast Cancer	Phase III—NCT04191499	Active
	serabelisib (INK-1117)	Solid Tumor	Phase II—NCT04073680	Active
	taselisib	Lymphoma, Myeloma, Solid Tumor	Phase II—NCT02465060	Active
PI3Kβ inhibitor	GSK2636771	Lymphoma, Myeloma, Solid Tumor	Phase II—NCT02465060	Active
PI3Kγ inhibitor	eganelisib (IPI-549)	Breast Cancer, Kidney Cancer	Phase II—NCT03961698	Active
PI3Kδ inhibitor	amdizalisib (HMPL-689)	Lymphoma	Phase II—NCT04849351	Active
	idelalisib	Leukemia, Lymphoma	—	Marketed
	IOA-244	Lymphoma, Melanoma, Solid Tumor	Phase I—NCT04328844	Active
	linperlisib (YY-20394)	Lymphoma	Phase II—NCT04370405, NCT04379167, NCT04500561, NCT04705090, NCT04948788	Active
	parsaclisib (INCB50465)	Lymphoma, Myelofibrosis	Phase III—NCT04551053, NCT04551066, NCT04796922, NCT04849715	Active
	SHC014748 (SH-748)	Lymphoma	Phase II—NCT04431089, NCT04470141	Active
	umbralisib	Lymphoma	-	Marketed
	zandelisib (PWT-143)	Lymphoma	Phase III—NCT04745832	Active

(Continued on following page)

10.3389/pore.2024.1611643

TABLE 2 (*Continued*) Classification, highest clinical phase, status, and application of PI3K/Akt/mTOR inhibitors in various tumor types based on the GlobalData database.

Target	Drug Name	Tumor types	Highest phase and ID number of the clinical trial	Status
Various targets	AMG319 (ACP-319), apitolisib, AZD-8835, bimiralisib (PQR309), dactolisib, dezapelisib (NCB-040093), nemiralisib (GSK2269557), pictilisib (GDC-0941), pilaralisib, SAR260301, seletalisib (UCB-5857), SF1126, sonolisib, voxtalisib, ZSTK-474etc.			Inactive/ Discontinued
mTOR inhibitors				
Allosteric mTOR inhibitor	everolimus	Breast Cancer, Central Nervous System Tumor, Endocrine Tumor, Kidney Cancer	—	Marketed
	sirolimus	Lymphangioleiomyomatosis	—	Marketed
	temsirolimus	Kidney Cancer	—	Marketed
mTOR-kinase inhibitor (inhibits both mTORC1 and mTORC2)	CC-115	Central Nervous System Tumor	Phase II—NCT02977780	Active
	onatasertib (ATG-008)	Solid Tumor	Phase II—NCT03591965, NCT04337463, NCT04518137, NCT04998760	Active
	sapanisertib (MLN0128)	Lymphoma, Myeloma, Solid Tumor	Phase II—NCT02465060	Active
	vistusertib	Lung Cancer	Phase II—NCT02664935, NCT03334617	Active
Various targets	apitolisib, AZD8055, bimiralisib (PQR309), dactolisib, ridaforolimus (Deforolimus, MK-8669), SF1126, voxtalisibetc.			Inactive/ Discontinued
Akt inhibitors				
Pan-Akt	afuresertib	Ovarian Cancer, Prostate Cancer	Phase II—NCT04060394, NCT04374630	Active
	capivasertib	Breast Cancer, Prostate Cancer	Phase III—NCT03997123, NCT04305496, NCT04493853, NCT04862663	Active
	ipatasertib	Breast Cancer, Prostate Cancer	Phase III—NCT03072238, NCT03337724, NCT04060862, NCT04177108, NCT04650581	Active
	MK-2206	Breast Cancer, Lung Cancer, Thymoma	Phase II—NCT01042379, NCT01306045	Active
	TAS-117	Solid Tumor	Phase II—NCT04770246	Active
	triciribine (PTX-200)	Leukemia	Phase II—NCT02930109	Active
	uprosertib	Myeloma, Solid Tumor	Phase II—NCT01902173, NCT01989598	Active
Various targets	COTI-2, LY-2503029, perifosineetc.			Inactive/ Discontinued

(Continued on following page)

10.3389/pore.2024.1611643

10.3389/pore.2024.1611643

TABLE 2 (*Continued*) Classification, highest clinical phase, status, and application of PI3K/Akt/mTOR inhibitors in various tumor types based on the GlobalData database.

Target	Drug Name	Tumor types	Highest phase and ID number of the clinical trial	Status
Dual inhibitors				
PI3K, mTOR dual inhibitor	gedatolisib	Breast Cancer	Phase II—NCT03698383, NCT03911973	Active
	paxalisib	Central Nervous System Tumor	Phase III—NCT03970447	Active
	samotolisib	Lymphoma, Solid Tumor	Phase II—NCT03155620, NCT03213678	Active

moderate, 25% low Rictor expression, and 38% were negative. The expression of p-Akt was high in 16%, moderate in 26%, and low in 35% of the cases, whereas in 23% of the tested samples, we could not detect the presence of the protein. Statistical analyses showed that Rictor immunohistochemistry had a sensitivity of 93% and a specificity of 73%; p-Akt immunohistochemistry had a sensitivity of 80% and a specificity of 65% compared to *RICTOR* FISH results. The presence or absence of *RICTOR* amplification was not associated with the overall survival data of the patients. However, higher *in situ* expression of Rictor and p-Akt proteins was significantly associated with shorter overall survival [46].

A rare lung disease, lymphangioleiomyomatosis (LAM), is caused by a loss-of-function mutation in the *TSC1/2* gene, resulting in lung tissue damage through proliferation, growth, and invasion of LAM cells [107, 108]. The therapeutic relevance of mTORC1 activity and the expression of downstream markers of the mTOR signaling pathway (e.g., p-p70S6K, p-S6, p-4EBP1) have been demonstrated by immunohistochemical studies [109, 110].

With the help of the Mayo Clinic, 11 cases of LAM were involved in our studies. Most of these (91%) showed high p-S6 protein expression, demonstrating increased mTORC1 activity and supporting mTOR inhibitor treatments. In parallel, high levels of Rictor expression were detected in addition to p-S6 in more than half of the cases (55%). This observation also highlights the role of the potential activity of the mTORC2 complex in this disease, which may explain the ineffectiveness of mTORC1 inhibitors in certain cases. This study was the first to examine both mTORC1 and mTORC2 activity in human LAM samples, and in addition to previously reported mTORC1 hyperactivity, we have also demonstrated increased mTORC2 complex presence and activity. Further studies demonstrating mTORC2 hyperactivity may suggest using other dual mTORC1 and mTORC2 inhibitors or dual mTOR inhibitors to slow the progression of this rare disease [47].

Our studies support the importance of characterizing mTOR activity in a wide range of tumors, which may indicate the clinical need for the appropriate use of mTOR inhibitors. In these cases, we recommend the immunohistochemical analysis of at least 3-4 *in situ* tissue markers [e.g., p-mTOR, p-S6, Rictor, and p-Akt (Ser473)] to provide a good representation of mTORC1 and mTORC2 activity in tumor tissue. It is important to note that first-generation mTORC1 inhibitors may be ineffective in the presence of high Rictor and p-Akt (Ser473) expression, as tumor cells with high mTORC2 activity may survive despite the administration of specific mTORC1 inhibitors [111].

Targeted therapeutic options in the presence of mTOR hyperactivity and/or *RICTOR* amplification

Over the past decades, the efficacy of several PI3K/Akt/mTOR signaling inhibitors has been investigated. Despite

TABLE 3 Ongoing therapies in combination with mTOR inhibitors and their highest clinical trial phase in various tumor types based on the GlobalData database.

Tumor types	Therapy	Highest phase and ID number of the clinical trial
Breast Tumors		
Marketed: Metastatic, hormone receptor+/HER2– Breast Cancer (everolimus)		
HER2+ (hormone receptor–/HER2+) Breast Cancer	chemotherapy + inetetamab + sirolimus	Phase III—NCT04736589
Luminal A (hormone receptor+/HER2–) Breast Cancer	AZD2014/everolimus + fulvestrant	Phase II—NCT02216786
	everolimus + paclitaxel	Phase II—NCT04355858
Triple-Negative Breast Cancer	AZD2014 + AZD6244 (MEKI)	Phase I/II — NCT02583542
	bevacizumab + doxorubicin + everolimus	Phase II—NCT02456857
	AZD6244 + temsirolimus	Phase I—NCT00600496
Central Nervous System Tumors		
Marketed: Astrocytoma (everolimus)		
	perifosine + temsirolimus	Phase I—NCT02238496
	cyclophosphamide + dasatinib + temsirolimus	Phase I—NCT02389309
	temsirolimus + vorinostat	Phase I—NCT02420613
	irinotecan + nab-rapamycin + temozolomide	Phase I—NCT02975882
	everolimus + trametinib	Phase I—NCT04485559
	celecoxib + cyclophosphamide + etoposide + sirolimus	Phase II—NCT02574728
	nab-rapamycin + standard therapy	Phase II—NCT03463265
Digestive System Tumors		
Colorectal Cancer	AZD6244 + temsirolimus	Phase I—NCT00600496
	bevacizumab + FOLFOX6 + nab-rapamycin	Phase I/II—NCT03439462
Hepatocellular Carcinoma	everolimus + lenvatinib + trametinib	Phase II—NCT04803318
Pancreatic Cancer	gedatolisib + palbociclib	Phase I — NCT03065062
Head and Neck Tumors		
	gedatolisib + palbociclib	Phase I—NCT03065062
Neuroendocrine Tumors		
Marketed: Neuroendocrine Tumors of the Lungs, Pancreas, or Intestines (everolimus)		
Neurofibromatosis	PLX3397 (MTKI) + sirolimus	Phase I/II—NCT02584647
	selumetinib (MEKI) + sirolimus	Phase II—NCT03433183
	bevacizumab + everolimus + octreotide acetate	Phase II—NCT01229943
	everolimus + lenvatinib	Phase II—NCT03950609
Other Tumors		
Advanced Tumor	sirolimus/everolimus/temsirolimus + vorinostat	Phase I—NCT01087554
	bevacizumab + carboplatin/sorafenib/paclitaxel + temsirolimus	Phase I—NCT01187199

(Continued on following page)

TABLE 3 (*Continued*) Ongoing therapies in combination with mTOR inhibitors and their highest clinical trial phase in various tumor types based on the GlobalData database.

Tumor types	Therapy	Highest phase and ID number of the clinical trial
	everolimus + vandetanib	Phase I—NCT01582191
	ceritinib + everolimus	Phase I—NCT02321501
	cemiplimab + sirolimus/everolimus + prednisone	Phase I—NCT04339062
Hepatoblastoma	chemotherapy + temsirolimus	Phase III—NCT00980460
Neuroblastoma	irinotecan + temozolomide + temsirolimus	Phase II—NCT01767194
Solid Tumor	ixabepilone + temsirolimus	Phase I—NCT01375829
	cyclophosphamide + dasatinib + temsirolimus	Phase I—NCT02389309
	bevacizumab + cyclophosphamide + temsirolimus + valproát	Phase I—NCT02446431
	irinotecan + nab-rapamycin + temozolomide	Phase I—NCT02975882
	gedatolisib + palbociclib	Phase I—NCT03065062
	epacadostat + sirolimus	Phase I—NCT03217669
	celecoxib + cyclophosphamide + etoposide + sirolimus	Phase II—NCT02574728
	everolimus + lenvatinib + trametinib	Phase II—NCT04803318
Vascular Tumor	prednisolone + sirolimus	Phase II—NCT03188068
Skin Tumors		
Melanoma	AZD6244 + temsirolimus	Phase I—NCT00600496
Soft Tissue and Bone Tumors		
	chemotherapy + everolimus + temsirolimus	Phase I—NCT04199026
	nab-rapamycin + pazopanib hydrochloride	Phase I/II—NCT03660930
	everolimus + ribociclib	Phase II—NCT03114527
	chemotherapy + temsirolimus	Phase III—NCT02567435
Thoracic Tumors		
Marketed: Sporadic Lymphangioleiomyomatosis (sirolimus)		
Non-Small Cell Lung Cancer	gedatolisib + palbociclib	Phase I—NCT03065062
	epacadostat + sirolimus	Phase I—NCT03217669
	durvalumab + sirolimus	Phase I—NCT04348292
	AZD2014 + AZD6244 (MEKI)	Phase I/II—NCT02583542
Non-Small Cell Lung Cancer + Small Cell Lung Cancer	AZD6244 + temsirolimus	Phase I—NCT00600496
	auranofin + sirolimus	Phase I/II—NCT01737502
Tumors of Haematopoietic and Lymphoid Tissues		
Marketed: Mantle Cell Lymphoma (temsirolimus)		
Hodgkin's Lymphoma	everolimus + itacitinib	Phase I/II—NCT03697408
Leukemia	decitabine + sirolimus	Phase I/II—NCT02109744
	azacitidine + sirolimus	Phase II—NCT01869114

(Continued on following page)

TABLE 3 (*Continued*) Ongoing therapies in combination with mTOR inhibitors and their highest clinical trial phase in various tumor types based on the GlobalData database.

Tumor types	Therapy	Highest phase and ID number of the clinical trial
	clofarabine + melphalan + sirolimus + tacrolimus	Phase II—NCT01885689
Urinary and Male Genital Tumors		
Marketed: Metastatic Kidney Cancer (everolimus, temsirolimus)		
Kidney Cancer	AZD6244 + temsirolimus	Phase I—NCT00600496
	DFF332 (HIF2αI) + everolimus	Phase I—NCT04895748
	sunitinib + temsirolimus	Phase II—NCT01517243
	everolimus + lenvatinib	Phase I—NCT03324373
		Phase II—NCT05012371
	anastrozol + AZD2014	Phase I/II—NCT02730923
	carboplatin + paclitaxel + temsirolimus	Phase II—NCT00977574
	everolimus + levonorgestrel	Phase II—NCT02397083
	everolimus + letrozole + ribociclib	Phase II—NCT03008408
	auranofin + sirolimus	Phase II—NCT03456700
	ATG008/ATG010	Phase II—NCT04998760

numerous clinical trials with inhibitors of this signaling pathway, therapeutic responses are often lower than expected; moreover, only a few new drugs have been introduced to treat various tumors. One possible reason for this could be an inadequate patient selection method and, in this context, the lack of reliable predictive markers. Sensitivity to mTOR inhibitors may be predicted by specific genetic abnormalities (e.g., *PIK3CA* mutation/amplification, *PTEN* loss-of-function mutation, *AKT* mutation, *RICTOR* amplification) or overexpression of the signaling pathway elements and their active targets (e.g., Rictor, p-S6, p-Akt). These markers can be well assessed at the tissue level, and their presence or absence should be evaluated/considered when designing targeted therapies before specific inhibitors are used [112, 113].

The best-known mTOR inhibitor, rapamycin (or sirolimus), also the eponymous inhibitor of mTOR kinase, was discovered by George Nogrady, a Hungarian-born bacteriologist, in the Chilean territory of Easter Island (Rapa Nui) in 1964 [114]. The compound was isolated as a microbial antibiotic and introduced as an immunosuppressant in 1975 [115]. Following the discovery of the specific target protein of rapamycin, mTOR kinase, allosteric mTOR inhibitors, rapamycin and its derivatives (rapalogs—everolimus, temsirolimus, etc.,) have been used with varying results in several types of tumors (e.g., breast, kidney, endocrine, central nervous system). Rapalogs inhibit the activity of mTORC1 by binding to the FRB domain of mTOR kinase through the FKBP12 protein. Due to the structural differences between the two complexes (see above), no direct effect of rapamycin is observed for the mTORC2 complex [111]. Further studies are needed to determine the possible impact of rapamycin on the mTORC2 complex.

In addition to rapalogs, double mTORC1 and mTORC2 inhibitors (e.g., CC-115, sapanisertib, vistusertib), as well as dual mTOR kinase and another signaling kinase (e.g., PI3K) inhibitors (e.g., gedatolisib, paxalisib, samatolisib) are currently under development. Other specific Akt inhibitors are also being tested (e.g., afuresertib, capivasertib, ipatasertib, MK-2206, TAS-117, triciribine, uprosertib) and are currently in phase II and III trials. Third-generation mTOR inhibitors (e.g., RapaLink-1) are also being developed for the treatment of various advanced cancers (e.g., renal, breast, mantle cell, and other high-grade lymphomas) [116]. Table 2 summarizes PI3K/Akt/mTOR inhibitors currently in use and development.

Developing potent and highly selective small molecules specific to the mTORC2 complex while preserving mTORC1 activity remains challenging. Among the specific inhibitors of mTORC2, only a few inhibitors based primarily on siRNA technology (e.g., Rictor si-NP, JR-AB2-011) are under preclinical testing [64, 117].

Despite the association between PI3K/Akt/mTOR hyperactivation and adverse prognosis, the efficacy of mTOR inhibitors used as monotherapy is very low, as is the case for most targeted therapeutic agents. However, combining mTOR inhibitors with other targeted therapies or conventional chemotherapy/radiotherapy may help sensitize different agents and overcome resistance mechanisms to treatment. This type of

combination therapy is also being developed for a wide range of malignancies (Table 3) [118]. However, the administration of these mTOR inhibitor combination therapies can also be limited by adverse effects and/or severe individual side effects that require very careful management by oncologists [119].

Future perspectives

Advances in personalized therapies and the increasing availability of molecular genetic data on malignancies, including our findings of mTORC1 and mTORC2 activity and *RICTOR* amplification in various tumors, highlight the importance of validated targets in common and rare malignancies. The efficacy of targeted therapies often fails to deliver the expected results due to inadequate patient selection. In a biomarker-driven umbrella study, patients were selected based on *RICTOR* amplification, demonstrating a promising strategy for personalized therapies by selecting patients most likely to respond to targeted treatments. In this clinical trial, two of the four SCLC patients treated with a vistusertib (dual mTORC1 and mTORC2 inhibitor) showed an increase in survival of almost 1 year [120].

In our work, we have developed a marker panel to determine tissue characteristics of mTOR activity in biopsy specimens, patient materials, and cell lines. Our results and other molecular findings will hopefully support and optimize future therapeutic decisions.

mTOR hyperactivity can be a targeted genetic alteration in different tumor types. In our studies, we present our findings on the activity of both complexes and the characterization and prognostic role of mTORC2 complex hyperactivity. In the future, we intend to investigate further the significance of mTOR hyperactivity and *RICTOR* amplification in several malignancies. Expanding next-generation sequencing into routine diagnostics will facilitate more accurate oncogenic and tumor suppressor gene alterations mapping. Molecular pathology results and molecular genetics data will become widely available, which may help to identify mutations affecting mTOR activity. This will also help to determine the importance of specific mutations in rare tumor types.

In summary, several third-generation PI3K/Akt/mTOR pathway inhibitors are already developing, and some of these are in clinical trials. Only a few inhibitors have been approved for treating various cancers compared to the enormous amount of research and money spent on their development. To increase this number and to achieve clinical translation of more mTOR inhibitors or other targeted inhibitors into personalized therapies, it is essential to identify predictive markers that can help therapeutic decision-making. In conclusion, for biomarker-driven patient selection, it is crucial to develop agents that are as effective as possible while maintaining a good safety profile and use rational drug combinations that improve quality of life and may be effective in overcoming primary or acquired resistance.

Footnotes

The figures in this review (Figures 1, 4, and 6) were edited using BioRender (https://biorender.com) under license from the Department of Pathology and Experimental Cancer Research, Semmelweis University.

Author contributions

All authors (DS, DM, GP, TD, FS, RM, VV, NN, GP, JP, IK, and AS) participated in the design and review of the manuscript. AS supervised the literature review and manuscript preparation. DS and IK wrote the manuscript. All authors contributed to the article and approved the submitted version.

Funding

A recent review has been funded by the National Research, Development and Innovation Office of Hungary (NKFIH); TKP2021-EGA-24, NKFI-K-142799.

Conflict of interest

The authors declare that the research was conducted in the absence of any commercial or financial relationships that could be construed as a potential conflict of interest.

References

1. Saxton RA, Sabatini DM. mTOR signaling in growth, metabolism, and disease. *Cell* (2017) 168:960–76. doi:10.1016/j.cell.2017.02.004

2. Wullschleger S, Loewith R, Hall MN. TOR signaling in growth and metabolism. *Cell* (2006) 124:471–84. doi:10.1016/j.cell.2006.01.016

3. Liu GY, Sabatini DM. mTOR at the nexus of nutrition, growth, ageing and disease. *Nat Rev Mol Cel Biol* (2020) 4:183–203. doi:10.1038/s41580-019-0199-y

4. Fu W, Hall MN. Regulation of mTORC2 signaling. *Genes (Basel)* (2020) 11: 1045. doi:10.3390/genes11091045

5. Sebestyén A, Dankó T, Sztankovics D, Moldvai D, Raffay R, Cervi C, et al. The role of metabolic ecosystem in cancer progression - metabolic plasticity and mTOR hyperactivity in tumor tissues. *Cancer Metastasis Rev* (2021) 40:989–1033. doi:10.1007/s10555-021-10006-2

6. Yamaguchi H, Kawazu M, Yasuda T, Soda M, Ueno T, Kojima S, et al. Transforming somatic mutations of mammalian target of rapamycin kinase in human cancer. *Cancer Sci* (2015) 106:1687–92. doi:10.1111/cas.12828

7. Grabiner BC, Nardi V, Birsoy K, Possemato R, Shen K, Sinha S, et al. A diverse array of cancer-associated MTOR mutations are hyperactivating and can predict rapamycin sensitivity. *Cancer Discov* (2014) 4:554–63. doi:10.1158/2159-8290.CD-13-0929

8. Wagle N, Grabiner BC, Van Allen EM, Amin-Mansour A, Taylor-Weiner A, Rosenberg M, et al. Response and acquired resistance to everolimus in anaplastic thyroid cancer. *N Engl J Med* (2014) 371:1426–33. doi:10.1056/NEJMoa1403352

9. Menon S, Manning BD. Common corruption of the mTOR signaling network in human tumors. *Oncogene* (2008) 27(Suppl. 2(0 2)):S43–51. doi:10.1038/onc.2009.352

10. Eng CP, Sehgal SN, Vézina C. Activity of rapamycin (AY-22,989) against transplanted tumors. *J Antibiot* (1984) 37:1231–7. doi:10.7164/antibiotics.37.1231

11. Choe G, Horvath S, Cloughesy TF, Crosby K, Seligson D, Palotie A, et al. Analysis of the phosphatidylinositol 3'-kinase signaling pathway in glioblastoma patients *in vivo*. *Cancer Res* (2003) 63:2742–6.

12. Zhou X, Tan M, Stone Hawthorne V, Klos KS, Lan KH, Yang Y, et al. Activation of the Akt/mammalian target of rapamycin/4E-BP1 pathway by ErbB2 overexpression predicts tumor progression in breast cancers. *Clin Cancer Res* (2004) 10:6779–88. doi:10.1158/1078-0432.CCR-04-0112

13. Nathan CO, Amirghahari N, Abreo F, Rong X, Caldito G, Jones ML, et al. Overexpressed eIF4E is functionally active in surgical margins of head and neck cancer patients via activation of the Akt/mammalian target of rapamycin pathway. *Clin Cancer Res* (2004) 10:5820–7. doi:10.1158/1078-0432.CCR-03-0483

14. Sahin F, Kannangai R, Adegbola O, Wang J, Su G, Torbenson M. mTOR and P70 S6 kinase expression in primary liver neoplasms. *Clin Cancer Res* (2004) 10:8421–5. doi:10.1158/1078-0432.CCR-04-0941

15. Balsara BR, Pei J, Mitsuuchi Y, Page R, Klein-Szanto A, Wang H, et al. Frequent activation of AKT in non-small cell lung carcinomas and preneoplastic bronchial lesions. *Carcinogenesis* (2004) 25:2053–9. doi:10.1093/carcin/bgh226

16. Xu G, Zhang W, Bertram P, Zheng XF, McLeod H. Pharmacogenomic profiling of the PI3K/PTEN-AKT-mTOR pathway in common human tumors. *Int J Oncol* (2004) 24:893–900. doi:10.3892/ijo.24.4.893

17. Nozawa H, Watanabe T, Nagawa H. Phosphorylation of ribosomal p70 S6 kinase and rapamycin sensitivity in human colorectal cancer. *Cancer Lett* (2007) 251:105–13. doi:10.1016/j.canlet.2006.11.008

18. Lin F, Zhang PL, Yang XJ, Prichard JW, Lun M, Brown RE. Morphoproteomic and molecular concomitants of an overexpressed and activated mTOR pathway in renal cell carcinomas. *Ann Clin Lab Sci* (2006) 36:283–93.

19. Kremer CL, Klein RR, Mendelson J, Browne W, Samadzedeh LK, Vanpatten K, et al. Expression of mTOR signaling pathway markers in prostate cancer progression. *Prostate* (2006) 66:1203–12. doi:10.1002/pros.20410

20. Liu Y, Hidayat S, Su WH, Deng X, Yu DH, Yu BZ. Expression and activity of mTOR and its substrates in different cell cycle phases and in oral squamous cell carcinomas of different malignant grade. *Cell Biochem Funct* (2007) 25:45–53. doi:10.1002/cbf.1332

21. Boone J, Ten Kate FJ, Offerhaus GJ, van Diest PJ, Rinkes IH, van Hillegersberg R. mTOR in squamous cell carcinoma of the oesophagus: a potential target for molecular therapy? *J Clin Pathol* (2008) 61:909–13. doi:10.1136/jcp.2008.055772

22. Karbowniczek M, Spittle CS, Morrison T, Wu H, Henske EP. mTOR is activated in the majority of malignant melanomas. *J Invest Dermatol* (2008) 128:980–7. doi:10.1038/sj.jid.5701074

23. Pham NA, Schwock J, Iakovlev V, Pond G, Hedley DW, Tsao MS. Immunohistochemical analysis of changes in signaling pathway activation downstream of growth factor receptors in pancreatic duct cell carcinogenesis. *BMC Cancer* (2008) 8:43. doi:10.1186/1471-2407-8-43

24. Feng W, Duan X, Liu J, Xiao J, Brown RE. Morphoproteomic evidence of constitutively activated and overexpressed mTOR pathway in cervical squamous carcinoma and high grade squamous intraepithelial lesions. *Int J Clin Exp Pathol* (2009) 2:249–60.

25. Yu G, Wang J, Chen Y, Wang X, Pan J, Li G, et al. Overexpression of phosphorylated mammalian target of rapamycin predicts lymph node metastasis and prognosis of Chinese patients with gastric cancer. *Clin Cancer Res* (2009) 15:1821–9. doi:10.1158/1078-0432.CCR-08-2138

26. Leseux L, Hamdi SM, Al Saati T, Capilla F, Recher C, Laurent G, et al. Syk-dependent mTOR activation in follicular lymphoma cells. *Blood* (2006) 108:4156–62. doi:10.1182/blood-2006-05-026203

27. Peponi E, Drakos E, Reyes G, Leventaki V, Rassidakis GZ, Medeiros LJ. Activation of mammalian target of rapamycin signaling promotes cell cycle progression and protects cells from apoptosis in mantle cell lymphoma. *Am J Pathol* (2006) 169:2171–80. doi:10.2353/ajpath.2006.051078

28. Follo MY, Mongiorgi S, Bosi C, Cappellini A, Finelli C, Chiarini F, et al. The Akt/mammalian target of rapamycin signal transduction pathway is activated in high-risk myelodysplastic syndromes and influences cell survival and proliferation. *Cancer Res* (2007) 67:4287–94. doi:10.1158/0008-5472.CAN-06-4409

29. Marzec M, Liu X, Kasprzycka M, Witkiewicz A, Raghunath PN, El-Salem M, et al. IL-2- and IL-15-induced activation of the rapamycin-sensitive mTORC1 pathway in malignant CD4+ T lymphocytes. *Blood* (2008) 111:2181–9. doi:10.1182/blood-2007-06-095182

30. Zhao MY, Auerbach A, D'Costa AM, Rapoport AP, Burger AM, Sausville EA, et al. Phospho-p70S6K/p85S6K and cdc2/cdk1 are novel targets for diffuse large B-cell lymphoma combination therapy. *Clin Cancer Res* (2009) 15:1708–20. doi:10.1158/1078-0432.CCR-08-1543

31. Mora J, Rodríguez E, de Torres C, Cardesa T, Ríos J, Hernández T, et al. Activated growth signaling pathway expression in Ewing sarcoma and clinical outcome. *Pediatr Blood Cancer* (2012) 58:532–8. doi:10.1002/pbc.23348

32. Iżycka-Świeszewska E, Drożyńska E, Rzepko R, Kobierska-Gulida G, Grajkowska W, Perek D, et al. Analysis of PI3K/AKT/mTOR signalling pathway in high risk neuroblastic tumours. *Pol J Pathol* (2010) 61:192–8.

33. Schmid K, Bago-Horvath Z, Berger W, Haitel A, Cejka D, Werzowa J, et al. Dual inhibition of EGFR and mTOR pathways in small cell lung cancer. *Br J Cancer* (2010) 103:622–8. doi:10.1038/sj.bjc.6605761

34. Liu J, Brown RE. Morphoproteomics demonstrates activation of mTOR pathway in anaplastic thyroid carcinoma: a preliminary observation. *Ann Clin Lab Sci* (2010) 40:211–7.

35. McCampbell AS, Harris HA, Crabtree JS, Winneker RC, Walker CL, Broaddus RR. Loss of inhibitory insulin receptor substrate-1 phosphorylation is an early event in mammalian target of rapamycin-dependent endometrial hyperplasia and carcinoma. *Cancer Prev Res (Phila)* (2010) 3:290–300. doi:10.1158/1940-6207.CAPR-09-0199

36. Tickoo SK, Milowsky MI, Dhar N, Dudas ME, Gallagher DJ, Al-Ahmadie H, et al. Hypoxia-inducible factor and mammalian target of rapamycin pathway markers in urothelial carcinoma of the bladder: possible therapeutic implications. *BJU Int* (2011) 107:844–9. doi:10.1111/j.1464-410X.2010.09517.x

37. Sápi Z, Füle T, Hajdu M, Matolcsy A, Moskovszky L, Márk A, et al. The activated targets of mTOR signaling pathway are characteristic for PDGFRA mutant and wild-type rather than KIT mutant GISTs. *Diagn Mol Pathol* (2011) 20:22–33. doi:10.1097/PDM.0b013e3181eb931b

38. Sebestyén A, Sticz TB, Márk A, Hajdu M, Timár B, Nemes K, et al. Activity and complexes of mTOR in diffuse large B-cell lymphomas--a tissue microarray study. *Mod Pathol* (2012) 25:1623–8. doi:10.1038/modpathol.2012.141

39. Suzuki S, Dobashi Y, Minato H, Tajiri R, Yoshizaki T, Ooi A. EGFR and HER2-Akt-mTOR signaling pathways are activated in subgroups of salivary gland carcinomas. *Virchows Arch* (2012) 461:271–82. doi:10.1007/s00428-012-1282-3

40. Nemes K, Sebestyén A, Márk A, Hajdu M, Kenessey I, Sticz T, et al. Mammalian target of rapamycin (mTOR) activity dependent phospho-protein expression in childhood acute lymphoblastic leukemia (ALL). *PLoS One* (2013) 8:e59335. doi:10.1371/journal.pone.0059335

41. Leal P, García P, Sandoval A, Letelier P, Brebi P, Ili C, et al. Immunohistochemical expression of phospho-mTOR is associated with poor prognosis in patients with gallbladder adenocarcinoma. *Arch Pathol Lab Med* (2013) 137:552–7. doi:10.5858/arpa.2012-0032-OA

42. Márk Á, Hajdu M, Váradi Z, Sticz TB, Nagy N, Csomor J, et al. Characteristic mTOR activity in Hodgkin-lymphomas offers a potential therapeutic target in high risk disease--a combined tissue microarray, *in vitro* and *in vivo* study. *BMC Cancer* (2013) 13:250. doi:10.1186/1471-2407-13-250

43. Pócza T, Sebestyén A, Turányi E, Krenács T, Márk A, Sticz TB, et al. mTOR pathway as a potential target in a subset of human medulloblastoma. *Pathol Oncol Res* (2014) 20:893–900. doi:10.1007/s12253-014-9771-0

44. Sticz T, Molnár A, Márk Á, Hajdu M, Nagy N, Végső G, et al. mTOR activity and its prognostic significance in human colorectal carcinoma depending on C1 and C2 complex-related protein expression. *J Clin Pathol* (2017) 70:410–6. doi:10.1136/jclinpath-2016-203913

45. Krencz I, Sebestyén A, Fábián K, Márk Á, Moldvay J, Khoor A, et al. Expression of mTORC1/2-related proteins in primary and brain metastatic lung adenocarcinoma. *Hum Pathol* (2017) 62:66–73. doi:10.1016/j.humpath.2016.12.012

46. Krencz I, Sebestyen A, Papay J, Lou Y, Lutz GF, Majewicz TL, et al. Correlation between immunohistochemistry and RICTOR fluorescence *in situ* hybridization amplification in small cell lung carcinoma. *Hum Pathol* (2019) 93:74–80. doi:10.1016/j.humpath.2019.08.018

47. Krencz I, Sebestyen A, Papay J, Jeney A, Hujber Z, Burger CD, et al. *In situ* analysis of mTORC1/2 and cellular metabolism-related proteins in human Lymphangioleiomyomatosis. *Hum Pathol* (2018) 79:199–207. doi:10.1016/j.humpath.2018.05.018

48. Petővári G, Dankó T, Tőkés AM, Vetlényi E, Krencz I, Raffay R, et al. *In situ* metabolic characterisation of breast cancer and its potential impact on therapy. *Cancers (Basel)* (2020) 12:2492. doi:10.3390/cancers12092492

49. Petővári G, Dankó T, Krencz I, Hujber Z, Rajnai H, Vetlényi E, et al. Inhibition of metabolic shift can decrease therapy resistance in human high-grade glioma cells. *Pathol Oncol Res* (2020) 26:23–33. doi:10.1007/s12253-019-00677-2

50. Felkai L, Krencz I, Kiss DJ, Nagy N, Petővári G, Dankó T, et al. Characterization of mTOR activity and metabolic profile in pediatric rhabdomyosarcoma. *Cancers (Basel)* (2020) 12:1947. doi:10.3390/cancers12071947

51. Krencz I, Vetlényi E, Dankó T, Petővári G, Moldvai D, Sztankovics D, et al. Metabolic adaptation as potential target in papillary renal cell carcinomas based on their *in situ* metabolic characteristics. *Int J Mol Sci* (2022) 23:10587. doi:10.3390/ijms231810587

52. Mohás A, Krencz I, Váradi Z, Arató G, Felkai L, Kiss DJ, et al. *In situ* analysis of mTORC1/C2 and metabolism-related proteins in pediatric osteosarcoma. *Pathol Oncol Res* (2022) 28:1610231. doi:10.3389/pore.2022.1610231

53. Hujber Z, Petővári G, Szoboszlai N, Dankó T, Nagy N, Kriston C, et al. Rapamycin (mTORC1 inhibitor) reduces the production of lactate and 2-hydroxyglutarate oncometabolites in IDH1 mutant fibrosarcoma cells. *J Exp Clin Cancer Res* (2017) 36:74. doi:10.1186/s13046-017-0544-y

54. Shaw RJ, Cantley LC. Ras, PI(3)K and mTOR signalling controls tumour cell growth. *Nature* (2006) 441:424–30. doi:10.1038/nature04869

55. Gkountakos A, Pilotto S, Mafficini A, Vicentini C, Simbolo M, Milella M, et al. Unmasking the impact of Rictor in cancer: novel insights of mTORC2 complex. *Carcinogenesis* (2018) 39:971–80. doi:10.1093/carcin/bgy086

56. Krencz I, Sebestyen A, Khoor A. mTOR in lung neoplasms. *Pathol Oncol Res* (2020) 26:35–48. doi:10.1007/s12253-020-00796-1

57. Jiang WJ, Feng RX, Liu JT, Fan LL, Wang H, Sun GP. RICTOR expression in esophageal squamous cell carcinoma and its clinical significance. *Med Oncol* (2017) 34:32. doi:10.1007/s12032-017-0894-5

58. Wazir U, Newbold RF, Jiang WG, Sharma AK, Mokbel K. Prognostic and therapeutic implications of mTORC1 and Rictor expression in human breast cancer. *Oncol Rep* (2013) 29:1969–74. doi:10.3892/or.2013.2346

59. Driscoll DR, Karim SA, Sano M, Gay DM, Jacob W, Yu J, et al. mTORC2 signaling drives the development and progression of pancreatic cancer. *Cancer Res* (2016) 76:6911–23. doi:10.1158/0008-5472.CAN-16-0810

60. Joechle K, Guenzle J, Hellerbrand C, Strnad P, Cramer T, Neumann UP, et al. Role of mammalian target of rapamycin complex 2 in primary and secondary liver cancer. *World J Gastrointest Oncol* (2021) 13:1632–47. doi:10.4251/wjgo.v13.i11.1632

61. Jebali A, Battistella M, Lebbé C, Dumaz N. RICTOR affects melanoma tumorigenesis and its resistance to targeted therapy. *Biomedicines* (2021) 9:1498. doi:10.3390/biomedicines9101498

62. Morrison Joly M, Hicks DJ, Jones B, Sanchez V, Estrada MV, Young C, et al. Rictor/mTORC2 drives progression and therapeutic resistance of HER2-amplified breast cancers. *Cancer Res* (2016) 76:4752–64. doi:10.1158/0008-5472.CAN-15-3393

63. Morrison Joly M, Williams MM, Hicks DJ, Jones B, Sanchez V, Young CD, et al. Two distinct mTORC2-dependent pathways converge on Rac1 to drive breast cancer metastasis. *Breast Cancer Res* (2017) 19:74. doi:10.1186/s13058-017-0868-8

64. Werfel TA, Wang S, Jackson MA, Kavanaugh TE, Joly MM, Lee LH, et al. Selective mTORC2 inhibitor therapeutically blocks breast cancer cell growth and survival. *Cancer Res* (2018) 78:1845–58. doi:10.1158/0008-5472.CAN-17-2388

65. Zhang F, Zhang X, Li M, Chen P, Zhang B, Guo H, et al. mTOR complex component Rictor interacts with PKCzeta and regulates cancer cell metastasis. *Cancer Res* (2010) 70:9360–70. doi:10.1158/0008-5472.CAN-10-0207

66. Liu Y, Lu Y, Li A, Celiku O, Han S, Qian M, et al. mTORC2/Rac1 pathway predisposes cancer aggressiveness in IDH1-mutated glioma. *Cancers (Basel)* (2020) 12:787. doi:10.3390/cancers12040787

67. Alvarenga AW, Machado LE, Rodrigues BR, Lupinacci FC, Sanemastu P, Matta E, et al. Evaluation of Akt and RICTOR expression levels in astrocytomas of all grades. *J Histochem Cytochem* (2017) 65:93–103. doi:10.1369/0022155416675850

68. Petővári G, Hujber Z, Krencz I, Dankó T, Nagy N, Tóth F, et al. Targeting cellular metabolism using rapamycin and/or doxycycline enhances anti-tumour effects in human glioma cells. *Cancer Cel Int* (2018) 18:211. doi:10.1186/s12935-018-0710-0

69. Akgül S, Li Y, Zheng S, Kool M, Treisman DM, Li C, et al. Opposing tumor-promoting and -suppressive functions of rictor/mTORC2 signaling in adult glioma and pediatric SHH medulloblastoma. *Cell Rep* (2018) 24:463–78. doi:10.1016/j.celrep.2018.06.050

70. Gulhati P, Bowen KA, Liu J, Stevens PD, Rychahou PG, Chen M, et al. mTORC1 and mTORC2 regulate EMT, motility, and metastasis of colorectal cancer via RhoA and Rac1 signaling pathways. *Cancer Res* (2011) 71:3246–56. doi:10.1158/0008-5472.CAN-10-4058

71. Wen FF, Li XY, Li YY, He S, Xu XY, Liu YH, et al. Expression of Raptor and Rictor and their relationships with angiogenesis in colorectal cancer. *Neoplasma* (2020) 67:501–8. doi:10.4149/neo_2020_190705N597

72. Wang L, Qi J, Yu J, Chen H, Zou Z, Lin X, et al. Overexpression of Rictor protein in colorectal cancer is correlated with tumor progression and prognosis. *Oncol Lett* (2017) 14:6198–202. doi:10.3892/ol.2017.6936

73. Bang H, Ahn S, Ji Kim E, Kim ST, Park HY, Lee J, et al. Correlation between RICTOR overexpression and amplification in advanced solid tumors. *Pathol Res Pract* (2020) 216:152734. doi:10.1016/j.prp.2019.152734

74. Kim ST, Kim SY, Klempner SJ, Yoon J, Kim N, Ahn S, et al. Rapamycin-insensitive companion of mTOR (RICTOR) amplification defines a subset of advanced gastric cancer and is sensitive to AZD2014-mediated mTORC1/2 inhibition. *Ann Oncol* (2017) 28:547–54. doi:10.1093/annonc/mdw669

75. Cao RZ, Min L, Liu S, Tian RY, Jiang HY, Liu J, et al. Rictor activates cav 1 through the Akt signaling pathway to inhibit the apoptosis of gastric cancer cells. *Front Oncol* (2021) 11:641453. doi:10.3389/fonc.2021.641453

76. Kaibori M, Shikata N, Sakaguchi T, Ishizaki M, Matsui K, Iida H, et al. Influence of rictor and raptor expression of mTOR signaling on long-term outcomes of patients with hepatocellular carcinoma. *Dig Dis Sci* (2015) 60:919–28. doi:10.1007/s10620-014-3417-7

77. Villanueva A, Chiang DY, Newell P, Peix J, Thung S, Alsinet C, et al. Pivotal role of mTOR signaling in hepatocellular carcinoma. *Gastroenterology* (2008) 135:1972–83. doi:10.1053/j.gastro.2008.08.008

78. Schmidt KM, Hellerbrand C, Ruemmele P, Michalski CW, Kong B, Kroemer A, et al. Inhibition of mTORC2 component RICTOR impairs tumor growth in pancreatic cancer models. *Oncotarget* (2017) 8:24491–505. doi:10.18632/oncotarget.15524

79. Wen SY, Li CH, Zhang YL, Bian YH, Ma L, Ge QL, et al. Rictor is an independent prognostic factor for endometrial carcinoma. *Int J Clin Exp Pathol* (2014) 7:2068–78.

80. Naruse T, Yanamoto S, Okuyama K, Yamashita K, Omori K, Nakao Y, et al. Therapeutic implication of mTORC2 in oral squamous cell carcinoma. *Oral Oncol* (2017) 65:23–32. doi:10.1016/j.oraloncology.2016.12.012

81. Ruicci KM, Plantinga P, Pinto N, Khan MI, Stecho W, Dhaliwal SS, et al. Disruption of the RICTOR/mTORC2 complex enhances the response of head and neck squamous cell carcinoma cells to PI3K inhibition. *Mol Oncol* (2019) 13:2160–77. doi:10.1002/1878-0261.12558

82. Kawasaki G, Naruse T, Furukawa K, Umeda M. mTORC1 and mTORC2 expression levels in oral squamous cell carcinoma: an immunohistochemical and clinicopathological study. *Anticancer Res* (2018) 38:1623–8. doi:10.21873/anticanres.12393

83. Kondo S, Hirakawa H, Ikegami T, Uehara T, Agena S, Uezato J, et al. Raptor and rictor expression in patients with human papillomavirus-related oropharyngeal squamous cell carcinoma. *BMC Cancer* (2021) 21:87. doi:10.1186/s12885-021-07794-9

84. Zhang X, Wang X, Xu T, Zhong S, Shen Z. Targeting of mTORC2 may have advantages over selective targeting of mTORC1 in the treatment of malignant pheochromocytoma. *Tumour Biol* (2015) 36:5273–81. doi:10.1007/s13277-015-3187-7

85. Schmidt KM, Dietrich P, Hackl C, Guenzle J, Bronsert P, Wagner C, et al. Inhibition of mTORC2/RICTOR impairs melanoma hepatic metastasis. *Neoplasia* (2018) 20:1198–208. doi:10.1016/j.neo.2018.10.001

86. Gibault L, Ferreira C, Pérot G, Audebourg A, Chibon F, Bonnin S, et al. From PTEN loss of expression to RICTOR role in smooth muscle differentiation: complex involvement of the mTOR pathway in leiomyosarcomas and pleomorphic sarcomas. *Mod Pathol* (2012) 25:197–211. doi:10.1038/modpathol.2011.163

87. Okada T, Lee AY, Qin LX, Agaram N, Mimae T, Shen Y, et al. Integrin-α10 dependency identifies RAC and RICTOR as therapeutic targets in high-grade myxofibrosarcoma. *Cancer Discov* (2016) 6:1148–65. doi:10.1158/2159-8290.CD-15-1481

88. Ross JS, Wang K, Elkadi OR, Tarasen A, Foulke L, Sheehan CE, et al. Next-generation sequencing reveals frequent consistent genomic alterations in small cell undifferentiated lung cancer. *J Clin Pathol* (2014) 67:772–6. doi:10.1136/jclinpath-2014-202447

89. Umemura S, Mimaki S, Makinoshima H, Tada S, Ishii G, Ohmatsu H, et al. Therapeutic priority of the PI3K/AKT/mTOR pathway in small cell lung cancers as revealed by a comprehensive genomic analysis. *J Thorac Oncol* (2014) 9:1324–31. doi:10.1097/JTO.0000000000000250

90. Sakre N, Wildey G, Behtaj M, Kresak A, Yang M, Fu P, et al. RICTOR amplification identifies a subgroup in small cell lung cancer and predicts response to drugs targeting mTOR. *Oncotarget* (2017) 8:5992–6002. doi:10.18632/oncotarget.13362

91. Zeng Z, Sarbassov dos D, Samudio IJ, Yee KW, Munsell MF, Ellen Jackson C, et al. Rapamycin derivatives reduce mTORC2 signaling and inhibit AKT activation in AML. *Blood* (2007) 109:3509–12. doi:10.1182/blood-2006-06-030833

92. Zhuang J, Hawkins SF, Glenn MA, Lin K, Johnson GG, Carter A, et al. Akt is activated in chronic lymphocytic leukemia cells and delivers a pro-survival signal: the therapeutic potential of Akt inhibition. *Haematologica* (2010) 95:110–8. doi:10.3324/haematol.2009.010272

93. Simioni C, Martelli AM, Zauli G, Melloni E, Neri LM. Targeting mTOR in acute lymphoblastic leukemia. *Cells* (2019) 8:190. doi:10.3390/cells8020190

94. Müller A, Zang C, Chumduri C, Dörken B, Daniel PT, Scholz CW. Concurrent inhibition of PI3K and mTORC1/mTORC2 overcomes resistance to rapamycin induced apoptosis by down-regulation of Mcl-1 in mantle cell lymphoma. *Int J Cancer* (2013) 133:1813–24. doi:10.1002/ijc.28206

95. Sahu D, Huan J, Wang H, Sahoo D, Casteel DE, Klemke RL, et al. Bladder cancer invasion is mediated by mammalian target of rapamycin complex 2-driven regulation of nitric oxide and invadopodia formation. *Am J Pathol* (2021) 191: 2203–18. doi:10.1016/j.ajpath.2021.08.002

96. Juengel E, Kim D, Makarević J, Reiter M, Tsaur I, Bartsch G, et al. Molecular analysis of sunitinib resistant renal cell carcinoma cells after sequential treatment with RAD001 (everolimus) or sorafenib. *J Cel Mol Med* (2015) 19:430–41. doi:10.1111/jcmm.12471

97. Sztankovics D, Krencz I, Moldvai D, Dankó T, Nagy Á, Nagy N, et al. Novel RICTOR amplification harbouring entities: FISH validation of RICTOR amplification in tumour tissue after next-generation sequencing. *Sci Rep* (2023) 13:19610. doi:10.1038/s41598-023-46927-x

98. Tian T, Li X, Zhang J. mTOR signaling in cancer and mTOR inhibitors in solid tumor targeting therapy. *Int J Mol Sci* (2019) 20:755. doi:10.3390/ijms20030755

99. Dobashi Y, Watanabe Y, Miwa C, Suzuki S, Koyama S. Mammalian target of rapamycin: a central node of complex signaling cascades. *Int J Clin Exp Pathol* (2011) 4:476–95.

100. Chen B, Tan Z, Gao J, Wu W, Liu L, Jin W, et al. Hyperphosphorylation of ribosomal protein S6 predicts unfavorable clinical survival in non-small cell lung cancer. *J Exp Clin Cancer Res* (2015) 34:126. doi:10.1186/s13046-015-0239-1

101. Ekman S, Wynes MW, Hirsch FR. The mTOR pathway in lung cancer and implications for therapy and biomarker analysis. *J Thorac Oncol* (2012) 7:947–53. doi:10.1097/JTO.0b013e31825581bd

102. Spoerke JM, O'Brien C, Huw L, Koeppen H, Fridlyand J, Brachmann RK, et al. Phosphoinositide 3-kinase (PI3K) pathway alterations are associated with histologic subtypes and are predictive of sensitivity to PI3K inhibitors in lung cancer preclinical models. *Clin Cancer Res* (2012) 18:6771–83. doi:10.1158/1078-0432.CCR-12-2347

103. Szalai F, Sztankovics D, Krencz I, Moldvai D, Pápay J, Sebestyén A, et al. Rictor—a mediator of progression and metastasis in lung cancer. *Cancers* (2024) 16: 543. doi:10.3390/cancers16030543

104. Conde E, Angulo B, Tang M, Morente M, Torres-Lanzas J, Lopez-Encuentra A, et al. Molecular context of the EGFR mutations: evidence for the activation of mTOR/S6K signaling. *Clin Cancer Res* (2006) 12:710–7. doi:10.1158/1078-0432.CCR-05-1362

105. Hendifar AE, Marchevsky AM, Tuli R. Neuroendocrine tumors of the lung: current challenges and advances in the diagnosis and management of well-differentiated disease. *J Thorac Oncol* (2017) 12:425–36. doi:10.1016/j.jtho.2016.11.2222

106. Krencz I, Sztankovics D, Danko T, Sebestyen A, Khoor A. Progression and metastasis of small cell lung carcinoma: the role of the PI3K/Akt/mTOR pathway and metabolic alterations. *Cancer Metastasis Rev* (2021) 40:1141–57. doi:10.1007/s10555-021-10012-4

107. Glasgow CG, Steagall WK, Taveira-Dasilva A, Pacheco-Rodriguez G, Cai X, El-Chemaly S, et al. Lymphangioleiomyomatosis (LAM): molecular insights lead to targeted therapies. *Respir Med* (2010) 104:S45–S58. doi:10.1016/j.rmed.2010.03.017

108. Henske EP, McCormack FX. Lymphangioleiomyomatosis - a wolf in sheep's clothing. *J Clin Invest* (2012) 122:3807–16. doi:10.1172/JCI58709

109. Adachi K, Miki Y, Saito R, Hata S, Yamauchi M, Mikami Y, et al. Intracrine steroid production and mammalian target of rapamycin pathways in pulmonary lymphangioleiomyomatosis. *Hum Pathol* (2015) 46:1685–93. doi:10.1016/j.humpath.2015.02.019

110. Hayashi T, Kumasaka T, Mitani K, Okada Y, Kondo T, Date H, et al. Bronchial involvement in advanced stage lymphangioleiomyomatosis: histopathologic and molecular analyses. *Hum Pathol* (2016) 50:34–42. doi:10.1016/j.humpath.2015.11.002

111. Sarbassov DD, Guertin DA, Ali SM, Sabatini DM. Phosphorylation and regulation of Akt/PKB by the rictor-mTOR complex. *Science* (2005) 307:1098–101. doi:10.1126/science.1106148

112. Janku F, Yap TA, Meric-Bernstam F. Targeting the PI3K pathway in cancer: are we making headway? *Nat Rev Clin Oncol* (2018) 15:273–91. doi:10.1038/nrclinonc.2018.28

113. Owonikoko TK, Khuri FR. Targeting the PI3K/AKT/mTOR pathway: biomarkers of success and tribulation. *Am Soc Clin Oncol Educ Book* (2013) 10: e395–401. doi:10.14694/EdBook_AM.2013.33.e395

114. Hobby G, Clark R, Woywodt A. A treasure from a barren island: the discovery of rapamycin. *Clin Kidney J* (2022) 15:1971–2. doi:10.1093/ckj/sfac116

115. Sehgal SN, Baker H, Vézina C. Rapamycin (AY-22,989), a new antifungal antibiotic. II. Fermentation, isolation and characterization. *J Antibiot* (1975) 28: 727–32. doi:10.7164/antibiotics.28.727

116. Mao B, Zhang Q, Ma L, Zhao DS, Zhao P, Yan P. Overview of research into mTOR inhibitors. *Molecules* (2022) 27:5295. doi:10.3390/molecules27165295

117. Guenzle J, Akasaka H, Joechle K, Reichardt W, Venkatasamy A, Hoeppner J, et al. Pharmacological inhibition of mTORC2 reduces migration and metastasis in melanoma. *Int J Mol Sci* (2020) 22:30. doi:10.3390/ijms22010030

118. Conciatori F, Ciuffreda L, Bazzichetto C, Falcone I, Pilotto S, Bria E, et al. mTOR cross-talk in cancer and potential for combination therapy. *Cancers (Basel)* (2018) 10:23. doi:10.3390/cancers10010023

119. Ali ES, Mitra K, Akter S, Ramproshad S, Mondal B, Khan IN, et al. Recent advances and limitations of mTOR inhibitors in the treatment of cancer. *Cancer Cel Int* (2022) 22:284. doi:10.1186/s12935-022-02706-8

120. Park S, Shim J, Mortimer PGS, Smith SA, Godin RE, Hollingsworth SJ, et al. Biomarker-driven phase 2 umbrella trial study for patients with recurrent small cell lung cancer failing platinum-based chemotherapy. *Cancer* (2020) 126:4002–12. doi:10.1002/cncr.33048

Pathology & Oncology Research | frontiers

TYPE Review
PUBLISHED 21 May 2024
DOI 10.3389/pore.2024.1611774

Check for updates

OPEN ACCESS

EDITED BY
Nora Bittner,
National Koranyi Institute of TB and Pulmonology, Hungary

*CORRESPONDENCE
Zsolt Pápai-Székely,
zsoltpapai@yahoo.com

RECEIVED 22 March 2024
ACCEPTED 24 April 2024
PUBLISHED 21 May 2024

CITATION
Pápai-Székely Z, Grmela G and Sárosi V (2024), Novel diagnostic processes and challenges in bronchoscopy. *Pathol. Oncol. Res.* 30:1611774. doi: 10.3389/pore.2024.1611774

COPYRIGHT
© 2024 Pápai-Székely, Grmela and Sárosi. This is an open-access article distributed under the terms of the Creative Commons Attribution License (CC BY). The use, distribution or reproduction in other forums is permitted, provided the original author(s) and the copyright owner(s) are credited and that the original publication in this journal is cited, in accordance with accepted academic practice. No use, distribution or reproduction is permitted which does not comply with these terms.

Novel diagnostic processes and challenges in bronchoscopy

Zsolt Pápai-Székely[1]*, Gábor Grmela[1] and Veronika Sárosi[2]

[1]Department of Pulmonology, Szent György University Teaching Hospital of Fejér County, Székesfehérvár, Hungary, [2]Department of Pulmonology, Pécs Medical School, Pécs, Hungary

Diagnostic bronchoscopy is a minimally invasive procedure that plays a crucial role in the diagnosis and management of various respiratory conditions. This paper explores the advancements in technology that have revolutionized the field and focuses on the new diagnostic procedures in bronchoscopy that have emerged in recent years. These innovative techniques have expanded the diagnostic capabilities of bronchoscopy, allowing for more accurate and comprehensive evaluation of respiratory conditions. This paper will also discuss the challenges in the diagnostic process with bronchoscope.

KEYWORDS

diagnostic bronchoscopy, respiratory medicine, endobronchial ultrasound, virtual bronchoscopy, autofluorescence bronchoscopy

Introduction

Diagnostic bronchoscopy is a minimally invasive procedure that allows for direct visualization and sampling of the airways, providing valuable diagnostic information in the evaluation of various respiratory conditions. Technological advancements have revolutionized the field of diagnostic bronchoscopy. Flexible bronchoscopes have replaced rigid instruments, enabling easier access to peripheral airways [1]. Endoscopic ultrasound techniques revolutionized the diagnostic work-up, due to their extreme importance we leave it to be discussed in a separate paper. Virtual bronchoscopy and navigation systems provide enhanced visualization and guidance during the procedure. Optical coherence tomography and confocal laser endomicroscopy offer real-time imaging of the airway mucosa, aiding in the detection of early neoplastic lesions. The field of diagnostic bronchoscopy continues to evolve, with ongoing research and development of advanced imaging techniques, biomarkers, and molecular testing. The integration of artificial intelligence in bronchoscopy holds promise for improving diagnostic accuracy and efficiency.

Autofluorescence bronchoscopy (AFB)

Autofluorescence bronchoscopy (AFB) is a technique that utilizes the natural fluorescence properties of bronchial tissue to detect early changes associated with pre-malignant and malignant lesions. It involves the use of a specialized bronchoscope equipped with a light source that emits specific wavelengths of light to excite the fluorophores in the tissue.

Indications and applications of AFB

AFB is primarily used for the detection and surveillance of pre-malignant and early-stage lung cancer. It can identify subtle changes in the bronchial mucosa that may not be visible under white light bronchoscopy. AFB is particularly useful in patients with a high risk of developing lung cancer, such as smokers or individuals with a history of occupational exposure to carcinogens [2].

In addition to lung cancer, AFB has shown promise in the evaluation of other respiratory conditions, such as bronchial dysplasia, chronic obstructive pulmonary disease (COPD), and interstitial lung diseases. It can aid in the early detection and characterization of these conditions, allowing for timely intervention and management.

Technique and procedure of AFB

AFB is performed using a specialized bronchoscope that emits blue or ultraviolet light to excite the fluorophores in the bronchial tissue. The emitted fluorescence is then visualized and interpreted by a bronchoscopist. Areas of abnormal fluorescence, such as loss of autofluorescence or increased fluorescence intensity, may indicate the presence of pre-malignant or malignant lesions.

The procedure is typically performed under conscious sedation or general anesthesia, depending on the patient's tolerance and the complexity of the case. AFB requires specialized training and expertise to accurately interpret the fluorescence patterns and differentiate between normal and abnormal findings.

Confocal laser endomicroscopy (CLE)

Confocal laser endomicroscopy (CLE) is a real-time imaging technique that allows for microscopic visualization of the bronchial mucosa during bronchoscopy. It involves the use of a miniaturized confocal microscope probe that can be inserted through the working channel of a standard bronchoscope [3].

Indications and applications of CLE

CLE is primarily used for the evaluation of bronchial mucosal abnormalities, such as pre-malignant lesions, inflammatory conditions, and infectious processes. It provides high-resolution images of the cellular and subcellular structures of the bronchial mucosa, allowing for detailed assessment and characterization of these abnormalities.

CLE has shown promise in the early detection and surveillance of lung cancer, as well as the evaluation of other respiratory conditions, such as asthma, COPD, and interstitial lung diseases. It can aid in the identification of specific cellular features, such as cellular atypia or inflammatory cell infiltrates, that may not be visible under white light bronchoscopy. It can be used as a guiding system to find optimal cryobiopsy location in interstitial lung diseases [4].

Technique and procedure of CLE

CLE is performed using a specialized bronchoscope equipped with a confocal microscope probe. The probe is inserted through the working channel of the bronchoscope and positioned adjacent to the target area of interest. Laser light is then emitted from the probe and focused on the bronchial mucosa, while the emitted fluorescent signals are captured and processed to generate real-time microscopic images.

The procedure is typically performed under conscious sedation or general anesthesia, depending on the patient's tolerance and the complexity of the case. CLE requires specialized training and expertise to accurately interpret the microscopic images and differentiate between normal and abnormal findings.

Optical coherence tomography (OCT)

Optical coherence tomography (OCT) is an imaging technique that utilizes light waves to generate cross-sectional images of the bronchial mucosa. It provides high-resolution images of the tissue architecture, allowing for the assessment of cellular and structural abnormalities.

Indications and applications of OCT

OCT is primarily used for the evaluation of bronchial mucosal abnormalities, such as pre-malignant lesions, inflammatory conditions, and airway remodeling. It can aid in the early detection and surveillance of lung cancer, as well as the evaluation of other respiratory conditions, such as asthma, COPD, and bronchiectasis.

OCT has also shown potential in guiding therapeutic interventions, such as laser ablation or photodynamic therapy, by providing real-time feedback on the depth and extent of tissue involvement. It can help optimize treatment planning and improve treatment outcomes.

Technique and procedure of OCT

OCT is performed using a specialized bronchoscope equipped with an OCT imaging probe. The probe is inserted

through the working channel of the bronchoscope and positioned adjacent to the target area of interest. Low-coherence light waves are emitted from the probe and directed onto the bronchial mucosa, while the reflected light is captured and processed to generate cross-sectional images.

The procedure is typically performed under conscious sedation or general anesthesia, depending on the patient's tolerance and the complexity of the case. OCT requires specialized training and expertise to accurately interpret the cross-sectional images and differentiate between normal and abnormal findings.

New diagnostic procedures in bronchoscopy, such as autofluorescence bronchoscopy (AFB), confocal laser endomicroscopy (CLE), and optical coherence tomography (OCT), have expanded the diagnostic capabilities of bronchoscopy by providing real-time imaging and characterization of bronchial mucosal abnormalities. These techniques offer the potential for early detection, precise characterization, and targeted management of respiratory conditions, including pre-malignant and malignant lesions. Understanding the indications, techniques, and limitations of these new diagnostic procedures is essential for healthcare professionals involved in bronchoscopy and respiratory care.

Ultrathin bronchoscopy: advancements in minimally invasive diagnostic techniques

Ultrathin bronchoscopy is a minimally invasive diagnostic technique that utilizes a thin and flexible bronchoscope to visualize and access the airways. This chapter explores the advancements in ultrathin bronchoscopy, its applications, benefits, and limitations in the field of respiratory medicine [5].

Ultrathin bronchoscopy: an overview

Ultrathin bronchoscopy involves the use of a bronchoscope with a small diameter, typically ranging from 2.2 to 3.0 mm. This slim and flexible design allows for easier navigation through the airways, including the peripheral regions. The bronchoscopist can visualize the airways and perform diagnostic procedures with minimal discomfort to the patient.

Applications of ultrathin bronchoscopy

Peripheral lung lesions

One of the primary applications of ultrathin bronchoscopy is the evaluation of peripheral lung lesions. These lesions are often challenging to access using traditional bronchoscopic techniques due to their location in the smaller airways. Ultrathin bronchoscopy provides improved maneuverability and visualization in these areas, allowing for targeted biopsies and sampling of peripheral lesions [6].

Airway assessment and management

Ultrathin bronchoscopy is also useful for assessing and managing various airway conditions. It can be used to evaluate airway stenosis, granulation tissue, and other abnormalities. Additionally, it allows for the placement of stents or other therapeutic interventions in the airways, providing relief for patients with obstructive airway diseases [7].

Pediatric bronchoscopy

Ultrathin bronchoscopy is particularly valuable in pediatric patients. The small diameter of the bronchoscope reduces discomfort and the risk of complications in children. It allows for thorough evaluation of the airways and facilitates diagnostic procedures, such as bronchoalveolar lavage and transbronchial lung biopsy, in pediatric populations.

Benefits of ultrathin bronchoscopy

Minimally invasive procedure

Ultrathin bronchoscopy offers a minimally invasive alternative to traditional bronchoscopy. The small diameter of the bronchoscope reduces patient discomfort and the risk of complications, such as bleeding or pneumothorax. It allows for outpatient procedures and faster recovery times.

Improved access to peripheral lesions

The slim and flexible design of the ultrathin bronchoscope enables better access to peripheral lung lesions. It can navigate through narrow and tortuous airways, reaching areas that may be challenging to visualize and sample with larger bronchoscopes. This improves the diagnostic yield and reduces the need for more invasive procedures, such as surgical lung biopsy.

Enhanced patient tolerance

Ultrathin bronchoscopy is better tolerated by patients, especially those with sensitive airways or respiratory conditions. The small diameter and flexibility of the bronchoscope cause less irritation and discomfort during the procedure, making it more suitable for patients with compromised lung function or heightened airway sensitivity.

Limitations and challenges of ultrathin bronchoscopy

Limited instrumentation and maneuverability

The small diameter of the ultrathin bronchoscope limits the availability of specialized instruments and accessories. This may

restrict certain diagnostic and therapeutic procedures that require large instruments or tools. Additionally, the flexibility of the bronchoscope may limit its maneuverability in some cases.

Reduced visualization and image quality

Ultrathin bronchoscopes may have limitations in image quality and visualization compared to large bronchoscopes. The small diameter can result in reduced light transmission and image resolution. However, advancements in technology have led to improvements in image quality, mitigating this limitation to some extent.

Learning curve and expertise

Ultrathin bronchoscopy requires specialized training and expertise. The bronchoscopist must develop skills in navigating through the smaller airways and performing procedures with the limited instrumentation available. Adequate training and experience are crucial to ensure safe and effective use of ultrathin bronchoscopy.

Future directions and conclusion

Ultrathin bronchoscopy has emerged as a valuable tool in the field of respiratory medicine, offering a minimally invasive approach to diagnose and manage various airway conditions. Ongoing advancements in technology and instrumentation are expected to further improve the capabilities and image quality of ultrathin bronchoscopes. With continued research and training, ultrathin bronchoscopy has the potential to become a standard diagnostic technique, providing safer and more comfortable procedures for patients while maintaining diagnostic accuracy.

Electromagnetic navigation bronchoscopy (ENB)

Electromagnetic navigation bronchoscopy (ENB) is a technique that allows for the navigation and sampling of peripheral lung lesions that are not easily accessible by conventional bronchoscopy. It utilizes electromagnetic technology to create a virtual 3D map of the patient's airways, guiding the bronchoscope to the target lesion [8].

Indications and applications of ENB

ENB is primarily used for the diagnosis and staging of peripheral lung lesions, particularly when other diagnostic modalities, such as CT-guided biopsy or surgical resection, are not feasible or desirable. It allows for the sampling of small or inaccessible lesions, providing valuable information for treatment planning and prognosis.

ENB can also be used for the placement of fiducial markers for radiation therapy, as well as the delivery of therapeutic agents, such as brachytherapy or photodynamic therapy, to peripheral lung lesions. It offers a less invasive alternative to surgical resection for selected patients with early-stage lung cancer.

Technique and procedure of ENB

ENB involves the use of a specialized bronchoscope equipped with electromagnetic sensors and a working channel for biopsy instruments. Prior to the procedure, a CT scan of the patient's chest is obtained, which is then used to create a virtual 3D map of the airways and target lesion.

During the procedure, the bronchoscope is navigated through the airways using real-time electromagnetic guidance. The virtual 3D map is overlaid onto the live bronchoscopic images, allowing the operator to accurately guide the bronchoscope to the target lesion. Biopsy instruments can then be advanced through the working channel to obtain tissue samples for diagnosis [9].

Virtual bronchoscopy: a non-invasive approach to airway visualization and assessment

Virtual bronchoscopy is a non-invasive imaging technique that utilizes computed tomography (CT) or magnetic resonance imaging (MRI) data to create a three-dimensional virtual representation of the airways. This chapter explores the advancements in virtual bronchoscopy, its applications, benefits, and limitations in the field of respiratory medicine [10].

Virtual bronchoscopy: an overview

Virtual bronchoscopy involves the use of advanced imaging software to generate a virtual model of the airways based on CT or MRI scans. The virtual model allows for a detailed visualization of the airway anatomy, providing valuable information for diagnostic and therapeutic purposes [11].

Applications of virtual bronchoscopy

Airway assessment and pathology detection

Virtual bronchoscopy is primarily used for the assessment of airway anatomy and the detection of various pathologies. It allows for a comprehensive evaluation of the airways, including the detection of tumors, stenosis, strictures, and other abnormalities. Virtual bronchoscopy can aid in the diagnosis and planning of treatment for conditions such as lung cancer, bronchiectasis, and tracheobronchomalacia.

Preoperative planning and simulation

Virtual bronchoscopy is valuable in preoperative planning for airway interventions. It enables the bronchoscopist to assess the feasibility and optimal approach for procedures such as bronchial stenting, laser therapy, or endobronchial valve placement. Virtual bronchoscopy can simulate the procedure, allowing for precise planning and reducing the risk of complications.

Patient education and communication

Virtual bronchoscopy provides a visual representation of the airways that can be easily understood by patients. It can be used as a tool for patient education, allowing them to visualize their airway condition and understand the proposed treatment plan. Virtual bronchoscopy enhances communication between the healthcare provider and the patient, leading to better patient engagement and informed decision-making.

Benefits of virtual bronchoscopy

Non-invasive and radiation-free

Virtual bronchoscopy is a non-invasive imaging technique that does not require the insertion of a bronchoscope into the airways. This eliminates the need for sedation or anesthesia and reduces the risk of complications associated with invasive procedures. Additionally, virtual bronchoscopy does not involve ionizing radiation, making it a safer alternative to traditional bronchoscopy or CT scans.

Comprehensive airway visualization

Virtual bronchoscopy provides a comprehensive visualization of the airways, allowing for a detailed assessment of the anatomy and pathology. The three-dimensional virtual model offers a panoramic view of the airways, enabling the bronchoscopist to explore different angles and perspectives. This enhances the diagnostic accuracy and aids in treatment planning.

Time and cost efficiency

Virtual bronchoscopy can be performed using existing CT or MRI scans, eliminating the need for additional imaging procedures. This saves time and reduces healthcare costs associated with multiple imaging studies. Virtual bronchoscopy also allows for efficient preoperative planning, optimizing the use of resources and minimizing procedural delays.

Limitations and challenges of virtual bronchoscopy

Limited functional information

Virtual bronchoscopy provides detailed anatomical information but lacks functional data. It cannot assess dynamic airway collapse, airflow obstruction, or mucosal abnormalities that may be observed during traditional bronchoscopy. Therefore, virtual bronchoscopy should be used in conjunction with other diagnostic modalities to obtain a comprehensive evaluation of the airways.

Dependence on high-quality imaging

The accuracy and reliability of virtual bronchoscopy depend on the quality of the CT or MRI scans used to generate the virtual model. Suboptimal image quality, artifacts, or motion artifacts can affect the accuracy of the virtual model and limit its diagnostic value. Therefore, it is essential to ensure high-quality imaging for optimal results.

Operator experience and interpretation

Virtual bronchoscopy requires expertise in image interpretation and manipulation. The bronchoscopist must be familiar with the software and techniques used to generate and navigate the virtual model. Adequate training and experience are necessary to accurately interpret the virtual bronchoscopy images and make informed clinical decisions.

Future directions and conclusion

Virtual bronchoscopy has emerged as a valuable non-invasive tool in the field of respiratory medicine, providing detailed visualization of the airways and aiding in diagnosis, treatment planning, and patient communication. Ongoing advancements in imaging technology and software algorithms are expected to further enhance the capabilities of virtual bronchoscopy. With continued research and development, virtual bronchoscopy has the potential to become an integral part of the diagnostic and therapeutic armamentarium, improving patient care and outcomes in respiratory medicine.

Cone beam CT in bronchoscopy: advancements in imaging and navigation

Cone Beam CT (CBCT) is a three-dimensional imaging technique that has revolutionized the field of bronchoscopy. This chapter explores the advancements in CBCT technology, its applications, benefits, and limitations in the context of bronchoscopy [12].

Cone beam CT: an overview

Cone Beam CT is a specialized imaging technique that utilizes a cone-shaped X-ray beam and a flat-panel detector to capture high-resolution, three-dimensional images of the airways. Unlike traditional CT scans, CBCT provides real-time imaging during

bronchoscopy procedures, allowing for improved navigation and accurate localization of lesions.

Applications of cone beam CT in bronchoscopy

Localization of peripheral lung lesions

One of the primary applications of CBCT in bronchoscopy is the localization of peripheral lung lesions. CBCT provides real-time imaging of the airways and allows the bronchoscopist to precisely locate and target lesions that may be difficult to visualize with traditional bronchoscopic techniques. This improves the accuracy of diagnostic procedures and reduces the need for additional invasive interventions.

Guidance for biopsy and sampling

CBCT can guide the bronchoscopist during biopsy and sampling procedures. The real-time imaging provided by CBCT helps in accurately positioning the bronchoscope and instruments, ensuring optimal sampling of the target lesion. This improves the diagnostic yield and reduces the risk of complications associated with blind biopsies.

Assessment of airway anatomy and pathology

CBCT allows for detailed assessment of airway anatomy and pathology. It provides high-resolution images that can reveal structural abnormalities, such as stenosis, strictures, or tumors, which may not be easily visible with traditional bronchoscopic techniques. This aids in pre-procedural planning and enhances the bronchoscopist's understanding of the patient's airway condition.

Benefits of cone beam CT in bronchoscopy

Real-time imaging and navigation

The real-time imaging capability of CBCT provides immediate feedback to the bronchoscopist during the procedure. This allows for precise navigation through the airways, reducing the risk of complications and improving the efficiency of the procedure. The bronchoscopist can visualize the position of the bronchoscope and instruments in relation to the target lesion, ensuring accurate sampling and minimizing damage to healthy tissue.

Improved lesion localization

CBCT enables accurate localization of peripheral lung lesions, even in challenging anatomical locations. The three-dimensional imaging provides a clear visualization of the lesion's position relative to the airway, facilitating targeted biopsies and reducing the need for additional procedures.

Reduced radiation exposure

Compared to traditional CT scans, CBCT in bronchoscopy typically involves lower radiation doses. The cone-shaped X-ray beam used in CBCT focuses on the area of interest, minimizing radiation exposure to surrounding tissues. This is particularly beneficial for patients who require multiple imaging procedures or have a higher risk of radiation-related complications.

Limitations and challenges of cone beam CT in bronchoscopy

Equipment and infrastructure requirements

CBCT requires specialized equipment and infrastructure, including a dedicated CBCT system and a flat-panel detector. These requirements may limit the availability of CBCT in certain healthcare settings, particularly smaller clinics or facilities with limited resources.

Learning curve and interpretation

The interpretation of CBCT images requires specialized training and expertise. Bronchoscopists need to develop skills in navigating and interpreting three-dimensional images to effectively utilize CBCT during procedures. Adequate training and experience are essential to ensure accurate interpretation and optimal utilization of CBCT in bronchoscopy.

Cost considerations

The cost of CBCT equipment and maintenance can be a limiting factor for widespread adoption. The initial investment and ongoing expenses associated with CBCT may pose challenges for healthcare institutions, particularly those with limited budgets.

Future directions and conclusion

Cone Beam CT has emerged as a valuable tool in bronchoscopy, providing real-time imaging and navigation capabilities. Ongoing advancements in CBCT technology, such as improved image quality and reduced radiation doses, are expected to further enhance its utility in the field. With continued research and development, CBCT has the potential to become a standard imaging modality in bronchoscopy, enabling more accurate diagnoses, targeted interventions, and improved patient outcomes.

Robotic bronchoscopy: advancements in diagnostic techniques

Robotic bronchoscopy is an emerging technology that combines the precision of robotics with the diagnostic capabilities of bronchoscopy. This chapter explores the

advancements in robotic bronchoscopy, its applications, benefits, and limitations in the field of respiratory medicine. Robotic bronchoscopy involves the use of a robotic system to navigate and manipulate a bronchoscope within the airways. The robotic system consists of a robotic arm, a control console, and specialized instruments. The bronchoscopist operates the system from the console, which provides a 3D visualization of the airways and precise control of the robotic arm [13].

Applications of robotic bronchoscopy

Peripheral lung lesions

One of the primary applications of robotic bronchoscopy is the diagnosis and management of peripheral lung lesions. These lesions are often challenging to access using traditional bronchoscopic techniques. Robotic bronchoscopy allows for improved navigation and maneuverability within the peripheral airways, enabling the bronchoscopist to reach and sample these lesions more effectively [14, 15].

Mediastinal lymph node sampling

Robotic bronchoscopy also offers advantages in mediastinal lymph node sampling. The robotic system provides enhanced visualization and precise control, allowing for accurate targeting and sampling of lymph nodes. This is particularly beneficial in cases where lymph nodes are in difficult-to-reach areas or when there is a need for precise sampling for staging of lung cancer.

Interventional procedures

In addition to diagnostic purposes, robotic bronchoscopy can be used for interventional procedures. The robotic system enables the bronchoscopist to perform procedures such as endobronchial biopsy, endobronchial ultrasound-guided transbronchial needle aspiration (EBUS-TBNA), and laser ablation with increased precision and control. This opens new possibilities for minimally invasive treatment options [16].

Benefits of robotic bronchoscopy

Improved access and navigation

Robotic bronchoscopy provides improved access to peripheral lung lesions and challenging anatomical locations. The robotic arm can navigate through narrow and tortuous airways with greater precision, reducing the risk of complications and improving the diagnostic yield.

Enhanced visualization

The 3D visualization provided by the robotic system enhances the bronchoscopist's ability to visualize the airways and target lesions. This improved visualization allows for more accurate targeting and sampling, leading to better diagnostic outcomes.

Increased precision and control

The robotic system offers increased precision and control during bronchoscopy procedures. The robotic arm can perform precise movements and manipulations, reducing the risk of tissue damage and improving the safety of the procedure.

Limitations and challenges of robotic bronchoscopy

Cost and availability

One of the main limitations of robotic bronchoscopy is its cost and availability. The robotic systems and associated instruments are expensive, making them less accessible in certain healthcare settings. Additionally, the expertise required to operate the robotic system may be limited to specialized centers with trained personnel.

Learning curve

Robotic bronchoscopy requires specialized training and expertise. The learning curve for mastering the robotic system and its associated techniques can be steep. Adequate training and proctoring are essential to ensure safe and effective use of the technology.

Technical limitations

While robotic bronchoscopy offers many advantages, it also has some technical limitations. The size of the robotic arm and instruments may limit access to certain areas of the airways. Additionally, the robotic system may not be suitable for all patients, such as those with severe airway abnormalities or significant comorbidities.

Future directions and conclusion

Robotic bronchoscopy is a promising advancement in the field of respiratory medicine. As technology continues to evolve, we can expect further improvements in robotic systems, including miniaturization of instruments and enhanced capabilities. With ongoing research and development, robotic bronchoscopy has the potential to revolutionize the diagnostic and interventional management of respiratory conditions, providing safer and more precise procedures for patients.

Challenges in the diagnostic process of bronchoscopy

Bronchoscopy is a valuable diagnostic tool for evaluating respiratory conditions. However, the diagnostic process of bronchoscopy is not without challenges. We will discuss some of the common challenges encountered during bronchoscopy and strategies to overcome them, ensuring a successful diagnostic outcome.

Technical challenges

Limited access to peripheral lesions

One of the major challenges in bronchoscopy is accessing peripheral lung lesions. These lesions are located deep within the lung tissue and may be difficult to reach using a standard bronchoscope. Traditional bronchoscopic techniques, such as transbronchial biopsy, may have limited success in obtaining adequate tissue samples from these lesions.

To overcome this challenge, various advanced techniques have been developed, including electromagnetic navigation bronchoscopy (ENB) and radial endobronchial ultrasound (EBUS). These techniques provide real-time imaging guidance, allowing for accurate navigation to peripheral lesions and increasing the diagnostic yield.

Inadequate visualization

Another challenge in bronchoscopy is inadequate visualization of the airway and target lesions. Factors such as excessive secretions, blood, or poor lighting can hinder the bronchoscopist's ability to clearly visualize the airway and obtain accurate diagnostic information.

To address this challenge, proper airway preparation is essential. Pre-bronchoscopy measures, such as bronchial hygiene techniques and administration of mucolytic agents, can help reduce secretions and improve visualization. Adequate suctioning and irrigation during the procedure can also help clear the airway and improve visualization.

Diagnostic challenges

Sampling error

Sampling error is a common challenge in bronchoscopy, particularly when obtaining tissue samples for histopathological examination. The bronchoscopist must ensure that the biopsy samples are representative of the target lesion to obtain an accurate diagnosis.

To minimize sampling error, it is important to carefully select the biopsy site based on radiological findings and bronchoscopic assessment. Techniques such as transbronchial needle aspiration (TBNA) and endobronchial ultrasound-guided transbronchial needle aspiration (EBUS-TBNA) can provide more targeted sampling of mediastinal lymph nodes and peripheral lesions, improving the diagnostic yield.

False-negative results

Obtaining false-negative results is another challenge in bronchoscopy. In some cases, the bronchoscopist may not be able to visualize or sample the lesion adequately, leading to a negative diagnostic outcome despite the presence of pathology.

To address this challenge, a multidisciplinary approach is crucial. Collaboration with radiologists, pathologists, and other specialists can help correlate clinical, radiological, and pathological findings to ensure a comprehensive diagnostic evaluation. Repeat bronchoscopy or alternative diagnostic procedures may be considered if there is a high suspicion of pathology despite initial negative results.

Safety challenges

Complications and adverse events

Bronchoscopy, like any invasive procedure, carries the risk of complications and adverse events. These can range from minor complications such as bleeding or pneumothorax to more serious events such as respiratory distress or cardiac arrhythmias.

To mitigate these risks, it is important to adhere to strict safety protocols and guidelines. Proper patient selection, thorough pre-procedure assessment, and appropriate monitoring during and after the procedure are essential. Adequate training and expertise in bronchoscopy, as well as prompt recognition and management of complications, are crucial for ensuring patient safety.

Infection control

Infection control is a significant challenge in bronchoscopy due to the potential for cross-contamination and transmission of infectious agents. The bronchoscope and associated accessories can harbor bacteria or other pathogens, posing a risk of infection to both patients and healthcare providers.

To address this challenge, strict adherence to infection control practices is essential. This includes proper cleaning and disinfection or sterilization of bronchoscopes and accessories, adherence to hand hygiene protocols, and use of personal protective equipment. Regular monitoring and auditing of infection control practices can help identify and address any gaps or deficiencies.

Conclusion

The diagnostic process of bronchoscopy is not without challenges. Technical challenges, such as limited access to peripheral lesions and inadequate visualization, can impact the diagnostic yield. Diagnostic challenges, including sampling error and false-negative results, require a multidisciplinary approach and careful consideration of alternative diagnostic procedures. Safety challenges, such as complications and infection control, necessitate adherence to

strict protocols and guidelines. By recognizing and addressing these challenges, healthcare professionals can optimize the diagnostic process of bronchoscopy and improve patient outcomes.

Author contributions

All authors listed have made a substantial, direct, and intellectual contribution to the work and approved it for publication.

Funding

The author(s) declare that no financial support was received for the research, authorship, and/or publication of this article.

Conflict of interest

The authors declare that the research was conducted in the absence of any commercial or financial relationships that could be construed as a potential conflict of interest.

References

1. Silvestri GA, Gonzalez AV, Jantz MA, Margolis ML, Gould MK, Tanoue LT, et al. Methods for staging non-small cell lung cancer: diagnosis and management of lung cancer, 3rd ed: American College of Chest Physicians evidence-based clinical practice guidelines. *Chest* (2013) 143(Suppl. 5):e211S–e250S. doi:10.1378/chest.12-2355

2. Lam B, Wong MP, Fung SL, Lam DC, Wong PC, Mok TY, et al. The clinical value of autofluorescence bronchoscopy for the diagnosis of lung cancer. *Eur Respir J* (2006) 28(5):915–9. doi:10.1183/09031936.06.00131405

3. Goorsenberg A, Kalverda KA, Annema J, Bonta P. Advances in optical coherence tomography and confocal laser endomicroscopy in pulmonary diseases. *Respiration* (2020) 99(3):190–205. doi:10.1159/000503261

4. Zheng Y, Zhang L, Lou Y, Fan B, Cui Y, Wu X, et al. The cryobiopsy in interstitial lung diseases guided by probe-based confocal laser endomicroscopy is feasible. *Clin Respir J* (2023) 17(10):998–1005. doi:10.1111/crj.13669

5. Burks AC, Akulian J. Bronchoscopic diagnostic procedures available to the pulmonologist. *Clin Chest Med* (2020) 41:129–44. doi:10.1016/j.ccm.2019.11.002

6. Kalanjeri S, Holladay RC, Gildea TR. State-of-the-Art modalities for peripheral lung nodule biopsy. *Clin Chest Med* (2018) 39:125–38. doi:10.1016/j.ccm.2017.11.007

7. Oki M, Saka H, Ando M, Asano F, Kurimoto N, Morita K, et al. Ultrathin bronchoscopy with multimodal devices for peripheral pulmonary lesions. A randomized trial. *Am J Respir Crit Care Med* (2015) 192:468–76. doi:10.1164/rccm.201502-0205OC

8. Jiang S, Xie F, Mao X, Ma H, Sun J. The value of navigation bronchoscopy in the diagnosis of peripheral pulmonary lesions: a meta-analysis. *Thorac Cancer* (2020) 11:1191–201. doi:10.1111/1759-7714.13373

9. Cherian SV, Kaur S, Karanth S, Xian JZ, Estrada-Y-Martin RM. Diagnostic yield of electromagnetic navigational bronchoscopy: a safety net community-based hospital experience in the United States. *Ann Thorac Med* (2021) 16:102–9. doi:10.4103/atm.ATM_388_20

10. Kato A, Yasuo M, Tokoro Y, Kobayashi T, Ichiyama T, Tateishi K, et al. Virtual bronchoscopic navigation as an aid to CT-guided transbronchial biopsy improves the diagnostic yield for small peripheral pulmonary lesions. *Respirology* (2018) 23:1049–54. doi:10.1111/resp.13377

11. Giri M, Puri A, Wang T, Huang G, Guo S. Virtual bronchoscopic navigation versus non-virtual bronchoscopic navigation assisted bronchoscopy for the diagnosis of peripheral pulmonary lesions: a systematic review and meta-analysis. *Ther Adv Respir Dis* (2021) 15:17534666211017048. doi:10.1177/17534666211017048

12. Casal RF. Cone beam CT-guided bronchoscopy: here to stay? *J Bronchol Interv Pulmonol* (2018) 25:255–6. doi:10.1097/LBR.0000000000000546

13. Murgu SD. Robotic assisted-bronchoscopy: technical tips and lessons learned from the initial experience with sampling peripheral lung lesions. *BMC Pulm Med* (2019) 19:89–8. doi:10.1186/s12890-019-0857-z

14. Fielding DI, Bashirzadeh F, Son JH, Todman M, Chin A, Tan L, et al. First human use of a new robotic-assisted fiber optic sensing navigation system for small peripheral pulmonary nodules. *Respiration* (2019) 98:142–50. doi:10.1159/000498951

15. Rojas-Solano JR, Ugalde-Gamboa L, Machuzak M. Robotic bronchoscopy for diagnosis of suspected lung cancer: a feasibility study. *J Bronchol Interv Pulmonol* (2018) 25:168–75. doi:10.1097/LBR.0000000000000499

16. Chaddha U, Hogarth DK, Murgu S Bronchoscopic ablative therapies for malignant central airway obstruction and peripheral lung tumors. *Ann Am Thorac Soc* (2019) 16:1220–9. doi:10.1513/AnnalsATS.201812-892CME

Pathology & Oncology Research | frontiers

TYPE Original Research
PUBLISHED 05 March 2024
DOI 10.3389/pore.2024.1611454

Check for updates

OPEN ACCESS

EDITED BY
József Tímár,
Semmelweis University, Hungary

*CORRESPONDENCE
Miklós Bély,
dr.bely.miklos@gmail.com

RECEIVED 17 August 2023
ACCEPTED 16 February 2024
PUBLISHED 05 March 2024

CITATION
Bély M and Apáthy Á (2024), Crystal induced arthropathies—a comparative study of 40 patients with apatite rheumatism, chondrocalcinosis and primary synovial chondromatosis. *Pathol. Oncol. Res.* 30:1611454. doi: 10.3389/pore.2024.1611454

COPYRIGHT
© 2024 Bély and Apáthy. This is an open-access article distributed under the terms of the Creative Commons Attribution License (CC BY). The use, distribution or reproduction in other forums is permitted, provided the original author(s) and the copyright owner(s) are credited and that the original publication in this journal is cited, in accordance with accepted academic practice. No use, distribution or reproduction is permitted which does not comply with these terms.

Crystal induced arthropathies—a comparative study of 40 patients with apatite rheumatism, chondrocalcinosis and primary synovial chondromatosis

Miklós Bély [1]* and Ágnes Apáthy[2]

[1]Department of Pathology, Hospital of the Order of the Brothers of Saint John of God in Budapest, Budapest, Hungary, [2]Department of Rheumatology, St. Margaret Clinic, Budapest, Hungary

Introduction: Apatite rheumatism (AR), chondrocalcinosis (Ch-C), and primary synovial chondromatosis (prSynCh) are regarded as distinct clinical entities. The introduction of the non-staining technique by Bély and Apáthy (2013) opened a new era in the microscopic diagnosis of crystal induced diseases, allowing the analysis of MSU (monosodium urate monohydrate) HA (calcium hydroxyapatite), CPPD (calcium pyrophosphate dihydrate) crystals, cholesterol, crystalline liquid lipid droplets, and other crystals in unstained sections of conventionally proceeded (aqueous formaldehyde fixed, paraffin-embedded) tissue samples. The aim of this study was to describe the characteristic histology of crystal deposits in AR, Ch-C, and prSynCh with traditional stains and histochemical reactions comparing with unstained tissue sections according to Bély and Apáthy (2013).

Patients and methods: Tissue samples of 4 with apatite rheumatism (Milwaukee syndrome), 16 with chondrocalcinosis, and 20 with clinically diagnosed primary synovial chondromatosis were analyzed.

Results and conclusion: Apatite rheumatism, chondrocalcinosis, and primary synovial chondromatosis are related metabolic disorders with HA and CPPD depositions. The authors assume that AR and Ch-C are different stages of the same metabolic disorder, which differ from prSynCh in amorphous mineral production, furthermore in the production of chondroid, osteoid and/or bone. prSynCh is a defective variant of HA and CPPD induced metabolic disorders with reduced mineralization capabilities, where the deficient mineralization is replaced by chondroid and/or bone formation. The non-staining technique

Abbreviations: AR, Apatite rheumatism; Ch-C, Chondrocalcinosis; prSynCh, primary synovial chondromatosis; HA, Calcium hydroxyapatite—[$Ca_5(PO_4)_3(OH)$]; CPPD, Calcium pyrophosphate dihydrate—[$Ca_2P_2O_7.2H_2O$]; CC, Cholesterol crystals—[$C_{27}H_{46}O$]; CL, Crystalline liquid lipid spherules; HE, Hematoxylin Eosin; Ts, Tissue samples; Pr. n^0/y, Protocol number/year.

of Bély and Apáthy proved to be a much more effective method for the demonstration of crystals in metabolic diseases than conventional stains and histochemical reactions.

KEYWORDS

apatite rheumatism, chondrocalcinosis, primary synovial chondromatosis, conventional stains, non-staining technique

Introduction

Serendipity—the unexpected and incidental discovery

Legs amputated because of Mönckeberg's sclerosis and/or atherosclerosis were studied by the authors [1, 2]. They observed unstained tissue sections of the conventionally processed surgical specimens viewed with polarized light; variable amounts of cholesterol (CC—[$C_{27}H_{46}O$]), crystalline liquid lipid droplets (CL), calcium hydroxyapatite (HA—[$Ca_5(PO_4)_3(OH)$]) and calcium pyrophosphate dihydrate (CPPD—[$Ca_2P_2O_7.2H_2O$]) crystals were detectable.

It is generally accepted that CC and CL cannot be detect in conventionally processed tissue samples stained with HE or other aqueous dyes; only empty spaces indicate the previous presence of cholesterol and crystalline lipids [3].

Lipid complexes can exceptionally remain in traditionally processed HE-stained sections, if these complexes did not dissolve in conventional fat solvents (ethyl alcohol, acetone, xylene, chloroform, methanol) or in aqueous dye solutions.

In HE stained sections of traditionally processed surgical specimens the small and soluble, weakly birefringent HA crystals are not visible with a conventional light microscope [4] or under polarized light [5, 6]. Some authors believe that HA crystals are identical with the amorphous mineral deposits stained with Alizarin red S [6–10], although Alizarin red S staining is not specific for HA crystals [11]. Moreover, calcium and phosphorus in crystalline structure do not stain with Alizarin red S or with the von Kossa reaction [12–16].

Using a professional polarizing microscope with high brightness (at least 100-Watt illumination) the weak birefringent HA crystals can be detected exceptionally in HE stained sections viewed under polarized light [15, 16], while the large and less soluble CPPD crystals with a relatively strong birefringence are more often demonstrated, and are usually well identifiable [15–17].

In contrast to the classical staining methods the unstained technique is much more effective in the detection of crystals and crystalline structures of various metabolic disorders [1, 12–16].

Objective

The authors wished to ascertain with their sensitive non-staining technique the presence of various crystals in conventionally processed tissue samples of patients with the clinical diagnosis of apatite rheumatism (AR), chondrocalcinosis (Ch-C), and primary synovial chondromatosis (prSynCh).

Patients and methods

Between 1985 and 2010 surgical specimens of 101,855 patients were processed in the Department of Pathology of the National Institute of Rheumatology (ORFI) and of the Hospital of the Order of Brothers of Saint John of God (BIK).

Among these, apatite rheumatism (Milwaukee syndrome) was diagnosed clinically in 4 (0.0039%), chondrocalcinosis in 16 (0.016%), and primary synovial chondromatosis in 20 (0.020%) patients.

Sixteen (16) paraffin embedded tissue blocks of the 4 patients with apatite rheumatism, 40 of the 16 patients with chondrocalcinosis, and 37 blocks of the 20 patients with prSynCh were available.

The tissue samples were fixed in an 8% aqueous solution of formaldehyde at pH 7.6 for at least 24 h at room temperature (20°C) and embedded in paraffin.

Serial sections were examined without staining [1, 12–16], with HE staining [18], as well as with special stains recommended in the literature, and were examined with the light microscope and under polarized light, respectively.

Amorphous calcium phosphate [$Ca_3(PO_4)_2$] and/or calcium carbonate [CaCO3] deposits—characteristically accompanying HA and CPPD crystal deposits—were identified with Alizarin red S staining (specific for calcium) [19, 20] and the von Kossa reaction (specific for phosphate and/or carbonate) [19, 21].

Conventionally stained tissue sections were compared with unstained sections according to Bély and Apáthy (2013) (description of non-staining method see as Appendix at the end of the manuscript).

The amount of amorphous mineral deposits, chondroid, osteoid and/or bone formations were assessed by conventional stains and reactions using a semiquantitative score system: "0"—no mineral deposits, chondroid and/or bone formation, "1"—minimal mineral deposits, chondroid and/or bone formation, "2"—moderate mineral deposits, chondroid and/or bone formation, "3"—abundant (massive) mineral deposits, chondroid and/or bone formation [15, 16]. The differences

TABLE 1 Sex, mean age with SD and range (in years) of 40 patients with clinically diagnosed G, AR, Ch-C or prSynCh.

Clinical diagnosis	Number of patients (tissue samples)	Mean age in years at surgery ± SD	Range (In years)
Apatite rheumatism (HA)	4 (16)	74.00 ± 7.70	66–82
Female	3 (12)	76.67 ± 6.81	69–82
Male	1 (4)	66.0	66.0
Chondrocalcinosis (CPPD)	16 (40)	63.67 ± 21.17	39–81
Female	14 (34)	62.08 ± 14.02	39–81
Male	2 (6)	74.00 ± 1.41	73–75
Primary synovial chondromatosis	20 (37)	50.20 ± 12.51	30–76
Female	13 (22)	53.15 ± 10.49	40–74
Male	7 (15)	44.71 ± 14.90	30–76

Combined (co-existent) diseases did not occur in our patient cohorts with gout, apatite rheumatism, chondrocalcinosis, and primary synovial chondromatosis.

TABLE 2 Level of significance ("p" value < 0.05) comparing the mean age of 40 patients with clinically diagnosed AR, Ch-C or prSynCh.

Clinical diagnosis number of patients	Mean age of patients	$p < 0.05$	Mean age of females	$p < 0.05$	Mean age of males	$p < 0.05$
AR $n = 4$ vs. Ch-C $n = 16$	74.00 vs. 63.67	0.8440	76.67 vs. 62.08	0.0361	66.00 vs. 74.00	—
AR $n = 4$ vs. prSynCh $n = 20$	74.00 vs. 50.20	0.0018	76.67 vs. 53.15	0.0061	66.00 vs. 44.71	—
Ch-C $n = 16$ vs. prSynCh $n = 20$	63.67 vs. 50.20	0.0074	62.08 vs. 53.15	0.0920	74.00 vs. 44.71	0.0018

Differences were not calculated between male patients with the clinical diagnosis of AR and Ch-C, because of a zero divisor.

were calculated and compared with the student (Welch) T-probe [22].

Demographics of the patients with the clinical diagnosis of AR, Ch-C and prSynCh were compared with the Student (Welch) T-probe [22].

The effectivity of non-staining technique was characterized with Pearson's chi-squared (χ^2) test comparing the prevalence of deposited crystals in unstained tissue sections with HE [22]. The difference between two cohorts of samples was regarded "significant" at an alpha level of 0.05.

Standard and unstained sections were examined with a professional high-brightness (100-Watt) microscope (Olympus BX51); in selected cases, electron microscopy and electron diffraction were also performed (JEM 100CX).

Results

Demographics of patients with clinically diagnosed apatite rheumatism, chondrocalcinosis and primary synovial chondromatosis

The mean age of patients with the clinical diagnosis of prSynCh (50.20 years) was low at the time of surgery.

The mean age of patients with AR was high at the time of surgery compared to the patients with the clinical diagnosis of prSynCh (74.0 years versus 50.20 years; $p < 0.0001$) (Tables 1, 2).

There was no significant difference between patient cohorts with AR and Ch-C (74.0 years versus 63.67 years; $p < 0.0840$), except the women (76.67 years versus 62.028 years; $p < 0.0361$).

Table 1 summarizes the demographics of patient cohorts with the clinical diagnosis of AR ($n = 4$), Ch-C ($n = 16$) or prSynCh ($n = 20$).

Table 2 summarizes the "p" values of significance (at an alpha level of 0.05) comparing the mean age of patient cohorts with the clinical diagnosis of AR ($n = 4$), Ch-C ($n = 16$) or prSynCh ($n = 20$).

Microscopic characteristics of apatite rheumatism, chondrocalcinosis and primary synovial chondromatosis

Microscopic characteristics of HA (hydroxyapatite [$Ca_5(PO_4)_3(OH)$]) crystal deposits in patients with clinically diagnosed apatite rheumatism

Apatite rheumatism was characterized histologically by intra- or periarticular accumulation of HA [$Ca_5(PO_4)_3(OH)$] crystals (with or without CPPD), typically in association with amorphous calcium phosphate

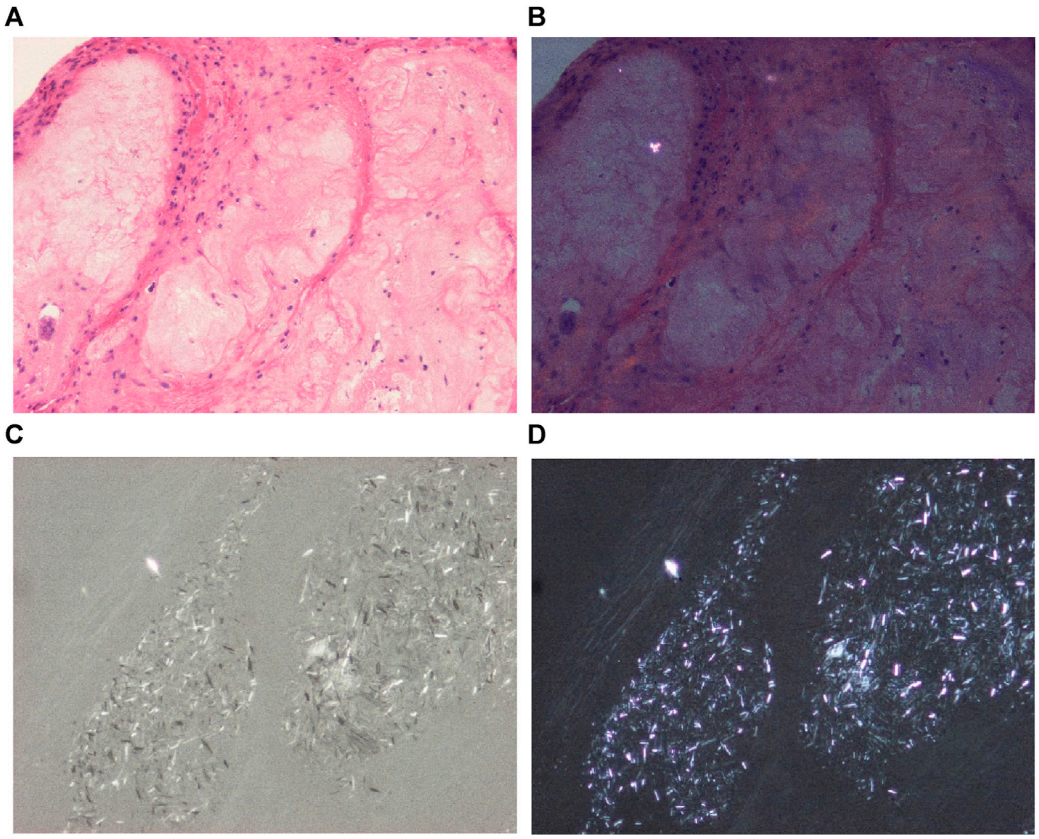

FIGURE 1
Hydroxyapatite arthropathy (Milwaukee syndrome, apatite rheumatism) induced by hydroxyapatite (HA) crystals, viewed with the light microscope and under polarized light, respectively. The weakly birefringent small HA crystals are readily soluble and are not detected in conventionally fixed tissue specimens stained with HE. **(A)** HE, viewed with the light microscope, ×100, **(B)** HE, viewed under polarized light (birefringent particle is a remnant of paraffin), same as **(A)** ×100. Mixed HA, CPPD, and unidentified needle-shaped crystals at high brightness illumination (100-Watt); less illumination (60-Watt) deceptively highlights the dominant (more birefringent) crystals. **(C)** Unstained section, viewed under polarized light with high brightness illumination (100-Watt), same microscopic field as **(A)** ×100, **(D)** same as **(C)** with 60-Watt illumination.

$[Ca_3(PO_4)_2]$, and/or calcium carbonate $[CaCO_3]$ deposits of irregular shape (Figures 2A–D).

According to our semi-objective score system, in AR the mineral deposition was 1.063 per tissue sections, accompanied with minimal chondroid formation (0.063 per tissue sections); osteoid or newly formed bone tissue was not detected [23].

The nearly complete absence of inflammation (with or without adjacent fibrosis) was characteristic for amorphous mineral deposits associated with HA [11, 14, 15, 24, 25].

The individual HA crystals in the synovial membrane caused acute inflammation, and provoked phagocytosis of neutrophilic leukocytes in all cases [24, 25].

Acute inflammation of joints was accompanied with severe clinical symptoms: sudden onset of severe pain, synovial fluid effusion, swelling, tenderness, restricted motion, joint destruction of rapid progression, deformity and instability of joints [23–25].

In unstained sections, using a professional polarizing microscope with high, at least 100-Watt brightness, the clusters (1–5 μm) of HA crystals were visible, and were birefringent under polarized light (×100) [13, 14]. The clusters formed aggregates of 100 μm or larger, which were visible with an objective of ×40 with non-staining techniques [13, 14].

The birefringence of HA prisms was weakly positive (δ = 0.007) compared to the stronger positive birefringence of CPPD crystals (δ = 0.017); the large and strongly birefringent CPPD crystals dominated deceptively the microscopic fields, in cases of coexisting HA and CPPD crystals at 60-Watt illumination, or using a Red I compensator (the Red I compensator notably reduces the intensity of illumination) [13, 14].

In our previous study we examined 16 tissue samples of 4 patients with clinically diagnosed apatite rheumatism; 9 joints were operated: 5 knees, 3 shoulders and 1 hip.

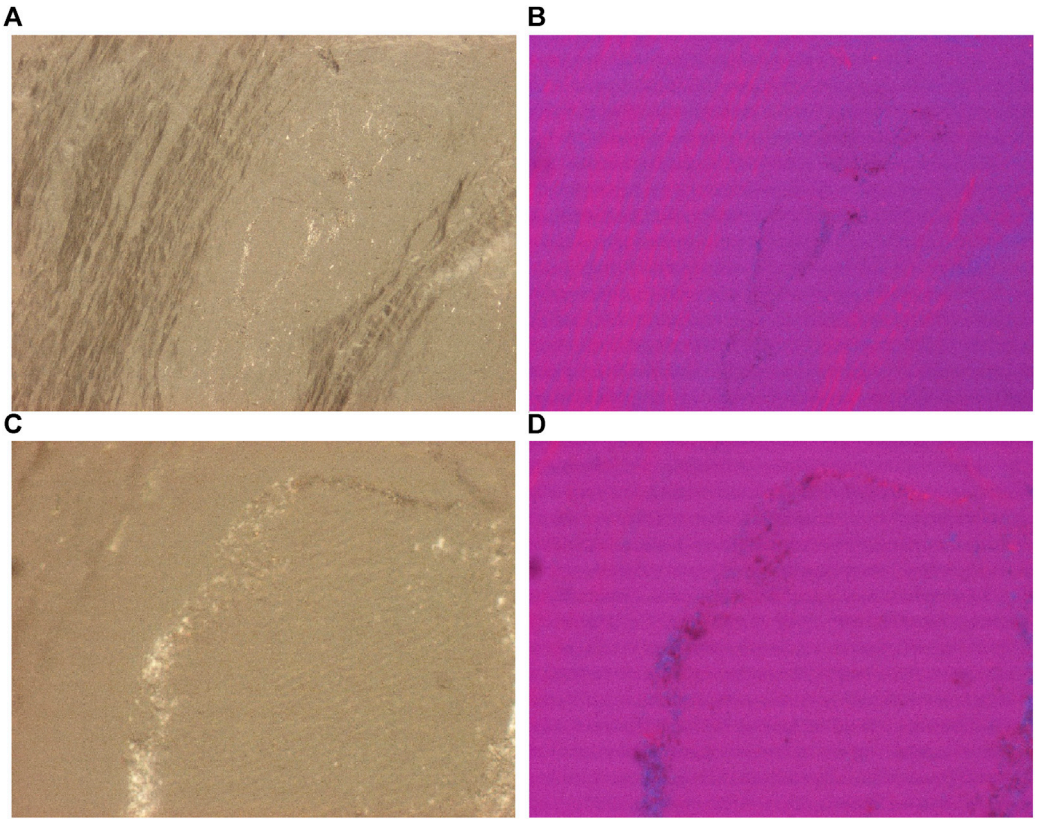

FIGURE 2
Prepatellar bursa, hydroxyapatite arthropathy, HA crystal prisms, unstained section, viewed under polarized light. HA crystals are colorless, translucent fragments or small (50–500 nm) rod-shaped prisms. Under polarized light with Red I. compensator the birefringence of **HA** crystals is weak and positive. **(A)** HA crystals, unstained sections, viewed under polarized light, ×100, **(C)** same as **(A)** ×600. **(B)** HA crystals, unstained sections, viewed under polarized light, using Red I compensator, ×100, **(D)** same as **(B)** ×600.

In traditionally fixed and processed tissue sections stained with HE, Alizarin red S or with the von Kossa reaction, HA crystals were not found.

With non-staining techniques HA crystals were present in all 4 patients, and were detected in 10 (62.5%) of the 16 unstained sections (with or without CPPD crystals) [16].

In HE stained tissue section cholesterol crystals (CC—$[C_{27}H_{46}O]$) were not found, but in unstained sections CC crystals were detected in 3 of 4 patients [23].

The characteristics of HA crystal deposits are demonstrated in Figures 1, 2.

Microscopic characteristics of CPPD (calcium pyrophosphate dihydrate $[Ca_2P_2O_7.2H_2O]$) crystal deposits in patients with clinically diagnosed chondrocalcinosis

CPPD crystal deposition was accompanied with more or less amorphous calcium phosphate $[Ca_3(PO_4)_2]$ and/or calcium carbonate $[CaCO_3]$ deposits of irregular shape [16, 24, 25].

Based on our semi-objective score system in Ch-C the mineral deposition was 1.054 per tissue sections, accompanied by minimal chondroid formation (0.054 per tissue sections); osteoid or newly formed bone tissue was not detected [23].

In synovium, menisci or hyaline cartilage, etc. the CPPD crystals were often asymptomatic, the inflammatory reaction around mineral deposits were usually moderate or absent.

Occasionally CPPD crystals provoked a cellular reaction (with or without macrophages) and also caused joint damage; the affected joints were usually swollen, warm, and severely painful [24].

CPPD crystals were less soluble in an 8% aqueous formaldehyde solution or water containing dyes than HA crystals; in tissue sections stained with HE, Alizarin red S or with the von Kossa reaction, occasionally some CPPD crystals remained back and were demonstrable with polarized light.

Large amounts of amorphous mineral deposits obscured CPPD crystals, but the crystals not stained with Alizarin red S or with the von Kossa reaction [14].

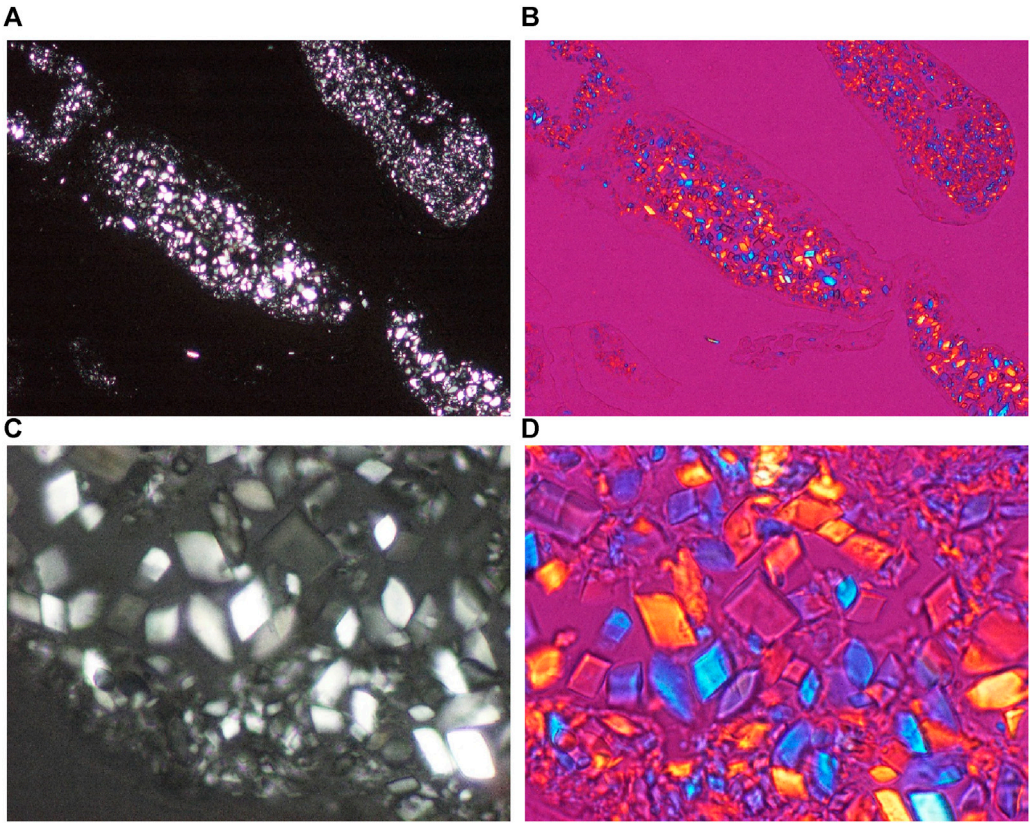

FIGURE 3
Chondrocalcinosis, knee joint, synovial membrane, unstained section, viewed under polarized light. CPPD plane crystals are of hexagonal, rhomboid, trapezoid, parallelogram-shape or fragments of these, they range in size from submicroscopic to 40 μm, and show a relatively strong positive birefringence according to the long axis of the crystals with Red I. compensator. **(A)** CPPD crystals, unstained sections, viewed under polarized light, ×100, **(C)** ×600. **(B)** CPPD crystals, unstained sections, viewed under polarized light, using Red I compensator, same as **(A)**, ×100, **(D)** ×600.

CPPD typically showed plane crystals of hexagonal, rhomboid, trapezoid, parallelogram-shape or fragments of these (Figures 3A–D).

With Red I compensator the CPPD crystals showed a relative strong positive birefringence ($\delta = 0.017$), in contrast to the weak positive birefringence of HA crystals ($\delta = 0.007$).

In our previous study we examined 40 tissue samples of 16 patients with clinically diagnosed chondrocalcinosis; 16 joints were operated: 8 knees, 4 hips, 2 wrists, 1 shoulder, and 1 elbow.

In traditionally fixed and processed tissue sections stained with HE, Alizarin red S or with the von Kossa reaction, CPPD crystals were found in 5 of 16 (31.25%) patients, and were detected in 8 (20.0%) of the 40 tissue sections.

With non-staining techniques CPPD crystals were present in all 16 patients, and were detected in 22 (55.0%) of the 40 unstained sections (with or without HA crystals) [16, 24, 25].

In HE stained tissue section cholesterol crystals (CC—$[C_{27}H_{46}O]$) were not found, and in unstained sections CC crystals were detected in 11 of 16 patients [23].

Figures 3A–D demonstrates characteristic CPPD crystal deposits in a patient with clinically diagnosed chondrocalcinosis.

Microscopic characteristics of HA and/or CPPD crystal deposits in patients with clinically diagnosed primary synovial chondromatosis

Primary synovial chondromatosis (prSynCh) was characterized clinically by slow progression of symptoms: joint pain, and swelling, stiffness, limited motion of the affected joint, intraarticular fluid, tenderness and creaking, grinding, or popping noise during movement (crepitus) or locking of the joint.

Abundant chondroid and/or bone formation (with or without true medullary spaces) was usually accompanied only with minimal amorphous calcium phosphate $[Ca_3(PO_4)_2]$ and/or calcium carbonate $[CaCO_3]$ deposition [15, 16].

Calculated by our semi-objective score system in prSynCh the average chondroid and/or bone formation was 2.135 per tissue sections, accompanied with minimal mineral deposition (0.270 per tissue sections) [23].

In our previous study we examined 37 tissue samples of 17 patients with clinically diagnosed prSynCh; 18 joints were operated: 12 knees, 4 hips, 2 elbows.

In traditionally fixed and processed tissue sections stained with hematoxylin eosin HA crystals were not detected, CPPD

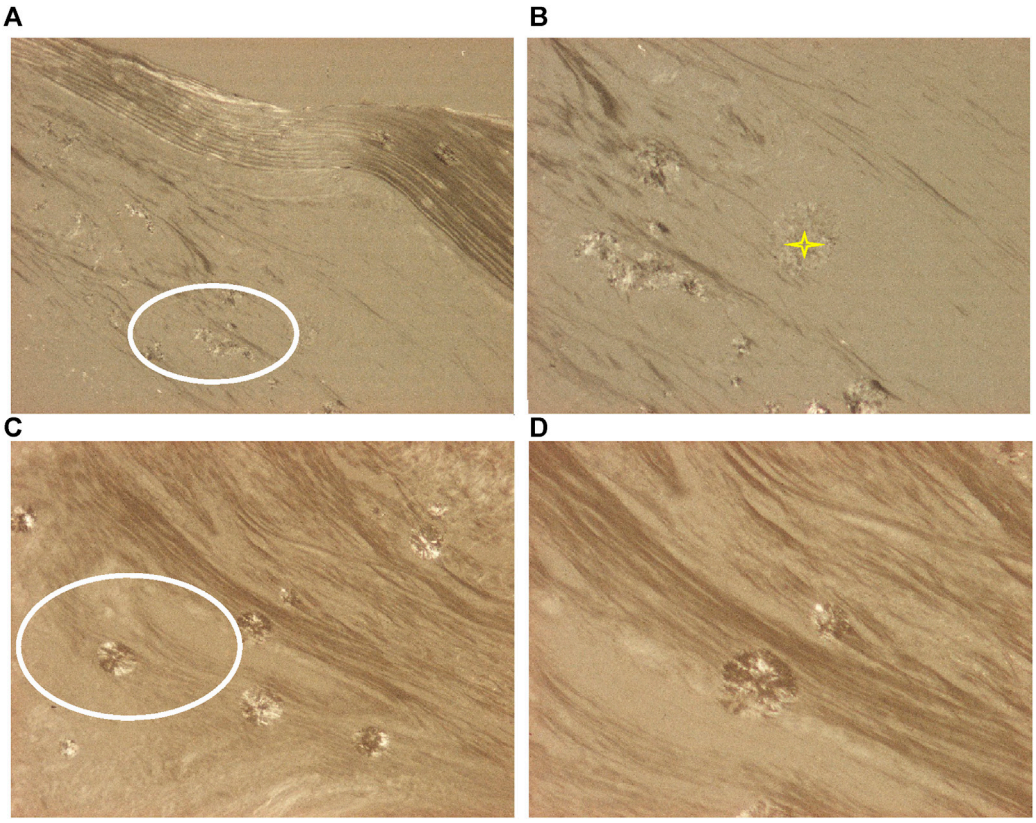

FIGURE 4
Synovial osteo-chondromatosis, knee joint, HA crystal prisms and clusters. The small prisms of HA crystals (white ellipses) are arranged in larger spheroid microaggregates (yellow stars). Under polarized light the direction of birefringence is positive according to the long axis of HA crystals, like that of collagen fibers. **(A)** HA crystals, unstained sections, viewed under polarized light, ×100, **(B)** ×200, **(C)** ×100, **(D)** ×200.

TABLE 3 Forty-three operated joints of 37 patients with available 93 tissue samples.

Cl Dx/Patients	Sample	Knee	Hip	Shoulder	Elbow	Wrist	Surgery
AR n = 4	16	5	1	3	0	0	9
Ch-C n = 16	40	8	4	1	1	2	16
prSynCh n = 17	37	12	4	0	2	0	18
Total n = 37	93	25	9	4	3	2	43
In % of total		58.14	20.93	9.30	6.98	4.65	100.0

Tissue samples of 3 patients with clinically diagnosed prSynCh were not available; Table 3 summarizes only the 18 operated joints of 17 patient with 37 tissue samples.
The most common indication for surgery was registered in the case of the knee (58.14%), followed by the hip (20.93%), shoulder (9.30%), elbow (6.98%), and wrist (4.65%).
AR, Apatite rheumatism; Ch-C, Chondrocalcinosis; prSynCh, primary synovialis chondromatosis; Cl Dx, Clinical Diagnosis; Pts, Patients; Ts, Tissue sample.

crystals were found in 4 of 17 (23.53%) patients, and in 4 of 37 (10.81%) tissue sections.

With the non-staining technique only 17 tissue sections of 8 patients were examined; HA and CPPD crystals were present in all patients and in 12 of 17 tissue sections [15, 16].

In HE stained tissue sections of prSynCh no cholesterol crystals (CC—[$C_{27}H_{46}O$]) were not found, but in unstained sections CC crystals were detected in 2 of 8 patients [23].

Figures 4A–D demonstrates characteristic HA crystal deposits in a patient with clinically diagnosed primary synovial chondromatosis.

TABLE 4 Amorphous mineral deposits, chondroid, osteoid and/or bone formation in tissue samples of patients with clinically diagnosed AR, Ch-C, and prSynCh.

Clinical diagnosis patients	Tissue samples	Calcification	Calcification/Tissue samples	Chondroid and/or bone formation	Chondroid and/or bone formation/Tissue samples
AR $n = 4$	16	17	1.063	1	0.063
Ch-C $n = 16$	37	39	1.054	2	0.054
prSynCh $n = 17$	37	10	0.270	79	2.135
Total of patients $n = 37$	90	66	0.733	82	0.911

The amount of calcium phosphate [$Ca_3(PO_4)_2$] and/or calcium carbonate [$CaCO_3$], furthermore chondroid, osteoid and/or bone formation was determined in 37 of 40 tissue samples with chondrocalcinosis; three tissue samples of one patient with clinically diagnosed Ch-C were not available for histological evaluation (tissue samples were too small).
In prSynCh the mineral deposits, chondroid, osteoid and/or bone formation were analyzed in 37 tissue samples of 17 patients.

TABLE 5 Distribution of HA and CPPD crystals in various tissue structures of different joints in unstained sections ($n = 73$) of patients with clinically diagnosed AR, Ch-C, and prSynCh.

Clinical diagnosis	Synovial membrane	Capsule	Bome/Cart	Bursa	Tendon	∑ of Ts
Apatite rheumatism						
Number of tissue samples	7	5	2	2	0	16
HA positivity	7	1	0	2	0	10
in %	100	20	0	100	0	62.50
CPPD positivity	7	0	0	2	0	9
in %	100	0	0	100	0	56.25
Chondrocalcinosis						
N of tissue samples	15	15	5	3	2	40
HA positivity	15	7	2	1	1	26
in %	100	33	0	33	50	65.00
CPPD positivity	15	5	0	1	1	22
in %	18	18	1	0	0	55.00
prSynCh						
Number of tissue samples	8	8	1	0	0	17
HA positivity	8	4	0	0	0	12
in %	100	50	0	zero divisor	zero divisor	70.59
CPPD positivity	8	4	0	0	0	12
in %	100	50	0	zero divisor	zero divisor	70.59
Total number of Ts	30	28	8	5	2	73
In % of ∑ of Ts	41.10	38.36	10.96	6.85	2.74	100.00

The prevalence of HA and/or CPPD was determined with polarized light in 73 unstained tissue sections of 28 patients.
prSynCh, primary synovialis chondromatosis; Ts, Tissue sample.

Comparative histological analyses of apatite rheumatism, chondrocalcinosis and primary synovial chondromatosis

Apatite rheumatism, chondrocalcinosis and primary synovial chondromatosis were equally characterized by the accumulation of HA and CPPD crystals in various tissues of different joints (with or without amorphous mineral deposition, and with or without chondroid, osteoid and/or bone formation).

Forty-three (43) joints (knee 25, hip 9, shoulder 4, elbow 3 and wrist 2) of 37 patients were operated; 93 tissue samples of

TABLE 6 Distribution of HA and CPPD crystals in tissue sections stained with HE (n = 93) compared to unstained sections (n = 73).

Staining technics clinical diagnosis	HE stained tissue sections prevalence n (%)		Unstained tissue sections prevalence n (%)	
	HA	CPPD	HA	CPPD
Apatite rheumatism				
Patients n = 4	0 (0% of 4)	3 (75.0% of 4)	4 (100% of 4)	4 (100% of 4)
Tissue samples n = 16	0 (0% of 16)	3 (18.75% of 16)	10 (62.5% of 16)	9 (56.25% of 16)
Chondrocalcinosis				
Patients n = 16	0 (0% of 16)	5 (31.25% of 16)	16 (100% of 16)	16 (100% of 16)
Tissue samples n = 40	0 (0% of 40)	8 (20.0% of 40)	26 (65% of 40)	22 (55% of 40)
Primary synovial chondromatosis				
Patients n = 17 of 20[a]	0 (0% of 17)	4 (23.53% of 17	8 (100% of 8)	8 (100% of 8)
Tissue samples n = 37 of 17 Pts[b]	0 (0% of 37)	4 (10.81% of 37)	12 (70.59% of 17)	12 (70.59% of 17)
Total n of patients n = 37[a]	0 (0% of 37)	12 (32.43% of 37)	n = 28 (73.68% of 38)	n = 28 (100% of 38)
Total n of tissue sections n = 93[b]	0 (0% of 93)	18 (19.35% of 93)	n = 48 (65.75% of 73)	n = 43 (58.90% of 73)

HA or CPPD crystal fragments in traces with uncertain birefringence were regarded negative.

[a]Tissue samples of 3 patients with clinically diagnosed prSynCh were not available therefore only 17 of 20 patients were taken into account.

[b]Prevalence of HA and CPPD crystals was determined in 37 HE stained tissue sections of 17 patients, and in 17 unstained tissue sections of 8 patients with prSynCh; 20 tissue sections of 9 patients with prSynCh were not analyzed with the non-staining technique.

37 patients were available and were examined with the light microscope.

The surgeries of patients with clinically diagnosed apatite rheumatism, chondrocalcinosis and primary synovial chondromatosis are summarized in Table 3.

Massive amorphous calcium phosphate [$Ca_3(PO_4)_2$] and/or calcium carbonate [$CaCO_3$] deposition characterized apatite rheumatism and chondrocalcinosis, chondroid formation was minimal (osteoid and/or bone formation was not detected).

Abundant chondroid, osteoid and/or bone formation was characteristic of primary synovial chondromatosis; amorphous mineral deposition occurred occasionally and was minimal.

The average mineral deposits, chondroid, osteoid and/or bone formation in tissue sections of patients with clinically diagnosed apatite rheumatism, chondrocalcinosis and primary synovial chondromatosis are summarized in Table 4.

Seventy-three (73) unstained tissue sections of 28 patients were examined with polarized light.

In unstained tissue sections of various tissues of joints HA and CPPD crystals existed side by side with different prevalence.

HA crystals were detected in 48, and CPPD in 43 cases of 73 unstained tissue sections.

HA crystals were observed without CPPD crystals in some cases, but usually were accompanied with some CPPD crystals.

CPPD crystals were not found without HA crystals (using Red I compensator the HA crystals with weak birefringence were not always detected because of the reduced illumination).

Table 5 summarizes the prevalence of HA and CPPD crystals in various tissue structures of different joints of 28 patients with the clinical diagnosis of apatite rheumatism, chondrocalcinosis and primary synovial chondromatosis.

Prevalence of HA and CPPD crystals was detected in 93 HE stained tissue sections of 37 patients.

In contrast to the HE stained sections the prevalence of HA and CPPD crystals was detected only in 73 unstained tissue sections of 28 patients; 20 tissue samples of 9 patients with prSynCh were not available for analysis.

Demonstration of HA and CPPD crystals was more effectively expressed in percent of positive cases by the non-staining technique according to Bély and Apáthy (2013) than with conventional HE stains.

Table 6 summarizes the occurrence of HA and CPPD crystals in 93 HE stained tissue sections of 37 patients with the clinical diagnosis of AR, Ch-C, and prSynCh, compared to the 73 unstained tissue sections of 28 patients.

In HE stained tissue sections of MSU, AR, Ch-C or prSynCh cholesterol crystals (CC—[$C_{27}H_{46}O$]), and/or crystalline liquid lipid droplets (CL) were not found.

Variable amounts of cholesterol (CC—[$C_{27}H_{46}O$]), and crystalline liquid lipid droplets (CL) were demonstrated with

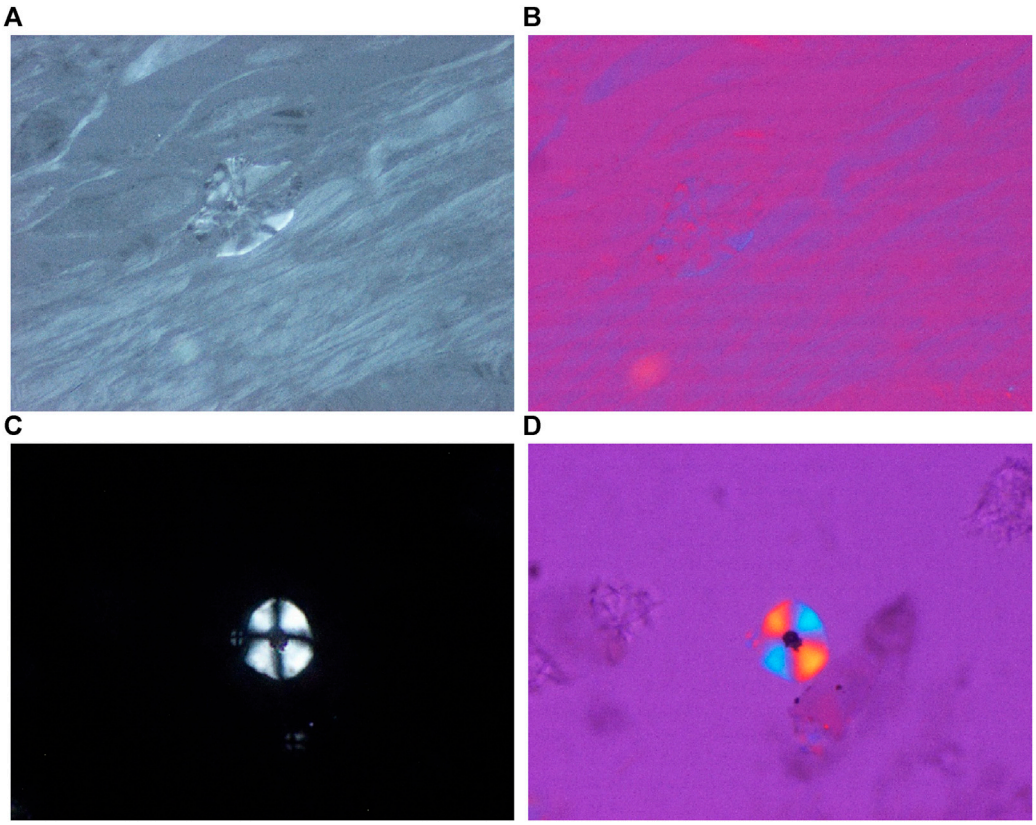

FIGURE 5
Apatite rheumatism, synovial membrane, semiliquid cholesterol crystals; unstained tissue section, viewed by polarized light, with and without Red 1 compensator. The birefringence of semiliquid cholesterol and lipid liquid crystals is identical with the birefringence of collagen fibers, and is positive in **(A,B)**. **(A)** Semiliquid cholesterol crystal, unstained sections, viewed under polarized light without Red I. compensator, ×200, **(B)** with Red 1 compensator, same as **(A)** ×200, **(C)** Lipid liquid crystals, stained for cholesterol according to Schultz, viewed under polarized light, without Red I. compensator, ×600, **(D)** with Red 1 compensator, same as **(C)** ×600.

Bély and Apáthy's non-staining technique (2013) in 3 of 4 with AR, in 11 of 16 with Ch-C, and in 2 of 8 patients with clinical diagnosis of prSynCh.

Figures 5A–D demonstrates characteristic semiliquid cholesterol and crystalline liquid lipid droplets.

In unstained sections of 5 patients the typical HA and CPPD crystals were accompanied with crystals of different shapes, sizes, and arrangements like a hair braid or reminiscent of a shingle roof.

Crystals with such different shapes, sizes and arrangements occurred in all three patient groups; in 1 patient with the clinical diagnosis of AR, in 2 with Ch-C, and in further 2 patients with prSynCh.

The birefringence of these crystals was stronger than that of HA crystals, and weaker than that of CPPD. The birefringence of the closely fitting parallel crystals was positive and negative in the same axis position.

Figure 6 demonstrates rod-shaped crystals of different sizes and arrangement than that of HA or CPPD crystals.

Discussion

Apatite rheumatism (apatite rheumatism, apatite rheumatism, hydroxyapatite arthritis, calcifying tenosynovitis, Milwaukee syndrome, frozen shoulder, calcific tendinitis) is a HA crystal induced arthropathy, while chondrocalcinosis [pseudogout, calcific gout, polyarticular (familial) chondrocalcinosis, pyrophosphate arthropathy] is thought to be a CPPD crystal induced arthropathy.

These metabolic diseases are regarded as different clinical entities [26–37], although the clinical symptoms are the same, the most frequently affected joints overlap, and there is currently no difference in their treatment [37–40].

Bywaters (1972) reported coexistent CPPD and HA crystal deposits in the synovial membrane in rheumatoid arthritis without suspicion of a single metabolic disease [41].

Hayes and Conway (1990) described co-occurrence of CPPD and HA crystals in periarticular soft tissues, especially in tendons; the co-occurrence of HA and CPPD were regarded as a mixed metabolic

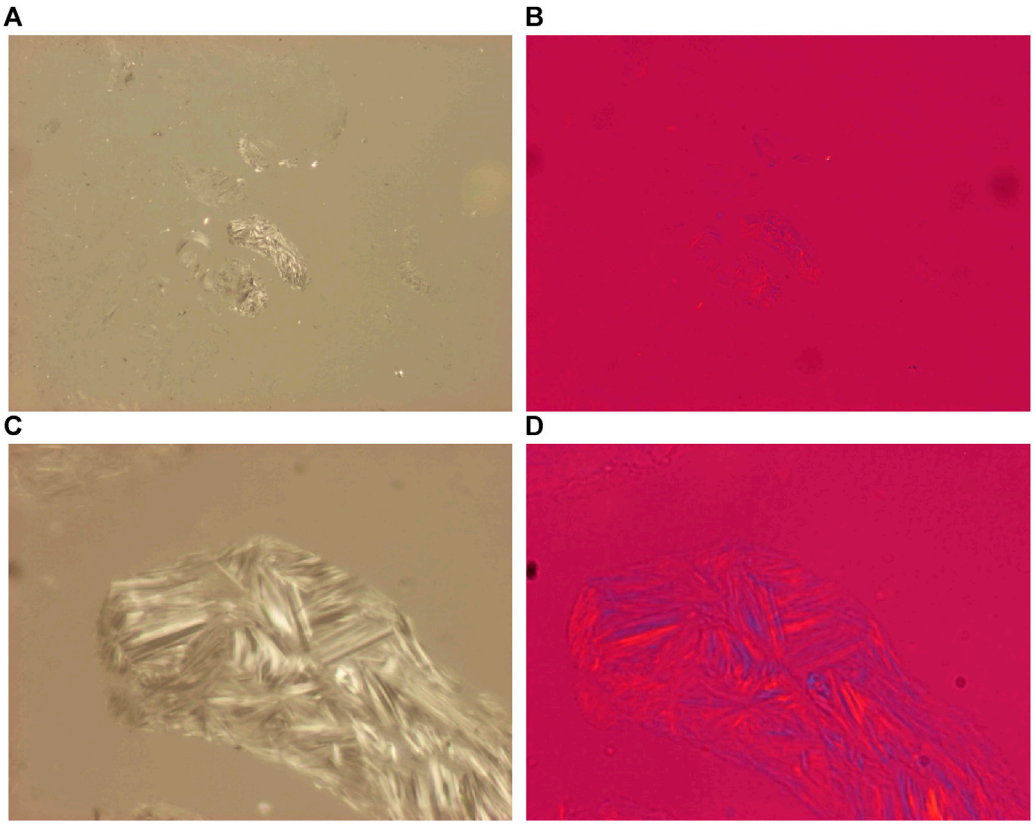

FIGURE 6
Apatite rheumatism, knee joint synovial membrane, unidentified rod-shaped crystals in a hair braid (vortex) like arrangement. The shape, size and arrangement of these tightly fitting unidentified crystals differs from that of HA and/or CPPD crystals. The birefringence of these crystals is positive and negative parallel to the long axis of the crystals. The rod shape of the crystals is supported by the birefringence in the dark-light band of the same width. **(A)** HA crystals, unstained sections, viewed under polarized light, ×100, **(C)** ×600. **(B)** HA crystals, unstained sections, viewed under polarized light, using Red I compensator [same field as **(A)**, ×100, **(D)** ×600].

malady of apatite rheumatism and calcium phosphate crystal deposition disease [42] quoting Resnick [43].

Using the Bély and Apáthy non-staining technique (2013) varying amounts of HA and CPPD crystals were observed side by side in apatite rheumatism and in chondrocalcinosis [24, 25].

These studies indicate that apatite rheumatism and chondrocalcinosis are HA and CPPD induced maladies, of the same basic metabolic disorder [24, 25].

The classic clinical diagnosis should be based on the presence of the dominant crystals in the deposits and not on the clinical symptoms or their localization.

Primary synovial chondromatosis (Reichel disease) of unknown origin is considered to be a distinct clinical entity [27, 30, 44, 45].

The constant presence of HA and CPPD crystals demonstrated with the unstained technique in primary synovial chondromatosis suggests that prSynCh and apatite rheumatism or chondrocalcinosis are related, but distinct metabolic diseases, which belong to the same group of metabolic maladies.

HA and CPPD crystals in apatite rheumatism or chondrocalcinosis were accompanied in most cases with abundant calcium phosphate [$Ca_3(PO_4)_2$] and/or calcium carbonate [$CaCO_3$] deposits, while chondroid and/or osteoid formation is rare and minimal (Table 5).

The presence of HA and CPPD crystals in prSynCh was characterized by conspicuous chondroid and/or bone formation in contrast to AR or Ch-C, while the amorphous calcium phosphate [$Ca_3(PO_4)_2$] and/or calcium carbonate [$CaCO_3$] deposition was rare and minimal (Table 5).

An inflammatory reaction was inhibited or moderated in the presence of amorphous minerals in AR or Ch-C, and inhibited or moderated in the presence of chondroid, osteoid and/or bone formation in prSynCh.

We consider amorphous calcium deposition a first-line response, and chondroid and/or osteoid formation a second-line defense mechanism against the crystals, reducing or moderating inflammation.

In our view the prSynCh is a defective variant of HA and CPPD induced metabolic disorders, where the deficient mineralization is replaced by chondroid and/or bone formation. These abilities may be determined by genetic or

other, unidentified factors, respectively influenced by intrinsic and/or extrinsic causes.

The relatively high mean age of patients with clinically diagnosed AR (74.00 years) at the time of surgery compared with the relatively lower mean age of patients with clinically diagnosed Ch-C (63.67 years) suggests that the small, more soluble, phagocytosed HA crystals are more tolerable for a longer period of time, and provoke lesser clinical symptoms than the larger, less soluble, more irritative CPPD crystal deposits.

There was no significant difference in mean age between patient cohorts with AR and Ch-C ($p < 0.844$) supporting the possibility that AR and Ch-C represent the same metabolic disorder.

The mean age of the patients with the clinical diagnosis of prSynCh was low in comparison with AR or Ch-C, probably caused by the synovial calcified and/or ossified loose bodies.

Crystal induced arthropathies are progressive maladies.

All diseases characterized by progressive deposition of crystals or proteins (amyloid), fat, etc., begin in organs and on tissue structures that are frequently involved by marked deposits; deposition starts later where deposits are infrequent or less marked.

In connection with systemic amyloidosis this general rule was analyzed in detail and confirmed in our previous studies [46–49].

According to the Wald sequence analysis [50], the "most common deposit is the earliest deposit."

A disease with progressive cumulative depositions probably starts where small early deposits are the most common.

This is a fundamental rule for all progressive cumulative disorders, including crystal induced arthropathies.

In patients with clinically diagnosed AR, Ch-C, and prSynCh the most commonly involved joint was the knee 25 (58.14% of 43 surgeries), followed by the hip 9 (20.93%), shoulder 4 (9.30%), elbow 3 (6.98%), and wrist 2 (4.65%) (Table 4).

Regarding the tissue structures of the joints, the most commonly involved tissues were the synovial membranes (41.10%), followed by the capsules (38.36%), bone and/or cartilage (10.96%), bursae (6.85%), and tendons (2.74%) (Table 6).

These data support the theory that *crystal deposition begins in all three metabolic maladies in the synovial membrane of the knee, succeeded by other structures and other joints*.

Unstained sections of 73 surgical samples of 37 patients showed more frequent, and more marked HA crystal deposition than CPPD crystal deposition; HA crystals were present in 48 (65.75%), while CPPD only in 43 (58.90%) of 73 tissue samples (Table 6).

In our patients with clinically diagnosed AR, Ch-C or prSynCh the crystal deposition appears to have begun with HA crystal deposition, followed by CPPD deposition.

This histologically outlined progressive process is also reflected in the clinically recognized stages of crystal-induced diseases.

These were recommended for chondrocalcinosis: asymptomatic CPP disease ("asymptomatic CPPD"), acute CPP crystal arthritis ("pseudogout"), and chronic CPP crystal inflammatory arthritis ("pseudo-RA") [37], and for apatite rheumatism: pre-calcific, formative, resting phases, including resorptive phase characterized by inflammation, and post-calcific phase characterized by reparative processes [51].

Conclusion

The non-staining technique of Bély and Apáthy is a much more effective method for the demonstration of crystals in metabolic diseases than the conventional stains and reactions.

Apatite rheumatism, chondrocalcinosis, and primary synovial chondromatosis are related metabolic disorders, provoked by HA and CPPD depositions.

AR and Ch-C are different stages of the same metabolic disorder, which differ from the prSynCh in amorphous mineral production, furthermore in the production of chondroid, osteoid and/or bone in prSynCh.

The authors assume that the prSynCh is a defective variant of HA and CPPD induced metabolic disorders with reduced mineralization capabilities, where the deficient mineralization is replaced by chondroid and/or bone formation.

Data availability statement

All relevant data is contained within the article and supplementary material. The original clinical and histological documents were filed in the authors' department, but due to reconstruction of the institute are no longer available. Any further inquiries can be directed to corresponding author.

Ethics statement

The studies involving human participants were reviewed and approved by the Ethics Committee of Buda Hospital of the Hospitalier Order of Saint John of God. The requirement for written informed consent to participate in this study was waived because it was a retrospective study.

Author contributions

ÁA (rheumatologist, neurologist) controlled the clinical diagnosis and the clinical data. MB (histopathologist) analyzed the surgical specimens and tissue sections. All authors contributed to the article and approved the submitted version.

Conflict of interest

The authors declare that the research was conducted in the absence of any commercial or financial relationships that could be construed as a potential conflict of interest.

References

1. Bély M, Apáthy Á. Mönckeberg sclerosis – kristály indukálta angiopathia (Mönckeberg"s sclerosis: crystal-induced angiopathy). *Orvosi Hetilap* (2013) 154(23):908–13. doi:10.1556/OH.2013.29628

2. Bély M, Apáthy Á. Vascular calcification and crystal deposition diseases - a comparative study on 67 amputated legs with atherosclerosis and/or Mönckeberg sclerosis. *EC Cardiol* (2021) 8(10):01–19.

3. Pearse AGE. Fat soluble colorant methods. In: Pearse AGE, editor. *Histochemistry theoretical and applied. Volume one: p. 129-131, Volume two: analytical technology, Lipids, lipoproteins and proteolipids. Ch. 16, p. 786-849*. Edinburgh, London, Melbourne and New York: Churchill Livingstone (1985).

4. Swan A, Chapman B, Heap P, Dieppe P. Submicroscopic crystals in osteoarthritic synovial fluids. *Ann Rheum Dis* (1994) 53(7):467–70. doi:10.1136/ard.53.7.467

5. Pay S, Terkeltaub R. Calcium pyrophosphate dihydrate and hydroxyapatite crystal deposition in the joint: new developments relevant to the clinician. *Curr Rheumatol Rep* (2003) 5(3):235–43. doi:10.1007/s11926-003-0073-x

6. Shidham V, Chivukula M, Basir Z, Shidham G. Evaluation of crystals in formalin-fixed, paraffin-embedded tissue sections for the differential diagnosis of pseudogout, gout, and tumoral calcinosis. *Mod Pathol* (2001) 14(8):806–10. doi:10.1038/modpathol.3880394

7. Forster CJ, Oglesby RJ, Szkutnik AJ, Roberts JR. Positive alizarin red clumps in Milwaukee shoulder syndrome. *J Rheumatol* (2009) 36(12):2853. doi:10.3899/jrheum.090163

8. Gatter RA, Schumacher HR. "Microscopic findings under compensated polarized light and phase light" in: gatter RA. In: Schumacher HR, editor. *A practical handbook of joint synovial fluid analysis*. Philadelphia, London: Lea & Febiger (1991). p. 46.

9. Paul H, Reginato AJ, Schumacher HR. Alizarin red S staining as a screening test to detect calcium compounds in synovial fluid. *Arthritis Rheum* (1983) 26(2):191–200. PMID: 6186260. doi:10.1002/art.1780260211

10. Shoji K. Alizarin red S staining of calcium compound crystals in synovial fluid. *Nihon Seikeigeka Gakkai Zasshi* (1993) 67(4):201–10. PMID: 7686572.

11. Yang JH, Oh KJ, Pandher DS. Hydroxyapatite crystal deposition causing rapidly destructive arthropathy of the hip joint. *Indian J Orthopaedics* (2011) 45:569–72. doi:10.4103/0019-5413.87139

12. Bély M, Apáthy Á. A simple method of diagnostic pathology for identification of crystal deposits in metabolic and crystal induced diseases (2022). Available from: http://structural-crystallography.imedpub.com/archive.php (Accessed February 15, 2016).

13. Bély M, Apáthy A. Metabolic diseases and crystal induced arthropathies technic of non-staining histologic sections - a comparative study of standard stains and histochemical reactions. *Clin Arch Bone Jt Dis* (2018) 1(2). doi:10.23937/cabjd-2017/1710007

14. Bély M, Apáthy A. Crystal deposits in tissue of patients with chondrocalcinosis and apatite rheumatism – microscopic identification of CPPD and HA with the non-staining technique of Bely and Apáthy. *BAOJ Clin Trials* (2018) 4(1):018.

15. Apáthy Á, Bély M. AB1262 amorphous mineralization, chondroid and/or osteoid formation in crystal induced metabolic disorders – a comparative study of apatite rheumatism, chondrocalcinosis and primary synovial chondromatosis apatite rheumatism, chondrocalcinosis, primary synovial chondromatosis. *Ann Rheum Dis* (2023) 82(1):1857–8. doi:10.1136/annrheumdis-2023-eular.193

16. Bély M, Apáthy Á. A comparative microscopic study of apatite rheumatism, chondrocalcinosis and synovial chondromatosis – HA and CPPD induced metabolic disorders. *EC Pulmonology Respir Med* (2023) 12(6):01–17.

17. Ohira T, Ishikawa K. Preservation of calcium pyrophosphate dihydrate crystals: effect of Mayer's haematoxylin staining period. *Ann Rheum Dis* (2001) 60(1):80–2. PMID 11114290. doi:10.1136/ard.60.1.80

18. Carson FL. "Mayer's hematoxylin" In: carson FL. In: *Histotechnology*. Chicago: ASCP Press (1990). p. 100–5.

19. McManus JFA, Mowry RW. Methods of general utility for the routine study of tissues, sodium Alizarin sulfonate stain for calcium and Von Kossa's method for phosphates and carbonates. In: McManus JFA, Mowry RW, editors. *Staining methods, histologic and histochemical*. New York: Hoeber PB Inc (1960). p. 55–72.

20. Vacca LL. Alizarin red S. In: Vacca LL, editor. *Laboratory manual of histochemistry*. New York: Raven Press (1985). p. 333–4.

21. Lillie RD. Von Kóssa's method. In: Lillie RD, editor. *Histpathologic technic and practical histochemistry*. New York, Toronto, London: The Blakiston Division McGraw-Hill Book Company (1954). p. 264–5.

22. Lentner C. "Statistical methods" volume 2. In: Lentner C, Diem K, Seldrup J, editors. *Geigy scientific tables*. Basle, Switzerland: Ciba-Geigy Limited (1982). p. 227.

23. Bély M, Apáthy A. Metabolikus megbetegedések – a kristályok csodálatos világa (Metabolic disorders – the wonderful world of crystals). *Orvostovábbképző Szemle* (2023) 9:66–81.

24. Bély M, Apáthy A. Crystal deposits in apatite rheumatism and chondrocalcinosis – microscopic identification of hydroxyapatite and calcium pyrophosphate dihydrate crystals with standard stains and histochemical reactions and with the nonstaining technique of Bély and Apáthy. *EC Pulmonology* (2022) 1:03–24.

25. Bély M, Apáthy Á. Apatite rheumatism and chondrocalcinosis are different stages of the same metabolic disorder – a clinicopathologic study of 21 patients with clinically diagnosed apatite rheumatism or chondrocalcinosis. *J Interdiscip Histopathology* (2022) 10:1–14.

26. Reginato AM, Yuvienco C. Hydroxyapatite crystal-induced rheumatology (2022). Available from: https://www.rheumatologyadvisor.com/home/decision-support-in-medicine/rheumatology/hydroxyapatite-crystal-induced/ (Accessed November 15, 2022).

27. Mohr W. Kalziumpirophosphat-arthropathie, apatitkrankheiten, primäre synoviale osteochondromatose. In: Mohr W, editor. *Gelenkpathologie, historische Grundlagen, Ursachen und Entwicklungen von Gelenkleiden und ihre Pathomorphologie*. Berlin, Heidelberg: Springer-Verlag (2000). p. 193–212.

28. Reginato AJ, Reginato AM. Diseases associated with deposition of calcium pyrophosphate or hydroxyapatite. In: Ruddy S, Harris ED, Sledge CB, editors. *Crystal-associated synovitis, section XV, kelly's textbook of rheumatology*. 6th ed. Philadelphia, London, New York, St. Louis, Sydney, Toronto: WB Saunders Company: A division of Harcourt Brace & Company (2001). p. 1377–90. Ch. 90.

29. Žitňan D, Sitaj Š. Chondrocalcinosis articularis Section L clinical and radiological study. *Ann Rheum Dis* (1963) 22:142–52. doi:10.1136/ard.22.3.142

30. Gardner DL, McClure J. Metabolic, nutritional and endocrine diseases of connective tissue, synovial osteochondromatosis. In: Arnold E, editor. *Pathological basis of the connective tissue diseases*. 1st ed. London, Melbourne, Auckland: Great Britain (1992). p. 984–6. Ch. 24.

31. McCarty DJ, Lehr RJ, Halverson PB. Crystal populations in human synovial fluid. Identification of apatite, octacalcium phosphate, and tricalcium phosphate. *Arthritis Rheum* (1983) 26:1220–4. doi:10.1002/art.1780261008

32. Fassbender HG. *Crystal-associated arthropathies" in Pathology and pathobiology of rheumatic diseases*. 2nd ed. Berlin, Heidelberg, New York, Germany: Springer-Verlag (2002). p. 353–69. ch. 17.

33. Gupta SJ. Crystal induced arthritis: an overview. INJR (Indian Journal of Rheumatology - formerly). *J Indian Rheumatol Assoc* (2002) 10:5–13.

34. Rosenthal AK, Ryan LM. Calcium pyrophosphate deposition disease. *New Engl J Med* (2016) 374:2575–84. doi:10.1056/NEJMra1511117

35. Dieppe PA, Crocker P, Huskisson EC, Willoughby DA. Apatite deposition disease. A new arthropathy. *Lancet* (1976) 307:266–9. doi:10.1016/S0140-6736(76)91400-8

36. Dieppe PA. Milwaukee shoulder. *Br Med J (Clin Res Ed).* (1981) 283(6305):1488–9. PMC1507904. doi:10.1136/bmj.283.6305.1488

37. Rosenthal A, Dalbeth N, Romain PL. *Clinical manifestations and diagnosis of calcium pyrophosphate crystal deposition (CPPD) disease"*. Wolters Kluwer Canada (2024). Available from: https://www.uptodate.com/contents/clinical-manifestations-and-diagnosis-of-calcium-pyrophosphate-crystal-deposition-cppd-disease (Accessed November 01, 2023).

38. Bachmann D, Resnick D. "Calcium pyrophosphate dihydrate crystal deposition disease" and "Calcium hydroxyapatite crystal deposition disease". In: Bachmann D, Resnick D, editors. *Radiological atlas of rheumatological diseases*. Basel, Switzerland: Hoffmann-La Roche Ltd. (1994). p. 108–23.

39. mayoclinic. *Pseudogout* (2022). Available from: https://www.mayoclinic.org/diseases-conditions/pseudogout/symptoms-causes/syc-20376983 (Accessed July 28, 2022).

40. Pálinkás M, Poór G. Kristályatrthritisek. In: Szekanecz Z, Nagy G, editors. *Reumatológia*. Budapest: Medicina könyvkiadó Zrt (2019). p. 572. Ch. 41.

41. Bywaters EGL. Calcium pyrophosphate deposits in synovial membrane. *Ann Rheum Dis* (1972) 31(3):219–21. doi:10.1136/ard.31.3.219-b

42. Hayes CW, Conway WF. Calcium hydroxyapatite deposition disease. *RadioGraphics* (1990) 10:1031–48. doi:10.1148/radiographics.10.6.2175444

43. Resnick D. Calcium hydroxyapatite crystal deposition disease. In: Resnick D, Niawayama G, editors. *Diagnosis of bone and joint disorders*. 2nd ed. Saunders Philadelphia (1988). p. 1733–64.

44. GARD. *Synovial chondromatosis – gard* (2023). Available from: https://rarediseases.info.nih.gov/diseases/6054/synovial-chondromatosis (Accessed February, 2023).

45. AAOS. *Synovial chondromatosis - OrthoInfo – AAOS* (2022). Available from: https://orthoinfo.aaos.org/en/diseases–conditions/synovial-chondromatosis (Accessed January 2022).

46. Bely M, Apathy A, Pinter T, Ratko J. Generalized secondary amyloidosis in rheumatoid arthritis. *Acta morphologica Hungarica* (1992) 40:49–69.

47. Bély M. "Identification of amyloid deposits by histochemical methods of romhányi" in: bély M, guest editor. *Amyloid* (2001) 8.2:177–82.

48. Bély M, Apáthy Á. *Clinical pathology of rheumatoid arthritis: cause of death, lethal complications and associated diseases in rheumatoid arthritis*. Budapest: Akadémiai Kiadó (2012). p. 1–440.

49. Bély M, Apáthy Á. Formal pathogenesis of systemic and localized amyloidosis. *EC Cardiol* (2019) 6(5):444–69.

50. Wald A. *Sequential analysis*. New York: Wiley Mathematical Statistics Series, Chapman & Hall (1947).

51. Uhthoff HK, Loehr JW. Calcific tendinopathy of the rotator cuff: pathogenesis, diagnosis, and management. *J Am Acad Orthopaedic Surgeons* (1997) 5(4):183–91. doi:10.5435/00124635-199707000-00001

AppendixBély and Apáthy's "non-staining" technique

1. Tissue blocks of surgically removed specimens are fixed in 8% neutral buffered formalin (at pH 7.6 for >24 h at 20°C room temperature) [1, 12–16].
2. Tissue blocks are dehydrated in ethyl alcohol, and are embedded in paraffin using acetone as well as xylene—5 μm sections are cut.
3. Prolonged deparaffinization (3–5 days) in a thermostat at 56°C (daily changing xylene)
4. Chloroform–methanol I. (1:1) solution for 1 h
5. Chloroform–methanol II. (1:1) solution for 1 h or overnight
6. Dehydration in ethyl alcohol (two changes of 96% alcohol I-II. 30–30 min), and using terpene xylene, as well as xylene, mounting in Canada balsam, cover slip.

Results

In deparaffinized tissue sections of formaldehyde fixed and paraffin embedded surgical specimens—without staining with aqueous dyes—the cholesterol crystals and crystalline lipids, furthermore the HA crystals are preserved, and are well detectable with polarized light.

In unstained sections MSU and CPPD crystals are more abundant than in sections stained with HE or with other staining.

Pathology & Oncology Research | frontiers

TYPE Review
PUBLISHED 09 May 2024
DOI 10.3389/pore.2024.1611635

Check for updates

OPEN ACCESS

EDITED BY
Gábor Méhes,
University of Debrecen, Hungary

*CORRESPONDENCE
Anna Kerpel-Fronius,
kerpel.anna@koranyi.hu

RECEIVED 11 December 2023
ACCEPTED 24 April 2024
PUBLISHED 09 May 2024

CITATION
Kerpel-Fronius A and Bogos K (2024), HUNCHEST projects—advancing low-dose CT lung cancer screening in Hungary.
Pathol. Oncol. Res. 30:1611635.
doi: 10.3389/pore.2024.1611635

COPYRIGHT
© 2024 Kerpel-Fronius and Bogos. This is an open-access article distributed under the terms of the Creative Commons Attribution License (CC BY). The use, distribution or reproduction in other forums is permitted, provided the original author(s) and the copyright owner(s) are credited and that the original publication in this journal is cited, in accordance with accepted academic practice. No use, distribution or reproduction is permitted which does not comply with these terms.

HUNCHEST projects—advancing low-dose CT lung cancer screening in Hungary

Anna Kerpel-Fronius[1]* and Krisztina Bogos[2]

[1]Department of Radiology, National Korányi Institute for Pulmonology, Budapest, Hungary, [2]Director of the National Korányi Institute for Pulmonology, Budapest, Hungary

Lung cancer, the leading cause of malignancy-related deaths worldwide, demands proactive measures to mitigate its impact. Low-dose computer tomography (LDCT) has emerged as a promising tool for secondary prevention through lung cancer screening (LCS). The HUNCHEST study, inspired by the success of international trials, including the National Lung Cancer Screening Trial and the Dutch NELSON study, embarked on the first LDCT-based LCS program in Hungary. The initiative assessed the screening efficiency, incorporating lung function tests and exploring the interplay between lung cancer and chronic obstructive pulmonary disease (COPD). Building upon this foundation, an implementation trial involving 18 Hungarian centers supported by the Ministry of Human Capacities demonstrated the feasibility of LCS within a multicentric framework. These centers, equipped with radiology capabilities, collaborated with multidisciplinary oncology teams, ensuring optimal patient pathways. However, a critical challenge remained the patient recruitment. To address this, the HUNCHEST 3 project, initiated in 2023, seeks to engage general practitioners (GPs) to reach out to eligible patients within a municipality collective of 60 thousand inhabitants. The project's ultimate success is contingent upon the willingness of eligible individuals to undergo LDCT scans. In conclusion, the HUNCHEST program represents a crucial step in advancing lung cancer screening in Hungary. With a focus on efficiency, multidisciplinary collaboration, and innovative patient recruitment strategies, it endeavors to contribute to the reduction of lung cancer mortality and serve as a blueprint for potential nationwide LCS programs.

KEYWORDS

lung cancer, screening, LDCT, pulmonary nodules, implementation

Abbreviations: COPD, chronic obstructive pulmonary disorder; CXR, Chest X-ray; HC1, HUNCHEST I; HC2, HUNCHEST II; LCS, Lung cancer screening; LDCT, low dose computer tomography; MDT, multidisciplinary team; NELSON, Nederlands–Leuvens Longkanker Screenings Onderzoek (Dutch–Belgian lung-cancer screening trial); OKPI, Országos Korányi Pulmonológiai Intézet (National Korányi Institute for Pulmonolgy); NLST, National Lung Screening Trial; SOLACE, Strengthening the screening of Lung Cancer in Europe; VDT, Volume doubling time.

Introduction

The year 1912 marked the beginning of formal documentation of lung cancer cases, with Isaac Adler publishing a review that identified 374 documented instances [1]. Fast forward to the present, and lung cancer annually claims the lives of 1.7 million people globally, with Hungary alone witnessing about 10,000 new cases each year [2].

Regrettably, by the time lung cancer becomes symptomatic, it often presents in an advanced or metastatic stage. Presently, surgery remains the sole curative option, but without early detection, only 15%–25% of cases are operable [3].

The disease has witnessed significant progress in the realm of early detection and prevention. This article focuses on the role of low-dose computer tomography (LDCT) in identifying the disease in its earliest, most treatable stages. While primary prevention through smoking cessation programs is essential to reduce new cases, secondary prevention, in the form of screening, plays a vital role in reducing mortality rates.

Early screening efforts initially centred on conventional radiography, utilizing chest X-rays (CXR) since they were widely accessible. In the 1960 s, several controlled trials were conducted, such as the Czechoslovakian and the Mayo Lung Project, which used chest X-rays, and the Johns Hopkins trial, which employed sputum cytology [4–6]. The final significant trial employing chest X-rays was the Prostate, Lung, Colorectal, and Ovarian trial, which followed over 150,000 patients for 13 years, but failed to show a reduction in mortality [7]. In Hungary, lung CXRs were a part of the fight against tuberculosis—the mandatory nature was later revoked, but still a large proportion of adults view CXRs as part of a health check [8]. Nearly 1,000 lung cancer cases are still detected this way in a population of 10 million. These patients have approximately twice the number of resectable LCS than their symptomatically detected counterparts [9].

The true breakthrough came with advancements in medical imaging technology. In 1992, the Early Lung Cancer Action Project (ELCAP) was launched in the United States of Amerika, by Claudia Henschke and her team, with a focus on LDCT screening. Over 31,000 asymptomatic individuals were screened, resulting in the diagnosis of 484 lung cancers, 85% of which were at Stage I. This was the first large-scale trial to demonstrate the potential of LDCT screening in lung cancer [10].

In the United States, the National Lung Cancer Screening Trial (NLST), initiated in 2002, proved to be a game-changer. It was a control-armed, prospective trial, involving 53,454 high-risk individuals. The results announced in 2013 revealed a 20% mortality reduction in the LDCT screening arm [11]. This compelling data led to the United States Preventive Services Task Force (USPSTF) in 2013 recommending LDCT lung cancer screening for individuals between 55–80 years of age with a smoking history of at least 30 pack-years who are active smokers or quit within the last 15 years—based on clinical data. This was modified in 2021 to include individuals as young as 50 years of age with a 20 pack-year history [12]. Medicare coverage was provided for at-risk individuals, although uptake remained low [13].

In Europe, the Dutch-Belgian Randomized Lung Cancer Screening Trial (NELSON) is the largest concluded lung cancer screening study to date. Data presented in 2018 showed a 26% reduction in mortality for high-risk males, and even more significant benefits for women. The introduction of an "indeterminate for cancer" category reduced the number of false positives in comparison to the NLST [14].

In 2015, the European Respiratory Society and the European Society of Radiologists published a joint statement followed by the European position statement on lung cancer screening in 2017 [15, 16]. These documents emphasize the importance of risk stratification, patient education, quality assurance, and a clear pathway for managing screen-detected nodules.

In Hungary, the first prospective LDCT lung cancer screening project started as early as in 2013. In this article the authors present a brief review of the results of the finished screening projects, and introduce the ongoing LDCT-LCS projects.

HUNCHEST I

The HUNCHEST (Hungarian Chest Screening) pilot initiative, spearheaded by the National Korányi Institute for Pulmonology in Budapest, sought to evaluate the efficacy of LDCT in detecting lung cancer in asymptomatic individuals, regardless of established risk factors [17].

Initially conceived as a single-center study, the program aimed to establish screening protocols, reporting mechanisms, and ensure comprehensive patient follow-up. In 2015, additional thoracic centers specializing in lung cancer imaging joined the initiative, bringing the total to six active centers contributing to screening efforts. Each center employed adaptable recruitment strategies, leveraging media campaigns, websites, posters, newspaper advertisements, and informational leaflets to encourage voluntary participation.

The study encompassed individuals undergoing the first screening round between October 2013 and January 2020. Inclusion criteria targeted asymptomatic individuals aged between 50 and 79 years of age, irrespective of known risk factors. Participants with a history of smoking received smoking cessation counseling at recruitment. Exclusion criteria, in line with the NELSON trial and study protocol, excluded individuals with specific health conditions, self-reported moderate or poor health, permanent oxygen therapy needs, body weight of 140 kg or more, a history of cancer within the past 5 years, previous lung surgery, or chest CT examinations within the last 2 years. Written informed consent was

mandatory, and those unable to provide it were excluded. Participants were categorized based on smoking habits and comorbidities.

The HUNCHEST program included lung function tests (spirometry) for all applicants to identify undiagnosed chronic obstructive pulmonary disease (COPD), with specific criteria for diagnosis and severity assessment.

LDCT protocols were tailored to the scanner model, with scans conducted during suspended maximal inspiration in a single breath-hold, covering the entire lungs. Radiation exposure was controlled, and imaging conditions were standardized across sites. Two independent radiologists read all scans with semiautomatic segmentation of nodules and manual measurements conducted as needed. The Siemens SyngoVia MM Oncology Lung Computer-Aided Detection (CAD) software played a crucial role in matching previously detected nodules and calculating the volume doubling time (VDT) for nodule growth assessment.

Nodules were categorized based on their VDT into likely benign (VDT >600 days), suspicious (VDT <400 days), inflammatory (VDT <40 days), and indeterminate (VDT between 400 and 600 days), necessitating further evaluation.

The number of screen-detected malignancies and positive predictive values in the study aligned with internationally published studies. Similarly to the NELSON protocol, the study incorporated not only positive/negative categories, but also an indeterminate category, optimizing nodule management. A web-based structured reporting platform facilitated clear pathways post a positive screen, enabling cost-effectiveness calculations and providing vital data for endorsing a nationwide risk group-based screening program.

Notably, the trial included never-smokers in its cohort, both with and without COPD as a comorbidity. This pioneering aspect positioned the initiative among the first to comprehensively evaluate Caucasian never-smoker participants concerning COPD within the context of a low-dose CT screening project. Despite acknowledged limitations, including the absence of a detailed evaluation on why non-smokers were sensitized for screening, the trial's outcomes offered a unique vantage point for assessing the cost-effectiveness within this specific subgroup. Participants who tested positive during screening were referred to specialized pulmonologists. These experts assessed the necessity for further diagnostic measures or treatments based on available guidelines. These measures included full-dose contrast-enhanced chest or comprehensive staging CT scans, PET-CT scans, bronchoscopy, transthoracic needle biopsy (TNB), or video-assisted thoracoscopic surgery (VATS). The study meticulously documented the diagnosis, stage, pathology, and treatment plan for each case of lung cancer.

In conclusion, 1.5% of participants were diagnosed with histologically proven lung cancer, a percentage consistent with international data within the study population, ranging between 0.8%–2.2%.

The HUNCHEST study provided answers to health economy questions, revealing the annual costs of both screened and unscreened populations [18]. In the initial year, lung cancer screening with LDCT incurs an additional annual cost of approximately 3.3 billion HUF. By the 5th year, there is a yearly surplus cost of 1.9 billion HUF, considering a 10% participation rate of the affected population. The direct additional costs associated with screening amount to roughly 2.6 billion HUF per year. In the first 3 years of screening, the therapy for newly detected patients is more expensive than for those without screening. However, in the 4th and 5th years, the cost of treating later-stage, more expensive, and less effectively managed patients in the unscreened group surpasses the therapeutic cost of screened patients. By year ten screening is not only cost effective, but cost-saving.

HUNCHEST-II

The HUNCHEST II extended implementation study model examination was launched in 2019 with the proposal and support of the State Secretariat for Healthcare of the Ministry of Human Resources. The study included 18 centers, following a uniform protocol, applying the same patient follow-up scheme after positive screening results. The goal was to shed light on how a LDCT lung cancer screening program could be expanded nationwide. The key question during the study was whether it could be proven that lung cancer is more likely to be detected in symptom-free, early stages among 50–74-year-olds who are current or former heavy smokers participating in the program. Another aim was to conduct a cost-effectiveness and budgetary impact analysis based on the real-life data obtained during patient care in HUNCHEST II [19].

A cornerstone of the study was the uniform nodule tracking protocol, with the expectation of minimizing regional healthcare disparities. The recommendation and implementation of smoking cessation support for active smokers was carried out according to the specified professional guidelines using the methods outlined for smoking cessation support. The task of expediting the examination of highlighted patients fell under the responsibility of the territorial pulmonary department. Special diagnostic teams dedicated to handling the diagnostic pathway of nodules detected during lung cancer screening had to be established at the examination centers. Initially, these teams were closely associated with the oncology multi-disciplinary team (MDT) and in cases of confirmed lung cancer diagnosis, the routine MDT consultation decided on the patient's further course. (Internationally, it is recommended to establish a MDT for discussing solitary pulmonary nodules—approximately 70% of the cases identified are ultimately non-tumorous, and unnecessary invasive investigations can be reduced through MDT discussions).

During the examination, the designated radiologist at each center evaluated LDCT images on-site or through remote reporting. In addition, a central core Computer-Aided Detection (CAD) system provided by Aidence, the Veye Lung software provides the necessary secondary reporting. The images are automatically sent from the examination center's PACS system to CoreCAD for central processing, and almost in real-time (expectedly within 5–10 min), CoreCAD provides a diagnosis established by the computer. The radiologist had this data available by the time she started the reporting process -this also replaced the need for the resource-intensive dual radiologist reporting.

AI tools have become a necessity in LCS programs—the correct volume measurements require computer assistance, and the correct assessment of VDT also relies on CAD system. These cannot however be applied as first readers, as it suggests in the name these "aid the diagnosis." Deep learning (DL) systems are also developed in the field of LCS—in a recent metaanalysis, their specificity was 0.63 and sensitivity 0.93. The biggest question behind these systems that it is unclear how the machine calculates these results, so while promising, they are not yet accepted as part of non-study based screening projects [20].

Each center reported screenings to the National Korányi Institute for Pulmonology through an online data submission platform designed for this purpose, in compliance with GDPR regulations. The online interface is based on the tuberculosis surveillance system recorded by the National Korányi Institute for Pulmonology (OKPI) Methodology Department but is separate from it. Not only did it monitor the completion and results of controls in indeterminate screenings, but also, in the case of a positive screen it recorded the results of all necessary investigations. In the event of a lung cancer diagnosis, the histological type, stage, and the therapy suggested by the MDT was also documented. In the event of an alternative diagnosis, diagnosis and a brief description of the diagnostic pathway leading to it (bronchoscopy, PET/CT, biopsy, surgical intervention) was also noted.

In the clinical trial, data from more than 4,000 individuals were analyzed, with an average age of around 61 at the time of enrollment. Among the participants, the baseline LDCT examination result was negative in nearly 75% of all cases, and positive in 4%. The remaining group required LDCT follow-up, predominantly resulting in negative findings. In cases with positive results, every individual underwent a pulmonary specialist examination. Those with suspected tumors were appropriately referred to the local MDT for further assessment according to the protocol. Ultimately, 61 individuals were confirmed to have malignant lung tumors based on histopathology and/or clinical and radiological images.

Comparing the stage-wise distribution of new lung cancer patients participating in the HUNCHEST II program with those treated in the National Korányi Institute for Pulmonology (same time frame, same age range, confirmed smokers), it became evident that the HUNCHEST II study more frequently succeeded in detecting lung cancer in early stages. According to OKPI data, nearly 70% of patients presenting with symptoms were inoperable, while in HUNCHEST II, this was only the case for 20% of screen-detected tumor patients (Table 1).

Comparing the statistics between HUNCHEST I and HUNCHEST II reveals several differences in participant characteristics during the 1st round of screening. The average age in HUNCHEST I was 63.2, slightly higher than the average age of 61.3 in HUNCHEST II. The female percentage among current smokers was similar in both studies. The number of former or never smokers was comparable between the two studies, with slight differences in age and gender distribution. The prevalence of COPD as a comorbidity was higher in HUNCHEST I (18.6%) compared to HUNCHEST II (13.2%) This was due to the proactive screening for COPD in the first study with standard lung function testing, whereas in HUNCHEST II self-reporting of the disease was noted. In summary, HUNCHEST II involved a larger and slightly younger cohort, with a lower prevalence of COPD, as a comorbidity. The gender distribution varied slightly, and HUNCHEST II had a higher number of participants with a positive screen in the 1st round compared to HUNCHEST I.

The examination of lung cancer histological subtypes within the screening programs HUNCHEST I (HC1) and HUNCHEST II (HC2), alongside data from OKPI, unveils intriguing variations. In the screening-focused HC1, adenocarcinomas prevailed at 62.1%, contrasting with HC2 at 56.2%. OKPI reported 50% in 2022 and 47% in 2019. HC2 exhibited a higher frequency of squamous cell carcinomas (31.2%) compared to HC1 (24.1%), closely mirroring OKPI's 23% in 2022 and 24% in 2019—the lower incidence of this subtype in HUNCHEST I is possibly due to the fact that this program included never smokers, where squamous cell carcinomas are not common. For small cell carcinomas, HC1 was at 6.9%, HC2 at 6.2%, OKPI 2022 at 13%, and OKPI 2019 at 14%—the number of small cell carcinomas are usually lower in screening programs than in real life data, due to its more aggressive nature—the tumor grows much faster, thus making screening for it difficult. Other subtypes (including large cell tumors and carcinoids) constituted 6.9% in HC1, 10.4% in HC2, 5% in OKPI 2022, and 6% in OKPI 2019. These observations underscore the nuanced prevalence of lung cancer subtypes in screening programs, emphasizing the importance of considering diverse datasets in clinical and research contexts, particularly in the context of screening efforts (Table 2).

Lung cancer screening projects in central Europe

In the past decade more and more European initiatives have started, most of them pilots—including Italy (MILD) and France (CASCADE), to name a few [21]. In the UK, regional programs have

TABLE 1 Comparison of histological subtypes of screen detected and incidental lung cancer.

	All[d]	Adenocc	Squamousc.cc	Small cell Cc	Other[e]
HC1[a]	29	18 (62.1%)	7 (24.1%)	2 (6.9%)	2 (6.9%)
HC2[b]	48	27 (56.2%)	15 (31.2%)	3 (6.2%)	5 (10.4%)
OKPI[c] data 2022	NA	50%	23%	13%	5%
OKPI[c] data 2019	NA	47%	24%	14%	6%

[a]HUNCHEST I.
[b]HUNCHEST II.
[c]National Korányi Institute for Pulmonology.
[d]In case of HC2 26 patients withdrew from follow-up, exact histological data cannot be collected, therefore excluded.
[e]In both 2019 and 2022 9% of OKPI patients had no exact histological classification.

TABLE 2 Comparison of characteristics of participants in 1st round of screening in HUNCHEST I and II.

	All participants		People who currently smoke		Former or never smokers		Positive screen in 1st round	
	HC1[a]	HC2[b]	HC1	HC2	HC1	HC2	HC1	HC2
Number of participants	1890	4,215	870	3,284	1,020	931	70	174
Age	63.2	61.3	64.5	60.6	62.1	63.1		
Females	1,071 (56.7%)	2,254 (53.5%)	0,564 (55.3%)	1811 (55.1%)	507 (58.3%)	443 (47.6%)	38	97
COPD[c] as comorbidity	351 (18.6%)	556 (13.2%)	258 (24.3%)	439 (13.4%)	103 (11.8%)	117 (12.6%)	19	34

[a]HUNCHEST I.
[b]HUNCHEST II.
[c]Chronic obstructive pulmonary disease.

developed in such an extent, that today the Targeted Lung Health Checks are covering England by 2024 [22]. In 2020 Croatia was the first European country to roll out a nationwide screening project, with enrollment standing at over 29 thousand as the end of 2023 [23]. Historically Poland has a long standing history with LCS starting in 2008—today Poland has also started a nationwide project, based on the voivodeship system [24]. In the Czech Republic the nationwide system is based on pulmonologist, they refer patients in case of existing risk factors to the radiology departments [25]. These efforts reflect a comprehensive approach to lung cancer prevention and early detection across Europe. In Austria, Slovakia, Slovenia, Romania and Serbia no nationwide pilots were rolled out as of date, smaller studies such as the Vojvodina project in Serbia have been established, or in case of Slovakia, a comprehensive white paper has been formulated. Many of these countries, however, are part of the SOLACE project, thus implementation might start in these countries too [26–29].

Ongoing programs

HUNCHEST-III

In anticipation of a potential nationwide screening program, further studies are still necessary. The HUNCHEST I and II programs have provided compelling evidence supporting the cost-effectiveness of LDCT lung cancer screening within the appropriate risk group in Hungary. Notably, these initiatives were characterized by voluntary and opportunistic screening methodologies, focusing on modeling patient pathways post-screening rather than elucidating the routes leading to screening. Recognizing the significance of clarifying pre-screening patient journeys, we recommend a more nuanced approach by modeling primary care patient selection within a more confined population.

The primary dilemma facing lung cancer screening programs is their departure from age-specific screening, unlike other public health screenings, adopting a risk-based approach instead. Currently, there is available literature data regarding the effectiveness of screening individuals aged 50 (55)–75 (80) years with a significant smoking history (25–30 pack-years). Given this, the initiation of screening for this group is imperative. Unfortunately, obtaining precise smoking history is not readily available in most places, making the traditional invitation system based on residency records, as used in other screenings (e.g., breast cancer screening), unsuitable for lung cancer screening.

Illustrating the challenges faced in real-world, non-trial screenings, Kinsinger et al. conducted screening in Veterans Health Administration hospitals from 2013 to 2015, utilizing

NLST criteria. Initially identifying 93,033 individuals meeting the initial screening criteria (age between 55–80 years, no serious comorbidities, and life expectancy of more than 6 months), nurses reviewed their histories, seeking individuals with at least a 30 pack-year smoking history, either current smokers or those who quit within the last 15 years. Due to missing data, 36,555 individuals were excluded, and an additional 38,395 lacked a smoking history suitable for screening. Among the remaining 18,083 individuals, doctors did not assess 13,084 cases, while 789 were deemed unsuitable for LDCT screening. Out of the remaining 4,246 patients, 1,794 declined screening, and eventually, 2,106 screenings were completed within the timeframe. Of these, 59.7% had a positive result based on NLST criteria, detecting suspicious lesions in 73 patients, ultimately confirming lung cancer in 31 cases. The false-positive rate was remarkably high at 97.5%. Additionally, 40.7% of patients had incidental findings, most commonly emphysema and coronary atherosclerosis [30].

Among those who participated in the screening, 1,120 individuals, according to NLST criteria, were expected to attend a follow-up examination after 1 year. Despite repeated invitations via written and telephone communication, only 870 individuals attended. This was less than 78%, significantly lower than the 95% recall success rate assumed in NLST's public health calculations. These challenges underscore the complexities faced in implementing effective lung cancer screening programs, particularly in identifying and engaging the target population.

Thus, the aim of the final HUNCHEST project is to test prescreening pathways. To that effect a smaller, well described population based study was called for. Demographic overview encompassing the settlements affiliated with the "Budakörnyéki egészségprogram" Peri-Budapest Healthcare Program—Biatorbágy, Budajenő, Budakeszi, Herceghalom, Nagykovácsi, Páty, Perbál, Pilisjászfalu, Remeteszőlős, Telki, Tinnye, Tök collectively house approximately 60–65,000 residents. Within this demographic, an estimated 12,000 individuals fall within the 50–75 age bracket, with an anticipated 3,500–4,000 individuals exhibiting a substantial history of tobacco use. The overarching objective is to meticulously map the smoking history of all individuals within the specified age group, facilitating the identification and subsequent invitation of those at risk for LDCT screening.

The success of the screening program hinges upon the active involvement of general practitioners and their assistants. Their pivotal role involves assessing the smoking history of individuals aged 50–75 in their respective areas and discerning those deemed suitable for screening. Furthermore, at this juncture, a targeted smoking minimal intervention is administered. Following this initial phase, coordination with the Comprehensive Cancer Center's coordinator ensues, whereby the collected information is meticulously recorded within the HUNCHEST platform.

We anticipate that 20% of screened patients will be recalled for a 3-month follow-up assessment based on our previous pilots. Based on the HUNCHEST program, the lung cancer identification rate is projected to range between 1.5%–2% in Hungary. This implies the potential detection of approximately 80 cases of lung cancer, with a substantial majority—around 70%—being identified in the early stages. This comprehensive approach holds the promise that approximately 65 patients may receive a genuine opportunity for long-term survival.

The HUNCHEST-III project is currently in the active recruitment phase, screening started in September 2023, preliminary results are excepted in early 2025.

SOLACE

In 2022, the EU4Health project introduced a groundbreaking initiative aligned with Europe's Beating Cancer Plan—the Strengthening the screening of Lung Cancer in Europe (SOLACE) project [31]. This innovative endeavor aims to streamline the implementation of lung cancer screening programs across Europe, ensuring equitable access for individuals from diverse social and economic backgrounds. Representing a significant stride in comprehensive lung cancer screening, SOLACE is dedicated to developing, testing, and disseminating tools that address identified obstacles and health inequalities in various European countries.

The primary goal of SOLACE is to provide a versatile toolbox for personalized approaches to lung cancer screening, applicable on both national and regional scales. The project specifically focuses on facilitating and supporting the structured implementation of LDCT lung cancer screening programs throughout Europe. By doing so, SOLACE aims to enhance the overall quality of lung cancer screening practices, while also improving accessibility, benefit-harm balance, and cost-effectiveness.

A key feature of SOLACE involves unprecedented collaboration among key stakeholders essential for designing, planning, and implementing sustainable lung cancer screening programs in member states. To ensure the lasting impact of the project, the proposal includes the establishment of the European Lung Cancer Screening Alliance (ELCSA).

Hungary actively participates in SOLACE with three centers, notably including the OKPI. Over the next 18 months, the project will test various recruitment strategies to measure their effectiveness in targeting different groups, with a special focus on the socio-economically deprived and on those with preexisting pulmonary comorbidities. Notably, the project places a particular emphasis on women, recognizing the insufficient data on lung cancer screening strategies in the female population.

TABLE 3 Comparison of the different HUNCHEST studies.

	HUNCHEST I	HUNCHEST II	HUNCHEST III
aim	Demonstrating the feasibility of LCS in Hungary	Establishing patient pathways	Modelling population wide screening (estimated 4,000 at risk—determining efficacy of invitation methods)
date	2013-20	2019-22	2023-ongoing
criteria	50–79 both smokers and neversmokers	50–75 20 + pys	50–75 20 + pys
participants	1,890	4,215	TBA
Lung cancers found	1.5%	1.8%	TBA

Conclusion

With the 3 HUNCHEST projects, we have modeled the three pillars of screening: the technical implementation of screening, the design of patient pathways post-screening, and the identification and invitation of high-risk patients, as seen in Table 3. The next step is to determine the feasibility of a potential public health screening. In the meantime, it may be advisable for the health administration to create a means allowing high-risk individuals to participate in LDCT screening once a year.

Considering the future of large-scale LDCT screenings, key questions arise regarding the application of artificial intelligence (AI) and deep learning models to address human resource challenges. Furthermore, there is a need to determine additional biomarkers for individuals currently not in high-risk groups, such as non-smokers or young individuals, in order to develop screening in potentially identifiable risk groups, while adhering a thorough cost/benefit analysis.

The integration of AI and deep learning models in LDCT screenings presents a promising avenue for enhancing efficiency and accuracy in diagnosis. This technological advancement can alleviate human resource constraints by automating the analysis of LDCT results, and enabling quicker and more precise identification of potential tumors. Adequate training for healthcare professionals in collaboration with AI systems will be crucial to optimize this integration.

Identifying biomarkers beyond the current high-risk groups is essential. Research efforts should focus on exploring additional biomarkers that can aid in identifying low-risk groups more accurately. Factors such as genetic predispositions, environmental exposures, and other elements should be considered to refine the screening criteria and ensure a more targeted approach.

Conducting comprehensive cost/benefit analyses is imperative for shaping effective screening programs. Evaluating the costs against potential savings and improvements in patients' quality of life will provide insights into the economic viability of such programs. Considering the long-term health and economic impacts is crucial in making informed decisions.

Author contributions

All authors participated in the design, interpretation of the studies and analysis of the data and review of the manuscript, AK-F was responsible for writing the article, with KB editing.

Funding

The author(s) declare(s) that no financial support was received for the research, authorship, and/or publication of this article.

Conflict of interest

The authors declare that the research was conducted in the absence of any commercial or financial relationships that could be construed as a potential conflict of interest.

Acknowledgments

The authors would like to thank the team of the National Korányi Institute for Pulmonology for their continuous support of the LDCT-LCS effort.

References

1. Timmermann C. Lung cancer and consumption in the nineteenth century: bodies, tissues, cells and the making of a rare disease. In: *A history of lung cancer. Science, technology and medicine in modern history*. London: Palgrave Macmillan (2014).

2. Központi Statisztikai Hivatal *4.1.1.25. Reported new malignant neoplasms** (2023). Available from: https://www.ksh.hu/stadat_files/ege/hu/ege0025.html (Accessed December 1, 2023).

3. Blandin Knight S, Crosbie PA, Balata H, Chudziak J, Hussell T, Dive C. Progress and prospects of early detection in lung cancer. *Open Biol* (2017) 7:170070. doi:10.1098/rsob.170070

4. Kubik A, Parkin DM, Khlat M, Erban J, Polak J, Adamec M. Lack of benefit from semi-annual screening for cancer of the lung: follow-up report of a randomized controlled trial on a population of high-risk males in Czechoslovakia. *Int J Cancer* (1990) 45(1):26–33. doi:10.1002/ijc.2910450107

5. Tockman MS. Survival and mortality from lung cancer in a screened population. *CHEST* (1986) 89(4):324S–5S. doi:10.1378/chest.89.4_Supplement.324S-a

6. Fontana RS, Sanderson DR, Woolner LB, Taylor WF, Miller WE, Muhm JR. Lung cancer screening: the Mayo program. *J Occup Med* (1986) 28(8):746–50. doi:10.1097/00043764-198608000-00038

7. National Cancer Institute *Prostate, lung, colorectal, and ovarian cancer screening trial (PLCO)* (2023). Available from: https://prevention.cancer.gov/major-programs/prostate-lung-colorectal-and-ovarian-cancer-screening-trial-plco (Accessed December 1, 2023).

8. Ostoros G, Ajkay Z, Böszörményi NG, Kovács G. Gondolatok a tüdőrák szűrővizsgálatáról. *Orvosi Hetilap* (1998) 139(42):2491–4.

9. Korányi Bulletin *Korányi bulletin* (2023). Available from: https://szakmai.koranyi.hu/bulletin/ (Accessed December 1, 2023).

10. Henschke CI, McCauley DI, Yankelevitz DF, Naidich DP, McGuinness G, Miettinen OS, et al. Early Lung Cancer Action Project: overall design and findings from baseline screening. *Lancet* (1999) 354:99–105. doi:10.1016/S0140-6736(99)06093-6

11. The National Lung Screening Trial Research TeamAberle DR, Adams AM, Berg CD, Black WC, Clapp JD, et al. Reduced lung-cancer mortality with low-dose computed tomographic screening. *N Engl J Med* (2011) 365:395–409. doi:10.1056/NEJMoa1102873

12. U.S. Preventive Services Task Force (USPSTF) *Lung cancer: scrrening* (2021). Available from: https://www.uspreventiveservicestaskforce.org/uspstf/recommendation/lung-cancer-screening (Accessed December 1, 2023).

13. Yong PC, Sigel K, Rehmani S, Wisnivesky J, Kale MS. Lung cancer screening uptake in the United States. *Chest* (2020) 157(1):236–8. doi:10.1016/j.chest.2019.08.2176

14. de Koning HJ, van der Aalst CM, de Jong PA, Scholten ET, Nackaerts K, Heuvelmans MA, et al. Reduced lung-cancer mortality with volume CT screening in a randomized trial. *N Engl J Med* (2020) 382(6):503–13. doi:10.1056/NEJMoa1911793

15. Kauczor HU, Bonomo L, Gaga M, Nackaerts K, Peled N, Prokop M, et al. ESR/ERS white paper on lung cancer screening. *Eur Radiol* (2015) 25(9):2519–31. doi:10.1007/s00330-015-3697-0

16. Oudkerk M, Devaraj A, Vliegenthart R, Henzler T, Prosch H, Heussel CP, et al. European position statement on lung cancer screening. *Lancet Oncol* (2017) 18(12):e754–66. doi:10.1016/S1470-2045(17)30861-6

17. Kerpel-Fronius A, Monostori Z, Kovacs G, Ostoros G, Horvath I, Solymosi D, et al. Nationwide lung cancer screening with low-dose computed tomography: implementation and first results of the HUNCHEST screening program. *Eur Radiol* (2022) 32:4457–67. doi:10.1007/s00330-022-08589-7

18. Nagy B, Szilberhorn L, Győrbíró DM, Moizs M, Bajzik G, Kerpel-Fronius A, et al. Shall we screen lung cancer with low-dose computed tomography? Cost-effectiveness in Hungary. *Value Health Reg Issues* (2023) 34:55–64. doi:10.1016/j.vhri.2022.10.002

19. Kerpel-Fronius A, Megyesfalvi Z, Markóczy Z, Solymosi D, Csányi P, Tisza J, et al. HUNCHEST-II contributes to a shift to earlier-stage lung cancer detection: final results of a nationwide screening program. *Eur Radiol* (2023). doi:10.1007/s00330-023-10379-8

20. Forte GC, Altmayer S, Silva RF, Stefani MT, Libermann LL, Cavion CC, et al. Deep learning algorithms for diagnosis of lung cancer: a systematic review and meta-analysis. *Cancers* (2022) 14:3856. doi:10.3390/cancers14163856

21. Wait S, Alvarez-Rosete A, Osama T, Bancroft D, Cornelissen R, Marušić A, et al. Implementing lung cancer screening in Europe: taking a systems approach. *JTO Clin Res Rep* (2022) 3(5):100329. doi:10.1016/j.jtocrr.2022.100329

22. NHS *Blog* (2024). Available from: https://www.england.nhs.uk/blog/rolling-out-targeted-lung-health-checks/ (Accessed April 1, 2024).

23. Schmidt S *Sebastian Schmidt: lung cancer screening – results from Croatia* (2024). Available from: https://oncodaily.com/blog/38363.html (Accessed April 1, 2024).

24. Lung Cancer Policy Network *LDCT screening pilots in Poland* (2022). Available from: https://www.lungcancerpolicynetwork.com/lung-cancer-screening-in-poland/ (Accessed April 1, 2024).

25. Prevenceproplice *Prevenceproplice* (2024). Available from: https://www.prevenceproplice.cz/en/about/ (Accessed April 1, 2024).

26. Pirker R, Prosch H, Popper H, Klepetko W, Dieckmann K, Burghuber OC, et al. Lung cancer in Austria. *J Thorac Oncol* (2021) 16(5):725–33. doi:10.1016/j.jtho.2020.10.158

27. Juskanic D, Sandor F, Denkova L, Juhos P, Janik M, Hontzas J, et al. Lung cancer screening initiative in Slovakia: guidelines of screening implementation. *Bratisl Lek Listy* (2023) 124(2):109–15. doi:10.4149/BLL_2023_016

28. Štupnik T. Thoracic surgery in Slovenia. *J Thorac Dis* (2022) 14(6):2326–34. doi:10.21037/jtd-21-1172

29. Cavic M, Kovacevic T, Zaric B, Stojiljkovic D, Korda NJ, Rancic M, et al. Lung cancer in Serbia. *J Thorac Oncol* (2022) 17(7):867–72. doi:10.1016/j.jtho.2022.04.010

30. Kinsinger LS, Anderson C, Kim J, Larson M, Chan SH, King HA, et al. Implementation of lung cancer screening in the Veterans health administration. *JAMA Intern Med* (2017) 177(3):399–406. doi:10.1001/jamainternmed.2016.9022

31. SOLACE *Strengthening the screening of lung cancer in Europe* (2023). Available from: https://europeanlung.org/solace/ (Accessed December 1, 2023).

Pathology & Oncology Research | frontiers

TYPE Brief Research Report
PUBLISHED 14 July 2023
DOI 10.3389/pore.2023.1611167

Check for updates

OPEN ACCESS

EDITED BY
Krenács Tibor,
Semmelweis University, Hungary

*CORRESPONDENCE
Beryl Rabindran,
baugustine@perimetermed.com

RECEIVED 08 March 2023
ACCEPTED 05 July 2023
PUBLISHED 14 July 2023

CITATION
Rabindran B and Corben AD (2023), Wide-field optical coherence tomography for microstructural analysis of key tissue types: a proof-of-concept evaluation.
Pathol. Oncol. Res. 29:1611167.
doi: 10.3389/pore.2023.1611167

COPYRIGHT
© 2023 Rabindran and Corben. This is an open-access article distributed under the terms of the Creative Commons Attribution License (CC BY). The use, distribution or reproduction in other forums is permitted, provided the original author(s) and the copyright owner(s) are credited and that the original publication in this journal is cited, in accordance with accepted academic practice. No use, distribution or reproduction is permitted which does not comply with these terms.

Wide-field optical coherence tomography for microstructural analysis of key tissue types: a proof-of-concept evaluation

Beryl Rabindran[1]* and Adriana D. Corben[2]

[1]Perimeter Medical Imaging AI, Toronto, ON, Canada, [2]Icahn School of Medicine at Mount Sinai, Mount Sinai Hospital, New York, NY, United States

Introduction: The presence of positive margins following tumor resection is a frequent cause of re-excision surgery. Nondestructive, real-time intraoperative histopathological imaging methods may improve margin status assessment at the time of surgery; optical coherence tomography (OCT) has been identified as a potential solution but has not been tested with the most common tissue types in surgical oncology using a single, standardized platform.

Methods: This was a proof-of-concept evaluation of a novel device that employs wide-field OCT (WF-OCT; OTIS 2.0 System) to image tissue specimens. Various cadaveric tissues were obtained from a single autopsy and were imaged with WF-OCT then processed for permanent histology. The quality and resolution of the WF-OCT images were evaluated and compared to histology and with images in previous literature.

Results: A total of 30 specimens were collected and tissue-specific microarchitecture consistent with previous literature were identified on both WF-OCT images and histology slides for all specimens, and corresponding sections were correlated. Application of vacuum pressure during scanning did not affect specimen integrity. On average, specimens were scanned at a speed of 10.3 s/cm^2 with approximately three features observed per tissue type.

Conclusion: The WF-OCT images captured in this study displayed the key features of the most common human tissue types encountered in surgical oncology with utility comparable to histology, confirming the utility of an FDA-cleared imaging platform. With further study, WF-OCT may have the potential to bridge the gap between the immediate information needs of the operating room and the longer timeline inherent to histology workflow.

KEYWORDS

histopathology, breast-conserving surgery, histology, optical coherence tomography, intraoperative margin assessment

Abbreviations: BCS, breast-conserving surgery; FDA, food and drug administration; OCT, optical coherence tomography; WF-OCT, wide-field optical coherence tomography.

Introduction

Surgical excision remains the first-line treatment for localized, early-stage solid tumors arising from cancers of the breast, colon and rectum, kidney, lung, thyroid, and those of other tissues and organs [1, 2]. Its effectiveness is dependent upon the complete removal of diseased tissue, ideally encapsulated within a safe margin of healthy, normal tissue. In breast-conserving surgery (BCS), for example, histopathologically "clear" or "negative" tumor margins have been associated with a twofold decrease in tumor recurrence [3, 4], which in turn has a significant favorable impact on overall morbidity, mortality, and the economics of managing breast cancer [3–5].

When, on pathological examination, cancerous cells are found at or near the margin of the tumor, additional tissue must be removed from the resection bed to reduce the risk of disease recurrence [6]. For example, in BCS, re-excision for positive or close margins is indicated when disease is detected within 2 mm from the tumor surface for *in situ* disease, and less than 1 mm for invasive disease [4, 5, 7]. Unfortunately, the typical timeframe for standard-of-care histological analysis of excised tissue is on the order of days to weeks; therefore, a positive margin generally necessitates a return to the operating room for a second surgery. Re-excision has been estimated to occur in greater than 20% of cases on average and has been independently associated with poorer clinical outcomes, higher costs of care, and reduced patient satisfaction with treatment [8–12].

Methods that can provide a rapid, thorough, and non-destructive intraoperative assessment of excisional tissue margins have the potential to improve the overall success of primary tumor resection, minimize the incidence of re-excision surgeries and local tumor recurrence, and improve costs of care [6]. Their development is, accordingly, of paramount importance for patients, surgeons, healthcare systems, and payors [13].

Optical coherence tomography (OCT) is one of the oldest and most extensively studied tomographic modalities for imaging of human tissues on a microscopic scale [14]. First described for imaging of the retina and coronary arteries in the 1990s [15], OCT uses near infra-red interferometry to produce cross-sectional images of biological tissues. The underlying principle is analogous to ultrasound imaging; in the case of OCT, light (1,250–1,350 nm) responds to differences in refractive index and optical scattering and absorption properties associated with the structures found in biological tissues [14, 16, 17]. The echo and time delay of the reflected, backscattered light are exploited to generate images with an axial resolution of 6–15 μm at a penetration depth up to 2 mm. Thus, OCT facilitates rapid, non-destructive visualization of clinically relevant tissue microarchitecture at or near the surface of a tissue sample without sectioning, labeling, or other preparation. OCT has a long history of use in ophthalmology [14, 18], and has been adapted to intravascular assessment of atherosclerotic disease [14, 16, 19].

In 2016, a wide-field optical coherence tomography (WF-OCT) imaging platform (OTIS 1.0 System, Perimeter Medical Imaging AI, Inc. Toronto, Canada) was cleared to market by the US FDA for general imaging of tissue microstructure. With WF-OCT a user can view real-time, high-resolution, cross-sectional tissue images up to 2 mm in depth from the tissue surface. Image resolution is approximately 30 μm and imaging requires no use of chemicals or radiolabeling and does not affect the sample quality for subsequent histology [20–23]. The system has previously demonstrated the ability to evaluate tissue specimens in oropharyngeal cancer resections prior to routine pathology, including margin assessment without specimen damage or disruption of workflow, in addition to utility in imaging the margin of resected breast tissue at the time of surgery [20–23, 23, 24]. Other studies of the system with single and multiple readers have demonstrated a high degree of concordance between breast tissue margin assessment based on WF-OCT and the corresponding histology slides, with greater than 85% sensitivity and specificity for identifying tissue changes suspicious for malignancy. There remains, however, a greater need to investigate the comparability of WF-OCT images to histology in more tissue types, in both normal and pathological states, on a single, standardized platform. Accordingly, we conducted a proof-of-concept study to assess whether WF-OCT images from the system had sufficient quality and resolution to identify tissue microstructures unique to the most common tissue types encountered in surgical oncology, as assessed by qualified clinicians.

Materials and methods

This was a proof-of-concept study using a commercial WF-OCT system on multiple tissue types obtained from a single autopsy. The study objective was to assess whether images generated by the system were sufficiently detailed to allow qualified clinician reviewers to resolve near-surface tissue microstructures on the order of 50 μm, identify key strata therein (e.g., epithelial, adipose, and stromal tissue), and correlate them to histology slides of the same sample. The study was also intended to investigate whether or not specimen integrity and viability for standard pathology processing were compromised during system use, and that the user interface adequately enabled the reviewers to interact with acquired scans.

Ethics

The deidentified human tissue used for this study was procured via autopsy by the Biorepository of the Icahn School of Medicine at Mount Sinai Hospital (New York, NY, United States), from a cadaver donated for research purposes. Ethical approval was obtained by the Biorepository at the Icahn School of Medicine

for the use of the human cadaver in this study, including informed written consent from the legally authorized representative. The protocol was granted an exemption from ethics approval by the Institutional Review Board of Mount Sinai Hospital. The study sponsor did not have access to protected health information.

WF-OCT system

A newer version of the original system was used in this study (OTIS 2.1 System); the device received FDA 510(k) clearance in 2021 for use as an imaging tool in the evaluation of excised human tissue microstructure by providing two-dimensional, cross-sectional, real-time depth visualization, with image review manipulation software for identifying and annotating regions of interest. The device can obtain OCT images with sufficient image quality to identify tissue microstructure in thyroid, colon, ovary, uterus, cervix, skin and breast tissue; however, the system has a general indication in the US and is not specifically indicated for use in any tissue types. The system comprises a console for specimen scanning and a disposable component for specimen handling. The console is a mobile cart that provides automated OCT scanning of individual margins of the excised specimen. To scan, the user positions the specimen against the flat, OCT-transparent imaging window of the consumable set. A user-adjustable level of vacuum is applied to secure the tissue in place. The vacuum pressure also reduces the gap between the glass surface and the tissue, thereby ensuring good image quality. The scanner employs an automated image probe positioning mechanism to enable rapid capture of multiple, small, conventional OCT images from excised tissue surfaces. The software tiles these images into stacks for review by the user, providing microscopic visualization of cross-sectional images at a depth of up to 2 mm below the surface of a sample, with a maximum size of 9 cm × 9 cm at approximately 30 μm resolution.

The console has a user interface system with a touch screen that allows for data input and clinician review of collected images. The OCT images are paired with photographic surface images via review software that allows clinicians to identify, manipulate, and annotate regions of interest.

Study procedures

Specimen preparation, imaging, and histology

The study was conducted at Mount Sinai Hospital on excised, cadaveric human tissue retained for research purposes and procured within 24 h following death.

The specimen preparation workflow is summarized in Supplementary Figure S1. Tissue samples were resected and grossed using standard methodology at the autopsy laboratory. A total of three specimens were excised for each tissue type. For WF-OCT image acquisition, each sample was dotted with specimen ink to mark orientation, placed in a disposable tray, and positioned on the specimen window. Each specimen was then photographed for documentation purposes and secured in place using either low, high, or no vacuum pressure to compare the effect of vacuum on specimen integrity (one specimen per tissue type at each vacuum setting). After scanning, each specimen was again photographed and palpated by the pathologist to assess tissue integrity after vacuum application.

Following photography and OCT image capture, each of the three specimens was fully inked, grossed, placed in a specimen cassette, and fixed in neutral buffered formalin. Specimens were then transported to the Biorepository CoRE lab at Mount Sinai Medical Center, where they were processed into slides, stained with hematoxylin and eosin (H&E), and then digitized for further analysis.

Specimen review and correlations

A pathologist from Mount Sinai Hospital (ADC) reviewed and annotated the digitized histology slides using CaseViewer (version 2.2, 3DHISTECH Ltd., Budapest, Hungary), noting the microstructures and other features pertinent to each specific tissue type.

Separately, WF-OCT images were reviewed and annotated by a lead clinical scientist (BR) from the study sponsor, using the OTIS software (version 2.0.10, loaded on a Windows-based workstation), as well as a clinical leader from the sponsor to validate the annotations. To assist review, the clinical scientist used reference images from a number of prior publications showing correlations between swept-source or other OCT approaches and histology for some of the tissue types used in this study [25–32].

Once the separate reviews were complete, the histology slides were correlated with the OCT images that displayed corresponding layers and microstructures and the B-scan number (optical "slice") of each OCT image was noted. This correlation work enabled the creation of an atlas of the appearance of tissue-specific layers and microstructures in the OCT images.

Data analysis

This was a proof-of-concept evaluation. The time taken to scan each tissue specimen as well as the sizes of the specimens were noted (Table 1). The features observed in each tissue type were tabulated and displayed descriptively. The features observed in reference images [25–32] were also tabulated, providing a side-by-side comparison of previous studies with this device (Table 2).

Results

Tissue preparation, OCT imaging, and tissue integrity

All tissues for this study were excised from a deceased, 68-year-old female donor secondary to hemorrhagic and septic

TABLE 1 Specimen sizes and scan times.

Tissue type	#	Vacuum level	Specimen sizes (cm) L, B, W			Scan area selected (cm) L, B		Total scan area (cm^2)	Scan time (sec)	Scan time/area (sec/cm^2)
			L	B	W	L	B			
Breast	1	Control	5	5	0.5	N/A	N/A	N/A	N/A	N/A
		Low	5	7	0.5	2	3	6	58	9.67
		High	4.5	6	0.5	2	2	4	39	9.75
Heart	2	Control	6	2	0.5	N/A	N/A	N/A	N/A	N/A
		Low	5	3	0.5	2	2	4	39	9.75
		High	6	3	1	2	1	2	20	10.00
Kidney	3	Control	3.5	2.5	1	N/A	N/A	N/A	N/A	N/A
		Low	3	1.5	1	2	1	2	20	10.00
		High	3	1.5	0.5	2	1	2	20	10.00
Spleen	4	Control	8	6.5	1	N/A	N/A	N/A	N/A	N/A
		Low	8	5	1	3	3	9	86	9.56
		High	8	5	1	3	3	9	86	9.56
Thyroid	5	Control	2	1.5	0.5	N/A	N/A	N/A	N/A	N/A
		Low	4	1.8	0.5	1	3	3	30	10.00
		High	2	1	0.5	1	2	2	20	10.00
Adrenal	6	Control	2	1.5	0.5	N/A	N/A	N/A	N/A	N/A
		Low	2.5	2	0.5	2	2	4	39	9.75
		High	3	2.5	0.5	1	2	2	20	10.00
Pancreas	7	Control	3.5	2.5	1	N/A	N/A	N/A	N/A	N/A
		Low	2.5	3.5	1	1	2	2	39	19.50
		High	6.5	2	2	2	2	4	39	9.75
Liver	8	Control	10	4.5	1.5	N/A	N/A	N/A	N/A	N/A
		Low	10	7	1	3	3	9	86	9.56
		High	11	6.5	1	3	3	9	86	9.56
Lung	9	Control	2	3	0.5	N/A	N/A	N/A	N/A	N/A
		Low	3.5	2	0.5	2	2	4	39	9.75
		High	3.5	2.5	0.5	2	2	4	39	9.75
Colon	10	Control	6	2	0.3	N/A	N/A	N/A	N/A	N/A
		Low	7.5	3.5	0.3	2	2	4	39	9.75
		High	4.5	2	0.5	3	2	6	58	9.67
Average			**5.03**	**3.31**	**0.74**	**2.05**	**2.15**	**4.55**	**45.10**	**10.27**

The table above shows the sizes of the different tissue specimens scanned. The scan areas and scan times for the specimens scanned on low and high vacuum pressure are shown as well. The control specimen was not scanned and used as a control to compare specimen integrity with the specimens scanned on low and high vacuum.
Tissue type: Type of tissue scanned using WF-OCT; #: Number; Vacuum level: Vacuum setting on WF-OCT device used to secure the specimen in place; Specimen sizes (cm) L, B, W: Size of specimen scanned using WF-OCT. L-Length, B-Breadth, W- Width; Scan area selected (cm) L, B: Dimensions of scan area selected on the WF-OCT device for scanning. L- Length, B-Breadth; Total scan area (cm^2): L*B from column 5 (scan area selected); corresponds to the total area scanned on the specimen; Scan time (sec): Time taken to scan this area on the specimen; Scan time/area (sec/cm^2): Time taken to scan per cm^2 of the specimen.

TABLE 2 Summary of features resolvable in reference publications and WF-OCT.

#	Tissue	References	Layers/Features resolved in literature	Layers/Features resolved in WF-OCT	Number of features resolved in literature	Number of features resolved in WF-OCT
1	Breast	[27]	Adipose tissue, Fibrous tissue (stroma), Duct	Adipose tissue, Fibrous tissue (stroma), Duct	3	3
2	Heart	[26]	Adipose Tissue, Collagen, Myocardium	Adipose tissue, Muscle	3	2
3	Kidney	[31]	Glomerulus, Tubules	Glomerulus, Vessel	2	2
4	Thyroid	[25]	Follicles, Stroma, Capsule	Follicles, Stroma, Capsule, Cyst, Vessel	3	5
5	Pancreas	[29]	Cysts	Vessel, Adipose tissue, Parenchyma	1	3
6	Liver	[32]	Vessel, Connective tissue layers, Serosa, Epithelium	Vessel, Fibrosis, Duct	4	3
7	Lung	[28]	Necrosis, Fibrosis	Vessel, Alveoli	2	2
8	Colon	[30]	Upper-Mucosa, Muscularis Mucosae, Sub-Mucosa, Muscularis propria, Crypts	Upper-Mucosa, Sub-Mucosa, Muscularis propria	5	3
	Average				2.875	2.875

The table above provides a summary of the features observed in each of the tissue types against those in reference publications. It also shows a comparison of the number of features observed in literature for each tissue type and the number of features observed using WF-OCT. Two tissue types were not included in the table because no reference publications showing the OCT images for these tissue types were available—Spleen and Adrenal Glands.

shock from a bacterial infection. Her past medical history was significant for renal failure, liver cirrhosis, and emphysema. Tissue specimens were excised and imaged within 24 h of death.

Ten tissue types were scanned from this patient, with three specimens taken per tissue type. These three specimens were scanned at no vacuum, low vacuum and high vacuum pressure respectively, for each tissue type. Table 1 shows the sizes of all 30 specimens, along with the scan areas of the specimens scanned at low and high vacuum. The average size of the specimen scanned was 5.0 cm × 3.3 cm × 0.74 cm. For an average scan area of 2.0 × 2.2 cm^2, the average scan time was 45.1 s, at the rate of 10.3 s/cm^2.

All 30 of the specimens included in the primary evaluation were successfully scanned and processed. The pathologist confirmed that specimen integrity and viability for routine pathology processing was not compromised when specimens were scanned under vacuum at any setting, showing that using vacuum is safe for specimen scanning using this WF-OCT device for the ten tissue types scanned in this study. Images of the gross, unprocessed specimens before and after OCT scanning are displayed in the Supplementary Material.

For all 10 tissue types, we looked at previous literature to determine what other features had been observed in similar studies using OCT [25–32]. We tabulated the features seen previously using OCT against the features we saw using WF-OCT (Table 2). We found references for eight tissue types; spleen and adrenal glands did not have any prior publications showing OCT images. For the eight tissue types that we compared, on average 2.875 features/tissue type were observed in literature. This was the same as the average number of features observed in WF-OCT, with no significant difference in the number of features observed in previous studies vs. in this study ($p > 0.05$).

Comparative histology

The pathologist confirmed that the appearance of both healthy and diseased tissue in the histology slides was as expected in clinical practice, given the tissue donor's health status at time of death. Further, the observed tissue architecture was comparable between the WF-OCT images and the corresponding histology, both for healthy and diseased tissue types.

Representative image correlations between the WF-OCT images and histology slides from each tissue type are displayed in Figures 1, 2. Adipose tissue, fibrous tissue (stroma), and ducts were observed in the breast tissue in both WF-OCT images and histology slides (Figure 1). The thyroid specimens displayed follicles, stroma, capsule, a cyst, and a vessel (Figure 1).

Glomeruli and vessels could be observed in the kidney specimens, both by histology and WF-OCT (Figure 1). Tubules were not observed with WF-OCT, and histology showed dying/necrotic tubules with lack of discernible nuclei, consistent with renal failure. The liver was fibrotic due to cirrhotic disease, and although the fibrotic tissue structure could be observed in both histology and WF-OCT, neither method was able to detect connective tissue nor serosa layers. However, vessels and ducts were observed in both histology and WF-OCT images (Figure 1). Both WF-OCT and histology images displayed normal lung features such as alveoli and vessels, with evidence of localized inflammation and damaged alveoli characteristic of emphysema (Figure 1).

In the colon specimens, the upper mucosa, submucosa, and muscularis propria layers were identified in both histology and WF-OCT images (Figure 2). Crypts were not observed by either

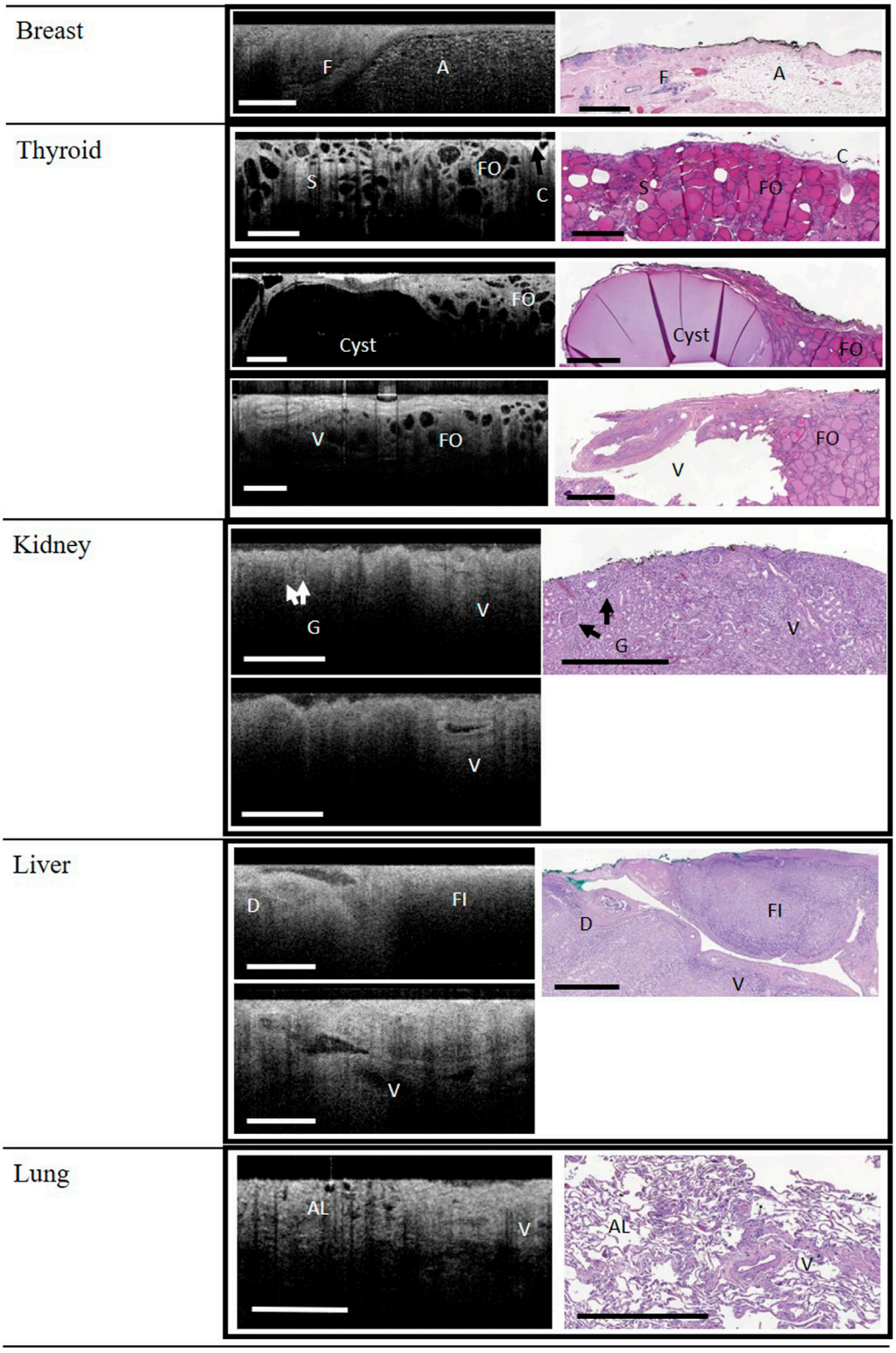

FIGURE 1
WF-OCT images and correlated histology from Breast, Thyroid, Kidney, Liver and Lung. Reference images for kidney and liver (lower panels) demonstrate that vessels (V) could be followed across multiple WF-OCT image slices. Abbreviations: A, adipose tissue; C, Capsule; F, fibrous tissue; FO, follicle; S, Stroma; AL, alveoli; D, Duct; Fl, fibrosis; G, glomerulus; V, vessel; WF-OCT, wide-field optical coherence tomography. Scale bar: 1 mm.

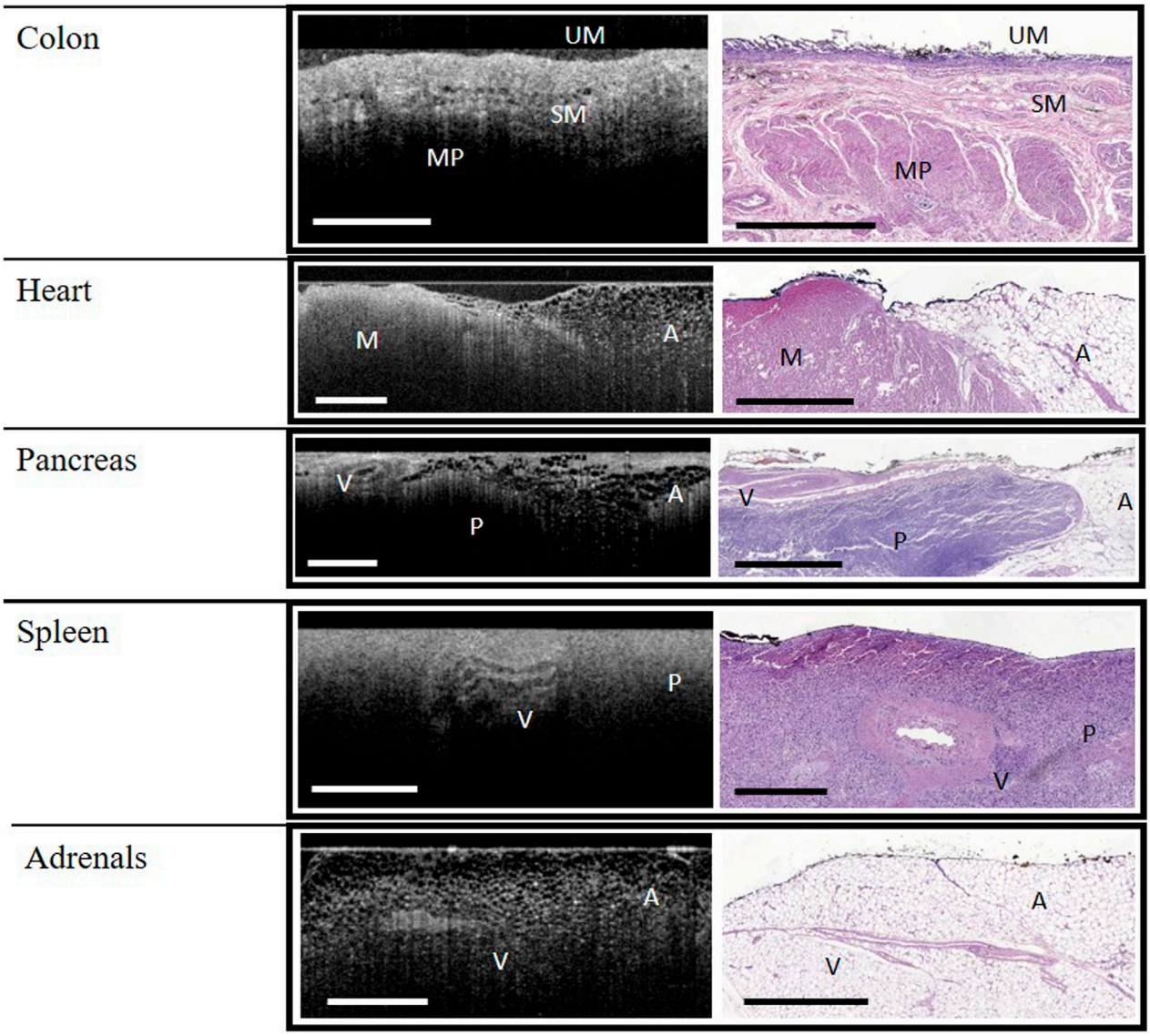

FIGURE 2
WF-OCT images and correlated histology from Colon, Heart, Pancreas, Spleen and Adrenal Glands. Abbreviations: A, adipose tissue; M, muscle; MP, muscularis propria; P, parenchyma; SM, submucosa; UM, upper mucosa; V, vessel; WF-OCT, wide-field optical coherence tomography. Scale bar: 1 mm.

method, and a lower-than-expected density of glands on the tissue surface was attributed to autolysis. While both adipose and muscle tissues were observed in the heart specimens, collagen and myocardium layers were not observed by either method (Figure 2). Features observed in the pancreas specimens, by both histology and WF-OCT imaging, were adipose tissue, parenchyma, and vessels (Figure 2).

The features observed in both histology and WF-OCT images of the spleen were vessels and parenchyma. Vessels and adipose tissue were observed in the adrenal tissue (Figure 2).

General usability and image quality

A notable feature of the WF-OCT analysis on this system was the ability to "scroll" between multiple image slices rapidly, in essence allowing the evaluator to visualize microstructures through a 3-dimensional volume of tissue. Indeed, as shown in Figures 1, 2, the pathway of vessels in thyroid, kidney, and liver specimens could be followed through the specimen. Video examples of this feature are shown in Supplementary Videos S1–S3.

The evaluators noted an anecdotal observation that the quality of the WF-OCT images acquired for this study were at

least comparable to and in most cases of higher quality than those generated by swept-source devices as found in the literature [25–32], and overall image quality contributed to the ease of interpretation of the images.

Discussion

In this proof-of-concept study of a standardized platform for WF-OCT imaging, trained clinicians were consistently able to identify normal and pathologic tissue-specific layers, features, and microstructures in 10 different tissue types, collected via autopsy of a donor with a known clinical course. In some cases—especially in the kidneys, liver, and lungs—the tissue microarchitecture was observably abnormal, secondary to ongoing disease processes at the donor's time of death; however, it is notable that by histology, the observed changes were consistent with the clinical course and that they could be correlated to corresponding features observed in the WF-OCT images. In other words, the WF-OCT images and histology slides demonstrated both normal and pathological tissue features consistent with the donor's clinical history. Thus, the objectives of the study were met.

Although none of the tissue types analyzed in the present study were malignant, this study has important implications for the use of WF-OCT as an adjunctive imaging technique for real-time review of tissue microarchitecture. At this time, there are a number of adjunctive techniques and technologies for assessing intraoperative margin status, but each has limitations that affect overall utility for clinical management [6, 33]. For example, while intraoperative frozen section analysis has demonstrated high sensitivity and specificity, the technique is costly, technically difficult, and may compromise the sample's integrity for histology [6, 33]. Imprint cytology is moderately sensitive and specific but requires specialized expertise in sample preparation and interpretation and is not able to distinguish *in situ* vs. invasive disease, or measure margin depth [33]. Specimen radiography and intraoperative ultrasound have also demonstrated high intraoperative utility, however neither is able to reliably detect noncalcified nor nonpalpable lesions, respectively, and microscopic analysis at the margin is impossible with these methods [6, 33]. Finally, although a radiofrequency spectroscopy device (Margin Probe, Dune Medical, Alpharetta, Georgia) was previously cleared by the FDA to differentiate benign from malignant breast tissue at the margin, the device's pivotal trial to market clearance demonstrated that the low overall specificity (46.4%; 95% CI: 42.9–49.9) of the technology led to a tripling of the false-positive rate (53.6% vs. 16.6% for the device and control arms, respectively) and an unacceptably high number of unnecessary cavity shaves to remove additional tissue at the margins [34, 35].

Already in use for ophthalmic and intravascular clinical and translational applications [36–39], OCT capitalizes on the light-scattering properties of biologic tissues to generate cross-sectional images of microscopic features and structures, in both nontransparent and transparent tissues [17, 39]. There are several important rationales for using this technique to assess tumor surface features during surgery. First, OCT specimen preparation is nondestructive and label-free, and does not expose patients or clinicians to ionizing radiation. Second, images are generated in real time, at a clinically relevant depth and resolution [6, 17]. Lastly, because OCT is non-destructive, it does not affect downstream histology, and as shown in this report and others, the images generated by WF-OCT can be matched, correlated to, and validated against the permanent histology in both healthy and diseased tissue [20–23].

Regarding its use for real-time intraoperative margin assessment while the primary excision procedure is in progress, the rationale arises from the effort and time required to process and interpret specimens using histology, as well as from the limitations of other current intraoperative methods [6, 33]. For frozen section and imprint cytology margin assessment, due to the additional time (estimated by one group to be approximately 30 min) and inflexible staffing requirement of having a specially-trained pathologist in proximity to the operating room, institutional and surgeon uptake has been poor [6, 33]. OCT is attractive as an alternative as it can be completed rapidly, can scan a large specimen surface area within a timeframe compatible with surgery, and has the potential to be interpreted by the surgeon after training. Preclinical and clinical studies have thus far bolstered the contention that OCT may provide a high degree of accuracy compared to histology and other intraoperative imaging technologies presently in use, such as radiography and ultrasound [6, 33]. Previous work has demonstrated comparability to histology in both intraoperative and postoperative settings [17, 20–32, 37–40]. More recently, results from four studies related to the WF-OCT system evaluated in this report have been published, including three studies in human breast tissue and one in tissues of the head and neck [20–23].

The present report builds on these prior studies by demonstrating that normal and abnormal tissue from organs other than the breast may be successfully imaged and correlated to permanent histology by the OTIS 2.0 system. Although this study was performed using tissue obtained post-mortem, we do not currently see a use for this technology in a post-mortem setting. The study was performed here because it gave us access to multiple tissue specimens and organs which would have been difficult to obtain through normal, standard-of-care pathology processing.

Our discussion focuses on the use of this technology in breast and head-and-neck tissue types, because currently these represent the biggest unmet need in intraoperative specimen analysis and is where the largest body of work in this field has been performed. There is definitely a need in other tissue types and many of them leverage intraoperative frozen sectioning. Breast conserving surgery seldom uses frozen sectioning as it is very difficult to freeze breast tissue, creating the larger need in those types of surgeries.

We acknowledge several limitations to this study. First, the study's generalizability is limited by its design, with a small number of evaluators, and using *postmortem* tissues from a single donor with ongoing disease processes at autopsy. Although a single-subject design that contains both normal and abnormal pathology provides some unique benefits, further study of fresh, non-diseased tissues from multiple donors and with additional readers is warranted to confirm that correlation of histology and WF-OCT remains consistent and robust across other settings. Second, the effect of WF-OCT imaging and analysis on timing and convenience of operative workflow was not assessed in this study, though others have found the impact to be minimal [20–23]. As the time required to scan and interpret images is not immaterial, this is an important metric for all future studies of intraoperative utility. Lastly, although the WF-OCT system evaluated in this study is FDA-cleared in the United States and available worldwide, no clinical trial has yet investigated its efficacy in reducing reoperations for positive margins. A prospective multi-center, randomized, controlled study to investigate this question in breast conserving surgery is currently under way. Considering the above limitations, the results presented here add to the body of evidence that WF-OCT imaging using the system can be used to identify and characterize the microarchitecture of normal and pathological tissue from a variety of human organ types.

In closing, in this autopsy-based study, both a trained pathologist and a clinical scientist were able to use WF-OCT images to identify key normal and pathological features and layers across a variety of tissue types using a single, FDA-cleared device, with direct correlation to the same features and layers observed by standard-of-care histology. Although limited to a single subject, these results are foundational in enabling the design and execution of larger clinical trials to assess if WF-OCT has the potential to bridge the gap between the immediate information needs of the operating room and the time delay inherent to tissue processing and pathology. Further clinical study of the utility of WF-OCT imaging for margin assessment at the time of surgical resection is warranted.

Data availability statement

The raw data supporting the conclusion of this article will be made available by the authors, without undue reservation.

Ethics statement

Ethical approval was obtained by the Biorepository at the Icahn School of Medicine for the use of the human cadaver in this study, including informed written consent from the legally authorized representative. The protocol was granted an exemption from ethics approval by the Institutional Review Board of Mount Sinai Hospital. The study sponsor did not have access to protected health information.

Author contributions

AC and BR are listed as authors, and all authors certify that they have participated sufficiently in the work to take public responsibility for the content, including participation in the concept, design, analysis, writing, or revision of the manuscript. Furthermore, each author certifies that this material or similar material has not been and will not be submitted to or published in any other publication. All authors contributed to the article and approved the submitted version.

Acknowledgments

The authors thank Biolexica Health Science Communications for professional medical writing assistance with manuscript preparation and the Biorepository at the Icahn School of Medicine for providing the donor tissue for this study.

Conflict of interest

BR is a former employee and current consultant for Perimeter Medical Imaging AI. AC received a fee for service from Perimeter Medical Imaging AI in an amount consistent with customary pathology practice.

The authors declare that this study received funding from Perimeter Medical Imaging. Perimeter Medical Imaging funded lab services and professional medical writing assistance with manuscript preparation. Perimeter was involved in the study design, collection, analysis, interpretation of data, the writing of this article, and the decision to submit it for publication.

Supplementary material

The Supplementary Material for this article can be found online at: https://www.por-journal.com/articles/10.3389/pore.2023.1611167/full#supplementary-material

References

1. American Cancer Society. *Cancer facts & Figures 2021* (2021). Available from: https://www.cancer.org/research/cancer-facts-statistics/all-cancer-facts-figures/cancer-facts-figures-2022.html (Accessed January 4, 2023).

2. Miller KD, Nogueira L, Mariotto AB, Rowland JH, Yabroff KR, Alfano CM, et al. Cancer treatment and survivorship statistics, 2019. *CA Cancer J Clin* (2019) 69: 363–85. doi:10.3322/caac.21565

3. Clarke M, Collins R, Darby S, Davies C, Elphinstone P, Evans V, et al. Effects of radiotherapy and of differences in the extent of surgery for early breast cancer on local recurrence and 15-year survival: An overview of the randomised trials. *Lancet* (2005) 366:2087–106. doi:10.1016/S0140-6736(05)67887-7

4. Moran MS, Schnitt SJ, Giuliano AE, Harris JR, Khan SA, Horton J, et al. Society of Surgical Oncology-American Society for Radiation Oncology consensus guideline on margins for breast-conserving surgery with whole-breast irradiation in stages I and II invasive breast cancer. *Ann Surg Oncol* (2014) 21: 704–16. doi:10.1245/s10434-014-3481-4

5. Morrow M, Van Zee KJ, Solin LJ, Houssami N, Chavez-MacGregor M, Harris JR, et al. Society of surgical oncology-American society for radiation oncology-American society of clinical oncology consensus guideline on margins for breast-conserving surgery with whole-breast irradiation in ductal carcinoma *in situ*. *Ann Surg Oncol* (2016) 23:3801–10. doi:10.1245/s10434-016-5449-z

6. Voskuil FJ, Vonk J, van der Vegt B, Kruijff S, Ntziachristos V, van der Zaag PJ, et al. Intraoperative imaging in pathology-assisted surgery. *Nat Biomed Eng* (2022) 6:503–14. doi:10.1038/s41551-021-00808-8

7. Schnitt SJ, Moran MS, Giuliano AE. Lumpectomy margins for invasive breast cancer and ductal carcinoma *in situ*: Current guideline recommendations, their implications, and impact. *J Clin Oncol* (2020) 38:2240–5. doi:10.1200/JCO.19.03213

8. Atkins J, Al Mushawah F, Appleton CM, Cyr AE, Gillanders WE, Aft RL, et al. Positive margin rates following breast-conserving surgery for stage I-iii breast cancer: Palpable versus nonpalpable tumors. *J Surg Res* (2012) 177:109–15. doi:10.1016/j.jss.2012.03.045

9. Balch GC, Mithani SK, Simpson JF, Kelley MC. Accuracy of intraoperative gross examination of surgical margin status in women undergoing partial mastectomy for breast malignancy. *Am Surg* (2005) 71:22–8. doi:10.1177/000313480507100104

10. Brown JQ, Bydlon TM, Richards LM, Yu B, Kennedy SA, Geradts J, et al. Optical assessment of tumor resection margins in the breast. *IEEE J Sel Top Quan Electron* (2010) 16:530–44. doi:10.1109/jstqe.2009.2033257

11. Fleming FJ, Hill AD, Mc Dermott EW, O'Doherty A, O'Higgins NJ, Quinn CM. Intraoperative margin assessment and re-excision rate in breast conserving surgery. *Eur J Surg Oncol* (2004) 30:233–7. doi:10.1016/j.ejso.2003.11.008

12. McCahill LE, Single RM, Aiello Bowles EJ, Feigelson HS, James TA, Barney T, et al. Variability in reexcision following breast conservation surgery. *JAMA* (2012) 307:467–75. doi:10.1001/jama.2012.43

13. Bolshinsky V, Lin MJ, Serpell J, Leung M, Wolfe R, McLean C, et al. Frequency of residual melanoma in wide local excision (WLE) specimens after complete excisional biopsy. *J Am Acad Dermatol* (2016) 74:102–7. doi:10.1016/j.jaad.2015.08.065

14. Drexler W, Fujimoto JG. *Optical coherence tomography: Technology and applications*. Switzerland AG: Springer International Publishing (2015).

15. Huang D, Swanson EA, Lin CP, Schuman JS, Stinson WG, Chang W, et al. Optical coherence tomography. *Science* (1991) 254:1178–81. doi:10.1126/science.1957169

16. Subban V, Raffel OC. Optical coherence tomography: Fundamentals and clinical utility. *Cardiovasc Diagn Ther* (2020) 10:1389–414. doi:10.21037/cdt-20-253

17. Wang J, Xu Y, Boppart SA. Review of optical coherence tomography in oncology. *J Biomed Opt* (2017) 22:1–23. doi:10.1117/1.JBO.22.12.121711

18. Zysk AM, Nguyen FT, Oldenburg AL, Marks DL, Boppart SA. Optical coherence tomography: A review of clinical development from bench to bedside. *J Biomed Opt* (2007) 12:051403. doi:10.1117/1.2793736

19. Tung ET, Yim KHC, Li CL, Cheung CY, Chan YC. Optical coherence tomography in peripheral arterial disease: A systematic review. *Int J Clin Pract* (2021) 75:e14628. doi:10.1111/ijcp.14628

20. Badhey AK, Schwarz JS, Laitman BM, Veremis BM, Westra WH, Yao M, et al. Intraoperative use of wide-field optical coherence tomography to evaluate tissue microstructure in the oral cavity and oropharynx. *JAMA Otolaryngol Head Neck Surg* (2022) 149:71–8. doi:10.1001/jamaoto.2022.3763

21. DuPree BB, Papez MJ, Pirruccello E, Hassenflug A. Potential utility of adjunct imaging with wide-field optical coherence tomography for gross and microscopic evaluation of breast specimens in real-time in the operating suite. *Indian J Surg* (2021) 84:751–6. doi:10.1007/s12262-021-03079-4

22. Schmidt H, Connolly C, Jaffer S, Oza T, Weltz CR, Port ER, et al. Evaluation of surgically excised breast tissue microstructure using wide-field optical coherence tomography. *Breast J* (2020) 26:917–23. doi:10.1111/tbj.13663

23. Ha R, Friedlander LC, Hibshoosh H, Hendon C, Feldman S, Ahn S, et al. Optical coherence tomography: A novel imaging method for post-lumpectomy breast margin assessment-a multi-reader study. *Acad Radiol* (2018) 25:279–87. doi:10.1016/j.acra.2017.09.018

24. Erickson-Bhatt SJ, Nolan RM, Shemonski ND, Adie SG, Putney J, Darga D, et al. Real-time imaging of the resection bed using a handheld probe to reduce incidence of microscopic positive margins in cancer surgery. *Cancer Res* (2015) 75: 3706–12. doi:10.1158/0008-5472.CAN-15-0464

25. Conti de Freitas LC, Phelan E, Liu L, Gardecki J, Namati E, Warger WC, et al. Optical coherence tomography imaging during thyroid and parathyroid surgery: A novel system of tissue identification and differentiation to obviate tissue resection and frozen section. *Head Neck* (2014) 36:1329–34. doi:10.1002/hed.23452

26. Gan Y, Tsay D, Amir SB, Marboe CC, Hendon CP. Automated classification of optical coherence tomography images of human atrial tissue. *J Biomed Opt* (2016) 21:101407. doi:10.1117/1.JBO.21.10.101407

27. Gan Y, Yao X, Chang E, Amir SB, Hibshoosh H, Feldman S, et al. Comparative study of texture features in OCT images at different scales for human breast tissue classification. In: 2016 38th Annual International Conference of the IEEE Engineering in Medicine and Biology Society; 16-20 August 2016; Orlando, FL, USA (2016). p. 3926–9.

28. Hariri LP, Mino-Kenudson M, Lanuti M, Miller AJ, Mark EJ, Suter MJ. Diagnosing lung carcinomas with optical coherence tomography. *Ann Am Thorac Soc* (2015) 12:193–201. doi:10.1513/AnnalsATS.201408-370OC

29. Iftimia N, Cizginer S, Deshpande V, Pitman M, Tatli S, Iftimia NA, et al. Differentiation of pancreatic cysts with optical coherence tomography (OCT) imaging: An *ex vivo* pilot study. *Biomed Opt Express* (2011) 2:2372–82. doi:10.1364/BOE.2.002372

30. Jäckle S, Gladkova N, Feldchtein F, Terentieva A, Brand B, Gelikonov G, et al. *In vivo* endoscopic optical coherence tomography of the human gastrointestinal tract-toward optical biopsy. *Endoscopy* (2000) 32:743–9. doi:10.1055/s-2000-7711

31. Lee HC, Zhou C, Cohen DW, Mondelblatt AE, Wang Y, Aguirre AD, et al. Integrated optical coherence tomography and optical coherence microscopy imaging of *ex vivo* human renal tissues. *J Urol* (2012) 187:691–9. doi:10.1016/j.juro.2011.09.149

32. Poneros JM, Tearney GJ, Shiskov M, Kelsey PB, Lauwers GY, Nishioka NS, et al. Optical coherence tomography of the biliary tree during ERCP. *Gastrointest Endosc* (2002) 55:84–8. doi:10.1067/mge.2002.120098

33. St John ER, Al-Khudairi R, Ashrafian H, Athanasiou T, Takats Z, Hadjiminas DJ, et al. Diagnostic accuracy of intraoperative techniques for margin assessment in breast cancer surgery: A meta-analysis. *Ann Surg* (2017) 265:300–10. doi:10.1097/SLA.0000000000001897

34. Gray RJ, Pockaj BA, Garvey E, Blair S. Intraoperative margin management in breast-conserving surgery: A systematic review of the literature. *Ann Surg Oncol* (2018) 25:18–27. doi:10.1245/s10434-016-5756-4

35. Schnabel F, Boolbol SK, Gittleman M, Karni T, Tafra L, Feldman S, et al. A randomized prospective study of lumpectomy margin assessment with use of MarginProbe in patients with nonpalpable breast malignancies. *Ann Surg Oncol* (2014) 21:1589–95. doi:10.1245/s10434-014-3602-0

36. Ali ZA, Karimi Galougahi K, Maehara A, Shlofmitz RA, Ben-Yehuda O, Mintz GS, et al. Intracoronary optical coherence tomography 2018: Current status and future directions. *JACC Cardiovasc Interv* (2017) 10:2473–87. doi:10.1016/j.jcin.2017.09.042

37. Ang M, Tan ACS, Cheung CMG, Keane PA, Dolz-Marco R, Sng CCA, et al. Optical coherence tomography angiography: A review of current and future clinical applications. *Graefes Arch Clin Exp Ophthalmol* (2018) 256:237–45. doi:10.1007/s00417-017-3896-2

38. Fujii K, Kawakami R, Hirota S. Histopathological validation of optical coherence tomography findings of the coronary arteries. *J Cardiol* (2018) 72: 179–85. doi:10.1016/j.jjcc.2018.03.003

39. Vakoc BJ, Fukumura D, Jain RK, Bouma BE. Cancer imaging by optical coherence tomography: Preclinical progress and clinical potential. *Nat Rev Cancer* (2012) 12:363–8. doi:10.1038/nrc3235

40. Nguyen FT, Zysk AM, Chaney EJ, Kotynek JG, Oliphant UJ, Bellafiore FJ, et al. Intraoperative evaluation of breast tumor margins with optical coherence tomography. *Cancer Res* (2009) 69:8790–6. doi:10.1158/0008-5472.CAN-08-4340

Pathology & Oncology Research | frontiers

TYPE Original Research
PUBLISHED 01 August 2024
DOI 10.3389/pore.2024.1611813

Check for updates

OPEN ACCESS

EDITED BY
József Tímár,
Semmelweis University, Hungary

*CORRESPONDENCE
László Baráti,
barati.laszlo@pte.hu

RECEIVED 30 April 2024
ACCEPTED 19 July 2024
PUBLISHED 01 August 2024

CITATION
Baráti L, Maász A, Mikó A, Bércesi É, Kalbani SA, Bene J, Kovács S, Mangel L and Hadzsiev K (2024), Molecular genetic investigation of hereditary breast and ovarian cancer patients in the Southern Transdanubian region: widening the mutation spectrum and searching for new pathogenic variants using next-generation methods. *Pathol. Oncol. Res.* 30:1611813. doi: 10.3389/pore.2024.1611813

COPYRIGHT
© 2024 Baráti, Maász, Mikó, Bércesi, Kalbani, Bene, Kovács, Mangel and Hadzsiev. This is an open-access article distributed under the terms of the Creative Commons Attribution License (CC BY). The use, distribution or reproduction in other forums is permitted, provided the original author(s) and the copyright owner(s) are credited and that the original publication in this journal is cited, in accordance with accepted academic practice. No use, distribution or reproduction is permitted which does not comply with these terms.

Molecular genetic investigation of hereditary breast and ovarian cancer patients in the Southern Transdanubian region: widening the mutation spectrum and searching for new pathogenic variants using next-generation methods

László Baráti[1]*, Anita Maász[1], Alexandra Mikó[1,2], Éva Bércesi[3], Sultan Al Kalbani[1], Judit Bene[1], Sebestyén Kovács[4], László Mangel[3] and Kinga Hadzsiev[1]

[1]Department of Medical Genetics, Clinical Centre, Medical School, University of Pécs, Pécs, Hungary, [2]Institute for Translational Medicine, Medical School, University of Pécs, Pécs, Hungary, [3]Department of Oncotherapy, Clinical Centre, Medical School, University of Pécs, Pécs, Hungary, [4]Urology Clinic, Clinical Centre, University of Pécs, Pécs, Hungary

Hereditary breast and ovarian cancer is a well-known genetic condition, inherited mainly in an autosomal dominant way, which elevates the risk of developing malignancies at a young age in heterozygous carriers. Advances in new generation sequencing have enabled medical professionals to determine whether a patient is harbouring mutations in moderate- or high penetrance susceptibility genes. We conducted a retrospective analysis among 275 patients who underwent genetic counselling and multigene panel testing for hereditary breast and ovarian cancer syndrome in our department. From these patients 74.5% (205/275) were affected by some type of malignancy, while the remaining 25.5% (70/275) had a positive family history of different cancers, suggesting a genetic predisposition. These tests confirmed a genetic variant in 29.8% and 28.6% of these patient groups respectively. The results also mirrored our general knowledge concerning the genetic background of hereditary breast and ovarian cancer, as variants in either one of the *BRCA1* and *BRCA2* genes proved to be the most common cause among our patients with 41.5%. Our test also detected a novel mutation in the *CDH1* gene and three patients with double heterozygosity in two different susceptibility genes. This study demonstrates

the relevance of genetic counselling and non-*BRCA* gene sequencing among cancer patients and patients who fulfil the criteria for genetic testing, while also providing important details about the genetic profile of Hungarian patients.

KEYWORDS

HBOC, new generation sequencing, multigene panel testing, BRCA1, BRCA2

Introduction

Cancer is among the leading causes of mortality all over the world. Over the last decade, the incidence of malignancies has been growing worldwide, resulting in an estimated 20 million new cases and 9.7 million deaths in 2022. In most types of cancer, mortality has decreased due to preventive measures, improved diagnostic tests, screening programmes and more effective treatment options [1, 2]. Unfortunately, predictions lead us to believe, that we can expect a steady increase in the number of new cases in the upcoming years [3].

In Hungary, breast cancer is the third most common malignancy after lung cancer and colorectal cancer, and the leading cause of cancer incidence in the female population, resulting in approximately 8,000 new cases and 2,000 deaths every year according to the Hungarian Cancer Registry [4].

Until recently, environmental causes were viewed as the main reason for the occurrence of malignancies. Akin to most multifactorial diseases, breast cancer is known to be associated with certain factors, that affect one's risk to develop the disease in their lifetime. Modifiable risk factors include obesity, consumption of tobacco and alcohol, and taking hormones, while reproductive history, increasing age and a positive family history belong to non-modifiable risk factors [5–7].

In recent decades it has become apparent, that genetic variants play a considerable role in the development of breast- and ovarian cancer. While malignancies in general are usually a result of somatic mutations [8, 9], approximately 5%–10% are caused by germline mutations in moderate- or high penetrance cancer susceptibility genes [10]. These predisposing genetic traits usually follow an autosomal dominant inheritance, leading to patients having a highly elevated cumulative risk of developing different types of malignancies, and a 50% chance of passing the mutation onto their offspring [11].

Over the last few decades, diagnosis of hereditary cancer syndromes has shown promising progress. With rapid advances in molecular testing and next-generation sequencing, a great number of individuals and families have been identified, who are affected by mutations in cancer susceptibility genes. While the BRCA-related hereditary breast- and ovarian cancer (HBOC) is among the most well-known tumour syndromes, one cannot skim over the importance of other, less common predisposition genes.

Due to a lack of data on genetic spectrum of the Hungarian HBOC population, we aimed to determine the prevalence of genetic variants of HBOC-associated genes in the Hungarian patient cohort and in healthy relatives with family history of cancer; to evaluate the associations of detected variants with clinical features; to evaluate how worthwhile it is to use a larger gene panel (including other genes beside *BRCA*s) in routine genetic diagnostics of Hungarians; and to evaluate the association between familial history of cancer and familial accumulation of the genetic variants in the cohort.

Subjects and methods

Subjects

The examinations related to this retrospective study were carried out in the Department of Medical Genetics in the University of Pécs. The patients and relatives that were involved into this study derived from the joint genetic counselling facility of Department of Medical Genetics and Department of Oncotherapy at the University of Pécs (Oncogenetic Counselling and Family Screening Centre). Patients' data (personal history of cancer, tumour type, and age at diagnosis) were obtained from clinical records, while the family history of cancer was obtained from interviews with the probands. People referred to the genetic counselling went through a cancer genetic risk assessment. The purpose was to identify individuals at elevated cancer risk who may benefit from genetic testing, additional screening or preventive interventions. Using clues from the personal and family history, the genetic counsellor classified individuals as average (general population), increased (moderate), or high (strong) risk patients according to the widely accepted National Comprehensive Cancer Centre (NCCN) Clinical Practice Guidelines in Oncology, which are available online for experts[1]. After risk assessment, individuals classified into the average risk level group were excluded from the study. We highlight the genetic risk stratification for HBOC in Table 1.

Blood samples were taken from individuals with increased (moderate) and high (strong) risk for cancer and they were included in the study and for further examination. We collected 370 samples from patients with any cancer type. We classified the

1 www.nccn.org

TABLE 1 Genetic risk stratification for HBOC patients.

Risk level	Personal and family history evidence
Average	No first- or second-degree relatives[a] with breast or ovarian cancer; OR
	More distant relatives with a breast cancer diagnosis or diagnoses after age 50
Increased (moderate)	Prior history of breast cancer, lobular neoplasia (LCIS/ALH), or atypical ductal hyperplasia
	5-year risk ≥1.7% in women ≥35 years using the Gail model, or ≥20% lifetime risk defined by risk models
	Thoracic radiotherapy <30 years
	One or two first- or second-degree relatives with breast cancer diagnosis after age 50
High (strong)	Known pathogenic variant (mutation) in the family
	Somatic tumor testing suggesting a hereditary cancer syndrome
	Patient or first-degree relative diagnosed with exocrine pancreatic cancer
	Diagnosis in patient, or first- or second-degree relative with
	breast cancer at age 45 or younger
	triple negative breast cancer diagnosed at any age
	multiple primary breast cancers
	ovarian, certain prostate cancers, or male breast cancer at any age
	breast cancer or prostate cancer diagnosis at any age and Ashkenazi Jewish ancestry
	Two or more first- or second-degree relatives on same side of family with breast cancer, if at least one was diagnosed ≤ age 50
	Three or more total diagnoses of breast cancer in patient, first- or second-degree relatives on the same side of the family

[a]First-degree relatives are parents, children, and siblings. Second-degree relatives are grandparents, grandchildren, uncles and aunts.

samples according to cancer types and we assorted 205 HBOC patients for further examination. Patients with other cancer types were excluded from the current analyses. Besides, we involved 70 healthy persons with a positive family history of HBOC-related cancer, e.g., breast, ovarian, prostate or pancreatic cancer into our examination.

All individuals gave their consent to genetic testing and biobanking, which were conducted following the WMA Declaration of Helsinki - Ethical principles for medical research involving human subjects (2013) and the Hungarian genetic law (XXI/2008). The study was approved by the Regional Research Ethics Committee of the University of Pécs (8770-PTE2021) and by the Medical Research Council (IV/3831-3/2021/EKU).

Methods

Whole peripheral blood samples were taken from all patients. DNA was extracted from the blood leukocytes using E.Z.N.A. Blood DNA Maxi Kit (Omega Biotek, Norcross, GA, United States) according to the protocol. QubitTM 2.0 Fluorometric Quantitation system (Thermo Fisher Scientific Inc., Waltham, MA United States) was used to calculate the quantity and quality of genomic DNA samples (Qubit™ 1X dsDNA HS (High Sensitivity) Assay Kits) according to the protocol. The DNA samples were deposited into the biobank of the department.

The patients were examined using Agilent SureMASTR Hereditary Cancer Kit previously, which was no longer manufactured (Agilent Technologies, Santa Clara, CA United States), thereafter we used TruSight Hereditary Cancer Kit (Illumina Inc., San Diego, CA United States). Both Kits are targeted sequencing panels. The SureMASTR Hereditary Cancer Kit contained 26 cancer-associated genes (*ATM*, *BARD1*, *BLM*, *BRCA1*, *BRCA2*, *BRIP1*, *CDH1*, *CHEK2*, *EPCAM (3'UTR)*, *FAM175A*, *MEN1*, *MLH1*, *MRE11A*, *MSH2*, *MSH6*, *MUTYH*, *NBN*, *PALB2*, *PMS2*, *PTEN*, *RAD50*, *RAD51C*, *RAD51D*, *STK11*, *TP53*, and *XRCC2*), the TruSight Hereditary Cancer Kit designed to assess germline mutations across 113 genes (*ACD*, *AIP*, *AKT1*, *APC*, *ATM*, *BAP1*, *BARD1*, *BLM*, *BMPR1A*, *BRCA1*, *BRCA2*, *BRIP1*, *CASR*, *CDC73*, *CDH1*, *CDK4*, *CDKN1B*, *CDKN2A*, *CEBPA*, *CHEK2*, *CTRC*, *DDB2*, *DICER1*, *DIS3L2*, *EPCAM*, *ERCC1*, *ERCC2*, *ERCC3*, *ERCC4*, *ERCC5*, *FAM175A*, *FANCA*,

FANCB, FANCC, FANCD2, FANCE, FANCF, FANCG, FANCI, FANCL, FANCM, FH, FLCN, GALNT12, GATA2, GPC3, GREM1, HOXB13, KIF1B, KIT, LZTR1, MAX, MEN1, MET, MITF, MLH1, MRE11A, MSH2, MSH3, MSH6, MUTYH, NBN, NF1, NF2, NSD1, NTHL1, PALB2, PDGFRA, PHOX2B, PIK3CA, PMS2, POLD1, POLE, POT1, PRKAR1A, PTCH1, PTEN, RAD50, RAD51, RAD51B, RAD51C, RAD51D, RB1, RECQL4, RET, RHBDF2, RINT1, RUNX1, SDHA, SDHAF2, SDHB, SDHC, SDHD, SLX4, SMAD4, SMARCA4, SMARCB1, SMARCE1, SPINK1, SPRED1, STK11, SUFU, TERF2IP, TERT, TMEM127, TP53, TSC1, TSC2, VHL, WT1, XPA, XPC, and *XRCC2*) commonly associated with hereditary predisposition to several cancers like breast, ovarian, colon, and gastric and tumour associated syndromes like tuberous sclerosis and neurofibromatosis. The SureMASTR Hereditary Cancer Kit assay uses amplicon sequencing method. The TruSight Hereditary Cancer Kit assay uses hybrid-capture chemistry integrated with Nextera Flex for Enrichment. We performed the assays according to the description of the manufacturer.

After sequencing reactions base called raw sequencing data was transformed into FASTQ format using Illumina's software (bcl2fastq). Sequence reads of each sample were mapped to the human reference genome (GRCh37/hg19). Burrows-Wheeler Aligner (BWA-MEM) software was used for reading alignment. Duplicate read marking, local realignment around indels, base quality score recalibration and variant calling were performed using GATK algorithms (Sentieon Inc., California, United States). Variant data was annotated using a collection of tools (VcfAnno and VEP) with a variety of public variant databases including but not limited to gnomAD[2], ClinVar[3] and HGMD[4]. The variants detected were adapted to available public databases, depositories like Ensembl[5], Varsome[6], Franklin[7]; and HGMD[8] and were classified according to the latest guidelines and interpretation criteria established by the American College of Medical Genetics and Genomics. The variants received were matched to the clinical features of the patients and the persons with positive family history.

We used PCR for validation of variants detected by NGS. The accession numbers of the gene reference sequences applied for designing methods were summarized in Supplementary Table S1 (Supplementary Material). For amplification of the region of interest, we designed specific primers (Integrated DNA Technologies Inc., Coralville, IA, United States) using the NCBI-PRIMER-BLAST tool (NCBI, Bethesda, MD, United States). The sequences of the applied oligonucleotide primers were summarized in Supplementary Table S1 (Supplementary Material).

We performed PCR reactions according to the protocol below:

Final volume was 50 μL, which contained 200 μM of each dNTP (1 μL), 0.2 mM of each primer (1–1 μL), 5 μL of reaction buffer (containing 500 mM KCl, 10 mM Tris-HCl, 14 mmol/L MgCl2, pH 9.0), 1 U of Taq polymerase (1 μL of 10 U/μL) and

TABLE 2 Patient cohorts' characteristics.

Cohort of HBOC patients[a]	
Gender n (%)	
Female	193 (94.1%)
Male	12 (5.85%)
total	205
Age (years)	
Average ±SD	56.0 ± 15.0
Min–max	21–84
Age at diagnosis (years)	
Average ±SD	46.3 ± 11.7
Min–max	15–78
≤45	n = 105 (51.2%)
45–60	n = 70 (34.2%)
>60	n = 30 (14.6%)
Tumour types n (%)	
Breast cancer	179 (87.3%)
Ovarian cancer	16 (7.81%)
Uterus cancer	3 (1.47%)
Prostate cancer	6 (2.93%)
Endocervix	1 (0.49%)
Cohort of non-HBOC persons[b]	
Gender n (%)	
Female	60 (85.7%)
Male	10 (14.3%)
total	70
Age (years)	
Average ±SD	49.0 ± 14.0
Min–max	20–81

[a]HBOC, cohort: hereditary breast and ovarian cancer.
[b]non-HBOC: healthy persons with hereditary cancer relatives.

2 https://gnomad.broadinstitute.org/
3 https://www.ncbi.nlm.nih.gov/clinvar/
4 https://www.hgmd.cf.ac.uk/ac/index.php
5 https://ensemble.org
6 https://varsome.com/
7 https://franklin.genoox.com/clinical-db/home
8 http://www.hgmd.cf.ac.uk/ac/index.php

TABLE 3 Distribution of carriers and non-carriers in the cohorts.

			Age at diagnosis	
		Number of cases n (%)	Average ±SD (years)	Min–max (years)
HBOC patients (n = 205)	Variant carriers	62 (29.8)	44.1 ± 10.9	25–72
	Non-carriers	143 (70.2)	47.3 ± 11.9	15–78
non-HBOC persons (n = 70)	Variant carriers	20 (28.6)	-	-
	Non-carriers	50 (71.4)	-	-
All participants (n = 275)	Variant carriers	82 (29.8)	-	-
	Non-carriers	193 (70.2)	-	-

1 μg extracted DNA as template (1 μL). The conditions of the polymerase chain reactions for the detection of HBOC variants were as follows: initial denaturation at 96°C followed by 35 cycles of 30 s at 95°C; 30 s at the annealing temperature; 30 s at 72°C and a final extension at 72°C. The annealing temperatures applied for certain variants are indicated in Supplementary Table S1 (Supplementary Material). The polymerase chain reactions were carried out using a SensoQuest Labcycler (SensoQuest GmBH, Göttingen, Germany).

After the amplification reaction, the products were electrophoresed through an ethidium-bromide-stained 1.5%–2% agarose gel and visualized by UVIdoc gel documentation system (UVITEC, Cambridge, UK).

The sequencing reactions were performed by Sanger sequencing on an Applied BiosystemsTM 3500 Genetic Analyzer (Thermo Fisher Scientific Inc., Waltham, MA, United States) using BigDye Terminator Chemistry. The sequence alignments were made using the Winstar genetic program (DNASTAR Inc., Madison, WI, United States).

Results

General characterization

We summarized the general characteristics of the study groups in Table 2. We have analysed a total of 275 samples with targeted next-generation sequencing panels of which, 205 agreed with HBOC criteria (HBOC cohort) and 70 were the sample of healthy persons with a positive family history of different cancers (non-HBOC cohort). The samples derived from non-consanguineous Hungarian people. HBOC patients' data (age, tumour type and age at diagnosis) and non-HBOC person's data were summarized in Table 2. Among the HBOC cases, 193 (94.1%) were females and 12 (5.85%) were males, all with a history of HBOC-related cancer. The average age of HBOC cases was 56.0 ± 15.0 years. The lowest age discovered was 21 years while the highest was 84 years. The average age at diagnosis for HBOC cases was 46.3 ± 11.7 years (range = 15–78 years). Among HBOC patients, 51.2% had their primary cancer diagnosis at age 45 years or younger. The types of cancers identified within the HBOC group were breast cancer (n = 179; 87.3%), ovarian cancer (n = 16; 7.81%), prostate cancer (n = 6; 2.93%), uterus cancer (n = 3; 1.47%) and endocervix cancer (n = 1; 0.49%).

Among the healthy non-HBOC cases, there were 60 (85.7%) females and 10 (14.3%) males, all without personal breast and ovarian cancer history but with a positive family history of any cancer. The average age of non-HBOC cases was 49.0 ± 14.0 years, ranging from 20 to 81 years.

In Table 3, we summarized the distribution of genetic variants in all cohorts and the age at diagnosis in the HBOC cohort. The average age at diagnosis in the carrier HBOC group was 44.1 ± 10.9 years, where 25 years was the minimum and 72 years was the maximum age at diagnosis. The average age at diagnosis in non-carriers was 47.3 ± 11.9 years. The minimum age at diagnosis was 15 years; however, the maximum age at diagnosis was 78 years. There was no significant difference in the age at diagnosis between carrier and non-carrier HBOC groups.

Mutational profile of HBOC and non-HBOC study groups

The number of cases of HBOC patients carrying any genetic variants were 61, which is 29.8% of all HBOC patients tested. In the non-HBOC study group, 20 individuals were found carrying any genetic variant in association of cancer predisposition, which is 28.6% of the tested non-HBOC persons. The total number of all variant carriers was 82 cases, which is the 29.8% of all cases.

The complete record of the positive results of different tumour types is summarized in Table 4. The table shows the genes in which we detected variants and it contains the most prevalent variants, as well. Breast cancer was diagnosed in most of our cases (179/205; 87.3%), of which we identified genetic variants in 51 cases, representing 28.5% of the breast cancer patients: twelve *BRCA2* (6.70%), eight *CHEK2* (4.47%), eight *BRCA1* (4.47%), seven *ATM* (3.91%), three *PALB2* (1.68%), and 2-2 variants in *BARD1, FANCI* and *RAD51C* genes (1.12%), and

TABLE 4 Carriers of pathogenic/likely pathogenic variants and variants of uncertain significance (VUS) according to tumour types in the HBOC cohort.

Tumour types	Gene Variant detected	All carriers n (%)	Carriers of p/LP n (%)	Carriers of VUS n (%)
Breast cancer (n = 179)		51 (28.5)	34 (19.0)	17 (9.50)
	BRCA2	12 (6.70)	9 (5.03)	3 (1.68)
	BRCA1	8 (4.47)	8 (4.47)	0
	BRCA1 c.5266dupC	3 (1.68)		
	CHEK2	8 (4.47)	7 (3.91)	1 (0.56)
	CHEK2 c.599T>C	3 (1.68)		
	ATM	7 (3.91)	4 (2.23)	3 (1.68)
	PALB2	3 (1.68)	1 (0.56)	2 (1.12)
	BARD1	2 (1.12)	1 (0.56)	1 (0.56)
	FANCI	2 (1.12)	1 (0.56)	1 (0.56)
	RAD51C	2 (1.12)	1 (0.56)	1 (0.56)
	APC	1 (0.56)	0	1 (0.56)
	BLM	1 (0.56)	1 (0.56)	0
	CDH1	1 (0.56)	1 (0.56)	0
	ERCC2	1 (0.56)	1 (0.56)	0
	KIT	1 (0.56)	0	1 (0.56)
	MSH6	1 (0.56)	0	1 (0.56)
	PMS2	1 (0.56)	0	1 (0.56)
	RAD50	1 (0.56)	0	1 (0.56)
	RAD51B	1 (0.56)	0	1 (0.56)
	RET	1 (0.56)	0	1 (0.56)
Ovarian cancer (n = 16)		9 (56.3)	7 (43.8)	2 (12.5)
	BRCA1	6 (37.5)	5 (31.3)	1 (6.25)
	BRCA1 c.5266dupC	3 (18.8)		
	RAD51C	2 (12.5)	1 (6.25)	1 (6.25)
	BRCA2	1 (6.25)	1 (6.25)	0
Prostate cancer (n = 6)	*CHEK2*	1 (16.7)	1 (16.7)	0
Uterus cancer (n = 3)	*BRCA1*	1 (33.3)	1 (33.3)	0
Endocervix (n = 1)		0	0	0

1-1 variant in *APC, BLM, CDH1, ERCC2, KIT, MSH6,, PMS2, RAD50, RAD51B,* and *RET* genes (0.56%). Besides, 9 out of 16 ovarian cancer cases (56.3%) harboured genetic variants: six *BRCA1* (37.5%), two *RAD51C* (12.5%) and in one case *BRCA2* (6.25%). The most prevalent variant was *BRCA1* c.5266dupC in the cohorts. Of the six prostate cancer cases, only one carried a genetic variant in the oncogenes (16.7%). From the three cases diagnosed with uterus cancer, only one case revealed positivity, where a pathogenic variant was found in the *BRCA1* gene. We could not detect any genetic alteration in the patients diagnosed with endocervix cancer by oncogenetic testing.

The identified genetic variants in the HBOC and non-HBOC groups are listed in Supplementary Table S2 (Supplementary Material). The table contains the clinical significance of the variants, which were predicted by the ClinVar database and Franklin interpretation tool. The clinical significance of most of

the variants can be determined unanimously based on the data from ClinVar and Franklin. In some cases, there were discrepancies between the interpretation of ClinVar and Franklin (pathogenic-likely pathogenic, pathogenic-VUS). Based on the analysis, Franklin proved to be more permissive in most cases. In the ClinVar database, no records were found for the *CDH1* c.2499delT variant; however, after classification according to the ACMG guidelines, we interpreted it as a likely pathogenic/pathogenic variant, as was predicted by the Franklin prediction tool.

We identified pathogenic/likely pathogenic and VUS genetic variants in *APC, ATM*, *BARD1*, *BLM, BRCA1*, *BRCA2*, *CHEK2*, *CDH1*, *ERCC2, FANCI, KIT*, *MSH6*, *PALB2*, *PMS2*, *RAD50, RAD51B, RAD51C,* and *RET* in the HBOC group. The non-HBOC patients harbour pathogenic/likely pathogenic and VUS genetic variants in *BRCA1*, *BRCA2*, *CHEK2*, *EPCAM, ERCC3, FANCD2, MSH6*, *MUTYH, PALB2*, *POLE, PTCH1,* and *RAD51C*. Genetic variants in *BARD1*, *CDH1*, *PMS2*, *KIT* and *RET* genes were identified in HBOC patients only. Variants in *MUTYH*, *EPCAM*, *FANCD2*, *POLE*, *ERCC3,* and *PTCH1* were reported in the non-HBOC persons only. Overall, we identified 67 unique pathogenic/likely pathogenic variants and VUS carried by 82 individuals: 35 missense (52.2%), 15 frameshift (22.4%), 10 nonsense (14.9%), 2 synonymous (2.99%), 4 splice site variants (5.97%) and one three basepair deletion (1.49%), which cause one amino acid deletion, but not frameshift.

For *BRCA2*, 16 distinct variants in the association of cancer were identified in 17 individuals. The majority of the variants had pathogenic or likely pathogenic clinical significance. Only two variants were VUS (c.1012 G>A; c.3042 T>G). The most prevalent variant was the c.1408dupG, which were detected in two breast cancer cases, representing 2.98% of all variants detected.

For *BRCA1*, 10 different variants in association of cancer were identified in 17 individuals. Almost all variants were predicted to be pathogenic, and only one was predicted to be VUS (c.734 A>T). In the case of c.845 C>T, Franklin predicted it as VUS; however, it was mentioned as pathogenic in ClinVar. One of the variants (c.5266dupC) was present in seven samples, representing approximately 10.4% of all variants detected.

CHEK2 is the third gene, in which we most frequently identified variants in association with cancer. We detected 6 different variants in 11 individuals, from which five were pathogenic/likely pathogenic, one was VUS (c.1039 A>G) and one had conflicting interpretations of pathogenicity (c.1684 C>G; ClinVar: pathogenic/likely pathogenic, Franklin: VUS). One of the variants (c.599 T>C) was present in six samples, representing approximately 8.96% of all variants detected.

For *ATM* gene, 7 distinct variants in the association of cancer were identified in 7 individuals, from which three were pathogenic/likely pathogenic and four were VUS according to ClinVar and Franklin.

We compared the numbers of detected cases and allele frequencies of the pathogenic/likely pathogenic variants for each gene in the study groups, which are summarized in Table 5. Pathogenic/likely pathogenic variants of *BRCA1* and *BRCA2* showed similar allele frequencies, which shared the highest frequencies among the genes in the HBOC cohort. In the non-HBOC group, *BRCA1* showed the highest frequency. Additionally, we assessed the allele frequencies of the genes in the gnomAD non-cancer cohort (n = 134 187), which showed significant differences in *BRCA1, BRCA2, CHEK2, MUTYH, MSH6, POLE, and ERCC3* genes in comparison to our non-HBOC groups.

Remarkably, *BRCA1* and *BRCA2* are the genes that explain almost half of the positive cases (17 + 17/82; 41.5%). *BRCA1* and *BRCA2* were the genes with the highest rate of pathogenic/likely pathogenic variants. Three patients diagnosed with breast cancer in the HBOC group harboured two genetic variants concomitantly (double heterozygotes; DH): 1. patient: *BRCA1* c.5266dupC het, p.Gln1756Profs*74 and *BLM* c.1642C>T het, p.Gln548Ter, which are known pathogenic variants; the patient was diagnosed with Grade 3 triple negative, invasive ductal carcinoma at the age of 32 years. 2. patient: *BRCA2* c.7976G>A het, p.Arg2659Lys and *RAD50* c.287T>C het, p.Val96Ala, which are pathogenic and VUS, respectively; the patient has been receiving treatment for Grade 3 triple negative, invasive ductal carcinoma as well, which was diagnosed at the age of 29 years. 3. patient: *BRCA2* c.3042T>G het, p.Asn1014Lys and *ATM* c.5890A>G het, p.Lys1964Glu, which are VUSs. The patient was first diagnosed with Grade 3 triple negative invasive ductal carcinoma at the age of 35 years, and a contralateral Grade 3 triple negative ductal breast cancer at the age of 44 years. Though there were suspicions for causality based on the patient's phenotype, the initial classification of these variants remained unchanged upon reevaluation.

Besides, we identified other variants with benign clinical significance by next-generation testing, which were not confirmed by Sanger sequencing and they are not the part of this study.

Discussion

Over the last decade, the spreading of new techniques such as NGS that allows the simultaneous analysis of multiple genes in panels as well as whole exome/genome are more cost-effective and efficient compared to Sanger sequencing. The use of these techniques probably contributes to faster recognition of the genetic cause of rare or ultra-rare disorders and to broadening the genetic screening of certain disorders, like cancers, where rapid diagnosis is extremely important for further care and the selection of appropriate therapy.

TABLE 5 Detection ratio of *BRCA1, BRCA2, PALB2, ATM, CHEK2, MUTYH, MSH6, RAD51C, BARD1, CDH1, POLE and ERCC3* P/LP variants in the study groups and gnomAD non-cancer population.

Gene name	HBOC cohort (n = 205)		Non-HBOC cohort (n = 70)		All participants (n = 275)		GnomAD non-cancer cohort (n = 134 187)	
	Detected cases	Allele frequency	Detected cases	Allele frequency	Detected cases	Allele frequency	Detected cases	Allele frequency
BRCA1	13	0.03170	3	0.02143[a]	16	0.02909	295	0.00110
BRCA2	13	0.03170	2	0.01429[a]	15	0.02727	411	0.00153
PALB2	1	0.00244	0	0	1	0.00182	200	0.00075
ATM	3	0.00730	0	0	3	0.00545	428	0.00160
CHEK2	8	0.01950	1	0.00714[a]	9	0.01636	207	0.00077
MUTYH	0	0	1	0.01429[a]	1	0.00182	1,536	0.00572
MSH6	0	0	2	0.01429[a]	2	0.00363	119	0.00044
RAD51C	1	0.00244	0	0	1	0.00182	118	0.00044
BARD1	1	0.00244	0	0	1	0.00182	84	0.00031
CDH1	1	0.00244	0	0	1	0.00182	9	0.00003
POLE	0	0	1	0.00714[a]	1	0.00182	48	0.00018
ERCC3	0	0	1	0.00714[a]	1	0.00182	247	0.00092
FANCI	1	0.00244	0	0	1	0.00182		
ERCC2	1	0.00244	0	0	1	0.00182		
BLM	1		0	0	1	0.00182		

All individuals carried the variants in heterozygous form.

[a]Chi-square tests were used for comparison of the allele frequencies between GnomAD, Non-Cancer Group and our non-HBOC, group.

In our work, NGS allows us to determine the prevalence of genetic variants of HBOC-associated genes in the Hungarian patient cohort. Such data were not available for the Hungarian population, so far. We focused on the prevalence of genetic variants, predominantly pathogenic/likely pathogenic variants in cancer susceptibility genes in a Hungarian patient cohort selected from gathering increased (moderate) and high (strong) risk criteria for HBOC and a healthy individual's cohort, whose family history was positive for any cancer.

Pathogenic/likely pathogenic variants and VUSs were found in almost 50% of all individuals in HBOC as well as in non-HBOC groups. We found variants in the following genes: *APC*, *ATM*, *BARD1*, *BLM*, *BRCA1* and *BRCA2, CDH1, CHEK2, EPCAM, ERCC3, FANCD2, KIT, MSH6, MUTYH, PALB2, PMS2, POLE, PTCH1, RAD, RAD51B, RAD51C,* and *RET*. These genes are involved in repairing DNA damage and maintaining the stability of the cell's genetic material [12]. Some of these genes play important roles particularly in the homologous recombination-, base excision- and mismatch repair pathway (HRR, BER, MMR), which are important for maintaining genomic stability [13–15].

It is well-established that due to pathogenic germline variants detected in these genes, cells can grow uncontrolled and carrying these variants can confer predisposition for the development of hereditary cancer syndromes, which affects 5% of all HBOC cases. In the Hungarian HBOC group, *BRCA1* and *BRCA2* genes proved to be highly penetrant genes with their pathogenic detection rate of 6.34% (13/205, each). While *CHEK2* and *ATM* have moderate penetrance in HBOC (3.90%, 8/205; 1.46%, 3/205, respectively); in turn, the *PALB2* gene has a lower detection rate of 0.48% (1/205). These results are consistent with others' findings in European populations with HBOC [16, 17]. In the non-HBOC group, we obtained similar results regarding the *BRCA1* gene (4.29%, 3/70); however, there are differences in the prevalence of other genes. These differences can result from the fact, that in this group there were healthy people, who have a positive family history with a wide range of tumour spectrum including colorectal, pancreatic or gastric cancers, which have been associated with other genes such as *MUTYH* and *MSH6*.

Furthermore, the HBOC group was divided into subgroups according to the type of cancer: breast, ovarian, prostate, uterus and endocervix subgroups, and we evaluated the prevalence of genetic variants in each group. In the breast cancer subgroup, variants in *BRCA2* and *BRCA1* were the most frequently detected. In the ovarian cancer subgroup, *BRCA1* variants,

mainly c.5266dupC was found. Besides, rare variants in other genes like *ATM*, *CHEK2*, *CDH1*, *PALB2*, *RAD50,* and *RAD51C* have been detected mainly in the breast cancer subgroup. Most of these variants detected are variants of uncertain significance (VUS). In clinical practice, VUSs represent a challenge, because they must be indicated on medical results; however, - according to ACMG recommendations - VUSs are not used to guide clinical management until the clarification of their exact role [18]. Almost all of the VUSs detected in the study are located within important regions of the genes or functional domains of the proteins and could affect biochemical properties and biological functions. Even though we cannot determine their clinical significance with current evidence, functional studies on these variants would be necessary to explore their phenotype consequences. In our study, these variants of uncertain significance account for high percentage of the positive cases, furthermore we detected a surprising number of pathogenic variants in moderate-, and low penetrant genes. There are differences among European countries in the judgement of involving low penetrance genes in the first-line genetic HBOC screening. In some countries (e.g., Austria, Estonia, Finland, Poland), the hotspot and/or founder variants of BRCA or HBOC genes are tested first. In other countries like Finland and the Netherland, WES is executed and evaluated as an oncogenetic panel. However, it may vary among laboratories within a given country. Our findings highlight the possible benefits of including other genes besides *BRCA*s in routine genetic testing. However, incorporation testing of several genes into multigene (*PMS2, RET, KIT*) for which the evidence of risk-association is weak or absent can result in information that might not be clinically relevant to the affected patients and their families [19, 20].

In the Hungarian cohorts, the c.5266dupC in the *BRCA1* gene was detected most frequently (7/82, 8.54%). This variant is an insertion of one cytosine resulting in a frameshift and the creation of a novel translational termination codon after 74 amino acid residues. It is predicted to encode a truncated non-functional protein due to nonsense-mediated mRNA decay, which is a commonly known mechanism for disease. Functional studies have shown activity of the protein is significantly impaired by this variant [21]. This mutation has been described in individuals with HBOC, including individuals with male breast cancer, pancreatic cancer, and prostate cancer [22–27], and has been shown to be a founder mutation in several ethnic groups [28]. The high prevalence of this variant in our cohort and the fact that this variant has been reported several times in the literature state the probability of being a founder mutation of our population or maybe for a specific ethnicity; however, we did not collect information about the patient's origin. To confirm this hypothesis, further studies are required.

To evaluate the association between familial history of cancer and accumulation of the genetic variants, we assessed allele frequency data between our non-HBOC group and the gnomAD non-cancer non-Finnish European population as a group of healthy (non-cancer) individuals without any family history of cancer [29]. The findings revealed significant differences in allele frequencies between the two study groups, so the healthy persons with elevated risk for cancer (because of positive family history) carry the pathogenic variants in a higher proportion than people in the average population. Generally, indications of testing for high-penetrance susceptibility genes include a personal history of cancer at a young age, triple-negative or male breast cancer, epithelial ovarian cancer, multiple primary malignancies, or a positive family anamnesis. Based on these facts, genetic screening of predisposing genes in healthy but elevated-risk persons would be necessary to prevent developing tumours. After screening, healthy carriers can be easily managed and can be involved in surveillance programs and preventive follow-up care. Recognizing at-risk patients who carry the aforementioned genetic variants has important consequences on an individual level and on a larger scale as well. Affected individuals, who are already undergoing treatment can receive targeted therapy based on their genetic results, which usually leads to better outcomes and higher probability of long-term survival. Since their risk for developing other malignancies is also elevated, a positive genetic result also warrants a multidisciplinary approach to their surveillance. Identification of healthy carriers offers patients an opportunity to attend regular screening from a young age and the possibility of certain, primary preventive measures, including chemoprevention and risk-reducing surgery [30–33]. These surveillance strategies lead to earlier detection and better prognosis, reducing premature mortality and prolonged disability, while also easing the strain of costs on the healthcare system.

Besides, we detected a novel germline variant (*CDH1* c.2499delT), which is not yet recorded in variant databases. We interpreted and classified this sequence variant according to the standards and guidelines published by the American College of Medical Genetics and Genomics and Association for Molecular Pathology (ACMG-AMP) [34, 35]. This variant is predicted to cause loss of normal protein function either through protein truncation or nonsense-mediated mRNA decay resulting in an absent or non-functional protein product (PVS1). Other frameshift variants in the nearby region have been reported in individuals with hereditary cancer-predisposing syndrome, and Familial cancer of breast, loss-of-function of *CDH1* is a well-established mechanism leading to the disorder. This variant has not been observed in the large reference population cohorts of the Genome Aggregation Database (gnomAD, n > 120 000 exomes and n > 15 000 genomes) (PM2). To our knowledge, the variant has not been published in the relevant medical literature or reported in disease-related variation databases such as HGMD or ClinVar. To assess the impact of the missense change, we applied

a combination of some of the most widely used "*in silico*" computational prediction tools like PolyPhen, Provean and MutationTaster [36]. These algorithms support obvious evidence that the c.2499delT variant is a protein damaging, disease-causing variant (PP3). To our best knowledge, there are no "*in vitro*" functional studies which investigate the damaging effect of this variant on the gene product (PS3). The classification of this *CDH1* variant provides strong evidence of pathogenicity. The patient was diagnosed with metastasizing lobular breast carcinoma at the age of 48 years. The histological subtype of her tumour suggests furthermore, that there is a cause-effect relation between her illness and the detected germline variant.

Double heterozygosity (DH) in a high-, or moderate penetrance gene is a rare event; however, its number is likely to increase due to the use of NGS. In our study, we report three breast cancer cases (3/205; 1.46%) with (1) two VUSs in *BRCA2* and *ATM* genes; (2) one pathogenic variant in the *BRCA2* gene and one VUS in the *RAD50* gene; (3) two pathogenic variant in *BRCA1* gene. Some studies showed no significant differences in risk for HBOC in DH carriers when compared with those carrying only one germline variant [37, 38]. Others suggest that this genotype is not associated with early disease onset or a more severe phenotype [38]. In regards to our patients, all three were diagnosed with high grade, triple negative ductal carcinoma at a very young age. However, ethnic differences have been described as Caucasian DH females might develop breast cancer at an earlier age and have more severe disease in contrast to e.g., Ashkenazi Jewish females [37]. However, despite the little information about phenotype of DH carriers, we should not ignore their assumed risk modifier role and their possible cumulative impact on the development of the phenotype supporting a polygenic risk that should be considered in risk prediction in genetic counselling. Furthermore, DHs should be involved in more intensive surveillance programs/follow-up care and may need more severe prophylactic surgery [39].

The limitation of our study is the small number of individuals in certain groups with cancer types, which does not allow us to make profound genotype-phenotype associations. Besides, associations assumed in this study can be reliably assessed with information on other extrinsic contributing factors like smoking, alcohol consumption and dietary habits of the patients. These should be evaluated on a larger cohort of cancer patients.

Conclusion

The prevalence of hereditary mutations in breast, ovarian, endometrial and prostate cancer highlights the significance of genetic counselling and molecular genetic testing concerning these malignancies. Our study demonstrates a considerable percentage of pathogenic mutation carriers, emphasizing the benefits of molecular screening tests. The expansions of the diagnostic field revealed many other pathogenic variants associated with HBOC cancer that could have been missed if only *BRCA1* and *BRCA2* genes had been analysed. In this context, the appearance of next-generation sequencing methods has great potential. Thanks to its expansion, many new variants have been discovered in previously undiagnosed patients. Besides, comprehensive genetic diagnostics have long-term clinical benefits like increased patient cure rates, better patient surveillance, reduced cancer mortality rates, more effective treatments, and rapid recognition of high-risk families to reduce the risk of developing cancer. However, new challenges are generated in emerging next-generation sequencing like the interpretation of the huge amount of data derived from NGS, which highlights the need for highly skilled professionals in genetic counselling and molecular diagnostics with close cooperation of a multidisciplinary team.

Our results provide important new information to ethnic-specific cancer risk profiling and to determining even polygenic risk scores for HBOC, which can increase the sensitivity and specificity of cancer diagnostics as well as lowering the cost. However, several rare variants were identified with uncertain clinical significance, evaluation of the biological impact of these variants, further functional assays or robust segregation studies are needed.

Data availability statement

The datasets presented in this study can be found in online repositories. The names of the repository/repositories and accession number(s) can be found in the article/Supplementary Material.

Ethics statement

The studies involving humans were approved by the Regional Research Ethics Committee of the University of Pécs (8770-PTE2021) and by the Medical Research Council (IV/3831-3/2021/EKU). The studies were conducted in accordance with the local legislation and institutional requirements. The participants provided their written informed consent to participate in this study.

Author contributions

AnM and KH devised the main conceptual ideas and the outlines of the manuscript. AlM, LB, and KH conducted genetic counsultations, AnM and JB conducted sample preparation and genetic testing. Data collection about patient cohort and genetic results was performed mainly by SK. Patients of the cohort were referred to our institution by LM and EB as well. Manuscript

written mainly by SK, AnM, AlM, LB, and KH. All authors contributed to the article and approved the submitted version.

Funding

The author(s) declare that financial support was received for the research, authorship, and/or publication of this article. This work is supported (not financially) by the European Reference Network on Genetic Tumour Risk Syndromes (ERN GENTURIS). This study was supported by the Medical School of the University of Pécs, "ÁOK-KA" Research Program; KA-2023-22.

Conflict of interest

The authors declare that the research was conducted in the absence of any commercial or financial relationships that could be construed as a potential conflict of interest.

Supplementary material

The Supplementary Material for this article can be found online at: https://www.por-journal.com/articles/10.3389/pore.2024.1611813/full#supplementary-material

References

1. Mattiuzzi C, Lippi G. Current cancer epidemiology. *J Epidemiol Glob Health* (2019) 9(4):217–22. doi:10.2991/jegh.k.191008.001

2. Sung H, Ferlay J, Siegel RL, Laversanne M, Soerjomataram I, Jemal A, et al. Global cancer statistics 2020: GLOBOCAN estimates of incidence and mortality worldwide for 36 cancers in 185 countries. *CA: a Cancer J clinicians* (2021) 71(3): 209–49. doi:10.3322/caac.21660

3. Garner WB, Smith BD, Ludmir EB, Wakefield DV, Shabason J, Williams GR, et al. Predicting future cancer incidence by age, race, ethnicity, and sex. *J Geriatr Oncol* (2023) 14(1):101393. doi:10.1016/j.jgo.2022.10.008

4. Nemzeti Rákregiszter. *Nemzeti rákregiszter* (2022). Available from: http://stat.nrr.hu/ (Accessed May 26, 2022).

5. Howell A, Anderson AS, Clarke RB, Duffy SW, Evans DG, Garcia-Closas M, et al. Risk determination and prevention of breast cancer. *Breast Cancer Res : BCR* (2014) 16(5):446. doi:10.1186/s13058-014-0446-2

6. Kruk J, Aboul-Enein HY. Environmental exposure, and other behavioral risk factors in breast cancer. *Curr Cancer Ther Rev* (2006) 2:3–21. doi:10.2174/157339406775471795

7. Momenimovahed Z, Salehiniya H. Epidemiological characteristics of and risk factors for breast cancer in the world. *Breast Cancer (Dove Med Press)* (2019) 11: 151–64. doi:10.2147/BCTT.S176070

8. Greenman C, Stephens P, Smith R, Dalgliesh GL, Hunter C, Bignell G, et al. Patterns of somatic mutation in human cancer genomes. *Nature* (2007) 446(7132): 153–8. doi:10.1038/nature05610

9. Tate JG, Bamford S, Jubb HC, Sondka Z, Beare DM, Bindal N, et al. COSMIC: the catalogue of somatic mutations in cancer. *Nucleic Acids Res* (2019) 47(D1): D941–947. doi:10.1093/nar/gky1015

10. Fan X, Wynn J, Shang N, Liu C, Fedotov A, Hallquist MLG, et al. Penetrance of breast cancer susceptibility genes from the eMERGE III Network. *JNCI Cancer Spectr* (2021) 5(4):pkab044. doi:10.1093/jncics/pkab044

11. Garber JE, Offit K. Hereditary cancer predisposition syndromes. *J Clin Oncol* (2005) 23(2):276–92. doi:10.1200/JCO.2005.10.042

12. Rebbeck TR, Friebel TM, Mitra N, Wan F, Chen S, Andrulis IL, et al. Inheritance of deleterious mutations at both BRCA1 and BRCA2 in an international sample of 32,295 women. *Breast Cancer Res : BCR* (2016) 18(1):112. doi:10.1186/s13058-016-0768-3

13. Gohil D, Sarker AH, Roy R. Base excision repair: mechanisms and impact in biology, disease, and medicine. *Int J Mol Sci* (2023) 24(18):14186. doi:10.3390/ijms241814186

14. Hirai Y, Banno K, Suzuki M, Ichikawa Y, Udagawa Y, Sugano K, et al. Molecular epidemiological and mutational analysis of DNA mismatch repair (MMR) genes in endometrial cancer patients with HNPCC-associated familial predisposition to cancer. *Cancer Sci* (2008) 99(9):1715–9. doi:10.1111/j.1349-7006.2008.00886.x

15. Shao C, Wan J, Lam FC, Tang H, Marley AR, Song Y, et al. A comprehensive literature review and meta-analysis of the prevalence of pan-cancer BRCA mutations, homologous recombination repair gene mutations, and homologous recombination deficiencies. *Environ Mol mutagenesis* (2022) 63(6):308–16. doi:10.1002/em.22505

16. Butz H, Nagy P, Papp J, Bozsik A, Grolmusz VK, Pócza T, et al. PALB2 variants extend the mutational profile of Hungarian patients with breast and ovarian cancer. *Cancers* (2023) 15(17):4350. doi:10.3390/cancers15174350

17. Slavin TP, Maxwell KN, Lilyquist J, Vijai J, Neuhausen SL, Hart SN, et al. The contribution of pathogenic variants in breast cancer susceptibility genes to familial breast cancer risk. *NPJ breast cancer* (2017) 3:22. doi:10.1038/s41523-017-0024-8

18. Tischkowitz M, Balmaña J, Foulkes WD, James P, Ngeow J, Schmutzler R, et al. Management of individuals with germline variants in PALB2: a clinical practice resource of the American College of Medical Genetics and Genomics (ACMG). *Genet Med* (2021) 23(8):1416–23. doi:10.1038/s41436-021-01151-8

19. Graffeo R, Rana HQ, Conforti F, Bonanni B, Cardoso MJ, Paluch-Shimon S, et al. Moderate penetrance genes complicate genetic testing for breast cancer diagnosis: ATM, CHEK2, BARD1 and RAD51D. *Breast (Edinburgh, Scotland)* (2022) 65:32–40. doi:10.1016/j.breast.2022.06.003

20. Grafodatskaya D, O'Rielly DD, Bedard K, Butcher DT, Howlett CJ, Lytwyn A, et al. Practice guidelines for BRCA1/2 tumour testing in ovarian cancer. *J Med Genet* (2022) 59(8):727–36. doi:10.1136/jmedgenet-2021-108238

21. Bouwman P, van der Gulden H, van der Heijden I, Drost R, Klijn CN, Prasetyanti P, et al. A high-throughput functional complementation assay for classification of BRCA1 missense variants. *Cancer Discov* (2013) 3(10):1142–55. doi:10.1158/2159-8290.CD-13-0094

22. Antoniou AC, Pharoah PD, Narod S, Risch HA, Eyfjord JE, Hopper JL, et al. Breast and ovarian cancer risks to carriers of the BRCA1 5382insC and 185delAG and BRCA2 6174delT mutations: a combined analysis of 22 population based studies. *J Med Genet* (2005) 42(7):602–3. doi:10.1136/jmg.2004.024133

23. Finkelman BS, Rubinstein WS, Friedman S, Friebel TM, Dubitsky S, Schonberger NS, et al. Breast and ovarian cancer risk and risk reduction in Jewish BRCA1/2 mutation carriers. *J Clin Oncol* (2012) 30(12):1321–8. doi:10.1200/jco.2011.37.8133

24. Fostira F, Saloustros E, Apostolou P, Vagena A, Kalfakakou D, Mauri D, et al. Germline deleterious mutations in genes other than BRCA2 are infrequent in male breast cancer. *Breast Cancer Res Treat* (2018) 169(1):105–13. doi:10.1007/s10549-018-4661-x

25. Kluz T, Jasiewicz A, Marczyk E, Jach R, Jakubowska A, Lubiński J, et al. Frequency of BRCA1 and BRCA2 causative founder variants in ovarian cancer patients in South-East Poland. *Hereditary Cancer Clin Pract* (2018) 16:6. doi:10.1186/s13053-018-0089-x

26. Pritchard CC, Mateo J, Walsh MF, De Sarkar N, Abida W, Beltran H, et al. Inherited DNA-repair gene mutations in men with metastatic prostate cancer. *New Engl J Med* (2016) 375(5):443–53. doi:10.1056/NEJMoa1603144

27. Yurgelun MB, Chittenden AB, Morales-Oyarvide V, Rubinson DA, Dunne RF, Kozak MM, et al. Germline cancer susceptibility gene variants, somatic second hits, and survival outcomes in patients with resected pancreatic cancer. *Genet Med* (2019) 21(1):213–23. doi:10.1038/s41436-018-0009-5

28. Ladopoulou A, Kroupis C, Konstantopoulou I, Ioannidou-Mouzaka L, Schofield AC, Pantazidis A, et al. Germ line BRCA1 & BRCA2 mutations in Greek breast/ovarian cancer families: 5382insC is the most frequent mutation observed. *Cancer Lett* (2002) 185(1):61–70. doi:10.1016/s0304-3835(01)00845-x

29. Chen S, Francioli LC, Goodrich JK, Collins RL, Kanai M, Wang Q, et al. A genomic mutational constraint map using variation in 76,156 human genomes. *Nature* (2024) 625(7993):92–100. doi:10.1038/s41586-023-06045-0

30. Campeau PM, Foulkes WD, Tischkowitz MD. Hereditary breast cancer: new genetic developments, new therapeutic avenues. *Hum Genet* (2008) 124(1):31–42. doi:10.1007/s00439-008-0529-1

31. Marmolejo DH, Wong MYZ, Bajalica-Lagercrantz S, Tischkowitz M, Balmaña J, extended ERN-GENTURIS Thematic Group 3. Overview of hereditary breast and ovarian cancer (HBOC) guidelines across Europe. *Eur J Med Genet* (2021) 64(12): 104350. doi:10.1016/j.ejmg.2021.104350

32. Owens DK, Davidson KW, Krist AH, Barry MJ, Cabana M, Caughey AB, et al. Risk assessment, genetic counseling, and genetic testing for BRCA-related cancer: US preventive services task force recommendation statement. *Jama* (2019) 322(7): 652–65. doi:10.1001/jama.2019.10987

33. Pashayan N, Antoniou AC, Ivanus U, Esserman LJ, Easton DF, French D, et al. Personalized early detection and prevention of breast cancer: ENVISION consensus statement. *Nat Rev Clin Oncol* (2020) 17(11):687–705. doi:10.1038/s41571-020-0388-9

34. Miller DT, Lee K, Abul-Husn NS, Amendola LM, Brothers K, Chung WK, et al. ACMG SF v3.1 list for reporting of secondary findings in clinical exome and genome sequencing: a policy statement of the American College of Medical Genetics and Genomics (ACMG). *Genet Med* (2022) 24(7):1407–14. doi:10.1016/j.gim.2022.04.006

35. Richards S, Aziz N, Bale S, Bick D, Das S, Gastier-Foster J, et al. Standards and guidelines for the interpretation of sequence variants: a joint consensus recommendation of the American College of medical genetics and genomics and the association for molecular Pathology. *Genet Med* (2015) 17(5):405–24. doi:10.1038/gim.2015.30

36. Adzhubei IA, Schmidt S, Peshkin L, Ramensky VE, Gerasimova A, Bork P, et al. A method and server for predicting damaging missense mutations. *Nat Methods* (2010) 7(4):248–9. doi:10.1038/nmeth0410-248

37. Laish I, Friedman E, Levi-Reznick G, Kedar I, Katz L, Levi Z, et al. Double heterozygotes of BRCA1/BRCA2 and mismatch repair gene pathogenic variants: case series and clinical implications. *Breast Cancer Res Treat* (2021) 188(3):685–94. doi:10.1007/s10549-021-06258-9

38. Megid TBC, Barros-Filho MC, Pisani JP, Achatz MI. Double heterozygous pathogenic variants prevalence in a cohort of patients with hereditary breast cancer. *Front Oncol* (2022) 12:873395. doi:10.3389/fonc.2022.873395

39. Vos JR, Giepmans L, Röhl C, Geverink N, Hoogerbrugge N, ERN GENTURIS. Boosting care and knowledge about hereditary cancer: European reference Network on genetic tumour risk syndromes. *Fam Cancer* (2019) 18(2):281–4. doi:10.1007/s10689-018-0110-6

Pathology & Oncology Research | frontiers

TYPE Original Research
PUBLISHED 15 May 2023
DOI 10.3389/pore.2023.1610905

Check for updates

OPEN ACCESS

EDITED BY
Andrea Ladányi,
National Institute of Oncology (NIO), Hungary

*CORRESPONDENCE
Attila Zalatnai,
zalatnai.attila@med.semmelweis-univ.hu

RECEIVED 28 October 2022
ACCEPTED 25 April 2023
PUBLISHED 15 May 2023

CITATION
Janka M and Zalatnai A (2023), Correlations between the histopathological alterations in minor salivary glands and the clinically suspected Sjögren's syndrome. *Pathol. Oncol. Res.* 29:1610905. doi: 10.3389/pore.2023.1610905

COPYRIGHT
© 2023 Janka and Zalatnai. This is an open-access article distributed under the terms of the Creative Commons Attribution License (CC BY). The use, distribution or reproduction in other forums is permitted, provided the original author(s) and the copyright owner(s) are credited and that the original publication in this journal is cited, in accordance with accepted academic practice. No use, distribution or reproduction is permitted which does not comply with these terms.

Correlations between the histopathological alterations in minor salivary glands and the clinically suspected Sjögren's syndrome

Mária Janka and Attila Zalatnai*

Department of Pathology and Experimental Cancer Research, Faculty of Medicine, Semmelweis University, Budapest, Hungary

In sicca syndrome patients the xerostomia, xerophthalmia and the serological findings may strongly suggest the autoimmune Sjögren's syndrome, but the histological findings in the labial salivary gland biopsies do not always justify the suspected diagnosis. The aim of this study was to compare the histomorphological changes and the clinical findings in patients with pathologically established Sjögren's syndrome and in cases with negative histology. A total of 133 labial biopsies have been retrospectively evaluated from 2015 to May 2022, and the characteristic Sjögren's lesions were found in 67 cases. According to the clinical data, 34 cases proved to be primary, and 33 were associated ("secondary") forms. In 66 cases, the histology did not justify Sjögren's syndrome; a significant acinar loss, fibrolipomatous infiltration, and mild sialadenitis had led to the clinical symptoms. In Sjögren's histologies, the acinar loss was detected in just 31.8% of cases, which might indicate that the diminished saliva production represents immune-mediated hypofunction rather than direct damage of the acini. This is the first systemic study in Hungary investigating the correlation between pathological alterations and clinical findings.

KEYWORDS

immunohistochemistry, clinicopathology, retrospective study, Sjögren syndrome, labial gland biopsy

Introduction

Sjögren's syndrome (SS)—named after a Swedish ophthalmologist—is a treatable, but not curable autoimmune disease affecting primarily the salivary and the lacrimal glands, but in about 50% of patients, other immune-mediated diseases are also detected. The primary Sjögren's syndrome is not associated with other disorders, while the other types are coupled with systemic connective tissue diseases, such as SLE, rheumatoid arthritis, or systemic sclerosis [1]. Although its frequency may vary considerably depending on the classification criteria used, on the clinical or pathological settings, or on the age groups studied, the estimated prevalence of the primary forms in a US population-based cohort

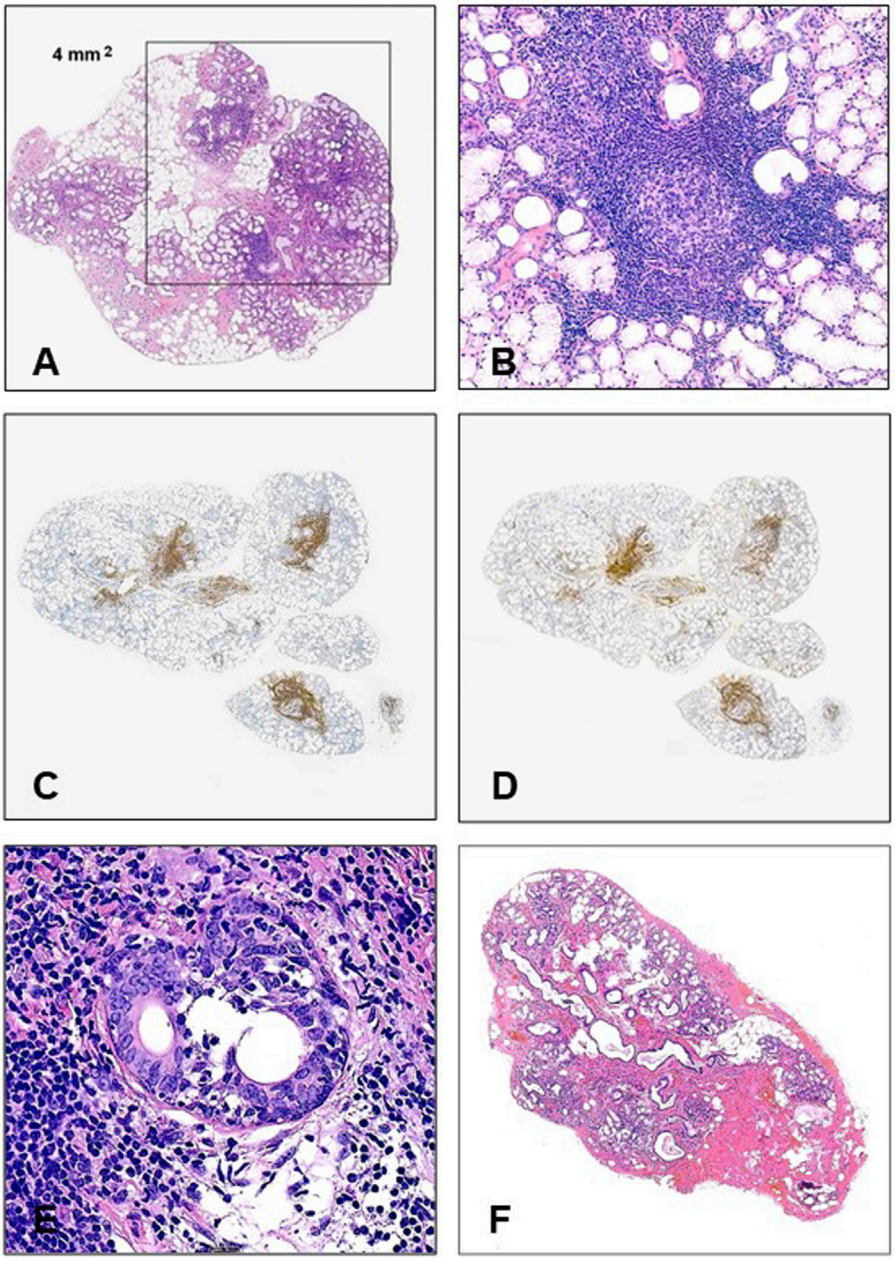

FIGURE 1
(A) For the histological establishment of Sjögren's syndrome in labial biopsy materials, at least 1 lymphoid focus containing a minimum of 50 mature lymphocytes should be identified in 4 mm^2 (HE, ×20). **(B)** Germinal center in a minor salivary gland (HE, ×200). **(C)** CD20 positivity in the small labial gland (×20). **(D)** CD3 positivity in small labial gland (×20). **(E)** Small duct is infiltrated by mature lymphocytes (HE, ×400). **(F)** Typical histology in a non-Sjögren's labial biopsy (HE, x20).

was reported as 22/100,000 inhabitants [2], but this figure in Europe is around 39/100,000 [3]. A recent report in Hungary claimed a lower incidence (16/100,000) of newly diagnosed SS cases [4].

Since the autoimmune process harms salivation and tear production, the classical clinical symptoms are characterized by xerostomia and xerophthalmia (sicca syndrome), but sometimes other mucosal dryness can also be experienced (in the digestive tract, vagina, etc.). However, because dry symptoms can also be found in other conditions, such as a side effect of antihypertensive drugs or chemotherapeutic agents, in old age or in diabetes mellitus [5], correct diagnosis of Sjögren's

syndrome requires well-defined criteria. Over the years, several schemes have been proposed both for the primary and the associated forms [6, 7]. In the actual ACR-EULAR classification, the diagnosis is based on the combination of the clinical symptoms, the autoimmune markers, and the histopathological findings, but the SS-A/Ro/positivity and the labial salivary gland biopsy results have higher scores [8].

Although the presenting clinical symptoms indicating Sjögren's syndrome are usually highly suggestive, salivary gland biopsy is indicated when a patient experiences long-standing (over 3 months) ocular and/or oral dryness with or without accompanied systemic autoimmune diseases to reinforce the diagnosis. The clinical symptoms may poorly correlate with the overt Sjögren's syndrome [9]. The primary and associated forms may show similar manifestations in SLE, for example, definitive SS is just diagnosed in around 14%–18% [1]. Similarly, in rheumatoid arthritis dry eye, dry mouth, or ocular foreign body sensations were seen in 78%, 68%, or 17% of patients, respectively, however, only 8.7% of patients proved to be Sjögren's syndrome [10]. Moreover, SS-A/SS-B antibodies can also be detected in a general population (up to 16%) without displaying any autoimmune disease [11].

The major salivary glands are responsible for over 95% of saliva production, while the minor salivary glands have just an ancillary role, but their continuous secretion is important in the moistening of the oral cavity [12]. The histological sampling of the major salivary glands, however, is just exceptionally practiced [13, 14]. The generally accepted method is the labial biopsy. This sensitive technique was introduced by *Chisholm* and *Mason* [15], and they showed a definite association between the clinically suspected SS and the lymphocytic foci in the minor salivary glands. The actual standard diagnostic criteria of the primary Sjögren's syndrome have been defined by the ACR-EULAR classification [8].

In this classification scheme the anti-SSA/Ro positivity and the labial biopsy results have the highest weight. Histologically, the diffuse lymphocytic infiltration is not a feature, it represents just an aspecific sialadenitis; for establishing Sjögren's pathology the mature lymphoid cells (at least 50) must be arranged in foci, at least one focus per 4 square mm (Figure 1A), sometimes with secondary follicle formation with germinal center (Figure 1B). Although many innate and adaptive immune cells play a role in the damage of the glandular structures [16], the foci are composed of subsets of B-cells associated with T-cell population [17, 18] (Figures 1C, D). In the glandular damage the interplay between the immune cells and the glandular elements seems to be important [19], but the hypofunction rather than destruction is regarded as the main mechanism of the secretory failure [20].

Although by definition the histological hallmark of Sjögren's syndrome in labial biopsies is ≥1 focus per 4 square mm, it would be worth investigating other morphological alterations in the glands, moreover, whether the extent of the lymphoid accumulation correlates with the clinical symptoms.

Materials and methods

Between 2015 and May 2022, 133 labial biopsies have been evaluated at the (1st) Department of Pathology and Experimental Cancer Research. The patients with clinically suspected Sjögren's syndrome had an average age of 58.5 (25–82) years. The vast majority of patients were female (125/133 = 94%). The clinical data have been collected from the Semmelweis University electronic archives and all patients provided their written informed consent. The patients with previous head/neck irradiation, the HCV-, IgG4-, COVID-19 or HIV-positive cases, the organ-, or bone marrow transplanted patients have been excluded, and similarly, those who regularly took antidepressants or anticholinergic drugs. Non-insulin-dependent, but well-controlled diabetes mellitus was mentioned in 6 cases. Malignant tumors were diagnosed in three patients (breast cancer, malignant melanoma, and MALT-lymphoma), but none of them were on an actual chemotherapeutic regimen. Before taking a labial gland biopsy, a detailed immunological checkup was accomplished and in the oral cavity no preneoplastic or infective conditions were detected. During the histological evaluation the following features were assessed: the number of lobules, the percentage of the infiltrating fat and connective tissue, the rate of the acinar loss, the ductular changes, the small vessels, and the lymphocytic foci. The proportions of the components have been assessed by either routine ×20 microscopic field and calculated to square mm, or the scanned slides were evaluated by using a SlideViewer program (P1000 Scanner with Panoramic 1,000 software; 3D Histech Ltd., Budapest). Both investigators (MJ, AZ) double-checked the histological findings. The establishment of Sjögren's histology was based on the internationally accepted consensus [21] (Figure 1A), and among the 133 biopsies, 67 specimens (50.4%) fulfilled these criteria. In the remaining 66 cases, the clinical settings indicated SS, but in the labial biopsies, the required criteria were not found. In both groups the focus scores have been calculated for 4 square mm glandular areas.

The aim of this study was to evaluate the morphological changes of labial gland biopsies in patients with clinically suspected sicca syndrome, to compare the findings with Sjögren's and non-Sjögren's cases, and to analyze the relevant clinical data.

Results

Sjögren's histologies

The histological changes are presented in Table 1. The labial glands contained 2–16 lobules. The histologically visible glandular damages were highly inconstant, with the only universal finding being the presence of the diagnostic (≥1) lymphoid foci. The average number of foci per gland

TABLE 1 Histopathological findings of labial gland biopsies in Sjögren's and non-Sjögren's syndrome patients.

	Sjögren's syndrome	Percent	Non-Sjögren's syndrome	Percent	P
Focus score ≥1	67/67 average focus number: 3.6 (1–11)	100	0/66	0	
Acinar loss	21/67 (5%–80%)	31.3	50/66 (20%–60%)	75.8	0.025[a]
Fat infiltration	45/67 median area: 32.5% (0–85)	67.2	60/66 median area: 25% (15–60)	91	NS
Fibrosis	60/67 median area: 22.5% (0–50)	89.5	64/66 median area: 50% (40–67)	97	NS
Ductectasia	37/67	55.2	49/66	74.2	NS
Vasculitis	4/67	6	0/66	0	
Aspecific chronic sialadenitis	0/67	0	50/66	75.8	
Normal histology	0/67	0	7/66	10.6	

[a]Calculated by chi-square test.

was 3.6, varying between 1 and 11, and the lymphoid accumulations were arranged around the moderately distended ductules (Figure 1A). In two cases germinal centers were also formed (Figure 1B). The foci have been composed of proportional $CD20^+$ and $CD3^+$ mature lymphocytes (Figures 1C, D), among the T-cells with the helper ($CD4^+$) predominance. In a single, severe case the lymphocytes invaded some ductular cells (Figure 1E), but the attack of the acinar elements was not the feature. Loss of the acini was detected in about one-third of cases and these areas were mainly replaced by fibrosis (89.5% of cases) and partly by fat tissue (67.1%). The extent of the glandular injury was highly variable, ranging from 5 to 80 percent. The remaining glands were structurally preserved, and no apoptotic activity was seen. The accumulation of connective tissue led to dilatation of the small ducts in about half of the cases, accompanied by inspissated secreted material. In four samples, mild vasculitis was also seen close to the lymphoid foci.

Non-Sjögren's histologies

There were 66 patients who complained of chronic xerostomia and/or xerophthalmia and were clinically suspected of having Sjögren's syndrome, but the labial gland biopsies did not show the diagnostic lymphoid foci (Table 1; Figure 1F). Instead, a frequent finding was the mild, aspecific sialadenitis in the stroma, displaying a loose, but diffuse lymphoplasmocytic infiltration, without neutrophils. The inflammatory cells did not attack the acinar elements. The predominating histological finding was the significant accumulation of the fibrolipomatous stroma, the small ducts had been dilated in two-thirds of samples, and more than two-thirds of the acini had been severely atrophied or disappeared. Signs of necrosis or apoptosis were not seen. In seven samples (10.6%), no histological abnormalities were found at all.

TABLE 2 Clinicopathological findings in patients with or without typical Sjögren-histologies.

	Sjögren (N = 67)		Non-Sjögren (N = 66)		
	No.	%	No.	%	P
Hyposalivation	19/67	28 Sensitivity: 28.3% Specificity: 92%	5/66	8	<0.005
Xerophthalmia	43/67	64 Sensitivity: 64.2% Specificity: 51.5%	32/66	48	<0.05
Schirmer-pos.	39/67	58 Sensitivity: 58.2% Specificity: 81.8%	12/66	18	<0.001
SS-A (Ro52)	42/67	62 Sensitivity: 62.7% Specificity: 93.9%	4/66	6	<0.0001
SS-B (La)	13/67	19 Sensitivity: 19.4% Specificity: 97%	2/66	3	<0.005
ANA	15/67	23 Sensitivity: 22.4% Specificity: 86.3%	9/66	13	NS
RF	10/67	15 Sensitivity: 14.9% Specificity: 97%	2/66	3	<0.025

Clinical and laboratory findings in patients with Sjögren's histologies

The relevant clinical data are illustrated in Table 2 and in Figure 2. Although all patients complained of subjective chronic dry mouth sensation, however, objective hyposalivation measured by unstimulated sialometry was only found in less than one-third of cases. Xerophthalmia was also a rather common symptom, which was

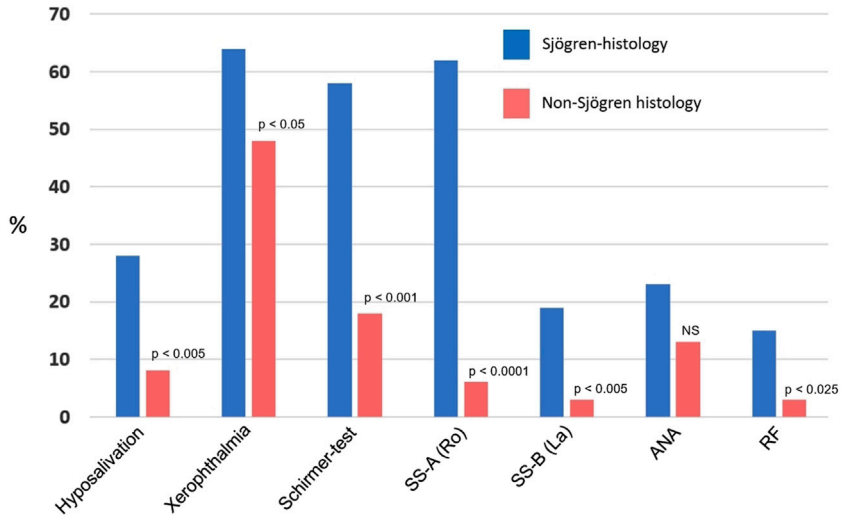

FIGURE 2
Clinical and laboratory findings in patients with histologically proven Sjögren's syndrome and in non-Sjögren's histologies. ANA, antinuclear antibody; RF, rheumatoid factor (Significances were calculated by Chi-Square test).

frequently evidenced by the Schirmer-test (reduced tear production). Interestingly, the ocular symptoms were not always equally affecting both eyes. The presence of the SS-A autoantibody was a frequent, but not a constant finding in all patients (62%), but the SS-B (which is a less sensitive marker), being detectable just in 19%. The non-specific antibodies (ANA, RF) were identified in 23% and 15%, respectively, however, among them no SLE or rheumatoid arthritis were diagnosed.

In all the 67 labial gland biopsies the focus score fulfilled the diagnostic criteria, however, it was found that the number of lymphoid foci was rather variable. Therefore, we compared this figure with the clinical data but no correlation was found. The dry symptoms occurred at the same frequency irrespective of the extent of the lymphoid infiltration. The SS-A-positivities did not differ either.

Although prolonged xerostomia is also a frequent finding in poorly controlled diabetes mellitus, among primary Sjögren's patients only one, well-managed diabetic patient was noted. Other, occasional, probably unrelated diseases were: polyneuropathy (n = 1), trigeminal neuropathy (n = 1), primary biliary cholangitis (n = 1), idiopathic thrombocytopenic purpura (n = 1), or antiphospholipid syndrome (n = 1). The overwhelming majority of our cases were not associated with systemic autoimmune conditions.

Clinical and laboratory findings in patients with non-Sjögren's histologies

Although the presenting signs were also chronic dryness in the mouth, objective hyposalivation was seen in less than 10% of cases (Figure 2). Albeit xerophthalmia was a frequent complaint (48%), it was objectively reinforced by Schirmer-test in just 18% of cases. SS-A and SS-B have rarely been detected (6% and 3%, respectively), and similarly, rheumatoid factor was seldom noticed. All these figures differed significantly from those of the values seen in Sjögren's histologies. Antinuclear antibody was a relatively frequent finding (13%).

Within these patients, none of them took antidepressants or anticholinergic drugs. Diabetes mellitus was only diagnosed in five cases, but autoimmune diseases were frequently mentioned: 8 rheumatoid arthritis, 3 SLE, 1 DLE, 2 Hashimoto thyroiditis, 11 hypothyroidisms, and 5 non-differentiated autoimmune disease. In addition, 13 patients complained of various rheumatic symptoms, but without evidenced autoimmune background.

Discussion

No single clinical or laboratory finding is characteristic for Sjögren's syndrome. The diagnosis is based on a subjective and objective decrease of saliva and tear productions, the presence of specific autoantibodies (SS-A, SS-B), and pathological evaluation of the minor salivary glands. All these findings are scored (summing up 6 points), and the disease can be established, when the scores are ≥4. Although the positive labial biopsy scored 3, histology alone is not a gold standard, but it serves a pivotal role in the diagnostic workup; the most important morphological sign is the presence of ≥1 lymphoid focus per 4 square mm, but other, additional features are also useful suggesting signs. Based on a large scale, prospective cohort study (1726 labial gland biopsies), however, the clinical/lab findings may not always correlate with the morphological alterations [22]. Similar data have also been provided by a Hungarian study [4], where a positive focus score was only found in 109 cases (31.8%) out of 342 biopsies from patients with Sicca symptoms.

In our study, loss of the acini in Sjögren's patients was noted in about one-third of cases, but its extent proved to be highly variable. Although the accumulation of the connective tissue and the fat cells was a very frequent finding, they seemed to be consecutive and not causative events. The lymphoid foci, containing equally $CD20^+$ and $CD3^+$ lymphocytes, were situated mostly in periductular localization, no direct contact was observable with the acinar structures, and morphological signs of necrosis/apoptosis were not seen either. Direct invasion of the small duct was just seen in a single, severe case (Figure 1D). The clinical symptoms or the SS-A positivity did not correlate with the severity of the focus score. These findings are consistent with those by *Venables* [20], who claimed that hypofunction rather than the direct glandular destruction can be regarded as the main mechanism in the disease.

In Sjögren's disease the characteristic lymphoid foci are comprised of many types of immune cells and their interaction with the epithelial elements is an important issue regarding glandular destruction [16, 20, 23]. The proportion of the T-and B lymphocytes, however, is not constant throughout the disease course: in the early stage $CD4^+$ cells predominate, and the B-cells appear later, but they mutually interact [19]. The interferon-γ, IL-17, IL-21, or the overstimulated B-cell products (excessive amounts of various antibodies) play multifaceted roles [24], and these findings have initiated therapeutic attempts at B-cell depletion. Although these strategies are logical and encouraging, the results are still indecisive [18, 25, 26]. Moreover, some innovative and promising novel trials are also under investigation [27].

In 66 labial gland biopsies, focal lymphoid collections were never seen, just a diffusely occurring, mild, aspecific sialadenitis, albeit in these patients the clinical symptoms suggested Sjögren's syndrome. While in Sjögren-histologies acinar loss was a feature in only approximately one-third of cases (21/67), in non-Sjögren's biopsies the acini did disappear in around 76% of cases (50/66), replaced by fibrolipomatous stromal elements in 91%–97%. Due to the compression effect, the small ducts were dilated, with some secreted material in their lumina. Interestingly, in 7 out of 66 biopsies (10.6%) the labial glands displayed a normal morphology.

It seemed to be perplexing the detection of the SS-A(Ro) antibody in patients whose labial biopsies did not show the histological features of Sjögren's syndrome (4/66, 6%), raising the likelihood that these cases could have been misdiagnosed. However, this antibody is not an absolute marker, it can often be detected in other autoimmune disorders [28–30]. Moreover, some authors have found that anti-SSA or anti-SSB antibodies can be present at a high percentage in the early phase of Sjögren's syndrome, even years before the clinically manifested disease, or in seemingly healthy people [27, 31]. In our study, among the cases presenting dry syndromes and SS-A(Ro) positivity but where the labial gland biopsy failed to show ≥1 focus score, there were patients suffering from various rheumatic complaints but definite autoimmune diseases have not been diagnosed. This might explain the unexpected lab finding.

In conclusion, the clinical symptoms suggesting Sjögren's syndrome always require histological investigation of the small labial salivary glands to evaluate the morphological alterations reinforcing or excluding the supposed diagnosis. It was clear from the clinicopathological findings that neither the objective measurements of the saliva or tear production or the presence of autoantibodies reached high sensitivities alone, although xerophthalmia and the SS-A had a highest suggestive value. For that reason, in the ACR/EULAR consensus the Ro antibody and the histology get the highest weight (3-3 points each).

While in Sjögren's histologies acinar loss was seen in just one-third of cases, no direct contact was found between the glands and the lymphoid foci, and because no necrosis or apoptosis were the feature of damage, it is presumable that the hyposalivation resulted from the indirect effect of the lymphoid foci. This view is further reinforced by the negative connection between the clinical signs and the number of foci. When the biopsies did not justify the sicca syndrome, definitive reduction of the acinar structures and heavy accumulation of fibrolipomatous tissue led to decreased saliva production.

This research is the first systemic study in Hungary investigating the correlation between pathological alterations and the clinical findings.

Data availability statement

The raw data supporting the conclusion of this article will be made available by the authors, without undue reservation.

Ethics statement

Ethical review and approval was not required for the study on human participants in accordance with the local legislation and institutional requirements. The patients/participants provided their written informed consent to participate in this study.

Author contributions

All authors listed have made a substantial, direct, and intellectual contribution to the work and approved it for publication.

Conflict of interest

The authors declare that the research was conducted in the absence of any commercial or financial relationships that could be construed as a potential conflict of interest.

References

1. Pasoto SG, deOliveira Martins VA, Bonfa E. Sjögren's syndrome and systemic lupus erythematosus: Links and risks. *Open Access Rheumatol* (2019) 11:33–45. doi:10.2147/OARRR.S167783

2. Maciel G, Crowson CS, Matteson L, Cornec D. Prevalence of primary sjögren's syndrome in a US population-based cohort. *Arthritis Care Res (Hoboken)* (2017) 69: 1612–6. doi:10.1002/acr.23173

3. Cornec D, Chiche L. Is primary sjögren's syndrome an orphan disease? A critical appraisal of prevalence studies in Europe. *Ann Rheum Dis* (2015) 74:e25. doi:10.1136/annrheumdis-2014-206860

4. Dézsi AJ, Erdei C, Demeter T, Kovács A, Nagy G, Mensch K, et al. Prevalence of Sjögren's syndrome in patients with dry mouth in the region of Central Hungary. *Oral Dis* (2022). doi:10.1111/odi.14264

5. Yousefi H, Abdollahi M. An update on drug-induced oral reactions. *J Pharm Pharm Sci* (2018) 21:171–83. doi:10.18433/jpps29893

6. Parisis D, Chivasso C, Perret J, Soyfoo MS, Delporte C. Current state of knowledge on primary Sjögren's syndrome, an autoimmune exocrinopathy. *J Clin Med* (2020) 9:2299. doi:10.3390/jcm9072299

7. Negrini S, Emmi G, Greco M, Borro M, Sardanelli F, Murdaca G, et al. Sjögren's syndrome: A systemic autoimmune disease. *Clin Exp Med* (2022) 22:9–25. doi:10.1007/s10238-021-00728-6

8. Shiboski CH, Shiboski SC, Seror R, Criswell LA, Labetoulle M, Lietman TM, et al. 2016 American college of rheumatology/European league against rheumatism classification criteria for primary sjögren's syndrome: A consensus and data-driven methodology involving three international patient cohorts. *Arthritis Rheumatol* (2017) 69:35–45. doi:10.1002/art.39859

9. Alunno A, Bartoloni E, Valentini V, La Paglia GMC, Valentini E, Leone MC, et al. Discrepancy between subjective symptoms, objective measures and disease activity indexes: The lesson of primary sjögren's syndrome. *Clin Exp Rheumatol* (2018) 36:210–4.

10. Kim H, Cho SK, Kim HW, Han J, Kim Y, Hwang KG, et al. The prevalence of sjögren's syndrome in rheumatoid arthritis patients and their clinical features. *Korean Med Sci* (2020) 35:e369. doi:10.3346/jkms.2020.35.e369

11. Metsküla K, Salur L, Mandel M, Uibo R. Demonstration of high prevalence of SS-A antibodies in a general population: Association with HLA-DR and enterovirus antibodies. *Immunol Lett* (2006) 106:14–8. doi:10.1016/j.imlet.2006.03.005

12. Shen D, Ono K, Do Q, Ohyama H, Nakamura K, Obata K, et al. Clinical anatomy of the inferior labial gland: A narrative review. *Gland Surg* (2021) 10: 2284–92. doi:10.21037/gs-21-143

13. Soyfoo MS, Catteau X, Delporte C. Parotid gland biopsy as an additional diagnostic tool for supporting the diagnosis of sjögren's syndrome. *Int J Rheumatol* (2011) 2011:302527. doi:10.1155/2011/302527

14. Spijkervet FK, Haacke E, Kroese FG, Bootsma H, Vissink A. Parotid gland biopsy, the alternative way to diagnose sjögren syndrome. *Rheum Dis Clin North Am* (2016) 42:485–99. doi:10.1016/j.rdc.2016.03.007

15. Chisholm DM, Mason DK. Labial salivary gland biopsy in Sjögren's disease. *J Clin Pathol* (1968) 21:656–60. doi:10.1136/jcp.21.5.656

16. Witas R, Gupta S, Nguyen CQ. Contributions of major cell populations to sjögren's syndrome. *J Clin Med* (2020) 9:3057. doi:10.3390/jcm9093057

17. Zhou H, Yang J, Tian J, Wang S. CD8(+) T lymphocytes: Crucial players in sjögren's syndrome. *Front Immunol* (2021) 11:602823. doi:10.3389/fimmu.2020.602823

18. Hamza N, Bos NA, Kallenberg CG. B-cell populations and sub-populations in Sjögren's syndrome. *Presse Med* (2012) 41:e475–83. doi:10.1016/j.lpm.2012.05.021

19. Verstappen GM, Pringle S, Bootsma H, Kroese FGM. Epithelial-immune cell interplay in primary Sjögren syndrome salivary gland pathogenesis. *Nat Rev Rheumatol* (2012) 17:333–48. doi:10.1038/s41584-021-00605-2

20. Venables PJ. Sjögren's syndrome. *Best Pract Res Clin Rheumatol* (2004) 18: 313–29. doi:10.1016/j.berh.2004.02.010

21. Shiboski SC, Shiboski CH, Criswell L, Baer A, Challacombe S, Lanfranchi H, et al. Sjögren's international collaborative clinical alliance (SICCA) research groups (2012) American college of rheumatology classification criteria for sjögren's syndrome: A data-driven, expert consensus approach in the sjögren's international collaborative clinical alliance cohort. *Arthritis Care Res (Hoboken)* 64 :475–87. doi:10.1002/acr.21591

22. Daniels TE, Cox D, Shiboski CH, Schiødt M, Wu A, Lanfranchi H, et al. Sjögren's International Collaborative Clinical Alliance Research Groups (2011) Associations between salivary gland histopathologic diagnoses and phenotypic features of Sjögren's syndrome among 1,726 registry participants. *Arthritis Rheum* 63: 2021–30. doi:10.1002/art.30381

23. Nordmark G, Alm GV, Rönnblom L. Mechanisms of disease: Primary sjögren's syndrome and the type I interferon system. *Nat Clin Pract Rheumatol* (2006) 2:262–9. doi:10.1038/ncprheum0173

24. Cornec D, Devauchelle-Pensec V, Tobón GJ, Pers JO, Jousse-Joulin S, Saraux A. B cells in sjögren's syndrome: From pathophysiology to diagnosis and treatment. *J Autoimmun* (2012) 39:161–7. doi:10.1016/j.jaut.2012.05.014

25. Chen YH, Wang XY, Jin X1, Yang Z1, Xu J. Rituximab therapy for primary sjögren's syndrome. *Front Pharmacol* (2021) 12:731122. doi:10.3389/fphar.2021.731122

26. Gandolfo S, De Vita S. Double anti-B cell and anti-BAFF targeting for the treatment of primary Sjögren's syndrome. *Clin Exp Rheumatol* (2019) 37: 199–208.

27. Zandonella Callegher S, Giovannini I, Zenz S, Manfrè V, Stradner MH, Hocevar A, et al. Sjögren syndrome: Looking forward to the future. *Ther Adv Musculoskelet Dis* (2022) 14:1759720X221100295. doi:10.1177/1759720X221100295

28. Menéndez A, Gómez J, Caminal-Montero L, Díaz-López JB, Cabezas-Rodríguez I, Mozo L. Common and specific associations of anti-SSA/Ro60 and anti-Ro52/TRIM21 antibodies in systemic lupus erythematosus. *Sci World J* (2013) 2013:832789. doi:10.1155/2013/832789

29. Sánchez-Montalvá A, Fernández-Luque A, Simeón CP, Fonollosa-Plà V, Marín A, Guillén A, et al. Anti-SSA/Ro52 autoantibodies in scleroderma: Results of an observational, cross-sectional study. *Clin Exp Rheumatol* (2014) 32:177–82.

30. Smeele HTW, Schreurs MWJ, Costedoat-Chalumeau N, Cornette JMJ, Dolhain RJEM. Low prevalence of anti-SSA (anti-Ro) and anti-SSB (anti-La) autoantibodies in female patients with rheumatoid arthritis with a wish to conceive. *RMD Open* (2021) 7:e001727. doi:10.1136/rmdopen-2021-001727

31. Theander E, Jonsson R, Sjöström B, Brokstad K, Olsson P, Henriksson G. Prediction of Sjögren's syndrome years before diagnosis and identification of patients with early onset and severe disease course by autoantibody profiling. *Arthritis Rheumatol* (2015) 67:2427–36. doi:10.1002/art.39214

Pathology & Oncology Research | frontiers

TYPE Original Research
PUBLISHED 17 April 2024
DOI 10.3389/pore.2024.1611744

Check for updates

OPEN ACCESS

EDITED BY
Andrea Ladányi,
National Institute of Oncology (NIO), Hungary

*CORRESPONDENCE
Gizem Kaval,
gizemkaval1@istanbul.edu.tr

RECEIVED 24 February 2024
ACCEPTED 03 April 2024
PUBLISHED 17 April 2024

CITATION
Kaval G, Dagoglu Kartal MG, Azamat S, Cingoz E, Ertas G, Karaman S, Kurtuldu B, Keskin M, Berker N, Karabulut S, Oral EN and Dagoglu Sakin N (2024), Evaluating complete response prediction rates in locally advanced rectal cancer with different radiomics segmentation approaches. *Pathol. Oncol. Res.* 30:1611744. doi: 10.3389/pore.2024.1611744

COPYRIGHT
© 2024 Kaval, Dagoglu Kartal, Azamat, Cingoz, Ertas, Karaman, Kurtuldu, Keskin, Berker, Karabulut, Oral and Dagoglu Sakin. This is an open-access article distributed under the terms of the Creative Commons Attribution License (CC BY). The use, distribution or reproduction in other forums is permitted, provided the original author(s) and the copyright owner(s) are credited and that the original publication in this journal is cited, in accordance with accepted academic practice. No use, distribution or reproduction is permitted which does not comply with these terms.

Evaluating complete response prediction rates in locally advanced rectal cancer with different radiomics segmentation approaches

Gizem Kaval[1]*, Merve Gulbiz Dagoglu Kartal[2], Sena Azamat[3], Eda Cingoz[4], Gokhan Ertas[5], Sule Karaman[1], Basak Kurtuldu[6], Metin Keskin[7], Neslihan Berker[8], Senem Karabulut[9], Ethem Nezih Oral[1] and Nergiz Dagoglu Sakin[1]

[1]Department of Radiation Oncology, Istanbul Faculty of Medicine, Istanbul University, Istanbul, Türkiye, [2]Department of Radiology, Istanbul Faculty of Medicine, Istanbul University, Istanbul, Türkiye, [3]Department of Radiology, Cam and Sakura City Hospital, Istanbul, Türkiye, [4]Department of Radiology, Bagcilar Training and Research Hospital, Istanbul, Türkiye, [5]Department of Biomedical Engineering, Yeditepe University, Istanbul, Türkiye, [6]Department of Emergency, Hackalibaba Hospital, Trabzon, Türkiye, [7]Department of General Surgery, Istanbul Faculty of Medicine, Istanbul University, Istanbul, Türkiye, [8]Department of Pathology, Istanbul Faculty of Medicine, Istanbul University, Istanbul, Türkiye, [9]Department of Medical Oncology, Istanbul Faculty of Medicine, Istanbul University, Istanbul, Türkiye

Purpose: Studies examining prediction of complete response (CR) in locally advanced rectum cancer (LARC) from pre/post chemoradiotherapy (CRT) magnetic resonance imaging (MRI) are performed mostly with segmentations of the tumor, whereas only in two studies segmentation included tumor and mesorectum. Additionally, pelvic extramesorectal region, which is included in the clinical target volume (CTV) of radiotherapy, may contain information. Therefore, we aimed to compare predictive rates of radiomics analysis with features extracted from segmentations of tumor, tumor+mesorectum, and CTV.

Methods and materials: Ninety-three LARC patients who underwent CRT in our institution between 2012 and 2019 were retrospectively scanned. Patients were divided into CR and non-CR groups. Tumor, tumor+mesorectum and CTV were segmented on T2 preCRT MRI images. Extracted features were compared for best area under the curve (AUC) of CR prediction with 15 machine-learning models.

Results: CR was observed in 25 patients (26.8%), of whom 13 had pathological, and 12 had clinical complete response. For tumor, tumor+mesorectum and CTV segmentations, the best AUC were 0.84, 0.81, 0.77 in the training set and 0.85, 0.83 and 0.72 in the test set, respectively; sensitivity and specificity for the test set were 76%, 90%, 76% and 71%, 67% and 62%, respectively.

Conclusion: Although the highest AUC result is obtained from the tumor segmentation, the highest accuracy and sensitivity are detected with tumor+mesorectum segmentation and these findings align with previous

studies, suggesting that the mesorectum contains valuable insights for CR. The lowest result is obtained with CTV segmentation. More studies with mesorectum and pelvic nodal regions included in segmentation are needed.

KEYWORDS

rectal cancer, watch and wait, radiomics, radiotherapy, pathological complete response ratio

Introduction

Colorectal cancer is the third most common malignancy among all [1]. Recently, the recommended treatment of locally advanced rectum cancer (LARC) is "total neoadjuvant therapy," which consists of long-term chemoradiotherapy (CRT) or short-term radiotherapy (RT) and consolidation or induction chemotherapy in suitable patients, followed by total mesorectal excision (TME) or "watch-and-wait" [2–4]. Pathological complete response (pCR) is observed at a rate of 15%–30% and it is important to truly detect these patients before surgery, who may be candidates for "watch-and-wait" [5].

Endoscopy and imaging are the most common methods for assessing treatment response. True prediction of clinical complete response (cCR) by endoscopy is approximately 85%, yet it does not discern extraluminal lesions [6]. The most suitable imaging method is magnetic resonance imaging (MRI) as it does not emit ionizing radiation and shows soft tissue with high resonance. If fibrosis develops inside the tumor after CRT, the viable tumor tissue under the fibrotic scar may not be detected with MRI [7, 8]. Diverse treatment responses necessitate an individualized treatment approach [9]. It is critical to develop markers that will predict unresponsive or more sensitive patients. Tumor heterogeneity, recognized as a potential mechanism contributing to resistance to CRT, arises from the phenomenon wherein neoplastic cells, stemming from a common progenitor undergo various mutations. This process leads to the emergence of distinct subpopulations within the tumor [10]. Furthermore, tumor cells may have molecular interactions with adipocytes in the peritumoral tissue and mesorectum, which support tumor progression and metastasis [11, 12]. Alongside their limitations, current diagnostic methods lack the capacity to comprehensively assess both intratumoral heterogeneity and peritumoral interactions that influence tumor behavior.

Radiomics is an innovative method developed with the aim of providing additional information that may affect the clinical approach derived from the reflections of the underlying pathophysiological features and intratumoral heterogeneity from medical images [13].

Radiomics studies in LARC have emphasized the noninvasive prediction of patients with complete response (CR) through preCRT and/or postCRT MRI [14] scans. Radiomics analysis was performed by segmenting only the tumor region in most of these studies. A study conducted by Shaish et al. in 2020, where they compared radiomics analyzes with different segmentations, is the first study to examine the predictive rate of pCR analysis with mesorectum segmentation. Segmented regions were tumor-only, mesorectum-only and tumor+mesorectum. The highest result was obtained from the radiomics analysis of mesorectum-only segmentation for pCR evaluation. In another study conducted in 2022, radiomics analysis from mesorectal fatty tissue segmentation was examined [15, 16]. Based on these studies, analysis of mesorectal tissue seems to be informative for pCR. In addition to the mesorectum, the pelvic extramesorectal region, which is encompassed within the clinical target volume (CTV) of RT due to the occasional presence of nodal metastases may also provide valuable insights of disease behaviour. Regarding the issue, we aimed to compare CR predictive rates of radiomics analysis operated with features extracted from segmentations of tumor-only, tumor+mesorectum, and CTV.

Methods

Patients

In our study, patients who were referred to our institution with a histopathologically confirmed diagnosis of LARC between 2012 and 2019 were retrospectively screened. The stage was determined following endoscopic and radiological assessments. The study cohort comprised patients who underwent CRT and surgery afterwards or those who remained under surveillance without recurrence, adhering to the "watch-and-wait" approach. Patients lacking appropriate protocol images were excluded from the study. MRI images were retrieved from the Picture Archiving and Communication System.

Patients who attained a pathological stage of ypT0N0 were classified as pCR, while patients who met the criteria for the "watch-and-wait" strategy and remained recurrence-free for 4 years were categorized as cCR. In both instances, these patients were collectively evaluated as demonstrating CR.

Neoadjuvant treatment and response evaluation

We conduct simulation computed tomography (SCT) scans with a cross-sectional interval of 0.3 cm for RT planning. CTV

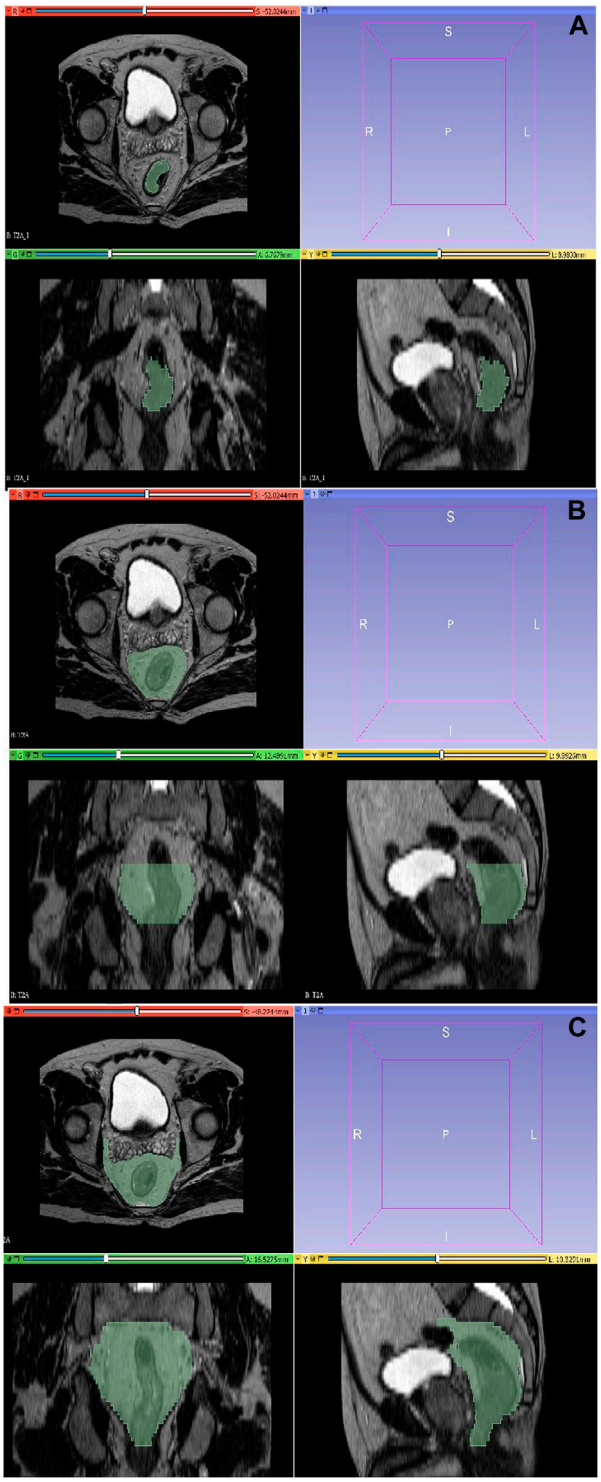

FIGURE 1
Segmentation with 3D-Slicer. **(A)** Tumor region. **(B)** Combined tumor-mesorectum. **(C)** CTV region.

and gross tumor volume (GTV) are delineated following the RTOG contouring atlas [17].

RT is administered at a dose of 45–50.4 Gray (Gy) in 25–28 fractions. RT planning techniques were either three-dimensional conformal RT or intensity-modulated RT via Varian and Eclipse planning systems. Treatments are carried out with linear accelerator devices.

Simultaneously with RT, all patients were administered either capecitabine (825 mg/m^2 orally in two daily doses, daily) or 5-fluorouracil (daily dose ranging from 200 to 225 mg/m^2 by infusion) through a port.

Subsequent to neoadjuvant treatment, patients underwent evaluation via endoscopic techniques and MRI scans at 6–8 weeks. Surgical interventions were scheduled within a window of 6–10 weeks. Dworak Regression Score was employed to assess tumor regression [18]. Adjuvant chemotherapy was administered based on the pathology findings.

As for adjuvant therapy, 19 patients received 6–8 cycles of CAPOX (capecitabine+oxaliplatin), and 53 patients received 8–2 cycles of FOLFOX (5 Fluorouracil+oxaliplatin). Adjuvant chemotherapy was not administered to 20 patients. Notably, all patients enrolled in the "watch-and-wait" approach received at least 8 cycles of FOLFOX regimen.

Patients who met the specified criteria, as outlined in the trial conducted by Maas, were categorized as having achieved cCR [19].

Image data acquisition and segmentation

MRI images were acquired utilizing 1.5 Tesla MRI devices, the Philips Achieva (Philips Medical Systems, Netherlands), and Symphoni (Siemens, Erlangen, Germany) models. The standard MRI imaging protocols for Turbo-spin-eco, T2-weighted sequences in the axial plane are as follows: TR/TE is 3,000/100 msec, image matrix of 348 × 278, a field of view measuring 210 × 228, and a cross-section thickness of 3 mm. Furthermore, the administration of iohexol contrast agent was performed at a dosage of 0.2 mL per kilogram during the MRI procedure.

A total of 93 contrast-enhanced abdominal preCRT MRI images from two MRI devices were anonymized, uploaded to MRIcron program in DICOM format, and converted to "nii.gz" format. Subsequently, the segmentation process was conducted through manual delineation using the 3D Slicer program. This collaborative effort involved radiation oncology (G.K.) and radiology (E.C.) residents with 6 years of experience and an associate professor radiologist (M.G.D.K.) with 16 (See Figure 1).

The segmentation of the tumor region was executed on T2 sequences, encompassing its complete volumetric extent while excluding vascular structures, calcifications, and air

densities. This segmentation preserved the three-dimensional structural representation of the tumor as visualized in axial sections. Concurrently, the mesorectal region was delineated, incorporating the rectum and the adjacent mesorectal tissues along the craniocaudal extension of the tumor, without encompassing adjacent organs in the vicinity. The recommended CTV definition entails the inclusion of the entire mesorectum, perirectal area, presacral region, and the internal iliac lymph node regions in the axial plane and craniocaudally commences from the promontory and extends downward to a point 2 cm below the tumor. The delineation of the CTV was performed in a manner that excluded adjacent organs.

Feature extraction and selection

The PyRadiomics 2.2.0, an extension of the open-source Python program for feature extraction,[1] was employed in the study. Prior to analysis, N4 bias correction was applied to the data. The image discretization bin width was set at 5, voxel array shift at 300, normalization scale at 100, and resampling at 3 mm × 3 mm × 3 mm. The extracted features encompassed both first-order characteristics such as mean gray value level, entropy, standard deviation, skewness (a measure of asymmetry around the mean), and kurtosis (a measure of histogram flatness) and high-order features derived from gray-level co-occurrence, gray-level dependence, gray-level run-length and gray-level size zone matrixes, and wavelet and Laplacian of Gaussian filters.

The analysis continued within the Python 2.3 environment, utilizing Jupyter Notebook and the PyCaret Library. The data underwent Z-score normalization as a preprocessing step. A multicollinearity threshold of 0.9 and an outlier removing threshold of 0.05 were applied. The dataset was divided into training and test sets, adhering to a ratio of 0.7 for training and 0.3 for testing. Cross-validation was performed five times. For feature selection, the "classical" technique was chosen and applied.

Machine learning

To address the imbalanced distribution within the dataset, the Synthetic Minority Over-sampling Technique (SMOTE) was employed. Subsequently, a Pearson correlation test was conducted, and correlation matrixes were obtained. For features from each three segmentations, machine-learning models were independently evaluated using the training dataset to predict the two groups. Subsequently, the method that yielded the most favorable AUC result was further assessed using the test dataset.

1 Accessible at http:/radiomics.io/pyradiomics.html

TABLE 1 Patients characteristics.

	n = 93	%
Median Age	58 (26–80)	
Male	70	75
Female	23	25
Tumor Localisation		
Distal	41	44
Middle	42	45
Proximal	10	11
cT		
T2	7	7
T3a	23	25
T3b	23	25
T3c	24	26
T3d	1	1
T4a	6	6
T4b	9	10
cN		
N0	15	16
N1	26	28
N1c	4	4
N2	48	52
CRM		
Negative	62	66
Positive	31	34

CRM, circumferential resection margin; cT, clinical T stage; cN, clinical N stage.

Results

Patient and treatment characteristics

Among 93 patients, 23 (25%) were female, and 70 (75%) were male. The median age at diagnosis was 58 years, with a median follow-up period of 70 months (8–125). Eighty-one patients underwent TME. Among these surgical cases, 64 patients underwent Low Anterior Resection, while 17 patients underwent Abdominoperineal Resection. pCR was observed in 13 of the surgically treated patients, accounting for 16% of this subgroup. Information regarding the patients' initial stage as

TABLE 2 AUC, sensitivity, specifity, positive odds ratio, negative odds ratio, positive and negative predictive values and accuracy results of the test set.

Segmentation Type	AUC	Sensitivity	Specificity	Positive Odds Ratio	Negative Odds Ratio	Positive Predictive Value	Negative Predictive Value	Accuracy
Tumor	0.85	76%	71%	2.67	0.33	73%	7%5	74%
Tumor + Mesorectum	0.83	90%	67%	2.71	0.14	73%	87,5%	79%
CTV	0.72	76%	62%	2.00	0.38	67%	72%	69%

AUC, area under curve; CTV, clinical target volume.

determined by MRI and colonoscopy, as well as other characteristics, is presented in Table 1. Furthermore, 12 patients were determined to be cCR based on the results of MRI, PET/CT, and colonoscopy examinations and were managed according to the "watch-and-wait" protocol. During their follow-up, these patients underwent digital rectal examinations every 3 months, colonoscopies and MRI assessments every 6 months. None of these patients exhibited recurrence over the course of the 4-year follow-up period. In summary, CR, encompassing both pCR and cCR categories, was observed in 26.88% of all patients.

Feature selection and construction of the radiomics model

A total of 1,132 radiomics features were extracted from each three different segmentations. Following normalization, the SMOTE and Pearson correlation test was conducted. For each radiomics features derived from three different segmentations, 15 machine-learning models were evaluated for the best AUC result, respectively.

Performances of radiomics models operated with features from different segmentations

The "Light Gradient Boosting Machine Classifier" demonstrated the highest AUC value (AUC:0.84) for the analysis of tumor region segmentation. For the analysis of tumor+mesorectum segmentation, the "Logistic Regression" model exhibited the highest AUC in the training set (AUC: 0.81). Meanwhile, for analysis of the CTV segmentation, the "Gaussian Naïve Bayes" model yielded the highest AUC value (AUC: 0.77).

In the test set, the highest AUC values for these analyzes of these respective segmentations were as follows: 0.85 for the tumor segmentation, 0.83 for the tumor+mesorectum segmentation, and 0.72 for the CTV segmentation.

Sensitivity and specificity rates in the test set were measured as 76% and 71% for tumor segmentation, 90% and 67% for tumor+mesorectum segmentation, and 76% and 62% for CTV segmentation, respectively.

Table 2 presents the calculated values, including AUC, sensitivity, specificity, positive odds ratio, negative odds ratio, positive predictive value (PPV), negative predictive value (NPV), and accuracy, obtained from each three analyzes with different segmentations. See Figures 2, 3 for selected features and ROC curves.

Discussion

In our research, we focused on comparing radiomics analyzes for predicting CR based on preCRT MRI images derived from the segmentation of the tumor, tumor+mesorectum, and CTV regions in LARC patients who underwent neoadjuvant therapy. Our findings revealed that the highest AUC was achieved when analyzing solely the tumor segmentation.

The AUC values in the training set for analyzing three segmentations were as follows: 0.84 for tumor-only, 0.81 for tumor+mesorectum and 0.77 for CTV. In the test set, these AUC values were found to be 0.85 for tumor-only, 0.83 for tumor+mesorectum, and 0.72 for CTV segmentations, respectively. Regarding sensitivity, the test set yielded values of 76% for tumor-only, 90% for tumor+mesorectum, and 76% for CTV segmentations. In terms of specificity, the test set exhibited 71% for tumor-only, 67% for tumor+mesorectum, and 62% for CTV segmentations.

Radiomics for LARC has been evaluated in many studies. Models have been developed for the prediction of pCR, survival, and recurrence using preCRT and/or postCRT MRI images [14]. In the realm of rectal cancer, where locally advanced stages can still yield prolonged survival outcomes, there is a growing emphasis on personalized treatment strategies aimed at minimizing side effects. The ability to predict pCR based on preCRT MRI data has emerged as a valuable guiding marker for tailoring individualized treatment approaches.

Studies to date have mostly focused on pCR prediction through radiomics analysis of tumor region segmentations from preCRT MRI images. It is noteworthy that the behavior of rectal tumors is not solely dictated by the tumor itself; it is profoundly influenced by the transformation of peritumoral

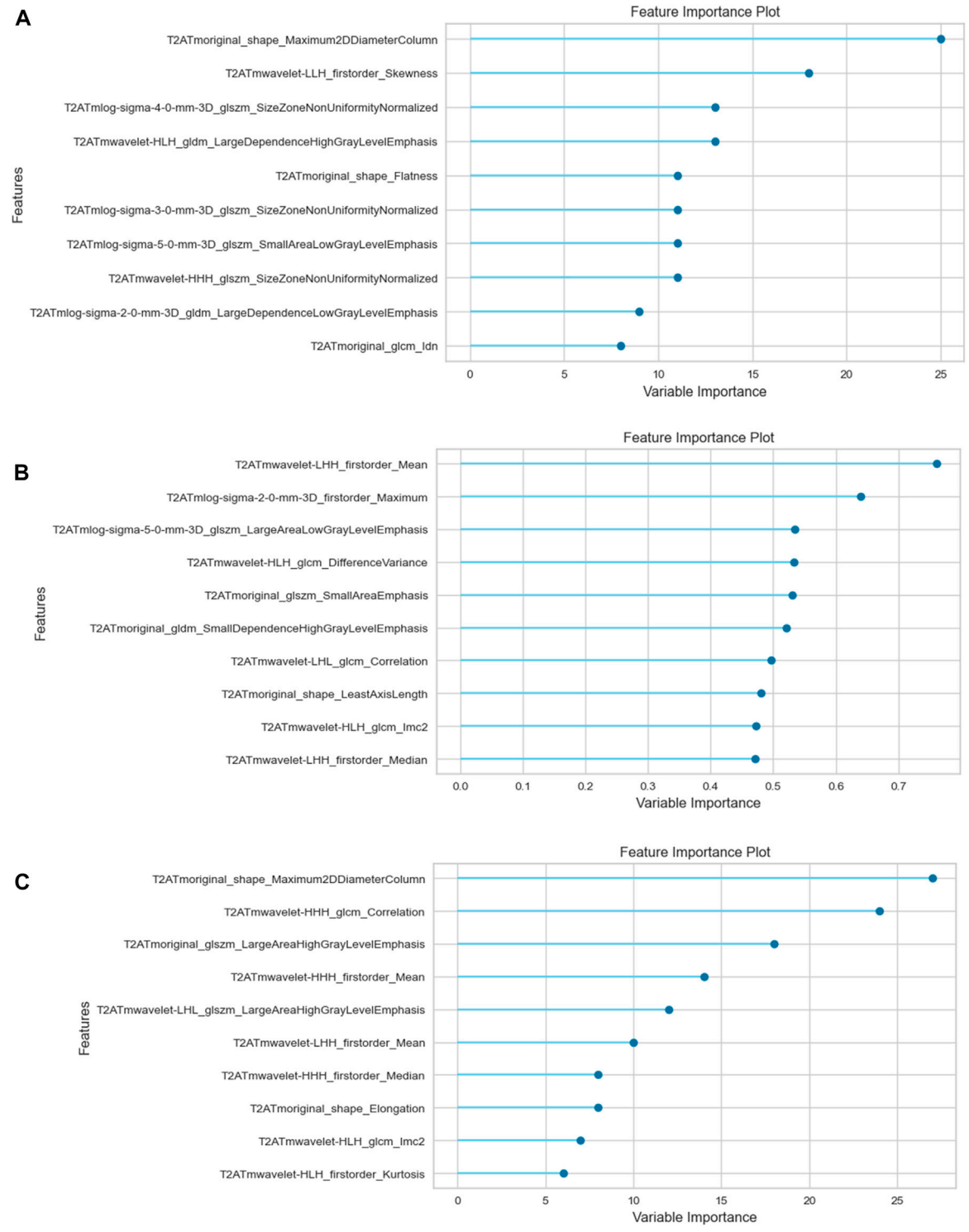

FIGURE 2
Feature importance plots. **(A)** Tumor. **(B)** Tumor+Mesorectum. **(C)** CTV.

stromal tissue and the resultant alterations in the microenvironment [11, 12]. Consequently, the mesorectal tissue is deemed to harbor crucial insights into the disease. However, only two studies incorporated the mesorectum within the segmentation region [15, 16]. In 2020, Shaish et al. conducted a comparative analysis of radiomics, exploring various

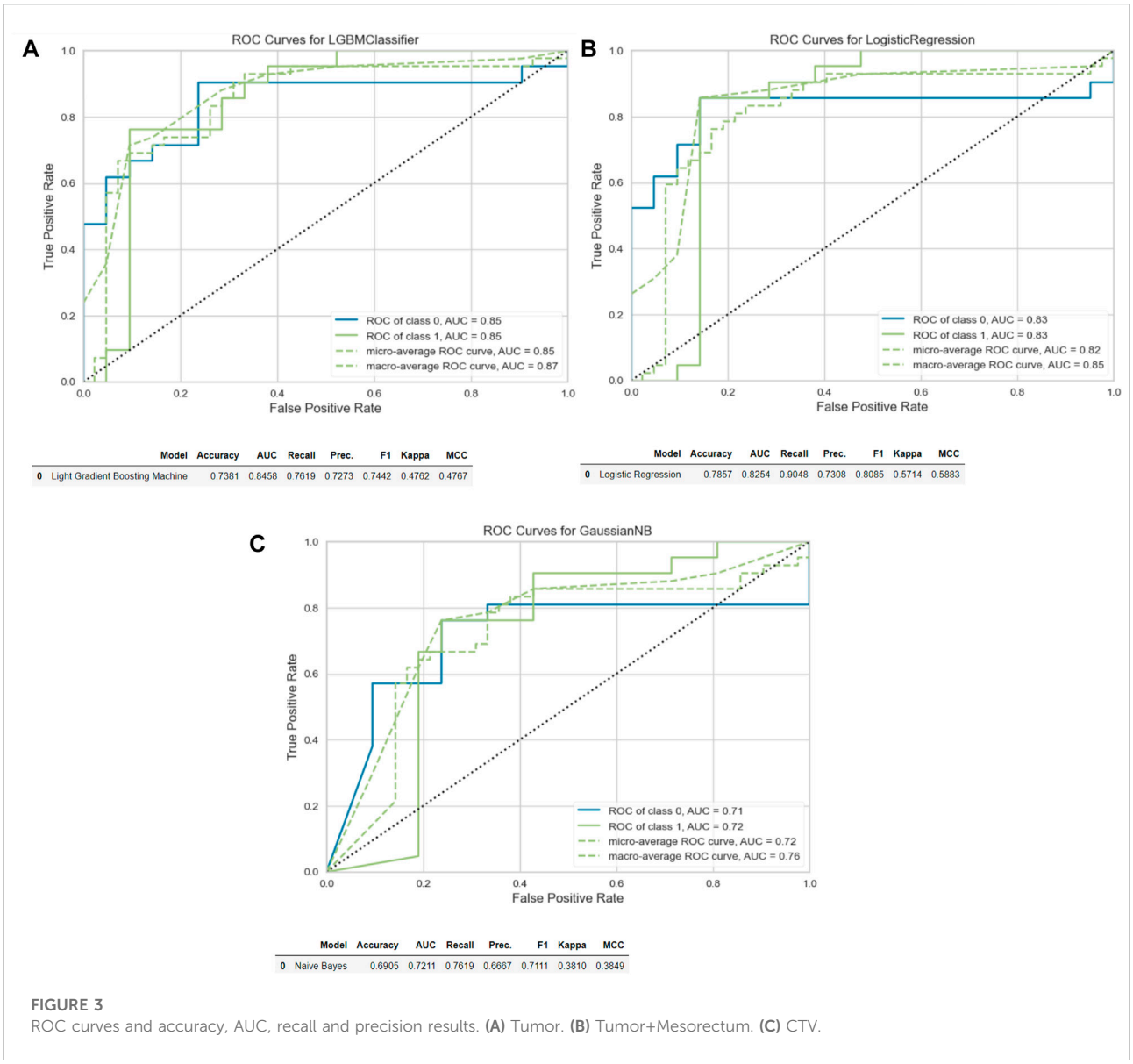

FIGURE 3
ROC curves and accuracy, AUC, recall and precision results. **(A)** Tumor. **(B)** Tumor+Mesorectum. **(C)** CTV.

segmentation approaches encompassing tumor, mesorectum, and tumor+mesorectum regions. Their study reported that analysis from tumor+mesorectum segmentation achieved the highest AUC score (AUC: 0.80) for tumor regression scoring, underlining its significance. Subsequently, in 2022, Jayaprakasam et al. conducted analysis with mesorectal fatty tissue segmentation and achieved a AUC result of 0.89.

In datasets characterized by non-uniform distributions, such as the dataset in this study, the commonly employed parameter for assessing outcomes is the AUC. Consequently, AUC results were employed in our investigation for comparative analysis. It is important to acknowledge, however, that certain literature sources posit that metrics such as recall (sensitivity) and precision (PPV) may carry enhanced significance in certain contexts [20]. Accordingly, our study aimed to contextualize our findings by incorporating these metrics into our analysis.

Based on the AUC results, radiomics analysis of tumor segmentation exhibited the most favorable performance in both training and test datasets. Nevertheless, it is noteworthy that segmentation of tumor+mesorectum demonstrated superior accuracy, sensitivity, and PPV in the test, and superior sensitivity in the training set. This observation leads us to assert that the incorporation of mesorectal segmentation into future response assessment studies for LARC may harbor considerable potential.

In the context of the "watch-and-wait" protocol, an imperative prerequisite for patients to qualify as cCR is the identification of a negative lymph node on MRI [19]. Notably, while not encountered within our patient cohort, cases featuring

ypT0N1 status have been reported in literature [21]. It is pertinent to emphasize that relying on radiomics based solely on tumor segmentation may prove insufficient in predicting CR. This aspect assumes significance as radiomics is being explored as a potential imaging-based biomarker guiding the selection of optimal neoadjuvant treatment regimens. To this end, a solitary study has undertaken radiomics analysis inclusive of lymph node segmentation on preCRT MRI scans. The outcomes of this study revealed an AUC of 0.91, underscoring the feasibility of accurately detecting a nodal CR from preCRT MRI [22] images.

Considering these findings, we posited that radiomics analysis with CTV region segmentation, encompassing both tumor and pelvic lymph node regions, could yield meaningful insights. However, the resultant AUC of 0.71 was found to be lower than that achieved through tumor-only and tumor+mesorectum segmentations. It is conceivable that, the presence of the tumor-free rectal region within the delineated CTV during segmentation, may have affected the obtained results negatively. In subsequent studies, it is advisable to consider a multi-sequence approach and to exclude the tumor-free rectum from the CTV region during the segmentation process.

Local recurrence rate after TME and neoadjuvant treatments generally falls within the range of 5%–10%, varying across different studies. A substantial proportion of such recurrences manifest within the extramesorectal lateral pelvic nodal region. The implementation of lateral pelvic nodal dissection remains a subject of controversy within the existing literature [23]. Consequently, while analysis with mesorectal segmentation has yielded the most favorable outcomes in terms of accuracy and sensitivity, there is a rationale to consider the assessment of the lateral pelvic nodal region within response evaluation studies with radiomics analysis, as it may offer valuable guidance for tailoring individualized treatment strategies.

It is important to note that, focus of most studies lies in the inclusion of patients who have attained a pCR, excluding patients with cCR. This practice carries the accidental risk of omitting a segment of patients who have indeed achieved a CR from the evaluative framework. In an effort to mitigate this potential limitation and maintain consistency, our study encompassed patients who exhibited cCR and have, to date, remained free from any relapse during the follow-up period.

Furthermore, it is worth highlighting that our study adopted a distinctive approach by not restricting the patient cohort to data acquired from a single MRI device, unlike most studies. Instead, we performed radiomics analysis using heterogeneous MRI data from two devices, resulting in an AUC value of 0.84.

Several limitations are worth acknowledging in our study. Firstly, its retrospective nature may be considered a potential limitation. Nonetheless, it is essential to emphasize that patient evaluations were conducted prospectively. Furthermore, the absence of an assessment regarding multiple readers and the lack of an interobserver reproducibility evaluation can be perceived as a limitation. Nevertheless, it is plausible that for volumes characterized by such standardized boundaries, such as CTV, the interreader variations are likely to be less pronounced compared to tumor segmentation. This aspect, however, could serve as a topic for future investigations. Moreover, it should be acknowledged that the models developed in our study were not subjected to evaluation using an external validation dataset. The primary rationale behind this decision lies in the objective of our study, which primarily aimed to compare outcomes across analyzes of different region segmentations rather than constructing a predictive model. Therefore, external validation was not prioritized for the specific research objectives of this study.

Conclusion

In our research, we conducted a comparative analysis of radiomics assessments based on preCRT MRI images, focusing on three distinct segmentation areas: tumor-only, tumor combined with the mesorectum, and CTV. Although the highest AUC result was achieved with radiomics analysis of tumor segmentation, our investigation revealed that the highest accuracy and sensitivity were observed with radiomics analysis of combined tumor and mesorectum segmentations. Our findings align with previous studies, suggesting that the mesorectum contains valuable insights for the prediction of CR.

Finally, although the lowest predictive performance was observed with the analysis of CTV segmentation, predictive results of this region could be improved within further trials, considering the fact that lateral pelvic nodal region is also a possible local metastasis area and should be involved in CR prediction analyzes of LARC. There is a need for further research, encompassing larger patient cohorts and involving multiple readers with different segmentation methods to explore the inclusion of the mesorectum and pelvic nodal regions within the segmentation area for the prediction of CR as well as distant metastasis and prognosis in LARC.

Data availability statement

The raw data supporting the conclusion of this article will be made available by the authors, without undue reservation.

Ethics statement

The studies involving humans were approved by the Istanbul Medical Faculty Clinical Research Ethics Committee. The studies were conducted in accordance with the local legislation and institutional requirements. Written informed consent for participation was not required from the participants or the participants' legal guardians/next of kin in accordance with the national legislation and institutional requirements.

Author contributions

GK, SA, MD, ND, EC, BK, GE, and SuK: concept, design, definition of intellectual content, literature search, data analysis and interpretation of data, statistical analysis, drafting the article, manuscript preparation, editing and review, final approval. SeK, NB, MK, and EO: concept, design, definition of intellectual content, literature search, manuscript editing, revising and advising intellectual content, final approval. All authors contributed to the article and approved the submitted version.

Funding

The authors declare that no financial support was received for the research, authorship, and/or publication of this article.

Conflict of interest

The authors declare that the research was conducted in the absence of any commercial or financial relationships that could be construed as a potential conflict of interest.

References

1. GLOBOCAN. *Estimated age-standardized incidence rates (World) in 2020, rectum*. France: GLOBOCAN (2020). Available from: https://gco.iarc.fr/ (Accessed February 2023).

2. Bahadoer RR, Dijkstra EA, van Etten B, Marijnen CAM, Putter H, Kranenbarg EM, et al. Short-course radiotherapy followed by chemotherapy before total mesorectal excision (TME) versus preoperative chemoradiotherapy, TME, and optional adjuvant chemotherapy in locally advanced rectal cancer (RAPIDO): a randomised, open-label, phase 3 trial. *Lancet Oncol* (2021) 22:29–42. doi:10.1016/S1470-2045(20)30555-6

3. Cisel B, Pietrzak L, Michalski W, Wyrwicz L, Rutkowski A, Kosakowska E, et al. Long-course preoperative chemoradiation versus 5 × 5 Gy and consolidation chemotherapy for clinical T4 and fixed clinical T3 rectal cancer: long-term results of the randomized Polish II study. *Ann Oncol* (2019) 30:1298–303. doi:10.1093/annonc/mdz186

4. Jin J, Tang Y, Hu C, Jiang LM, Jiang J, Li N, et al. Multicenter, randomized, phase III trial of short-term radiotherapy plus chemotherapy versus long-term chemoradiotherapy in locally advanced rectal cancer (STELLAR). *J Clin Oncol* (2022) 40:1681–92. doi:10.1200/JCO.21.01667

5. Maas M, Nelemans PJ, Valentini V, Das P, Rödel C, Kuo L-J, et al. Long-term outcome in patients with a pathological complete response after chemoradiation for rectal cancer: a pooled analysis of individual patient data. *Lancet Oncol* (2010) 11:835–44. doi:10.1016/S1470-2045(10)70172-8

6. Maas M, Lambregts DM, Nelemans PJ, Heijnen LA, Martens MH, Leijtens JW, et al. Assessment of clinical complete response after chemoradiation for rectal cancer with digital rectal examination, endoscopy, and MRI: selection for organ-saving treatment. *Ann Surg Oncol* (2015) 22:3873–80. doi:10.1245/s10434-015-4687-9

7. Lambregts DM, Beets GL, Maas M, Curvo-Semedo L, Kessels AG, Thywissen T, et al. Tumour ADC measurements in rectal cancer: effect of ROI methods on ADC values and interobserver variability. *Eur Radiol* (2011) 21:2567–74. doi:10.1007/s00330-011-2220-5

8. Sassen S, de Booij M, Sosef M, Berendsen R, Lammering G, Clarijs R, et al. Locally advanced rectal cancer: is diffusion weighted MRI helpful for the identification of complete responders (ypT0N0) after neoadjuvant chemoradiation therapy? *Eur Radiol* (2013) 23:3440–9. doi:10.1007/s00330-013-2956-1

9. Dattani M, Marijnen C, Moran B, Tait D, Cunningham C, Rodriguez-Bigas M, et al. Session 4: shaping radiotherapy for rectal cancer: should this be personalized? *Colorectal Dis* (2018) 20(Suppl. 1):92–6. doi:10.1111/codi.14087

10. Hardiman KM, Ulintz PJ, Kuick RD, Hovelson DH, Gates CM, Bhasi A, et al. Intra-tumor genetic heterogeneity in rectal cancer. *Lab Invest* (2016) 96:4–15. doi:10.1038/labinvest.2015.131

11. Chu K, Bos SA, Gill CM, Torriani M, Bredella MA. Brown adipose tissue and cancer progression. *Skeletal Radiol* (2020) 49:635–9. doi:10.1007/s00256-019-03322-w

12. Conti G, Calderan L, Quintero Sierra LA, Conti A, Ossanna R, Boschi F, et al. Tumor and peritumoral adipose tissue crosstalk: de-differentiated adipocytes influence spread of colon carcinoma cells. *Tissue Cell* (2023) 80:101990. doi:10.1016/j.tice.2022.101990

13. Gillies RJ, Kinahan PE, Hricak H. Radiomics: images are more than pictures, they are data. *Radiology* (2016) 278:563–77. doi:10.1148/radiol.2015151169

14. Miranda J, Horvat N, Araujo-Filho JAB, Albuquerque KS, Charbel C, Trindade BMC, et al. The role of radiomics in rectal cancer. *J Gastrointest Cancer* (2023) 54:1158–80. doi:10.1007/s12029-022-00909-w

15. Jayaprakasam VS, Paroder V, Gibbs P, Bajwa R, Gangai N, Sosa RE, et al. MRI radiomics features of mesorectal fat can predict response to neoadjuvant chemoradiation therapy and tumor recurrence in patients with locally advanced rectal cancer. *Eur Radiol* (2022) 32:971–80. doi:10.1007/s00330-021-08144-w

16. Shaish H, Aukerman A, Vanguri R, Spinelli A, Armenta P, Jambawalikar S, et al. Radiomics of MRI for pretreatment prediction of pathologic complete response, tumor regression grade, and neoadjuvant rectal score in patients with locally advanced rectal cancer undergoing neoadjuvant chemoradiation: an international multicenter study. *Eur Radiol* (2020) 30:6263–73. doi:10.1007/s00330-020-06968-6

17. Myerson RJ, Garofalo MC, El Naqa I, Abrams RA, Apte A, Bosch WR, et al. Elective clinical target volumes for conformal therapy in anorectal cancer: a radiation therapy oncology group consensus panel contouring atlas. *Int J Radiat Oncol Biol Phys* (2009) 74:824–30. doi:10.1016/j.ijrobp.2008.08.070

18. Dworak Lk O, Hoffmann A. Pathological features of rectal cancer after preoperative radiochemotherapy. *Int J Colorectal Dis* (1997) 12:19–23. doi:10.1007/s003840050072

19. Maas M, Beets-Tan RG, Lambregts DM, Lammering G, Nelemans PJ, Engelen SM, et al. Wait-and-see policy for clinical complete responders after chemoradiation for rectal cancer. *J Clin Oncol* (2011) 29:4633–40. doi:10.1200/JCO.2011.37.7176

20. Saito T, Rehmsmeier M. The precision-recall plot is more informative than the ROC plot when evaluating binary classifiers on imbalanced datasets. *PLoS One* (2015) 10:e0118432. doi:10.1371/journal.pone.0118432

21. Kim SH, Chang HJ, Kim DY, Park JW, Baek JY, Kim SY, et al. What is the ideal tumor regression grading system in rectal cancer patients after preoperative chemoradiotherapy? *Cancer Res Treat* (2016) 48:998–1009. doi:10.4143/crt.2015.254

22. Zhang S, Tang B, Yu M, He L, Zheng P, Yan C, et al. Development and validation of a radiomics model based on lymph-node regression grading after neoadjuvant chemoradiotherapy in locally advanced rectal cancer. *Int J Radiat Oncol Biol Phys* (2023) 117:821–33. doi:10.1016/j.ijrobp.2023.05.027

23. Otero de Pablos J, Mayol J. Controversies in the management of lateral pelvic lymph nodes in patients with advanced rectal cancer: east or west? *Front Surg* (2019) 6:79. doi:10.3389/fsurg.2019.00079

Pathology & Oncology Research | frontiers

TYPE Brief Research Report
PUBLISHED 22 June 2023
DOI 10.3389/pore.2023.1611284

Check for updates

OPEN ACCESS

EDITED BY
Anna Sebestyén,
Semmelweis University, Hungary

*CORRESPONDENCE
Tadashi Yoshizawa,
tyoshi@hirosaki-u.ac.jp

RECEIVED 05 May 2023
ACCEPTED 14 June 2023
PUBLISHED 22 June 2023

CITATION
Ogasawara H, Yoshizawa T, Oshima K, Ogasawara K, Kubota S, Goto S, Morohashi S, Wakiya T, Kimura N, Ishido K, Kijima H and Hakamada K (2023), Three-dimensional analysis of perineural invasion in extrahepatic cholangiocarcinoma using tissue clearing.
Pathol. Oncol. Res. 29:1611284.
doi: 10.3389/pore.2023.1611284

COPYRIGHT
© 2023 Ogasawara, Yoshizawa, Oshima, Ogasawara, Kubota, Goto, Morohashi, Wakiya, Kimura, Ishido, Kijima and Hakamada. This is an open-access article distributed under the terms of the Creative Commons Attribution License (CC BY). The use, distribution or reproduction in other forums is permitted, provided the original author(s) and the copyright owner(s) are credited and that the original publication in this journal is cited, in accordance with accepted academic practice. No use, distribution or reproduction is permitted which does not comply with these terms.

Three-dimensional analysis of perineural invasion in extrahepatic cholangiocarcinoma using tissue clearing

Hirokazu Ogasawara[1,2], Tadashi Yoshizawa[1]*, Kiyoko Oshima[3], Kenta Ogasawara[1,2], Shunsuke Kubota[1,2], Shintaro Goto[1], Satoko Morohashi[1], Taiichi Wakiya[2], Norihisa Kimura[2], Keinosuke Ishido[2], Hiroshi Kijima[1] and Kenichi Hakamada[2]

[1]Department of Pathology and Bioscience, Hirosaki University Graduate School of Medicine, Hirosaki, Aomori, Japan, [2]Department of Gastroenterological Surgery, Hirosaki University Graduate School of Medicine, Hirosaki, Aomori, Japan, [3]Department of Pathology, Johns Hopkins University School of Medicine, Baltimore, MD, United States

Perineural invasion (PNI) is a characteristic invasion pattern of distal cholangiocarcinoma (DCC). Conventional histopathologic examination is a challenging approach to analyze the spatial relationship between cancer and neural tissue in full-thickness bile duct specimens. Therefore, we used a tissue clearing method to examine PNI in DCC with three-dimensional (3D) structural analysis. The immunolabeling-enabled 3D imaging of solvent-cleared organs method was performed to examine 20 DCC specimens from five patients and 8 non-neoplastic bile duct specimens from two controls. The bile duct epithelium and neural tissue were labeled with CK19 and S100 antibodies, respectively. Two-dimensional hematoxylin/eosin staining revealed only PNI around thick nerve fibers in the deep layer of the bile duct, whereas PNI was not identified in the superficial layer. 3D analysis revealed that the parts of DCC closer to the mucosa exhibited more nerves than the normal bile duct. The nerve fibers were continuously branched and connected with thick nerve fibers in the deep layer of the bile duct. DCC formed a tubular structure invading from the epithelium and extending around thin nerve fibers in the superficial layer. DCC exhibited continuous infiltration around the thick nerve fibers in the deep layer. This is the first study using a tissue clearing method to examine the PNI of DCC, providing new insights into the underlying mechanisms.

KEYWORDS

tissue clearing, three-dimensional, perineural invasion, cholangiocarcinoma, iDISCO

Introduction

Distal cholangiocarcinoma (DCC) is often diagnosed at advanced stage and has poor prognosis [1, 2]. Surgery is a curative treatment option in patients with DCC; however, the prognosis remains poor even after radical resection. Perineural invasion (PNI) is an independent poor prognostic factor after surgery in patients with DCC. Studies examining PNI, a characteristic invasion pattern observed in cholangiocarcinoma as well as in pancreatic cancer [3–5], have revealed that the molecular mechanisms underlying PNI include the activation of nerve growth factor, L1 cell adhesion molecule, matrix metalloproteinases, M3 muscarinic acetylcholine receptor, and hepatocyte growth factor [6–10]. On the other hand, few studies conducted three-dimensional (3D) morphologic analysis of PNI. Maxwell et al. analyzed PNI in extrahepatic cholangiocarcinoma using the 3D construction of serial sections and showed that DCC exhibited continuous branching in the perineural space. However, the resolution of 3D analysis was low, and the observation was limited to a small area around the nerve fibers [11]. Miyashita et al. examined the 3D structure of PNI in Auerbach's plexus in a cohort of patients with colorectal cancer using the reconstruction of serial sections and reported the presence of two PNI types, PNI with preserved nerve structure and PNI with damaged the nerve structure [12]. However, the structural relationship between nerve fibers and cancer across the full thickness of the bile duct wall using 3D imaging methods has not yet been examined.

In recent years, detailed observation of 3D structures has become possible with the development of tissue clearing methods [13], which have been utilized in pancreatic cancer [14, 15] and extrahepatic cholangiocarcinoma [16] to elucidate invasion mechanisms by 3D observation. In the present study, we aimed to clarify the morphologic characteristics of PNI in DCC using 3D structural analysis with a tissue clearing method.

Materials and methods

Patients and tissue samples

A total of 20 cancer tissue specimens, measuring up to 1.5 cm × 1.5 cm × 0.5 cm, in dimensions collected from five patients with DCC, including three and two patients with well-differentiated and moderately differentiated adenocarcinoma, were examined. Additionally, eight non-neoplastic distal bile duct tissue specimens collected from two patients, including one patient with duodenal cancer confined to the mucosa and one patient with duodenal adenoma, were examined as negative controls.

Fresh tissue preparation

A total of 28 freshly collected bile duct tissue specimens were processed as previously described [14–16]. Briefly, the tissue specimens were fixed in 80% methanol/20% dimethyl sulfoxide (DMSO) overnight. The next day, the specimens were placed in 4% paraformaldehyde and incubated at 4°C for 24 h, followed by dehydration with a series of methanol washes (once each in 50%, 80%, and 90% methanol, and three times in 100% methanol). The specimens were then incubated at 4°C for 60 min, followed by overnight incubation in 66% dichloromethane/33% methanol at room temperature. Next, the specimens were washed twice with 100% methanol and incubated in methanol with 5% hydrogen peroxide at 4°C overnight to oxidize endogenous pigments and autofluorescent proteins. The specimens were rehydrated with a series of washes (90%, 80%, and 50% methanol), washed once with phosphate-buffered saline (PBS), and washed twice, 1 h each, in 1 × PBS/0.2%Triton X-100 (Millipore Sigma, St. Louis, MO, United States). Finally, the specimens were incubated in a permeabilization solution (1 × PBS/20% DMSO/0.2%Triton X-100/0.3 M glycine) at 37°C for 2 days and in a blocking reagent including 1 × PBS/0.2%Triton X-100/10%DMSO/6% donkey serum at 37°C for 2 days.

Immunolabeling

The specimens were immunolabeled with a mouse monoclonal antibody against S100 (1:250; clone, 4C4.9; cat. no., ab4066; Abcam, Cambridge, United Kingdom) and a rabbit monoclonal antibody against cytokeratin 19 (CK19) (1:200; clone, EP1580Y; cat. no., ab52625; Abcam). For both antibodies, the antibody concentration was gradually increased over 4 days to allow antibody penetration. Additionally, the centrifugal flow was used to promote antibody penetration. The specimens were centrifuged at 300 *g* for 12 h and shaken at 37°C for 12 h, alternating between centrifugation and shaking, during 4 days of antibody incubation. Next, the specimens were washed five times with 1 × PBS/0.2% Tween-20 supplemented with 10 mg/mL heparin, for 60 min each, at room temperature, followed by incubation with Alexa Fluor 488-conjugated AffiniPure F (ab') 2 fragment donkey antirabbit immunoglobulin G antibody and cyanine 3-conjugated AffiniPure F (ab') 2 fragment donkey antimouse immunoglobulin G antibody, both from Jackson ImmunoResearch Laboratories (West Grove, PA, United States) for 3 days with protection from light. During immunolabeling with the secondary antibodies, the specimens were centrifuged at 300 *g* for 12 h and shaken at 37°C for 12 h, alternating between centrifugation and shaking. Finally, the specimens were washed five times with 1 × PBS/0.2% Tween-20 supplemented with 10 mg/mL heparin, for 60 min each, at room temperature.

Tissue clearing

The tissues were dehydrated using a series of methanol washes (once each in 50%, 80%, and 90% methanol, and three times in 100% methanol), for 60 min each, followed incubation in 66% dichloromethane/33% methanol once for 3 h and incubation in 100% dichloromethane twice for 15 min. Finally, the tissues were transferred to dibenzyl ether and incubated at 4°C overnight.

Tissue imaging and analysis

Images of immunolabeled and cleared tissue specimens were acquired with a CellVoyager CQ1 benchtop high-content analysis system (Yokogawa, Tokyo, Japan) using ×4, ×10, and ×20 objectives. The Alexa Fluor 488 signals were visualized using a bandpass filter set with an excitation range of 421/50 nm and an emission range of 480/40 nm to visualize CK19-labeled epithelial cells in normal bile duct and neoplastic cells. The cyanine 3 signals were visualized using a filter set with an excitation range of 550/40 nm and an emission range of 570/50 nm to visualize S100-labeled Schwann cells. Autofluorescence detected with an excitation range of 405/40 nm and an emission range of 460/50 nm was used to visualize the bile duct wall. 3D and surface-rendering image construction was performed using IMARIS software (version 9.4; Bitplane, Zurich, Switzerland).

Immunohistochemistry

Routinely collected specimens were processed to prepare formalin-fixed/paraffin-embedded (FFPE) tissue blocks, and 4-μm-thick sections were prepared, which were then mounted on saline-coated glass slides for histologic examination. Immunohistochemical examination was performed on deparaffinized sections using the standard avidin-biotin-peroxidase complex method with a BenchMark XT automated immunostainer (Ventana Medical Systems, Tucson, AZ, United States). Neural tissue was identified based on the presence of Schwann cells, which were labeled using a primary rabbit monoclonal antibody against S100 (1:1; clone, EP32; Leica Biosystems, Newcastle, United Kingdom). The sections were washed four times with PBS and incubated with the BOND Polymer Refine Detection reagent (Leica Biosystems) for secondary immunostaining.

Validation of observations made in cleared tissues

In cases with available fresh tissue, sections next to the fresh tissue harvested for clearing were processed to prepare FFPE blocks, which were sectioned at 4-μm thickness and stained with hematoxylin and eosin (H&E) and S100 for optical microscopic examination. The area of nerve distribution or PNI was marked on H&E-stained sections, and the same lesion in fresh tissue or FFPE tissue was evaluated using 3D images.

This study was performed in accordance with the Declaration of Helsinki for Human Research and was approved by the Ethics Committee of Hirosaki University Graduate School of Medicine (protocol no. 2020-173).

Results

Clearing and labeling with antibodies

All 28 specimens were successfully cleared and immunolabeled to observe the 3D morphology (Figure 1). Fluorescent immunostaining for CK19 allowed us to observe neoplastic and nonneoplastic bile duct epithelium. Neural tissue was also confirmed by observing the presence of S100-labeled Schwann cells coating the periaxonal area. Additionally, the structure of the bile duct wall was observed by autofluorescence. Image acquisition was possible at depths of approximately 200–500 μm.

2D and 3D imaging of the normal bile duct wall

The bile duct in control cases lined with columnar epithelium was observed in 2D H&E-stained sections. Several thick bundles of neural tissue were noted in the deep layer of the bile duct wall adjacent to the pancreas (Figure 2A). S100 immunostaining highlighted the neural tissue in the deep layer of the bile duct; however, detecting it on the superficial layer of the bile duct wall was challenging (Figure 2B). In the 3D images, CK19 fluorescent staining highlighted the biliary epithelium of the bile duct wall. Peribiliary glands, characterized as aggregates of glands, were present beneath the epithelium. The separated bundles of nerve fibers observed in 2D images were continuous in the deep bile duct wall in 3D images. The thin nerve fibers branching from the thick nerve fibers extending toward the mucosal surface was also observed in 3D images (Figures 2C, D).

DCC in the superficial layer of the bile duct

In 2D H&E-stained images, DCC forming glands infiltrated the bile duct wall (Figure 3A). Additionally, S100 immunostaining revealed multiple separated bundles of neural tissue within the deep layer of the bile duct; however, superficial nerve tissue was difficult to observe (Figure 3B). In the 3D images, nerve fibers were widely distributed in the superficial layer of the bile duct wall. DCC appeared to form complex interconnecting tubes in the 3D images. The nerve fibers were continuous and branched to form thin nerve

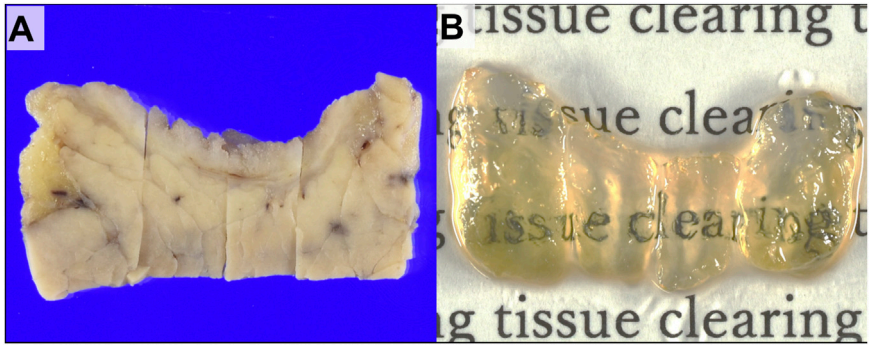

FIGURE 1
Gross images of the extrahepatic bile duct wall with cholangiocarcinoma. **(A)** Gross appearance of distal cholangiocarcinoma (DCC) before tissue clearing. **(B)** Gross appearance of the specimen after tissue clearing.

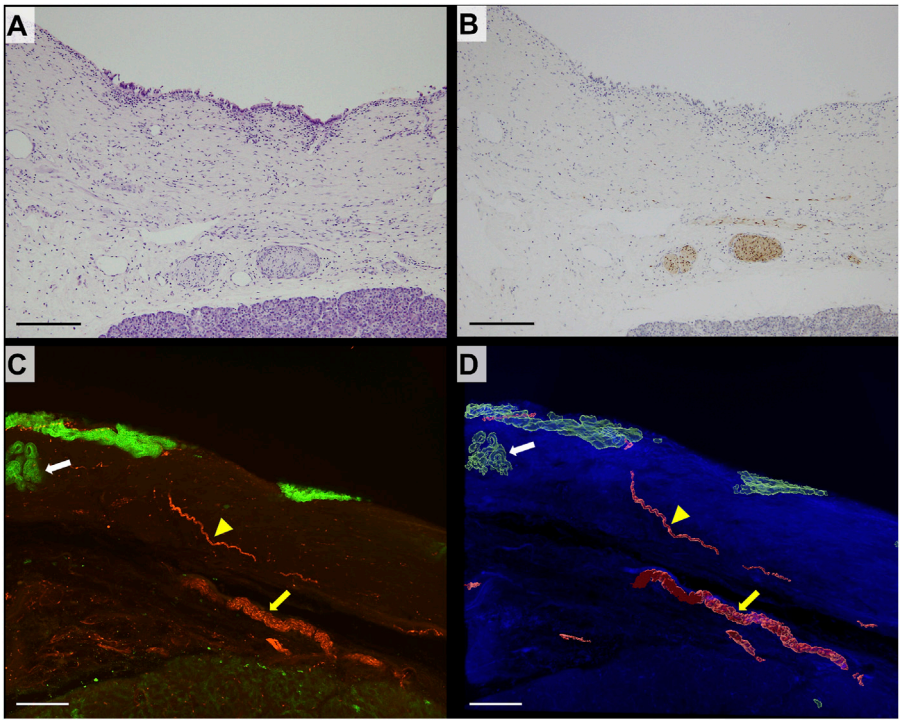

FIGURE 2
2D and 3D images of nonneoplastic distal bile duct wall. **(A)** 2D image of the hematoxylin/eosin (H&E)-stained section of a non-neoplastic distal bile duct (scale bar, 200 μm). **(B)** 2D image of a section immunohistochemically stained for S100 (scale bar, 200 μm). Thick nerve fibers positive for S100 are seen in the deep layer of the bile duct. **(C)** 3D confocal microscopic images (CK19, green; S100, red; scale bar, 200 μm). **(D)** 3D-rendered image (autofluorescence, blue; scale bar, 200 μm). The large nerve exhibits continuity in the deep layer of the bile duct (yellow arrow). Thin neural fibers extend toward the mucosal surface (yellow arrowhead). Peribiliary glands are identified under the mucosal epithelium (white arrow).

fibers widely distributed in the superficial layer of the bile duct wall in 3D images. The thin neural fibers were distributed inside the DCC with a reticular pattern (Figures 3C–E). IMARIS software used to obtain images at higher magnification, and surface rendering was performed to observe the specimens in more detail. As shown in Figures 3F–I, DCC infiltrating along the thin nerve fibers was continuously branching and an area of thick nerve fibers transected by cancer was observed (Supplementary Movie S1).

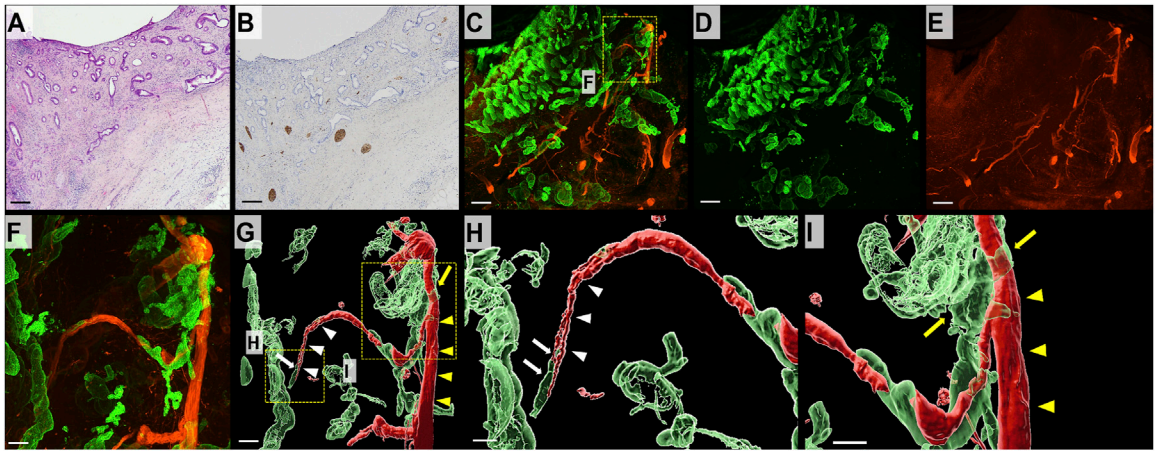

FIGURE 3
2D and 3D images of the bile duct wall in DCC. **(A)** 2D H&E-stained image of DCC (scale bar, 500 μm). DCC forming tubular structures is infiltrating the bile duct wall. **(B)** 2D image of a section immunohistochemically stained for S100 (scale bar, 500 μm). Thick neural tissue is observed in the deep layer of the bile duct wall. It is difficult to observe neural tissue in the superficial layers. **(C)** 3D microscopic image showing DCC (CK19, green) in combination with neural tissue (S100, red; scale bar, 500 μm). **(D)** DCC forms an interconnecting tubule and invades from the mucosal surface to the deeper layers of the bile duct wall (CK19, green). **(E)** 3D image of neural tissue (S100, red). The bile duct wall with DCC has an extensive network of thin neural tissue. **(F)** Magnified 3D confocal microscopic image (scale bar, 100 μm). **(G)** 3D-rendered image (scale bar, 100 μm). **(H,I)** Magnified 3D-rendered image (scale bar, 150 μm). Thin nerve fibers (white arrowhead) branch from a thick nerve (yellow arrowhead) in the deep mucosal layer. DCC is observed around the thin nerve fiber (white arrow) and exhibits continuous thick nerve fiber (yellow arrow).

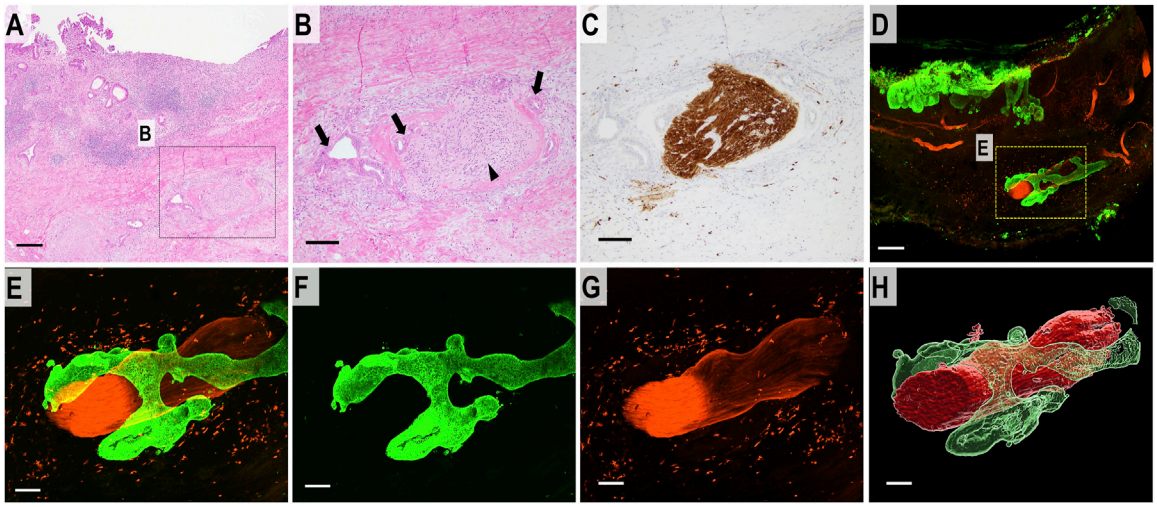

FIGURE 4
2D and 3D images of DCC with perineural invasion. **(A)** 2D H&E staining image of perineural invasion (scale bar, 500 μm). **(B)** High-magnification 2D image (scale bar, 100 μm). DCC (arrow) is forming glands which infiltrate around the neural tissue (arrowhead). **(C)** 2D image of a section immunohistochemically stained for S100 showing neural tissue in the deep bile duct wall (scale bar, 100 μm). **(D)** Merged 3D confocal microscopic images of perineural invasion. DCC in the full thickness of the bile duct wall (CK19, green). Neural tissue is immunostained with S100 (red) (scale bar, 500 μm). **(E)** Higher-magnification merged 3D confocal microscopic images showing perineural invasion. **(F)** 3D confocal microscopic image of DCC (CK19, green). **(G)** 3D confocal microscopic image of neural tissue (S100, red). **(H)** 3D-rendered image of DCC continuously invading the surrounding perineurium (scale bar, 150 μm).

DCC in the deep layer of the bile duct

The 2D H&E-stained images showed separate large bundles of nerve fibers in the deep layer of the bile duct. DCC forming glands were present adjacent to the nerve fibers and confirmed the diagnosis of PNI. S100 immunostaining showed thick bundles of neural tissue (Figures 4A–C). The 3D images revealed that the separate bundles of neural tissue observed in the 2D images were continuous in the deep layer of the bile duct wall. DCC surrounded and extended along the neural tissue in the bile duct wall (Figures 4D–H) (Supplementary Movie S2).

Discussion

This was possibly the first study to examine the 3D structural relationship of DCC and nerve fibers in full-thickness bile duct specimens, and the results have revealed several findings. First, although the 2D analysis of H&E-stained sections showed PNI limited to the thick nerve fibers in the deep layer, the 3D analysis of the tissue specimens processed with tissue clearing revealed that DCC had more complex nerve fibers on the surface of the bile duct than in the normal bile duct wall and that these structures continuously branched from thick nerve fibers in the deep layer of the bile duct. Second, DCC invaded the bile duct wall by forming an interconnecting tube from the epithelium and extended around the thin nerve fibers in the superficial layer. Finally, DCC exhibited a contiguously invasive pattern by surrounding the thick nerve fibers in the deep layer of the bile duct.

A previous 2D study reported that the nerve fibers are abundantly distributed within the deep layer of the distal bile duct but that only a small amount of nerve fibers were identified within the superficial layer [17]. PNI in the superficial bile duct wall was not considered a frequent finding, and that it was reported to occur mainly in the deep layer [17]. However, our 3D analysis has revealed that more nerve fibers are distributed in the superficial layer of the bile duct in DCC samples compared with the non-neoplastic bile duct wall; PNI was observed even in the superficial layer. Through 2D and 3D reconstruction of prostatectomy specimens, Ayala et al. reported that mouse dorsal root ganglia extended neural tissue toward prostate cancer and formed prostate cancer-associated axons with nerve enlargement or increased nerve density [18, 19]. These studies indicated that the mechanism of PNI involved active and reciprocal interactions between cancer cells and adjacent nerves/ganglions during cancer progression. Although the small number of cases in the present study did not allow statistical analysis to compare the distribution of nerve fibers in the bile duct wall between the normal and DCC cases, our findings are consistent with their experimental results.

Previous studies using 3D imaging analysis of extrahepatic cholangiocarcinoma using reconstruction of serial sections demonstrated that cancer cells extended in a perineural space continuum [11, 19]. However, the area visible by the 3D construction of the serial sections in these studies was small and could not fully reveal the architecture of the entire thickness of the bile duct. Our 3D analysis using specimens processed with tissue clearing enabled the analysis of the full thickness of the bile duct wall from the surface to the deep layer and clarified that the thin nerve fibers was widely distributed on the mucosal side and that cancer cells infiltrated this thin nerve fibers. Additionally, the cancer cells continuously wrapped around the nerve fibers and spread widely into the bile duct wall alongside the thick nerve fibers in the deep layer. Our 3D observations raise the possibility that DCC, while invisible in H&E-stained sections, might remain around the thin nerve fibers at the surface of the bile duct wall in cases where PNI is present near the margin of bile duct resection, explaining the poor prognosis associated with PNI in patients with DCC.

The pathways of abdominal spread of gastrointestinal cancer can be direct, perineural, lymphatic, hematogenous, or peritoneal. Whether the perineural space is an independent compartment or is connected to a lymphatic channel has not yet been confirmed. A 3D study using the reconstruction of serial sections demonstrated the relationship between the nerve fibers and adjacent lymphatics and suggested that DCC in the perineural space was a result of direct invasion from the lymphatics. The authors reported tumor cell clusters floating within the dilated lymphatic vessel adjacent to the nerve fibers and hypothesized that these cells broke into the perineural space [20]. However, the resolution of the reconstructed 3D images of the serial tissue sections was not sufficient to visualize the tumor cell clusters breaking into this perineural space. The present study did not analyze the structural relationship between PNI and lymphatics; however, the 3D images showed the continuous infiltration of DCC in the perineural area, suggesting that PNI was an independent route distinct from invasion through lymphatic vessels or vessels or direct invasion and that PNI provided a favorable environment for DCC spread Future studies should include the comprehensive analysis of the relationship between DCC and neural, lymphatic, and vascular structures using 3D images of specimen after tissue clearing, which may provide new insights into the mechanism of PNI.

Data availability statement

The raw data supporting the conclusion of this article will be made available by the authors, without undue reservation.

Ethics statement

The studies involving human participants were reviewed and approved by Ethics Committee of Hirosaki University Graduate School of Medicine (protocol no. 2020-173). The patients/participants provided their written informed consent to participate in this study.

Author contributions

HO, TY, KOs, and SM designed the experiments. HO, TY, KOg, and SK performed the experiments. HO, TY, KOs, SM, TW, NK, KI, HK, and KH performed the data analysis. HO, TY, and KOs wrote the main manuscript text, and prepared the figures. TY, SG, SM, and HK contributed to histological evaluation. KOs, HK, and KH critically revised the manuscript. TY and HK confirm the authenticity of all the raw data. All authors contributed to the article and approved the submitted version.

Funding

The present study was supported by Japan Society for the Promotion of Science Kakenhi (grant no. JP21K15396) and The Sakurai Memorial Fund for Medical Research.

Conflict of interest

The authors declare that the research was conducted in the absence of any commercial or financial relationships that could be construed as a potential conflict of interest.

Supplementary material

The Supplementary Material for this article can be found online at: https://www.por-journal.com/articles/10.3389/pore.2023.1611284/full#supplementary-material

SUPPLEMENTARY MOVIE S1
Perineural invasion of the images in the superficial layer of the bile duct.

SUPPLEMENTARY MOVIE S2
Perineural invasion of the images in the deep layer of the bile duct.

References

1. Wu R, Zhang G, Feng J, Zhang L, Yang Z. Proposal of the optimal numbers of examined and positive lymph nodes to the 8th edition of American joint committee on cancer (AJCC) staging for 758 patients with distal cholangiocarcinoma. *PLOS ONE* (2020) 15:e0234464. doi:10.1371/journal.pone.0234464

2. Kijima H, Wu Y, Yosizawa T, Suzuki T, Tsugeno Y, Haga T, et al. Pathological characteristics of early to advanced gallbladder carcinoma and extrahepatic cholangiocarcinoma. *J Hepato-bil Pancreat Sci* (2014) 21:453–8. doi:10.1002/jhbp.72

3. Bhuiya MR, Nimura Y, Kamiya J, Kondo S, Fukata S, Hayakawa N, et al. Clinicopathologic studies on perineural invasion of bile duct carcinoma. *Ann Surg* (1992) 215:344–9. doi:10.1097/00000658-199204000-00007

4. Wellner UF, Shen Y, Keck T, Jin W, Xu Z. The survival outcome and prognostic factors for distal cholangiocarcinoma following surgical resection: A meta-analysis for the 5-year survival. *Surg Today* (2017) 47:271–9. doi:10.1007/s00595-016-1362-0

5. Kondo N, Murakami Y, Uemura K, Hashimoto Y, Nakagawa N, Sasaki H, et al. An increased number of perineural invasions is independently associated with poor survival of patients with resectable pancreatic ductal adenocarcinoma. *Pancreas* (2015) 44:1345–51. doi:10.1097/MPA.0000000000000413

6. Ma J, Jiang Y, Jiang Y, Sun Y, Zhao X. Expression of nerve growth factor and tyrosine kinase receptor A and correlation with perineural invasion in pancreatic cancer. *J Gastroenterol Hepatol* (2008) 23:1852–9. doi:10.1111/j.1440-1746.2008.05579.x

7. Li S, Jo YS, Lee JH, Min JK, Lee ES, Park T, et al. L1 cell adhesion molecule is a novel independent poor prognostic factor of extrahepatic cholangiocarcinoma. *Clin Cancer Res* (2009) 15:7345–51. doi:10.1158/1078-0432.CCR-09-0959

8. Na'ara S, Amit M, Gil Z. L1CAM induces perineural invasion of pancreas cancer cells by upregulation of metalloproteinase expression. *Oncogene* (2019) 38:596–608. doi:10.1038/s41388-018-0458-y

9. Feng Y, Hu X, Liu G, Lu L, Zhao W, Shen F, et al. M3 muscarinic acetylcholine receptors regulate epithelial-mesenchymal transition, perineural invasion, and migration/metastasis in cholangiocarcinoma through the AKT pathway. *Cancer Cell Int* (2018) 18:173. doi:10.1186/s12935-018-0667-z

10. Nan L, Qin T, Xiao Y, Qian W, Li J, Wang Z, et al. Pancreatic stellate cells facilitate perineural invasion of pancreatic cancer via HGF/c-met pathway. *Cell Transpl* (2019) 28(9-10):1289–98. doi:10.1177/0963689719851772

11. Maxwell P, Hamilton PW, Sloan JM. Three-dimensional reconstruction of perineural invasion in carcinoma of the extrahepatic bile ducts. *J Pathol* (1996) 180:142–5. doi:10.1002/(SICI)1096-9896(199610)180:2<142::AID-PATH618>3.0.CO;2-6

12. Miyashita Y, Ikeda T, Shinto E, Okano S, Korehisa S, Shimazaki H, et al. Three-dimensional imaging of intramural perineural invasion in colorectal cancer: Three-dimensional reconstruction approach with multiple immunohistochemically stained sections. *Pathol Int* (2022) 72:293–9. doi:10.1111/pin.13222

13. Renier N, Wu Z, Simon DJ, Yang J, Ariel P, Tessier-Lavigne M. iDISCO: A simple, rapid method to immunolabel large tissue samples for volume imaging. *Cell* (2014) 159:896–910. doi:10.1016/j.cell.2014.10.010

14. Noë M, Rezaee N, Asrani K, Skaro M, Groot VP, Wu PH, et al. Immunolabeling of cleared human pancreata provides insights into three-dimensional pancreatic anatomy and pathology. *Am J Pathol* (2018) 188:1530–5. doi:10.1016/j.ajpath.2018.04.002

15. Hong SM, Jung D, Kiemen A, Gaida MM, Yoshizawa T, Braxton AM, et al. Three-dimensional visualization of cleared human pancreas cancer reveals that sustained epithelial-to-mesenchymal transition is not required for venous invasion. *Mod Pathol* (2020) 33:639–47. doi:10.1038/s41379-019-0409-3

16. Yoshizawa T, Hong SM, Jung D, Noë M, Kiemen A, Wu PH, et al. Three-dimensional analysis of extrahepatic cholangiocarcinoma and tumor budding. *J Pathol* (2020) 251:400–10. doi:10.1002/path.5474

17. Hashiguchi G. Studies on perineural invasion of the extrahepatic bile duct cancer. *Tokyo Jikeikai Med J* (1984) 99:687–98.

18. Ayala GE, Wheeler TM, Shine HD, Schmelz M, Frolov A, Chakraborty S, et al. *In vitro* dorsal root ganglia and human prostate cell line interaction: Redefining perineural invasion in prostate cancer. *Prostate* (2001) 49:213–23. doi:10.1002/pros.1137

19. Ayala GE, Dai H, Powell M, Li R, Ding Y, Wheeler TM, et al. Cancer-related axonogenesis and neurogenesis in prostate cancer. *Clin Cancer Res* (2008) 14:7593–603. doi:10.1158/1078-0432.CCR-08-1164

20. Suzuki M, Takahashi T, Ouchi K, Matsuno S. Perineural tumor invasion and its relation with the lymphogenous spread in human and experimental carcinoma of bile duct. A computer-aided 3-D reconstruction study. *Tohoku J Exp Med* (1994) 172:17–28. doi:10.1620/tjem.172.17

Pathology & Oncology Research | frontiers

TYPE Original Research
PUBLISHED 05 June 2023
DOI 10.3389/pore.2023.1611001

Check for updates

OPEN ACCESS

EDITED BY
Anna Sebestyén,
Semmelweis University, Hungary

*CORRESPONDENCE
Zengxin Lu,
luzx777@163.com

RECEIVED 07 December 2022
ACCEPTED 24 May 2023
PUBLISHED 05 June 2023

CITATION
Huang H, Li Z, Xia Y, Zhao Z, Wang D, Jin H, Liu F, Yang Y, Shen L and Lu Z (2023), Association between radiomics features of DCE-MRI and CD8$^+$ and CD4$^+$ TILs in advanced gastric cancer. *Pathol. Oncol. Res.* 29:1611001. doi: 10.3389/pore.2023.1611001

COPYRIGHT
© 2023 Huang, Li, Xia, Zhao, Wang, Jin, Liu, Yang, Shen and Lu. This is an open-access article distributed under the terms of the Creative Commons Attribution License (CC BY). The use, distribution or reproduction in other forums is permitted, provided the original author(s) and the copyright owner(s) are credited and that the original publication in this journal is cited, in accordance with accepted academic practice. No use, distribution or reproduction is permitted which does not comply with these terms.

Association between radiomics features of DCE-MRI and CD8$^+$ and CD4$^+$ TILs in advanced gastric cancer

Huizhen Huang[1], Zhiheng Li[2], Yue Xia[1], Zhenhua Zhao[3], Dandan Wang[3], Hongyan Jin[4], Fang Liu[4], Ye Yang[4], Liyijing Shen[3] and Zengxin Lu[3,5]*

[1]Shaoxing of Medicine, Shaoxing University, Shaoxing, China, [2]Department of Radiology, Anhui Provincial Hospital, Hefei, China, [3]Department of Radiology, Shaoxing People's Hospital, Shaoxing, China, [4]Country Department of Pathology, Shaoxing People's Hospital, Shaoxing, China, [5]The First Affiliated Hospital of Shaoxing University, Shaoxing, China

Objective: The aim of this investigation was to explore the correlation between the levels of tumor-infiltrating CD8$^+$ and CD4$^+$ T cells and the quantitative pharmacokinetic parameters of dynamic contrast-enhanced magnetic resonance imaging (DCE-MRI) in patients with advanced gastric cancer.

Methods: We retrospectively analyzed the data of 103 patients with histopathologically confirmed advanced gastric cancer (AGC). Three pharmacokinetic parameters, K_{ep}, K^{trans}, and V_e, and their radiomics characteristics were obtained by Omni Kinetics software. Immunohistochemical staining was used to determine CD4$^+$ and CD8$^+$ TILs. Statistical analysis was subsequently performed to assess the correlation between radiomics characteristics and CD4$^+$ and CD8$^+$ TIL density.

Results: All patients included in this study were finally divided into either a CD8$^+$ TILs low-density group (n = 51) (CD8$^+$ TILs < 138) or a high-density group (n = 52) (CD8$^+$ TILs ≥ 138), and a CD4$^+$ TILs low-density group (n = 51) (CD4$^+$ TILs < 87) or a high-density group (n = 52) (CD4$^+$ TILs ≥ 87). ClusterShade and Skewness based on K_{ep} and Skewness based on K^{trans} both showed moderate negative correlation with CD8$^+$ TIL levels (r = 0.630–0.349, p < 0.001), with ClusterShade based on K_{ep} having the highest negative correlation (r = −0.630, p < 0.001). Inertia-based K_{ep} showed a moderate positive correlation with the CD4$^+$ TIL level (r = 0.549, p < 0.001), and the Correlation based on K_{ep} showed a moderate negative correlation with the CD4$^+$ TIL level, which also had the highest correlation coefficient (r = −0.616, p < 0.001). The diagnostic efficacy of the above features was assessed by ROC curves. For CD8$^+$ TILs, ClusterShade of K_{ep} had the highest mean area under the curve (AUC) (0.863). For CD4$^+$ TILs, the Correlation of K_{ep} had the highest mean AUC (0.856).

Conclusion: The radiomics features of DCE-MRI are associated with the expression of tumor-infiltrating CD8$^+$ and CD4$^+$ T cells in AGC, which have

the potential to noninvasively evaluate the expression of $CD8^+$ and $CD4^+$ TILs in AGC patients.

KEYWORDS

radiomics, $CD4^+$, $CD8^+$, advanced gastric cancer (AGC), dynamic contrast-enhanced magnetic resonance imaging (DCE-MRI)

Introduction

Although the incidence and mortality of gastric cancer have declined over the past decades, gastric cancer remains the fourth most prevalent cancer worldwide [1]. Traditional surgical resection remains the main treatment for gastric cancer [2]. However, most patients with gastric cancer are usually diagnosed at an advanced stage, and thus less than 30% are suitable for radical resection [3]. In recent years, there have been new research advances in the treatment of advanced gastric cancer (AGC), and immunotherapy based on blocking immune checkpoint inhibitors (ICIs) has made a great promise for gastric cancer patients [4]. While immune checkpoint blockade significantly extends the survival of patients with AGC, only a small percentage of patients can benefit from treatment, in part because tumor-immune interactions in the tumor immune microenvironment (TIME) suppress the efficacy of ICI [5]. Furthermore, cell adoptive therapy based on tumor-infiltrating lymphocytes has shown promising results in the treatment of advanced solid tumors [6]. This is an immunotherapy that eliminates tumor cells by using immune cells in the tumor microenvironment.

Tumor-infiltrating lymphocytes (TILs) are an important part of the TME and are related to the metabolism of tumor cells and the local immune response. The number of T lymphocyte subsets is considered to be not only closely related to the metastasis, progression, and growth of malignant tumors, but also related to immune dysfunction, a key factor affecting the effect of tumor immunotherapy [7–9]. T lymphocytes are mainly divided into different functional subsets: $CD4^+$ T cells, effector ($CD8^+$) T cells, and other types of cells such as natural killer T (NKT) cells. CD8 is a marker of cytotoxic T cells and is the main antitumor effector cell, as it can recognize and kill tumor cells. The majority of $CD4^+$ T cells are helper T lymphocytes. $CD4^+$ T cells that promote their activation and proliferation and their synergistic antitumor activity are considered to be essential for tumor surveillance. Studies have shown that monitoring the changes in T lymphocytes in tumor patients is of great significance for the timely reflection of immune function and the prognosis of therapeutic effects in tumor patients. In addition, $CD4^+$ and $CD8^+$ T cells are closely associated with an improved response to immunotherapy in patients with advanced gastric cancer [10, 11]. Immune checkpoint inhibitor (ICI) therapy aims to prevent tumor cells from suppressing the immune system, thus enabling the immune system to attack tumor cells more effectively. However, the effectiveness of ICI therapy may be diminished if a patient has a low number of $CD4^+$ and $CD8^+$ T cells, as these cells are responsible for recognizing and killing cancer cells. Consequently, the number of $CD4^+$ and $CD8^+$ T cells may impact the efficacy of ICI therapy [12]. The gold standard for TIL quantification is the evaluation of biopsy specimens by immunohistochemistry. However, this approach is limited by its invasiveness, no reproducibility, and inability to reflect intra- and intertumoral heterogeneity. These shortcomings indicate an urgent need to comprehensively assess TIL levels in a dynamic and noninvasive biomarker manner.

Radiomics is an emerging field in which subtle information contained in medical imaging is extracted and transformed into quantitative features that represent the underlying tissue attributes of a tumor. Radiomics has the potential to improve our understanding of tumor biology and guide the choice of clinical treatment options [4, 13, 14]. Several studies have confirmed that radiomics is very effective for the diagnosis and classification of gastric cancer as well as the identification of other molecules and is potentially a biomarker to assess immunohistochemical features, thereby helping to guide the treatment of patients [15–17]. Several studies have discussed the correspondence between DCE-MRI and EGFR and VEGF expression levels; however, few studies have discussed radiomics assessment at the TIL level based on preoperative DCE-MRI in patients with advanced gastric cancer. Therefore, this study aims to preliminarily explore the correlation between the radiomics features of DCE-MRI and the infiltration degree of $CD8^+$ and $CD4^+$ tumor-infiltrating T lymphocytes and lay the foundation for future research.

Materials and methods

Patient demographics

Informed consent did not need to be obtained by patients in this retrospective study after the Ethics Committee of Shaoxing People's Hospital approved it. We enrolled patients with advanced gastric cancer admitted to Shaoxing People's Hospital between April 2018 and July 2022, and we collected their imaging data before treatment. The following criteria were used for inclusion: 1) surgery or gastroscopic biopsy confirmed GC; 2) there were no absolute contraindications to MRI; and 3) prior to DCE-MRI, no antitumor therapy was administered. The following criteria were used for exclusion: 1) heavy image artifacts, which seriously affected the delineation of the lesion;

2) maximum tumor diameter <1 cm; and 3) contraindications to surgery or puncture. According to the study's findings, 103 patients participated, 77 males and 26 females, with an average age of 67.7 years (range 33–88 years).

DCE-MRI examination

All patients were prepared as follows: 1) patients fasted for 8 h before examination and underwent respiratory training 30 min before the examination; 2) intramuscular anisodamine injection (Hangzhou Minsheng Pharmaceutical Co., Ltd., China) was injected 10 min before the examination to prevent gastrointestinal motility; and 3) 5 min before the MRI, patients drank 800–1,000 mL of tepid water to fill their stomachs.

A 3.0 T magnetic resonance scanner (Verio, Siemens, Germany) with a 12-channel phased-array surface coil was used for scanning. The patient was evaluated while lying flat, and the entire stomach was scanned. T1WI, T2WI, and DCE-MRI were all part of the scan's overall sequence, and DCE-MRI was carried out while the patient was breathing freely. Initially, multi-flip angle cross-sectional T1WI was performed, and a fast 3D volume interpolation gas fat-suppression sequence was used. These were the precise specifications: slice thickness is 5 mm, the field of view is 350 mm by 284 mm, the matrix is 288 × 164, and the repetition time is 3.25 ms. Different flip angles (5°, 10°, 15°) were used to scan one stage, each cycle was 6.5 s, and the total time was 19.5 s. The gradient echo volume interpolation fat-suppression sequence was used. The flip angle was 10°, a total of 35 phases were scanned, and the imaging time was 227.5 s. The other variables were the same as for the cross-sectional T1WI with several flips. In the third phase, gadodiamide (Omniscan, GE Healthcare, China) was given at a dose of 0.1 mmol/kg and an injection rate of 3.5 mL/s. Normal saline was then flushed with 20 mL at the same flow rate.

Image information evaluation

The raw images of all eligible AGC patients were imported into the hemodynamic software Omni. Kinetics (GE Healthcare, China). Nonrigid 3D registration was used to preprocess the DCE images and Omni. Kinetics software was used to post-process the multi-flip angle (5°, 10°, 15°) and correct the dynamically enhanced images. The abdominal aorta was chosen as the entry artery. The perfusion parameters were calculated using the Tofts pharmacokinetic model (Ktrans, Kep, and Ve). The study area was chosen to avoid cystic degeneration, necrosis, and normal gastric wall tissue. Two senior radiologists delineated the contours by hand. The AGC lesion was delineated layer by layer and then fused to form a 3D ROI. From the three perfusion maps, the software generated 231 radiomics features, including Haralick, first-order, histogram, gray-level cooccurrence matrix, and run-length matrix. The final measurements were all the mean values obtained by repeating three calculations. In Figure 1, the workflow is displayed.

Immunohistochemical staining and evaluation

The main immunohistochemistry (IHC) staining and quantitative analysis of $CD4^+$ and $CD8^+$ T cells was carried out in accordance with previous research [10, 18]. Gastric cancer specimens were obtained by surgery or gastroscopic biopsy. All gastric cancer specimens were cut into 4-μm-thick slices after paraffin embedding. All slices were deparaffinized and hydrated before antigen retrieval. Endogenous peroxidase activity was then inhibited in a 3% H_2O_2 solution for 10 min at 37°C (H36021693, Nanchang Baiyun Pharmaceutical Co., Ltd., Nanchang, China). Sections were immunohistochemically stained with rabbit anti-CD4 monoclonal antibody (GT219102, Gene Tech, Shanghai, China) or mouse anti-CD8 monoclonal antibody (GT211202, Gene Tech, Shanghai, China), and stored in the refrigerator at 4°C overnight. Sections were subsequently stained with secondary antibodies (K5009, Dako, Beijing, China) and then incubated at 37°C for 10 min. Diaminobenzidine (DAB) staining, hematoxylin counterstaining. The slides were examined under a microscope after dehydration, transparency, and mounting. The immunohistochemical results were reviewed by two experienced pathologists in a double-blind manner. The whole field of tissue was observed under a low-power microscope, and then five fields were randomly selected under high-power fields (X40) in each case (Figure 2). The counting field of view included cancer cell nests within the tumor tissue and the surrounding stroma. Then, according to previous studies [18], the expression of $CD4^+$ and $CD8^+$ TIL was evaluated according to the average number of positively stained cells, and then patients were divided into high and low groups according to the median.

Statistical analyses

The data analysis and image drawing processes used SPSS (version 24, IBM Corporation, United States) and GraphPad Prism 8.0 (GraphPad Prism Software Inc., San Diego, CA, United States). The Mann–Whitney U test or independent sample Student's t-test was applied depending on the circumstances. Measurement data are expressed as the mean and standard deviation. When appropriate, Fisher's exact probability method or the chi-square test was employed to describe count data as frequency (%). Due to the nonnormal distribution of continuous variables, Spearman correlation was employed to examine the relationship between each DCE-MRI

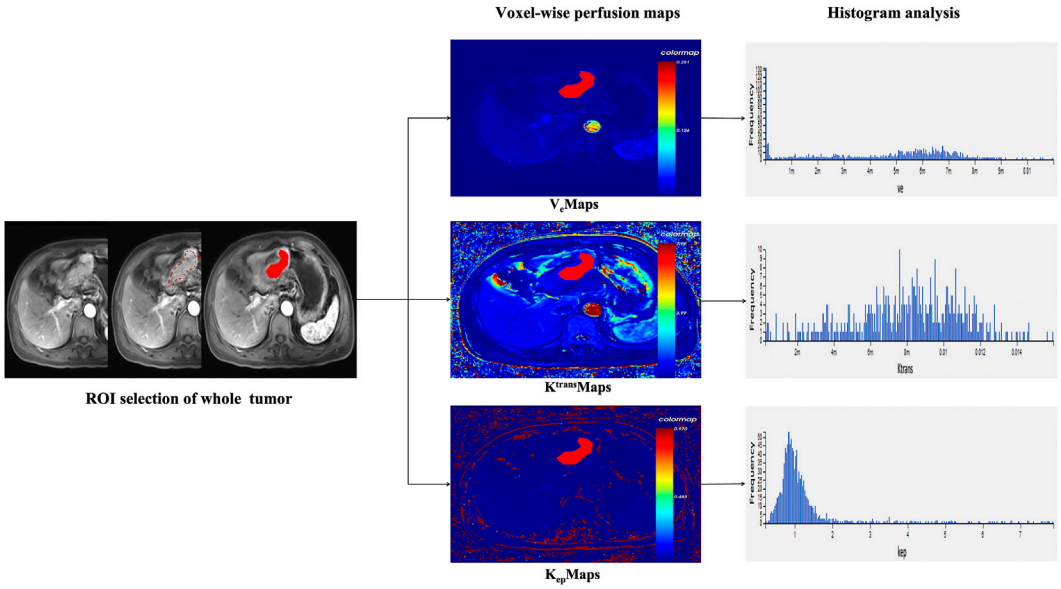

FIGURE 1
Voxel-wise analysis of the entire tumor is shown in the research's overall flow chart.

perfusion parameter and the degree of $CD4^+$ and $CD8^+$ TIL infiltration. For all statistics, two-sided probability tests were employed. Statistics were judged significant at $p < 0.05$.

Results

The study included 103 patients with advanced gastric cancer who presented to Shaoxing People's Hospital between the ages of 33 and 88. The median value of $CD4^+$ and $CD8^+$ TILs was 87 and 138, respectively. As shown in Table 1, the study results revealed no significant differences in gender, age, BMI, tumor location, differentiation level, CEA level, CA199 level, and CA125 level between cohorts with high and low infiltration levels of CD4 and CD8.

Several radiomics profiles of DCE-MRI pharmacokinetic parameters significantly associated with the infiltration of $CD4^+$ and $CD8^+$ TILs are summarized in Figure 3 and Tables 2, 3. ClusterShade of Kep had the greatest correlation coefficient with CD8 ($r = -0.630$, $p < 0.001$), and the Correlation of Kep had the highest correlation value with CD4 ($r = -0.616$, $p < 0.001$).

ROC curve analysis was performed to evaluate the diagnostic performance of radiomics parameters in distinguishing high and low expression of CD8 and CD4 in AGC. For CD8 expression, the radiomics parameters SkewnessKtrans, SkewnessKep, and ClusterShadeKep exhibited good discriminatory ability with AUC values of 0.702, 0.737, and 0.863, respectively. These parameters showed promising sensitivity, specificity, accuracy, and predictive values (Table 4 and Figure 4). Similarly, for CD4 expression, the radiomics parameters UniformityKtrans, InertiaKep, and CorrelationKep demonstrated effective discrimination with AUC values of 0.778, 0.817, and 0.856, respectively. These parameters achieved high sensitivity, specificity, accuracy, and predictive values (Table 5 and Figure 4). Overall, the results of the ROC curve analysis highlight the potential of these radiomics parameters in differentiating between high and low expression of CD8 and CD4 in AGC patients.

Among the above DCE-MRI radiomics parameters and the clinicopathological data included in this study, only Ktrans (Skewness) was positively correlated with CEA level ($r = 0.197$, $p = 0.046$, Table 6).

Discussion

To our knowledge, this is the first study to distinguish the degree of CD4 and CD8 tumor-infiltrating lymphocyte infiltration in AGC patients based on DCE-MRI radiomics characteristics. It has been found that radiomics parameters based on DCE-MRI perfusion maps have good diagnostic performance in distinguishing the degree of CD4 and CD8 infiltration. It is inferred that this approach may help guide the clinical identification of immune therapy beneficiaries and the selection of appropriate treatment options for patients with AGC.

Various biomarkers are currently employed in routine clinical practice, as they can reveal tumor characteristics in a

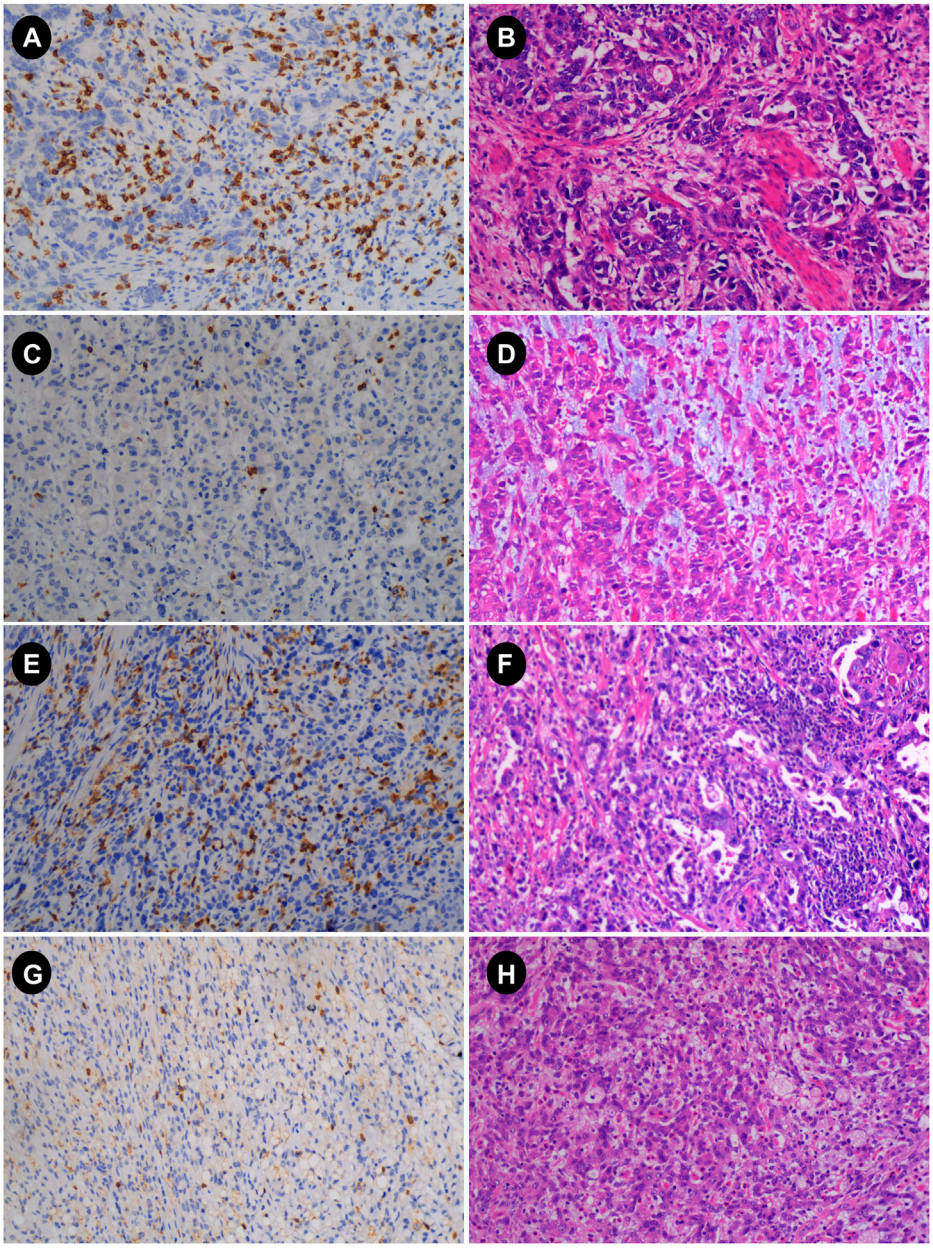

FIGURE 2
Immunohistochemistry (IHC) and hematoxylin-eosin (HE) images of advanced gastric cancer. **(A,B)** IHC and HE plots with high CD8; **(C,D)** IHC and HE plots with low CD8; **(E,F)** IHC and HE plots with high CD4; **(G,H)** IHC and HE plots with low CD4 (magnification: 10 × 40) HE, hematoxylin and eosin staining; IHC, immunohistochemistry.

variety of ways [19]. Imaging is a critical examination method for determining the occurrence and progression of tumors. The development of computer algorithms and other technologies has led to the emergence of radiomics. This approach enables the quantification of the pixel and spatial distribution of medical images, and extracted features describe not only the gray level, and texture, but also other information [20]. Most studies have shown that it can reflect tumor heterogeneity and thus be used to evaluate biomarkers noninvasively [21–23]. In this study, we used DCE-MRI to extract radiomics features. Different from traditional MRI imaging techniques, DCE-MRI has the advantage of assessing the tumor vascular microenvironment. DCE-MRI has been applied to several tumor studies and achieved satisfactory results [15]. Therefore, we established DCE-MRI-based radiomics features to identify CD4 and CD8 expression and achieved satisfactory results.

TABLE 1 Advanced gastric cancer patients' clinical features.

Characteristic	$CD8^+$ TILs status			$CD4^+$ TILs status		
	High (n = 52)	Low (n = 51)	P	High (n = 52)	Low (n = 51)	P
Age (years, mean ± SD)	67.673 ± 11.206	69.863 ± 9.210	0.286	68.096 ± 10.417	69.431 ± 10.185	0.516
BMI (Kg/m^2, mean ± SD)	22.965 ± 2.887	22.383 ± 3.314	0.348	22.148 ± 2.619	23.215 ± 3.476	0.084
Gender			0.954			0.609
Male	39	38		40	37	
Female	13	13		12	14	
Location			0.211			0.091
Cardia	11	6		8	9	
Body	13	20		12	21	
Antrum	28	25		32	21	
Differentiation level			0.494			0.280
High/Moderate	30	26		31	25	
Poor	22	25		21	26	
CEA level (ng/mL)			0.945			0.442
Normal	35	34		33	36	
Elevated	17	17		19	15	
CA199 level (μ/mL)			0.238			0.777
Normal	41	35		39	37	
Elevated	11	16		13	14	
CA125 level (μ/mL)			0.446			0.854
Normal	42	38		40	40	
Elevated	10	13		12	11	

With a high incidence and poor prognosis, gastric cancer is a malignant tumor developing from the stomach mucosal epithelium [24]. In recent years, the host tumor's local immune response has gradually become a hot research topic [25–27]. Tumor-infiltrating immune cells play a crucial role in this response, and TILs make up the majority of this immune cell [27, 28]. TILs, tumor-infiltrating lymphocytes, are a crucial part of the tumor microenvironment and lymphocytes that leave the bloodstream to infiltrate the tumor. TILs are often linked to a higher immunotherapy response and prognosis, according to a number of studies [29–31]. The number of TILs may be a significant predictor of the response to cytotoxic treatments such as chemotherapy and radiotherapy and is assumed to be associated with the mechanisms regulating cancer growth, progression, and metastasis [32–34]. TILs have major subtypes, $CD4^+$ and $CD8^+$, which have a significant impact on the prognosis of AGC [35]. Understanding the expression and differences in $CD4^+$ and $CD8^+$ TILs in patients with advanced gastric cancer can help identify patients, provide reasonable and personalized treatment, and contribute to the advancement of precision medicine. Hyein Ahn et al. discovered that texture features extracted from FDG PET/CT are correlated with $CD8^+$ T lymphocytes, which can provide histopathological characteristics of the immune microenvironment and predict cancer patients' recurrence-free survival [36]. Bian, Y et al. used contrast-enhanced CT to predict tumor $CD8^+$ TIL levels and developed an XGBoot classifier with AUCs of 0.75 and 0.67 in the training and validation sets, respectively [37]. Compared to CT and PET/CT, MRI has better resolution and contrast in soft tissue imaging without the need for radiotracers. In this study, MRI-based methods were used, which reflect more functional information about the tumor.

DCE-MRI is an oncology functional imaging technique that measures tumor blood flow, vascular permeability, and vascular and interstitial volume [38]. DCE-MRI has some utility in predicting the expression of various proteins in gastric cancer and assessing gastric cancer angiogenesis [15]. Traditional DCE-MRI parameters are inadequate for assessing intratumoral heterogeneity. Instead of conventional DCE-MRI parameters, a histogram analysis method based on DCE-MRI was used in this study to obtain radiomics parameters. Histogram analysis is a technique for analyzing the gray level distribution on biomedical images and producing metrics that reflect the frequency with which pixels display gray level in a given interval [39, 40]. As a result, radiomics parameters based on histograms are more likely to reflect tumor heterogeneity. DCE-MRI has previously been shown to predict the expression of tumor-infiltrating

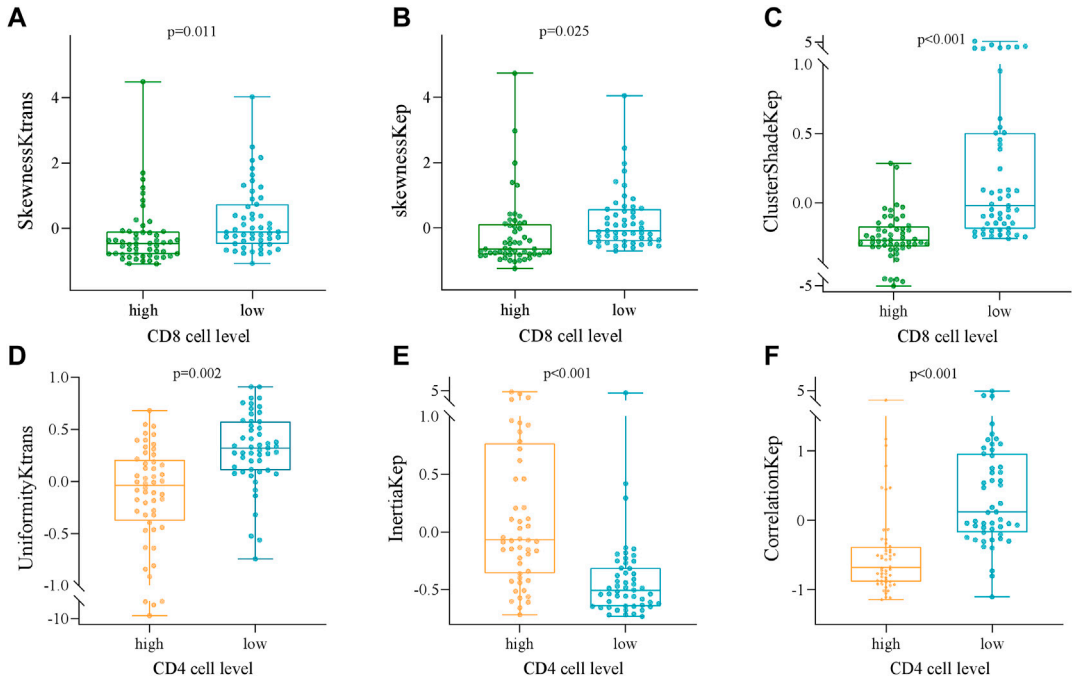

FIGURE 3
Box and whisker plots showing the relationships between the expression of CD8 and CD4 TILs and the DCE-MRI-based phenotypes. **(A)** SkewnessKtrans, **(B)** skewnessKep, **(C)** ClusterShadeKep, **(D)** UniformityKtrans, **(E)** InertiaKep, and **(F)** CorrelationKep.

TABLE 2 Correlation analysis between DCE-MRI parameters and $CD8^+$ TILs in patients with advanced gastric cancer.

Kinetic parameter	Parameter	*r* value	*p*-value
Ktrans	Skewness	−0.349	<0.001
Kep	Skewness	−0.411	<0.001
	ClusterShade	−0.630	<0.001

Note: *r*, correlation coefficient.

TABLE 3 Correlation analysis between DCE-MRI parameters and $CD4^+$ TILs in patients with advanced gastric cancer.

Kinetic parameter	Parameter	*r* value	*p*-value
Ktrans	Uniformity	−0.481	<0.001
Kep	Inertia	0.549	<0.001
	Correlation	−0.616	<0.001

Note: *r*, correlation coefficient.

lymphocytes in breast cancer, lung cancer, and melanoma [41, 42]. According to the findings, radiomics features extracted from DCE-MRI have some utility in identifying the expression of tumor-infiltrating lymphocytes. The feasibility of using DCE-MRI to predict the expression of tumor-infiltrating lymphocyte subsets in AGC patients has not been investigated.

In our study, some pharmacokinetic radiomics parameters based on perfusion maps were found to have good diagnostic performance in distinguishing the different densities of $CD4^+$ and $CD8^+$ TILs in AGC patients. In this study, ROC curve analysis revealed that ClusterShade of Kep (0.557), skewness of Kep (0.518), and skewness of Ktrans (0.360) provided the perfect combination of sensitivity (0.980, 0.980, and 0.725), specificity (0.558, 0.519, and 0.615), PPV (0.685, 0.667, and 0.649), and NPV (0.967, 0.964, and 0.696) for distinguishing the different densities of $CD8^+$ TILs in AGC ($p < 0.001$, respectively). We found that ClusterShade of Kep exhibited the most negative association with $CD8^+$ TILs ($r = -0.630$). ClusterShade is one of the texture features of the gray level co-occurrence matrix (GLCM), which is used to describe the distribution of cluster shadows in images. In medical image analysis, ClusterShade is frequently used to analyze heterogeneity and changes in tissue structure, reflecting the distribution of different types of cells within the tissue [39]. The larger the cluster shadow value of Kep indicates the larger the difference in the distribution of different types of cells and the higher the heterogeneity within the tissue [15]. The relationship with $CD8^+$ TILs may indicate cell density and arrangement in tumor tissue, thereby having an impact on immune cell infiltration and anti-tumor immune responses. Some studies have shown that tumor cells line more loosely and irregularly tumor tissue, are more easily attacked by immune cells, and

TABLE 4 ROC curve analysis of radiomics parameters for differentiating CD8 high expression from low expression in AGC.

Parameter	Cut-off	Sensitivity	Specificity	Accuracy	PPV	NPV	AUC	P
SkewnessKtrans	0.360	0.725	0.615	0.670	0.649	0.696	0.702	<0.001
SkewnessKep	0.518	0.980	0.519	0.748	0.667	0.964	0.737	<0.001
ClusterShadeKep	0.557	0.980	0.558	0.767	0.685	0.967	0.863	<0.001

Note: AUC, the area under curve.

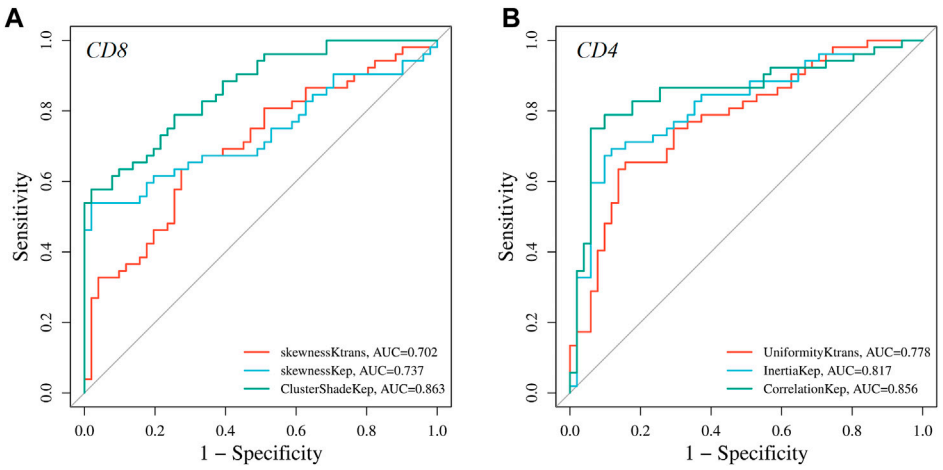

FIGURE 4
Graphs showing the receiver operating characteristic curves (ROC) of DCE-MRI parameters for differentiating high and low **(A)** CD8 and **(B)** CD4 expressions.

TABLE 5 ROC curve analysis of radiomics parameters for differentiating CD4 high expression from low expression in AGC.

Parameter	Cut-off	Sensitivity	Specificity	Accuracy	PPV	NPV	AUC	P
UniformityKtrans	0.498	0.863	0.635	0.748	0.698	0.825	0.778	<0.001
InertiaKep	0.575	0.902	0.673	0.786	0.730	0.875	0.817	<0.001
CorrelationKep	0.691	0.941	0.731	0.835	0.774	0.927	0.856	<0.001

Note: AUC, the area under the curve.

TABLE 6 Correlation between DCE-MRI parameters and CEA level of AGC.

Kinetic parameter	Parameter	*r* value	*p*-value
Ktrans	Skewness	0.197	0.046*
	Uniformity	−0.149	0.132
Kep	Correlation	−0.039	0.697
	Skewness	−0.007	0.945
	ClusterShade	−0.003	0.972
	Inertia	0.090	0.368

Note: *r*, correlation coefficient. * indicates significance at $p < 0.05$. CEA, carcinoembryonic antigen.

achieve better immunotherapeutic responses [29]. Therefore, Kep.ClusterShade may be a potential biomarker to predict response to immunotherapy.

As for CD4, the ideal combination of sensitivity (0.941, 0.902, and 0.863), specificity (0.731, 0.673, and 0.635), PPV (0.774, 0.730, and 0.698), and NPV (0.927, 0.875, and 0.825) was Correlation of Kep (0.557), Inertia of Kep (0.518), and Uniformity of Ktrans (0.360). ($p < 0.001$), respectively. The negative connection between Kep and $CD4^+$ TILs was the strongest ($r = -0.616$). Kep represents the transfer rate constant between plasma and extracellular space, and it is a reflection of extravascular interstitial permeability. Previous studies have suggested that Kep may reflect

microvessel density characteristics such as vessel area [43]. A higher K_{ep} value represents an increase in tumor perfusion and vascular permeability, which is attributed to an increased number of nascent tumor vessels [44]. $CD4^+$ T cells play an important role in the tumor microenvironment, and there is no direct evidence that $CD4^+$ T cells directly inhibit tumor angiogenesis. However, it has been shown that $CD4^+$ T cells can also secrete some cytokines, such as IL-10, which can inhibit tumor angiogenesis through a variety of pathways, such as inhibiting endothelial cell proliferation and migration, and reducing the secretion of vascular endothelial growth factor [9]. Lower CD4 numbers may indirectly lead to more aggressive tumors and more angiogenesis, thus resulting in a negative correlation between Kep and CD4. The mechanism still needs further study in the future. Previous studies have shown that an insufficient number of $CD8^+$ T lymphocytes can cause tumor cell proliferation, invasion, and metastasis, resulting in rapid tumor progression [45–47]. Numerous studies have demonstrated that a positive prognosis for gastric cancer is related to high expression of TILs (CD4, CD8) [35, 48]We find that the derived parameters of gray level co-occurrence matrix (GLCM) play an important role. GLCM played an important role in predicting $CD8^+$ TIL density, which is consistent with previous reports that radiomics metrics of GLCM were dominant in models predicting $CD8^+$ TIL density in renal clear cells [49]. This study also found a close relationship between the radiomics parameters of GLCM and $CD4^+$TILs.

In addition, a correlation was observed between Ktrans (skewness) and CEA levels (r = 0.197, p = 0.046) in our study. Carcinoembryonic antigen (CEA) is a widely used tumor marker in patients with gastrointestinal cancer before treatment and during follow-up. Previous studies have found that patients with high pretreatment serum CEA levels have a poor prognosis [50]. Currently, the mechanism by which elevated CEA levels lead to worse survival remains unclear. One possible explanation is that CEA acts indirectly in cell-cell adhesion between tumor cells and vascular endothelial cells, thereby contributing to tumor invasion and metastasis [51]. Patients with higher CEA levels in this study had higher Ktrans (skewness) values relative to patients with normal CEA levels. Higher Ktrans (skewness) values in tumor tissue represent a more heterogeneous distribution of tumor vessels, that is, more heterogeneous vascularity [15]. The association between them may therefore be plausible, however, to better elucidate this association, we should investigate this association further.

This study has certain limitations. Firstly, the TIL subtypes investigated in this study included only CD4 and CD8, and other subtypes were not included. Future studies should include other subtypes associated with immunotherapy to more comprehensively assess the tumor immune microenvironment. Secondly, the study did not include other molecular expression data, such as EBV or MSI status. The inclusion of these data allows better patient stratification and may provide a basis for precision immunotherapy. In future investigations, we plan to include these additional molecular expression data to further enrich the study and strengthen its clinical relevance. Thirdly, it is important to highlight that the current study lacks clinical validation. While our findings provide valuable insights, further studies with larger sample sizes and prospective designs are needed to validate the results in a clinical setting. Clinical validation would help assess the practical utility and generalizability of our findings, ensuring their applicability in real-world clinical practice. Last but not least, this study is a single-center retrospective study with possible selection bias, and more patients (based on existing studies) will be included in the future for further multicenter studies to verify. These limitations should be considered when interpreting the results of our study and provide directions for future research to overcome these limitations and further advance the field. In conclusion, our study showed that some quantitative pharmacokinetic parameters obtained from DCE-MRI have the potential to assess the levels of $CD8^+$ and $CD4^+$ TILs infiltration. The identification of $CD8^+$ and $CD4^+$ TIL infiltration levels is helpful for the development of precision medicine and provides more information for clinical practice to assist clinical decision-making. In the future, machine learning methods will be introduced to establish better evaluation models.

Conclusion

In several cases, the expression of $CD4^+$ and $CD8^+$ TILs in AGC patients correlated with DCE-MRI quantitative perfusion histogram characteristics. Quantitative perfusion histogram parameters using DCE-MRI can be utilized as imaging biomarkers to noninvasively reflect $CD4^+$ and $CD8^+$ TIL expression in AGC patients and serve as a reference for customized treatment of AGC patients.

Data availability statement

The raw data supporting the conclusion of this article will be made available by the authors, without undue reservation.

Ethics statement

The Ethics Committee of Shaoxing People's Hospital, Shaoxing, China, examined and approved the experiments involving human subjects. The need for written informed consent was waived by the ethics committee. Any potentially identifiable photographs or data included in this article were published without obtaining the individual's (written) informed consent.

Author contributions

ZLu and ZZ designed the study and helped to revise the manuscript. HH conducted the study and collected important

background data. HH was the main writer of the manuscript. HH and LS performed the statistical analysis of the data. YX, DW, LS, and ZLi collected the clinical data. HJ, YY, and FL performed immunohistochemistry. All authors contributed to the article and approved the submitted version.

Funding

This work was made possible thanks to funding from the General Project of Zhejiang Province Health Science and Technology Plan (grant numbers, 2021KY1140, 2021KY1150, 2022KY1296, and 2022KY1291).

Conflict of interest

The authors declare that the research was conducted in the absence of any commercial or financial relationships that could be construed as a potential conflict of interest.

Acknowledgments

We sincerely appreciate the Key Laboratory of Functional Molecular Imaging of Tumor (Shaoxing People's Hospital, Shaoxing, Zhejiang, China) for their financial and technical support of this effort.

References

1. Xie J, Fu L, Jin L. Immunotherapy of gastric cancer: Past, future perspective and challenges. *Pathol Res Pract* (2021) 218:218153322. doi:10.1016/j.prp.2020.153322

2. Emaan H, Abdullah E, Ibrahim M, Haneen S, Maen A. Recent trends and advancements in the diagnosis and management of gastric cancer. *Cancers* (2022) 14(22):5615. doi:10.3390/cancers14225615

3. Meng X, Wang L, Zhu B, Sun T, Guo S, Wang Y, et al. Totally laparoscopic gastrectomy versus laparoscopic-assisted gastrectomy for gastric cancer: A systematic review and meta-analysis. *J Laparoendosc Adv Surg Tech A* (2021) 31(6):676–691. doi:10.1089/lap.2020.0566

4. Cui Q, Mao Y, Wu D, Hu Y, Ma D, Zhang L, et al. Apatinib combined with PD-1 antibody for third-line or later treatment of advanced gastric cancer. *Front Oncol* (2022) 12:12952494. doi:10.3389/fonc.2022.952494

5. El Helali A, Tao J, Wong CHL, Chan WW, Mok KC, Wu WF, et al. A meta-analysis with systematic review: Efficacy and safety of immune checkpoint inhibitors in patients with advanced gastric cancer. *Front Oncol* (2022) 12:908026. doi:10.3389/fonc.2022.908026

6. Granhøj JS, Witness Præst Jensen A, Presti M, Met Ö, Svane IM, Donia M. Tumor-infiltrating lymphocytes for adoptive cell therapy: Recent advances, challenges, and future directions. *Expert Opin Biol Ther* (2022) 22(5):627–641. doi:10.1080/14712598.2022.2064711

7. Zhang D, He W, Wu C, Tan Y, He Y, Xu B, et al. Scoring system for tumor-infiltrating lymphocytes and its prognostic value for gastric cancer. *Front Immunol* (2019) 10:1071. doi:10.3389/fimmu.2019.00071

8. Escors D, Bocanegra A, Chocarro L, Blanco E, Piñeiro-Hermida S, Garnica M, et al. Systemic CD4 immunity and PD-L1/PD-1 blockade immunotherapy. *Int J Mol Sci* (2022) 23(21):13241. doi:10.3390/ijms232113241

9. Hung K, Hayashi R, Lafond-Walker A, Lowenstein C, Pardoll D, Levitsky H. The central role of CD4(+) T cells in the antitumor immune response. *J Exp Med* (1998) 188(12):2357–68. doi:10.1084/jem.188.12.2357

10. Zhang N, Wang D, Hu X, Zhang G, Li Z, Zhao Y, et al. Analysis of immune status in gastric adenocarcinoma with different infiltrating patterns and origin sites. *Front Immunol* (2022) 13:13978715. doi:10.3389/fimmu.2022.978715

11. Zhao L, Liu Y, Zhang S, Wei L, Cheng H, Wang J, et al. Impacts and mechanisms of metabolic reprogramming of tumor microenvironment for immunotherapy in gastric cancer. *Cell Death Dis* (2022) 13(4):378. doi:10.1038/s41419-022-04821-w

12. He J, Xiong X, Yang H, Li D, Liu X, Li S, et al. Defined tumor antigen-specific T cells potentiate personalized TCR-T cell therapy and prediction of immunotherapy response. *Cell Res* (2022) 32(6):530–542. doi:10.1038/s41422-022-00627-9

13. Liao H, Zhang Z, Chen J, Liao M, Xu L, Wu Z, et al. Preoperative radiomic approach to evaluate tumor-infiltrating CD8+ T cells in hepatocellular carcinoma patients using contrast-enhanced computed tomography. *Ann Surg Oncol* (2019) 26(13):4537–47. doi:10.1245/s10434-019-07815-9

14. El Naqa I, Ten Haken RK. Can radiomics personalise immunotherapy? *Lancet Oncol* (2018) 19(9):1138–9. doi:10.1016/S1470-2045(18)30429-7

15. Li Z, Zhao Z, Wang C, Wang D, Mao H, Liu F, et al. Association between DCE-MRI perfusion histogram parameters and EGFR and VEGF expressions in different lauren classifications of advanced gastric cancer. *Pathol Oncol Res* (2021) 27:271610001. doi:10.3389/pore.2021.1610001

16. Braman N, Prasanna P, Whitney J, Singh S, Beig N, Etesami M, et al. Association of peritumoral radiomics with tumor biology and pathologic response to preoperative targeted therapy for HER2 (ERBB2)-Positive breast cancer. *JAMA Netw Open* (2019) 2(4):e192561. doi:10.1001/jamanetworkopen.2019.2561

17. Jiang Y, Wang H, Wu J, Chen C, Yuan Q, Huang W, et al. Noninvasive imaging evaluation of tumor immune microenvironment to predict outcomes in gastric cancer. *Ann Oncol* (2020) 31(6):760–768. doi:10.1016/j.annonc.2020.03.295

18. Lee HE, Chae SW, Lee YJ, Kim MA, Lee HS, Lee BL, et al. Prognostic implications of type and density of tumour-infiltrating lymphocytes in gastric cancer. *Br J Cancer* (2008) 99(10):1704–11. doi:10.1038/sj.bjc.6604738

19. Sarhadi VK, Armengol G. Molecular biomarkers in cancer. *Biomolecules* (2022) 12(8):1021. doi:10.3390/biom12081021

20. Mayerhoefer ME, Materka A, Langs G, Häggström I, Szczypiński P, Gibbs P, et al. Introduction to radiomics. *J Nucl Med* (2020) 61(4):488–95. doi:10.2967/jnumed.118.222893

21. Chetan MR, Gleeson FV. Radiomics in predicting treatment response in non-small-cell lung cancer: Current status, challenges and future perspectives. *Eur Radiol* (2021) 31(2):1049–1058. doi:10.1007/s00330-020-07141-9

22. Fiz F, Viganò L, Gennaro N, Costa G, La Bella L, Boichuk A, et al. Radiomics of liver metastases: A systematic review. *Cancers (Basel)* (2020) 12(10):2881. doi:10.3390/cancers12102881

23. Yu Y, He Z, Ouyang J, Tan Y, Chen Y, Gu Y, et al. Magnetic resonance imaging radiomics predicts preoperative axillary lymph node metastasis to support surgical decisions and is associated with tumor microenvironment in invasive breast cancer: A machine learning, multicenter study. *EBioMedicine* (2021) 69:69103460. doi:10.1016/j.ebiom.2021.103460

24. Smyth EC, Nilsson M, Grabsch HI, van Grieken NC, Lordick F. Gastric cancer. *Lancet* (2020) 396(10251):635–48. doi:10.1016/S0140-6736(20)31288-5

25. Ruffin AT, Li H, Vujanovic L, Zandberg DP, Ferris RL, Bruno TC. Improving head and neck cancer therapies by immunomodulation of the tumour microenvironment. *Nat Rev Cancer* (2022) 23:173–188. doi:10.1038/s41568-022-00531-9

26. Park S, Cha H, Kim HS, Lee B, Kim S, Kim TM, et al. Transcriptional upregulation of CXCL13 is correlated with a favorable response to immune checkpoint inhibitors in lung adenocarcinoma. *Cancer Med* (2022) 12:7639–7650. doi:10.1002/cam4.5460

27. Cho H, Kim JE, Hong YS, Kim SY, Kim J, Ryu YM, et al. Comprehensive evaluation of the tumor immune microenvironment and its dynamic changes in patients with locally advanced rectal cancer treated with preoperative chemoradiotherapy: From the phase II ADORE study. *Oncoimmunology* (2022) 11(1):2148374. doi:10.1080/2162402X.2022.2148374

28. Liang Y, Tan Y, Guan B, Guo B, Xia M, Li J, et al. Single-cell atlases link macrophages and CD8+ T-cell subpopulations to disease progression and immunotherapy response in urothelial carcinoma. *Theranostics* (2022) 12(18):7745–7759. doi:10.7150/thno.77281

29. Mehrdad R, Elio A, Biagio R, Lynette MS, Weiwei S, Joao VA, et al. Association of machine learning-based assessment of tumor-infiltrating lymphocytes on standard histologic images with outcomes of immunotherapy in

patients with NSCLC. *JAMA Oncol* (2022) 9(1):51–60. doi:10.1001/jamaoncol.2022.4933

30. Smith JD, Bellile EL, Ellsperman SE, Heft-Neal ME, Mann JE, Birkeland AC, et al. Prognostic value of CD103+ tumor-infiltrating lymphocytes and programmed death ligand-1 (PD-L1) combined positive score in recurrent laryngeal squamous cell carcinoma. *Oral Oncol* (2022) 135:135106226. doi:10.1016/j.oraloncology.2022.106226

31. Zhang C, Sun Y, Li S, Shen L, Teng X, Xiao Y, et al. Autophagic flux restoration enhances the antitumor efficacy of tumor infiltrating lymphocytes. *J Immunother Cancer* (2022) 10(10):e004868. doi:10.1136/jitc-2022-004868

32. Wang XR, Zhao WP, He LH, Wang SL, Li WD, Wang J, et al. dNLR and TILS can be used as indicators for prognosis and efficacy evaluation of neo-adjuvant chemotherapy in breast cancer. *Am J translational Res* (2021) 13(11):13093–13098. Available from: https://pubmed.ncbi.nlm.nih.gov/34956528/(Accessed December 4, 2022).

33. Anaïs JR, Daniel NÁ, Carmen DA, Luis ÁV. Synthetic TILs: Engineered tumor-infiltrating lymphocytes with improved therapeutic potential. *Front Oncol* (2021) 10:593848. doi:10.3389/fonc.2020.593848

34. Okcu O, Öztürk SD, Öztürk Ç, Şen B, Yasin Aİ, Bedir R. Tumor-infiltrating lymphocytes (TILs)/volume and prognosis: The value of TILs for survival in HER2 and TN breast cancer patients treated with chemotherapy. *Ann Diagn Pathol* (2022) 58:151930. doi:10.1016/j.anndiagpath.2022.151930

35. Li F, Sun Y, Huang J, Xu W, Liu J, Yuan Z. CD4/CD8 + T cells, DC subsets, Foxp3, and Ido expression are predictive indictors of gastric cancer prognosis. *Cancer Med* (2019) 8(17):7330–44. doi:10.1002/cam4.2596

36. Ahn H, Song GJ, Jang S-H, Lee HJ, Lee M-S, Lee J-H, et al. Relationship of FDG PET/CT textural features with the tumor microenvironment and recurrence risks in patients with advanced gastric cancers. *Cancers (Basel)* (2022) 14(16):3936. doi:10.3390/cancers14163936

37. Li J, Shi Z, Liu F, Fang X, Cao K, Meng Y, et al. XGBoost classifier based on computed tomography radiomics for prediction of tumor-infiltrating CD8+ T-cells in patients with pancreatic ductal adenocarcinoma. *Front Oncol* (2021) 11:11671333. doi:10.3389/fonc.2021.671333

38. Albano D, Bruno F, Agostini A, Angileri SA, Benenati M, Bicchierai G, et al. Dynamic contrast-enhanced (DCE) imaging: State of the art and applications in whole-body imaging. *Jpn J Radiol* (2022) 40(4):341–366. doi:10.1007/s11604-021-01223-4

39. Li Z, Huang H, Wang C, Zhao Z, Ma W, Wang D, et al. DCE-MRI radiomics models predicting the expression of radioresistant-related factors of LRP-1 and survivin in locally advanced rectal cancer. *Front Oncol* (2022) 12:12881341. doi:10.3389/fonc.2022.881341

40. Lambin P, Leijenaar RTH, Deist TM, Peerlings J, de Jong EEC, van Timmeren J, et al. Radiomics: The bridge between medical imaging and personalized medicine. *Nat Rev Clin Oncol* (2017) 14(12):749–62. doi:10.1038/nrclinonc.2017.141

41. Tang W, Kong Q, Cheng Z, Liang Y, Jin Z, Chen L, et al. Performance of radiomics models for tumour-infiltrating lymphocyte (TIL) prediction in breast cancer: The role of the dynamic contrast-enhanced (DCE) MRI phase. *Eur Radiol* (2022) 32(2):864–875. doi:10.1007/s00330-021-08173-5

42. Wu J, Li X, Teng X, Rubin DL, Napel S, Daniel BL, et al. Magnetic resonance imaging and molecular features associated with tumor-infiltrating lymphocytes in breast cancer. *Breast Cancer Res* (2018) 20(1):101. doi:10.1186/s13058-018-1039-2

43. Li X, Hu Y, Xie Y, Lu R, Li Q, Tao H, et al. Whole-tumor histogram analysis of diffusion-weighted imaging and dynamic contrast-enhanced MRI for soft tissue sarcoma: Correlation with HIF-1alpha expression. *Eur Radiol* (2022) 33:3961–3973. doi:10.1007/s00330-022-09296-z

44. Kang SR, Kim HW, Kim HS. Evaluating the relationship between dynamic contrast-enhanced MRI (DCE-MRI) parameters and pathological characteristics in breast cancer. *J Magn Reson Imaging* (2020) 52(5):1360–73. doi:10.1002/jmri.27241

45. Dolina JS, Van Braeckel-Budimir N, Thomas GD, Salek-Ardakani S. CD8+ T cell exhaustion in cancer. *Front Immunol* (2021) 12:715234. doi:10.3389/fimmu.2021.715234

46. Reading JL, Gálvez-Cancino F, Swanton C, Lladser A, Peggs KS, Quezada SA. The function and dysfunction of memory CD8+ T cells in tumor immunity. *Immunol Rev* (2018) 283(1):194–212. doi:10.1111/imr.12657

47. van der Leun AM, Thommen DS, Schumacher TN. CD8+ T cell states in human cancer: Insights from single-cell analysis. *Nat Rev Cancer* (2020) 20(4):218–32. doi:10.1038/s41568-019-0235-4

48. Wang S, Shi Q, Zhao Y, Song Y, Qiao G, Liu G, et al. Expansion of CD3+CD8+PD1+ T lymphocytes and TCR repertoire diversity predict clinical responses to adoptive cell therapy in advanced gastric cancer. *Am J Cancer Res* (2022) 12(5):2203–2215.

49. Ahn H, Song GJ, Jang S-H, Son MW, Lee HJ, Lee M-S, et al. Predicting the recurrence of gastric cancer using the textural features of perigastric adipose tissue on [18F] FDG PET/CT. *Int J Mol Sci* (2022) 23(19):11985. doi:10.3390/ijms231911985

50. Chen D, Fu M, Chi L, Lin L, Cheng J, Xue W, et al. Prognostic and predictive value of a pathomics signature in gastric cancer. *Nat Commun* (2022) 13(1):6903. doi:10.1038/s41467-022-34703-w

51. Thomas SN, Zhu F, Schnaar RL, Alves CS, Konstantopoulos K. Carcinoembryonic antigen and CD44 variant isoforms cooperate to mediate colon carcinoma cell adhesion to E- and L-selectin in shear flow. *J Biol Chem* (2008) 283(23):15647–55. doi:10.1074/jbc.M800543200

Pathology & Oncology Research | frontiers

TYPE Original Research
PUBLISHED 30 October 2024
DOI 10.3389/pore.2024.1611815

Check for updates

OPEN ACCESS

EDITED BY
Tamás Micsik,
Semmelweis University, Hungary

*CORRESPONDENCE
Yukako Yagi,
yagiy@mskcc.org

†These authors have contributed equally to this work and share first authorship

RECEIVED 01 May 2024
ACCEPTED 15 October 2024
PUBLISHED 30 October 2024

CITATION
Bakoglu N, Cesmecioglu E, Sakamoto H, Yoshida M, Ohnishi T, Lee S-Y, Smith L and Yagi Y (2024) Artificial intelligence-based automated determination in breast and colon cancer and distinction between atypical and typical mitosis using a cloud-based platform. *Pathol. Oncol. Res.* 30:1611815. doi: 10.3389/pore.2024.1611815

COPYRIGHT
© 2024 Bakoglu, Cesmecioglu, Sakamoto, Yoshida, Ohnishi, Lee, Smith and Yagi. This is an open-access article distributed under the terms of the Creative Commons Attribution License (CC BY). The use, distribution or reproduction in other forums is permitted, provided the original author(s) and the copyright owner(s) are credited and that the original publication in this journal is cited, in accordance with accepted academic practice. No use, distribution or reproduction is permitted which does not comply with these terms.

Artificial intelligence-based automated determination in breast and colon cancer and distinction between atypical and typical mitosis using a cloud-based platform

Nilay Bakoglu[1†], Emine Cesmecioglu[2†], Hirotsugu Sakamoto[3], Masao Yoshida[4], Takashi Ohnishi[1], Seung-Yi Lee[5], Lindsey Smith[6] and Yukako Yagi[1*]

[1]Department of Pathology, Laboratory Medicine, Memorial Sloan Kettering Cancer Center, New York, NY, United States, [2]Department of Pathology, Marmara University Research and Education Hospital, Istanbul, Türkiye, [3]Department of Medicine, Division of Gastroenterology, Jichi Medical University, Tochigi, Japan, [4]Division of Endoscopy, Shizuoka Cancer Center, Shizuoka, Japan, [5]Aiforia Technologies, Cambridge, MA, United States, [6]Flywheel.io, Minneapolis, MN, United States

Artificial intelligence (AI) technology in pathology has been utilized in many areas and requires supervised machine learning. Notably, the annotations that define the ground truth for the identification of different confusing process pathologies, vary from study to study. In this study, we present our findings in the detection of invasive breast cancer for the IHC/ISH assessment system, along with the automated analysis of each tissue layer, cancer type, etc. in colorectal specimens. Additionally, models for the detection of atypical and typical mitosis in several organs were developed using existing whole-slide image (WSI) sets from other AI projects. All H&E slides were scanned by different scanners with a resolution of 0.12–0.50 µm/pixel, and then uploaded to a cloud-based AI platform. Convolutional neural networks (CNN) training sets consisted of invasive carcinoma, atypical and typical mitosis, and colonic tissue elements (mucosa-epithelium, lamina propria, muscularis mucosa, submucosa, muscularis propria, subserosa, vessels, and lymph nodes). In total, 59 WSIs from 59 breast cases, 217 WSIs from 54 colon cases, and 28 WSIs from 23 different types of tumor cases with relatively higher amounts of mitosis were annotated for the training. The harmonic average of precision and sensitivity was scored as F1 by AI. The final AI models of the Breast Project showed an F1 score of 94.49% for Invasive carcinoma. The mitosis project showed F1 scores of 80.18%, 97.40%, and 97.68% for mitosis, atypical, and typical mitosis layers, respectively. Overall F1 scores for the current results of the colon project were 90.02% for invasive carcinoma, 94.81% for the submucosa layer, and 98.02% for vessels and lymph nodes. After the training and optimization of the AI models and validation of each model, external validators evaluated the results of the AI models via blind-reader tasks. The AI models developed in this study were able to identify tumor foci, distinguish *in situ* areas, define colonic layers, detect vessels and lymph nodes, and catch the difference between atypical and

typical mitosis. All results were exported for integration into our in-house applications for breast cancer and AI model development for both whole-block and whole-slide image-based 3D imaging assessment.

KEYWORDS

mitosis, colon adenecarcinoma, breast, artificial intelligence, invasive carcinoma

Introduction

In recent years, machine learning-based image analysis methodologies have been actively developed in the field of digital pathology to aid the quantification of diagnostic parameters in histology and tumor morphology [1]. Specifically, deep learning is a machine learning methodology that has an accelerated ability to assist in pathological diagnosis [2]. It can provide objective and common metrics for uncertain diagnoses, and more importantly, it has the potential to add new information that could not have been quantified previously by pathologists. Recent studies support that the majority of histopathological malignancies can be diagnosed with high accuracy with deep learning methods [3].

Artificial intelligence (AI) in pathology has important implications not only for diagnostics, but also for cancer research, clinical trials and AI-enabled therapeutic targeting [4]. The involvement of AI in a number of diagnostic tasks using WSIs has expanded rapidly in the last year [5–7]. Achieving the identification of cancer is remarkable. In a study conducted by Bejnordi and colleagues in 2017, out of 32 AI models developed for breast cancer detection in lymph nodes, the best model achieved a human-like area under the curve (AUC) of 0.994 (95% CI 0.983–0.999) [8]. In 2020, Thakur et al reviewed 30 studies related to colorectal cancer, some of which showed high diagnostic accuracy, but the overall study size was limited [9].

AI and other neural networks have made great progress in capturing the detection of morphological diagnoses by pathologists with digital platforms [10]. Diagnostic protocols focus equally on efficiency and accuracy [11]. Recently, code-free and user-friendly solutions have become commercially available to assist in the design, training, validation, and deployment of AI models for pathologists without prior knowledge of machine learning and image processing. Our research group has utilized these code-free solutions to develop in-house AI models using Aiforia's cloud-based platform. We also investigated their availability, convenience, performance, and expansivity in general digital pathology applications. We chose Aiforia because it is easy to use, accessible, fast, and integrated for our research studies. In this paper, we report three AI models that aided the analysis of prognostic parameters detection of Breast and Colon cancer specimens, and mitosis detection in several organs.

Breast cancer is the most common cancer in women [12]. One of the factors determining the treatment of breast carcinomas is the results of molecular tests performed in invasive carcinoma areas [13]. The assessment of HER2 gene amplification, a key molecular test, is made under a microscope using the *in situ* hybridization (ISH) method in invasive tumor areas [14]. Separating the invasive tumor area from the non-invasive area in the breast tissue is important because it determines the diagnosis and grade of the tumor, and most importantly, it determines the targeted therapy based on the HER-2 status in the tumor cells [15]. Digital pathology provides a cutting-edge solution where algorithms can recognize and select invasive tumor areas. Even more powerful is the ability to combine the above pan-tumor detection with immunohistochemistry (IHC) and ISH studies, considering the studies on semi-automated HER2 gene amplification diagnosis made in invasive tumor areas [16].

Colorectal carcinoma is the third most common cancer and the second most deadly cancer in the world [12]. Endoscopic submucosal dissection (ESD) is a method that makes an early diagnosis and treatment of colorectal and gastric neoplasms [17]. ESD maintains its superiority for lesions with superficial submucosal invasion [18]. The depth of the invasion less than 1,000 μm below the muscularis mucosa is suggested as a cure by The Japan Gastroenterological Endoscopy Society [19]. The factors that determine the pathological stage classification of colorectal cancer are tumor extension in the colonic layers, lymph node metastasis and tumor deposits, distant metastasis, tumor budding, lymph vascular invasion, and perineural invasion, in addition to histological type and grade. With the help of AI model-assisted analysis, we aimed to identify prognostic quantitative parameters on colon resection specimens and integrate the algorithm into our 3D tools (Micro-CT) to improve the quality of virtual H&E.

Mitotic count in histological preparations is associated with tumor growth and grading, has prognostic importance [20], and remains a fundamental part of pathology reports from diagnosis to treatment in all cancers [21]. Currently, the number of mitotic cells is determined by manual counting under the microscope, which is encumbered by inter- and intra-observer variability [22]. This variability causes not only the rate of variability among the mitotic counts by pathologists to differ but also contributes to methodological diversity [23, 24]. Atypical mitotic figures are frequently seen in proliferative and aggressive tumors and, in practice, play an important role in the distinction between benign and malignant tumors [25]. To avoid subjective and laborious counting of mitoses, and to predict prognosis, we developed an

TABLE 1 Dataset of each project.

Projects	Cases	Diagnosis	Scanner	Total WSI	Trained WSI	Tested WSI	Validated WSI
Mitosis	23	Multiple tumors[a]	P1000	40	28	8	4 (20)[b]
Breast-Invasive	141	Invasive carcinoma	P250 P1000 GT450	141	59	73	9 (19)
Breast Benign	10	Benign breast tissue	GT450	10	—	10	—
Colon-ESD	41	LGD, HGD, Adenocarcinoma	S60	65	53	12	5 (30)
Colon-Resection	13	Mucinous adenocarcinoma	P1000 S60	102	200[c]	55	15 (19 × 10) (CRP-1) 16 (20 × 2) (CRP-2)

WSI, whole slide image; ESD, endoscopic submucosal dissection; LGD, Low-Grade Dysplasia; HGD, High-Grade Dysplasia; CRP, Colorectal project.
[a]Four splenic Neuroendocrine Tumors (NETs), four pancreatic NETs, five soft tissue-bone tumors, and ten breast tumors.
[b]The number in the parentheses represents the number of ROIs validated in the WSIs (20 ROIs in 4 images were validated and scored by external validators in the mitosis project).
[c]Colon Resection specimens were prepared as Whole Mount Slides, scanned by S60 and p1000 scanners, and trained, tested, and validated as WMIs. Some of the same slides were trained for different layers in the project.

AI model to detect mitoses and to distinguish between atypical and typical mitoses.

In this study, we describe how we have been developing AI models using Aiforia's cloud-based AI solutions for breast and colorectal cancer diagnosis, mitosis detection, and in-house AI application development for our integration of AI-based applications and 3D imaging systems.

Materials and methods

Dataset

The studies involving human participants were reviewed and approved by the Institutional Review Board at Memorial Sloan Kettering 18-013. The patients provided written informed consent to participate in this study. Cases were diagnosed and reported by pathologists at the Department of Pathology at Memorial Sloan Kettering Cancer Center. In total, 65 digital slides of 41 ESD specimens diagnosed as low-grade dysplasia (LGD), high-grade dysplasia (HGD), and adenocarcinoma, 102 digital slides of 13 colon resection specimens diagnosed as Mucinous adenocarcinoma for the Colon Project, 141 digital slides of 141 breast specimens diagnosed as Breast Invasive carcinoma, 10 digital slides of 10 breast specimens diagnosed as Benign breast parenchyma for the Breast Project, 40 digital slides of 23 multi-organ tumor specimens (four spleen Neuroendocrine tumors (NETs), four pancreatic NETs, five soft tissue-bone tumors, and ten breast tumors) for the Mitosis Project were used in our study cohort. In total 358 digital slides were trained (348 digital slides were used- some of the same slides were trained in different projects), 158 digital slides were tested, and 49 digital slides were validated across all projects. The same slides were used for training in different projects in the colon resection project (Supplementary Table S1) and some of the slides tested in the colon ESD and Colon resection Projects were also used for validation (Table 1).

Sample digitization

All the slides were prepared from archival formalin-fixed paraffin-embedded (FFPE) tissue blocks sectioned at 4 μm and stained with Hematoxylin and Eosin (H&E). All H&E slides for all three projects were digitized by four different scanners by depending on availability. The first scanner was a Panoramic P250 (3DHistech Ltd., Budapest, Hungary), which was used with a ×20 objective (NA 0.8) and a pixel resolution of 0.17 μm. The second scanner was a Panoramic P1000 (3DHistech Ltd., Budapest, Hungary), which was used with a ×40 objective (NA 0.95) and a pixel resolution of 0.13 μm. The third scanner was the Aperio GT 450 (Leica Biosystems, Illinois, United States), which was used at ×40 equivalent magnification with a pixel resolution of 0.26 μm. The fourth scanner was a NanoZoomer S60 (Hamamatsu Photonics K.K., Shizuoka, Japan) used at ×40 equivalent magnification with a pixel resolution of 0.23 μm. Especially, in the case of colorectal samples, whole mount slides, whose size is twice the size of regular slides, were used and scanned by NanoZoomer S60 and Panoramic P1000.

Development of the AI model

For AI model development, Aiforia's cloud-based platform (Aiforia Technologies, Cambridge, MA, United States) was used. The AI-model training dataset representing the entire dataset was carefully selected. These whole slide images were uploaded to Aiforia's cloud platform in their native file formats (mrxs, svs, or ndpi) and automatically converted into platform-compatible file types. Using the training dataset, AI projects were created, and

TABLE 2 Breast project verification and validation results.

	Precision (%)	Sensitivity (%)	F1 score (%)	Area error (%)
Tissue	99.60	99.34	99.47	0.26
Invasive	92.26	96.84	94.49	1.12
Non-invasive	99.65	98.73	99.19	1.45

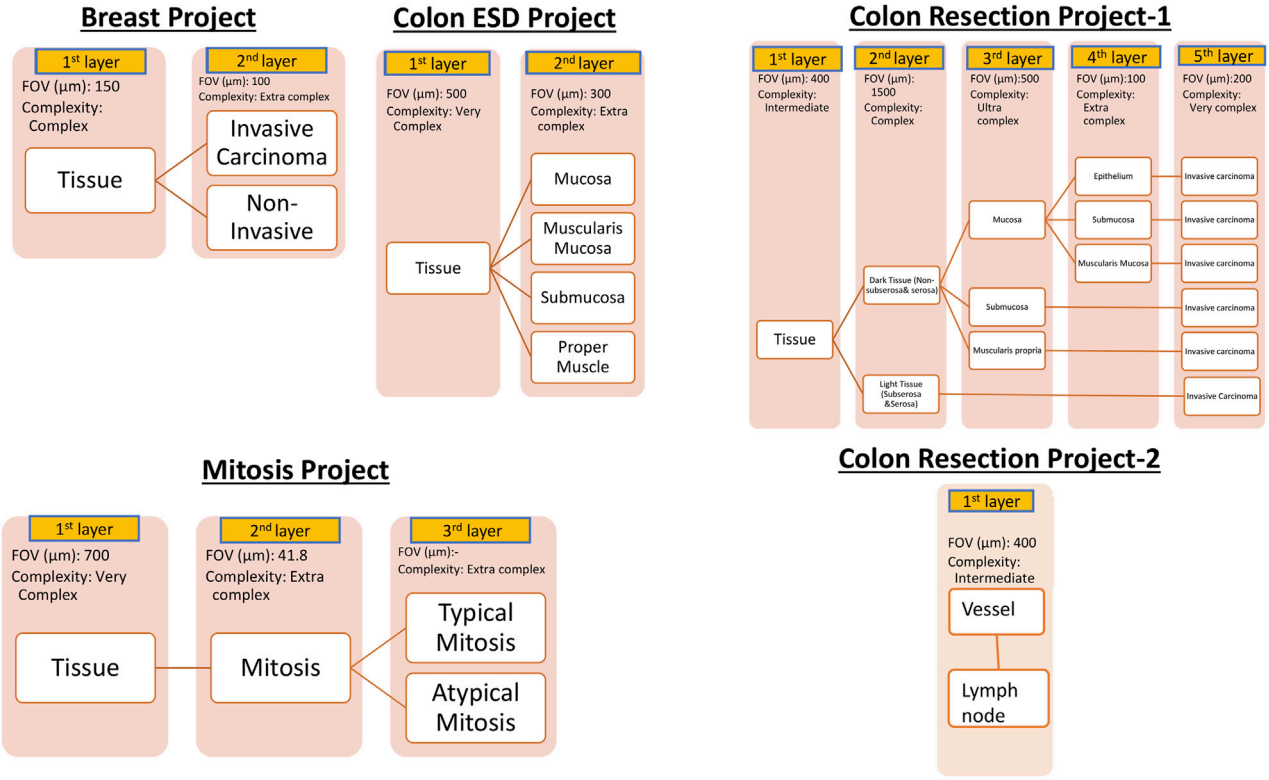

FIGURE 1
Hierarchical layered structure of AI models. Yellow colors represent each child layer. White colors correspond to the analytical results shown in the results session. User-adjustable parameters on the Aiforia platform are listed below the layer boxes. Augmentation was utilized to further improve the AI model as needed.

the AI models were custom-designed and presented as a graphic layer tree. Each layer consists of an individual convolutional neural network (CNN) that performs a task (segmentation or object detection) with adjustable parameters, such as field of view, and resolution of the input patch image. The structure of the AI models is shown in Figure 1. The Breast Carcinoma AI model was built with three classes: Tissue, Invasive tumor, and non-invasive tumor. The invasive tumor area included IHC/ISH target cells, and the Non-invasive tumor area consisted of tumor stroma, necrosis, non-neoplastic breast, and non-invasive lesions. For the Colon ESD project, mucosa, muscularis mucosa, submucosa, and proper muscle annotations were added under tissue layer as a child layers. The Colon Resection Project consisted of five separate projects: 1. Invasive tumor, 2. Tissue, and Tissue sublayers-1 3. Tissue sublayers 2 “Dark Tissue and Light Tissue” [Light Tissue represents the Subserosa layer of the colon, and Dark tissue represents all the other layers of the colon (mucosa, submucosa, and muscularis propria). Dark and Light Tissues were created to make a reliable distinction between subserosa and serosa and other layers to avoid false positives of subserosa in the submucosa layer because of the similarity of histomorphology], 4. Mucosal Subregions (Mucosa, Submucosa, Muscularis mucosa), 5. Vessels, and Lymph nodes. Supplementary Table S1 shows the trained WSI dataset for each Colon Resection Project. The same whole mount slide images were taught separately for all five

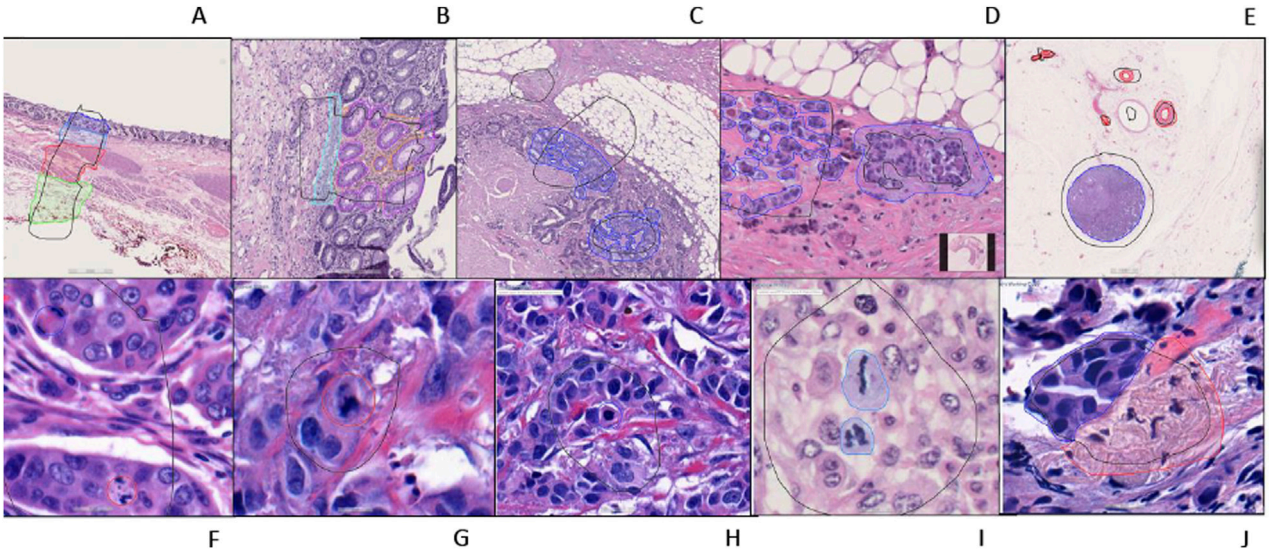

FIGURE 2
An example of training regions and training annotations **(A–I)**. First row from left to right: **(A–E)**, second row from left to right: **(F–J)**. **(A):** Location type annotation of colonic layers, **(B)**: Colon mucosa layers annotations, **(C, D)**: Colon invasive carcinoma annotations **(E)**: Whole shape lymph node and vessel annotations **(F–H)**: Atypical and typical mitosis annotations (Red: atypical; Blue typical) **(I)**: Mitosis annotation **(J)**: Breast invasive carcinoma annotation [**(A–E, J)** are semantic segmentation annotations, **(F–H)** are object annotations].

separate projects. Ultimately, we made two projects. Only the Vessels and Lymph node Project was separated from the others. The algorithm consisted of three layers and four classes: 1-Tissue, 2-Mitosis, 3a-Atypical Mitosis, and 3b-Typical Mitosis for the Mitosis Project. Object detection was used for the mitosis, atypical mitosis, and typical mitosis layers. The mitosis layer was built to exclude mitosis mimics like apoptosis, necrotic tumor cells, stromal cells, etc. Annotations were made by a pathologist for each classifier in all three projects (Figure 2). Supplementary Table S2 shows the number of total semantic segmentation areas and objects that were annotated for each project and each layer.

Image analysis by an AI model was hierarchically conducted from the top layer to the final layer. In the case of our mitosis project, the first layer was designed as a binary semantic segmentation model that detects tissue regions. The second layer was an object detection model that counted mitosis within the tissue regions identified by the first layer. Finally, the detected mitotic cells were classified into typical and atypical by the third layer.

The accuracy of the trained AI model was calculated based on verification statistics, which were derived from the comparison of the AI-model predictions to the original input training annotations for each feature (false positive, false negative, total error, precision, sensitivity, and F1-Score). The F1 score is a statistical measure utilized to quantify the degree of overlap between two data sets [26] and represents the harmonic average of precision and sensitivity. If the area error was higher than 5%, and the confidence was less than 80%, the tested results were evaluated, then annotations were added or modified by a pathologist, and the AI model was retrained. These test-to-retrain processes were repeated until all layers reached satisfactory accuracy.

Training, testing, and validation

In view of our future projects, all annotations were made by a pathologist, after AI models were created according to the corresponding pathological histological structures. The size and number of annotations were decided by the application specialist and pathologist together in each training round and proceeded accordingly. The cloud-based platform provided results in the "Verification and Validation" tool in comparison to the human-generated annotations, after the analysis. The results included false positives (regions that were annotated, and were found in the verification); percentage of the total area of all training regions-detection of non-invasive areas as invasive tumors in breast and colon tumors, false negatives (regions that were annotated and were not found in the verification), percentage of the total area of all training regions-undetected invasive areas, precision (space-dependent overlap of analysis results with human annotations), sensitivity (space-independent overlap of analysis results with annotations), and F measure (the harmonic mean of precision and sensitivity).

TABLE 3 Colon ESD project tissue sublayers verification and validation results.

	Precision (%)	Sensitivity (%)	F1 score (%)	Area error (%)
Mucosa	96.80	97.47	97.13	1.40
Muscularis mucosa	84.65	84.63	84.64	0.56
Submucosa	98.06	92.98	95.46	1.41
Proper muscle	97.04	99.11	98.06	0.09

TABLE 4 Mitosis project verification and validation results.

	Precision (%)	Sensitivity (%)	F1 score (%)	Area error (%)
Tissue	99.59	99.79	99.69	0.16
Total mitosis	67.85	97.97	80.18	0.17
Typical mitosis	97.74	97.07	97.40	
Atypical mitosis	98.18	97.19	97.68	

When the AI models achieved satisfactory accuracy, we released the latest models and tested them on untrained images. If the results were not sufficiently accurate, we did not release the model and kept training. Our criteria for success was to reach at least 90% of the F1 score. Once we reached satisfactory accuracy according to ground-truth pathologists the area error was less than 5% and the confidence was more than 80% for the AI models, with the validators agreeing on at least "very good" accuracy; therefore, we stopped training. All results were exported to be used as annotations for our applications.

Validators were invited to evaluate the results and rate the accuracy of the AI model for each project. Three pathologists were used for the evaluation of specific ROIs for each breast, mitosis, and colon project (Merve Basar, Irem Isgor, and Hulya Sahin Ozturk). They scored each feature blindly and independently of each other and the AI model. The validators evaluated the analysis results as a percentage with the classification, which we divided into four categories. The features of the segmentation area were rated for accuracy using the following scale: 1. Perfect or nearly perfect accuracy (95%–100%, no significant errors) 2. Very good accuracy (80%–95%, only minor errors) 3. Good accuracy (70%–80%, significant errors but still capturing the feature well) 4. Insufficient accuracy (less than 70%, significant errors compromising feature recognition).

Results

Breast project

After four runs, our final training results for the breast project were 0.10% false positive, and 0.16% false negative for the tissue layer, 0.56% false positive, and 0.73% false negative for invasive and non-invasive layers. Table 2 shows the results for each layer of the Breast Project, and Figure 3 shows the image analysis results for invasive carcinoma.

External validator results of breast project

In total, 9 untrained images including 19 ROIs were sent to three pathologists. The external validator results showed that rating scores for invasive carcinoma (2) were in the range of "very good," for tissue (1.1) and for non-invasive (1.9) were in the range of "very good" to "perfect or nearly perfect" (Figure 4). However, the median values were Score 1 (Perfect or nearly perfect accuracy) for Tissue and Invasive tumors and Score 2 (Very good accuracy) for Non-invasive layers.

Colon ESD project

The final AI model results were 0.18% total area error, 0.12% false positivity, 0.06% false negativity, 99.36% precision, 99.71% sensitivity, and 99.54% F1 score for tissue class, 3.47% total area error, 0.36% false positivity, 0.51% false negativity, 96.74% precision, 95.42% sensitivity, 96.08%, F1 score, and 0.87% area error for tissue subregions. By looking a Table 3 we can see the other results for each layer.

External validator results of the colon ESD project

This AI model was validated by three reviewers. Specifically, the reviewers were asked to draw annotations on the 30 validation regions. Their annotations were

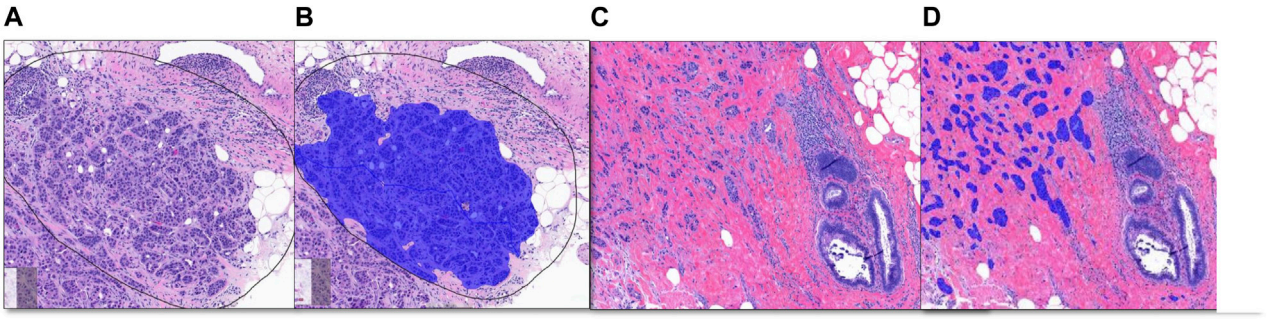

FIGURE 3
Breast Project results [From left to right **(A–D)**]. **(A, C)** are untrained images. **(A)** includes selected ROI (black line) for validation. **(B, D)** are image analysis results. **(B)**: Invasive tumor detection (blue) in selected ROI, **(D)**: The non-invasive region consisting of benign mammary glands and the invasive tumor detection (blue) are shown together.

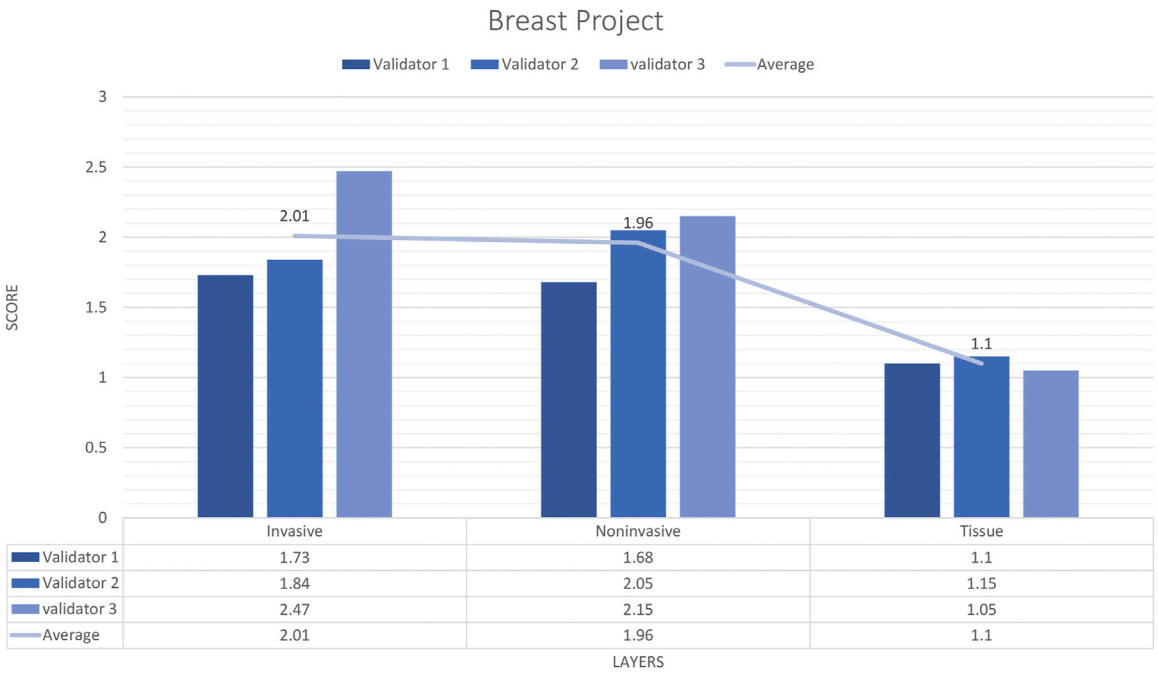

FIGURE 4
Breast carcinoma project external validator results. The evaluation of tissue, non-invasive, and invasive carcinoma detection in breast carcinoma cases by three pathologists. Segmentation area features were rated for accuracy using the following scale: 1. Perfect or nearly perfect accuracy (95%–100%, no significant errors) 2. Very good accuracy (80%–95%, only minor errors) 3. Good accuracy (70%–80%, significant errors but still captures the feature well) 4. Insufficient accuracy (less than 70%, significant errors compromising feature recognition). The average value for tissue and invasive carcinoma detection is in the range of 1 (Perfect or nearly perfect accuracy), and non-invasive layer detection is in the range of 2 (very good accuracy).

compared using intersection-over-union analysis against the AI model, on a pixel-by-pixel basis. Once the AI model performance reached 80% confidence, it was used to analyze the remaining 27 WSIs from the dataset. The final AI model showed a false positive rate of 0.18%, a false negative rate of 0.29%, a precision of 97.41%, a sensitivity of 95.89%, and an F1 score of 96.65%, respectively. External validation showed a false positive rate of 0.15%, a false negative rate of 0.058%, a precision of 92.01%, a sensitivity of 95.91%, and an F1 score of 97.57%, respectively. The image analysis generated by the final AI model showed correct discrimination of each layer with high confidence (Figure 5).



FIGURE 5
Tissue and subregion recognition feature of the ESD specimens by AI model **(A–C)**. **(A)**: An original H&E stain (×20 magnification) showing low-grade dysplasia in a colon ESD specimen; **(B)** and automated tissue (yellow) and **(C)** and automated colonic layer segmentation (mucosa: blue, muscularis mucosa: red, submucosa: green) original magnification [**(B, C)**, ×20].

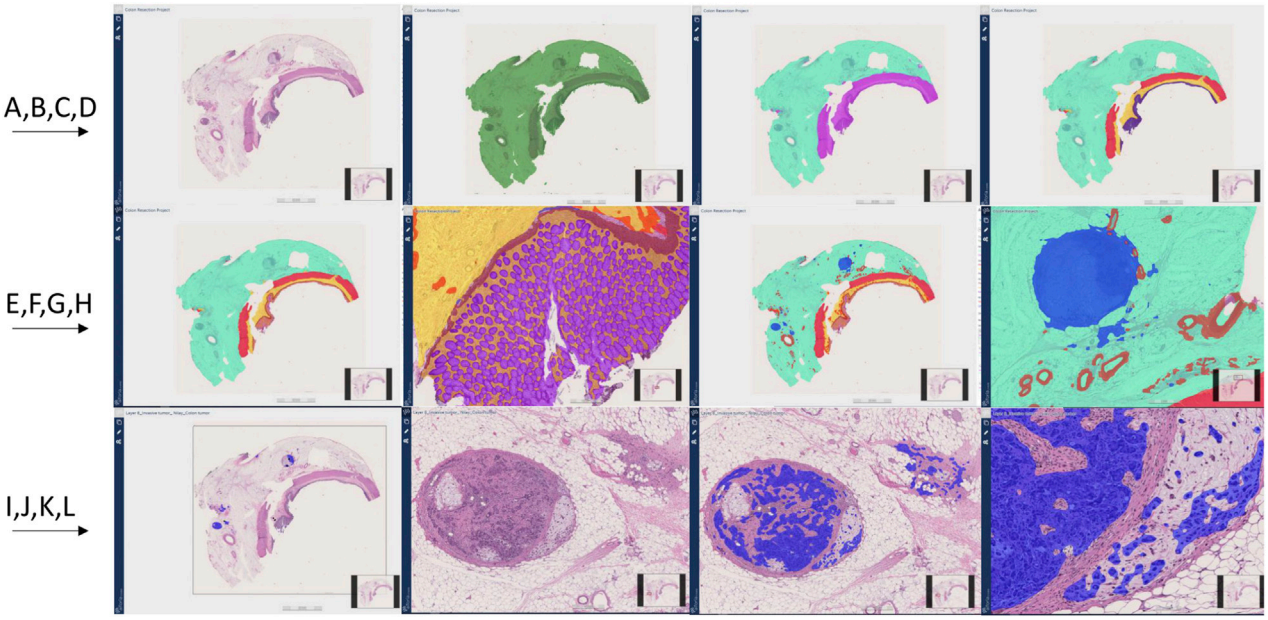

FIGURE 6
Colon resection project steps and image Analysis results **(A–J)**. First row from left to right **(A–D)**, Second row from left to right **(E–H)**, Third row from left to right **(I–L)**. **(A)**: Original whole slide image H&E stain (×20 magnification), **(B)**: Tissue detection (Green) **(C)**: Light and dark tissue detection [Light tissue (Subserosa and serosa): Light green, Dark tissue (muscular propria, submucosa, and mucosa): Purple] **(D)**: Subserosa and serosa (green), muscularis propria (red), submucosa (yellow), mucosa (purple) detection **(E, F)**: Mucosa subregions detection: Epithelium (Purple), Lamina propria (Yellow), muscularis mucosa (Brown) **(G, H)**: Vessel and lymph node detection (Red: Vessels, Blue: Lymph nodes) **(I)**: Invasive tumor detection (Blue) **(J)**: Metastatic lymph node and tumor focus in subserosa H&E, **(K, L)**: Invasive tumor detection (Blue) in metastatic lymph node and serosal fat tissue.

Colon resection projects

All layers showed over 90% F1-scores. Supplementary Table S3 shows the performance of the final AI model results for each layer and their child layers compared to the original annotations for the colon resection project. Figure 6 shows all detected layers by the AI models.

External validator results of the colon resection project_1

In total, 15 images and 19 ROIs were evaluated for Colon Resection Project_1 by three experienced pathologists. The results showed that the rating scores for tissue (1.12), dark tissue (1.47), light tissue (1.56), mucosa (1.91), muscularis

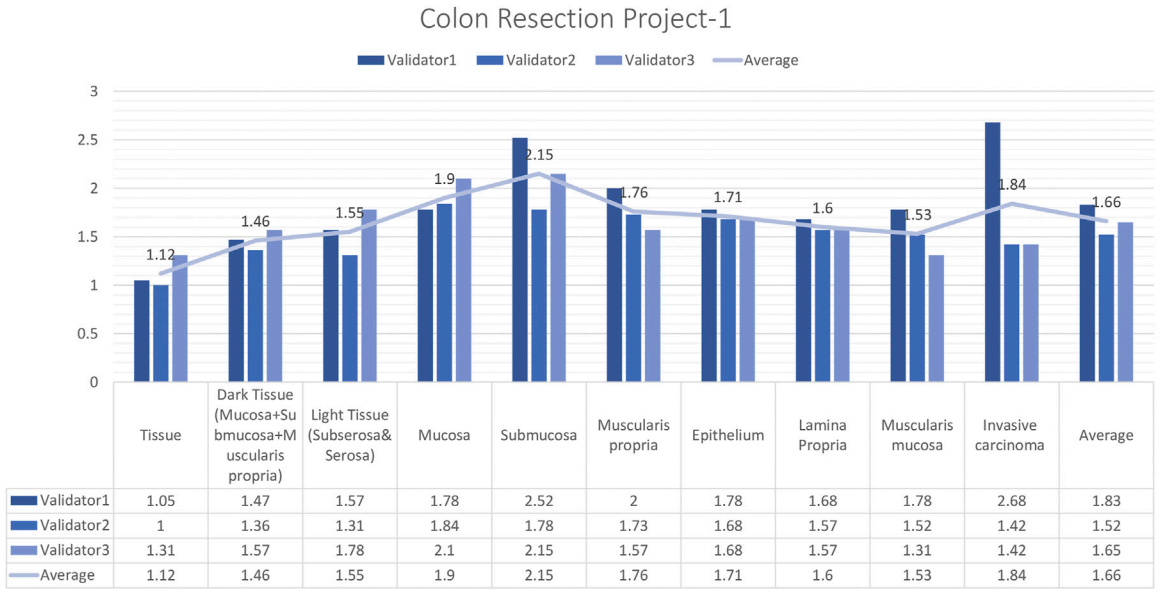

	Tissue	Dark Tissue (Mucosa+Submucosa+Muscularis propria)	Light Tissue (Subserosa& Serosa)	Mucosa	Submucosa	Muscularis propria	Epithelium	Lamina Propria	Muscularis mucosa	Invasive carcinoma	Average
Validator1	1.05	1.47	1.57	1.78	2.52	2	1.78	1.68	1.78	2.68	1.83
Validator2	1	1.36	1.31	1.84	1.78	1.73	1.68	1.57	1.52	1.42	1.52
Validator3	1.31	1.57	1.78	2.1	2.15	1.57	1.68	1.57	1.31	1.42	1.65
Average	1.12	1.46	1.55	1.9	2.15	1.76	1.71	1.6	1.53	1.84	1.66

FIGURE 7
Colon Resection Project-1 External Validators Results. Scoring of all layers by three pathologists. Segmentation area features were rated for accuracy using the following scale: 1. Perfect or nearly perfect accuracy (95%–100%, no significant errors) 2. Very good accuracy (80%–95%, only minor errors) 3. Good accuracy (70%–80%, significant errors but still captures the feature well) 4. Insufficient accuracy (less than 70%, significant errors compromising feature recognition). The median value of vessel and lymph node detection is in the range of 1(Perfect or nearly perfect accuracy).

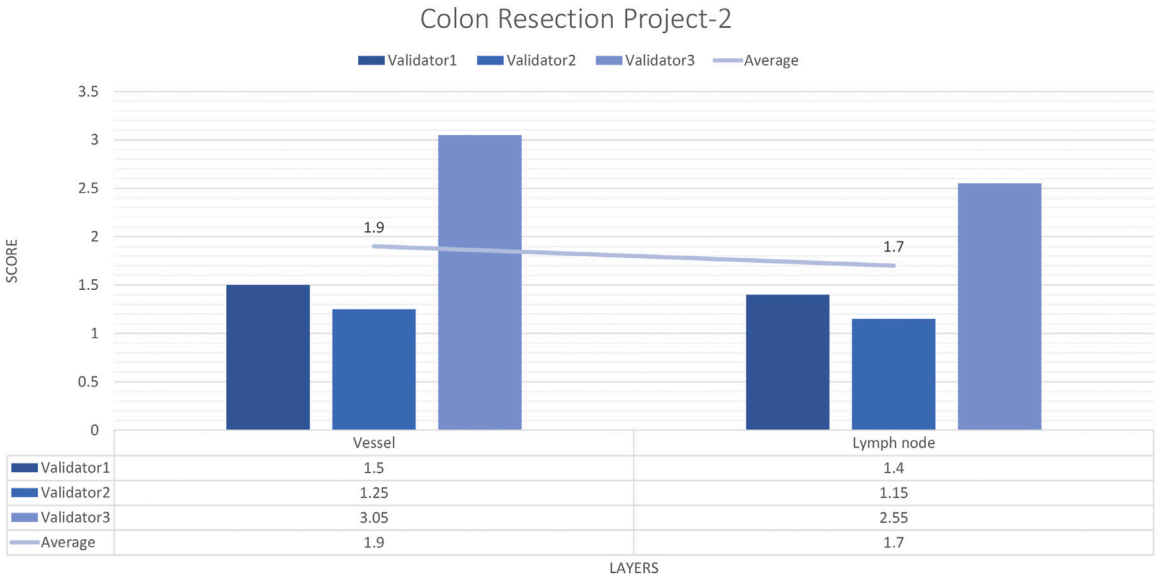

	Vessel	Lymph node
Validator1	1.5	1.4
Validator2	1.25	1.15
Validator3	3.05	2.55
Average	1.9	1.7

FIGURE 8
Colon Resection Project-2 external validators results. Evaluation of vessel and lymph node detection by three pathologists. Segmentation area features were rated for accuracy using the following scale: 1. Perfect or nearly perfect accuracy (95%–100%, no significant errors) 2. Very good accuracy (80%–95%, only minor errors) 3. Good accuracy (70%–80%, significant errors but still captures the feature well) 4. Insufficient accuracy (less than 70%, significant errors compromising feature recognition). The median value of vessel and lymph node detection is in the range of 1 (Perfect or nearly perfect accuracy).

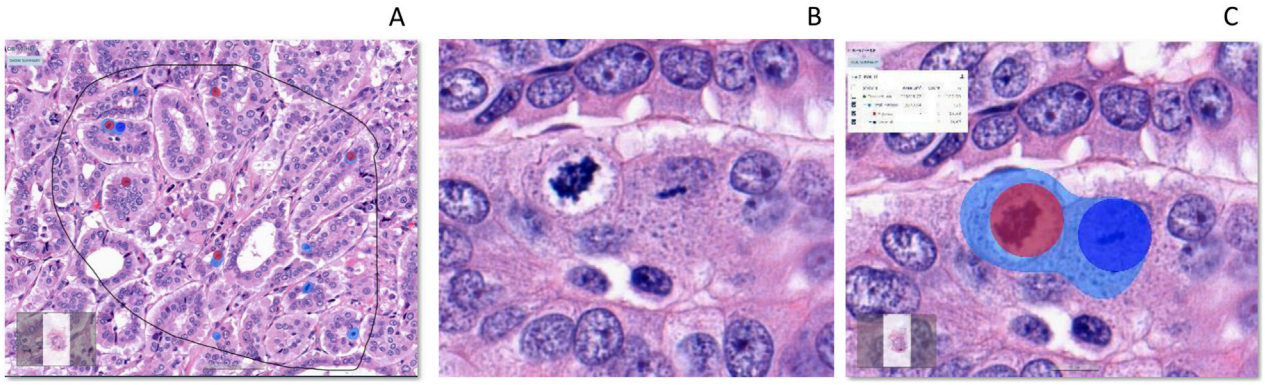

FIGURE 9
Detection of total mitosis, atypical and typical mitosis [From left to right **(A–C)**]. **(A)**: H&E, Invasive carcinoma breast, Selected ROI, **(B)**: Atypical and typical mitosis **(C)**: Detection of mitosis (Light Blue), Atypical mitosis (Red Circle) and Typical mitosis (Dark Blue Circle). IA, Image analysis; H&E, hematoxylin, and eosin.

propria (1.77), the epithelium (1.71), lamina propria (1.61), muscularis mucosa (1.54), and invasive carcinoma (1.84), were in the "perfect or nearly perfect" range and submucosa (2.15) was in the "very good" range (Figure 7). The most frequently assigned score in terms of average and median value was Score 1 (Perfect or nearly perfect) for all layers.

External validator results of the colon resection project_2

For each vessel and lymph node project, 16 images and 20 ROIs were evaluated by three experienced pathologists. The external validator results showed that the rating scores for vessels (1.9) and lymph nodes (1.4) were in the "perfect or nearly perfect" range. The most frequently assigned score in terms of average and median value was Score 1 (Perfect or nearly perfect accuracy) (Figure 8).

Mitosis project

Atypical and typical mitosis layers showed over 97% F1-scores. Table 4 shows the results of the mitosis project tree for each layer and class. The algorithm captured both typical and atypical mitotic figures (Figure 9).

External validator results of the mitosis project

Three pathologists evaluated 20 carefully selected ROIs in 4 WSIs. The external validator results showed that the rating scores for tissue (1) were in the "perfect or nearly perfect" range, but mitosis (2.83), atypical mitosis (2.45), and typical mitosis (2.5) were rated between "good and very good" accuracy. The highest score given by the three pathologists on average was 2 (Very good accuracy) for the Mitosis layer, Atypical Mitosis, and Typical Mitosis, and 1 (Perfect accuracy) for the Tissue layer. Therefore, the evaluation of all external validators as "total mitosis, atypical, and typical mitosis detection by AI" was classified in the "Very good" range. The validators agreed that AI could detect mitosis with at least 80%–95% accuracy (Figure 10).

Discussion

AI models were built by pathologists with the help of application specialists, depending on the significant findings of histomorphology for each tissue. Models were trained and tested individually until the application reached reliability according to its own standards determined by pathologists, and then models include selected specific ROIs shared with validators (external pathologists) for validation. Finally, external pathologists who evaluated the models rated each model as having at least very good accuracy (80%–95%, only minor errors). Our findings showed that we were able to extract clinically relevant information from H&E slides with neural networks in line with the literature [2, 27]. AI algorithms exist in the literature that show that all tiles in each heatmap were assigned as hotspots for cancer detection [28] or any other histologic parameters [29]. Instead of using hot spots to recognize objects or segments, the algorithm we employed in our study displays the entire picture of histomorphology with extremely clear boundaries. It also examined each learned layer by separating it from other areas that the pathologists are not interested in. To use an example, children's painting styles in coloring books vary according to their age. As they age, the frequency of coloring outside the lines in a coloring book rises. Through advanced analyses, our algorithm makes it possible to add molecular studies into

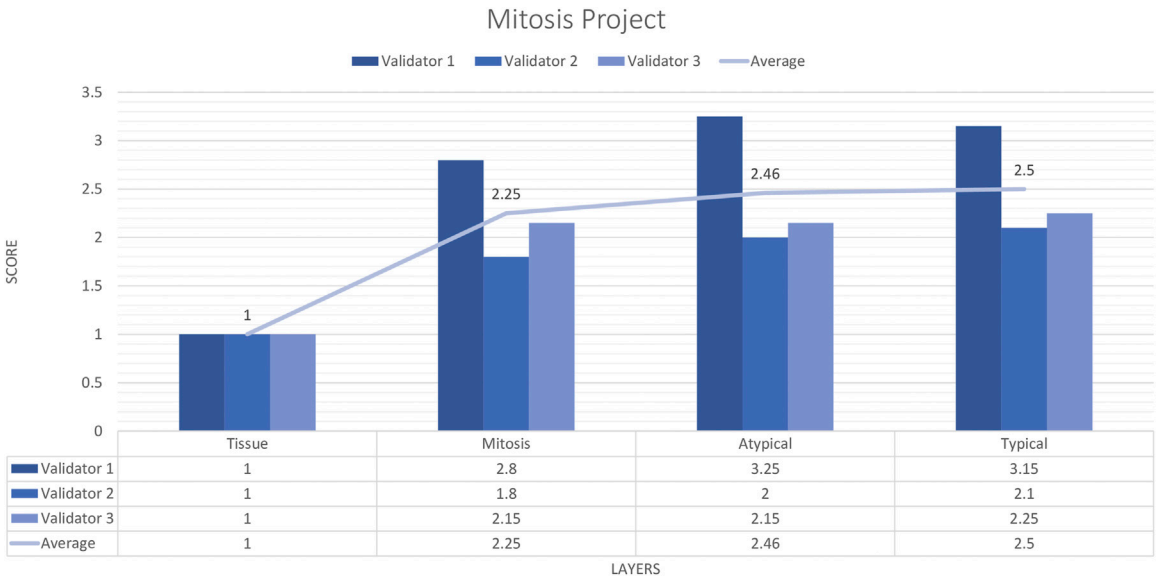

FIGURE 10
Mitosis project external validators results. Evaluation of tissue, mitosis, atypical and typical mitosis detection by three pathologists. Segmentation area features were rated for accuracy using the following scale: 1. Perfect or nearly perfect accuracy (95%–100%, no significant errors) 2. Very good accuracy (80%–95%, only minor errors) 3. Good accuracy (70%–80%, significant errors but still captures the feature well) 4. Insufficient accuracy (less than 70%, significant errors compromising feature recognition). The average value for tissue is in the range of 1 (Perfect or nearly perfect accuracy), and the detection of mitosis, atypical mitosis, and typical mitosis is in the range of 2 (very good accuracy).

these more accurate sharp boundaries in future projects, such as our breast project, in accordance with its morphology analyses.

In the Breast project, 59 images were trained with 18,777 iterations, the CNN complexity was set to extra complex, and the field of view was 100 μm. False positive areas consisted of desmoplastic tumor stroma, proliferative endothelial cells, and some empty spaces in tumor clusters. The location of false positive areas in the algorithm was the *in situ* area. In total, 54 untrained images and 10 benign breast tissues were tested by the final model of AI. In the benign 10 breast tissue images the false positive detection of invasive carcinoma ranged from 0.02% to 1.48%. Some groups of cells with hyperchromatic nuclei and areas of adenosis were detected as invasive carcinoma at an average rate of 1%. Considering that there are areas of cancer that can be detected by AI that may be overlooked by pathologists in some studies [30], it appears that this rate can be reduced to 0% in future studies. While two pathologists evaluated the diagnosis of invasive carcinoma by AI as nearly perfect (95%–100% accuracy) in all ROIs, the 3rd pathologist focused on Score 2 (80%–95% accuracy) in this evaluation. We checked and learned that the two validators who scored in a similar way were trained in the same medical school, whereas the third pathologist was educated in a different medical school. This is a good example of the need for artificial intelligence, which can provide an objective solution to the subjective perspective gained through education while making the diagnosis. Ultimately, three pathologists agreed that AI can detect breast-invasive tumors with at least 80%–95% accuracy.

Three different scanners were used for breast carcinoma, but we could not get satisfactory results due to low-quality images. We used image augmentation tools, but it was not enough. These images needed more annotations to detect invasive carcinoma areas compared to images from other scanners. Our results show that scanner and image quality affect the detection by AI, but we know it is fixable if we teach the AI when the resolution changes. Cross-verification of different scanners and different resolutions is beyond the scope of this publication. We need the AI to function for all images of our scanner lineup, but the AI algorithm is not required to support all scanners except our own in this study, as we used available scanners in real-world situations and it was sufficient to create accurate models and verify the results. For the mitosis detection model, we did not use 20× magnification (0.5 um/pixel resolution). We trained the AI until it could understand all formats. We see the potential for future evaluation between scanners and resolutions with the goal of AI becoming more objective and supporting all digital platforms to make a more accurate diagnosis.

Although the muscularis mucosa is a sublayer of the mucosa, it was used as a separate layer from the mucosa in the ESD Project due to its importance in terms of depth of invasion. However, when the results of the tissue and mucosa layers were examined after 53 images were trained, only the F1 score of the muscularis

mucosa was less than 90% (84%). As for the colon resection project, the F1 scores of all colon project layers, including the muscularis mucosa, were above 90%. The differences were as follows: the ESD project was the only project where the evaluators made their own annotations (they were not pathologists), the colon resection project was created and trained by the pathologist for histologically correct positioning of the muscularis mucosa, and more importantly, the trained area was 36 times larger (Supplementary Table S2). A pathologist is vital to the success of the digital image analysis project, as the denotative analysis algorithm could not have been invented without their specialized expertise [31].

In the colon resection project tissue detection was as good as in the breast and ESD projects. The AI was able to detect any type of tissue layer, regardless of which organ it belonged to. In terms of accuracy, only the submucosal layer detection scoring was in the range between very good and good accuracy, while the other layers in the colon resection project were in the range of perfect accuracy. The vascular structures and loose connective tissue histology of the submucosa and subserosa are the same. Due to this similarity, we obtained false positive and false negative results in the separation of the two layers. To eliminate this overlap and confusion, we divided the colonic layers into two categories: light tissues as subserosa and dark tissues as other layers. Although we separated the subserosa from the submucosa, there were still negative areas and missing parts in the submucosal layer of the colon. However, it was satisfactory that we achieved high accuracy in the subserosa layer, which has an important place in prognosis and staging in the context of understanding tumor infiltration, detecting vascular invasion, and catching metastatic lymph nodes, and tumor deposits.

In total, 22 images were trained with 5,000 iterations, with CNN complexity set to extra complex and 50 μm field of view in the invasive carcinoma detection in the colon project. After 5 runs we reached the accurate analysis results. In the first model, false positive cells were located in normal mucosa. We changed the FOV (50 μm) and complexity (extra) by comparing the false positive areas between the AI models. With a lower FOV (200 μm) and complexity (very), fewer false positive cells were detected in normal mucosa. In the new model, false positives were found in the tumor stroma and lumen, and AI was able to separate the invasive tumor region from the non-invasive region.

The results of the lymph nodes and vessels project showed high accuracy in identifying vessels and lymph nodes. We used whole shape annotations to train for vessels and lymph nodes in the subserosa and serosa layers. The results showed that the detection was nearly perfect. The challenge for AI was that the muscularis propria layer also consisted of muscles like the vessel walls. In addition, we tried to do annotations with all the construction drawings for vessels. The handicap for lymph node identification was the difficulty in distinguishing epithelial cells in the mucosa. However, by using high iterations and adding background annotations, we fixed the majority of these problems in 4–5 training rounds, and the true positive rates became quite high.

Mitotic counting is a time-consuming process in pathology reporting, but it is just as important in nearly all carcinoma types to determine grade and prognosis. Even when counted again by the pathologist, there is a difference in mitotic rates, while it is an indisputable fact that this difference between pathologists is obvious [32]. We would like to implement clinical to count mitosis for pathologists to help to avoid time consuming processes. It is important to determine the best area for mitotic counting. A study showed that the use of High Power Fields (HPF) should be abandoned and replaced by standardized international (SI) units; the use of square millimeters (mm^2) provides a properly standardized unit for area measurement, and the calculation of mitosis per mm^2 becomes easier. The data obtained are not related to the microscope and magnification used [33]. The article cited referred to digital platforms that facilitate the development of mitotic counting algorithms that use the evaluation of the entire tumor, as in our algorithm, indicating that we can measure the mitotic index only in certain tumor types more accurately and find new ways to classify tumors. An AI application that will standardize the mitotic rate is very important for pathologists and other clinicians to determine treatment. In a recent study, a semi-automated image processing algorithm generated datasets directly from H&E and pHH3-stained tile images with a new U-Net-based mitosis detection model that learned mitotic features from annotated images proposed in a simple and highly efficient way according to classical methods without performing annotations [34]. The segmentation model was re-trained for the confusing cells called mitosis look-alikes (MLAs) to reduce false positives. In our study, the mitotic layer was the only layer with an F1 score below 90% in all projects. The mitotic layer was added later to the detection of atypical and typical mitotic objects to exclude artifacts. The aim was to reach an F1 score of 90% for atypical and typical mitosis. However, mitosis training was discontinued when accuracy in distinguishing atypical and typical mitosis increased. It should be recognized that it is not easy for AI to detect mitosis due to it being confused with dark hyperchromatic nuclei, lymphocytes, and other inflammatory cells, artifacts, pigments, and crushed cells [25]. However, the detection of atypical and typically distinctive mitosis offered an above-average detection rate in our study. One of our future plans is to define prognostic differences between atypical and typical mitotic counts and/or to determine whether there are any effects between these two classes in determining staging or grading in cancer types, specifically pancreatic cancer [35]. Another plan is to provide a measurement of mitotic count, rate, and index using mitosis detection by AI. Our shortcoming in this project, which serves as a step toward new research, was that we needed more data.

Additionally, as a part of future work, we exported the analysis results from the Aiforia platform to an image server in a JSON format. Because the exported files contain only coordinates of an outline of segmented or detected regions, each region was reconstructed on the local computer by our software, which confirmed that the segmentation results could be successfully reconstructed on the local computer. Based on this result, the analysis result obtained by the AI developed on the Aiforia platform may be used on other applications. For example, in the case of the breast cancer assessment, immunohistochemistry (IHC) and fluorescence and bright field *in situ* hybridization (ISH) slides are used together with H&E slides to determine the human epidermal growth factor receptor 2 (HER2) status. If invasive areas are automatically identified on H&E images by an AI model, an additional in-house machine-learning-based image analysis application may help in the subsequent assessment of IHC, and ISH images. This would reduce manual tedious operations and replace the assessment from subjective to objective. In addition, if AI accomplishes adequate accuracy on the Aiforia platform, these results may be used as annotations for additional development of in-house image analysis algorithms and/or AI models.

Some of our 3D pathology imaging applications use micro-computed tomography (Micro CT) to scan entire FFPE blocks or resected tissue non-destructively. Whole Block Imaging (WBI) and Whole Tissue Imaging (WTI) by a Micro-CT scanner are novel non-invasive imaging techniques that detect histomorphological features [36]. A recent study proposed 3D vessel detection using a deep neural network for micro-CT images. In addition to vessel detection, the purpose of the study was to detect tumor lesions, measure tumor invasion depth, and identify metastatic lymph nodes [37]. To improve the efficiency of this processing, it is necessary to integrate all the functions by applying methods such as ours, which were created for the Colon Project. We believe that by using AI-cloud-based platforms, we will be able to reach at least 80% accuracy for histomorphological features of samples, which will allow us to be able to integrate the 3D imaging tools and provide a broad spectrum, giving the pathologist the freedom to use all the tools in the process of achieving the most accurate diagnosis.

Currently, 3D imaging, and image analysis applications are highly desired. Some research groups have proposed machine-learning-based 3D analysis applications and the complexity of annotation has been pointed out as an important problem. In particular manual annotations of hundreds of serial sections of the same block is an extremely time-consuming and laborious task. If the developed AI model works on 3D imaging modalities such as micro-computed tomography or light sheet microscopy, we will develop an efficient AI model for 3D image analysis more easily. It should be kept in mind that specific cross- or multimodal image analysis strategies are required to seamlessly implement the deployment of 3D imaging devices and their integration with H&E images.

Conclusion

This study aimed to develop a deep-learning segmentation algorithm that can define invasive carcinomas in the breast and colon, identify colonic layers in colon specimens, and distinguish between atypical and typical mitoses. The final step was to validate the output against interpretations by a pathologist and in an independent test cohort and finally to use the algorithm as an application in our software programs.

Our developed AI models showed excellent performance for tissue detection in all organ types. The AI models identified tumor areas well even in the presence of different tumor grades and *in situ* areas, in breast carcinomas, detected the invasive carcinoma and colonic layers, and recognized vessels and lymph nodes in colon specimens.

We will continue to create a new project for colorectal carcinoma resection specimens to teach AI to define prognostically significant findings in whole-mount images to apply it to Whole block 3D imaging and use the exported data from breast carcinomas to achieve the IHC/ISH assessment system.

Data availability statement

The original contributions presented in the study are included in the article/Supplementary Material, further inquiries can be directed to the corresponding author.

Ethics statement

The study was approved by the Memorial Sloan Kettering Cancer Center Institutional Review Board (Protocol #18-013) and has been performed in accordance with the ethical standards as laid down in the 1964 Declaration of Helsinki and its later amendments. The requirement for written informed consent was waived as the study was retrospective, all data was deidentified, and the research contained no more than minimal risk to the participants or their privacy.

Author contributions

Conception and design: YY, NB, and EC. Collection and assembly of data: NB, EC, MY, and HS. Data analysis and interpretation: NB, EC, TO, S-YL, and LS. All authors contributed to the article and approved the submitted version.

Funding

The author(s) declare that financial support was received for the research, authorship, and/or publication of this article. This

study was supported by the Cancer Center Support Grant from the National Institutes of Health/National Cancer Institute under award number P30CA008748.

Acknowledgments

The authors acknowledge the assistance of Hamamatsu Photonics, K.K. Japan and 3DHistech Ltd. Budapest, Hungary.

Conflict of interest

Authors S-YL and LS were employed by the company Aiforia Technologies at the time of the study. YY serves on the scientific advisory board and reports on receiving consultancy fees from Aiforia Technologies. Author LS was employed by the company Flywheel.io.

The remaining authors declare that the research was conducted in the absence of any commercial or financial relationships that could be construed as a potential conflict of interest.

Author disclaimer

The content is solely the responsibility of the authors and does not necessarily represent the official views of the National Institutes of Health.

Supplementary material

The Supplementary Material for this article can be found online at: https://www.por-journal.com/articles/10.3389/pore.2024.1611815/full#supplementary-material

References

1. Laury AR, Blom S, Ropponen T, Virtanen A, Carpén OM. Artificial intelligence-based image analysis can predict outcome in high-grade serous carcinoma via histology alone. *Scientific Rep* (2021) 11(1):19165. doi:10.1038/s41598-021-98480-0

2. Coudray N, Ocampo PS, Sakellaropoulos T, Narula N, Snuderl M, Fenyö D, et al. Classification, and mutation prediction from non–small cell lung cancer histopathology images using deep learning. *Nat Med* (2018) 24(10):1559–67. doi:10.1038/s41591-018-0177-5

3. Arvaniti E, Fricker KS, Moret M, Rupp N, Hermanns T, Fankhauser C, et al. Automated Gleason grading of prostate cancer tissue microarrays via deep learning. *Scientific Rep* (2018) 8(1):12054. doi:10.1038/s41598-018-30535-1

4. Baxi V, Edwards R, Montalto M, Saha S. Digital pathology and artificial intelligence in translational medicine and clinical practice. *Mod Pathol* (2022) 35(1):23–32. doi:10.1038/s41379-021-00919-2

5. Tizhoosh HR, Pantanowitz L. Artificial intelligence and digital pathology: challenges and opportunities. *J Pathol Inform* (2018) 9(1):38. doi:10.4103/jpi.jpi_53_18

6. Pantanowitz L, Sharma A, Carter AB, Kurc T, Sussman A, Saltz J. Twenty years of digital pathology: an overview of the road travelled, what is on the horizon, and the emergence of vendor-neutral archives. *J Pathol Inform* (2018) 9(1):40. doi:10.4103/jpi.jpi_69_18

7. Colling R, Pitman H, Oien K, Rajpoot N, Macklin P, Snead D, et al. Artificial intelligence in digital pathology: a roadmap to routine use in clinical practice. *The J Pathol* (2019) 249(2):143–50. doi:10.1002/path.5310

8. Ehteshami BB, Veta M, Diest PJvan, Ginneken B, van KN, Litjens G, et al. Diagnostic assessment of deep learning algorithms for detection of lymph node metastases in women with breast cancer. *JAMA* (2017) 318:2199–0. doi:10.1001/jama.2017.14585

9. Thakur N, Yoon H, Chong Y. Current trends of artificial intelligence for colorectal cancer pathology image analysis: a systematic review. *Cancers* (2020) 12(7):1884. doi:10.3390/cancers12071884

10. Van der Laak J, Litjens G, Ciompi F. Deep learning in histopathology: the path to the clinic. *Nat Med* (2021) 27(5):775–84. doi:10.1038/s41591-021-01343-4

11. Litjens G, Sánchez CI, Timofeeva N, Hermsen M, Nagtegaal I, Kovacs I, et al. Deep learning as a tool for increased accuracy and efficiency of histopathological diagnosis. *Sci Rep* (2016) 6:26286. doi:10.1038/srep26286

12. Deo SV, Sharma J, Kumar S. GLOBOCAN 2020 report on global cancer burden: challenges and opportunities for surgical oncologists. *Ann Surg Oncol* (2022) 29(11):6497–500. doi:10.1245/s10434-022-12151-6

13. Giordano SH, Franzoi MA, Temin S, Anders CK, Chandarlapaty S, Crews JR, et al. Systemic therapy for advanced human epidermal growth factor receptor 2–positive breast cancer: ASCO guideline update. *J Clin Oncol* (2022) 40(23):2612–35. doi:10.1200/JCO.22.00519

14. Lim TH, Lim AS, Tien SL, Tan PH. Impact of the updated 2018 American Society of Clinical Oncology/College of American Pathologists (ASCO/CAP) guidelines on Human Epidermal Growth Factor Receptor 2 (HER2) gene testing in invasive breast cancers: a single center study. *Ann Diagn Pathol* (2022) 58:151935. doi:10.1016/j.anndiagpath.2022.151935

15. Cardoso F, Kyriakides S, Ohno S, Penault-Llorca F, Poortmans P, Rubio IT, et al. Early breast cancer: ESMO Clinical Practice Guidelines for diagnosis, treatment, and follow-up. *Ann Oncol* (2019) 30(8):1194–220. doi:10.1093/annonc/mdz173

16. Hossain MS, Hanna MG, Uraoka N, Nakamura T, Edelweiss M, Brogi E, et al. Automatic quantification of HER2 gene amplification in invasive breast cancer from chromogenic *in situ* hybridization whole slide images. *J Med Imaging* (2019) 6(4):047501. doi:10.1117/1.JMI.6.4.047501

17. Yu Z, Jiang D, Huang W, Luo R, Wang H, Su J, et al. Comparison of two pathological processing methods for large endoscopic submucosal dissection (ESD) specimens. *J Clin Pathol* (2023) 76(11):757–62. doi:10.1136/jcp-2022-208491

18. Ahmed Y, Othman M. EMR/ESD: techniques, complications, and evidence. *Curr Gastroenterol Rep* (2020) 22:39–2. doi:10.1007/s11894-020-00777-z

19. Ishihara R, Arima M, Iizuka T, Oyama T, Katada C, Kato M, et al. Endoscopic submucosal dissection/endoscopic mucosal resection guidelines for esophageal cancer. *Dig Endosc* (2020) 32(4):452–93. doi:10.1111/den.13654

20. Mathew T, Kini JR, Rajan J. Computational methods for automated mitosis detection in histopathology images: a review. *Biocybernetics Biomed Eng* (2021) 41(1):64–82. doi:10.1016/j.bbe.2020.11.005

21. Li C, Wang X, Liu W, Latecki LJ. DeepMitosis: mitosis detection via deep detection, verification and segmentation networks. *Med image Anal* (2018) 45:121–33. doi:10.1016/j.media.2017.12.002

22. Zehra T, Anjum S, Mahmood T, Shams M, Sultan BA, Ahmad Z, et al. A novel deep learning-based mitosis recognition approach and dataset for uterine leiomyosarcoma histopathology. *Cancers* (2022) 14(15):3785. doi:10.3390/cancers14153785

23. Ibrahim A, Lashen AG, Katayama A, Mihai R, Ball G, Toss MS, et al. Defining the area of mitoses counting in invasive breast cancer using whole slide image. *Mod Pathol* (2022) 35(6):739–48. doi:10.1038/s41379-021-00981-w

24. Lakshmanan B, Priyadharsini S, Selvakumar B. Computer assisted mitotic figure detection in histopathology images based on DenseNetPCA framework. *Mater Today Proc* (2022) 62:4936–9. doi:10.1016/j.matpr.2022.03.683

25. Ibrahim A, Lashen A, Toss M, Mihai R, Rakha E. Assessment of mitotic activity in breast cancer: revisited in the digital pathology era. *J Clin Pathol* (2021) 23:365–72. doi:10.1136/jclinpath-2021-207742

26. Anttila TT, Aspinen S, Pierides G, Haapamäki V, Laitinen MK, Ryhänen J. Enchondroma detection from hand radiographs with an interactive deep learning segmentation tool—a feasibility study. *J Clin Med* (2023) 12(22):7129. doi:10.3390/jcm12227129

27. Kather JN, Heij LR, Grabsch HI, Loeffler C, Echle A, Muti HS, et al. Pan-cancer image-based detection of clinically actionable genetic alterations. *Nat Cancer* (2020) 1(8):789–99. doi:10.1038/s43018-020-0087-6

28. Satturwar S, Parwani AV. Artificial intelligence-enabled prostate cancer diagnosis and prognosis: current state and future implications. *Adv Anat Pathol* (2024) 31(2):136–44. doi:10.1097/PAP.0000000000000425

29. Bakoglu N, Cesmecioglu E, Ohnishi T, Ohnishi C, Ross DR, Yagi Y *Evaluation of AI-integrated HER-2 dual ISH detection systems in invasive breast carcinoma*, 104. Modern Pathology: Laboratory Investigation (2024). p. S115–117. Issue3, Suppl 1, 100428.

30. Ozkan TA, Eruyar AT, Cebeci OO, Memik O, Ozcan L, Kuskonmaz I. Interobserver variability in Gleason histological grading of prostate cancer. *Scand J Urol* (2016) 50(6):420–4. doi:10.1080/21681805.2016.1206619

31. Aeffner F, Wilson K, Bolon B, Kanaly S, Mahrt CR, Rudmann D, et al. Commentary: roles for pathologists in a high-throughput image analysis team. *Toxicologic Pathol* (2016) 44(6):825–34. doi:10.1177/0192623316653492

32. Çayır S, Solmaz G, Kusetogullari H, Tokat F, Bozaba E, Karakaya S, et al. MITNET: a novel dataset and a two-stage deep learning approach for mitosis recognition in whole slide images of breast cancer tissue. *Neural Comput Appl* (2022) 34(20):17837–51. doi:10.1007/s00521-022-07441-9

33. Cree IA, Tan PH, Travis WD, Wesseling P, Yagi Y, White VA, et al. Counting mitoses: SI (ze) matters! *Mod Pathol.* 2021;34(9):1651–7. doi:10.1038/s41379-021-00825-7

34. Li J, Adachi T, Takeyama S, Yamaguchi M, Yagi Y. U-Net based mitosis detection from H&E-stained images with the semi-automatic annotation using pHH3 IHC-stained images. In: Medical imaging 2022: image processing. SPIE (2022), 12032:669–681.

35. Matsuda Y, Yoshimura H, Ishiwata T, Sumiyoshi H, Matsushita A, Nakamura Y, et al. Mitotic index and multipolar mitosis in routine histologic sections as prognostic markers of pancreatic cancers: a clinicopathological study. *Pancreatology* (2016) 16(1):127–32. doi:10.1016/j.pan.2015.10.005

36. Xu B, Teplov A, Ibrahim K, Inoue T, Stueben B, Katabi N, et al. Detection and assessment of capsular invasion, vascular invasion and lymph node metastasis volume in thyroid carcinoma using microCT scanning of paraffin tissue blocks (3D whole block imaging): a proof of concept. *Mod Pathol* (2020) 33(12):2449–57. doi:10.1038/s41379-020-0605-1

37. Ohnishi T, Teplov A, Kawata N, Ibrahim K, Ntiamoah P, Firat C, et al. Three-dimensional vessel segmentation in whole-tissue and whole-block imaging using a deep neural network: proof-of-concept study. *The Am J Pathol* (2021) 191(3):463–74. doi:10.1016/j.ajpath.2020.12.008

Pathology & Oncology Research | frontiers

TYPE Original Research
PUBLISHED 22 January 2024
DOI 10.3389/pore.2024.1611553

Check for updates

OPEN ACCESS

EDITED BY
Andrea Ladányi,
National Institute of Oncology (NIO), Hungary

*CORRESPONDENCE
Ioannis Panagopoulos,
ioannis.panagopoulos@rr-research.no

RECEIVED 16 October 2023
ACCEPTED 10 January 2024
PUBLISHED 22 January 2024

CITATION
Hatchett WJ, Brunetti M, Andersen K, Tandsæther MR, Lobmaier I, Lund-Iversen M, Lien-Dahl T, Micci F and Panagopoulos I (2024), Genetic characterization of intramuscular myxomas. *Pathol. Oncol. Res.* 30:1611553. doi: 10.3389/pore.2024.1611553

COPYRIGHT
© 2024 Hatchett, Brunetti, Andersen, Tandsæther, Lobmaier, Lund-Iversen, Lien-Dahl, Micci and Panagopoulos. This is an open-access article distributed under the terms of the Creative Commons Attribution License (CC BY). The use, distribution or reproduction in other forums is permitted, provided the original author(s) and the copyright owner(s) are credited and that the original publication in this journal is cited, in accordance with accepted academic practice. No use, distribution or reproduction is permitted which does not comply with these terms.

Genetic characterization of intramuscular myxomas

William John Hatchett[1], Marta Brunetti[1], Kristin Andersen[1], Maren Randi Tandsæther[1], Ingvild Lobmaier[2], Marius Lund-Iversen[2], Thomas Lien-Dahl[2], Francesca Micci[1] and Ioannis Panagopoulos[1]*

[1]Section for Cancer Cytogenetics, Institute for Cancer Genetics and Informatics, The Norwegian Radium Hospital, Oslo University Hospital, Oslo, Norway, [2]Department of Pathology, The Norwegian Radium Hospital, Oslo University Hospital, Oslo, Norway

Introduction: Intramuscular myxomas are benign tumors that are challenging to diagnose, especially on core needle biopsies. Acquired chromosomal aberrations and pathogenic variants in codon 201 or codon 227 in GNAS complex locus gene (*GNAS*) have been reported in these tumors. Here we present our genetic findings in a series of 22 intramuscular myxomas.

Materials and methods: The tumors were investigated for the presence of acquired chromosomal aberrations using G-banding and karyotyping. Pathogenic variants in codon 201 or codon 227 of *GNAS* were assessed using direct cycle Sanger sequencing and Ion AmpliSeq Cancer Hotspot Panel v2 methodologies.

Results: Eleven tumors carried chromosomal abnormalities. Six tumors had numerical, four had structural, and one had both numerical and structural chromosomal aberrations. Gains of chromosomes 7 and 8 were the most common abnormalities being found in five and four tumors respectively. Pathogenic variants in *GNAS* were detected in 19 myxomas (86%) with both methodologies. The detected pathogenic variants were p.R201H in nine cases (seven with abnormal and two with normal karyotypes), p.R201C in five cases, all with normal karyotypes, p.R201S in three cases (two with abnormal and one with normal karyotype), p.R201G in one case with a normal karyotype, and p.Q227E in one case with a normal karyotype.

Conclusion: Firstly, our data indicate a possible association between chromosomal abnormalities and *GNAS* pathogenic variants in intramuscular myxomas. Secondly, the presence of the rare pathogenic variants R201S, p.R201G and p.Q227E in 26% (5 out of 19) of myxomas with *GNAS* pathogenic variants shows that methodologies designed to detect only the common "hotspot" of p.R201C and p.R201H will give false negative results. Finally, a comparison between Ion AmpliSeq Cancer Hotspot Panel v2 and direct cycle Sanger sequencing showed that direct cycle Sanger sequencing

provides a quick, reliable, and relatively cheap method to detect *GNAS* pathogenic variants, matching even the most cutting-edge sequencing methods.

KEYWORDS

intramuscular myxoma, chromosomal aberrations, GNAS, codon 201, codon 227, Sanger sequencing, Ion torrent

Introduction

Intramuscular myxomas are rare benign soft tissue tumors, characterized by stellate and/or spindle-shaped cells embedded in a hypo-vascular, abundant myxoid stroma. They were first pathologically described by Enzinginer in 1965 [1] and the description has since been validated in later studies [2–6]. The reported annual incidence rate of intramuscular myxoma is 0.10–0.13/100,000 and mostly occurs in adults, with women having a predisposition for the condition (~60–70%) [7–9]. Intramuscular myxoma is a somatic disorder with the majority of patients presenting asymptomatically with painless, palpable, well-defined tumors that slowly enlarge to around 2–15 cm in diameter [9]. They are mostly located in the thigh, and do not recur after a simple excision [8]. Multiple intramuscular myxomas are rare, generally occurring as an isolated lesion not associated with other clinical abnormalities [8]. However, multiple intramuscular myxomas in combination with polyostotic fibrous dysplasia can be associated with Mazabraud's syndrome [7, 9]. Intramuscular myxoma, Mazabraud's syndrome and the closely related McCune-Albright syndrome (also associated with fibrous dysplasia, café au lait macules and endocrine disorders) are mostly caused by the activating missense mutations in codon 201 or codon 227 of the GNAS complex locus gene (*GNAS*) [10–14].

Pathogenic variants in codon 201 of the *GNAS* gene on chromosome 20 are one of the primary cancer-causing variants in heterotrimeric G proteins and is one of the leading causes of oncogenesis in a variety of low-grade malignant and benign tumors [15]. The *GNAS* gene encodes the stimulatory G-alpha subunit of the heterotrimeric G-protein complex, which regulates the activation of adenylyl cyclase that converts adenosine triphosphate into cyclic adenosine monophosphate. When a cell has a *GNAS* pathogenic variant, there is an overproduction of cyclic adenosine monophosphate and activation of downstream signaling pathways [16–22]. The first description of a somatic *GNAS* pathogenic variant in intramuscular myxomas was published by Okamoto et al. in 2000 [10]. Thereafter, many studies have shown *GNAS* pathogenic variants occurring frequently in sporadic intramuscular myxomas [10, 18–22]. Additionally, *GNAS* pathogenic variants are absent in low-grade myxofibrosarcoma, which can be used as a malignant differential diagnosis to intramuscular myxomas [23, 24]. A precise diagnosis between these two is essential for the correct treatment; low-grade myxofibrosarcomas commonly recur and require wide excisions, whereas a more precise or marginal excision is sufficient to treat intramuscular myxomas [24, 25].

Intramuscular myxomas are challenging to diagnose, especially on core needle biopsies [26]. Also, they have a broad differential diagnosis at a morphological level and no clear karyotypic diagnosis [22, 27]. Additionally, there are many different types of *GNAS* pathogenic variants found in intramuscular myxomas, located on either codon 201, in exon 8, or codon 227, in exon 9. *GNAS* also has a low range of pathogenic allele frequencies in intramuscular myxomas, ranging between ~ 5–30%. The most common pathogenic variants are p.R201H (c.602G>A) and p.R201C (c.601C>T), making up approximately 80%–90% of all cases [10, 19, 20, 22]. This has influenced the design of some diagnostic methods to only detect common pathogenic variants, and not the rarer ones [28, 29]. Depending on the method, *GNAS* pathogenic variants were found in ~30–80% of intramuscular myxomas [20–22].

The gold standard for sensitive screening for genes that can predispose a patient to particular cancer types, such as pathogenic variants in *GNAS*, was PCR amplification, followed by sequencing, e.g., Sanger sequencing (also known as dideoxy chain termination method) of the amplified product [30–34]. However, in the last two decades, next-generation sequencing (NGS, also known as high throughput sequencing and massive parallel sequencing) has become common practice in cancer genetic screening [35]. Methods such as whole genome sequencing, exome sequencing, and transcriptome sequencing can provide more sensitive and accurate results. The main difference between Sanger sequencing and NGS is the sequencing volume. The Sanger methodology can only sequence a single DNA fragment at a time, whereas NGS simultaneously sequences millions of fragments per run. Thus, NGS results in hundreds to thousands of genes being sequenced simultaneously. Additionally, NGS can start with relatively low input DNA compared to that of Sanger methodology and provides enhanced detection capabilities to detect novel or rare variants through deep sequencing. Comparing the results obtained from NGS and Sanger sequencing there is close to 100% concordance between these methodologies [36–38]. NGS-based gene panels have also been developed to target specific genes or pathogenic variants (hotspots) that are associated to a particular cancer type [39–41]. These panels are nowadays used in clinical cancer genetics, providing accurate information on oncogenic drivers and actionable genetic alterations for a variety of genes [39–41]. The commercially available Ion AmpliSeq Cancer Hotspot Panel v2 (ThermoFisher Scientific, Waltham, MA, United States) covers approximately 2,800 pathogenic variants which are found in the Catalogue Of Somatic Mutations In Cancer (COSMIC) [42]. The pathogenic variants detected by Ion AmpliSeq Cancer Hotspot Panel v2 are

TABLE 1 Clinicopathological data, karyotypes, and status of pathogenic variants of the *GNAS* gene on the intramuscular myxomas.

Case	Sex/ Age	Location	Karyotypes	Amino acid sequence change[a]	Nucleotide sequence change[b]	Allele frequency[c]
1	F/55	Thigh	47,XX,+8 [2]/46,XX [24]	p.R201H	c.602G>A	7.80%
2	F/45	Thigh	46,XX,t (6; 13) (p23; q14)[3]/46,XX [22]	p.R201H	c.602G>A	11.40%
3	F/66	Upper arm	46,XX,inv (12) (q13q21)[2]/46,XX [23]	p.R201H	c.602G>A	8.20%
4	F/49	Thigh	46,XX,t (10; 22) (q24; q13)[3]/46,XX [22]	p.R201H	c.602G>A	7.90%
5	F/39	Buttock	46,XX	p.R201H	c.602G>A	13.50%
6	M/74	Thigh	46–47,X,-Y,+X,add (8) (p?11),+9 [cp5]/ 46,XY [15]	p.R201H	c.602G>A	16.70%
7	F/78	Back	49,XX,+X,+7,+8 [5]/46,XX [5]	p.R201H	c.602G>A	4.30%
8	F/58	Thigh	47,XX,+7 [3]/46,XX [10]	p.R201H	c.602G>A	5.20%
9	F/52	Thigh	46,XX	p.R201H	c.602G>A	33%
10	F/56	Thigh	46,XX	p.R201C	c.601C>T	7.40%
11	F/54	Thigh	46,XX	p.R201C	c.601C>T	28%
12	M/64	Thigh	46,XY	p.R201C	c.601C>T	21.90%
13	F/46	Thigh	46,XX	p.R201C	c.601C>T	10.10%
14	F/58	Upper arm	46,XX	p.R201C	c.601C>T	13.70%
15	F/67	Buttock	46,XX	p.R201S	c.601C>A	15.90%
16	F/71	Hip	50,XX,+7,+8,+8,+20 [8]/46,XX [2]	p.R201S	c.601C>A	7%
17	F/80	Leg	47–48,XX,+7 [cp3]/48,XX,+7,+8 [4]/46,X,-X,+5 [4]/46,XX [22]	p.R201S	c.601C>A	5.30%
18	M/66	Thigh	46,XY	p.R201G	c.601C>G	18.40%
19	M/71	Thigh	46,XY,add (15) (p11~13)[2]/46,XY [8]	p.Q227E	c.679C>G	11.60%
20	M/69	Thigh	48,XY,+7,+9 [5]/46,XY [20]	No pathogenic variant	—	—
21	F/58	Thigh	46,XX	No pathogenic variant	—	—
22	F/79	Back	46,XX	No pathogenic variant	—	—

[a]Based on GNAS reference sequence NP_000507.1.
[b]Based on *GNAS* reference sequence: NM_000516.7.
[c]Allele frequency obtained with Ion torrent/Ion AmpliSeq Cancer Hotspot Panel v2. It is defined as the ratio between allele coverage and total coverage.

from 50 oncogenes and tumor suppressor genes, including those at codons 201 and 227 of *GNAS*.

In the present study, we cytogenetically analyzed intramuscular myxomas and compared a PCR based/Sanger sequencing methodology with the above-mentioned panel for the detection of *GNAS* pathogenic variants in codons 201 and 227.

Materials and methods

Patients

Our materials consisted of 22 intramuscular myxomas (Table 1) and all samples were collected at the Norwegian Radium Hospital between 2015 and 2023. The patients were 17 females and five males between the ages of 39 and 80. The study was approved by the Regional Committees for Medical Research Ethics South East Norway.

G-banding and karyotyping

A representative tumor area was investigated cytogenetically as previously described [27, 43]. Material for cytogenetic examination was available from all 22 samples. After mechanical and enzymatic disaggregation of the tissue sample, the resulting cells were short-term cultured, harvested, and processed for cytogenetic examination. To obtain G-banding

TABLE 2 Designation, sequence (5′->3′), and position in reference sequence of the forward (F) and reverse (R) primers used for BigDye™ Direct Cycle Sequencing of exons 8 and 9 of the *GNAS* gene.

Primer designation	Sequence (5′->3′)	Reference sequence: Position
M13For-GNASint7-F1	***TGTAAAACGACGGCCAGT*** ACTGTTTCGGTTGGCTTTGGTGA	NG_016194.2: 74,561–74583
M13Rev-GNASint8-R1	***CAGGAAACAGCTATGACC*** CAGAGGGACTGGGGTGAATGTCA	NG_016194.2: 74,752–74730
M13For-GNASint8-F1	***TGTAAAACGACGGCCAGT*** TGACATTCACCCCAGTCCCTCTG	NG_016194.2: 74,730–74752
M13Rev-GNASint9-R1	**CAGGAAACAGCTATGACC** AGCGACCCTGATCCCTAACAACAC	NG_016194.2: 74,910–74887

The forward primers have the **M13** (highlighted in bold) forward primer sequence TGTAAAACGACGGCCAGT at their 5′-end. The reverse primers had the M13 reverse primer sequence CAGGAAACAGCTATGACC at their 5′-end.

of chromosomes, Wright's stain was used (Sigma Aldrich; St Louis, MO, United States). The subsequent cytogenetic analysis and karyotype description followed the recommendations of the International System for Human Cytogenomic Nomenclature (ISCN) 2020 guidelines [44].

DNA extraction from tumor and FFPE tissue samples

Frozen (−80°C) tumor tissue adjacent to that used for cytogenetic analysis and histologic examination was available for 21 myxomas (Table 1; Supplementary Table S1) and formalin-fixed, paraffin-embedded (FFPE) sample was used for case 14 (Supplementary Table S1). DNA was extracted from the frozen tumor samples, using the Maxwell RSC Tissue DNA Kit and the Maxwell RSC Instrument (Promega, Madison, WI, United States). For FFPE sample, DNA was extracted using the QIAamp DNA FFPE Tissue Kit (Qiagen, Hilden, Germany). The DNA concentration was then estimated for each sample, using the QuantiFluor ONE dsDNA System using Quantus™ Fluorometer (Promega).

Sequencing of *GNAS* pathogenic variants using Sanger sequencing

The primers used for PCR amplification and Sanger sequencing are listed in Table 2. The BigDye Direct Cycle Sequencing Kit was used for PCR/cycle (Sanger) sequencing according to the company's recommendations (ThermoFisher Scientific, Waltham, MA, United States). The primer combination M13For-GNASint7-F1 and M13Rev-GNASint8-R1 was used for amplification and sequencing of exon 8 of *GNAS* to detect possible pathogenic variants at the codon 201 (p.R201) (Table 2). The primer combination M13For-GNASint8-F1 and M13Rev-GNASint9-R1 was used for amplification and sequencing of exon 9 of *GNAS* to detect possible pathogenic variants at codon 227 (p.Q227) (Table 2). Sequencing was run on the Applied Biosystems SeqStudio Genetic Analyzer system (ThermoFisher Scientific). For analysis of sequence data, the basic local alignment search tool (BLAST) software[1] was used [45]. The obtained sequences were aligned against the *GNAS* reference sequences NM_000516.7 and NG_016194.2 corresponding to GNAS complex locus (*GNAS*) transcript variant 1 and RefSeqGene on chromosome 20, respectively. Codons 201 (p.R201) and 227 (p.Q227) are based on the NCBI reference sequence NP_000507.1 which corresponds to protein GNAS isoform GNASL.

Sequencing of *GNAS* pathogenic variants using Ion AmpliSeq Cancer Hotspot Panel v2

The Ion Ampliseq™ Cancer Hotspot Panel v2 Chef-Ready Kit was used to detect *GNAS* pathogenic variants following the company's recommendations (ThermoFisher Scientific). DNA samples were diluted to between 0.4 and 1.6 ng/μL or used as is when the sample concentration was below 0.6 ng/μL. All runs on the Ion Chief and Ion torrent were created in TorrenSuite™ (ThermoFisher Scientific). Libraries were prepared using Ion Ampliseq™ Cancer Hotspot Research Panel v2 primers and by using the Ion AmpliSeq™ Kit for Chef DL8 and were run using recommended setting from the company (ThermoFisher Scientific). All samples were templated via the automated template preparation protocol Ion 540™ Kit—Chef (ThermoFisher Scientific), which was then sequenced on the Ion GeneStudio S5 following the company's recommendations (ThermoFisher Scientific).

Results

Cytogenetics

The cytogenetic data are presented in Table 1. Normal karyotypes were found in 11 intramuscular myxomas and

1 https://blast.ncbi.nlm.nih.gov/Blast.cgi

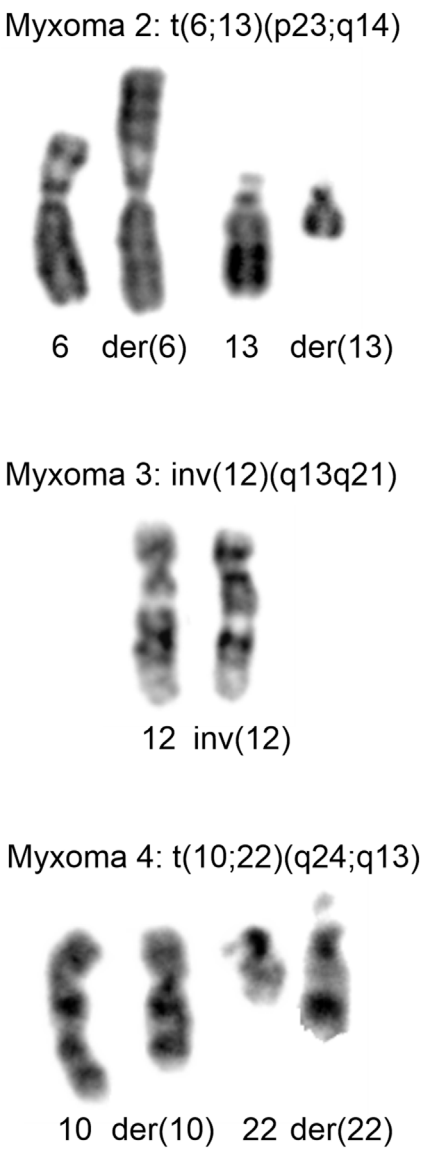

FIGURE 1
Cytogenetic analysis of myxomas 2, 3, and 4. Partial Karyotypes showing the abnormal chromosomes together with the corresponding normal chromosome homologs. For myxoma 2, der (6) and der (13), together with chromosomes 6 and 13 are shown. For myxoma 3, inv (12) together with normal 12 are shown. For myxoma 4, der (10) and der (22), together with chromosomes 10 and 22 are shown.

were abnormal in 11 tumors. Six abnormal karyotypes had numerical chromosomal aberrations, involving one or more of chromosomes X, 7, 8, 9, 20, and four tumors had structural aberration, and one had both numerical and structural aberrations (Table 1). Gains of chromosome 7 were the most frequent abnormalities found in five myxomas, followed by gains of chromosome 8, which were found in four tumors. No recurrent structural aberration was found (Table 1). The structural aberrations were t (6; 13) (p23; q14), inv (12) (q13q21), t (10; 22) (q24; q13), add (15) (p11~13), and add (8) (p?11) (Figure 1; Table 1).

Sanger sequencing

DNA was successfully extracted from all tumor samples. Pathogenic variants in the *GNAS* gene were detected in 19 out of 22 myxomas (86%) (Supplementary Table S1). The detected pathogenic variants were p.R201H in nine cases which were found in seven myxomas with abnormal karyotypes and two with a normal karyotype, p.R201C in five cases all of them with normal karyotypes, p.R201S in three cases which two of them had abnormal karyotype and one had a normal karyotype, p.R201G in one case with a normal karyotype, and p.Q227E in one case with an abnormal karyotype (Table 1; Figure 2).

Ion AmpliSeq Cancer Hotspot Panel v2

The Ion torrent results were the same as that of Sanger sequencing (Supplementary Table S1) and are therefore both represented in Table 1 for each case. Pathogenic variants in the *GNAS* gene were detected in the same 19 samples in which were detected by Sanger sequencing. Ion torrent also provided the allele frequencies of the mutated alleles ranging from 4.3%–33%, with an average of 13% (Table 1).

Discussion

Over 40,000 new GNAS p.R201 pathogenic variant cases were reported in 2021 in the United States alone, illustrating the high prevalence of this genetic abnormality and importance of detecting this genetic abnormality [15]. Diagnosing myxoma is difficult as there are no useful immunohistochemical markers to distinguish intramuscular myxomas from low-grade myxofibrosarcomas, both have an abundant myxoid matrix, and both may express the CD34 molecule [22, 46, 47]. Detection of acquired genetic abnormalities in combination with histopathology, can be a powerful diagnostic tool to help distinguish between morphologically similar neoplasms, such as intramuscular myxomas and low-grade myxofibrosarcomas [18, 23, 24]. Morphologically, myxofibrosacomas have more prominent blood vessels and nuclear atypia, but cellular myxomas share similar features, so morphology alone is not always sufficient to make a definite diagnosis, especially in small biopsies. Additionally, small biopsies may also create issues with pathogenic variants detection which can be hampered by low frequency of pathogenic variants alleles, i.e., sequences of mutated alleles “diluted” by wild-type sequences. For pathogenic variant detection it is recommended to analyses at least 50% lesioned tissue. This may require painstaking and time-

10.3389/pore.2024.1611553

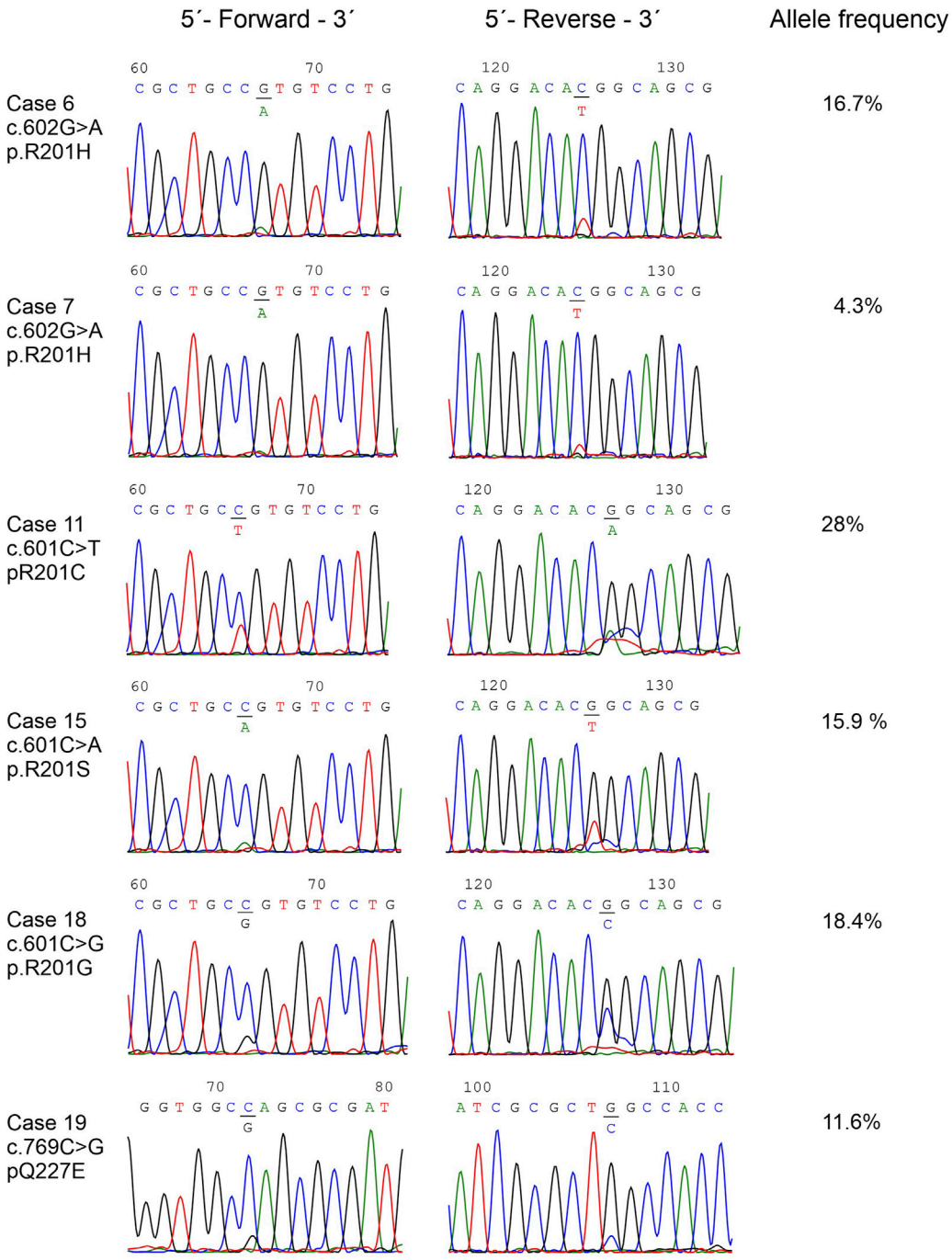

FIGURE 2
The detected *GNAS* pathogenic variants. Partial chromatograms showing the *GNAS* pathogenic variants in cases 10, 11, 13, 16, 18, and 19. Chromatograms from both forward and reverse sequencing are shown. The frequencies of mutated alleles, found with the Ion Ampliseq™ Cancer Hotspot Panel v2, are also shown.

consuming micro-dissection of the relevant tissue and can be difficult to achieve in samples from needle biopsies [18, 21]. It has been suggested that a minimum of 10% tumor cell fraction is required to detect *GNAS* pathogenic variants [22], but the tumor cell fraction may have not been estimated accurately [48, 49]. This is especially difficult in intramuscular myxoma tumors, even when using fully excised tumors, as there is low amounts of DNA available for extraction and a generally low level of pathogenic

variants which could easily become diluted by wild-type sequences [18].

Another complication is that there are no pathognomonic chromosomal aberrations for intermuscular myxomas [27]. The abnormal karyotypes, which were found in 11 out of 22 myxomas (Table 1), confirmed the result and conclusion of our previous study [27]. Abnormalities of chromosomes 7 and 8, both mainly trisomy, were the most common aberrations. These abnormalities lack specificity and are found in a variety of different neoplasms [50–55] and trisomy 7 is also seen in non-neoplastic lesions [27, 56] Furthermore, the observed structural chromosomal aberrations were not recurrent (Table 1; [27]). Even though "acquisition of clonal chromosome aberrations is an integral part of the disease process" in intermuscular myxomas, the cytogenetic information cannot be used for the diagnosis of myxomas (Table 1, [27]).

A useful tool for the diagnosis of intramuscular myxomas is that intramuscular myxomas often carry a somatic *GNAS* pathogenic variants. Since *GNAS* pathogenic variants are absent in low-grade myxofibrosarcoma, detection of these pathogenic variants can be a useful differential diagnosis [10, 18–24]. Detecting pathogenic variants within the *GNAS* gene in intramuscular myxoma can be difficult due to the poor cellularity of the tumor and the low frequency of mutated alleles, which was found to be between 5% and 30%, [3, 18, 20–22]. A further complication for *GNAS* pathogenic variant detection is that PCR-based methods can produce varying results. Okamato et al. (2000) detected *GNAS* pathogenic variants in five out of six (83%) intramuscular myxomas (60% p.R201H and 40% p.R201C) using PCR methodology together with single strand conformation polymorphism [10, 57]. Delaney et al. (2009) detected pathogenic variants in eight out of 28 (29%) intramuscular myxomas using PCR followed by pathogenic variant-specific restriction enzyme digestion [18]. However, they found *GNAS* pathogenic variants in 17 out of 28 (61%) intramuscular myxomas with COLD-PCR followed by pathogenic variant-specific restriction enzyme digestion [18]. Walther et al. (2014) detected pathogenic variants in 23 out of 63 (36%) intramuscular myxomas (52% p.R201C and 48% p.R201H) using PCR and direct sequencing [19]. In the present work, we detected *GNAS* pathogenic variants in 19 out of 22 samples (86%) using direct cycle Sanger sequencing with primers tailed on their 5′-end with M13 universal primer sequences (Table 2). We detected a total of five different pathogenic variants: p.R201H (47.3%), p.R201C (26.3%), p.R201S (16%), p.Q227E (5.2%), and the rare pathogenic variant p.R201G (5.2%) (Table 1; Figure 2). The p.R201G pathogenic variants has so far only been reported in one patient with McCune-Albright Syndrome over 20 years ago [58]. One complication when using Sanger sequencing is that it can be hard to detect allele frequencies below 15%. Intramuscular myxomas tumors have low allele frequencies of GNAS pathogenic variants and in our investigation, we found an average allele frequency of 13% (Table 1). To combat this a positive result from both bidirectional Sanger sequencing is mandatory, and reruns are used to confirm if only one direction is positive. Additionally, Sanger sequencing cannot accurately determine the allele frequency and is only used as a qualitative method (Yes/No) whereas NGS can be used as both qualitative and quantitative (Yes/No and frequency of various alleles) (Table 1; Figure 2).

NGS has also been used to detect *GNAS* pathogenic variants in intramuscular myxomas [20–22]. Sunitsch et al. (2018) detected *GNAS* pathogenic variants in 12 out of 13 (92%) specimens (four cases with p.R201C, six cases with p.R201H and two cases with p.Q227E) using Ion Ampliseq primer panel and Ion torrent sequencing [21]. Bekers et al. (2019) detected *GNAS* pathogenic variants in 16 out of 28 (57%) samples with frequency of the mutant allele between 5% and 27% using single molecule tagged molecular inversion probe assay and Illumina NextSeq sequencing [20]. In addition to p.R201H and p.R201C, which were detected in 44% and 31% of the samples respectively, four other *GNAS* pathogenic variants were found in intramuscular myxomas; p.R201S, p.R201L, p.R201P and p.Q227R [20]. Libbrecht et al. (2019) detected eight out of nine (89%) intramuscular myxomas to have a *GNAS* pathogenic variants (62.5% p.R201H and 37.5% p. R201C) with frequency of the mutant allele ranging between 5% and 28% using TruSight Tumor 26 panel [22]. In the present study, we detected five different *GNAS* pathogenic variants in 19 out of 22 samples 83%, with frequency of the mutated allele to ranging between 4.3% and 28% (Table 1) using the Ion Ampliseq™ Cancer Hotspot Panel v2. Our data obtained with the NGS panel were similar to the above-mentioned studies. We also found that results obtained from the NGS panel were identical to those obtained by direct cycle Sanger sequencing, indicating that the latter methodology is a highly sensitive technique to detect *GNAS* pathogenic variants. The present study (Table 1) together with the studies published by Bekers et al. (2019) and Sunitsch et al. (2019) showed that approximately 23% of myxomas with *GNAS* pathogenic variants carried variants in other locations other than the "hotspot" variants p.R201C and p.R201H. Thus, assays targeting only these pathogenic variants, p.R201C and p.R201H, such as pyrosequencing, quantitative real-time PCR, and digital PCR should be used with caution for the detection of *GNAS* pathogenic variants in intramuscular myxomas [20, 21, 59, 60].

Even though cytogenetic information cannot be used for the diagnosis of myxomas, we found an association between karyotypes and specific *GNAS* pathogenic variant. The pathogenic variant p.R201H was detected in seven tumors carrying abnormal karyotype and in only two tumors with normal karyotype. The detected p.R201C pathogenic variants were found in five tumors with only normal karyotype (Table 1). To the best of our knowledge, this association

between cytogenetic and molecular aberrations in intramuscular myxomas is reported for the first time in the present study. Although the number of cases in this report make up to few to draw any conclusions, our data may imply functional variations between the different pathogenic variants. Very little is known about possible functional differences between *GNAS* pathogenic variants. All constitutive pathogenic variants activate Gsα adenylate cyclase with overproduction of cyclic adenosine monophosphate (cAMP) and are therefore often treated as one and the same [61–63]. *GNAS* pathogenic variants are associated with upregulation of Wnt/beta-catening signaling [64–66] and were found in many tumors [15, 67]. In murine models, either p.R201C or p. R201H resulted in fibrous dysplasia [64, 68]. In patients with fibrous dysplasia/McCune-Albright syndrome carrying p.R201H or p.R201C, no clear genotype-phenotype correlation was found [69, 70]. Additionally, in patients with fibrous dysplasia no association was found between age, site, size, specimen type and *GNAS* mutational status [71]. A pan-cancer cohort of patients from 1050 *GNAS* mutant tumors showed a heavy disposition to the p.R201 codon, with a classic gain-of-function mutation. Both p.R201H and p.R201C pathogenic variants were found to drive tumor cell growth both *in vitro* and *in vivo* [15]. *GNAS* was overexpressed in the LS174T cell line using a doxycycline-inducible promoter, and the resulting effect on clonogenic capacity was assessed [15]. In another study, the basal and maximal adenylyl cyclase activity (cAMP accumulation) dose response under isoproterenol stimulation was found to be higher in p.R201H than that of p.R201C [72]. However, the authors have suggested that the *GNAS* expression was not stringently controlled, and this result could be a technical issue. This warranted further experimentation with both pathogenic variants and wildtype alleles to further elucidate functional variation like our karyotype results suggest.

It has been suggested that there can be notable variability found in phenotypes, pathogenicity and oncogenic effects, based on the specific substitution at a single location [73–75]. For example, the pathogenic missense variants which alter codon 336 in the *GARS1* gene that results in different phenotypic expression in a range of genetic neuropathies [73]. Two pathogenic variants resulting in a missense modifying amino acid at codon 336 in the catalytic domain of *GARS1*, were found in two unrelated patients - one a female with infantile spinal muscular atrophy; and the second, a male with Charcot–Marie–Tooth disease type 2D [73]. Exchanges in amino acids that change the pH of the residue have also been linked to cancers [75]. White et al. (2017) found that the pathogenic variants resulting in a change from arginine residue to a histidine residue produced a rise in intracellular pH, which in turn, conferred these mutants with oncogenic effects [75]. This is the same change in amino acid residue we see in the amino acid pathogenic variant p.R201H which could suggest functional variations between the different pathogenic variants in *GNAS*.

In conclusion, acquired genomic abnormalities, both at chromosomal and molecular levels, are found in intramuscular myxomas. However, the detected chromosomal aberrations are not pathognomonic for myxomas since they lack specificity and are found in various neoplasms or even in non-neoplastic cells. In our experiment, we reliably detected somatic *GNAS* pathogenic variants at the molecular level. Together with H&E stain morphology and immunohistochemistry, we can reliably diagnose and detect the majority of intramuscular myxomas, which in turn leads to the appropriate treatment. The two methods used, i.e., direct cycle Sanger sequencing (BigDye Direct Cycle Sequencing Kit) and NGS panel (Ion AmpliSeq Cancer Hotspot Panel v2) gave identical results detected *GNAS* pathogenic variant in 83% of the examined myxomas. In 26% of the myxomas which carried *GNAS* pathogenic variants, both methods detected pathogenic variants other than the common "hotspot" of p.R201C and p.R201H. This shows that methods designed to detect only "hotspot" variants might give false negative results. Direct cycle Sanger sequencing is a quick, reliable, and relatively cheap method to detect the *GNAS* pathogenic variants, matching even the most cutting-edge of sequencing methods while only lacking the detection of frequency of mutant allele, not required for diagnostic purposes. Ultimately, this will allow laboratories that do not have the funding for expensive NGS methods to accurately diagnose *GNAS* pathogenic variants. This will find application not only in intramuscular myxomas but other tumor types as well.

Data availability statement

The original contributions presented in the study are included in the article/Supplementary Material, further inquiries can be directed to the corresponding author.

Ethics statement

The studies involving humans were approved by the Regional Committees for Medical Research Ethics South East Norway. The studies were conducted in accordance with the local legislation and institutional requirements. The participants provided their written informed consent to participate in this study.

Author contributions

IP planned and designed the experiment, WH, MB, KA, MT, and IP conducted genetic/cytogenetic diagnostics and IL, ML-I, and TL-D conducted pathological examinations. WH, MB, KA, and IP did the experiment, WH and IP did data analysis, and wrote the manuscript. Finally, WH, MB, KA, MT, IL, ML-I, TL-D, FM, and IP edited the manuscript. All authors contributed to the article and approved the submitted version.

Conflict of interest

The authors declare that the research was conducted in the absence of any commercial or financial relationships that could be construed as a potential conflict of interest.

Supplementary material

The Supplementary Material for this article can be found online at: https://www.por-journal.com/articles/10.3389/pore.2024.1611553/full#supplementary-material

References

1. Enzinger FM. Intramuscular myxoma: a review and follow-up study of 34 cases. *Am J Clin Pathol* (1965) 43:104–13. doi:10.1093/ajcp/43.2.104

2. Miettinen M, Markku M. *Modern soft tissue pathology: tumors and non-neoplastic conditions*. Cambridge University Press (2016). p. 1062. Available from: https://www.cambridge.org/core/product/716C3345EDB53691CEE30DB640C84E7E (Accessed June 13, 2023).

3. Nielsen GP, O'Connell JX, Rosenberg AE. Intramuscular myxoma: a clinicopathologic study of 51 cases with emphasis on hypercellular and hypervascular variants. *Am J Surg Pathol* (1998) 22:1222–7. doi:10.1097/00000478-199810000-00007

4. Kindblom L-G, Stener B, Angervall L. Intramuscular myxoma. *Cancer* (1974) 34:1737–44. doi:10.1002/1097-0142(197411)34:5<1737::AID-CNCR2820340523>3.0.CO;2-U

5. Miettinen M, Höckerstedt K, Reitamo J, Tötterman S. Intramuscular myxoma—a clinicopathological study of twenty-three cases. *Am J Clin Pathol* (1985) 84:265–72. doi:10.1093/ajcp/84.3.265

6. Hashimoto H, Tsuneyoshi M, Daimaru Y, Enjoji M, Shinohara N. Intramuscular myxoma: a clinicopathologic, immunohistochemical, and electron microscopic study. *Cancer* (1986) 58:740–7. doi:10.1002/1097-0142(19860801)58:3<740::AID-CNCR2820580322>3.0.CO;2-K

7. Heymans O, Gebhart M, Alexiou J, de Saint Aubain N, Larsimont D. Intramuscular myxoma. *Acta Chir Belg* (1998) 98:120–2. doi:10.1080/00015458.1998.12098394

8. Allen PW. Myxoma is not a single entity: a review of the concept of myxoma. *Ann Diagn Pathol* (2000) 4:99–123. doi:10.1016/S1092-9134(00)90019-4

9. Murphey MD, McRae GA, Fanburg-Smith JC, Temple HT, Levine AM, Aboulafia AJ. Imaging of soft-tissue myxoma with emphasis on CT and MR and comparison of radiologic and pathologic findings. *Radiology* (2002) 225:215–24. doi:10.1148/radiol.2251011627

10. Okamoto S, Hisaoka M, Ushijima M, Nakahara S, Toyoshima S, Hashimoto H. Activating Gs(alpha) mutation in intramuscular myxomas with and without fibrous dysplasia of bone. *Virchows Archiv* (2000) 437:133–7. doi:10.1007/s004280000217

11. Schwindinger WF, Francomano CA, Levine MA. Identification of a mutation in the gene encoding the alpha subunit of the stimulatory G protein of adenylyl cyclase in McCune-Albright syndrome. *Proc Natl Acad Sci* (1992) 89:5152–6. doi:10.1073/pnas.89.11.5152

12. Shenker A, Weinstein LS, Moran A, Pescovitz OH, Charest NJ, Boney CM, et al. Severe endocrine and nonendocrine manifestations of the McCune-Albright syndrome associated with activating mutations of stimulatory G protein Gs. *J Pediatr* (1993) 123:509–18. doi:10.1016/S0022-3476(05)80943-6

13. Shenker A, Weinstein LS, Sweet DE, Spiegel AM. An activating Gs alpha mutation is present in fibrous dysplasia of bone in the McCune-Albright syndrome. *J Clin Endocrinol Metab* (1994) 79:750–5. doi:10.1210/jcem.79.3.8077356

14. Weinstein LS, Shenker A, Gejman PV, Merino MJ, Friedman E, Spiegel AM. Activating mutations of the stimulatory G protein in the McCune–albright syndrome. *New Engl J Med* (1991) 325:1688–95. doi:10.1056/NEJM199112123252403

15. More A, Ito I, Haridas V, Chowdhury S, Gu Y, Dickson P, et al. Oncogene addiction to GNAS in GNASR201 mutant tumors. *Oncogene* (2022) 41:4159–68. doi:10.1038/s41388-022-02388-6

16. O'Hayre M, Vázquez-Prado J, Kufareva I, Stawiski EW, Handel TM, Seshagiri S, et al. The emerging mutational landscape of G proteins and G-protein-coupled receptors in cancer. *Nat Rev Cancer* (2013) 13:412–24. doi:10.1038/nrc3521

17. Weinstein LS, Chen M, Xie T, Liu J. Genetic diseases associated with heterotrimeric G proteins. *Trends Pharmacol Sci* (2006) 27:260–6. doi:10.1016/j.tips.2006.03.005

18. Delaney D, Diss TC, Presneau N, Hing S, Berisha F, Idowu BD, et al. GNAS1 mutations occur more commonly than previously thought in intramuscular myxoma. *Mod Pathol* (2009) 22:718–24. doi:10.1038/modpathol.2009.32

19. Walther I, Walther BM, Chen Y, Petersen I. Analysis of GNAS1 mutations in myxoid soft tissue and bone tumors. *Pathol Res Pract* (2014) 210:1–4. doi:10.1016/j.prp.2013.09.003

20. Bekers EM, Eijkelenboom A, Rombout P, van Zwam P, Mol S, Ruijter E, et al. Identification of novel GNAS mutations in intramuscular myxoma using next-generation sequencing with single-molecule tagged molecular inversion probes. *Diagn Pathol* (2019) 14:15. doi:10.1186/s13000-019-0787-3

21. Sunitsch S, Gilg MM, Kashofer K, Gollowitsch F, Leithner A, Liegl-Atzwanger B. Detection of GNAS mutations in intramuscular/cellular myxomas as diagnostic tool in the classification of myxoid soft tissue tumors. *Diagn Pathol* (2018) 13:52. doi:10.1186/s13000-018-0734-8

22. Libbrecht L, Bempt IV, Schubert T, Sciot R, Galant C. Next generation sequencing for GNAS uncovers CD34 as a sensitive marker for intramuscular myxoma. *Ann Diagn Pathol* (2019) 43:151409. doi:10.1016/j.anndiagpath.2019.151409

23. Bartuma H, Möller E, Collin A, Domanski HA, Von Steyern FV, Mandahl N, et al. Fusion of the FUS and CREB3L2 genes in a supernumerary ring chromosome in low-grade fibromyxoid sarcoma. *Cancer Genet Cytogenet* (2010) 199:143–6. doi:10.1016/j.cancergencyto.2010.02.011

24. Mertens F, Fletcher CDM, Antonescu CR, Coindre J-M, Colecchia M, Domanski HA, et al. Clinicopathologic and molecular genetic characterization of low-grade fibromyxoid sarcoma, and cloning of a novel FUS/CREB3L1 fusion gene. *Lab Invest* (2005) 85:408–15. doi:10.1038/labinvest.3700230

25. Mentzel T, Calonje E, Wadden C, Camplejohn RS, Beham A, Smith MA, et al. Myxofibrosarcoma. Clinicopathologic analysis of 75 cases with emphasis on the low-grade variant. *Am J Surg Pathol* (1996) 20:391–405. doi:10.1097/00000478-199604000-00001

26. Ogilvie CM, Torbert JT, Finstein JL, Fox EJ, Lackman RD. Clinical utility of percutaneous biopsies of musculoskeletal tumors. *Clin Orthop Relat Res* (2006) 450:95–100. doi:10.1097/01.blo.0000229302.52147.c7

27. Panagopoulos I, Gorunova L, Lobmaier I, Bjerkehagen B, Heim S. Karyotyping and analysis of GNAS locus in intramuscular myxomas. *Oncotarget* (2017) 8:22086–94. doi:10.18632/oncotarget.14986

28. Fecteau RE, Lutterbaugh J, Markowitz SD, Willis J, Guda K. GNAS mutations identify a set of right-sided, RAS mutant, villous colon cancers. *PLoS One* (2014) 9:e87966. doi:10.1371/journal.pone.0087966

29. Dal Molin M, Matthaei H, Wu J, Blackford A, Debeljak M, Rezaee N, et al. Clinicopathological correlates of activating GNAS mutations in intraductal papillary mucinous neoplasm (IPMN) of the pancreas. *Ann Surg Oncol* (2013) 20:3802–8. doi:10.1245/s10434-013-3096-1

30. Gal S. Sequencing of double-stranded PCR products. In: Graham CA, Hill AJM, editors. *DNA sequencing protocols*. New Jersey: Humana Press (1993). p. 183–90. doi:10.1385/0-89603-248-5:183

31. Dorit RL, Ohara O, Hwang CB-C, Kim JB, Blackshaw S. Direct DNA sequencing of PCR products. In: Ausubel FM, Brent R, Kingston RE, Moore DD, Seidman JG, Struhl K, editors. *Current protocols in molecular biology*. Hoboken, NJ, USA: John Wiley and Sons, Inc. (2001). doi:10.1002/0471142727.mb1502s56

32. Sanger F, Nicklen S, Coulson AR. DNA sequencing with chain-terminating inhibitors. *Proc Natl Acad Sci U S A* (1977) 74:5463–7. doi:10.1073/pnas.74.12.5463

33. Bevan IS, Rapley R, Walker MR. Sequencing of PCR-amplified DNA. *PCR Methods Appl* (1992) 1:222–8. doi:10.1101/gr.1.4.222

34. Kretz K, Callen W, Hedden V. Cycle sequencing. *PCR Methods Appl* (1994) 3:S107–12. doi:10.1101/gr.3.5.s107

35. Mardis ER. The impact of next-generation sequencing on cancer genomics: from discovery to clinic. *Cold Spring Harb Perspect Med* (2019) 9:a036269. doi:10.1101/cshperspect.a036269

36. Baudhuin LM, Lagerstedt SA, Klee EW, Fadra N, Oglesbee D, Ferber MJ. Confirming variants in next-generation sequencing panel testing by sanger sequencing. *J Mol Diagn* (2015) 17:456–61. doi:10.1016/j.jmoldx.2015.03.004

37. Mu W, Lu H-M, Chen J, Li S, Elliott AM. Sanger confirmation is required to achieve optimal sensitivity and specificity in next-generation sequencing panel testing. *J Mol Diagn* (2016) 18:923–32. doi:10.1016/j.jmoldx.2016.07.006

38. De Cario R, Kura A, Suraci S, Magi A, Volta A, Marcucci R, et al. Sanger validation of high-throughput sequencing in genetic diagnosis: still the best practice? *Front Genet* (2020) 11:592588. doi:10.3389/fgene.2020.592588

39. Nagahashi M, Shimada Y, Ichikawa H, Kameyama H, Takabe K, Okuda S, et al. Next generation sequencing-based gene panel tests for the management of solid tumors. *Cancer Sci* (2019) 110:6–15. doi:10.1111/cas.13837

40. Colomer R, Miranda J, Romero-Laorden N, Hornedo J, González-Cortijo L, Mouron S, et al. Usefulness and real-world outcomes of next generation sequencing testing in patients with cancer: an observational study on the impact of selection based on clinical judgement. *EClinicalMedicine* (2023) 60:102029. doi:10.1016/j.eclinm.2023.102029

41. Mauer CB, Pirzadeh-Miller SM, Robinson LD, Euhus DM. The integration of next-generation sequencing panels in the clinical cancer genetics practice: an institutional experience. *Genet Med* (2014) 16:407–12. doi:10.1038/gim.2013.160

42. Tate JG, Bamford S, Jubb HC, Sondka Z, Beare DM, Bindal N, et al. COSMIC: the Catalogue of somatic mutations in cancer. *Nucleic Acids Res* (2019) 47: D941–D947. doi:10.1093/nar/gky1015

43. Panagopoulos I, Gorunova L, Lund-Iversen M, Andersen K, Andersen HK, Lobmaier I, et al. Cytogenetics of spindle cell/pleomorphic lipomas: karyotyping and FISH analysis of 31 tumors. *Cancer Genomics Proteomics* (2018) 15:193–200. doi:10.21873/cgp.20077

44. McGowan-Jordan J, Hastings R, Moore S, editors. *ISCN 2020: an international System for human cytogenomic nomenclature*. Karger (2020). p. 164. doi:10.1159/isbn.978-3-318-06867-2

45. Altschul SF, Gish W, Miller W, Myers EW, Lipman DJ. Basic local alignment search tool. *J Mol Biol* (1990) 215:403–10. doi:10.1016/S0022-2836(05)80360-2

46. Smith SC, Poznanski AA, Fullen DR, Ma L, McHugh JB, Lucas DR, et al. CD34-positive superficial myxofibrosarcoma: a potential diagnostic pitfall. *J Cutan Pathol* (2013) 40:639–45. doi:10.1111/cup.12158

47. Sugiura Y, Machinami R, Matsumoto S, Kanda H, Ae K, Takazawa Y, et al. Prognostic value of CD34 expression status in patients with myxofibrosarcomas and undifferentiated pleomorphic sarcomas. *Sci Rep* (2021) 11:15494. doi:10.1038/s41598-021-94834-w

48. Smits AJJ, Kummer JA, de Bruin PC, Bol M, van den Tweel JG, Seldenrijk KA, et al. The estimation of tumor cell percentage for molecular testing by pathologists is not accurate. *Mod Pathol* (2014) 27:168–74. doi:10.1038/modpathol.2013.134

49. Lhermitte B, Egele C, Weingertner N, Ambrosetti D, Dadone B, Kubiniek V, et al. Adequately defining tumor cell proportion in tissue samples for molecular testing improves interobserver reproducibility of its assessment. *Virchows Archiv* (2017) 470:21–7. doi:10.1007/s00428-016-2042-6

50. Sreekantaiah C, Karakousis CP, Leong SP, Sandberg AA. Trisomy 8 as a nonrandom secondary change in myxoid liposarcoma. *Cancer Genet Cytogenet* (1991) 51:195–205. doi:10.1016/0165-4608(91)90132-e

51. Bridge JA, Swarts SJ, Buresh C, Nelson M, Degenhardt JM, Spanier S, et al. Trisomies 8 and 20 characterize a subgroup of benign fibrous lesions arising in both soft tissue and bone. *Am J Pathol* (1999) 154:729–33. doi:10.1016/S0002-9440(10)65319-9

52. Paulsson K, Johansson B. Trisomy 8 as the sole chromosomal aberration in acute myeloid leukemia and myelodysplastic syndromes. *Pathol Biol (Paris)* (2007) 55:37–48. doi:10.1016/j.patbio.2006.04.007

53. Hemsing AL, Hovland R, Tsykunova G, Reikvam H. Trisomy 8 in acute myeloid leukemia. *Expert Rev Hematol* (2019) 12:947–58. doi:10.1080/17474086.2019.1657400

54. Broberg K, Toksvig-Larsen S, Lindstrand A, Mertens F. Trisomy 7 accumulates with age in solid tumors and non-neoplastic synovia. *Genes Chromosomes Cancer* (2001) 30:310–5. doi:10.1002/1098-2264(2000)9999:9999<::aid-gcc1096>3.0.co;2-c

55. Swansbury J. Cytogenetic and genetic studies in solid tumors: background. *Methods Mol Biol* (2003) 220:125–33. doi:10.1385/1-59259-363-1:125

56. Johansson B, Heim S, Mandahl N, Mertens F, Mitelman F. Trisomy 7 in nonneoplastic cells. *Genes Chromosomes Cancer* (1993) 6:199–205. doi:10.1002/gcc.2870060402

57. Hayashi K. PCR-SSCP: a simple and sensitive method for detection of mutations in the genomic DNA. *PCR Methods Appl* (1991) 1:34–8. doi:10.1101/gr.1.1.34

58. Riminucci M, Fisher LW, Majolagbe A, Corsi A, Lala R, De Sanctis C, et al. A novel GNAS1 mutation, R201G, in McCune-albright syndrome. *J Bone Mineral Res* (1999) 14:1987–9. doi:10.1359/jbmr.1999.14.11.1987

59. Liang Q, Wei M, Hodge L, Fanburg-Smith JC, Nelson A, Miettinen M, et al. Quantitative analysis of activating alpha subunit of the G protein (Gsα) mutation by pyrosequencing in fibrous dysplasia and other bone lesions. *J Mol Diagn* (2011) 13:137–42. doi:10.1016/j.jmoldx.2010.10.003

60. Romanet P, Philibert P, Fina F, Cuny T, Roche C, Ouafik L, et al. Using digital droplet polymerase chain reaction to detect the mosaic GNAS mutations in whole blood DNA or circulating cell-free DNA in fibrous dysplasia and McCune-albright syndrome. *J Pediatr* (2019) 205:281–5. doi:10.1016/j.jpeds.2018.09.070

61. Lin Y-L, Ma R, Li Y. The biological basis and function of GNAS mutation in pseudomyxoma peritonei: a review. *J Cancer Res Clin Oncol* (2020) 146:2179–88. doi:10.1007/s00432-020-03321-8

62. Weinstein LS, Liu J, Sakamoto A, Xie T, Chen M. Minireview: GNAS: normal and abnormal functions. *Endocrinology* (2004) 145:5459–64. doi:10.1210/en.2004-0865

63. Weinstein LS, Yu S, Warner DR, Liu J. Endocrine manifestations of stimulatory G protein alpha-subunit mutations and the role of genomic imprinting. *Endocr Rev* (2001) 22:675–705. doi:10.1210/edrv.22.5.0439

64. Khan SK, Yadav PS, Elliott G, Hu DZ, Xu R, Yang Y. Induced GnasR201H expression from the endogenous Gnas locus causes fibrous dysplasia by up-regulating Wnt/β-catenin signaling. *Proc Natl Acad Sci U S A* (2018) 115:E418–E427. doi:10.1073/pnas.1714313114

65. Nomura R, Saito T, Mitomi H, Hidaka Y, Lee S, Watanabe S, et al. GNAS mutation as an alternative mechanism of activation of the Wnt/β-catenin signaling pathway in gastric adenocarcinoma of the fundic gland type. *Hum Pathol* (2014) 45:2488–96. doi:10.1016/j.humpath.2014.08.016

66. Wilson CH, McIntyre RE, Arends MJ, Adams DJ. The activating mutation R201C in GNAS promotes intestinal tumourigenesis in Apc(Min/+) mice through activation of Wnt and ERK1/2 MAPK pathways. *Oncogene* (2010) 29:4567–75. doi:10.1038/onc.2010.202

67. Tirosh A, Jin DX, De Marco L, Laitman Y, Friedman E. Activating genomic alterations in the Gs alpha gene (GNAS) in 274 694 tumors. *Genes Chromosomes Cancer* (2020) 59:503–16. doi:10.1002/gcc.22854

68. Zhao X, Deng P, Iglesias-Bartolome R, Amornphimoltham P, Steffen DJ, Jin Y, et al. Expression of an active Gαs mutant in skeletal stem cells is sufficient and necessary for fibrous dysplasia initiation and maintenance. *Proc Natl Acad Sci U S A* (2018) 115:E428–E437. doi:10.1073/pnas.1713710115

69. Zhadina M, Roszko KL, Geels RES, de Castro LF, Collins MT, Boyce AM. Genotype-phenotype correlation in fibrous dysplasia/McCune-albright syndrome. *J Clin Endocrinol Metab* (2021) 106:1482–90. doi:10.1210/clinem/dgab053

70. Lumbroso S, Paris F, Sultan CEuropean Collaborative Study. Activating Gsalpha mutations: analysis of 113 patients with signs of McCune-Albright syndrome--a European Collaborative Study. *J Clin Endocrinol Metab* (2004) 89:2107–13. doi:10.1210/jc.2003-031225

71. Jour G, Oultache A, Sadowska J, Mitchell T, Healey J, Nafa K, et al. GNAS mutations in fibrous dysplasia: a comparative study of standard sequencing and locked nucleic acid PCR sequencing on decalcified and nondecalcified formalin-fixed paraffin-embedded tissues. *Appl Immunohistochem Mol Morphol* (2016) 24:660–7. doi:10.1097/PAI.0000000000000242

72. Wheeler EC, Vora S, Mayer D, Kotini AG, Olszewska M, Park SS, et al. Integrative RNA-omics discovers *GNAS* alternative splicing as a phenotypic driver of splicing factor–mutant neoplasms. *Cancer Discov* (2022) 12:836–55. doi:10.1158/2159-8290.CD-21-0508

73. Meyer AP, Forrest ME, Nicolau S, Wiszniewski W, Bland MP, Tsao C, et al. Pathogenic missense variants altering codon 336 of *GARS1* lead to divergent dominant phenotypes. *Hum Mutat* (2022) 43:869–76. doi:10.1002/humu.24372

74. Roeber S, Grasbon-Frodl E-M, Windl O, Krebs B, Xiang W, Vollmert C, et al. Evidence for a pathogenic role of different mutations at codon 188 of PRNP. *PLoS One* (2008) 3:e2147. doi:10.1371/journal.pone.0002147

75. White KA, Ruiz DG, Szpiech ZA, Strauli NB, Hernandez RD, Jacobson MP, et al. Cancer-associated arginine-to-histidine mutations confer a gain in pH sensing to mutant proteins. *Sci Signal* (2017) 10:eaam9931. doi:10.1126/scisignal.aam9931

Pathology & Oncology Research | frontiers

TYPE Original Research
PUBLISHED 28 March 2024
DOI 10.3389/pore.2024.1611590

Check for updates

OPEN ACCESS

EDITED BY
József Tímár,
Semmelweis University, Hungary

*CORRESPONDENCE
Jörg Kumbrink,
joerg.kumbrink@med.uni-muenchen.de

RECEIVED 16 November 2023
ACCEPTED 15 March 2024
PUBLISHED 28 March 2024

CITATION
Kumbrink J, Demes M-C, Jeroch J, Bräuninger A, Hartung K, Gerstenmaier U, Marienfeld R, Hillmer A, Bohn N, Lehning C, Ferch F, Wild P, Gattenlöhner S, Möller P, Klauschen F and Jung A (2024), Development, testing and validation of a targeted NGS-panel for the detection of actionable mutations in lung cancer (NSCLC) using anchored multiplex PCR technology in a multicentric setting. *Pathol. Oncol. Res.* 30:1611590. doi: 10.3389/pore.2024.1611590

COPYRIGHT
© 2024 Kumbrink, Demes, Jeroch, Bräuninger, Hartung, Gerstenmaier, Marienfeld, Hillmer, Bohn, Lehning, Ferch, Wild, Gattenlöhner, Möller, Klauschen and Jung. This is an open-access article distributed under the terms of the Creative Commons Attribution License (CC BY). The use, distribution or reproduction in other forums is permitted, provided the original author(s) and the copyright owner(s) are credited and that the original publication in this journal is cited, in accordance with accepted academic practice. No use, distribution or reproduction is permitted which does not comply with these terms.

Development, testing and validation of a targeted NGS-panel for the detection of actionable mutations in lung cancer (NSCLC) using anchored multiplex PCR technology in a multicentric setting

Jörg Kumbrink[1,2]*, Melanie-Christin Demes[3], Jan Jeroch[3], Andreas Bräuninger[4], Kristin Hartung[4], Uwe Gerstenmaier[5], Ralf Marienfeld[5], Axel Hillmer[6], Nadine Bohn[7], Christina Lehning[7], Ferdinand Ferch[7], Peter Wild[3], Stefan Gattenlöhner[4], Peter Möller[5], Frederick Klauschen[1,2] and Andreas Jung[1,2]

[1]Institute of Pathology, Faculty of Medicine, Ludwig Maximilian University of Munich (LMU), Munich, Germany, [2]German Cancer Consortium (DKTK), Partner Site Munich, Munich, Germany, [3]Dr. Senckenberg Institute of Pathology, University Hospital Frankfurt, Frankfurt, Germany, [4]Institute of Pathology, Justus Liebig University Giessen, Giessen, Germany, [5]Institute of Pathology, University Ulm, Ulm, Germany, [6]Institute of Pathology, University Hospital Cologne, Cologne, Germany, [7]Archer, Boulder, CO, United States

Lung cancer is a paradigm for a genetically driven tumor. A variety of drugs were developed targeting specific biomarkers requiring testing for tumor genetic alterations in relevant biomarkers. Different next-generation sequencing technologies are available for library generation: 1) anchored multiplex-, 2) amplicon based- and 3) hybrid capture-based-PCR. Anchored multiplex PCR-based sequencing was investigated for routine molecular testing within the national Network Genomic Medicine Lung Cancer (nNGM). Four centers applied the anchored multiplex ArcherDX-Variantplex nNGMv2 panel to re-analyze samples pre-tested during routine diagnostics. Data analyses were performed by each center and compiled centrally according to study design. Pre-defined standards were utilized, and panel sensitivity was determined by dilution experiments. nNGMv2 panel sequencing was successful in 98.9% of the samples (N = 90). With default filter settings, all but two potential *MET* exon 14 skipping variants were identified at similar allele frequencies. Both *MET* variants were found with an adapted calling filter. Three additional variants (*KEAP1*, *STK11*, *TP53*) were called that were not identified in pre-testing analyses. Only total DNA amount but not a qPCR-based DNA quality score correlated with average coverage. Analysis was successful with a DNA input as low as 6.25 ng. Anchored multiplex PCR-based sequencing (nNGMv2) and a

sophisticated user-friendly Archer-Analysis pipeline is a robust and specific technology to detect tumor genetic mutations for precision medicine of lung cancer patients.

KEYWORDS

lung cancer, targeted therapy, next-generation sequencing panel, anchored multiplex PCR, actionable mutations

Introduction

Lung cancer, specifically non-small cell lung cancer (NSCLC), covering the large entity of adenocarcinomas of the lung, is a paradigm for precision medicine as there are several tumor drivers known for which targeted drugs have been developed, tested and approved by legal bodies, e.g., EMA (European Medicines Agency), FDA (Food and Drug Administration) and many others [1, 2]. In precision medicine, therapies are patient tailored (personalized medicine) depending on the genetic make-up of the tumor which has to be determined by molecular diagnostics also known as companion diagnostic or theranostic in this context [3–5]. Due to the many known tumor genetic alterations found in lung cancer on the one hand and low amounts of tissue (biopsy, aspirates) on the other hand it is of great advantage to run molecular pathological analyses using multiplexing systems. Thus, NGS (next-generation sequencing) is a good choice and therefore used by many laboratories [6].

In Germany, the national consortium nNGM (national Network Genomic Medicine lung cancer) was established to provide central high quality and continuously advanced diagnostic testing of lung cancer patients from university hospitals, specialized lung clinics and local practices by more than 20 regional university pathology centers. This structure warrants both expertise and up to date molecular pathological diagnostics for the daily care of lung cancer patients [7].

The nNGM follows the strategy to provide a cost-effective analysis of genes/biomarkers that are associated with therapeutic options (EMA approved drugs) or are investigated in German clinical trials which can be reimbursed by German health insurances. However, the reimbursement contract hardly covers the costs for utilization of larger NGS panels. Therefore, a small panel covering mutation hotspots/biomarkers in NSCLC was designed.

The nNGM algorithm includes besides immunostaining of certain markers (e.g., PD-L1) the parallel analyses for single and small multi nucleotide variants on DNA level as well as testing for gene fusions/translocations. Currently, the nNGM guidelines require on the one hand the NGS analysis of pre-defined genomic regions within 26 genes on DNA level. However, the NGS technology of choice is not mandatory. On the other hand, the method of choice for gene fusion/translocation/isoform analyses (*ALK*, *MET* exon 14 skipping, *NTRK1/2/3*, *ROS1*, *RET*) is not stipulated, accepting results from various validated methods including FISH (fluorescence *in situ* hybridization) and NGS (DNA- or RNA-based).

Since different methods, besides NGS, are allowed for gene fusion determination, here we only focus on the cost-effective NGS nNGM DNA panel for the determination of single nucleotide variants, insertions/deletions, duplications and splice site variants. The second version of the nNGM panel (nNGMv2) comprises: *ALK*, *BRAF*, *CTNNB1*, *EGFR*, *ERBB2*, *FGFR1*, *FGFR2*, *FGFR3*, *FGFR4*, *HRAS*, *IDH1*, *IDH2*, *KEAP1*, *KRAS*, *MAP2K1*, *MET*, *NRAS*, *NTRK1*, *NTRK2*, *NTRK3*, *PIK3CA*, *PTEN*, *RET*, *ROS1*, *STK11* and *TP53*.

Different NGS technologies are available for library generation: 1) anchored multiplex- (AMP), 2) amplicon based- (AMPL) and 3) hybrid capture-based (HCP) -PCR [8, 9].

Archer's VariantPlex technology is based on AMP and has several advantages including low required DNA-amount, high specificity, fast hands-on protocol and easy parallel sample-handling [9]. Moreover, a free sophisticated analysis pipeline is available (Archer Analysis suite, Archer DX). AMP utilizes primer extension and represents an efficient way for specific amplification of DNA (either genomic or cDNA). This technique takes advantage of two different gene specific primers (GSP1, GSP2) per target and allows the amplification of DNA of low quality and or at low amounts [9].

The aim of this multiccentric study was to establish and validate an AMP based cost-efficient NGS panel (ArcherDX VariantPlex nNGMv2), fulfilling the minimum requirements of the nNGM. Therefore, a panel was defined by the nNGM, subsequently designed by ArcherDX and finally tested and validated in a joint effort of four nNGM centers.

Materials and methods

Study design and samples

The study design is depicted in Figure 1. Briefly, the German Institutes of Pathology of the Goethe University (Frankfurt)—center CA, Justus-Liebig University Giessen (Giessen)—center CB, Ludwig-Maximilians-University (Munich)—center CC and University of Ulm (Ulm)—center CD participated in this study. Each center selected 21 to 26 DNA samples (in total 93 samples) from its archives that had been previously analyzed during routine diagnostics by panel sequencing/NGS. DNA had been isolated from formalin fixed paraffin embedded (FFPE) NSCLC

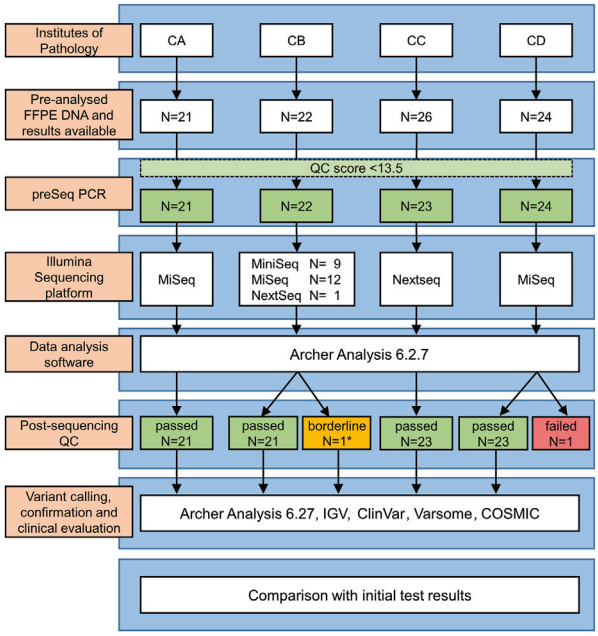

FIGURE 1
Study design. *Low leftover DNA volume (~1/3 of the recommended volume).

tumor samples. The samples were selected to 1) encompass a large repertoire of different tumor genetic variants [SNV (single nucleotide variants); ins (insertions); del (deletions); delins, dup (duplications); splice site variants; rare variants] relevant in NSCLC treatment, 2) comprise a spectrum of low to high DNA concentrations (1–392 ng/μL, median = 23 ng/μL) as well as 3) to cover a broad range of tumor cell contents (2%–90%, median = 50%). The same DNA samples which had been used for the initial routine diagnostics were enrolled in the present validation of our custom ArcherDX VariantPlex nNGMv2 panel (for simplicity mentioned from now on as nNGMv2 panel, ArcherDX, Boulder, CO, United States). In addition, two patient samples (CC-02-28 and CC-03-29) were utilized for serial DNA dilution/reduction experiments for investigating sensitivity and reproducibility. Finally, the commercial Horizon OncoSpan FFPE control (Catalog ID: HD832; Horizon Discovery Ltd., Cambridge, United Kingdom) containing 26 variants verified by NGS and digital droplet PCR of which 13 were covered by our custom panel were analyzed by two centers.

Histopathological samples and DNA extraction

Leftover DNA isolated from tissue samples of NSCLC patients was used after completion of all diagnostic analyses. Originally, sections from FFPE tissue samples were prepared followed by hematoxylin-eosin (H&E) staining of a representative slide. Areas containing appropriate densities of tumor cells (Supplementary Table S1) were defined and marked by expert pathologists and used as blueprints for transferring marked areas onto unstained serial tissue sections. Marked areas were microdissected under microscopic control and genomic DNA was subsequently isolated using QIAamp DNA Micro Kits (Qiagen, Hilden, Germany; Center CA), Maxwell RSC FFPE Plus DNA Kits (Promega, Madison, WI, United States; Center CB), GeneRead DNA FFPE Kits (Qiagen; Center CC) or Qiagen FFPE AllPrep Kits (Qiagen; Center CD) according to the respective manufacturer's instructions. DNA concentrations were measured using Qubit3 (Centers CB, CC) or −4 (Centers CA, CD) fluorimeters (Thermo Fisher Scientific, Waltham, MA, United States) (Supplementary Table S1).

Next-generation-sequencing (NGS) analyses

The routine pre-analyses were performed using Illumina or IonTorrent sequencing instruments together with different panels and analysis pipelines. All analyses used the human reference genome version 19 (hg19) for the alignment and annotation processes. The establishment/validation of the custom nNGMv2 panel analyses were conducted as follows. Briefly, the DNA quality control score (DNA QC Score) of each sample was analyzed using Archer PreSeq DNA QC KITs (ArcherDX) using 5 μL of 1 ng/μL DNA as input. A DNA QC score limit of a maximum of 13.5 was chosen. The recommended DNA input (9.4–359.0 ng; median 102.0 ng) for library preparation based on the QC score was calculated using the PreSeq Calculator.[1] NGS library preparations were performed according to the Archer VariantPlex Somatic Protocol for Illumina. Library concentration and quality were measured employing Qubit3- (Centers CC, CB) or −4 fluorimeters (Centers CA, CC, CD) (Thermo Fisher Scientific) and 2100 Bioanalyzer (Center CB, CD) or Tapestation instruments (Center CA) (Agilent Technologies, Santa Clara, CA, United States). Subsequently, libraries were sequenced on different Illumina instruments using appropriate flow cells, different library loading concentrations, cluster densities and clusters passing filters. FastQ files were generated from raw sequencing data employing Local Run Manager off-instrument 2.0 (Centers CC, CD; Illumina) and compiled to a single FastQ file per read direction per case by using a self-written python-script (FASTQ Merger v.1.0, CC) or other applications. All further analyses, including quality control and variant calling,

1 https://eu.idtdna.com/pages/support/archer-support

were performed applying the cloud-based instance Archer Analysis Unlimited Version 6.2.7. Amongst others, the following sequencing quality metrics were applied: 1) mean target coverage ≥ 100; 2) unique fragment filtered on target percent ≥ 80%; 3) unique fragment total ≥ 150,000; 4) average unique DNA start sites per GSP2 ≥ 50. Analyses that did not pass all four quality limits were evaluated individually by including additional parameters presented in Supplementary Table S2.

Variant calling, annotation and evaluation

For the initial routine analysis different analysis software and variant calling tools were used. The cut offs for minimum allele frequencies (AF) of previously reported variants were: Center CA 5%, CB 2% (1% at low tumor cell content), CC 3% and CD 5%.

During the validation of the custom nNGMv2 panel the Archer Analysis 6.2.7 default "somatic" filter applying a minimum AF of 2.7% was used. For the detection of *MET* intron variants potentially resulting in *MET* exon 14 skipping a custom filter was used with the following additional settings: Filter Consequence like "intron_variant"; Symbol is *MET*. No filter was used for variants reported in the initial routine analysis with AF below 2.7%.

Variant annotation was performed using the Archer Analysis 6.2.7 as well as the IGV (Integrative Genomics Viewer, Broad Institute, Boston, MA, United States [10]) and the COSMIC (catalogue of somatic mutations in cancer (Sanger-Cancer Center, Cambridge, United Kingdom [11]) database.

Clinical relevance of the identified tumor variants was classified by the standard evaluation algorithm of each center including the ClinVar [12], COSMIC [11] JAX CKB,[2] OncoKB [13] and Varsome [14] databases/tools. Only likely pathogenic, pathogenic and VUS (variant of unknown significance) variants were reported. Gene variants being a predictive biomarker for EMA or FDA approved targeted therapies were considered "clinically relevant." Detailed information on identified variants can be found in Supplementary Table S1.

Statistical analysis

For the correlation of sequencing parameters Spearman's test was applied using Graphpad Prism 8 (GraphPad Software, Inc., San Diego, CA, United States). Rank correlation values were considered as: very strong relationship: >0.7, strong: 0.40–0.69, moderate: 0.30–0.39, weak: 0.20–0.29. *p*-values lower than 5% ($p < 0.05$, two-sided) were defined as statistically significant.

2 https://ckb.jax.org/

Results

Design and specifications of the custom ArcherDX VariantPlex nNGMv2 panel

The nNGM (national Network Genomic Medicine lung cancer) demands the detection of defined areas including variant hot spots in 26 Genes (*ALK*, *BRAF*, *CTNNB1*, *EGFR*, *ERBB2*, *FGFR1*, *FGFR2*, *FGFR3*, *FGFR4*, *HRAS*, *IDH1*, *IDH2*, *KEAP1*, *KRAS*, *MAP2K1*, *MET*, *NRAS*, *NTRK1*, *NTRK2*, *NTRK3*, *PIK3CA*, *PTEN*, *RET*, *ROS1*, *STK11*, *TP53*). Alterations in these genes are associated with targeted therapies either approved for NSCLC or other solid tumor entities (off-label options) by the EMA, being studied in clinical trials or having other clinical indications (*TP53*). Biomarkers and associated EMA approved drugs or targeted inhibitors are summarized in Table 1.

Notably, for the detection of variants resulting in exon 14 skipping of the *MET* gene coverage of the whole intron 13 and exon 14 as well as 100 bp of intron 14 of the *MET* gene are required to cover also non canonical splice site variants located more distant from the consensus splice sites. Moreover, the nNGMv2 panel covers 12 additional single nucleotide polymorphisms [SNP, rs17793354, rs987640, rs2269355, rs321198, rs338882, rs3780962, rs6444724, rs6811238, rs9951171, rs233214 (X-Chr), rs4829207 (X-Chr), Yp11.2 (Y-Chr)] for genetic identification and verification of tissue (ID-marking) especially in situations of multiple or resistance testing.

Therefore, a specific genomic content (exons, chromosomal regions) was defined on behalf of the nNGM (AH, Cologne) and subsequently converted into the custom nNGMv2 sequencing panel based on the Archer AMP technology by Archer's design team. This panel includes unique molecular identifiers (UMIs) and was validated by the molecular pathology laboratories of the four nNGM centers University of Frankfurt (center CA), Giessen (CB), Munich (CC) and Ulm (CD). Detailed information on the covered genes, exons/introns and exact chromosomal areas are presented in Supplementary Table S3.

Study design and validation approach

The study design is depicted in Figure 1. First, each center assembled a list of NSCLCs which were pre-analyzed during routine diagnostics following nNGM regulations. A subset of cases ($N = 93$) was selected encompassing a large repertoire of tumor genetic variants relevant in NSCLC treatment and the majority of genes present in the nNGMv2 panel. Second, DNA quality was determined by qPCR (Archer PreSeq DNA QC, quality score had to be $C_T \leq 13.5$) allowing $N = 90$ (96.8%) to pass to the third step, the NGS of the samples using the newly designed nNGMv2 panel. MiniSeq (CB), MiSeq (CA, CB, CD) or NextSeq500/550 (CB, CC) sequencing devices (all Illumina) were

TABLE 1 Covered genes and associated EMA approved drugs or targeted inhibitors.

Gene	Marker	Drugs	Approved/off-label	nNGM trials
ALK	Gene fusion/translocation	Crizotinib, Alectinib, Brigatinib, Ceritinib, Lorlatinib	EMA	Yes
ALK	Resistance mutation	Brigatinib, Ceritinib, Lorlatinib	EMA	Yes
BRAF	V600	Dabrafenib/Trametinib	EMA	
BRAF	Activating mutation (non-V600)	RAF/MEK/FAK inhibitors	—	Yes
CTNNB1	Activating mutation	—	—	—
EGFR	Activating/resistance mutation	Afatinib, Dacomitinib, Erlotinib, Gefitinib, Osimertinib	EMA	Yes
EGFR	Exon 20 insertion	Amivantamab	EMA	Yes
ERBB2	Activating mutation	Trastuzumab deruxtecan	EMA (CHMP)	Yes
FGFR1	Activating mutation	FGFR inhibitors	Off-label EMA	Yes
FGFR2	Activating mutation	Pemigatinib, Erdafitinib	Off-label EMA (Pemi.)	Yes
FGFR2	Gene fusion	Pemigatinib, Futibatinib, Erdafitinib	Off-label EMA (Pemi./Futi.)	Yes
FGFR3	Activating mutation	FGFR inhibitors	Off-label EMA	Yes
FGFR4	Activating mutation	FGFR inhibitors	Off-label EMA	Yes
HRAS	Activating mutation	MEK/farnesyl transferase inhibitors	—	—
IDH1	R132	Ivosidenib	Off-label EMA	—
IDH2	Activating mutation	Enasidenib	Off-label FDA	—
KEAP1	Inactivating mutation	—	—	—
KRAS	G12C	Sotorasib	EMA	Yes
KRAS	Activating mutation	MEK/FAK inhibitors	—	Yes
MAP2K1	Activating mutation	Cobimetinib, Trametininb	Off-label EMA	—
MET	Exon 14 skipping mutation	Capmatinib, Tepotinib	EMA	Yes
NRAS	Activating mutation	MEK inhibitors	—	—
NTRK1/2/3	Gene fusion/translocation	Entrectinib, Larotrectinib	EMA	Yes
NTRK1/2/3	Resistance mutation	Larotrectinib, ALK/RET/ROS1 RTK inhibitors	(Off-label) EMA	Yes
PIK3CA	Activating mutation	PI3K/AKT inhibitors	—	—
PTEN	Inactivating mutation	—	—	—
RET	Gene fusion/translocation	Selpercatinib, Pralsetinib	EMA	Yes
RET	Activating/resistance mutation	ALK/RET/ROS1 RTK inhibitors	Off-label EMA	Yes
ROS1	Gene fusion/translocation	Crizotinib, Entrectinib	EMA	—
ROS1	Resistance mutation	ALK/RET/ROS1 RTK inhibitors	Off-label EMA	—
STK11	Inactivating mutation	—	—	Yes (ICI)
TP53	Gain/loss of funtion mutation	—	—	—

CHMP, committee for medicinal products for human use; ICI, immune checkpoint inhibitor; RTK, receptor tyrosine kinase.

used (Table 2). Fourth, for reasons of comparability, all results were analyzed applying the same Archer Analysis 6.2.7 software. $N = 89$ (98.9%) of the tested cases passed the Archer analysis pipeline and study internal quality requirements (Table 3, average values from all samples; Supplementary Table S2, values for each sample). Fifth, the resulting variant calls were annotated and evaluated for clinical relevance using not only Archer Suite's built-in annotation algorithm, but also IGV,

TABLE 2 Technical parameters.

Center	Nucleic acid extraction method	Cases (N)	Pre-testing				Archer NSCLC panel testing					
			Instrument used	Panel	Cases (N)	Analysis software	Illumina instrument used	Flow cell	Cases (N)	Loading conc. (pM)	Cluster density (K/mm^2)	Clusters passing filter (%)
CA	QIAamp® DNA Micro Kit (50) (Qiagen)	21	Ion Torrent GeneStudio S5	Thermo Fisher nNGMv2	21	Ion Reporter 5.18.4.0	MiSeq	V3	7	10	972	93.68
								V3	7	10	918	95.13
								V3	7	8	1,008	93.37
CB	Maxwell RSC FFPE Plus DNA Kit (Promega)	22	Illumina MiniSeq/ MiSeq	Qiagen nNGMv2	19	CLC Genomics Workbench 20	MiniSeq	Mid Output	5	0.8	232–274	80.77–85.21
			Illumina MiniSeq/ MiSeq	Thermo Fisher nNGMv2	3	BaseSpace Variant Interpreter	MiniSeq	High Output	4	0.8	274–309	70.96–84.48
							MiSeq	V2	1	1.7	549	97.81
							MiSeq	V2 Micro	8	1.7	861–1,571	41.40–93.14
							MiSeq	V3	3	1.7	913–1,621	79.81–94.02
							NextSeq	Mid Output	1	1.5	271	71.03
CC	GeneRead DNA FFPE Kit (Qiagen)	23	Ion Torrent GeneStudio S5 prime	Oncomine Comprehensive Assay v3	17	Ion Reporter 5.10 and in-house pipeline	NextSeq	Mid Output	23	1.6	220	87.62
			Illumina Nextseq 500	AmpliSeq forIllumina Comprehensive Panel v3	6	Local Run Manager OFF-Instrument 2.0 and in-house pipeline						
CD	AllPrep DNA/ RNA FFPE Kit (Qiagen)	22	Illumina MiSeq	Qiagen nNGMv1	6	CLC Genomics Workbench 5	MiSeq	V2	8	6.5	823	97.42
	GeneRead DNA FFPE Kit (Qiagen)	2	Illumina MiSeq	Qiagen nNGMv2	18	CLC Genomics Workbench 20.0.4		V3	16	7.5	647	98.79

10.3389/pore.2024.1611590

TABLE 3 Summary of quality control parameters of all samples.

Parameter	N	Minimum	Maximum	Confidence interval (95%)	Median	Mean	SD (mean)
DNA concentration (ng/μL)	92	1.17	392	29.49–55.3	23	42.4	61.97
DNA QC Score	92	6.64	13.24	9.762–10.31	10.02	10.04	1.321
recommended amount of DNA (ng)	92	7	332	114.9–146.5	116	130.7	75.76
DNA input quantity (ng)	92	9.4	359	99.37–128.9	102	114.1	70.97
Avg. coverage	92	19.61	6,638	2,171–2,730	2,377	2,450	1,350
Coverage 100x	92	0	100	97.9–98.53	98.67	97.3	11.36
Coverage 10x	92	50.67	100	97.71–99.87	100	98.79	5.221
Uniformity (%)	92	91	100	94.94–99.65	99	98.22	1.518
Molbar total num reads	92	7,125	7,051,206	2,215,000–2,937,000	2,019,687	2,575,975	1,744,923
Unique fragment total	92	6,460	2,833,423	828,199–1,060,000	866,423	944,007	559,209
Raw fragment filtered on target (%)	92	84.65	93.7	90.4–91.11	91.09	90.76	1.711
Unique fragment filtered on target (%)	92	79.67	92.25	86.73–87.98	88	87.36	3.016
On target deduplication ratio	92	1	8.92	2.356–3.065	2.155	2.71	1.712
Unique fragment mean length (bp)	92	80.91	217.4	144.8–155.3	152.4	150	25.46
Average unique DNA start sites per GSP2	92	12.72	909	271.6–312.2	297.9	291.9	98.2

COSMIC, Clinvar, JAX CKB, OnkoKB and Varsome. Sixth, in a final step these results were compared to those of the original analyses (Figure 1). Finally, for the determination of sensitivity and robustness of the nNGMv2-panel 1) serial DNA dilution experiments of two cases (center CC) and 2) the Horizon OncoSpan FFPE standard (centers CB and CC) were included, respectively.

Testing

All participating nNGM centers applied their own standard workflow during routine pre-testing and nNGMv2 analyses starting from nucleic acids extraction and ending with calling/annotation/evaluation of variants (Supplementary Table S1). Each center contributed more than 20 cases (21–26, average 22.5 per center, total $N = 93$, Figure 1 and Table 2) to this validation study. Subsequently, DNA quality was determined with Archer PreSeq DNA QC qPCR kits and the resulting DNA QC scores were transformed into DNA input as described in Materials and Methods. $N = 90$ (96.8%) DNA passed the test and were thus used as an input for NGS library preparation using nNGMv2 kits, sequencing, data processing and cloud-based Archer Analysis 6.2.7 as mentioned in Materials and Methods.

The Archer Analysis software 6.2.7 is available as an 1) on-premise installable virtual machine (VM, UNIX system) or 2) cloud-based instance (Archer Analysis Unlimited Version 6.2.7). In this study, a study-private instance of the cloud-based v6.2.7 was utilized for the analysis of each case. Resulting variants and annotations were revised according to the HGVS (Human Genome Variation Society [15]) nomenclature using IGV and COSMIC, which was especially necessary for variants affecting more than one base pair [multi-nucleotide variants (MNV), del, delins, dup, ins]. As mentioned above, each center evaluated the clinical/biological relevance based on their default classification system. In addition, variants, complying with HGVS rules, from all centers were submitted together with their reference NM-ID (MANE sequence) to ClinVar retrieving their pathogenic potential based on ClinVar evaluation criteria utilizing a NCBI Application Programming Interface (API)[3] in an iterative manner applying a self-written python-code (PathInfony v.1.4.4, CC) (Supplementary Table S1).

Quality control (QC)

As DNA isolated from FFPE tissue is usually of lower quality compared to fresh tissue it might be important to know the usefulness of individual DNA isolates. Information about the isolated DNA can be obtained from different parameters including DNA concentration measurement and DNA QC scores (Archer PreSeq DNA QC). Parameters indicating the

3 https://www.ncbi.nlm.nih.gov/home/develop/api/

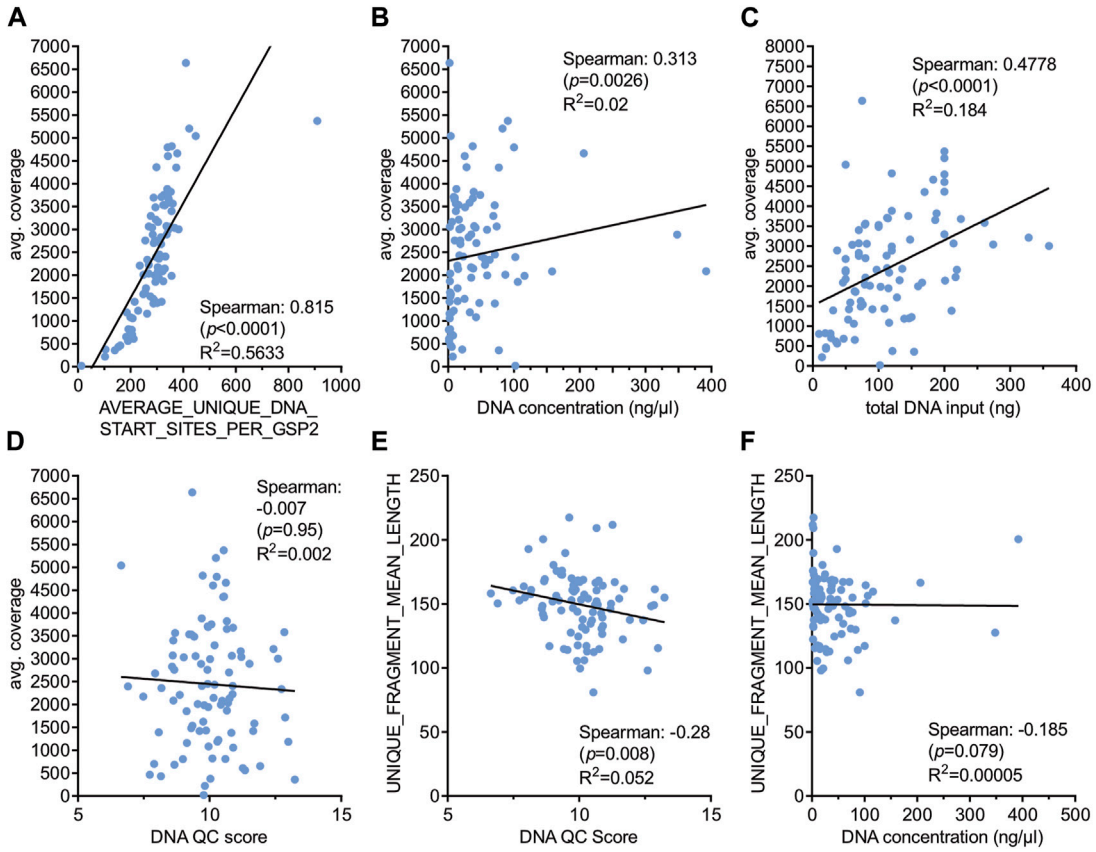

FIGURE 2
Correlation of various technical parameters with sequencing quality. Spearman correlation was performed with the indicated parameters **(A–F)** and correlation coefficients, *p*-values and R^2 values are shown. DNA QC score was determined with the Archer PreSeq DNA QC KIT as described in Materials and Methods.

quality of NGS libraries are amongst others *average coverage* and *mean length of unique fragments* of the libraries (Table 3). Expectedly, the *average number of unique start sites per GSP2* (gene specific primer) displayed a very strong correlation with *average coverage* (Spearman coefficient 0.815, $p < 0.0001$, Figure 2A) indicating the usefulness of these parameters given by the Archer analysis pipeline. Neither *DNA concentration* nor *DNA QC score* correlated with *average coverage* (Figures 2B, D) nor *fragment length* (Figures 2E, F). Only *total amounts of DNA* used as input for NGS library preparation showed a strong correlation with *average coverage* (Spearman coefficient 0.48, $p < 0.0001$, Figure 2C).

Characteristics of the VariantPlex nNGMv2 panel

To test whether reduced DNA concentration but similar total DNA input amounts influence the performance of the panel (Figure 3, Supplementary Table S4) a serial dilution of DNA from case CC-02-28, harboring a KRAS G12C alteration, was performed (44.0, 4.4, 2.6 and 0.9 ng/µL) and similar amounts of total DNA from each dilution were used for library preparation. No substantial changes regarding 1) *average coverage* (Figure 3A), 2) on *target deduplication* (Figure 3C) and 3) other parameters (Figure 3B) as well as 4) the KRAS G12C specific coverage and AF (Figure 3D) were observed indicating a high robustness of this panel. Next, a serial reduction of total input DNA (about 200, 100, 50, 25, 12.5 and 6.25 ng) of case CC-03-29 with an *EGFR* Exon 19 deletion was conducted (Figure 4, Supplementary Table S4). As expected, a continuous coverage reduction at lower DNA amounts was observed. However, even at 6.25 ng total input DNA an average UMI coverage of 494 (Figure 4A) and a target specific coverage for the *EGFR* Exon 19 deletion, much higher than the nNGM requirements for UMI panels (~100), of 697 at similar AF (Figure 4D) were achieved. Expectedly, deduplication rates, an indirect measure for the multiplicity of genomes, increased notably below 25 ng DNA input (Figure 4C). Inversely corresponding, *average unique DNA start sites per GSP2* were greatly reduced below 25 ng DNA to

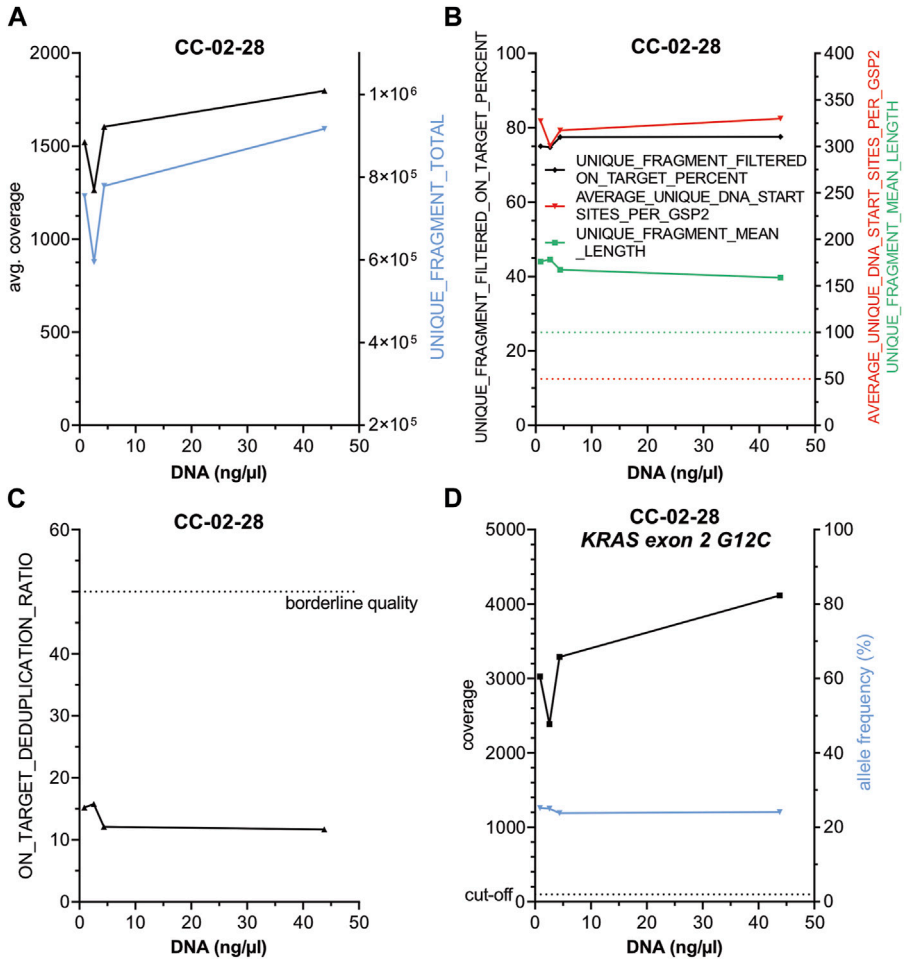

FIGURE 3
Reduction of DNA concentration does not influence the performance of the nNGMv2 panel. DNA from CC-02-28, harboring a KRAS G12C alteration, was diluted to 44, 4.4, 2.6 and 0.9 ng/µl and similar total amounts of DNA (44–50 ng) were used for library preparation. DNA concentration was plotted against the indicated sequencing quality parameters **(A–D)**. Dashed lines, cut-offs of the shown parameters.

134 at 6.25 ng but still much higher than the threshold of 50 (Figure 4B).

Taken together, these data indicate that the nNGMv2 panel performance is excellent and stable covering a broad range of DNA input conditions starting with an input as low as an equivalent of 1,000 cells in a reliable manner even in situations where the input material is of lower quality.

Performance of the nNGMv2 Archer analysis pipeline—testing of a pre-defined FFPE control tissue

In order to evaluate accuracy and specificity of the nNGMv2 panel two centers (CB and CC) subjected the Horizon OncoSpan FFPE control, comprising 13 variants that were cross validated by Horizon with NGS and digital droplet PCR and covered by this panel, to NGS (Supplementary Table S5). All 13 alterations, including three deletions, were identified by both centers and the majority of the variants (80.8%) were detected at AF within the acceptance criteria. Only one variant (PIK3CA E545K) was called by both centers at AF outside the acceptance range (7.00%–10.60%; CB, −3.71%; CC, +18.01%).

Performance of the nNGMv2 Archer analysis pipeline—comparison with pre-testing results

To investigate the performance, including specificity (variant calling) and precision (AF), of the nNGMv2 panel, the results of the Archer Analysis pipeline were compared with the outcomes of the previous routine diagnostics (N = 89; Table 4). QC parameters and variant calling limits as well as the variant

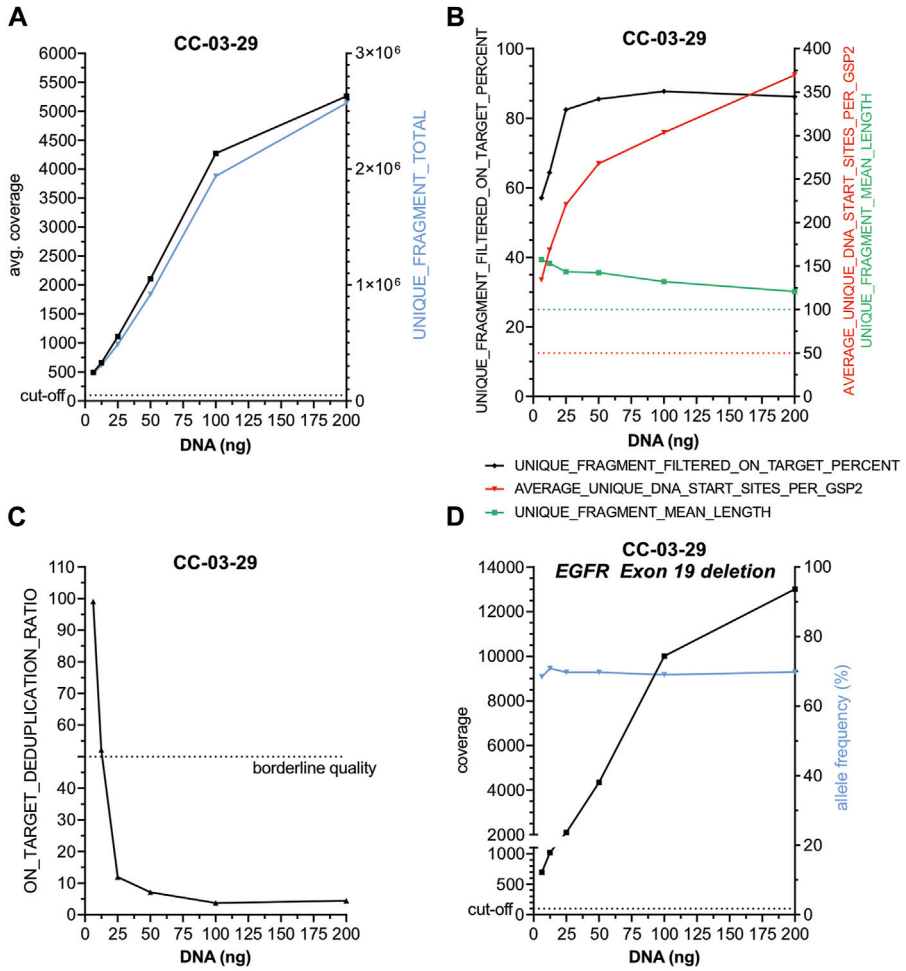

FIGURE 4
The AMP nNGMv2 panel delivers robust sequencing results with DNA input as low as 6.25 ng. Two hundred, 100, 50, 25, 12.5 and 6.25 ng DNA from case CC-03-29 harboring an EGFR Exon 19 deletion were used for library preparation. DNA amount was plotted against the indicated sequencing quality parameters **(A–D)**. Dashed lines, cut-offs of the shown parameters.

evaluation algorithm are described in detail in Materials and Methods. The pre-testing of the cases included different analysis pipelines including IonReporter, Qiagen CLC Workbench and an in-house Illumina pipeline (Tables 2, 4). Sequencing quality of the nNGMv2 panel analyses and of the various utilized Illumina systems are presented in Table 2 per center. The analyzed samples displayed tumor cell contents ranging from 2% to 90% (median = 50%) (Supplementary Table S1). In total, 192 variants were called in the pre-testing analyses in almost all (24—*ALK* and *HRAS* missing) of the 26 genes present in the nNGMv2 panel including 25 deletions (*EGFR*, *KEAP1*, *MET*, *PIK3CA*, *PTEN*, *STK11*, *TP53*), nine deletion insertions (*EGFR*, *FGFR2*, *IDH1*, *KRAS*, *MET*, *TP53*), six duplications (*EGFR*, *KEAP1*, *STK11*, *ERBB2*) and seven splice site variants (*MET*, *TP53*). All alterations but two *MET* intron 13 non-consensus splice variants that might be leading to exon 14 skipping (not confirmed on RNA level) were identified with the Archer Analysis default filter settings. When applying an adapted filter for *MET* intron variants (see Methods) both variants were called. Moreover, three additional variants that were in principle covered by the employed NGS panel (KEAP1 and STK11 truncation variants and a *TP53* point mutation) but not called during pre-testing by the utilized algorithms were identified with the nNGMv2 panel. An excellent precision of the developed panel regarding AF of the variants was also observed. The median AF difference was 0.29% and only 13 variants displayed a difference in AF greater than 10%. In summary of all validation steps, the nNGMv2 panel displayed an excellent specificity, precision as well as robustness. The panel was successfully applied to samples with low cell numbers/DNA content. However, an adapted/

TABLE 4 Summary: comparison with previous results.

		Previous analyses				Archer analyses (6.2.7)								
Center	Cases (N)	Previous analysis method	Min. % AF[a]	No. of reported variants	Wildtype cases	Successful analyses	Min. % AF[b]	Wildtype cases	No. of reported variants	Discrepant results/ variants (%)	Missing clinically relevant variants (targeted therapy)	Missing clinically relevant (targeted therapy) variants with default "somatic" filter	Additional variants	Additional variants clinically relevant (targeted therapy)
CA	21	- TF nNGMv2, AmpliSeq 2.0; IonReporter 5.18.4.0	5	36	1	21/21 (100%)	2.7	1	38	2.7	0	0	1 (+1 not covered in previous panel)	0
CB	22	- QIAseq nNGMv2; CLC20 - TF nNGMv2 Ampliseq for Illumina; basespace (3 cases)	2	67	—	22/22 (100%)	2.7	—	68	1.49	0	1**	0 (+1 not covered in previous panel)	0
CC	23	- Oncomine Comprehensive Assay v3; IonReporter 5.10 and in-house pipeline (17 cases) - AmpliSeq forIllumina Comprehensive Panel v3; Local Run Manager OFF-Instrument 2.0.0 and in-house pipeline (6 cases)	3	41	2	23/23 (100%)	2.7	2	44	2.5	0	0	1 (+4 not covered in previous panel)	0
CD	24	- Qiagen nNGM V1; CLC5 (6 cases) - Qiagen nNGM V2; CLC 20.0.4 (18 cases)	5	48	3	23/24 (95.8%)	2.7	2 (+1 wildtype failed)	47	4.26	0	1*	1	0

(Continued on following page)

10.3389/pore.2024.1611590

10.3389/pore.2024.1611590

TABLE 4 (*Continued*) Summary: comparison with previous results.

Center	Cases (N)	Previous analyses					Archer analyses (6.2.7)									
		Previous analysis method	Min. % AF[a]	No. of reported variants	Wildtype cases	Successful analyses	Min. % AF[b]	Wildtype cases	No. of reported variants	Discrepant results/ variants (%)	Missing clinically relevant variants (targeted therapy)	Missing clinically relevant (targeted therapy) variants with default "somatic" filter	Additional variants	Additional variants clinically relevant (targeted therapy)		
										Sample ID	Gene-ID	HGVS_c	HGVS_p	AF (%)		
										*CD-B2-09	MET	c.2942-21_2942-17delinsAGAA	Splicesite	19		
										**CB-02-12	MET	c.2942-35_2942-31del	Splicesite	13		

AF, allele frequency.
[a]Reduced at low tumor cell content.
[b]Default somatic filter.

second filter was required for the detection of certain more distant non-canonic *MET* exon 14 splice site alterations [16].

Discussion

Here, the AMP-based nNGMv2 panel was established and validated in a multicentric approach for potential diagnostic testing of NSCLC patient samples fulfilling the nNGM analysis requirements [7].

The AMP technique applies sample and molecular (unique molecular identifier) barcode adapter ligation to the DNA followed by usually two subsequent semi-nested PCRs each employing a different gene-specific primer (GSP1, GSP2) in combination with universal primers [9]. AMP offers several advantages compared to AMPL and HCP: 1) amplification is highly specific due to a semi-nested approach with two GSPs reducing off-target amplification, 2) easy multiplexing significantly increasing throughput and cost-effectiveness of NGS library preparation. 3) works with reduced input requirements (both amounts and quality) which is particularly beneficial when working with limited FFPE NSCLC biopsies routinely employed for molecular pathology analyses. 4) high flexibility in target selection making it easy to adapt existing panels, 5) high uniformity of libraries, 6) simple hands-on protocol. Therefore, AMP 7) is easily scalable, 8) has a fast turnaround time as summarized by Zheng et al. [9].

Here, we compare results obtained with the AMP approach (nNGMv2 panel) to results from previous analyses performed during routine testing with AMPL techniques. A direct head-to-head comparison of the techniques was not possible due to lack of sufficient DNA amounts. Nevertheless, both the pre and the AMP nNGMv2 panel testing were performed with the same DNA. Initially, 24–30 samples were selected out of more than 200 recently pre-tested (AMPL) DNAs per center. The samples were selected to encompass various different tumor genetic variants, including complex insertions/deletions and splice site variants, as well as a broad range of DNA concentrations/amounts and tumor cell contents. Moreover, sensitivity (DNA input/cell number) and precision (allele frequency) of the panel were determined by library preparation from serial dilutions of DNA from two cases or a Horizon standard, respectively. We confirmed that the AMP-based nNGMv2 panel in combination with the Archer analysis suite provides specific, reliable and robust results at high uniformity of the sequencing results even with small amounts of input material (DNA input as low as 6.25 ng/~1,000 cells).

Sequencing was successful in 98.9% of the samples ($N = 90$) even though small biopsies resulting in low DNA concentrations of <5 ng/μL (mean 42.4 ng/μL) in 21% of the samples were included. The sequencing analysis of one sample at a high DNA concentration (102 ng/μL) failed probably due to technical problems. Since all samples were previously tested at

least at acceptable quality values and thus preselected, a comparison of both techniques (AMP vs. AMPL) regarding performance cannot be performed. However, after completion of the validation study, Center CC used the AMP-based nNGMv2 panel for routine testing of about 1,000 NSCLC cases until the end of 2022. Initially, extracted DNAs from all FFPE samples were used independent of DNA concentrations for library preparation and subsequent sequencing. Nevertheless, after re-evaluation of the sequencing qualities of the first 100 cases the minimum DNA concentration threshold was set to 2 ng/μL for subsequent cases achieving >96% successful analyses (data not shown). This success rate is high in comparison with the experiences at center CC with various Ion Torrent Oncomine Assays where only 85%–90% of the sequencing analyses were successful at the same DNA concentration cutoff (data not shown). Moreover, it is possible to mix AMP NGS libraries prepared with different techniques, e.g., nNGMv2 or other panels of this type (AMP), Ampliseq for Illumina BRCA- (AMPL) as well as TSO500 HRD-panels (HCP) on a single flow cell in parallel thereby increasing flexibility. Nevertheless, it is recommendable to develop a system specific (Illumina device, flow cell, number of samples) dilution protocol before pooling all libraries as undiluted Archer AMP libraries may lead to irregular clustering depending on the amount of samples.

All but two potential *MET* exon 14 skipping variants were identified at similar allele frequencies with default filter settings in the Archer analysis suite. Both *MET* variants were found with an adapted calling filter showing that, as experienced with analysis pipelines from other sequencing systems, adjustment/refinement of the analysis algorithm is also required to obtain correct/complete results. Three additional variants (*KEAP1*, *STK11*, *TP53*) were called with the nNGMv2 panel that were not identified in the pre-testing analyses. For example, the STK11 truncation variant was not called by the Ion Reporter (5.10) although clearly present in IGV (coverage 1,463, AF 18.9%). Although all three variants do not represent direct targets for approved targeted therapies their detection is important because they might influence the efficacy of immune checkpoint inhibitors in the context of other mutations [17–19]. In this context, our results showed a similar if not even slightly better performance of the Archer analysis suite compared with analysis systems utilized in pre-testing.

It is still an often-discussed question if and how to control quality of input material for generation of NGS-libraries. Several different approaches are available including qPCR measurements of various genes, DNA bio-analyzer profile, DNA ladder amplification and/or DNA quantification [20]. In our study, we demonstrated that using total amounts of DNA as quality determining parameter is superior to a real time PCR based approach (here: Archer PreSeq DNA QC KIT). If this situation is different when applying other qPCR kits or approaches has to be tested experimentally.

Our validation study has clear limitations which are majorly due to the lack of tissue and sufficient DNA amounts as well as the high cost of NGS analyses. 1) For these reasons, a direct head-to-head comparison of the techniques (pre and AMP test) was not feasible, an inter-laboratory exchange (ring trial) was not performed and only limited intra or inter reproducibility tests were included [21]. However, the results obtained with our study design clearly showed the excellent performance of the VariantPlex nNGMv2 panel. Moreover, center CC successfully completed various external ring trials hosted by the Quality in Pathology (QuIP, Berlin, Germany) and the required internal nNGM performance and proficiency tests (including the multigene ring trial) applying the VariantPlex nNGMv2 panel. 2) The VariantPlex system does not cover the detection of gene fusions/translocations and thus is insufficient as a stand-alone biomarker test for NSCLC. Therefore, the nNGM algorithm includes parallel analysis systems for gene fusion detection such as ArcherDx FusionPlex NGS tests or FISH. Recently, ArcherDx expanded the FusionPlex system to perform parallel testing for small nucleotide variants and fusions on RNA level [22]. However, in our hands the coverage of key driver mutations is not optimal, and the corresponding allele frequencies differ significantly from those obtained on DNA level (data not shown). Since the FusionPlex Lung v2 panel is performed in parallel to DNA analysis for detection of relevant gene fusions (ALK, MET, NTRK1/2/2, RET, ROS1), it is rather recommendable for confirmation of variants identified with the VariantPlex analysis.

Taken together, we show that the AMP technology is not only versatile and easy to be used in daily routine diagnostics of NGS-panel based detection of actionable variants in lung cancer but is also a robust technique which can handle DNA of different sources and a broad range of qualities. Thus, AMP represents a suitable workhorse in the daily routine care of molecular pathology.

Data availability statement

The raw data supporting the conclusion of this article will be made available by the authors, without undue reservation.

Ethics statement

The studies involving human participants were reviewed and approved by the ethics committees of the faculties of medicine of the LMU Munich (project number: 19-542) and the Goethe University Frankfurt (project number: 19-425). The patients provided written informed consent to participate in this study. The study was conducted in accordance with the Declaration of Helsinki.

Author contributions

JK: Conceptualization, data curation, formal analysis, investigation, methodology, project administration, supervision, writing—original draft. M-CD: Conceptualization, data curation, formal analysis, investigation, methodology, writing—review editing. JJ: data curation, formal analysis, investigation. AB: Conceptualization, data curation, formal analysis, investigation, methodology, writing—review editing. KH: data curation, formal analysis, investigation. UG: Conceptualization, data curation, formal analysis, investigation, methodology, writing—review editing. RM: Conceptualization, investigation, writing—review editing. AH: formal analysis, investigation, panel design. NB, CL, and FF: Conceptualization, investigation, methodology, resources, writing—review editing. PW, SG, PM, and FK: Conceptualization, resources, writing—review editing. AJ: Conceptualization, investigation, methodology, project administration, supervision, writing—original draft.

Funding

Archer VariantPlex nNGMv2 sequencing kits, Archer PreSeq DNA QC kits and Horizon OncoSpan controls were provided by ArcherDx.

Conflict of interest

AJ received honoraria for scientific talks, participance in adboards and reimbursement of travel as well as accommodation expenses from Amgen, AstraZeneca, Bayer Pharmaceuticals, BMS, Biocartis, Boehringer Ingelheim, Merck KgA, Lilly, MSD, Novartis, QuIP GmbH, Roche Pharma, Stemline, Takeda. M-CD has received consulting fees and honoraria for lectures by Biocartis, Roche, Bayer, Janssen-Cilag, Novartis, Thermo Fisher Scientific, Molecular Health, Qiagen and Astra Zeneca. Research Support was provided by Astra Zeneca, Roche and Thermo Fisher. RM received a research grant from BMS and participated in adboards from BMS and AstraZeneca. CL, FF, and NB are affiliated with ArcherDx which supported the study.

The remaining authors declare that the research was conducted in the absence of any commercial or financial relationships that could be construed as a potential conflict of interest.

Author disclaimer

The authors are fully responsible for the content of this paper, and the views and opinions described in the publication solely reflect those of the authors.

Acknowledgments

We thank Konstanze Schleich for technical and organizational support.

Supplementary material

The Supplementary Material for this article can be found online at: https://www.por-journal.com/articles/10.3389/pore.2024.1611590/full#supplementary-material

References

1. Falcone R, Lombardi P, Filetti M, Duranti S, Pietragalla A, Fabi A, et al. Oncologic drugs approval in europe for solid tumors: overview of the last 6 years. *Cancers (Basel)* (2022) 14:889. doi:10.3390/cancers14040889

2. Oda Y, Narukawa M. Response rate of anticancer drugs approved by the Food and Drug Administration based on a single-arm trial. *BMC Cancer* (2022) 22:277. doi:10.1186/s12885-022-09383-w

3. Turner JH. An introduction to the clinical practice of theranostics in oncology. *Br J Radiol* (2018) 91:20180440. doi:10.1259/bjr.20180440

4. Herrera-Juarez M, Serrano-Gomez C, Bote-de-Cabo H, Paz-Ares L. Targeted therapy for lung cancer: beyond EGFR and ALK. *Cancer* (2023) 129:1803–20. doi:10.1002/cncr.34757

5. Khadela A, Postwala H, Rana D, Dave H, Ranch K, Boddu SHS. A review of recent advances in the novel therapeutic targets and immunotherapy for lung cancer. *Immunotherapy Lung Cancer Med Oncol* (2023) 40:152. doi:10.1007/s12032-023-02005-w

6. Morash M, Mitchell H, Beltran H, Elemento O, Pathak J. The role of next-generation sequencing in precision medicine: a review of outcomes in oncology. *J Pers Med* (2018) 8:30. doi:10.3390/jpm8030030

7. Buttner R, Wolf J, Kron A, Nationales Netzwerk Genomische M. The national Network Genomic Medicine (nNGM): model for innovative diagnostics and therapy of lung cancer within a public healthcare system. *Pathologe* (2019) 40:276–80. doi:10.1007/s00292-019-0605-4

8. Singh RR. Target enrichment approaches for next-generation sequencing applications in oncology. *Diagnostics (Basel)* (2022) 12:1539. doi:10.3390/diagnostics12071539

9. Zheng Z, Liebers M, Zhelyazkova B, Cao Y, Panditi D, Lynch KD, et al. Anchored multiplex PCR for targeted next-generation sequencing. *Nat Med* (2014) 20:1479–84. doi:10.1038/nm.3729

10. Robinson JT, Thorvaldsdottir H, Wenger AM, Zehir A, Mesirov JP. Variant review with the integrative genomics viewer. *Cancer Res* (2017) 77:e31–4. doi:10.1158/0008-5472.CAN-17-0337

11. Tate JG, Bamford S, Jubb HC, Sondka Z, Beare DM, Bindal N, et al. COSMIC: the catalogue of somatic mutations. *Cancer Nucleic Acids Res* (2019) 47:D941–D947. doi:10.1093/nar/gky1015

12. Landrum MJ, Lee JM, Benson M, Brown GR, Chao C, Chitipiralla S, et al. ClinVar: improving access to variant interpretations and supporting evidence. *Nucleic Acids Res* (2018) 46:D1062–D1067. doi:10.1093/nar/gkx1153

13. Chakravarty D, Gao J, Phillips SM, Kundra R, Zhang H, Wang J, et al. OncoKB: a precision oncology knowledge base. *JCO Precis Oncol* (2017) 2017:1–16. doi:10.1200/PO.17.00011

14. Kopanos C, Tsiolkas V, Kouris A, Chapple CE, Albarca Aguilera M, Meyer R, et al. VarSome: the human genomic variant search engine. *Bioinformatics* (2019) 35: 1978–80. doi:10.1093/bioinformatics/bty897

15. den Dunnen JT, Dalgleish R, Maglott DR, Hart RK, Greenblatt MS, McGowan-Jordan J, et al. HGVS recommendations for the description of sequence variants: 2016 update. *Hum Mutat* (2016) 37:564–9. doi:10.1002/humu.22981

16. Awad MM, Oxnard GR, Jackman DM, Savukoski DO, Hall D, Shivdasani P, et al. MET exon 14 mutations in non-small-cell lung cancer are associated with advanced age and stage-dependent MET genomic amplification and c-met overexpression. *J Clin Oncol* (2016) 34:721–30. doi:10.1200/JCO.2015.63.4600

17. West HJ, McCleland M, Cappuzzo F, Reck M, Mok TS, Jotte RM, et al. Clinical efficacy of atezolizumab plus bevacizumab and chemotherapy in KRAS-mutated non-small cell lung cancer with STK11, KEAP1, or TP53 comutations: subgroup results from the phase III IMpower150 trial. *J Immunother Cancer* (2022) 10: e003027. doi:10.1136/jitc-2021-003027

18. Marinelli D, Mazzotta M, Scalera S, Terrenato I, Sperati F, D'Ambrosio L, et al. KEAP1-driven co-mutations in lung adenocarcinoma unresponsive to immunotherapy despite high tumor mutational burden. *Ann Oncol* (2020) 31: 1746–54. doi:10.1016/j.annonc.2020.08.2105

19. Ricciuti B, Arbour KC, Lin JJ, Vajdi A, Vokes N, Hong L, et al. Diminished efficacy of programmed death-(ligand)1 inhibition in STK11- and KEAP1-mutant lung adenocarcinoma is affected by KRAS mutation status. *J Thorac Oncol* (2022) 17:399–410. doi:10.1016/j.jtho.2021.10.013

20. Dang J, Mendez P, Lee S, Kim JW, Yoon JH, Kim TW, et al. Development of a robust DNA quality and quantity assessment qPCR assay for targeted next-generation sequencing library preparation. *Int J Oncol* (2016) 49:1755–65. doi:10.3892/ijo.2016.3654

21. Jennings LJ, Arcila ME, Corless C, Kamel-Reid S, Lubin IM, Pfeifer J, et al. Guidelines for validation of next-generation sequencing-based oncology panels: a joint consensus recommendation of the association for molecular pathology and college of American pathologists. *J Mol Diagn* (2017) 19:341–65. doi:10.1016/j.jmoldx.2017.01.011

22. Desmeules P, Boudreau DK, Bastien N, Boulanger MC, Bosse Y, Joubert P, et al. Performance of an RNA-based next-generation sequencing assay for combined detection of clinically actionable fusions and hotspot mutations in NSCLC. *JTO Clin Res Rep* (2022) 3:100276. doi:10.1016/j.jtocrr.2022.100276

Pathology & Oncology Research | frontiers

TYPE Brief Research Report
PUBLISHED 29 October 2024
DOI 10.3389/pore.2024.1611875

Check for updates

OPEN ACCESS

EDITED BY
Anna Sebestyén,
Semmelweis University, Hungary

*CORRESPONDENCE
Zuzana Zemanova,
zuzana.zemanova@vfn.cz

†These authors have contributed equally to this work

RECEIVED 13 June 2024
ACCEPTED 14 October 2024
PUBLISHED 29 October 2024

CITATION
Aghova T, Lhotska H, Lizcova L, Svobodova K, Hodanova L, Janeckova K, Vucinic K, Gregor M, Konecna D, Kramar F, Soukup J, Netuka D and Zemanova Z (2024) Diagnostic challenges in complicated case of glioblastoma.
Pathol. Oncol. Res. 30:1611875.
doi: 10.3389/pore.2024.1611875

COPYRIGHT
© 2024 Aghova, Lhotska, Lizcova, Svobodova, Hodanova, Janeckova, Vucinic, Gregor, Konecna, Kramar, Soukup, Netuka and Zemanova. This is an open-access article distributed under the terms of the Creative Commons Attribution License (CC BY). The use, distribution or reproduction in other forums is permitted, provided the original author(s) and the copyright owner(s) are credited and that the original publication in this journal is cited, in accordance with accepted academic practice. No use, distribution or reproduction is permitted which does not comply with these terms.

Diagnostic challenges in complicated case of glioblastoma

Tatiana Aghova[1†], Halka Lhotska[1†], Libuse Lizcova[1], Karla Svobodova[1], Lucie Hodanova[1], Karolina Janeckova[1], Kim Vucinic[2], Martin Gregor[3], Dora Konecna[4], Filip Kramar[4], Jiri Soukup[5,6,7], David Netuka[4] and Zuzana Zemanova[1]*

[1]Center of Oncocytogenomics, Institute of Medical Biochemistry and Laboratory Diagnostics, General University Hospital and 1st Faculty of Medicine of Charles University in Prague, Prague, Czechia, [2]Laboratory of Genomics and Bioinformatics, Institute of Molecular Genetics of the Czech Academy of Sciences, Prague, Czechia, [3]Laboratory of Integrative Biology, Institute of Molecular Genetics of the Czech Academy of Sciences, Prague, Czechia, [4]Department of Neurosurgery, 1st Faculty of Medicine of Charles University and Military University Hospital Prague, Prague, Czechia, [5]Department of Pathology, 1st Faculty of Medicine of Charles University and Military University Hospital Prague, Prague, Czechia, [6]The Fingerland Department of Pathology, Charles University, Faculty of Medicine in Hradec Králové and University Hospital Hradec Králové, Hradec Králové, Czechia, [7]Department of Pathology, Charles University, First Faculty of Medicine and General University Hospital in Prague, Prague, Czechia

Glioblastoma is the commonest primary malignant brain tumor, with a very poor prognosis and short overall survival. It is characterized by its high intra- and intertumoral heterogeneity, in terms of both the level of single-nucleotide variants, copy number alterations, and aneuploidy. Therefore, routine diagnosis can be challenging in some cases. We present a complicated case of glioblastoma, which was characterized with five cytogenomic methods: interphase fluorescence *in situ* hybridization, multiplex ligation-dependent probe amplification, comparative genomic hybridization array and single-nucleotide polymorphism, targeted gene panel, and whole-genome sequencing. These cytogenomic methods revealed classical findings associated with glioblastoma, such as a lack of *IDH* and *TERT* mutations, gain of chromosome 7, and loss of chromosome 10. At least three pathological clones were identified, including one with whole-genome duplication, and one with loss of 1p and suspected loss of 19q. Deletion and mutation of the *TP53* gene were detected with numerous breakends on 17p and 20q. Based on these findings, we recommend a combined approach to the diagnosis of glioblastoma involving the detection of copy number alterations, mutations, and aneuploidy. The choice of the best combination of methods is based on cost, time required, staff expertise, and laboratory equipment. This integrated strategy could contribute directly to tangible improvements in the diagnosis, prognosis, and prediction of the therapeutic responses of patients with brain tumors.

KEYWORDS

diagnostics, cytogenomics, MLPA, I-FISH, aCGH/SNP, gene panel, WGS

Introduction

Glioblastoma is the commonest primary malignant brain tumor, and has a very poor prognosis [1] and short overall survival [2]. Historically, glioblastoma has been routinely diagnosed and classified based on its histopathology, according to a microscopic evaluation and its clinical behavior [3–5]. In recent decades, new diagnostic tools have been introduced that produce diagnostic and prognostic information that is more accurate, including interphase fluorescence *in situ* hybridization (I-FISH), multiplex ligation-dependent probe amplification (MLPA), and comparative genomic hybridization array and single-nucleotide polymorphism (aCGH/SNP) analyses [6]. Since 2008, with the introduction of next-generation sequencing (NGS) and its application to numerous diagnostic methods (e.g., whole-genome sequencing [WGS] and targeted gene panels), the simultaneous sequencing of several markers associated with tumors has become possible. The World Health Organization (WHO) and the European Association of Neuro-Oncology (EANO) recently implemented molecular diagnostic guidelines for the classification, treatment, and follow-up of glioblastoma [7, 8].

According to the current classification, glioblastoma (WHO grade 4) is defined by the following molecular features: lack of mutations in isocitrate dehydrogenase (*IDH*) genes, absence of G34R/V or K27M mutations in *H3F3A/H3F3B*, presence of mutations in the telomerase reverse transcriptase *(TERT)* gene promoter, amplification of the epidermal growth factor receptor (*EGFR)* gene, and the combined gain of chromosome 7 and loss of chromosome 10 [7, 8].

Another characteristic feature of glioblastoma is its high intra- and intertumoral heterogeneity [9, 10]. The level of intratumor genetic diversity has been shown to correlate with cancer progression and mortality [11–14]. Many types of genetic heterogeneity are associated with cancer, including single-nucleotide variants (SNVs), copy-neutral loss of heterozygosity (CN-LOH), copy number alterations (CNAs), and aneuploidy [15]. Therefore, the diagnosis of glioblastoma often poses significant challenges, requiring the integration of multiple advanced cytogenomic techniques to achieve diagnostic clarity.

Here, we present a complex case of a patient with glioblastoma. Samples obtained during routine neurosurgery were analyzed with WGS and several other cytogenomic approaches used in the routine diagnosis of brain tumors. A comparison of the results allowed us to define the advantages and limitations of these methods and to discuss any ambivalent results. This overview provides not only theoretical, but also practical insight into the complexity of glioblastoma diagnosis.

Materials and methods

Biopsy processing

The patient with glioblastoma underwent neurosurgical resection at the Department of Neurosurgery, Military University Hospital, Prague, Czech Republic. The patient gave his written consent for his biological material to be used for research purposes, in accordance with the ethical standards of the local ethic committees (Ref. No. 108/15-33/2020). Two biopsies were taken from a similar region of the brain tumor during the routine neurosurgical procedure, for diagnostic and experimental purposes. The first was used for the histopathological diagnosis of the tumor mass. The second biopsy sample was immersed in phosphate-buffered saline (PBS) containing 1% heparin (Zentiva, Prague, Czech Republic) and transferred to the Center of Oncocytogenomics, General University Hospital, Prague, Czech Republic) for further analysis. The biopsy sample was homogenized at medium speed for 45 s with a homogenizer (Minilys, Bertin Instruments, Montigny-le-Bretonneux, France), and then divided into two parts. The first part was fixed and used for I-FISH (see I-FISH protocol). The other part was centrifuged (24,000 × *g*, 5 min, 4°C) and the pellet was used for isolating genomic DNA (gDNA). The patient's peripheral blood, taken after the procedure, was placed in Vacuette 2 mL K3-EDTA tubes (Dialab, Prague, Czech Republic). The gDNA was isolated and used as a control to eliminate germline variants and copy number changes.

gDNA isolation and quantification

The gDNA was isolated from the tumor sample with the DNeasy Blood and Tissue Kit (Qiagen, Valencia, CA, United States), according to the manufacturer's protocol. The GenElute Blood Genomic DNA Kit (MERC, Darmstad, Germany) was used to isolate the peripheral blood gDNA, according to manufacturer's instructions.

The quality and quantity of gDNA were assessed with a spectrophotometer (NanoDrop 2000, Thermo Fisher Scientific, Waltham, MA, United States) and a fluorometer (Qubit 4.0, Life Technologies, Carlsbad, CA, United States). The quality of the gDNA was confirmed on 1% agarose gel, after visualization with a gel imaging system (Essential V6, Uvitec Cambridge, Cambridge, United Kingdom).

Interphase fluorescence *in situ* hybridization (I-FISH)

The homogenized tissues in PBS containing heparin were processed further with standard cytogenetic procedures (hypotonia, fixation in methanol/acetic acid). Microscopy

samples for I-FISH were prepared from fixed cell suspensions. Dual-color interphase FISH was performed with the DNA probes Vysis LSI 1p36 SpO/1q25 SpG, LSI 19q13 SpO/19p13 SpG, LSI PTEN/CEP 10, LSI TP53/CEP 17, LSI 13 (RB1)/13q34, CEP X SpO/Y SpG (Abbott Molecular, Des Plaines, IL, United States), XL EGFR amp, XL 6q21/6q23/6cen, XL CDKN2A (MetaSystems, Altlussheim, Germany), and MGMT-20-OR (Empire Genomics, Williamsville, NY, United States), according to the manufacturers' recommendations, to detect the biomarkers for glioblastoma categorization and to confirm the findings of the other methods. The slides were analyzed with an fluorescence microscope (Axio Imager Z2, Zeiss, Oberkochen, Germany) by two independent observers. The cut-off values were defined as 5% for deletions and 2.5% for gains, as described in a previous study [16].

Multiplex ligation-dependent probe amplification (MLPA)

The MLPA probe mixes (MRC Holland, Amsterdam, Netherlands) p370 BRAF-IDH1-IDH2 (version C1), p150 Glioma2 (version D3), and p088 Oligodendroglioma 1p-19q (version D1) were used to detect CNAs and selected variants of the *IDH1*, *IDH2*, and *BRAF* genes. The methylation-specific MLPA probe mix ME012 MGMT-IDH1–IDH2 (version A1) (MRC Holland, Amsterdam, Netherlands) was used to detect the methylation of the *MGMT* promoter and selected mutations in the *IDH* genes, according to the manufacturer's instructions. The PCR amplicons were analyzed with the SeqStudio Genetic Analyzer System (Applied Biosystems, Waltham, MA, United States). The acquired fragmentation data were analyzed with Coffalyser.Net (MRC Holland). MLPA probes with scores of ≥1.3 were deemed to show gains/amplifications, and those with scores of 1.15–1.29 were deemed to be the suspected gains/amplifications. MLPA probes with scores of ≤0.7 were deemed to show losses/deletions and those with scores of 0.71–0.85 were deemed to show suspected losses.

Comparative genomic hybridization array and single-nucleotide polymorphism (aCGH/SNP)

A microarray analysis (aCGH/SNP) was performed with the SurePrint G3 Human CGH Microarray Kit, 4 × 180K (Agilent Technologies, Santa Clara, CA, United States) to detect unbalanced chromosomal changes and CN-LOH. The final product was scanned with a microarray scanner system (G2565CA, Agilent Technologies) and analyzed with the CytoGenomics 5.2.0.20 software (Agilent Technologies). Unbalanced chromosomal abnormalities of >350 kb and CN-LOH regions of >10 Mb are reported.

Targeted gene panel

The Archer VariantPlex Solid Tumor Kit (IDT, Coralville, IA, United States), which detects SNVs and CNAs in 67 genes associated with solid tumors, was used to analyze the tumor samples, according to the manufacturer's recommendations. Final quantification was performed with the KAPA Library Quantification Kit (Roche, Basel, Switzerland), followed by sequencing with the NextSeq 500/550 Mid Output Kit v2 (300 Cycles) (Illumina, San Diego, CA, United States). The quality of runs was examined with Sequencing Analysis Viewer v2.4.7 (Illumina) and FASTQC v0.11.9 [17]. The analysis was performed in Archer software v7 (IDT). Only variants that met our criteria (allele frequency > 5%, quality score > 1,000, depth > 500) were considered further. The variants from the peripheral blood were compared with the variants from the glioma samples and only somatic variants were analyzed further (Supplementary Table S4).

Whole-genome sequencing (WGS)

DNA was fragmented with an ultrasonicator (M220, Covaris, Woburn, MA, United States) with the program set up for 500–600-bp fragments. The fragment length distribution was controlled with an Agilent Bioanalyzer 2100 (High Sensitivity DNA Kit) (Agilent). Sequencing libraries were prepared from the fragmented DNA (40 ng) with the NEBNext Ultra II DNA Library Prep Kit for Illumina (New England BioLabs, Ipswich, MA, United States). NEBNext Multiplex Oligos for Illumina (Dual Index Set 1) (New England BioLabs, Ipswich, MA, United States) was used to barcode the libraries. The final PCR amplification of the library included six cycles and the products were cleaned up with SPRIselect beads (Beckman Coulter, Brea, CA, United States). The library length profiles and concentrations were controlled with the Agilent Bioanalyzer (High Sensitivity DNA Kit) and fluorometer (Qubit 2.0, Life Technologies, Carlsbad, CA, United States), respectively. The libraries were mixed in equimolar ratios and commercially sequenced on a sequencing system (NovaSeq 6000, Illumina) to obtain a minimum of 5000 paired-end reads (150 bp × 150 bp).

The data analysis workflow consisted of quality control, alignment, and somatic variant calling. The analysis was performed with the nf-core/sarek pipeline v2.7.1 [18] with the default options, unless otherwise stated. Read quality was assessed with FastQC v0.11.9 [17], and the reports were combined with MultiQC v1.12 [19]. The reads were aligned to the GRCh38 human reference genome [20]. The somatic variant calling of SNVs was performed with GATK MuTect2 v4.1.7.0, Strelka v2.9.10, and the best-practice modification of Strelka, called "StrelkaBP" [21]. Structural variants (SVs) were

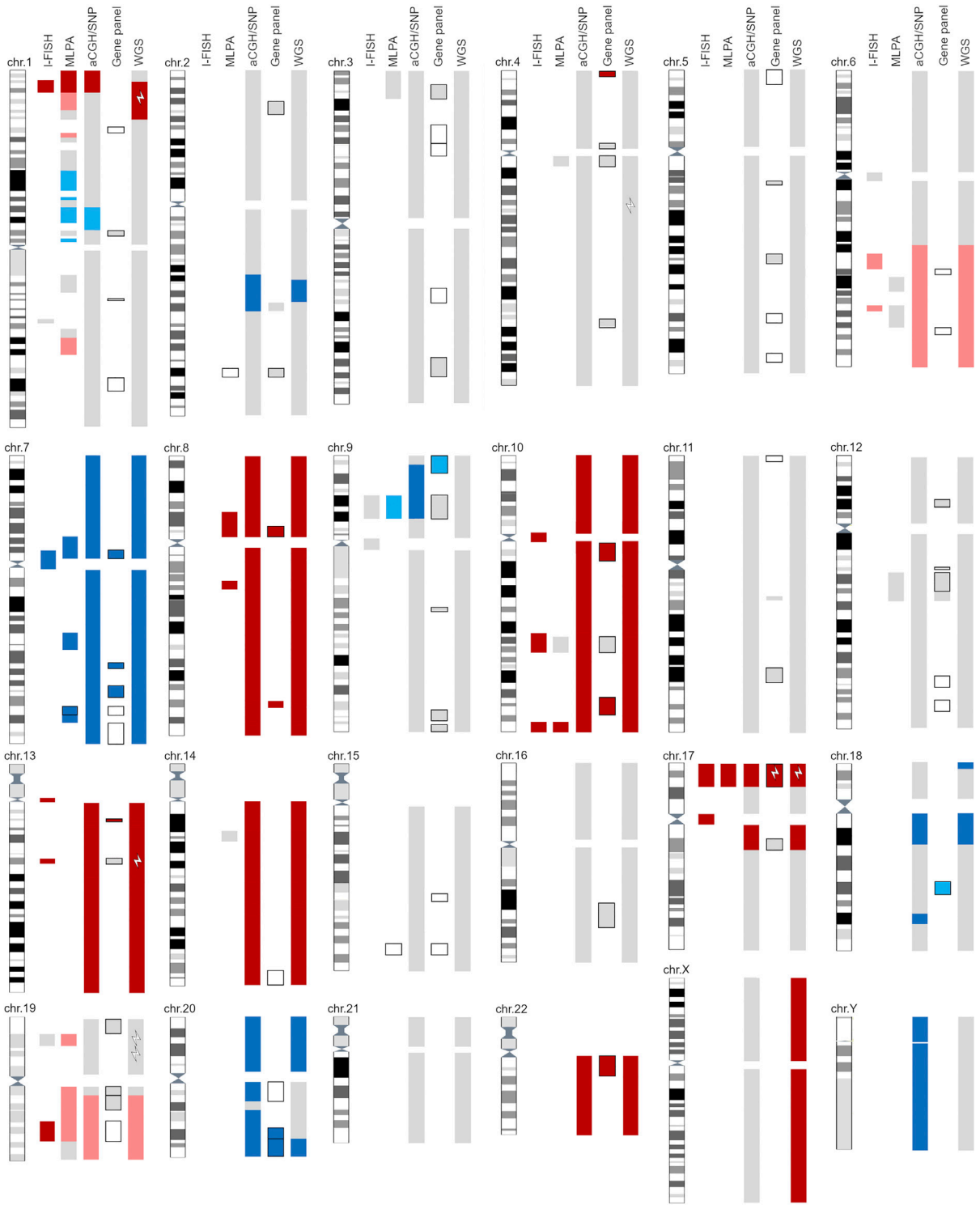

FIGURE 1
Graphic representation of all reported findings with five cytogenomics methods. Light gray—area with normal findings investigated with selected method. Dark blue—gain/amplification of designated area; light blue—suspected gain of marked area (at the border of detection limit). Dark red—loss/deletion of designated area; light red—suspected loss of marker area (at the border of detection limit). Black outlined areas indicate detection of SNVs with gene panel and/or MLPA. White lightning bolts represent positive gene mutations detected with the selected method. For detailed information, see Supplementary Material.

TABLE 1 Comparison of different cytogenomic methods for glioblastoma diagnosis.

	I-FISH	MLPA	aCGH/SNP	Gene panel	WGS
Input material	200 nuclei	15–450 ng DNA	1,000 ng DNA	1–100 ng DNA	5–100 ng DNA
PCR	No	Yes	No	Yes	Yes/no
Sequencing	No	Capillary electrophoresis	No	Illumina/others	Illumina/others
Analysis					
Wet-laboratory time	<2 days	<2 days	2–3 days	3–5 days	3–5 days
Analysis time	20 min	10 min	30 min	3 h	>3 h[a]
Analysis software	Fluorescence microscope, ISIS (MetaSystems)	Coffalyser (MRC Holland)	CytoGenomics (Agilent); GenomeStudio Software (Illumina); BlueGnome (Illumina); CytoSure Interpret Software (OGT)	Archer Software (ITD); BaseSpace (Illumina); SOPHiA DDM Platform (Sophia Genetic)	Bioinformatic pipelines
Time for interpretation of results	5 min	30 min	2 h	10 min–2 h	>2 h[a]
SNVs/mutations					
IDH1	No	Yes	No	Yes	Yes
IDH2	No	Yes	No	Yes	Yes
BRAF	No	Yes	No	Yes	Yes
EGFR	No	No	No	Yes	Yes
TP53	No	No	No	Yes	Yes
H3F3A	No	No	No	Yes	Yes
TERT promoter	No	Yes (ME012)	No	Yes	Yes
CNAs					
1p/19q co-deletion	Yes	Yes	Yes	Yes	Yes
chr 7 gain (*EGFR*)	Yes	Yes	Yes	Yes	Yes
chr 9 loss (*CDKN2A/CDKN2B*)	Yes	Yes	Yes	Yes	Yes
chr 10 loss (*PTEN, MGMT*)	Yes	Yes	Yes	Yes	Yes
ATRX loss	Yes	Yes (P013)	Yes	Yes	Yes
Polyploidy	Yes	No	No	No	Yes
CN-LOH	No	No	Yes	No	Yes
SVs	No	No	No	Yes (only specific SV)	Yes

The criteria for comparison were the input material and laboratory equipment, time for wet laboratory testing, time for analysis and interpretation, detections of the single-nucleotide variants (SNVs), copy number alterations (CNAs), copy-neutral loss of heterozygosity (CN-LOH), and structural variants (SVs).
[a]It can take from several hours up to a few days, depending on the data, analyst expertise and bioinformatic pipeline.

determined with Manta v1.6.0 [22]. CNVs, LOH, and neutral events were detected with both Control-FREEC v11.6 [23] and ASCAT v2.5.2 [24]. ASCAT was used to estimate ploidy and tumor heterogeneity. SNVs were annotated with snpEff v4.3t [25] and Ensembl Variant Effect Predictor (VEP) v99.2 [26], whereas SVs were only annotated with VEP. Both tools used the ENSEMBL annotation file GRCh38 v99. Data manipulation, report generation, and the creation of several plots were performed in R v4.1.3 [27]. Circos v0.69.8 software [28] was used to visualize the SV and CNV data in circos plot.

Results

Case presentation

In December 2020, a 65-year-old male patient experienced an epileptic seizure with postictal right-sided hemiparesis and was diagnosed with glioblastoma of the left parietal lobe. Surgery was postponed because the patient became infected with SARS-CoV-2. Two months later, the patient underwent subtotal resection of the tumor, and minimal residue was detected on a postoperative MRI scan. The patient's recovery was uncomplicated, but slight right-sided hemiparesis persisted. After the results of the histological analysis were received—glioblastoma, *IDH*-wildtype – concomitant chemoradiotherapy was recommended and begun at the end of February 2021. However, the tumor had recurred at the first check-up, 4 months after surgery. The Karnofsky performance score of the patient was 50–60. Given the rapid decline in the patient's condition, further surgery was not recommended and adjuvant chemotherapy with temozolomide was suggested as the best option. Despite oncological treatment, the tumor continued to grow. The patient died in March 2022.

A microscopic examination showed brain tissue infiltrated by a highly cellular diffuse glioma, with prominent nuclear atypia and high proliferative activity (5–6 mitoses per high-power field, including atypical mitoses). Foci of microvascular proliferation and areas of necrosis were present, with a palisade-like arrangement of tumor cells at the periphery. Immunochemistry revealed that the nuclear expression of *ATRX* was retained in all the tumor cells, there was no R132H mutation in the *IDH1* gene, loss of p53 immunoreactivity and the Ki67 index was up to 25% in highly proliferative areas (data not shown).

Cytogenomic findings

The genetic aberrations specific for glioblastoma were detected with a combination of cytogenomic methods, and the diagnosis was confirmed with histopathological analyses (Figure 1, Supplementary Tables S1–S7). No mutation of *IDH1/IDH2* was identified; nor was the G34R/V or K27M mutation in *H3F3A* or any mutation in the *TERT* promoter detected. Gain of chromosome 7 (including the *EGFR* gene) was observed (trisomy–hexasomy on I-FISH, and up to eight copies were detected with WGS). Monosomy of chromosome 10 was observed with I-FISH, aCGH/SNP, and WGS, although MLPA and the gene panel indicated an intact *PTEN* gene (Figure 1, Supplementary Table S2). Methylation of the *MGMT* promoter was not confirmed (Supplementary Table S2).

As well as glioblastoma-specific cytogenomic aberrations, additional SNAs, CNVs, SVs, and aneuploidy were detected. I-FISH and WGS detected at least three pathological clones, one of which was near-tetraploid (5%–15% interphase nuclei, depending on the selected probe; ploidy = 3.83). I-FISH detected the deletion of 1p36 and 19q13 (Figure 1, Supplementary Table S1). Other methods (MLPA, aCGH/SNP, and WGS) only identified the deletion of 1p36, and a suspected deletion of 19p (below the cut-off limit; Figure 1, Supplementary Tables S2, S3, S7).

In the near-tetraploid clone, two types of chromosomal losses were identified based on the WGS results: 1) chromosome losses with a homozygous allelotype (two copies instead of four), such as chromosomes 8, 10, 13, 14 and 22; and 2) chromosome losses with a heterozygous allelotype (three copies instead of four), such as the long arm of chromosome 6 and the loss of chromosomes 19 and 21. The same mechanism was also observed for gains (five chromosomes instead of four), such as the gain of one copy each of chromosomes 1, 9, 13 and 18 (Supplementary Figure S1).

The loss of 17p was confirmed with all the methods used. Moreover, the I-FISH analysis revealed monosomy 17 in a small cell clone (Figure 1, Supplementary Table S1). The pathogenic variant R196* of the *TP53* gene was subsequently detected with the gene panel and WGS (Supplementary Tables S4, S6).

The WGS data revealed seven SNVs that were classified as pathogenic or likely pathogenic (Tiers I/II) and 13 variants of unknown significance (Tier III) (Supplementary Table S6). WGS also confirmed SVs on nearly all chromosomes, except chromosomes 13 and 14. Among these, deletions (n = 88) were most frequent, followed by breakends (BNDs; n = 80), duplication events (n = 42), and insertions (n = 4). Two chromosomes showed the most BNDs: the short arm of chromosome 17 (17p13.1 and 17p12) with 14 BNDs (10 BNDs and 2 interchromosomal translocations) and chromosome 20 with 29 BND events (19 BNDs and 5 interchromosomal translocations) (Supplementary Figures S2, S3). Detailed results of the SV analysis are given in the Supplementary Figures S1–S3 and Supplementary Tables S6, S7.

Discussion

The findings in glioblastoma patients are usually very complex, ranging from clinically significant aberrations to complex structural rearrangements that are detectable only with methods such as WGS. In this study, we represent one case that was selected as an ideal candidate for methods presentation due to the complexity of his findings, which thoroughly tested our laboratory methodologies.

One of the most important factors influencing the prognosis of glioblastoma patients is CNAs [29], followed by SNVs [30]. Recent data have shown that gene fusions and

rearrangements are also important drivers in some brain tumors [6, 31]. All methods compared in this study detected CNAs, although with considerable differences in the numbers detected, based on their detection limits (Figure 1, Table 1, Supplementary Material). I-FISH and MLPA required several probes or kits to detect all the CNAs necessary for a molecular diagnosis of glioblastoma (Table 1). Other methods (aCGH/SNP, gene panel, WGS) detected all the important CNAs in one assay. However, in general, NGS methods (gene panels, WGS) are not optimal for large CNAs, such as the gain or deletion of whole chromosomes or chromosomal arms [32]. In our patient, the gene panel detected partial deletions of chromosomes 10 and 13, but not monosomies of the whole chromosomes (Figure 1). CNA-recognition software is based on the coverage of amplicons and the detection of outliers after the appropriate normalization step. Therefore, it is crucial to analyze several samples together, ideally with reference samples as the negative controls, and thereby improve the detection of large CNAs with gene panels.

I-FISH is the standard diagnostic method for detecting the unbalanced whole-arm translocation t(1; 19)(q10; p10), which is a typical finding in oligodendroglial tumors [7]. This rearrangement results in the whole arm 1p/19q co-deletion, which is used as an important diagnostic marker [33]. However, FISH probes only allow targeted detection of the loss of specific chromosomal regions 1p36 and 19q13 [34, 35] but do not provide information on the extent and origin of these deletions. Thus, they can lead to false-positive findings. Similarly in our patient, I-FISH detected deletion of 1p36 and 19q13, i.e., a suspected 1p/19q co-deletion. However, MLPA, aCGH/SNP and WGS analyses revealed only partial loss of the short arm of chromosome 1 (1p35p36) and the hole long arm of chromosome 19 (Figure 1), so the origin of the deletions was likely different from the recurrent t(1; 19)(q10; p10) translocation. These losses are a relatively common finding in astrocytic tumors [36, 37]. According to published data, the frequency of false-positive FISH findings of 1p/19q co-deletion in diffuse astrocytomas is estimated to be approximately 3.6% [38]. Therefore, in *IDH*-mutated gliomas, it is beneficial to investigate the 1p/19q co-deletion with two independent methods to refine the type of these deletions, as recommended by Brandner [39]. The loss of chromosome 10 was observed, although MLPA and the gene panel indicated an intact *PTEN* gene. This ambivalent result may be caused by the presence of small polyploid clones. The presence of more than two copies of chromosome 10 may affect the relative ratio calculated with these methods. The LOH on the short arm of chromosome 17 frequently occurs in human cancers, often including the region containing the *TP53* tumor suppressor gene (17p13.1; [1]). *TP53* mutations or deletions are observed in 23%–28% of patients with primary glioblastoma [40, 41]. The complete loss of the *TP53* gene is commonly associated with t(17; 20) reciprocal translocations in glioblastoma [42]. Our data confirms the translocation breakpoints at loci on 17p and 20q (Supplementary Figure S3). *TP53* alterations have been shown to be mutually exclusive with the amplifications of the *MDM* family genes *(MDM1/2/4)* and *CDKN2A* [40], which is consistent with our findings. The pathogenic variant *TP53* R196*, which was detected in our patient, was previously described by Shiraishi et al. [43].

Concurrent *TP53* mutations are twice as common in the presence of whole-genome duplication (WGD), although *TP53* dysfunction is not an obligatory event for WGD [44]. One of the most important findings that caused ambiguous results was the presence of several clones, one of which was a small near-tetraploid clone (7% of cells). Only two methods (I-FISH, WGS) could reliably detect aneuploidy. WGD leads to tetraploidy and is a common macroevolutionary event occurring early in tumorigenesis [44, 45]. Its frequency is reported to range from 11% [45, 46] to 25% in glioblastoma [47]. WGD has been associated with several molecular and clinical features, including a higher mutational burden, increased proliferation signatures, worse overall survival, and resistance to radiation therapy and chemotherapy [44, 46, 48]. WGD may also contribute to intratumor heterogeneity. Intratumoral heterogeneity has been well documented with single-cell RNA-sequencing experiments, which revealed cross-talk among four different cellular states [49, 50]. We were unable to assign our finding to these states, but at least three clones were observed based on the I-FISH and WGS results (Supplementary Figure S1). Moreover, the same pathological clone, discovered with I-FISH in diploid cells, was also present after its duplication in near-tetraploid (Supplementary Figure S1). The remaining methods (MLPA, aCGH/SNP, and gene panel) detected only the changes present in most tumor cells, and in targeted chromosomal regions (such as the long arm of chromosome 6 and the short arm of chromosome 9), so the presence of several clones with various findings led to inconclusive results.

The diagnostic routine for solid tumors currently requires that the results be delivered within 14 days of the receipt of the sample [41]. The time required for the laboratory processing range from several hours or days (I-FISH, MLPA) to ≥3 days (aCGH/SNP, gene panels, WGS), depending on the number of samples, the amount of sample delivered, and the complexity of each sample (Table 1). In terms of the time required to interpret the results, the methods that are based on gDNA analyses and that can only detect the most abundant aberrations (such as MLPA and gene panels) are less time-consuming. The time required to interpret an I-FISH analysis can be influenced by the number of pathological clones present in the sample. The challenge of WGS is the expertise and time required to interpret the full spectrum of SNAs, CNVs, and SVs [51]. Analysis and interpretation can take several hours or up to several days, depending upon the quality of the data and the number of SNVs and CNVs. Another important component of diagnostic testing is the cost of the analysis performed, which may be linked

to insurance reimbursement [52]. The most economically efficient procedure is MLPA, followed by I-FISH and aCGH/SNP. Gene panels are more cost-effective than WGS, because WGS inherently requires substantially more sequencing capacity than gene panels, and thus is more expensive. Protocols for WGS at very low depth have recently been established to reduce costs (e.g., [53]). The availability or selection of a sequencing instrument with high throughput capacity can dramatically reduce the cost of methods based on NGS. However, for small laboratories, the number of samples could also be a limitation. The time required to collect sufficient samples for NGS-based approaches or even aCGH/SNP can prolong the delivery of the results to neurosurgeons and increase the sequencing cost.

The methods compared in our study detected CNAs, SNVs, SVs, and aneuploidy, either alone or in combination. Nevertheless, these methods cannot detect the exact number of pathogenic clones, microsatellite instability, the expression of genes, and/or translocations. There are many technologies available today, including Single-cell DNA sequencing, Single-cell RNA sequencing, epigenetic profiling, optical genome mapping and circulating and tumor cell enumeration, that can together provide a comprehensive "snapshot" of an individual cancer. However, this is not economically feasible for routine practice yet.

The prevailing diagnostic method for glioblastoma is based on an investigation of several selected aberrations in a relatively short period so that the patient's treatment can begin as soon as possible. The treatment approach recommended by the National Comprehensive Cancer network (NCCN) guidelines for glioblastoma patients with good performance status (PS) includes maximal surgical removal, followed by radiotherapy and chemotherapy with temozolomide and/or participation in clinical trial [54]. The genomic findings in this case, particularly the detection of *TP53* mutations, *EGFR* amplification, and chromosomal alterations such as gain of chromosome 7 and loss of chromosome 10, carry important implications for treatment. The p53 pathway (TP53/MDM2/P14$^{arf\zeta}$) and PI3K/AKT/mTOR pathway (activated by *EGFR* gene amplification) are the main signalling pathways involved in glioblastoma tumorigenesis and are associated with resistance to standard treatments [55, 56]. Therapies targeting the *TP53* gene aim to restore normal level of p53 tumor suppressor protein through inhibition of p53/MDM2 complex [57] or MDM2 itself [58]. Similarly, *EGFR* amplification opens the potential for targeted therapies, including three generations of EGFR inhibitors [59, 60] or EGFR antibodies [61]. However, the heterogeneity observed in the tumor complicates treatment decisions, as the presence of multiple clones with varying genetic profiles suggests that single-target therapies may not be sufficient. Comprehensive molecular profiling in glioblastoma cases, as demonstrated in this study, is crucial for tailoring personalized treatment strategies and potentially improving patient outcomes.

We have shown that although the presence of several pathological clones and aneuploidy can complicate the examination of the sample, it is feasible to use a combination of modern molecular diagnostic methods. Based on the findings presented here, a combined approach involving the detection of CNAs (I-FISH, MLPA, aCGH/SNP), mutations (MLPA, gene panel), and aneuploidy (I-FISH) is recommended for routine diagnosis. The great promise for the future looks to be WGS, which can detect the most sensitive SNAs, CNVs and aneuplodies in a single analysis. The choice of the best combination of methods will be based on price, time required, staff expertise, and laboratory equipment available. This integrated strategy could contribute directly to a tangible improvement in the diagnosis, prognosis, and prediction of the therapeutic responses of patients with brain tumors.

Data availability statement

All data generated or analyzed during this study are included in this published article (and in its Supplementary Material).

Ethics statement

The studies involving humans were approved by the local ethic committee (Ref. No. 108/15-33/2020). The studies were conducted in accordance with the local legislation and institutional requirements. The participants provided their written informed consent to participate in this study. Written informed consent was obtained from the individual(s) for the publication of any potentially identifiable images or data included in this article.

Author contributions

TA, HL, and ZZ conceived and designed the study; TA, HL, LL, KS, LH, and KJ performed the cytogenomic analysis; KV and MG performed WGS; DK, DN, and FK were responsible for neurosurgical resection; JS performed the histopathological analysis; TA, HL, and ZZ wrote the first version of the manuscript. All authors contributed to the article and approved the submitted version.

Funding

The author(s) declare that financial support was received for the research, authorship, and/or publication of this article. This work was supported by grants of the Ministry of Health of Czech Republic: AZV NU21-04-00100 and MH CZ-DRO-VFN64165. Also by the Institutional Research Project of the Czech Academy

of Sciences (RVO 68378050) and the project National Institute for Cancer Research (Programme EXCELES, ID Project No. LX22NPO5102) - Funded by the European Union - Next-Generation EU.

Acknowledgments

We would like to thank all our colleagues at the Center of Oncocytogenomics. We acknowledge the department of Genomics and Bioinformatics, Institute of Molecular Genetics of the Czech Academy of Sciences for their support.

Conflict of interest

The authors declare that the research was conducted in the absence of any commercial or financial relationships that could be construed as a potential conflict of interest.

Supplementary material

The Supplementary Material for this article can be found online at: https://www.por-journal.com/articles/10.3389/pore.2024.1611875/full#supplementary-material

References

1. Rasras S, Zibara K, Vosughi T, Zayeri Z. Genetics and epigenetics of glioblastoma: therapeutic challenges. *Clin Cancer Invest J* (2018) 7:43–9. doi:10.4103/ccij.ccij_82_17

2. Stupp R, Mason WP, Van Den Bent MJ, Weller M, Fisher B, Taphoorn MJ, et al. Radiotherapy plus concomitant and adjuvant temozolomide for glioblastoma. *N Engl J Med* (2005) 352:987–96. doi:10.1056/nejmoa043330

3. Park SH, Won J, Kim SI, Lee Y, Park CK, Kim SK, et al. Molecular testing of brain tumor. *J Pathol Transl Med* (2017) 51:205–23. doi:10.4132/jptm.2017.03.08

4. Perry A, Wesseling P. Histologic classification of gliomas. *Handbook Clin Neurol* (2016) 134:71–95. doi:10.1016/B978-0-12-802997-8.00005-0

5. Pessôa IA, Amorim CK, Ferreira WAS, Sagica F, Brito JR, Othman M, et al. Detection and correlation of single and concomitant *TP53*, *PTEN*, and *CDKN2A* alterations in gliomas. *Int J Mol Sci* (2019) 20:2658–20. doi:10.3390/ijms20112658

6. Horbinski C, Ligon KL, Brastianos P, Huse JT, Venere M, Chang S, et al. The medical necessity of advanced molecular testing in the diagnosis and treatment of brain tumor patients. *Neuro-Oncol* (2019) 21:1498–508. doi:10.1093/neuonc/noz119

7. Louis DN, Perry A, Wesseling P, Brat DJ, Cree IA, Figarella-Branger D, et al. The 2021 WHO classification of tumors of the central nervous system: a summary. *Neuro-Oncol* (2021) 23:1231–51. doi:10.1093/neuonc/noab106

8. Weller M, van den Bent M, Preusser M, Le Rhun E, Tonn JC, Minniti G, et al. EANO guidelines on the diagnosis and treatment of diffuse gliomas of adulthood. *Nat Rev Clin Oncol* (2021) 18:170–86. doi:10.1038/s41571-020-00447-z

9. DeCordova S, Shastri A, Tsolaki AG, Yasmin H, Klein L, Singh SK, et al. Molecular heterogeneity and immunosuppressive microenvironment in glioblastoma. *Front Immunol* (2020) 11:1402–18. doi:10.3389/fimmu.2020.01402

10. Patel AP, Tirosh I, Trombetta JJ, Shalek AK, Gillespie SM, Wakimoto H, et al. Single-cell RNA-seq highlights intratumoral heterogeneity in primary glioblastoma. *Science* (2014) 344:1396–401. doi:10.1126/science.1254257

11. Almendro V, Marusyk A, Polyak K. Cellular heterogeneity and molecular evolution in cancer. *Ann Rev Pathol* (2013) 8:277–302. doi:10.1146/annurev-pathol-020712-163923

12. Maley CC, Galipeau PC, Finley JC, Wongsurawat VJ, Li X, Sanchez CA, et al. Genetic clonal diversity predicts progression to esophageal adenocarcinoma. *Nat Genet* (2006) 38:468–73. doi:10.1038/ng1768

13. Marusyk A, Almendro V, Polyak K. Intra-tumour heterogeneity: a looking glass for cancer? *Nat Rev Cancer* (2012) 12:323–34. doi:10.1038/nrc3261

14. Park SY, Gönen M, Kim HJ, Michor F, Polyak K. Cellular and genetic diversity in the progression of *in situ* human breast carcinomas to an invasive phenotype. *J Clin Invest* (2010) 120:636–44. doi:10.1172/JCI40724

15. Albertson DG, Pinkel D. Genomic microarrays in human genetic disease and cancer. *Hum Mol Genet* (2003) 12:145–52. doi:10.1093/hmg/ddg261

16. Zemanova Z, Michalova K, Babicka L, Pavlistova L, Jarosova M, Holzerova M, et al. Clinical relevance of complex chromosomal aberrations in bone marrow cells of 107 children with *ETV6/RUNX1* positive acute lymphoblastic leukemia (ALL). *Blood* (2006) 108:2278. doi:10.1182/blood.v108.11.2278.2278

17. Andrews S. FastQC: a quality control tool for high throughput sequence data (2010). Available from: http://www.bioinformatics.babraham.ac.uk/projects/fastqc (Accessed February 2, 2024).

18. Garcia M, Juhos S, Larsson M, Olason PI, Martin M, Eisfeldt J, et al. Sarek: a portable workflow for whole-genome sequencing analysis of germline and somatic variants. *F1000Res* (2020) 9:63. doi:10.12688/f1000research.16665.1

19. Ewels P, Magnusson M, Lundin S, Käller M. MultiQC: summarize analysis results for multiple tools and samples in a single report. *Bioinformatics* (2016) 32:3047–8. doi:10.1093/bioinformatics/btw354

20. Schneider VA, Graves-Lindsay T, Howe K, Bouk N, Chen HC, Kitts PA, et al. Evaluation of GRCh38 and *de novo* haploid genome assemblies demonstrates the enduring quality of the reference assembly. *Genome Res* (2017) 27:849–64. doi:10.1101/gr.213611.116

21. Kim S, Scheffler K, Halpern AL, Bekritsky MA, Noh E, Kallberg M, et al. Strelka2: fast and accurate calling of germline and somatic variants. *Nat Methods* (2018) 15:591–4. doi:10.1038/s41592-018-0051-x

22. Chen X, Schulz-Trieglaff O, Shaw R, Barnes B, Schlesinger F, Kallberg M, et al. Manta: rapid detection of structural variants and indels for germline and cancer sequencing applications. *Bioinformatics* (2016) 32:1220–2. doi:10.1093/bioinformatics/btv710

23. Boeva V, Popova T, Bleakley K, Chiche P, Cappo J, Schleiermacher G, et al. Control-FREEC: a tool for assessing copy number and allelic content using next-generation sequencing data. *Bioinformatics* (2012) 28:423–5. doi:10.1093/bioinformatics/btr670

24. Van Loo P, Nordgard SH, Lingjaerde OC, Russnes HG, Rye IH, Sun W, et al. Allele-specific copy number analysis of tumors. *Proc Natl Acad Sci USA* (2010) 107:16910–5. doi:10.1073/pnas.1009843107

25. Cingolani P, Platts A, Wang LL, Coon M, Nguyen T, Wang L, et al. A program for annotating and predicting the effects of single nucleotide polymorphisms, SnpEff: SNPs in the Genome of *Drosophila melanogaster* Strain w1118; iso-2; iso-3. *Fly (Austin)* (2012) 6:80–92. doi:10.4161/fly.19695

26. McLaren W, Gil L, Hunt SE, Riat HS, Ritchie GR, Thormann A, et al. The Ensembl variant Effect predictor. *Genome Biol* (2016) 17:122. doi:10.1186/s13059-016-0974-4

27. The R Development Core Team. R: a language and environment for statistical computing. 2022.

28. Krzywinski M, Schein J, Birol I, Connors J, Gascoyne R, Horsman D, et al. Circos: an information aesthetic for comparative genomics. *Genome Res* (2009) 19:1639–45. doi:10.1101/gr.092759.109

29. Xiao J, Jin X, Zhang C, Zou H, Chang Z, Han N, et al. Systematic analysis of enhancer regulatory circuit perturbation driven by copy number variations in malignant glioma. *Theranostics* (2021) 11:3060–73. doi:10.7150/THNO.54150

30. Eckel-Passow JE, Decker PA, Kosel ML, Kollmeyer TM, Molinaro AM, Rice T, et al. Using germline variants to estimate glioma and subtype risks. *Neuro-Oncol* (2019) 21:451–61. doi:10.1093/neuonc/noz009

31. Clarke M, Mackay A, Ismer B, Pickles JC, Tatevossian RG, Newman S, et al. Infant high-grade gliomas comprise multiple subgroups characterized by novel targetable gene fusions and favorable outcomes. *Cancer Discov* (2020) 10:942–63. doi:10.1158/2159-8290.CD-19-1030

32. Zheng C, Miao X, Li Y, Huang Y, Ruan J, Ma X, et al. Determination of genomic copy number alteration emphasizing a restriction site-based strategy of genome re-sequencing. *Bioinformatics* (2013) 29:2813–21. doi:10.1093/bioinformatics/btt481

33. Jenkins RB, Blair H, Ballman KV, Giannini C, Arusell RM, Law M, et al. A t(1; 19)(q10; p10) mediates the combined deletions of 1p and 19q and predicts a better prognosis of patients with oligodendroglioma. *Cancer Res* (2006) 66:9852–61. doi:10.1158/0008-5472.CAN-06-1796

34. Felsberg J, Erkwoh A, Sabel MC, Kirsch L, Fimmers R, Blaschke B, et al. Oligodendroglial tumors: refinement of candidate regions on chromosome arm 1p and correlation of 1p/19q status with survival. *Brain Pathol* (2004) 14:121–30. doi:10.1111/j.1750-3639.2004.tb00044.x

35. Smith J, Alderete B, Minn Y, Borell TJ, Perry A, Mohapatra G, et al. Localization of common deletion regions on 1p and 19q in human gliomas and their association with histological subtype. *Oncogene* (1999) 18:4144–52. doi:10.1038/sj.onc.1202759

36. Henrich KO, Schwab M, Westermann F. 1p36 tumor suppression—a matter of dosage? *Cancer Res* (2012) 72:6079–88. doi:10.1158/0008-5472.CAN-12-2230

37. Ichimura K, Vogazianou AP, Liu L, Pearson DM, Bäcklund LM, Plant K, et al. 1p36 is a preferential target of chromosome 1 deletions in astrocytic tumours and homozygously deleted in a subset of glioblastomas. *Oncogene* (2008) 27:2097–108. doi:10.1038/sj.onc.1210848

38. Ball MK, Kollmeyer TM, Praska CE, McKenna ML, Giannini C, Raghunathan A, et al. Frequency of false-positive FISH 1p/19q codeletion in adult diffuse astrocytic gliomas. *Neuro-oncol Adv* (2020) 2:vdaa109. doi:10.1093/noajnl/vdaa109

39. Brandner S. Molecular diagnostics of adult gliomas in neuropathological practice. *Acta Med Acad* (2021) 50:29–46. doi:10.5644/ama2006-124.324

40. Brennan CW, Verhaak RGW, McKenna A, Campos B, Noushmehr H, Salama SR, et al. The somatic genomic landscape of glioblastoma. *Cell* (2013) 155:462–77. doi:10.1016/j.cell.2013.09.034

41. Zacher A, Kaulich K, Stepanow S, Wolter M, Köhrer K, Felsberg J, et al. Molecular diagnostics of gliomas using next generation sequencing of a glioma-tailored gene panel. *Brain Pathol* (2017) 27:146–59. doi:10.1111/bpa.12367

42. Albertoni M, Daub DM, Arden KC, Viars CS, Powell C, Van Meir EG. Genetic instability leads to loss of both p53 alleles in a human glioblastoma. *Oncogene* (1998) 16:321–6. doi:10.1038/sj.onc.1201544

43. Shiraishi S, Tada K, Nakamura H, Makino K, Kochi M, Saya H, et al. Influence of p53 mutations on prognosis of patients with glioblastoma. *Cancer* (2002) 95:249–57. doi:10.1002/cncr.10677

44. Bielski CM, Zehir A, Penson AV, Donoghue MTA, Chatila W, Armenia J, et al. Genome doubling shapes the evolution and prognosis of advanced cancers. *Nat Genet* (2018) 50:1189–95. doi:10.1038/s41588-018-0165-1

45. Zack TI, Schumacher SE, Carter SL, Cherniack AD, Saksena G, Tabak B, et al. Pan-cancer patterns of somatic copy number alteration. *Nat Genet* (2013) 45:1134–40. doi:10.1038/ng.2760

46. Boisselier B, Dugay F, Belaud-Rotureau M-A, Coutolleau A, Garcion E, Menei P, et al. Whole genome duplication is an early event leading to aneuploidy in *IDH*-wild type glioblastoma. *Oncotarget* (2018) 9:36017–28. doi:10.18632/oncotarget.26330

47. Carter SL, Cibulskis K, Helman E, McKenna A, Shen H, Zack T, et al. Absolute quantification of somatic DNA alterations in human cancer. *Nat Biotechnol* (2012) 30:413–21. doi:10.1038/nbt.2203

48. Quinton RJ, DiDomizio A, Vittoria MA, Kotýnková K, Ticas CJ, Patel S, et al. Whole-genome doubling confers unique genetic vulnerabilities on tumour cells. *Nature* (2021) 590:492–7. doi:10.1038/s41586-020-03133-3

49. Neftel C, Laffy J, Filbin MG, Hara T, Shore ME, Rahme GJ, et al. An integrative model of cellular states, plasticity, and genetics for glioblastoma. *Cell* (2019) 178:835–49. doi:10.1016/j.cell.2019.06.024

50. Wang T, Li B, Nelson CE, Nabavi S. Comparative analysis of differential gene expression analysis tools for single-cell RNA sequencing data. *BMC Bioinformatics* (2019) 20:40–16. doi:10.1186/s12859-019-2599-6

51. Wrzeszczynski KO, Frank MO, Koyama T, Rhrissorrakrai K, Robine N, Utro F, et al. Comparing sequencing assays and human-machine analyses in actionable genomics for glioblastoma. *Neurol Genet* (2017) 3:e164–8. doi:10.1212/NXG.0000000000000164

52. Gray PN, Dunlop CL, Elliott AM. Not all next generation sequencing diagnostics are created equal: understanding the nuances of solid tumor assay design for somatic mutation detection. *Cancers* (2015) 7:1313–32. doi:10.3390/cancers7030837

53. Gilly A, Southam L, Suveges D, Kuchenbaecker K, Moore R, Melloni GEM, et al. Very low-depth whole-genome sequencing in complex trait association studies. *Bioinformatics* (2019) 35:2555–61. doi:10.1093/bioinformatics/bty1032

54. NCCN. The NCCN clinical practice guidelines in oncology (NCCN Guidelines®) for guideline central nervous system cancers version 3.2024 © national comprehensive cancer network, inc. 2024. All rights reserved. Available from: https://www.nccn.org/ (Accessed October 3, 2024).

55. Diplas BH, He X, Brosnan-Cashman JA, Liu H, Chen LH, Wang Z, et al. The genomic landscape of TERT promoter wildtype-IDH wildtype glioblastoma. *Nat Commun* (2018) 9:2087. doi:10.1038/s41467-018-04448-6

56. Yeo AT, Shah R, Aliazis K, Pal R, Xu T, Zhang P, et al. Driver mutations dictate the immunologic landscape and response to checkpoint immunotherapy of glioblastoma. *Cancer Immunol Res* (2023) 11:629–45. doi:10.1158/2326-6066.cir-22-0655

57. Klein AM, De Queiroz RM, Venkatesh D, Prives C. The roles and regulation of MDM2 and MDMX: it is not just about P53. *Genes Dev* (2021) 35:575–601. doi:10.1101/gad.347872.120

58. Pellot Ortiz KI, Rechberger JS, Nonnenbroich LF, Daniels DJ, Sarkaria JN. MDM2 inhibition in the treatment of glioblastoma: from concept to clinical investigation. *Biomedicines* (2023) 11:1879. doi:10.3390/biomedicines11071879

59. An Z, Aksoy O, Zheng T, Fan Q-W, Weiss WA. Epidermal growth factor receptor (EGFR) and EGFRvIII in glioblastoma (GBM): signaling pathways and targeted therapies. *Oncogene* (2018) 37:1561–75. doi:10.1038/s41388-017-0045-7

60. Liu X, Chen X, Shi L, Shan Q, Cao Q, Yue C, et al. The third-generation EGFR inhibitor AZD9291 overcomes primary resistance by continuously blocking ERK signaling in glioblastoma. *J Exp Clin Cancer Res* (2019) 38:219. doi:10.1186/s13046-019-1235-7

61. Choi SW, Jung HA, Cho H-J, Kim TM, Park C-K, Nam D-H, et al. A multicenter, phase II trial of GC1118, a novel anti-EGFR antibody, for recurrent glioblastoma patients with EGFR amplification. *Cancer Med* (2023) 12:15788–96. doi:10.1002/cam4.6213

Pathology & Oncology Research | frontiers

TYPE Original Research
PUBLISHED 10 October 2024
DOI 10.3389/pore.2024.1611881

Check for updates

OPEN ACCESS

EDITED BY
Aniko Maraz,
University of Szeged, Hungary

*CORRESPONDENCE
György Gyimesi,
drgyimesigy@gmail.com

RECEIVED 17 June 2024
ACCEPTED 26 September 2024
PUBLISHED 10 October 2024

CITATION
Gyimesi G, Keczer B, Rein P, Horváth M, Szűcs Á, Marjai T, Szijártó A and Hritz I (2024) Diagnostic performance of intracystic carcinoembryonic antigen (CEA) versus glucose in differentiation of mucinous and non-mucinous pancreatic cysts.
Pathol. Oncol. Res. 30:1611881.
doi: 10.3389/pore.2024.1611881

COPYRIGHT
© 2024 Gyimesi, Keczer, Rein, Horváth, Szűcs, Marjai, Szijártó and Hritz. This is an open-access article distributed under the terms of the Creative Commons Attribution License (CC BY). The use, distribution or reproduction in other forums is permitted, provided the original author(s) and the copyright owner(s) are credited and that the original publication in this journal is cited, in accordance with accepted academic practice. No use, distribution or reproduction is permitted which does not comply with these terms.

Diagnostic performance of intracystic carcinoembryonic antigen (CEA) versus glucose in differentiation of mucinous and non-mucinous pancreatic cysts

György Gyimesi[1,2]*, Bánk Keczer[3], Péter Rein[3], Miklós Horváth[4], Ákos Szűcs[3], Tamás Marjai[3], Attila Szijártó[3] and István Hritz[4]

[1]School of Doctoral Studies, Semmelweis University, Budapest, Hungary, [2]Department of Gastroenterology, Spital Thurgau AG, Münsterlingen, Switzerland, [3]Department of Surgery, Transplantation and Gastroenterology, Semmelweis University, Budapest, Hungary, [4]Department of Surgery, Transplantation and Gastroenterology, Division of Interventional Gastroenterology, Semmelweis University, Budapest, Hungary

Background and Objectives: Pancreatic cysts have various potential for malignant transformation. Differentiating mucinous from non-mucinous cysts is crucial to make the right decision about further management, since mucinous cysts carry the risk of malignancy. Using endoscopic ultrasound (EUS) guided fine needle aspiration to determine intracystic carcinoembryonic antigen (CEA) levels is the recommended method for identifying mucinous cysts, although intracystic glucose assessment has also proved to be an effective tool. This study aims to compare the diagnostic performance of intracystic glucose and CEA in distinguishing between mucinous and non-mucinous pancreatic cystic lesions.

Methods: In this single center study, we prospectively collected and analyzed the data of 91 consecutive patients who underwent endoscopic ultrasound (EUS)-guided fine-needle aspiration (FNA) with cytological analysis and measurement of intracystic CEA and glucose levels. The cyst type was classified based on radiological and EUS morphology, string sign, CEA, cytological and histological findings in resected cases. The diagnosis was established retrospectively by three experienced gastroenterologists blinded for glucose level in cases without definitive cytology or histology. We calculated the sensitivity, specificity, the positive- and negative predictive value of glucose and CEA respectively, and compared the two methods.

Results: The sensitivity of intracystic glucose versus CEA proved to be 96.2% vs. 69.2% in identifying mucinous cysts, while the specificity of glucose was shown to be 79.5%, compared to 100% for CEA.

Conclusion: Intracystic glucose is a sensitive, easily accessible biomarker in identifying mucinous pancreatic cysts, however, the specificity is lower compared to CEA. The measurement of intracystic glucose level could help

in decision-making in daily clinical practice, however the diagnostic performance of the method remains inferior to "through-the-needle" techniques, such as confocal laser endomicroscopy and Moray forceps biopsy.

KEYWORDS

pancreatic cyst, endosonography, FNA, intracystic CEA, intracystic glucose

Introduction

The widespread use of abdominal ultrasound and cross-sectional imaging with computed tomography (CT) and magnetic resonance imaging (MRI) has led to an increased diagnosis of asymptomatic pancreatic cysts. Studies reported a detection rate of 0.7%–36% in asymptomatic populations [1, 2]. Since pancreatic cysts have various potential for malignant transformation, it is of great importance to differentiate between the different types of cystic lesions.

Unfortunately, there is no single method or combination of diagnostic techniques which would grant a definitive diagnosis. This can be verified only after surgical resection or by positive intracystic fluid cytology for adenocarcinoma or neuroendocrine tumor.

In general, to guide the patient's management, we need to utilize the patient's previous history (e.g., pancreatitis), imaging modalities (such as CT, MRI) and evaluation of intracystic fluid samples obtained by EUS-guided fine needle aspiration (FNA). It is crucial to differentiate between mucinous and non-mucinous cysts since mucinous lesions are potentially malignant and require surgical resection or long-term follow up according to current international guidelines [3–5].

The accuracy of CT/Magnetic Resonance Cholangiopancreatography (MRCP) in determining a definitive diagnosis is merely about 50% [6, 7]. EUS-FNA, with the possibility of obtaining intracystic fluid for analysis of intracystic cytology and biomarkers, plays an outstanding role in diagnosing pancreatic cystic lesions. Cytology has a high specificity but a low sensitivity in detecting malignancy, and its role in differentiating cysts is limited. In three current meta-analyses of differentiating mucinous from non-mucinous cysts, the sensitivity and specificity of intracystic CEA (cut-off value 192 ng/mL) was shown to be 56%–67% and 80%–96%, while the sensitivity and specificity of glucose (cut-off value 50 mg/dL) was 91% and 75%–86% [8–10], respectively.

In our present study, we evaluated the sensitivity, specificity, diagnostic accuracy and positive and negative predictive value of CEA and glucose in the differentiation of mucinous from non-mucinous cystic lesions.

Methods and materials

This study was approved by the Ethics Committee of the Semmelweis University of Budapest (Ethical approval number: 1121-1/2020/EKU). All patients provided informed consent prior to the procedure for obtaining intracystic fluid by EUS-FNA. The clinical records, EUS, CT/MRI reports and images, laboratory results, cytology, pathology and surgical reports included are all well documented and reliable. We collected the data in a prospective manner between September 2020 and December 2023. The endosonography scans were performed by two expert endoscopists (I.H. and M.H.), each with an overall experience of more than 1000 pancreatic EUS. A UCT-180 linear echoendoscope and an EU-ME2 Premium endoscopic ultrasound processor (Olympus GmbH) were used to visualize the EUS-morphology of the lesions. All the cysts were punctured with a 19/22/25 G EchoTip Ultra FNA needle (Cook Co., Boston, United States) and a 10 mL syringe vacuum suction was applied. "String sign" was documented in 52 cases (57.1%) and the collected fluid samples were used for cytological analysis and for assessment of intracystic amylase, CEA and glucose levels. Only cysts with successfully measured both CEA and glucose level were included in the study. No complications were observed in relation to the EUS-FNA. The specific cyst type was defined based on previous clinical follow-up, cyst morphology on cross-sectional imaging and EUS, "string sign," intracystic amylase level, cytological characteristics, definitive cytology (5 cases, 5.5%) and post-operative histology (13 cases, 14.3%) in resected cases. The CEA cut-off level for mucinous cysts was determined by > 192 ng/mL. The diagnosis was established retrospectively by three experienced gastroenterologists (GG, IH, and MH) blinded for glucose level in cases without definitive cytology or histology. The study cohort consisted of patients who underwent EUS FNA and cyst fluid analysis, where the cyst type was unclear and where the results were likely to alter the management. Cysts with obvious morphological signs of malignancy were not included in the study. Patients were excluded if a consensual final diagnosis between the three experts could not be established. The mean follow-up time was 921 days.

EUS, CT/MRI morphology

During EUS, we assessed and documented the localization, size, number of cysts, lobularity, cyst wall thickness, septa, nodules, solid masses associated with the cyst, pancreatic duct diameter, communication of the cyst with the pancreatic duct and lymphadenopathy. Multidetector computed tomography

(MDCT) or MRI/MRCP were also performed in each patient. The same morphological criteria were used during cross-sectional imaging to define the cyst type as for EUS. All cysts were initially assessed by three experienced pancreatologists (IH, MH, and GG) and a consensual decision was made about the suspected diagnosis. Cases with a suspicion of a premalignant or malignant lesion were also discussed in an interdisciplinary pancreatic board meeting (e.g., Pancreas Team).

String sign

The "String Sign" test involved placing a sample of intracystic fluid between the index finger and thumb, and measuring the distance before the string broke when separating the fingers at a minimum length of 3–4 mm and lasting for at least 1 second.

Cytology

Cytological analysis was performed using haematoxylin-eosin and Papanicolaou staining. The presence of malignant cells, cells with atypia, mucin-containing cells or glycogen-containing cells was assessed. Presence of extracellular mucin and inflammatory cells was also documented.

CEA and glucose

The obtained fluid samples were immediately transferred to the laboratory and measurements took place within 4 h. Both CEA (by electro-chemiluminescence using an enzyme-labelled sandwich immunoassay) and glucose (by spectrophotometric assessment using Hexokinase) measurements were performed by the Clinical Laboratory of Semmelweis University of Budapest. Regarding intracystic CEA, we applied the standardized cut-off value of 192 ng/mL according to the classic study of Brugge et al. [11], and cut-off for the glucose level was defined as 50 mg/dL (2.8 mmol/L) based on the studies of Zikos et al. [12], to differentiate between mucinous and non-mucinous cysts.

Amylase

We applied amylase level under 250 U/L as a criterion to exclude pseudocysts.

Statistical analysis

Data collection, evaluation, and figure generation were performed using the IBM SPSS Statistics 25, GraphPad Prism and Microsoft Office Excel software. Normality tests (Anderson–Darling, D'Agostino and Pearson, Shapiro–Wilk, Kolmogorov–Smirnov) were performed to determine the normality level of the samples. In instances where a normal distribution was observed, independent two-sample *t*-test was employed for intergroup comparisons. For continuous variables that deviated from a normal distribution, non-parametric tests were utilized for comparative investigations. Categorical variables were characterized by specifying the number of elements in the corresponding category and calculating the percentage distribution. For statistical analyses, we utilized the χ^2 test or, in cases of low (less than 5) expected values, the Fisher's exact test. Continuous variables were presented as mean ± standard deviation (SD) or median with range, as appropriate for the data distribution. All statistical tests were conducted assuming a two-tailed distribution, with a significance threshold set at $p < 0.05$.

Results

In total, pancreatic cystic fluid was obtained from 97 patients and analyzed for cytology, amylase, CEA and glucose content. 4 cases were excluded from the analysis because of obvious signs of infected cyst fluid (cytological or microbiological testing) and 2 other cases because of significant blood content in the fluid (by macroscopic assessment), since these conditions may lead to false glucose and CEA levels, respectively.

Of the 91 patients, 28 (30.8%) were male and 63 (69.2%) were female. The median age was 72.4 years (SD 12.18) in the mucinous group and 56.4 years (SD 15.48) in the non-mucinous group ($p < 0.0001$). The median cyst diameter on endosonography was 28 mm in the mucinous group and 38 mm in the non-mucinous group (p 0.054). 43 cysts were unilocular and 48 were multilocular. 28 cysts were localized in the uncinate process and in the pancreatic head, 59 in the body and 4 in the tail. The patient and cyst characteristics are presented in Table 1.

13 cases (14.3%) were diagnosed by post-operative histology and 5 cases (5.5%) by definitive fluid cytology. The remaining cysts were assessed using clinical and radiological evaluation, cytological characteristics, the "string sign" and clinical follow-up as standard reference. The diagnosis was made by the consensus-based decision of three experienced pancreatologists (IH, MH, and GG). We identified 52 mucinous cysts, including 33 intraductal papillary mucinous neoplasms (IPMNs), 12 mucinous cystadenomas and 7 adenocarcinomas. The remaining 39 cases were non-mucinous cysts, including 21 pseudocysts, 16 serous cystadenomas, 1 neuroendocrine tumor and 1 lymphoepithelial cyst (Table 2).

The median CEA level measured in the mucinous group was 449.5 ng/mL and 3 ng/mL ($p < 0.0001$, CI 95%) in the non-mucinous group. The median glucose level was shown to be 8.1 mg/dL in the mucinous group and 100.9 mg/dL in the non-

TABLE 1 Population demographics and cyst characteristics.

	Mucinous	Non-Mucinous	*p*-value
Gender			
Male, n (%)	18 (35)	10 (26)	
Female, n (%)	34 (65)	29 (74)	
Age in years, median (IQR)	72.4 (76.58–65.95)	56.4 (71.2–42.6)	*<0.0001*
Cyst characteristics	**Mucinous**	**Non-Mucinous**	***p*-value**
Localization of the largest cyst, n, (%)			
Uncinate process	3 (6)	0 (0)	
Head	12 (23)	13 (33)	
Genu of pancreas	8 (15)	8 (21)	
Body	16 (30)	14 (36)	
Body-tail border	11 (21)	2 (5)	
Tail	2 (4)	2 (5)	
Largest cyst diameter in mm, median (95% CI)	28 (24–32)	38 (25–41)	*0.054*
Unilocular cyst, n (%)	24 (46)	19 (49)	
Multilocular cyst, n (%)	28 (54)	20 (51)	

TABLE 2 Disease characteristics.

	Mucinous	Non-mucinous
Diagnosis based on	**Number of cysts (%)**	**Number of cysts (%)**
Follow up, Imaging	37 (71)	36 (92)
Postoperative histopathology	12 (23)	1 (3)
EUS guided FNA – definitive cytopathology	3 (6)	2 (5)
Diagnosis	**Number of cysts (%)**	**Number of cysts (%)**
IPMN	33 (63.5)	—
MCN	12 (23)	—
Adenocarcinoma	7 (13.5)	—
SCN	—	16 (41)
Pseudocyst	—	21 (54)
NET	—	1 (2.5)
Lymphoepithelial cyst	—	1 (2.5)

mucinous group ($p < 0.0001$, CI 95%). CEA was above the cut-off level (192 ng/mL) in 36 of 52 mucinous cysts, resulting in a sensitivity of 69.2% for the differentiation of mucinous lesions. The intracystic glucose level was under the cut-off value (50 mg/dL) in 50 of 52 mucinous cysts, meaning a sensitivity of 96.2% in this regard. The specificity of CEA was shown to be 100%, while the specificity of glucose was 79.5%. The combination of the two methods (either CEA >192 ng/mL or glucose <50 mg/dL) improved the sensitivity to 100%, while the specificity was lower than that of CEA alone (79.5% vs. 100%). The results, including positive and negative predictive values, are presented in Table 3.

TABLE 3 Diagnostic performance of CEA, Glucose and CEA with Glucose combined.

	Mucinous	Non-Mucinous	*p*-value
CEA (Cutoff 192 ng/mL)			
CEA level, median (95% CI)	449.5 (209.2–873.8)	3 (3–14.4)	*<0.0001*
Elevated/non-elevated	35/17	1/38	
Glucose (Cutoff 50 mg/dL)			
Glucose level, median (95%CI)	8.1 (3.6–10.8)	100.9 (79.2–108.1)	*<0.0001*
Elevated/non-elevated	3/49	30/9	
CEA and Glucose			
(either CEA elevated or Glucose non-elevated)	52/0	6/33	
Amylase (Cutoff 250 IU/L)			
Amylase level, median (95%CI)	2.445 (1.011–8.825)	10.360 (173–52.800)	
Elevated/non-elevated	40/12	23/16	
	CEA	**Glucose**	**CEA and glucose**
Sensitivity	67.3%	94.2%	100%
Specificity	97.5%	81.3%	84.6%
PPV	0.97	0.85	0.89
NPV	0.69	0.91	0.94

Discussion

Differentiation between mucinous and non-mucinous pancreatic cysts remains challenging. Even if best practice according to the clinical guidelines is applied, only 72% of pancreatic cystic neoplasms are diagnosed correctly and adequate differentiation of mucinous cysts is made in 86% of cases [13]. Analysis of intracystic fluid obtained by EUS-FNA is an effective tool in improving the diagnostic accuracy for detecting mucinous cysts. Although current guidelines recommend the use of cytology and intracystic CEA for this purpose, CEA has a relatively low sensitivity (56%–67%) at a standardized cut-off value of 192 ng/mL, while the specificity has been shown to be 80%–95% in systematic reviews [8–10].

The optimal cut-off value of CEA is still unclear. A value of 20 ng/mL achieved the highest diagnostic accuracy with a sensitivity of 91% (95% Cl 88%–94%) and specificity of 85% (95% Cl 72%–93%) [14].

In 2013, a study of pancreatic cyst fluid analysis by Park et al. found glucose as a promising tool for identifying mucinous pancreatic cystic lesions [15]. In contrast to CEA, glucose level analysis has been well established in various biological fluids (serum, plasma, cerebrospinal fluid, urine) with good reproducibility, while the CEA assay is validated only in serum and its value in pancreatic cysts can vary across laboratories and assay kits [16]. Moreover, determining the level of glucose requires a significantly lower volume of intracystic fluid than the CEA assay (50 μL vs. at least 200 μL) [9].

The disadvantage of intracystic glucose measurement is that an infection of the cyst could cause, similar to mucinous cysts, a higher glucose consumption which could lead to a lower intracystic glucose level. Cysts with signs of infection on cytological or microbiological testing were therefore excluded from statistical analysis in our study.

Additionally, DNA markers, particularly mutation analysis of GNAS and KRAS, may be applied for identifying mucin-producing cysts with high sensitivity. According to the European Guideline on pancreatic cystic neoplasms, in cases in which the diagnosis is unclear and a change in diagnosis will alter management, analysis of these mutations may be considered. The minimal volume to perform molecular analysis is 0.2–0.5 mL, although in some samples the amount of DNA is insufficient to perform the analysis [17–19]. Furthermore, next-generation sequencing is costly and requires specialized experience, which limits the widespread use of this method.

Diagnostic performance of advanced EUS guided "through-the-needle" techniques, such as confocal laser endomicroscopy and Moray forceps biopsy is superior to intracystic biomarker measurements [20], however, the availability of these methods is limited to highly specialized centers.

A limitation of our study is that it is a single center series containing cysts with diagnosis mainly based on clinical follow-up, imaging and cytological features, with low proportion of cysts diagnosed by positive cytology (cystic adenocarcinoma or neuroendocrine tumor) or postoperative histology. Reliability of the final diagnosis in the remaining cases is equivocal. However, the assessed cysts in our study represent a wide spectrum of lesions with various sizes and morphology. Furthermore, a relatively small proportion of cysts require surgical resection in clinical practice and cytological testing rarely leads to a definitive diagnosis.

Another limitation is the mean follow up time of 921 days, which is a relatively short period in case of undefined pancreatic cystic lesions.

Our results are in accordance with the literature demonstrating an outstanding sensitivity of intracystic glucose in the differentiation of mucinous cysts. Our study shows that the highest sensitivity can be reached by using the combination of elevated intracystic CEA and lowered glucose levels. The specificity of the combined method proved to be higher than that of glucose, but lower than that of CEA alone.

Conclusion

Current guidelines do not contain any recommendation regarding determination of intracystic glucose levels in the differentiation of mucinous versus non-mucinous pancreatic cysts. However, there have been several trials published in the last 10 years with conclusive results. In these, such as in our present study, glucose has been shown to be a cost effective, easily accessible, reliable cystic biomarker with a higher sensitivity in identifying mucinous pancreatic cysts compared to CEA. On the other hand, this study confirms the data in the literature regarding the low specificity of glucose, which diagnostic performance for pancreatic cystic lesions remains inferior to "through-the-needle" techniques, such as confocal laser endomicroscopy and Moray forceps biopsy [20]. However, glucose is more sensitive than CEA, and may be efficiently used as an additional biomarker in centers not equipped with "through-the-needle" techniques.

Nevertheless, further research and multicentric, randomized studies are needed to confirm the data regarding the usefulness of intracystic glucose measurement. If the results of these are congruent with the data from this and previously published studies, intracystic glucose assessment may be integrated into routine clinical practice and international guidelines.

Data availability statement

The raw data supporting the conclusions of this article will be made available by the authors, without undue reservation.

Ethics statement

This study was approved by the Ethics Committee of the Semmelweis University of Budapest (Ethical approval number: 1121-1/2020/EKU). All patients provided informed consent prior to the procedure for obtaining intracystic fluid by EUS-FNA.

Author contributions

Biological sample collection was performed by IH and MH. Cyst morphology and diagnosis assessed on imaging by GG, IH, and MH, in cooperation with the members of the pancreatic tumor-board ÁkS, TM, and AtS. Data collection and analysis by PR, GG, and BK. The manuscript was written by GG, IH, and BK. All authors contributed to the article and approved the submitted version.

Funding

The author(s) declare that no financial support was received for the research, authorship, and/or publication of this article.

Conflict of interest

IH received consultation fee from Olympus GmbH. Author GG was employed by Spital Thurgau AG Münsterlingen.

The remaining authors declare that the research was conducted in the absence of any commercial or financial relationships that could be construed as a potential conflict of interest.

References

1. Becker WF, Welsh RA, Pratt HS. Cystadenoma and cystadenocarcinoma of the pancreas. *Ann Surg* (1965) 161(6):845–63. doi:10.1097/00000658-196506000-00005

2. Zhang XM, Mitchell DG, Dohke M, Holland GA, Parker L. Pancreatic cysts: depiction on single-shot fast spin-echo MR images. *Radiology* (2002) 223(2): 547–53. doi:10.1148/radiol.22320108153

3. Diagnosis and management of cystic pancreatic lesions. European evidence-based guidelines on pancreatic cystic neoplasms. *Gut* (2018) 67:789–804. doi:10.1136/gutjnl-2018-316027

4. Tanaka M, Fernandez-Del Castillo C, Kamisawa T, Jang JY, Levy P, Ohtsuka T, et al. Revisions of international consensus Fukuoka guidelines for the management of IPMN of the pancreas. *Pancreatology* (2017) 17:738–53. doi:10.1016/j.pan.2017.07.007

5. Ohtsuka T, Del Castillo CF, Furukawa T, Hijioka S, Jang J-Y, Lennon AM, et al. International evidence-based Kyoto guidelines for the management of intraductal papillary mucinous neoplasm of the pancreas 2024;24(2):255–70. doi:10.1016/j.pan.2023.12.009

6. Dushyant VS, Kambadakone A, Macari M, Takahashi N, Chari S, Fernandez-del Castillo C. Diagnosis and management of cystic pancreatic lesions Am. *J Roentgenol* (2013) 200(2):343–54. doi:10.2214/AJR.12.8862

7. Brendan CV1, Yeh BM, Qayyum A, Way LW, McCulloch CE, Coakley FV. Characterization of cystic pancreatic masses: relative accuracy of CT and MRI. *Am J Roentgenol* (2007) 189(3):648–56. doi:10.2214/AJR.07.2365

8. McCarty TR, Garg R, Rustagi T. Pancreatic cyst fluid glucose in differentiating mucinous from nonmucinous pancreatic cysts: a systematic review and meta-analysis. *Gastrointest Endosc* (2021) 94(698–712):698–712.e6. doi:10.1016/j.gie.2021.04.025

9. Faias S, Cravo M, Chaves PL. Comparative analysis of glucose and carcinoembryonic antigen in the diagnosis of pancreatic mucinous cysts: a systematic review and meta-analysis. *Gastrointest Endosc* (2021) 94(2):235–47. doi:10.1016/j.gie.2021.03.935

10. Guzmán CE, Martinez MB, Casellas JA, Sparicio JR. Intracystic glucose levels appear useful for diagnosis of pancreatic cystic lesions: a systematic review and meta-analysis. *Dig Dis Sci* (2022) 67(6):2562–70. doi:10.1007/s10620-021-07035-w

11. Brugge WR, Lewandrowski K, Lee-Lewandrowski E, Centeno BA, Szydlo T, Regan S, et al. Diagnosis of pancreatic cystic neoplasms: a report of the cooperative pancreatic cyst study. *Gastroenterology* (2004) 126:1330–6. doi:10.1053/j.gastro.2004.02.013

12. Zikos T, Pham K, Bowen R, Chen AM, Banerjee S, Friedland S, et al. Cyst fluid glucose is rapidly feasible and accurate in diagnosing mucinous pancreatic cysts. *Am J Gastroenterol* (2015) 110:909–14. doi:10.1038/ajg.2015.148

13. Lekkerkerker SJ, Besselink MG, Busch OR, Verheij J, Engelbrecht MR, Rauws EA, et al. Comparing 3 guidelines on the management of surgically removed pancreatic cysts with regard to pathological outcome. *Gastrointest Endosc* (2017) 85(5):1025–31. doi:10.1016/j.gie.2016.09.027

14. van Huijgevoort NCM, Hoogenboom SA, Lekkerkerker SJ, Topazian M, Chandrasekhara V, Morris-Stif G, et al. The diagnostic accuracy of carcinoembryonic antigen in differentiating mucinous and non-mucinous pancreatic cystic neoplasms—a systematic review and individual patient data meta-analysis. In: *ESGE days 2018 accepted abstracts*. Budapest, Hungary, New York City, NY: Endoscopy (2018).

15. Park WG, Wu M, Bowen R, Zheng M, Fitch WL, Pai RK, et al. Metabolomic-derived novel cyst fluid biomarkers for pancreatic cysts: glucose and kynurenine. *Gastrointest Endosc* (2013) 78(2):295–302. doi:10.1016/j.gie.2013.02.037

16. Boot C. A review of pancreatic cyst fluid analysis in the differential diagnosis of pancreatic cyst lesions. *Ann Clin Biochem* (2014) 51:151–66. doi:10.1177/0004563213503819

17. Singhi AD, McGrath K, Brand RE, Khalid A, Zeh HJ, Chennat JS, et al. Preoperative next-generation sequencing of pancreatic cyst fluid is highly accurate in cyst classification and detection of advanced neoplasia. *Gut* (2018) 67:2131–41. doi:10.1136/gutjnl-2016-313586

18. Rockacy MJ, Zahid M, McGrath KM, Fasanella KE, Khalid A. Association between KRASmutation, detected in pancreatic cyst fluid, and long-term outcomes of patients. *Clin Gastroenterol Hepatol* (2013) 11:425–9. doi:10.1016/j.cgh.2012.12.008

19. Nikiforova MN, Khalid A, Fasanella KE, McGrath KM, Brand RE, Chennat JS, et al. Integration of KRAS testing in the diagnosis of pancreatic cystic lesions: a clinical experience of 618 pancreatic cysts. *Mod Pathol* (2013) 26:1478–87. doi:10.1038/modpathol.2013.91

20. Li S-Y, Wang Z-J, Pan C-Y, Wu C, Li Z-S, Jin Z-D, et al. Comparative performance of endoscopic ultrasound-based techniques in patients with pancreatic cystic lesions: a network meta-analysis. *Am J Gastroenterol* (2023) 118(2):243–55. doi:10.14309/ajg.0000000000002088

Pathology & Oncology Research | frontiers

TYPE Original Research
PUBLISHED 29 August 2024
DOI 10.3389/pore.2024.1611826

Check for updates

OPEN ACCESS

EDITED BY
Tamás Micsik,
Semmelweis University, Hungary

*CORRESPONDENCE
Dara S. Ross,
rossd@mskcc.org

RECEIVED 10 May 2024
ACCEPTED 09 August 2024
PUBLISHED 29 August 2024

CITATION
Liao C-HC, Bakoglu N, Cesmecioglu E, Hanna M, Pareja F, Wen HY, D'Alfonso TM, Brogi E, Yagi Y and Ross DS (2024) Semi-automated analysis of HER2 immunohistochemistry in invasive breast carcinoma using whole slide images: utility for interpretation in clinical practice.
Pathol. Oncol. Res. 30:1611826.
doi: 10.3389/pore.2024.1611826

COPYRIGHT
© 2024 Liao, Bakoglu, Cesmecioglu, Hanna, Pareja, Wen, D'Alfonso, Brogi, Yagi and Ross. This is an open-access article distributed under the terms of the Creative Commons Attribution License (CC BY). The use, distribution or reproduction in other forums is permitted, provided the original author(s) and the copyright owner(s) are credited and that the original publication in this journal is cited, in accordance with accepted academic practice. No use, distribution or reproduction is permitted which does not comply with these terms.

Semi-automated analysis of HER2 immunohistochemistry in invasive breast carcinoma using whole slide images: utility for interpretation in clinical practice

Chiu-Hsiang Connie Liao, Nilay Bakoglu, Emine Cesmecioglu, Matthew Hanna, Fresia Pareja, Hannah Y. Wen, Timothy M. D'Alfonso, Edi Brogi, Yukako Yagi and Dara S. Ross*

Department of Pathology and Laboratory Medicine, Memorial Sloan Kettering Cancer Center, New York, NY, United States

Human epidermal growth factor receptor 2 (*HER2*) gene amplification and subsequent protein overexpression is a strong prognostic and predictive biomarker in invasive breast carcinoma (IBC). ASCO/CAP recommended tests for HER2 assessment include immunohistochemistry (IHC) and/or *in situ* hybridization (ISH). Accurate HER2 IHC scoring (0, 1+, 2+, 3+) is key for appropriate classification and treatment of IBC. HER2-targeted therapies, including anti-HER2 monoclonal antibodies and antibody drug conjugates (ADC), have revolutionized the treatment of HER2-positive IBC. Recently, ADC have also been approved for treatment of HER2-low (IHC 1+, IHC 2+/ISH-) advanced breast carcinoma, making a distinction between IHC 0 and 1+ crucial. In this focused study, 32 IBC with HER2 IHC scores from 0 to 3+ and HER2 FISH results formed a calibration dataset, and 77 IBC with HER2 IHC score 2+ and paired FISH results (27 amplified, 50 non-amplified) formed a validation dataset. H&E and HER2 IHC whole slide images (WSI) were scanned. Regions of interest were manually annotated and IHC scores generated by the software QuantCenter (MembraneQuant application) by 3DHISTECH Ltd. (Budapest, Hungary) and compared to the microscopic IHC score. H-scores [(3×%IHC3+) +(2×%IHC2+) +(1×%IHC1+)] were calculated for semi-automated (MembraneQuant) analysis. Concordance between microscopic IHC scoring and 3DHISTECH MembraneQuant semi-automated scoring in the calibration dataset showed a Kappa value of 0.77 (standard error 0.09). Microscopic IHC and MembraneQuant image analysis for the detection of *HER2* amplification yielded a sensitivity of 100% for both and a specificity of 56% and 61%, respectively. In the validation set of IHC 2+ cases, only 13 of 77 cases (17%) had discordant results between microscopic and MembraneQuant images, and various artifacts limiting the interpretation of HER2 IHC, including cytoplasmic/granular staining and crush artifact were noted. Semi-automated analysis using WSI and microscopic evaluation yielded similar HER2 IHC scores, demonstrating the potential utility of this tool for interpretation in clinical practice and subsequent

accurate treatment. In this study, it was shown that semi-automatic HER2 IHC interpretation provides an objective approach to a test known to be quite subjective.

KEYWORDS

HER2, immunohistochemistry, breast carcinoma, whole slide imaging, semi-automated analysis

Introduction

Human epidermal growth factor receptor 2 (*HER2*) gene amplification and subsequent protein overexpression is a strong prognostic and predictive biomarker in invasive breast carcinoma (IBC), assessed by immunohistochemistry (IHC) and/or *in situ* hybridization (ISH) per the guidelines issued by the American Society of Clinical Oncology/College of American Pathologists (ASCO/CAP) [1]. HER2 IHC is generally performed first in IBC to assess for HER2 protein expression and ISH is subsequently performed in cases with equivocal IHC results [score 2+: weak to moderate complete membrane staining in >10% of tumor cells, complete membrane staining that is intense but within ≤10% of tumor cells, or moderate to intense but incomplete membrane staining (basolateral or lateral)] [1] to further assess the *HER2* gene amplification status. Although HER2 IHC is cost-effective with a fast turnaround time, this semiquantitative detection method is subjective and requires special training and expertise for accurate reporting and proper patient management [2]. The ASCO/CAP HER2 IHC scoring algorithm incorporates the percentage, completeness, intensity, and uniformity of membrane staining in IBC, with scores 0 or 1+ (negative), 2+ (equivocal) and 3+ (positive). *HER2* overexpression/amplification in IBC and the subsequent classification of HER2-positive disease is predictive of response to HER2-directed therapies in the neoadjuvant, adjuvant or metastatic settings [1]. The treatment of HER2-positive IBC has been revolutionized by the FDA approval of targeted therapies in the appropriate clinical settings, including the monoclonal antibodies trastuzumab and pertuzumab, the antibody-drug conjugates (ADC) trastuzumab emtansine (T-DM1) and fam-trastuzumab deruxtecan-nxki (T-DXd), and the tyrosine kinase inhibitors lapatinib and neratinib. Recent clinical trials have shown a benefit of ADCs in HER2 low-expressing IBC, defined as IHC 1+ or IHC 2+/ISH- [3, 4].

Targeted treatment for IBC was previously dependent upon a dichotomous HER2-positive or HER2-negative result. Now the distinction between the scores in the lower end of HER2 protein expression (IHC 0, 1+ and 2+/ISH-) becomes increasingly more crucial from a therapeutic standpoint [5]. Unfortunately, there are many challenges in HER2 testing and detection of HER2-low breast carcinoma, particularly when distinguishing between IHC scores of 0 and 1+ [6], as IHC companion diagnostic tests were optimized for the accurate detection of high HER2 protein expression levels [7]. The aim of this focused study is to validate a semi-automated computational model to assist in HER2 IHC interpretation using the QuantCenter (MembraneQuant) software developed by 3DHISTECH Ltd. (Budapest, Hungary) and provide a platform for larger studies going forward to aid in the subsequent HER2 classification and appropriate treatment of IBC.

Materials and methods

Case selection, HER2 testing and clinicopathologic data collection

This study was conducted under institutional review board approval (Protocol #18-013). A calibration dataset of breast biopsies and resection specimens with HER2 IHC scores 0 to 3+ and paired HER2 fluorescence *in situ* hybridization (FISH) were collected (n = 32). HER2 IHC staining (PATHWAY anti–HER2/neu [4B5], Ventana Medical Systems Inc., Tucson, Arizona, U *ultra*View PATHWAY HER2 4B5 staining procedure) was performed and clinically reported on all cases of IBC at the time of diagnosis. HER2 FISH (HER2 IQFISH pharmDx, Dako, Carpinteria, California) was performed on HER2 IHC equivocal (2+) cases in accordance with the ASCO/CAP guidelines and the standard practices at our institution. Select HER2 IHC negative (0, 1+) or positive (3+) cases were also assessed by FISH as per clinician request or for the purpose of this study. HER2 IHC and FISH were reported in accordance with the 2018 ASCO/CAP guidelines which were affirmed in the 2023 update; HER2 IHC was scored as 0, 1+, 2+, 3+ and HER2 FISH was classified into 5 groups (Group 1, HER2/CEP17 ≥2.0 and average HER2 copy number ≥4.0; Group 2, HER2/CEP17 ratio ≥2.0 and average HER2 copy number <4.0; Group 3, HER2/CEP17 ratio <2.0 and average HER2 copy number ≥6.0; Group 4, HER2/CEP17 <2.0 and average HER2 copy number ≥4.0 and <6.0; Group 5, HER2/CEP17 <2.0 and average HER2 copy number <4.0) [1]. A validation dataset of HER2 IHC 2+ cases was also collected (n = 77), consisting of IBC cases that were reported and sent for HER2 FISH between January 2021 and June 2021. The pathologic features of the cases were obtained from the clinical pathology reports.

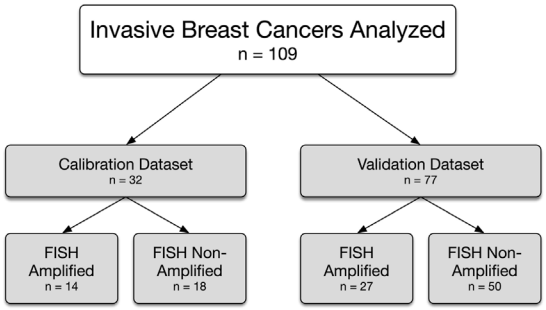

FIGURE 1
Invasive breast cancers analyzed and the HER2 FISH status.

Semi-automated analysis

Hematoxylin and eosin (H&E) and HER2 IHC slides, with a tissue thickness of 5 microns, were scanned at 20× (0.5 um/pixel) by Leica AT2 for diagnostic use; whole slide images (WSI) were downloaded and converted into a 3DHISTECH software-compatible format. Analyses were conducted using MembraneQuant which is a function of QuantCenter by 3DHISTECH Ltd. (Budapest, Hungary). Prior to analysis, IBC regions of interest (ROI) were manually annotated by a pathologist, which included all areas of invasive carcinoma on the WSI, with areas of *in situ* carcinoma, abundant lymphoid aggregates and stromal cells avoided when possible. All annotated areas of IBC were analyzed by the software. A minimum of at least 5 to 6 tumor cells was required for analysis. The determination of the threshold for IHC scores 0, 1+, 2+, and 3+ in MembraneQuant was manually set by the study pathologist based on the calibration dataset in this study and all subsequent analyses by MembraneQuant used the same parameters and thresholds. MembraneQuant measurement parameters include membrane detection, membrane filters, nucleus detection, nucleus filters and score. Final HER2 IHC scores were generated by MembraneQuant. HER2 H-scores [(3×%IHC3+) +(2×%IHC2+) +(1×%IHC1+)] were calculated for semi-automated (MembraneQuant) analysis. Comparison of H-scores was performed using two-tailed Student's t-test (statistical significance $p < 0.05$). On semi-automatic analysis, HER2 scores are distinguished by four colors: cells with HER2 score of 3+ are displayed in red, score of 2+ are in orange, score of 1+ are in yellow and score of 0 are in blue. The primary endpoint was the comparison of HER2 IHC microscopic/manual scoring with HER2 semi-automated scoring by MembraneQuant. Kappa values were calculated using the R studio statistical software. For the validation dataset of HER2 IHC 2+ cases, the H&E and HER2 IHC slides were scanned and analyzed using the same parameters/thresholds as in the calibration dataset. HER2 IHC scores were generated by MembraneQuant. For cases with discordant scores between MembraneQuant and microscopic scoring, the physical H&E and HER2 IHC slides were subsequently re-reviewed microscopically by three pathologists (DR, FP, TD).

Results

The calibration dataset was composed of 32 IBC samples (27 excisions, 5 biopsies) with both HER2 IHC and FISH results available (Figure 1). The calibration dataset included 14 HER2 amplified cases (44%) (ASCO/CAP Group 1, n = 14) and 18 HER2 non-amplified cases (56%) (ASCO/CAP Group 5, n = 17; Group 4, n = 1) by FISH. The breakdown of the HER2 IHC microscopic and MembraneQuant scores within both the HER2 amplified and non-amplified groups are shown in Table 1. The agreement between microscopic IHC and MembraneQuant scoring in the calibration dataset was found to be substantial ($\kappa = 0.77 \pm 0.09$ SE). The overall concordance between the two scoring modalities is shown in Table 2 A. Of the 14 cases that were HER2 amplified by FISH, 9 cases (64%) were scored as HER2 IHC 3+ by microscopic review and were also scored as 3+ by MembraneQuant. The remaining 5 cases (36%) in the HER2 amplified group were microscopically scored as 2+; MembraneQuant scored 4 (29%) of these cases as 2+ and 1 (7%) as 3+ (Table 2 B). Out of the 18 cases that were HER2 non-amplified by FISH, 8 cases (45%) were interpreted as 2+ by microscopic scoring, while MembraneQuant scored 7 (39%) of these cases as 2+ and 1 (6%) as 1+. Four cases (22%) were scored as IHC 1+ microscopically and concordantly MembraneQuant scored all as 1+ (22%). For the 6 cases (33%) that were microscopically scored as IHC 0, 3 of these cases (16.5%) were scored as 1+ by MembraneQuant and 3 (16.5%) were scored as 0 (Table 2 C). Microscopic IHC and MembraneQuant image analysis showed a specificity of 56% and 61%, respectively, and a sensitivity of 100% for the detection of HER2 amplification (Table 3). Representative micrographs of IBCs displaying HER2 IHC scores of 0, 1+, 2+ and 3+, as well as the corresponding MembraneQuant quantification overlay are shown in Figure 2. Representative images of microscopic/MembraneQuant discordant cases (0/1+, 2+/1+ and 2+/3+) from the calibration dataset are shown in Figure 3.

The validation dataset was composed of 77 IBC samples, each clinically scored as HER2 IHC 2+ and subjected to HER2 FISH testing (51 excisions, 26 biopsies; Figure 1). Twenty-seven (35%) cases were HER2 amplified [ASCO/CAP Group 1, n = 24 (31%); Group 3, n = 3 (4%)] and 50 (65%) cases were HER2 non-amplified [ASCO/CAP Group 5, n = 37 (48%); Group 4, n = 12 (16%); Group 2, n = 1 (1%)] by FISH. In the HER2 amplified group (n = 27), MembraneQuant scored 19 cases (71%) as 2+ (ASCO/CAP Group 1, n = 16; Group 3, n = 3), 2 cases (7%) as 1+ (ASCO/CAP Group 1, n = 2) and 6 cases (22%) as 3+ (ASCO/CAP Group 1, n = 6); in the FISH amplified group, discordant

TABLE 1 Comparison of HER2 IHC scores by microscopic and semi-automated analysis for calibration dataset (N = 32).

FISH	Microscopic HER2 IHC score				MembraneQuant HER2 IHC score			
	0	1+	2+	3+	0	1+	2+	3+
AMPLIFIED, N (%)	0 (0%)	0 (0%)	5 (16%)	9 (28%)	0 (0%)	0 (0%)	4 (12%)	10 (32%)
NON-AMPLIFIED, N (%)	6 (19%)	4 (12%)	8 (25%)	0 (0%)	3 (9%)	8 (25%)	7 (22%)	0 (0%)

TABLE 2 Concordance and discordance between microscopic (Mx) IHC scoring and 3DHISTECH MembraneQuant semi-automated scoring for calibration dataset (N = 32) (A). Cases are also separated based on FISH amplification status of HER2 amplified (amp) (N = 14) (B) and HER2 non-amplified (non-amp) (N = 18) (C).

A.	MembraneQuant HER2 IHC score					B.	MembraneQuant HER2 IHC score					C.	MembraneQuant HER2 IHC score				
Mx HER2 IHC Score, N = 32		0	1+	2+	3+	Mx HER2 IHC Score, N = 14 (amp)		0	1+	2+	3+	Mx HER2 IHC Score, N = 18 (non-amp)		0	1+	2+	3+
	0	3	3	0	0		0	0	0	0	0		0	3	3	0	0
	1+	0	4	0	0		1+	0	0	0	0		1+	0	4	0	0
	2+	0	1	11	1		2+	0	0	4	1		2+	0	1	7	0
	3+	0	0	0	9		3+	0	0	0	9		3+	0	0	0	0

Kappa value based on results in Table 2 A is 0.77 with standard error of 0.09.

TABLE 3 Confusion matrix of true positive (TP, IHC 2+ or 3+ and HER2 amplified), true negative (TN, IHC 0 or 1+, HER2 non-amplified), false positive (FP, IHC 2+ or 3+, HER2 non-amplified) and false negative (FN, IHC 0 or 1+, HER2 amplified) for microscopic (Mx) and MembraneQuant HER2 IHC score.

A.	HER2 amplification status		B.	HER2 amplification status	
Mx HER2 IHC score		Amp	Non-Amp	MembraneQuant HER2 IHC score		Amp	Non-Amp
	2+ or 3+	14	8		2+ or 3+	14	7
	0+ or 1+	0	10		0+ or 1+	0	11

The sensitivity and specificity for microscopic HER2 analysis are 100% and 56%, and for MembraneQuant are 100% and 61%.

microscopic/MembraneQuant results were observed in 8/27 (30%) cases. In the HER2 non-amplified group (n = 50), MembraneQuant scored 45 cases (90%) as 2+ (ASCO/CAP Group 5, n = 34; Group 4, n = 11), 2 cases (4%) as 1+ (ASCO/CAP Group 5, n = 2), and 3 cases (6%) as 3+ (ASCO/CAP Group 5, n = 1; Group 4, n = 1; Group 2, n = 1), with discordant microscopic/MembraneQuant results observed in 5/50 (10%) cases. Table 4 displays the HER2 IHC score called by MembraneQuant and the HER2 amplification status by FISH.

The semi-automated H-scores for the calibration and validation datasets are listed in Table 5. The H-score mean for the calibration dataset in the amplified group is: 135 (range 99–185) for IHC 2+ and 162 (range 88–191) for IHC 3+, whereas in the non-amplified group it is 45 (range 18–81) for IHC 1+ and 109 (range 62–157) for IHC 2+. The H-score mean for the validation dataset in the amplified group is: 128 (range 95–161) for IHC 2+, 157 (range 118–188) for IHC 3+, whereas in the non-amplified group it is 75 (56–94) for IHC 1+, 129 (82–190) for IHC 2+, and 184 (171–198) for IHC 3+. For the MembraneQuant IHC 2+ cases in the calibration dataset, no statistical significance was appreciated between the H-scores for the FISH amplified and FISH non-amplified groups ($p = 0.27$). In addition, for the FISH amplified cases in the calibration dataset, no statistical significance was appreciated between the H-scores for the MembraneQuant IHC 2+ or IHC 3+ cases ($p = 0.18$). For the FISH amplified cases in the validation dataset, there was a statistical difference between the H-scores for the MembraneQuant IHC 2+ and MembraneQuant IHC 3+ cases ($p = 0.008$). In addition, for the FISH non-amplified cases in the validation dataset, there was a statistical difference between the H-scores for the MembraneQuant IHC 2+ and MembraneQuant IHC 3+ cases ($p = 0.00073$).

The glass H&E and HER2 IHC slides of the 13 discordant microscopic/MembraneQuant cases in the validation dataset

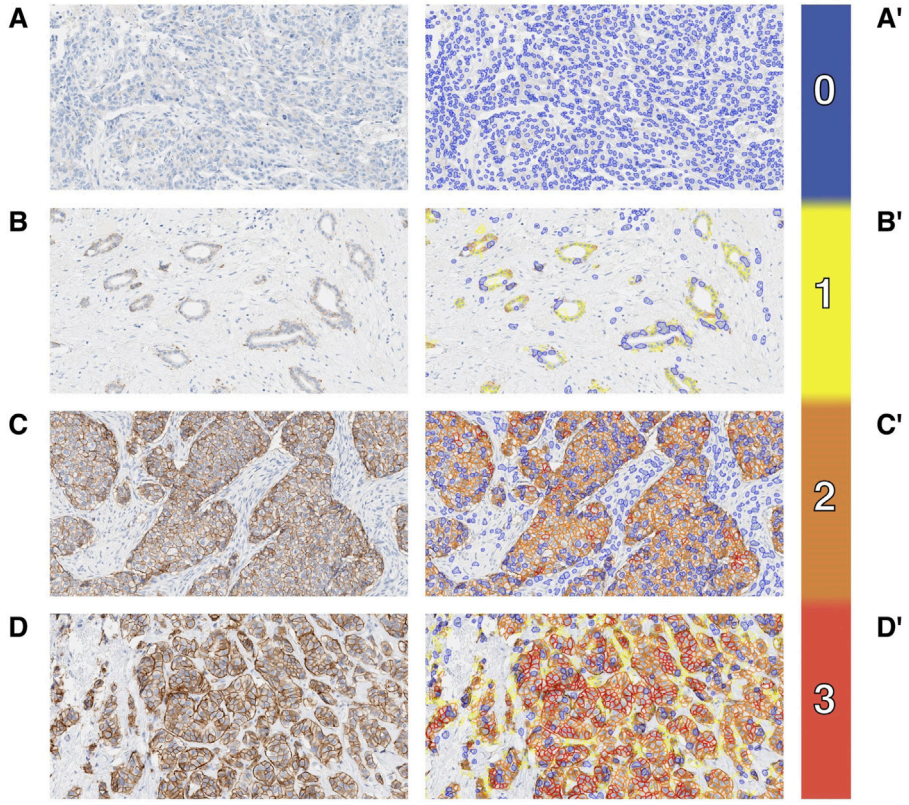

FIGURE 2
Case examples. IBC HER2 IHC with microscopic score 0 **(A)**, 1+ **(B)**, 2+ **(C)** and 3+ **(D)** and corresponding overlay from MembraneQuant by 3DHISTECH **(A′, B′, C′, D′)** with score 3 highlighted by red, score 2 orange, score 1 yellow and score 0 blue.

originally clinically reported as HER2 IHC 2+ were re-reviewed by three pathologists (DR, FP, TD) and their microscopic HER2 IHC scores are listed in Table 6. These 13 discordant cases included 11 primary tumors and 2 metastatic tumors. The primary tumors were all invasive breast carcinoma of no special type (ductal), including three with note of dense tumor infiltrating lymphocytes. Artifacts and limitations to analysis were appreciated during review in 8/13 discordant cases, most notably including cytoplasmic and granular IHC staining as well as areas of crush artifact. Few other limitations noted included abundant lymphocytes which impacted selection of the ROI, a case status post neoadjuvant therapy with tumor in a background of treatment effect, and a metastatic case with artifactual staining in stromal mucin associated with tumor cells. Cases with any artifacts or limitations were included in the overall analysis however notes were taken during the review. Overall, the re-review among three pathologists yielded agreement (between at least two out of three pathologists) with the original microscopic HER2 IHC score in 7 of 13 cases (54%) and MembraneQuant score in 5 of 13 cases (38%). In 11 of 13 cases (85%), MembraneQuant scored the same as at least one pathologist upon re-review. In one case, interpretation was limited by intratumoral heterogeneity (case 9, Table 6). This case was HER2 amplified by FISH and called 2+ with heterogeneity manually and 3+ by MembraneQuant. On re-review of glass slides, this case showed significant variation in the score, ranging from 0 to 2+. This case highlights the importance of ROI selection in cases where there is significant HER2 IHC staining heterogeneity. Additional images showing various artifacts limiting the interpretation of HER2 IHC, by microscopic review and MembraneQuant, including crush artifact, cytoplasmic and granular staining, and chatter from histologic sectioning, are shown in Figure 4.

Discussion

The availability of WSI and digital pathology is becoming more widespread in clinical practice and advancements have led to the creation of ancillary software tools that can assist with interpretation and diagnosis. In this study, we sought to determine the performance of a semi-automated HER2 IHC

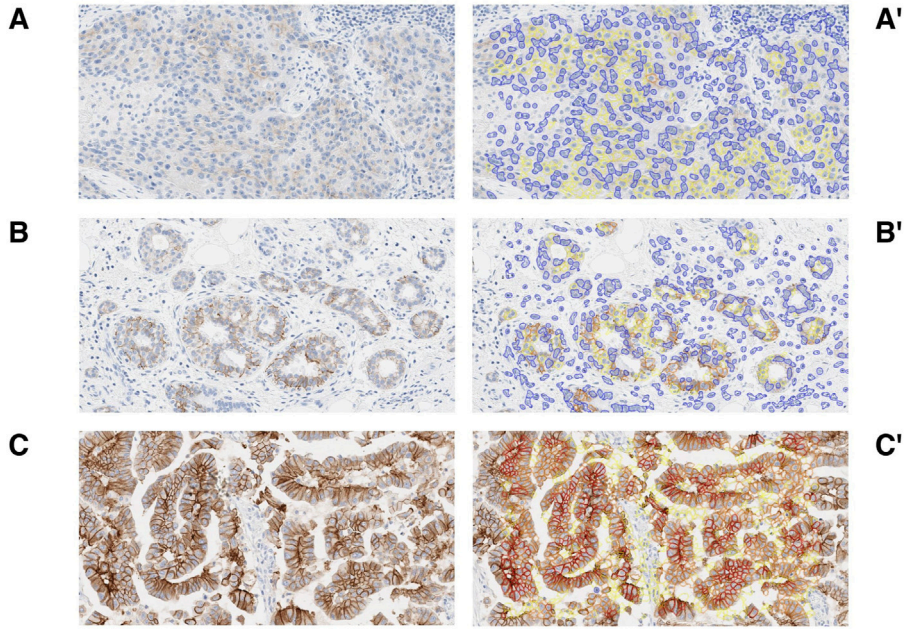

FIGURE 3
Discordant cases. Examples of discordance between microscopic IHC scoring and QuantCenter (MembraneQuant) by 3DHISTECH semi-automated scoring. Microscopic IHC 0 scored as 1+ by MembraneQuant **(A)** and corresponding overlay **(A')**. Microscopic IHC 2+ scored as 1+ by MembraneQuant **(B)** and corresponding overlay **(B')**. Microscopic IHC 2+ scored as 3+ by MembraneQuant **(C)** and corresponding overlay **(C')**.

TABLE 4 Validation dataset (composed of HER2 IHC 2+ cases) showing the MembraneQuant IHC score by FISH amplification status (N = 77).

FISH	MembraneQuant HER2 IHC score			
	0	1+	2+	3+
AMPLIFIED, N (%)	0 (0%)	2 (2.5%)	19 (25%)	6 (8%)
NON-AMPLIFIED, N (%)	0 (0%)	2 (2.5%)	45 (58%)	3 (4%)

algorithm for IHC assessment which is quite subjective in daily practice. According to Wu et al.'s systematic review and meta-analysis study on automatic evaluation of HER2 IHC status in breast cancer, the diagnostic performance of artificial intelligence (AI) shows high sensitivity and specificity with the diagnosis rendered by pathologists, and while these programs are able to distinguish between different HER2 IHC scores, the ability of AI to identify HER2 IHC scores of 2+ was slightly lower compared to recognition of scores of 0/1+ and 3+ [8]. The findings from the HER2 IHC 2+ validation dataset in our study demonstrate the wide range of HER2 IHC staining patterns that may be classified as 2+ by pathologists. The threshold for calling IHC 3+ microscopically is also variable, highlighted by the 6 HER2 amplified cases that were called 2+ on microscopic review but classified as 3+ by MembraneQuant. In clinical practice, in addition to the ASCO/CAP algorithm for evaluation, factors that impact the threshold for assigning a HER2 IHC score of 3+ include the quality of positive and negative controls, tissue quality, and staining characteristics. In the 6 HER2 amplified cases that were upgraded to 3+ by MembraneQuant, the IHC slide showed artifacts or non-membranous staining patterns in 4/6 cases, including crush and cytoplasmic/granular staining. Artifacts strongly impact a pathologist's IHC interpretation and even with strong HER2 intensity, the threshold for calling 3+ is generally higher due to treatment implications and FISH is frequently ordered in these cases. According to ASCO/CAP guidelines, edge artifact, cytoplasmic positivity, overstaining, and misinterpretation of ductal carcinoma *in situ* (DCIS) can lead to false positive results [9]. Chatter artifacts caused when cutting on the microtome also impact interpretation. In addition, prolonged cold ischemia time, tumor heterogeneity, and improper antibody titration can lead to false negative HER2 IHC results [10]. Additionally, the performance of AI algorithms relies heavily on the quality of HER2 IHC digital images and is affected by factors such as IHC slide quality and digital slide imaging. [11, 12] These pre-analytic and analytic variables that affect the test results always need to be considered and repeat testing should be performed when indicated [1]. The study of Palm et al. further

TABLE 5 Semi-automatic H-scores generated by MembraneQuant for calibration (N = 32) and validation (N = 77) datasets.

FISH	Calibration dataset MembraneQuant HER2 IHC score				Validation dataset MembraneQuant HER2 IHC score			
	0	1+	2+	3+	0	1+	2+	3+
AMPLIFIED, N (%)	0 (0%)	0 (0%)	4 (12%)	10 (32%)	0 (0%)	2 (2.5%)	19 (25%)	6 (8%)
H-SCORE, Mean (Range)	N/A	N/A	135 (99–185)	162 (88–191)	N/A	53 (53–53)	128 (95–161)	157 (118–188)
NON-AMPLIFIED, N (%)	3 (9%)	8 (25%)	7 (22%)	0 (0%)	0 (0%)	2 (2.5%)	45 (58%)	3 (4%)
H-SCORE, Mean (Range)	0 (0–5)	45 (18–81)	109 (62–157)	N/A	N/A	75 (56–94)	129 (82–190)	184 (171–198)

TABLE 6 Discordant cases in the validation HER2 IHC 2+ dataset (N = 13).

Case	HER2 Score	MembQt IHC score	HER2 FISH (ASCO/CAP group)	Path 1	Path 2	Path 3	Specimen type	Histologic subtype	Limitations
1	2+	1+	AMP (Group 1)	Focal 2+	2+	1+	EX	IDC, dense TIL	Abundant TIL
2	2+	1+	AMP (Group 1)	2+	2+	1+	EX	IDC	Post NAC
3	2+	1+	NONAMP (Group 5)	1+	2+	1+	BX	IDC, dense TIL	Crush, cytoplasmic/ granular staining
4	2+	1+	NONAMP (Group 5)	2+	2+	1+	BX	IDC, dense TIL	N/A
5	2+	3+	AMP (Group 1)	2+	3+	2+	EX	IDC	Crush, cytoplasmic/ granular staining
6	2+	3+	AMP (Group 1)	2+	3+	3+	BX	IDC	Crush, cytoplasmic/ granular staining
7	2+	3+	AMP (Group 1)	2+	3+	3+	EX	IDC	N/A
8	2+	3+	AMP (Group 1)	2+	2+	3+	BX	IDC	Crush, cytoplasmic/ granular staining
9	2+	3+	AMP (Group 1)	0	2+	1-2+	EX	IDC	Intratumoral heterogeneity, crush, cytoplasmic/granular staining
10	2+	3+	AMP (Group 1)	2+	3+	3+	EX	IDC	N/A
11	2+	3+	NONAMP (Group 4)	2+	3+	3+	EX	IDC	N/A
12	2+	3+	NONAMP (Group 5)	2+	3+	2+	BX	Mucinous and micropapillary	Staining in stromal mucin
13	2+	3+	NONAMP (Group 2)	2+	2+	2+	BX	IDC	N/A

MembQt, MembraneQuant; ASCO/CAP, American Society of Clinical Oncology/College of American Pathologists; AMP, amplified; NONAMP, non-amplified; BX, biopsy; EX, excision; IDC, invasive breast carcinoma no special type (ductal); TIL, tumor infiltrating lymphocytes; NAC, neoadjuvant chemotherapy; N/A, not applicable.

demonstrated the importance of pre-analytic variables, as it showed the agreement in HER2 IHC evaluation between AI and pathologists increased from 38.3% to 77.6% after adjustments for Ultra Cell Conditioning Solution (CC1) incubation time, antibody incubation time and counterstaining time [13]. In the one case that was classified as 1+ by MembraneQuant but was HER2 amplified by FISH in our study, the sample was status post neoadjuvant chemotherapy, with prior biopsy result of IHC 2+/FISH amplified. In the neoadjuvant setting, HER2 IHC staining has been reported to be less intense [14], either due to a true decrease in staining intensity or secondary to changes in cytomorphology. Overall, the above factors need to be taken into account when assessing IHC microscopically and especially by semi-automated analysis.

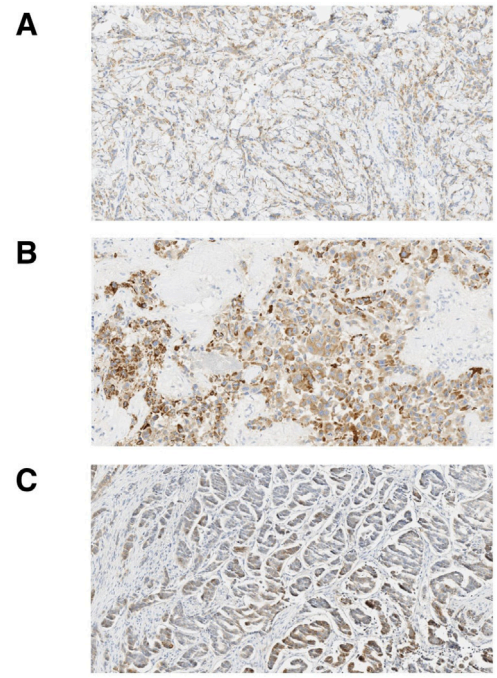

FIGURE 4
Artifacts seen with HER2 IHC staining. Examples of artifacts confounding interpretation of HER2 IHC **(A)** crush artifact, **(B)** cytoplasmic and granular staining and **(C)** chatter artifact.

The review of the discordant HER2 IHC 2+ cohort in this study by three additional pathologists further highlights the interobserver variability in borderline cases and the need for objective tools. Distinguishing between HER2 IHC scores of 0 and 1+, which is crucial in the current HER2-low IBC era, is challenging. Fernandez et al. showed an interrater agreement lower than 70% between all HER2 IHC scores, but mostly 0 and 1+, in 19% of cases (15/80) [6]. The assessment of HER2 IHC 0 and 1+ cases was limited to the calibration dataset in this analysis with only few cases, which is a limitation of the current study. Four out of 18 non-amplified cases (22%) were scored as IHC 1+ microscopically and concordantly MembraneQuant scored all as 1+ (22%). However for the 6 out of 18 non-amplified cases (33%) that were microscopically scored as IHC 0, 3 cases were scored as 1+ by MembraneQuant and 3 were scored as 0. Distinguishing HER2 IHC 0 from 1+ remains challenging, even with computational tools, highlighting the limitations of existing HER2 assays in detecting HER2-low IBC. Wu et al. analyzed data from four studies focusing on AI's ability to discriminate between HER2 IHC scores of 0 and 1+ and found that the performance of AI was relatively poor [8]. It is important to note that many prior concordance studies assessing digital image analysis for HER2 IHC scoring considered scores of 0 and 1+ as a single entity as, until recently, there were no clinical outcomes associated with distinguishing between these negative results [9]; Holten-Rossing et al. for example, combined 0/1+ IHC scores into a single group (HER2 negative) for analysis in their 2015 publication [15].

While MembraneQuant provides more objective parameters that are applied in a uniform manner to all slides, there are several limitations with the program. First, the software at the time of this analysis does not reliably distinguish between tumor cells and background stromal cells or tumor infiltrating lymphocytes. For this study, we used the same nuclear size cut off for each scanned slide for consistency, however adjusting the nuclear size in the program to a set threshold for individual cases may help with reducing interference from background stromal cells in the interpretation of HER2 IHC using MembraneQuant. Second, the internal scoring algorithm of MembraneQuant is weighted more heavily on the intensity of staining rather than the completeness and pattern of staining. The issue of intensity was highlighted in a separate study by Jung et al., where Al-powered ER/PR and HER2 analyzers of the breast based on a digital learning algorithm were developed, each containing both a cell detection model and a tissue segmentation model. By combining the results from both cell and tissue models, some tumor cells incorrectly detected in areas outside the ROI could be excluded. Discrepancies in the cell detection model were observed, mainly in cell classes, where the AI analyzer assessment differed by a single degree of intensity, such as changing from a HER2 IHC 2+ tumor cell to a 1+ tumor cell. In contrast, cases in which the AI analyzer misjudged the intensity by more than two grades, such as HER2 IHC 3+ tumor cell to negative (0) tumor cell, were less common [16]. Moreover, while MembraneQuant can calculate an H-score based on the fraction of cells scored with each intensity, only one overall HER2 IHC score is actually assigned. In the MembraneQuant's calculation, scoring is purely assessed by cellularity and percentage, and the ASCO/CAP recommendation of scoring tumor cells within a contiguous area appreciable at low power [9] is not incorporated and can contribute to overscoring of HER2 IHC. In addition, a limitation of MembraneQuant is that it depends on both ROI annotation and overall H-score generation. However, most algorithms do not handle tasks with parameters beyond specific training sets due to a lack of robustness, and more importantly, they may require human intervention to annotate ROIs [17–19]. In one study by Selcuk et al., a digital learning-based method that utilizes pyramid sampling was used to automate the classification of HER2 status in IHC-stained slides. This method of analyzing features across multiple special scales addresses the challenge of HER2 expression heterogeneity without ROI selection prior to model training. The quantitative analysis involving 523 core images from 300 patients included in the study resulted in a classification accuracy of 84.70% compared to the consensus scores obtained from 5 board-certified pathologists [20].

In the present study, significant differences in H-scores were observed only in the validation set (n = 77, HER2 IHC 2+), specifically between the 2+ and 3+ scored cases by MembraneQuant, and interestingly regardless of the FISH amplification result (amplified or non-amplified), raising the question of its utility in clinical practice and alluding to some of

the previously raised limitations of H-score calculation. The three MembraneQuant IHC 3+ cases that were non-amplified by FISH were notably categorized in ASCO/CAP group 2 (n = 1), group 4 (n = 1), and group 5 (n = 1). These three cases would be clinically managed as HER2-negative based on a combined FISH result and clinical IHC 2+ score, but it does highlight the need to further assess the more uncommon ASCO/CAP groups 2, 3 and 4 with semi-automated software tools. While no significant difference was observed in HER2 2+ and 3+ cases in the calibration set, this is likely due to the small number of cases evaluated. Further studies are needed to assess the value of H-scores in discriminating between cases categorized as HER2-low.

Lastly, significant time is required to run each analysis even following ROI selection. Analysis of a small biopsy at the time of this study takes on average 2–5 min and analysis of a large resection specimen takes 10–15 min. This is a significant amount of time compared to the manual review of a HER2 IHC analysis by an experienced pathologist. There is however great potential of this software for pathologists in training looking to set their own internal threshold and this should be explored further.

Previous studies have addressed issues regarding color consistency of WSI between different scanners. The inconsistency in contrast/brightness may alter visibility and impact the assessment of HER2 membrane expression as intensity/brightness is a crucial factor in scoring [21]. In regards to HER2 IHC scoring on WSI, it has been reported to show stronger intensity and higher scores than that conducted on glass slides due to possible increased color contrast on WSI [22]. However, a recent study comparing the performance of glass slides to digital slides for biomarker assessment of breast cytology specimens showed good concordance between the two methods and a good kappa correlation between glass slides and WSI for each study pathologist [23].

Conclusion

Semi-automated analysis using WSI yielded a sensitivity of 100% and specificity of 61% in the calibration dataset and 84% of IHC 2+ cases in the validation set showed 100% agreement with microscopic analysis. In discordant cases which were also re-reviewed by three pathologists, MembraneQuant showed 85% (11/13) agreement with at least one pathologist scoring. There are inherent limitations in current HER2 tests, particularly in the detection of HER2-low IBC, that semi-automatic HER2 IHC interpretation cannot resolve at this time, however there is great value in providing an objective computational tool for a test known to be quite subjective. This software also neutralizes the experience factor in IHC scoring, raising all observers to approximately the same level and diminishing interobserver variability. Based on the results of this study, future prospective studies using semi-automated immunohistochemical analysis tools on a wider range of HER2 IHC scores are warranted.

Data availability statement

The raw data supporting the conclusions of this article will be made available by the authors, without undue reservation.

Ethics statement

The study was approved by the Memorial Sloan Kettering Cancer Center Institutional Review Board (Protocol #18-013) and has been performed in accordance with the ethical standards as laid down in the 1964 Declaration of Helsinki and its later amendments. The requirement for written informed consent was waived as the study was retrospective, all data was deidentified, and the research contained no more than minimal risk to the participants or their privacy.

Author contributions

DR and YY conceptualized the project. CL, NB, EC, YY, and DR performed data curation and formal analysis. CL and DR wrote the original draft of manuscript. CL, NB, MH, FP, HW, TD, EB, and YY reviewed and edited the final draft. All authors contributed to the article and approved the submitted version.

Funding

The authors declare that financial support was received for the research, authorship, and/or publication of this article. This research was funded in part through the NIH/NCI Cancer Center Support Grant P30 CA008748. FP is funded in part by an NIH/NCI P50 CA24779 01 grant and by a Starr Cancer Consortium Grant.

Acknowledgments

This work would not have been possible without the technical assistance of 3DHISTECH Ltd. (Budapest, Hungary). We also acknowledge the assistance of Kareem Ibrahim in YY's Digital Pathology Laboratory.

Conflict of interest

FP is a member of the scientific advisory board of Multiplex DX. In addition, FP serves on the diagnostic advisory board and reports receiving consultancy fees from AstraZeneca.

The remaining authors declare that the research was conducted in the absence of any commercial or financial relationships that could be construed as a potential conflict of interest.

References

1. Wolff AC, Somerfield MR, Dowsett M, Hammond ME, Hayes DF, McShane LM, et al. Human epidermal growth factor receptor 2 testing in breast cancer: ASCO–College of American Pathologists Guideline Update. *J Clin Oncol* (2023) 41(22):3867–72. doi:10.1200/JCO.22.02864

2. Hechtman JF, Ross DS. The past, present, and future of HER2 (ERBB2) in cancer: approaches to molecular testing and an evolving role in targeted therapy. *Cancer Cytopathology* (2019) 127(7):428–31. doi:10.1002/cncy.22124

3. Modi S, Park H, Murthy RK, Iwata H, Tamura K, Tsurutani J, et al. Antitumor activity and safety of trastuzumab deruxtecan in patients with HER2-low–expressing advanced breast cancer: results from a phase Ib study. *J Clin Oncol* (2020) 38(17):1887–96. doi:10.1200/JCO.19.02318

4. Modi S, Jacot W, Yamashita T, Sohn J, Vidal M, Tokunaga E, et al. Trastuzumab deruxtecan in previously treated HER2-low advanced breast cancer. *New Engl J Med* (2022) 387(1):9–20. doi:10.1056/NEJMoa2203690

5. Tarantino P, Hamilton E, Tolaney SM, Cortes J, Morganti S, Ferraro E, et al. HER2-low breast cancer: pathological and clinical landscape. *J Clin Oncol* (2020) 38(17):1951–62. doi:10.1200/JCO.19.02488

6. Fernandez AI, Liu M, Bellizzi A, Brock J, Fadare O, Hanley K, et al. Examination of low ERBB2 protein expression in breast cancer tissue. *JAMA Oncol* (2022) 8(4):1–4. doi:10.1001/jamaoncol.2021.7239

7. Zhang H, Katerji H, Turner BM, Hicks DG. HER2-low breast cancers: new opportunities and challenges. *Am J Clin Pathol* (2022) 157(3):328–36. doi:10.1093/ajcp/aqab117

8. Wu S, Li X, Miao J, Xian D, Yue M, Liu H, et al. Artificial intelligence for assisted HER2 immunohistochemistry evaluation of breast cancer: a systematic review and meta-analysis. *Pathology-Research Pract* (2024) 16:155472. doi:10.1016/j.prp.2024.155472

9. Wolff AC, Hammond ME, Allison KH, Harvey BE, McShane LM, Dowsett M. HER2 testing in breast cancer: American Society of Clinical Oncology/College of American Pathologists clinical practice guideline focused update summary. *J Oncol Pract* (2018) 14(7):437–41. doi:10.1200/JOP.18.00206

10. Allison KH, Hammond ME, Dowsett M, McKernin SE, Carey LA, Fitzgibbons PL, et al. Estrogen and progesterone receptor testing in breast cancer: American Society of Clinical Oncology/College of American Pathologists guideline update. *Arch Pathol and Lab Med* (2020) 144(5):545–63. doi:10.5858/arpa.2019-0904-SA

11. Smith B, Hermsen M, Lesser E, Ravichandar D, Kremers W. Developing image analysis pipelines of whole-slide images: pre-and post-processing. *J Clin Translational Sci* (2021) 5(1):e38. doi:10.1017/cts.2020.531

12. Manuel C, Zehnder P, Kaya S, Sullivan R, Hu F. Impact of color augmentation and tissue type in deep learning for hematoxylin and eosin image super resolution. *J Pathol Inform* (2022) 13:100148. doi:10.1016/j.jpi.2022.100148

13. Palm C, Connolly CE, Masser R, Padberg Sgier B, Karamitopoulou E, Simon Q, et al. Determining HER2 status by artificial intelligence: an investigation of primary, metastatic, and HER2 low breast tumors. *Diagnostics* (2023) 13(1):168. doi:10.3390/diagnostics13010168

14. Guarneri V, Dieci MV, Barbieri E, Piacentini F, Omarini C, Ficarra G, et al. Loss of HER2 positivity and prognosis after neoadjuvant therapy in HER2-positive breast cancer patients. *Ann Oncol* (2013) 24(12):2990–4. doi:10.1093/annonc/mdt364

15. Holten-Rossing H, Møller Talman ML, Kristensson M, Vainer B. Optimizing HER2 assessment in breast cancer: application of automated image analysis. *Breast Cancer Res Treat* (2015) 152:367–75. doi:10.1007/s10549-015-3475-3

16. Jung M, Song SG, Cho SI, Shin S, Lee T, Jung W, et al. Augmented interpretation of HER2, ER, and PR in breast cancer by artificial intelligence analyzer: enhancing interobserver agreement through a reader study of 201 cases. *Breast Cancer Res* (2024) 26:31. doi:10.1186/s13058-024-01784-y

17. Gokhale S, Rosen D, Sneige N, Diaz LK, Resetkova E, Sahin A, et al. Assessment of two automated imaging systems in evaluating estrogen receptor status in breast carcinoma. *Appl Immunohistochem and Mol Morphol* (2007) 15(4):451–5. doi:10.1097/PAI.0b013e31802ee998

18. Gandomkar Z, Brennan PC, Mello-Thoms C (2016). Computer-based image analysis in breast pathology. *J Pathol Inform*, 7(1), 43. doi:10.4103/2153-3539.192814

19. Faratian D, Kay C, Robson T, Campbell FM, Grant M, Rea D, et al. Automated image analysis for high-throughput quantitative detection of ER and PR expression levels in large-scale clinical studies: the TEAM Trial Experience. *Histopathology* (2009) 55(5):587–93. doi:10.1111/j.1365-2559.2009.03419.x

20. Selcuk SY, Yang X, Bai B, Zhang Y, Li Y, Aydin M, et al. Automated HER2 scoring in breast cancer images using deep learning and pyramid sampling. *BMEF (BME Frontiers)* (2024) 5:0048. doi:10.34133/bmef.0048

21. Ohnishi C, Ohnishi T, Ntiamoah P, Ross DS, Yamaguchi M, Yagi Y. Standardizing HER2 immunohistochemistry assessment: calibration of color and intensity variation in whole slide imaging caused by staining and scanning. *Appl Microsc* (2023) 53(1):8. doi:10.1186/s42649-023-00091-8

22. Kondo Y, Iijima T, Noguchi M. Evaluation of immunohistochemical staining using whole-slide imaging for HER2 scoring of breast cancer in comparison with real glass slides. *Pathol Int* (2012) 62(9):592–9. doi:10.1111/j.1440-1827.2012.02847.x

23. Hanna MG, Parwani A, Sirintrapun SJ. Whole slide imaging: technology and applications. *Adv Anat Pathol* (2020) 27(4):251–9. doi:10.1097/PAP.0000000000000273

Pathology & Oncology Research | frontiers

TYPE Original Research
PUBLISHED 29 August 2024
DOI 10.3389/pore.2024.1611853

Check for updates

OPEN ACCESS

EDITED BY
Andrea Ladányi,
National Institute of Oncology (NIO), Hungary

*CORRESPONDENCE
Lorand Lakatos,
lakatoslorandl@gmail.com

RECEIVED 29 May 2024
ACCEPTED 19 July 2024
PUBLISHED 29 August 2024

CITATION
Lakatos L, Illyes I, Budai A, Bencze V, Szijarto A, Kiss A and Banky B (2024), Feasibility of indocyanine green (ICG) fluorescence in *ex vivo* pathological dissection of colorectal lymph nodes—a pilot study.
Pathol. Oncol. Res. 30:1611853.
doi: 10.3389/pore.2024.1611853

COPYRIGHT
© 2024 Lakatos, Illyes, Budai, Bencze, Szijarto, Kiss and Banky. This is an open-access article distributed under the terms of the Creative Commons Attribution License (CC BY). The use, distribution or reproduction in other forums is permitted, provided the original author(s) and the copyright owner(s) are credited and that the original publication in this journal is cited, in accordance with accepted academic practice. No use, distribution or reproduction is permitted which does not comply with these terms.

Feasibility of indocyanine green (ICG) fluorescence in *ex vivo* pathological dissection of colorectal lymph nodes—a pilot study

Lorand Lakatos[1]*, Ildiko Illyes[2], Andras Budai[2], Viktoria Bencze[1], Attila Szijarto[1], Andras Kiss[2] and Balazs Banky[1]

[1]Department of Surgery, Transplantation and Gastroenterology, Semmelweis University, Budapest, Hungary, [2]Department of Pathology, Forensic and Insurance Medicine, Semmelweis University, Budapest, Hungary

Accurate lymph node (LN) retrieval during colorectal carcinoma resection is pivotal for precise N-staging and the determination of adjuvant therapy. Current guidelines recommend the examination of at least 12 mesocolic or mesorectal lymph nodes for accurate staging. Traditional histological processing techniques, reliant on visual inspection and palpation, are time-consuming and heavily dependent on the examiner's expertise and availability. Various methods have been documented to enhance LN retrieval from colorectal specimens, including intra-arterial *ex vivo* methylene blue injection. Recent studies have explored the utility of indocyanine green (ICG) fluorescence imaging for visualizing pericolic lymph nodes and identifying sentinel lymph nodes in colorectal malignancies. This study included 10 patients who underwent colon resection for malignant tumors. During surgery, intravenous ICG dye and an endoscopic camera were employed to assess intestinal perfusion. Post-resection, *ex vivo* intra-arterial administration of ICG dye was performed on the specimens, followed by routine histological processing and an ICG-assisted lymph node dissection. The objective was to evaluate whether ICG imaging could identify additional lymph nodes compared to routine manual dissection and to assess the clinical relevance of these findings. For each patient, a minimum of 12 lymph nodes (median = 25.5, interquartile range = 12.25, maximum = 33) were examined. ICG imaging facilitated the detection of a median of three additional lymph nodes not identified during routine processing. Metastatic lymph nodes were found in four patients however no additional metastatic nodes were detected with ICG assistance. Our findings suggest that *ex vivo* intra-arterial administration of indocyanine green dye can augment lymph node dissection, particularly in cases where the number of lymph nodes retrieved is below the recommended threshold of 12.

KEYWORDS

indocyanine green, colorectal cancer, lymph node, *ex vivo*, colorectal resection

Introduction

Following the resection for colorectal carcinoma, the number of retrieved regional lymph nodes is important for determining the stage and adjuvant therapy. For accurate N-staging, as many as possible, but at least 12 mesocolic or mesorectal lymph nodes need to be histologically examined [1].

In the pathological processing of colorectal specimens, the traditional dissection "performed by visual inspection and palpation" is a time-consuming method. In addition, the effectiveness of lymph node harvesting significantly depends on the experience of the examiner and the time available. The technical difficulty is well illustrated by the fact that 80% of mesenteric lymph nodes are less than 3 mm in diameter, and 50% of metastatic lymph nodes are less than 5 mm in diameter [2].

Additionally, in rectal cancer cases, post-neoadjuvant total mesorectal excision (TME) dissection results in a typically low number of extracted lymph nodes, making even the threshold of 12 hard to achieve [3].

There are many methods known in the literature to facilitate the extraction of lymph nodes from a colorectal specimen, including intra-arterial *ex vivo* Methylene Blue specimen loading [4], fat-clearance techniques [5], and even the employment of extra pathology assistant staff [6].

In vivo, intraoperative fluorescence imaging of subserosal-injected indocyanine green (ICG) has recently been proven to be a promising method for imaging lymphatic vessels and lymph nodes [7]. Several studies have investigated peritumoral submucosal ICG injection by endoscopy to identify sentinel lymph nodes in colorectal cancer; however, the results are still controversial [8].

ICG, on the other hand, has been introduced as an effective tool to qualitatively and quantitatively verify adequate blood supply to the resection lines during colorectal resection [9]. Under near-infrared excitation (with the help of a laser light source and image processing suitable for fluorescence detection), intravenous injection of ICG solution helps to differentiate between well- and under-perfused tissues.

ICG has a relatively short half-life in the blood (approximately 2–4 min) and is quickly distributed to various tissues through systemic circulation. Combining the two phenomena that intra-arterial dyes accumulate in mesenteric lymph nodes (as in methylene blue studies) [10], and that ICG can be used for lymph node detection, we postulated that lymph node harvesting in histologic specimen processing may be enhanced by the ICG fluorescence technique. The aim of this study was to evaluate the feasibility and efficacy of the intraarterial ICG technique to facilitate lymph node dissection in colorectal resection.

Materials and methods

In our pilot study, we enrolled ten consecutive patients with colorectal cancer who underwent colorectal resection. We used the Medtronic Elevision™ IR platform imaging system with Verdye™ indocyanine dye as a fluorophore, to perform ICG fluorescence imaging (ICG-FI). The dye in powder form was dissolved in sterile distilled water for injection according to the manufacturer's instructions, and a bolus intravenous injection of 0.05 mg/kg ICG dye was administered during surgery before colorectal resection as a routine perfusion check. After specimen extraction, arterial cannulation and a second shot of 0.05 mg/kg dose of direct intraarterial ICG were performed *ex vivo* under fluorescence imaging (Figure 1).



FIGURE 1
Cannulation of the supplying artery and ICG perfusion of the extracted specimen Ensure that all the figures, tables, and captions are correct, and that all figures are of the highest quality/resolution. You may upload improved figures to the Production Forum. If so, please describe in visual terms the exact changes(s) made to help us confirm that the updated version has been used in the finalized proof. Please note that figures and tables must be cited sequentially, per the author guidelines.

The specimen was then routinely processed after a 24-hour incubation in a 4% buffered formaldehyde solution and sent for traditional pathology grossing. After conventional lymph node dissection carried out by a pathologist under naked eye control and traditional palpation technique, each specimen was re-examined using ICG-FI. This was possible as formaldehyde does not compromise fluorescence excitability [11]. The additionally identified lymph nodes were sent for further pathological examination (Figure 2). The lymph node numbers of the primary (conventional) harvesting and the ICG-fluorescence-enhanced extra lymph node numbers were recorded. Lymph node sizes were measured as well during



FIGURE 2
Fluorescence imaging of the extra harvested lymph nodes.

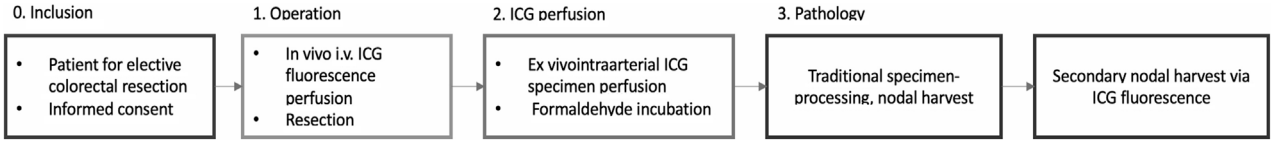

FIGURE 3
Study design.

the pathological routine workup using a conventional light microscope.

A summary of the study design is shown in Figure 3.

In order to exclude or highlight the Hawthorne effect [12] we compared lymph node yields to a historical cohort of 30 consecutive patients with colorectal cancer with similar patient and clinical characteristics (propensity-matched cases).

TABLE 1 Patient characteristics.

Mean age	73
Sex ratio	1:1
Right hemicolectomy	3
Transverse colon resection	1
Rectal resection	6

Statistical work-up

Demographic data, cancer characteristics, lymph node numbers and lymph node sizes were analyzed. The normality of the distributions of continuous variables was tested with the Shapiro-Wilk test. Comparisons were made using the Student's paired sample T-test for normally distributed variables and the Mann-Whitney U-test for non-Gaussian distributed ones. Differences with $p < 0.05$ were considered significant. The propensity score was calculated by binal logarithmic regression, covariates were T and N stages, neoadjuvant therapy and type of resection. After propensity score matching we carried out the Mann-Whitney U test using mean ranks to determine whether there was a significant increase in lymph node yield with ICG assistance in addition to traditional harvesting. Statistical analysis was performed using SPSS (IBM© SPSS© statistics 27) software.

TABLE 2 Tumor characteristics.

Patient #	T stage	N stage	Neoadjuvant therapy
1	3	0	Yes
2	4a	1b	No
3	3	1b	No
4	1	0	Yes
5	2	0	Yes
6	3	2a	No
7	2	0	No
8	2	0	Yes
9	4a	1a	No
10	4b	0	No

Results

Patient characteristics and tumor characteristics are shown in Tables 1, 2.

Number of harvested lymph nodes

A median of 21.5 lymph nodes was identified in the experimental population by the initial conventional pathological workup which was supplemented by ICG fluorescence imaging to a median of 25.5 lymph nodes (Figure 6).

ICG fluorescence imaging identified an additional 34 lymph nodes in 10 cases that were not detected by traditional pathological examination (Figure 4).

Metastatic lymph nodes

A total of 11 metastatic lymph nodes were identified in 4 out of 10 specimens. No metastatic lymph node was identified by ICG.

Size of harvested lymph nodes

Of all metastatic lymph nodes, 50% were smaller than 5 mm in diameter. The median size of lymph nodes harvested by the traditional pathological examination was 3 mm and 1.8 mm for lymph nodes identified with ICG (Figure 5).

The mean size of lymph nodes extracted by ICG assistance following traditional lymph node harvesting was half that of lymph nodes identified with conventional dissection (3.70 vs. 1.76 mm, SD 2.05 vs. 0.73 mm). We found that the smaller lymph nodes, which are more difficult to detect with traditional dissection methods, were more likely to be identified with ICG-FI.

Historical cohort

After propensity score matching, the median lymph node yield was significantly higher in the study group even without ICG assistance than in the control group of a historical cohort (Figure 6) (median of 21.5 vs. 13, $p = 0.052$, U = 24, r = 0.6). In total, 30% of the cases in the historical cohort had suboptimal nodal staging (less than 12 lymph nodes assessed), while only 2 cases (20%) had inaccurate nodal staging in the traditional work-up during the study period, both of which were improved above 12 nodes with ICG supplementation.

In our current study, the accuracy was 80%, in the propensity-matched historical cohort it was 70%.

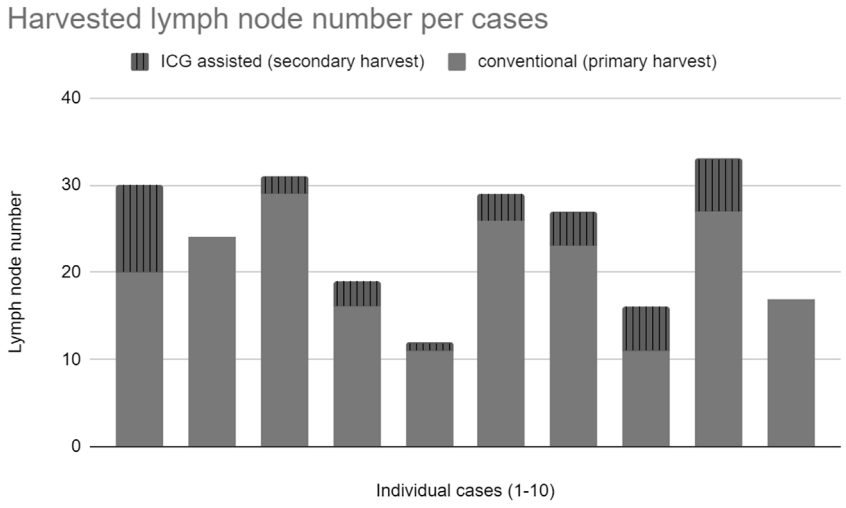

FIGURE 4
Total harvested lymph nodes.

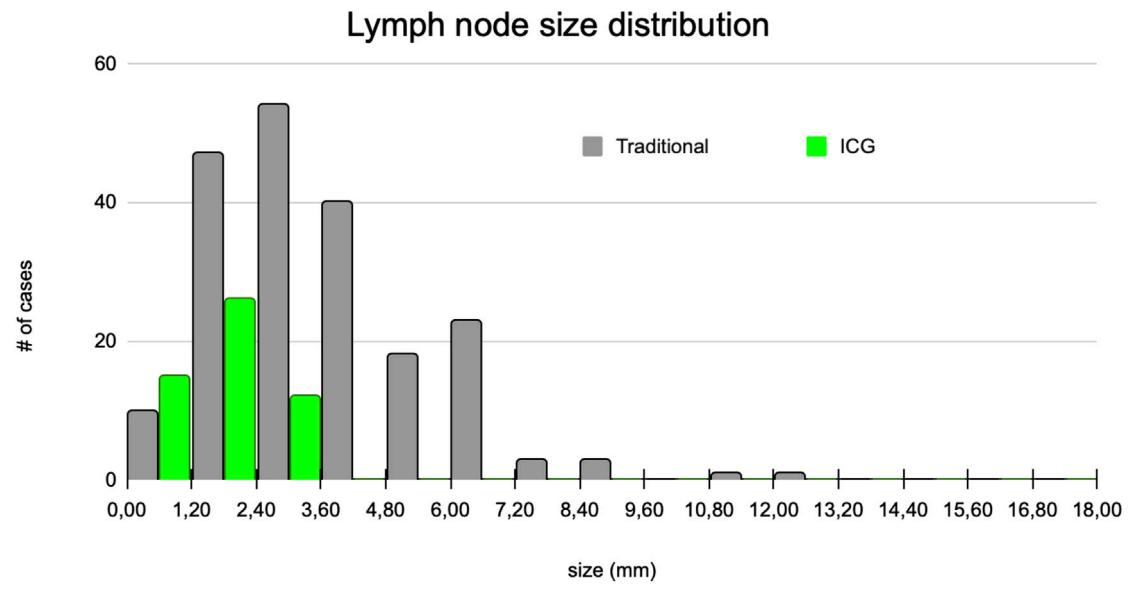

FIGURE 5
Lymph node size distributions.

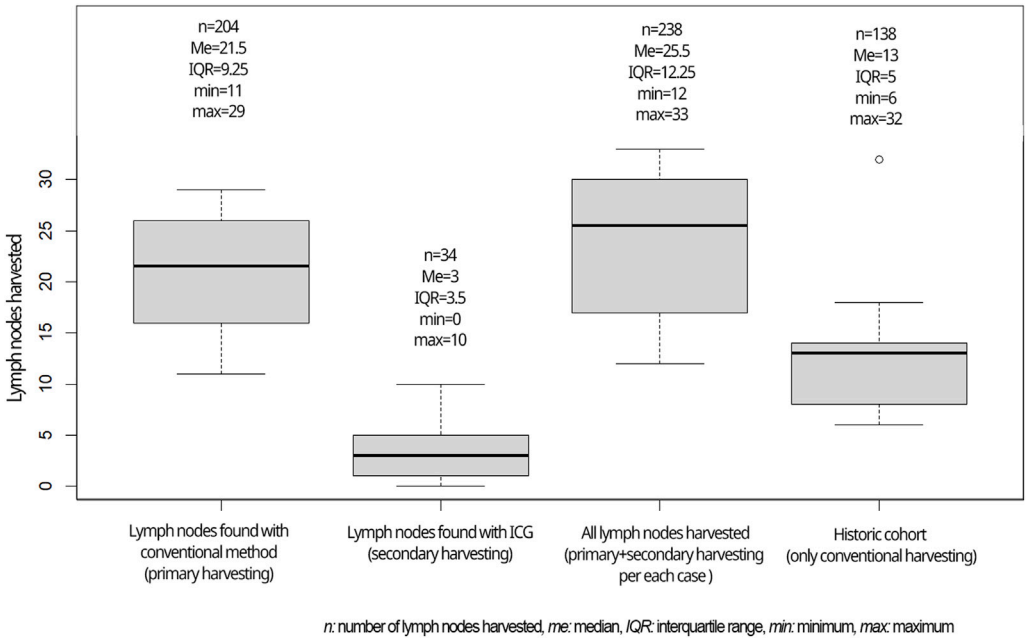

FIGURE 6
Lymph nodes harvested in the current study compared to the historical cohort.

Adverse events

Because ICG-assisted lymph node dissection was performed *ex vivo*, no adverse events were recorded regarding the assessments. Given that a single vial of ICG is sufficient for intraoperative perfusion assessment and *ex vivo* lymph node identification, the technique has no additional cost.

Discussion

Indocyanine green as a fluorescent dye is commonly used in medical imaging and diagnostic procedures. It absorbs light in the near-infrared range (wavelengths of 700–900 nm), which is beyond the visible spectrum. Near-infrared light is less scattered and absorbed by tissues compared to visible light, resulting in deeper tissue penetration. The present study aimed to evaluate the feasibility and performance of *ex vivo* intraarterial ICG perfusion-based fluorescence lymph node identification in colorectal cancer.

The number of examined lymph nodes is highly prognostic [13] in addition to being a strong predictive factor affecting the postoperative multidisciplinary team decision regarding oncotherapy [14]. In cases of inaccurate N0 staging (examined nodes less than 12), patients may fail to receive the beneficial adjuvant therapy (which is routine in Hungarian oncological practice) or may be the target of unnecessary overtreatment (in some Western-European countries) [15].

In our pilot study of 10 consecutive cases of colorectal resection, ICG-FI significantly improved the number of retrieved lymph nodes, however the number of positive (metastatic) lymph nodes was not affected. Considering that the minimum lymph node yield for accurate staging according to the AJCC Cancer Staging System is at least 12, our data show that even without the help of ICG, this requirement is fulfilled in the majority of the current study. This makes the beneficial effect of ICG-FI even more impressive.

Our results show a significantly higher lymph node yield when compared to our retrospectively analyzed past results of conventional (manual) tissue harvesting. Therefore we have proved that the high success rate of lymph node retrieval within the study is at least partly due to a Hawthorne effect.

Consequently, the use of the ICG FI technique may be beneficial due to the higher number of identified lymph nodes, which in turn will result in more precise staging where accurate lymph node staging is more difficult to achieve on a regular basis.

Our results support the finding of other researchers that a significant proportion (up to 50%) of metastatic lymph nodes are smaller than or equal to 5 mm in diameter [16]. Therefore, the easy-to-perform ICG-FI is well expected to increase the positive lymph node yield.

Accuracy in pathological staging is defined as at least 12 non-metastatic lymph nodes found or any number of lymph nodes but with N1-2 stage [6, 17]. This is the primary requirement for the appropriate decision on the need for adjuvant chemotherapy, therefore it can also have a long-term oncological impact [18–20].

Although ICG-FI requires special equipment (laser, camera, dye), the same setup can be used for a variety of tasks. There is a good possibility that it will be used routinely both in the operating room and for pathological examinations in the future.

Conclusion

ICG fluorescence can improve the accuracy of lymph node staging. It identified additional lymph nodes that were not detected by traditional pathological examination, indicating that this technique has the potential to help optimize treatment planning and improve patient outcomes.

Centers with a lower number of routinely retrieved lymph nodes after colorectal resection, in addition to cases following neoadjuvant chemo-irradiation may benefit most from this technique.

Larger studies are needed to validate these findings and to determine the optimal protocol for using ICG fluorescence to improve histologic specimen processing after colorectal surgery.

Comparison of ICG-FI with other techniques for the same purpose (methylene blue intra-arterial injection, fat clearance techniques, use of pathology assistants, etc.) will be a task for the future.

Data availability statement

The raw data supporting the conclusions of this article will be made available by the authors, without undue reservation.

Ethics statement

The studies involving humans were approved by Egészségügyi Tudományos Tanács Tudományos és Kutatásetikai Bizottság. The studies were conducted in accordance with the local legislation and institutional requirements. The participants provided their written informed consent to participate in this study. Written informed consent was obtained from the individual(s) for the publication of any potentially identifiable images or data included in this article.

Author contributions

LL, VB, II, and AB conducted the experiments, LL and BB wrote the manuscript. All authors contributed to the article and approved the submitted version.

Funding

The authors declare that no financial support was received for the research, authorship, and/or publication of this article.

Conflict of interest

The authors declare that the research was conducted in the absence of any commercial or financial relationships that could be construed as a potential conflict of interest.

References

1. Kim J, Huynh R, Abraham I, Kim E, Kumar RR. Number of lymph nodes examined and its impact on colorectal cancer staging. *The Am surgeon* (2006) 72(10):902–5. doi:10.1177/000313480607201013

2. Markl B, Roessle J, Arnholdt HM, Schaller T, Krammer I, Cacchi C, et al. The clinical significance of lymph node size in colon cancer. *Mod Pathol* (2012) 25: 1413–22. doi:10.1038/modpathol.2012.92

3. Destri GL, Di Carlo I, Scilletta R, Scilletta B, Puleo S. Colorectal cancer and lymph nodes: the obsession with the number 12. *World J Gastroenterol WJG* (2014) 20(8):1951–60. doi:10.3748/wjg.v20.i8.1951

4. Borowski DW, Banky B, Banerjee AK, Agarwal AK, Tabaqchali MA, Garg DK, et al. Intra-arterial methylene blue injection into *ex vivo* colorectal cancer specimens improves lymph node staging accuracy: a randomized controlled trial. *Colorectal Dis* (2014) 16(9):681–9. PMID: 24911342. doi:10.1111/codi.12681

5. Gregurek SF, Wu HH. Can GEWF solution improve the retrieval of lymph nodes from colorectal cancer resections? *Arch Pathol Lab Med* (2009) 133(1):83–6. PMID: 19123742. doi:10.1043/1543-2165-133.1.83

6. Schofield JB, Mounter NA, Mallett R, Haboubi NY. The importance of accurate pathological assessment of lymph node involvement in colorectal cancer. *Colorectal Dis* (2006) 8(6):460–70. doi:10.1111/j.1463-1318.2006.01044.x

7. Chand M, Keller DS, Joshi HM, Devoto L, Rodriguez-Justo M, Cohen R. Feasibility of fluorescence lymph node imaging in colon cancer: FLICC. *Tech Coloproctol* (2018) 22(4):271–7. Epub 2018 Mar 17. PMID: 29551004. doi:10.1007/s10151-018-1773-6

8. Sposito C, Maspero M, Belotti P, Simonotti N, Altomare M, Ciana P, et al. Indocyanine green fluorescence-guided surgery for gastrointestinal tumors: a systematic review. *Ann Surg Open* (2022) 3(3):e190. PMID: 37601143; PMCID: PMC10431291. doi:10.1097/AS9.0000000000000190

9. Watanabe J, Ota M, Suwa Y, Suzuki S, Suwa H, Momiyama M, et al. Evaluation of the intestinal blood flow near the rectosigmoid junction using the indocyanine green fluorescence method in a colorectal cancer surgery. *Int J colorectal Dis* (2015) 30:329–35. doi:10.1007/s00384-015-2129-6

10. Märkl B, Arnholdt HM, Jähnig H, Spatz H, Anthuber M, Oruzio DV, et al. A new concept for the role of *ex vivo* sentinel lymph nodes in node-negative colorectal cancer. *Ann Surg Oncol* (2010) 17:2647–55. doi:10.1245/s10434-010-1030-3

11. Leiloglou M, Kedrzycki MS, Chalau V, Chiarini N, Thiruchelvam PT, Hadjiminas DJ, et al. Indocyanine green fluorescence image processing techniques for breast cancer macroscopic demarcation. *Scientific Rep* (2022) 12(1):8607. doi:10.1038/s41598-022-12504-x

12. Fry DE. The Hawthorne effect revisited. *Dis Colon Rectum* (2018) 61(1):6–7. PMID: 29219914. doi:10.1097/DCR.0000000000000928

13. Edler D, Öhrling K, Hallström M, Karlberg M, Ragnhammar P. The number of analyzed lymph nodes–a prognostic factor in colorectal cancer. *Acta Oncologica* (2007) 46(7):975–81. doi:10.1080/02841860701203537

14. Keller DS, Berho M, Perez RO, Wexner SD, Chand M. The multidisciplinary management of rectal cancer. *Nat Rev Gastroenterol Hepatol* (2020) 17(7):414–29. doi:10.1038/s41575-020-0275-y

15. Brouwer NP, Stijns RC, Lemmens VE, Nagtegaal ID, Beets-Tan RG, Fütterer JJ, et al. Clinical lymph node staging in colorectal cancer; a flip of the coin? *Eur J Surg Oncol* (2018) 44(8):1241–6. doi:10.1016/j.ejso.2018.04.008

16. Rodriguez-Bigas MA, Maamoun S, Weber TK, Penetrante RB, Blumenson LE, Petrelli NJ. Clinical significance of colorectal cancer: metastases in lymph nodes< 5 mm in size. *Ann Surg Oncol* (1996) 3:124–30. doi:10.1007/BF02305790

17. Suszták N, Besznyák I, Almási K, Bursics A, Kelemen D, Borowski DW, et al. Improved accuracy of lymph node staging and long-term survival benefit in colorectal cancer with *ex vivo* arterial methylene blue infiltration. *Pathol Oncol Res* (2022) 28: 1610742. PMID: 36330051; PMCID: PMC9624224. doi:10.3389/pore.2022.1610742

18. Tan L, Liu ZL, Ma Z, He Z, Tang LH, Liu YL, et al. Prognostic impact of at least 12 lymph nodes after neoadjuvant therapy in rectal cancer: a meta-analysis. *World J Gastrointest Oncol* (2020) 12(12):1443–55. PMID: 33362914; PMCID: PMC7739152. doi:10.4251/wjgo.v12.i12.1443

19. Lykke J, Jess P, Roikjaer O, Danish Colorectal Cancer Group. Increased lymph node yield is associated with improved survival in rectal cancer irrespective of neoadjuvant treatment: results from a national cohort study. *Dis Colon Rectum* (2015) 58:823–30. doi:10.1097/DCR.0000000000000429

20. Parnaby CN, Scott NW, Ramsay G, MacKay C, Samuel L, Murray GI, et al. Prognostic value of lymph node ratio and extramural vascular invasion on survival for patients undergoing curative colon cancer resection. *Br J Cancer* (2015) 113(2):212–9. Epub 2015 Jun 16. PMID: 26079302; PMCID: PMC4506392. doi:10.1038/bjc.2015.211

Pathology & Oncology Research | frontiers

TYPE Original Research
PUBLISHED 08 August 2023
DOI 10.3389/pore.2023.1611163

Check for updates

OPEN ACCESS

EDITED BY
József Tímár,
Semmelweis University, Hungary

*CORRESPONDENCE
K. Greimelmaier,
greimelmaierkr@diako.de

RECEIVED 05 March 2023
ACCEPTED 27 July 2023
PUBLISHED 08 August 2023

CITATION
Greimelmaier K, Klopp N, Mairinger E, Wessolly M, Borchert S, Steinborn J, Schmid KW, Wohlschlaeger J and Mairinger FD (2023), Fibroblast activation protein-α expression in fibroblasts is common in the tumor microenvironment of colorectal cancer and may serve as a therapeutic target. *Pathol. Oncol. Res.* 29:1611163. doi: 10.3389/pore.2023.1611163

COPYRIGHT
© 2023 Greimelmaier, Klopp, Mairinger, Wessolly, Borchert, Steinborn, Schmid, Wohlschlaeger and Mairinger. This is an open-access article distributed under the terms of the Creative Commons Attribution License (CC BY). The use, distribution or reproduction in other forums is permitted, provided the original author(s) and the copyright owner(s) are credited and that the original publication in this journal is cited, in accordance with accepted academic practice. No use, distribution or reproduction is permitted which does not comply with these terms.

Fibroblast activation protein-α expression in fibroblasts is common in the tumor microenvironment of colorectal cancer and may serve as a therapeutic target

K. Greimelmaier[1]*, N. Klopp[2], E. Mairinger[2], M. Wessolly[2], S. Borchert[2], J. Steinborn[2], K. W. Schmid[2], J. Wohlschlaeger[1] and F. D. Mairinger[2]

[1]Institut für Pathologie, Diakonissenkrankenhaus Flensburg, Flensburg, Germany, [2]Institut für Pathologie, Universitätsklinikum Essen, Essen, Germany

Background: Colorectal cancer (CRC) is still one of the leading causes of cancer death worldwide, emphasizing the need for further diagnostic and therapeutic approaches. Cancer invasion and metastasis are affected by the tumor microenvironment (TME), with cancer-associated fibroblasts (CAF) being the predominant cellular component. An important marker for CAF is fibroblast activation protein-α (FAP) which has been evaluated as therapeutic target for, e.g., radioligand therapy. The aim of this study was to examine CRC regarding the FAP expression as a candidate for targeted therapy.

Methods: 67 CRC, 24 adenomas, 18 tissue samples of inflammation sites and 28 non-neoplastic, non-inflammatory tissue samples of colonic mucosa were evaluated for immunohistochemical FAP expression of CAF in tissue microarrays. The results were correlated with clinicopathological data, tumor biology and concurrent expression of additional immunohistochemical parameters.

Results: 53/67 (79%) CRC and 6/18 (33%) inflammatory tissue specimens showed expression of FAP. However, FAP was only present in 1/24 (4%) adenomas and absent in normal mucosa (0/28). Thus, FAP expression in CRC was significantly higher than in the other investigated groups. Within the CRC cohort, expression of FAP did not correlate with tumor stage, grading or the MSI status. However, it was observed that tumors exhibiting high immunohistochemical expression of Ki-67, CD3, p53, and β-Catenin showed a significantly higher incidence of FAP expression.

Abbreviations: CRC, colorectal cancer; CAF, cancer-associated fibroblasts; ECM, extracellular matrix; FAP, fibroblast activation protein-α; IHC, immunohistochemistry; IRS, immunoreactivity score; MSI, microsatellite instability; MSI-H, High microsatellite instability; MSS, microsatellite stability; MMR, mismatch repair; PDGF-R, platelet-derived growth factor receptor; TMA, tissue microarray; TME, tumor microenvironment.

Conclusion: In the crosstalk between tumor cells and TME, CAF play a key role in carcinogenesis and metastatic spread. Expression of FAP was detectable in the majority of CRC but nearly absent in precursor lesions and non-neoplastic, non-inflammatory tissue. This finding indicates that FAP has the potential to emerge as a target for new diagnostic and therapeutic concepts in CRC. Additionally, the association between FAP expression and other immunohistochemical parameters displays the interaction between different components of the TME and demands further investigation.

KEYWORDS

colorectal cancer, tumor microenvironment, cancer-associated fibroblasts, fibroblast-activation protein, radioligand therapy

Introduction

Colorectal cancer (CRC) is one of the most common malignancies and accounts for 9.2% of cancer-related deaths worldwide [1]. The majority of cancer patients die from metastatic disease. Despite increased efforts in screening programs, more than half of the patients with CRC show advanced disease and metastases at the time of diagnosis [2], emphasizing the need for further therapeutic approaches. Cancer invasion and metastatic spread are affected by different cells and pathological reactions in the tumor microenvironment (TME). Among tumor stromal cell types, cancer-associated fibroblasts (CAF) proved to be the predominant component in TME [3, 4]. Fibroblasts in general synthesize the extracellular matrix (ECM) of connective tissue and are essential for tissue repair after damage. Activated fibroblasts in the TME, i.e., activated CAF contribute to the regulation and initiation of crucial steps for malignant progression of tumors. Especially in tumors with high levels of desmoplasia such as pancreatic ductal adenocarcinoma and colorectal adenocarcinoma, recruitment and activation of CAF play a key role in carcinogenesis [5, 6]. CAF can produce and modulate the ECM of tumors and are involved in the recruitment of other cell types and the production of different enzymes, immunomodulatory cytokines and growth factors [7, 8]. They are able to induce invasive growth and tumor proliferation by promoting epithelial-mesenchymal transition of tumor cells as well as initiate metastasis [9–11].

Although the origin of CAF and the mechanism of transformation from normal fibroblasts to activated CAF remains unknown, there are several markers to identify CAF in the TME [12]. Among α-smooth muscle actin (SMA), and platelet-derived growth factor receptor (PDGF-R), fibroblast activation protein-α (FAP) proved to be a reliable marker for activated CAF [3, 4, 8, 13]. FAP is a type II transmembrane glycoprotein of the group of plasma membrane-bound serine proteases that is upregulated in fibroblasts at sites of active tissue remodeling, including wound healing and fibrosis. While FAP is absent in normal tissue [14–16], high expression of FAP has been detected in several solid tumors such as CRC [8, 13, 17]. Previous studies have demonstrated that high FAP expression is associated with an increased risk of metastases and poor survival in CRC and thus proposed FAP as a possible biomarker for disease progression [4, 8, 17, 18]. Furthermore, FAP has been discussed as both a novel therapeutic target and diagnostic tool. Although there are some studies examining the use of FAP-targeted radioligands for *in-vivo* imaging and targeted nucleotide therapy for a variety of cancers, including CRC [19–22], this field of research has yet to be fully developed.

The aim of this study was to examine CRC regarding the expression of FAP as a potential candidate for targeted imaging and therapy and to correlate the results with other immunohistochemical parameters in the TME such as p53, β-catenin, Ki-67 and CD3.

Certain aspects of this study have already been presented at a conference [23].

Materials and methods

Identification of patients and biopsies

A total of 76 colorectal adenocarcinomas from 72 adult patients that underwent radical surgical resection at University Hospital Essen in the period from 2001 to 2020 were included in this study. The collected specimens encompassed colorectal adenocarcinomas with pathological stages ranging from pT1-4b, pN0-2b, pM0-1, and grading G1-3. Furthermore, 24 colorectal adenomas with low-grade or high-grade dysplasia were included for evaluation. In addition, samples of inflamed tissue from the colorectal tract (i.e., diverticulitis, colitis) as well as non-neoplastic, non-inflammatory tissue (e.g., cases of diverticulosis) were examined as control cohorts.

Histological review and tissue microarrays (TMA)

Formalin-fixed, paraffin-embedded tissue were retrieved from the archives of the Department of Pathology of the University Essen. Four μm sections were cut and stained with

haematoxylin and eosin to define representative tumor regions (i.e., tumor center). Two core tissue biopsies with a diameter of 0.6 mm were punched from selected areas of each case using a thin-wall stainless steel tube and brought into a new paraffin block. Evaluation of the TMA confirmed that the tumor tissue cores correspond to the original block. Cores without viable tumor or artefacts were excluded. All specimens were reviewed by two experienced pathologists (KG and JW).

Immunohistochemistry

Tissue sections of thickness 4 µm were prepared from buffered formalin-fixed, paraffin-embedded tissue blocks. Immunohistochemistry (IHC) for fibroblast activating protein (FAP) was performed on the tissue sections with a primary monoclonal antibody (clone SP325, abcam, dilution 1:100) on an automated staining system (Ventana Discovery XT, Munich, Germany) according to standard protocol using the OptiView DAB detection kit. Briefly, pretreatment for antigen retrieval was performed by heating in citrate buffer (Ultra Cell Conditioning Solution II, Ventana Medical Systems, Basel, CH) at pH 6, 90°C for 48 min followed by antibody incubation for 60 min at 36°C. Assessment of immunohistochemical staining of the TMAs were evaluated by two different pathologists who were both blinded regarding the clinical data and outcome of the patients. The number of FAP-positive staining was counted in the whole tissue cores and the percentage of positive cells was calculated. As suggested by Henry et al. [24] immunoreactivity was evaluated semi-quantitatively, considering greater than 1% and less than 10% FAP-positivity in stromal cells as low expression and samples with at least 10% FAP-positive cells as high expression. Additionally, for each case the immunoreactive score (IRS) was determined, which is a multiplication score combining staining intensity and percentage of positive cells. The FAP staining intensity was visually scored and stratified as follows: 0 (negative), 1 (weak), 2 (moderate) and 3 (strong). Points for the percentage of positive cells were assigned as follows: 0: none, 1: 1%–10%, 2: 11%–50%, 3: 51%–80%, and 4: 81%–100%. These two values were then multiplied together to determine the IRS (ranging from 0 to a maximum of 12). IRS value 0 was considered FAP-negative whereas IRS values 1 to 4 were used to define the low expression group and values 5 to 12 the high expression group of FAP.

To determine the MSI status, IHC analysis was conducted according to established protocols, as previously described using standard techniques [25]. The specimens were categorized as MMR-proficient or MMR-deficient based on the presence or absence of nuclear stains of MMR proteins (MSH2, MSH6, MLH1 and PMS2). In certain cases, additional polymerase chain reaction (PCR) was performed using a commercially available five-marker MSI testing kit (Promega, United States). Evaluation of p53, β-catenin (BCAT) and Ki67 was depicted with the percentage of stained cells. Evaluation of CD3 was performed with a four-tier score: 0 described no infiltration, 1 described low infiltration, 2 described intermediate infiltration and 3 described high infiltration. Additionally, nuclear β-catenin aberrance was evaluated. An overview of all used clones, dilutions and pretreatments is given in Supplementary Table S1.

Statistical analysis

Statistical analysis was performed using the R statistical programming environment V 4.0.2. Before starting exploratory data analysis, normal distribution of each data set was tested by Shapiro-Wilks-test taking ordinal as well as metric variables into account. Either two-sided Students's t-test (parametric) or Wilcoxon rank-sum test (non-parametric) was used for dichotomous variables. To compare factors with more than two groups or variables with ordinal character, either ANOVA (parametric) or Kruskal-Wallis test (non-parametric) was performed.

Analysis of double dichotomous contingency tables was carried out using Fisher's exact test. Pearson's Chi-squared test was used to assess dependency of ranked parameters with more than two groups.

Due to the use of multiple statistical tests the p-values were adjusted by using the false discovery rate (FDR). A value of $p \leq 0.05$ after adjustment was considered statistically significant.

Results

To evaluate the overall FAP expression in CRC, a cohort of resected adenocarcinomas, low- and high-grade adenomas, along with tissue samples of inflammation sites as well as non-inflammatory, non-neoplastic specimens of colonic mucosa were analyzed by immunohistochemistry. The quality of study material was heterogeneous, resulting in a variable subset of the cohort (n = 137) being evaluable for IHC analysis. Evaluable samples were available from 67 adenocarcinomas, 24 adenomas, 18 colonic inflammation specimens and 28 non-neoplastic, non-inflammatory tissue samples.

FAP expression was observed in 53 of 67 (79%) CRC cases, while positive FAP expression was also detected in 6 of 18 (33%) inflammatory tissue specimens. However, FAP was only present in 1 of 24 (4%) adenomas and absent in non-neoplastic, non-inflammatory tissue (0/28). Thus, FAP expression was significantly higher in CRC than in the other investigated groups ($p < 0.0001$; Pearson's Chi-squared Test). In more detail, significant differences in FAP expression were observed when considering negative, low positive, and high positive cases. These differences were evident between CRC and adenomas ($p < 0.0001$; $\chi^2 = 41.8$), CRC and inflammation specimens ($p < 0.0001$; $\chi^2 = 28.9$), as well as CRC and non-neoplastic, non-inflammatory tissue ($p < 0.0001$; $\chi^2 =$

TABLE 1 FAP expression in different investigated groups.

Specimen	Cases (n)	FAP Expression semi-quantitatively total (%)		Positive FAP Expression (semi-quantitatively)		FAP Expression IRS total (%)		Positive FAP Expression (IRS)	
		Positive	Negative	High	Low	Positive	Negative	High	Low
Carcinoma	67	53 (79.1)	14 (20.9)	41	12	42 (62.7)	25 (37.3)	28	14
Adenoma	24	1 (4.2)	23 (95.8)	0	1	0 (0)	24 (100)	0	0
Inflammation	18	6 (33.3)	12 (66.6)	4	2	6 (33.3)	12 (66.6)	1	5
Non-neoplastic, non-inflammatory tissue	28	0 (0)	28 (100)	0	0	0 (0)	28 (100)	0	0

Immunoreactivity was evaluated semi-quantitatively, considering greater than 1% and less than 10 % FAP-positivity in stromal cells as low expression and samples with at least 10% FAP-positive cells as high expression. The immunoreactive score (IRS) was determined by multiplying the ratio of positive-stained fibroblasts (0: none, 1: 1%–10%, 2: 11%–50%, 3: 51%–80%, and 4: 81%–100%) and the staining intensity (0: no staining, 1: weak, 2: moderate, and 3: strong). The total IRS ranges from 0 to 12. IRS value 0 was considered FAP-negative whereas IRS values 1–4 were used to define the low expression group and values 5–12 the high expression group of FAP.

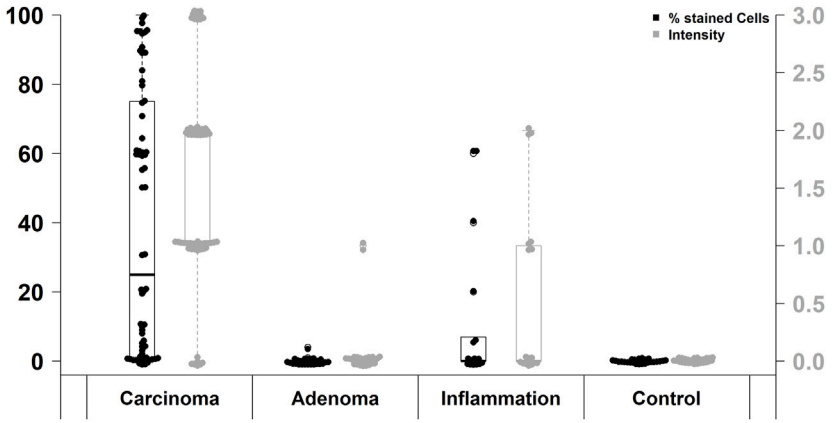

FIGURE 1
Immunohistochemical FAP staining levels in different investigated groups.

35.8). Moreover, there was a significantly higher level of FAP expression in inflammatory sites compared to adenomas (p = 0.02905; χ^2 = 7.1). Results are presented in Table 1 and Figure 1.

41 of 53 (77%) FAP-positive CRC showed high expression levels and 12 (23%) showed low expression in semi-quantitative evaluation. Regarding the immunoreactive score (IRS), only 42 of 67 (63%) CRC specimens were classified as FAP-positive, of which 28 (67%) had a high expression and 14 (33%) a low expression of FAP. The difference between high and low FAP expression was neither in semi-quantitative assessment nor in IRS evaluation statistically significant (Table 1). In the evaluation of the percentual expression of FAP in the two different tumor cores on the TMA, a deviation of more than 5% was detectable in 29 CRC cases (43%). Figure 2 shows representative examples of high and low immunohistochemical expression of FAP in CRC.

Within the CRC cohort, expression of FAP did not correlate with tumor stage or grading (Supplementary Table S2). FAP positive specimens more frequently showed lymph node metastases, however, the difference was not statistically significant (21/45, 47% and 2/11, 18%, respectively, p = 0.074; Wilcoxon rank-sum test). Equally, no significant difference in the occurrence of distant metastases could be shown (11/31, 35% and 1/2, 50%, respectively, p = 0.2; Wilcoxon rank-sum test).

There was no correlation observed between FAP expression and the patients' age, gender, or the primary site of the tumor (Supplementary Table S2). However, CRC tumor cores with positive expression of FAP also showed higher expression of other immunohistochemical parameters: There was a significant correlation between percentual FAP positivity and the expression of tumor protein p53 (p < 0.0001, Wilcoxon rank-sum test with continuous TP53 values; p < 0.0001, Fisher's exact test with grouped TP53 values (aberrant/non-aberrant)). Similarly, a significant correlation was found between FAP positivity and the expression of Ki-67, a nuclear protein that is associated with cellular

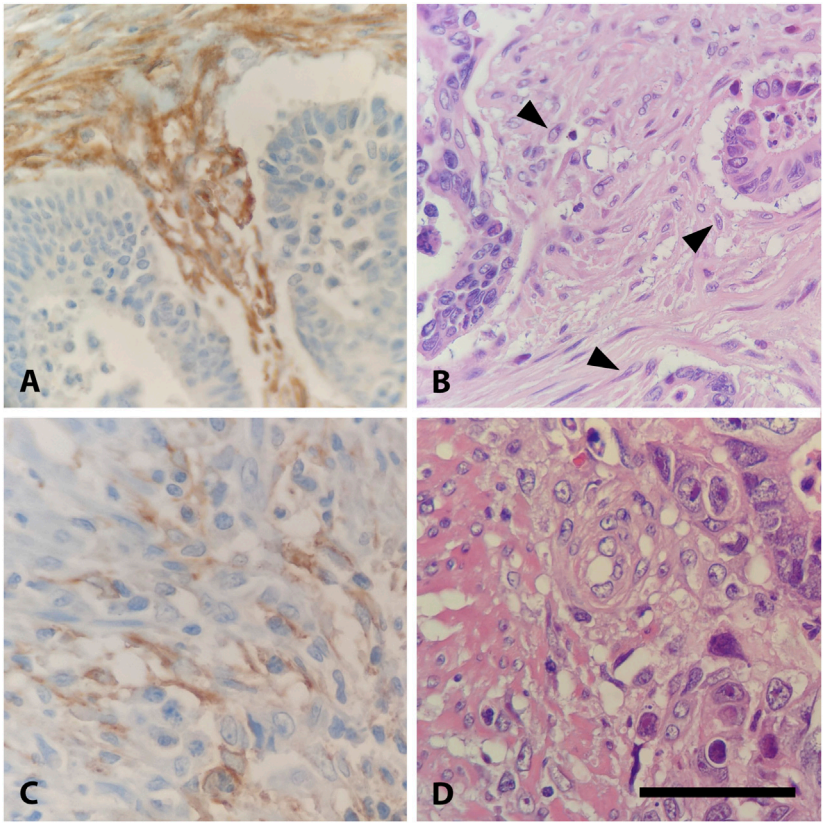

FIGURE 2
Expression of FAP in CRC. **(A)** High FAP expression in stromal fibroblasts of an intermediate grade adenocarcinoma, ×400. **(B)** Hematoxylin and Eosin (H&E) stain of **(A)** with activated fibroblasts, identified by typical morphological features: increased cell size, altered nuclear morphology, and enhanced cytoplasmic basophilia (highlighted with arrowhead), ×400. **(C)** Low stromal expression of FAP in an intermediate grade adenocarcinoma, ×400. **(D)** Hematoxylin and Eosin (H&E) stain of C, ×400. Scalebar is 50 µm.

proliferation ($p < 0.0001$, Wilcoxon rank-sum test with continuous Ki67 values; $p = 0.0019$, Fisher's exact test with grouped Ki67 values (high/low)). Additionally, FAP positive tumors more frequently displayed elevated numbers of tumor-infiltrating CD3-positive T-lymphocytes [$p = 0.014$; Wilcoxon rank-sum test with ordinal CD3 values; $p = 0.027$, Fisher's exact test with grouped CD3 values (high/low)]. This trend was also observed when comparing cases with high and low IRS ($p = 0.049$, Fisher's exact test). Regarding the immunohistochemical expression of β-Catenin, higher levels were observed in FAP-positive tumors on a continuous scale of expression intensity ($p = 0.02$; Pearson's LM/Product Moment Correlation). However, this association could not be confirmed when comparing samples with aberrant and normal expression patterns of BCAT, where the localization of BCAT (nuclear vs. cytoplasmic) needed to be considered ($p = 0.76$, Fisher's exact test). An overview of statistical results of the immunohistochemical markers are presented in Figure 3. Regarding the association between FAP expression and the microsatellite instability (MSI) status of the tumors, no significant correlation could be shown (Supplementary Table S2). Out of the 52 FAP positive tumors with available immunohistochemical MSI status, 8 (15%) exhibited deficient MMR protein expression. Conversely, among the 11 tumors with negative FAP expression, 2 (18%) were also diagnosed as MMR-deficient ($p = 0.6732$, Fisher's Exact Test). PCR results for MSI status were only available for a subset of colorectal carcinomas ($n = 14$). Among this subset, 8 out of 13 FAP positive carcinomas displayed high microsatellite instability (MSI-high). Nonetheless, it is worth noting that also one FAP negative tumor with available PCR results was classified as MSI-high, so no significant difference could be observed. Representative examples of immunohistochemistry corresponding to FAP expression are shown in Figure 4.

Discussion

In the context of developing new therapeutic approaches for combating CRC, the focus of attention lies not merely on the neoplastic cells anymore but also on the TME and the crosstalk between tumoral and stromal cells. FAP expressing cancer-

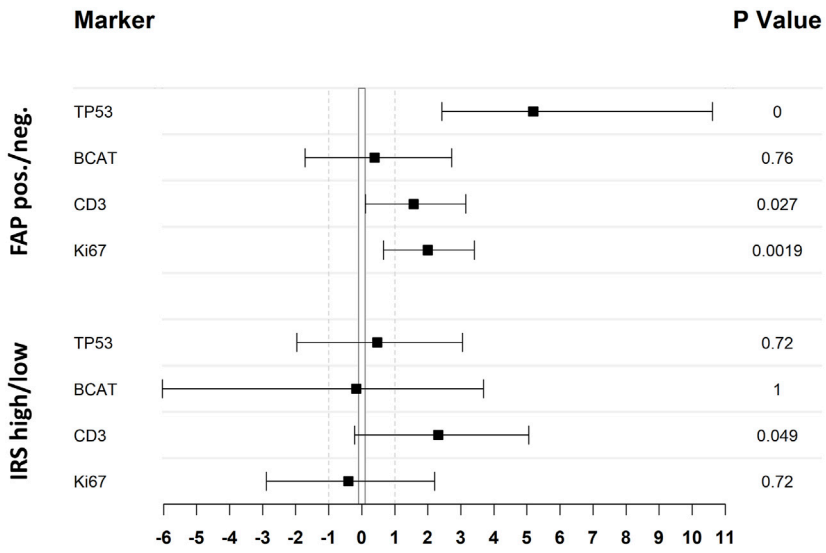

FIGURE 3
Statistical analysis of the association between expression of investigated IHC markers and FAP expression illustrated as odds-ratio forest plot. Black squares indicate the odds ratio (log2 transformed) whereas the black lines refer to the 95% CI. Upper four lines result from a comparison of FAP positive and negative cases, lower four lines differentiate between cases with low or high IRS score as stated in the material and methods section. TP53 and BCAT expression has been classified as aberrant and not-aberrant, whereas CD3 and Ki67 has been grouped in high and low expression (cut-off CD3: > 1; cut-off Ki67: > mean [47.1]) to achieve double-dichotomous contingency tables. All *p*-values where calculated by Fisher's exact test.

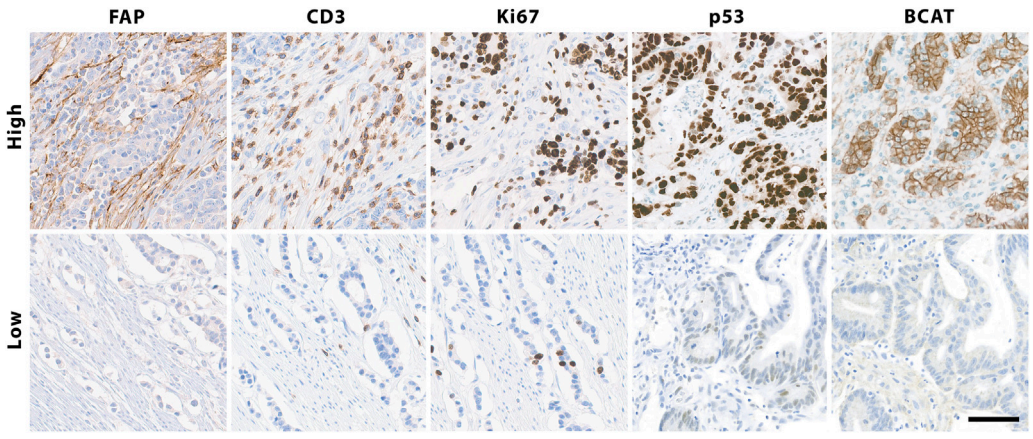

FIGURE 4
Immunohistochemical staining of colorectal cancer tissue for FAP, analyzed as either high or low expression, considering greater than 1% and less than 10% FAP-positivity in stromal cells as low expression and samples with at least 10% FAP-positive cells as high expression, as well as high and low levels of Ki-67, CD3, p53 and β-Catenin, exemplified in top boxes, ×200. Scalebar is 50 µm.

associated fibroblasts (CAF) are the predominant component in the stroma of CRC and have been recognized as co-responsible for tumor growth and metastasis.

The objective of this study was to investigate FAP expression of CAF in the tumor microenvironment of CRC and to evaluate FAP as a candidate for targeted imaging and therapy.

Consistent with previous reports, expression of FAP was detectable in the majority of CRC but nearly absent in precursor lesions (i.e., adenomas) and non-neoplastic, non-inflammatory tissue [8, 26, 27]. This finding supports the role of FAP in tumor growth and invasion. Moreover, in this study, a positive correlation between FAP expression and several

immunohistochemical markers that are involved in carcinogenesis could be shown.

Tumors with expression of FAP significantly more often displayed high expression of Ki-67, a nuclear protein that is associated with cellular proliferation. Similarly, an association with immunohistochemical expression of p53 was detected. This has previously also been reported for non-small cell adenocarcinomas of the lung [28]. p53 is a tumor suppressor protein that regulates cell growth by promoting cell apoptosis and DNA repair. When becoming mutated p53 loses its function which results in accumulation of the protein in the cell promoting an abnormal cell proliferation and tumor progression [29]. This emphasizes the involvement of FAP in crucial processes of tumor development. Another parameter associated with positive FAP expression in this study was β-Catenin. It is involved in regulation and coordination of cell–cell adhesion and gene transcription and acts as an intracellular signal transducer in the Wnt-signaling pathway as a subunit of the cadherin protein complex [30]. Moreover, Wnt-signaling has been shown to be a key feature in the crosstalk between activated myofibroblasts and cancer cells. Overexpression of β-catenin is associated with many cancers, including CRC [30]. Studies have demonstrated that FAP expression in the membrane of CAF induced this β-Catenin related pathway in CRC [3, 18]. Previous investigations also displayed that combined expression of FAP and β-Catenin was independently associated with the occurrence of metastasis [18].

In addition to the findings above, in this study FAP positivity also correlated with high expression of CD3 on T-lymphocytes in the tumor stroma of CRC. Several studies have indicated that FAP expression is associated with a shift in immune cell populations within the tumor, thereby promoting a pro-tumorigenic environment [31, 32]. Here, only one immune cell parameter has been evaluated, so no final conclusions can be drawn. But the results point out the value of further investigating the link between CAF and immunoreactivity in CRC. The described association between FAP and the expression of the immunohistochemical parameters mentioned above displays the interaction between different components of the TME. Interestingly, while a positive correlation was observed between FAP expression and other immunohistochemical parameters, no significant association between FAP expression and MSI status of the tumors was found in this investigation. It should be noted that the number of CRC cases with microsatellite instability in this study was relatively small (9 MSI-H tumors detected in PCR and 10 MMR-deficient tumors detected in IHC, respectively), which may have influenced the lack of correlation. On the other hand, CRC with MSI are generally less aggressive than MSS tumors and exhibit a lower incidence of lymph node metastases or distant spread [26], which could potentially explain the lower expression of FAP in these tumors. To clarify this coherence, further investigation is needed.

In line with other studies that evaluated FAP expression by IHC [8, 27], FAP was not correlated to age and gender of the patients nor to the primary site of the tumor. In this study, no correlation between FAP expression and the tumor stage and grading could be found and no significant correlation was observed between FAP expression and the occurrence of lymph node or distant metastases. However, it should be noted that the number of metastatic events, particularly in the group of FAP negative tumors, was limited, making it difficult to draw definitive conclusions.

Despite the fact that FAP was widely present in carcinomas but nearly absent even in high-grade adenomas and not detectable in non-neoplastic, non-inflammatory tissue, it could serve as a diagnostic marker in routine diagnostics of early CRC and be helpful to discriminate invasive carcinoma from high-grade dysplasia in small biopsies or adenomatous polyps. In the recent years, there is an increasing use of nanomedicine in cancer including radionuclide-based approaches for targeted therapy. Recently, the FDA approved 68Ga-PSMA as first PSMA-targeted PET drug in potentially curable patients with metastatic prostate cancer [33]. In addition, endo-radioligand therapy with Lu177-PSMA has been proven powerful in therapy of advanced prostate cancer [34]. Beside PSMA, there are multiple other targets discussed for their potency in PET/CT diagnostics or radioligand therapy. PET imaging using a 64Cu- or 89Zr-labeled monoclonal antibody against mesothelin as well as therapeutical usage of antibody-drug conjugate treatment has shown promising results in pancreatic and/or ovarian cancer [35, 36]. 68Ga-Pentixafor as radio ligand for CXCR4 has been proven an alternative to 18F-FDG PET, showing clearly higher detection rates and better tumor-to-background contrast [37]. It also has to be discussed as potential candidate for directed endo-radiotherapy [38].

The fibroblast activating protein (FAP) is used in 68Ga-FAPI PET/CT [39, 40] as well as 64Cu- and 225Ac-labeled FAPI combined in a “theranostics” approach [41]. Surprisingly, Kratochwil et al. [42] demonstrated colorectal and pancreatic carcinomas only with intermediate 68Ga-FAPI uptake, although they showed highest amounts of DSR histologically. However, they reported significant lower hepatic background compared to 18F-FDG and therefore an advantage for the detection of liver metastases. A case report using [68Ga]Ga-DOTA.SA.FAPI PET/CT-guided [177Lu]Lu-DOTA.SA.FAPI radionuclide therapy in a patient with metastatic (lung, liver, bones and brain) end-stage breast cancer showed intense radiotracer accumulation in all lesions in concordance to PET/CT [43]. As post treatments, symptoms and laboratory parameters decreased with no treatment-related adverse events, the authors concluded this as new opportunity in breast cancer therapy for patients refractory to conventional treatment options. Additionally, in head and neck cancer, evidence of diagnostic and therapeutic potential of FAPI ligands could

be proven, although no histopathological DSR correlate or FAP IHC has been evaluated in upfront diagnostics [44]. In recent studies, FAPI tracers are already successfully developed for SPECT imaging and combined therapy in a theranostics setting, since SPECT is a lower-cost and broader available technology compared to PET [45]. Of note, "next-generation" of FAPI tracers are on their way, showing improved tumor retention and pharmacokinetics [46].

Given the fact that FAP proved to be a reliable marker of activated CAF, and that high expression of FAP almost exclusively occurs in invasive carcinomas but not in adenomas or non-neoplastic, non-inflammatory tissue, FAP has the potential to emerge as a powerful target for new diagnostic and therapeutic concepts in CRC. However, because the amount of available data is limited, further research in this field is necessary. When considering FAP as a promising tool in new cancer diagnostics and therapeutics, one should also take into account the immunohistochemical scoring system that is used to quantify the FAP expression. Up until now, there is no standard quantification score for an objective evaluation of CAF activation markers such as FAP, so studies lack comparability. In the present study, there were different results depending on the scoring method that was used. In particular, the positive rate (including high and low expression) of FAP in CRC was 62.6% using the IRS system to quantify the immunohistochemical expression which was different from the 79.1% positivity using the semi-quantitative grading system suggested by Henry et al. [24] (Table 1). Regarding the FAP positivity in inflammation sites there was no difference between the scoring systems. Although examination of FAP positivity on TMAs has proved to be a fast and reliable procedure [8, 27], for further research and for establishing a standardized scoring system whole slide evaluation of FAP should be preferred.

Conclusion

In the crosstalk between tumor cells and TME, FAP expressing CAF play a key role in carcinogenesis and metastatic spread. In this study, FAP proved to be a suitable marker for activated CAF in CRC. With regard to the urgent need for new strategies in cancer treatment, FAP may serve as a possible target for new diagnostics and targeted therapy of CRC in the near future.

Data availability statement

The raw data supporting the conclusion of this article will be made available by the authors, without undue reservation.

Ethics statement

The study conforms to the principles outlined in the declaration of Helsinki and was approved by the local Ethics Committee of the Medical Faculty of the University Duisburg-Essen (protocol no. 20-9141-BO). As no clinical data has been used for analysis and due to the retrospective nature of the study, the need for additional informed consent has been waived.

Author contributions

The authors confirm contribution to the paper as follows: study conception and design: KG, FM, and KS; data collection: KG, NK, EM, MW, JS, and SB; analysis and interpretation of results: KG, FM, SB, KS, and JW; draft manuscript preparation: KG, FM, JW, and KS. All authors contributed to the article and approved the submitted version.

Conflict of interest

The authors declare that the research was conducted in the absence of any commercial or financial relationships that could be construed as a potential conflict of interest.

Supplementary material

The Supplementary Material for this article can be found online at: https://www.por-journal.com/articles/10.3389/pore.2023.1611163/full#supplementary-material

References

1. Bray F, Ferlay J, Soerjomataram I, Siegel RL, Torre LA, Jemal A. Global cancer statistics 2018: GLOBOCAN estimates of incidence and mortality worldwide for 36 cancers in 185 countries. *CA Cancer J Clin* (2018) 68(6):394–424. doi:10.3322/caac.21492

2. Siegel RL, Miller KD, Jemal A. Cancer statistics. *CA Cancer J Clin* (2018) 68(1):7–30. doi:10.3322/caac.21442

3. Yoshida GJ. Regulation of heterogeneous cancer-associated fibroblasts: the molecular pathology of activated signaling pathways. *J Exp Clin Cancer Res* (2020) 39(1):112. doi:10.1186/s13046-020-01611-0

4. Nurmik M, Ullmann P, Rodriguez F, Haan S, Letellier E. In search of definitions: Cancer-associated fibroblasts and their markers. *Int J Cancer* (2020) 146(4):895–905. doi:10.1002/ijc.32193

5. Sperb N, Tsesmelis M, Wirth T. Crosstalk between tumor and stromal cells in pancreatic ductal adenocarcinoma. *Int J Mol Sci* (2020) 21(15):5486. doi:10.3390/ijms21155486

6. Chan TS, Shaked Y, Tsai KK. Targeting the interplay between cancer fibroblasts, mesenchymal stem cells, and cancer stem cells in desmoplastic cancers. *Front Oncol* (2019) 9:688. doi:10.3389/fonc.2019.00688

7. Erdogan B, Webb DJ. Cancer-associated fibroblasts modulate growth factor signaling and extracellular matrix remodeling to regulate tumor metastasis. *Biochem Soc Trans* (2017) 45(1):229–36. doi:10.1042/bst20160387

8. Coto-Llerena M, Ercan C, Kancherla V, Taha-Mehlitz S, Eppenberger-Castori S, Soysal SD, et al. High expression of FAP in colorectal cancer is associated with angiogenesis and immunoregulation processes. *Front Oncol* (2020) 10:979. doi:10.3389/fonc.2020.00979

9. Hurtado P, Martínez-Pena I, Piñeiro R. Dangerous liaisons: circulating tumor cells (CTCs) and cancer-associated fibroblasts (CAFs). *Cancers* (2020) 12(10):2861. doi:10.3390/cancers12102861

10. Gonzalez-Villarreal CA, Quiroz-Reyes AG, Islas JF, Garza-Treviño EN. Colorectal cancer stem cells in the progression to liver metastasis. *Front Oncol* (2020) 10:1511. doi:10.3389/fonc.2020.01511

11. Hu JL, Wang W, Lan XL, Zeng ZC, Liang YS, Yan YR, et al. CAFs secreted exosomes promote metastasis and chemotherapy resistance by enhancing cell stemness and epithelial-mesenchymal transition in colorectal cancer. *Mol Cancer* (2019) 18(1):91. doi:10.1186/s12943-019-1019-x

12. Kanzaki R, Pietras K. Heterogeneity of cancer-associated fibroblasts: opportunities for precision medicine. *Cancer Sci* (2020) 111(8):2708–17. doi:10.1111/cas.14537

13. Lindner T, Loktev A, Giesel F, Kratochwil C, Altmann A, Haberkorn U. Targeting of activated fibroblasts for imaging and therapy. *EJNMMI Radiopharmacy Chem* (2019) 4(1):16. doi:10.1186/s41181-019-0069-0

14. Fitzgerald AA, Weiner LM. The role of fibroblast activation protein in health and malignancy. *Cancer Metastasis Rev* (2020) 39(3):783–803. doi:10.1007/s10555-020-09909-3

15. Jacob M, Chang L, Puré E. Fibroblast activation protein in remodeling tissues. *Curr Mol Med* (2012) 12(10):1220–43. doi:10.2174/156652412803833607

16. Rovedatti L, Di Sabatino A, Knowles CH, Sengupta N, Biancheri P, Corazza GR, et al. Fibroblast activation protein expression in Crohn's disease strictures. *Inflamm Bowel Dis* (2011) 17(5):1251–3. doi:10.1002/ibd.21446

17. Liu F, Qi L, Liu B, Liu J, Zhang H, Che D, et al. Fibroblast activation protein overexpression and clinical implications in solid tumors: a meta-analysis. *PloS one* (2015) 10(3):e0116683. doi:10.1371/journal.pone.0116683

18. Solano-Iturri JD, Beitia M, Errarte P, Calvete-Candenas J, Etxezarraga MC, Loizate A, et al. Altered expression of fibroblast activation protein-α (FAP) in colorectal adenoma-carcinoma sequence and in lymph node and liver metastases. *Aging* (2020) 12(11):10337–58. doi:10.18632/aging.103261

19. Loktev A, Lindner T, Mier W, Debus J, Altmann A, Jäger D, et al. A tumor-imaging method targeting cancer-associated fibroblasts. *J Nucl Med* (2018) 59(9):1423–9. doi:10.2967/jnumed.118.210435

20. Paauwe M, Schoonderwoerd MJA, Helderman R, Harryvan TJ, Groenewoud A, van Pelt GW, et al. Endoglin expression on cancer-associated fibroblasts regulates invasion and stimulates colorectal cancer metastasis. *Clin Cancer Res* (2018) 24(24):6331–44. doi:10.1158/1078-0432.Ccr-18-0329

21. Barrett RL, Puré E. Cancer-associated fibroblasts and their influence on tumor immunity and immunotherapy. *eLife* (2020) 9:e57243. doi:10.7554/eLife.57243

22. Yang M, Li J, Gu P, Fan X. The application of nanoparticles in cancer immunotherapy: targeting tumor microenvironment. *Bioact Mater* (2021) 6(7):1973–87. doi:10.1016/j.bioactmat.2020.12.010

23. Greimelmaier K. Fibroblast activation protein-α expressing fibroblasts are common in and may serve as a therapeutic target in colorectal cancer. *Deutsche Gesellschaft für Pathologie e.V.* (2021) 2021:307–8.

24. Henry LR, Lee HO, Lee JS, Klein-Szanto A, Watts P, Ross EA, et al. Clinical implications of fibroblast activation protein in patients with colon cancer. *Clin Cancer Res* (2007) 13(6):1736–41. doi:10.1158/1078-0432.Ccr-06-1746

25. Stone JG, Robertson D, Houlston RS. Immunohistochemistry for MSH2 and MHL1: a method for identifying mismatch repair deficient colorectal cancer. *J Clin Pathol* (2001) 54(6):484–7. doi:10.1136/jcp.54.6.484

26. Wikberg ML, Edin S, Lundberg IV, Van Guelpen B, Dahlin AM, Rutegård J, et al. High intratumoral expression of fibroblast activation protein (FAP) in colon cancer is associated with poorer patient prognosis. *Tumour Biol* (2013) 34(2):1013–20. doi:10.1007/s13277-012-0638-2

27. Son GM, Kwon MS, Shin DH, Shin N, Ryu D, Kang CD. Comparisons of cancer-associated fibroblasts in the intratumoral stroma and invasive front in colorectal cancer. *Medicine* (2019) 98(18):e15164. doi:10.1097/md.0000000000015164

28. Moreno-Ruiz P, Corvigno S, Te Grootenhuis NC, La Fleur L, Backman M, Strell C, et al. Stromal FAP is an independent poor prognosis marker in non-small cell lung adenocarcinoma and associated with p53 mutation. *Lung Cancer (Amsterdam, Netherlands)* (2021) 155:10–9. doi:10.1016/j.lungcan.2021.02.028

29. Kanapathipillai M. Treating p53 mutant aggregation-associated cancer. *Cancers* (2018) 10(6):154. doi:10.3390/cancers10060154

30. Taciak B, Pruszynska I, Kiraga L, Bialasek M, Krol M. Wnt signaling pathway in development and cancer. *J Physiol Pharmacol.* (2018) 69(2). doi:10.26402/jpp.2018.2.07

31. Herrera M, Mezheyeuski A, Villabona L, Corvigno S, Strell C, Klein C, et al. Prognostic interactions between FAP+ fibroblasts and CD8a+ T cells in colon cancer. *Cancers* (2020) 12(11):3238. doi:10.3390/cancers12113238

32. Puré E, Blomberg R. Pro-tumorigenic roles of fibroblast activation protein in cancer: Back to the basics. *Oncogene.* (2018) 37(32):4343–57. doi:10.1038/s41388-018-0275-3

33. FDA. 2021 SNMMI highlights lecture: oncology and therapy, Part 2. *J Nucl Med* (2021) 62(2):11N–16N.

34. Gupta M, Karthikeyan G, Choudhury PS, Babu Koyyala VP, Sharma M, Jain P, et al. A walk with Lu-177 PSMA: how close we have reached from bench to bedside? *Cancer Invest* (2020) 38(8-9):486–92. doi:10.1080/07357907.2020.1811301

35. Lamberts LE, Menke-van der Houven van Oordt CW, ter Weele EJ, Bensch F, Smeenk MM, Voortman J, et al. ImmunoPET with anti-mesothelin antibody in patients with pancreatic and ovarian cancer before anti-mesothelin antibody-drug conjugate treatment. *Clin Cancer Res* (2016) 22(7):1642–52. doi:10.1158/1078-0432.CCR-15-1272

36. Kobayashi K, Sasaki T, Takenaka F, Yakushiji H, Fujii Y, Kishi Y, et al. A novel PET imaging using (6) (4)Cu-labeled monoclonal antibody against mesothelin commonly expressed on cancer cells. *J Immunol Res* (2015) 2015:268172. doi:10.1155/2015/268172

37. Mayerhoefer ME, Raderer M, Lamm W, Pichler V, Pfaff S, Weber M, et al. CXCR4 PET imaging of mantle cell lymphoma using [(68)Ga]pentixafor: Comparison with [(18)F]FDG-PET. *Theranostics* (2021) 11(2):567–78. doi:10.7150/thno.48620

38. Walenkamp AME, Lapa C, Herrmann K, Wester HJ. CXCR4 ligands: the next big hit? *J Nucl Med* (2017) 58(2):77S–82S. doi:10.2967/jnumed.116.186874

39. Hayrapetian A, Girgis MD, Yanagawa J, French SW, Schelbert HR, Auerbach MS, et al. Incidental detection of elastofibroma dorsi with 68Ga-FAPI-46 and 18F-fdg PET/CT in a patient with esophageal cancer. *Clin Nucl Med* (2021) 46(2):e86–e87. doi:10.1097/RLU.0000000000003218

40. Pang Y, Wei J, Shang Q, Zhao L, Chen H. 68Ga-Fibroblast activation protein inhibitor, a promising radiopharmaceutical in PET/CT to detect the primary and metastatic lesions of chromophobe renal cell carcinoma. *Clin Nucl Med* (2021) 46(2):177–9. doi:10.1097/RLU.0000000000003454

41. Watabe T, Liu Y, Kaneda-Nakashima K, Shirakami Y, Lindner T, Ooe K, et al. Theranostics targeting fibroblast activation protein in the tumor stroma: (64)Cu- and (225)Ac-labeled FAPI-04 in pancreatic cancer xenograft mouse models. *J Nucl Med* (2020) 61(4):563–9. doi:10.2967/jnumed.119.233122

42. Kratochwil C, Flechsig P, Lindner T, Abderrahim L, Altmann A, Mier W, et al. 68Ga-FAPI PET/CT: tracer uptake in 28 different kinds of cancer. *J Nucl Med* (2019) 60(6):801–5. doi:10.2967/jnumed.119.227967

43. Ballal S, Yadav MP, Kramer V, Moon ES, Roesch F, Tripathi M, et al. A theranostic approach of [(68)Ga]Ga-DOTA.SA.FAPi PET/CT-guided [(177)Lu]Lu-DOTA.SA.FAPi radionuclide therapy in an end-stage breast cancer patient: new frontier in targeted radionuclide therapy. *Eur J Nucl Med Mol Imaging* (2021) 48(3):942–4. doi:10.1007/s00259-020-04990-w

44. Syed M, Flechsig P, Liermann J, Windisch P, Staudinger F, Akbaba S, et al. Fibroblast activation protein inhibitor (FAPI) PET for diagnostics and advanced targeted radiotherapy in head and neck cancers. *Eur J Nucl Med Mol Imaging* (2020) 47(12):2836–45. doi:10.1007/s00259-020-04859-y

45. Lindner T, Altmann A, Krämer S, Kleist C, Loktev A, Kratochwil C, et al. Design and development of (99m)Tc-labeled FAPI tracers for SPECT imaging and (188)Re therapy. *J Nucl Med* (2020) 61(10):1507–13. doi:10.2967/jnumed.119.239731

46. Loktev A, Lindner T, Burger EM, Altmann A, Giesel F, Kratochwil C, et al. Development of fibroblast activation protein-targeted radiotracers with improved tumor retention. *J Nucl Med* (2019) 60(10):1421–9. doi:10.2967/jnumed.118.224469

Pathology & Oncology Research | frontiers

TYPE Original Research
PUBLISHED 19 April 2023
DOI 10.3389/pore.2023.1611014

Check for updates

OPEN ACCESS

EDITED BY
Andrea Ladányi,
National Institute of Oncology (NIO), Hungary

*CORRESPONDENCE
Bochao Zhao,
summerain2010@126.com
Kewei Meng,
doctormkw1969@126.com

RECEIVED 12 December 2022
ACCEPTED 06 April 2023
PUBLISHED 19 April 2023

CITATION
Zhao B, Wang J, Ma Z, Ye H, Yang T and Meng K (2023), Development and validation of a prognostic nomogram for rectal cancer patients who underwent surgical resection. *Pathol. Oncol. Res.* 29:1611014. doi: 10.3389/pore.2023.1611014

COPYRIGHT
© 2023 Zhao, Wang, Ma, Ye, Yang and Meng. This is an open-access article distributed under the terms of the Creative Commons Attribution License (CC BY). The use, distribution or reproduction in other forums is permitted, provided the original author(s) and the copyright owner(s) are credited and that the original publication in this journal is cited, in accordance with accepted academic practice. No use, distribution or reproduction is permitted which does not comply with these terms.

Development and validation of a prognostic nomogram for rectal cancer patients who underwent surgical resection

Bochao Zhao*, Jingchao Wang, Zhicheng Ma, Haikun Ye, Tao Yang and Kewei Meng*

Department of Gastrointestinal Surgery, Tianjin First Central Hospital, Tianjin, China

Objective: The purpose of this study was to develop and validate a nomogram model for the prediction of survival outcome in rectal cancer patients who underwent surgical resection.

Methods: A total of 9,919 consecutive patients were retrospectively identified using the Surveillance, Epidemiology, and End Results (SEER) database. Significant prognostic factors were determined by the univariate and multivariate Cox analysis. The nomogram model for the prediction of cancer-specific survival (CSS) in rectal cancer patients were developed based on these prognostic variables, and its predictive power was assessed by the concordance index (C-index). Calibration curves were plotted to evaluate the associations between predicted probabilities and actual observations. The internal and external cohort were used to further validate the predictive performance of the prognostic nomogram.

Results: All patients from the SEER database were randomly split into a training cohort (n = 6,944) and an internal validation cohort (n = 2,975). The baseline characteristics of two cohorts was comparable. Independent prognostic factors were identified as age, pT stage, lymph node metastasis, serum CEA level, tumor size, differentiation type, perineural invasion, circumferential resection margin involvement and inadequate lymph node yield. In the training cohort, the C-index of the nomogram was 0.719 (95% CI: 0.696–0.742), which was significantly higher than that of the TNM staging system (C-index: 0.606, 95% CI: 0.583–0.629). The nomogram had a C-index of 0.726 (95% CI: 0.691–0.761) for the internal validation cohort, indicating a good predictive power. In addition, an independent cohort composed of 202 rectal cancer patients from our institution were enrolled as the external validation. Compared with the TNM staging system (C-index: 0.573, 95% CI: 0.492–0.654), the prognostic nomogram still showed a better predictive performance, with the C-index of 0.704 (95% CI: 0.626–0.782). Calibration plots showed a good consistency between predicted probability and the actual observation in the training and two validation cohorts.

Conclusion: The nomogram showed an excellent predictive ability for survival outcome of rectal cancer patients, and it might provide an accurate prognostic stratification and help clinicians determine individualized treatment strategies.

KEYWORDS

survival, prognostic, nomogram, SEER, rectal cancer

Introduction

Colorectal cancer (CRC) is one of the most prevalent malignancies and a major cause of cancer-related mortality in both Eastern and Western populations (1, 2). Despite considerable advancements in cancer prevention and early detection, a high proportion of CRC patients were diagnosed at a locally advanced stage. To date, preoperative chemoradiotherapy and surgical resection with total mesorectal excision (TME) have become the standard treatment strategy for locally advanced rectal cancer patients (3–5). Multidisciplinary treatment modalities reduced the rate of locoregional recurrence, but overall survival of rectal cancer patients was still unsatisfactory (6, 7). Adjuvant chemotherapy following the curative resection is expected to improve the survival outcome of these patients, but a few evidence have shown that rectal cancer patients could not gain a survival benefit from adjuvant chemotherapy, particularly for those patients underwent preoperative chemoradiotherapy (8, 9).

The tumor, node, metastasis (TNM) classification of the American Joint Commission on Cancer (AJCC) is a widely used staging system for prognostic evaluation and treatment decision-making of rectal cancer patients. However, many well-established prognostic factors, such as serum carcinoembryonic antigen (CEA) level, differentiation type, lymphovascular invasion (LVI), perineural invasion (), circumferential resection margin (CRM), and the number of lymph node harvest, are not considered in the current staging system. Its predictive value for the survival outcome of rectal cancer patients might be limited in the precision medicine era. Therefore, appropriate prognostic stratification is warranted to determine who might benefit from the individualized treatment.

The nomogram is an intuitive graph of statistical model that generates a numerical probability of clinical event by incorporating important predictive factors. Recently, several nomogram models have been developed to predict the survival outcome of rectal cancer patients and shown an excellent prognostic performance (10–12). However, the development and validation of the nomogram models were limited by the sample size. In the present study, we identified independent prognostic factors for rectal cancer patients using a large population-based database, and develop a prognostic nomogram to help establish a risk stratification and make decision on therapeutic protocol.

Materials and methods

Patients and follow-up

All patients were retrospectively identified from the Surveillance, Epidemiology, and End Results (SEER) 18 Registries Research database (1973–2016). The eligibility criteria of enrolled individuals were as follows: (1). The surgical resection for primary rectal cancer was performed (2). The diagnosis of rectal cancer was confirmed by histopathology (3). No distant metastasis at presentation (3). No neoadjuvant chemotherapy and/or radiotherapy before surgery (4). Patient age ≥18 years old (5). The clinicopathological records were completed and follow-up duration was at least 1 month. Ultimately, a total of 9,919 consecutive patients who underwent surgical resection for rectal cancer between January 2010 and December 2015 were included in this analysis.

To test the predictive value of the prognostic nomogram, 202 rectal cancer patients who underwent curative resection in our institution from January 2015 and December 2019 were recruited as an independent cohort for the external validation. This study was approved by the Ethics Committee of Tianjin First Central Hospital (No. 2023000503), and was conducted under the principles of the Helsinki Declaration.

Demographic, clinicopathologic and survival data, including patient age, sex, race, year of diagnosis, preoperative carcinoembryonic antigen (CEA) level, pathological T category (pT stage), pathological N category (pN stage), pTNM stage, tumor size, differentiation type, histological classification, PNI, circumferential resection margin (CRM), lymph node yield, follow-up duration and vital status, were systematically collected and analyzed. The SEER database was accessed *via* free public website at www.seer.cancer.gov, and relevant data were extracted using the SEER*Stat software (version 8.3.6). Investigators received permission from the SEER program to access the original data.

The pTNM stage of rectal cancer patients was recorded according to the 7th edition of the TNM classification of the AJCC. In the current study cohort, the median period of follow-up was 33 months (range, 1–71 months). The primary outcome of survival analysis was cancer-specific survival (CSS), which was defined as the period from the date of diagnosis to the date of death owing to cancer-related causes. The observations of patients who died of other causes or were alive at the end of follow-up were defined as censored events.

Statistical analysis

Categorical variables were reported as frequency distributions and were summarized in a descriptive table, and they were compared by Pearson's chi-square test or Fisher's exact test as appropriate. Continuous variables were expressed as median with range unless indicated otherwise and were compared using an unpaired Student's

TABLE 1 Clinicopathological characteristics of rectal cancer patients in the training cohort and internal validation cohort.

Characteristics	Patients (%)	Patient cohort		
		Training (n = 6,944)	Internal validation (n = 2,975)	p-value
Age (years old)				0.433
<60	4,262 (43.0%)	2,966 (42.7%)	1,296 (43.6%)	
≥60	5,657 (57.0%)	3,978 (57.3%)	1,679 (56.4%)	
Sex				0.816
Female	3,995 (40.3%)	2,802 (38.3%)	1,193 (40.1%)	
Male	5,924 (59.7%)	4,142 (61.7%)	1782 (59.9%)	
Race				0.193
Black	766 (7.7%)	516 (7.4%)	250 (8.4%)	
White	7,933 (80.0%)	5,582 (80.4%)	2,351 (79.0%)	
Other	1,220 (12.3%)	846 (12.2%)	374 (12.6%)	
CEA level				0.571
Normal	5,957 (60.1%)	4,183 (60.2%)	1,774 (59.6%)	
Elevated	3,962 (39.9%)	2,761 (39.8%)	1,201 (40.4%)	
Differentiation type				0.448
WD/MD	8,606 (86.8%)	6,027 (86.8%)	2,579 (86.7%)	
PD	1,081 (10.9%)	747 (10.8%)	334 (11.2%)	
UD	232 (2.3%)	170 (2.4%)	62 (2.1%)	
Histological type				0.558
Adenocarcinoma	9,261 (93.4%)	6,490 (93.5%)	2,771 (93.1%)	
MUC/SRC	658 (6.6%)	454 (6.5%)	204 (6.9%)	
pT stage				0.104
T1-2	2,350 (23.7%)	1,686 (24.3%)	664 (22.3%)	
T3	6,526 (65.8%)	4,529 (65.2%)	1,997 (67.1%)	
T4	1,043 (10.5%)	729 (10.5%)	314 (10.6%)	
pN stage				0.117
N0	5,803 (58.7%)	4,123 (59.4%)	1,700 (57.1%)	
N1	2,823 (28.3%)	1,932 (27.8%)	871 (29.3%)	
N2	1,293 (13.0%)	889 (12.8%)	404 (13.6%)	
Tumor size (cm)				0.713
≤5	5,934 (59.8%)	4,146 (59.7%)	1,788 (60.1%)	
>5	3,985 (40.2%)	2,798 (40.3%)	1,187 (39.9%)	
CRM				0.804
Negative	8,266 (83.3%)	5,791 (83.4%)	2,475 (83.2%)	
Positive	1,653 (16.7%)	1,153 (16.6%)	500 (16.8%)	
Perineural invasion				0.922
No	8,647 (87.2%)	6,055 (87.2%)	2,592 (87.1%)	
Yes	1,272 (12.8%)	889 (12.8%)	383 (12.9%)	
Lymph node yield				0.549
<12	1,950 (19.7%)	1,376 (19.8%)	574 (19.3%)	
≥12	7,969 (80.3%)	5,568 (80.2%)	2,401 (80.7%)	

CEA: carcinoembryonic antigen; WD: well-differentiated; MD: moderately differentiated; PD: poorly differentiated; UD: undifferentiated; MUC: mucinous adenocarcinoma; SRC: signet-ring cell carcinoma; CRM: circumferential resection margin.

TABLE 2 Clinicopathological characteristics of 202 rectal cancer patients in the external validation cohort.

Characteristics	Patients (%)
Age (years old)	
<60	88 (43.6%)
≥60	114 (56.4%)
Sex	
Female	63 (31.2%)
Male	139 (68.8%)
CEA level	
Normal	143 (70.8%)
Elevated	59 (29.2%)
Differentiation type	
WD/MD	184 (91.1%)
PD	16 (7.9%)
UD	2 (1.0%)
pT stage	
T1-2	29 (14.4%)
T3	155 (76.7%)
T4	18 (8.9%)
pN stage	
N0	59 (29.2%)
N1	101 (50.0%)
N2	42 (20.8%)
Tumor size (cm)	
≤5	126 (62.4%)
>5	76 (37.6%)
CRM	
Negative	180 (89.1%)
Positive	22 (10.9%)
Perineural invasion	
No	145 (71.8%)
Yes	57 (28.2%)
Lymph node yield	
<12	24 (11.9%)
≥12	178 (88.1%)

CEA: carcinoembryonic antigen; WD: well-differentiated; MD: moderately differentiated; PD: poorly differentiated; UD: undifferentiated; CRM: circumferential resection margin.

t-test or Mann-Whitney test. The prognostic significance of clinicopathologic factors was assessed using the univariate Cox regression analysis, and the variables at a significant level (p-value <0.05) were candidates for the multivariate analysis. A Cox proportional hazard model with a backward stepwise selection procedure was used to determine independent prognostic factors for rectal cancer patients. Results for significant prognostic factors were presented as hazard ratio (HR) and its 95% confidence interval (CI).

Based on the regression coefficients estimated by the multivariate Cox analysis, the nomogram was established to predict the survival probabilities at 1-year, 3-year and 5-year. The predictive ability of the nomogram was assessed by calculating the concordance index (C-index), which estimates the probability of concordance between predicted and observed outcomes and is equivalent to the area under curve value of the receiver operating characteristic (ROC) (13). The value of the C-index should fall between 0.5 and 1.0. The maximum value of the C-index is 1.0, indicating a perfect prediction, whereas a C-index of 0.5 indicates that the nomogram model does not have sufficient predictive power (13). Calibration curves were plotted to evaluate the associations between predicted probabilities and the observed outcomes. In the calibration curve, the vertical axis represented the actual observations, whereas the horizontal one is the predicted probabilities. To reduce the overfit bias, the predictive performances of the nomogram were evaluated by bootstrapping method, in which the datasets were tested 1,000 times with random resampling each time. All statistical analyses were conducted using the statistical package for SPSS 22.0 (IBM Inc., New York, USA) and R software program with version 4.2.1 (http://www.r-project.org), and the statistical significance was accepted at a p-value <0.05.

Results

Patient characteristics

The entire cohort consisted of 5,924 males (59.7%) and 3,995 females (40.3%), and the proportion of patients aged 60 or older was 57.0% (5,657/9,919). Among 9,919 patients, 39.9% (3,962/9,919) had an elevated CEA level before surgery. The prevalence of lymph node metastasis in rectal cancer patients was 41.5% (4,116/9,919), and the median of metastatic lymph nodes was 2 (range, 1–36). The median of retrieved lymph nodes was 16 (range, 1–90), and 80.3% (7,969/9,919) of patients had at least 12 lymph nodes yield. Histologically, the proportion of well/moderately differentiated (WD/MD), poorly differentiated (PD) and undifferentiated (UD) adenocarcinoma were 86.8% (8,606/9,919), 10.9% (1,081/9,919) and 2.3% (232/9,919), respectively. According to the 7th edition of pTNM classification, the proportion of stage I, stage II and stage III patients were 17.9% (1,777/9,919), 40.6% (4,026/9,919) and 41.5% (4,116/9,919), respectively. The presence of PNI was detected in 1,272 patients (12.8%), and the incidence of CRM involvement was 16.7% (1,653/9,919) in rectal cancer patients.

In this analysis, 9,919 patients were randomly split into a training cohort (n = 6,944) and an internal validation cohort (n = 2,975) with a ratio of 7:3. Clinicopathologic characteristics of the two cohorts were summarized in Table1. The results indicated

TABLE 3 Univariate and multivariate Cox regression analysis of prognostic factors for rectal cancer patients in the training cohort.

Factor	Univariate analysis		Multivariate analysis	
	HR (95% CI)	*p*-value	HR (95% CI)	*p*-value
Age (years old)				
<60	Reference		Reference	
≥60	2.015 (1.746–2.325)	< **0.001**	2.236 (1.935–2.583)	< **0.001**
Sex				
Female	Reference		-	
Male	1.094 (0.892–1.341)	0.389	-	
Race				
Black	Reference		Reference	
White	0.789 (0.630–0.989)	**0.040**	0.847 (0.675–1.063)	0.153
Other	0.766 (0.577–1.018)	0.066	0.805 (0.605–1.070)	0.135
CEA level				
Normal	Reference		Reference	
Elevated	1.720 (1.512–1.957)	< **0.001**	1.358 (1.188–1.551)	< **0.001**
Differentiation type				
WD/MD	Reference		Reference	
PD	1.976 (1.670–2.339)	< **0.001**	1.341 (1.126–1.597)	< **0.001**
UD	2.443 (1.802–3.312)	< **0.001**	1.746 (1.283–2.375)	< **0.001**
Histological type				
Adenocarcinoma	Reference		Reference	
MUC/SRC	2.081 (1.700–2.548)	< **0.001**	1.711 (0.975–1.407)	0.092
pT stage				
T1-2	Reference		Reference	
T3	1.917 (1.586–2.316)	< **0.001**	1.355 (1.111–1.654)	**0.003**
T4	4.033 (3.218–5.054)	< **0.001**	2.027 (1.580–2.601)	< **0.001**
pN stage				
N0	Reference		Reference	
N1	1.860 (1.603–2.158)	< **0.001**	1.589 (1.362–1.854)	< **0.001**
N2	3.042 (2.581–3.585)	< **0.001**	2.371 (1.979–2.840)	< **0.001**
Tumor size (cm)				
≤5	Reference		Reference	
>5	1.515 (1.332–1.724)	< **0.001**	1.207 (1.054–1.382)	**0.007**
CRM				
Negative	Reference		Reference	
Positive	2.292 (1.993–2.636)	< **0.001**	1.609 (1.387–1.866)	< **0.001**
Perineural invasion				
No	Reference		Reference	
Yes	2.572 (2.211–2.992)	< **0.001**	1.557 (1.321–1.835)	< **0.001**
Lymph node yield				
<12	Reference		Reference	
≥12	0.857 (0.737–0.995)	**0.043**	0.771 (0.661–0.898)	**0.001**

The bold value represent a statistical significance ($p < 0.05$).

that the distributions of baseline characteristics between the training and validation cohort were comparable. The data split provided a balanced statistical power to develop and validate a prognostic nomogram for rectal cancer patients. Furthermore, 202 rectal cancer patients who underwent curative resection in our institution were recruited as an independent cohort for the external validation. The baseline characteristics of these patients were listed in the Table 2.

Univariate and multivariate analysis of prognostic factors for rectal cancer patients

The prognostic significance of clinicopathologic variables for rectal cancer patients in the training cohort was evaluated by the univariate and multivariate Cox analysis. In the univariate analysis, patient age ($p < 0.001$), race ($p = 0.040$), preoperative CEA level ($p < 0.001$), differentiation type ($p < 0.001$), histological classification ($p < 0.001$), tumor size ($p < 0.001$), pT stage ($p < 0.001$), pN stage ($p < 0.001$), the presence of PNI ($p < 0.001$), CRM involvement ($p < 0.001$) and lymph node yield ($p = 0.043$) were significantly associated with survival outcome of rectal cancer patients. After adjusting for potential covariates, age ($p < 0.001$), advanced pT stage (pT3 vs. pT1-T2 stage, $p = 0.003$; pT4 vs. pT1-T2 stage, $p < 0.001$), lymph node metastasis (pN1 vs. pN0 stage, $p < 0.001$; pN2 vs. pN0 stage, $p < 0.001$), elevated CEA level ($p < 0.001$), tumor size ≥5 cm ($p = 0.007$), PD or UD ($p < 0.001$), PNI ($p < 0.001$), CRM involvement ($p < 0.001$) and at least 12 lymph nodes yield ($p = 0.001$) were identified as independent prognostic factors (Table 3).

Development and validation of the prognostic nomogram

The nomogram was developed using identified 9 prognostic variables. As shown in Figure 1, the nomogram determined the survival probabilities of rectal cancer patients by assigning a score to each prognostic variable. The sum of these scores corresponds to the survival probability of patients. Higher total points in the nomogram, poorer survival for rectal cancer patients. In this predictive model, pN2 stage was the most important prognostic factor for rectal cancer patients followed by patient age and pT4 stage. pN1 and pN2 stage were assigned 53 points and 100 points, respectively. Similarly, patient age over 60 years old was assigned 92 points. pT3 and pT4 stage were assigned 34 points and 79 points, respectively. For example, a 55 years old patient with pT2N0 stage, elevated CEA level (for 35 points), tumor size of 7 cm (for 23 points), the presence of PNI (for 51 points), CRM involvement (for 55 points), undifferentiated type (for 64 points) and 10 lymph nodes harvest (for 31 points) had a total of 259 points. The predicted 3-year and 5-year CSS rates of this patient were 73.3% and 58.2%, respectively.

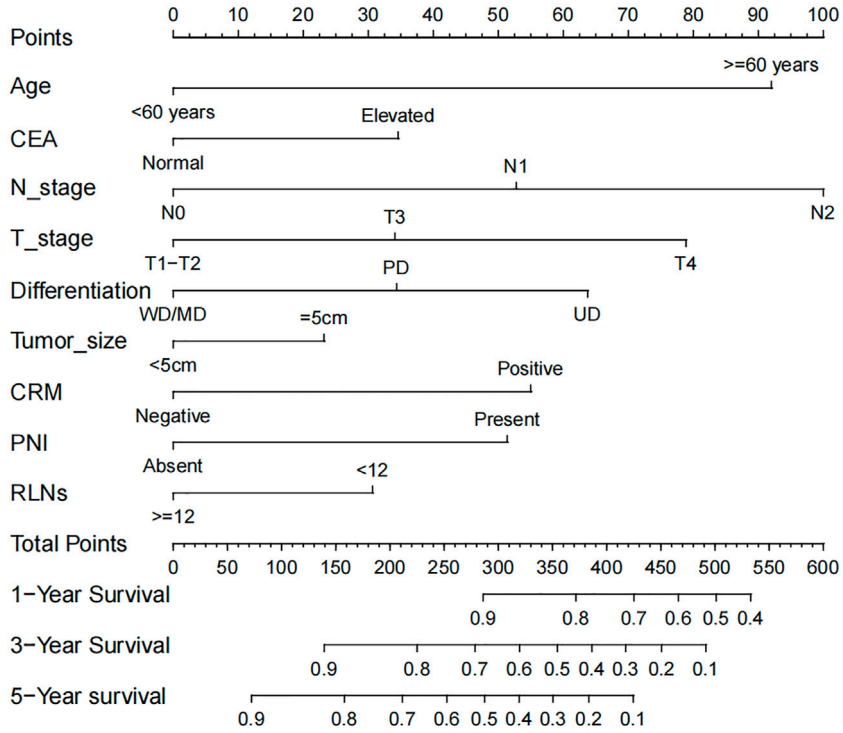

FIGURE 1
The prognostic nomogram of rectal cancer patients.

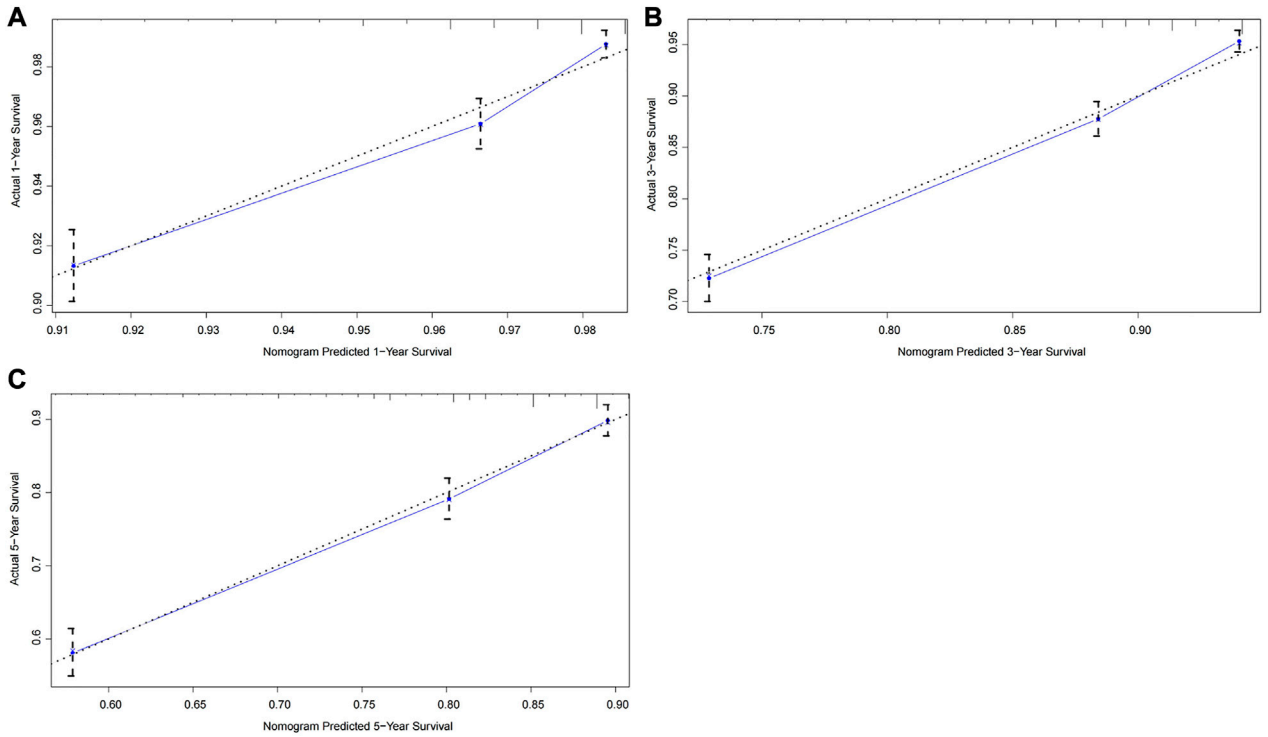

FIGURE 2
Calibration curves of the prognostic nomogram for the training cohort. **(A)** Predicted 1-year survival; **(B)** Predicted 3-year survival; **(C)** Predicted 5-year survival.

The C-index of the nomogram in the training cohort was 0.719 (95% CI: 0.696–0.742), which was significantly higher than that of the TNM staging system (C-index: 0.606, 95% CI: 0.583–0.629). Figure 2 illustrated calibration plots for the prediction of 1-year, 3-year and 5-year CSS in the training cohort. For a well-calibrated model, predicted outcomes should fall on a 45-degree diagonal line through the origin. As shwon in the calibration plots, a satisfactory conformance between the predicted and actual probability was observed (Figure 2). The nomogram had a C-index of 0.726 (95% CI: 0.691–0.761) for the internal validation cohort. There was no significant difference between the training and validation cohort for predictive performance, suggesting that the bias of model overfit was less evident. In addition, the nomogram had a higher C-index than the TNM staging system (C-index: 0.612, 95% CI: 0.577–0.647) for the prediction of survival outcome.

To further test the generalisability and clinical availability of the prognostic nomogram, an independent cohort composed of 202 rectal cancer patients were enrolled as the external validation. Compared with the TNM staging system (C-index: 0.573, 95% CI: 0.492–0.654), the prognostic nomogram still showed a better predictive performance, with the C-index of 0.704 (95% CI: 0.626–0.782). The calibration plots showed a good consistency between predicted probability and the actual observation in the internal and external validation cohort (Figures 3, 4).

Discussion

Accurate risk stratification is crucial to prognostic assessment and subsequent treatment decisions for rectal cancer patients. In the precision medicine era, the single TNM staging system is insufficient to meet the therapeutic needs of all patients. Identifying as many prognostic variables as possible is helpful to determine individualized treatment strategies. In the present study, independent prognostic factors for rectal cancer patients were identified as age, pT stage, lymph node metastasis, elevated CEA level, tumor size, poorly differentiated/undifferentiated adenocarcinoma, PNI, CRM involvement, and inadequate lymph nodes yield, which have been reported in previous studies (14–20). Based on these data, we developed and validated a prognostic nomogram for rectal cancer patients. The results indicated that the nomogram had a higher C-index than the TNM staging

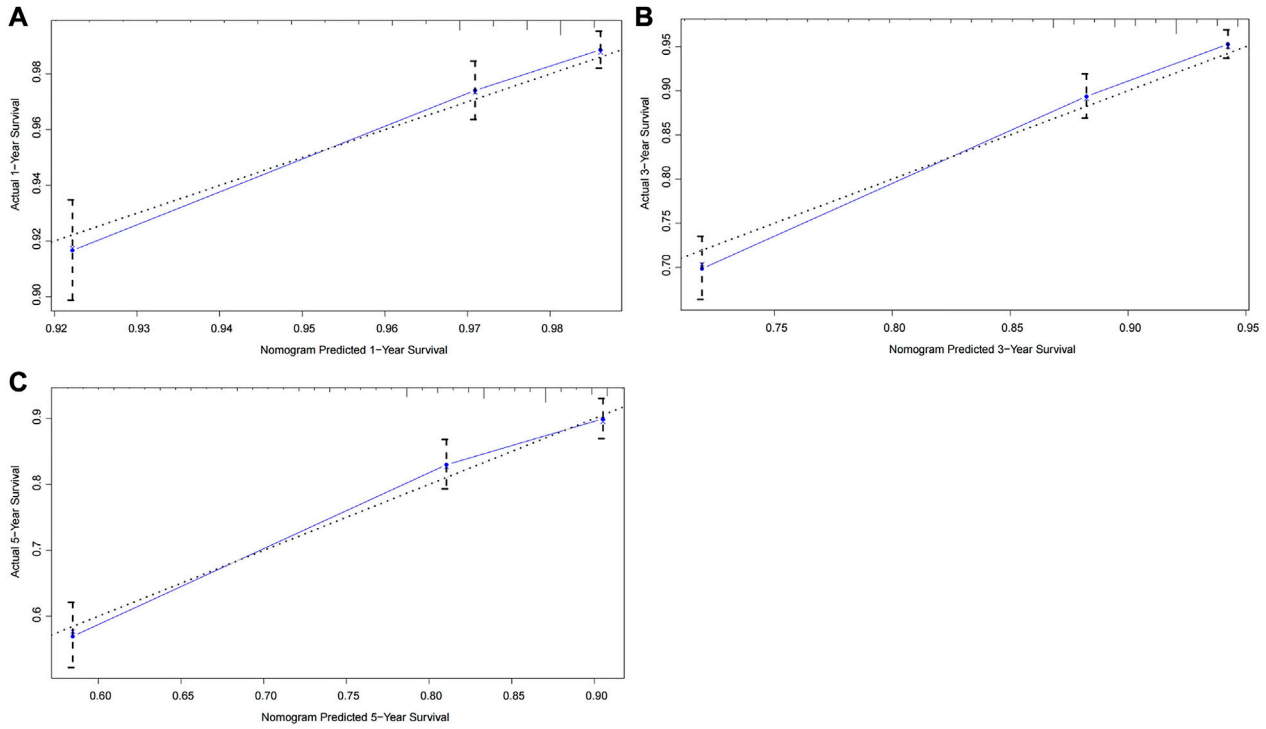

FIGURE 3
Calibration curves of the prognostic nomogram for the internal validation cohort. **(A)** Predicted 1-year survival; **(B)** Predicted 3-year survival; **(C)** Predicted 5-year survival.

system for the survival prediction (0.719 vs. 0.606), suggesting a better predictive ability. More importantly, its predictive performance was fruther validatd in an independent internal (C-index: 0.726 vs. 0.612) and external cohort (C-index: 0.704 vs. 0.573). These findings suggested that the nomogram model provided more accurate prognostic stratification for rectal cancer patients.

To date, there have been several nomogram models for survival prediction of rectal cancer patients. Using individual data from five large European randomized clinical trials, Valentini et al developed nomogram models that could predict local recurrence, distant metastasis and overall survival in locally advanced rectal cancer patients (10). After variable selection, patient age, pT stage, pN stage, surgical procedure, and adjuvant treatment were incorporated into the prognostic nomogram to evaluate the risk of recurrence and death. The C-index of the nomogram for the predictions of local recurrence, distant metastasis and overall survival were 0.68, 0.73 and 0.70, respectively (10). However, Shen et al reported that the predicted probabilities of relevant outcomes for a Chinese patient cohort could be overestimated by the nomogram model (21). The discrepancy may be interpreted as demographic heterogeneity and different treatment methods between Eastern and Western populations. On the other hand, the predictive performance of the nomogram for rectal cancer patients needs to be further optimized by introducing additional prognostic variables. Recently, Fan et al developed a prognostic nomogram incorporated clinicopathologic factors (patient age, pT stage, pN stage, differentiation type, PNI, tumor deposits) with serum biomarkers (CEA and CA19-9 level) to predict survival outcome of rectal cancer patients (12). The data indicated that the nomogram model had a better predictive performance than the TNM staging system (C-index: 0.71 vs. 0.58), and this finding was successfully validated by an external cohort (C-index: 0.69 vs. 0.57) (12). In the current study, several prognostic variables such as tumor size, CRM involvement and lymph node yield were further included in the nomogram model, and the results revealed a better predictive value. To avoid overfitting of the predictive model, it is essential to verify the generality of the nomogram. Using an internal cohort from the SEER database and an independent external cohort from our institution, the analytical results further supported the reliability and reproducibility of the prognostic nomogram.

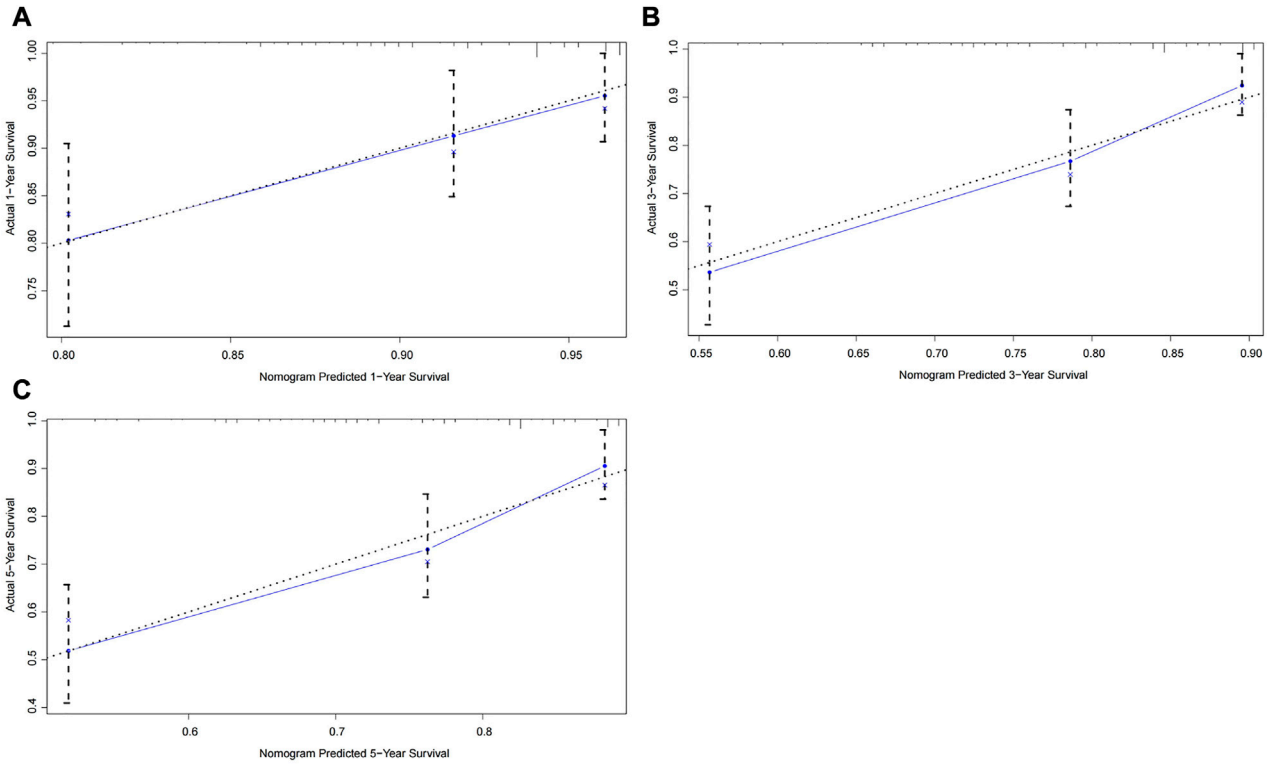

FIGURE 4
Calibration curves of the prognostic nomogram for the external validation cohort. **(A)** Predicted 1-year survival; **(B)** Predicted 3-year survival; **(C)** Predicted 5-year survival.

Several limitations of this study require further discussion. Firstly, only those patients with complete clinicopathologic data were analyzed, which could introduce the potential selection bias. Secondly, adjuvant chemoradiotherapy and several well-established molecular variables such as microsatellite instability (MSI), KRAS and BRAF mutations were not included in this analysis since they were unavailable in the public SEER database. This is a major shortcoming of the current analysis. Thirdly, therapeutic protocols for rectal cancer patients have been evolved over the recent decade. Preoperative chemoradiotherapy followed by surgical resection with TME technique has become the standard treatment strategy for locally advanced rectal cancer (cT3/cT4 stage or lymph nodes involvement). However, the current analysis did not include patients who underwent neoadjuvant chemoradiotherapy, which limited the application of the nomogram for these individuals.

Despite the above-mentioned limitations, the prognostic nomogram was successfully developed by a large scale of real-world populations and was validated by an independent external cohort. Our data suggested that the nomogram model had an excellent predictive performance for the survival outcome of rectal cancer patients. It might provide an accurate prognostic stratification for rectal cancer patients and help clinicians make a decision on individualized treatment strategies.

Data availability statement

The supportive data of this manuscript are available from the Supplementary Material.

Ethics statement

The studies involving human participants were reviewed and approved the Ethics Committee of Tianjin First Central Hospital. The ethics committee waived the requirement of written informed consent for participation.

Author contributions

BZ designed this study, conducted data analysis and drafted the original manuscript; JW and ZM were responsible for data collection and result interpretation; HY contributed to the editing and preparation of the final manuscript; TY and KM critically reviewed this manuscript.

Funding

This work was supported by the Tianjin Health Science and Technology Project (No. ZC20213).

Conflict of interest

The authors declare that the research was conducted in the absence of any commercial or financial relationships that could be construed as a potential conflict of interest.

Supplementary material

The Supplementary Material for this article can be found online at: https://www.por-journal.com/articles/10.3389/pore.2023.1611014/full#supplementary-material

References

1. Siegel RL, Miller KD, Goding Sauer A, Fedewa SA, Butterly LF, Anderson JC, et al. Colorectal cancer statistics, 2020. *CA Cancer J Clin* (2020) 70:145–64. doi:10.3322/caac.21601

2. Siegel RL, Miller KD, Fuchs HE, Jemal A. Cancer statistics. *CA Cancer J Clin* (2022) 72:7–33. doi:10.3322/caac.21708

3. Benson AB, Venook AP, Al-Hawary MM, Cederquist L, Chen YJ, Ciombor KK, et al. Rectal cancer, version 2.2018, NCCN clinical practice guidelines in Oncology. *J Natl Compr Canc Netw* (2018) 16:874–901. doi:10.6004/jnccn.2018.0061

4. Schmoll HJ, Van Cutsem E, Stein A, Valentini V, Glimelius B, Haustermans K, et al. ESMO Consensus Guidelines for management of patients with colon and rectal cancer. a personalized approach to clinical decision making. *Ann Oncol* (2012) 23:2479–516. doi:10.1093/annonc/mds236

5. van Gijn W, Marijnen CA, Nagtegaal ID, Kranenbarg EM, Putter H, Wiggers T, et al. Preoperative radiotherapy combined with total mesorectal excision for resectable rectal cancer: 12-year follow-up of the multicentre, randomised controlled TME trial. *Lancet Oncol* (2011) 12:575–82. doi:10.1016/S1470-2045(11)70097-3

6. Engelen SM, Maas M, Lahaye MJ, Leijtens JW, van Berlo CL, Jansen RL, et al. Modern multidisciplinary treatment of rectal cancer based on staging with magnetic resonance imaging leads to excellent local control, but distant control remains a challenge. *Eur J Cancer* (2013) 49:2311–20. doi:10.1016/j.ejca.2013.03.006

7. Nikberg M, Kindler C, Chabok A, Letocha H, Shetye J, Smedh K. Circumferential resection margin as a prognostic marker in the modern multidisciplinary management of rectal cancer. *Dis Colon Rectum* (2015) 58:275–82. doi:10.1097/DCR.0000000000000250

8. Bosset JF, Calais G, Mineur L, Maingon P, Stojanovic-Rundic S, Bensadoun RJ, et al. Fluorouracil-based adjuvant chemotherapy after preoperative chemoradiotherapy in rectal cancer: Long-term results of the EORTC 22921 randomised study. *Lancet Oncol* (2014) 15:184–90. doi:10.1016/S1470-2045(13)70599-0

9. Breugom AJ, Swets M, Bosset JF, Collette L, Sainato A, Cionini L, et al. Adjuvant chemotherapy after preoperative (chemo)radiotherapy and surgery for patients with rectal cancer: A systematic review and meta-analysis of individual patient data. *Lancet Oncol* (2015) 16:200–7. doi:10.1016/S1470-2045(14)71199-4

10. Valentini V, van Stiphout RG, Lammering G, Gambacorta MA, Barba MC, Bebenek M, et al. Nomograms for predicting local recurrence, distant metastases, and overall survival for patients with locally advanced rectal cancer on the basis of European randomized clinical trials. *J Clin Oncol* (2011) 29:3163–72. doi:10.1200/JCO.2010.33.1595

11. Li ZH, Xie PY, Zhang DF, Li YJ, Wu L, Dong J, et al. Nomogram for predicting disease-free survival among a multicenter cohort of Chinese patients with locally advanced rectal cancer. *Cancer Manag Res* (2019) 11:2471–83. doi:10.2147/CMAR.S196614

12. Fan S, Li T, Zhou P, Peng Q, Zhu Y. Development and validation of nomogram combining serum biomarker for predicting survival in patients with resected rectal cancer. *Biosci Rep* (2019) 39:BSR20192636. doi:10.1042/BSR20192636

13. Iasonos A, Schrag D, Raj GV, Panageas KS. How to build and interpret a nomogram for cancer prognosis. *J Clin Oncol* (2008) 26:1364–70. doi:10.1200/JCO.2007.12.9791

14. Kim KH, Yang SS, Yoon YS, Lim SB, Yu CS, Kim JC. Validation of the seventh edition of the American Joint committee on cancer tumor-node-metastasis (AJCC TNM) staging in patients with stage II and stage III colorectal carcinoma: Analysis of 2511 cases from a medical centre in korea. *Colorectal Dis* (2011) 13:e220–6. doi:10.1111/j.1463-1318.2011.02625.x

15. Tarantino I, Warschkow R, Worni M, Merati-Kashani K, Köberle D, Schmied BM, et al. Elevated preoperative CEA is associated with worse survival in stage I-III rectal cancer patients. *Br J Cancer* (2012) 107:266–74. doi:10.1038/bjc.2012.267

16. Tayyab M, Razack A, Sharma A, Gunn J, Hartley JE. Correlation of rectal tumor volumes with oncological outcomes for low rectal cancers: Does tumor size matter. *Surg Today* (2015) 45:826–33. doi:10.1007/s00595-014-1068-0

17. Hyngstrom JR, Hu CY, Xing Y, You YN, Feig BW, Skibber JM, et al. Clinicopathology and outcomes for mucinous and signet ring colorectal adenocarcinoma: Analysis from the national cancer data base. *Ann Surg Oncol* (2012) 19:2814–21. doi:10.1245/s10434-012-2321-7

18. Song JH, Yu M, Kang KM, Lee JH, Kim SH, Nam TK, et al. Significance of perineural and lymphovascular invasion in locally advanced rectal cancer treated by preoperative chemoradiotherapy and radical surgery: Can perineural invasion be an indication of adjuvant chemotherapy. *Radiother Oncol* (2019) 133:125–31. doi:10.1016/j.radonc.2019.01.002

19. Bernstein TE, Endreseth BH, Romundstad P, Wibe ANorwegian Colorectal Cancer Group. Circumferential resection margin as a prognostic factor in rectal cancer. *Br J Surg* (2009) 96:1348–57. doi:10.1002/bjs.6739

20. Lykke J, Jess P, Roikjaer ODanish Colorectal Cancer Group. Increased lymph node yield is associated with improved survival in rectal cancer irrespective of neoadjuvant treatment: Results from a national cohort study. *Dis Colon Rectum* (2015) 58:823–30. doi:10.1097/DCR.0000000000000429

21. Shen L, van Soest J, Wang J, Yu J, Hu W, Gong YU, et al. Validation of a rectal cancer outcome prediction model with a cohort of Chinese patients. *Oncotarget* (2015) 6:38327–35. doi:10.18632/oncotarget.5195

Pathology & Oncology Research | frontiers

TYPE Hypothesis & Theory
PUBLISHED 24 February 2023
DOI 10.3389/pore.2023.1611016

Check for updates

OPEN ACCESS

EDITED BY
Jozsef Dudas,
Innsbruck Medical University, Austria

*CORRESPONDENCE
Wenjing Zhang,
wenjing_zhang1@163.com

RECEIVED 13 December 2022
ACCEPTED 14 February 2023
PUBLISHED 24 February 2023

CITATION
Zhang Y, Li Y, Zuo Z, Li T, An Y and Zhang W (2023), An epithelial–mesenchymal transition-related mRNA signature associated with the prognosis, immune infiltration and therapeutic response of colon adenocarcinoma.
Pathol. Oncol. Res. 29:1611016.
doi: 10.3389/pore.2023.1611016

COPYRIGHT
© 2023 Zhang, Li, Zuo, Li, An and Zhang. This is an open-access article distributed under the terms of the Creative Commons Attribution License (CC BY). The use, distribution or reproduction in other forums is permitted, provided the original author(s) and the copyright owner(s) are credited and that the original publication in this journal is cited, in accordance with accepted academic practice. No use, distribution or reproduction is permitted which does not comply with these terms.

An epithelial–mesenchymal transition-related mRNA signature associated with the prognosis, immune infiltration and therapeutic response of colon adenocarcinoma

Yu Zhang[1,2], Yan Li[1,2], Zan Zuo[1,2], Ting Li[1,2], Ying An[1,2] and Wenjing Zhang[3,4]*

[1]Department of Gastroenterology, The First People's Hospital of Yunnan Province, Affiliated Hospital of Kunming University of Science and Technology, Kunming, China, [2]Yunnan Digestive Endoscopy Clinical Medical Center, Kunming, China, [3]Faculty of Medicine, Kunming University of Science and Technology, Kunming, China, [4]Department of Medical Oncology, The First People's Hospital of Yunnan Province, Affiliated Hospital of Kunming University of Science and Technology, Kunming, China

Background: Epithelial-mesenchymal transition (EMT) is closely associated with cancer cell metastasis. Colon adenocarcinoma (COAD) is one of the most common malignancies in the world, and its metastasis leading to poor prognosis remains a challenge for clinicians. The purpose of this study was to explore the prognostic value of EMT-related genes (EMTRGs) by bioinformatics analysis and to develop a new EMTRGs prognostic signature for COAD.

Methods: The TCGA-COAD dataset was downloaded from the TCGA portal as the training cohort, and the GSE17538 and GSE29621 datasets were obtained from the GEO database as the validation cohort. The best EMTRGs prognostic signature was constructed by differential expression analysis, Cox, and LASSO regression analysis. Gene set enrichment analysis (GSEA) is used to reveal pathways that are enriched in high-risk and low-risk groups. Differences in tumor immune cell levels were analyzed using microenvironmental cell population counter and single sample gene set enrichment analysis. Subclass mapping analysis and Genomics of Drug Sensitivity in Cancer were applied for prediction of immunotherapy response and chemotherapy response, respectively.

Results: A total of 77 differentially expressed EMTRGs were identified in the TCGA-COAD cohort, and they were significantly associated with functions and pathways related to cancer cell metastasis, proliferation, and apoptosis. We constructed EMTRGs prognostic signature with COMP, MYL9, PCOLCE2, SCG2, and TIMP1 as new COAD prognostic biomarkers. The high-risk group had a poorer prognosis with enhanced immune cell infiltration. The GSEA demonstrated that the high-risk group was involved in "ECM Receptor Interaction," "WNT Signaling Pathway" and "Colorectal Cancer." Furthermore,

patients with high risk scores may respond to anti-CTLA4 therapy and may be more resistant to targeted therapy agents BI 2536 and ABT-888.

Conclusion: Together, we developed a new EMTRGs prognostic signature that can be an independent prognostic factor for COAD. This study has guiding implications for individualized counseling and treatment of COAD patients.

KEYWORDS

epithelial-mesenchymal transition, bioinformatics, prognostic signature, tumor immune microenvironment, colon adenocarcinoma

Introduction

Colon adenocarcinoma (COAD), as one of the common gastrointestinal malignancies, has the top incidence and mortality rate among common cancers worldwide. According to the Global Cancer Statistics report published in 2020 (1), colorectal cancer (CRC) has the third highest incidence and the second highest mortality rate of all malignancies. The mortality and morbidity rate of COAD in China is also increasing year by year, which has posed a serious threat to the health of the residents, and caused a heavy burden on the families of patients financially (2). Early-stage COAD can be treated well with surgical resection or with radiotherapy. However, due to the insidious onset of COAD, most patients are diagnosed at the medium or advanced stage with tumor infiltration and metastasis. Notably, approximately 90% of cancer-related mortality is caused by cancer metastasis (3). Consequently, an in-depth exploration of biomarkers in the development and metastasis of COAD will help to establish new diagnostic and therapeutic approaches for COAD.

Epithelial-mesenchymal transition (EMT) is considered to be one of the main mechanisms determining the spread of infiltrative and metastatic cancer cells, a dynamic and reversible process of increased motility and invasiveness of cancer cells. During EMT, epithelial cells gradually lose intercellular adhesion and apical-basal polarity, thus transforming into mesenchymal cells with migratory and invasive abilities (4). On the one hand, EMT plays an important role in the generation of neural crest delamination, gastrula, and a variety of cell and tissue types (4, 5). On the other hand, for cancer cells to acquire an invasive phenotype for metastasis, EMT is aberrantly activated in cancer cells and facilitates their spread from the primary tumor into the circulation, leading to enhanced cell stemness and immune resistance of tumor cells to resist various therapeutic attacks (4, 6). The role of EMT in COAD metastasis has been well demonstrated. Wang et al. (7) showed that Cinobufacini can inhibit EMT to restrain invasion and metastasis of COAD by suppressing Wnt/β-catenin signaling pathway activation *in vivo* and *in vitro*. ACLY can stabilize β-catenin by mutual interaction thus promoting nuclear translocation of β-catenin, which contributes to the EMT process exacerbating COAD metastasis (8). In recent years, with the continuous exploitation of sequencing data, the development of EMT-related genes (EMTRG) prognostic signatures based on public datasets such as TCGA and GEO has been well studied in a variety of malignancies including endometrial cancer (9), bladder cancer (BC) (10, 11), hepatocellular carcinoma (HCC) (12), and pancreatic cancer (13, 14). Nevertheless, the EMTRG prognostic signature in COAD remains to be investigated in depth.

Based on this, we propose to search for new EMTRG prognostic signatures of COAD through public data in TCGA and GEO databases. The aim is to provide potential therapeutic targets and new insights into the mechanisms and functions of EMT in the development of COAD and to explore new prognostic biomarkers for the diagnosis and treatment of metastases in COAD patients.

Materials and methods

Data source

The COAD-related data used in this study were obtained from the freely available TCGA (https://portal.gdc.cancer.gov/) and GEO (https://www.ncbi.nlm.nih.gov/geo/) databases. We obtained RNA-seq sequencing data and clinical data of COAD from the TCGA database. The mRNA and lncRNA expression matrices were obtained for 163 TCGA-COAD and 10 normal samples, and miRNA expression profiles were achieved for 158 TCGA-COAD and 3 normal samples. Of the 163 TCGA-COAD samples, those with incomplete survival information and missing clinical data were excluded, and the remaining 154 TCGA-COAD samples were used as the training cohort for screening prognostic genes and evaluating prognostic models in this study.

A total of five COAD-related datasets were downloaded through the GEO database, namely GSE17538, GSE29621, GSE39582, GSE44076, and GSE74602. Among them, the GSE17538 (n = 232) and GSE29621 (n = 65) datasets containing complete survival information of COAD patients were used as independent external validation cohorts for the validation of the constructed prognostic models. The GSE39582 (566 COAD and 19 normal samples), GSE44076 (98 COAD

samples and 148 normal samples), and GSE74602 (30 COAD and 30 normal samples) datasets were used to validate the prognostic gene expression.

The clinical characteristics of COAD patients in the TCGA cohort, GSE17538 dataset, GSE29621 dataset, GSE39582 dataset, GSE44076 dataset, and GSE74602 dataset were shown in Supplementary Table S1.

Differential expression analysis

Differential expression analysis of mRNA, miRNA, and lncRNA in COAD and normal samples were performed using R package limma. Significance thresholds were set to adjust (adj.) $p < 0.05$ and $|\log_2$ fold change (FC)$| > 1$. *P*-values were corrected for multiple testing using the Benjamini & Hochberg method.

The 200 EMTRGs were obtained from the Molecular Signatures Database (MSigDB; http://www.gsea-msigdb.org). Briefly, genes retrieved in MSigDB using the keyword "Epithelial-mesenchymal transition" were defined as EMTRGs. The overlapping genes of EMTRGs and differentially expressed mRNAs (DE-mRNAs), defined as DE-EMTRGs (Supplementary Table S2), were obtained by intersection analysis. Intersection analysis was performed using the Jvenn online tool (http://jvenn.toulouse.inra.fr/app/example.html).

Construction and confirmation of an EMTRGs prognostic signature

The training cohort containing complete clinical information was first analyzed using univariate Cox regression to select prognostically relevant DE-EMTRGs. After initial screening, a LASSO analysis was established to select candidate DE-EMTRGs with a penalty parameter tuning adjusted by 20 times cross-validation, then a signature based on these well-selected DE-EMTRGs was developed. These prognostically relevant EMTRGs were analyzed by multivariate Cox regression analysis to calculate their respective expression levels and regression coefficients to obtain risk scores. The risk scores were calculated as follows:

$$risk\ score = \sum_{n=1}^{n} (coef_i \times x_i)$$

where $coef_i$ denotes the multivariate Cox regression coefficient of the *i*th gene, x_i denotes the relative expression of the *i*th gene, and *n* denotes the number of genes in model. The risk score of each patient was calculated according to this formula, and patients were divided into high-risk and low-risk groups according to the median of the risk scores. Kaplan-Meier (K-M) analysis and log-rank test were used to compare survival differences between the high-risk and low-risk groups. Then, in the R package SURVIVALROC, time-dependent receiver operating characteristic (ROC) analysis was used to calculate the area under the curve (AUC) for 1-, 3-, and 5-year overall survival (OS), and to determine the predictive accuracy of the model. The above method was used to further validate the predictive performance of the EMTRGs prognostic signature in validation cohort (GSE17538 and GSE29621).

Independent prognostic analysis

To determine whether this prognostic model was significant among other clinical characteristics, all clinicopathological characteristics in the TCGA-COAD dataset ($n = 154$), including age, gender, pathological T stage, pathological N stage, and pathological M stage, were performed with univariate and multivariate Cox regression analyses to identify the independent clinical prognostic factors using the survival package in R with $p < 0.05$ as the threshold for significance.

Construction and evaluation of the nomogram

The nomogram and calibration curves were created using the rms package in the R software. The time-dependent ROC curves were used to determine the prognostic performance of the nomogram model with R package survival ROC. Calibration curves were plotted to assess the discrimination of the nomogram and the 45° dotted line indicates the optimal prediction. In addition, decision curve analysis (DCA) was performed to evaluate the clinical usefulness and to compare the established nomogram with the separately identified independent prognostic factors.

Gene set enrichment analysis (GSEA)

To explore the biological signaling pathways, GSEA was performed on the high-risk and low-risk groups of TCGA-COAD samples, respectively. The filtered KEGG gene set (c2.cp.kegg.v7.4.symbols.gmt) was downloaded from MSigDB. GSEA analysis was performed on the downloaded gene sets using GSEA software (v4.0.3) (15). KEGG pathways with significant enrichment results were demonstrated based on NES (net enrichment score) and *P* value. Gene sets with $|NES| > 1$, NOM $p < 0.05$, and FDR $q < 0.25$ were considered significantly enriched.

ESTIMATE analysis

The immune score and stromal cell score were calculated by the ESTIMATE package (16) in the R software, thereby

quantifying the proportion of immune stromal components in the tumor microenvironment for each sample. The results were expressed in the form of three scores:ImmuneScore, StromalScore, and ESTIMATEScore, which were positively correlated with the proportion of immune, stromal, and the sum of both, respectively, which means that the higher the respective score, the greater the proportion of the corresponding component in the tumor microenvironment. The Wilcoxon test was used to assess the difference between the three scores of the high-risk and low-risk groups in the TCGA-COAD database.

Infiltration of immune cells

To further understand the composition of the tumor immune microenvironment (TIME) between the high- and low-risk groups in the TCGA database, we used a microenvironment cell population counter (MCP-counter) (17) to quantify the number of immune cells, fibroblasts and epithelial cells per COAD sample according to marker genes. Then single-sample gene set enrichment analysis (ssGSEA) was performed on tumor tissue infiltrating immune cells, and 28 immune cell types were obtained (16, 18, 19). The significant differences in immune cell numbers were identified by the Wilcoxon test. Furthermore, the correlation between prognostic genes and immune cells was analyzed by the Spearman method. The significance threshold was set at $|r| > 0.5$ and $p < 0.05$.

Immunotherapy and chemotherapy response prediction

The subclass mapping (SubMap) modules (20) of GenePattern were used to predict the response of all 154 COAD samples to immune checkpoints. The pRRophetic algorithm (21) based on the Genomics of Drug Sensitivity in Cancer (GDSC) pharmacogenomic database (21) was used to predict chemotherapy response per 154 COAD samples. The half-maximal inhibitory concentration (IC_{50}) was estimated by ridge regression, and the prediction accuracy was evaluated by 10-fold cross-validation.

Construction of ceRNA network

The miRNAs were predicted by miRwalk database, and 504 mRNA-miRNA pairs of 5 prognostic genes were predicted. Overlap analysis of the identified DE-miRNAs and predicted miRNAs obtained 84 DE-miRNAs and 154 mRNA-miRNAs pairs. Subsequently, 18,987 lncRNAs of 89 DE-miRNAs were predicted using the lncbaseV2.0 database with a score >0.6. Of these, 133 predicted lncRNAs were previously obtained DE-lncRNAs. Considering the mechanism of ceRNA, we excluded DE-lncRNAs with an opposite trend of prognostic gene expression in COAD, and obtained a total of 32 mRNA-miRNA relationship pairs (5 mRNAs and 29 miRNAs) and 152 miRNA-lncRNA relationship pairs (29 miRNAs and 76 lncRNAs). Based on $r > 0.3$, $p < 0.05$, Pearson correlation analysis screened 169 pairs of lncRNA-mRNA positive regulatory relationships (5 mRNA and 65 lncRNA). Finally, the above relationship pairs were combined to visualize the lncRNA-miRNA-mRNA ceRNA network by Cytoscape software.

Statistical analysis

All statistical calculations in this study were performed in R software (version 3.6.1). The Cox proportional hazards regression model was used for univariate and multivariate analyses. The log-rank test was used for K-M survival analyses. The AUC was used as an indicator of prognostic accuracy. Wilcoxon test was used for comparing immune cells and IC50 of drugs between the low-risk and high-risk groups. If not otherwise specified, $p < 0.05$ was a statistically significant threshold.

Result

Identification of DE-EMTRGs in the TCGA COAD cohort

The analysis flow chart of this study is shown in Figure 1. Principal component analysis (PCA) exhibited that the mRNA, miRNA and lncRNA expression data were distributed in different directions in the healthy population and COAD samples (Figures 2A–C). Based on expression data from the TCGA-COAD cohort, a total of 1989 DE-mRNAs containing 1168 down-regulated and 821 up-regulated DE-mRNAs (Figures 2D, E), 585 DE-miRNAs containing 330 down-regulated and 255 upregulated DE-miRNAs (Supplementary Figures S1A, B), and 149 DE-lncRNAs containing 68 downregulated and 81 upregulated DE-lncRNAs (Supplementary Figures S1C, D) were identified. Further, 200 EMTRGs were retrieved through the MSigDB database. Venn diagram displayed the presence of 40 down-regulated and 37 up-regulated DE-EMTRGs in DE-mRNA, respectively (Figure 2F). These DE-EMTRGs are mainly involved in functions and pathways related to cell migration, proliferation and apoptosis such as “negative regulation of cell migration,” “leukocyte migration,” “negative regulation of cell proliferation” and “negative regulation of apoptotic process” (Supplementary Figure S2).

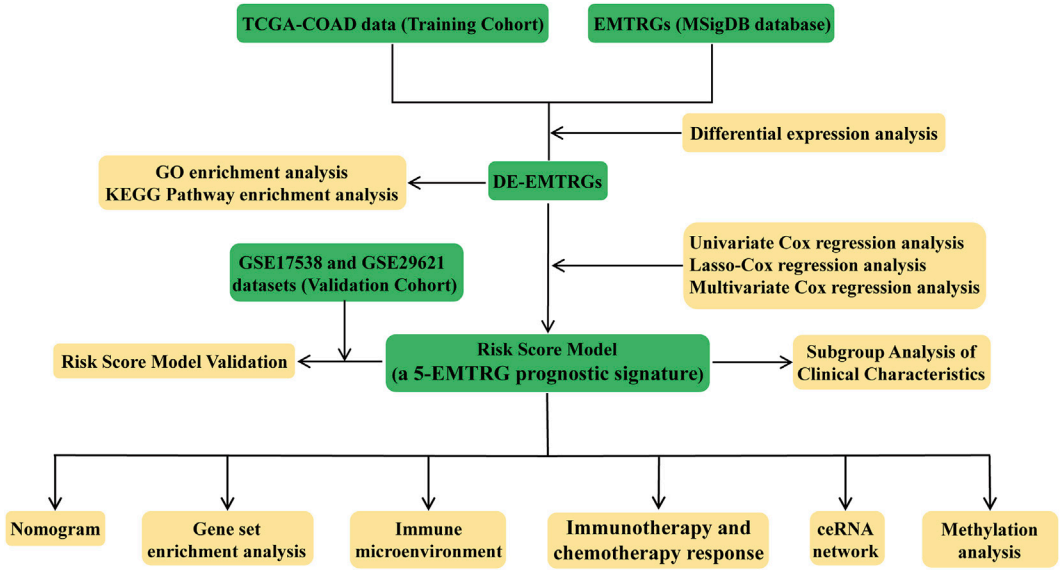

FIGURE 1
Flow chart of this study.

Establishment and validation of a five-EMTRG prognostic signature for predicting patient-specific survival in COAD

The TCGA COAD cohort was used as the training cohort, and the GSE17538 and GSE29621 datasets were used as the validation cohort to construct and validate the Risk scoring (RS) model for DE-EMTRGs in COAD, respectively. Eight DE-mRNAs associated with survival in COAD patients were identified in 77 DE-EMTRGs by univariate Cox regression analysis (Figure 3A). Lasso regression analysis further screened 5 prognostic biomarkers (COMP, MYL9, PCOLCE2, SCG2, TIMP1; Figures 3B, C). A multivariate Cox analysis was performed based on five prognostic biomarkers, and the coefficient of each biomarker was calculated, and used to construct the RS model. The 154 COAD patients in the training cohort were distinguished by a median risk score of 2.966300771 into high- and low-risk groups containing 77 COAD samples each. K-M curves revealed that OS of COAD patients in the high-risk group was significantly lower than in the low-risk group (p = 0.012; Figure 3D). The ROC showed that the AUC of the RS model was 0.766, 0.673 and 0.73 at 1, 3 and 5 years for patients, respectively (Figure 3E), which indicates that this RS has good predictive performance for the prognosis of COAD patients. The expression patterns of the five genes in the high- and low-risk groups are shown in Figure 3F, and COAD patients with higher risk scores had lower survival outcomes (Figure 3G). The GSE17538 and GSE29621 datasets were brought into the RS model for validation, and this five-EMTRG signature has moderate performance for the prognosis of COAD patients with all AUC values greater than 0.6 (Supplementary Figure S3).

COMP and TIMP1 were significantly upregulated, and MYL9, PCOLCE2 and SCG2 were significantly downregulated in TCGA-COAD cohort of the five-EMTRG prognostic signature (Supplementary Figure S4A). In addition, we validated the five-EMTRG prognostic signature in GSE39582, GSE44076 and GSE74602 datasets, and obtained results consistent with the TCGA training cohort (Supplementary Figures S4B–D). Further, we explored the relationship between the RS model and clinicopathological features. The results showed that the risk scores were significantly different at stage I–II and stage III–IV (Supplementary Figure S4G), T1-2 and T3-4 (Supplementary Figure S5H), and N0 and N1-2 (Supplementary Figure S4I), respectively ($p < 0.05$). We also constructed a lncRNA-miRNA-mRNA ceRNA network containing DE-lncRNA and DE-miRNA associated with five-EMTRG prognostic signature. The ceRNA network contained 63 lncRNA-miRNA-mRNA relationship pairs which contained 29 lncRNAs, 18 miRNAs and 4 mRNAs (Supplementary Figure S5).

It is suggested that this five-EMTRG prognostic signature has high specificity and sensitivity for the prediction of survival in COAD, and has good applicability in clinical practice.

Five-EMTRG prognostic signature is an independent prognostic factor for COAD

To explore independent prognostic factors of COAD, we integrated clinicopathological characteristics of the TCGA

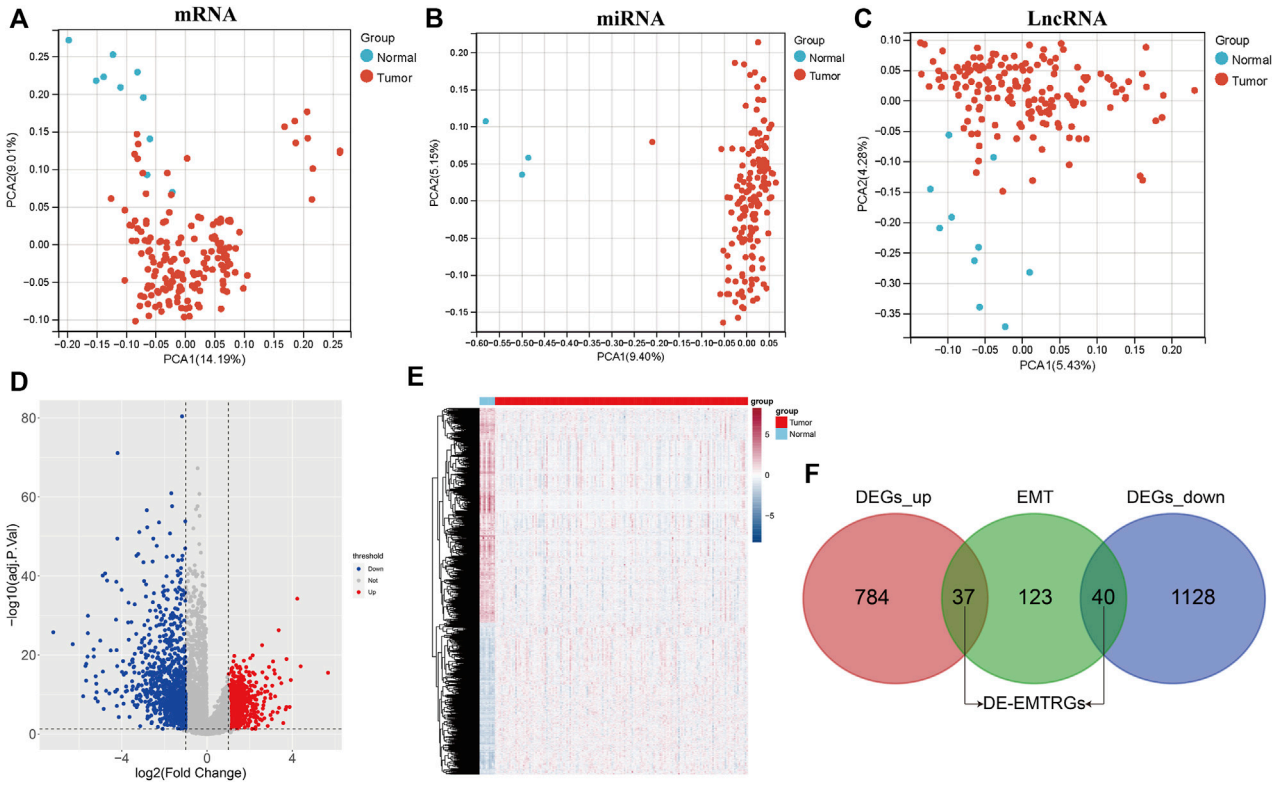

FIGURE 2
Identification of differentially expressed epithelial-mesenchymal transition related genes (DE-EMTRGs) in COAD. **(A–C)** Principal component analysis reveals differences between expression data of healthy population and COAD samples in TCGA. From left to right are mRNA, miRNA and lncRNA. **(D)** Volcano plot **(E)** and heatmap of differentially expressed mRNA (DE-mRNA) in healthy population and COAD samples in TCGA. **(F)** Venn diagram displayed the number of DE-EMTRGs. Difference thresholds: adj. $p < 0.05$ and $|\log_2\text{Fold Change}| > 1$.

COAD cohort, including age, gender, pathologic T, pathologic M, and pathologic N, for univariate Cox regression analysis, and the results showed that age ($p = 0.016$), pathologic M ($p = 0.005$), pathologic N ($p = 0.010$), and risk score ($p < 0.001$) were significantly associated with the survival of COAD patients (Figure 4A). Subsequently, the results of univariate Cox regression analysis were enrolled in multivariate Cox regression analysis and demonstrated that age ($p = 0.024$) and risk score ($p = 0.028$) were independent prognostic factors (Figure 4B). Cox regression analyses were also performed in GSE17538 and GSE29621 datasets and found that risk score also was an independent prognostic factor (Supplementary Figures S6A, B). As shown in Figure 4C, we constructed nomogram including age and RS to predict the survival of patients. The calibration curves implied that the 1-year and 3-year patient survival predicted by the nomogram may be similar to the actual survival time, but the 5-year prediction was poor (Figure 4D). The AUC values of 1, 3, and 5 years in the nomogram model were above 0.7, indicating the validity of the constructed nomogram (Figure 4E). The DCA displayed that "nomogram" was higher than the "all," "age" and "risk score" curves (Figure 4F), indicating that the nomogram model was beneficial within the high-risk threshold range of 0–1, and that the clinical benefit of the nomogram model was higher than the "age" and "risk score" curves. The above results demonstrate that five-EMTRG prognostic signature can be used as an independent prognostic factor for COAD and has the potential for high clinical utility.

Identification of signaling pathways associated with RS models

Considering the negative correlation between RS and prognosis in COAD patients, we performed GSEA for the high-risk and low-risk groups. The results revealed that the main enriched pathways in the high-risk group include "Focal Adhesion," "Leukocyte Transendothelial Migration," "Regulation of Actin Cytoskeleton," "Tight Junction" and "Viral Myocarditis" (Figure 5A). As expected, classical pathways associated with EMT occurrence ("ECM Receptor Interaction," "TGF Beta Signaling Pathway," "WNT Signaling Pathway") and

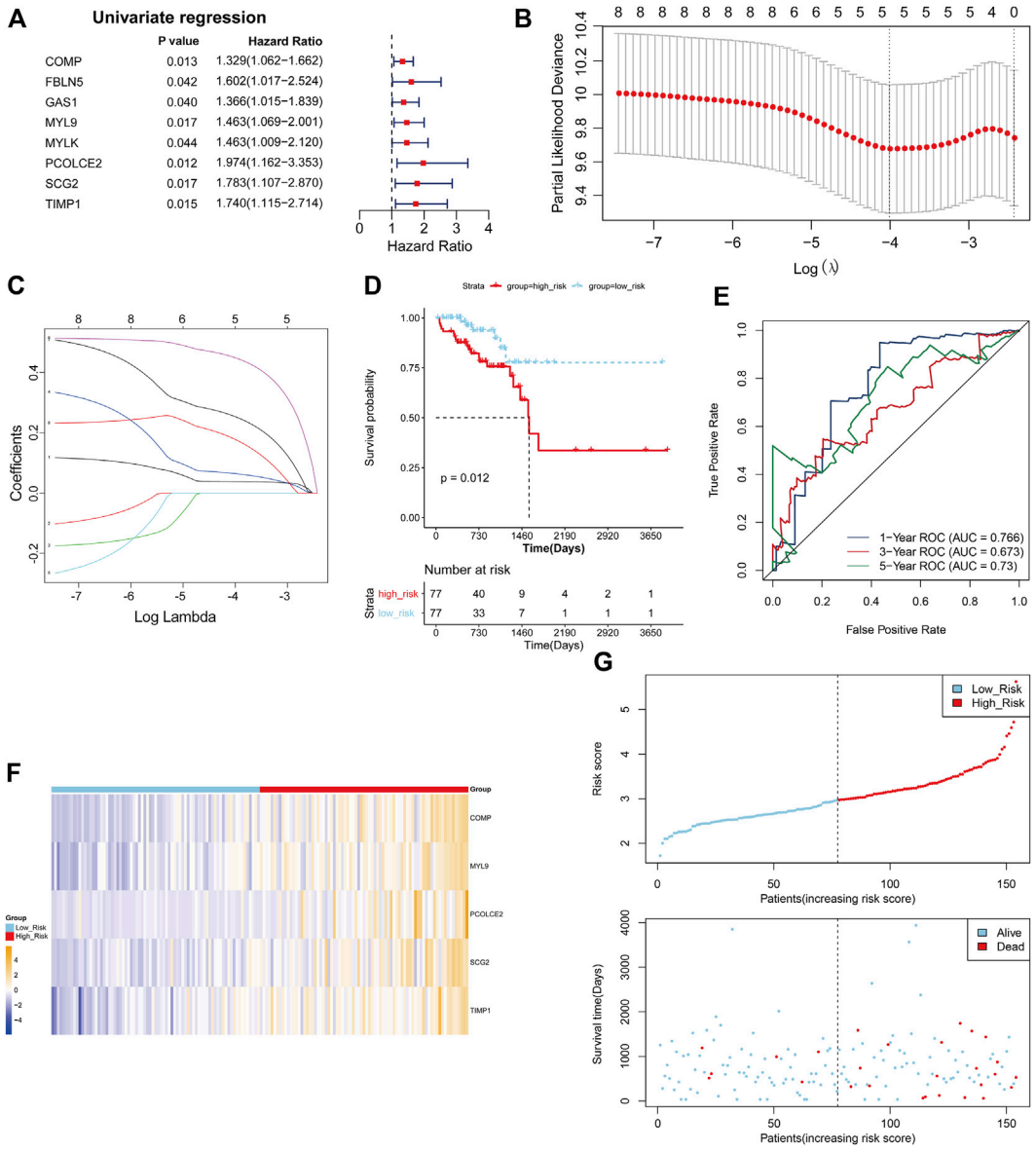

FIGURE 3
Establishment of a five epithelial-mesenchymal transition-related genes (EMTRGs) prognostic signature for predicting patient-specific survival in COAD. **(A)** Forest plot for univariate Cox regression analysis. **(B)** Penalty maps of the Lasso model for 8 prognostic genes in COAD. The best optimal parameter (λ) was selected by 10-fold cross-validation as 0.01817085. **(C)** LASSO coefficient mapping of 8 prognostic genes. Each curve corresponds to a gene. **(D)** Kaplan-Meier curves indicating the OS in high- and low-risk groups. **(E)** Receiver operating characteristic curves for validating the prognostic performance of risk scores in TCGA training cohort. **(F)** Heatmap of the expression of five-EMTRG prognostic signature in the TCGA training cohort. **(G)** (top) Distribution of risk scores in TCGA training cohort, and (bottom) survival status and time of COAD patients in high- and low-risk groups.

"Colorectal Cancer" pathway were also significantly enriched in the high-risk group. "Base Excision Repair," "Butanoate Metabolism," "Citrate Cycle Tca Cycle" and "Pyruvate Metabolism" were activated mainly in the low-risk group (Figure 5B). Most of the enriched pathways were associated with tumor metastasis, which demonstrated the validity of our five-EMTRG prognostic signature constructed in tumor EMT.

Correlation of RS model with COAD TIME

To investigate the relevance of the RS model to the TIME of COAD, we used the Estimate algorithm to evaluate the high- and low-risk groups. The results showed that risk scores were strongly correlated with immune scores, stromal scores, and estimate scores, and presented a positive correlation (Figure 6A). Compared to the

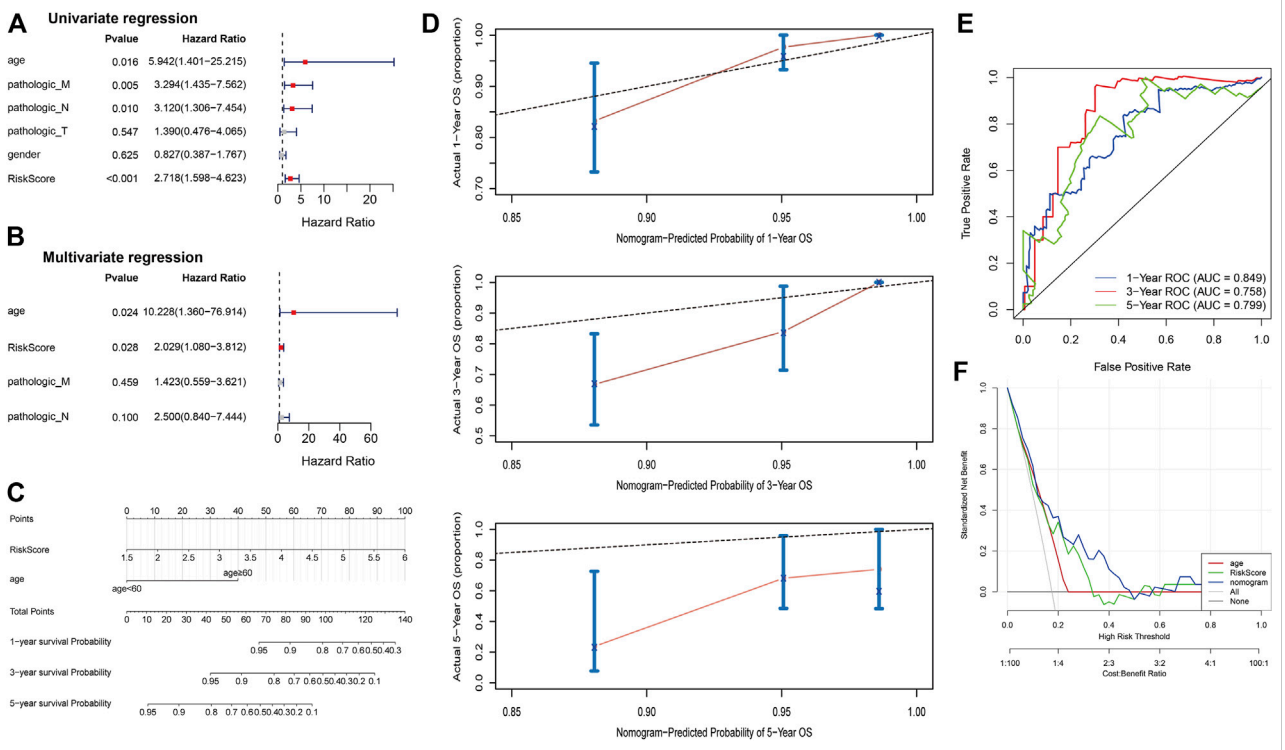

FIGURE 4
Five epithelial-mesenchymal transition-related genes (EMTRGs) prognostic signature is an independent prognostic factor for COAD. **(A)** Univariate and **(B)** multivariate Cox regression analyses for the identification of independent prognostic factors in the TCGA COAD cohort. **(C)** The nomogram based on independent prognostic factors "age" and "risk score." **(D)** Calibration plots to assess the accuracy of nomogram predicting (top) 1-, (middle) 3-, and (bottom) 5-year survival rates. **(E)** Receiver operating characteristic curves used to validate the prognostic performance of the nomogram. **(F)** Decision curve analysis for assessing the clinical utility of "nomogram," "age" and "risk score."

high-risk group, the immune score (Figure 6B), stromal score (Figure 6C) and estimate score (Figure 6D) were significantly lower in the low-risk group ($p < 0.001$). To observe the difference of immune cells in the high- and low-risk groups, both MCP-counter algorithm and ssGSEA algorithm were used to infer the abundance of immune cell infiltration, respectively. In the MCP-counter algorithm, COMP exhibited the most significant positive correlation with fibroblasts, MYL9 presented the most significant positive correlation with endothelial cells and fibroblasts, respectively, and TIMP1 displayed the most positive correlation with fibroblasts (Figure 6E). In the ssGSEA algorithm, COMP showed the most significant positive correlation with natural killer cell, natural killer T cell, MYL9 showed the most significantly positively correlated with natural killer cell and natural killer T cell, and SCG2 showed the most significantly positive correlation with effector memory CD4 T cell (Figure 6H). In addition, there were 5 immune cell types that differed between high- and low-risk groups in the MCP-counter algorithm ($p < 0.01$; Figures 6F, G) and 18 in the ssGSEA algorithm ($p < 0.05$; Figures 6I, J).

Immunotherapy response and targeted therapy agents prediction

The subclass mapping analysis was used to predict the efficacy of anti-PD1 and anti-CTLA4 treatments. As shown in Figure 7A, we discovered that patient with high risk score may respond to anti-CTLA4 therapy (nominal $p = 0.011$; Figure 7A). Using the pRRophetic algorithm, a ridge regression model was constructed to predict the IC_{50} of targeted therapy agents based on cell line expression profiles and TCGA gene expression profiles from the GDSC database, and the IC_{50} of patients in high- and low-risk groups for these two common targeted therapy agents (BI 2536 and ABT-888) was predicted. The results suggested that patients in the high-risk group may be more resistant to both BI 2536 and ABT-888 compared to the low-risk group ($p < 0.05$; Figures 7B, C). Thus, the 5-EMTRGs prognostic signature could act as a potential predictor for immunotherapies and chemotherapies.

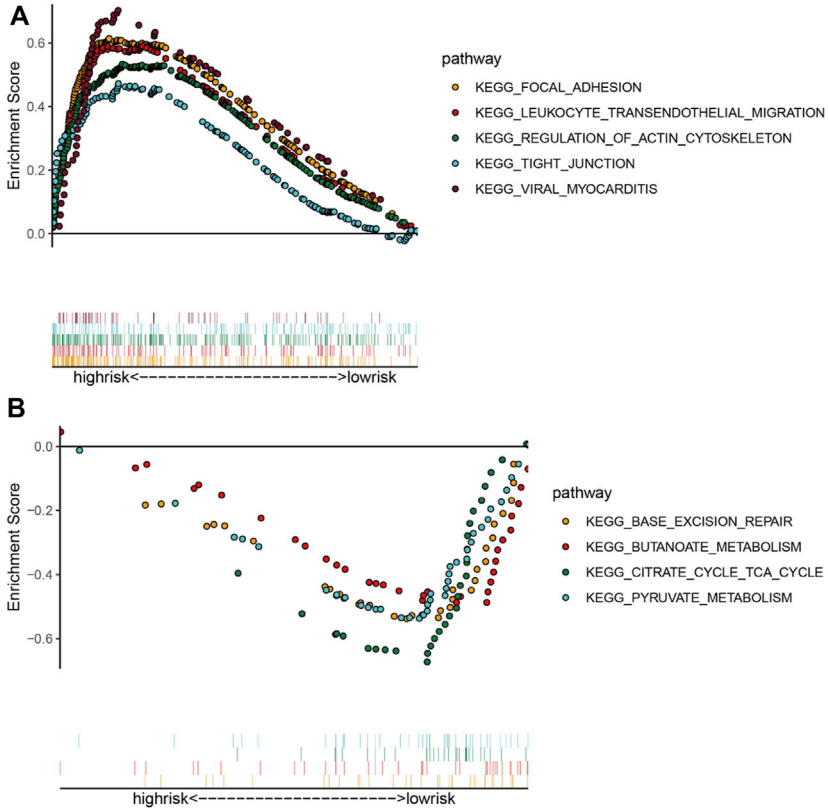

FIGURE 5
Identification of signaling pathways associated with risk scoring models. The main signaling pathways involved in the **(A)** high- and **(B)** low-risk groups obtained by gene set enrichment analysis. The dots of each color in the upper part of the figure indicate one pathway, and the vertical lines in the lower part indicate the genes covered under each pathway.

Discussion

In the present study, we identified 77 DE-EMTRGs in the TCGA-cohort, and they were involved in EMT-related terms, including "negative regulation of cell migration" and "leukocyte migration." Based on 77 DE-EMTRGs, we developed an RS model consisting of 5 prognostic biomarkers (COMP, MYL9, PCOLCE2, SCG2, TIMP1), and demonstrated that the five-EMTRG prognostic signature can be used as an independent prognostic factor for COAD patients with good clinical utility. We further performed GSEA, and revealed that five-EMTRG prognostic signature was enriched to the pathway associated with tumor metastasis. Furthermore, five-EMTRG prognostic signature correlated with the infiltration abundance of immune cells including Natural killer cells, Natural killer T cells and Effector memory CD4 T cells, and with immune drug CTLA4 inhibitors and targeted therapy agents BI 2536 and ABT-888.

In fact, five biomarkers from the five-EMTRG prognostic signature have been demonstrated to be associated with EMT in a variety of malignancies, including COAD. COMP is an extracellular matrix protein that has been shown to contribute to fibrosis in a variety of visceral organs (22). In CRC, Zhong et al. (23) indicated that COMP is aberrantly highly expressed in CRC tissues, and that it interacts with TAGLN *in vivo* and *in vitro*, leading to cytoskeleton remodeling to promote the EMT process. A bioinformatic analysis showed that COMP is co-expressed with EMT markers in COAD, and is associated with poor patient survival (24). This suggests that COMP contributes to EMT, which also supports the accuracy of the five-EMTRG prognostic signature in COAD. MYL9 is the regulatory light chain that makes up myosin, and its phosphorylation is involved in the tail contraction propulsion of cell migration (25). Previous studies have shown that high expression of MYL9 is associated with poorer prognosis in patients with early-onset CRC (26, 27), epithelial ovarian cancer (28), esophageal squamous cell carcinoma (29) and glioma (30). In contrast to them, Huang et al. (31) showed that downregulation of MYL9 predicted poor biochemical recurrence-free survival in prostate cance, and was significantly associated with prostate cancer cell metastasis. In CRC, MYL9 activates Hippo signaling by binding to YAP1, thereby promoting CRC cell proliferation and metastasis (32).

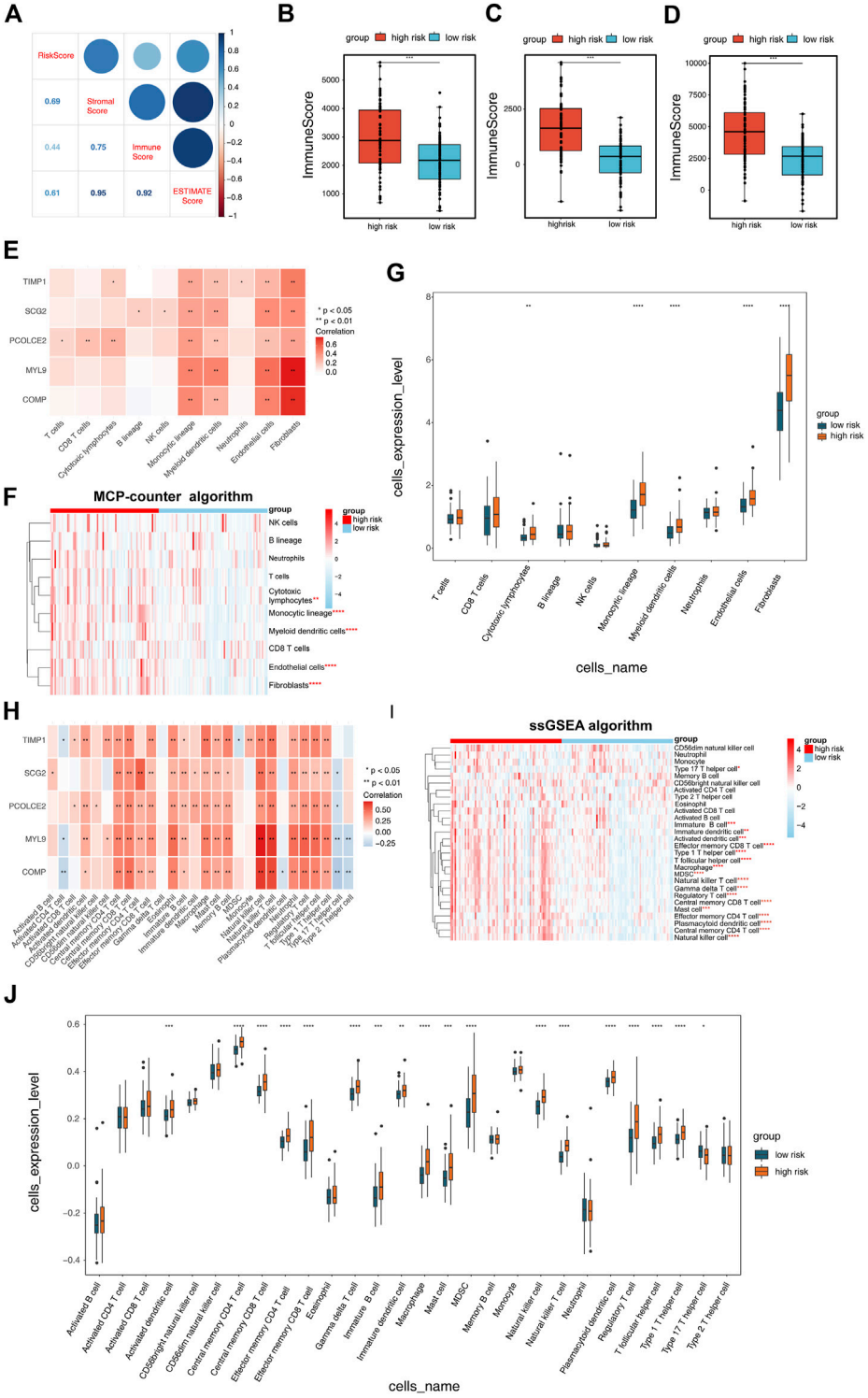

FIGURE 6
Correlation of risk scoring model with COAD tumor immune microenvironment (TIME). **(A)** The Estimate algorithm was applied to analyze the correlation between risk scores and immune scores, stromal scores, and ESTIMATE scores. Differences in **(B)** ImmuneScores, **(C)** StromalScores and **(D)** ESTIMATEScores of the high and low risk groups obtained from the Estimate algorithm analysis. **(E)** Correlation of risk scoring model with 10 immune cell types was performed by MCP-counter algorithm analysis. **(F)** Heatmap exhibited the enrichment of immune cells in high- and low-risk groups obtained by the MCP-counter algorithm analysis. **(G)** Box plot demonstrated the immune cells with differences in the high- and low-risk groups obtained by the MCP-counter algorithm analysis. **(H)** Correlation of five Epithelial-mesenchymal transition-related genes prognostic signature with 28 immune cell types calculated by single-sample gene set enrichment analysis (ssGSEA) algorithm. **(I)** Heatmap and **(J)** box plot showing the immune cells with differences in the high- and low-risk groups as calculated by the ssGSEA algorithm.

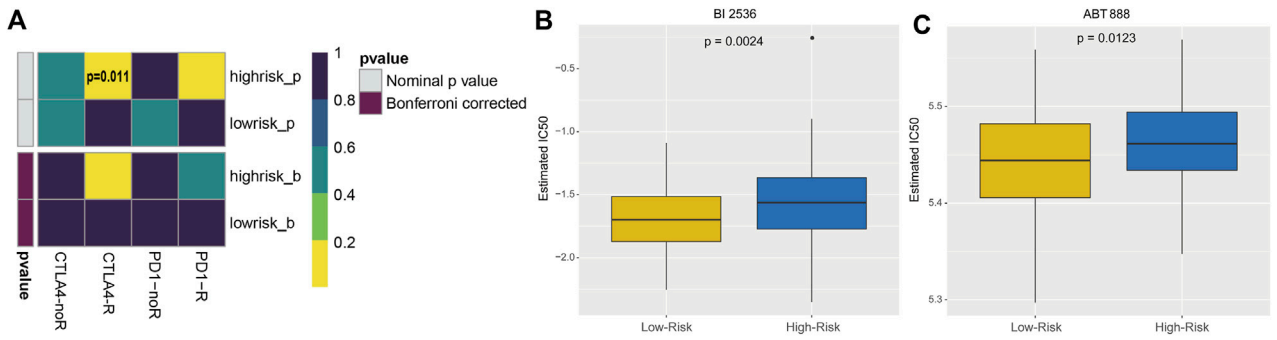

FIGURE 7
Analysis of risk scoring model-related immunotherapy and chemotherapy prediction. **(A)** Heatmap of the difference in immunotherapy sensitivity between the high- and low-risk groups. Differential IC_{50} of **(B)** BI 2536 and **(C)** ABT-888 in the high- and low-risk groups.

Zhu et al. (33) demonstrated that MYL9 is involved in regulating proliferation and metastasis of CRC stem cells as a downstream of the LncRNA MBNL1-AS1/miR-412-3p axis. PCOLCE2 has been demonstrated to be a prognostically relevant biomarker for CRC (34–36), gastric cancer (37), bladder cancer (38), head and neck squamous cell carcinoma (39), and thyroid cancer (40). However, PCOLCE2 remains to be validated *in vivo* and *in vitro* for its specific mechanism in the EMT process of COAD. SCG2 has been identified as a prognostic biomarker associated with immune infiltration in CRC (41, 42), bladder cancer (43, 44), breast cancer (45), and lung adenocarcinoma (46). Wet assays revealed that SCG2 is lowly expressed in CRC, and inhibits the growth and angiogenesis of CRC cells by promoting the degradation of HIF-1α (47). As an epithelial cell marker, the role of TIMP1 in the tumor EMT process has been well documented (48, 49), and it was identified as a biomarker affecting the prognosis of COAD patients (50). The above study demonstrates the potential and availability of five genes in our five-EMTRG prognostic signature as prognostic biomarkers for COAD.

TME consists mainly of tumor cells, their surrounding tumor-associated fibroblasts (CAFs), inflammatory and immune cells, and non-cellular components including cellular matrix, inflammatory factors and cytokines, and is an extremely complex cellular microenvironment that is considered to be an important factor in tumor development (51, 52). In the course of tumor development, EMT and TIME are mutually crosstalked. It was found that EMT-related genes such as ZEB1 and Snail enrich immunosuppressive cells and inhibit the expression of immunosuppressive molecules through chemokines, leading to the formation of an immunosuppressive microenvironment (53). In turn, immunosuppressive factors lead to tumorigenic EMT (53). The role of TIME in CRC has been well studied. For example, CAFs are abundantly infiltrated with M2 macrophages in CRC, and their markers are poor prognostic factors for CRC (54). Yamila et al. (55) showed that in CRC, the phenotype of natural killer (NK) cells is altered and their receptor expression is drastically reduced, which leads to a reduction in the ability of NK cells to kill cancer cells, and consequently immune escape of tumor cells. In the present study, we found that five-EMTRG prognostic signature was significantly associated with fibroblasts, endothelial cells, NK cells and effector memory CD4 T cells. Notably, the role of the five markers in the five-EMTRG prognostic signature in relation to TIME has been previously reported. For example, COMP correlates with TIME in prostate cancer (56, 57) and bladder cancer (58) and can be a prognostic biomarkers. Zhou et al. (59) revealed by single-cell multi-omics sequencing that MYL9 can serve as a specific biomarker for CAFs, and predicts a poor prognosis for CRC. The nine-gene prognostic signature containing PCOLCE2 constructed by Liu et al. (35) was identified to be associated with CRC TIME. SCG2 was identified as a prognostic biomarker associated with macrophage polarization and immune cell infiltration in CRC (42). Nevertheless, as in the present study, the above-mentioned studies only investigated the correlation between prognostic biomarkers and TIME, but the specific mechanisms of these 5 prognostic biomarkers in EMT and TIME of COAD still need to be further explored.

BI 2536 and ABT-888 are two novel targeted therapy agents that are specific inhibitors of PLK1 and PARP, respectively, and are currently in clinical trials (60, 61). It was shown that BI 2536 effectively impedes mitosis of COAD *in vivo* and *in vitro*, and can synergize with simvastatin for treatment (62) and has a sensitizing effect on radiotherapy (63). ABT-888 has been applied in a phase II clinical trial, and its combination with capecitabine (64), temozolomide (65) and FOLFIRI ± bevacizumab (66) alleviates metastatic colorectal cancer with no unexpected safety concerns. CTLA-4 is a member of the immunoglobulin-associated receptor family, which mediates the suppression of T-cell activation. Ipilimumab (67, 68) and tremelimumab (69,70), which are CTLA4 inhibitors, were

effective for improving the survival of patients with metastatic colorectal cancer in phase II clinical trials. The present study found that the high-risk group may be more tolerant to treatment with BI 2536, ABT 888 and CTLA4 inhibitors than the low-risk group in the RS model. Notably, to investigate the possible molecular mechanisms of five biomarkers in the COAD process, we constructed a five-EMTRG prognostic signature-related ceRNA network based on the identified DE-lncRNA and DE-miRNA. The network contains 63 lncRNA-miRNA-mRNA relationship pairs, and some of these DE-lncRNAs and DE-miRNAs have been demonstrated to be involved in COAD. Hsa-miR-16-5p (71, 72), hsa-miR-188-5p (73, 74), lncRNA ADAMTS9-AS1 (75) and LncRNA HAND2-AS1 (76), which are anti-cancer factors, and hsa-miR-192-3p (77), lncRNA MAFG-AS1 (78,79) and lncRNA HAGLR (80), which are pro-cancer factors, are involved in the COAD process by regulating proliferation, apoptosis and EMT phenotype. However, the role of these lncRNA-miRNA-mRNA axes in the COAD process remains to be further validated. It is worth noting that previous studies have identified prognostic expression of signatures associated with EMT in CRC (81–85). In contrast to these studies, only COAD was investigated in this study, and the five-EMTRG prognostic signature was constructed differently from these studies and proved to have a high clinical potential. Furthermore, compared with the studies of Liu (82), Wang (83) and Liao (84) et al., we more comprehensively analyzed the correlation between five-EMTRG prognostic signature and TIME and immunotherapy and chemotherapy response, and constructed the ceRNA network associated with it. Nevertheless, this study has many shortcomings. The sample size of this study is small, including only 163 TCGA-COAD samples from the TCGA-COAD data as the training cohort, and external datasets other than the GEO database are needed for further validation of our model. The lack of *in vivo* and *in vitro* wet experiments to validate the specific regulatory mechanisms of the five biomarkers in the five-EMTRG prognostic signature on the COAD EMT process, which is the focus of our subsequent studies.

In conclusion, we construct a novel five-EMTRG prognostic signature, that can be applied to predict the prognosis of COAD patients, and can be a critical factor in TIME and immunotherapy and chemotherapy. Our results provide greater insight into the role of these key prognostic factors in COAD, and provide a basis for their future use as potential diagnostic and therapeutic biomarkers for COAD.

Data availability statement

The original contributions presented in the study are included in the article/Supplementary Material, further inquiries can be directed to the corresponding author.

Author contributions

WZ and TL designed the study. YZ, YL, and ZZ did interpretation and analysis of data. YZ and YA wrote the manuscript.

Funding

This study was supported by grant from the National Natural Science Foundation of China (81860522, 81860509), Young Academic Talents Cultivation Foundation of Yunnan Province (202205AC160070), Yunnan Medical Training Program (YNWR-QNBJ-2019-147).

Conflict of interest

The authors declare that the research was conducted in the absence of any commercial or financial relationships that could be construed as a potential conflict of interest.

Supplementary material

The Supplementary Material for this article can be found online at: https://www.por-journal.com/articles/10.3389/pore.2023.1611016/full#supplementary-material

References

1. Sung H, Ferlay J, Siegel RL, Laversanne M, Soerjomataram I, Jemal A, et al. Global cancer Statistics 2020: GLOBOCAN estimates of incidence and mortality worldwide for 36 cancers in 185 countries. *CA Cancer J Clin* (2021) 71(3):209–49. doi:10.3322/caac.21660

2. Shi JF, Wang L, Ran JC, Wang H, Liu CC, Zhang HZ, et al. Clinical characteristics, medical service utilization, and expenditure for colorectal cancer in China, 2005 to 2014: Overall design and results from a multicenter retrospective epidemiologic survey. *Cancer* (2021) 127(11):1880–93. doi:10.1002/cncr.33445

3. Ganesh K, Massagué J. Targeting metastatic cancer. *Nat Med* (2021) 27(1): 34–44. doi:10.1038/s41591-020-01195-4

4. Derynck R, Weinberg RA. EMT and cancer: More than meets the eye. *Dev Cel* (2019) 49(3):313–6. doi:10.1016/j.devcel.2019.04.026

5. Dongre A, Weinberg RA. New insights into the mechanisms of epithelial-mesenchymal transition and implications for cancer. *Nat Rev Mol Cel Biol* (2019) 20(2):69–84. doi:10.1038/s41580-018-0080-4

6. Bakir B, Chiarella AM, Pitarresi JR, Rustgi AK. EMT, MET, plasticity, and tumor metastasis. *Trends Cel Biol* (2020) 30(10):764–76. doi:10.1016/j.tcb.2020.07.003

7. Wang J, Cai H, Liu Q, Xia Y, Xing L, Zuo Q, et al. Cinobufacini inhibits colon cancer invasion and metastasis via suppressing wnt/β-catenin signaling pathway and EMT. *Am J Chin Med* (2020) 48(3):703–18. doi:10.1142/S0192415X20500354

8. Wen J, Min X, Shen M, Hua Q, Han Y, Zhao L, et al. ACLY facilitates colon cancer cell metastasis by CTNNB1. *J Exp Clin Cancer Res* (2019) 38(1):401. doi:10.1186/s13046-019-1391-9

9. Cai L, Hu C, Yu S, Liu L, Zhao J, Zhao Y, et al. Identification of EMT-related gene signatures to predict the prognosis of patients with endometrial cancer. *Front Genet* (2020) 11:582274. doi:10.3389/fgene.2020.582274

10. Tong H, Li T, Gao S, Yin H, Cao H, He W. An epithelial-mesenchymal transition-related long noncoding RNA signature correlates with the prognosis and progression in patients with bladder cancer. *Biosci Rep* (2021) 41(1). doi:10.1042/BSR20203944

11. Xu F, Tang Q, Wang Y, Qian K, Ju L, Xiao Y Development and validation of a six-gene prognostic signature for bladder cancer. *Front Genet* (2021) 12:758612. doi:10.3389/fgene.2021.758612

12. Xu BH, Jiang JH, Luo T, Jiang ZJ, Liu XY, Li LQ. Signature of prognostic epithelial-mesenchymal transition related long noncoding RNAs (ERLs) in hepatocellular carcinoma. *Medicine (Baltimore)* (2021) 100(30):e26762. doi:10.1097/MD.0000000000026762

13. Zhang Z, Gu J, Yin M, Wang D, Ma C, Du J, et al. Establishment and investigation of a multiple gene expression signature to predict long-term survival in pancreatic cancer. *Biomed Res Int* (2020) 2020:1570862. doi:10.1155/2020/1570862

14. Xue K, Zheng H, Qian X, Chen Z, Gu Y, Hu Z, et al. Identification of key mRNAs as prediction models for early metastasis of pancreatic cancer based on LASSO. *Front Bioeng Biotechnol* (2021) 9:701039. doi:10.3389/fbioe.2021.701039

15. Subramanian A, Tamayo P, Mootha VK, Mukherjee S, Ebert BL, Gillette MA, et al. Gene set enrichment analysis: a knowledge-based approach for interpreting genome-wide expression profiles. *Proc Natl Acad Sci U S A* (2005) 102(43):15545–50. doi:10.1073/pnas.0506580102

16. Yoshihara K, Shahmoradgoli M, Martínez E, Vegesna R, Kim H, Torres-Garcia W, et al. Inferring tumour purity and stromal and immune cell admixture from expression data. *Nat Commun* (2013) 4:2612. doi:10.1038/ncomms3612

17. Becht E, Giraldo NA, Lacroix L, Buttard B, Elarouci N, Petitprez F, et al. Estimating the population abundance of tissue-infiltrating immune and stromal cell populations using gene expression. *Genome Biol* (2016) 17(1):218. doi:10.1186/s13059-016-1070-5

18. Finotello F, Trajanoski Z. Quantifying tumor-infiltrating immune cells from transcriptomics data. *Cancer Immunol Immunother* (2018) 67(7):1031–40. doi:10.1007/s00262-018-2150-z

19. Thorsson V, Gibbs DL, Brown SD, Wolf D, Bortone DS, Ou Yang TH, et al. The immune landscape of cancer. *Immunity* (2018) 48(4):812–30.e14. doi:10.1016/j.immuni.2018.03.023

20. Hoshida Y, Brunet JP, Tamayo P, Golub TR, Mesirov JP. Subclass mapping: identifying common subtypes in independent disease data sets. *PLoS One* (2007) 2(11):e1195. doi:10.1371/journal.pone.0001195

21. Geeleher P, Cox N, Huang RS. pRRophetic: an R package for prediction of clinical chemotherapeutic response from tumor gene expression levels. *PLoS One* (2014) 9(9):e107468. doi:10.1371/journal.pone.0107468

22. Zachou K, Gabeta S, Shums Z, Gatselis NK, Koukoulis GK, Norman GL, et al. COMP serum levels: A new non-invasive biomarker of liver fibrosis in patients with chronic viral hepatitis. *Eur J Intern Med* (2017) 38:83–8. doi:10.1016/j.ejim.2017.01.007

23. Zhong W, Hou H, Liu T, Su S, Xi X, Liao Y, et al. Cartilage oligomeric matrix protein promotes epithelial-mesenchymal transition by interacting with transgelin in colorectal cancer. *Theranostics* (2020) 10(19):8790–806. doi:10.7150/thno.44456

24. Nfonsam VN, Nfonsam LE, Chen D, Omesiete PN, Cruz A, Runyan RB, et al. COMP gene coexpresses with EMT genes and is associated with poor survival in colon cancer patients. *J Surg Res* (2019) 233:297–303. doi:10.1016/j.jss.2018.08.021

25. Kimura MY, Koyama-Nasu R, Yagi R, Nakayama T. A new therapeutic target: the CD69-myl9 system in immune responses. *Semin Immunopathol* (2019) 41(3):349–58. doi:10.1007/s00281-019-00734-7

26. Zhao B, Baloch Z, Ma Y, Wan Z, Huo Y, Li F, et al. Identification of potential key genes and pathways in early-onset colorectal cancer through bioinformatics analysis. *Cancer Control* (2019) 26(1):1073274819831260. doi:10.1177/1073274819831260

27. Qiu X, Cheng SH, Xu F, Yin JW, Wang LY, Zhang XY. Weighted gene co-expression network analysis identified MYL9 and CNN1 are associated with recurrence in colorectal cancer. *J Cancer* (2020) 11(8):2348–59. doi:10.7150/jca.39723

28. Deng Y, Liu L, Feng W, Lin Z, Ning Y, Luo X. High expression of MYL9 indicates poor clinical prognosis of epithelial ovarian cancer. *Recent Pat Anticancer Drug Discov* (2021) 16(4):533–9. doi:10.2174/1574891X16666210706153740

29. Wang JH, Zhang L, Huang ST, Xu J, Zhou Y, Yu XJ, et al. Expression and prognostic significance of MYL9 in esophageal squamous cell carcinoma. *PLoS One* (2017) 12(4):e0175280. doi:10.1371/journal.pone.0175280

30. Kruthika BS, Sugur H, Nandaki K, Arimappamagan A, Paturu K, Santosh V. Expression pattern and prognostic significance of myosin light chain 9 (MYL9): a novel biomarker in glioblastoma. *J Clin Pathol* (2019) 72(10):677–81. doi:10.1136/jclinpath-2019-205834

31. Huang YQ, Han ZD, Liang YX, Lin ZY, Ling XH, Fu X, et al. Decreased expression of myosin light chain MYL9 in stroma predicts malignant progression and poor biochemical recurrence-free survival in prostate cancer. *Med Oncol* (2014) 31(1):820. doi:10.1007/s12032-013-0820-4

32. Feng M, Dong N, Zhou X, Ma L, Xiang R. Myosin light chain 9 promotes the proliferation, invasion, migration and angiogenesis of colorectal cancer cells by binding to Yes-associated protein 1 and regulating Hippo signaling. *Bioengineered* (2022) 13(1):96–106. doi:10.1080/21655979.2021.2008641

33. Zhu K, Wang Y, Liu L, Li S, Yu W. Long non-coding RNA MBNL1-AS1 regulates proliferation, migration, and invasion of cancer stem cells in colon cancer by interacting with MYL9 via sponging microRNA-412-3p. *Clin Res Hepatol Gastroenterol* (2020) 44(1):101–14. doi:10.1016/j.clinre.2019.05.001

34. Shi C, Xie Y, Li X, Li G, Liu W, Pei W, et al. Identification of ferroptosis-related genes signature predicting the efficiency of invasion and metastasis ability in colon adenocarcinoma. *Front Cel Dev Biol* (2021) 9:815104. doi:10.3389/fcell.2021.815104

35. Liu J, Lan Y, Tian G, Yang J. A systematic framework for identifying prognostic genes in the tumor microenvironment of colon cancer. *Front Oncol* (2022) 12:899156. doi:10.3389/fonc.2022.899156

36. Yao H, Li C, Tan X. An age stratified analysis of the biomarkers in patients with colorectal cancer. *Sci Rep* (2021) 11(1):22464. doi:10.1038/s41598-021-01850-x

37. Xu H, Wan H, Zhu M, Feng L, Zhang H, Su F. Discovery and validation of an epithelial-mesenchymal transition-based signature in gastric cancer by Genomics and prognosis analysis. *Biomed Res Int* (2021) 2021:9026918. doi:10.1155/2021/9026918

38. Chen Q, Cai L, Liang J. Construction of prognosis model of bladder cancer based on transcriptome. *J Zhejiang Da Xue Xue Bao Yi Xue Ban* (2021) 50(7):1–9.

39. Tian S, Meng G, Zhang W. A six-mRNA prognostic model to predict survival in head and neck squamous cell carcinoma. *Cancer Manag Res* (2019) 11:131–42. doi:10.2147/CMAR.S185875

40. Luo Y, Chen R, Ning Z, Fu N, Xie M. Identification of a four-gene signature for determining the prognosis of papillary thyroid carcinoma by integrated bioinformatics analysis. *Int J Gen Med* (2022) 15:1147–60. doi:10.2147/IJGM.S346058

41. Liu JW, Yu F, Tan YF, Huo JP, Liu Z, Wang XJ, et al. Profiling of tumor microenvironment components identifies five stroma-related genes with prognostic implications in colorectal cancer. *Cancer Biother Radiopharm* (2022) 37:882–92. doi:10.1089/cbr.2020.4118

42. Wang H, Yin J, Hong Y, Ren A, Li M, Zhao Q, et al. SCG2 is a prognostic biomarker associated with immune infiltration and macrophage polarization in colorectal cancer. *Front Cel Dev Biol* (2021) 9:795133. doi:10.3389/fcell.2021.795133

43. Wang C, Chen S, Li S, Mi H. A prognostic model for predicting tumor mutation burden and tumor-infiltrating immune cells in bladder urothelial carcinoma. *Front Genet* (2022) 13:708003. doi:10.3389/fgene.2022.708003

44. Luo Y, Chen L, Zhou Q, Xiong Y, Wang G, Liu X, et al. Identification of a prognostic gene signature based on an immunogenomic landscape analysis of bladder cancer. *J Cel Mol Med* (2020) 24(22):13370–82. doi:10.1111/jcmm.15960

45. Tao D, Wang Y, Zhang X, Wang C, Yang D, Chen J, et al. Identification of angiogenesis-related prognostic biomarkers associated with immune cell infiltration in breast cancer. *Front Cel Dev Biol* (2022) 10:853324. doi:10.3389/fcell.2022.853324

46. Ma C, Li F, Wang Z, Luo H. A novel immune-related gene signature predicts prognosis of lung adenocarcinoma. *Biomed Res Int* (2022) 2022:4995874. doi:10.1155/2022/4995874

47. Fang C, Dai L, Wang C, Fan C, Yu Y, Yang L, et al. Secretogranin II impairs tumor growth and angiogenesis by promoting degradation of hypoxia-inducible factor-1α in colorectal cancer. *Mol Oncol* (2021) 15(12):3513–26. doi:10.1002/1878-0261.13044

48. Justo BL, Jasiulionis MG. Characteristics of TIMP1, CD63, and β1-integrin and the functional impact of their interaction in cancer. *Int J Mol Sci* (2021) 22(17):9319. doi:10.3390/ijms22179319

49. Cabral-Pacheco GA, Garza-Veloz I, Castruita-De La Rosa C, Ramirez-Acuna JM, Perez-Romero BA, Guerrero-Rodriguez JF, et al. The roles of matrix metalloproteinases and their inhibitors in human diseases. *Int J Mol Sci* (2020) 21(24):9739. doi:10.3390/ijms21249739

50. Zeng C, Chen Y. HTR1D, TIMP1, SERPINE1, MMP3 and CNR2 affect the survival of patients with colon adenocarcinoma. *Oncol Lett* (2019) 18(3):2448–54. doi:10.3892/ol.2019.10545

51. Wu T, Dai Y. Tumor microenvironment and therapeutic response[J]. *Cancer Lett* (2017) 387:61–8.

52. Hui L, Chen Y. Tumor microenvironment: Sanctuary of the devil. *Cancer Lett* (2015) 368(1):7–13. doi:10.1016/j.canlet.2015.07.039

53. Taki M, Abiko K, Ukita M, Murakami R, Yamanoi K, Yamaguchi K, et al. Tumor immune microenvironment during epithelial-mesenchymal transition. *Clin Cancer Res* (2021) 27(17):4669–79. doi:10.1158/1078-0432.CCR-20-4459

54. Hanus M, Parada-Venegas D, Landskron G, Wielandt AM, Hurtado C, Alvarez K, et al. Immune system, microbiota, and microbial metabolites: The unresolved triad in colorectal cancer microenvironment. *Front Immunol* (2021) 12: 612826. doi:10.3389/fimmu.2021.612826

55. Rocca YS, Roberti MP, Arriaga JM, Amat M, Bruno L, Pampena MB, et al. Altered phenotype in peripheral blood and tumor-associated NK cells from colorectal cancer patients. *Innate Immun* (2013) 19(1):76–85. doi:10.1177/1753425912453187

56. Ren X, Chen X, Zhang X, Jiang S, Zhang T, Li G, et al. Immune microenvironment and response in prostate cancer using large population cohorts. *Front Immunol* (2021) 12:686809. doi:10.3389/fimmu.2021.686809

57. Lv D, Wu X, Chen X, Yang S, Wang M, Liu Y, et al. A novel immune-related gene-based prognostic signature to predict biochemical recurrence in patients with prostate cancer after radical prostatectomy. *Cancer Immunol Immunother* (2021) 70(12):3587–602. doi:10.1007/s00262-021-02923-6

58. Li F, Teng H, Liu M, Liu B, Zhang D, Xu Z, et al. Prognostic value of immune-related genes in the tumor microenvironment of bladder cancer. *Front Oncol* (2020) 10:1302. doi:10.3389/fonc.2020.01302

59. Zhou Y, Bian S, Zhou X, Cui Y, Wang W, Wen L, et al. Single-cell multiomics sequencing reveals prevalent genomic alterations in tumor stromal cells of human colorectal cancer. *Cancer Cell* (2020) 38(6):818–28.e5. doi:10.1016/j.ccell.2020.09.015

60. Gutteridge RE, Ndiaye MA, Liu X, Ahmad N. Plk1 inhibitors in cancer therapy: From laboratory to clinics. *Mol Cancer Ther* (2016) 15(7):1427–35. doi:10.1158/1535-7163.MCT-15-0897

61. Wagner LM. Profile of veliparib and its potential in the treatment of solid tumors. *Onco Targets Ther* (2015) 8:1931–9. doi:10.2147/OTT.S69935

62. Solanes-Casado S, Cebrián A, Rodríguez-Remírez M, Mahillo I, Garcia-Garcia L, Rio-Vilarino A, et al. Overcoming PLK1 inhibitor resistance by targeting mevalonate pathway to impair AXL-TWIST axis in colorectal cancer. *Biomed Pharmacother* (2021) 144:112347. doi:10.1016/j.biopha.2021.112347

63. Lund-Andersen C, Patzke S, Nähse-Kumpf V, Syljuasen RG. PLK1-inhibition can cause radiosensitization or radioresistance dependent on the treatment schedule. *Radiother Oncol* (2014) 110(2):355–61. doi:10.1016/j.radonc.2013.12.014

64. Czito BG, Deming DA, Jameson GS, Mulcahy MF, Vaghefi H, Dudley MW, et al. Safety and tolerability of veliparib combined with capecitabine plus radiotherapy in patients with locally advanced rectal cancer: a phase 1b study. *Lancet Gastroenterol Hepatol* (2017) 2(6):418–26. doi:10.1016/S2468-1253(17)30012-2

65. Pishvaian MJ, Slack RS, Jiang W, Hwang JJ, Hankin A, Dorsch-Vogel K, et al. A phase 2 study of the PARP inhibitor veliparib plus temozolomide in patients with heavily pretreated metastatic colorectal cancer. *Cancer* (2018) 124(11):2337–46. doi:10.1002/cncr.31309

66. Gorbunova V, Beck JT, Hofheinz RD, Garcia-Alfonso P, Nechaeva M, Cubillo Gracian A, et al. A phase 2 randomised study of veliparib plus FOLFIRI±bevacizumab versus placebo plus FOLFIRI±bevacizumab in metastatic colorectal cancer. *Br J Cancer* (2019) 120(2):183–9. doi:10.1038/s41416-018-0343-z

67. Morano F, Raimondi A, Pagani F, Lonardi S, Salvatore L, Cremolini C, et al. Temozolomide followed by combination with low-dose ipilimumab and nivolumab in patients with microsatellite-stable, O^6-methylguanine-DNA methyltransferase-silenced metastatic colorectal cancer: The MAYA trial. *J Clin Oncol* (2022) 40(14): 1562–73. doi:10.1200/JCO.21.02583

68. Parikh AR, Szabolcs A, Allen JN, Clark JW, Wo JY, Raabe M, et al. Radiation therapy enhances immunotherapy response in microsatellite stable colorectal and pancreatic adenocarcinoma in a phase II trial. *Nat Cancer* (2021) 2(11):1124–35. doi:10.1038/s43018-021-00269-7

69. Kanikarla Marie P, Haymaker C, Parra ER, Kim YU, Lazcano R, Gite S, et al. Pilot clinical trial of perioperative durvalumab and tremelimumab in the treatment of resectable colorectal cancer liver metastases. *Clin Cancer Res* (2021) 27(11): 3039–49. doi:10.1158/1078-0432.CCR-21-0163

70. Chung KY, Gore I, Fong L, Venook A, Beck SB, Dorazio P, et al. Phase II study of the anti-cytotoxic T-lymphocyte-associated antigen 4 monoclonal antibody, tremelimumab, in patients with refractory metastatic colorectal cancer. *J Clin Oncol* (2010) 28(21):3485–90. doi:10.1200/JCO.2010.28.3994

71. Huang X, Hou Y, Weng X, Pang W, Hou L, Liang Y, et al. Diethyldithiocarbamate-copper complex (CuET) inhibits colorectal cancer progression via miR-16-5p and 15b-5p/ALDH1A3/PKM2 axis-mediated aerobic glycolysis pathway. *Oncogenesis* (2021) 10(1):4. doi:10.1038/s41389-020-00295-7

72. Wu H, Wei M, Jiang X, Tan J, Xu W, Fan X, et al. lncRNA PVT1 promotes tumorigenesis of colorectal cancer by stabilizing miR-16-5p and interacting with the VEGFA/VEGFR1/AKT Axis. *Mol Ther Nucleic Acids* (2020) 20:438–50. doi:10.1016/j.omtn.2020.03.006

73. Yan S, Yue Y, Wang J, Li W, Sun M, Gu C, et al. LINC00668 promotes tumorigenesis and progression through sponging miR-188-5p and regulating USP47 in colorectal cancer. *Eur J Pharmacol* (2019) 858:172464. doi:10.1016/j.ejphar.2019.172464

74. Si M, Song Y, Wang X, Wang D, Liu X, Qu X, et al. CXCL12/CXCR7/β-arrestin1 biased signal promotes epithelial-to-mesenchymal transition of colorectal cancer by repressing miRNAs through YAP1 nuclear translocation. *Cell Biosci* (2022) 12(1):171. doi:10.1186/s13578-022-00908-1

75. Li N, Li J, Mi Q, Xie Y, Li P, Wang L, et al. Long non-coding RNA ADAMTS9-AS1 suppresses colorectal cancer by inhibiting the Wnt/β-catenin signalling pathway and is a potential diagnostic biomarker. *J Cel Mol Med* (2020) 24(19): 11318–29. doi:10.1111/jcmm.15713

76. Zhou J, Lin J, Zhang H, Zhu F, Xie R. LncRNA HAND2-AS1 sponging miR-1275 suppresses colorectal cancer progression by upregulating KLF14. *Biochem Biophys Res Commun* (2018) 503(3):1848–53. doi:10.1016/j.bbrc.2018.07.125

77. Krattinger R, Boström A, Schiöth HB, Thasler WE, Mwinyi J, Kullak-Ublick GA. microRNA-192 suppresses the expression of the farnesoid X receptor. *Am J Physiol Gastrointest Liver Physiol* (2016) 310(11):G1044–51. doi:10.1152/ajpgi.00297.2015

78. Cui S, Yang X, Zhang L, Zhao Y, Yan W. LncRNA MAFG-AS1 promotes the progression of colorectal cancer by sponging miR-147b and activation of NDUFA4. *Biochem Biophys Res Commun* (2018) 506(1):251–8. doi:10.1016/j.bbrc.2018.10.112

79. Chen T, Huang B, Pan Y. Long non-coding RNA MAFG-AS1 promotes cell proliferation, migration, and EMT by miR-3196/STRN4 in drug-resistant cells of liver cancer. *Front Cel Dev Biol* (2021) 9:688603. doi:10.3389/fcell.2021.688603

80. Sun W, Nie W, Wang Z, Zhang H, Li Y, Fang X. Lnc HAGLR promotes colon cancer progression through sponging miR-185-5p and activating CDK4 and CDK6 *in vitro* and *in vivo*. *Onco Targets Ther* (2020) 13:5913–25. doi:10.2147/OTT.S246092

81. Yang Y, Feng M, Bai L, Liao W, Zhou K, Zhang M, et al. Comprehensive analysis of EMT-related genes and lncRNAs in the prognosis, immunity, and drug treatment of colorectal cancer. *J Transl Med* (2021) 19(1):391. doi:10.1186/s12967-021-03065-0

82. Liu H, Tian Y, Li J, Zhang G, Liu Q, Yang M, et al. Identification and functional analysis of lncRNAs and mRNAs between tumorigenesis and metastasis in CRC. *J Aging (Albany Ny)* (2021) 13(24):25859–85. doi:10.18632/aging.203775

83. Wang K, Song K, Ma Z, Yao Y, Liu C, Yang J, et al. Identification of EMT-related high-risk stage II colorectal cancer and characterisation of metastasis-related genes. *Br J Cancer* (2020) 123(3):410–7. doi:10.1038/s41416-020-0902-y

84. Wang L, Liu D, Liu S, Liao T, Jiao Y, Jiang X, et al. Identification of IMPA2 as the hub gene associated with colorectal cancer and liver metastasis by integrated bioinformatics analysis. *Transl Oncol* (2022) 21:101435. doi:10.1016/j.tranon.2022.101435

85. Zhang Z, Zheng S, Lin Y, Sun J, Ding N, Chen J, et al. Genomics and prognosis analysis of epithelial-mesenchymal transition in colorectal cancer patients. *BMC Cancer* (2020) 20(1):1135. doi:10.1186/s12885-020-07615-5

Pathology & Oncology Research | frontiers

TYPE Original Research
PUBLISHED 06 June 2024
DOI 10.3389/pore.2024.1611789

Check for updates

OPEN ACCESS

EDITED BY
Andrea Ladányi,
National Institute of Oncology (NIO), Hungary

*CORRESPONDENCE
Nauryzbay M. Imanbayev,
dr.imanbayev@gmail.com

RECEIVED 04 April 2024
ACCEPTED 21 May 2024
PUBLISHED 06 June 2024

CITATION
Imanbayev NM, Iztleuov YM, Kamyshanskiy YK and Zhumasheva AV (2024), Diagnostic and prognostic significance of keloid-like collagen remodeling patterns in the extracellular matrix of colorectal cancer.
Pathol. Oncol. Res. 30:1611789.
doi: 10.3389/pore.2024.1611789

COPYRIGHT
© 2024 Imanbayev, Iztleuov, Kamyshanskiy and Zhumasheva. This is an open-access article distributed under the terms of the Creative Commons Attribution License (CC BY). The use, distribution or reproduction in other forums is permitted, provided the original author(s) and the copyright owner(s) are credited and that the original publication in this journal is cited, in accordance with accepted academic practice. No use, distribution or reproduction is permitted which does not comply with these terms.

Diagnostic and prognostic significance of keloid-like collagen remodeling patterns in the extracellular matrix of colorectal cancer

Nauryzbay M. Imanbayev [1]*, Yerbolat M. Iztleuov [2], Yevgeniy K. Kamyshanskiy [3] and Aigul V. Zhumasheva [4]

[1]Department of Oncology, West Kazakhstan Marat Ospanov Medical University, Aktobe, Kazakhstan, [2]Department of Radiology, West Kazakhstan Marat Ospanov Medical University, Aktobe, Kazakhstan, [3]Department of Pathology, Karaganda Medical University, Karaganda, Kazakhstan, [4]Department of Pathomorphology, Medical Centre of West Kazakhstan Marat Ospanov Medical University, Aktobe, Kazakhstan

Background: The desmoplastic reaction is considered a promising prognostic parameter for colorectal cancer. However, intermediate desmoplastic reaction is characterized by sizeable stromal heterogeneity, including both small amounts of keloid-like collagen (KC) in the fibrotic stroma and thick tufts of KC circumferentially surrounding cancer nests and occupying most of the fields of view. The present study aimed to evaluate the diagnostic and prognostic significance of KC histophenotyping with a quantitative visual assessment of its presence in the stroma of the invasive margin of TNM (The "tumor-node-metastasis" classification) stage II/III colorectal cancer (CRC).

Methods and results: 175 resected tumors from patients with TNM stage II/III CRC were examined. Keloid-like collagen was assessed according to Ueno H. criteria. KC was assessed at the primary tumor invasive margin using Hematoxylin & Eosin and Masson's trichrome staining. The cut-off point for KC was examined using "the best cutoff approach by log-rank test." Using a cutoff point of 30%, we histologically divided fibrous stroma in the invasive area into two groups: "type A"—KC ≤ 0.3 and "type B"—KC>0.3. Type A stroma was observed in 48% of patients, type B—in 52%. The association between collagen amount and 5-year recurrence-free survival (5-RFS) was assessed using Cox regression analysis. Kaplan-Meier analysis and log-rank tests were used to assess the significance of survival analysis. Analysis of categorical variables showed that increased KC in CRC stroma predicted adverse outcomes for 5-RFS (hazard ratio [HR] = 3.143, 95%,

confidence interval [CI] = 1.643–6.012, p = 0.001). Moreover, in Kaplan-Meier analysis, the log-rank test showed that type B exhibited worse 5-RFS than type A (p = 0.000).

Conclusion: KC is an independent predictor of 5-year overall and RFS in patients with TNM stage II/III CRC treated with surgery, with worse survival rates when the amount of KC increases by >30%.

KEYWORDS

colorectal cancer, intermediate desmoplastic reaction, keloid-like collagen, desmoplastic reaction, extracellular matrix of colorectal cancer

Introduction

Colorectal cancer (CRC) is a disease with high morbidity and mortality, ranking third in prevalence worldwide [1]. One basis for making clinical decisions about the treatment of cancer patients, including patients with CRC, is the TNM classification [2]. However, patients with the same stage of CRC, according to the TNM classification, have different clinical outcomes. In this regard, searching for additional prognostic markers to stratify patients and improve clinical decisions is exceptionally relevant. Histological examination is highly reliable and inexpensive, so identifying additional histological criteria is a promising strategy.

Traditionally, the leading place in histological studies was occupied by the epithelial component, but modern research paradigms have gradually shifted from the tumor epithelium to the stroma [3–5]. Even Masson P. drew attention to proliferating fibroblasts among the inflammatory infiltrate of the tumor and described the reactions of the tumor stroma depending on the time of their appearance [6]. The prognostic value of the stroma of the invasive tumor margin was demonstrated by Ueno H [5, 7, 8]. The desmoplastic reaction is considered a promising prognostic parameter for colorectal cancer. However, the intermediate desmoplastic reaction is characterized by sizeable stromal heterogeneity, including both small amounts of keloid-like collagen in the fibrotic stroma and thick tufts of colloid-like collagen circumferentially surrounding cancer nests and occupying most of the visual fields.

Recent studies have shown that tumors can directly exploit extracellular matrix remodeling to create a microenvironment that promotes tumorigenesis and metastasis [9, 10]. The dominant component of the extracellular matrix is collagen, and its structure is increasingly recognized as a reliable biomarker for establishing the prognosis of various types of tumors, such as prostate cancer and gastric cancer [11, 12]. In addition, previous studies have shown that different histopatterns of extracellular collagen matrix is associated with different therapy response in colorectal and breast cancer [13–15]. Collagen I fibers influence the movement of macromolecules in the tumor extracellular matrix [16], and the structural characteristics of these fibers can promote or hinder cancer cell migration [17]. Collagen changes in the tumor microenvironment correlate with cancer dissemination and prognosis. Collagen regulates tumor-associated immune infiltration and is required for tumor angiogenesis, histological features of the Collagen I matrix can lead to significantly enhanced tumor metastatic potential [18, 19]. Moreover, radial alignment of collagen at the tumor-stroma interface increases the invasiveness of cancer cells [20, 21]. Histologically, abnormal collagen remodeling mainly results in excessive deposition and changes in the proportions and localization of collagen [22–24]. These morphological changes may reflect important tumor characteristics that influence patient prognosis.

Pathologists can identify stromal components, but their description and quantification is not routine and stromal factors are not always considered when making treatment decisions. This leads to different approaches in understanding the nature of individual tumors between the laboratory and the clinic. Additional evaluation of sections stained with hematoxylin and eosin does not always allow for the best determination of the various elements of the extracellular matrix. The purpose of the work was to evaluate the diagnostic and prognostic significance of histophenotyping of keloid-like collagen with a quantitative visual assessment of its presence in the stroma of the invasive margin of TNM stage II-III colorectal cancer.

Materials and methods

Tissue samples and study cohort selection

This monocentric retrospective cohort study consecutively included resected colorectal cancer specimens with keloid-like collagen at the invasive tumor margin from all patients who underwent complete oncologic resection for TNM stage II or III colon adenocarcinoma in Aktobe (Kazakhstan) during the period since January 2001 until December 2019 All patients were observed for 5 years from the date of surgical resection.

Exclusion criteria: 1) histological diagnosis other than adenocarcinoma; 2) tumor-stroma ratio less than 50%; 3) desmoplastic reaction of the invasive tumor margin, classified as “immature,” myxoid stroma according to Ueno H. criteria [5]; 4) radiation therapy before surgery;

5) Patient death within 30 days after surgery; 6) history of malignancy within 5 years before the diagnosis of colorectal

TABLE 1 Clinicopathological characteristics of the investigated groups.

Parameters	Categories	Total *n* = 175	Type A *n* = 84	Type B *n* = 91	*p*-value
Age (years)	ME ± SD	61.8 ± 9.9	60.9 ± 10.6	62.7 ± 9.4	0.332
	Range	[38; 89]	[38; 81]	[40; 89]	
	≤65 years	107 (61.1)	54 (64.3)	53 (58.2)	
	>65 years	68 (38.9)	30 (35.7)	38 (41.8)	
Gender, n (%)	Male	85 (48.6)	40 (47.6)	45 (49.5)	0.809
	Female	90 (51.4)	44 (52.4)	46 (50.5)	
Race, n (%)	White	43 (24.6)	26 (31.0)	17 (18.7)	0.060
	Asian	132 (75.4)	58 (69.0)	74 (81.3)	
	Other	—	—	—	
CCI Score	≤3	109 (62.3)	48 (57.1)	61 (67.0)	0.178
	>3	66 (37.7)	36 (42.9)	30 (33.0)	
Family history of cancer, n (%)	No	148 (84.6)	71 (84.5)	77 (84.6)	0.987
	Yes	27 (15.4)	13 (15.5)	14 (15.4)	
Date of diagnosis	2001–2005	20 (11.4)	8 (9.5)	12 (12.4)	0.553
	2006–2010	35 (20.0)	14 (16.7)	21 (21.6)	
	2011–2015	57 (32.6)	30 (35.7)	27 (27.8)	
	2016–2019	63 (36.0)	32 (38.1)	31 (31.9)	
Tumor site, n (%)	Right	68 (38.9)	30 (35.7)	38 (41.8)	0.413
	Left	107 (61.1)	54 (64.3)	53 (58.2)	
T-stage, n (%)	T2	127 (72.6)	68 (81.0)	59 (64.8)	**0.017**
	T3	48 (27.4)	16 (19.0)	32 (35.2)	
Tumor differentiation, n (%)	G1	2 (1.1)	1 (1.2)	1 (1.1)	**0.020**
	G2	134 (76.6)	72 (85.7)	62 (68.1)	
	G3	39 (22.3)	11 (13.1)	28 (30.8)	
Tumor budding	BD1	69 (39.4)	39 (46.4)	30 (33.0)	**0.036**
	BD2	67 (38.3)	33 (39.3)	34 (37.4)	
	BD3	39 (22.2)	12 (14.3)	27 (29.6)	
Lymphatic invasion	Negative	132 (75.4)	70 (83.3)	62 (68.1)	**0.020**
	Positive	43 (24.6)	14 (16.7)	29 (31.9)	
Venous invasion	Negative	130 (74.3)	69 (82.1)	61 (67.0)	**0.023**
	Positive	45 (25.7)	15 (17.9)	30 (33.0)	
Perineural invasion, n (%)	No	159 (90.9)	75 (89.3)	84 (92.3)	0.489
	Yes	16 (9.1)	9 (10.7)	7 (7.7)	
KRAS status, n (%)	Mutant	100 (57.1)	47 (56.0)	53 (58.2)	0.760
	Wild-type	75 (42.9)	37 (44.0)	38 (41.8)	
Chemotherapy in postoperative period	No	43 (24.6)	17 (20.2)	26 (26.8)	0.352

(Continued on following page)

TABLE 1 (*Continued*) Clinicopathological characteristics of the investigated groups.

Parameters	Categories	Total *n* = 175	Type A *n* = 84	Type B *n* = 91	*p*-value
	Yes	51 (29.2)	24 (28.6)	27 (27.8)	
	No data	81 (46.3)	43 (51.2)	38 (39.2)	

Type A—Keloid-like Collagen ≤ 0.3, Type B—Keloid-like Collagen > 0.3; CCI, Charlson Comorbidity Index; *p*- value—A chi-square test was performed to compare categorical data. Analysis of variance was performed to compare continuous variables, **bold** indicates values with a significant difference, $p < 0.05$.

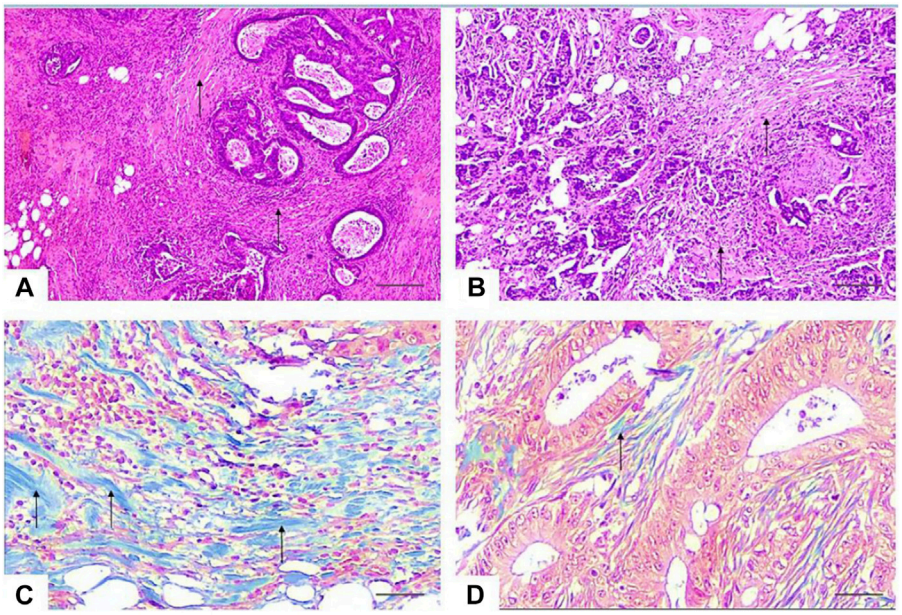

FIGURE 1
Photomicrographs of representative sections of the invasive tumor margin. **(A, B)**—the stroma-to-tumor ratio is more than 50%, the stroma is dense with multiple bundles of keloid-like collagen (arrows) with bright eosinophilic hyalinization around tumor nests and focal infiltration by immune cells. HE × 40. Scale bar, 500 μm **(C)**—stromal keloid-like collagen histopattern type B—thick tufts of hypocellular keloid-like collagen (arrows) of a homogeneous blue color, occupy more than a third of the stroma of the invasive margin of the tumor. Masson's trichrome × 400. Scale bar, 50 μm. **(D)**—Stromal mature collagen histopattern type A—thin mature collagen fibers (arrows) and single keloid-like collagen fibers. Masson's trichrome 400. Scale bar, 50 μm.

cancer (except basal cell carcinoma or cervical cancer *in situ*); 7) patient refusal of treatment, highly severe clinical condition of the patient, or old age (>90 years). All tissues selected for the study were re-evaluated independently by two pathologists without their knowledge of the clinical information. All samples were anonymized before the start of the study.

Keloid-like collagen was assessed at the invasive margin of the primary tumor using hematoxylin & eosin and Masson's trichrome staining.

In all our cases, two pathologists (Y.K.K. and A.V.Z.) with more than 10 years of experience identified the most invasive part of the removed tumor ("the invasion front"), defined as the area with the deepest tumor infiltration or the area where tumor tissue meets non-tumor tissue. On a microslide of the most invasive edge of the tumor 10 fields of microscopic view with ×40 objective magnification were selected, and then the relative amount of keloid-like collagen was calculated for each case. The cut-off point for keloid-like collagen was examined using "the best cut-off approach by log-rank test" and 30% was determined as the cut-off point. All cases, based on the ratio of colloid-like collagen in the stroma of the invasive edge of the tumor, were divided into groups "type A" (Keloid-like Collagen ≤ 0.3) and "type B" (Keloid-like Collagen > 0.3) (Table 1; Figure 1).

Clinical data

Clinical data were collected using software in an integrated health information system from patient medical records. These data included the sex and age of the patients, comorbidities, family history of colorectal cancer, date of surgery, data on concomitant diseases and comorbidities before surgery, localization of the tumor in the right or left side of the colon, occurrence of recurrence, date of its discovery and treatment provided.

Endpoints and definitions

The primary endpoint of this study was recurrence-free survival (RFS). RFS was defined as the time in months between the date of surgery and the date of cancer recurrence (defined as the first date of radiographic or histological diagnosis of local tumor recurrence or metastasis of colon cancer) or the date of last follow-up (with a maximum period of 5 years). Standard examinations were performed following national cancer surveillance guidelines for colon cancer after curative resection for 5 years after surgery [25]. Patients dying without cancer recurrence were censored at the date of death.

Overall survival was defined as the duration from surgery to death or last follow-up. Patients alive at the last follow-up were recorded as censored events.

Surgical resection was defined as complete single-stage removal of all gross tumors with negative surgical margins on microscopic examination. Distant metastases were determined by preoperative abdominal ultrasound or computed tomography, chest radiography or MRI (Magnetic Resonance Imaging), and intraoperative examination.

The "tumor-node-metastasis" (TNM) classification was used to determine the primary tumor stage according to the edition in effect at the time of cancer diagnosis.

Tumor budding was defined as an isolated cancer cell or cluster comprising <5 cells at the invasive front and classified into grades BD1, BD2, and BD3 according to international criteria [26, 27].

Vascular invasion was defined as the presence of tumor cells in the muscular layer of blood vessels or invasion of the muscular vascular endothelium; lymphatic invasion was defined as the presence of nests of tumor cells in the lymphatic cavity [28].

Perineural invasion was defined as the presence of tumor cells in three layers of the nerve sheath or in close proximity to the nerve, affecting at least 33% of its entire circumference [29–31].

Tumor marker KRAS

Tissue blocks from all study participants were obtained from the initial surgical resection and assessed for KRAS mutational status. Sequencing of KRAS, representative tumor portions were marked histologically, and the corresponding areas on unstained tissue slides were then subjected to manual microdissection. The dissected tissues were collected into microtubes containing lysis buffer and proteinase K and incubated at 55°C for up to 2 days. KRAS mutations were determined by standard PCR followed by Sanger sequencing of exons 2 and 3 of KRAS.

Histological examination

Before the histological examination, tissue samples were fixed in 10% formaldehyde at 4°C for 24 h, washed with tap water, and dehydrated using a series of alcohols of increasing concentration (70%, 90%, 95%, 100%). The tissue samples were then immersed in xylene and embedded in paraffin blocks. Tissue sections 3 μm thick were cut using a microtome and placed on a glass slide. The slides were then deparaffinized and stained.

Hematoxylin and eosin staining procedure. Tissue sections were immersed in Mayer's hematoxylin for 15 min and then washed with water for 5 min. After this, the sections were subjected to 1-min eosin staining.

From the tissue block, we carefully selected plain HE-stained sections that showed the representative invasive part of the primary tumor.

Masson's trichrome staining procedure. For staining with Masson's trichrome, a commercial kit [Trichrome dye (Masson) Bio-Optica (Italy)] was used according to the standard protocol. Collagen fibers were defined as dark-blue fibers with black nuclei.

Morphological criteria

Morphological variables were obtained as a result of repeated review of histological specimens of the tumor (surgical material) and also collected from pathologists' reports, including tumor differentiation, tumor budding, lymphatic, venous, and perineural invasion.

Ethics statement

Due to the retrospective nature of this study, ethical review and approval was not required in accordance with the local legislation and institutional requirements.

Statistical analysis

Statistical analysis was performed using Statistica 10.0 and IBM SPSS Statistic 25.0 software (v.25.00, IBM Statistics, Armonk/NY, United States). No formal sample size calculation was performed. All eligible patients were included in the analysis. Descriptive statistics were used to present the data. Qualitative and quantitative variables were compared using the χ^2 or Student's t-test, respectively (Mann-Whitney or Kruskal-Wallis test when the reliability conditions of Student's t-test and χ^2 test were not met). A p-value <0.05 was considered statistically significant. The Kaplan-Meier method was used to calculate overall (OS) and relapse-free (RFS) survival. Univariate and multivariate analyses using the Cox proportional hazards regression model were performed to calculate HRs and 95% CI. The log-rank test, Kaplan-Meier method, and Cox regression (univariate) were used to estimate the cutoff value.

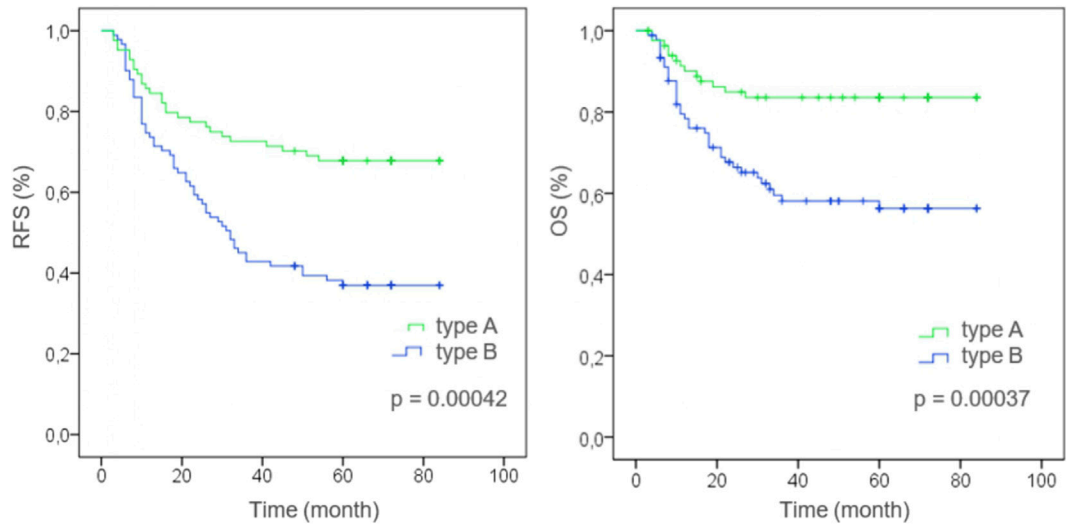

FIGURE 2
Kaplan-Meier curve features in the investigated groups [stratified by histophenotype of stromal collagen (Type A or Type B) in the colorectal cancer]. RFS—Recurrence-free survival of patients, OS—Overall survival of patients, Type A—Keloid-like Collagen less than 30% of stromal collagen fibers in the invasive tumor front (≤0.3), Type B—Keloid-like Collagen more than 30% of stromal collagen fibers in the invasive tumor front (>0.3).

Results

Study population

The clinicopathological characteristics of the study groups of patients are presented in Table 1.

Patients were divided into groups "type A" (Keloid-like Collagen ≤0.3) and "type B" (Keloid-like Collagen > 0.3). Based on the cut-off point, 84 (48%) patients were identified as cases with a reduced amount of keloid-like collagen (type A), and 91 (52%) patients were identified as cases with an increased amount of keloid-like collagen (type B). Representative examples of images with stroma type A and type B histophenotypes are shown in Figure 1.

Survival analyses of overall survival and recurrence-free survival

The results of the Kaplan-Meier analysis of survival curves are presented in Figure 2.

In the group with the structural pattern of mature thin-structured collagen stroma type A, the following survival rates (RFS) were determined: on the 1st year it was 84.5%, on the 3rd year—72.6%, on the 5th year—67.9%; OS in the 1st year was 90.5%, in the 3rd year—84.5%, in the 5th year—84.5%.

In the group with the structural pattern of intermediate keloid-like collagen stroma type B, the following survival rates (RFS) were determined: on the 1st year it was 74.7%, on the 3rd year—48.4%, on the 5th year—37.4%; OS in the 1st year was 80.2%, in the 3rd year—63.7%, in the 5th year—59.4%.

Univariate and multivariate analysis of prognostic factors

Univariate Cox regression was performed to evaluate the prognostic significance of all clinicopathological data and keloid-like collagen assessed on all slides containing the invasive tumor margin (Table 2).

Univariate analysis showed that among the prespecified clinicopathological prognostic factors assessed in this study, the T-stage had a significant impact on RFS: in patients with the T3 stage, the hazard ratio was 2.345 (95% CI: 1.054–5.215; p = 0.037) compared to patients at stage T2. Lymphatic invasion [HR, 2.533 (1.238–5.183), p = 0.011] and venous invasion [HR, 3.509 (1.682–7.323), p = 0.001] were also significant prognostic factors for RFS. Patients with stromal histophenotype Type B (Keloid-like Collagen > 0.3) had a significantly higher risk of relapse [HR, 3.539 (1.895–6.609), p = 0.001] than patients with stromal histophenotype Type A. In a univariate analysis, it was found that several factors, such as age, sex, race, family history of cancer, and tumor differentiation grade, did not have a statistically significant effect on RFS in patients with stage II-III colorectal cancer.

After univariate analysis, significant factors were further assessed using a multivariate Cox regression model to determine their independent prognostic value for RFS.

TABLE 2 Univariate and multivariate analyses of RFS using the Cox proportional-hazards regression model in the investigated groups.

		Univariate analysis		Multivariate analysis	
		HR (95% CI)	*p*-value	HR (95% CI)	*p*-value
Age (years)	≤65 years				
	>65 years	1.140 (0.620–2.095)	0.673	—	—
Gender, n (%)	Male				
	Female	1.204 (0.539–2.446)	0.607	—	—
Race, n (%)	White				
	Asian	0.845 (0.425–1.683)	0.633	—	—
CCI Score	≤3				
	>3	2.127 (0.962–4.701)	0.062	—	—
Family history of cancer, n (%)	No				
	Yes	1.212 (0.504–2.916)	0.668	—	—
Tumor site, n (%)	Right				
	Left	0.406 (0.213–1.087)	0.068	—	—
T-stage, n (%)	T2				
	T3	2.345 (1.054–5.215)	**0.037**	1.654 (0.695–3.939)	0.256
Tumor differentiation, n (%)	G1				
	G2	0.375 (0.022–6.484)	0.500	—	—
	G3	1.417 (0.645–3.114)	0.386	—	—
Tumor budding	BD1				
	BD2	2.326 (0.959–5.641)	0.062	—	—
	BD3	1.355 (0.576–3.190)	0.487	—	—
Lymphatic invasion	Negative				
	Positive	2.533 (1.238–5.183)	**0.011**	1.420 (0.495–4.070)	0.514
Venous invasion	Negative				
	Positive	3.509 (1.682–7.323)	**0.001**	1.696 (0.624–4.609)	0.301
Perineural invasion, n (%)	No				
	Yes	2.592 (0.861–7.803)	0.090	—	—
KRAS status, n (%)	Mutant				
	Wild-type	1.046 (0.575–1.902)	0.884	—	—
Keloid-like Collagen	Type A				
	Type B	3.539 (1.895–6.609)	**0.000**	3.143 (1.643–6.012)	**0.001**

Type A—Keloid-like Collagen ≤0.3, Type B—Keloid-like Collagen >0.3; CCI, Charlson Comorbidity Index; *p*-value—**bold** indicates values with a significant difference, $p < 0.05$.

After adjustment for other covariates, T stage [HR: 1.654, 95% CI: (0.695–3.939); $p = 0.256$], lymphatic invasion (HR: 1.420, 95% CI: 0.495–4.070; $p = 0.514$) and venous invasion (HR: 1.696, 95% CI: 0.624–4.609; $p = 0.301$) were not predictive of poor outcome, in contrast to the structural pattern of keloid-like collagen. Multivariate analysis showed that stromal histophenotype Type B (Keloid-like Collagen >0.3) was an independent factor significantly associated with worse RFS [HR, 3.143 (1.643–6.012), $p = 0.001$] in multivariate analysis (Table 2).

Discussion

In this study, we examined the diagnostic and prognostic significance of structural histochemical patterns of keloid-like collagen in the stroma of colorectal cancer. We analyzed the impact of clinical and histopathological prognostic factors on metastasis and survival of patients with colorectal cancer. The histopathological pattern of colon cancer between the left and right parts of the large intestine did not show significant differences, therefore, in this study, the main results of the comparative clinical and morphological assessment are presented as general data from all parts of the large intestine with a relatively uniform number of cases (Table 1).

First, our results showed that increased content of keloid-like collagen in the stroma of the invasive tumor margin correlates with the presence of aggressive features, such as tumor differentiation (G3) ($p = 0.020$), tumor budding (BD3) ($p = 0.036$), lymphatic invasion ($p = 0.020$) and venous invasion ($p = 0.023$).

Second, we found that the categorization of keloid-like collagen at the invasive margin of colorectal cancer stratifies the risk of recurrence in this group of patients. Multivariate models analysis showed that the increase in keloid-like collagen in the stroma is an independent factor of postoperative relapse in patients with stage II-III colon cancer. In particular, distant metastases and postoperative relapses within 5 years after surgery in the group with a keloid-like collagen content of more than 30% were detected in 39.5% of patients, and in the group with a keloid-like collagen content of less than 30% in 15.5% of patients. These results are consistent with scientific research [32–34] and suggest a close relationship between keloid-like collagen and the metastatic behavior of cancer cells.

The mechanism leading to a worsening prognosis in patients with increased keloid-like collagen in the stroma is not yet fully understood. As colorectal cancer progresses the increase in the number of thick collagen fibers may initially be associated with a primary fibroproliferative reaction and, in later stages, with abnormal collagen production and defective maturation, which may promote tumor growth [35]. We believe that the tumor stroma is initially capable of exerting an inhibitory effect on malignant cells.

With continued growth, the tumor can exploit its stroma, for example, by changing its composition, which is morphologically manifested by changes in the quantitative and qualitative characteristics of collagen, in order to stimulate tumor growth and metastasis. This process occurs parallel to tumor progression and is characterized by a complex bidirectional communication between the tumor and its stroma [36–38]. The different rates of progression, relapse, and continued growth suggest that the in some cases tumor progression in the group with increased amount of keloid-like collagen stroma may be caused by primary stromal changes causing *de novo* tumor development. However, this assumption is speculative and requires further research.

Third, Kaplan-Meier analysis revealed that patients with more than 30% keloid-like collagen in the stroma of the invasive tumor margin had a significantly worse survival rate than patients with less than 30% keloid-like collagen ($p < 0.01$). Our results indicate that the predictive power of keloid-like collagen categorization at the invasive margin of colorectal cancer may be independent of the anatomical TNM grade of the disease. These results suggest that stromal classification may provide reliable prognostic features and improve TNM classification for colorectal cancer. In addition, integrating histophenotype into multivariate analysis showed improved predictive capabilities, indicating that this histophenotype may be a potential addition to an outcome prediction system while simultaneously facilitating improved risk stratification for adverse outcomes. The evolving knowledge that tumor stroma plays an active role in cancer progression as it interacts with tumor and benign cells at different stages, from tumor initiation to invasion and metastasis [39, 40], explains our findings. We recommend recording the presence of keloid-like collagen stroma as a high grade of malignancy if it constitutes more than a third of the entire extracellular matrix of the tumor's invasive margin. Future studies are needed to discover additional features of the collagen matrix that could more accurately predict patient treatment outcomes.

The strengths of this study are the homogeneous study population and a single geographic area where diagnosis and treatment were performed in the same hospital without selection bias. Other strengths were the comprehensive histological evaluation by specialized pathologists and the availability of detailed clinicopathological information. Limitations include the relatively small sample size compared to other studies in this area and the lack of detailed cancer treatment data. However, we adjusted multivariate models for clinical and demographic characteristics. In addition, because data on the histopattern of stromal collagen were not generally available to treating physicians, treatment decisions were not made based on the specific structural patterns of collagens in the desmoplastic reaction. This study also included patients from 5 to 10 years ago, and developments in colorectal cancer treatments during this period may have influenced prognosis. For these reasons, extensive multicenter studies are needed to explore trends further. Manual assessment of the relative amount of keloid-like collagen could have a relatively high variability of results, so in the future, digital assessment of colorectal cancer extracellular matrix proteins will significantly increase accuracy and reduce the variability of results.

Conclusion

In summary, the results of this study indicate that keloid-like collagen stroma type B, when the relative amount of keloid-like

collagen increases by more than 30% of the entire extracellular matrix in the tumor invasive front, is an independent prognostic factor in patients with TNM stage II or III colorectal cancer treated with surgery, with worse overall and recurrence-free survival rates. Determining the histophenotype of stromal keloid-like collagen will help stratify risk groups of patients and improve individual therapeutic strategies for colorectal cancer. Furthermore, these results suggest that stromal classification, in particular for stromal collagen histophenotype, may provide reliable prognostic features and improve TNM classification for colorectal cancer.

Data availability statement

The raw data supporting the conclusion of this article will be made available by the authors, without undue reservation.

Ethics statement

The studies involving human participants were reviewed and approved by the local commission on bioethics of the NJSC West Kazakhstan Medical University Named After Marat Ospanov. The requirement for written informed consent to participate in this study was waived by the committee due to the retrospective nature of the study.

Author contributions

Conceptualization, NI and YI; Data curation, NI, YI, YK, and AZ; Formal analysis, NI, YI, and YK; Methodology, NI, AZ, and YK; Project administration, NI; Resources, NI and YK; Software, NI, YI, YK, and AZ; Supervision, NI and YI; Validation, NI, YI, and YK; Visualization, AZ and YK; Writing, original draft, NI; Writing, review and editing, NI, YI, YK, and AZ. All authors contributed to the article and approved the submitted version.

Funding

The authors declare that no financial support was received for the research, authorship, and/or publication of this article.

Conflict of interest

The authors declare that the research was conducted in the absence of any commercial or financial relationships that could be construed as a potential conflict of interest.

References

1. Sung H, Ferlay J, Siegel RL, Laversanne M, Soerjomataram I, Jemal A, et al. Global cancer statistics 2020: GLOBOCAN estimates of incidence and mortality worldwide for 36 cancers in 185 countries. *CA Cancer J Clin* (2021) 71(3):209–49. doi:10.3322/caac.21660

2. Li J, Yi CH, Hu YT, Yuan Y, Zhang SZ, Zheng S, et al. TNM staging of colorectal cancer should be reconsidered according to weighting of the T stage: verification based on a 25-year follow-up. *Medicine (Baltimore)* (2016) 95(6):e2711. doi:10.1097/MD.0000000000002711

3. Son GM, Kwon MS, Shin DH, Shin N, Ryu D, Kang CD. Comparisons of cancer-associated fibroblasts in the intratumoral stroma and invasive front in colorectal cancer. *Medicine (Baltimore)* (2019) 98(18):e15164. doi:10.1097/MD.0000000000015164

4. Nearchou IP, Kajiwara Y, Mochizuki S, Harrison DJ, Caie PD, Ueno H. Novel internationally verified method reports desmoplastic reaction as the most significant prognostic feature for disease-specific survival in stage II colorectal cancer. *Am J Surg Pathol* (2019) 43(9):1239–48. doi:10.1097/PAS.0000000000001304

5. Ueno H, Kajiwara Y, Ajioka Y, Sugai T, Sekine S, Ishiguro M, et al. Histopathological atlas of desmoplastic reaction characterization in colorectal cancer. *Jpn J Clin Oncol* (2021) 51(6):1004–12. doi:10.1093/jjco/hyab040

6. Masson P *Human tumors: histology, diagnosis, and technique. 2d ed., rev. And enl. Translated by sidney D. Kobernick*. Wayne State University Press (1970).

7. Ueno H, Jones AM, Wilkinson KH, Jass JR, Talbot IC. Histological categorisation of fibrotic cancer stroma in advanced rectal cancer. *Gut* (2004) 53(4):581–6. doi:10.1136/gut.2003.028365

8. Shin N, Son GM, Shin DH, Kwon MS, Park BS, Kim HS, et al. Cancer-associated fibroblasts and desmoplastic reactions related to cancer invasiveness in patients with colorectal cancer. *Ann Coloproctol* (2019) 35(1):36–46. doi:10.3393/ac.2018.09.10

9. Winkler J, Abisoye-Ogunniyan A, Metcalf KJ, Werb Z. Concepts of extracellular matrix remodelling in tumour progression and metastasis. *Nat Commun* (2020) 11(1):5120. Published 2020 Oct 9. doi:10.1038/s41467-020-18794-x

10. Theocharis AD, Skandalis SS, Gialeli C, Karamanos NK. Extracellular matrix structure. *Adv Drug Deliv Rev* (2016) 97:4–27. doi:10.1016/j.addr.2015.11.001

11. Penet MF, Kakkad S, Pathak AP, Krishnamachary B, Mironchik Y, Raman V, et al. Structure and function of a prostate cancer dissemination-permissive extracellular matrix. *Clin Cancer Res* (2017) 23(9):2245–54. doi:10.1158/1078-0432.CCR-16-1516

12. Chen D, Liu Z, Liu W, Fu M, Jiang W, Xu S, et al. Predicting postoperative peritoneal metastasis in gastric cancer with serosal invasion using a collagen nomogram. *Nat Commun* (2021) 12(1):179. Published 2021 Jan 8. doi:10.1038/s41467-020-20429-0

13. Desa DE, Bhanote M, Hill RL, Majeski JB, Buscaglia B, D'Aguiar M, et al. Second-harmonic generation directionality is associated with neoadjuvant chemotherapy response in breast cancer core needle biopsies. *J Biomed Opt* (2019) 24(8):1–9. doi:10.1117/1.JBO.24.8.086503

14. Jiang W, Li M, Tan J, Feng M, Zheng J, Chen D, et al. A nomogram based on a collagen feature support vector machine for predicting the treatment response to neoadjuvant chemoradiotherapy in rectal cancer patients. *Ann Surg Oncol* (2021) 28(11):6408–21. doi:10.1245/s10434-021-10218-4

15. Jiang W, Wang S, Wan J, Zheng J, Dong X, Liu Z, et al. Association of the collagen signature with pathological complete response in rectal cancer patients. *Cancer Sci* (2022) 113(7):2409–24. doi:10.1111/cas.15385

16. Kakkad SM, Penet MF, Akhbardeh A, Pathak AP, Solaiyappan M, Raman V, et al. Hypoxic tumor environments exhibit disrupted collagen I fibers and low macromolecular transport. *PLoS One* (2013) 8(12):e81869. Published 2013 Dec 12. doi:10.1371/journal.pone.0081869

17. Wolf K, Alexander S, Schacht V, Coussens LM, von Andrian UH, van Rheenen J, et al. Collagen-based cell migration models *in vitro* and *in vivo*. *Semin Cel Dev Biol* (2009) 20(8):931–41. doi:10.1016/j.semcdb.2009.08.005

18. Egeblad M, Ewald AJ, Askautrud HA, Truitt ML, Welm BE, Bainbridge E, et al. Visualizing stromal cell dynamics in different tumor microenvironments by spinning disk confocal microscopy. *Dis Model Mech* (2008) 1(2- 3):155–67. doi:10.1242/dmm.000596

19. Han W, Chen S, Yuan W, Fan Q, Tian J, Wang X, et al. Oriented collagen fibers direct tumor cell intravasation. *Proc Natl Acad Sci U S A* (2016) 113(40):11208–13. doi:10.1073/pnas.1610347113

20. Conklin MW, Gangnon RE, Sprague BL, Van Gemert L, Hampton JM, Eliceiri KW, et al. Collagen alignment as a predictor of recurrence after ductal carcinoma *in situ*. *Cancer Epidemiol Biomarkers Prev* (2018) 27(2):138–45. doi:10.1158/1055-9965.EPI-17-0720

21. Conklin MW, Eickhoff JC, Riching KM, Pehlke CA, Eliceiri KW, Provenzano PP, et al. Aligned collagen is a prognostic signature for survival in human breast carcinoma. *Am J Pathol* (2011) 178(3):1221–32. doi:10.1016/j.ajpath.2010.11.076

22. Najafi M, Farhood B, Mortezaee K. Extracellular matrix (ECM) stiffness and degradation as cancer drivers. *J Cel Biochem* (2019) 120(3):2782–90. doi:10.1002/jcb.27681

23. Brauchle E, Kasper J, Daum R, Schierbaum N, Falch C, Kirschniak A, et al. Biomechanical and biomolecular characterization of extracellular matrix structures in human colon carcinomas. *Matrix Biol* (2018) 68-69:180–93. doi:10.1016/j.matbio.2018.03.016

24. Paul CD, Hruska A, Staunton JR, Burr HA, Daly KM, Kim J, et al. Probing cellular response to topography in three dimensions. *Biomaterials* (2019) 197:101–18. doi:10.1016/j.biomaterials.2019.01.009

25. Joint Commission on the Quality of Medical Services of the Ministry of Health of the Republic of Kazakhstan. *Clinical protocol for diagnosis and treatment of malignant tumors of the colon was approved by the joint commission on the quality of medical services of the ministry of health of the republic of Kazakhstan dated july 1, 2022 protocol No. 164* (2022).

26. Imai T. Histological comparison of cancer of the stomach in autopsy and operation cases. *Jpn J Cancer Res* (1949) 40:199–201.

27. Lugli A, Kirsch R, Ajioka Y, Bosman F, Cathomas G, Dawson H, et al. Recommendations for reporting tumor budding in colorectal cancer based on the International Tumor Budding Consensus Conference (ITBCC) 2016. *Mod Pathol* (2017) 30:1299–311. doi:10.1038/modpathol.2017.46

28. Lim SB, Yu CS, Jang SJ, Kim TW, Kim JH, Kim JC. Prognostic significance of lymphovascular invasion in sporadic colorectal cancer. *Dis Colon Rectum* (2010) 53(4):377–84. doi:10.1007/DCR.0b013e3181cf8ae5

29. Huh JW, Kim HR, Kim YJ. Prognostic value of perineural invasion in patients with stage II colorectal cancer. *Ann Surg Oncol* (2010) 17(8):2066–72. doi:10.1245/s10434-010-0982-7

30. Fagan JJ, Collins B, Barnes L, D'Amico F, Myers EN, Johnson JT. Perineural invasion in squamous cell carcinoma of the head and neck. *Arch Otolaryngol Head Neck Surg* (1998) 124(6):637–40. doi:10.1001/archotol.124.6.637

31. Yilmaz T, Hosal AS, Gedikoğlu G, Onerci M, Gürsel B. Prognostic significance of vascular and perineural invasion in cancer of the larynx. *Am J Otolaryngol* (1998) 19(2):83–8. doi:10.1016/s0196-0709(98)90100-4

32. Akimoto N, Väyrynen JP, Zhao M, Ugai T, Fujiyoshi K, Borowsky J, et al. Desmoplastic reaction, immune cell response, and prognosis in colorectal cancer. *Front Immunol* (2022) 13:840198. Published 2022 Mar 22. doi:10.3389/fimmu.2022.840198

33. Sandberg TP, Stuart MPME, Oosting J, Tollenaar RAEM, Sier CFM, Mesker WE. Increased expression of cancer-associated fibroblast markers at the invasive front and its association with tumor-stroma ratio in colorectal cancer. *BMC Cancer* (2019) 19(1):284. Published 2019 Mar 29. doi:10.1186/s12885-019-5462-2

34. Brown KM, Xue A, Smith RC, Samra JS, Gill AJ, Hugh TJ. Cancer-associated stroma reveals prognostic biomarkers and novel insights into the tumour microenvironment of colorectal cancer and colorectal liver metastases. *Cancer Med* (2022) 11(2):492–506. doi:10.1002/cam4.4452

35. Arun Gopinathan P, Kokila G, Jyothi M, Ananjan C, Pradeep L, Humaira Nazir S. Study of collagen birefringence in different grades of oral squamous cell carcinoma using picrosirius red and polarized light microscopy. *Scientifica (Cairo).* (2015) 2015:802980. doi:10.1155/2015/802980

36. Joyce JA, Pollard JW. Microenvironmental regulation of metastasis. *Nat Rev Cancer* (2009) 9(4):239–52. doi:10.1038/nrc2618

37. Bissell MJ, Radisky D. Putting tumours in context. *Nat Rev Cancer* (2001) 1(1):46–54. doi:10.1038/35094059

38. Beacham DA, Cukierman E. Stromagenesis: the changing face of fibroblastic microenvironments during tumor progression. *Semin Cancer Biol* (2005) 15(5):329–41. doi:10.1016/j.semcancer.2005.05.003

39. Guinney J, Dienstmann R, Wang X, de Reyniès A, Schlicker A, Soneson C, et al. The consensus molecular subtypes of colorectal cancer. *Nat Med* (2015) 21(11):1350–6. doi:10.1038/nm.3967

40. Quail DF, Joyce JA. Microenvironmental regulation of tumor progression and metastasis. *Nat Med* (2013) 19(11):1423–37. doi:10.1038/nm.3394

Pathology & Oncology Research | frontiers

TYPE Original Research
PUBLISHED 24 February 2023
DOI 10.3389/pore.2023.1610874

Check for updates

OPEN ACCESS

EDITED BY
Anna Sebestyén,
Semmelweis University, Hungary

*CORRESPONDENCE
Hongbo Wei,
zssyweihb@163.com
Tufeng Chen,
chentuf@mail.sysu.edu.cn

†These authors have contributed equally to this work

RECEIVED 09 October 2022
ACCEPTED 14 February 2023
PUBLISHED 24 February 2023

CITATION
Jia G, Lei P, Zhang Y, Zheng Z, Fang J, Yang X, Wei H and Chen T (2023), New staging systems for left-sided colon cancer based on the number of retrieved and metastatic lymph nodes provide a more accurate prognosis. *Pathol. Oncol. Res.* 29:1610874. doi: 10.3389/pore.2023.1610874

COPYRIGHT
© 2023 Jia, Lei, Zhang, Zheng, Fang, Yang, Wei and Chen. This is an open-access article distributed under the terms of the Creative Commons Attribution License (CC BY). The use, distribution or reproduction in other forums is permitted, provided the original author(s) and the copyright owner(s) are credited and that the original publication in this journal is cited, in accordance with accepted academic practice. No use, distribution or reproduction is permitted which does not comply with these terms.

New staging systems for left-sided colon cancer based on the number of retrieved and metastatic lymph nodes provide a more accurate prognosis

Guiru Jia†, Purun Lei†, Yanru Zhang, Zongheng Zheng, Jiafeng Fang, Xiaofeng Yang, Hongbo Wei* and Tufeng Chen*

Department of Gastrointestinal Surgery, The Third Affiliated Hospital, Sun Yat-sen University, Guangzhou, China

Objectives: We aimed to explore reasonable lymph node classification strategies for left-sided colon cancer (LCC) patients.

Methods: 48,425 LCC patients from 2010 to 2015 were identified in the US Surveillance, Epidemiology, and End Results database. We proposed an innovative revised nodal (rN) staging of the 8th American Joint Committee on Cancer (AJCC) Tumor/Node/Metastasis (TNM) classification based on the cut-off value of retrieved lymph nodes and survival analyses in patients with LCC. Log odds of positive lymph nodes (LODDS) stage is a numerical classification strategy obtained by a formula that incorporates the numbers of retrieved and positive lymph nodes. To develop the TrN or TLODDS classification, patients with similar survival rates were grouped by combining T and rN or LODDS stage. The TrN or TLODDS classification was further evaluated in a validation set of 12,436 LCC patients from 2016 to 2017 in the same database and a Chinese application set of 958 LCC patients.

Results: We developed novel TrN and TLODDS classifications for LCC patients that incorporated 7 stages with reference to the AJCC staging system. In comparison to the 8th AJCC TNM and TrN classifications, TLODDS classification demonstrated significantly better discrimination (area under the receiver operating characteristic curve, 0.650 vs. 0.656 vs. 0.661, $p < 0.001$), better model-fitting (Akaike information criteria, 309,287 vs. 308,767 vs. 308,467), and superior net benefits. The predictive performance of the TrN and TLODDS classifications was further verified in the validation and application sets.

Conclusion: Both the TrN and TLODDS classifications have better discriminatory ability, model-fitting, and net benefits than the existing TNM classification, and represent an alternative to the current TNM classification for LCC patients.

KEYWORDS

left-sided colon cancer, retrieved lymph nodes, log odds of positive lymph nodes, revised nodal stage, staging system

Introduction

Colorectal cancer (CRC) is the third most common cancer worldwide and the second most common cause of cancer-specific mortality (1). CRC continues to present challenges to patients and clinicians worldwide. Tumors originating in the distal third of the transverse colon, descending, sigmoid colon, and rectum are classified as left-sided colon cancer (LCC) tumors, whereas tumors originating in the caecum, ascending, and proximal two-thirds of the transverse colon are classified as right-sided colon cancer (RCC) tumors (2, 3). Recent in-depth research on CRC reported differences in clinical manifestations and patient prognosis between LCC and RCC (4–6). In the left-sided tumors, researchers observed chromosomal instability pathway-related mutations, such as KRAS, p53, APC, PIK3CA mutations, and demonstrate polypoid-like morphology (5–8). LCC and RCC have been identified as two different types of solid tumors. Evaluating LCC separately will have a positive impact on the application of individualized treatments to corresponding patients.

An accurate staging system is critical for clinical practice. Furthermore, the status of lymph nodes (N stage) is regarded as the most important predictor of survival (9). The American Joint Committee on Cancer (AJCC) Tumor/Node/Metastasis (TNM) classification is worldwide applied to assess the prognosis of patients with LCC. The American Society of Clinical Oncology and the National Comprehensive Cancer Network have issued guidelines for AJCC N staging of LCC requiring clinical physicians to evaluate at least 12 lymph nodes in clinical work (10). An increase in the number of retrieved lymph nodes (LNs) is known to be associated with a survival benefit for both node-negative and node-positive LCC patients (11). Nevertheless, insufficient lymph node sampling may lead to under-staging and subsequent misestimation of the prognosis (12). We aimed to investigate a more acceptable lymph node staging strategy for LCC, taking into account the quantity of retrieved LNs and metastatic status. We stratified the AJCC N staging based on the lymph node cut-off value and combined subgroups with similar survival rates to establish a revised nodal (rN) staging. Log odds of positive lymph nodes (LODDS) is another potential option as this could be applied to multiple types of cancers (13–15). LODDS has been proved to have a prognostic advantage for CRC (15).

The difference in prognosis between LCC and RCC indicates their different requirements for the staging system. So far, there are no reports exploring the prognostic value of the new staging system for LCC. In this study, we aimed to develop TrN and TLODDS classifications for LCC using a training set acquired from the US Surveillance, Epidemiology, and End Results (SEER) database. We compared the discrimination, model-fitting, and net benefits of the novel classifications to the 8th AJCC TNM classification to determine whether they could improve survival stratification. Finally, we investigated the predictive performance of new models in a validation set from the same database and an application set from a Chinese hospital.

Materials and methods

Data sources and screening criteria

48,425 cases of LCC from 2010 to 2015 were identified in the SEER database (National Cancer Institute, https://seer.cancer.gov/) to act as a training set, and 12,436 cases from 2016 to 2017 were considered as a validation set. We determined the codes from the International Classification of Diseases for Oncology for eligible patients: C185, C186, C187, C199 and C209 for LCC patients, and C180, C182, C183 and C184 for RCC patients (3). Data from the SEER database was exempted from informed consent and ethics committee review. We also incorporated an application set of LCC patients from The Third Affiliated Hospital of Sun Yat-sen University (SYSU). The latest follow-up was July 2021. The Institute Ethics Committee approved the study. The flow chart for patient selection is shown in Supplementary Figure S1.

TABLE 1 5-year overall survival (OS) rates of corresponding N0 to N2b of >14 LNs vs. ≤14 LNs cohorts.

The 8th AJCC pN stage	5-Year OS rate (%)	
	The number of LNs retrieved >14 (Adequate set)	The number of LNs retrieved ≤14 (Inadequate set)
pN0	82.0	78.1
pN1a	78.3	70.6
pN1b	73.1	65.1
pN1c	71.0	55.6
pN2a	68.9	57.1
pN2b	53.8	46.1

TABLE 2 The rN staging for LCC in the training set according to the 8th AJCC pN classification stratified into Adequate (>14 LNs) and Inadequate (≤14 LNs) set.

The 8th AJCC pN stage	rN stage	
	Adequate set(No.)	Inadequate set (No.)
pN0	rN0 (n = 15,989)	rN1a (n = 13,338)
pN1a	rN1a (n = 3,601)	rN1c(n = 2,648)
pN1b	rN1b(n = 3,578)	rN2a (n = 2,280)
pN1c	rN1c(n = 464)	rN2b(n = 451)
pN2a	rN2a (n = 2,322)	rN2b(n = 1,163)
pN2b	rN2b(n = 2060)	rN2b(n = 531)

TABLE 3 The development of the TrN classification for patients with LCC in the training set.

TrN staging system	5-Y OS, % (95% CI)	HR (95% CI)	Log-rank (Mantel-Cox)	
			χ^2-value	*p*-value
Stage I				
T1rN0	90.2 (89.1–91.3)	1.00(Ref.)	-	-
Stage IIA				
T1rN1	87.8 (86.9–88.7)	1.20 (1.07–1.35)	9.024	0.003
Stage IIB				
T2rN0	86.9 (85.7–88.1)	1.40 (1.24–1.59)	9.294	0.002
T1rN2a	83.8 (79.2–88.8)	1.66 (1.25–2.20)	1.307	0.253
T2rN1	81.8 (80.6–83.0)	1.89 (1.69–2.11)	0.891	0.345
T2rN2a	79.0 (75.3–82.8)	1.92 (1.57–2.35)	0.035	0.852
T3rN0	80.1 (79.2–81.0)	2.05 (1.84–2.27)	0.494	0.482
Stage IIC				
T1rN2b	70.9 (61.7–81.5)	2.59 (1.77–3.80)	1.52	0.218
T3rN1	73.7 (72.9–74.5)	2.68 (2.42–2.97)	0.028	0.867
T2rN2b	71.8 (66.1–77.9)	2.91 (2.30–3.68)	0.52	0.471
T3rN2a	67.9 (66.3–69.6)	3.30 (2.95–3.68)	1.266	0.26
T4arN0	67.3 (63.9–71.0)	3.39 (2.91–3.95)	0.165	0.684
T4brN0	65.1 (61.8–68.5)	3.64 (3.15–4.20)	0.726	0.394
Stage IIIA				
T4arN1	58.5 (55.9–61.2)	4.48 (3.96–5.07)	9.074	0.003
T3rN2b	56.8 (55.0–58.7)	4.76 (4.26–5.30)	1.615	0.204
Stage IIIB				
T4brN1	54.3 (51.2–57.5)	5.33 (4.69–6.05)	4.953	0.026
T4arN2a	53.3 (48.9–58.0)	5.34 (4.58–6.23)	0.003	0.957
Stage IIIC				
T4brN2a	43.8 (37.9–50.6)	6.79 (5.64–8.18)	5.479	0.019
T4arN2b	41.2 (37.6–45.2)	7.84 (6.86–8.96)	2.441	0.118
T4brN2b	36.6 (31.5–42.4)	8.87 (7.52–10.46)	2.108	0.146

Inclusion criteria: a positive follow-up; the primary tumor was located in the left-sided colon; being AJCC stage I–III.

Exclusion criteria: patients with incomplete clinicopathological information such as numbers of retrieved and positive lymph nodes, TN stage and primary site; patients who died during the first postoperative month.

Development of TrN and TLODDS staging systems

Lymph node involvement was classified according to the 8th AJCC pathological N (pN) classification (pN0: no metastasis; pN1a: 1 metastatic lymph node; pN1b: 2-3 metastatic LNs; pN1c: no metastatic lymph node, but there are tumor deposits (TD) in subserosal, mesenteric, pericolonic or perirectal tissue; pN2a: 4-6 metastatic LNs; pN2b: 7 and more metastatic LNs) (9). The optimal cut-off value of retrieved LNs in patients with LCC calculated by X-tile software in the training set was 14. Then, we developed a lymph node staging strategy called rN staging to homogenize the nodal classification of LCC cohorts comprising of both >14 (Adequate set) and ≤14 (Inadequate set) LNs. Six pN substages from pN0 to pN2b were obtained by using the 8th AJCC pN stage in Inadequate and Adequate sets, respectively. Table 1 shows the detailed overall survival (OS) rates of the 8th AJCC pN stage. By dividing it into its respective Inadequate set and Adequate set, we found that the 5-year OS rates of $N0_{inadequate}$ to $N2a_{inadequate}$ were closer to that of $N1a_{adequate}$ to $N2b_{adequate}$, rather than their corresponding $N0_{adequate}$ to $N2a_{adequate}$. As displayed in Figure 2, there was no significant difference between Kaplan–Meier OS curves of patients under $pN0_{inadequate}$ and $pN1a_{adequate}$ (p = 0.73), $pN1a_{inadequate}$ and $pN1c_{adequate}$ (p = 0.59), $pN1c_{inadequate}$ and $pN2b_{adequate}$ (p = 0.39). The p-value of survival curves of $pN1b_{inadequate}$ and $pN2a_{adequate}$

TABLE 4 LODDS staging for patients with LCC in the training set.

LODDS-value	Log-rank (Mantel-Cox)	
	χ^2-value	*p*-value
≤−1.9	-	-
−1.9~−1.7	1.576	0.209
−1.7~−1.5	0.748	0.387
−1.5~−1.3	**27.887**	**<0.001**
−1.3~−1.1	4.786	0.029
−1.1~−0.9	7.783	0.005
−0.9~−0.7	**12.928**	**<0.001**
−0.7~−0.5	5.101	0.024
−0.5~−0.3	1.615	0.204
−0.3~-0.1	**29.759**	**<0.001**
−0.1~0.1	5.236	0.022
0.1~0.3	**7.974**	**0.005**
0.3~0.5	0.127	0.721
0.5~0.7	1.405	0.236
0.7~0.9	2.62	0.106
0.9~1.1	0.058	0.81
1.1~1.3	5.808	0.016
1.3~1.5	0.851	0.356
1.5~1.7	2.435	0.119
>1.7	0.151	0.697

The chi-square values in bold represent 4 peaks as the cut-off values. The *p* values in bold are the *p* values corresponding to the cutoff values.

was less than that of $pN1b_{inadequate}$ and $pN1c_{adequate}$. Table 2 showed that subgroups with similar survival rates were then aggregated to determine the rN stage. Next, we replaced the pN classification of the 8th AJCC pTNM staging system with our rN classification to form the pTrNM classification. Log-rank tests for OS were conducted between two neighboring substages and 19 χ^2 values were generated (Table 3). The Cox proportional hazards model was used to estimate hazard ratio (HR) values for per substage (using the HR of T1rN0 as a reference), and all substages were sorted by HR values from the lowest (T1rN0) to the highest (T4brN2b). Five peak cutoff χ^2 values (9.024, 9.294, 9.074, 4.953, 5.479) were identified in LCC patients, and merge substages between neighboring peak cutoff χ^2 values. But there were far too many substages from substage T2rN0 to T4brN0. We chose substage T1rN2b to be stopped in the middle depending on the survival curve and HR value of each substage (Figure 3A; Table 3). We developed seven categories for the TrN classification (I, IIA, IIB, IIC, IIIA, IIIB, IIIC).

LODDS was estimated by: $\mathrm{LODDS} = log\frac{\mathrm{pLNs}+0.5}{\mathrm{LNs}-\mathrm{pLNs}+0.5}$, where the pLNs is the number of positive lymph nodes and LNs is the total number of retrieved lymph nodes, and 0.5 is added to both numerator and denomination to avoid singularity(16). In the training set, patients with LCC were classified into 20 substages (divided by unit 0.2, as shown in Table 4). HR values were ordered from the lowest (using LODDS ≤ −1.9 as a reference) to the highest (LODDS>1.7). Log-rank tests were conducted between two neighboring LODDS substages and 19 χ^2 values were generated. Four peaks of χ^2 values were identified as the cutoff values. Using the four identified cutoff values for LODDS, a novel LODDS stage with five categories was developed (LODDS1≤−1.5; −1.5<LODDS2≤−0.9; −0.9<LODDS3≤−0.3; −0.3<LODDS4≤0.1; LODDS5>0.1). We replaced the pN classification of the 8th AJCC pTNM staging system with our LODDS classification to form the pTLODDSM classification. Log-rank tests for OS were conducted between two neighboring substages and 25 χ^2 values were generated (Table 5). Six peak cutoff χ^2 values (16.814, 22.778, 76.608, 7.771, 8.919, 8.414) were identified. We merged substages between neighboring peak cutoff χ^2 values, so as to obtain seven categories for the TLODDS classification (I, IIA, IIB, IIC, IIIA, IIIB, IIIC).

Statistical analysis

We conducted a descriptive analysis of the study population. Continuous variables were expressed as median (interquartile range), while categorical variables were expressed as count and percentage. Their clinical characteristics were compared using Pearson's χ^2 test. The Kaplan–Meier method was used to calculate OS, and log-rank tests were used to compare survival differences between the groups. A cox proportional regression hazard model was used to identify risk factors significantly associated with OS. X-Tile software (https://medicine.yale.edu/lab/rimm/research/software.aspx) was used to identify the potential cut-off values for each LN group based on minimal probability (P) values (17). The predictive accuracy of the model was evaluated by the value of area under the receiver operating characteristic curve (AUC). A larger AUC value represented a more accurate model prediction. The linear trend χ^2 test was used to measure the discriminatory ability and gradient monotonicity. The likelihood ratio χ^2 test was used to assess the homogeneity (no significant differences in survival among patients with the same stage) within each stage. A higher linear trend chi-square score showed better discriminatory ability and monotonicity, while higher likelihood ratio chi-square scores meant better homogeneity. Akaike information criteria (AIC) and Bayesian information criterion (BIC) represented the model fitting level (18). A smaller AIC or BIC value indicated a more desirable model for prediction of OS outcomes. Clinical benefits were assessed by decision curve analyses (DCAs) (19, 20).

All analyses were performed with the R software (version 4.1.1; R Foundation for Statistical Computing, Vienna, Austria) and SPSS version 22.0 for Windows (IBM Corporation, Chicago, IL, USA), and a two-tailed *p*-value <0.05 was considered statistically significant.

TABLE 5 The development of the TLODDS classification for patients with LCC in the training set.

TLODDS staging system	5-Y OS, % (95% CI)	HR (95% CI)	Log-rank (Mantel-Cox)	
			χ^2-value	*p*-value
Stage I				
T1LODDS1	91.0 (89.9–92.2)	1.00(Ref.)	-	-
Stage IIA				
T1LODDS2	87.6 (86.6–88.6)	1.31 (1.15–1.49)	16.814	<0.001
T1LODDS3	86.9 (84.8–89.1)	1.46 (1.22–1.75)	1.598	0.206
T2LODDS1	86.8 (85.6–88.1)	1.54 (1.34–1.76)	0.567	0.451
Stage IIB				
T2LODDS2	82.6 (81.4–83.9)	1.98 (1.75–2.24)	22.778	<0.001
T2LODDS3	80.0 (77.7–82.4)	2.13 (1.82–2.49)	1.164	0.281
T3LODDS1	80.5 (79.7–81.4)	2.17 (1.93–2.44)	0.154	0.695
Stage IIC				
T3LODDS2	75.1 (74.2–75.9)	2.77 (2.48–3.11)	76.608	<0.001
T2LODDS4	70.7 (64.1–78.0)	3.12 (2.37–4.10)	0.842	0.359
T1LODDS4	72.4 (62.6–83.8)	3.20 (2.15–4.77)	0.016	0.899
T2LODDS5	66.1 (55.7–78.4)	3.51 (2.39–5.17)	0.076	0.783
T3LODDS3	68.2 (67.0–69.5)	3.58 (3.19–4.02)	0.006	0.937
T1LODDS5	69.7 (57.1–85.0)	3.70 (2.30–5.94)	0.026	0.873
T4aLODDS1	66.3 (62.8–70.0)	3.75 (3.20–4.40)	0	0.999
T4bLODDS1	65.9 (62.6–69.3)	3.91 (3.36–4.56)	0.286	0.593
Stage IIIA				
T4aLODDS2	59.9 (57.0–63.0)	4.79 (4.16–5.51)	7.771	0.005
T3LODDS4	58.3 (55.9–60.8)	4.80 (4.22–5.46)	0.021	0.883
T4aLODDS3	54.4 (51.1–57.9)	5.55 (4.81–6.39)	5.48	0.019
T4bLODDS2	55.0 (51.7–58.6)	5.56 (4.82–6.41)	0.012	0.914
Stage IIIB				
T4aLODDS4	46.7 (41.5–52.6)	7.25 (6.08–8.64)	8.919	0.003
T4bLODDS3	45.3 (40.8–50.4)	7.37 (6.28–8.65)	0.018	0.893
T3LODDS5	44.6 (41.4–48.0)	7.42 (6.48–8.51)	0.037	0.848
T4bLODDS4	40.7 (33.5–49.5)	7.985 (6.361–10.023)	0.361	0.548
Stage IIIC				
T4aLODDS5	30.8 (25.6–37.0)	11.91 (9.99–14.19)	8.414	0.004
T4bLODDS5	26.4 (19.6–35.5)	14.02 (11.20–17.55)	2.455	0.117

Result

Relationships between the number of retrieved LNs and prognosis

Supplementary Table S1 shows the demographic and pathological characteristics of the eligible patients. The median number of retrieved LNs in LCC patients was larger than 12 (16 in the training set, 17 in the validation set, and 17 in the application set), implying that the number of LNs retrieved according to the guidelines was even less.

We used X-tile software to determine the best cut-off value for the number of LNs retrieved by LCC and RCC. According to descriptive statistics, the optimal minimum number of retrieved LNs of RCC is higher than that of LCC (18 vs. 14, as shown in Figure 1; Supplementary Figure S2). It is crucial to develop a lymph node staging system that distinguishes between LCC and RCC. Evaluation of LCC alone can more accurately evaluate the prognosis characteristics of LCC population. By comparing the number of LNs and cut-off value, LCC study population was divided into two categories, and the survival curves of LNs >14 (Adequate set) and LNs ≤14 (Inadequate set) were drawn, respectively. Two subgroups showed significant differences in survival prognosis ($p < 0.0001$, as shown in Figure 1B).

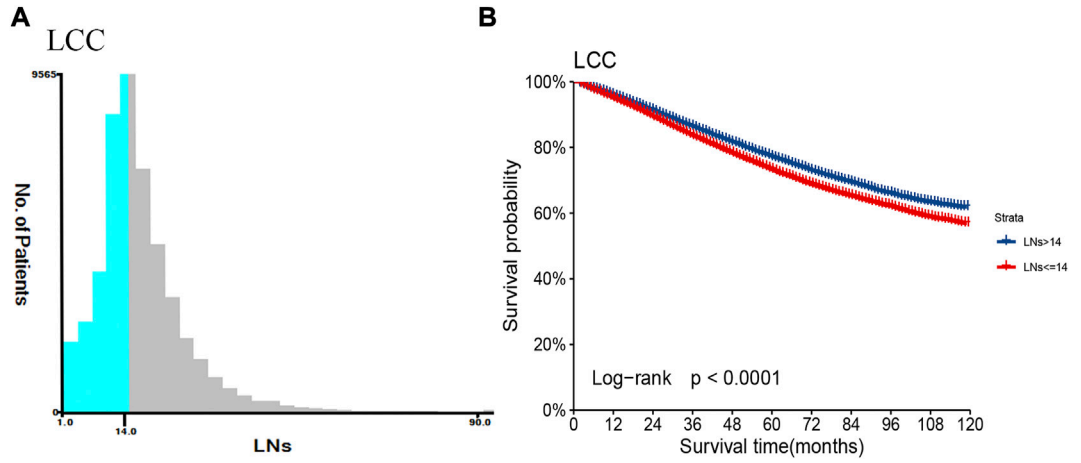

FIGURE 1
The number of retrieved LNs and prognosis difference between patients with LCC in the training set. **(A)** Based on the results of X-tile software, the best cut-off point of regional lymph node count in patients with LCC was determined. **(B)** The Kaplan-Meier survival curves of patients with LCC were depicted using the retrieved optimal thresholds of the two groups of retrieved LNs.

Development of rN classification and TrN staging system

We stratified 6 pN stages in the training set based on the LNs cutoff value and established rN stages by merging subgroups with similar survival rates. The initial six pN subgroups with LNs>14 (Adequate set) were labeled as rN0-rN2b. Subgroups with no significant difference in OS between LNs≤14 (Inadequate set) and LNs>14 (Adequate set) were combined (Figure 2; Table 2).

Referring to the 8th AJCC TNM stage, the three subgroups of pN1 have no effect on the overall TNM staging results, hence we consolidated rN1a-c into rN1 for subsequent analysis. Five peak cutoff χ^2 values (9.024, 9.294, 9.074, 4.953, 5.479) were identified in LCC patients. Then we merged substages between neighboring peak cutoff χ^2 values. A trouble was shown in Table 3. There were far too many substages from substage T2rN0 to T4brN0. We chose substage T1rN2b to be stopped in the middle, depending on the survival curve and HR value of each substage (Figure 3A; Table 3). Twenty substages were clustered into a novel TrN classification of seven clusters (Figure 3B).

Development of LODDS classification and TLODDS staging system

First, we calculated the LODDS value of each LCC patient in the training set, and then divided the study population into 20 subgroups according to the unit of 0.2. We used the log-rank (Mantel-Cox) test between adjacent subgroups to identify 19 cutoff χ^2values. We chose four peak cutoff χ^2 values (27.887, 12.928, 29.759 and 7.974) to distinguish the cut-off values of LODDS (−1.5, −0.9, −0.3 and 0.1) (Table 4). We created a LODDS stage consisting of five categories: (1) LODDS1≤−1.5; (2) −1.5< LODDS2≤−0.9; (3) −0.9< LODDS3≤−0.3; (4) −0.3< LODDS4≤0.1 and (5) LODDS5>0.1.

25 substages (T1-4bLODDS1-5) were created by merging the T and LODDS classifications. HR values were ranked from lowest to highest (using T1LODDS1 as a reference, HR = 1.00). We used the log-rank (Mantel-Cox) test between adjacent substages to identify 24 cutoff χ^2 values. The six peak cutoff χ^2 values (16.814, 22.778, 76.608, 7.771, 8.919, 8.414) whose corresponding *p* values were less than 0.05 between two neighboring substages were chosen. According to the six peak cutoff χ^2 values, 25 substages were clustered into a novel TLODDS classification of seven categories (I, IIA, IIB, IIC, IIIA, IIIB, IIIC) (Table 5). Kaplan-Meier curves with log-rank tests and details of the novel TLODDS classification are shown in Figure 4.

Comparison of the three staging systems

In the training set, the 8th AJCC TNM classification displayed an unreasonable predictive performance in that stage IIIA and IIIB had higher 5-year survival rates than stage IIA and IIB (Supplementary Table S2). However, the 5-year OS rates for LCC patients according to the TrN or TLODDS classification showed steadily decreasing trends as the stage increased (5-year OS, stages I to IIIC, 90.2%, 87.8%, 81.9%, 71.9%, 57.3%, 54.0% and 40.6% according to TrN classification; 91.0%, 87.3%, 81.1%, 72.0%, 57.3%, 44.8% and 29.4% according to TLODDS classification). Furthermore, HRs exhibited consistently increasing tendencies as the stage increased (HRs, stages I to IIIC, 1.0, 1.2, 1.9, 2.9, 4.7, 5.4 and 7.9 according to TrN classification; 1.0, 1.4, 2.1, 3.1, 5.1, 7.5 and 12.6 according to TLODDS classification). The TLODDS and TrN

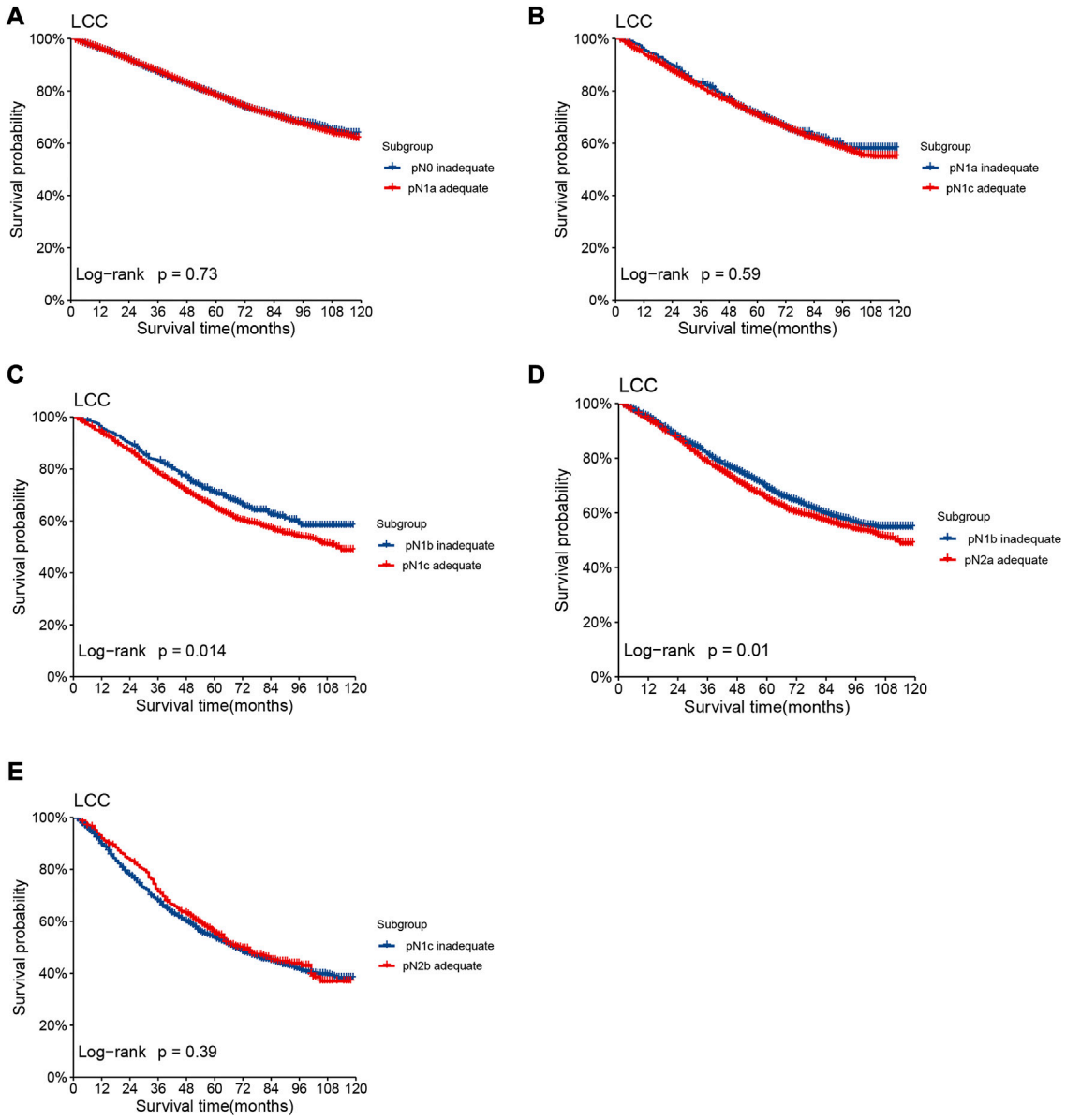

FIGURE 2
Kaplan–Meier OS curves of patients under different pN stages assigned to Inadequate set and Adequate set. Subgroup **(A)** $pN0_{inadequate}$ vs. $pN1a_{adequate}$, **(B)** $pN1a_{inadequate}$ vs. $pN1c_{adequate}$, **(C)** $pN1b_{inadequate}$ vs. $pN1c_{adequate}$, **(D)** $pN1b_{inadequate}$ vs. $pN2a_{adequate}$, **(E)** $pN1c_{inadequate}$ vs. $pN2b_{adequate}$ of patients with LCC in the training set.

classifications also showed better prognostic discrimination (AUC, 0.661 vs. 0.656 vs. 0.650; Liner trend χ^2 score, 3,104.5 vs. 2,851.6 vs. 1,504.4, $p < 0.001$), better model-fitting (AIC, 308,467 vs. 308,767 vs. 309,287), and superior net benefits than the TNM classification (Figure 5; Table 6).

The predictive performance of TrN and TLODDS classifications was validated in the validation or application set. As demonstrated in Figures 6, 7, both TrN and TLODDS classifications identify I-IIIC stages effectively in the validation or application set for patients with LCC, with significant differences in OS between neighboring stages. The TLODDS classification showed the best prognosis discrimination across the three staging systems (Figures 6C, 7C), as well as the best model fit and net benefit (Figures 6D, 7D; Table 6).

Discussion

Tumor staging is a key criterion for evaluating the severity of the cancer, formulating treatment strategies, predicting the

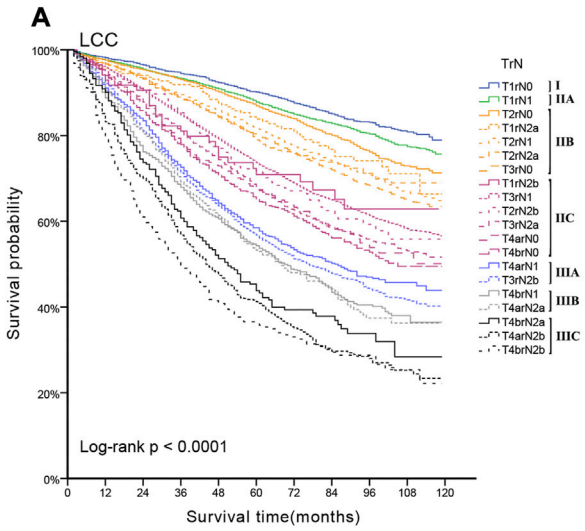

B

(LCC)TrN	rN0	rN1a	rN1b	rN1c	rN2a	rN2b
T1	I	IIA	IIA	IIA	IIB	IIC
T2	IIB	IIB	IIB	IIB	IIB	IIC
T3	IIB	IIC	IIC	IIC	IIC	IIIA
T4a	IIC	IIIA	IIIA	IIIA	IIIB	IIIC
T4b	IIC	IIIB	IIIB	IIIB	IIIC	IIIC

FIGURE 3
(A) Kaplan-Meier estimates for the novel classification of LCC characterized by T-stage and rN stage. **(B)** Details of the novel LCC TrN classification.

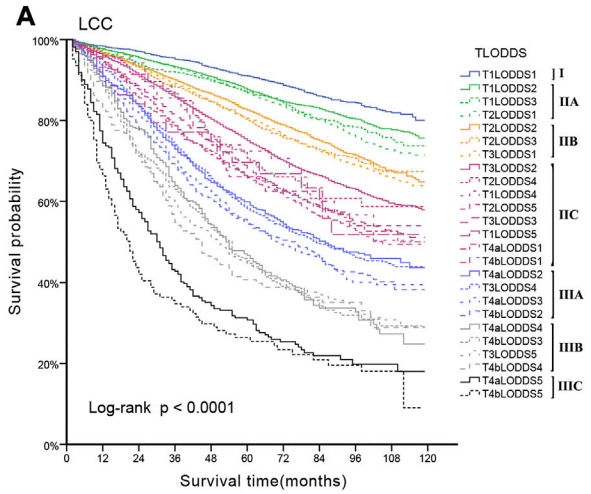

B

LODDS value	≤-1.5	-1.5 ~ -0.9	-0.9 ~ -0.3	-0.3 ~ 0.1	>0.1
(LCC)TLODDS	LODDS1	LODDS2	LODDS3	LODDS4	LODDS5
T1	I	IIA	IIA	IIC	IIC
T2	IIA	IIB	IIB	IIC	IIC
T3	IIB	IIC	IIC	IIIA	IIIB
T4a	IIC	IIIA	IIIA	IIIB	IIIC
T4b	IIC	IIIA	IIIB	IIIB	IIIC

FIGURE 4
(A) Kaplan-Meier estimates for the novel classification of LCC characterized by T-stage and LODDS stage. **(B)** Details of the novel LCC TLODDS classification.

recurrence risk and long-term survival of patients. Accurate staging allows cross-sectional comparisons of cohort data from different countries and centers. Currently, stage III of LCC patients even showed a trend of better prognosis than stage II patients according to the 8th AJCC TNM staging system used worldwide. It is crucial to develop new classifications to better stratify LCC survival. The primary flaw of the number-based AJCC pN classification is that the accuracy of the predicted prognosis was significantly influenced by the total number of retrieved LNs (11). The distinct requirements of LCC and RCC patients for the amount of retrieved LNs prompted us to investigate the

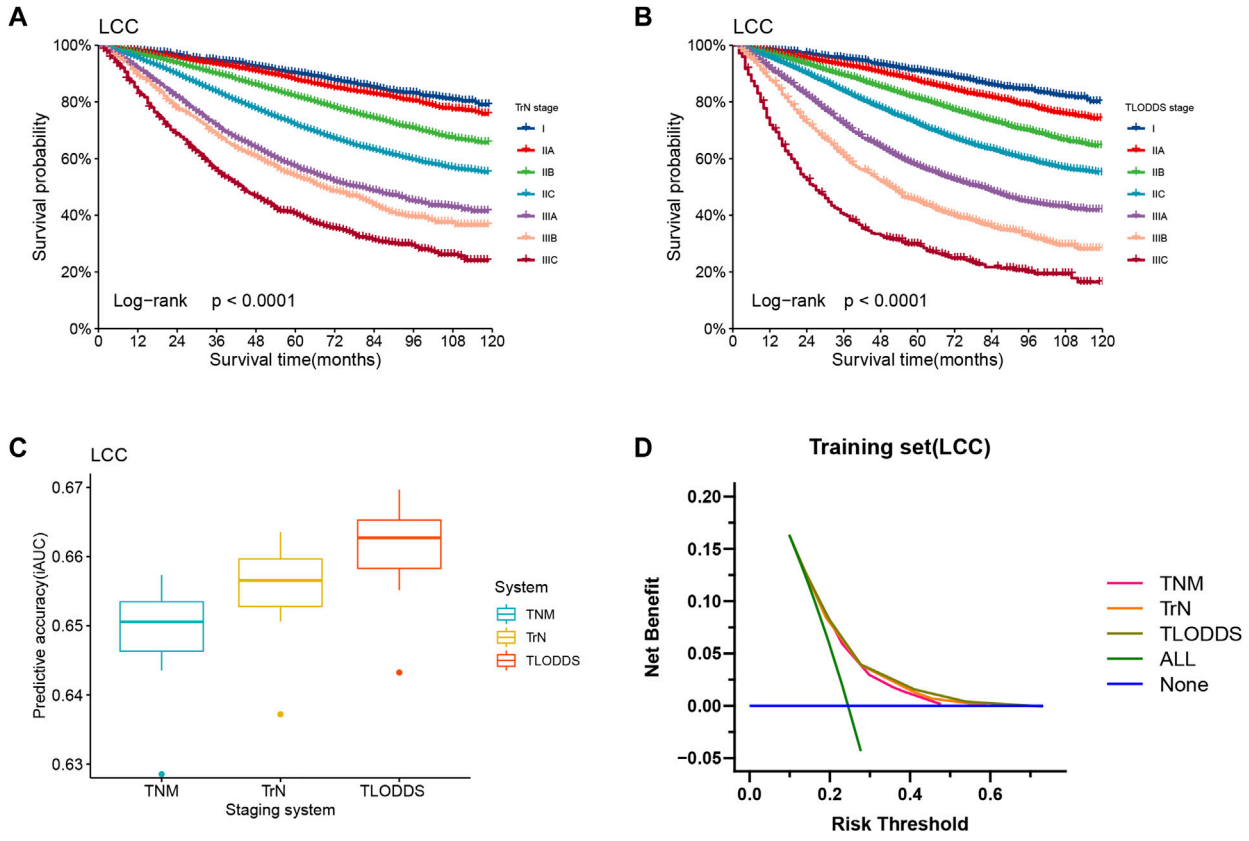

FIGURE 5
Model evaluation of three staging systems for patients with LCC in the training set. The Kaplan-Meier survival curves of patients with LCC in the training set were depicted according to the **(A)** TrN or **(B)** TLODDS staging system. **(C)** Performance of the TrN and TLODDS staging systems compared with the AJCC TNM staging system. **(D)** Decision curve analyses to compare the estimation of OS among the AJCC TNM, TrN and TLODDS classifications.

TABLE 6 Comparison of the performance of the 8th AJCC TNM, TrN and TLODDS staging systems in predicting prognosis of LCC.

Staging system	Liner trend χ2	Likelihood ratio χ2	AIC	BIC
Training set				
AJCC TNM	1,504.392($p < 0.001$)	2,449.929($p < 0.001$)	309,286.9	309,332.5
TrN	2,851.613($p < 0.001$)	2,942.981($p < 0.001$)	308,766.6	308,812.3
TLODDS	3,104.469($p < 0.001$)	3,212.848($p < 0.001$)	308,466.7	308,512.4
Validation set				
AJCC TNM	292.980($p < 0.001$)	475.225($p < 0.001$)	28,625.5	28,657.8
TrN	590.186($p < 0.001$)	579.894($p < 0.001$)	28,512.8	28,545.1
TLODDS	614.707($p < 0.001$)	621.676($p < 0.001$)	28,472.0	28,504.3
Application set				
AJCC TNM	85.284($p < 0.001$)	100.564($p < 0.001$)	2004.4	2023.2
TrN	92.347($p < 0.001$)	100.258($p < 0.001$)	2004.2	2019.9
TLODDS	94.823($p < 0.001$)	115.049($p < 0.001$)	1987.5	2003.2

lymph node staging of the two types of cancer (3). Scholars attempted to use the lymph node ratio (LNR, the ratio of the metastatic LNs and the total retrieved LNs) to predict patient outcomes (21). However, LNR cannot identify individuals without metastatic LNs, and its value is influenced by the overall number of LNs, hence it is not widely used. The

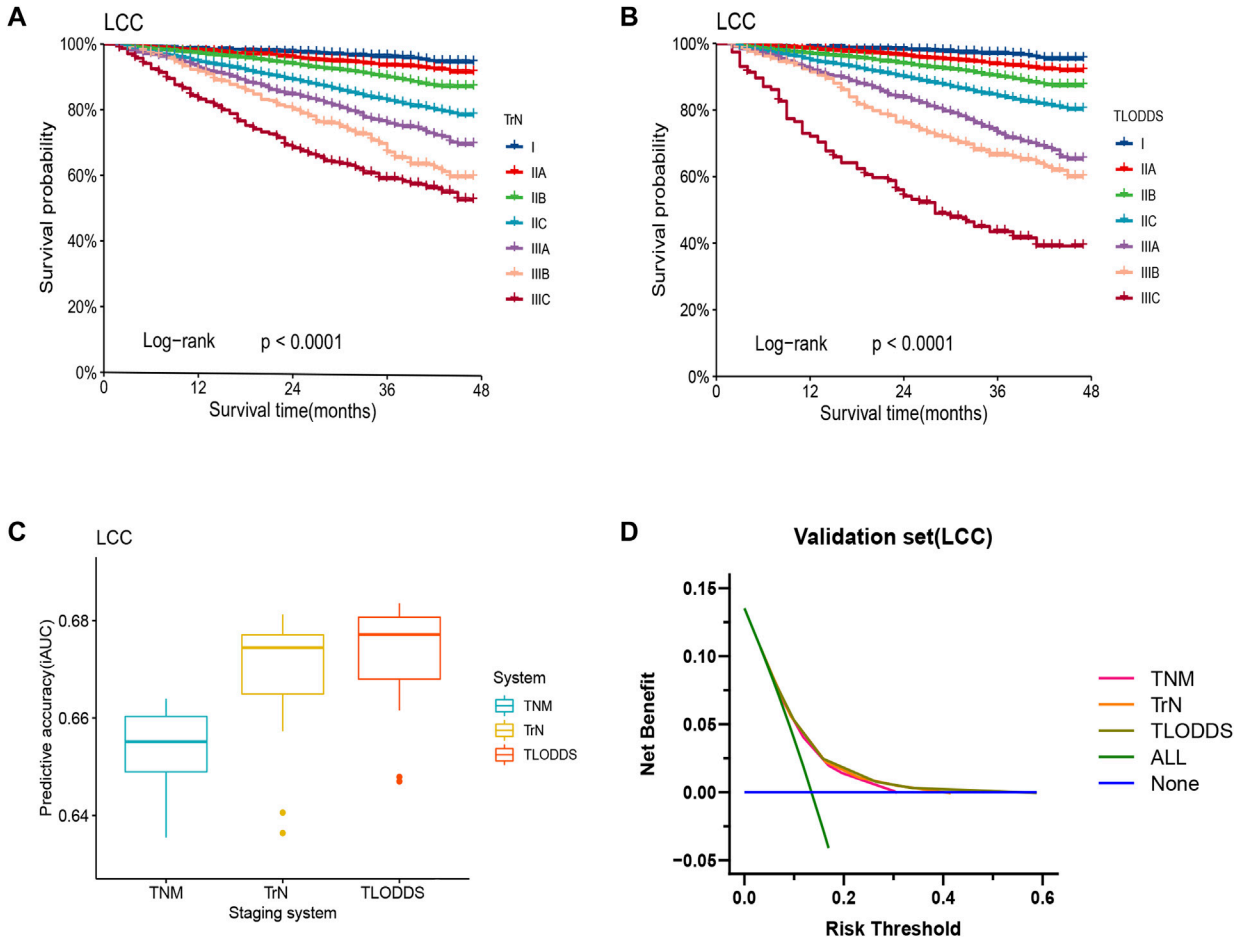

FIGURE 6
Model evaluation of three staging systems for patients with LCC in the validation set. The Kaplan-Meier survival curves of patients with LCC in the validation set were depicted according to the **(A)** TrN or **(B)** TLODDS staging system. **(C)** Performance of the TrN and TLODDS staging systems compared with the AJCC TNM staging system. **(D)** Decision curve analyses to compare the estimation of OS among the AJCC TNM, TrN and TLODDS classifications.

recently proposed LODDS has demonstrated high prediction capacity in a variety of cancers (13–15). Andrea et al. and Persiani et al. proved that LODDS classification outperformed AJCC pN and LNR classifications (22, 23).

More researches focused on the prognostic factors of RCC patients while disregarding those of LCC patients. In this study, we developed a TLODDS staging utilizing AJCC T-stage combined with LODDS classification to stratify LCC patients into different survival groups. The TLODDS staging performed better in terms of prognosis discrimination, model fitting, and net benefit. However, the computation of LODDS is relatively complicated, which increases the complexity of clinical application. Furthermore, there are other factors that may affect prognosis, including CEA markers, adjuvant treatments, microsatellite instability, KRAS and BRAF mutation status, etc. (24–26) By integrating these factors, it is possible to further improve our new classification. To successfully apply the TLODDS classification in clinical practice, the development of corresponding clinical calculators and predictive models may be an effective approach. The AJCC pN classification solely takes into account the amount of positive LNs and cannot identify individuals who do not have metastatic LNs. But it is only grouped by counting, which has undoubted advantages in clinical practice. We developed rN classification with the aim of improving prognostic stratification without increasing computational complexity. The rN classification was obtained directly by simple calculations based on postoperative pathology reports. Compared with TLODDS staging, the TrN staging system has the advantages of simpler operation in clinical practice. This suggests that TrN may be a better alternative to the AJCC TNM or TLODDS classification. Both TrN and TLODDS staging systems performed well with regard to distinguishing survival

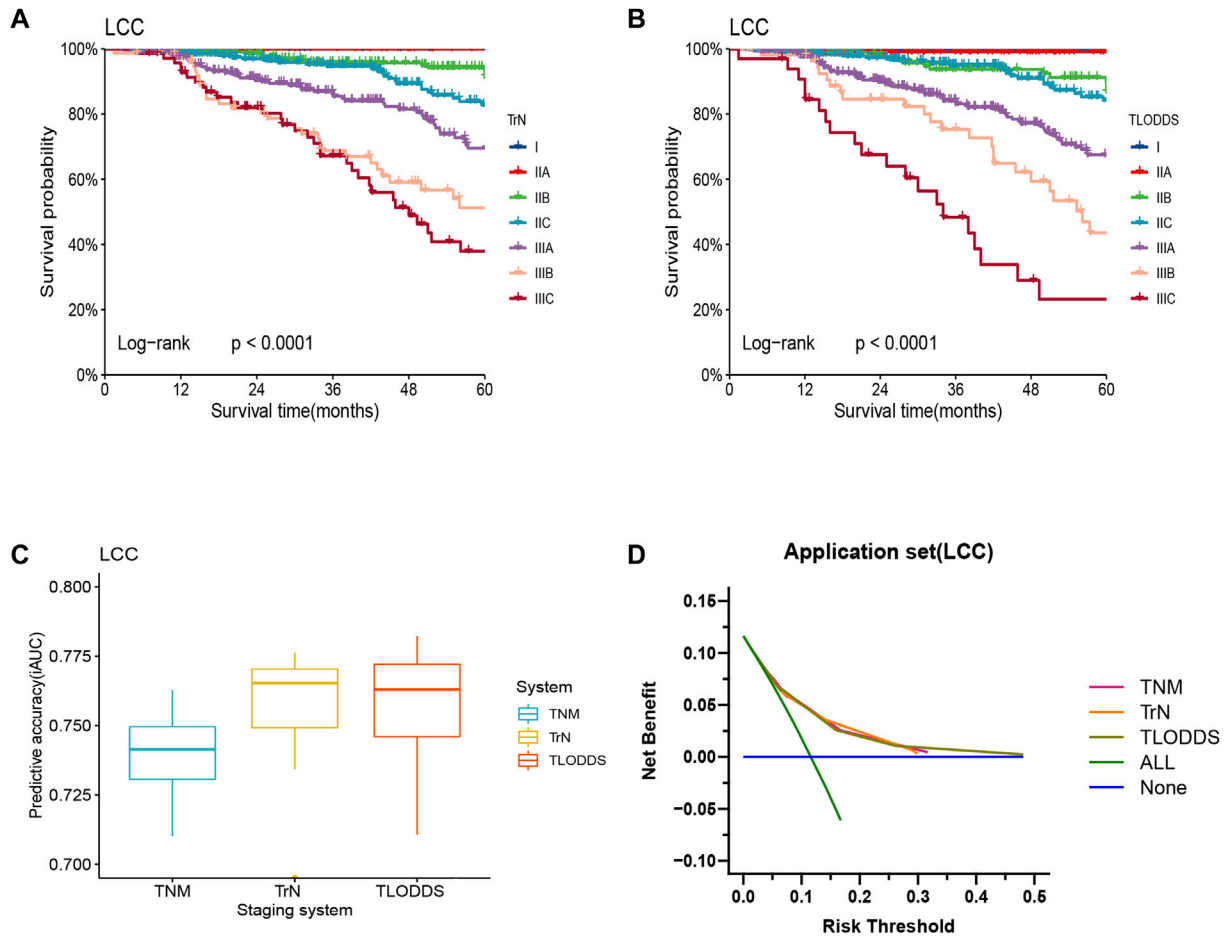

FIGURE 7
Model evaluation of three staging systems for patients with LCC in the application set. The Kaplan-Meier survival curves of patients with LCC in the application set were depicted according to the **(A)** TrN or **(B)** TLODDS staging system. **(C)** Performance of the TrN and TLODDS staging systems compared with the AJCC TNM staging system. **(D)** Decision curve analyses to compare the estimation of OS among the AJCC TNM, TrN and TLODDS classifications.

differences among different sub-stages, reflecting their general applicability. These findings were confirmed in the validation set.

However, this study has some shortcomings. The SEER 22 enrollment data represents only 28% of the U.S. population, and these data were not randomly selected, making the analysis biased (27). Additionally, there was an unavoidable unknown bias owing to the retrospective experimental design. Validation in large, multi-center, prospective clinical trials is needed to obtain more reliable results.

Conclusion

In conclusion, the TrN and TLODDS staging systems can effectively distinguish the survival differences, and more accurately predict the 5-year OS rate of patients undergoing coloproctectomy with insufficient numbers of retrieved LNs compared with that of the TNM staging system.

Data availability statement

The original contributions presented in the study are included in the article/Supplementary Material, further inquiries can be directed to the corresponding authors.

Ethics statement

The studies involving human participants were reviewed and approved by Ethics Committee of the Third Affiliated Hospital of Sun Yat-sen University. Written informed consent from the participants or their legal guardian/next of kin was not

required to participate in this study in accordance with the national legislation and the institutional requirements.

Author contributions

GJ and PL analysed the data and wrote the manuscript. YZ, XY, and JF were responsible for collecting data. ZZ had some advices for revisions. TC and HW designed the study and participated in data analysis and interpretation. All authors approved the paper.

Funding

This study is supported by the Medical Scientific Research Foundation of Guangdong Province, China (NO. A2021163) and the Clinical Medical Research 5010 Program of Sun Yat-sen University (2018023).

Conflict of interest

The authors declare that the research was conducted in the absence of any commercial or financial relationships that could be construed as a potential conflict of interest.

Supplementary material

The Supplementary Material for this article can be found online at: https://www.por-journal.com/articles/10.3389/pore.2023.1610874/full#supplementary-material

References

1. Keum N, Giovannucci E. Global burden of colorectal cancer: Emerging trends, risk factors and prevention strategies. *Nat Rev Gastroenterol Hepatol* (2019) 16: 713–32. doi:10.1038/s41575-019-0189-8

2. Gervaz P, Bucher P, Morel P. Two colons-two cancers: Paradigm shift and clinical implications. *J Surg Oncol* (2004) 88:261–6. doi:10.1002/jso.20156

3. Wu W, Li D, Ma W, Zheng S, Han D, Xu F, et al. Examining more lymph nodes may improve the prognosis of patients with right colon cancer: Determining the optimal minimum lymph node count. *Cancer Control* (2021) 28: 10732748211064034. doi:10.1177/10732748211064034

4. Glebov OK, Rodriguez LM, Nakahara K, Jenkins J, Cliatt J, Humbyrd CJ, et al. Distinguishing right from left colon by the pattern of gene expression. *Cancer Epidemiol Biomarkers Prev* (2003) 12:755–62.

5. Baran B, Mert ON, Yerli TN, Acar E, Bekcioglu O, Baskin Y. Difference between left-sided and right-sided colorectal cancer: A focused review of literature. *Gastroenterol Res* (2018) 11:264–73. doi:10.14740/gr1062w

6. Marzouk O, Schofield J. Review of histopathological and molecular prognostic features in colorectal cancer. *Cancers (Basel)* (2011) 3:2767–810. doi:10.3390/cancers3022767

7. Gualco G, Reissenweber N, Cliche I, Bacchi CE. Flat elevated lesions of the colon and rectum: A spectrum of neoplastic and nonneoplastic entities. *Ann Diagn Pathol* (2006) 10:333–8. doi:10.1016/j.anndiagpath.2006.03.003

8. Nawa T, Kato J, Kawamoto H, Okada H, Yamamoto H, Kohno H, et al. Differences between right- and left-sided colon cancer in patient characteristics, cancer morphology and histology. *J Gastroenterol Hepatol* (2008) 23:418–23. doi:10.1111/j.1440-1746.2007.04923.x

9. Amin MB, Greene FL, Edge SB, Compton CC, Gershenwald JE, Brookland RK, et al. The Eighth Edition AJCC Cancer Staging Manual: Continuing to build a bridge from a population-based to a more "personalized" approach to cancer staging. *CA Cancer J Clin* (2017) 67: 93–9. doi:10.3322/caac.21388

10. Li DG, Di Carlo I, Scilletta R, Scilletta B, Puleo S. Colorectal cancer and lymph nodes: The obsession with the number 12. *World J Gastroenterol* (2014) 20:1951–60. doi:10.3748/wjg.v20.i8.1951

11. Le Voyer TE, Sigurdson ER, Hanlon AL, Mayer RJ, Macdonald JS, Catalano PJ, et al. Colon cancer survival is associated with increasing number of lymph nodes analyzed: A secondary survey of intergroup trial INT-0089. *J Clin Oncol* (2003) 21: 2912–9. doi:10.1200/JCO.2003.05.062

12. Xie D, Song X, Tong L. Stage migration resulting from inadequate number of examined lymph nodes impacts prognosis in stage II colon cancer after radical surgery. *Int J Colorectal Dis* (2021) 36:959–69. doi:10.1007/s00384-020-03794-6

13. Deng W, Xu T, Wang Y, Xu Y, Yang P, Gomez D, et al. Log odds of positive lymph nodes may predict survival benefit in patients with node-positive non-small cell lung cancer. *Lung Cancer* (2018) 122:60–6. doi:10.1016/j.lungcan.2018.05.016

14. Xu Z, Jing J, Ma G. Development and validation of prognostic nomogram based on log odds of positive lymph nodes for patients with gastric signet ring cell carcinoma. *Chin J Cancer Res* (2020) 32:778–93. doi:10.21147/j.issn.1000-9604.2020.06.11

15. Pei JP, Zhao ZM, Sun Z, Gu WJ, Zhu J, Zhu J, et al. Development and validation of a novel classification scheme for combining pathological T stage and log odds of positive lymph nodes for colon cancer. *Eur J Surg Oncol* (2022) 48: 228–36. doi:10.1016/j.ejso.2021.09.005

16. Wang J, Hassett JM, Dayton MT, Kulaylat MN. The prognostic superiority of log odds of positive lymph nodes in stage III colon cancer. *J Gastrointest Surg* (2008) 12:1790–6. doi:10.1007/s11605-008-0651-3

17. Camp RL, Dolled-Filhart M, Rimm DL. X-Tile: A new bio-informatics tool for biomarker assessment and outcome-based cut-point optimization. *Clin Cancer Res* (2004) 10:7252–9. doi:10.1158/1078-0432.CCR-04-0713

18. Akaike H. A new look at the statistical model identification. *Ieee T Automat Contr* (1974) 6:716–23. doi:10.1109/tac.1974.1100705

19. Fitzgerald M, Saville BR, Lewis RJ. Decision curve analysis. *JAMA* (2015) 313: 409–10. doi:10.1001/jama.2015.37

20. Vickers AJ, Elkin EB. Decision curve analysis: A novel method for evaluating prediction models. *Med Decis Making* (2006) 26:565–74. doi:10.1177/0272989X06295361

21. Greenberg R, Itah R, Ghinea R, Sacham-Shmueli E, Inbar R, Avital S. Metastatic lymph node ratio (LNR) as a prognostic variable in colorectal cancer patients undergoing laparoscopic resection. *Tech Coloproctol* (2011) 15:273–9. doi:10.1007/s10151-011-0701-9

22. Scarinci A, Di Cesare T, Cavaniglia D, Neri T, Colletti M, Cosenza G, et al. The impact of log odds of positive lymph nodes (LODDS) in colon and rectal cancer patient stratification: A single-center analysis of 323 patients. *Updates Surg* (2018) 70:23–31. doi:10.1007/s13304-018-0519-3

23. Persiani R, Cananzi FC, Biondi A, Paliani G, Tufo A, Ferrara F, et al. Log odds of positive lymph nodes in colon cancer: A meaningful ratio-based lymph node classification system. *World J Surg* (2012) 36:667–74. doi:10.1007/s00268-011-1415-x

24. Zhang C, Mei Z, Pei J, Abe M, Zeng X, Huang Q, et al. A modified tumor-node-metastasis classification for primary operable colorectal cancer. *JNCI Cancer Spectr* (2021) 5:pkaa093. doi:10.1093/jncics/pkaa093

25. Imamura Y, Lochhead P, Yamauchi M, Kuchiba A, Qian ZR, Liao X, et al. Analyses of clinicopathological, molecular, and prognostic associations of KRAS codon 61 and codon 146 mutations in colorectal cancer: Cohort study and literature review. *Mol Cancer* (2014) 13:135. doi:10.1186/1476-4598-13-135

26. Kosumi K, Hamada T, Zhang S, Liu L, da Silva A, Koh H, et al. Prognostic association of PTGS2 (COX-2) over-expression according to BRAF mutation status in colorectal cancer: Results from two prospective cohorts and CALGB 89803 (Alliance) trial. *Eur J Cancer* (2019) 111:82–93. doi:10.1016/j.ejca.2019.01.022

27. Park HS, Lloyd S, Decker RH, Wilson LD, Yu JB. Limitations and biases of the surveillance, Epidemiology, and End results database. *Curr Probl Cancer* (2012) 36: 216–24. doi:10.1016/j.currproblcancer.2012.03.011

Pathology & Oncology Research | frontiers

TYPE Original Research
PUBLISHED 31 May 2023
DOI 10.3389/pore.2023.1610908

Check for updates

OPEN ACCESS

EDITED BY
József Tímár,
Semmelweis University, Hungary

*CORRESPONDENCE
Ivan Vlahović,
ivan_vlahovic@hotmail.com

RECEIVED 29 October 2022
ACCEPTED 16 May 2023
PUBLISHED 31 May 2023

CITATION
Vlahović I, Rajc J, Švagelj I, Šolić K and Švagelj D (2023), Potential predictors for CDX2 expression loss and mismatch repair deficiency in colorectal cancer. *Pathol. Oncol. Res.* 29:1610908. doi: 10.3389/pore.2023.1610908

COPYRIGHT
© 2023 Vlahović, Rajc, Švagelj, Šolić and Švagelj. This is an open-access article distributed under the terms of the Creative Commons Attribution License (CC BY). The use, distribution or reproduction in other forums is permitted, provided the original author(s) and the copyright owner(s) are credited and that the original publication in this journal is cited, in accordance with accepted academic practice. No use, distribution or reproduction is permitted which does not comply with these terms.

Potential predictors for CDX2 expression loss and mismatch repair deficiency in colorectal cancer

Ivan Vlahović[1]*, Jasmina Rajc[2], Ivan Švagelj[3], Krešimir Šolić[4] and Dražen Švagelj[3]

[1]Department of Abdominal Surgery, Clinical Hospital Center Osijek, Faculty of Medicine, University of Osijek, Osijek, Croatia, [2]Department of Pathology and Forensic Medicine, Clinical Hospital Center Osijek, Faculty of Medicine, University of Osijek, Osijek, Croatia, [3]Department of Pathology and Cytology, General County Hospital Vinkovci, Vinkovci, Croatia, [4]Department of Medical Statistics and Medical Informatics, Faculty of Medicine, University of Osijek, Osijek, Croatia

CDX2 expression loss is commonly associated with mismatch repair deficiency (dMMR) in colorectal cancer (CRC). However, there are only a few studies that have attempted to correlate CDX2 expression loss with specific MMR genes (*MLH1, MSH2, MSH6, PMS2*). This is a retrospective study of 327 patients who underwent surgery due to CRC. Nine patients (2.9%) had two synchronous CRCs, making the total sample 336 CRC. Histopathological data such as tumor type, tumor grade, perineural, lymphatic, and vascular invasion, pT stage, pN stage, peritumoral and intratumoral lymphocytic infiltration were collected and recorded in the database. After immunohistochemical analysis, CDX2 expression, MLH1, MSH2, MSH6, and PMS2 deficiency were also recorded. CDX2 expression loss was detected in 19 out of 336 CRCs (5.9%) and was associated with ascending colon CRC, partially mucinous adenocarcinoma, poorly differentiated carcinoma, and dMMR. Forty-four (13.1%) of CRCs were dMMR. We found a statistically significant association between CDX2 expression loss and MLH1 and PMS2 deficiency. Considering that most expression phenotypes include pairs of MMR genes, we analyzed MLH1/PMS2 and MSH2/MSH6 as heterodimers. Analysis of heterodimers showed a similar result, namely, that MLH1/PMS2 heterodimer deficiency was significantly associated with CDX2 expression loss. We also constructed a regression model for CDX2 expression loss and for dMMR. Poor tumor differentiation and MLH1/PMS2 heterodimer deficiency have been identified as potential predictors for CDX2 expression loss. CRC in the ascending colon and CDX2 expression loss have been identified as positive potential predictors of dMMR with rectal cancer as negative potential predictor of dMMR. Our study showed a significant association between CDX2 expression loss and MLH1 and PMS2 deficiency in CRC. We also managed to produce a regression model for CDX2 expression and showed that poor tumor differentiation and MLH1/PMS2 heterodimer deficiency are independent factors for CDX2 expression loss. We were the first to include CDX2 expression in a regression model for dMMR and showed that CDX2 expression loss can be used as a predictive factor for dMMR, which should be confirmed by further studies.

KEYWORDS

immunohistochemistry, colorectal cancer (CRC), CDX2, dMMR, regression model

Introduction

Colorectal cancer (CRC) is the third most common malignant tumor worldwide and the second leading cause of tumor death. It is a major public health problem, especially in developed countries [1].

CRC is treated by surgical resection, neoadjuvant therapy in some cases of rectal cancer, and adjuvant chemotherapy. Many research groups are trying to find new biomarkers that would distinguish the group of patients who benefit from adjuvant chemotherapy from the group of patients in whom chemotherapy has no effect.

One of these biomarkers is caudal homeobox 2 (CDX2). The gene encoding CDX2 is located on chromosome 13q12-13. It is a transcription factor that regulates intestinal epithelial cell differentiation. CDX2 induces differentiation and inhibits proliferation at the level of gene transcription [2]. Its expression is almost completely restricted to the gastrointestinal tract. In routine daily diagnostic practice, CDX2 is used as a marker for the identification of tumors of intestinal origin. It has been claimed that CDX2 is a tumor suppressor gene, but since it is expressed in 70%–95% of all CRC, this claim is controversial [3, 4]. Loss of CDX2 expression is associated with poor prognosis in CRC patients, as described in the publications by Dawson et al. and Bae et al. [5, 6]. Dalerba et al. analysed whether patients with CDX2 expression loss will benefit from adjuvant chemotherapy treatment. Their conclusion was that both stage II and stage III CRC patients with CDX2 expression loss might benefit from adjuvant chemotherapy. This is especially important in stage II patients who are commonly treated with surgery alone [7]. In 2022 Alarid-Escudero et al. published a cost-effectiveness analysis of CDX2 expression testing and adjuvant chemotherapy implementation for stage II colon cancer. Their conclusion was that identifying a group of stage II colon cancer patients for targeted chemotherapy based on CDX2 expression loss was a cost-effective strategy [8].

Mismatch repair system (MMR) analysis in CRC cells is part of standard pathohistological practice worldwide. *MLH1*, *MSH2*, *MSH6*, and *PMS2* are genes responsible for the mismatch repair system. A mutation in any of these genes results in mismatch repair deficiency. Immunohistochemically, CRC can be mismatch-deficient (dMMR) or mismatch-proficient (pMMR). A deficient mismatch repair system leads to microsatellite instability (MSI), which is characterized by unstable microsatellites, a type of simple DNA sequence repeat. dMMR develops in 15% of CRCs—3% in autosomal dominant Lynch syndrome and 12%–15% sporadically.

The association between CDX2 expression loss and dMMR in CRC has been described previously and is well established. In our study, we will try to find the relationship between the expression of specific MMR proteins (MLH1, MSH2, MSH6, PMS2) and CDX2 expression loss. We will also try to find potential predictors of CDX2 expression loss and dMMR.

Materials and methods

Patients

This is a single-institution retrospective study done at General County Hospital Vinkovci in Croatia. The patient cohort consisted of 327 patients who underwent surgery at the Department of Abdominal Surgery between 1 January 2016 and 31 December 2021. All patients underwent surgical resection for colorectal cancer. Nine patients had two synchronous tumors at the time of surgery so 336 tumor specimens were included in this study. Histopathological and immunohistochemical analysis was performed at the Department of Pathology and Cytology.

Clinical data such as age, gender, tumor location, and tumor diameter were recorded in the database. Histopathological data such as tumor type, tumor grade, perineural, lymphatic, and vascular invasion, pT stage, pN stage, peritumoral and intratumoral lymphocytic infiltration were also recorded and stored in the database. The TNM8 classification of malignant tumors was used for tumor staging [9]. Adenocarcinoma with >50% lesion composed of pools of extracellular mucin was defined as mucinous adenocarcinoma. Lesions that contain extracellular mucin but <50% were defined as partially mucinous adenocarcinoma [10]. After immunohistochemical analysis, CDX2 expression, MLH1, MSH2, MSH6, and PMS2 deficiency were also recorded. Because family history information was not available, no attempt was made to divide patients into Lynch syndrome and sporadic dMMR.

Immunohistochemistry

Immunohistochemical analysis was performed on 4-μm sections of paraffin-embedded tissue samples. Tissue sections were incubated at 60°C for 180 min. The slides were cooled down and deparaffinized 2 min × 5 min, according to the manufacturer's protocol with paraffin cleaning agent Tissue-Tek (Sakura, Torrance, CA, United Sates), followed by: 1 min × 5 min wash with 2-propanol, 1 min × 5 min wash with 96% ethanol, 1 min × 5 min wash with 70% ethanol and 1 × 5 min wash with deionized water. The immunohistochemical procedure was performed according to the manufacturer's recommendations (Dako, Glostrup, Denmark). Slides were briefly prewarmed to 65°C with Dako PT Link in Target Retrieval Solution, pH 9, heated to 95°C for 20 min, and then cooled to 65°C. Slides were incubated in Washing Buffer (Dako Glostrup, Denmark), loaded into a Dako Autostainer and stained according to the standard method: Peroxidase Blocking Reagent (Dako Glostrup, Denmark), for 5 min, Washing Buffer; and primary antibodies as follows: Monoclonal mouse Anti-human CDX-2 Clone DAK-CDX2, FLEX Monoclonal Mouse Anti-

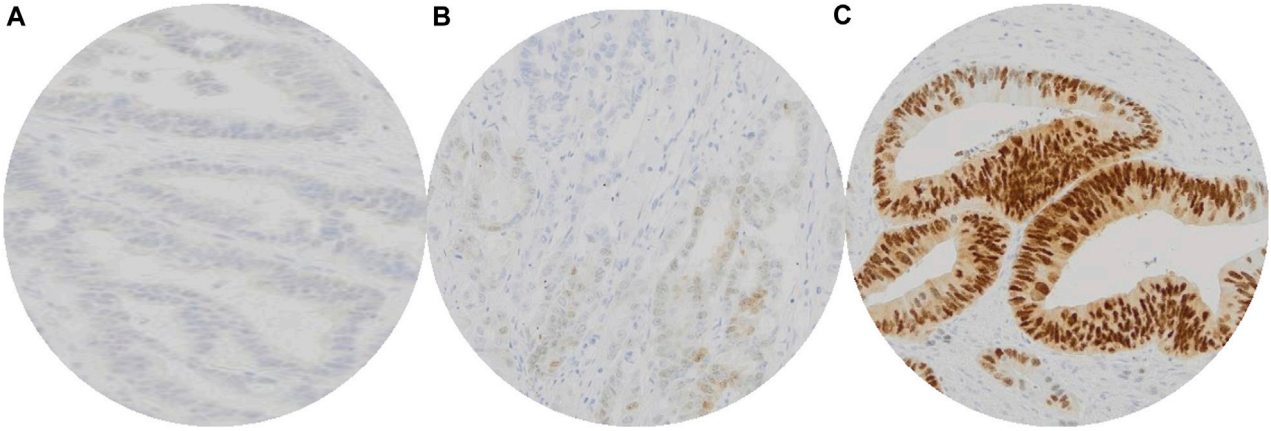

FIGURE 1
Interpretation of immunohistochemical staining of CDX2: No staining of CDX2 in colorectal carcinoma cells, valuated as score 0 **(A)**. Weak CDX2 positivity in minority (~20%) of colorectal carcinoma cells, valuated as score 1 **(B)**. Moderate/strong CDX2 positivity of colorectal carcinoma cells, valuated as score 2 **(C)**. Tumors with scores 0 and 1 were considered negative (CDX2 expression loss) while score 2 was considered positive (normal CDX2 expression).

Human MutL Protein Homolog 1 Clone ES05, FLEX Monoclonal Rabbit Anti-Human MutS Protein Homolog 2 Clone FE11, FLEX Monoclonal Rabbit Anti-Human MutS Protein Homolog 6 EP49, FLEX Monoclonal Rabbit Anti-Human Postmeiotic Segregation Increased 2 Clone EP51, 20 min. After washing, the slides were treated with Dako REAL EnVision/HRP for 30 min and stained with Dako REAL DAB + Chromogen. All sections were counterstained with Mayer's hematoxylin. Slides were evaluated independently by two pathologists. The staining pattern was nuclear. One strongly positive sample of colon cancer tissue served as a positive control. Negative controls were performed by replacing the primary antibody with PBS.

All immunohistochemical staining was evaluated by two independent observers (IŠ and DŠ). CDX2 expression was evaluated in accordance with Dalerba et al. and Hesteun et al. [7, 11]. Cases were divided in three groups: score 0—no staining (0%–5% positive cells), score 1—weak staining in majority of cells (5%–49% positive cells) and score 2—moderate/strong staining in a majority of cells (50%–100% positive cells). Tumors with scores 0 and 1 were considered negative (CDX2 expression loss) while score 2 was considered positive (normal CDX2 expression) (Figure 1). Weak positivity in the majority of the cells (>50%) was considered positive CDX2 staining.

CDX2 expression was immunohistochemically analysed on the same tissue samples as MMR. Independently of CDX2 expression being positive or negative the analysis was not expanded on other tissue samples of the same carcinoma so we could not exclude CDX2 expression heterogeneity.

Carcinoma was considered dMMR when there was absence of nuclear staining for at least one protein. Adjacent normal colonic epithelium, lymphocytes, and stromal cells served as positive internal controls. According to the CAP protocol for immunohistochemistry interpretation, any nuclear staining, even patchy, is taken as "no loss of expression" and only absolute absence of nuclear staining was considered "loss of expression," provided internal controls are positive [12]. Expression of proteins was then grouped into six categories: no loss of expression, loss of expression of all four proteins, combined loss of MLH1/PMS2, combined loss of MSH2/MSH6, and isolated loss of MSH6 and PMS2.

Statistical analysis

Standard statistical methods were used for statistical analysis. All collected categorical data were presented with absolute and relative frequencies, while numerical data were presented with arithmetic mean and standard deviation or with median and interquartile range if the distribution did not follow the Gaussian normal distribution. Results are presented in tables or graphical figures and explained in the text below. Differences between two independent sets of numerical data were tested using the parametric Student's t-test or the nonparametric Mann-Whitney U test. Differences between categorical data were tested with Chi-Square Test or with Fisher's Exact Test, if needed, whereas pairs of categorical data were tested with McNemar Test. In addition, Cramér's V was calculated as a measure of association between two nominal variables when deficiency of a particular MMR gene was analyzed. Exploratory Multivariate Binary Logistic Regression was applied to the variables that were significantly different in order to identify potential predictors. Statistical analysis was performed using either MedCalc (release 19.1.3, MedCalc Software by) or IBM SPSS

TABLE 1 Clinicopathological variables and their association with CDX2 expression and MMR.

	Overall	CDX2−	CDX2+	*p*-value	dMMR	pMMR	*p*-value
Age/mean (SD)							
	67.6 (11.6)	69.1 (10.2)	67.5 (11.7)	0.57*	66.7 (12.2)	67.7 (11.5)	0.59*
Gender/*n* (%)							
Male	200 (61.2)	11 (5.3)	197 (94.7)	0.71[a]	25 (12.0)	183 (88.0)	0.46[a]
Female	127 (38.8)	8 (6.3)	120 (93.8)		19 (14.8)	109 (85.2)	
T status/*n* (%)							
1	8 (2.4)	0	8 (2.5)	>0.99[b]	0	8 (2.7)	0.45[b]
2	41 (12.2)	2 (10.5)	39 (12.3)		8 (18.2)	33 (11.3)	
3	273 (81.2)	17 (89.5)	256 (80.8)		34 (77.3)	239 (81.8)	
4a	4 (1.2)	0	4 (1.3)		0	4 (1.4)	
4b	10 (3.0)	0	10 (3.1)		2 (4.5)	8 (2.7)	
N status/*n* (%)							
0	189 (56.2)	13 (68.4)	176 (55.5)	0.50[b]	27 (61.4)	162 (55.5)	0.35[b]
1a	48 (14.3)	1 (5.3)	47 (14.8)		5 (11.4)	43 (14.7)	
1b	55 (16.4)	3 (15.8)	52 (16.4)		9 (20.5)	46 (15.8)	
2a	21 (6.2)	2 (10.5)	19 (6.0)		0	21 (7.2)	
2b	23 (6.8)	0	23 (7.3)		3 (6.8)	20 (6.8)	
Tumor location/*n* (%)							
A	92 (27.4)	10 (52.6)	82 (25.9)	**0.03**[b]	33 (75.0)	59 (20.2)	**<0.001**[b]
T	12 (3.6)	1 (5.3)	11 (3.5)		1 (2.3)	11 (3.8)	
D	48 (14.3)	4 (21.1)	44 (13.9)		1 (2.3)	47 (16.1)	
S	68 (20.2)	1 (5.3)	67 (21.1)		7 (15.9)	61 (20.9)	
R	116 (34.5)	3 (15.8)	113 (35.6)		2 (4.5)	114 (39.0)	
Tumor diameter/median (25%–75%)							
	4 (3–5)	4.3 (3–6.2)	4 (3–5)	0.46[c]	5 (4–6.8)	4 (3–5)	**<0.001**[c]
Tumor type/*n* (%)							
Ac	250 (74.4)	10 (52.6)	240 (75.7)	**0.04**[b]	18 (40.9)	232 (79.5)	**<0.001**[a]
MAc	36 (10.7)	3 (15.8)	33 (10.4)		13 (29.5)	23 (7.9)	
PMAc	50 (14.9)	6 (31.6)	44 (13.9)		13 (29.5)	37 (12.7)	
Tumor differentiation/*n* (%)							
WD	43 (12.8)	1 (5.3)	42 (13.2)	**<0.001**[b]	6 (13.6)	37 (12.7)	**<0.001**[a]
MD	279 (83.0)	9 (47.4)	270 (85.2)		29 (65.9)	250 (85.6)	
PD	14 (4.2)	9 (47.4)	5 (1.6)		9 (20.5)	5 (1.7)	
Peritumoral lymphocytic infiltration/*n* (%)							
Absent	180 (53.6)	10 (52.6)	170 (53.6)	0.67[a]	16 (36.4)	164 (56.2)	**0.002**[a]
Focal	100 (29.8)	7 (36.8)	93 (29.3)		13 (29.5)	87 (29.8)	
Present	56 (16.7)	2 (10.5)	54 (17.0)		15 (34.1)	41 (14.0)	
Intratumoral lymphocytic infiltration/*n* (%)							
Absent	125 (37.2)	8 (42.1)	117 (36.9)	0.30[a]	16 (36.4)	109 (37.3)	0.20[a]
Focal	157 (46.7)	6 (31.6)	151 (47.6)		17 (38.6)	140 (47.9)	
Present	54 (16.1)	5 (26.3)	49 (15.5)		11 (25.5)	43 (14.7)	

(Continued on following page)

TABLE 1 (*Continued*) Clinicopathological variables and their association with CDX2 expression and MMR.

	Overall	CDX2−	CDX2+	*p*-value	dMMR	pMMR	*p*-value
Vascular invasion/*n* (%)							
Absent	325 (96.7)	18 (94.7)	307 (96.8)	0.48[b]	44 (100.0)	281 (96.2)	0.37[b]
Present	11 (3.3)	1 (5.3)	10 (3.2)		0	11 (3.8)	
Lymphatic invasion/*n* (%)							
Absent	305 (90.8)	17 (89.5)	288 (90.9)	0.69[b]	41 (93.2)	264 (90.4)	0.78[b]
Present	31 (9.2)	2 (10.5)	29 (9.1)		3 (6.8)	28 (9.6)	
Perineural infiltration/*n* (%)							
Absent	276 (82.1)	15 (78.9)	261 (82.3)	0.76[b]	39 (88.6)	237 (81.2)	0.23[a]
Present	60 (17.9)	4 (21.1)	56 (17.7)		5 (11.4)	55 (18.8)	
Total	336 (100.0)	19 (100.0)	317 (100.0)		44 (100.0)	292 (100.0)	

Abbreviations: A, ascending colon; T, transverse colon; D, descending colon, S, sigmoid colon, R, rectum, Ac, adenocarcinoma; Mac, mucinous adenocarcinoma, PMAc, partially mucinous adenocarcinoma; WD, well differentiated; MD, moderately differentiated; PD, poorly differentiated.
*Student's T-Test.
[a]Chi-Square Test.
[b]Fisher's Exact Test.
[c]Mann-Whitney U Test.
Bold values are statistically significant.

Statistics (release 24.0.0.0) software tools, with statistical significance defined as $\alpha = 0.05$, where all p values were two-tailed.

Results

A total of 327 patients with CRC were included (mean age was 67.6, SD = 11.6). As mentioned previously, nine patients (2.9%) had two synchronous CRCs, making the total sample 336 CRCs. Clinicopathologic characteristics are listed in Table 1. Almost two-thirds of the patients were male (Chi-Square Test, $p = 0.004$). Most tumors were pT3 and N0 according to the TNM8 classification. Tumors were most commonly located in the rectum (34.5%), were 4 cm in diameter, moderately differentiated, and lacked perineural, vascular, and lymphatic invasion. The most common tumor type was adenocarcinoma (Table 1).

CDX2 expression loss in relation to pathological and clinical features

CDX2 expression loss was identified in 19 out of 336 CRCs (5.9%). There was no difference in age or gender between CDX2-negative and CDX2-positive patients. Through standard statistical analysis we identified significant differences regarding CDX2 expression loss for several examined variables. CDX2 expression loss was associated with ascending colon ($p = 0.03$), partially mucinous adenocarcinoma ($p = 0.04$), poorly differentiated carcinoma ($p < 0.001$) and dMMR (Fisher's Exact Test, $p < 0.001$). There was no statistically significant difference regarding CDX2 expression status and pT, pN, tumor diameter, peritumoral and intratumoral lymphocytic infiltration, lymphatic, vascular, and perineural invasion (Table 1).

dMMR in relation to pathological and clinical features

dMMR was identified in 44 out of 336 CRCs (13.1%). MLH1 deficiency was found in 32 (9.1%) patients, MSH2 deficiency in nine (2.7%), MHS6 deficiency in 10 (3%), and PMS2 deficiency in 34 (10.1%) patients (Table 2). dMMR was significantly associated with ascending colon ($p < 0.001$), mucinous adenocarcinoma ($p < 0.001$) poorly differentiated carcinoma ($p < 0.001$), peritumoral lymphocytic infiltration ($p = 0.002$) and CDX2 expression loss (Fisher's Exact Test, $p < 0.001$). Compared to pMMR, there was a statistically significant difference in tumor diameter. dMMR has, on average, 1 cm wider diameter than pMMR (Mann-Whitney U Test, $p < 0.001$). There was no statistically significant difference regarding dMMR and pT, pN, peritumoral and intratumoral lymphocytic infiltration, lymphatic, vascular, and perineural invasion (Table 1).

CDX2 loss in relation to MLH1, MSH2, MSH6, and PMS2

There was a statistically significant association between CDX2 expression loss and MLH1 and PMS2 deficiency (Fisher's Exact Test, $p < 0.001$). Although statistically not significant, the

TABLE 2 Association between CXD2 expression loss and deficiency of specific MMR gene.

	CDX2−	CDX2+	*p*-value	Cramer's V	Overall	*p*-value
MLH1/*n* (%)						
0	8 (42.1)	24 (7.6)	**<0.001***	0.272	32 (9.5)	**<0.001**[a]
1	11 (57.9)	293 (92.4)			304 (90.5)	
MSH2/*n* (%)						
0	2 (10.5)	7 (2.2)	0.09*	0.119	9 (2.7)	**<0.001**[a]
1	17 (89.5)	310 (97.8)			327 (97.3)	
MSH6/*n* (%)						
0	2 (10.5)	8 (2.5)	0.10*	0.109	10 (3.0)	**<0.001**[a]
1	17 (89.5)	309 (97.5)			326 (97.0)	
PMS2/*n* (%)						
0	9 (47.4)	25 (7.9)	**<0.001***	0.302	34 (10.1)	**<0.001**[a]
1	10 (52.6)	292 (92.1)			302 (89.9)	
MMR/*n* (%)						
dMMR	10 (52.6)	34 (10.7)	**<0.001***	0.287	44 (13.1)	**<0.001**[a]
pMMR	9 (47.4)	283 (89.6)			292 (86.9)	
MLH1/PMS2/*n* (%)						
0	9 (47.4)	26 (8.2)	**<0.001***	0.296	35 (10.4)	**<0.001**[a]
1	10 (52.6)	291 (91.8)			301 (89.6)	
MSH2/MSH6/*n* (%)						
0	2 (10.5)	8 (2.5)	0.104	0.109	10 (3.0)	**<0.001**[a]
1	17 (89.5)	309 (97.5)			326 (97.0)	
Total	19 (100,0)	317 (100.0)			336 (100.0)	

*Fisher's Exact Test.
[a]Chi-Square Test.
Bold values are statistically significant.

association between CDX2 expression loss and MSH2 and MSH6 deficiency was four to five times higher (Table 2).

In our patient cohort, 44 (13.1%) CRCs were dMMR. Regarding the fact that most expression phenotypes include pairs of MMR genes, we further analyzed MLH1/PMS2 and MSH2/MSH6 as heterodimers. Analysis of heterodimers showed a similar result in the way that MLH1/PMS2 heterodimer deficiency was significantly associated with CDX2 expression loss (Fisher's Exact Test, $p < 0.001$), while MSH2/MSH6 heterodimer was not (Figure 2). Additionally, Cramér's V coefficient (0.296) shows the highest association when comparing MLH1/PMS2 as a heterodimer (Table 2).

Synchronous tumors in relation to CDX2 expression loss and dMMR

Nine patients in the sample had synchronous CRC (2.9%). One patient had CDX2 expression loss and it was detected only in one of his synchronous tumors. As mentioned previously CDX2 expression loss was detected in 5.9% of tumors in the whole sample (19 out of 336) and in this group of tumors in 5.5% (1 out of 18).

Two patients had dMMR and it was detected in both of their synchronous tumors. dMMR was detected in 13.1% of tumors in the whole sample (44 out of 336) and in this group in 22.2% (4 out of 18). Results of Fisher Exact test has not shown this difference as statistically significant ($p = 0.3$). Both of the patients had the same MMR protein deficiency in their synchronous tumors. One patient had MSH2 and MSH6 deficiency in both of his synchronous tumors and the other patient had PMS2 deficiency in both of the tumors.

Regression model for CDX2 and dMMR

The next step in statistical analysis was to make a regression model for CDX2 expression loss and dMMR. All variables that were identified as significant for CDX2 expression loss (Table 1), including MLH1/PMS2 heterodimer (Table 2) were included in the regression model.

10.3389/pore.2023.1610908

TABLE 3 Potential predictors for CDX2 expression loss and dMMR.

	Coefficient	SE	Wald	*p**	OR	95% CI of OR
Potential predictors for CDX2 expression loss						
CRC location—ascending colon	−0.36	0.72	0.25	0.62	0.70	0.17–2.87
Moderately differentiated CRC	0.39	1.09	0.13	0.72	1.48	0.18–12.45
Poorly differentiated CRC	4.03	1.20	11.32	**<0.001**	56.46	5.39–591.67
Adenocarcinoma	3.99	19244894.27	0.00	>0.99	53.95	
Mucinous adenocarcinoma	4.03	19244894.27	0.00	>0.99	56.29	
Partially mucinous adenocarcinoma	3.99	19244894.27	0.00	>0.99	54.53	
MLH1/PMS2 heterodimer deficiency	1.89	0.74	6.48	**0.011**	6.60	1.54–28.18
Constant	−8.03	19244894.27	0.00	>0.99		
Potential predictors for dMMR						
CRC location—ascending colon	1.17	0.48	5.91	**0.015**	3.22	1.25–8.27
CRC location—descending colon	−1.91	1.15	2.77	0.096	0.15	0.02–1.40
CRC location - rectum	−1.91	0.84	5.22	**0.022**	0.15	0.03–0.76
Adenocarcinoma	−0.63	15713390.37	0.00	>0.99	0.53	
Mucinous adenocarcinoma	0.91	15713390.37	0.00	>0.99	2.48	
Partially mucinous adenocarcinoma	0.57	15713390.37	0.00	>0.99	1.78	
Tumor diameter	0.11	0.10	1.21	0.271	1.11	0.92–1.35
Moderately differentiated CRC	0.29	0.59	0.24	0.623	1.33	0.42–4.21
Poorly differentiated CRC	1.28	1.00	1.62	0.203	3.58	0.50–25.57
Peritumoral lymphocytic infiltration—absent	−0.32	0.52	0.39	0.535	0.73	0.26–2.00
Peritumoral lymphocytic infiltration—present	0.66	0.54	1.48	0.224	1.94	0.67–5.61
CDX2 expression loss	1.85	0.84	4.89	**0.027**	6.34	1.23–32.58
Constant	−2.85	15713390.37	0.00	>0.99		

*Logistic regresion, Method: Enter.
Bold values are statistically significant.

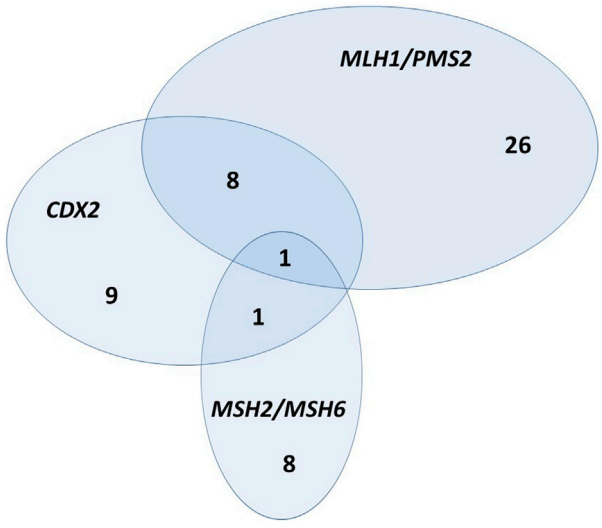

FIGURE 2
Euclid's diagram—relationship between CDX2 expression loss, MLH1/PMS2 heterodimer, and MSH2/MSH6 heterodimer.

The result was a statistically significant model ($p < 0.001$, Chi-Squared = 45.9, Cox & Snell $R^2 = 0.128$, Nagelkerke $R^2 = 0.362$) identifying poor tumor differentiation and MLH1/PMS2 heterodimer deficiency as potential predictors for CDX2 expression loss (Table 3) [95.83% of all cases were correctly classified (Hosmer and Lemeshow test, $p = 0.567$)].

In the regression model for dMMR, we included all variables that were identified as significant for dMMR, including CDX2 expression loss (Table 1). We got a statistically significant model ($p < 0.001$, Chi-Squard 94.1, Cox & Snell $R^2 = 0.244$, Nagelkerke $R^2 = 0.453$) identifying three variables as potential predictors for dMMR: CRC located in the ascending colon and CDX2 expression loss are positive potential predictors while CRC located in rectum is negative potential predictor for dMMR (Table 3) [91.37% of all cases were correctly classified (Hosmer and Lemeshow test, $p = 0.512$)].

Discussion

CDX2 is an emerging biomarker in CRC research. In our study, CDX2 expression loss was found in 5.9% of the CRCs

included in the research. According to other research groups, CDX2 expression loss ranged from 4% to 35% [3, 4, 6, 11, 13–24]. The study with the largest series of patients regarding CDX2 expression loss was performed by Dalerba et al. on 2115 patients. They found a CDX2 expression loss of 4.1%, and their result is similar to our findings [7].

In our study, CDX2 expression loss was significantly associated with CRC in ascending colon, dMMR, partially mucinous, and poorly differentiated (high grade) adenocarcinoma (Table 1). These findings are consistent with the results of other research groups. Their results showed that CDX2 expression loss was related to the right side of the colon [3–6, 11, 14, 16, 17, 19, 20, 22, 23, 25–29], dMMR [3–6, 11, 14, 16–18, 20–23, 25, 28, 29], poorly differentiated (high grade) CRC [3–5, 11, 14, 15, 17–19, 21, 23, 25] and mucinous CRC [3, 5, 6, 29]. According to the literature, some authors found an association between CDX2 expression loss and the female sex [3, 17, 18, 23, 27]. Our results show that CDX2 expression loss is not associated with age or gender, and similar results were published by Shigematsu et al, Slik et al, and Neuman et al. [13, 19, 22].

In 2018, Tomasello et al. published a systematic review and meta-analysis of the association of CDX2 expression with survival in early CRC. The result of their analysis was that CDX2 expression loss was negatively associated with survival [30]. Our results show that there is no association between CDX2 expression loss and the classical pathohistological features of worse survival such as high pT and pN stage, vascular, neural, and lymphatic invasion. Further research on our sample is needed to find a possible association between CDX2 expression, pathohistological features, and survival rate.

As opposed to CDX2, dMMR is an already established biomarker and an important decision factor for choosing treatment options in CRC therapy. It is present in 15% of CRCs, according to the literature, and our study shows a similar result −13.1% (Table 2). Our results show that dMMR is significantly associated with ascending colon location, mucinous adenocarcinoma, poorly differentiated carcinoma, and peritumoral lymphocytic infiltration (Table 1). These results are consistent with review articles of dMMR/MSI and CRC published by de'Angelis et al. and Boland et al. [31, 32].

We further analyzed individual deficiency of MMR proteins (MLH1, MSH2, MSH6, and PMS2) and their association with CDX2 expression. There is a statistically significant association between CDX2 expression loss and deficiency of MLH1 and PMS2 ($p < 0.001$) (Table 2). There is also an association between CDX2 expression loss and MSH2 and MSH6 deficiency, but it is not statistically significant ($p = 0.09$, $p = 0.10$) (Table 2).

According to the literature, there are two research groups that have studied the relationship between individual MMR protein deficiency and CDX2 expression loss in CRC. Sayar et al. published a study on 111 patients and examined only colon cancer, while rectal cancers were left out of the study. They found a strong association between CDX2 expression loss and PMS2 deficiency. All of the patients who had CDX2 expression loss had synchronous PMS2 deficiency [33]. Melincovici et al. found a similar result. In their study on 31 patients, PMS2 deficiency was significantly correlated to CDX2 expression loss, while there was no correlation between CDX2 expression loss and other MMR protein deficiency [24]. Our results are partially different from the results of these two research groups, but our sample is much bigger (336 CRCs vs. 111 and 31 CRCs).

Tóth et al. analyzed the relationship between CDX2 expression loss and individual MMR protein deficiency in CRC liver metastasis. They found that CDX2 expression loss is in a significant relationship with the deficiency of all four MMR proteins. It is hard to compare our results with theirs because of the different samples (primary CRC vs. CRC liver metastases), but it also shows the association between CDX2 expression loss and individual MMR protein deficiency [34].

The major role of the normal DNA MMR system is performed by MutSα and MutLα complexes. MutSα complex compromises MSH2/MSH6 heterodimer and MutLα MLH1/PMS2 heterodimer [35]. Therefore, we further analyzed MMR proteins as heterodimers and their relationship with CDX2 expression. As shown in Table 2, there is a statistically significant association between CDX2 expression loss and MLH1/PMS2 heterodimer deficiency, while there is no association between CDX2 expression loss and MSH2/MSH6 heterodimer deficiency. A graphical summary of this association is shown in Euclid's diagram (Figure 2). This diagram shows that, in absolute numbers, eight CRCs have synchronous CDX2 expression loss and MLH1/PMS2 heterodimer deficiency, while only one CRC has synchronous CDX2 expression loss and MSH2/MSH6 heterodimer deficiency. One CRC has CDX2 expression loss and deficiency of both heterodimers. According to our extensive literature research, no study has analyzed the relationship between CDX2 expression and MMR heterodimer deficiency. Further research is needed to find out the possibility that the same molecular mechanism is responsible for CDX2 expression loss and MLH1/PMS2 heterodimer deficiency.

Furthermore, synchronous tumors were separated from the whole sample and analysed as a group. We found no difference in CDX2 expression loss when comparing group of synchronous tumors with the whole sample (5.9% vs. 5.5%) but the difference in more obvious, although not statistically significant ($p = 0.3$) when comparing this two groups regarding MMR (22.2% vs. 13.1%). It is likely that the

larger sample size would reveal this difference as statistically significant (which should be proven in a further studies). Lee et al. made an analysis on a sample of 8,368 patients with CRC and found that 2.6% of patients had synchronous tumors which is similar to our result (2.9%) [36]. Among other CRC characteristics analysed in their study they found that patients with synchronous tumors had higher proportion of dMMR/MSI then patients with single cancer (12.8% vs. 6.6%) which is also similar to our result.

We further developed a regression model for the prediction of CDX2 expression loss and dMMR. We analyzed all variables that were significantly associated with CDX2 expression loss. Only two of them are potential predictors for CDX2 expression loss according to our regression model: poorly differentiated CRC and MLH1/PMS2 heterodimer deficiency. As CDX2 is a transcription factor that regulates intestinal epithelial cell differentiation, it is expected that poor differentiation of CRC is a predictor for CDX2 expression loss. Why the MLH1/PMS2 heterodimer deficiency is a predictor for CDX2 expression loss has to be analyzed by further molecular and (epi)genetic research. To our knowledge, this is the first published regression model for prediction of CDX2 expression loss. As mentioned in introduction Alarid-Escudero et al. published a cost-effectiveness analysis of CDX2 expression testing and adjuvant chemotherapy implementation for stage II colon cancer [8]. Based on our analysis CDX2 expression could be immunohistochemically tested only in patients with poorly differentiated CRC and MLH1/PMS2 heterodimer deficiency resulting in even less expensive immunohistochemical analysis.

All statistically significant variables according to dMMR were analyzed in the second regression model. Positive potential predictors for dMMR in CRC are CRC in ascending colon and CDX2 expression loss while CRC in rectum is negative potential predictor. According to the literature, there are five published prediction models for dMMR/MSI in CRC [37–41]. Fujiyosi et al. and Chikanati et al. made a prediction model for Japanese patients. In Asia, the incidence of dMMR/MSI is 4%–5%, in contrast to Western countries where the incidence is 10%–15%, so the sample could be different than our sample [37]. Jenkins et al. developed the "MsPath" model for patients younger than 50 years of age. Greenson et al. and Román et al. developed prediction models independent of age and with a similar population to our study sample. They found mucinous pattern to be predictor for dMMR. In our study mucinous adenocarcinoma was significantly associated with dMMR but it was not a potential predictor according to our regression model. They also found tumor infiltrating lymphocytes (TIL) to be a predictive factor. In our regression model, we did not include TIL because it was not significantly associated with dMMR in our sample. They both found Chron's-like reaction to be a predictive factor for dMMR/MSI, but this factor was not included in our analysis, which is one of the limitations of our study. We were the first group to include CDX2 expression loss in the regression model for dMMR. We found CDX2 to be an independent prognostic factor for dMMR with a 6.34 OR. Both of these research groups found that proximal tumor location is independent prediction factor for dMMR/MSI, which is similar to our results. They divided CRC location on the right/proximal and left/distal location. In our study we divided CRC location in five categories (ascending, transversal, descending, sigmoid colon and rectum) which is more precise and found rectal cancer to be a negative potential predictor for dMMR. In 2022, Cercek et al. published that treatment of dMMR rectal cancer with anti-PD-1 monoclonal antibody Dostarlimab for 6 months resulted in complete response in all of the 12 patients included in study [41]. According to our finding that rectal cancer location is negative predictive factor for dMMR, only a minority of rectal cancer patients would be appropriate for Dostarlimab treatment and researchers would more benefit in treating proximal CRC with this cancer treatment.

We should consider the limitations of the present study. This is a single-institution study. In addition to that, we included only patients who underwent CRC resection, while patients with unresectable and uncurable tumors were left out. Another limitation of this study is the relatively low number of patients with both dMMR and CDX2 expression loss.

Conclusion

Our study showed a significant association between CDX2 expression loss and MLH1 and PMS2 deficiency in CRC. To our knowledge, this is only the third study that compares CDX2 expression with individual mismatch protein deficiency in CRC, but with a much bigger sample than previous studies. According to our extensive literature research, we were the first to produce a regression model for CDX2 expression loss which showed that poor tumor differentiation and MLH1/PMS2 heterodimer deficiency are independent factors for CDX2 expression loss. We were also the first to include CDX2 expression in the regression model for dMMR and show that CDX2 expression loss could be used as a prediction factor for dMMR.

Data availability statement

The original contributions presented in the study are included in the article/supplementary material, further inquiries can be directed to the corresponding author.

Ethics statement

The ethics committees of General County Hospital Vinkovci approved the use of patient data and tumor material for this study.

Author contributions

IV, JR, and DŠ designed the study. IŠ and DŠ performed histopathological and immunohistochemical analysis. IV obtained clinical data. KŠ performed statistical evaluation. IV wrote the manuscript. JR, IŠ, and DŠ edited the manuscript. All authors contributed to the article and approved the submitted version.

Conflict of interest

The authors declare that the research was conducted in the absence of any commercial or financial relationships that could be construed as a potential conflict of interest.

References

1. Sung H, Ferlay J, Siegel RL, Laversanne M, Soerjomataram I, Jemal A, et al. Global cancer Statistics 2020: GLOBOCAN estimates of incidence and mortality worldwide for 36 cancers in 185 countries. *CA Cancer J Clin* (2021) 71(3):209–49. doi:10.3322/caac.21660

2. Saad RS, Ghorab Z, Khalifa MA, Xu M. CDX2 as a marker for intestinal differentiation: Its utility and limitations. *World J Gastrointest Surg* (2011) 3(11): 159–66. doi:10.4240/wjgs.v3.i11.159

3. Asgari-Karchekani S, Karimian M, Mazoochi T, Taheri MA, Khamehchian T. CDX2 protein expression in colorectal cancer and ItsCorrelation with clinical and pathological characteristics, prognosis, and survival rate of patients. *J Gastrointest Cancer* (2020) 51(3):844–9. doi:10.1007/s12029-019-00314-w

4. Olsen J, Eiholm S, Kirkeby LT, Espersen MLM, Jess P, Gögenür I, et al. CDX2 downregulation is associated with poor differentiation and MMR deficiency in colon cancer. *Exp Mol Pathol* (2016) 100(1):59–66. doi:10.1016/j.yexmp.2015.11.009

5. Dawson H, Koelzer VH, Lukesch AC, Mallaev M, Inderbitzin D, Lugli A, et al. Loss of Cdx2 expression in primary tumors and lymph node metastases is specific for mismatch repair-deficiency in colorectal cancer. *Front Oncol* (2013) 3:265–6. doi:10.3389/fonc.2013.00265

6. Bae JM, Lee TH, Cho NY, Kim TY, Kang GH. Loss of CDX2 expression is associated with poor prognosis in colorectal cancer patients. *World J Gastroenterol* (2015) 21(5):1457–67. doi:10.3748/wjg.v21.i5.1457

7. Dalerba P, Sahoo D, Paik S, Guo X, Yothers G, Song N, et al. CDX2 as a prognostic biomarker in stage II and stage III colon cancer. *N Engl J Med* (2016) 374(3):211–22. doi:10.1056/NEJMoa1506597

8. Alarid-Escudero F, Schrag D, Kuntz KM. CDX2 biomarker testing and adjuvant therapy for stage II colon cancer: An exploratory cost-effectiveness analysis. *Value Heal* (2022) 25(3):409–18. doi:10.1016/j.jval.2021.07.019

9. Brierly JD, Gospodarowicz MKWC. *TNM classification of malignant tumours*. 8th ed. New Jersey, United States: Wiley (2017).

10. Nagtegaal ID, Odze RD, Klimstra D, Paradis V, Rugge M, Schirmacher P, et al. The 2019 WHO classification of tumours of the digestive system. *Histopathology* (2020) 76(2):182–8. doi:10.1111/his.13975

11. Hestetun KE, Aasebø K, Rosenlund NB, Müller Y, Dahl O, Myklebust MP. Mismatch repair phenotype determines the implications of tumor grade and CDX2 expression in stage II–III colon cancer. *Mod Pathol* (2021) 34(1):161–70. doi:10.1038/s41379-020-0634-9

12. Hashmi AA, Ali R, Hussain ZF, Faridi N, Khan EY, Bakar SMA, et al. Mismatch repair deficiency screening in colorectal carcinoma by a four-antibody immunohistochemical panel in Pakistani population and its correlation with histopathological parameters. *World J Surg Oncol* (2017) 15(1):116. doi:10.1186/s12957-017-1158-8

13. Neumann J, Heinemann V, Engel J, Kirchner T, Stintzing S. The prognostic impact of CDX2 correlates with the underlying mismatch repair status and BRAF mutational status but not with distant metastasis in colorectal cancer. *Virchows Arch* (2018) 473(2):199–207. doi:10.1007/s00428-018-2360-y

14. Konukiewitz B, Schmitt M, Silva M, Pohl J, Lang C, Steiger K, et al. Loss of CDX2 in colorectal cancer is associated with histopathologic subtypes and microsatellite instability but is prognostically inferior to hematoxylin–eosin-based morphologic parameters from the WHO classification. *Br J Cancer* (2021) 125(12):1632–46. doi:10.1038/s41416-021-01553-0

15. Kim JH, Rhee YY, Bae JM, Cho NY, Kang GH. Loss of CDX2/CK20 expression is associated with poorly differentiated carcinoma, the CpG island methylator phenotype, and adverse prognosis in microsatellite-unstable colorectal cancer. *Am J Surg Pathol* (2013) 37(10):1532–41. doi:10.1097/PAS.0b013e31829ab1c1

16. Bruun J, Sveen A, Barros R, Eide PW, Eilertsen I, Kolberg M, et al. Prognostic, predictive, and pharmacogenomic assessments of CDX2 refine stratification of colorectal cancer. *Mol Oncol* (2018) 12(9):1639–55. doi:10.1002/1878-0261.12347

17. Baba Y, Nosho K, Shima K, Freed E, Irahara N, Philips J, et al. Relationship of CDX2 loss with molecular features and prognosis in colorectal cancer. *Clin Cancer Res* (2009) 15(14):4665–73. doi:10.1158/1078-0432.CCR-09-0401

18. Ribeirinho-Soares S, Pádua D, Amaral AL, Valentini E, Azevedo D, Marques C, et al. Prognostic significance of MUC2, CDX2 and SOX2 in stage II colorectal cancer patients. *BMC Cancer* (2021) 21(1):359–13. doi:10.1186/s12885-021-08070-6

19. Shigematsu Y, Inamura K, Mise Y, Saiura A, Rehnberg E, Yamamoto N, et al. CDX2 expression is concordant between primary colorectal cancer lesions and corresponding liver metastases independent of chemotherapy: A single-center retrospective study in Japan. *Oncotarget* (2018) 9(24):17056–65. doi:10.18632/oncotarget.24842

20. Pilati C, Taieb J, Balogoun R, Marisa L, de Reyniès A, Laurent-Puig P. CDX2 prognostic value in stage II/III resected colon cancer is related to CMS classification. *Ann Oncol Off J Eur Soc Med Oncol* (2017) 28(5):1032–5. doi:10.1093/annonc/mdx066

21. Shigematsu Y, Inamura K, Yamamoto N, Mise Y, Saiura A, Ishikawa Y, et al. Impact of CDX2 expression status on the survival of patients after curative resection for colorectal cancer liver metastasis 11 Medical and Health Sciences 1112 Oncology and Carcinogenesis. *BMC Cancer* (2018) 18(1):980. doi:10.1186/s12885-018-4902-8

22. Slik K, Turkki R, Carpén O, Kurki S, Korkeila E, Sundstrom J, et al. CDX2 loss with microsatellite stable phenotype predicts poor clinical outcome in stage II colorectal carcinoma. *Am J Surg Pathol* (2019) 43(11):1473–82. doi:10.1097/PAS.0000000000001356

23. Graule J, Uth K, Fischer E, Centeno I, Galván JA, Eichmann M, et al. CDX2 in colorectal cancer is an independent prognostic factor and regulated by promoter methylation and histone deacetylation in tumors of the serrated pathway. *Clin Epigenetics* (2018) 10(1):120. doi:10.1186/s13148-018-0548-2

24. Melincovici CS, Boşca AB, Şuşman S, Cutaş A, Mărginean M, Ilea A, et al. Assessment of mismatch repair deficiency, CDX2, beta-catenin and E-cadherin expression in colon cancer: Molecular characteristics and impact on prognosis and survival - an immunohistochemical study. *Rom J Morphol Embryol* (2020) 61(3): 715–27. doi:10.47162/RJME.61.3.10

25. Rozek LS, Lipkin SM, Fearon ER, Hanash S, Giordano TJ, Greenson JK, et al. CDX2 polymorphisms, RNA expression, and risk of colorectal cancer. *Cancer Res* (2005) 65(13):5488–92. doi:10.1158/0008-5472.CAN-04-3645

26. Ohki D, Yamamichi N, Sakaguchi Y, Takahashi Y, Kageyama-Yahara N, Yamamichi M, et al. Transcriptome of sessile serrated adenoma/polyps is associated with MSI- high colorectal cancer and decreased expression of CDX2. *Cancer Med* (2022) 1–13:5066–5078. doi:10.1002/cam4.4810

27. Ryan ÉJ, Creavin B, Khaw YL, Kelly ME, Mohan HM, Geraghty R, et al. Effects of CDX2 on prognosis and chemotherapy responsiveness in mismatch repair-deficient colorectal cancer. *BJS Open* (2018) 2(6):456–63. doi:10.1002/bjs5.91

28. Lugli A, Tzankov A, Zlobec I, Terracciano LM. Differential diagnostic and functional role of the multi-marker phenotype CDX2/CK20/CK7 in colorectal cancer stratified by mismatch repair status. *Mod Pathol* (2008) 21(11):1403–12. doi:10.1038/modpathol.2008.117

29. Dawson H, Galván JA, Helbling M, Muller DE, Karamitopoulou E, Koelzer VH, et al. Possible role of Cdx2 in the serrated pathway of colorectal cancer characterized by BRAF mutation, high-level CpG Island methylator phenotype and mismatch repair-deficiency. *Int J Cancer* (2014) 134(10):2342–51. doi:10.1002/ijc.28564

30. Tomasello G, Barni S, Turati L, Ghidini M, Pezzica E, Passalacqua R, et al. Association of CDX2 expression with survival in early colorectal cancer: A systematic review and meta-analysis. *Clin Colorectal Cancer* (2018) 17(2):97–103. doi:10.1016/j.clcc.2018.02.001

31. De'angelis GL, Bottarelli L, Azzoni C, De'angelis N, Leandro G, Di Mario F, et al. Microsatellite instability in colorectal cancer. *Acta Biomed* (2018) 89(6):97–101. doi:10.23750/abm.v89i9-S.7960

32. Boland CR, Goel A. Microsatellite instability in colorectal cancer. *Gastroenterology* (2010) 138(6):2073–87. doi:10.1053/j.gastro.2009.12.064

33. Sayar I, Akbas EM, Isik A, Gokce A, Peker K, Demirtas L, et al. Relationship among mismatch repair deficiency, CDX2 loss, p53 and E-cadherin in colon carcinoma and suitability of using a double panel of mismatch repair proteins by immunohistochemistry. *Polish J Pathol* (2015) 66(3):246–53. doi:10.5114/pjp.2015.54958

34. Tóth C, Sükösd F, Valicsek E, Herpel E, Schirmacher P, Tiszlavicz L. Loss of CDX2 gene expression is associated with DNA repair proteins and is a crucial member of the Wnt signaling pathway in liver metastasis of colorectal cancer. *Oncol Lett* (2018) 15(3):3586–93. doi:10.3892/ol.2018.7756

35. Kim JH, Kang GH. Molecular and prognostic heterogeneity of microsatellite-unstable colorectal cancer. *World J Gastroenterol* (2014) 20(15):4230–43. doi:10.3748/wjg.v20.i15.4230

36. Lee BC, Yu CS, Kim J, Lee JL, Kim CW, Yoon YS, et al. Clinicopathological features and surgical options for synchronous colorectal cancer. *Med (United States)* (2017) 96(9):e6224. doi:10.1097/MD.0000000000006224

37. Chikatani K, Chika N, Suzuki O, Sakimoto T, Ishibashi K, Eguchi H, et al. A model for Predicting DNA mismatch repair-deficient colorectal cancer. *Anticancer Res* (2020) 40(8):4379–85. doi:10.21873/anticanres.14441

38. Jenkins MA, Hayashi S, O'Shea AM, Burgart LJ, Smyrk TC, Shimizu D, et al. Pathology features in bethesda guidelines predict colorectal cancer microsatellite instability: A population-based study. *Gastroenterology* (2007) 133(1):48–56. doi:10.1053/j.gastro.2007.04.044

39. Fujiyoshi K, Yamaguchi T, Kakuta M, Takahashi A, Arai Y, Yamada M, et al. Predictive model for high-frequency microsatellite instability in colorectal cancer patients over 50 years of age. *Cancer Med* (2017) 6(6):1255–63. doi:10.1002/cam4.1088

40. Román R, Verdú M, Calvo M, Vidal A, Sanjuan X, Jimeno M, et al. Microsatellite instability of the colorectal carcinoma can be predicted in the conventional pathologic examination. A prospective multicentric study and the statistical analysis of 615 cases consolidate our previously proposed logistic regression model. *Virchows Arch* (2010) 456(5):533–41. doi:10.1007/s00428-010-0896-6

41. Greenson JK, Huang SC, Herron C, Moreno V, Bonner JD, Tomsho LP, et al. Pathologic predictors of microsatellite instability in colorectal cancer. *Am J Surg Pathol* (2009) 33(1):126–33. doi:10.1097/PAS.0b013e31817ec2b1

Pathology & Oncology Research | frontiers

TYPE Original Research
PUBLISHED 02 June 2023
DOI 10.3389/pore.2023.1611179

Check for updates

OPEN ACCESS

EDITED BY
Anna Sebestyén,
Semmelweis University, Hungary

*CORRESPONDENCE
Jinsong Zhang,
stspine@163.com
Qing Qiao,
qqing44@fmmu.edu.cn

†These authors have contributed equally to this work and share first authorship

RECEIVED 13 March 2023
ACCEPTED 24 May 2023
PUBLISHED 02 June 2023

CITATION
Zhang G, Hao Y, Chen L, Li Z, Gao L, Tian J, Qiao Q and Zhang J (2023), Expression of aquaporin 1, 3 and 5 in colorectal carcinoma: correlation with clinicopathological characteristics and prognosis.
Pathol. Oncol. Res. 29:1611179.
doi: 10.3389/pore.2023.1611179

COPYRIGHT
© 2023 Zhang, Hao, Chen, Li, Gao, Tian, Qiao and Zhang. This is an open-access article distributed under the terms of the Creative Commons Attribution License (CC BY). The use, distribution or reproduction in other forums is permitted, provided the original author(s) and the copyright owner(s) are credited and that the original publication in this journal is cited, in accordance with accepted academic practice. No use, distribution or reproduction is permitted which does not comply with these terms.

Expression of aquaporin 1, 3 and 5 in colorectal carcinoma: correlation with clinicopathological characteristics and prognosis

Guangwen Zhang[1†], Yongfei Hao[1,2†], Ling Chen[3], Zengshan Li[3], Langlang Gao[1], Jian Tian[1], Qing Qiao[4*] and Jinsong Zhang[1*]

[1]Department of Radiology, Xijing Hospital, Fourth Military Medical University, Xi'an, Shaanxi, China, [2]School of Medicine, Yan'an University, Yan'an, Shaanxi, China, [3]Department of Pathology, Xijing Hospital, Fourth Military Medical University, Xi'an, Shaanxi, China, [4]Department of General Surgery, Tangdu Hospital, Fourth Military Medical University, Xi'an, Shaanxi, China

Background: Prognostic biomarkers in colorectal carcinoma (CRC) have an important role in therapeutic strategy. Studies have shown that high expression of Aquaporin (AQP) is associated with poor prognosis in a variety of human tumors. AQP is involved in the initiation and development of CRC. The present study aimed to investigate the correlation between the expression of AQP1, 3 and 5 and clinicopathological features or prognosis in CRC.

Methods: The AQP1, 3 and 5 expressions were analyzed based on the immunohistochemical staining of tissue microarray specimens including 112 patients with CRC between June 2006 and November 2008. The expression score of AQP (Allred_score and H_score) was digitally obtained with Qupath software. Patients were divided into high or low expression subgroups based on the optimal cut-off values. The relationship between expression of AQP and clinicopathological characteristics were evaluated using chi-square test, t-test, or one-way ANOVA, when appropriate. Survival analysis of 5-year progression free survival (PFS) and overall survival (OS) was performed with time-dependent ROC, Kaplan-Meier curves, univariate and multivariate COX analysis.

Results: The AQP1, 3 and 5 expressions were associated with regional lymph node metastasis, histological grading, and tumor location in CRC, respectively ($p < 0.05$). Kaplan-Meier curves showed that patients with high AQP1 expression had worse 5-year PFS than those with low AQP1 expression (Allred_score: 47% vs. 72%, $p = 0.015$; H_score: 52% vs. 78% $p = 0.006$), as well as 5-year OS (Allred_score: 51% vs. 75%, $p = 0.005$; H_score: 56% vs. 80%, $p = 0.002$). Multivariate Cox regression analysis indicated that AQP1 expression was an independent risk prognostic factor ($p = 0.033$, HR = 2.274, HR95% CI: 1.069–4.836). There was no significant correlation between the expression of AQP3 and 5 and the prognosis.

Conclusion: The AQP1, 3 and 5 expressions correlate with different clinicopathological characteristics and the AQP1 expression may be a potential biomarker of prognosis in CRC.

KEYWORDS

biomarker, prognosis, clinical features, colorectal cancer, aquaporin

Introduction

Colorectal carcinoma (CRC) is the second most deadly cancer and the third most prevalent malignant tumor worldwide [1]. In the past few decades, despite aggressive surgery and advances in chemotherapy, the prognosis for CRC remains unsatisfactory, the 5-year survival rate of CRC patients is still less than 64% [2, 3]. Previous studies have shown that the effectiveness of postoperative chemotherapy and patient survival was closely related to tumor biology [4, 5]. Therefore, the discovery of potential biomarkers is imperative to predict the prognosis of CRC.

Aquaporins (AQPs), a family of transmembrane proteins, are widely distributed on the membrane of nucleated cells. The fluid transfer interceded by AQPs is the primary method for water entry into the cells or outside the cells [6]. At present, it is known that 13 kinds of AQPs can be expressed in humans, of which AQP0, AQP1, AQP2, AQP4, AQP5, AQP6, and AQP8 play a major role in selectively transporting water molecules; AQP3, AQP7, AQP9, and AQP10 can transport glycerol and other small molecular solutes [7], while AQP11 and AQP12 are responsible for the transport of H_2O_2 in the endoplasmic reticulum [8]. Some clinical studies have indicated that AQPs play an important role in maintaining osmotic pressure, regulating tumor cell migration, cell-matrix adhesion and cell proliferation, and promoting tumor neovascularization [9]. In addition, AQPs have extensive interactions with oncogenes and proteins [10]. Recent research has proved that AQPs were strongly expressed in a variety of human tumors, including, renal cell carcinoma [11], prostate cancer [12], breast cancer [13], pancreatic adenocarcinoma [14], and lung cancer [15].

Although previous studies have confirmed that AQP1 was strongly associated with the prognosis of CRC, a consensus has not been reached until now. Yoshida et al [16] showed that AQP1 was an independent poor prognostic factor for overall survival (OS, $p = 0.03$). On the contrary, Byung et al [17]found that AQP1 was suggested as not an independent prognostic factor for progression free survival (PFS) and OS. Likewise, Imaizumi et al [18] demonstrated that AQP1 expression was not related to the PFS. In our previous research, we found that the ultra-high b-value DWI could match AQP1 expression of tumor and accordingly speculate AQP1 may be a potential biomarker for prognosis [19]. Up until now, few studies have used two expression scores to evaluate the possible correlation between AQP1, 3 and 5 expression and clinicopathological characteristics or prognosis in CRC. Since the AQPs with high expression in CRC are mainly AQP1, 3 and 5 [20], We therefore hope to determine whether AQP1, 3 and 5 could be used as specific biomarkers indicating that CRC has different clinicopathological features and prognosis.

Materials and methods

Patients

This study was approved by the Ethics Committee of Xijing Hospital and informed consent was acquired for patient specimens and follow-up information. A total of 191 patients with CRC who had undergone surgical resection between June 2006 and November 2008 were investigated and followed up until 2016 in this study. According to the following inclusion and exclusion criteria (Figure 1), the postoperative specimens of 112 patients were involved. The inclusion criteria included: 1) histologically confirmed colorectal adenocarcinoma; 2) age ≥ 18; 3) without other malignant tumors. The exclusion criteria included: 1) non-adenocarcinoma ($n = 15$); 2) received preoperative anti-tumor therapies ($n = 48$); 3) follow-up data unavailable ($n = 16$); 4) unqualified specimens (AQP1, $n = 9$; AQP3, $n = 5$; AQP5, $n = 3$). Lastly, the total number of specimens evaluated for AQP1 expression was 103, AQP3 expression was 107 and AQP5 expression was 109. The main indicators were PFS and OS. PFS was defined as the period of time from the patient's diagnosis date until any tumor progression, such as metastasis, recurrence, or death. OS was defined as the period of time from the diagnostic date until death from any cause.

Immunohistochemical staining of AQP1, 3 and 5

Each TMA contained 17 patients' tissues including 2 cores of tumor tissue and 1 core of paracancerous tissue for one patient. The core diameter of TMA was 1.6 mm. The immunohistochemical staining was performed on a Leica BOND-MAX autoimmunostainer (Leica Instrument Co., Ltd.). The tissue chips were first cut into 4-μm-thick slices using a microtome, attached to slides, dried, and baked at 60°C for 24 h before use. The prepared slices were dewaxed with xylene, rehydrated with different concentrations of ethanol (100% and 95%), rinsed with distilled water, and repaired with heat-induced antigen. Finally, the antigen

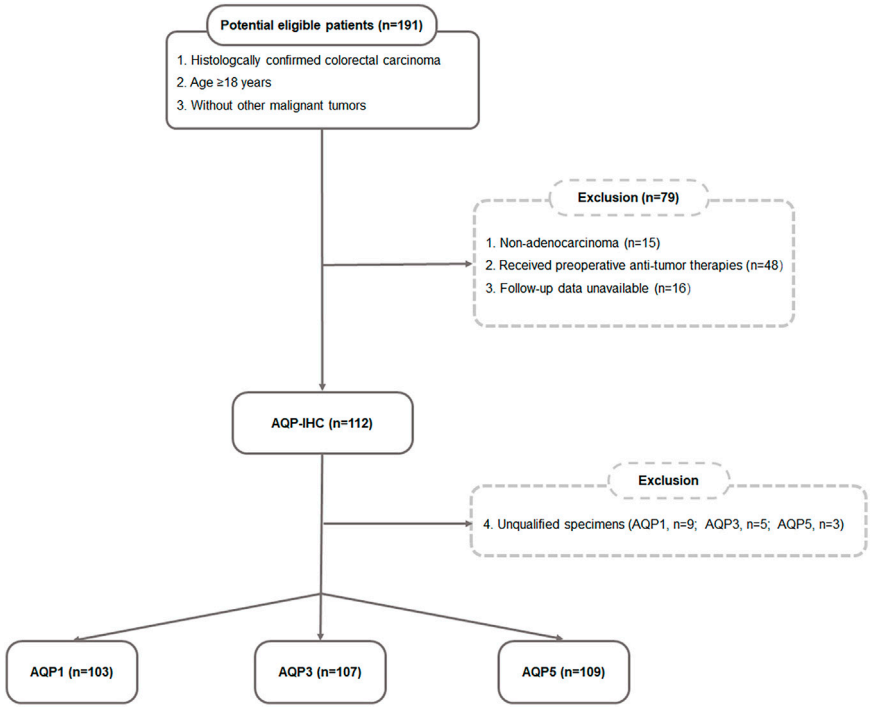

FIGURE 1
Flow chart of the eligible patient's selection.

was detected by an automatic staining machine (Benchmark) and Bond Polymer Purification Detection Kit (LeicaInstrumentCo., Ltd.). The primary antibodies (Abcam) were diluted as follows: anti-AQP1 (ab168387, 1:1,000), anti-AQP3 (ab125219, 1:500), and anti-AQP5 (ab92320, 1:200).

Scoring of AQP immunohistochemical staining

All slides were scanned with a Nano Zoomer SQ (HAMAMATSU, Japan). The expression levels of AQP1, 3 and 5 in the tumor region of each core of TMA were evaluated by Qupath software (Quantitative Pathology, version 0.2.0) and corresponding scores (Allred_score [21]and H_score [22]) were obtained. The average score of two tumor cores from the same patient was submitted for statistical analysis.

The combination of the values for staining intensity and the percentage of positively stained cells produced an Allred score that ranged from 0 to 8. The intensity was given a score between 0 and 3, with 0 representing no staining, 1 representing weak staining, 2 representing moderate staining, and 3 representing high staining Scores representing the proportion of positively stained tumor cells were stratified as 0 (no positive tumor cells), 1 (<1%), 2 (1%–10%), 3 (10%–33%), 4 (33%–67%) and 5 (67%–100%).

The H_score which ranged from 0 to 300 was calculated with the following equation: H_score = $\sum (PI \times I)$ = (percentage of cells with weak intensity × 1) + (percentage of cells with moderate intensity × 2) + (percentage of cells with strong intensity × 3). The terms *PI* and *I* in the formula represent the proportion of positive cells to all cells and the staining intensity (0–3), respectively.

Statistical analysis

All analyses were completed using the statistical programming language R (version 4.1.2, 6.1, www.r-project.org) and SPSS (version 26.0, IBM, Armonk, NY). For all statistical tests, differences were considered statistically significant when the *p*-value was <0.05 (two-tailed).

The correlations between AQP expression and clinicopathological characteristics were investigated with chi-square test, *t*-test, or one-way ANOVA, when appropriate. The optimal cut-off values of AQP (Allred_score and H_score) to distinguish high AQP1, 3 and 5 expressions from low expression were determined separately using time-dependent ROC curves (R package "survival ROC"). The Kaplan-Meier curves and log-rank tests were used to perform survival analysis of AQP expression by R package "survival." The

TABLE 1 Clinicopathological characteristics of patients in AQP1, 3 and 5 groups.

Characteristics	AQP1 (n = 103)	AQP3 (n = 107)	AQP5 (n = 109)
Age, years (mean ± SD), n (%)	59.5 ± 13.4	58.8 ± 14.0	58.9 ± 14.0
<60	50 (48.5%)	53 (49.5%)	54 (49.5%)
≥60	53 (51.5%)	54 (50.5%)	55 (50.5%)
Gender, n (%)			
Male	66 (64.1%)	67 (62.6%)	68 (62.4%)
Female	37 (35.9%)	40 (37.4%)	41 (37.6%)
Primary tumor site, n (%)			
Left colon	61 (59.2%)	60 (56.1%)	62 (56.9%)
Right colon	42 (40.8%)	47 (43.9%)	47 (43.1%)
Histological grade, n (%)			
Well differentiated	33 (32.0%)	35 (32.7%)	36 (33.0%)
Moderate differentiated	62 (60.2%)	61 (57.0%)	62 (56.9%)
Poor differentiated	8 (7.8%)	11 (10.3%)	11 (10.1%)
TNM stage, n (%)			
I	22 (21.4%)	24 (22.4%)	24 (22.0%)
II	42 (40.8%)	40 (37.4%)	42 (38.6%)
III	22 (21.4%)	25 (23.4%)	25 (22.9%)
IV	17 (16.5%)	18 (16.8%)	18 (16.5%)
T stage, n (%)			
T2	25 (24.3%)	27 (25.2%)	27 (24.8%)
T3	26 (25.2%)	27 (25.2%)	28 (25.7%)
T4	52 (50.5%)	53 (49.5%)	54 (49.5%)
N stage, n (%)			
N–	69 (67%)	70 (65.4%)	72 (66.1%)
N+	34 (33%)	37 (34.6%)	37 (33.9%)
M stage, n (%)			
M–	86 (83.5%)	89 (83.2%)	91 (83.5%)
M+	17 (16.5%)	18 (16.8%)	18 (16.5%)
Treatment strategy, n (%)			
Surgery only	31 (30.1%)	33 (30.8%)	34 (31.2%)
Surgery + other treatment	72 (69.9%)	74 (69.2%)	75 (68.8%)
Survival rate, n (%)			
3-year PFS	68%	68%	67%
3-year OS	70%	70%	69%
5-year PFS	60%	60%	59%
5-year OS	61%	62%	61%

Abbreviations: PFS, progression free survival; OS, overall survival. The pathological stage was determined by the pathologist according to the 7th edition of AJCC.

Cox proportional hazard regression models were used to conduct both univariate and multivariate survival analyses.

Results

Patient characteristics

A total of 112 patients were eventually enrolled in this retrospective study. The AQP1 group contained 103 consecutive patients (66 males, 37 females; mean age, 59.5 ± 13.4 years; mean follow-up, 78 months, range: 1–128 months). The AQP3 group contained 107 consecutive patients (67 males, 40 females; mean age, 58.8 ± 14.0 years; mean follow-up, 79 months, range: 1–128 months). The AQP5 group contained 109 consecutive patients (68 males, 41 females; mean age, 58.9 ± 14.0 years; mean follow-up, 78 months, range: 1–128 months). The other clinical characteristics of patients were presented in Table 1.

Patients were divided into high or low expression subgroups according to the optimal cut-off values (Allred_score and H_score)

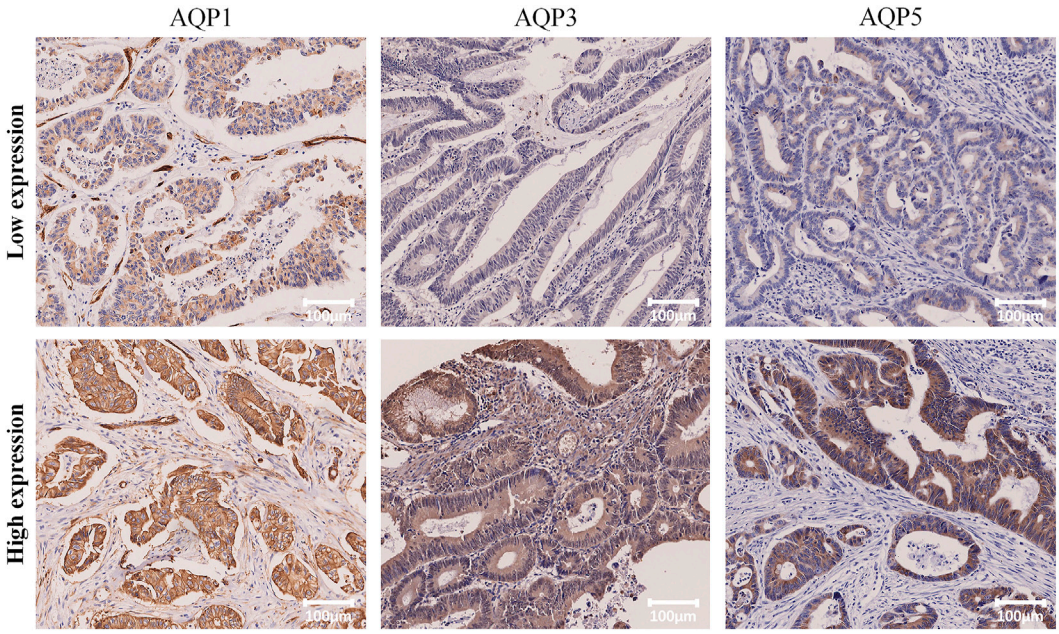

FIGURE 2
Representative IHC staining of high and low expression of AQP1, AQP3 and AQP5 (×100).

of AQP1, 3 and 5 expressions which were determined by time-dependent ROC curves according to the 5-year PFS. The optimal cut-off values for AQP1 (Allred_score) and AQP1 (H_score) were 6.0 and 116.17, respectively. The optimal cut-off values for AQP3 (Allred_score) and AQP3 (H_score) were 5.5 and 115.64, respectively. The optimal cut-off values for AQP5 (Allred_score) and AQP5 (H_score) were 6.0 and 18.64, respectively. Accordingly, Immunohistochemical examples of low and high expression of AQP1, 3 and 5 were shown in Figure 2.

Associations between AQP1, 3 and 5 expressions and clinicopathological characteristics

This study investigated the relationship between AQP1, 3 and 5 expression and gender, age, primary tumor site, histological grading, and TNM stage. For Allred_score, the rate of AQP1 high expression in the positive lymph node group was significantly more common than that in the negative lymph node group (79.4% vs. 58.0%, $\chi^2 = 4.605$, $p = 0.032$, Figure 3). For H_score, the expression of AQP1 was significantly higher in positive lymph node group than that in negative lymph node group (134.81 ± 44.573 vs. 105.978 ± 46.122, $t = 3.016$, $p = 0.003$, Figure 4).

The AQP3(Allred_score) was significantly correlated with the histological grading of CRC. ($\chi^2 = 10.773$, $p = 0.005$, Supplementary Figure S1), AQP3 (H_score) had a similar conclusion ($F = 4.212$, $p = 0.017$, Supplementary Figure S2). In multiple comparisons between groups, AQP3 expression (H_score) was found to be significantly higher in well-differentiated group than in moderate-differentiated group ($p = 0.005$, Supplementary Figure S2), while no statistically significant differences in AQP3 expression were found between the well-differentiated group and poor-differentiated group, as well as moderate-differentiated group and poor-differentiated group ($p = 0.233$ and 0.542, respectively).

The AQP5 (Allred_score) was apparently associated with the tumor location of colorectal carcinoma ($\chi^2 = 8.123$, $p = 0.004$, Supplementary Figure S3), AQP5 (H_score) had a similar conclusion, resulting in significantly lower AQP5 expression in the left hemicolectomy than in the right hemicolectomy (50.473 ± 54.175 vs. 90.052 ± 62.624, $t = -3.531$, $p = 0.001$, Supplementary Figure S4).

Kaplan-Meier survival curves with AQP1, 3 and 5 expressions

Kaplan-Meier survival curves demonstrated that the patient with high expression of the AQP1 had poorer 5-year PFS than patients with low expression of the AQP1 (Allred_score, 5-year PFS = 47% vs. 72%, $p = 0.015$, Figure 5A; H_score, 5-year PFS = 52% vs. 78%, $p = 0.006$; Figure 5B). Likewise, the survival rate of patients with high AQP1 expression in 5-year OS was significantly lower compared to that of patients with low AQP1 expression in 5-year OS (Allred_score, 5-year OS = 51% vs. 75%, $p = 0.005$, Figure 5C; H_score, 5-year OS = 56%



FIGURE 3
Percentage bar graph about the correlation between AQP1 (Allred_score) expression and clinicopathological characteristics. The AQP1 expression was significantly correlated with the N stage of CRC (χ^2 = 4.605, p = 0.032).

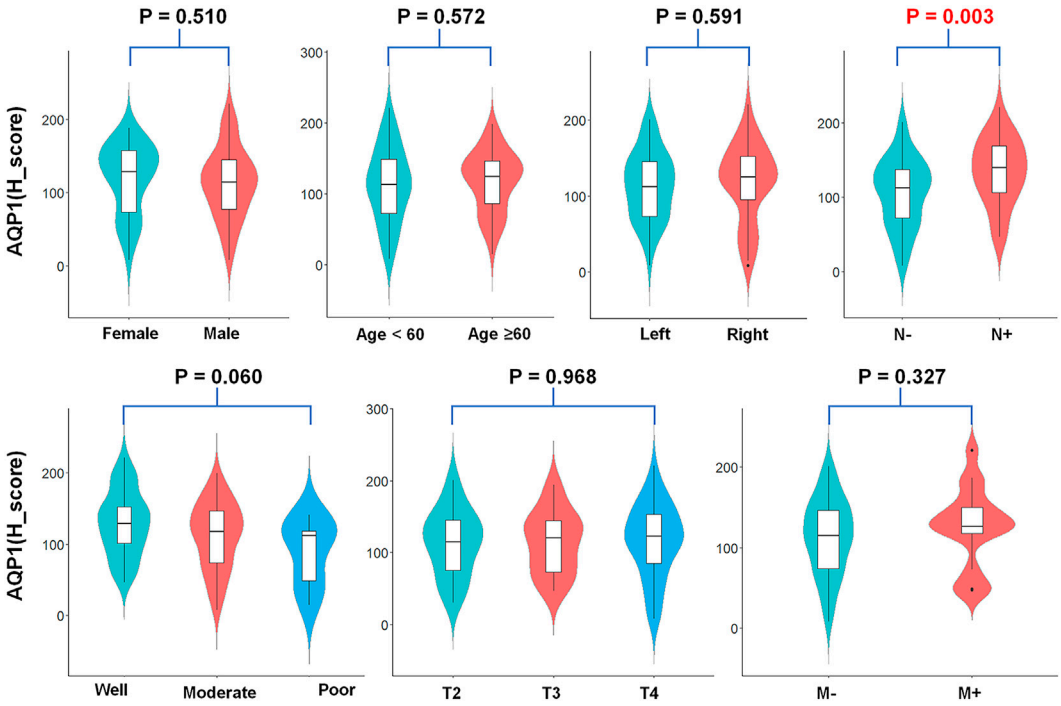

FIGURE 4
Violin plots about AQP1 (H_score) expression and clinicopathological characteristics. The AQP1 (H_score) expression was significantly correlated with the N stage of CRC (t = 3.016, p = 0.003).

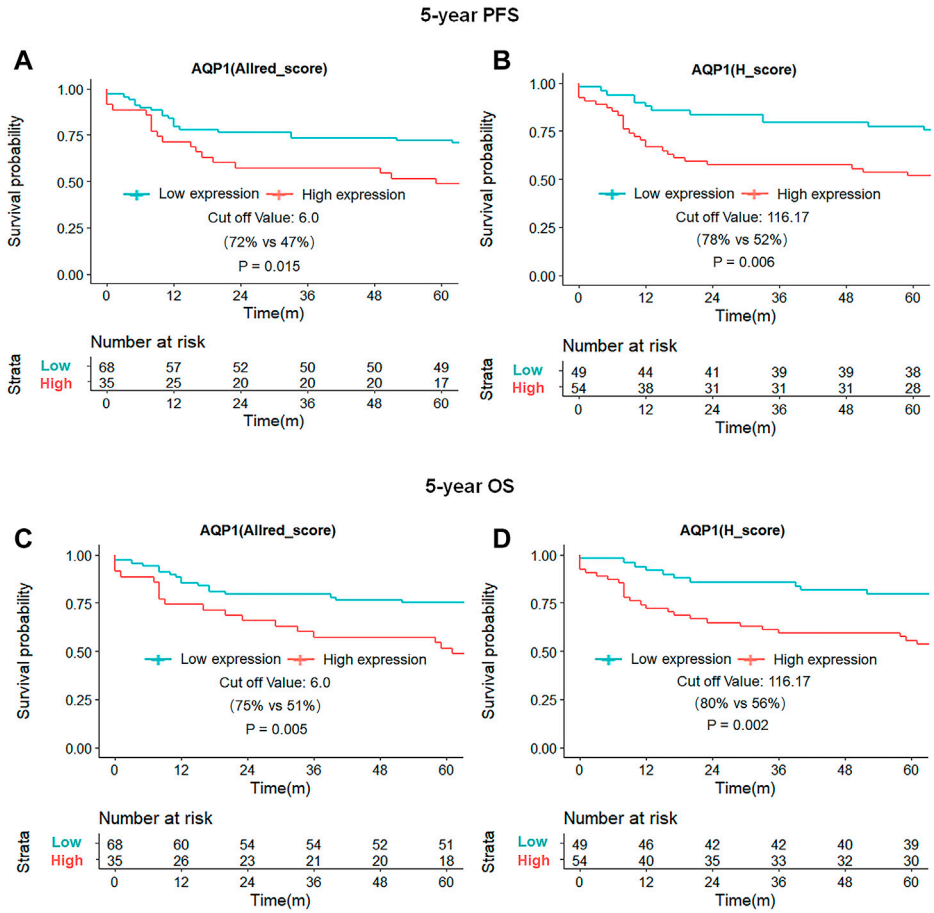

FIGURE 5
Kaplan-Meier survival curves of 5-year PFS and OS for patients based on AQP1 expression. Patients with high AQP (Allred_score) expression had worse 5-year PFS and OS than those with low AQP (Allred_score) expression [47% vs. 72%, p = 0.015, **(A)**; 51% vs. 75%, p = 0.005; **(C)**], with similar results for AQP1 (H_score) expression [52% vs. 78%, p = 0.006, **(B)**; 56% vs. 80%, p = 0.002; **(D)**].

vs. 80%, p = 0.002; Figure 5D). However, Kaplan-Meier survival curves presented that the 5-year PFS and OS of patients in high or low AQP3 and 5 expression groups had no statistical difference. (p > 0.05, Supplementary Figures S5, S6).

Univariate and multivariate COX regression analysis of the prognosis

The AQP1, 3 and 5 expression and clinicopathologic factors, including age, gender, primary tumor site, histological grading, TNM-stage and treatment strategy, were submitted into univariate and multivariate COX regression analysis. The univariate Cox regression analysis showed that AQP1 (Allred_score and H_score), age, and TNM-stage were risk factors of 5-year PFS and OS for CRC (p < 0.05), while the expression of AQP 3 and AQP5 were not correlated with 5-year PFS and OS (p > 0.05, Table 2).

Since the Allred_score and H_score were two indicators to evaluate the same protein expression and the univariate COX analysis showed that the H_score was more significant than Allred_score in PFS and OS assessment (PFS, p = 0.008 vs. 0.017; OS, p = 0.003 vs. 0.008), the multivariate COX regression analysis was performed using H_score of AQP1 and indicated that AQP1 was no longer an independent risk factor for 5-year PFS (p = 0.086, HR = 1.866, HR95% CI: 0.916–3.800), but an independent risk factor for 5-year OS (p = 0.033, HR = 2.274, HR95% CI: 1.069–4.836, Table 3).

Discussion

In the present study, we investigated the correlation between AQP1, AQP3 and AQP5 expression and clinicopathological features or prognosis in 121 patients with CRC. The AQP1 expression, AQP3 expression and AQP5 expression

TABLE 2 Univariate cox regression analysis for prognosis of colorectal carcinoma.

Variate	PFS		OS	
	P	HR (95% CI)	*P*	HR (95% CI)
AQP1 (Allred_score ≥6)	**0.017**	2.144 (1.143–4.021)	**0.007**	2.433 (1.276–4.641)
AQP3 (Allred_score ≥5.5)	0.588	1.187 (0.638–2.211)	0.405	1.319 (0.688–2.528)
AQP5 (Allred_score ≥6)	0.349	1.402 (0.691–2.845)	0.897	1.043 (0.550–1.979)
AQP1 (H_score ≥116.17)	**0.008**	2.532 (1.282–5.004)	**0.003**	3.041 (1.471–6.288)
AQP3 (H_score ≥115.64)	0.458	1.283 (0.664–2.478)	0.495	1.248 (0.660–2.361)
AQP5 (H_score ≥18.64)	0.368	1.385 (0.682–2.809)	0.521	1.264 (0.618–2.586)
Gender (male)	0.656	0.859 (0.442–0.163)	0.898	0.957 (0.487–1.880)
Age (≥60)	**0.042**	1.971 (1.024–3.794)	**0.030**	2.115 (1.076–4.157)
Primary tumor site (left)	0.969	0.988 (0.522–1.870)	0.673	0.869 (0.454–1.666)
Histological grade (low)	0.475	1.219 (0.708–2.100)	0.213	1.428 (0.815–2.501)
TNM-stage (III–IV)	**<0.001**	3.084 (1.624–5.858)	**<0.001**	3.122 (1.614–6.038)
Treatment (comprehensive)	0.064	0.544 (0.287–1.037)	0.130	0.598 (0.308–1.163)

Abbreviations: PFS, progression-free survival; OS, overall survival; HR (95% CI), hazard ratio and its 95% confidence interval. Univariate and multivariate COX regression analyses of clinicopathological characteristics were performed based on the data of the AQP1 group. The score of AQP expression (<cut-off value), age (<60 years old), gender (female), primary tumor site (right), histological grade (high and moderate), TNM-stage (I–II) and treatment modality (surgery only) were set as references in COX regression analyses. Comprehensive treatment indicated that patients received surgery plus with neoadjuvant therapy and or adjuvant therapy.
Bold values are significant at $p < 0.05$.

TABLE 3 Multivariate cox regression analysis for prognosis of colorectal carcinoma.

Variate	PFS		OS	
	P	HR95% CI	*P*	HR95% CI
Age (≥60 years)	0.252	1.483 (0.756–2.911)	0.229	1.533 (0.764–3.076)
TNM stage (III-IV)	**0.007**	2.494 (1.285–4.839)	**0.010**	2.450 (1.243–4.827)
AQP1 (H_score ≥116.17)	0.086	1.866 (0.916–3.800)	**0.033**	2.274 (1.069–4.836)

Abbreviations: PFS, progression free survival; OS, overall survival; HR (95% CI), 95% confidence interval of the hazard ratio. Multivariate COX regression analysis of clinicopathological characteristics was conducted using AQP1 group data. The age (<60 years), TNM stage (I–II) and AQP1 (H_score <116.17) were set as references in COX regression analyses.
Bold values are significant at $p < 0.05$.

were related to regional lymph node metastasis, histological grading, and tumor location of CRC, respectively. In survival analysis, the AQP1 high expression was related to poor 5-year PFS and OS and was an independent prognostic factor for 5-year OS, but the AQP3 and AQP5 expression were not significantly correlated with prognosis in CRC.

This study found that AQP1 (H_score) expression was significantly higher in the positive lymph node group than negative lymph node group (134.81 ± 44.573 vs. 105.978 ± 46.122, $p = 0.003$) and AQP1 (H_score) high expression group had significantly worse 5-year PFS than that of the AQP1 low expression group (52% vs. 78%, $p = 0.006$). These results were similar to the work by Yoshida et al. [16] who found that high AQP1 expression in stage II/III colon cancer was strongly associated with regional lymph node metastasis and the 5-year survival rate was significantly lower in the positive AQP1 expression group than the negative group (73.7% vs. 87.9%, $p = 0.03$). In contrast, Byung et al. [17] showed that patients with AQP1 high expression are less likely to develop regional lymph node metastasis which was inconsistent with the theory that high AQP1 expression can promote tumor invasion and metastasis.

Although the molecular mechanism of AQP1 in cancer biology is not fully understood, numerous studies have indicated that AQP1 is involved in the angiogenesis, migration, and proliferation of tumor cells, which plays an important role in the development of cancer [23]. Potential downstream effectors in the signaling pathways involved in AQP1-mediated tumor progression include β-linked protein, Lin-7, FAK, MMP2, MMP9, and histone proteinase B [24]. A representative study reported that AQP1 may enhance the migratory ability and invasiveness of tumor cells by mediating the Wnt/β-catenin signaling pathway and stabilizing the cadherin/β-catenin/Lin-7/F-actin complex on cell membranes [25, 26]. β-catenin as an intracellular signal transducer in the canonical Wnt signaling pathway regulates the

expression of downstream genes (c-Myc, cyclinD1, c-Jun, and FRA1), which leads to cell proliferation, differentiation, and inhibition of apoptosis [27]. Therefore, regional lymph node metastasis should be associated with high AQP1 expression, rather than low expression. The high AQP1 expression was strongly associated with worse 5-year PFS and OS, which supports that high AQP1 expression can promote tumor invasion and reduce patient survival. There was no significant correlation between AQP1 expression and other clinicopathological characteristics (gender, age, tumor location, histological grading, T stage, and M stage).

The high expression of AQP3 has been observed in several cancers, which promotes to metastasis, proliferation, and epithelial-to-mesenchymal transition (EMT) [28]. Despite previous studies found that the high expression of AQP3 was related to the degree of lymphatic metastasis and differentiation of CRC [29], this study only found that the expression of AQP3 was related to the histological grading of CRC. Specifically, there was no linear relationship between AQP3 expression and histological grading which may be partially attributed to the small sample size of patients with low differentiation (n = 11). Further studies with more low differentiation of sample sizes are needed to validate the result.

In a recent study, Byung et al. [17] showed that AQP5 was not associated with PFS and OS of CRC. This outcome is contrary to that of Tao Shan et al. [30] who found that AQP5 was closely correlated with poor prognosis. According to our current study, the expression of AQP5 was related to the location of the tumor which might remind us that AQP5 played a different role in left and right-sided CRC. There was no significant correlation between AQP5 expression and other clinicopathological characteristics (age, gender, histological grading, and TNM stage).

Although both Allred_score and H_score are semi-quantitative indicators for evaluating protein expression, the range of H_score (0–300) is significantly higher than that of Allred_score (0–8). Therefore, H_score can be analyzed as a continuous variate. As the statistical efficiency of the H_score was generally better than Allred_score in this study, it was considered that H_score could describe AQP expression more accurately than Allred_score and was a better indicator for evaluating protein immunohistochemical results. Qupath is a free open-source digital pathological analysis software developed by the Center for Cancer Research and Cell Biology of Queen's University in Belfast, which has been widely used all over the world [31]. Several studies published in Nature [32], Cell [33], and Science [34] have demonstrated that quantitative analysis of biomarkers using Qupath software has good reliability and repeatability.

This study has some potential limitations. Firstly, it had a retrospective nature and a relatively small number of patients. In particular, there were only 11 cases of poor-differentiated CRC, more subjects need to be included in further evaluation. Secondly, the heterogeneity of staining may be affected by different sampling methods (TMA vs. whole slides), which is a possible reason that may contribute to different results in the literature. In this study, two tissue cores were carefully selected by a pathologist with 16-year experiences in gastrointestinal cancer, which may compensate for the insufficient representativity of TMA to some extent. Furthermore, we performed a long-time follow-up and digital scoring method for IHC staining, which may supply solid support for the conclusion of this study.

In conclusion, our data suggested that the expression levels of AQP1, AQP3 and AQP5 were associated with regional lymph node metastasis, histological grading, and tumor location of CRC, respectively. However, only AQP1 expression level was an independent risk factor for the prognosis of CRC.

Data availability statement

The original contributions presented in the study are included in the article/Supplementary Material, further inquiries can be directed to the corresponding authors.

Ethics statement

The studies involving human participants were reviewed and approved by Ethics Committee of Xijing Hospital. The patients/participants provided their written informed consent to participate in this study. Written informed consent was obtained from the individual(s) for the publication of any potentially identifiable images or data included in this article.

Author contributions

JZ, GZ, and YH designed the study, analyzed the data, and wrote the article. JZ and QQ were the supervisor of the study and revised the paper. LC and ZL collated the pathological data of patients and prepared the tables. LG and JT performed digital data analysis work and made the figures. All authors contributed to the article and approved the submitted version.

Funding

This study was funded by Key Research and Development Projects in Shaanxi (2018ZDXM-SF-059).

Conflict of interest

The authors declare that the research was conducted in the absence of any commercial or financial relationships that could be construed as a potential conflict of interest.

Acknowledgments

The author thanks Prof. Jing Zhang from Department of Pathology at Xijing Hospital for providing language assistance.

Supplementary material

The Supplementary Material for this article can be found online at: https://www.por-journal.com/articles/10.3389/pore.2023.1611179/full#supplementary-material

References

1. Sung H, Ferlay J, Siegel RL, Laversanne M, Soerjomataram I, Jemal A, et al. Global cancer statistics 2020: GLOBOCAN estimates of incidence and mortality worldwide for 36 cancers in 185 countries. *CA Cancer J Clin* (2021) 71:209–49. doi:10.3322/caac.21660

2. Bender U, Rho YS, Barrera I, Aghajanyan S, Acoba J, Kavan P. Adjuvant therapy for stages II and III colon cancer: Risk stratification, treatment duration, and future directions. *Curr Oncol* (2019) 26:S43–s52. doi:10.3747/co.26.5605

3. Siegel RL, Miller KD, Sauer AG, Fedewa SA, Butterly LF, Anderson JC, et al. Colorectal cancer statistics, 2020. *Ca-a Cancer J Clinicians* (2020) 70:145–64. doi:10.3322/caac.21601

4. Malki A, Abu ElRuz R, Gupta I, Allouch A, Vranic S, Al Moustafa AE. Molecular mechanisms of colon cancer progression and metastasis: Recent insights and advancements. *Int J Mol Sci* (2021) 22:130. doi:10.3390/ijms22010130

5. Bregni G, Telli TA, Camera S, Deleporte A, Moretti L, Bali AM, et al. Adjuvant chemotherapy for rectal cancer: Current evidence and recommendations for clinical practice. *Cancer Treat Rev* (2020) 83:101948. doi:10.1016/j.ctrv.2019.101948

6. Ribatti D, Ranieri G, Annese T, Nico B. Aquaporins in cancer. *Biochim Biophys Acta* (2014) 1840:1550–3. doi:10.1016/j.bbagen.2013.09.025

7. Zannetti A, Benga G, Brunetti A, Napolitano F, Avallone L, Pelagalli A. Role of aquaporins in the physiological functions of mesenchymal stem cells. *Cells* (2020) 9:2678. doi:10.3390/cells9122678

8. Prata C, Hrelia S, Fiorentini D. Peroxiporins in cancer. *Int J Mol Sci* (2019) 20:1371. doi:10.3390/ijms20061371

9. Moon CS, Moon D, Kang SK. Aquaporins in cancer biology. *Front Oncol* (2022) 12:782829. doi:10.3389/fonc.2022.782829

10. Papadopoulos MC, Saadoun S. Key roles of aquaporins in tumor biology. *Biochim Biophys Acta-Biomembranes* (2015) 1848:2576–83. doi:10.1016/j.bbamem.2014.09.001

11. Morrissey JJ, Mellnick VM, Luo J, Siegel MJ, Figenshau RS, Bhayani S, et al. Evaluation of urine aquaporin-1 and perilipin-2 concentrations as biomarkers to screen for renal cell carcinoma A prospective cohort study. *Jama Oncol* (2015) 1:204–12. doi:10.1001/jamaoncol.2015.0213

12. Kushwaha PP, Verma S, Gupta S. Aquaporins as prognostic biomarker in prostate cancer. *Cancers (Basel)* (2023) 15:331. doi:10.3390/cancers15020331

13. Rodrigues C, Milkovic L, Bujak IT, Tomljanovic M, Soveral G, Cipak Gasparovic A. Lipid profile and aquaporin expression under oxidative stress in breast cancer cells of different malignancies. *Oxid Med Cell Longev* (2019) 2019:2061830. doi:10.1155/2019/2061830

14. Chen G, Song H, Yang Z, Du T, Zheng Y, Lu Z, et al. AQP5 is a novel prognostic biomarker in pancreatic adenocarcinoma. *Front Oncol* (2022) 12:890193. doi:10.3389/fonc.2022.890193

15. Kao YC, Jheng JR, Pan HJ, Liao WY, Lee CH, Kuo PL. Elevated hydrostatic pressure enhances the motility and enlarges the size of the lung cancer cells through aquaporin upregulation mediated by caveolin-1 and ERK1/2 signaling. *Oncogene* (2017) 36:863–74. doi:10.1038/onc.2016.255

16. Yoshida T, Hojo S, Sekine S, Sawada S, Okumura T, Nagata T, et al. Expression of aquaporin-1 is a poor prognostic factor for stage II and III colon cancer. *Mol Clin Oncol* (2013) 1:953–8. doi:10.3892/mco.2013.165

17. Kang BW, Kim JG, Lee SJ, Chae YS, Jeong JY, Yoon GS, et al. Expression of aquaporin-1, aquaporin-3, and aquaporin-5 correlates with nodal metastasis in colon cancer. *Oncology* (2015) 88:369–76. doi:10.1159/000369073

18. Imaizumi H, Ishibashi K, Takenoshita S, Ishida H. Aquaporin 1 expression is associated with response to adjuvant chemotherapy in stage II and III colorectal cancer. *Oncol Lett* (2018) 15:6450–6. doi:10.3892/ol.2018.8170

19. Zhang G, Ma W, Dong H, Shu J, Hou W, Guo Y, et al. Based on histogram analysis: ADC(aqp) derived from ultra-high b-value DWI could be a non-invasive specific biomarker for rectal cancer prognosis. *Sci Rep* (2020) 10:10158. doi:10.1038/s41598-020-67263-4

20. Moosavi MS, Elham Y. Aquaporins 1, 3 and 5 in different tumors, their expression, prognosis value and role as new therapeutic targets. *Pathol Oncol Res* (2020) 26:615–25. doi:10.1007/s12253-019-00646-9

21. Harvey JM, Clark GM, Osborne CK, Allred DC. Estrogen receptor status by immunohistochemistry is superior to the ligand-binding assay for predicting response to adjuvant endocrine therapy in breast cancer. *J Clin Oncol* (1999) 17:1474–81. doi:10.1200/jco.1999.17.5.1474

22. McCarty KS, Jr, Miller LS, Cox EB, Konrath J, McCarty KS. Estrogen receptor analyses. Correlation of biochemical and immunohistochemical methods using monoclonal antireceptor antibodies. *Arch Pathol Lab Med* (1985) 109:716–21.

23. Ribatti D, Ranieri G, Annese T, Nico B. Aquaporins in cancer. *Biochim Biophys Acta-General Subjects* (2014) 1840:1550–3. doi:10.1016/j.bbagen.2013.09.025

24. Tomita Y, Dorward H, Yool AJ, Smith E, Townsend AR, Price TJ, et al. Role of aquaporin 1 signalling in cancer development and progression. *Int J Mol Sci* (2017) 18:299. doi:10.3390/ijms18020299

25. Meng FB, Rui YF, Xu LL, Wan C, Jiang XH, Li G. Aqp1 enhances migration of bone marrow mesenchymal stem cells through regulation of FAK and beta-catenin. *Stem Cell Development* (2014) 23:66–75. doi:10.1089/scd.2013.0185

26. Clevers H, Nusse R. Wnt/β-catenin signaling and disease. *Cell* (2012) 149:1192–205. doi:10.1016/j.cell.2012.05.012

27. Tetsu O, McCormick F. Beta-catenin regulates expression of cyclin D1 in colon carcinoma cells. *Nature* (1999) 398:422–6. doi:10.1038/18884

28. Marlar S, Jensen HH, Login FH, Nejsum LN. Aquaporin-3 in cancer. *Int J Mol Sci* (2017) 18:2106. doi:10.3390/ijms18102106

29. Li A, Lu DH, Zhang YP, Li J, Fang Y, Li F, et al. Critical role of aquaporin-3 in epidermal growth factor-induced migration of colorectal carcinoma cells and its clinical significance. *Oncol Rep* (2013) 29:535–40. doi:10.3892/or.2012.2144

30. Shan T, Cui X, Li W, Lin W, Li Y. AQP5: A novel biomarker that predicts poor clinical outcome in colorectal cancer. *Oncol Rep* (2014) 32:1564–70. doi:10.3892/or.2014.3377

31. Humphries MP, Maxwell P, Salto-Tellez M, QuPath: The global impact of an open source digital pathology system. *Comput Struct Biotechnol J* (2021) 19:852–9. doi:10.1016/j.csbj.2021.01.022

32. Roberti MP, Yonekura S, Duong CPM, Picard M, Ferrere G, Alou MT, et al. Chemotherapy-induced ileal crypt apoptosis and the ileal microbiome shape immunosurveillance and prognosis of proximal colon cancer. *Nat Med* (2020) 26:919–31. doi:10.1038/s41591-020-0882-8

33. Choudhury SR, Babes L, Rahn JJ, Ahn BY, Goring KAR, King JC, et al. Dipeptidase-1 is an adhesion receptor for neutrophil recruitment in lungs and liver. *Cell* (2019) 178:1205–21. doi:10.1016/j.cell.2019.07.017

34. Nejman D, Livyatan I, Fuks G, Gavert N, Zwang Y, Geller LT, et al. The human tumor microbiome is composed of tumor type-specific intracellular bacteria. *Science* (2020) 368:973–80. doi:10.1126/science.aay9189

Pathology & Oncology Research | frontiers

TYPE Original Research
PUBLISHED 12 April 2023
DOI 10.3389/pore.2023.1611082

Check for updates

OPEN ACCESS

EDITED BY
Andrea Ladányi,
National Institute of Oncology (NIO), Hungary

*CORRESPONDENCE
Weizhong Tang,
tangweizhong@gxmu.edu.cn

†These authors have contributed equally to this work and share first authorship

RECEIVED 28 January 2023
ACCEPTED 03 April 2023
PUBLISHED 12 April 2023

CITATION
Long J, Cong F, Wei Y, Liu J and Tang W (2023), Increased Kremen2 predicts worse prognosis in colon cancer. *Pathol. Oncol. Res.* 29:1611082. doi: 10.3389/pore.2023.1611082

COPYRIGHT
© 2023 Long, Cong, Wei, Liu and Tang. This is an open-access article distributed under the terms of the Creative Commons Attribution License (CC BY). The use, distribution or reproduction in other forums is permitted, provided the original author(s) and the copyright owner(s) are credited and that the original publication in this journal is cited, in accordance with accepted academic practice. No use, distribution or reproduction is permitted which does not comply with these terms.

Increased Kremen2 predicts worse prognosis in colon cancer

Junxian Long[1,2†], Fengyun Cong[1,3†], Yousheng Wei[4], Jungang Liu[1,5] and Weizhong Tang[1,5*]

[1]Division of Colorectal and Anal Surgery, Department of Gastrointestinal Surgery, Guangxi Medical University Cancer Hospital, Nanning, Guangxi, China, [2]Department of Breast and Thyroid Surgery, The Fifth Affiliated Hospital of Guangxi Medical University, Nanning, Guangxi, China, [3]Department of Gastroenteroanal Surgery, The Fifth Affiliated Hospital of Guangxi Medical University, Nanning, Guangxi, China, [4]Department of Gynecologic Oncology, Guangxi Medical University Cancer Hospital, Nanning, Guangxi, China, [5]Guangxi Clinical Research Center for Colorectal Cancer, Nanning, Guangxi, China

Background: Colon cancer (CC) is the fifth most prevalent cancer around the globe and poses a major risk to human health. Even though Kremen2 serves as a prognostic indicator in individuals with malignant tumours, its role in evaluating the prognosis of individuals with colon cancer has not been confirmed.

Methods: Here, we examined the protein expression of Kremen2 in CC tissues and paired adjacent normal tissues by immunohistochemistry (IHC), then analyzed the clinical and RNA-seq data presented in The Cancer Genome Atlas (TCGA) database to confirm the relationship between Kremen2 levels and CC. In addition, the associations between Kremen2 mRNA expression and infiltrating immune cells were examined.

Results: The study showed that the mRNA expression and protein level of Kremen2 were increased in CC tissues compared with adjacent normal tissues. According to Kaplan–Meier analysis, high Kremen2 expression in CC was linked to poor overall survival and progression-free survival. Clinical correlation analysis highlighted that a high level of Kremen2 expression was strongly linked with tumour progression, particularly lymph node metastasis. Cox regression analysis highlighted that Kremen2 was an independent prognostic indicator for CC. Bioinformatic studies highlighted that Kremen2 might be associated with the immune status in CC.

Conclusion: Increased Kremen2 could serve as a potential prognostic CC biomarker.

KEYWORDS

colon cancer, prognosis, bioinformatic, Kremen2, tumour infiltrating cells

Introduction

Colon cancer (CC) is a prevalent malignant tumour, with rising morbidity and ranking fifth globally in cancer-associated mortality (1). According to previous research, in 2020, approximately 1.2 million individuals were diagnosed with CC, and over 570,000 mortalities occurred globally (1). Data from China's National Central Cancer Registry show that in 2015,

there were approximately 376 per 100,000 new cases and 191 per 100,000 cancer deaths because of CC (2). Despite advancements in treatment over the last decades, tumour recurrence is common. There are various causative factors for CC, and the accumulation of genetic and epigenetic changes is the main cause of CC (3). Numerous genetic alterations that occur during colon carcinogenesis have been found by molecular investigations, but the particular genetic alterations that cause CC to develop and grow are yet to be elucidated (4–6). Therefore, discovering additional diagnostic and prognostic biomarkers and therapeutic targets to help improve long-term outcomes for patients with CC is a priority.

Kringle domain-containing protein Kremen was first discovered to have homologous triple-disulphide-linked peptide repeats in the blood coagulation factor prothrombin (7). Mammalian Kremen1 is a dependence receptor that regulates cell death pathways to eliminate aberrant or undesired cells, and Kremen2 is a very potent inhibitor that blocks the homodimerisation of Kremen1 (8). In addition, Kremen1 and Kremen2 are high-affinity secreted protein Dickkopf1 (Dkk1) receptors that work with Dkk1 to inhibit canonical Wnt (Wnt/β-catenin) signalling (9). Two receptor families transduce the Wnt/β-catenin signalling through the β-catenin pathway. By stabilising intracellular β-catenin, frizzled proteins and low-density lipoprotein receptor-related protein (LRP) 5 or LRP6 (LRP5/6) bind Wnts and transmit their signal (10). With Dkk1 and LRP6, Kremen2 forms a ternary complex, inducing rapid endocytosis, and eliminating the Wnt receptor LRP6 from the cellular membrane.

Kremen2 involvement in the development of the embryo, bone, neural ridge, and tumours has been demonstrated by several studies (11, 12). According to The Cancer Genome Atlas (TCGA) data, more than 65% of the tissue samples in 18 different types of cancer, revealed that Kremen2 expression in cancerous tissues was greater in comparison to that in paired normal tissues. This was particularly observed in squamous cell carcinoma of the lung, where the median increase was ten times greater (8). However, Kremen2's role and expression in CC are yet unclear. In order to understand the regulatory role of Kremen2 in the advancement and metastasis of CC and its link to patients' pathological characteristics, this study looked at Kremen2 expression in CC. It also laid the foundation for the development of novel therapeutic targets for CC.

Methodology

Patients and tissue samples

We collected paraffin specimens from individuals with CC after radical resection at the Department of Gastrointestinal Surgery, Guangxi Medical University Cancer Hospital, between November 2014 and February 2021. In this study, we included 46 adjacent normal tissues and 113 patients with primary CC. The patients underwent radical resection before radiotherapy and chemotherapy, and the diagnosis was established by two pathologists after evaluating the paraffin specimens. The 2019 World Health Organisation Classification of Tumours of the Digestive System was used to guide all pathological diagnoses. Data on survival were collected through telephonic follow-ups. In addition, we collected detailed clinical information, including age, sex, carcinoembryonic antigen (CEA), tumour size, differentiation, peripheral nerve invasion, lymphovascular invasion, deoxyribonucleic acid mismatch repair (MMR), and the American Joint Committee on Cancer tumour node metastasis (TNM) staging system (seventh edition). All participants provided written consent for this research, and this study was approved by the ethics committee of Guangxi Medical University Cancer Hospital (approval number: LW2022123).

TABLE 1 Characteristics of patients with CC based on TCGA.

Characteristics	Number of cases	Percentages (%)
Sex		
Male	172	54.43
Female	144	45.57
Age		
≥55	257	81.33
<55	59	18.67
T stage		
T1	7	2.22
T2	58	18.35
T3	218	68.99
T4	33	10.44
N stage		
N0	191	60.44
N1	72	22.78
N2	53	16.77
M stage		
M0	266	84.18
M1	50	15.82

T: tumour; N: node; M: metastasis.

Immunohistochemical (IHC) staining

The sections that had been embedded in paraffin underwent IHC staining. In summary, sections (4 mm thick) were formalin-fixed, paraffin-embedded, regularly deparaffinised, rehydrated, and heated in antigen retrieval citrate buffer (pH 6.0). After that, non-specific antigens were blocked for 20 min with 10% normal goat serum at 37°C and endogenous peroxidase for 20 min with 3% hydrogen peroxide. Subsequently, the rabbit polyclonal antibody anti-KREMEN2 (orb185896; 1:100 dilution; Biorbyt, Cambridge, UK) was incubated at room temperature for 1 h. This was followed by conjugation to the secondary antibody (KIT-5010; Maixin Inc., Fujian, China) and 3, 3′-diaminobenzidine (DAB) (DAB-1031; Maixin Inc., Fujian, China) staining. A

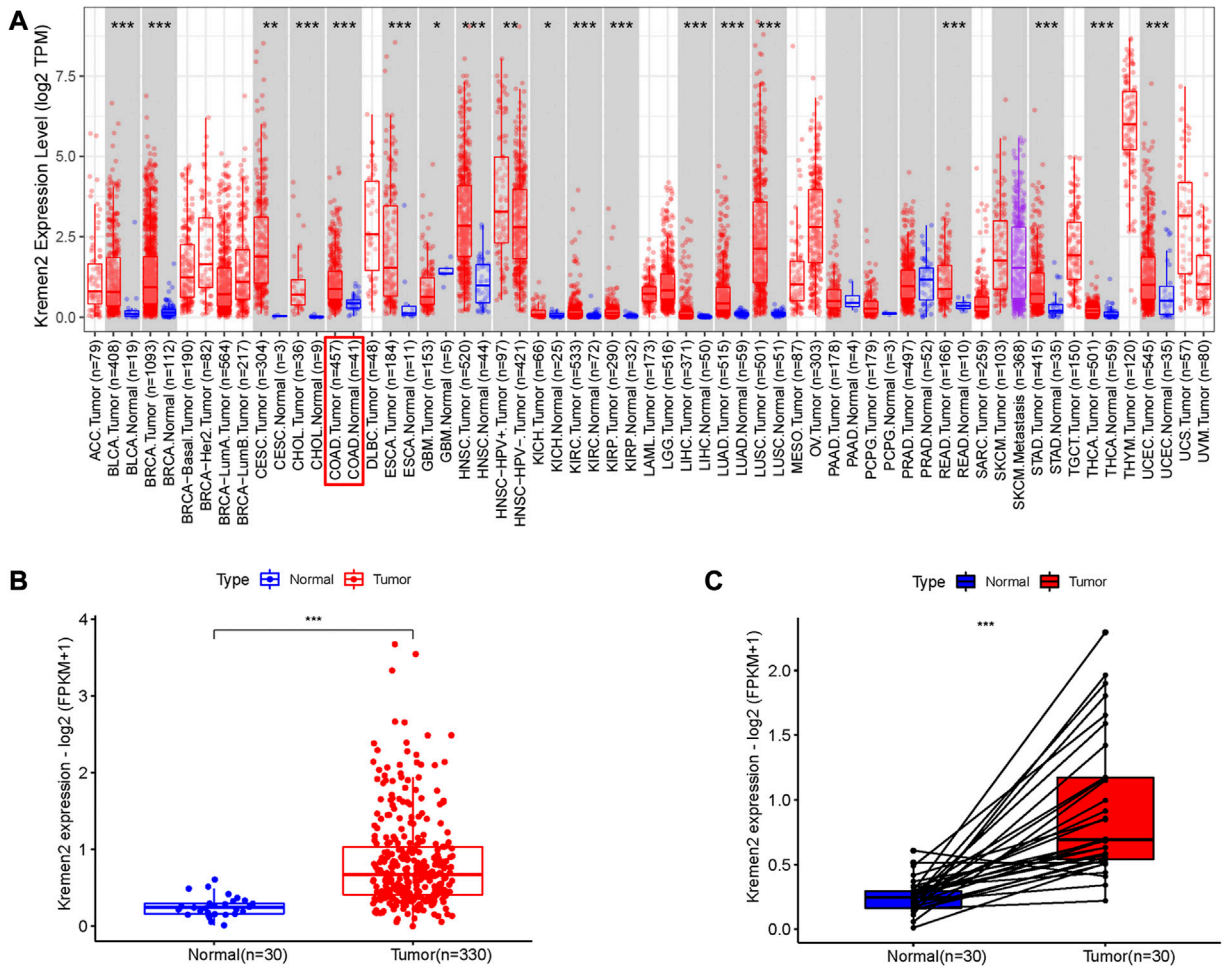

FIGURE 1
The mRNA expression of Kremen2 in different tumours base on TIMER database and in the COAD base on TCGA database. **(A)** The Kremen2 mRNA expression in different kinds of tumours. **(B)** Unpaired comparison: Kremen2 mRNA expression was elevated in COAD tissues compare to adjacent normal tissues. **(C)** Paired comparison: Kremen2 mRNA expression was elevated in COAD tissues compare to adjacent normal tissues. *: $p < 0.05$, **: $p < 0.01$, ***: $p < 0.001$.

primary antibody that had been replaced with phosphate-buffered saline buffer was employed as a negative control.

IHC staining evaluation

Independent evaluation and scoring of the IHC data were performed by two researchers who were unaware of the clinicopathological characteristics of the individuals. A semi-quantitative scoring method based on intensity scores (InSs) and proportion scores (PSs) was used to assess protein expression. The InSs were stated as follows: 0, no staining; 1, light brown; 2, brown; 3, dark brown. The PSs of stained epithelial cells were as stated: 0% (0), 1%–25% (1), 26%–50% (2), 51%–75% (3), and 76%–100% (4). The formula IS = PS × InS was used to determine the final IHC scores (ISs). Lastly, according to the Kremen2 protein expression, the samples were sorted into high and low expression groups (IS ≥ 8 and IS < 8, respectively).

Gene expression analysis in the TCGA database

First, we collected gene expression information of different types of tumours in the Tumour IMmune Estimation Resource (TIMER) database (http://timer.cistrome.org/). Further, we downloaded messenger ribonucleic acid sequencing (mRNA-seq) (level 3, HTSeq-Fragments Per Kilobase of transcript per Million mapped reads data) of the colon adenocarcinoma (COAD) cohort and relevant clinical data from TCGA

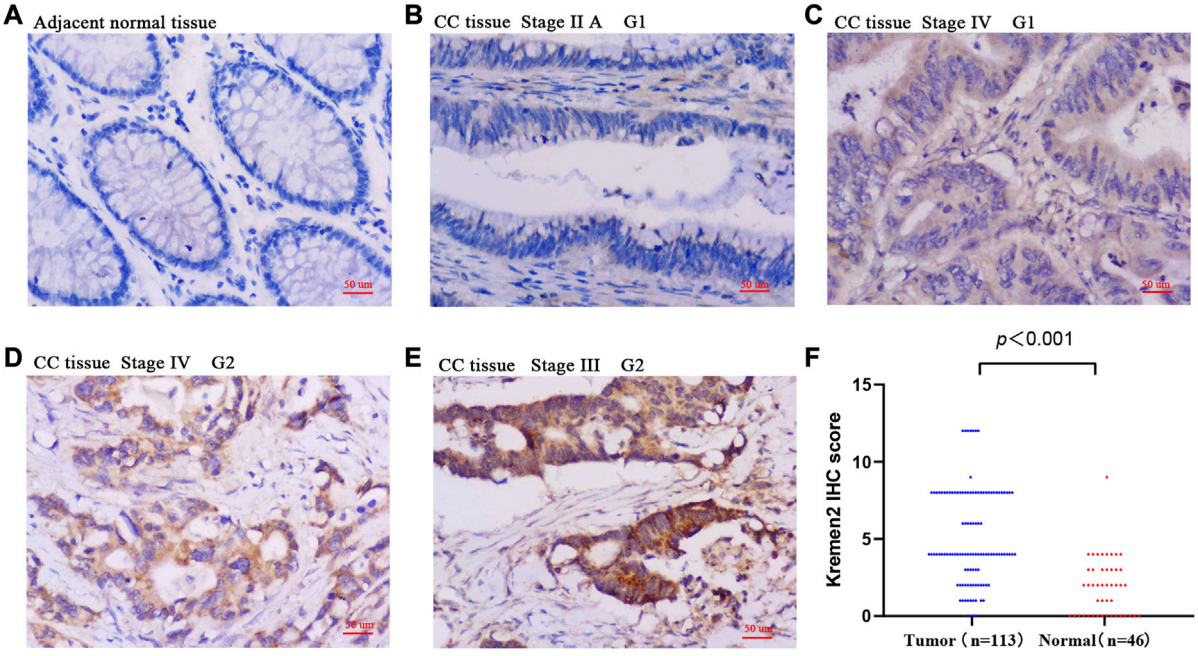

FIGURE 2
The protein expression of Kremen2 in colon cancer and adjacent normal tissues by using IHC analysis. **(A)** Adjacent normal tissue InS = 0. **(B)** High differentiation (G1), tumour tissue InS = 0. **(C)** High differentiation (G1), tumour tissue InS = 1. **(D)** Moderate differentiation (G2), tumour tissue InS = 2. **(E)** Moderate differentiation (G2), tumour tissue InS = 3. **(F)** The IHC score of Kremen2 protein was elevated in tumour tissues. Magnification ×200, scale bar = 50 μm. InS: intensity scores, IHC: immunohistochemical, CC: colon cancer.

(https://portal.gdc.cancer.gov/). These data were obtained from 30 normal colon tissue samples, 330 colon tumour tissue samples, and 316 patients with CC (basic information, including age, sex, and the TNM stage, while cases without mRNA-seq data and cases with incomplete clinical data and overall survival (OS) of <30 days were excluded). The characteristics of CC patients are shown in Table 1. Perl was used for data processing. Data processing comprised Integration and normalisation of the transcriptome profiling data, the extraction of clinical information, and the merging of the mRNA data.

R packages "ggpubr" and "limma" were used to compare Kremen2 mRNA expression between the colon tumour and normal tissue samples (13). On the basis of the levels of Kremen2 mRNA expression in tumour tissues, 316 patients were subsequently enrolled and separated into two groups (the high-expression and low-expression groups). R packages "ggpubr," "limma," "survival," and "survminer" were employed to assess the significance of the Kremen2 mRNA expression level with different pieces of clinical information and the role of Kremen2 in predicting OS (14). Whether the Kremen2 mRNA expression level could independently predict survival in patients with CC was analysed using a multivariate Cox regression model. Our research complied with the TCGA publication guidelines.

Infiltrating immune cell estimation

The differences between 22 immune cell subtypes in patients with CC belonging to the high- and low-expression groups were analysed with the CIBERSORT method combined with the LM22 feature matrix to estimate the infiltration status of immune cells (15, 16). The association of the Kremen2 mRNA expression level with immune cell infiltration was analysed using the Spearman correlation coefficient.

Statistical analysis

R software v4.1, Statistical Package for the Social Sciences v21.0, and GraphPad Prism 8 were utilized to perform the statistical analysis. A non-parametric test was employed to determine the variation in Kremen2 protein expression between CC and adjacent normal tissues. The association of the Kremen2 protein expression level with different pieces of clinical information was analysed with the help of Chi-square or Fisher's exact tests. The Kaplan–Meier (K–M) analysis was employed to assess the role of Kremen2 in predicting the OS. Receiver operating characteristic (ROC) curves were utilised for measuring the prognostic capacity of Kremen2 protein

expression. In order to determine if Kremen2 might be employed as an independent prognostic indicator in individuals with CC, univariate and multivariate Cox regression analyses were carried out. $p < 0.05$ was considered a significant value.

Results

Kremen2 is overexpressed in CC

Based on the TIMER data, we observed Kremen2 mRNA overexpression in various tumours, including CC ($p < 0.001$) (Figure 1A). TCGA data analysis revealed that Kremen2 mRNA levels were significantly elevated in CC tissues (Figures 1B, C, $p < 0.001$). We analysed the ISs in 113 tumour tissues and 46 paired adjacent normal tissues to verify Kremen2 protein expression in CC. Using the non-parametric test, we observed that Kremen2 protein expression in CC was remarkably higher in comparison to the adjacent normal tissues ($p < 0.001$) (Figure 2).

Relationship between Kremen2 protein expression and the clinicopathological features of individuals with CC

Subgroup analysis was performed based on the age, sex, tumour site, TNM stage, CEA, tumour size, differentiation, peripheral nerve invasion, lymphovascular invasion, and MMR for determining the association of Kremen2 protein expression and clinicopathological parameters. In contrast with individuals with CC having no lymph node metastasis, individuals with CC having lymph node metastasis had substantially greater levels of Kremen2 protein expression ($p = 0.036$). In addition, we observed that Kremen2 protein correlated with sex and age in patients with CC. Female patients ($p = 0.025$) and patients aged <55 years ($p = 0.013$) tended to have a high Kremen2 protein expression. However, there was no considerable association between Kremen2 protein expression in CC and other clinicopathological parameters ($p > 0.05$) (Table 2).

TABLE 2 The correlation between Kremen2 protein expression and clinicopathological parameters of CC.

Parameters	Kremen2		
	High	Low	*p*
Sex			0.025
Male	20	52	
Female	20	21	
Age			0.013
<55	21	21	
≥55	19	52	
Tumour size (cm)			0.438
≤5	26	42	
>5	14	31	
T stage			0.221
Tis/T1/T2	1	8	
T3/T4	39	65	
N stage			0.036
N0	17	46	
N1/N2	23	27	
M stage			0.129
M0	32	67	
M1	8	6	
Differentiation			0.163
High/Moderate	29	61	
Poorly	11	12	
Peripheral nerve invasion			0.547
Positive	21	34	
Negative	19	39	
Lymphovascular invasion			0.890
Positive	12	21	
Negative	28	52	
CEA (ng/mL)			0.362
≤5	20	43	
>5	20	30	
MMR			0.708
DMMR	5	11	
PMMR	35	62	

MMR: DNA mismatch repair; dMMR: defective DNA mismatch repair; pMMR: proficient DNA mismatch repair.

The relationship between Kremen2 mRNA expression and clinical properties

When we examined the relationship between clinicopathological parameters and Kremen2 mRNA expression in patients with CC based on TCGA, we observed that high Kremen2 mRNA expression was linked to tumour N stage (from N0 to N2 and from N1 to N2) ($p = 0.005$, 0.012) (Figure 3A). In terms of the T stage, progression from T2 to T3 was correlated with elevated Kremen2 mRNA expression levels ($p = 0.032$) (Figure 3B). However, Kremen2 mRNA expression was not related to sex, age, or the M stage (Figures 3C–E).

High Kremen2 expression in CC was linked to a poor prognosis

The K–M survival curve was implemented to determine the association of Kremen2 expression and survival in CC. As per the

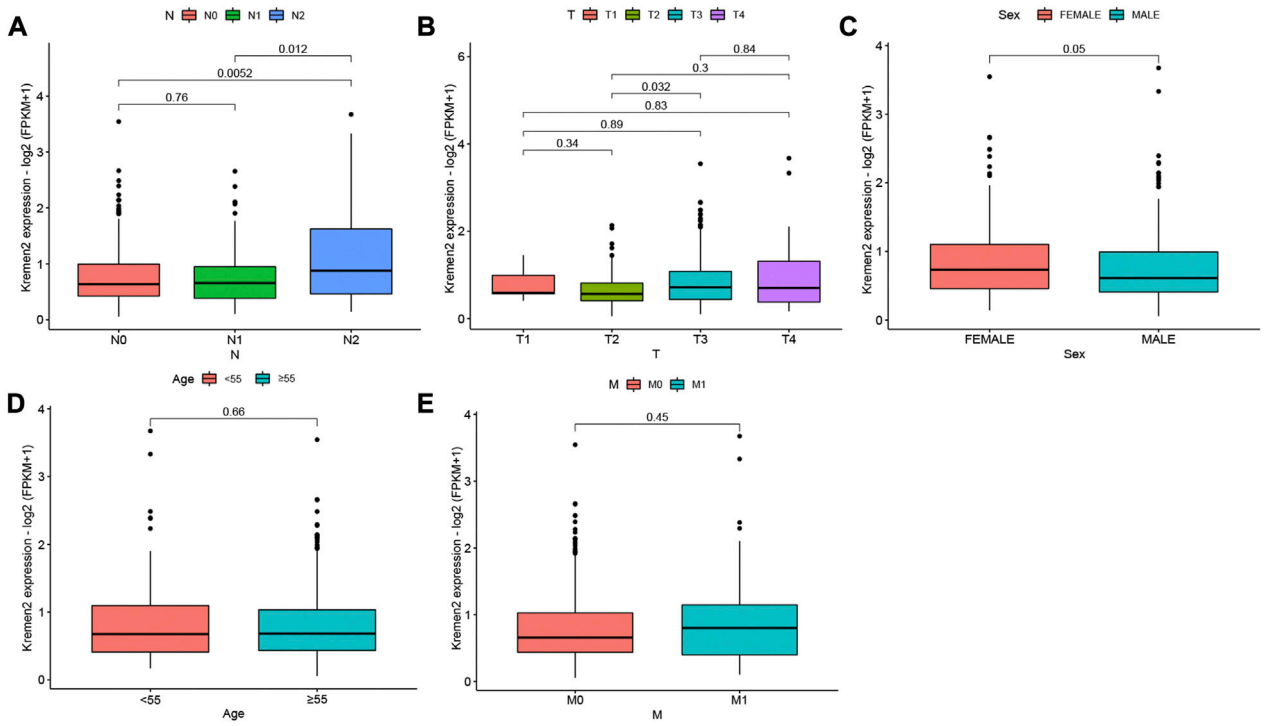

FIGURE 3
Relationship between Kremen2 mRNA expression and clinicopathological characteristics of CC patients based on TCGA. Box plot showing the relation of Kremen2 mRNA to **(A)** N stage, **(B)** T stage, **(C)** sex, **(D)** age and **(E)** M stage.

K–M chart, CC cases with elevated Kremen2 mRNA expression had a shorter OS (TCGA, $p = 0.043$) (Figure 4A) and progression-free survival (TCGA, $p = 0.041$) (Figure 4B). The K–M survival curve also revealed that high Kremen2 protein expression was linked to a poor prognosis (IHC, $p = 0.013$) (Figure 4C). Subsequently, the ROC curve analysis was employed to analyse the predictive value of Kremen2 protein expression, promising a prognosis value of the signature for CC over survival. The area under the curve scores over 1, 3, and 5 years (0.769, 0.636, and 0.651, respectively), were observed on the ROC curves (Figure 4D).

Kremen2 protein expression is an independent prognostic factor for patients with CC

Using clinical data from TCGA, we observed that age ($p = 0.014$), the T stage ($p = 0.007$), the N stage ($p = 0.012$), and the M stage ($p < 0.001$) were independent risk factors for the prognosis of individuals with CC (Figure 5). As per the univariate analysis results, high Kremen2 mRNA expression was strongly related to poor prognosis ($p = 0.001$), while it was not correlated in the multivariate analysis ($p = 0.107$). In addition, the univariate Cox regression analysis revealed a substantial correlation between high Kremen2 protein expression and a poor prognosis ($p = 0.017$). Other clinical parameters, including the N stage ($p = 0.009$), the M stage ($p = 0.000$), and peripheral nerve invasion ($p = 0.018$), were linked to a poor prognosis (Table 3). Furthermore, the multivariate analysis revealed that high Kremen2 protein expression ($p = 0.036$) and the M stage ($p = 0.001$) were independently linked with a poor prognosis (Table 3).

Correlation between Kremen2 mRNA levels and immune cell infiltration levels

Tumour-infiltrating lymphocytes can independently reflect cancer survival (17). Herein, we assessed the link between Kremen2 mRNA expression and the infiltration of 22 immune cell subtypes in TCGA-COAD. Regulatory T cells (Tregs) ($p = 0.034$) and activated natural killer (NK) cells ($p = 0.020$) were the immune cells with a substantially higher infiltration level in the high-expression group. $CD4^+$ memory resting T cell infiltration level was substantially higher in the low-expression group in

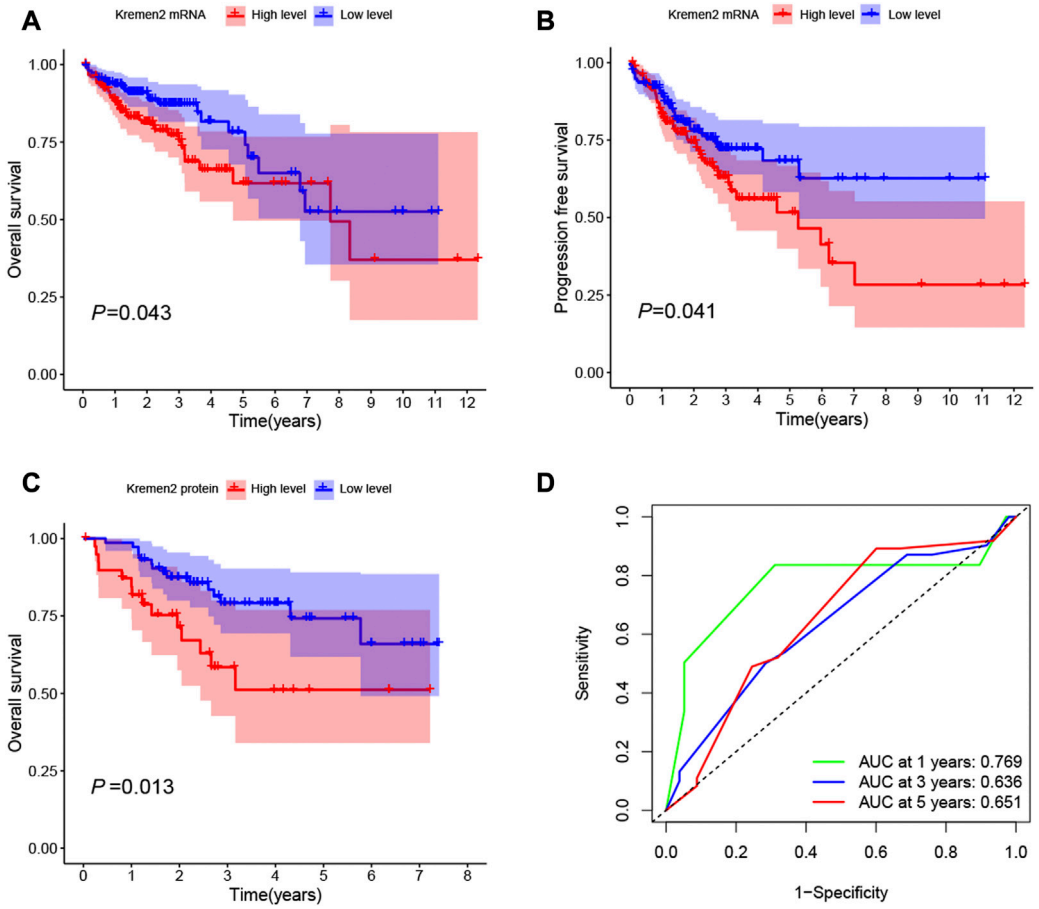

FIGURE 4
Kaplan-Meier survival curves of CC patients with high and low Kremen2 expression levels. **(A)** OS in CC patients with differential Kremen2 mRNA expression. **(B)** Progression free survival in CC patients with differential Kremen2 mRNA expression. **(C)** OS in CC patients with differential Kremen2 protein expression. **(D)** The AUC score at 1, 3, 5 years in Kremen2 protein expression. AUC, area under the ROC curve.

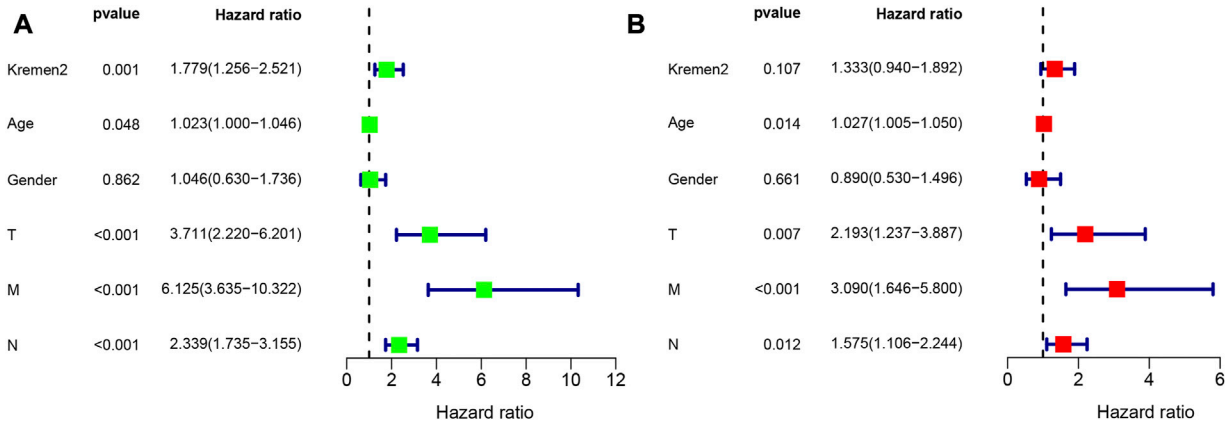

FIGURE 5
Univariate and multivariate Cox regression analyses of OS for CC patients in the TCGA. **(A)** Univariate Cox analyses. **(B)** Multivariate Cox analyses.

TABLE 3 Univariate and multivariate Cox regression analyses of OS for CC patients in the IHC cohort.

Parameters	Univariate analysis			Multivariate analysis		
	P	HR	95% CI	*P*	HR	95% CI
Sex (Male vs. Female)	0.158	0.590	0.283–1.228			
Age (≥55 vs. < 55)	0.426	1.378	0.626–3.032			
T stage (T3/T4 vs. Tis/T1/T2)	0.246	3.263	0.442–24.065			
N stage (N1/N2 vs. N0)	0.009	2.742	1.283–5.858	0.698	1.202	0.475–3.038
M stage (M1 vs. M0)	0.000	6.354	2.851–14.161	0.001	4.942	1.945–12.555
CEA (ng/mL) (>5 vs. ≤5)	0.077	1.943	0.930–4.060			
Tumour size (cm) (>5 vs. ≤5)	0.699	0.860	0.400–1.850			
Differentiation (High/Moderate vs. Poorly)	0.396	0.701	0.309–1.590			
Peripheral nerve invasion (Positive vs. Negative)	0.018	2.605	1.182–5.738	0.089	2.057	0.895–4.728
Lymphovascular invasion (Positive vs. Negative)	0.090	1.888	0.906–3.936			
Kremen2 protein (High vs. Low)	0.017	2.446	1.177–5.084	0.036	2.231	1.052–4.730
MMR (dMMR vs. pMMR)	0.202	0.392	0.093–1.653			

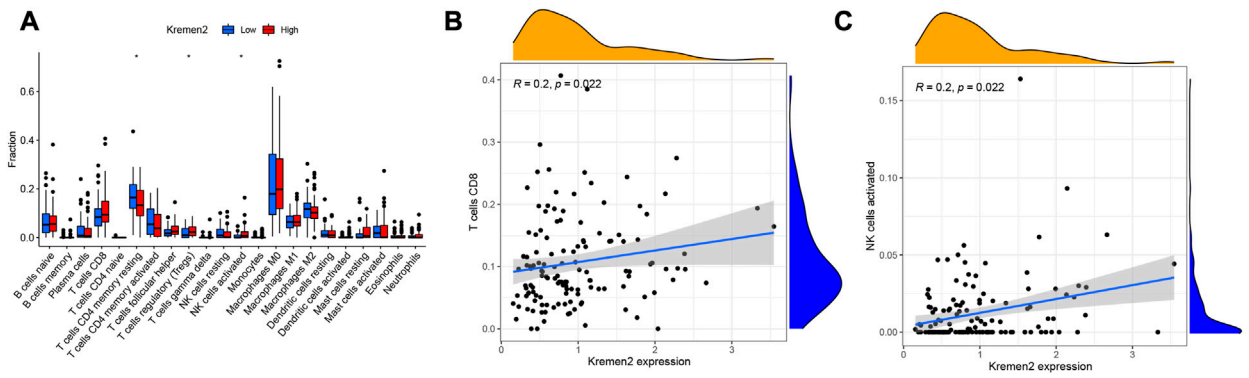

FIGURE 6
Association analysis between the Kremen2 mRNA levels and immune cells infiltration levels. **(A)** The immune cells between high-expression and low-expression groups; *$p < 0.05$. **(B)** The correlation between CD8 T cells and Kremen2 mRNA level. **(C)** The correlation between activated NK cells and Kremen2 mRNA level.

comparison to that in the high-expression group ($p = 0.031$) (Figure 6A). According to the correlation analyses, $CD8^+$ T cell and activated NK cell infiltration were positively linked to Kremen2 mRNA expression (Figures 6B, C, r = 0.2, $p = 0.022$; r = 0.2, $p = 0.022$).

Discussion

CC is among the most common cancers globally, and its treatment and rehabilitation cause significant pain to patients (18). Despite advancements in diagnostic and treatment modalities, judging the prognosis of individuals with CC needs further research (19, 20). Therefore, it is essential to further define the underlying mechanism of CC, particularly in terms of the prognostic molecular markers. Currently, there is growing interest in studying the mechanism of Kremen2 in tumorigenesis and tumour development.

Kremen2 plays a crucial role in neural crest induction (11), bone formation (12, 21), and tumorigenesis (8, 22). Kremen2 inhibits cell apoptosis by inhibiting homodimerisation of Kremen1. Conversely, Kremen2 functions as a receptor of Dkk1, forming a trimer with LRP5/6 protein to internalise LRP5/6, and block the Wnt-LRP5/6-frizzled complex formation, thus enhancing the Dkk1-mediated suppression of the Wnt/β-catenin signalling pathway. Another research discovered that Kremen2 might bind to LRP5/6 and sustain its presence on the cellular membrane in the absence of the Dkk1 protein, activating

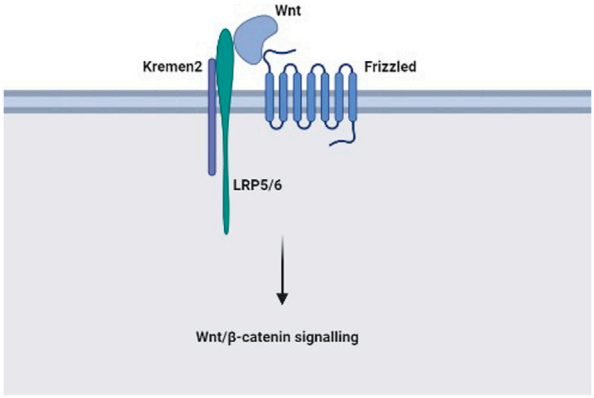

FIGURE 7
The possible mechanism of Kremen2 in colon cancer disease progression: In the absence of Dkk1, Kremen2 activates the Wnt/β-catenin signalling pathway by maintaining LRP5 or LRP6 at the plasma membrane.

the Wnt/β-catenin signalling pathway (23). In conclusion, Kremen2 exhibits biological effects in a variety of biological environments. Recent research reveals that Kremen2 is upregulated in various tumours, such as renal clear cell carcinoma, breast invasive carcinoma, COAD, and stomach adenocarcinoma, in comparison to that in normal tissues (8). Dkk1 and Kremen expression in combination may act as indicators of the osteoblastic response to breast and prostate cancer bone metastases in cancer cells (24). The proliferation of gastric cancer cells was considerably inhibited after knocking down Kremen2, indicating that Kremen2 may exert oncogene-like functions, thus promoting gastric cancer proliferation (25).

However, the role and expression of Kremen2 in CC are yet unclear. In the present investigation, using TCGA-COAD, we observed that Kremen2 mRNA expression was substantially higher in CC tissues in comparison to that in normal tissues. Subsequently, the IHC results also revealed that Kremen2 protein was upregulated in CC tissues, suggesting Kremen2's involvement in CC carcinogenesis. Prognostic data from TCGA-COAD and the IHC cohort revealed that high Kremen2 expression was strongly linked to poor prognosis in patients regardless of the mRNA or protein levels. This further confirmed the possibility of Kremen2 serving as a prognostic molecule for CC.

Lymph node staging is crucial for determining the prognosis and therapy stratification in CC (26, 27). Lymph node metastasis is associated with an adverse clinical course and is an indication of adjuvant chemotherapy (28). According to the clinicopathological data-based correlation study, Kremen2 mRNA expression was strongly linked to the N stage. Using the IHC cohort, we then verified the association of Kremen2 protein expression with the clinicopathological data and observed that elevated Kremen2 protein expression levels also predicted a poor N stage. The relatively higher Kremen2 expression in the advanced N stage indicated that it could be linked to tumour progression in CC.

According to the univariate and multivariate Cox regression analyses, Kremen2 protein expression can serve as an independent prognostic factor for individuals with CC, the same as the M stage. Consequently, we believed that Kremen2 could serve as a reference for prognostic prediction in individuals with CC. However, further research and clarification regarding the specific mechanism *via* which Kremen2 functions is warranted.

Increasing evidence suggests that malignant tumours rely on tumour cells and the tumour microenvironment, such as extracellular matrix molecules, inflammatory mediators, and immune cells (29, 30). Tumour-infiltrating immune cells are valuable for CC diagnosis and progression and prognosis determination (31–33). Prior research has highlighted that the efficacy of immunotherapy decreases because of the antitumor immune effects of Tregs, thereby promoting immune evasion and cancer progression (34). Therefore, anti-Treg immunotherapy may be highly effective in individuals with CC. NK cells have been reported as natural lymphocytes that may eliminate cancer cells or viral infections (35). Imai et al. (36) observed that tumour progression was linked to a reduced killing capacity of NK cells in peripheral blood. As a result, NK cells are promising targets for anti-CC immunotherapy because they control tumorigenesis. The individuals with CC having a higher proportion of $CD4^+$ memory resting T cells and activated NK cells had a better prognosis. On the other hand, a lower proportion of $CD8^+$ T cells had a worse prognosis (37). Herein, we observed that Tregs and activated NK cell infiltration levels were significantly higher in the Kremen2 mRNA high-expression group, with attenuated $CD4^+$ memory resting T cell infiltration. According to the correlation analysis, $CD8^+$ T cell and activated NK cell infiltration were positively linked with Kremen2 mRNA expression, but the association is weak. These results imply that Kremen2 may be associated with the immune status in CC. However, more studies on the association between Kremen2 and CC immune infiltration are warranted.

Conclusion

In summary, this research highlighted that Kremen2 expression was upregulated in CC tissues and was strongly linked to tumour progression and prognosis in individuals with CC. This shows that Kremen2 could be a new CC biomarker. Furthermore, a high Kremen2 expression level might predict a poor prognosis, and Kremen2 protein expression level could serve as an independent prognostic factor. Furthermore, Kremen2 may be associated with the immune status in CC. The specific mechanism of Kremen2 in CC disease progression is still unclear. According to relevant

literature and this study, Kremen2 may be involved in CC disease progression by activating the Wnt/β-catenin signalling pathway, and the possible mechanism is shown in Figure 7. However, our results are only based on bioinformatic analysis and tissue validation, and further *in vitro* as well as *in vivo* studies are warranted to investigate the biological relationship and function of Kremen2.

Data availability statement

The original contributions presented in the study are included in the article/supplementary material, further inquiries can be directed to the corresponding author.

Ethics statement

All participants provided written consent for this research, and this study was approved by the ethics committee of Guangxi Medical University Cancer Hospital (approval number: LW2022123).

Author contributions

JL and FC completed the paper writing and experiments, YW completed the data analysis, JL and WT completed the experimental design and project support. All authors contributed to the article and approved the submitted version.

Funding

This work was supported by Guangxi Science and Technology Project (AD19245197), and the Guangxi Scientific Research and Technology Development Project (Guike AB18126033).

Conflict of interest

The authors declare that the research was conducted in the absence of any commercial or financial relationships that could be construed as a potential conflict of interest.

References

1. Sung H, Ferlay J, Siegel RL, Laversanne M, Soerjomataram I, Jemal A, et al. Global cancer statistics 2020: GLOBOCAN estimates of incidence and mortality worldwide for 36 cancers in 185 countries. *CA Cancer J Clin* (2021) 71(3):209–49. doi:10.3322/caac.21660

2. Chen W, Zheng R, Baade PD, Zhang S, Zeng H, Bray F, et al. Cancer statistics in China, 2015. *CA Cancer J Clin* (2016) 66(2):115–32. doi:10.3322/caac.21338

3. Puccini A, Berger MD, Naseem M, Tokunaga R, Battaglin F, Cao S, et al. Colorectal cancer: Epigenetic alterations and their clinical implications. *Biochim Biophys Acta Rev Cancer* (2017) 1868(2):439–48. doi:10.1016/j.bbcan.2017.09.003

4. Uppada SB, Gowrikumar S, Ahmad R, Kumar B, Szeglin B, Chen X, et al. MASTL induces Colon Cancer progression and Chemoresistance by promoting Wnt/β-catenin signaling. *Mol Cancer* (2018) 17(1):111. doi:10.1186/s12943-018-0848-3

5. Kaprio T, Lindström AM, Rasila T, Saavalainen O, Beilmann-Lehtonen I, Mustonen H, et al. Elevated tumor expression of Astroprincin (FAM171A1) is an independent marker of poor prognosis in colon cancer. *BMC Gastroenterol* (2021) 21(1):341. doi:10.1186/s12876-021-01918-y

6. Mengjie L, Xiao F, Lili J, Jiequn M, Xiaoqiang Z, Shuhong W, et al. Colon cancer cells secreted CXCL11 via RBP-Jκ to facilitated tumour-associated macrophage-induced cancer metastasis. *J Cell Mol Med* (2021) 25(22):10575–90. doi:10.1111/jcmm.16989

7. Nakamura T, Aoki S, Kitajima K, Takahashi T, Matsumoto K, Nakamura T. Molecular cloning and characterization of Kremen, a novel kringle-containing transmembrane protein. *Biochim Biophys Acta* (2001) 1518(1-2):63–72. doi:10.1016/s0167-4781(01)00168-3

8. Sumia I, Pierani A. Kremen1-induced cell death is regulated by homo- and heterodimerization. *Cell Death Discov* (2019) 5:591. doi:10.1038/s41420-019-0175-5

9. Mao B, Wu W, Davidson G, Marhold J, Li M, Mechler BM, et al. Kremen proteins are Dickkopf receptors that regulate Wnt/beta-catenin signalling. *Nature* (2002) 417(6889):664–7. doi:10.1038/nature756

10. Mao B, Wu W, Li Y, Hoppe D, Stannek P, Glinka A, et al. LDL-receptor-related protein 6 is a receptor for Dickkopf proteins. *Nature* (2001) 411(6835):321–5. doi:10.1038/35077108

11. Hassler C, Cruciat CM, Huang YL, Kuriyama S, Mayor R. Kremen is required for neural crest induction in Xenopus and promotes LRP6-mediated Wnt signaling. *Development* (2007) 134(23):4255–63. doi:10.1242/dev.005942

12. Schulze J, Seitz S, Saito H, Schneebauer M, Marshall RP, Baranowsky A, et al. Negative regulation of bone formation by the transmembrane Wnt antagonist Kremen-2. *PLoS One* (2010) 5(4):e10309. doi:10.1371/journal.pone.0010309

13. Wen L. Identification and validation of xenobiotic metabolism-associated prognostic signature based on five genes to evaluate immune microenvironment in colon cancer. *J Gastrointest Oncol* (2021) 12(6):2788–802. doi:10.21037/jgo-21-655

14. Wang K, Feng X, Zheng L, Chai Z, Yu J, You X, et al. TRPV4 is a prognostic biomarker that correlates with the immunosuppressive microenvironment and chemoresistance of anti-cancer drugs. *Front Mol Biosci* (2021) 8:8690500. doi:10.3389/fmolb.2021.690500

15. Chong W, Shang L, Liu J, Fang Z, Du F, Wu H, et al. m(6 A regulator-based methylation modification patterns characterized by distinct tumor microenvironment immune profiles in colon cancer. *Theranostics* (2021) 11(5):2201–17. doi:10.7150/thno.52717

16. Lu J, Wang Z, Maimaiti M, Hui W, Abudourexiti A, Gao F. Identification of diagnostic signatures in ulcerative colitis patients via bioinformatic analysis integrated with machine learning. *Hum Cel* (2022) 35(1):179–88. doi:10.1007/s13577-021-00641-w

17. Mou Y, Wu J, Zhang Y, Abdihamid O, Duan C, Li B. Low expression of ferritinophagy-related NCOA4 gene in relation to unfavorable outcome and defective immune cells infiltration in clear cell renal carcinoma. *BMC Cancer* (2021) 21(1):18. doi:10.1186/s12885-020-07726-z

18. Wong M, Huang J, Lok V, Wang J, Fung F, Ding H, et al. Differences in incidence and mortality trends of colorectal cancer worldwide based on sex, age, and anatomic location. *Clin Gastroenterol Hepatol* (2021) 19(5):955–66.e61. doi:10.1016/j.cgh.2020.02.026

19. Chen EX, Jonker DJ, Loree JM, Kennecke HF, Berry SR, Couture F, et al. Effect of combined immune checkpoint inhibition vs best supportive care alone in patients with advanced colorectal cancer: The Canadian cancer trials group CO.26 study. *JAMA Oncol* (2020) 6(6):831–8. doi:10.1001/jamaoncol.2020.0910

20. Deng J, Chen X, Zhan T, Chen M, Yan X, Huang X. CRYAB predicts clinical prognosis and is associated with immunocyte infiltration in colorectal cancer. *PeerJ* (2021) 9:e12578. doi:10.7717/peerj.12578

21. Plotkin LI. Molecular signaling in bone cells: Regulation of cell differentiation and survival. *Adv Protein Chem Struct Biol* (2019) 116:116237–281. doi:10.1016/bs.apcsb.2019.01.002

22. Zhou Q, Wang C, Zhu Y, Wu Q, Jiang Y, Huang Y, et al. Key genes and pathways controlled by E2F1 in human castration-resistant prostate cancer cells. *Onco Targets Ther* (2019) 12:128961–8976. doi:10.2147/OTT.S217347

23. Cselenyi CS, Lee E. Context-dependent activation or inhibition of Wnt-beta-catenin signaling by Kremen. *Sci Signal* (2008) 1(8):pe10. doi:10.1126/stke.18pe10

24. Clines KL. DKK1 and kremen expression predicts the osteoblastic response to bone metastasis. *Transl Oncol* (2018) 11(4):873–82. doi:10.1016/j.tranon.2018.04.013

25. Chen B, Wang SQ, Huang J, Xu W, Lv H, Nie C, et al. Knockdown of Kremen2 inhibits tumor growth and migration in gastric cancer. *Front Oncol* (2020) 10:10534095. doi:10.3389/fonc.2020.534095

26. Xu Y, Huang Y, Wang X, Sun Y, Ye D, Chi P. Prognostic significance of lymph node yield in patients with synchronous colorectal carcinomas. *Int J Colorectal Dis* (2020) 35(12):2273–82. doi:10.1007/s00384-020-03700-0

27. İmamoğlu Gİ, Oğuz A, Cimen S, Eren T, Karacin C, Colak D, et al. The impact of lymph node ratio on overall survival in patients with colorectal cancer. *J Cancer Res Ther* (2021) 17(4):1069–74. doi:10.4103/jcrt.JCRT_11_19

28. Kim HJ. Clinical implications of lymph node metastasis in colorectal cancer: Current status and future perspectives. *Ann Coloproctol* (2019) 35(3):109–17. doi:10.3393/ac.2019.06.12

29. Giannone G, Ghisoni E, Genta S, Scotto G, Tuninetti V, Turinetto M, et al. Immuno-Metabolism and microenvironment in cancer: Key players for immunotherapy. *Int J Mol Sci* (2020) 21(12):4414. doi:10.3390/ijms21124414

30. Freeman JW. Structural biology of the tumor microenvironment. *Adv Exp Med Biol* (2021) 1350:135091–100. doi:10.1007/978-3-030-83282-7_4

31. Ye L, Zhang T, Kang Z, Guo G, Sun Y, Lin K, et al. Tumor-infiltrating immune cells act as a marker for prognosis in colorectal cancer. *Front Immunol* (2019) 10:102368. doi:10.3389/fimmu.2019.02368

32. Zhou R, Zhang J, Zeng D, Sun H, Rong X, Shi M, et al. Immune cell infiltration as a biomarker for the diagnosis and prognosis of stage I-III colon cancer. *Cancer Immunol Immunother* (2019) 68(3):433–42. doi:10.1007/s00262-018-2289-7

33. Zhang N, Ning F, Guo R, Pei J, Qiao Y, Fan J, et al. Prognostic values of preoperative inflammatory and nutritional markers for colorectal cancer. *Front Oncol* (2020) 10:10585083. doi:10.3389/fonc.2020.585083

34. Shitara K, Nishikawa H. Regulatory T cells: A potential target in cancer immunotherapy. *Ann N Y Acad Sci* (2018) 1417(1):104–15. doi:10.1111/nyas.13625

35. Myers JA, Miller JS. Exploring the NK cell platform for cancer immunotherapy. *Nat Rev Clin Oncol* (2021) 18(2):85–100. doi:10.1038/s41571-020-0426-7

36. Imai K, Matsuyama S, Miyake S, Suga K, Nakachi K. Natural cytotoxic activity of peripheral-blood lymphocytes and cancer incidence: An 11-year follow-up study of a general population. *Lancet* (2000) 356(9244):1795–9. doi:10.1016/S0140-6736(00)03231-1

37. Katayama C, Yokobori T, Ozawa N, Suga K, Shiraishi T, Okada T, et al. Low level of stromal lectin-like oxidized LDL receptor 1 and CD8(+) cytotoxic T-lymphocytes indicate poor prognosis of colorectal cancer. *Cancer Rep (Hoboken)* (2021) 4(4):e1364. doi:10.1002/cnr2.1364

Pathology & Oncology Research | frontiers

TYPE Original Research
PUBLISHED 30 November 2023
DOI 10.3389/pore.2023.1611396

Check for updates

OPEN ACCESS

EDITED BY
Gabor Cserni,
University of Szeged, Hungary

*CORRESPONDENCE
Peng Xia,
805451046@qq.com

RECEIVED 11 July 2023
ACCEPTED 20 November 2023
PUBLISHED 30 November 2023

CITATION
Zhang F, Wang X, Zhu Y and Xia P (2023), Conjoint analysis of clinical, imaging, and pathological features of schistosomiasis and colorectal cancer. *Pathol. Oncol. Res.* 29:1611396. doi: 10.3389/pore.2023.1611396

COPYRIGHT
© 2023 Zhang, Wang, Zhu and Xia. This is an open-access article distributed under the terms of the Creative Commons Attribution License (CC BY). The use, distribution or reproduction in other forums is permitted, provided the original author(s) and the copyright owner(s) are credited and that the original publication in this journal is cited, in accordance with accepted academic practice. No use, distribution or reproduction is permitted which does not comply with these terms.

Conjoint analysis of clinical, imaging, and pathological features of schistosomiasis and colorectal cancer

Fang Zhang[1], XiaoShuang Wang[1], YuanTing Zhu[2] and Peng Xia[3]*

[1]Department of Radiology, Jingzhou Hospital Affiliated to Yangtze University, Jingzhou, China, [2]Department of Pathology, Jingzhou Hospital Affiliated to Yangtze University, Jingzhou, China, [3]Department of Parasitology, School of Basic Medicine, Health Science Center, Yangtze University, Jingzhou, China

This study aims to examine and compare clinical, radiological, and pathological data between colorectal cancer (CRC) patients with and without schistosomiasis and uncover distinctive CRC characteristics when accompanied by schistosomiasis. This retrospective study is based on data collected from 341 patients diagnosed with CRC post-surgery and pathology. Of these patients, 101 (Group A) were diagnosed with colorectal cancer co-occurring with schistosomiasis (CRC-S), while 240 patients (Group B) were diagnosed with colorectal cancer without concurrent schistosomiasis (CRC-NS). Both groups were compared and analyzed based on their clinical data, imaging-based TNM staging, lymph node metastasis, nerve invasion, vascular cancer thrombus, and histopathological differentiation. A Chi-squared test revealed a significant difference in gender distribution between the patients with CRC-S (Group A) and CRC-NS (Group B), with a p -value of 0.043 and χ^2 = 4.115. Specifically, a higher incidence rate was observed among males in Group A. There was a difference in the overall distribution of TNM staging between the two groups (p = 0.034, χ^2 = 6.764). After pairwise comparison, a statistically significant difference was observed in the T3 stage (p <0.05). The proportion of the T3 stage in Group A was significantly higher than that in Group B, indicating certain advantages. There was a difference in postoperative histopathological grading between the two groups (p = 0.005, χ^2 = 10.626). After pairwise comparison, a statistically significant difference was observed between the well-differentiated adenocarcinoma and the moderately and poorly differentiated adenocarcinoma (p <0.05), with a higher proportion of welldifferentiated patients in Group A compared to Group B. There was no significant difference in age, lymph node metastasis, nerve invasion, and vascular invasion between the two groups of patients (p > 0.05). Among the 101 patients with CRC-S, 87 (86%) showed linear calcification on CT imaging. Patients with CRC-S are mainly male, with tumor staging mostly in the middle stage, high tumor differentiation, and low malignancy. CT imaging can help

identify the presence of lumps and linear calcification indicative of schistosome deposits. MRI can early clarify TNM staging and determine the presence of lymph node metastasis and nerve and vascular invasion.

KEYWORDS

schistosomiasis, colorectal cancer, imaging, t stage, pathology

Introduction

CRC ranks third among the most prevalent cancers worldwide, constituting 8.5% of all cancer mortalities [1]. The underlying causes of CRC remain undefined; however, epidemiological and pathological evidence proposes its association with schistosomiasis [2–4]. However, a series of chronic intestinal diseases caused by schistosomiases, such as intestinal fibrosis and ulcers, are considered precancerous lesions [5]. Compared with CRC-NS, CRC-S has different clinical and pathological features, which are complex. Therefore, it is necessary to diagnose CRC-S accurately. The clinical history of schistosomiasis infection, elevated serum CA-125 levels, and imaging examinations have important guiding significance for diagnosing CRC-S. Currently, surgical treatment is considered one of the most effective treatment methods for CRC. Imaging can accurately carry out TNM staging of CRC and has the characteristics of multi-directional and high-resolution imaging. In terms of morphology, it can clearly show the related anatomical structure of CRC and reflect the characteristics of molecular diffusion and blood flow perfusion of pathological water in terms of function. It plays a critical role in the selection and evaluation of preoperative methods of clinical surgery, as well as the formulation of postoperative radiotherapy and chemotherapy treatment plans and the evaluation of efficacy. This study comprehensively analyzes the characteristics of CRC-S disease from clinical and imaging aspects combined with postoperative pathology.

Materials and methods

Patients

From January 2020 to December 2022, a total of 341 cases of colorectal cancer diagnosed pathologically were collected from our hospital. Out of these, 101 cases (group A), including 73 males and 28 females, aged 45–88 years, were diagnosed with colorectal cancer complicated with schistosomiasis by pathological examination after the operation. The remaining 240 patients had colorectal cancer without schistosomiasis (group B), including 144 males and 96 females, aged 35–82 years. Regardless of whether neoadjuvant radiotherapy and chemotherapy were performed before surgery, both groups of patients should undergo CT and 3.0T high-resolution MRI before surgery and neoadjuvant radiotherapy and chemotherapy. The Ethics Committee of the Faculty of Medicine of Yangtze University reviewed and approved this study (ethical code: KY202320), and the informed consent forms of tissue specimens, medical history, and data were signed.

Imaging examination

Routine scanning was carried out using the Philips Brilliance CT 64 Slice scanner and the GE Discovery MR 750 3.0T MRI. The abdominal CT employed a plain scan and enhancement, with scan/reconstruction layer thickness set at 5.0 mm and 1.0 mm, respectively, and a scanning interval of 0.7 mm. All images were subsequently transmitted to the workstation for further evaluation. The MRI sequences employed included FSE axial T1WI, axial T2WI, sagittal T2WI, coronal T2WI, and DWI. All sequences covered the entire tumor, and the images were subsequently forwarded to the ADW4.6 workstation for post-processing to observe the tumor lesion's location, size, and TNM staging.

Data analysis

The TNM staging for CRC in this study adheres to the criteria provided by the American Joint Commission on Cancer (AJCC)/Union for International Cancer Control (UICC)/TNM staging system for CRC, as per the eighth edition in 2017: T1 stage tumors invade the mucosa and submucosa, T2 stage tumors invade the intrinsic muscle layer, T3 stage tumors penetrate the intrinsic muscle layer to the subserosal layer, or invade colorectal tissue without peritoneal coverage, T4 stage tumors penetrate the peritoneal visceral layer, or directly invade or adhere to other organs or structures. The histopathological grading for CRC follows the WHO 2010 edition: High differentiation implies >95% glandular duct formation; Middle differentiation: 50%–95% glandular duct formation; Low differentiation: 0%–49% glandular duct formation. Two highly experienced physicians, each with years of expertise in abdominal and pelvic imaging diagnosis, conducted a joint review and analysis of the tumor's location, CT and MRI imaging characteristics, and its potential invasion of surrounding intestinal structures. If there was any disagreement, a consensus was reached through discussion. All cases

TABLE 1 Comparison of clinical, imaging, and pathological data between two groups of patients.

Parameter	Colorectal cancer		χ^2	*p*-value
	Group A	Group B		
All cases	101	240		
Age (≤50/>50)	8/93	28/212	0.697	0.404
gender (male/female)	73/28	144/96	4.115	0.043
Imaging TNM staging (T1-2/T3/T4)	22/73/6	66/141/33	6.764	0.034
Imaging TNM staging T1-2/T4	22/6	66/33	1.454	0.228
Imaging TNM staging T1-2/T3	22/73	66/141	2.401	0.121
Imaging TNM staging T3/T4	73/6	141/33	5.387	0.020
Histologic grade (high/medium/low)	23/71/7	23/196/21	10.626	0.005
Histologic grade high/medium	23/71	23/196	10.232	0.001
Histologic grade high/low	23/7	23/21	4.513	0.034
Histologic grade medium/low	71/7	196/21	0.033	0.856
LN metastasis (Yes/No)	38/63	87/153	0.0138	0.907
Peripheral invasion (Yes/No)	30/71	62/178	0.362	0.548
Vascular invasion (Yes/No)	20/81	52/188	0.0576	0.810

underwent surgical and pathological diagnosis, and the staging, pathological tissue grading, presence or absence of lymph node metastasis, nerve invasion, and vascular cancer thrombus of the rectal tumor were recorded.

Statistics

The statistical software SPSS 26.0 was used to compare various parameters, including age, gender, imaging TNM staging, presence or absence of lymph node metastasis, nerve and vascular invasion, and histopathological grading between patients in Group A (CRC-S) and Group B (CRC-NS). The collected data underwent subsequent analysis and processing. We employed the Chi-squared (χ^2) test to compare usage rates, with a statistically significant result set at $p < 0.05$.

Results

This study compared Group A and Group B based on age, gender, imaging TNM staging, lymph node metastasis, nerve and vascular invasion, and histopathological grading. Group A showed significant differences ($p < 0.05$) compared to Group B in terms of gender, imaging TNM staging, and histopathological grading, with statistical significance ($p < 0.05$) (Table 1). There was a difference in the overall distribution of TNM staging between the two groups ($p = 0.034$, $\chi^2 = 6.764$). After pairwise comparison, a statistically significant difference was observed in the T3 stage ($p < 0.05$). The proportion of the T3 stage in Group A was significantly higher than that in Group B, indicating certain advantages. There was a difference in postoperative histopathological grading between the two groups ($p = 0.005$, $\chi^2 = 10.626$). After pairwise comparison, a statistically significant difference was observed between the well-differentiated adenocarcinoma and the moderately and poorly differentiated adenocarcinoma ($p < 0.05$), and the proportion of well-differentiated patients in group A was higher than that in group B (Table 1). CT showed thickening of the lower rectal duct wall with significant linear calcification indicative of Schistosoma (Figure 1A), MRI images clearly showed T3 staging (Figures 1B–D), and pathological images (Figure 1E) showed deposition of Schistosoma eggs within the tumor. In some cases, CT shows a clear mass with calcification in the rectal area (Figures 2A, B), while MRI images clearly show that the tumor has broken through the muscular layer in the T3 phase. The intestinal wall appeared significantly thickened with irregular masses, and there was evidence of infiltration into the fat spaces around the rectum and lymph node metastasis (Figures 2C, D). Pathological images (Figures 2E, F) further confirmed the presence of Schistosoma eggs and tumor tissue.

Discussion

Schistosomiasis has been classified as a clear Carcinogen for humans (Class I Carcinogen), and Schistosoma japonicum is

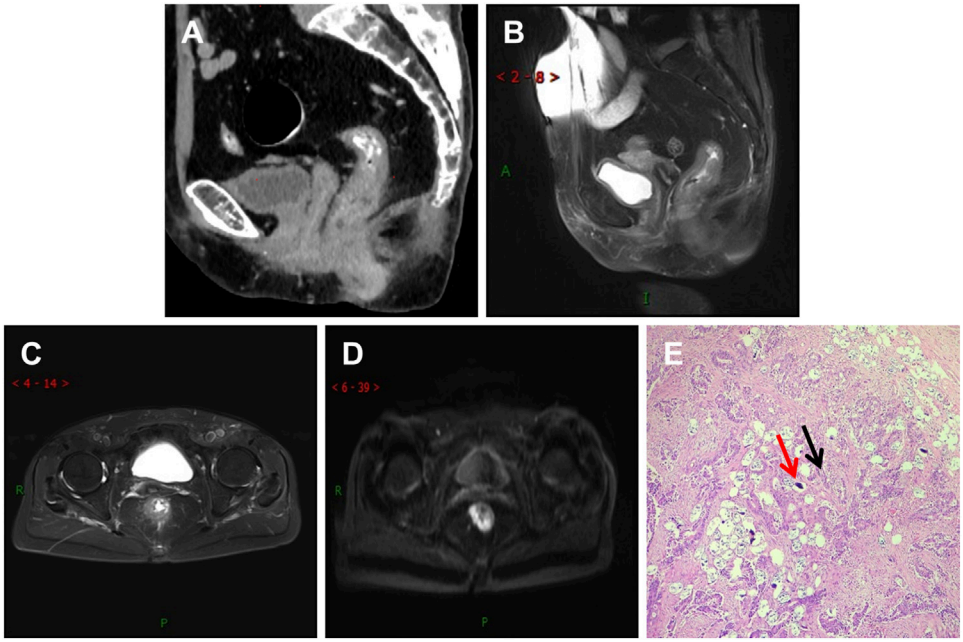

FIGURE 1
Differentiated adenocarcinoma of the rectum, where the tumor penetrates the intrinsic muscle layer to the exterior of the intestinal wall (T3N0MX stage). **(A)** CT shows significant thickening of the lower rectal wall and narrowing of the lumen, with multiple spotted and small strip-shaped calcifications visible within it; **(B,C)** T2WI sagittal and transverse images showed that the rectal tumor presented low signal intensity, thickening of the intestinal wall, rough edges, burry changes, incomplete muscularis mucosa lining, involvement of more than ½ circle of the intestinal cavity, and no lymph node shadow in the surrounding Mesentery fat space area; **(D)** The DWI sequence showed significantly high signal intensity in tumors; **(E)** In the pathological picture, the red arrow indicates Schistosoma eggs and the black arrow indicates tumor tissue. Schistosoma eggs are distributed in the tumor tissue.

considered a possible Carcinogen for humans (Class 2B Carcinogen) [6]. Schistosoma japonicum is the most prevalent in China, mainly concentrated in the middle and lower reaches of the Yangtze River. In recent years, significant progress has been made in controlling schistosomiasis, owing to advancements in national sanitary conditions and effective management. Studies have shown that [7, 8] because Schistosoma eggs deposit in the intestinal submucosa, the local inflammatory reaction forms Granuloma, and long-term repeated stimulation eventually leads to tissue proliferation, fibrosis, inflammatory polyps, and even the adenoma formation, which is consistent with the evolution process of colorectal tumors. Therefore, the inflammatory response caused by schistosomiasis plays an important role in cancer development. Various studies [9, 10] have affirmed schistosomiasis as an autonomous etiological factor for CRC. Current research endeavors have pivoted towards understanding the molecular dynamics associated with CRC-S. The prevalence of CRC-S is low, leading to a dearth of public awareness about routine health check-ups. Consequently, this lack of awareness contributes to significant delays in the initial diagnosis of CRC-S.

Findings from the current investigation reveal a male predominance in CRC-S cases, corroborating several domestic and international studies [11–13]. This trend is potentially linked to the increased likelihood of males encountering contaminated farmland water [14, 15]. Another research study [16] postulates an association with female hormone secretion, such as estrogen and progesterone. It has been reported [17, 18] that CRC-S mainly occurs in the rectum, followed by the Sigmoid colon, which is consistent with the results of this study. Age discrepancies among CRC-S and CRC-NS patients have varied in the literature; some suggest that CRC-NS patients tend to be older by 6–16 years compared to their CRC-S counterparts [15, 19], whereas others propose that CRC-S patients are typically older [20]. However, no substantial age differences were observed between the two cohorts in our study.

Surgical treatment of CRC is the primary clinical approach and also serves as a critical adjuvant therapy for advanced rectal cancer stages T3 and beyond. It holds the potential to prognosticate patient outcomes effectively. Routine check-ups, colonoscopies, and barium enemas can establish an initial CRC diagnosis without staging. Endoscopic ultrasound enables detailed visualization of local tumor invasion, yet its scope is restricted. If a tumor results in lumen constriction, the endoscope's passage becomes hindered, precluding examination. Submucosal dissection via endoscopy has gained traction as a common early-stage CRC treatment, although it cannot detect deeper lesions, lymph node metastasis in the

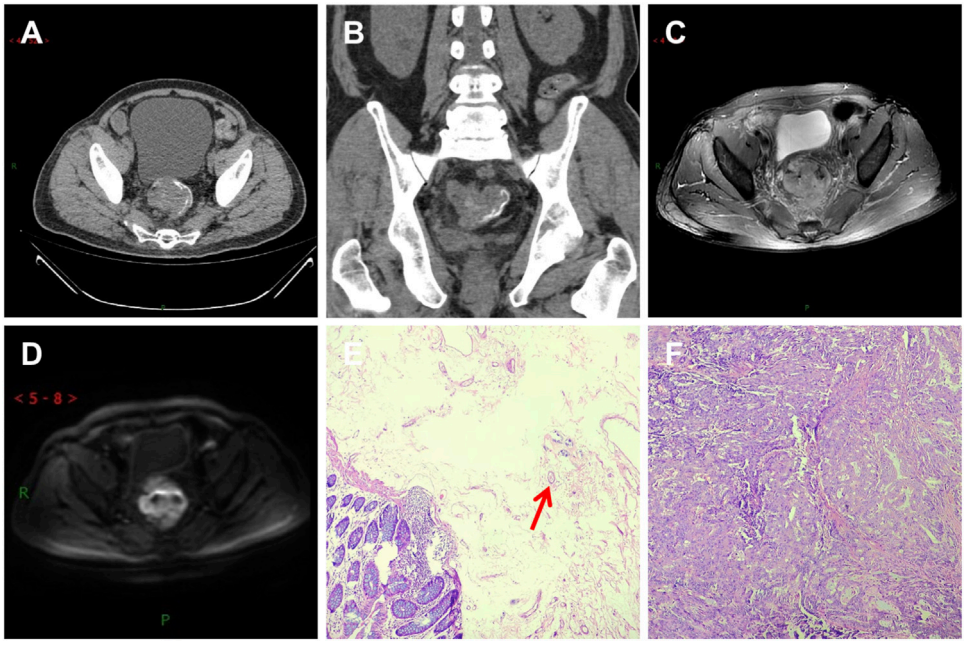

FIGURE 2
A patient with moderately differentiated adenocarcinoma of the rectum, with the tumor invading the entire intestinal wall and lymph node metastasis visible outside the intestinal wall (T3N1MX stage). **(A)** CT shows soft tissue mass shadows in the rectal area, linear calcification shadows in the submucosa of the intestinal wall, and lymph node shadows in the surrounding area; **(B,C)** T2WI transverse and sagittal images showed that the lesion involved all rectal walls and broke through the muscular layer. Burr-like and flocculent shadows were seen around the lesion. The boundary between the lesion and surrounding Mesentery fat was unclear. Slightly high signal lymph node shadows were seen in the rectal mesentery fat; **(D)** The DWI sequence showed significantly high signal intensity in the tumor; **(E)** In the pathological picture, the red arrow indicates the Schistosoma egg; **(F)** Tumor tissue.

intestinal periphery, or vascular invasion. Hence, MRI has emerged as the benchmark imaging modality for evaluating CRC [21].

Out of the 101 CRC-S patients in this retrospective analysis, 87 (86%) exhibited linear calcification on CT imaging, 92 (91%) displayed marked intestinal wall thickening, and 9 (9%) had pronounced masses. Zhang et al. [22] compared CT findings with pathological attributes, identifying irregular intestinal wall thickening in 95% of patients and soft tissue masses in 5%. Among these patients, 80% or 104 presented with linear, patchy, and minor calcifications, while unclear margins were observed in 96 out of 130 patients. The study by Hao Feng et al. [23] aligns with our findings, as their 26 patients demonstrated CT-detected intestinal wall thickening accompanied by linear calcification.

This study used a 3.0T high-resolution MRI sequence to carry out T staging of CRC, including the degree of intestinal wall thickening, stenosis, peritubular invasion, mesorectal fascia invasion, lymph node metastasis, vascular tumor thrombus, and nerve invasion. T staging indicates the primary tumor's growth range and the degree of its invasion into surrounding tissues. For CRC visualized via MRI, distinguishing between stages T2 and T3 proves crucial and challenging for preoperative clinical staging. A determining factor is whether the tumor breaches the serous layer of the mesorectum, that is, the completeness of the low signal ring within the rectal muscle layer, clarity of surrounding fat spaces, and involvement of the mesorectum. Occasionally, the boundary between the rectal tumor edge and the muscularis can appear indistinct and irregular, forming low signal, needle-like, or spiny extensions in the surrounding area, often misconstrued as tumor invasion of the rectal mesothelium. However, it may be a response reflecting proliferative connective tissue in the rectal tumor's surrounding mesothelium, devoid of tumor cell invasion [24]. Various factors, such as the depth of tumor infiltration, lymph node metastasis, and differentiation degree, directly impact the prognosis of rectal cancer.

Schistosoma has little effect in the early stage of T1-2 in different clinical stages, while patients with T3-4 stage tumors complicated with lymph node metastasis have a certain risk in the late clinical stage. There was a difference in the overall distribution of TNM staging between the two groups ($p = 0.034$, $\chi^2 = 6.764$). After pairwise comparison, a statistically significant difference was observed in the T3 stage ($p < 0.05$). The proportion of the T3 stage in Group A was significantly higher than that in Group B, thus indicating certain advantages. This is roughly similar to the findings of the previously reported study [12]. Another previous study [14] has indicated an older average age among schistosomiasis

patients, with most CRC-S patients found in stages T1-3, predominantly in the early and middle stages, which is largely consistent with this study. In these cases, clinicians initially assess the presence of calcification, intestinal thickening, or mass of Schistosoma japonicum using CT scans. Following this, a high-resolution MRI can be employed to determine whether the rectal tumor has invaded the muscularis, assess the integrity of the muscularis, and identify whether the tumor has broken through the muscularis and the depth of infiltration, identify the presence of cancerous nodules in the surrounding mesorectum, and ascertain if there is an invasion of the mesorectal fascia and peritoneum. In general, total mesorectal excision (TME) is often used for direct resection in T2-stage cases. Patients with advanced stage T3 and above mainly require neoadjuvant radiotherapy and chemotherapy before surgery. This aims to reduce the staging, enhance the rate of complete tumor resection, and reduce the potential risk of recurrence, which might otherwise impact the rate of anus-preserving procedures. Accurately distinguishing T2/3 colorectal cancer helps determine whether patients need preoperative radiotherapy and chemotherapy. For patients who do not need these treatments, it helps reduce the complications associated with them, lessen the economic burden on patients, and save treatment time. For patients who need preoperative radiotherapy and chemotherapy, TME after neoadjuvant radiotherapy and chemotherapy can significantly improve the tumor resection rate and reduce the risk of postoperative recurrence. The similarity between imaging and pathological results implies that imaging examinations for comprehensive analysis, evaluation, and prognosis of CRC-S patients preoperatively can significantly enhance clinical diagnostic efficacy, reduce patient treatment duration, and provide compelling evidence for preoperative treatment plans.

Previous research suggests [25] that CRC-S exhibits a lower risk of lymph node metastasis, which may be associated with the development of submucosal fibrous tissue in the intestinal wall, forming a restrictive band that impedes the metastasis of cancer cells *via* lymphatic channels. Another explanation could be the presence of Schistosoma egg granulomas in tissue vessels and lymphatic nodes, which may obstruct or damage their structure, resulting in intestinal wall fibrosis and lymphatic vessel occlusion, thereby making tumor metastasis rare. However, other studies [11, 12] report a higher predisposition toward lymph node metastasis in CRC-S. The results of this investigation indicate that the likelihood of lymph node metastasis in CRC-S is not significantly different from that in CRC-NS, possibly due to the stage, number, and clinical pathological changes of the CRC-S cases examined. No significant differences were observed between the two patient groups concerning lymph node metastasis, neural invasion, and vascular cancer thrombosis, suggesting that a schistosomiasis infection may not elevate the risk of neural and vascular invasion in CRC. There was a difference in postoperative histopathological grading between the two groups ($p = 0.005$, $\chi^2 = 10.626$). After pairwise comparison, a statistically significant difference was observed between the well-differentiated adenocarcinoma and the moderately and poorly differentiated adenocarcinoma ($p < 0.05$), and the proportion of well-differentiated patients in group A was higher than that in group B. This suggests that the degree of differentiation in CRC-S is higher, potentially leading to a better prognosis.

Schistosoma japonicum infection is considered an important risk factor for CRC and can increase the mortality of CRC patients [17], but the exact pathogenesis is still unclear. It is widely believed that chronic inflammatory processes and oxidative stress are the reasons for the carcinogenic effect of schistosomiasis infection [26]. Research reports using the AOM/DSS model demonstrate that the protein Sj E16.7 secreted by Schistosoma eggs can promote cancer progression [27]. In addition to immune response, various other factors, such as oncogene activation, tumor suppressor gene inhibition, changes in normal microRNA expression patterns, genetic factors, and gut microbiota, are all involved in developing CRC [28]. Multivariate analysis revealed that schistosomiasis impacted cancer patients' disease-free and overall survival rates. It has been suggested that the prognosis for CRC-S is poorer than that for CRC [29]. Conversely, another study [14] reported a significantly higher 5 years survival rate in CRC-S, compared to the CRC-NS group, as determined through follow-up surveys. While there is inconsistency in the literature regarding the prognosis for these two groups, the author posits that this discrepancy may be due to factors such as the study cases being drawn from differing periods and alterations in various pathological processes. Therefore, irrespective of the prognosis, early accurate diagnosis, staging, and treatment planning are critical for patients with CRC-S.

There are certain limitations to this study. Due to the retrospective analysis, there may be bias in selecting patients. However, schistosomiasis does have adverse effects on CRC patients, and a large amount of data has not yet been collected using methods such as CT and MRI for preoperative staging of rectal cancer and their comparison. Further improvement is needed in future research.

In summary, compared to CRC-NS, CRC-S is more common in males and predominantly at the mid-stages as assessed by imaging and pathology. The level of pathological differentiation tends to be high, and the risk of lymph node metastasis is not increased. CT imaging and high-resolution MRI serve as critical tools in the accurate and early staging of patients with CRC-S. These techniques are integral in prognostic evaluation before surgery, including assessing the tumor size, potential invasion of surrounding mesorectal fascia, lymph node metastasis, vascular tumor thrombosis, and nerve invasion. Such insights guide

clinical surgeons in selecting surgical procedures and rationally applying postoperative treatment plans.

Data availability statement

The original contributions presented in the study are included in the article/supplementary material, further inquiries can be directed to the corresponding author.

Ethics statement

The studies involving humans were approved by Ethics Committee of Medical College of Yangtze University (ethics code: KY202320). The studies were conducted in accordance with the local legislation and institutional requirements. The participants provided their written informed consent to participate in this study. Written informed consent was obtained from the individual(s) for the publication of any potentially identifiable images or data included in this article.

Author contributions

FZ is responsible for data collection, methodology, statistical analysis, preparation of graphs and tables, literature review and manuscript writing; XW is responsible for machine operation and data analysis: YZ is responsible for all histological examinations and necessary revisions to the previous paraffin blocks; PX is responsible for research design and direction, methodology and visualization. All authors contributed to the article and approved the submitted version.

Funding

This study is funded by the joint development fund for medical research of Yangtze University in 2019 (wj2019-36). The present study was supported by the Nature Science Foundation of Hubei Province (grant no. 2015CFA018).

Conflict of interest

The authors declare that the research was conducted in the absence of any commercial or financial relationships that could be construed as a potential conflict of interest.

Acknowledgments

We would like to thank all the reviewers MS, SS, and SM who participated in the review, as well as MJEditor (www.mjeditor.com) for providing English editing services during the preparation of this manuscript.

References

1. Bray F, Ferlay J, Soerjomataram I, Siegel RL, Torre LA, Jemal A. Global cancer statistics 2018: GLOBOCAN estimates of incidence and mortality worldwide for 36 cancers in 185 countries. *CA Cancer J Clin* (2018) 68(6):394–424. doi:10.3322/caac.21492

2. Liu W, Zeng HZ, Wang QM, Yi H, Mou Y, Wu CC, et al. Schistosomiasis combined with colorectal carcinoma diagnosed based on endoscopic findings and clinicopathological characteristics: a report on 32 cases. *Asian Pac J Cancer Prev* (2013) 14(8):4839–42. doi:10.7314/apjcp.2013.14.8.4839

3. Darre T, Djiwa T, Dare S, Alassani F, Napo-Koura G. Difficult causality relationship between colorectal cancer and schistosomiasis. *Pathol Oncol Res* (2020) 26(1):597–8. doi:10.1007/s12253-018-00566-0

4. Canepa M, Fanta PT, Weidner N, Peterson MR. Schistosomiasis and signet ring cell carcinoma of the rectum. *Ann Diagn Pathol* (2012) 16(5):385–7. doi:10.1016/j.anndiagpath.2010.12.008

5. Wang M, Wu QB, He WB, Wang ZQ. Clinicopathological characteristics and prognosis of schistosomal colorectal cancer. *Colorectal Dis* (2016) 18(10):1005–9. doi:10.1111/codi.13317

6. Vennervald BJ, Polman K. Helminths and malignancy. *Parasite Immunol* (2009) 31(11):686–96. doi:10.1111/j.1365-3024.2009.01163.x

7. Imai J, Ichikawa H, Mizukami H, Suzuki T, Watanabe N, Mine T. Colonic high-grade tubular adenomas associated with schistosoma japonicum. *Tokai J Exp Clin Med* (2016) 41(1):22–3.

8. Abe T, Yunokizaki H, lijima H, Tamura K, Lee ZL, Higashi D, et al. Schistosoma japonicum showing flat colon polyp Appearance. *Gastrointest Endosc* (2011) 73(4):8202–2. doi:10.1016/j.gie.2010.10.038

9. Regula J, Rupinski M, Kraszewska E, Polkowski M, Pachlewski J, Orlowska J, et al. Colonoscopy in colorectal-cancer screening for detection of advanced neoplasia. *N Engl J Med* (2006) 355(18):1863–72. doi:10.1056/NEJMoa054967

10. Wang ZJ, Yang JH. Effect of schistosomiasis japonica on the development of gastric andcolorectal cancer. *Zhong guo Xue Xi Chong Bing Fang Zhi Za Zhi* (2020) 32(2):148–53. doi:10.16250/j.32.1374.2019240

11. Wu C, WangGao YHL, Zhang Y, Dai M, Li S. Relationship between salt-inducible kinase 2 (SIK2) and lymph node metastasis in colorectal cancer patients complicated with chronic schistosomiasis. *Zhejiang Da Xue Xue Bao Yi Xue Ban* (2021) 50(5):607–13. doi:10.3724/zdxbyxb-2021-0157

12. Wang W, Lu K, Wang LM, Jing H, Pan W, Huang S, et al. Comparison of non-schistosomal colorectal cancer and schistosomal colorectal cancer. *Comp Study World J Surg Oncol* (2020) 18(1):149. doi:10.1186/s12957-020-01925-5

13. Zheng N, WangYu HQ, Wang C, Bai C, Pan A Changing trends, clinicopathological characteristics, surgical treatment patterns, and prognosis of schistosomiasis-associated versus non-schistosomiasis-associated colorectal cancer: a large retrospective cohort study of 31 153 cases in Shanghai, China (2001-2021). *Int J Surg* (2023) 109(4):772–84. doi:10.1097/js9.0000000000000293

14. Wang Z, Du Z, Liu Y, Wang W, Liang M, Zhang A, et al. Comparison of the clinicopathological features and prognoses of patients with schistosomal and nonschistosomal colorectal cancer. *Oncol Lett* (2020) 19(3):2375–83. doi:10.3892/ol.2020.11331

15. Hamid HKS. Schistosoma japonicum-associated colorectal cancer: a review. *Am J Trop Med Hyg* (2019) 100(3):501–5. doi:10.4269/ajtmh.18-0807

16. Xiao R, Li F, Zou X. Correlation analysis between chronic schistosomiasis and colorectal cancer. *J Clin Surg* (2019) 27(9):779–81.

17. Barsoum RS, Esmat G, Ei-Baz T. Human schistosomiasis: clinical perspective review. *J Adv Res* (2013) 4(5):433–44. doi:10.1016/j.jare.2013.01.005

18. Qin X, Liu CY, Xiong YL, Bai T, Zhang L, Hou XH, et al. The clinical features of chronic intestinal schistosomiasis-related intestinal lesions. *BMC Gastroenterol* (2021) 21(1):12. doi:10.1186/s12876-020-01591-7

19. Yosry A. Schistosomiasis and neoplasia. *Contrib Microbiol* (2006) 13:81–100. doi:10.1159/000092967

20. Chen YB, Liu Z, Qian J, Feng HY, Li DC, Fan YT. Expression difference of DNA mismatch repair gene hMLH1 and hMSH2 between schistomiasis-associated colorectal cancer and sporadic colorectal cancer. *Zhonghua Wei Chang Wai Ke Za Zhi* (2016) 19(1):75–9.

21. Benson AB, Venook AP, Al-Hawary MM, Cederquist L, Chen YJ, Ciombor KK, et al. Rectal cancer, version 2.2018,NCCN clinical practice guidelines in Oncology. *J Natl Compr Canc Netw* (2018) 16(7):874–901. doi:10.6004/jnccn.2018.0061

22. Zhang W, Wang PJ, Shen X, Wang GL, Zhao XH, Seema SF, et al. CT presentations of colorectal cancer with chronic schistosomiasis: a comparative study with pathological findings. *Eur J Radiol* (2012) 81:835–43. doi:10.1016/j.ejrad.2012.02.020

23. Feng H, Lu AG, Zhao XW, Han DP, Zhao JK, Shi L, et al. Comparison of non-schistosomal rectosigmoid cancer and schistosomal rectosigmoid cancer. *World J Gastroenterol* (2015) 21(23):7225–32. doi:10.3748/wjg.v21.i23.7225

24. Samdani T, Garcia-Aguilar J. Imaging in rectal cancer: magnetic resonance imaging versus endorectal ultrasonography. *Surg Oncol Clin North America* (2014) 23(1):59–77. doi:10.1016/j.soc.2013.09.011

25. Cheever AW. Schistosomiasis and colon cancer. *Lancet* (1981) 1(8234):1369–70. doi:10.1016/s0140-6736(81)92547-2

26. Van Tong H, Brindley PJ, Meyer CG, Velavan TP. Parasite infection, carcinogenesis and human malignancy. *EBioMedicine* (2017) 15:12–23. doi:10.1016/j.ebiom.2016.11.034

27. Wu CY, Du XY, Tang LL, Wu JH, Zhao W, Guo XK, et al. Schistosoma japonicum SJE16.7 protein promotes tumor development via the receptor for advanced glycation end products(RAGE). *Front Immunol* (2020) 11:1767. doi:10.3389/fimmu.2020.01767

28. Snider AJ, Bialkowska AB, Ghaleb AM, Yang VW, Obeid LM, Hannun YA. Murine model for colitis-associated cancer of the colon. *Methods Mol Biol* (2016) 1438:245–54. doi:10.1007/978-1-4939-3661-8_14

29. Wang M, Zhang YC, Yang XY, Wang ZQ. Prognostic analysis of schistosomal rectal cancer. *Astan Pac J Cancer Prev* (2014) 15(21):9271–5. doi:10.7314/apjcp.2014.15.21.9271

Pathology & Oncology Research | frontiers

TYPE Original Research
PUBLISHED 24 April 2023
DOI 10.3389/pore.2023.1611081

Check for updates

OPEN ACCESS

EDITED BY
Anna Sebestyén,
Semmelweis University, Hungary

*CORRESPONDENCE
Kuisheng Chen,
chenksh2002@163.com
Miaomiao Sun,
sunmiaomiaohd@163.com

†These authors have contributed equally to this work and share first authorship

RECEIVED 27 January 2023
ACCEPTED 11 April 2023
PUBLISHED 24 April 2023

CITATION
Li H, Yang C, Chen K and Sun M (2023), Expression significance of Emi1, UBCH10 and CyclinB1 in esophageal squamous cell carcinoma.
Pathol. Oncol. Res. 29:1611081.
doi: 10.3389/pore.2023.1611081

COPYRIGHT
© 2023 Li, Yang, Chen and Sun. This is an open-access article distributed under the terms of the Creative Commons Attribution License (CC BY). The use, distribution or reproduction in other forums is permitted, provided the original author(s) and the copyright owner(s) are credited and that the original publication in this journal is cited, in accordance with accepted academic practice. No use, distribution or reproduction is permitted which does not comply with these terms.

Expression significance of Emi1, UBCH10 and CyclinB1 in esophageal squamous cell carcinoma

Hui Li[1,2†], Chenbo Yang[1,2†], Kuisheng Chen[1,2*] and Miaomiao Sun[1,2*]

[1]Department of Pathology, The First Affiliated Hospital of Zhengzhou University, Zhengzhou, China, [2]Henan Key Laboratory of Tumor Pathology, Zhengzhou University, Zhengzhou, China

Despite significant advances in the diagnosis and treatment of esophageal squamous cell carcinoma (ESCC), esophageal cancer is still a heavy social and medical burden due to its high incidence. Uncontrolled division and proliferation is one of the characteristics of tumor cells, which will promote rapid tumor growth and metastasis. Early mitotic inhibitor 1 (Emi1), ubiquitin-conjugating enzyme 10 (UBCH10) and CyclinB1 are important proteins involved in the regulation of cell cycle. In this study, the expression of Emi1, UBCH10 and CyclinB1 in ESCC tissues and adjacent normal tissues will be analyzed by immunohistochemistry and *in-situ* hybridization techniques, and their relationship with tumor proliferation and apoptosis will be analyzed. The results showed that Emi1, UBCH10 and CyclinB1 genes and proteins were highly expressed in tumor tissues, which were correlated with tumor grade, lymph node metastasis and pathological stage, and positively correlated with tumor proliferation. Emi1, UBCH10 and CyclinB1 are also positively correlated. It is speculated that Emi1, UBCH10 and CyclinB1 genes synergically promote tumor proliferation and inhibit apoptosis, which may be potential diagnostic and therapeutic targets for ESCC.

KEYWORDS

tumor proliferation, Emi1, UBCH10, CyclinB1, tumor apoptosis

Introduction

Esophageal cancer is characterized by insidious onset, and patients often seek medical treatment in the middle and late stages, leading to poor prognosis and short survival time (1). Esophageal squamous cell carcinoma (ESCC) is a highly common subtype of esophageal carcinoma, so it is urgent to further explore the molecular pathology and the mechanism of malignant progression of ESCC. The uncontrolled proliferation of tumor cells is the result of dysregulation of cell cycle (2). Early mitotic inhibitor 1 (Emi1) mainly plays a role in promoting endogenous inhibitor of anaphase-promoting complex/cyclosome (APC/C), promoting the accumulation of S and G2 related mitotic Cyclin (3). Ubiquitin-conjugating enzyme 10 (UBCH10) is involved in the degradation of target proteins by the ubiquitin-proteasome

system and thus plays a role in regulating the cell cycle (4). CyclinB1 belongs to the Cyclin family, which plays an important role in regulating the whole process of cell division and proliferation. Abnormal expression of cyclinB1 will cause the cell cycle to stall or exit, and the cell division and proliferation cannot be completed (5).

Currently, it is known that CyclinB1 is the target protein of ubiquitination protein degradation system, in which Emi1 and UBCH10 are participants. Studies have confirmed that Emi1, UBCH10 and CyclinB1 are abnormally expressed in a variety of tumors, and are closely related to the occurrence of tumors (6, 7). However, the expressions of Emi1, UBCH10 and CyclinB1 in ESCC, as well as whether there is interaction among them to jointly regulate the cell cycle process, are still unknown. Therefore, by exploring the expression of three proteins in ESCC and their correlation with tumor growth, we deeply understand the cell cycle process and regulatory mechanism of ESCC, hoping to provide a new theoretical basis for improving the therapeutic effect and prognosis of ESCC.

Methods

Tissue sample

All histological specimens were collected from confirmed ESCC and paracancer normal mucosal tissues from the Department of Pathology, the First Affiliated Hospital of Zhengzhou University from June 2020 to June 2021. All patients had not received radiotherapy or chemotherapy before surgery, and clinicopathologic data were complete. Among the 50 patients with ESCC, 29 were males and 21 were females. They ranged in age from 48 to 83, with a mean age of 60; 16 cases were classified as grade I-II and 34 cases as grade III. There were 23 cases with lymph node metastasis and 27 cases without lymph node metastasis. There were 27 cases of stage I to stage II and 23 cases of stage III to stage IV. Pathological staging was determined according to the TNM staging criteria for esophageal cancer (8th Edition) jointly published by the International Union Against Cancer (UICC) and the American Cancer Federation (AJCC) in 2017.

Reagents

Rabbit anti-human Emi1 polyclonal antibody and rabbit anti-human UBCH10 polyclonal antibody were purchased from Proteintech, United States. Rabbit anti-human CyclinB1 monoclonal antibody was purchased from Shanghai Biyuntian Biotechnology Co., LTD. Rabbit anti-human Ki-67 monoclonal antibody was purchased from Shanghai Gene Technology Co., LTD. TUNEL test kit was purchased from Jiangsu Kaiji Biotechnology Co., LTD. *In situ* hybridization biotin labeled probe was designed and synthesized by Shanghai GenePharma Technology Co., LTD.

Immunohistochemistry (IHC)

The slices were baked in a 61°C drying oven for 150min, and then dewaxed and hydrated. High pressure heating was used for antigen repair. Slices were added with appropriate 3% H_2O_2 drops, and then normal goat serum working solution was added. Add appropriate amount of primary antibody working solution and put the wet box in the refrigerator at 4°C overnight. On the second day, biotin labeled secondary antibody was added, then horseradish peroxidase labeled chain enzyme ovalbumin was added, and DAB working solution was added finally. ESCC tissue slices with known positive expressions of Emi1, UBCH10, CyclinB1 and Ki-67 were used as positive controls. PBS buffer will be used instead of primary antibody as the negative control.

Score by number of positive cells/percentage of observed cells. <1% is 0 point, 1%–25% is 1 point, 26%–50% is 2 point, 51%–75% is 3 point, >76% is 4 point. Score according to cell staining intensity: no color development is 0 point, light yellow is 1 point, brown and yellow is 2 point, tan is 3 point. Finally, the percentage score of positive cells was multiplied by the score of cell staining intensity to obtain the final score. The score ≤4 is negative, and the score >4 is positive.

In-situ hybridization (ISH)

The *in-situ* hybridization biotin labeled probe sequence is shown below. Emi1 probe sequence: 5′-CAACTATCCGAGGGT CGAGG-3′. UBCH10 probe sequence: 5′-CAGGGCTCCTGG CTGGTGACCTGCTT-3′. CyclinB1 probe sequence: 5′-CAG TGACTTCCCGACCCAGTAGGTATTT-3′.

The slices were baked in a 61°C drying oven for 150 min, and then dewaxed and hydrated. The slices were then dripped with an appropriate amount of 3% H_2O_2, followed by 0.3% Triton-X100. After pepsin was added, the pre-hybridization solution was added and incubated at 40°C for 3 h in a wet box. Biotin-labeled oligonucleotide probes were added and incubated overnight in a wet box at 42°C. On the second day, wash with SSC solution, add appropriate amount of sealing solution, and incubate in a wet box at 37°C for 30 min. Appropriate amount of SA-AP was added and incubated in a wet box at 37°C for 30 min. Appropriate amount of BCIP/NBT color developing working solution was added and incubated at 37°C in a wet box for 30–60 min. Appropriate amount of nuclear solid red dye solution was added to restain the nucleus for 5–15 min. ESCC slices with known positive expressions of Emi1, UBCH10 and CyclinB1 were used as positive controls. Hybridization solution without probe was used as negative control.

Score by number of positive cells/percentage of observed cells. <10% is 1 point, 11%–30% is 2 point, 31%–70% is 3 point, >70% is 4 point. Score according to cell staining intensity: no color development is 0 point, light blue is

TABLE 1 The expression difference of Emi1, UBCH10 and CyclinB1 proteins in ESCC and paracancer tissues.

Group	Number of cases	Emi1				UBCH10				CyclinB1			
		+	−	χ^2	*p*	+	−	χ^2	p	+	−	χ^2	*p*
ESCC	50	43	7	46.314	0.000*	44	6	54.782	0.000*	43	7	54.782	0.000*
Paracancer	50	9	41			7	43			6	44		

*$p < 0.05$.

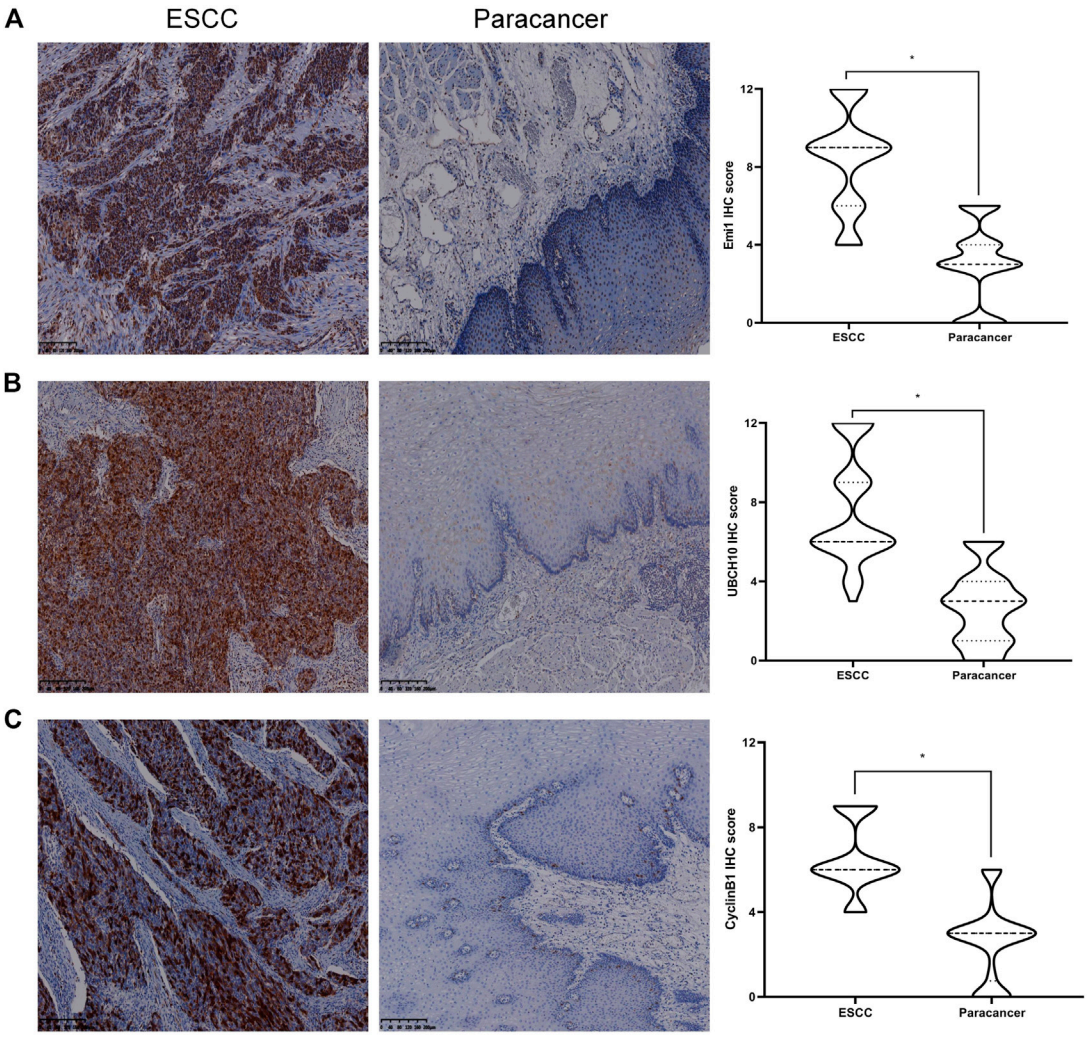

FIGURE 1
Expression of Emi1, UBCH10 and CyclinB1 proteins in ESCC and paracancer tissues. **(A)** Emi1 protein expression; **(B)** UBCH10 protein expression; **(C)** CyclinB1 protein expression (DAB color development, ×100).

1 point, darker purple blue is 2 point, deep purple blue is 3 point. Finally, the percentage score of positive cells was multiplied by the score of cell staining intensity to obtain the final score. The score <1 is negative, and the score ≥1 is positive.

In-situ end labeling (TUNEL)

The slices were baked in a 61°C drying oven for 150 min, and then dewaxed and hydrated. Microwave heating was used

TABLE 2 The expression difference of Emi1, UBCH10 and CyclinB1 mRNA in ESCC and paracancer tissues.

Group	Number of cases	Emi1				UBCH10				CyclinB1			
		+	−	χ^2	p	+	−	χ^2	p	+	−	χ^2	p
ESCC	50	43	7	54.782	0.000*	44	6	51.923	0.000*	41	9	46.314	0.000*
Paracancer	50	6	44			8	42			7	43		

*$p < 0.05$.

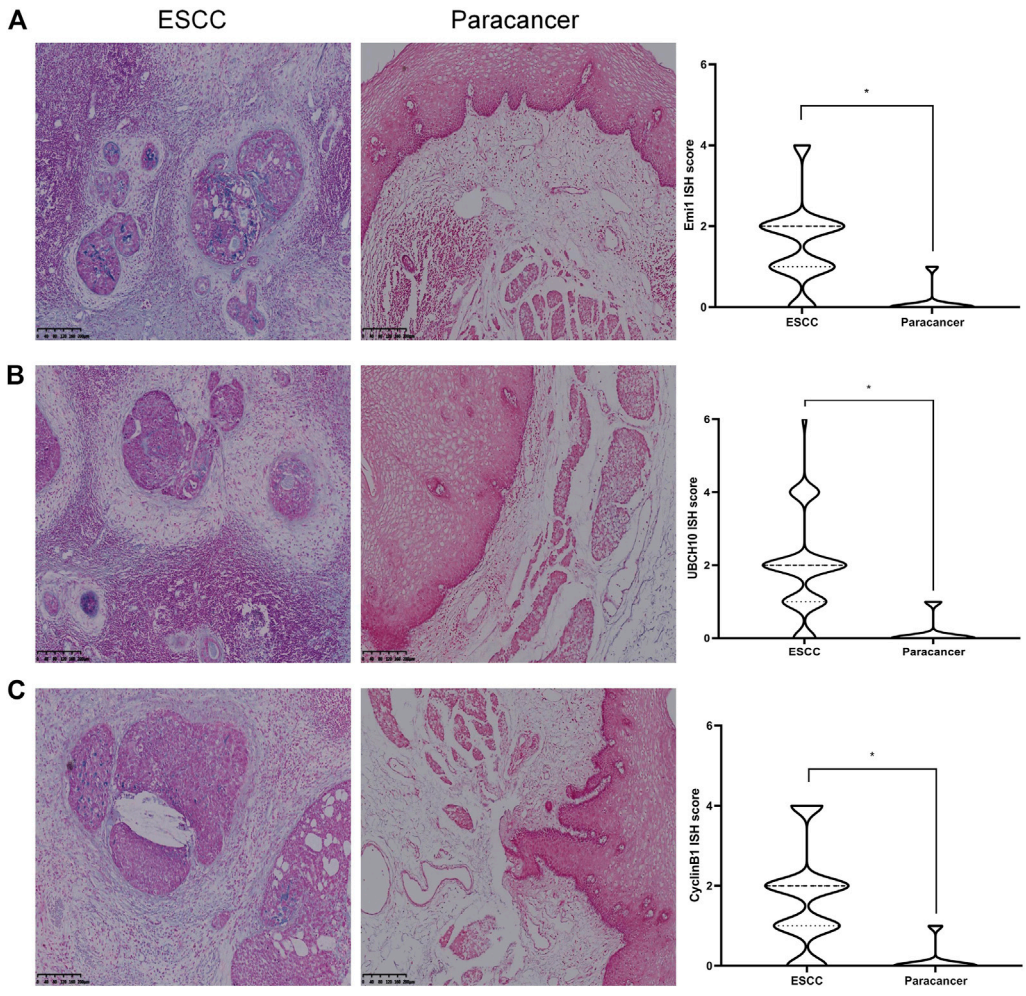

FIGURE 2
Expression of Emi1, UBCH10 and CyclinB1 mRNA in ESCC and paracancer tissues. **(A)** Emi1 mRNA expression; **(B)** UBCH10 mRNA expression; **(C)** CyclinB1 mRNA expression (BCIP/NBT color development, ×100).

to repair antigen. The slices was dripped with 3% H_2O_2, and then the sealer was dripped. Add TdT enzyme working solution and incubate at 37°C for 60 min in the dark. Streptavidin-HRP working solution was added and incubated at 37°C for 30 min in the dark. DAB working solution was added and color was developed for 3–7 min. The known positive tissue slices were treated with Dnase I as positive control. Reaction solution without TDT enzyme was used as negative control.

The degree of apoptosis was suggested by the apoptosis index (AI), which was calculated according to the number of positive cells/percentage of observed cells: AI = number of positive cells/200*100%.

TABLE 3 Correlation between the expressions of Emi1 and clinicopathological indexes.

Clinicopathological indexes	Number of cases	Emi1 protein				Emi1 mRNA			
		Positive (%)	Negative (%)	χ^2	*p*	Positive (%)	Negative (%)	χ^2	*p*
Gender									
Male	29	27 (93.10)	2 (6.90)	1.659	0.198	27 (93.10)	2 (6.90)	1.659	0.198
Female	21	16 (76.19)	5 (23.81)			16 (76.19)	5 (23.81)		
Age									
<60	17	16 (94.12)	1 (5.88)	0.573	0.449	14 (82.35)	3 (17.65)	0.011	0.918
≥60	33	27 (81.82)	6 (18.18)			29 (87.88)	4 (12.12)		
Tumor diameter (cm)									
<3	16	13 (81.25)	3 (18.75)	0.052	0.820	13 (81.25)	3 (18.75)	0.052	0.820
≥3	34	30 (88.24)	4 (11.76)			30 (88.24)	4 (11.76)		
Tissue grade									
G1–G2	16	11 (68.75)	5 (31.25)	3.899	0.048*	11 (68.75)	5 (31.25)	3.899	0.048*
G3	34	32 (94.12)	2 (5.88)			32 (94.12)	2 (5.88)		
Depth of invasion									
T1–T2	21	17 (80.95)	4 (19.05)	0.214	0.644	18 (85.71)	3 (14.29)	0.000	1.000
T3–T4	29	26 (89.66)	3 (10.34)			25 (86.21)	4 (13.79)		
Lymph node metastasis									
N^-	27	20 (74.07)	7 (25.93)	6.934	0.011*	20 (74.07)	7 (25.93)	6.934	0.011*
N^+	23	23 (100)	0 (0)			23 (100)	0 (0)		
Pathological stage									
I–II	27	20 (74.07)	7 (25.93)	6.934	0.011*	20 (74.07)	7 (25.93)	6.934	0.011*
III–IV	23	23 (100)	0 (0)			23 (100)	0 (0)		

N^+, Lymph node metastasis; N^-, No lymph node metastasis. *$p < 0.05$.

Statistical analysis

SPSS21.0 (United States) software was used for statistical analysis. Measurement data were expressed as $\bar{X} \pm S$, and *t*-test was used to compare the differences between the two groups. Comparison of count data were performed by χ^2 test or Fisher's exact probability method, and correlation analysis was performed by Spearman method. Test level $\alpha = 0.05$, $p < 0.05$ was considered statistically significant.

Results

The expression difference of Emi1, UBCH10 and CyclinB1 proteins in ESCC and paracancer tissues

The expressions of Emi1, UBCH10 and CyclinB1 proteins in ESCC and paracancer tissues were detected by IHC. The results showed that Emi1, UBCH10 and CyclinB1 proteins were highly expressed in ESCC tissues, as shown in Table 1 and Figure 1. There were significant differences in protein expression between ESCC and paracancer tissues ($p < 0.05$).

The expression difference of Emi1, UBCH10 and CyclinB1 mRNA in ESCC and paracancer tissues

The expressions of Emi1, UBCH10 and CyclinB1 mRNA in ESCC and paracancer tissues were detected by ISH. The results showed that Emi1, UBCH10 and CyclinB1 mRNA were highly expressed in ESCC tissues, as shown in Table 2 and Figure 2. mRNA expression was significantly different between ESCC and paracancer tissues ($p < 0.05$).

Correlation between the expressions of Emi1, UBCH10, CyclinB1 and clinicopathological indexes

The correlation between Emi1, UBCH10, CyclinB1 and clinicopathological indexes was analyzed, including gender, age, tumor diameter, tissue grade, depth of invasion, lymph node metastasis, and pathological stage. The results showed that the expression of Emi1 protein and mRNA were correlated with tissue grade, lymph node metastasis and pathological stage ($p < 0.05$), as shown in Table 3.

TABLE 4 Correlation between the expressions of UBCH10 and clinicopathological indexes.

Clinicopathological indexes	Number of cases	UBCH10 protein				UBCH10 mRNA			
		Positive (%)	Negative (%)	χ^2	p	Positive (%)	Negative (%)	χ^2	p
Gender									
Male	29	28 (96.55)	1 (3.45)	3.048	0.081	26 (89.66)	3 (10.34)	0.000	1.000
Female	21	16 (76.19)	5 (23.81)			18 (85.71)	3 (14.29)		
Age									
<60	17	15 (88.24)	2 (11.76)	0.001	1.000	15 (88.24)	2 (11.76)	0.000	1.000
≥60	33	29 (87.88)	4 (12.12)			29 (87.88)	4 (12.12)		
Tumor diameter (cm)									
<3	16	15 (93.75)	1 (6.25)	0.154	0.695	13 (81.25)	3 (18.75)	0.293	0.588
≥3	34	29 (85.29)	5 (14.71)			31 (91.18)	3 (8.82)		
Tissue grade									
G1–G2	16	11 (68.75)	5 (31.25)	5.794	0.016*	11 (68.75)	5 (31.25)	5.794	0.016*
G3	34	33 (97.06)	1 (2.94)			33 (97.06)	1 (2.94)		
Depth of invasion									
T1–T2	21	16 (76.19)	5 (23.81)	3.048	0.081	18 (85.71)	3 (14.29)	0.000	1.000
T3–T4	29	28 (96.55)	1 (3.45)			26 (89.66)	3 (10.34)		
Lymph node metastasis									
N^-	27	21 (77.78)	6 (22.22)	5.808	0.025*	21 (77.78)	6 (22.22)	5.808	0.025*
N^+	23	23 (100)	0 (0)			23 (100)	0 (0)		
Pathological stage									
I–II	27	21 (77.78)	6 (22.22)	5.808	0.025*	21 (77.78)	6 (22.22)	5.808	0.025*
III–IV	23	23 (100)	0 (0)			23 (100)	0 (0)		

N^+, Lymph node metastasis; N^-, No lymph node metastasis. *$p < 0.05$.

UBCH10 protein and mRNA expression were correlated with tissue grade, lymph node metastasis and pathological stage ($p < 0.05$), as shown in Table 4. CyclinB1 protein is correlated with tissue grade, lymph node metastasis, and pathological stage, while CyclinB1 mRNA is only correlated with tissue grade ($p < 0.05$). The difference between CyclinB1 protein and mRNA may be related to the small tissue sample size, as shown in Table 5.

Correlation of Emi1, UBCH10 and CyclinB1 expression

The correlation of protein expression among Emi1, UBCH10 and CyclinB1 in ESCC tissues was analyzed, as shown in Figure 3. The results showed that Emi1 was positively correlated with UBCH10 protein expression ($r = 0.5418$, $p < 0.0001$). Emi1 was positively correlated with the expression of CyclinB1 ($r = 0.5539$, $p < 0.0001$). UBCH10 was positively correlated with the expression of CyclinB1 ($r = 0.6020$, $p < 0.0001$).

The mRNA expression correlation among Emi1, UBCH10 and CyclinB1 in ESCC tissues was further analyzed, as shown in Figure 3. The results showed that Emi1 was positively correlated with UBCH10 mRNA expression ($r = 0.4181$, $p = 0.0025$). Emi1 was positively correlated with the expression of CyclinB1 mRNA ($r = 0.7357$, $p < 0.0001$). UBCH10 was positively correlated with the expression of CyclinB1 mRNA ($r = 0.5997$, $p < 0.0001$).

Proliferation and apoptosis in ESCC and paracancer tissues

The expression of Ki-67 protein in ESCC and paracancer tissues was detected by IHC. Ki-67 is a nuclear antigen closely related to cell proliferation. The proliferation index was determined by evaluating the expression of Ki-67 in ESCC and paracancer tissues, as shown in Table 6 and Figure 4. The results showed that the ESCC tissue presented a very obvious high proliferation index, with a mean of 60.40%, while the proliferation index of the paracancer tissue was significantly reduced, about 11.90%, compared with the tumor tissue ($p < 0.05$).

Apoptosis in ESCC and paracancer tissues was determined by TUNEL technique, as shown in Table 6 and Figure 4. The results showed that the apoptotic index was about 29.60% in

TABLE 5 Correlation between the expressions of CyclinB1 and clinicopathological indexes.

Clinicopathological indexes	Number of cases	CyclinB1 protein				CyclinB1 mRNA			
		Positive (%)	Negative (%)	χ^2	p	Positive (%)	Negative (%)	χ^2	p
Gender									
Male	29	27 (93.10)	2 (6.90)	1.659	0.198	26 (89.66)	3 (10.34)	1.646	0.200
Female	21	16 (76.19)	5 (23.81)			15 (71.43)	6 (28.57)		
Age									
<60	17	16 (94.12)	1 (5.88)	0.573	0.449	14 (82.35)	3 (17.65)	0.000	1.000
≥60	33	27 (81.82)	6 (18.18)			27 (81.82)	6 (18.18)		
Tumor diameter (cm)									
<3	16	14 (87.50)	2 (12.50)	0.000	1.000	12 (75.00)	4 (25.00)	0.239	0.625
≥3	34	29 (85.29)	5 (14.71)			29 (85.29)	5 (14.71)		
Tissue grade									
G1–G2	16	11 (68.75)	5 (31.25)	3.899	0.048*	9 (56.25)	7 (43.75)	8.160	0.004*
G3	34	32 (94.12)	2 (5.88)			32 (94.12)	2 (5.88)		
Depth of invasion									
T1–T2	21	16 (76.19)	5 (23.81)	1.659	0.198	17 (80.95)	4 (19.05)	0.000	1.000
T3–T4	29	27 (93.10)	2 (6.90)			24 (82.76)	5 (17.24)		
Lymph node metastasis									
N^-	27	20 (74.07)	7 (25.93)	6.934	0.011*	19 (70.37)	8 (29.63)	3.802	0.051
N^+	23	23 (100)	0 (0)			22 (95.65)	1 (4.35)		
Pathological stage									
I–II	27	20 (74.07)	7 (25.93)	6.934	0.011*	19 (70.37)	8 (29.63)	3.802	0.051
III–IV	23	23 (100)	0 (0)			22 (95.65)	1 (4.35)		

N^+, Lymph node metastasis; N^-, No lymph node metastasis. *$p < 0.05$.

ESCC tissue and 42.20% in paracarcinoma tissue, and the apoptotic index was lower in ESCC tissue. The proliferation and apoptosis indexes of ESCC and paracancer tissues were significantly different ($p < 0.05$).

Correlation between Emi1, UBCH10, CyclinB1 expression and tumor proliferation

The correlation between Emi1, UBCH10 and CyclinB1 protein expression and proliferation index in ESCC tissues was analyzed, as shown in Figure 5. The results showed that the protein expression of Emi1, UBCH10 and CyclinB1 was positively correlated with the proliferation index ($r = 0.4561$, $p = 0.0009$) ($r = 0.4082$, $p = 0.0033$) ($r = 0.4300$, $p = 0.0018$).

The correlation between Emi1, UBCH10 and CyclinB1 mRNA expression and proliferation index in ESCC tissues was analyzed, as shown in Figure 5. The results showed that the mRNA expression of Emi1, UBCH10 and CyclinB1 was positively correlated with the proliferation index ($r = 0.5326$, $p < 0.0001$) ($r = 0.5764$, $p < 0.0001$) ($r = 0.6794$, $p < 0.0001$).

Correlation between expression of Emi1, UBCH10, CyclinB1 and tumor apoptosis

The correlation between Emi1, UBCH10, CyclinB1 protein expression and apoptosis index in ESCC tissues was analyzed, as shown in Figure 6. The results showed that the protein expressions of Emi1, UBCH10 and CyclinB1 were negatively correlated with the apoptosis index ($r = -0.5737$, $p < 0.0001$) ($r = -0.4178$, $p = 0.0025$) ($r = -0.4939$, $p = 0.0018$).

The correlation between Emi1, UBCH10 and CyclinB1 mRNA expression and apoptosis index in ESCC tissues was analyzed, as shown in Figure 6. The results showed that the mRNA expressions of Emi1, UBCH10 and CyclinB1 were negatively correlated with the apoptosis index ($r = -0.4614$, $p = 0.0007$) ($r = -0.3450$, $p = 0.0141$) ($r = -0.4742$, $p = 0.0005$).

Discussion

Although a series of early screening work has been carried out in areas with high incidence of esophageal cancer, showing preliminary tumor prevention and control effect, the tumor burden of esophageal cancer is still very large.

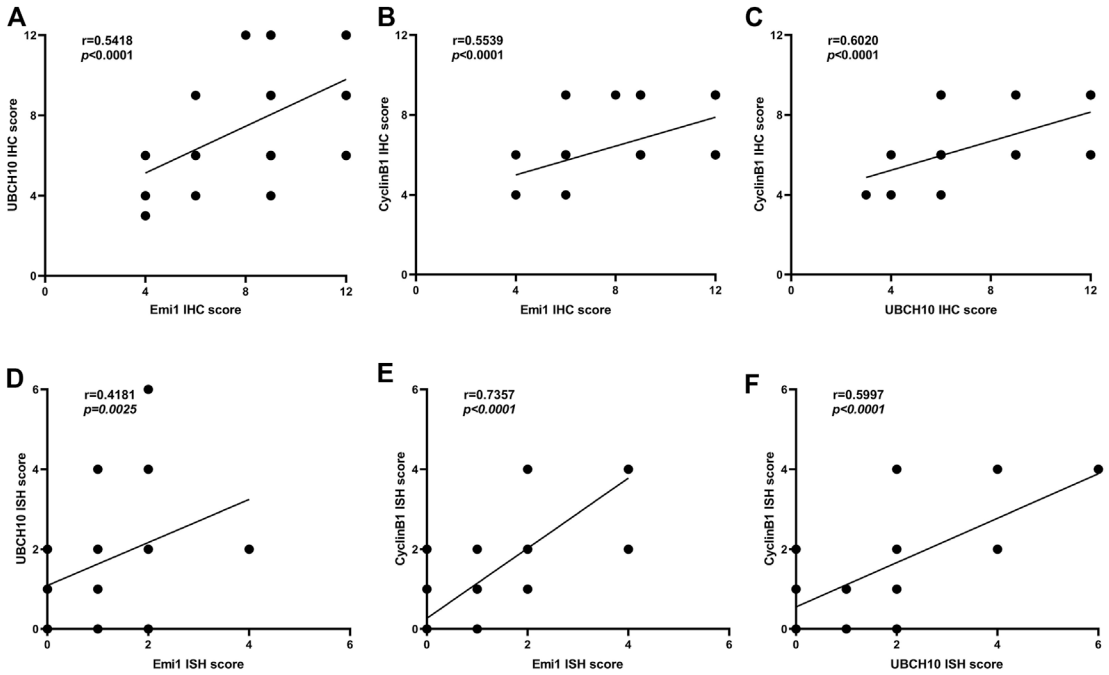

FIGURE 3
Correlation between Emi1, UBCH10 and CyclinB1 expression (A dot may represent multiple samples with the same score). **(A)** Protein expression between Emi1 and UBCH10; **(B)** Protein expression between Emi1 and CyclinB1; **(C)** Protein expression between UBCH10 and CyclinB1; **(D)** mRNA expression between Emi1 and UBCH10; **(E)** mRNA expression between Emi1 and CyclinB1; **(F)** mRNA expression between UBCH10 and CyclinB1.

TABLE 6 Proliferation index and apoptosis index in ESCC and paracancer tissue ($\bar{X} \pm S$) (%).

Group	Number of cases	Proliferation index		Apoptosis index	
		Mean ± s.d	*p*	Mean ± s.d	*p*
ESCC	50	60.40 ± 15.08	0.000*	29.60 ± 20.89	0.002*
Paracancer	50	11.90 ± 6.84		42.20 ± 18.98	

*$p < 0.05$.

Finding new genes and proteins that may play an important role in the occurrence and development of ESCC and elucidating their related molecular mechanisms will be of great significance in the diagnosis and treatment of ESCC. Normal cells proliferate through mitosis and are regulated by a variety of cyclins, Cyclin-dependent protein kinases (CDKs), cell cycle checkpoints and cell cycle signaling pathways (8). The level of cyclin determines the mitotic process of cells. When the level of cyclin decreases, the cell cycle will actively stop or even exit the mitotic process. Protein ubiquitination plays an important role in the stabilization of cyclin levels (9).

Emi1 was initially thought to be a protein involved in the regulation of cell cycle. However, with the development of tumor research, researchers found that the "identity" of Emi1 in the development of tumor was actually oncogene (10). However, there are few reports on the expression of Emi1 in ESCC tissues, so this study started from exploring the expression of Emi1 gene in ESCC. We found that Emi1 mRNA and protein expressions in ESCC tumor tissues were higher than those in paracancer normal esophageal mucosa tissues, confirming the view that Emi1 is an oncogenic gene. Moreover, Emi1 expression was correlated with tumor differentiation, lymph node metastasis, and pathological stage, and was positively correlated with proliferation and

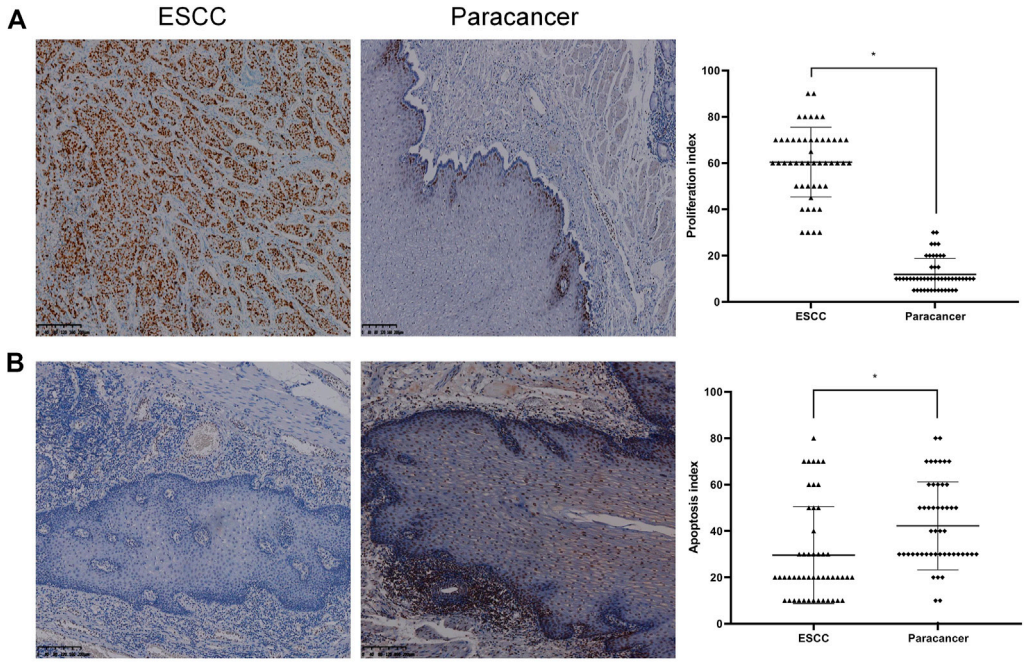

FIGURE 4
Proliferation and apoptosis in ESCC and paracancer tissues [**(A)** Proliferation in ESCC and paracancer tissue; **(B)** Apoptosis in ESCC and paracancer tissues] (DAB color development, ×100).

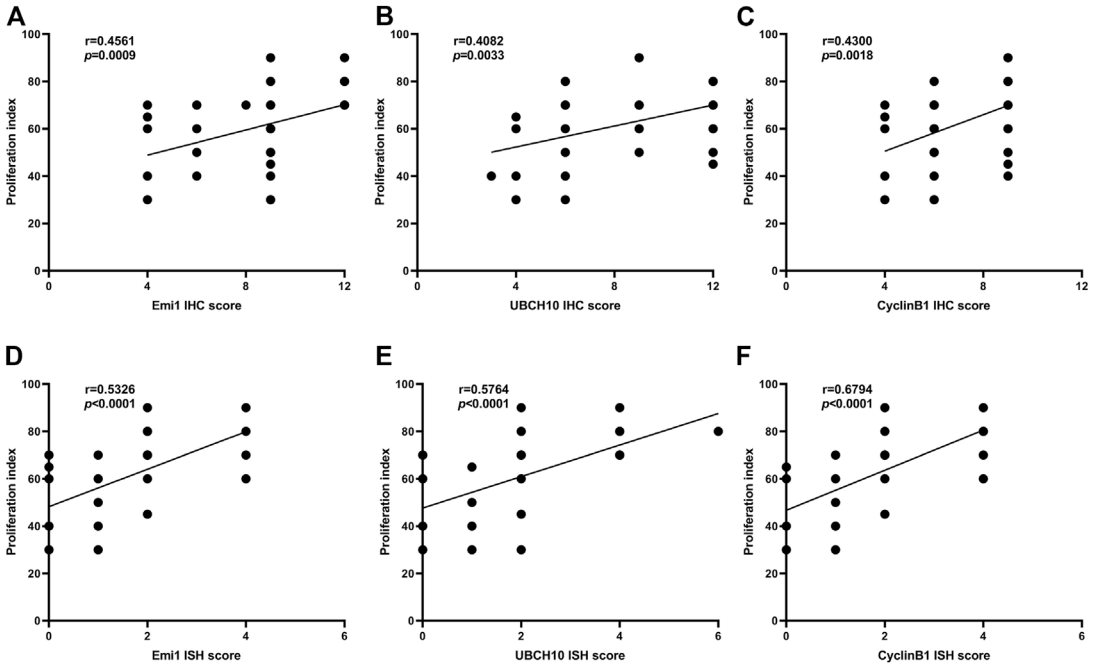

FIGURE 5
Correlation between Emi1, UBCH10, CyclinB1 and proliferation index (A dot may represent multiple samples with the same score). **(A)** Correlation between Emi1 protein and proliferation index; **(B)** Correlation between UBCH10 protein and proliferation index; **(C)** Correlation between CyclinB1 protein and proliferation index; **(D)** Correlation between Emi1 mRNA and proliferation index; **(E)** Correlation between UBCH10 mRNA and proliferation index; **(F)** Correlation between CyclinB1 mRNA and proliferation index.

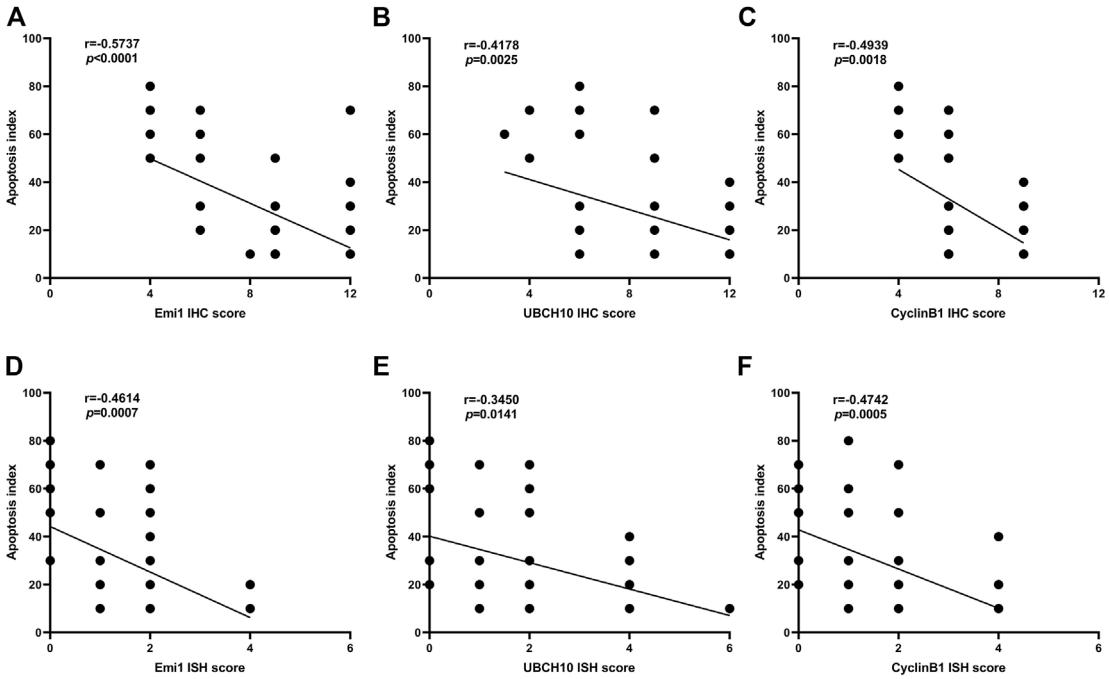

FIGURE 6
Correlation between Emi1, UBCH10, CyclinB1 and apoptosis index (A dot may represent multiple samples with the same score). **(A)** Correlation between Emi1 protein and apoptosis index; **(B)** Correlation between UBCH10 protein and apoptosis index; **(C)** Correlation between CyclinB1 protein and apoptosis index; **(D)** Correlation between Emi1 mRNA and apoptosis index; **(E)** Correlation between UBCH10 mRNA and apoptosis index; **(F)** Correlation between CyclinB1 mRNA and apoptosis index.

negatively correlated with apoptosis, suggesting that Emi1 played an important role in the malignant process of ESCC. The findings of Emi1 in breast cancer are similar to our findings, Emi1 mediates the anti-apoptotic and pro-proliferative carcinogenicity of Skp2 through PI3K/Akt signaling pathway (11).

UBCH10 is an active protein in ubiquitin-proteasome. However, in addition to regulating ubiquitination degradation of protein, UBCH10 is also closely related to tumor proliferation and metastasis, and may be a new tumor marker or therapeutic target (4). Our study found that UBCH10 was significantly highly expressed in ESCC, which was related to tumor differentiation, lymph node metastasis, and pathological stage, and was positively correlated with tumor proliferation index and negatively correlated with apoptosis index, suggesting that UBCH10 could promote tumor proliferation and inhibit tumor apoptosis in ESCC. Compared with ESCC, UBCH10 has been extensively studied in other tumors. In glioma, UBCH10 expression increases with the increase of tumor malignancy. After siRNA silencing UBCH10, glioma cells show growth inhibition, cell cycle arrest and increased apoptosis (12, 13). UBCH10 in lung cancer is also related to tumor differentiation and patient survival, and UBCH10 can lead to P53 and EGFR gene mutations, resulting in loss of tumor inhibitory effect of P53 gene and enhancement of growth promoting effect of EGFR, while the proliferation of lung cancer cells and drug resistance of chemotherapy drugs are weakened after UBCH10 gene silencing (14, 15). UBCH10 is associated with ER and Ki-67 in breast cancer. Silencing UBCH10 can inhibit the proliferation of tumor cells and increase the sensitivity to chemotherapy. UBCH10 has also been detected in circulating tumor cells, suggesting that it can be used as an indicator for early screening and diagnosis of breast cancer (16).

CyclinB1 is a "star molecule" in the cyclin family and a core protein that regulates the G2 phase of the cell cycle. Similar to UBCH10, CyclinB1 not only has cell cycle regulation function, but also is an oncogenic gene associated with abnormal tumor proliferation. Through the detection of CyclinB1 mRNA and protein in ESCC tissues, it was found that the high expression of CyclinB1 in ESCC tissues was positively correlated with the proliferation index and negatively correlated with the apoptosis index. The expression of CyclinB1 protein was correlated with tumor grade, lymph node metastasis and pathological stage. Other researchers have found evidence that confirms our results, The expression of CyclinB1 was downregulated in cervical cancer cells, and it was found that tumor progression was inhibited and cell cycle was stagnated in G2/M phase, which ultimately delayed the process of tumor development (17, 18). When the level of CyclinB1 was reduced in

breast cancer cells, the proliferation and migration of tumor cells were inhibited, and the cell cycle was stagnated in G2/M phase (7).

Emi1 is involved in cell cycle regulation by acting as an endogenous inhibitor of APC/C and hindering the degradation of its substrates by APC/C (19). UBCH10, as a member of ubiquitin binding enzyme E2 family, binds to ubiquitin ligase E3 to form a complex to initiate ubiquitin-proteasome degradation pathway, degrades APC/C substrate CyclinB, and finally plays a role in regulating cell cycle (20). CyclinB1 is mainly involved in the regulation of G2 phase of the cell cycle. In late mitosis, CyclinB1 combines with CDK1 to form a complex, Cyclinb1-CDK1, which phosphorylates APC/C and then promotes the degradation of CyclinB1 (21). Emi1, UBCH10 and CyclinB1 are all participants in the cell cycle regulation mechanism and are key points in the APC/C molecular mechanism network. By analyzing the correlation between the expressions of Emi1, UBCH10 and CyclinB1, the results confirmed that there was a positive correlation between Emi1, UBCH10 and CyclinB1 at both protein level and mRNA level. The degradation of cyclins is mainly dependent on ubiquitination, among which APC/C is an important ubiquitin-binding enzyme E3, and the degradation substrates of APC/C include a variety of proteins such as CyclinA and CyclinB. The silencing of Emi1 in cells will cause a large number of ubiquitination substrate proteins of APC/C, resulting in ubiquitination degradation of CyclinA and CyclinB, and insufficient accumulation of cyclin in cells, which cannot enter the next phase, and eventually lead to cell cycle arrest (22). However, overexpression of Emi1 in cells will block the catalytic site of APC/C and competitively prevent APC/C substrate proteins from binding to APC/C co-receptors, resulting in increased CyclinA and CyclinB levels and disorder of cell proliferation cycle (19). Normal cell cycle arrest and cell physiological apoptosis can not be carried out, which further leads to malignant cell proliferation, promotes cell proliferation and inhibits cell apoptosis. In-depth analysis of the inhibitory effect and mechanism of Emi1 revealed that Emi1 protein contains a variety of domains that block the substrate binding site of APC/C and inhibit the formation of ubiquitin chains (23). As ubiquitin binding enzyme E2, UBCH10 has the function of forming and extending ubiquitin chains, which can connect the substrate protein and ubiquitin ligase E3 through the ubiquitin chain, label ubiquitin on the substrate protein, and initiate the ubiquitination degradation process (24). In normal cells, Emi1 can effectively inhibit UBCH10 ubiquitin chain extension, thus effectively stabilizing the level of substrate protein (25).

At present, the specific molecular mechanism of Emi1, UBCH10 and CyclinB1 genes in promoting tumor proliferation and inhibiting apoptosis has not been reported. Combined with our experimental results, we conjectured that Emi1 reduced UBCH10 consumption by inhibiting ubiquitin chain extension between UBCH10 and CyclinB1, and inhibited the ubiquitination degradation of CyclinB1 protein, resulting in high expression of Emi1, UBCH10 and CyclinB1 in tumor tissues. Cell cycle regulation is a complex and huge mechanism network. In addition to the influence of UBCH10 and CyclinB1 proteins, Emi1 may also have other molecular effects, which requires further discussion.

Data availability statement

The original contributions presented in the study are included in the article/Supplementary Material, further inquiries can be directed to the corresponding authors.

Ethics statement

The studies involving human participants were reviewed and approved by Life Science Ethics Review Committee of Zhengzhou University. The patients/participants provided their written informed consent to participate in this study. Written informed consent was obtained from the individual(s) for the publication of any potentially identifiable images or data included in this article.

Author contributions

KC and MS designed the research study and approved the final version of the manuscript for publication. HL completed the experiment. CY conducted the research and wrote the paper. All authors read and approved the final manuscript.

Funding

National Natural Science Foundation of China (81873455); Training Program for young and middle-aged Health Science and Technology innovation Leaders in Henan Province (YXKC2022015).

Conflict of interest

The authors declare that the research was conducted in the absence of any commercial or financial relationships that could be construed as a potential conflict of interest.

Supplementary material

The Supplementary Material for this article can be found online at: https://www.por-journal.com/articles/10.3389/pore.2023.1611081/full#supplementary-material

References

1. Arnold M, Abnet CC, Neale RE, Vignat J, Giovannucci EL, McGlynn KA, et al. Global burden of 5 major types of gastrointestinal cancer. *Gastroenterology* (2020) 159:335–49. doi:10.1053/j.gastro.2020.02.068

2. Lezaja A, Altmeyer M. Dealing with DNA lesions: When one cell cycle is not enough. *Curr Opin Cel Biol* (2021) 70:27–36. doi:10.1016/j.ceb.2020.11.001

3. Zhao Y, Tang Q, Ni R, Huang X, Wang Y, Lu C, et al. Early mitotic inhibitor-1, an anaphase-promoting complex/cyclosome inhibitor, can control tumor cell proliferation in hepatocellular carcinoma: Correlation with Skp2 stability and degradation of p27(kip1). *Hum Pathol* (2013) 44:365–73. doi:10.1016/j.humpath.2012.03.030

4. Presta I, Novellino F, Donato A, La Torre D, Palleria C, Russo E, et al. UbcH10 a major actor in cancerogenesis and a potential tool for diagnosis and therapy. *Int J Mol Sci* (2020) 21:2041. doi:10.3390/ijms21062041

5. Wood DJ, Endicott JA. Structural insights into the functional diversity of the CDK-cyclin family. *Open Biol* (2018) 8:180112. doi:10.1098/rsob.180112

6. Lei H, Wang K, Jiang T, Lu J, Dong X, Wang F, et al. KIAA0101 and UbcH10 interact to regulate non-small cell lung cancer cell proliferation by disrupting the function of the spindle assembly checkpoint. *BMC Cancer* (2020) 20:957. doi:10.1186/s12885-020-07463-3

7. Liu B, Liu Y, Wang Y, Xie C, Gan M, Han T, et al. CyclinB1 deubiquitination by USP14 regulates cell cycle progression in breast cancer. *Pathol Res Pract* (2019) 215:152592. doi:10.1016/j.prp.2019.152592

8. Sun Y, Liu Y, Ma X, Hu H. The influence of cell cycle regulation on chemotherapy. *Int J Mol Sci* (2021) 22:6923. doi:10.3390/ijms22136923

9. Peters JM. The anaphase promoting complex/cyclosome: A machine designed to destroy. *Nat Rev Mol Cel Biol.* (2006) 7:644–56. doi:10.1038/nrm1988

10. Yamano H. EMI1, a three-in-one ubiquitylation inhibitor. *Nat Struct Mol Biol* (2013) 20:773–4. doi:10.1038/nsmb.2626

11. Liu X, Wang H, Ma J, Xu J, Sheng C, Yang S, et al. The expression and prognosis of Emi1 and Skp2 in breast carcinoma: Associated with PI3K/akt pathway and cell proliferation. *Med Oncol* (2013) 30:735. doi:10.1007/s12032-013-0735-0

12. Donato G, Iofrida G, Lavano A, Volpentesta G, Signorelli F, Pallante PL, et al. Analysis of UbcH10 expression represents a useful tool for the diagnosis and therapy of astrocytic tumors. *Clin Neuropathol* (2008) 27:219–23. doi:10.5414/npp27219

13. Jiang L, Bao Y, Luo C, Hu G, Huang C, Ding X, et al. Knockdown of ubiquitin-conjugating enzyme E2C/UbcH10 expression by RNA interference inhibits glioma cell proliferation and enhances cell apoptosis *in vitro*. *J Cancer Res Clin Oncol* (2010) 136:211–7. doi:10.1007/s00432-009-0651-z

14. Perrotta I, Bruno L, Maltese L, Russo E, Donato A, Donato G. Immunohistochemical analysis of the ubiquitin-conjugating enzyme UbcH10 in lung cancer: A useful tool for diagnosis and therapy. *J Histochem Cytochem* (2012) 60:359–65. doi:10.1369/0022155412439717

15. Pallante P, Malapelle U, Berlingieri MT, Bellevicine C, Sepe R, Federico A, et al. UbcH10 overexpression in human lung carcinomas and its correlation with EGFR and p53 mutational status. *Eur J Cancer* (2013) 49:1117–26. doi:10.1016/j.ejca.2012.09.033

16. Wang C, Pan YH, Shan M, Xu M, Bao JL, Zhao LM. Knockdown of UbcH10 enhances the chemosensitivity of dual drug resistant breast cancer cells to epirubicin and docetaxel. *Int J Mol Sci* (2015) 16:4698–712. doi:10.3390/ijms16034698

17. Zhu B, Zhang Q, Wu Y, Luo J, Zheng X, Xu L, et al. SNAP23 suppresses cervical cancer progression via modulating the cell cycle. *Gene* (2018) 673:217–24. doi:10.1016/j.gene.2018.06.028

18. Cheng YM, Tsai CC, Hsu YC. Sulforaphane, a dietary isothiocyanate, induces G2/M arrest in cervical cancer cells through CyclinB1 downregulation and gadd45β/CDC2 association. *Int J Mol Sci* (2016) 17:1530. doi:10.3390/ijms17091530

19. Vaidyanathan S, Cato K, Tang L, Pavey S, Haass NK, Gabrielli BG, et al. *In vivo* overexpression of Emi1 promotes chromosome instability and tumorigenesis. *Oncogene* (2016) 35:5446–55. doi:10.1038/onc.2016.94

20. van Ree JH, Jeganathan KB, Malureanu L, van Deursen JM. Overexpression of the E2 ubiquitin-conjugating enzyme UbcH10 causes chromosome missegregation and tumor formation. *J Cel Biol* (2010) 188:83–100. doi:10.1083/jcb.200906147

21. Gavet O, Pines J. Progressive activation of CyclinB1-Cdk1 coordinates entry to mitosis. *Dev Cel* (2010) 18:533–43. doi:10.1016/j.devcel.2010.02.013

22. Lee H, Lee DJ, Oh SP, Park HD, Nam HH, Kim JM, et al. Mouse emi1 has an essential function in mitotic progression during early embryogenesis. *Mol Cel Biol* (2006) 26:5373–81. doi:10.1128/mcb.00043-06

23. Frye JJ, Brown NG, Petzold G, Watson ER, Grace CR, Nourse A, et al. Electron microscopy structure of human APC/C(CDH1)-EMI1 reveals multimodal mechanism of E3 ligase shutdown. *Nat Struct Mol Biol* (2013) 20:827–35. doi:10.1038/nsmb.2593

24. Bonacci T, Emanuele MJ. Impressionist portraits of mitotic exit: APC/C, K11-linked ubiquitin chains and cezanne. *Cell Cycle (Georgetown, Tex.)* (2019) 18:652–60. doi:10.1080/15384101.2019.1593646

25. Wang W, Kirschner MW. Emi1 preferentially inhibits ubiquitin chain elongation by the anaphase-promoting complex. *Nat Cel Biol* (2013) 15:797–806. doi:10.1038/ncb2755

Pathology & Oncology Research | frontiers

TYPE Hypothesis & Theory
PUBLISHED 19 January 2023
DOI 10.3389/pore.2023.1610893

Check for updates

OPEN ACCESS

EDITED BY
József Tímár,
Semmelweis University, Hungary

*CORRESPONDENCE
Youcheng Zhang,
zhangyouchengphd@163.com

RECEIVED 20 October 2022
ACCEPTED 09 January 2023
PUBLISHED 19 January 2023

CITATION
Deng H, Li T, Wei F, Han W, Xu X and Zhang Y (2023), High expression of TMEM200A is associated with a poor prognosis and immune infiltration in gastric cancer.
Pathol. Oncol. Res. 29:1610893.
doi: 10.3389/pore.2023.1610893

COPYRIGHT
© 2023 Deng, Li, Wei, Han, Xu and Zhang. This is an open-access article distributed under the terms of the Creative Commons Attribution License (CC BY). The use, distribution or reproduction in other forums is permitted, provided the original author(s) and the copyright owner(s) are credited and that the original publication in this journal is cited, in accordance with accepted academic practice. No use, distribution or reproduction is permitted which does not comply with these terms.

High expression of TMEM200A is associated with a poor prognosis and immune infiltration in gastric cancer

Hongyang Deng, Tengfei Li, Fengxian Wei, Wei Han, Xiaodong Xu and Youcheng Zhang*

Department of General Surgery, Hepatic-Biliary-Pancreatic Institute, Lanzhou University Second Hospital, Lanzhou, China

Background: Gastric cancer (GC) is one of the global malignant tumors with high incidence and poor prognosis. Exploring new GC molecular markers is important to improve GC prognosis. Transmembrane protein 200A (TMEM200A) is a member of the family of transmembrane proteins (TMEM). This study is the first to investigate the potential function of TMEM200A and its relationship with immune infiltration in GC.

Methods: The differential expression of TMEM200A was determined through the Cancer Genome Atlas (TCGA) and Gene Expression Omnibus (GEO) databases. The receiver operating characteristic (ROC) curve was drawn to assess the diagnostic value of TMEM200A for GC. The relationship between TMEM200A and the clinical characteristics of patients with GC was investigated using the Wilcoxon test and the Kruskal-Wallis test. The effect of TMEM200A on overall survival (OS) was identified using the Kaplan-Meier method, the Log-rank test, the univariate/multivariate Cox regression analysis, and the nomogram prediction model. The co-expressed genes and gene set enrichment analysis (GSEA) were used to explore the potential biological functions of TMEM200A. We used the Tumor Immune Estimation Resource (TIMER) database and the ssGSEA algorithm to estimate the relationship between TMEM200A and immune cell infiltration. Furthermore, we investigated the correlation of TMEM200A with immune checkpoint/immune cell surface markers using the TCGA-STAD data set. Finally, we identified prognosis-related methylation sites in TMEM200A using MethSurv.

Results: TMEM200A was highly expressed in GC tissues. TMEM200A had a good diagnostic value for GC. High expression of TMEM200A may shorten the OS of GC patients and may be an independent risk factor for OS in GC patients. TMEM200A participates in the construction of a predictive model with a good predictive effect on the survival rate of GC patients at 1, 3, and 5 years. Co-expressed genes and GSEA indicated that TMEM200A may be an adhesion molecule closely associated with tumor invasion and metastasis. In addition, TMEM200A may be significantly associated with immune cell infiltration and immune checkpoint expression. We also found that TMEM200A contains three methylation sites associated with a poor prognosis.

Conclusion: Upregulated TMEM200A may be a promising prognostic marker for GC and is closely associated with the tumor microenvironment (TME).

KEYWORDS

bioinformatics, gastric cancer, prognostic, immune infiltration, TMEM200A

Introduction

Gastric cancer (GC) is common cancer worldwide, with more than one million new cases each year (1, 2). It has the sixth highest number of new cancers diagnoses in the world by 2020 (2). Furthermore, patients with GC are often diagnosed at an advanced stage and therefore do not have a high 5-year survival rate, making it the third leading cause of cancer-related death after lung and liver cancer (2). GC is most prevalent in East Asia, North East Asia, and North Africa (2). Surgery and platinum chemotherapy combined with fluorouracil are the mainstays of GC treatment, but the median overall survival (OS) after chemotherapy in patients with unresectable or metastatic GC is only less than 1 year (3). Despite the benefit seen with trastuzumab in combination with chemotherapy targeting the HER2 gene over chemotherapy alone (4), HER2 gene overexpression occurs in only 10%–20% of GC patients (5). Therefore, the development of new GC biomarkers or specific therapeutic targets may improve the prognosis of patients with GC.

The transmembrane protein (TMEM) family genes encode a large class of proteins that span the lipid bilayer of the cell membrane. Due to their transmembrane properties, TMEM proteins play a role in signal transduction, ion transport, and cell adhesion (6). Although some studies (7) suggested that genes in the TMEM family are essential for tumor metastasis. Different families of TMEM gene play cancer promoting or cancer suppressing roles in different cancers (8–10). In general, current knowledge of the biological functions and mechanisms of action of TMEM genes is limited (11). A deeper understanding of the function of TMEM genes may be a promising direction for the development of new therapeutic targets for tumors.

Transmembrane protein 200A (TMEM200A) (Ensembl ID: ENSG00000164484) is also a member of the TMEM gene family, located on chromosome 6q23.1, with a total length of 77.536 Kb and comprising 8 exons. Recent studies have shown that TMEM200A can regulate adipose morphology by affecting adipogenesis (12). Tan et al. (13) found that the expression of TMEM200A in familial pancreatic cancer was lower than in sporadic pancreatic cancer. Furthermore, 6q23.1, where TMEM200A is located, was identified to be associated with cleft palate and cleft lip (14). Bioinformatics analysis based on the Cancer Genome Atlas (TCGA) and Gene Expression Omnibus (GEO) databases showed that (15) TMEM200A could be used to construct a risk score for the prognosis of acute myeloid leukemia (AML) and could effectively predict the OS of patients with AML. Zhang et al. (16) analyzed somatic mutations and RNA prognostic markers in GC and initially found that TMEM200A may have a prognostic value in GC. However, the role of TMEM200A in GC is still unknown.

This study compared the differential expression of TMEM200A between GC tissues and adjacent/normal gastric mucosal tissues based on TCGA and GEO databases. Subsequently, Kaplan-Meier method, univariate/multivariate Cox regression analysis confirmed the effect of TMEM200A on the prognosis of patients with GC and used the expression of TMEM200A and clinical characteristics of patients with GC to construct a nomogram model to predict the prognosis. In addition, co-expression of genes and GSEA explored the possible biological functions and signaling pathways involved in TMEM200A. In addition, we calculated the relationship between TMEM200A and 28 immune cell infiltrates using the ssGSEA algorithm. We also explored the correlation between TMEM200A expression and immune checkpoint expression to further understand the impact of TMEM200A on the tumor microenvironment (TME). Finally, we analyzed the effect of TMEM200A on the sensitivity of common chemotherapeutic drugs and DNA methylation sites.

Materials and methods

Expression analysis of TMEM200A in pan-cancer

The Tumor Immune Estimation Resource (TIMER) database (https://cistrome.shinyapps.io/timer/) is based on the TCGA database (https://portal.gdc.cancer.gov/) of 10,897 cancer patients from 32 types of cancer and can be used to calculate differences in gene expression in cancer and adjacent tissues, correlations between genes and levels of immune cell infiltration (17). The GEPIA database (http://gepia.cancer-pku.cn/detail.php) contains gene expression data for 9736 tumor tissues from the TCGA database and 8587 normal tissues from the GTEx database (18). We used these two databases to assess the differential expression of TMEM200A in different kinds of tumor.

Expression analysis of TMEM200A in GC

We downloaded RNA sequencing (RNA-Seq) data in TPM format for GC samples and adjacent samples from the TCGA database. The combined RNA-Seq data from the TCGA GC and GTEx databases of normal gastric tissue were downloaded from

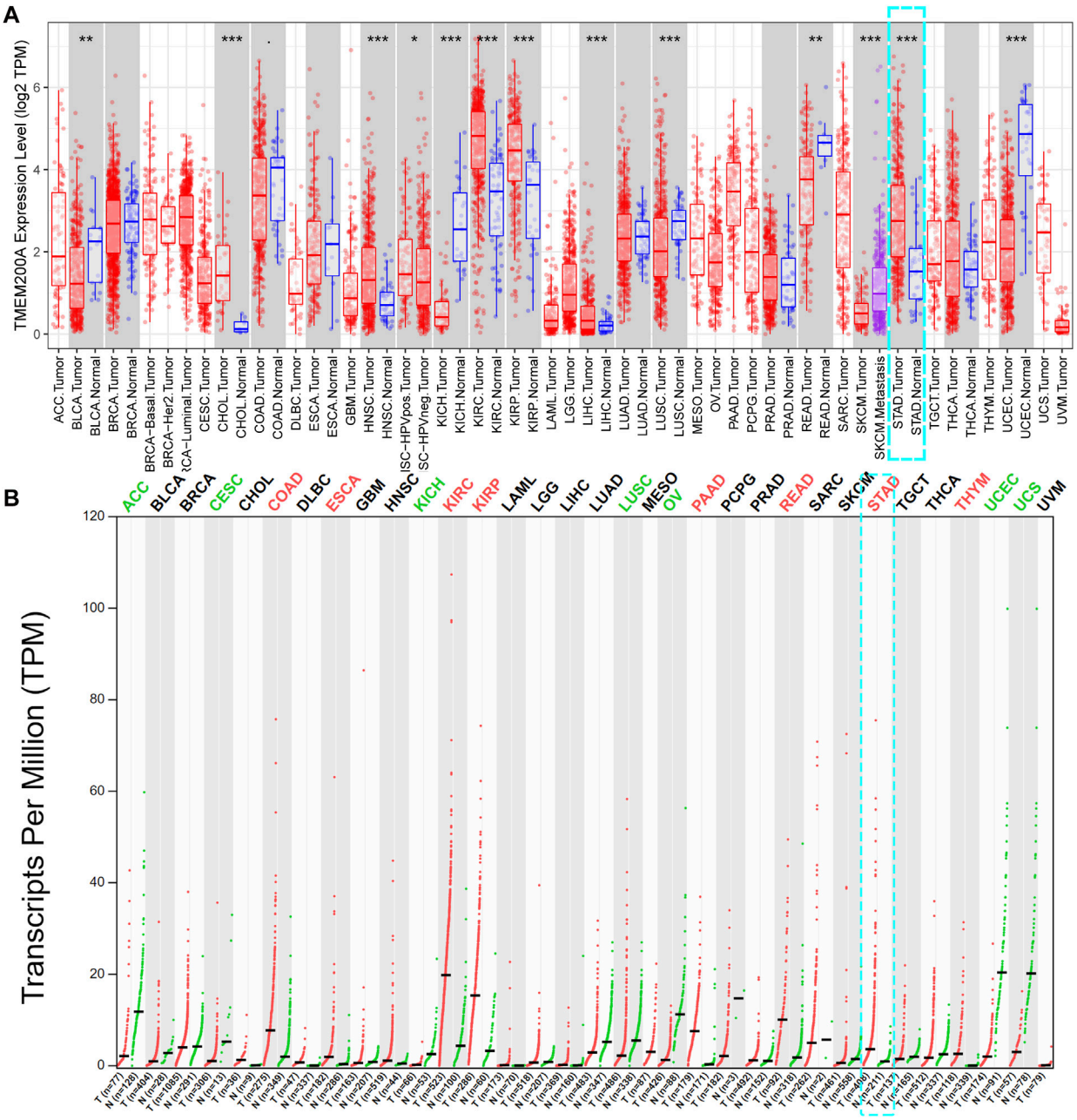

FIGURE 1
Pan-cancer analysis of TMEM200A expression levels. **(A)** Expression of TMEM200A in different kinds of tumor and adjacent tissues in the TIMER database. **(B)** Expression of TMEM200A in different kinds of tumor and normal tissues from the GEPIA database. *, $p < 0.05$; **, $p < 0.01$; ***, $p < 0.001$.

the UCSC database (https://xenabrowser.net/datapages/) (19), and the TCGA-STAD data set relating the clinical profile and survival information. In addition, we acquired GEO database to obtain GSE54129 and GSE66229 (20) as expression validation datasets. The receiver operating characteristic (ROC) curve was drawn to evaluate the diagnostic ability of the TMEM200A to identify GC tissue.

Association of TMEM200A expression with clinical characteristics and prognosis of patients with GC

Excluding samples with partially missing data, we used RNA-Seq data for TMEM200A from 350 patients with GC in the TCGA-STAD dataset and the corresponding clinical information to assess

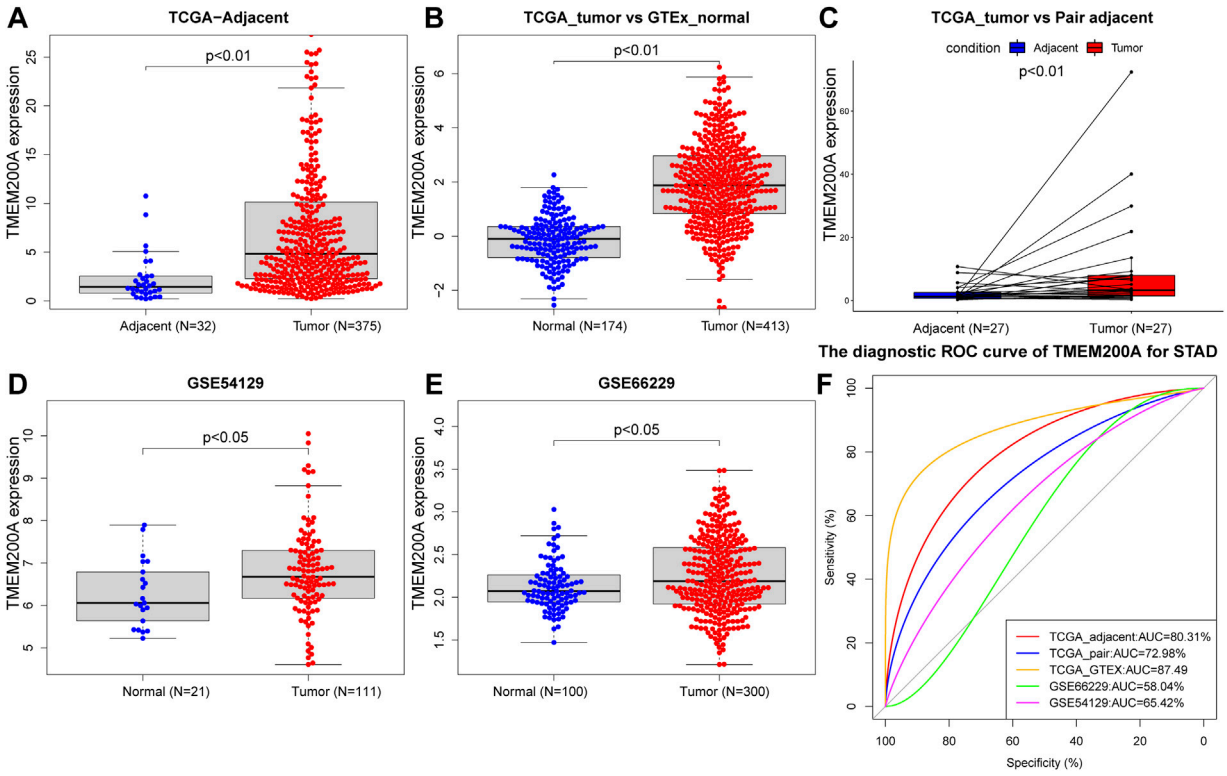

FIGURE 2
Expression level and diagnostic value of TMEM200A in GC. **(A)** TMEM200A expression levels in GC tissue (n = 375) and adjacent tissue (n = 32) in the TCGA-STAD data set. **(B)** Expression levels of TMEM200A in TCGA-STAD GC tissues (n = 413) and GTEx normal gastric tissues (n = 174). **(C)** TMEM200A expression levels in GC tissues (n = 27) and adjacent tissues (n = 27) of paired samples in the TCGA-STAD dataset. **(D)** Expression levels of TMEM200A in GC tissues (n = 111) and normal tissues (n = 21) of the GSE54129 dataset. **(E)** TMEM200A expression levels in GC tissues (n = 100) and normal tissues (n = 300) of the GSE66229 data set. **(F)** ROC curve of TMEM200A for identifying GC tissues.

the prognostic impact of TMEM200A. The median expression value of TMEM200A was used to divide the GC samples into high and low expression groups. We used Kaplan-Meier curves to visualize the effect of TMEM200A on the OS of patients with GC and calculated the p-value using the Log-Rank test. To evaluate the independence of the prognostic impact of TMEM200A, we performed a univariate/multivariate Cox regression analysis of patient clinical information such as age, sex, and stage with TMEM200A expression. Furthermore, we evaluated the efficacy of TMEM200A in predicting the prognosis of patients with gastric cancer using the nomogram prediction model and assessed the effect of the model by the C-index and the calibration curve. GSE15459 (21) contains RNA-Seq and survival information from 192 GC patients as an external validation cohort.

Analysis of TMEM200A co-expressed genes in GC

The LinkedOmics database (http://www.linkedomics.org/login.php/) collects clinical characteristics, RNA-Seq, methylation and other multi-omics data from 32 TCGA cancer cohorts and 10 CPTAC cancer cohorts (22). We used it to calculate the co-expressed genes of TMEM200A, using volcano plot to represent all co-expressed genes and heat map to represent the top 50 genes positively and negatively correlated with TMEM200A. The Pearson correlation test was used to calculate the correlation coefficient, and genes with $p < 0.05$ and correlation coefficients greater than or equal to 0.3 were selected for Gene Ontology (GO) and Kyoto Encyclopedia of Genes and Genomes (KEGG) enrichment analysis by using the clusterProfiler (23) package R.

Gene set enrichment analysis

MSigDB (http://www.gsea-msigdb.org/gsea/index.jsp) collects various annotated gene sets, and gene set enrichment analysis (GSEA) is an algorithm to calculate the variability of these gene sets between two different phenotypes (24). We made the log(TPM+1) normalized TCGA-STAD dataset as input RNA-Seq data and used TMEM200A as the phenotypic label

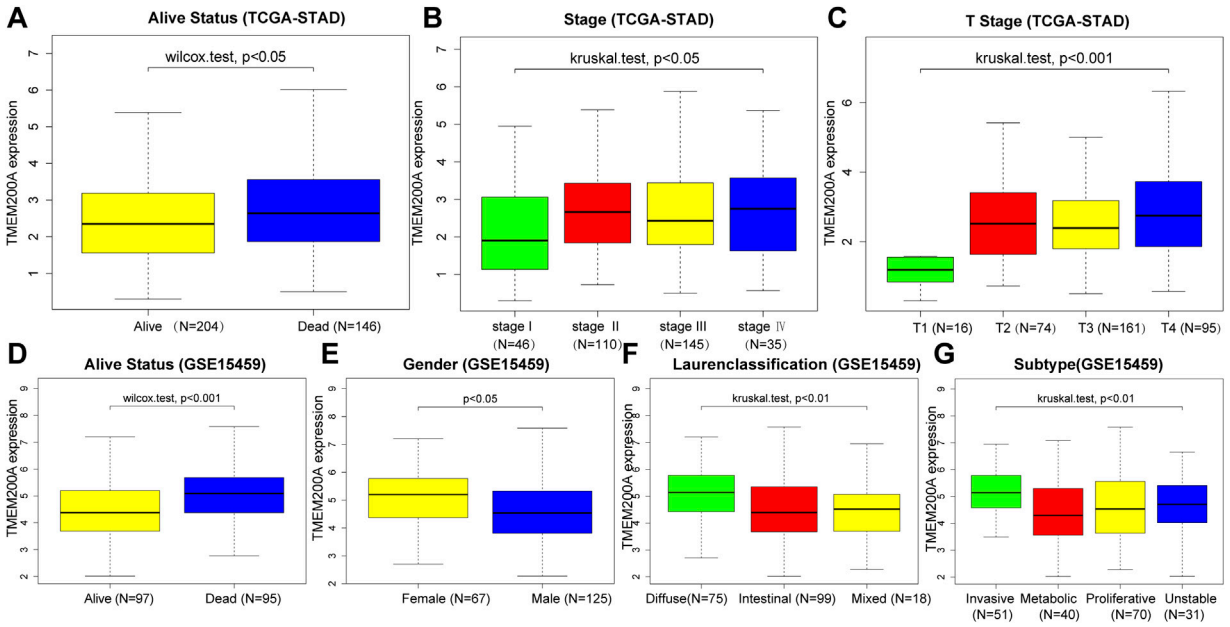

FIGURE 3
Correlation between the expression of TMEM200A and the clinical characteristics of patients with GC. TCGA-STAD cohort: **(A)** alive Status, **(B)** stage, **(C)** stage T. GSE15459 cohort: **(D)** alive Status, **(E)** gender, **(F)** Lauren-Classification, **(G)** Subtype.

and permutation tests 1000 times and considered statistically significant at $p < 0.05$ and FDR <0.05. The reference gene sets were c5.go.bp.v2002.1.Hs.symbols.gmt, c5.go.cc.v2002.1.Hs.symbols.gmt, c5.go.mf.v2002.1.Hs.symbols.gmt, and c2.cp.kegg.v2022.1.Hs. symbols.gmt. All results were sorted by NES value from largest to smallest.

Correlation analysis between TMEM200A and immune cell infiltration

The TIMER database was used to estimate the relationship between TMEM200A and the abundance of six immune cell infiltrates. Subsequently, we further calculated the relationship between TMEM200A and 28 subtypes of immune cell infiltration by the ssGSEA algorithm of the GSVA (25) R package, and the results were presented in box plots. Finally, we explored the correlation of TMEM200A expression with immune checkpoint and immune cell surface marker expression in GC tissues using the TCGA-STAD dataset with adjacent excluded samples, and the results were visualised by radar plots.

Drug sensitivity

We calculated the semi-inhibitory concentrations (IC50) of chemotherapeutic agents for each sample in the TCGA-STAD dataset using the pRRophetic R package. The patients were divided into high and low TMEM200A expression groups by median TMEM200A expression values and the difference in IC50 of these chemotherapeutic agents between the two groups was analyzed by the Wilcoxon test.

Methylation analysis of TMEM200A

DNA methylation is a process of epigenetic modification of genes in which methyl groups are mounted on DNA cytosines. Aberrant DNA methylation plays a key role in cancer development. MethSurv (https://biit.cs.ut.ee/methsurv/) (26) is a database for DNA methylation survival analysis based on 7,358 patients of 25 different cancers in TCGA. We used MethSurv to analyze the methylation sites of TMEM200A and the impact of these methylation sites on the survival of patients with GC.

Statistical analysis

The R software (version 4.1.2) and its packages were applied to test and visualize. *p*-values less than 0.05 were considered statistically significant.

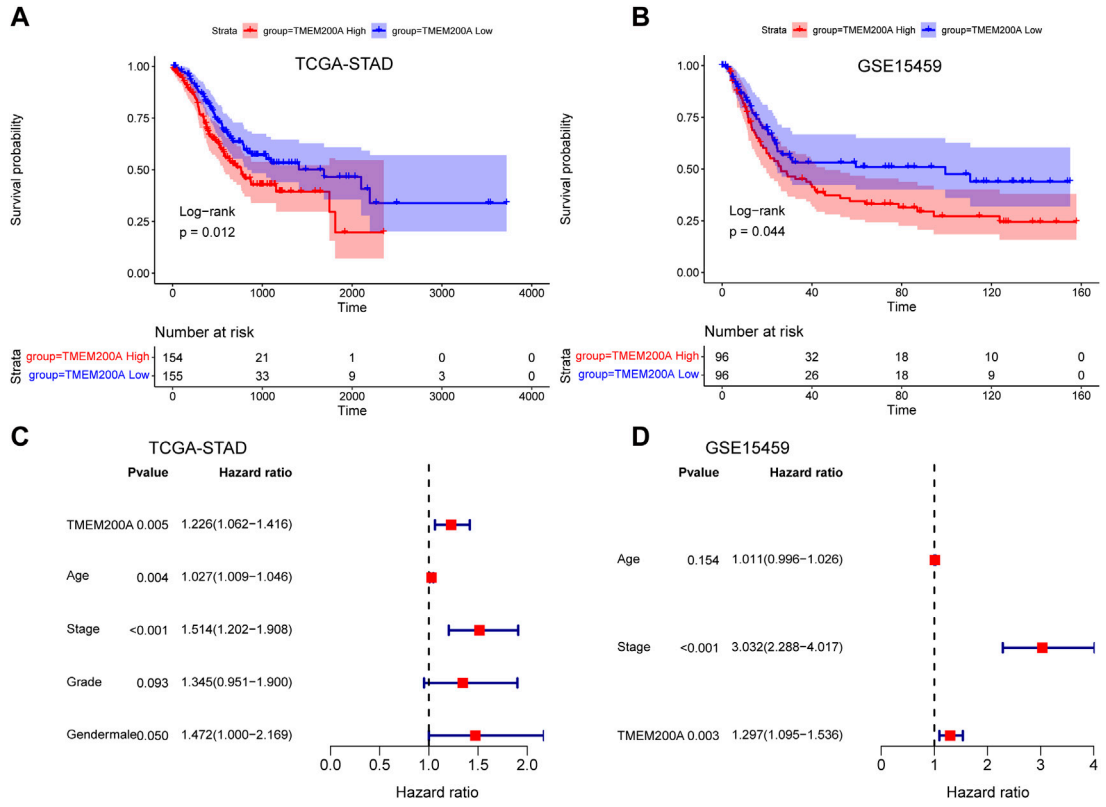

FIGURE 4
Analysis of the prognostic value of TMEM200A in GC. **(A)** Kaplan-Meier curves for OS of patients in the TCGA-STAD cohort. **(B)** Kaplan-Meier curves for OS of patients in the GSE15459 cohort. **(C)** Forest plot of the results of the TCGA-STAD cohort multifactorial Cox regression analysis. **(D)** Forest plot of the results of the multifactorial Cox regression analysis of the GSE15459 cohort.

Results

TMEM200A is aberrantly expressed in a variety of cancers

TIMER database analysis showed that TMEM200A was significantly more expressed in cholangiocarcinoma (CHOL), head and neck squamous carcinoma (HNSC), kidney renal clear cell carcinoma (KIRC), kidney renal papillary cell carcinoma (KIRP), liver hepatocellular carcinoma (LIHC), stomach adenocarcinoma (STAD) and less expressed in bladder urothelial carcinoma (BLCA), kidney chromophobe (KICH), lung squamous cell carcinoma (LUSC), rectum adenocarcinoma (READ), skin cutaneous melanoma (SKCM) and uterine corpus endometrial carcinoma (UCEC) compared to paraneoplastic tissues (Figure 1A). The results of GEPIA database analysis suggested that TMEM200A was highly expressed in colon adenocarcinoma (CODA), esophageal carcinoma (ESCA), KIRC, KIRP, pancreatic adenocarcinoma (PADD), READ, STAD and thymoma (THYM) and low in adrenocortical carcinoma (ACC), cervical squamous cell carcinoma and endocervical adenocarcinoma (CESC), KICH, LUSC, ovarian serous cystadenocarcinoma (OV), UCEC, uterine carcinosarcoma (UCS) compared to normal tissues (Figure 1B). Interestingly, we found that TMEM200A was significantly upregulated in GC tissues compared to both adjacent and normal tissues.

TMEM200A is significantly highly expressed in GC and has diagnostic value

After comparison, we further confirmed that the expression of TMEM200A in 375 GC samples was significantly higher than that in 32 adjacent tissues in the TCGA-STAD dataset ($p < 0.01$) (Figure 2A). Moreover, the expression of TMEM200A in 413 GC tissues was also significantly higher than that in 174 normal tissues ($p < 0.01$) (Figure 2B). Subsequently, the TCGA dataset of 27 paired GC and adjacent tissues ($p < 0.01$) (Figure 2C) and the GSE54129 ($p < 0.05$) (Figure 2D) and GEE66229 ($p < 0.01$) (Figure 2E) datasets also found that TMEM200A was significantly elevated in GC. ROC analysis revealed that

TABLE 1 Clinicopathologic characteristics of GC patients in TCGA-STAD and GSE15459 datasets.

Characteristics	TCGA-STAD (N = 350) N (%)	GSE15459 (N = 192) N (%)
Alive status		
Alive	204 (58.29)	97 (50.52)
Dead	146 (41.71)	95 (49.48)
Gender		
Female	124 (35.43)	67 (34.9)
Male	226 (64.57)	125 (65.1)
Age		
≥55	289 (83.29)	152 (79.17)
<55	58 (16.71)	40 (20.83)
Unkown	3	0
Stage		
I	46 (13.14)	31 (16.15)
II	110 (31.43)	29 (15.1)
III	145 (41.43)	72 (37.5)
IV	35 (10)	60 (31.25)
Unkown	14 (4)	0
Subtype		
Invasive	—	51 (26.56)
Metabolic	—	40 (20.83)
Proliferative	—	70 (36.46)
Unstable	—	31 (16.15)
Laurenclassification		
Diffuse	—	75 (39.06)
Intestinal	—	99 (51.56)
Mixed	—	18 (9.38)
Grade		
G1	9 (2.57)	—
G2	125 (35.71)	—
G3	207 (59.14)	—
Unkown	9 (2.57)	—
M stage		
M0	312 (89.14)	—
M1	23 (6.57)	—
Unkown	15 (4.29)	—
N stage		
N0	103 (29.43)	—
N1	93 (26.57)	—
N2	72 (20.57)	—
N3	71 (20.29)	—
Unkown	11 (3.14)	—
T stage		
T1	16 (4.57)	—
T2	74 (21.14)	—
T3	161 (46)	—
T4	95 (27.14)	—
Unkown	4 (1.14)	—

(Continued in next column)

TABLE 1 (*Continued*) Clinicopathologic characteristics of GC patients in TCGA-STAD and GSE15459 datasets.

TMEM200A had a strong value in the diagnosis of GC. The AUC of TMEM200A in TCGA-STAD, TCGA-STAD paired samples, TCGA-GTEx dataset, GSE54129 and GSE66229 dataset were 0.803, 0.730, 0.875, 0.580, and 0.654 (Figure 2F). These results indicated that TMEM200A was abnormally upregulated in GC.

Correlation between TMEM200A and the clinical characteristics of GC patients

Table 1 summarized the clinical characteristics of all GC patients in the TCGA-STAD and GSE15459 data sets. As shown in Figures 3A–G, highly expressed TMEM200A is distributed in dead patients (TCGA-STAD, alive vs. dead, $p < 0.05$) (GSE15459, alive vs. dead, $p < 0.001$) and female patients (GSE15459, female vs. male, $p < 0.05$). Furthermore, the expression of TMEM200A tends to increase with increasing clinical stage (TCGA-STAD, stage I vs. stage II vs. stage III vs. stage IV, $p < 0.05$) and T stage (TCGA-STAD, T1 vs. T2 vs. T3 vs. T4, $p < 0.001$). The distribution of TMEM200A expression varies between Lauren-classification and subtypes, with the highest expression in the diffuse and invasive types of GC. These results suggested that the high expression of TMEM200A appears to accelerate the progression of GC and contribute to its more aggressive nature.

Upregulated TMEM200A has GC prognostic value

In the TCGA-STAD cohort ($n = 309$), the calculation of the Kaplan-Meier method showed that patients with GC with high expression of TMEM200A had significantly lower OS than those with low expression of TMEM200A ($p = 0.012$) (Figure 4A). Univariable/multifactor Cox regression analysis illustrates that TMEM200A was an independent risk factor for OS in GC patients (HR = 1.226, 95%CI = 1.062–1.416, $p = 0.005$) (Figure 4C) (Table 2). Based on the results of multifactor Cox analysis, we selected factors with p less than 0.05 to construct a nomogram prediction model for predicting the survival rate of

TABLE 2 Results of a univariable/multivariate Cox regression analysis based on the TCGA-STAD dataset.

	Univariate cox regression		Multivariate cox regression	
Factors	**HR (95%CI)**	***p*-value**	**HR (95%CI)**	***p*-value**
TMEM200A	1.244 (1.082–1.431)	0.002	1.226 (1.062–1.416)	0.005
Age	1.021 (1.004–1.040)	0.017	1.027 (1.009–1.046)	0.004
Stage	1.474 (1.191–1.825)	<0.001	1.514 (1.202–1.908)	<0.001
Grade	1.377 (0.974–1.946)	0.070	1.345 (0.951–.900)	0.093
M Stage	1.675 (0.877–3.200)	0.118	—	—
N Stage	1.308 (1.118–1.530)	<0.001	—	—
T Stage	1.299 (1.040–1.622)	0.021	—	—
Gender	1.464 (0.998–2.147)	0.051	1.472 (0.999–2.169)	>0.05

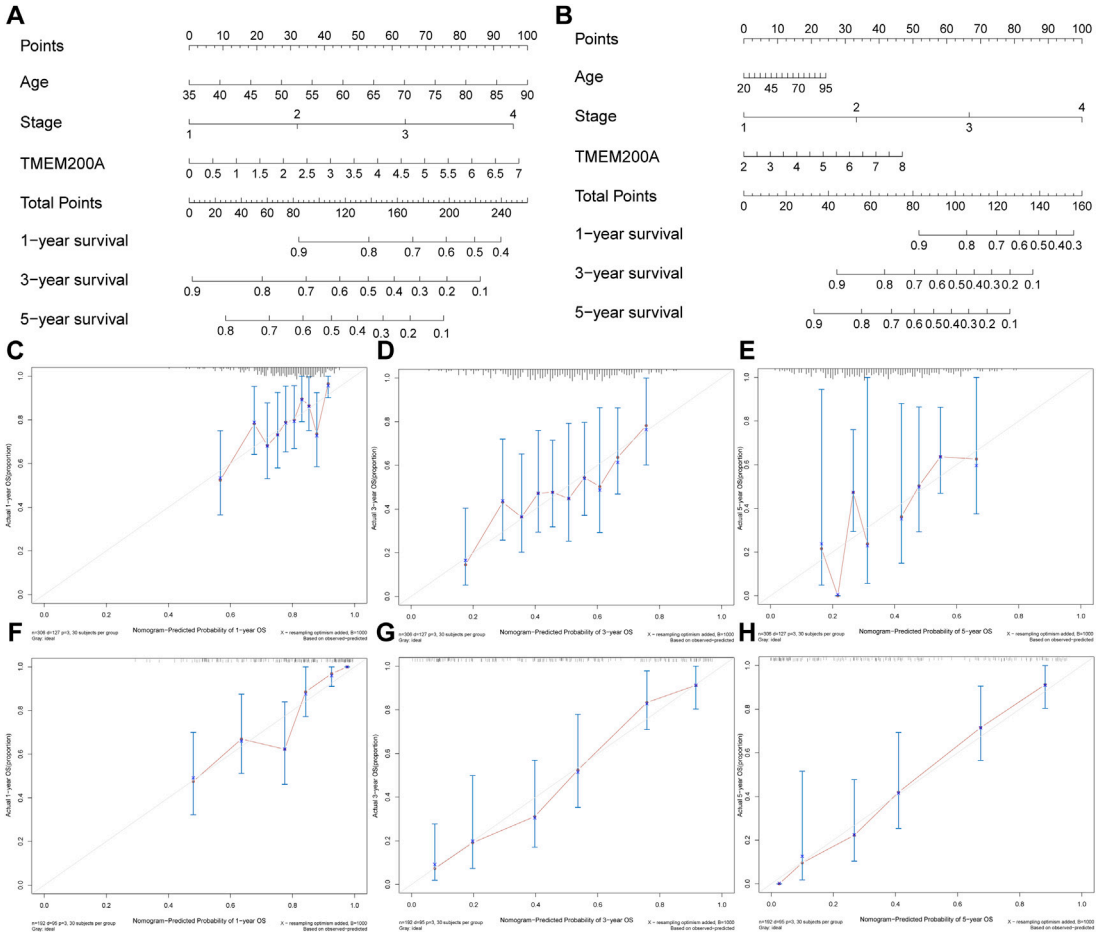

FIGURE 5
Nomogram plots of combining TMEM200A and clinical features evaluated survival in GC. **(A)** Nomogram for predicting OS in TCGA-STAD dataset. **(B)** Nomogram for predicting OS in the GSE15459 dataset. **(C–E)** The calibration curve of the nomogram for one, three, and 5 years of OS prediction in TCGA-STAD dataset. **(F–H)** The calibration curve of the nomogram for one, three, and 5 years of OS prediction in GSE15459 dataset.

TABLE 3 Results of a univariable/multivariate Cox regression analysis based on the GSE15459 dataset.

	Univariate cox regression		Multivariate cox regression	
Factors	**HR (95%CI)**	***p*-value**	**HR (95%CI)**	***p*-value**
TMEM200A	1.197 (1.010–1.420)	0.038	1.297 (1.095–1.536)	0.003
Age	0.999 (0.984–1.016)	0.969	1.011 (0.996–1.026)	0.154
Stage	2.790 (2.140–3.635)	<0.001	3.031 (2.288–4.017)	<0.001
Gender	1.402 (0.908–2.165)	0.127	—	—

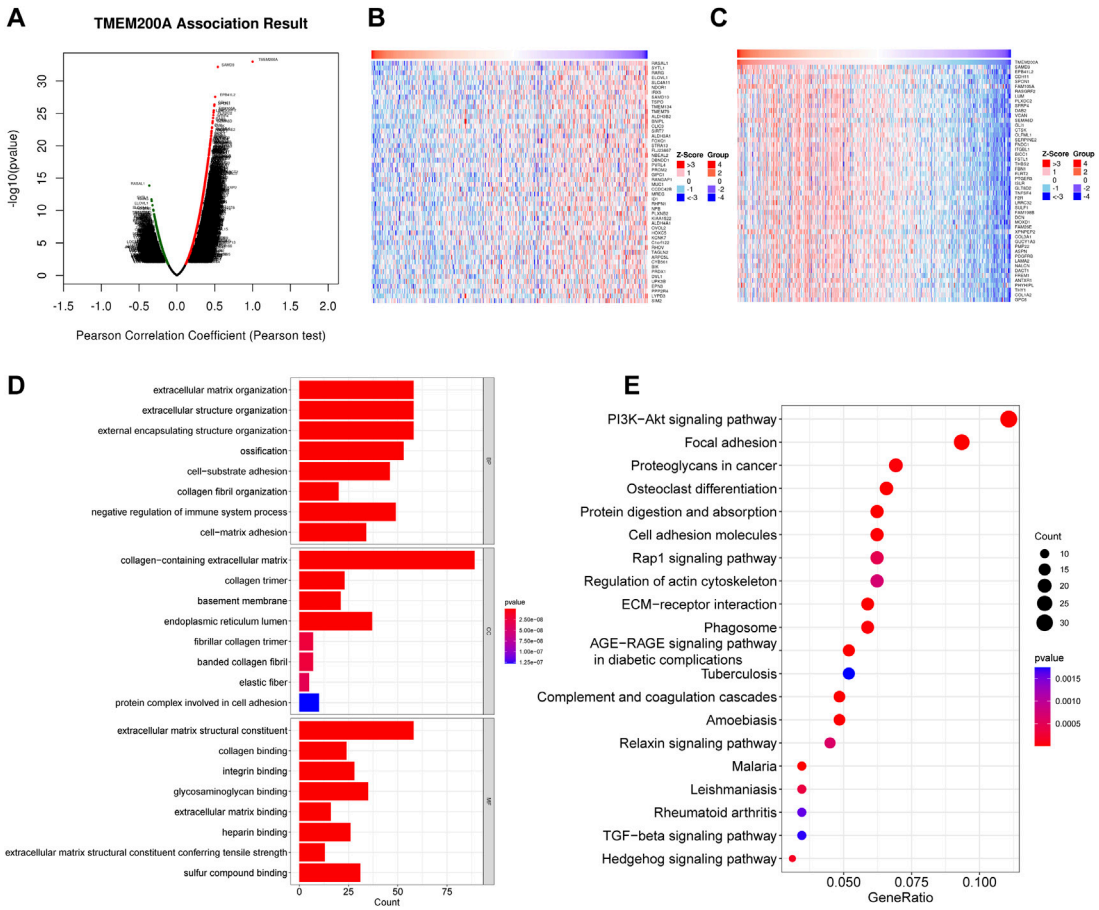

FIGURE 6
Co-expression of genes and functional enrichment of TMEM200A. **(A)** Volcano map of 8492 co-expressed genes of TMEM200A. **(B)** Heat map of the top 50 TMEM200A negatively related genes. **(C)** Heat map of the top 50 TMEM200A positively related genes. **(D)** GO enrichment analysis. **(E)** KEGG enrichment analysis.

GC patients at 1, 3 and 5 years. The C-index of the model is 0.635 (95% CI = 0.608–0.662) (Figure 5A), indicating good predictive performance. The calibration curves show a good fit between the probability of predicting OS at 1, 3 and 5 years in GC patients and the actual probability of occurrence on the column graphs (Figures 5C–E).

Furthermore, we further validated the effect of TMEM200A on the survival of patients with GC by analyzing the GSE15459 dataset (n = 192). Similarly, GC patients with high TMEM200A expression have lower OS than those with low TMEM200A expression (p = 0.044) (Figure 4B). Meanwhile, TMEM200A is an independent risk factor for the prognosis of patients with GC

(HR = 1.297, 95%CI = 1.095–1.536, p = 0.003) (Figure 4D) (Table 3). We also used TMEM200A in conjunction with age and stage to build the nomogram prediction model (Figure 5B), which also had excellent prediction performance (C-index = 0.766, 95%CI = 0.745–0.787) (Figures 5F–H). In conclusion, our study showed that upregulation of TMEM200A expression promoted GC progression and shortened the OS of GC patients.

Co-expression gene analysis of TMEM200A

LinkedOmics identified a total of 8492 TMEM200A related genes (Figure 6A) of which 3,074 were negatively related (Figure 6B) and 5,418 were positively related (Figure 6C). The total number of TMEM200A positively correlated genes with correlation coefficients greater than or equal to 0.3 was 705. In general, co-expressed genes have similar biological functions. The results of GO analysis suggested that the co-expressed genes of TMEM200A might be part of the cytoskeleton and were associated with ECM and adhesion (Figure 6D). KEGG pathway enrichment analysis revealed that co-expressed genes of TMEM200A could be involved in the P13K-Akt signaling pathway, focal adhesion, cell adhesion molecules, Rap1 signaling pathway, regulation of actin cytoskeleton, ECM-receptor interaction, phagosome, relaxin signaling pathway, TGF-beta signaling pathway, and Hedgehog signaling pathway (Figure 6E). These results suggested that TMEM200A may promote the progression of GC through these pathways.

GSEA

GSEA unraveled that extracellular matrix assembly, FC receptor signaling pathway, phagocytic vesicle, extracellular matrix structural constituent, fibronectin binding, transforming growth factor beta binding, B cell receptor signaling pathway, cell adhesion molecules CAMs, ECM receptor interaction, focal adhesion, T cell receptor signaling pathway, TGF-beta signaling pathway and ubiquitin-mediated proteolysis (Figures 7A, B), indicating that elevated TMEM200A could participate in the occurrence and progression of GC through these pathway. This is similar to the results of the co-expression gene enrichment analysis of TMEM200A, suggesting that TMEM200A may be an important adhesion molecule in extracellular information traffic and may be relevant to tumor immunity.

TMEM200A is associated with immune cell infiltration in GC

We found a positive correlation between TMEM200A and $CD4^+$ T cells (r = 0.284, p = 3.18e−08), macrophages (r = 0.337, p = 2.88e−11), neutrophils (r = 0.179, p = 5.36e−04) and DC (r = 0.278, p = 5.37e−08) based on TIMER (Figure 8A). Furthermore, 23 of the 28 immune cell subtypes could be regulated by TMEM200A expression in GC tissues (Figure 8B). In addition, we found that TMEM200A is positively correlated with 17 common surface markers of the immune cell (Table 4). Interestingly, TMEM200A was positively correlated with the expression of 12 immune checkpoints in GC (Figure 8C), such as PDCD1, TIGIT, LAG3, CD40, etc. The above results suggested that TMEM200A probably modulated the tumor immune microenvironment (TIME) of GC, promoted the infiltration of immune cells and upregulates the expression of various immune checkpoints, which helped GC cells to immune escape and thus promoted the progression of GC.

Drug sensitivity analysis

After estimated the IC50 of 138 drugs in TCGA-STAD patients, we discovered that GC patients with high TMEM200A expression might gradually tolerate for AKT.inhibitor.VIII, Afatinib, Gefitinib, Lapatinib, and Metformin, while All-trans Retinoic Acid, Cytarabine, Nilotinib, and Crizotinib may have better therapeutic effects in these patients (Figure 9).

DNA methylation sites of TMEM200A

Six TMEM200A methylation sites were identified by using MethSury tool (Figure 10A), all of which had high methylation levels. Hypermethylation at three of these methylation sites was positively associated with a poor prognosis in patients with GC (Figures 10B–D). These results suggested that methylated of TMEM200A may be a potential method to inhibit the progression of GC.

Discussion

Several members of the TMEM family gene have been shown to be associated with the progression of digestive cancers. For example, interference with TMEM45B expression inhibited the proliferation migration and invasive ability of GC cells (27). TMEM106C is highly expressed in LIHC and suppresses LIHC proliferation and metastasis after knockdown (28). High TMEM180 expression have been shown to predict low survival in COAD (29). Therefore, the intrinsic link between the members of the TMEM family gene and the tumors of digestive system deserves further exploration.

To the best of our knowledge, the expression and biological function of TMEM200A in GC and the relationship with TIME have not been reported. In this study, we found that TMEM200A was upregulated in GC tissues and shortened the OS of GC

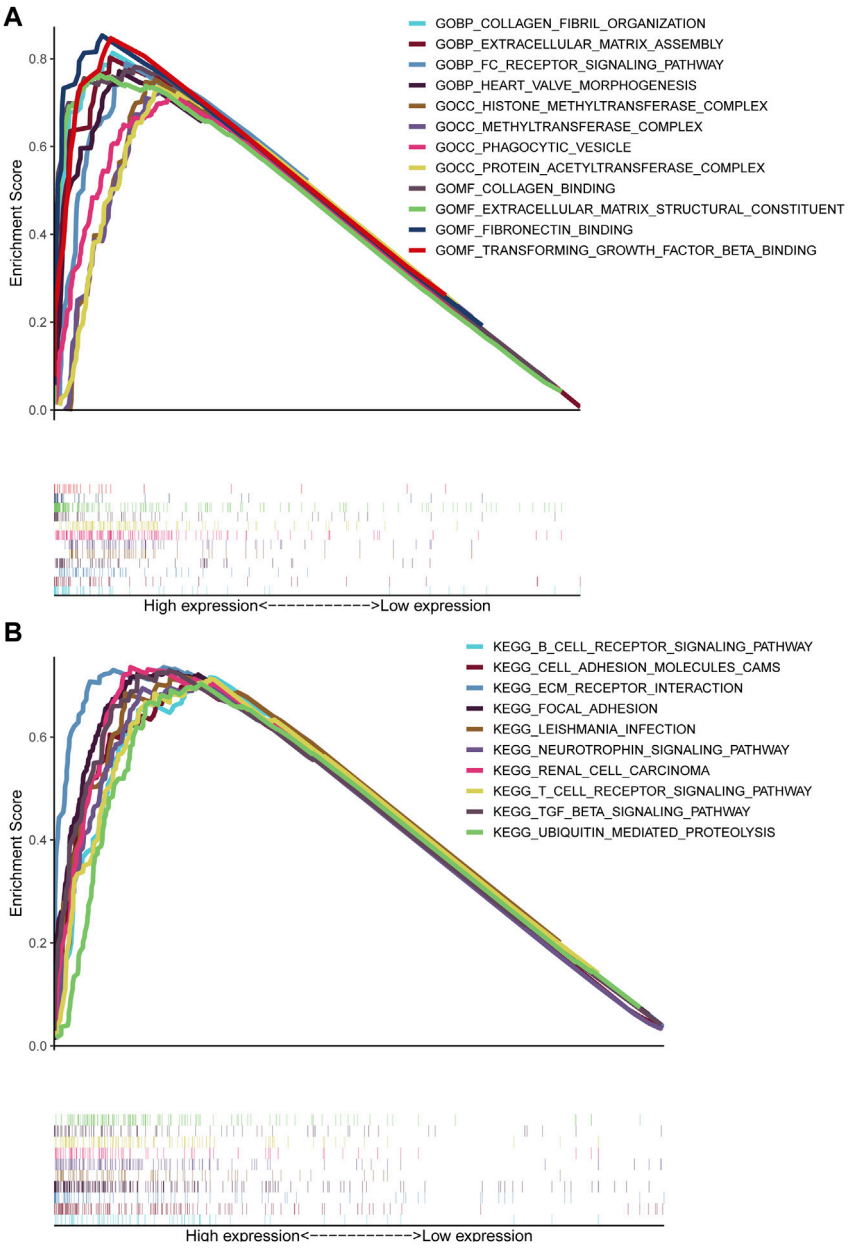

FIGURE 7
Results of the GSEA analysis of TMEM200A. **(A)** GSEA of GO. **(B)** GSEA of KEGG.

patients by calculating multiple data sets. Meanwhile, we also believe that the expression of TMEM200A increased with increasing staging. More importantly, univariable/multifactor cox regression analysis based on two independent data sets showed that TMEM200A was an independent risk factor for OS in patients with GC. Based on the results of multifactor Cox regression analysis, we constructed a nomogram prediction model using TMEM200A in combination with the clinical characteristics of GC patients, which had excellent predictive power for 1-year, 3-year and 5-year survival rates of GC patients. It is reasonable to assume that high expression TMEM200A promotes the progression of GC and is a valid prognostic indicator of GC. Therefore, it is necessary to further clarify the pathways through which it can exert its cancer-promoting effects.

Enrichment analysis of TMEM200A co-expressed genes revealed that TMEM200A could act as a cell membrane adhesion molecule possibly involved in the P13K-AKT pathway, focal adhesion, cell adhesion molecules,

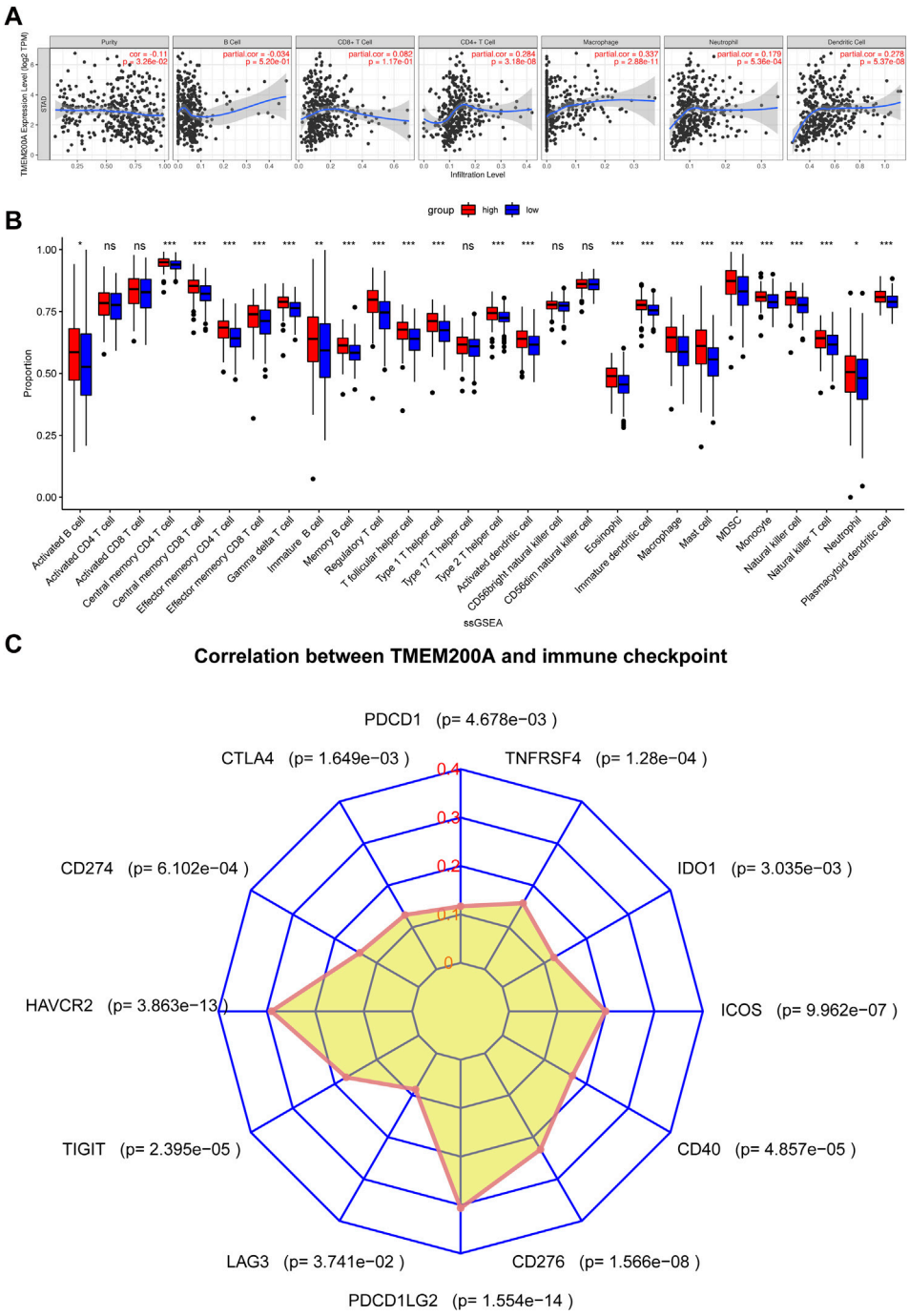

FIGURE 8
Results of TMEM200A and tumor immunological correlation analysis. **(A)** Correlation analysis of TMEM200A with the level of infiltration of six types of immune cells in the TIMER database. **(B)** Correlation analysis of TMEM200A with 28 immune cell subtypes calculated using the ssGSEA algorithm. **(C)** Correlation analysis of TMEM200A and immune checkpoint expression.

Rap1 signaling pathway, regulation of actin cytoskeleton, ECM-receptor interaction, phagosome, relaxin signaling pathway, TGF-beta signaling pathway, and Hedgehog signaling pathway. It has been shown (30) that the P13-AKT pathway can promote GC cells proliferation and invasion. Rap1, which has a high sequence similarity to the Ras oncoprotein, is an important Ras regulator and has been shown to be highly associated with cell adhesion and integrin function (31).

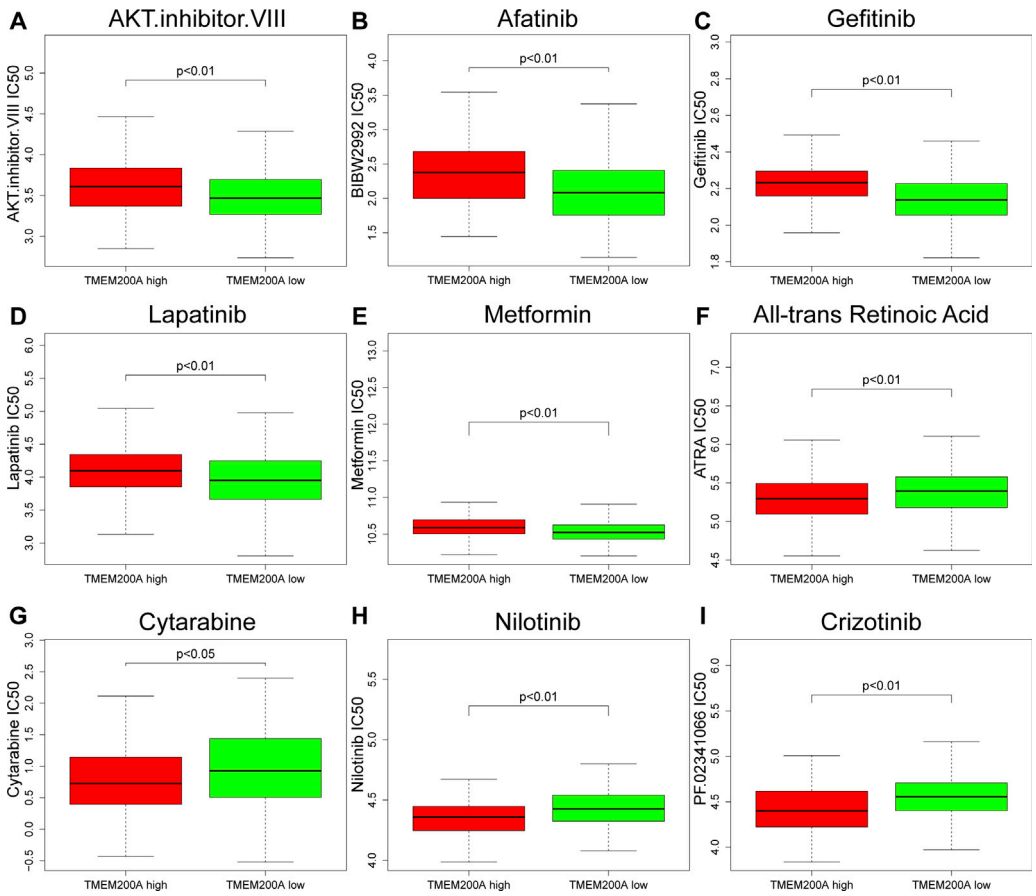

FIGURE 9
Correlation between the expression level of TMEM200A and the IC50 of chemotherapy drugs. **(A)** AKT.inhibitor.VIII, **(B)** Afatinib, **(C)** Gefitinib, **(D)** Lapatinib, **(E)** Metformin, **(F)** All-trans Retinoic Acid, **(G)** Cytarabine, **(H)** Nilotinib, and **(I)** Crizotinib.

Relaxin signaling promotes the proliferation, migration, invasion, and adhesion of prostate cancer cells (32) and is associated with ECM remodeling (33). The TGF-beta pathway is involved in the construction of an immunosuppressive microenvironment that assists in the immune escape of tumor cells (34). Organoid models of GC confirmed (35) that the Hedgehog signaling pathway mediates PD-L1 expression in GC cells *via* mTOR. Focal adhesion is part of the integrin adhesion complex and plays an important role in cell migration, cell cycle and cell proliferation (36). Similarly, cell migration is regulated by the cytoskeleton (37). In addition, it has been shown (38) that ECM is a key mediator of the metastatic spread of cancer cells. Overall, these findings demonstrated that TMEM200A may act as an adhesion molecule and be an accomplice in increased aggressiveness and metastasis of GC cells. These results were also corroborated by the GSEA results. Interestingly, we observed an additional enrichment of GSEA for the transforming growth factor beta binding, the B cell receptor signaling pathway, and the T cell receptor signaling pathway, suggesting that TMEM200A may be closely associated with the TIME.

The TIME, which includes tumor cells, immune cells and cytokines (39), has long been implicated in the progression, metastasis and recurrence of cancer (40). Our study found a positive correlation between TMEM200A and $CD4^+$ T cell infiltration, macrophages, neutrophils, and DCs. $CD4^+$ T cells are known to function through cytokines that help immune cells such as $CD8^+$ T. However, $CD4^+CD25^+$ Treg cells, a subpopulation of $CD4^+$ T cells, suppress effector T cells and thereby impair anti-tumor immunity (41, 42). Tumor-associated macrophages (TAM) are key regulators of GC progression (43). Especially, M2 TAMs promote GC angiogenesis and participate in the construction of TIME (43). Neutrophils are the main line of defense against exogenous agents, but their release of neutrophil extracellular traps (NETs) is one of the key regulatory players in promoting tumor recurrence and metastasis (44). In addition, we found that TMEM200A high expression samples were infiltrated by 23 more immune cell

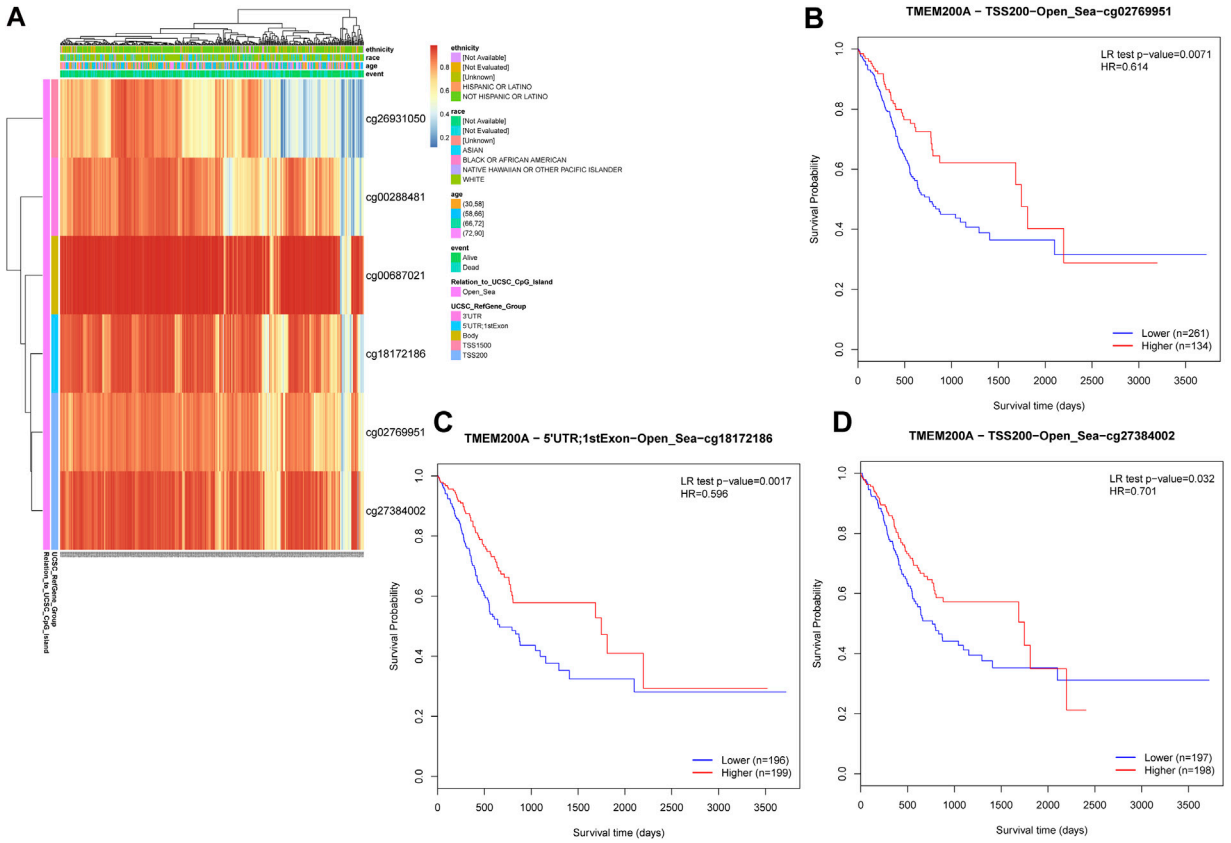

FIGURE 10
DNA methylation sites of TMEM200A. **(A)** Red to blue means that the methylation level goes from high to low. The different colored boxes represent ethnicity, race, age, event, relation to UCSC CpG Island, and UCSC RefGene Group. **(B)** The Kaplan-Meier curve of TMEM200A-TSS200-Open_Sea-cg02769951 in patients with GC. **(C)** The Kaplan-Meier curve of TMEM200A-5′UTR; 1stExon-Open_Sea-cg18172186 in patients with GC. **(D)** The Kaplan-Meier curve of TMEM200A-TSS200-Open_Sea-cg27384002 in patients with GC.

subtypes, which was also confirmed by correlation analysis of immune cell surface markers with TMEM200A. Collectively, these results suggested that TMEM200A is closely related to immune cells and likely induces immune cell infiltration that affects the prognosis of patients with GC.

Immune checkpoints are involved in creating an immunosuppressive microenvironment that promotes tumor immune escape. Our study revealed that TMEM200A is positively correlated with the expression of 12 common immune checkpoints, with HAVCR2, TIGIT, PDCD1LG2, CD276, and ICOS being the most significant. HAVCR2 (TIM-3) and TIGIT are co-inhibitory receptors expressed on T cells, $Foxp3^+$ Treg cells, macrophages and DC cells that can cause T cell failure (45). PDCD1LG2 (PD-L2), the second ligand of PD-1, inhibits antitumor immunity by suppressing T-cell activation (46). It has been shown (47), that CD276 expression on the surface of tumor stem cells can promote their evasion of immune responses and epithelial mesenchymal transformation. T cells expressing ICOS can inhibit the proliferation of $CD8^+$ T cells (48). These results demonstrated that although TMEM200A may induce immune cell infiltration in GC tissues. On the other hand, TMEM200A may inhibit antitumor immunity by up-regulating immune checkpoints.

Chemotherapy is a postoperative adjuvant treatment for patients undergoing surgery for GC and a dividend treatment for patients with advanced disease (5), but the ensuing resistance of tumor cells is also a cause of metastasis and recurrence (49). This study found that GC patients with high TMEM200A expression may be sensitive to All-trans Retinoic Acid, Cytarabine, Nilotinib, and Crizotinib, but may be resistant to AKT.inhibitor.VIII, Afatinib, Gefitinib, Lapatinib, and Metformin. These findings may help reduce drug resistance and improve the prognosis of GC patients. DNA methylation is considered to be one of the causes of tumorigenesis (50). As DNA methylation is reversible, regulation of DNA methylation has been suggested to be a promising direction for cancer therapy. Finally, we identified three TMEM200A methylation sites that were negatively associated with the prognosis of GC

TABLE 4 Results of correlation analysis of TMEM200A and immune cell surface markers.

Cell type	Marker	Cor	*p*-value
$CD8^+$T cell	CD8A	0.174	**7.28E-04**
	CD8B	0.164	**1.45E-03**
$CD4^+$T cell	CD4	0.37	**1.24E-13**
	CD40LG	0.276	**5.66E-08**
	CXCR4	0.287	**1.62E-08**
T cell (general)	CD2	0.254	**6.17E-07**
	CD3E	0.199	**1.09E-04**
	CD3D	0.184	**3.44E-04**
	CD6	0.25	**9.63E-07**
	SH2D1A	0.249	**1.09E-06**
	TRAT1	0.225	**1.07E-05**
	CD3G	0.24	**2.66E-06**
B cell	CD19	0.123	**1.76E-02**
	CD79A	0.136	**8.51E-03**
Monocyte	CD86	0.371	**1.12E-13**
	CSF1R	0.392	**3.19E-15**
TAM	CD68	0.057	2.71E-01
	CCL2	0.287	**1.51E-08**
	IL10	0.287	**1.47E-08**
M1 macrophage	IRF5	0.183	**3.79E-04**
	PTGS2	0.196	**1.37E-04**
M2 macrophage	CD163	0.385	**1.02E-14**
	VSIG4	0.347	**4.82E-12**
	MS4A4A	0.378	**3.57E-14**
Neutrophil	S100A12	0.028	5.91E-01
	CEACAM3	0.132	**1.06E-02**
	CCR7	0.208	**4.74E-05**
	FPR1	0.31	**9.07E-10**
	SIGLEC5	0.251	**8.12E-07**
	CSF3R	0.266	**1.78E-07**
	FCAR	0.198	**1.12E-04**
	FCGR3B	0.136	**8.19E-03**
Nature killer cell	KIR2DL1	0.078	1.31E-01
	KIR2DL3	0.118	**2.25E-02**
	KIR2DL4	−0.017	7.38E-01
	KIR3DL1	0.101	**4.97E-02**
	KIR3DL2	0.063	2.24E-01
	KIR3DL3	−0.083	1.11E-01
	XCL1	0.122	**1.85E-02**
	XCL2	0.139	**7.19E-03**
	NCR1	0.055	2.84E-01
DC	ITGAX	0.375	**5.38E-14**
	HLA-DPA1	0.18	**4.58E-04**
	HLA-DRA	0.2	**9.68E-05**
	HLA-DQB1	0.105	**4.23E-02**
	HLA-DPB1	0.15	**3.64E-03**
	CCL13	0.225	**1.09E-05**
	HSD11B1	0.407	**2.23E-16**
Th1	TBX21	0.167	**1.18E-03**
	TNF	0.063	2.20E-01
	STAT1	0.196	**1.29E-04**
	STAT4	0.269	**1.25E-07**
Th2	IL13	0.131	**1.11E-02**
	GATA3	0.126	**1.44E-02**
	STAT5A	0.325	**1.11E-10**
	STAT6	0.281	**3.14E-08**
Tfh	VSIG4	0.347	**4.82E-12**
Th17	STAT3	0.302	**2.32E-09**
Treg	TGFB1	0.324	**1.24E-10**
	STAT5B	0.455	**1.57E-20**
	CCR8	0.371	**1.17E-13**
	FOXP3	0.292	**8.44E-09**
T cell exhaustion	TIGIT	0.216	**2.40E-05**
	GZMB	0.113	**2.90E-02**
	TOX	0.302	**2.33E-09**
	HAVCR2	0.363	**3.86E-13**
	LAG3	0.108	**3.74E-02**
	CTLA4	0.162	**1.65E-03**
	PDCD1	0.146	**4.68E-03**

(Continued in next column)

TABLE 4 (*Continued*) Results of correlation analysis of TMEM200A and immune cell surface markers.

The meaning of the bold values is p<0.05.

patients. Increasing the degree of methylation of these sites may provide new ideas for GC therapy.

Conclusion

In conclusion, we found that TMEM200A was upregulated in GC and that high TMEM200A expression predicted poor prognosis. TMEM200A may play a role as an adhesion molecule regulating the GC immune microenvironment and promoting the invasive metastasis of GC cells. In addition, TMEM200A may upregulate immune checkpoints to help GC cells evade anti-tumor immune responses. Our study elucidated the potential role of TMEM200A in GC for the first time. We believed that TMEM200A deserves further study.

Data availability statement

Publicly available datasets were analyzed in this study. This data can be found here: All data generated or analysed during this study are available in the TCGA (https://portal.gdc.cancer.gov) and GEO (https://www.ncbi.nlm.nih.gov/geo/). The names of the repositories and accession number be found in the article/Materials and Methods, TCGA-STAD GSE54129, GSE66229, and GSE15459.

Author contributions

HD analyzed the data and wrote the manuscript. TL refined the language and logic. FW, WH, and XX revised the manuscript. YZ is the corresponding author and provided ideas and study design. All the authors contributed directly, substantially, and intellectually to this manuscript and approved the submitted version.

Funding

This work was supported by National Natural Science Foundation of China (82060800), the Science and Technique Innovation Project of Lanzhou University Second Hospital (CY2022-MS11), the Doctoral Supervisors Research Fund of Lanzhou University Second Hospital (bdkyjj-04), and Gansu Provincial Science Foundation for Young Scholars of China (21JR1RA161, 21JR1RA149, and 21JR11RA114).

Conflict of interest

The authors declare that the research was conducted in the absence of any commercial or financial relationships that could be construed as a potential conflict of interest.

References

1. Bray F, Ferlay J, Soerjomataram I, Siegel RL, Torre LA, Jemal A. Global cancer statistics 2018: GLOBOCAN estimates of incidence and mortality worldwide for 36 cancers in 185 countries. *CA Cancer J Clin* (2018) 68(6):394–424. doi:10.3322/caac.21492

2. Sung H, Ferlay J, Siegel RL, Laversanne M, Soerjomataram I, Jemal A, et al. Global cancer statistics 2020: GLOBOCAN estimates of incidence and mortality worldwide for 36 cancers in 185 countries. *CA Cancer J Clin* (2021) 71(3):209–49. doi:10.3322/caac.21660

3. Smyth EC, Nilsson M, Grabsch HI, van Grieken NC, Lordick F. Gastric cancer. *Lancet* (2020) 396(10251):635–48. doi:10.1016/S0140-6736(20)31288-5

4. Bang YJ, Van Cutsem E, Feyereislova A, Chung HC, Shen L, Sawaki A, et al. Trastuzumab in combination with chemotherapy versus chemotherapy alone for treatment of HER2-positive advanced gastric or gastro-oesophageal junction cancer (ToGA): A phase 3, open-label, randomised controlled trial. *Lancet* (2010) 376(9742):687–97. doi:10.1016/S0140-6736(10)61121-X

5. Lordick F, Carneiro F, Cascinu S, Fleitas T, Haustermans K, Piessen G, et al. Gastric cancer: ESMO clinical practice guideline for diagnosis, treatment and follow-up. *Ann Oncol* (2022) 33(10):1005–20. doi:10.1016/j.annonc.2022.07.004

6. Zhao Y, Zhang K, Pan H, Wang Y, Zhou X, Xiang Y, et al. Genetic analysis of six transmembrane protein family genes in Parkinson's disease in a large Chinese cohort. *Front Aging Neurosci* (2022) 14:889057. doi:10.3389/fnagi.2022.889057

7. Marx S, Dal Maso T, Chen JW, Bury M, Wouters J, Michiels C, et al. Transmembrane (TMEM) protein family members: Poorly characterized even if essential for the metastatic process. *Semin Cancer Biol* (2020) 60:96–106. doi:10.1016/j.semcancer.2019.08.018

8. Zhuang J, Huang Y, Zheng W, Yang S, Zhu G, Wang J, et al. TMEM100 expression suppresses metastasis and enhances sensitivity to chemotherapy in gastric cancer. *Biol Chem* (2020) 401(2):285–96. doi:10.1515/hsz-2019-0161

9. Schmit K, Michiels C. TMEM proteins in cancer: A review. *Front Pharmacol* (2018) 9:1345. doi:10.3389/fphar.2018.01345

10. Zhang S, Dai H, Li W, Wang R, Wu H, Shen M, et al. TMEM116 is required for lung cancer cell motility and metastasis through PDK1 signaling pathway. *Cell Death Dis* (2021) 12(12):1086. doi:10.1038/s41419-021-04369-1

11. Koteluk O, Bielicka A, Lemańska Ż, Jóźwiak K, Klawiter W, Mackiewicz A, et al. The landscape of transmembrane protein family members in head and neck cancers: Their biological role and diagnostic utility. *Cancers (Basel)* (2021) 13(19):4737. doi:10.3390/cancers13194737

12. Lundbäck V, Kulyté A, Arner P, Strawbridge RJ, Dahlman I. Genome-Wide association study of diabetogenic adipose morphology in the GENetics of adipocyte lipolysis (GENiAL) cohort. *[J] Cell* (2020) 9(5):1085. doi:10.3390/cells9051085

13. Tan M, Schaffalitzky De Muckadell OB, Jøergensen MT. Gene expression network analysis of precursor lesions in familial pancreatic cancer. *J Pancreat Cancer* (2020) 6(1):73–84. doi:10.1089/pancan.2020.0007

14. Vieira AR, de Carvalho FM, Johnson L, DeVos L, Swailes AL, Weber ML, et al. Fine mapping of 6q23.1 identifies TULP4 as contributing to clefts. *Cleft Palate Craniofac J* (2015) 52(2):128–34. doi:10.1597/13-023

15. Nie L, Zhang Y, You Y, Lin C, Li Q, Deng W, et al. The signature based on seven genomic instability-related genes could predict the prognosis of acute myeloid leukemia patients. *Hematology* (2022) 27(1):840–8. doi:10.1080/16078454.2022.2107970

16. Zhang X, Zheng P, Li Z, Gao S, Liu G. The somatic mutation landscape and RNA prognostic markers in stomach adenocarcinoma. *Onco Targets Ther* (2020) 13:7735–46. doi:10.2147/OTT.S263733

17. Li T, Fan J, Wang B, Traugh N, Chen Q, Liu JS, et al. Timer: A web server for comprehensive analysis of tumor-infiltrating immune cells. *Cancer Res* (2017) 77(21):e108–10. doi:10.1158/0008-5472.CAN-17-0307

18. Tang Z, Li C, Kang B, Gao G, Li C, Zhang Z. Gepia: A web server for cancer and normal gene expression profiling and interactive analyses. *Nucleic Acids Res* (2017) 45(W1):W98–W102. doi:10.1093/nar/gkx247

19. Goldman MJ, Craft B, Hastie M, Repečka K, McDade F, Kamath A, et al. Visualizing and interpreting cancer genomics data via the Xena platform. *Nat Biotechnol* (2020) 38(6):675–8. doi:10.1038/s41587-020-0546-8

20. Oh SC, Sohn BH, Cheong JH, Kim SB, Lee JE, Park KC, et al. Clinical and genomic landscape of gastric cancer with a mesenchymal phenotype. *Nat Commun* (2018) 9(1):1777. doi:10.1038/s41467-018-04179-8

21. Ooi CH, Ivanova T, Wu J, Lee M, Tan IB, Tao J, et al. Oncogenic pathway combinations predict clinical prognosis in gastric cancer. *Plos Genet* (2009) 5(10):e1000676. doi:10.1371/journal.pgen.1000676

22. Vasaikar SV, Straub P, Wang J, Zhang B. LinkedOmics: Analyzing multi-omics data within and across 32 cancer types. *Nucleic Acids Res* (2018) 46(D1):D956–d963. doi:10.1093/nar/gkx1090

23. Yu G, Wang LG, Han Y, He QY. clusterProfiler: an R package for comparing biological themes among gene clusters. *Omics* (2012) 16(5):284–7. doi:10.1089/omi.2011.0118

24. Subramanian A, Tamayo P, Mootha VK, Mukherjee S, Ebert BL, Gillette MA, et al. Gene set enrichment analysis: A knowledge-based approach for interpreting genome-wide expression profiles. *Proc Natl Acad Sci U S A* (2005) 102(43):15545–50. doi:10.1073/pnas.0506580102

25. Hänzelmann S, Castelo R, Guinney J. Gsva: Gene set variation analysis for microarray and RNA-seq data. *BMC Bioinformatics* (2013) 14:7. doi:10.1186/1471-2105-14-7

26. Modhukur V, Iljasenko T, Metsalu T, Lokk K, Laisk-Podar T, Vilo J. MethSurv: A web tool to perform multivariable survival analysis using DNA methylation data. *Epigenomics* (2018) 10(3):277–88. doi:10.2217/epi-2017-0118

27. Shen K, Yu W, Yu Y, Liu X, Cui X. Knockdown of TMEM45B inhibits cell proliferation and invasion in gastric cancer. *Biomed Pharmacother* (2018) 104:576–81. doi:10.1016/j.biopha.2018.05.016

28. Duan J, Qian Y, Fu X, Chen M, Liu K, Liu H, et al. TMEM106C contributes to the malignant characteristics and poor prognosis of hepatocellular carcinoma. *Aging (Albany NY)* (2021) 13(4):5585–606. doi:10.18632/aging.202487

29. Shiraishi T, Ikeda K, Tsukada Y, Nishizawa Y, Sasaki T, Ito M, et al. High expression of TMEM180, a novel tumour marker, is associated with poor survival in stage III colorectal cancer. *BMC Cancer* (2021) 21(1):302. doi:10.1186/s12885-021-08046-6

30. Chen ZF, Wang J, Yu Y, Wei W. MicroRNA-936 promotes proliferation and invasion of gastric cancer cells by down-regulating FGF2 expression and activating

P13K/Akt signaling pathway. *Eur Rev Med Pharmacol Sci* (2020) 24(12):6707–15. doi:10.26355/eurrev_202006_21658

31. Shah S, Brock EJ, Ji K, Mattingly RR. Ras and Rap1: A tale of two GTPases. *Semin Cancer Biol* (2019) 54:29–39. doi:10.1016/j.semcancer.2018.03.005

32. Feng S, Agoulnik IU, Li Z, Han HD, Lopez-Berestein G, Sood A, et al. Relaxin/RXFP1 signaling in prostate cancer progression. *Ann N Y Acad Sci* (2009) 1160: 379–80. doi:10.1111/j.1749-6632.2008.03793.x

33. Ng HH, Shen M, Samuel CS, Schlossmann J, Bennett RG. Relaxin and extracellular matrix remodeling: Mechanisms and signaling pathways. *Mol Cel Endocrinol* (2019) 487:59–65. doi:10.1016/j.mce.2019.01.015

34. Peng D, Fu M, Wang M, Wei Y, Wei X. Targeting TGF-β signal transduction for fibrosis and cancer therapy. *Mol Cancer* (2022) 21(1):104. doi:10.1186/s12943-022-01569-x

35. Koh V, Chakrabarti J, Torvund M, Steele N, Hawkins JA, Ito Y, et al. Hedgehog transcriptional effector GLI mediates mTOR-Induced PD-L1 expression in gastric cancer organoids. *Cancer Lett* (2021) 518:59–71. doi:10.1016/j.canlet.2021.06.007

36. Mishra YG, Manavathi B. Focal adhesion dynamics in cellular function and disease. *Cell Signal* (2021) 85:110046. doi:10.1016/j.cellsig.2021.110046

37. Seetharaman S, Etienne-Manneville S. Cytoskeletal crosstalk in cell migration. *Trends Cel Biol* (2020) 30(9):720–35. doi:10.1016/j.tcb.2020.06.004

38. Gilkes DM, Semenza GL, Wirtz D. Hypoxia and the extracellular matrix: Drivers of tumour metastasis. *Nat Rev Cancer* (2014) 14(6):430–9. doi:10.1038/nrc3726

39. Lv B, Wang Y, Ma D, Cheng W, Liu J, Yong T, et al. Immunotherapy: Reshape the tumor immune microenvironment. *Front Immunol* (2022) 13:844142. doi:10.3389/fimmu.2022.844142

40. Fu T, Dai LJ, Wu SY, Xiao Y, Ma D, Jiang YZ, et al. Spatial architecture of the immune microenvironment orchestrates tumor immunity and therapeutic response. *J Hematol Oncol* (2021) 14(1):98. doi:10.1186/s13045-021-01103-4

41. Granito A, Muratori L, Lalanne C, Quarneti C, Ferri S, Guidi M, et al. Hepatocellular carcinoma in viral and autoimmune liver diseases: Role of $CD4^+$ $CD25^+$ $Foxp3^+$ regulatory T cells in the immune microenvironment [J]. *World J Gastroenterol* (2021) 27(22):2994–3009. doi:10.3748/wjg.v27.i22.2994

42. Shen LS, Wang J, Shen DF, Yuan XL, Dong P, Li MX, et al. $CD4(^+)CD25(^+)$ CD127(low/-) regulatory T cells express Foxp3 and suppress effector T cell proliferation and contribute to gastric cancers progression [J]. *Clin Immunol* (2009) 131(1):109–18. doi:10.1016/j.clim.2008.11.010

43. Gambardella V, Castillo J, Tarazona N, Gimeno-Valiente F, Martínez-Ciarpaglini C, Cabeza-Segura M, et al. The role of tumor-associated macrophages in gastric cancer development and their potential as a therapeutic target. *Cancer Treat Rev* (2020) 86:102015. doi:10.1016/j.ctrv.2020.102015

44. Demkow U. Neutrophil extracellular traps (NETs) in cancer invasion, evasion and metastasis. *Cancers (Basel)* (2021) 13(17):4495. doi:10.3390/cancers13174495

45. Das M, Zhu C, Kuchroo VK. Tim-3 and its role in regulating anti-tumor immunity. *Immunol Rev* (2017) 276(1):97–111. doi:10.1111/imr.12520

46. Latchman Y, Wood CR, Chernova T, Chaudhary D, Borde M, Chernova I, et al. PD-L2 is a second ligand for PD-1 and inhibits T cell activation. *Nat Immunol* (2001) 2(3):261–8. doi:10.1038/85330

47. Wang C, Li Y, Jia L, Kim JK, Li J, Deng P, et al. CD276 expression enables squamous cell carcinoma stem cells to evade immune surveillance. *Cell Stem Cell* (2021) 28(9):1597–613.e7. e7. doi:10.1016/j.stem.2021.04.011

48. Nagase H, Takeoka T, Urakawa S, Morimoto-Okazawa A, Kawashima A, Iwahori K, et al. $ICOS(^+)$ $Foxp3(^+)$ TILs in gastric cancer are prognostic markers and effector regulatory T cells associated with *Helicobacter pylori* [J]. *Int J Cancer* (2017) 140(3):686–95. doi:10.1002/ijc.30475

49. Zhang X, Xie K, Zhou H, Wu Y, Li C, Liu Y, et al. Role of non-coding RNAs and RNA modifiers in cancer therapy resistance. *Mol Cancer* (2020) 19(1):47. doi:10.1186/s12943-020-01171-z

50. Das PM, Singal R. DNA methylation and cancer. *J Clin Oncol* (2004) 22(22): 4632–42. doi:10.1200/JCO.2004.07.151

Glossary

GC gastric cancer
OS overall survival
TMEM transmembrane protein
TMEM200A transmembrane protein 200A
TCGA the cancer genome atlas
GEO gene expression omnibus
ROC receiver operating characteristic curve
TME tumor microenvironment
TIMER tumor immune estimation resource
RNA-Seq RNA sequencing
CHOL cholangiocarcinoma
HNSC head and neck squamous carcinoma
KIRC kidney renal clear cell carcinoma
KIRP kidney renal papillary cell carcinoma
LIHC liver hepatocellular carcinoma
STAD stomach adenocarcinoma
BLCA less expressed in bladder urothelial carcinoma
KICH kidney chromophobe
LUSC lung squamous cell carcinoma
READ rectum adenocarcinoma
SKCM skin cutaneous melanoma
UCEC uterine corpus endometrial carcinoma
CODA colon adenocarcinoma
ESCA esophageal carcinoma
PADD pancreatic adenocarcinoma
THYM thymoma
ACC adrenocortical carcinoma
CESC cervical squamous cell carcinoma and endocervical adenocarcinoma
OV ovarian serous cystadenocarcinoma
UCS uterine carcinosarcoma
GO gene ontology
KEGG kyoto encyclopedia of genes and genomes
GSEA gene set enrichment analysis
IC50 semi-inhibitory concentrations
TIME tumor immune microenvironment
TAMs tumor-associated macrophages
NETs neutrophil extracellular traps

Pathology & Oncology Research | frontiers

TYPE Original Research
PUBLISHED 09 January 2023
DOI 10.3389/pore.2022.1610824

Check for updates

OPEN ACCESS

EDITED BY
József Tímár,
Semmelweis University, Hungary

*CORRESPONDENCE
Yingyong Hou,
hou.yingyong@zs-hospital.sh.cn

RECEIVED 13 September 2022
ACCEPTED 20 December 2022
PUBLISHED 09 January 2023

CITATION
Deng M, Luo R, Huang J, Luo Y, Song Q, Liang H, Xu C, Yuan W and Hou Y (2023), Clinicopathologic features of gastric glomus tumor: A report of 15 cases and literature review.
Pathol. Oncol. Res. 28:1610824.
doi: 10.3389/pore.2022.1610824

COPYRIGHT
© 2023 Deng, Luo, Huang, Luo, Song, Liang, Xu, Yuan and Hou. This is an open-access article distributed under the terms of the Creative Commons Attribution License (CC BY). The use, distribution or reproduction in other forums is permitted, provided the original author(s) and the copyright owner(s) are credited and that the original publication in this journal is cited, in accordance with accepted academic practice. No use, distribution or reproduction is permitted which does not comply with these terms.

Clinicopathologic features of gastric glomus tumor: A report of 15 cases and literature review

Minying Deng[1], Rongkui Luo[1], Jie Huang[1], Yuanlong Luo[2], Qi Song[1], Huaiyu Liang[1], Chen Xu[1], Wei Yuan[1] and Yingyong Hou[1]*

[1]Department of Pathology, Zhongshan Hospital, Fudan University, Shanghai, China, [2]Shanghai University of Traditional Chinese Medicine, Shanghai, China

Objective: Glomus tumor is a relatively uncommon soft tissue neoplasm predominantly occurring in upper extremity (fingers), less reported in stomach. This study aimed to discuss the clinicopathologic features of gastric glomus tumor (GGT) and then provide reference for clinical practice.

Methods: A retrospective analysis of all cases pathologically diagnosed of GGT was performed, pathological findings were correlated with clinical information, immunohistochemical studies, next-generation sequencing, and patient follow-ups. A review of literature by searching similar cases was conducted to summarize previous knowledge of GGTs.

Results: Our study identified 15 GGTs included 5 males and 10 females, aged between 35–75 years old (median, 49 years old). The tumor was located to the gastric corpus in 6 cases (40%) and to the antrum in 9 cases (60%). The maximum tumor diameter ranged between 1–4 cm (median, 1.5 cm). There were 11 cases (73%) of solid glomus tumor, 3 cases (20%) of mixture of solid glomus tumor and glomangioma, and 1 case (7%) of glomangiomyoma. Partial spindle cell area was observed in 3 cases (20%), moderate cellular atypia in 1 case (7%), atypical mitosis in 1 case (7%), vascular invasion in 5 cases (33%), neural invasion in 6 cases (40%) and tumor necrosis in 1 case (7%). Tumor cells expressed Collagen type IV, α-smooth muscle actin (α-SMA), and synaptophysin in most cases. The Ki67 index varied from 1% to 30%. Next-generation sequencing reported *EGFR, PIK3CA, KEAP1* and *TP53* mutation. The outcome information was obtained in 12 (80%) cases, followed for 6–63 months, 11 patients (92%) had tumor-free survival and 1 patient (8%) developed liver metastasis 26 months after surgery. Literature review obtained 16 previously reported malignant GGT cases. In terms of the total 31 cases, univariate analysis revealed that the atypical mitosis (OS: $p = 0.009$; DFS: $p = 0.010$) and severe cellular atypia (OS: $p = 0.007$; DFS: $p = 0.004$) were significantly associated with poor prognosis (patient death).

Conclusion: GGT is indolent, while long-term close follow-up should be required in the presence of increasing number of risk factors. Malignant GGT is relatively uncommon and predisposes to liver metastasis, calling for accumulation of large-sample data and experience.

KEYWORDS

glomus tumor, gastric tumor, immunohistochemistry, molecular genetics, prognosis

Introduction

Glomus tumor (GT) is a type of mesenchymal neoplasm originating from the glomus cells. It is rare and mainly occurs in the extremities and peripheral soft tissues, rarely in visceral organs. Gastric glomus tumor (GGT) was first reported by Talijeva et al. [1] in 1928. The present study retrospectively analyzed the clinicopathologic characteristics, immunohistochemical features, gene mutation, and prognosis in 15 cases of GGT from Zhongshan hospital. Additionally, literature review was performed to obtain the previous 16 reports of malignant GGT cases, and statistical analysis was conducted, so as to raise the awareness about this disease and provide reference for clinical practice.

Materials and methods

Clinical data

Fifteen patients who were histopathologically diagnosed with GGT by the Pathology of Zhongshan Hospital, Fudan University between January 2014 and April 2022 were included. Basic clinical data, including age, sex, tumor site, tumor size, clinical symptom, and previous history, were collected.

Hematoxylin & Eosin (HE) and immunohistochemical (IHC) staining

HE staining: All specimens were fixed by 10% neutral formalin, regularly dehydrated, paraffin-embedded, sectioned into 3-μm sections, and processed for HE staining. IHC staining: IHC staining was performed using the EnVision two-step strategy. Primary antibody information: CD117, HMB45, Desmin, synaptophysin, chromograninA, S100 protein, wide-spectrum cytokeratin, Ki67, and vimentin (DAKO); Bcl2, P53, CD56, CD57 (LEICA); muscle specific actin (MSA), CD34, H-caldesmon (LongIsland); SOX10, INI1, DOG-1 (Gene Tech); somatostatin receptor 2 (SSTR2), somatostatin receptor 5 (SSTR5) (Abcam); α-smooth muscle actin (α-SMA) (Thermo); ATRX (Sigma); calponin, Collagen type IV (MXB Biotechnologies); BRAF V600E (ZSGB Biotechnology). The dilutions, clone and sources of these antibodies were listed in Table 1.

Next-generation sequencing

DNA was extracted from the paraffin-embedded tissue samples of 15 GGT, and then processed for analysis on *BRAF* gene using the PCR-Sanger sequencing and amplification refractory mutation system (ARMS) using the ABI3500Dx sequencing platform and ABI7500 sequencing platform, respectively. At the same time, the Illumina Nextseq CN500 detection platform was used to amplify 15 cases of GGT (Amplicon-based NGS).

Histological assessment

The HE-stained sections were assessed from the following aspects: 1) histological type; 2) growth pattern (infiltrative/expansive): infiltrative growth was defined by unclear borders between tumor tissues and surrounding normal tissues, and the growth of tumor tissues between intermuscular or interfascial spaces; expansive growth was defined by clear borders between tumor tissues and surrounding normal tissues; 3) infiltration level: muscular infiltration was defined by tumor cells growing to smooth muscle fibers in a nested, lingual, or patchy manner; 4) myxoid degeneration of the stroma; 5) spindle cell area; 6) cellular atypia: the degree of cellular (nuclear) atypia was determined by previous experience and the study of Folpe et al. [2]. Mild atypia: tumor cells are similar to the normal glomus cells, presenting with a small regular nucleus with an unobvious nucleolus, or a transverse diameter of the tumor cell nucleus ≤ diameter of 1 lymphocyte; moderate atypia: occasional nucleolus, or diameter of 1 lymphocyte < transverse diameter of the tumor cell nucleus ≤ diameter of 2 lymphocytes; severe atypia: the tumor cell nucleus is 2–3 times larger than the normal glomus cells and is significantly irregular with an obvious nucleolus, or transverse diameter of the tumor cell nucleus > diameter of 2 lymphocytes [2, 3]; 7) mitotic counts from 50 high power fields (HPFs), magnification of 400 (OLYMPUS BX43, FN = 22 or LEICA DM2000, FN = 22) (50HPFs = 12 mm^2); 8) atypical mitosis; 9) vascular invasion; 10) neural invasion; 11) tumor necrosis; 12) mucosal erosion or ulceration; 13) hemorrhage; 14) calcification.

Literature retrieval

The second part of this study was made up of 16 malignant GGT cases between 2001–2022 retrieved from the PubMed and Wanfang databases from different hospitals and institutes. The same basic and clinicopathologic data of all retrieved cases as those analysed in our series of cases were collected by going through the original reference [2–16].

Follow-up

Data about follow-up were obtained by review of medical records and telephone interviews. Patients were followed up in

TABLE 1 Primary antibodies used in this study.

Antigen	Clone	Catalogue numbers	Dilution	Source
CD117	Poly	A4502	1: 300	DAKO
HMB45	HMB45	M0634	1: 100	DAKO
Desmin	D33	M0760	1: 100	DAKO
Synaptophysin	DAK-SYNAP	IR660	working fluid	DAKO
S100 protein	Poly	IR504	working fluid	DAKO
wide-spectrum CK	AE1/AE3	M3515	1: 200	DAKO
Ki67	MIB1	RMA-0731	1: 200	DAKO
Vim	V9	M0725	1: 200	DAKO
chromograninA	DAK-A3	M-0202	1: 200	DAKO
Bcl2	3.1	NCL-L-Bcl2	1: 100	LEICA
p53	DO-7	NCL-L-P53-DO7	1: 500	LEICA
CD56	1B6	NCL-CD56-1B6	1: 100	LEICA
CD57	NK-1	NCL-NK1	1: 200	LEICA
MSA	HHF35	M-0002	1: 100	LongIsland
CD34	QBEnd/10	M-0117	1: 100	LongIsland
H-caldesmon	TD107	M-0061	1: 50	LongIsland
SOX10	SDM2	Gt221029	1: 100	Gene Tech
INI-1	25	GT225729	1: 100	Gene Tech
DOG-1	SP31	GT205429	1: 100	Gene Tech
SSTR2	UMB1	ab134152	1: 200	Abcam
SSTR5	UMB4	ab109495	1: 200	Abcam
SMA	1A4	MS-113-P	1: 100	Thermo
ATRX	Poly	HPA001906	1: 500	SIGMA
Calponin	CALP	GM355629	1: 200	MXB Biotechnologies
Collagen type	IV	MAB0781	working fluid	MXB Biotechnologies
BRAF V600E	RMD15	ZM-0632	working fluid	ZSGB Biotechnology

months from the day after pathological confirmation to 27 May 2022. Termination of the follow-up was determined by loss-to-follow-up or death. Primary endpoints were overall survival (OS) and disease-free survival (DFS). DFS is defined by the time period from the date of surgery to the date of the first tumor metastasis/recurrence or the last follow-up visit. OS is defined by the time period from the date of surgery to the date of death from tumor or the last follow-up visit.

Statistical analysis

IBM SPSS Statistics 25 (IBM, China) software was used for statistical analysis. Pearson correlation analysis was applied to assess the correlation between continuous data (including age, maximum tumor diameter, and mitotic count). Other clinicopathologic data were analyzed by Crosstabs and Fisher exact probability test, and non-parametric Spearman test was used for correlation analysis. Prognostic significance of the clinicopathologic parameters for the clinical outcomes of the disease (recurrence/metastasis, death) was assessed by Kaplan-Meier survival curve together with Log-rank test. Multivariate analysis was performed using the Cox proportional hazard regression analysis. $p < 0.05$ was considered as statistically significant. p-value for trend was between 0.05–0.1. The range of r value for the correlation coefficient is between −1 and 1, and the larger the absolute value, the stronger the correlation.

Results

Clinical characteristics

Of the 15 GGT patients from Zhongshan hospital, there were 5 males (33%) and 10 females (67%). The age of onset was between 35–75 years old (median, 49 years; average, 51.6 years). Tumor sites were the gastric corpus ($n = 6$, 40%) and the antrum ($n = 9$, 60%). One patient (7%) was admitted for repeated hematemesis with black stool for half a month, 1 (7%) for progressive elevation of carcinoembryonic antigen (CEA) for 5 years (Pre-operative >9 ng/mL, post-operative 7–8 ng/mL), 4 (27%) for recurrent upper abdominal discomfort, and 9 (60%) for

TABLE 2 Clinical symptom and surgical procedures of the 15 GGTs from Zhongshan hospital.

Case	Sex	Age(y)	Clinical symptom	Preoperative diagnosis	Surgical procedure
1	F	59	A 10-year stomach-occupying lesion found on physical examination	GIST	Subtotal gastrectomy
2	F	49	Half-month recurrent hematemesis with black stool	Gastric malignancy with hemorrhage	Radical gastrectomy
3	F	57	Over 4 years of recurrent upper abdominal discomfort	A submucosal benign mass of the antrum	EFTR
4	M	65	An 8-month gastric submucosal mass found on physical examination	GIST	EFTR
5	M	49	A 10-year stomach-occupying lesion found on physical examination	GIST	Laparoscopic gastrectomy
6	F	35	2-year gastric submucosal protrusion on physical examination	GIST	ESD
7	M	50	5-year progressive CEA elevation on physical examination	Neuroendocrine neoplasm	ESD + subtotal gastrectomy + sentinel lymph-node dissection
8	M	62	A 2-month gastric mass on physical examination	Lipoma	EFTR
9	F	75	A stomach-occupying lesion found on physical examination	GIST	EFTR
10	M	58	Intermittent abdominal pain with no predisposing factors, accompanying postprandial acid regurgitation for over half a year	Neuroendocrine neoplasm	Subtotal antrectomy + subtotal duodenostomy
11	F	41	Left upper abdominal pain for over 3 years and exacerbation for 4 years	GIST	Laparoscopic gastrectomy
12	F	41	A 4-month submucosal mass localized to the posterior wall of the antrum found on physical examination	GIST	ESD
13	F	51	3-year submucosal protrusion of the antrum on physical examination	GIST, hemangioma	ESD
14	F	36	A stomach-occupying lesion found on physical examination	SMT of the gastric corpus	Subtotal gastrectomy
15	F	46	Upper abdominal pain for over 2 months	SMT of the gastric corpus	ESD

a stomach-occupying lesion found on physical examination. Previous histories included alcohol consumption (n = 3, 20%), smoking (n = 2, 13%), hypertension (n = 1, 7%), diabetes (n = 1, 7%), malignant thyroid tumor (n = 1, 7%), meningioma (n = 1, 7%), and duodenal gastrointestinal stromal tumor (GIST) with hypertension, hypokalaemia and thymoma, without any GIST familiar predisposition, Carney syndrome or anamnestic data regarding genetic background (n = 1, 7%) (Table 2).

Imaging and surgical procedures

Nine patients (60%) underwent preoperative CT, and 8 of them manifested spindle or circle soft-tissue density shadow in the gastric wall, which was significantly enhanced after enhanced scan (Figure 1A). Six patients (40%) were examined by endoscopic ultrasonography preoperatively, showing a gastric wall submucosal tumor (SMT) originating from the submucosal layer or the muscularis propria (Figure 1B). Eleven patients (73%) received preoperative endoscopy and presented with mucosal protrusion in the gastric wall, which had a smooth surface and was complicated by partial hemorrhage. Combined with imaging and clinical presentations, 8 patients (53%) were diagnosed with GIST, 2 (13%) with neuroendocrine tumor, and 1 (7%) with lipoma before surgery. Additionally, 1 patient (7%) was considered as having gastric malignancy, while the other 3 patients (20%) were considered as having gastric SMT on imaging before surgery. Surgical procedures were endoscopic full-thickness resection (EFTR) under general anesthesia in 4 patients (27%), endoscopic submucosal dissection (ESD) in 4 patients (27%), subtotal gastrectomy in 2 patients (13%), radical gastrectomy in 1 patient (7%), laparoscopic gastric tumor resection in 2 patients (13%), subtotal antrectomy plus subtotal duodenostomy for concurrent occupying lesions in the stomach (GGT) and duodenum (GIST) in 1 patient (7%), and tumor resection followed by subtotal gastrectomy plus sentinel lymph-node dissection in 1 patient (7%) (neuroendocrine tumor was considered by biopsy pathology, and the resection margin was positive) (Figure 1C) (Table 2).

Pathologic features

Gross examination

Tumors of 14 patients (93%) were single and nodular, presenting with greyish white and yellow sections with partially colored greyish red, a soft and tough texture, and clear borders. The tumor of the other 1 patient (7%) was polypoid colored grayish brown, without a well-defined base. None of the tumors had erosion or ulceration. The maximum tumor diameter ranged between 1–4 cm (median, 1.5 cm; average, 1.89 cm), less than 2 cm in 9 patients (60%) while between 2–5 cm in 6 patients (40%).

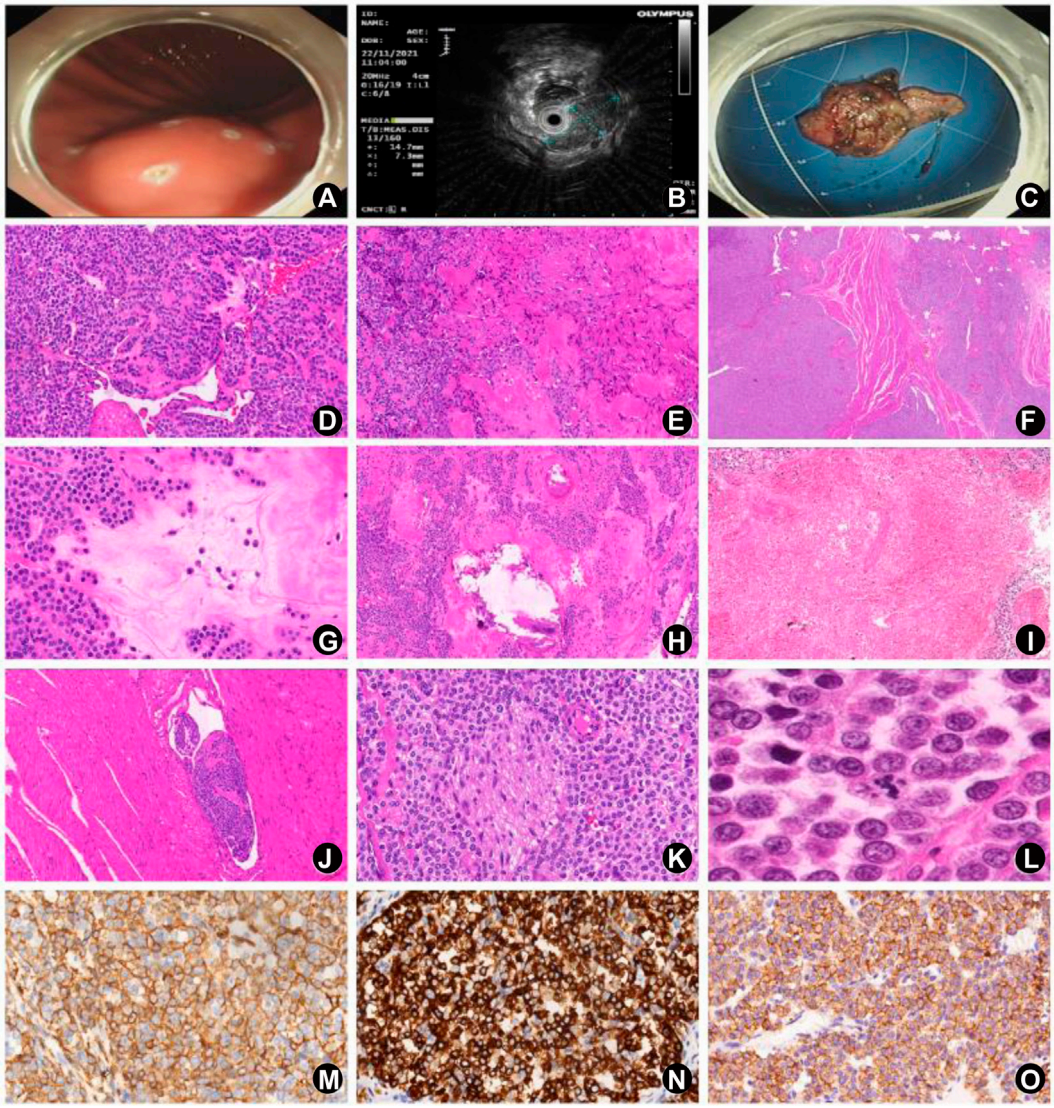

FIGURE 1
Clinical features, HE, and IHC results of the 15 GGT cases. **(A)** Case 15: a 2-cm submucosal protrusion localized to the posterior wall of the upper part of the gastric corpus on gastroscopic examination, with a smooth surface and a soft texture. **(B)** Case 15: a 15 x 8 mm uniformed hypoechoic occupying lesion on ultrasound gastroscopy, with clear borders, originating from the submucosal layer with intact posterior mucosal layer. **(C)** Case 15: endoscopic full-thickness resection (EFTR) of the mass, with absence of partial muscular layer. **(D)** Case 10: solid glomus tumor growing surrounding the blood vessels in a patchy consolidation pattern (HE, high magnification). **(E)** Case 4: glomangiomyoma showing a transition state of glomus cells and smooth muscle cells (HE, high magnification). **(F)** Case 1: solid glomus tumor invading to the muscular layer (HE, medium magnification). **(G)** Case 10: myxoid degeneration of the partial stroma (HE, high magnification). **(H)** Case 10: calcification in part of the tumor (HE, high magnification). **(I)** Case 14: necrosis in part of the tumor (HE, medium magnification). **(J)** Case 10: vascular invasion (HE, medium magnification). **(K)** Case 1: neural invasion (HE, high magnification). **(L)** Case 14: visible atypical mitosis (HE, high magnification); **(M)** Diffuse expression of α-SMA by tumor cells (EnVision, high magnification). **(N)** Diffuse expression of synaptophysin by tumor cells (EnVision, high magnification). **(O)** Diffuse expression of SSTR2 by tumor cells (EnVision, high magnification).

Microscopic examination

At low magnification, gastric mucosal tissues were absent in 6 cases (40%), possibly because it was not removed during the surgical section or taking the pathological specimen. Gastric mucosal tissues were observed in 9 cases (60%), but none of them had mucosal erosions. The muscularis propria layer and the subserosal layer of the gastric wall were involved in 12 cases (80%) and 2 cases (13%), respectively. It was impossible to judge on the involvement in the other 1 case (7%) because of the fragmented specimen without proper histological orientation. Tumors in 6 cases (40%) presented with an expansive growth pattern, and tumors in 8 cases (53%) showed an infiltrative growth pattern,

TABLE 3 Clinicopathologic features of the 15 GGTs from Zhongshan Hospital.

Case	Gastric site	Size (cm)	Location	Infiltrative growth	Mitoses/ 50HPF	Risk indicator							Diffuse growth inside the tumor	Myxoid degeneration of the stroma	Mucosal erosion or ulceration	Histological subtype	Follow-up
						Severe atypia	Mitoses>5/ 50 HPF	Atypical mitoses	Vascular invasion	Neural invasion	Tumor necrosis	Cumulative number					
1	Corpus	1.5	Muscularis propria	No	0	No	No	No	No	Yes	No	1	No	Yes, 5%	Yes	solid glomus tumor	Loss-to- follow-up
2	Antrum	2.7	Muscularis propria	Yes	0	No	No	No	Yes	No	No	1	No	Yes, 30%	No	solid glomus tumor	ANED, 63 months
3	Antrum	2.5	Muscularis propria	Yes	0	No	No	No	No	No	No	0	No	Yes, 20%	No	solid glomus tumor	ANED, 59 months
4	Antrum	1.2	Muscularis propria	Yes	0	No	No	No	No	No	No	0	No	Yes, 30%	No mucosa	Glomangiomyoma	ANED, 61 months
5	Corpus	2.3	Subserosa	Yes	1	No	No	No	Yes	No	No	1	No	No	No	solid glomus tumor	Loss-to-follow-up
6	Antrum	1	—	—	0	No	No	No	No	No	No	0	No	Yes, 10%	No	solid glomus tumor + glomangioma	ANED, 57 months
7	Corpus	1	Muscularis propria	No	0	No	No	No	No	Yes	No	1	No	Yes, 20%	No mucosa	solid glomus tumor + glomangioma	ANED, 46 months
8	Antrum	1.2	Muscularis propria	No	0	No	No	No	No	Yes	No	1	No	Yes, 2%	No	solid glomus tumor	ANED, 37 months
9	Corpus	4	Muscularis propria	No	0	No	No	No	No	No	No	0	No	Yes, 5%	No	solid glomus tumor	ANED, 26 months
10	Antrum	1	Muscularis propria	Yes	0	No	No	No	Yes	Yes	No	2	No	Yes, 10%	No mucosa	solid glomus tumor	ANED, 27 months
11	Antrum	2	Muscularis propria	Yes	0	No	No	No	No	Yes	No	1	No	Yes, 2%	No mucosa	solid glomus tumor+ glomangioma	Loss-to-follow-up
12	Antrum	1.5	Muscularis propria	No	2	No	No	No	Yes	No	No	1	No	Yes, 2%	No mucosa	solid glomus tumor	ANED, 16 months
13	Antrum	1	Muscularis propria	Yes	1	No	No	No	No	Yes	No	1	No	Yes, 5%	No mucosa	solid glomus tumor	ANED, 9 months
14	Corpus	4	Subserosa	Yes	6	No(moderate)	Yes	Yes	Yes	No	Yes, 10%	4	Yes, 40%	Yes, 5%	No	solid glomus tumor	ANED, 31 months; liver metastasis, 26 months postoperatively
15	Corpus	1.5	Muscularis propria	No	2	No	No	No	No	No	No	0	No	Yes, 2%	No	solid glomus tumor	ANED, 6 months

Note: —: Non-evaluable due to the fragmented tissues and absence of normal tissue surrounding the tumor; ANED: alive with no evidence of disease; No mucosa: Not seen under the microscope and not clear whether caused by ulceration.

10.3389/pore.2022.1610824

TABLE 4 Immunohistochemical and molecular results of 15 GGTs from Zhongshan hospital.

Case	1	2	3	4	5	6	7	8	9	10	11	12	13	14	15	Positive/total (% of positive cases)
Molecular genetics	EGFR	–	–	PIK3CA, MSI	–	–	TP53	–	–	–	–	–	–	KEAP1	–	
α-SMA	+/–	70%+	70%+	80%+	100%+	80%++	70%+	30%+	90%+	60%+	40%+	10%+	80%+	60%+	70%+	14/15 (93)
MSA	10%+	90%+	80%+	–	90%++	60%+	–	50%+	80%+	70%+	–	60%+	50%+	30%+	80%+	12/15 (80)
Vimentin	90%++	90%+	70%+	70%+	100%++	80%+	70%+	90%+	70%+	80%+	80%+	20%+	70%+	80%+	30%+	15/15 (100)
H-caldesmon	80%+	30%+	30%+	70%++	20%+	–	–	40%+	30%+	30%++	20%+	30%+	60%+	5%+	20%+	13/15 (87)
calponin	30%+	–	20%+	–	10%+	70%+	–	30%+	–	10%+	–	10%+	10%+	–	30%+	9/15 (60)
Collagen type IV	40%+	100%+	100%++	80%+	60%+	70%+	40%+	90%+–++	100%+	100%++	100%++	80%+	100%+	100%++	90%++	15/15 (100)
CD34	–	15%+	–	–	–	–	–	–	–	–	–	–	20%+	–	–	2/15 (13)
Desmin	–	–	–	–	–	–	–	–	–	–	–	–	–	–	5%+	1/15 (7)
S100 protein	–	–	–	–	–	20%+	–	–	–	–	–	–	–	–	–	1/15 (7)
wide-spectrum cytokeratin	–	–	–	–	–	–	–	–	–	–	–	–	–	–	–	0/15 (0)
Synaptophysin	100%++	–	60%+	10%+	80%+	70%+	80%+	60%+	80%+	80%+	40%+	50%+	–	90%+	70%+	13/15 (87)
CgA	–	–	–	–	–	–	–	–	–	–	–	–	20%+	–	–	1/15 (7)
CD56	–	–	–	–	–	–	–	–	–	–	–	10%+	–	–	5%+	2/15 (13)
Bcl2	–	–	–	5%+	100%++	70%+	50%+	–	40%+	–	30%+	2%+	60%+	80%+	70%+	10/15 (67)
P53	2%+	20%+	60%+	10%+	40%+	60%+	–	5%+	20%+	5%+	5%+	10%+	30%+	–	70%+	
Braf(V600E)	–	–	–	–	–	–	–	–	–	–	–	–	–	–	–	0/15 (0)
INI1	90%+	70%+	90%+	80%+	90%+	80%+	80%+	50%+	80%+	90%+	90%+	90%+	90%+	90%+	100%+	15/15 (100)
CD57	–	20%+	70%+	80%+	–	70%+	40%+	80%+	70%+	80%+	80%+	10%+	60%+	100%+	30%+	12/15 (80)
Ki67	1%	5%	Dense area 10%	1%	5%	2%	3%	5%	5%	5%	3%	5%	2%	10%	5%	
SSTR2	80%+	70%+	70%+	50%++	10%+	60%+	–	80%+	95%++	80%+	70%+	100%++	95%++	10%+	90%+	14/15 (93)
SSTR5	–	–	–	–	–	–	–	–	–	–	–	–	–	–	–	0/15 (0)
CD117	–	–	–	–	–	–	10%+	–	–	–	–	–	–	–	–	1/15 (7)
DOG-1	–	–	–	–	–	–	–	10%+	–	10%+	5%+	20%+	–	–	10%+	5/15 (33)
SOX10	–	–	–	–	–	–	–	–	–	–	–	–	–	–	–	0/15 (0)
HMB45	–	–	–	10%+	–	–	–	–	–	–	–	–	–	–	–	1/15 (7)

10.3389/pore.2022.1610824

TABLE 5 Clinicopathologic features of the 16 previously reported cases of malignant GGT from different institutes.

Case	Author	Publication year	Sex	Age(y)	Tumor site	Diameter (cm)	Location	Nuclear grade	Risk indicator						Spindle cell area	Myxoid degeneration of the stroma	Ki67-index	Follow-up
									Severe atypia	Mitoses/ 10 or 50 HPF	Atypical mitoses	Vascular invasion	Neural invasion	Tumor necrosis	Cumulative number			
1	Folpe[2]	2001	M	69	Stomach	8.5	NA	Mild	No	3/50	No	Yes	NA	No	1	No	NA	NA	DOD, 36 months; liver metastasis in the same month
2	Miettinen [3]	2002	M	69	Antrum	6.5	Serosa	Mild	No	1/50	NA	Yes	NA	NA	1	Yes	NA	2%	DOD, 50 months; liver metastasis, 33 months postoperatively
3	Bray[4]	2009	M	58	Stomach	17	Serosa	Moderate	No	>15/50	NA	Yes	NA	NA	2	NA	NA	NA	DOD, 72 months; liver, lung, brain, scalp metastases in the same month
4	Lee[5]	2009	F	65	Gastric fundus	3	NA	High	Yes	2/50	Yes	NA	NA	NA	2	NA	NA	NA	DOD, 8 months; kidney and brain metastases at the same time, bone metastasis 4 months postoperatively
5	Lee[5]	2009	M	63	Gastric corpus	9	NA	High	Yes	NA	NA	Yes	NA	NA	2	NA	NA	NA	DOD, 2 months; liver metastasis at the same time
6	Zhang[6]	2009	F	18	Greater curvature in the posterior wall	5	NA	High	NA	2–3/50	NA	NA	NA	NA	0	Yes	Yes	NA	Survival 72 months postoperatively; metastasis to left upper uterus and greater omentum in the same month
7	Song[7]	2010	F	65	Gastric fundus	3	Muscularis propria	Moderate	Yes	2/50	Yes	NA	NA	NA	2	Yes	NA	NA	DOD, 7 months; bone, epididymis, and bilateral lung metastases 1 month postoperatively; brain metastasis 6 months postoperatively
8	Teng[8]	2012	F	66	Antrum	5.3	Muscularis propria	High	No	4/50	NA	Yes	NA	NA	1	Yes	NA	NA	ANED, 9 months
9	Yao[9]	2013	F	52	Antrum	2	NA	High	Yes	0	NA	NA	NA	NA	1	NA	Yes	NA	ANED, 13 months
10	Tao[10]	2013	F	36	Antrum	4	Muscularis propria	High	NA	<5/50	NA	NA	NA	NA	0	NA	NA	NA	ANED, 10 months
11	Zaidi[11]	2016	F	53	Gastric fundus	10	Submucosa	High	Yes	10/50	Yes	NA	NA	Yes	4	NA	NA	15%	ANED, 15 months
12	Li[12]	2017	M	53	Antrum	3	Muscularis propria	NA	Yes	NA	NA	Yes	NA	NA	2	NA	NA	10%	NA
13	Bodolan [13]	2018	F	80	Antrum	7.1	NA	High	No	28/10	NA	No	NA	No	1	NA	NA	NA	ANED, 6 days; introoperative liver metastasis
14	Toti[14]	2019	M	72	Gastric corpus	6	NA	Moderate	Yes	14/10	NA	NA	NA	Yes	3	Yes	NA	25%	Survival 3 months postoperatively; liver metastasis before diagnosis of the primary tumor
15	Kong[15]	2019	F	63	Antrum	2.4	Muscularis mucosa	Moderate	Yes	9/10	NA	No	No	NA	2	NA	NA	40%	NA
16	Alsahwan [16]	2021	M	56	Stomach	7	NA	NA	No	12/10	Yes	NA	NA	NA	2	Yes	NA	30%	ANED, 6 months

Note: M, male; F, female; NA, not available; ANED, alive with no evidence of disease; DOD, died of diseases.

10.3389/pore.2022.1610824

TABLE 6 Kaplan-Meier analysis of DFS and OS in total 31 GGT cases.

Parameter	*p*-value (DFS)	*p*-value (OS)
Atypical mitosis	0.010	0.009
Vascular invasion	0.115	0.175
Tumor necrosis	0.665	0.665
Spindle cell area	0.289	0.534
Gender	0.454	0.388
Severe cellular atypia	0.004	0.007
Maximum tumor diameter ≥5 cm	0.073	0.090
Myxoid degeneration of the stroma	—	—
Neural invasion	—	—
Muscularis propria layer involvement	0.819	0.803
Subserosal layer involvement	0.351	0.495
Growth pattern (infiltrative/expansive)	—	—

Note: —: not be statistically analyzed with the available data.

including the tumor in 1 case exhibiting patchy consolidation (40%) for not abundant blood sinus inside the tumor (Figure 1F). The other 1 case (7%) was unable to be assessed due to the crushed tumor tissues and absence of normal tissues surrounding the tumor. There were 11 cases (73%) of typical solid glomus tumor, 3 cases (20%) of mixture of solid glomus tumor and glomangioma, and 1 case (7%) of glomangiomyoma (Figures 1D,E). Hemorrhage was seen from the inner area or margin of the tumor in 3 cases (20%), and small focal calcification was observed in the inner part of the tumor in 3 cases (20%) (Figure 1H). Hyalinosis or myxoid degeneration of the stroma (2%–30%) were detected in 13 cases (87%), and spindle cell areas in partial parts of the tumor (2%–5%) were noticed in 3 cases (20%) (Figure 1G). At high magnification, 14 cases (93%) exhibited mild nuclear atypia, and the other one case (7%) showed moderate atypia. Mitosis was readily visible in 5 cases (33%) (1-6 mitoses/50 HPFs or 12 mm^2), including atypical mitosis in only 1 case (Figure 1L). Vascular invasion and neural invasion were observed in 5 cases (33%) and 6 cases (40%), respectively (Figures 1J,K). Only one case (7%) presented with focal tumor necrosis (about 10%) (Figure 1I). Ten cases (67%) showed visible neuroendocrine tumor-like cells surrounding the tumor (2%–20%), which had scanty cytoplasm, hyperchromatic nuclei and fine chromatin. Three cases (20%) had tumor tissues in the resected margin (Table 3).

Immunophenotype

The immunohistochemical results are summarized in Table 4 and Figures 1M–O. Vimentin was expressed by all the 15 cases (100%); α-SMA and SSTR2 were expressed by 14 cases (93%). Variable Collagen type IV positivity (median percentage of positive cells 90%) was seen in all 15 cases. Positive expression of H-caldesmon and synaptophysin were detected in 13 cases (87%), of which synaptophysin positivity varied from 10% of tumor cells to global immunoreactivity (median of positive tumor cells 70%). CD57 and MSA was expressed in 12 cases (80%); ten of 15 tumors (67%) had different positivity for Bcl2 in 2%–100% of tumor cells. Calponin were expressed in 9 cases (60%) (median 20% of positive cells); partial or focal expression of DOG-1 was observed in 5 cases (33%), varying from 5% of tumor cells to 20%, whereas of those cases CD117 negative and Collagen type IV positive, so it could be differentiated from GIST. Focal expression of CD34 and CD56 was noted in 2 cases (13%), of which Collagen type IV was positive in CD34-positive partly cases, so it could be differentiated from solitary fibrous tumor. S-100 protein, desmin, chromograninA, CD117 and HMB45 were slightly expressed by 1 case (7%). Wide-spectrum cytokeratin, SSTR5, Braf (V600E) and SOX10 were negative in all the 15 cases (100%). The Ki67 index ranged between 1%–30%.

Molecular genetics

Sanger sequencing and ARMS testing demonstrated no *BRAF V600E* mutation in all 15 cases (100%). High-throughput sequencing technology found one case of *EGFR* gene exon 21 R831H missense mutation. One case detected the *PIK3CA* gene exon 10 E545K missense mutation, and found microsatellite instability (MSI). One case found a *TP53* gene exon 5 T150Afs*16 frameshift mutation. One case found that exon 3 of the *KEAP1* gene P384 = synonymous mutation (Table 4).

Follow-up and prognosis

None of the 15 patients from Zhongshan hospital underwent postoperative radiotherapy or chemotherapy. Twelve patients (80%) completed follow-up by telephone interviews or outpatient visit, and the follow-up time period was between 6–63 months. Of the 12 patients, 1 patient underwent hepatectomy for localized liver metastases 26 months postoperatively and survived after 31 months. The other 11 patients had tumor-free survival. Two of them underwent ESD and one was treated by EFTR under general anesthesia. All the three patients had visible tumor tissues in the resected margin endoscopically, and survived 57, 37, and 9 months postoperatively without recurrence or metastasis (Table 3).

Clinical pathological and follow-up data of 16 cases of malignant GGT reported in the literature

Literature review of the current study obtained 16 cases of malignant GGT reported domestically and abroad between 2001 and 2022, together with their clinicopathologic and follow-up data [2–16]. Among the 16 patients, there were

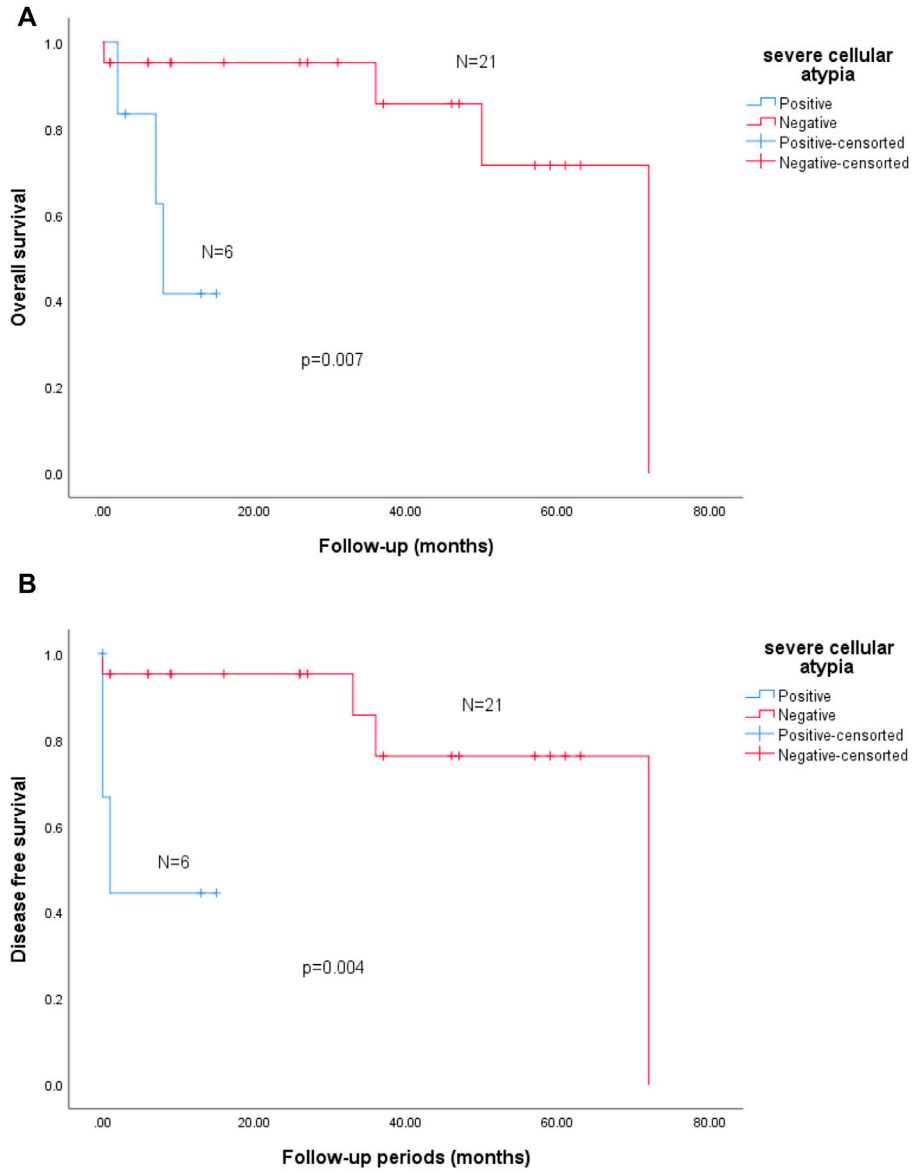

FIGURE 2
(Continued).

7 males (44%) and 9 females (56%) (male-to-female ratio = 1: 1.3), aged between 18–80 years old (median, 63 years). The tumors were localized to the gastric antrum (n = 7, 44%), the corpus (n = 3, 19%), and the fundus (n = 3, 19%). No specific tumor site was reported in the other 3 cases (19%). The maximum tumor diameter ranged between 2–17 cm (median, 5.65 cm). Involved sites included the muscularis propria (n = 4, 25%), the serosal layer (n = 2, 13%), the mucosal muscle layer (n = 1, 6%), and the submucosal layer (n = 1, 6%) of the gastric wall. No specific involvement was mentioned in the reports of the other 8 cases (50%). Mucosal erosion or ulceration was visible in 5 cases (31%), myxoid degeneration of the stroma in 2 cases (13%), partial spindle cell areas in 6 cases (38%), partial tumor necrosis in 2 cases (15%), and vascular invasion in 6 cases (38%). None of the 16 cases reported neural invasion. In terms of the cellular atypia, it was presented as severe in 8 cases (50%), moderate in 4 cases (25%), and mild in 2 cases (13%). In the other two cases, cellular atypia was not available from primary literature. 13 cases (81%) showed mitosis, of which 9 cases used 50HPF count with the range of 1-15/50HPF, and 4 cases used 10HPF count with the range of 9-28/10HPF. Mitosis was not easy to find in one case (6%) and was not mentioned in the other 2 cases (13%) in the original data of literature. Ki67 cell proliferation

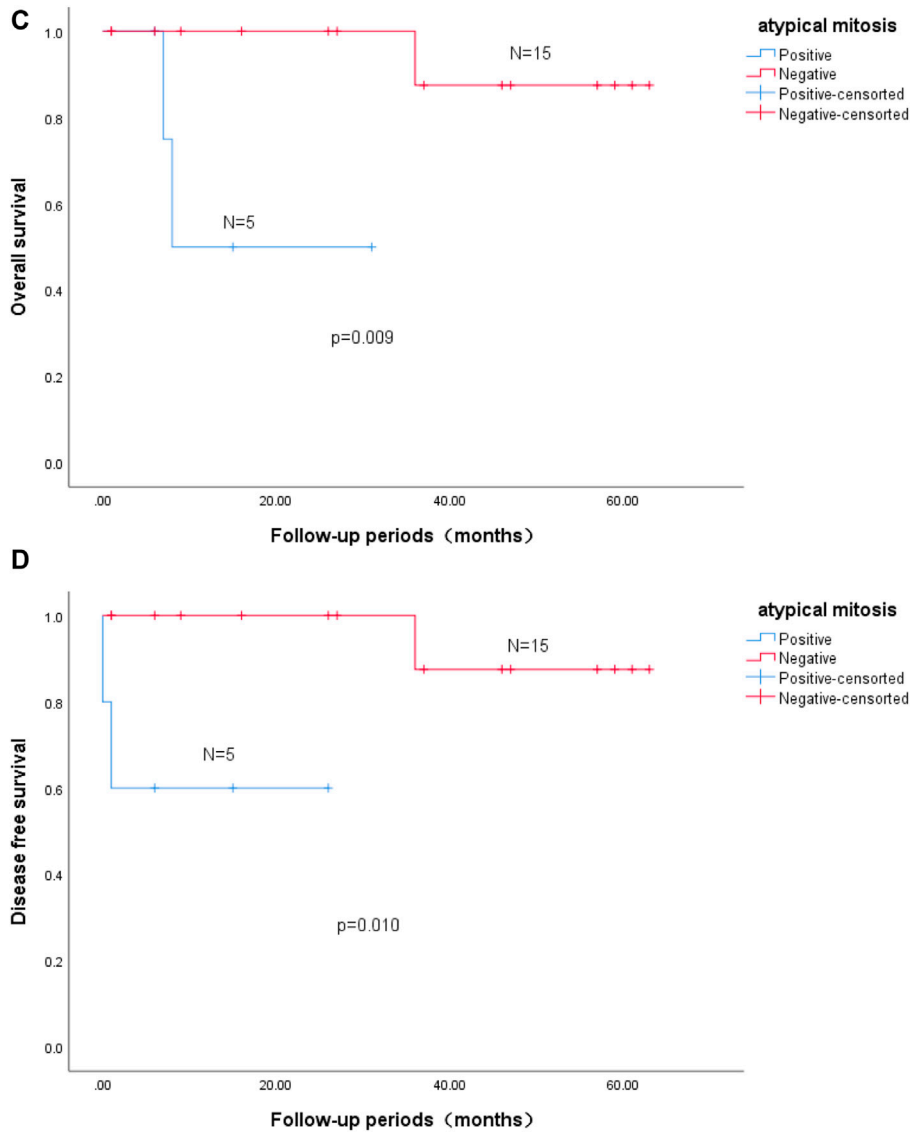

FIGURE 2
(Continued). Survival analysis. Kaplan-Meier estimation of overall survival (OS) by severe cellular atypia in GGT (n = 27, **(A,B)**). Severe cellular atypia positive group exhibited a shorter DFS (p = 0.004, log-rank, n = 27, **(B)**) and a significant tendency towards a poor OS (p = 0.007, log-rank, n = 27, **(A)**). Kaplan-Meier estimation of overall survival (OS) by atypical mitosis in GGT (n = 20, **(C,D)**). Atypical mitosis positive group exhibited a shorter DFS (p = 0.010, log-rank, n = 20, **(D)**) and a significant tendency towards a poor OS (p = 0.009, log-rank, n = 20, **(C)**).

index was reported in 5 cases, ranging from 10% to 40%. Follow-up was completed in 14 cases (88%), ranging between 0.2–72 months (median, 9.5 months; average, 21.7 months). Nine patients (56%) experienced metastasis, majorly to the liver (the most common), lung, brain, kidney, scalp, humerus, epididymis, and greater omentum. One patient developed liver metastasis 36 months postoperatively and eventually died. Another one patient suffered from multiple metastases to the liver, lung, brain, and scalp, and eventually died as well (Table 5).

Correlation between clinicopathologic parameters

The total 31 cases, including 15 cases analyzed in the present study from Zhongshan hospital and 16 previously reported cases from literature review between 2001–2022, were analyzed collectively from the following aspects: age, sex, maximum tumor diameter, involvement level, growth pattern, patchy consolidation, cellular atypia, mitotic count, atypical mitosis, vascular invasion, neural invasion, tumor necrosis, spindle cell

area, and myxoid degeneration of the stroma. Statistically, significant positive associations were demonstrated between maximum tumor diameter and cellular atypia (p = 0.002, r = 0.546), maximum tumor diameter ≥5 cm and spindle cell area (p = 0.023, r = 0.528), severe atypia and atypical mitosis (p = 0.009, r = 0.728), severe atypia and tumor necrosis (p = 0.018, r = 0.792), atypical mitosis and spindle cell area (p = 0.012, r = 0.721), tumor necrosis and spindle cell area (p = 0.044, r = 0.658). Additionally, remarkable negative associations were indicated between subserosal involvement and myxoid degeneration of the stroma (p = 0.011, r = −1.00), and between muscular involvement and severe cellular atypia (p = 0.029, r = −0.669).

Correlation between clinicopathologic parameters and clinical outcome

Associations between the clinicopathologic parameters and clinical outcomes of patients were analyzed in the total 31 cases (Table 6). The results demonstrated that patients with severe cellular atypia predicted shorter OS (p = 0.007) and DFS (p = 0.004) than patients without severe cellular atypia (Figures 2A,B). In addition, atypical mitosis tended to have shorter OS (p = 0.009) and DFS (p = 0.010) (Figures 2C,D). Univariate analysis indicated that maximum tumor diameter ≥5 cm was significantly positively associated with the death outcome in patients (p = 0.030, r = 0.438). While in multivariate analysis, no statistical significance was found in associations between the adverse clinical outcomes of the disease and the clinicopathologic parameters.

Discussion

GT is derived from glomus cells that is rare and comprises less than 2% of all soft tissue tumors [17]. It was first reported by Masson et al. [18] in 1924. Together with cutaneous leiomyoma, angiolipoma, and traumatic neuroma, it is also known as "painful subcutaneous nodule." GT commonly occurs in the extremities and peripheral soft tissues, such as the glomus cell-rich parts including figure, toe, and nail bed, rarely seen in the visceral regions that have fewer glomus cells (approximately 1/4) [19].

GGT is extremely rare accounting for approximately 2.2% of the total gastric tumors while 1% of the gastric mesenchymal tumors [20, 21]. It was first reported by Talijeva et al. [1] in 1928, followed by Kay et al. [22] in 1951, who reported 3 GGT cases. According to the literature, GGT is prevalent in females, with the age of onset ranging between 19–90 years old (median, 55 years; average, 53 years) and the common site being the gastric antrum [3]. The majority of GGT cases have non-specific clinical symptoms, mainly presenting with varying degrees of upper abdominal discomfort, abdominal distension, gastrointestinal bleeding, black stool, and vomiting. Additionally, GGT cases can also be asymptomatic and be found incidentally on physical examination. In the 15 GGT patients reported here from Zhongshan hospital, the male-to-female ratio was 1:2, the age of onset was between 35–75 years old (median, 49 years), and the tumor site was more common in the gastric antrum (n = 9), consistent with the literature above. With reference to the cause of admission, 5 patients were admitted for gastrointestinal symptoms, 1 patient for progressive CEA elevation, and 9 patients for a stomach-occupying lesion incidentally found on physical examination, which might be attributed to the popularization of endoscopic examination and the increasing health awareness in people. Usually, GGT patients more often present with mucosal protrusion on gastroscopic examination; a submucosal or muscular uniform hypoechoic mass on ultrasound gastroscopic examination; low-density shadow on CT scan, with clear borders and regular shape, and arterial-phase hyperenhancement after enhanced scan. The imaging presentations of the 15 cases reported here are in line with the literature report. Furthermore, 8 patients (53%) were preoperatively diagnosed with GIST, 2 (13%) with neuroendocrine tumor, and 1 (7%) with lipoma. Additionally, 1 patient (7%) was considered as having gastric malignancy, while the other 3 patients (20%) were considered as having SMT. As GGT is relatively rare, we believed that the clinical symptoms and preoperative imaging presentations mentioned above are not sufficient to make a definite diagnosis of GGT. Instead, histopathology is required. However, GGT should also be well distinguished from the neuroendocrine tumor, GIST, solitary fibrous tumor, paraganglioma, epidermal leiomyoma, or clear cell leiomyoma in their pathology patterns.

Literature has reported that the maximum tumor diameter of GGT is between 2–5 cm (median, 2–3 cm). In most cases, the GGT tumors are solitary with clear borders, greyish red section, and a slightly tough texture, accompanying partial hemorrhage or calcification [3, 23]. In the present study, the maximum tumor diameter of the 15 cases ranged between 1–4 cm (median, 1.5 cm). GGT shares a similar histological pattern with other GTs originating from soft tissues and can be classified as solid glomus tumor, glomangioma, and glomangiomyoma. Here, there were 11 (73%) cases of solid glomus tumor, 3 (20%) cases of mixture of solid glomus tumor and glomangioma, and 1 (7%) case of glomangiomyoma. Hyalinosis or myxoid degeneration of the stroma (2%–30%) were detected in 13 cases (87%), and calcification was observed in 3 cases (20%). By now, there has been no literature reporting the practical significance of the histological subtype and myxoid degeneration of the stroma in clinical prognosis of GGT.

The majority of GGT cases are reported as benign, and malignant GGT is relatively rare. For the first time, Kirschbaum et al. [24] reported a case of malignant GGT in 1939. Subsequently, Yannopoulos et al. [25] reported a 12-year-old girl suffering from malignant GGT in 1962. It has not been established about the standard for definite diagnosis of malignant GGT because of the rare cases. In 2001, Folpe et al. [2] retrospectively analyzed the clinicopathologic parameters of 52 malignant GT cases, including tumor size, infiltration depth, growth pattern, cellular atypia, mitotic

count/50 HPFs, atypical mitosis, vascular invasion, and tumor necrosis. Of the 52 patients, 35 patients were followed up for 5 months to 23 years (average, 5.5 years), including 7 patients having recurrence, 8 patients with metastasis, and 7 deaths. Following statistical analysis, they proposed a standard for the diagnosis of malignant GT, including the following three criteria: 1) the tumor localized to the fascia or viscera, with the maximum diameter >2 cm; or 2) visible atypical mitosis; or 3) moderate-to-severe nuclear atypia, and mitotic count ≥5/50 HPFs. The authors noted that patients could be diagnosed with atypical GT if they met one of the following criteria: 1) a deep tumor site; or 2) diameter >2 cm; or 3) a shallow tumor site and mitotic count ≥5/50 HPFs. However, whether this standard is applicable for discrimination between benign and malignant GGT needs to be further validated.

GGT is relatively rare. Previous reports are mostly dominated by one case, while the reports of a series of cases have gradually increased in recent years [26, 27]. It remains on debate whether the standard proposed by Folpe et al. [2] is applicable for GGT. To explore the prognostic significance of the clinicopathologic features, we statistically analyzed the clinicopathologic parameters of the total 31 cases, including the age, gender, maximum tumor diameter, involvement level, growth pattern, patchy consolidation, cellular atypia, atypical mitosis, vascular invasion, neural invasion, tumor necrosis, spindle cell area, and myxoid degeneration of the stroma. Univariate analysis revealed that patients with atypical mitosis and severe cellular atypia had shorter OS ($p = 0.009$, $p = 0.007$) and DFS ($p = 0.010$, $p = 0.004$), as compared to corresponding controls. Nevertheless, neither atypical mitosis nor severe cellular atypia exhibited prognostic significance for adverse clinical outcome of GGT patients in multivariate analysis. We believed that the prognostic significance of atypical mitosis and severe atypia for GGT is still worthy of further exploration, and the non-significant result might be associated with the low incidence of malignant GGT, requiring further large-scale studies. However, it is important to note that the assessment of nuclear atypia is subjective, and metastatic GGT has previously reported only mild cytologic atypia and a small amount of mitosis [3]. Therefore, Pansa et al. [26] believed that the absence of severe cell atypia and mitosis do not exclude malignant potential.

Some scholars pointed out that the stomach is a deep organ and over half the gastric tumors have a maximum diameter >2 cm (median, 2–3 cm) [3, 20]. Thus, they thought the standard mentioned above is not suitable for diagnosis of benign and malignant GGT. Miettinen et al. [3] believed that maximum tumor diameter >5 cm would increase the risk of developing recurrence/metastasis. Papke et al. [27] also recently conducted clinicopathological analysis on 26 cases of gastroesophageal glomus tumor, and proposed a new malignant criterion for gastroesophageal glomus tumor: 1) the maximum diameter of the tumor ≥5cm; or 2) both nuclear atypia and mitoses ≥2/10HPF. In the 15 cases reported here from Zhongshan hospital, the maximum tumor diameter was between 1–4 cm (average, 1.89 cm). One case had liver metastasis, while the maximum tumor diameter was 4 cm <5 cm. Of the 16 previously reported cases from different hospitals in the literature, the maximum tumor diameter ranged between 2–17 cm (median, 5.65 cm). While in the 9 cases developing metastasis, the maximum tumor diameter was between 3–17 cm (median, 6.5 cm; average, 7.23 cm). Besides, both the uni- and multi-variate analyses demonstrated that maximum tumor diameter ≥5 cm was not statistically associated with the adverse outcome of GGT. Perhaps more data may need to be accumulated to clarify the meaning. The prognostic significance of mitotic count was not covered in the current study, as the counting method for mitosis was not uniformed in the previously reported 16 cases from literature coverage (partial 10 HPFs, and partial 50 HPFs). The 16 cases of GGT reported in the previous literature did not mention the microscope model used, so only the data could be compiled for description. In all, the standard for differentiation between benign and malignant GT put forward by Folpe et al. [2] or Papke et al. [27] has certain limitations when applied for GGT cases.

In experience, vascular invasion, neural invasion, tumor necrosis, and presence of significant spindle cell area are potential indicators that predict the malignancy of tumor [28]. However, these appear to be less applicable in diagnosis of GGT cases. Haque et al. [29] held the view that the vascular invasion after GGT was not identical to the traditional vascular invasion with different clinical implications, and they believed that it was not applicable for predicting the malignancy of GGT. Among the 15 cases reported in the present study from Zhongshan hospital, 5 cases (20%) had vascular invasion, 6 cases (40%) experienced neural invasion, 1 case (7%) developed focal tumor necrosis, and 3 cases (20%) were detected with spindle cell areas in some tumor parts. While in the 16 previously reported cases of malignant GGT from literature coverage, 6 cases (38%) had partial spindle cell areas, 2 cases (15%) had partial tumor necrosis, and 6 cases (38%) developed vascular invasion. Our statistical analysis indicated that none of the events mentioned above had significant prognostic value for the adverse outcomes of GGT, but this can be also caused by the low number of involved cases. Of the 31 cases so far, 11 have vascular invasion, but the statistical results are not significant. We speculated that vascular invasion shown by GGT may only be a manifestation of local invasion of tumor tissue, but the potential to cause the planting and growth of corresponding organs is relatively limited. In addition, the 16 previously reported cases from literature review are dominated by single cases, resulting in incomplete morphological description. Besides, the fundamental cases of GGT and the incidence of patients developing adverse outcomes (recurrence/metastasis/death) within a certain period of time from the multi-center is not available, which leads to data deficiency or incompleteness. The conditions mentioned above increase certain difficulty of exploring the benign and malignant judgment criteria of GGT. In this context, the morphology of GGT is of certain clinical value that may potentially predict the adverse biological behaviors. Miettinen et al. [3] reported 32 gastrointestinal GT cases diagnosed from 1970 to 1998, including 31 GGT cases and 1 cecum GT case.

Only one case had liver metastasis 33 months postoperatively and died 50 months postoperatively, histologically presenting with mild cellular atypia, spindle cell foci, vascular invasion, and 1 mitosis/50 HPFs. While in the 15 cases (2014–2022) reported here from Zhongshan hospital, 1 case had postoperative liver metastasis and histologically presented with vascular invasion, tumor necrosis, mitosis >5/50HPFs (12 mm^2), and atypical mitosis. The above findings imply that GGT has a low incidence with few cases reported and has relatively indolent biological behaviors. Besides, more attention should be paid in cases displaying more high-risk indicators, which may predict the probability of developing adverse outcomes. In the meantime, close follow-up is also on demand to accumulate more data and experience to facilitate prediction of the biological behaviors of GGT.

Consistent with the present study, Luzar et al. [30] believed that the mitotic count at 50 HPFs was hard to be achieved in cutaneous GT due to the small tumor size in most cases, and that the standard proposed by Folpe et al. was not easily to be applied in cases of cutaneous GT. Similarly, Zhu et al. [31] reported a case of bronchial GT presenting with local infiltration, and mitotic count >5/50 HPFs (12-19 mitoses/50 HPFs, there was no evidence of recurrence or metastasis during the 2-year follow-up. This also indicated that the standard proposed by Folpe et al. is limited in predicting the biological behaviors of deep organs.

GGT shares similar IHC features with other GTs derived from soft tissues, majorly expressing α-SMA, vimentin, h-Caldesmon, calponin, and type IV collagen, partially expressing synaptophysin and CD34, and rarely expressing wide-spectrum cytokeratin, S-100 protein, CD117, desmin, CD56, and chromograninA, etc. [3, 32, 33]. Synaptophysin is mainly expressed in GGT but has not been reported in the GT of other sites, and there has been no literature reporting its prognostic significance [34]. Consistently, synaptophysin was expressed in 13 out of the 15 cases reported in the present study.

From the perspective of molecular genetics, previous study adopted fluorescent *in situ* hybridization (FISH) method and detected *NOTCH* gene rearrangement, dominated by *NOTCH2-MIR143* fusion gene (73%), in approximately 50% of GT cases [35]. Recent research reports that *CARMN-NOTCH2* fusion is also common (58%) [27]. Since fusion gene detection of *NOTCH* was not covered by our applied next-generation sequencing panel, there is no information in the present study. Another study found that approximately 6% malignant GT or atypical GT had *BRAF V600E* mutation, and *BRAF* gene was believed to be a potential therapeutic target [36]. To further clarify the genetic difference between benign and malignant GGT, the present study applied Sanger sequencing and ARMS testing but found no *BRAF V600E* mutation in either of the 15 cases. We reasoned that this might be due to the few cases of malignant GGT with liver metastasis (only 1 case here). Moreover, none of the 16 malignant GGT cases reported gene testing result, probably because the researchers were not aware of the prognostic significance of the *BRAF* gene in GT or due to the limited objective detection technique at that time. Next-generation sequencing reported *EGFR, PIK3CA, KEAP1* and *TP53* gene mutation. However, previous literature had not reported any prognostic significance of above gene mutations in GGT, so our study can only describe them.

To sum up, GGT is relatively indolent with good prognosis and usually managed by surgical resection in clinic. Notably, more attention should be paid to the presence of increasing morphological risk factors, which may predict the probability of developing adverse outcomes. In the meantime, long-term close follow-up is required to help timely find metastasis and thereby to increase the chance of prolonging survival time by surgical resection.

Data availability statement

The data supporting the findings of this study are available within the article and its supplementary material.

Ethics statement

The studies involving human participants were reviewed and approved by Zhongshan Ethics Committee of Fudan University. Written informed consent to participate in this study was provided by the participants' legal guardian/next of kin. Written informed consent was obtained from the individual(s), and minor(s)' legal guardian/next of kin, for the publication of any potentially identifiable images or data included in this article.

Author contributions

Conception and design, YH, RL, and MD; Methodology, JH; Performed experiment and data collection, JH, YL, MD, and RL; Data analysis, MD, HL, and WY; Writing, MD and HL; Patient sample management, MD, CX and WY; Supervision, YH and CX. All authors contributed to data interpretation, manuscript editing, and revision.

Funding

This work was supported by Shanghai Science and Technology Development Fund (19MC1911000), (19441904000), Shanghai Municipal Clinical Specialty (shslczdzk01302).

Conflict of interest

The authors declare that the research was conducted in the absence of any commercial or financial relationships that could be construed as a potential conflict of interest.

References

1. Smol'iannikov AA. Glomus tumors. *Vopr Onkol* (1974) 20(10):104–16.

2. Folpe AL, Fanburg-Smith JC, Miettinen M, Weiss SW. Atypical and malignant glomus tumors: Analysis of 52 cases, with a proposal for the reclassification of glomus tumors. *Am J Surg Pathol* (2001) 25(1):1–12. doi:10.1097/00000478-200101000-00001

3. Miettinen M, Paal E, Lasota J, Sobin LH. Gastrointestinal glomus tumors: A clinicopathologic, immunohistochemical, and molecular genetic study of 32 cases. *Am J Surg Pathol* (2002) 26(3):301–11. doi:10.1097/00000478-200203000-00003

4. Bray AP, Wong NA, Narayan S. Cutaneous metastasis from gastric glomus tumour. *Clin Exp Dermatol* (2009) 34(8):e719–21. doi:10.1111/j.1365-2230.2009.03445.x

5. Lee H, Choi YS, Oh SC, Park JJ, Kim CW, Kim HC, et al. Malignant glomus tumors of the stomach - a report of 2 cases with multiple metastases. *Korean J Pathol* (2009) 43(4):358–563. doi:10.4132/KoreanJPathol.2009.43.4.358

6. Zhang Q, Zhang CS, Liu GQ, Yu WT, Ma Z. Malignant gastric glomus tumor and literature review. *Chin J Digestion* (2009) 29(9):573–4. doi:10.3760/cma.j.issn.0254-1432.2009.09.019

7. Song SE, Lee CH, Kim KA, Lee HJ, Park CM. Malignant glomus tumor of the stomach with multiorgan metastases: Report of a case. *Surg Today* (2010) 40(7):662–7. doi:10.1007/s00595-008-4113-z

8. Teng TH, Huang SH, Liang CW. Malignant gastric glomus tumour mimicking GIST. *Pathology* (2012) 44(3):261–3. doi:10.1097/PAT.0b013e3283514067

9. Yao XF. A case of malignant gastric glomus tumor. *Chin J Diagn Pathol* (2013) 20(6):380–1. doi:10.3969/j.issn.1007-8096.2013.06.018

10. Tao YL, Wang ZJ, Han JG, Wei GH, Yi BQ, Wei P. A case of gastric malignant glomus tumor complicated by acute gastrointestinal bleeding. *Cancer Res Clinic* (2013) 25(3):214–5. doi:10.3760/cma.j.issn.1006-9801.2013.03.025

11. Zaidi S, Arafah M. Malignant gastric glomus tumor: A case report and literature review of a rare entity. *Oman Med J* (2016) 31(1):60–4. doi:10.5001/omj.2016.11

12. Li CX, Jiang HC, Wang QG. A case of gastric malignant glomus tumor. *Chin J Med Imaging Technol* (2017) 33(3):483. doi:10.13929/j.1003-3289.201608147

13. Bodolan AA, Wilcox R, Yang MX. Malignant glomus tumor of the gastric antrum with hepatic metastases: A case report and literature review. *Hum Pathol Case Rep* (2018) 14:81–4. doi:10.1016/j.ehpc.2018.09.004

14. Toti L, Manzia TM, Roma S, Meucci R, Blasi F, Ferlosio A, et al. Rare malignant glomus tumor of the stomach with liver metastases. *Radiol Case Rep* (2019) 14(4):463–7. doi:10.1016/j.radcr.2019.01.012

15. Kong FH, Chen LQ, Gao SM, Xu GD, Zhang YX. A case of malignant gastric glomus tumor. *Chin J Diagn Pathol* (2019) 26(3):175178. doi:10.3969/j.issn.1007-8096.2019.03.011

16. Alsahwan AG, Alfaraj ZM, AlSafwani J, Bunaiyan AH, AlKhalifah RH, Al-Saba'a SA, et al. Rare gastric neoplasm: Malignant glomus tumor of the stomach. A case report. *Int J Surg Case Rep* (2021) 81:105802. doi:10.1016/j.ijscr.2021.105802

17. Shugart RR, Soule EH, Johnson EW, Jr. Glomus tumor. *Surg Gynecol Obstet* (1963) 117:334–40.

18. Masson P. Le glomus neuromyoarterial des regions tactiles et ses tumeurs. *Lyon Chir* (1924) 21:257–80.

19. Lamba G, Rafiyath SM, Kaur H, Khan S, Singh P, Hamilton AM, et al. Malignant glomus tumor of kidney: The first reported case and review of literature. *Hum Pathol* (2011) 42(8):1200–3. doi:10.1016/j.humpath.2010.11.009

20. Kang G, Park HJ, Kim JY, Choi D, Min BH, Lee JH, et al. Glomus tumor of the stomach: A clinicopathologic analysis of 10 cases and review of the literature. *Gut Liver* (2012) 6(1):52–7. doi:10.5009/gnl.2012.6.1.52

21. Wang X, Hanif S, Wang B, Chai C. Management of gastric glomus tumor: A case report. *Medicine (Baltimore)* (2019) 98(38):e16980. doi:10.1097/MD.0000000000016980

22. Kay S, Callahan WP, Jr, Murray MR, Randall HT, Stout AP. Glomus tumors of the stomach. *Cancer* (1951) 4(4):726–36. doi:10.1002/1097-0142(195107)4:4<726:aid-cncr2820040410>3.0.co;2-z

23. Cao JX, Wang LQ, Li J. Clinicopathologic features of gastric glomus tumor. *Chin J Diagn Pathol* (2021) 28(2):94–7. doi:10.3969/j.issn.1007-8096.2021.02.004

24. Kirshbaum JD, Teitelman SL. Malignant tumor of the greater omentum simulating a glomangioma. *Arch Path* (1939) 27:95–103.

25. Yannopoulos K, Stout AP. Smooth muscle tumors in children. *Cancer* (1962) 15:958–71. doi:10.1002/1097-0142(196209/10)15:5<958:aid-cncr2820150511>3.0.co;2-u

26. Pansa A, Samà L, Ruspi L, Sicoli F, Cananzi FCM, Quagliuolo V. Glomus tumor of the stomach: A systematic review and illustrative case report. *Dig Dis* (2022). doi:10.1159/000525513

27. Papke DJ, Jr, Sholl LM, Doyle LA, Fletcher C, Hornick JL. Gastroesophageal glomus tumors: Clinicopathologic and molecular genetic analysis of 26 cases with a proposal for malignancy criteria. *Am J Surg Pathol* (2022) 46(10):1436–46. doi:10.1097/PAS.0000000000001925

28. Wu TT, Wu CL, Yang QX, Cai F, Zhang FR. Clinical and pathological features of gastric glomus tumor. *Chin J Diagn Pathol* (2013) 20(7):410–3. doi:10.3969/j.issn.1007-8096.2013.07.009

29. Haque S, Modlin IM, West AB. Multiple glomus tumors of the stomach with intravascular spread. *Am J Surg Pathol* (1992) 16(3):291–9. doi:10.1097/00000478-199203000-00010

30. Luzar B, Martin B, Fisher C, Calonje E. Cutaneous malignant glomus tumours: Applicability of currently established malignancy criteria for tumours occurring in the skin. *Pathology* (2018) 50(7):711–7. doi:10.1016/j.pathol.2018.08.005

31. Zhu YZ, Li WP, Wang ZY, Yang HF, He QL, Zhu HG, et al. Glomus tumor of uncertain malignant potential arising in the bronchus. *J Cardiothorac Surg* (2013) 8:146. doi:10.1186/1749-8090-8-146

32. Matevossian E, Brücher BL, Nährig J, Feußner H, Hüser N. Glomus tumor of the stomach simulating a gastrointestinal stromal tumor: A case report and review of literature. *Case Rep Gastroenterol* (2008) 2(1):1–5. doi:10.1159/000112862

33. Xu XD, Lu XH, Ye GX, Hu XR. Immunohistochemical analysis and biological behaviour of gastric glomus tumours: A case report and review of the literature. *J Int Med Res* (2010) 38(4):1539–46. doi:10.1177/147323001003800438

34. Wang JC, Jin XF, Weng SX, Xu C, Gan MF. Gastric glomus tumors expressing synaptophysin: Clinicopathologic and immunohistochemical analyses. *Zhonghua Bing Li Xue Za zhi= Chin J Pathol* (2017) 46(11):756–9. doi:10.3760/cma.j.issn.0529-5807.2017.11.004

35. Agaram NP, Zhang L, Jungbluth AA, Dickson BC, Antonescu CR. A molecular reappraisal of glomus tumors and related pericytic neoplasms with emphasis on NOTCH-gene fusions. *Am J Surg Pathol* (2020) 44(11):1556–62. doi:10.1097/PAS.0000000000001531

36. Karamzadeh Dashti N, Bahrami A, Lee SJ, Jenkins SM, Rodriguez FJ, Folpe AL, et al. BRAF V600E mutations occur in a subset of glomus tumors, and are associated with malignant histologic characteristics. *Am J Surg Pathol* (2017) 41(11):1532–41. doi:10.1097/PAS.0000000000000913

Pathology & Oncology Research | frontiers

TYPE Systematic Review
PUBLISHED 06 August 2024
DOI 10.3389/pore.2024.1611823

Check for updates

OPEN ACCESS

EDITED BY
Andrea Ladányi,
National Institute of Oncology (NIO), Hungary

*CORRESPONDENCE
Armand Csontos,
csontos.armand@pte.hu

RECEIVED 08 May 2024
ACCEPTED 19 July 2024
PUBLISHED 06 August 2024

CITATION
Csontos A, Németh D, Szakó L, Berke G, Sindler DL, Berki D, Papp C, Hegyi P, Vereczkei A and Papp A (2024), Intraoperative pyloric drainage is unnecessary during esophagectomies: a meta-analysis and systematic review of randomized controlled trials. *Pathol. Oncol. Res.* 30:1611823. doi: 10.3389/pore.2024.1611823

COPYRIGHT
© 2024 Csontos, Németh, Szakó, Berke, Sindler, Berki, Papp, Hegyi, Vereczkei and Papp. This is an open-access article distributed under the terms of the Creative Commons Attribution License (CC BY). The use, distribution or reproduction in other forums is permitted, provided the original author(s) and the copyright owner(s) are credited and that the original publication in this journal is cited, in accordance with accepted academic practice. No use, distribution or reproduction is permitted which does not comply with these terms.

Intraoperative pyloric drainage is unnecessary during esophagectomies: a meta-analysis and systematic review of randomized controlled trials

Armand Csontos[1,2]*, Dávid Németh[2,3], Lajos Szakó[2,4,5], Gergő Berke[2], Dóra Lili Sindler[1], Dávid Berki[6], Csenge Papp[1], Péter Hegyi[2,7,8,9], András Vereczkei[1] and András Papp[1]

[1]Department of Surgery, Clinical Center, Medical School, University of Pécs, Pécs, Hungary, [2]Institute for Translational Medicine, Medical School, University of Pécs, Pécs, Hungary, [3]Institute of Bioanalysis, Medical School, University of Pécs, Pécs, Hungary, [4]János Szentágothai Research Centre, Medical School, University of Pécs, Pécs, Hungary, [5]Department of Emergency Medicine, Medical School, University of Pécs, Pécs, Hungary, [6]First Department of Surgery, Military Hospital Medical Centre, Hungarian Defense Forces, Budapest, Hungary, [7]First Department of Medicine, Medical School, University of Szeged, Szeged, Hungary, [8]Hungary Centre for Translational Medicine, Semmelweis University, Budapest, Hungary, [9]Division of Pancreatic Diseases, Heart and Vascular Center, Semmelweis University, Budapest, Hungary

Objective: The topic of this meta-analysis is the comparison of gastric conduit esophageal reconstructions with or without pyloroplasty.

Background: Surgical procedures, especially minimal invasive esophagectomy (MIE) can be a curative treatment in the early stages of esophageal cancer. Previously, intraoperative pyloroplasty was routinely performed, but nowadays it became debated again in the light of minimally invasive esophagectomy.

Methods: A comprehensive search was performed in multiple databases to identify randomized controlled trials investigating the topic. Two independent authors performed the selection based on predefined criteria. Statistical analysis was performed to assess any significant difference, then the bias and quality of the data were estimated.

Results: Nine relevant RCTs consisting of 529 patients with esophageal cancer were identified. No significance was found in mortality [odds ratio (OR): 0.85; p = 0.642], anastomosis leakage (OR: 0.57; p = 0.254), respiratory morbidity (OR: 0.51; p = 0.214) and vomiting (OR: 0.74; p = 0.520), however the results about gastric emptying time (GET) were controversial (weighted mean difference (WMD): −67.71; p = 0.009, OR: 2.75; p = 0.072). Significant heterogeneity was not detected except for GET. Trial sequential analyses (TSA) show that a certain conclusion would require more data except in the binary variables of GET.

Conclusion: We conclude that the pyloric drainage procedure is not routinely necessary, but further well-designed studies would be needed, especially in Europe.

KEYWORDS

esophageal cancer, esophagectomy, esophageal surgery, pyloroplasty, minimal invasive

Introduction

Esophageal cancer is the 8th most common malignancy in the world with more than 600,000 cases (3.1% of all) and it is responsible for more than 500,000 deaths (5.5% of all) on a yearly basis, thus being the 6th most common cause of cancer mortality. The worldwide prevalence in the 1-, 3-, and 5-year-periods are 2.4%, 1.6%, and 1.3%, respectively [1].

The two histological subtypes are squamous cell cancer (SCC) and adenocarcinoma (AC). In 2012 the incidences were estimated to be more than 398,000 (5.2 per 100,000 people) for SCC and 52,000 (0.7 per 100,000 people) for AC globally. Although SCC is still the leading histological form, the number of AC in the Western world is gradually increasing, including Hungary [2]. Esophageal cancer is more common among men, the male-to-female ratios being 2.7 and 4.4 in SCC and AC, respectively [3].

Nowadays esophagus carcinoma still has a poor 5-year survival rate, which is estimated at around 19% in the United States and 12% in Europe [4, 5]. According to tumors, under 3 cm, in stage I–III, the 5-year survival rate can be estimated at 86%–22%. However, in the case of a larger tumor the prognosis is significantly worse, around 27%–8% [6]. As presented, esophageal cancer itself is accompanied by significant mortality and morbidity, to which the possibility of early metastases also contributes. Therefore surgical treatment may also show poor outcomes which depend on the stage of the tumor, the condition of the patients, and the skill of the surgeon [7].

To treat esophageal cancer, the 8th edition of the UICC-AJCC TNM Classification recommends esophagectomy in stages I-IIB, when the operation can be a curative treatment, especially with minimal invasive esophagectomy (MIE) or a robot assisted minimal invasive esophagectomy (RAMIE), both are becoming the gold standard procedures [8, 9]. Performing intraoperative pyloric drainage has long been considered an integral part of the elective esophagectomy, but its application along minimally invasive resections, lead to technical difficulties and prolonged operation time, therefore the necessity of pyloric drainage procedures became debated again [10]. The importance of the topic is also supported by the fact, that new articles are published nowadays, but the literature is still controversial [11–13].

Before the spread of minimal invasive techniques, performing pyloroplasty or pyloromyotomy during esophagectomy was recommended with the aim of reducing gastric stasis, furthermore, providing a better quality of life [14]. From this aspect pyloric drainage can prevent anastomosis leakage, and postoperative pulmonary complications, which can lead to shorter hospital stays, and a lower risk of overall perioperative mortality [15].

Contrary to this, other authors demonstrated that the long-term complications of pyloric interventions facilitate biliary reflux and reflux esophagitis, which can lead to poor quality of life [16]. Therefore, pyloric drainage should be avoided as it is ineffective on the gastric emptying time and may also cause biliary reflux esophagitis [17].

Several papers describe, that pyloroplasty has no benefit in terms of mortality or any sort- and long-term complications, however, the effects of pyloroplasty on the relative risk of delayed gastric emptying is still controversial [16, 18, 19].

Our aim was to investigate whether pyloric drainage procedures are advantageous compared to the omission of these interventions in terms of mortality, gastric emptying time, anastomosis leakage, vomiting, and aspiration pneumonia by performing a meta-analysis according to the latest methodologies. Only the highest quality randomized controlled trials were selected for the most accurate and reliable results.

Methods

We registered our protocol to the medRxiv server in advance, under the number 10.1101/2022.08.24.22279164 [20].

Search strategy

We included studies, which reported on patients treated with esophagectomy due to esophageal cancer. We excluded patients with esophageal resections due to any other causes. The investigational group of our analysis consisted of those with any kind of intraoperative pylorus drainage procedure, while those without it formed the control group. The investigated outcomes were mortality, gastric emptying time (GET), anastomosis leakage, aspiration, vomiting, and respiratory complications. Although our trial was registered in 2022, an up-to-date systematic search was conducted on the 18th of March 2024 to renew our database, allowing us to find the latest RCTs. We searched the following databases: MEDLINE

(via PubMed), Embase, Cochrane Library, Web of Science, and Scopus. We did not use any restrictions. The search phrase was defined as "[(esophagus OR oesophagus OR esophageal OR oesophageal) AND (surgery OR surgical OR operative OR operation OR resection)] OR (esophagectomy OR oesophagectomy OR minimal invasive OR MIE OR RAMIE) AND (pyloroplasty OR pyloromyotomy OR drain*)."

Selection

The selection was performed by two independent authors (A. C. and L. S.) and the disagreements were resolved by a third author (A. P.). EndNote (EndNote X9.3.3, Alfasoft AB, Göteborg, Sweden) was used for the selection steps, which was done by the title, abstract and full-text. We included randomized clinical trials with esophageal cancer patients, who were treated by esophagectomy and pyloric drainage. The trial also had to contain a control group in which no pyloric drainage procedure was performed. References of included articles and former meta-analyses were screened for additional publications. The reasons for exclusion were the retrospective study design, lack of randomization or control group, pediatric trials or animal studies, non-malignant esophageal pathologies, additional surgical interventions, and postoperative pylorus drainage procedure (e.g., balloon dilatation, botulinum toxin injection) or peroral endoscopic myotomy (POEM).

Data extraction

Two independent authors (A. C. and L. S.) extracted data from the articles based on pre-agreed criteria using an Excel data sheet (Office 365, Microsoft, Redmond, WA, United States) for collection and methodization. Data on publication, demography, pathology, operation, and investigated outcomes were extracted.

Statistical analysis

The meta-analytic calculations were performed using the STATA statistical software package (StataCorp. 2017. Stata Statistical Software: Release 15. College Station, TX: StataCorp LLC). Recommendations of the working group of the Cochrane Collaborations were used during the data synthesis. From raw data, pooled odds ratios (ORs) with their 95% confidence intervals (CIs) in the case of dichotomous variables were calculated. In the case of continuous variables, weighted mean differences (WMD) with their 95% confidence intervals were calculated. The random effect model with the estimation of DerSimonian and Laird [21] was used, and the results were displayed on a forest plot. Cochrane's Q and the I^2 statistics were used to assess heterogeneity. Statistical significance was achieved in the case of $p < 0.05$. Trial sequential analysis was performed to assess the necessary number of cases to obtain conclusive evidence in each outcome using the trial sequential analysis tool from Copenhagen Trial Unit (Centre for Clinical Intervention Research, Denmark).

Risk of bias assessment

Two independent authors (A. C. and L. S.) used the Risk of Bias Assessment Tool version 2 by Cochrane to assess the possible biases, and the disagreements were resolved by a third author (A. P.) [22].

Certainty of evidence

To assess the certainty of evidence the GRADE approach was applied by two independent authors (A. C. and L. S.) and a third author (A. P.) to resolve the disagreements [23].

Result

Results of the selection process

In five databases 11,141 articles were identified. After the selection procedures eight articles were included [18, 24–30]. One additional article was found from the references of former meta-analysis [31]. In summary, nine relevant articles were included in the quantitative synthesis [18, 24–31].

We excluded four articles because of a missing control group, and in the case of three articles, full-text articles could not be obtained, even by contacting the authors [32–38].

The detailed results of the selection are presented below (Figure 1).

Characteristics of the studies included

All these nine studies were randomized controlled trials published between 1985 at 2016. Table 1 shows the details of these studies.

Characteristics of the patients

The studied population consisted of 529 patients diagnosed with esophageal cancer, where malignant tumors were confirmed in 524 (99%) cases. 257 (48.6%) patients were randomly assigned to the intraoperative pyloric drainage group, where 253 (98.4%) pyloroplasties and 4 (1.6%) pyloromyotomies were performed. The weighted average age of the population was 58.6 years, and

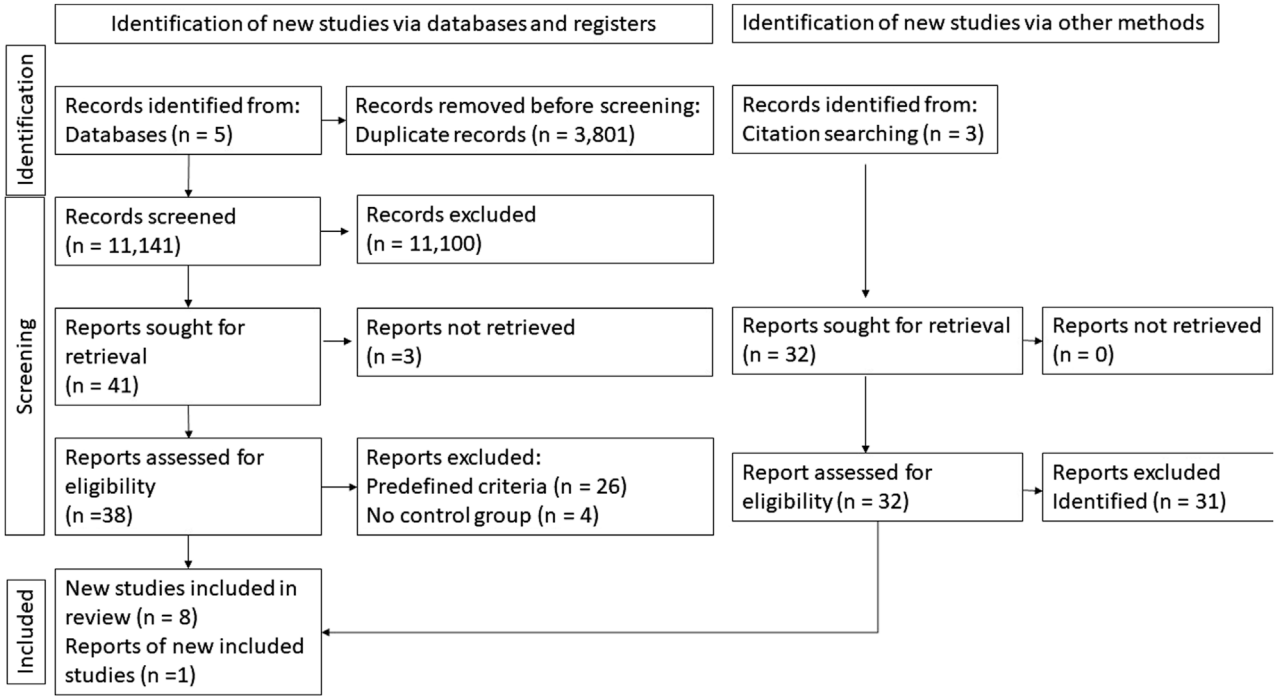

FIGURE 1
Selection flow chart.

TABLE 1 The characteristic of the study.

Author	Year of publication	Country	No. of patients	Man/ Woman	Age	Type of pyloroplasty	Follow-up (mean)
Huang et al. [31]	1985	China	52	—	—	Heineke - Mikulicz	—
Gupta et al. [30]	1989	India	24	—	—	Heineke - Mikulicz	—
Mannel et al. [25]	1990	South Africa	40	—	53.0	Aust	5 MTH
Chattopadhyay et al. [26]	1991	India	24	—	—	Heineke - Mikulicz	—
Fok et al. [24]	1991	Hong Kong	200	9.5	61.0	Heineke - Mikulicz	17 MTH
Chattopadhyay et al. [27]	1993	India	24	3.8	49.0	Heineke - Mikulicz	6 MTH
Kao et al. [29]	1994	China	38	3.8	62.3	Pyloroplasty (n = 15) Pyloromyotomy (n = 4)	—
Zieren et al. [28]	1995	Germany	107	3.9	57.5	Pyloroplasty	6 MTH (median)
Mohajeri et al. [18]	2016	United Arab Emirates	20	2.3	57.4	Pyloroplasty	—

Table 1 is containing the character of the studies. No, number; n, number of patients who underwent intervention; MTH, month. An empty cell means no information is mentioned.

there were 6.7 times more men than women. The patients were in 20% European, 73% Asian, and 7% African. Data on follow-up were very heterogeneous. Patients were followed-up from 2 weeks to 15 years, but the average follow-up time was at 1 year.

Mortality

We included 347 patients from three RCTs in the analysis [25, 28, 30]. No difference was found between the pyloroplasty

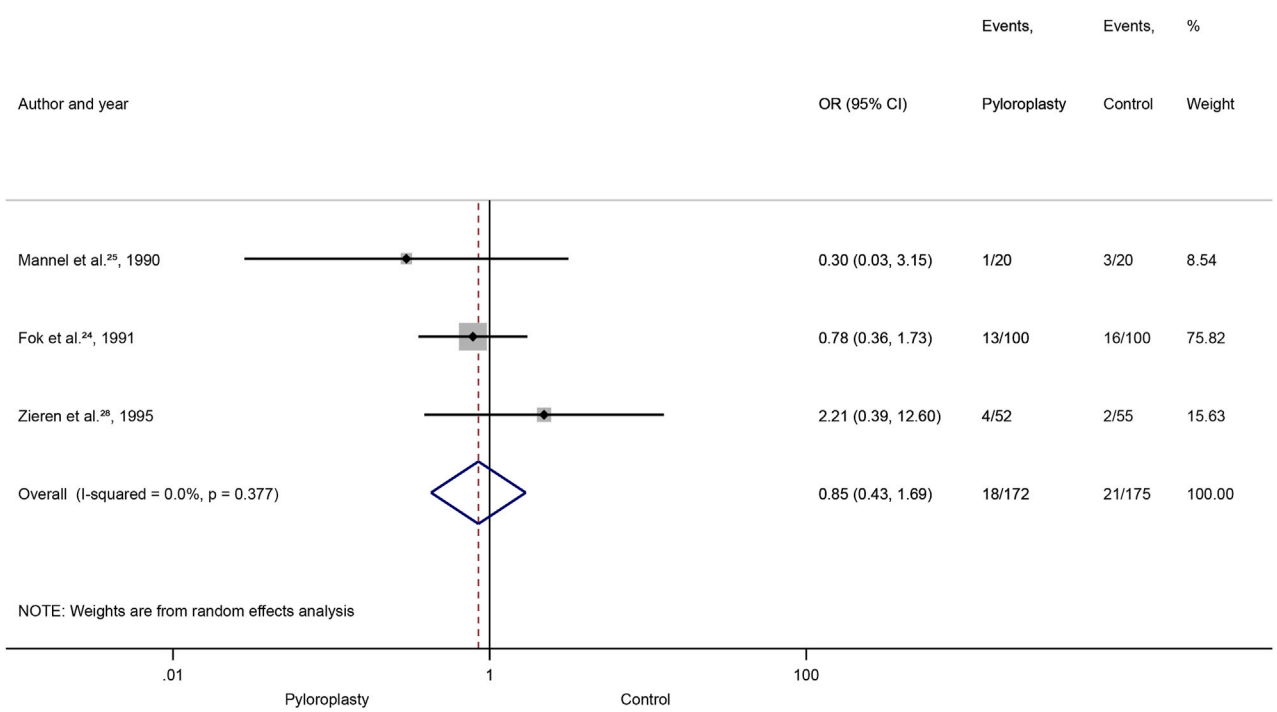

FIGURE 2
Mortality, Forrest plot, OR: odds ratio: CI: confidence interval.

and the control group (OR: 0.85, 95% CI: [0.43, 1.69], p = 0.642), and significant heterogeneity was not detected (I^2 = 0%, p = 0.37) (Figure 2). The TSA analysis could not be performed as the insufficient difference between the two groups were detected.

Anastomosis leakage

367 patients from four RCTs were included [18, 25, 28, 30], and no difference was found between the pyloroplasty and the control group (OR: 0.57, 95% CI: [0.21, 1.51], p = 0.254), and significant heterogeneity was not detected (I^2 = 41%, p = 0.16), however, according to the TSA analysis 2006 patients would have been needed to conclude (Supplementary Figures S1, S2).

Respiratory morbidity

We had 196 patients in three RCTs [25, 26, 30]. No difference was found between the pyloroplasty and the control group (OR: 0.51, 95% CI: [0.18, 1.48], p = 0.214), and significant heterogeneity was not detected (I^2 = 0%, p = 0.47), however, 534 patients would have been required, based on the TSA analysis (Supplementary Figures S3, S4).

Vomiting

The four included RCTs provided 316 patients [25, 27, 30, 31]. No difference was found between the pyloroplasty and the control group (OR: 0.74, 95% CI: [0.30, 1.84], p = 0.520), and significant heterogeneity was not detected (I^2 = 0%, p = 0.62) however, 5,043 patients would have been required to make a conclusive statement (Supplementary Figures S5, S6).

Gastric emptying time

We had 245 patients from four RCTs for dichotomous data [18, 28–30]. The results of the statistical analysis showed that patients in the control group had a significantly, 2.75-fold higher chance for the delayed GET than the pyloroplasty group (OR: 2.75, 95% CI: [1.28, 5.91], p = 0.009), and significant heterogeneity was not detected (I^2 = 0%, p = 0.48) (Figure 3). According to the TSA analysis, the required number of patients was achieved (Supplementary Figure S7).

We had 253 patients from seven RCTs for continuous data [18, 24–26, 28, 29, 31]. No difference was found between the two groups (WMD: −67.71, 95% CI: [−141.60, 6.18], p = 0.072), and significant heterogeneity was detected (I^2 = 99%, p < 0.001), however 623 patients would have been required for this outcome to be conclusive (Supplementary Figures S8, S9).

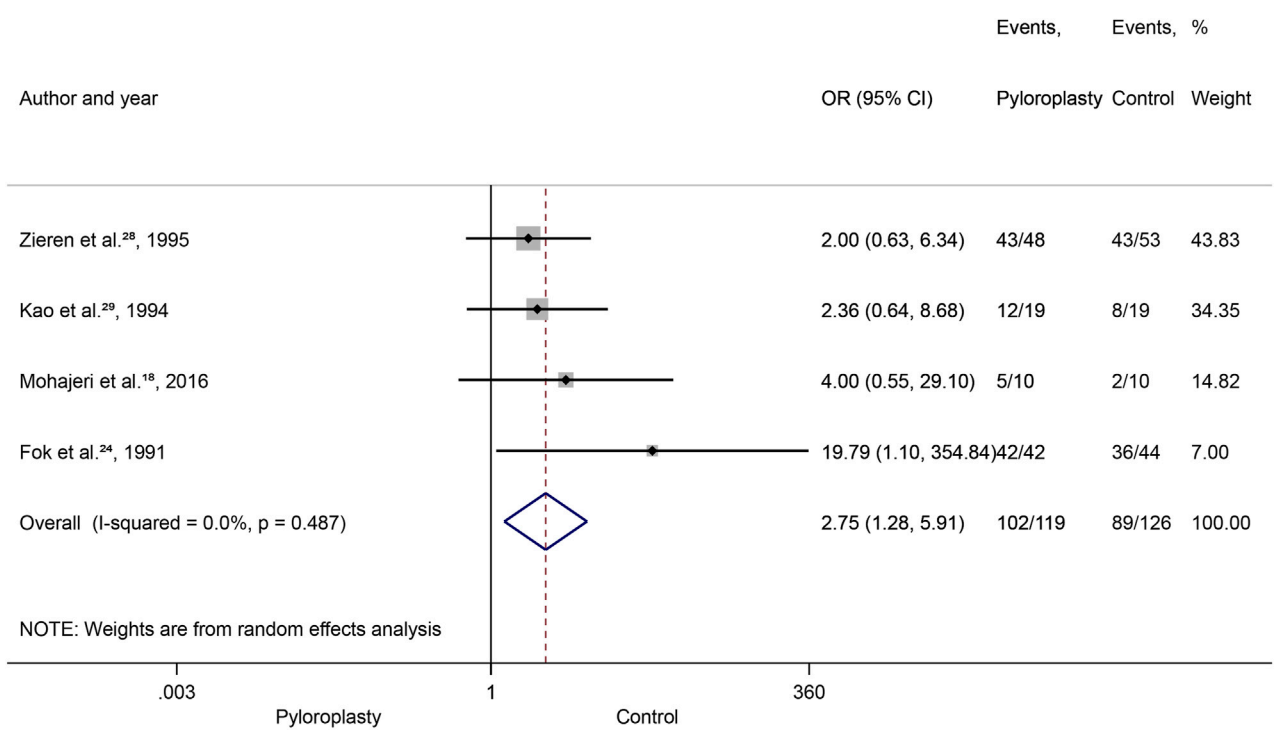

FIGURE 3
Gastric emptying time (GET) dichotomic data, Forrest plot, OR: odds ratio, CI: confidence interval.

Risk of bias

We used Risk of Bias Assessment Tool 2, which estimated all outcomes as low risk (Table 2) [22].

Certainty of evidence

The quality of the evidence (GRADE) of mortality, anastomosis leakage, respiratory morbidity, vomiting, and the dichotomic data of gastric emptying time, were estimated as moderate, due to older articles and the fact, that most of the studies were conducted in an Asian country. The continuous data of the gastric emptying time was low quality, therefore, it should be interpreted accordingly (Supplementary Table S1) [23].

Discussion

Although the debate about the benefit of pyloroplasty is an old-school topic, new articles are still being written about the subject [11–13]. Pyloroplasty following esophagectomy in elective esophageal surgery is still recommended as a routine procedure by many authors, but recommendations apply for a modified version of the technique [11, 13, 39, 40]. In contrast, our investigation has demonstrated, that this step of esophagectomy has no benefits in the practice. In other words, its omission can significantly shorten the surgical time, which can be beneficial for the patient. This fact can be especially important in relation to minimal invasive techniques, which is supported by Nobel et al. with their retrospective study [12].

Minimally invasive esophagectomy (MIE) appears to be beneficial and is increasingly moving towards robot-assisted techniques and has become the gold standard procedure with widespread use [41]. These techniques have many advantages, and only come with negligible limitations. Siaw-Acheampong et al. compared laparoscopic, thoracoscopic, totally minimally invasive, and robotic esophagectomy and they found decreased perioperative morbidity and hospitalization period against open surgery, while MIE did not influence perioperative mortality. Szakó et al. also confirmed these findings in terms of pulmonary complications [41]. On the other hand, these procedures are associated with technical difficulties and prolonged operation time [10]. This is the reason why intraoperative pyloroplasty itself is an additional intervention which can logically extend the otherwise prolonged operation, which may even generate perioperative complications, therefore the debate about the necessity of pyloroplasty arose again.

Through technical developments new postoperative methods have emerged, such as balloon dilatation, pyloric bouginage, endoscopic myotomy, or botulinum toxin injection [11, 13, 18, 42]. Although all are safe and accessible, and can be performed instead of surgical pyloroplasty in some cases,

TABLE 2 The result of risk of bias tool 2.

Outcome	Article	Randomization process	Deviations from the intended interventions	Missing outcome data	Measurement of the outcome	Selection of the reported result	Overall
Mortality	Mannel et al. [25], 1990	+	+	+	+	+	+
	Fok et al. [24], 1991	+	+	+	+	+	+
	Zieren et al. [28], 1995	+	+	+	+	+	+
Anastomosis Leakage	Mannel et al. [25], 1990	+	+	+	+	+	+
	Fok et al. [24], 1991	+	+	+	+	+	+
	Zieren et al. [28], 1995	+	+	+	+	+	+
	Mohajeri et al. [18], 2016	+	+	+	+	+	+
Respiratory Morbidity	Mannel et al. [25], 1990	+	+	+	+	+	+
	Chattopadhyay et al. [26], 1991	+	+	+	+	+	+
	Zieren et al. [28], 1995	+	+	+	+	+	+
Vomiting	Huang et al. [31], 1985	+	+	+	+	+	+
	Mannel et al. [25], 1990	+	+	+	+	+	+
	Chattopadhyay et al. [26], 1991	+	+	+	+	+	+
	Zieren et al. [28], 1995	+	+	+	+	+	+
Gastric Emptying Time (dichotomic)	Fok et al. [24], 1991	+	+	+	+	+	+
	Kao et al. [29], 1994	+	+	+	+	+	+
	Zieren et al. [28], 1995	+	+	+	+	+	+
	Mohajeri et al. [18], 2016	+	+	+	+	+	+
Gastric Emptying Time (continuous)	Huang et al. [31], 1985	+	+	+	+	+	+
	Gupta et al. [30], 1989	+	+	+	+	+	+
	Mannel et al. [25], 1990	+	+	+	+	+	+
	Chattopadhyay et al. [26], 1991	+	+	+	+	+	+
	Fok et al. [24], 1991	+	+	+	+	+	+

(Continued on following page)

TABLE 2 (*Continued*) The result of risk of bias tool 2.

Outcome	Article	Randomization process	Deviations from the intended interventions	Missing outcome data	Measurement of the outcome	Selection of the reported result	Overall
	Kao et al. [29], 1994	+	+	+	+	+	+
	Mohajeri et al. [18], 2016	+	+	+	+	+	+

Table 2 is containing the results of Risk of Bias Tool 2, which resulted in low risk in all outcomes. +: Low risk; !: Some concerns; -: high risk.

there are still limitations and no evidence about routine usage. Per-oral gastric pyloromyotomy (GPOP), which was developed in the pattern of per-oral endoscopic myotomy (POEM), may be useful in case of resistance to balloon dilatation or botulinum toxin injection, however, it has limitations due to its technical difficulties [43]. In the case of botulinum toxin injection there are data about an increased chance of reoperation [44]. Despite their limitations, all these methods are available, safe, and quick, therefore potentially may replace intraoperative pyloroplasty. Based on these, our focus of interest is highlighted again [12, 32, 44].

Clear evidence is still missing, considering the best type of minimally invasive pyloric drainage procedure or whether pyloric drainage should be recommended during surgery or not [11, 12, 44].

Almost a decade ago, Gaur et al. and Khan et al. stated that the omission of pyloroplasty had no benefits and proposed the technique [15, 39]. Later, Arya et al. found no significant difference between the pyloroplasty and the control groups in their work, although the strength of these findings had limitations, because only seven RCTs were included in addition to 18 lower quality articles [16]. Other limitation were the small number of patients and the high heterogeneity of the definitions of outcomes in the enrolled studies.

In our meta-analysis, we provide the most precise and objective evidence available to date on the topic, due to the strict inclusion criteria of our work. Although the previous meta-analyses' partial results confirm our findings, they overall favored intraoperative pyloroplasty or had a significant heterogeneity, therefore, we considered this rediscussion necessary. We used the latest protocol in our study, and only the latest randomized controlled studies were included to minimize the risk of bias.

As expected, **mortality** remained low in both arms in the individual enrolled studies, as esophagectomy is usually performed as an elective intervention. Based on our analysis, performing pyloric drainage combine with esophagectomy does not carry additional advantage compared to the omission of pyloric drainage ($p = 0.642$). This finding is also supported by the former systematic analyses ($p = 0.86$) [19]. Despite the fact, that mortality is the strongest investigated outcome, this might not present a clear view of the benefits and harms of such an intervention due to the formerly mentioned reasons. On the other hand, cancer-specific and overall survival should be investigated more thoroughly by future studies.

Anastomotic leakage is one of the most common complications of any kind of surgical resection. The additional operation can be associated with mortality and morbidity, therefore may influence this outcome. However, neither our analysis ($p = 0.254$) nor previous works ($p = 0.12$; $p = 0.77$) described such an effect or difference [16, 19].

Besides anastomotic leakage, another common complication of surgical procedures is **pulmonary morbidity**. Since none of the existing systematic reviews and meta-analyses found a significant difference ($p = 0.214$) ($p = 0.31$; $p = 0.15$) [16, 19], and Urschel et al. also have not reported any significant difference in risk of **fatal pulmonary aspiration** ($p = 0.14$), therefore pyloric drainage is not superior from this aspect [19].

Relative risk of **pyloric drainage complication** was reported ($p = 0.33$) [19], and we also have not found any benefit in terms of **vomiting** ($p = 0.520$). Although Urschel et al. found no evidence of biliary complications [19], but in the opinion of other authors, pyloric interventions may increase long-term **biliary reflux** ($p = 0.069$) and **reflux esophagitis** ($p < 0.05$), which can lead to poor quality of life, however, this long-term complication could not be analysed in this meta-analysis [15, 16].

Multiple methods can be used for examining the **gastric emptying time**; therefore, the results carry notable limitations. Arya et al. found only six comparative studies out of twenty-four, and they found no significant difference between the control and pyloroplasty groups in delayed gastric emptying ($p = 0.22$) [16]. Urschel et al. found that the 0.53 drainage versus no drainage ratio expressed a shorter emptying time in scintigraphy examination, but the semiquantitative analysis found no significance in gastric emptying [19]. However, we also found in seven RCTs shorter gastric emptying time, in the case of continuous data ($p = 0.009$), but in the dichotomic analysis, we found no significant difference based on four RCTs ($p = 0.072$) [18, 28–30].

Gaur et al. used delayed **gastric emptying and gastric outlet obstruction ratio**, which did not show a significant difference between the control and the pyloric drainage group (DGE/GOO of 8.1%, 13.2%) [15].

Although not clearly detailed, Urschel et al. found relative risk for **gastric outlet obstruction**, based on three RCTs [25, 28, 30]. (RR: 0.18, 95% CI, 0.03, 0.97; $p = 0.046$), but the semiquantitative analysis found no significant difference in **obstructive foregut symptoms** (−0.84) and **food intake** and

nutritional status (+1.02) [19]. According to Gaur et al. pyloric drainage was ineffective in **dumping syndrome** [15].

The population and outcomes of our analysis are homogeneous. Due to the enrolment of randomized controlled trials the risk of bias is low. The TSA analysis is limited according to the recent guidelines, therefore they should be interpreted accordingly. In the case of some outcomes, the evidence is not conclusive, based on our TSA results. In these cases, further randomized clinical trials are needed. RCTs should focus on survival rather than mortality, as it provides a clearer picture of the most relevant outcome.

Limitations were caused by the rigorous inclusion criteria, which resulted in fewer clinical trials being available, thus a low number of patients. The other limitation is the date of the trials. The median year of origin of the articles was 1991, which carries a bias, due to development of the esophageal surgical procedures.

The proportion of available data of the demographic parameters about age, sex, stage, type of surgery, and resection were 66%, 55%, 22%, and 44%, respectively, which may affect the examined outcomes.

The population of the patients was overwhelmingly Asian while Europeans and South Africans were represented by only one article each [25, 30]. Thus, the application of these results to European and American populations is limited due to the seven Asian articles, in detail China, Hong Kong and India [24, 26–29, 31]. United Arab Emirates was also represented [18].

Another possible limitation is that certain outcomes were very heterogenic. The measurement of gastric emptying time used different methods and protocols (barium or isotope protocol), and some morbidity groups did not have clear clusters or artificial limit value was defined and the subjective sensations were also not clarified or not scanned at all.

Conclusion

In conclusion, pyloroplasty during esophagectomy in elective surgery especially MIE has no substantial benefit based on our results, therefore it should be routinely omitted to reduce operating time. It does not affect mortality, anastomosis leakage, respiratory or another morbidity like vomiting, or reflux, but it has possible risks. Its effect on shorter gastric emptying time is unclear, and the beneficial consequence is questionable. If symptoms of gastric stasis occur, available postoperative pyloric drainage procedures are good options.

Data availability statement

The original contributions presented in the study are included in the article/Supplementary Material, further inquiries can be directed to the corresponding author.

Author contributions

AC contributed to the conception, search, data interpretation, creating figures, tables and writing the manuscript. DN contributed to statistical analysis and writing the manuscript. LS contributed to the conception, search, data interpretation and writing the manuscript. GB contributed to the revision of the conception and writing the manuscript. DS contributed to the data interpretation and writing of the manuscript. DB contributed to the data interpretation and writing of the manuscript. CP contributed to the data interpretation and writing of the manuscript. PH contributed to the methodological revision of the analysis. AV contributed to the professional and linguistic revision. AP contributed to the conception, data interpretation, writing of the manuscript and the professional and linguistic revision. All authors contributed to the article and approved the submitted version.

Funding

The authors declare that no financial support was received for the research, authorship, and/or publication of this article.

Conflict of interest

The authors declare that the research was conducted in the absence of any commercial or financial relationships that could be construed as a potential conflict of interest.

Supplementary material

The Supplementary Material for this article can be found online at: https://www.por-journal.com/articles/10.3389/pore.2024.1611823/full#supplementary-material

SUPPLEMENTARY FIGURE S1
Anastomosis leakage, Forrest plot, OR: odds ratio, CI: confidence interval.

SUPPLEMENTARY FIGURE S2
Anastomosis leakage, trial sequential analysis (TSA) analysis.

SUPPLEMENTARY FIGURE S3
Respiratory morbidity, Forrest plot, OR: odds ratio, CI: confidence interval.

SUPPLEMENTARY FIGURE S4
Respiratory morbidity, trial sequential analysis (TSA) analysis.

SUPPLEMENTARY FIGURE S5
Vomiting, Forrest plot, OR: odds ratio, CI: confidence interval.

SUPPLEMENTARY FIGURE S6
Vomiting, trial sequential analysis (TSA) analysis.

SUPPLEMENTARY FIGURE S7
Gastric emptying time (GET) dichotomic data, trial sequential analysis (TSA) analysis.

SUPPLEMENTARY FIGURE S8
Gastric emptying time (GET) continuous data, Forrest plot, WMD: weighted mean difference, SD: standard deviation.

SUPPLEMENTARY FIGURE S9
Gastric emptying time (GET) continuous data, trial sequential analysis (TSA) analysis.

References

1. GLOBOCAN. *Cancer today - IARC, 150 cours Albert Thomas, 69372 Lyon CEDEX 08, France - Tel: +33 (0)4 72 73 84 85 - powered by GLOBOCAN* (2020).

2. Tinusz B, Szapáry LB, Paládi B, Papp A, Bogner B, Hegedűs I, et al. The esophageal adenocarcinoma epidemic has reached Hungary: a multicenter, cross-sectional study. *Front Oncol* (2020) 10:541794. doi:10.3389/fonc.2020.541794

3. Arnold M, Soerjomataram I, Ferlay J, Forman D. Global incidence of oesophageal cancer by histological subtype in 2012. *Gut* (2015) 64(3):381–7. doi:10.1136/gutjnl-2014-308124

4. Siegel R, Ma J, Zou Z, Jemal A. Cancer statistics, 2014. *CA Cancer J Clin* (2014) 64(1):9–29. Epub 2014 Jan 7. Erratum in: CA Cancer J Clin. 2014 Sep-Oct; 64(5): 364. doi:10.3322/caac.21208

5. De Angelis R, Sant M, Coleman MP, Francisci S, Baili P, Pierannunzio D, et al. Cancer survival in Europe 1999–2007 by country and age: results of EUROCARE--5-a population-based study. *Lancet Oncol* (2014) 15(1):23–34. doi:10.1016/S1470-2045(13)70546-1

6. Yendamuri S, Swisher SG, Correa AM, Hofstetter W, Ajani JA, Francis A, et al. Esophageal tumor length is independently associated with long-term survival. *Cancer* (2009) 115(3):508–16. doi:10.1002/cncr.24062

7. Kim SH, Lee KS, Shim YM, Kim K, Yang PS, Kim TS. Esophageal resection: indications, techniques, and radiologic assessment. *Radiographics* (2001) 21(5): 1119–37. discussion 1138-40. doi:10.1148/radiographics.21.5.g01se031119

8. Rice TW, Patil DT, Blackstone EH. 8th edition AJCC/UICC staging of cancers of the esophagus and esophagogastric junction: application to clinical practice. *Ann Cardiothorac Surg* (2017) 6(2):119–30. doi:10.21037/acs.2017.03.14

9. Noordman BJ, Gisbertz SS. Minimally invasive oesophagectomy as standard of care. *Br J Surg* (2023) 13:1118–9. doi:10.1093/bjs/znad209

10. Siaw-Acheampong K, Kamarajah SK, Gujjuri R, Bundred JR, Singh P, Griffiths EA. Minimally invasive techniques for transthoracic oesophagectomy for oesophageal cancer: systematic review and network meta-analysis. *BJS Open* (2020) 4(5):787–803. doi:10.1002/bjs5.50330

11. Nevo Y, Calderone A, Kammili A, Boulila C, Renaud S, Cools-Lartigue J, et al. Endoscopic pyloromyotomy in minimally invasive esophagectomy: a novel approach. *Surg Endosc* (2022) 36(4):2341–8. doi:10.1007/s00464-021-08511-0

12. Nobel T, Tan KS, Barbetta A, Adusumilli P, Bains M, Bott M, et al. Does pyloric drainage have a role in the era of minimally invasive esophagectomy? *Surg Endosc* (2019) 33(10):3218–27. doi:10.1007/s00464-018-06607-8

13. Kim D. The optimal pyloric procedure: a collective review. *Korean J Thorac Cardiovasc Surg* (2020) 53(4):233–41. doi:10.5090/kjtcs.2020.53.4.233

14. Hagen JA, Peyre CG. Gastric emptying procedures after esophagectomy. In: Ferguson MK, editor. *Difficult decisions in thoracic surgery*. London: Springer (2007). doi:10.1007/978-1-84628-474-8_30

15. Gaur P, Swanson SJ. Should we continue to drain the pylorus in patients undergoing an esophagectomy? *Dis Esophagus* (2014) 27(6):568–73. doi:10.1111/dote.12035

16. Arya S, Markar SR, Karthikesalingam A, Hanna GB. The impact of pyloric drainage on clinical outcome following esophagectomy: a systematic review. *Dis Esophagus* (2015) 28(4):326–35. doi:10.1111/dote.12191

17. Palmes D, Weilinghoff M, Colombo-Benkmann M, Senninger N, Bruewer M. Effect of pyloric drainage procedures on gastric passage and bile reflux after esophagectomy with gastric conduit reconstruction. *Langenbecks Arch Surg* (2007) 392(2):135–41. doi:10.1007/s00423-006-0119-4

18. Mohajeri G, Tabatabaei SA, Hashemi SM, Hemmati H. Comparison of pyloromyotomy, pyloric buginage, and intact pylorus on gastric drainage in gastric pull-up surgery after esophagectomy. *J Res Med Sci* (2016) 21:33. doi:10.4103/1735-1995.181993

19. Urschel JD, Blewett CJ, Young JE, Miller JD, Bennett WF. Pyloric drainage (pyloroplasty) or no drainage in gastric reconstruction after esophagectomy: a meta-analysis of randomized controlled trials. *Dig Surg* (2002) 19(3):160–4. doi:10.1159/000064206

20. Csontos A, Németh D, Szakó L, Berke G, Sindler DL, Hegyi P, et al. (2022). The necessity of pyloric drainage in esophagectomies: protocol of a meta-analysis and a systematic review of randomized controlled trials. Available from: https://www.medrxiv.org/. doi:10.1101/2022.08.24.22279164

21. DerSimonian R, Laird N. Meta-analysis in clinical trials. *Control Clin Trials* (1986) 7(3):177–88. doi:10.1016/0197-2456(86)90046-2

22. Higgins JP, Altman DG, Gøtzsche PC, Jüni P, Moher D, Oxman AD, et al. The Cochrane collaboration's tool for assessing risk of bias in randomised trials. *BMJ* (2011) 343:d5928. doi:10.1136/bmj.d5928

23. Brozek JL, Akl EA, Alonso-Coello P, Lang D, Jaeschke R, Williams JW, et al. Grading quality of evidence and strength of recommendations in clinical practice guidelines. Part 1 of 3. An overview of the GRADE approach and grading quality of evidence about interventions. *Allergy* (2009) 64(5):669–77. doi:10.1111/j.1398-9995.2009.01973.x

24. Fok M, Cheng SW, Wong J. Pyloroplasty versus no drainage in gastric replacement of the esophagus. *Am J Surg* (1991) 162(5):447–52. doi:10.1016/0002-9610(91)90258-f

25. Mannell A, McKnight A, Esser JD. Role of pyloroplasty in the retrosternal stomach: results of a prospective, randomized, controlled trial. *Br J Surg* (1990) 77(1):57–9. doi:10.1002/bjs.1800770120

26. Chattopadhyay TK, Gupta S, Padhy AK, Kapoor VK. Is pyloroplasty necessary following intrathoracic transposition of stomach? Results of a prospective clinical study. *Aust N Z J Surg* (1991) 61(5):366–9. doi:10.1111/j.1445-2197.1991.tb00236.x

27. Chattopadhyay TK, Shad SK, Kumar A. Intragastric bile acid and symptoms in patients with an intrathoracic stomach after oesophagectomy. *Br J Surg* (1993) 80(3):371–3. doi:10.1002/bjs.1800800336

28. Zieren HU, Müller JM, Jacobi CA, Pichlmaier H. Soll beim magenhochzug nach subtotaler oesophagektomie mit oesophago-gastraler anastomose am hals eine pyloroplastik durchgeführt werden? Eine prospektiv randomisierte studie should a pyloroplasty be carried out in stomach transposition after subtotal esophagectomy with esophago-gastric anastomosis at the neck? A prospective randomized study. *Chirurg* (1995) 66(4):319–25.

29. Kao CH, Chen CY, Chen CL, Wang SJ, Yeh SH. Gastric emptying of the intrathoracic stomach as oesophageal replacement for oesophageal carcinomas. *Nucl Med Commun* (1994) 15(3):152–5. doi:10.1097/00006231-199403000-00006

30. Gupta S, Chattopadhyay TK, Gopinath PG, Kapoor VK, Sharma LK. Emptying of the intrathoracic stomach with and without pyloroplasty. *Am J Gastroenterol* (1989) 84(8):921–3.

31. Huang GJ, Zhang DC, Zhang DW. A Comparative study of resection of carcinoma of the esophagus with and without pyloroplasty. In: Demeester TR, Skinner DB, editors. *Esophageal disorder: pathophysiology and therapy*. New York, NY: Raven Press (1985). p. 383.

32. Manjari R, Padhy AK, Chattopadhyay TK. Emptying of the intrathoracic stomach using three different pylorus drainage procedures--results of a comparative study. *Surg Today* (1996) 26(8):581–5. doi:10.1007/BF00311660

33. Bagheri R, Fattahi SH, Haghi SZ, Aryana K, Aryanniya A, Akhlaghi S, et al. Botulinum toxin for prevention of delayed gastric emptying after esophagectomy. *Asian Cardiovasc Thorac Ann* (2013) 21(6):689–92. doi:10.1177/0218492312468438

34. Law S, Cheung MC, Fok M, Chu KM, Wong J. Pyloroplasty and pyloromyotomy in gastric replacement of the esophagus after esophagectomy: a randomized controlled trial. *J Am Coll Surg* (1997) 184(6):630–6.

35. Nikbakhsh N, Hashemi R, Noorbaran A. Esophagectomy without pyloroplasty or pyloromyotomy. *J Isfahan Med Sch* (2014) 32(277).

36. Nakamura Y, Nakayama T, Mitomi T, Ueda M, Kaitsu N. Clinical study on pyloroplasty and myotomy of the pylorus in surgery of esophageal cancer. *Shujutsu* (1967) 21(9):899–910.

37. Cheung HC, Siu KF, Wong J. Is pyloroplasty necessary in esophageal replacement by stomach? A prospective, randomized controlled trial. *Surgery* (1987) 102(1):19–24.

38. Kobayashi A, Ide H, Eguchi R, Nakamura T, Hayashi K, Hanyu F. The efficacy of pyloroplasty affecting to oral-intake quality of life using reconstruction with gastric tube post esophagectomy. *Nihon Kyobu Geka Gakkai Zasshi* (1996) 44(6): 770–8.

39. Khan OA, Manners J, Rengarajan A, Dunning J. Does pyloroplasty following esophagectomy improve early clinical outcomes? *Interact Cardiovasc Thorac Surg* (2007) 6(2):247–50. doi:10.1510/icvts.2006.149500

40. Oezcelik A, DeMeester SR, Hindoyan K, Leers JM, Ayazi S, Abate E, et al. Circular stapled pyloroplasty: a fast and effective technique for pyloric disruption during esophagectomy with gastric pull-up. *Dis Esophagus* (2011) 24(6):423–9. doi:10.1111/j.1442-2050.2010.01169.x

41. Szakó L, Németh D, Farkas N, Kiss S, Dömötör RZ, Engh MA, et al. Network meta-analysis of randomized controlled trials on esophagectomies in esophageal cancer: the superiority of minimally invasive surgery. *World J Gastroenterol* (2022) 28(30):4201–10. doi:10.3748/wjg.v28.i30.4201

42. Fuchs HF, Broderick RC, Harnsberger CR, Divo FA, Coker AM, Jacobsen GR, et al. Intraoperative endoscopic botox injection during total esophagectomy prevents the need for pyloromyotomy or dilatation. *J Laparoendosc Adv Surg Tech A* (2016) 26(6):433–8. doi:10.1089/lap.2015.0575

43. Anderson MJ, Sippey M, Marks J. Gastric per oral pyloromyotomy for post-vagotomy-induced gastroparesis following esophagectomy. *J Gastrointest Surg* (2020) 24(3):715–9. doi:10.1007/s11605-019-04418-3

44. Giugliano DN, Berger AC, Meidl H, Pucci MJ, Rosato EL, Keith SW, et al. Do intraoperative pyloric interventions predict the need for postoperative endoscopic interventions after minimally invasive esophagectomy? *Dis Esophagus* (2017) 30(4): 1–8. doi:10.1093/dote/dow034

Pathology & Oncology Research | frontiers

TYPE Systematic Review
PUBLISHED 11 October 2024
DOI 10.3389/pore.2024.1611844

Check for updates

OPEN ACCESS

EDITED BY
Judit Kocsis,
Bács-Kiskun County Hospital, Hungary

*CORRESPONDENCE
Yan Wang,
wangyanxw@wchscu.cn
Chao Cheng,
505162410@qq.com

†These authors have contributed equally to this work

RECEIVED 22 May 2024
ACCEPTED 19 September 2024
PUBLISHED 11 October 2024

CITATION
Chen P, Chen M, Bu Y, Che G, Cheng C and Wang Y (2024) Prognostic role of lymph node regression in patients with esophageal cancer undergoing neoadjuvant therapy.
Pathol. Oncol. Res. 30:1611844.
doi: 10.3389/pore.2024.1611844

COPYRIGHT
© 2024 Chen, Chen, Bu, Che, Cheng and Wang. This is an open-access article distributed under the terms of the Creative Commons Attribution License (CC BY). The use, distribution or reproduction in other forums is permitted, provided the original author(s) and the copyright owner(s) are credited and that the original publication in this journal is cited, in accordance with accepted academic practice. No use, distribution or reproduction is permitted which does not comply with these terms.

Prognostic role of lymph node regression in patients with esophageal cancer undergoing neoadjuvant therapy

Pingrun Chen[1†], Maojia Chen[2†], Yijie Bu[3], Guowei Che[4], Chao Cheng[3*] and Yan Wang[3*]

[1]Department of Gastroenterology and Hepatology, West China Hospital, Sichuan University, Chengdu, China, [2]Animal Experiment Center, West China Hospital, Sichuan University, Chengdu, China, [3]Department of Thoracic Surgery, West China Hospital, Sichuan University, Chengdu, China, [4]Department of Thoracic Surgery/Lung Cancer Center, West China Hospital, Sichuan University, Chengdu, China

Purpose: To clarify the prognostic value of lymph node regression (LNR) status including the lymph node regression grade (LNRG) and N downstaging in patients with esophageal cancer receiving neoadjuvant therapy based on available evidence.

Methods: Several databases were searched up to 25 March 2024. The main outcomes included overall survival (OS), disease-free survival (DFS) and cancer-specific survival (CSS). Hazard ratios (HRs) and 95% confidence intervals (CIs) were combined. Subgroup analyses based on the neoadjuvant therapy and pathological type were also conducted.

Results: In total, 14 retrospective studies with 3,212 participants were included. Nine and five studies explored the relationship between LNRG and N downstaging and survival, respectively. Pooled results indicated that complete LNR predicted significantly improved OS (HR = 0.47, 95% CI: 0.41–0.55, P < 0.001) and DFS (HR = 0.42, 95% CI: 0.32–0.55, P < 0.001) and subgroup analysis based on neoadjuvant therapy and pathological type manifested similar results. Besides, N downstaging was also significantly related to improved OS (HR = 0.40, 95% CI: 0.21–0.77, P = 0.006) and CSS (HR = 0.27, 95% CI: 0.12–0.60, P < 0.001).

Conclusion: LNR could serve as a novel and reliable prognostic factor in patients with esophageal cancer receiving neoadjuvant therapy and complete LNR and N downstaging predict better survival.

KEYWORDS

lymph node regression, esophageal cancer, neoadjuvant therapy, survival, meta-analysis

Introduction

Esophageal cancer ranks as the fourth leading cause of cancer-related deaths, comprising predominantly squamous cell carcinoma and adenocarcinoma, with an overall poor prognosis [1, 2]. In recent years, the clinical role of neoadjuvant therapy in the treatment of esophageal cancer has become increasingly prominent and neoadjuvant therapy combined with surgery significantly improves the prognosis for the majority of patients with locally advanced esophageal cancer [3]. Recent studies have demonstrated the superiority of neoadjuvant chemoradiotherapy over neoadjuvant chemotherapy in terms of long-term survival outcomes in locally advanced esophageal cancer [4]. Even with similar adverse effects, neoadjuvant chemoradiotherapy provides superior short-term benefits compared to neoadjuvant chemotherapy [4]. Moreover, neoadjuvant chemoradiotherapy is associated with impressive rates of pathological complete response, and survival [5, 6]. In addition, the role of neoadjuvant immunotherapy is gradually being elucidated in the clinic [7]. Thus, neoadjuvant therapy holds an indispensable position in the comprehensive antitumor therapy of esophageal cancer.

Furthermore, with the incorporation of adjuvant therapy, the TNM stage appears to be less reliable in predicting the prognosis of neoadjuvant therapy compared to surgery alone. Therefore, to aid in prognosis evaluation, imaging and pathological approaches to assess tumor regression are considered vital evaluation tools. However, pathological criteria undoubtedly offer greater objectivity. The widely adopted tumor regression grade (TRG) system categorizes residual tumors after treatment-induced regression based on parameters such as quantity, proportion, tumor cell condition, and extent and distribution of fibrosis [8]. Nevertheless, there exist multiple variations of TRG [9, 10]. While the majority of evaluation systems are generally regarded as good indicators for predicting short-term therapeutic effects and estimating the risk of recurrence, each grade only reflects the therapeutic effect on the primary tumors [9, 10]. However, it has been reported that the response of primary lesions and lymph nodes to neoadjuvant therapy differs [9]. Furthermore, some studies have indicated that lymph node metastasis status is more strongly associated with prognosis than primary lesion invasion, whether after surgery or neoadjuvant therapy [11]. Consequently, lymph nodes must be individually evaluated and the prognostic role of lymph node regression (LNR) in patients with esophageal cancer should be further determined. For LNR grade (LNRG) assessment, dissected lymph nodes are usually stained with hematoxylin and eosin and analyzed microscopically for metastatic disease in clinics. Currently, there is no standardized protocol for evaluating LNR. Lymph node downstaging is usually defined as any regional lymph node that is positive on clinical evaluation (cN+) and subsequently has no evidence of pathologic regional lymph node disease. To date, the prognostic role of LNR in esophageal cancer patients undergoing neoadjuvant therapy remains uncertain.

Therefore, this study aimed to identify the predictive role of LNR status in locally advanced patients with esophageal cancer who received neoadjuvant therapy based on current evidence.

Materials and methods

This study was performed according to the Preferred Reporting Items for Systematic Review and Meta-Analyses 2020 [12].

Literature search

The Medline, EMBASE, and Web of Science databases were searched from their inception up to 25 March 2024. The following terms were used: esophageal, esophagus, tumor, cancer, neoplasm, carcinoma, survival, prognostic, prognosis, neoadjuvant, lymph node regression, and N downstaging. A detailed search strategy in Medline is provided in Supplementary file 1. References to the included studies were also reviewed.

Inclusion criteria

Studies were included if they met the following criteria: 1) patients were pathologically diagnosed with primary esophageal cancer; 2) patients received neoadjuvant therapy including chemotherapy, radiotherapy, immunotherapy, or combined therapy; 3) lymph node status was evaluated before and after neoadjuvant therapy; 4) patients in the complete/subtotal response group and partial/no response group and patients in the N downstaging group (ypN0) and ypN+ group were compared separately; 5) overall survival (OS), disease-free survival (DFS) or (and) was compared between groups; 6) hazard ratios (HRs) with 95% confidence intervals (CIs) were reported, or the Kaplan-Meier survival curves were provided; 7) full texts were available in English.

Exclusion criteria

Studies were excluded if they met the following criteria: 1) insufficient, duplicated, or overlapping data; 2) animal studies, editorials, letters, meeting abstracts or case reports.

Data extraction

The following information was collected: the first author, publication year, country, sample size, c-tumor-node-metastasis

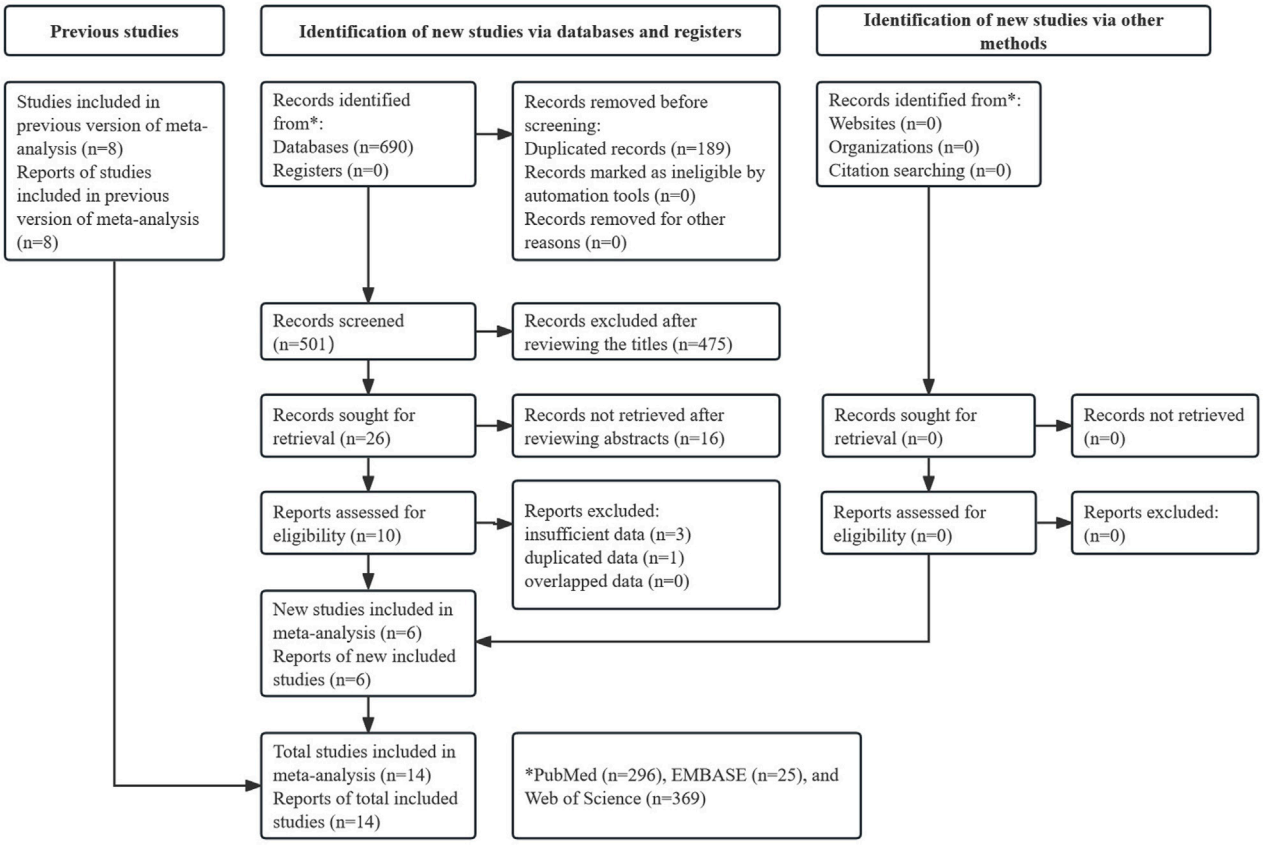

FIGURE 1
Prisma flow diagram of this meta-analysis.

(cTNM) stage, type of neoadjuvant therapy, pathological type, type of LNR, definition of LNRG or N downstaging, source of HR, follow-up time, outcome, and HR with 95% CI.

Quality evaluation

The Newcastle-Ottawa scale (NOS) was used to evaluate the quality of included retrospective studies and studies with an NOS score ≥6 were regarded as high-quality studies [13].

The literature search, selection, data extraction, and quality evaluation were all performed by two authors independently and all disagreements were resolved by team discussion.

Statistical analysis

All statistical analyses were conducted using STATA 15.0 software. HR with 95% CI was combined to identify the association between LNR and survival in patients with esophageal cancer undergoing neoadjuvant therapy. Heterogeneity among included studies was evaluated by I^2 statistics and Q tests. When significant heterogeneity was observed, presenting as $I^2 > 50\%$ or $P < 0.1$, the random-effects model was applied; otherwise, the fixed-effects model was used [14]. Subgroup analysis focusing on neoadjuvant therapy and pathological type was also conducted. Sensitivity analysis was conducted to evaluate the stability of the pooled results. Begg's funnel plot and Egger's test were conducted to detect publication bias [15, 16]. Significant publication bias was defined as $P < 0.05$.

Results

Literature search and selection

As shown in Figure 1, 690 records were identified from three databases and 189 duplicate records were removed. After reviewing the titles and abstracts, 491 records were excluded. Finally, 14 studies were included after reviewing the full text of the remaining publications [17–30]. Notably, eight studies were included in a previous similar meta-analysis by Hagens et al. [31]. Therefore, six new studies were included in this updated meta-analysis.

TABLE 1 Basic characteristics of the included studies.

Author	Year	Country	Sample size	cTNM stage	Neoadjuvant therapy	Pathological type	LNR type	Definition of LNRG/N downstaging	Source of HR	Follow-up period	Endpoint	NOS score
Bollschweiler [18]	2011	Germany	40	cT3/4N+	CRT	Mixed	LNRG	Low-risk: no LNM and less than three LNs with central fibrosis; medium-risk: no LNM and three or more LNs with central fibrosis *or* LNM with an LN ratio less than 0.05; high-risk: LNM	R	5.5 (4.2–7.6) years (median)	OS	6
Nieman [20]	2015	USA	90	cIB-cIIIA	CRT	AC	LNRG	Complete response: without evidence of metastatic disease; partial response: with evidence of previous cancer involvement but no currently viable cancer cells; no response: involved with malignancy	R	27 (13.4–40.1) months (median)	OS	7
Philippron [21]	2016	Germany	222	cT3N + M0	CRT	Mixed	LNRG	High-LN response: without LNM showing central fibrosis in fewer than three LNs; medium-LN response: central fibrosis in three or more LNs of ypN0 or LNM with an LN ratio of less than 0.05; Low-LN response: other	R	4.5 (1.0–11.2) years (median)	OS	7
Davies [25]	2018	Sweden	183	cT2-4N+	CT	AC	LNRG	Score 1: complete response; Score 2: <10% residual tumor; Score 3: 10%–50% residual tumor; Score 4: >50% viable tumor; Score 5: no response	R	NR	OS, DFS	7
Hsu [26]	2021	China	115	cT1-4N−/+	CRT	SCC	LNRG	Score 0: N (−) with no evidence of tumor involvement or regression; score 1: N (−) with evidence of complete regression; score 2: N (+) with\50% viable tumor; score 3: N (+) with >50% viable tumor	R	NR	OS, DFS	7
Koemans [27]	2021	Netherlands	117	cIB–IIIC	CRT	Mixed	LNRG	Class A: no tumor, no signs of regression; B: tumor without regression; C: viable tumor and regression; D: complete response	R	37 (29–44) months (median)	OS	7
Evans [28]	2022	Italy	130	cT2-4N+	CT	AC	LNRG	Complete response: any of the following features with no residual tumor cells: the presence of foamy or hemosiderin-laden macrophages with or without dystrophic calcification, (ii) lakes of acellular mucin, and/or (iii)	R	NR	OS, DFS	7

(Continued on following page)

10.3389/pore.2024.1611844

TABLE 1 (*Continued*) Basic characteristics of the included studies.

Author	Year	Country	Sample size	cTNM stage	Neoadjuvant therapy	Pathological type	LNR type	Definition of LNRG/N downstaging	Source of HR	Follow-up period	Endpoint	NOS score
								the presence of substantial fibrosis or tumor necrosis; partial response: with features of nodal regression and persistent tumor cells; no response: with LN metastasis but no features of regression				
Moore [29]	2023	UK	763	cT1-4N−/+	CT	AC	LNRG	Score 1: complete response; score 2: <10% residual tumor; score 3: 10%–50% residual tumor; score 4: >50% residual tumor; score 5: no response	R	NR	OS, DFS	8
Yehan [30]	2024	China	112	cN+	CRT	SCC	LNRG	Score 1: 0% of total viable tumor area; score 2: <10% of total viable tumor area; score 3: 10%–50% of total viable tumor area; score 4: >50% of total viable tumor area	R	29.6 months (median)	DFS	7
Rice [17]	2001	USA	69	cN+	NR	Mixed	N downstaging	cN1 to ypN0	R	26 ± 15 months (mean)	OS	6
Donohoe [19]	2013	Ireland	155	cN+	CRT	Mixed	N downstaging	cN+ to ypN0	R	48 (6–273) months (median)	OS	6
Zanoni [22]	2016	Italy	55	cN+	CRT	Mixed	N downstaging	cN+ to ypN0	R	44 (11–131) months (median)	OS, CSS	6
Noble [23]	2017	UK	981	NR	CRT	AC	N downstaging	cN+ to ypN0	R	NR	OS	6
Shapiro [24]	2017	Netherland	180	cN+	CRT	Mixed	N downstaging	cN+ to ypN0	R	NR	OS	6

TNM: tumor-node-metastasis; CRT: chemoradiotherapy; CT: chemotherapy; LNR: lymph node regression; LNRG: lymph node regression grade; LNM: lymph node metastasis; LN: lymph node; AC: adenocarcinoma; SCC: squamous cell carcinoma; R: reported; OS: overall survival; DFS: disease-free survival; CSS: cancer-specific survival; NOS: Newcastle-Ottawa Scale.

10.3389/pore.2024.1611844

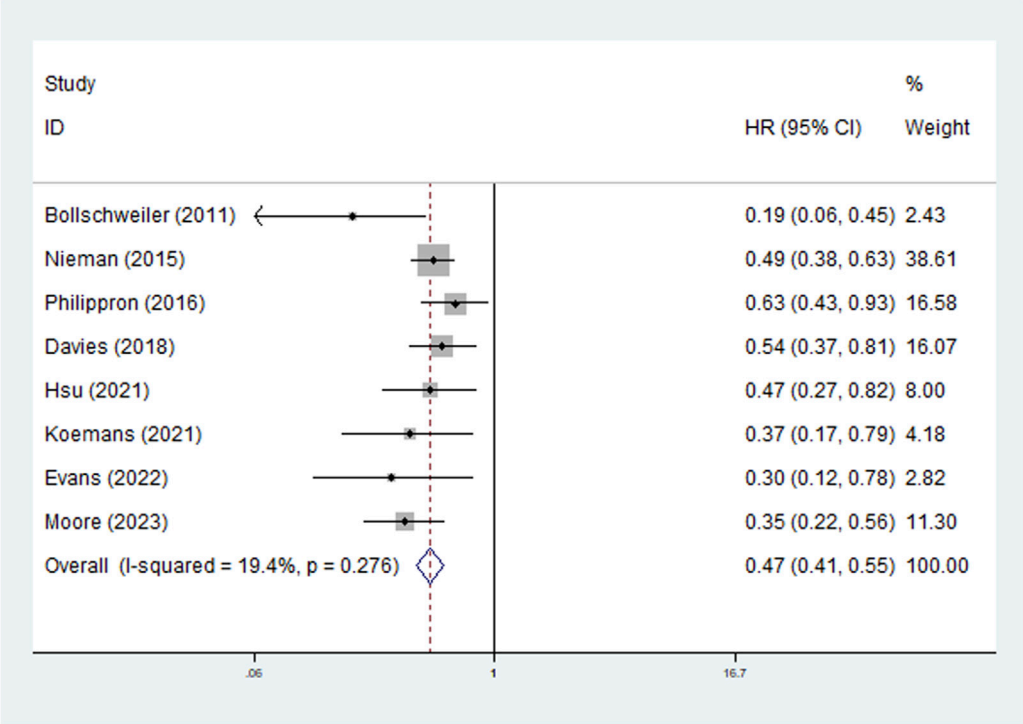

FIGURE 2
The association between lymph node regression grade and overall survival in patients with esophageal cancer undergoing neoadjuvant therapy.

Baseline characteristics of included studies

Among the 14 included retrospective studies, 3,212 patients were enrolled. Nine studies explored the relationship between LNRG and prognosis [18, 20, 21, 25–30], while the other five studies identified the predictive role of N downstaging for survival [17, 19, 22–24]. The sample sizes ranged from 40 to 981 subjects. The majority of patients received chemoradiotherapy as neoadjuvant therapy. Notably, neoadjuvant therapy was not incorporated in all included studies. All included studies directly reported HRs with 95% CIs and were high-quality studies with the NOS score ≥6. Further detailed information is presented in Table 1.

Association of LNRG with survival in patients with esophageal cancer receiving neoadjuvant therapy

The survival of patients with complete (or subtotal) lymph node response and with partial (or no) lymph node response was compared in the included studies. Eight studies explored the predictive role of LNRG for OS, and the pooled results demonstrated that complete LNR predicted significantly improved OS (HR = 0.47, 95% CI: 0.41–0.55, P < 0.001; I^2 = 19.4%, P = 0.276) (Figure 2). Then, subgroup analysis stratified by neoadjuvant therapy (chemoradiotherapy: HR = 0.49, 95% CI: 0.41–0.59, P < 0.001; chemotherapy: HR = 0.43, 95% CI: 0.33–0.58, P < 0.001) and pathological type (adenocarcinoma: HR = 0.46, 95% CI: 0.38–0.56, P < 0.001; squamous cell carcinoma: HR = 0.47, 95% CI: 0.27–0.82, P = 0.008) showed similar results (Table 2).

Five studies explored the relationship between LNRG and DFS and the pooled results indicated that LNRG was significantly associated with DFS (HR = 0.42, 95% CI: 0.32–0.55, P < 0.001; I^2 = 30.0%, P = 0.221) (Figure 3). Similarly, subgroups based on neoadjuvant therapy (chemoradiotherapy: HR = 0.53, 95% CI: 0.33–0.87, P = 0.011; chemotherapy: HR = 0.38, 95% CI: 0.28–0.52, P < 0.001) and pathological type (adenocarcinoma: HR = 0.53, 95% CI: 0.33–0.87, P = 0.011; squamous cell carcinoma: HR = 0.38, 95% CI: 0.28–0.52, P < 0.001) identified the association of complete LNR with improved DFS (Table 2).

Association of N downstaging with survival in patients with esophageal cancer receiving neoadjuvant therapy

All included studies defined the N downstaging as cN+ to ypN0. Five studies clarified the predictive role of N downstaging

TABLE 2 Results of the meta-analysis.

	No. of studies	HR	95% CI	p-Value	I^2 (%)	$P_{heterogeneity}$
LNRG						
Overall survival	8	0.47	0.41–0.55	<0.001	19.4	0.276
Type of neoadjuvant therapy						
Chemoradiotherapy	5	0.49	0.41–0.59	<0.001	28.1	0.234
Chemotherapy	3	0.43	0.33–0.58	<0.001	23.3	0.271
Pathological type						
Adenocarcinoma	4	0.46	0.38–0.56	<0.001	0.0	0.394
Squamous cell carcinoma	1	0.47	0.27–0.82	0.008	-	-
Disease-free survival	5	0.42	0.32–0.55	<0.001	30.0	0.221
Type of neoadjuvant therapy						
Chemoradiotherapy	2	0.53	0.33–0.87	0.011	70.9	0.064
Chemotherapy	3	0.38	0.28–0.52	<0.001	0.0	0.605
Pathological type						
Adenocarcinoma	2	0.53	0.33–0.87	0.011	70.9	0.064
Squamous cell carcinoma	3	0.38	0.28–0.52	<0.001	0.0	0.605
N downstaging						
Overall survival	5	0.40	0.21–0.77	0.006	96.6	<0.001
Cancer-specific survival	1	0.27	0.12–0.60	<0.001	-	-

HR, hazard ratio; CI, confidence interval.

for OS and the pooled results demonstrated that N downstaging predicted significantly worse OS (HR = 0.40, 95% CI: 0.21–0.77, p = 0.006; I^2 = 96.6%, P < 0.001) (Figure 4). However, due to the limited data available, it was not possible to conduct a more detailed subgroup analysis on N downstaging for OS.

Furthermore, Zanoni et al. reported that N downstaging was also significantly associated with improved CSS (HR = 0.27, 95% CI: 0.12–0.60, P < 0.001) (Table 2).

Sensitivity analysis and publication bias

We conducted a sensitivity analysis on LNRG for OS. As shown in Figure 5, the pooled results of this meta-analysis were stable and reliable.

Meanwhile, Begg's funnel plot (Figure 6) and Egger's test (P = 0.064) indicated that there was no obvious publication bias.

Discussion

According to this meta-analysis, LNR is significantly associated with long-term survival among patients with esophageal cancer who receive neoadjuvant therapy and patients with complete (or subtotal) LNR or (and) N downstaging are more likely to experience a better prognosis. Therefore, LNR should be carefully considered as a prognostic indicator in this group of patients.

Hagens et al. conducted a similar meta-analysis to explore the prognostic role of LNR in esophageal cancer [31]. They included eight studies, three of which assessed LNRG and five of which assessed N downstaging. According to their results, N downstaging was associated with improved survival (HR = 0.41, 95% CI: 0.22–0.77, P = 0.005). However, no significant association was observed between LNRG and survival (HR = 0.52, 95% CI: 0.26–1.06). Furthermore, a more detailed analysis was not performed in their meta-analysis [31]. Therefore, we conducted the current meta-analysis to further identify the prognostic relevance of LNR on survival in patients with esophageal cancer undergoing neoadjuvant therapy and to provide more evidence on the prognostic role of LNR in this group of patients.

The response to chemoradiotherapy may differ between lymph node metastases and primary lesions in esophageal cancer. First, cancer cells in primary lesions and metastases may exhibit different levels of differentiation [32]. Typically,

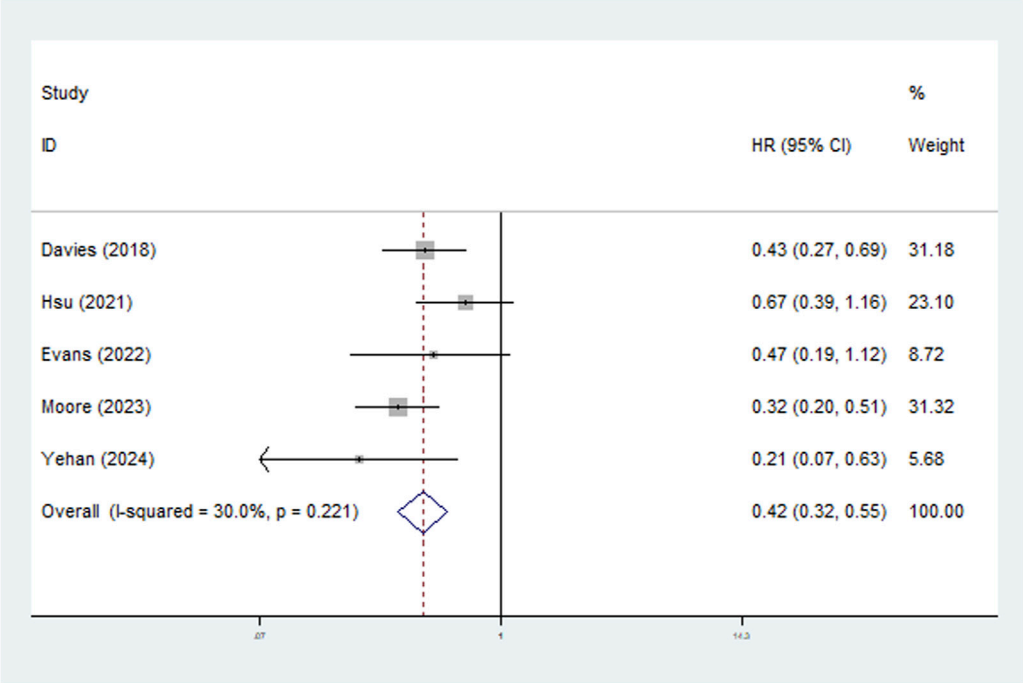

FIGURE 3
The association between lymph node regression grade and disease-free survival in patients with esophageal cancer undergoing neoadjuvant therapy.

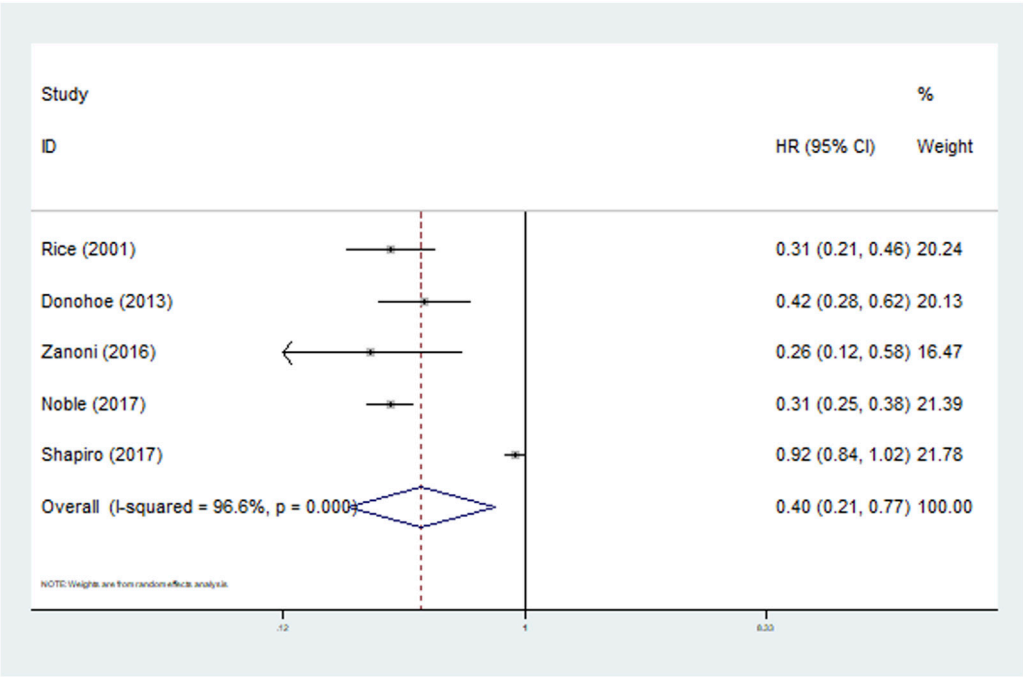

FIGURE 4
The association between N downstaging and overall survival in patients with esophageal cancer undergoing neoadjuvant therapy.

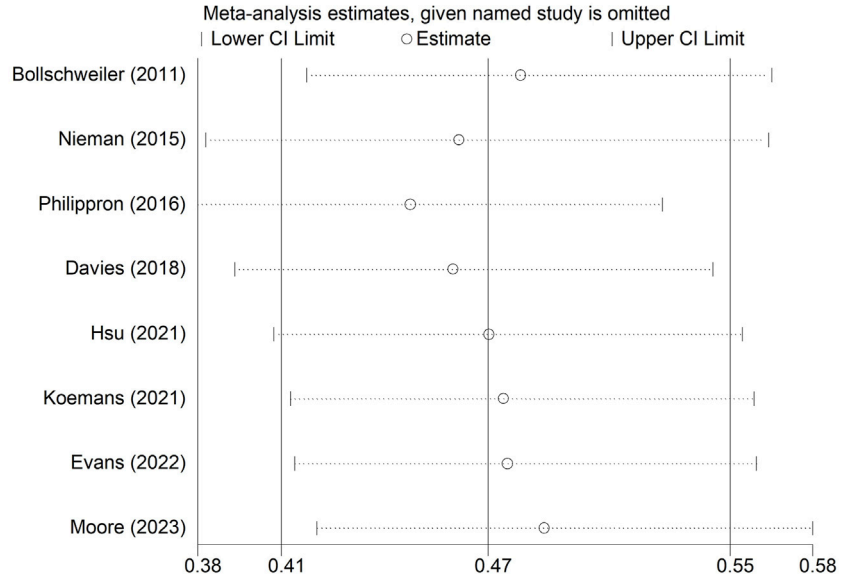

FIGURE 5
Sensitivity analysis for the association between lymph node regression grade and overall survival in patients with esophageal cancer undergoing neoadjuvant therapy.

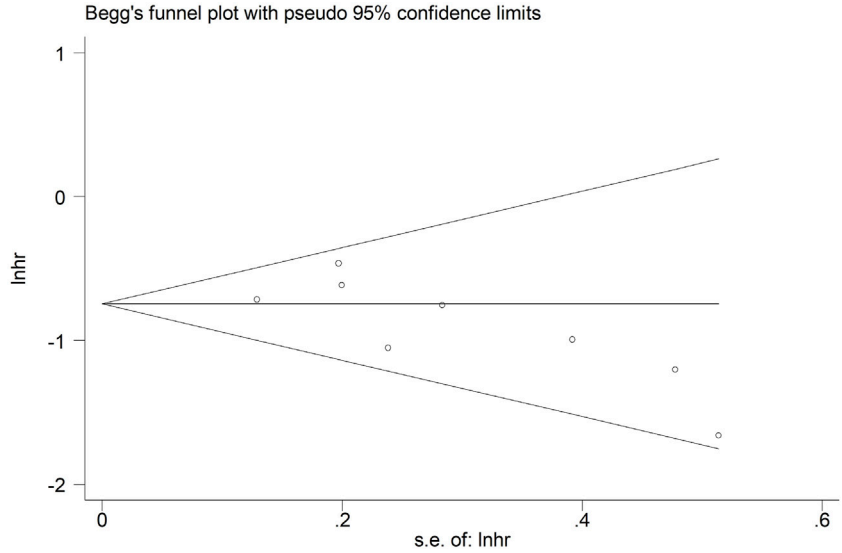

FIGURE 6
Begg's funnel plot for the association between lymph node regression grade and overall survival in patients with esophageal cancer undergoing neoadjuvant therapy.

cancer cells in primary lesions may be more differentiated, while those in metastases may be more unstable, heterogeneous, and may even contain more stem cell-like cells [33, 34]. This could lead to an increased resistance of metastases to chemotherapy [34]. Second, there may be differences in the microenvironment between metastatic lymph nodes and primary tumors, such as oxygen concentration, nutrient supply, and immune cell infiltration [35, 36]. These microenvironmental differences may affect the sensitivity of cancer cells to chemoradiotherapy [37]. Additionally, metastases may accumulate genetic mutations

different from those in primary lesions, which may affect the sensitivity of cancer cells to anti-tumor drugs [38]. Specifically, metastases may develop resistance mutations to certain drugs [38]. While previous studies have often assessed the efficacy of neoadjuvant therapy based on changes in primary tumors, the evaluation of LNR status is also crucial in practice.

However, there is currently no standardized protocol for evaluating LNR, leading to variations in the grading systems used in the included studies, which needs to be further elucidated in future studies. At the same time, we believe it is also crucial to compare and assess the role of regression in primary tumors and lymph node metastases in predicting the prognosis of patients with esophageal cancer undergoing neoadjuvant therapy or to investigate the prognostic significance of joint evaluation of regression in primary tumors and lymph node metastases in response to neoadjuvant therapy. As reported by Yun et al., the combined evaluation of TRG and lymph node status demonstrated greater clinical value in predicting the prognosis of patients with esophageal cancer undergoing neoadjuvant therapy compared to TNM stage, TRG, and LNR [9]. Furthermore, whether LNR status contributes to guiding the formulation of postoperative adjuvant therapy or treatment strategies after recurrence in patients with esophageal cancer also needs to be explored.

Our meta-analysis has several limitations. First, the sample size was relatively small and all included studies were retrospective. Second, there were some confounding factors such as the surgical procedures, definition of LNRG, tumor stage, etc. Third, regarding LNRG, some studies included a small number of cN- patients, but did not specify whether these patients were excluded during the analysis, which may introduce a slight bias. Fourth, data from other countries were missing, more studies in other countries are still needed to verify our findings. Fifth, the neoadjuvant immunotherapy was not considered in all included studies. The association of LNR with prognosis in patients with esophageal cancer receiving neoadjuvant immunotherapy should be further investigated. Sixth, the optimal neoadjuvant chemotherapy or chemoradiotherapy regimen remains controversial, especially in patients with different clinical characteristics.

Conclusion

Overall, LNR could serve as a novel and reliable prognostic factor in patients with esophageal cancer undergoing neoadjuvant therapy and complete LNR and N downstaging predict better prognosis.

Data availability statement

The original contributions presented in the study are included in the article/Supplementary Material, further inquiries can be directed to the corresponding authors.

Author contributions

YW and CC conceived the study idea and designed the search strategy. PC and MC screened studies for eligibility and extracted data. PC and YB double appraised the results of studies for risk of bias. PC and MC undertook the data synthesis and analysis. PC and MC wrote the first drafts of the figures, tables, and appendices. PC and MC wrote the first draft of the manuscript. MC, YB, and GC interpreted the data analysis and critically revised the manuscript. YW and CC were the guarantors. The corresponding authors attest that all listed authors meet authorship criteria and that no others meeting the criteria have been omitted. All authors contributed to the article and approved the submitted version.

Funding

The author(s) declare that no financial support was received for the research, authorship, and/or publication of this article.

Conflict of interest

The authors declare that the research was conducted in the absence of any commercial or financial relationships that could be construed as a potential conflict of interest.

Supplementary material

The Supplementary Material for this article can be found online at: https://www.por-journal.com/articles/10.3389/pore.2024.1611844/full#supplementary-material

References

1. Ju W, Zheng R, Zhang S, Zeng H, Sun K, Wang S, et al. Cancer statistics in Chinese older people, 2022: current burden, time trends, and comparisons with the US, Japan, and the Republic of Korea. *Sci China Life Sci* (2023) 66(5):1079–91. doi:10.1007/s11427-022-2218-x

2. Xia C, Dong X, Li H, Cao M, Sun D, He S, et al. Cancer statistics in China and United States, 2022: profiles, trends, and determinants. *Chin Med J (Engl)* (2022) 135(5):584–90. doi:10.1097/CM9.0000000000002108

3. Yang W, Niu Y, Sun Y. Current neoadjuvant therapy for operable locally advanced esophageal cancer. *Med Oncol* (2023) 40(9):252. doi:10.1007/s12032-023-02097-4

4. Liang Z, Chen T, Li W, Lai H, Li L, Wu J, et al. Efficacy and safety of neoadjuvant chemoradiotherapy versus neoadjuvant chemotherapy in locally advanced esophageal cancer: an updated meta-analysis. *Medicine (Baltimore)* (2024) 103(3):e36785. doi:10.1097/MD.0000000000036785

5. Tang H, Wang H, Fang Y, Zhu JY, Yin J, Shen YX, et al. Neoadjuvant chemoradiotherapy versus neoadjuvant chemotherapy followed by minimally invasive esophagectomy for locally advanced esophageal squamous cell carcinoma: a prospective multicenter randomized clinical trial. *Ann Oncol* (2023) 34(2):163–72. doi:10.1016/j.annonc.2022.10.508

6. Eyck BM, van Lanschot JJB, Hulshof M, van der Wilk BJ, Shapiro J, van Hagen P, et al. Ten-year outcome of neoadjuvant chemoradiotherapy plus surgery for esophageal cancer: the randomized controlled CROSS trial. *J Clin Oncol* (2021) 39(18):1995–2004. doi:10.1200/JCO.20.03614

7. Li Q, Liu T, Ding Z. Neoadjuvant immunotherapy for resectable esophageal cancer: a review. *Front Immunol* (2022) 13:1051841. doi:10.3389/fimmu.2022.1051841

8. Baksh K, Prithviraj G, Kim Y, Hoffe S, Shridhar R, Coppola D, et al. Correlation between standardized uptake value in preneoadjuvant and postneoadjuvant chemoradiotherapy and tumor regression grade in patients with locally advanced esophageal cancer. *Am J Clin Oncol* (2018) 41(3):254–8. doi:10.1097/COC.0000000000000258

9. Yun JK, Kim Y, Lee GD, Choi S, Kim YH, Kim DK, et al. Tumor regression grade combined with lymph node status in esophageal squamous cell carcinoma after neoadjuvant chemoradiotherapy. *Cancer Med* (2022) 11(19):3623–32. doi:10.1002/cam4.4748

10. Gu YM, Lyu SM, Shang QX, Zhang HL, Yang YS, Wang WP, et al. Is tumor regression grade sufficient to predict survival in esophageal cancer with trimodal therapy? *J Invest Surg* (2022) 35(11-12):1818–23. doi:10.1080/08941939.2022.2127036

11. Yasuda T, Yano M, Miyata H, Yamasaki M, Takiguchi S, Fujiwara Y, et al. Prognostic significance of (18)F-fluorodeoxyglucose positron emission tomography (FDG-PET)-Positive lymph nodes following neoadjuvant chemotherapy and surgery for resectable thoracic esophageal squamous cell carcinoma. *Ann Surg Oncol* (2015) 22(8):2599–607. doi:10.1245/s10434-014-4299-9

12. Zhang X, Tan R, Lam WC, Yao L, Wang X, Cheng CW, et al. PRISMA (preferred reporting Items for systematic reviews and meta-analyses) extension for Chinese herbal medicines 2020 (PRISMA-CHM 2020). *Am J Chin Med* (2020) 48(6):1279–313. doi:10.1142/S0192415X20500639

13. Wang Y, Li J, Chang S, Dong Y, Che G. Risk and influencing factors for subsequent primary lung cancer after treatment of breast cancer: a systematic review and two meta-analyses based on four million cases. *J Thorac Oncol : official Publ Int Assoc Study Lung Cancer* (2021) 16(11):1893–908. doi:10.1016/j.jtho.2021.07.001

14. Barili F, Parolari A, Kappetein PA, Freemantle N. Statistical Primer: heterogeneity, random- or fixed-effects model analyses? *Interact Cardiovasc Thorac Surg* (2018) 27(3):317–21. doi:10.1093/icvts/ivy163

15. Begg CB, Mazumdar M. Operating characteristics of a rank correlation test for publication bias. *Biometrics* (1994) 50(4):1088–101. doi:10.2307/2533446

16. Egger M, Davey Smith G, Schneider M, Minder C. Bias in meta-analysis detected by a simple, graphical test. *BMJ (Clinical research ed)* (1997) 315(7109):629–34. doi:10.1136/bmj.315.7109.629

17. Rice TW, Blackstone EH, Adelstein DJ, Zuccaro G, Jr, Vargo JJ, Goldblum JR, et al. N1 esophageal carcinoma: the importance of staging and downstaging. *J Thorac Cardiovasc Surg* (2001) 121(3):454–64. doi:10.1067/mtc.2001.112470

18. Bollschweiler E, Hoelscher AH, Metzger R, Besch S, Moenig SP, Baldus SE, et al. Prognostic significance of a new grading system of lymph node morphology after neoadjuvant radiochemotherapy for esophageal. *Ann Thorac Surg* (2011) 92(6):2020–7. doi:10.1016/j.athoracsur.2011.06.091

19. Donohoe CL, O'Farrell NJ, Grant T, King S, Clarke L, Muldoon C, et al. Classification of pathologic response to neoadjuvant therapy in esophageal and junctional cancer: assessment of existing measures and proposal of a novel 3-point standard. *Ann Surg* (2013) 258(5):784–92. discussion 792. doi:10.1097/SLA.0b013e3182a66588

20. Nieman DR, Peyre CG, Watson TJ, Cao W, Lunt MD, Lada MJ, et al. Neoadjuvant treatment response in negative nodes is an important prognosticator after esophagectomy. *Ann Thorac Surg* (2015) 99(1):277–83. doi:10.1016/j.athoracsur.2014.07.037

21. Philippron A, Bollschweiler E, Kunikata A, Plum P, Schmidt C, Favi F, et al. Prognostic relevance of lymph node regression after neoadjuvant chemoradiation for esophageal cancer. *Semin Thorac Cardiovasc Surg* (2016) 28(2):549–58. doi:10.1053/j.semtcvs.2016.04.003

22. Zanoni A, Verlato G, Giacopuzzi S, Motton M, Casella F, Weindelmayer J, et al. ypN0: does it matter how you get there? Nodal downstaging in esophageal cancer. *Ann Surg Oncol* (2016) 23(Suppl. 5):998–1004. doi:10.1245/s10434-016-5440-8

23. Noble F, Lloyd MA, Turkington R, Griffiths E, O'Donovan M, O'Neill JR, et al. Multicentre cohort study to define and validate pathological assessment of response to neoadjuvant therapy in oesophagogastric adenocarcinoma. *Br J Surg* (2017) 104(13):1816–28. doi:10.1002/bjs.10627

24. Shapiro J, Biermann K, van Klaveren D, Offerhaus GJ, Ten Kate FJ, Meijer SL, et al. Prognostic value of pretreatment pathological tumor extent in patients treated with neoadjuvant chemoradiotherapy plus surgery for esophageal or junctional cancer. *Ann Surg* (2017) 265(2):356–62. doi:10.1097/SLA.0000000000001630

25. Davies AR, Myoteri D, Zylstra J, Baker CR, Wulaningsih W, Van Hemelrijck M, et al. Lymph node regression and survival following neoadjuvant chemotherapy in oesophageal adenocarcinoma. *Br J Surg* (2018) 105(12):1639–49. doi:10.1002/bjs.10900

26. Hsu P-K, Yeh Y-C, Chien L-I, Huang C-S, Hsu H-S. Clinicopathological significance of pathologic complete lymph node regression after neoadjuvant chemoradiotherapy in esophageal squamous cell carcinoma. *Ann Surg Oncol* (2021) 28(4):2048–58. doi:10.1245/s10434-020-09363-z

27. Koemans WJ, Larue R, Kloft M, Ruisch JE, Compter I, Riedl RG, et al. Lymph node response to chemoradiotherapy in oesophageal cancer patients: relationship with radiotherapy fields. *Esophagus* (2021) 18(1):100–10. doi:10.1007/s10388-020-00777-y

28. Evans RP, Kamarajah SK, Kunene V, Zardo D, Elshafie M, Griffiths EA. Impact of neoadjuvant chemotherapy on nodal regression and survival in oesophageal adenocarcinoma. *Eur J Surg Oncol* (2022) 48(5):1001–10. doi:10.1016/j.ejso.2021.12.021

29. Moore JL, Green M, Santaolalla A, Deere H, Evans RPT, Elshafie M, et al. Pathologic lymph node regression after neoadjuvant chemotherapy predicts recurrence and survival in esophageal adenocarcinoma: a multicenter study in the United Kingdom. *J Clin Oncol* (2023) 41(28):4522–34. doi:10.1200/JCO.23.00139

30. Yehan Z, Ying L, Peng G, Zongyao H, Chengmin Z, Hong Y, et al. Prognostic significance of positive lymph node regression grade to neoadjuvant chemoradiation for esophageal squamous cell carcinoma. *J Surg Oncol* (2024) 129(4):708–17. doi:10.1002/jso.27555

31. Hagens E, Tukanova K, Jamel S, van Berge Henegouwen M, Hanna GB, Gisbertz S, et al. Prognostic relevance of lymph node regression on survival in esophageal cancer: a systematic review and meta-analysis. *Dis Esophagus* (2022) 35(1):doab021. doi:10.1093/dote/doab021

32. Walter D, Harter PN, Battke F, Winkelmann R, Schneider M, Holzer K, et al. Genetic heterogeneity of primary lesion and metastasis in small intestine neuroendocrine tumors. *Sci Rep* (2018) 8(1):3811. doi:10.1038/s41598-018-22115-0

33. Choi JY, Lee YS, Shim DM, Lee YK, Seo SW. GNAQ knockdown promotes bone metastasis through epithelial-mesenchymal transition in lung cancer cells. *Bone Joint Res* (2021) 10(5):310–20. doi:10.1302/2046-3758.105.BJR-2020-0262.R3

34. Fischer HP. Regression and therapy-resistance of primary liver tumors and liver metastases after regional chemotherapy and local tumor ablation. *Pathologe* (2005) 26(3):191–200. doi:10.1007/s00292-005-0749-2

35. Popper H. Primary tumor and metastasis-sectioning the different steps of the metastatic cascade. *Transl Lung Cancer Res* (2020) 9(5):2277–300. doi:10.21037/tlcr-20-175

36. Cacho-Díaz B, García-Botello DR, Wegman-Ostrosky T, Reyes-Soto G, Ortiz-Sánchez E, Herrera-Montalvo LA. Tumor microenvironment differences between primary tumor and brain metastases. *J Transl Med* (2020) 18(1):1. doi:10.1186/s12967-019-02189-8

37. Wood SL, Pernemalm M, Crosbie PA, Whetton AD. The role of the tumor-microenvironment in lung cancer-metastasis and its relationship to potential therapeutic targets. *Cancer Treat Rev* (2014) 40(4):558–66. doi:10.1016/j.ctrv.2013.10.001

38. Xu CW, Wang WX, Wu MJ, Zhu YC, Zhuang W, Lin G, et al. Comparison of the c-MET gene amplification between primary tumor and metastatic lymph nodes in non-small cell lung cancer. *Thorac Cancer* (2017) 8(5):417–22. doi:10.1111/1759-7714.12455

Pathology & Oncology Research | frontiers

TYPE Original Research
PUBLISHED 02 June 2023
DOI 10.3389/pore.2023.1610897

Check for updates

OPEN ACCESS

EDITED BY
Anna Sebestyén,
Semmelweis University, Hungary

*CORRESPONDENCE
Wei-guo Xu,
xwg853@163.com

†These authors have contributed equally to this work

RECEIVED 22 October 2022
ACCEPTED 16 May 2023
PUBLISHED 02 June 2023

CITATION
Liu Y-h, Meng R, Zhu B, Zhan Q-q, Yang X, Ding G-y, Jia C-l, Liu Q-y and Xu W-g (2023), Integrated oxidative stress score for predicting prognosis in stage III gastric cancer undergoing surgery.
Pathol. Oncol. Res. 29:1610897.
doi: 10.3389/pore.2023.1610897

COPYRIGHT
© 2023 Liu, Meng, Zhu, Zhan, Yang, Ding, Jia, Liu and Xu. This is an open-access article distributed under the terms of the Creative Commons Attribution License (CC BY). The use, distribution or reproduction in other forums is permitted, provided the original author(s) and the copyright owner(s) are credited and that the original publication in this journal is cited, in accordance with accepted academic practice. No use, distribution or reproduction is permitted which does not comply with these terms.

Integrated oxidative stress score for predicting prognosis in stage III gastric cancer undergoing surgery

Yu-hang Liu[1†], Rui Meng[2†], Bing Zhu[3], Qi-qi Zhan[4], Xin Yang[4], Guan-yi Ding[3], Chun-liang Jia[5], Qian-yu Liu[4] and Wei-guo Xu[4,6*]

[1]School of Clinical Medicine, North China University of Science and Technology, Tangshan, China, [2]Department of Emergency Intensive Care Unit, Yangpu Hospital, Tongji University, Shanghai, China, [3]Tangshan Gongren Hospital, Tangshan, China, [4]North China University of Science and Technology Affiliated Hospital, Tangshan, China, [5]Tangshan People's Hospital, Tangshan, China, [6]Department of Gastrointestinal Surgery, China Hospital Medical Sciences, Shenzhen, China

Objective: This study aimed to develop a novel scoring system, named the integrated oxidative stress score (IOSS), based on oxidative stress indices to predict the prognosis in stage III gastric cancer.

Methods: Retrospective analysis of stage III gastric cancer patients who were operated on between January 2014 and December 2016 were enrolled into this research. IOSS is a comprehensive index based on an achievable oxidative stress index, comprising albumin, blood urea nitrogen, and direct bilirubin. The patients were divided according to receiver operating characteristic curve into two groups of low IOSS (IOSS ≤ 2.00) and high IOSS (IOSS > 2.00). The grouping variable was performed by Chi-square test or Fisher's precision probability test. The continuous variables were evaluated by t-test. The disease free survival (DFS) and overall survival (OS) were performed by Kaplan-Meier and Log-Rank tests. Univariate Cox proportional hazards regression models and stepwise multivariate Cox proportional hazards regression analysis were determined to appraise the potential prognostic factors for DFS and OS. A nomogram of the potential prognostic factors by the multivariate analysis for DFS and OS was established with R software. In order to assess the accuracy of the nomogram in forecasting prognosis, the calibration curve and decision curve analysis were produced, contrasting the observed outcomes with the predicted outcomes.

Results: The IOSS was significantly correlated with the DFS and OS, and was a potential prognostic factor in patients with stage III gastric cancer. Patients with low IOSS had longer survival (DFS: χ^2 = 6.632, p = 0.010; OS: χ^2 = 6.519, p = 0.011), and higher survival rates. According to the univariate and multivariate analyses, the IOSS was a potential prognostic factor. The nomograms were conducted on the potential prognostic factors to improve the correctness of survival prediction and evaluate the prognosis in stage III gastric cancer patients. The calibration curve indicated a good agreement in 1-, 3-, 5-year lifetime rates. The decision curve analysis indicated that the nomogram's predictive clinical utility for clinical decision was better than IOSS.

Conclusion: IOSS is a nonspecific tumor predictor based on available oxidative stress index, and low IOSS is found to be a vigorous factor of better prognosis in stage III gastric cancer.

KEYWORDS

gastric cancer, oxidative stress, albumin, bilirubin, blood urea nitrogen

Introduction

Gastric cancer ranked sixth among the global cancer burdens in both females and males in 2020, and remains one of the prime causes of cancer-related morbidity and cancer-related death in the world [1, 2]. The incidence of gastric cancer is highest in Eastern Asia, such as South Korea and China, and is largely dependent on *Helicobacter pylori* infection, co-infection by Epstein-Barr virus (EBV), gastroesophageal reflux disease, and obesity [3, 4]. Despite changes in dietary habits and improvements in living conditions, the mortality of gastric cancer is still high in recent decades [5, 6]. Currently, the surgical operation remains the primary curative therapy for early-stage gastric cancer [7]. Complex treatment, such as chemotherapy, radiotherapy, targeted therapy and immunotherapy, is used for gastric cancer or metastatic disease [8]. Although these treatments have significantly improved the overall survival of gastric cancer patients, unfortunately, the long-term survival rate is unsatisfactory. Approximately 70% of gastric cancer patients have distant metastasis or recurrence within 5 years [9]. As a result of geographical, genetic, and dietary differences, predicting the survival and prognosis of gastric cancer patients can be challenging [10, 11]. However, the precise prediction of prognosis is crucial for treatment election and doctor-patient communication. Consequently, it is very important to look for the potential prognostic factor for gastric cancer.

Previous studies have indicated that systemic inflammation, malnutrition, and TNM staging system can usually predict survival of gastric cancer patients [12–14]. Nevertheless, gastric cancer is a heterogeneous disorder. Even if the patients are at the same stage of disease, they may have different prognoses [15]. The present TNM staging system is uniform and simple, and does not consider several noteworthy variables that may influence the survival of gastric cancer patients, comprising clinicopathological characteristics and adjuvant treatment. Hence, the prognosis of gastric cancer patients cannot be accurately predicted. Currently, the long-term prognosis of gastric cancer is still poor, and warranting an effective and reasonable predictive model is needed to evaluate the long-term prognosis of gastric cancer patients.

Oxidative stress, which is defined as an imbalance between reactive metabolites and free radicals, interacts with the occurrence, development, and progression of malignant tumors [16, 17]. Previous studies have shown that foods such as vegetables, fruits, seeds, and whole grains can counteract oxidative stress and inflammation, and may also be beneficial to cancer patients [18]. Henriksen HB et al. found that a healthy diet played a critical role in suppressing oxidative stress and inflammation, affecting survival time and outcome in colorectal cancer patients [19]. Moreover, the progression-related hub oxidative stress genes were confirmed to be conspicuously related to the progression of gastric cancer according to the weighted gene co-expression network analysis (WGCNA) and Gene Expression Omnibus (GEO) database [20]. Early assessment of oxidative stress for patients with gastric cancer can ameliorate the clinical outcomes. One study has indicated that the oxidative stress genes, such as NQO1 and PON1, were the noteworthy prognostic factors in metastatic gastric cancer patients treated with chemotherapy; and the oxidative stress-related genetic variants may facilitate optimization of individualized chemotherapy in clinical practice [21]. Another study indicated that the CRC-Integrated Oxidative Stress Score (CIOSS) based on the combination of available oxidative stress indices (albumin, direct bilirubin, and blood urea nitrogen) was significantly associated with survival in CRC patients; and the CIOSS was a powerful indicator of poor prognosis in CRC patients [22]. Taking into consideration the important function of oxidative stress in the development of gastric cancer, we tried to study the potential prognostic implication of oxidative stress correlated indicators. In the current study, we validated a gastric cancer Integrated Oxidative Stress Score (IOSS), and aimed to determine the prognostic significance of IOSS in stage III gastric cancer. Furthermore, we compared the relevance between IOSS and clinicopathological characteristics.

Materials and methods

Patients and study design

198 patients with gastric cancer who were treated at the North China University of Science and Technology Affiliated Hospital between January 2014 and December 2016 were brought into this study. We excluded patients with clinical evidence of inflammatory, infectious, and hematological diseases, and without complete clinical data. This study was authorized by the Ethics Review Committee of the North China University of Science and Technology Affiliated Hospital, and it meets the criteria of the Declaration of Helsinki and its later

revised drafts. All enrolled patients signed the agreement, and individual patient information has been protected and not been shown.

The inclusion criteria were as follows: 1) confirmed gastric cancer by histopathology; 2) received primary tumor resection without evidence of distant metastasis; 3) without inflammatory, infectious, and hematological diseases; 4) availability of whole clinical and pathological data. Participants were considered ineligible if they were gastric cancer patients who had: 1) multiple primary malignant tumors or blood disease; 2) presence of kidney dysfunction, metabolic diseases, or cardiovascular disease; 3) received anti-inflammatory drugs prior to surgery; 4) no follow-up information.

Integrated oxidative stress score (IOSS)

The blood routine and biochemical detection were performed from the first day of admission for gastric cancer patients. In the previous study, the oxidative stress indicators (albumin, bilirubin, and blood urea nitrogen) were found to be independent risk factors and significantly correlated with OS or DFS by performing Cox regression in CRC patients [22]. The Integrated Oxidative Stress Score (IOSS) in our study comprised albumin (ALB), blood urea nitrogen (BUN), and direct bilirubin (DBIL). The IOSS was calculated as follows: 0.074 × albumin (g/L)–0.094 × bilirubin (μmol/L)–0.099 × blood urea nitrogen (mmol/L), according to the previous study [22].

Follow-up

The follow-up data were gathered through telephone interviews or inpatient and outpatient check-ups, and were obtained every 3 months. In this study, disease free survival (DFS) was defined as the time from operation to local recurrence of tumor, or death or last follow-up. Overall survival (OS) was defined as the time from operation to death or last follow-up. The last follow-up was assessed in June 2022.

Statistical analysis

SPSS 22.0 (SPSS Inc., Chicago, IL, United States) and R 4.1.2 software (Institute for Statistics and Mathematics, Vienna, Austria) were used to perform all statistical analyses. The optimal cutoff value for IOSS was performed by the receiver operating characteristic (ROC) curve analysis. The nominal variables were assessed by Chi-square test or Fisher's precision probability test. The continuous variables were evaluated by t-test. The DFS and OS time were performed by Kaplan-Meier method and Log-Rank test. Univariate and multivariate Cox proportional hazards regression models were determined to evaluate the potential prognostic factors for DFS and OS. The nomogram model of the potential prognostic factors by the multivariate analysis for DFS and OS were established with R software. In order to assess the precision of the nomogram model in forecasting prognosis, the calibration curve and decision curve analysis were generated comparing the observations with the predictions. p values of <0.05 were considered statistically significant.

Results

Study population

In total, 198 patients with gastric cancer from North China University of Science and Technology Affiliated Hospital were included in this research. There were 128 males (64.6%) and 70 females (35.4%). The average age was 59.37 ± 11.10 years, and ranged from 30 to 80 years. The optimal cutoff value for IOSS was performed by ROC, and the value was 2.00. Based on the optimal cutoff value, all cases were divided into two groups: low IOSS group (IOSS ≤ 2.00) and high IOSS group (IOSS > 2.00). The clinical characteristics of gastric cancer patients were given in Table 1. Compared to the patients' clinical and histopathological features, IOSS indicated significant relationship with age, radical resection, and tumor size ($p < 0.05$).

IOSS and blood parameters

The blood routine and biochemical parameters were enrolled into this research and the median values were used to group these indicators. Table 2 has shown the associations of IOSS and the blood routine and biochemical parameters. According to the patient characteristics of blood routine and biochemical parameters, IOSS indicated a significant relationship with total protein (TP), albumin (ALB), prealbumin (PALB), blood urea nitrogen (BUN), triglyceride (TRIG), hemoglobin (Hb), and red blood cell R) ($p < 0.05$).

IOSS and pathological characteristics

In this study, human epidermal growth factor receptor-2 (HER-2) positive means IHC (+++) or IHC (++) and FISH (+). We further investigated the association between IOSS and pathological characteristics. The results displayed that IOSS was related to the HER2 and perineural invasion (PNI) ($p < 0.05$). However, IOSS was not significantly correlated with lymphatic vessel invasion (LVI) ($p > 0.05$). Table 3 has shown the relationships of IOSS and the pathological characteristics parameters.

TABLE 1 Association of IOSS and patient characteristics.

Characteristics	Level	Low IOSS	High IOSS	*p*
n		**91**	**107**	
Sex	Male	64 (70.3)	64 (59.8)	0.163
	Female	27 (29.7)	43 (40.2)	
Age	≤60	33 (36.3)	64 (59.8)	**0.002**
	>60	58 (63.7)	43 (40.2)	
Profession	White collar workers	21 (23.1)	18 (16.8)	0.356
	Blue collar workers	70 (76.9)	89 (83.2)	
BMI	≤22.0	49 (53.8)	46 (43.0)	0.167
	>22.0	42 (46.2)	61 (57.0)	
Radical resection	R0	69 (75.8)	93 (86.9)	**<0.001**
	R1	20 (22.0)	3 (2.8)	
	R2	2 (2.2)	11 (10.3)	
Type of surgery	distal gastrectomy	77 (84.6)	81 (75.7)	0.296
	proximal gastrectomy	3 (3.3)	6 (5.6)	
	total gastrectomy	11 (12.1)	20 (18.7)	
Primary tumor site	upper 1/3	8 (8.8)	10 (9.3)	0.456
	middle 1/3	8 (8.8)	13 (12.1)	
	low 1/3	66 (72.5)	67 (62.6)	
	whole	9 (9.9)	17 (15.9)	
Borrmann type	Borrmann 0	0 (0.0)	2 (1.9)	0.189
	Borrmann I	4 (4.4)	3 (2.8)	
	Borrmann II	19 (20.9)	18 (16.8)	
	Borrmann III	63 (69.2)	69 (64.5)	
	Borrmann IV	3 (3.3)	13 (12.1)	
	Borrmann V	2 (2.2)	2 (1.9)	
Tumor size	≤20 mm	14 (15.4)	21 (19.6)	**0.020**
	>20 and <50 mm	51 (56.0)	39 (36.4)	
	≥50 mm	26 (28.6)	47 (43.9)	
Differentiation	poorly differentiated	38 (41.8)	61 (57.0)	0.101
	moderately differentiated	52 (57.1)	45 (42.1)	
	well differentiated	1 (1.1)	1 (0.9)	
Pathology	adenocarcinoma	37 (40.7)	33 (30.8)	0.314
	mucinous carcinoma	4 (4.4)	4 (3.7)	
	signet ring cell carcinoma	2 (2.2)	6 (5.6)	
	mixed carcinoma	48 (52.7)	62 (57.9)	
	others	0 (0.0)	2 (1.9)	
pTNM stage	IIIA	35 (38.5)	40 (37.4)	0.956
	IIIB	38 (41.8)	44 (41.1)	
	IIIC	18 (19.8)	23 (21.5)	
pT stage	T2	1 (1.1)	2 (1.9)	0.437
	T3	53 (58.2)	50 (46.7)	
	T4a	29 (31.9)	42 (39.3)	
	T4b	8 (8.8)	13 (12.1)	
pN stage	N0	1 (1.1)	6 (5.6)	0.389
	N1	11 (12.1)	12 (11.2)	
	N2	32 (35.2)	43 (40.2)	
	N3a	33 (36.3)	34 (31.8)	
	N3b	14 (15.4)	12 (11.2)	

(Continued on following page)

TABLE 1 (*Continued*) Association of IOSS and patient characteristics.

Characteristics	Level	Low IOSS	High IOSS	*p*
n		**91**	**107**	
Lauren type	Intestinal	43 (47.3)	44 (41.1)	0.687
	Diffuse	22 (24.2)	29 (27.1)	
	Mixed	26 (28.6)	34 (31.8)	
Postoperative chemotherapy	No	39 (42.9)	55 (51.4)	0.290
	Yes	52 (57.1)	52 (48.6)	

Abbreviation: BMI, body mass index; TNM, tumor node metastasis. Bold values are primarily used to identify meaningful variables.

The potential independent prognostic factors of DFS and OS for stage III gastric cancer patients who underwent curative resection

To further identify potential independent prognostic predictors of DFS and OS, we enrolled the common parameters into Cox proportional hazard regression model for univariate and multivariate analysis. The univariate and multivariate Cox regression analysis has shown that IOSS, PALB (prealbumin), TLN (total lymph node), tumor size, and postoperative chemotherapy were authenticated as potential independent factors to determine the DFS. Moreover, the IOSS, age, A/G (Albumin/Globulin), PALB (prealbumin), FIB (fibrinogen), TLN (total lymph node), and tumor size were authenticated as potential independent factors to determine the OS. The detailed information were shown in Table 4.

Association of IOSS with DFS and OS

To determine the prognostic ability of IOSS in forecasting DFS and OS, the 198 stage III gastric cancer patients were separated into two groups: low IOSS ≤2.00 (N = 91) and high IOSS >2.00 (N = 107). The median DFS and OS in the low IOSS group were evidently longer than those in the high IOSS group (χ^2 = 6.632, p = 0.010; χ^2 = 6.519, p = 0.011). In terms of DFS, patients with low IOSS had higher 1-, 3-, and 5-year DFS rates [84.50% (95% CI: 0.773–0.923), 72.40% (95% CI: 0.636–0.825), and 64.1% (95% CI: 0.545–0.755) vs. 76.30% (95% CI: 0.686–0.849), 51.8% (95% CI: 0.428–0.626), and 46.9% (95% CI: 0.380–0.581)]. In terms of OS, patients with low IOSS had higher 1-, 3-, and 5-year OS rates [94.50% (95% CI: 0.899–0.993), 73.20% (95% CI: 0.645–0.830), and 65.9% (95% CI: 0.567–0.767) vs 81.30% (95% CI: 0.742–0.890), 59.8% (95% CI: 0.512–0.698), and 51.6% (95% CI: 0.428–0.622)]. Cumulative survival is shown in Figure 1.

Nomogram development and validation

Nomograms of the potential prognostic factors by the multivariate analysis for DFS and OS were established (Figure 2). The enrolled factors for DFS included IOSS, PALB (prealbumin), TLN (total lymph node), tumor size, and postoperative chemotherapy; and for OS included IOSS, age, A/G (Albumin/Globulin), PALB (prealbumin), FIB (fibrinogen), TLN (total lymph node), and tumor size via the multivariate analysis. Moreover, the calibration curve was performed to test predictive performance for DFS and OS after curative resection. The calibration curve has shown good agreement between predicted and actual probability at different survival time points (Figure 3). To further test predictive clinical utility, the decision curve analysis was applied to measure the net benefits under different threshold value probabilities. Compared to only IOSS, the constructed nomogram model (the nomogram incorporating the respective potential prognostic factors by the multivariate analysis) generated the best net benefit within the threshold probability for 1-, 3-, and 5-year survival time. Furthermore, the constructed nomogram model's predictive clinical utility for clinical decision was better than IOSS (Figure 4).

Discussion

Despite routine treatment with radical surgery and adjuvant therapy, the survival outcome remains unsatisfactory in gastric cancer, especially in stage III gastric cancer [23, 24]. According to the research report, half of gastric cancer patients will develop recurrence or metastasis within 5 years of systemic treatment [25]. At present, it is said that the damage of the antioxidant system will lead to the development of cancer, and the high oxidative stress status will increase risk of gastrointestinal malignancy [26]. Oxidative stress participates in the advancement of malignant tumors, including gastric cancer, however, it is not clear in gastric cancer prognosis [27, 28].

TABLE 2 Association between IOSS and blood routine and biochemical parameters.

Parameters	Level	Low IOSS	High IOSS	*p*
n		91	107	
Alanine aminotransferase	≤18.0	50 (54.9)	47 (43.9)	0.161
	>18.0	41 (45.1)	60 (56.1)	
Aspartate aminotransferase	≤20.0	39 (42.9)	53 (49.5)	0.426
	>20.0	52 (57.1)	54 (50.5)	
γ-glutamyl transferase	≤14.0	47 (51.6)	50 (46.7)	0.584
	>14.0	44 (48.4)	57 (53.3)	
Lactate dehydrogenase	≤165.0	46 (50.5)	52 (48.6)	0.896
	>165.0	45 (49.5)	55 (51.4)	
Total bilirubin	≤10.2	44 (48.4)	54 (50.5)	0.878
	>10.2	47 (51.6)	53 (49.5)	
Direct bilirubin	≤3.8	41 (45.1)	57 (53.3)	0.313
	>3.8	50 (54.9)	50 (46.7)	
Indirect bilirubin	≤6.5	46 (50.5)	53 (49.5)	1.000
	>6.5	45 (49.5)	54 (50.5)	
Total protein	≤65.0	65 (71.4)	33 (30.8)	**<0.001**
	>65.0	26 (28.6)	74 (69.2)	
Albumin	≤40.0	66 (72.5)	23 (21.5)	**<0.001**
	>40.0	25 (27.5)	84 (78.5)	
Globulin	≤25.0	44 (48.4)	41 (38.3)	0.201
	>25.0	47 (51.6)	66 (61.7)	
Albumin/Globulin (A/G)	≤1.5	49 (53.8)	47 (43.9)	0.212
	>1.5	42 (46.2)	60 (56.1)	
Prealbumin	≤230.0	58 (63.7)	40 (37.4)	**<0.001**
	>230.0	33 (36.3)	67 (62.6)	
Blood urea nitrogen	≤5.5	31 (34.1)	61 (57.0)	**0.002**
	>5.5	60 (65.9)	46 (43.0)	
Alkaline phosphatase	≤73.0	43 (47.3)	55 (51.4)	0.660
	>73.0	48 (52.7)	52 (48.6)	
Glucose	≤5.1	48 (52.7)	46 (43.0)	0.220
	>5.1	43 (47.3)	61 (57.0)	
Cholesterol	≤4.2	51 (56.0)	46 (43.0)	0.091
	>4.2	40 (44.0)	61 (57.0)	
Triglyceride	≤1.1	55 (60.4)	42 (39.3)	**0.005**
	>1.1	36 (39.6)	65 (60.7)	
ABO blood type	A	28 (30.8)	46 (43.0)	0.229
	B	37 (40.7)	30 (28.0)	
	O	19 (20.9)	22 (20.6)	
	AB	7 (7.7)	9 (8.4)	
White blood cell	≤6.5	50 (54.9)	48 (44.9)	0.203
	>6.5	41 (45.1)	59 (55.1)	
Neutrophils	≤3.7	46 (50.5)	53 (49.5)	1.000
	>3.7	45 (49.5)	54 (50.5)	
Lymphocyte	≤1.9	47 (51.6)	48 (44.9)	0.418
	>1.9	44 (48.4)	59 (55.1)	
Monocyte	≤0.5	48 (52.7)	50 (46.7)	0.483
	>0.5	43 (47.3)	57 (53.3)	

(Continued on following page)

TABLE 2 (*Continued*) Association between IOSS and blood routine and biochemical parameters.

Parameters	Level	Low IOSS	High IOSS	*p*
n		**91**	**107**	
Eosinophils	≤0.1	43 (47.3)	55 (51.4)	0.660
	>0.1	48 (52.7)	52 (48.6)	
Basophil	≤0.03	37 (40.7)	50 (46.7)	0.475
	>0.03	54 (59.3)	57 (53.3)	
Hemoglobin	≤135	61 (67.0)	38 (35.5)	**<0.001**
	>135	30 (33.0)	69 (64.5)	
Red blood cell	≤4.3	56 (61.5)	41 (38.3)	**0.002**
	>4.3	35 (38.5)	66 (61.7)	
Platelet	≤255.0	48 (52.7)	50 (46.7)	0.483
	>255.0	43 (47.3)	57 (53.3)	
International normalized ratio	≤1.0	42 (46.2)	52 (48.6)	0.841
	>1.0	49 (53.8)	55 (51.4)	
Fibrinogen	≤3.0	43 (47.3)	57 (53.3)	0.483
	>3.0	48 (52.7)	50 (46.7)	
Carcinoembryonic antigen	≤2.1	41 (45.1)	58 (54.2)	0.254
	>2.1	50 (54.9)	49 (45.8)	
Alpha fetoprotein	≤2.7	47 (51.6)	51 (47.7)	0.677
	>2.7	44 (48.4)	56 (52.3)	
Carbohydrate antigen199	≤12.8	48 (52.7)	53 (49.5)	0.758
	>12.8	43 (47.3)	54 (50.5)	
Carbohydrate antigen724	≤2.5	49 (53.8)	51 (47.7)	0.469
	>2.5	42 (46.2)	56 (52.3)	

Abbreviation: ALT, alanine aminotransferase; AST, aspartate aminotransferase; GGT, γ-glutamyl transferase; LDH, lactate dehydrogenase; TBIL, total bilirubin; DBIL, direct bilirubin; IDBIL, indirect bilirubin; TP, total protein; ALB, albumin; GLOB, globulin; PALB, prealbumin; A/G, ALB/GLOB; BUN, blood urea nitrogen; ALP, alkaline phosphatase; Glu, glucose; CHOL, cholesterol; TRIG, triglyceride; W, white blood cell; N, neutrophils; L, lymphocyte; M, monocyte; E, eosinophils; B, basophil; Hb, hemoglobin; R, red blood cell; P, platelet; INR, international normalized ratio; FIB, fibrinogen; CEA, carcinoembryonic antigen; AFP, alpha fetoprotein; CA199, Carbohydrate antigen199; CA724, Carbohydrate antigen724. Bold values are primarily used to identify meaningful variables.

TABLE 3 The relationships of IOSS and the pathological characteristics parameters.

Parameters	Level	Low IOSS	High IOSS	*p*
n		**91**	**107**	
TLN	≤25	40 (44.0)	55 (51.4)	0.367
	>25	51 (56.0)	52 (48.6)	
pN	≤5	42 (46.2)	58 (54.2)	0.324
	>5	49 (53.8)	49 (45.8)	
HER2	Negative	80 (87.9)	105 (98.1)	**0.009**
	Positive	11 (12.1)	2 (1.9)	
Lymphatic vessel invasion	No	48 (52.7)	60 (56.1)	0.745
	Yes	43 (47.3)	47 (43.9)	
Perineural invasion	No	49 (53.8)	75 (70.1)	**0.027**
	Yes	42 (46.2)	32 (29.9)	

Abbreviation: TLN, total lymph node; pN, positive lymph node; HER2, human epidermal growth factor receptor-2; LVI, lymphatic vessel invasion; PNI, perineural invasion. Bold values are primarily used to identify meaningful variables.

Therefore, accurate risk assessment is essential for supervising postoperative treatment and recurrence monitoring.

In the current research, we established a comprehensive score, IOSS, based on ALB (albumin), DBIL (direct bilirubin), and BUN (blood urea nitrogen), to predict the prognosis of stage III gastric cancer. We investigated the relationship between clinicopathological parameters and prognosis of gastric cancer. IOSS was related to age, radical resection, and tumor size. For elderly patients with gastric cancer, the probability of anemia, body mass decline, and malnutrition is high. The albumin is reflected by the nutritional status. Furthermore, the liver function is also affected by the gastric cancer disease, and the elderly patients with stage III gastric cancer are prone to liver dysfunction. The possibility of radical resection was low in patients with later TNM stage, and after surgery, the incidence rate of postoperative complications is high as well as poor nutritional status. According to univariate and multivariate Cox proportional hazard regression analysis, the result indicated that IOSS was a potential prognostic factor

TABLE 4 The univariate and multivariate Cox proportional hazard regression analysis.

Characteristics	DFS						OS					
	Univariate			Multivariate			Univariate			Multivariate		
	HR	95% CI	*p*	HR	95% CI	*p*	HR	95% CI	*p*	HR	95% CI	*p*
IOSS	1.785	1.141–2.792	**0.011**	3.107	1.828–5.280	**0.000**	1.776	1.136–2.776	**0.012**	4.355	2.429–7.808	**0.000**
Sex	1.248	0.805–1.934	0.321				1.230	0.793–1.905	0.355			
Age	1.543	0.996–2.391	0.052				1.706	1.101–2.645	**0.017**	1.881	1.139–3.108	**0.01**4
BMI	1.197	0.779–1.840	0.412				1.195	0.778–1.838	0.416			
Alanine aminotransferase	0.814	0.530–1.250	0.347				0.789	0.514–1.211	0.278			
Aspartate aminotransferase	0.795	0.518–1.221	0.295				0.804	0.524–1.235	0.319			
γ-Glutamyl Transferase	0.903	0.588–1.386	0.640				0.903	0.589–1.386	0.642			
Tactate dehydrogenase	0.747	0.486–1.149	0.184				0.740	0.481–1.137	0.170			
Direct bilirubin	1.015	0.661–1.557	0.947				1.047	0.682–1.606	0.833			
Indirect bilirubin	0.786	0.512–1.209	0.273				0.769	0.500–1.181	0.230			
Total protein	1.211	0.789–1.858	0.382				1.216	0.792–1.866	0.372			
Albumin	0.974	0.633–1.497	0.903				0.980	0.638–1.507	0.928			
Globulin	1.550	0.994–2.415	0.053				1.499	0.962–2.335	0.074			
Albumin/Globulin (A/G)	0.538	0.348–0.831	0.005	0.745	0.442–1.254	0.268	0.553	0.358–0.853	0.007	0.690	0.406–1.171	0.169
Prealbumin	0.484	0.310–0.754	**0.001**	0.529	0.310–0.901	**0.019**	0.486	0.312–0.757	**0.001**	0.489	0.284–0.839	**0.009**
Blood urea nitrogen	1.261	0.818–1.943	0.294				1.273	0.826–1.962	0.275			
Alkaline phosphatase	0.978	0.637–1.500	0.919				1.071	0.698–1.643	0.754			
Glucose	1.024	0.667–1.574	0.912				1.048	0.683–1.610	0.829			
Cholesterol	1.080	0.704–1.658	0.724				1.095	0.714–1.680	0.678			
Triglyceride	1.106	0.721–1.698	0.644				1.134	0.739–1.741	0.565			
ABO blood type	1.150	0.914–1.446	0.232				1.149	0.914–1.445	0.234			
White blood cell	0.973	0.634–1.492	0.899				0.948	0.618–1.455	0.807			
Neutrophils	1.007	0.656–1.545	0.975				0.961	0.626–1.475	0.856			
Lymphocyte	0.833	0.543–1.279	0.405				0.865	0.564–1.328	0.507			
Monocyte	0.785	0.511–1.205	0.268				0.805	0.524–1.237	0.322			
Eosinophils	0.623	0.403–0.964	0.033	0.862	0.533–1.394	0.544	0.583	0.377–0.902	0.015	0.777	0.480–1.255	0.302
Basophil	0.900	0.586–1.381	0.628				0.883	0.575–1.355	0.568			
Hemoglobin	1.277	0.831–1.961	0.264				1.232	0.802–1.892	0.340			
Red blood cell	1.025	0.668–1.573	0.910				1.001	0.653–1.536	0.995			
Platelet	0.746	0.485–1.147	0.182				0.727	0.473–1.119	0.147			
International normalized ratio	1.214	0.789–1.869	0.378				1.246	0.809–1.917	0.318			
Fibrinogen	1.804	1.166–2.791	0.008	1.467	0.917–2.348	0.110	1.831	1.184–2.833	**0.007**	1.611	1.005–2.582	**0.048**
Carcinoembryonic antigen	0.862	0.561–1.324	0.499				0.888	0.578–1.364	0.587			
Alpha fetoprotein	0.853	0.556–1.308	0.466				0.838	0.546–1.286	0.418			
Carbohydrate antigen199	1.236	0.805–1.897	0.332				1.231	0.802–1.889	0.342			
Carbohydrate antigen724	1.066	0.695–1.635	0.770				1.069	0.697–1.64	0.761			
Radical resection	1.536	1.100–2.146	0.012	1.368	0.942–1.987	0.100	1.626	1.161–2.278	0.005	1.378	0.945–2.011	0.096
Type of surgery	1.214	0.937–1.573	0.141				1.298	1.003–1.681	0.048	1.295	0.968–1.734	0.082
Primary tumor site	1.118	0.836–1.496	0.452				1.076	0.800–1.447	0.628			
Borrmann type	1.332	0.988–1.795	0.060				1.308	0.977–1.751	0.071			
TLN	0.634	0.412–0.976	**0.038**	0.489	0.295–0.810	**0.005**	0.592	0.384–0.911	**0.017**	0.401	0.240–0.670	**0.000**
pN	1.160	0.756–1.780	0.496				1.099	0.717–1.686	0.664			
Tumor size	1.752	1.275–2.407	**0.001**	1.839	1.273–2.657	**0.001**	1.693	1.229–2.332	**0.001**	1.852	1.258–2.726	**0.002**
Differentiation	1.269	0.839–1.919	0.259				1.343	0.888–2.031	0.162			

(Continued on following page)

TABLE 4 (*Continued*) The univariate and multivariate Cox proportional hazard regression analysis.

Characteristics	DFS						OS					
	Univariate			Multivariate			Univariate			Multivariate		
	HR	95% CI	*p*	HR	95% CI	*p*	HR	95% CI	*p*	HR	95% CI	*p*
Pathology	0.915	0.790–1.059	0.231				0.918	0.792–1.064	0.257			
pTNM stage	1.256	0.957–1.649	0.101				1.275	0.967–1.681	0.085			
pT stage	1.234	0.917–1.661	0.165				1.288	0.956–1.736	0.096			
pN stage	1.032	0.821–1.296	0.790				1.014	0.809–1.270	0.906			
Lauren type	0.895	0.697–1.149	0.383				0.883	0.686–1.138	0.338			
HER2	0.750	0.303–1.852	0.532				0.834	0.338–2.059	0.694			
Lymphatic vessel invasion	1.027	0.669–1.577	0.902				1.031	0.671–1.583	0.890			
Perineural invasion	2.464	1.136–5.346	0.022	1.341	0.595–3.020	0.479	2.393	1.103–5.191	0.027	1.306	0.581–2.936	0.519
Postoperative chemotherapy	1.654	1.067–2.564	**0.024**	1.587	1.003–2.510	**0.049**	1.726	1.113–2.677	0.015	1.469	0.910–2.373	0.116

Abbreviation: BMI, body mass index; TNM, tumor node metastasis; ALT, alanine aminotransferase; AST, aspartate aminotransferase; GGT, γ-glutamyl transferase; LDH, lactate dehydrogenase; TBIL, total bilirubin; DBIL, direct bilirubin; IDBIL, indirect bilirubin; TP, total protein; ALB, albumin; GLOB, globulin; PALB, prealbumin; A/G, ALB/GLOB; BUN, blood urea nitrogen; ALP, alkaline phosphatase; Glu, glucose; CHOL, cholesterol; TRIG, triglyceride; W, white blood cell; N, neutrophils; L, lymphocyte; M, monocyte; E, eosinophils; B, basophil; Hb, hemoglobin; R, red blood cell; P, platelet; INR, international normalized ratio; FIB, fibrinogen; CEA, carcinoembryonic antigen; AFP, alpha fetoprotein; CA199, Carbohydrate antigen199; CA724, Carbohydrate antigen724; TLN, total lymph node; pN, positive lymph node; HER2, human epidermal growth factor receptor-2; LVI, lymphatic vessel invasion; PNI, perineural invasion. Bold values are primarily used to identify meaningful variables.

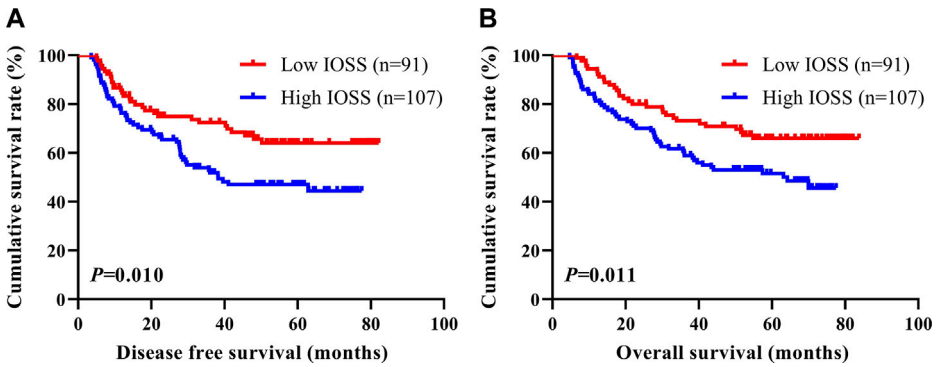

FIGURE 1
DFS and OS of patients with stage III gastric cancer. **(A)** Kaplan-Meier analysis of DFS for the IOSS, **(B)** Kaplan-Meier analysis of OS for the IOSS.

in gastric cancer patients. The prognostic value of IOSS was further analyzed, and indicated that patients with low IOSS survived longer, and with higher 1-, 3-, and 5-year survival rates. Moreover, the IOSS was significantly associated with age, radical resection, and tumor size. IOSS was also significantly associated with total protein (TP), albumin (ALB), prealbumin (PALB), blood urea nitrogen (BUN), triglyceride (TRIG), hemoglobin (Hb), and red blood cell (R). Furthermore, IOSS was significantly associated with HER2 and perineural invasion. These results indicated that oxidative stress had a critical influence on the prognosis in gastric cancer patients. Predicting metastasis and recurrence following curative resection is important for the management of stage III gastric cancer. At present, there are still no highly reliable and convenient biomarkers to predict metastasis and recurrence of gastric cancer.

In order to establish a pin-point accurate DFS and OS forecasting model, the potential prognostic factors from univariate analysis were taken a step further by multivariate analysis. The five valuable factors, IOSS, PALB (prealbumin), TLN (total lymph node), tumor size, and postoperative chemotherapy were used to conduct the predictive DFS model. The seven valuable factors, IOSS, age, A/G (Albumin/Globulin), PALB (prealbumin), FIB (fibrinogen), TLN (total

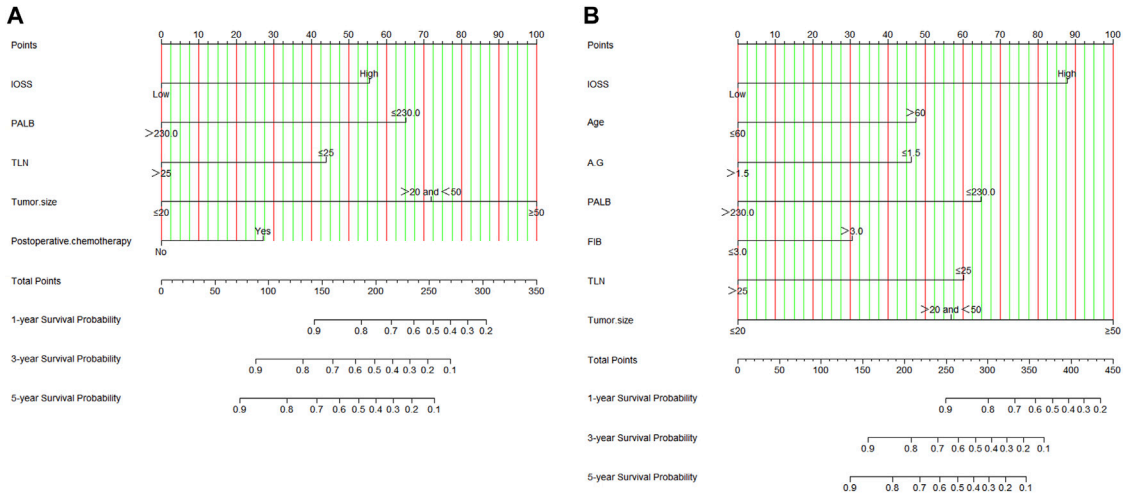

FIGURE 2
Nomograms by multivariate Cox proportional hazard regression analysis for predicting DFS and OS. **(A)** Nomogram for predicting DFS; **(B)** Nomogram for predicting OS.

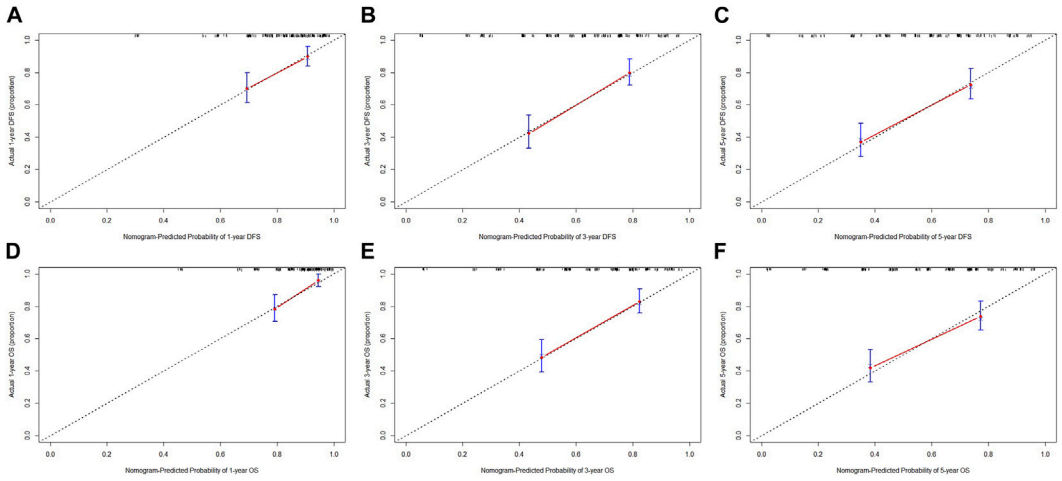

FIGURE 3
Calibration curve for evaluating the 1-, 3-, and 5-year DFS and OS rates. **(A)** Calibration curve for evaluating 1-year DFS rate; **(B)** Calibration curve for evaluating 3-year DFS rate; **(C)** Calibration curve for evaluating 5-year DFS rate; **(D)** Calibration curve for evaluating 1-year OS rate; **(E)** Calibration curve for evaluating 3-year OS rate; **(F)** Calibration curve for evaluating 5-year OS rate.

lymph node), and tumor size were used to conduct the predictive OS model. The nomograms combine clinical characteristics from the multivariate analysis on DFS and OS to increase the accuracy of survival prediction, and were used to evaluate the prognosis in gastric cancer patients. The calibration curve has shown a good homogeneity between predicted and actual probability at different survival time points, including 1-, 3-, and 5-year survival rates. The decision curve analysis was used to quantify the net benefits under different threshold value probabilities, and the predictive clinical utility of the nomogram for clinical decision was better than IOSS.

Assessment of antioxidant administration and oxidative stress is very important for the prevention and treatment of gastric cancer [29–31]. The current study indicated that the oxidative stress was related to the initiation and development of gastric cancer. IOSS was a potential factor to improve the degree of accuracy of gastric cancer prognosis. Several plausible mechanisms are used to explain the association between IOSS and prognosis of stage III gastric cancer.

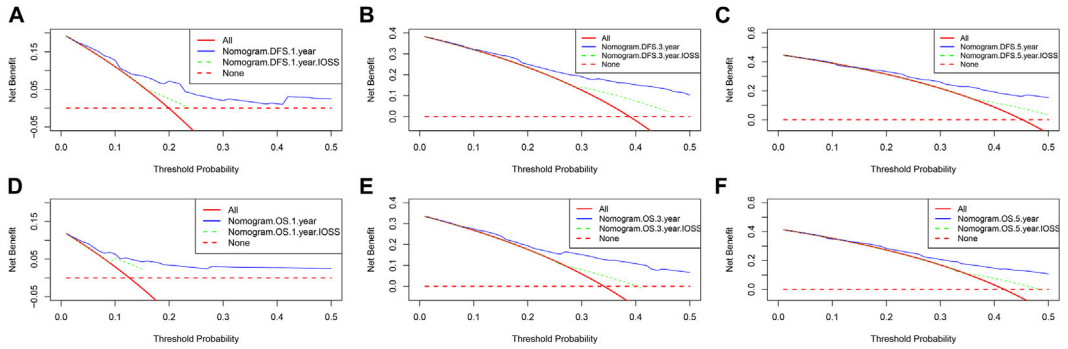

FIGURE 4
Decision curve analysis for the nomogram and only IOSS. **(A)** Decision curve analysis for 1-year DFS; **(B)** Decision curve analysis for 3-year DFS; **(C)** Decision curve analysis for 5-year DFS; **(D)** Decision curve analysis for 1-year OS; **(E)** Decision curve analysis for 3-year OS; **(F)** Decision curve analysis for 5-year OS.

Albumin is the most abundant plasma protein, accounting for one-half of the total protein content [32]. Low concentration of albumin may reflect a worse nutritional status, and the undernutrition may weaken the immune system and have an adverse impact on the prognosis of cancer patients [33]. Albumin is also an important factor in systemic inflammatory response [34]. Bile acid is the end-product of cholesterol decomposition, and consists of two forms in hepatocytes and peripheral blood, comprising direct bilirubin (DBIL) and indirect bilirubin (IDBIL) [35]. Serum bilirubin is the final product of blood metabolism, and has lots of barrier properties, including anticancer, antioxidant, and anti-inflammatory activities [36–38]. Furthermore, the bilirubin is negatively related to the risk of many of cancers, such as lung cancer, breast cancer, and gastrointestinal cancer [39–41]. Blood urea nitrogen (BUN) is manufactured by the metabolism of amino acids and protein in the body, and influences the physiological responses of human protein intake and metabolism [42]. Moreover, blood urea nitrogen (BUN) is a major factor reporting the association between nutritional status and renal status, and is associated with mortality [43].

A number of limitations for the current research should be considered. Firstly, this research was a retrospective single center study with a small number of patients. To go a step further to enrich the references, a prospective, multicenter, and well-designed study with more patients is needed. Secondly, multiple treatment measures were received by reason of tumor recurrence or metastasis during the follow-up periods, and might affect OS. The different postoperative treatments were not fully enrolled into the assessment of prognostic factors. Thirdly, even though the patients were chosen according to inclusion and exclusion criteria, selection bias was still inevitable. Finally, owing to the clinical record boundedness, the oxidative stress markers were not completely contained. Large-scale clinical research with more clinicopathological parameters carried out on multiple centers should be further studied to test and verify our findings.

Conclusion

IOSS is a nonspecific tumor predictor based on procurable oxidative stress index, comprising ALB (albumin), DBIL (direct bilirubin), and BUN (blood urea nitrogen). Low IOSS is discovered to be a vigorous indicator of better prognosis. A nomogram conducted by combining the IOSS with other potential prognostic factors can predict the prognosis of gastric cancer patients.

Data availability statement

The raw data supporting the conclusion of this article will be made available by the authors, without undue reservation.

Ethics statement

The studies involving human participants were reviewed and approved by North China University of Science and Technology Affiliated Hospital. The patients/participants provided their written informed consent to participate in this study.

Author contributions

Y-HL and RM drafted and revised the manuscript. BZ and Q-QZ conducted the data analysis. XY, GD, and C-LJ prepared all the figures and tables. Q-YL and W-GX

supervised the project. All authors contributed to the article and approved the submitted version.

Funding

This research was funded by the Natural Science Foundation of Hebei (No. H2020209309); Key Project of Medical Science Research of Hebei (No. 20160736); Project of introducing overseas students of Human Resources and Social Security of Hebei (No. CY201721); Project of Beijing, Tianjin, and Hebei Basic Research Cooperation (No. J200016).

Conflict of interest

The authors declare that the research was conducted in the absence of any commercial or financial relationships that could be construed as a potential conflict of interest.

References

1. Sung H, Ferlay J, Siegel RL, Laversanne M, Soerjomataram I, Jemal A, et al. Global cancer statistics 2020: GLOBOCAN estimates of incidence and mortality worldwide for 36 cancers in 185 countries. *CA Cancer J Clin* (2021) 71(3):209–249. doi:10.3322/caac.21660

2. Zheng X, Wang Y, Chen Y. Gastric cancer subtypes in tumour and nontumour tissues by immunologic and hallmark gene sets. *J Oncol* (2022) 2022:7887711. doi:10.1155/2022/7887711

3. Cao W, Chen HD, Yu YW, Li N, Chen WQ. Changing profiles of cancer burden worldwide and in China: A secondary analysis of the global cancer statistics 2020. *Chin Med J (Engl)* (2021) 134(7):783–791. doi:10.1097/CM9.0000000000001474

4. Arnold M, Ferlay J, van Berge Henegouwen MI, Soerjomataram I. Global burden of oesophageal and gastric cancer by histology and subsite in 2018. *Gut* (2020) 69(9):1564–1571. doi:10.1136/gutjnl-2020-321600

5. Japanese Gastric Cancer Association. Japanese gastric cancer treatment guidelines 2018 (5th edition). *Gastric Cancer* (2021) 24(1):1–21. doi:10.1007/s10120-020-01042-y

6. Sekiguchi M, Oda I, Matsuda T, Saito Y. Epidemiological trends and future perspectives of gastric cancer in eastern Asia. *Digestion* (2022) 103(1):22–28. doi:10.1159/000518483

7. Young E, Philpott H, Singh R. Endoscopic diagnosis and treatment of gastric dysplasia and early cancer: Current evidence and what the future may hold. *World J Gastroenterol* (2021) 27(31):5126–5151. doi:10.3748/wjg.v27.i31.5126

8. Komatsu Y, Hironaka S, Tanizawa Y, Cai Z, Piao Y, Boku N. Treatment pattern for advanced gastric cancer in Japan and factors associated with sequential treatment: A retrospective administrative claims database study. *Adv Ther* (2022) 39(1):296–313. doi:10.1007/s12325-021-01931-3

9. Kung CH, Jestin Hannan C, Linder G, Johansson J, Nilsson M, Hedberg J, et al. Impact of surgical resection rate on survival in gastric cancer: Nationwide study. *BJS Open* (2021) 5(2):zraa017. doi:10.1093/bjsopen/zraa017

10. Lyons K, Le LC, Pham YT, Borron C, Park JY, Tran CTD, et al. Gastric cancer: Epidemiology, biology, and prevention: A mini review. *Eur J Cancer Prev* (2019) 28(5):397–412. doi:10.1097/CEJ.0000000000000480

11. Sexton RE, Hallak MNA, Uddin MH, Diab M, Azmi AS. Gastric cancer heterogeneity and clinical outcomes. *Technol Cancer Res Treat* (2020) 19:1533033820935477. doi:10.1177/1533033820935477

12. Hirahara N, Tajima Y, Matsubara T, Fujii Y, Kaji S, Kawabata Y, et al. Systemic immune-inflammation index predicts overall survival in patients with gastric cancer: A propensity score-matched analysis. *J Gastrointest Surg* (2021) 25(5):1124–1133. doi:10.1007/s11605-020-04710-7

13. Li Q, Zhang X, Tang M, Song M, Zhang Q, Zhang K, et al. Different muscle mass indices of the Global Leadership Initiative on Malnutrition in diagnosing malnutrition and predicting survival of patients with gastric cancer. *Nutrition* (2021) 89:111286. doi:10.1016/j.nut.2021.111286

14. Sano T, Coit DG, Kim HH, Roviello F, Kassab P, Wittekind C, et al. Proposal of a new stage grouping of gastric cancer for TNM classification: International Gastric Cancer Association staging project. *Gastric Cancer* (2017) 20(2):217–225. doi:10.1007/s10120-016-0601-9

15. Smyth EC, Nilsson M, Grabsch HI, van Grieken NC, Lordick F. Gastric cancer. *Lancet* (2020) 396(10251):635–648. doi:10.1016/S0140-6736(20)31288-5

16. Jelic MD, Mandic AD, Maricic SM, Srdjenovic BU. Oxidative stress and its role in cancer. *J Cancer Res Ther* (2021) 17(1):22–28. doi:10.4103/jcrt.JCRT_862_16

17. Yun HR, Jo YH, Kim J, Shin Y, Kim SS, Choi TG. Roles of autophagy in oxidative stress. *Int J Mol Sci* (2020) 21(9):3289. doi:10.3390/ijms21093289

18. Szczuko M, Kikut J, Szczuko U, Szydłowska I, Nawrocka-Rutkowska J, Ziętek M, et al. Nutrition strategy and life style in polycystic ovary syndrome-narrative review. *Nutrients* (2021) 13(7):2452. doi:10.3390/nu13072452

19. Henriksen HB, Ræder H, Bøhn SK, Paur I, Kværner AS, Billington SÅ, et al. The Norwegian dietary guidelines and colorectal cancer survival (CRC-NORDIET) study: A food-based multicentre randomized controlled trial. *BMC Cancer* (2017) 17(1):83. doi:10.1186/s12885-017-3072-4

20. Wu Z, Wang L, Wen Z, Yao J. Integrated analysis identifies oxidative stress genes associated with progression and prognosis in gastric cancer. *Sci Rep* (2021) 11(1):3292. doi:10.1038/s41598-021-82976-w

21. Geng R, Chen Z, Zhao X, Qiu L, Liu X, Liu R, et al. Oxidative stress-related genetic polymorphisms are associated with the prognosis of metastatic gastric cancer patients treated with epirubicin, oxaliplatin and 5-fluorouracil combination chemotherapy. *PLoS One* (2014) 9(12):e116027. doi:10.1371/journal.pone.0116027

22. Cao Y, Deng S, Yan L, Gu J, Mao F, Xue Y, et al. An oxidative stress index-based score for prognostic prediction in colorectal cancer patients undergoing surgery. *Oxid Med Cell Longev* (2021) 2021:6693707. doi:10.1155/2021/6693707

23. Joharatnam-Hogan N, Shiu KK, Khan K. Challenges in the treatment of gastric cancer in the older patient. *Cancer Treat Rev* (2020) 85:101980. doi:10.1016/j.ctrv.2020.101980

24. Stocker G, Thieme R, Lordick F. Neoadjuvant and perioperative treatment of gastric cancer, current studies and new biomarkers. *Chirurg* (2021) 92(6):499–505. doi:10.1007/s00104-021-01355-3

25. Chen D, Liu Z, Liu W, Fu M, Jiang W, Xu S, et al. Predicting postoperative peritoneal metastasis in gastric cancer with serosal invasion using a collagen nomogram. *Nat Commun* (2021) 12(1):179. doi:10.1038/s41467-020-20429-0

26. Sczepanik FSC, Grossi ML, Casati M, Goldberg M, Glogauer M, Fine N, et al. Periodontitis is an inflammatory disease of oxidative stress: We should treat it that way. *Periodontol* (2020) 84(1):45–68. doi:10.1111/prd.12342

27. O'Malley J, Kumar R, Inigo J, Yadava N, Chandra D. Mitochondrial stress response and cancer. *Trends Cancer* (2020) 6(8):688–701. doi:10.1016/j.trecan.2020.04.009

28. Li T, Zhang T, Gao H, Liu R, Gu M, Yang Y, et al. Tempol ameliorates polycystic ovary syndrome through attenuating intestinal oxidative stress and modulating of gut microbiota composition-serum metabolites interaction. *Redox Biol* (2021) 41:101886. doi:10.1016/j.redox.2021.101886

29. Tumer AA, Rashid FA. The relationship between circulating irisin and oxidative stress in gastric and colorectal cancer patients. *Asian Pac J Cancer Prev* (2022) 23(8):2649–2654. doi:10.31557/APJCP.2022.23.8.2649

30. Jakubik JA, Kołodziejczyk-Czepas J, Kędzierska M, Kaczmarek M, Nowak P, Potemski P, et al. A preliminary evaluation of oxidative stress in patients with gastric cancer before chemotherapy. *Arch Med Sci* (2021) 18(2):440–447. doi:10.5114/aoms/102344

31. Danis N, Ozkan AE, Karatas F, Cakici C, Yigitbasi T, Sevencan NO, et al. The importance of antioxidant status in gastric intestinal metaplasia. *J Med Biochem* (2021) 40(4):378–383. doi:10.5937/jomb0-29349

32. Terhaar HM, Allbaugh RA, Mochel JP, Sebbag L. Serum albumin and total protein concentration in the tear film of horses with healthy or diseased eyes. *Vet Ophthalmol* (2021) 24(1):20–27. doi:10.1111/vop.12822

33. Lei J, Wang Y, Guo X, Yan S, Ma D, Wang P, et al. Low preoperative serum ALB level is independently associated with poor overall survival in endometrial cancer patients. *Future Oncol* (2020) 16(8):307–316. doi:10.2217/fon-2019-0732

34. Cattaneo L, Lopreiato V, Piccioli-Cappelli F, Trevisi E, Minuti A. Plasma albumin-to-globulin ratio before dry-off as a possible index of inflammatory status and performance in the subsequent lactation in dairy cows. *J Dairy Sci* (2021) 104(7):8228–8242. doi:10.3168/jds.2020-19944

35. Li ZZ, Huang Q, Yang XL, Zeng J, Wang QH, Tang HM, et al. Cholesterol metabolic markers for differential evaluation of patients with hyperlipidemia and familial hypercholesterolemia. *Dis Markers* (2022) 2022:2008556. doi:10.1155/2022/2008556

36. Jia Z, Zhu Z, Wang Y, Ding J, Lin Z, Zhang Y, et al. The prognostic value of serum bilirubin in colorectal cancer patients with surgical resection. *Int J Biol Markers* (2021) 36(2):17246008211036128. doi:10.1177/17246008211036128

37. Turkmen D. Serum bilirubin and uric acid antioxidant levels in rosacea patients. *J Cosmet Dermatol* (2020) 19(10):2717–2720. doi:10.1111/jocd.13395

38. Zhang L, Zhang C, Meng Z, Gong L, Pang C, Liu X, et al. Serum bilirubin is negatively associated with white blood cell count. *Clinics (Sao Paulo)* (2019) 74:e775. doi:10.6061/clinics/2019/e775

39. Jiang D, Shi J, Yuan M, Duan X, Li L, Li Q. Levels of serum bilirubin in small cell lung cancer and non-small cell lung cancer patients. *Cell Mol Biol (Noisy-le-grand)* (2018) 64(6):71–76.

40. Monroy-Iglesias MJ, Moss C, Beckmann K, Hammar N, Walldius G, Bosco C, et al. Serum total bilirubin and risk of cancer: A Swedish cohort study and meta-analysis. *Cancers (Basel)* (2021) 13(21):5540. doi:10.3390/cancers13215540

41. Yang L, Ge LY, Yu T, Liang Y, Yin Y, Chen H. The prognostic impact of serum bilirubin in stage IV colorectal cancer patients. *J Clin Lab Anal* (2018) 32(2):e22272. doi:10.1002/jcla.22272

42. Shen S, Yan X, Xu B. The blood urea nitrogen/creatinine (BUN/cre) ratio was U-shaped associated with all-cause mortality in general population. *Ren Fail* (2022) 44(1):184–190. doi:10.1080/0886022X.2022.2030359

43. Peng X, Huang Y, Fu H, Zhang Z, He A, Luo R. Prognostic value of blood urea nitrogen to serum albumin ratio in intensive care unit patients with lung cancer. *Int J Gen Med* (2021) 14:7349–7359. doi:10.2147/IJGM.S337822

Pathology & Oncology Research | frontiers

TYPE Original Research
PUBLISHED 30 May 2024
DOI 10.3389/pore.2024.1611734

Check for updates

OPEN ACCESS

EDITED BY
Andrea Ladányi,
National Institute of Oncology (NIO), Hungary

*CORRESPONDENCE
Houqiang Li,
docli254@126.com

†These authors have contributed equally to this work

RECEIVED 19 February 2024
ACCEPTED 13 May 2024
PUBLISHED 30 May 2024

CITATION
Li H, Zheng L, Zhong G, Yu X, Zhang X, Chen L and Chen X (2024), Gastric epithelial neoplasm of fundic-gland mucosa lineage: representative of the low atypia differentiated gastric tumor and Ki67 may help in their identification. *Pathol. Oncol. Res.* 30:1611734. doi: 10.3389/pore.2024.1611734

COPYRIGHT
© 2024 Li, Zheng, Zhong, Yu, Zhang, Chen and Chen. This is an open-access article distributed under the terms of the Creative Commons Attribution License (CC BY). The use, distribution or reproduction in other forums is permitted, provided the original author(s) and the copyright owner(s) are credited and that the original publication in this journal is cited, in accordance with accepted academic practice. No use, distribution or reproduction is permitted which does not comply with these terms.

Gastric epithelial neoplasm of fundic-gland mucosa lineage: representative of the low atypia differentiated gastric tumor and Ki67 may help in their identification

Houqiang Li[1,2*†], Lanqing Zheng[1,2†], Guodong Zhong[3], Xunbin Yu[1,2], Xia Zhang[1,2], Linying Chen[4] and Xin Chen[1,2]

[1]Shengli Clinical Medical College of Fujian Medical University, Fuzhou, China, [2]Fujian Provincial Hospital, Fuzhou, China, [3]The Second Affiliated Hospital of Fujian Traditional Chinese Medical University, Fuzhou, China, [4]The First Affiliated Hospital of Fujian Medical University, Fuzhou, Fujian, China

Background: Gastric epithelial neoplasm of the fundic-gland mucosa lineages (GEN-FGMLs) are rare forms of gastric tumors that encompass oxyntic gland adenoma (OGA), gastric adenocarcinoma of the fundic-gland type (GA-FG), and gastric adenocarcinoma of the fundic-gland mucosa type (GA-FGM). There is no consensus on the cause, classification, and clinicopathological features of GEN-FGMLs, and misdiagnosis is common because of similarities in symptoms.

Methods: 37 cases diagnosed with GEN-FGMLs were included in this study. H&E-stained slides were reviewed and clinicopathological parameters were recorded. Immunohistochemical staining was conducted for MUC2, MUC5AC, MUC6, CD10, CD56, synaptophysin, chromograninA, p53, Ki67, pepsinogen-I, H^+/K^+-ATPase and Desmin.

Results: The patients' ages ranged from 42 to 79 years, with a median age of 60. 17 were male and 20 were female. Morphologically, 19 OGAs, 16 GA-FGs, and two GA-FGMs were identified. Histopathological similarities exist between OGA, GA-FG, and GA-FGM. The tumors demonstrated well-formed glands, expanding with dense growth patterns comprising pale, blue-grey columnar cells with mild nuclear atypia. These cells resembled fundic gland cells. None of the OGA invaded the submucosal layer. The normal gastric pit epithelium covered the entire surface of the OGA and GA-FG, but the dysplasia pit epithelium covered the GA-FGM. Non-atrophic gastritis was observed in more than half of the background mucosa. All cases were diffusely positive for MUC6 and pepsinogen-I on immunohistochemistry. H^+/K^+-ATPase staining was negative or showed a scattered pattern in most cases. MUC5AC was expressed on the surface of GA-FGMs. p53 was focally expressed and the Ki67 index was low (1%–20%). Compared with OGA, GA-FG and GA-FGM were more prominent in the macroscopic view ($p < 0.05$) and had larger sizes ($p < 0.0001$). Additionally, GA-FG and GA-FGM exhibited higher Ki67 indices than

OGA ($p < 0.0001$). Specimens with Ki-67 proliferation indices >2.5% and size >4.5 mm are more likely to be diagnosed with GA-FG and GA-FGM than OGA.

Conclusion: GEN-FGMLs are group of well-differentiated gastric tumors with favourable biological behaviours, low cellular atypia, and low proliferation. Immunohistochemistry is critical for confirming diagnosis. Compared with OGA, GA-FG and GA-FGM have larger sizes and higher Ki67 proliferation indices, indicating that they play a critical role in the identification of GEN-FGML. Pathologists and endoscopists should be cautious to prevent misdiagnosis and overtreatment, especially in biopsy specimens.

KEYWORDS

gastric cancer, gastric adenocarcinoma of fundic-gland type, gastric adenocarcinoma of fundic-gland mucosa type, oxyntic gland adenoma, low-grade differentiated gastric tumors

Introduction

Gastric cancer (GC) is one of the most common malignant tumors of the digestive system worldwide [1]. Benefiting from the improvement and popularization of endoscopic technology in recent years, researchers have discovered many low-grade well differentiated gastric tumors, such as the gastric epithelial neoplasm of the fundic-gland mucosa lineages (GEN-FGML). GEN-FGMLs are rare tumors that differentiate from gastric mucosa to fundic glands, including oxyntic gland adenoma (OGA), gastric adenocarcinoma of the fundic-gland type (GA-FG), and gastric adenocarcinoma of the fundic-gland mucosa type (GA-FGM) [2–4]. OGA and GA-FG are defined as well-differentiated neoplasms composed of parietal cell-like tumor cells with mild morphologic atypia that are positive for pepsinogen I and/or H^+/K^+-ATPase. GA-FG can be divided into three subcategories according to the tumor composition: chief cell predominant, parietal cell predominant, and mixed phenotype [2]. The histologic features of GA-FGM are similar to those of GA-FG, but the gastric pit epithelium is atypical and malignant [5, 6]. GA-FGM was also divided into three subtypes (Type 1, Type 2, and Type 3) according to the mucosal structure of the pit epithelium and fundic gland [4]. GEN-FGML can be easily misdiagnosed. GA-FG is known as an oxyntic mucosal polyp/adenoma in the West [7], whereas Japanese scholars believe that OGA is the intramucosal stage of GA-FG. Japanese scholars divided fundic gland tumors into GA-FG and GA-FGM, and GA-FGM is believed to have more malignant potential [6, 8]. In addition, OGA and GA-FG were officially listed as new gastric neoplasms in the World Health Organization (WHO) classification of tumors in 2019 [9]. GA-FG is diagnosed when OGA invades the submucosal layer. GEN-FGMLs, particularly OGA and GA-FG, have a good prognosis [2]. Unlike other low-grade well differentiated gastric tumors, GEN-FGMLs have a high frequency of GNAS mutations, which are a characteristic genetic feature of GEN-FGMLs [4]. Here, we report the clinicopathological features of 37 cases of GEN-FGMLs, helping pathologists and endoscopists diagnose GEN-FGMLs.

Materials and methods

Data collection

Between January 2019 and December 2023, 43 specimens from 37 patients pathologically diagnosed with GEN-FGMLs, including 19 OGAs, 16 GA-FGs, and two GA-FGMs, were included from Fujian Provincial Hospital. All original H&E slides were reviewed, and patients' clinicopathologic parameters were extracted from the hospital medical record system. These parameters included age, sex, tumor location, morphology, depth of invasion, vascular invasion, and nerve invasion. The background mucosa was also recorded. The diagnosis of the disease were based on the 5th edition of the WHO Health Organization tumor classification and the 6th edition of the Japanese Gastric Carcinoma Classification. All pathologic diagnoses were reviewed by 2 senior pathologists and were followed up until April 2024.

Histology and immunohistochemistry

Histopathological analyses were performed on the basis of the following factors: histological subcategories (OGA, GA-FG, and GA-FGM), architectural patterns, presence of cytonuclear atypia, depth of invasion, and atrophy or intestinal metaplasia of the background. The presence of MUC2, CD10, MUC5AC, MUC6, Ki67, chromograninA (CgA), synaptophysin (Syn), CD56, p53, pepsinogen-I, H^+/K^+-ATPase, and Desmin was measured using specific antibodies and analyzed using the Lumatas platform (Maixin Biotechnology Co. LTD, China).

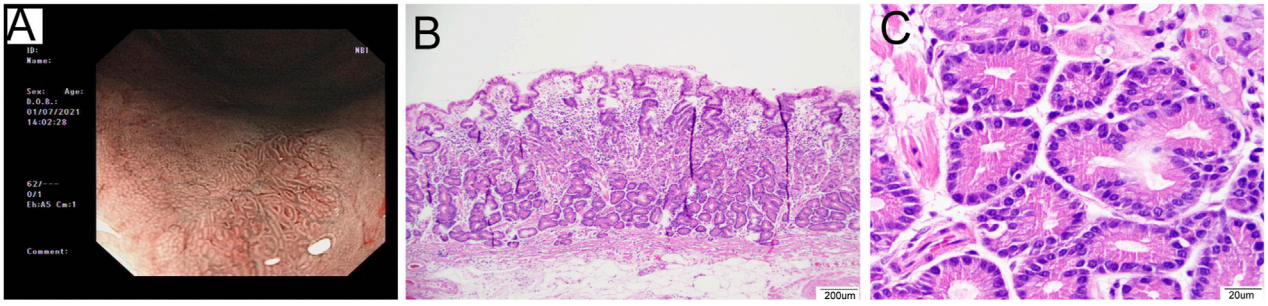

FIGURE 1
Representative images of a 53-year-old male patient diagnosed with OGA. **(A)**: The image of NBI shows fundus mucosa observed as a flat lesion in the macroscopic view. **(B)**: The lesion was clearly defined on the mucosa layer. The lesion covered normal gastric pit epithelium and glands exhibited branching, expanding arrangement (40×). **(C)**: The glands were composed of columnar cells with mild nuclear atypia, similar to fundic gland cells. The nuclei were slightly enlarged (400×).

Immunostaining results were considered positive if ≥ 10% of neoplastic cells were stained. Details of the antibodies, incubation conditions, and antigen retrieval are listed in Supplementary Table S1. PBS was used as a negative control. The histopathological diagnosis and immunostaining results were confirmed by two pathologists. A consensus review under a multi-head microscope was performed when facing inconsistent results.

Statistical analysis

Graphs and statistical analysis were administered using GraphPad Prism 9.0 (La Jolla, CA, United States). Continuous data were compared using the Mann-Whitney U test. Categorical variables were analyzed using Fisher's exact test. A p-value < 0.05 was considered statistically significant.

Results

Clinicopathologic characterization of GEN-FGMLs

All patients were 42–79 years old, with a median age of 60. Of all patients, 17 were male (45.95%) and 20 were female (54.05%), and the male-to-female ratio was approximately 4: 5. Endoscopic findings indicated 15 lesions in the fundus and 22 in the gastric body. 12 cases of OGA and five cases of GA-FG were observed as flatting lesions in the macroscopic view (Figure 1A). While, six cases of OGA, 11 cases of GA-FG, and all two cases of GA-FGM were observed as protruding lesions in the macroscopic view (Figures 2A, B; 3A, B). Of all GEN-FGMLs, 36 cases were available for the follow-up survey, 15 cases were biopsied, 22 cases were endoscopically resected, and one case underwent additional surgical resection. Endoscopic resection was performed in 17 patients with GA-FG and GA-FGM. The average follow-up time for cases in this group was 20.6 months (ranging from 5 to 41 months). During the follow-up period, one patient of GA-FG presented with 1 lymph node metastasis and underwent additional surgical resection. There was no recurrence, metastasis, or gastric cancer-specific death in all others (Table 1).

Of all patients, 14 were diagnosed with OGA due to limitations in evaluating mucosal layer depth, 16 were diagnosed with GA-FG, and two cases were diagnosed with GA-FGM. Four patients were misdiagnosed with OGA based on pathological biopsy before endoscopic resection. The tumors classified as GEN-FGMLs were solitary, with sizes ranging from 2 mm to 17 mm (average = 6.3 mm). The average size of GA-FG and GA-FGM tumours is larger than OGA tumours (3.8 mm for OGA vs. 8.7 mm for GA-FG and GA-FGM, $p < 0.0001$). Moreover, OGA had a flattened form, whereas GA-FG and GA-FGM commonly had a protruded form ($p = 0.044$). No significant differences were found between OGA, GA-FG, and GA-FGM with respect to other variables, such as sex, age, location, and atrophic gastritis of the peripheral mucosa (Table 1).

From a histological perspective, OGA, GA-FG, and GA-FGM have similar morphologies. At low magnification, all of the tumors showed an expansive and dense growth pattern, with clear demarcation, but without migrating (Figures 1B, 2C, 3C). Normal gastric pit epithelium covered the entire surface of OGA and GA-FG (Figures 1B, 2D). However, dysplastic/cancerous pit epithelium covered GA-FGM (Figure 3E). At high magnification, GEN-FGMLs tumor cell exhibited mild cellular and structural atypia with well-formed glands displaying expansive and dense growth patterns. The glands were composed of pale gray-blue basophilic columnar cells with mild nuclear atypia, similar to

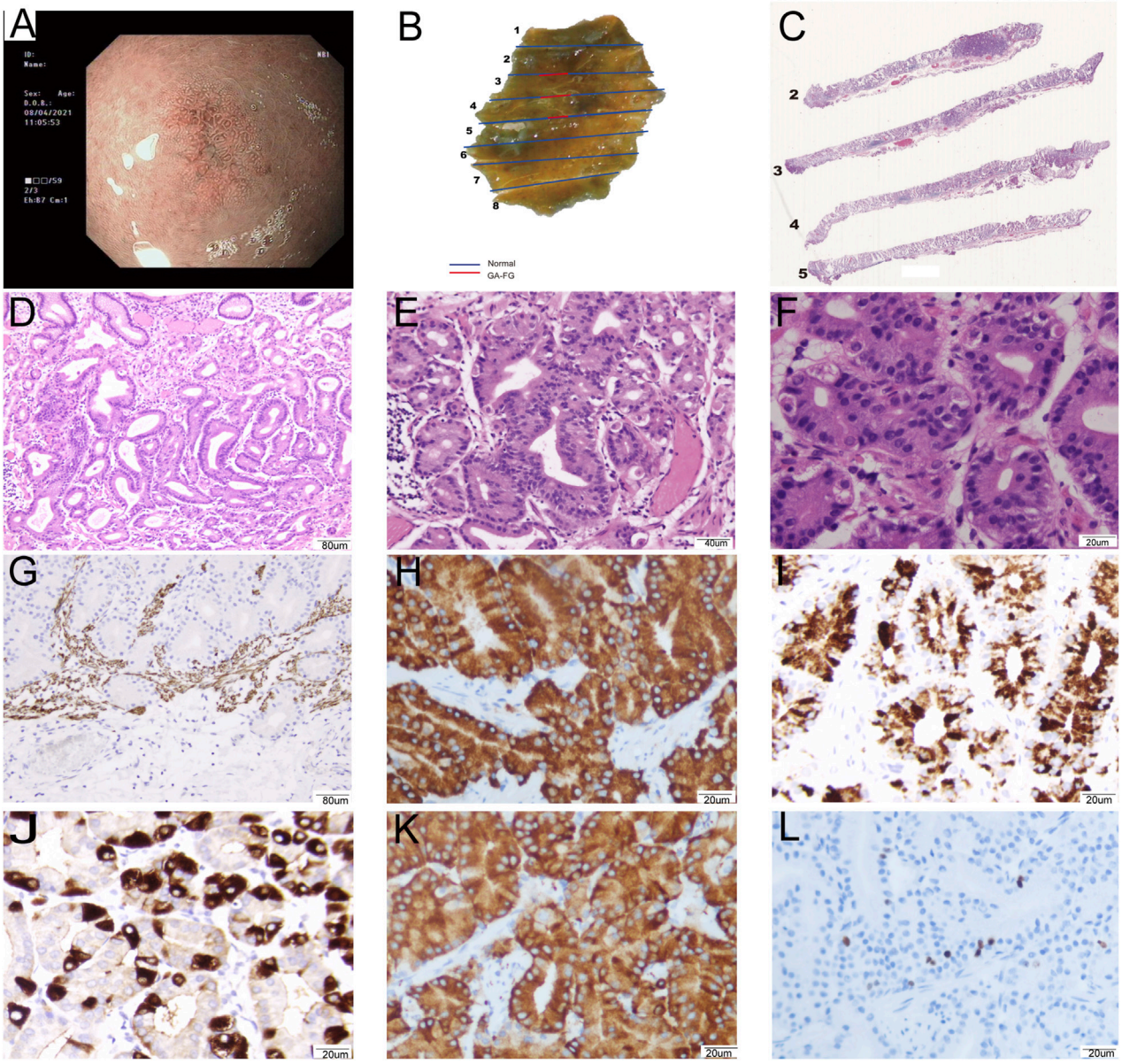

FIGURE 2
Representative images of a 63-year-old female patient diagnosed with GA-FG: 0-IIb, Tub1>tub2 (SM1), Ly0, V0, UL (–), pHM0, pVM0. **(A)**: The image of NBI shows background fundus mucosa without *H. pylori* infection and non-atrophic gastritis. The 0–IIb lesion had a blurred border with irregularly arranged marginal crypt epithelium with asymmetric distribution. The lesion consisted of microvessels with dendritic vasculature. **(B)**: Macroscopic findings of the resected specimen showing a protruding submucosal lesion. **(C)**: The lesion was clearly defined and infiltrated into the submucosa. **(D)** The lesion covered normal gastric pit epithelium and glands and exhibited branching, expanding arrangement, and fusion (100×). **(E)**: The tumors exhibited mild cellular and structural atypia with well-formed glands, similar to fundic gland cells (200×). **(F)**: The glands were composed of pale grey-blue, basophilic columnar cells with mild nuclear atypia. The nuclei had hyperchromatic chromatin and were slightly enlarged (400×). **(G–L)**: Immunohistochemical analysis. **(G)** Desmin showed carcinoma invasion of the submucosal layer (100×). Carcinoma was diffusely positivity for MUC6 (H, 400×), pepsinogen-I (I, 400×), and Syn (K, 400×), focally positivity for H+/K + -ATPase (J, 400×), and Ki67 index was 3% (L, 400×).

fundic gland cells. The glands exhibited branching, expansion, a back-to-back arrangement, and fusion. The nuclei were arranged in a crowded round or ovoid shape, with small nucleoli, hyperchromatic chromatin, and slight enlargement (Figures 1C, 2E, F). However, GA-FGM showed more atypia than GA-FG and OGA (Figures 3F, G). Mitosis and necrosis were not observed in any case. IHC staining showed that MUC6 and pepsinogen I were positive in all cases (Figures 2H, I). While the

10.3389/pore.2024.1611734

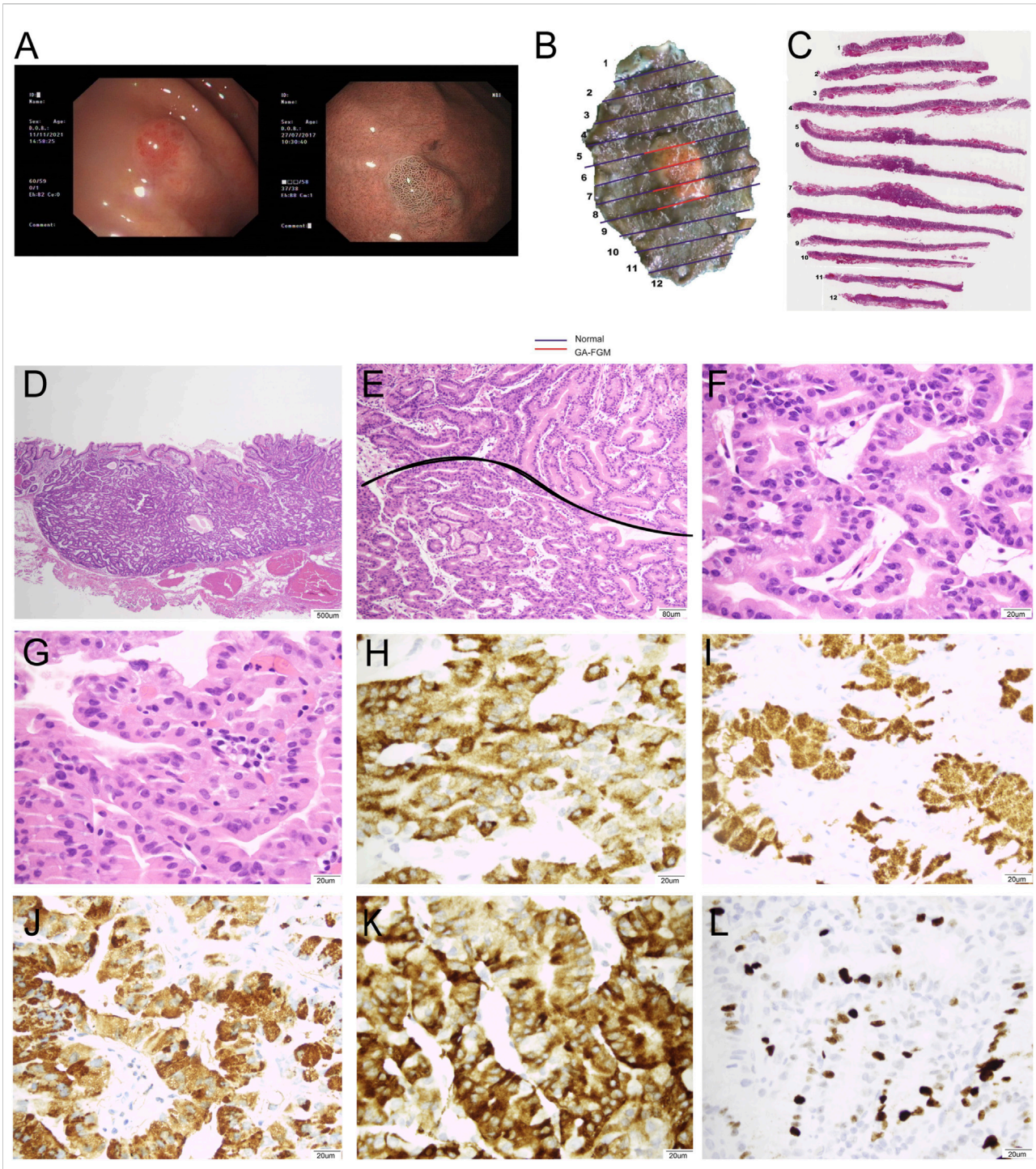

FIGURE 3
Representative images of a 71-year-old female patient diagnosed with GA-FGM: 0-IIa, Tub1>tub2 (SM2), Ly0, V0, UL (–), pHM0, and pVM0. **(A)**: Conventional endoscopy revealed a smooth, reddish lesion in the gastric fundus with distinct borders. The background mucosa did not show *H. pylori* infection and non-atrophic gastritis. The lesion exhibited significant changes in microvascular and microsurface patterns. The marginal crypt epithelium had a complex ripple-like pattern that was wider and irregularly arranged compared to that of the background mucosa. **(B,C)**: Macroscopic findings of the resected specimen showing a protruding lesion. **(C,D)**: The lesion was well-defined and infiltrated into the submucosa (20×). **(E)**: The pit epithelium exhibited cellular atypia, and glands exhibited branching, expanding arrangement, and fusion (400×). **(F)**: The tumors exhibited marked cellular and structural atypia. The glands were composed of pale grey-blue and basophilic columnar cells (40×). **(G)**: The pit epithelium exhibited obvious cellular and structural atypia (400×). **(H–L)**: Immunohistochemical analysis (400×). Carcinoma was diffusely positive for MUC6 **(H)** and pepsinogen-I **(I)**. The pit epithelium was positive for MUCAC **(J)** and diffusely positive for Syn **(K)**, and Ki67 index was 15% **(L)**.

TABLE 1 Clinicopathological characteristics, immunohistochemical analysis of GA-FGMLs.

Clinicopathological characteristics	OGA (n = 19)	GA-FG/GA-FGM (n = 18)	p-val
Sex (male: female)	8:11	9:9	0.75
Age (Median: years)	61 (range: 42–69)	58 (range: 45–79)	0.49
Location	B: F = 13:6	B: F = 9:9	0.32
Macroscopic type (Flat: Protruded)	12:6	5:13	0.044
Size of tumor (average: mm)	3.8 (2–8), 18cases	8.7 (4–17), 17cases	<0.0001
Depth of invasion (SM1:SM2)	NA	16:2	NA
Lymphatic and venous invasion	NA	5.88% (1/17)	NA
Perineural invasion	NA	0% (0/17)	NA
Atrophic gastritis	43.75% (7/16)	44.44% (8/18)	>0.99
Follow up time (months)	20.7 (range: 5–41)	20.5 (range: 5–39)	>0.99
Outcome	19 cases: SWD	17 cases: SWD Lymph node metastasis in one case	NA
Immunohistochemical analysis			
pepsinogen-I	100% (11/11)	100% (14/14)	>0.99
H/K-ATPase	0% (0/11)	14.3% (2/14)	0.50
MUC2	0% (0/11)	0% (0/16)	>0.99
MUC5AC	0% (0/11)	12.5% (2/16)	0.51
MUC6	100% (11/11)	100% (16/16)	>0.99
CD10	0% (0/10)	0% (0/16)	>0.99
CgA	0% (0/11)	0% (0/15)	>0.99
Syn	100% (11/11)	100% (15/15)	>0.99
CD56	100% (11/11)	100% (15/15)	>0.99
p53	4.7% (1%–20%), 14 cases	4.2% (1%–30%), 15 cases	>0.99
Ki-67	1.9% (1%–5%), 16 cases	7.5% (2%–20%), 16 cases	<0.0001

B: gastric body; F: fundus; NA: date not available; SWD: survive without disease.

H^+/K^+-ATPase staining was negative or showed a scattered pattern (<10% of neoplastic cells were stained) in most of the cases. Positive staining was observed in one GA-FG and one GA-FGM case (Figure 2J). MUC5AC staining was positive in the pit epithelium and GA-FGM surface tumor cells (Figure 3J). MUC2 and CD10 were negative in all the cases. Regarding neuroendocrine markers, CD56 and Syn were positive in staining (Figures 2K, 3K), but CgA was negative. Additionally, GA-FG and GA-FGM exhibited higher Ki-67 proliferation indices (p < 0.0001) than OGA (Table 1) (Figures 2L, 3L). However, no significant findings were reported for other markers. None of the patients exhibited p53 overexpression. The desmin staining (Figure 2G) showed the invasion of the carcinoma into the submucosal layer. GA-FG invaded the submucosal layer at a depth of < 500 μm (SM1) in 15 cases, and GA-FGM invaded the submucosal layer at a depth of > 500 μm (SM2) in one case. Furthermore, We used receiver operating characteristics (ROC) analysis to calculate the optimal cut-off value of the Ki-67 proliferation indices (>2.5%) and lesion size (>4.5 mm) in GEN-FGMLs diagnosis and revealed that the Ki-67 proliferation indices and lesion size serve as a good indicator for differentiating GEN-FGMLs (Figure 4) (Table 2).

Discussion

Recently, the incidence of early gastric cancer has increased significantly with the application of narrow-band imaging (NBI) magnifying endoscopy [10]. Many *H. Pylori*-negative gastric adenocarcinomas, including GEN-FGML, have been reported [2, 6, 10–17]. In 2021, GEN-FGML was classified into OGA, GA-FG, and GA-FGM, based on cell differentiation and histological features [4]. Furthermore,

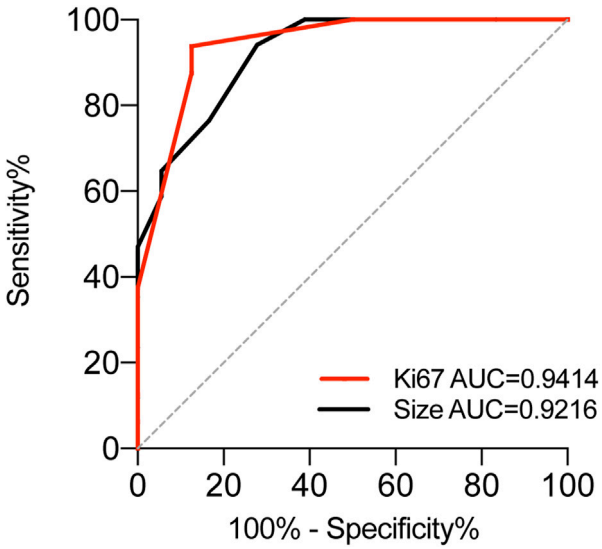

FIGURE 4
ROC analysis to assess the specificity and sensitivity of Ki-67 and Size to differentiate between OGA GA-FG and GA-FGM in GA-FGML.

GA-FG can be divided into three subcategories according to the tumor composition: chief cell predominant, parietal cell predominant, and mixed phenotype [9]. And GA-FGM was also divided into three subtypes (Type 1, Type 2, and Type 3) according to the mucosal structure of the pit epithelium and fundic gland [4].

In our study, we present 37 cases of GEN-FGMLs, including 19 cases of OGA, 16 cases of GA-FG, and two cases of GA-FGM. Previous studies in Japan have shown that GEN-FGMLs are predominantly observed in males [4]. However, our results showed that GEN-FGMLs are more common in females in China. In the present study, GEN-FGMLs were different based on their sizes. GA-FG and GA-FGM had larger diameters, with an average of 8.8 mm, than OGA, with an average diameter of 5 mm. Furthermore, our study demonstrated that GA-FG and GA-FGM had proliferation indices with Ki-67 than OGA, suggesting that Ki-67 plays a crucial role in the diagnosis of GEN-FGML. Previous studies showed that the background mucosa of GEN-FGML shows no atrophic changes and intestinal metaplasia [4, 16]. In the present study, over 40% of patients had slight atrophic gastritis in the adjacent mucosa.

Histopathological assessment is essential for confirming the diagnosis of GEN-FGMLs. According to the WHO classification, the depth of invasion differentiates between OGA and GA-FG [9]. Based on the Japanese diagnostic criteria, despite showing low-grade atypia and invading the submucosal layer, many stomach neoplasms are diagnosed as invasive carcinomas in the absence of an obvious desmoplastic response [2, 18, 19]. Thus, Japanese scholars have proposed that OGA is the intramucosal stage of GA-FG, and OGA and GA-FG

TABLE 2 Summary of clinicopathologic characteristics of GA-FGMLs.

Parameters	OGA	GA-FG	GA-FGM
Size[a]	≤4.5 mm	>4.5 mm	
Macroscopic type	Flat	Protruded	
Submucosal invasion	Absent	Present	
Growth pattern	Demonstrated expansive and dense growth pattern, with clear demarcation.Tumor glands exhibited branching, expanding arrangement and fusion		
Tumor cell differentiation	Dominated by chief cell differentiation or mixed with parietal cells differentiation		Dominated by chief cell differentiation and mixed with gastric pit epithelium differentiation
Tumor heterogeneity	Exhibited mild cellular and structural atypia, similar to fundic gland cells		Exhibited marked cellular and structural atypia. The pit epithelium is atypical and malignant
Gastric pit epithelium	Normal		Atypical proliferation or carcinogenesis
Synaptophysin	Positive	Positive	
Pepsinogen-I	Positive	Positive	
MUC6	Positive	Positive	
MUC5AC	Negative		Positive
Ki67[b]	≤2.5%	>2.5%	

[a]Sensitivity% = 94.12%,Specificity% = 72.22%, Youden Index = 0.6634.
[b]Sensitivity% = 93.75%,Specificity% = 87.5%, Youden Index = 0.8125.

represent different developmental stages of the same tumor [8]. The identification of OGA and GA-FG as intramucosal adenomas or low-grade gastric adenocarcinomas relies on whether the pathologist uses the Western or Japanese diagnostic criteria. In this cohort study, our diagnosis followed the WHO criteria, as we believe that overdiagnosis may cause unnecessary overtreatment in patients in China.

OGA and GA-FG are well-differentiated tumors with expansive and dense growth, composed of pale gray-blue basophilic columnar cells with mild nuclear atypia and slightly enlarged fundic gland cells. IHC staining revealed that they were positive for pepsinogen-I. The surface of the lesions was covered with a normal gastric pit epithelium. In addition, the deep part of the tumor was irregularly branched or dendritic. The tumor gland and background mucosa were demarcated without migrating. The histological features of GA-FGM were similar to those of GA-FG. However, GA-FGM is always accompanied by differentiation to the fundic glands and pit mucous cells and occasionally progresses into tumors consisting of pyloric glands. Differentiation into fundic glands and pit mucous cells suggests that GA-FGM presumably possesses multilineage differentiation potential. GA-FGM is a unique type of complex gastric adenocarcinoma with differentiated fundic glands [2]. Our study revealed histological characteristics similar to those of GEN-FGMLs. Compared to OGA and GA-FG, GA-FGM exhibits greater cellular atypia and malignant transformation of the pit epithelium [6]. GA-FGM showed the highest malignant potential due to higher rates of vascular invasion and lymph node metastasis [2]. Owing to the limited sample size, we did not observe lymphatic invasion and vascular invasion in GA-FGM. However, lymph node metastasis was observed in one GA-FG case. The IHC staining results were consistent with those of previous studies. In the gastric mucosa, pit mucous cells express MUC5AC, gland mucous cells express MUC6, chief cells express pepsinogen I, and parietal cells express H^+/K^+-ATPase. GEN-FGMLs mainly consist of tumor components with chief cell-like differentiation, whereas gland mucous cells were previously thought to be the precursors of chief cells [20]. All GEN-FGML samples were positive for MUC6 and pepsinogen-I, indicating that the GEN-FGMLs originated from immature chief cells. MUC5AC was expressed in the pit epithelium and GA-FGM surface, whereas MUC2 and CD10 were not detected. GEN-FGMLs also expressed neuroendocrine markers (Syn and CD56) but not CgA. GEN-FGMLs had a low Ki-67/MIB1 proliferation index and lacked p53 protein.

GEN-FGMLs contain *GNAS* mutation, which is thought to be a characteristic genetic feature [4]. Ueyama *et al.* [4] showed that GEN-FGMLs belong to the same genetic lineage, and that GA-FGM may be the final stage of OGA and GA-FG. In addition to *GNAS* mutations, GEN-FGMLs have genetic mutations associated with *Wnt/β-catenin*, *KRAS*, *PIK3CA*, and sonic hedgehog signalling pathways, but not with *TP53* [6, 21–25]. Thus, *Wnt/β-catenin* signalling pathway may play a role in the development and progression of GEN-FGMLs [6], suggesting that targeting the *Wnt/β-catenin* pathway or *GNAS* mutations may be a potential therapeutic strategy for treating GEN-FGMLs. Further studies are needed to fully understand the molecular mechanisms underlying GEN-FGML.

Previous studies on the origin of GEN-FGMLs have not been consistent and have suggested that spasmolytic polypeptide-expressing metaplasia (SPEM) is fundamental to the development of intestinal metaplasia and gastric cancer, and that mature chief cells cannot dedifferentiate into SPEM. However, recent findings suggest that chief cells undergo differentiation into SPEM [26]. Leushacker *et al.* [27] hypothesized that $Lgr5^+$ chief cells are the major origin of gastric cancer because $Lgr5^+$ cells play an essential role in maintaining homeostatic stem cells. It has been shown that chief cells can dedifferentiate into different types of gastric mucosal epithelium, such as pit mucosal cells and gland cells. These results suggest that GEN-FGMLs may be derived from malignant transformation of the chief cells. Recent studies have indicated that intramucosal gastric carcinoma (IGC), OGA, and SPEM are derived from common ancestral glands. IGC and OGA originate from the KRAS-mutated SPEM [28]. However, the specific mechanism needs to be investigated further.

It is crucial to distinguish GEN-FGMLs from other gastric tumors. MUC6 and pepsinogen-I co-expression are crucial for the diagnosis of GEN-FGMLs, but the use of simple IHC markers may result in misdiagnosis. All participants in this study were positive for CD56 and Syn, and negative for CgA. These results could have led to the misdiagnosis of neuroendocrine tumors. Gastric neuroendocrine tumors are organ-like structures with basophilic tumor cells, accompanied by significant interstitial microvascular hyperplasia and CgA expression compared to GEN-FGMLs, which do not express CgA [29]. Distinguishing between GEN-FGMLs and pyloric gland adenomas (PGAs) is also challenging. Both PGA and GEN-FGMLs develop in the gastric fundus mucosa and express MUC6, pepsinogen-I, and MUC5AC. Nonetheless, PGAs show polypoid proliferation of pyloric-type glands with cuboidal/columnar cells and foamy ground-glass cytoplasm. Kushima *et al.* revealed that the outer tumor cells in PGAs are taller than the inner cells [25]. Differentiated adenocarcinoma with low atypia was related to GA-FG, but it lacked chief or parietal cells and showed an aggressive growth pattern despite the low atypia. Owing to the rarity of GEN-FGMLs and lack of awareness, most of our cases were primarily misdiagnosed as fundic gland polyps (FGPs). Both FGPs and GEN-FGMLs originate from fundic glands and exhibit similar features, such as the presence of hyperplastic glandular structures, cystic dilation, and distortion of glandular architecture. Typically, FGPs are benign lesions with less than 5 mm in diameter, consisting of dilated oxynitic glands, foveolar hypoplasia, and parietal hyperplasia [9]. However, GEN-FGMLs originate from the fundic glands of the stomach and display glandular or tubular structures with a monoclonal shape. FGPs can also exhibit intraepithelial

neoplasia and dysplasia [30]. Notably, dysplasia or adenocarcinoma in fundic gland polyps originates from the foveolar epithelium and not from the fundic glands. It is difficult to diagnose GEN-FGMLs based on biopsy specimens because the mucosal muscle may be indiscernible in such samples. Previous studies and our study have shown that GEN-FGML lesions with larger sizes are more often diagnosed as GA-FG or GA-FGM [4, 16]. Furthermore, our study demonstrated that GA-FG and GA-FGM had higher proliferation indices with Ki-67 than OGA, suggesting that Ki-67 plays a crucial role in the diagnosis of GEN-FGML, especially in biopsy specimens. Specimens with Ki-67 proliferation indices >2.5% and lesion size >4.5 mm are more likely to be diagnosed with GA-FG and GA-FGM than OGA. Moreover, endoscopic findings resemble those of early undifferentiated carcinoma and mucosa-associated lymphoid tissue. Endoscopy plays a limited role in the differential diagnosis. NBI is a promising technique for the diagnosis of GA-FGM and GA-FG. There are distinctive differences between GA-FGM and GA-FG in conventional endoscopy and NBI, including indigo carmine dye spraying, demarcation line, peculiar microvascular pattern, irregular microsurface pattern, and wider marginal crypt epithelium [13].

GEN-FGMLs are lower aggressive than other GCs as they possess minor cellular atypia, less vascular invasion and proliferation, and lack *TP53* mutations. GA-FGM, particularly type 2 GA-FGM, displays the highest malignant potential owing to strong vascular invasion, lymph node metastasis, and deep submucosal invasion [4]. Standard indications for endoscopic and surgical treatment of GEN-FGMLs are urgently needed. Two retrospective analyses from Japan have shown that endoscopic resection is currently the most common and appropriate initial treatment for GEN-FGMLs [4, 16]. Iwamuro *et al.* [16] indicated that GA-FG with an invasion depth of > 500 μm will not recur, even if endoscopic resection is the only treatment, as muscle infiltration and vascular invasion are uncommon in GA-FG. Ueyama *et al.* [4] demonstrated that no cases of GEN-FGMLs (including GA-FGM) that underwent endoscopic resection experienced recurrence, metastasis, or death. The Japanese Gastric Cancer Treatment Guidelines (6th edition) stipulate that radical tumor removal must be performed in differentiated gastric cancer when the invasion depth is > 500 μm [3]. Thus, the treatment of GEN FGML is challenging. On the one hand, surgical resection may not be an advisable treatment for GA-FG with an invasive depth of > 500 μm [16]. In contrast, GA-FGM was more aggressive than GA-FG. Therefore, endoscopic treatment guidelines for common gastric adenocarcinomas should be followed to treat GA-FGM. Hence, future studies on GEN-FGMLs should establish standardized endoscopic treatment and follow-up protocols.

Conclusion

In conclusion, GEN-FGML is a rare type of well-differentiated tumors possibly originating from dedifferentiated chief cells, with typical histopathological and molecular features. GEN-FGMLs are a group of well-differentiated gastric tumors with favorable biological behaviors, low cellular atypia, and low proliferation. It can be divided into OGA, GA-FG, and GA-FGM subtypes. Immunohistochemistry is critical for confirming diagnosis. The Ki-67 proliferation indices and lesion size may help differentiate between OGA, GA-FG, and GA-FGM, especially in biopsy specimens. Close cooperation between pathologists and endoscopists is required to avoid misdiagnosis and overtreatment. Endoscopic resection is currently the mainstream initial treatment for GEN-FGMLs.

Data availability statement

The raw data supporting the conclusion of this article will be made available by the authors, without undue reservation.

Ethics statement

The studies involving humans were approved by the Fujian Provincial Hospital ethics committee. The studies were conducted in accordance with the local legislation and institutional requirements. The participants provided their written informed consent to participate in this study.

Author contributions

Conceived and designed the experiments: HL and LZ. Performed the experiments: HL, LZ, GZ, XY, and XZ. Analyzed the data: HL and LZ. Contributed reagents/materials/analysis tools: HL, LZ, GZ, XY, XZ, LC, and XC. Wrote the paper: QL and LZ. All authors contributed to the article and approved the submitted version.

Funding

The author(s) declare that financial support was received for the research, authorship, and/or publication of this article. This study was supported by the Startup Fund for Scientific Research, Fujian Medical University (grant number: 2020QH1168).

Conflict of interest

The authors declare that the research was conducted in the absence of any commercial or financial relationships that could be construed as a potential conflict of interest.

Acknowledgments

The authors express their gratitude to EditSprings (https://www.editsprings.cn) for providing expert linguistic services.

Supplementary material

The Supplementary Material for this article can be found online at: https://www.por-journal.com/articles/10.3389/pore.2024.1611734/full#supplementary-material

References

1. Sung H, Ferlay J, Siegel RL, Laversanne M, Soerjomataram I, Jemal A, et al. Global cancer statistics 2020: GLOBOCAN estimates of incidence and mortality worldwide for 36 cancers in 185 countries. *CA Cancer J Clin* (2021) 71(3):209–49. doi:10.3322/caac.21660

2. Ueyama H, Yao T, Nakashima Y, Hirakawa K, Oshiro Y, Hirahashi M, et al. Gastric adenocarcinoma of fundic gland type (chief cell predominant type): proposal for a new entity of gastric adenocarcinoma. *Am J Surg Pathol* (2010) 34:609–19. doi:10.1097/PAS.0b013e3181d94d53

3. Japanese Gastric Cancer Association. Japanese gastric cancer treatment guidelines 2021 (6th edition). *Gastric Cancer* (2023) 26(1):1–25. doi:10.1007/s10120-022-01331-8

4. Ueyama H, Yao T, Akazawa Y, Hayashi T, Kurahara K, Oshiro Y, et al. Gastric epithelial neoplasm of fundic-gland mucosa lineage: proposal for a new classification in association with gastric adenocarcinoma of fundic-gland type. *J Gastroenterol* (2021) 56(9):814–28. doi:10.1007/s00535-021-01813-z

5. Tanabe H, Iwashita A, Ikeda K. Histopathological characteristics of gastric adenocarcinoma of fundic gland type. *StomachIntest* (2015) 50:1521–31.

6. Ushiku T, Kunita A, Kuroda R, Shinozaki-Ushiku A, Yamazawa S, Tsuji Y, et al. Oxyntic gland neoplasm of the stomach: expanding the spectrum and proposal of terminology. *Mod Pathol* (2020) 33:206–16. doi:10.1038/s41379-019-0338-1

7. Singhi AD, Lazenby AJ, Montgomery EA. Gastric adenocarcinoma with chief cell differentiation: a proposal for reclassification as oxyntic gland polyp/adenoma. *Am J Surg Pathol* (2012) 36(7):1030–5. doi:10.1097/PAS.0b013e31825033e7

8. Okumura Y, Takamatsu M, Ohashi M, Yamamoto Y, Yamamoto N, Kawachi H, et al. Gastric adenocarcinoma of fundic gland type with aggressive transformation and lymph node metastasis: a case report. *J Gastric Cancer* (2018) 18:409–16. doi:10.5230/jgc.2018.18.e22

9. IARC. *WHO classification of tumours editorial board: WHO classification of tumours, 5th edn, vol 1 digestive system tumours*. Lyon: IARC (2019).

10. Kanesaka T, Uedo N, Yao K, Tanabe H, Yamasaki Y, Takeuchi Y, et al. New subtype of gastric adenocarcinoma: mixed fundic and pyloric mucosa-type adenocarcinoma. *Clin J Gastroenterol* (2017) 10:224–8. doi:10.1007/s12328-017-0727-2

11. Kai K, Satake M, Tokunaga O. Gastric adenocarcinoma of fundic gland type with signet-ring cell carcinoma component: a case report and review of the literature. *World J Gastroenterol* (2018) 24:2915–20. doi:10.3748/wjg.v24.i26.2915

12. Li C, Wu X, Yang S, Yao J, Zheng H. Gastric adenocarcinoma of the fundic gland type: clinicopathological features of eight patients treated with endoscopic submucosal dissection. *Diagn Pathol* (2020) 15(1):131. doi:10.1186/s13000-020-01047-2

13. Imamura K, Yao K, Nimura S, Tanabe H, Kanemitsu T, Miyaoka M, et al. Characteristic endoscopic findings of gastric adenocarcinoma of fundic-gland mucosa type. *Gastric Cancer* (2021) 24(6):1307–19. doi:10.1007/s10120-021-01208-2

14. Sun WW, Zhang L, Gu MM, Zhang YQ, Qiu CM, Da Q. Gastric adenocarcinoma of the fundic gland type: clinicopathological analysis of six cases. *Chin J Pathol* (2020) 49(4):343–7. doi:10.3760/cma.j.cn112151-20190720-00404

15. Shen FY, Zhuang HJ, Bai DY, Li NN, Zhang HF. Clinicopathological characteristics of 18 cases of oxyntic gland neoplasm from gastric fundic gland. *Chin J Pathol* (2023) 52(7):718–20. doi:10.3760/cma.j.cn112151-20221027-00891

16. Iwamuro M, Kusumoto C, Nakagawa M, Kobayashi S, Yoshioka M, Inaba T, et al. Endoscopic resection is a suitable initial treatment strategy for oxyntic gland adenoma or gastric adenocarcinoma of the fundic gland type. *Sci Rep* (2021) 11(1):7375. doi:10.1038/s41598-021-86893-w

17. Iwamuro M, Kusumoto C, Nakagawa M, Matsueda K, Kobayashi S, Yoshioka M, et al. Endoscopic features of oxyntic gland adenoma and gastric adenocarcinoma of the fundic gland type differ between patients with and without *Helicobacter pylori* infection: a retrospective observational study. *BMC Gastroenterol* (2022) 22(1):294. doi:10.1186/s12876-022-02368-w

18. Zhou WX, Chen J. Consideration of diagnosing extremely well differentiated adenocarcinoma of gastrointestinal tract. *Chin J Pathol* (2022) 51(8):693–5. doi:10.3760/cma.j.cn112151-20220517-00425

19. Hou WH, Duan XK, Hou WD, Liu YX, Wang JH, Wang XZ, et al. Clinicopathological features of very well-differentiated adenocarcinoma of the stomach. *Chin J Pathol* (2022) 51(2):96–102. doi:10.3760/cma.j.cn112151-20210723-00525

20. Karam SM, Leblond CP. Identifying and counting epithelial cell types in the "corpus" of the mouse stomach. *Anat Rec* (1992) 232(2):231–46. doi:10.1002/ar.1092320208

21. Lee SY, Saito T, Mitomi H, Hidaka Y, Murakami T, Nomura R, et al. Mutation spectrum in the Wnt/β-catenin signaling pathway in gastric fundic gland-associated neoplasms/polyps. *Virchows Arch* (2015) 467(1):27–38. doi:10.1007/s00428-015-1753-4

22. Murakami T, Mitomi H, Yao T, Saito T, Shibuya T, Watanabe S. Epigenetic regulation of Wnt/β-catenin signal-associated genes in gastric neoplasia of the fundic gland (chief cell-predominant) type. *Pathol Int* (2017) 67:147–55. doi:10.1111/pin.12509

23. Tajima Y, Murakami T, Saito T, Hiromoto T, Akazawa Y, Sasahara N, et al. Distinct involvement of the sonic Hedgehog signaling pathway in gastric adenocarcinoma of fundic gland type and conventional gastric adenocarcinoma. *Digestion* (2017) 96:81–91. doi:10.1159/000478999

24. Matsubara A, Sekine S, Kushima R, Ogawa R, Taniguchi H, Tsuda H, et al. Frequent GNAS and Kras mutations in pyloric gland adenoma of the stomach and duodenum. *J Pathol* (2013) 229:579–87. doi:10.1002/path.4153

25. Kushima R, Sekine S, Matsubara A, Taniguchi H, Ikegami M, Tsuda H. Gastric adenocarcinoma of the fundic gland type shares common genetic and phenotypic features with pyloric gland adenoma. *Pathol Int* (2013) 63:318–25. doi:10.1111/pin.12070

26. Nam KT, Lee HJ, Sousa JF, Weis VG, O'Neal RL, Finke PE, et al. Mature chief cells are cryptic progenitors for metaplasia in the stomach. *Gastroenterology* (2010) 139(6):2028–37. doi:10.1053/j.gastro.2010.09.005

27. Leushacke M, Tan SH, Wong A, Swathi Y, Hajamohideen A, Tan LT, et al. Lgr5-expressing chief cells drive epithelial regeneration and cancer in the oxyntic stomach. *Nat Cell Biol* (2017) 19(7):774–86. doi:10.1038/ncb3541

28. Kumagai K, Shimizu T, Nikaido M, Hirano T, Kakiuchi N, Takeuchi Y, et al. On the origin of gastric tumours: analysis of a case with intramucosal gastric carcinoma and oxyntic gland adenoma. *J Pathol* (2023) 259(4):362–8. doi:10.1002/path.6050

29. Fahrenkamp AG, Wibbeke C, Winde G, Ofner D, Böcker W, Fischer-Colbrie R, et al. Immunohistochemical distribution of chromogranins A and B and secretogranin II in neuroendocrine tumours of the gastrointestinal tract. *Virchows Arch* (1995) 426(4):361–7. doi:10.1007/BF00191345

30. Sano W, Inoue F, Hirata D, Iwatate D, Hattori S, Fujita M, et al. Sporadic fundic gland polyps with dysplasia or carcinoma: clinical and endoscopic characteristics. *World J Gastrointest Oncol* (2021) 13(7):662–72. doi:10.4251/wjgo.v13.i7.662

Pathology & Oncology Research | frontiers

TYPE Original Research
PUBLISHED 29 June 2023
DOI 10.3389/pore.2023.1611270

Check for updates

OPEN ACCESS

EDITED BY
Anna Sebestyén,
Semmelweis University, Hungary

*CORRESPONDENCE
Dezső Tóth,
dr.toth.dezso@med.unideb.hu

RECEIVED 24 April 2023
ACCEPTED 21 June 2023
PUBLISHED 29 June 2023

CITATION
Varga Z, Bíró A, Török M and Tóth D (2023), A combined approach for individualized lymphadenectomy in gastric cancer patients.
Pathol. Oncol. Res. 29:1611270.
doi: 10.3389/pore.2023.1611270

COPYRIGHT
© 2023 Varga, Bíró, Török and Tóth. This is an open-access article distributed under the terms of the Creative Commons Attribution License (CC BY). The use, distribution or reproduction in other forums is permitted, provided the original author(s) and the copyright owner(s) are credited and that the original publication in this journal is cited, in accordance with accepted academic practice. No use, distribution or reproduction is permitted which does not comply with these terms.

A combined approach for individualized lymphadenectomy in gastric cancer patients

Zsolt Varga[1], Adrienn Bíró[2], Miklós Török[3] and Dezső Tóth[1]*

[1]Department of Surgery, University of Debrecen, Debrecen, Hungary, [2]Department of Surgery, Moritz Kaposi General Hospital, Kaposvár, Hungary, [3]Department of Pathology, University of Debrecen, Debrecen, Hungary

Introduction: Gastric cancer ranks as the fifth most common cancer globally. The presence of lymph node metastasis is a significant prognostic factor influencing survival. Postoperative morbidity and nodal staging accuracy are heavily affected by the extent of lymph node dissection. Our study aimed to explore the potential integration of two contemporary methods, sentinel node navigation surgery (SNNS) and the Maruyama Computer Program (MCP), to improve the accuracy of nodal staging.

Materials and methods: We conducted a prospective data collection involving patients with gastric adenocarcinoma from 2008 to 2018 at the Department of Surgery, University of Debrecen, Hungary. Data from 100 consecutive patients were collected. The primary and secondary endpoints included evaluating the rate of node-negative patients and the diagnostic accuracy of our combined approach.

Results: Sentinel node mapping was successful in 97 out of 100 patients. We found that using the threshold value of the Maruyama Index (MI) ≥ 28, all metastatic stations of sentinel-node-negative patients could be identified. Our method achieved 100% sensitivity and negative predictive value, with a specificity of 60.42% (95% CI = 46.31%–72.98%).

Discussion: The combined application of SNNS and MCP has proven to be an effective diagnostic technique in the synergistic approach for identifying metastasis-positive lymph node stations. Despite its limitations, this combination may assist clinicians in customizing lymphadenectomy for gastric cancer patients.

KEYWORDS

gastric cancer, surgery, lymphadenectomy, sentinel, Maruyama

Abbreviations: EGD, esophagogastroduodenoscopy; HE, hematoxylin and eosin; ICG, indocyanine green; JCGC, Japanese Classification of Gastric Carcinoma; MCP, Maruyama Computer Program; MI, Maruyama Index; OSNA, one-step nucleic acid amplification; pN+, positive pathologic lymph node staging; pN–, negative pathologic lymph node staging; QoL, quality of life; RT-PCR, reverse transcription polymerase chain; SLN, sentinel lymph node; SLNB, sentinel lymph node biopsy; SNNS, sentinel node navigation surgery; 95% CI, 95% confidence interval.

Introduction

According to the recent GLOBOCAN 2020 estimation, gastric cancer is the fifth most common cancer worldwide [1]. The diagnosis is often made at an advanced stage, resulting in a high mortality rate. One of the most important prognostic factors after curative resection in patients with gastric adenocarcinoma is the presence of lymph node metastases.

In 1881, Theodor Billroth (1829–1894) performed the first successful gastric resection for gastric cancer. Despite scientific and technological advancements, including the development of the multimodal treatment approach, resection still remains at the forefront of curative management in gastric cancer [2]. The clinical stage determines the treatment approach since a stage-adapted, individualized treatment is crucial to achieve optimal oncological outcomes.

Surgery aims to establish local control through free surgical resection margins and the clearance of regional lymph nodes. Though, a significant proportion of patients have no nodal involvement after R0 resection. Postoperative morbidity and the accuracy of nodal staging are heavily influenced by the extent of lymph node dissection, although the optimal extent of lymph node dissection has been debated over the last decades. Insufficient lymphadenectomy may result in the understaging and undertreatment of a patient. Conversely, unnecessary lymph node dissection may have higher rates of postoperative complications [3–5].

Conventional preoperative imaging techniques, such as computed tomography (CT), magnetic resonance imaging (MRI), endoscopic ultrasound (EUS), and positron emission tomography (PET), provide an accurate T and M stage, but there is significant uncertainty regarding the N stage [6]. These techniques predominantly depend on size criteria for the detection of lymph node metastasis. However, metastatic lymph nodes that do not result in significant enlargement could be overlooked, as the resolution provided by CT, MRI, and PET scans might not be adequate to detect such small metastatic lymph nodes [7]. PET scans identify metabolic activity, but not all metastatic lymph nodes in gastric cancer display increased metabolic activity. Given the relatively poor spatial resolution, which makes distinguishing nodes from the primary tumor itself challenging, and the fact that inflammation can also result in higher metabolic activity, the utility of PET scans in this context may be limited [8]. EUS primarily assesses perigastric lymph nodes, and thus, may not detect skipping metastases that have spread directly to the D2 compartment, bypassing the perigastric area. In a study, the incidence of such metastases was found to be 4.8% among the overall gastric cancer population [9]. The differentiation between benign and malignant lymphadenopathy is merely based on morphological characteristics, which include size (greater than 5 mm), shape (round), echo pattern (hypoechoic), and border (smooth) [10].

In a comparative study, the detection rate of lymph node metastasis by CT scan was 71.7%, with a sensitivity of 44.6% and a specificity of 85.4%. The performance of endoscopic ultrasonography was similar, providing a detection rate of 70.4%, a sensitivity of 19.3%, and a specificity of 96.3% [11].

In 1973, the Japanese Research Society for Gastric Cancer described the lymphatic drainage pattern of the stomach in the first edition of their manual. They identified 16 unique lymph node stations based on anatomical locations and introduced a system for quantifying the extent of lymphadenectomy, namely, D1, D2, and D3. Since its inception, this guideline has undergone numerous revisions [12].

The sentinel lymph node (SLN) is defined as the first node to receive lymphatic flow from a tumor, theoretically representing the status of the other regional lymph nodes. Sentinel node navigation surgery (SNNS) is a type of surgical technique in which the SLN is removed and examined for the presence of cancer cells [13]. During SNNS, a tracer substance is injected near the tumor which then travels through the lymph vessels and ends up in the sentinel node(s). In gastric cancer surgery, various tracers have been used: blue dye, indocyanine green (ICG), radiocolloids, and their combinations [14]. The extent of lymph node dissection might be determined according to the status of the SLN. If the sentinel lymph node is free of metastases, a gastrectomy, and D2 lymph node dissection may not be necessary. This promising approach may lead to a lesser extent of resection and lymph node dissection, resulting in organ preservation, faster postoperative recovery, and better quality of life (QoL) without compromising oncological safety [14]. It can also increase the surgeons' awareness of critical lymph node stations, thereby improving the effectiveness of lymphadenectomy for each patient. Unfortunately, metastatic lymph nodes are not always stained by the tracer, and conversely, stained nodes are not necessarily metastatic. In practice, there are several challenges, particularly when dealing with gastric cancer. The process of identifying and sampling the sentinel lymph node(s) is technically demanding, requiring careful procedural execution and pathological analysis. Errors or variations in the surgeon's technique can lead to missed sentinel nodes [15]. Furthermore, lymphatic drainage patterns can significantly differ between individuals, and even within different regions of the same tumor [16]. This variability can sometimes lead to unpredictable sentinel nodes, which could potentially be missed. If cancer has spread to a lymph node and has blocked the lymphatic drainage pathway, the tracer used to identify the sentinel lymph node may be diverted to a different lymph node, leading to a false-negative result [17]. On top of that, micrometastases or isolated tumor cells might not be detected during routine pathological examination of the sentinel lymph node, also potentially leading to a false-negative result [18]. The concept of sentinel (lymphatic) basin dissection was introduced to address many of the limitations associated with previous techniques. This approach was first introduced by Miwa et al.

in 2003 [15]. Their technique entailed not just the removal of the stained sentinel node, but also the associated nodal compartment (basin), thereby achieving an accuracy of 98.0%.

There are two large-scale ongoing randomized clinical trials to determine the role of SNNS in gastric cancer surgery. The SENORITA trial failed to show non-inferiority of SNNS compared with laparoscopic standard gastrectomy in terms of 3-year disease-free survival (DFS) [19]. Still, the 5-year disease-free survival and overall survival did not reveal the statistical difference between the two groups [20]. This concept has yet to be proven in a broader clinical setting. It is worth noting, that its' strict inclusion criteria might compromise its general applicability to the Western population.

The Maruyama Computer Program (MCP), developed by Keiichi Maruyama and released in 1989, is a tool designed to estimate the likelihood of lymph node involvement in stations No. 1–16, based on several prognostic factors [21]. These factors include seven preoperative variables: sex, age, tumor type, depth of invasion, tumor location, primary tumor diameter, and histological type. After providing these elements, the software is computing a numerical value for each station. MCP was initially validated in a Japanese patient cohort, where it achieved a predictive accuracy of lymph node involvement in 94% of cases [22]. The program's precision was further enhanced from 66% to 93% through the application of an artificial neural network [23].

In our previous work, we proved the high reliability of MCP, achieving a sensitivity of 90.2%, a specificity of 63.3%, and an overall accuracy of 78.4%. We also demonstrated that MCP's predictive capabilities for lymph node metastases were superior to those of standard pre-operative imaging techniques [24].

The MCP has traditionally served as an effective tool for projecting long-term oncological results. The term "Maruyama Index" (MI) was coined by Hundahl et al. [25] in the aftermath of the Intergroup 0116 Trial. They conducted a blinded re-evaluation of the Dutch D1-D2 trial using autopsy findings and demonstrated that surgeries characterized as "low MI" (which entails not leaving behind any lymphatic stations with high MI) had a more beneficial impact on survival compared to surgeries guided solely by D-levels [26].

Our objective was to explore the potential integration of the MCP and SNNS to improve the accuracy of detecting nodal involvement and to identify a possible method that could make tailored lymphadenectomy safer. We aimed to evaluate the individual efficacy of these techniques and determine MI values that could optimally supplement SNNS in a synergetic manner.

Materials and methods

A prospective data collection of patients operated on with a curative intention of gastric adenocarcinoma was conducted from 2008 until 2018 (Figure 1). It was a single-center study, with every procedure being performed at the Department of Surgery, University of Debrecen, Hungary. Adult patients (>18 years of age) who were willing and able to provide written informed consent were included. Another requirement was that the patient had a histologically confirmed adenocarcinoma in the stomach sampled by preoperative esophagogastroduodenoscopy (EGD). Complete oncological staging (including chest-, abdomen-, and pelvis CT scan) and evaluation of fitness for surgery were required.

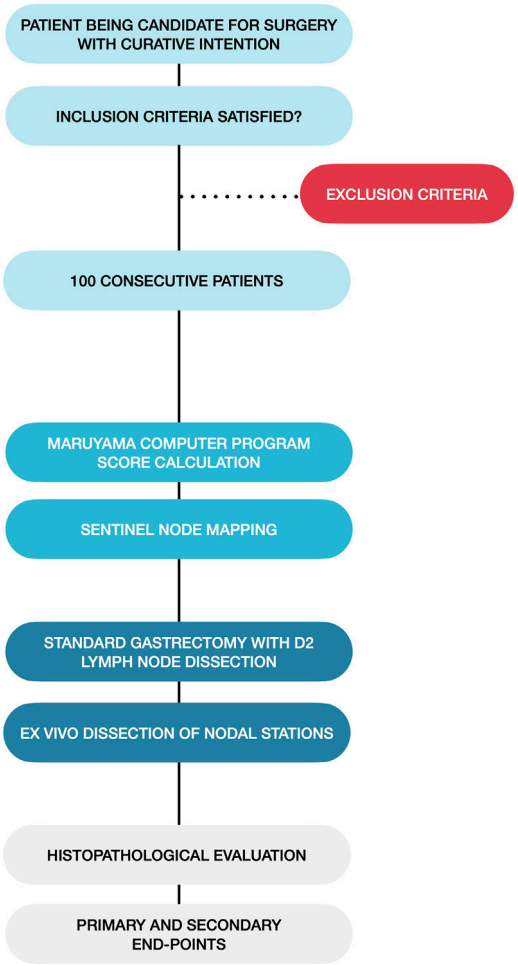

FIGURE 1
Flowchart of the patient management and data collection process.

Exclusion criteria were gross (macroscopic) serosal or nearby organ invasion, history of gastric resection, cancer of the gastric cardia (<5 cm distance from the gastroesophageal junction), and distant metastases. Patients with macroscopic serosal invasion had only a peritoneal lavage at the index procedure, without any resection. The cytological examination was carried out later as the peritoneal fluid sample was processed. Positive cytology was

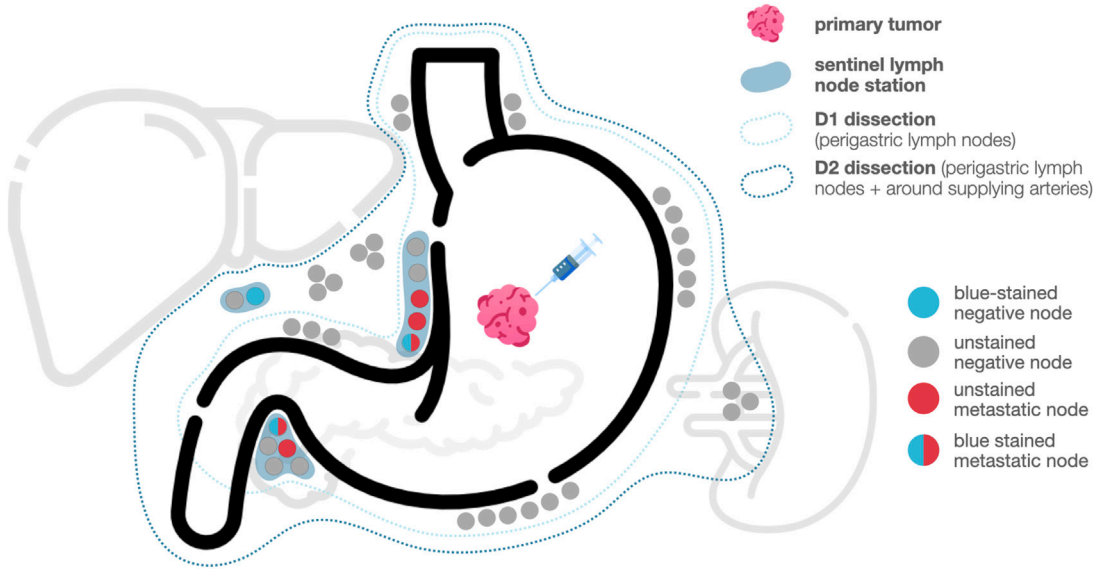

FIGURE 2
Types of nodal involvement in sentinel node navigation surgery.

taken as verification of peritoneal dissemination and M1 stage disease. These patients were treated accordingly.

Before 2018, neoadjuvant treatment was not frequently used for non-cardia gastric cancer in Hungary. However, as this approach became routine, we chose to finish our data and patient collection to prevent any systematic bias that could be introduced with the inclusion of patients undergoing neoadjuvant therapy. There is considerable controversy about the degree and significance of nodal regression after neoadjuvant treatment [27–29]. Our study population could be one of the last cohorts of patients with locally advanced gastric cancer, who did not receive any preoperative oncological treatment, in which the unharmed lymphatic drainage of gastric cancer could be observed.

Our primary and secondary end-points were the assessment of the rate of node-negative patients and the accuracy of our combined technique.

We collected data for 100 consecutive patients. Patient information, such as age, gender, comorbidities, location, histological type, and clinical and pathological stage of the tumor was recorded. Meanwhile, three different (sixth, seventh, and eighth) editions of the UICC TNM classification of malignant tumors had been in use. These editions have well-known differentiating factors in the staging of gastric cancer. To consolidate our findings, all previous documents were revised by a medical oncologist and a pathologist and reported according to the eighth edition.

Before the surgical intervention, the Maruyama Computer Program (MCP; WinEstimate v2.5 Gastric cancer diagnosis and treatment. An interactive training program. Windows Version. CD-ROM) was used to assess the probability of lymph node metastasis in each nodal station. The software-generated Maruyama Index (MI) was noted for each lymphatic station. During the procedure, peritumoral–subserosal or submucosal injection of 2 mL blue dye (Bleu Patente V 2.5/100 mg, Guerbet, France) was used for sentinel node mapping (Figure 2). After the injection, a 10-min waiting period was given to allow lymphatic drainage. Then a conventional (total, subtotal, or distal) open or laparoscopic gastrectomy with standard D2 lymphadenectomy was performed. The blue-stained sentinel lymph nodes were assessed with intraoperative frozen sections. The D3 compartment (stations 13–16) and station 10 nodes were sampled only if clinical suspicion was high for metastasis.

After completing the surgery, *ex vivo* dissection and categorization of the lymph nodes were carried out. The anatomical position of each lymph node station was labeled according to the Japanese Classification of Gastric Carcinoma (JCGC). The presence of a (blue-colored) sentinel node in a station was marked for the pathologist.

All dissected lymph nodes were sent for postoperative histopathologic evaluation, following a protocol similar to the one used in the SENORITA trial [30]. Nodes from the blue-stained stations were examined for micrometastases using 0.2 mm sections. Otherwise, a slice was made at 2-mm intervals parallel to the long axis. Hematoxylin and eosin (HE) staining and pan-cytokeratin immunohistochemistry examinations were performed (Monoclonal Mouse Anti-Human Cytokeratin, Clones AE1/AE3; DAKO, Denmark).

All patient data collected during this study was recorded in a standalone offline Microsoft Excel database.

TABLE 1 Descriptive data of patients included in the study.

Factors	Results
Number of patients (n)	100
Gender	
Female	53
Male	47
Median age (range; in years)	67 (48–82)
Median body mass index (BMI; kg/m^2)	23 (17.5–36.0)
Tumor location	
Upper third	13
Middle third	21
Lower third	66
Histological subtype	
Signet-ring cell carcinoma	31
Poorly differentiated adenocarcinoma	27
Moderately differentiated adenocarcinoma	38
Well-differentiated adenocarcinoma	4
Surgical technique	
Open surgery	73
Laparoscopic surgery	27
Pathological T-stage	
T1a	8
T1b	13
T2	16
T3	33
T4a	30
Pathological N-stage	
N0	48
N1	19
N2	17
N3	16
Total number of dissected lymph nodes	2083
Median number of dissected lymph nodes (range)	20 (9–42)

Continuous variables were tested for normality by the Shapiro-Wilk test. Data with normal distribution are shown as mean ± standard deviation or medians with a range for non-Gaussian distribution. They were analyzed by the Student's t-test and ANOVA test, or an appropriate non-parametric method (Mann–Whitney U-test or Kruskal–Wallis).

Categorical variables shown as counts and percentages were analyzed by Fisher's exact test. The level of statistical significance was set at $p < 0.05$ for all analyses.

The sentinel node detection rate was defined as the number of patients with a successful marking of the sentinel lymph node, divided by the total number of patients. The sensitivity and specificity in sentinel node mapping were calculated according to the number of patients with metastatic lymph nodes in the sentinel station, and the number of patients with metastatic lymph nodes.

All statistical analyses were performed using IBM SPSS Statistics for Macintosh, Version 28.0 (Released 2021. Armonk, NY: IBM Corp).

Results

There were 53 women and 47 men among the enrolled patients. Their median age was 67 (48–82) years. The median BMI was 23.0 (17.5–36.0) kg/m^2. The tumor was located in the upper third in 13 cases (13%), in the middle third in 21 (21%) cases, and in the lower third in 66 cases (66%). 38 patients had a moderately differentiated adenocarcinoma, 31 patients had signet-ring cell carcinoma, 27 patients had poorly differentiated adenocarcinoma, and 4 patients had well-differentiated adenocarcinoma. Table 1 shows the descriptive data of these patients. We performed a total gastrectomy on 39 patients, and a distal gastrectomy on 61 patients. The laparoscopic technique was used in 27 cases (3 total gastrectomies, 24 laparoscopic-assisted distal gastrectomies). Despite gross serosal or nearby organ invasion being in the exclusion criteria, the histopathology report showed 30 patients with pT4a stage. After the revision of these patients' data, we decided not to exclude their results from the analysis as they could prove beneficial in understanding the behavior of advanced gastric cancer. The total number of removed lymph nodes was 2083, and the median number of dissected nodes from a patient was 20 (range: 9–42).

The sentinel node mapping was successful in 97 of the 100 patients, resulting in a 97.0% detection rate. The median number of blue-stained (sentinel) nodes was 7 (range: 0–19) and the median number of labeled stations was 2 (0–6). The number of labeled nodes was not associated with the BMI of the patient ($p = 0.705$), location ($p = 0.254$), the histological subtype of the tumor ($p = 0.891$), pT stage ($p = 0.227$), or operative (open or laparoscopic) technique ($p = 0.393$). The location of the sentinel nodes was in the D1 compartment in 80 cases (82.47%), both in the D1 and D2 compartments in 16 cases (16.50%), and exclusively in the D2 compartment in 1 case (1.03%).

We explored the connection between the pT stage of the tumor, the success rate of sentinel node mapping, and the presence of lymph node metastases.

Among the 21 patients with pT1 stage tumors, most (18 patients, or 85.71%) had no lymph node metastases. The remaining three patients had metastases confined to the stations containing the sentinel nodes, with no involvement of any other lymph node stations. In two cases, sentinel node mapping was not successful; however, these patients were found to be without lymph node involvement (pN0 stage).

In the group of patients with pT2 tumors (totaling 16), more than half (nine patients, or 56.25%) had no lymph node metastases. When lymph node metastases were present, they were always located within the sentinel nodes. Sentinel node

TABLE 2 The ability of SNNS to find metastatic lymph node stations.

Patients	pN+	pN−
SLNB negative	3	45
SLNB not informative/positive	49	3
Total	52	48
Identification of metastatic lymph node stations by SLNB (not informative/positive)	**Value**	**95% CI**
Sensitivity	94.23%	84.36%–98.43%
Specificity	93.75%	83.16%–97.85%
Positive predictive value	94.23%	84.36%–98.43%
Negative predictive value	93.75%	83.16%–97.85%
		$p < 0.001$

SLNB, sentinel lymph node biopsy; pN+, positive pathologic lymph node staging; pN−, negative pathologic lymph node staging; 95% CI, 95% confidence interval.

mapping was successfully carried out for all patients in this group, identifying seven patients with lymph node metastases. In each case, the metastases were exclusively situated within the blue-stained D1 station.

Among the 33 patients with pT3 stage tumors, 14 (42.42%) were found to have no lymph node involvement. Of the remaining 19 patients with lymph node involvement, all but one had metastases within the sentinel nodes. There was a single instance of a non-sentinel station showing positivity, and one patient had no labeled station.

As for the patients with pT4a stage tumors ($n = 30$), seven cases (23.33%) had no lymph node metastases. When lymph node metastases were present, they were almost always (21 out of 23 cases, or 91.30%) confined to the same station as the sentinel node.

The overall sensitivity of sentinel node mapping in patients with successful labeling ($n = 97$) was 94.23% (95% CI = 84.36%–98.43%) with 100% specificity (95% CI = 92.73%–100%), $p < 0.001$ (Table 2). This level of sensitivity is considered excellent, however, relying solely on this technique would have resulted in overlooking nodal metastases in three patients. Of the 48 sentinel node-negative patients, all 3 patients had macrometastasis, and no micrometastasis was found in the sentinel nodes.

To improve this 93.75% negative predictive value, we combined the results of the sentinel node mapping technique with the Maruyama Computer Program.

In our previous research, we used receiver operating characteristic (ROC) curve analysis to fine-tune the cut-off value for the Maruyama Index [24]. In this current investigation, we aimed to achieve a sensitivity of 100% (thus eliminating any false negative cases) using the combined technique. This goal, however, led to a reduction in specificity (resulting in more false positives). Upon evaluating the results of the MCP predictions and histological reports, we found that an MI cut-off value of 28 or higher could deliver the desired level of sensitivity. Using the MCP alone with this threshold, we correctly identified 44 of the 52 patients with at least one node-positive station. The sensitivity of the MCP alone was 84.62% (95% CI = 72.48%–91.99%), and its specificity was 52.08% (95% CI = 38.33%–65.53%), Table 3. The positive predictive value was 65.57% (95% CI = 53.73%–75.91%), and the negative predictive value was 75.76% (95% CI = 58.98%–87.17%).

In our effort to integrate the two techniques, for patients who were sentinel node negative, we set a threshold for the Maruyama Index at ≥28 (Figure 3). This allowed us to identify all metastatic stations. With this approach, we were able to attain a sensitivity and negative predictive value of 100% (95% CI = 93.12%–100% and 88.30%–100%, respectively), as well as a specificity of 60.42% (95% CI = 46.31%–72.98%). The positive predictive value was determined to be 73.42% (95% CI = 61.95%–82.15%) (Table 4). The median number of additional stations (those that were non-stained and had a Maruyama Index ≥28) that needed to be dissected was 1, with a range of 1–5.

30 of the 79 (37.97%) pT2-4a stage patients were node-negative and had unnecessary complete D2 lymphadenectomy. All node-positive patients and their metastatic stations were correctly identified with 100% accuracy (refer to Table 4) using the combination method. Using this synergetic approach, these 30 patients would have a median number of 4 stations (range: 1–7) removed. We found no side effects in the blue dye mapping.

Discussion

The predicted prognosis of any gastrointestinal cancer is significantly influenced by the presence of lymph node metastases. A sufficient level of lymphadenectomy helps to avoid both stage migration and the undertreatment of patients, however unnecessary lymph node dissection can result in a higher risk for iatrogenic injuries and higher

TABLE 3 The ability of MCP to find metastatic lymph node stations.

Patients	pN+	pN−
MI < 28	8	25
MI ≥ 28	44	23
Total	52	48
Identification of metastatic lymph node stations by MI ≥ 28	**Value**	**95% CI**
Sensitivity	84.62%	72.48%–91.99%
Specificity	52.08%	38.33%–65.53%
Positive predictive value	65.57%	53.73%–75.91%
Negative predictive value	75.76%	58.98%–87.17%
		$p < 0.001$

MI, maruyama index; pN+, positive pathologic lymph node staging; pN−, negative pathologic lymph node staging; 95% CI, 95% confidence interval.

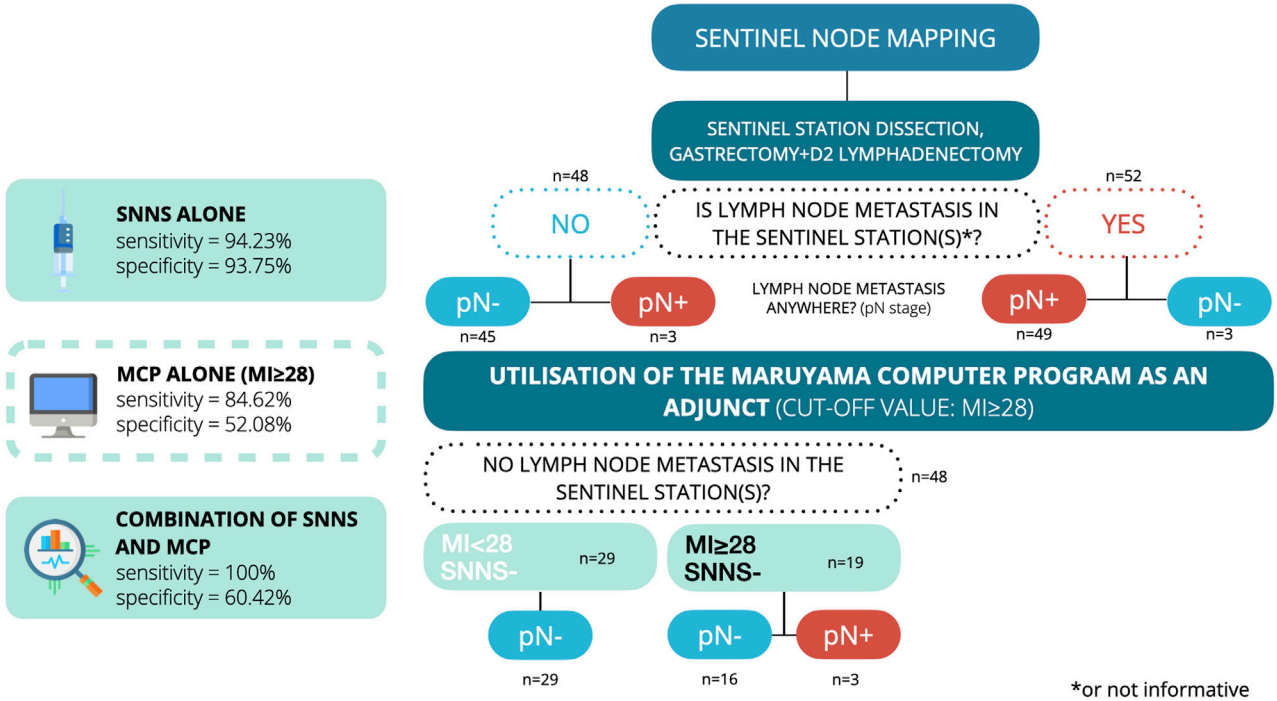

FIGURE 3
Flowchart for the diagnostic accuracy of the combined technique.

postoperative morbidity. Accurate prediction of the presence and location of lymph node metastasis is necessary to reduce the extent of lymphadenectomy, without undermining the oncological safety.

The JCOG0302 trial in Japan had to be discontinued due to the unexpectedly high false-negative rate of 46.4% [31]. The study began in May 2004 but was halted in September 2005 after enrolling 440 patients. The explanation for this termination was the discovery of false negative results in 13 patients. The main reason for this unreliability was the single-plane frozen section. To avoid these issues, we adopted a protocol similar to that used in the Korean SENORITA trial [30]. According to this protocol, nodes thicker than 4 mm are sliced at 2 mm intervals along the long axis to ensure that macrometastasis is not overlooked. The results of the intraoperative frozen section correlated with the postoperative pathological findings in all the cases, as in our previous study [32]. In a previous study of ours, submucosal and subserosal marking methods were proven to be equivalent in

TABLE 4 The ability of the combination of SNNS and MCP to find metastatic lymph node stations.

Patients	pN+	pN−
SLNB negative and MI < 28	0	29
SLNB not informative/positive and/or MI ≥ 28	52	19
Total	52	48
Identification of metastatic lymph node stations by SLNB (not informative/positive) and/or MI ≥ 28	**Value**	**95% CI**
Sensitivity	100%	93.12%–100%
Specificity	60.42%	46.31%–72.98%
Positive predictive value	73.24%	61.95%–82.15%
Negative predictive value	100%	88.30%–100%
		$p < 0.001$

SLNB, sentinel lymph node biopsy; MI, maruyama index; pN+, positive pathologic lymph node staging; pN−, negative pathologic lymph node staging; 95% CI, 95% confidence interval.

detection rate. The sensitivity and specificity were 100% in the submucosal group, and 100% and 92.3% in the subserosal group, respectively [33].

For the safe implementation of nodal staging based on SN mapping results, particularly in an intraoperative setting, it is crucial to accurately detect lymph node metastases. Compared to HE and IHC staining, molecular biology methods like reverse transcription polymerase chain reaction (RT-PCR) can provide more accuracy by allowing examination of the entire lymph node. Multiple RT-PCR methods have proven suitable for intraoperative detection of (micro) metastases, but their application can be time-consuming. The one-step nucleic acid amplification (OSNA) assay emerges as a quicker, appealing alternative diagnostic tool for identifying SN metastases in gastric cancer patients [34].

In gastric adenocarcinoma, the lymphatic drainage of the tumor can be complicated. A significant amount of patient data has been collected over the past decades to find consistency among the results. The Maruyama Computer Program was invented based on this predictability. It is usually utilized in advanced gastric cancer to explore potential lymph node metastases preoperatively. Sentinel node navigation surgery is another tool that helps us to find potential metastatic lymph nodes. By combining these two approaches, we synthesized an efficient way to detect those stations and identify those patients who need extended lymphadenectomy with 100% sensitivity and 60.42% specificity. The exceptionally high level of sensitivity in our model needs to be further validated by independent studies.

Several limitations of our study require further discussion. The selection criteria for patients could potentially lead to a selection bias. It is particularly true for pT4a stage cases, since some of them may not be included in our investigation by the macroscopic serosal invasion.

Some well-established predictive factors for lymph node metastasis, such as grade, tumor size, or lymphovascular invasion were not included in the analysis. This is because the route of lymphatic drainage is not influenced by them, thus the number and location of the involved stations are independent of their existence.

In an era of routine perioperative chemotherapy for cT2/N+ gastric cancer, our findings emphasize a personalized approach. This enables us to pay more attention to potentially affected stations, irrespective of the level of lymph node dissection. The data collection for evaluating the survival outcomes is in progress.

We demonstrated that the flaws of each of these modern techniques could be overcome by their combination, making it a powerful method. We are not advocating for the omission of preoperative nodal clinical staging or the standard D2 lymphadenectomy. Instead, our goal is to draw attention to a potentially beneficial tool that can enhance surgeons' awareness of critical lymph node stations. Nevertheless, in selected cases, the extent of lymphadenectomy could potentially be safely reduced using this method. Despite these limitations, this synergic approach of sentinel node mapping with the Maruyama Computer Program may help clinicians tailor lymphadenectomy for gastric cancer patients.

Data availability statement

The raw data supporting the conclusion of this article will be made available by the authors, without undue reservation.

Ethics statement

All procedures followed were in accordance with the ethical standards of the responsible committee on human experimentation (institutional and national) and with the Helsinki Declaration of 1964 and later versions. Informed consent to be included in the study, or the equivalent, was

obtained from all patients. The study protocol was approved by the local ethical committee in 2008.

Author contributions

DT contributed to the study design, data interpretation, and preparation of this manuscript; ZV contributed to data analysis, data interpretation, prepared figures and drafted the manuscript; AB contributed to data collection; MT performed all the histological examinations and the necessary revision of previous paraffin blocks. All authors contributed to the article and approved the submitted version.

Conflict of interest

The authors declare that the research was conducted in the absence of any commercial or financial relationships that could be construed as a potential conflict of interest.

References

1. Sung H, Ferlay J, Siegel RL, Laversanne M, Soerjomataram I, Jemal A, et al. Global cancer Statistics 2020: Globocan estimates of incidence and mortality worldwide for 36 cancers in 185 countries. *CA Cancer J Clin* (2021) 71(3): 209–49. doi:10.3322/caac.21660

2. Eom SS, Choi W, Eom BW, Park SH, Kim SJ, Kim YI, et al. A comprehensive and comparative review of global gastric cancer treatment guidelines. *J Gastric Cancer* (2022) 22(1):3–23. doi:10.5230/jgc.2022.22.e10

3. Hartgrink HH, van de Velde CJ, Putter H, Bonenkamp JJ, Klein Kranenbarg E, Songun I, et al. Extended lymph node dissection for gastric cancer: Who may benefit? Final results of the randomized Dutch gastric cancer group trial. *J Clin Oncol* (2004) 22(11):2069–77. doi:10.1200/JCO.2004.08.026

4. Degiuli M, Reddavid R, Tomatis M, Ponti A, Morino M, Sasako M, et al. D2 dissection improves disease-specific survival in advanced gastric cancer patients: 15-Year follow-up results of the Italian gastric cancer study group D1 versus D2 randomised controlled trial. *Eur J Cancer* (2021) 150:10–22. doi:10.1016/j.ejca.2021.03.031

5. Songun I, Putter H, Kranenbarg EM, Sasako M, van de Velde CJ. Surgical treatment of gastric cancer: 15-Year follow-up results of the randomised nationwide Dutch D1d2 trial. *Lancet Oncol* (2010) 11(5):439–49. doi:10.1016/S1470-2045(10)70070-X

6. Habermann CR, Weiss F, Riecken R, Honarpisheh H, Bohnacker S, Staedtler C, et al. Preoperative staging of gastric adenocarcinoma: Comparison of helical ct and endoscopic us. *Radiology* (2004) 230(2):465–71. doi:10.1148/radiol.2302020828

7. Kim HJ, Kim AY, Oh ST, Kim JS, Kim KW, Kim PN, et al. Gastric cancer staging at multi-detector row ct gastrography: Comparison of transverse and volumetric ct scanning. *Radiology* (2005) 236(3):879–85. doi:10.1148/radiol.2363041101

8. Findlay JM, Antonowicz S, Segaran A, El Kafsi J, Zhang A, Bradley KM, et al. Routinely staging gastric cancer with (18)F-fdg pet-ct detects additional metastases and predicts early recurrence and death after surgery. *Eur Radiol* (2019) 29(5): 2490–8. doi:10.1007/s00330-018-5904-2

9. Choi YY, An JY, Guner A, Kang DR, Cho I, Kwon IG, et al. Skip lymph node metastasis in gastric cancer: Is it skipping or skipped? *Gastric Cancer* (2016) 19(1): 206–15. doi:10.1007/s10120-015-0472-5

10. Faige DO. Eus in patients with benign and malignant lymphadenopathy. *Gastrointest Endosc* (2001) 53(6):593–8. doi:10.1067/mge.2001.114060

11. Hwang SW, Lee DH, Lee SH, Park YS, Hwang JH, Kim JW, et al. Preoperative staging of gastric cancer by endoscopic ultrasonography and multidetector-row computed tomography. *J Gastroenterol Hepatol* (2010) 25(3):512–8. doi:10.1111/j.1440-1746.2009.06106.x

12. Japanese Gastric Cancer A. Japanese gastric cancer treatment guidelines 2018 (5th edition). *Gastric Cancer* (2021) 24(1):1–21. doi:10.1007/s10120-020-01042-y

13. Ohdaira H, Nimura H, Mitsumori N, Takahashi N, Kashiwagi H, Yanaga K. Validity of modified gastrectomy combined with sentinel node navigation surgery for early gastric cancer. *Gastric Cancer* (2007) 10(2):117–22. doi:10.1007/s10120-007-0419-6

14. Wei J, Bu Z. Sentinel lymph node detection for gastric cancer: Promise or pitfall? *Surg Oncol* (2020) 33:1–6. doi:10.1016/j.suronc.2019.12.005

15. Miwa K, Kinami S, Taniguchi K, Fushida S, Fujimura T, Nonomura A. Mapping sentinel nodes in patients with early-stage gastric carcinoma. *Br J Surg* (2003) 90(2):178–82. doi:10.1002/bjs.4031

16. Lee SE, Lee JH, Ryu KW, Cho SJ, Lee JY, Kim CG, et al. Sentinel node mapping and skip metastases in patients with early gastric cancer. *Ann Surg Oncol* (2009) 16(3):603–8. doi:10.1245/s10434-008-0283-6

17. Liu JY, Deng JY, Zhang NN, Liu HF, Sun WL, He WT, et al. Clinical significance of skip lymph-node metastasis in Pn1 gastric-cancer patients after curative surgery. *Gastroenterol Rep (Oxf)* (2019) 7(3):193–8. doi:10.1093/gastro/goz008

18. Jeuck TL, Wittekind C. Gastric carcinoma: Stage migration by immunohistochemically detected lymph node micrometastases. *Gastric Cancer* (2015) 18(1):100–8. doi:10.1007/s10120-014-0352-4

19. Ryu KW, Kim YW, Min JS, An JY, Yoon HM, Eom BW, et al. Laparoscopic sentinel node navigation surgery versus laparoscopic standard gastrectomy with lymph node dissection in early gastric cancer: Final three-year survival results of multicenter randomized controlled phase iii trial (senorita trial). *J Clin Oncol* (2020) 38(15):4510. doi:10.1200/JCO.2020.38.15_suppl.4510

20. Hur H, Lee YJ, Kim Y-W, Min J-S, Yoon HM, An JY, et al. Clinical efficacy of laparoscopic sentinel node navigation surgery for early gastric cancer: Five-year results of senorita trial. *J Clin Oncol* (2022) 40(16):4050. doi:10.1200/JCO.2022.40.16_suppl.4050

21. Kampschoer GH, Maruyama K, van de Velde CJ, Sasako M, Kinoshita T, Okabayashi K. Computer analysis in making preoperative decisions: A rational approach to lymph node dissection in gastric cancer patients. *Br J Surg* (1989) 76(9): 905–8. doi:10.1002/bjs.1800760910

22. Maruyama K, Gunven P, Okabayashi K, Sasako M, Kinoshita T. Lymph node metastases of gastric cancer. General pattern in 1931 patients. *Ann Surg* (1989) 210(5):596–602. doi:10.1097/00000658-198911000-00005

23. Bollschweiler EH, Monig SP, Hensler K, Baldus SE, Maruyama K, Holscher AH. Artificial neural network for prediction of lymph node metastases in gastric cancer: A phase ii diagnostic study. *Ann Surg Oncol* (2004) 11(5):506–11. doi:10.1245/ASO.2004.04.018

24. Toth D, Torok M, Kincses Z, Damjanovich L. Prospective, comparative study for the evaluation of lymph node involvement in gastric cancer: Maruyama computer program versus sentinel lymph node biopsy. *Gastric Cancer* (2013) 16(2):201–7. doi:10.1007/s10120-012-0170-5

25. Hundahl SA, Macdonald JS, Benedetti J, Fitzsimmons TSouthwest Oncology Group and the Gastric Intergroup. Surgical treatment variation in a prospective, randomized trial of chemoradiotherapy in gastric cancer: The effect of undertreatment. *Ann Surg Oncol* (2002) 9(3):278–86. doi:10.1007/BF02573066

26. Peeters KC, Hundahl SA, Kranenbarg EK, Hartgrink H, van de Velde CJ. Low Maruyama index surgery for gastric cancer: Blinded reanalysis of the Dutch D1-D2 trial. *World J Surg* (2005) 29(12):1576–84. doi:10.1007/s00268-005-7907-9

27. Athauda A, Nankivell M, Langer R, Pritchard S, Langley RE, von Loga K, et al. Pathological regression of primary tumour and metastatic lymph nodes following chemotherapy in resectable og cancer: Pooled analysis of two trials. *Br J Cancer* (2023) 128(11):2036–43. doi:10.1038/s41416-023-02217-x

28. Zhu YL, Sun YK, Xue XM, Yue JY, Yang L, Xue LY. Unnecessity of lymph node regression evaluation for predicting gastric adenocarcinoma outcome after neoadjuvant chemotherapy. *World J Gastrointest Oncol* (2019) 11(1):48–58. doi:10.4251/wjgo.v11.i1.48

29. Pereira MA, Ramos M, Dias AR, Cardili L, Ribeiro RRE, Charruf AZ, et al. Lymph node regression after neoadjuvant chemotherapy: A predictor of survival in gastric cancer. *J Surg Oncol* (2020) 121(5):795–803. doi:10.1002/jso.25785

30. Park JY, Kim YW, Ryu KW, Nam BH, Lee YJ, Jeong SH, et al. Assessment of laparoscopic stomach preserving surgery with sentinel basin dissection versus standard gastrectomy with lymphadenectomy in early gastric cancer-a multicenter randomized phase iii clinical trial (senorita trial) protocol. *BMC Cancer* (2016) 16:340. doi:10.1186/s12885-016-2336-8

31. Miyashiro I, Hiratsuka M, Sasako M, Sano T, Mizusawa J, Nakamura K, et al. High false-negative proportion of intraoperative histological examination as a serious problem for clinical application of sentinel node biopsy for early gastric cancer: Final results of the Japan clinical oncology group multicenter trial Jcog0302. *Gastric Cancer* (2014) 17(2):316–23. doi:10.1007/s10120-013-0285-3

32. Toth D, Kincses Z, Plosz J, Torok M, Kovacs I, Kiss C, et al. Value of sentinel lymph node mapping using a blue dye-only method in gastric cancer: A single-center experience from north-east Hungary. *Gastric Cancer* (2011) 14(4):360–4. doi:10.1007/s10120-011-0048-y

33. Toth D, Kathy S, Csoban T, Kincses Z, Torok M, Plosz J, et al. Gyomortumorok őrszemnyirokcsomó-jelölésének prospektív, összehasonlító vizsgálata – submucosus kontra subserosus jelölés. *Magy Seb* (2012) 65(1):3–8. doi:10.1556/MaSeb.65.2012.1.1

34. Shimada A, Takeuchi H, Nishi T, Mayanagi S, Fukuda K, Suda K, et al. Utility of the one-step nucleic acid amplification assay in sentinel node mapping for early gastric cancer patients. *Gastric Cancer* (2020) 23(3):418–25. doi:10.1007/s10120-019-01016-9

Pathology & Oncology Research | frontiers

TYPE Systematic Review
PUBLISHED 27 June 2023
DOI 10.3389/pore.2023.1611221

Check for updates

OPEN ACCESS

EDITED BY
Andrea Ladányi,
National Institute of Oncology (NIO), Hungary

*CORRESPONDENCE
Caihong Hu,
523161885@qq.com

RECEIVED 02 April 2023
ACCEPTED 14 June 2023
PUBLISHED 27 June 2023

CITATION
Lv J, Chen P, Wu J and Hu C (2023), Prognostic value of pretreatment Controlling Nutritional Status score in esophageal cancer: a meta-analysis. *Pathol. Oncol. Res.* 29:1611221. doi: 10.3389/pore.2023.1611221

COPYRIGHT
© 2023 Lv, Chen, Wu and Hu. This is an open-access article distributed under the terms of the Creative Commons Attribution License (CC BY). The use, distribution or reproduction in other forums is permitted, provided the original author(s) and the copyright owner(s) are credited and that the original publication in this journal is cited, in accordance with accepted academic practice. No use, distribution or reproduction is permitted which does not comply with these terms.

Prognostic value of pretreatment Controlling Nutritional Status score in esophageal cancer: a meta-analysis

Jing Lv, Peirui Chen, Jianqiang Wu and Caihong Hu*

Department of Thoracic Surgery, People's Hospital of Deyang City, Deyang, China

Background and purpose: The association between the pretreatment Controlling Nutritional Status (CONUT) score and the prognosis of esophageal cancer patients remains unclear. The aim of this meta-analysis was to further elucidate the prognostic role of the pretreatment CONUT score in esophageal cancer based on current evidence.

Methods: The PubMed, Embase, Web of Science and CNKI databases were searched up to 27 September 2022. The primary and secondary outcomes were overall survival (OS) and progression-free survival (PFS)/cancer-specific survival (CSS), and the hazard ratio (HR) and 95% confidence interval (CI) were pooled for analysis.

Results: A total of 11 retrospective studies involving 3,783 participants were included. The pooled results demonstrated that a higher pretreatment CONUT score was significantly related to poor OS (HR = 1.82, 95% CI: 1.31–2.54, $p < 0.001$), and subgroup analysis stratified by pathological type showed similar results. In addition, the pretreatment CONUT score was associated with poor PFS (HR = 1.19, 95% CI: 1.10–1.28, $p < 0.001$) and CSS (HR = 2.67, 95% CI: 1.77–4.02, $p < 0.001$).

Conclusion: The pretreatment CONUT score was predictive of worse prognosis in esophageal cancer, and patients with a higher CONUT score showed worse survival.

KEYWORDS

meta-analysis, prognosis, esophageal cancer, pretreatment, Controlling Nutritional Status score

Introduction

Esophageal carcinoma is one of the most common malignant cancers worldwide, ranking sixth and seventh in terms of mortality and incidence [1, 2]. To date, the prognosis of patients with esophageal cancer remains extremely poor despite considerable advances in surgical technologies, neoadjuvant chemotherapy and immunotherapy [3]. The TNM stage is regarded as the prognostic indicator for esophageal cancer and contributes substantially to the formulation of a treatment

strategy. However, increasing evidence indicates that a number of host parameters affect the long-term survival of esophageal cancer [4].

In particular, nutritional status has been verified as an essential prognostic factor in cancers, and it has been reported that impaired nutritional conditions have a negative impact on survival in cancer patients [5]. Thus, a number of nutritional indicators based on laboratory data have been investigated, and the prognostic role of several indices has been explored in recent years, including the prognostic nutritional index (PNI) [6], nutritional risk index (NRI) [7], geriatric nutritional risk index (GNRI) [8] and modified Glasgow Prognostic Score (mGPS) [9]. Some of them have been shown to be significantly associated with the prognosis of esophageal carcinoma patients [6, 8, 9]. The Controlling Nutritional Status (CONUT) score is a novel nutritional indicator that has been described in the past several years [10]. It is calculated by scoring serum, albumin concentration, lymphocyte count and total cholesterol level [11], and the association of CONUT score and perioperative surgical risk in esophageal cancer has been reported [12]. In addition, the relationship between the pretreatment CONUT score and survival has also been manifested in several types of tumors by meta-analyses, including renal cell carcinoma, pancreatic cancer, lung cancer and colorectal cancer [13–16]. However, whether the pretreatment CONUT score could serve as a reliable prognostic factor in esophageal cancer is unclear.

Therefore, this meta-analysis aimed to further elucidate the association of the pretreatment CONUT score with long-term survival in esophageal cancer, which might contribute to the treatment strategy for esophageal cancer patients.

Materials and methods

This meta-analysis was performed according to the Preferred Reporting Items for Systematic Review and Meta-Analyses 2020 [17].

Literature search

The PubMed, Embase, Web of Science and CNKI databases were searched up to 27 September 2022, for studies investigating the prognostic role of the pretreatment CONUT score in esophageal cancer. The following terms were used during the search: Controlling Nutritional Status score, CONUT, esophageal, esophagus, cancer, tumor, carcinoma, neoplasm, survival, prognostic and prognosis. The specific search strategy was as follows: (Controlling Nutritional Status score OR CONUT) AND (esophageal OR esophagus) AND (cancer OR tumor OR carcinoma OR neoplasm) AND (survival OR prognostic OR prognosis). Additionally, all references cited in the included studies were also screened.

Inclusion criteria

The inclusion criteria were as follows: 1) patients were diagnosed with primary esophageal cancer pathologically; 2) the CONUT score was calculated based on the serum albumin concentration, peripheral total lymphocyte count and cholesterol level before antitumor treatment as previously described: serum albumin levels≥3.50 g/dL, 3.00–3.49 g/dL, 2.50–3.49 g/dL and <2.50 g/dL [18] were separately defined as score 0, 2, 4 and 6, the total cholesterol levels≥180 mg/dL, 140–179 mg/dL, 100–139 mg/dL and<100 mg/dL were scored 0, 1, 2 and 3 and the total lymphocyte counts ≥1,600/μL, 1,200–1,599/μL, 800–1,199/μL and<800/μL were scored 0, 1, 2 and 3, respectively; 3) patients were divided into two groups based on the CONUT score and the association between pretreatment CONUT score and prognosis presenting as the overall survival (OS), progression-free survival (PFS) or cancer-specific survival (CSS); 4) the hazard ratios (HRs) and 95% confidence intervals (CIs) for the above endpoints were provided in the papers or the Kaplan–Meier survival curves were presented; and 5) high-quality studies with a Newcastle–Ottawa Scale (NOS) score >5 [19].

Exclusion criteria

The exclusion criteria were as follows: 1) publications with letters, editorials, case reports, reviews or animal trials; 2) overlapped or duplicated data; and 3) the HRs with corresponding 95% CIs were not available.

Data collection

The following information was extracted: the name of the first author, publication year, sample size, country, tumor-node-metastasis (TNM) stage, treatment (surgical or nonsurgical therapy), pathological type, definition and comparison of CONUT score, endpoint, HR and 95% CI.

Methodological quality assessment

The quality was assessed according to the NOS score tool, and only high-quality studies with an NOS score ≥5 were ultimately included [19].

The literature search, selection, data collection and quality assessment were all conducted by two authors independently, and any disagreement was resolved by discussion.

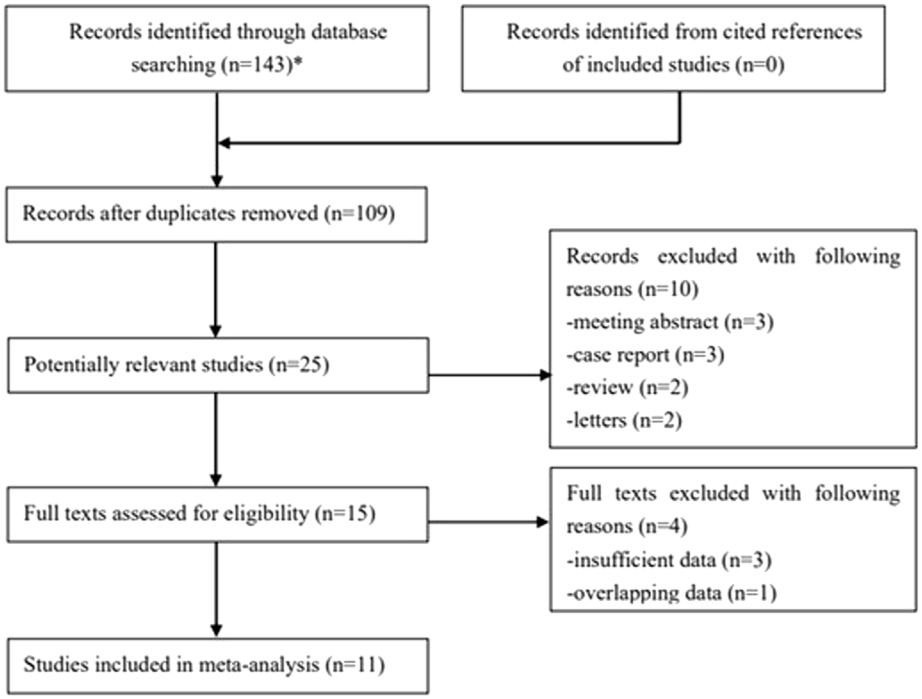

FIGURE 1
The flow diagram of this meta-analysis.

Statistical analysis

All statistical analyses were performed using STATA 15.0 software. The HRs and 95% CIs were calculated to evaluate the association between the pretreatment CONUT score and the prognosis of esophageal cancer patients. Heterogeneity among the included studies was evaluated using I^2 statistics and the Q-test. If obvious heterogeneity was observed, representing $I^2 > 50\%$ and/or $p < 0.1$, the random effects model was applied; otherwise, the fixed effects model was used. Sensitivity analysis was performed to clarify sources of heterogeneity and evaluate the stability of the pooled results. Additionally, Begg's test and Egger's test were conducted to detect publication bias, and significant publication bias was defined as $p < 0.05$ [20, 21]. If we detected significant publication bias, then the nonparametric trim-and-fill method was used to re-estimate a corrective effect size after publication bias was adjusted [22].

Results

Literature search and selection

One hundred forty-three records were searched from databases, and 34 duplicated publications were removed. Then, 25 potentially relevant studies were further reviewed after excluding 84 irrelevant publications by reading the titles. The full texts of the remaining 15 studies were carefully reviewed after excluding 10 publications. Ultimately, 11 retrospective studies were included [23–33]. The specific process is displayed in Figure 1.

Basic characteristics of the included studies

A total of 3,783 patients were enrolled, and most (7/11) studies were from Japan [23–25, 27–30]. Except for the study by Chang et al. [33], the other studies included operated patients. In addition, six studies focused on esophageal squamous cell carcinoma (ESCC) patients [23, 25, 26, 29, 31, 32]. The other detailed characteristics are presented in Table 1.

Predictive effect of the pretreatment CONUT score for OS

Ten studies explored the predictive effect of the pretreatment CONUT score on OS in esophageal cancer [23, 24, 26–33]. The results demonstrated that a higher pretreatment CONUT score was obviously related to poorer

TABLE 1 Basic characteristics of included studies.

Author	Year	Sample size	Country	TNM stage	Treatment	Pathological type	Definition of CONUT score and comparison	Endpoint	NOS
Toyokawa [23]	2016	185	Japan	I-IV	Surgery	SCC	Albumin (g/dL): ≥3.50: 0, 3.00–3.49: 2, 2.50–2.99: 4, <2.50: 6; lymphocyte count (/mm^3): ≥1,600: 0, 1,200–1,599: 1, 800–1,199: 2, <800: 3; cholesterol (mg/dL): ≥180: 0, 140–179: 1, 100–139: 2, <100: 3; CONUT 0–1 vs. ≥ 2	OS, PFS	7
Yoshida [24]	2017	373	Japan	I-IV	Surgery	EC	Albumin (g/dL): ≥3.50: 0, 3.00–3.49: 2, 2.50–2.99: 4, <2.50: 6; lymphocyte count (/mm^3): ≥1,600: 0, 1,200–1,599: 1, 800–1,199: 2, <800: 3; cholesterol (mg/dL): ≥180: 0, 140–179: 1, 100–139: 2, <100: 3; NR	OS, CSS	7
Hirahara [25]	2018	148	Japan	I-III	Surgery	SCC	Albumin (g/dL): ≥3.50: 0, 3.00–3.49: 2, 2.50–2.99: 4, <2.50: 6; lymphocyte count (/mm^3): ≥1,600: 0, 1,200–1,599: 1, 800–1,199: 2, <800: 3; cholesterol (mg/dL): ≥180: 0, 140–179: 1, 100–139: 2, <100: 3; CONUT 0–1 vs. 2–4 vs. 5–12	CSS	7
Xu [26]	2018	510	China	I-IV	Surgery	SCC	Albumin (g/dL): ≥3.50: 0, 3.00–3.49: 2, 2.50–2.99: 4, <2.50: 6; lymphocyte count (/mm^3): ≥1,600: 0, 1,200–1,599: 1, 800–1,199: 2, <800: 3; cholesterol (mg/dL): ≥180: 0, 140–179: 1, 100–139: 2, <100: 3; CONUT 0–1 vs. ≥ 2	OS	6
Hikage [27]	2019	141	Japan	I-IV	Surgery	EC	Albumin (g/dL): ≥3.50: 0, 3.00–3.49: 2, 2.50–2.99: 4, <2.50: 6; lymphocyte count (/mm^3): ≥1,600: 0, 1,200–1,599: 1, 800–1,199: 2, <800: 3; cholesterol (mg/dL): ≥180: 0, 140–179: 1, 100–139: 2, <100: 3; CONUT 0–4 vs. 5–12	OS, PFS	6
Sakai [28]	2020	105	Japan	I-IV	Surgery	EC	Albumin (g/dL): ≥3.50: 0, 3.00–3.49: 2, 2.50–2.99: 4, <2.50: 6; lymphocyte count (/mm^3): ≥1,600: 0, 1,200–1,599: 1, 800–1,199: 2, <800: 3; cholesterol (mg/dL): ≥180: 0, 140–179: 1, 100–139: 2, <100: 3; CONUT <3 vs. ≥ 4	OS	6
Suzuki [29]	2021	241	Japan	I	Surgery	SCC	Albumin (g/dL): ≥3.50: 0, 3.00–3.49: 2, 2.50–2.99: 4, <2.50: 6; lymphocyte count (/mm^3): ≥1,600: 0, 1,200–1,599: 1, 800–1,199: 2, <800: 3; cholesterol (mg/dL): ≥180: 0, 140–179: 1, 100–139: 2, <100: 3; CONUT 0–1 vs. ≥ 2	OS	6
Urabe [30]	2021	224	Japan	NR	Surgery	EC	Albumin (g/dL): ≥3.50: 0, 3.00–3.49: 2, 2.50–2.99: 4, <2.50: 6; lymphocyte count (/mm^3): ≥1,600: 0, 1,200–1,599: 1, 800–1,199: 2, <800: 3; cholesterol (mg/dL): ≥180: 0, 140–179: 1, 100–139: 2, <100: 3; CONUT 0–1 vs. 2–4 vs. 5–12	OS, CSS	8
Xu [31]	2021	522	China	I-IV	Surgery	SCC	Albumin (g/dL): ≥3.50: 0, 3.00–3.49: 2, 2.50–2.99: 4, <2.50: 6; lymphocyte count (/mm^3): ≥1,600: 0, 1,200–1,599: 1, 800–1,199: 2, <800: 3; cholesterol (mg/dL): ≥180: 0, 140–179: 1, 100–139: 2, <100: 3; CONUT 0–1 vs. ≥ 2	OS	6
Yoon [32]	2021	1265	Korea	I-IV	Surgery	SCC	Albumin (g/dL): ≥3.50: 0, 3.00–3.49: 2, 2.50–2.99: 4, <2.50: 6; lymphocyte count (/mm^3): ≥1,600: 0, 1,200–1,599: 1, 800–1,199: 2, <800: 3; cholesterol (mg/dL): ≥180: 0, 140–179: 1, 100–139: 2, <100: 3; CONUT 0–2 vs. ≥ 3	OS, PFS	7

(Continued on following page)

TABLE 1 (*Continued*) Basic characteristics of included studies.

Author	Year	Sample size	Country	TNM stage	Treatment	Pathological type	Definition of CONUT score and comparison	Endpoint	NOS
Chang [33]	2022	69	China	Advanced	Non-surgery	EC	Albumin (g/dL): ≥3.50: 0, 3.00–3.49: 2, 2.50–2.99: 4, <2.50: 6; lymphocyte count (/mm^3): ≥1,600: 0, 1,200–1,599: 1, 800–1,199: 2, <800: 3; cholesterol (mg/dL): ≥180: 0, 140–179: 1, 100–139: 2, <100: 3; CONUT 0–1 vs. ≥ 2	OS, PFS	7

NR, not reported; SCC, squamous cell carcinoma; EC, esophageal cancer; CONUT, controlling nutritional status; OS, overall survival; PFS, progression-free survival; CSS, cancer-specific survival; NOS, Newcastle-Ottawa Scale.

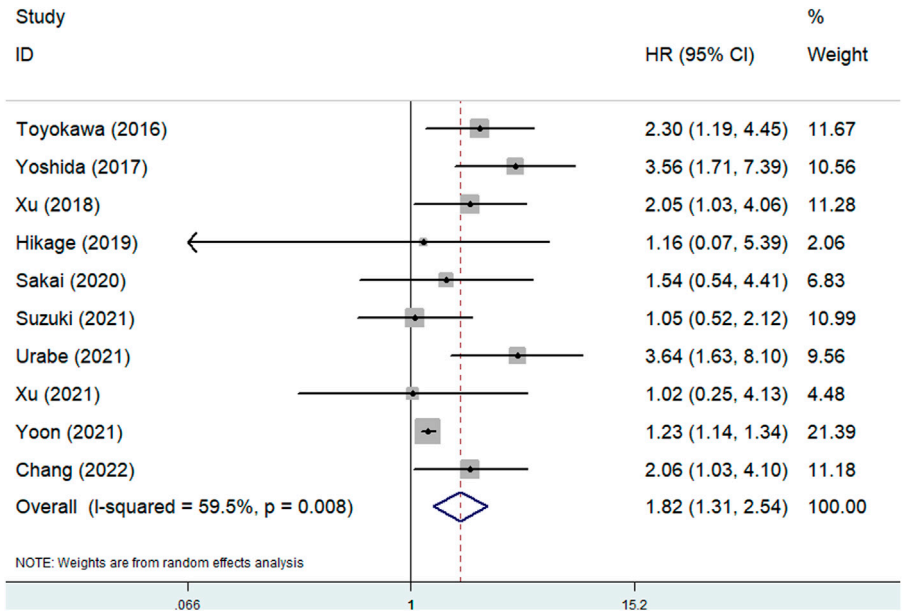

FIGURE 2
The association between pretreatment CONUT score and overall survival of esophageal cancer patients.

TABLE 2 Results of included studies.

	No. of studies	Hazard ratio	95% confidence interval	*p*-value	I^2 (%)	*p*-value
Overall survival	10 [23, 24, 26–33]	1.82	1.31–2.54	<0.001	59.5	0.008
Pathological type						
Squamous cell carcinoma	5 [23, 26, 29, 31, 32]	1.40	1.06–1.85	0.019	30.7	0.217
Esophageal cancer	5 [24, 27, 28, 30, 33]	2.59	1.76–3.82	<0.001	0.0	0.509
Progression-free survival	4 [23, 27, 32, 33]	1.19	1.10–1.28	<0.001	19.9	0.290
Cancer-specific survival	3 [24, 25, 30]	2.67	1.77–4.02	<0.001	0.0	0.494

OS (HR = 1.82, 95% CI: 1.31–2.54, $p < 0.001$; $I^2 = 59.5\%$, $p = 0.008$) (Figure 2). Subgroup analysis based on the pathological type showed similar results (ESCC: HR = 1.40, 95% CI: 1.06–1.85, $p = 0.019$; esophageal cancer: HR = 2.59, 95% CI: 1.76–3.82, $p < 0.001$) (Table 2).

Predictive effect of pretreatment CONUT score on PFS and CSS

Four [23, 27, 32, 33] and three [24, 25, 30] studies explored the association between pretreatment CONUT score and PFS and CSS,

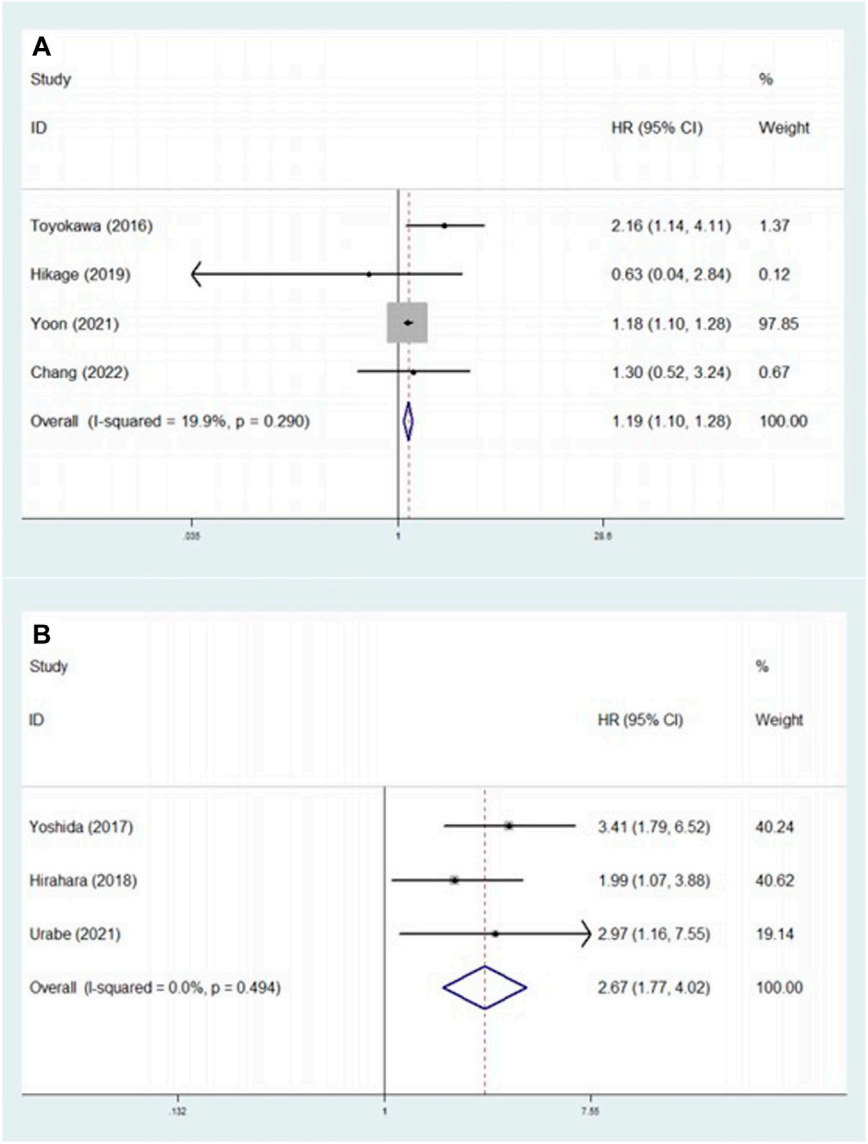

FIGURE 3
(A) The association between pretreatment CONUT score and progression-free survival of esophageal cancer patients. **(B)** The association between pretreatment CONUT score and cancer-specific survival of esophageal cancer patients.

respectively. The pooled results indicated that a higher pretreatment CONUT score predicted worse PFS (HR = 1.19, 95% CI: 1.10–1.28, $p < 0.001$; $I^2 = 19.9\%$, $p = 0.290$) and CSS (HR = 2.67, 95% CI: 1.77–4.02, $p < 0.001$; $I^2 = 0.0\%$, $p = 0.494$) (Figures 3A, B; Table 2).

Sensitivity analysis and publication bias

Sensitivity analysis for OS showed that the results of the current meta-analysis were reliable and stable, and none of the included studies showed an obvious impact on the overall results (Figure 4). However, based on the asymmetric Begg's funnel plot (Figure 5A) and $p = 0.050$ of Egger's test, significant publication bias was revealed. Thus, the nonparametric trim-and-fill method was conducted, and only one potentially "unpublished" study was revealed (Figure 5B), but this study did not affect the overall results (filled HR = 1.69, 95% CI: 1.24–2.30, $p = 0.001$).

Discussion

This meta-analysis showed that the pretreatment CONUT score was associated with the prognosis of esophageal cancer patients, and patients with a higher pretreatment CONUT score

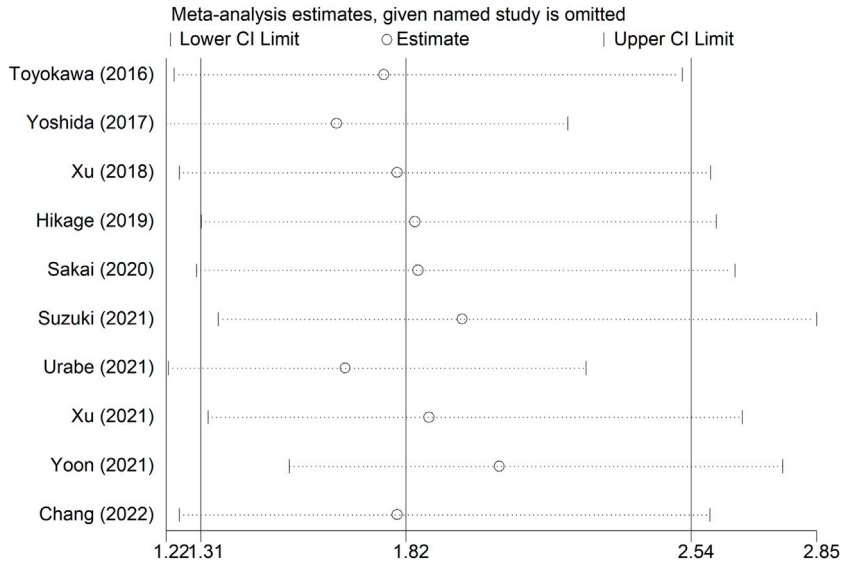

FIGURE 4
Sensitivity analysis for the overall survival.

experienced poorer OS, PFS and CSS based on current evidence. Therefore, the pretreatment CONUT might contribute to the evaluation of long-term survival and formulation of therapy strategies for esophageal cancer patients. However, because of limitations in this meta-analysis, more high-quality prospective studies are needed to verify the above findings.

The CONUT score consisted of serum albumin concentration, total cholesterol level and total lymphocyte count in peripheral blood. Serum albumin usually reflects the ability of the body to synthesize protein, total cholesterol level reflects the ability of the body to metabolize lipids, and peripheral total lymphocyte count mainly reflects the immune condition of the body [23]. Previous studies have well demonstrated that the nutritional and immune-inflammatory status is closely associated with the development, progression and prognosis of cancers. As mentioned above, the serum and cholesterol and lymphocyte count are good indicators for nutritional and immune-inflammatory status of patients, respectively. Therefore, CONUT score is indicated to be closely related to prognosis of esophageal cancer patients. Overall, the CONUT score is an easier and more objective assessment of nutritional status than the Subjective Global Assessment and the Full Nutritional Assessment [34]. In addition, we deem that the CONUT score might have some advantages over other nutritional indicators, such as the PNI, NRI and GNRI, mentioned above. PNI was calculated as follows: PNI = 10 × serum albumin (g/dL) + 0.005 × total lymphocyte count (per mm^3) [6], NRI was calculated according to the following formula: NRI = 1.519 × albumin (g/dL) + 41.7 × present weight/usual weight [35], and GNRI was calculated as follows: GNRI = 1.489 × albumin (g/dL) + 41.7 × present weight/ideal weight [36]. First, cholesterol plays an essential role in the progression and prognosis of esophageal cancer patients. It has been verified that the cholesterol level in tumor tissues is higher than that in normal tissues and that the cholesterol metabolite 27-hydroxycholesterol promotes the proliferation and migration of tumor cells [37, 38]. Tao et al. demonstrated that Lysophosphatidylcholine acyltransferase 1 (LPCAT1) reprograms tumor cells cholesterol metabolism in esophageal cancer and could be applied as a potential treatment target against esophageal carcinoma [39]. Furthermore, total cholesterol level was reported as a prognostic factor in esophageal cancer patients [40]. Thus, the cholesterol level in the peripheral blood, reflecting the condition of cholesterol metabolism to some extent, contributes to the evaluation of tumor progression and prognosis. In addition, the effect of body weight on the prognosis of cancer patients is polarizing. In detail, both overweight and low body weight are significantly associated with poor survival in cancer patients [41, 42]. Furthermore, the muscle content could objectively reflect the nutritional status of the body, and several indices, such as the skeletal muscle mass index (SMI), are reported to have high prognostic value in esophageal cancer [43, 44]. However, they are calculated from CT images in a relatively complicated way, which limits their application in clinics.

The prognostic role of the pretreatment CONUT score has been verified in several types of cancers. Ma et al. included seven studies with 2,294 patients and showed that an elevated CONUT

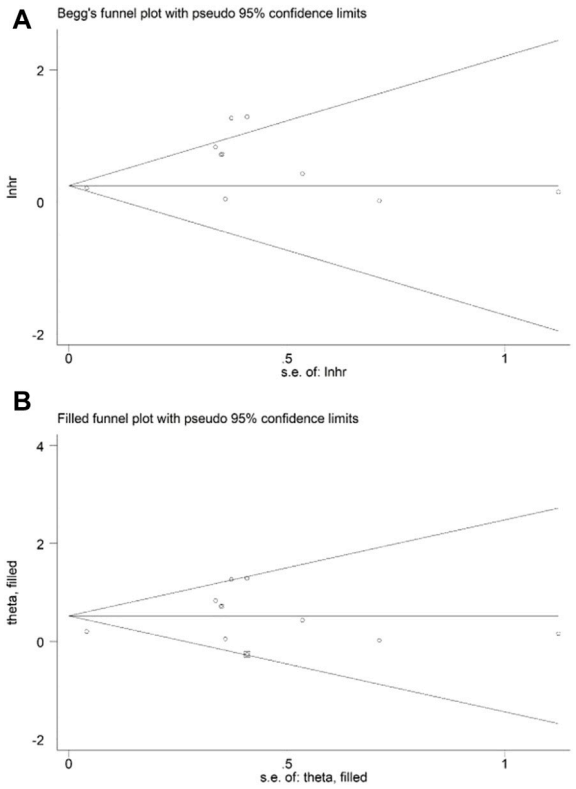

FIGURE 5
Begg's **(A)** and filled Begg's **(B)** funnel plots.

score was related to poor OS (HR = 1.56, $p = 0.007$) in pancreatic cancer [14]. In addition, Takagi et al. demonstrated that a high CONUT score was related to poor OS (HR = 1.97, $p < 0.001$), CSS (HR = 3.64, $p < 0.001$) and PFS (HR = 1.68, $p = 0.001$) after reviewing 2,601 participants [13]. Furthermore, the association between the CONUT score and the prognosis of lung cancer patients was also identified in a meta-analysis by Zhang et al. [15]. Our meta-analysis further verified the predictive role of the CONUT score for the long-term survival of esophageal cancer patients.

There are still several fields about the prognostic value of the CONUT score in esophageal cancer that need further investigation. First, only the relationship between pretreatment CONUT score and survival was identified in most relevant studies. The posttreatment CONUT score and changes in the CONUT score during antitumor treatment might also contribute to the prediction of the therapeutic effect and long-term survival of esophageal cancer. In addition, it is necessary to identify the clinical value of moderately lowering the CONUT score before or during antitumor treatment. For example, whether reducing CONUT scores by consuming cholesterol-high foods and supplementing with albumin could improve the therapeutic effect to antitumor therapy remains unclear. Furthermore, it is also worth investigating whether increasing lymphocyte count before and during the anti-tumor treatment can improve patient outcomes.

There are several limitations in this meta-analysis. First, all included studies were retrospective, and the overall sample size was relatively small. Thus, some bias might exist and should be considered. Second, all patients were from Asian countries, which might limit the generalizability of our conclusions. Third, due to the lack of original data, we were unable to conduct subgroup analysis based on other important parameters, such as TNM stage and age.

Conclusion

The pretreatment CONUT score was predictive of worse prognosis in esophageal cancer, and patients with a higher CONUT score showed worse survival. However, more high-quality prospective studies are still needed to verify our findings.

Data availability statement

The original contributions presented in the study are included in the article/supplementary material, further inquiries can be directed to the corresponding author.

Author contributions

CH designed this meta-analysis. JL and PC performed the literature search and selection, collected data and wrote the paper. JL and JW performed the statistical analysis and revised the manuscript. All authors contributed to the article and approved the submitted version.

Funding

This work was funded by the Research project of Sichuan Provincial Health Commission (20PJ248).

Conflict of interest

The authors declare that the research was conducted in the absence of any commercial or financial relationships that could be construed as a potential conflict of interest.

References

1. Siegel RL, Miller KD, Fuchs HE, Jemal A. Cancer statistics, 2022. *CA: a Cancer J clinicians* (2022) 72(1):7–33. doi:10.3322/caac.21708

2. Xia C, Dong X, Li H, Cao M, Sun D, He S, et al. Cancer statistics in China and United States, 2022: Profiles, trends, and determinants. *Chin Med J* (2022) 135(5): 584–90. doi:10.1097/CM9.0000000000002108

3. Bray F, Ferlay J, Soerjomataram I, Siegel RL, Torre LA, Jemal A. Global cancer statistics 2018: GLOBOCAN estimates of incidence and mortality worldwide for 36 cancers in 185 countries. *CA: a Cancer J clinicians* (2018) 68(6):394–424. doi:10.3322/caac.21492

4. Hursting SD, Berger NA. Energy balance, host-related factors, and cancer progression. *J Clin Oncol : official J Am Soc Clin Oncol* (2010) 28(26):4058–65. doi:10.1200/JCO.2010.27.9935

5. Norman K, Pichard C, Lochs H, Pirlich M. Prognostic impact of disease-related malnutrition. *Clin Nutr (Edinburgh, Scotland)* (2008) 27(1):5–15. doi:10.1016/j.clnu.2007.10.007

6. Liao G, Zhao Z, Yang H, Chen M, Li X. Can prognostic nutritional index be a prediction factor in esophageal cancer?: A meta-analysis. *Nutr Cancer* (2020) 72(2): 187–93. doi:10.1080/01635581.2019.1631859

7. Ma LX, Taylor K, Espin-Garcia O, Anconina R, Suzuki C, Allen MJ, et al. Prognostic significance of nutritional markers in metastatic gastric and esophageal adenocarcinoma. *Cancer Med* (2021) 10(1):199–207. doi:10.1002/cam4.3604

8. Yu J, Zhang W, Wang C, Hu Y. The prognostic value of pretreatment geriatric nutritional risk index in esophageal cancer: A meta-analysis. *Nutr Cancer* (2022) 74(9):3202–10. doi:10.1080/01635581.2022.2069273

9. Wang Y, Chen L, Wu Y, Li P, Che G. The prognostic value of modified Glasgow prognostic score in patients with esophageal squamous cell cancer: A meta-analysis. *Nutr Cancer* (2020) 72(7):1146–54. doi:10.1080/01635581.2019.1677925

10. López-Larramona G, Lucendo AJ, Tenías JM. Association between nutritional screening via the Controlling Nutritional Status index and bone mineral density in chronic liver disease of various etiologies. *Hepatol Res : official J Jpn Soc Hepatol* (2015) 45(6):618–28. doi:10.1111/hepr.12395

11. Iseki Y, Shibutani M, Maeda K, Nagahara H, Ohtani H, Sugano K, et al. Impact of the preoperative controlling nutritional status (CONUT) score on the survival after curative surgery for colorectal cancer. *PloS one* (2015) 10(7):e0132488. doi:10.1371/journal.pone.0132488

12. Yoshida N, Baba Y, Shigaki H, Harada K, Iwatsuki M, Kurashige J, et al. Preoperative nutritional assessment by controlling nutritional status (CONUT) is useful to estimate postoperative morbidity after esophagectomy for esophageal cancer. *World J Surg* (2016) 40(8):1910–7. doi:10.1007/s00268-016-3549-3

13. Takagi K, Buettner S, Ijzermans JNM. Prognostic significance of the controlling nutritional status (CONUT) score in patients with colorectal cancer: A systematic review and meta-analysis. *Int J Surg (London, England)* (2020) 78: 91–6. doi:10.1016/j.ijsu.2020.04.046

14. Ma X, Zou W, Sun Y. Prognostic value of pretreatment controlling nutritional status score for patients with pancreatic cancer: A meta-analysis. *Front Oncol* (2021) 11:770894. doi:10.3389/fonc.2021.770894

15. Zhang C, Li XK, Cong ZZ, Zheng C, Luo C, Xie K, et al. Controlling nutritional status is a prognostic factor for patients with lung cancer: A systematic review and meta-analysis. *Ann Palliat Med* (2021) 10(4): 3896–905. doi:10.21037/apm-20-2328

16. Peng L, Meng C, Li J, You C, Du Y, Xiong W, et al. The prognostic significance of controlling nutritional status (CONUT) score for surgically treated renal cell cancer and upper urinary tract urothelial cancer: A systematic review and meta-analysis. *Eur J Clin Nutr* (2022) 76(6):801–10. doi:10.1038/s41430-021-01014-0

17. Page MJ, McKenzie JE, Bossuyt PM, Boutron I, Hoffmann TC, Mulrow CD, et al. The PRISMA 2020 statement: An updated guideline for reporting systematic reviews. *BMJ (Clinical research ed)* (2021) 372:790–9. doi:10.1016/j.rec.2021.07.010

18. Takagi K, Buettner S, Ijzermans JNM, Wijnhoven BPL. Systematic review on the controlling nutritional status (CONUT) score in patients undergoing esophagectomy for esophageal cancer. *Anticancer Res* (2020) 40(10):5343–9. doi:10.21873/anticanres.14541

19. Wang Y, Li J, Chang S, Dong Y, Che G. Risk and influencing factors for subsequent primary lung cancer after treatment of breast cancer: A systematic review and two meta-analyses based on four million cases. *J Thorac Oncol : official Publ Int Assoc Study Lung Cancer* (2021) 16(11):1893–908. doi:10.1016/j.jtho.2021.07.001

20. Begg CB, Mazumdar M. Operating characteristics of a rank correlation test for publication bias. *Biometrics* (1994) 50(4):1088–101. doi:10.2307/2533446

21. Egger M, Davey Smith G, Schneider M, Minder C. Bias in meta-analysis detected by a simple, graphical test. *BMJ (Clinical research ed)* (1997) 315(7109): 629–34. doi:10.1136/bmj.315.7109.629

22. Wang Y, Huang D, Xu WY, Wang YW, Che GW. Prognostic value of pretreatment lymphocyte-to-monocyte ratio in non-small cell lung cancer: A meta-analysis. *Oncol Res Treat* (2019) 42(10):523–31. doi:10.1159/000501726

23. Toyokawa T, Kubo N, Tamura T, Sakurai K, Amano R, Tanaka H, et al. The pretreatment Controlling Nutritional Status (CONUT) score is an independent prognostic factor in patients with resectable thoracic esophageal squamous cell carcinoma: Results from a retrospective study. *BMC cancer* (2016) 16(1):722. doi:10.1186/s12885-016-2696-0

24. Yoshida N, Harada K, Baba Y, Kosumi K, Iwatsuki M, Kinoshita K, et al. Preoperative controlling nutritional status (CONUT) is useful to estimate the prognosis after esophagectomy for esophageal cancer. *Langenbeck's Arch Surg* (2017) 402(2):333–41. doi:10.1007/s00423-017-1553-1

25. Hirahara N, Matsubara T, Hayashi H, Takai K, Nakada S, Tajima Y. Prognostic importance of controlling nutritional status in patients undergoing curative thoracoscopic esophagectomy for esophageal cancer. *Am J Ther* (2018) 25(5):E524–E532. doi:10.1097/MJT.0000000000000414

26. Xu J. *Analysis of preoperative nutritional data and prognostic model of esophageal squamous cell carcinoma*. Doctor. Hangzhou, China: Zhejiang University (2018).

27. Hikage M, Taniyama Y, Sakurai T, Sato C, Takaya K, Okamoto H, et al. The influence of the perioperative nutritional status on the survival outcomes for esophageal cancer patients with neoadjuvant chemotherapy. *Ann Surg Oncol* (2019) 26(13):4744–53. doi:10.1245/s10434-019-07742-9

28. Sakai M, Sohda M, Saito H, Ubukata Y, Nakazawa N, Kuriyama K, et al. Comparative analysis of immunoinflammatory and nutritional measures in surgically resected esophageal cancer: A single-center retrospective study. *vivo (Athens, Greece)* (2020) 34(2):881–7. doi:10.21873/invivo.11853

29. Suzuki T, Furukawa K, Funasaka K, Ishikawa E, Sawada T, Maeda K, et al. Long-term prognostic predictors of esophageal squamous cell carcinoma potentially indicated for endoscopic submucosal dissection. *Digestion* (2021) 102(4):563–71. doi:10.1159/000510091

30. Urabe M, Ueno M, Ogawa Y, Yago A, Shimoyama H, Honda A, et al. Comparative analysis of the prognostic utility of preoperative nutritional parameters in patients with resectable esophageal carcinoma. *Gen Thorac Cardiovasc Surg* (2021) 69(2):326–35. doi:10.1007/s11748-020-01555-4

31. Xu D. *Inflammatory and nutritional indicators and circRNA in the prognosis of esophageal cancer*. Nanjing, China: Nanjing Medical University (2021). 硕士.

32. Yoon JP, Nam JS, Abidin M, Kim SO, Lee EH, Choi IC, et al. Comparison of preoperative nutritional indexes for outcomes after primary esophageal surgery for esophageal squamous cell carcinoma. *Nutrients* (2021) 13(11):4086. doi:10.3390/nu13114086

33. Chang L, Cheng Q, Ma Y, Wu C, Zhang X, Ma Q, et al. Prognostic effect of the controlling nutritional status score in patients with esophageal cancer treated with immune checkpoint inhibitor. *J Immunother* (2022) 45:415–22. doi:10.1097/CJI.0000000000000438

34. Tsunematsu M, Haruki K, Fujiwara Y, Furukawa K, Onda S, Matsumoto M, et al. Preoperative controlling nutritional status (CONUT) score predicts long-term outcomes in patients with non-B non-C hepatocellular carcinoma after curative hepatic resection. *Langenbeck's Arch Surg* (2021) 406(1):99–107. doi:10.1007/s00423-020-01987-9

35. Poulia KA, Yannakoulia M, Karageorgou D, Gamaletsou M, Panagiotakos DB, Sipsas NV, et al. Evaluation of the efficacy of six nutritional screening tools to predict malnutrition in the elderly. *Clin Nutr (Edinburgh, Scotland)* (2012) 31(3): 378–85. doi:10.1016/j.clnu.2011.11.017

36. Bouillanne O, Morineau G, Dupont C, Coulombel I, Vincent JP, Nicolis I, et al. Geriatric nutritional risk index: A new index for evaluating at-risk elderly medical patients. *Am J Clin Nutr* (2005) 82(4):777–83. doi:10.1093/ajcn/82.4.777

37. Loosen SH, Kostev K, Luedde M, Luedde T, Roderburg C. Low blood levels of high-density lipoprotein (HDL) cholesterol are positively associated with cancer. *J Cancer Res Clin Oncol* (2022) 148(11):3039–46. doi:10.1007/s00432-021-03867-1

38. Tang Q, Liang B, Zhang L, Li X, Li H, Jing W, et al. Enhanced CHOLESTEROL biosynthesis promotes breast cancer metastasis via modulating CCDC25 expression and neutrophil extracellular traps formation. *Scientific Rep* (2022) 12(1):17350. doi:10.1038/s41598-022-22410-x

39. Tao M, Luo J, Gu T, Yu X, Song Z, Jun Y, et al. LPCAT1 reprogramming cholesterol metabolism promotes the progression of esophageal squamous cell carcinoma. *Cell Death Dis* (2021) 12(9):845. doi:10.1038/s41419-021-04132-6

40. Li Y, Luo H, Ye B, Zhang K, Liu C, Zu R, et al. Prognostic value of nutritional and inflammatory indicators in females with esophageal squamous cell cancer: A propensity score matching study. *Front Genet* (2022) 13:1026685. doi:10.3389/fgene.2022.1026685

41. Harborg S, Zachariae R, Olsen J, Johannsen M, Cronin-Fenton D, Bøggild H, et al. Overweight and prognosis in triple-negative breast cancer patients: A systematic review and meta-analysis. *NPJ breast cancer* (2021) 7(1):119. doi:10.1038/s41523-021-00325-6

42. Simillis C, Taylor B, Ahmad A, Lal N, Afxentiou T, Powar MP, et al. A systematic review and meta-analysis assessing the impact of body mass index on long-term survival outcomes after surgery for colorectal cancer. *Eur J Cancer* (2022) 172:237–51. doi:10.1016/j.ejca.2022.05.020

43. Yao L, Wang L, Yin Y, Che G, Yang M. Prognostic value of pretreatment skeletal muscle mass index in esophageal cancer patients: A meta-analysis. *Nutr Cancer* (2022) 74(10):3592–600. doi:10.1080/01635581.2022.2088814

44. Nishimura E, Kawakubo H, Matsuda S, Fukuda K, Nakamura R, Kitagawa Y. Long-term variation in psoas muscle mass index is affected by short-term loss after esophagectomy in survivors of esophageal cancer. *Dis esophagus : official J Int Soc Dis Esophagus* (2022) 36:doac053. doi:10.1093/dote/doac053

Pathology & Oncology Research | frontiers

TYPE Systematic Review
PUBLISHED 21 February 2024
DOI 10.3389/pore.2024.1611595

Check for updates

OPEN ACCESS

EDITED BY
Andrea Ladányi,
National Institute of Oncology (NIO), Hungary

*CORRESPONDENCE
Lushun Zhang,
zhangls2012@cmc.edu.cn
Li Cheng,
852649464@qq.com

†These authors have contributed equally to this work

RECEIVED 18 November 2023
ACCEPTED 07 February 2024
PUBLISHED 21 February 2024

CITATION
Wu J, Wang Y, Cheng Y, Cheng L and Zhang L (2024), Comprehensive landscape and future perspectives of non-coding RNAs in esophageal squamous cell carcinoma, a bibliometric analysis from 2008 to 2023. *Pathol. Oncol. Res.* 30:1611595. doi: 10.3389/pore.2024.1611595

COPYRIGHT
© 2024 Wu, Wang, Cheng, Cheng and Zhang. This is an open-access article distributed under the terms of the Creative Commons Attribution License (CC BY). The use, distribution or reproduction in other forums is permitted, provided the original author(s) and the copyright owner(s) are credited and that the original publication in this journal is cited, in accordance with accepted academic practice. No use, distribution or reproduction is permitted which does not comply with these terms.

Comprehensive landscape and future perspectives of non-coding RNAs in esophageal squamous cell carcinoma, a bibliometric analysis from 2008 to 2023

Jiaxin Wu[1†], Yuanying Wang[1†], Yi Cheng[2†], Li Cheng[3*] and Lushun Zhang[3*]

[1]Graduate School, Chengdu Medical College, Chengdu, China, [2]Department of Radiology, People's Hospital of Lushan County, Ya'an, China, [3]Department of Pathology and Pathophysiology, Chengdu Medical College, Chengdu, China

Objectives: Summarize the progress and hot topic evolution of non-coding RNAs (ncRNAs) research in esophageal squamous cell carcinoma (ESCC) in recent years and predict future research directions.

Methods: Relevant articles from the Web of Science until 31 October 2023 were obtained. Bibliometric analysis of included articles was performed using software (VOSviewer, CiteSpace, and Bibliometrix). The volume and citation of publications, as well as the country, institution, author, journal, keywords of the articles were used as variables to analyze the research trends and hot spot evolution.

Results: 1,118 literature from 2008 to 2023 were retrieved from database, with 25 countries/regions, 793 institutions, 5,426 authors, 261 journals involved. Global cooperation was centered on China, Japan, and the United States. Zhengzhou University, an institution from China, had the highest publication. The most prolific author was Guo Wei, and the most prolific journal was Oncology Letters. Analysis of keywords revealed that the research in this field revolved around the role of ncRNAs in the occurrence, development, diagnosis, treatment, and prognosis of ESCC, mainly including micro RNAs, long non-coding RNAs, and then circular RNAs.

Conclusion: Overall, research on ncRNAs in ESCC remains strong. Previous research has mainly focused on the basic research, with a focus on the mechanism of ncRNAs in the occurrence, development, diagnosis, treatment, and prognosis of ESCC. Combining current research with emerging disciplines to

further explore its mechanisms of action or shifting the focus of research from preclinical research to clinical research based on diagnosis, treatment, and prognosis, will be the main breakthrough in this field in the future.

KEYWORDS

novel biomarker, non-coding RNAs, digestive system cancer, bibliometric analysis, VOSviewer

Introduction

Esophageal squamous cell carcinoma (ESCC) is a highly aggressive malignancy with the seventh incidence rate and a leading cause of cancer-related deaths around the world [1]. Despite significant advancements in surgical techniques, chemotherapy, and radiation therapy, as well as the emergence of new targeted therapy and immunotherapy, the five-year survival rate of ESCC patients remains low at only 10%–25% [2]. Thus, the identification of novel biomarkers and therapeutic targets is essential. Non-coding RNAs (ncRNAs) constitute 98%–99% of the transcriptome, and do not encode proteins. Instead, they play crucial roles in various biological functions [3]. In recent years, ncRNAs have emerged as promising diagnostic and prognostic biomarkers, and as potential therapeutic targets in ESCC, and the most widely studied ncRNAs are microRNAs (miRNAs), long non-coding RNAs (lncRNAs) and circular RNAs (circRNAs). These ncRNAs are abnormally expressed in ESCC and participate in various biological functions such as gene expression, cell cycle, and epithelial-mesenchymal transition (EMT) through multiple mechanisms, promoting the occurrence and development of ESCC [4–6].

Bibliometrics is a method of quantitative analysis and evaluation based on the use of literature database records. It is employed to analyze the production efficiency and characteristics of publications in a particular field, assess the quality and impact of academic outcomes, and forecast trends and directions [7, 8]. So far, bibliometric has been widely used in the fields of biosciences and clinical medicine and has provided a new horizon for research in related fields [9–11].

Currently, there has been a large amount of previous research on ncRNAs associated with ESCC worldwide, and numerous research achievements have been obtained. However, the research progress and hot spot evolution in the field are still unclear. Therefore, a comprehensive bibliometric visualization analysis of the research on ncRNAs in ESCC is warranted. This study analyzed previous studies on ncRNAs associated with ESCC using bibliometric approach and visualized the results in an effort to gain insight into the past and current research status, identify potential directions for the future research in this area.

Methods

Literature acquisition and data collection strategy

To guarantee comprehensive and accurate data retrieval, literature was searched in the Web of Science Core Collection Science Citation Index Expanded (SCIE) database until 31 October 2023 and exported as "plain text" format. Two reviewers conducted a systematic literature search independently. A senior investigator made final decisions concerning any discrepancies between the two independent reviewers. As shown in Figure 1, after obtaining literature from database, data cleaning was carried out. Duplicate documents were first excluded, followed by document type that were not articles (including review, letter, meeting summary, editorial material, book, etc.). Finally, the content of the literature was reviewed and those that did not meet the research theme were also excluded. The search formula was as follows:

#1: TS = ("esophageal squamous cell carcinoma" OR "oesophageal squamous cell carcinoma").

#2: TS = ("non-coding RNA" OR "noncoding RNA" OR "ncRNA" OR "microRNA" OR "miRNA" OR "small RNA" OR "snoRNA" OR "snRNA" OR "long non-coding RNA" OR "lncRNA" OR "circular RNA" OR "circRNA" OR "piwi-interacting RNA" OR "piRNA").

#3: **#1** AND **#2**.

Bibliometric analysis and visualization

We mainly used VOSviewer (ver. 1.6.19), CiteSpace (ver. 6.1.R 2), and R package Bibliometrix (ver. 4.1.2) for the analysis and visualization of the retrieved data [12]. Annual volume of publications as well as keywords with the strongest citation burst were obtained using CiteSpace. Publication information of the source journals and high-citation articles were obtained using VOSviewer. The co-authorship analysis of country/region, organization, and author were analyzed and visualized using VOSviewer. A world map enabling visualization of the volume of publications and cooperation between countries was drawn using R package Bibliometrix. After manually standardized keywords with different spellings but same meanings, the 100 keywords

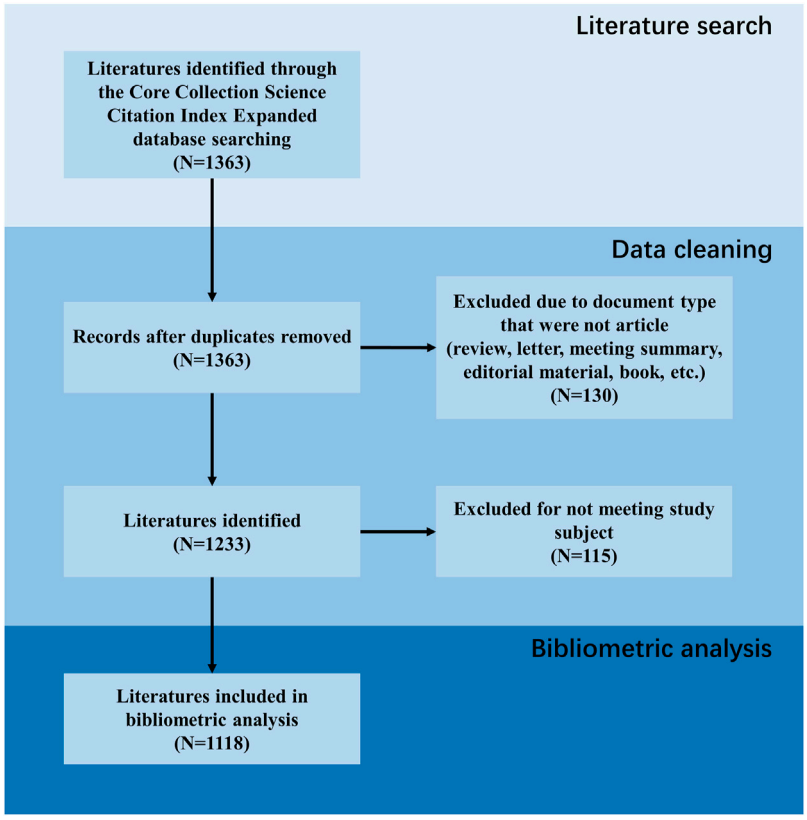

FIGURE 1
Flow diagram of literature inclusion.

with the highest frequency of occurrence were obtained using VOSviewer and visualized according to the strength of association and average year of occurrence.

Results

The annual trend in publications

We obtained literature from the SCIE database according to the developed search strategy and removed records that did not meet the inclusion criteria. The above process is presented in Figure 1, identifying a total of 1,118 articles included in this study.

As shown in Figure 2, over the past 15 years, there had been an annual increase in publications on ncRNAs associated with ESCC. Since the first publication in 2008, the annual publications had begun to climb. In 2014, the number breached 50, and in 2018 it surpassed 100. The peak was reached in 2019 with 152 publications. However, the volume of publications declined in the following 3 years compared with 2019. In addition, the increasing trend of total citations was not as robust as the volume of publications, and it showed a decreasing trend after peaking in 2015. Notably, the mean citation of papers in the field was high at first but decreased year after year, apart from a transient rise in 2010 and 2015.

The co-authorship analysis of countries and organizations

There were 25 countries/regions that have conducted relevant research, Supplementary Table S1 lists the countries with the top 10 publications. Among them, China had the highest publications, with a total of 980 articles published, followed by Japan (N = 66) and the United States (N = 57). Countries with more than 10 publications were Iran, Australia, South Korea and Germany, the remaining countries had either 10 publications or no previous publications. As for the average citation, the highest ranking was in the order of Japan (N = 65.20), Australia (N = 49.71), South Korea (N = 38.18). To gain further insight into regional cooperation in

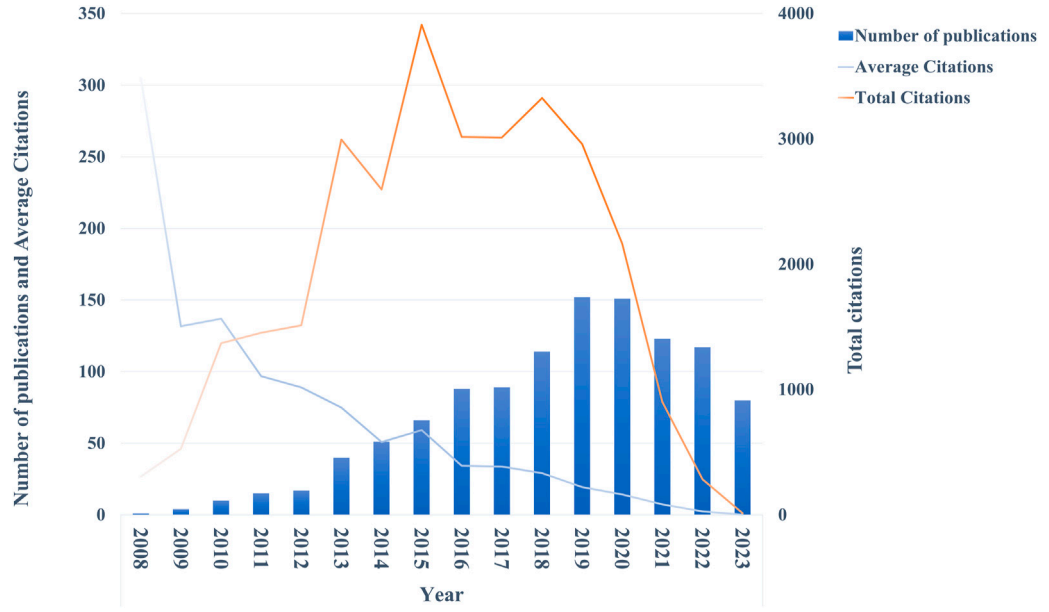

FIGURE 2
Annual publications trend chart.

publications, we conducted a co-authorship analysis and visualized the results. In Figure 3A, it can be seen that Asia, represented by China and Japan, and North America, represented by the United States, became the center of the current research, countries from other continents also participated in the study through direct or indirect collaboration. Figure 3B further validates this claim through a cooperation network of the world map.

A total of 793 organizations worldwide had participated in the field. Zhengzhou University had the largest number of publications (N = 118), followed by Nanjing Medical University (N = 110) and Hebei Medical University (N = 55). We included in Supplementary Table S2 the organizations with the top 10 publications, all of them were Chinese institutions. We performed co-authorship analysis in order to better understand publication cooperation between organizations (Figure 3C). Compared with other countries, the institutes within China were numerous and more cooperative. Among them, Zhengzhou University, Nanjing Medical University, and Hebei Medical University were the most active in cooperative research.

The co-authorship analysis of authors and co-cited authors

A total of 5,426 authors took part in the relevant research over the past 15 years. We listed the top 10 high productive authors in Supplementary Table S3. The first three scholars, all from Hebei Medical University, were Guo Wei, Dong Zhiming, Guo Yanli. It also can be found that these high-yielding scholars were all from China, suggesting the important contributions made by Chinese scholars in the current field. To reveal the contribution and cooperation of authors, the co-authorship analysis of top 100 authors was conducted (Figure 4A). By visualizing the network according to the mean publication year, two largest clusters can be found to be representative: the earlier conducted studies by the red cluster have authors Bai Yun, Li Juan, and Wang Kai, while the currently active purple cluster in the field have authors Guo Wei, Dong Zhiming, and Guo Yanli (Figure 4B).

By analyzing co-cited authors, we learn about the impact and contribution of authors in this academia, as well as examining interdigitation and collaboration in different disciplinary areas. Supplementary Table S3 demonstrates the top 10 co-cited authors. The first three authors were David P Bartel from Howard Hughes Medical Institute (United States), George A Calin from Ohio State University (United States), and Chen Wanqing from National Cancer Center (China). It can be found that most of these authors were from the United States, illustrating the founder contribution that American scholars have made to the development of this field. Furthermore, the authors come from different fields, embodying that modern scientific research is the product of the intersection of different disciplines.

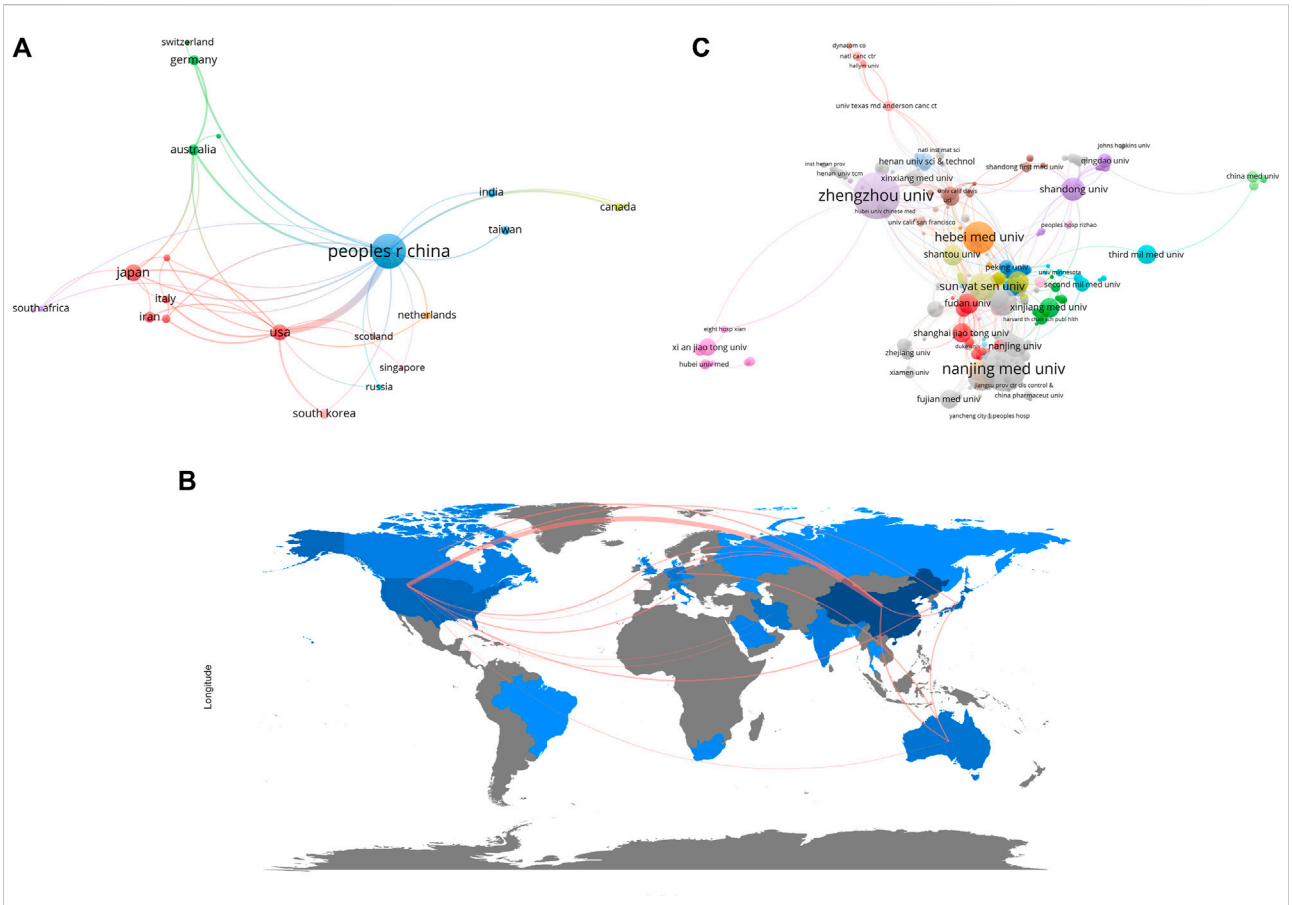

FIGURE 3
The co-authorship analysis of ncRNAs associated with ESCC. **(A)** Network plot of co-authorship analysis of countries/regions. **(B)** World map of co-authorship analysis of countries/regions. **(C)** Network plot of co-authorship analysis of organizations. The size of the circles or the depth of map color blocks represents the number of publications, and the thickness of the lines between the circles or the map color blocks represents the degree of collaboration.

The distribution of source journals and highly cited articles

A total of 261 journals had published articles on ncRNAs associated with ESCC. Among them, *Oncology Letters* published the most article (N = 31), followed by *Oncotarget* (N = 30), *Oncology Reports* (N = 28). From the total citations, the number one was *Oncotarget* (N = 1958), followed by *Tumor Biology* (N = 719) and *Oncology Reports* (N = 623). Supplementary Table S4 lists the top 10 journals with the largest number of publications. Of these, one journal had an impact factor greater than 5: *Biomedicine & Pharmacotherapy* (IF = 7.419). Additionally, *Oncotarget* and *International Journal of Clinical and Experimental Pathology* had no impact factor because they were not currently included in the SCIE database since 2018 and 2020, respectively.

The citations of a paper can reflect its impact and visibility in the field to some extent. The total number of citations for the 1,118 articles were 30,340, with an average of 29 citations per article. The top 10 most cited articles are shown in Supplementary Table S5, with frequencies ranging from 237 to 551. These articles were published between 2008 and 2015, with the 2008 publication titled *Distinctive microRNA profiles relating to patient survival in esophageal squamous cell* carcinoma being the earliest in the field, the prelude to the research on ncRNAs associated with ESCC has since been revealed. Articles titled *Circular RNA ITCH has inhibitory effect on ESCC by suppressing the Wnt/β-catenin pathway*, published in 2015, was the most highly cited with up to 551 citations. Furthermore, these articles were authored by scholars from Japan and China, with 7 articles authored by Chinese scholars and 3 articles authored by Japanese scholars.

Keywords analysis

We conducted cluster analysis of the top 100 keywords according to the frequency of their occurrence (each keyword appeared at least 12 times). In Figure 4C, analyzing the

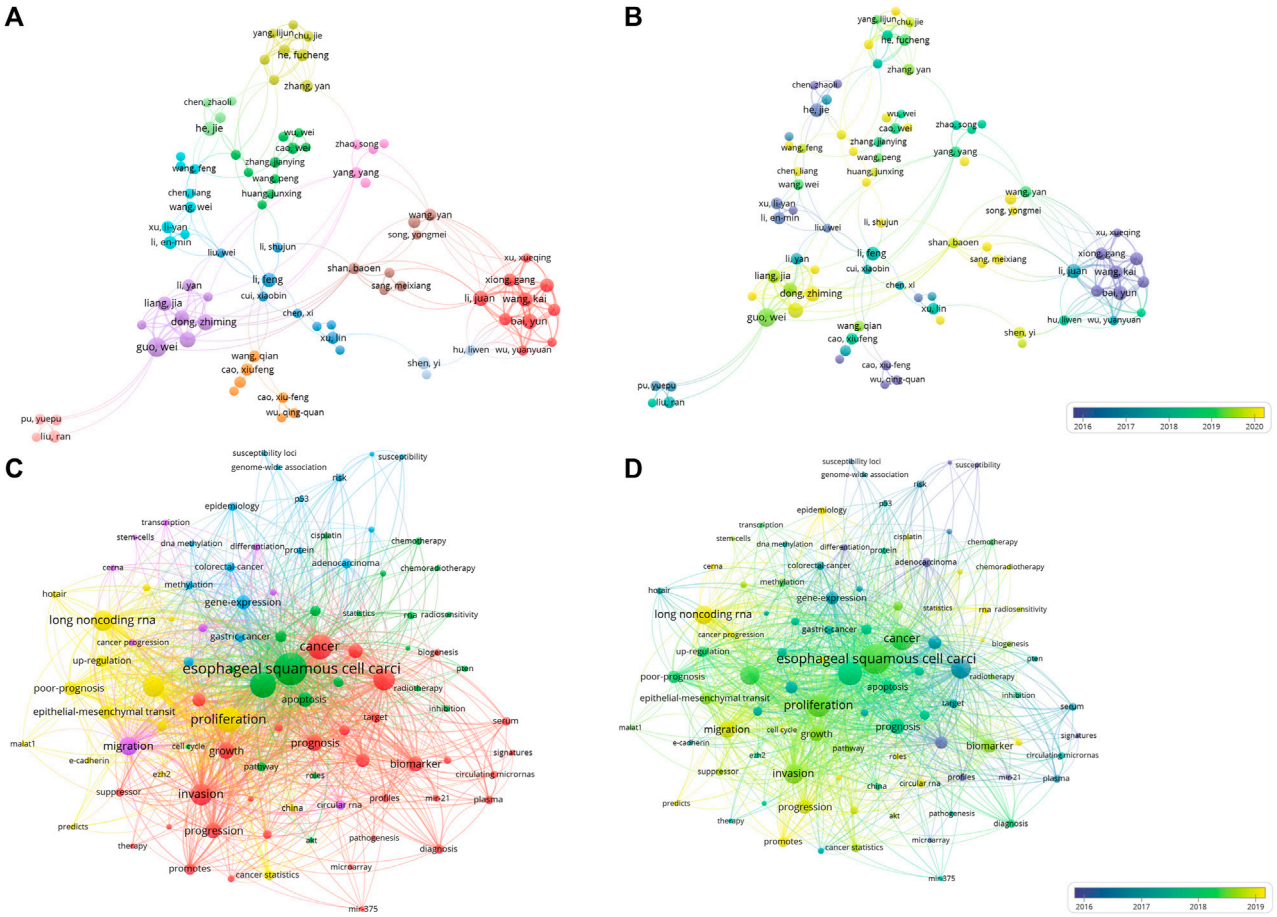

FIGURE 4
The co-authorship analysis and co-occurrence analysis of ncRNAs associated with ESCC. **(A)** Network plot of co-authorship analysis of authors. **(B)** Overlay map of co-authorship analysis of authors. **(C)** Network plot of co-occurrence analysis of top 100 keywords. **(D)** Overlay map of co-occurrence analysis of top 100 keywords. In network plot, a circle represents an author or a keyword. The larger the circle, the more articles the author has published or the more frequently the keyword appears. The thickness of the connecting line between circles represents the strength of the association. In overlay map, cold colors indicate that the author was active earlier or the keywords appeared earlier, while warm colors indicate that the author was active more recently or the keywords appeared more recently.

clusters reveals that the 100 keywords are mainly divided into five clusters. The red cluster mainly includes keywords such as microRNA, biomarker, tumor-growth, prognosis and invasion, this suggests that miRNAs are potential biomarkers for ESCC, and their expression levels correlate with the occurrence and development of ESCC. Using these miRNAs as biomarkers could aid in the diagnosis and treatment of ESCC. The green cluster mainly includes ESCC, cancer cell, apoptosis, autophagy, mechanism, radiosensitivity, uncovering the cellular and molecular mechanisms by which ncRNAs participate in the development and progression of ESCC, and the association between ncRNAs and radiotherapy sensitivity of ESCC. The yellow cluster mainly includes long non-coding RNAs, metastasis and EMT, indicating the important roles and regulatory mechanisms of lncRNAs in the development and progression of ESCC. The purple cluster mainly includes migration, circular RNA and ceRNA, this suggests that circRNAs as ceRNA (competing endogenous RNA) involved in the development and progression of ESCC. The blue cluster mainly includes gene-express, DNA methylation, protein and susceptibility loci, these have implicated related molecular mechanisms in the regulation of ncRNAs in ESCC.

According to the average publication year, overlay visualization of the co-occurrence network of 100 keywords can reveal the prevalence trends of keywords. Cool colors denote earlier published keywords, whereas warm colors indicate later ones. As shown in Figure 4D, it is not difficult to find that the earliest keywords to appear were polymorphism, susceptibility, tumor-suppressor gene, profiles, mir-21,

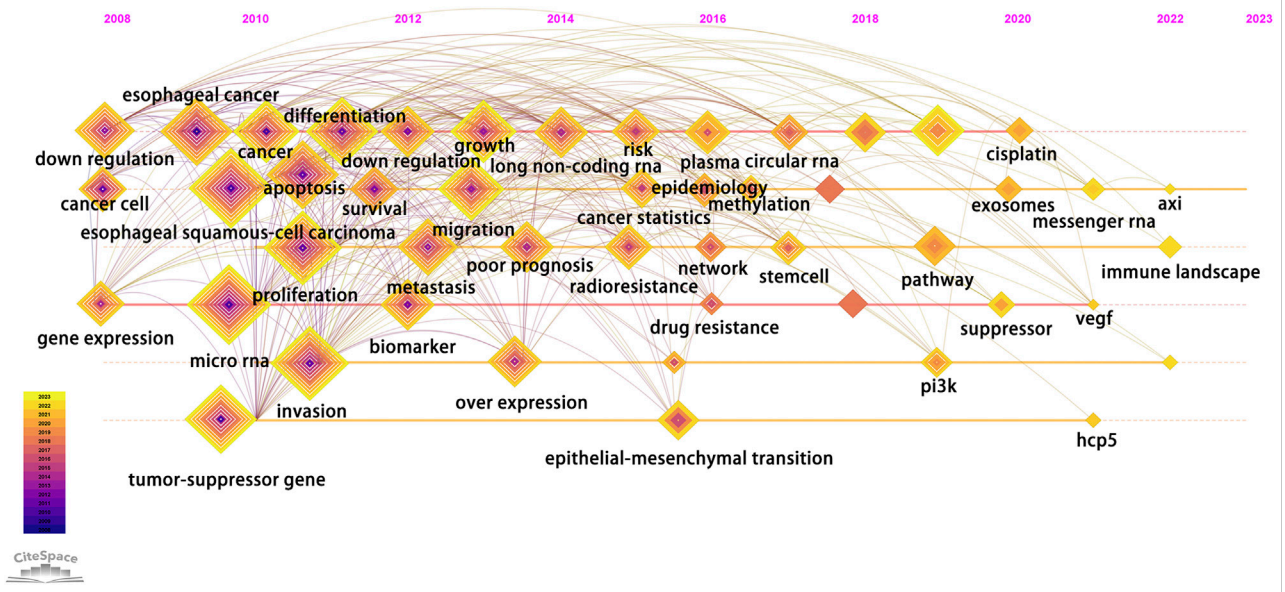

FIGURE 5
Timeline chart of keywords. Each diamond represents a keyword, and its position on the timeline represents the time it appeared. In addition, the size of the diamond represents the number of times it appears in the total time period, while each layer inside the diamond represents the number of times it appears in the corresponding year.

signatures, microarray, and the latest keywords were ceRNA, cancer progression, circular RNA, exosome. To explore the variation and trend of keywords in this field, we plotted a timeline for the high-frequency keywords that appear each year. As shown in Figure 5, It can be found that the early focus of this field was on the expression profile of ncRNAs, as well as the biological process of ncRNAs on the differentiation and apoptosis of ESCC cells, and on predicting the survival of ESCC patients. At this point, the main focus of attention on ncRNAs was miRNAs (2008–2012). In the mid-term stage of this field, more attention had been paid to the mechanisms by which ncRNAs participate in the occurrence and development of ESCC, including EMT, migration, etc. In addition, attention had been paid to the role of ncRNAs in the treatment and prognosis of ESCC. During this stage, lncRNAs gradually gained attention (2012–2016). At the present stage, based on the long-term research on the role of ncRNAs in the occurrence, development, diagnosis, treatment and prognosis of ESCC, circRNAs began to receive attention. And the recent keywords in this field were vegf, pi3k and hcp5 (2016–2022). In order to further understand the outbreak range of hotspots, we identified the top 25 keywords with the strongest citation burst in Figure 6. Focusing on these keywords, it can be observed that researchers have extensively concentrated on the role of ncRNAs in the development, progression, and prognosis of ESCC, along with the related mechanisms of their regulation. It can also be seen that the earliest ncRNAs that had received attention were miRNAs with the citation burst in 2010–2013, while circRNAs and lncRNAs are the current and future research trend with the citation burst in 2020–2023.

Discussion

Our study delved into the research of ncRNAs associated with ESCC through a bibliometric analysis that reviewed 1,118 relevant articles indexed in the SCIE database from 2008 to 2023. We scrutinized annual publication trends, affiliations, authors, co-cited authors, source journals, highly cited articles, keywords, and further investigated the current development trends and hot topics in this area.

General overview

By analyzing the trends in annual publications, the development of the research field can be divided into three phases: slow rise in the early stage (2008–2012), rapid rise stage (2013–2019), and stagnation in the later stage (2020–2023) (Figure 2). The trends in the first two stages may be attributed to the development of high-throughput sequencing technology. The article titled *Distinctive microRNA profiles relating to patient survival in esophageal squamous cell carcinoma* published by Guo Y et al. was the first publication in the field and one of the most highly cited articles [13] (Supplementary Table S3). The authors used

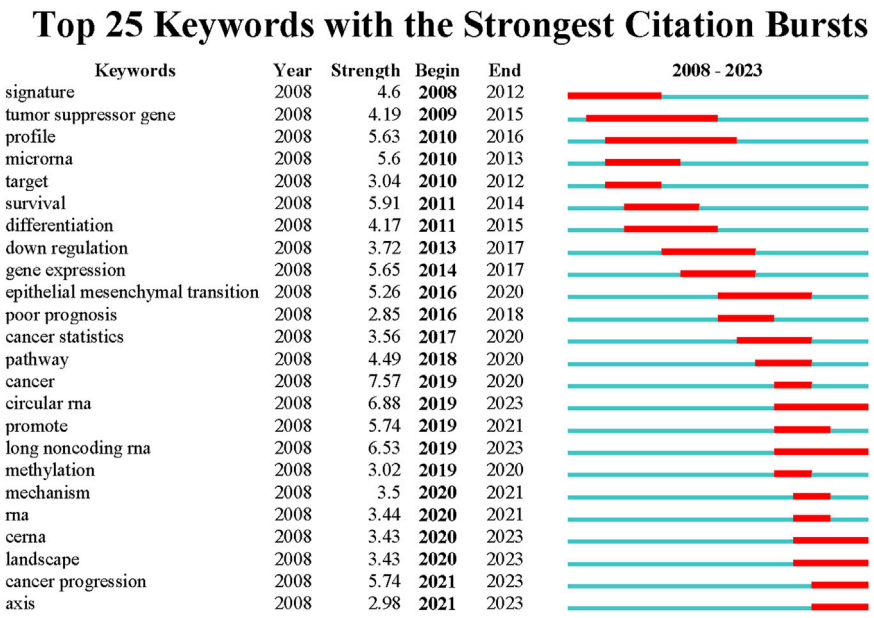

FIGURE 6
Top 25 keywords with the strongest citation burst. Blue lines indicate the time period in which the keywords appeared and ended, and red lines indicate the time period in which the keywords at high frequencies.

advanced microRNA microarray technology to study the expression of miRNAs in esophageal cancer tissue and identified 46 RNAs that were specifically expressed in tumor tissues. Thereafter, lncRNAs and circRNAs expression profiles in ESCC were sequentially revealed [14, 15]. Building on previous work from these studies, researchers can move to deeper studies around ncRNAs and ESCC. For example, mining sequencing results through bioinformatics technology and annotating differential genes can help reveal the molecular mechanism of ncRNAs in ESCC [16, 17]. Another possible reason why research on ncRNAs in ESCC had been so popular is that ncRNAs are numerous of the transcriptome and are involved in many cellular processes [3], yet previous research in this area has been lacking. Therefore, it attracted the attention from researchers. However, the third stage of annual publications perhaps indicating that research in the field had encountered bottlenecks. The possible explanations for why there is a trend towards stagnation when it comes to investigating the mechanism of ncRNAs in ESCC could be several. Firstly, previous studies had exhaustively investigated the role of ncRNAs in ESCC, leading to the exhaustion of the field. Secondly, the research conducted so far has almost been limited to basic research, which had hindered the translation of the research results into clinical applications. Thirdly, the ncRNAs mechanism in ESCC is complex, and the field is striving to find new insights into this diverse mechanism. However, the current research model is tending towards homogenization.

In this field, China had the largest number of organizations and the most prolific authors engaged in relevant research, which had resulted in the highest productions. Japanese papers had the highest average citation rate, while the greatest number of co-cited authors cited were from the United States (Supplementary Tables S1–S3). This indicated that China was at the forefront in terms of the high yield in the field. Japanese and American research achievements in this field had a high level of influence and recognition. It can be explained by the fact that Japan and China are high-risk countries for esophageal cancer, both countries attach great importance to research on esophageal cancer [1]. And the United States holds strong strength for biomedical research [18]. In addition, the Matthew effect can also be used as a possible explanation, as these high-yielding countries have more output compared to other countries with fewer resources due to their existing research funding support or research capabilities [19]. It is worth noting that despite having the highest publication volume, China's average citation of papers was not optimistic, indicating the need for further efforts to enhance the quality of research. As shown in Figure 3, 25 countries had participated in this research area, and a research center has been formed with China, Japan, and the United States, but the situation is that there was more frequent domestic cooperation in each respective country. The reason for this phenomenon may be that language and cultural differences between different countries may cause

difficulties in communication and cooperation. On the other hand, research institutions and scientists in different countries may have varying resource and interest needs, leading to difficulties in balancing cooperation between countries. Therefore, we also look forward to closer cooperation between countries in order to produce more high-quality research.

Based on publications and citations, *Oncotarget* was the most influential journal in this field (Supplementary Table S4). However, the journal was not indexed by SCIE in 2018 due to excessive self-citation and potentially unjustified co-authored research. Similarly, *International Journal of Clinical and Experimental Pathology* was not indexed by SCIE in 2020. After excluding these two journals, *Tumor Biology* had the highest average citation count, establishing it as the most influential journal in this field. It is an open access journal focused on tumor related research, which also suggests that open access journals have become increasingly popular in recent years as they provide free and unrestricted access to research articles, making it easier for researchers and academics to access and share knowledge. This has helped to increase the visibility and impact of research and has also promoted greater collaboration and exchange of ideas within the academic community. Therefore, many researchers and institutions are now recognizing the value of open access publishing and are choosing to publish their research in open access journals. Highly cited articles, to some extent, also reflect hot topics of concern in the field of scientific research, and their published journals also have an undeniable influence in this field. In addition to the aforementioned journals, the articles published in the following journals rank among the top ten in terms of citation: *International Journal of Cancer, Cancer, Gut, Cancer Research, Molecular Cancer, Clinical Chemistry, Journal of Biological Chemistry, and Clinical Cancer Research.* These journals are positioned in fields such as oncology, molecular biology, pharmacy, and clinical medicine, reflecting the long-standing and future scientific research model of multidisciplinary cooperation.

Research hotspots

We employed co-occurrence analysis of keyword networks (Figures 4C, D) and timeline charts (Figure 5) to unveil the distribution of research focus in the field. Additionally, we analyzed keywords with the strongest citation burst to further uncover the evolving trends of research hotspots (Figure 6). Based on the above results, we can divide the research process in this field into three parts: 1. ncRNAs as a diagnostic and prognostic marker of ESCC; 2. ncRNAs participates in the occurrence and development of ESCC; 3. the therapeutic potential of ncRNAs on ESCC. The main studied ncRNAs include miRNAs, lncRNAs, and circRNAs.

One of the most promising research parts for ncRNAs in ESCC is its potential as a diagnostic and prognostic biomarker, which has been highly valued since the beginning of research in this field. Compared to normal physiological conditions, the levels of specific ncRNAs produced by cancer cells may undergo significant alterations. The detection of their expression can yield valuable biological information [20]. Furthermore, certain ncRNAs exhibit widespread stability in bodily fluids, such as blood, saliva, and urine [21]. This forms the basis for efficient, non-invasive, and cost-effective detection methods Studies have demonstrated the utility of ncRNAs as prognostic and diagnostic biomarkers for ESCC, with miRNAs being the most well-studied in this regard. For example, studies have shown that high expression of miR-1246, miR-766-3p, miR-20b-5p, and miR-1290 in the serum of ESCC patients has strong diagnostic and prognostic potential [22–25]. Similarly, lncRNAs such as HOTAIR, MALAT1, CCAT2, and PCAT-1, and circRNAs such as circ-SLC7A, circ-SMAD7, circ_000194, and circ-GSK3β, have also been identified as potential diagnostic and prognostic biomarkers for ESCC [15, 26–32]. In addition, there is a study that has taken a step further towards the identification of miRNAs (miRNA-103, miRNA-106b, miRNA-151, miRNA-17, miRNA-181a, miRNA-21, miRNA-2 and miRNA-93) with diagnostic implications in a retrospective and prospective multicenter cohort study. The results demonstrate higher specificity and sensitivity of miRNAs markers compared with traditional tumor markers including SCC Ag, CEA and CYFRA21-1, further confirming the practical significance of serum miRNAs used as diagnostic markers for early-stage ESCC [33].

Another part of research on ncRNAs in ESCC is their role in the initiation and progression of the disease. Studies have shown that ncRNAs can act as tumor promoters or suppressors in ESCC by regulating several biological processes such as proliferation, metastasis, apoptosis, cell cycle, DNA damage repair, and EMT [34–37]. Many miRNAs play a role by binding to the 3′UTR of the target gene, blocking its translation and leading to its inactivation at the mRNA level, or participating in the related pathways of G protein coupled receptors [38–40]. LncRNAs can recruit chromatin remodeling factors or inhibit transcription factors of target gene promoters to exert its effects [41]. Recently, it was found that lncRNAs can regulate the expression of related miRNAs and then participate in the occurrence and development of ESCC. For example, lncRNA FAM83A-AS1 downregulated the expression of miRNA-214, which indirectly deregulated the repression of CDC25B by miRNA-214, and thus participated in ESCC progression [42]. Similarly, circRNAs such as circRUNX1, ciRS-7, and LPAR3 function as ceRNAs of their counterpart miRNAs, contributing to the development of ESCC [4, 43, 44]. The term “ceRNA” refers to the ability of circRNAs to serve as miRNA sponges by sequestering them and inhibiting their regulatory effects on downstream targets, thus exerting their own regulatory roles.

The third part of research on ncRNAs in ESCC is their potential for use in treatment. NcRNAs may be able to improve the efficacy of existing therapies, such as chemotherapy and radiotherapy, or act as novel therapeutic targets. The main chemotherapy regimen for ESCC patients mainly includes cis-diamminedichloro-platinum (CDDP), 5-fluorouracil, and gefitinib. If the patient is not sensitive to these anticancer drugs, it may lead to unsatisfactory treatment effectiveness [45–47]. Studies have shown that high-risk ncRNAs, such as miR-624, miR-140-3P, lncRNA NORAD, lncRNA CASC8, and hsa_circ_0000277, can increase chemotherapy resistance in ESCC patients. Therefore, reversing the expression of high-risk ncRNAs may have a positive effect on reducing chemotherapy resistance, thereby improving treatment efficacy [5, 6, 48–50]. For instance, re-expression of circRNA-cdopey2 decreased the amount of anti-apoptotic protein Mcl-1 expression, which in turn enhanced the apoptosis of ESCC cells and enhanced the killing ability of CDDP on cancer cells [51]. Jin et al. showed that the overexpression of miR-141-3p can promote acquired chemotherapy resistance of 5-fluorouracil by regulating tumor suppressor PTEN [46]. In addition, lncRNAs (such as AFAP1-AS1 and LINC01014) participate in Wnt/β-Catenin and PI3K/Akt/mTOR signaling pathways reduced the effectiveness of chemotherapy drugs including gefitinib [52]. Radiotherapy is a radical treatment modality for ESCC, but studies have found that ncRNAs are involved in the sensitivity of ESCC cells to radiation. Dysregulation of ncRNAs such as miRNA-4443 and miRNA-21 can affect cell cycle, apoptosis, and DNA damage repair, making them potential targets for improving ESCC radiosensitivity [37, 53]. The abundance of miRNA-21 can be decreased by upregulating lncRNA gas5, which further upregulates expression of a transformation repressor named RECK to enhance ESCC cell radiosensitivity [53]. Similarly, circvrk1 was found to be under expressed in ESCC tissues and cell lines compared with controls. Radiation resistance of ESCC cells could be alleviated by overexpression of circvrk1, the mechanism is that circvrk1, as the ceRNA of mir-624-3p, upregulates PTEN and exhibits a role in reducing radiation resistance [54]. In summary, ncRNAs have great potential in the field of ESCC treatment. Unfortunately, as of now, there are no large-scale, high-quality randomized controlled clinical studies to further validate.

With the emergence of new technologies, research on ncRNAs in ESCC has been further explored based on previous research models. For example, relevant research focuses on ncRNAs in exosomes, because as a subgroup of tumor microenvironment, it promotes cell communication by transmitting various biological molecules [55]. Exosomes carrying ncRNAs, due to their stability and widespread presence in body fluids, along with advancements in exosome separation technology, are expected to make the detection of ncRNAs for screening ESCC patients non-invasive, convenient, and efficient [56]. In addition, studies have also focused on the immune landscape related to ncRNAs in ESCC, which will be of great significance in revealing the tumor immune microenvironment. The continuous evolution of research on the immune landscape has given rise to a variety of novel technologies, providing more in-depth and comprehensive insights. These encompass single-cell RNA sequencing, bioinformatics, and machine learning. The integrated application of these emerging technologies enables researchers to gain a more comprehensive and profound understanding of the intricacies of the immune landscape, particularly in relation to ncRNAs [57, 58].

Therefore, it can be said that the study of ncRNAs in ESCC has opened up new avenues for the development of novel diagnostic, prognostic, and therapeutic approaches. Our study can also provide insights into the focus of future studies. On the one hand, future studies can further apply new technologies (e.g., Mendelian randomization and network pharmacology) to explore the role of ncRNAs in ESCC based on current research model. On the other hand, more in-depth studies, especially clinical studies are needed to validate the value of ncRNAs in the practical clinical application of ESCC.

Limitation

Our study utilized bibliometrics to comprehensively analyze the progression of research on ncRNAs associated with ESCC. However, we must be aware of potential limitations. Firstly, considering the completeness and authenticity of the data obtained, we used only the SCIE database to retrieve related articles. Secondly, quality assessment was not conducted due to the large volume of included literature, potentially leading to variations in article quality. Thirdly, due to the unavoidable issue of inconsistent spelling or identical names among authors, the author names automatically extracted by software may differ slightly from the actual situation, and currently, there is no effective method for bulk correction.

Conclusion

In summary, exploring the roles and mechanisms of ncRNAs in ESCC has paved the way for the discovery of novel diagnostic, prognostic, and therapeutic approaches. However, the current research paradigm in this field tends towards homogeneity. Future investigations should focus on providing more nuanced explanations for the functions of ncRNAs, aiming to gain a deeper understanding of its role in ESCC. This involves a concerted effort to translate these findings into clinical research, validating the specificity, sensitivity, and clinical feasibility of ncRNAs in ESCC.

Integrating novel interdisciplinary elements into the existing research framework or shifting the research emphasis from preclinical studies to clinical investigations centered on diagnosis, treatment, and prognosis will likely constitute the primary avenues for breakthroughs in this field.

Data availability statement

The data used in this study comes from published studies, and all data related to the research results are included in the main text. For more information, please consult the corresponding authors.

Author contributions

JW was responsible for the concept and design of the project, as well as the drafting of the manuscript. YW and YC were involved in the acquisition, analysis, and interpretation of the data. LC and LZ provided administrative, technical, and material support throughout the project, and also supervised the overall process. All authors contributed to the article and approved the submitted version.

Funding

This work was supported by the Project of Chengdu Medical College Graduate Innovative Scientific Research Foundation (Grant Nos. YCX2022-01-02 and YCX2023-02-06).

Conflict of interest

The authors declare that the research was conducted in the absence of any commercial or financial relationships that could be construed as a potential conflict of interest.

Acknowledgments

Jingxin Yan provided inspiration to this paper.

Supplementary material

The Supplementary Material for this article can be found online at: https://www.por-journal.com/articles/10.3389/pore.2024.1611595/full#supplementary-material

References

1. Sung H, Ferlay J, Siegel RL, Laversanne M, Soerjomataram I, Jemal A, et al. Global cancer statistics 2020: GLOBOCAN estimates of incidence and mortality worldwide for 36 cancers in 185 countries. *CA: a Cancer J clinicians* (2021) 71(3): 209–49. doi:10.3322/caac.21660

2. Huang J, Koulaouzidis A, Marlicz W, Lok V, Chu C, Ngai CH, et al. Global burden, risk factors, and trends of esophageal cancer: an analysis of cancer registries from 48 countries. *Cancers* (2021) 13(1):141. doi:10.3390/cancers13010141

3. Moore JE, Purcaro MJ, Pratt HE, Epstein CB, Shoresh N, Adrian J, et al. Expanded encyclopaedias of DNA elements in the human and mouse genomes. *Nature* (2020) 583(7818):699–710. doi:10.1038/s41586-020-2493-4

4. Wang C, Zhou M, Zhu P, Ju C, Sheng J, Du D, et al. IGF2BP2-induced circRUNX1 facilitates the growth and metastasis of esophageal squamous cell carcinoma through miR-449b-5p/FOXP3 axis. *J Exp Clin Cancer Res : CR* (2022) 41(1):347. doi:10.1186/s13046-022-02550-8

5. Wu Q, Zhang H, Yang D, Min Q, Wang Y, Zhang W, et al. The m6A-induced lncRNA CASC8 promotes proliferation and chemoresistance via upregulation of hnRNPL in esophageal squamous cell carcinoma. *Int J Biol Sci* (2022) 18(13): 4824–36. doi:10.7150/ijbs.71234

6. Song B, Liu X, Dong H, Roy R. miR-140-3P induces chemotherapy resistance in esophageal carcinoma by targeting the NFYA-MDR1 Axis. *Appl Biochem Biotechnol* (2023) 195(2):973–91. doi:10.1007/s12010-022-04139-5

7. Ninkov A, Frank JR, Maggio LA. Bibliometrics: methods for studying academic publishing. *Perspect Med Educ* (2022) 11(3):173–6. doi:10.1007/s40037-021-00695-4

8. Okubo Y. "Bibliometric indicators and analysis of research systems: methods and examples," in *OECD science, technology and industry working papers*, No. 1997/01. Paris: OECD Publishing (1997). doi:10.1787/208277770603

9. Ge Y, Chao T, Sun J, Liu W, Chen Y, Wang C. Frontiers and hotspots evolution in psycho-cardiology: a bibliometric analysis from 2004 to 2022. *Curr Probl Cardiol* (2022) 47(12):101361. doi:10.1016/j.cpcardiol.2022.101361

10. Ahmad P, Slots J. A bibliometric analysis of periodontology. *Periodontol 2000* (2021) 85(1):237–40. doi:10.1111/prd.12376

11. Hassan W, Zafar M, Duarte AE, Kamdem JP, Teixeira da Rocha JB. Pharmacological Research: a bibliometric analysis from 1989 to 2019. *Pharmacol Res* (2021) 169:105645. doi:10.1016/j.phrs.2021.105645

12. Aria M, Cuccurullo C. bibliometrix: an R-tool for comprehensive science mapping analysis. *J Informetrics* (2017) 11(4):959–75. doi:10.1016/j.joi.2017.08.007

13. Guo Y, Chen Z, Zhang L, Zhou F, Shi S, Feng X, et al. Distinctive microRNA profiles relating to patient survival in esophageal squamous cell carcinoma. *Cancer Res* (2008) 68(1):26–33. doi:10.1158/0008-5472.CAN-06-4418

14. Li CQ, Huang GW, Wu ZY, Xu YJ, Li XC, Xue YJ, et al. Integrative analyses of transcriptome sequencing identify novel functional lncRNAs in esophageal squamous cell carcinoma. *Oncogenesis* (2017) 6(2):e297. doi:10.1038/oncsis.2017.1

15. Fan L, Cao Q, Liu J, Zhang J, Li B. Circular RNA profiling and its potential for esophageal squamous cell cancer diagnosis and prognosis. *Mol Cancer* (2019) 18(1): 16. doi:10.1186/s12943-018-0936-4

16. Su H, Lin F, Deng X, Shen L, Fang Y, Fei Z, et al. Profiling and bioinformatics analyses reveal differential circular RNA expression in radioresistant esophageal cancer cells. *J translational Med* (2016) 14(1):225. doi:10.1186/s12967-016-0977-7

17. Liu H, Zhang Q, Lou Q, Zhang X, Cui Y, Wang P, et al. Differential analysis of lncRNA, miRNA and mRNA expression profiles and the prognostic value of lncRNA in esophageal cancer. *Pathol Oncol Res : POR* (2020) 26(2):1029–39. doi:10.1007/s12253-019-00655-8

18. Wagner CS, Jonkers K. Open countries have strong science. *Nature* (2017) 550(7674):32–3. doi:10.1038/550032a

19. Bol T, de Vaan M, van de Rijt A. The Matthew effect in science funding. *Proc Natl Acad Sci USA* (2018) 115(19):4887–90. doi:10.1073/pnas.1719557115

20. Zhou H, Hao X, Zhang P, He S. Noncoding RNA mutations in cancer. *Wiley Interdiscip Rev RNA* (2023) 14(6):e1812. doi:10.1002/wrna.1812

21. Yan H, Bu P. Non-coding RNA in cancer. *Essays Biochem* (2021) 65(4): 625–39. doi:10.1042/EBC20200032

22. Takeshita N, Hoshino I, Mori M, Akutsu Y, Hanari N, Yoneyama Y, et al. Serum microRNA expression profile: miR-1246 as a novel diagnostic and prognostic biomarker for oesophageal squamous cell carcinoma. *Br J Cancer* (2013) 108(3):644–52. doi:10.1038/bjc.2013.8

23. Liu S, Lin Z, Zheng Z, Rao W, Lin Y, Chen H, et al. Serum exosomal microRNA-766-3p expression is associated with poor prognosis of esophageal

squamous cell carcinoma. *Cancer Sci* (2020) 111(10):3881–92. doi:10.1111/cas.14550

24. Huang Z, Zhang L, Zhu D, Shan X, Zhou X, Qi LW, et al. A novel serum microRNA signature to screen esophageal squamous cell carcinoma. *Cancer Med* (2017) 6(1):109–19. doi:10.1002/cam4.973

25. Sun H, Wang L, Zhao Q, Dai J. Diagnostic and prognostic value of serum miRNA-1290 in human esophageal squamous cell carcinoma. *Cancer biomarkers : section A Dis markers* (2019) 25(4):381–7. doi:10.3233/CBM-190007

26. Chen FJ, Sun M, Li SQ, Wu QQ, Ji L, Liu ZL, et al. Upregulation of the long non-coding RNA HOTAIR promotes esophageal squamous cell carcinoma metastasis and poor prognosis. *Mol carcinogenesis* (2013) 52(11):908–15. doi:10.1002/mc.21944

27. Cao X, Zhao R, Chen Q, Zhao Y, Zhang B, Zhang Y, et al. MALAT1 might be a predictive marker of poor prognosis in patients who underwent radical resection of middle thoracic esophageal squamous cell carcinoma. *Cancer biomarkers : section A Dis markers* (2015) 15(6):717–23. doi:10.3233/CBM-150513

28. Zhang X, Xu Y, He C, Guo X, Zhang J, He C, et al. Elevated expression of CCAT2 is associated with poor prognosis in esophageal squamous cell carcinoma. *J Surg Oncol* (2015) 111(7):834–9. doi:10.1002/jso.23888

29. Shi WH, Wu QQ, Li SQ, Yang TX, Liu ZH, Tong YS, et al. Upregulation of the long noncoding RNA PCAT-1 correlates with advanced clinical stage and poor prognosis in esophageal squamous carcinoma. *Tumour Biol : J Int Soc Oncodevelopmental Biol Med* (2015) 36(4):2501–7. doi:10.1007/s13277-014-2863-3

30. Huang E, Fu J, Yu Q, Xie P, Yang Z, Ji H, et al. CircRNA hsa_circ_0004771 promotes esophageal squamous cell cancer progression via miR-339-5p/CDC25A axis. *Epigenomics* (2020) 12(7):587–603. doi:10.2217/epi-2019-0404

31. Zhang Y, Wang Q, Zhu D, Rong J, Shi W, Cao X. Up-regulation of circ-SMAD7 inhibits tumor proliferation and migration in esophageal squamous cell carcinoma. *Biomed Pharmacother* (2019) 111:596–601. doi:10.1016/j.biopha.2018.12.116

32. Hu X, Wu D, He X, Zhao H, He Z, Lin J, et al. circGSK3β promotes metastasis in esophageal squamous cell carcinoma by augmenting β-catenin signaling. *Mol Cancer* (2019) 18(1):160. doi:10.1186/s12943-019-1095-y

33. Miyoshi J, Zhu Z, Luo A, Toden S, Zhou X, Izumi D, et al. A microRNA-based liquid biopsy signature for the early detection of esophageal squamous cell carcinoma: a retrospective, prospective and multicenter study. *Mol Cancer* (2022) 21(1):44. doi:10.1186/s12943-022-01507-x

34. Qiao G, Dai C, He Y, Shi J, Xu C. Effects of miR-106b-3p on cell proliferation and epithelial-mesenchymal transition, and targeting of ZNRF3 in esophageal squamous cell carcinoma. *Int J Mol Med* (2019) 43(4):1817–29. doi:10.3892/ijmm.2019.4107

35. Guo Y, Sun P, Guo W, Yin Q, Han J, Sheng S, et al. LncRNA DDX11 antisense RNA 1 promotes EMT process of esophageal squamous cell carcinoma by sponging miR-30d-5p to regulate SNAI1/ZEB2 expression and Wnt/β-catenin pathway. *Bioengineered* (2021) 12(2):11425–40. doi:10.1080/21655979.2021.2008759

36. Gu L, Sang Y, Nan X, Zheng Y, Liu F, Meng L, et al. circCYP24A1 facilitates esophageal squamous cell carcinoma progression through binding PKM2 to regulate NF-κB-induced CCL5 secretion. *Mol Cancer* (2022) 21(1):217. doi:10.1186/s12943-022-01686-7

37. Shi X, Liu X, Huang S, Hao Y, Pan S, Ke Y, et al. miR-4443 promotes radiation resistance of esophageal squamous cell carcinoma via targeting PTPRJ. *J translational Med* (2022) 20(1):626. doi:10.1186/s12967-022-03818-5

38. Lu HB. MicroRNA-556-3p promotes the progression of esophageal cancer via targeting DAB2IP. *Eur Rev Med Pharmacol Sci* (2018) 22(20):6816–23. doi:10.26355/eurrev_201810_16149

39. Tan X, Ren S, Fu MZ, Ren S, Yang C, Wu X, et al. microRNA-196b promotes esophageal squamous cell carcinogenesis and chemoradioresistance by inhibiting EPHA7, thereby restoring EPHA2 activity. *Am J Cancer Res* (2021) 11(7):3594–610.

40. Xu C, Li B, Zhao S, Jin B, Jia R, Ge J, et al. MicroRNA-186-5p inhibits proliferation and metastasis of esophageal cancer by mediating HOXA9. *OncoTargets Ther* (2019) 12:8905–14. doi:10.2147/OTT.S227920

41. Wang N, Yu Y, Xu B, Zhang M, Li Q, Miao L. Pivotal prognostic and diagnostic role of the long non-coding RNA colon cancer-associated transcript 1 expression in human cancer (Review). *Mol Med Rep* (2019) 19(2):771–82. doi:10.3892/mmr.2018.9721

42. Jia J, Li H, Chu J, Sheng J, Wang C, Jia Z, et al. LncRNA FAM83A-AS1 promotes ESCC progression by regulating miR-214/CDC25B axis. *J Cancer* (2021) 12(4):1200–11. doi:10.7150/jca.54007

43. Sang M, Meng L, Sang Y, Liu S, Ding P, Ju Y, et al. Circular RNA ciRS-7 accelerates ESCC progression through acting as a miR-876-5p sponge to enhance MAGE-A family expression. *Cancer Lett* (2018) 426:37–46. doi:10.1016/j.canlet.2018.03.049

44. Shi Y, Fang N, Li Y, Guo Z, Jiang W, He Y, et al. Circular RNA LPAR3 sponges microRNA-198 to facilitate esophageal cancer migration, invasion, and metastasis. *Cancer Sci* (2020) 111(8):2824–36. doi:10.1111/cas.14511

45. Toshimitsu H, Hashimoto K, Tangoku A, Iizuka N, Yamamoto K, Kawauchi S, et al. Molecular signature linked to acquired resistance to cisplatin in esophageal cancer cells. *Cancer Lett* (2004) 211(1):69–78. doi:10.1016/j.canlet.2004.01.038

46. Jin YY, Chen QJ, Xu K, Ren HT, Bao X, Ma YN, et al. Involvement of microRNA-141-3p in 5-fluorouracil and oxaliplatin chemo-resistance in esophageal cancer cells via regulation of PTEN. *Mol Cell Biochem* (2016) 422(1-2):161–70. doi:10.1007/s11010-016-2816-9

47. Zhu H, Du F, Cao C. Restoration of circPSMC3 sensitizes gefitinib-resistant esophageal squamous cell carcinoma cells to gefitinib by regulating miR-10a-5p/PTEN axis. *Cel Biol Int* (2021) 45(1):107–16. doi:10.1002/cbin.11473

48. Jia Y, Tian C, Wang H, Yu F, Lv W, Duan Y, et al. Long non-coding RNA NORAD/miR-224-3p/MTDH axis contributes to CDDP resistance of esophageal squamous cell carcinoma by promoting nuclear accumulation of β-catenin. *Mol Cancer* (2021) 20(1):162. doi:10.1186/s12943-021-01455-y

49. Yan J, Shi L, Lin S, Li Y. MicroRNA-624-mediated ARRDC3/YAP/HIF1α axis enhances esophageal squamous cell carcinoma cell resistance to cisplatin and paclitaxel. *Bioengineered* (2021) 12(1):5334–47. doi:10.1080/21655979.2021.1938497

50. Cheng J, Zhang R, Yan M, Li Y. Circular RNA hsa_circ_0000277 promotes tumor progression and DDP resistance in esophageal squamous cell carcinoma. *BMC cancer* (2022) 22(1):238. doi:10.1186/s12885-022-09241-9

51. Liu Z, Gu S, Wu K, Li L, Dong C, Wang W, et al. CircRNA-DOPEY2 enhances the chemosensitivity of esophageal cancer cells by inhibiting CPEB4-mediated Mcl-1 translation. *J Exp Clin Cancer Res : CR* (2021) 40(1):361. doi:10.1186/s13046-021-02149-5

52. Sharma U, Murmu M, Barwal TS, Tuli HS, Jain M, Prakash H, et al. A pleiotropic role of long non-coding RNAs in the modulation of wnt/β-catenin and PI3K/Akt/mTOR signaling pathways in esophageal squamous cell carcinoma: implication in chemotherapeutic drug response. *Curr Oncol (Toronto, Ont)* (2022) 29(4):2326–49. doi:10.3390/curroncol29040189

53. Lin J, Liu Z, Liao S, Li E, Wu X, Zeng W. Elevation of long non-coding RNA GAS5 and knockdown of microRNA-21 up-regulate RECK expression to enhance esophageal squamous cell carcinoma cell radio-sensitivity after radiotherapy. *Genomics* (2020) 112(3):2173–85. doi:10.1016/j.ygeno.2019.12.013

54. He Y, Mingyan E, Wang C, Liu G, Shi M, Liu S. CircVRK1 regulates tumor progression and radioresistance in esophageal squamous cell carcinoma by regulating miR-624-3p/PTEN/PI3K/AKT signaling pathway. *Int J Biol macromolecules* (2019) 125:116–23. doi:10.1016/j.ijbiomac.2018.11.273

55. Yao W, Jia X, Zhu L, Xu L, Zhang Q, Xia T, et al. Exosomal circ_0026611 contributes to lymphangiogenesis by reducing PROX1 acetylation and ubiquitination in human lymphatic endothelial cells (HLECs). *Cell Mol Biol Lett* (2023) 28(1):13. doi:10.1186/s11658-022-00410-z

56. Zhao L, Yu L, Wang X, He J, Zhu X, Zhang R, et al. Mechanisms of function and clinical potential of exosomes in esophageal squamous cell carcinoma. *Cancer Lett* (2023) 553:215993. doi:10.1016/j.canlet.2022.215993

57. Zhao F, Li Z, Dong Z, Wang Z, Guo P, Zhang D, et al. Exploring the potential of exosome-related LncRNA pairs as predictors for immune microenvironment, survival outcome, and microbiotain landscape in esophageal squamous cell carcinoma. *Front Immunol* (2022) 13:918154. doi:10.3389/fimmu.2022.918154

58. Zheng Y, Chen Z, Han Y, Han L, Zou X, Zhou B, et al. Immune suppressive landscape in the human esophageal squamous cell carcinoma microenvironment. *Nat Commun* (2020) 11(1):6268. doi:10.1038/s41467-020-20019-0

Pathology & Oncology Research | frontiers

TYPE Brief Research Report
PUBLISHED 07 February 2023
DOI 10.3389/pore.2023.1610909

Check for updates

OPEN ACCESS

EDITED BY
Andrea Ladányi,
National Institute of Oncology (NIO), Hungary

REVIEWED BY
Tamás Micsik,
Semmelweis University, Hungary
János Tibor Fekete,
Semmelweis University, Hungary

*CORRESPONDENCE
Lining Wang,
wanglining1001@126.com

†These authors have contributed equally to this work

RECEIVED 30 October 2022
ACCEPTED 26 January 2023
PUBLISHED 07 February 2023

CITATION
Kong L, Yang M, Wan Z and Wang L (2023), Cohort size required for prognostic genes analysis of stage II/III esophageal squamous cell carcinoma. *Pathol. Oncol. Res.* 29:1610909. doi: 10.3389/pore.2023.1610909

COPYRIGHT
© 2023 Kong, Yang, Wan and Wang. This is an open-access article distributed under the terms of the Creative Commons Attribution License (CC BY). The use, distribution or reproduction in other forums is permitted, provided the original author(s) and the copyright owner(s) are credited and that the original publication in this journal is cited, in accordance with accepted academic practice. No use, distribution or reproduction is permitted which does not comply with these terms.

Cohort size required for prognostic genes analysis of stage II/III esophageal squamous cell carcinoma

Linghong Kong[1†], Ming Yang[2†], Zhiyi Wan[1] and Lining Wang[1*]

[1]Department of Pathology, Beijing Chuiyangliu Hospital, Beijing, China, [2]Hepato-Pancreato-Biliary Center, Beijing Tsinghua Changgung Hospital, School of Clinical Medicine, Tsinghua University, Beijing, China

Background: Few overlaps between prognostic biomarkers are observed among different independently performed genomic studies of esophageal squamous cell carcinoma (ESCC). One of the reasons for this is the insufficient cohort size. How many cases are needed to prognostic genes analysis in ESCC?

Methods: Here, based on 387 stage II/III ESCC cases analyzed by whole-genome sequencing from one single center, effects of cohort size on prognostic genes analysis were investigated. Prognostic genes analysis was performed in 100 replicates at each cohort size level using a random resampling method.

Results: The number of prognostic genes followed a power-law increase with cohort size in ESCC patients with stage II and stage III, with exponents of 2.27 and 2.25, respectively. Power-law curves with increasing events number were also observed in stage II and III ESCC, respectively, and they almost overlapped. The probability of obtaining statistically significant prognostic genes shows a logistic cumulative distribution function with respect to cohort size. To achieve a 100% probability of obtaining statistically significant prognostic genes, the minimum cohort sizes required in stage II and III ESCC were approximately 95 and 60, respectively, corresponding to a number of outcome events of 33 and 36, respectively.

Conclusion: In summary, the number of prognostic genes follows a power-law growth with the cohort size or events number in ESCC. The minimum events number required to achieve a 100% probability of obtaining a statistically significant prognostic gene is approximately 35.

KEYWORDS

esophageal squamous cell carcinoma, prognostic genes analysis, power-law, events number, cohort size

Background

Esophageal squamous cell carcinoma (ESCC) is the most common histologic subtype of esophageal cancer and characterized by a high degree of clinical and genetic heterogeneity [1–3]. A reliable set of prognostic genes will contribute to a better understanding of the molecular mechanisms of ESCC progression and is crucial to guide clinical management. With the development of high-throughput sequencing technology, whole-exome sequencing (WES) or whole-genome sequencing (WGS) has been widely used for prognostic markers analysis in ESCC [4–11]. Over 1,000 ESCC exomes have been sequenced in the past years, however, little overlap between prognostic genes has been seen in the different ESCC studies [4–11]. The most straightforward explanation for this phenomenon is usually attributed to the fact that the cohorts used in different studies differed in certain potentially relevant factors (such as stage, gender, and genetic context). However, sample size is also an important influencing factor [12].

Somatic mutations have been detected in the coding regions of approximately 14,000 genes in ESCC, of which 65 genes showed mutation frequency of >5% [8]. In prognostic survival analysis, the number of outcome events should be sufficient relative to predictors [13]. For the identification of prognosis-related genes, the cohort size should be larger than the number of mutated genes. However, the cohort size for different genomic studies in ESCC is usually in the tens to hundreds. In addition, the number of outcome events is also an important factor for prognostic genes analysis. The statistical power of survival analysis actually depends on the number of outcome events rather than the total cohort size [14, 15].

Here, our aim is to define how many cases are needed to identify prognosis-related genes in ESCC? To exclude other influencing factors, such as genetic context, follow-up time, and staging, we have focused here on a single ESCC dataset from one center and investigated the effect of cohort size on prognostic genes using random resampling methods.

Methods

Study data

Somatic mutation data and clinical information of ESCC cases were obtained from the published study [8]. Of the patients, a total of 222 ESCC patients with stage II and 165 ESCC patients with stage III from one center had overall survival (OS) data and were selected for further analysis. The median follow-up time for stage II and III patients was 34 and 27 months, respectively. The number of OS outcome events for stage II and III patients was 77 and 99, respectively.

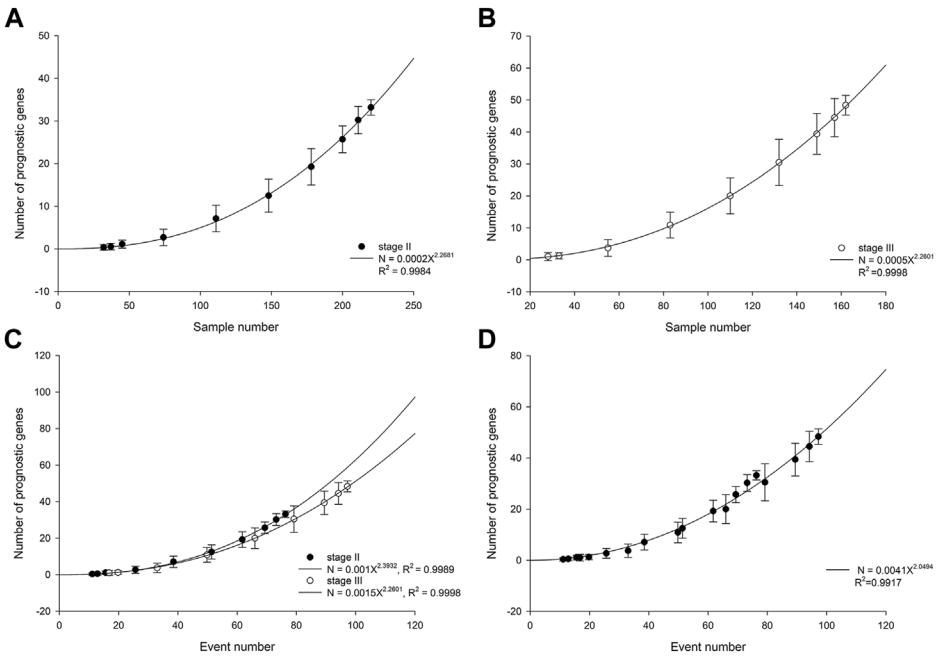

FIGURE 1
Number of prognostic genes increases with cohort size in stage II ESCC **(A)** and stage III ESCC **(B)**. The lines are best-fit results for power-law growth $N = 0.0002X^{2.2681}$ in stage II ESCC and $N = 0.0005X^{2.2601}$ in stage III ESCC, respectively. **(C)** Number of prognostic genes increases with events number. The lines are best-fit results for power-law growth $N = 0.001X^{2.3932}$ in stage II ESCC and $N = 0.0015X^{2.2601}$ in stage III ESCC, respectively. **(D)** Mixing data from stage II and stage III, simulated number of prognostic genes increases with events number. The line is best-fit result for power-law growth $N = 0.0041X^{2.0494}$.

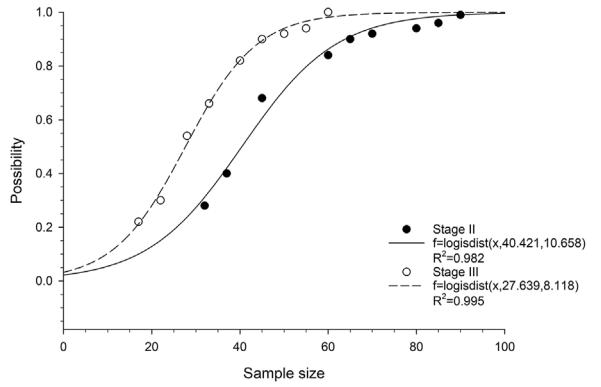

FIGURE 2
Correlation between probability of obtaining at least one prognostic gene and cohort size in ESCC patients. The fitted curves are based on logistic cumulative distribution functions.

Prognostic genes analysis

Random resampling was performed by randomly selecting n cases in the dataset of stage II patients and the dataset of stage III patients, respectively. The cohort size n ranged from 1/7%–95% of all cases, with each cohort size being randomly sampled 100 times. Predictive analyses for prognostic genes associated with OS were also repeatedly performed 100 times for each cohort size level using the "maftools" package [16]. Survival analyses were determined using the Kaplan-Meier method and compared by the log-rank test. Differential genes with $p < 0.05$ were considered significant.

Statistical analysis

Statistical analysis was carried out using SPSS 22.0 software (SPSS, Inc., Chicago, IL, United States) or R statistical software (v4.1.0; R Core Team 2021). All results were presented as means ± standard error.

Results

In patients with stage II ESCC, the number of statistically significant prognostic genes increased with cohort size in a power-law with an exponent of 2.27 (Figure 1A). The power-law growth curve was also observed in patients with stage III ESCC and was generally consistent with the growth exponent of patients with stage II ESCC (Figure 1B). We further analyzed the relationship between the number of prognostic genes and the number of outcome events. Power-law growth curves were observed again for stage II and stage III ESCC, respectively, and they almost overlapped (Figure 1C). We then simulated and analyzed the relationship between the number of prognostic genes and the events number by mixing data from stage II and stage III ESCC. The best-fit curve also conformed to the power-law growth with R^2 of 0.9917 (Figure 1D).

We then analyzed the probability of obtaining at least one statistically significant prognostic gene in relation to cohort size. Logistic cumulative distribution curves were observed in both stage II and stage III ESCC patients (Figure 2). To achieve a 90% probability of obtaining statistically at least one statistically significant prognostic gene, the minimum cohort sizes required for stage II and III ESCC were approximately 65 and 45, respectively (Figure 2), which correspond to a number of events of 23 and 27, respectively. To achieve a 100% probability of obtaining at least one statistically significant prognostic gene, the minimum cohort sizes required for stage II and III ESCC were approximately 95 and 60, respectively (Figure 2), which correspond to a number of events of 33 and 36, respectively.

Discussion

Prognosis is one of the core principles of medical practice. A number of studies have been conducted on the prediction of OS in ESCC based on WGS or WES [4–11]. However, few studies investigate the cohort size needed for prognostic genes studies. The prognostic genes identified by different studies showed very little overlap [4–11]. One reason is the inadequate cohort size. In this paper, we focused on a single ESCC dataset from one center and investigated the effect of cohort size on prognostic genes using random resampling methods. This cohort is the largest ESCC cohort to date from a single clinical center and includes 437 ESCC cases from Han population of Shanxi, China [8]. This cohort nicely excludes the interference of genetic background differences. A total of 387 patients with stage II/III ESCC were enrolled in the study after verification of clinical information.

In both stage II and stage III ESCC patients, the number of prognostic genes showed a power-law relationship with increasing cohort size, although the specific parameters of the formula differed. However, prognostic analysis is based on time-to-event data [17]. The events number is more critical than cohort size in prognostic analysis. Relative to the events number, the growth curves of the number of prognostic genes in patients with stage II and stage III ESCC largely overlapped. Although the cohort sizes required for prognostic genes analysis of stage II and stage III ESCC are different, the number of outcome events required is essentially the same. These results indicated that the power-law growth of the number of prognostic genes with cohort size is common in ESCC, independent of stage.

Prognostic studies are usually retrospective and cohort sizes are rarely considered prior to analysis [18]. However, the prognostic genes obtained on limited data are nothing but misleading. Our results showed that at least 35 outcome events are required in ESCC to ensure the acquisition of statistically significant prognostic genes.

A limitation of this study is that the number of ESCC patients from one center (99 outcome events) is still insufficient, resulting in the plateau in the number of prognostic genes not reached. Enrolling more patients will detect more mutated genes, thereby increasing the number of prognostic genes. However, theoretically there should be a plateau in the number of prognostic genes. The number of cases or events needed to reach this plateau still needs to be further explored.

Conclusion

In summary, the number of prognostic genes takes a power-law growth with cohort size in ESCC. Our results suggest that at least 35 outcome events are required for genomic mutation-based prognostic studies in ESCC. These results will help to the trial design of prognostic genes analysis in ESCC.

Data availability statement

The original contributions presented in the study are included in the article/supplementary material, further inquiries can be directed to the corresponding author.

Ethics statement

The original data analyzed in this study are publicly available and come from the published study (PMID: 32398863). Ethical review and approval were not required for the study on human participants in accordance with the local legislation and institutional requirements. This study did not require informed consent for participation in accordance with the national legislation and institutional requirements.

Author contributions

LW conceived the study and reviewed the manuscript. LK, MY, and ZW contributed to data collection and statistical analysis. LK and MY drafted the manuscript. All authors read and approved the final manuscript.

Conflict of interest

The authors declare that the research was conducted in the absence of any commercial or financial relationships that could be construed as a potential conflict of interest.

References

1. Lam AK. Molecular biology of esophageal squamous cell carcinoma. *Crit Rev Oncol Hematol* (2000) 33:71–90. doi:10.1016/s1040-8428(99)00054-2

2. Arnal MJD, Arenas ÁF, Arbeloa ÁL. Esophageal cancer: Risk factors, screening and endoscopic treatment in Western and Eastern countries. *World J Gastroenterol* (2015) 21:7933–43. doi:10.3748/wjg.v21.i26.7933

3. Lin DC, Wang MR, Koeffler HP. Genomic and epigenomic aberrations in esophageal squamous cell carcinoma and implications for patients. *Gastroenterology* (2018) 154:374–89. doi:10.1053/j.gastro.2017.06.066

4. Lin DC, Hao JJ, Nagata Y, Xu L, Shang L, Meng X, et al. Genomic and molecular characterization of esophageal squamous cell carcinoma. *Nat Genet* (2014) 46: 467–73. doi:10.1038/ng.2935

5. Gao YB, Chen ZL, Li JG, Hu XD, Shi XJ, Sun ZM, et al. Genetic landscape of esophageal squamous cell carcinoma. *Nat Genet* (2014) 46:1097–102. doi:10.1038/ng.3076

6. The Cancer Genome Atlas Research Network. Integrated genomic characterization of oesophageal carcinoma. *Nature* (2017) 541:169–75. doi:10.1038/nature20805

7. Moody S, Senkin S, Islam SMA, Wang J, Nasrollahzadeh D, Cortez Cardoso Penha R, et al. Mutational signatures in esophageal squamous cell carcinoma from eight countries with varying incidence. *Nat Genet* (2021) 53:1553–63. doi:10.1038/s41588-021-00928-6

8. Cui Y, Chen H, Xi R, Cui H, Zhao Y, Xu E, et al. Whole-genome sequencing of 508 patients identifies key molecular features associated with poor prognosis in esophageal squamous cell carcinoma. *Cell Res* (2020) 30:902–13. doi:10.1038/s41422-020-0333-6

9. Song Y, Li L, Ou Y, Gao Z, Li E, Li X, et al. Identification of genomic alterations in oesophageal squamous cell cancer. *Nature* (2014) 509:91–5. doi:10.1038/nature13176

10. Sawada G, Niida A, Uchi R, Hirata H, Shimamura T, Suzuki Y, et al. Genomic landscape of esophageal squamous cell carcinoma in a Japanese population. *Gastroenterology* (2016) 150:1171–82. doi:10.1053/j.gastro.2016.01.035

11. Zhang N, Shi J, Shi X, Chen W, Liu J. Mutational characterization and potential prognostic biomarkers of Chinese patients with esophageal squamous cell carcinoma. *Onco Targets Ther* (2020) 13:12797–809. doi:10.2147/OTT.S275688

12. Ein-Dor L, Kela I, Getz G, Givol D, Domany E. Outcome signature genes in breast cancer: Is there a unique set? *Bioinformatics* (2005) 21:171–8. doi:10.1093/bioinformatics/bth469

13. Riley RD, Snell KI, Ensor J, Burke DL, Harrell FE, Jr, Moons KG, et al. Minimum sample size for developing a multivariable prediction model: PART II - binary and time-to-event outcomes. *Stat Med* (2019) 38:1276–96. doi:10.1002/sim.7992

14. Schober P, Vetter TR. Survival analysis and interpretation of time-to-event data: The tortoise and the hare. *Anesth Analg* (2018) 127:792–8. doi:10.1213/ANE.0000000000003653

15. In J, Lee DK. Survival analysis: Part II - applied clinical data analysis. *Korean J Anesthesiol* (2019) 72:441–57. doi:10.4097/kja.19183

16. Mayakonda A, Lin DC, Assenov Y, Plass C, Koeffler HP. Maftools: Efficient and comprehensive analysis of somatic variants in cancer. *Genome Res* (2018) 28: 1747–56. doi:10.1101/gr.239244.118

17. Moons KG, Royston P, Vergouwe Y, Grobbee DE, Altman DG. Prognosis and prognostic research: What, why, and how? *Bmj* (2009) 338:b375. doi:10.1136/bmj.b375

18. Jinks RC, Royston P, Parmar MK. Discrimination-based sample size calculations for multivariable prognostic models for time-to-event data. *BMC Med Res Methodol* (2015) 15:82. doi:10.1186/s12874-015-0078-y

Pathology & Oncology Research | frontiers

TYPE Original Research
PUBLISHED 03 July 2023
DOI 10.3389/pore.2023.1611114

Check for updates

OPEN ACCESS

EDITED BY
Judit Kocsis,
Bács-Kiskun Megyei Kórház, Hungary

*CORRESPONDENCE
Shenzha Liu,
zhazha.liu.md@hotmail.com
Min Tao,
taomin@suda.edu.cn

RECEIVED 13 February 2023
ACCEPTED 21 June 2023
PUBLISHED 03 July 2023

CITATION
Han G, Sun C, Cui L, Huang Y, Yu L, Liu S and Tao M (2023), Efficacy of the low dose apatinib plus deep hyperthermia as third-line or later treatment in HER-2 negative advanced gastric cancer. *Pathol. Oncol. Res.* 29:1611114. doi: 10.3389/pore.2023.1611114

COPYRIGHT
© 2023 Han, Sun, Cui, Huang, Yu, Liu and Tao. This is an open-access article distributed under the terms of the Creative Commons Attribution License (CC BY). The use, distribution or reproduction in other forums is permitted, provided the original author(s) and the copyright owner(s) are credited and that the original publication in this journal is cited, in accordance with accepted academic practice. No use, distribution or reproduction is permitted which does not comply with these terms.

Efficacy of the low dose apatinib plus deep hyperthermia as third-line or later treatment in HER-2 negative advanced gastric cancer

Guohu Han[1,2], Changchun Sun[2], Lihua Cui[2], Yufeng Huang[2], Lijiang Yu[2], Shenzha Liu[2]* and Min Tao[1,3]*

[1]Department of Oncology, Dushu Lake Hospital Affiliated to Soochow University, Suzhou, Jiangsu, China, [2]Department of Oncology, Jingjiang People's Hospital, The Seventh Affiliated Hospital of Yangzhou University, Jingjiang, Jiangsu, China, [3]Department of Oncology, The First Affiliated Hospital of Soochow University, Suzhou, Jiangsu, China

Aim: To observe the efficacy of the low dose apatinib plus deep hyperthermia as third-line or later treatment for patients with human epidermal growth factor receptor 2 (HER-2) negative advanced gastric cancer.

Methods: 80 eligible patients with HER-2 negative advanced gastric cancer admitted to Jingjiang People's Hospital Affiliated with Yangzhou University-from March 2021 to March 2022 were selected, and they were divided into the control group (n = 40, apatinib) and experimental group (n = 40, apatinib plus deep hyperthermia) on the basis of random number table method. The levels of serum carcinoembryonic antigen (CEA), carbohydrate antigen 199 (CA199), and vascular endothelial growth factor (VEGF) were monitored, and the efficacy of the two groups was analyzed by referring to Karnofsky performance status (KPS), overall survival (OS) and disease control rate (DCR) before and after treatment.

Results: The levels of CEA, CA199, and VEGF in both groups were lower after treatment than before ($p < 0.05$), and lower (CEA: 8.85 ± 1.36 vs. 12.87 ± 1.23, CA199: 34.19 ± 4.68 vs. 50.11 ± 5.73, VEGF: 124.8 ± 18.03 vs. 205.9 ± 19.91) in the experimental group than in the control group ($p < 0.05$). The DCR and KPS of the patients in the experimental group were significantly higher (DCR: 62.50% vs. 40.00%; KPS: 83.25 ± 1.15 vs. 76.25 ± 1.17) than in the control group ($p < 0.05$). In survival analysis, patients with control group had shorter OS than the experimental group. (median 5.65 vs. 6.50 months; hazard ratio [HR], 1.63 [95% confidence interval (CI) 1.02–2.60], p = 0.0396).

Conclusion: The application of low-dose apatinib plus deep hyperthermia for patients with HER-2 negative gastric cancer who failed second-line treatment should be a promising option.

KEYWORDS
apatinib, deep hyperthermia, gastric cancer, efficacy evaluation, prognosis

Introduction

Advanced gastric cancer is one of the common malignant tumors in the gastrointestinal tract or gastrointestinum, which presents a high mortality rate and poses a threat to human public health [1–3]. The absolute majority of patients have entered the advanced stage and lost the opportunity for surgery once diagnosed, and it is difficult to treat [4, 5]. For these patients, the first- and second-line treatment is mainly based on platinum, fluorouracil, and taxane-based chemotherapy [6]. However, due to the low efficacy and side effects of chemotherapy, researchers have been considering trying new drugs. Under such a circumstance, apatinib is a novel antiangiogenic agent that can highly selectively inhibit vascular endothelial growth factor (VEGF) receptor and block tumor angioneogenesis to achieve antitumor effect [7].

In recent years, deep hyperthermia as a new type of antitumor treatment has gradually become another tumor treatment method after surgery, chemotherapy, and targeted therapy [8]. Because of its safety, effectiveness and low adverse reactions, it may produce synergistic effects when added to conventional therapy [8, 9]. However, no studies have definitively determined the efficacy of deep hyperthermia and apatinib in advanced gastric cancer. In the present study, we intend to explore the therapeutic effect to provide references for patients with human epidermal growth factor receptor 2 (HER-2) negative gastric cancer who have failed second-line treatment.

Materials and methods

Baseline data

80 patients with HER-2 negative gastric cancer who had failed second-line treatment in our hospital from March 2021 to March 2022 were selected and were divided into two groups. Before enrollment, all the clinical baseline information of patients was relatively balanced in terms of sex, age, site of primary tumor, histology and number of prior chemotherapy regimens between the two groups (all $p > 0.05$), as shown in Table 1. This study had been approved by the Ethics Committee of Jingjiang People's Hospital Affiliated with Yangzhou University (No. 2021-03-029). All subjects in this study provided their written informed consent consistent with the Declaration of Helsinki.

Inclusion and exclusion criteria

Inclusion criteria were as follows: [1] patients confirmed to have HER-2 negative advanced gastric cancer, and the metastatic disease was confirmed by clinical, imaging, histological, or cytological measures. [2] patients who failed after second-line treatment [3], patients with expected survival time greater than 3 months [4], patients with sound heart, lung, liver and kidney functions [5], patients with no second primary tumor, and [6] patients who

TABLE 1 Baseline patient characteristics (n (%)).

Characteristic	Control group (n = 40)	Experimental group (n = 40)	χ^2	P
Sex				
Male	25 (62.50%)	28 (70.00%)	0.503	0.478
Female	15 (37.50%)	12 (30.00%)		
Age (years)				
<65	23 (57.50%)	21 (52.50%)	0.202	0.653
≥65	17 (42.50%)	19 (47.50%)		
Site of primary tumor				
Fundus	9 (22.50%)	6 (15.00%)	1.533	0.675
Body	9 (22.50%)	11 (27.50%)		
Antrum	16 (40.00%)	14 (35.00%)		
Cardia	6 (15.00%)	9 (22.50%)		
Histology				
Well differentiated	0 (0.00%)	1 (2.50%)	1.671	0.434
Moderately differentiated	21 (52.50%)	24 (60.00%)		
Poorly differentiated	19 (47.50%)	15 (37.50%)		
Number of prior chemotherapy regimens				
2	29 (72.50%)	31 (77.50%)	0.267	0.606
≥3	11 (27.50%)	9 (22.50%)		

TABLE 2 Karnofsky performance status.

Conditions	Percentage	Comments
A: Able to perform normal daily activities and work. No special care is necessary	100	Normal, without symptoms or signs of disease
	90	Ability to perform normal daily activities, minor symptoms or signs of disease
	80	perform normal daily activities with some effort, some symptoms or signs of disease
B: Ability to live at home and take care of most personal needs. Assistance is needed to varying degrees	70	Can take care of self, unable to do work or maintain normal daily activities. Such as cooking, playing football, and driving a car
	60	Can take care of self the most of the time, but occasionally required considerable assistance
	50	Required considerable assistance frequently
C: Unable to take care of self. Hospital care is required. Disease can advance rapidly	40	Disabled, requires medical care and assistance, in bed ≥50% of the time
	30	Seriously disabled, unable to take care of themselves, almost always in bed
	20	Seriously bedfast, hospitalization necessary, requiring active supportive treatment
	10	Moribund, comatose or difficult to wake up
	0	Dead

TABLE 3 Comparison of serum CEA expression level (mean ± standard deviation).

Groups	*n*	Before treatment	After treatment	*T*	*P*
Control group	40	15.79 ± 0.81	12.87 ± 1.23	2.818	0.008
Experimental group	40	16.58 ± 1.14	8.85 ± 1.36	3.538	0.001
t		0.569	2.199		
P		0.571	0.031		

Note: CEA, carcinoembryonic antigen (μg/L).

voluntarily provided informed consent. Exclusion criteria were as follows: [1] patients with hypertension (systolic blood pressure>140 mm Hg, diastolic blood pressure>90 mm Hg) that could not be reduced to the normal range by antihypertensive drug treatment [2], patients with coagulation dysfunction [3], patients with disease [4], patients who did not coordinate with clinical follow-up [5], patients with a clear tendency to gastrointestinal bleeding, and [6] patients with incomplete clinical and pathological data.

Treatment methods

Control group: patients received 250 mg/d of apatinib (Jiangsu Hengrui Medicine Co., Ltd., SFDA approval No. H20140103, 0.25 g) orally. Experimental group: on the basis of apatinib regimen in the control group, patients received deep hyperthermia (Nanjing Hengpu Weiye Technology Co., LTD, NO. HY7000-1). The method of deep hyperthermia: before hyperthermia, the location and size of the tumor should be determined according to the results of CT, B-ultrasound or MRI examination. The tumor should be taken as the central point for positioning, appropriate plate and body position should be selected, and water bags with appropriate size and temperature should be selected according to the individual situation of the patient. The patient was supine. After adjusting the position, a water bag was placed on the skin of the corresponding treatment site (covering the treatment site), and the plate was lowered to make it close to the water bag. The treatment was carried out under the computer monitoring. Deep hyperthermia device with a power of 400–800 W for twice a week, and a preset temperature of 42°C–43°C, and each treatment lasted for 30 min, and each deep hyperthermia was performed within 1 h after oral apatinib. Antitumor treatment was 8 consecutive weeks long.

Outcome measures

Tumor biomarkers determination: Sera were obtained through centrifuging fasting venous blood, employing an automatic electrochemiluminometer E170® and assorted kits (Roche™, Switzerland). Serum free vascular epidermal growth factor (VEGF) was detected by ELISA kit (R&D Systems Inc., Minneapolis, MN, USA) according to the instructions. References ranged as follows: CEA <3.5 ng/mL, CA199 <39 U/Ml, VEGF: 6.25–142.2 pg/mL.

The efficacy was assessed by referring to Response Evaluation Criteria In Solid Tumors (RECIST) [6]. Complete remission (CR): all targeted lesions disappeared without new ones were found for more than 1 month; partial remission (PR): the total diameter of the target

TABLE 4 Comparison of serum CA199 expression level (mean ± standard deviation).

Groups	*n*	Before treatment	After treatment	*t*	*P*
Control group	40	93.59 ± 8.62	50.11 ± 5.73	3.524	0.001
Experimental group	40	89.45 ± 3.03	34.19 ± 4.68	8.705	<0.001
t		0.453	2.153		
P		0.652	0.034		

Note: CA199, carbohydrate antigen 199, (U/Ml).

TABLE 5 Comparison of serum VEGF expression level (mean ± standard deviation).

Groups	*n*	Before treatment	After treatment	*t*	*P*
Control group	40	292.8 ± 11.90	205.9 ± 19.91	3.382	0.002
Experimental group	40	299.6 ± 11.39	124.8 ± 18.03	6.719	<0.001
t		0.416	3.018		
P		0.679	0.003		

Note: VEGF, Vascular endothelial growth factor, (pg/mL).

lesions was decreased in volume at least 30%, and no new lesions were found for more than 1 month; progressive disease (PD): the total diameter of the target lesions increased at least 20%, or new lesions were found; stable disease (SD): Neither sufficient shrinkage to qualify PR nor sufficient increase to qualify for PD; disease control rate (DCR)= (number of CR cases+ number of PR cases+ number of SD cases)/total number of cases × 100%. The clinical outcome of OS was calculated as the time from the first treatment to the date of death.

The percentage of the Karnofsky performance status (KPS) was used to describe the physical health by three conditions: A (0%–40%), B (50%–70%), and C (80%–100%). KPS scores range from 0 to 100, and 100 is fully capable of in daily activities without clinical evidence of disease (signs or symptoms), 0 means death (Table 2).

The adverse reactions were graded by the National Cancer Institute's Common Terminology Criteria for Adverse Events version 4.0 (NCI-CTCAE v4.0).

Statistical analysis

SAS version 9.2 (SAS Institute, Inc., Cary, NC) and GraphPad Prism 8.02 (GraphPad Software, Inc.) software were performed for statistical analyses. Fisher's exact test or chi-square test, correction of continuity chi-square test were used to compare categorical data for baseline characteristics and adverse reactions between the control group and the experimental group. The continuous data were presented by mean ± standard deviations (mean ± SD), and the comparison of the mean ± SD before and after treatment in the same group was performed by paired samples *t*-test, and the comparison of the mean ± SD of the two groups was performed by Unpaired independent samples *t*-test. Overall survival description was illustrated by the Kaplan-Meier curves, with *p*-value determined by a log-rank test, and the 95% CI for the median time to each event was computed. $p < 0.05$ was considered indicating a statistically significant difference (2-sided).

Results

Comparison of the levels of CEA, CA199, and VEGF before and after treatment between the two groups

After treatment, the levels of CEA, CA199, and VEGF were significantly reduced than before treatment in the control group (CEA: 12.87 ± 1.23 vs. 15.79 ± 0.81, CA199: 50.11 ± 5.73 vs. 93.59 ± 8.62, VEGF: 205.9 ± 19.91 vs. 292.8 ± 11.90) and experimental group (CEA: 8.85 ± 1.36 vs. 16.58 ± 1.14, CA199: 34.19 ± 4.68 vs. 89.45 ± 3.03, VEGF: 124.8 ± 18.03 vs. 299.6 ± 11.39). After treatment, the levels of these indicators in the experimental group were significantly lower (CEA: 8.85 ± 1.36 vs. 12.87 ± 1.23, CA199: 34.19 ± 4.68 vs. 50.11 ± 5.73, VEGF: 124.8 ± 18.03 vs. 205.9 ± 19.91) than in the control group (all $p < 0.05$, Tables 3–5).

Comparison of the percentages of the Karnofsky performance status (KPS) and incidence of adverse reactions before and after treatment between the two groups

After treatment, the percentages of the KPS were significantly increased than before treatment in the control group (76.25 ± 1.17 vs. 71.00 ± 1.67) and experimental group (83.25 ± 1.15 vs. 72.75 ± 1.64). After treatment, the

percentage of the KPS in the experimental group was significantly higher (83.25 ± 1.15 vs. 76.25 ± 1.17) than in the control group (all $p < 0.05$, Table 6). After treatment, there were no statistical significance in the incidence of adverse reactions between the control group and the experimental group (all $p > 0.05$, Table 7).

Comparison of clinical efficacy before and after treatment between the two groups

After treatment, the experimental group was superior to the control group in the matter of DCR (62.50% 25/40% vs. 40.00% 16/40) ($p < 0.05$, Table 8). The median OS of the control group and experimental group were 5.65 months (95% CI, 4.50–6.30) vs. 6.50 months (95% CI, 5.60–7.40) respectively, and the OS in the control group was shorter than the experimental group ($p = 0.0396$, Figure 1).

Discussion

Gastric cancer has become one of the malignant tumors that has impacted on human life span [1, 2]. Despite its worldwide decline in incidence over the past century, gastric cancer remains a major killer across the globe [10]. For the treatment of patients with advanced gastric cancer, the development from traditional chemotherapy to molecular precision targeted therapy has extended the survival period of patients and improved the quality of life [11]. The principle of hyperthermia is to utilize the thermal sensitivity of tumor cells to increase the permeability of the membrane structure of tumor cells so that the concentration of anti-tumor drugs in the tumor increases, and the death of tumor cells is accelerated, but the normal tissue around the lesion will not be damaged because of its normal blood flow and good heat dissipation [12].

Apatinib, a novel receptor tyrosine kinase inhibitor that highly selectively inhibits the binding of VEGF and vascular epidermal growth factor-2 (VEGFR-2), blocking the activation of mitogen-activated protein kinase (MAPK) signaling pathway, achieving the purpose of anti-tumor neovascularization and preventing further proliferation and metastasis of tumor cells [13]. Since 2014, apatinib has been approved by Chinese Society of Clinical Oncology (CSCO) guideline as a third-line or follow-up treatment for advanced gastric cancer and gastroesophageal junction adenocarcinoma in China [14], providing an important basis for clinical medication guidance. For the third-line treatment of patients with advanced gastric cancer, although apatinib is recommended by the guidelines, there are still some patients who refuse to receive apatinib, because of potential side effects requiring dietary restriction, severe hypertension with poor drug control, as well as intolerance to apatinib [15–17]. Therefore, low-dose apatinib was selected in this study for patients who had failed second-line and late treatment.

A previous study showed a highly positive correlation between the level of VEGF and tumor progression of patients with gastric cancer [18]. VEGF was highly expressed in gastric cancer, closely related to TNM staging and lymph node metastasis, which predicted worse prognosis of gastric cancer patients [19]. In addition to VEGF, serum CEA is a well-characterized glycoprotein, which is associated with depth of tumor invasion, lymph node metastasis and tumor metastasis, and is usually used to diagnose gastrointestinal malignancies and monitor of therapeutic effects in gastric cancer, esophageal cancer and breast cancer [20, 21]. Raised serum CA199 level was positively related to poor prognosis, tumor size, metastasis and invasion in gastric cancer patients [20, 21]. Nevertheless, the

TABLE 6 Comparison of KPS scores (mean ± standard deviation).

Groups	*n*	Before treatment	After treatment	*t*	*P*
Control group	40	71.00 ± 1.67	76.25 ± 1.17	3.667	0.001
Experimental group	40	72.75 ± 1.64	83.25 ± 1.15	9.802	<0.001
T		0.747	4.259		
P		0.457	<0.001		

Note: KPS, Karnofsky performance status.

TABLE 7 Comparison of adverse reactions of patients (n (%)).

Groups	*n*	Hypertension	Albuminuria	Bone marrow suppression	Diarrhea
Control group	40	18 (45.00%)	11 (27.50%)	15 (37.50%)	18 (45.00%)
Experimental group	40	15 (37.50%)	9 (22.50%)	13 (32.50%)	21 (52.50%)
χ^2		0.464	0.267	0.220	0.450
P		0.496	0.606	0.639	0.502

Note: Bone marrow suppression: Neutropenia or Anemia or Thrombocytopenia.

TABLE 8 Comparison of clinical efficacy (n (%)).

Groups	Control group (n = 40)	Experimental group (n = 40)	χ^2	P
CR	0 (0.00%)	0 (0.00%)		
PR	3 (7.50%)	8 (20.00%)		
SD	13 (32.50%)	17 (42.50%)		
PD	24 (60.00%)	15 (37.50%)		
DCR	16 (40.00%)	25 (62.50%)	4.053	0.044

Note: CR, complete response; PD, progressive disease; PR, partial response; SD, stable disease; DCR, disease control rate.

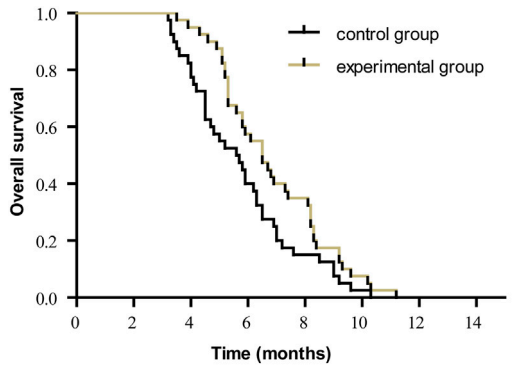

	control group (n=40)	experimental group (n=40)
Median OS, months (95% CI)	5.65 (4.50-6.30)	6.50 (5.60-7.40)
HR (95% CI)	1.63 (1.02-2.60)	
p value	0.0396	

FIGURE 1
Kaplan-Meier survival curve of the overall survival (OS) in all patients. Note: OS, overall survival; CI, confidence interval; HR, hazard ratio.

merge effect of these tumor markers on apatinib plus deep hyperthermia in advanced gastric cancer is unclear. In our study, the results showed that after treatment, the levels of serum CEA, CA199, and VEGF were significantly reduced than before treatment in the control group and experimental group. At the same time, compared with single apatinib, the levels of these indicators in the experimental group were much lower. Thus, deep hyperthermia plus apatinib may become a novel strategy for the treatment of advanced gastric cancer.

In a real-world study, 747 patients who had failed at least second-line therapy treated with low-dose apatinib (250 or 500 mg/d). Four patients achieved CR, 47 achieved PR, and 374 achieved SD. The DCR was 56.89% [22]. Moreover, following the result of a previous meta-analysis: concerning DCR, apatinib (odds ratio 7.84, 95% CI 4.12–16.50) was the best treatment for the third-line treatment of advanced gastric cancer in contrast to the third-line chemotherapy [23]. The study suggests that low dose apatinib is an effective treatment for advanced gastric cancer. Hyperthermia in advanced gastric cancer improved survival and clinical outcomes (DCR), and reduced recurrence according to a meta-analysis of studies [24]. Hyperthermia can enhance the chemotherapeutic efficacy of cisplatin-based therapy in gastric cancer [25]. A recent study showed that 500 mg of apatinib combined with chemotherapy obtained significantly higher DCR and KPS scores of compared with the chemotherapy group ($p < 0.05$) [26]. In this study, after treatment, the experimental group was superior to the control group in the matter of DCR, OS and KPS. The incidence of adverse reactions was similar between the two groups, and the overall tolerance was good. Although this study did not find statistically significant differences in the incidence of the above adverse reactions between the two groups, it still needs clinical attention. The results showed that apatinib plus deep hyperthermia displayed a synergistic effect. Its mechanism of action is that apatinib accelerates the thermal sensitivity of tumor cells. After the tumor tissue is heated, the gene expression and protein synthesis of VEGF are significantly inhibited, inhibiting the proliferation of endothelial cells and the formation of tumor neovascularization, while increasing the permeability of the cell membrane, making it easy for drugs to enter the tumor cells, and maintaining a high concentration of drugs in the cells, thereby improving the killing effect of tumors [27, 28]. On the other hand, Apatinib inhibits neovascularization and reduces repair ability of tumor tissue; Moreover, high-temperature causes protein denaturation and coagulative necrosis of local tumor cells, causing tumor tissue to fall off, affecting the synthesis and repair function of tumor cells, thus damaging cells and achieving the purpose of controlling tumors [29, 30]. Although numerous studies have continuously confirmed the clinical value of deep hyperthermia, the current clinical technology of hyperthermia is poor, and accurate deep hyperthermia cannot be realized, sometimes it has little effect, which leads to some scholars skeptical of tumor hyperthermia.

The features and innovations of this study are as follows [1]: Through comparative analysis of apatinib combined with deep hyperthermia, to explore the feasibility of combined therapy [2]; By comparing the total effective rate and quality of life of different subjects, the excellent performance of apatinib combined with deep hyperthermia in the treatment of advanced gastric cancer was discussed, and the clinical significance and application value of the above therapy for advanced gastric cancer was generally evaluated, revealing the prospect of clinical application. Although there are different opinions on the third-line treatment for patients with advanced gastric cancer, our study is designed only to explore an effective treatment method. Our study is the first to use apatinib plus deep hyperthermia in the treatment of gastric cancer, so some limitations that still merit attention.

This study had several limitations. First, the effective sample capacity was small owing to the study included only 80 patients. Second, long-term complications, such as hoarseness and hand-foot syndrome, were not assessed because of the short follow-up period and short treatment cycle. Third, no observation of progression free survival time, further verification of multi-center, large-sample clinical trial is still needed in the future.

Conclusion

In conclusion, apatinib with deep hyperthermia is superior to apatinib alone in advanced gastric cancers cases, which can effectively reduce the levels of tumor markers, significantly improve clinical response rate, enhance the quality of life, demonstrate longer OS in patients. Besides, deep hyperthermia is a non-invasive therapy, and patients are psychologically willing to accept it with good compliance, which is worth promoting diligently.

Data availability statement

The original contributions presented in the study are included in the article/supplementary material, further inquiries can be directed to the corresponding authors.

Ethics statement

This study had been approved by the Ethics Committee of Jingjiang people's hospital (No. 2021-03-029). All subjects in this study provided their written informed consent consistent with the Declaration of Helsinki.

Author contributions

SL, MT, and LY designed the research topics. GH, CS, and LC performed the experiments. GH and YH analyzed the data and prepared the figure and table. GH, MT, CS, and SL drafted the manuscript and revised it for academic content. MT and SL reviewed the conduct of the study. At least three authors saw all the raw data. All authors contributed to the article and approved the submitted version.

Conflict of interest

The authors declare that the research was conducted in the absence of any commercial or financial relationships that could be construed as a potential conflict of interest.

References

1. Kawazoe A, Shitara K, Boku N, Yoshikawa T, Terashima M. Current status of immunotherapy for advanced gastric cancer. *Jpn J Clin Oncol* (2021) 51(1):20–7. doi:10.1093/jjco/hyaa202

2. Leiting JL, Grotz TE. Advancements and challenges in treating advanced gastric cancer in the West. *World J Gastrointest Oncol* (2019) 11(9):652–64. doi:10.4251/wjgo.v11.i9.652

3. van Amelsfoort RM, van der Sluis K, Schats W, Jansen E, van Sandick JW, Verheij M, et al. Health-related quality of life in locally advanced gastric cancer: A systematic review. *Cancers (Basel)* (2021) 13(23):5934. doi:10.3390/cancers13235934

4. Chen ZD, Zhang PF, Xi HQ, Wei B, Chen L, Tang Y. Recent advances in the diagnosis, staging, treatment, and prognosis of advanced gastric cancer: A literature review. *Front Med (Lausanne)* (2021) 8:744839. doi:10.3389/fmed.2021.744839

5. Izumi D, Nunobe S. How to decide approaches and procedures for early and advanced gastric cancer? *Can J Gastroenterol Hepatol* (2022) 2022:8324242. doi:10.1155/2022/8324242

6. Wagner AD, Syn NL, Moehler M, Grothe W, Yong WP, Tai BC, et al. Chemotherapy for advanced gastric cancer. *Cochrane Database Syst Rev* (2017) 8(8):CD004064. doi:10.1002/14651858.CD004064.pub4

7. Tian Z, Niu X, Yao W. Efficacy and response biomarkers of apatinib in the treatment of malignancies in China: A review. *Front Oncol* (2021) 11:749083. doi:10.3389/fonc.2021.749083

8. Lindner LH, Blay JY, Eggermont A, Issels RD. Perioperative chemotherapy and regional hyperthermia for high-risk adult-type soft tissue sarcomas. *Eur J Cancer* (2021) 147:164–9. doi:10.1016/j.ejca.2021.02.002

9. Gronau F, Jara M, Feldbrugge L, Wolf V, Oeff A, Rau B. Cytoreductive surgery and hyperthermic intraperitoneal chemotherapy in gastric cancer. *Chirurg* (2021) 92:522–7. doi:10.1007/s00104-021-01371-3

10. Sun D, Li H, Cao M, He S, Lei L, Peng J, et al. Cancer burden in China: Trends, risk factors and prevention. *Cancer Biol Med* (2020) 17(4):879–95. doi:10.20892/j.issn.2095-3941.2020.0387

11. Song Z, Wu Y, Yang J, Yang D, Fang X. Progress in the treatment of advanced gastric cancer. *Tumour Biol* (2017) 39(7):1010428317714626. doi:10.1177/1010428317714626

12. Westermann AM, Grosen EA, Katschinski DM, Jager D, Rietbroek R, Schink JC, et al. A pilot study of whole body hyperthermia and carboplatin in platinum-resistant ovarian cancer. *Eur J Cancer* (2001) 37(9):1111–7. doi:10.1016/s0959-8049(01)00074-0

13. Teng F, Xu Z, Chen J, Zheng G, Zheng G, Lv H, et al. DUSP1 induces apatinib resistance by activating the MAPK pathway in gastric cancer. *Oncol Rep* (2018) 40(3):1203–22. doi:10.3892/or.2018.6520

14. Scott LJ. Apatinib: A review in advanced gastric cancer and other advanced cancers. *Drugs* (2018) 78(7):747–58. doi:10.1007/s40265-018-0903-9

15. Zhang Y, Gou M, Han C, Li J, Wang L, Qiao Q, et al. Efficacy and safety of apatinib as second-line therapy for advanced gastric cancer: A single-center observational study. *Anticancer Drugs* (2018) 29(2):184–9. doi:10.1097/CAD.0000000000000582

16. Chen D, Zhong X, Lin L, Xie J, Lian Y, Xu L. Comparative efficacy and adverse reactions of apatinib-chemotherapy combinations versus chemotherapy alone for treatment of advanced colorectal cancer: A meta-analysis of randomized controlled trials. *Am J Transl Res* (2022) 14(9):6703–11.

17. Xue JM, Astere M, Zhong MX, Lin H, Shen J, Zhu YX. Efficacy and safety of apatinib treatment for gastric cancer, hepatocellular carcinoma and non-small cell lung cancer: A meta-analysis. *Onco Targets Ther* (2018) 11:6119–28. doi:10.2147/OTT.S172717

18. Dong CR, Hu DX, Liu SC, Luo HL, Zhang WJ. AKT/GSK-3beta/VEGF signaling is involved in P2RY2 activation-induced the proliferation and metastasis of gastric cancer. *Carcinogenesis* (2023) 44(1):65–79. doi:10.1093/carcin/bgac095

19. Pang L, Wang J, Fan Y, Xu R, Bai Y, Bai L. Correlations of TNM staging and lymph node metastasis of gastric cancer with MRI features and VEGF expression. *Cancer Biomark* (2018) 23(1):53–9. doi:10.3233/CBM-181287

20. Ning S, Wei W, Li J, Hou B, Zhong J, Xie Y, et al. Clinical significance and diagnostic capacity of serum TK1, CEA, CA 19-9 and CA 72-4 levels in gastric and colorectal cancer patients. *J Cancer* (2018) 9(3):494–501. doi:10.7150/jca.21562

21. Sun Z, Zhang N. Clinical evaluation of CEA, CA19-9, CA72-4 and CA125 in gastric cancer patients with neoadjuvant chemotherapy. *World J Surg Oncol* (2014) 12:397. doi:10.1186/1477-7819-12-397

22. Du Y, Cao Q, Jiang C, Liang H, Ning Z, Ji C, et al. Effectiveness and safety of low-dose apatinib in advanced gastric cancer: A real-world study. *Cancer Med* (2020) 9(14):5008–14. doi:10.1002/cam4.3105

23. Huang M, Li J, Yu X, Xu Q, Zhang X, Dai X, et al. Comparison of efficacy and safety of third-line treatments for advanced gastric cancer: A systematic review with bayesian network meta-analysis. *Front Oncol* (2021) 11:734323. doi:10.3389/fonc.2021.734323

24. Mi DH, Li Z, Yang KH, Cao N, Lethaby A, Tian JH, et al. Surgery combined with intraoperative hyperthermic intraperitoneal chemotherapy (IHIC) for gastric cancer: A systematic review and meta-analysis of randomised controlled trials. *Int J Hyperthermia* (2013) 29(2):156–67. doi:10.3109/02656736.2013.768359

25. Cesna V, Sukovas A, Jasukaitiene A, Naginiene R, Barauskas G, Dambrauskas Z, et al. Narrow line between benefit and harm: Additivity of hyperthermia to cisplatin cytotoxicity in different gastrointestinal cancer cells. *World J Gastroenterol* (2018) 24(10):1072–83. doi:10.3748/wjg.v24.i10.1072

26. Gao S, Li X, Shi W, Huo L, Liu H. Efficacy of the low dose apatinib plus chemotherapy on advanced gastric carcinoma. *J Oncol* (2022) 2022:3009494. doi:10.1155/2022/3009494

27. Sawaji Y, Sato T, Takeuchi A, Hirata M, Ito A. Anti-angiogenic action of hyperthermia by suppressing gene expression and production of tumour-derived vascular endothelial growth factor *in vivo* and *in vitro*. *Br J Cancer* (2022) 86(10):1597–603. doi:10.1038/sj.bjc.6600268

28. Andresen TL, Jensen SS, Jørgensen K. Advanced strategies in liposomal cancer therapy: Problems and prospects of active and tumor specific drug release. *Prog Lipid Res* (2005) 44(1):68–97. doi:10.1016/j.plipres.2004.12.001

29. Wust P, Hildebrandt B, Sreenivasa G, Rau B, Gellermann J, Riess H, et al. Hyperthermia in combined treatment of cancer. *Lancet Oncol* (2002) 3(8):487–97. doi:10.1016/s1470-2045(02)00818-5

30. Falk MH, Issels RD. Hyperthermia in oncology. *Int J Hyperthermia* (2001) 17(1):1–18. doi:10.1080/02656730150201552

Pathology & Oncology Research | frontiers

TYPE Systematic Review
PUBLISHED 24 April 2023
DOI 10.3389/pore.2023.1611055

Check for updates

OPEN ACCESS

EDITED BY
Aniko Maraz,
University of Szeged, Hungary

*CORRESPONDENCE
Yue Gou,
396812462@qq.com
Dan Jia,
417522774@qq.com

RECEIVED 11 January 2023
ACCEPTED 12 April 2023
PUBLISHED 24 April 2023

CITATION
He X, Zhou S, Li H, Gou Y and Jia D (2023), Prognostic role of pretreatment skeletal muscle index in gastric cancer patients: A meta-analysis.
Pathol. Oncol. Res. 29:1611055.
doi: 10.3389/pore.2023.1611055

COPYRIGHT
© 2023 He, Zhou, Li, Gou and Jia. This is an open-access article distributed under the terms of the Creative Commons Attribution License (CC BY). The use, distribution or reproduction in other forums is permitted, provided the original author(s) and the copyright owner(s) are credited and that the original publication in this journal is cited, in accordance with accepted academic practice. No use, distribution or reproduction is permitted which does not comply with these terms.

Prognostic role of pretreatment skeletal muscle index in gastric cancer patients: A meta-analysis

Xiaohong He[1,2], Sicheng Zhou[2], Hongjun Li[2], Yue Gou[2]* and Dan Jia[2]*

[1]Cancer Center, West China Hospital, Sichuan University, Chengdu, China, [2]Outpatient Department, West China Hospital, Sichuan University/West China School of Nusing Sichuan University, Chengdu, China

Background: The association between pretreatment skeletal muscle index (SMI) and long-term survival of gastric cancer patients remains unclear up to now. The aim of this meta-analysis was to identify the prognostic value of pretreatment SMI in gastric cancer.

Methods: The PubMed, EMBASE and Web of Science electronic databases were searched up to 5 June 2022 for relevant studies. The primary outcome was overall survival (OS) and the second outcomes were disease-free survival (DFS) and cancer-specific survival (CSS). The hazard ratios (HRs) and 95% confidence intervals (CIs) were combined to assess the relationship between pretreatment SMI and survival of gastric cancer patients. All statistical analyses were conducted by STATA 15.0 software.

Results: A total of 31 retrospective studies involving 12,434 patients were enrolled in this meta-analysis. The pooled results demonstrated that lower pretreatment was significantly associated with poorer OS (HR = 1.53, $p < 0.001$). Besides, lower pretreatment SMI was also related with worse DFS (HR = 1.39, $p < 0.001$) and CSS (HR = 1.96, $p < 0.001$).

Conclusion: Pretreatment SMI was significantly associated with prognosis of gastric cancer patients and lower SMI predicted worse survival. However, more prospective high-quality studies are still needed to verify our findings.

KEYWORDS

meta-analysis, prognosis, gastric cancer, pretreatment, skeletal muscle index

Introduction

Gastric cancer remains the sixth highest incidence of all cancer worldwide with over none million newly diagnosed cases every year and is also the second-leading cause of cancer-related death (1). Despite of the great advances in the early diagnosis and treatment strategies including the screening of gastroscopy, surgical techniques and neoadjuvant chemoradiotherapy, the prognosis of gastric cancer patients remains extremely poor and about half of gastric cancer patients may recur after curative treatment, which is a severe global health problem needing to be solved (2, 3). It is

still necessary to identify more valuable and reliable clinical indicators to precisely estimate the prognosis of gastric cancer patients.

It is well known that the nutrition condition of the body plays an essential role in the development and progression of cancers. In overall, a poor nutrition condition could promote the occurrence and progression of cancers and malnutrition leads to a decline in the antineoplastic ability of patients (4, 5). Besides, the nutritional status could help predict long-term survival of cancer patients (4, 5). In recent years, a number of clinical parameters which could reflect the nutritional status to a certain extent have been introduced and reported to show high prognostic value in gastric cancer such as the controlling nutritional status (CONUT) score, prognostic nutritional index (PNI) and geriatric nutritional risk index (GNRI) (6–8). Unfortunately, none of these parameters are widely applied in clinics because they are unstable and could be affected by many factors.

Skeletal muscle loss is a strong and reliable indicator for poor nutritional status and closely related with survival of cancer patients (9–11). In recent years, skeletal muscle index has been introduced and it is calculated based on the third lumbar vertebra (L3) level skeletal muscle area and squared height (12). Meanwhile, the skeletal muscles in the L3 level include the e psoas muscles, the para-spinal muscles, and the abdominal wall muscles. Furthermore, the prognostic value of pretreatment SMI in several cancers has been well verified such as the epithelial ovarian cancer, colorectal cancer and hepatocellular carcinoma (13–15). However, the prognostic role of pretreatment SMI in gastric cancer remains unclear.

Thus, the aim of this meta-analysis was to demonstrate the prognostic value of pretreatment SMI in gastric cancer, which might contribute to predicting and improving the clinical outcomes of gastric cancer patients.

Materials and methods

This systematic review and meta-analysis were conducted according to the Preferred Reporting Items for Systematic Reviews and Meta-Analyses guidelines (16).

Literature search

The PubMed, EMBASE and Web of Science electronic databases were searched up to 5 June 2022. The following key words were used during the search: skeletal muscle index, SMI, stomach, gastric, neoplasm, cancer, tumor, carcinoma, survival, prognosis and prognostic. A combination of subject terms and free words was applied. The detailed search strategy was as follows: (skeletal muscle index OR SMI) AND (stomach OR gastric) AND (cancer OR tumor OR neoplasm OR carcinoma) AND (prognosis OR survival OR prognostic). Besides, the references cited in included studies were also reviewed for eligibility.

Inclusion and exclusion criteria

The inclusion criteria were as follows: 1) patients were pathologically diagnosed with primary gastric cancer; 2) the SMI was calculated before any anti-tumor treatment such as the surgery, chemotherapy and radiotherapy; 3) the association between pretreatment SMI and survival of gastric cancer patients were explored and the corresponding hazard ratios (HRs) and 95% confidence intervals (CIs) were reported in articles directly; 4) the outcomes included at least one of the following endpoints: overall survival (OS), disease-free survival (DFS) and cancer-specific survival (CSS).

The exclusion criteria were as follows: 1) meeting abstracts, animal trials, case reports, reviews or editorials; 2) HRs with corresponding 95% CIs were unavailable; 3) full texts were not available; 4) low-quality studies with the Newcastle-Ottawa Scale (NOS) score of 5 or lower (17).

Data collection and quality assessment

In this meta-analysis, the following information was collected from included studies: the name of first author, publication year, sample size, country, threshold of SMI, tumor-node-metastasis (TNM) stage, treatment, endpoint, HR and corresponding 95% CI.

The NOS was applied to evaluate the quality of included studies and only high-quality studies with a NOS score of 6 or higher were included (17).

The literature search, selection, data collection and quality assessment were all performed by two authors independently.

Statistical analysis

All statistical analyses were conducted with STATA 15.0 software. The HRs with corresponding 95% CIs were calculated to evaluate the association between pretreatment SMI and prognosis of gastric cancer patients. The heterogeneity among the included studies was evaluated by I^2 statistics and Q test. When significant heterogeneity was observed representing as $I^2 > 50\%$ and (or) $p < 0.1$, the random effects model was applied; otherwise, the fix effects model was used. The sensitivity analysis was performed to detect the sources of heterogeneity and evaluate the stability of pooled results. Furthermore, the Begg's funnel plot and Egger's test were conducted to detect publication bias and significant publication bias was defined as $p < 0.05$ (18, 19) If significant

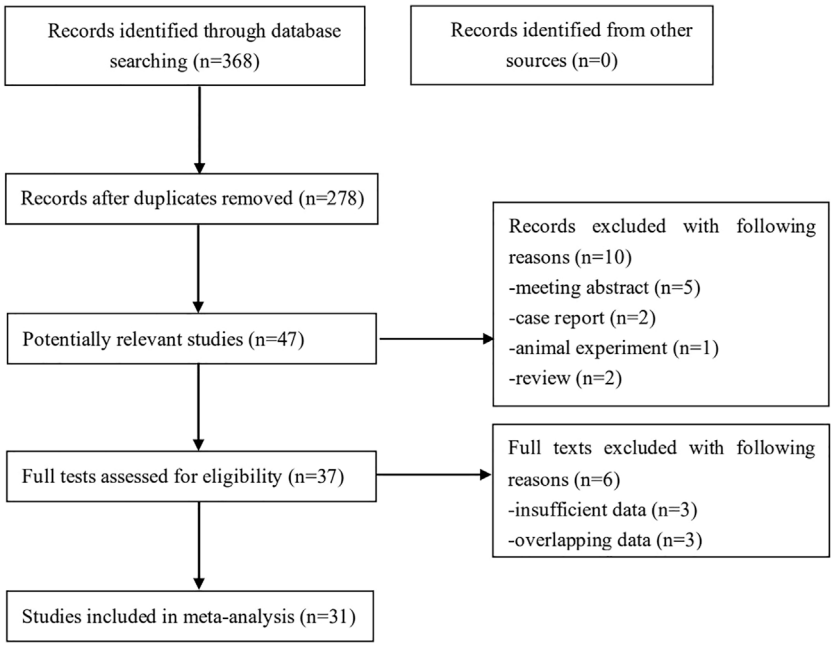

FIGURE 1
The flow diagram of this meta-analysis.

publication bias was detected, then the nonparametric trim-and-fill method was applied to re-estimate a corrective effect size after publication bias was adjusted (20).

Results

Literature search

Initially, 368 records were identified from several databases and 90 duplicated records were removed. Then 47 potentially relevant publications were further reviewed and ten records were excluded. Eventually, 29 articles were included (21–49). However, in the studies conducted by (29) and Wang et al. (32), two different populations were enrolled. Thus, we considered them as two studies separately and a total of 31 studies were included. The detailed literature search process was presented in Figure 1.

Basic characteristics of included studies

Among these 31 studies, 12,434 patients were enrolled and the sample size ranged from 40 to 1801. These studies were reported from 2016 to 2022. Most of patients were from Asian countries (26/31) and received surgical treatment (25/31). All included studies were high-quality studies with a NOS score ≥6. The other detailed characteristics were presented in Table 1.

The association between pretreatment SMI and OS of gastric cancer patients

All included studies explored the predictive role of pretreatment SMI for OS of gastric cancer patients (21–49). The pooled results demonstrated that lower pretreatment SMI was significantly associated with poorer OS (HR = 1.53, 95% CI: 1.36–1.72, $p < 0.001$; $I^2 = 85.0\%$, $p < 0.001$) (Figure 2).

Furthermore, the subgroup analysis based on the country (non-China: HR = 1.56, 95% CI: 1.27–1.91, $p < 0.001$; China: HR = 1.61, 95% CI: 1.29–2.01, $p < 0.001$) and treatment (non-surgery: HR = 1.56, 95% CI: 1.25–1.95, $p < 0.001$; surgery: HR = 1.53, 95% CI: 1.35–1.73, $p < 0.001$) were also conducted and similar results were observed (Table 2).

The association between pretreatment SMI and DFS of gastric cancer patients

Only 13 included studies involving 5,803 patients explored the predictive role of pretreatment SMI for DFS (22, 23, 26, 32, 34–37, 40, 41, 47, 49). The pooled results indicated that lower

TABLE 1 Basic characteristics of included studies.

Author	Year	Sample size	Country	Threshold of SMI	TNM	Treatment	Endpoint	NOS
Hayashi (21)	2016	53	Japan	41 cm^2/m^2 for women, 43/53 cm^2/m^2 for men	Advanced	Non-surgery	OS	6
Zhuang (22)	2016	937	China	34.9cm2/m2 for women, 40.8cm2/m2 for men	I-III	Surgery	OS, DFS	7
Zheng (23)	2017	924	China	28.6 cm^2/m^2 for women, 32.5 cm^2/m^2 for men	NR	Surgery	OS, DFS	7
Lee (24)	2018	140	South Korea	31 cm^2/m^2 for women, 49 cm^2/m^2 for men	Advanced	Non-surgery	OS	7
O'Brien (25)	2018	56	Ireland	38.5 cm^2/m^2 for women, 52.4 cm^2/m^2 for men	I-III	Surgery	OS	8
Park (26)	2018	136	Korea	49.4 cm^2/m^2	II-III	Surgery	OS	7
Sugiyama (27)	2018	231	Japan	38.5 cm^2/m^2 for women, 53.4 cm^2/m^2 for men	IV	Non-surgery	OS	6
Sierzega (28)	2019	138	Poland	38.5 cm^2/m^2 for women, 52.4 cm^2/m^2 for men	I-IV	Surgery	OS	7
Zhuang (29)	2019	150	China	34.9 cm^2/m^2 for women, 40.8 cm^2/m^2 for men	I-III	Surgery	OS, DFS	7
Zhuang (29)	2019	167	China	34.9 cm^2/m^2 for women, 40.8 cm^2/m^2 for men	I-III	Surgery	OS, DFS	7
Kim (30)	2020	305	Korea	53.6 cm^2/m^2 for women, 56.2 cm^2/m^2 for men	I-III	Surgery	OS	6
Il Yu (31)	2020	440	Republic of Korea	31 cm^2/m^2 for women, 49 cm^2/m^2 for men	NR	Surgery	OS, DFS	6
Dong (32)	2020	1,147	China	34.9 cm^2/m^2 for women, 40.8 cm^2/m^2 for men	I-III	Surgery	OS, DFS	6
Yang (33)	2020	182	China	38.5 cm^2/m^2 for women, 52.4 cm^2/m^2 for men	NR	Surgery	OS	7
Wang (34)	2020	64	China	32.4 cm^2/m^2 for women, 44.3 cm^2/m^2 for men	NR	Surgery	OS, DFS	6
Wang (34)	2020	74	China	32.4 cm^2/m^2 for women, 44.3 cm^2/m^2 for men	NR	Surgery	OS, DFS	6
An (35)	2021	339	Republic of Korea	40.77 cm^2/m^2 for women, 46.48 cm^2/m^2 for men	I-III	Surgery	OS, DFS	7
Alnimri (36)	2021	62	Australia	41 cm^2/m^2 for women, 43/53 cm^2/m^2 for men	I-IV	Surgery	OS, DFS	7
Huang (37)	2021	597	China	34.9 cm^2/m^2 for women, 40.8 cm^2/m^2 for men	I-III	Surgery	OS, DFS	6
Kim J (38)	2021	840	South Korea	31 cm^2/m^2 for women, 49 cm^2/m^2 for men	I-IV	Surgery	OS	7
Kim KW (39)	2021	958	South Korea	None	IIA-IIIC	Surgery	OS	6
Kim YY (40)	2021	149	Korea	31 cm^2/m^2 for women, 49 cm^2/m^2 for men	Advanced	Non-surgery	OS, PFS	7
Matsunaga (41)	2021	83	Japan	34.7 cm^2/m^2 for women, 43.9 cm^2/m^2 for men	Advanced	Non-surgery	OS	7
Lee (42)	2021	1801	South Korea	34.1 cm^2/m^2 for women, 44.4 cm^2/m^2 for men	I-III	Surgery	OS, DFS	7
Rimini (43)	2021	40	Italy	41 cm^2/m^2 for women, 43/53 cm^2/m^2 for men	IV	Non-surgery	OS	6
Sakurai (44)	2021	1,054	Japan	34.9 cm^2/m^2 for women, 40.8 cm^2/m^2 for men	I-III	Surgery	OS, CSS	7
Taki (45)	2021	257	Japan	37.3 cm^2/m^2 for women, 39.0 cm^2/m^2 for men	I-III	Surgery	OS	7
Matsui (46)	2022	512	Japan	34.04 cm^2/m^2 for women, 41.87 cm^2/m^2 for men	I-IV	Surgery	OS	7
Ricciardolo (47)	2022	55	Italy	38.5 cm^2/m^2 for women, 52.4 cm^2/m^2 for men	I-IV	Surgery	OS, DFS	7
Tan (48)	2022	318	China	37.81 cm^2/m^2 for women, 43.13 cm^2/m^2 for men	I-III	Surgery	OS, DFS	7
Xiong (49)	2022	225	China	34.9 cm^2/m^2 for women, 40.8 cm^2/m^2 for men	I-III	Surgery	OS, DFS	6

NR, not reported; OS, overall survival; DFS, disease-free survival; CSS, cancer-specific survival; NOS, Newcastle-Ottawa Scale.

pretreatment SMI was related with worse DFS (HR = 1.39, 95% CI: 1.13–1.69, $p < 0.001$; $I^2 = 58.5\%$, $p = 0.004$) (Figure 3).

Besides, subgroup analysis based on the country (non-China: HR = 1.22 95% CI: 0.92–1.62, $p = 0.001$; China: HR = 1.57, 95% CI: 1.19–2.06, $p = 0.176$) and treatment (surgery: HR = 1.42, 95% CI: 1.15–1.75, $p = 0.001$) were also performed and similar results were observed (Table 2).

The association between pretreatment SMI and CSS of gastric cancer patients

Only one study involving 1,054 patients explored the predictive role of pretreatment SMI for CSS (44). The results manifested that patients with a lower pretreatment SMI showed significantly worse CSS (HR = 1.96, 95% CI: 1.42–2.68, $p < 0.001$) (Table 2).

Sensitivity analysis and publication bias

The sensitivity analysis was conducted by excluding each included studies at one time, which indicated that the pooled results of this meta-analysis were stable and reliable and none of each included studies had a significantly impact on the overall results (Figure 4).

Significant publication bias was observed in our meta-analysis representing as asymmetric Begg's funnel plot (Figure 5) and $p < 0.001$ in Egger's test. Therefore, the trim-and-fill method was further applied. As a result, there

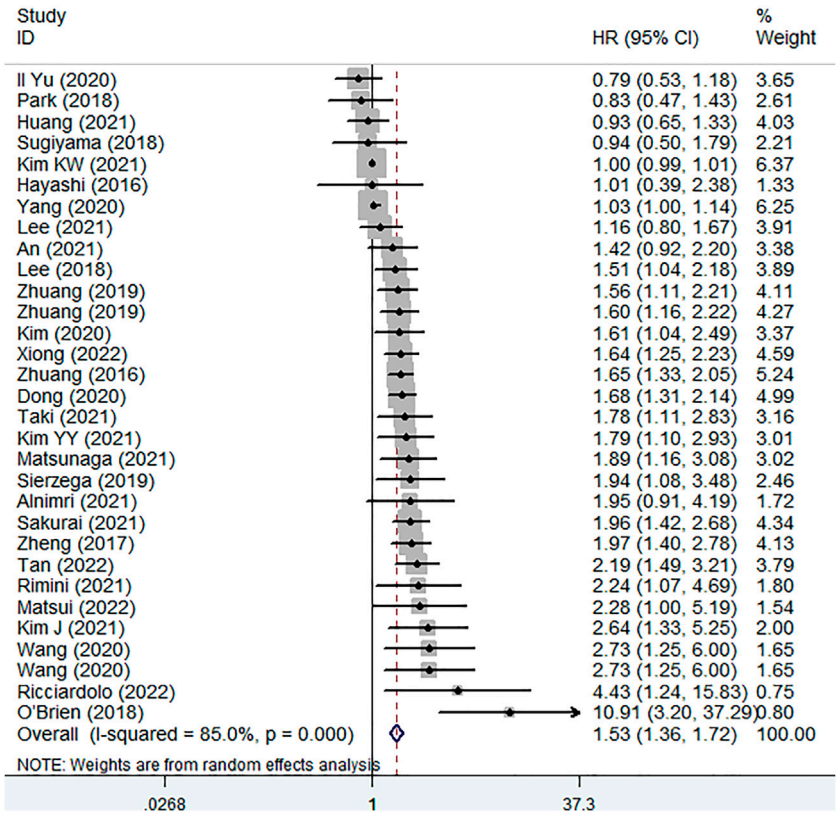

FIGURE 2
The association between pretreatment skeletal muscle index and overall survival in gastric cancer.

TABLE 2 Results of meta-analysis.

	No. of studies	HR	95% CI	*p*-value	I^2 (%)	*p*-value
Overall survival	31	1.53	1.36–1.72	<0.001	85.0	<0.001
Country						
Non-China	20	1.56	1.27–1.91	<0.001	79.5	<0.001
China	11	1.61	1.29–2.01	<0.001	86.5	<0.001
Treatment						
Non-surgery	6	1.56	1.25–1.95	<0.001	2.8	0.399
Surgery	25	1.53	1.35–1.73	<0.001	86.6	<0.001
Disease-free survival	13	1.39	1.13–1.69	0.001	58.5	0.004
Cancer-specific survival	1	1.96	1.42–2.68	<0.001	—	—

HR, hazard ratio; CI, confidence interval.

were five studies hypothetically remained unpublished for the association between pretreatment SMI and OS (Figure 6). The recalculated result did not change significantly (HR = 1.44, 95% CI: 1.28–1.61, $p < 0.001$), which indicated the stability of the results.

Discussion

The current meta-analysis demonstrated that pretreatment SMI was significantly associated with OS, DFS and CSS of gastric cancer patients and patients with a lower pretreatment SMI

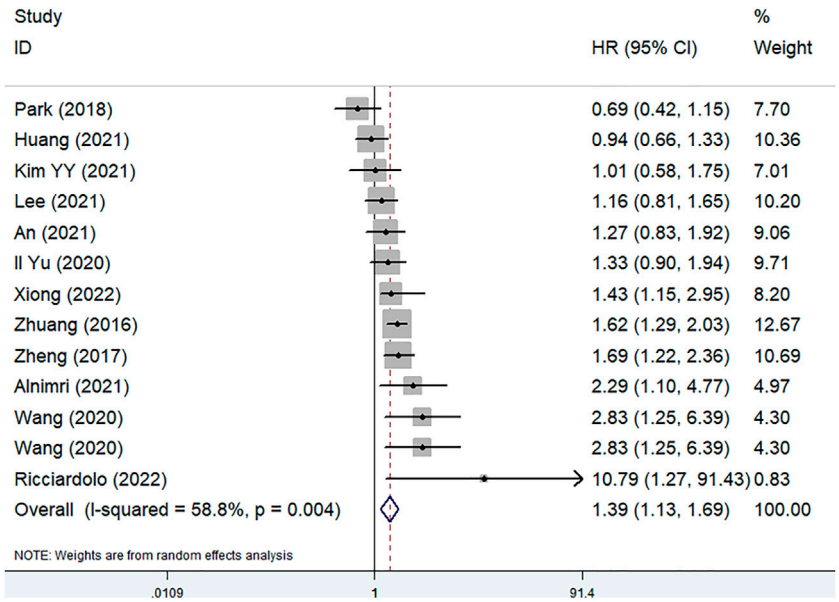

FIGURE 3
The association between pretreatment skeletal muscle index and disease free survival in gastric cancer.

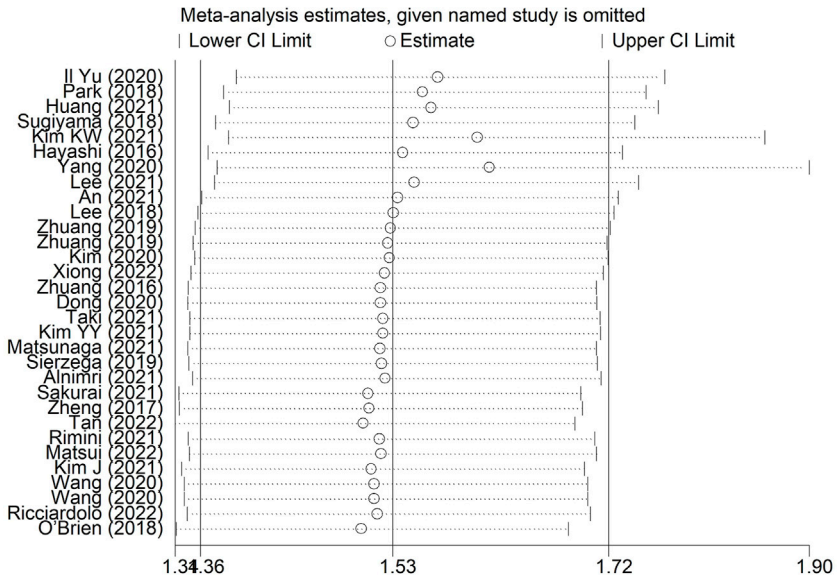

FIGURE 4
Sensitivity analysis about the association between pretreatment skeletal muscle index and overall survival in gastric cancer.

suffered from poorer prognosis after reviewing 31 retrospective studies involving 12,434 patients. Thus, the pretreatment SMI should be considered during the prediction of long-term survival and formulation of appropriate treatment strategies. However, more prospective high-quality studies are still needed to verify above findings.

The SMI is usually applied to define the sarcopenia and a lot of previous literature have showed that SMI is one of the most

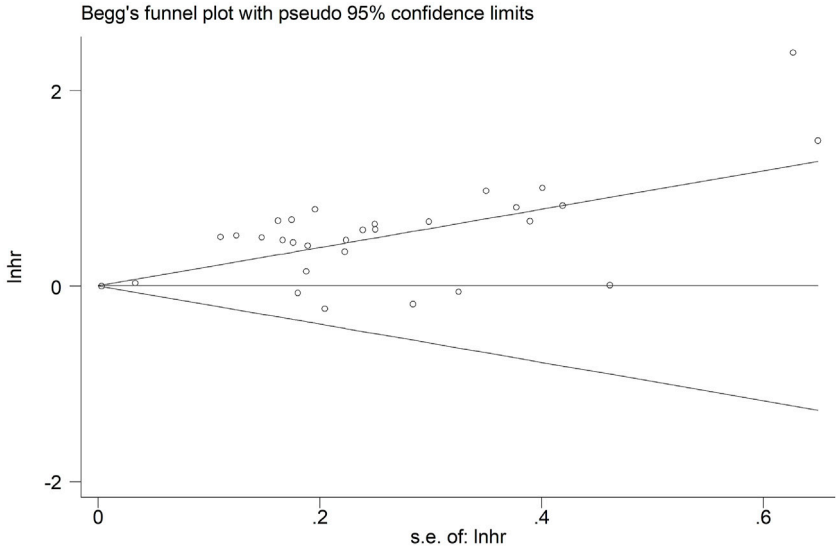

FIGURE 5
Begg's funnel plot.

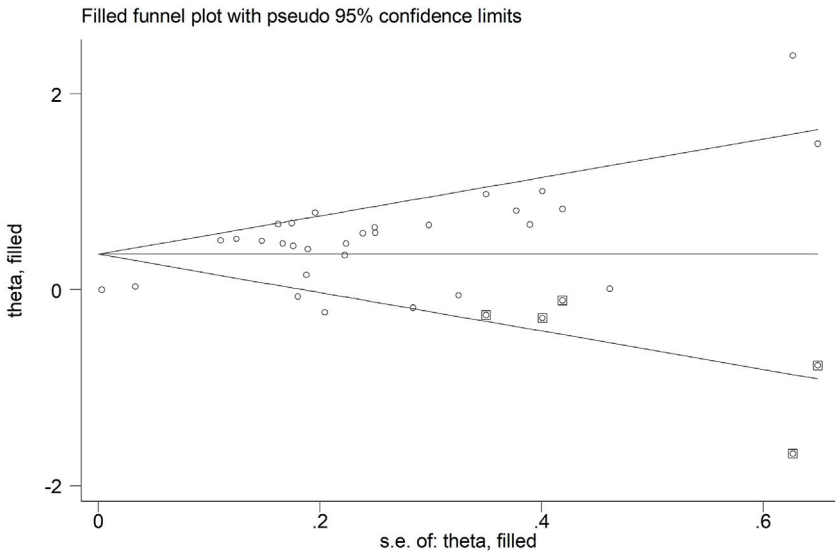

FIGURE 6
Filled Begg's funnel plot.

authoritative indicators to determine the existence of sarcopenia (14, 50, 51). Sarcopenia is a condition characterized by loss of muscle mass and strength, typically associated with aging. Cachexia, on the other hand, is a multifactorial syndrome characterized by loss of muscle mass, weight loss, and systemic inflammation, often seen in chronic diseases such as cancer, heart failure, and AIDS. While both conditions involve loss of muscle mass, cachexia is a more severe and systemic condition that can cause significant morbidity and mortality. In cancer patients, sarcopenia is relatively common compared with cachexia (52). Furthermore, it has been reported that sarcopenia is frequently seen among gastric cancer patients with the

incidence of 7%–57.4% in gastric cancer patients (53). Meanwhile, sarcopenia is closely related with worse prognosis of cancer patients (54–56). There are several possible causes to explain why sarcopenia worsens the survival of cancer patients. First, muscle wasting leads to increased inflammatory response (57, 58). Muscle tissue is the largest protein reservoir in the body, and when muscle wasting occurs, a large amount of protein and amino acids are released. These proteins and amino acids enter the bloodstream and stimulate an increase in the inflammatory response, which can promote tumor growth and metastasis (57, 58). Second, muscle wasting leads to decreased nutrient uptake and metabolic capacity (59). Muscle tissue has high energy and nutrient demands, and when muscle wasting occurs, the body's metabolic rate and energy expenditure also decrease. Moreover, muscle tissue can break down protein to produce amino acids, which are essential building blocks for protein synthesis and cellular function. Muscle wasting can therefore result in amino acid deficiency, which can further affect tumor cell growth and division (59, 60). Third, muscle wasting leads to decreased immune function (61). Muscle tissue is a major reservoir for immune cells, and when muscle wasting occurs, the body's immune function also decreases. Muscle wasting can also cause immune cells to migrate and impair their function, which reduces the body's ability to monitor and clear cancer cells (61). Fourth, muscle wasting leads to decreased physical activity (62, 63). Muscle tissue is the primary organ for movement in the body, and when muscle wasting occurs, physical activity also decreases. Muscle wasting can also result in decreased cardiovascular and pulmonary function and reduced endurance, which can lower tolerance for cancer treatment (62, 63). Five, skeletal muscle plays an important role in enduring the chemotherapy and the chemotherapy could cause a significantly increased risk for sarcopenia (64). Thus, cancer patients with sarcopenia show a lower tolerance to chemotherapy and may experience worse therapeutic effects (65). Besides, postoperative skeletal muscle mass loss is also related to more chemotherapy modifications like the dose reduction, delay or termination and has been identified as a risk factor for worse prognosis after gastric cancer surgery, which leads to poorer tumor control and worse survival (48). Furthermore, several studies have indicated that sarcopenia is an independent predictor for worse survival of gastric cancer patients and patient with sarcopenia should be treated more positively (66–69).

Measuring and monitoring a patient's SMI can help physicians better evaluate a gastric cancer patient's physical condition and treatment response, and detect and intervene early in cases of malnutrition and muscle rehabilitation issues. In addition, for patients with low SMI, interventions such as reasonable nutritional support and muscle rehabilitation training can improve patients' quality of life and treatment outcomes. Therefore, SMI can serve as an important indicator for the clinical treatment of gastric cancer patients, guiding and optimizing patients' treatment plans and nutritional support strategies.

Actually, there are still some valuable fields about the SMI in gastric cancer needing more in-depth investigations. As mentioned above, low SMI is closely related to the adverse events of chemotherapy. Thus, we speculated that the change of SMI during the adjuvant or neoadjuvant chemoradiotherapy may also play an important role in the prediction of long-term survival of gastric cancer patients. Most of relevant studies specified the cutoff values of SMI by sex. However, age is also believed to be an essential factor that significantly affect the baseline condition of skeletal muscle mass. Therefore, more detailed and distinguishing optimal critical values of SMI are wanted, which might contribute to the clinical application of SMI. Besides, a combination of SMI and other valuable prognostic factors like the TNM stage may show higher prognostic value than a single indicator.

There are several limitations in this meta-analysis. First, all included studies are retrospective and the sample size is relatively small. Second, most studies are from Asian countries, which may limit the generalizability of the conclusions. Third, the cut off values of pretreatment SMI differ in included studies, but we could not determine the optimal critical value in this meta-analysis. Fourth, we were unable to conduct more subgroup analysis based on other important parameters such as the age, sex, and TNM stage due to the lack of original data.

Conclusion

Pretreatment SMI was significantly related with prognosis of gastric cancer patients and lower pretreatment SMI predicted much worse survival. However, more prospective high-quality studies are still needed to verify above findings.

Data availability statement

The original contributions presented in the study are included in the article/supplementary material, further inquiries can be directed to the corresponding authors.

Author contributions

YG and DJ conceived and designed the analyses. XH and HL, performed the literature search and selection, collected data, and wrote the paper. XH and SZ performed statistical analyses. All authors contributed substantially to its revision.

Conflict of interest

The authors declare that the research was conducted in the absence of any commercial or financial relationships that could be construed as a potential conflict of interest.

References

1. Bray F, Ferlay J, Soerjomataram I, Siegel RL, Torre LA, Jemal A. Global cancer statistics 2018: GLOBOCAN estimates of incidence and mortality worldwide for 36 cancers in 185 countries. *CA: a Cancer J Clin* (2018) 68(6):394–424. doi:10.3322/caac.21492

2. Cao W, Chen HD, Yu YW, Li N, Chen WQ. Changing profiles of cancer burden worldwide and in China: A secondary analysis of the global cancer statistics 2020. *Chin Med J* (2021) 134(7):783–91. doi:10.1097/CM9.0000000000001474

3. Sung H, Ferlay J, Siegel RL, Laversanne M, Soerjomataram I, Jemal A, et al. Global cancer statistics 2020: GLOBOCAN estimates of incidence and mortality worldwide for 36 cancers in 185 countries. *CA: a Cancer J Clin* (2021) 71(3):209–49. doi:10.3322/caac.21660

4. Porro C, La Torre ME, Tartaglia N, Benameur T, Santini M, Ambrosi A, et al. The potential role of nutrition in lung cancer establishment and progression. *Life (Basel, Switzerland)* (2022) 12(2):270. doi:10.3390/life12020270

5. Supportive PDQ. Palliative care editorial B: Nutrition in cancer care (PDQ®): Health professional version. In: *PDQ cancer information summaries*. edn. Bethesda (MD): National Cancer Institute US (2002).

6. Takagi K, Domagala P, Polak WG, Buettner S, Wijnhoven BPL, Ijzermans JNM. Prognostic significance of the controlling nutritional status (CONUT) score in patients undergoing gastrectomy for gastric cancer: A systematic review and meta-analysis. *BMC Surg* (2019) 19(1):129. doi:10.1186/s12893-019-0593-6

7. Wang SH, Zhai ST, Lin H. Role of prognostic nutritional index in patients with gastric cancer: A meta-analysis. *Minerva Med* (2016) 107(5):322–7.

8. Yang Y, Gao P, Song Y, Sun J, Chen X, Zhao J, et al. The prognostic nutritional index is a predictive indicator of prognosis and postoperative complications in gastric cancer: A meta-analysis. *Eur J Surg Oncol* (2016) 42(8):1176–82. doi:10.1016/j.ejso.2016.05.029

9. Lee J, Lin JB, Chen TC, Jan YT, Sun FJ, Chen YJ, et al. Progressive skeletal muscle loss after surgery and adjuvant radiotherapy impact survival outcomes in patients with early stage cervical cancer. *Front Nutr* (2021) 8:773506. doi:10.3389/fnut.2021.773506

10. Nose Y, Yamashita K, Takeoka T, Momose K, Saito T, Tanaka K, et al. Perioperative ghrelin administration attenuates postoperative skeletal muscle loss in patients undergoing esophagectomy for esophageal cancer: Secondary analysis of a randomized controlled trial. *Ann Surg Oncol* (2022) 29:3604–12. doi:10.1245/s10434-022-11436-0

11. Okamoto A, Aikou S, Iwata R, Oya S, Kawasaki K, Okumura Y, et al. The type of gastrectomy affects skeletal muscle loss and the long-term outcomes of elderly patients with gastric cancer: A retrospective study using computed tomography images. *Surg Today* (2021) 52:812–21. doi:10.1007/s00595-021-02414-2

12. Tang R, Deng JP, Zhang L, Zhang WW, Sun JY, Chi F, et al. Prognostic significance of the skeletal muscle index and systemic inflammatory index in patients with lymph node-positive breast cancer after radical mastectomy. *BMC Cancer* (2022) 22(1):234. doi:10.1186/s12885-022-09312-x

13. Di Giorgio A, Rotolo S, Cintoni M, Rinninella E, Pulcini G, Schena CA, et al. The prognostic value of skeletal muscle index on clinical and survival outcomes after cytoreduction and HIPEC for peritoneal metastases from colorectal cancer: A systematic review and meta-analysis. *Eur J Surg Oncol* (2022) 48(3):649–56. doi:10.1016/j.ejso.2021.10.008

14. Tranoulis A, Kwong FLA, Lakhiani A, Georgiou D, Yap J, Balega J. Prevalence of computed tomography-based sarcopenia and the prognostic value of skeletal muscle index and muscle attenuation amongst women with epithelial ovarian malignancy: A systematic review and meta-analysis. *Eur J Surg Oncol* (2022) 48:1441–54. doi:10.1016/j.ejso.2022.02.024

15. Xu L, Jing Y, Zhao C, Zhang Q, Zhao X, Yang J, et al. Preoperative computed tomography-assessed skeletal muscle index is a novel prognostic factor in patients with hepatocellular carcinoma following hepatectomy: A meta-analysis. *J Gastrointest Oncol* (2020) 11(5):1040–53. doi:10.21037/jgo-20-122

16. McLeroy KR, Northridge ME, Balcazar H, Greenberg MR, Landers SJ. Reporting guidelines and the American journal of public health's adoption of preferred reporting Items for systematic reviews and meta-analyses. *Am J Public Health* (2012) 102(5):780–4. doi:10.2105/AJPH.2011.300630

17. Stang A. Critical evaluation of the Newcastle-Ottawa scale for the assessment of the quality of nonrandomized studies in meta-analyses. *Eur J Epidemiol* (2010) 25(9):603–5. doi:10.1007/s10654-010-9491-z

18. Begg CB, Mazumdar M. Operating characteristics of a rank correlation test for publication bias. *Biometrics* (1994) 50(4):1088–101. doi:10.2307/2533446

19. Egger M, Davey Smith G, Schneider M, Minder C. Bias in meta-analysis detected by a simple, graphical test. *BMJ (Clinical research ed)* (1997) 315(7109):629–34. doi:10.1136/bmj.315.7109.629

20. Wang Y, Huang D, Xu WY, Wang YW, Che GW. Prognostic value of pretreatment lymphocyte-to-monocyte ratio in non-small cell lung cancer: A meta-analysis. *Oncol Res Treat* (2019) 42(10):523–31. doi:10.1159/000501726

21. Hayashi N, Ando Y, Gyawali B, Shimokata T, Maeda O, Fukaya M, et al. Low skeletal muscle density is associated with poor survival in patients who receive chemotherapy for metastatic gastric cancer. *Oncol Rep* (2016) 35(3):1727–31. doi:10.3892/or.2015.4475

22. Zhuang CL, Huang DD, Pang WY, Zhou CJ, Wang SL, Lou N, et al. Sarcopenia is an independent predictor of severe postoperative complications and long-term survival after radical gastrectomy for gastric cancer: Analysis from a large-scale cohort. *Medicine (Baltimore)* (2016) 95(13):e3164. doi:10.1097/MD.0000000000003164

23. Zheng ZF, Lu J, Zheng CH, Li P, Xie JW, Wang JB, et al. A novel prognostic scoring system based on preoperative sarcopenia predicts the long-term outcome for patients after R0 resection for gastric cancer: Experiences of a high-volume center. *Ann Surg Oncol* (2017) 24(7):1795–803. doi:10.1245/s10434-017-5813-7

24. Lee JS, Kim YS, Kim EY, Jin W. Prognostic significance of CT-determined sarcopenia in patients with advanced gastric cancer. *Plos One* (2018) 13(8):e0202700. doi:10.1371/journal.pone.0202700

25. O'Brien S, Twomey M, Moloney F, Kavanagh RG, Carey BW, Power D, et al. Sarcopenia and post-operative morbidity and mortality in patients with gastric cancer. *J Gastric Cancer* (2018) 18(3):242–52. doi:10.5230/jgc.2018.18.e25

26. Park HS, Kim HS, Beom SH, Rha SY, Chung HC, Kim JH, et al. Marked loss of muscle, visceral fat, or subcutaneous fat after gastrectomy predicts poor survival in advanced gastric cancer: Single-center study from the CLASSIC trial. *Ann Surg Oncol* (2018) 25(11):3222–30. doi:10.1245/s10434-018-6624-1

27. Sugiyama K, Narita Y, Mitani S, Honda K, Masuishi T, Taniguchi H, et al. Baseline sarcopenia and skeletal muscle loss during chemotherapy affect survival outcomes in metastatic gastric cancer. *Anticancer Res* (2018) 38(10):5859–66. doi:10.21873/anticanres.12928

28. Sierzega M, Chrzan R, Wiktorowicz M, Kolodziejczyk P, Richter P. Prognostic and predictive implications of sarcopenia in Western patients undergoing gastric resections for carcinoma of the stomach. *J Surg Oncol* (2019) 120(3):473–82. doi:10.1002/jso.25509

29. Zhuang CL, Shen X, Zou HB, Dong QT, Cai HY, Chen XL, et al. EWGSOP2 versus EWGSOP1 for sarcopenia to predict prognosis in patients with gastric cancer after radical gastrectomy: Analysis from a large-scale prospective study. *Clin Nutr (Edinburgh, Scotland)* (2019) 39(7):2301–10. doi:10.1016/j.clnu.2019.10.024

30. Dong QT, Cai HY, Zhang Z, Zou HB, Dong WX, Wang WB, et al. Influence of body composition, muscle strength, and physical performance on the postoperative complications and survival after radical gastrectomy for gastric cancer: A comprehensive analysis from a large-scale prospective study. *Clin Nutr (Edinburgh, Scotland)* (2020) 40(5):3360–9. doi:10.1016/j.clnu.2020.11.007

31. Kim EY, Jun KH, Kim SY, Chin HM. Body mass index and skeletal muscle index are useful prognostic factors for overall survival after gastrectomy for gastric cancer Retrospective cohort study. *Medicine* (2020) 99(47):e23363. doi:10.1097/MD.0000000000023363

32. Wang JB, Xue Z, Lu J, He QL, Zheng ZF, Xu BB, et al. Effect of sarcopenia on short- and long-term outcomes in patients with gastric neuroendocrine neoplasms after radical gastrectomy: Results from a large, two-institution series. *BMC Cancer* (2020) 20(1):1002. doi:10.1186/s12885-020-07506-9

33. Yang W, Xia F, Wang J, Zhou M, Li G, Shen L, et al. Quantifying skeletal muscle wasting during chemoradiotherapy with Jacobian calculations for the prediction of survival and toxicity in patients with gastric cancer. *Ejso* (2020) 46(7):1254–61. doi:10.1016/j.ejso.2020.03.223

34. Yu JI, Choi C, Lee J, Kang WK, Park SH, Kim ST, et al. Effect of baseline sarcopenia on adjuvant treatment for D2 dissected gastric cancer: Analysis of the ARTIST phase III trial. *Radiother Oncol : J Eur Soc Ther Radiol Oncol* (2020) 152:19–25. doi:10.1016/j.radonc.2020.07.043

35. Alnimri F, Sivakumar J, Sutherland T, Johnson MA, Ward S, Chong L, et al. Pre-operative low muscle mass is associated with major complications and lower recurrence-free survival after gastric cancer surgery. *Anz J Surg* (2021) 91(3):316–22. doi:10.1111/ans.16590

36. An S, Eo W, Kim Y-J. Muscle-related parameters as determinants of survival in patients with stage I-III gastric cancer undergoing gastrectomy. *J Cancer* (2021) 12(18):5664–73. doi:10.7150/jca.61199

37. Huang DD, Yu DY, Song HN, Wang WB, Luo X, Wu GF, et al. The relationship between the GLIM-defined malnutrition, body composition and functional parameters, and clinical outcomes in elderly patients undergoing

radical gastrectomy for gastric cancer. *Eur J Surg Oncol* (2021) 47(9):2323–31. doi:10.1016/j.ejso.2021.02.032

38. Kim J, Han SH, Kim H-I. Detection of sarcopenic obesity and prediction of long-term survival in patients with gastric cancer using preoperative computed tomography and machine learning. *J Surg Oncol* (2021) 124(8):1347–55. doi:10.1002/jso.26668

39. Kim KW, Lee K, Lee JB, Park T, Khang S, Jeong H, et al. Preoperative nutritional risk index and postoperative one-year skeletal muscle loss can predict the prognosis of patients with gastric adenocarcinoma: A registry-based study. *BMC Cancer* (2021) 21(1):157. doi:10.1186/s12885-021-07885-7

40. Kim YY, Lee J, Jeong WK, Kim ST, Kim JH, Hong JY, et al. Prognostic significance of sarcopenia in microsatellite-stable gastric cancer patients treated with programmed death-1 inhibitors. *Gastric Cancer* (2021) 24(2):457–66. doi:10.1007/s10120-020-01124-x

41. Lee JK, Park YS, Lee K, Youn SI, Won Y, Min SH, et al. Prognostic significance of surgery-induced sarcopenia in the survival of gastric cancer patients: A sex-specific analysis. *J Cachexia Sarcopenia Muscle* (2021) 12(6):1897–907. doi:10.1002/jcsm.12793

42. Matsunaga T, Saito H, Miyauchi W, Shishido Y, Miyatani K, Morimoto M, et al. Impact of skeletal muscle mass in patients with unresectable gastric cancer who received palliative first-line chemotherapy based on 5-fluorouracil. *Bmc Cancer* (2021) 21(1):1219. doi:10.1186/s12885-021-08953-8

43. Rimini M, Pecchi A, Prampolini F, Bussei C, Salati M, Forni D, et al. The prognostic role of early skeletal muscle mass depletion in multimodality management of patients with advanced gastric cancer treated with first line chemotherapy: A pilot experience from modena cancer center. *J Clin Med* (2021) 10(8):1705. doi:10.3390/jcm10081705

44. Sakurai K, Kubo N, Tamamori Y, Aomatsu N, Nishii T, Tachimori A, et al. Depletion of skeletal muscle mass adversely affects long-term outcomes for men undergoing gastrectomy for gastric cancer. *Plos One* (2021) 16(8):e0256365. doi:10.1371/journal.pone.0256365

45. Taki Y, Sato S, Nakatani E, Higashizono K, Nagai E, Nishida M, et al. Preoperative skeletal muscle index and visceral-to-subcutaneous fat area ratio are associated with long-term outcomes of elderly gastric cancer patients after gastrectomy. *Langenbecks Arch Surg* (2021) 406(2):463–71. doi:10.1007/s00423-021-02092-1

46. Matsui R, Inaki N, Tsuji T. Impact of diabetes mellitus on long-term prognosis after gastrectomy for advanced gastric cancer: A propensity score matching analysis. *Surg Today* (2022) 52:1382–91. doi:10.1007/s00595-022-02482-y

47. Ricciardolo AA, De Ruvo N, Serra F, Prampolini F, Solaini L, Battisti S, et al. Strong impact of sarcopenia as a risk factor of survival in resected gastric cancer patients: First Italian report of a bicentric study. *Updates Surg* (2022) 74(1):283–93. doi:10.1007/s13304-021-01175-4

48. Tan S, Zhuang Q, Zhang Z, Li S, Xu J, Wang J, et al. Postoperative loss of skeletal muscle mass predicts poor survival after gastric cancer surgery. *Front Nutr* (2022) 9:794576. doi:10.3389/fnut.2022.794576

49. Xiong J, Hu H, Kang W, Shao X, Li Y, Jin P, et al. Association of sarcopenia and expression of interleukin-16 in gastric cancer survival. *Nutrients* (2022) 14(4):838. doi:10.3390/nu14040838

50. Chen F, Chi J, Zhao B, Mei F, Gao Q, Zhao L, et al. Impact of preoperative sarcopenia on postoperative complications and survival outcomes of patients with esophageal cancer: A meta-analysis of cohort studies. *Dis Esophagus : Off J Int Soc Dis Esophagus* (2022) 35:doab100. doi:10.1093/dote/doab100

51. Li S, Wang T, Lai W, Zhang M, Cheng B, Wang S, et al. Prognostic impact of sarcopenia on immune-related adverse events in malignancies received immune checkpoint inhibitors: A systematic review and meta-analysis. *Transl Cancer Res* (2021) 10(12):5150–8. doi:10.21037/tcr-21-1470

52. Dolin TG, Mikkelsen MK, Jakobsen HL, Vinther A, Zerahn B, Nielsen DL, et al. The prevalence of sarcopenia and cachexia in older patients with localized colorectal cancer. *J Geriatr Oncol* (2023) 14(1):101402. doi:10.1016/j.jgo.2022.11.001

53. Petermann-Rocha F, Balntzi V, Gray SR, Lara J, Ho FK, Pell JP, et al. Global prevalence of sarcopenia and severe sarcopenia: A systematic review and meta-analysis. *J Cachexia Sarcopenia Muscle* (2022) 13(1):86–99. doi:10.1002/jcsm.12783

54. Takenaka Y, Takemoto N, Oya R, Inohara H. Prognostic impact of sarcopenia in patients with head and neck cancer treated with surgery or radiation: A meta-analysis. *PLoS One* (2021) 16(10):e0259288. doi:10.1371/journal.pone.0259288

55. Waalboer RB, Meyer YM, Galjart B, Olthof PB, van Vugt JLA, Grünhagen DJ, et al. Sarcopenia and long-term survival outcomes after local therapy for colorectal liver metastasis: A meta-analysis. *HPB : Off J Int Hepato Pancreato Biliary Assoc* (2022) 24(1):9–16. doi:10.1016/j.hpb.2021.08.947

56. Watanabe J, Matsui R, Sasanuma H, Ishizaki Y, Fukunaga T, Kotani K, et al. Body composition assessment and sarcopenia in patients with biliary tract cancer: A systematic review and meta-analysis. *Clin Nutr (Edinburgh, Scotland)* (2022) 41(2):321–8. doi:10.1016/j.clnu.2021.12.005

57. Schiaffino S, Dyar KA, Ciciliot S, Blaauw B, Sandri M. Mechanisms regulating skeletal muscle growth and atrophy. *FEBS J* (2013) 280(17):4294–314. doi:10.1111/febs.12253

58. Webster JM, Kempen L, Hardy RS, Langen RCJ. Inflammation and skeletal muscle wasting during cachexia. *Front Physiol* (2020) 11:597675. doi:10.3389/fphys.2020.597675

59. Ekramzadeh M, Santoro D, Kopple JD. The effect of nutrition and exercise on body composition, exercise capacity, and physical functioning in advanced CKD patients. *Nutrients* (2022) 14(10):2129. doi:10.3390/nu14102129

60. Dasarathy S, Merli M. Sarcopenia from mechanism to diagnosis and treatment in liver disease. *J Hepatol* (2016) 65(6):1232–44. doi:10.1016/j.jhep.2016.07.040

61. Tian J, Chung HK, Moon JS, Nga HT, Lee HY, Kim JT, et al. Skeletal muscle mitoribosomal defects are linked to low bone mass caused by bone marrow inflammation in male mice. *J Cachexia Sarcopenia Muscle* (2022) 13(3):1785–99. doi:10.1002/jcsm.12975

62. Nishikawa H, Fukunishi S, Asai A, Yokohama K, Nishiguchi S, Higuchi K. Pathophysiology and mechanisms of primary sarcopenia (Review). *Int J Mol Med* (2021) 48(2):156. doi:10.3892/ijmm.2021.4989

63. Pár A, Hegyi JP, Váncsa S, Pár G. Sarcopenia - 2021: Pathophysiology, diagnosis, therapy. *Orvosi Hetilap* (2021) 162(1):3–12. doi:10.1556/650.2021.32015

64. Awad S, Tan BH, Cui H, Bhalla A, Fearon KC, Parsons SL, et al. Marked changes in body composition following neoadjuvant chemotherapy for oesophagogastric cancer. *Clin Nutr (Edinburgh, Scotland)* (2012) 31(1):74–7. doi:10.1016/j.clnu.2011.08.008

65. Palmela C, Velho S, Agostinho L, Branco F, Santos M, Santos MP, et al. Body composition as a prognostic factor of neoadjuvant chemotherapy toxicity and outcome in patients with locally advanced gastric cancer. *J Gastric Cancer* (2017) 17(1):74–87. doi:10.5230/jgc.2017.17.e8

66. Erkul O, Cekic AB, Cansu A, Yildirim R, Guner A. Effects of sarcopenia on postoperative outcomes in patients who underwent gastrectomy for gastric cancer. *J Surg Res* (2022) 274:196–206. doi:10.1016/j.jss.2021.12.051

67. Hisada H, Tamura N, Tsuji Y, Nagao S, Fukagawa K, Miura Y, et al. The impact of sarcopenia on adverse events associated with gastric endoscopic submucosal dissection. *Surg Endosc* (2022) 36:6387–95. doi:10.1007/s00464-021-08965-2

68. Huang ZX, Zhang HH, Zhang WT, Shi MM, Ren JH, Xu LB, et al. Effect of short-term preoperative parenteral nutrition support for gastric cancer patients with sarcopenia: A propensity score matching analysis. *J Gastrointest Surg* (2022) 26:1362–72. doi:10.1007/s11605-021-05185-w

69. Kim HJ, Lee ES, Kim BJ, Kim WS, Park JY, Kim JG, et al. Risk factors and clinical outcomes of postgastrectomy sarcopenia newly developed after curative resection for gastric cancer. *Medicine (Baltimore)* (2022) 101(6):e28699. doi:10.1097/MD.0000000000028699

Pathology & Oncology Research | frontiers

TYPE Hypothesis & Theory
PUBLISHED 08 March 2023
DOI 10.3389/pore.2023.1610976

Check for updates

OPEN ACCESS

EDITED BY
Jozsef Dudas,
Innsbruck Medical University, Austria

*CORRESPONDENCE
Xiying Cao,
xiyingcao@163.com
Hui Li,
huilee@vip.sina.com

RECEIVED 26 November 2022
ACCEPTED 22 February 2023
PUBLISHED 08 March 2023

CITATION
Cao X, Wu B, Guo S, Zhong W, Zhu S, Zhang Z, Gu L and Li H (2023), APOC1 predicts a worse prognosis for esophageal squamous cell carcinoma and is associated with tumor immune infiltration during tumorigenesis. *Pathol. Oncol. Res.* 29:1610976. doi: 10.3389/pore.2023.1610976

COPYRIGHT
© 2023 Cao, Wu, Guo, Zhong, Zhu, Zhang, Gu and Li. This is an open-access article distributed under the terms of the Creative Commons Attribution License (CC BY). The use, distribution or reproduction in other forums is permitted, provided the original author(s) and the copyright owner(s) are credited and that the original publication in this journal is cited, in accordance with accepted academic practice. No use, distribution or reproduction is permitted which does not comply with these terms.

APOC1 predicts a worse prognosis for esophageal squamous cell carcinoma and is associated with tumor immune infiltration during tumorigenesis

Xiying Cao[1,2]*, Bingqun Wu[3], Shaoming Guo[2], Weixiang Zhong[2], Shenyu Zhu[2], Zuxiong Zhang[2], Liang Gu[2] and Hui Li[1]*

[1]Department of Thoracic Surgery, Beijing Chao-Yang Hospital, Capital Medical University, Beijing, China, [2]Department of Thoracic Surgery, The First Affiliated Hospital of Gannan Medical University, Ganzhou, Jiangxi, China, [3]Department of Thoracic Surgery, Huaxin Hospital, First Hospital of Tsinghua University Beijing, Beijing, China

Background: Esophageal carcinoma (ESCA), a common malignant tumor of the digestive tract with insidious onset, is a serious threat to human health. Despite multiple treatment modalities for patients with ESCA, the overall prognosis remains poor. Apolipoprotein C1 (APOC1) is involved in tumorigenesis as an inflammation-related molecule, and its role in esophageal cancer is still unknown.

Methods: We downloaded documents and clinical data using The Cancer Genome Atlas (TCGA)and Gene Expression Omnibus (GEO) databases. We also conducted bioinformatics studies on the diagnostic value, prognostic value, and correlation between APOC1 and immune infiltrating cells in ESCA through STRING (https://cn.string-db.org/), the TISIDB (http://cis.hku.hk/TISIDB/) website, and various other analysis tools.

Results: In patients with ESCA, APOC1 was significantly more highly expressed in tumor tissues than in normal tissues ($p < 0.001$). APOC1 could diagnose ESCA more accurately and determine the TNM stage and disease classification with high accuracy (area under the curve, AUC≥0.807). The results of the Kaplan–Meier curve analysis showed that APOC1 has prognostic value for esophageal squamous carcinoma (ESCC) ($p = 0.043$). Univariate analysis showed that high APOC1 expression in ESCC was significantly associated

Abbreviations: APOC1, Apolipoprotein C1; AUC, area under the curve; ACC, adrenocortical carcinoma; BLCA, bladder urothelial carcinoma; BRCA, Breast invasive carcinoma; CESC, endocervical adenocarcinoma; CHOL, paraneoplastic tissues in cholangiocarcinoma; COAD, Colon adenocarcinoma; EAC, esophageal adenocarcinoma; ESCC, esophageal squamous cell carcinoma; GEO, Gene Expression Omnibus; GO, gene ontology; GSEA, gene set enrichment analysis; GSVA, gene set variation analysis; HNSC, neck squamous cell carcinoma; KEGG, kyoto encyclopedia of genes and genomes; KIRC, kidney renal clear cell carcinoma; KICH, kidney chromophobe; KIRP, kidney renal papillary cell carcinoma; LUAD, lung adenocarcinoma; LUSC, lung squamous cell carcinoma; OS, overall survival; OV, ovarian serous cystadenocarcinoma; PRAD, prostate adenocarcinoma; STAD, stomach adenocarcinoma; TCGA, the cancer genome atlas; THCA, thyroid carcinoma; TILs, tumor-infiltrating lymphocytes; UCEC, uterine corpus endometrial carcinoma.

with worse overall survival (OS) (p = 0.043), and multivariate analysis shows that high APOC1 expression was an independent risk factor for the OS of patients with ESCC (p = 0.030). In addition, the GO (gene ontology)/KEGG (Kyoto encyclopedia of genes and genomes) analysis showed a concentration of gene enrichment in the regulation of T-cell activation, cornification, cytolysis, external side of the plasma membrane, MHC protein complex, MHC class II protein complex, serine-type peptidase activity, serine-type endopeptidase activity, *Staphylococcus aureus* infection, antigen processing and presentation, and graft-versus-host disease (all $p < 0.001$). GSEA (gene set enrichment analysis) showed that enrichment pathways such as immunoregulatory-interactions between a lymphoid and non-lymphoid cell (NES = 1.493, p. adj = 0.023, FDR = 0.017) and FCERI-mediated NF-KB activation (NES = 1.437, p. adj = 0.023, FDR = 0.017) were significantly enriched in APOC1-related phenotypes. In addition, APOC1 was significantly associated with tumor immune infiltrating cells and immune chemokines.

Conclusion: APOC1 can be used as a prognostic biomarker for esophageal cancer. Furthermore, as a novel prognostic marker for patients with ESCC, it may have potential value for further investigation regarding the diagnosis and treatment of this group of patients.

KEYWORDS

bioinformatics, prognosis, expression, APOC1, ESCA

Introduction

Esophageal carcinoma (ESCA) currently ranks seventh and sixth in the world in terms of incidence and overall mortality, respectively (1). The main tissue types of ESCA are esophageal squamous cell carcinoma (ESCC) and esophageal adenocarcinoma (EAC) (2). Worldwide, ESCC accounts for approximately 90% of all patients with ESCA (3). East Asian countries including China have a high incidence of ESCA, and the dominant histological type is ESCC (4). Although multiple treatment modalities exist for patients with ESCA, the overall survival (OS) rate of patients remains poor, with a low (20%) 5-year survival rate (5, 6). Owing to the disease characteristics of ESCA itself and the complexity of the causative factors (7), failure to diagnose early lesions in time also has an important impact on the prognosis of patients (8).

In recent years, immunotherapy has been applied to the treatment of lung cancer, breast cancer, and other tumors with variable efficiency (9), and it is also highly anticipated that immunotherapy will benefit more patients with more tumor types (10). The safety of immunotherapy combined with radiotherapy in the treatment of ESCA is also under study (11). However, some patients do not respond to immunotherapy because of the multiple immune evasion mechanisms of the tumor (12). Current research has focused on radiotherapy, chemotherapy, and combination radiotherapy and immunotherapy, but there are no specific targeted molecules for the treatment of this malignancy (13). Therefore, it is particularly important to identify a biomarker that has high diagnostic sensitivity for ESCA and prognostic predictive value, and one that can be used to clarify the molecular mechanism of tumors and therapeutic targets.

APOC1 is a member of the apolipoprotein C family, with a size of 6.6 kD, and its coding gene region is located at 19q13.32 on chromosome 19 and is mainly synthesized by the liver (14). In recent years, several studies on the prognostic value of APOC1 in a variety of tumors have emerged (15-17). Some studies have shown that APOC1 regulates the development of various tumors such as renal cell carcinoma, colorectal cancer, and pancreatic cancer (18-21), which in turn affects the disease progression of many tumors.

It is well known that there is a strong link between inflammation and tumors (22), and infiltration of inflammatory cells is very common in tumor histopathology (23). The growth of tumors relies on the support of a complex mixture of organismal stroma containing inflammatory cells (24), and inflammatory indicators can predict the risk of postoperative tumor complications (25). Therefore, we hypothesized that the study of inflammation-related cells and proteins in the body could be used to predict tumor development. Studies have shown that several inflammation-related protein molecules including APOC1 are involved in the inflammatory response (26). Related studies have also shown that APOC1 may influence tumor progression in patients with kidney cancer (19) and colon cancer (18) by regulating gene expression and may be a potential prognostic marker for tumors such as gastric cancer (15) and lung cancer (17). However, to our knowledge, the expression and biological role of APOC1 in ESCA has not yet been reported except the study by Guo, Q et al. (27).

In this study, we applied several databases such as The Cancer Genome Atlas (TCGA), Gene Expression Omnibus (GEO), and the Genotype-Tissue Expression (GETx) (28-30); bioinformatics algorithms; and web tools such as the Search Tool for the Retrieval of Interacting Genes/Proteins (STRING) (31) and TISIDB(an integrated repository portal for tumor-immune system interactions) (32) to analyze the correlation between APOC1 and the tumor microenvironment of ESCA and to clarify the diagnostic and prognostic value, tumorigenic mechanism, and immune response regulation of APOC1 in ESCA.

At the beginning of this study, we analyzed the relationship between the expression of APOC1 in various tumors and disease prognosis from TCGA and GEO databases and specifically analyzed APOC1 expression in ESCA. Then, the diagnostic and prognostic value of APOC1 in esophageal cancer was evaluated, and finally, the relationship between APOC1 and tumor immune infiltrating cells was analyzed. With these results, we may be able to better understand the biological role of APOC1 in tumorigenesis and immunotherapeutic response in ESCA and ESCC.

Materials and methods

Data sources

We simultaneously extracted APOC1 expression and clinical data from the TCGA (https://portal.gdc.cancer.gov/) and GTEx (https://gtexportal.org/) databases in ESCA tissues, adjacent tumor tissues, and normal tissues to analyze the differences in APOC1 expression between tumor and normal tissues and the relationship between the expression of APOC1 and clinical characteristics. The data sets GSE161533 (84 paired normal tissues, para-tumor tissues, and tumor tissues from 28 ESCC patients microarray experiments performed by microarray analysis), GSE20347 (RNA was extracted from 17 paired tumor tissues and matched normal adjacent tissue from ESCC patients using the PureLink Micro-to-Midi Total RNA Purification System), and GSE29001(Gene expression from twelve cases of patient-matched normal basal epithelial cells, normal differentiated squamous epithelium, and cancer by expression microarrays.) were downloaded from the GEO (https://www.ncbi.nlm.nih.gov/gds/) database for the analysis of APOC1 expression differences between tumor and normal tissues and between tumor and adjacent tissues, respectively.

Analysis of receiver operating characteristic (ROC) curve

After analyzing the difference between APOC1 expression in ESCA tissues and normal tissues, we performed a ROC curve analysis to detect the diagnostic ability of APOC1 for ESCA.

Analysis of OS

Following the analysis of the diagnostic value of APOC1 for ESCA, we used Kaplan–Meier (KM) curves to analyze the influence of APOC1 expression status on the prognosis of patients with ESCA.

Analysis of univariate and multivariate logistic regression

We compared the relationship between APOC1 expression status and the overall prognosis of ESCA patients by univariate and multifactorial analyses. We also analyzed whether APOC1 expression is an independent risk factor for the poor prognosis of ESCC patients. The significant criterion for COX analysis was set at $p < 0.05$.

Analysis of functional enrichment

Differential analysis of APOC1 expression data (|log2 (fold change|) ≥1, adj. $p < 0.05$) was performed using the R (version 3.6.3) (R Core Team (2021). R: A language and environment for statistical computing. R Foundation for Statistical Computing, Vienna, Austria. URL https://www.R-project.org/) limma package. Gene Ontology/Kyoto Encyclopedia of Genes and Genome (GO/KEGG) analysis was used to obtain the correlation between APOC1 and ESCC, (adj. $p < 0.05$ was considered statistically significant), and the above results were visualized by applying the ggplot2 package (https://CRAN.R-project.org/package=ggplot2).

Analysis of gene enrichment

Gene Set Enrichment Analysis (GSEA) was performed using the R (version 3.6.3) cluster profiler and ggplot2 packages. Statistical analysis with |NES| ((normalized enrichment score)) >1, $p < 0.05$, and FDR (false discovery rate) > 0.25 was considered to indicate statistically significant differences.

Analysis of protein interactions

In the protein interaction analysis, we used STRING online tool (31) to study and analyze the protein-protein binding to APOC1 protein-protein interaction (PPI) with APOC1. The network was operated to obtain 50 proteins that bind to APOC1, and the genes encoding these 50 proteins were intersected with the differentially expressed genes associated with APOC1 in ESCA tissues. We then analyzed the correlation analysis of APOC1 with these intersecting genes

separately using Spearman's relationship analysis. Statistical significance was considered at $p < 0.05$.

Analysis of APOC1 expression and immune infiltration

We used the TISIDB (32) (http://cis.hku.hk/TISIDB/browse.php?gene=APOC1) web tool and Gene Set Variation Analysis (GSVA) method to analyze the relationship between the expression of APOC1 and tumor-infiltrating lymphocytes (TILs). The correlation between APOC1 and immune checkpoint genes in ESCA tissues was also analyzed, and the link between APOC1 expression and migration of immune cells was analyzed by chemokine and chemokine receptor modules.

Statistics

We performed statistical analysis using the R (version 3.6.3) and plotted receiver operating characteristic (ROC) curves. The correlation between APOC1 mRNA expression and clinical characteristics of ESCA patients was tested using a chi-square test.

Results

Clinical characteristics of patients with ESCA

We extracted clinical data from the TCGA-GTEx database for 173 patients (162 patients with tumors and 11 healthy controls). The clinical information is shown in Table 1.

Expression of APOC1 in various tumors and ESCA

To understand the expression status of APOC1 in tumor tissues, adjacent tumor tissues, and normal tissues, we analyzed the expression of APOC1 in various types of tumors from the TCGA(10534 patients) and GTEx (15776 patients) databases. As shown in Figures 1A, B, the expression of APOC1 was significantly upregulated in tumor tissue compared with normal tissue in Breast invasive carcinoma (BRCA), Cervical squamous cell carcinoma and endocervical adenocarcinoma (CESC), Colon adenocarcinoma (COAD), ESCA, Kidney Chromophobe (KICH), Kidney renal clear cell carcinoma (KIRC), Kidney renal papillary cell carcinoma (KIRP), and Ovarian serous cystadenocarcinoma (OV). However, the expression level of APOC1 in tumors was

TABLE 1 Clinical characteristics of esophageal carcinoma (ESCA) patients.

Characteristic	Low expression of APOC1	High expression of APOC1	*p*
N	81	81	
Age, n (%)			0.346
<=60	45 (27.8%)	38 (23.5%)	
>60	36 (22.2%)	43 (26.5%)	
Gender, n (%)			0.177
Female	15 (9.3%)	8 (4.9%)	
Male	66 (40.7%)	73 (45.1%)	
Tumor central location, n (%)			0.168
Distal	55 (34.2%)	58 (36%)	
Mid	24 (14.9%)	18 (11.2%)	
Proximal	1 (0.6%)	5 (3.1%)	
T stage, n (%)			0.012
T1	18 (12.4%)	9 (6.2%)	
T2	21 (14.5%)	16 (11%)	
T3	31 (21.4%)	46 (31.7%)	
T4	0 (0%)	4 (2.8%)	
N stage, n (%)			0.424
N0	37 (25.7%)	29 (20.1%)	
N1	29 (20.1%)	34 (23.6%)	
N2	3 (2.1%)	6 (4.2%)	
N3	2 (1.4%)	4 (2.8%)	
M stage, n (%)			1.000
M0	57 (44.2%)	64 (49.6%)	
M1	4 (3.1%)	4 (3.1%)	
Histological type, n (%)			0.157
Adenocarcinoma	35 (21.6%)	45 (27.8%)	
Squamous Cell Carcinoma	46 (28.4%)	36 (22.2%)	
Pathologic stage, n (%)			0.005
Stage I	13 (9.2%)	3 (2.1%)	
Stage II	36 (25.4%)	33 (23.2%)	
Stage III	16 (11.3%)	33 (23.2%)	
Stage IV	4 (2.8%)	4 (2.8%)	
BMI, n (%)			0.040
<=25	36 (23.5%)	48 (31.4%)	
>25	42 (27.5%)	27 (17.6%)	
Reflux history, n (%)			0.967
No	42 (30.9%)	42 (30.9%)	
Yes	25 (18.4%)	27 (19.9%)	
Barrett's esophagus, n (%)			0.511
No	51 (38.6%)	55 (41.7%)	
Yes	15 (11.4%)	11 (8.3%)	
Alcohol history, n (%)			0.635
No	21 (13.2%)	25 (15.7%)	
Yes	58 (36.5%)	55 (34.6%)	

(Continued on following page)

TABLE 1 (*Continued*) Clinical characteristics of esophageal carcinoma (ESCA) patients.

Characteristic	Low expression of APOC1	High expression of APOC1	*p*
Age, mean ± SD	61.32 ± 11.84	63.16 ± 12.2	0.332
BMI, median (IQR)	25.49 (22.12, 28.73)	23.74 (20.87, 26.61)	0.027

significantly lower than in normal tissues in Adrenocortical carcinoma (ACC). APOC1 expression was not significantly different between Lung adenocarcinoma (LUAD) and normal tissues. We also analyzed APOC1 expression in various tumor tissues and tumor-adjacent tissues. APOC1 was more highly expressed in tumor tissues than tumor adjacent in Bladder Urothelial Carcinoma (BLCA), COAD, Head and Neck squamous cell carcinoma (HNSC), KICH, KIRC, KIRP, Prostate adenocarcinoma (PRAD), Stomach adenocarcinoma (STAD), Thyroid carcinoma (THCA), and Uterine Corpus Endometrial Carcinoma (UCEC), while it was less expressed in tumor tissues than tumor adjacent tissues in Cholangiocarcinoma (CHOL), LUAD, and LUSC(lung squamous cell carcinoma), with no significant difference in expression in reading (Figures 1C, D). Next, we analyzed the transcription levels of APOC1 with the TCGA, GTEx, and GEO databases. The analysis showed that APOC1 mRNA expression was significantly upregulated in ESCA tissues compared with normal tissues ($p < 0.001$) (Figure 2A), and the expression of APOC1 mRNA was also significantly increased in ESCA tissues compared with tumor adjacent tissues ($p < 0.01$) (Figure 2B).

Diagnostic value of APOC1 mRNA in ESCA

The diagnostic value of APOC1 mRNA expression in ESCA was analyzed in our study using the ROC method. Our results showed that the area under the curve (AUC) was 0.887. We also analyzed the diagnostic value of APOC1 mRNA expression in different stages, grading, lymph node metastasis, and distant metastasis. The AUC values were 0.808, 0.895, 0.926, and 0.898 by stage I, stage II, stage III, and stage IV, respectively; 0.862, 0.899, 0.900, and 1.000 by T stage T1, T2, T3, and T4, respectively; 0.884, 0.890, 0.949, and 0.955 by lymph node metastasis stages N0, N1, N2, and N3, respectively; and 0.898 for both M0 and M1 according to M staging (Supplementary Figure S1).

Expression of APOC1 is an independent risk factor for poor outcomes in patients with ESCC

We applied the K-M survival curve to analyze the prognostic impact of APOC1 mRNA expression on patients with ESCA. The results showed that APOC1 mRNA expression had no significant effect on all tumors including EAC ($p = 0.052$) (Figure 3A) and EAC alone ($p = 0.09$) (Figure 3B), while patients with ESCC who overexpressed APOC1 mRNA in their tissues had a worse survival prognosis ($p = 0.043$) (Figure 3C). Overexpression of APOC1 mRNA also significantly affected the OS of patients with ESCC at T-stage (T1 and T2) ($p = 0.023$) (Figure 3D), pathological stage (TNM-stage, AJCC prognostic stage) (stage I and stage II) ($p = 0.039$) (Figure 3E), tumor histological grade (grade 1 and grade 2) ($p = 0.009$) (Figure 3F), and columnar metaplasia ($p = 0.027$) ESCC (Figure 3G), while the effect was not significant in T-stage (T3 and T4) ($p = 0.282$) (Figure 3H) and pathological stage (TNM-stage, AJCC prognostic stage) (Stage III and Stage IV) ($p = 0.544$) (Figure 3I) as shown in the subgroup analysis. Univariate and multifactorial analyses showed that high expression of APOC1mRNA, lymph node metastasis, and sex were associated with OS of patients with ESCC, and APOC1 mRNA was likely an independent prognostic risk factor for OS in patients with ESCC (Table 2; Figure 4).

Functional analysis of APOC1 in ESCC

GO functional annotation analysis revealed that APOC1 co-expressed genes in ESCC were mainly involved in the following aspects: regulation of T cell activation, cornification, cytolysis, external side of plasma membrane, MHC protein complex, MHC class II protein complex, serine–type peptidase activity, serine-type endopeptidase activity (Supplementary Table S1; Figure 5A). The KEGG pathway enrichment analysis showed that co-expressed genes of APOC1 were mainly enriched in *Staphylococcus aureus* infection, antigen processing and presentation, and graft-versus-host disease pathways (Supplementary Table S2; Figure 5B).

Identification of APOC1-related signaling pathways by GSEA analysis

The signaling pathways associated with ESCC were analyzed by the GSEA method. The results showed that immunoregulatory interactions between a lymphoid and a non-lymphoid cell and FCERI-mediated NF-KB activation were significantly enriched in APOC1-related phenotypes were significantly enriched (Figure 6).

Establishment of protein interactions signaling network

Through the establishment of protein interactions signaling network, we can understand the metabolic and molecular

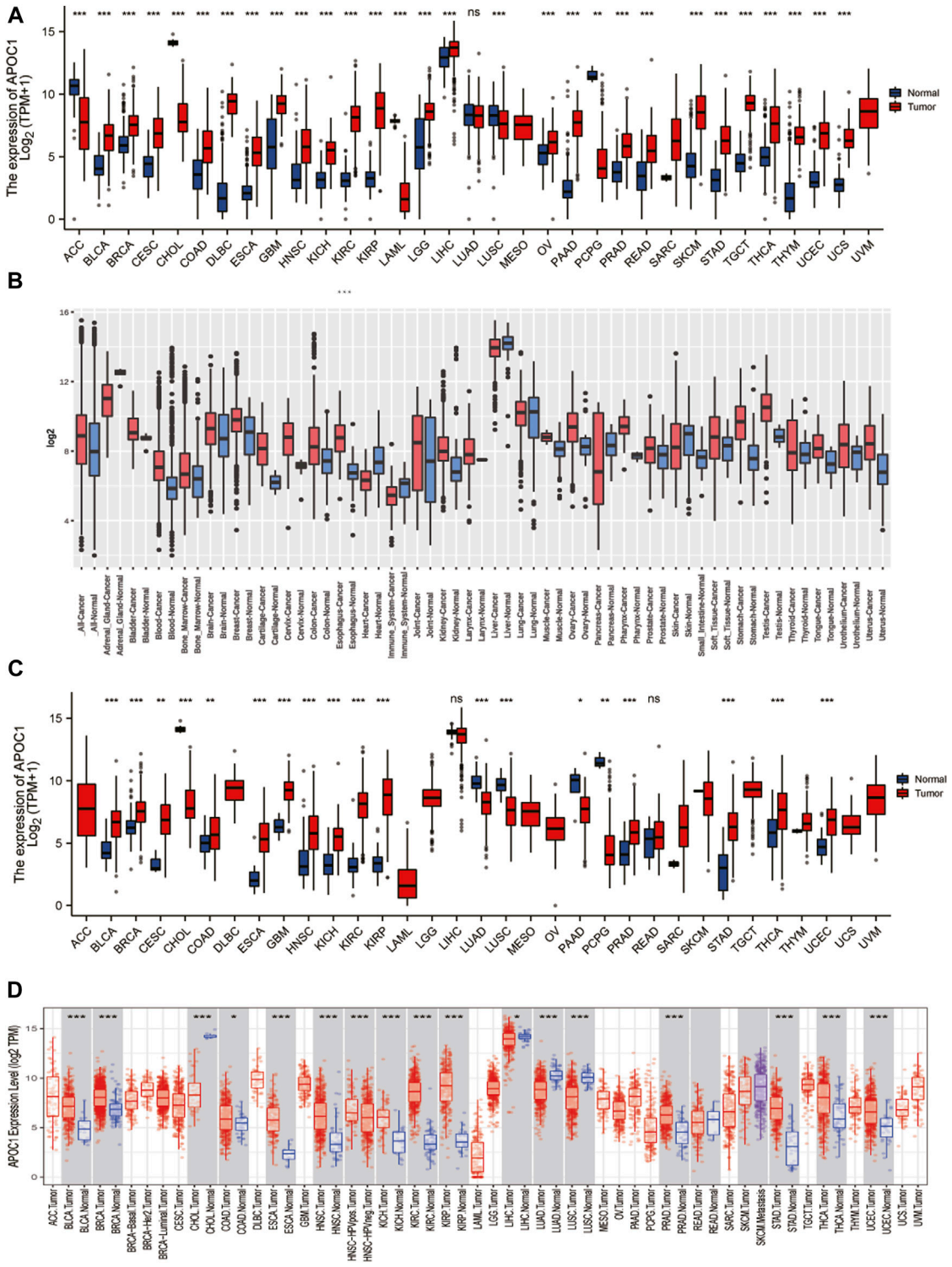

FIGURE 1
The expression of apolipoprotein C1 (APOC1) in various tumors including esophageal carcinoma (ESCA). Expression of APOC1 in tumor versus normal tissues based on the cancer genome atlas (TCGA) database from the genotype-tissue expression (GETx) **(A)** and the GEO platform 96 (GPL96) database from the gene expression database of normal and tumor tissues (GENT2) website **(B)**. The expression of APOC1 mRNA in tumor versus adjacent tissues based on the TCGA database from GTEx**(C)** and TCGA databases from the tumor immune estimation resource (TIMER) website**(D)**. *$p < 0.05$, **$p < 0.01$, ***$p < 0.001$.

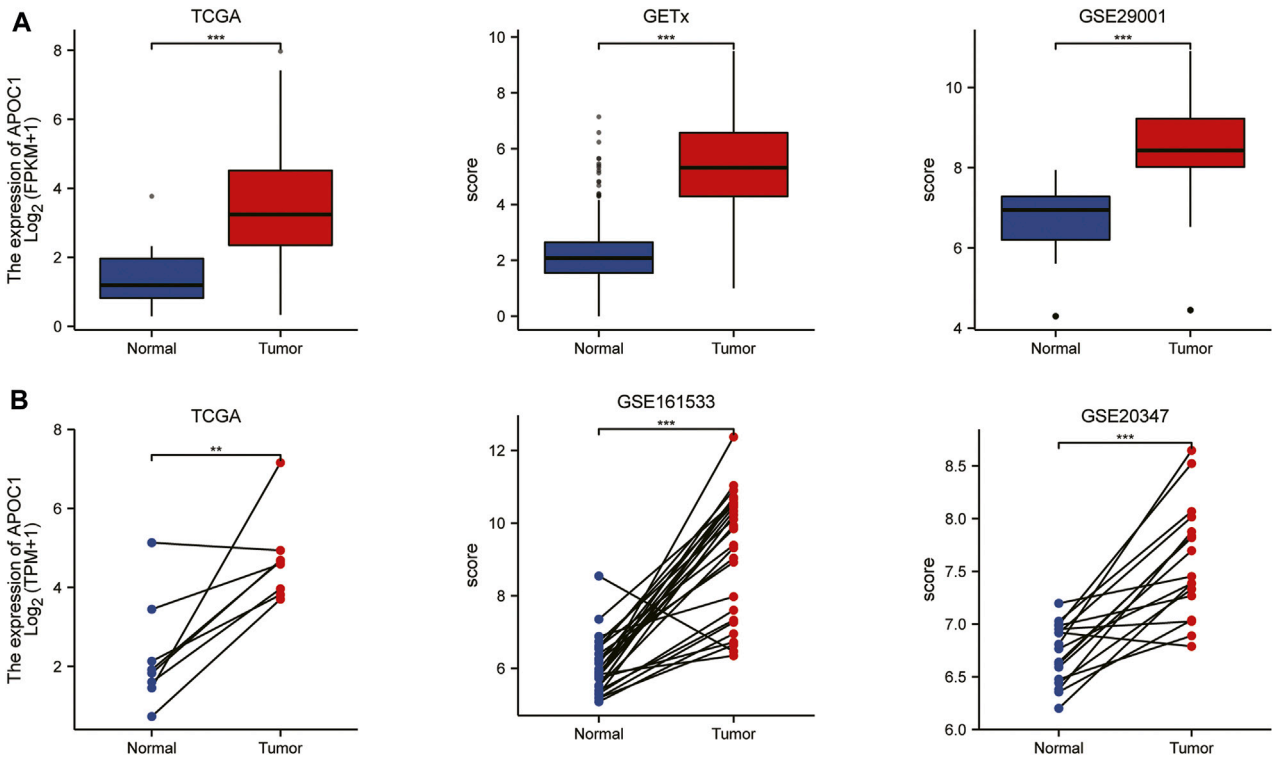

FIGURE 2
The expression of apolipoprotein C1 (APOC1) in esophageal carcinoma (ESCA) based on the cancer genome atlas (TCGA), Genotype-tissue expression (GTEx), and Gene expression omnibus (GEO) databases. The expression of APOC1 mRNA in ESCA and normal tissues **(A)**. The expression of APOC1 mRNA in ESCA and tumor adjacent tissues **(B)**. *$p < 0.05$, **$p < 0.01$, ***$p < 0.001$.

mechanism of ESCC. Therefore, we analyzed the interaction of APOC1 in ESCC through the STRING website protein PPI network. First, on the STING website, we set the parameters for text mining and experimental evidence identification, and then we obtained the APOC1-related protein interactions network (Figure 7A). In addition, we also took the proteins interacting with APOC1 and the differential proteins associated with APOC1 expression in ESCC for intersection analysis and screened the common proteins as APOE, SAA1, APOF, LPL, APOC2, respectively (Figure 7B). Next, we analyzed the correlation between the expression of APOC1 and that of these common proteins, and the results showed that APOC1 had a significant positive correlation with the expression of APOE (r = 0.324, $p = 0.003$); APOF (r = 0.932, $p < 0.001$); LPL (r = 0.550, $p < 0.001$); and APOC2 (r = 0.729, $p < 0.001$) (Figures 7C–F).

Correlation between the expression of APOC1 and the level of immune infiltration

The results of this study showed that in ESCC tissue, a variety of immune infiltrating cells were positively correlated with APOC1 expression such as T cells (r = 0.376, $p < 0.001$); aDC (antibody-dependent cytotoxicity) (r = 0.411, $p < 0.001$); CD8T cells (r = 0.402, $p < 0.001$), cytotoxic cells (r = 0.463, $p < 0.001$), iDC (immature dendritic cell) (r = 0.507, $p < 0.001$), macrophages (r = 0.551, $p < 0.001$), NK CD56 dim cells (r = 0.381, $p < 0.001$), Th1 cells (r = 0.346, $p = 0.002$), and Treg (r = 0.460, $p < 0.001$) (Figures 8A, B). Moreover, cell grouping analysis and individual cell analysis showed a significant positive correlation between APOC1 and immune infiltrating cells (Figures 8C–K). To further explore the relationship between APOC1 expression and tumor-infiltrating lymphocytes (TILs), we examined the relationship between TILs and APOC1 expression through the TISIDB website. The results showed a significant positive correlation between APOC1 and multiple TILs cells in ESCA (Supplementary Figure S2). Given that current targeted drug therapy against tumors benefits patients with a wide range of tumors (33), in this study we also analyzed the relationship between APOC1 and various tumor control-related genes. Our results showed that tumor targeting-related immune checkpoint genes such as CD274 ($p = 0.0137$), TGFB1 ($p = 0.0175$), PDCD1 ($p < 0.001$), CTLA4 ($p < 0.001$), and LAG3 ($p < 0.001$) were significantly associated with APOC1

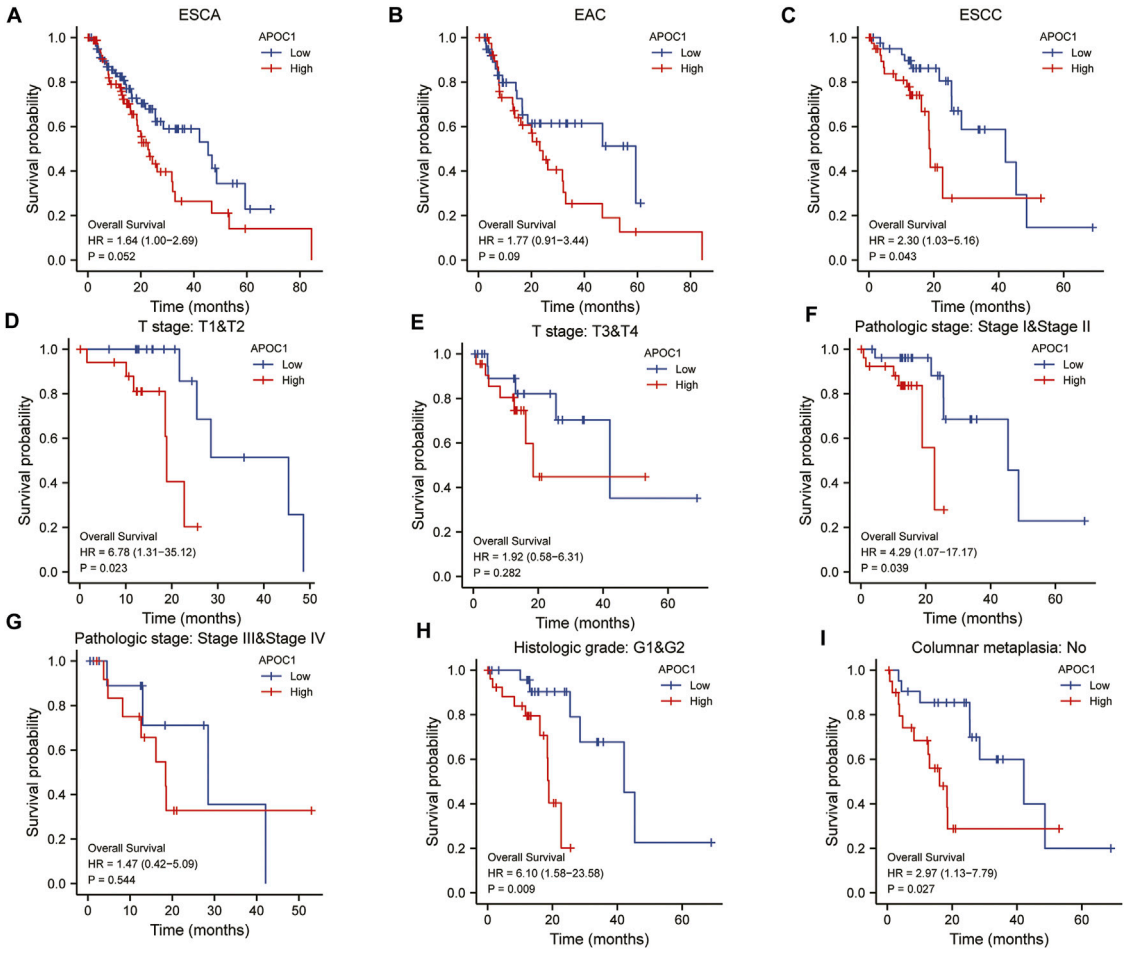

FIGURE 3
Analysis of overall survival (OS) with apolipoprotein C1 (APOC1) mRNA expression in esophageal carcinoma (ESCA), esophageal adenocarcinoma (EAC), and esophageal squamous cell carcinoma (ESCC) **(A–C)**. Subgroup analysis of overall survival with APOC1 mRNA in ESCC **(D–I)**.

(Figure 9). These significant correlations may be related to the poorer prognosis of patients with ESCC owing to high expression of APOC1. Interestingly, APOC1 expression was also significantly correlated with inflammatory factors such as IL10 ($p < 0.001$) (Figure 9). In addition, we also analyzed the relationship between APOC1 expression and chemokines (Supplementary Figure S3) and chemokine receptor (Supplementary Figure S4). The analysis showed a significant positive correlation between APOC1 and a large variety of immune chemokines and chemokine receptors. Combined with the results of correlation analysis of APOC1 expression with target molecules, immune-related molecules, and inflammatory chemokines, AOPC1 may be involved in immune infiltration and inflammatory responses in the tumor microenvironment and tumorigenesis and development.

Discussion

In the present study, we found that consistent with the findings on the role of APOC1 in other cancers, APOC1 also showed significantly higher expression in ESCA tissues than in normal tissues and tumor-adjacent tissues. Therefore, we hypothesized that APOC1 may play an important role in the development of ESCA. Subsequently, we found by ROC analysis that the expression of APOC1 in different patient stages of ESCA also has some diagnostic value. In subsequent survival analysis, it was shown that high APOC1 expression was significantly associated with poorer OS in patients with ESCC. Based on these findings, we concluded that APOC1 could be used as a biomarker for the staging determination and prognosis of patients with ESCA, especially ESCC.

TABLE 2 Cox proportional hazards regression model analysis for OS of ESCC patients.

Characteristics	Total (N)	Univariate analysis		Multivariate analysis	
		Hazard ratio (95% CI)	*p* value	Hazard ratio (95% CI)	*p* value
T stage	79				
T1&T2	35	Reference			
T3&T4	44	0.942 (0.414–2.142)	0.887		
N stage	78				
N0	46	Reference			
N1	26	1.960 (0.789–4.869)	0.147	1.315 (0.353–4.896)	0.684
N2&N3	6	4.310 (1.301–14.279)	**0.017**	7.977 (1.200–53.005)	**0.032**
M stage	73				
M0	70	Reference			
M1	3	3.197 (0.909–11.238)	0.070	4.643 (0.878–24.553)	0.071
APOC1	82				
Low	41	Reference			
High	41	2.302 (1.027–5.158)	**0.043**	3.210 (1.119–9.208)	**0.030**
Gender	82				
Female	12	Reference			
Male	70	10.030 (1.323–76.071)	**0.026**	191838562.424 (0.000–Inf)	0.998
Pathologic stage	79				
Stage I&Stage II	54	Reference			
Stage IV&Stage III	25	2.178 (0.958–4.952)	0.063	0.512 (0.123–2.133)	0.358
Age	82				
<=60	53	Reference			
>60	29	1.592 (0.676–3.749)	0.288		

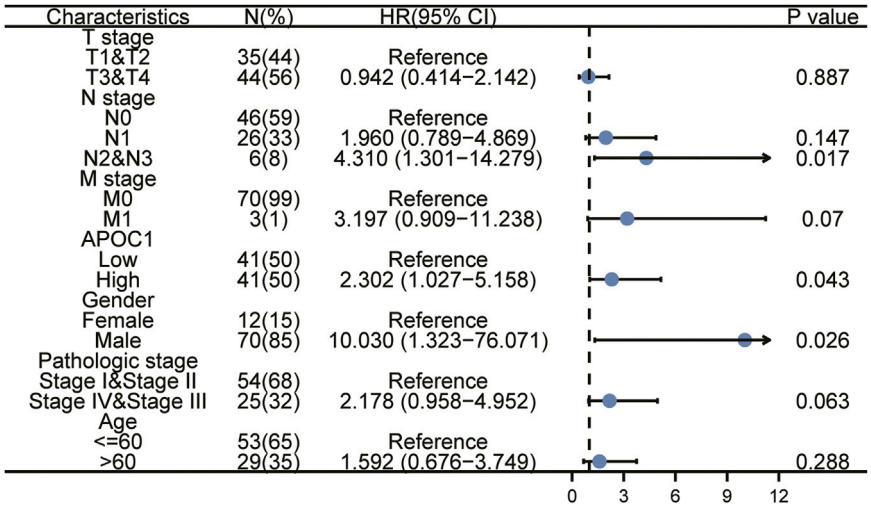

FIGURE 4
Univariate and multivariate regression analysis of apolipoprotein C1 (APOC1) and characteristics with overall survival (OS) in ESCC patients.

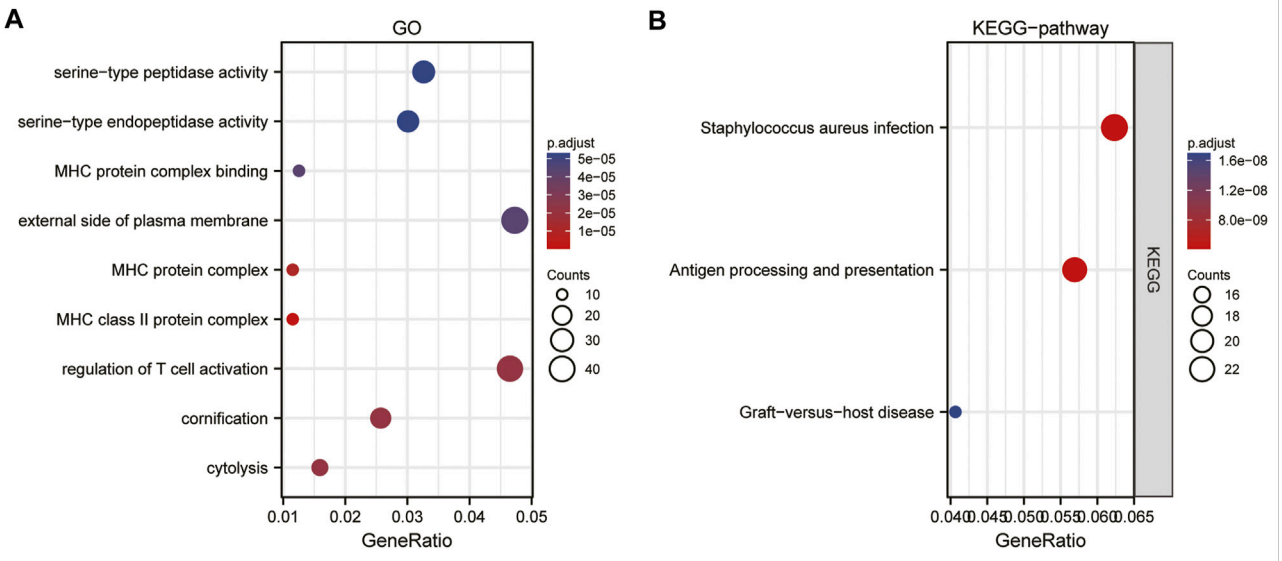

FIGURE 5
Gene ontology (GO)**(A)** and kyoto encyclopedia of genes and genome (KEGG) **(B)**enrichment analysis of apolipoprotein C1 (APOC1) expression correlated different expression genes in esophageal squamous cell carcinoma (ESCC).

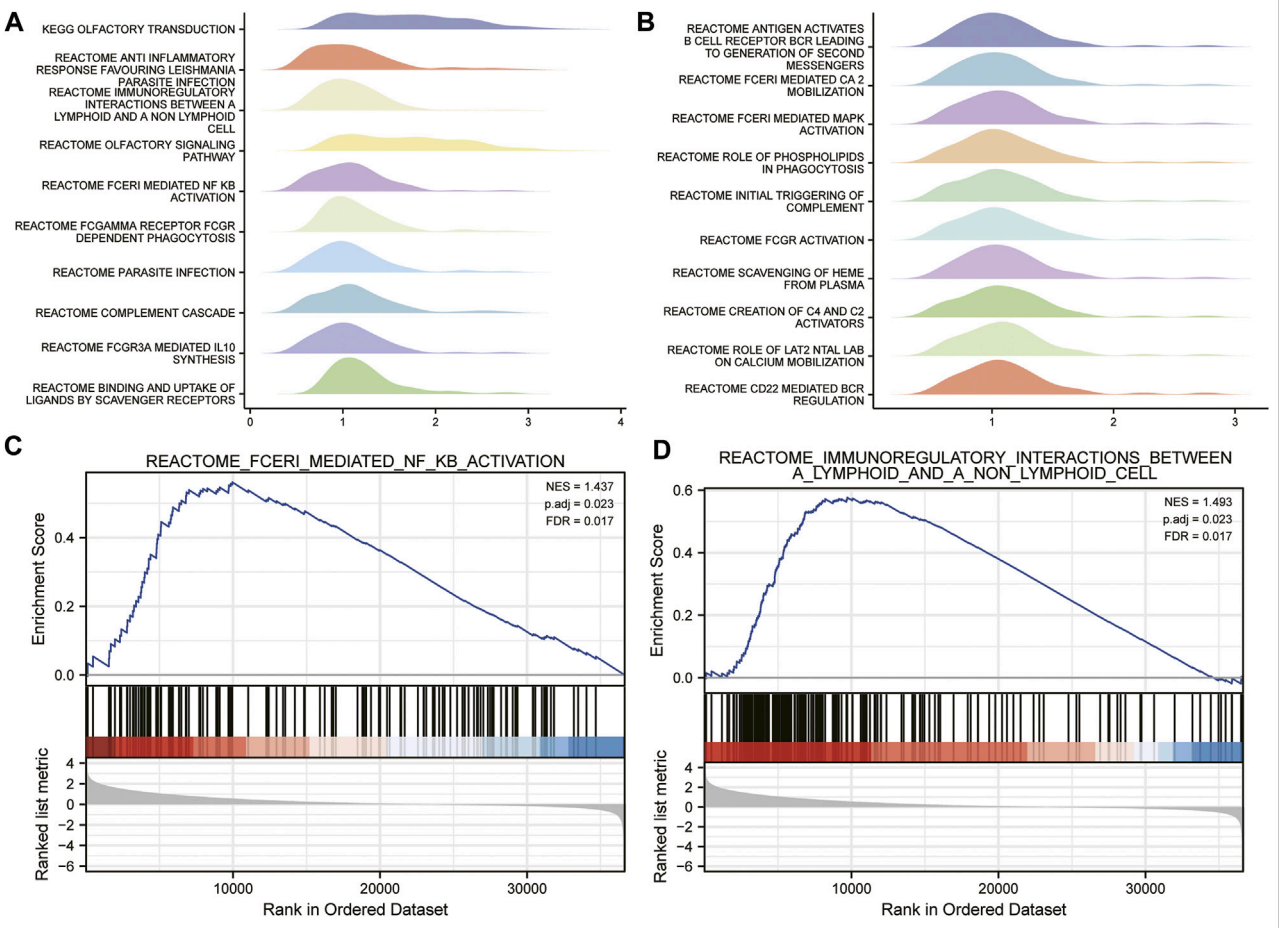

FIGURE 6
Identification of apolipoprotein C1 (APOC1) related signaling pathways by gene set enrichment analysis (GSEA) analysis **(A,B)**. Fceri mediated nuclear factor kappa B (NFKB) activation **(C)**. Immuno-regulatory interactions between a lymphoid and a non-lymphoid cell **(D)**.

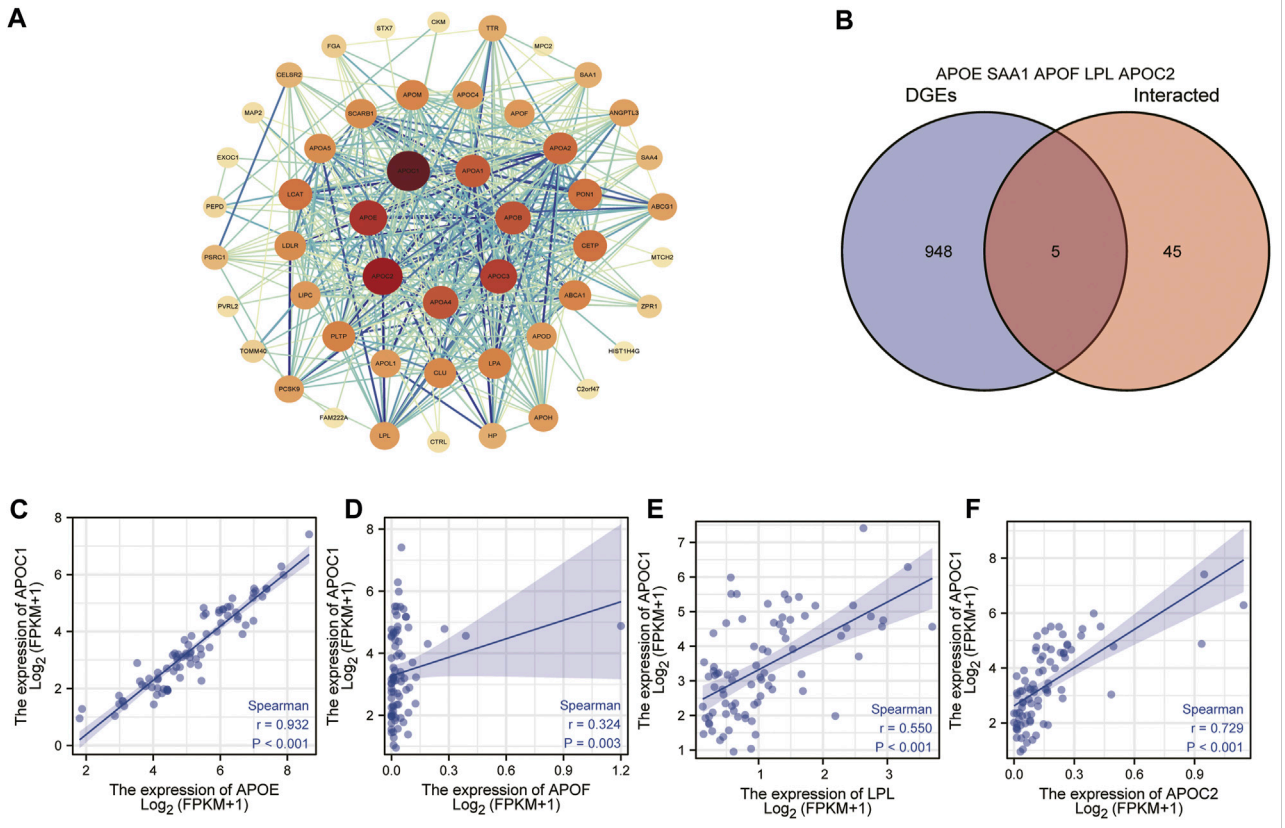

FIGURE 7
Establishment of apolipoprotein C1 (APOC1) related genes protein interactions signaling network. Protein-protein interaction (PPI) network obtained from the search tool for the retrieval of interacting genes/proteins (STRING) **(A)**. Common proteins screened by taking intersections between APOC1-interacting proteins and APOC1 expression-related differential gene proteins **(B)**. Correlation of APOC1 with common proteins **(C–F)**.

Tumorigenesis and the development of tumors depend on the tumor microenvironment (TME), and tumors are also involved in the composition, regulation, and development of the TME (34). The effectiveness of tumor immunotherapy is related not only to the tumor, but also to the immune microenvironment, which is external to the tumor (35). By contrast, tumor-infiltrating lymphocytes with a predictive role for immune checkpoint inhibitors in ESCA immunotherapy have not yet been reported. In the present study, we analyzed the correlation of APOC1 expression with immune checkpoint markers and tumor immune infiltrating lymphocytes. Our results showed that APOC1 expression was significantly and positively correlated with aDC ($r = 0.411$, $p < 0.001$); CD8 T cells ($r = 0.402$, $p < 0.001$); and cytotoxic cells ($r = 0.463$, $p < 0.001$), especially macrophages ($r = 0.551$, $p < 0.001$). Further analysis showed that APOC1 had significant positive correlations with IL10 ($p < 0.001$), CSF1R ($p < 0.001$), CD274 (PD-L1) ($p = 0.0137$), TGFB1 ($p = 0.0175$), PDCD1 (PD-1) ($p < 0.001$), PDCD1LG2 (PD-L2) ($p < 0.001$), CTLA4($p < 0.001$), and LAG3($p < 0.001$). This may be because the TME with high APOC1 expression affects the polarization of macrophages, causing macrophages to secrete substances such as IL10, which in turn causes pro-tumorigenic effects of macrophages on ESCA cells, leading to tumor development (36). It was inferred that APOC1 expression was significantly correlated with multiple immune markers and immune infiltration levels, which is consistent with previous findings (37). Because APOC1 has a close relationship with both tumor internal factors and tumor external factors of the tumor immune microenvironment (TIME), we hypothesized that the expression level of APOC1 may be a potential predictive biomarker for application as an immune checkpoint inhibitor. According to the results of GSEA analysis, immunoregulatory interactions between a lymphoid and a non-lymphoid cell and FCERI-mediated NF-KB activation are potential signaling pathways, suggesting that APOC1 may be closely related to both cellular and humoral immune

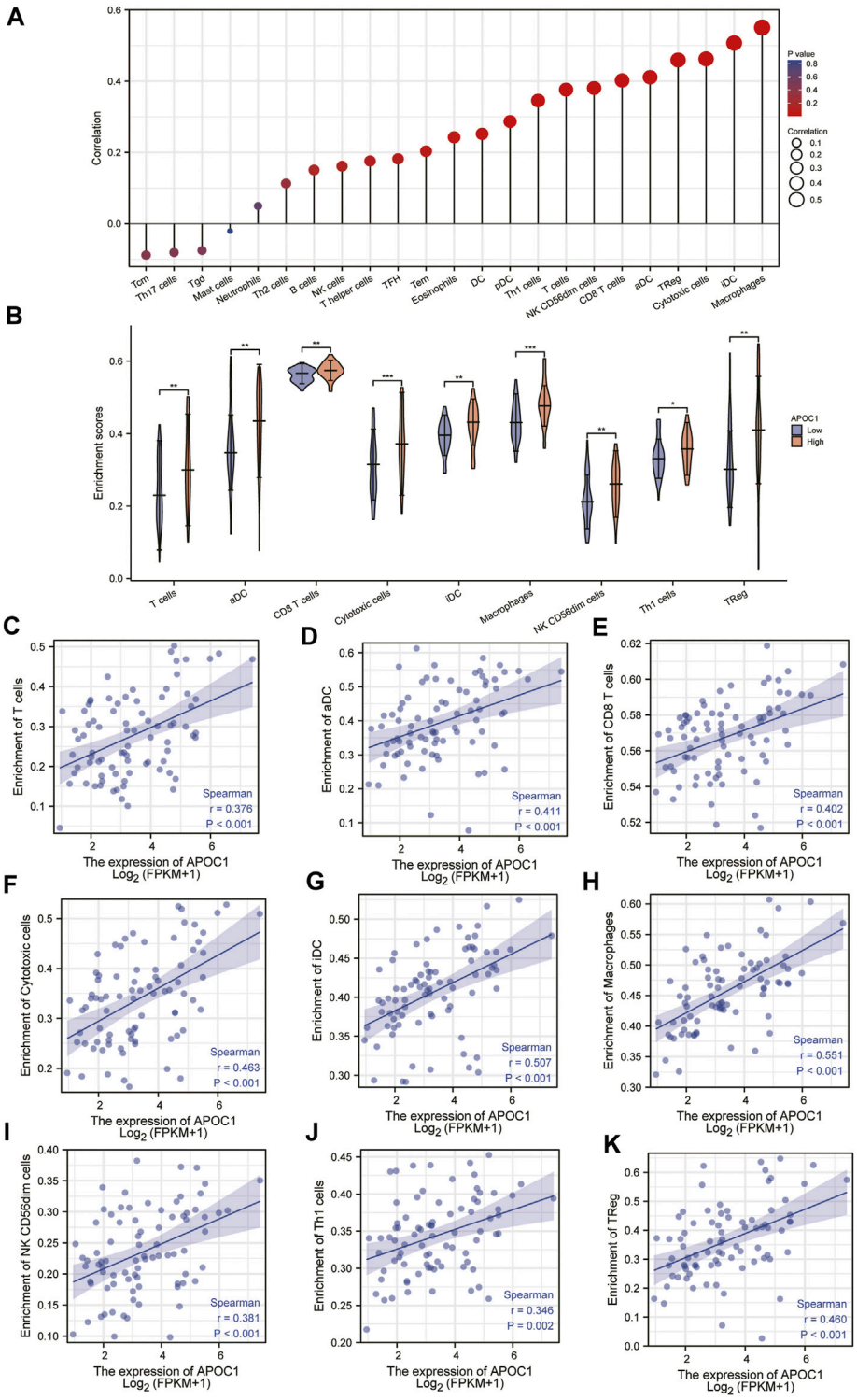

FIGURE 8
Correlation between the expression of apolipoprotein C1 (APOC1) and immune infiltration level in esophageal squamous cell carcinoma (ESCC) **(A,B)**. Positive correlation between APOC1 and various immune infiltrating cells **(C–K)**.

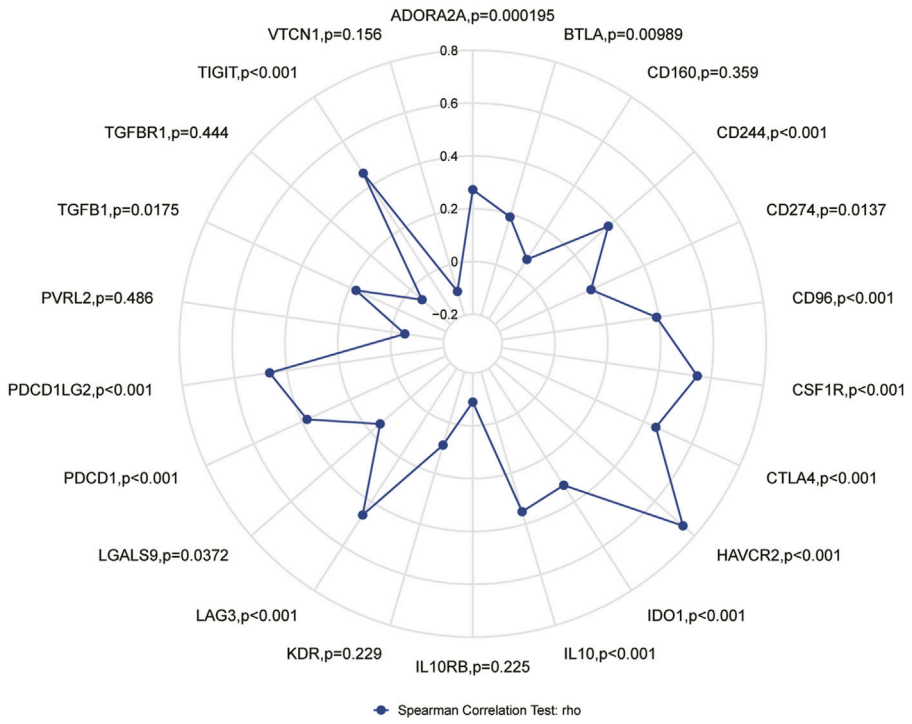

FIGURE 9
Correlation of apolipoprotein C1 (APOC1) expression with immune checkpoint genes.

responses during esophageal carcinogenesis. This may also be a potential mechanism for the association of APOC1 with poorer prognosis in patients with ESCA. Meanwhile, the analysis of the relationship between APOC1 expression and related immune chemokines showed that APOC1 was significantly and positively correlated with most of the immune chemokines, and chemokines regulate lymphocyte recruitment(38), which may be associated with poorer prognosis of ESCA. However, thus far to our knowledge, no experiments have been conducted to verify this inference, which is a limitation of our study. Further basic and clinical experiments are needed to fully elucidate the biological function of APOC1 in ESCA.

Conclusion

In conclusion, APOC1 may be used as a diagnostic biomarker for esophageal cancer. In addition, as a new prognostic marker in ESCC patients, it positively correlates with T cells, CD8T cells, cytotoxic cells and is closely related to NF-KB, and may be potentially valuable for further investigation of the diagnosis and treatment of ESCC patients.

Data availability statement

The original contributions presented in the study are included in the article/Supplementary Material, further inquiries can be directed to the corresponding authors.

Ethics statement

Ethical review and approval was not required for the study on human participants in accordance with the local legislation and institutional requirements. Written informed consent for participation was not required for this study in accordance with the national legislation and the institutional requirements.

Author contributions

XC and BW were involved in data curation, data analysis, investigation, methodology, and writing; HL was involved in project administration, supervision, and writing—review. SG, WZ, SY, ZZ, and LG were involved in data analysis, investigation and writing; All authors read and approved the final manuscript.

Funding

The study is supported by the Doctoral Start-up Fund from the First Affiliated Hospital of Gannan Medical University, QD202214.

Conflict of interest

The authors declare that the research was conducted in the absence of any commercial or financial relationships that could be construed as a potential conflict of interest.

Acknowledgments

We acknowledge the GEO, TCGA, GTEx, STRING, and TISIDB databases freely used online.

Supplementary material

The Supplementary Material for this article can be found online at: https://www.por-journal.com/articles/10.3389/pore.2023.1610976/full#supplementary-material

References

1. Sung H, Ferlay J, Siegel RL, Laversanne M, Soerjomataram I, Jemal A, et al. Global cancer statistics 2020: GLOBOCAN estimates of incidence and mortality worldwide for 36 cancers in 185 countries. *CA Cancer J Clin* (2021) 71(3):209–49. doi:10.3322/caac.21660

2. Pennathur A, Gibson MK, Jobe BA, Luketich JD. Oesophageal carcinoma. *Lancet* (2013) 381(9864):400–12. doi:10.1016/S0140-6736(12)60643-6

3. Arnold M, Soerjomataram I, Ferlay J, Forman D. Global incidence of oesophageal cancer by histological subtype in 2012. *Gut* (2015) 64(3):381–7. doi:10.1136/gutjnl-2014-308124

4. Lin Y, Totsuka Y, He Y, Kikuchi S, Qiao Y, Ueda J, et al. Epidemiology of esophageal cancer in Japan and China. *J Epidemiol* (2013) 23(4):233–42. doi:10.2188/jea.je20120162

5. Graham AJ, Shrive FM, Ghali WA, Manns BJ, Grondin SC, Finley RJ, et al. Defining the optimal treatment of locally advanced esophageal cancer: A systematic review and decision analysis. *Ann Thorac Surg* (2007) 83(4):1257–64. doi:10.1016/j.athoracsur.2006.11.061

6. Smyth EC, Lagergren J, Fitzgerald RC, Lordick F, Shah MA, Lagergren P, et al. Oesophageal cancer. *Nat Rev Dis Primers* (2017) 3:17048. doi:10.1038/nrdp.2017.48

7. Chen W, Zheng R, Zeng H, Zhang S. The updated incidences and mortalities of major cancers in China, 2011. *Chin J Cancer* (2015) 34(11):502–7. doi:10.1186/s40880-015-0042-6

8. Chen G, Wang Z, Liu XY, Liu FY. Recurrence pattern of squamous cell carcinoma in the middle thoracic esophagus after modified Ivor-Lewis esophagectomy. *World J Surg* (2007) 31(5):1107–14. doi:10.1007/s00268-006-0551-1

9. Homet Moreno B, Ribas A. Anti-programmed cell death protein-1/ligand-1 therapy in different cancers. *Br J Cancer* (2015) 112(9):1421–7. doi:10.1038/bjc.2015.124

10. Riley RS, June CH, Langer R, Mitchell MJ. Delivery technologies for cancer immunotherapy. *Nat Rev Drug Discov* (2019) 18(3):175–96. doi:10.1038/s41573-018-0006-z

11. Zhang W, Yan C, Gao X, Li X, Cao F, Zhao G, et al. Safety and feasibility of radiotherapy plus camrelizumab for locally advanced esophageal squamous cell carcinoma. *Oncologist* (2021) 26:e1110–e1124. doi:10.1002/onco.13797

12. Chouaib S. EMT in immuno-resistance. *Oncoscience* (2015) 2:841–2. doi:10.18632/oncoscience.226

13. Yamamura K, Izumi D, Kandimalla R, Sonohara F, Baba Y, Yoshida N, et al. Intratumoral fusobacteriukm nucleatum levels predict therapeutic response to neoadjuvant chemotherapy in esophageal squamous cell carcinoma. *Clin Cancer Res* (2019) 25:6170–9. doi:10.1158/1078-0432.CCR-19-0318

14. Jong MC, Hofker MH, Havekes LM. Role of ApoCs in lipoprotein metabolism: Functional differences between ApoC1, ApoC2, and ApoC3, *Arterioscler Thromb Vasc Biol* (1999) 19(3):472–84. doi:10.1161/01.atv.19.3.472

15. Yi J, Ren L, Wu J, Li W, Zheng X, Du G, et al. Apolipoprotein C1 (APOC1) as a novel diagnostic and prognostic biomarker for gastric cancer, *Ann Transl Med* (2019) 7(16):380. doi:10.21037/atm.2019.07.59

16. Zhang J, Guo F, Wang L, Zhao W, Zhang D, Yang H, et al. Identification of apolipoprotein C-I as a potential Wilms' tumor marker after excluding inflammatory factors. *Int J Mol Sci* (2014) 15(9):16186–95. doi:10.3390/ijms150916186

17. Ko HL, Wang YS, Fong WL, Chi MS, Chi KH, Kao SJ. Apolipoprotein C1 (APOC1) as a novel diagnostic and prognostic biomarker for lung cancer: A marker phase I trial. *Thorac Cancer* (2014) 5:500–8. doi:10.1111/1759-7714.12117

18. Ren H, Chen Z, Yang L, Xiong W, Yang H, Xu K, et al. Apolipoprotein C1 (APOC1) promotes tumor progression via MAPK signaling pathways in colorectal cancer. *Cancer Manag Res* (2019) 11(1):4917–30. doi:10.2147/CMAR.S192529

19. Jiang H, Tang JY, Xue D, Chen YM, Wu TC, Zhuang QF, et al. Apolipoprotein C1 stimulates the malignant process of renal cell carcinoma via the Wnt3a signaling, *Cancer Cel Int* (2021) 21(1):41. doi:10.1186/s12935-020-01713-x

20. Moore LE, Brennan P, Karami S, Menashe I, Berndt SI, Dong LM, et al. Apolipoprotein E/C1 locus variants modify renal cell carcinoma risk. *Cancer Res* (2009) 69(20):8001–8. doi:10.1158/0008-5472.CAN-09-1734

21. Takano S, Yoshitomi H, Togawa A, Sogawa K, Shida T, Kimura F, et al. Apolipoprotein C-1 maintains cell survival by preventing from apoptosis in pancreatic cancer cells. *Oncogene* (2008) 27(20):2810–22. doi:10.1038/sj.onc.1210951

22. Dvorak HF. Tumors: Wounds that do not heal. Similarities between tumor stroma generation and wound healing. *N Engl J Med* (1986) 315(26):1650–9. doi:10.1056/NEJM198612253152606

23. Chechlinska M, Kowalewska M, Nowak R. Systemic inflammation as a confounding factor in cancer biomarker discovery and validation. *Nat Rev Cancer* (2010) 10(1):2–3. doi:10.1038/nrc2782

24. Dvorak HF. Tumors: Wounds that do not heal-redux. *Cancer Immunol Res* (2015) 3(1):1–11. doi:10.1158/2326-6066.CIR-14-0209

25. Wu CX, Rao DY, Sang CP, Zhu SY, Gu L, Wu YY, et al. Peripheral blood inflammation indices are effective predictors of anastomotic leakage in elective esophageal surgery. *J Gastrointest Oncol* (2021) 12, 2675–84. doi:10.21037/jgo-21-812

26. Berbée JFP, Havekes LM, Rensen PCN. Apolipoproteins modulate the inflammatory response to lipopolysaccharide. *SAGE* (2005) 112:97–103. doi:10.1177/09680519050110020501

27. Guo Q, Liu XL, Jiang N, Zhang WJ, Guo SW, Yang H, et al. Decreased APOC1 expression inhibited cancer progression and was associated with better prognosis and immune microenvironment in esophageal cancer. *Am J Cancer Res* (2022) 12(11):4904–29.

28. Clough E, Barrett T. The gene expression omnibus database. *Methods Mol Biol* (2016) 1418:93–110. doi:10.1007/978-1-4939-3578-9_5

29. Tomczak K, Czerwinska P, Wiznerowicz M. The cancer genome atlas (TCGA): An immeasurable source of knowledge. *Contemp Oncol (Pozn)* (2015) 19:A68–77. doi:10.5114/wo.2014.47136

30. Consortium GT. The genotype-tissue expression (GTEx) project. *Nat Genet* (2013) 45(6):580–5. doi:10.1038/ng.2653

31. Szklarczyk D, Gable AL, Lyon D, Junge A, Wyder S, Huerta-Cepas J, et al. STRING v11: Protein-protein association networks with increased coverage, supporting functional discovery in genome-wide experimental datasets. *Nucleic Acids Res* (2019) 47:D607–D613. doi:10.1093/nar/gky1131

32. Ru B, Wong CN, Tong Y, Zhong JY, Zhong SSW, Wu WC, et al. Tisidb: An integrated repository portal for tumor-immune system interactions. *Bioinformatics* (2019) 35(20):4200–2. doi:10.1093/bioinformatics/btz210

33. Topalian SL, Drake CG, Pardoll DM. Immune checkpoint blockade: A common denominator approach to cancer therapy. *Cancer Cell* (2015) 27(4): 450–61. doi:10.1016/j.ccell.2015.03.001

34. Hanahan D, Coussens LM. Accessories to the crime: Functions of cells recruited to the tumor microenvironment. *Cancer Cell* (2012) 21(3):309–22. doi:10.1016/j.ccr.2012.02.022

35. Gibney GT, Weiner LM, Atkins MB, Predictive biomarkers for checkpoint inhibitor-based immunotherapy. *Lancet Oncol* (2016) 17(3):e542–51. doi:10.1016/S1470-2045(16)30406-5

36. Mantovani A, Sozzani S, Locati M, Allavena P, Sica A. Macrophage polarization: Tumor-associated macrophages as a paradigm for polarized M2 mononuclear phagocytes. *Trends Immunol* (2002) 23:549–55. doi:10.1016/s1471-4906(02)02302-5

37. Mi X, Xu R, Hong S, Xu T, Zhang W, Liu M. Macrophage-derived exosomal lncRNA AFAP1-AS1 and MicroRNA-26a affect cell migration and metastasis in esophageal cancer. *Mol Ther Nucleic Acids* (2020) 22:779–90. doi:10.1016/j.omtn.2020.09.035

38. Mitchem JB, Brennan DJ, Knolhoff BL, Belt BA, Zhu Y, Sanford DE, et al. Targeting tumor-infiltrating macrophages decreases tumor-initiating cells, relieves immunosuppression, and improves chemotherapeutic responses. *Cancer Res* (2013) 73:1128–41. doi:10.1158/0008-5472.CAN-12-2731

Pathology & Oncology Research | frontiers

TYPE Review
PUBLISHED 07 February 2023
DOI 10.3389/pore.2023.1610931

Check for updates

OPEN ACCESS

EDITED BY
Anna Sebestyén,
Semmelweis University, Hungary

*CORRESPONDENCE
Aiqin Sun,
aiqinsun@ujs.edu.cn
Qiong Lin,
qlin@ujs.edu.cn

RECEIVED 07 November 2022
ACCEPTED 16 January 2023
PUBLISHED 07 February 2023

CITATION
Sun A, Tian X, Chen Y, Yang W and Lin Q (2023), Emerging roles of the HECT E3 ubiquitin ligases in gastric cancer. *Pathol. Oncol. Res.* 29:1610931. doi: 10.3389/pore.2023.1610931

COPYRIGHT
© 2023 Sun, Tian, Chen, Yang and Lin. This is an open-access article distributed under the terms of the Creative Commons Attribution License (CC BY). The use, distribution or reproduction in other forums is permitted, provided the original author(s) and the copyright owner(s) are credited and that the original publication in this journal is cited, in accordance with accepted academic practice. No use, distribution or reproduction is permitted which does not comply with these terms.

Emerging roles of the HECT E3 ubiquitin ligases in gastric cancer

Aiqin Sun[1,2]*, Xianyan Tian[1], Yifei Chen[1], Wannian Yang[1] and Qiong Lin[1]*

[1]School of Medicine, Jiangsu University, Zhenjiang, China, [2]Department of laboratory Medicine, School of Medicine, Jiangsu University, Zhenjiang, China

Gastric cancer (GC) is one of the most pernicious gastrointestinal tumors with extraordinarily high incidence and mortality. Ubiquitination modification of cellular signaling proteins has been shown to play important roles in GC tumorigenesis, progression, and prognosis. The E3 ubiquitin ligase is the crucial enzyme in the ubiquitination reaction and determines the specificity of ubiquitination substrates, and thus, the cellular effects. The HECT E3 ligases are the second largest E3 ubiquitin ligase family characterized by containing a HECT domain that has E3 ubiquitin ligase activity. The HECT E3 ubiquitin ligases have been found to engage in GC progression. However, whether HECT E3 ligases function as tumor promoters or tumor suppressors in GC remains controversial. In this review, we will focus on recent discoveries about the role of the HECT E3 ubiquitin ligases, especially members of the NEDD4 and other HECT E3 ligase subfamilies, in GC.

KEYWORDS

gastric cancer, ubiquitination, tumor suppressor, HECT E3 ubiquitin ligases, oncoprotein

Introduction

Ubiquitin is an evolutionarily conserved 76-amino acid polypeptide, which serves as a modifier molecule that covalently binds to target proteins for degradation or non-degradative signaling (1). The process attaches ubiquitin to specific substrate proteins, which is called ubiquitination, and is one of the most important protein post-translational modifications. Ubiquitination has been shown to regulate and maintain basic biological functions, including cell cycle, cell differentiation, cell localization, cell survival, apoptosis, signal transduction, and the inflammatory response (2-4). Ubiquitination, including activating, conjugating, and ligating, is a highly orchestrated enzymatic cascade involved in the multistep processes catalyzed by activating enzymes (E1), conjugating enzymes (E2), and ubiquitin ligases (E3) (5). In the human genome, two E1s, 38-40 E2s, and more than 600 E3 ubiquitin ligases have been identified (6,7). E3 ubiquitin ligases are remarkable enzymes, which directly medicate the interaction between ubiquitin and substrates, and mainly determine the substrate specificity and versatility for ubiquitination modification (8,9). In mammalian cells, E3 ligases are usually the

TABLE 1 HECT E3 ligases in human gastric cancer.

E3	Expression	Substrates	Adaptors/ Regulators	Pathway	Functions	Role in GC	Reference
NEDD4	upregulation	unknown	Unknown	unknown	regulates proliferation, migration and invasion	dual	(17–20)
NEDD4L	downregulation	unknown	HIF-1α	unknown	unknown	tumor suppressor	(21, 22)
ITCH	downregulation	SMAD7	ASSP2 miR-17 Cir-ITCH	TGF-β pathway Wnt/β-catenin pathway	relates to invasion and TGF-β1-induced EMT	dual	(23–25)
WWP1	upregulation	unknown	miR-584-5p miR-129-5p miR-129-3p	TGF-β pathwayPTEN/AKT pathway	increases tumor growth and decreases apoptosis	oncoprotein	(26–28)
WWP2	upregulation	unknown	unknown	PTEN/PI3K/AKT pathway	promotes proliferation	oncoprotein	(29)
SMURF1	upregulation	MEKK2	miR-424 miR-1254 Kir2.1 STK38	PI3K/AKT pathway MEK1/2–ERK1/2 pathway	participates in metastasis and EMT	dual	(30–33)
HUWE1	upregulation	TGFBR2	unknown	unknown	promotes proliferation, migration, and invasion	oncoprotein	(34)
HACE1	downregulation hypermethylation	cyclin C	unknown	Wnt/β-catenin pathway	suppresses proliferation and migration, enhances apoptosis	tumor suppressor	(35–37)
UBR5	upregulation frameshift mutations	GKN1	unknown	unknown	enhances cell growth, migration, and invasion	oncoprotein	(38–40)
UBE3C	upregulation	P53 AXIN1	RAD18	Wnt/β-catenin pathway P53 pathway	promotes proliferation and inhibits apoptosis	oncoprotein	(41, 42)
HECTD3	upregulation	c-MYC	unknown	unknown	facilitates proliferation and inhibits apoptosis	oncoprotein	(43)

prominent focal point of cell regulation, which makes them the most attractive targets for disease treatment and intervention (10,11). HECT E3 ligase activity and substrate specificity can be regulated by a wide variety of mechanisms, such as different post-translational modifications or protein–protein interactions (12). There are several approaches for targeting the HECT E3s, however specific inhibitors of the HECT E3s have still not been exploited.

Gastric cancer (GC) is an extremely aggressive tumor and is estimated to be a major cause of cancer-related death worldwide (13,14). The pathogenetic mechanisms of gastric cancer are complex and heterogeneous, involving environmental factors, gene mutations, copy number variants, and epigenetic changes (15,16). Recently, the HECT E3 ligases have received considerable attention due to their multiple roles in the occurrence and development of GC. Due to the scarcity of studies concentrating on the potential contributions of HERC subfamily E3 ligases to GC, in this review we focus on the roles of NEDD4 subfamily and other HECT E3 ligases in GC development (Table 1).

The HECT E3 ubiquitin ligases

Based on their structures and catalytic mechanism, E3 ubiquitin ligases can be categorized into three groups: HECT (Homologous to E6-associated protein C-terminus) E3s (44-46), RING (really interesting new gene) E3s (47,48), and RBR (RING-between-RING) E3s (49,50). RING E3s, which make up 95% of E3 ligases, act as scaffold proteins, performing a single-step ubiquitin transfer from the ubiquitin-charging E2 enzyme to the substrates (45). Unlike RING E3s, HECT and RBR E3 ligases contain catalytic cysteine residue, forming an intermediate thioester bond with ubiquitin before the transfer of ubiquitin to lysine residue on the substrates (51).

HECT E3 ligases have a total of 28 members, typically with a conserved ~40 kDa HECT domain, which can be further divided into three subgroups on the basis of their domain architecture in the N-terminus:NEDD4 subfamily with C2 and WW domains, HERC subfamily with RLD domains, and "Other" HECT E3 subfamily which contains neither C2 and WW domains nor RLD domains (12,52) (Figure 1).

The NEDD4 subfamily is the most famous and has been studied most in-depth of the HECT E3 ligases, consisting of 9 proteins in humans: NEDD4 (NEDD4-1), NEDD4L (NEDD4-2), ITCH (AIP4), WWP1 (AIP5), WWP2 (AIP2), SMURF1, SMURF2, NEDL1 (HECW1) and NEDL2 (HECW2) (53). Structurally, NEDD4 subfamily proteins contain an N-terminal C2 domain, two to four WW domains in the central region, and a C-terminal HECT domain (Figure 1). The C2 domain is defined as a Ca^{2+} and is a phospholipid binder involved in protein-protein interactions, regulating the

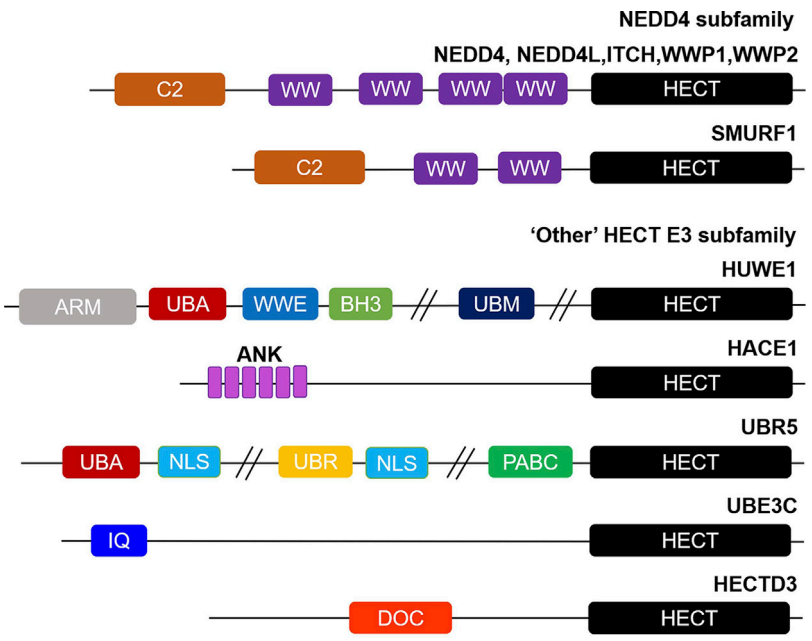

FIGURE 1
Overview of structural domain organization of HECT E3 family members. HECT E3 ubiquitin ligases are grouped into three subfamilies: NEDD4, HERC, and "Other" HECT E3 subfamily on the basis of their N-terminal structural properties to the HECT domain. The NEDD4 subfamily is characterized by C2 and WW domains, and "Other" HECT E3 subfamily carries a myriad of structural domains in their N-terminal region. The domain abbreviations used are as follows: C2, Calcium-dependent lipid binding domain; WW, WW domain; HECT, homologous to E6AP C-terminus; ARM, armadillo repeat-containing domain; UBA, ubiquitin-associated domain; WWE, WWE domain; BH3, Bcl-2 homology 3 domain; UBM, ubiquitin-binding motif; ANK, Ankyrin repeat-containing domain; NLS, nuclear localization sequence; UBR, ubiquitin-recognin box; PABC//MLLE, polyadenylate-binding protein C-terminal domain; IQ, IQ motif/EF-hand binding site; DOC, APC10/DOC domain.

activity of the HECT domain, as well as membrane binding (54-58). The WW domains have two conserved tryptophan residues, which are thought to be mainly responsible for protein-protein interactions *via* interacting with proline rich PPXY motifs and phosphorylated Ser/Thr residues in substrates (59-61). Whereas the HECT domain exhibits catalytic E3 activity and catalyzes the transfer of ubiquitin to substrates. The HERC subfamily can be divided into large and small HERCs. The large HERCs include HERC1 and HERC2 that contain more than one RLD domain and additional predicted domains. Whereas the four small HERCs, named HERC3~6, only have a single RLD domain. RLD domains can interact with chromatin through histones H2A and H2B, in addition to functioning as a guanine nucleotide exchange factor (GEF) to regulate the small GTPase Ran (62,63). Finally, the 13 members of other HECT E3s carry a myriad of structural domains in their N-terminal region that are responsible for binding and recruiting substrates (64) (Figure 1). EA6P, HUWE1, UBR5 (EDD), TRIP12 (ULF), and HACE1 are the best studied of other HECT E3 ligases. It is worth emphasizing that with the development of sequencing technology, it may be possible to further subdivide the 'other' HECT E3s into subfamilies according to their genetic evolutionary histories in the near future (65,66).

NEDD4 subfamily

NEDD4

Neuronal precursor cell-expressed developmentally downregulated 4 (NEDD4, also known as NEDD4-1) is the ancestral and prototypic member of the NEDD4 family, and has been unveiled as a versatile E3 ligase with an extensive range of target substrates. NEDD4 is thought to be implicated in various human diseases, from cardiovascular disease (Liddle's syndrome) to cancers (61,67). Interestingly, the relationship of NEDD4 to GC appears to be rather complicated. One study showed that overexpression of NEDD4 was detected in 75% GC tissues (17). Surprisingly, there is no association between NEDD4 levels and invasion, metastasis, or stage. However, another study found that NEDD4 is upregulated in advanced GC tissues and associated with metastasis (18). In accordance with the study, we found that gastric cardia adenocarcinoma patients have a high expression of NEDD4, which was associated with metastasis occurrence and negative prognosis of patients (19). Unexpectedly, Yang et al. observed no upregulation of NEDD4 and no correlation with PTEN expression in GC tumor samples (20). The

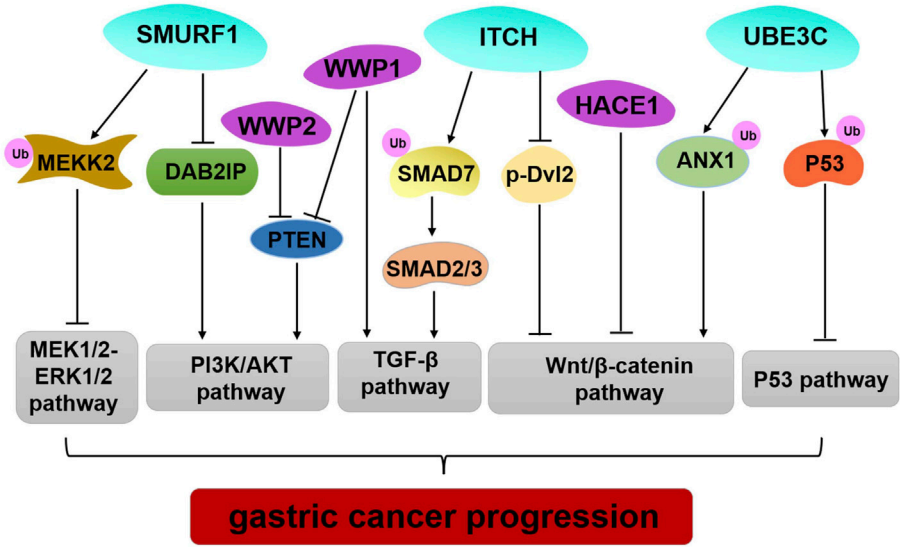

FIGURE 2
Regulation of important signaling pathways by HECT E3 ligases in GC. SMURF1 mediated pluripotency degradation of MEKK2, which resulted in inactivation of MEK1/2–ERK1/2 signaling. SMURF1, WWP1, and WWP2 have similar functions by regulating PIAK/AKT signaling pathway. Limiting ITCH activity causes accumulation of SMAD7 and blocks TGF- β1 signal transduction to inhibit GC progression. ITCH also exerts tumor-suppressive functions by down-regulating the protein level of β-catenin and p-Dvl2. HACE1 executes its regulation of the Wnt/β-catenin signaling pathway through its E3 ligase activity. UBE3C promotes ubiquitination and degradation ANX1 to activate the WNT/β-catenin signaling in GC development. UBE3C directly binds to p53, and it mediates p53 degradation to inhibit the p53 pathway in GC.

discrepancy may be due to the differences in gastric tumor types, stages, or sample numbers. Therefore, it is worth exploring the role of NEDD4 in GC further.

NEDD4L

Neural precursor cell-expressed developmentally downregulated 4-like (NEDD4L, also known as NEDD4-2) is highly homologous to NEDD4 and is thought to have originated later in evolution, as it has a different substrate repertoire from NEDD4 (68). To date, NEDD4L has been implicated in carcinogenesis and tumor progression by regulation of multiple central pathways, including TGF-β, PI3K-AKT, Wnt, and EGFR signaling pathways (69-72). GC patients were observed to express low levels of NEDD4L with an aggressive clinical course and poor clinical outcomes (21). Additionally, NEDD4L is an independent predictor for GC metastasis and survival. At the same time, the expression of NEDD4L protein in GC tissues is negatively correlated with HIF-1α, suggesting that NEDD4L may, together with HIF-1α, contribute to metastasis of GC (22), but the underlying molecular mechanism remains unclear.

ITCH

ITCH, also known as AIP4, was initially identified as an important immune system regulator (73). Emerging studies have revealed a critical connection between ITCH and tumorigenesis, and GC as well. ITCH is reported to ubiquitinate and degrade SMAD7 (74,75). Gen et al. have demonstrated ITCH activity is restricted *via* its interaction with ASSP2 that exerts an inhibitory competitive action on the recruitment of SMAD7, a key gene in TGF-β1-SMAD2/3 signaling, which in turn inactivates TGF-β1-SMAD2/3 signaling to inhibit invasion and TGF-β1-induced EMT in diffuse-type GC (23). However, a recent study found Cir-ITCH may increase ITCH expression by sponging miR-17 (24). Moreover, Cir-ITCH significantly decreases the protein level of β-catenin and p-Dvl2 and two Wnt target genes c-Myc and cyclin D1, thus attenuating the cell proliferation, migration, and invasion in GC (24). Clinically, GC patients expressing low levels of Cir-ITCH and ITCH with metastasis have shorter overall survival times (24,25). Thus, the true role of ITCH in GC is still controversial and further studies will be necessary to identify the downstream substrates and mechanisms.

WWP1

WW domain-containing E3 ubiquitin protein ligase 1 (WWP1, also known as AIP5 or TIUL1) is related to NEDD4 family members, contains four WW domains, and is primarily involved in inflammation, neurological disorders, cardiovascular diseases, and malignancies (76) (Figure 1). Elevated expression of WWP1 has been detected in human GC tissues and cells, and has been shown to be associated with poor clinicopathological characteristics and worse survival (26). Besides, downregulation of WWP1 leads to

compromised tumor proliferation, as well as enhanced G0/G1-phase arrest and apoptosis by governing the PTEN/AKT signaling pathway (26). Its similar oncogenic activity has also been confirmed in subsequent studies, evidenced by the fact that WWP1 is a direct target of miR-584-5p, miR-129-5p, and miR-129-3p, and these miRNAs inhibit GC tumor growth by targeting WWP1 (27,28). All of these studies indicate that WWP1 is an important tumor promoter and promising target in GC.

WWP2

WWP2 (also known as AIP2) functions as an E3 to regulate a myriad of cellular activities (77), which is interestingly emerging to have a role in carcinogenesis. At present, only one study has provided insight into the role of WWP2 in GC. WWP2 was found to be upregulated in GC tissues compared with paired adjacent non-tumor tissues (29). In patients with GC, the upregulated expression of WWP2 contributed to an unfavorable prognosis (29). In addition, depletion of WWP2 increases PTEN protein levels and decreases AKT phosphorylation level, thereby inhibiting the proliferation of GC cells both *in vitro* and *in vivo* (29). However, whether WWP2 regulates PTEN/PI3K/AKT pathway through its E3 ligase activity remains elusive.

SMURF1

Like other NEDD4 family members, SMAD-specific E3 ubiquitin protein ligase 1 (SMURF1) interacts with many potential targets and plays a role in different cellular functions including bone homeostasis, embryogenesis, autophagy, and carcinogenesis (78). Deregulated expression of SMURF1 has been reported in several human cancers, and its increased expression is frequently associated with disease progression and prognosis (79). Interestingly, SMURF1 appears to have a dual role in carcinogenesis, the majority of the studies assign SMURF1 a role of oncogenic factor. In GC, highly expressed SMURF1 has been observed in tumor tissues and cell lines, which was associated to malignant phenotypes and decreased survival (30). The pro-tumor property of SMURF1 was attributed to suppress the expression of DAB2IP and subsequently enhances activation of the PI3K/AKT pathway (30). Besides, SMURF1 has been reported to be a target of miR-424, thereby regulating cisplatin-resistant advanced GC (31). Similarly, Jiang et al. have unveiled that miR-1254 could target the 3′-UTR of SMURF1 and inhibit its protein expression to inactivate the PI3K/AKT pathway, thus repressing the proliferation, migration, invasion, and EMT of GC cells (32). Together, the above results point to SMURF1 as an activator of the PI3K/AKT pathway and suggest that it functions as a tumor promoter in GC. Interestingly, SMURF1 mediated pluripotency degradation of MEKK2 was attenuated by the interaction of Kir2.1 with STK38, which resulted in activation of MEK1/2–ERK1/2 signaling also stimulating GC cell invasion and metastasis (33).

Other HECT E3 ligases

HUWE1

The HECT, UBA, and WWE domain-containing E3 ubiquitin protein ligase 1 (HUWE1, also known as Mule, HectH9, ARF-BP1, HSPC272, Ib772, URE-B1, E3Histone, and LASU1) is a large and evolutionarily conserved E3 belonging to the other HECT subfamily (64) (Figure 1). In most cases, HUWE1 could regulate many biological processes, such as DNA damage repair, transcription, cell proliferation, differentiation, autophagy, and apoptosis (80). Available evidence shows that HUWE1 is interestingly emerging to have a role in tumorigenesis, and in GC as well. Very little was known about how HUWE1 regulates GC, until recently, when He et al. reported the role and mechanistic studies of HUWE1 in GC. The results showed that GC patients expressed high levels of HUWE1 and low protein levels of TGFBR2 (34). In addition, overexpression of HUWE1 promoted the proliferative activity, migratory, and invasive potential of GC cells (34). Mechanistically, HUWE1 can degrade the tumor suppressor TGFBR2 through ubiquitination, leading to the malignant progression of GC (34). The extent of HUWE1 contribution to gastric malignancies is still far from being understood.

HACE1

In addition to HECT domain, the E3 ligase HACE1 harbors six ankyrin repeats that function to mediate protein-protein interactions (Figure 1). HACE1 has attracted much attention in recent years because of its involvement in the development of human malignancies, in which it acts as a tumor suppressor (81). Chen et al. found that HACE1 was significantly reduced in GC tissues and cell lines, and it was closely correlated with tumor pathological differentiation (35). Accordingly, lower HACE1 expression is associated with better overall survival rate in TNM stages I-IIIa GC patients (35). In addition, overexpression of HACE1 suppressed the ability of proliferation and migration of GC cells, and enhanced cell apoptosis (35). Mechanistically, HACE1 can downregulate the expression of β-catenin, which in turn inhibits the activity of the Wnt signal to impede the malignant progression of GC (35). Furthermore, the authors demonstrated HACE1 executes its regulation of the Wnt/β-catenin signaling through its E3 ligase activity (35). However, the specific substrates in the Wnt/β-catenin signaling of HACE1 in GC are still largely unknown. Besides, HACE1 has been reported to cause ubiquitination of cyclin C in the non-proteolytic K11 linkage form, which led to the cisplatin-induced nuclear–mitochondrial translocation of cyclin C and finally promoted apoptosis of GC cells (36). The investigation of Sakata M et al. showed that hypermethylation of the HACE1 gene is associated with reduced expression of HACE1 (37), which points out that demethylation of HACE1 may be a new strategy for the treatment of GC.

UBR5

The other HECT E3 ligase UBR5 (also known as EDD1, EDD, DD5, HYD, or KIAA0896), consists of a ubiquitin-binding UBA domain, a zinc finger-like UBR domain involved in N-rule substrate recognition, two nuclear localization sequences, a PABC/MLLE domain for protein–protein interaction, and a C-terminal HECT (82) (Figure 1). UBR5 has been related to the regulation of DNA damage response, translation, metabolism, transcription, and apoptosis (83). Recent evidence has unveiled a critical role of UBR5 (38)in the progression of multiple cancer types, including GC. UBR5 was mutated in 27.8% of GC, and GC patients with high UBR5 expression had a poor prognosis (39,40). Moreover, Knockdown of UBR5 in GC cells was shown to suppress cell growth, migration and invasion, which is mainly due to the inhibition of protein stability of tumor suppressor GKN1 through ubiquitination (84).

UBE3C

UBE3C, also known as RAUL, contains an N-terminal IQ motif and a C-terminal HECT domain (Figure 1), and is able to assemble K48 and less preponderant K29 and K11 linkages (85). A study identified the N-terminal region just preceding the HECT domain is crucial for the stabilization and enzymatic activity of UBE3C (86). Accumulating evidence indicated that UBE3C is implicated in several tumors, including glioma, melanoma, renal cell carcinoma, hepatocellular carcinoma, breast cancer, lung cancer, and gastric cancer (41,42,87-91). And the role of UBE3C in gastric cancer has only recently begun to be explored. Zhao et al. discovered that LINC00355, as a tumor promoter, promotes the malignant progression of GC by enhancing the association of E3 ubiquitin ligases UBE3C and RAD18 with P53, facilitating its ubiquitination and degradation (43). Furthermore, another study identified that the protein and mRNA levels of UBE3C in GC were both heightened and inversely correlated with patient outcomes. UBE3C could interact directly with and downregulate AXIN1, thus activating β-catenin signaling and promoting the development and progression of GC (42).

HECTD3

Homologous to the E6-associated protein carboxyl terminus domain containing 3 (HECTD3) is an under-investigated other HECT E3 ligase and characterized by an N-terminal DOC domain (Figure 1). Recently, Zhang et al. discovered the abnormal activation of HECTD3 in GC cells, which was correlated with poor outcomes of patients (92). Also, HECTD3 could facilitate the malignant proliferation and tumorigenesis of GC cells, and inhibit the cell apoptosis, suggesting that it serves as a tumor promoter in GC. Mechanistically, HECTD can stabilize expression of c-MYC by interacting with c-MYC and mediating K29 linked polyubiquitination of c-MYC (92).

Conclusion and perspective

The data reviewed here illustrate genetic alteration, abnormal expression, or dysfunction of HECT E3 ligases that may contribute to GC occurrence and progression (Table 1; Figure 2). However, several HECT E3 ligases have been reported to play a dual role in GC (Table 1). The concrete mechanisms have not been fully explored. Currently, E3 ubiquitin ligases become important therapeutic targets for cancer treatment (10,93). Many inhibitors of the RING family E3 ligases have been developed for cancer therapy, while only limited efforts have been made regarding the HECT E3 ligases. With the better understanding of the mechanism underlying regulation of the HECT E3 ubiquitin ligases, and advances in research technology, such as high-throughput screenings and PROTAC (proteolysis targeting chimera) technology, we will be able to develop more drugs that target the HECT E3 ligases for GC therapy.

Author contributions

AS, WY, and QL wrote this manuscript. XT and YC prepared the figures and tables. All authors contributed to the article and approved the final version of the manuscript.

Funding

This work was supported by the National Natural Science Foundation of China (Nos. 82002581, 81871888, and 82172942), China Postdoctoral Science Foundation (No. 2020M671375), Jiangsu Province Postdoctoral Research Funding Scheme (No. 2020Z261).

Conflict of interest

The authors declare that the research was conducted in the absence of any commercial or financial relationships that could be construed as a potential conflict of interest.

References

1. Hershko A. Ubiquitin: Roles in protein modification and breakdown. *Cell* (1983) 34:11–2. doi:10.1016/0092-8674(83)90131-9

2. Pickart CM. Mechanisms underlying ubiquitination. *Annu Rev Biochem* (2001) 70:503–33. doi:10.1146/annurev.biochem.70.1.503

3. Rape M. Ubiquitylation at the crossroads of development and disease. *Nat Rev Mol Cel Biol* (2018) 19:59–70. doi:10.1038/nrm.2017.83

4. Kwon YT, Ciechanover A. The ubiquitin code in the ubiquitin-proteasome system and autophagy. *Trends Biochemical Sciences* (2017) 42:873–86. doi:10.1016/j.tibs.2017.09.002

5. Ciechanover A. The unravelling of the ubiquitin system. *Nat Rev Mol Cel Biol* (2015) 16:322–4. doi:10.1038/nrm3982

6. Schulman BA, Harper JW. Ubiquitin-like protein activation by E1 enzymes: The apex for downstream signalling pathways. *Nat Rev Mol Cel Biol* (2009) 10:319–31. doi:10.1038/nrm2673

7. Ye Y, Rape M. Building ubiquitin chains: E2 enzymes at work. *Nat Rev Mol Cel Biol* (2009) 10:755–64. doi:10.1038/nrm2780

8. Yang Q, Zhao J, Chen D, Wang Y. E3 ubiquitin ligases: Styles, structures and functions. *Mol Biomed* (2021) 2:23. doi:10.1186/s43556-021-00043-2

9. Buetow L, Huang DT. Structural insights into the catalysis and regulation of E3 ubiquitin ligases. *Nat Rev Mol Cel Biol* (2016) 17:626–42. doi:10.1038/nrm.2016.91

10. Deng L, Meng T, Chen L, Wei W, Wang P. The role of ubiquitination in tumorigenesis and targeted drug discovery. *Signal Transduction Targeted Therapy* (2020) 5:11. doi:10.1038/s41392-020-0107-0

11. Senft D, Qi J, Ronai ZA. Ubiquitin ligases in oncogenic transformation and cancer therapy. *Nat Rev Cancer* (2018) 18:69–88. doi:10.1038/nrc.2017.105

12. Sluimer J, Distel B. Regulating the human HECT E3 ligases. *Cell Mol Life Sci : CMLS* (2018) 75:3121–41. doi:10.1007/s00018-018-2848-2

13. Sung H, Ferlay J, Siegel RL, Laversanne M, Soerjomataram I, Jemal A, et al. Global cancer statistics 2020: GLOBOCAN estimates of incidence and mortality worldwide for 36 cancers in 185 countries. *CA: a Cancer J clinicians* (2021) 71:209–49. doi:10.3322/caac.21660

14. Arnold M, Abnet CC, Neale RE, Vignat J, Giovannucci EL, McGlynn KA, et al. Global burden of 5 major types of gastrointestinal cancer. *Gastroenterology* (2020) 159:335–49. doi:10.1053/j.gastro.2020.02.068

15. Shi J, Qu YP, Hou P. Pathogenetic mechanisms in gastric cancer. *World J Gastroenterol* (2014) 20:13804–19. doi:10.3748/wjg.v20.i38.13804

16. Shimizu D, Kanda M, Kodera Y. Review of recent molecular landscape knowledge of gastric cancer. *Histology and histopathology* (2018) 33:11–26. doi:10.14670/hh-11-898

17. Kim SS, Yoo NJ, Jeong EG, Kim MS, Lee SH. Expression of NEDD4-1, a PTEN regulator, in gastric and colorectal carcinomas. *APMIS : Acta pathologica, microbiologica, immunologica Scand* (2008) 116:779–84. doi:10.1111/j.1600-0463.2008.00999.x

18. Wang YY, Ye ZY, Zhao ZS, Tao HQ, Li SG. Systems biology approach to identification of biomarkers for metastatic progression in gastric cancer. *J Cancer Res Clin Oncol* (2010) 136:135–41. doi:10.1007/s00432-009-0644-y

19. Sun A, Yu G, Dou X, Yan X, Yang W, Lin Q. Nedd4-1 is an exceptional prognostic biomarker for gastric cardia adenocarcinoma and functionally associated with metastasis. *Mol Cancer* (2014) 13:248. doi:10.1186/1476-4598-13-248

20. Yang Z, Yuan XG, Chen J, Lu NH. Is NEDD4-1 a negative regulator of phosphatase and tensin homolog in gastric carcinogenesis? *World J Gastroenterol* (2012) 18:6345–8. doi:10.3748/wjg.v18.i43.6345

21. Gao C, Pang L, Ren C, Ma T. Decreased expression of Nedd4L correlates with poor prognosis in gastric cancer patient. *Med Oncol (Northwood, Lond England)* (2012) 29:1733–8. doi:10.1007/s12032-011-0061-3

22. Jiang X, Zhang S, Yin Z, Sheng Y, Yan Q, Sun R, et al. The correlation between NEDD4L and HIF-1α levels as a gastric cancer prognostic marker. *Int J Med Sci* (2019) 16:1517–24. doi:10.7150/ijms.34646

23. Gen Y, Yasui K, Kitaichi T, Iwai N, Terasaki K, Dohi O, et al. ASPP2 suppresses invasion and TGF-β1-induced epithelial-mesenchymal transition by inhibiting Smad7 degradation mediated by E3 ubiquitin ligase ITCH in gastric cancer. *Cancer Lett* (2017) 398:52–61. doi:10.1016/j.canlet.2017.04.002

24. Peng Y, Wang HH. Cir-ITCH inhibits gastric cancer migration, invasion and proliferation by regulating the Wnt/β-catenin pathway. *Scientific Rep* (2020) 10:17443. doi:10.1038/s41598-020-74452-8

25. Ghasemi S, Emadi-Baygi M, Nikpour P. Down-regulation of circular RNA ITCH and circHIPK3 in gastric cancer tissues. *Turkish J Med Sci* (2019) 49:687–95. doi:10.3906/sag-1806-50

26. Zhang L, Wu Z, Ma Z, Liu H, Wu Y, Zhang Q. WWP1 as a potential tumor oncogene regulates PTEN-Akt signaling pathway in human gastric carcinoma. *Tumour Biol : J Int Soc Oncodevelopmental Biol Med* (2015) 36:787–98. doi:10.1007/s13277-014-2696-0

27. Li Q, Li Z, Wei S, Wang W, Chen Z, Zhang L, et al. Overexpression of miR-584-5p inhibits proliferation and induces apoptosis by targeting WW domain-containing E3 ubiquitin protein ligase 1 in gastric cancer. *J Exp Clin Cancer Res : CR* (2017) 36:59. doi:10.1186/s13046-017-0532-2

28. Ma L, Chen X, Li C, Cheng R, Gao Z, Meng X, et al. miR-129-5p and -3p co-target WWP1 to suppress gastric cancer proliferation and migration. *J Cell Biochem* (2018) 120:7527–38. doi:10.1002/jcb.28027

29. Wang K, Liu J, Zhao X, Li H, Luo G, Yu Y, et al. WWP2 regulates proliferation of gastric cancer cells in a PTEN-dependent manner. *Biochem biophysical Res Commun* (2020) 521:652–9. doi:10.1016/j.bbrc.2019.10.179

30. Tao Y, Sun C, Zhang T, Song Y. SMURF1 promotes the proliferation, migration and invasion of gastric cancer cells. *Oncol Rep* (2017) 38:1806–14. doi:10.3892/or.2017.5825

31. Lu L, Wu M, Lu Y, Zhao Z, Liu T, Fu W, et al. MicroRNA-424 regulates cisplatin resistance of gastric cancer by targeting SMURF1 based on GEO database and primary validation in human gastric cancer tissues. *OncoTargets Ther* (2019) 12:7623–36. doi:10.2147/ott.S208275

32. Jiang M, Shi L, Yang C, Ge Y, Lin L, Fan H, et al. miR-1254 inhibits cell proliferation, migration, and invasion by down-regulating Smurf1 in gastric cancer. *Cel Death Dis* (2019) 10:32. doi:10.1038/s41419-018-1262-x

33. Ji CD, Wang YX, Xiang DF, Liu Q, Zhou ZH, Qian F, et al. Kir2.1 interaction with Stk38 promotes invasion and metastasis of human gastric cancer by enhancing MEKK2-MEK1/2-ERK1/2 signaling. *Cancer Res* (2018) 78:3041–53. doi:10.1158/0008-5472.Can-17-3776

34. He Y, Zhou J, Wan Q. The E3 ligase HUWE1 mediates TGFBR2 ubiquitination and promotes gastric cancer cell proliferation, migration, and invasion. *Invest New Drugs* (2021) 39:713–23. doi:10.1007/s10637-020-01041-x

35. Chen YL, Li DP, Jiang HY, Yang Y, Xu LL, Zhang SC, et al. Overexpression of HACE1 in gastric cancer inhibits tumor aggressiveness by impeding cell proliferation and migration. *Cancer Med* (2018) 7:2472–84. doi:10.1002/cam4.1496

36. Jiang HY, Chen YL, Xu XX, Li CY, Chen Y, Li DP, et al. Ubiquitylation of cyclin C by HACE1 regulates cisplatin-associated sensitivity in gastric cancer. *Clin translational Med* (2022) 12:e770. doi:10.1002/ctm2.770

37. Sakata M, Kitamura YH, Sakuraba K, Goto T, Mizukami H, Saito M, et al. Methylation of HACE1 in gastric carcinoma. *Anticancer Res* (2009) 29:2231–3.

38. Adhikary S, Marinoni F, Hock A, Hulleman E, Popov N, Beier R, et al. The ubiquitin ligase HectH9 regulates transcriptional activation by Myc and is essential for tumor cell proliferation. *Cell* (2005) 123:409–21. doi:10.1016/j.cell.2005.08.016

39. Kim MS, Oh JE, Eom HS, Yoo NJ, Lee SH. Mutational analysis of UBR5 gene encoding an E3 ubiquitin ligase in common human cancers. *Pathology* (2010) 42:93–4. doi:10.3109/00313020903434322

40. Ding F, Zhu X, Song X, Yuan P, Ren L, Chai C, et al. UBR5 oncogene as an indicator of poor prognosis in gastric cancer. *Exp Ther Med* (2020) 20:7. doi:10.3892/etm.2020.9135

41. Gu J, Mao W, Ren W, Xu F, Zhu Q, Lu C, et al. Ubiquitin-protein ligase E3C maintains non-small-cell lung cancer stemness by targeting AHNAK-p53 complex. *Cancer Lett* (2019) 443:125–34. doi:10.1016/j.canlet.2018.11.029

42. Zhang Y, Xu J, Fu H, Wei Z, Yang D, Yan R. UBE3C promotes proliferation and inhibits apoptosis by activating the β-catenin signaling via degradation of AXIN1 in gastric cancer. *Carcinogenesis* (2021) 42:285–93. doi:10.1093/carcin/bgaa098

43. Zhao W, Jin Y, Wu P, Yang J, Chen Y, Yang Q, et al. LINC00355 induces gastric cancer proliferation and invasion through promoting ubiquitination of P53. *Cel Death Discov* (2020) 6:99. doi:10.1038/s41420-020-00332-9

44. Rotin D, Kumar S. Physiological functions of the HECT family of ubiquitin ligases. *Nat Rev Mol Cel Biol* (2009) 10:398–409. doi:10.1038/nrm2690

45. Berndsen CE, Wolberger C. New insights into ubiquitin E3 ligase mechanism. *Nat Struct Mol Biol* (2014) 21:301–7. doi:10.1038/nsmb.2780

46. Scheffner M, Kumar S. Mammalian HECT ubiquitin-protein ligases: Biological and pathophysiological aspects. *Biochim Biophys Acta* (2014) 1843:61–74. doi:10.1016/j.bbamcr.2013.03.024

47. Deshaies RJ, Joazeiro CA. RING domain E3 ubiquitin ligases. *Annu Rev Biochem* (2009) 78:399–434. doi:10.1146/annurev.biochem.78.101807.093809

48. Metzger MB, Pruneda JN, Klevit RE, Weissman AM. RING-Type E3 ligases: Master manipulators of E2 ubiquitin-conjugating enzymes and ubiquitination. *Biochim Biophys Acta* (2014) 1843:47–60. doi:10.1016/j.bbamcr.2013.05.026

49. Spratt DE, Walden H, Shaw GS. RBR E3 ubiquitin ligases: New structures, new insights, new questions. *Biochem J* (2014) 458:421–37. doi:10.1042/bj20140006

50. Walden H, Rittinger K. RBR ligase-mediated ubiquitin transfer: A tale with many twists and turns. *Nat Struct Mol Biol* (2018) 25:440–5. doi:10.1038/s41594-018-0063-3

51. Zheng N, Shabek N. Ubiquitin ligases: Structure, function, and regulation. *Annu Rev Biochem* (2017) 86:129–57. doi:10.1146/annurev-biochem-060815-014922

52. Wang Y, Argiles-Castillo D, Kane EI, Zhou A, Spratt DE. HECT E3 ubiquitin ligases - emerging insights into their biological roles and disease relevance. *J Cel Sci* (2020) 133:jcs228072. doi:10.1242/jcs.228072

53. Zou X, Levy-Cohen G, Blank M. Molecular functions of NEDD4 E3 ubiquitin ligases in cancer. *Biochim Biophys Acta* (2015) 1856:91–106. doi:10.1016/j.bbcan.2015.06.005

54. Plant PJ, Yeger H, Staub O, Howard P, Rotin D. The C2 domain of the ubiquitin protein ligase Nedd4 mediates Ca2+-dependent plasma membrane localization. *J Biol Chem* (1997) 272:32329–36. doi:10.1074/jbc.272.51.32329

55. Yamaguchi K, Ohara O, Ando A, Nagase T. Smurf1 directly targets hPEM-2, a GEF for Cdc42, via a novel combination of protein interaction modules in the ubiquitin-proteasome pathway. *Biol Chem* (2008) 389:405–13. doi:10.1515/bc.2008.036

56. Tian M, Bai C, Lin Q, Lin H, Liu M, Ding F, et al. Binding of RhoA by the C2 domain of E3 ligase Smurf1 is essential for Smurf1-regulated RhoA ubiquitination and cell protrusive activity. *FEBS Lett* (2011) 585:2199–204. doi:10.1016/j.febslet.2011.06.016

57. Wiesner S, Ogunjimi AA, Wang HR, Rotin D, Sicheri F, Wrana JL, et al. Autoinhibition of the HECT-type ubiquitin ligase Smurf2 through its C2 domain. *Cell* (2007) 130:651–62. doi:10.1016/j.cell.2007.06.050

58. Dunn R, Klos DA, Adler AS, Hicke L. The C2 domain of the Rsp5 ubiquitin ligase binds membrane phosphoinositides and directs ubiquitination of endosomal cargo. *J Cel Biol* (2004) 165:135–44. doi:10.1083/jcb.200309026

59. Dodson EJ, Fishbain-Yoskovitz V, Rotem-Bamberger S, Schueler-Furman O. Versatile communication strategies among tandem WW domain repeats. *Exp Biol Med (Maywood, N.J.)* (2015) 240:351–60. doi:10.1177/1535370214566558

60. Bork P, Sudol M. The WW domain: A signalling site in dystrophin? *Trends Biochemical Sciences* (1994) 19:531–3. doi:10.1016/0968-0004(94)90053-1

61. Staub O, Dho S, Henry P, Correa J, Ishikawa T, McGlade J, et al. WW domains of Nedd4 bind to the proline-rich PY motifs in the epithelial Na+ channel deleted in Liddle's syndrome. *EMBO J* (1996) 15:2371–80. doi:10.1002/j.1460-2075.1996.tb00593.x

62. Nemergut ME, Mizzen CA, Stukenberg T, Allis CD, Macara IG. Chromatin docking and exchange activity enhancement of RCC1 by histones H2A and H2B. *Science (New York, N.Y.)* (2001) 292:1540–3. doi:10.1126/science.292.5521.1540

63. Zhang C, Clarke PR. Chromatin-independent nuclear envelope assembly induced by Ran GTPase in Xenopus egg extracts. *Science (New York, N.Y.)* (2000) 288:1429–32. doi:10.1126/science.288.5470.1429

64. Singh S, Ng J, Sivaraman J. Exploring the "Other" subfamily of HECT E3-ligases for therapeutic intervention. *Pharmacol Ther* (2021) 224:107809. doi:10.1016/j.pharmthera.2021.107809

65. Grau-Bové X, Sebé-Pedrós A, Ruiz-Trillo I. A genomic survey of HECT ubiquitin ligases in eukaryotes reveals independent expansions of the HECT system in several lineages. *Genome Biol Evol* (2013) 5:833–47. doi:10.1093/gbe/evt052

66. Marín I. Animal HECT ubiquitin ligases: Evolution and functional implications. *BMC Evol Biol* (2010) 10:56. doi:10.1186/1471-2148-10-56

67. Wang ZW, Hu X, Ye M, Lin M, Chu M, Shen X. NEDD4 E3 ligase: Functions and mechanism in human cancer. *Semin Cancer Biol* (2020) 67:92–101. doi:10.1016/j.semcancer.2020.03.006

68. Yang B, Kumar S. Nedd4 and nedd4-2: Closely related ubiquitin-protein ligases with distinct physiological functions. *Cel Death Differ* (2010) 17:68–77. doi:10.1038/cdd.2009.84

69. Gao S, Alarcón C, Sapkota G, Rahman S, Chen PY, Goerner N, et al. Ubiquitin ligase Nedd4L targets activated Smad2/3 to limit TGF-beta signaling. *Mol Cel* (2009) 36:457–68. doi:10.1016/j.molcel.2009.09.043

70. Wang Z, Dang T, Liu T, Chen S, Li L, Huang S, et al. NEDD4L protein catalyzes ubiquitination of PIK3CA protein and regulates PI3K-AKT signaling. *J Biol Chem* (2016) 291:17467–77. doi:10.1074/jbc.M116.726083

71. Ding Y, Zhang Y, Xu C, Tao QH, Chen YG. HECT domain-containing E3 ubiquitin ligase NEDD4L negatively regulates Wnt signaling by targeting dishevelled for proteasomal degradation. *J Biol Chem* (2013) 288:8289–98. doi:10.1074/jbc.M112.433185

72. Chan W, Tian R, Lee YF, Sit ST, Lim L, Manser E. Down-regulation of active ACK1 is mediated by association with the E3 ubiquitin ligase Nedd4-2. *J Biol Chem* (2009) 284:8185–94. doi:10.1074/jbc.M806877200

73. Melino G, Gallagher E, Aqeilan RI, Knight R, Peschiaroli A, Rossi M, et al. Itch: A HECT-type E3 ligase regulating immunity, skin and cancer. *Cel Death Differ* (2008) 15:1103–12. doi:10.1038/cdd.2008.60

74. Lallemand F, Seo SR, Ferrand N, Pessah M, L'Hoste S, Rawadi G, et al. AIP4 restricts transforming growth factor-beta signaling through a ubiquitination-independent mechanism. *J Biol Chem* (2005) 280:27645–53. doi:10.1074/jbc.M500188200

75. Park SH, Jung EH, Kim GY, Kim BC, Lim JH, Woo CH. Itch E3 ubiquitin ligase positively regulates TGF-β signaling to EMT via Smad7 ubiquitination. *Mol Cell* (2015) 38:20–5. doi:10.14348/molcells.2015.2120

76. Zhi X, Chen C. WWP1: A versatile ubiquitin E3 ligase in signaling and diseases. *Cell Mol Life Sci : CMLS* (2012) 69:1425–34. doi:10.1007/s00018-011-0871-7

77. Chen W, Jiang X, Luo Z. WWP2: A multifunctional ubiquitin ligase gene. *Pathol Oncol Res : POR* (2014) 20:799–803. doi:10.1007/s12253-014-9838-y

78. Cao Y, Zhang L. A Smurf1 tale: Function and regulation of an ubiquitin ligase in multiple cellular networks. *Cell Mol Life Sci : CMLS* (2013) 70:2305–17. doi:10.1007/s00018-012-1170-7

79. Fu L, Cui CP, Zhang X, Zhang L. The functions and regulation of Smurfs in cancers. *Semin Cancer Biol* (2020) 67:102–16. doi:10.1016/j.semcancer.2019.12.023

80. Qi L, Xu X, Qi X. The giant E3 ligase HUWE1 is linked to tumorigenesis, spermatogenesis, intellectual disability, and inflammatory diseases. *Front Cell Infect Microbiol* (2022) 12:905906. doi:10.3389/fcimb.2022.905906

81. Zhang L, Anglesio MS, O'Sullivan M, Zhang F, Yang G, Sarao R, et al. The E3 ligase HACE1 is a critical chromosome 6q21 tumor suppressor involved in multiple cancers. *Nat Med* (2007) 13:1060–9. doi:10.1038/nm1621

82. Matta-Camacho E, Kozlov G, Menade M, Gehring K. Structure of the HECT C-lobe of the UBR5 E3 ubiquitin ligase. *Acta Crystallographica Section F, Struct Biol crystallization Commun* (2012) 68:1158–63. doi:10.1107/s1744309112036937

83. Shearer RF, Iconomou M, Watts CK, Saunders DN. Functional roles of the E3 ubiquitin ligase UBR5 in cancer. *Mol Cancer Res : MCR* (2015) 13:1523–32. doi:10.1158/1541-7786.Mcr-15-0383

84. Yang M, Jiang N, Cao QW, Ma MQ, Sun Q. The E3 ligase UBR5 regulates gastric cancer cell growth by destabilizing the tumor suppressor GKN1. *Biochem biophysical Res Commun* (2016) 478:1624–9. doi:10.1016/j.bbrc.2016.08.170

85. Michel MA, Elliott PR, Swatek KN, Simicek M, Pruneda JN, Wagstaff JL, et al. Assembly and specific recognition of k29-and k33-linked polyubiquitin. *Mol Cel* (2015) 58:95–109. doi:10.1016/j.molcel.2015.01.042

86. Singh S, Sivaraman J. Crystal structure of HECT domain of UBE3C E3 ligase and its ubiquitination activity. *Biochem J* (2020) 477:905–23. doi:10.1042/bcj20200027

87. Pan SJ, Zhan SK, Ji WZ, Pan YX, Liu W, Li DY, et al. Ubiquitin-protein ligase E3C promotes glioma progression by mediating the ubiquitination and degrading of Annexin A7. *Scientific Rep* (2015) 5:11066. doi:10.1038/srep11066

88. Tang L, Yi XM, Chen J, Chen FJ, Lou W, Gao YL, et al. Ubiquitin ligase UBE3C promotes melanoma progression by increasing epithelial-mesenchymal transition in melanoma cells. *Oncotarget* (2016) 7:15738–46. doi:10.18632/oncotarget.7393

89. Wen JL, Wen XF, Li RB, Jin YC, Wang XL, Zhou L, et al. UBE3C promotes growth and metastasis of renal cell carcinoma via activating Wnt/β-catenin pathway. *PloS one* (2015) 10:e0115622. doi:10.1371/journal.pone.0115622

90. Jiang JH, Liu YF, Ke AW, Gu FM, Yu Y, Dai Z, et al. Clinical significance of the ubiquitin ligase UBE3C in hepatocellular carcinoma revealed by exome sequencing. *Hepatol (Baltimore, Md* (2014) 59:2216–27. doi:10.1002/hep.27012

91. Xiong J, Wei B, Ye Q, Liu W. MiR-30a-5p/UBE3C axis regulates breast cancer cell proliferation and migration. *Biochem biophysical Res Commun* (2019) 516:1013–8. doi:10.1016/j.bbrc.2016.03.069

92. Zhang G, Zhu Q, Yan X, Ci M, Zhao E, Hou J, et al. HECTD3 promotes gastric cancer progression by mediating the polyubiquitination of c-MYC. *Cel Death Discov* (2022) 8:185. doi:10.1038/s41420-022-01001-9

93. Duan S, Pagano M. Ubiquitin ligases in cancer: Functions and clinical potentials. *Cel Chem Biol* (2021) 28:918–33. doi:10.1016/j.chembiol.2021.04.008

Pathology & Oncology Research | frontiers

TYPE Original Research
PUBLISHED 21 December 2023
DOI 10.3389/pore.2023.1611456

Check for updates

OPEN ACCESS

EDITED BY
Aniko Maraz,
University of Szeged, Hungary

*CORRESPONDENCE
Ferenc Lakosi,
lakosiferenc@yahoo.com

RECEIVED 21 August 2023
ACCEPTED 14 November 2023
PUBLISHED 21 December 2023

CITATION
Kisivan K, Farkas A, Kovacs P, Glavak C, Lukacs G, Mahr K, Szabo Z, Csima MP, Gulyban A, Toth Z, Kaposztas Z and Lakosi F (2023), Pancreatic SABR using peritumoral fiducials, triggered imaging and breath-hold.
Pathol. Oncol. Res. 29:1611456.
doi: 10.3389/pore.2023.1611456

COPYRIGHT
© 2023 Kisivan, Farkas, Kovacs, Glavak, Lukacs, Mahr, Szabo, Csima, Gulyban, Toth, Kaposztas and Lakosi. This is an open-access article distributed under the terms of the Creative Commons Attribution License (CC BY). The use, distribution or reproduction in other forums is permitted, provided the original author(s) and the copyright owner(s) are credited and that the original publication in this journal is cited, in accordance with accepted academic practice. No use, distribution or reproduction is permitted which does not comply with these terms.

Pancreatic SABR using peritumoral fiducials, triggered imaging and breath-hold

Katalin Kisivan[1], Andrea Farkas[1], Peter Kovacs[1], Csaba Glavak[1], Gabor Lukacs[2], Karoly Mahr[3], Zsolt Szabo[3], Melinda Petone Csima[4,5], Akos Gulyban[6,7], Zoltan Toth[8,9], Zsolt Kaposztas[10] and Ferenc Lakosi[1,5]*

[1]Department of Radiotherapy, Somogy County Kaposi Mór Teaching Hospital, Kaposvár, Hungary, [2]Department of Medical Oncology, Somogy County Kaposi Mór Teaching Hospital, Kaposvár, Hungary, [3]Department of Medical Oncology, Zala County Szent Raphael Hospital, Zalaegerszeg, Hungary, [4]Institute of Education, Hungarian University of Agricultural and Life Sciences, Gödöllő, Hungary, [5]Faculty of Health Sciences, University of Pecs, Pecs, Hungary, [6]Department of Medical Physics, Institut Jules Bordet, Brussels, Belgium, [7]Radiophysics and MRI Physics Laboratory, Université Libre De Bruxelles (ULB), Brussels, Belgium, [8]Medicopus Nonprofit Ltd., Somogy County Kaposi Mór Teaching Hospital, Kaposvár, Hungary, [9]PET Center, Somogy County Kaposi Mór Teaching Hospital, Kaposvár, Hungary, [10]Department of Surgery, Somogy County Kaposi Mór Teaching Hospital, Kaposvár, Hungary

Background: We aim to present our linear accelerator-based workflow for pancreatic stereotactic ablative radiotherapy (SABR) in order to address the following issues: intrafractional organ motion management, Cone Beam CT (CBCT) image quality, residual errors with dosimetric consequences, treatment time, and clinical results.

Methods: Between 2016 and 2021, 14 patients with locally advanced pancreatic cancer were treated with induction chemotherapy and SABR using volumetric modulated arc therapy (VMAT). Internal target volume (ITV) concept (5), phase-gated (4), or breath hold (5) techniques were used. Treatment was verified by CBCT before and after irradiation, while tumor motion was monitored and controlled by kV triggered imaging and beam hold using peritumoral surgical clips. Beam interruptions and treatment time were recorded. The CBCT image quality was scored and supplemented by an agreement analysis (Krippendorff's-α) of breath-hold CBCT images to determine the position of OARs relative to the planning risk volumes (PRV). Residual errors and their dosimetry impact were also calculated. Progression free (PFS) and overall survival (OS) were assessed by the Kaplan-Meier analysis with acute and late toxicity reporting (CTCAEv4).

Results: On average, beams were interrupted once (range: 0–3) per treatment session on triggered imaging. The total median treatment time was 16.7 ± 10.8 min, significantly less for breath-hold vs. phase-gated sessions (18.8 ± 6.2 vs. 26.5 ± 13.4, $p < 0.001$). The best image quality was achieved by breath hold CBCT. The Krippendorff's-α test showed a strong agreement among five radiation therapists (mean K-α value: 0.8 (97.5%). The mean residual errors were <0.2 cm in each direction resulting in an average difference of <2% in dosimetry for OAR and target volume. Two patients received offline adaptation. The median OS/PFS after induction chemotherapy and SABR was 20/12 months and 15/8 months. No Gr. ≥2 acute/late RT-related toxicity was noted.

Conclusion: Linear accelerator based pancreatic SABR with the combination of CBCT and triggered imaging + beam hold is feasible. Peritumoral fiducials improve utility while breath-hold CBCT provides the best image quality at a reasonable treatment time with offline adaptation possibilities. In well-selected cases, it can be an effective alternative in clinics where CBCT/MRI-guided online adaptive workflow is not available.

KEYWORDS

motion control, pancreatic cancer, triggered imaging, stereotactic ablative radiotherapy, deep inspiration breath hold

Introduction

Pancreatic cancer (PC) is the seventh leading cause of cancer-related deaths worldwide, with a 5 years survival rate of less than 10% [1–4]. Currently, complete resection is the only curative approach, however only 10%–15% of patients are diagnosed with resectable disease. Gemcitabine or 5-fluorouracil, leucovorin, irinotecan, and oxaliplatin (Folfirinox)-based induction chemotherapy (iCT) followed by radio-chemotherapy (RCT) is the mainstay of treatment for the remaining subset of patients presenting with either locally advanced (LAPC) or borderline resectable disease [1, 2]. Dose escalated RT/RCT, or stereotactic ablative radiotherapy (SABR), have emerged as effective treatment options in recent years. Prospective and retrospective data showed an impressive median overall survival of 13.9–26 months with an acceptable ≥ Grade (Gr.) 3 morbidity of 6%–12.8% [5–15].

Delivery of high doses is challenging during LAPC-SABR due to the close vicinity of organs at risk (OARs) (duodenum, gastric wall, small/large bowels) with their large intra- and interfractional positional and volumetric changes. This could potentially increase the dose to these organs and may be responsible for serious late toxicity [6, 16, 17]. Hence, both the visualization of OARs and intrafraction organ motion management are cornerstones during LAPC-SABR. MRI linear accelerator (Linac), with its superior soft tissue contrast, in conjunction with daily adaptation and real-time organ motion management has great potential [14], however, it is not yet widely available. Alternatively, CT-on rail [12] or CBCT based adaptive workflows (Ethos, Varian Medical Systems, Palo Alto, CA, United States) could be used for similar purposes [18]. Still, one should explore and address the above-mentioned needs on conventional Linacs equipped with cone beam CT (CBCT) where no adaptive workflows are available.

The image quality of abdominal CBCT on Linacs—especially in 4D mode—is suboptimal due to motion and gas artefacts, necessitating the use of fiducials and a better selection of CBCT acquisitions [19, 20]. Fiducials also form the backbone of any intrafraction X-ray based image-guided radiation therapy (IGRT). Most commonly, intra-tumoral fiducials are used. However, they have the disadvantage of not providing any spatial information or landmarks for the positions of the target and OARs. Time efficiency is also a crucial factor since advanced techniques such as gating or tracking are prone to have longer treatment times and consequently more room for errors.

Our goal was to find the most appropriate and time efficient IGRT workflow on our TrueBeam linear accelerator (Varian Medical Systems, Palo Alto, CA, United States) equipped with the Advanced IGRT & Motion Package, allowing intrafractional kilovoltage triggered imaging and Beam Hold.

This system is able to acquire repetitive 2D kV image images during SABR, autodetect different type of fiducials, and hold the treatment beam if their positions do not meet the pre-defined deviation limit [21]. We investigated the image quality and time efficiency of deep inspiration breath-hold (DIBH) technique as the most promising candidate for achieving improved image quality [22] and, as a consequence, offline adaptation. We also introduced peritumoral fiducials, which could potentially expand the utility of fiducial based IGRT. Finally, we combined these techniques with the whole available spectra of 3D/4D CBCTs acquired before (pre-CBCT), and after (post-CBCT) pancreatic SABR. As far as we are aware, this kind of workflow has never been published before.

In this report our primary aim was to present this IGRT workflow for pancreatic SABR, including motion management strategies, CBCT image quality, and time efficiency, especially focusing on breath-hold technique and its offline adaptive aspects. Secondarily, clinical efficacy was also demonstrated.

Methods and materials

Between 2016 and 2021, fifteen patients with primary or recurrent LAPC were treated with volumetric-modulated arc therapy (VMAT) as a five-fraction SABR or hypofractionated dose-escalated RT (DE-RT). Patients with large (>6 cm) tumors with infiltration of luminal structures and/or were unresponsive to iCT with persistently elevated post-CT carbohydrate antigen (CA19-9) (>300 IU/mL) or extensive nodal disease were not eligible and directed to conventional RCT with capecitabine or systemic treatment. Patients were treated based on the approval of the Central Ethics Committee (OGYÉI/5301/2018). Finally, 14/15 patients were analyzed since one patient refused neoadjuvant chemotherapy and progressed only 3 months after SABR.

The workflow is characterized by the use of fiducials followed by multimodal imaging in the supine position for contouring and

planning purposes. A minimum of two types of imaging at two different time points were acquired to obtain relevant information on movement patterns and filling status of OARs. This is the most reliable way of creating internal target volumes (ITV) and planning Organs at risk volumes (PRV_OARs) to select the most appropriate verification protocol for the patient: ITV-based RT with abdominal compression +TI, Phase-gated RT with abdominal compression + triggered imaging or breath-hold RT+ triggered imaging. Pretreatment imaging may include cine MRIs (Siemens Biograph mMRI, 3T, TR 351 ms, TE 1 ms, Flip Angle (FA) 8°, field of view (FOV) 350 mm, Slice thickness/spacing 20/0 mm, one slice, 50 measures, 18 s) in sagittal and coronal planes completed with T2-weighted axial images in the treatment planning position. Initial diagnostic scans were also co-registered with the planning CT (Figure 1).

Different types of fiducials were used: lipiodol, titanium clips, bile duct stent. Titanium clips were either already present in the postoperative bed (in case of local relapses) or placed around the tumor at the OARs interfaces during a surgical exploration. The latter provides a proper target volume delineation on CT and allows for multidimensional visualization on TI. It also helps recognize positional and volumetric changes of OARs (Figure 2). While functioning as an indirect surrogate for OARs on intrafractional kV imaging (Figure 3). Lipiodol was injected into the tumor via a transabdominal route. In a minority of the cases a surrogate structure, such as a biliary stent, was used for daily image guidance. Proton -pump inhibitors, antiemetics, and prokinetics were also used as part of the treatment protocol. Patients were simulated in the supine position with arms up after a minimum of 2–3 h fasting. 3D/4D CT scan with abdominal compression [thermoplastic mask with underneath Styrofoam block, from 2019 Zfix (Qfix, Avondale, PA, United States)] or breath-hold CT was performed with Real-time Position Management (RPM). Candidates for breath-hold had a training session at the Linac before simulation to evaluate patient suitability and achievable and reproducible breath-hold levels. Minimum eligibility criteria required the patients to be able to hold their breaths for a minimum of 20 s. During breath-hold-SABR only audio-coaching was available.

Target definition followed international recommendations [23, 24]. The GTVp was defined on a tri-phase contrast-CT. Any major vessel within 5 mm of the tumor had its full circumference included. Fibrotic areas near vessels were also included in the GTVp. Initial diagnostic scans were also co-registered and together with the fiducials helped to finalize GTVp (Figure 2). ITV was created by using motion information from breath hold scans and/or 4D-CT. An ITV-to-PTV margin of 5 mm was applied to generate the PTV. A high dose area within PTV consisted of subtracting the gastrointestinal PRV from the GTVp without margin. GI PRV represents all positional/volumetric changes on different scans with a 3–5 mm expansion. GTVn was also defined as present. Elective nodes (elective nodal irradiation, ENI) were included if nodal disease was present after ICT.

SABR was delivered in five daily fractions for 1.5–2 weeks, prescribing 33 Gy (BED_{10}:55 Gy) to the PTV. At the beginning of

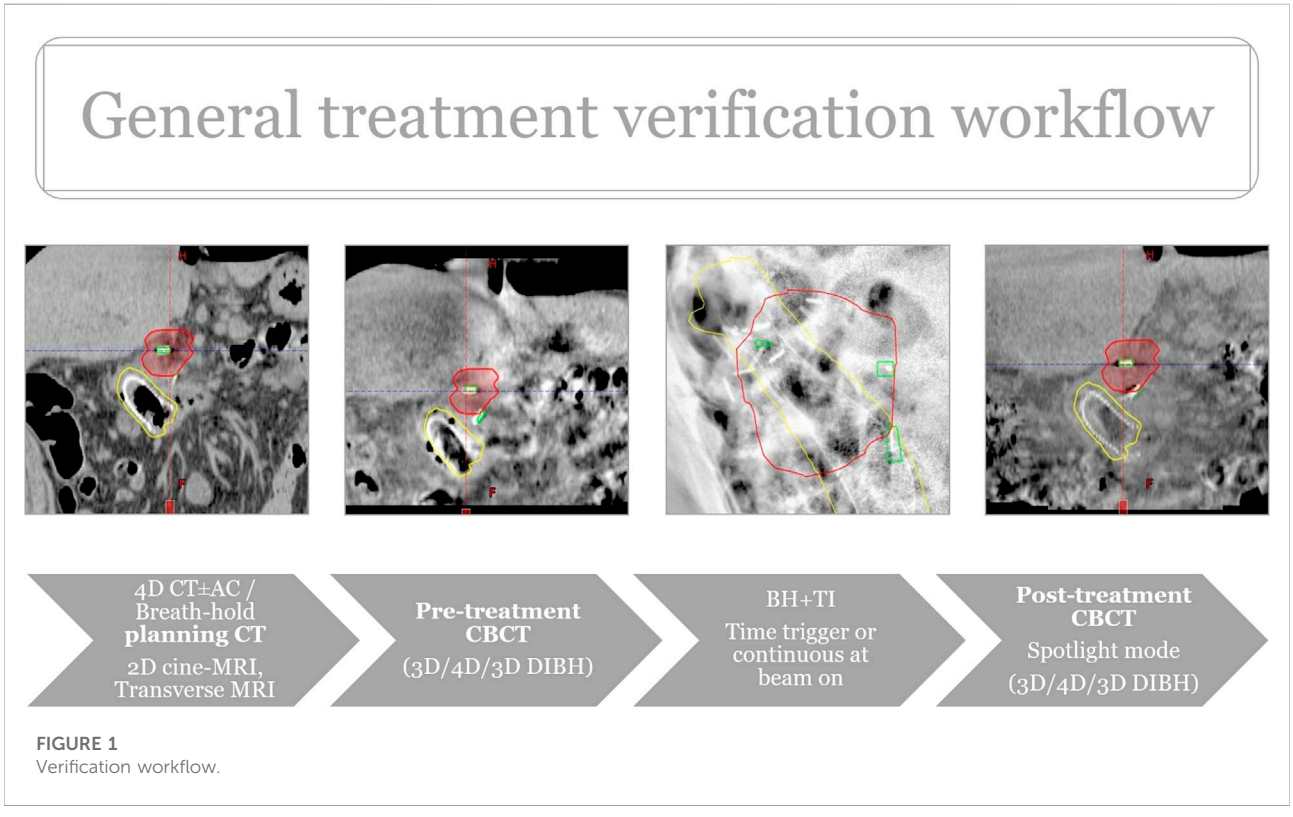

FIGURE 1
Verification workflow.

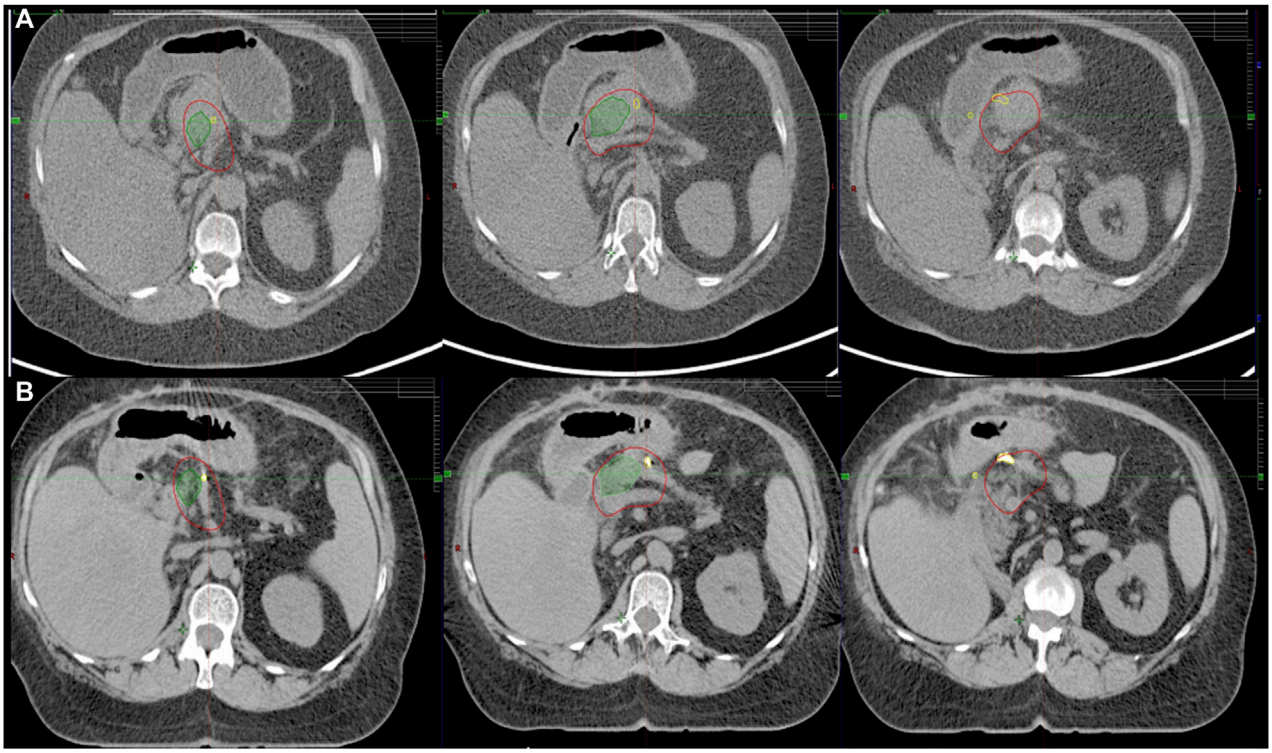

FIGURE 2
Corresponding axial CT slices on diagnostic scan **(A)** and treatment planning CT **(B)** fused by rigid registration. LAPC with abutment of gastric wall. Residual tumor (green), CTV (red). Note the implanted titanium clips (yellow) between the target volume and OARs assisting in target volume delineation.

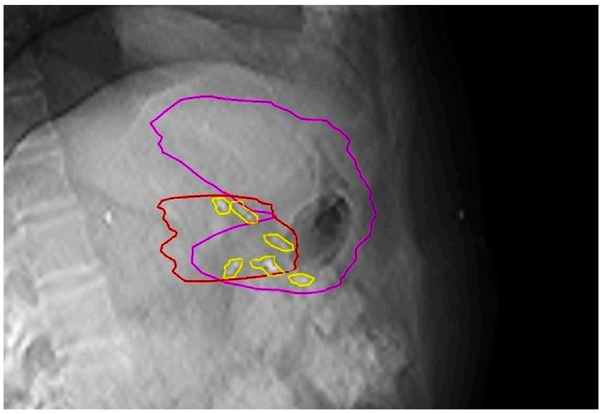

FIGURE 3
Multiple peritumoral fiducials (yellow) provide multidimensional visualization of the tumor (red) on triggered imaging, while certain clips indirectly represent the preserved gastric wall (purple).

our learning curve, a homogeneous dose prescription was applied (N: 9). With further experience, a dose escalation was carried out to the high-dose area with SIB approach up to 40 Gy (33/40Gy BED_{10}:55/72 Gy, N:4). The prescribed dose was reduced to 25 (D99 > 25 Gy) on the overlap area between the PTV and PRV if necessary. In one patient with extensive nodal disease even after iCT, a hypofractionated regimen was applied, consisting of 15 consecutive fractions up to a total dose of 37.5 (elective node)/52.5/60 Gy (macroscopic tumor, BED_{10}: 84 Gy). Initially, the normal tissue constraints followed those used in the Herman trial [7], and thereafter followed the recommendation of the UK SABR consortium guideline and published American recommendations [23, 24]. Treatment plans were designed and optimized according to two 6-MV full volumetric modulated arcs (VMAT; TrueBeam v2.7) using flattening filter free (1400 MU/min) photon beams.

Treatment verification started with 3D/4D CBCTs (3D Thorax mode, Slice thickness: 2 mm, 125 kVp and 270 mAs, 4D Thorax mode, Slice thickness: 2 mm, 125 kVp and 672 mAs) followed by triggered imaging and Beam Hold. In the case of breath, breath-hold-CBCT was acquired. Matching was based on fiducials with OAR verification at the same time. During treatment the radiation therapists (RTT) were responsible for manual beam hold (passive beam hold). Time triggering with 3s frequency was applied continuously or when the beam was on (Supplementary Video S1). Overlay structures served as the deviation limit for triggered imaging: 1) breath-hold: Fiducials plus 3 mm, 2) ITV- or Phase-gated SABR: summation of clips' contours from each or selected breathing phases. In the case of deviation limit violation, treatment

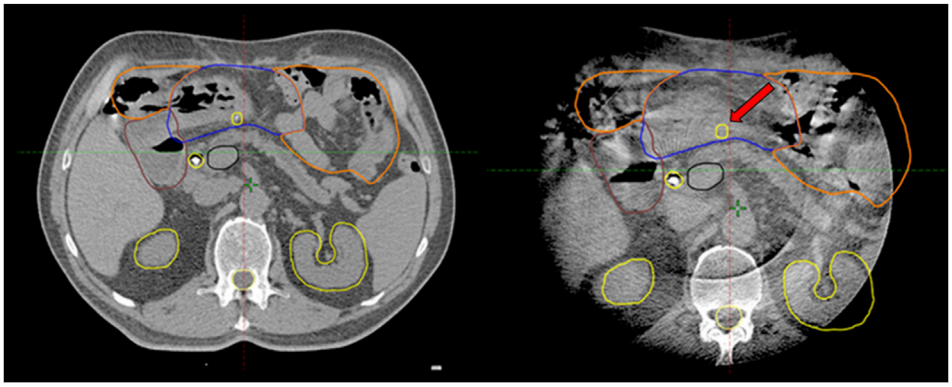

FIGURE 4
Corresponding axial slices on planning breath-hold-CT and breath-hold-CBCT (half fan mode): Systematic posterior displacement of the stomach (blue) and clip (arrow) was observed during the 1–4th fractions becoming closer to the high-dose area. Consequences/conclusions: 1. The position of this clip (arrow) is no longer relevant during intrafractional triggered imaging 2. This simultaneously alerts radiation therapists to the anatomical changes on CBCT.

delivery was manually interrupted and corrections using additional imaging (2D/3D match ± CBCT), or an adjustment of the gating threshold, was performed. The post-CBCT consisted of a faster half fan mode (Spotlight mode, Slice thickness: 2 mm, 125 kVp and 750 mAs, time 33 s) (Figure 4). In two breath-hold cases OARs were systematically delineated on each pre-and post-CBCTs with offline dose prediction per fraction. If dose constraint per fraction was not fulfilled, a new PRV was generated using CBCT contours and a dose re-optimization was done. If PRVs were violated on pre-CBCT, treatment was prohibited, and the same protocol was applied. Then, patients were treated according to the most appropriate plan based on the actual OARs anatomy (Plan of the day approach). The accumulated D0.5cc for OARs and D98%, D2% for the target was calculated as the mean of each DVH parameter across all CBCT contours in each patient.

Descriptive statistics were given for clinical variables, toxicity, and outcomes.

CBCT image quality for OARs was evaluated on a scale of 1–4 (1: inadequate, 2: doubtful, 3: acceptable, 4: excellent) on full arc pre-CBCT and half fan post CBCTs. Image quality of different CBCT modes (Free breathing, 3D CBCT breath-hold, 4D CBCT AIP, and 4D CBCT MIP) was compared between with Kruskal-Wallis H test and Mann-Whitney U test with a significance level of $p < 0.05$. Furthermore, we performed a Krippendorff agreement analysis among five radiation therapists (RTT) on 4 LAPC cases retrospectively. They were asked to judge whether the OARs respect their PRV on 40 CBCTs (yes/no). The pre-CBCT was a full arc, while the post-CBCT was a half fan acquisition. The Krippendorff's-α coefficient ($\alpha \geq 0.8$) [25] was calculated and compared between the two image acquisition types (McNemar's test at a significance level of $p < 0.05$).

Treatment time was compared between ITV-, phase gated- and breath-hold-gated SABR with Kruskal-Wallis H test and Mann-Whitney U test with a significance level of $p < 0.05$. The average

TABLE 1 Patient and tumor characteristics.

No of Pts	15
Age, y, median (range)	67 (52–83)
Male/female	5/10
ECOG, median, (range)	1 (0–1)
Tumor size, mm, (range)	38 (25–60)
Primary	11
Recurrence (post-op)	4
T stage, *N*, (%)	
T3	1
T4	14
N+	3
Induction CT, (%)	14 (93)
Folfirinox/Gemcitabine (%)	10 (67)/4(33)
Regression/SD post-ICT	7 (50)/7 (50)
Number of CT cycles, median, (range)	7 (2–13)
Initial CA19-9, mean, U/mL (range)	308 (15–1,000)
Post-ICT CA19-9, mean, U/mL (range)	146 (0.6–395)

times of the workflow were extracted from ARIA: 1) total treatment time (from the start of pre-CBCT to the end of post-CBCT); 2) treatment delivery time (from the start of the first arc to the end of the second arc); 3) "beam on" time + triggering time; and 4) time for 2D/3D match ± other operational time (CBCT analysis, couch movements, settings for Beam Hold, treatment field selection, etc.) Beam interruptions and treatment time were also recorded. Correlation analysis (Spearman) was also performed between the different time spans and number of corrections.

Overall survival (OS), Progression free survival (PFS), and Local progression free survival (LPFS) were calculated and described by the Kaplan-Meier analysis and reported, both from the start of iCT and the end of SABR. OS/PFS/LPFS were defined as the period from the start date of ICT and end date of SABR to the date of any death/

progression/local progression. Acute and late toxicity side effects were evaluated using the Common Toxicity Criteria for Adverse Events version 4.0 (CTCAEv4U.S. Department of Health and Human Services, National Institutes of Health, National Cancer Institute, 2009).

Statistical evaluation was performed using Statistical Package for the Social Sciences (SPSS) version 25.0 (IBM Corporation, Armonk, NY), and scipy (1.6.3) and lifelines (0.26.0) python (3.7) packages (Python Software Foundation, Beaverton OR, United States).

Results

Patient and tumor characteristics

Patient characteristics are shown in Table 1. All patients had locally advanced and/or node positive disease. Ninety-three percent of the patients received iCT dominantly with Folfirinox. Seventy-three percent of the patients had primary disease, while the remaining had local recurrences after a Whipple operation. The mean CA19-9 value before SABR was 146 IU/mL on average.

Treatment characteristics/treatment time

Seventy-one percent (10/14) of the patients had titanium surgical clips, with an average number of 6 (1–10). One patient had lipiodol labelling, while three patients had bile duct stents. There were no intervention-related side effects.

ITV-based (5), phase-gated (5), or breath-hold (4) techniques were applied (Table 2). The median treatment time was 16.6 ± 11 min. On average, beams were interrupted once (range: 0–3) per treatment session. Treatment time and number of corrections were moderately correlated ($R = 0.43$, $p < 0.01$). The shortest treatment

TABLE 2 Characteristics of treatment verification, treatment time analysis.

Imaging for treatment planning	Dynamics/cine MRI	5/14
	4D CT, N/Σ	6/14
	4D CBCT, N/Σ	–
	DIBH CT	6/14
Intrafractional triggered kV imaging, N/Σ		14/14
Post-CBCT, N/Σ		12/14
Motion-management technique	ITV concept	5/14
	Respiratory gated	4/14
	DIBH technique	6/14
Total treatment time[a], median ± SD, min	Σ	16.7 ± 10.8
	ITV concept (N:5)	12.1 ± 9.2
	Respiratory gated (N:5)	26.5 ± 13.4
	DIBH technique (N:5)	18.8 ± 6.2
Treatment delivery time[b], median ± SD, min	Σ	7.3 ± 7
	ITV concept	3.8 ± 8
	Respiratory gated	10.5 ± 6.4
	DIBH technique	9.8 ± 4.3
Beam on time + triggering time, median ± SD, min	Σ	4 ± 2.5
	ITV concept	2.5 ± 0.5
	Respiratory gated	8.3 ± 1.1
	DIBH technique	5 ± 2
Time for 2D/3D ± other operational time, median ± SD, min	Σ	2.4 ± 6.1
	ITV concept	1.4 ± 7.9
	Respiratory gated	2.9 ± 5.8
	DIBH technique	4 ± 3.4
Correction time, median ± SD, min[c]	CBCT	4.9 ± 4
	Triggered imaging	1.5 ± 0.7
Number of corrections, mean (range)		1 (0–3)
Number of subjects, *N*		65
Imaging modality of corrections	CBCT, *N*	17/64
	Triggered imaging, *N*	48/65

[a]Kruskal-Wallis H is 43.61 and is highly statistically significant with $p < 0.001$.
[b]From the start of the first arc to the end of the second arc.
[c]Mann-Whitney U is 15 and is highly statistically significant with $p < 0.001$.

time was achieved by ITV-based treatment, however breath-hold-SABR required significantly less time compared to phase-gated treatment (18.8 ± 6.2 vs. 26.5 ± 13.4, $p < 0.001$).

There was a significant difference ($p < 0.001$) between the image quality of different CBCT modes. The best image quality was achieved by breath-hold CBCT (median: 3) compared to other modalities (DIBH vs. FB: 3 vs. 2, $p = 0.002$, DIBH vs. AIP: 3 vs. 1, $p < 0.001$, DIBH vs. MIP: 3 vs. 1, $p < 0.001$) (Figure 5). There was no significant difference ($p > 0.05$) between FB, AIP, and MIP CBCT. The global mean K-α value was 0.8 (97.5%), and for pre- and post-CBCT was 0.8 (97%) and 0.9 (98%), respectively, showing strong agreement among the five independent RTTs. The lowest agreement was achieved for the lower part of the duodenum (Table 3). There was no significant difference ($p > 0.05$) between pre-(full fan) and post (half fan) CBCT except for the middle part of the duodenum ($p = 0.007$).

Dose-volume parameters are shown in Table 4. The average residual errors on pre-and post-breath-hold CBCTs were the following: vertical: 0 (0–0.34) cm, longitudinal: 0.2 (0–0.61) cm, lateral: 0.1 (0–0.37) cm. Consequently, the average (±SD) dose deviations from the original plan for D0.5cc of the duodenum, stomach, bowel, and high-dose PTV D2, D98 were −0.1% ± 1.2%, −1.1% ± 3.3%, 0.8% ± 3.3%, −1.6% ± 1.7%, and −0.3% ± 0.2%, respectively.

In two patients (15 fraction DE-RT, and 5 fraction-SABR) offline treatment adaptations were made due to substantial volume and systemic positional changes of the stomach (Figure 4; Supplementary Figure S1). In both cases the stomach moved toward the high-dose area, violating the dose per fraction limit or the original PRV. Based on the CBCTs, delineations of the stomach's new PRV-s were created, and re-optimization took place. One patient had a single treatment modification after the first four fractions, while in the second case two offline adaptations were required to fulfill the dose/fraction limit for the whole course of the treatment. In both cases only the adaptive plans were used for the remaining fractions. Dose-volume parameters per fraction for offline adaptive cases presented in Supplementary Figures S1–S3.

Clinical outcome

Median OS and PFS_{iCT} was 20 (9–46) and 12 months (1–41), while OS/PFS_{SABR} was 15 (4–37) and 8 months (1–32), respectively (Figure 6). Five (36%) patients reached a minimum of 20 months survival [22–46 months (iCT), 22–37 months (SABR)]. The dominant pattern of failure (12/14) was distant metastasis (peritoneum: 12, liver: 3, lung: 3, pleura: 1). Eleven patients died of cancer, one patient died of cardiac decompensation during the re-induction of Folfirinox. The two adaptive cases are still alive after 28 and 36 months from the start of iCT without any sign of progression or toxicity. Eight patients (57%) recurred locally, half of them after 12 months, all but one with massive simultaneous systemic relapse. The 1-y $LC_{iCT/sabr}$ was 78/70%, while the 2-y $LC_{iCT/sabr}$ was 58/52% (Figure 6). The acute side effects were minimal with only Gr.1 nausea/vomiting/diarrhea/bloating in a single case with gastric abutment by the tumor (Figure 2). There was no late RT-related toxicity (diarrhea, GI bleeding/obstruction).

Discussion

Our paper highlights an innovative Linac-based workflow for pancreatic SABR combining peritumoral fiducial-guided triggered imaging with gated or non-gated CBCT. Our ultimate goals were to develop full control of the entire workflow, improve time efficiency, and exploit the best CBCT image quality for better visualization of OARs and target with adaptation possibilities. From all these aspects we found that the breath-hold technique would be the first choice for pancreatic IGRT for SABR.

Pancreatic SABR requires the visualization of the tumor and OARs to increase dose delivery and maximize normal tissue protection. MRI-guided radiotherapy [14], with its excellent soft tissue contrast, combined with daily—even during fractional adaptation—real-time organ motion visualization, is already considered the treatment of choice for pancreatic SABR among all available technologies. As the incidence of LAPC increases, the need for pancreatic SABR is also growing. Unfortunately, MRI or CT-on-rail or CBCT based adaptive workflows are not widely available, mainly due to their elevated costs, reimbursement challenges and high resource requirements. The biggest disincentive from pancreatic SABR on conventional Linacs is the fear of side effects, which can be handled in two ways. Firstly, more careful patient selection compared to the advanced technologies and secondly, the development of a workflow that can address the above-mentioned challenges and ensures high dose delivery with minimized toxicity. Since direct visualization of OARS and tumor is not possible on Linac during treatment, we used fiducials as indirect surrogates, whose movement was controlled by kV images guided by a built-in software of the Linac. The rationale of using peritumoral fiducials was severalfold. Surgical exploration may detect peritoneal deposits, thus excluding these patients from further local treatment. It could also improve target definition on planning CT by incorporation of intraoperative findings, while allowing a multidimensional visualization of the target on triggered imaging, hence improving precision of our treatment (Figures 2, 3). Furthermore, the displacement of fiducials could also signal a positional and/or volumetric changes of duodenum/stomach on CBCT or on triggered imaging as they are inserted at the tumor/OAR interfaces (Figure 4). Each long-term survivor in our cohort had surgically implanted fiducials.

Treatment time is a crucial factor during SABR since prolonged radiation delivery is prone to have more errors. As

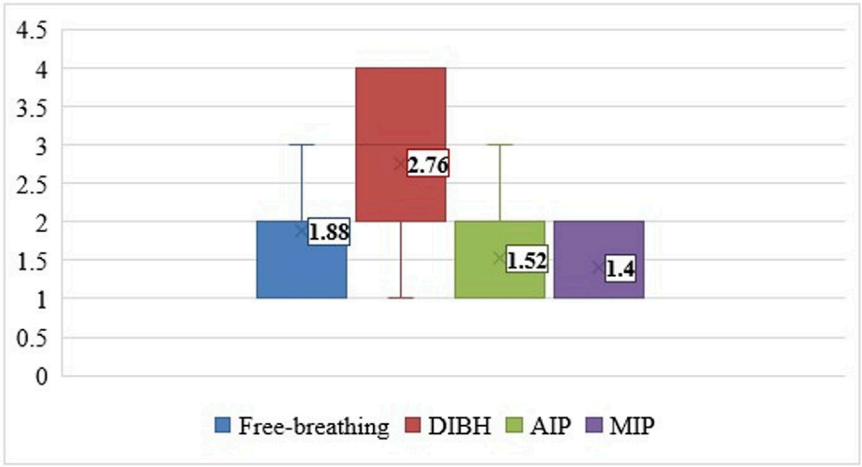

Structures	Imaging			
	3D CBCT		4D CBCT	
	FB	DIBH	AIP	MIP
Duodenum				
Upper part	2 (1-3)	3 (1-4)	1 (1-2)	1 (1-2)
Middle part	2 (1-3)	3 (1-4)	1 (1-2)	1 (1-2)
Lower part	2 (1-3)	4 (2-4)	2 (1-3)	1 (1-2)
Stomach	2 (1-3)	3 (1-4)	1 (1-2)	1 (1-2)
Bowel	1 (1-2)	3 (1-4)	1 (1-2)	1 (1-2)

FIGURE 5
Image quality assessment of different CBCT modes. FB, free breathing; DIBH, deep inspiration breath hold; AIP, average intensity projection; MIP, maximum intensity projection.

TABLE 3 The degree of agreement between the RTTs' evaluations.

	Organs at risk	Pre-CBCT			Post-CBCT		
		K-α	%	95% CI	K-α	%	95% CI
OAR position relative to PRV	Duodenum						
	Upper	1	100	1	1	100	1
	Middle	0.88	99	0.76–0.97	0.77	97	0.65–0.87
	Lower	0.78	94	0.68–0.88	0.71	94	0.59–0.82
	Stomach	0.89	99	0.82–0.96	0.86	98	0.75–0.95
	Bowel	0.82	98	0.69–0.93	0.75	96	0.63–0.86

Abbreviations: K-α, Krippendorff's alpha; %, in % of Krippendorff's alpha; 95% CI, the 95% confidence intervals; CBCT, cone beam computed tomography.

expected, ITV-based treatment with abdominal compression was the most time efficient due to its lower complexity, mostly due to the benefit of non-moving targets such as retroperitoneal recurrences. Interestingly, breath-hold-SABR took only 18 min on average, 25% less than free breathing phase-gated treatment in addition to clearly better image quality. This can be explained by careful selection and training of breath-hold patients, as well as the time triggering feature of beam hold. During treatment, the Auto-beam hold function was switched off, so the radiation therapist was responsible for the beam control, which allows the number of breaths to be reduced. When the beam is held during time triggering, the system keeps shooting, providing a dynamic movement analysis just before or any time during radiation delivery. First, this fast confirmation of the fiducials could decide whether the breath-hold threshold should be fine-tuned or not. Second, the radiation therapist can give short verbal

TABLE 4 Dosimetric results.

Target and OARs		5-fx SABR, (N:4)		5-fx SABR, (N:5)		5-fx SABR, (N:4)		15-fx DERT, (N:1)
		Mean	SD	Mean	SD	Mean	SD	Value
PTVlow	D98.00 [Gy]	28.3	6.2	25.4	2.8	31.0	3.5	37.6
	D2.00 [Gy]	33.4	5.1	37.4	2.6	45.7	4.8	56.7
PTVhigh	D98.00 [Gy]	31.0	4.7	32.7	4.4	40.3	3.0	57.4
	D2.00 [Gy]	33.4	5.2	37.7	2.6	46.1	4.9	60.1
Duodenum	D0.50cc [Gy]	15.8	4.8	27.8	5.5	32.1	0.6	44.3
Stomach	D0.50cc [Gy]	12.0	9.9	16.5	7.9	23.1	7.3	43.2
Bowel	D0.50cc [Gy]	23.5	8.5	23.5	8.5	23.5	8.5	43.2
Spinal Cord	D1.00cc [Gy]	8.0	2.2	8.0	2.2	8.0	2.2	19.2
Left Kidney	Mean dose	3.8	1.6	3.8	1.6	3.8	1.6	8.8
Right Kidney	Mean dose	4.4	1.8	4.4	1.8	4.4	1.8	8.1
Kidneys	Mean dose	4.0	1.3	4.0	1.3	4.0	1.3	8.4

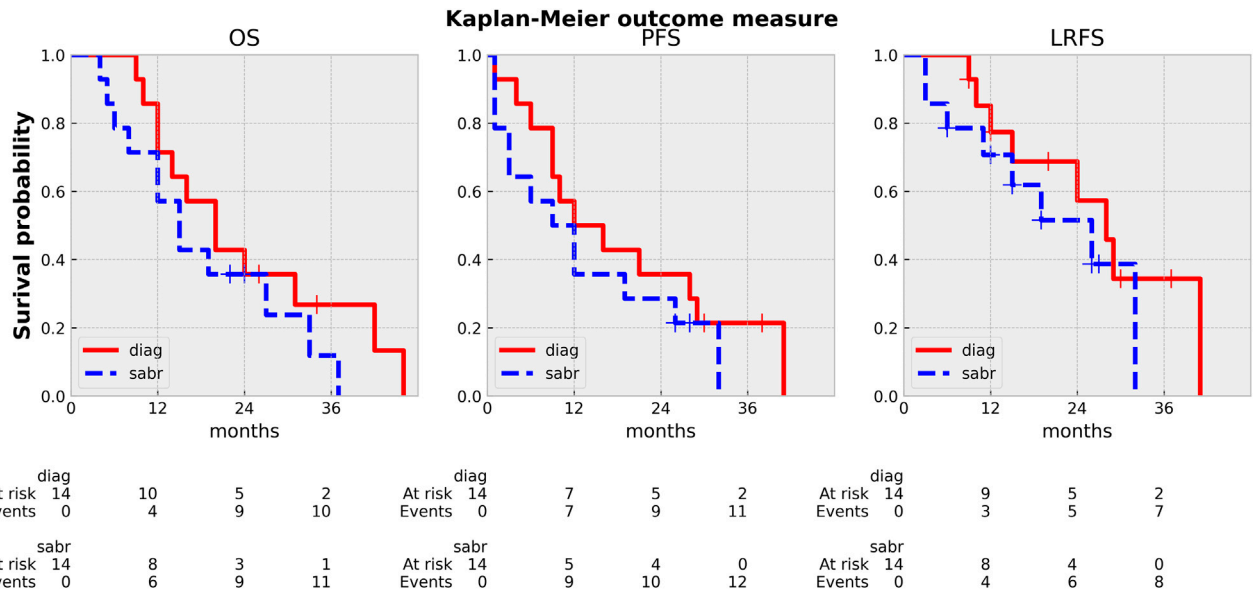

FIGURE 6
Kaplan Meier curves: OS (overall survival), PFS (progression free survival), LPFS (local-progression free survival). diag: from the start of induction CT, sabr: from the end of SABR.

instructions ("breathe in or breathe out a little more/less") to the patient, which permits continuous treatment and avoids unnecessary cessation of radiation delivery and consequently, the early exhaustion of the patient. Third, fiducial overlap or random displacement of the fiducials may occur, resulting in an undetectable or tilted position of the markers on triggered imaging, which would inevitably lead to an immediate interruption of radiation delivery if auto beam hold mode were active. It should be mentioned that during these treatments, no visual coaching device was available, so treatment time could be further decreased. Due to its complexity, considerably longer treatment time was reported with MR Linacs ranging between 83–90 min on average, decreasing toward 60 min with the introduction of audio feedback [26, 27]. However, it is counterbalanced by the intrafractional soft tissue visualization. Even with online adaptive CBCT based treatments, a total treatment time of 70 min was reported (18). CT equivalent CBCT embraced

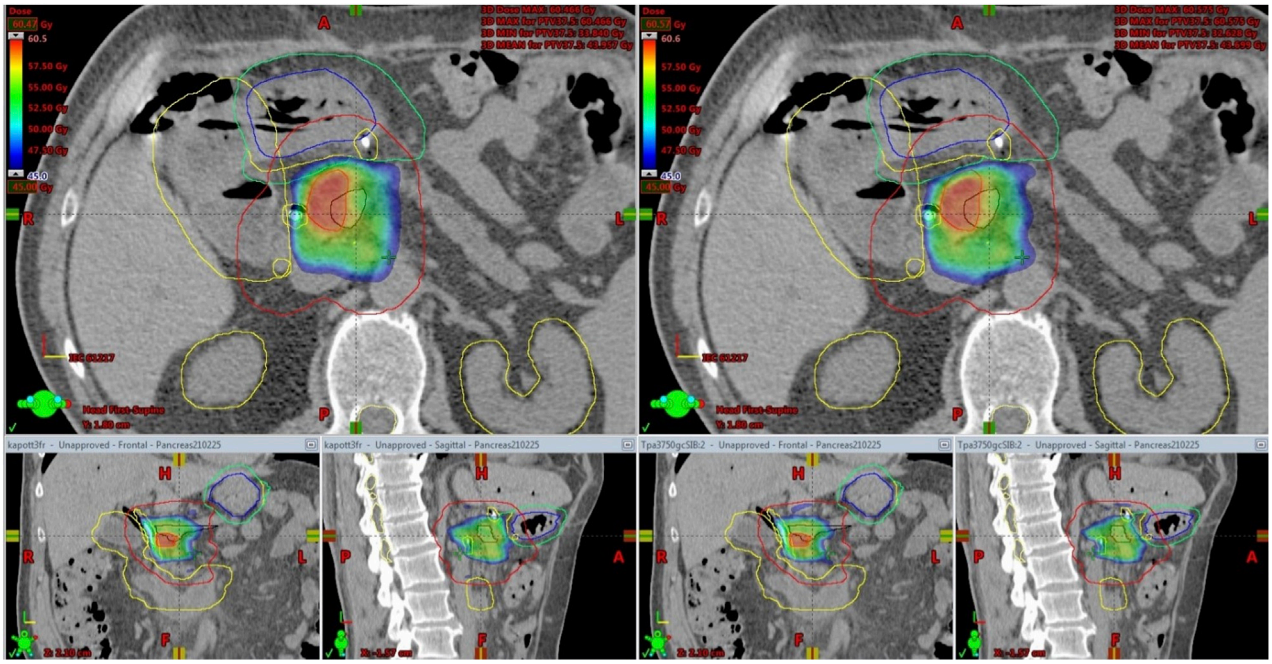

FIGURE 7
Offline treatment plan re-optimization based on CBCT contouring of the stomach (Blue: original stomach, yellow: original PRV, green: new PRV).

with ultrarapid image acquisition (6s) is coming up on the latest version of Halcyon.

Again, CBCT may not be competitive with MRI, but tailored protocols can go a long way to improving image quality by reducing gas and internal motion artifacts and reducing treatment time. However, free breathing acquired images still suffer from respiration induced artefacts even with abdominal compression. In this aspect, breath-hold seems to be a good alternative. Moreover, reproducibility is not influenced by an abdominal compressor, which could cause even higher positional variations of the pancreas or OARs. In contrast, the technique needs careful patient selection and training. Our first experiences with breath-hold were very positive [22]. Instead of using only a descriptive 1–4-point scale to measure image quality, we sought to evaluate an offline treatment simulation of the visibility of OARs. Based on the opinion of five independent RTTs, breath-hold-CBCT can be used to reliably determine OAR position relative to PRV [K-α = 0.85 (0.71–1)]. Surprisingly, the agreement was the lowest for the lower part of the duodenum. The CBCT acquisition type was only an influencing factor for the mid-part of the duodenum, favoring the full arc mode. However, in the case of Spotlight mode, it is still above the minimum criteria value of K-α (0.66), and we consider that clinically acceptable. This means that breath-hold image quality is sufficient to monitor PRVs during treatment and capable of triggering offline treatment adaptation as we did in our two cases (Figure 4, 7). Moreover, Spotlight mode (Figure 4) reduces image acquisition time by half per CBCT, further reducing the number of breath-holds and the total treatment time.

Our clinical results (OS, PFS, LC) are comparable to those using the similar fractionation scheme [7]. In more than one-third of our cases, exceptionally good clinical outcomes were achieved including four patients with no evidence of progression >24 months (26–41) from the start date of ICT. Two of them are still alive without any sign of progression. In both adaptive cases (Figure 4, 7) there was a substantial response of the tumor and CA19-9 to polychemotherapy, and the prescribed dose was also the highest in these cases (Table 4). As expected, distant metastasis represented the dominant pattern of failure. It should be also mentioned that half of these patients had simultaneous local progression as well. We had only one patient with local-only recurrence as first failure. Recent studies demonstrated that dose escalation beyond a BED of 70 Gy was associated with improved OS [12, 14]. Moreover, BED higher than 100 Gy seems to further boost these clinical results [24, 28–30] beyond a median OS of 18 months, however prospective randomized trials are still warranted. In light of these results, the dose we prescribe can be considered conservative. We did not have either Grade 3 acute or late side effects which is impressive even with these conservative SABR doses. Notably, in trials using the same dose levels, Gr. 3 GI toxicity of 6%–10% was reported including Gr. 5 events as well [7, 13, 30]. We believe that our

feasible toxicity profile is partly attributed to our advanced image verification workflow as well. Isotoxic high-dose SABR with improved or maintained serious side effects could be realized on MR-Linac. The SMART Pancreas study, applying 50Gy/5 BED100 Gy, met its primary objective with zero incidences of acute grade 3+ GI toxicity [14, 31, 32].

The limited number of cases, as well as heterogeneous, continuously evolving protocol, are potential weaknesses of our paper. On the other hand, on Linac, this advanced end-to-end workflow has never been presented and it is supported by comprehensive image quality and time efficiency assessments with the introduction of offline adaptive cases. We hope that our protocol could serve as an example to be followed by other Institutions with similar technologies.

In conclusion, Linac-based pancreatic SABR with triggered imaging and beam-hold is feasible. Peritumoral fiducials with time triggering improve utility and time efficiency. Breath-hold-CBCT provides the best image quality at a reasonable treatment time span with offline adaptation possibilities and should be considered as a first choice IGRT technique for pancreatic SABR. Clinical outcome is promising with negligible side effects. In selected cases, this workflow may be a viable alternative in clinics where MR-guided and/or online adaptive CBCT/CT technology is not available.

Data availability statement

The raw data supporting the conclusion of this article will be made available by the authors, without undue reservation.

Ethics statement

The studies involving humans were approved by the Hungarian National Institute of Pharmacy and Nutrition under permission number OGYÉI/5301/2018. The studies were conducted in accordance with the local legislation and institutional requirements. The participants provided their written informed consent to participate in this study.

Author contributions

Conceptualization: FL and KK. Methodology: AG, PK, and CG. Analysis: MC and KK. Investigation: FL and KK. Data curation: AF, GL, KM, ZS, and ZK. Writing: FL, AG, and KK. All authors contributed to the article and approved the submitted version.

Conflict of interest

Author ZT was employed by the company Medicopus Nonprofit Ltd.

The remaining authors declare that the research was conducted in the absence of any commercial or financial relationships that could be construed as a potential conflict of interest.

Supplementary material

The Supplementary Material for this article can be found online at: https://www.por-journal.com/articles/10.3389/pore.2023.1611456/full#supplementary-material

SUPPLEMENTARY FIGURE S1
Offline adaptive cases. Case 1: 5 fraction SABR. Due to increased volume changes of the stomach during breath-hold **(A)** there was a clear trend of increased dose of the stomach on pre-and especially post-CBCT compared to the reference.

SUPPLEMENTARY FIGURE S2
Dose deviations of the Target (D2, D98) and Stomach (D0.5cc) from the original plan considering offline adaptations and residual errors. As a worst-case scenario (post-CBCT) a 5% increase in D0.5 cc of the stomach (from 32.1 to 33.9 Gy) and 8% decrease in D98 (from 34.95 to 32.08 Gy) could be estimated while still meeting hard constraints.

SUPPLEMENTARY FIGURE S3
Offline adaptive case 2: 15-fraction dose escalated treatment. Evolution of dose per fraction of OARs during the whole course of the treatment. After the 4th fraction, a single adaptation was applied and used consequently for the remaining fractions to avoid overtreatment of the gastro-duodenal junction.

References

1. Chiorean EG, Chiaro MD, Tempero MA, Malafa MP, Benson AB, Cardin DB, et al. Ampullary adenocarcinoma, version 1.2023, NCCN clinical practice guidelines in oncology. *JNCCN J Natl Compr Cancer Netw* (2023) 21(7):753–82. doi:10.6004/jnccn.2023.0034

2. Balaban EP, Mangu PB, Yee NS Locally advanced unresectable pancreatic cancer: American society of clinical oncology clinical practice guideline summary. *J Oncol Pract* (2017) 13(4):265–9. doi:10.1200/JOP.2016.017376

3. Ferlay J, Colombet M, Soerjomataram I, Parkin DM, Piñeros M, Znaor A, et al. Cancer statistics for the year 2020: an overview. *Int J Cancer* (2021) 149(4):778–89. doi:10.1002/ijc.33588

4. Versteijne E, Van Dam JL, Suker M, Janssen QP, Groothuis K, Akkermans-Vogelaar JM, et al. Neoadjuvant chemoradiotherapy versus upfront surgery for resectable and borderline resectable pancreatic cancer: long-term results of the dutch randomized PREOPANC trial. *J Clin Oncol* (2022) 40(11):1220–30. doi:10.1200/JCO.21.02233

5. Comito T, Cozzi L, Clerici E, Franzese C, Tozzi A, Iftode C, et al. Can stereotactic body radiation therapy be a viable and efficient therapeutic option for unresectable locally advanced pancreatic adenocarcinoma? results of a phase 2 study. *Tech Cancer Res Treat* (2017) 16(3):295–301. doi:10.1177/1533034616650778

6. Panje C, Andratschke N, Brunner TB, Niyazi M, Guckenberger M Stereotactic body radiotherapy for renal cell cancer and pancreatic cancer: literature review and practice recommendations of the DEGRO working group on stereotactic radiotherapy. *Strahlentherapie Und Onkologie* (2016) 192(12):875–85. doi:10.1007/s00066-016-1053-1

7. Herman JM, Chang DT, Goodman KA, Dholakia AS, Raman SP, Hacker-Prietz A, et al. Phase 2 multi-institutional trial evaluating gemcitabine and stereotactic

body radiotherapy for patients with locally advanced unresectable pancreatic adenocarcinoma. *Cancer* (2015) 121(7):1128–37. doi:10.1002/cncr.29161

8. Petrelli F, Comito T, Ghidini A, Torri V, Scorsetti M, Barni S Stereotactic body radiation therapy for locally advanced pancreatic cancer: a systematic review and pooled analysis of 19 trials. *Int J Radiat Oncol Biol Phys* (2017) 97(2):313–22. doi:10.1016/j.ijrobp.2016.10.030

9. Rossi G, Simoni N, Paiella S, Rossi R, Venezia M, Micera R, et al. Risk adapted ablative radiotherapy after intensive chemotherapy for locally advanced pancreatic cancer. *Front Oncol* (2021) 11(April):662205–9. doi:10.3389/fonc.2021.662205

10. Manderlier M, Navez J, Hein M, Engelholm J, Closset J, Bali MA, et al. Isotoxic high-dose stereotactic body radiotherapy (iHD-SBRT) versus conventional chemoradiotherapy for localized pancreatic cancer: a single cancer center evaluation. *Cancers* (2022) 14(23):5730. doi:10.3390/cancers14235730

11. Reyngold M, O'Reilly EM, Varghese AM, Fiasconaro M, Zinovoy M, Romesser PB, et al. Association of ablative radiation therapy with survival among patients with inoperable pancreatic cancer. *JAMA Oncol* (2021) 7(5):735–8. doi:10.1001/jamaoncol.2021.0057

12. Krishnan S, Chadha AS, Suh Y, Chen HC, Rao A, Das P, et al. Focal radiation therapy dose escalation improves overall survival in locally advanced pancreatic cancer patients receiving induction chemotherapy and consolidative chemoradiation. *Int J Radiat Oncol Biol Phys* (2016) 94(4):755–65. doi:10.1016/j.ijrobp.2015.12.003

13. Teriaca MA, Loi M, Suker M, Eskens FALM, van Eijck CHJ, Nuyttens JJ A phase II study of stereotactic radiotherapy after FOLFIRINOX for locally advanced pancreatic cancer (LAPC-1 trial): long-term outcome. *Radiother Oncol* (2021) 155:232–6. doi:10.1016/j.radonc.2020.11.006

14. Rudra S, Jiang N, Rosenberg SA, Olsen JR, Roach MC, Wan L, et al. Using adaptive magnetic resonance image-guided radiation therapy for treatment of inoperable pancreatic cancer. *Cancer Med* (2019) 8(5):2123–32. doi:10.1002/cam4.2100

15. Palta M, Godfrey D, Goodman KA, Hoffe S, Dawson LA, Dessert D, et al. Radiation therapy for pancreatic cancer: executive summary of an ASTRO clinical practice guideline. *Pract Radiat Oncol* (2019) 9(5):322–32. doi:10.1016/j.prro.2019.06.016

16. Loi M, Magallon-Baro A, Suker M, van Eijck C, Sharma A, Hoogeman M, et al. Pancreatic cancer treated with SBRT: effect of anatomical interfraction variations on dose to organs at risk. *Radiother Oncol* (2019) 134:67–73. doi:10.1016/j.radonc.2019.01.020

17. Tyran M, Jiang N, Cao M, Raldow A, Lamb JM, Low D, et al. Retrospective evaluation of decision-making for pancreatic stereotactic MR-guided adaptive radiotherapy. *Radiother Oncol* (2018) 129(2):319–25. doi:10.1016/j.radonc.2018.08.009

18. Kim M, Schiff JP, Price A, Laugeman E, Samson PP, Kim H, et al. The first reported case of a patient with pancreatic cancer treated with cone beam computed tomography-guided stereotactic adaptive radiotherapy (CT-STAR). *Radiat Oncol* (2022) 17(1):157–11. doi:10.1186/s13014-022-02125-z

19. Khan M, Sandhu N, Naeem M, Ealden R, Pearson M, Ali A, et al. Implementation of a comprehensive set of optimised CBCT protocols and validation through imaging quality and dose audit. *Br J Radiol* (2022) 95(1139):20220070. doi:10.1259/bjr.20220070

20. Kawahara D, Ozawa S, Nakashima T, Suzuki T, Tsuneda M, Tanaka S, et al. Absorbed dose and image quality of varian TrueBeam CBCT compared with OBI CBCT. *Physica Med* (2016) 32(12):1628–33. doi:10.1016/j.ejmp.2016.11.118

21. Kaur G, Lehmann J, Greer P, Simpson J Assessment of the accuracy of truebeam intrafraction motion review (IMR) system for prostate treatment guidance. *Australas Phys Eng Sci Med* (2019) 42(2):585–98. doi:10.1007/s13246-019-00760-7

22. Kisiván K, Erdélyesi D, Gutyina D, Sajti P, Gugyerás D, Farkas A, et al. Hasnyálmirigyrák lineáris gyorsító alapú sztereotaxiás sugárterápiája kezelés alatti tumorkövetéssel. *Magyar Onkológia* (2021) 65(1):6–13.

23. Hanna GG, Murray L, Patel R, Jain S, Aitken KL, Franks KN, et al. UK consensus on normal tissue dose constraints for stereotactic radiotherapy. *Clin Oncol* (2018) 30(1):5–14. doi:10.1016/j.clon.2017.09.007

24. Koay EJ, Hanania AN, Hall WA, Taniguchi CM, Rebueno N, Myrehaug S, et al. Dose-escalated radiation therapy for pancreatic cancer: a simultaneous integrated boost approach. *Pract Radiat Oncol* (2020) 10(6):e495–e507. doi:10.1016/j.prro.2020.01.012

25. Krippendorff K Agreement and information in the reliability of coding. *Commun Methods Measures* (2011) 5(2):93–112. doi:10.1080/19312458.2011.568376

26. Gaya A, Camilleri P, Nash A, Hughes D, Good J Implementation of stereotactic MRI-guided adaptive radiotherapy (SMART) for hepatobiliary and pancreatic cancers in the United Kingdom – fifty in five. *Cureus* (2021) 13(5):e15075. doi:10.7759/cureus.15075

27. Chuong MD, Bryant J, Mittauer KE, Hall M, Kotecha R, Alvarez D, et al. Ablative 5-fraction stereotactic magnetic resonance–guided radiation therapy with on-table adaptive replanning and elective nodal irradiation for inoperable pancreas cancer. *Pract Radiat Oncol* (2021) 11(2):134–47. doi:10.1016/j.prro.2020.09.005

28. Reyngold M, Parikh P, Crane CH Ablative radiation therapy for locally advanced pancreatic cancer: techniques and results. *Radiat Oncol* (2019) 14(1):95. doi:10.1186/s13014-019-1309-x

29. Colbert LE, Rebueno N, Moningi S, Beddar S, Sawakuchi GO, Herman JM, et al. Dose escalation for locally advanced pancreatic cancer: how high can we go? *Adv Radiat Oncol* (2018) 3(4):693–700. doi:10.1016/j.adro.2018.07.008

30. Zaorsky NG, Lehrer EJ, Handorf E, Meyer JE Dose escalation in stereotactic body radiation therapy for pancreatic cancer: a meta-analysis. *Am J Clin Oncol Cancer Clin Trials* (2019) 42(1):46–55. doi:10.1097/COC.0000000000000472

31. Chuong MD, Kirsch C, Herrera R, Rubens M, Gungor G, Schaff EM, et al. Long-term multi-institutional outcomes of 5-fraction ablative stereotactic MR-guided adaptive radiation therapy (SMART) for inoperable pancreas cancer with median prescribed biologically effective dose of 100 Gy10. *Int J Radiat Oncol. Biol. Phys.* (2021) 111(3):S147–8. doi:10.1016/j.ijrobp.2021.07.330

32. Parikh PJ, Lee P, Low D, Kim J, Mittauer KE, Bassetti MF, et al. Stereotactic MR-guided on-table adaptive radiation therapy (SMART) for patients with borderline or locally advanced pancreatic cancer: primary endpoint outcomes of a prospective phase II multi-center international trial. *Int J Radiat Oncol. Biol. Phys.* (2022) 114(5):1062–3. doi:10.1016/j.ijrobp.2022.09.010

Pathology & Oncology Research | frontiers

TYPE Original Research
PUBLISHED 30 May 2023
DOI 10.3389/pore.2023.1611175

Check for updates

OPEN ACCESS

EDITED BY
Anna Sebestyén,
Semmelweis University, Hungary

*CORRESPONDENCE
Wen Cheng,
chengwen@hrbmu.edu.cn

†These authors have contributed equally to this work

RECEIVED 11 March 2023
ACCEPTED 10 May 2023
PUBLISHED 30 May 2023

CITATION
Zhang L, Zhang X, Wu B, Han X, Guo C, Li B, Jing H and Cheng W (2023), Prognostic value of albumin-bilirubin score in pancreatic cancer patients after pancreatoduodenectomy with liver metastasis following radiofrequency ablation.
Pathol. Oncol. Res. 29:1611175.
doi: 10.3389/pore.2023.1611175

COPYRIGHT
© 2023 Zhang, Zhang, Wu, Han, Guo, Li, Jing and Cheng. This is an open-access article distributed under the terms of the Creative Commons Attribution License (CC BY). The use, distribution or reproduction in other forums is permitted, provided the original author(s) and the copyright owner(s) are credited and that the original publication in this journal is cited, in accordance with accepted academic practice. No use, distribution or reproduction is permitted which does not comply with these terms.

Prognostic value of albumin-bilirubin score in pancreatic cancer patients after pancreatoduodenectomy with liver metastasis following radiofrequency ablation

Lei Zhang[1,2†], Xuefei Zhang[1,2†], Bolin Wu[1,2], Xue Han[1], Cunli Guo[1], Bo Li[1], Hui Jing[1] and Wen Cheng[1,2*]

[1]Department of Ultrasound, Harbin Medical University Cancer Hospital, Harbin, China, [2]Interventional Ultrasound Ward, Harbin Medical University Cancer Hospital, Harbin, China

Objective: The current study aimed to investigate the prognostic value of albumin-bilirubin (ALBI) score in predicting clinical outcomes of pancreatic cancer patients after pancreatoduodenectomy with liver metastasis following radiofrequency ablation.

Methods: This retrospective study included 90 pancreatic cancer patients after pancreatoduodenectomy with liver metastasis from January 2012 to December 2018. In this study, the Chi-square or Fisher's exact tests, the receiver operating characteristic (ROC) curve, Kaplan-Meier method and Log-rank test, univariate and multivariate Cox proportional hazard regression analyses, nomogram, calibration curves and decision curve analysis were used for all statistical analysis.

Results: We analyzed the optimal cut-off value of ALBI by ROC curve, and the optimal cut-off value was −2.60. According to ALBI score, these patients were divided into two groups: low ALBI group (n = 33) and high ALBI group (n = 57). Patients with low ALBI score was significantly related to longer progression free survival (PFS) (p = 0.0002, HR: 3.039, 95% CI: 1.772–5.210) and overall survival (OS) (p = 0.0005, HR: 2.697, 95% CI: 1.539–4.720). The 1-, 3-, and 5-year PFS and OS rates in low ALBI group were higher than those in high ALBI group. ALBI was a potential independent prognostic factor for pancreatic cancer patients after pancreatoduodenectomy with liver metastasis following radiofrequency ablation. Moreover, the nomogram was used to predict the 1-, 3-, and 5-year survival probabilities of PFS and OS. The calibration curve shown that the prediction line matched the reference line well for postoperative 3-year PFS and OS. The DCA shown that nomogram model was better than the only ALBI, and indicated the ability for clinical decision-making, especially in 1-year PFS, and 3-, 5-year OS.

Conclusion: ALBI is a potential independent factor for PFS and OS, and can predict the prognosis of pancreatic cancer patients after

pancreatoduodenectomy with liver metastasis following radiofrequency ablation.

KEYWORDS

chemotherapy, pancreatic cancer, liver metastasis, radiofrequency ablation, pancreatoduodenectomy

Introduction

Pancreatic cancer is the fourteenth leading cause of cancer-related incidence and the seventh leading cause of cancer-related deaths all over the world [1]. As a result of the changes in lifestyle, the incidence has been increasing in developed countries, especially in western countries [2]. Surgery is the primary treatment for early and resectable pancreatic cancer. With the progress of surgical technology, adjuvant treatment, and the improvement of perioperative management are now continuously increasing [3]. However, due to delay diagnosis, ineffective treatment, no obvious symptom, the majority of the patients are not appropriate candidates for operation [4]. Despite the progress in the detection and treatment of pancreatic cancer, the 1-year survival rate is about 24%, and the 5-year survival rate is about 6% [5]. Liver is the most common site of metastasis, and synchronous liver metastasis reportedly occurs in approximately 50% of pancreatic cancer patients at the time of initial diagnosis, and postoperative liver metastasis accounts for 40%–90% [6, 7]. Although the simultaneous resection of pancreatic cancer and liver metastasis are technically feasible, and liver metastasis is still considered to be the main cause of death in patients with pancreatic cancer [8].

Radiofrequency ablation (RFA) is a non-surgical treatment for liver metastasis of pancreatic cancer with unresectable liver metastases or complications [9]. Compared with systemic chemotherapy, hepatectomy can increase the local disease control rate, improve progression free survival (PFS) and have better overall survival (OS) [10]. However, not all pancreatic cancer patients with liver metastases can benefit from hepatectomy due to the aggressive tumor behavior, limited surgical operation indications or frequent liver failure after liver resection [11]. In order to improve the survival outcomes of pancreatic cancer with liver metastases, the hepatic arterial infusion chemotherapy, systemic chemotherapy, RFA and radiotherapy have been practiced in the clinical setting [12–15].

Tumor associated systemic inflammation plays an important role in the development and metastasis of tumor cells [16]. Previous studies have revealed that systemic inflammation biomarkers, such as neutrophil-to-lymphocyte ratio (NLR), lymphocyte-to-monocyte ratio (LMR), and platelet-to-lymphocyte ratio (PLR), were closely associated with tumor prognosis [17, 18]. A novel inflammation-related marker, albumin-bilirubin (ALBI) score, calculated from albumin and bilirubin, has been identified for the first time as estimating the degree of liver function in patients with hepatocellular carcinoma [19]. ALBI has been gradually emerged as an independent predictor in some tumors, such as colon cancer, high-grade gliomas, and hepatocellular carcinoma [20–22]. However, there are few studies on the role of ALBI in pancreatic cancer after pancreatoduodenectomy with liver metastasis. Hence, the aim of our study was to investigate the association of ALBI with clinicopathological indicators and survival outcomes in pancreatic cancer patients after pancreatoduodenectomy with liver metastasis following radiofrequency ablation.

Materials and methods

Patients section

The inclusion criteria were as follows: 1) pancreatic cancer confirmed by histopathology after pancreatoduodenectomy; 2) positron emission tomography computer tomography (PETCT)/multi-detector computed tomography (MDCT) imaging diagnosis confirmed liver metastasis, and without extrahepatic diffusion; 3) single or multiple liver metastases (less than five lesions), and the maximum size of the largest liver lesion less than 5 cm; 4) Eastern Cooperative Oncology Group (ECOG) < 2 scores and Karnofsky (KPS) ≥70 scores, and could bear the risk of the treatment; 5) with complete follow-up data. The exclusion criteria were as follows: 1) with organ metastasis or other tumors; 2) with serious complications, such as infection, active bleeding, coagulation abnormalities; 3) with any severe comorbidities, such as respiratory failure, renal failure or heart failure; 4) with poor clinical compliance.

Process of RFA and chemotherapy regimens

RFA therapeutic instrument with multiple probe approaches for the RFA operation. RFA was conducted under the guidance of B-type ultrasound. Intraoperative ultrasound and magnetic resonance imaging (MRI) were used to detect whether the liver metastases were completely necrotic by the latest guidelines of National Comprehensive Cancer Network (NCCN) and Chinese Society of Clinical Oncology (CSCO). According to the size and location of the tumor, single needle or multi needle electrodes with 2 or 3 cm tip were used during the operation. Depending on the size of the tumor, each ablation

TABLE 1 Characteristics of patients with liver metastasis after pancreatoduodenectomy.

Parameters	Level	Overall	Low ALBI	High ALBI	*p*
Cases (n)		**90**	**33**	**57**	
Sex	Male	45 (50.0)	15 (45.5)	30 (52.6)	0.662
	Female	45 (50.0)	18 (54.5)	27 (47.4)	
Age	<57	44 (48.9)	13 (39.4)	31 (54.4)	0.249
	≥57	46 (51.1)	20 (60.6)	26 (45.6)	
Differentiation	Poorly	21 (23.3)	7 (21.2)	14 (24.6)	0.460
	Moderately	60 (66.7)	21 (63.6)	39 (68.4)	
	Well	9 (10.0)	5 (15.2)	4 (7.0)	
Pathological type	Adenocarcinoma	78 (86.7)	30 (90.9)	48 (84.2)	0.563
	Mucinous carcinoma	12 (13.3)	3 (9.1)	9 (15.8)	
Underlying disease	Yes	28 (31.1)	15 (45.5)	13 (22.8)	0.045
	No	62 (68.9)	18 (54.5)	44 (77.2)	
Liver metastases	Single	32 (35.6)	18 (54.5)	14 (24.6)	0.008
	Multiple	58 (64.4)	15 (45.5)	43 (75.4)	
Size of liver metastases	≤2 cm	27 (30.0)	13 (39.4)	14 (24.6)	0.215
	>2 cm	63 (70.0)	20 (60.6)	43 (75.4)	
Chemotherapy	No	21 (23.3)	8 (24.2)	13 (22.8)	1.000
	Yes	69 (76.7)	25 (75.8)	44 (77.2)	

cycle lasted 6–12 minutes. Patients need to undergo one or more RFA treatments. At the end of the treatment, the puncture pathway was solidified to avoid bleeding during needle extraction. All hepatic metastasis were imaged by B-type ultrasound to detect whether abnormal enhancement or not. When all related adverse events of RFA were resolved and the liver metastases were confirmed to be completely removed, the patients were given systemic chemotherapy after RFA intervention for 2–4 weeks. The chemotherapy regimen included GO regimen (Gemcitabine and Oxaliplatin combination); GT regimen (Gemcitabine and Tegafur combination). All patients could tolerate the side effects of chemotherapy.

Follow up

All patients were regularly followed up after RFA. The progression free survival (PFS) was defined as the time from RFA to intrahepatic or extrahepatic recurrence or progression. The overall survival (OS) was defined as the time from RFA to death or last follow up.

Calculation of the ALBI score

The blood routine and biochemical tests were obtained at the first day of admission in our hospital. The albumin-bilirubin (ALBI) score was evaluated by albumin and direct bilirubin measurements, the direct bilirubin is in μmol/L, and albumin is in g/L. The ALBI score was as follows: ALBI score = 0.660× log10 direct bilirubin - 0.085×albumin. The ALBI score was referred to the previous literature [19]. According to the receiver operating characteristic (ROC) curve, we analyzed the optimal cut-off value of ALBI. In our study, we divided these patients into two groups: low ALBI group (≤−2.60) and high ALBI group (>−2.60).

Statistical analysis

Baseline characteristics were described as numbers (%) for categorical variables. The Chi-square or Fisher's exact tests were used to compare categorical variables. The Kaplan-Meier and Log-rank test were constructed to determine the survival curve. The hazard ratio (HR) and 95% Confidence Interval (CI) were performed to evaluate the association between ALBI score and prognosis. The univariate and multivariate Cox proportional hazard regression analyses were used to evaluate the potential independent factors. The prognostic nomogram were conducted according to the multivariate analyses. The calibration curves and decision curve analysis were performed to evaluate the predictive performance. All statistical analysis were performed by R (version 3.6.0), SPSS Statistics software (version 22.0) and GraphPad prism software (version 8.0), and a two-tailed $p < 0.05$ was considered statistically significant.

10.3389/pore.2023.1611175

TABLE 2 Associations between blood parameters and ALBI score.

Parameters	Level	Overall	Low ALBI	High ALBI	*p*
Cases (n)		90	33	57	
CA199	≤19.91	45 (50.0)	16 (48.5)	29 (50.9)	1.000
	>19.91	45 (50.0)	17 (51.5)	28 (49.1)	
CEA	≤0.45	50 (55.6)	13 (39.4)	37 (64.9)	0.033
	>0.45	40 (44.4)	20 (60.6)	20 (35.1)	
ALT	≤65.50	47 (52.2)	21 (63.6)	26 (45.6)	0.153
	>65.50	43 (47.8)	12 (36.4)	31 (54.4)	
AST	≤53.50	45 (50.0)	24 (72.7)	21 (36.8)	0.002
	>53.50	45 (50.0)	9 (27.3)	36 (63.2)	
r-GT	≤32.70	46 (51.1)	18 (54.5)	28 (49.1)	0.782
	>32.70	44 (48.9)	15 (45.5)	29 (50.9)	
Alkaline phosphatase	≤100.0	46 (51.1)	17 (51.5)	29 (50.9)	1.000
	>100.0	44 (48.9)	16 (48.5)	28 (49.1)	
Total protein	≤66.25	45 (50.0)	11 (33.3)	34 (59.6)	0.029
	>66.25	45 (50.0)	22 (66.7)	23 (40.4)	
Albumin	≤37.40	47 (52.2)	11 (33.3)	36 (63.2)	0.012
	>37.40	43 (47.8)	22 (66.7)	21 (36.8)	
Total bilirubin	≤11.94	45 (50.0)	22 (66.7)	23 (40.4)	0.029
	>11.94	45 (50.0)	11 (33.3)	34 (59.6)	
Direct bilirubin	≤5.79	46 (51.1)	23 (69.7)	23 (40.4)	0.014
	>5.79	44 (48.9)	10 (30.3)	34 (59.6)	
Creatinine	≤62.00	46 (51.1)	11 (33.3)	35 (61.4)	0.019
	>62.00	44 (48.9)	22 (66.7)	22 (38.6)	
Glucose	≤5.80	49 (54.4)	17 (51.5)	32 (56.1)	0.838
	>5.80	41 (45.6)	16 (48.5)	25 (43.9)	
Hemoglobin	≤112	46 (51.1)	15 (45.5)	31 (54.4)	0.550
	>112	44 (48.9)	18 (54.5)	26 (45.6)	
Platelet	≤175	46 (51.1)	16 (48.5)	30 (52.6)	0.873
	>175	44 (48.9)	17 (51.5)	27 (47.4)	
Lymphocyte	≤1.30	47 (52.2)	14 (42.4)	33 (57.9)	0.231
	>1.30	43 (47.8)	19 (57.6)	24 (42.1)	
White blood cell	≤8.22	45 (50.0)	21 (63.6)	24 (42.1)	0.080
	>8.22	45 (50.0)	12 (36.4)	33 (57.9)	
Neutrophils	≤8.22	47 (52.2)	25 (75.8)	22 (38.6)	0.001
	>8.22	43 (47.8)	8 (24.2)	35 (61.4)	
Red blood cell	≤3.85	57 (63.3)	24 (72.7)	33 (57.9)	0.238
	>3.85	33 (36.7)	9 (27.3)	24 (42.1)	
Prothrombin time	≤11.90	70 (77.8)	24 (72.7)	46 (80.7)	0.539
	>11.90	20 (22.2)	9 (27.3)	11 (19.3)	
Prothrombin activity	≤98.00	68 (75.6)	22 (66.7)	46 (80.7)	0.216
	>98.00	22 (24.4)	11 (33.3)	11 (19.3)	
INR	≤0.89	70 (77.8)	24 (72.7)	46 (80.7)	0.539
	>0.89	20 (22.2)	9 (27.3)	11 (19.3)	

CA199, carbohydrate antigen199; CEA, carcinoembryonic antigen; ALT, alanine aminotransferase; AST, aspartate aminotransferase; r-GT, r-glutamyltransferase.

TABLE 3 Univariate and multivariate analysis of progression free survival and overall survival.

Characteristics	PFS						OS					
	HR	Univariate 95% CI	*p*	HR	Multivariate 95% CI	*p*	HR	Univariate 95% CI	*p*	HR	Multivariate 95% CI	*p*
Sex (Male vs. Female)	0.476	0.274–0.827	0.008	0.596	0.330–1.076	0.086	0.536	0.309–0.931	0.027	0.811	0.442–1.488	0.498
Age (<57 vs. ≥57 years)	1.127	0.656–1.937	0.665				1.108	0.645–1.906	0.710			
Differentiation (Poorly vs. Moderately + Well)	0.784	0.485–1.267	0.320				0.767	0.466–1.263	0.298			
Pathological type (Adenocarcinoma vs. Mucinous)	1.481	0.742–2.957	0.265				2.352	1.173–4.717	0.016	1.961	0.790–4.865	0.147
Underlying disease (Yes vs. No)	1.267	0.685–2.342	0.450				1.340	0.725–2.477	0.351			
Liver metastases (Single vs. Multiple)	1.098	0.621–1.943	0.747				1.249	0.706–2.211	0.444			
Size of liver metastases (≤2 vs. >2 cm)	1.067	0.592–1.923	0.829				1.043	0.579–1.880	0.888			
CA199 (≤19.91 vs. >19.91)	0.832	0.483–1.435	0.509				0.775	0.449–1.335	0.358			
CEA (≤0.45 vs. >0.45)	0.615	0.350–1.079	0.090				0.623	0.355–1.093	0.099			
ALT (≤65.50 vs. >65.50)	1.292	0.752–2.218	0.353				1.234	0.717–2.125	0.448			
AST (≤53.50 vs. >53.50)	1.868	1.068–3.270	0.029	0.337	0.140–0.811	0.015	1.914	1.092–3.353	0.023	0.288	0.107–0.770	0.013
r.GT (≤32.70 vs. >32.70)	1.157	0.674–1.986	0.597				1.090	0.636–1.870	0.754			
Alkaline phosphatase (≤100.0 vs. >100.0)	1.948	1.125–3.373	0.017	2.088	1.175–3.712	0.012	2.137	1.231–3.709	0.007	2.634	1.319–5.258	0.006
Total protein (≤66.25 vs. >66.25)	1.047	0.611–1.794	0.868				0.887	0.518–1.521	0.664			
Albumin (≤37.40 vs. >37.40)	1.155	0.673–1.982	0.602				1.327	0.773–2.276	0.305			
Total bilirubin (≤11.94 vs. >11.94)	1.430	0.830–2.461	0.197				1.421	0.826–2.446	0.204			
Direct bilirubin (≤5.79 vs. >5.79)	1.318	0.767–2.266	0.318				1.257	0.732–2.158	0.407			
Creatinine (≤62.00 vs. >62.00)	0.563	0.322–0.983	0.043	0.581	0.303–1.113	0.102	0.518	0.297–0.906	0.021	0.414	0.212–0.807	0.010
Glucose (≤5.80 vs. >5.80)	0.987	0.570–1.708	0.962				0.869	0.502–1.504	0.616			
Hemoglobin (≤112 vs. >112)	0.721	0.418–1.244	0.240				0.710	0.412–1.224	0.217			
Platelet (≤175 vs. >175)	1.113	0.649–1.909	0.698				0.983	0.572–1.687	0.949			
Lymphocyte (≤1.30 vs. >1.30)	0.984	0.574–1.687	0.953				1.127	0.657–1.933	0.664			
White blood cell (≤8.22 vs. >8.22)	0.866	0.504–1.490	0.604				0.808	0.470–1.389	0.441			
Neutrophils (≤6.21 vs. >6.21)	1.816	1.051–3.139	0.033	1.481	0.743–2.950	0.264	1.764	1.022–3.044	0.041	1.855	0.763–4.510	0.173
Red blood cell (≤3.85 vs. >3.85)	1.151	0.663–1.998	0.618				1.178	0.679–2.045	0.561			
Prothrombin time (≤11.90 vs. >11.90)	0.317	0.135–0.744	0.008	0.099	0.023–0.430	0.002	0.326	0.139–0.767	0.010	0.067	0.015–0.301	0.000

(Continued on following page)

TABLE 3 (*Continued*) Univariate and multivariate analysis of progression free survival and overall survival.

Characteristics	PFS						OS					
	HR	Univariate 95% CI	*p*	HR	Multivariate 95% CI	*p*	HR	Univariate 95% CI	*p*	HR	Multivariate 95% CI	*p*
Prothrombin activity (≤98.00 vs. >98.00)	1.678	0.919–3.064	0.092				1.538	0.845–2.800	0.159			
ALBI (Low vs. High)	3.257	1.684–6.301	0.000	4.417	1.781–10.956	0.001	3.070	1.582–5.960	0.001	3.722	1.645–8.425	0.002
Chemotherapy (No vs. Yes)	0.421	0.189–0.935	0.034	1.621	0.411–6.386	0.490	0.425	0.191–0.947	0.036	2.027	0.496–8.291	0.325

Results

Baseline clinicopathologic characteristics

Ninety pancreatic cancer after pancreatoduodenectomy with liver metastasis were recruited for this study. These patients were received RFA treatment, and 69 patients were received chemotherapy after RFA. There were 45 males and 45 females in this study. The mean age was 55 years, with the range from 34 to 73 years, and the median age was 57 years. Of all patients, 21 patients with poorly differentiated pancreatic cancer, 60 patients with moderately differentiated pancreatic cancer, and 9 patients with well differentiated pancreatic cancer, respectively. Adenocarcinoma is the main pathological type, accounting for 86.7% (78/90). The baseline clinicopathologic characteristics were listed in Table 1. According to ALBI score, these patients were divided into two groups: low ALBI group ($n = 33$) and high ALBI group ($n = 57$). Compared to these characteristics, ALBI was associated with underlying disease ($p = 0.045$) and liver metastases ($p = 0.008$).

Associations between blood parameters and ALBI score

The blood parameters were obtained before RFA. We analyzed blood parameters by median value. Compared with two groups, there were significant differences in carcinoembryonic antigen (CEA) ($p = 0.033$), aspartate aminotransferase (AST) ($p = 0.002$), total protein ($p = 0.029$), albumin ($p = 0.012$), total bilirubin ($p = 0.029$), direct bilirubin ($p = 0.014$), creatinine ($p = 0.019$), neutrophils ($p = 0.001$), respectively. The detail information were shown in Table 2.

Univariate and multivariate analysis

The univariate analysis revealed that sex, AST, alkaline phosphatase, creatinine, neutrophils, prothrombin time, ALBI and chemotherapy were related to the prognosis for PFS, however, the multivariate analysis revealed that AST, alkaline phosphatase, prothrombin time and ALBI were the potential independent prognostic factors for PFS. Moreover, the univariate analysis revealed that sex, pathological type, AST, alkaline phosphatase, creatinine, neutrophils, prothrombin time, ALBI and chemotherapy were related to the prognosis for OS, however, the multivariate analysis revealed that AST, alkaline phosphatase, creatinine, prothrombin time and ALBI were the potential independent prognostic factors for OS. The detail information was shown in Table 3. The multivariate analysis results were displayed using forest plots (Figure 1).

Survival analysis by ABLI score

In low ABLI group, the median PFS and OS were 40.17 (95% CI: 29.97–53.80) and 54.07 (95% CI: 38.57–79.10) months. In high ABLI group, the median PFS and OS were 11.30 (95% CI: 10.47–16.00) and 23.83 (95% CI: 20.03–28.53) months. Compared with high ABLI group, the median PFS and OS in low ABLI group were survived longer and had better prognosis (PFS, $p = 0.0002$; OS, $p = 0.0005$) (Figure 2). Moreover, the 1-, 3- and 5-year PFS rates were 84.8% (95% CI: 0.735–0.980), 69.7% (95% CI: 0.557–0.873), 58.1% (95% CI: 0.414–0.815) in low ABLI group, and the 1-, 3- and 5-year PFS rates were 49.1% (95% CI: 0.377–0.640), 28.1% (95% CI: 0.185–0.425), 0% (95% CI: 0.000–0.000) in high ABLI group. Furthermore, the 1-, 3- and 5-year OS rates were 93.9% (95% CI: 0.861–1.000), 69.7% (95% CI: 0.557–0.873), 69.7% (95% CI: 0.557–0.873) in low ABLI group, and the 1-, 3- and 5-year PFS rates were 87.7% (95% CI: 0.796–0.967), 32.7% (95% CI: 0.225–0.477), 25.3% (95% CI: 0.156–0.408) in high ABLI group.

Nomogram for PFS and OS

Though the multivariate analysis, we constructed a nomogram for individualized assessment of PFS and OS. By the nomogram, every enrolled variable was imputed a

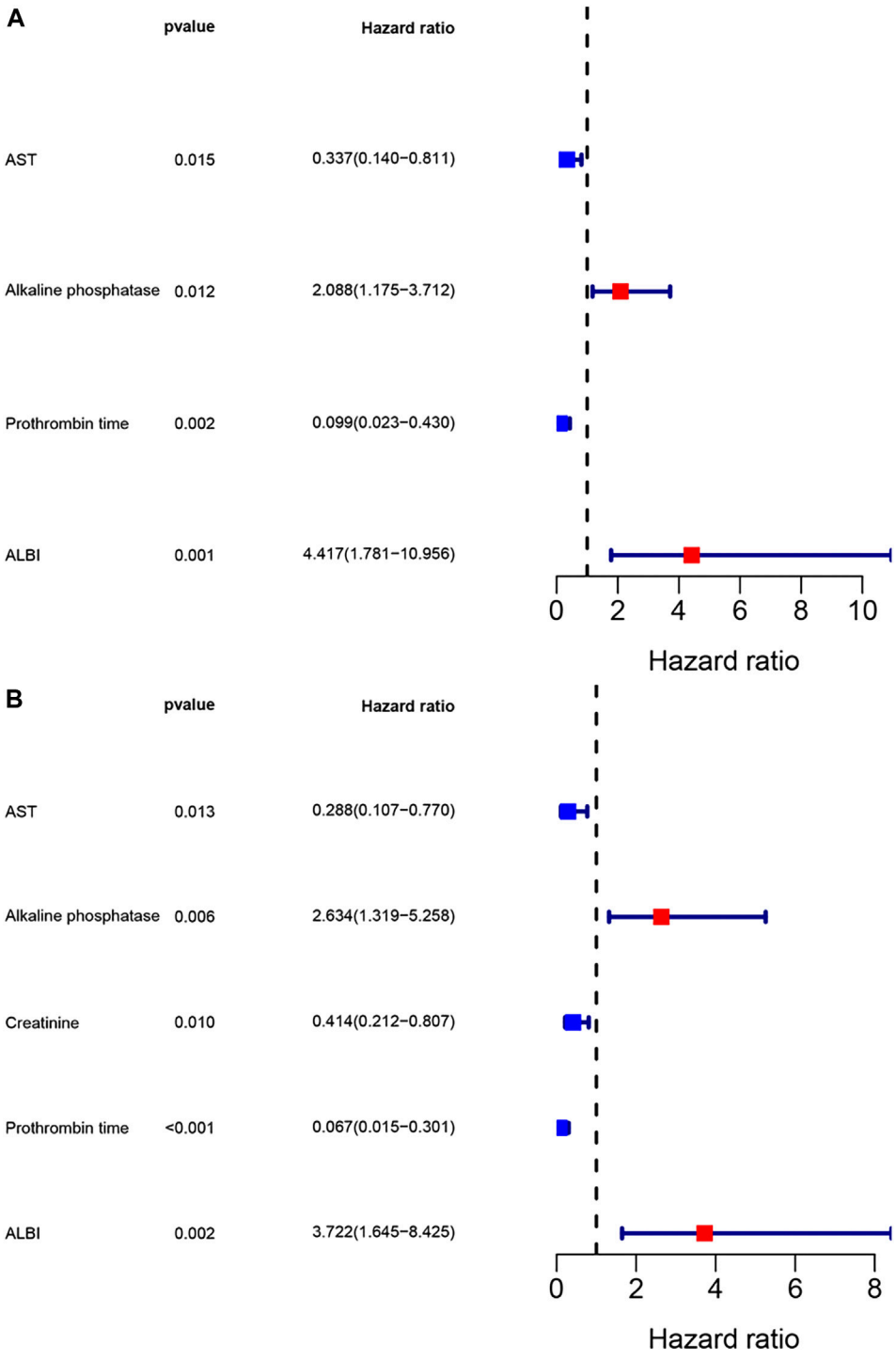

FIGURE 1
Forest plots for multivariate analysis. **(A)** Multivariate analysis for progression free survival; **(B)** Multivariate analysis for overall survival.

weighted point, and the sum of the points could predict 1-, 3- and 5-year survival probabilities for PFS and OS. The nomogram for PFS had integrated AST, alkaline phosphatase, prothrombin time and ALBI; and the OS had integrated AST, alkaline phosphatase, creatinine, prothrombin time and ALBI (Figure 3). The patients with

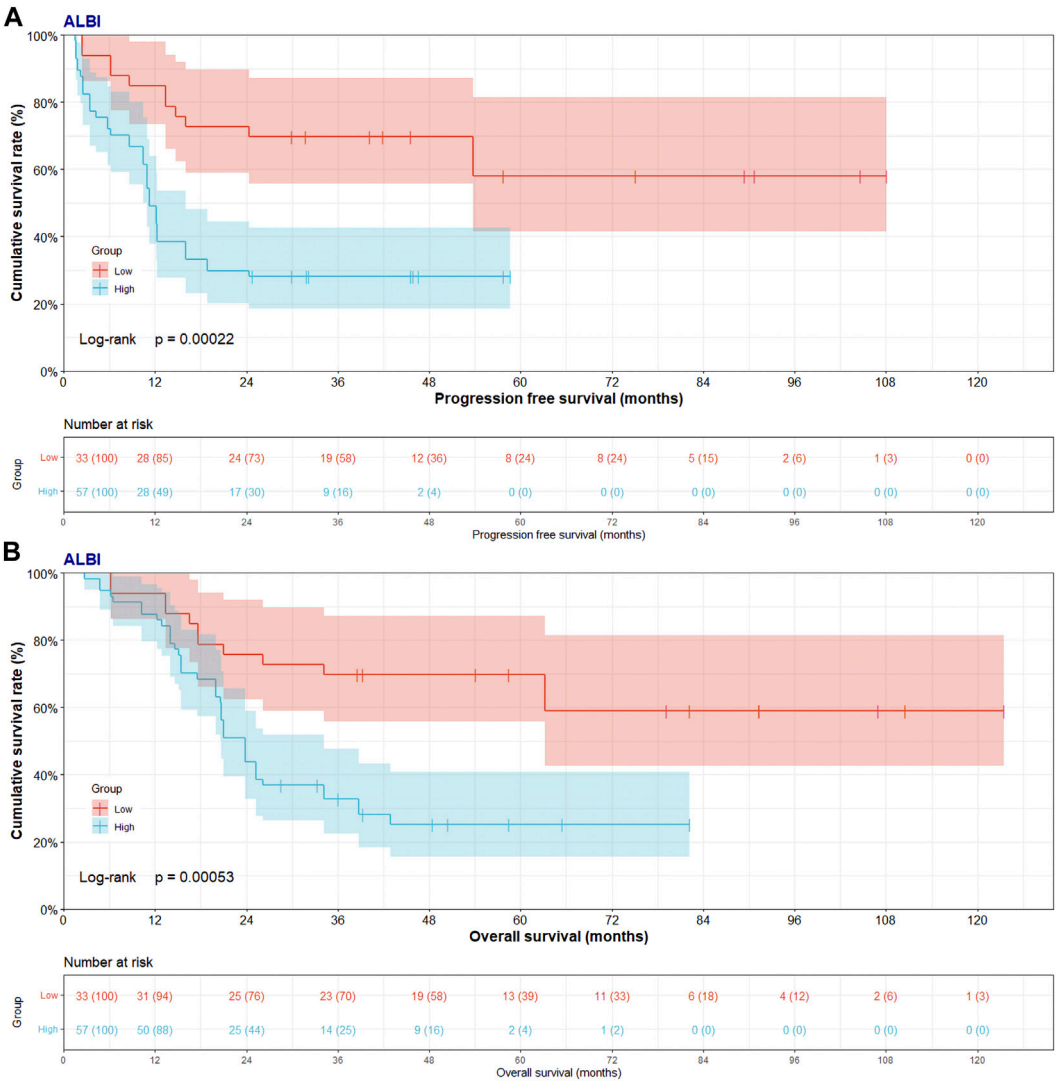

FIGURE 2
Progress free survival (PFS) and overall survival (OS) of patients with pancreatic cancer after pancreatoduodenectomy with liver metastasis treated with RFA by ALBI score. **(A)** Kaplan-Meier analysis of PFS for patients treated with RFA by ALBI score; **(B)** Kaplan-Meier analysis of OS for patients treated with RFA by ALBI score.

high grade were related to a lower survival probability. Moreover, we used the calibration curve to determine the nomogram for the predicted and actual probability of PFS and OS. The prediction line matched the reference line well for 3-year PFS and OS (Figure 4). Furthermore, we also used the decision curve analysis to determine the clinical utility between nomogram (the potential independent prognostic factors by multivariate analysis) and ALBI by quantifying the net benefits at different threshold probabilities. The nomogram model was better than the only ALBI, and shown the ability for clinical decision-making, especially in 1-year PFS, and 3-, 5-year OS (Figure 5).

Discussion

Metastatic disease is the cause of over 90% of solid tumor related mortality, however, it is still the least known component of cancer pathogenesis [23, 24]. Liver is highly metastatic organ, as for its unique and diverse structure, cell composition enables the liver to undertake many special functions, and liver metastases are more common than primary hepatic tumors [25, 26]. The biological characteristics of liver, especially its hemodynamic characteristics and unique microenvironment, make the liver essentially suitable for disseminated tumor cells. The

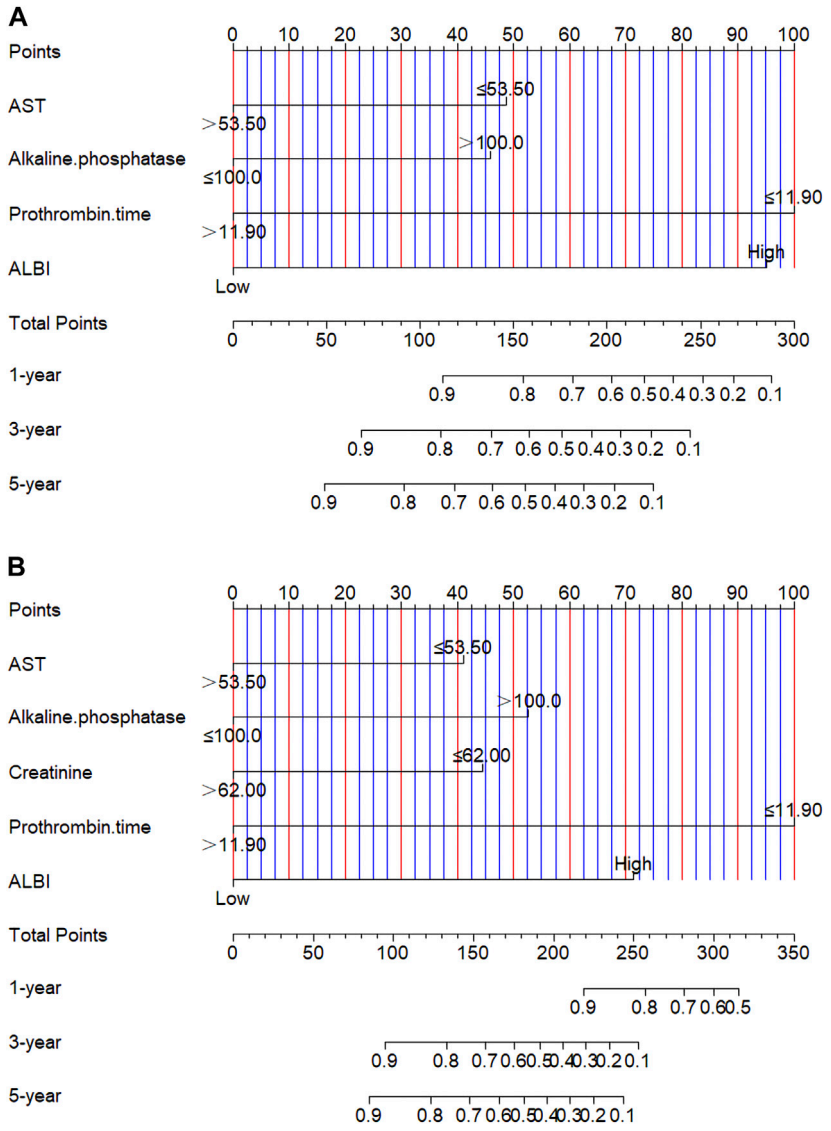

FIGURE 3
Nomogram for predicting progress free survival (PFS) and overall survival (OS). **(A)** Nomogram for predicting PFS; **(B)** Nomogram for predicting OS.

primary tumors, such as breast cancer, colorectal cancer, neuroendocrine tumors, prostate carcinomas, gastric cancer, uveal melanoma and pancreatic cancer, were easy to spread to the liver [27–33]. Moreover, the studies indicated that the prognosis of patients with liver metastasis was worse than that of patients without liver metastasis [8]. At present, about 30%–70% of patients was to die of liver metastasis disease, and increased the costs and spending obviously [34]. Various treatments, including surgery (liver resection), chemotherapy, RFA, trans arterial chemoembolization (TACE), hepatic arterial infusion chemotherapy, have been used in clinical practice. Pancreatic cancer has a very poor prognosis. Pancreatoduodenectomy is the main treatment approach, however, less than 20% of patients can survive more than 5 years [35]. Many pancreatic cancer patients have liver metastasis even after pancreatoduodenectomy. The chemotherapy are used for the treatment of pancreatic cancer or after pancreatoduodenectomy [36, 37]. However, as a result of the serious adverse reactions, damage the quality of life, not all patients can benefit from chemotherapy [38, 39]. Some studies have pointed out that RFA was an appropriate choice for patients with solitary liver metastasis of malignant tumors,

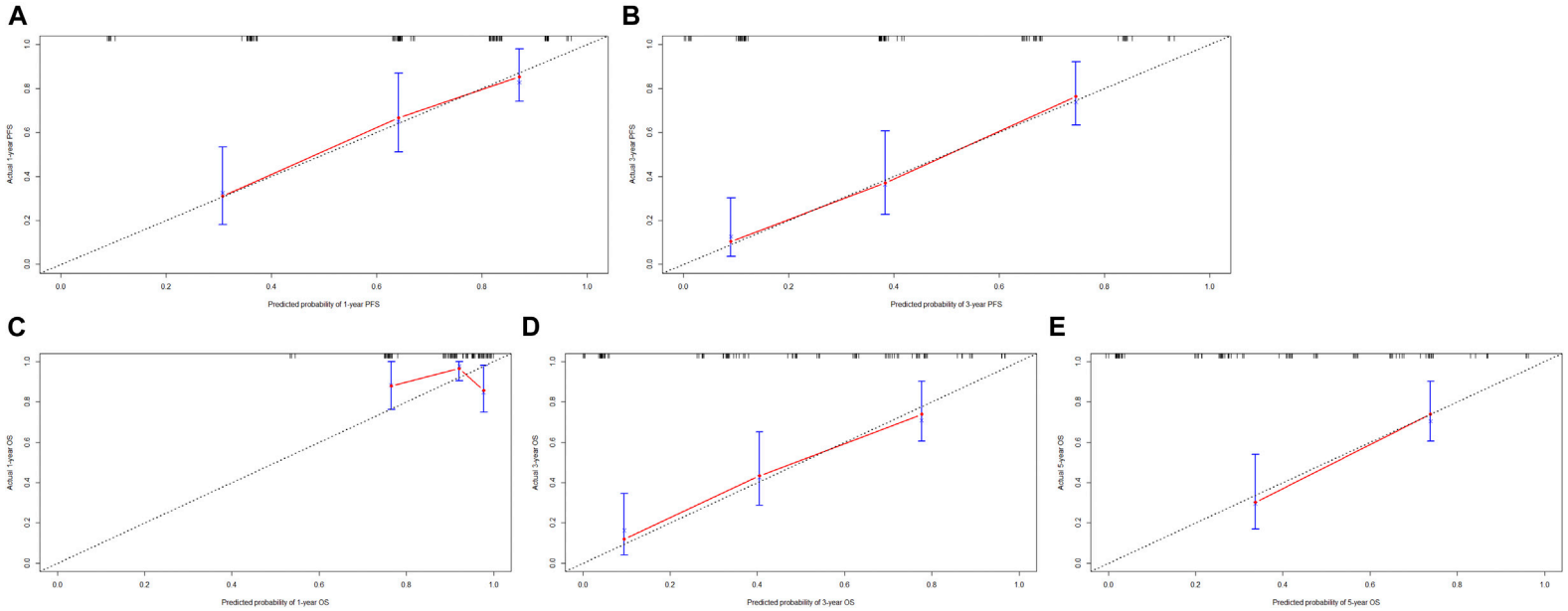

FIGURE 4
The calibration curves for predicting the 1-, 3-, 5-year PFS and OS rates. **(A)** The calibration curves for predicting the 1-year PFS rate; **(B)** The calibration curves for predicting the 3-year PFS rate; **(C)** The calibration curves for predicting the 1-year OS rate; **(D)** The calibration curves for predicting the 3-year OS rate; **(E)** The calibration curves for predicting the 5-year OS rate.

10.3389/pore.2023.1611175

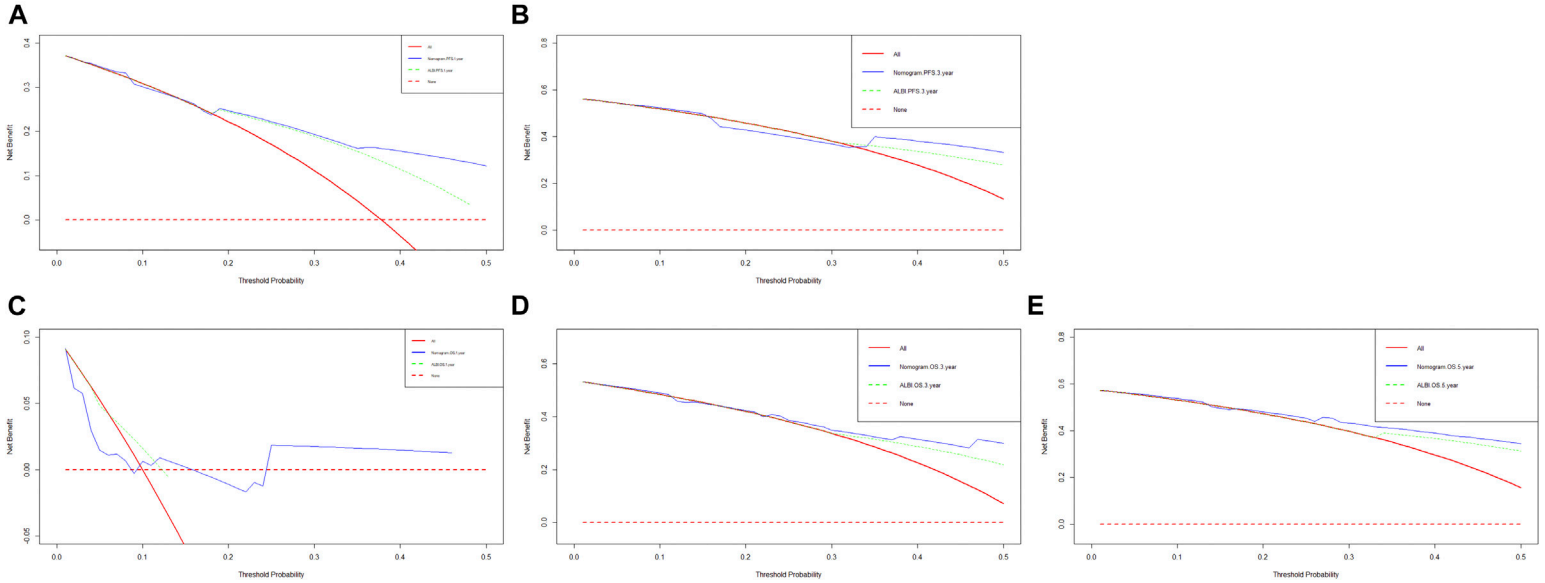

FIGURE 5
Decision curve analysis (DCA) of the nomogram (the independent prognostic factors by multivariate analysis) and only ALBI score for predicting progress free survival (PFS) and overall survival (OS). **(A)** DCA of the nomogram and treatment for predicting the 1-year PFS; **(B)** DCA of the nomogram and treatment for predicting the 3-year PFS; **(C)** DCA of the nomogram and treatment for predicting the 1-year OS; **(D)** DCA of the nomogram and treatment for predicting the 3-year OS; **(E)** DCA of the nomogram and treatment for predicting the 5-year OS.

10.3389/pore.2023.1611175

and could effectively inhibit the growth and metastasis of cancer cells [40, 41]. However, the effectively predictors which used to evaluate the prognosis of pancreatic cancer was still not clear. Therefore, it is necessary to find prognostic biomarkers for pancreatic cancer patients after pancreatoduodenectomy with liver metastasis.

ALBI is a new marker of malignant tumor recently described, which is specifically characterized by a comprehensive assessment of nutritional status and liver function. Nevertheless, few studies have studied the relationship between ALBI and prognosis in pancreatic cancer. It is reported that low ALBI is a positive indicator for better survival in pancreatic cancer patients [42]. ALBI was independently correlated with overall survival in multivariate analysis [42]. Other study also shown that the median progression free survival and median overall survival in low ALBI was longer than those in high ALBI in pancreatic cancer patients with liver metastasis [43].

In this study, we found that low ALBI was significantly related to longer PFS (p = 0.0002, HR: 3.039, 95% CI: 1.772–5.210) and OS (p = 0.0005, HR: 2.697, 95% CI: 1.539–4.720). The 1-, 3- and 5-year PFS and OS rates in low ALBI group were higher than those in high ALBI group. In the present study, underlying disease, liver metastases, CEA, AST, total protein, albumin, total bilirubin, direct bilirubin, creatinine and neutrophils were found to be significantly related to ALBI score. One study proved that liver status, CEA and CA199 were the important predictor in pancreatic cancer patients after pancreaticoduodenectomy [44]. Other study indicated that systemic inflammation response index, based on peripheral neutrophil, monocyte, and lymphocyte, was associated with pancreatic cancer patients survival, and could improve treatment outcomes by identifying candidates for active treatment [45]. According to univariate and multivariate analysis, the AST, alkaline phosphatase, prothrombin time and ALBI were the potential independent protective factor for PFS; and the AST, alkaline phosphatase, creatinine, prothrombin time and ALBI were the potential independent protective factor for OS. In the current study, multivariate analysis shown ALBI was an potential independent prognostic factor for liver metastasis of pancreatic cancer after pancreatoduodenectomy. Moreover, we constructed a nomogram by the potential prognostic factors by the multivariate analysis. The nomogram was used to predict the 1-, 3- and 5-year survival probabilities of PFS and OS. The calibration curve shown that the prediction line matched the reference line well for 3-year PFS and OS. Furthermore, the DCA shown that nomogram model was better than the only ALBI, and indicated the ability for clinical decision-making, especially in 1-year PFS, and 3-, 5-year OS.

The biological mechanism of ALBI as a potential prognostic factor of pancreatic cancer has not been clearly explained. We try to explain the relevance of each component of ALBI score. Albumin is composed in the liver, and can be used to reflect people's nutritional condition [46]. The serum albumin concentration will be reduced when the nutritional condition is poor or liver function is impaired. The increase in bilirubin may be caused by biliary obstruction, and the impairment of liver can also cause the dysregulation of bilirubin. Moreover, the bilirubin can enter the brain interstitium freely and cause neurotoxicity.

The study has several limitations. Firstly, this study was a retrospective study, and a small number of patients were included in the study. And more of patients should be enrolled into study. Secondly, the small sample size is biased to guide the decisive conclusion of other potential prognostic factors. Finally, more homogeneous groups should be analyzed to validate this valuable conclusion in the future study. Therefore, multi-center and prospective studies should be enrolled to evaluate the prognostic value of ALBI score for pancreatic cancer patients after pancreatoduodenectomy with liver metastasis following radiofrequency ablation.

Conclusion

ALBI is a potential independent factor for PFS and OS, and can predict the prognosis of pancreatic cancer patients after pancreatoduodenectomy with liver metastasis following radiofrequency ablation. Patients with low ALBI score have better prognosis and longer survival time. The nomogram model with ALBI may be a predictive stratification tool to facilitate clinical decisions.

Data availability statement

The raw data supporting the conclusion of this article will be made available by the authors, without undue reservation.

Ethics statement

This retrospective cohort study received approval from Institutional Review Board of Harbin Medical University Cancer Hospital (No. 2019H099) and was performed in accordance with the Declaration of 1964 Helsinki as well as its later amendments. Ninety patients who underwent

pancreatoduodenectomy with liver metastasis were enrolled into this study from January 2012 to December 2018, and these patients were received radiofrequency ablation after surgery. All patients were waived the written consent because of the retrospective nature of the research.

Author contributions

LZ and XZ wrote and reviewed the manuscript; BW and XH collected and summarized the patients' information; CG and BL analyzed the results; HJ and WC provided resources and acquired funding.

Funding

This work was supported by grants from the Science Foundation of Heilongjiang Province (grant no. LH2019H099); and Youth Project of the National Natural Science Foundation of China (grant no. 82003067).

Conflict of interest

The authors declare that the research was conducted in the absence of any commercial or financial relationships that could be construed as a potential conflict of interest.

References

1. Sung H, Ferlay J, Siegel RL, Laversanne M, Soerjomataram I, Jemal A, et al. Global cancer Statistics 2020: GLOBOCAN estimates of incidence and mortality worldwide for 36 cancers in 185 countries. *CA Cancer J Clin* (2021) 71(3):209–49. doi:10.3322/caac.21660

2. Neoptolemos JP, Kleeff J, Michl P, Costello E, Greenhalf W, Palmer DH. Therapeutic developments in pancreatic cancer: Current and future perspectives. *Nat Rev Gastroenterol Hepatol* (2018) 15(6):333–48. doi:10.1038/s41575-018-0005-x

3. Hackert T, Klaiber U, Pausch T, Mihaljevic AL, Büchler MW. Fifty years of surgery for pancreatic cancer. *Pancreas* (2020) 49(8):1005–13. doi:10.1097/MPA.0000000000001634

4. McGuigan A, Kelly P, Turkington RC, Jones C, Coleman HG, McCain RS. Pancreatic cancer: A review of clinical diagnosis, epidemiology, treatment and outcomes. *World J Gastroenterol* (2018) 24(43):4846–61. doi:10.3748/wjg.v24.i43.4846

5. McGuire S. World cancer report 2014. Geneva, Switzerland: World health organization, international agency for research on cancer, WHO press, 2015. *Adv Nutr* (2016) 7(2):418–9. doi:10.3945/an.116.012211

6. David M, Lepage C, Jouve JL, Jooste V, Chauvenet M, Faivre J, et al. Management and prognosis of pancreatic cancer over a 30-year period. *Br J Cancer* (2009) 101(2):215–8. doi:10.1038/sj.bjc.6605150

7. Hayashibe A, Kameyama M, Shinbo M, Makimoto S. Clinical results on intra-arterial adjuvant chemotherapy for prevention of liver metastasis following curative resection of pancreatic cancer. *Ann Surg Oncol* (2007) 14(1):190–4. doi:10.1245/s10434-006-9110-0

8. Horn SR, Stoltzfus KC, Lehrer EJ, Dawson LA, Tchelebi L, Gusani NJ, et al. Epidemiology of liver metastases. *Cancer Epidemiol* (2020) 67:101760. doi:10.1016/j.canep.2020.101760

9. Paiella S, De Pastena M, Romeo F, D'onofrio M, Fontana M, Pea A, et al. Ablation treatments in unresectable pancreatic cancer. *Minerva Chir* (2019) 74(3):263–9. doi:10.23736/S0026-4733.18.07881-1

10. Hua YQ, Wang P, Zhu XY, Shen YH, Wang K, Shi WD, et al. Radiofrequency ablation for hepatic oligometastatic pancreatic cancer: An analysis of safety and efficacy. *Pancreatology* (2017) 17(6):967–73. doi:10.1016/j.pan.2017.08.072

11. Andreou A, Knitter S, Klein F, Malinka T, Schmelzle M, Struecker B, et al. The role of hepatectomy for synchronous liver metastases from pancreatic adenocarcinoma. *Surg Oncol* (2018) 27(4):688–94. doi:10.1016/j.suronc.2018.09.004

12. Macedo FI, Ryon E, Maithel SK, Lee RM, Kooby DA, Fields RC, et al. Survival outcomes associated with clinical and pathological response following neoadjuvant FOLFIRINOX or gemcitabine/nab-paclitaxel chemotherapy in resected pancreatic cancer. *Ann Surg* (2019) 270(3):400–13. doi:10.1097/SLA.0000000000003468

13. Akahori T, Sho M, Tanaka T, Nishiofuku H, Kinoshita S, Nagai M, et al. Significant efficacy of new transcatheter arterial chemoembolization technique for hepatic metastases of pancreatic neuroendocrine tumors. *Anticancer Res* (2013) 33(8):3355–8. doi:10.3109/0284186X.2013.806820

14. Hlavsa J, Procházka V, Andrasina T, Pavlík T, Penka I, Kala Z. Radiofrequency ablation in pancreatic cancer. *Rozhl Chir* (2019) 98(11):441–9. doi:10.33699/PIS.2019.98.11.441-449

15. de Geus SWL, Eskander MF, Kasumova GG, Ng SC, Kent TS, Mancias JD, et al. Stereotactic body radiotherapy for unresected pancreatic cancer: A nationwide review. *Cancer* (2017) 123(21):4158–67. doi:10.1002/cncr.30856

16. Wellenstein MD, Coffelt SB, Duits DEM, van Miltenburg MH, Slagter M, de Rink I, et al. Loss of p53 triggers WNT-dependent systemic inflammation to drive breast cancer metastasis. *Nature* (2019) 572(7770):538–42. doi:10.1038/s41586-019-1450-6

17. Cupp MA, Cariolou M, Tzoulaki I, Aune D, Evangelou E, Berlanga-Taylor AJ. Neutrophil to lymphocyte ratio and cancer prognosis: An umbrella review of systematic reviews and meta-analyses of observational studies. *BMC Med* (2020) 18(1):360. doi:10.1186/s12916-020-01817-1

18. Kasahara K, Ishizaki T, Enomoto M, Mazaki J, Okazaki N, Tago T, et al. Preoperative lymphocyte-to-monocyte ratio in the prognostication of advanced resectable colon cancer: A retrospective observational study. *Indian J Surg Oncol* (2021) 12(3):498–506. doi:10.1007/s13193-021-01356-y

19. Johnson PJ, Berhane S, Kagebayashi C, Satomura S, Teng M, Reeves HL, et al. Assessment of liver function in patients with hepatocellular carcinoma: A new evidence-based approach-the ALBI grade. *J Clin Oncol* (2015) 33(6):550–8. doi:10.1200/JCO.2014.57.9151

20. Lee HG, Lim SB, Lee JL, Kim CW, Yoon YS, Park IJ, et al. Preoperative albumin-bilirubin score as a prognostic indicator in patients with stage III colon cancer. *Sci Rep* (2022) 12(1):14910. doi:10.1038/s41598-022-19329-8

21. Zhang J, Xu Q, Zhang H, Zhang Y, Yang Y, Luo H, et al. High preoperative albumin-bilirubin score predicts poor survival in patients with newly diagnosed high-grade gliomas. *Transl Oncol* (2021) 14(4):101038. doi:10.1016/j.tranon.2021.101038

22. Park HJ, Seo KI, Kim SJ, Lee SU, Yun BC, Han BH, et al. Effectiveness of albumin-bilirubin score as a predictor of post-hepatectomy liver failure in patients with hepatocellular carcinoma. *Korean J Gastroenterol* (2021) 77(3):115–22. doi:10.4166/kjg.2020.148

23. Gupta GP, Massagué J. Cancer metastasis: Building a framework. *Cell* (2006) 127(4):679–95. doi:10.1016/j.cell.2006.11.001

24. Chaffer CL, Weinberg RA. A perspective on cancer cell metastasis. *Science* (2011) 331(6024):1559–64. doi:10.1126/science.1203543

25. Clark AM, Ma B, Taylor DL, Griffith L, Wells A. Liver metastases: Microenvironments and *ex-vivo* models. *Exp Biol Med (Maywood)* (2016) 241(15):1639–52. doi:10.1177/1535370216658144

26. Mielgo A, Schmid MC. Liver tropism in cancer: The hepatic metastatic niche. *Cold Spring Harb Perspect Med* (2020) 10(3):a037259. doi:10.1101/cshperspect.a037259

27. Ma R, Feng Y, Lin S, Chen J, Lin H, Liang X, et al. Mechanisms involved in breast cancer liver metastasis. *J Transl Med* (2015) 13:64. doi:10.1186/s12967-015-0425-0

28. Engstrand J, Nilsson H, Strömberg C, Jonas E, Freedman J. Colorectal cancer liver metastases - a population-based study on incidence, management and survival. *BMC Cancer* (2018) 18(1):78. doi:10.1186/s12885-017-3925-x

29. Riihimäki M, Hemminki A, Sundquist K, Sundquist J, Hemminki K. The epidemiology of metastases in neuroendocrine tumors. *Int J Cancer* (2016) 139(12): 2679–86. doi:10.1002/ijc.30400

30. van Roekel C, Jonges TGN, Lock TMTW. What are the odds? Prostate metastases to ureter and peritoneum. *BMJ Case Rep* (2018) 2018:bcr2018225730. doi:10.1136/bcr-2018-225730

31. Kawahara K, Makino H, Kametaka H, Hoshino I, Fukada T, Seike K, et al. Outcomes of surgical resection for gastric cancer liver metastases: A retrospective analysis. *World J Surg Oncol* (2020) 18(1):41. doi:10.1186/s12957-020-01816-9

32. Rowcroft A, Loveday BPT, Thomson BNJ, Banting S, Knowles B. Systematic review of liver directed therapy for uveal melanoma hepatic metastases. *HPB (Oxford)* (2020) 22(4):497–505. doi:10.1016/j.hpb.2019.11.002

33. Saade Lemus P, Anderson K, Smith M, Bullock A. Spontaneous regression of pancreatic cancer with liver metastases. *BMJ Case Rep* (2019) 12(5):e229619. doi:10.1136/bcr-2019-229619

34. Gilbert BK. The 26th annual bowditch lecture: New computer technologies and their potential for expanded vistas in biomedicine. *Physiologist* (1982) 25(1):2–18.

35. Stoop TF, Ateeb Z, Ghorbani P, Scholten L, Arnelo U, Besselink MG, et al. Surgical outcomes after total pancreatectomy: A high-volume center experience. *Ann Surg Oncol* (2021) 28(3):1543–51. doi:10.1245/s10434-020-08957-x

36. Seufferlein T, Bachet JB, Van Cutsem E, Rougier PESMO Guidelines Working Group. Pancreatic adenocarcinoma: ESMO-ESDO clinical practice guidelines for diagnosis, treatment and follow-up. *Ann Oncol* (2012) 23(7):vii33–40. doi:10.1093/annonc/mds224

37. Alemi F, Alseidi A, Scott Helton W, Rocha FG. Multidisciplinary management of locally advanced pancreatic ductal adenocarcinoma. *Curr Probl Surg* (2015) 52(9):362–98. doi:10.1067/j.cpsurg.2015.07.003

38. Khushman M, Dempsey N, Maldonado JC, Loaiza-Bonilla A, Velez M, Carcas L, et al. Full dose neoadjuvant FOLFIRINOX is associated with prolonged survival in patients with locally advanced pancreatic adenocarcinoma. *Pancreatology* (2015) 15(6):667–73. doi:10.1016/j.pan.2015.08.010

39. Syed AR, Carleton NM, Horne Z, Dhawan A, Bedi G, Kochhar G, et al. Survival trends for resectable pancreatic cancer using a multidisciplinary conference: The impact of post-operative chemotherapy. *J Gastrointest Cancer* (2020) 51(3):836–43. doi:10.1007/s12029-019-00303-z

40. Wang H, Ding W, Shi H, Bao H, Lu Y, Jiang TA. Combination therapy with low-frequency ultrasound irradiation and radiofrequency ablation as a synergistic treatment for pancreatic cancer. *Bioengineered* (2021) 12(2):9832–46. doi:10.1080/21655979.2021.1995581

41. Deng Q, He M, Fu C, Feng K, Ma K, Zhang L. Radiofrequency ablation in the treatment of hepatocellular carcinoma. *Int J Hyperthermia* (2022) 39(1):1052–63. doi:10.1080/02656736.2022.2059581

42. Zhang TN, Yin RH, Wang LW. The prognostic and predictive value of the albumin-bilirubin score in advanced pancreatic cancer. *Medicine (Baltimore)* (2020) 99(28):e20654. doi:10.1097/MD.0000000000020654

43. Sakin A, Sahin S, Sakin A, Atci MM, Yasar N, Arici S, et al. Assessment of pretreatment albumin-bilirubin grade in pancreatic cancer patients with liver metastasis. *J BUON* (2020) 25(4):1941–6.

44. El Nakeeb A, El Shobary M, El Dosoky M, Nabeh A, El Sorogy M, El Eneen AA, et al. Prognostic factors affecting survival after pancreaticoduodenectomy for pancreatic adenocarcinoma (single center experience). *Hepatogastroenterology* (2014) 61(133):1426–38. doi:10.5754/hge13579

45. Qi Q, Zhuang L, Shen Y, Geng Y, Yu S, Chen H, et al. A novel systemic inflammation response index (SIRI) for predicting the survival of patients with pancreatic cancer after chemotherapy. *Cancer* (2016) 122(14):2158–67. doi:10.1002/cncr.30057

46. Wang Y, Li C, Wang W, Wang J, Li J, Qian S, et al. Serum albumin to globulin ratio is associated with the presence and severity of inflammatory bowel disease. *J Inflamm Res* (2022) 15:1907–20. doi:10.2147/JIR.S347161

Pathology & Oncology Research | frontiers

TYPE Original Research
PUBLISHED 18 May 2023
DOI 10.3389/pore.2023.1611216

Check for updates

OPEN ACCESS

EDITED BY
Gabor Cserni,
University of Szeged, Hungary

*CORRESPONDENCE
Ji Hyun Ahn,
jvcjh@hanmail.net

RECEIVED 30 March 2023
ACCEPTED 08 May 2023
PUBLISHED 18 May 2023

CITATION
Kim KB, Ahn JH, Kwon SW, Lee SJ, Lee Y, Park SY, Kim A, Choi KU, Lee CH and Huh GY (2023), Tumor budding as a predictor of disease-free survival in patients with cholangiocarcinoma. *Pathol. Oncol. Res.* 29:1611216. doi: 10.3389/pore.2023.1611216

COPYRIGHT
© 2023 Kim, Ahn, Kwon, Lee, Lee, Park, Kim, Choi, Lee and Huh. This is an open-access article distributed under the terms of the Creative Commons Attribution License (CC BY). The use, distribution or reproduction in other forums is permitted, provided the original author(s) and the copyright owner(s) are credited and that the original publication in this journal is cited, in accordance with accepted academic practice. No use, distribution or reproduction is permitted which does not comply with these terms.

Tumor budding as a predictor of disease-free survival in patients with cholangiocarcinoma

Kyung Bin Kim[1], Ji Hyun Ahn[1]*, Soon Wook Kwon[1], Su Ji Lee[1], Yury Lee[1], Seo Young Park[1], Ahrong Kim[1,2], Kyung Un Choi[1,2], Chang Hun Lee[1,2] and Gi Yeong Huh[1,2]

[1]Department of Pathology, Pusan National University Hospital, Busan, Republic of Korea, [2]Department of Pathology, Pusan National University School of Medicine, Yangsan-si, Gyeongsangnamdo, Republic of Korea

Background: Tumor budding is considered a prognostic factor in several solid cancer types. However, we lack comprehensive information on the importance of tumor budding in cholangiocarcinoma. Therefore, we aimed to assess the prognostic value of tumor budding in intrahepatic and extrahepatic cholangiocarcinomas and to evaluate its correlations with other clinicopathological parameters.

Methods: We monitored 219 patients who underwent surgery for intrahepatic or extrahepatic cholangiocarcinoma at the Pusan National University Hospital between 2012 and 2021. Tumor budding was evaluated using the International Tumor Budding Consensus Conference scoring system. Tumor budding was classified into low (0–4), intermediate (5–9), and high (≥10). For statistical analysis, tumor budding was divided into two groups based on the cut-off value of 10 (lower: 0–9 vs. higher: ≥10). The correlations between clinicopathological parameters were examined using the chi-square and Fisher's exact test. The prognostic values of the variables were analyzed using the log-rank test and Cox regression analysis.

Results: Low, intermediate, and high tumor buddings were identified in 135 (61.6%), 63 (28.8), and 21 (9.6%), patients, respectively. Higher tumor budding was related to the presence of lymphatic invasion (p = 0.017), higher tumor grade (p = 0.001), higher N category (p = 0.034). In the univariable and multivariable analyses, higher tumor budding was associated with shorter disease-free survival in 97 (44.3%) patients who underwent R0 resection (p < 0.001 and p = 0.011). Tumor budding did not significantly correlate with disease-specific survival in entire patients.

Conclusion: Tumor budding may serve as a prognostic factor for intrahepatic and extrahepatic cholangiocarcinomas treated with R0 resection.

KEYWORDS

prognosis, cholangiocarcinoma, tumor budding, prediction, disease-free survival

Introduction

Cholangiocarcinoma (CC) is a malignant neoplasm originating from epithelial cells lining the biliary tract. CC is divided into intrahepatic CC (iCC) and extrahepatic CC (eCC) depending on its anatomical location. Over the past few decades, the overall incidence of CC, particularly iCC, has gradually increased worldwide [1]. CC is associated with a poor prognosis, with a 5-year survival rate of 10%–49% for iCC and 20%–40% for eCC [2]. However, the prognostic factors for CC remained poorly understood.

Tumor budding (TB) is defined as a single tumor cell or a cluster of fewer than 5 cells that are observed separately from the tumor mass exhibiting invasion [3]. TB is a histopathological phenomenon of the epithelial-mesenchymal transition (EMT), the process by which epithelial cells are transformed into mesenchymal stem cells. During this process, the cells tend to migrate and invade instead of losing cell polarity and intercellular adhesion. EMT is a crucial developmental process; however, in the case of solid tumors, it promotes tumor growth by increasing invasive and metastatic activity. Since Imai et al. [4] mentioned it first, TB has been actively investigated mainly in patient with colorectal cancer. TB is associated with lymph node metastasis, distant metastasis, local recurrence, and poor prognosis regardless of the TNM stage in patients with colorectal cancer [5]. In 2016, a consensus was reached to objectively and accurately measure TB in patients with colorectal cancer [6]. By introducing this concept, studies on the prognostic significance of TB in various cancer types, such as pancreatic, gallbladder, esophageal, and gastric cancers, have been conducted [7–10]. Although relevant studies have recently been performed to evaluate the importance of TB in CC, the number remains limited, and only 10 papers have been published to date (as of March 2023) [11–19].

Hence, we aimed to investigate the relationship between TB and clinicopathological parameters and the prognostic significance of TB in iCC and eCCs.

Materials and methods

Case selection

Based on the medical records, we selected patients who underwent surgery and histopathological examination for biliary tract cancer at Pusan National University Hospital from January 2012 to December 2021 through the medical records. Patients diagnosed with cholangiocarcinoma arising in the intrahepatic, perihilar, and distal extrahepatic bile ducts were included in this study. Patients diagnosed with gallbladder or cystic duct cancer were excluded. Patients who received neoadjuvant chemotherapy; were diagnosed with cancers, such as undifferentiated, squamous cell, or neuroendocrine carcinomas other than adenocarcinomas, and with missing data were excluded.

Clinicopathological parameters

Data on age, sex, date of local recurrence, distant metastasis, date of last hospital visit or death, and cause of death were obtained. One pathologist (J.H.Ahn) reviewed all available hematoxylin and eosin (H&E) slides with pathologic reports to determine the tumor location, size, histologic grade, lymphatic invasion status, venous invasion status, perineural invasion status, and resection marginal status. Depending on the tumor location, each patient was classified into the iCC group or eCC group. The eCC group included the CC arising from the perihilar and distal extrahepatic bile ducts. Pathologic TNM categories and overall stages were reassessed according to the eighth edition of the American Joint Committee on Cancer [20].

Evaluation of tumor budding

TB was basically evaluated according to the criteria recommended by the 2016 International Tumor Budding Consensus (ITBCC) [6]. The H&E-stained slide with the highest degree of budding at the invasive front was selected. Hotspots were identified at low magnification, and the number of TB was counted at ×200 magnification. Patients with TB were classified into the low (0–4), intermediate [5–9], and high (≥10) groups. For statistical analysis, TB was reclassified into lower (0–9) and higher (≥10) groups. Two pathologists (K. B. Kim and J. H. Ahn) independently evaluated all available slides containing the tumor samples of each patient. However, they were blinded to all clinical data and the assessment results of the other pathologist. The concordance rate was 89.4%. In cases of disagreement, the two pathologists discussed and reached a consensus.

Statistical analysis

The correlations between TB and other parameters were evaluated using the chi-square and Fisher's exact test. Kaplan-Meier analysis was performed to compare the differences in disease-free survival (DFS) and disease-specific survival (DSS) between the TB groups. Univariable Cox regression analysis was performed to identify the parameters that could affect the DFS and DSS. Multivariable Cox regression analysis was performed using parameters considered significant result in

TABLE 1 Clinicopathological characteristics.

Parameter	N = 219	%
Age (mean; range) (yr)	74.3; 45–96	
< 60	17	7.8
≧ 60	202	92.2
Sex		
Male	137	62.6
Female	82	37.4
Location		
Intrahepatic	49	22.4
Extrahepatic	170	77.6
Size (mean; range) (mm)	37.21; 3–152	
<50	174	79.5
≧50	45	20.5
Grade		
Well differentiated	44	20.1
Moderately differentiated	138	63.0
Poorly differentiated	37	16.9
Lymphatic invasion		
No	136	62.1
Yes	81	37.9
Venous invasion		
No	116	53.0
Yes	103	47.0
Perineural invasion		
No	47	21.5
Yes	172	78.5
Resection marginal status		
Negative (R0)	97	44.3
Positive (R1 or R2)	122	55.7
Tumor budding		
Low (0–4)	135	61.6
Intermediate (5–9)	63	28.8
High (≥10)	21	9.6
T category		
1	66	30.1
2	93	42.5
3	57	26.0
4	3	1.4
N category		
0	147	67.1
1	53	24.2
2	19	8.7
Overall stage		
I	53	24.2
II	121	55.3
III	40	18.3
IV	5	2.3

the univariable analysis. All statistical analyses were performed using IBM SPSS Statistics (version 27.0; IBM Corp., New York, United States). A p-value <0.05 was considered significant.

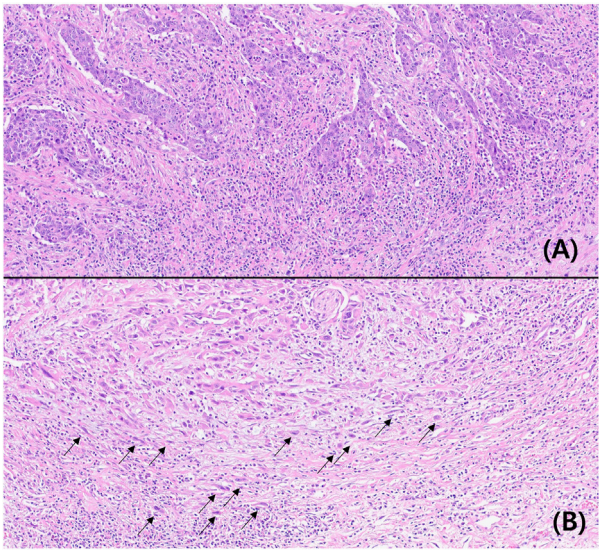

FIGURE 1
Microscopic findings of low **(A)** and high **(B)** tumor buddings (Hematoxylin-eosin, ×200, arrow: tumor budding).

Research ethics

This study was approved by the Institutional Review Board of Pusan National University Hospital (approval number 2302-001-123) and performed in accordance with the Declaration of Helsinki.

Results

Clinicopathologic characteristics

Table 1 shows the clinicopathologic characteristics of the entire cohort of this study. This study included 219 patients with a mean age was 74.3 years (range: 45 and 96 years). Of the total patients, 137 (62.6%) were male and 82 (37.4%) were female. A total of 49 (22.4%) patients had iCC, while 170 (77.6%) had eCC. Forty-four (20.1%), 138 (63.0%), and 37 (16.9%) patients had well, moderately, and poorly differentiated adenocarcinomas, respectively. Lymphatic, venous, and perineural invasions were identified in 81 (37.9%), 103 (47.0%), and 172 (78.5%) patients, respectively. A total of 97 (44.3%) patients underwent R0 resection. A total of 66 (30.1%) patients had the T1 category, 93 (42.5%) with the T2 category, 57 (26.0%) with the T3 category, and 3 (1.4%) with the T4 category. N0, N1, and N2 categories were identified in 147 (67.1%), 53 (24.2%), and 19 (8.7%) patients, respectively. According to the AJCC staging system, 53 (24.2%) patients had stage I CC, 121 (55.3%) had stage II CC, 40 (18.3%) had stage III CC, and 5 (2.3%) had stage IV CC.

TABLE 2 Association between tumor budding and clinicopathological parameters.

Parameter	Lower TB[a] (%) (*n* = 198, 90.4%)	Higher TB (%) (*n* = 21, 9.6%)	*p*-value
Age (mean; range) (yr)			
<60	15 (88.2)	2 (11.8)	*0.670*
≧60	183 (90.6)	19 (9.4)	
Sex			*0.095*
Male	120 (87.6)	17 (12.4)	
Female	78 (95.1)	4 (4.9)	
Location			*0.423*
Intrahepatic	46 (93.9)	3 (6.1)	
Extrahepatic	152 (89.4)	18 (10.6)	
Size (mean; range) (mm)			0.228
<50	155 (91.7)	14 (8.3)	
≧50	43 (86.0)	7 (14.0)	
Grade			*0.001**
Well differentiated	44 (100.0)	0 (0.0)	
Moderately differentiated	126 (91.3)	12 (8.7)	
Poorly differentiated	28 (75.7)	9 (24.3)	
Lymphatic invasion			*0.017**
No	128 (94.1)	8 (5.9)	
Yes	70 (84.3)	13 (15.7)	
Venous invasion			*0.058*
No	109 (94.0)	7 (6.0)	
Yes	89 (86.4)	14 (13.6)	
Perineural invasion			*0.052*
No	46 (97.9)	1 (2.1)	
Yes	152 (88.4)	20 (11.6)	
Resection marginal status			*0.127*
Negative (R0)	91 (93.8)	6 (6.2)	
Positive (R1 or R2)	107 (87.7)	15 (12.3)	
T category			*0.505*
1	62 (93.9)	4 (6.1)	
2	84 (90.3)	9 (9.7)	
3	49 (86.0)	8 (14.0)	
4	3 (100.0)	0 (0.0)	
N category			*0.034**
0	138 (93.9)	9 (6.1)	
1	45 (84.9)	8 (15.1)	
2	15 (78.9)	4 (21.1)	
Overall stage			*0.130*
I	50 (94.3)	3 (5.7)	
II	108 (89.3)	13 (10.7)	
III	37 (92.5)	3 (7.5)	
IV	3 (60.0)	2 (40.0)	

[a]Tumor budding.

Tumor budding

TB was not observed in 41 patients. At least one tumor bud was observed in 178 patients. Based on the ITBCC scoring system, 135 (61.6%), 63 (28.8%), and 21 (9.6%) patients had low, intermediate, and high TB, respectively. According to the TB classification for statistical analysis, the lower and higher TB groups were 198 (90.4%) and 21 (9.6%) patients. The typical findings are shown in Figure 1.

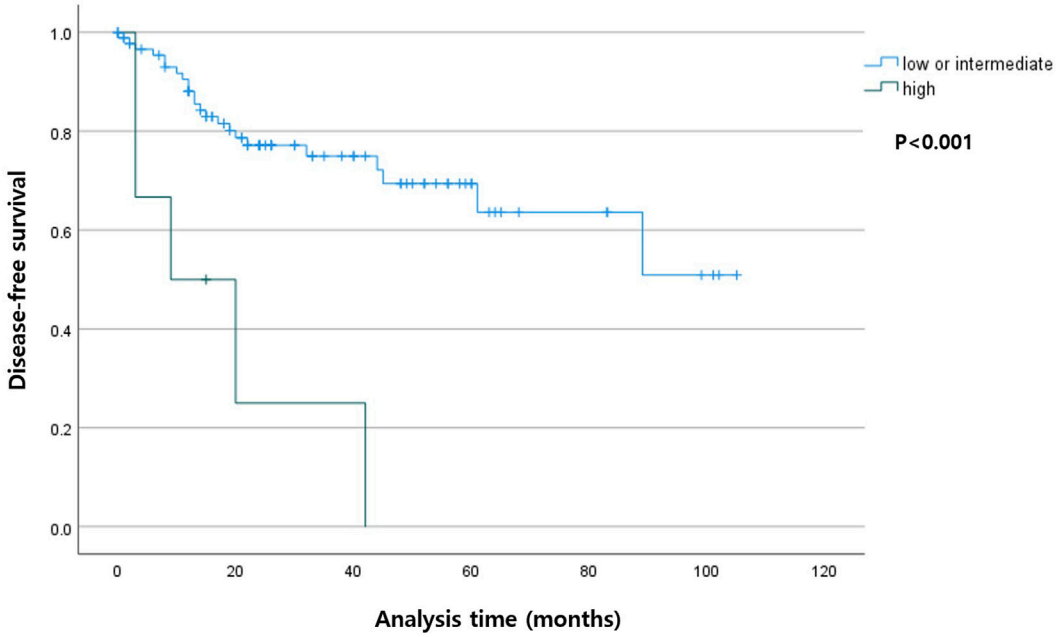

FIGURE 2
Kaplan-Meier curve depicting disease-free survival according to the tumor budding status in patients with R0 resection.

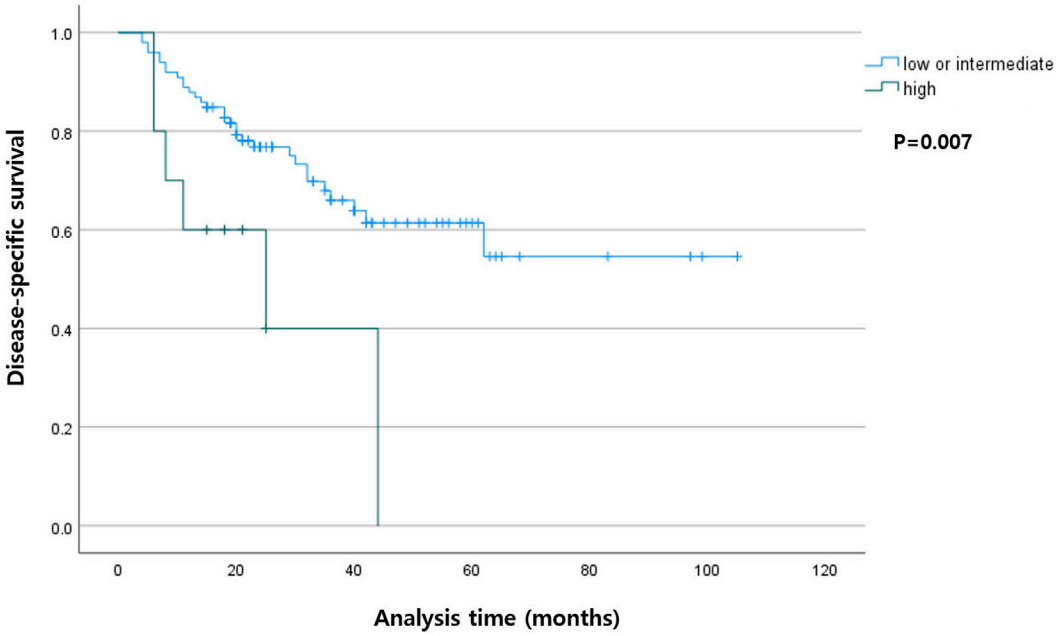

FIGURE 3
Kaplan-Meier curve showing disease-specific survival according to the tumor budding status in the entire cohort.

TABLE 3 Factors associated with disease-free survival in patients with R0 resection.

	Univariable analysis			Multivariable analysis		
	HR[a]	95% CI[b]	*p*-value	HR	95% CI	*p*-value
Age (yr)						
(<60/≧60)	1.148	0.271–4.861	*0.851*			
Sex						
(male/female)	0.977	0.428–2.230	*0.955*			
Location						
(intra-/extra-hepatic)	1.601	0.679–3.775	*0.282*			
Size						
(<50/≧50)	2.048	0.861–4.871	*0.098*			
Grade						
Well differentiated	Reference			Reference		
Moderately differentiated	1.547	0.522–4.588	*0.431*	0.723	0.217–2.412	*0.598*
Poorly differentiated	3.993	1.099–14.508	*0.035**	1.802	0.420–7.727	*0.428*
Lymphatic invasion						
(no/yes)	1.927	0.881–4.213	*0.095*			
Venous invasion						
(no/yes)	3.989	1.829–8.700	*<0.001**	2.887	1.259–6.621	*0.012**
Perineural invasion						
(no/yes)	1.302	0.587–2.884	*0.515*			
Tumor budding						
(lower/higher)	5.755	2.133–15.529	*<0.001**	3.969	1.375–11.455	*0.011**
T category						
1	Reference			Reference		
2	1.936	0.798–4.698	*0.144*	1.229	0.463–3.261	*0.679*
3–4	2.712	1.018–7.228	*0.046**	1.076	0.301–3.843	*0.910*
N category						
0	Reference			Reference		
1	3.379	1.387–8.237	*0.007**	2.635	1.045–6.647	*0.040**
2	4.040	1.158–14.090	*0.028**	4.440	1.234–15.970	*0.022**
Overall stage						
I	Reference					
II	2.174	0.927–5.101	*0.074*			
III–IV	3.116	0.795–12.220	*0.103*			

[a]Hazard ratio.
[b]Confidence interval.

Association between tumor budding and other parameters

The correlations between TB and clinicopathological parameters are presented in Table 2. Higher TB was associated with higher tumor grade ($p = 0.001$), lymphatic invasion ($p = 0.017$), and higher N category ($p = 0.034$). In patients who had venous and perineural invasion, a higher TB tended to be more prevalent, but the difference was not significant ($p = 0.058$ and 0.050, respectively). Age, sex, tumor location, size, resection marginal status, T category, and the overall stage had no correlation with TB.

Survival according to tumor budding

Among the patients with R0 resection, the higher TB group had shorter DSS ($p < 0.001$) compared with that in the lower TB groups. In the entire cohort, the higher TB patients had shorter

TABLE 4 Factors associated with disease-specific survival.

	Univariable analysis			Multivariable analysis		
	HR[a]	95% CI[b]	*p*-value	HR	95% CI	*p*-value
Age (yr)						
(<60/≧60)	0.538	0.223–1.300	*0.162*			
Sex						
(male/female)	0.892	0.462–1.724	*0.734*			
Location						
(intra-/extra-hepatic)	1.107	0.486–2.525	*0.808*			
Size						
(<50/≧50)	1.201	0.592–2.437	*0.611*			
Grade						
Well differentiated	Reference					
Moderately differentiated	1.108	0.490–2.509	*0.805*			
Poorly differentiated	2.249	0.835–6.060	*0.109*			
Lymphatic invasion						
(no/yes)	2.493	1.287–4.829	*0.005**	1.175	0.423–3.266	*0.757*
Venous invasion						
(no/yes)	4.246	2.032–8.875	*<0.001**	1.947	0.820–4.624	*0.131*
Perineural invasion						
(no/yes)	5.115	1.566–16.707	*0.003**	0.713	0.169–3.014	*0.645*
Resection marginal status						
(negative/positive)	6.926	2.684–17.857	*0.000**	4.893	1.613–15.092	*0.002**
Tumor budding						
(lower/higher)	3.134	1.291–7.608	*0.008**	1.428	0.494–4.128	*0.511*
T category						
1	Reference			Reference		
2	3.126	1.044–9.356	*0.042**	3.374	1.061–10.737	*0.039**
3–4	7.229	2.414–21.652	*<0.001**	5.262	1.618–17.112	*0.006**
N category						
0	Reference			Reference		
1	3.462	1.668–7.187	*0.001**	1.670	0.733–3.807	*0.222*
2	9.629	3.750–24.725	*<0.001**	6.667	2.284–19.461	*0.001**
Overall stage						
I	Reference			Reference		
II	9.076	1.217–67.697	*0.031**	2.262	0.159–32.243	*0.547*
III–IV	28.414	3.659–218.591	*0.001**	2.740	0.173–43.473	*0.475*

[a]Hazard ratio.
[b]Confidence interval.

DFS ($p = 0.007$). The Kaplan-Meier curves for DSS and DFS are presented in Figures 2, 3, respectively.

Factors associated with disease-free survival

Table 3 shows the association between the clinicopathological parameters and DFS in 97 patients who underwent R0 resection. In the univariable analysis, poor differentiation, venous invasion, TB, advanced [3, 4] T category, and N category were associated with DFS. In multivariable analysis, the presence of venous invasion, and higher TB and N category were related to shorter DFS.

Factors associated with disease-specific survival

Table 4 presents the association between the clinicopathological parameters and DSS in all 219 patients. In

the univariable analysis, lymphatic, venous, and perineural invasion status; resection marginal status; TB; and T and N categories and overall stages were correlated with DSS. In the multivariable analysis, positive resection marginal status and higher T category were associated with shorter DSS. However, TB was not correlated with DSS in the multivariable analysis.

Discussion

Our findings suggested that a higher TB was related to factors indicating aggressiveness, such as lymphatic invasion, higher tumor grade, and higher N category. In patients who underwent R0 resection, the higher TB group showed a shorter DFS compared with that of the lower TB group.

TB is an EMT phenotype. Anchorage-dependent cells undergo a programmed cell death process, called anoikis, when separated from the surrounding extracellular matrix. EMT provides the characteristics of stem cells, while destroying the intercellular junctions and avoiding anoikis in the tumor microenvironment, thus resulting in the acquisition of mobility and invasive phenotypes. TB cells in colorectal and gastric cancers overexpress tyrosine kinase receptor B (TrkB), an indicator of anoikis resistance, which allows TB cells to survive [21, 22]. Surviving TB cells are inevitably associated with invasiveness. Microscopically, TB cells are often observed near the lymphatic or blood vessels, which suggests the possibility of intravasation and spreading to distant tissues [22]. Lugli et al. suggested that TB is a good indicator of aggressiveness in rectal cancer, demonstrating that it is associated with the number of involved nodes, extramural spread, lymphocytic infiltration, and tumor differentiation [3]. Okudo et al. reported that TB occurs more frequently observed in the cases of poor differentiation at the invasive front of biliary tract cancer [16]. Agostini-Vulaj et al. also reported that TB is associated with high tumor grade, lymphovascular invasion, and perineural invasion in iCC and eCCs [11]. In this study, TB was significantly associated with lymphatic invasion, and higher tumor grade and N category. Higher TB was associated with the presence of venous and perineural invasion but did not show statistical significance in this study.

Okudo et al. are the first team to evaluate the prognostic impact of TB in the CC [16]. They demonstrated that the ≧5 TB foci were as an independent predictor in overall survival. Ogino et al. also reported that patients with perihilar and distal duct CC who had a high TB grade had a short postoperative overall survival [15]. Ito et al. reported that high TB was correlated with poor DSS in patients with perihilar CC; moreover, the DSS rate in the high TB group was similar to that of the group without resection [12]. In this study, DSS was not correlated with TB in the entire cohort. However, the DFS was significantly associated with TB in patients who underwent R0 resection.

All studies investigating TB in patients with CC published thus far graded the TB based on ITBCC scoring system [11–15, 17–19, 23]. Most of these studies classified TB into low and intermediate/high groups based on the cut-off value of 5 [11, 12, 14, 15, 18]. Conversely, Kosaka et al. reported a difference in the survival outcomes between low/intermediate and high TB groups, using a cut-off value of 10 in their multicenter study [13]. As in Kosaka's study, we divided patients with TB into low/intermediate and high groups. Findings from previous studies and the present study suggest that the ITBCC method is appropriate for TB cell counting in cholangiocarcinoma. Higher TB levels were correlated with worse survival. However, few studies had revealed the correlation between TB and survival when patients with TB were divided into three groups according to the ITBCC scoring system. Previous studies had demonstrated a good correlation with survival when TB was divided into two groups based on a cut-off value of 5 or 10. Therefore, for CC, further investigation is required to confirm whether the ITBCC scoring system should be applied as it is or whether a revised system should be established.

Recently, Zlobec et al. proposed the revised ITBCC scoring system [24]. They reported that dividing TB into four categories, including "zero-buds," is more informative on tumor behavior than the previous ITBCC scoring system. This study included 41 (18.7%) patients with zero buds. However, in this study, there was no difference between DFS and DSS in the zero-buds and lower-TB (1–9) groups (Supplementary Material S1).

Ogino et al. reported differences in prognostic stratification with TB in perihilar CC and distal CC [15]. These differences were in term of anatomical location and histological characteristics; for example, the connective tissue surrounding the proximal bile duct is less dense than the distal bile duct. On the contrary, Agostini-Vulaj et al. reported that TB occurred more in eCC than iCC [11]. In this study, there was no difference in the frequency of TB according to the anatomical location. Therefore, one cannot conclude on the difference in the frequency of TB.

This study has several limitations. First, we investigated the eCC and iCC, including large- and small-duct types. CCs may have varying carcinogenic mechanisms depending on their location. Particularly, in iCC, the large duct type is similar to perihilar CC, while the small duct type is similar to the adenocarcinoma component of combined hepatocellular-cholangiocarcinoma. However, considering these differences, the number of cases in each location was insufficient to conduct this study according to the tumor location. Second, patients who had incomplete resection accounted for over half of the cohort in this study. Therefore, the data used for analyzing the DFS were limited. Hence, further investigations are required to address these limitations.

In conclusion, our findings suggested that higher TB levels in patients with CC are associated with aggressiveness and worse DFS. Moreover, TB may have prognostic implications in CC.

Data availability statement

The raw data supporting the conclusion of this article will be made available by the authors, without undue reservation.

Ethics statement

The studies involving human participants were reviewed and approved by the Institutional Review Board of Pusan National University Hospital (approval number 2302-001-123). The patients/participants or their legal guardian/next of kin provided written informed consent to participate in this study.

Author contributions

Conceptualization: JA. Data curation: SK, SL, YL, and SP. Formal analysis: KK and JA. Funding acquisition: JA. Investigation: KK and JA. Methodology: KK, JA, and AK. Project administration: JA, AK, and KC. Resources: AK, KC, CL, and GH. Software: SK. Supervision: AK and KC. Validation: KK, JA, and AK. Visualization: KK and JA. Writing-original draft: KK. Writing-review and editing: JA. All authors contributed to the article and approved the submitted version.

Funding

This study was supported by Biomedical Research Institute Grant (202300130001), Pusan National University Hospital.

Conflict of interest

The authors declare that the research was conducted in the absence of any commercial or financial relationships that could be construed as a potential conflict of interest.

Supplementary material

The Supplementary Material for this article can be found online at: https://www.por-journal.com/articles/10.3389/pore.2023.1611216/full#supplementary-material

References

1. Khan SA, Tavolari S, Brandi G. Cholangiocarcinoma: Epidemiology and risk factors. *Liver Int* (2019) 39:19–31. doi:10.1111/liv.14095

2. Khan AS, Dageforde LA. Cholangiocarcinoma. *Surg Clin North Am* (2019) 99(2):315–35. doi:10.1016/j.suc.2018.12.004

3. Ueno H, Murphy J, Jass JR, Mochizuki H, Talbot IC. Tumour 'budding' as an index to estimate the potential of aggressiveness in rectal cancer. *Histopathology* (2002) 40(2):127–32. doi:10.1046/j.1365-2559.2002.01324.x

4. Imai T. The growth of human carcinoma: A morphological analysis. *Fukuoka Igaku Zasshi* (1954) 45:72–102.

5. De Smedt L, Palmans S, Sagaert X. Tumour budding in colorectal cancer: What do we know and what can we do? *Virchows Arch* (2016) 468(4):397–408. doi:10.1007/s00428-015-1886-5

6. Lugli A, Kirsch R, Ajioka Y, Bosman F, Cathomas G, Dawson H, et al. Recommendations for reporting tumor budding in colorectal cancer based on the International Tumor Budding Consensus Conference (ITBCC) 2016. *Mod Pathol* (2017) 30(9):1299–311. doi:10.1038/modpathol.2017.46

7. Karamitopoulou E, Wartenberg M, Zlobec I, Cibin S, Worni M, Gloor B, et al. Tumour budding in pancreatic cancer revisited: Validation of the ITBCC scoring system. *Histopathology* (2018) 73(1):137–46. doi:10.1111/his.13508

8. Kim HN, Lee SY, Kim BH, Kim CY, Kim A, Kim H. Prognostic value of tumor budding in gallbladder cancer: Application of the international tumor budding consensus conference scoring system. *Virchows Arch* (2021) 478(6):1071–8. doi:10.1007/s00428-020-03012-2

9. Lohneis P, Hieggelke L, Gebauer F, Ball M, Bruns C, Büttner R, et al. Tumor budding assessed according to the criteria of the International Tumor Budding Consensus Conference determines prognosis in resected esophageal adenocarcinoma. *Virchows Arch* (2021) 478(3):393–400. doi:10.1007/s00428-020-02897-3

10. Szalai L, Jakab Á, Kocsmár I, Szirtes I, Kenessey I, Szijártó A, et al. Prognostic ability of tumor budding outperforms poorly differentiated clusters in gastric cancer. *Cancers (Basel)* (2022) 14(19):4731. doi:10.3390/cancers14194731

11. Agostini-Vulaj D, Cates JMM, Bratton LE, Gonzalez RS. Increasing tumor budding in cholangiocarcinoma is associated with decreased disease-specific survival. *Hum Pathol* (2021) 111:75–83. doi:10.1016/j.humpath.2021.03.004

12. Ito T, Kuriyama N, Kozuka Y, Komatsubara H, Ichikawa K, Noguchi D, et al. High tumor budding is a strong predictor of poor prognosis in the resected perihilar cholangiocarcinoma patients regardless of neoadjuvant therapy, showing survival similar to those without resection. *BMC Cancer* (2020) 20(1):209. doi:10.1186/s12885-020-6695-9

13. Kosaka H, Ishida M, Ueno M, Komeda K, Hokutou D, Iida H, et al. Tumor budding may be a promising prognostic indicator in intrahepatic cholangiocarcinoma: A multicenter retrospective study. *Ann Gastroenterol Surg* (2023) 7(1):138–46. doi:10.1002/ags3.12605

14. Nakayama G, Hisaka T, Sakai H, Akashi M, Yuichi G, Sato T, et al. Tumour budding as an independent prognostic factor for survival in patients with distal bile duct cancer. *Anticancer Res* (2022) 42(8):4079–87. doi:10.21873/anticanres.15905

15. Ogino M, Nakanishi Y, Mitsuhashi T, Hatanaka Y, Amano T, Marukawa K, et al. Impact of tumour budding grade in 310 patients who underwent surgical resection for extrahepatic cholangiocarcinoma. *Histopathology* (2019) 74(6):861–72. doi:10.1111/his.13827

16. Okubo S, Mitsunaga S, Kato Y, Kojima M, Sugimoto M, Gotohda N, et al. The prognostic impact of differentiation at the invasive front of biliary tract cancer. *J Surg Oncol* (2018) 117(6):1278–87. doi:10.1002/jso.24946

17. Regmi P, Paudyal A, Paudyal P, Hu HJ, Liu F, Ma WJ, et al. Prognostic significance of tumor budding in biliary tract cancer. *Eur J Surg Oncol* (2022) 48(1):160–8. doi:10.1016/j.ejso.2021.08.008

18. Tanaka M, Yamauchi N, Ushiku T, Shibahara J, Hayashi A, Misumi K, et al. Tumor budding in intrahepatic cholangiocarcinoma: A predictor of postsurgery

outcomes. *Am J Surg Pathol* (2019) 43(9):1180–90. doi:10.1097/PAS.0000000000001332

19. Yoshizawa T, Hong SM, Jung D, Noë M, Kiemen A, Wu PH, et al. Three-dimensional analysis of extrahepatic cholangiocarcinoma and tumor budding. *J Pathol* (2020) 251(4):400–10. doi:10.1002/path.5474

20. Amin MB, Edge SB, Greene FL, Byrd DR, Brookland RK, Washington MK, et al. *AJCC cancer staging manual*. 8th ed. New York: Springer (2017).

21. Cao Z, Livas T, Kyprianou N. Anoikis and EMT: Lethal "liaisons" during cancer progression. *Crit Rev Oncog* (2016) 21(3-4):155–68. doi:10.1615/CritRevOncog.2016016955

22. Lugli A, Zlobec I, Berger MD, Kirsch R, Nagtegaal ID. Tumour budding in solid cancers. *Nat Rev Clin Oncol* (2021) 18(2):101–15. doi:10.1038/s41571-020-0422-y

23. Tanaka M, Kunita A, Yamagishi M, Katoh H, Ishikawa S, Yamamoto H, et al. KRAS mutation in intrahepatic cholangiocarcinoma: Linkage with metastasis-free survival and reduced E-cadherin expression. *Liver Int* (2022) 42(10):2329–40. doi:10.1111/liv.15366

24. Zlobec I, Bächli M, Galuppini F, Berger MD, Dawson HE, Nagtegaal ID, et al. Refining the ITBCC tumor budding scoring system with a "zero-budding" category in colorectal cancer. *Virchows Arch* (2021) 479(6):1085–90. doi:10.1007/s00428-021-03090-w

Pathology & Oncology Research | frontiers

TYPE Original Research
PUBLISHED 04 January 2023
DOI 10.3389/pore.2022.1610818

Check for updates

OPEN ACCESS

EDITED BY
Andrea Ladányi,
National Institute of Oncology (NIO), Hungary

*CORRESPONDENCE
Peizhong Shang,
spz251@163.com

RECEIVED 08 September 2022
ACCEPTED 16 December 2022
PUBLISHED 04 January 2023

CITATION
Fan Z, Liu B and Shang P (2023), Development and validation of a nomogram prediction model based on albumin-to-alkaline phosphatase ratio for predicting the prognosis of gallbladder carcinoma.
Pathol. Oncol. Res. 28:1610818.
doi: 10.3389/pore.2022.1610818

COPYRIGHT
© 2023 Fan, Liu and Shang. This is an open-access article distributed under the terms of the Creative Commons Attribution License (CC BY). The use, distribution or reproduction in other forums is permitted, provided the original author(s) and the copyright owner(s) are credited and that the original publication in this journal is cited, in accordance with accepted academic practice. No use, distribution or reproduction is permitted which does not comply with these terms.

Development and validation of a nomogram prediction model based on albumin-to-alkaline phosphatase ratio for predicting the prognosis of gallbladder carcinoma

Zizheng Fan[1], Bing Liu[2] and Peizhong Shang[2]*

[1]Department of Graduate School, Hebei North University, Zhangjiakou, China, [2]Department of Hepatobiliary Surgery, The Hospital of 81st Group Army PLA, Zhangjiakou, China

Gallbladder carcinoma (GBC) is a rare biliary tract cancer with a high recurrence rate and a poor prognosis. Albumin-alkaline phosphatase ratio (AAPR) has been demonstrated to be a prognostic predictor for several cancers, but its predictive value for GBC patients remains unknown. The aim of this study was to investigate the predictive role of AAPR in GBC patients and to develop a novel nomogram prediction model for GBC patients. We retrospectively collected data from 80 patients who underwent surgery at the Hospital of 81st Group Army PLA as a training cohort. Data were collected from 70 patients with the same diagnosis who underwent surgery at the First Affiliated Hospital of Hebei North University as an external verification cohort. The optimal cut-off value of AAPR was determined using X-tile software. A nomogram for the overall survival (OS) based on multivariate Cox regression analysis was developed and validated using calibration curves, Harrell's concordance index, the receiver operating characteristic curves, and decisive curve analyses. The optimal cut-off value of AAPR was .20. Univariate and multivariate Cox regression analyses demonstrated that BMI (p = .043), R0 resection (p = .001), TNM stage (p = .005), and AAPR (p = .017) were independent risk factors for GBC patients. In terms of consistency, discrimination, and net benefit, the nomogram incorporating these four independent risk factors performed admirably. AAPR is an independent predictor of GBC patients undergoing surgery, and a novel nomogram prediction model based on AAPR showed superior predictive ability.

KEYWORDS

prognosis, nomogram, gallbladder carcinoma, independent risk factors, AAPR

Introduction

Gallbladder carcinoma (GBC) is the most common malignant tumor of the biliary system, and its incidence ranks sixth among malignant tumors of the digestive system [1]. According to the latest GLOBOCAN 2020 database [2], the number of new cancer cases and cancer deaths in 2020 for GBC are 115,949 and 84,695, respectively. Due to the atypical clinical symptoms in the early stage, GBC is often misdiagnosed as biliary colic or chronic cholecystitis. Therefore, most GBC patients are in an advanced stage at the time of diagnosis. To date, radical resection remains the only effective treatment for patients with GBC [3]. The 5-year survival rate remains low due to high postoperative recurrence and metastasis rates [4]. Therefore, it is of great importance to establish a prognostic model for GBC patients to ensure timely treatment.

The concept of albumin-alkaline phosphatase ratio (AAPR) was originally proposed by Chan et al, who demonstrated that AAPR is an independent prognostic indicator of OS in hepatocellular carcinoma patients who underwent radical surgery [5]. In 2018, Tan et al. [6] proposed the predictive value of AAPR in patients with upper tract urothelial carcinoma. Subsequently, several studies demonstrated that AAPR is a clinical prognostic indicator for non-small cell lung cancer [7] and combined hepatocellular-cholangiocarcinoma [8]. Recently, a study was performed by Li et al. [9], who developed a nomogram model after radical cystectomy of bladder cancer, and considered that AAPR could be conducive to clinical decision-making and risk stratification in those patients. Nevertheless, AAPR, as a novel inflammation-related ratio index, has not been explored in GBC. Thus, it is valuable to study the potential application of AAPR in GBC.

This study aimed to investigate the prognostic value of AAPR in GBC patients and combine AAPR with other three independent risk factors to establish a nomogram prediction model for the prognosis of GBC patients.

Patients and methods

Patients

We retrospectively reviewed the medical records of GBC patients at the Hospital of the 81st Group Army PLA from January 2014 to May 2022 and the medical records of GBC patients at the First Affiliated Hospital of Hebei North University from March 2016 to March 2022. The inclusion criteria were as follows: 1) GBC confirmed by pathological examination; 2) Patients who underwent surgery; 3) No other malignant tumors; and 4) Complete medical records and follow-up data. Patients with incomplete medical records, missing follow-up data, or other malignant tumors were excluded from this study. This study was reviewed and approved by the ethics committee of the Hospital of 81st Group Army PLA (JTJYY-202207) and the First Affiliated Hospital of Hebei North University (W2021036).

Data collection and definition

We collected clinical information of the two cohorts from the medical records including age, gender, body mass index (BMI), jaundice, gallbladder stone, diabetes mellitus, R0 resection, tumor location, tumor size, tumor number, tumor differentiation, TNM stage, Nevin stage, intraoperative blood loss, and survival time. Clinical staging was graded in accordance with the American Joint Committee on Cancer (AJCC) 8th edition of the GBC TNM staging system and the Nevin staging system. Albumin (ALB) and alkaline phosphatase (ALP) were obtained from preoperative blood biochemical tests. AAPR was the ratio obtained by dividing ALB by ALP.

Statistical analysis

X-tile software (Rimm Laboratory, Yale School of Medicine, New Haven, CT, United States) was employed to determine the optimal cut-off value of AAPR [10]. The same method identified the optimal cut-off values for other associated factors. Differences in the unordered categorical variables and the ordinal categorical variables in the training cohort and verification cohort were determined using the Chi-square test and the Mann-Whitney U test, respectively. The relationship between AAPR and the clinical characteristics of patients was compared using the Chi-square test or Fisher's exact test, as appropriate. The Kaplan-Meier method and the log-rank test were employed to calculate survival analyses. Univariate and multivariate Cox regression analyses were performed to analyze independent risk factors. A multicollinearity test was performed to assess the correlation between variables. Nomogram was constructed based on the results of multivariate Cox regression analysis, and the performance of the nomogram was evaluated using calibration curves, Harrell's consistency index (C-index), the receiver operating characteristic (ROC) curves, and decisive curve analyses (DCA). In the present study, statistical analyses were carried out using the Statistical Package for the Social Sciences version 25.0 software (IBM Corp., Armonk, United States) and R software 4.2.0 (http://www.r-project.org/). p-value < .05 was considered statistically significant.

Results

Patients' characteristics

The training cohort consisted of 60 (75.00%) females and 20 (25.00%) males, with a mean age of 65.95 ± 9.71 years. There were 52 (65.00%) patients with well or moderate cancer cell differentiation and 28 (35.00%) patients with poor cancer cell differentiation, respectively. According to the eighth edition of the AJCC TNM staging system, 3 (3.75%), 14 (17.50%), 3 (3.75%), 49 (61.25%), and 11 (13.50%) GBC patients were categorized as stage 0, I, II, III, and IV, respectively. The verification cohort included 53 (75.71%) females and 17 (24.29%)

TABLE 1 Clinicopathological characteristics of 150 patients with gallbladder carcinoma in the training cohort and verification cohort.

Characteristics	Training cohort (%)	Verification cohort (%)	*P*-value
Number of patients	80	70	
Age, yr			.568
≤65	34 (42.50)	33 (47.14)	
>65	46 (57.50)	37 (52.86)	
Gender			.919
Male	20 (25.00)	17 (24.29)	
Female	60 (75.00)	53 (75.71)	
BMI, kg/m^2			.563
≤25.3	55 (68.75)	45 (64.29)	
>25.3	25 (31.25)	25 (35.71)	
Jaundice			.598
No	58 (72.50)	48 (68.57)	
Yes	22 (27.50)	22 (31.43)	
Gallbladder stone			.349
No	31 (38.75)	22 (31.43)	
Yes	49 (61.25)	48 (68.57)	
Diabetes mellitus			.095
No	70 (87.50)	54 (77.14)	
Yes	10 (12.50)	16 (22.86)	
R0 resection			.453
No	31 (38.75)	23 (32.86)	
Yes	49 (61.25)	47 (67.14)	
Tumor differentiation			.063
Well or Moderate	52 (65.00)	35 (50.00)	
Poor	28 (35.00)	35 (50.00)	
TNM stage			.256
0	3 (3.75)	7 (10.00)	
I	14 (17.5)	11 (15.71)	
II	3 (3.75)	3 (4.29)	
III	49 (61.25)	43 (61.43)	
IV	11 (13.75)	6 (8.57)	
Nevin stage			
I	5 (6.25)	8 (11.43)	.261
II	13 (16.25)	17 (24.29)	
III	41 (51.25)	26 (37.14)	
IV	9 (11.25)	10 (14.28)	
V	12 (15.00)	9 (12.86)	
Tumor size, cm			.527
≤3	64 (80.00)	53 (75.71)	
>3	16 (20.00)	17 (24.29)	
Tumor location			.131
Body, bottom	72 (90.00)	57 (81.43)	
Neck, other	8 (10.00)	13 (18.57)	
Tumor number			.153
Single	67 (83.75)	52 (74.29)	
Multiple	13 (16.25)	18 (25.71)	
Intraoperative blood loss, ml			.965
≤50	46 (57.50)	40 (57.14)	

(Continued on following page)

TABLE 1 (*Continued*) Clinicopathological characteristics of 150 patients with gallbladder carcinoma in the training cohort and verification cohort.

Characteristics	Training cohort (%)	Verification cohort (%)	*P*-value
>50	34 (42.50)	30 (42.86)	
AAPR			.707
≤.20	24 (30.00)	23 (32.86)	
>.20	56 (70.00)	47 (67.14)	

Abbreviations: yr, year; BMI, body mass index; AAPR, albumin to alkaline phosphatase ratio.

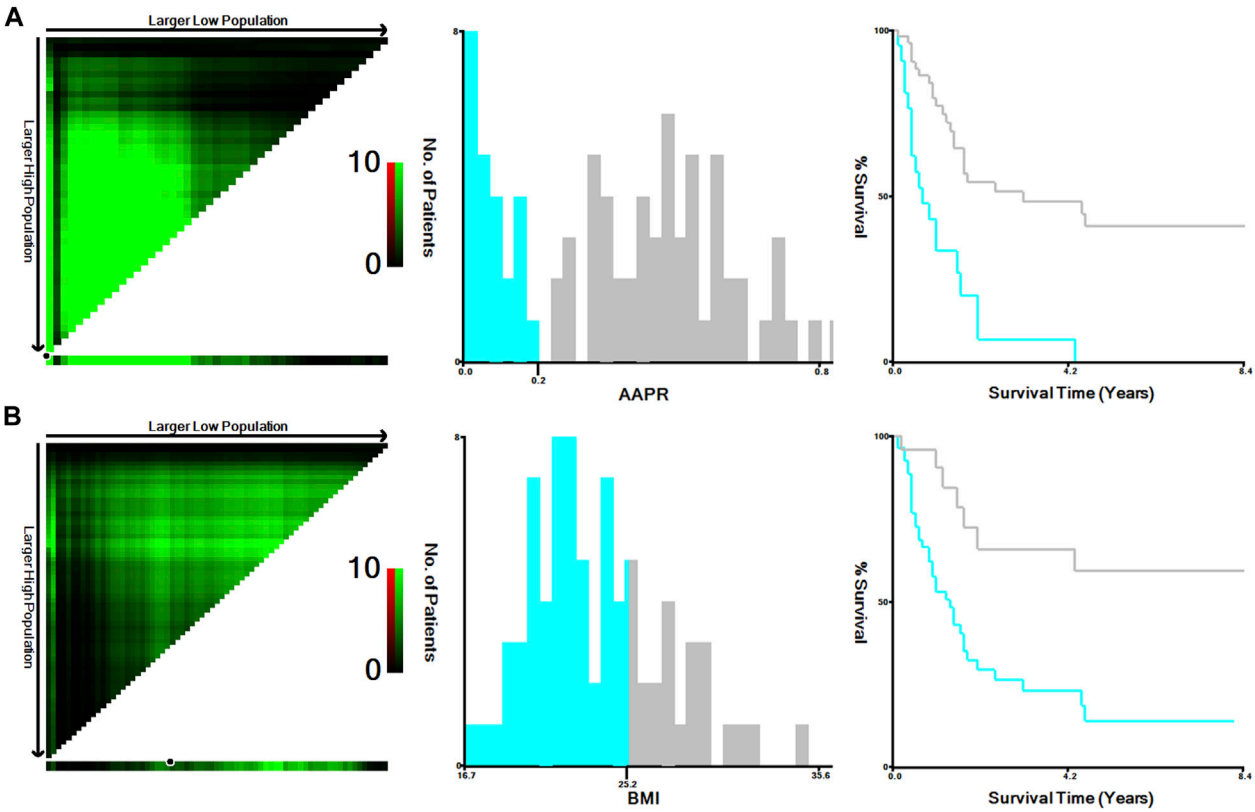

FIGURE 1
Calculation of optimal cut-off values of AAPR **(A)** and BMI **(B)** of the training cohort using X-tile software. Abbreviations: AAPR, albumin-to-alkaline phosphatase ratio; BMI, body mass index.

males, with a mean age of 64.11 ± 9.84 years. There were 35 (50.00%) patients with well or moderate cancer cell differentiation and 35 (50.00%) patients with poor cancer cell differentiation, respectively. According to the eighth edition of the AJCC TNM staging system, 7 (10.00%), 11 (15.71%), 3 (4.29%), 43 (61.43%), and 6 (8.57%) GBC patients were classified as stage 0, I, II, III, and IV, respectively.

In the training cohort, 43 (53.75%) patients died with a median OS of 20 months, The 1-, 3-, and 5-year OS rates were 64.40%, 36.60%, and 29.10%, respectively. In the verification cohort, 43 (61.43%) died with a median OS of 16 months. The 1- and 3-year OS rates were 57.90% and 30.10%, respectively. The clinicopathological characteristics of the patients in the training and verification cohorts were detailed in Table 1.

Relationship between AAPR and patients' clinical characteristics in the training cohort

The optimal cutoff values for AAPR and BMI obtained with the X-tile software were 0.20 and 25.30, respectively (Figure 1). Patients were categorized into a low group (AAPR ≤ .20, n = 24) and a high group (AAPR > .20, n =

TABLE 2 Clinical characteristics of the patients according to albumin-to-alkaline phosphatase ratio in the training cohort.

Characteristics	AAPR≤.20, *n* (%)	AAPR>.20 *n* (%)	X^2	*P*-value
Age, yr			.789	.374
≤65	12 (50)	22 (39.29)		
>65	12 (50)	34 (60.71)		
Gender			7.937	**.005**
Male	11 (45.83)	9 (16.07)		
Female	13 (54.17)	47 (83.93)		
BMI, kg/m^2			1.732	.188
≤25.2	19 (79.17)	36 (64.29)		
>25.2	5 (20.83)	20 (35.71)		
Jaundice			53.608	**<.001**
No	4 (16.67)	54 (96.43)		
Yes	20 (83.33)	2 (3.57)		
Gallbladder stone			.123	.726
No	10 (41.67)	21 (37.50)		
Yes	14 (58.33)	35 (62.50)		
Diabetes mellitus			.136	.712
No	22 (91.67)	48 (85.71)		
Yes	2 (8.33)	8 (14.29)		
R0 resection			8.148	**.004**
No	15 (62.50)	16 (28.57)		
Yes	9 (37.50)	40 (71.43)		
Tumor differentiation			3.391	.066
Well or Moderate	12 (50)	40 (71.43)		
Poor	12 (50)	16 (28.57)		
TNM stage			1.270	.260
0–II	4 (16.67)	16 (28.57)		
III–IV	20 (83.33)	40 (71.43)		
Nevin stage			1.966	.161
I–II	3 (12.50)	15 (26.79)		
III–V	21 (87.50)	41 (73.21)		
Tumor size, cm			5.093	**.024**
≤3	15 (62.50)	49 (87.50)		
>3	9 (37.50)	7 (12.50)		
Tumor location			.800	.371
Neck	4 (16.67)	4 (7.14)		
Body, bottom	20 (83.33)	52 (92.86)		
Tumor number			.157	.692
Single	19 (79.17)	48 (85.71)		
Multiple	5 (20.83)	8 (14.29)		
Intraoperative blood loss, ml			11.263	**.001**
≤50	7 (29.17)	39 (69.64)		
>50	17 (70.83)	17 (30.36)		

Abbreviations: yr, year; BMI, body mass index; AAPR, albumin to alkaline phosphatase ratio. Indicate statistically significant.

56) on the basis of the optimal cutoff value of AAPR. In the high AAPR group, the frequency of females was higher. Jaundice occurred more frequently in the low AAPR group compared to the high AAPR group, and the proportion of patients with R0 resection was greater in the high AAPR group than in the low AAPR group. The high AAPR group had a larger number of patients with tumor size less than 3 cm compared to the low AAPR group. Patients in the low AAPR group suffered more intraoperative blood loss than those in the high AAPR

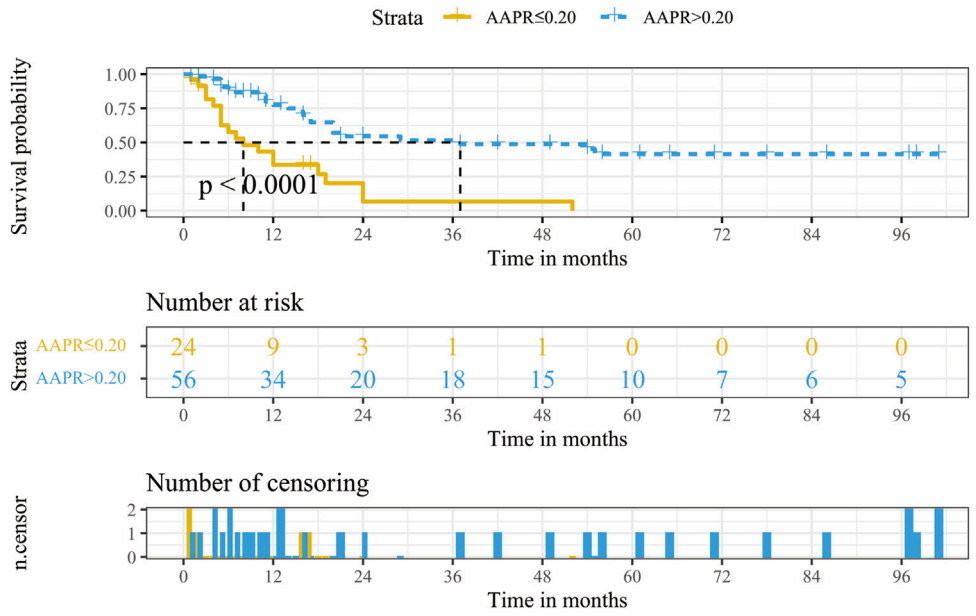

FIGURE 2
Kaplan-Meier survival analysis for OS stratified according to AAPR in the training cohort. Abbreviations: OS, overall survival; AAPR, albumin-to-alkaline phosphatase ratio.

group. In the present study, AAPR seems to be not associated with BMI, TNM stage, and Nevin stage. The relationship between AAPR and other clinicopathological features is detailed in Table 2.

The Kaplan-Meier curve of AAPR is presented in Figure 2. The median OS of the low AAPR group and the high AAPR group were 8 and 37 months, respectively ($p < .0001$).

Independent prognostic factors in the training cohort

Univariate Cox analysis revealed that gender, jaundice, tumor differentiation, BMI, R0 resection, intraoperative blood loss, TNM stage, Nevin stage, tumor size, and AAPR were significantly associated with the prognosis of GBC patients (Table 3). The multicollinearity test revealed a strong relationship between the Nevin stage and the TNM stage (Tables 2, 3). As a result, the Nevin stage was excluded from the multivariate Cox model, and the TNM stage, which is more commonly used in clinical practice, was selected. The multivariate Cox analysis demonstrated that BMI [hazard ratio (HR) = .413, 95% confidence interval (CI): .175–.971; $p = .043$], R0 resection (HR = 3.096, 95%CI: 1.558–6.151; $p = .001$), TNM stage (HR = 4.921, 95%CI: 1.631–14.849; $p = .005$), and AAPR (HR = .212, 95%CI: .060–.757; $p = .017$) were independent risk factors for GBC patients (Table 3).

Establishment and verification of the nomogram

The results of multivariate Cox analysis showed that BMI, R0 resection, TNM stage, and AAPR were independent risk factors for predicting GBC patients after surgery (Table 3). Using the R software "RMS" package, a nomogram prediction model was developed by combining these four independent risk factors (Figure 3), and 1- and 3-year calibration curves of the training and verification cohorts were plotted, which demonstrated that results predicted by the nomogram prediction model were in good agreement with the actual observations in the calibration curves of the training and verification cohorts (Figure 4).

Comparing different prediction models

According to the ROC analysis in the training cohort, the area under the curve (AUC) at 1 year was .862, .727, and .779 for the nomogram prediction model, TNM staging system, and Nevin staging system, respectively, and the AUC at 3 years was .898, .762, and .795, respectively (Figure 5A). The C-index of the nomogram prediction model, TNM staging system, and Nevin staging system were .821, .716, and .745, respectively (Table 4). In the verification cohort, the nomogram prediction model's 1- and 3-year AUCs were .946 and .955, respectively, which were significantly higher than those of the

10.3389/pore.2022.1610818

TABLE 3 Univariate and multivariate Cox proportional hazard analyses of factors associated with overall survival in the training cohort.

	Univariate test			Multivariate test		
	HR	**95% CI**	***P*-value**	**HR**	**95% CI**	***P*-value**
Age, yr						
≤65						
>65	1.040	.563–1.919	.901			
Gender						
Male						
Female	.522	.278–.978	**.043**	1.192	.580–2.446	.633
BMI, kg/m^2						
≤25.2						
>25.2	.275	.121–.625	**.002**	.413	.175–.971	**.043**
Jaundice						
No						
Yes	2.853	1.521–5.350	**.001**	.512	.143–1.829	.303
Gallbladder stone						
No						
Yes	.853	.467–1.561	.607			
Diabetes mellitus						
No						
Yes	.727	.285–1.854	.505			
R0 resection						
Yes						
No	4.374	2.363–8.096	**<.001**	3.096	1.558–6.151	**.001**
Tumor differentiation						
Moderate-well						
Poor	2.079	1.136–3.805	**.018**	.905	.448–1.829	.781
TNM stage						
0–II						
III–IV	5.645	2.006–15.886	**.001**	4.921	1.631–14.849	**.005**
Nevin stage						
I–II						
III–V	5.477	1.944–15.430	**.001**[a]			
Tumor size, cm						
≤3						
>3	2.369	1.204–4.663	**.013**	1.085	.487–2.415	.842
Tumor location						
Neck						
Body, bottom	.709	.252–1.994	.514			
Tumor number						
Single						
Multiple	1.158	.536–2.501	.708			
Intraoperative blood loss, ml						
≤50						
>50	3.011	1.621–5.595	**<.001**	1.645	.711–3.804	.245
AAPR						
≤.20						
>.20	.266	.142–.499	**<.001**	.212	.060–.757	**.017**

[a]Nevin stage was excluded from the multivariate Cox regression due to the multicollinearity between the TNM, stage and the Nevin stage (VIF >5). Abbreviations: yr, year; BMI, body mass index; AAPR, albumin to alkaline phosphatase ratio. Indicate statistically significant.

TABLE 4 Comparisons of the performance and discriminative ability between different prognosis prediction models in the training cohort and verification cohort.

	Training cohort			Verification cohort		
	Nomogram	TNM stage	Nevin stage	Nomogram	TNM stage	Nevin stage
1-yr AUC	.862	.727	.779	.946	.771	.817
3-yr AUC	.898	.762	.795	.955	.853	.859
C-index	.821	.716	.745	.888	.694	.690

Abbreviations: yr, year; AUC, area under the curve.

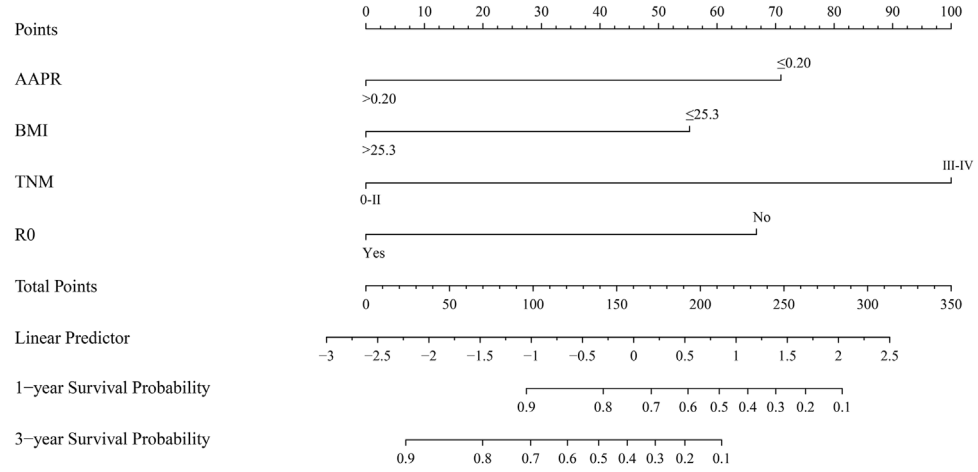

FIGURE 3
Nomogram based on AAPR, BMI, TNM stage, and R0 resection for predicting OS of GBC patients. Abbreviations: AAPR, albumin-to-alkaline phosphatase ratio; BMI, body mass index; OS, overall survival; GBC, gallbladder carcinoma.

TNM and Nevin staging systems (Figure 5B). The AUCs and C-index in the training cohort and verification cohort were summarized in Table 4.

In addition, to estimate the value of the clinical application of the nomogram prediction model, DCA was employed to compare the net benefit of the nomogram prediction model with the TNM and Nevin staging systems in the training cohort and the verification cohort (Figure 6). The results suggested that the nomogram prediction model generated more net benefit at 3 years after surgery in both the training and verification cohorts, across a wide range of threshold probabilities, which indicates that the nomogram prediction model may have great potential and application in clinical practice.

The Establishment of the risk stratification model

In the present study, a novel risk stratification model was developed based on the total nomogram score of each patient in the training cohort and verification cohort. Patients in both cohorts were divided into the low-risk, middle-risk, and high-risk groups, respectively. In the training cohort, the median OS of the middle-risk and high-risk groups was 20 and 6 months, respectively (Figure 7A). In the verification cohort, the median OS was 16 and 3 months for the middle-risk and high-risk groups, respectively (Figure 7B). Patients in the high-risk group had a lower OS rate than those within the low-risk or middle-risk group, indicating that the risk stratification model based on the nomogram was also predictive.

Discussion

GBC is a rare malignancy of the gastrointestinal tract, accounting for 1.2% of all malignancies and 50% of biliary tract malignancies worldwide [11]. Because of the late presentation of clinical manifestations and poor prognosis, it

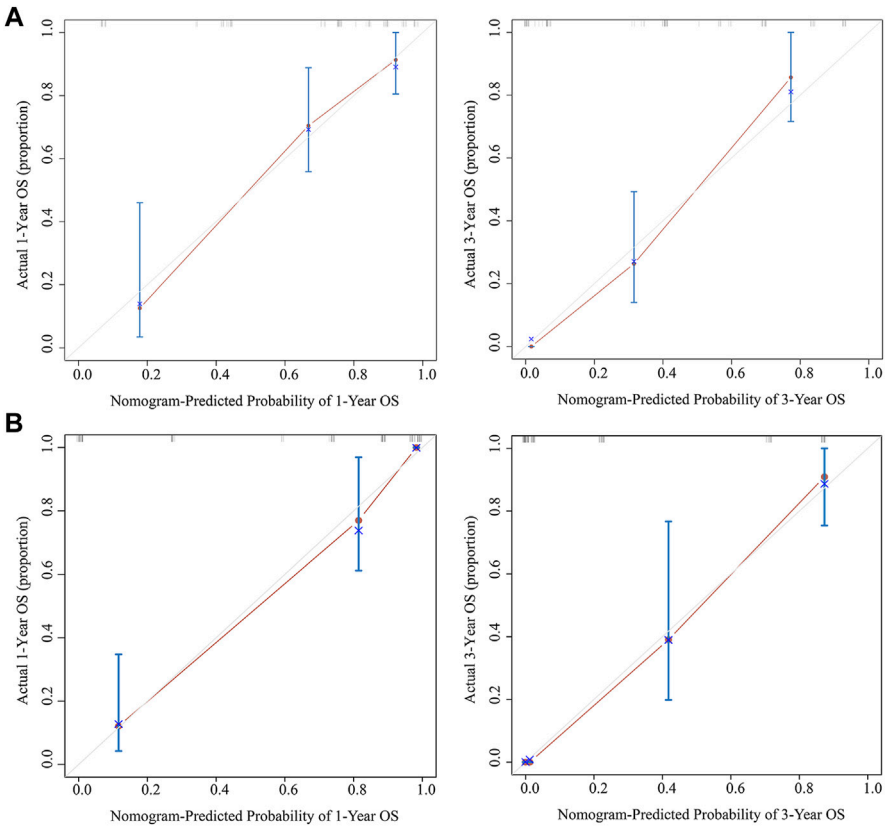

FIGURE 4
Calibration curves of the nomogram predicting 1- and 3-year OS for the training cohort **(A)** and verification cohort **(B)**. Abbreviation: OS, overall survival.

is often at an advanced stage at the time of diagnosis, and the 5-year survival rate for GBC is 5%–10% [12]. Therefore, accurately predicting the prognosis of GBC helps clinical decision-making for individualized postoperative treatment and then using the targeted treatment for different patient groups after surgery, which in turn improves the prognosis of patients. In this study, we aimed to evaluate the predictive value of AAPR and to develop a prognostic prediction model as a nomogram for GBC patients. This nomogram can be used as a reference for clinical decision-making and patient risk stratification, which has promising prospects for clinical use.

Serum ALB is a protein synthesized in the liver, consisting of 585 amino acid residues, which plays an important role in maintaining oncotic pressure, transporting nutrients, and other microenvironmental systems. Recent studies have revealed the ability of ALB in stabilizing cell proliferation, DNA replication, and exerting antioxidant reactions for anti-carcinogenesis [13–15]. Meanwhile, ALB is an important indicator to assess the nutritional status of the organism and can also reflect the systemic inflammatory response of the patient. Malnutrition can affect the body's defense mechanisms, which in turn increases tumorigenesis [16]. Previous studies have illustrated that ALB has anti-inflammatory and immunomodulatory attributes and that inflammation-induced reductions in ALB synthesis may have an impact on immune defense [17, 18]. The body's inflammatory response is closely related to carcinogenesis, tumor progression, and metastasis, and inflammatory factors cause damage to the body and promote the malignant progression of tumors. A growing number of studies have shown that serum ALB levels are associated with poor prognosis in a variety of malignancies [19–21]. Wheler et al. [22] discovered that low serum ALB levels in patients with metastatic breast cancer were significantly associated with shorter survival. And another study found that endometrial cancer patients with low serum ALB levels had a significantly shorter survival time [23]. Furthermore, a recently published study found that low serum ALB levels predicted a worse prognosis for patients with metastatic gastric cancer [24]. ALP, mainly concentrating in the liver, kidney, and bones, is a hydrolytic enzyme widely distributed in the body. A previous study has shown that ALP plays an important role in enhancing cancer cell proliferation, vascular invasion, and distant metastasis

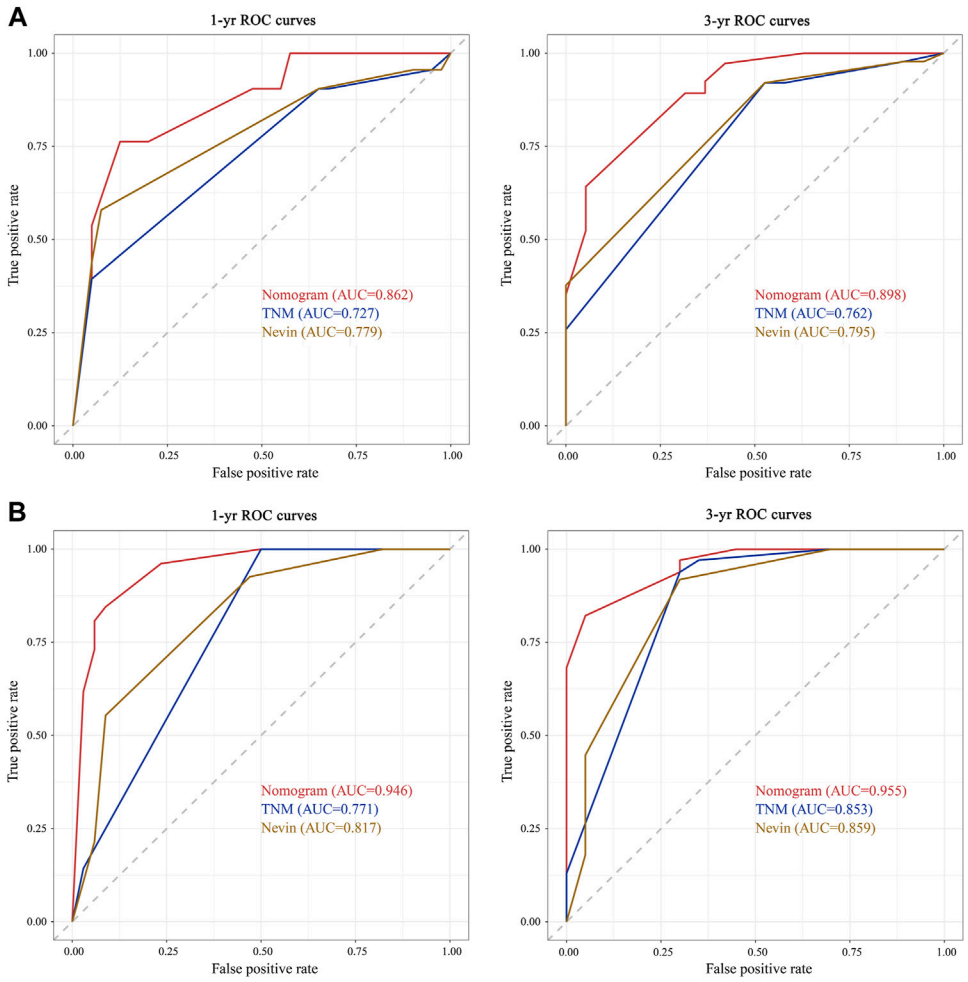

FIGURE 5
Comparisons of ROC curves of the nomogram prediction model, TNM staging system, and Nevin staging system for 1- and 3-year overall survival in the training cohort **(A)** and verification cohort **(B)**. Abbreviations: yr, year; AUC, area under the curve; ROC, receiver operating characteristic; OS, overall survival.

[25]. In addition, ALP has also been reported as an independent prognostic factor in patients with hepatocellular carcinoma, skeletal metastatic nasopharyngeal carcinoma, hypertrophic cardiomyopathy, and periampullary carcinoma [26–29]. AAPR is the ratio of ALB to ALP. Several studies have demonstrated that low AAPR is strongly associated with poor prognosis in malignancies [6, 30–33].

Currently, the prognostic indicators of GBC commonly used in clinical practice, such as the TNM staging system, Nevin staging system, and the histological grade, are mainly obtained from postoperative examination of tumor tissues. Although widely employed in clinical practice, the AJCC TNM staging system has inherent drawbacks. Because it only takes the conditions of the primary tumor, lymph nodes, and metastasis into consideration and lacks a personal examination reference for individual patients. According to a recent study, a nomogram prediction model based on the albumin-γ-glutamyl transferase ratio outperformed the TNM staging system [34]. Unfortunately, the Nevin staging system was not included in the study. In this study, we developed a novel nomogram prediction model based on AAPR and compared it with TNM staging system and Nevin staging system. The results of the ROC curve, C-index, and DCA revealed that the nomogram prediction model based on AAPR had significantly better predictive performance than the TNM staging system and the Nevin staging system, as well as greater clinical application value.

In the present study, we discovered that AAPR, a novel inflammation-related ratio index defined by preoperative levels of ALB and ALP, is an independent risk factor for GBC patients, with AAPR levels less than .20 having a lower OS. Previous studies have shown that AAPR is an excellent predictor of the prognosis of several types of cancer. However, its value in GBC has not been

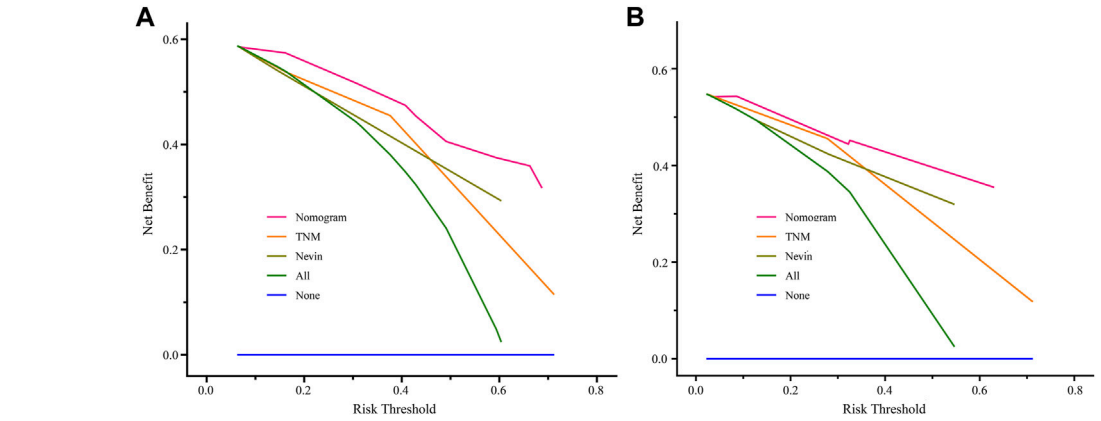

FIGURE 6
Comparisons of DCA of the nomogram prediction model, TNM staging system, and Nevin staging system for predicting 3-year survival probability in the training cohort **(A)** and verification cohort **(B)**. Abbreviation: DCA, decisive curve analysis.

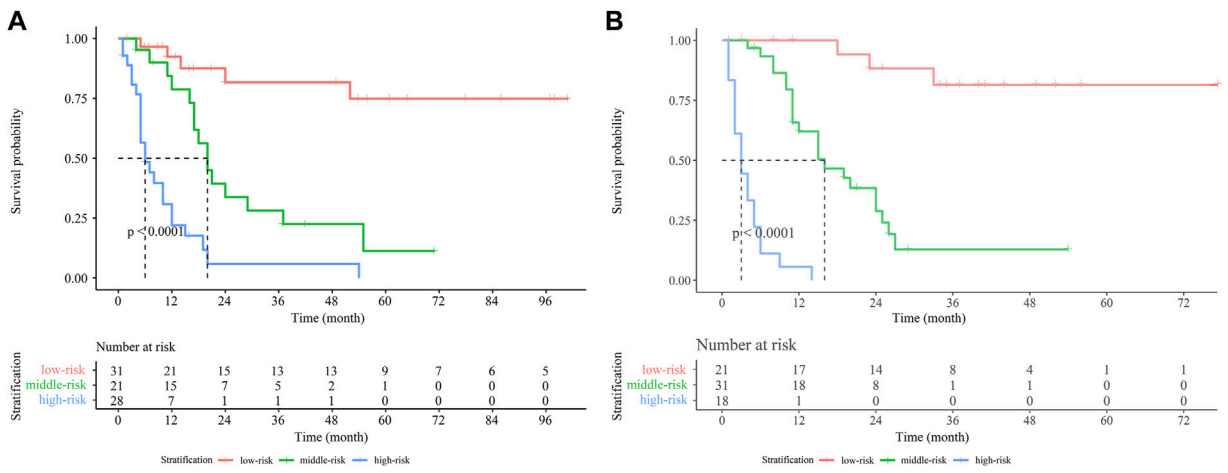

FIGURE 7
Kaplan-Meier survival curves for GBC patients stratified by the nomogram score in the training cohort **(A)** and verification cohort **(B)**. Abbreviation: GBC, gallbladder carcinoma.

reported yet. To the best of our knowledge, this is the first study analyzing the predictive value of AAPR in GBC patients who received surgery. This study found that AAPR was associated with several clinicopathological characteristics, such as gender, jaundice, R0 resection, tumor size, and intraoperative blood loss. A high level of AAPR indicates a better prognosis and a longer OS. GBC patients with AAPR high-level had significantly higher 1- and 3-year OS rates than GBC patients with AAPR low-level. Meanwhile, we integrated AAPR with the other three independent prognostic factors, including BMI, R0 resection, and TNM stage, to develop a predictive nomogram for 1-, and 3-year survival probability. The nomogram achieved considerable prognostic performance in terms of consistency, discrimination, and net benefit, and AAPR was demonstrated to have superior predictive ability for GBC patients. The current nomogram also showed better discrimination and more net benefit compared with TNM and Nevin staging systems for GBC patients. In addition, we developed a risk stratification model according to the nomogram to assist clinicians in identifying GBC patients at high risk and provide early warning for a better individualized and precise treatment.

In this study, we demonstrated for the first time the prognostic value of AAPR in GBC patients and validated using external data. However, this study has some limitations. First, it was a retrospective study. Second, due to the fact that GBC is a relatively rare malignancy, the sample size enrolled was

relatively limited. Finally, AAPR as a potentially valuable prognostic indicator needs to be further confirmed in future prospective studies for its prognostic value in GBC.

Conclusion

In summary, our study revealed that the AAPR was an independent predictive factor for the prognosis of GBC patients. According to this finding, we developed a nomogram based on AAPR for a prognostic prediction model and further clinical decision-making in GBC patients.

Data availability statement

The original contributions presented in the study are included in the article/Supplementary Material, further inquiries can be directed to the corresponding author.

Ethics statement

The studies involving human participants were reviewed and approved by the ethics committee of the Hospital of 81st Group Army PLA and the First Affiliated Hospital of Hebei North University.

Author contributions

ZF contributed to the conception, the acquisition of data, drafting, statistical analyses, and writing of the manuscript. BL and PS were responsible for supervision and revisions for important intellectual content. All authors approved the final manuscript.

Conflict of interest

The authors declare that the research was conducted in the absence of any commercial or financial relationships that could be construed as a potential conflict of interest.

Acknowledgments

The authors thank Xiantao Huang for his effort in collecting the verification cohort data.

Supplementary material

The Supplementary Material for this article can be found online at: https://www.por-journal.com/articles/10.3389/pore.2022.1610818/full#supplementary-material

References

1. Chen W, Zheng R, Baade PD, Zhang S, Zeng H, Bray F, et al. Cancer statistics in China, 2015. *CA Cancer J Clin* (2016) 66:115–32. doi:10.3322/caac.21338

2. Sung H, Ferlay J, Siegel RL, Laversanne M, Soerjomataram I, Jemal A, et al. Global cancer statistics 2020: GLOBOCAN estimates of incidence and mortality worldwide for 36 cancers in 185 countries. *CA Cancer J Clin* (2021) 71:209–49. doi:10.3322/caac.21660

3. Kakaei F, Beheshtirouy S, Nejatollahi SM, Zarrintan S, Mafi MR. Surgical treatment of gallbladder carcinoma: A critical review. *Updates Surg* (2015) 67: 339–51. doi:10.1007/s13304-015-0328-x

4. Kanthan R, Senger JL, Ahmed S, Kanthan SC. Gallbladder cancer in the 21st century. *J Oncol* (2015) 2015:967472. doi:10.1155/2015/967472

5. Chan AW, Chan SL, Mo FK, Wong GL, Wong VW, Cheung YS, et al. Albumin-to-alkaline phosphatase ratio: A novel prognostic index for hepatocellular carcinoma. *Dis Markers* (2015) 2015:564057. doi:10.1155/2015/564057

6. Tan P, Xie N, Ai J, Xu H, Xu H, Liu L, et al. The prognostic significance of Albumin-to-Alkaline Phosphatase Ratio in upper tract urothelial carcinoma. *Sci Rep* (2018) 8:12311. doi:10.1038/s41598-018-29833-5

7. Zhang L, Zhang H, Yue D, Wei W, Chen Y, Zhao X, et al. The prognostic value of the preoperative albumin to alkaline phosphatase ratio in patients with non-small cell lung cancer after surgery. *Thorac Cancer* (2019) 10:1581–9. doi:10.1111/1759-7714.13107

8. Zhang F, Lu S, Tian M, Hu K, Chen R, Zhang B, et al. Albumin-to-Alkaline phosphatase ratio is an independent prognostic indicator in combined hepatocellular and cholangiocarcinoma. *J Cancer* (2020) 11:5177–86. doi:10.7150/jca.45633

9. Li S, Lu S, Liu X, Chen X. Association between the pretreatment albumin-to-alkaline phosphatase ratio and clinical outcomes in patients with bladder cancer treated with radical cystectomy: A retrospective cohort study. *Front Oncol* (2021) 11:664392. doi:10.3389/fonc.2021.664392

10. Camp RL, Dolled-Filhart M, Rimm DL. X-Tile: A new bio-informatics tool for biomarker assessment and outcome-based cut-point optimization. *Clin Cancer Res* (2004) 10:7252–9. doi:10.1158/1078-0432.CCR-04-0713

11. Bray F, Ferlay J, Soerjomataram I, Siegel RL, Torre LA, Jemal A. Global cancer statistics 2018: GLOBOCAN estimates of incidence and mortality worldwide for 36 cancers in 185 countries. *CA Cancer J Clin* (2018) 68:394–424. doi:10.3322/caac.21492

12. Kasumova GG, Tabatabaie O, Najarian RM, Callery MP, Ng SC, Bullock AJ, et al. Surgical management of gallbladder cancer: Simple versus extended cholecystectomy and the role of adjuvant therapy. *Ann Surg* (2017) 266:625–31. doi:10.1097/SLA.0000000000002385

13. Zhou T, Yu ST, Chen WZ, Xie R, Yu JC. Pretreatment albumin globulin ratio has a superior prognostic value in laryngeal squamous cell carcinoma patients: A comparison study. *J Cancer* (2019) 10:594–601. doi:10.7150/jca.28817

14. Nojiri S, Joh T. Albumin suppresses human hepatocellular carcinoma proliferation and the cell cycle. *Int J Mol Sci* (2014) 15:5163–74. doi:10.3390/ijms15035163

15. Reebye V, Sætrom P, Mintz PJ, Huang KW, Swiderski P, Peng L, et al. Novel RNA oligonucleotide improves liver function and inhibits liver carcinogenesis *in vivo*. *Hepatology* (2014) 59:216–27. doi:10.1002/hep.26669

16. Shirai Y, Shiba H, Haruki K, Horiuchi T, Saito N, Fujiwara Y, et al. Preoperative platelet-to-albumin ratio predicts prognosis of patients with pancreatic ductal adenocarcinoma after pancreatic resection. *Anticancer Res* (2017) 37:787–93. doi:10.21873/anticanres.11378

17. Chen Z, Shao Y, Yao H, Zhuang Q, Wang K, Xing Z, et al. Preoperative albumin to globulin ratio predicts survival in clear cell renal cell carcinoma patients. *Oncotarget* (2017) 8:48291–302. doi:10.18632/oncotarget.15162

18. He X, Guo S, Chen D, Yang G, Chen X, Zhang Y, et al. Preoperative albumin to globulin ratio (AGR) as prognostic factor in renal cell carcinoma. *J Cancer* (2017) 8: 258–65. doi:10.7150/jca.16525

19. Bağırsakçı E, Şahin E, Atabey N, Erdal E, Guerra V, Carr BI. Role of albumin in growth inhibition in hepatocellular carcinoma. *Oncology* (2017) 93:136–42. doi:10.1159/000471807

20. Zhang H, Ren P, Ma M, Zhu X, Zhu K, Xiao W, et al. Prognostic significance of the preoperative albumin/fibrinogen ratio in patients with esophageal squamous cell carcinoma after surgical resection. *J Cancer* (2021) 12:5025–34. doi:10.7150/jca.58022

21. Gupta D, Lis CG. Pretreatment serum albumin as a predictor of cancer survival: A systematic review of the epidemiological literature. *Nutr J* (2010) 9:69. doi:10.1186/1475-2891-9-69

22. Wheler J, Tsimberidou AM, Moulder S, Cristofanilli M, Hong D, Naing A, et al. Clinical outcomes of patients with breast cancer in a phase I clinic: The M. D. Anderson cancer center experience. *Clin Breast Cancer* (2010) 10:46–51. doi:10.3816/CBC.2010.n.006

23. Lei J, Wang Y, Guo X, Yan S, Ma D, Wang P, et al. Low preoperative serum ALB level is independently associated with poor overall survival in endometrial cancer patients. *Future Oncol* (2020) 16:307–16. doi:10.2217/fon-2019-0732

24. Li YT, Zhou XS, Han XM, Tian J, Qin Y, Zhang T, et al. Pretreatment serum albumin-to-alkaline phosphatase ratio is an independent prognosticator of survival in patients with metastatic gastric cancer. *World J Gastrointest Oncol* (2022) 14:1002–13. doi:10.4251/wjgo.v14.i5.1002

25. Yu MC, Chan KM, Lee CF, Lee YS, Eldeen FZ, Chou HS, et al. Alkaline phosphatase: Does it have a role in predicting hepatocellular carcinoma recurrence. *J Gastrointest Surg* (2011) 15:1440–9. doi:10.1007/s11605-011-1537-3

26. Xu XS, Wan Y, Song SD, Chen W, Miao RC, Zhou YY, et al. Model based on γ-glutamyltransferase and alkaline phosphatase for hepatocellular carcinoma prognosis. *World J Gastroenterol* (2014) 20:10944–52. doi:10.3748/wjg.v20.i31.10944

27. Jin Y, Yuan MQ, Chen JQ, Zhang YP. Serum alkaline phosphatase predicts survival outcomes in patients with skeletal metastatic nasopharyngeal carcinoma. *Clinics (Sao Paulo)* (2015) 70:264–72. doi:10.6061/clinics/2015(04)08

28. Liu L, Xu Y, Jia S, Chen X, He S. Prognostic significance of serum alkaline phosphatase for all-cause mortality in patients with hypertrophic cardiomyopathy: A cohort of the hospitalized population. *Ann Clin Biochem* (2022) 59:387–95. doi:10.1177/00045632221113986

29. Dang C, Deng YH, Qin RY. Prognostic value of ALP and LDH in periampullary carcinoma patients undergoing surgery. *Curr Med Sci* (2022) 42:150–8. doi:10.1007/s11596-021-2452-9

30. Wang Y, Xiong F, Yang J, Xia T, Jia Z, Shen J, et al. Decreased albumin-to-alkaline phosphatase ratio predicted poor survival of resectable gastric cancer patients. *J Gastrointest Oncol* (2021) 12:1338–50. doi:10.21037/jgo-21-430

31. Liu X, Li Y, Zhao Q, Jiang H, Ni J, Cai H. Albumin-to-alkaline phosphatase ratio: A novel prognostic index for patients with driver mutation-negative advanced non-small cell lung cancer. *Clin Respir J* (2021) 15:540–9. doi:10.1111/crj.13339

32. Li J, Zuo M, Zhou X, Xiang Y, Zhang S, Feng W, et al. Prognostic significance of preoperative albumin to alkaline phosphatase ratio in patients with glioblastoma. *J Cancer* (2021) 12:5950–9. doi:10.7150/jca.61866

33. Acikgoz Y, Bal O, Dogan M. Albumin-to-Alkaline phosphatase ratio: Does it predict survival in grade 1 and grade 2 neuroendocrine tumors. *Pancreas* (2021) 50:111–7. doi:10.1097/MPA.0000000000001720

34. Sun L, Ke X, Wang D, Yin H, Jin B, Xu H, et al. Prognostic value of the albumin-to-γ-glutamyltransferase ratio for gallbladder cancer patients and establishing a nomogram for overall survival. *J Cancer* (2021) 12:4172–82. doi:10.7150/jca.49242

Pathology & Oncology Research | frontiers

TYPE Original Research
PUBLISHED 21 April 2023
DOI 10.3389/pore.2023.1611077

Check for updates

OPEN ACCESS

EDITED BY
Andrea Ladányi,
National Institute of Oncology (NIO), Hungary

*CORRESPONDENCE
Aniko Maraz,
dr.aniko.maraz@gmail.com

RECEIVED 24 January 2023
ACCEPTED 04 April 2023
PUBLISHED 21 April 2023

CITATION
Revesz J, Posfai B, Pajor L, Papdan T, Varga L, Paczona VR, Varga Z, Sukosd F and Maraz A (2023), Correlation between fibroblast growth factor receptor mutation, programmed death ligand-1 expression and survival in urinary bladder cancer based on real-world data.
Pathol. Oncol. Res. 29:1611077.
doi: 10.3389/pore.2023.1611077

COPYRIGHT
© 2023 Revesz, Posfai, Pajor, Papdan, Varga, Paczona, Varga, Sukosd and Maraz. This is an open-access article distributed under the terms of the Creative Commons Attribution License (CC BY). The use, distribution or reproduction in other forums is permitted, provided the original author(s) and the copyright owner(s) are credited and that the original publication in this journal is cited, in accordance with accepted academic practice. No use, distribution or reproduction is permitted which does not comply with these terms.

Correlation between fibroblast growth factor receptor mutation, programmed death ligand-1 expression and survival in urinary bladder cancer based on real-world data

Janos Revesz[1], Boglarka Posfai[2], Laszlo Pajor[3], Timea Papdan[2], Linda Varga[2], Viktor R. Paczona[2], Zoltan Varga[2], Farkas Sukosd[4] and Aniko Maraz[2]*

[1]PhD School, University of Szeged, Szeged, Hungary, [2]Department of Oncotherapy, University of Szeged, Szeged, Hungary, [3]Department of Urology, University of Szeged, Szeged, Hungary, [4]Department of Pathology, University of Szeged, Szeged, Hungary

Background: Programmed cell death (PD)-1/PD-ligand 1 (PD-L1) inhibitors have made a breakthrough in the therapy of advanced urothelial bladder cancer (UBC). The impact of Fibroblast Growth Factor Receptor 3 (FGFR3) mutation on the effectiveness of PD-L1 treatment remains still unclear. Objective: Our study aimed to investigate the frequency of FGFR mutations at different tumor stages, and their relation to PD-L1 status and survival.

Methods: 310 patients with urothelial bladder cancer and subsequent radical cystectomy were included in a retrospective study over a 10-year study period at the University of Szeged, Hungary. FGFR3 mutations from the most infiltrative areas of the tumor were analyzed by targeted next-generation sequencing and PD-L1 (28-8 DAKO) tests (tumor positive score -TPS and combined positives score–CPS). In T0 cases FGFR3 mutations were analyzed from the earlier resection samples. Survival and oncological treatment data were collected from the National Health Insurance Fund (NHIF). Neoadjuvant, adjuvant and palliative conventional chemotherapies were allowed; immunotherapies were not. The relationship between the covariates was tested using chi-square tests, and survival analysis was performed using the Kaplan-Meier model and Cox proportional hazards regression.

Abbreviations: CD8, cluster of differentiation 8; CPS, combined positive score; FFPE, formalin-fixed paraffin-embedded; FGFR, fibroblast growth factor receptor; HR, hazard ratio; IHC, immunohistochemistry; LCL, lower control limit; MIBC, muscle-invasive; NGS, next-generation sequencing; NMIBC, non-invasive; NWT, no wild type; OS, overall survival; PCR, polymerase chain reaction; PD-1, programmed cell death-1; PD-L1, programmed cell death-ligand 1; St, stage; TCGA, the cancer genom atlas; TNM, tumour, node, metastasis; TPS, tumor positive score; TUR, transurethral resection; UBC, urothelial bladder cancer; UCL, upper control limit; WT, wild type.

Results: PD-L1 and FGFR could be tested successfully in 215 of the 310 UBC samples [$pT0_{cyst}$ 19 (8.8%); St.0-I 43 (20%); St.II 41 (19%); St.III-IV 112 (52%)]. Significant pairwise dependency was found between tumor stage, FGFR3 mutation status and PD-L1 expression ($p < 0.01$). Samples with FGFR mutation were more common in less advanced stages and were also less likely to demonstrate PD-L1 expression. The effect of all investigated factors on survival was found to correlate with tumor stage.

Conclusion: FGFR alteration frequency varied between the different stages of cancer. Higher positivity rates were observed at early stages, but lower levels of PD-L1 expression were detected in patients with FGFR mutations across at all stages of the disease.

KEYWORDS

urinary bladder cancer, fibroblast growth factor receptor, FGFR mutation, programmed death-ligand 1 expression, combined positive score

Introduction

Bladder cancer is the tenth most common cancer worldwide with approximately 550,000 new cases annually (1). The depth of tumor invasion is the most important prognostic factor from a clinical standpoint and is divided into non-muscle-invasive bladder cancer (NMIBC) and the prognostically less favorable muscle-invasive cancer (MIBC) types (2). The rate of occurrence of MIBC capable of forming distant metastases is 25%–42%, while that of the disseminated stage is 4%–15% (1, 3). Localized MIBCs become disseminated in almost 50% over the course of the disease despite the radical cystectomy or locoregional trimodal therapy (3). In the treatment of advanced disease, for decades only combined chemotherapy was available, with relatively low efficacy and significant toxicity—moreover, molecular markers did not exist for predicting treatment ineffectiveness.

In recent years, checkpoint inhibitor immunotherapy has revolutionised the treatment of advanced urothelial bladder cancer (3). However, the role of potential biomarkers predicting the effectiveness of immunotherapy remains incompletely understood, and many factors that assume an immunogenic mechanism are currently under investigations.

In some studies, the presence of tumor infiltrating lymphocytes such as $CD8^+$ (cluster of differentiation 8) T cells, as well as interferons and chemokines has been found to result in improved response to immunotherapies (4); however the prognostic value of programmed cell death ligand-1 (PD-L1) in urothelial cancer remains controversial (5). Based on several previous analyses, it can be assumed that patients with tumor cells showing PD-L1 positivity have a better response to anti-PD-1/PD-L1 monotherapy (6). The predictive effect of high PD-L1 expression on pembrolizumab immunotherapy has been confirmed in the first-line treatment of metastatic patients unfit for cisplatin (7, 8), as high combined positive score (CPS) of ≥10% was associated with a prolonged median overall survival (OS) (8).

In addition to immune mechanisms, the mutations responsible for bladder tumor progression are also the focus of genetic analyses. The mutation rate of urothelial carcinomas was published in The Cancer Genom Atlas (TCGA), however the possibilities and actual effectiveness of targeted drug treatments against mutations remain low (9). MIBC is a molecularly diverse disease with heterogeneous clinical outcomes (10, 11). Several reports have highlighted the clinical significance of molecular stratification of MIBC. A Consensus Molecular Classification of MIBC identified six different molecular classes with the occurrence of the following possible mutations: luminal papillary (24%)—FGFR3, KDM6A, STAG2; luminal non-specified (8%)—ELF3; luminal unstable (15%)—TP53, ERCC2, TMB+, APCBEC+; stroma-rich (15%), basal/squamous (35%)—EGFR+, TP53+, RB1+; and neuroendocrine-like (3%)—TP53-, RB1, by suggesting that responses to immunotherapy and chemotherapy may be enriched in specific subtypes (10). Because of the molecular heterogeneity of bladder cancer, molecular characterization is a very dynamically developing area.

In recent years, due to the emergence of FGFR inhibitor therapy, the clinical significance of FGFR mutation has come into view. Fibroblast growth factor receptor 3 (FGFR3) is a member of protein tyrosine kinase family, which consists of four transmembrane receptors, (FGFR1–4), and the alteration of the receptors induces an oncogenic signaling pathway (12). The aberrations in FGFR1–4—are detected in 5%–10% of all human cancers, although some types, such as urothelial cancer and intrahepatic cholangiocarcinoma display an increased (10%–30%) frequency of FGFR aberrations. Amongst these aberrations, the FGFR3 activating point mutation is the most frequently occurring one (10%–60%), mainly present in low grade, early stage NMIBC, while FGFR3 fusion and FGFR1 amplification can also occur in 6% and 7%, respectively (13).

However point mutation is rarely associated with MIBC, as nearly the half of advanced stage tumors bear wild-type FGFR3 gene (14). The FGFR pathway is an appealing targeted treatment option, and in the case of its alteration, phase 2 results of the multiple receptor inhibitor erdafitinib therapy are already available (15).

Sweis et al categorised bladder cancer into two subgroups using immune gene profiling; T-cell-inflamed tumors and non-T-cell-inflamed tumors. In the non-T-cell-inflamed subgroup, which is mostly associated with luminal-papillary subtype (or cluster I subtype), they identified some exclusively typical somatic mutation, where FGFR3 was the most common molecular alteration (16, 17). Lower response rates and shortened OS following anti–PD-L1 therapy was observed in patients with FGFR alterations (18).

Based on the published data, the ratio of PD-L1 expression, CPS score, and FGFR expression in each tumor stage is not clear, nor is the prognostic or predictive effect of their relation to each other.

The aim of our study was to demonstrate the frequency of FGFR3 mutation in different tumor stages of cystectomy samples, and to reveal a possible relationship between the FGFR status, PD-L1 status, CPS score, tumour-stages and the survival of patients.

Material and methods

Patients and demographic characterization

Prospective next-generation sequencing (NGS) of tumor tissues, and retrospective collections and analyses of clinical data were performed by the collaboration between University of Szeged, and the Szeged Biology Research Institute, with the use of Hungarian National Health Insurance Fund Database. Enrolled patients were previously diagnosed with urothelial bladder cancer and underwent radical operation during a 10-year period (before the immunotherapy era, between 2006 and 2016) at the University of Szeged, Hungary. Patients were included after partial or radical cystectomy, without known metastatic disease. The indication for the majority of cystectomies was primarily diagnosed muscle invasive transitional cell bladder cancer. In a smaller proportion of cases, extensive, multiple recurrent, non-muscle-invasive tumors were also indications for surgery, based on the guidelines. Neoadjuvant chemotherapy was allowed. The pT0 cases based on cystectomy specimens were called $pT0_{cyst}$. In these cases the biomarker analysis was performed from the initial sampling tissues, but the stage was not redefined based on the less accurate result of the baseline transurethral resection (TUR) samples. Patients were excluded from the current analysis in the following cases: sequenced samples without clinical information or patients with clinical informations without sequencing results; uncertain sequencing outcomes (due to technical reasons); neuroendocrine histology; immunotherapy or anti-FGFR therapy after progression (to avoid a potential influence on survival data).

The main clinical and demographic data included gender, age, stage and previous therapies. The surgical specimen was graded according to WHO classification and staged by the 7th TNM criteria. The patients' basic pathological (histology, pT, pN, demography, age, gender), clinical, oncological treatment and outcome data were collected from the pathological and medical documents of University of Szeged, and the overall survival data from the National Health Insurance Fund database, respectively. All data of patients from different databases were linked at the patient level then de-identified. Overall survival (OS) was defined from the date of cystectomy to the date of death.

Tissue sample testing

Two tests were performed on easch tissue sample. The service provider together with University of Szeged performed FGFR next-generation sequencing (NGS) for mutations and PD-L1 stain with DAKO 28-8 tests.

This sample collection was supplemented with a retrospectively analyzed anonymized patient's follow up database from the medical reports and funder data.

Only the FGFR3 mutation status (wild type -WT, non-wild type—NWT) was recorded, the exact type of mutation (point mutation, deletion, insertion, etc.) was not analyzed. The PD-L1 (IHC) expression level of the samples was given in percentages, and the samples were considered positive if the expression level was at least 1% and negative otherwise.

PD-L1 positivity was defined if the PD-L1 expressed tumor cell count was at least 1% (tumor positive score—TPS). Nowadays, a more relevant CPS score in clinical application has also been defined as the ratio of the number of all PD-L1–expressing cells (tumor cells, lymphocytes, macrophages) to the number of all tumor cells (high level ≥10) (9).

A detailed description of histological and molecular analyses can be found in the Supplementary Material.

Formation of analyzed groups

In our study 392 surgical samples were collected, of which 82 patients were excluded on the basis of insufficient information. The data of 310 patients were considered for analysis. Three subgroups were formed based on possible testing for FGFR, PD-L1 and CPS score: in the first subgroup of patients, FGFR mutation testing of histological samples were performed; in the second subgroup, PD-L1 analysis was available; while in the third subgroup, both tests (PD-L1 and FGFR) were also performed. The data on the interaction of biomarkers and their role in survival were evaluated in the last subgroup in which all results were available (Figure 1).

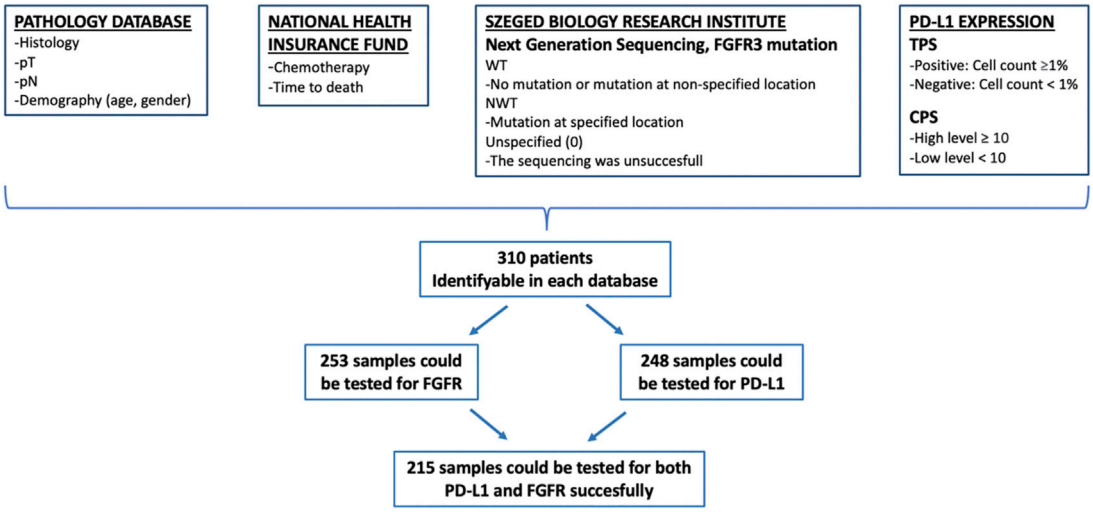

FIGURE 1
Method of data collection. CPS, combined positive score; FGFR, fibroblast growth factor receptor; NWT, non wild type; PD-L1, programmed cell death ligand 1; pN, pathologic lymph node stage; pT, pathologic tumor stage; TPS, tumor positive score; WT, wild type.

Statistical analysis

Demographic data were characterized using gender, median age, TNM stage and different biomarkers. The independence between the stratifying variables was analyzed using chi-square test for independence. Fischer's Exact test was used to examine the relationship between binary variables. P values <0.05 were considered significant.

Survival analysis was performed to analyze overall survival, Kaplan-Meier estimators were used to characterize the survival function. The effect of TNM, FGFR mutation, and PD-L1 expression on overall survival (OS) was evaluated independently using univariate stratification of the Kaplan-Meier estimation. During survival analyses, Bonferroni correction was used for pairwise comparisons in the case of variables with more than 2 groups. Univariate and multivariate (with forward likelihood ratio method) Cox proportional hazard models were used to estimate the effect of certain covariates on the overal survival from cystectomy. The following variables were used in the Cox models as predictors: gender, age of the patient at the time of cystectomy (dichotomized as under 65 years vs. at least 65 years), TNM stage, FGFR mutation (WT/NWT), PD-L1 expression (positive/negative), chemotherapy (yes/no). Model reference values were the following: gender–male, age–lower than 65 years, chemotherapy–no, TNM stage–$pT0_{cyst}$ pN0, FGFR–NWT, PD-L1—negative.

SPSS 25.0 for Windows (SPSS Inc., Chicago, IL, United States) was used for statistical analysis. Survival analyses (Kaplan-Meier plots) were carried out using the statistical software R 4.2.2 (R Core Team 2021).

Results

Baseline characteristics, TNM stage, FGFR and PD-L1 results

The data of 310 patients were considered for analysis, of 236 (76.1%) were male and 74 (23.9%) female. The median age of the entire patient population was 62.8 years, women were slightly younger (median age 61.5 years) than men (median age 63.1 years) (Table 1). 253 samples could be tested for FGFR mutation, 248 samples for PD-L1 and CPS score, and 215 samples for both PD-L1 and FGFR succesfully. The characteristics of the patients were similar in the entire population, as in the further analyzed subgroup in which both biomarkers could be evaluated (Figure 1 and Table 1).

Results of FGFR alteration testing were categorized into subgroups based on the non-wild type or wild type, PD-L1 immunostaining data as TPS negative or positive, and CPS <10 or CPS ≥10, respectively (Table 1).

Test of independence of TNM stage, FGFR and PD-L1 status

There was a strong correlation between TNM stage and FGFR mutation ($p < 0.001$), i.e., higher stage had a lower NWT ratio. The positive PD-L1 rate was significantly ($p = 0.005$) lower in the NWT group (19.4% vs. 44.1%) than in the WT, similar to the CPS ≥10 rate ($p = 0.003$). Significant relationship was also found between stage and PD-L1 expression based on TPS ($p = 0.070$) or CPS ($p = 0.002$), in

TABLE 1 The baseline characteristics.

	All patients (%) [valid %]	Both FGFR and PD-L1 available (%)
Number	310 (100)	215 (69.4 of all pts)
Gender		
Male	236 (76.1)	171 (79.5)
Female	74 (23.9)	44 (20.5)
Age		
Median age (months)	62.8	62.9
Patients over 65 years (%)	112 (36.1)	80 (37.2)
Stage (%)		
$pT0_{cyst}$ pN0	20 (6.5)	19 (8.8)
St.0-I (pTa, pTis, pT1 pN0)	54 (17.4)	43 (20.0)
St.II (pT2a, pT2b pN0)	60 (19.3)	41 (19.1)
St.III-IV (pT3a, pT3b, pT4/pN+)	176 (56.8)	112 (52.1)
Any chemotherapy performed (%)	87 (28.1)	59 (27.4)
Neoadjuvant (NA) chemotherapy (%)	18 (5.8)	12 (5.6)
Any chemotherapy except NA (%)	69 (22.3)	47 (21.8)
FGFR		
Missing or unsuccesful	95 (30.7)	NA
Non-wilde type (NWT)	36 (11.6) [16.7]	36 (16.7)
Wilde type (WT)	179 (57.7) [83.3]	179 (83.3)
PD-L1 (TPS)		
Missing or unsuccesful	62 (20.0)	NA
PD-L1 negative (<1%)	146 (47.1) [58.9]	129 (60.0)
PD-L1 positive (≥1%)	102 (32.9) [41.1]	86 (40.0)
PD-L1 (CPS)		
Missing or unsuccesful	62 (20.0)	NA
CPS < 10	169 (54.5) [68.1]	146 (67.9)
CPS ≥ 10	79 (25.5) [31.9]	69 (32.1)

CPS, combined positive score; FGFR, fibroblast growth factor receptor; NA, not applicable; NWT, non-wilde type; PD-L1, programmed cell death ligand 1; pts, patients; St, stage; TPS, tumor positive score; WT, wilde type.

TABLE 2 Correlations between the FGFR mutation and the TNM stage.

		FGFR alteration		*p*-value
		NWT	WT	
		***n* = 36**	***n* = 179**	
TNM stage	$pT0_{cyst}$ (%)	5 (26.3)	14 (73.7)	**<0.001**
	St.I (%)	16 (37.2)	27 (62.8)	
	St.II (%)	7 (17.1)	34 (82.9)	
	St.III-IV (%)	8 (7.1)	104 (92.9)	

more advanced stages the frequency of PD-L1 positivity was higher (Tables 2–4).

We focused primarily on the correlation between FGFR and PD-L1 (TPS and CPS) status, where we found that the more likely the samples were FGFR mutated, the less likely they were PD-L1 positive. Our results show that TNM stage has a strong significant effect on FGFR mutation and PD-L1 expression.

Effect of TNM stage on survival

Stratifying the patients based on the TNM stage at the time of cystectomy showed that the survival at more advanced stages was worse than at earlier cases. Survival of locally advanced patients with TNM stage III-IV at the time of cystectomy was significantly the most unfavorable factor (median: 17.97 months, $p < 0.001$). Although this is not unexpected, this finding verifies the validity of the model (Figure 2 and Table 5).

Based on the pairwise comparison, we found that the survival of the TNM stage III-IV group was significantly worse compared to the other groups, while no difference could be detected between the groups with a better prognosis.

TABLE 3 Correlations between the FGFR mutation and the PD-L1 expression (TPS, CPS).

		FGFR alteration		*p*-value
		NWT	WT	
		n = 36 (%)	*n* = 179 (%)	
PD-L1 expression (TPS)	Negative (<1%)	29 (80.6)	100 (55.9)	**0.005**
	Positive (≥1%)	7 (19.4)	79 (44.1)	
PD-L1 expression (CPS)	<10	32 (88.9)	114 (63.7)	**0.003**
	≥10	4 (11.1)	65 (36.3)	

TABLE 4 Correlations between the TNM stage and the PD-L1 expression (TPS, CPS).

		PD-L1 expression					
		TPS < 1%	TPS ≥ 1%	*p*-value	CPS < 10	CPS ≥ 10	*p*-value
		n = 129	*n* = 86		*n* = 146	*n* = 69	
TNM stage	$pT0_{cyst}$	12 (63.2)	7 (36.8)	**0.07**	14 (73.7)	5 (26.3)	**0.002**
	St.I	33 (76.7)	10 (23.3)		39 (90.7)	4 (9.3)	
	St.II	24 (58.5)	17 (41.5)		23 (56.1)	18 (43.9)	
	St.III-IV	60 (53.6)	52 (46.4)		70 (62.5)	42 (37.5)	

The effects of analyzed biomarkers on survival

We found that the survival was longer in FGFR positive, mutant (NWT - median OS 56.7 months, 95% CI 38.9-NA), than in FGFR wild type (WT—median OS 23.2 months, 95% CI 15.6–30.9) patients ($p = 0.024$) (Figure 3 and Table 6).

There was no difference detected in median overall survival between patients with PD-L1 positive or negative (30.07 vs. 29.03, $p = 0.81$) based on TPS, and high or low level of CPS (31.63 vs. 29.03, $p = 0.28$) (Figures 4A, B).

Based on our data, FGFR NWT vs. WT was a factor affecting patient survival, while PD-L1 negativity vs. positivity or CPS low vs. high level was not found significant. Our data showed that the stage proved to be a significant independent factor for survival, the close connection with FGFR had no independent effect. As in case of TNM, the independency of these variables were rejected with high probability here too.

The gender (male vs. female, HR: 1.18, $p = 0.52$), age (older than 65 vs. younger, HR: 1.48, $p = 0.07$) of the patients and the chemotherapy use (no versus yes, HR: 0.793, $p = 0.18$) did not affect survival.

There was a significant correlation between all variables (TNM, FGFR status, PD-L1 status). All covariates were associated with TNM stage and their impact on survival is through the TNM stage. It is not possible to evaluate the impact of any of the covariates independently from each other, based on multivariate Cox model the only exception is TNM stage.

Hazard ratios for the covariates in univariate and multivariate analysis from Cox model are summed in Table 7.

Discussion

It is well-known that urothelial tumors of the bladder predominantly develop in older adults, owing to the influence of environmental factors. However, such tumors have begun to appear more and more often in younger age groups (19). In our analysis, the average age of patients was 63 years; 36% were over 65 years old, and women were slightly younger than men.

The standard treatment of muscle-invasive, non-metastatic tumors is cystectomy. Surgery may or may not be preceded by neoadjuvant chemotherapy, depending on eligibility to receive cisplatin (1, 3). Neoadjuvant cisplatin-based chemotherapy results in a 5% benefit in 5-year overall survival and a 9% benefit in 5-year disease-free survival based on a meta-analysis (11 trials, 3,005 patients) (20). Most of our analyzed cases were locally advanced, but the use of chemotherapy was still detected

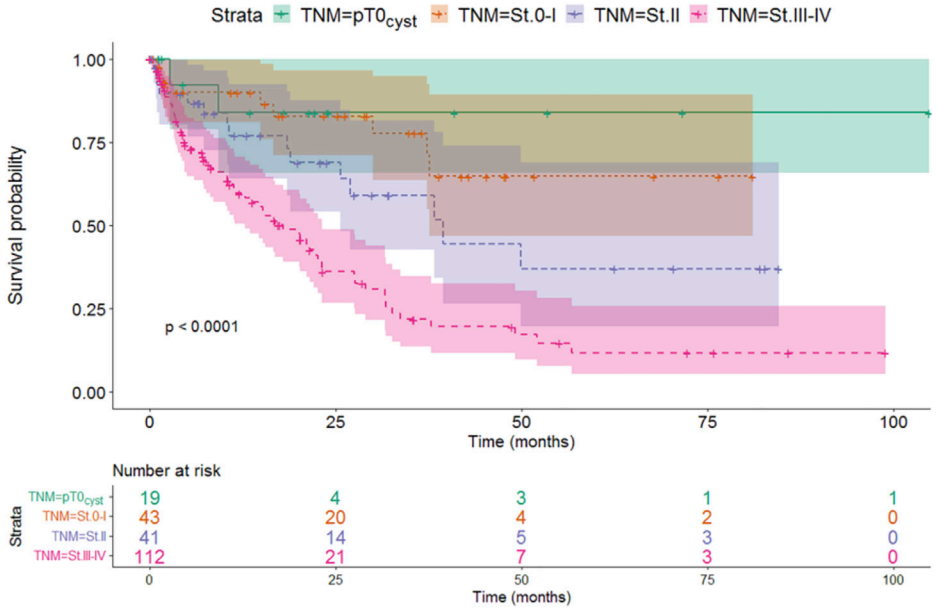

FIGURE 2
The effect of TNM stages on survival.

TABLE 5 Connection with TNM stages and median survival.

TNM stage	Median survival (months)	95% CI LL	95% CI UL	*p*-value
$pT0_{cyst}$	Not reached	NA	NA	<0.001
St.0-I	Not reached	37.86	NA	
St.II	39.50	20.25	58.75	
St.III-IV	17.97	11.98	23.96	

CI, confidence interval; LL, lower limit; St, stage; TNM, Tumor, Node, Metastasis; UL, upper limit.

at a very low rate. This may be due to the fact that in the period covered, the only treatment option available was the toxic platinum-based chemotherapy combination, which generally yielded little success. As a result, it was used with great caution and viewed with skepticism by both patients and urologists (21). In our study, the use of chemotherapy did not provide a survival advantage in the entire population. Since the focus of our work was the investigation of biomarkers and the number of patients receiving chemotherapy was small, it was not possible to search for further relevant correlations related to chemotherapy.

In recent years, the appearance of immunotherapy has been a breakthrough in the treatment of UBC, nowadays clinical trials are also taking place with the use of neoadjuvant indications (22). Radical surgery can also be recommended in the case of multiple recurring, non-muscle invasive tumors, as was the case in 18.7% of our results, if the patient's general condition allowed it (1, 3).

The indication for cystectomy is mainly the muscle invasive diagnosis based on TUR. However, it is possible that tumor tissue is no longer detectable in the cystectomy sample (pT0), e.g., due to the ablative effect of TUR or even the effectiveness of neoadjuvant treatment. The life expectancy of these patients is more favorable based on literature data (23). pT0 tumor status occurred in 6.5% of our samples, the survival of these patients was the best amongst all stages, similar to the international multicenter results of Tilki et al (23).

PD-L1 expression and FGFR alterations are the most frequently investigated biomarkers in connection with the treatment of advanced bladder tumors today, due to the clinical need related to therapeutic options. Immunotherapies are mostly used in advanced urothelial cancer after platinum-based chemotherapy, regardless of biomarker analysis, but they are also effective and approved as a first choice in case of high PD-L1 (CPS–combined positive score or IC–immune cell score)

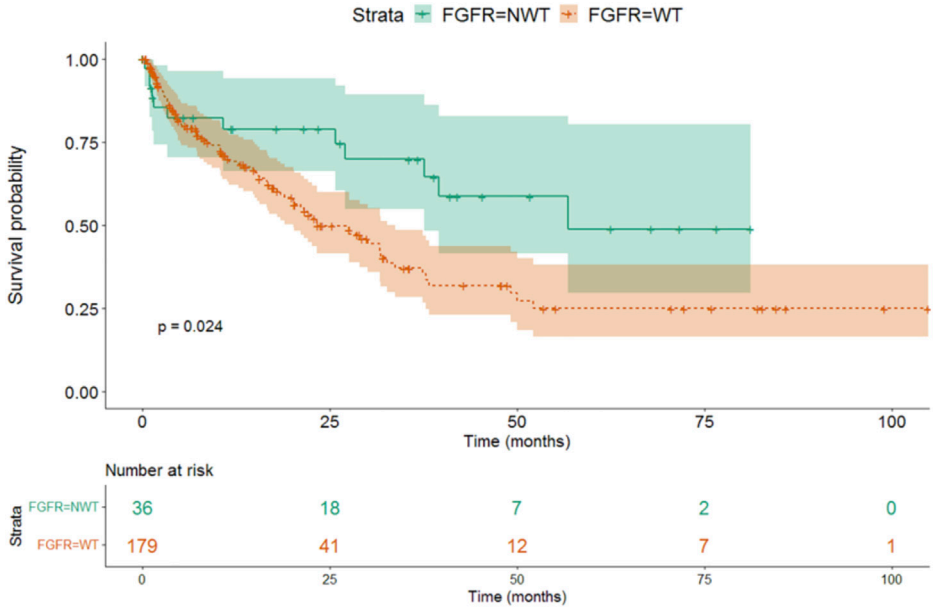

FIGURE 3
The effect of different FGFR mutations on survival.

TABLE 6 Connection with FGFR mutations and median survival.

FGFR	Median survival (months)	95% CI LL	95% CI UL	*p*-value
NWT	56.73	38.95	NA	0.024
WT	23.23	15.59	30.87	

CI, confidence interval; FGFR, fibroblast growth factor receptor; LL, lower limit; NA, not available; NWT, non-wild type; WT, wild type; UL, upper limit.

status (1, 3). In our work, PD-L1 status was determined based on TPS and CPS as well. Their effect on the outcome of the disease had a similar prognostic value. PD-L1 expression on urothelial tumor cells was associated with muscle-invasive disease and with worse overall survival (24).

TCGA project supports the high molecular heterogenity of MIBC such as in non-small cell lung cancer and in melanoma (25). The most common form of bladder cancer is NMIBC at diagnosis. Histologically these tumors are papillary tumors, they recur in more than the half of the cases, but have rare progression tendency (26). Approximately 70% of low-grade non-invasive papillary tumors show FGFR3 mutation in literature (27). In our study, patients with superficial bladder tumors (20%) who underwent cystectomy were included after a recurrence or if the disease could not be controlled by transurethral resection. Even in this higher-risk superficial group, the proportion of FGFR mutant patients was 37.2%, lower than in published data, but higher than in our analyzed muscle-invasive or locally advanced group (30). The strongest correlation could be observed between TNM stage and FGFR mutation. Our results represent the high frequency of FGFR3 mutation in earlier stages. Previous studies support our data, and it has been demonstrated that over half of pTa tumors recur, accordingly FGFR alteration is a possible signaling pathway in the development of these tumors (27). Compared to the literature (26), our findings suggest an oncogenic relationship, as FGFR3 mutation is mostly seen in non-invasive tumors, and less frequently at more advanced stages. Fernandez et al. found FGFR genomic alterations as an independent factor associated with the survival and as a relevant biomarker of mUC that may influence response to systemic therapy (28).

Advanced stage tumors have worse survival than early stage, and stratifying the patients according to TNM stage, we found also significant difference in survival from cystectomy between NWT and WT patients. Our data is similar to other published results that have reported an association between favorable prognosis and FGFR mutation status (29). The real prognostic effect of FGFR mutation is questionable because of the strong

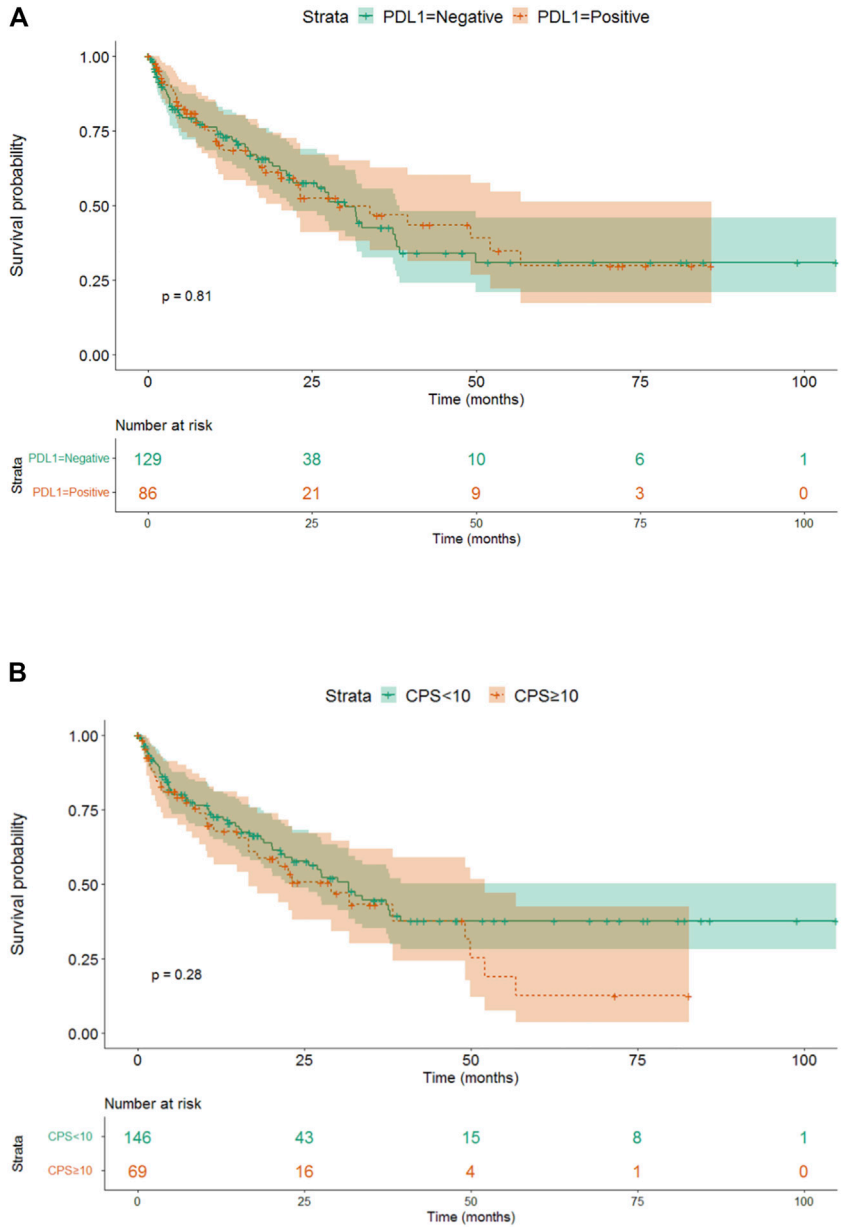

FIGURE 4
(A) The effect of different 256 PD-L1 expressions (TPS) on survival. **(B)** The effect of different PD-L1 expressions (CPS) on survival.

correlation with low stage tumors. Based on our results, FGFR alteration is not an independent prognostic parameter for survival, but occurs more often at lower stages, which is why it affects the overall survival of patients through the stage.

We detected across TNM stages that tumors with high ratio of FGFR3 mutation are less likely associated with positive PD-L1 expression. Regarding the covariates examined with the cox regression model, we found that their occurrence is not independent of each other. Based on the results obtained, a very strong correlation could be identified between the individual parameters, but the database analysis method and the limited number of elements found in each subgroup did not allow the matching of the individual elements and the adjustment of the data.

Even if there is an assumable connection between these results, there is no clear evidence that FGFR3 alteration would enhance a resistance mechanism against immune checkpoint inhibitors. Some previous studies verified mutated FGFR3 with increased FGFR3 gene expression and an association with decreased T-cell infiltration, but in this publication there was no significant difference in response rate or OS with

TABLE 7 Hazard ratios for the covariates in univariate and multivariate analysis.

Covariate	Univariate				Multivariate			
	HR	95% CI LL	95% CI UL	*p*-value	HR	95% CI LL	95% CI UL	*p*-value
TNM stage								
$pT0_{cyst}$	References							
St.0-I	1.612	0.348	7.469	0.541	1.612	0.348	7.469	0.541
St.II	3.156	0.721	13.803	0.127	3.156	0.721	13.803	0.127
St.III-IV	6.812	1.665	27.857	0.008	6.812	1.665	27.857	0.008
FGFR								
NWT	References							
WT	1.997	1.082	3.685	0.027	NA			0.718
PD-L1								
TPS < 1%	References							
TPS ≥ 1%	1.052	0.693	1.596	0.813	NA			0.231
CPS < 10	References							
CPS ≥ 10	1.265	0.825	1.938	0.281	NA			0.776

CI, confidence interval; CPS, combined positive score; FGFR, fibroblast growth factor receptor; HR, hazard ratio; LL, lower limit; NA, not available; NWT, non-wild type; PD-L1, programmed cell death ligand 1; St, stage; UL, upper limit; WT, wild type.

immunecheckpoint inhibitors in FGFR3 separated groups, possibly due to the lower stromal-mediated immune suppression (17). The controversial manifestation of FGFR3 and PD-L1 in various stages of the examined cystectomic samples in our study suggest a deeper stratification in molecular and immunological status in urothelial carcinomas.

The T-cell based subtyping of bladder cancers shows that tumors with high FGFR3 expression are associated with lower T-cell infiltration based on the count of the $CD8^+$ T-cells (16). These findings may propose a negative or immunosuppressive effect of FGFR3 alterations on T-cell gene mechanism. Based on one of the latest retrospective analyses with a relatively high number of patients available in the literature, a lower response rates and shorter OS was observed in patients with FGFR alteratations following anti-PD-L1 immunotherapy (18).

Our aim was to investigate whether FGFR mutation is a possible independent prognostic factor of survival. Reflect on many controversial survival and response data in the anti-PD-L1 treated FGFR mutated patient group (15, 18, 30–33), according to other studies we consider a larger investigation of special non-invasive subtypes to be necessary in order to verify its predictive and prognostic value. In addition, we consider it forward-looking waiting for the results of the phase 3 prospective THOR (NCT03390504) study, which compares the effects of erdafitinib and pembrolizumab in patients with advanced mUC, to clarify the real therapeutic significance of FGFR alterations (34).

Limitations of our study include that we could not obtain retrospective relevant clinical data in almost 1/3 of the cystectomized patients, and molecular analysis was unsuccessful in 15% of the samples suitable for FGFR analysis. Another limitation is that although a strong correlation was detected between the individual investigated parameters, due to the limited number of elements of each subgroup, and the type of database analysis method, matching the individual elements and the adjustment of the data was not feasible.

The strength of our work is that it processes the real-life results of a relatively large number of bladder tumor patients who have undergone cystectomy (35). Another advantage of our work is that we also evaluated the CPS data in relation to PD-L1 expression, used better in the daily practice during first line immunotherapies nowadays, which would provide the opportunity for further potentially predictive conclusions. It should also be emphasized that it was possible to connect the data available in the clinical and pathological medical systems precisely and individually with the survival results available in the funder's database, thus facilitating the accuracy of our work.

Our results highlight the high FGFR alteration rate in non-muscle invasive tumors, thereby pointing to a potentially new area for future analysis of the effect of FGFR inhibitors. The higher rate of PD-L1 expression in more advanced stages also confirms the immune mechanism of bladder tumors. Although the survival of FGFR mutant patients was more favorable than wild-type, this effect was established through the tumor stage.

In summary, based on all of our results, the role of tumor stage can be highlighted as the strongest survival factor in this group of patients.

While molecular subtyping of urothelial cancers has yet to find its exact place in managing the disease, more and more data are being collected on the molecular profile of each subtype. The goal of newer clinical trials is to combine immunotherapy with modern, antigen-drug conjugates, and to find a place for targeted therapies against individual genetic abnormalities. Although immunotherapy is now the standard treatment for UBC, the frequency of FGFR3 alterations in NMIBC underscores the importance of a new molecular classification for the future of targeted therapy. FGFR inhibitors may represent an additional solution in the treatment of urothelial cancer, perhaps in a possible combination of immune and molecularly targeted therapies, or in halting the progression of early-stage FGFR-mutant tumors.

Data availability statement

The raw data supporting the conclusion of this article will be made available by the authors, without undue reservation.

Ethics statement

"The genetic classification of urinary bladder cancer and research on molecular diagnostic and prognostic markers" study had the permission of the Hungarian Medical Research Council under (1011/16, 2017/EKU and 20090/2016 EKU) numbers. The samples were anonymized according to the Bio Bank Regulation (250/C-2/2017K.K) of the University of Szeged.

Author contributions

Study concept: AM, FS, LP, and JR; study design: AM, FS, and LP; data acquisition: JR, BP, TP, LV, AM, and FS; quality control of data and algorithms: AM and ZV; data analysis and interpretation: ZV, AM, and FS; statistical analysis: ZV; manuscript preparation: JR, BP, TP, LV, VP, ZV, FS, and AM; editing: JR, BP, ZV, and AM; manuscript review: JR, BP, LP, ZV, FS, and AM.

Funding

University of Szeged Open Access Fund Grant Number 6080 supported the publication of the manuscript, Janssen-Cilag Hungary and Janssen EMEA supported the FGFR mutation analysis.

Conflict of interest

The authors declare that the research was conducted in the absence of any commercial or financial relationships that could be construed as a potential conflict of interest.

Supplementary material

The Supplementary Material for this article can be found online at: https://www.por-journal.com/articles/10.3389/pore.2023.1611077/full#supplementary-material

References

1. Richters A, Aben KKH, Kiemeney LALM. The global burden of urinary bladder cancer: An update. *World J Urol* (2020) 38:1895–904. doi:10.1007/s00345-019-02984-4

2. Witjes JA, Bruins HM, Cathomas R, Hernández V, Neuzillet Y, Compérat EM, et al. The importance of hospital and surgeon volume as major determinants of morbidity and mortality after radical cystectomy for bladder cancer: A systematic review and recommendations by the European association of urology muscle-invasive and metastatic bladder cancer guideline panel. *Eur Urol Oncol* (2020) 3:131–44. doi:10.1016/j.euo.2019.11.005

3. Flaig TW, Spiess PE, Abern M. *NCCN Guidelines® insights: Bladder cancer* (2022). Version 2.2022. doi:10.6004/jnccn.2022.0041

4. Gajewski TF, Woo SR, Zha Y, Spaapen R, Zheng Y, Corrales L, et al. Cancer immunotherapy strategies based on overcoming barriers within the tumor microenvironment. *Curr Opin Immunol* (2013) 2:268–76. doi:10.1016/j.coi.2013.02.009

5. Ding X, Chen Q, Yang Z, Li J, Zhan H, Lu N, et al. Clinicopathological and prognostic value of PD-L1 in urothelial carcinoma: A meta-analysis. *Cancer Manag Res* (2019) 11:4171–84. doi:10.2147/CMAR.S176937

6. Liu J, Zhang C, Hu J, Tian Q, Wang X, Gu H, et al. Effectiveness of anti-PD-1/PD-L1 antibodies in urothelial carcinoma patients with different PD-L1 expression levels: A meta-analysis. *Oncotarget* (2018) 9:12400–7. doi:10.18632/oncotarget.24249

7. Balar AV, Castellano D, O'Donnell PH, Grivas P, Vuky J, Powles T, et al. First-line pembrolizumab in cisplatin-ineligible patients with locally advanced and unresectable or metastatic urothelial cancer (KEYNOTE-052): A multicentre, single-arm, phase 2 study. *Lancet Oncol* (2017) 18:1483–92. doi:10.1016/S1470-2045(17)30616-2

8. O'Donnell PH, Balar AV, Vuky J, Bellmunt J, Powles T, Bajorin DF, et al. First-line pembrolizumab (pembro) in cisplatin-ineligible patients with advanced urothelial cancer (UC): Response and survival results up to five years from the KEYNOTE-052 phase 2 study. *JCO* (2021) 39:4508. doi:10.1200/JCO.2021.39.15_suppl.4508

9. Cancer Genome Atlas Research Network. Comprehensive molecular characterization of urothelial bladder carcinoma. *Nature* (2014) 507:315–22. doi:10.1038/nature12965

10. Kamoun A, de Reynies A, Allory Y, Sjödahl G, Robertson AG, Seiler R, et al. A Consensus molecular classification of muscle-invasive bladder cancer. *Cancer Eur Urol* (2020) 77:420–33. doi:10.1016/j.eururo.2019.09.006

11. Robertson AG, Kim J, Al-Ahmadie H, Bellmunt J, Guo G, Cherniack AD, et al. Comprehensive molecular characterization of muscle-invasive bladder cancer. *Cel* (2017) 171:540–56.e25. doi:10.1016/j.cell.2017.09.007

12. Turner N. Fibroblast growth factor signalling: From development to cancer. *Nat Rev Cancer* (2010) 10:116–29. doi:10.1038/nrc2780

13. Krook MA, Reeser JW, Barker H, Wilberding M, Li G. Fibroblast growth factor receptors in cancer: Genetic alterations, diagnostics, therapeutic targets and mechanisms of resistance. *Br J Cancer* (2021) 124:880–92. doi:10.1038/s41416-020-01157-0

14. di Martino E, Tomlinson DC, Williams SV, Knowles MA. A place for precision medicine in bladder cancer: Targeting the FGFRs. *Future Oncol* (2016) 12:2243–63. doi:10.2217/fon-2016-0042

15. Siefker-Radtke A, Necchi A, Rosenbaum E, Culine S, Burgess EF, O'Donnell PH, et al. Efficacy of programmed death 1 (PD-1) and programmed death 1 ligand (PD-L1) inhibitors in patients with FGFR mutations and gene fusions: Results from

a data analysis of an ongoing phase 2 study of erdafitinib (JNJ-42756493) in patients (pts) with advanced urothelial cancer (UC). *J Oncol* (2018) 36:450. doi:10.1200/jco.2018.36.6_suppl.450

16. Sweis RF, Spranger S, Bao R, Paner GP, Stadler WM, Steinberg G, et al. Molecular drivers of the non-T-cell-inflamed tumor microenvironment in urothelial bladder cancer. *Cancer Immunol Res* (2016) 4:563–8. doi:10.1158/2326-6066.CIR-15-0274

17. Wang L, Gong Y, Saci A, Szabo PM, Martini A, Necchi A, et al. Fibroblast growth factor receptor 3 alterations and response to PD-1/PD-L1 blockade in patients with metastatic urothelial cancer. *Eur Urol* (2019) 76:599–603. doi:10.1016/j.eururo.2019.06.025

18. Kalebasty AR, Benjamin DJ, Loriot Y, Papantoniou D, Siefker-Radtke AO, Necchi A, et al. Outcomes of patients with advanced urothelial carcinoma after anti-programmed death-(ligand) 1 therapy by fibroblast growth factor receptor gene alteration status: An observational study. *Eur Urol Open Sci* (2023) 47:48–57. doi:10.1016/j.euros.2022.11.001

19. Palumbo C, Pecoraro A, Rosiello G, Luzzago S, Deuker M, Stolzenbach F, et al. Bladder cancer incidence rates and trends in young adults aged 20-39 years. *Urol Oncol Semin Orig* (2020) 38:934.e11–934.934.e19. doi:10.1016/j.urolonc.2020.06.009

20. Yin M, Joshi M, Meier RP, Glantz M, Holder S, Harvey HA, Neoadjuvant chemotherapy for muscle-invasive bladder cancer: A systematic review and two-step meta-analysis. *Oncologist*, 21 (2016). p. 708–15. doi:10.1634/theoncologist.2015-0440

21. Maráz A, Varga L, Pósfai B, Géczi L, Küronya Z. New aspects of chemotherapy and indications for maintenance immuno-therapy in urothelial cancers. *Magy Onkol* (2021) 65:329–37.

22. Necchi A, Raggi D, Gallina A, Madison R, Colecchia M, Lucianò R, et al. Updated results of PURE-01 with preliminary activity of neoadjuvant pembrolizumab in patients with muscle-invasive bladder carcinoma with variant histologies. *Eur Urol* (2020) 77:439–46. doi:10.1016/j.eururo.2019.10.026

23. Tilki D, Svatek RS, Novara G, Seitz M, Godoy G, Karakiewicz PI, et al. Stage pT0 at radical cystectomy confers improved survival: An international study of 4,430 patients. *J Urol* (2010) 184:888–94. doi:10.1016/j.juro.2010.04.081

24. Ding X, Chen Q, Yang Z, Li J, Zhan H, Lu N, et al. Clinicopathological and prognostic value of PD-L1 in urothelial carcinoma: A meta-analysis. *Cancer Manag Res* (2019) 11:4171–84. doi:10.2147/CMAR.S176937

25. Lawrence MS, Stojanov P, Polak P, Kryukov GV, Cibulskis K, Sivachenko A, et al. Mutational heterogeneity in cancer and the search for new cancer-associated genes. *Nature* (2013) 499:214–8. doi:10.1038/nature12213

26. Billerey C, Chopin D, Aubriot-Lorton MH, Ricol D, Gil Diez de Medina S, Van Rhijn B, et al. Frequent FGFR3 mutations in papillary non-invasive bladder (pTa) tumors. *Am J Pathol* (2001) 158:1955–9. doi:10.1016/S0002-9440(10)64665-2

27. Kawahara T, Kojima T, Kandori S, Kurobe M, Yoshino T, Kimura T, et al. TP53 codon 72 polymorphism is associated with FGFR3 and RAS mutation in non-muscle-invasive bladder cancer. *PLoS One* (2019) 14:e0220173. doi:10.1371/journal.pone.0220173

28. Fernández S, Lacalle M, Moreno R, Barquín García A, Yagüe Fernández M, Navarro Alcaraz P, et al. Prognostic value and clinical significance of FGFR genomic alterations (GAs) in metastatic urothelial cancer patients. *J Clin Med* (2022) 11:4483. doi:10.3390/jcm11154483

29. Hernández S, López-Knowles E, Lloreta J, Kogevinas M, Amorós A, Tardón A, et al. Prospective study of FGFR3 mutations as a prognostic factor in nonmuscle invasive urothelial bladder carcinomas. *J Clin Oncol* (2006) 24:3664–71. doi:10.1200/JCO.2005.05.1771

30. Casadei C, Dizman N, Schepisi G, Cursano MC, Basso U, Santini D, et al. Targeted therapies for advanced bladder cancer: New strategies with FGFR inhibitors. *Ther Adv Med Oncol* (2019) 11:1758835919890285. doi:10.1177/1758835919890285

31. Kim J, Kwiatkowski D, McConkey DJ, Meeks JJ, Freeman SS, Bellmunt J, et al. The cancer genome Atlas expression subtypes stratify response to checkpoint inhibition in advanced urothelial cancer and identify a subset of patients with high survival probability. *Eur Urol* (2019) 75(6):961–4. doi:10.1016/j.eururo.2019.02.017

32. Joerger M, Cassier P, Penel N, Cathomas R, Richly H, Schostak M, et al. Rogaratinib treatment of patients with advanced urothelial carcinomas prescreened for tumor FGFR mRNA expression. *J Clin Oncol* (2018) 36(6):494. doi:10.1200/jco.2018.36.6_suppl.494

33. Kim WJ, Rose TL, Roghmann F, Eckstein M, Jarczyk J, Zengerling F, et al. Predictive value of fibroblast growth factor receptor (FGFR) alterations on anti-PD-(L)1 treatment outcomes in patients (Pts) with advanced urothelial cancer (UC): Pooled analysis of real-world data. *J Clin Oncol* (2020) 38(6):493. doi:10.1200/jco.2020.38.6_suppl.493

34. Loriot Y, Necchi A, Park SH, Huddart R, Burgess E, Zhong B, et al. Erdafitinib compared with vinflunine or docetaxel or pembrolizumab in patients (pts) with metastatic or surgically unresectable (M/UR) urothelial carcinoma (UC) and selected fgfr gene alterations (FGFRalt): The phase III THOR study. *Ann Oncol* (2018) 29:viii327–8. doi:10.1093/annonc/mdy283.129

35. Maraz A, Takacs P, Lawson J, Santiago-Walker A, Pajor L, Sukosd F, et al. Correlation between FGFR mutation and PD-L1 expression of urinary bladder cancers: A real-world based biomarker study. *J Clin Oncol Oncol* (2019) 37:e16030. doi:10.1200/jco.2019.37.15_suppl.e16030

Pathology & Oncology Research | frontiers

TYPE Original Research
PUBLISHED 21 June 2023
DOI 10.3389/pore.2023.1611157

Check for updates

OPEN ACCESS

EDITED BY
József Tímár,
Semmelweis University, Hungary

*CORRESPONDENCE
Sarolta Molnár,
molnar.sarolta@med.unideb.hu

RECEIVED 28 February 2023
ACCEPTED 12 June 2023
PUBLISHED 21 June 2023

CITATION
Korpás KL, Beke L, Varga D, Bidiga L, Méhes G and Molnár S (2023), Grade Group accuracy is improved by extensive prostate biopsy sampling, but unrelated to prostatectomy specimen sampling or use of immunohistochemistry.
Pathol. Oncol. Res. 29:1611157.
doi: 10.3389/pore.2023.1611157

COPYRIGHT
© 2023 Korpás, Beke, Varga, Bidiga, Méhes and Molnár. This is an open-access article distributed under the terms of the Creative Commons Attribution License (CC BY). The use, distribution or reproduction in other forums is permitted, provided the original author(s) and the copyright owner(s) are credited and that the original publication in this journal is cited, in accordance with accepted academic practice. No use, distribution or reproduction is permitted which does not comply with these terms.

Grade Group accuracy is improved by extensive prostate biopsy sampling, but unrelated to prostatectomy specimen sampling or use of immunohistochemistry

Kristóf Levente Korpás[1], Lívia Beke[1], Dániel Varga[2], László Bidiga[1], Gábor Méhes[1] and Sarolta Molnár[1]*

[1]Department of Pathology, Clinical Centre, University of Debrecen, Debrecen, Hungary, [2]Department of Urology, Clinical Centre, University of Debrecen, Debrecen, Hungary

Assessing the accurate Grade Group of a prostate needle biopsy specimen is essential for choosing the adequate therapeutic modality for prostate cancer patients. However, it is well-known that biopsy Grade Group tends to up- or downgrade significantly at radical prostatectomy. We aimed to investigate the correlation between accuracy and biopsy core number, performed immunohistochemical staining (IHC) or prostatectomy specimen sampling, with the latest also being correlated with higher detection rates of adverse pathological features, e.g., positive surgical margins, higher pathological stage or presence of perineural invasion (PnI status). The study cohort consisted of 315 consecutive patients diagnosed with prostate adenocarcinoma via transrectal ultrasound-guided needle biopsy who later underwent radical prostatectomy. We grouped and compared patients based on Grade Group accuracy, presence of IHC on biopsy, margin status, pathological stage, and PnI status. Inter-observer reproducibility was also calculated. Statistical analyzes included ANOVA, Tukey's multiple comparisons *post hoc* test, Chi-squared test, and Fleiss kappa statistics. Undergraded cases harboured a significantly lower number of biopsy cores ($p < 0.05$), than accurately graded cases. Using IHC did not affect grading accuracy significantly, nor did the number of slides from prostatectomy specimens. The mean number of slides was virtually identical when margin status, pathological stage and PnI status of prostatectomy specimens were compared. Inter-observer reproducibility at our institute was calculated as fair (overall kappa = 0.29). Grade Group accuracy is significantly improved by obtaining more cores at biopsy but is unrelated to performed IHC. The extent of sampling prostatectomy specimens, however, did not affect accuracy and failed to significantly improve detection of adverse pathological features.

Abbreviations: AMACR, α-methylacyl-CoA racemase; GG, Grade Group; IHC, immunohistochemistry; ISUP, International Society of Urological Pathologists; RP, radical prostatectomy.

KEYWORDS
prostate cancer, needle biopsy, prostatectomy, grade group, pathology

Introduction

In 2020, prostate cancer was the second most commonly diagnosed malignancy of males; with the repertoire of screening and treating modalities available today, 375,304 deaths were still reported worldwide [1]. Nowadays, diagnoses are almost exclusively made early, following the revolutionary introduction of prostate-specific antigen screening in the late eighties. Treatment options for localized or locally advanced prostate cancer include hormonal ablation therapy, radiotherapy and radical prostatectomy (RP). Guidelines indicate choosing a treatment modality based on the patient's risk for disease progression: RP is the gold standard for high-risk patients, while it is most beneficial for low- or very low-risk patients to choose active surveillance. Besides clinical stage, PSA level and comorbidity-adjusted life expectancy, the pathological grade is a primary determinant of patient risk [2]. For the assessment of pathological grade, the Gleason score-based Grade Group system established at the 2014 International Society of Urological Pathology (ISUP) Consensus Conference is used, primarily on needle biopsy specimens [3]. Recent papers suggest that Grade Group (GG) is likely to be a static parameter set early in tumorigenesis, and grade progression is uncommon [4, 5]. However, the question of grade progression has remained controversial [6, 7].

It is beneficial, if not essential, to perform immunohistochemical staining on biopsy samples to ensure the spotting of malignant glands. The most commonly used target antigens are basal cell markers p63 and 34βE12 and neoplastic acinar cell marker α-methylacyl-CoA racemase (AMACR) [8]. For patients undergoing RP, post-RP treatment depends on various clinical and pathological data, including pathological stage, surgical margin status, and final GG.

In the present study, we aimed to see whether an extended number of cores obtained at biopsy, extended RP specimen sampling or performing AMACR/34βE12/p63 IHC on biopsy specimens improves concordance between biopsy and RP GGs. In addition, we hypothesized that extended specimen sampling at pathology results in a higher detection rate of adverse features, e.g., positive surgical margins, perineural invasion, and higher pathological stage (presence of extraprostatic extension or seminal vesicle invasion).

At our institute and in most community settings, biopsy samples are taken by several urologists and evaluated by numerous general pathologists; thus, inter-observer reproducibility frequently biases the accurate grading of biopsy or RP samples. That is why our aims included calculating the inter-observer reproducibility at our institute and identifying morphological pitfalls that could lead to over- or undergrading different prostate samples.

Materials and methods

Study settings

In this retrospective study, we analyzed data of men diagnosed with prostatic adenocarcinoma via transrectal ultrasound-guided needle biopsy who later underwent RP at our institute during the period from January 2016 to November 2021. Cases with pre-RP neoadjuvant treatment and more than 1 year between biopsy and RP were excluded. Eventually, a total of 315 consecutive cases met the inclusion criteria. These cases were then grouped based on the concordance between biopsy and RP GGs into accurately graded (n = 143), undergraded (n = 153) and overgraded (n = 19) groups. We compared the number of obtained biopsy cores, presence of IHC on biopsy and multiple factors regarding RP specimens (e.g., slide number, specimen weight, slide/weight ratio, largest tumor diameter) in these three groups. The number of slides was also correlated with adverse pathological features, e.g., presence of positive surgical margin, perineural invasion and higher pT stage. The correction factor for whole-mount slides was 3 (the mean area of tissue embedded in a whole-mount slide equaled three standard slides).

Regarding the RP specimen, the method of processing (total versus partial embedding) was correlated with the weight of the RP specimen and the greatest diameter of the largest tumor nodule. Despite the small number of totally processed cases (n = 14), significant differences were found between the two processing methods regarding both parameters. Due to these findings, totally embedded cases were excluded from the statistics regarding specimen sampling, and statistics were done only on partially embedded cases (n = 301) to prevent bias of the processing method. As a pre-test analysis to assess whether slide number can be considered an independent variable, it was correlated with the weight of the RP specimen and the greatest diameter of the largest tumor nodule, as one can assume that the extent of the embedding is biased by these two parameters. R^2 values from both tests indicated no significant correlation with either parameter (Supplementary Figure S1).

Biopsy procedure

Transrectal ultrasound-guided biopsies were taken using DP-8800 Plus ultrasound machine (Mindray, Shenzhen, Guangdong, China) with an end-fired 7.5 MHz ultrasound probe. The spring-loaded core biopsy gun was equipped with an 18 G needle and notch length of 15 mm. Prior to the procedure, antibiotic prophylaxis with ciprofloxacin was given.

Pathological processing

Biopsy samples were received in 4% phosphate-buffered formaldehyde solution (cat. no.: HT501640-19L, Sigma-Aldrich Chemie GmbH, Taufkirchen, Germany) mainly in two containers per patient, with cores from each prostate lobe. Cores were transferred into two cassettes and underwent routine formalin-fixed paraffin-embedded processing. 3 μm sections were then made on silanized slides from the selected blocks, stained with hematoxylin and eosin and microscopically evaluated by one of ten general pathologists. Ancillary testing was optional. Histopathological report included the diagnosis, number of cores sent, number of cores containing tumor, GG, estimated percentage of tumor volume in the biopsy specimen, and adverse features, if present. When both lobes were tumorous, the highest GG was reported.

RP specimens were fixed in 4% phosphate-buffered formaldehyde solution overnight, measured and inked. The prostate was sliced in the plane perpendicular to the urethra. Apical and basal (bladder neck) resection margin was then sliced in the sagittal plane and embedded entirely. From this point there was no departmental protocol for further processing of RP specimens, however only 14 RP specimens were totally and 301 partially embedded. Vast majority of partially processed specimens were embedded at least in 50%. Slides were then submitted for further histopathological evaluation. 3 μm sections were hematoxylin and eosin-stained and microscopically evaluated by one of ten general pathologists. Pathological report included size of prostate, the number and location of tissue blocks, tumor focality, localization and size, the estimated percentage of tumor volume in the specimen, histological diagnosis, GG, presence or absence of adverse features (intraductal carcinoma, capsule infiltration, extraprostatic extension and its localization, bladder neck, seminal vesicle, lymphovascular and perineural invasion), surgical margin status and pathological stage.

Immunohistochemistry

We also analyzed the effect of IHC on GG accuracy. Either single AMACR, 34βE12, p63 staining or a dual or triple cocktail of those was performed. For simplicity purposes, the triple staining protocol is described herein. Routine formalin-fixed paraffin-embedded processing of biopsy samples was done as detailed earlier. Immunohistochemical staining was performed in a BenchMark Ultra immunostaining machine (Roche Diagnostics GmbH, Penzberg, Germany). The deparaffinization of the sections was automated. Antigen retrieval was performed in Cell Conditioning Solution (ULTRA CC1) Tris-based buffer (pH 8.5, cat. no.: 950-224, Roche Diagnostics GmbH, Penzberg, Germany) for 48 min at 100°C. IHC staining started with p63 mouse monoclonal antibody (clone: DAK-p63, cat. no.: M731701-2, Dako, an Agilent Technologies Company, Glostrup, Denmark) and 34βE12 mouse monoclonal antibody (clone: 34βE12, cat. no.: M063001-2, Dako, an Agilent Technologies Company, Glostrup, Denmark) cocktail at a dilution of 1/200 for both p63 and 34βE12. The incubation lasted for 48 min at 37°C. The immunohistochemical reaction was detected with OptiView DAB IHC Detection kit (cat. no.: 760–700, Roche Diagnostics GmbH, Penzberg, Germany). After the first IHC staining, incubation was continued with AMACR mouse monoclonal antibody (clone: 13H4, cat. no.: M361601-2, Dako, an Agilent Technologies Company, Glostrup, Denmark) at a dilution of 1/200. The sections were detected using the ultraView Universal Alkaline Phosphatase Red Detection Kit (cat. no.: 05269814001, Roche Diagnostics GmbH, Penzberg, Germany), and overstaining was done using Hematoxylin II solution (cat. no.: 790–2208, Roche Diagnostics GmbH, Penzberg, Germany) according to the manufacturer's instructions.

Inter-observer reproducibility

To assess inter-observer reproducibility, three pathologists evaluated GGs of 20 consecutive prostate biopsies with 12 cores from the study cohort. Only the final given GG of each case was considered. The degree of agreement was defined as *Landis et Koch* described: a kappa value of <0 indicates no agreement, 0–0.20 indicates slight, 0.21–0.40 indicates fair agreement, while a kappa value of 0.41–0.60 means moderate, 0.61–0.80 means substantial, and 0.81–1 means near-perfect agreement [9].

Visualization

Ten random cases were chosen from the undergraded and overgraded groups and examined thoroughly, looking for possible pitfalls for misgrading. Examples were then photographed using Nikon Eclipse E200 light microscope (Nikon Corporation, Tokyo, Japan), TrueChrome Metrics camera and TCapture 5.1.1 software (Tucsen Photonics Co., Ltd., Fujian, China).

Statistical analyses

One-way ANOVA with Tukey's multiple comparisons *post hoc* test were used to calculate the significance of difference among accurately graded, under-, and overgraded groups. To assess the difference between groups of adverse features, unpaired t-test was used. Chi-squared and Fisher's exact test was the test of choice when comparison of stained and unstained groups. Interobserver reproducibility was calculated using Fleiss kappa. All statistical analyses were performed using GraphPad

TABLE 1 Grade Group distribution among biopsy and radical prostatectomy specimens (n = 315).

		n (%)
Biopsy specimens		
	Grade Group 1	203 (*64.4%*)
	Grade Group 2	75 (*23.8%*)
	Grade Group 3	8 (*2.5%*)
	Grade Group 4	24 (*7.6%*)
	Grade Group 5	5 (*1.6%*)
Radical prostatectomy specimens		
	Grade Group 1	91 (*28.9%*)
	Grade Group 2	135 (*42.9%*)
	Grade Group 3	32 (*10.2%*)
	Grade Group 4	33 (*10.5%*)
	Grade Group 5	24 (*7.6%*)

Italic refers to percentage (%) of the total

TABLE 2 Concordance of biopsy and radical prostatectomy Grade Groups in our study (n = 315).

Concordance		n (%)
Accurately graded		143 (*45.4%*)
Undergraded total		153 (*48.6%*)
	Undergraded by 1 Grade Group	103 (*32.7%*)
	Undergraded by 2 Grade Groups	22 (*7.0%*)
	Undergraded by 3 Grade Groups	20 (*6.4%*)
	Undergraded by 4 Grade Groups	8 (*2.5%*)
Overgraded total		19 (*6.0%*)
	Overgraded by 1 Grade Group	11 (*3.5%*)
	Overgraded by 2 Grade Groups	7 (*2.2%*)
	Overgraded by 3 Grade Groups	1 (*0.3%*)

Italic refers to percentage (%) of the total

Prism 9.4.1 (GraphPad Software, Inc., San Diego, CA, United States) and $p < 0.05$ was considered significant.

Results

The distribution of ISUP GGs is demonstrated in Table 1. The majority of biopsy samples were graded as GG 1 (64.4%), while in the case of RP specimens, the most commonly given GG was 2 (42.9%).

As presented in Table 2, 45.4% of all cases were graded accurately at biopsy, whereas 48.6% were under-, and 6.0% were overgraded. 81.6% of all cases were graded accurately or within one GG.

The mean number of cores obtained at biopsy was 12.58 ± 2.84, 11.84 ± 1.97 and 13.11 ± 3.41 (range 7–25) in accurately, under-, and overgraded groups, respectively. The difference between these three groups appeared to be significant (p = 0.0132). In cases with concordant biopsy and RP GGs, the number of cores obtained at biopsy was significantly higher than in undergraded cases (p = 0.0313). The mean number of biopsy cores in the overgraded group was higher than in the other two groups, however, it did not reach statistical significance (Figure 1A). The tendency of overgraded cases harbouring higher and undergraded cases harbouring lower biopsy core numbers than accurately graded cases can be viewed in Figure 1B.

As far as the extent of RP specimen processing is concerned, pre-test analyzes needed to be run to assess whether total versus partial processing depends on the size of the RP specimen and the greatest diameter of the largest tumor nodule. Totally embedded specimens were significantly less of weight, than those embedded partially (p = 0.0094), and the largest diameter of the tumor was significantly smaller (p = 0.0424) in the group of totally embedded specimens. Due to these findings, and the relatively small number of cases in the totally embedded group (n = 14), we decided to exclude these cases from further statistics and focused only on the group of partially embedded specimens (n = 301). The extent of partial RP specimen processing was also correlated with the parameters mentioned above. R^2 values from both tests indicated no significant correlation with either parameter (Supplementary Figure S1). The mean number of slides was 17.79 ± 4.31, 17.88 ± 4.50 and 18.37 ± 3.37 (range 11–37) in accurately, under-, and overgraded groups, respectively. In terms of accuracy, the number of slides, weight of the specimen and weight/slide ratio indicated no differences between the groups and so did the greatest diameter of the largest tumor nodule (Figure 2).

An annual breakdown of biopsy core and RP slide numbers were also performed. Biopsy core numbers did not change significantly between 2016 and 2021, but had a temporary setback in 2019. In contrast, the number of slides made from prostatectomy specimens showed an increasing tendency between 2016 and 2021 (Figures 3A, B). The annual trend of the fraction of accurately graded biopsies follows the annual trend of biopsy core numbers: the latter reached a nadir in 2019, while the fraction of accurately graded cases had a setback in the same and following year (Figure 3C).

Using AMACR/p63/34βE12 IHC on biopsy samples did not affect grading accuracy significantly (p = 0.1976). We found, however, a slightly larger proportion of accurately graded biopsies when IHC was performed. Another tendency revealed was the diminished ratio of overgraded cases in the IHC-performed group (4.8% vs. 10.8%; p = 0.0823) (Figure 4).

Detailed data regarding adverse pathological features of RP specimens in partially embedded group (n = 301) are shown in Table 3. The mean number of slides was virtually identical in the case of surgical margin status and pathological stage. Similarly, an extended number of slides did not result in significant difference regarding perineural invasion.

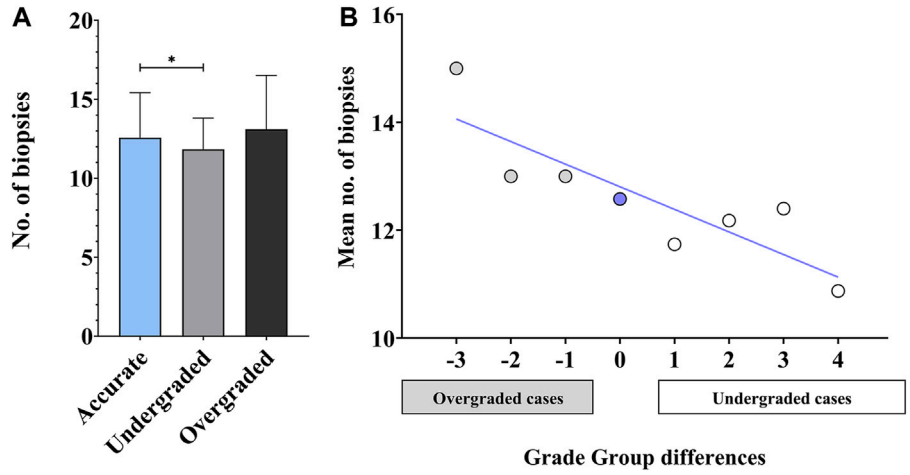

FIGURE 1
Accuracy of biopsy and radical prostatectomy Grade Groups—biopsy core numbers. **(A)** Statistical comparison of biopsy core numbers in accurately, under-, and overgraded groups. (n = 315; mean ± SD; ANOVA, Tukey's multiple comparisons test; *$p < 0.05$) **(B)** Mean number of biopsy cores plotted against Grade Group differences (calculated as [*prostatectomy Grade Group*]−[*biopsy Grade Group*]) (n = 315; blue line: linear fit; R^2 = 0.74).

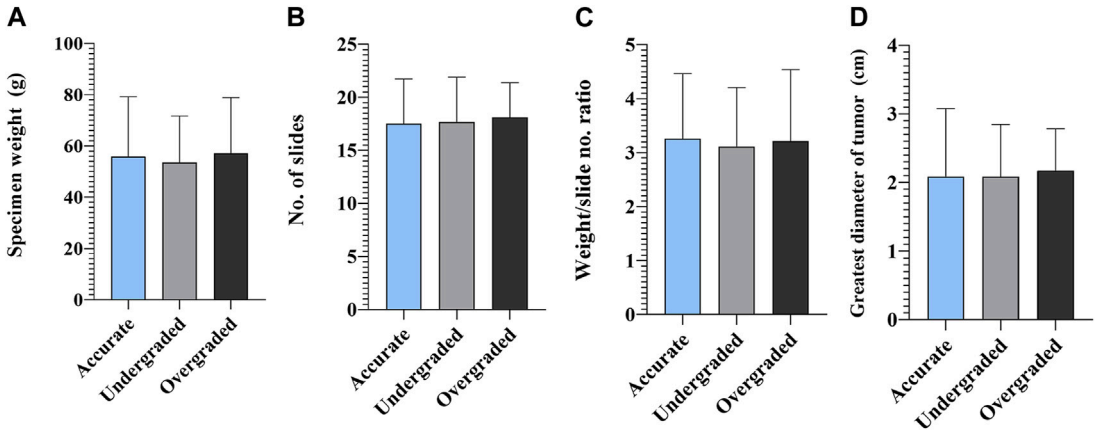

FIGURE 2
Accuracy of biopsy and radical prostatectomy Grade Groups—radical prostatectomy specimens. **(A)** Statistical comparison of specimen weight, **(B)** number of slides made from prostatectomy specimens, **(C)** specimen weight/slide number ratio and **(D)** greatest diameter of tumor in accurately, under-, and overgraded groups (n = 301; mean ± SD).

Among the three pathologists involved in this study, consensus on GGs of biopsy samples was reached in 35%, and the overall Fleiss kappa was calculated as 0.29, which indicates only fair agreement. Of cases with perfect agreement among all three pathologists, the majority was GG 1 (4/7; 57%).

After evaluating 10 randomly chosen samples, we identified the following five morphological patterns that might be misleading when grading prostate needle biopsy or RP specimens:

- Evaluating necrosis within malignant glands with cribriform patterns may be challenging due to the resemblance of necrotic debris to actual glandular secretions. Cribriform pattern with necrosis is Gleason pattern 5, whereas without necrosis, it is Gleason pattern 4 (Figures 5A, B).
- Differentiating between cribriform high-grade prostatic intraepithelial neoplasia and invasive glands with cribriform patterns can be hard, especially when the

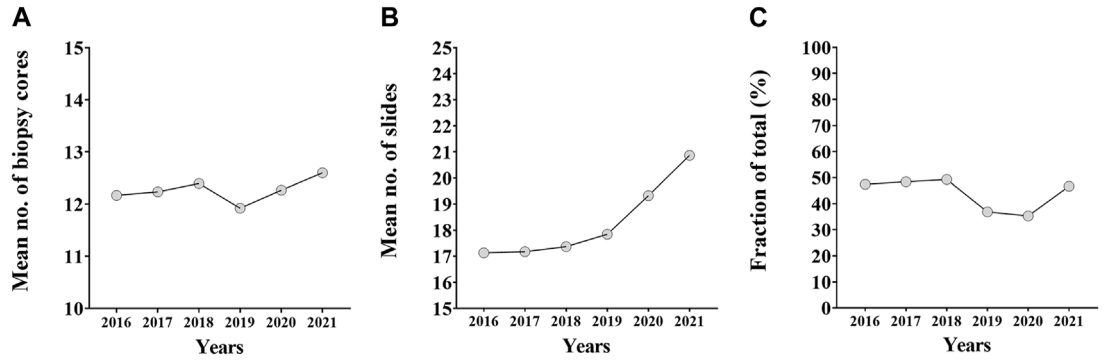

FIGURE 3
The annual breakdown of biopsy core numbers, prostatectomy specimen slide numbers and fraction of accurately graded cases. **(A)** The annual trend of biopsy core numbers between 2016 and 2021. **(B)** The annual trend of number of slides made from prostatectomy specimens between 2016 and 2021. **(C)** The annual trend of the fraction of accurately graded biopsies between 2016 and 2021.

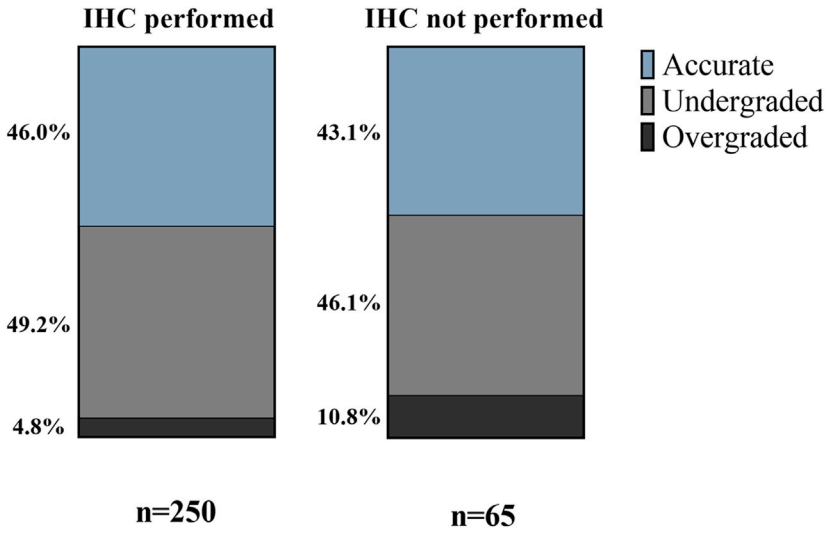

FIGURE 4
Effect of immunohistochemical staining on Grade Group accuracy—percentages of accurately, under- and overgraded cases in IHC groups.

basal cell layer shows focal integrity deficits. This can lead to invalid reported percentages of pattern 4 glands and may change the final GG (Figure 5C).

- Small lumina may be overlooked in areas with closely packed glands. A solid sheet of cells is Gleason pattern 5, while the presence of abortive glands is Gleason pattern 4 (Figure 5D).
- Gleason pattern 4-equivalent glomeruloid structures are also not easy to identify, especially at low power magnification, when intermixed with Gleason pattern 3 glands (Figure 5E).
- Cohesive cells containing intracellular mucin are frequently encountered in prostate samples. In nested or glandular patterns, they can mimic small cribriform glands. Invasive glands harbouring cribriform pattern equals Gleason pattern 4, whereas non-cribriform structures are considered Gleason pattern 3 or less (Figure 5F).

Discussion

Accurately grading prostate biopsy samples is essential for choosing the best treatment option for prostate cancer. It saves patients eligible for active surveillance from RP and its side effects and also from undertreatment and progressing into locally advanced or metastatic disease.

TABLE 3 Adverse features evaluated in radical prostatectomy specimens (n = 301).

Feature		n (%)	[a]mean ± SD	*p*-value
Margin status				
	Positive	73 (*24.3%*)	17.78 ± 4.315	0.7218
	Negative	228 (*75.7%*)	17.58 ± 4.127	
[b]Pathological stage				
	pT3	120 (*39.9%*)	17.80 ± 4.428	0.5627
	pT2	181 (*60.1%*)	17.51 ± 3.990	
Perineural invasion				
	Pn0	36 (*12.0%*)	18.31 ± 4.006	0.3000
	Pn1	265 (*88.0%*)	17.54 ± 4.188	

SD, standard deviation.
Italic refers to percentage (%) of the total
[a]Means of the number of slides in each subgroup are shown.
[b]All cases were of stage pT2 or pT3.

Undergrading and overgrading prostate needle biopsies is a well-known phenomenon. A meta-analysis of 16 studies with nearly fifteen thousand patients by Cohen et al. demonstrated an overall accuracy of 63% (range 53%–74%). Undergrading occurred in 30% (range 6%–36%), and overgrading was found in 7% (range 4%–28%) of the cases [10]. In the present study, overall accuracy was found to be 45%, which is markedly inferior to the meta-analysis results; samples were undergraded in 49% and overgraded in 6% of all cases. This may be due to the fact that at our institute—similarly to other minor academic or community centres—mainly general pathologists evaluate and grade prostate samples instead of specified urogenital pathologists. In addition, as Danneman et al. suggested, the newly introduced GG system, in which Gleason score 7 is divided into GG 2 (3 + 4) and 3 (4 + 3), plays a role in poorer accuracy [11].

We found a significant difference in the number of biopsy cores between accurately, under-, and overgraded cases. The group of accurately graded cases harboured a significantly higher mean number of cores than the group of undergraded cases, but interestingly had a lower mean number of cores than the group of overgraded cases. The current prostate biopsy evaluation protocol could be one possible explanation for why overgraded cases harbour higher core numbers: besides the most common Gleason pattern in the sample, the highest-graded pattern also needs to be considered to calculate the GG of each case. When a high number of biopsy cores are taken, the chances of sampling a small focal high-grade pattern are greater. Since the generally poor accuracy of biopsy GG to predict RP GG, several studies have addressed the question of extended biopsy schemes and their effects on concordance. Many of them reported findings consistent with ours [12–15].

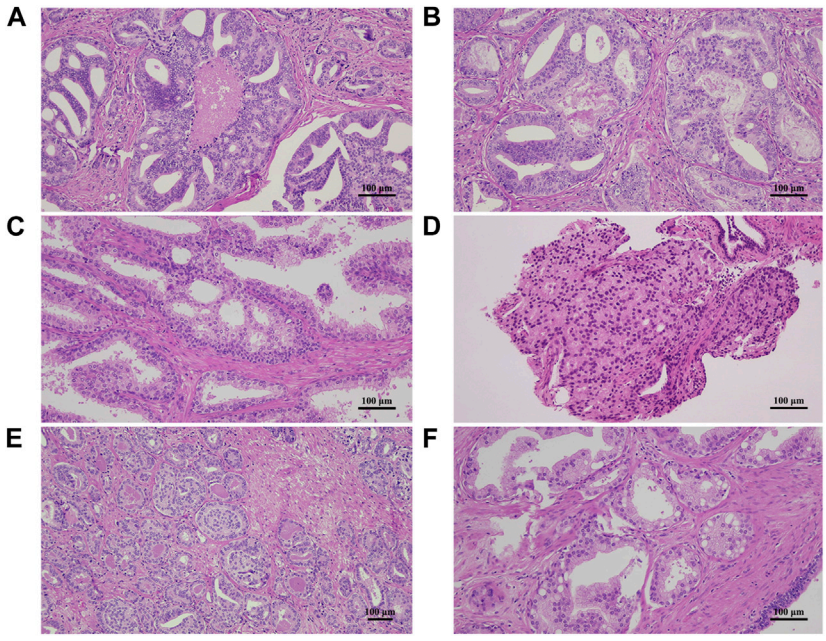

FIGURE 5
Hematoxylin and eosin-stained sections demonstrating morphologic pitfalls for misgrading prostate adenocarcinoma samples. **(A,B)** Necrotic debris and secretion in a gland with cribriform pattern may be hard to distinguish. **(C)** High-grade prostatic intraepithelial neoplasia may mimic invasive pattern 4 glands, especially with inconsistent basal cell layer and no immunohistochemical stains. **(D)** Closely-packed glands with small lumina can be hard to differentiate from a solid sheet of cells. **(E)** Glomeruloid structures may not be easy to identify when intermixed with pattern 3 glands. **(F)** Cells containing intracellular mucin in a nested or glandular pattern may give the impression of a cribriform gland.

However, other studies have failed to show significant improvement in accuracy when using extended biopsy schemes [16, 17]. Miyake et al. grouped cases based on the biopsy core number and found significantly more concordant cases in the group with 10 or more cores, than in the group with less than 10 cores. When subdividing the groups according to initial Gleason scores, this correlation proved to be significant only in specimens with Gleason score of 6 and below (equivalent to GG 1), but the core number did not affect accuracy significantly in cases with higher GGs [18]. A prostate volume-controlled study conducted by Antunes et al. also reported significantly better concordance in the group of 10 or more cores than in groups with 6 or 8 cores, but only in cases of prostates below 50 cm^3 [19].

Immunohistochemical staining of prostate carcinoma marker AMACR and basal cell markers p63 and 34βE12 are widely-used tools in detecting neoplastic prostate glands lacking basal cell layer. Detection rates have been reported higher when a double or triple cocktail was used, but single staining is also accepted when encountering small foci of suspicious glands, according to the 2014 ISUP recommendations [8, 20–22]. While several studies have addressed the role of IHC in detecting prostate cancer and its mimickers, there are no studies, to date, that have investigated the effects of IHC on the grading accuracy of biopsy samples. Since cribriform pattern equals Gleason pattern 4, noting areas of cribriform high-grade prostatic intraepithelial neoplasia as invasive malignant glands or *vice versa* can lead to over- and underestimating Gleason pattern 4 percentage, resulting in potential under- or overgrading of biopsy samples. In the present study, we failed to demonstrate significantly improved accuracy when IHC was performed. However, a slightly larger proportion of accurately graded cases were found in the group with IHC. A more noticeable finding was the diminished ratio of overgraded cases in the IHC-performed group, which leads to the assumption that not performing IHC is more likely to result in evaluating a suspicious cribriform area rather invasive than non-invasive, thus calculating its pattern into the GG.

In recent decades, multiple studies with numerous approaches have investigated different sampling and processing methods (various partial versus total embedding, standard versus whole-mount slides) for RP specimens. The need for cost-effectiveness and decreased workload at pathology laboratories opposes the need for as little loss of essential information as possible. In most reports, the extent of lost important information, e.g., adverse pathological features, was in primary focus. In a recent paper by Collette et al., the findings of a dozen studies have been summed [23]. Seven of them reported no significant information loss when using partial or alternate slice sampling, thus favouring this RP handling method; [24–30]. The rest promoted total embedding [31–35]. Of those, Desai et al. reported poorer patient outcomes with partial embedding [31]. Inconsistent results from these studies have contributed to the fact that an overall consensus has failed to be made; however, most guidelines recommend total embedding with large-format histology [36, 37]. In our study, specimens were either totally or partially embedded, because there was no departmental protocol for RP specimen handling. However, the former group contained only a small number of cases and the processing type appeared to be biased by the weight of the specimen and the greatest diameter of the largest tumor nodule. Because of these factors we chose not to include totally embedded cases into further statistical analyses and focused only on the partially embedded group. Since the number of slides made from RP specimens acted as an independent variable in our settings, we used this parameter for comparison and found virtually no difference between groups of pT2 and pT3 cases, positive and negative surgical margin cases or Pn0 and Pn1 cases. Furthermore, we found no significant difference in the number of slides in accurately, under- or overgraded groups. These findings suggest that generally when a relatively large specimen and/or tumor is partially embedded (preferably alternating slices), the extent of sampling and processing does not necessarily affect detection rates of adverse pathological features or GG accuracy.

Subjectivity is an intrinsic feature of grading systems, and the Grade Group system is no exception. In centres where numerous general, non-specialized pathologists evaluate specimens of all kinds, inter-observer variability is an inevitable phenomenon that applies to all types of samples. In an optimal case, pathologists work with perfect intra- and inter-observer reproducibility; however, in reality, inter-observer reproducibility of most centres leans towards being moderate. In a publication by Ozkan et al., 407 slides from 34 consecutive cases were evaluated and scored by two general pathologists, who both were trained on the 2005 ISUP Gleason grading system and Epstein's modification; inter-observer reproducibility was found moderate (overall kappa value of 0.39) [38]. Similarly, another study where 23 general pathologists scored biopsy samples from 37 patients also reported moderate reproducibility of the Gleason grading system (overall kappa = 0.49) [39]. Singh et al. conducted a study in which 20 biopsy/transurethral prostate resection samples were evaluated by 21 general pathologists and showed fair to moderate reproducibility among professionals [40]. Substantial reproducibility (overall kappa = 0.68) was found among six specialised urogenital pathologists, whereas reproducibility among eight general pathologists was moderate (overall kappa = 0.44) in a study by Oyama et al. [41] With a conclusion of tutorials and training being highly beneficial, Mulay et al. showed that reproducibility between four pathologists improved after completing a web-based tutorial session; the original kappa value of 0.459 increased to 0.538 [42]. In the current study, three general pathologists

evaluated 20 biopsy samples, and the overall kappa value was 0.29, which indicated only fair agreement.

Limitations

A final comment should be made on the limitations of the present study. When testing accuracy, only the number of obtained biopsy cores was taken into consideration instead of their summed length. In addition, we corrected the number of slides in cases of whole-mount sectioning, as 1 whole-mount slide equaled 3 standard slides, since most—although not all—pathologists claimed using this ratio when doing large-format histology at our institute. Furthermore, as mentioned earlier, our inter-observer reproducibility in Gleason grading was fair, which may bias the results on improved accuracy. Finally, IHC was not performed uniformly: in some cases, only AMACR or one of the basal cell-specific markers was used, whereas in other cases, a cocktail of two or three of them was applied.

Conclusion

In conclusion, this study reveals that obtaining more cores (at least 6-6 from both lobes) at prostate needle biopsy of men with high serum PSA levels or lesions suspicious for malignancy results in a better concordance between biopsy and RP GGs. The importance lies in the fact that with accurate grading at biopsy, patients eligible for active surveillance are saved from RP and its side effects, and patients with actual high-grade cancer are saved from potential insufficient treatment and progressing into locally advanced or metastatic disease.

We recommend to use a departmental protocol for handling RP specimens. Small specimens (e.g., below 30 g) should not be processed partially. For higher cost-effectivity, larger specimens could be processed partially, with the acclaimed risk of information being lost, since it is questionably essential for further therapeutic decisions. Alternating slice sampling (with additional sampling of basal and apical slices) can decrease this risk.

Although performing IHC on biopsy cores does not affect GG accuracy, it is well known, that IHC improves detection of prostate cancer. Therefore, we recommend including IHC in the biopsy processing protocols.

Data availability statement

The raw data supporting the conclusion of this article will be made available by the authors, without undue reservation.

Ethics statement

I declare that the study meets general ethical standards (Helsinki Declaration), since it doesn't include any identifiable personal data, statements or macroscopic photographs of the patients. This is a retrospective analysis not requiring any new examinations run on the preexisting samples.

Author contributions

KK: data collection, methodology, statistical analyses, figure and table preparation, literature review, manuscript writing; LBe and DV: methodology; LBi: contribution to calculating inter-observer reproducibility; GM: supervision; SM: study design and direction, methodology, visualization. All authors contributed to the article and approved the submitted version.

Conflict of interest

The authors declare that the research was conducted in the absence of any commercial or financial relationships that could be construed as a potential conflict of interest.

Supplementary material

The Supplementary Material for this article can be found online at: https://www.por-journal.com/articles/10.3389/pore.2023.1611157/full#supplementary-material

SUPPLEMENTARY FIGURE S1
Correlations to assess whether slide number is independent of the weight of the specimen and the greatest diameter of the tumor. **(A)** Correlation between number of slides from radical prostatectomy specimens and weight of specimens (n = 301; blue line: linear fit; R^2 is noted). **(B)** Correlation between number of slides from radical prostatectomy specimens and greatest diameter of the tumor (n = 185; blue line: linear fit; R^2 is noted).

References

1. Sung H, Ferlay J, Siegel RL, Laversanne M, Soerjomataram I, Jemal A, et al. Global cancer statistics 2020: GLOBOCAN estimates of incidence and mortality worldwide for 36 cancers in 185 countries. *CA Cancer J Clin* (2021) 71(3):209–49. doi:10.3322/caac.21660

2. Brawley S, Mohan R, Nein CD. Localized prostate cancer: Treatment options. *Am Fam Physician* (2018) 97(12):798–805.

3. Epstein JI, Egevad L, Amin MB, Delahunt B, Srigley JR, Humphrey PA, et al. The 2014 international society of urological pathology (ISUP) consensus conference on Gleason grading of prostatic carcinoma: Definition of grading patterns and proposal for a new grading system. *Am J Surg Pathol* (2016) 40(2):244–52. doi:10.1097/PAS.0000000000000530

4. Penney KL, Stampfer MJ, Jahn JL, Sinnott JA, Flavin R, Rider JR, et al. Gleason grade progression is uncommon. *Cancer Res* (2013) 73(16):5163–8. doi:10.1158/0008-5472.CAN-13-0427

5. Freedland SJ, Kane CJ, Amling CL, Aronson WJ, Presti JC, Terris MK, et al. Delay of radical prostatectomy and risk of biochemical progression in men with low

risk prostate cancer. *J Urol* (2006) 175(4):1298–302. doi:10.1016/S0022-5347(05)00646-4

6. Sampurno F, Earnest A, Millar J, Frydenberg M, Murphy D, Delprado W, et al. Population-based study of grade progression in patients who harboured Gleason 3 + 3. *World J Urol* (2017) 35(11):1689–99. doi:10.1007/s00345-017-2047-z

7. Inoue LY, Trock BJ, Partin AW, Carter HB, Etzioni R. Modeling grade progression in an active surveillance study. *Stat Med* (2014) 33(6):930–9. doi:10.1002/sim.6003

8. Epstein JI, Egevad L, Humphrey PA, Montironi R, Group MotIIiDUP. Best practices recommendations in the application of immunohistochemistry in the prostate: Report from the international society of urologic pathology consensus conference. *Am J Surg Pathol* (2014) 38(8):e6–e19. doi:10.1097/PAS.0000000000000238

9. Landis JR, Koch GG. The measurement of observer agreement for categorical data. *Biometrics* (1977) 33(1):159–74. doi:10.2307/2529310

10. Cohen MS, Hanley RS, Kurteva T, Ruthazer R, Silverman ML, Sorcini A, et al. Comparing the Gleason prostate biopsy and Gleason prostatectomy grading system: The lahey clinic medical center experience and an international meta-analysis. *Eur Urol* (2008) 54(2):371–81. doi:10.1016/j.eururo.2008.03.049

11. Danneman D, Drevin L, Delahunt B, Samaratunga H, Robinson D, Bratt O, et al. Accuracy of prostate biopsies for predicting Gleason score in radical prostatectomy specimens: Nationwide trends 2000-2012. *BJU Int* (2017) 119(1):50–6. doi:10.1111/bju.13458

12. San Francisco IF, DeWolf WC, Rosen S, Upton M, Olumi AF. Extended prostate needle biopsy improves concordance of Gleason grading between prostate needle biopsy and radical prostatectomy. *J Urol* (2003) 169(1):136–40. doi:10.1097/01.ju.0000042811.83736.04

13. Mian BM, Lehr DJ, Moore CK, Fisher HA, Kaufman RP, Ross JS, et al. Role of prostate biopsy schemes in accurate prediction of Gleason scores. *Urology* (2006) 67(2):379–83. doi:10.1016/j.urology.2005.08.018

14. Coogan CL, Latchamsetty KC, Greenfield J, Corman JM, Lynch B, Porter CR. Increasing the number of biopsy cores improves the concordance of biopsy Gleason score to prostatectomy Gleason score. *BJU Int* (2005) 96(3):324–7. doi:10.1111/j.1464-410X.2005.05624.x

15. Athanazio D, Gotto G, Shea-Budgell M, Yilmaz A, Trpkov K. Global Gleason grade groups in prostate cancer: Concordance of biopsy and radical prostatectomy grades and predictors of upgrade and downgrade. *Histopathology* (2017) 70(7):1098–106. doi:10.1111/his.13179

16. Chun FK, Briganti A, Shariat SF, Graefen M, Montorsi F, Erbersdobler A, et al. Significant upgrading affects a third of men diagnosed with prostate cancer: Predictive nomogram and internal validation. *BJU Int* (2006) 98(2):329–34. doi:10.1111/j.1464-410X.2006.06262.x

17. Egevad L, Norlén BJ, Norberg M. The value of multiple core biopsies for predicting the Gleason score of prostate cancer. *BJU Int* (2001) 88(7):716–21. doi:10.1046/j.1464-4096.2001.02419.x

18. Miyake H, Kurahashi T, Takenaka A, Hara I, Fujisawa M. Improved accuracy for predicting the Gleason score of prostate cancer by increasing the number of transrectal biopsy cores. *Urol Int* (2007) 79(4):302–6. doi:10.1159/000109713

19. Antunes AA, Leite KR, Dall'Oglio MF, Cury J, Srougi M. The effect of the number of biopsy cores on the concordance between prostate biopsy and prostatectomy Gleason score: A prostate volume-controlled study. *Arch Pathol Lab Med* (2008) 132(6):989–92. doi:10.1043/1543-2165(2008)132[989:TEOTNO]2.0.CO;2

20. Jiang Z, Li C, Fischer A, Dresser K, Woda BA. Using an AMACR (P504S)/34betaE12/p63 cocktail for the detection of small focal prostate carcinoma in needle biopsy specimens. *Am J Clin Pathol* (2005) 123(2):231–6. doi:10.1309/1g1nk9dbgfnb792l

21. Yu T, Zhu SX, Zheng S, Chen SP. Detection of AMACR (P504S), P63 and 34betaE12 cocktail in the early diagnosis of prostate cancer. *Zhonghua Nan Ke Xue* (2007) 13(3):222–5.

22. Paner GP, Luthringer DJ, Amin MB. Best practice in diagnostic immunohistochemistry: Prostate carcinoma and its mimics in needle core biopsies. *Arch Pathol Lab Med* (2008) 132(9):1388–96. doi:10.1043/1543-2165(2008)132[1388:BPIDIP]2.0.CO;2

23. Collette ERP, den Bakker MA, Klaver SO, Vis AN, Kliffen M. Partial versus complete prostatectomy specimen sampling: Prospective non-inferiority study for pT3a tumours and surgical margin involvement. *BMJ Open* (2019) 9(4):e024524. doi:10.1136/bmjopen-2018-024524

24. Hall GS, Kramer CE, Epstein JI. Evaluation of radical prostatectomy specimens. A comparative analysis of sampling methods. *Am J Surg Pathol* (1992) 16(4):315–24. doi:10.1097/00000478-199204000-00001

25. Cohen MB, Soloway MS, Murphy WM. Sampling of radical prostatectomy specimens. How much is adequate? *Am J Clin Pathol* (1994) 101(3):250–2. doi:10.1093/ajcp/101.3.250

26. Hollenbeck BK, Bassily N, Wei JT, Montie JE, Hayasaka S, Taylor JM, et al. Whole mounted radical prostatectomy specimens do not increase detection of adverse pathological features. *J Urol* (2000) 164(5):1583–6. doi:10.1016/s0022-5347(05)67033-4

27. Sehdev AE, Pan CC, Epstein JI. Comparative analysis of sampling methods for grossing radical prostatectomy specimens performed for nonpalpable (stage T1c) prostatic adenocarcinoma. *Hum Pathol* (2001) 32(5):494–9. doi:10.1053/hupa.2001.24322

28. Vainer B, Toft BG, Olsen KE, Jacobsen GK, Marcussen N. Handling of radical prostatectomy specimens: Total or partial embedding? *Histopathology* (2011) 58(2):211–6. doi:10.1111/j.1365-2559.2011.03741.x

29. Llanos CA, Blieden C, Vernon SE. Processing radical prostatectomies: An alternate-slice method is comparable with total embedding. *Ann Diagn Pathol* (2012) 16(4):284–7. doi:10.1016/j.anndiagpath.2011.10.004

30. Kim K, Pak PJ, Ro JY, Shin D, Huh SJ, Cho YM. Limited sampling of radical prostatectomy specimens with excellent preservation of prognostic parameters of prostate cancer. *Arch Pathol Lab Med* (2009) 133(8):1278–84. doi:10.1043/1543-2165-133.8.1278

31. Desai A, Wu H, Sun L, Sesterhenn IA, Mostofi FK, McLeod D, et al. Complete embedding and close step-sectioning of radical prostatectomy specimens both increase detection of extra-prostatic extension, and correlate with increased disease-free survival by stage of prostate cancer patients. *Prostate Cancer Prostatic Dis* (2002) 5(3):212–8. doi:10.1038/sj.pcan.4500600

32. Fadul LC, da Silva MT, de Freitas LA, Athanazio DA. Assessment of the circumferential margins, extraprostatic extension and Gleason score in radical prostatectomy specimens: Comparison of a partial embedding method with supplemental total inclusion of peripheral tissues. *Pathol Res Pract* (2016) 212(3):217–21. doi:10.1016/j.prp.2015.12.014

33. Grossfeld GD, Chang JJ, Broering JM, Miller DP, Yu J, Flanders SC, et al. Does the completeness of prostate sampling predict outcome for patients undergoing radical prostatectomy?: Data from the CAPSURE database. *Urology* (2000) 56(3):430–5. doi:10.1016/s0090-4295(00)00705-6

34. Iremashvili V, Lokeshwar SD, Jorda M, Pelaez L, Soloway MS. Prognostic implications of partial sampling of radical prostatectomy specimens: Comparison of 3 methods. *J Urol* (2013) 190(1):84–90. doi:10.1016/j.juro.2012.12.021

35. Iremashvili V, Lokeshwar SD, Soloway MS, Pelaez L, Umar SA, Manoharan M, et al. Partial sampling of radical prostatectomy specimens: Detection of positive margins and extraprostatic extension. *Am J Surg Pathol* (2013) 37(2):219–25. doi:10.1097/PAS.0b013e318268ccc1

36. Mottet N, Bellmunt J, Bolla M, Briers E, Cumberbatch MG, De Santis M, et al. EAU-ESTRO-SIOG guidelines on prostate cancer. Part 1: Screening, diagnosis, and local treatment with curative intent. *Eur Urol* (2017) 71(4):618–29. doi:10.1016/j.eururo.2016.08.003

37. Samaratunga H, Montironi R, True L, Epstein JI, Griffiths DF, Humphrey PA, et al. International society of urological pathology (ISUP) consensus conference on handling and staging of radical prostatectomy specimens. Working group 1: Specimen handling. *Mod Pathol* (2011) 24(1):6–15. doi:10.1038/modpathol.2010.178

38. Ozkan TA, Eruyar AT, Cebeci OO, Memik O, Ozcan L, Kuskonmaz I. Interobserver variability in Gleason histological grading of prostate cancer. *Scand J Urol* (2016) 50(6):420–4. doi:10.1080/21681805.2016.1206619

39. Bori R, Salamon F, Móczár C, Cserni G. Interobserver reproducibility of Gleason grading in prostate biopsy samples. *Orv Hetil* (2013) 154(31):1219–25. doi:10.1556/OH.2013.29659

40. Singh RV, Agashe SR, Gosavi AV, Sulhyan KR. Interobserver reproducibility of Gleason grading of prostatic adenocarcinoma among general pathologists. *Indian J Cancer* (2011) 48(4):488–95. doi:10.4103/0019-509X.92277

41. Oyama T, Allsbrook WC, Kurokawa K, Matsuda H, Segawa A, Sano T, et al. A comparison of interobserver reproducibility of Gleason grading of prostatic carcinoma in Japan and the United States. *Arch Pathol Lab Med* (2005) 129(8):1004–10. doi:10.1043/1543-2165(2005)129[1004:ACOIRO]2.0.CO;2

42. Mulay K, Swain M, Jaiman S, Gowrishankar S. Gleason scoring of prostatic carcinoma: Impact of a web-based tutorial on inter- and intra-observer variability. *Indian J Pathol Microbiol* (2008) 51(1):22–5. doi:10.4103/0377-4929.40385

Pathology & Oncology Research | frontiers

TYPE Original Research
PUBLISHED 01 February 2023
DOI 10.3389/pore.2023.1610852

Check for updates

OPEN ACCESS

EDITED BY
Gabor Cserni,
University of Szeged, Hungary

*CORRESPONDENCE
Yan Peng,
pengyan871005@163.com

RECEIVED 29 September 2022
ACCEPTED 12 January 2023
PUBLISHED 01 February 2023

CITATION
Chen T, Peng Y, Lei T, Wu C, Wang H and Shi Y (2023), Low-grade oncocytic tumour (LOT) of the kidney is characterised by GATA3 positivity, FOXI1 negativity and mTOR pathway mutations.
Pathol. Oncol. Res. 29:1610852.
doi: 10.3389/pore.2023.1610852

COPYRIGHT
© 2023 Chen, Peng, Lei, Wu, Wang and Shi. This is an open-access article distributed under the terms of the Creative Commons Attribution License (CC BY). The use, distribution or reproduction in other forums is permitted, provided the original author(s) and the copyright owner(s) are credited and that the original publication in this journal is cited, in accordance with accepted academic practice. No use, distribution or reproduction is permitted which does not comply with these terms.

Low-grade oncocytic tumour (LOT) of the kidney is characterised by GATA3 positivity, FOXI1 negativity and mTOR pathway mutations

Tongbing Chen, Yan Peng*, Ting Lei, Chao Wu, Hui Wang and Yongqiang Shi

Department of Pathology, The Third Affiliated Hospital of Soochow University, Changzhou First People's Hospital, Changzhou, China

Aims: We present a 5-case series of low-grade oncocytic tumour of the kidney to further discuss their clinicopathological characteristics.

Methods and results: Five patients were included in this study. There were three females and two males aged 45–66 years, with a median age of 65 years. Four tumours were located in the right kidney, and one was located in the left kidney. Most of the tumour sections were yellow-brown in colour. Tumour sizes ranged from 2.5 to 4.5 cm, with a median size of 3 cm. Microscopically, the tumours were well-circumscribed but lacked a fibrous capsule; the tumours consisted of monomorphous oncocytic cells arranged mainly in solid and nested architectural patterns. The tumour cells had uniformly round to oval nuclei and often had perinuclear halos but lacked significant irregularities. Immunohistochemically, the tumour cells showed a diffuse and strong positivity for CK7 and were negative for CD117. The tumour cells were also positive for GATA3, E-cadherin, Pax-8, Succinate dehydrogenase B (SDHB) and Fumarate hydratase (FH), and negative for vimentin, Carbonic anhydrase 9 (CA9), CD10, P504s, CK20, TFE3, TFEB, HMB45, ALK and Forkhead box protein I1 (FOXI1). Next-generation sequencing identified genetic variations in these tumours, including *MTOR* gene mutations (4/5) and *PIK3CA* gene mutation (1/5). All patients were alive without disease progression at a median follow-up of 32 months (range 10–57 months).

Conclusion: LOT is an emerging renal entity of indolent behaviour that has morphologic overlap with some renal tumours with eosinophilic cytoplasm, primarily with oncocytoma and eosinophilic variant of chromophobe renal cell carcinoma. Familiarity with the distinctive morphological features, immunophenotype and molecular genetics of LOT helps avoid misdiagnosis.

KEYWORDS

immunohistochemistry, clinicopathological characteristics, mTOR, differential diagnosis, low-grade oncocytic tumour (LOT) of the kidney

Introduction

Low-grade oncocytic tumour (LOT) of the kidney is an emerging renal entity that was first described by Trpkov K and Hes O in 2019 (1). This low-grade entity is composed of oncocytic tumour cells, and characterized by a CK7-positive/CD117-negative immunoprofile (2). Several case series have been reported. In the current study, we present five patients with LOT, and the clinical, histological, immunophenotypic and molecular features were analysed. The aim of our study was to further discuss the clinicopathological features and differential diagnosis of LOT.

Materials and methods

Case selection

From 2017 to 2021, 876 renal tumours were processed in The Third Affiliated Hospital of Soochow University/Changzhou First People's Hospital. A series of 62 oncocytic renal tumours were identified, including 19 cases of eosinophilic variant of chromophobe renal cell carcinoma (E-ChRCC), 13 cases of renal oncocytoma, 16 cases of papillary renal cell carcinoma (PRCC) with eosinophilic features, 8 cases of clear cell renal cell carcinoma (CCRCC) with eosinophilic features, and 6 cases of unclassified oncocytic renal tumour. We only identified 5 tumours as LOT characterized by CK7 positivity and CD117 negativity. Of the five cases, four were originally diagnosed as E-ChRCC, and one as renal oncocytoma. The clinical and pathological findings were obtained from the medical records and pathology reports. Follow-up information was obtained by direct telephone communication with the patients and/or their relatives.

Immunohistochemical analysis

Immunohistochemical staining was performed on 4-μm-thick formalin-fixed, paraffin-embedded (FFPE) tissue sections using a Roche Benchmark XT Automated Staining System. The antibodies used in this study (Supplementary Table S1) included CK7 (EP16, prediluted, ZSGB-BIO), CD117 (YR145, prediluted, MXB Biotechnologies), Carbonic anhydrase 9 (CA9) (H-11, prediluted, ZSGB-BIO), CD10 (MX002, prediluted, MXB Biotechnologies), P504s (13H4, prediluted, ZSGB-BIO), Pax-8 (EP298, prediluted, MXB Biotechnologies), vimentin (UMAB159, prediluted, ZSGB-BIO), E-cadherin (MX020, prediluted, MXB Biotechnologies), HMB45 (HMB45, prediluted, MXB Biotechnologies), CK20 (EP23, prediluted, ZSGB-BIO), Succinate dehydrogenase B(SDHB) (OTI1H6, prediluted, ZSGB-BIO), Fumarate hydratase(FH) (OTI1F10, prediluted, ZSGB-BIO), ALK (5A4, prediluted, MXB Biotechnologies), TFE3 (EP285, prediluted, ZSGB-BIO), TFEB (OTI2C1, 1:500, OriGene), GATA3 (EP368, prediluted, ZSGB-BIO), Forkhead box protein I1 (FOXI1) (EPR22940-151, 1:100, Abcam) and Ki-67 (UMAB107, prediluted, ZSGB-BIO). Positive and negative controls were used for each antibody. Immunoreactivity was scored by the percentage of positive tumour cells as follows: <1% (negative), 1%–50% (focal positive), and > 50% (diffusely positive).

Next-generation sequencing

Next-generation sequencing (NGS) was performed by Illumina MiSeq (Illumina). The tissue DNA was extracted from FFPE tumour tissues using QIAamp DNA FFPE tissue kit (Qiagen, Hilden, Germany). Fragments between 200 and 400 bp from the sheared tissue DNA were purified (Agencourt AMPure XP Kit, Beckman Coulter, CA, United States), hybridized with capture probes baits, selected with magnetic beads, and amplified. Target capture was performed using a commercial panel consisting of 520 genes (Supplementary Table S2) chosen by Guangzhou Burning Rock Biotech Ltd. Sequence data were mapped to the reference human genome (hg19) using Burrows-Wheeler Aligner version 0.7.10. Local alignment optimization, duplication marking and variant calling were performed using Genome Analysis Tool Kit version 3.2, and VarScan version 2.4.3. Base calling in tissue samples required at least 8 supporting reads for single nucleotide variations (SNVs) and 2 and 5 supporting reads for insertion-deletion variations (Indels), respectively. Copy number variations (CNVs) were analyzed based on the depth of coverage data of capture intervals.

Results

Clinical features

The clinical features of the five patients are summarized in Table 1. There were three females and two males with ages ranging from 45 to 66 years (mean, 59 years; median, 65 years). All tumours were detected during a physical examination. Three patients underwent partial nephrectomy, and two patients underwent radical nephrectomy. Four tumours were located in the right kidney, and one was located in the left kidney. The tumour's cut surface was mostly yellow–brown in colour. Tumour size ranged from 2.5 to 4.5 cm in the maximal diameter (mean, 3.3 cm; median, 3 cm). No adjunctive treatment was administered. All patients had no evidence of local recurrence or distant metastasis during follow-up, which ranged from 10 to 57 months (mean, 34 months; median, 32 months).

Pathological features

Histologically, all tumours were well circumscribed but lacked a fibrous capsule. The growth patterns included solid,

TABLE 1 Clinicopathological features of low-grade oncocytic tumour (LOT) of the kidney.

Case	Age	Sex	Site	Size (mm)	Type of surgery	Status	Follow up (months)
1	45	Female	Right	25	Partial	Alive no evidence of disease	57
2	65	Male	Right	30	Partial	Alive no evidence of disease	53
3	66	Female	Right	35	Radical	Alive no evidence of disease	32
4	56	Male	Left	45	Partial	Alive no evidence of disease	21
5	65	Female	Right	30	Radical	Alive no evidence of disease	10

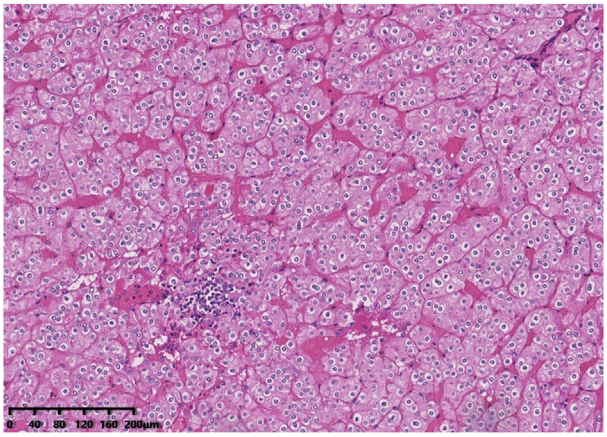

FIGURE 1
Histological features of low-grade oncocytic tumour (LOT) of the kidney. The tumour cells demonstrated a nested growth pattern. There are abundant thin-walled vessels around the tumour cell nest. Lymphocytic clusters were seen in this area. The tumour cells had perinuclear halos but lacked significant irregularities. The nucleoli were slightly conspicuous.

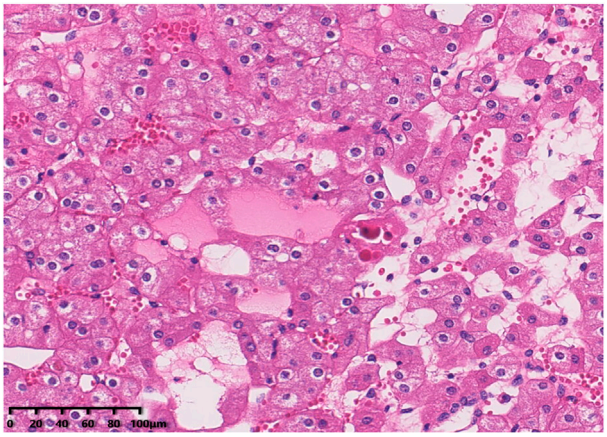

FIGURE 2
The tumour cells demonstrated a microcytic growth pattern.

nested (Figure 1), trabecular and microcystic growth (Figure 2). There were abundant thin-walled vessels around the tumour cell nest (Figure 1). Lymphocytic clusters (Figure 1) were observed in one tumour (Case 3). One tumour (Case 4) exhibited thick-walled vessels. Oedematous stromal areas were seen in two tumours (Case 2 and Case 4), with scattered single-cell arrangement in these areas (Figure 3). Focal fresh haemorrhage was also noted in three tumours (Cases 2, 3 and 4). No necrosis was observed in any of the tumours. The tumour cells had indistinct cell membranes, monomorphous oncocytic cytoplasm, and uniformly round to oval nuclei without mitotic activity. The tumour cells had perinuclear halos (Figure 1) but lacked significant irregularities. The nucleoli were slightly conspicuous (Figure 1).

Immunohistochemically, all tumours showed diffuse and strong positivity for CK7 and were negative for CD117. GATA binding protein 3 (GATA3) (Figure 4), E-cadherin and Pax-8 were also present in all neoplasms. SDHB and FH were retained. All tumour cells were negative for vimentin, CA9, CD10, P504s, CK20, TFE3, TFEB, HMB45, ALK and FOXI1. The Ki-67 index was less than 3%. NGS identified genetic variations in these tumours (Table 2). Four tumours had a *MTOR* gene exon 53 p.L2427Q mutation [c.7280T>A (p.Leu2427Gln)], and one tumour had a *PIK3CA* gene exon 10 p.E542K mutation [c.1624G>A (p.Glu542Lys)].

Discussion

Low-grade oncocytic tumour (LOT) of the kidney has emerged as a new diagnostic entity in renal tumour pathology in recent years (2–13). LOT is now enrolled in a new tumour subgroup called other oncocytic tumours of the kidney in the fifth edition of the WHO classification of urinary and male genital tumours (14), and is defined as a neoplasm with bland low-grade nuclei, diffuse strong CK7 labelling, and negative CD117 labelling. From 2017 to 2021, the incidence rates of LOT in our hospital were approximately 0.57% among renal tumours and 8% among oncocytic tumours in our study, while the incidence rates reported previously were 0.18% (4), 0.35% (5) and 0.17% (7) among renal cell tumours, respectively.

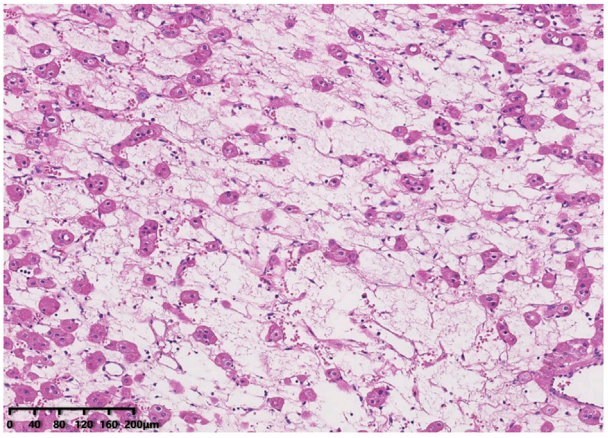

FIGURE 3
Oedematous stromal areas are presented, with scattered single-cell arrangement in these areas.

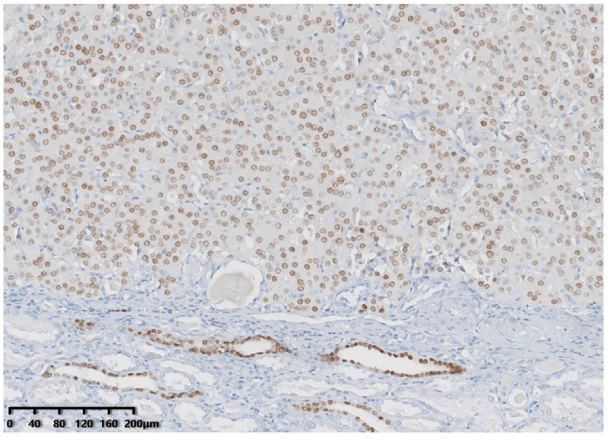

FIGURE 4
GATA3 showed consistent positivity in low-grade oncocytic tumour (LOT) of the kidney.

The clinicopathological features of LOT in this study are highly consistent with those of previously published cases. The tumours are found accidentally during physical examination in older patients as a single tumour, have a slight female predilection and have an indolent behaviour. Several LOTs have been reported in patients with tuberous sclerosis complex (TSC) (5, 6, 8) or end-stage renal disease (ESRD) (5). Multiple and/or bilateral renal tumours have been discovered (5, 6). Individual patients have died from unrelated diseases (5, 8, 12). The neoplasms in this study were typically well-circumscribed solid tumours consisting of monomorphous oncocytic cells arranged mainly in solid and nested architectural patterns, with no papillary growth pattern. The tumour cells were monomorphous with indistinct cell membranes and had an eosinophilic cytoplasm and prominent round to oval nuclei that lacked significant irregularities and often had perinuclear halos. Cystic change and central scarring are only seen in larger tumours (3) in general. Individual neoplasms have perirenal fat infiltration (3). Renal tubules can be entrapped at the periphery in individual tumours (4). Spindle elongated tumour cells are also observed, especially in hypocellular areas with oedematous stroma, such as cell culture growth. Muller–Mowry colloidal iron staining of LOT was either negative or only luminally positive (2, 3).

All the five tumours in this study had a typical immunophenotype characterized by diffuse positivity for CK7 and negativity for CD117, and were also positive for PAX-8, E-cadherin, FH and SDHB, but negative for vimentin, CD10, P504s, CA9, CK20, TFE3, TFEB, HMB45, and ALK. Rare neoplasms can show weak focal CD117 staining (2). Vimentin, CD10 and P504s can be focally positive (3, 4). BerEP4 (2, 4), MOC31 (2), CyclinD1 (4), 4EBP1 and S6K (8, 9) are also positive in LOT. Morini et al. (9) found no expression of FOXI1 in LOT. FOXI1 is a member of the forkhead transcription factor family, and high expression of FOXI1 has been found in restricted normal cell types, such as renal intercalated cells (ICs). Research has shown that FOXI1 is a potential biomarker of IC-related renal tumours, such as ChRCC and renal oncocytoma (15). We also identified negativity for FOXI1 in the current study. GATA3 belongs to the family of transcription factors that recognizes G-A-T-A nucleotide sequences in the target gene and is mostly used as a marker for breast and urothelial carcinomas. Studies (16) have found that GATA3 is expressed in distal nephrons, 51% of ChRCCs and 17% of oncocytomas. GATA3-positive reactions have also been documented in clear cell papillary renal cell tumour (17) and the recently recognized papillary renal neoplasm with reverse polarity (18). Therefore, GATA3 is not an entirely specific marker for one entity of renal cell neoplasms. Researches (12, 19) recently noted consistent GATA3 immunohistochemical positivity in LOT. We also observed GATA3 positivity in this study. Therefore, it can be inferred that the findings of FOXI1 negativity and consistent GATA3 positivity further expand the expected pattern of immunohistochemical markers in LOT.

Reports on the genetic analysis and molecular pathology of LOT are limited. Trpkov et al. (2) initially found that there were deletions at 19p13.3, 1p36.33 and 19q13.11 in some LOT patients by using array comparative genomic hybridization (ACGH). *CCND1* rearrangements were not found in LOT by using fluorescence *in situ* hybridization (FISH) (5). An increasing number of genetic tests have identified genetic mutations in LOT patients, including *RHEB* (8), *MTOR* (7–13), *TSC1* (6–9, 11–13), *TSC2* (11, 12), and *PIK3CA* (12), which are primarily involved in the *mTOR* pathway. The *PI3K/AKT/mTOR* signalling pathway plays a key role in cell survival and growth, *mTOR* is the master regulator of cell metabolism and growth, and acts through two different multiprotein complexes, namely, mTOR complex 1 (mTORC1) and mTOR complex 2 (mTORC2). mTORC1 is

TABLE 2 Genetic variations in the five adults with low-grade oncocytic tumour (LOT) of the kidney.

Case	Gene	Mutation_type	Description	Allele fraction (%)	Depth	Exon_number	Chromosome	Position	Hgvs_c	Hgvs_p
1	PRKDC	synonymous_variant	p.Y2483=	43.70	1389	55	8	48752579	c.7449C>T	p.Tyr2483=
	APC	stop_gained	p.R283*	17.26	2132	9	5	112151204	c.847C>T	p.Arg283*
	KDR	missense_variant	p.I519V	47.06	1719	12	4	55972089	c.1555A>G	p.Ile519Val
	EP300	missense_variant	p.P210S	45.35	3063	2	22	41513724	c.628C>T	p.Pro210Ser
	MTOR	missense_variant	p.L2427Q	20.92	2510	53	1	11174395	c.7280T>A	p.Leu2427Gln
	SPEN	missense_variant	p.D303V	47.95	1293	4	1	16235842	c.908A>T	p.Asp303Val
2	MTOR	missense_variant	p.L2427Q	9.34	1413	53	1	11174395	c.7280T>A	p.Leu2427Gln
3	MTOR	missense_variant	p.L2427Q	18.62	1847	53	1	11174395	c.7280T>A	p.Leu2427Gln
4	PIK3CA	missense_variant	p.E542K	24.85	1356	10	3	178936082	c.1624G>A	p.Glu542Lys
	CDK4	synonymous_variant	p.A16=	35.69	1303	2	12	58145453	c.48C>T	p.Ala16=
5	PDGFRB	synonymous_variant	p.V480=	44.71	2098	10	5	149509459	c.1440G>A	p.Val480=
	MTOR	missense_variant	p.L2427Q	17.73	1743	53	1	11174395	c.7280T>A	p.Leu2427Gln
	JAK3	splice_acceptor_variant	c.1787-2A>G	52.48	747	14	19	17946862	c.1787-2A>G	
	FAT1	intron_variant	c.13139-7C>T	43.38	989	27	4	187510381	c.13139-7C>T	

Abbreviations: Hgvs, human genome variation society.

10.3389/pore.2023.1610852

regulated by the tuberous sclerosis complex (TSC) (12). 4EBP1 and S6K expressed in LOT are the main downstream effectors of mTORC1 (20). All of these results confirm that LOT is a *mTOR* pathway mutation-associated renal tumour. We also found *MTOR* gene mutations in four tumours and an uncommon *PIK3CA* gene mutation in one tumour in this study.

Pivovarcikova et al. (21) discussed three TSC/mTOR pathway mutation-associated eosinophilic renal tumours, including eosinophilic solid and cystic renal cell carcinoma (ESC RCC), eosinophilic vacuolated tumours (EVT) and LOT. ESC RCC (22) is arranged in solid areas of eosinophilic cells with cytoplasmic stippling combined with cystic spaces lined by similar cells with a hobnail-shaped configuration. The tumour typically demonstrates the CK7-/CD117-/CK20+/vimentin+ immunophenotype. EVT demonstrates a solid growth architecture, large eosinophilic cells with distinct intracytoplasmic vacuoles, prominent cell membranes, large nuclei with prominent nucleoli, a CK7-/CD117+/CD10+/cathepsin K+ immunophenotype (23), and sporadic *TSC/MTOR* mutations (24). Recently, Xia et al. (13) further explored the molecular characteristics of *TSC/MTOR*-associated eosinophilic renal tumours, which included ESC RCC, EVT, LOT and unclassified renal tumours with *TSC/MTOR* mutations (*TSC-mt* RCC-NOS). They observed a specific trend in *TSC/MTOR* mutation in different tumours. ESC RCC and *TSC*-mt RCC-NOS displayed consistent *TSC1/TSC2* mutations, EVT demonstrated equal mutation distributions in *TSC* and *MTOR* genes, and all LOT cases but one bearing *TSC1* mutation displayed *MTOR* gene mutations.

LOT shows some similarities with oncocytoma and E-ChRCC. Oncocytoma often contains the CD117+/CK7− immunophenotype, and commonly exhibits recurrent chromosomal losses (1, 14, 21, X, Y) (14). E-ChRCC is characterized by eosinophilic tumour cells with raisinoid nuclei and perinuclear haloes and demonstrates CK7+/CD117+ immunophenotype. Some tumours are associated with Birt-Hogg-Dubé (BHD) syndrome harbouring *FLCN* germline mutations. Hybrid oncocytic/chromophobe tumour (HOCT) was initially described in patients with BHD syndrome harbouring *FLCN* gene mutations (14). The other differential entities include SDH-deficient RCC, TFEB translocation RCC, and oncocytic type of FH-deficient RCC. SDH-deficient RCC is negative for CK7, and loss of SDHB protein as determined by IHC (25). TFEB translocation RCC (26) is positive for cathepsin K, HMB45, Melan A, and TFEB. Molecular genetic analyses may detect *TFEB* gene expression. A new oncocytic type of FH-deficient RCC (27) exhibits variable cytoplasmic vacuolation, IHC shows strong nucleocytoplasmic 2SC positivity, PAX8 positivity and loss of FH expression, and can identify *FH* gene mutations. The broader differential types include epithelioid angiomyolipoma, CCRCC and PRCC with eosinophilic features, which are usually easily distinguished from LOT.

In summary, we present a 5-case series of LOT, an emerging entity of renal tumour with indolent clinical behaviour, which often presents a diagnostic challenge because renal tumours with oncocytic cytoplasm have a wide morphologic spectrum. The remarkable morphological features, immunohistochemical profile positive for CK7 and GATA3, and absent (or rarely weak) expression of CD117 and FOXI1 may help to avoid misdiagnosis. In challenging cases, the molecular genetic features of *TSC/mTOR* pathway mutations help to make the correct diagnosis.

Data availability statement

The datasets presented in this study can be found in online repositories. The names of the repository/repositories and accession number(s) can be found in the article/Supplementary Material.

Ethics statement

Written informed consent was obtained from the individual(s) for the publication of any potentially identifiable images or data included in this article.

Author contributions

TC: Design of the study and writing-original draft; TL and CW: Data acquisition and investigation; HW and YS: Data analysis and methodology; YP: Design of the study, writing-editing and reviewing. All authors contributed to the article and approved the submitted version.

Conflict of interest

The authors declare that the research was conducted in the absence of any commercial or financial relationships that could be construed as a potential conflict of interest.

Supplementary material

The Supplementary Material for this article can be found online at: https://www.por-journal.com/articles/10.3389/pore.2023.1610852/full#supplementary-material

References

1. Trpkov K, Hes O. New and emerging renal entities: A perspective post-WHO 2016 classification. *Histopathology* (2019) 74(1):31–59. doi:10.1111/his.13727

2. Trpkov K, Williamson SR, Gao Y, Martinek P, Cheng L, Sangoi AR, et al. Low-grade oncocytic tumour of kidney (CD117-negative, cytokeratin 7-positive): A distinct entity? *Histopathology* (2019) 75(2):174–84. doi:10.1111/his.13865

3. Akgul M, Al-Obaidy KI, Cheng L, Idrees MT. Low-grade oncocytic tumour expands the spectrum of renal oncocytic tumours and deserves separate classification: A review of 23 cases from a single tertiary institute. *J Clin Pathol* (2021) 75:772–5. doi:10.1136/jclinpath-2021-207478

4. Guo Q, Liu N, Wang F, Guo Y, Yang B, Cao Z, et al. Characterization of a distinct low-grade oncocytic renal tumor (CD117-negative and cytokeratin 7-positive) based on a tertiary oncology center experience: The new evidence from China. *Virchows Arch* (2021) 478(3):449–58. doi:10.1007/s00428-020-02927-0

5. Kravtsov O, Gupta S, Cheville JC, Sukov WR, Rowsey R, Herrera-Hernandez LP, et al. Low-Grade Oncocytic Tumor of Kidney (CK7-Positive, CD117-Negative): Incidence in a single institutional experience with clinicopathological and molecular characteristics. *Hum Pathol* (2021) 114:9–18. doi:10.1016/j.humpath.2021.04.013

6. Lerma LA, Schade GR, Tretiakova MS. Co-existence of ESC-RCC, EVT, and LOT as synchronous and metachronous tumors in six patients with multifocal neoplasia but without clinical features of tuberous sclerosis complex. *Hum Pathol* (2021) 116:1–11. doi:10.1016/j.humpath.2021.06.002

7. Bai YF, Chang CD, Wang B, Zhao M, Teng XD. CK7+/CD117-low grade oncocytic tumor of the kidney: A clinicopathological analysis. *Zhonghua Bing Li Xue Za Zhi* (2022) 51(10):976–80. doi:10.3760/cma.j.cn112151-20220719-00627

8. Kapur P, Gao M, Zhong H, Chintalapati S, Mitui M, Barnes SD, et al. Germline and sporadic mTOR pathway mutations in low-grade oncocytic tumor of the kidney. *Mod Pathol* (2022) 35(3):333–43. doi:10.1038/s41379-021-00896-6

9. Morini A, Drossart T, Timsit MO, Sibony M, Vasiliu V, Gimenez-Roqueplo AP, et al. Low-grade oncocytic renal tumor (LOT): Mutations in mTOR pathway genes and low expression of FOXI1. *Mod Pathol* (2022) 35(3):352–60. doi:10.1038/s41379-021-00906-7

10. Xie B, Cheng LC, Yin GL, Liu BA, Hu ZL, Tong K. Clinicopathological features of low-grade oncocytic renal tumor (CD117-negative, cytokeratin 7-positive): Report of seven cases. *Zhonghua Bing Li Xue Za Zhi* (2022) 51(8):719–25. doi:10.3760/cma.j.cn112151-20220410-00263

11. Zhang HZ, Xia QY, Wang SY, Shi MJ. Low-grade oncocytic tumor of kidney harboring TSC/MTOR mutation: Clinicopathologic, immunohistochemical and molecular characteristics support a distinct entity. *Virchows Arch* (2022) 480(5):999–1008. doi:10.1007/s00428-022-03283-x

12. Williamson SR, Hes O, Trpkov K, Aggarwal A, Satapathy A, Mishra S, et al. Low-grade oncocytic tumour of the kidney is characterised by genetic alterations of TSC1, TSC2, MTOR or PIK3CA and consistent GATA3 positivity. *Histopathology* (2022) 82:296–304. doi:10.1111/his.14816

13. Xia QY, Wang XT, Zhao M, He HY, Fang R, Ye SB, et al. TSC/MTOR -associated eosinophilic renal tumors exhibit a heterogeneous clinicopathologic spectrum: A targeted next-generation sequencing and gene expression profiling study. *Am J Surg Pathol* (2022) 46(11):1562–76. doi:10.1097/PAS.0000000000001955

14. WHO Classification of Tumours. *Urinary and male genital tumors*. 5th ed. Lyon (France): International Agency for Research on Cancer (2022).

15. Tong K, Hu Z. FOXI1 expression in chromophobe renal cell carcinoma and renal oncocytoma: A study of the cancer genome atlas transcriptome-based outlier mining and immunohistochemistry. *Virchows Arch* (2021) 478(4):647–58. doi:10.1007/s00428-020-02900-x

16. Miettinen M, McCue PA, Sarlomo-Rikala M, Rys J, Czapiewski P, Wazny K, et al. GATA3: A multispecific but potentially useful marker in surgical pathology: A systematic analysis of 2500 epithelial and nonepithelial tumors. *Am J Surg Pathol* (2014) 38(1):13–22. doi:10.1097/PAS.0b013e3182a0218f

17. Mantilla JG, Antic T, Tretiakova M. GATA3 as a valuable marker to distinguish clear cell papillary renal cell carcinomas from morphologic mimics. *Hum Pathol* (2017) 66:152–8. doi:10.1016/j.humpath.2017.06.016

18. Al-Obaidy KI, Eble JN, Cheng L, Williamson SR, Sakr WA, Gupta N, et al. Papillary renal neoplasm with reverse polarity: A morphologic, immunohistochemical, and molecular study. *Am J Surg Pathol* (2019) 43(8):1099–111. doi:10.1097/PAS.0000000000001288

19. Mansoor M, Siadat F, Trpkov K. Low-grade oncocytic tumor (LOT) - a new renal entity ready for a prime time: An updated review. *Histol Histopathol* (2022) 37(5):405–13. doi:10.14670/HH-18-435

20. Miricescu D, Balan DG, Tulin A, Stiru O, Vacaroiu IA, Mihai DA, et al. PI3K/AKT/mTOR signalling pathway involvement in renal cell carcinoma pathogenesis (Review). *Exp Ther Med* (2021) 21(5):540. doi:10.3892/etm.2021.9972

21. Pivovarcikova K, Alaghehbandan R, Vanecek T, Ohashi R, Pitra T, Hes O. TSC/mTOR pathway mutation associated eosinophilic/oncocytic renal neoplasms: A heterogeneous group of tumors with distinct morphology, immunohistochemical profile, and similar genetic background. *Biomedicines* (2022) 10(2):322. doi:10.3390/biomedicines10020322

22. Trpkov K, Abou-Ouf H, Hes O, Lopez JI, Nesi G, Comperat E, et al. Eosinophilic solid and cystic renal cell carcinoma (ESC RCC): Further morphologic and molecular characterization of ESC RCC as a distinct entity. *Am J Surg Pathol* (2017) 41(10):1299–308. doi:10.1097/PAS.0000000000000838

23. He H, Trpkov K, Martinek P, Isikci OT, Maggi-Galuzzi C, Alaghehbandan R, et al. High-grade oncocytic renal tumor": Morphologic, immunohistochemical, and molecular genetic study of 14 cases. *Virchows Arch* (2018) 473(6):725–38. doi:10.1007/s00428-018-2456-4

24. Farcas M, Gatalica Z, Trpkov K, Swensen J, Zhou M, Alaghehbandan R, et al. Eosinophilic vacuolated tumor (EVT) of kidney demonstrates sporadic TSC/MTOR mutations: Next-generation sequencing multi-institutional study of 19 cases. *Mod Pathol* (2022) 35(3):344–51. doi:10.1038/s41379-021-00923-6

25. Tsai TH, Lee WY. Succinate dehydrogenase-deficient renal cell carcinoma. *Arch Pathol Lab Med* (2019) 143(5):643–7. doi:10.5858/arpa.2018-0024-RS

26. Xia QY, Wang XT, Fang R, Wang Z, Zhao M, Chen H, et al. Clinicopathologic and molecular analysis of the TFEB fusion variant reveals new members of TFEB translocation renal cell carcinomas (RCCs): Expanding the genomic spectrum. *Am J Surg Pathol* (2020) 44(4):477–89. doi:10.1097/PAS.0000000000001408

27. Smith SC, Sirohi D, Ohe C, McHugh JB, Hornick JL, Kalariya J, et al. A distinctive, low-grade oncocytic fumarate hydratase-deficient renal cell carcinoma, morphologically reminiscent of succinate dehydrogenase-deficient renal cell carcinoma. *Histopathology* (2017) 71(1):42–52. doi:10.1111/his.13183

Pathology & Oncology Research | frontiers

TYPE Original Research
PUBLISHED 09 January 2023
DOI 10.3389/pore.2022.1610831

Check for updates

OPEN ACCESS

EDITED BY
József Tímár,
Semmelweis University, Hungary

*CORRESPONDENCE
Levente Kuthi,
kuthi.levente@med.u-szeged.hu

RECEIVED 19 September 2022
ACCEPTED 20 December 2022
PUBLISHED 09 January 2023

CITATION
Fejes Z, Sánta F, Jenei A, Király IE, Varga L and Kuthi L (2023), Angiomyolipoma of the kidney—Clinicopathological analysis of 52 cases.
Pathol. Oncol. Res. 28:1610831.
doi: 10.3389/pore.2022.1610831

COPYRIGHT
© 2023 Fejes, Sánta, Jenei, Király, Varga and Kuthi. This is an open-access article distributed under the terms of the Creative Commons Attribution License (CC BY). The use, distribution or reproduction in other forums is permitted, provided the original author(s) and the copyright owner(s) are credited and that the original publication in this journal is cited, in accordance with accepted academic practice. No use, distribution or reproduction is permitted which does not comply with these terms.

Angiomyolipoma of the kidney—Clinicopathological analysis of 52 cases

Zsuzsanna Fejes[1], Fanni Sánta[2], Alex Jenei[3], István Előd Király[4], Linda Varga[5] and Levente Kuthi[2]*

[1]Department of Radiology, Albert Szent-Györgyi Medical School, University of Szeged, Szeged, Hungary, [2]Department of Pathology, Albert Szent-Györgyi Medical School, University of Szeged, Szeged, Hungary, [3]Department of Pathology and Experimental Cancer Research, Semmelweis University, Budapest, Hungary, [4]Department of Urology, Albert Szent-Györgyi Medical School, University of Szeged, Szeged, Hungary, [5]Department of Oncotherapy, Albert Szent-Györgyi Medical School, University of Szeged, Szeged, Hungary

The renal angiomyolipoma (AML) is a benign tumor characteristically composed of fat, smooth muscle tissue, and vessels. We collected AMLs from our nephrectomy database, reclassified them according to their histological appearance, recorded the demographic, clinical, and pathological parameters, and compared them with oncocytoma (RO) and renal cell carcinoma (RCC). Immunohistochemistry was ordered in 41 cases. In 2224 nephrectomies, we found 52 AMLs with a 53 mm median size. The mean age was 52.76. Forty-eight tumors were sporadic, while four were hereditary. The revision resulted in 31 classic, 13 leiomyoma-like, five lipoma-like, two epithelioid, and one AML with epithelial cysts. SMA was diffusely positive, except for the epithelioid type, while MelanA harbored stronger expression than HMB45. AML was more frequent in females and appeared ten and 7 years earlier than RO and RCC, respectively. The follow-up time was 7.42 years, and neither tumor-related death nor relapse occurred. AML is rare in nephrectomies and develops primarily in females in their 50s with an average size of 50–60 mm at the surgery. The histological appearance in order of frequency is classic, leiomyoma-like, lipoma-like, epithelioid, and cystic. The MelanA, HMB45, and SMA immunohistochemistry can support the light-microscopic findings.

KEYWORDS

AML, angiomyolipoma, kidney tumor, tuberous sclerosis, nephrectomy

Introduction

The angiomyolipoma (AML) is a benign tumor occurring mainly in the kidney and belongs to the perivascular epithelioid cell tumors (PEComa) [1, 2]. Generally, AML is composed of thick-walled vessels, adipose, and smooth muscle tissue in various distributions [3], but occasionally, the tumor has cystic, leiomyoma-like, lipoma-like, or epithelioid appearance [4]. In contrast to classic AML, the latter has malignant potential, and a certain number of these cases may relapse or give distant metastasis [4]. AML can be sporadic or hereditary and linked to tuberous sclerosis (TSC) [5]. Sporadic tumors are four times more frequent in females, related to hormonal causes [6,

7]. Hereditary cases develop in younger individuals and have no gender predilection [4, 8]. Genetically speaking, AMLs are characterized by the biallelic inactivation of *TSC1* or *TSC2* genes [5, 9], which encode the hamartin and tuberin, respectively [5, 10]. These proteins, along with TBC1D7, build up the TSC1-TSC2 complex that regulates the cellular metabolism, protein synthesis, and cell cycle *via* the mTOR pathway [11]. AML occurs approximately in 1% of the nephrectomy specimens [4]. Most of the sporadic cases are discovered accidentally, but infrequently (2.2%), they may cause hemorrhage, which positively correlates with the tumor size [12, 13]. In a typical clinical scenario, the imaging technics can differentiate AMLs from renal cell tumors [14, 15], and for these cases, the radiologic follow-up might be adequate and beneficial. However, the usual sensitivity of radiological techniques is inappropriate in epithelioid and leiomyoma-like morphology [16]. Surgical removal is needed for tumor-related symptoms, compression of the adjacent structures, and hemorrhagic complications [17]. If applicable, nephron-sparing techniques should be used [17]. For classic AML, the pathological diagnosis is usually straightforward [4], but tumors with epithelioid [18] and leiomyoma-like [4] morphology often require extensive immunohistochemical examinations to exclude renal cell carcinoma (RCC), metastasis, and sarcoma. Multifocality and bilaterality are worrisome features for TSC; consequently, in the cases, clinical genetic consultation along with the investigation of the *TSC1* and *TSC2* are necessary [19]. Peripheral blood and buccal smear can be the source for the germline testing of the genes mentioned above [19]. We collected 52 consecutively removed AMLs and analyzed the patients' clinical characteristics and the tumors' pathological features.

Materials and methods

Case selection and pathological revision

AML cases were collected from the archive of the Department of Pathology, Albert Szent-Györgyi Medical School, University of Szeged. Two pathologists (AJ and LK) reviewed all hematoxylin eosin-stained slides and available immunohistochemical staining. They reclassified the cases according to the current classification scheme, and the subtypes were as follows: classic AML, AML with epithelial cysts (AMLEC), lipoma-like AML, leiomyoma-like AML, oncocytic AML, and epithelioid AML (eAML) [4]. In this study, solely nephrectomy samples were enrolled; therefore, biopsy and autopsy cases were excluded. The demographic data (age and gender) along with the main clinical features (symptoms and syndromic background) were collected. The tumors' size, laterality, and multifocality were registered based on the original pathology report. These characteristics were compared with renal cell carcinoma (RCC) and oncocytoma (RO).



FIGURE 1
Ruptured angiomyolipoma with hemorrhage. There is a fatty tumor on the cut surface with several foci of hemorrhage (red arrow). On the other hand, several smaller tumor nodules are present (black arrow). The renal parenchyma is hard to recognize (asterisks).

Immunohistochemistry

All immunohistochemical stains available in 22 tumors were reviewed. By using tissue microarray technique, another 19 AMLs were stained by MelanA (Labvision, clone A103, mouse monoclonal antibody, dilution 1:200), HMB45 (Cell Marque, clone hmb-45, mouse monoclonal antibody, dilution: 1:200), and SMA (Cell Marque, clone 1a4, mouse monoclonal antibody, dilution: 1:300). Two 2-mm-thick tissue cores represented the tumors. The reactions were evaluated in a semiquantitative fashion (0% positivity = negative; 1%–50% positivity = +; 51%–100% positivity = ++). The FFPE blocks were unavailable in eleven cases; hence, no immunohistochemistry was performed for these tumors.

Statistical analysis

For parametric and non-parametric tests, the SPSS software package was applied, and the differences were deemed significant if $p < .05$.

Results

Clinical aspects

Fifty-two AML cases were diagnosed from 2224 nephrectomy specimens. The mean age of all patients was 52.76 years (range 27–76 years). In males, 7 tumors, while, in females, 45 AMLs occurred (female-to-male ratio:

TABLE 1 The clinical features of the cases investigated.

Case	Age	Sex	Signs/Circumstances of discovery	Tuberous sclerosis	Surgery	Additional data
1	52	F	No data	No	Radical nephrectomy	-
2	66	F	Incidental finding at cholecystectomy	No	Tumor resection	-
3	73	F	Tumor rupture	No	Total nephrectomy	-
4	36	F	No data	No	Total nephrectomy	-
5	46	F	Tumor rupture	No	Total nephrectomy	-
6	55	F	Tumor rupture	No	Total nephrectomy	-
7	58	F	Retroperitoneal hemorrhage	No	Total nephrectomy	-
8	33	F	No data	Yes	Total nephrectomy	-
9	26	F	No data	No	Total nephrectomy	-
10	49	F	No data	No	Tumor resection	-
11	26	F	Surgical finding at kidney transplantation	No	Total nephrectomy	-
12	45	F	Incidental finding at SLE examination	No	Tumor resection	-
13	34	F	No data	Yes	Radical nephrectomy	-
14	46	F	No data	No	Total nephrectomy	-
15	53	F	No data	No	Radical nephrectomy	-
16	47	F	No data	No	Tumor resection	-
17	62	F	No data	No	Total nephrectomy	-
18	60	F	No data	No	Total nephrectomy	-
19	52	F	Tumor rupture	No	Radical nephrectomy	-
20	49	F	Incidental finding on abdominal US	No	Total nephrectomy	-
21	49	F	At the examination of hemorrhoids	No	Radical nephrectomy	-
22	60	F	Tumor rupture	No	Total nephrectomy	-
23	57	F	No data	No	Radical nephrectomy	-
24	60	F	Hematuria	No	Total nephrectomy	-
25	67	F	No data	No	Total nephrectomy	-
26	35	F	No data	No	Total nephrectomy	-
27	56	M	At the examination of kidney stones	No	Tumor resection	-
28	31	F	At the examination of PCOS	No	Tumor resection	-
29*	40	F	Hemorrhagic shock	Yes	Total nephrectomy	-
30	58	F	Tumor rupture	No	Total nephrectomy	Evolved in horseshoe kidney
31	43	M	At the examination for kidney transplantation	No	Radical nephrectomy	Evolved in polycystic kidney
32	66	F	No data	No	Total nephrectomy	-
33	73	M	At the examination of BPH	No	Tumor resection	-
34	76	F	Incidental finding on abdominal US	No	Tumor resection	-
35	54	M	At graft kidney's follow-up	No	Tumor resection	Evolved in graft kidney
36	65	F	No data	No	Total nephrectomy	-
37	68	M	No data	No	Total nephrectomy	-
38	68	F	No data	No	Total nephrectomy	-
39	46	M	At the examination of urethral discharge	No	Total nephrectomy	-
40	75	F	No data	No	Total nephrectomy	Ipsilateral RO is present
41	69	F	No data	No	Tumor resection	-
42	56	F	No data	No	Tumor resection	-
43	74	F	No data	No	Total nephrectomy	Ipsilateral ccRCC is present
44*	43	F	Renal pain, tumor rupture	Yes	Radical nephrectomy	-
45	65	F	No data	No	Tumor resection	-
46	33	F	No data	No	Tumor resection	-
47	31	M	No data	No	Total nephrectomy	-
48	57	F	No data	No	Total nephrectomy	-

(Continued on following page)

TABLE 1 (*Continued*) The clinical features of the cases investigated.

Case	Age	Sex	Signs/Circumstances of discovery	Tuberous sclerosis	Surgery	Additional data
49	46	F	Renal colic	No	Total nephrectomy	Ipsilateral HOCT and ccRCC are present
50	60	F	At gastrointestinal examination	No	Tumor resection	-
51	54	F	Subcostal pain	No	Total nephrectomy	-
52	41	F	Incidental finding on abdominal US	No	Tumor resection	-

F, Female; M, Male; SLE, Systemic lupus erythematosus; US, Ultrasound; PCOS, Polycystic ovary syndrome; BPH, Benign prostatic hyperplasia; RO, Renal oncocytoma; ccRCC, Clear cell renal cell carcinoma; RCC-U, Renal cell carcinoma unclassified. * Case #29 and #44 are from the same patient.

6.42:1). Forty-eight tumors were sporadic in our data set, and four were linked to TSC. The mean ages of sporadic and TSC cases were 54.04 and 37.75, respectively. One tumor developed in polycystic kidney disease, and another one evolved in a graft kidney. Tumor rupture and hemorrhagic complications occurred in eight patients (shown in Figure 1), and in one case, a hemorrhagic shock was developed as well. Fourteen tumors were resected, while total and radical nephrectomy was carried out in 30 and 8 patients, respectively. The median follow-up time was 2.64 years, and neither local relapse nor tumor-related death was registered. The patients' clinical characteristics are summarized in Table 1.

Pathological aspects

The median size of all tumors was 53 mm (range: 4–300 mm), but in cases with tuberous sclerosis, it was found to be 260 mm. The revision of the cases resulted in thirty-one classic, thirteen leiomyoma-like, five lipoma-like, two epithelioid, and one AMLEC. No oncocytic AML was seen. Synchronous tumors were observed in four cases (Table 1). Seven AMLs were multifocal. A renal sinus invasion was present in case #37 and #51 along with the infiltration of the renal vein in the latter. Both cases harbored epithelioid morphology. Besides, microscopic tumor necrosis was solely present in eAMLs. At least one melanocytic and smooth muscle marker was expressed in every case. Diffuse SMA-positivity was seen in all tumors except the eAMLs. Among the melanocytic markers, the MelanA was stronger (+ = 16; ++ = 18) compared to HMB45 (+ = 27, ++ = 7). Ki67 immunohistochemistry was available for six tumors, and the mean proliferation activity was about 1%. The morphological aspects are summarized in Table 2.

Classic AML

Classic AML was the most common subtype (59.61%). Two tumors occurred in males (case #31 and #33). In case #35, the tumor developed in damaged kidney parenchyma (polycystic kidney), while, in case #33, the patient used finasteride to treat benign prostatic hyperplasia. All TSC-linked cases showed classic morphology. Figure 2 presents the morphological features of this subtype. Here, the median size of the tumors was 52 mm (range: 4–300 mm).

Leiomyoma-like AML

This morphology was seen in 25% of the AMLs investigated. These tumors contained only a small amount of fat tissue; therefore, macroscopically, they caused no impression of AML (shown in Figure 3).

Lipoma-like AML

We registered a lipoma-like appearance in five cases, and case #35 evolved in a transplanted kidney. Figure 4 summarizes the morphological characteristics of this subtype.

Epithelioid AML

We diagnosed two tumors as eAML. This subtype required several immunohistochemical staining at the original histological diagnosis. Invasion, mitotic activity, and tumor cell necrosis were exclusively seen in these tumors (shown in Figure 5).

AML with epithelial cysts

This tumor was discovered in a 46-years-old male. The relatively small lesion was accidentally noticed during a urological investigation. Histologically, the tumor shared some characteristics with metanephric stromal tumor, and the tumor cells were estrogen and progesterone receptor-positive. We have no data on any hormonal treatment. Figure 6 represents the histological features of AMLEC.

Correlation with different renal neoplasms

We compared the gender, age and tumor size of AML patients with those, who were operated with oncocytoma (RO)

TABLE 2 The pathological characteristics of the cases investigated.

Case	Laterality	Focality	Size (mm)	Histological subtype	Immunohistochemistry
1	Right	Unifocal	20	Leiomyoma-like	MelanA: ++, HMB45: +, SMA: ++
2	Right	Unifocal	6	Leiomyoma-like	MelanA: ++, HMB45: +, SMA: ++
3	Right	Unifocal	No data	Classic	MelanA: -, HMB45: +, SMA: ++
4	Left	Unifocal	40	Classic	MelanA: +, HMB45: +, SMA: ++
5	Left	Unifocal	75	Classic	MelanA: ++, HMB45: +, SMA: ++
6	Right	Unifocal	20	Classic	MelanA: ++, HMB45: −, SMA: ++
7	Right	Unifocal	39	Leiomyoma-like	MelanA: ++, HMB45: +, SMA: ++
8	Left	Multifocal	No data	Classic	MelanA: ++, HMB45: ++, SMA: ++
9	Right	Unifocal	36	Leiomyoma-like	MelanA: ++, HMB45: ++, SMA: ++
10	Left	Unifocal	70	Lipoma-like	MelanA: +, HMB45: +, SMA: ++
11	Left	Multifocal	No data	Classic	Not performed
12	Right	Unifocal	22	Classic	MelanA: +, HMB45: +, SMA: ++
13	Left	Multifocal	200	Classic	MelanA: ++, HMB45: ++, SMA: ++
14	Left	Multifocal	25	Classic	Not performed
15	Right	Unifocal	90	Classic	Not performed
16	Right	Unifocal	20	Classic	Not performed
17	Left	Unifocal	17	Leiomyoma-like	HMB45: +, SMA: ++
18	Left	Unifocal	25	Classic	Not performed
19	Left	Unifocal	46	Classic	MelanA: ++, HMB45: ++, SMA: ++
20	Right	Unifocal	170	Lipoma-like	Not performed
21	Left	Unifocal	65	Classic	Not performed
22	Left	Unifocal	245	Classic	Not performed
23	Left	Unifocal	100	Classic	MelanA: +, HMB45: +, SMA: ++
24	Right	Unifocal	30	Leiomyoma-like	Not performed
25	Right	Unifocal	40	Classic	MelanA: +, HMB45: −, SMA: ++
26	Left	Unifocal	80	Classic	MelanA: −, HMB45: +, SMA: ++
27	Left	Unifocal	37	Leiomyoma-like	HMB45: +, SMA: ++
28	Right	Unifocal	40	Classic	MelanA: ++, HMB45: ++, SMA: ++, CD1a: −, Ki67: 1%
29	Right	Multifocal	300	Classic	MelanA: +, HMB45: +, SMA: ++
30	Right	Unifocal	155	Classic	MelanA: +, HMB45: +, SMA: ++
31	Left	Multifocal	6	Classic	MelanA: ++, HMB45: +, SMA: ++
32	Left	Unifocal	42	Leiomyoma-like	MelanA: +, HMB45: +, SMA: ++, h-Caldesmon: ++
33	Left	Unifocal	20	Classic	MelanA: +, HMB45: +, SMA: ++, CathepsinK: +
34	Left	Unifocal	31	Leiomyoma-like	MelanA: ++, HMB45: ++, SMA: ++ CD1a: −
35	Right	Unifocal	45	Lipoma-like	MelanA: ++, HMB45: ++, SMA: ++
36	Right	Unifocal	No data	Classic	Not performed
37	Left	Unifocal	40	Epitheloid	MelanA: +, HMB45: +, SMA: +, EMA: −, PAX2: −, S100: −, CD56: −, Ki67: 1%
38	Left	Unifocal	69	Classic	MelanA: ++, HMB45: -, SMA: ++
39	Right	Unifocal	20	Cystic	Epithel: CK7: ++, PAX8: ++, MNF116: ++, Stroma: MelanA: +, HMB45: +, SMA: ++, ER: +, PR: +, TLE1: −, S100: −, CD34: −, Ki67: <1%
40	Right	Unifocal	4	Classic	MelanA: +, HMB45: +, SMA: ++
41	Left	Unifocal	23	Leiomyoma-like	MelanA: +, HMB45: −, SMA: ++
42	Left	Unifocal	46	Classic	MelanA: ++, HMB45: −, SOX10: -, SMA: ++
43	Right	Unifocal	11	Leiomyoma-like	MelanA: +, HMB45: −, SMA: ++
44	Left	Unifocal	260	Classic	MelanA: ++, HMB45: +, SMA: ++
45	Right	Unifocal	30	Lipoma-like	Not performed
46	Graft	Unifocal	5	Lipoma-like	MelanA: +, HMB45: +, SMA: ++, S100: ++, CD34: -, Ki67: <1%
47	Left	Unifocal	52	Leiomyoma-like	HMB45: +, SMA: ++, CD117: +, Ki67: 1%–2%

(Continued on following page)

TABLE 2 (*Continued*) The pathological characteristics of the cases investigated.

Case	Laterality	Focality	Size (mm)	Histological subtype	Immunohistochemistry
48	Right	Unifocal	28	Classic	HMB45: +, SMA: ++
49	Left	Multifocal	4	Classic	MelanA: −, HMB45: ++, PAX8: −, SDHB: ++, β-Catenin: ++ (membrane), SMA: ++
50	Left	Unifocal	15	Leiomyoma-like	MelanA: ++, HMB45: +, SMA: ++, Ki67: 1%–2%
					MelanA: +, HMB45: -, SMA: +, CD68: +, CathepsinK: +, CD117: +, PAX2: −
51	Left	Unifocal	42	Epitheloid	PAX8: −, FH: ++, SDHB: ++, CA9: −, CK7: −, CD10: −, TFE3: −, GATA3: −
					PBRM1: ++, BAP1: ++
52	Left	Unifocal	55	Classic	MelanA: ++, HMB45: +, SMA: ++

− = negative (0% positivity), + = 1%–50% positivity, ++ = 51%–100% positivity.
HMB45, Human melanoma black 45; SMA, Smooth muscle actin; CD, Cluster of differentiation; EMA, Epithelial membrane antigen; PAX, Paired-box; ER, Estrogen receptor; PR, Progesterone receptor; TLE1, Transducin-like enhancer of split 1; SOX10, SRY-related HMG-box 10; SDHB, Succinate dehydrogenase B subunit; FH, Fumarate hydratase; CA9, Carbonic anhydrase 9; CK7, Cytokeratin 7; TFE3, Transcription factor 3E; GATA3, GATA-binding factor 3; PBRM1, Polybromo 1; BAP1, BRCA1 associated protein 1.

and renal cell carcinoma (RCC). The AML is more common in females (AML vs. RO; $p < .001$; AML vs. RCC $p < .001$). Concerning the age among AML, onocytoma and RCC patients, the AML occurs 10 years and 7 years prior to the two aforementioned tumors, respectively (AML [mean age = 52.76] vs. RO [mean age = 62.41], $p < .001$; AML [mean age = 52.76] vs. RCC [mean age = 59.58], $p < .001$). There is no difference in terms of the tumor size among the three tumors (AML [mean size = 59.56 mm] vs. RO [mean size = 48.3 mm], $p = .78$; AML [mean size = 59.56 mm] vs. RCC [mean size = 62.61 mm], $p = .571$).

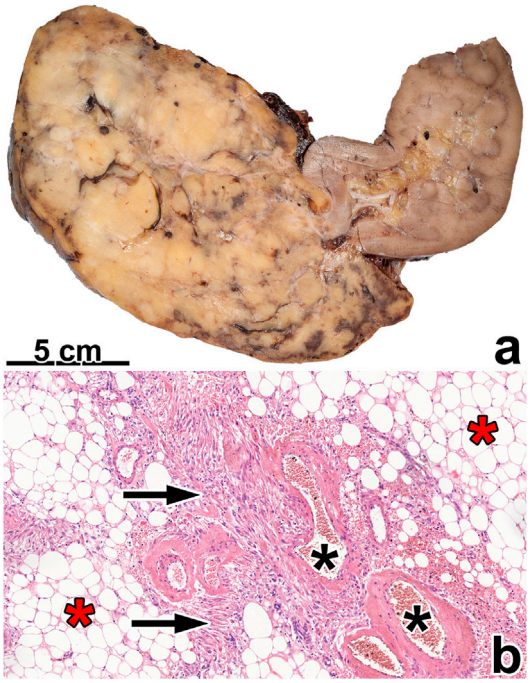

FIGURE 2
Classic angiomyolipoma. **(A)** The tumor is separated from the kidney parenchyma and has a fat tissue-like appearance. **(B)** Histologically, the tumor contains fat tissue (red asterisks), smooth muscle cells (black arrow), and thick blood vessels with hyaline walls (black asterisks). The image has a magnification factor of ×100.

Discussion

Oncocytoma and AML are the most common benign tumors of the kidney [4]. The former originates from the collecting ducts, while the latter comes from the perivascular epithelioid cells; hence it belongs to the PEComa tumor group [4]. PEComas include lymphangioleiomyomatosis, lung clear cell (sugar) tumor, and abdominopelvic PEComa [20, 21]. These tumors have a myomelanocytic differentiation with an expression of smooth muscle and melanocytic markers [1,2,3,4]. Based on the literature data, approximately 1% of nephrectomies are carried out due to AML [14]. We had a slightly higher incidence rate (2.33%). The difference might have two causes. At first, the specimens studied are collected for a relatively long period of time (1978–2021), and secondly, during nearly 45 years, the availability and sensitivity of the imaging techniques evolved significantly. The AML can be sporadic or linked to TSC [4]. The former is more frequent in females (female-to-male ratio = approximately 4:1) [22, 23]. This difference might have hormonal causes since the tumor cells in AML can express hormone receptors; moreover, in pregnant, the underlying AMLs can start a rapid enlargement [6, 7, 24]. We also found female dominance in our material with a female-to-male ratio of 6.14:1. Some authors suggest the syndromic cases lack the gender difference [12], while others state the opposite [4]. In our case set, all AMLs linked to TSC involved females. AML can occur at any age, but sporadic cases are mostly diagnosed at the end of the fourth or in the beginning of the fifth decades [6, 8]. We had a similar observation: our sporadic cases' mean age was 52.76, and on the other hand, TSC-linked AMLs developed 15 years earlier

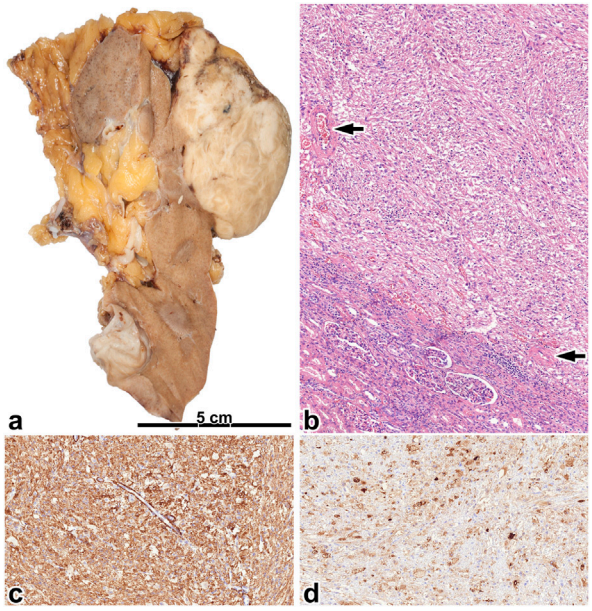

FIGURE 3
Leiomyoma-like angiomyolipoma. **(A)** Here, a greyish and whitish mass is present in the upper pole of the kidney, which is separated from the renal parenchyma and penetrates expansively to the adipose capsule. **(B)** The tumor is built up of spindle-shaped cells and blood vessels with thick walls (black arrow). The image has a magnification factor of ×100. **(C,D)** The SMA and MelanA immunostainings are diffusely positive. The two images have a magnification factor of ×200.

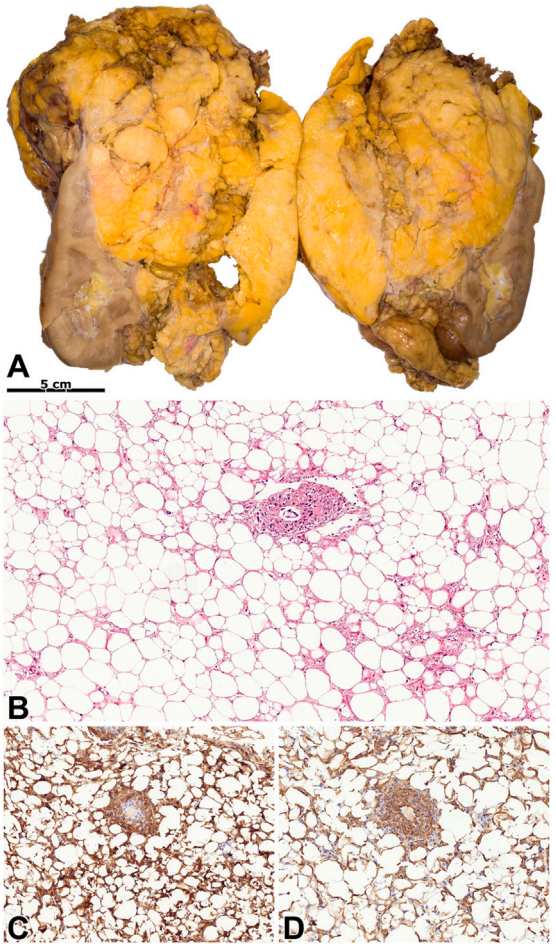

FIGURE 4
Lipoma-like angiomyolipoma. **(A)** An extensive mass with a fat-like appearance can be seen on the kidney's cut surface. **(B)** The tumor histologically resembles lipoma, and blood vessels are occasionally seen. Besides, there are foci of smooth muscle cells among the adipocytes. The image has a magnification factor of ×100. **(C,D)** The tumor cells have diffuse co-expression (insert) of SMA and MelanA. The two images have a magnification factor of ×200.

(mean age: 37.75). Also, we found that the sporadic AMLs appear approximately 10 years earlier than RCC; therefore, in unsure renal tumor cases, for female patients in this age group, a renal biopsy can be advised to achieve the best patient care. For childhood AML cases, genetic consultation and studies are required [8]. AMLs usually have no symptoms, and they are incidental findings of examinations for other underlying disorders (i.e., hypertension, staging of malignant tumor) [4, 25]. According to the literature data, tumors larger than 40 mm induce symptoms in 80% of the cases. The common symptoms are groin pain, hematuria, and newly recognized high blood pressure [26]. Hemorrhagic complications are detected more frequently in tumors larger than 40 mm [12, 25, 27]. Limited anamnestic data were available in our study. A hemorrhagic complication was reported in eight patients, one of whom developed a life-threatening hemorrhagic shock. The average size of such tumors in our material was 110 mm. Most AMLs are radiologically safe to diagnose. Like the pathological classification, imaging diagnostics classify AML into several groups, including fat tissue-rich AML, fat tissue-poor AML, and fat tissue-invisible [28]. The fat tissue-rich AML is the largest group, corresponding to the classical type known from the pathological classification. By B-mode ultrasound, fat tissue-rich AML is described as a typical, homogeneous, hyperechoic lesion with no signs of necrosis or calcification [28]. The non-enhanced CT scan also gives a typical picture (shown in Figure 7) because one can measure fat density, i.e., values below -10 HU [29]. The MRI examination may help to distinguish between AML and RCC, as the loss of signal intensity between in-phase and out-of-phase sequences indicates the presence of microscopic fat tissue [30]. The tumor is usually separated from the kidney parenchyma, renal sinus, and adipose capsule but may appear in the renal vein or the regional lymph nodes [26, 31, 32]. The latter refers to a multicentric origin rather than metastasis [33]. The composition of the tumor influences the

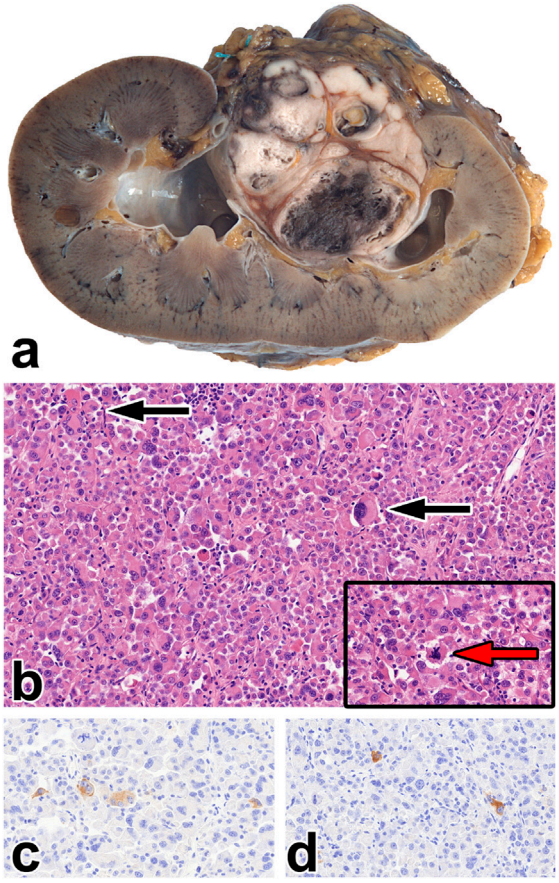

FIGURE 5
Epithelioid angiomyolipoma. **(A)** The gross picture shows a necrotic, hemorrhagic tumor located deeply in the renal sinus. **(B)** The tumor is made up of rhabdomyoblast-like cells. Besides, giant cells can be seen (black arrow), along with atypical mitosis (insert red arrow). The images have a magnification factor of ×200 and ×600, respectively. **(C,D)** MelanA and SMA co-expression is observed in some tumor cells. The two images have a magnification factor of ×400.

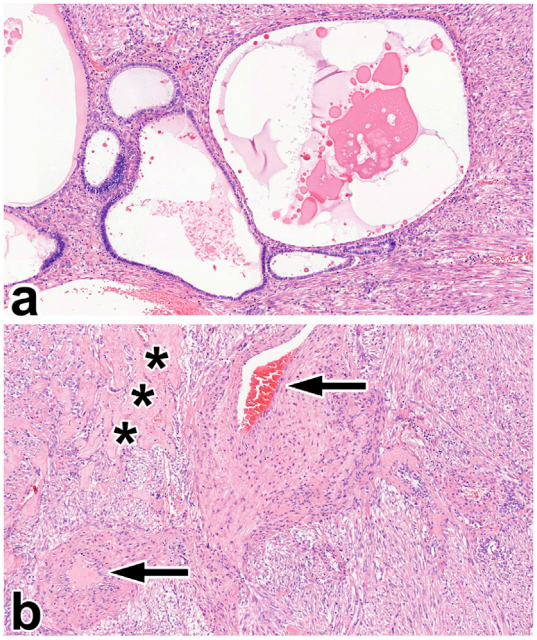

FIGURE 6
Angiomyolipoma with epithelial cysts. **(A)** The two-component tumor is built up of varying cysts in size and smooth muscle-rich stroma. **(B)** Apart from the smooth muscle cells, the stroma contains thick-walled blood vessels (black arrow) and sclerotic foci (black asterisks). All images have a magnification factor of ×100.

macroscopic appearance. The classic and lipoma-like AMLs have an adipose tissue-like cut surface, whereas leiomyoma-like AML and AMLEC mostly form a greyish-whitish mass [34]. The tumor is usually unilateral and unifocal, but 1/3 of the cases are multifocal, and 15% of the AMLs are bilateral [35]. Seven of our cases had multiple foci, and one patient with TSC had a bilateral tumor. In classic AML, the tumor consists of fat tissue, smooth muscle tissue, and thick-walled, irregular blood vessels in nearly similar proportions [36]. The adipose component corresponds to mature fat tissue, but sometimes vacuolated cells resembling lipoblasts can be detected. The smooth muscle cells typically form irregular fascicles and circular growth from the vessel wall [37]. The cytological atypia is usually mild, but sometimes, bizarre and multinucleated cells are present. The vascular component resembles thick-walled artery-like vessels with a thin elastic layer [4, 38]. The pathological diagnosis is straightforward in classic morphology, and immunostainings are unnecessary. Leiomyoma-like AMLs are often located below the fibrous capsule [39]. Because of the low-degree fat tissue component, the possibility of leiomyoma or schwannoma may arise; however, these, like other benign soft tissue tumors, are rare in the kidney and lack a myomelanocytic immunophenotype [40, 41]. In contrast to the former subtype, in the lipoma-like AML, the smooth muscle component may have a small amount, and the tumor is composed almost exclusively of fat tissue [42]. Such tumors are often associated with the adipose capsule and should be discriminated from lipoma or atypical lipomatous tumor [43]. These tumors are not characterized by myomelanocytic immunophenotype; furthermore, overexpression of MDM2 and CDK4 are seen in the latter [44]. The AMLEC is composed of stromal and epithelial components. The former is neoplastic, typically with irregular, smooth muscle bundles. The epithelial component forms cysts of varying size, but these most likely correspond to entrapped and dilated nephron segments [45, 46]. Currently, the term of angiomyolipoma with epithelial cysts is used instead

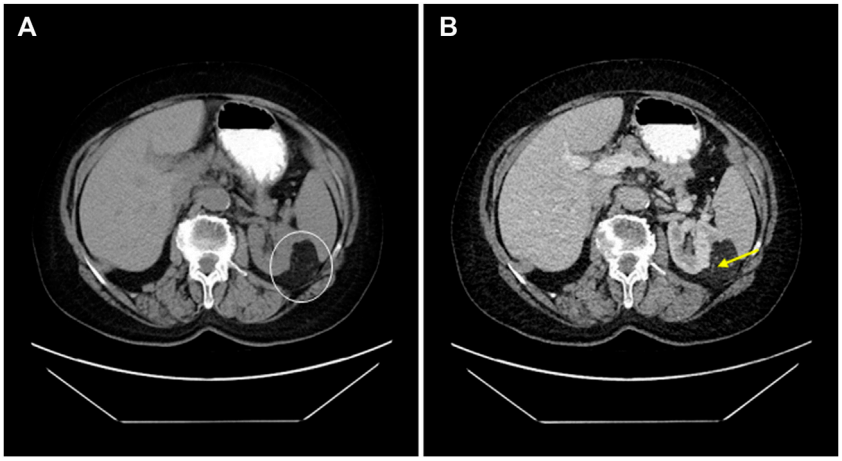

FIGURE 7
68-year-old female patient's CT scan accidentally reveals an angiomyolipoma. **(A)** A native CT scan shows a lobulated 54 mm maximal axial diametric mass with a mean density of -79 HU (white circle). **(B)** In the same plane, the venous phasic cross-section shows that the difference does not change substantially; moreover, the thick-wall blood vessels become visible (yellow arrow).

of cystic AML [47]. This subtype is characterized by hormone receptor positivity, and accordingly, the tumor should be distinguished from the mixed epithelial and stromal tumor of the kidney (MESTK) [45]. The stroma of the two entities differs because, in MESTK, it mimics the ovarian stroma. Also, MESTK has no co-expression of melanocytic and smooth muscle markers [48]. From a clinical point of view, the identification of eAML is crucial, because in contrast to the subtypes discussed so far, this variant may recur in some cases and give metastases [49]. The incidence of malignant behavior is quite different in the literature, but the likelihood is approximately 5% based on two large-number studies [37, 49]. Some epithelioid component is present in all AMLs, but if its proportion is above 80%, the tumor must be diagnosed as eAML [49, 50]. The pure eAML is rare and can cause severe diagnostic difficulties as it should be distinguished mainly from rhabdoid RCC, translocation RCC, primary renal pleomorphic sarcoma, and metastasis; therefore, a large amount of immunohistochemistry is usually performed [51, 52]. Of note, the myomelanocytic phenotype can also be observed, but it is often present focally [49]. Genetically, all types of AML are characterized by the inactivation of the *TSC1* or *TSC2*, which impairs the regulation of the mTOR signaling pathway and leads to increased cell proliferation [53]. A *TP53* mutation has also been noted in eAML, possibly contributing to the malignant clinical course [54]. Genetic testing is only required if TSC is suspected. Immunomorphologically, AML is usually diffusely positive with SMA, and other muscle markers expression is seen in 50% of cases [49]. Expression of a melanocytic marker is also always observed, most commonly MelanA or HMB45. In a comparative study of 20 cases, all AMLs were diagnosed using these two markers, and other melanocytic markers (tyrosinase, CD117, NK1-C3, etc.) have little diagnostic benefit [55]. Focal SMA staining was present in our material only in eAML, and 75.6% of the study cases expressed both melanocytic markers, of which MelanA immunostaining was generally more extensive and more often positive. Immunohistochemistry of hamartin and tuberin has no diagnostic value [56]. The treatment is influenced by tumor size, bilaterality, and the possibility of malignancy. Asymptomatic tumors below 40 mm should be monitored by annual CT or MRI [57]. A closer observation is recommended in the range of 40–80 mm; usually, surgical treatment is performed in half of the patients due to complications [57]. Surgical removal should be advised in symptomatic cases, preferably using nephron-sparing techniques [58]. The tumors larger than 80 mm have a high risk of hemorrhagic complications and should be treated surgically or with radiologic intervention, such as selective arterial embolization or radiofrequency ablation [59]. The complications and stress are less severe in intervention, but these patients should be followed because tumors may recur [60]. To maintain renal function, a nephron-sparing resection is also preferred in bilateral cases [61]. In doubtful cases, a biopsy is required as a first step, and depending on the diagnosis, observation or surgery should be carried out [57, 62]. Systemic treatment is used for metastatic eAML, which may be chemotherapy, mTOR inhibitors, or immunotherapy [63, 64].

Conclusion

AML is rare in nephrectomy specimens, and it is either sporadic or associated with TSC. It typically develops in women around 50 years, and the average size of surgically treated cases is about 50–60 mm. Histologically, the tumor may be classic, leiomyoma-like, lipoma-like, epithelioid, or cystic, in order of frequency. The eAML may be malignant, so such tumors should be treated like RCC and closely monitored. The pathological diagnosis is usually problem-free, and the light-microscopic findings may be supplemented by MelanA, HMB45, and SMA immunostaining.

Data availability statement

The raw data supporting the conclusion of this article will be made available by the authors, without undue reservation.

Ethics statement

The studies involving human participants were reviewed and approved by Regional and Institutional Human Medical Biological Research Ethics Committee, University of Szeged. Written informed consent for participation was not required for this study in accordance with the national legislation and the institutional requirements.

Author contributions

ZF prepared the figures and wrote the manuscript. IK and LV provided the patient characteristics and follow-up data. AJ and FS performed the histological analysis and immunohistochemical evaluation. LK contributed to the study concept and final supervision of the manuscript.

Funding

The University of Szeged, Faculty of Medicine Research Fund-Hetényi Géza Grant (Grant No. 5S 340 A202) and the New National Excellence Program funded this research (Grant No. UNKP-21-4-SZTE-131, UNKP-22-4-SZTE-305).

Conflict of interest

The authors declare that the research was conducted in the absence of any commercial or financial relationships that could be construed as a potential conflict of interest.

Acknowledgments

The authors gratefully acknowledge the assistance of Vivien Sánta and Samir Martin in the language editing of the text.

References

1. Folpe AL, Kwiatkowski DJ. Perivascular epithelioid cell neoplasms: Pathology and pathogenesis. *Hum Pathol* (2010) 41(1):1–15. doi:10.1016/j.humpath.2009.05.011

2. Martignoni G, Pea M, Reghellin D, Zamboni G, Bonetti F. PEComas: The past, the present and the future. *Virchows Arch* (2008) 452(2):119–32. doi:10.1007/s00428-007-0509-1

3. Martignoni G, Pea M, Reghellin D, Zamboni G, Bonetti F. Perivascular epithelioid cell tumor (PEComa) in the genitourinary tract. *Adv Anat Pathol* (2007) 14(1):36–41. doi:10.1097/PAP.0b013e31802e0dc4

4. WHO Classification of Tumours Editorial Board. Urinary and male genital tumours. In: *WHO classification of tumours series*. 5th ed.; vol. 8. Lyon (France): International Agency for Research on Cancer (2022).

5. van Slegtenhorst M, de Hoogt R, Hermans C, Nellist M, Janssen B, Verhoef S, et al. Identification of the tuberous sclerosis gene *TSC1* on chromosome 9q34. *Science* (1997) 277(5327):805–8. doi:10.1126/science.277.5327.805

6. Eble JN. Angiomyolipoma of kidney. *Semin Diagn Pathol* (1998) 15(1):21–40.

7. Henske EP, Ao X, Short MP, Greenberg R, Neumann HP, Kwiatkowski DJ, et al. Frequent progesterone receptor immunoreactivity in tuberous sclerosis-associated renal angiomyolipomas. *Mod Pathol* (1998) 11(7):665.

8. Cook JA, Oliver K, Mueller RF, Sampson J. A cross sectional study of renal involvement in tuberous sclerosis. *J Med Genet* (1996) 33(6):480–4. doi:10.1136/jmg.33.6.480

9. Smolarek TA, Wessner LL, McCormack FX, Mylet JC, Menon AG, Henske EP, et al. Evidence that lymphangiomyomatosis is caused by *TSC2* mutations: Chromosome 16p13 loss of heterozygosity in angiomyolipomas and lymph nodes from women with lymphangiomyomatosis. *Am J Hum Genet* (1998) 62(4):810–5. doi:10.1086/301804

10. European Chromosome 16 Tuberous Sclerosis Consortium. Identification and characterization of the tuberous sclerosis gene on chromosome 16. *Cell* (1993) 75(7):1305–15. doi:10.1016/0092-8674(93)90618-z

11. Dibble CC, Elis W, Menon S, Qin W, Klekota J, Asara JM, et al. TBC1D7 is a third subunit of the TSC1-TSC2 complex upstream of mTORC1. *Mol Cel* (2012) 47(4):535–46. doi:10.1016/j.molcel.2012.06.009

12. Steiner MS, Goldman SM, Fishman EK, Marshall FF. The natural history of renal angiomyolipoma. *J Urol* (1993) 150(6):1782–6. doi:10.1016/s0022-5347(17)35895-0

13. Yamakado K, Tanaka N, Nakagawa T, Kobayashi S, Yanagawa M, Takeda K. Renal angiomyolipoma: Relationships between tumor size, aneurysm formation, and rupture. *Radiology* (2002) 225(1):78–82. doi:10.1148/radiol.2251011477

14. Fujii Y, Ajima J, Oka K, Tosaka A, Takehara Y. Benign renal tumors detected among healthy adults by abdominal ultrasonography. *Eur Urol* (1995) 27:124–7. doi:10.1159/000475142

15. Halpenny D, Snow A, McNeill G, Torreggiani WC. The radiological diagnosis and treatment of renal angiomyolipomacurrent status. *Clin Radiol* (2010) 65(2):99–108. doi:10.1016/j.crad.2009.09.014

16. Varma S, Gupta S, Talwar J, Forte F, Dhar M. Renal epithelioid angiomyolipoma: A malignant disease. *J Nephrol* (2011) 24(1):18–22. doi:10.5301/jn.2010.5451

17. Kyo CK, Won TK, Won SH, Jin SL, Hee JJ, Young DC. Trends of presentation and clinical outcome of treated renal angiomyolipoma. *Yonsei Med J* (2010) 51(5):728–34. doi:10.3349/ymj.2010.51.5.728

18. Zavala-Pompa A, Folpe AL, Jimenez RE, Lim SD, Cohen C, Eble JN, et al. Immunohistochemical study of microphthalmia transcription factor and tyrosinase in angiomyolipoma of the kidney, renal cell carcinoma, and renal and retroperitoneal sarcomas: Comparative evaluation with traditional diagnostic

markers. *Am J Surg Pathol* (2001) 25(1):65–70. doi:10.1097/00000478-200101000-00007

19. Amin S, Kingswood JC, Bolton PF, Elmslie F, Gale DP, Harland C, et al. The UK guidelines for management and surveillance of Tuberous Sclerosis Complex. *QJM* (2019) 112(3):171–82. doi:10.1093/qjmed/hcy215

20. Travis WD, Brambilla E, Nicholson AG, Yatabe Y, Austin JHM, Beasley MB, et al. The 2015 world health organization classification of lung tumors: Impact of genetic, clinical and radiologic advances since the 2004 classification. *J Thorac Oncol* (2015) 10(9):1243–60. doi:10.1097/JTO.0000000000000630

21. Bennett JA, Braga AC, Pinto A, Van de Vijver K, Cornejo K, Pesci A, et al. Uterine PEComas: A morphologic, immunohistochemical, and molecular analysis of 32 tumors. *Am J Surg Pathol* (2018) 42(10):1370–83. doi:10.1097/PAS.0000000000001119

22. Baniak N, Barletta JA, Hirsch MS. Key renal neoplasms with a female predominance. *Adv Anat Pathol* (2021) 28(4):228–50. doi:10.1097/PAP.0000000000000301

23. Jenei A, Hes O, Kuthi L. Provisional renal cell carcinoma subsets following the 2016 WHO classification. *Orv Hetil* (2020) 161(3):83–94. doi:10.1556/650.2020.31654

24. Yanai H, Sasagawa I, Kubota Y, Ishigooka M, Hashimoto T, Kaneko H, et al. Spontaneous hemorrhage during pregnancy secondary to renal angiomyolipoma. *Urol Int* (1996) 56(3):188–91. doi:10.1159/000282838

25. Oesterling JE, Fishman EK, Goldman SM, Marshall FF. The management of renal angiomyolipoma. *J Urol* (1986) 135(6):1121–4. doi:10.1016/s0022-5347(17)46013-7

26. Bakshi SS, Vishal K, Kalia V, Gill JS. Aggressive renal angiomyolipoma extending into the renal vein and inferior vena cava - an uncommon entity. *Br J Radiol* (2011) 84(1004):e166–8. doi:10.1259/bjr/98449202

27. Tong YC, Chieng PU, Tsai TC, Lin SN. Renal angiomyolipoma: Report of 24 cases. *Br J Urol* (1990) 66(6):585–9. doi:10.1111/j.1464-410x.1990.tb07187.x

28. Song S, Park BK, Park JJ. New radiologic classification of renal angiomyolipomas. *Eur J Radiol* (2016) 85(10):1835–42. doi:10.1016/j.ejrad.2016.08.012

29. Park BK. Renal angiomyolipoma: Radiologic classification and imaging features according to the amount of fat. *Am J Roentgenol* (2017) 209(4):826–35. doi:10.2214/AJR.17.17973

30. Shetty AS, Sipe AL, Zulfiqar M, Tsai R, Raptis DA, Raptis CA, et al. In-phase and opposed-phase imaging: Applications of chemical shift and magnetic susceptibility in the chest and abdomen. *Radiographics* (2019) 39(1):115–35. doi:10.1148/rg.2019180043

31. Shirotake S, Yoshimura I, Kosaka T, Matsuzaki S. A case of angiomyolipoma of the renal sinus. *Clin Exp Nephrol* (2011) 15(6):953–6. doi:10.1007/s10157-011-0519-9

32. Lin WY, Chuang CK, Ng KF, Liao SK. Renal angiomyolipoma with lymph node involvement: A case report and literature review. *Chang Gung Med J* (2003) 26(8):607.

33. Ackerman TE, Levi CS, Lindsay DJ, Greenberg HM, Gough JC. Angiomyolipoma with lymph node involvement. *Can Assoc Radiol J* (1994) 45(1):52.

34. Stone CH, Lee MW, Amin MB, Yaziji H, Gown AM, Ro JY, et al. Renal angiomyolipoma: Further immunophenotypic characterization of an expanding morphologic spectrum. *Arch Pathol Lab Med* (2001) 125(6):751–8. doi:10.1043/0003-9985(2001)125<0751:RA>2.0.CO;2

35. Sooriakumaran P, Gibbs P, Coughlin G, Attard V, Elmslie F, Kingswood C, et al. Angiomyolipomata: Challenges, solutions, and future prospects based on over 100 cases treated. *BJU Int* (2010) 105(1):101–6. doi:10.1111/j.1464-410X.2009.08649.x

36. Schieda N, Kielar AZ, Al Dandan O, McInnes MD, Flood TA. Ten uncommon and unusual variants of renal angiomyolipoma (AML): Radiologic-pathologic correlation. *Clin Radiol* (2015) 70(2):206–20. doi:10.1016/j.crad.2014.10.001

37. Aydin H, Magi-Galluzzi C, Lane BR, Sercia L, Lopez JI, Rini BI, et al. Renal angiomyolipoma: Clinicopathologic study of 194 cases with emphasis on the epithelioid histology and tuberous sclerosis association. *Am J Surg Pathol* (2009) 33(2):289–97. doi:10.1097/PAS.0b013e31817ed7a6

38. Katabathina VS, Vikram R, Nagar AM, Tamboli P, Menias CO, Prasad SR. Mesenchymal neoplasms of the kidney in adults: Imaging spectrum with radiologic-pathologic correlation. *Radiographics* (2010) 30(6):1525–40. doi:10.1148/rg.306105517

39. Di BA, Ferrara G, Gogglia P. Renal capsuloma: Description of a case with predominantly muscular differentiation. *Pathologica* (2003) 95(2):119.

40. Aldughiman AW, Alzahrani A, Alzahrani T. Renal leiomyoma: Case report and literature review. *J Endourol Case Rep* (2019) 5(4):181–3. doi:10.1089/cren.2019.0049

41. Gobbo S, Eble JN, Huang J, Grignon DJ, Wang M, Martignoni G, et al. Schwannoma of the kidney. *Mod Pathol* (2008) 21(6):779–83. doi:10.1038/modpathol.2008.52

42. Mehta V, Venkataraman G, Antic T, Rubinas TC, Le Poole IC, Picken MM. Renal angiomyolipoma, fat-poor variant - a clinicopathologic mimicker of malignancy. *Virchows Arch* (2013) 463(1):41–6. doi:10.1007/s00428-013-1432-2

43. Oh SD, Oh SJ, Suh BJ, Shin JY, Oh CK, Park JK, et al. A giant retroperitoneal liposarcoma encasing the entire left kidney and adherent to adjacent structures: A case report. *Case Rep Oncol* (2016) 9(2):368–72. doi:10.1159/000447488

44. Knebel C, Neumann J, Schwaiger BJ, Karampinos DC, Pfeiffer D, Specht K, et al. Differentiating atypical lipomatous tumors from lipomas with magnetic resonance imaging: A comparison with *MDM2* gene amplification status. *BMC Cancer* (2019) 19(1):309. doi:10.1186/s12885-019-5524-5

45. Davis CJ, Barton JH, Sesterhenn IA. Cystic angiomyolipoma of the kidney: A clinicopathologic description of 11 cases. *Mod Pathol* (2006) 19(5):669–74. doi:10.1038/modpathol.3800572

46. Fine SW, Reuter VE, Epstein JI, Argani P. Angiomyolipoma with epithelial cysts (AMLEC): A distinct cystic variant of angiomyolipoma. *Am J Surg Pathol* (2006) 30(5):593–9. doi:10.1097/01.pas.0000194298.19839.b4

47. Armah HB, Yin M, Rao UN, Parwani AV. Angiomyolipoma with epithelial cysts (AMLEC): A rare but distinct variant of angiomyolipoma. *Diagn Pathol* (2007) 2:11. doi:10.1186/1746-1596-2-11

48. Michal M, Hes O, Bisceglia M, Simpson RH, Spagnolo DV, Parma A, et al. Mixed epithelial and stromal tumors of the kidney. A report of 22 cases. *Virchows Arch* (2004) 445(4):359–67. doi:10.1007/s00428-004-1060-y

49. Nese N, Martignoni G, Fletcher CD, Gupta R, Pan CC, Kim H, et al. Pure epithelioid PEComas (so-called epithelioid angiomyolipoma) of the kidney: A clinicopathologic study of 41 cases: Detailed assessment of morphology and risk stratification. *Am J Surg Pathol* (2011) 35(2):161–76. doi:10.1097/PAS.0b013e318206f2a9

50. Brimo F, Robinson B, Guo C, Zhou M, Latour M, Epstein JI. Renal epithelioid angiomyolipoma with atypia: A series of 40 cases with emphasis on clinicopathologic prognostic indicators of malignancy. *Am J Surg Pathol* (2010) 34(5):715–22. doi:10.1097/PAS.0b013e3181d90370

51. He W, Cheville JC, Sadow PM, Gopalan A, Fine SW, Al-Ahmadie HA, et al. Epithelioid angiomyolipoma of the kidney: Pathological features and clinical outcome in a series of consecutively resected tumors. *Mod Pathol* (2013) 26(10):1355–64. doi:10.1038/modpathol.2013.72

52. Mete O, van der Kwast TH. Epithelioid angiomyolipoma: A morphologically distinct variant that mimics a variety of intra-abdominal neoplasms. *Arch Pathol Lab Med* (2011) 135(5):665–70. doi:10.1043/2009-0637-RSR.1

53. Giannikou K, Malinowska IA, Pugh TJ, Yan R, Tseng YY, Oh C, et al. Whole exome sequencing identifies TSC1/TSC2 biallelic loss as the primary and sufficient driver event for renal angiomyolipoma development. *Plos Genet* (2016) 12(8):e1006242. doi:10.1371/journal.pgen.1006242

54. Li W, Guo L, Bi X, Ma J, Zheng S. Immunohistochemistry of p53 and Ki-67 and p53 mutation analysis in renal epithelioid angiomyolipoma. *Int J Clin Exp Pathol* (2015) 8(8):9446.

55. Roma AA, Magi-Galluzzi C, Zhou M. Differential expression of melanocytic markers in myoid, lipomatous, and vascular components of renal angiomyolipomas. *Arch Pathol Lab Med* (2007) 131(1):122–5. doi:10.1043/1543-2165(2007)131[122:DEOMMI]2.0.CO;2

56. Bonsib SM, Boils C, Gokden N, Grignon D, Gu X, Higgins JP, et al. Tuberous sclerosis complex: Hamartin and tuberin expression in renal cysts and its discordant expression in renal neoplasms. *Pathol Res Pract* (2016) 212(11):972–9. doi:10.1016/j.prp.2016.04.005

57. Sobiborowicz A, Czarnecka AM, Szumera-Ciećkiewicz A, Rutkowski P, Świtaj T. Rozpoznanie i leczenie nowotworów typu angiomyolipoma (AML). *Oncol Clin Pract* (2020) 16(3):116–32. doi:10.5603/ocp.2020.0008

58. Ljungberg B, Albiges L, Abu-Ghanem Y, Bensalah K, Dabestani S, Fernández-Pello S, et al. European association of urology guidelines on renal cell carcinoma: The 2019 update. *Eur Urol* (2019) 75(5):799–810. doi:10.1016/j.eururo.2019.02.011

59. Fernández-Pello S, Hora M, Kuusk T, Tahbaz R, Dabestani S, Abu-Ghanem Y, et al. Management of sporadic renal angiomyolipomas: A systematic review of available evidence to guide recommendations from the European association of urology renal cell carcinoma guidelines panel. *Eur Urol Oncol* (2020) 3(1):57–72. doi:10.1016/j.euo.2019.04.005

60. Vos N, Oyen R. Renal angiomyolipoma: The good, the bad, and the ugly. *J Belg Soc Radiol* (2018) 102(1):41. doi:10.5334/jbsr.1536

61. Kuusk T, Biancari F, Lane B, Tobert C, Campbell S, Rimon U, et al. Treatment of renal angiomyolipoma: Pooled analysis of individual patient data. *BMC Urol* (2015) 15:123. doi:10.1186/s12894-015-0118-2

62. Bissler JJ, Kingswood JC. Renal angiomyolipomata. *Kidney Int* (2004) 66(3):924–34. doi:10.1111/j.1523-1755.2004.00838.x

63. Lei JH, Liu LR, Wei Q, Song TR, Yang L, Yuan HC, et al. A four-year follow-up study of renal epithelioid angiomyolipoma: A multi-center experience and literature review. *Sci Rep* (2015) 5:10030. doi:10.1038/srep10030

64. Lattanzi M, Deng FM, Chiriboga LA, Femia AN, Meehan SA, Iyer G, et al. Durable response to anti-PD-1 immunotherapy in epithelioid angiomyolipoma: A report on the successful treatment of a rare malignancy. *J Immunother Cancer* (2018) 6(1):97. doi:10.1186/s40425-018-0415-x

Pathology & Oncology Research | frontiers

TYPE Original Research
PUBLISHED 11 December 2023
DOI 10.3389/pore.2023.1611547

Check for updates

OPEN ACCESS

EDITED BY
Andrea Ladányi,
National Institute of Oncology (NIO), Hungary

*CORRESPONDENCE
Evelin Makk,
makk.evelin@gmail.com

RECEIVED 12 October 2023
ACCEPTED 28 November 2023
PUBLISHED 11 December 2023

CITATION
Makk E, Bohonyi N, Oszter A, Éles K, Tornóczky T, Tóth A, Kálmán E and Kovács K (2023), Comparative analysis of EZH2, p16 and p53 expression in uterine carcinosarcomas.
Pathol. Oncol. Res. 29:1611547.
doi: 10.3389/pore.2023.1611547

COPYRIGHT
© 2023 Makk, Bohonyi, Oszter, Éles, Tornóczky, Tóth, Kálmán and Kovács. This is an open-access article distributed under the terms of the Creative Commons Attribution License (CC BY). The use, distribution or reproduction in other forums is permitted, provided the original author(s) and the copyright owner(s) are credited and that the original publication in this journal is cited, in accordance with accepted academic practice. No use, distribution or reproduction is permitted which does not comply with these terms.

Comparative analysis of EZH2, p16 and p53 expression in uterine carcinosarcomas

Evelin Makk[1]*, Noémi Bohonyi[2], Angéla Oszter[1], Klára Éles[1], Tamás Tornóczky[1], Arnold Tóth[3], Endre Kálmán[1] and Krisztina Kovács[1]

[1]Department of Pathology, University of Pécs Medical School, Pécs, Hungary, [2]Department of Obstretrics and Gynaecology, University of Pécs Medical School, Pécs, Hungary, [3]Department of Medical Imaging, University of Pécs Medical School, Pécs, Hungary

Introduction: The role of p16 and p53 immunohistochemistry in the diagnosis of rare and aggressive uterine carcinosarcoma (UCS) has been well established. However, enhancer of zeste homolog 2 (EZH2), a histone methyltransferase and a member of the polycomb group family is a relatively new biomarker, with limited published data on its significance in this tumor type. The goal of this study was to examine EZH2 expression in UCS and its components, in correlation with morphological features, and p16 and p53 staining patterns.

Methods: Twenty-eight UCSs were included in the study. EZH2, p16 and p53 immunoreactivity were assessed independently by two pathologists in both tumor components (epithelial and mesenchymal). EZH2 and p16 immunostains were scored semiquantitatively: based on the percentage and intensity of tumor cell staining a binary staining index ("high- or low-expressing") was calculated. The p53 staining pattern was evaluated as wild-type or aberrant (diffuse nuclear, null, or cytoplasmic expression). Statistical tests were used to evaluate the correlation between staining patterns for all three markers and the different tumor components and histotypes.

Results: High EZH2 and p16 expression and aberrant p53 patterns were present in 89.3% 78.6% and 85.7% of the epithelial component and in 78.6%, 62.5% and 82.1% of the mesenchymal component, respectively. Differences among these expression rates were not found to be significant ($p > 0.05$). Regarding the epithelial component, aberrant p53 pattern was found to be significantly ($p = 0.0474$) more frequent in the serous (100%) than in endometrioid (66.6%) histotypes. Within the mesenchymal component, p53 null expression pattern occurred significantly ($p = 0.0257$) more frequently in heterologous sarcoma components (71.4%) compared to the homologous histotype (18.8%).

Abbreviations: MMMT: Malignant mixed Müllerian tumor; UCS: Uterine carcinosarcoma; EMT: Epithelial-mesenchymal transition; EZH2: Enhancer of zeste homologue 2; RMS: Rhabdomyosarcoma; IHC: Immunohistochemistry; ec: epithelial component; mc: mesenchymal component.

Conclusion: In conclusion, EZH2, p16 and p53 seem to play a universal role in the pathogenesis of UCS; however, a distinctive pattern of p53 expression appears to exist between the serous and endometrioid carcinoma components and also between the homologous and heterologous sarcoma components.

KEYWORDS

uterine cancer, carcinosarcoma, EZH2, p16, p53

Introduction

Uterine carcinosarcoma (UCS), or uterine malignant mixed Müllerian tumor (MMMT) is a very aggressive and rare neoplasm of the female genital tract, comprising less than 5% of endometrial malignancies [1].

This tumor has a biphasic morphology, containing both malignant epithelial (carcinomatous) and malignant mesenchymal (sarcomatous) components [2]. In most cases, it consists of a single carcinoma and a single homologous sarcoma histologic subtype. The former is usually serous carcinoma, followed by less common endometrioid, clear cell, undifferentiated, and mixed histotypes. The mesenchymal component is most often a homologous high grade sarcoma, and less often it consists of a heterologous rhabdomyosarcoma (RMS), chondrosarcoma, osteosarcoma, or liposarcoma [3, 4].

The majority of studies support the "metaplastic monoclonal or conversion theory," whereby UCS develops from the metaplastic transformation of a single neoplastic cell type [5]. As part of the process, epithelial-mesenchymal transition (EMT) allows a polarized epithelial cell to transmogrify into a mesenchymal cell phenotype, giving the ability for it to migrate away from its original epithelial layer [6]. The EMT theory is supported by high epithelial to mesenchymal transition gene signature scores and is likely due to epigenetic alterations at microRNA promoters and histone gene mutations and amplifications [7]. However, a small percentage of UCS seem to represent real collision tumors, since they are molecularly biclonal and most likely develop from two independent cell populations [8].

Carcinosarcomas exhibit a significantly poorer prognosis compared to other high-grade endometrial carcinomas such as grade 3 endometrioid carcinoma, serous carcinoma and clear cell carcinoma [9].

Polycomb group proteins are a group of important epigenetic regulators. Enhancer of zeste homologue 2 (EZH2), a histone lysin methyltransferase and a catalytic component of polycomb repressive complex 2 is involved in cell proliferation, cell differentiation and tumorigenesis by silencing the transcription of several tumor suppressor genes (including p21, p16 and p27) [10–13]. Accordingly, numerous studies have highlighted the role of EZH2 in cancer development and progression. Overexpression of EZH2 protein has been shown in various malignant tumors, including carcinomas of the breast [14], lung [15], stomach [16], colon [17], pancreatobiliary tract [18], liver [19], thyroid gland [20], prostate [21], and bladder [22]. EZH2 has been also studied in most common gynecologic malignancies such as cervical [23, 24], endometrial [25, 26] and ovarian cancer [27, 28].

In recent years, EZH2 expression has also been discovered in certain sarcomas, including Ewing sarcoma [29], RMS [30, 31], synovial sarcoma [32], osteosarcoma [33], and chondrosarcoma [34].

Strong evidence demonstrated that EZH2 could promote EMT [35, 36], therefore, we postulated that aberrant EZH2 overexpression may also be invoved in the pathogenesis of UCS.

Nevertheless, only limited data are available regarding EZH2 expression and its clinicopathological correlations in UCS. EZH2 positivity in UCS was previously only reported in one effusion cytology specimen [37].

p53 is a frequently used immunohistochemical marker in the diagnostic work-up of endometrial carcinomas, and based on The Cancer Genome Atlas database over 90% of UCS harbor TP53 mutation [38]. Similarly, the p16-RB pathway has also been previously implicated in the pathogenesis of UCS [39].

In this study, our goal was to investigate the potential role of EZH2 along with p16 and p53 biomarkers in the diagnosis and histogenesis of UCS components and their histotypes.

Materials and methods

Subjects

The study was approved by our institutional ethical committee (number of permission: KK/644-1/2020). Consecutive cases of UCS diagnosed from 2012 to 2019 were retrieved from the archives of the Department of Pathology, University of Pécs, Hungary.

Formalin-fixed and paraffin embedded tissue samples were collected from hysterectomy and biopsy (curettage) specimens. The original hematoxylin and eosin–stained slides from each case were reviewed, and representative blocks containing both malignant epithelial and mesenchymal components were selected for immunohistochemistry (IHC). The epithelial component was subclassified according to the current WHO classification [40] as serous, endometrioid, clear cell,

undifferentiated and mixed histotypes, while the mesenchymal component was classified as homologous or heterologous type.

Immunohistochemical analysis of EZH2, p16 and p53 expression

For IHC, 4 μm thick sections were cut from the formalin-fixed paraffin-embedded tissue specimens. Immunostaining for EZH2 (mouse monoclonal, clone 6A10, prediluted, Newcastle Upon Tyne, United Kingdom), for p16 (mouse monoclonal, clone E6H4; Ventana Medical System Inc., Tucson, AZ), and for p53 (rabbit monoclonal, clone SP5, prediluted; Thermo Scientific, United States) were performed with proper positive and negative controls using Leica Bond Max autostainer (Leica Biosystems, Bannockburn, IL) and Leica Bond Polymer Refine Detection Kit (Upon Tyne, United Kingdom). Immunoreactivity was evaluated in both the epithelial and mesenchymal components independently by two board-certified pathologists with over 15 years of professional experience (K.K., A.O.).

EZH2 and p16 expression were scored semiquantitatively according to the percentage of tumor cell nuclear staining: 1+: <10% of tumor cell nuclei, 2+: between 10% and 50% of tumor cell nuclei, 3+: >50% of tumor cell nuclei [24, 41–44], and staining intensity (0: no staining, 1+: weak, 2+: moderate, 3+: strong). As in the previous studies, a staining index was calculated as the product of staining percentage and intensity on a scale of 0–9 [45, 46]. The tumors were categorized as high-expressing (staining index >4) or low-expressing (staining index ≤4).

P53 immunoreactivity interpretation was conducted according to the recommendations by the International Society for Gynecological Pathologists [47]. The p53 staining pattern was evaluated as wild-type or aberrant (latter can be further classified as diffuse nuclear, null, or cytoplasmic expression) [48]. In more details, wild-type (normal) pattern is met when a scattered nuclear staining is present with no or weak cytoplasmic staining; Aberrant/diffuse nuclear pattern is met when 80% strong and diffuse nuclear staining is present (with or without any cytoplasmic staining), Aberrant/null pattern is met when a complete absence of nuclear staining in all cells is present without cytoplasmic staining; Aberrant/cytoplasmic pattern is met when a moderate to strong cytoplasmic staining is present in the absence of diffuse nuclear expression.

Statistical evaluation

For EZH2 and p16, the median staining index scores (low or high expression) of the two experts were calculated in both components. Regarding staining percentage and staining intensity, the ratings were summed up for further analysis. Discordant p53 pattern ratings were reevaluated and the final result was decided in consensus. The EZH2 and p16 expression indices and p53 staining patterns were compared between the epithelial and mesenchymal components, as well as between the serous and endometrioid carcinoma components, and between the homologous and heterologous sarcoma components. Mixed and undifferentiated epithelial histotypes were excluded from histotype comparisons due to the low case numbers. Depending on the sample size, Chi square or Fisher exact tests were used to compare categorical values (staining index and p53 staining pattern) while Mann-Whitney test was used to compare ordinal values (staining percentage and staining intensity). Concordance between epithelial and mesenchymal components were evaluated with kappa test. All statistical tests were run in Medcalc [49]. A p-value of <0.05 was considered statistically significant [50].

Results

This study included 28 women with uterine carcinosarcoma, with a median age of 70.5 years (range 53–85 years). Formalin-fixed and paraffin embedded tissue samples were available from 22 hysterectomy and 6 biopsy (curettage) specimens. Histologically, the epithelial component comprised of 14 (50%) serous, 9 (32.1%) endometrioid, 2 (7.1%) undifferentiated, and 3 mixed (serous and endometrioid) carcinomas (10.7%). The mesenchymal component contained heterologous elements in 7 cases (25%), and homologous elements in 21 samples (75%). Among the heterologous sarcoma components, 4 chondrosarcoma and 3 RMS occurred. The most common homologous components were endometrial stromal sarcoma (n = 14), followed by 3 leiomyosarcomas, 3 undifferentiated sarcomas, and 1 myxoid fibrosarcoma.

The immunoreactivity measures of EZH2 and p16 in the epithelial and mesenchymal components are shown in Table 1. High EZH2 expression was slightly more common in the epithelial (89.3%) than in the mesenchymal (78.6%) component. Similarly, p16 expression was slightly higher in the epithelial (78.6%) compared to the mesenchymal (62.5%) components. Based on Fisher's exact test, p16 and EZH2 expressions between the epithelial and mesenchymal components were not statistically different (for EZH2 p = 0.468; for p16 p = 0.248). Based on Mann-Whitney tests, marker staining percentages and intensities were also not statistically different between the epithelial and mesenchymal components (p = 0.074 and p = 0.076 for staining percentage of EZH2 and p16, respectively; p = 0.11 and p = 0.059 for staining intensity of EZH2 and p16, respectively).

Figure 1 shows representative cases of diffuse and strong immunoreactivity with EZH2 and p16 markers and diffuse nuclear p53 pattern.

TABLE 1 Immunoreactivity of EZH2 and p16 in UCSs based on the two independent experts' ratings (medians for staining index, sums for staining percentage and nuclear intensity).

	EZH2		p16	
	Epithelial component	Mesenchymal component	Epithelial component	Mesenchymal component
Staining index	n (%)			
Low[a]	3 (10.7)	6 (21.4)	6 (21.4)	10.5 (37.5)
High[b]	25 (89.3)	22 (78.6)	22 (78.6)	17.5 (62.5)
	average[c](SD)			
Staining percentage	5.68 (0.72)	5.18 (1.15)	4.96 (1.68)	4.32 (1.87)
Nuclear Intensity	5.64 (0.95)	5.18 (1.36)	5.21 (1.5)	4.46 (1.86)

[a]Staining index of ≤ 4.
[b]Staining index of > 4.
[c]Value range = 0-6.

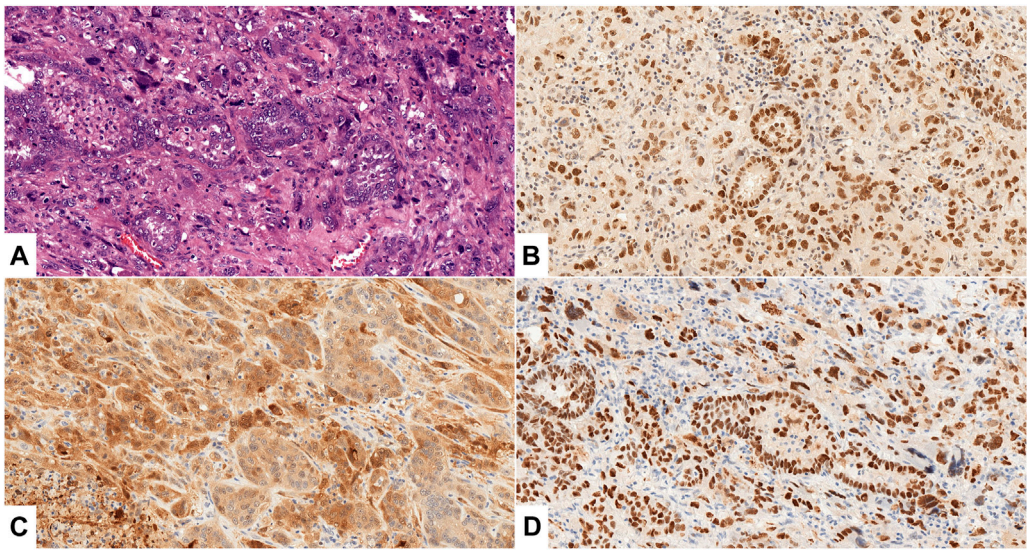

FIGURE 1
(A–D): Uterine carcinosarcoma, Case No. 26., ×200 magnification. **(A)** HE staining shows malignant epithelial (serous carcinoma) and mesenchymal (homologous undifferentiated sarcoma) components. **(B, C)** Diffuse, strong positive (3+) expression of EZH2 **(B)**, p16 **(C)** in both components; **(D)**: >80% strong and diffuse p53 nuclear staining in both components.

The immunoreactivity measures of EZH2 and p16, in the different carcinoma components are shown in Table 2. Both serous and endometrioid histotypes showed prominent staining with all markers. High expression of EZH2 was almost always present (89% for both endometrioid and serous carcinomas). High p16 expression was also very common (88% of endometroid, 79% of serous cases). There were no statistical differences in the EZH2 and p16 staining scores between the serous and endometrioid histotypes (Fisher exact test *p* values for staining index of EZH2 and p16 between the histotypes were 0.74 and 0.96 respectively. Mann-Whitney *p* values for staining percentages of EZH2 and p16 between the two carcinoma histotypes were 0.35 and 0.15, respectively. Mann-Whitney *p* values for EZH2 and p16 staining intensity between the two carcinoma histotypes were 0.37 and 0.26, respectively.)

The immunoreactivity measures of EZH2 and p16 in homologous and heterologous sarcoma components are shown in Table 3. Both sarcoma types showed similarly common high EZH2 expression (79% of the homologous elements, and 78.6% of the heterologous elements) and p16 expression (60% of the homologous elements and 72% of the heterologous elements). These markers showed no statistical differences (Fisher exact test *p* values for staining index of EZH2 and p16 between the two types were 1 and 0.66,

TABLE 2 Immunoreactivity of EZH2 and p16 in UCS epithelial component serous and endometrioid histotypes based on the two independent experts' ratings (medians for staining index, sums for staining percentage and nuclear intensity).

	EZH2				p16			
	Endometrioid	Serous	Mixed	Undiff.	Endometrioid	Serous	Mixed	Undiff.
Staining index	n (%)							
Low[a]	1 (11)	1.5 (10.7)	0.5 (16.7)	0 (0)	2 (22)	3 (21)	1 (33.3)	0 (0)
High[b]	8 (89)	12.5 (89.3)	2.5 (83.3)	2 (100)	7 (88)	11 (79)	2 (66.7)	2 (100)
	average[c] (SD)							
Staining percentage	5.77 (0.66)	5.57 (0.85)	5.66 (0.57)	6 (0)	4.88 (1.45)	4.93 (1.9)	4.66 (2.3)	6 (0)
Nuclear Intensity	5.44 (1.33)	5.71 (0.82)	5.66 (0.57)	6 (0)	5.11 (1.76)	5.28 (1.32)	4.66 (2.3)	6 (0)

[a]Staining index of ≤4.
[b]Staining index of >4.
[c]Value range = 0–6.

TABLE 3 Immunoreactivity of EZH2 and p16 in UCS mesenchymal component homologous and heterologous types based on the two independent experts' ratings (medians for staining index, sums for staining percentage and nuclear intensity).

	EZH2		p16	
	Homologous	Heterologous	Homologous	Heterologous
Staining index	n (%)			
Low[a]	4.5 (21)	1.5 (21.4)	8.5 (40)	2 (28)
High[b]	16.5 (79)	5.5 (78.6)	12.5 (60)	5 (72)
	average[c] (SD)			
Staining percentage	5.14 (1.23)	5.28 (0.95)	4.23 (1.92)	4.57 (1.81)
Nuclear Intensity	5.38 (1.28)	4.57 (1.51)	4.42 (1.98)	4.57 (1.51)

[a]Staining index of ≤4.
[b]Staining index of >4.
[c]Value range = 0–6.

TABLE 4 p53 staining patterns in UCS components and component types.

		Epithelial component					Mesenchymal component		
Expression		Endometrioid	Serous	Mixed	Undifferentiated	All	Homologous	Heterologous	All
Wild-type[a]		3/9 (33.3%)	0/14 (0%)	0/3 (0%)	1/2 (50%)	4/28 (14.3%)	5/21 (23.8%)	0/7 (0%)	5/28 (17.9%)
Aberrant[b]		6/9 (66.6%)	14/14 (100%)	3/3 (100%)	1/2 (50%)	24/28 (85.7%)	16/21 (76.2%)	7/7 (100%)	23/28 (82.1%)
Pattern	Diffuse nuclear	5/6 (83.3%)	11/14 (78.6%)	2/3 (66.7%)	0/1 (0%)	18/24 (75%)	13/16 (81.2%)	2/7 (28.6%)	15/23 (65.2%)
	Null	1/6 (16.7%)	3/14 (21.4%)	1/3 (33.3%)	1/1 (100%)	6/24 (25%)	3/16 (18.8%)	5/7 (71.4%)	8/23 (34.8%)
	Cytoplasmic	0/6 (0%)	0*/14 (0%)	0/3 (0%)	0/1 (0%)	0*/24 (0%)	0/16 (0%)	0/7 (0%)	0/23 (0%)

[a]Wild-type (normal) - scattered nuclear staining).
[b]Aberrant/Diffuse nuclear pattern: 80% strong and diffuse nuclear staining with ot without cytoplasmic staining, Aberrant/null pattern: complete absence of nuclear staining in all cells, Aberrant/cytoplasmic pattern: moderate to strong cytoplasmic staining in the absence of diffuse nuclear expression. *One serous case and two endometrioid cases presented weak to moderate cytoplasmic staining but also at least 80% strong and diffuse nuclear staining, therefore were attributed diffuse nuclear pattern (see Figure 2).

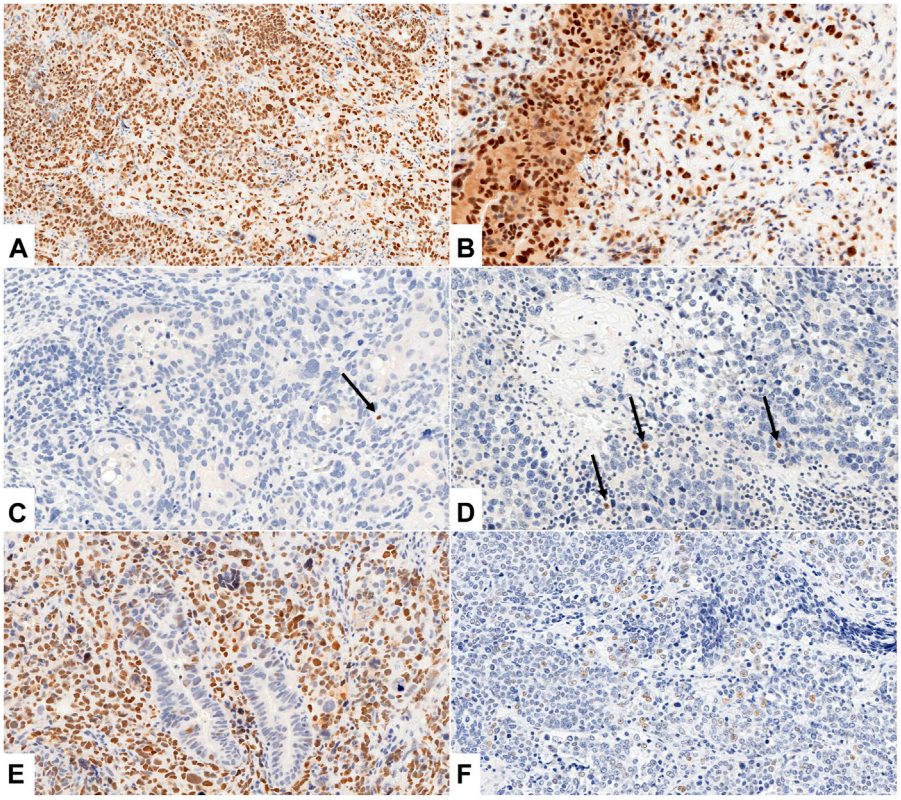

FIGURE 2
(A–F) Different patterns of p53 expression. **(A, B)** Aberrant, p53 diffuse nuclear pattern with weak **(A)** and weak to moderate **(B)** cytoplasmic staining in epithelial and mesenchymal components of UCS (**(A)**: Case No. 26., ×200 magnification, **(B)**: Case No. 5., ×400 magnification). **(C, D)** Aberrant, p53 null pattern with complete absence of nuclear staining in all cells of both components (**(C)**: Case No. 11., ×200 magnification, **(D)**: Case No. 21., ×200 magnification). Arrows indicate internal positive controls (lymphocytes). **(E, F)** Wild type p53 IHC pattern with scattered nuclear staining in epithelial **(E)** and mesenchymal **(F)** component, **(E)**: aberrant, p53 diffuse nuclear pattern in mesenchymal component (**(E)**: Case No. 19., ×200 magnification, **(F)**: Case No. 22., ×400 magnification).

respectively. Mann-Whitney *p* values for staining percentage of EZH2 and p16 between the two types were 0.37 and 0.4, respectively. Mann-Whitney *p* values for staining intensity of EZH2 and p16 between the two types were 0.1 and 0.48, respectively.)

P53 staining patterns are shown in Table 4. Aberrant p53 immunostaining was seen in 85.7% of the epithelial and 82.1% of the mesenchymal components. These values were statistically equal (Fischer test $p = 1$). P53 cytoplasmic staining was observed only focally in 3/28 cases, but none of the tumors showed aberrant cytoplasmic expression pattern. Within the epithelial components, aberrant p53 expression was found in 66.6% of the endometrioid and 100% of the serous carcinomas, which was statistically significant (Fisher test $p = 0.0474$). Regarding the mesenchymal components, homologous sarcomas showed aberrant p53 patterns in 76.2% of cases, while all heterologous sarcomas (100%) were p53 aberrant (no statistical difference, Fisher test $p = 0.29$). Aberrant null p53 pattern was observed in 71.4% of the heterologous sarcomas, whereas only 18.8% of the homologous sarcomas displayed this staining pattern (statistically significant difference, Fisher test $p = 0.0257$). Aberrant diffuse nuclear p53 expression was seen in 81.2% of the homologous sarcoma histotypes. No other significant differences were identified in p53 patterns among the UCS components and their different histotypes.

Figure 2 illustrates different patterns of p53 expression.

P53 was concordant between epithelial and mesenchymal components in 82.14% (Cohen's k: 0.34, fair agreement).

Discussion

Our results showed that EZH2 and p16 are similarly highly expressed, while p53 immunostaining is aberrant in the majority of uterine carcinosarcomas. Pattern differences were found between histotypes.

Previous studies have described various immunohistochemical profiles of carcinosarcomas.

EZH2 positivity in UCS was previously reported in a single effusion cytology specimen in one study [37], which investigated the utility of EZH2 as a single immunomarker in the diagnosis of metastatic carcinoma in effusion samples. A total of 108 pleural, peritoneal, and pericardial effusions/washings diagnosed as unequivocally reactive (n = 41) and metastatic carcinoma (n = 67) by cytomorphology over 18 months were reviewed. Among the metastatic carcinomas, 54 cases were adenocarcinoma and the remaining cases were squamous cell carcinoma (n = 1), carcinosarcoma (n = 1), and carcinoma of undefined histological subtypes (n = 11). Only one carcinosarcoma cytology specimen was included in this study that was a positive case.

The role of p16 and p53 immunohistochemistry as diagnostic and prognostic markers in UCS has been evaluated by a handful of prior studies. Engelsen et al. demonstrated that pathologic expression of p53 and p16 in endometrial curettings identifies high-risk endometrial carcinoma patients with poor prognosis [51]. Buza and Tavassoli reported p16 overexpression in the carcinomatous and sarcomatous components of uterine MMMTs, and observed that p16 immunohistochemical reaction was significantly more intense and diffuse than p53 immunostaining in both components. The concordance rates for p16 and p53 immunoreactivity for the two components within the same tumor were 83% and 90% of cases, respectively [39]. Xiaowei et al. examined the possible utility of p16, p53, and PAX8 IHC in the diagnosis of carcinosarcomas, and revealed almost equal staining in both components for p16 and p53. P16 staining showed almost equally high expression in the epithelial (74%) and mesenchymal components (71%), and p53 expression also was similar in the epithelial (48%) and mesenchymal (44%) components. High-expression of PAX8 was more common in the epithelial (73%) than in the mesenchymal (13%) components [46].

Compared to PAX8, EZH2 in our study shows not only a slightly higher expression rate in the epithelial component but is similarly highly expressed in the mesenchymal component as well.

Increased expression of EZH2 has been described in most common gynecologic malignancies such as cervical [23, 24], endometrial [25, 26] and ovarian cancer [27, 28]. Prognostic significance of EZH2 expression status has been also reported in patients with these tumours, because high expression of EZH2 was associated with tumor aggressiveness [52–54]. Therefore, EZH2 has been raised as a potential target for tumor therapy, and both preclinical and clinical studies on EZH2 inhibitors are intensively pursued [36, 55–58]. Regarding EZH2 as potential therapeutic target in UCS, no data exists in the literature.

Several further immunohistochemical markers have been studied as potential markers/adjuncts in the diagnosis of UCS as well, including p27, c-KIT, COX-2, EGFR, C-ErbB-2, the oncogene AKT [39, 59–63]. Recently, HER2 expression was also demonstrated in carcinosarcoma, as a potential therapeutic marker. Rates of HER2 overexpression or amplification were reported to be ranging from 6% to 25%. Intratumoural heterogeneity of HER2 expression/amplification and lower HER2 expression in the sarcoma component compared to the carcinoma component was also shown [62, 64, 65].

Regarding endometrial cancers in general, it is well-documented that the staining patterns of p53 and p16 are different between endometrial serous and endometrioid carcinomas [66–68]. The primary emphasis in most studies examining p53 in endometrial carcinomas is placed on the correlation between p53 overexpression and serous histology [69]. Mutations in TP53 are observable in intraepithelial carcinomas and are believed to occur at an early stage in the development of uterine serous carcinoma [70]. In a subset of endometrioid carcinomas, p53 overexpression has been documented, predominantly in tumors categorized as FIGO grade 3 endometrioid carcinomas [71]. In line with a 2018 recommendation, tumors exhibiting a double negative profile (p16-negative/p53-wild-type) are indicative of being primarily endometrioid, whereas tumors demonstrating a double positive profile (p53 aberrant/mutation-type and diffuse strong p16 positive) are more likely associated with serous histology [66]. This is consistent with the findings of the present study as we found significant more (p = 0.0474) p53 aberrant type serous than endometrioid subtype of the epithelial UCS components. The different p16 and p53 staining patterns between endometrial cancer types and UCS related epithelial component histotypes raise the possibility of their different pathomechanisms. In non-UCS related endometrial cancers, overexpression of EZH2 is well established [26, 72]. Gu et al [72] collected a total of 104 samples from patients with the diagnosis of endometrial cancer and analyzed the expression of EZH2 by immunohistochemical staining. The results showed that the positive expression rate of EZH2 was 68.27%, which was significantly higher than that in the adjacent tissue ($p < 0.05$). Krill et al [26] analysed 87 tissue specimens from sixty patients with both early and advanced stage endometrioid endometrial adenocarcinoma and 27 matched-normal tissue specimens. Their results showed that EZH2 mRNA ($p < .0001$) and protein expression ($p < .0001$) in tumor specimens were significantly higher than in the matched-normal tissue. In primary tumors, EZH2 protein expression was associated with lympho-vascular space invasion (p = .044), and EZH2 mRNA expression was associated with age (p = .037). However, these studies did not include specific cohorts of carcinosarcoma.

The pathogenesis of UCS is still debated. Authors largely agree that EMT seems to play role in its development [3, 5, 6, 73–75]. The EZH2-PRC2 complex regulates several target genes. EZH2 can directly bind to important tumor oncogenes and initiate signaling pathways for EMT events. Furthermore,

EZH2 can induce EMT. Ding et al. demonstrated that the EZH2 inhibitor GSK343 suppresses the progression of cervical cancer cells by inhibiting EMT. Their data also established that treatment with GSK343 leads to a suppression of EMT in xenograft tumours in nude mice. The observed EZH2–EMT-associated phenotypes and their underlying mechanisms have important implications for cervical cancer development and severity, which suggests that targeting this pathway through specific inhibitors would result in general epigenetic reprogramming [55]. Our data support the possible role of EZH2 in the pathogenesis of UCS along with the EMT theory.

The carcinomatous and sarcomatous components showed 85% concordance of p53 protein overexpression and 96% concordance of TP53 gene mutation, which points to a monoclonal origin of both components. P16 overexpression occurs in about 60% of UCS simultaneously with TP53 mutations. The concordance of p16 expression between the carcinomatous and sarcomatous components was approximately 85% in different series [39, 76].

P53 IHC is widely used as a surrogate for TP53 mutation testing in diagnostic gynecologic pathology [77]. P53 IHC is a reliable diagnostic adjunct for histotyping and molecular subtyping of endometrial carcinomas [48, 66, 78]. Another use of p53 IHC is triaging gynecological sarcomas for molecular testing based on the assumption that TP53-mutated gynecological sarcomas do not harbor cancer driving translocations [77]. Kunc et al. have observed high frequency of aberrant p53 IHC expression in extrauterine carcinosarcoma and high concordance between the carcinomatous and sarcomatous components [79]. Liu et al. reported p53 overexpression in 63% of UCS, with 47% and 77% overexpression in the homologous and heterologous tumors, respectively [80]. It has been recently noted that 46% of the epithelial and 53% of the mesenchymal components showed overexpression of p53, displaying a strong similarity of these tumor components [81]. In general, p53 diffuse positive cases indicate possible nonsynonymous missense mutations. In contrast, stopgain, indel or splicing mutations seem to result p53 null positive phenotype [82–84].

We observed a high frequency of aberrant p53 IHC expression in UCS with a fair concordance (82.14%, Cohen's $k = 0.34$) between the epithelial and mesenchymal components that is in line with previous reports [79–81, 85].

Cherniack et al. identified multiple somatic mutations and copy number alterations in UCSs that offer expanded therapeutic options including potential use of PARP, EZH2, cell cycle and PI3K pathway inhibitor [7]. Jones et al. in their study performed a complete exome analysis of 22 UCS and verified genetic alterations in chromatin remodelling genes. Overall, they identified 777 somatic mutations in 702 genes. Mutations in EZH2 were observed in 12% of the mutant tags [86].

The most frequently mutated genes in carcinosarcomas are TP53, PTEN, PIK3CA, RB1, PPP2R1A, FBXW7, KRAS and ARID1A [7]. In TCGA, over 90% of carcinosarcomas harbor a TP53 mutation [7]. Some carcinosarcomas share mutational profiles with the endometrioid lineage, e.g., PTEN mutation, indicating that, like serous carcinoma, an alternative route of carcinogenesis is via a low-grade endometrioid carcinoma and its precursors [87]. A comprehensive analysis of the genomic and proteomic profiles of 57 UCSs has unveiled disruptions in canonical pathways, notably the PI3K pathway. More than 75% of cases demonstrated mutations in FBXW7, loss of RB1, or amplification of CCNE1, suggesting dysregulation in cell cycle control [7].

Mutations in TP53 are frequently observed across various tumors, underscoring the pivotal involvement of the FBXW7, p53, and PI3K pathways in UCS. Among these pathways, FBXW7 stands out as a crucial driver in the development of this particular cancer [88]. Conclusive genetic evidence obtained through lineage tracing studies indicates that UCS originates from endometrial epithelial cells undergoing an epithelial-mesenchymal transition. This transition gives rise to a highly invasive phenotype, with FBXW7 identified as the specific driver in this process [89]. In accordance with the conversion theory, UCS are believed to originate in a monoclonal fashion, with carcinomatous subclones having the potential for metaplastic differentiation and subsequent transformation into sarcomatous cells [7]. Support for this theory stems from the concurrent expression of cytokeratins and epithelial membrane antigens in both carcinomatous and sarcomatous cells. Additionally, there is consistency in TP53 and KRAS mutations, identical patterns of X chromosome inactivation, and comparable loss of heterozygosity observed between the carcinomatous and sarcomatous components [7].

The main limitation of our study is that detailed molecular pathological exploration of EZH2, p53 and p16 and their interactions were not performed, which may be the focus of future research. In addition, statistical power may be impacted by the low case number, however, this is largely explained by the rarity of UCS. The applied cutoff values for defining EZH2 and p16 as low or high expressing are somewhat arbitrary and may affect case distributions. However, to date no standardized scoring has been adopted for these markers. So, instead of adjusting cutoff values for our study, we aimed to adhere to previous publications to achieve better reproducibility and comparability [24, 41–44]. Strengths of the study include that both components of UCS as well as their subtypes were analyzed.

In conclusion, EZH2, p16 and p53 seem to play a universal role in the pathogenesis of UCSs. However, a distinctive pattern of p53 expression appears to exist between the serous and endometrioid types of the epithelial component (aberrant vs. wild type) and also between the homologous and heterologous types of the mesenchymal component (diffuse nuclear aberrant vs. null aberrant). These pattern disparities may indicate unique genetical features and differentiation pathways warranting further molecular pathological studies.

Data availability statement

The raw data supporting the conclusion of this article will be made available by the authors, without undue reservation.

Ethics statement

The studies involving humans were approved by institutional ethical committee, University of Pécs (number of permission: KK/644-1/2020). The studies were conducted in accordance with the local legislation and institutional requirements. The ethics committee/institutional review board waived the requirement of written informed consent for participation from the participants or the participants' legal guardians/next of kin because the study was a retrospective analysis on non-identifiable data.

Author contributions

EM played a major role in literary research, data collection and overview, interpreted the data, edited and revised the manuscript for intellectual content. NB played a major role in literary research, interpreted the data and revised the manuscript for intellectual content. AO played a major role in data analysis, interpreted the data, and revised the manuscript for intellectual content. KÉ played a major role in data analysis, interpreted the data, and revised the manuscript for intellectual content. TT played a major role in the design and conception of the work, interpreted the data and revised the manuscript for intellectual content. AT played a major role in statistical data analysis, interpreted the data, edited and revised the manuscript for intellectual content. EK played a major role in conception of the work; analyzed the data, interpreted the data, edited and revised the manuscript for intellectual content. KK played a major role in conception of the work, analyzed the data, interpreted the data, edited and revised the manuscript for intellectual content. All authors contributed to the article and approved the submitted version.

Conflict of interest

The authors declare that the research was conducted in the absence of any commercial or financial relationships that could be construed as a potential conflict of interest.

Acknowledgments

The authors gratefully acknowledge the Immunopathology Laboratory, Department of Pathology, University of Pécs and for their technical assistance. The present scientific certification is dedicated to the 650th anniversary of the foundation of the University of Pécs, Hungary.

References

1. Loda M, Mucci LA, Mittelstadt ML, Hemelrijck MV, Cotter MB. *Pathology and epidemiology of cancer*. Cham: Springer International Publishing (2016). doi:10.1007/978-3-319-35153-7

2. Silverberg SG, Major FJ, Blessing JA, Fetter B, Askin FB, Liao SY, et al. Carcinosarcoma (malignant mixed mesodermal tumor) of the uterus: a gynecologic oncology group pathologic study of 203 cases. *Int J Gynecol Pathol* (1990) 9(1):1–19. doi:10.1097/00004347-199001000-00001

3. Artioli G, Wabersich J, Ludwig K, Gardiman MP, Borgato L, Garbin F. Rare uterine cancer: carcinosarcomas: review from histology to treatment. *Crit Rev Oncol Hematol* (2015) 94(1):98–104. doi:10.1016/j.critrevonc.2014.10.013

4. Leskela S, Pérez-Mies B, Rosa-Rosa JM, Cristobal E, Biscuola M, Palacios-Berraquero ML, et al. Molecular basis of tumor heterogeneity in endometrial carcinosarcoma. *Cancers (Basel)* (2019) 11:964. doi:10.3390/cancers11070964

5. Kernochan LE, Garcia RL. Carcinosarcomas (malignant mixed müllerian tumor) of the uterus: advances in elucidation of biologic and clinical characteristics. *J Natl Compr Cancer Netw* (2009) 7(5):550–6. doi:10.6004/jnccn.2009.0037

6. Kalluri R, Weinberg RA. The basics of epithelial-mesenchymal transition. *J Clin Invest* (2009) 119(6):1420–8. doi:10.1172/JCI39104

7. Cherniack AD, Shen H, Walter V, Stewart C, Murray BA, Bowlby R, et al. Integrated molecular characterization of uterine carcinosarcoma. *Cancer Cell* (2017) 31(3):411–23. doi:10.1016/j.ccell.2017.02.010

8. George E, Lillemoe TJ, Twiggs LB, Perrone T. Malignant mixed müllerian tumor versus high-grade endometrial carcinoma and aggressive variants of endometrial carcinoma: a comparative analysis of survival. *Int J Gynecol Pathol* (1995) 14(1):39–44. doi:10.1097/00004347-199501000-00007

9. Zhang C, Hu W, Jia N, Li Q, Hua K, Tao X, et al. Uterine carcinosarcoma and high-risk endometrial carcinomas: a clinicopathological comparison. *Int J Gynecol Cancer* (2015) 25(4):629–36. doi:10.1097/IGC.0000000000000350

10. Hock H. A complex Polycomb issue: the two faces of EZH2 in cancer. *Genes Dev* (2012) 26(8):751–5. doi:10.1101/gad.191163.112

11. Xie Z, Zhong C, Shen J, Jia Y, Duan S. LINC00963: a potential cancer diagnostic and therapeutic target. *Biomed Pharmacother* (2022) 150:113019. doi:10.1016/J.BIOPHA.2022.113019

12. Sasaki M, Nakanuma Y. Cellular senescence in biliary pathology. Special emphasis on expression of a polycomb group protein EZH2 and a senescent marker p16INK4a in bile ductular tumors and lesions. *Histol Histopathol* (2015) 30(3):267–75. doi:10.14670/HH-30.267

13. Said J. Biomarker discovery in urogenital cancer. *Biomarkers* (2005) 10(1):83–6. doi:10.1080/13547500500215050

14. Pourakbar S, Pluard TJ, Aaccurso AD, Farassati F. Ezh2, a novel target in detection and therapy of breast cancer. *Onco Targets Ther* (2017) 10:2685–7. doi:10.2147/OTT.S138777

15. Findeis-Hosey JJ, Huang J, Li F, Yang Q, McMahon LA, Xu H. High-grade neuroendocrine carcinomas of the lung highly express enhancer of zeste homolog 2, but carcinoids do not. *Hum Pathol* (2011) 42(6):867–72. doi:10.1016/j.humpath.2010.09.019

16. Choi JH, Song YS, Yoon JS, Song KW, Lee YY. Enhancer of zeste homolog 2 expression is associated with tumor cell proliferation and metastasis in gastric cancer. *APMIS* (2010) 118(3):196–202. doi:10.1111/j.1600-0463.2009.02579.x

17. Fluge O, Gravdal K, Carlsen E, Vonen B, Kjellevold K, Refsum S, et al. Expression of EZH2 and Ki-67 in colorectal cancer and associations with treatment response and prognosis. *Br J Cancer* (2009) 101(8):1282–9. doi:10.1038/sj.bjc.6605333

18. Toll AD, Dasgupta A, Potoczek M, Yeo CJ, Kleer CG, Brody JR, et al. Implications of enhancer of zeste homologue 2 expression in pancreatic ductal

adenocarcinoma. *Hum Pathol* (2010) 41(9):1205–9. doi:10.1016/j.humpath.2010.03.004

19. Zhai R, Tang F, Gong J, Zhang J, Lei B, Li B, et al. The relationship between the expression of USP22, BMI1, and EZH2 in hepatocellular carcinoma and their impacts on prognosis. *Onco Targets Ther* (2016) 9:6987–98. doi:10.2147/OTT.S110985

20. Borbone E, Troncone G, Ferraro A, Jasencakova Z, Stojic L, Esposito F, et al. Enhancer of zeste homolog 2 overexpression has a role in the development of anaplastic thyroid carcinomas. *J Clin Endocrinol Metab* (2011) 96(4):1029–38. doi:10.1210/jc.2010-1784

21. Aziza EA, Shimaa AA, Ragab AA. Prognostic value of twist-1, E-cadherin and EZH2 in prostate cancer: an immunohistochemical study. *Turk Patoloji Derg* (2017) 1:198–210. doi:10.5146/tjpath.2016.01392

22. Raman JD, Mongan NP, Tickoo SK, Boorjian SA, Scherr DS, Gudas LJ. Increased expression of the polycomb group gene, EZH2, in transitional cell carcinoma of the bladder. *Clin Cancer Res* (2005) 11(24):8570–6. doi:10.1158/1078-0432.CCR-05-1047

23. Jin M, Yang Z, Ye W, Yu X, Hua X. Prognostic significance of histone methyltransferase enhancer of zeste homolog 2 in patients with cervical squamous cell carcinoma. *Oncol Lett* (2015) 10(2):857–62. doi:10.3892/ol.2015.3319

24. Makk E, Bálint L, Cifra J, Tornóczky T, Oszter A, Tóth A, et al. Robust expression of EZH2 in endocervical neoplastic lesions. *Virchows Arch* (2019) 475(1):95–104. doi:10.1007/s00428-019-02550-8

25. Zhou J, Roh JW, Bandyopadhyay S, Chen Z, Munkarah AR, Hussein Y, et al. Overexpression of enhancer of zeste homolog 2 (EZH2) and focal adhesion kinase (FAK) in high grade endometrial carcinoma. *Gynecol Oncol* (2013) 128(2):344–8. doi:10.1016/j.ygyno.2012.07.128

26. Krill L, Deng W, Eskander R, Mutch D, Zweizig S, Hoang B, et al. Overexpression of enhance of zeste homolog 2 (EZH2) in endometrial carcinoma: an NRG oncology/gynecologic oncology group study. *Gynecol Oncol* (2020) 156(2):423–9. doi:10.1016/J.YGYNO.2019.12.003

27. Xu Y, Li X, Wang H, Xie P, Yan X, Bai Y, et al. Hypermethylation of CDH13, DKK3 and FOXL2 promoters and the expression of EZH2 in ovary granulosa cell tumors. *Mol Med Rep* (2016) 14(3):2739–45. doi:10.3892/mmr.2016.5521

28. Li H, Cai Q, Godwin AK, Zhang R. Enhancer of zeste homolog 2 promotes the proliferation and invasion of epithelial ovarian cancer cells. *Mol Cancer Res* (2010) 8(12):1610–8. doi:10.1158/1541-7786.MCR-10-0398

29. Ramaglia M, D'Angelo V, Iannotta A, Di Pinto D, Pota E, Affinita MC, et al. High EZH2 expression is correlated to metastatic disease in pediatric soft tissue sarcomas. *Cancer Cell Int* (2016) 16(1):59. doi:10.1186/S12935-016-0338-X

30. Adesso L, Leoncini PP, Dall'agnese A, Walters ZS, Verginelli F, Boldrini R, et al. The Polycomb group (PcG) protein EZH2 supports the survival of PAX3-FOXO1 alveolar rhabdomyosarcoma by repressing FBXO32 (Atrogin1/MAFbx). *Oncogene* (2014) 33:4173–84. doi:10.1038/onc.2013.471

31. Zhang N, Zeng Z, Li S, Wang F, Huang P. High expression of EZH2 as a marker for the differential diagnosis of malignant and benign myogenic tumors. *Sci Rep* (2018) 8:12331. doi:10.1038/s41598-018-30648-7

32. Shen JK, Cote GM, Gao Y, Choy E, Mankin HJ, Hornicek FJ, et al. Targeting EZH2-mediated methylation of H3K27 inhibits proliferation and migration of Synovial Sarcoma *in vitro*. *Sci Rep* (2016) 6:25239. doi:10.1038/srep25239

33. Sun R, Shen J, Gao Y, Zhou Y, Yu Z, Hornicek F, et al. Overexpression of EZH2 is associated with the poor prognosis in osteosarcoma and function analysis indicates a therapeutic potential. *Oncotarget* (2016) 7(25):38333–46. doi:10.18632/oncotarget.9518

34. Girard N, Bazille C, Lhuissier E, Benateau H, Llombart-Bosch A, Boumediene K, et al. 3-Deazaneplanocin A (DZNep), an inhibitor of the histone methyltransferase EZH2, induces apoptosis and reduces cell migration in chondrosarcoma cells. *PLoS One* (2014) 9(5):e98176. doi:10.1371/JOURNAL.PONE.0098176

35. Cao Q, Yu J, Dhanasekaran SM, Kim JH, Mani RS, Tomlins SA, et al. Repression of E-cadherin by the polycomb group protein EZH2 in cancer. *Oncogene* (2008) 27(58):7274–84. doi:10.1038/onc.2008.333

36. Ihira K, Dong P, Xiong Y, Watari H, Konno Y, Hanley SJB, et al. EZH2 inhibition suppresses endometrial cancer progression via miR-361/Twist axis. *Oncotarget* (2017) 8(8):13509–20. doi:10.18632/oncotarget.14586

37. Ang PP, Tan GC, Karim N, Wong YP. Diagnostic value of the EZH2 immunomarker in malignant effusion cytology. *Acta Cytol* (2020) 64(3):248–55. doi:10.1159/000501406

38. Huvila J, Pors J, Thompson EF, Gilks CB. Endometrial carcinoma: molecular subtypes, precursors and the role of pathology in early diagnosis. *J Pathol* (2021) 253(4):355–65. doi:10.1002/PATH.5608

39. Buza N, Tavassoli FA. Comparative analysis of P16 and P53 expression in uterine malignant mixed mullerian tumors. *Int J Gynecol Pathol* (2009) 28(6):514–21. doi:10.1097/PGP.0b013e3181a934e9

40. WHO Classification of Tumours Editorial Board. *Female genital tumours*. 5th ed. International Agency for Research on Cancer (2020). Volume 4. Available at: https://publications.iarc.fr/Book-And-Report-Series/Who-Classification-Of-Tumours/Female-Genital-Tumours-2020.

41. Bosari S, Lee AKC, Viale G, Heatley GJ, Coggi G. Abnormal p53 immunoreactivity and prognosis in node-negative breast carcinomas with long-term follow-up. *Virchows Arch A Pathol Anat Histopathol* (1992) 421(4):291–5. doi:10.1007/BF01660975

42. Bachmann IM, Halvorsen OJ, Collett K, Stefansson IM, Straume O, Haukaas SA, et al. EZH2 expression is associated with high proliferation rate and aggressive tumor subgroups in cutaneous melanoma and cancers of the endometrium, prostate, and breast. *J Clin Oncol* (2006) 24:268–73. doi:10.1200/JCO.2005.01.5180

43. Wagener N, Macher-Goeppinger S, Pritsch M, Hüsing J, Hoppe-Seyler K, Schirmacher P, et al. Enhancer of zeste homolog 2 (EZH2) expression is an independent prognostic factor in renal cell carcinoma. *BMC Cancer* (2010) 10(1):524. doi:10.1186/1471-2407-10-524

44. Sasaki M, Matsubara T, Kakuda Y, Sato Y, Nakanuma Y. Immunostaining for polycomb group protein EZH2 and senescent marker p16INK4a may be useful to differentiate cholangiolocellular carcinoma from ductular reaction and bile duct adenoma. *Am J Surg Pathol* (2014) 38(3):364–9. doi:10.1097/PAS.0000000000000125

45. Salvesen HB, Iversen OE, Akslen LA. Prognostic significance of angiogenesis and ki-67, p53, and p21 expression: a population-based endometrial carcinoma study. *J Clin Oncol* (1999) 17(5):1382–90. doi:10.1200/JCO.1999.17.5.1382

46. Chen X, Arend R, Hamele-Bena D, Tergas AI, Hawver M, Tong GX, et al. Uterine carcinosarcomas: clinical, histopathologic and immunohistochemical characteristics. *Int J Gynecol Pathol* (2017) 36(5):412–9. doi:10.1097/PGP.0000000000000346

47. Köbel M, Ronnett BM, Singh N, Soslow RA, Gilks CB, McCluggage WG. Interpretation of P53 immunohistochemistry in endometrial carcinomas: toward increased reproducibility. *Int J Gynecol Pathol* (2019) 38(1):S123–S131. doi:10.1097/PGP.0000000000000488

48. Rabban JT, Garg K, Ladwig NR, Zaloudek CJ, Devine WP. Cytoplasmic pattern p53 immunoexpression in pelvic and endometrial carcinomas with TP53 mutation involving nuclear localization domains: an uncommon but potential diagnostic pitfall with clinical implications. *Am J Surg Pathol* (2021) 45(11):1441–51. doi:10.1097/PAS.0000000000001713

49. Schoonjans F, Zalata A, Depuydt CE, Comhaire FH. MedCalc: a new computer program for medical statistics. *Comput Methods Programs Biomed* (1995) 48(3):257–62. doi:10.1016/0169-2607(95)01703-8

50. Cohen J. A coefficient of agreement for nominal scales. *Educ Psychol Meas* (1960) 20(1):37–46. doi:10.1177/001316446002000104

51. Engelsen IB, Stefansson I, Akslen LA, Salvesen HB. Pathologic expression of p53 or p16 in preoperative curettage specimens identifies high-risk endometrial carcinomas. *Am J Obstet Gynecol* (2006) 195(4):979–86. doi:10.1016/j.ajog.2006.02.045

52. Priya A, Chaurasia JK, P K, Panwar H, Yadav SK, Kapoor N. Evaluation of immunohistochemical expression of enhancer of zeste homolog 2 (EZH2) and its association with clinicopathological variables in carcinoma cervix. *Cureus* (2023) 15(3):e36946. doi:10.7759/CUREUS.36946

53. Oki S, Sone K, Oda K, Hamamoto R, Ikemura M, Maeda D, et al. Oncogenic histone methyltransferase EZH2: a novel prognostic marker with therapeutic potential in endometrial cancer. *Oncotarget* (2017) 8:40402–11. doi:10.18632/oncotarget.16316

54. Rao ZY, Cai MY, Yang GF, He LR, Mai SJ, Hua WF, et al. EZH2 supports ovarian carcinoma cell invasion and/or metastasis via regulation of TGF-beta1 and is a predictor of outcome in ovarian carcinoma patients. *Carcinogenesis* (2010) 31(9):1576–83. doi:10.1093/carcin/bgq150

55. Ding M, Zhang H, Li Z, Wang C, Chen J, Shi L, et al. The polycomb group protein enhancer of zeste 2 is a novel therapeutic target for cervical cancer. *Clin Exp Pharmacol Physiol* (2015) 42(5):458–64. doi:10.1111/1440-1681.12382

56. Bitler BG, Aird KM, Garipov A, Li H, Amatangelo M, Kossenkov AV, et al. Synthetic lethality by targeting EZH2 methyltransferase activity in ARID1A-mutated cancers. *Nat Med* (2015) 21(3):231–8. doi:10.1038/NM.3799

57. Roh JW, Eun Choi J, Dong Han H, Hu W, Matsuo K, Nishimura M, et al. Clinical and biological significance of EZH2 expression in endometrial cancer. *Cancer Biol Ther* (2019) 21:147–56. doi:10.1080/15384047.2019.1672455

58. Shi L, Zhang Q, Zhu S, Tang Q, Chen X, Lan R, et al. Pharmacological inhibition of EZH2 using a covalent inhibitor suppresses human ovarian cancer cell migration and invasion. *Mol Cell Biochem* (2023). doi:10.1007/S11010-023-04767-3

59. Abargel A, Avinoach I, Kravtsov V, Boaz M, Glezerman M, Menczer J. Expression of p27 and p53: comparative analysis of uterine carcinosarcoma and endometrial carcinoma. *Int J Gynecol Cancer* (2004) 14(2):354–9. doi:10.1111/j.1048-891x.2004.014221.x

60. Menczer J, Kravtsov V, Levy T, Berger E, Glezerman M, Avinoach I. Expression of c-kit in uterine carcinosarcoma. *Gynecol Oncol* (2005) 96(1):210–5. doi:10.1016/j.ygyno.2004.09.045

61. Menczer J, Schreiber L, Sukmanov O, Kravtsov V, Berger E, Golan A, et al. COX-2 expression in uterine carcinosarcoma. *Acta Obstet Gynecol Scand* (2010) 89(1):120–5. doi:10.3109/00016340903342006

62. Livasy CA, Reading FC, Moore DT, Boggess JF, Lininger RA. EGFR expression and HER2/neu overexpression/amplification in endometrial carcinosarcoma. *Gynecol Oncol* (2006) 100(1):101–6. doi:10.1016/j.ygyno.2005.07.124

63. Saglam O, Husain S, Toruner G. AKT, EGFR, C-ErbB-2, and C-kit expression in uterine carcinosarcoma. *Int J Gynecol Pathol* (2013) 32(5):493–500. doi:10.1097/PGP.0b013e31827fedef

64. Rottmann D, Snir OL, Wu X, Wong S, Hui P, Santin AD, et al. HER2 testing of gynecologic carcinosarcomas: tumor stratification for potential targeted therapy. *Mod Pathol* (2020) 33(1):118–27. doi:10.1038/S41379-019-0358-x

65. Jenkins TM, Cantrell LA, Stoler MH, Mills AM. HER2 overexpression and amplification in uterine carcinosarcomas with serous morphology. *Am J Surg Pathol* (2022) 46(4):435–42. doi:10.1097/PAS.0000000000001870

66. Murali R, Davidson B, Fadare O, Carlson JA, Crum CP, Gilks CB, et al. High-grade endometrial carcinomas: morphologic and immunohistochemical features, diagnostic challenges and recommendations. *Int J Gynecol Pathol* (2019) 38(1):S40–S63. doi:10.1097/PGP.0000000000000491

67. Yemelyanova A, Ji H, Shih IM, Wang TL, Wu LSF, Ronnett BM. Utility of p16 expression for distinction of uterine serous carcinomas from endometrial endometrioid and endocervical adenocarcinomas: immunohistochemical analysis of 201 cases. *Am J Surg Pathol* (2009) 33(10):1504–14. doi:10.1097/PAS.0B013E3181AC35F5

68. Gilks CB, Oliva E, Soslow RA. Poor interobserver reproducibility in the diagnosis of high-grade endometrial carcinoma. *Am J Surg Pathol* (2013) 37(6):874–81. doi:10.1097/PAS.0B013E31827F576A

69. Garg K, Leitao MM, Wynveen CA, Sica GL, Shia J, Shi W, et al. p53 overexpression in morphologically ambiguous endometrial carcinomas correlates with adverse clinical outcomes. *Mod Pathol* (2010) 23(1):80–92. doi:10.1038/MODPATHOL.2009.153

70. Tashiro H, Isacson C, Levine R, Kurman RJ, Cho KR, Hedrick L. p53 gene mutations are common in uterine serous carcinoma and occur early in their pathogenesis. *Am J Pathol* (1997) 150(1):177–85. Available from: https://www.ncbi.nlm.nih.gov/pmc/articles/PMC1858541/ (Accessed July 27, 2023).

71. Soslow RA, Shen PUF, Chung MH, Isacson C. Distinctive p53 and mdm2 immunohistochemical expression profiles suggest different pathogenetic pathways in poorly differentiated endometrial carcinoma. *Int J Gynecol Pathol* (1998) 17(2):129–34. doi:10.1097/00004347-199804000-00006

72. Gu Y, Zhang J, Guan H. Expression of EZH2 in endometrial carcinoma and its effects on proliferation and invasion of endometrial carcinoma cells. *Oncol Lett* (2017) 14(6):7191–6. doi:10.3892/ol.2017.7171

73. Castilla MÁ, Moreno-Bueno G, Romero-Pérez L, Van De Vijver K, Biscuola M, López-García MÁ, et al. Micro-RNA signature of the epithelial-mesenchymal transition in endometrial carcinosarcoma. *J Pathol* (2011) 223(1):72–80. doi:10.1002/PATH.2802

74. Chiyoda T, Tsuda H, Tanaka H, Kataoka F, Nomura H, Nishimura S, et al. Expression profiles of carcinosarcoma of the uterine corpus—are these similar to carcinoma or sarcoma? *Genes, Chromosom Cancer* (2012) 51(3):229–39. doi:10.1002/GCC.20947

75. McCluggage WG. Uterine carcinosarcomas (malignant mixed Mullerian tumors) are metaplastic carcinomas. *Int J Gynecol Cancer* (2002) 12(6):687–90. doi:10.1046/j.1525-1438.2002.01151.x

76. Kanthan R, Senger JLB, Diudea D. Malignant mixed Mullerian tumors of the uterus: histopathological evaluation of cell cycle and apoptotic regulatory proteins. *World J Surg Oncol* (2010) 8:60. doi:10.1186/1477-7819-8-60

77. Köbel M, Kang EY. The many uses of p53 immunohistochemistry in gynecological pathology: proceedings of the ISGyP companion society session at the 2020 USCAP annual9 meeting. *Int J Gynecol Pathol* (2021) 40(1):32–40. doi:10.1097/PGP.0000000000000725

78. Rabban JT, Blake Gilks C, Malpica A, Matias-Guiu X, Mittal K, Mutter GL, et al. Issues in the differential diagnosis of uterine low-grade endometrioid carcinoma, including mixed endometrial carcinomas: recommendations from the international society of gynecological pathologists. *Int J Gynecol Pathol* (2019) 38(1):S25–S39. doi:10.1097/PGP.0000000000000512

79. Kunc M, Gabrych A, Rekawiecki B, Gorczyński A, Haybaeck J, Biernat W, et al. Immunohistochemical evaluation of mismatch repair proteins and p53 expression in extrauterine carcinosarcoma/sarcomatoid carcinoma. *Wspolczesna Onkol* (2020) 24(1):1–4. doi:10.5114/WO.2020.94718

80. Liu FS, Kohler MF, Marks JR, Bast RC, Jr, Boyd J, Berchuck A. Mutation and overexpression of the P53 tumor suppressor gene frequently occurs in uterine and ovarian sarcomas. *Obstet Gynecol* (1994) 83(1):118–24.

81. De Jong RA, Nijman HW, Wijbrandi TF, Reyners AK, Boezen HM, Hollema H. Molecular markers and clinical behavior of uterine carcinosarcomas: focus on the epithelial tumor component. *Mod Pathol* (2011) 24(10):1368–79. doi:10.1038/MODPATHOL.2011.88

82. Köbel M, Piskorz AM, Lee S, Lui S, LePage C, Marass F, et al. Optimized p53 immunohistochemistry is an accurate predictor of TP53 mutation in ovarian carcinoma. *J Pathol Clin Res* (2016) 2(4):247–58. doi:10.1002/CJP2.53

83. da Costa LT, Dos Anjos LG, Kagohara LT, Torrezan GT, De Paula CAA, Baracat EC, et al. The mutational repertoire of uterine sarcomas and carcinosarcomas in a Brazilian cohort: a preliminary study. *Clinics* (2021) 76:e2324–15. doi:10.6061/CLINICS/2021/E2324

84. Zhao S, Bellone S, Lopez S, Thakral D, Schwab C, English DP, et al. Mutational landscape of uterine and ovarian carcinosarcomas implicates histone genes in epithelial-mesenchymal transition. *Proc Natl Acad Sci U S A* (2016) 113(43):12238–43. doi:10.1073/pnas.1614120113

85. Taylor NP, Zighelboim I, Huettner PC, Powell MA, Gibb RK, Rader JS, et al. DNA mismatch repair and TP53 defects are early events in uterine carcinosarcoma tumorigenesis. *Mod Pathol* (2006) 19:1333–8. doi:10.1038/modpathol.3800654

86. Jones S, Stransky N, McCord CL, Cerami E, Lagowski J, Kelly D, et al. Genomic analyses of gynaecologic carcinosarcomas reveal frequent mutations in chromatin remodelling genes. *Nat Commun* (2014) 5:5006. doi:10.1038/NCOMMS6006

87. McConechy MK, Ding J, Cheang MCU, Wiegand K, Senz J, Tone A, et al. Use of mutation profiles to refine the classification of endometrialcarcinomas. *J Pathol* (2012) 228(1):20–30. doi:10.1002/PATH.4056

88. Di Fiore R, Suleiman S, Drago-Ferrante R, Subbannayya Y, Vasileva-Slaveva M, Yordanov A, et al. The role of FBXW7 in gynecologic malignancies. *Cells* (2023) 12(10):1415. doi:10.3390/cells12101415

89. Cuevas IC, Sahoo SS, Kumar A, Zhang H, Westcott J, Aguilar M, et al. Fbxw7 is a driver of uterine carcinosarcoma by promoting epithelial-mesenchymal transition. *Proc Natl Acad Sci U S A* (2019) 116(51):25880–90. doi:10.1073/pnas.1911310116

Pathology & Oncology Research | frontiers

TYPE Brief Research Report
PUBLISHED 24 June 2024
DOI 10.3389/pore.2024.1611803

Check for updates

OPEN ACCESS

EDITED BY
Stefano Restaino,
Ospedale Santa Maria della Misericordia di Udine, Italy

*CORRESPONDENCE
Luigi Della Corte,
dellacorte.luigi25@gmail.com

RECEIVED 26 April 2024
ACCEPTED 11 June 2024
PUBLISHED 24 June 2024

CITATION
Della Corte L, Ascione M and Bifulco G (2024), Modified clock mapping biopsy sec. Della Corte-Bifulco in the preoperative assessment of excisional surgery for vulvar Paget's disease. *Pathol. Oncol. Res.* 30:1611803. doi: 10.3389/pore.2024.1611803

COPYRIGHT
© 2024 Della Corte, Ascione and Bifulco. This is an open-access article distributed under the terms of the Creative Commons Attribution License (CC BY). The use, distribution or reproduction in other forums is permitted, provided the original author(s) and the copyright owner(s) are credited and that the original publication in this journal is cited, in accordance with accepted academic practice. No use, distribution or reproduction is permitted which does not comply with these terms.

Modified clock mapping biopsy sec. Della Corte-Bifulco in the preoperative assessment of excisional surgery for vulvar Paget's disease

Luigi Della Corte[1]*, Mario Ascione[2] and Giuseppe Bifulco[2]

[1]Department of Neuroscience, Reproductive Sciences and Dentistry, School of Medicine, University of Naples Federico II, Naples, Italy, [2]Department of Public Health, University of Naples Federico II, Naples, Italy

We have developed a biopsy technique aimed at preoperative evaluating the extent of Paget's vulvar disease in order to plan subsequent radical vulvar surgery. The aim is to find all possible lesion sites that are not visible macroscopically, to obtain a clear evaluation of the disease spread and to tailor the radical surgical procedure to remove even microscopic lesions, avoiding recurrences and excessively destructive surgery, adopting as conservative an approach as possible. We used this procedure for the first time to establish the radicality of the surgical intervention in a 68-year-old patient initially suffering from a single invasive vulvar Paget's lesion.

KEYWORDS

gynecological cancer, extramammary Paget's disease of the vulva, vulvar malignant lesion, preoperative biopsy, new technique

Introduction

Extramammary Paget's disease of the vulva (EMPDV) is a rare non-squamous skin neoplasm, which is defined as an intraepithelial neoplasm of epithelial origin that expresses glandular characteristics. Histologically, it is characterized by the presence of large cells with prominent cytoplasm, called Paget cells [1, 2]. Vulvar localization accounts for 65% of cases of extramammary Paget's disease but constitutes only 1%–2% of genital neoplasms [3]. Due to its rarity and unclear clinical presentation, EMPDV is often diagnosed late, when the lesions are already quite extensive [4]. Although the lesions generally follow a slow and indolent evolution, in some cases the pathology may spread deeply, into the lymph nodes, and more rarely by the hematogenous route [5]. In the majority of cases of EMPDV, a discordance is established between the macroscopic and histological margins of the lesion: in fact, lesions may skip, be multifocal, or develop asymmetrically, which makes achieving negative surgical margins challenging [6]. Therefore, the perilesional satellite areas, which are macroscopically and clinically free, appear to be the site of disease on histopathological examination. For this reason, although surgical excision is the gold standard in the treatment of EMPDV, it

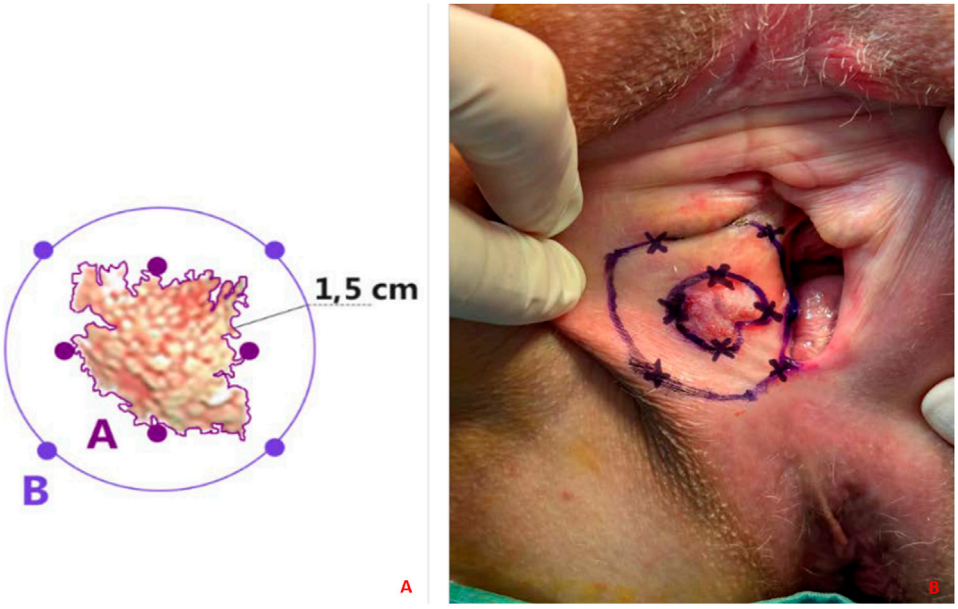

FIGURE 1
(A, B) Modified clock mapping technique. **(A)** A graphic representation of the sites where the biopsy should ideally be performed. The clinically evident edges of the lesion constitute perimeter A. Perimeter B is drawn 1.5 cm away from A; **(B)** *In vivo* application of clock mapping.



FIGURE 2
Final result of radical total vulvectomy.

is often insufficient in the evaluation of clinically occult lesions, leading to recurrence and the need for multiple excisional interventions with sometimes destructive and/or mutilating outcomes [7–9]. Other surgical techniques have been described in the literature aimed at pre-operatively evaluating the extent of the surface to be removed in order to minimize the possibility of recurrence. The Japanese experience had already highlighted how a biopsy mapping of the disease was superior over MMS (Mohs micrographic surgery), which instead aimed to practice a progressive excision of clinically evident lesions with an inevitably higher rate of recurrence [10]. Subsequently, Garganese et al. have proposed a "clock mapping" technique [11], which consists of performing multiple preoperative vulvovaginal biopsies at different sites both in the superficial vulvo-perineal area and in the central deep vaginal area, as follows:

- within the visible lesion, corresponding to any suspiciously thickened area;
- outside the visible lesion, at the level of each position of the clock, at three radial points defined as point A (corresponding to the margin of the lesion) and points B and C, respectively, which are at a distance of 2 and 4 cm from the edges of the lesion;
- at three vaginal levels for each cardinal point, i.e., at the vestibule and a distance of 2 and 4 cm from it.

However, despite the evidence reported in the literature regarding the prediction of the invasiveness and extension of EMPDV, this surgical strategy consists of 48 biopsy samples (36 in the vulvar region and 12 in the vaginal region) and,

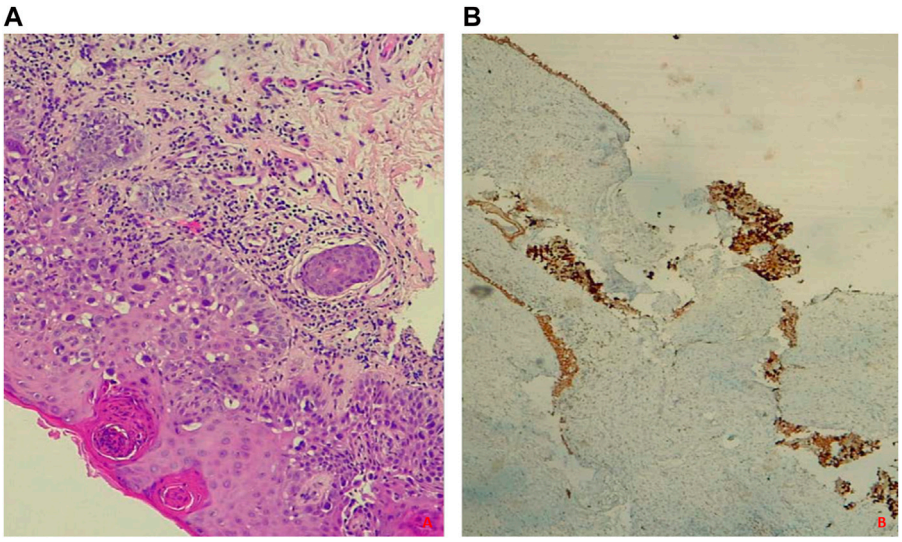

FIGURE 3
(A, B) Intraepithelial Paget's disease. **(A)** Hematoxylin-eosin staining shows atypical, polygonal, large glandular cells with abundant vacuolated cytoplasm, hyperchromic nuclei, and evident nucleoli resembling Paget's cells; **(B)** GATA3 Immunohistochemical Staining is positive.

therefore, requires the execution of a complex and time-consuming surgical procedure. From these considerations, we had the intuition to develop a new biopsy sampling technique to be proposed in the proper evaluation of EMPDV that is inspired by the models described so far in the literature but provides innovative and simplifying elements while maintaining adequate diagnostic efficiency.

Description of the surgical technique

Modified clock mapping biopsy sec. Della Corte-Bifulco consists of identifying the macroscopically evident lesion in the vulvar region, which represents the center of an imaginary clock. Biopsy samples are taken along two routes: perimeter A, corresponding to the margin of the clinically evident lesion, and perimeter B, 1.5 cm away from the first. Biopsy sampling is carried out as follows:

- Along perimeter A, four biopsy samples are taken at the four cardinal points, i.e., at 3, 6, 9, and 12 o'clock;
- Along perimeter B, four biopsy samples are obtained in such a way that they are misaligned with respect to the first ones. Specifically, the biopsy is taken at the midpoint between 1 and 2 h, then between 4 and 5 h, between 7 and 8 h, and finally between 10 and 11 h (Figure 1A).

Each biopsy sample must have an extension of at least 1 cm in diameter.

Application

A 68-year-old woman was referred to us after a vulvar biopsy was performed at another institution with a histological diagnosis of invasive EMPDV. She had been complaining of chronic itching for approximately 6 months. She had undergone bilateral mammography, colonoscopy, and urine cytology to exclude other EMPD localizations. The lesion appeared erythematous and ulcerated with a minute whitish nodule medially on the middle third of the right major labia, measuring 3 cm and 2 cm from the midline. Its edges appeared blurred. Preoperative Magnetic Resonance Imaging, and 18F-2-deoxy-2-fluoro-D-glucose Positron Emission Tomography were negative. Therefore, we decided to apply the "modified clock mapping" surgical technique in order to better understand its spread and to establish the tissue excision margins (Figure 1B). As described in the literature, this disease is characterized by the presence of "skip lesions," sometimes not macroscopically evident but responsible for recurrence. Thanks to our strategy, the invasive EMPDV was histologically confirmed at 9 o'clock (perimeter A) and, in addition, the pathologist discovered the presence of intraepithelial disease foci, 1.5 cm away from the main lesion, in particular at 7 o'clock (perimeter B) at the level of the posterior fourchette.

Finally, after detailed counseling and obtaining written informed consent, the surgeon (L.D.C.) performed a total radical vulvectomy with an ipsilateral inguinofemoral sentinel lymph node biopsy (Figure 2). Specifically, technetium(99) m-labeled microcolloid was injected intradermally at four locations around the tumor 5 h before the planned procedure.

Dynamic and static images were recorded using a gamma camera. The right SLN location was marked on the overlying skin. In the operating room, the SLN was identified at the beginning of the procedure using a handheld gamma-detection probe. Regarding the vulvar surgical time, the lesion was removed with 1 cm of free margin outside the 7 o'clock point.

The histological examination confirmed the dual vulvar diagnosis of invasive and non-invasive EMPDV with 1 cm of healthy surgical margin (Figures 3A, B), while the sentinel lymph node was negative. No early or late postoperative complications were recorded. After 6 months of follow-up, no recurrence has been described and the patient is in good health.

Conclusion

A high rate of invasiveness and recurrence characterizes EMPDV. Frequently, it manifests as skip lesions, which are not always clinically evident, as in our case. The "modified clock mapping" technique is feasible and safe for the preoperative evaluation of vulvar Paget's disease and avoids an excessive and sometimes unnecessary number of vulvar biopsies without the risk of underdiagnosis. It has allowed us to identify an area of satellite disease that otherwise would have remained unrecognized, leading to recurrence: this aspect is particularly important because it would avoid conservative treatment in the case of unknown lesions far from macroscopically evident ones, but also demolitive surgery when not necessary. Moreover, it could have a positive impact on the quality of life of the patients and a better aesthetic result. Further studies on a larger sample of patients are needed to estimate the impact of this surgical strategy in terms of recurrence-free survival in women with EMPDV.

Data availability statement

The raw data supporting the conclusion of this article will be made available by the authors, without undue reservation.

Ethics statement

The study was conducted according to the guidelines of the Declaration of Helsinki. The patient provided her written informed consent to participate in this study. Written informed consent was obtained from the individual for the publication of any potentially identifiable images or data included in this article.

Author contributions

Conceptualization: LDC; Methodology: LDC, GB; Formal analysis and investigation: MA; Writing–original draft preparation: LDC, MA; Writing–review and editing: LDC, GB; Supervision: GB. All authors contributed to the article and approved the submitted version.

Funding

The authors declare that no financial support was received for the research, authorship, and/or publication of this article.

Conflict of interest

The authors declare that the research was conducted in the absence of any commercial or financial relationships that could be construed as a potential conflict of interest.

References

1. Lloyd J, Flanagan A. Mammary and extramammary Paget's disease. *J Clin Pathol* (2000) 53:742–9. doi:10.1136/jcp.53.10.742

2. Lam C, Funaro D. Extramammary Paget's disease: summary of current knowledge. *Dermatol Clin* (2010) 28:807–26. doi:10.1016/j.det.2010.08.002

3. Noel A, Bhat RM, Rao SV, Fernandes S. An unusual secondary extramammary Paget's disease of vulva. *Indian J Sex Transm Dis AIDS* (2020) 41:210–2. doi:10.4103/ijstd.IJSTD_69_19

4. McDaniel B, Brown F, Crane JS. *Extramammary Paget disease*. Treasure Island, FL, USA: StatPearls Publishing (2022).

5. Della Corte L, Cafasso V, Conte C, Cuomo L, Giampaolinio P, Lavitola G, et al. Medical and surgical strategies in vulvar Paget disease: let's throw some light!. *J Pers Med* (2023) 13(1):100. doi:10.3390/jpm13010100

6. Zollo JD, Zeitouni NC. The roswell park cancer institute experience with extramammary Paget's disease. *Br J Dermatol* (2000) 142:59–65. doi:10.1046/j.1365-2133.2000.03242.x

7. Hatta N, Yamada M, Hirano T, Fujimoto A, Morita R. Extramammary Paget's disease: treatment, prognostic factors and outcome in 76 patients. *Br J Dermatol* (2008) 158(2):313–8. doi:10.1111/j.1365-2133.2007.08314.x

8. Borghi C, Bogani G, Ditto A, Martinelli F, Signorelli M, Chiappa V, et al. Invasive Paget disease of the vulva. *Int J Gynecol Cancer* (2018) 28(1):176–82. doi:10.1097/IGC.0000000000001131

9. Garganese G, Inzani F, Mantovani G, Santoro A, Valente M, Babini G, et al. The vulvar immunohistochemical panel (VIP) project: molecular profiles of vulvar Paget's disease. *J Cancer Res Clin Oncol* (2019) 145(9):2211–25. doi:10.1007/s00432-019-02975-3

10. Kato T, Fujimoto N, Fujii N, Tanaka T. Mapping biopsy with punch biopsies to determine surgical margin in extramammary Paget's disease. *J Dermatol* (2013) 40:968–72. doi:10.1111/1346-8138.12347

11. Garganese G, Anchora LP, Fragomeni SM, Mantovani G, Santoro A, Gentileschi S, et al. "Clock mapping" prior to excisional surgery in vulvar Paget's disease: tailoring the surgical plan. *Arch Gynecol Obstet* (2022) 306:473–80. doi:10.1007/s00404-022-06408-4

Pathology & Oncology Research | frontiers

TYPE Original Research
PUBLISHED 27 January 2023
DOI 10.3389/pore.2023.1610870

Check for updates

OPEN ACCESS

EDITED BY
Andrea Ladányi,
National Institute of Oncology (NIO), Hungary

*CORRESPONDENCE
Lihong Chen,
wscclh@163.com

RECEIVED 07 October 2022
ACCEPTED 20 January 2023
PUBLISHED 27 January 2023

CITATION
Wang S, Zheng Q, Wang J, Chen S and Chen L (2023), Long non-coding RNA MYU promotes ovarian cancer cell proliferation by sponging miR-6827-5p and upregulating HMGA1.
Pathol. Oncol. Res. 29:1610870.
doi: 10.3389/pore.2023.1610870

COPYRIGHT
© 2023 Wang, Zheng, Wang, Chen and Chen. This is an open-access article distributed under the terms of the Creative Commons Attribution License (CC BY). The use, distribution or reproduction in other forums is permitted, provided the original author(s) and the copyright owner(s) are credited and that the original publication in this journal is cited, in accordance with accepted academic practice. No use, distribution or reproduction is permitted which does not comply with these terms.

Long non-coding RNA MYU promotes ovarian cancer cell proliferation by sponging miR-6827-5p and upregulating HMGA1

Shaoyu Wang[1,2,3], Qiaomei Zheng[1,2,3], Jinhua Wang[1,2,3], Shaozhan Chen[1,2,3] and Lihong Chen[1,2,3]*

[1]Department of Obstetrics and Gynecology, The First Affiliated Hospital, Fujian Medical University, Fuzhou, China, [2]Department of Obstetrics and Gynecology, National Regional Medical Center, Binhai Campus of the First Affiliated Hospital, Fujian Medical University, Fuzhou, China, [3]Fujian Key Laboratory of Precision Medicine for Cancer, The First Affiliated Hospital, Fujian Medical University, Fuzhou, China

Background: Long non-coding RNAs (lncRNAs) have been confirmed to play vital roles in tumorigenesis. LncRNA MYU has recently been reported as an oncogene in several kinds of tumors. However, MYU's expression status and potential involvement in ovarian cancer (OC) remain unclear. In this study, we explored the underlying role of MYU in OC.

Methods and results: The expression of MYU was upregulated in OC tissues, and MYU's overexpression was significantly correlated with the FIGO stage and lymphatic metastasis. Knockdown of MYU inhibited cell proliferation in SKOV3 and A2780 cells. Mechanistically, MYU directly interacted with miR-6827-5p in OC cells; HMGA1 is a downstream target gene of miR-6827-5p. Furthermore, MYU knockdown increased the expression of miR-6827-5p and decreased the expression of HMGA1. Restoration of HMGA1 expression reversed the influence on cell proliferation caused by MYU knockdown.

Conclusion: MYU functions as a ceRNA that positively regulates HMGA1 expression by sponging miR-6827-5p in OC cells, which may provide a potential target and biomarker for the diagnosis or prognosis of OC.

KEYWORDS

lncRNA, ovarian cancer, HMGA1, MYU, miR-6827-5p

Introduction

Ovarian cancer (OC) is a common gynecological malignant tumor with the highest mortality rate. There will be approximately 57,090 newly diagnosed ovarian cancer cases and 39,306 deaths in China in 2022. Due to the insidious onset, there is no obvious clinical symptom at the early stage, 70% of patients are diagnosed at the advanced stage. Despite the improvements in surgery, chemotherapy, and maintenance therapy, the 5-year survival rate is still low, only about 47%. The

main causes of death are recurrence and distant metastasis. Therefore, there is an urgent need to further investigate the molecular mechanisms and find novel therapeutic targets in ovarian cancer (1-3).

The Human Genome Project has shown that only 1%–2% of nucleic acid sequences encode proteins. The rest without the ability to encode protein includes long non-coding RNAs (LncRNAs) and short RNAs represented by microRNA (miRNA) and siRNA (4). Numerous studies have confirmed that ncRNAs play critical roles in tumorigenesis and cancer progression. LncRNAs are a group of transcripts with a length of more than 200 nucleotides (nt) (5). LncRNAs can exert a tumor-promoting or tumor-suppressing effect in different cancers. MiRNAs are another endogenous short non-coding RNA with a length of approximately 17-25 nt. MiRNAs bind to the 3′-untranslated region (UTR) of target mRNA, leading to mRNA degradation or translation inhibition (6). Competitive endogenous RNA (ceRNA) is a typical post-transcriptional mechanism in which lncRNAs competitively sponge certain miRNAs and then positively regulate downstream mRNAs (7).

The c-Myc upregulated lncRNA MYU was named by Yoshihiro in 2016 (8). MYU is also annotated as VPS9D1-AS1 because it generates from the opposite strand of the *VPS9D1* gene, which is located in human chromosome 16 q24.3. It has been reported in several common types of human cancers in recent years. Several studies (8-14) have confirmed its critical role in the biological process of tumors, including cell proliferation, apoptosis, invasion, and migration. For instance, MYU interacted with RNA binding protein hnRNP-K to upregulate the CDK6 expression in colon cancer (8). In prostate cancer (PCa), MYU promoted tumorigenesis and progression by mediating the miR-184/c-Myc axis (9). Other researchers found it accelerated the cancer progression by sponging miR-4739 to upregulate MEF2D in PCa (10). In non-small cell lung cancer (NSCLC), the overexpression of MYU exhibited a robust correlation with the poor prognosis (11). The mechanism research revealed that MYU acted as a ceRNA to bind to miR-532-3p and upregulate the expression of HMGA2 in NSCLC (12). In acute lymphoblastic leukemia (ALL), MYU promoted cell proliferation by elevating GPX1 expression by sequestering miR-491-5p and miR-214-3p (13). MYU can also sponge miR-491-5p to upregulate SEC61A1 in hepatocellular carcinoma (14). However, to date, there have been no reports on the role or mechanism of MYU in OC.

The present study is the first to investigate the expression of MYU in OC tissue samples, and to observe the correlation between MYU expression and clinicopathologic features. Furthermore, we focused on the effects of MYU on cancer cell proliferation *in vitro*. These results will help us to clarify the role and potential involvement mechanism of MYU in OC.

Materials and methods

Sample collection

20 epithelial ovarian cancer tissue samples and 20 controls were obtained from patients who underwent surgical resection at the Department of Obstetrics and Gynecology, the First Affiliated Hospital of Fujian Medical University (Fujian, China) between March 2021 and January 2022. Normal ovarian tissue specimens were obtained from patients who underwent hysterectomy and bilateral salpingo-oophorectomy due to benign uterine diseases, including leiomyoma, adenomyosis, or uterine prolapse. The patients with ovarian cancer did not receive preoperative chemotherapy or have any concomitant gynecological cancer. Their clinical information is summarized in Table 1. All resected tissue samples were stored at −80°C after adding RNA Stabilization Reagent (Beyotime, Shanghai, China). This study was approved by the Ethics Committee of First Affiliated Hospital of Fujian Medical University (No. [2020]398). Informed consent was obtained from all patients included in the study.

Cell culture

Human ovarian cancer cell lines (SKOV3 and A2780) were obtained from the Fujian Key Laboratory of Precision Medicine for Cancer. The cells were cultured in RPMI-1640 medium supplemented with 10% fetal bovine serum (FBS) and 1% penicillin-streptomycin. The medium was renewed every 2 or 3 days. All cells were maintained in a humidified incubator containing 5% CO_2 at 37°C.

RNA extraction and quantitative real-time reverse-transcription polymerase chain reaction (qRT-PCR)

Trizol reagent (Beyotime, Shanghai, China) was used to extract total RNA from tissue samples and cell culture. The RNA concentration was determined by an ND5000 spectrophotometer (BioTeke, Beijing, China). RNA (1ug) was reverse transcribed to cDNA using a PrimeScript™ RT Master Mix (TaKaRa, Japan). Quantitative real-time polymerase chain reaction (PCR) was performed on 7500 Real-Time PCR systems (Applied Biosystems Life Technologies, United States). TB Green® Fast qPCR Mix (TaKaRa Bio, Otsu, Japan)was used to determine the mRNA expression, with GAPDH as control. For miRNA, RNAiso (TaKaRa, Japan) was used to extract miRNA and the Small RNA Cloning Kit (TaKaRa, Japan) was used for reverse transcription. Then Mir-X miRNA qRT-PCR TB Green® Kit (TaKaRa, Japan) was used to determine the expression of

TABLE 1 Relationship between MYU expression and clinicopathologic parameters of OC patients.

Characteristics	Number of cases	MYU expression		*p*-Value
		High (n = 10)	Low (n = 10)	
age (years)				0.07
≤55	9	2	7	
>55	11	8	3	
Histological type				0.303
Serous	15	9	6	
Others	5	1	4	
FIGO stage				0.005
I-II	11	2	9	
III-IV	9	8	1	
Lymph node metastasis				0.02
Positive	8	7	1	
Negative	12	3	9	

TABLE 2 Primer sequences used for RT-qPCR.

Gene		Primer sequences (5′–3′)
MYU	Forward	AGTGGCCGTTTTACAGAGACA
	Reverse	CATGCCAAGCTACGGGAAGG
HMGA1	Forward	AAGGGGCAGACCCAAAAA
	Reverse	TCCAGTCCCAGAAGGAAGC
GAPDH	Forward	GGAGCGAGATCCCTCCAAAAT
	Reverse	GGCTGTTGTCATACTTCTCATGG
miR-6827-5p	Forward	AAGCAACCCTTAACTCCAGA
	Reverse	CCAAGCAACCCTTAACTCCA
U6	Forward	CTCGCTTCGGCAGCACA
	Reverse	AACGCTTCACGAATTTGCGT

miRNA, with U6 as control. The relative expression of RNA was analyzed by the $2^{-\Delta\Delta CT}$ method. The primer sequences used for qRT-PCR were listed in Table 2.

shRNA transfection

The short-hairpin RNA (shRNA) lentiviruses targeting MYU and control shRNA lentiviruses were inserted into the pHBLV-CMV-MCS-3FLAG-EF1-ZsGreen-T2A-PURO vector (Hanbio Biotechnology, Shanghai, China). The combined plasmids were named sh-MYU-1#/2#/3#. The shRNA lentiviruses targeting miR-6827-5p were inserted into the pHBLV-CMV-ZsGreen-T2A-Puro vector (Hanbio Biotechnology, Shanghai, China). The combined plasmids were named miR-6827-5p inhibitor-1#/2#/3#. The sequences were shown in Table 3. The SKOV3 and A2780 cells were transfected with plasmids using PolyJet™ *In Vitro* DNA Transfection Reagent (SignaGen, MD, United States) according to the reagent protocol. Cells that were transfected with empty plasmids (sh-NC and NC inhibitor) served as controls. Transfected cells were obtained 2 days later and transfection efficiency was evaluated by qRT-PCR.

CCK-8 assay

CCK8 assay was performed to detect cell proliferation. Transfected SKOV3 and A2780 cells were seeded into 96-well plates (2×10^3 cells and 100ul each well) at 37°C for 24 h, 48 h, or 72 h. Then the cells were incubated with 10 μL Cell Counting Kit-8 (Fudebio, Hangzhou, China) solution for 4 h. The absorbance at 450 nm was determined by utilizing a SpectraMax iD3 multi-function reader (Molecular Devices, United States).

Dual-luciferase reporter assay

The sequence of miR-6827-5p was inserted into the PGL3-CMV-LUC-MCS vector (miR-6827-5p WT). The 5′UTR sequence of miR-6827-5p which contained the binding site of MYU was mutated and inserted into the same luciferase reporter vector (miR-6827-5p Mut). The recombinant plasmids were synthesized by Genomeditech (Shanghai, China). SKOV3 and A2780 cells were seeded in 24-well plates one night before the transfection. The miR-6827-5p WT or Mut recombinant plasmids and sh-MYU or sh-NC were co-transfected into SKOV3 and A2780 cells using a PolyJet *In Vitro* DNA Transfection Reagent (SignaGen, MD, United States). After 48 h transfection, the cells were collected, and then the luciferase activities were measured using a Dual-Luciferase

TABLE 3 The sequences of interference vectors.

Name		Sequences (5′–3′)
sh-MYU-1#	Top strand	GATCCGACCATGGACCTGCTCACACAGCCCTTCTTTCAAGAG AAGAAGGGCTGTGTGAGCAGGTCCATGGTCTTTTTTG
	Bottom strand	AATTCAAAAAAGACCATGGACCTGCTCACACAGCCCTTCTTC TCTTGAAAGAAGGGCTGTGTGAGCAGGTCCATGGTCG
sh-MYU-2#	Top strand	AGACCCCAGGAAGCCCAGTGGTGTCTGGACACCAGAGGAGT CTCTCTCATCCTCCCGGATTGCTCTGA GG CCAGGAGC
	Bottom strand	GCCTTCCCGTAGCTTGGCATGGAGCACCTCTGCGCGACCATG GACCTGCTCACACAGCCCTTCTGCGC GCCGTGGGAGC
sh-MYU-3#	Top strand	GATCCGCCACTGGAGTTCCTCTGTCTTCTGGGACTTCAAGAG AGTCCCAGAAGACAGAGGAACTCCAGTGGCTTTTTTG
	Bottom strand	AATTCAAAAAAGCCACTGGAGTTCCTCTGTCTTCTGGGACTC TCTTGAAGTCCCAGAAGACAGAGGAACTCCAGTGGCG
miR-6827-5p inhibitor1#		ACCCTCGGTTATTCCAGACACG
miR-6827-5p inhibitor2#		ACCCTCGGTACTAATAAACACG
miR-6827-5p inhibitor3#		ACCCTCGGTACTCCGTGATACG

Reporter Assay (Fudebio, Hangzhou, China). The activity of the firefly luciferase was normalized to that of the renilla luciferase.

Similarly, the 3′UTR sequence of HMGA1 which contained miR-6827-5p binding sites was inserted into the PGL3-CMV-LUC-MCS vector (HMGA1 WT). The 3′UTR sequence of HMGA1 which interacted with miR-6827-5p was mutated and inserted into the equivalent vector (HMGA1 Mut). The HMGA1 WT or Mut recombinant plasmids and miR-6827-5p inhibitor or NC inhibitor were co-transfected into SKOV3 and A2780 cells. The luciferase activities were measured in the same way.

Western blotting

Total protein was extracted from cells using a Protein Extraction Kit (Solarbio, Beijing, China). The concentration of protein was determined using a BCA Protein Assay Kit (Solarbio, Beijing, China) according to the manufacturer's instructions. Then protein samples (40ug) were separated on sodium dodecyl sulfate 10% polyacrylamide gel electrophoresis (SDS-PAGE, Fudebio, Hangzhou, China) and transferred onto polyvinylidene difluoride (PVDF) membrane (Thermo Scientific, MA, United States). After being incubated with 5% BSA for 1 h at room temperature, the membranes were incubated with primary antibodies targeting HMGA1 (29895-1-AP; dilution 1:10000; Proteintech Group, United States) or GAPDH (#5174; dilution 1:1000; Cell Signaling Technology, United States) at 4°C overnight. After Tris-buffered saline containing 0.1% Tween-20 (TBST) was washed three times, membranes were incubated with HRP-linked goat anti-rabbit secondary antibody (#7074; dilution 1:1000; Cell Signaling Technology, United States) at room temperature for 1 h. Protein bands were visualized using Pierce™ ECL Western Blotting Substrate (Thermo Scientific, MA, United States) with chemiluminescence detection system (ChemiDoc, Bio-Rad, United States). GAPDH was used as the loading control for relative protein expression.

Statistical analysis

All experiments were independently performed in triplicate with 3 repeats. SPSS 26(Chicago, IL, United States) or GraphPad Prism 9.0 software (GraphPad, San Diego, CA, United States) was used for data processing and analysis. Data were presented as mean ± standard deviation (SD). Pairwise comparisons were performed using Student's t-test. The differences among multiple groups (≥3) were carried out using one-way analysis of variance (ANOVA), followed by the *post hoc* Tukey's test, if appropriate. The correlation between MYU and clinicopathologic parameters of OC patients was analyzed using Fisher's exact tests. p-value < 0.05 was considered statistically significant.

Results

The expression of MYU in ovarian cancer tissues and its relationship with clinical significance

QRT-PCR was used to detect the expression of MYU in OC tissues and normal ovarian tissues. The expression of

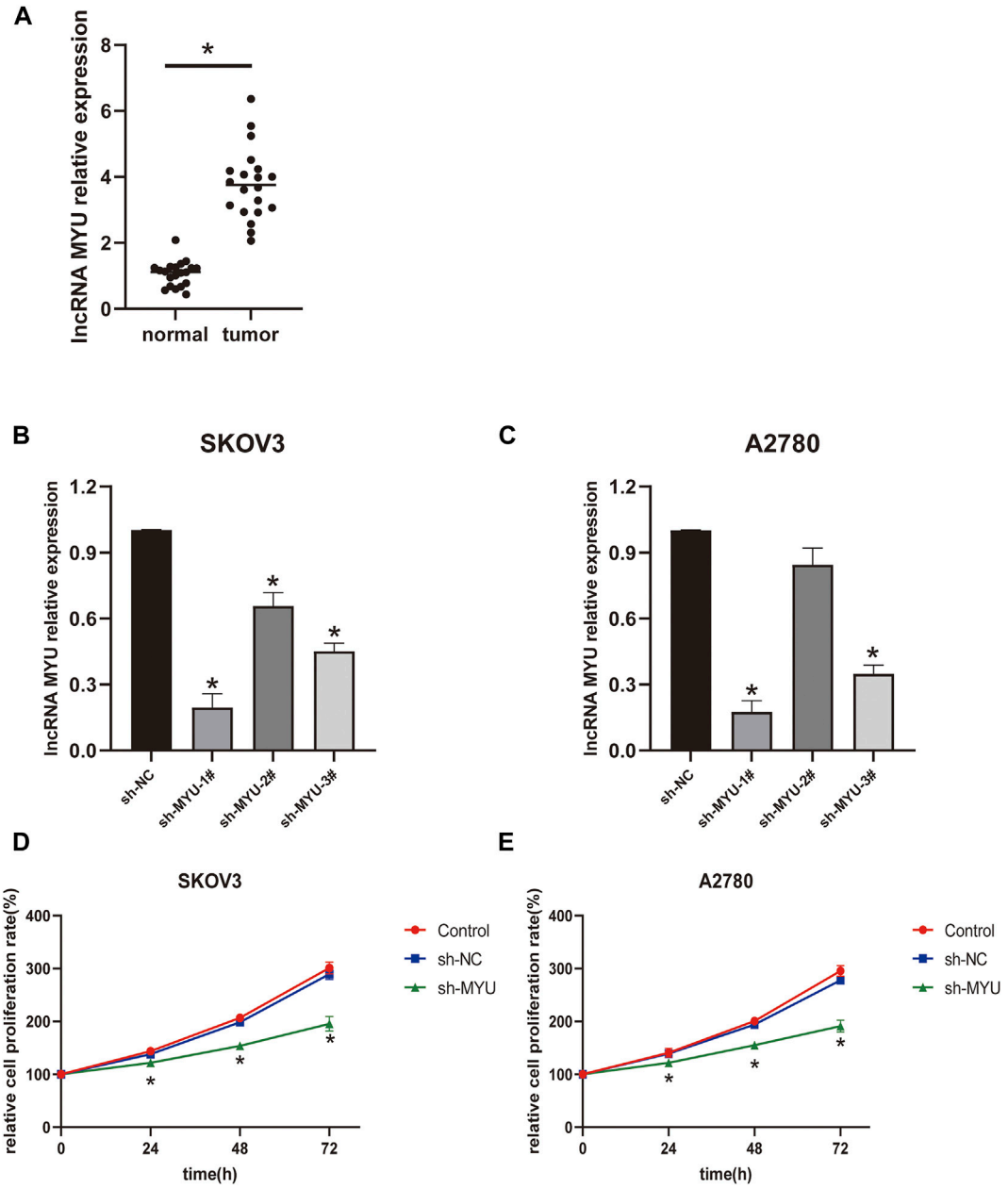

FIGURE 1
Relative expression of MYU in OC tissues and the effect of MYU on the proliferation of OC cell lines. **(A)** The expression level of MYU in OC tissues was higher than that in normal ovarian tissues by qRT-PCR. *$p < 0.05$, compared with normal tissue group. **(B, C)** The silencing efficiency of sh-MYU in SKOV3 and A2780 cells were detected by qRT-PCR; **(D, E)** Knockdown of MYU inhibited OC cell proliferation. *$p < 0.05$, compared with the sh-NC.

MYU was significantly higher in OC tissues than in normal tissues (Figure 1A). To further examine the significance of MYU expression in ovarian cancer, MYU expression was correlated with various clinicopathological features. Taking the median of MYU expression in OC tissues as the cut-off value, 20 OC patients were divided into MYU high expression group (n = 10) and MYU low expression group (n = 10) for clinicopathological correlation analysis. As shown in Table 1, the overexpression of MYU in OC was significantly correlated with the FIGO stage and lymphatic metastasis but was not correlated with patient age and histological type.

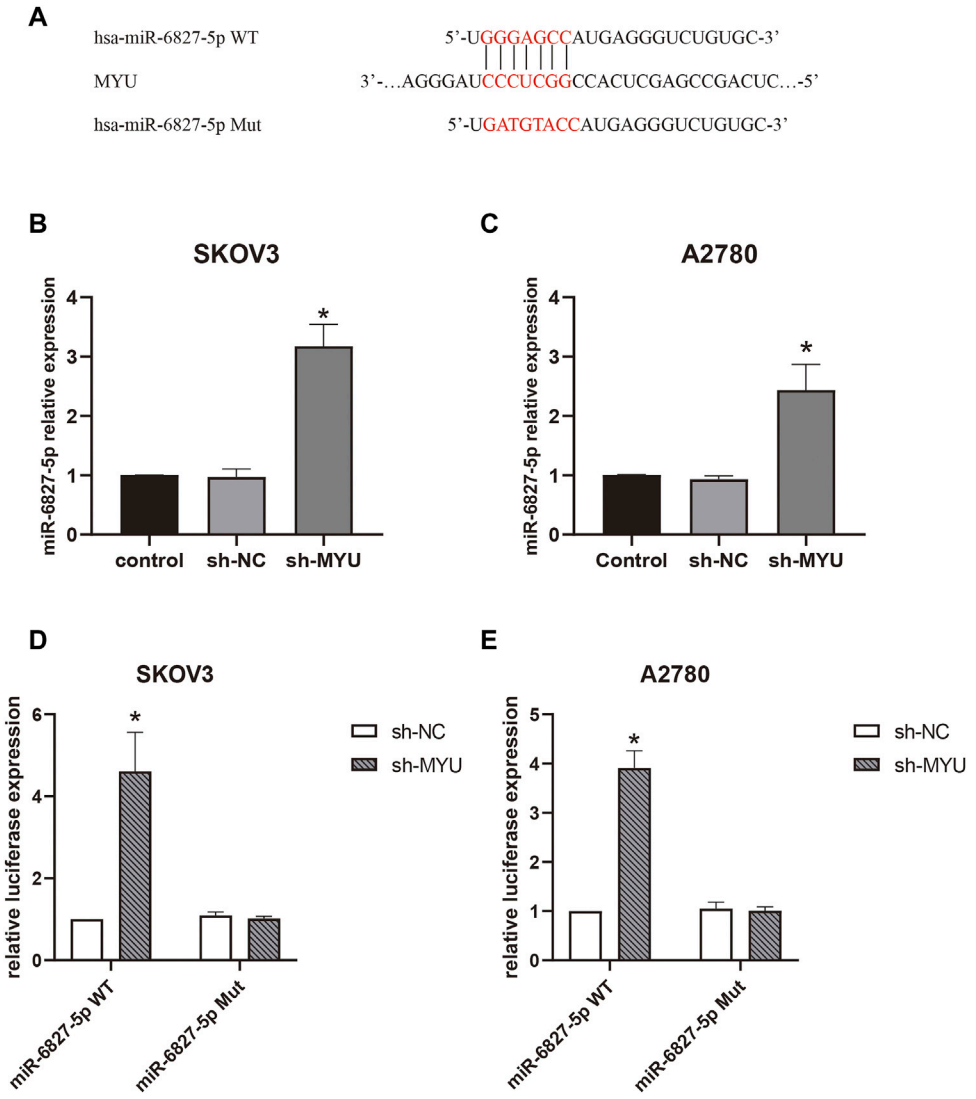

FIGURE 2
MYU functions as a sponge for miR-6827-5p in OC cells. **(A)** Wild-type and mutant MYU binding site in miR-6827-5p. **(B, C)** The relative expression of miR-6527-5p in SKOV3 and A2780 cells with MYU knockdown by qRT-PCR. **(D, E)** Interaction between MYU and miR-6827-5p in OC cells revealed by the luciferase reporter assay. SKOV3 and A2780 cells were co-transfected with a luciferase reporter plasmid carrying miR-6827-5p WT or Mut and sh-MYU or sh-NC. *$p < 0.05$, compared with the sh-NC.

MYU silencing inhibits ovarian cancer cell proliferation

The transfection efficiency of MYU was shown in Figures 1B, C; In SKOV3 cells, the silencing efficiency of the three types of sh-MYU was significantly higher than that of sh-NC. Sh-MYU-1# had the best silencing efficiency. In A2780 cells, the silencing efficiency of sh-MYU-1# and sh-MYU-3# were significant, and sh-MYU-1# was better. As a result, sh-MYU-1# was selected for further experiments. The results of the CCK8 assay revealed that MYU silencing significantly inhibited the viability and proliferation of SKOV3 and A2780 cells (Figures 1D, E).

MYU binds with miR-6827-5p and MYU silencing promotes its expression

Then we further investigated the molecular mechanism of MYU in ovarian cancer. Previous studies have revealed that MYU is mostly localized in the cytoplasm of cancer cells (10, 12-14), implying that it may function as a ceRNA by binding to specific miRNAs. To confirm this hypothesis, the bioinformatics tool miRDB (http://mirdb.org/) was used to predict the potential miRNA targets of MYU. There were 42 predicted miRNAs targeting MYU (Supplementary Table S1). The miRNA with the highest target score was miR-6827-5p in the list, so it was

chosen for our study. We found that miR-6827-5p had a potential binding sequence of MYU and MYU had 10 potential seed locations of miR-6827-5p. The potential binding sequence was shown in Figure 2A. Compared with sh-NC in qRT-PCR, knockdown of MYU dramatically increased the expression of miR-6827-5p (Figures 2B, C), indicating that MYU negatively regulated miR-6827-5p. Additionally, A luciferase reporter assay was performed. The luciferase activity was significantly increased in miR-6827-5p WT and sh-MYU co-transfected cells, compared with miR-6827-5p WT and sh-NC co-transfected cells. In contrast, the luciferase activity had no significant difference in miR-6827-5p Mut transfected cells (Figures 2D,E). The results revealed that MYU silencing promoted the expression of miR-6827-5p WT in SKOV3 and A2780 cells, while the regulatory effect of MYU disappeared when miR-6827-5p was mutated.

HMGA1 is a target gene of miR-6827-5p

Next, we wanted to explore the downstream target genes of miR-6827-5p in OC. By utilizing targetscan (https://www.targetscan.org/), 3944 transcripts containing a total of 5419 binding sites were predicted. HMGA1 was selected for further investigation because it was reported to be overexpressed in OC and correlated with cancer progression (15-17). We found that there were four potential binding sequences of miR-6827-5p in the 3′-UTR of HMGA1 mRNA. Three of the binding sequences of miR-6827-5p and HMGA1 were shown in Figure 3A. Firstly, the transfection efficiency of miR-6827-5p inhibitor was detected, and the silencing efficiency of miR-6827-5p inhibitor-3# was the best in SKOV3 and A2780 cells, so it was selected for further experiments (Figures 3B, C).

Then, a luciferase reporter assay was used to verify the binding of miR-6827-5p to 3′-UTR of HMGA1 mRNA. The results showed that luciferase activity was significantly increased in miR-6827-5p inhibitor and HMGA1 WT co-transfected cells, compared with NC inhibitor and HMGA1 WT co-transfected cells. In contrast, no evident changes were observed in cells co-transfected with HMGA1 Mut and miR-6827-5p inhibitor or NC inhibitor (Figures 3D, E).

MYU Positively Regulates HMGA1 Expression *via* Sponging miR-6827-5p

To further investigate whether MYU could modulate HMGA1 expression by sponging miR-6827-5p, rescue assays were carried out. As revealed by qRT-PCR(Figures 4A, B) and western blot (Figures 4C–F), the expression of HMGA1 mRNA and protein were decreased in SKOV3 and A2780 cells when MYU silencing, and the expression of HMGA1 mRNA and protein were remarkably increased when miR-6827-5p silencing. However, when co-transfecting with sh-MYU and miR-6827-5p inhibitor, the influence of MYU knockdown on HMGA1 mRNA and protein expression was abrogated. CCK-8 assay showed that knockdown of miR-6827-5p promoted OC cell proliferation. However, there was no significant change in cell proliferation after co-transfecting with sh-MYU and miR-6827-5p inhibitor. The results indicated that the restoration of HMGA1 expression reversed the effect of MYU knockdown on cell proliferation (Figures 4G, H). In other words, MYU sponged miR-6827-5p, thereby enhancing HMGA1 expression and promoting cell proliferation in OC.

Discussion

A growing number of studies have revealed that the aberrant expression of lncRNAs is closely related to the occurrence and development of tumors. LncRNAs are expected to become molecular markers and therapeutic targets for tumor diagnosis and prognosis (18). The function of several lncRNAs has been revealed in ovarian cancer, such as MALAT1 (19), HOTAIR (20), CCAT1 (21)、NEAT1 (22), MNX1-AS1 (23).

Although the oncogenic role of MYU in a variety of malignant tumors has been gradually discovered in recent years (8-14), the expression status and potential involvement of MYU in ovarian cancer remain unclear. In the present study, we investigated the expression of MYU in OC tissues and analyzed the clinical significance of MYU in OC. It is optimal to obtain tumor tissues and adjacent non-tumor tissues for evaluation from the same patients. However, in many cases, the ovarian tumor was large and the resected tissue samples should be stored at −80°C immediately. It is difficult to ensure that there is no infiltration of tumor cells if we collect the tissue adjacent to the tumor. Just like other studies (24, 25), we collected OC and normal ovarian tissue samples from different patients. We found that the MYU expression level was higher in OC tissues than that in normal ovarian tissues. The expression of MYU was positively associated with the FIGO stage and lymphatic metastasis. Moreover, shRNA-mediated knockdown of MYU significantly inhibited OC cell proliferation. Therefore, MYU exerts a tumor-promoting effect in OC and it might be a potential prognostic biomarker in OC patients.

Furthermore, we explored the molecular mechanism by which MYU contributed to tumorigenesis. In the recent decade, the ceRNA network has been extensively studied in the field of oncology (7). LncRNA can function as a ceRNA by competitively sponging miRNAs to release mRNAs from RNA-induced silencing complexes (RISCs). The bioinformatics tool was used to predict the potential miRNAs that interacted with MYU.

In the present study, miR-6827-5p expression was at a higher level after MYU knockdown compared with sh-NC in OC cells. It was also disclosed that the expression of miR-6827-5p was negatively regulated by MYU. Luciferase reporter assay verified the combination between MYU and miR-6827-

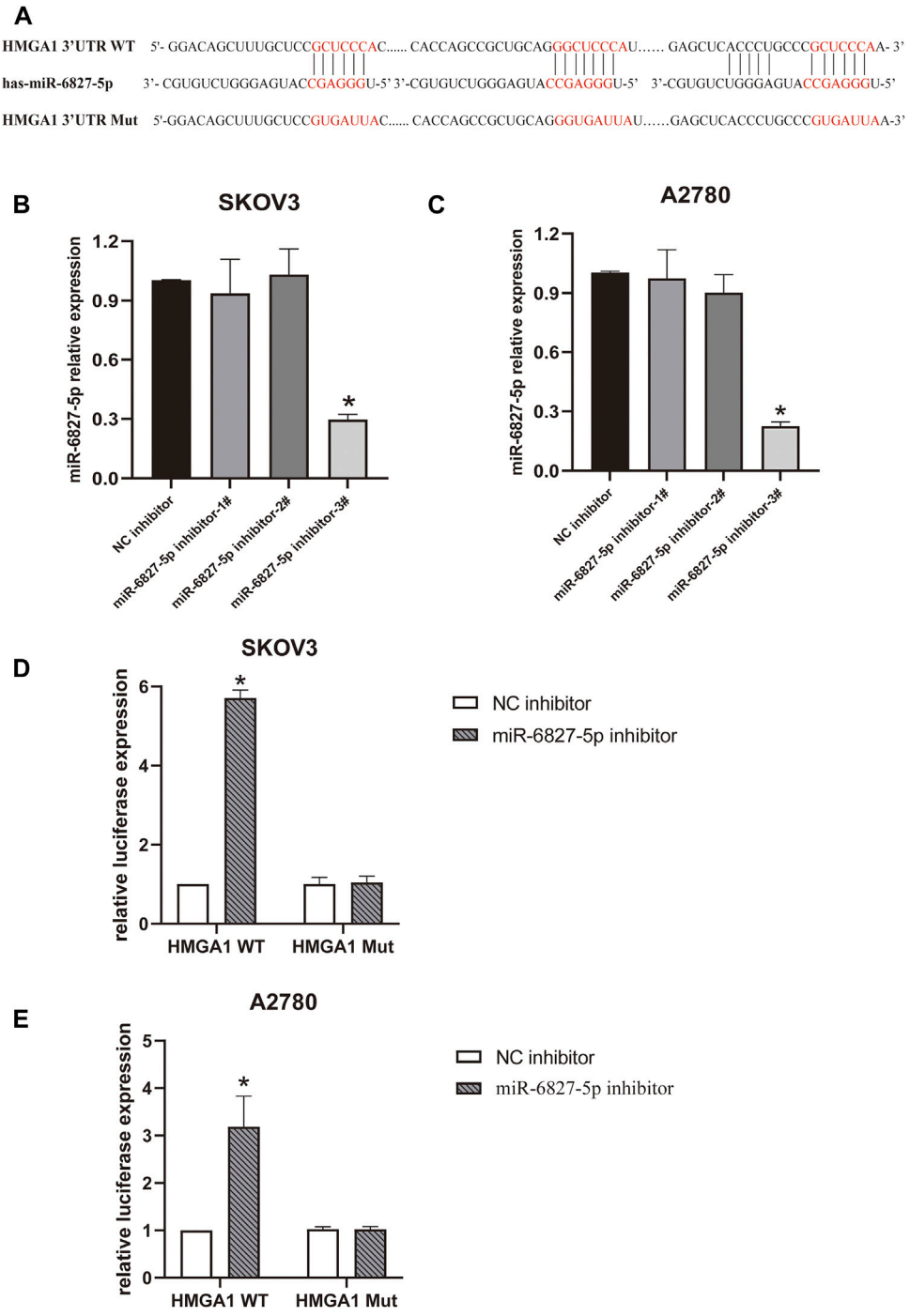

FIGURE 3
miR-6827-5p targets HMGA1 mRNA. **(A)** Wild-type and mutant miR-6827-5p binding site in the 3′-UTR of HMGA1 mRNA. **(B, C)** The silencing efficiency of miR-6827-5p inhibitor in SKOV3 and A2780 cells were detected by qRT-PCR. **(D, E)** Interaction between HMGA1 mRNA and miR-6827-5p in OC cells revealed by the luciferase reporter assay. SKOV3 and A2780 cells were co-transfected with a luciferase reporter plasmid carrying HMGA1 WT or Mut and miR-6827-5p inhibitor or NC inhibitor. *$p < 0.05$, compared with the NC inhibitor.

5p. Function test showed that knockdown of miR-6827-5p promoted cell proliferation. These results displayed that MYU promoted cell proliferation by sponging miR-6827-5p in OC.

Based on the bioinformatics website's predicted results, we found HMGA1 was a target gene of miR-6827-5p. HMGA1 is a member of the high mobility group (HMG) protein family and

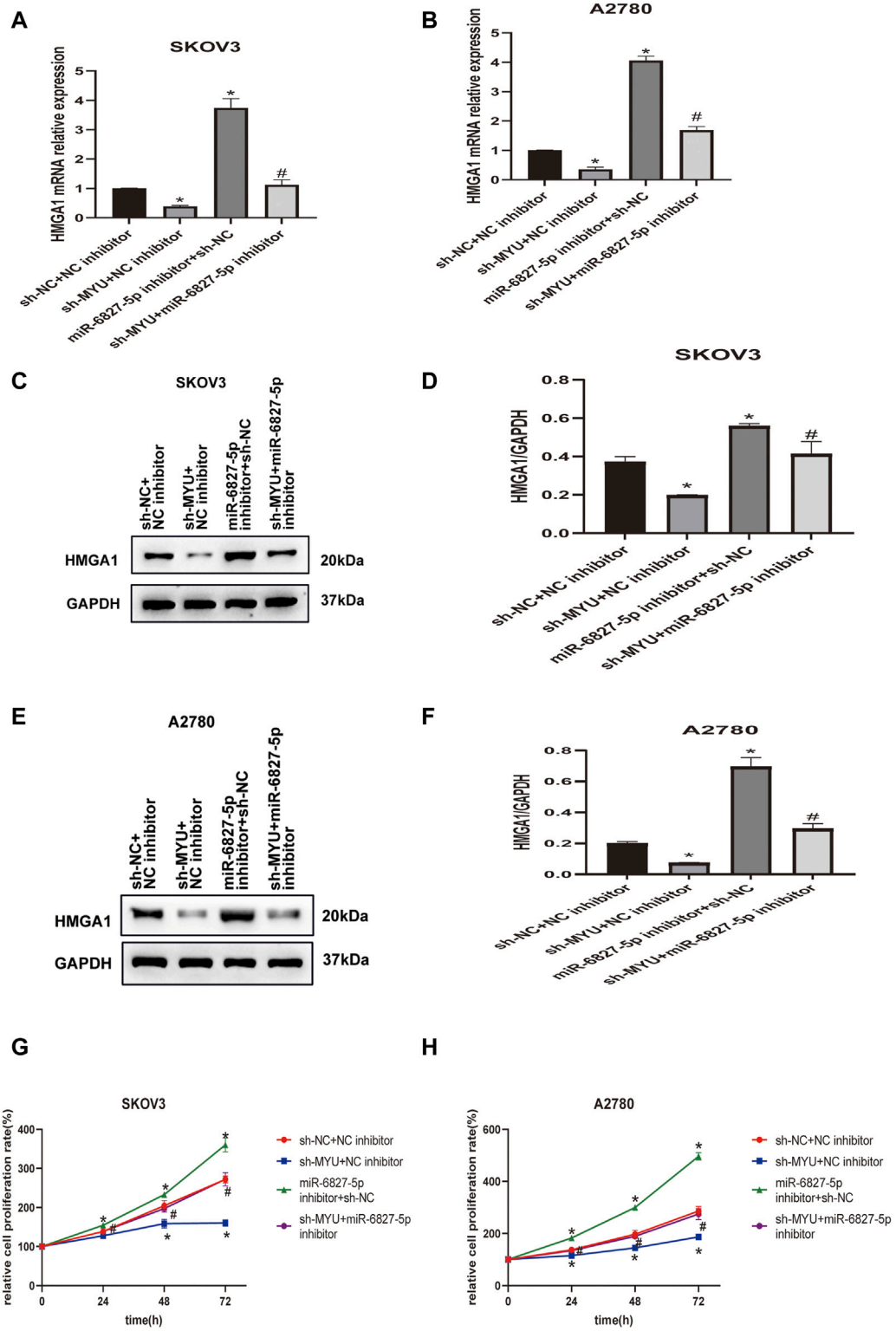

FIGURE 4
MYU acts as a ceRNA of miR-6827-5p and hence upregulates HMGA1 expression. **(A, B)** HMGA1 mRNA levels in SKOV3 and A2780 cells were determined by qRT-PCR after co-transfecting with sh-NC+ NC inhibitor, sh-MYU + NC inhibitor, miR-6827-5p inhibitor +sh-NC or sh-MYU + miR-6827-5p inhibitor. **(C–F)** HMGA1 protein levels in SKOV3 and A2780 cells were determined by western blot after co-transfecting with sh-NC+ NC inhibitor, sh-MYU + NC inhibitor, miR-6827-5p inhibitor +sh-NC or sh-MYU + miR-6827-5p inhibitor. **(G, H)** co-transfecting with sh-MYU and miR-6827-5p inhibitor reversed the influence on cell proliferation caused by MYU knockdown in SKOV3 and A2780 cells. $^{*}p < 0.05$, compared with the sh-NC + NC inhibitor. $^{\#}p < 0.05$, compared with the sh- MYU + NC inhibitor or miR-6827-5p inhibitor +sh-NC.

includes three isoforms: HMGA1a (107 amino acids, 11.7 kDa), HMGA1b (96 amino acids, 10.6 kDa) and HMGA1c (179 amino acids, 19.6 kDa) isoforms, which result from translation of alternative spliced forms of The *HMGA1* gene (26). HMGA1a and HMGA1b are identical in sequence except for the absence of a 11 amino acid region. HMGA1c has in common with HMGA1a only the first 64 amino acid, because of the alternative splicing using non-canonical splice donor and acceptor sites (27). HMGA1 protein binds to the A/T-rich DNA sequences and shows antagonistic actions against histone H1, leading to an open chromatin structure and promoting transcription (28).

HMGA1 is overexpressed in most cancers, including OC (15). The overexpression of HMGA1 is related to the malignant degree of the tumor, and knockdown of HMGA1 can reduce the proliferation and invasion ability of OC cells *in vitro* (17). In the present study, both the mRNA and protein expression of HMGA1 decreased when MYU was silenced, and there was a positive correlation between MYU and HMGA1 expression. These results suggested that MYU regulated HMGA1 expression in a post-transcriptional manner. Meanwhile, the mRNA and protein expression of HMGA1 increased when miR-6827-5p was silenced in OC cells. Luciferase reporter assay verified the interaction between miR-6827-5p and HMGA1 3′-UTR. The results of rescue experiments demonstrated that the effects of MYU knockdown on cell proliferation could be reversed by the upregulation of HMGA1. There was only one band of HMGA1 that could be observed in western blotting, and the molecular weight was about 20 KDa. Given the difference in molecular weight between HMGA1a, HMGA1b and HMGA1c, we speculated that it might be HMGA1c that regulated by the MYU/miR-6827-5p axis. In future studies, we will further explore the role of different HMGA1 protein isoforms on ovarian cancer.

Our study revealed that MYU was upregulated in ovarian cancer and it functioned as an oncogene, because knockdown of MYU can inhibit cell proliferation. However, there are limitations in our current study. First, whether MYU can promote OC cell migration and invasion remains to be explored. Second, the results of this study are limited to *in vitro* studies, tumor xenograft experiments are urgently needed. Third, lncRNA can regulate the expression of genes by sponging multiple different miRNAs and controlling transcriptional and post-transcriptional regulation by binding with proteins. A miRNA can regulate the expression of multiple target genes. Therefore, MYU/miR-6827-5p/HMGA1 is likely to be only one of the possible pathways in tumorigenesis of OC. We need to conduct more in-depth studies in the future.

Conclusion

In this study, we first elucidated that the aberrant overexpression of MYU promoted ovarian cancer cell proliferation by interacting with miR-6827-5p and upregulating HMGA1 expression. The novel ceRNA network composed of MYU, miR-6827-5p, and HMGA1 may provide potential targets and biomarkers for the diagnosis and prognosis of ovarian cancer.

Data availability statement

The raw data supporting the conclusion of this article will be made available by the authors, without undue reservation.

Ethics statement

The studies involving human participants were reviewed and approved by the Ethics Committee of First Affiliated Hospital of Fujian Medical University. The patients/participants provided their written informed consent to participate in this study. Written informed consent was obtained from the individual(s) for the publication of any potentially identifiable images or data included in this article.

Author contributions

ShW: Conceptualization, methodology, data curation, writing—original draft; QZ: Validation, supervision, formal analysis; JW: Project administration; ShC: Investigation, resources, visualization; LC: Writing—review and editing.

Funding

This research was supported by the Research Fund from the Education Department of Fujian Province (JAT200155) and Scientific Research Personnel Training Program of Fujian Province Health and Family Planning Committee (2018-CX-28).

Conflict of interest

The authors declare that the research was conducted in the absence of any commercial or financial relationships that could be construed as a potential conflict of interest.

Supplementary material

The Supplementary Material for this article can be found online at: https://www.por-journal.com/articles/10.3389/pore.2023.1610870/full#supplementary-material

References

1. Xia C, Dong X, Li H, Cao M, Sun D, He S, et al. Cancer statistics in China and United States, 2022: Profiles, trends, and determinants. *Chin Med J* (2022) 135(5): 584–90. doi:10.1097/cm9.0000000000002108

2. Moufarrij S, Dandapani M, Arthofer E, Gomez S, Srivastava A, Lopez-Acevedo M, et al. Epigenetic therapy for ovarian cancer: Promise and progress. *Clin epigenetics* (2019) 11(1):7. doi:10.1186/s13148-018-0602-0

3. Torre LA, Trabert B, DeSantis CE, Miller KD, Samimi G, Runowicz CD, et al. Ovarian cancer statistics. *CA Cancer J Clin* (2018) 68(4):284–96. doi:10.3322/caac.21456

4. Beermann J, Piccoli MT, Viereck J, Thum T. Non-coding RNAs in development and disease: Background, mechanisms, and therapeutic approaches. *Physiol Rev* (2016) 96(4):1297–325. doi:10.1152/physrev.00041.2015

5. Schaukowitch K, Kim TK. Emerging epigenetic mechanisms of long non-coding RNAs. *Neuroscience* (2014) 264:25–38. doi:10.1016/j.neuroscience.2013.12.009

6. Mendell J. MicroRNAs: Critical regulators of development, cellular physiology and malignancy. *Cell Cycle (Georgetown, Tex)* (2005) 4(9):1179–84. doi:10.4161/cc.4.9.2032

7. Qi X, Zhang DH, Wu N, Xiao JH, Wang X, Ma W. ceRNA in cancer: possible functions and clinical implications. *J Med Genet* (2015) 52(10):710–8. doi:10.1136/jmedgenet-2015-103334

8. Kawasaki Y, Komiya M, Matsumura K, Negishi L, Suda S, Okuno M, et al. MYU, a target lncRNA for wnt/c-myc signaling, mediates induction of CDK6 to promote cell cycle progression. *Cel Rep* (2016) 16(10):2554–64. doi:10.1016/j.celrep.2016.08.015

9. Wang J, Yang X, Li R, Wang L, Gu Y, Zhao Y, et al. Long non-coding RNA MYU promotes prostate cancer proliferation by mediating the miR-184/c-Myc axis. *Oncol Rep* (2018) 40:2814–25. doi:10.3892/or.2018.6661

10. Wang X, Chen Q, Wang X, Li W, Yu G, Zhu Z, et al. ZEB1 activated-VPS9D1-AS1 promotes the tumorigenesis and progression of prostate cancer by sponging miR-4739 to upregulate MEF2D. *Biomed Pharmacother* (2020) 122:109557. doi:10.1016/j.biopha.2019.109557

11. Tan J, Yang L. Long noncoding RNA VPS9D1-AS1 overexpression predicts a poor prognosis in non-small cell lung cancer. *Biomed Pharmacother* (2018) 106: 1600–6. doi:10.1016/j.biopha.2018.07.113

12. Han X, Huang T, Han J. Long noncoding RNA VPS9D1-AS1 augments the malignant phenotype of non-small cell lung cancer by sponging microRNA-532-3p and thereby enhancing HMGA2 expression. *Aging* (2020) 12(1):370–86. doi:10.18632/aging.102628

13. Xiao S, Xu N, Ding Q, Huang S, Zha Y, Zhu H. LncRNA VPS9D1-AS1 promotes cell proliferation in acute lymphoblastic leukemia through modulating GPX1 expression by miR-491-5p and miR-214-3p evasion. *Biosci Rep* (2020) 40. doi:10.1042/bsr20193461

14. Fa X, Song P, Fu Y, Deng Y, Liu K. Long non-coding RNA VPS9D1-AS1 facilitates cell proliferation, migration and stemness in hepatocellular carcinoma. *Cancer Cel Int* (2021) 21(1):131. doi:10.1186/s12935-020-01741-7

15. Masciullo V, Baldassarre G, Pentimalli F, Berlingieri MT, Boccia A, Chiappetta G, et al. HMGA1 protein over-expression is a frequent feature of epithelial ovarian carcinomas. *Carcinogenesis* (2003) 24(7):1191–8. doi:10.1093/carcin/bgg075

16. Kim DK, Seo EJ, Choi EJ, Lee SI, Kwon YW, Jang IH, et al. Crucial role of HMGA1 in the self-renewal and drug resistance of ovarian cancer stem cells. *Exp Mol Med* (2016) 48:e255. doi:10.1038/emm.2016.73

17. Liu Y, Wang Y, Zhang Y, Fu J, Zhang G. Knockdown of HMGA1 expression by short/small hairpin RNA inhibits growth of ovarian carcinoma cells. *Biotechnol Appl Biochem* (2012) 59(1):1–5. doi:10.1002/bab.56

18. Braga EA, Fridman MV, Moscovtsev AA, Filippova EA, Dmitriev AA, Kushlinskii NE. LncRNAs in ovarian cancer progression, metastasis, and main pathways: ceRNA and alternative mechanisms. *Int J Mol Sci* (2020) 21(22):8855. doi:10.3390/ijms21228855

19. Pa M, Naizaer G, Seyiti A, Kuerbang G. Long noncoding RNA MALAT1 functions as a sponge of MiR-200c in ovarian cancer. *Oncol Res* (2017). doi:10.3727/096504017X15049198963076

20. Zhang Y, Ai H, Fan X, Chen S, Wang Y, Liu L. Knockdown of long non-coding RNA HOTAIR reverses cisplatin resistance of ovarian cancer cells through inhibiting miR-138-5p-regulated EZH2 and SIRT1. *Biol Res* (2020) 53(1):18. doi:10.1186/s40659-020-00286-3

21. Cao Y, Shi H, Ren F, Jia Y, Zhang R. Long non-coding RNA CCAT1 promotes metastasis and poor prognosis in epithelial ovarian cancer. *Exp Cel Res* (2017) 359(1):185–94. doi:10.1016/j.yexcr.2017.07.030

22. Liu Y, Wang Y, Fu X, Lu Z. Long non-coding RNA NEAT1 promoted ovarian cancer cells' metastasis through regulation of miR-382-3p/ROCK1 axial. *Cancer Sci* (2018) 109(7):2188–98. doi:10.1111/cas.13647

23. Shen Y, Lv M, Fang Y, Lu J, Wu Y. LncRNA MNX1-AS1 promotes ovarian cancer process via targeting the miR-744-5p/SOX12 axis. *J Ovarian Res* (2021) 14(1):161. doi:10.1186/s13048-021-00910-0

24. Wu DD, Chen X, Sun KX, Wang LL, Chen S, Zhao Y. Role of the lncRNA ABHD11-AS1 in the tumorigenesis and progression of epithelial ovarian cancer through targeted regulation of RhoC. *Mol Cancer* (2017) 16(1):138. doi:10.1186/s12943-017-0709-5

25. Long X, Li L, Zhou Q, Wang H, Zou D, Wang D, et al. Long non-coding RNA LSINCT5 promotes ovarian cancer cell proliferation, migration and invasion by disrupting the CXCL12/CXCR4 signalling axis. *Oncol Lett* (2018) 15(5):7200–6. doi:10.3892/ol.2018.8241

26. Nagpal S, Ghosn C, DiSepio D, Molina Y, Sutter M, Klein ES, et al. Retinoid-dependent recruitment of a histone H1 displacement activity by retinoic acid receptor. *J Biol Chem* (1999) 274(32):22563–8. doi:10.1074/jbc.274.32.22563

27. Cleynen I, Van de Ven WJM. The HMGA proteins: A myriad of functions (Review). *Int J Oncol* (2008) 32(2):289–305. doi:10.3892/ijo.32.2.289

28. Benecke AG, Eilebrecht S. RNA-mediated regulation of HMGA1 function. *Biomolecules* (2015) 5(2):943–57. doi:10.3390/biom5020943

Pathology & Oncology Research | frontiers

TYPE Original Research
PUBLISHED 28 April 2023
DOI 10.3389/pore.2023.1611138

Check for updates

OPEN ACCESS

EDITED BY
Andrea Ladányi,
National Institute of Oncology (NIO), Hungary

*CORRESPONDENCE
Raksawan Deenonpoe,
raksde@kku.ac.th

RECEIVED 21 February 2023
ACCEPTED 18 April 2023
PUBLISHED 28 April 2023

CITATION
Khonrak T, Watcharadetwittaya S, Chamgramol Y, Intarawichian P and Deenonpoe R (2023), *RET* rearrangements are relevant to histopathologic subtypes and clinicopathological features in Thai papillary thyroid carcinoma patients. *Pathol. Oncol. Res.* 29:1611138. doi: 10.3389/pore.2023.1611138

COPYRIGHT
© 2023 Khonrak, Watcharadetwittaya, Chamgramol, Intarawichian and Deenonpoe. This is an open-access article distributed under the terms of the Creative Commons Attribution License (CC BY). The use, distribution or reproduction in other forums is permitted, provided the original author(s) and the copyright owner(s) are credited and that the original publication in this journal is cited, in accordance with accepted academic practice. No use, distribution or reproduction is permitted which does not comply with these terms.

RET rearrangements are relevant to histopathologic subtypes and clinicopathological features in Thai papillary thyroid carcinoma patients

Thitima Khonrak[1], Sasithorn Watcharadetwittaya[1,2], Yaovalux Chamgramol[1], Piyapharom Intarawichian[1,2] and Raksawan Deenonpoe[1,2]*

[1]Department of Pathology, Faculty of Medicine, Khon Kaen University, Khon Kaen, Thailand, [2]Cholangiocarcinoma Research Institute (CARI), Khon Kaen University, Khon Kaen, Thailand

Background: Papillary thyroid carcinoma (PTC) is the most common type of thyroid cancer. The *RET* gene rearrangements *CCDC6*::*RET* and *NCOA4*::*RET* are the most common *RET* gene rearrangements in PTC patients. Different *RET*::*PTC* rearrangements are associated with different PTC phenotypes.

Methods: Eighty-three formalin-fixed paraffin-embedded (FFPE) PTC samples were examined. The prevalence and expression levels of *CCDC6*::*RET* and *NCOA4*::*RET* were determined using semi-quantitative polymerase chain reaction (qRT-PCR). The association of these rearrangements with clinicopathological data was investigated.

Results: The presence of *CCDC6*::*RET* rearrangement was significantly associated with the classic subtype and absence of angio/lymphatic invasion ($p < 0.05$). While *NCOA4*::*RET* was associated with the tall-cell subtype, and presence of angio/lymphatic invasion and lymph node metastasis ($p < 0.05$). Multivariate analysis demonstrated that an absence of extrathyroidal extension and extranodal extension were independent predictive factors for *CCDC6*::*RET*, whereas the tall-cell subtype, large tumor size, angioinvasion, lymphatic invasion and perineural invasion were independent predictive factors for *NCOA4*::*RET* ($p < 0.05$). However, the mRNA expression level of *CCDC6*::*RET* and of *NCOA4*::*RET* were not significantly associated with clinicopathological data.

Conclusion: *CCDC6*::*RET* was correlated with an innocent PTC subtype and characteristics, but *NCOA4*::*RET* correlated with an aggressive phenotype of PTC. Therefore, these *RET* rearrangements strongly associated with clinicopathological phenotypes and can be used as predictive markers in PTC patients.

KEYWORDS

papillary thyroid carcinoma, RET rearrangements, *CCDC6*::*RET* rearrangement, *NCOA4*::*RET* rearrangement, gene rearrangements

Introduction

Papillary thyroid carcinoma (PTC) is the most common form of well-differentiated thyroid cancer, originating from thyroid follicular cells. PTC is also the most prevalent form of thyroid cancer overall, contributing to 75%–85% of thyroid-cancer cases (1). Although its incidence is rapidly increasing, PTC has the best overall prognosis of any type of thyroid cancer.

BRAF and *RAS* genes, as well as rearrangements of the *RET* gene are strongly associated with PTC, respectively. These mutations are associated with mitogen-activated protein kinase (MAPK) and phosphatidylinositol-3 kinase (PI3K)/AKT signaling pathways that affect proliferation and differentiation in cancer cells. *RET* fusions/rearrangements, are the most frequent molecular alterations reported in PTC, being present in about 10%–40% of cases worldwide, but in 45%–60% of cases involving adolescents and children with sporadic PTC (2–5). The major fusion partner genes in such rearrangements are *CCDC6* and *NCOA4* (also known as *ELE1*). These two fusions account for approximately 90% of such cases (6).

The *RET* (rearranged during transfection) gene is a proto-oncogene located on the long arm of chromosome 10 (10q11.2), and consists of three parts; the extracellular segment, transmembrane segment and an intracellular segment (7); the intracellular segment is an important part that causing of *RET*::*PTC* rearrangements. The fusion of tyrosine kinase domain with the 5′region of another gene such as *CCDC6* and *ELE1,* generates chimeric products collectively named *RET*::*PTCs*. These result in ligand-independent dimerization and constitutive activation of these chimeric proteins triggers *RAS* which activates *RAF* kinases, and the downstream signaling cascade, causing proliferation and differentiation in cancer cells.

CCDC6::*RET* is formed by fusion with the *CCDC6* (also designated *H4*) gene and *NCOA4*::*RET* by fusion with the *NCOA4* (also designated *ELE1*, *RFG* or *ARA70*). These rearrangements are associated with papillary thyroid carcinoma cases with different characteristics; *CCDC6*::*RET* is more associated with sporadic thyroid cancer (8, 9) and with older patients and classic subtypes of papillary carcinoma (8–10). The *NCOA4*::*RET* rearrangement correlates with a more aggressive phenotype and a more advanced stage of PTC. Those fusion genes are also strongly associated with short radiation latency and solid subtypes of PTC (8, 9, 11–13). *RET*::*PTC*-mediated signaling depends on a specific *RET* tyrosine residue, Y1062 (numbering refers to the full-length RET protein). Both types of *RET* fusion have comparable levels of Y1062 phosphorylation but, MAPK phosphorylation is higher in *NCOA4*::*RET* than in *CCDC6*::*RET* (14). Therefore, the two rearrangements have the same enzymatic activity and autophosphorylation levels, but activation of MAPK is greater by *NCOA4*::*RET* than *CCDC6*::*RET*.

Although the global prevalence of major *RET*::*PTC* fusions in PTC patients has been reported, but no data are available specifically for Thailand. Thus, this study aimed to determine the prevalence of *CCDC6*::*RET* and *NCOA4*::*RET* fusions in Thai papillary thyroid carcinoma patients. Prevalence and expression levels of *CCDC6*::*RET* and *NCOA4*::*RET* rearrangements in PTC patients were determined using semi-quantitative polymerase chain reaction (qRT-PCR). The association of these *RET*::*PTC* rearrangements with clinicopathological data was also investigated to test the hypothesis that *CCDC6*::*RET* and *NCOA4*::*RET* fusion genes are differently associated with aggressive characteristics in PTC.

Material and methods

Study population

The study was approved by the Ethics Committee for Human Research, Khon Kaen University (HE641011). Formal written informed consent was not required with a waiver by the appropriate IRB and/or national research ethics committee. Formalin-fixed paraffin-embedded (FFPE) tissue of patients (n = 83) who had been diagnosed with papillary thyroid carcinoma by pathologists at Pathology services, Department of Pathology in the years 2010–2014 were investigated. All cases were included for this study by clinical data from medical records at Srinagarind hospital,

TABLE 1 The primer sequences.

Name	Primers	Product size (bp)
GAPDH	F-GTCTCCTCTGACTTCAACAGCG	97
	R-ACCACCCTGTTGCTGTAGCCAA	
CCDC6::*RET*	F-ATACTGGAGAACAGGCCATCTG	207
	R-CGTTGCCTTGACCACTTTTCC	
NCOA4::*RET*	F-CCTTTCAGCGAATGGCTCCT	136
	R- ATTCCCACTTTGGATCCTCCT	

Nucleotide positions of the primers are based on the sequences deposited in GenBank: *CCDC6*::*RET* (accession no.AF395885.1) and *NCOA4*::*RET* (accession no. S71225.1).

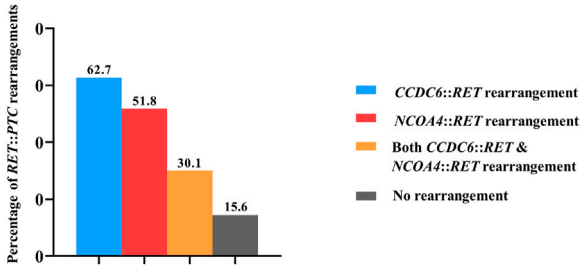

FIGURE 1
The frequency of *RET* rearrangements in PTC patients. In detail, *CCDC6*::*RET* rearrangements were detected in 62.7% (52/83), *NCOA4*::*RET* rearrangements in 51.8% (43/83), both *CCDC6*::*RET* and *NCOA4*::*RET* rearrangements co-occurred in 30.1% (25/83) and 15.6% (13/83) PTCs were negative for both *RET*::*PTC* rearrangements.

Khon Kaen, Thailand, including sex, age, clinicopathological information including size of tumor, subtype of PTC, angioinvasion, lymphatic invasion, perineural invasion, extrathyroidal extension, extranodal extension and lymph node metastasis. Data relating to lymph node metastasis and extranodal extension was missing for some patients. *BRAF* and *KRAS* mutations were not included in clinicopathological data according to genetic alterations were not performed in our routine service. As only morphologic features were investigated for pathological diagnosis.

FFPE slides preparation

Section of formalin-fixed, paraffin-embedded (FFPE) tissues from normal thyroid (n = 10), benign multinodular goiter (n = 10), PTC (n = 83) were stained with hematoxylin and eosin (H&E) and reviewed by two pathologists (SW & PI) to confirm the diagnoses and subclassify the subtypes of papillary carcinomas (Figure 2A). Paraffin blocks of each tumor were examined by pathologists to identify the extent of tumorous tissue. These were then used for RNA extraction.

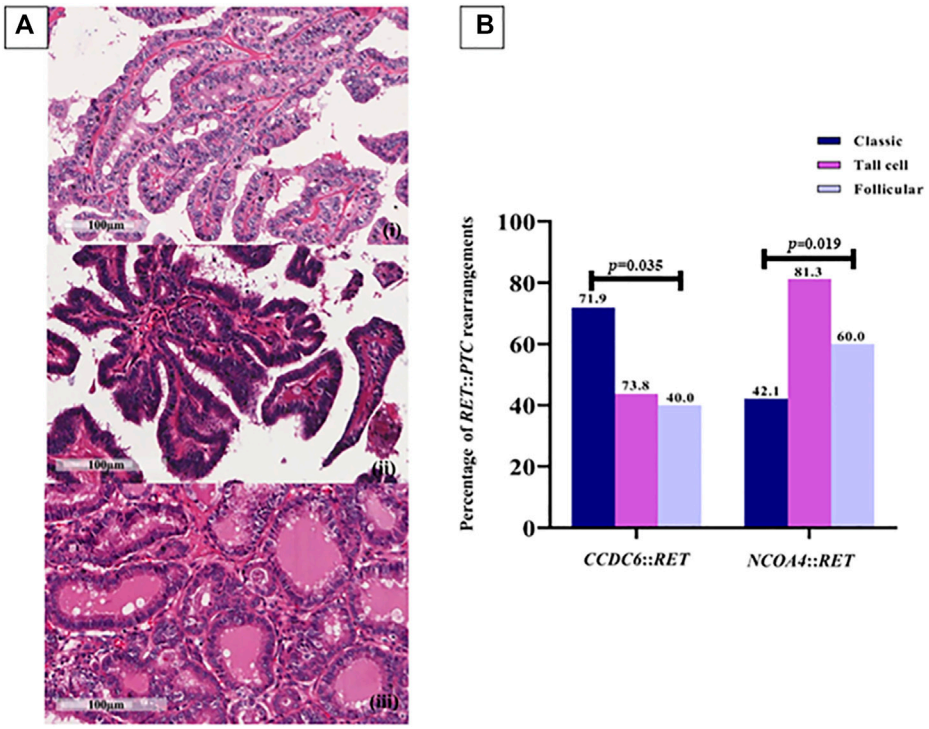

FIGURE 2
RET rearrangements in each PTC subtype. **(A)** Papillary thyroid carcinoma subtypes. (i) Classic PTC; consists of papillae with fibrovascular core line by neoplastic cell characterized by increased nuclear size, nuclear overlapping, nuclear features like clear, ground glass appearance and oval shape (400X, scale bar = 100 μm); (ii) Tall cell PTC; abundant eosinophilic cytoplasm and nuclear features characteristic of classic subtype (400X, scale bar = 100 μm); (iii) Follicular PTC; follicular architecture but enlarged nuclei with cytologic features of PTC (400X, scale bar = 100 μm). **(B)** The prevalence of *RET*::*PTC* rearrangements in each PTC subtype; 41 (71.9%) and 24 (42.1%) cases of the classic subtype are positive for *CCDC6*::*RET* and *NCOA4*::*RET*, respectively, 7 (43.8%) cases of the tall-cell subtype were positive for *CCDC6*::*RET* and 13 (81.3%) cases for *NCOA4*::*RET* rearrangement, 4 (40%) cases of follicular PTC for *CCDC6*::*RET* and 6 (60%) cases for *NCOA4*::*RET*. Either the frequency of *CCDC6*::*RET* or *NCOA4*::*RET* rearrangements are significantly different in those subtypes (p = 0.035, p = 0.019).

TABLE 2 Correlation between *RET* rearrangements and clinicopathological data using Chi-square analysis.

Variable	Category	N	*CCDC6*::*RET* rearrangement (%)	*p*	*NCOA4*::*RET* rearrangement (%)	*p*	*CCDC6*::*RET* and *NCOA4*::*RET* rearrangement (%)	*p*
Gender	Male	24	15 (62.5)	0.986	14 (58.3)	0.448	9 (37.5)	0.350
	Female	59	37 (62.7)		29 (49.2)		16 (27.1)	
Age	<55	53	39 (73.6)	**0.006**	25 (47.2)	0.261	17 (32.1)	0.606
	≥55	30	13 (43.3)		18 (60.0)		8 (26.7)	
Tumor size	≤1	7	5 (71.4)	0.311	4 (57.1)	0.501	3 (42.9)	0.746
	1 < T ≤ 2	18	13 (72.2)		8 (44.4)		5 (27.8)	
	2 < T ≤ 4	40	26 (65.0)		19 (47.5)		13 (32.5)	
	>4	18	8 (44.4)		12 (66.7)		4 (22.2)	
PTC subtype	Classic	57	41 (71.9)	**0.035**	24 (42.1)	**0.019**	14 (24.6)	0.258
	Tall cell	16	7 (43.8)		13 (81.3)		7 (43.8)	
	Follicular[a]	10	4 (40.0)		6 (60.0)		4 (40.0)	
Angioinvasion	Absent	43	33 (76.7)	**0.006**	15 (34.9)	**0.001**	13 (30.2)	0.982
	Present	40	19 (47.5)		28 (70.0)		12 (30.0)	
Lymphatic invasion	Absent	46	37 (80.4)	**<0.001**	17 (37.0)	**0.003**	16 (34.8)	0.343
	Present	37	15 (40.5)		26 (70.3)		9 (24.3)	
Perineural invasion	Absent	69	46 (66.7)	0.093	33 (47.8)	0.107	22 (31.9)	0.437
	Present	14	6 (42.9)		10 (71.4)		3 (21.4)	
Extrathyroidal extension	Absent	67	48 (71.6)	**<0.001**	29 (43.3)	**0.001**	21 (31.3)	0.619
	Present	16	4 (25.0)		14 (87.5)		4 (25.0)	
Lymph node metastasis[b]	Absent	12	9 (75.0)	0.129	4 (33.3)	**<0.001**	4 (33.3)	0.425
	Present	39	20 (51.3)		29 (74.4)		14 (35.9)	
Extranodal extension[b]	Absent	31	22 (71.0)	**0.030**	18 (58.1)	**0.013**	13 (41.9)	0.180
	Present	19	7 (36.8)		14 (73.7)		5 (26.3)	

[a]The follicular variant (n = 10) divided into 5 encapsulated FVPTC and 5 infiltrative FVPTC; 2 encapsulated FVPTC and 2 infiltrative FVPTC presented *CCDC6*::*RET*, 1 encapsulated FVPTC and 3 infiltrative FVPTC presented *NCOA4*::*RET*.
FVPTC, follicular variant of papillary thyroid carcinoma.
[b]Some missing data.
Bold values mean "statistical significant".

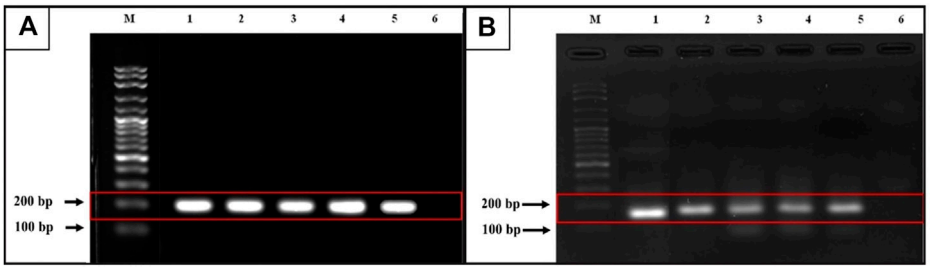

FIGURE 3
Gel electrophoresis from qRT-PCR products. **(A)** *CCDC6*::*RET* rearrangement (expected band size 207 bp). M = 100 bp ladder, lane 1 is a positive control, lanes 2 and 3 = classic subtype, lane 4 and lane 5 = follicular variant, lane 6 = undetectable case **(B)** *NCOA4*::*RET* rearrangement (expected band size 136 bp). M = 100 bp ladder, lane 1 is a positive control, lane 2 = classic subtype, lane 3 and 4 = tall-cell, lane 5 = follicular variant and lane 6 = undetectable case.

RNA extraction and cDNA synthesis

FFPE blocks of all PTC tissues, as well as, benign and normal thyroid, were cut to provide sections of approximately 10 μm in thickness. Ten ribbons from each sample were used for RNA extraction. Tissue deparaffinization was performed using xylene and ethanol (SAV Liquid Production GmbH, Flintsbach am Inn, Germany). RNA was extracted using TRIzol® Reagent (Thermofisher Waltham, Massachusetts, United States) with the addition of 0.2 mL of chloroform per 1 mL of TRIZOL

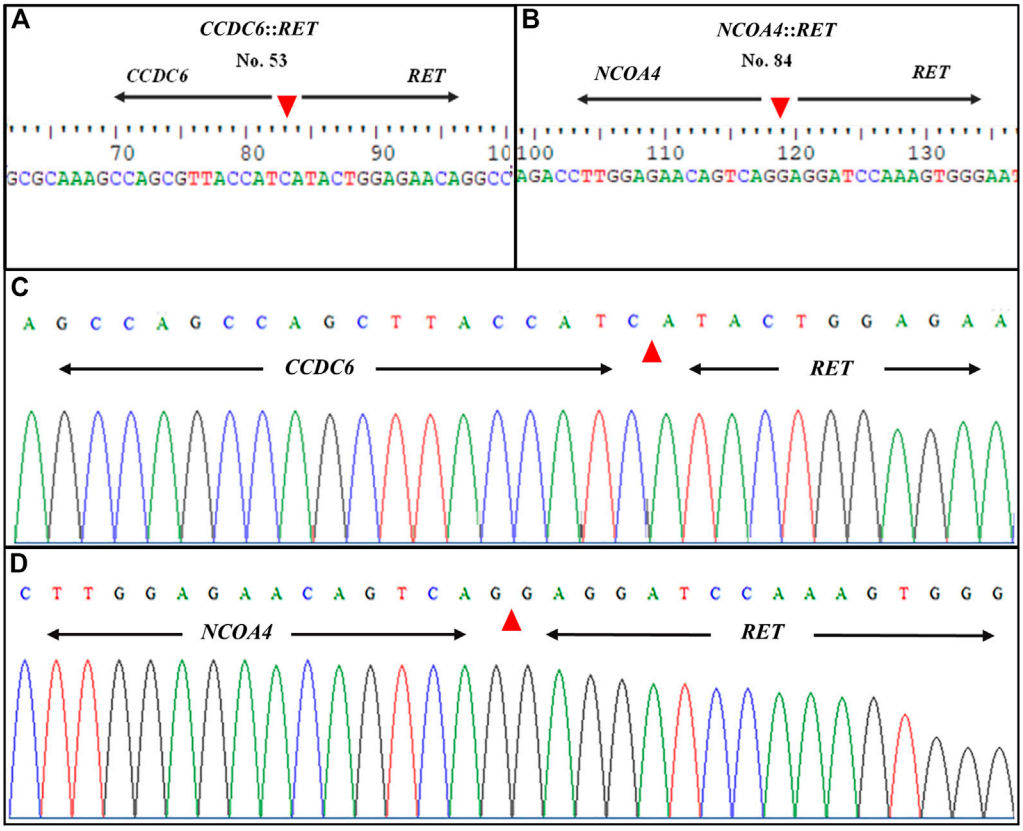

FIGURE 4
Representative sequence lengths of qRT-PCR products and electropherograms of *RET* rearrangements. **(A)** *CCDC6::RET; RET* fusion with the *CCDC6* gene and **(B)** *NCOA4::RET; RET* fusion with the *NCOA4* gene **(C)** Showing formed, distinctive single-coloured peaks of DNA electropherogram of *CCDC6::RET* and **(D)** *NCOA4::RET* rearrangements. The patient's identification number is listed at the top of each panel. Nucleotide sequences around the fusion points of the two different types of *RET* rearrangement transcripts are shown. Arrowheads indicate the fusion point.

reagent was added. Tissue sections were homogenized in 1 mL of TRIZOL reagent per 50–100 mg of tissue (1 ribbon with 10 µm ≈ 1 mg). Isopropanol per 1 mL TRIZOL reagent was used for precipitating the RNA. The concentration and purity of extracted RNA and protein were measured using a nanodrop spectrophotometer at wavelengths of 260 nm (A260) and 280 nm (A280), respectively. The concentration of RNA 50 µg/mL absorbed light at a wavelength of 260 nm in general. Complementary deoxyribonucleic acid (cDNA) was synthesized from messenger RNA using reverse transcription PCR and the RevertAid First Strand cDNA Synthesis Kit (Thermofisher Waltham, Massachusetts, United States) following the manufacturer's instructions. For oligo (dT) 18 or gene-specific primed cDNA synthesis, incubated for 60 min at 42°C. For random hexamer primed synthesis, incubated for 5 min at 25°C followed by 60 min at 42°C. Terminated the reaction by heating at 70°C for 5 min. The reverse transcription reaction product could be directly used in PCR applications or stored at −20°C for less than 1 week.

Semi-quantitative polymerase chain reaction (qRT-PCR)

Two specific primers were designed based on the sequences deposited in GenBank for *CCDC6::RET* and *NCOA4::RET* (Table 1). The nucleotide positions of those primers were synthesized as positive control. cDNA (50 ng/µL) and 23 µL of RT-PCR master mix [SYBR Green master mix qPCR kit (Thermo Scientific Ltd., United Kingdom)] were used for the qRT-PCR. The reactions were carried out in triplicate. GAPDH mRNA was used as an internal control and a no-template control (NTC) was included each time. The amplification of cDNA was performed using a Thermal kit (Thermo Scientific Ltd., United Kingdom) with the following 40 cycles of amplification conditions in Supplementary Table S1. The cuff off cycle threshold (Ct) value was 37th cycle. Cases with Ct values ≤37 were categorized as positive for the specific rearrangement. Post-PCR fluorescence melting curve analysis was done to

TABLE 3 Univariate and multivariate analysis of the clinicopathological factors with *RET* rearrangements by the simple logistic regression and multiple logistic regression.

Variable	Category	n (%)	*CCDC6*::*RET* rearrangement				n (%)	*NCOA4*::*RET* rearrangement			
			Univariate analysis		Multivariate analysis			Univariate analysis		Multivariate analysis	
			OR (95% CI)	*p*	OR (95% CI)	*p*		OR (95% CI)	*p*	OR (95% CI)	*p*
Gender	Male	15 (62.5)	1	0.986			14 (58.3)	1	0.449		
	Female	37 (62.7)	1.01 (0.38–2.69)				29 (49.2)	0.69 (0.26–1.80)			
Age	<55	39 (73.6)	1	**0.007**	1	0.159	25 (47.2)	1	0.263		
	≥55	13 (43.3)	0.27 (0.11–0.71)		0.27 (0.04–1.67)		18 (60.0)	1.68 (0.68–4.17)			
Tumor size	≤1	5 (71.4)	1		1	0.056	4 (57.1)	1		1	
	1 < T ≤ 2	13 (72.2)	1.04 (0.15–7.22)	0.968			8 (44.4)	0.60 (0.10–3.49)	0.570		
	2 < T ≤ 4	26 (65.0)	0.74 (0.13–4.33)	0.741			19 (47.5)	1.68 (0.13–3.43)	0.064	1.02 (0.00–1.53)	**0.020**
	>4	8 (44.4)	0.32 (0.05–2.11)	0.236	18.3 (0.93–361.64)		12 (66.7)	1.50 (0.25–8.98)	0.066	1.02 (0.00–1.87)	**0.042**
PTC subtype	Classic	41 (71.9)	1				24 (43.8)	1		1	
	Tall cell	7 (43.8)	0.30 (0.10–0.95)	**0.041**	0.75 (0.33–2.58)	0.07	13 (81.3)	5.96 (1.53–23.24)	**0.010**	6.06 (2.15–20.49)	**0.032**
	Follicular	4 (40.0)	1.18 (0.06–1.05)	0.058	1.09 (0.9–3.54)	0.121	6 (60.0)	2.06 (0.52–8.12)	0.300	0.03 (0.40–5.70)	0.173
Angioinvasion	Absent	33 (76.7)	1	**0.007**	0.48 (0.01–1.34)	0.086	15 (34.9)	1	**0.002**	1	**0.019**
	Present	19 (47.5)	0.27 (0.11–0.70)				28 (70.0)	4.36 (1.73–10.95)		16.29 (1.57–168.81)	
Lymphatic invasion	Absent	37 (80.4)	1	**<0.001**	1	0.078	17 (37.0)	1	**0.003**	1	**0.015**
	Present	15 (40.5)	0.17 (0.06–0.44)		0.25 (0.05–1.17)		26 (70.3)	4.03 (1.60–10.17)		44.11 (2.11–922.55)	
Perineural invasion	Absent	46 (66.7)	1	0.101	1	0.218	33 (47.8)	1	0.116	1	**0.039**
	Present	6 (42.9)	0.38 (0.12–1.21)		0.35 (0.07–1.86)		10 (71.4)	2.73 (0.78–9.54)		24.64 (1.18–515.96)	
Extrathyroidal extension	Absent	48 (71.6)	1	**0.001**	1	**0.032**	29 (43.3)	1	**0.005**	1	0.109
	Present	4 (25.0)	0.13 (0.04–0.46)		0.25 (0.02–0.84)		14 (87.5)	9.17 (1.93–43.58)		17.99 (0.53–613.89)	
Lymph node metastasis	Absent	9 (75.0)	1	0.157	0.89 (0.09–1.2)	0.123	4 (33.3)	1	**0.004**	1	0.058
	Present	20 (51.3)	0.35 (0.08–1.50)				29 (74.4)	8.7 (1.96–38.65)		9.03 (0.93–88.02)	
Extranodal extension	Absent	22 (71.0)	1	**0.021**	1	**0.026**	18 (58.1)	1	0.268		
	Present	7 (36.8)	0.24 (0.07–0.80)		0.16 (0.03–0.80)		14 (73.7)	2.02 (0.58–7.03)			

Bold values mean "statistical significant".

ensure that only a single product had been amplified. The CT values of *CCDC6*::*RET* and *NCOA4*::*RET* rearrangements were calculated, and data were expressed as the fold change of control (normal) using $2^{-(\Delta\Delta\ Ct)}$.

Gel electrophoresis and sequencing

PCR products from the cases positive according to qRT-PCR were analyzed by electrophoresis through a 2% gel electrophoresis

TABLE 4 Univariate and multivariate analysis of the clinicopathological factors with both *CCDC6*::*RET* and *NCOA4*::*RET* rearrangements group by the simple logistic regression and multiple logistic.

Variable	Category	n (%)	Univariate analysis		Multivariate analysis	
			OR (95% CI)	*p*	OR (95% CI)	*p*
Gender	Male	9 (37.5)	1	0.352		
	Female	16 (27.1)	0.62 (0.23–1.70)			
Age	<55	17 (32.1)	1	0.606		
	≥55	8 (26.7)	0.77 (0.29–2.08)			
Tumor size	≤1	3 (42.9)	1			
	1 < T ≤ 2	5 (27.8)	0.51 (0.08–3.16)	0.472		
	2 < T ≤ 4	13 (32.5)	0.64 (0.12–3.30)	0.596		
	>4	4 (22.2)	0.38 (0.06–2.46)	0.310		
PTC subtype	Classic	14 (24.6)	1			0.105
	Tall cell	7 (43.8)	2.39 (0.75–7.60)	0.140	1	
	Follicular	4 (40.0)	2.05 (0.50–8.32)	0.316	2.71 (0.81–9.04)	
Angioinvasion	Absent	13 (30.2)	1	0.982		
	Present	12 (30.0)	0.99 (0.39–2.53)			
Lymphatic invasion	Absent	16 (34.8)	1	0.304		
	Present	9 (24.3)	0.60 (0.23–1.58)			
Perineural invasion	Absent	22 (31.9)	1	0.441		
	Present	3 (21.4)	0.58 (0.15–2.30)			
Extrathyroidal extension	Absent	21 (31.3)	1	0.620		
	Present	4 (25.0)	0.73 (0.21–2.53)			
Lymph node metastasis	Absent	4 (33.3)	1	0.871		
	Present	14 (35.9)	1.12 (0.29–4.39)			
Extranodal extension	Absent	13 (41.9)	1	0.268		
	Present	5 (26.3)	0.49 (0.14–1.72)			

and visualized by ethidium bromide staining. The anticipated sizes of *CCDC6*::*RET* and *NCOA4*::*RET* products were 207 and 136 bp respectively. These bands were interpreted by visualization with a gel documentation system. Barcode-Tagged Sequencing (BTSeq ™) (U2Bio, Korea) was also applied for positive cases to obtain sequences of the PCR products.

Statistical analyses

Distributions of all continuous variables were tested for normality using the Shapiro-Wilk test. None was found to be normally distributed, requiring the use of non-parametric tests for further analysis. Comparison of categorical variables was carried out using Chi-square tests. Kruskal-Wallis tests and Mann-Whitney U tests to determine whether medians were different between comparison groups and to test for different expression levels between normal, benign goiter and PTC groups. Simple logistic regression and multiple logistic regression were used for backward stepwise univariate and multivariate analyses to identify independent prognostic factors for PTC patients using categorical data. Simple linear regression and multiple linear regression were used for continuous data. Variable factors with p value equal or less than 0.25 from univariate analysis were included to multivariate analysis to investigate the correlation between RET rearrangement and clinical characteristics.

The Ct values in the qRT-PCR assay of *CCDC6*::*RET* and *NCOA4*::*RET* levels were calculated, and data were expressed as the fold-change relative to controls using $2^{(-\Delta\Delta Ct)}$. Results were regarded as statistically significant at *p*-values lower than 0.05. The statistical analyses were done using IBM SPSS statistics software version 28.0 (IBM, Chicago, IL, United States).

Results

Prevalence of *RET* rearrangements

Eighty-three PTC patients included 59 females and 24 males with an average age of 48.21 years (range 17–79 years). Results from qRT-PCR showed the absence of *CCDC6*::*RET* or *NCOA4*::*RET* rearrangements in normal tissues (n = 10) and benign (multinodular goiter, n = 10) cases. On the other hand, *CCDC6*::*RET* rearrangements were detected in

10.3389/pore.2023.1611138

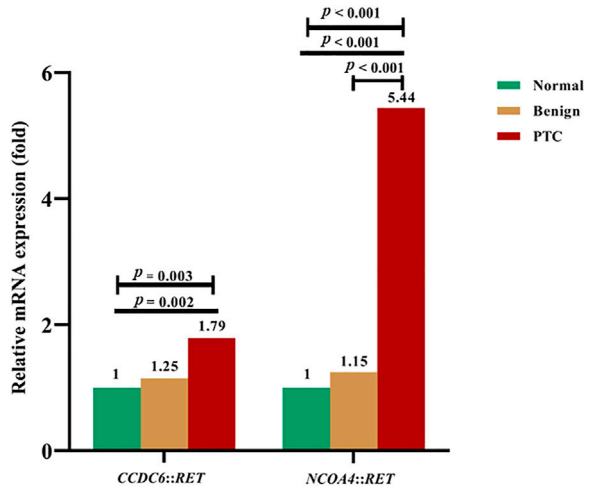

FIGURE 5
The relative fold-change of mRNA expression levels in *RET* rearrangements transcripts in normal, benign and PTC tissues. For *CCDC6::RET*, showing the differentiation of mRNA expression among PTC, benign compared to normal tissue (p = 0.003) by Kruskal-Wallis test. Expression of mRNA in PTC is greater than in normal thyroid tissue (p = 0.002) by Mann Whitney U test. The *NCOA4::RET* mRNA expression, showing the differentiation of mRNA expression among PTC, benign and normal tissues (p < 0.001), normal tissue compared to PTC (p < 0.001), and benign tissue compared to PTC (p < 0.001).

52 PTC cases (62.7%), and *NCOA4*::*RET* rearrangements in 43 cases (51.8%). Both *CCDC6*::*RET* and *NCOA4*::*RET* rearrangements co-occurred in 25 PTC tissues (30.1%). Thirteen PTCs (15.6%) tested negative for either *RET*::*PTC* rearrangement (Figure 1).

The association between *RET* rearrangements and clinicopathological data in PTC patients

PTCs have been categorized into classic, tall-cell subtypes and follicular variants. A correlation between the histological subtype and the type of *RET* rearrangement was observed; 71.93% of the classic subtype samples were positive for *CCDC6*::*RET* and 42.11% for *NCOA4*::*RET*, 43.75% of the tall-cell subtype tissues were positive for *CCDC6*::*RET* and 81.25% of them were *NCOA4*::*RET* positive. Both the frequency of *CCDC6*::*RET* and NCOA4::RET rearrangements were significantly different in those subtypes (OR = 0.27, 95% CI = 0.11–0.71) (Figure 2; Table 2).

Categorical variables were compared using Chi-square tests. Neither type of rearrangement was statistically significantly associated with gender. The *CCDC6*::*RET* rearrangement was significantly associated with patients younger than 55 years of age (p = 0.006) and classic subtype (p = 0.035). For clinicopathological markers, the *CCDC6*::*RET* rearrangement was significantly associated with an absence of angioinvasion (p = 0.006) and of lymphatic invasion extrathyroidal extension and extranodal extension (p= <0.001 and 0.030). *NCOA4*::*RET* rearrangements were statistically significantly associated with the tall cell subtype (p = 0.019) and angioinvasion (p = 0.001), lymphatic invasion (p = 0.003), lymph node metastasis (p= <0.001), extrathyroidal extension (p = 0.001) and extranodal extension (p = 0.013). Co-occurrence of *CCDC6*::*RET* and *NCOA4*::*RET* rearrangements was not significantly associated with clinicopathological data in PTC patients (Table 2).

Following gel electrophoresis and visualization, aliquots of each qRT-PCR product were sent to BTSeq ™ (U2Bio, Korea) for sequencing. The *CCDC6*::*RET* and *NCOA4*::*RET* products were 207 and 136 bp in length, respectively, as expected (Figure 3). The sequencing results showing the fusion points and sequencing electropherograms are shown in Figure 4.

Clinicopathological variables as predictive factors for *RET* rearrangements

Clinicopathological parameters of the 83 PTC patients were analyzed as dependent and independent predictive factors using simple logistic regression and multiple logistic regression with 95% CI values. Being younger than 55 years was a dependent predictive factor for the *CCDC6*::*RET* rearrangement (OR = 0.27, 95% CI = 0.11–0.71; p = 0.007). The absence of angioinvasion (OR = 0.27, 95% CI = 0.11–0.70; p = 0.007), absence of lymphatic invasion (OR = 0.17, 95% CI = 0.06–0.44; p < 0.001), of extrathyroidal extension (OR = 0.13, 95% CI = 0.04–0.46; p = 0.001) and of extranodal extension (OR = 0.24, 95% CI = 0.07–0.80; p = 0.021) were dependent predictive factors for *CCDC6*::*RET*. In multivariate analysis, controlling for the influence of other factors, an absence of extrathyroidal extension (OR = 0.25, 95% CI = 0.02–0.84, p = 0.032) and of extranodal extension (OR = 0.16, 95% CI = 0.03–0.80, p = 0.026) were significant independent predictive factors for *CCDC6*::*RET* (Table 3).

Tall-cell PTC (OR = 5.96, 95% CI = 1.53–23.24, p = 0.01), angioinvasion (OR = 4.36, 95% CI = 1.73–10.95; p = 0.002), lymphatic invasion (OR = 4.03, 95% CI = 1.60–10.17; p = 0.003), extrathyroidal extension (OR = 9.17, 95% CI = 1.93–43.58; p = 0.005) and lymph node metastasis (OR = 4.03 95% CI = 1.60–10.17; p = 0.004) were dependent predictive factors of the *NCOA4*::*RET* rearrangement. In multivariate analysis, the tall-cell subtype (OR = 6.06, 95% CI = 2.15–20.49, p = 0.032), tumor size 2 < T ≤ 4 cm and large tumor size >4 cm (OR = 1.02, 95% CI = 0.00–1.53, 0.00–0.87; p = 0.020 and 0.042, respectively), perineural invasion (OR = 24.64, 95% CI = 1.18–515.96; p = 0.039) lymphatic invasion (OR = 44.11, 95% CI = 2.11–922.55; p = 0.015), were significant independent predictive factors of *NCOA4*::*RET* (Table 3). However, co-occurrence of the two major *RET* fusions was not significantly associated with the clinicopathological data (Table 4).

TABLE 5 Mann-Whitney U tests and Kruskal-Wallis test of the predictive marker with relative *RET* mRNA expression levels in papillary thyroid carcinoma.

Variable	Category	n (%)	*CCDC6*::*RET* mRNA expression		n (%)	*NCOA4*::*RET* mRNA expression	
			Median	*p*		Median	*p*
Gender	Male	15 (62.5)	1.00 (0.20–17.23)	0.762	14 (58.3)	6.13 (1.00–162.38)	0.734
	Female	37 (62.7)	1.12 (0.48–328.60)		29 (49.2)	3.79 (0.69–95.52)	
Age	<55	39 (73.6)	1.31 (0.20–328.60)	0.485	25 (47.2)	3.38 (0.69–95.52)	0.722
	≥55	13 (43.3)	1.06 (0.55–2.63)		18 (60.0)	3.88 (0.97–162.38)	
Tumor size	≤1	5 (71.4)	1.67 (0.49–17.23)	0.100	4 (57.1)	1.92 (0.69–35.59)	0.508
	1 < T ≤ 2	13 (72.2)	1.00 (0.64–328.60)		8 (44.4)	2.94 (0.97–162.38)	
	2 < T ≤ 4	26 (65.0)	1.06 (0.20–61.12)		19 (47.5)	4.88 (0.98–62.24)	
	>4	8 (44.4)	0.90 (0.55–1.94)		12 (66.7)	5.19 (1.32–93.92)	
PTC subtype	Classic	41 (71.9)	1.94 (0.20–328.60)	0.761	24 (42.1)	3.37 (0.69–52.19)	0.294
	Tall cell	7 (43.8)	1.63 (0.64–17.23)		13 (81.3)	6.62 (0.69–162.38)	
	Follicular	4 (40.0)	0.80 (0.49–26.28)		6 (60.0)	3.18 (1.56–52.19)	
Angioinvasion	Absent	33 (76.7)	1.31 (0.53–328.60)	0.091	15 (34.9)	3.79 (0.69–62.24)	0.961
	Present	19 (47.5)	0.87 (0.20–18.48)		28 (70.0)	5.55 (0.69–162.38)	
Lymphatic invasion	Absent	37 (80.4)	1.12 (0.20–328.60)	0.770	17 (37.0)	3.79 (0.97–95.52)	0.377
	Present	15 (40.5)	1.04 (0.48–61.12)		26 (70.3)	2.86 (0.69–162.38)	
Perineural invasion	Absent	46 (66.7)	1.32 (0.20–328.60)	0.057	33 (47.8)	3.38 (0.69–162.38)	0.501
	Present	6 (42.9)	0.66 (0.49–8.07)		10 (71.4)	4.56 (1.06–93.92)	
Extrathyroidal extension	Absent	48 (71.6)	1.03 (0.20–328.60)	0.548	29 (43.3)	2.94 (0.69–95.52)	0.088
	Present	4 (25.0)	1.50 (1.04–2.63)		14 (87.5)	5.55 (1.36–162.38)	
Lymph node metastasis	Absent	9 (75.0)	0.92 (0.70–8.07)	0.814	4 (33.3)	5.39 (0.69–7.37)	0.934
	Present	20 (51.3)	1.18 (0.20–61.12)		29 (74.4)	3.18 (0.69–162.38)	
Extranodal extension	Absent	22 (71.0)	1.02 (0.20–61.12)	0.415	18 (58.1)	3.88 (0.69–93.92)	0.985
	Present	7 (36.8)	0.73 (0.48–4.29)		14 (73.7)	2.86 (0.97–162.38)	

Determination of mRNA expression levels of *RET* rearrangements in thyroid tissues

The mRNA expression levels of *CCDC6*::*RET* and *NCOA4*::*RET* rearrangements in PTC compared to benign (multinodular goiter) and normal thyroid tissue are shown in Figure 5. The median mRNA expression levels of *CCDC6*::*RET* transcripts were 0.61 (0.14–1.34), 0.76 (0.36–1.89) and 1.09 (0.20–328.60) in normal, benign and PTC tissues, respectively. The median mRNA expression levels of *NCOA4*::*RET* rearrangement were 0.66 (0.08–2.19), 0.76 (0.36–1.89) and 3.59 (0.69–162.38) in normal, benign and PTC tissues, respectively. The relative *CCDC6*::*RET* mRNA expression levels in PTC (1.79) and benign tissues (1.25) were significantly higher than in normal tissues ($p = 0.003$). The relative mRNA expression levels of *NCOA4*::*RET* transcripts were significantly higher in PTC tissues (5.44) than in benign tissues (1.15) or normal tissues ($p < 0.001$ in both cases) (Figure 5).

The associations between clinicopathological factors and relative mRNA expression levels of *RET* rearrangements in PTC patients

Associations between clinicopathological factors and mRNA expression levels of *RET* rearrangements were performed using Mann-Whitney U tests and Kruskal-Wallis tests. No statistically significant association with clinicopathological factors was found (Table 5).

In univariate analysis, the clinicopathological factors were not dependent predictive factors for *CCDC6*::*RET* and *NCOA4*::*RET* mRNA expression levels (Tables 6, 7).

Discussion

Papillary thyroid cancer (PTC) is the most common form of thyroid cancer. It is also rapidly increasing in incidence worldwide. This cancer has quite a good prognosis, with less

TABLE 6 Univariate analysis and multivariate analysis of the clinicopathological factors with relative *CCDC6*::*RET* mRNA expression level by simple linear regression and multiple linear regression.

Variable	Category	n (%)	Univariate analysis		Multivariate analysis	
			Mean diff (95% CI)	*p*	Mean diff (95% CI)	*p*
Gender	Male	15 (62.5)	1	0.416		
	Female	37 (62.7)	11.57 (−16.77–39.92)			
Age	<55	39 (73.6)	1	0.382		
	≥55	13 (43.3)	−13.02 (−42.62–16.60)			
Tumor size	≤1	5 (71.4)	1		1	
	1 < T ≤ 2	13 (72.2)	28.87 (−19.26–76.99)	0.234	−6.90 (−15.49–1.70)	0.111
	2 < T ≤ 4	26 (65.0)	0.37 (−44.29–45.02)	0.987		
	>4	8 (44.4)	−3.12 (−55.26–49.01)	0.905		
PTC subtype	Classic	41 (71.9)	1			
	Tall cell	7 (43.8)	−9.23 (−47.66–29.20)	0.632		
	Follicular	4 (40.0)	−5.68 (−54.91–43.54)	0.817		
Angioinvasion	Absent	33 (76.7)	1	0.295	1	
	Present	19 (47.5)	−13.99 (−40.54–12.57)			
Lymphatic invasion	Absent	37 (80.4)	1	0.659		
	Present	15 (40.5)	−6.30 (−34.78–22.18)			
Perineural invasion	Absent	46 (66.7)	1	0.607		
	Present	6 (42.9)	−10.40 (−50.76–29.96)			
Extrathyroidal extension	Absent	48 (71.6)	1	0.674		
	Present	4 (25.0)	−10.22 (−58.65–38.22)			
Lymph node metastasis	Absent	9 (75.0)	1	0.532		
	Present	20 (51.3)	2.88 (−6.46–12.21)			
Extranodal extension	Absent	22 (71.0)	1	0.515		
	Present	7 (36.8)	−3.24 (−13.33–6.84)			

than 2% mortality at 5 years. However, more than 25% of PTC patients suffer a recurrence in the long term (15).

Rearrangements of *BRAF*, *RAS*, *P53* and *RET* are all strongly associated with thyroid cancer. For *RET* rearrangements, *RET*::*PTC*s are the most frequent molecular alterations reported in PTC (2–5). Several fusion partner genes of *RET* in such rearrangements have been reported, but the major ones are *CCDC6*and *NCOA4* (accounting for more than 90%) (6).

We found that the prevalence of *CCDC6*::*RET*, *NCOA4*::*RET* rearrangements and co-occurrence of both in Thailand were 62.65%, 51.81%, and 30.12%, respectively. These rearrangements were not found in normal thyroid, or in benign tumors. Similarly, high frequencies of *RET*::*PTC* rearrangements have been reported from Taiwan (55%), New Caledonia (70%) and Australia (85%) (16, 17). On the other hand, studies from Korea (6.5%) and Japan (30%) showed low frequencies of *RET*::*PTC* rearrangements in PTC (18, 19). This heterogeneity in *RET*::*PTC* rearrangements may be due to ethnicity, different geographical location and/or differences in environmental exposure. The literature has reported that frequency of *RET* rearrangements in papillary carcinomas ranges from 0% to 87% (20, 21). These differences are partly explained by pre-selection of the analyzed cohort, geographical diversity and different sensitivities of the assays used for detection (20, 22). Naito et al. (23) reported that the prevalence of *RAS* gene mutations in Thai PTC patients was higher than in Japan. Being affected the RET rearrangements according to RET rearrangements/mutations and RAS family mutations are almost always mutually exclusive (23, 24).

This suggests that an existence of a specific environmental agent in northeast Thailand, presumably related to the high level of nitrates in the diet, particularly high salt-preserved fish; Pla-ra, Pla-som and also vegetables, water promotes the progression of thyroid papillary carcinomas (23). Apart from the forementioned majority factors, other putative carcinogens, for example, caffeine, ethanol, hypoxia are able to induce DNA double-strand breaks and generate RET/PTC rearrangements (26–28). As reported previously, the frequency of *CCDC6*::*RET* in sporadic thyroid cancer is higher than that of *NCOA4*::*RET* (8, 9). Moreover, our study revealed no major RET rearrangements in benign tumors, similar to previous studies (13, 21).

TABLE 7 Univariate analysis and multivariate analysis of the clinicopathological factors with relative *NCOA4*::*RET* mRNA expression level by simple linear regression and multiple linear regression.

Variable	Category	n (%)	Univariate analysis		Multivariate analysis	
			Mean diff (95% CI)	*p*	Mean diff (95% CI)	*p*
Gender	Male	14 (58.3)	1	0.363		
	Female	29 (49.2)	−9.55 (−30.49–11.40)			
Age	<55	25 (47.2)	1	0.356		
	≥55	18 (60.0)	9.10 (−10.59–28.79)			
Tumor size	≤1	4 (57.1)	1			
	1 < T ≤ 2	8 (44.4)	−10.76 (−51.46–29.94)	0.596		
	2 < T ≤ 4	19 (47.5)	0.73 (−35.68–37.13)	0.968		
	>4	12 (66.7)	−3.62 (−41.99–34.76)	0.850		
PTC subtype	Classic	24 (42.1)	1			0.051
	Tall cell	13 (81.3)	21.60 (0.02–43.18)	0.050	1	
	Follicular	6 (60.0)	9.74 (−18.95–38.43)	0.497	20.5 (0.23–40.77)	
Angioinvasion	Absent	15 (34.9)	1	0.374		
	Present	28 (70.0)	9.03 (−11.26–29.32)			
Lymphatic invasion	Absent	17 (37.0)	1	0.808		
	Present	26 (70.3)	2.43 (−17.60–22.45)			
Perineural invasion	Absent	33 (47.8)	1	0.829		
	Present	10 (71.4)	2.53 (−20.97–26.03)			
Extrathyroidal extension	Absent	29 (43.3)	1	0.123	1	0.082
	Present	14 (87.5)	15.74 (−4.46–35.94)		18.05 (−2.37–38.48)	
Lymph node metastasis	Absent	4 (33.3)	1	0.530		
	Present	29 (74.4)	11.12 (−24.6–46.85)			
Extranodal extension	Absent	18 (58.1)	1	0.558		
	Present	14 (73.7)	6.86 (−16.75–30.47)			

CCDC6::*RET* rearrangement was significantly associated with the classic histological subtype (41/57) ($p = 0.035$), a result in agreement with previous studies (8–10, 29). Similarly, Guerra et al (4) reported that *CCDC6*::*RET* was the dominant type within sporadic carcinomas and was strongly related to the classic subtype (4). *NCOA4*::*RET* rearrangement was significantly associated with the tall cell subtype (13/16) ($p = 0.019$). In term of clinicopathological markers, the *NCOA4*::*RET* rearrangement was significantly associated with angioinvasion ($p = 0.001$), lymphatic invasion ($p = 0.003$), extrathyroidal extension ($p = 0.001$), lymph node metastasis ($p < 0.001$) and extranodal extension ($p = 0.013$), respectively. This is in agreement with Sugg et al (12) and Mochizuki et al (30) who reported that *NCOA4*::*RET* may cause de-differentiation and more aggressive behavior in papillary thyroid carcinoma (12, 30). Certainly, *NCOA4*::*RET* correlates with a more aggressive phenotype and a more advanced stage of PTC (8, 9, 11–13). Galuppini et al (31), Khan et al (18) and Rogounovitch et al (32) reported that an *NCOA4*::*RET* rearrangement was associated with lymph node metastasis (18, 31, 32).

Univariate analysis revealed *CCDC6*::*RET* mRNA expression levels in patients with small tumor size (1 < T ≤ 2 cm) and the classic subtype was not significant that in contrast to with Rhoden et al. (21). Moreover, the other clinicopathological markers, such as extrathyroidal extension or metastases were not correlated with *CCDC6*::RET, in agreement with Tallini et al (33).

High expression levels of *NCOA4*::*RET* were found, but not significant in patients with the tall-cell subtype, extrathyroidal extension, lymph node metastasis and extranodal extension. Our findings are similar to those of from Powell et al (11) that showed the *NCOA4*::*RET* rearrangement was more frequent in tall-cell tumors: its expression in transgenic mice generated solid tumor subtypes of thyroid cancer with more aggressive and metastatic behavior (11). Martínez et al (34) reported that high detection or expression of *BRAFV600E* and low expression or absence of that *CCDC6*::*RET* rearrangement were associated with extrathyroidal extension. In contrast, a high activity of *RET* (presence of *CCDC6*::*RET* rearrangement or high expression) and low activity of *BRAF* (absence of *BRAFV600E* or its low expression) were associated with lymph node metastasis. It has been suggested that *BRAFV600E* and the *CCDC6*::*RET* rearrangement can predict aggressive PTC (34). The literature suggests that *RET*::*PTC* rearrangements, and especially *NCOA4*::*RET*, can be induced by radiation (23, 35). In such cases,

Nikiforov et al (8) and Rabes HM et al (9) reported that in radiation-induced PTC, *NCOA4*::*RET* has an equal or even higher prevalence than *CCDC6*::*RET* fusions (8, 9). Radiation exposure is often associated with *NCOA4*::*RET* and is more common in children 4 years of age or younger. In addition, the latest WHO classification 2022 emphasizes that the telomerase reverse transcriptase (*TERT*) gene mutation in PTC patients correlates with an increased risk of distant metastases and poor prognosis. Moreover, the gain of chromosome 1q in the *PLEKHS1* promoter (*PLEKSH1*p) may cause a poorer outcome in PTCs (36). Therefore, further investigation is required into more data on history of recurrence, radiation history, gene aberration, tumor focality among other aspects to enhance our understanding of *RET*::*PTC* rearrangements.

In our study, tumor tissues from 83 PTC patients were investigated to determine the prevalence of *CCDC6*::*RET* and *NCOA4*::*RET* rearrangements in Thailand and to explore the association between the mRNA expression of *CCDC6*::*RET* and *NCOA4*::*RET* rearrangements and clinicopathology. The *CCDC6*::*RET* rearrangement was significantly associated with less aggressive histological subtypes and absence of certain clinicopathological markers. Moreover, the absence of extrathyroidal and extranodal extension were independent predictive factors for *CCDC6*::*RET*.

In contrast, large tumor size, more aggressive types like the tall-cell type, angioinvasion, perineural invasion or extrathyroidal extension were independent predictive factors of *NCOA4*::*RET*. Briefly, *CCDC6*::*RET* correlated with less aggressive, but *NCOA4*::*RET* correlated with more aggressive phenotypes of PTC. In conclusion, the two rearrangements that we studied were strongly associated with particular clinicopathological phenotypes, particularly histological subtype.

Data availability statement

The datasets presented in this study can be found in online repositories. The names of the repository/repositories and accession number(s) can be found in the article/Supplementary Material.

Ethics statement

The study was approved by the Ethics Committee for Human Research, Khon Kaen University (HE641011). Formal written informed consent was not required with a waiver by the appropriate IRB and/or national research ethics committee.

Author contributions

TK: conceptualization, data curation, formal analysis, investigation, methodology, resources, software, validation and writing—original draft, writing—review and editing, and approval of the final manuscript. SW: methodology, visualization, writing—review and editing, and approval of the final manuscript. YC: validation, writing—review and editing, and approval of the final manuscript. PI: methodology, visualization, writing—review and editing, and approval of the final manuscript. RD: formal analysis, funding acquisition, methodology, project administration, resources, supervision, validation, visualization, conceptualization, writing—original draft, writing—review and editing, and approval of the final manuscript.

Funding

The study was supported by a postgraduate study support grant of Faculty of Medicine, Khon Kaen University and Invitation Research Fund from Faculty of Medicine No. IN64147 (date of approval 18 January 2021), Khon Kaen University, Thailand.

Conflict of interest

The authors declare that the research was conducted in the absence of any commercial or financial relationships that could be construed as a potential conflict of interest.

Acknowledgments

We would like to extend acknowledgment to Srinagarind Hospital for providing the specimens. We would like to acknowledge Prof. David Blair for editing the manuscript via Publication Clinic KKU, Thailand. We thank Mr. Suwit Balthaisong for preparation the slides from FFPE blocks that were used in this work. We thank Mr. Manop Sripa for molecular technique suggestions. We also thank Miss Piyanan Suparattanagool as the statistical expertise consultants.

Supplementary material

The Supplementary Material for this article can be found online at: https://www.por-journal.com/articles/10.3389/pore.2023.1611138/full#supplementary-material

References

1. Fagin JA, Wells SA, Jr. Biologic and clinical perspectives on thyroid cancer. *N Engl J Med* (2016) 375(11):1054–67. doi:10.1056/NEJMra1501993

2. Liu RT, Chou FF, Wang CH, Lin CL, Chao FP, Chung JC, et al. Low prevalence of *RET* rearrangements (*RET*/PTC1, *RET*/PTC2, *RET*/PTC3, and *ELKS-RET*) in sporadic papillary thyroid carcinomas in taiwan Chinese. *Thyroid* (2005) 15(4): 326–35. doi:10.1089/thy.2005.15.326

3. Fenton CL, Lukes Y, Nicholson D, Dinauer CA, Francis GL, Tuttle RM. The *ret*/PTC mutations are common in sporadic papillary thyroid carcinoma of children and young adults. *J Clin Endocrinol Metab* (2000) 85(3):1170–5. doi:10.1210/jcem.85.3.6472

4. Guerra A, Rosaria Sapio M, Marotta V, Campanile E, Ilaria Moretti M, Deandrea M, et al. Prevalence of RET/PTC rearrangement in benign and malignant thyroid nodules and its clinical application. *Endocr J* (2011) 58(1): 31–8. doi:10.1507/endocrj.k10e-260

5. Liu S, Gao A, Zhang B, Zhang Z, Zhao Y, Chen P, et al. Assessment of molecular testing in fine-needle aspiration biopsy samples: An experience in a Chinese population. *Exp Mol Pathol* (2014) 97(2):292–7. doi:10.1016/j.yexmp.2014.08.005

6. Staubitz JI, Musholt TJ, Schad A, Springer E, Lang H, Rajalingam K, et al. ANKRD26-RET - a novel gene fusion involving RET in papillary thyroid carcinoma. *Cancer Genet* (2019) 238:10–7. doi:10.1016/j.cancergen.2019.07.002

7. Santoro M, Carlomagno F. Central role of RET in thyroid cancer. *Cold Spring Harb Perspect Biol* (2013) 5(12):a009233. doi:10.1101/cshperspect.a009233

8. Nikiforov YE, Rowland JM, Bove KE, Monforte-Munoz H, Fagin JA. Distinct pattern of ret oncogene rearrangements in morphological variants of radiation-induced and sporadic thyroid papillary carcinomas in children. *Cancer Res* (1997) 57(9):1690–4.

9. Rabes HM, Demidchik EP, Sidorow JD, Lengfelder E, Beimfohr C, Hoelzel D, et al. Pattern of radiation-induced RET and NTRK1 rearrangements in 191 post-chernobyl papillary thyroid carcinomas: Biological, phenotypic, and clinical implications. *Clin Cancer Res* (2000) 6(3):1093–103.

10. Smida J, Salassidis K, Hieber L, Zitzelsberger H, Kellerer AM, Demidchik EP, et al. Distinct frequency of ret rearrangements in papillary thyroid carcinomas of children and adults from Belarus. *Int J Cancer* (1999) 80(1):32–8. doi:10.1002/(sici)1097-0215(19990105)80:1<32:aid-ijc7>3.0.co;2-l

11. Powell DJ, Russell J, Nibu K, Li G, Rhee E, Liao M, et al. The RET/PTC3 oncogene: Metastatic solid-type papillary carcinomas in murine thyroids. *Cancer Res* (1998) 58(23):5523–8.

12. Sugg SL, Ezzat S, Rosen IB, Freeman JL, Asa SL. Distinct multiple RET/PTC gene rearrangements in multifocal papillary thyroid neoplasia. *J Clin Endocrinol Metab* (1998) 83(11):4116–22. doi:10.1210/jcem.83.11.5271

13. Thomas GA, Bunnell H, Cook HA, Williams ED, Nerovnya A, Cherstvoy ED, et al. High prevalence of RET/PTC rearrangements in Ukrainian and belarussian post-chernobyl thyroid papillary carcinomas: A strong correlation between *RETPTC3* and the solid-follicular variant. *J Clin Endocrinol Metab* (1999) 84(11):4232–8. doi:10.1210/jcem.84.11.6129

14. Basolo F, Giannini R, Monaco C, Melillo RM, Carlomagno F, Pancrazi M, et al. Potent mitogenicity of the RET/PTC3 oncogene correlates with its prevalence in tall-cell variant of papillary thyroid carcinoma. *Am J Pathol* (2002) 160(1): 247–54. doi:10.1016/S0002-9440(10)64368-4

15. Abdullah MI, Junit SM, Ng KL, Jayapalan JJ, Karikalan B, Hashim OH. Papillary thyroid cancer: Genetic alterations and molecular biomarker investigations. *Int J Med Sci* (2019) 16(3):450–60. doi:10.7150/ijms.29935

16. Lee CH, Hsu LS, Chi CW, Chen GD, Yang AH, Chen JY. High frequency of rearrangement of the RET protooncogene (RET/PTC) in Chinese papillary thyroid carcinomas. *J Clin Endocrinol Metab* (1998) 83(5):1629–32. doi:10.1210/jcem.83.5.4774

17. Chua EL, Wu WM, Tran KT, Mccarthy SW, Lauer CS, Dubourdieu D, et al. Prevalence and distribution of RET/PTC 1, 2, and 3 in papillary thyroid carcinoma in New Caledonia and Australia. *J Clin Endocrinol Metab* (2000) 85(8):2733–9. doi:10.1210/jcem.85.8.6722

18. Khan MS, Qadri Q, Makhdoomi MJ, Wani MA, Malik AA, Niyaz M, et al. RET/PTC gene rearrangements in thyroid carcinogenesis: Assessment and clinico-pathological correlations. *Pathol Oncol Res* (2020) 26(1):507–13. doi:10.1007/s12253-018-0540-3

19. Chung JH, Hahm JR, Min YK, Lee MS, Lee MK, Kim KW, et al. Detection of RET/PTC oncogene rearrangements in Korean papillary thyroid carcinomas. *Thyroid* (1999) 9(12):1237–43. doi:10.1089/thy.1999.9.1237

20. Zhu Z, Ciampi R, Nikiforova MN, Gandhi M, Nikiforov YE. Prevalence of *RET*/*PTC* rearrangements in thyroid papillary carcinomas: Effects of the detection methods and genetic heterogeneity. *J Clin Endocrinol Metab* (2006) 91(9):3603–10. doi:10.1210/jc.2006-1006

21. Rhoden KJ, Johnson C, Brandao G, Howe JG, Smith BR, Tallini G. Real-time quantitative RT-PCR identifies distinct c-RET, *RET/PTC1* and *RET/PTC3* expression patterns in papillary thyroid carcinoma. *Lab Invest* (2004) 84(12): 1557–70. doi:10.1038/labinvest.3700198

22. Musholt TJ, Staubitz JI, Antonio Cámara RJ, Musholt PB, Humberg D, Springer E, et al. Detection of RET rearrangements in papillary thyroid carcinoma using RT-PCR and FISH techniques - a molecular and clinical analysis. *Eur J Surg Oncol* (2019) 45(6):1018–24. doi:10.1016/j.ejso.2018.11.009

23. Naito H, Pairojkul C, Kitahori Y, Yane K, Miyahara H, Konishi N, et al. Different ras gene mutational frequencies in thyroid papillary carcinomas in Japan and Thailand. *Cancer Lett* (1998) 131(2):171–5. doi:10.1016/s0304-3835(98)00149-9

24. Sherman SI, Clary DO, Elisei R, Schlumberger MJ, Cohen EW, Schöffski P, et al. Correlative analyses of RET and RAS mutations in a phase 3 trial of cabozantinib in patients with progressive, metastatic medullary thyroid cancer. *Cancer* (2016) 122(24):3856–64. doi:10.1002/cncr.30252

25. Melillo RM, Castellone MD, Guarino V, Falco VD, Cirafici AM, Salvatore G, et al. The RET/PTC-RAS-BRAF linear signaling cascade mediates the motile and mitogenic phenotype of thyroid cancer cells. *J Clin Invest* (2005) 115(4):1068–81. doi:10.1172/JCI22758

26. Romei C, Elisei R. RET/PTC translocations and clinico-pathological features in human papillary thyroid carcinoma. *Front Endocrinol* (2012) 3:54. doi:10.3389/fendo.2012.00054

27. Gandhi M, Dillon LW, Pramanik S, Nikiforov YE, Wang YH. DNA breaks at fragile sites generate oncogenic RET/PTC rearrangements in human thyroid cells. *Oncogene* (2010) 29(15):2272–80. doi:10.1038/onc.2009.502

28. Gandhi M, Evdokimova V, Nikiforov YE. Mechanisms of chromosomal rearrangements in solid tumors: The model of papillary thyroid carcinoma. *Mol Cel Endocrinol* (2010) 321(1):36–43. doi:10.1016/j.mce.2009.09.013

29. Adeniran AJ, Zhu Z, Gandhi M, Steward DL, Fidler JP, Giordano TJ, et al. Correlation between genetic alterations and microscopic features, clinical manifestations, and prognostic characteristics of thyroid papillary carcinomas. *Am J Surg Pathol* (2006) 30(2):216–22. doi:10.1097/01.pas.0000176432.73455.1b

30. Mochizuki K, Kondo T, Nakazawa T, Iwashina M, Kawasaki T, Nakamura N, et al. RET rearrangements and BRAF mutation in undifferentiated thyroid carcinomas having papillary carcinoma components: Genetic background of composite UTC. *Histopathology* (2010) 57(3):444–50. doi:10.1111/j.1365-2559.2010.03646.x

31. Galuppini F, Vianello F, Censi S, Barollo S, Bertazza L, Carducci S, et al. Differentiated thyroid carcinoma in pediatric age: Genetic and clinical scenario. *Front Endocrinol* (2019) 10:552. doi:10.3389/fendo.2019.00552

32. Rogounovitch TI, Mankovskaya SV, Fridman MV, Leonova TA, Kondratovitch VA, Konoplya NE, et al. Major oncogenic drivers and their clinicopathological correlations in sporadic childhood papillary thyroid carcinoma in Belarus. *Cancers* (2021) 13(13):3374. doi:10.3390/cancers13133374

33. Tallini G, Santoro M, Helie M, Carlomagno F, Salvatore G, Chiappetta G, et al. RET/PTC oncogene activation defines a subset of papillary thyroid carcinomas lacking evidence of progression to poorly differentiated or undifferentiated tumor phenotypes. *Clin Cancer Res Off J Am Assoc Cancer Res* (1998) 4(2):287–94.

34. Martínez JRW, Vargas-Salas S, Gamboa SU, Muñoz E, Domínguez JM, León A, et al. The combination of RET, BRAF and demographic data identifies subsets of patients with aggressive papillary thyroid cancer. *Horm Cancer* (2019) 10(2–3): 97–106. doi:10.1007/s12672-019-0359-8

35. Fugazzola L, Pilotti S, Pinchera A, Vorontsova TV, Mondellini P, Bongarzone I, et al. Oncogenic rearrangements of the RET proto-oncogene in papillary thyroid carcinomas from children exposed to the chernobyl nuclear accident. *Cancer Res* (1995) 55(23):5617–20.

36. Baloch ZW, Asa SL, Barletta JA, Ghossein RA, Juhlin CC, Jung CK, et al. Overview of the 2022 WHO classification of thyroid neoplasms. *Endocr Pathol* (2022) 33(1):27–63. doi:10.1007/s12022-022-09707-3

Pathology & Oncology Research | frontiers

TYPE Original Research
PUBLISHED 22 August 2023
DOI 10.3389/pore.2023.1611206

Check for updates

OPEN ACCESS

EDITED BY
Anna Sebestyén,
Semmelweis University, Hungary

*CORRESPONDENCE
Angéla Horváth,
horvathangela11@gmail.com

RECEIVED 26 March 2023
ACCEPTED 01 August 2023
PUBLISHED 22 August 2023

CITATION
Dános K, Horváth A, Halász J, Tamás L and Polony G (2023), Patient delay and its clinical significance among head and neck cancer patients in Hungary. *Pathol. Oncol. Res.* 29:1611206. doi: 10.3389/pore.2023.1611206

COPYRIGHT
© 2023 Dános, Horváth, Halász, Tamás and Polony. This is an open-access article distributed under the terms of the Creative Commons Attribution License (CC BY). The use, distribution or reproduction in other forums is permitted, provided the original author(s) and the copyright owner(s) are credited and that the original publication in this journal is cited, in accordance with accepted academic practice. No use, distribution or reproduction is permitted which does not comply with these terms.

Patient delay and its clinical significance among head and neck cancer patients in Hungary

Kornél Dános[1], Angéla Horváth[1,2]*, Judit Halász[2], László Tamás[1] and Gábor Polony[1]

[1]Department of Otorhinolaryngology, Head and Neck Surgery, Faculty of Medicine, Semmelweis University, Budapest, Hungary, [2]Department of Pathology, Forensic and Insurance Medicine, Faculty of Medicine, Semmelweis University, Budapest, Hungary

Introduction: Head and neck cancers represent a major health problem in Hungary. With their high incidence and mortality rates, Hungary is one of the world leaders in these indicators. The length of patient delay, defined as time from onset of symptoms to first medical consultation, is unknown in Hungarian patients with head and neck cancer. We aimed to use a representative sample of the Hungarian head and neck cancer patient population to determine patient delay according to disease localization and stage and to identify correlations with other clinical parameters.

Methods: In our retrospective study, we reviewed patient documentation. For the inclusion, the patients had to be diagnosed with malignant tumors of the oral cavity, oropharynx, hypopharynx or larynx at the Department Head and Neck Surgery of Semmelweis University between 2012 and 2017.

Results: We identified 236 patients who met the inclusion criteria. The median delay was 9.5 weeks (range 0–209 weeks) and the mean delay of patients was 17.57 weeks (SD 23.67). There was a significant difference in patient delay data by location. Among glottic cancers, the most common diagnosis was an early stage (67%), compared with other localizations, including most commonly the oropharynx (81%) and hypopharynx (80%), where a locoregionally advanced stage was more frequent.

Discussion: Compared to data from different countries, the delay of Hungarian patients with head and neck cancer is significantly longer, which may contribute to the high mortality in Hungary. Screening and patient education in high-risk groups could contribute to earlier diagnosis and thus improve prognosis.

KEYWORDS

survival, diagnosis, head and neck cancer, patient delay, symptom

Introduction

Hungary has the third highest incidence of head and neck squamous cell cancer (HNSCC) and the second worst cancer-related mortality in the world, causing an important health problem [1].

There are many articles in the international literature on patient delay as an important factor in late diagnosis, but no data are available for Hungary [2].

Diagnostic delay refers to the total period of time from the onset of symptoms to (histological and radiological) diagnosis. Diagnostic delay is generally separated into two phases: patient delay defined as the time period from the beginning of symptoms to the point where the patient seeks medical care and system delay is the elapsed time between first contact with a healthcare professional and the definitive diagnosis/treatment initiation [3].

In the case of suspected cancer, system delay can be shortened by accurate patient pathways, as such the "14-day rule," established by the Hungarian Government in 2014, aiming to reduce waiting times for staging-purpose imaging tests, and the 21 (30)-day rule which aims to shorten the time in which patients are referred to multidisciplinary tumor boards. Nevertheless, it is known that the length of time a patient waits from the first presentation of his/her first symptoms is crucial in treatment success, head and neck cancer patients very often seek medical attention for life-threatening symptoms only. It is also known that patient delay is multifactorial, including socioeconomic conditions, marital status, psychopathology, denial, and is therefore difficult to influence the time to first medical consultation [4]. No high-level evidence is available for HNSCC screening in the general population. Screening of patients with risk factors would be most recommended, but this patient group is difficult to access to make them adopt this awareness [5]. This underlines the importance of activities such as the Make Sense campaign launched by the European Head and Neck Cancer Society in 2013 to raise awareness of head and neck cancer [6].

The present study aimed to evaluate the patient delay in this specific and special Hungarian (based on incidence and mortality) patient population, and its correlations with clinical parameters.

Patients and methods

We aimed to enroll all patients in this retrospective, single-institution study after being diagnosed (histologically) with squamous cell cancer of the oral cavity, oropharynx, hypopharynx, or larynx between September 2012 and August 2017 at the Department of Otolaryngology and Head-Neck Surgery, Semmelweis University, Hungary.

The main exclusion criteria were: patients who were not diagnosed (by biopsy) at our tertiary referral center or had primaries in other head and neck sites (e.g., nasopharynx, nasal cavity, paranasal sinuses, salivary gland, or skin, furthermore those with unknown primaries) or had previous treatment for head and neck tumor or/and underwent oncological treatment in the last 5 years. Patients (22 cases) who had been diagnosed in other hospitals were excluded.

In our study, we evaluated retrospectively the patients' medical records (discharge summaries, multidisciplinary tumor board reports, histological reports, and imaging studies).

The TNM stages were defined using the seventh edition of the UICC TNM system [7].

To determine the HPV status in oropharyngeal cancers, as in the clinical practice and current guidelines, we used immunohistochemical (IHC) detection of the tumor suppressor $p16^{INK4}$ (Vitro Master Diagnostics, mouse anti-human p16-INK4A monoclonal antibody (MX007), 1:100). We used the primary antibody at 37°C with an incubation time of 10 min, at least 70% combined nuclear and cytoplasmic staining of the tumor tissue was necessary for positivity. This method is a reliable, surrogate marker for testing human papillomavirus (HPV) in oropharyngeal carcinoma [8].

For survival analyses, disease-specific survival was used: the statistical event was defined as death due to cancer or the presence of a tumor at the last check-up, while tumor-free control or death due to other diseases was not defined as an event.

Statistical analysis of the data—with descriptive statistics and correlation analyses—was performed using the Kruskal-Wallis test, Mann-Whitney U test, Chi-square test (Fisher's exact test), Kaplan-Meier estimates with log-rank tests.

We used SPSS Statistics for Mac v.28.0 (IBM Corp., Armonk, NY) for the analyses.

Patient delays were reported using the median values. We considered $p < 0.05$ as statistically significant.

Our research was carried out with the ethical permission of Semmelweis University (SE IKEB 105/2014).

Results

236 patients were identified meeting the criteria. We examined 198 men and 38 women. The mean age of the patients at the time of diagnosis was 61 years (40–92 years). The patient data is presented in Table 1. The median delay was 9.5 weeks (range 0–209 weeks), mean patient delay was 17.57 weeks (Std. deviation 23.67).

As for the tumor localizations in Table 2, the median delay was the longest in patients with supraglottic cancer, followed by glottic and transglottic tumors, while the patient delay was 8 weeks for oral and oropharyngeal cancers ($p = 0.004$).

Regarding the gender distribution of patient delay: we did not find a significant difference between the median patient delays by gender: men's median patient delay was 9 weeks, while it was 10 weeks among women ($p = 0.237$). In the women group, there was one remarkable outlier, who waited 209 weeks with her symptom, explaining the difference in the mean value (Table 3).

An overview of the symptoms by region shows the following (Table 4): in case of oral cancers, difficulty in swallowing (42.9%) was the most frequent symptom, 28.6% of this patient group had a sore throat and 14.3% reported weight loss, as significantly

TABLE 1 Descriptive statistics of patients involved in our study.

Clinicopathological features	All patients (N = 236)
Gender	
Male	198 (84%)
Female	38 (16%)
Alcohol consumption	
Never	59 (25%)
Previously	25 (10%)
Currently	105 (45%)
Not available	47 (20%)
Smoking	
Never	11 (4.7%)
Previously	46 (19.5%)
Currently	163 (69%)
Not available	16 (6.8%)
Age	61 years (40–92 years)
Stage	
T	
1	36 (15.2%)
2	53 (22.5%)
3	52 (22%)
4a	55 (23.4%)
4b	26 (11%)
Not available	14 (5.9%)
N	
N0	112 (47.4%)
N+	110 (46.6%)
Not available	14 (5.9%)
M	
M0	223 (94.5%)
M1	13 (5.5%)
Not available	0
Grade	
1	13 (5.5%)
2	66 (28%)
3	53 (22.5%)
Not available	104 (44%)
Sites	
Oral cavity	14 (5.93%)
Oropharynx p16 positive	28 (11.87%)
Oropharynx p16 negative	18 (7.63%)
Oropharynx p16 not available	29 (12.29%)
Hypopharynx	51 (21.62%)
Supraglottic larynx	24 (10.17%)
Glottic larynx	60 (25.42%)
Transglottic larynx	10 (4.23%)
Subglottic larynx	1 (0.42%)
Not assessable	1 (0.42%)

more common complaints than in other regions. We found that dysphagia was common among oropharyngeal cancer patients (40%), however, throat pain (48%) was even more frequent and neck mass was significantly more common than in other regions (32%).

Of all the regions, dysphagia was the most common among patients with hypopharyngeal cancer (47.1%), which was also found to be significant, but sore throat (25.5%), hoarseness (21.6%), neck mass (27.5%) and earache (19.6%) were also common symptoms in this group, of which earache showed to be significant, compared to other regions. In case of supraglottic tumors, the symptoms showed higher variability such as sore throat (29.2%), hoarseness (29.2%), dyspnea (25%), and neck mass (20.8%).

Patients with glottic and transglottic carcinoma presented significantly more often with hoarseness. The only subglottic cancer patient had hoarseness and dyspnea.

It is important to see what the median patient delay time was per region in light of the characteristic complaints.

Patients with a main complaint of hoarseness or difficulty in swallowing had significantly higher waiting times, compared to those without either of these two symptoms ($p < 0.001$ and $p = 0.022$, respectively). There were no differences in waiting times for sore throat, neck lump or earache. Due to the small number of patients, correlation analysis could not be performed for hemoptysis and trismus (Table 5).

The clinical stage at the time of the diagnosis is of utmost importance regarding the prognosis of head and neck cancers [9]. In our data, 67% of glottic cancers were diagnosed in the early stage, while the tumors in other localizations were diagnosed predominantly in a locoregionally advanced stage. In oropharyngeal and hypopharyngeal cancers, distant metastasis at the time of diagnosis occurred in 10% (Table 6).

Regarding survival data, we found a significant association between stage and disease-specific survival for both T, N and M status (Figures 1–3). Of particular note is the N status, where the localization and number of neck metastases do not influence survival as much as the presence or absence of cervical lymph node metastases at all (Figure 2). In cases of distant metastases, survival was significantly worse (Figure 3).

A significant correlation between tumor localization and survival was found. It is noteworthy that laryngeal cancers (with longer patient delay) have better survival rates compared to the oral cavity and pharyngeal cancers. Based on our previous data, it is remarkable that while the initial stage certainly predicts a high survival rate, in contrast, we found no significant direct association between the length of patient delay and survival (Figure 4).

When correlating quartiles of patient delay time (longest to shortest time interval in quartiles) to survival, we also found that

TABLE 2 Delay in weeks according to the region ($p = 0.004$).

Localization	Number	Mean patient delay (weeks)	Median patient delay (weeks)
Oral cavity	14	17.09	8
Oropharynx	75	11.18	8
Hypopharynx	51	13.9	11
Supraglottic larynx	24	27.75	*17.5*
Glottic larynx	60	25.9	15
Transglottic larynx	10	16.33	13
Subglottic larynx	1	Value = 4	

TABLE 3 Delay in weeks according to the gender.

Gender	Percent (%)	Mean patient delay	Median patient delay
Women	16.1	26.58 (1–209)	10
Men	83.9	15.79 (0–107)	9

TABLE 4 Symptoms (in percentage) with significance value and median patient delay (in weeks) according to the region.

Regions Complaints	Oral cavity	Oropharynx	Hypopharynx	Supraglottic larynx	Glottic larynx	Transglottic larynx	Subglottic larynx	*p*
Sore throat	28.6	*48.0*	25.5	29.2	3.3	0	0	<0.001
Hoarseness	0	4.0	21.6	29.2	*96.7*	60.0	*100*	<0.001
Neck mass	14.3	*32.0*	27.5	20.8	0	10.0	0	<0.001
Difficulty in swallowing	42.9	40.0	*47.1*	25.0	0	20.0	0	<0.001
Weight loss	*14.3*	4.0	9.8	4.2	0	0	0	0.149
Earache	7.1	13.3	*19.6*	4.2	0	10.0	0	0.027
Hemoptysis	0	0	2.0	4.2	0	0	0	0.513
Trismus	0	2.7	0	0	0	0	0	0.636
Dyspnea	0	5.3	5.9	4.2	3.3	20.0	100	<0.001
Median patient delay in weeks	8.0	8.0	11.0	17.5	15.0	13.0	4.0	

TABLE 5 Patients' delay time according to complaint in weeks $p < 0.05$.

Complaints	Median patient delay in weeks		*p*
	With symptom	Without symptom	
Sore throat	10	9	0.985
Hoarseness	15	8	*<0.001*
Neck mass	8	10	0.215
Difficulty in swallowing	8	11.5	*0.022*
Weight loss	7	10	—
Earache	8	10	0.140
Hemoptysis	0	10	—
Trismus	32	9.5	—
Dyspnea	6.5	10	—

TABLE 6 Cancer stage according to the cancer site: $p < 0.05$.

	Oral cavity	Oropharynx	Hypopharynx	Supraglottic larynx	Glottic larynx	Transglottic larynx
Early stage (T1-2N0M0)	3	7	5	8	*38*	3
	23%	10%	10%	36%	*67%*	30%
Locoregionally advanced stage (T3-4N0M0, T1-4N1-3M0)	10	*55*	*40*	13	18	*7*
	77%	*81%*	*80%*	59%	32%	70%
Distant metastasis (T1-4N1-3M1)	0	*6*	*5*	1	1	0
	0%	*10%*	*10%*	5%	2%	0%

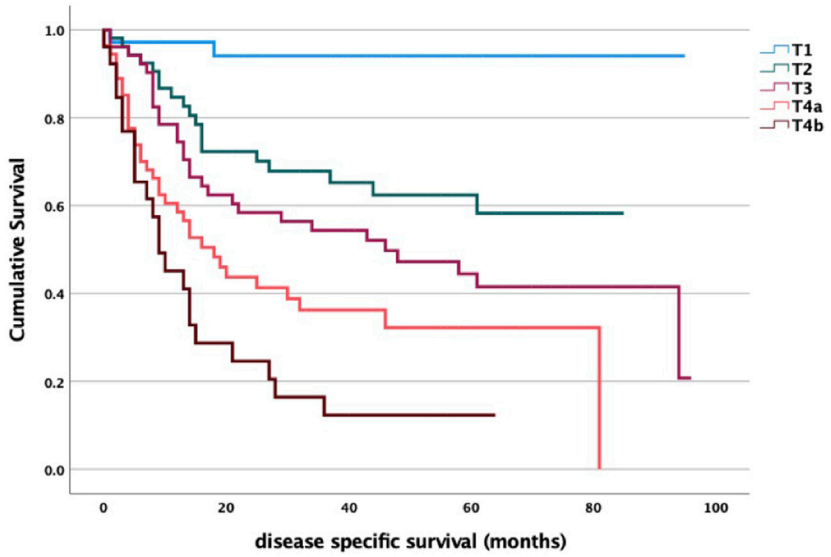

FIGURE 1
T stage and survival analysis log-rank $p < 0.001$. T1 vs. T2 $p = 0.025$; T1 vs. T3 $p < 0.001$; T1 vs. T4a $p = 0.003$; T1 vs. T4b $p < 0.001$; T2 vs. T3 $p = 0.099$; T2 vs. T4a $p = 0.105$; T2 vs. T4b $p = 0.005$; T3 vs. T4a $p = 0.805$; T3 vs. T4b $p = 0.108$; T4a vs. T4b $p = 0.316$.

patient waiting time did not significantly affect survival $p = 0.214$ (Figure 5).

We performed a multivariate regression analysis showing that while the prognostic role of stage remained significant, the patient delay was not a significant predictor of survival (Table 7).

Role of p16 status in oropharyngeal cancers

As for tumor biology, two groups of oropharyngeal cancers can be distinguished: here we present an overview of the symptoms according to the p16 status. In p16-positive oropharyngeal cancer patients, neck mass as presenting symptom was significantly more common than in p16-negative tumor cases ($p = 0.003$). There was no significant correlation between the patient delay and HPV-positivity status in the oropharyngeal cancer group ($p = 0.524$) (Table 8).

The p16 immunohistochemistry was available in forty-six out of seventy-six oropharyngeal cancer patients. Mean patient delay was more for p16 positive patients 14.47 weeks *versus* 9 weeks, while median delay did not differ: 8 weeks for both groups $p = 0.524$ (Table 9).

As expected, we found a significant correlation between HPV status and survival: p16-negative oropharyngeal cancers were associated with significantly worse survival (Figure 6).

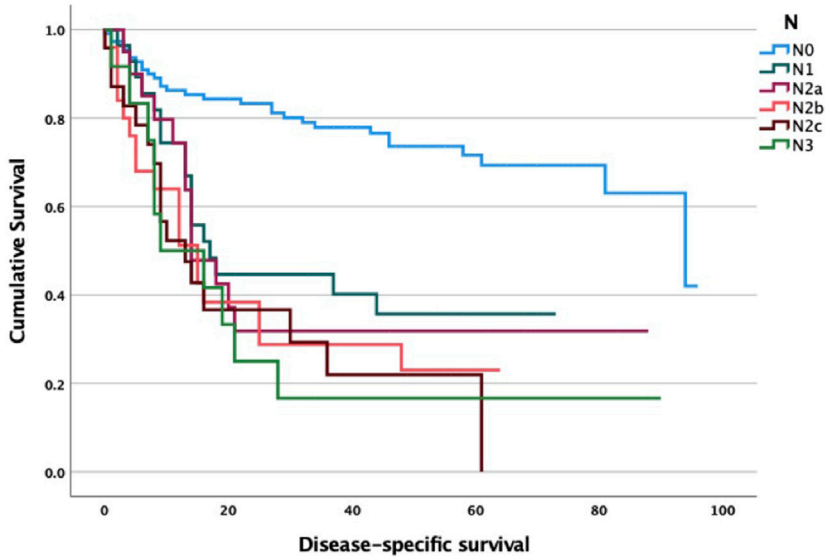

FIGURE 2
N stage and survival analysis log-rank $p < 0.001$. N0 vs. N1 $p < 0.001$; N0 vs. N2a $p = 0.005$; N0 vs. N2b $p < 0.001$; N0 vs. N2c $p < 0.001$; N0 vs. N3c $p = 0.049$; N1 vs. N2a $p = 0.957$; N1 vs. N2b $p = 0.433$; N1 vs. N2c $p = 0.103$; N1 vs. N3 $p = 0.791$.

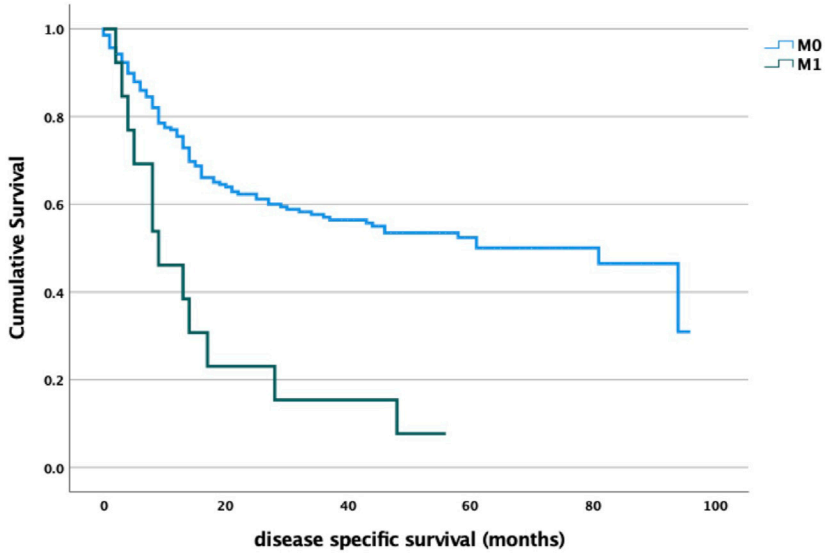

FIGURE 3
M stage and survival analysis log-rank $p < 0.001$.

Discussion

Head and neck cancers can cause a diversity of symptoms. These can be further classified into general symptoms, such as fatigue, weight loss, or site-specific ones, e.g., hoarseness, and sore throat.

Hoarseness can be due to the impaired function and structure of the cover-body system of the vocal cords, vocal fold movement problems associated with direct tumor spread to the paraglottic space or the thyroarytenoid joint, or infiltration of the recurrent laryngeal nerve [10]. Altered voice quality can also occur by structural abnormalities (i.e., presence of the tumor mass) in the

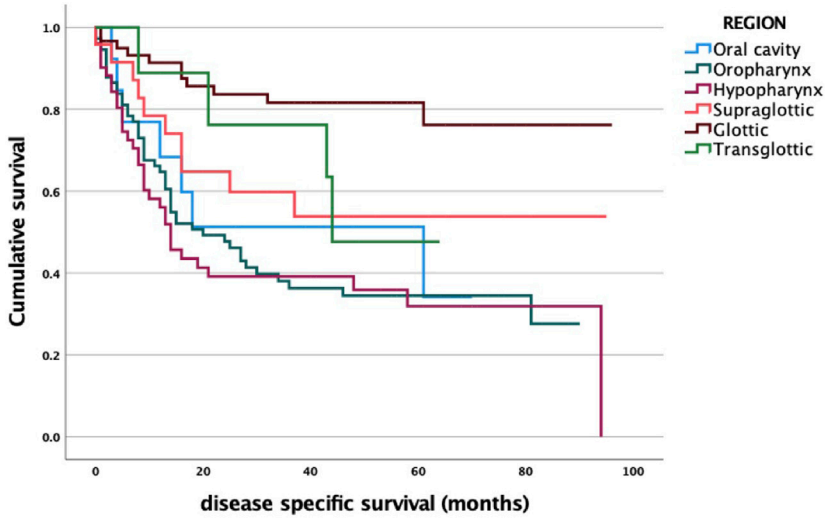

FIGURE 4
Primary tumor site and survival analysis log-rank $p < 0.001$. oral vs. orophar. $p = 0.906$; oral vs. hypophar. $p = 0.996$; oral vs. supraglot. $p = 0.860$; oral vs. glot. $p = 0.013$; oral vs. transglot. $p = 0.185$; orophar. vs. hypophar. $p = 0.985$; orophar. vs. supraglot. $p = 0.723$; orophar. vs. glot. $p < 0.001$; orophar. vs. transglot. $p = 0.144$; hypophar. vs. supraglot. $p = 0.603$; hypophar. vs. glot. $p < 0.001$; hypophar. vs. transglot. $p = 0.139$; supraglot. vs. glot. $p = 0.012$; supraglot. vs. transglot. $p = 0.215$; glot. vs. transglot. $p = 0.986$.

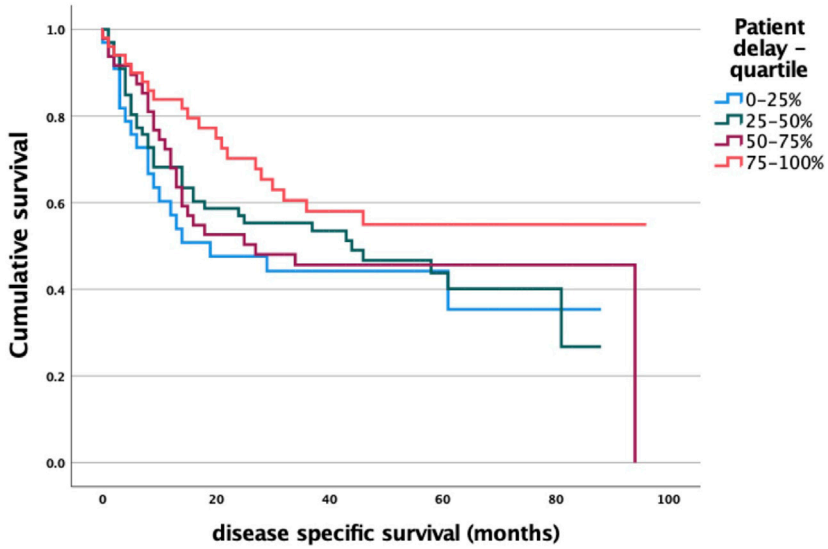

FIGURE 5
Patient delay and survival analysis log-rank $p = 0.214$.

pharynx and oral cavity. In our data set, hoarseness was significantly more common in cancers arising in the glottic and subglottic larynx, interestingly, the symptom was also significantly associated with longer patient delay. The latter might be associated with the better biological behavior of glottic cancers [11].

Referred ear pain can occur due to the involvement of the 5th (mainly in oral cancers), more commonly by the 9th and 10th cranial nerves [12]. We found a significant association between otalgia and tumor localization: hypopharyngeal cancers caused ear pain the most frequently.

TABLE 7 Multivariate regression analysis (Cox regression).

	p	HR	95% confidence interval (CI)	
			Lower	Upper
Stage	<0.001	5.075	2.756	9.347
Patient delay	0.265	0.990	0.974	1.007

cancer patients was 7.4 weeks [16], another localization of head and neck cancer was given as 12.3 weeks. In South India the median delay was only 4.29 weeks [17]. In the United States, from 1993 to 2004, this result (12.67 weeks) was less than in Hungary, but from 2005 to 2013 it was close to our rate (17.03 weeks) [18]. One-sample test was used to compare whether the difference in the delay times was significant. We found a significant difference between our data and the Brazilian and South Indian results.

TABLE 8 Oropharyngeal cancer symptoms according to p16 status.

	Presence of symptoms in percent		*p*
	p16 positive OPC	p16 negative OPC	
Sore throat	38.9	64.3	0.091
Hoarseness	5.6	3.6	1.0
Neck mass	61.1	17.9	*0.003*
Difficulty in swallowing	16.7	42.9	0.064
Weight loss	0	7.1	0.513
Earache	0	17.9	0.140
Hemoptysis	—	—	—
Trismus	5.6	3.6	1.0
Dyspnea	0	14.3	0.144
Median patient delay in weeks	8 weeks	8 weeks	0.524

TABLE 9 p16-positivity and patient delay in weeks in oropharyngeal cancers $p = 0.524$.

p16 status	Numbers (available patient delay scores)	Mean delay	Median delay
Positive	18 (17)	14.47 (2–56) weeks	8.00 weeks
Negative	28 (26)	9.81 (2–42) weeks	8.00 weeks
Not available	29		

Sore throat and neck mass, as presenting symptoms were significantly the most common in oropharyngeal cancers, and further analyzed by p16-status, HPV-positive cancer patients presented 3 times more common with neck lump as an initial sign of disease, which phenomenon is due to the often rapidly growing, cystic neck metastases of HPV-related head and neck cancers [13].

Regarding patient delay, when comparing the results of our study on a representative patient population in Hungary (17.57 weeks) with international data (Table 10), similar times were found (17.09 weeks) to the Canadian data [14]. However, the data from Brazil (43.48 weeks, median) were longer than our data [15]. This indicator was lower in the United Kingdom, where the mean patient delay for oral

In reviewing the factors that determine patient survival, one of the first to be mentioned is the size of the primary tumor, the presence of lymph node metastases and distant metastases. The TNM stage is a reliable predictor of survival, which increases with time, and thus with delay time. In advanced cancers, more drastic and radical surgery may be performed, and often the general condition of the patient, which also decreases with time, does not allow curative surgery. In advanced cancers, the side effects of chemo-radiation are also more pronounced. Delay time therefore indirectly determines patient survival [19].

Looking further at the components of survival, it is noted that some localized tumors have been found to have better survival rates despite longer waiting times. These were glottic and p16-

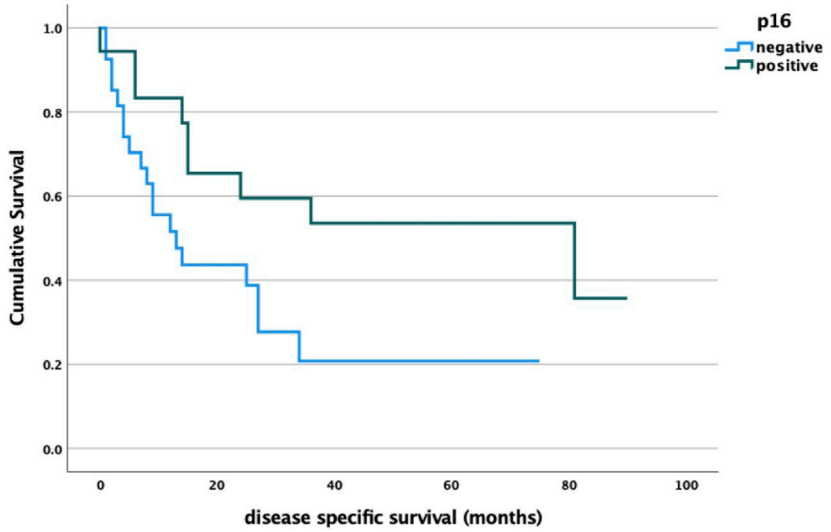

FIGURE 6
p16 status and survival analysis log rank p = 0.032.

TABLE 10 Patient delay times by country.

Country	Patient delay (weeks)	Period	Region	*p*-value
Our data	17.57 (mean)	2012–2017		
Canadian [14]	17.09 (mean)	2017–2018	All HNC	0.598
Brazil [15]	43.48 (median)	2011–2012	All HNC	*<0.001*
United Kingdom [16]	7.4 (mean)	1995–1996	Oral	0.307
	12.3 (mean)	1995–1996	All HNC ex. oral	*0.002*
South India [17]	4.29 (median)	2016–2017	All HNC	*<0.001*
United States [18]	12.67 (not reported)	1993–2004	All HNC	*0.001*
	17.03 (not reported)	2005–2013	All HNC	0.573
Iran [20]	23.05 (mean)	2004–2006	All HNC	*0.002*

positive oropharyngeal cancers. This suggests that the variable biological behavior of tumors with different localization is an important factor for patient survival. Glottic cancers grow more slowly and, due to their location, show obvious symptoms (hoarseness) even when small, which may trigger the patient to seek medical attention. However, our results show that they wait for a long time, which may be because their hoarseness does not cross their stimulus threshold, they probably think it is just a normal part of smoking. Furthermore, due to their lymphatic drainage, glottic tumors tend to metastasize only at an advanced stage.

The better survival of p16 oropharyngeal cancers can be explained by two factors: they have different tumor biology, which makes them more responsive to chemo-radiation, and they are younger, in a better general condition, with less smoking and alcohol-related diseases, so they can tolerate treatment better.

Tumors with different localizations and behaviors overlap in terms of symptoms, so this does not allow us to screen out patients with a more favorable biological behavior being likely to have a good chance in case of a delayed diagnosis. Instead of population-wide screening, the solution would be to screen patients with risk factors—smoking and drinking—so that tumors can be diagnosed and treated at an earlier stage.

A possible weakness of our study is the subjective matter of the patients' self reported date of symptom onset, however, there is no other option to assess the symptom onset which would be more accurate.

Data availability statement

The raw data supporting the conclusion of this article will be made available by the authors, without undue reservation.

Ethics statement

The studies involving human participants were reviewed and approved by SE IKEB 105/2014. Written informed consent for participation was not required for this study in accordance with the national legislation and the institutional requirements.

Author contributions

KD: study design, statistics. AH: data management, manuscript production. JH: immunohistochemistry, histopathology. LT and GP: scientific oversee, consultation. All authors contributed to the article and approved the submitted version.

Conflict of interest

The authors declare that the research was conducted in the absence of any commercial or financial relationships that could be construed as a potential conflict of interest.

References

1. International Agency for Research on Cancer. *Globocan: Global cancer observatory* (2020). Retrieved from: https://gco.iarc.fr/today/online-analysis-multibars?v=2020&mode=population&mode_population=countries&population=900&populations=900&key=crude_rate&sex=0&cancer=39&type=0&statistic=5&prevalence=0&population_group=0&ages_group%5B%5D=0&ages_group%5B%5D=17&nb_items=10&group_cancer=0&include_nmsc=0&include_nmsc_other=1&type_multiple=%257B%2522inc%2522%253Afalse%252C%2522mort%2522%253Atrue%252C%2522prev%2522%253Afalse%257D&orientation=horizontal&type_sort=1&type_nb_items=%257B%2522top%2522%253Atrue%252C%2522bottom%2522%253Afalse%257D#collapse-others (Accessed July 5, 2023).

2. Neal RD. Do diagnostic delays in cancer matter? *Br J Cancer* (2009) 101(2): S9–S12. doi:10.1038/sj.bjc.6605384

3. Goy J, Hall SF, Feldman-Stewart D, Groome PA. Diagnostic delay and disease stage in head and neck cancer: A systematic review. *Laryngoscope* (2009) 119(5): 889–98. doi:10.1002/lary.20185

4. Rozniatowski O, Reich M, Mallet Y, Penel N, Fournier C, Lefebvre JL. Psychosocial factors involved in delayed consultation by patients with head and neck cancer. *Head Neck* (2005) 27(4):274–80. doi:10.1002/hed.20157

5. Franceschi S, Barzan L, Talamini R. Screening for cancer of the head and neck: If not now, when? *Oral Oncol* (1997) 33(5):313–6. doi:10.1016/s1368-8375(97)00034-1

6. Reich M, Licitra L, Vermorken JB, Bernier J, Parmar S, Golusinski W, et al. Best practice guidelines in the psychosocial management of HPV-related head and neck cancer: Recommendations from the European head and neck cancer society's make Sense campaign. *Ann Oncol* (2016) 27(10):1848–54. doi:10.1093/annonc/mdw272

7. Edge SB, Compton CC. The American joint committee on cancer: The 7th edition of the AJCC cancer staging manual and the future of TNM. *Ann Surg Oncol* (2010) 17(6):1471–4. doi:10.1245/s10434-010-0985-4

8. Dok R, Nuyts S. HPV positive head and neck cancers: Molecular pathogenesis and evolving treatment strategies. *Cancers (Basel)* (2016) 8(4):41. doi:10.3390/cancers8040041

9. Teppo H, Alho OP. Relative importance of diagnostic delays in different head and neck cancers. *Clin Otolaryngol* (2008) 33(4):325–30. doi:10.1111/j.1749-4486.2008.01704.x

10. Ambrosch P, Fazel A. Functional organ preservation in laryngeal and hypopharyngeal cancer. GMS *Curr Top Otorhinolaryngol Head Neck Surg* (2011) 90(1):Doc02–109. Laryngorhinootologie. doi:10.3205/cto000075

11. Szentkúti G, Dános K, Brauswetter D, Kiszner G, Krenács T, Csákó L, et al. Correlations between prognosis and regional biomarker profiles in head and neck squamous cell carcinomas. *Pathol Oncol Res* (2015) 21(3):643–50. doi:10.1007/s12253-014-9869-4

12. Chen RC, Khorsandi AS, Shatzkes DR, Holliday RA. The radiology of referred otalgia. *AJNR Am J Neuroradiol* (2009) 30(10):1817–23. doi:10.3174/ajnr.A1605

13. Goldenberg D, Begum S, Westra WH, Khan Z, Sciubba J, Pai SI, et al. Cystic lymph node metastasis in patients with head and neck cancer: An HPV-associated phenomenon. *Head Neck* (2008) 30(7):898–903. doi:10.1002/hed.20796

14. Kassirian S, Dzioba A, Hamel S, Patel K, Sahovaler A, Palma DA, et al. Delay in diagnosis of patients with head-and-neck cancer in Canada: Impact of patient and provider delay. *Curr Oncol* (2020) 27(5):e467–e77. doi:10.3747/co.27.6547

15. Felippu AW, Freire EC, Silva Rde A, Guimaraes AV, Dedivitis RA. Impact of delay in the diagnosis and treatment of head and neck cancer. *Braz J Otorhinolaryngol* (2016) 82(2):140–3. doi:10.1016/j.bjorl.2015.10.009

16. Amir Z, Kwan SY, Landes D, Feber T, Williams SA. Diagnostic delays in head and neck cancers. *Eur J Cancer Care (Engl)* (1999) 8(4):198–203. doi:10.1046/j.1365-2354.1999.00165.x

17. Ganesan S, Sivagnanganesan S, Thulasingam M, Karunanithi G, Kalaiarasi K, Ravichandran S, et al. Diagnostic delay for head and neck cancer in South India: A mixed-methods study. *Asian Pac J Cancer Prev* (2020) 21(6):1673–8. doi:10.31557/APJCP.2020.21.6.1673

18. Smith MM, Abrol A, Gardner GM. Assessing delays in laryngeal cancer treatment. *Laryngoscope* (2016) 126(7):1612–5. doi:10.1002/lary.25734

19. Liao DZ, Schlecht NF, Rosenblatt G, Kinkhabwala CM, Leonard JA, Ference RS, et al. Association of delayed time to treatment initiation with overall survival and recurrence among patients with head and neck squamous cell carcinoma in an underserved urban population. *JAMA Otolaryngol Head Neck Surg* (2019) 145(11): 1001–9. doi:10.1001/jamaoto.2019.2414

20. Sargeran K, Murtomaa H, Safavi SM, Teronen O. Delayed diagnosis of oral cancer in Iran: Challenge for prevention. *Oral Health Prev Dent* (2009) 7(1):69–76. doi:10.3290/j.ohpd.a15270

Pathology & Oncology Research | frontiers

TYPE Original Research
PUBLISHED 15 March 2024
DOI 10.3389/pore.2024.1611664

Check for updates

OPEN ACCESS

EDITED BY
Anna Sebestyén,
Semmelweis University, Hungary

*CORRESPONDENCE
Andrea Molnár,
dr.molnarandrea.rd@gmail.com

RECEIVED 30 December 2023
ACCEPTED 28 February 2024
PUBLISHED 15 March 2024

CITATION
Molnár A, Pálfi E, Belák B, Blasszauer C, Reibl D and Lövey J (2024), Positive correlation between persistence of medical nutrition therapy and overall survival in patients with head and neck cancer.
Pathol. Oncol. Res. 30:1611664.
doi: 10.3389/pore.2024.1611664

COPYRIGHT
© 2024 Molnár, Pálfi, Belák, Blasszauer, Reibl and Lövey. This is an open-access article distributed under the terms of the Creative Commons Attribution License (CC BY). The use, distribution or reproduction in other forums is permitted, provided the original author(s) and the copyright owner(s) are credited and that the original publication in this journal is cited, in accordance with accepted academic practice. No use, distribution or reproduction is permitted which does not comply with these terms.

Positive correlation between persistence of medical nutrition therapy and overall survival in patients with head and neck cancer

Andrea Molnár[1,2,3]*, Erzsébet Pálfi[1,2,4], Barbara Belák[1,5], Célia Blasszauer[6], Dániel Reibl[6] and József Lövey[7,8]

[1]Health Sciences Division, Doctoral School of Semmelweis University, Budapest, Hungary, [2]Scientific Committee, National Association of Hungarian Dietitians, Budapest, Hungary, [3]Danone Hungary Kft., Budapest, Hungary, [4]Department of Dietetics and Nutritional Sciences, Semmelweis University, Budapest, Hungary, [5]Bacs-Kiskun County Hospital, Kecskemet, Hungary, [6]MedicalScan Kft., Budapest, Hungary, [7]National Tumour Biology Laboratory, National Institute of Oncology, Budapest, Hungary, [8]Department of Oncology, Semmelweis University, Budapest, Hungary

Background: Several factors can affect overall survival of head and neck cancer (HNC) patients, including characteristics of the cancer disease and response to treatments. However, patients' nutritional status and the effectiveness of medical nutrition therapy (MNT) can also impact overall survival. The primary goal of our research was to collect real-life data on the use of MNT in HNC patients and to specifically investigate the correlation between survival and the duration of uninterrupted (persistent) nutrition.

Method: The data of this retrospective, analytical, cohort study was collected from electronic healthcare records from the Hungarian National Health Insurance Fund Management. Overall, 38,675 HNC patients' data of the period between 2012 and 2021 was used. We applied multi-step exclusions to identify patient groups accurately and to avoid biasing factors. Statistical analysis was done by the Kaplan-Meier method, log-rank test, and Cox regression analysis.

Results: Throughout the investigated period 16,871 (64%) patients received MNT therapy out of 26,253 newly diagnosed patients (≥18 years). In terms of the persistence of MNT, we divided the patients into three groups (1–3; 4–6; ≥7-month duration of MNT). When comparing these groups, we found that patients receiving long-term (≥7 months) MNT had a significantly longer overall survival ($p < 0.0001$) than those who received MNT for a shorter duration, both in locally advanced and recurrent/metastatic cases.

Abbreviations: CI, Confidence interval; EN, enteral nutrition; HNC, head and neck cancer; HNHIFM, Hungarian National Health Insurance Fund Management; HR, hazard ratio; ICD, international classification of diseases; LA, locally advanced; MNT, medical nutrition therapy; ONS, oral nutritional supplement; QoL, quality of life; RWE, real-world evidence; R/M, recurrent/metastatic; TNM, Classification of Malignant Tumors; T, tumor size; N, degree of spread to regional lymph nodes; M, presence of distant metastasis.

Conclusion: The main outcome of the study is that there is a positive correlation between the persistence of MNT and the overall survival in HNC patients when nutritional intervention lasts several months. It highlights the responsibility of the specialists during the patient journey to use MNT early and to continue its use for as long as it is beneficial to the patients.

KEYWORDS

medical nutrition therapy, survival, real -word evidence, persistence of nutrition and survival, head and neck cancer

Introduction

Guidelines and clinical studies have shown that demographic characteristics (sex, age), cancer characteristics (stage, response to treatment), and nutritional status (presence of malnutrition, sarcopenia, cachexia and effectiveness of medical nutrition therapy (MNT) to treat them) can influence overall survival both independently and in relation to each other [1–7]. In the present article the authors address the issue of the effectiveness of MNT with a focus on the duration of uninterrupted MNT (referred to as *persistence*) and the survival in a head and neck cancer (HNC) patient population.

HNC is characterized by increasing incidence, prevalence, and still high mortality rates [8–12]. The 5- and 10-year survival rates are about 63% and 53%, respectively, and it is important to highlight that disease-specific deaths occur mainly in the first 2–3 years [8, 9]. One reason for the high mortality is that patients are often diagnosed at an advanced stage (due to diagnostic difficulties and lack of specific symptoms), and there is a high rate of local recurrence within 3 years (50%) [10, 13]. The more advanced the stage of HNC, the more invasive diagnostic and therapeutic procedures are required [14]. Treatment requires a multidisciplinary approach combining surgery, radiotherapy, and systemic therapy. These interventions on their own, and their combination even more, have short- and long-term consequences that have a significant impact on survival and other outcomes. While oncologists are looking for personalized therapeutic strategies to achieve more favorable outcomes, clinical expert guidelines highlight the need for early nutritional risk identification, early intervention (dietary advice, medical nutrition therapy when food intake is insufficient and escalation to tube feeding) [1, 2, 15].

The main aim of this study was to investigate the correlation between MNT persistence and overall survival. Another aim was to investigate the frequency and duration of uninterrupted MNT.

Material and method

The study was a retrospective, analytical, cohort study of HNC patients using data collected from the Hungarian National Health Insurance Fund Management (HNHIFM) electronic health records. Ethical approval number is BM/4245-1/2023. For data collection and reliable conclusions, we needed statistical processing of a large data set on the frequency (prevalence, incidence) of Hungarian HNC patients, the type of treatments, as well as the use of MNT, its frequency, persistence, and method of administration. The total number of patients included in the study and the sample size available for each subgroup analysis are shown in Figure 1. A total of ten filtering criteria were developed to define the subgroup breakdowns. The term "medical nutrition therapy" was used to refer to nutrition therapy interventions when the physician ordered oral nutritional supplement (ONS) or enteral tube feeding (enteral nutrition).

For the frequency of HNC, we used three restrictive criteria for the inclusion: the International Classification of Diseases (ICD) code, the examined interval, and the adult age. From ICD we selected patients with codes C00–C14 and C30–C32 who had presented at least four times in inpatient or outpatient care (thus excluding presumptive but not confirmed diagnoses). We chose 10 years between 2012 and 2021 as the period of analysis (as baseline prevalence data), and of these, we considered 9 years of time for new patients (as baseline incidence data). We excluded patients aged under 18 years.

In terms of treatment, we collected in detail who had and who had not received anti-cancer treatment, as well as the type of treatment they had received.

Data on the use of MNT were obtained from the prescribing data for foods for special medical purposes administered orally (ONS) or enteral tube-feeding (enteral formula). In determining the frequency of MNT, the selection was based on the three screening criteria mentioned above (for new patients) with the inclusion of the patient receiving nutrition therapy as a 4th criterion. For subgroup analyses on MNT persistence, we applied a 5th screening condition: we included only those who had also received antitumor therapy (thus eliminating the bias that could have been caused by shorter survival due to untreated status). In addition to the above, two further requirements were imposed: criterion 6th was that the interruption should not exceed 30 days to ensure continuity of MNT, and criterion 7th was that the patient should live for at least 1 year from the start of nutrition therapy. The latter criteria were necessary to exclude confounding factors that could rapidly shorten survival, such as very severe conditions that can no longer be controlled by anti-cancer treatment. We also

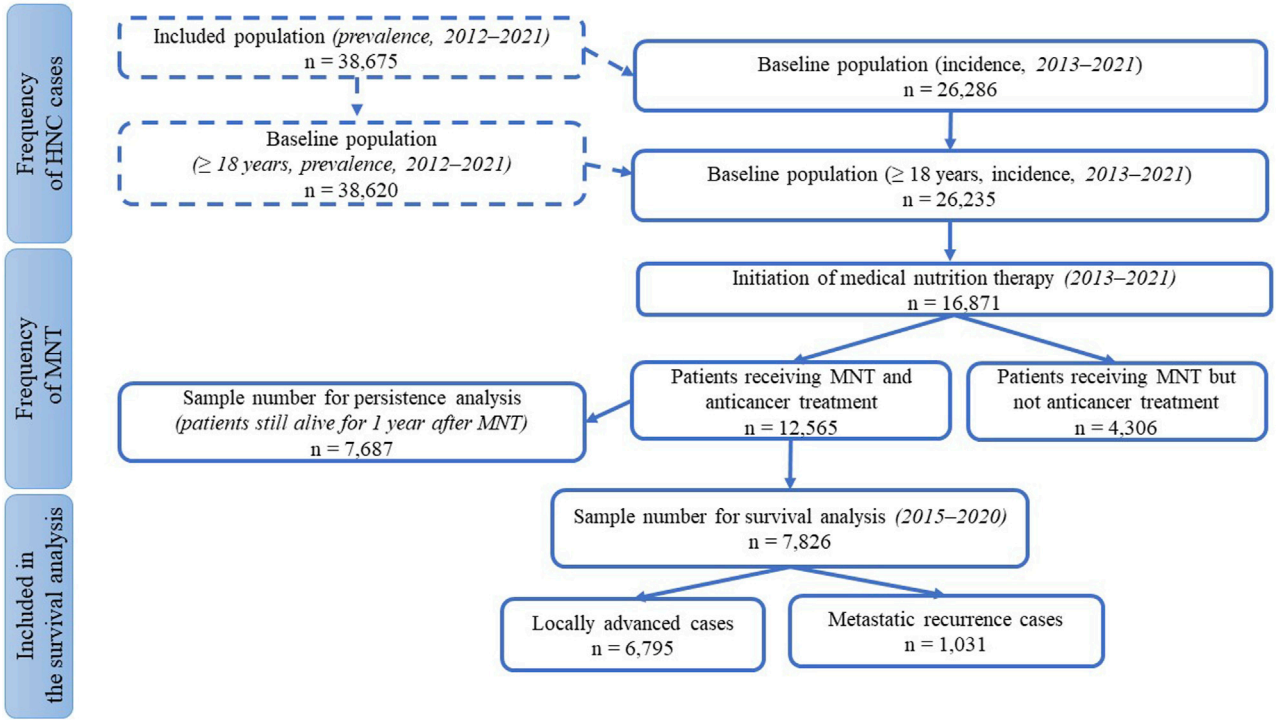

FIGURE 1
Patient numbers for subgroup analyses.

investigated the relationship between MNT persistence and survival in the two main groups of patients receiving anticancer treatment: locally advanced (LA) and recurrent/metastatic (R/M). Here, at inclusion, only the first 6 of the above criteria had to be met by the sample, not the 7th, i.e., there was no expectation that the patient would live for 1 year after starting MNT. We thus expanded the number of patients, but further narrowed it by testing two additional criteria: as screening criterion 8th, we only examined data at a slightly shorter time interval (2015–2020) to achieve a more homogeneous cohort; as criterion 9th, we used the data of patients with a minimum survival of 90 days to exclude bias caused by short term mortality. For survival analysis, we divided patients into three groups based on a 10th criterion depending on the duration of MNT: short (1–3 months), medium (4–6 months), and long-term (≥7 months) continuous nutritional therapy. These lengths were chosen because the usual follow-up period of the patients according to the data of the HNHIFM was 3 months, and in Hungary the physicians can prescribe ONS and tube feeding formulae for 3 months. Furthermore, in relation to MNT, observational studies follow patients for varying lengths of time, with 3–6 months being common and longer studies being rare [16–18], so we also chose to create groups of patients on nutrition therapy for 3 months, 6 months, or longer. Survival was followed here for 365 days.

Statistical analysis

The software "RStudio" was used to extract data from the HNHIFM database and to perform statistical analyses. Available data included socio-demographic data (e.g., age, gender), treatment and MNT information. Derived data were persistence and survival data. A p-value of 0.05 was set as the threshold for statistical significance (for Log-rank test and the other tests as well). The Kaplan-Meier method was used to estimate the probability of survival. Log-rank tests were used to assess the probability of mortality between groups. Cox regression model was used to evaluate the association between the survival time of patients and predictor variables, where the group receiving MNT for 1–3 months was the reference and compared with the group receiving MNT for 3–6 and ≥7 months.

Results

Summary of the results

Characteristics of the basic data used for the analyses (descriptive, categorization and distribution indicators): in Hungary, the prevalence of HNC is 38,675 patients for 10 years and the incidence is 26,286 patients for 9 years. The distribution of ICD codes based on prevalence data is presented

TABLE 1 The prevalence data of distribution of head and neck tumor diseases in Hungary between 2012 and 2021.

ICD codes	International classification of diseases (ICD), topographical codes	2012	2013	2014	2015	2016	2017	2018	2019	2020	2021	Summary
C00	Lip	217	273	256	273	265	279	236	294	237	239	**1,624**
C01	Base of tongue	702	737	794	764	751	720	704	703	642	604	**3,734**
C02	Other and unspecified parts of tongue	740	745	737	758	722	679	645	695	620	632	**3,749**
C03	Gum	140	149	132	128	146	154	146	149	127	165	**881**
C04	Floor of mouth	535	522	499	493	460	423	461	434	352	362	**2,430**
C05	Palate	275	272	293	282	266	238	278	274	188	203	**1,403**
C06	Other and unspecified parts of mouth	204	225	234	229	207	245	229	232	206	246	**1,397**
C07	Parotid gland	295	311	330	313	313	304	332	390	365	321	**1,775**
C08	Other and unspecified major salivary glands	103	122	139	145	133	122	125	158	116	137	**716**
C09	Tonsil	609	635	661	612	669	641	684	647	548	524	**3,056**
C10	Oropharynx	864	799	799	798	735	669	652	661	602	622	**4,054**
C11	Nasopharynx	277	287	285	299	283	289	283	294	236	240	**1,218**
C12	Pyriform sinus	103	130	123	117	109	96	106	94	81	82	**556**
C13	Hypopharynx	1,346	1,275	1,278	1,197	1,181	1,092	1,069	1,056	912	821	**5,952**
C14	Other and ill-defined sites in lip, oral cavity, and pharynx	783	834	876	889	884	978	867	887	835	777	**4,461**
C30	Nasal cavity and middle ear	120	117	115	125	137	128	140	147	144	151	**697**
C31	Accessory sinuses	155	155	167	146	163	134	136	141	123	129	**793**
C32	Larynx	3,225	3,229	3,225	3,171	3,028	2,917	2,838	2,752	2,384	2,378	**12,015**
Summary		**9,161**	**9,320**	**9,376**	**9,261**	**9,135**	**8,869**	**8,789**	**8,886**	**7,705**	**7,672**	**38,675**

Bold values indicate the local totals (subtotal values).

TABLE 2 Demographic characteristics of the study population.

Characteristic	Prevalence data		Incidence data	
	N	%	*N*	%
Sex				
Male	28,796	74.5	19,408	73.8
Female	9,879	25.5	6,878	26.2
Age (years)				
<18	55	0.1	51	0.2
18–65	21,816	56.4	16,149	61.4
>65	16,804	43.4	10,086	38.4

in Table 1. Demographic characteristics of the study population is shown in Table 2. Data on treatment: 58.5% (15,380) of new patients received anti-cancer treatment and 41.5% (10,906) did not receive such treatment. Data on the frequency of MNT use: 64.3% (16,871) of new patients (≥18 years) received nutrition therapy between 2013 and 2021.

Results of the correlation studies: After the examination of the persistence of MNT, the result of the relationship between the

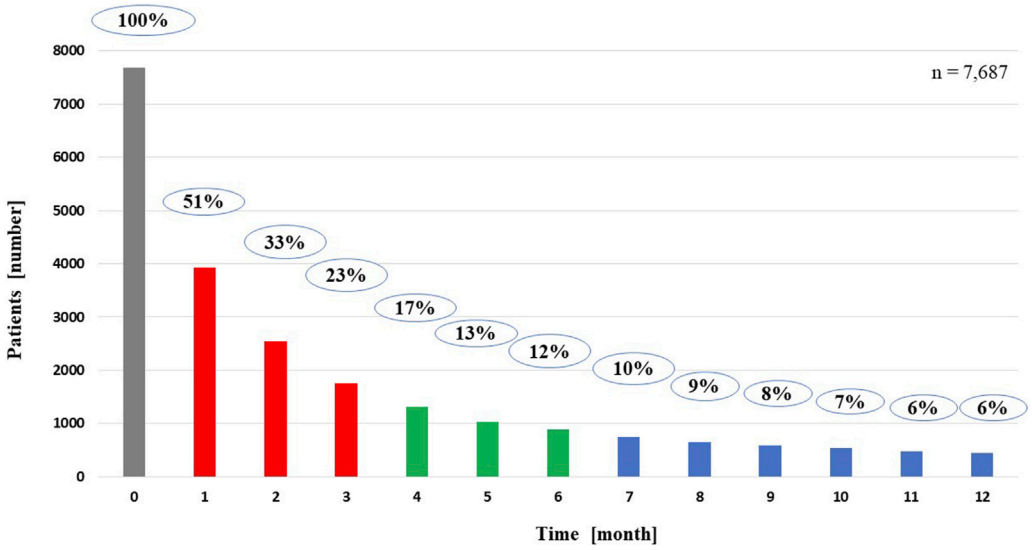

FIGURE 2
Persistence of medical nutrition therapy for patients living for 1 year from the start of nutrition therapy.

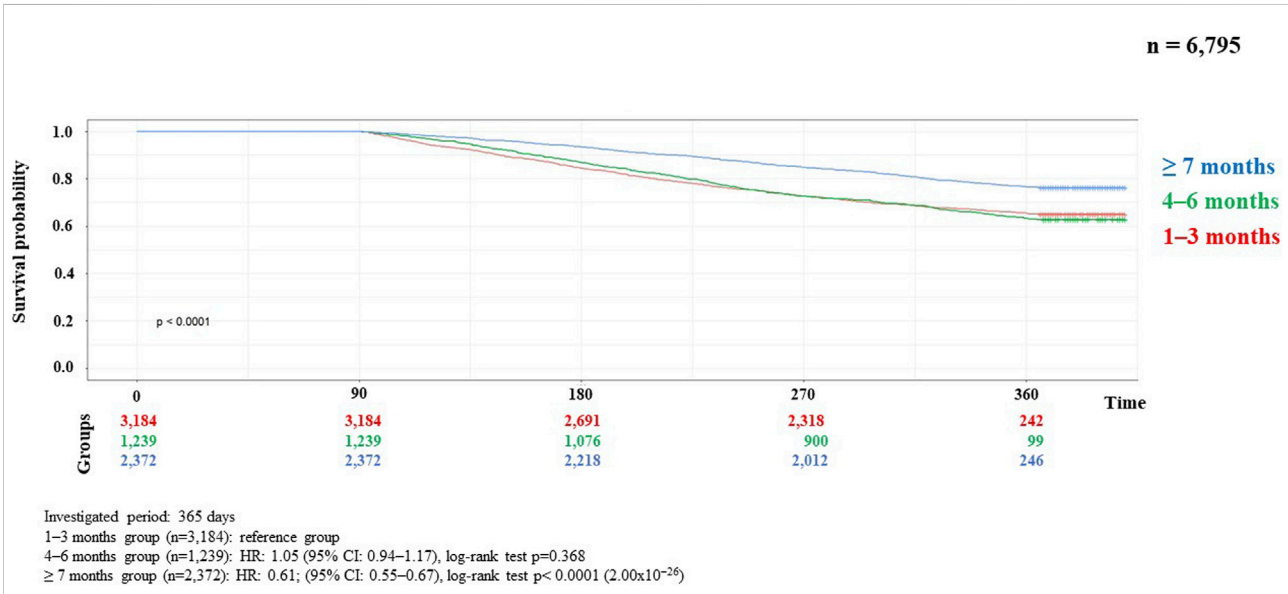

FIGURE 3
Kaplan-Meier curve of HNC survival probability in connection with persistence of MNT in locally advanced cases.

length of therapy and the decrease in the number of patients is presented in Figure 2, broken down by month and followed for 1 year. Initial number of patients: 7,687, followed by monthly decline: 3,928; 2,543; 1,762; 1,314; 1,027; 886; 744; 656; 584; 539; 482; 444. The main finding of the analyses examining the association between MNT duration and survival was that those receiving long-term (≥7 months) nutrition therapy had significantly better survival ($p < 0.0001$) than those receiving medium-term (4–6 months) ($p < 0.368$), compared to those receiving short-term (1–3 months) nutrition therapy. The results are presented in detail in Figures 3, 4.

Evaluation of the results

To determine the prevalence of HNC, we compared our data with the Hungarian population at the beginning and the end of the period. In both cases, a significant decrease was observed,

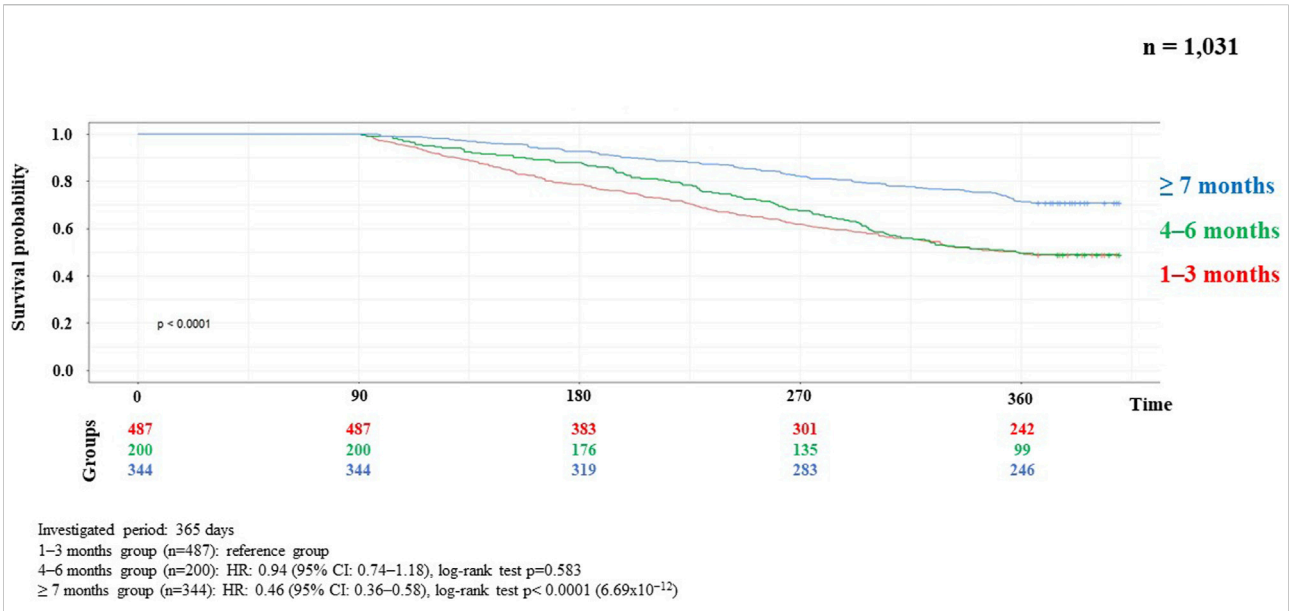

FIGURE 4
Kaplan-Meier curve of HNC survival probability in connection with persistence of MNT in metastatic recurrent cases.

with prevalence decreasing from 94 to 79 and incidence from 35 to 25 per 100,000 population. The lowest numbers were seen during the COVID epidemic (2020–2021), but it is likely that the decrease was not due to fewer patients, but to a lack of diagnosis. In terms of demographics, we found almost equal proportions of sex in the prevalence and incidence data, with a higher proportion of under-18s and lower proportions of older people in the incidence data in terms of age. When evaluating the prevalence data by ICD codes, it can be said that most of HNC patients (31.1%, 12,015) had the code C32 (laryngeal tumor).

For anti-cancer treatment, the proportion of untreated patients was high (41.5%, 10,906), which is why it was necessary to exclude untreated patients when examining the impact of MNT on survival, as the significant number of untreated patients and their high mortality would have distorted the assessment of effectiveness. In the group of patients receiving anti-cancer treatment, 71.4% received treatment corresponding to locally advanced stage, 18.3% to the metastatic stage, and 10.3% received induction treatment.

Regarding the frequency of MNT use, the data were further analyzed according to whether patients had received anti-cancer therapy in addition to MNT, given the relatively high prevalence (64.3%, 16,871 patients) of MNT. In total, 74.5% (12,565 patients) received both treatments, 25.5% (4,306 patients) received MNT but not anticancer therapy. It is assumed that MNT was used as part of palliative treatment in the latter patients. A further observation is that the initial relatively high MNT rate is followed by a short therapeutic period, i.e., the proportion of patients on MNT drops to 51% by the first month, 33% by the second month, 23% by the third month, 17% by the fourth month, 13% by the fifth month, 12% by the sixth month, 10% by the seventh month, and then it further decreases until the 12th month, when only 6% of the patients received MNT. Figure 2 shows the rapid decrease in the number of patients on MNT in a monthly breakdown.

Analyses of the persistence of MNT and survival showed that those receiving long-term (≥7 months) MNT had significantly better survival (both in the LA and R/M stage groups) compared to the group receiving MNT for 1–3 months (Figures 3, 4). There was no significant difference in expected survival for those receiving medium-term (4–6 months) nutrition therapy. Significant change ($p < 0.0001$) in survival in the figure was determined by the log-rank test and the null hypothesis that the survival probabilities are equal (i.e., there is no difference in survival probabilities among the groups), was rejected with 95% confidence. Based on the Cox regression calculation, we can state with 95% confidence that, compared to the MNT group of 1–3 months chosen as the reference, the 4–6 months group is not significantly different ($p < 0.368$), whereas the ≥7 months group is significantly different from the reference group ($p < 2 \times 10^{-16}$). One-year overall survival in the ≥7-month group was 76.3% for LA and 70.9% for R/M stage. Table 3 shows which specific treatments were used in the group breakdowns by the three treatment lengths. In further subgroup analyses we

TABLE 3 Treatments cases depending on the length of Medical Nutrition Therapy.

Length of MNT [months]	Type of treatments	Locally advanced cases [number of patients]	Metastatic recurrent cases [number of patients]
1–3	Chemotherapy		372
1–3	Radiotherapy	2,926	
1–3	Radio-chemotherapy	473	
1–3	Immunotherapy		166
1–3	Cetuximab therapy		132
1–3	**Summary**	**3,184**	**487**
4–6	Chemotherapy		152
4–6	Radiotherapy	1,155	
4–6	Radio-chemotherapy	152	
4–6	Immunotherapy		74
4–6	Cetuximab therapy		56
4–6	**Summary**	**1,239**	**200**
≥7	Chemotherapy		256
≥7	Radiotherapy	2,238	
≥7	Radio-chemotherapy	304	
≥7	Immunotherapy		161
≥7	Cetuximab therapy		115
≥7	**Summary**	**2,372**	**344**

Bold values indicate the local totals (subtotal values).

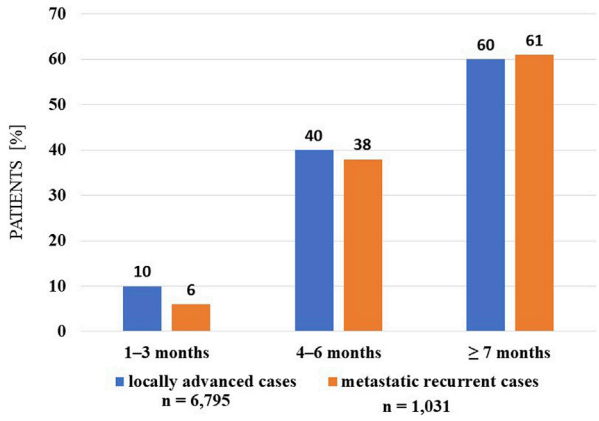

FIGURE 5
Percentage distribution of tube-fed patients in each therapeutic length group (investigated interval: 2015–2020).

examined the number and the proportion of patients on tube feeding in both LA and R/M stage and found that their proportion was highest in the long-term (≥7 months) MNT group, 60% and 61%, respectively (Figure 5).

Discussion

Research based on real-world evidence (RWE) has received increasing attention over the past decade and plays a major role in healthcare decisions, including anti-cancer treatments and MNT [19, 20]. Provided that the quality of the data is robust and transparent, the results of RWE-based research are valuable complements to randomized controlled trials for evaluating treatment effectiveness.

The nutritional status and nutrient intake of HNC patients can vary depending on a number of controllable and uncontrollable factors, and it is the responsibility of the oncology care team to change the controllable factors in a positive direction, as far as possible [15, 21]. Timely screenings (malnutrition, sarcopenia, cachexia) help identify controllable, influencing factors, and nutrition counselling, then MNT is necessary to improve nutritional status (which means that improved nutritional status has a positive effect on the outcome of the disease and survival). Nutritional counseling is needed to help and to encourage patients to comply with their nutritional support requirement, at this time dietitians can give various suggestions, such as a high-energy and high-protein diet providing adequate macro-, and micronutrients. MNT is advised

when the diet is not effective in reaching nutritional goals or if patients are unable to eat adequately (<50% of the requirement for >1 week or only 50%–75% of the requirement for >2 weeks). Enteral nutrition (EN) is recommended if oral nutrition remains inadequate despite ONS, and parenteral nutrition is recommended if EN is not sufficient or feasible [2]. Early introduction of MNT, including dietary counselling and the use of appropriate ONS with the proper daily dose and duration of therapy, are crucial for the effectiveness of the intervention [1, 2, 22, 23]. The majority of clinical research focus on early initiation and daily dosing, with length of therapy being a less researched area. In practice, there is clear evidence that the management of malnutrition in patients with chronic diseases is a continuous requirement along the patient journey and benefits of nutritional management are often only observed in the weeks and months following initiation. For cancer, no research has been done yet to investigate the relationship between the length of MNT and the expected survival in the particular types of cancer. However, for planning the duration of MNT, evidence is needed that shows, projected in months, the minimum intervention time that has a positive impact on survival.

Malnutrition is still under-diagnosed and under-treated in oncology patients, and international evidence-based research suggests that it is often prescribed as an end-of-life intervention or not used at all in oncology treatments [15, 20]. In a Hungarian study, Gallfy et al. also confirmed the above findings in a large sample population (1,616 patients) and found that 75.1% of patients would have required nutrition therapy intervention, but only 37.6% of patients received this intervention [24].

The uninterrupted duration of MNT is important in patients with cancer because achieving adequate nutritional intake is essential to support patients' nutritional status that is often challenged due to increased protein breakdown and systemic inflammation induced by the tumor [1, 2, 25, 26]. Clinical guidelines generally recommend long-term nutrition therapy for the treatment of malnutrition associated with chronic disease, but do not address the length of MNT for each disease that has been shown to have an impact on outcome or survival, probably due to the lack of good quality data [22, 23, 27, 28].

The introduction and use of prehabilitation could also help achieve long-term MNT in patients with HNC. This would allow for the identification of patients at risk before surgery and other anti-cancer treatments and the early introduction of MNT, thus prolonging the time to therapy [29–32]. Prehabilitation could also allow for intervention before the signs of malnutrition are present and prevent deterioration in nutritional status. The cancer cachexia clinical practice guideline of ESMO recommends early prophylactic/preventative nutritional intervention approach in patients planned for anticancer treatment with a high risk of inducing malnutrition (e.g., combined-modality treatments, high-dose chemotherapy, highly emetogenic agents) [1].

The authors of the present article were interested in examining the above-mentioned facts in relation to real-life data on MNT for HNC patients in Hungary, with particular reference to the frequency of MNT and the duration of therapy. Analysis of the data from the study presented in this article showed that newly diagnosed patients received MNT in only 64% of cases, which seems very inadequate considering that 80% of patients experience significant unintentional weight-loss during treatment [26, 33, 34]. This rate is even worse when looking at the persistence of MNT. There are no disease-specific guidelines on the length of MNT that should be used for each disease, but if we consider active anti-cancer treatment as the minimum nutrition therapy time for HNC patients, then MNT for at least 3 months would be necessary! Based on the analysis of the correlations in our study, it is likely that a much longer MNT would be required for a better survival in both LA and R/M HNC stages. This can be easily explained by the exclusion of early mortality from our analysis. But when we look at survival in the shorter period MNT groups, we see that patients in R/M stage show worse outcomes than LA stage. Since this is not a direct comparison, we do not know if this is a real difference, but it suggests that MNT may play an even more important role in R/M cases. Although several plausible explanations could be put forward to support these observations, these are only hypotheses generated by the data and will need to be confirmed by further studies. Another interesting finding is that the proportion of tube-fed patients is highest in the long-term (≥7 months) groups, 60% in LA and 61% in R/M cases. It cannot be directly assumed that tube feeding leads to better survival, but once the tube device is already inserted, the patients are usually fed through it, resulting in a more favorable nutritional status compared to ONS consumption. Clinical experience has shown that patients sometimes give up consuming ONS due to, for example, the narrow selection of flavors, further reducing adherence to the therapy. Procedures that can be used in everyday practice to improve ONS adherence: regular monitoring and follow up in patients with an ONS prescription, reviewing patients' acceptability and liking of the ONS they have been prescribed, and providing practical tips on how to incorporate ONS into daily life. In tube feeding adherence may be reduced by the extra care needed for the devices. In daily practice, it is observed that longer duration of MNT can be achieved with tube feeding, and this is confirmed by our research findings that the proportion of people receiving long-term nutrition therapy is higher than that of ONS users.

In conclusion, MNT is not used with sufficient frequency and duration of therapy in Hungarian HNC patients, and a correlation between long-term MNT and better overall survival was statistically demonstrated. In relation to these findings, we should mention the strengths and weaknesses of our data.

The obvious strength of our study is the robust sample size, which included a very large population with many patients. In Hungary, the most ONS and tube feeding formulas for MNT are

reimbursed by HNHIFM. The data are highly accurate and reflect real evidence, as they include data on all care provided to patients, as well as on the dispensing of prescribed, ONS and tube feeding formulas, in pharmacies.

On the other hand, our study suffers from the usual drawbacks of retrospective population-based studies, such as cancer registry analysis. We treated large groups of patients, but had little information on in-depth details and changes, such as stages, histological subgroups, or comorbidities and side effects. In order to obtain realistic results, we had to apply a number of post-processing methods to filter out statistical noise, which are described in detail in the previous sections of this article. Although these subgroupings based on overlapping criteria helped analyze the data more efficiently, they also had the potential to introduce bias. Finally, it is important to note that retrospective analyses can never establish causality with certainty.

Because of the results that significantly affect the outcome of the disease, the initial results of the research were presented in the form of an English-language poster at the ESPEN congress in 2023, and due to the great interest, the authors published the contents of the poster in the form of a short article in a Hungarian Oncology journal, in the Magyar Onkológia [35].

Conclusion

Our study has highlighted the fact that in Hungary head and neck cancer patients' medical nutrition therapy is not optimal, neither in terms of the number of patients nor in terms of the persistence of the MNT. Even allowing for possible bias in the analysis, the data suggest that adequate and sustained MNT can improve overall survival. Therefore, it is recommended to review and optimize the current practice of nutrition therapy management of HNC patients in Hungary for better treatment outcomes and longer survival.

Data availability statement

The original contributions presented in the study are included in the article/supplementary material, further inquiries can be directed to the corresponding author.

Ethics statement

The studies involving humans were approved by the Scientific and Research Ethics Committee of the Health Science Board (ETH Board TUKEB) (approval number BM/4245-1/2023) and in accordance with the Helsinki Declaration. The studies were conducted in accordance with the local legislation and institutional requirements. Written informed consent for participation was not required from the participants or the participants' legal guardians/next of kin because the data of this retrospective, analytical, cohort study was collected from electronic healthcare records from the Hungarian National Health Insurance Fund Management.

Author contributions

AM, CB, and JL were responsible for study concept and data interpretation. EP and BB contributed to the study design. CB and DR organized the database. DR performed the statistical analysis. AM and JL wrote the first draft of the manuscript. EP, BB, CB, and DR wrote sections of the manuscript. All authors contributed to the article and approved the submitted version.

Funding

The authors declare that this study received funding from Danone Hungary Kft. The funder was not involved in the study design, collection, analysis, interpretation of data, the writing of this article or the decision to submit it for publication.

Conflict of interest

AM is employed by Danone Hungary Kft. CB and DR were employed by MedicalScan Kft.

The remaining authors declare that the research was conducted in the absence of any commercial or financial relationships that could be construed as a potential conflict of interest.

References

1. Arends J, Strasser F, Gonella S, Solheim TS, Madeddu C, Ravasco P, et al. Cancer cachexia in adult patients: ESMO clinical practice guidelines. *ESMO Open* (2021) 6(3):100092. doi:10.1016/j.esmoop.2021.100092

2. Muscaritoli M, Arends J, Bachmann P, Baracos V, Barthelemy N, Bertz H, et al. ESPEN practical guideline: clinical Nutrition in cancer. *Clin Nutr* (2021) 40(5): 2898–913. doi:10.1016/j.clnu.2021.02.005

3. Seo Y, Eo W, Kim S, Shim B, Lee S. Can nutritional status predict overall survival in patients with advanced non-small cell lung cancer?. *Nutr Cancer* (2019) 71(7):1108–17. doi:10.1080/01635581.2019.1598564

4. Yu Y, Wu H, Qiu J, Ke D, Wu Y, Lin M, et al. A nutrition-related factor-based risk stratification for exploring the clinical benefits in the treatment of patients with locally advanced esophageal squamous cell carcinoma receiving definitive chemoradiotherapy: a retrospective cohort study. *Front Nutr* (2022) 9:896847. doi:10.3389/fnut.2022.896847

5. Migita K, Matsumoto S, Wakatsuki K, Ito M, Kunishige T, Nakade H, et al. A decrease in the prognostic nutritional index is associated with a worse long-term outcome in gastric cancer patients undergoing neoadjuvant chemotherapy. *Surg Today* (2017) 47(8):1018–26. doi:10.1007/s00595-017-1469-y

6. Mardas M, Madry R, Stelmach-Mardas M. Dietary intake variability in the cycle of cytotoxic chemotherapy. *Support Care Cancer* (2016) 24(6):2619–25. doi:10.1007/s00520-015-3072-3

7. Castillo-Martinez L, Castro-Eguiluz D, Copca-Mendoza ET, Perez-Camargo DA, Reyes-Torres CA, Avila EA, et al. Nutritional assessment tools for the identification of malnutrition and nutritional risk associated with cancer treatment. *Rev Invest Clin* (2018) 70(3):121–5. doi:10.24875/RIC.18002524

8. Koyama S, Tabuchi T, Okawa S, Taniyama Y, Nakata K, Morishima T, et al. Hospital volume and 5-year survival in head and neck cancer patients in Osaka, Japan. *Jpn J Clin Oncol* (2021) 51(10):1515–22. doi:10.1093/jjco/hyab132

9. Du E, Mazul AL, Farquhar D, Brennan P, Anantharaman D, Abedi-Ardekani B, et al. Long-term survival in head and neck cancer: impact of site, stage, smoking, and human papillomavirus status. *Laryngoscope* (2019) 129(11):2506–13. doi:10.1002/lary.27807

10. Guo K, Xiao W, Chen X, Zhao Z, Lin Y, Chen G. Epidemiological trends of head and neck cancer: a population-based study. *Biomed Res Int* (2021) 2021:1738932. doi:10.1155/2021/1738932

11. Golusinski P, Corry J, Poorten VV, Simo R, Sjogren E, Makitie A, et al. De-escalation studies in HPV-positive oropharyngeal cancer: how should we proceed? *Oral Oncol* (2021) 123:105620. doi:10.1016/j.oraloncology.2021.105620

12. Migliaro M, Massuh D, Infante MF, Brahm AM, San Martin MT, Ortuno D. Role of epstein-barr virus and human papilloma virus in the development of oropharyngeal cancer: a literature review. *Int J Dent* (2022) 2022:3191569. doi:10.1155/2022/3191569

13. Alterio D, Marvaso G, Ferrari A, Volpe S, Orecchia R, Jereczek-Fossa BA. Modern radiotherapy for head and neck cancer. *Semin Oncol* (2019) 46(3):233–45. doi:10.1053/j.seminoncol.2019.07.002

14. ESMO pocket gudeline. *Head and neck cancer* (2021). Available from: https://interactiveguidelines.esmo.org/esmo-web-app/toc/index.php?subjectAreaId=11&loadPdf=1 (Accessed December 26, 2023).

15. Bossi P, Delrio P, Mascheroni A, Zanetti M. The spectrum of malnutrition/cachexia/sarcopenia in oncology according to different cancer types and settings: a narrative review. *Nutrients* (2021) 13(6):1980. doi:10.3390/nu13061980

16. Cawood AL, Burden ST, Smith T, Stratton RJ. A systematic review and meta-analysis of the effects of community use of oral nutritional supplements on clinical outcomes. *Ageing Res Rev* (2023) 88:101953. doi:10.1016/j.arr.2023.101953

17. Molnar A, Csontos AA, Dako S, Hencz R, Anton DA, Palfi E, et al. Investigating the efficacy of nutrition therapy for outpatients with inflammatory bowel disease. *Orv Hetil* (2017) 158(19):731–9. doi:10.1556/650.2017.30719

18. Lovey J, Molnar A, Banky B. Long-term nutrition in patients candidate to neoadjuvant and adjuvant treatments. *Eur J Surg Oncol* (2023):106850. doi:10.1016/j.ejso.2023.02.007

19. Saesen R, Kantidakis G, Marinus A, Lacombe D, Huys I. How do cancer clinicians perceive real-world data and the evidence derived therefrom? Findings from an international survey of the European Organisation for Research and Treatment of Cancer. *Front Pharmacol* (2022) 13:969778. doi:10.3389/fphar.2022.969778

20. Caccialanza R, Goldwasser F, Marschal O, Ottery F, Schiefke I, Tilleul P, et al. Unmet needs in clinical nutrition in oncology: a multinational analysis of real-world evidence. *Ther Adv Med Oncol* (2020) 12:1758835919899852. doi:10.1177/1758835919899852

21. Martin L, Senesse P, Gioulbasanis I, Antoun S, Bozzetti F, Deans C, et al. Diagnostic criteria for the classification of cancer-associated weight loss. *J Clin Oncol* (2015) 33(1):90–9. doi:10.1200/JCO.2014.56.1894

22. Bischoff SC, Austin P, Boeykens K, Chourdakis M, Cuerda C, Jonkers-Schuitema C, et al. ESPEN practical guideline: home enteral nutrition. *Clin Nutr* (2022) 41(2):468–88. doi:10.1016/j.clnu.2021.10.018

23. Pironi L, Boeykens K, Bozzetti F, Joly F, Klek S, Lal S, et al. ESPEN practical guideline: home parenteral nutrition. *Clin Nutr* (2023) 42(3):411–30. doi:10.1016/j.clnu.2022.12.003

24. Galffy G, Molnar A, Blasszauer C, Komka I, Reibl D, Lovey J. Az alacsony testtömegindex és testtömeg csökkenés vizsgálata magyar tüdődaganatos betegek adatainak felhasználásáva. *Magy Onkol* (2022) 66(1):55–63.

25. de Oliveira Faria S, Alvim Moravia R, Howell D, Eluf Neto J. Adherence to nutritional interventions in head and neck cancer patients: a systematic scoping review of the literature. *J Hum Nutr Diet* (2021) 34(3):562–71. doi:10.1111/jhn.12848

26. Muller-Richter U, Betz C, Hartmann S, Brands RC. Nutrition management for head and neck cancer patients improves clinical outcome and survival. *Nutr Res* (2017) 48:1–8. doi:10.1016/j.nutres.2017.08.007

27. Wunderle C, Gomes F, Schuetz P, Stumpf F, Austin P, Ballesteros-Pomar MD, et al. ESPEN practical guideline: nutritional support for polymorbid medical inpatients. *Clin Nutr* (2024) 43(3):674–91. doi:10.1016/j.clnu.2024.01.008

28. Burgos R, Breton I, Cereda E, Desport JC, Dziewas R, Genton L, et al. ESPEN guideline clinical nutrition in neurology. *Clin Nutr* (2018) 37(1):354–96. doi:10.1016/j.clnu.2017.09.003

29. Cantwell LA, Fahy E, Walters ER, Patterson JM. Nutritional prehabilitation in head and neck cancer: a systematic review. *Support Care Cancer* (2022) 30(11):8831–43. doi:10.1007/s00520-022-07239-4

30. Loewen I, Jeffery CC, Rieger J, Constantinescu G. Prehabilitation in head and neck cancer patients: a literature review. *J Otolaryngol Head Neck Surg* (2021) 50(1):2. doi:10.1186/s40463-020-00486-7

31. Brady R, McSharry L, Lawson S, Regan J. The impact of dysphagia prehabilitation on swallowing outcomes post-chemoradiation therapy in head and neck cancer: a systematic review. *Eur J Cancer Care (Engl)* (2022) 31(3):e13549. doi:10.1111/ecc.13549

32. Furka A. Oncological prehabilitation. *Orv Hetil* (2022) 163(50):1975–81. doi:10.1556/650.2022.32646

33. Almada-Correia I, Neves PM, Makitie A, Ravasco P. Body composition evaluation in head and neck cancer patients: a review. *Front Oncol* (2019) 9:1112. doi:10.3389/fonc.2019.01112

34. Silver HJ, Dietrich MS, Murphy BA. Changes in body mass, energy balance, physical function, and inflammatory state in patients with locally advanced head and neck cancer treated with concurrent chemoradiation after low-dose induction chemotherapy. *Head Neck* (2007) 29(10):893–900. doi:10.1002/hed.20607

35. Belak B, Molnar A, Palfi E, Blasszauer C, Reibl D, Lovey J. Effect of long-term medical nutrition therapy on the survival of head and neck cancer patients - based on real-world data. *Magy Onkol* (2023) 67(4):341–4.

Pathology & Oncology Research | frontiers

TYPE Hypothesis & Theory
PUBLISHED 28 March 2023
DOI 10.3389/pore.2023.1610960

Check for updates

OPEN ACCESS

EDITED BY
Anna Sebestyén,
Semmelweis University, Hungary

*CORRESPONDENCE
Feng Wang,
wangfeng5024@126.com

†These authors have contributed equally to this work

RECEIVED 21 November 2022
ACCEPTED 06 March 2023
PUBLISHED 28 March 2023

CITATION
Chen H, Shi X, Ren L, Wan Y, Zhuo H, Zeng L, SangDan W and Wang F (2023), Screening of core genes and prediction of ceRNA regulation mechanism of circRNAs in nasopharyngeal carcinoma by bioinformatics analysis.
Pathol. Oncol. Res. 29:1610960.
doi: 10.3389/pore.2023.1610960

COPYRIGHT
© 2023 Chen, Shi, Ren, Wan, Zhuo, Zeng, SangDan and Wang. This is an open-access article distributed under the terms of the Creative Commons Attribution License (CC BY). The use, distribution or reproduction in other forums is permitted, provided the original author(s) and the copyright owner(s) are credited and that the original publication in this journal is cited, in accordance with accepted academic practice. No use, distribution or reproduction is permitted which does not comply with these terms.

Screening of core genes and prediction of ceRNA regulation mechanism of circRNAs in nasopharyngeal carcinoma by bioinformatics analysis

HongMin Chen[1†], XiaoXiao Shi[2†], Li Ren[3], YuMing Wan[1], HongYu Zhuo[1], Li Zeng[1], WangMu SangDan[4] and Feng Wang[1*]

[1]Department of Medical Oncology, Cancer Center, West China Hospital, West China, Medical School, Sichuan University, Sichuan, China, [2]Department of Medical Oncology, Chengdu Shangjin Nanfu Hospital, West China Hospital, Sichuan University, Chengdu, China, [3]Department of Thoracic Oncology, Cancer Center, West China Hospital, Sichuan University, Chengdu, China, [4]Department of Oncology, People's Hospital of Tibet Autonomous Region, Lhasa, China

Background: Nasopharyngeal carcinoma (NPC) represents a highly aggressive malignant tumor. Competing endogenous RNAs (ceRNA) regulation is a common regulatory mechanism in tumors. The ceRNA network links the functions between mRNAs and ncRNAs, thus playing an important regulatory role in diseases. This study screened the potential key genes in NPC and predicted regulatory mechanisms using bioinformatics analysis.

Methods: The merged microarray data of three NPC-related mRNA expression microarrays from the Gene Expression Omnibus (GEO) database and the expression data of tumor samples or normal samples from the nasopharynx and tonsil in The Cancer Genome Atlas (TCGA) database were both subjected to differential analysis and Weighted Gene Co-expression Network Analysis (WGCNA). The results from two different databases were intersected with WGCNA results to obtain potential regulatory genes in NPC, followed by Gene Ontology (GO) and Kyoto Encyclopedia of Genes and Genomes (KEGG) functional enrichment analyses. The hub-gene in candidate genes was discerned through Protein-Protein Interaction (PPI) analysis and its upstream regulatory mechanism was predicted by miRwalk and circbank databases.

Results: Totally 68 upregulated genes and 96 downregulated genes in NPC were screened through GEO and TCGA. According to WGCNA, the NPC-related modules were screened from GEO and TCGA analysis results, and the genes in the modules were obtained. After the results of differential analysis and WGCNA were intersected, 74 differentially expressed candidate genes associated with NPC were discerned. Finally, fibronectin 1 (FN1) was identified as a hub-gene in NPC. Prediction of upstream regulatory mechanisms of FN1 suggested that FN1 may be regulated by ceRNA mechanisms involving multiple circRNAs, thereby influencing NPC progression through ceRNA regulation.

Conclusion: FN1 is identified as a key regulator in NPC development and is likely to be regulated by numerous circRNA-mediated ceRNA mechanisms.

KEYWORDS

TCGA, nasopharyngeal carcinoma, weighted gene co-expression network analysis, GEO database, fibronectin 1

Introduction

Nasopharyngeal carcinoma (NPC) is a dominantly prevailing malignant tumor originating from the nasopharyngeal mucosal lining, and the tumor primarily occurs at the pharyngeal recess (1). In 2020, NPC contributes to approximately 133,000 new cases and 80,000 deaths worldwide (2). The 10-year survival rate can reach 98% for stage I NPC patients and 60% for stage II patients, but the median survival is merely 3 years for advanced stages (3). Due to the deep tumor location and absence of obvious clinical manifestations at the early stage, most patients have already advanced to the middle and late stages when diagnosed (4). Despite major advances in modern medicine, NPC remains one of the most difficult tumor types to distinguish and treat (5). At present, the potential modes and mechanisms of NPC development are still unclear. This underscores the need for identifying the molecular mechanisms underlying NPC initiation and development to efficiently diagnose and treat patients.

The functional screening of core genes contributing to cancer progression and structural characterization of cancer genomes provide novel and complementary insights into the essential molecular mechanisms and pathways behind diverse cancer types, which is of great value for the development of personalized therapies (6). Growing evidence unveils the involvement of numerous abnormally expressed non-coding RNAs in the initiation and progression of NPC (7, 8). Dysregulated circRNAs can act as tumor suppressors or oncogenes, controlling cell proliferation, migration, apoptosis, and tumor metastasis (9, 10), highlighting the imperative function of circRNAs in mediating carcinogenesis. Intrinsically, circRNA can exert vital roles as a competitive endovascular RNA (ceRNA) or protein-coding RNA, or interact with RNA-binding proteins to regulate tumor development and gene expression (11, 12). Nevertheless, the research on circRNAs related to NPC development is still scarce, and their potential mechanisms need to be clarified further.

Recently, with the development of molecular biotechnology, bioinformatics analysis has played a key role in screening tumor candidate biomarkers, providing a new direction for the study and prediction of tumor pathogenesis including NPC (13). For instance, Zhu et al. revealed in their work that curcumin can enhance NPC cell sensitivity to radiotherapy by mediating the ceRNA mechanism based on bioinformatics analysis (14). Zhang et al. identified several microRNAs (miRNAs) with potential as prognostic markers for NPC through miRNA microarrays and bioinformatics screening (15). Although researchers have conducted numerous studies on NPC, the core genes related to NPC and their regulatory mechanisms are still poorly understood. Therefore, we aimed to identify the hub-gene in NPC by performing the integrative analysis of Gene Expression Omnibus (GEO) and The Cancer Genome Atlas (TCGA) datasets as well as differential analysis and functional enrichment analysis of NPC-associated genes, so as to provide a new direction for comprehensively understanding the pathogenesis and potential regulatory mechanisms of NPC.

Materials and methods

GEO data acquisition and difference analysis

The NPC-related mRNA expression microarrays GSE13597, GSE34573, and GSE53819 (16–18) were downloaded from the GEO database. Among them, GSE13597 included 3 normal samples and 25 tumor samples, GSE34573 included 4 normal samples and 16 tumor samples, and GSE53819 included 18 normal samples and 18 tumor samples. All data were downloaded from the microarray expression data in GEO database. During gene annotation, if a gene corresponded to multiple probes, the average expression value of these probes was selected as the expression value of the gene. The R language "limma" package and "sva" package (19–21) were adopted to merge and batch-correct the data from the three chips (19), and an empirical Bayes framework was used to adjust for batch effects. Subsequently, with normal samples as the controls, differential analysis was performed using the "limma" package, and *p*-value was corrected using the false discovery rate (FDR) method, with $|logFC| > 1$ and adj. p.value <0.05 as the criteria to screen differentially expressed genes (DEGs). Meanwhile, the NPC-related miRNA expression microarray GSE70970 was obtained from GEO, which included 17 normal samples and 246 normal samples, and then the microarray was differentially analyzed using the "limma" package.

TCGA data acquisition and difference analysis

The expression data of NPC-related genes were downloaded from the TCGA GDC database. Specifically, only tumor sample expression data and normal sample expression data of selected nasopharyngeal tissues (including

the pharynx and tonsil) were downloaded. Subsequently, differential analysis was performed using the R language "limma" package and "edgeR" package (22–24), and normal samples were used as controls. The FDR method was utilized to correct the differential *p*-value, with |logFC| > 1 and adj.p.value <0.05 as screening criteria.

Weighted gene co-expression network analysis (WGCNA) analysis

The combined GEO gene expression data and TCGA data were analyzed by WGCNA using the R language "WGCNA" package (25), respectively. In brief, genes were divided into modules of different colors by analyzing the association between genes. The genes showing no association with other genes were classified into the gray module (a meaningless module). The module was recognized by dynamic clipping, the minimum number of genes in the module was set to 50, and the recommended soft threshold was automatically calculated by the soft threshold selection program. The similarity between modules was calculated based on eigengenes of modules using the cor function in R language, and the genes with high similarity were merged. Thereafter, the correlation between merged modules and sample phenotype was analyzed.

Functional enrichment analysis of candidate genes

Gene Ontology (GO) and Kyoto Encyclopedia of Genes and Genomes (KEGG) functional enrichment analyses of identified candidate genes were performed using "clusterprofile," "org.Hs.eg.db," "enrichplot," and "ggplot2" packages. Meanwhile, the functional enrichment bubble diagram was drawn. The *p*-value <0.05 indicated significant enrichment.

Protein-protein interaction (PPI) analysis

The interaction analysis of candidate genes was performed through the STRING database (https://cn.string-db.org/), and the gene interaction network was constructed using cytoscapev3.9.1. The degree value of each gene was calculated to obtain the hub-gene in the gene interaction network.

Prediction of upstream regulatory mechanisms of candidate genes

The upstream miRNAs of candidate genes were predicted using miRwalk database (http://mirwalk.umm.uni-heidelberg.de/), and the miRNA-mRNA regulatory network was mapped using cytoscape v3.8.1. The circRNA-miRNA regulation data were downloaded from the circBank database (http://www.circbank.cn/index.html), and the data with a prediction score greater than 500 points were retained for the subsequent prediction of the upstream circRNAs of candidate miRNAs. Subsequently, the circRNA-miRNA-mRNA regulation network diagram was drawn using "ggplot2," "ggalluvial," and "RColorBrewer" packages.

Results

Screening of DEGs in NPC

NPC-related expression microarrays GSE13597, GSE34573, and GSE53819 from the GEO database were merged, and the combined data were corrected in batch. Through differential analysis of integrated NPC gene expression data, 921 significant DEGs were identified, of which 431 genes were upregulated and 490 genes were downregulated in NPC samples (Figures 1A, B; Supplementary Table S1). Subsequently, the gene expression data of tumor samples and normal samples from selected tissues (such as the nasopharynx) were downloaded from TCGA database and then differentially analyzed. Consequently, 622 significant DEGs in NPC samples were discerned. Among them, 210 genes were highly expressed and 412 genes were weakly expressed in NPC samples (Figures 1C, D; Supplementary Table S2). To further screen genes that may exert an imperative regulatory role in NPC, the DEGs from GEO database and TCGA database were intersected. The upregulated genes in tumors from GEO analysis were intersected with upregulated genes in tumors from TCGA analysis (Figure 1E), and then 68 genes were identified to be highly expressed in both sets of tumor data, which may have the function of promoting tumorigenesis. Similarly, an intersection of significantly under-expressed genes in NPC (Figure 1F) identified 96 weakly expressed genes in both sets of tumor data, which may have the ability to inhibit tumor development.

Sample clustering and power value selection in WGCNA

Through WGCNA, genes could be grouped and divided into multiple different modules to understand the correlation between genes and clinical traits. The integrated GEO data and TCGA data were subjected to outlier detection of samples using the "WGCNA" package in R language (Figures 2A, C), and there were no obvious outliers. All samples were retained for subsequent analyses. In an attempt to identify gene modules

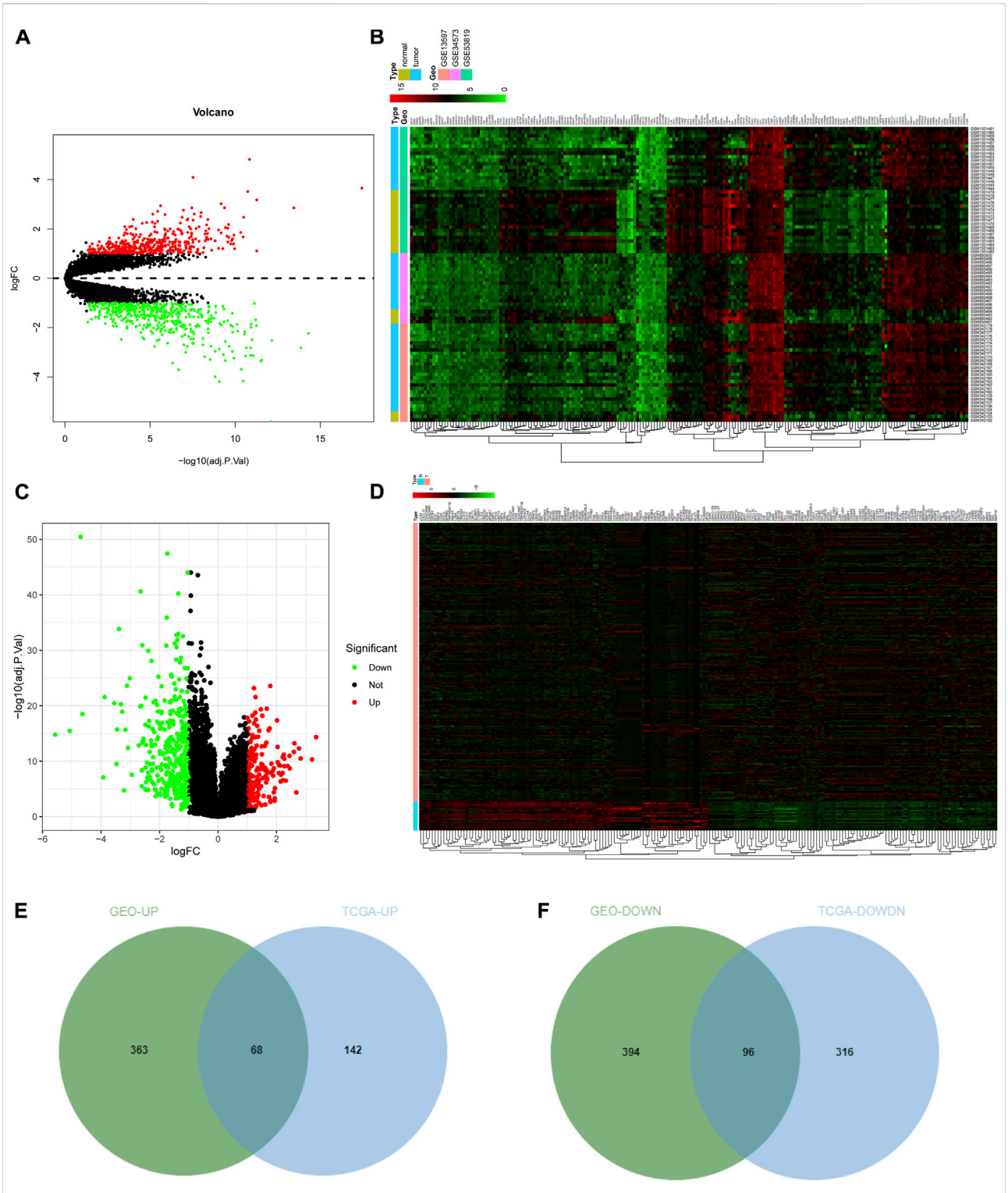

FIGURE 1
Screening of DEGs. **(A)** Volcano plot of DEGs in GEO database. The abscissa indicated the logFC, the ordinate indicated the −log10 (adj.p.val), red dots in the plot indicated significantly upregulated genes, and green dots indicated significantly downregulated genes in tumor samples; **(B)** Heat map of the top 100 significant DEGs in GEO. The abscissa represented the sample number, the ordinate represented the gene name, and the histogram in the upper right represented the color scale. **(C,D)** Volcano plot and heat map of DEGs from TCGA NPC dataset; **(E,F)** The intersection of significantly upregulated genes **(E)** or the intersection of significantly downregulated genes **(F)** from GEO and TCGA NPC datasets, respectively. The middle part indicated the intersection of the two datasets.

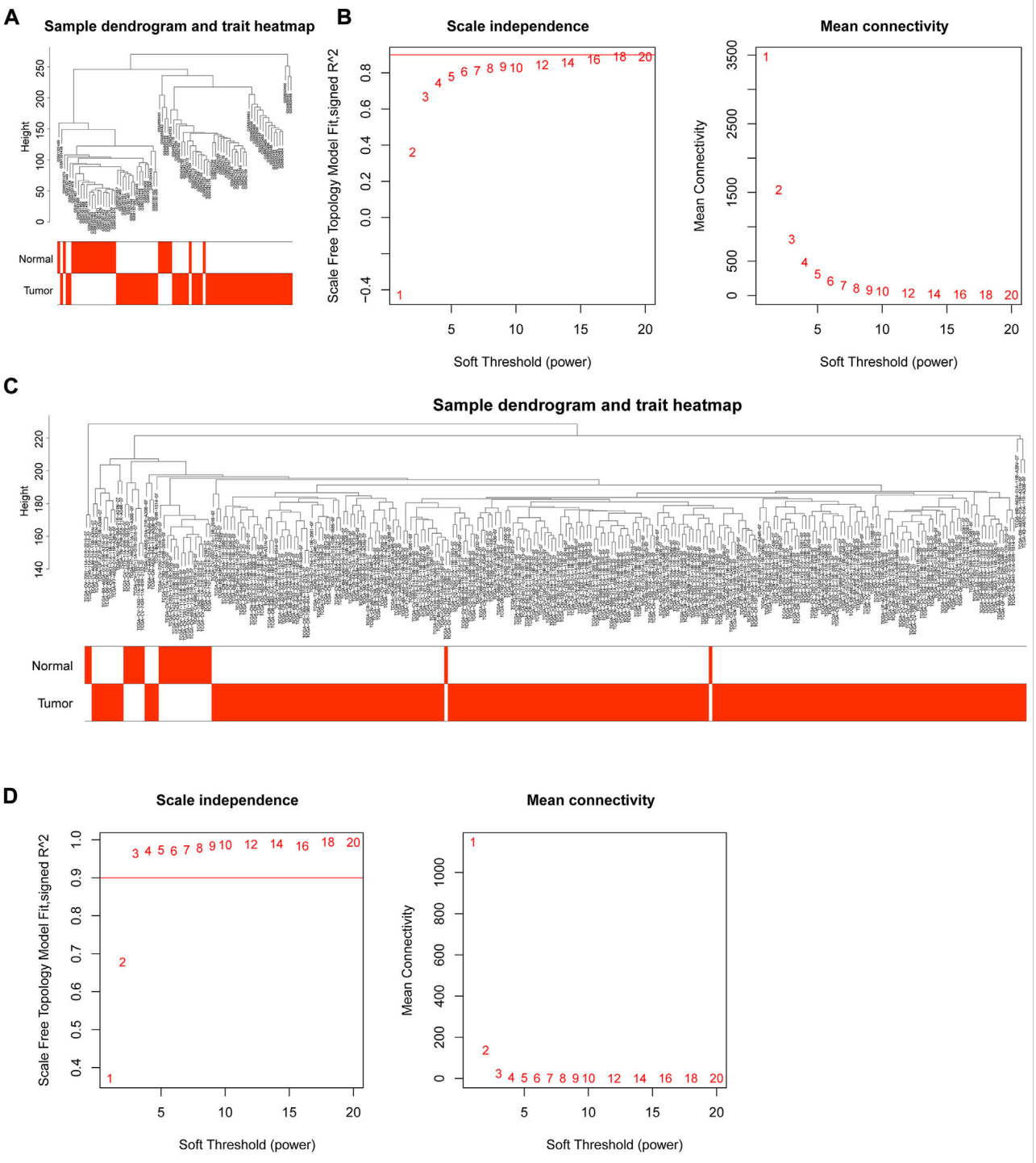

FIGURE 2
WGCNA of GEO and TCGA data. **(A)** Outlier detection of GEO samples; **(B)** Network topology for different soft threshold powers. The number indicated the corresponding soft threshold power. When soft threshold was 14, approximate scale-free topology could be obtained, indicating that this value was effective for gene partition; **(C)** Outlier detection of TCGA samples; **(D)** Screening of soft thresholds in TCGA data. The approximate scale-free topology could be acquired when soft threshold was 3.

associated with NPC, GEO and TCGA data module classifications were subjected to screening of soft thresholds, which showed that the optimal soft threshold was 14 in GEO data and the optimal soft threshold was 3 in TCGA data (Figures 2B, D). These two soft thresholds were chosen for subsequent gene module partition.

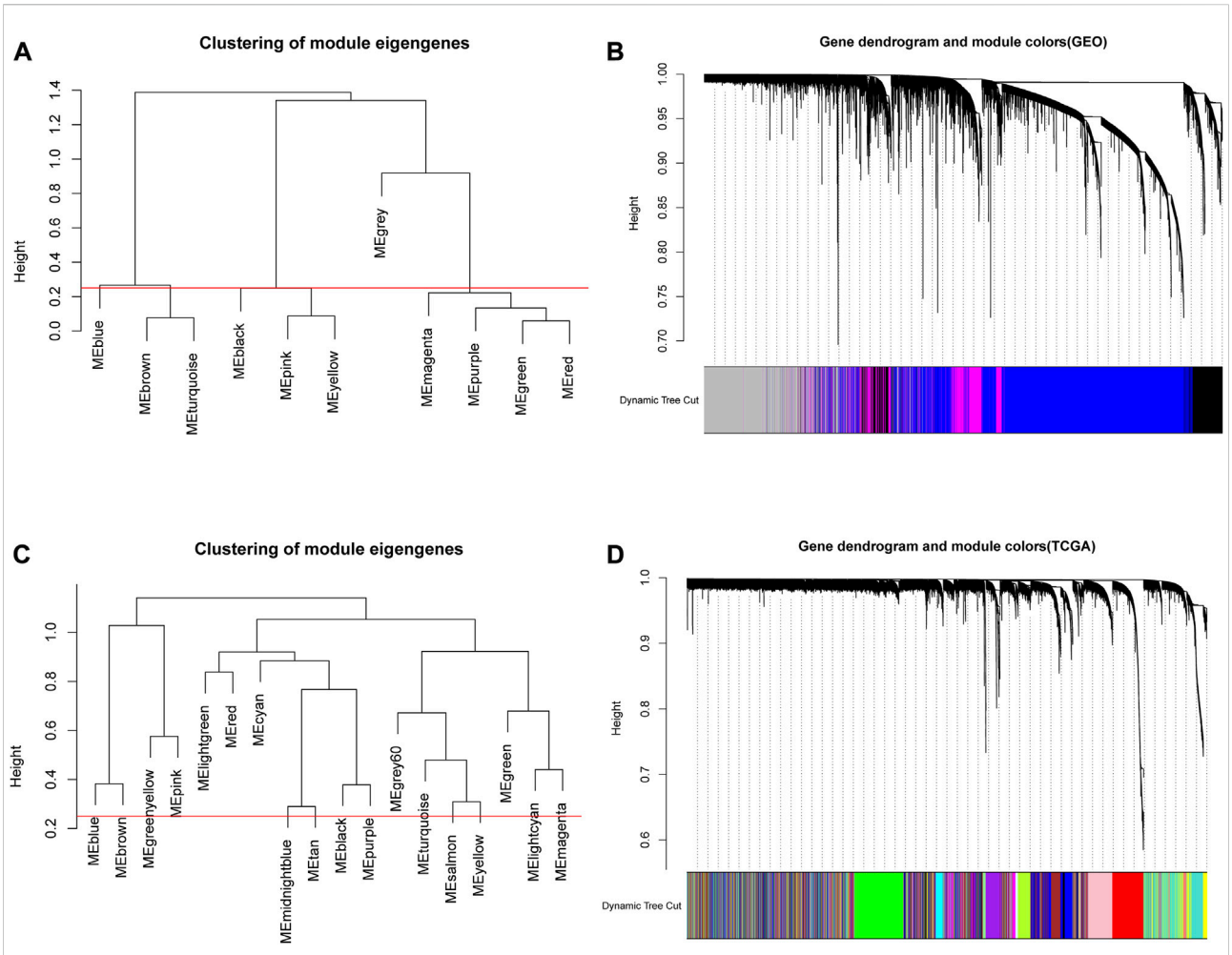

FIGURE 3
Module clustering in WGCNA. **(A,C)** The correlation analysis of modules prior to the merging of GEO and TCGA data. The ordinate indicated the similarity between modules and the low value indicated high similarity. Red lines indicated the shear height and 0.25 was selected as the shear height in this study (i.e., modules with similarity above 0.75 were merged); **(B,D)** Gene dendrogram of genes in corresponding modules in GEO and TCGA databases.

Module clustering in WGCNA

Based on the above analysis, the appropriate soft thresholds were selected for module partition of genes in GEO and TCGA data, respectively. The modules with similarity greater than 0.5 were merged, where gray modules were non-sense modules and genes in this module were mutually unrelated genes. In GEO data, a total of 11 gene modules of different colors were obtained (Figure 3A), and 4 modules of different colors were retained after merging (Figure 3B). Through the same approach, the genes in TCGA were subjected to module partition. A total of 18 gene modules with different colors were obtained (Figure 3C), and 18 modules with different colors remained after merging (Figure 3D).

Correlation analysis of WGCNA modules

After gene module partition, further clinical correlation analysis was performed on the WGCNA results of GEO data and TCGA data, respectively. In GEO analysis results, the correlation analysis between 4 gene modules and clinical traits revealed that the blue module was prominently positively correlated with tumors (Figure 4A; Supplementary Table S3), which implied that the genes in the blue module may promote tumor development. Based on the TCGA database, the black module and purple module were negatively correlated with the occurrence of tumors (Figure 4B; Supplementary Tables S4, S5), which indicated that the genes in these two modules may confer an inhibitory effect on the occurrence and development of tumors.

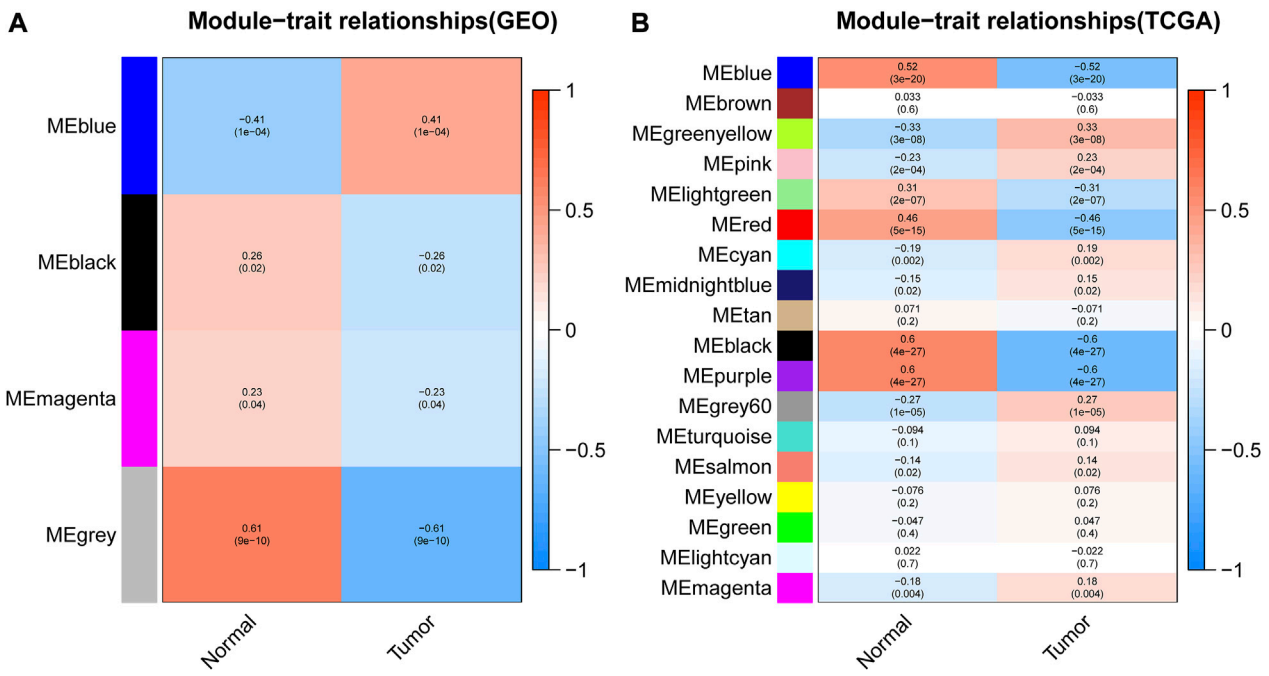

FIGURE 4
Correlation analysis between modules and clinical traits. **(A,B)** represented the correlation analysis between the modules obtained from the WGCNA analysis of GEO data or TCGA data with sample traits, respectively. The abscissa represented the trait type and different colors represented different correlations and *p* values.

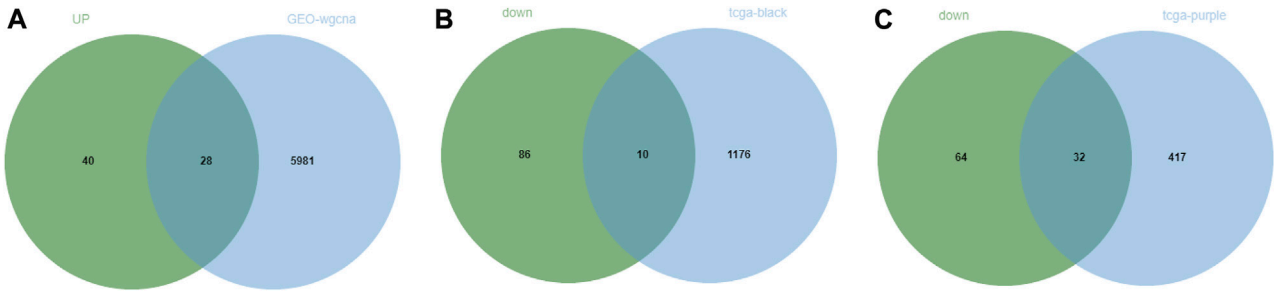

FIGURE 5
Screening of candidate genes in NPC. **(A)** The intersection between significantly highly expressed genes in NPC obtained from GEO database or TCGA database with genes in the module significantly positively correlated with tumor obtained by WGCNA of GEO data; **(B,C)** The intersection between significantly lowly expressed genes in NPC obtained from GEO database or TCGA database with genes in two modules significantly negatively correlated with tumor obtained by WGCNA of TCGA data.

Screening of candidate genes in NPC

Through the above differential analysis, 68 genes that were highly expressed in tumors were identified, which may have potential promoting effects on tumor development. Meanwhile, based on WGCNA, we found that the genes in the blue module may also have a tumor-promoting effect. Thereafter, an intersection of these two sets of genes was taken (Figure 5A) and consequently 32 candidate genes were identified, which may be crucial contributing factors to tumor development. Similarly, the 96 genes with significantly low expression in tumors were respectively intersected with genes in the two modules that were significantly negatively correlated with tumors obtained by WGCNA (Figures 5B, C), and finally, 10 and 32 candidate genes were discerned, respectively. These 42 genes may be suppressors of tumor development. In summary, we identified

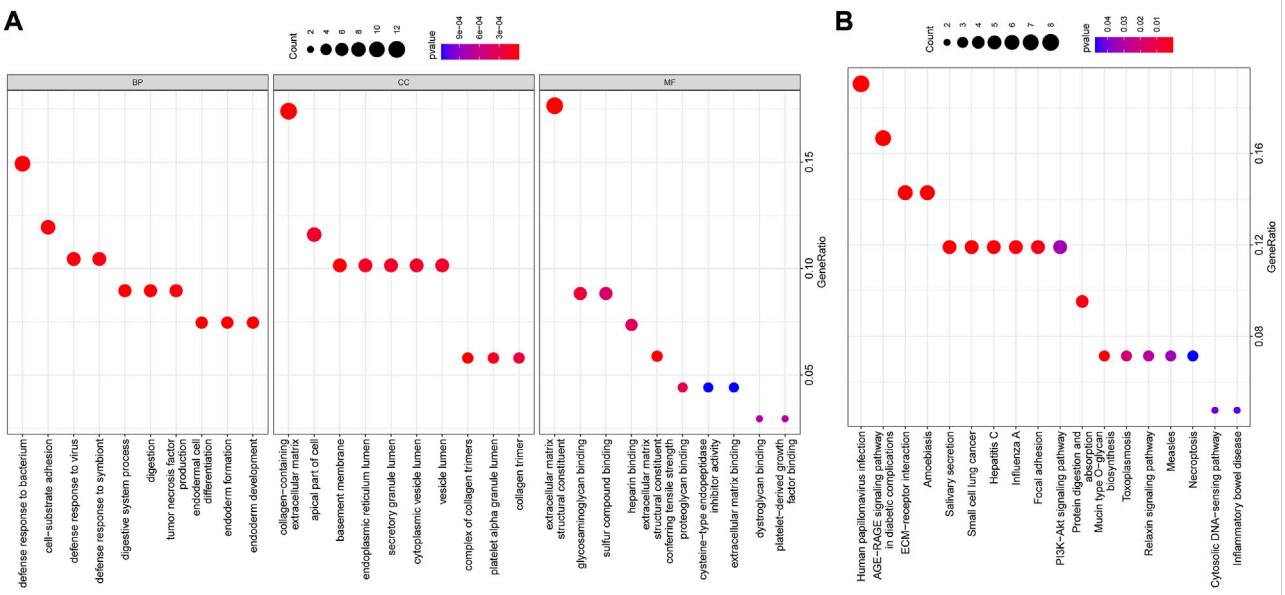

FIGURE 6
(A,B) GO and KEGG functional enrichment analyses of candidate genes. The abscissa indicated the GenerRatio, the ordinate indicated the functional item, circle size indicated the number of enriched genes, color indicated the enrichment p-value, and left histogram indicated the color scale.

74 DEGs (32 tumor-promoting genes and 42 tumor-suppressive genes) that were extensively associated with NPC as candidate genes.

Enrichment analysis

GO and KEGG functional enrichment analyses were further performed on the above 74 candidate genes. GO functional enrichment analysis revealed that these genes were enriched in relevant items such as "defense response to bacterium," "collagen-containing extracellular matrix," and "extracellular matrix structural constituent" (Figure 6A), indicating the underlying role of these functional items in NPC progression. KEGG pathway enrichment analysis unveiled that these genes were mainly enriched in related signaling pathways such as "human papillomavirus (HPV) infection" and "advanced glycation endproduct (AGE)-receptor for AGE (RAGE) signaling pathway in diabetic complications" (Figure 6B), suggesting that these signaling pathways may be one of the reasons for the development of NPC.

PPI analysis

To further screen potential regulatory genes in NPC, 74 candidate genes were subjected to interaction analysis, and a gene interaction network was constructed (Figure 7A). The interaction between genes was also analyzed to obtain the degree value of each gene (Figure 7B). The results revealed that the degree values of the genes in the top 10° values were all ≥8, indicating that there may be an interactive relationship between these 10 genes and at least 8 other genes. Importantly, the degree value of fibronectin 1 (FN1) was the largest, indicating that FN1 was the core in the gene interaction network and a hub-gene among these candidate genes. Therefore, FN1 may exert a crucial role in the development of NPC.

ceRNA prediction of FN1 gene

The differential expression of the identified hub-gene FN1 from GEO and TCGA was retrieved (Table 1), which revealed that FN1 was significantly upregulated in tumor samples. Meanwhile, a NPC-related miRNA expression microarray GSE70970 was acquired from GEO database. Differential analysis of miRNA expression in this microarray identified 29 upregulated miRNAs and 52 downregulated miRNAs in NPC (Figure 8A; Supplementary Table S6). Subsequently, the upstream miRNAs of FN1 were predicted, and the results were intersected with the significantly downregulated miRNAs in the microarray (Figure 8B), thus screening 5 potential upstream regulatory miRNAs. Further upstream circRNAs of the 5 miRNAs were predicted, 4 of which were involved in circRNA-mediated ceRNA regulation, and 60 potentially

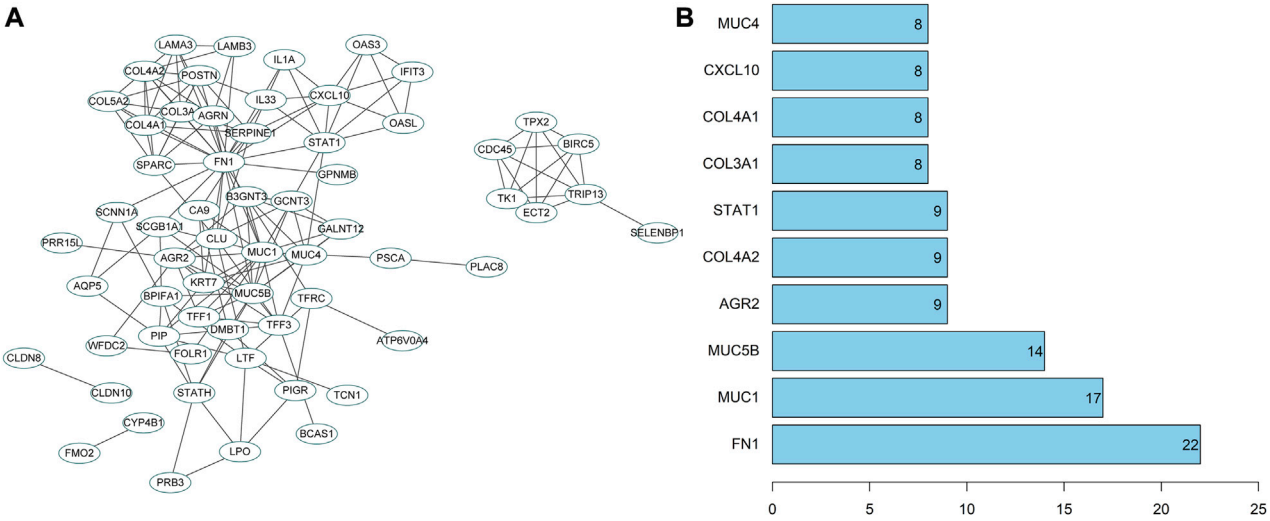

FIGURE 7
PPI analysis of candidate genes. **(A)** The interaction analysis of candidate genes. Each ellipse represented a gene, and the line between genes indicated the presence of interaction relation between genes; **(B)** The degree value of the top 10 genes. The abscissa represented the degree value, and the ordinate represented the gene name.

TABLE 1 Differential expression of the hub-gene.

Symbol	GEO-logFC	GEO-adjp	TCGA-logFC	TCGA-adjp
FN1	2.35	2.96E-08	2.14	4.57E-07

regulatory circRNAs were identified (Figure 8C; Supplementary Table S7), which meant that FN1 was very likely regulated by multiple circRNA-mediated ceRNA mechanisms, thus affecting the progression of NPC.

Discussion

NPC is chiefly characterized by recurrence and distant metastasis, making it an extremely life-threatening cancer worldwide (26). To make matters worse, NPC is difficult to identify and treat clinically because of early non-specific symptoms (27–29). Therefore, a better understanding of the mechanisms of NPC occurrence and progression and the identification of reliable markers of NPC are essential for the clinical diagnosis and treatment of NPC. In this study, we integrated three NPC-related microarrays from GEO database and retrieved the NPC samples included in TCGA. Subsequently, differential analysis and WGCNA of the obtained gene expression data were conducted to identify crucial genes associated with NPC, and their potential regulatory mechanisms were also preliminarily predicted.

It is noteworthy that increased oncogene expression and decreased tumor suppressor gene expression are indeed key factors in tumorigenesis (30). With the development of sequencing technology and chip technology, we can easily screen the expression levels of thousands of genes in the human genome simultaneously (30). In particular, WGCNA is an effective method for gene grouping through gene co-expression relationships to understand the association between genes and clinical traits (25), which is utilized to identify core modules and hub-genes associated with diabetic nephropathy (31) and breast cancer (32). In our current study, through differential analysis and WGCNA of NPC-related gene expression from GEO and TCGA datasets, 74 candidate genes were screened.

Furthermore, according to GO analysis, these genes unleashed crucial roles in extracellular matrix structural constituent, collagen-containing extracellular matrix, and defense response to bacterium. The extracellular matrix, composed of intercellular substance and basement membrane, functions as an essential tissue barrier for carcinoma metastasis, and cancer cells can degrade the matrix through secretion or activation of protein-degrading enzymes following their surface receptors' adhesion to various components of extracellular matrix, thus constituting channels for metastasis (33). Prior evidence has indicated a distinct change in the extracellular matrix remodeling pathway in NPC tissues (34). On the other hand, KEGG pathway enrichment analysis of these candidate genes showed that the main enriched pathways included the HPV infection and AGE-RAGE signaling pathway in diabetic complications. Viral infections, in particular HPV and Epstein-Barr virus (EBV), are considered crucial etiological agents for NPC

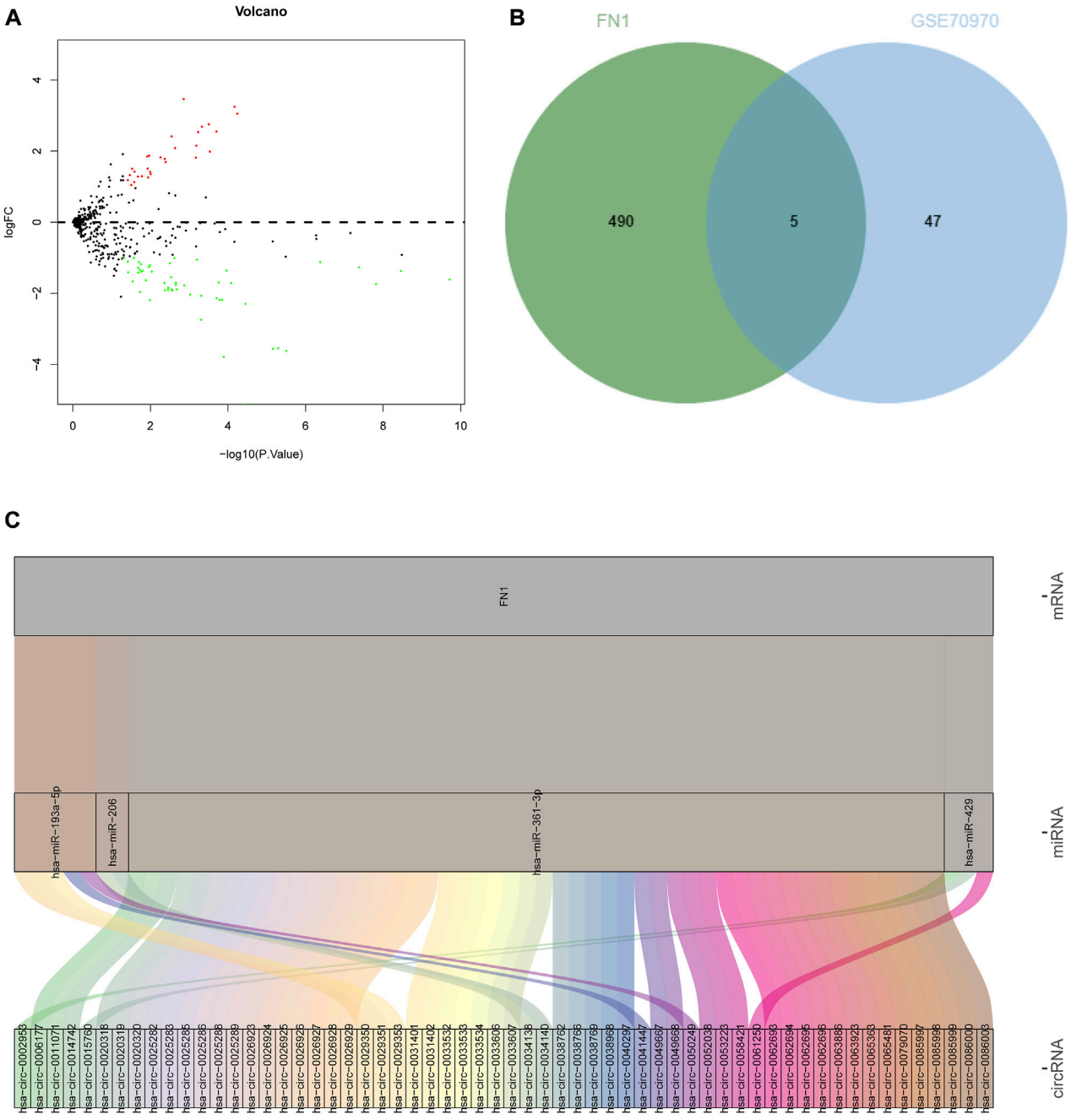

FIGURE 8
Prediction of upstream ceRNA mechanisms of the hub-gene. **(A)** Volcano plot of NPC-related miRNA microarray; **(B)** The intersection of the predicted upstream miRNAs of the hub-gene and significantly differentially expressed miRNAs in the microarray. The middle part indicated the intersection of the two groups of data; **(C)** Prediction of upstream circRNAs of the hub-gene. The leftmost part represented the circRNA, the middle represented the miRNA, the right represented the mRNA, and the line between the three represented a predicted regulatory relationship between them.

development, and HPV infection rate in NPC has been reported to range from 9% to 52.9%, largely depending on the geographic distribution and ethnicity of the population and viral detection methods (35). It is interesting to note that patients with HPV-positive NPC are afflicted by larger primary tumors and greater local symptoms than those with EBV-positive NPC (36). The

interaction between S100P and RAGE potentiates C666-1 cell proliferation and migration, and S100P-RAGE blockade is a potential therapeutic modality for NPC (37, 38). Therefore, GO and KEGG analyses can greatly help identify cellular components, molecular functions, biological processes, and crucial pathways underlying the occurrence and progression of NPC.

Further PPI analysis of 74 candidate genes revealed that the FN1 gene occupied a core position in the gene interaction network. FN1 is a glycoprotein that upregulates expression levels of matrix metalloproteinases to promote cancer cell local invasion and distant metastasis, and its overexpression in NPC is closely related to an advanced stage and poor survival (39). Of note, upregulation of FN1 impedes apoptosis by activating the NF-κB pathway and is also involved in facilitating proliferation, invasion, migration, and epithelial-mesenchymal transition in NPC cells (40, 41). These existing studies have further confirmed the role of FN1 as a hub gene in NPC.

The interaction between circRNAs and miRNAs has significant influences on key genes, thus disturbing the development of cancer (42, 43). Recently, the roles of various non-coding RNAs in mediating diverse biological pathways and functions in NPC have been extensively documented (44). Compelling evidence has revealed that circRNAs intrinsically mediate tumorigenesis and tumor cell proliferation and migration by competitively binding to miRNAs, thus participating in the pathogenesis of NPC (45, 46). Intriguingly, evidence suggests that FN1 serves as a direct transcriptional target of multiple miRNAs in tumors and circ0081534 has been pointed out to exert tumor oncogenic functions by manipulating the miR-508-5p/FN1 axis in NPC (47). Elevation of miR-9-3p suppresses the malignant behaviors of NPC cells by downregulating FN1 (40). Therefore, the potential upstream regulatory mechanisms of FN1 were predicted subsequently to provide a new research direction and theoretical basis for further understanding the detailed mechanisms of FN1 in NPC.

Although FN1 was previously studied in NPC, we further clarified the role and function of FN1 in the regulation of NPC through a comprehensive analysis of large NPC data from GEO and TCGA in this study. In addition, the detailed regulatory mechanism of FN1 in NPC was poorly studied. In this study, through differential analysis and WGCNA analysis of NPC-related gene expression, FN1 was finally identified as a possible key regulator in NPC. Meanwhile, the ceRNA axis controlled by multiple circRNAs and miRNAs upstream of FN1 was uncovered. This study provides a new research direction and theoretical references for further understanding the detailed mechanism of FN1 in NPC. Nevertheless, the selected microarray dataset is limited, probably leading to low statistical power and the identification of hub genes merely through bioinformatics is insufficient, and where FN1 is expressed in cells and its association with viruses are elusive. Additionally, the main finding of our study lacks clinically relevant information. The expression and function of FN1 in NPC warrant further experimental verification. It is of utmost importance to further delve into the mechanism of FN1 at the molecular, cellular, and biological levels by conducting molecular biological experiments. Additionally, other potential hub genes are worth exploring for the optimal management of NPC.

Conclusion

The FN1 gene was screened as a hub-gene by downloading NPC data from GEO and TCGA datasets and using WGCNA analysis and functional enrichment analysis. FN1 gene may be a key regulator in NPC development and regulated by ceRNA mechanisms involving multiple different circRNAs.

Data availability statement

The raw data supporting the conclusion of this article will be made available by the authors, without undue reservation.

Author contributions

HC is the guarantor of integrity of the entire study; XS, FW, and HZ contributed to the study concepts, study design, and definition of intellectual content; YW contributed to the literature research; XS contributed to the manuscript preparation; HC and FW contributed to the manuscript editing and review; HC and FW contributed to the clinical studies; HC, FW, and LZ contributed to the experimental studies and data acquisition; HC, LR, and WS contributed to the data analysis and statistical analysis. All authors read and approved the final manuscript.

Conflict of interest

The authors declare that the research was conducted in the absence of any commercial or financial relationships that could be construed as a potential conflict of interest.

Supplementary material

The Supplementary Material for this article can be found online at: https://www.por-journal.com/articles/10.3389/pore.2023.1610960/full#supplementary-material

References

1. Chen YP, Chan ATC, Le QT, Blanchard P, Sun Y, Ma J. Nasopharyngeal carcinoma. *Lancet* (2019) 394(10192):64–80. doi:10.1016/S0140-6736(19)30956-0

2. Sung H, Ferlay J, Siegel RL, Laversanne M, Soerjomataram I, Jemal A, et al. Global cancer statistics 2020: GLOBOCAN estimates of incidence and mortality worldwide for 36 cancers in 185 countries. *CA Cancer J Clin* (2021) 71(3):209–49. doi:10.3322/caac.21660

3. Wu L, Li C, Pan L. Nasopharyngeal carcinoma: A review of current updates. *Exp Ther Med* (2018) 15(4):3687–92. doi:10.3892/etm.2018.5878

4. Engku Nur Syafirah EAR, Irekeola AA, Yean Yean C. Diagnostic and prognostic indications of nasopharyngeal carcinoma. *Diagnostics (Basel)* (2020) 10(9):611. doi:10.3390/diagnostics10090611

5. Bruce JP, Yip K, Bratman SV, Ito E, Liu FF. Nasopharyngeal cancer: Molecular landscape. *J Clin Oncol* (2015) 33(29):3346–55. doi:10.1200/JCO.2015.60.7846

6. Tang J, Aittokallio T. Network pharmacology strategies toward multi-target anticancer therapies: From computational models to experimental design principles. *Curr Pharm Des* (2014) 20(1):23–36. doi:10.2174/13816128113199990470

7. Lee KT, Tan JK, Lam AK, Gan SY. MicroRNAs serving as potential biomarkers and therapeutic targets in nasopharyngeal carcinoma: A critical review. *Crit Rev Oncol Hematol* (2016) 103:1–9. doi:10.1016/j.critrevonc.2016.04.006

8. Wang H, Wang W, Fan S. Emerging roles of lncRNA in Nasopharyngeal Carcinoma and therapeutic opportunities. *Int J Biol Sci* (2022) 18(7):2714–28. doi:10.7150/ijbs.70292

9. Patop IL, Kadener S. circRNAs in Cancer. *Curr Opin Genet Dev* (2018) 48: 121–7. doi:10.1016/j.gde.2017.11.007

10. Yang M, Huang W. Circular RNAs in nasopharyngeal carcinoma. *Clin Chim Acta* (2020) 508:240–8. doi:10.1016/j.cca.2020.05.029

11. Chen N, Zhao G, Yan X, Lv Z, Yin H, Zhang S, et al. A novel FLI1 exonic circular RNA promotes metastasis in breast cancer by coordinately regulating TET1 and DNMT1. *Genome Biol* (2018) 19(1):218. doi:10.1186/s13059-018-1594-y

12. Greene JM, Larin Z, Taylor IC, Prentice H, Gwinn KA, Kingston RE. Multiple basal elements of a human hsp70 promoter function differently in human and rodent cell lines. *Mol Cel Biol* (1987) 7(10):3646–55. doi:10.1128/mcb.7.10.3646

13. Ye Z, Wang F, Yan F, Wang L, Li B, Liu T, et al. Bioinformatic identification of candidate biomarkers and related transcription factors in nasopharyngeal carcinoma. *World J Surg Oncol* (2019) 17(1):60. doi:10.1186/s12957-019-1605-9

14. Zhu D, Shao M, Yang J, Fang M, Liu S, Lou D, et al. Curcumin enhances radiosensitization of nasopharyngeal carcinoma via mediating regulation of tumor stem-like cells by a CircRNA network. *J Cancer* (2020) 11(8):2360–70. doi:10.7150/jca.39511

15. Zhang Z, Huang J, Wang G, Jin F, Zheng J, Xiao H, et al. Serum miRNAs, a potential prognosis marker of loco-regionally advanced nasopharyngeal carcinoma patients treated with CCRT. *BMC Cancer* (2020) 20(1):183. doi:10.1186/s12885-020-6689-7

16. Bao YN, Cao X, Luo DH, Sun R, Peng LX, Wang L, et al. Urokinase-type plasminogen activator receptor signaling is critical in nasopharyngeal carcinoma cell growth and metastasis. *Cell Cycle* (2014) 13(12):1958–69. doi:10.4161/cc.28921

17. Bose S, Yap LF, Fung M, Starzcynski J, Saleh A, Morgan S, et al. The ATM tumour suppressor gene is down-regulated in EBV-associated nasopharyngeal carcinoma. *J Pathol* (2009) 217(3):345–52. doi:10.1002/path.2487

18. Hu C, Wei W, Chen X, Woodman CB, Yao Y, Nicholls JM, et al. A global view of the oncogenic landscape in nasopharyngeal carcinoma: An integrated analysis at the genetic and expression levels. *PLoS One* (2012) 7(7):e41055. doi:10.1371/journal.pone.0041055

19. Ritchie ME, Phipson B, Wu D, Hu Y, Law CW, Shi W, et al. Limma powers differential expression analyses for RNA-sequencing and microarray studies. *Nucleic Acids Res* (2015) 43(7):e47. doi:10.1093/nar/gkv007

20. Leek JT, Storey JD. Capturing heterogeneity in gene expression studies by surrogate variable analysis. *Plos Genet* (2007) 3(9):1724–35. doi:10.1371/journal.pgen.0030161

21. Leek JT, Johnson WE, Parker HS, Jaffe AE, Storey JD. The sva package for removing batch effects and other unwanted variation in high-throughput experiments. *Bioinformatics* (2012) 28(6):882–3. doi:10.1093/bioinformatics/bts034

22. Robinson MD, McCarthy DJ, Smyth GK. edgeR: a Bioconductor package for differential expression analysis of digital gene expression data. *Bioinformatics* (2010) 26(1):139–40. doi:10.1093/bioinformatics/btp616

23. McCarthy DJ, Chen Y, Smyth GK. Differential expression analysis of multifactor RNA-Seq experiments with respect to biological variation. *Nucleic Acids Res* (2012) 40(10):4288–97. doi:10.1093/nar/gks042

24. Chen Y, Lun AT, Smyth GK. From reads to genes to pathways: Differential expression analysis of RNA-seq experiments using rsubread and the edgeR quasi-likelihood pipeline. *F1000Res* (2016) 5:1438. doi:10.12688/f1000research.8987.1

25. Langfelder P, Horvath S. Wgcna: an R package for weighted correlation network analysis. *BMC Bioinformatics* (2008) 9:559. doi:10.1186/1471-2105-9-559

26. Zhu Q, Zhang Q, Gu M, Zhang K, Xia T, Zhang S, et al. MIR106A-5p upregulation suppresses autophagy and accelerates malignant phenotype in nasopharyngeal carcinoma. *Autophagy* (2021) 17(7):1667–83. doi:10.1080/15548627.2020.1781368

27. Lee HM, Okuda KS, Gonzalez FE, Patel V. Current perspectives on nasopharyngeal carcinoma. *Adv Exp Med Biol* (2019) 1164:11–34. doi:10.1007/978-3-030-22254-3_2

28. Petersson F. Nasopharyngeal carcinoma: A review. *Semin Diagn Pathol* (2015) 32(1):54–73. doi:10.1053/j.semdp.2015.02.021

29. Tsao SW, Tsang CM, Lo KW. Epstein-Barr virus infection and nasopharyngeal carcinoma. *Philos Trans R Soc Lond B Biol Sci* (2017) 372(1732):20160270. doi:10.1098/rstb.2016.0270

30. Han B, Yang X, Zhang P, Zhang Y, Tu Y, He Z, et al. DNA methylation biomarkers for nasopharyngeal carcinoma. *PLoS One* (2020) 15(4):e0230524. doi:10.1371/journal.pone.0230524

31. Li G, Zhang J, Liu D, Wei Q, Wang H, Lv Y, et al. Identification of hub genes and potential ceRNA networks of diabetic nephropathy by weighted gene Co-expression network analysis. *Front Genet* (2021) 12:767654. doi:10.3389/fgene.2021.767654

32. Tian Z, He W, Tang J, Liao X, Yang Q, Wu Y, et al. Identification of important modules and biomarkers in breast cancer based on WGCNA. *Onco Targets Ther* (2020) 13:6805–17. doi:10.2147/OTT.S258439

33. Wen JY, Qin LT, Chen G, Huang HQ, Shen MJ, Pang JS, et al. Downregulation of MicroRNA-1 and its potential molecular mechanism in nasopharyngeal cancer: An investigation combined with in silico and in-house immunohistochemistry validation. *Dis Markers* (2022) 2022:7962220. doi:10.1155/2022/7962220

34. Chu Q, Huang H, Huang T, Cao L, Peng L, Shi S, et al. Extracellular serglycin upregulates the CD44 receptor in an autocrine manner to maintain self-renewal in nasopharyngeal carcinoma cells by reciprocally activating the MAPK/β-catenin axis. *Cell Death Dis* (2016) 7(11):e2456. doi:10.1038/cddis.2016.287

35. Verma N, Patel S, Osborn V, McBride S, Riaz N, Lee A, et al. Prognostic significance of human papillomavirus and Epstein-Bar virus in nasopharyngeal carcinoma. *Head Neck* (2020) 42(9):2364–74. doi:10.1002/hed.26245

36. Huang SH, Jacinto JCK, O'Sullivan B, Su J, Kim J, Ringash J, et al. Clinical presentation and outcome of human papillomavirus-positive nasopharyngeal carcinoma in a North American cohort. *Cancer* (2022) 128(15):2908–21. doi:10.1002/cncr.34266

37. Liu Y, Wang C, Shan X, Wu J, Liu H, Liu H, et al. S100P is associated with proliferation and migration in nasopharyngeal carcinoma. *Oncol Lett* (2017) 14(1): 525–32. doi:10.3892/ol.2017.6198

38. Wang C, Wang X, Han A, Wang Y, Jiang H. Proof-of-concept study investigating the role of S100P-RAGE in nasopharyngeal carcinoma. *Exp Ther Med* (2021) 21(5):470. doi:10.3892/etm.2021.9901

39. Yu Y, Lin ZX, Li HW, Luo HQ, Yang DH, Zhou HC, et al. Circulating tumor cells and fibronectin 1 in the prognosis of nasopharyngeal carcinoma. *Technol Cancer Res Treat* (2020) 19:1533033820909911. doi:10.1177/1533033820909911

40. Ding Y, Pan Y, Liu S, Jiang F, Jiao J. Elevation of MiR-9-3p suppresses the epithelial-mesenchymal transition of nasopharyngeal carcinoma cells via down-regulating FN1, ITGB1 and ITGAV. *Cancer Biol Ther* (2017) 18(6):414–24. doi:10.1080/15384047.2017.1323585

41. Wang J, Deng L, Huang J, Cai R, Zhu X, Liu F, et al. High expression of Fibronectin 1 suppresses apoptosis through the NF-κB pathway and is associated with migration in nasopharyngeal carcinoma. *Am J Transl Res* (2017) 9(10):4502–11.

42. Liu Q, Zhang W, Wu Z, Liu H, Hu H, Shi H, et al. Construction of a circular RNA-microRNA-messengerRNA regulatory network in stomach adenocarcinoma. *J Cel Biochem* (2020) 121(2):1317–31. doi:10.1002/jcb.29368

43. Peng Y, Croce CM. The role of MicroRNAs in human cancer. *Signal Transduct Target Ther* (2016) 1:15004. doi:10.1038/sigtrans.2015.4

44. Lin X, Wang S, Lin K, Zong J, Zheng Q, Su Y, et al. Competitive endogenous RNA landscape in epstein-barr virus associated nasopharyngeal carcinoma. *Front Cel Dev Biol* (2021) 9:782473. doi:10.3389/fcell.2021.782473

45. Pamudurti NR, Bartok O, Jens M, Ashwal-Fluss R, Stottmeister C, Ruhe L, et al. Translation of CircRNAs. *Mol Cel* (2017) 66(1):9–21. doi:10.1016/j.molcel.2017.02.021

46. Zhang S, Li Y, Xin S, Yang L, Jiang M, Xin Y, et al. Insight into LncRNA- and CircRNA-mediated CeRNAs: Regulatory network and implications in nasopharyngeal carcinoma-A narrative literature review. *Cancers (Basel).* (2022) 14(19):4564. doi:10.3390/cancers14194564

47. Li S, Wang Q. Hsa_circ_0081534 increases the proliferation and invasion of nasopharyngeal carcinoma cells through regulating the miR-508-5p/FN1 axis. *Aging (Albany NY)* (2020) 12(20):20645–57. doi:10.18632/aging.103963

Pathology & Oncology Research | frontiers

TYPE Original Research
PUBLISHED 24 April 2023
DOI 10.3389/pore.2023.1611123

Check for updates

OPEN ACCESS

EDITED BY
Andrea Ladányi,
National Institute of Oncology (NIO), Hungary

*CORRESPONDENCE
Zoltán Takácsi-Nagy,
takacsi.zoltan@oncol.hu

RECEIVED 16 February 2023
ACCEPTED 11 April 2023
PUBLISHED 24 April 2023

CITATION
Révész M, Oberna F, Slezák A, Ferenczi Ö, Kenessey I and Takácsi-Nagy Z (2023), The characteristics of head and neck squamous cell cancer in young adults: A retrospective single-center study. *Pathol. Oncol. Res.* 29:1611123. doi: 10.3389/pore.2023.1611123

COPYRIGHT
© 2023 Révész, Oberna, Slezák, Ferenczi, Kenessey and Takácsi-Nagy. This is an open-access article distributed under the terms of the Creative Commons Attribution License (CC BY). The use, distribution or reproduction in other forums is permitted, provided the original author(s) and the copyright owner(s) are credited and that the original publication in this journal is cited, in accordance with accepted academic practice. No use, distribution or reproduction is permitted which does not comply with these terms.

The characteristics of head and neck squamous cell cancer in young adults: A retrospective single-center study

Mónika Révész[1], Ferenc Oberna[1], András Slezák[2], Örs Ferenczi[3], István Kenessey[4,5,6] and Zoltán Takácsi-Nagy[3,6,7]*

[1]Multidisciplinary Head and Neck Cancer Center, National Institute of Oncology (NIO), Budapest, Hungary, [2]Center of Tumor Pathology Department, National Institute of Oncology (NIO), Budapest, Hungary, [3]Center of Radiotherapy, National Institute of Oncology (NIO), Budapest, Hungary, [4]Hungarian Cancer Registry, National Tumor Laboratory Project, National Institute of Oncology (NIO), Budapest, Hungary, [5]Department of Pathology, Forensic and Insurance Medicine, Semmelweis University, Budapest, Hungary, [6]National Tumor Laboratory Project, Budapest, Hungary, [7]Department of Oncology, Semmelweis University, Budapest, Hungary

We aimed to characterize clinical and prognostical factors of primary head and neck squamous cell carcinoma (HNSCC) in 85 young patients (≤39 years, median age: 37 years; between 2000–2018) in comparison with 140 institutional general HNSCC patients (median age: 61.5 years). The patient's medical records were collected from the institutional database. The prevalence of smoking and alcohol consumption (65.8% and 48.1%) in the young group exceeded the regional population average but was below the institutional (86.4% and 55%) general HNSCC patient population. Primary tumor sites in the group of young patients were as follows: oral cavity (56.4%), oropharynx (17.6%), hypopharynx (11.7%), and larynx (14.1%). Cumulative five-year overall survival was 44.2% in the young group, but significantly better with early T (T1-2 vs. T3-4: 52.6% vs. 26.7%; p = 0.0058) and N0 status (N0 vs. N+: 65.2% vs. 32.3%; p = 0.0013). Young age, abstinence, earlier stage and laryngeal tumor site might predict a better prognosis. The age distribution and the high prevalence of traditional risk factors among the young patients as well as the predominance of oral cavity tumor localization suggest that the early onset of tumor development could be originated from the premature failure of the intrinsic protective mechanisms.

KEYWORDS

survival, risk factors, prognostic factors, head and neck cancer, young adults

Introduction

Head and neck squamous cell carcinoma (HNSCC) was estimated as the sixth most common cancer with approximately 800,000 new cases yearly worldwide based on the GLOBOCAN database (1). The annual incidence of 17.2/100,000 in Hungary is the highest in Europe (2). Although HNSCC usually occurs in patients over 60 years, in the past half century the incidence also increased in young adults. According to the literature,

oral cancers constitute approximately 0.4%–3.6% of all cancers in patients under 40 years, and 6.7% under the age of 45 (3, 4). The cause of early-onset HNSCC is yet unclear (5). Certain authors indicated that traditional extrinsic risk factors (e.g., tobacco and alcohol consumption) may be similarly prevalent among older and younger individuals; however, the duration of the exposure in younger patients might not be sufficient to significantly increase the risk (5). The role of human papillomavirus (HPV) might also come into consideration (6, 7). Various factors might also play a role in the development of HNSCC in younger patients, such as genetic predisposition (e.g., Li-Fraumeni syndrome, Bloom's syndrome, Fanconi anaemia, Wiskott-Aldrich syndrome, dyskeratosis congenita or further factors suggested by positive family history for HNSCC), an immunocompromised status, previous chemotherapy or irradiation, poor oral hygiene and dietary components, but their true relevance is yet unclear (6, 8). However, the increasing incidence might suggest the role of non-predetermined factors. Even the definition of young patient seems to be arbitrary, and varies between different reports (5, 9). Several studies aimed to compare the prognosis of young and older patients, but the results are conflicting (5, 9, 10). According to our knowledge, only few comprehensive reports have been published involving all sites of HNSCC (oral cavity, oropharynx, hypopharynx, larynx) in young patients. Our aim was to characterize the clinical features, the age distribution and the prevalence of classical risk factors in the young patient group in comparison with a non-preselected institutional general HNSCC population. In addition we would like to determine the impact of age and certain etiologic factors and tumor variables on 5-year survival rates and prognosis.

Materials and methods

Patients and study design

We summarized and analyzed the medical records of 85 young patients with histologically verified HNSCC between 2000 and 2018 based on the institutional medical database of *National Institute of Oncology, Budapest, Hungary*. Patients diagnosed under 40 years (≤39) of age were accepted as young, according to National Comprehensive Cancer Network (NCCN) Adolescent and Young Adult (AYA) Oncology's guideline (11). We involved patients diagnosed and primarily treated in the *Multidisciplinary Head and Neck Cancer Center or Center of Radiotherapy*, as well as those who were admitted for adjuvant therapy (postoperative irradiation or chemoirradiation). According to the 10th revision of *International Classification of Diseases (ICD-10)* lip (C00), oral cavity (C01-C06), pharynx (C09; C10; C12; C13) and larynx (C32), with histologically verified squamous cell cancer morphology codes were included in our study (12). Patients with metastases of unknown primary tumors, as well as non-HNSCC (e.g., nasopharyngeal, salivary gland tumors, sinonasal carcinomas, thyroid tumors, lymphomas) tumors were excluded. Patient data (i.e., age, gender, drug and clinical history, tobacco and alcohol consumption, tumor site, stage, grade, and nodal status at the time of the diagnosis, time of death) were extracted from the hospital information system and the *National Cancer Registry*. Only those who had never smoked were considered non-smokers. Drinkers were defined as alcohol consumption at or above the *World Health Organization (WHO)* medium risk category (>40 g alcohol for men, or >20 g for women), which constitutes approximately a bottle of beer or >2–3 dL of wine on a daily basis (13). Each tumor was staged according to the 7th edition of TNM criteria of the Union for International Cancer Control (UICC) (14) and WHO classification was used to assess histological type and grading (12). Paraffin-embedded tissue sections were also used for the confirmation of the diagnosis and immunohistochemical staining for $p16^{INK4a}$ antigen with Roche CINtec® p16 ($E6H4^{TM}$) antibody for detection of this antigen (used according to the manufacturer's recommendation, Roche, Basle, Switzerland) in the *Center of Tumor Pathology Department of National Institute of Oncology*. The clinicopathological data of our study population were compared with an institutional group of 140 consecutive general HNSCC patients from year 2014.

The study was conducted under the ethical permission of the Scientific and Research Ethics Committee of the Medical Research Council (approval number: BMEÜ/3719- 1 2022/ EKU) in accordance with the Helsinki Declaration of 1975, as revised in 2008.

Follow-up

Recurrence was defined as the local or regional return of cancer after the patient was declared disease-free. Residual tumor was defined as histologically positive resection margins after surgical therapy, or tumor suspect soft tissue detected by radiological imaging (Computed tomography/CT/, Magnetic resonance imaging/MRI/, Positron emission tomography/PET/-CT) within 3 months from the end of the radio(chemo)therapy or other conservative treatment (in certain cases the residual tumor was also proved by histology). We also diagnosed locoregional residual disease if the locoregional recurrence occurred within 3 months after the first surgical treatment regardless of the surgical margin status. Overall survival (OS) was determined as months between the date of initial diagnosis and the last follow-up or death.

Statistical analysis

Chi-square test (CS) was used to compare the composition of groups. Fisher's exact test (FE) with Bonferroni correction of the alpha values was used as a post-hoc test for multiple

TABLE 1 Clinical characteristics and treatment methods of the young patients and the institutional control group.

	Young patients (n = 85)	Control group (n = 140)	p (Chi-square)
Sex			0.44
Male	67 (78.8%)	104 (74.3%)	
Female	18 (21.2%)	36 (25.7%)	
Median age (yr)	37	61.5	**0.001**
Interquartile range (yr)	33–39	56.75–67	
Smoking history			**$9.3*10^{-5}$**
pos	52 (65.8%)	123 (87.9%)	
neg	27 (34.1%)	17 (12.1%)	
NA	6	0	
Alcohol consumption			0.235
pos	38 (48.1%)	79 (56.4%)	
neg	41 (51.8%)	61 (43.6%)	
NA	6	0	
Localization			**$2.1*10^{-7}$**
Lip, oral cavity	48 (56.5%)	27 (19.3%)	
Mesopharynx	15 (17.6%)	35 (25%)	
Hypopharynx	10 (11.8%)	34 (24.3%)	
Larynx	12 (14.1%)	44 (31.4%)	
Primary tumor size			**0.037**
T1	24 (28.2%)	28 (20%)	
T2	33 (38.8%)	38 (27.1%)	
T3	12 (14.1%)	30 (21.4%)	
T4	16 (18.8%)	44 (31.4%)	
Nodal status			0.83
N0	31 (36.5%)	49 (35%)	
N1	16 (18.8%)	24 (17.1%)	
N2	33 (38.8%)	54 (38.6%)	
N3	5 (5.9%)	13 (9.3%)	
Stage			0.375
I	16 (18.8%)	16 (11.4%)	
II	8 (9.4%)	10 (7.1%)	
III	18 (21.2%)	31 (22.1%)	
IV	43 (50.5%)	83 (59.3%)	
Grade			**0.043**
1–2	55 (75.3%)	73 (61.3%)	
3–4	18 (24.7%)	46 (38.6%)	
NA	12	21	
Perineural spread			0.37
Pos	13 (38.2%)	17 (29.3%)	
Neg	21 (61.8%)	41 (70.7%)	
NA	51	82	
Vascular invasion			0.23
Pos	10 (28.6%)	24 (40.7%)	
Neg	25 (71.4%)	35 (59.3%)	
NA	50	81	
Primary treatment			0.11
Surgery	15 (17.6%)	12 (8.6%)	
non-surgery	28 (32.9%)	46 (32.8%)	
Combined	42 (49.4%)	82 (58.5%)	

NA: not available.
The significant values were marked with bold characters.

comparisons. Kolmogorov-Smirnov test was used to assess the normality of distributions. Student's t-test or Mann-Whitney U-test (MWU-test) was used to compare independent variables with normal or non-normal distribution, respectively. Survival curves were depicted according to the Kaplan-Meier method (KM), significance was analyzed by log-rank statistics (LR). Univariate and multivariate analyses of prognostic factors were done using the Cox's regression model. A p-value < 0.05 was accepted as statistically significant. KyPlot 5.0 (KyensLab Inc., Tokyo, Japan) and Statistica 14.0.1.25 (TIBCO Software Inc., Palo Alto, CO) were used for statistical analysis.

Results

Tumor characteristics of young patients

Among young patients male predominance (78.9%, male/female: 67/18) was found. The median age at the time of the diagnosis was 37 years (range 21–39) and two-third of the patients were 35–39 years old. For comparison we involved an institutional general HNSCC group (male/female: 104/36; median age: 61.5 years, range 34–88). The most common primary tumor locations were the lip and the oral cavity in contrast to the general patient population (48/85 [56.47%] vs. 27/140 [19.28%]; $p < 0.001$, CS). The most common subsite was the tongue in contrast to the oral cavity tumors of the general HNSCC patients (26/48, [54.1%] vs. 6/27, [22.2%], $p < 0.007$, CS). In the oral cavity subgroup 6 of 48 young patients (12.5%) and 3 of 27 general HNSCC patients (11.1%) presented with lip cancer, the difference was none-significant ($p = 0.85$, Chi-square test). Fifty-seven of 85 young patients had early (T1-T2) primary tumor status at the time of the diagnosis, which is significantly different from the control group (57/85 [67%] vs. 66/140 [47.1%], respectively, $p < 0.037$). Fifty-four (63.5%) had cervical lymph node involvement (N+) according to the physical examination and radiological imaging (ultrasound, CT scan, MRI). Lymph nodes were seldom involved in laryngeal cancer (N0: 83.3%, 10 of 12). None of the patients had distant metastasis (M) at the time of the diagnosis. Well-differentiated tumors are significantly more common among young patients than in the control group (55/73 [75.3%] vs. 73/119 [61.3%], respectively, $p < 0.05$). Detailed characteristics of all study groups are reported in Table 1.

Prevalence of potential risk factors in young patients

Data on smoking and alcohol consumption could be found in the medical records of 79 young patients. Fifty-two (65.8%) of them were (current or previous) smokers, 38 (48.1%) consumed alcohol and 33 (41.7%) enjoyed both risk factors. However, smoking was significantly less prevalent in the young group than in the general HNSCC patient population (65.8% vs. 86.4% respectively, $p < 0.001$, CS). In contrast, the alcohol consumption was similar in the young and the general HNSCC group (48.1% vs. 55.0%, respectively, $p < 0.0001$ CS) (Table 1). The p16 status was tested in 65 young and 36 control patients. The rate of positivity was 20% ($n = 13$) and 11.1% ($n = 4$) respectively, no significant difference was shown between the two groups ($p = 0.25$, Chi-square test).

Front-line therapy and histological parameters

Fifty-seven of the 85 patients (67%) underwent surgical therapy, 85.4% of those with lip and oral cavity cancer, 75% with laryngeal cancer, 40% with hypopharynx, 20% with mesopharynx cancer. Forty (70.2%) of the 57 patients underwent R0 resection, among them 10 patients with close R0 resection (the free margin is < 5 mm). In 29.8% ($n = 17$) of patients R1 resection was performed.

Two patients (20%) with close R0 resection, and 6 patients (35.2%) with R1 resection underwent a follow-up operation. The indications for postoperative irradiation were pT3 or pT4 stage, perineural spreading, vascular invasion, extranodal extension and close or positive surgical resection margins. Altogether 42 patients (73.6%; $n = 31$ patients with R0; $n = 11$ with R1 resection) received adjuvant therapy after the surgical therapy (Table 1.).

Overall survival (OS) of young patients

The median follow-up time since the diagnosis of cancer was 28.5 months (range 3–228). Cumulative five-year OS for all head and neck sites was 44.2% (Figure 1A), 44.9% for lip and oral cavity ($n = 47$), 58.3% for oropharynx ($n = 15$), 0% for hypopharynx ($n = 10$) and 62.8% for larynx ($n = 12$) carcinoma. Only the subgroup with hypopharynx carcinoma differed significantly from all others (Figure 1B).

The 5-year OS was analyzed according to risk factors. Significantly better OS was observed in the alcohol abstinent group (59.6% vs. 32.7%; $p = 0.0297$). The 5-year OS was significantly better in patients with early, than in advanced T status (T1-2: 52.6% vs. T3-4: 26.7%; $p = 0.0058$) (Figure 1C) and in patients with N0 vs. N+ nodal status (65.2% vs. 32.3% respectively; $p = 0.0013$) (Figure 1D).

The cumulative 5-year survival for all tumor sites was significantly better in the young than in the control group (44.2% vs. 32% respectively, $p = 0.005$).

Univariate Cox regression model for the entire study population revealed that young age, a non-smoker or abstinent status, as well as laryngeal tumor site might predict a significantly better prognosis. Data adjustment for multivariate Cox regression model proved that from the aforementioned parameters young age, abstinence and earlier stage remained

10.3389/pore.2023.1611123

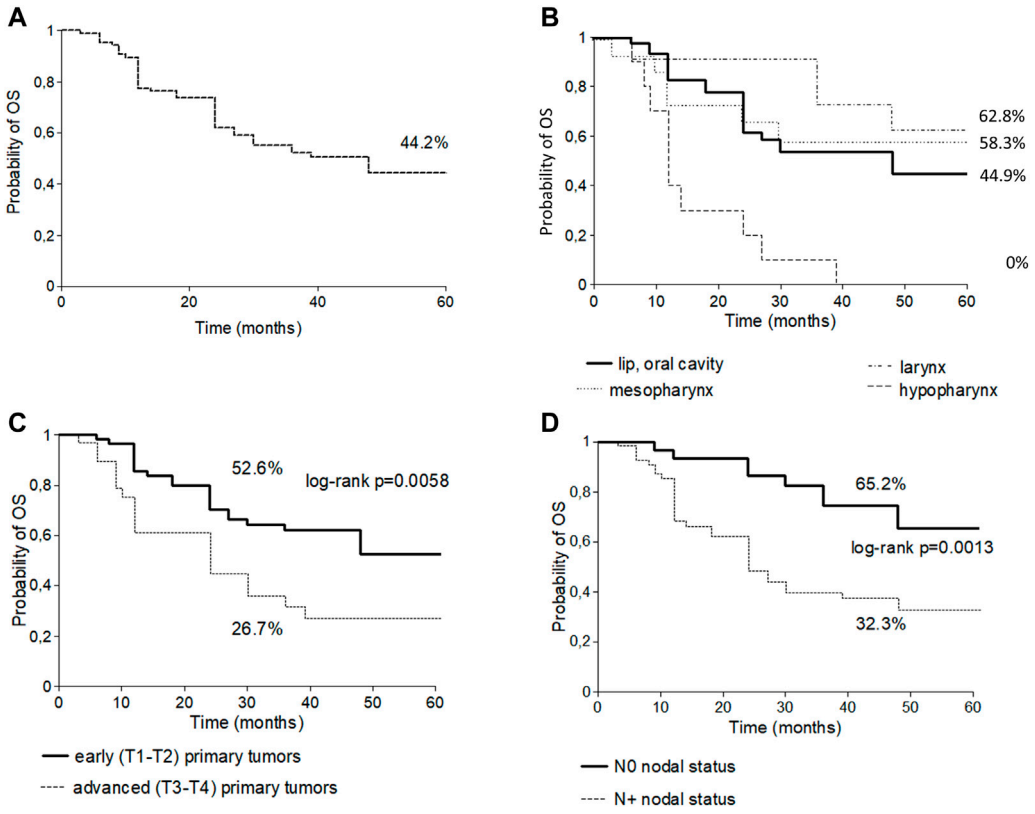

FIGURE 1
Five-year overall survival curve of all sites of head and neck cancers in young patients **(A)**; Five-year overall survival curve of subtypes of head and neck cancers in young patients **(B)**; Five-year overall survival curve stratified by T stage in young patients **(C)**; Five-year overall survival curve stratified by N stage in young patients **(D)**.

TABLE 2 Univariate and multivariate Cox regression model for the assessment of prognostic factors in the entire (young patients and control group) study population (RR = relative risk).

	Univariate model		Multivariate model	
	RR (95% CI)	*p*	RR (95% CI)	*p*
Young group (vs. control)	0.497 (0.309–0.797)	0.004	0.617 (0.426–0.894)	0.011
Male sex (vs. female)	0.837 (0.525–1.334)	0.454	0.708 (0.474–1.057)	0.091
Smokers (vs. non-smokers)	1.799 (1.037–3.121)	0.037		
Alcohol (vs. abstinent)	1.641 (1.073–2.508)	0.022	2.007 (1.394–2.888)	$1.8*10^{-4}$
Localization (vs. oral cavity)				
mesopharynx	0.877 (0.448–1.714)	0.308		
hypopharynx	0.814 (0.456–1.453)	0.164		
Larynx	0.398 (0.221–0.718)	0.005		
Grade 3/4 (vs. 1/2)	0.854 (0.581–1.255)	0.421		
Stage IV (vs. I-III)	2.454 (1.605–3.752)	$3.4*10^{-5}$	1.883 (1.343–2.64)	$2.4*10^{-4}$

TABLE 3 Univariate and multivariate Cox regression model for the assessment of prognostic factors among young head and neck squamous cancer patients.

	Univariate model		Multivariate model	
	RR (95% CI)	*p*	RR (95% CI)	*p*
Male sex (vs. female)	1.146 (0.531–2.472)	0.728	0.592 (0.208–1.688)	0.327
Smokers (vs. non-smokers)	1.796 (0.85–3.797)	0.125	1.746 (0.664–4.589)	0.258
Alcohol (vs. abstinent)	1.973 (1.029–3.783)	0.041	1.433 (0.61–3.369)	0.409
Tumor site (vs. oral cavity)				
mesopharynx	1.683 (0.464–6.113)	0.282	0.434 (0.05–3.79)	0.043
hypopharynx	4.08 (1.898–8.769)	$3.1*10^{-5}$	3.602 (1.404–9.244)	$3.9*10^{-5}$
Larynx	0.546 (0.188–1.582)	0.063	0.325 (0.071–1.491)	0.189
Grade 3/4 (vs. 1/2)	0.734 (0.333–1.618)	0.444	0.939 (0.396–2.227)	0.887
Stage IV (vs. I-III)	1.904 (1.026–3.535)	0.041	1.948 (0.908–4.179)	0.087

independent prognostic parameters, which were associated with more favorable outcome (Table 2). Contrarily, alcohol consumption, older age and advanced stage almost doubled the relative risk. When analyzing the young group separately, an alcohol-abstinent status, as well as advanced stage proved significant predictors of the prognosis. All the significancies and trends in the young age group were in line with those in the entire study group (Table 3).

Locoregional control

Residual disease was reported in 42.3% (n = 36) of the 85 patients. The histological analysis of the surgical materials showed positive margins in 17 cases, and residual disease was also detected in 15 cases after the completion of other treatment modalities (e.g., definitive radio(chemo)therapy, induction chemotherapy+ radio(chemo)therapy) by radiological imaging. We also considered four further cases of locoregional recurrences to constitute residual disease, as recurrence occured within 3 months (average of 10 weeks, range: 8–12) after surgical treatment with tumor-free margin (R0) status.

Recurrent disease was observed in 24.7% (n = 21) of the 85 patients (12 local, 4 regional, 3 distant metastasis and 2 locoregional recurrence) after that the patient was defined as disease free, and occurred within an average of 24 months after the diagnosis (local: 15.14 months/range 4–48/; regional: 9 months/range 4–20/; distant: 20 months/range 14–24/). The incidence of second primary cancers (lung, oropharynx and tongue) was 4.7% (n = 4).

Discussion

Previous studies confirmed that smoking, alcohol consumption and HPV are the most important risk factors of HNSCC (5, 6). However, these carcinogens are known for their delayed effect. As the time of exposure is limited in young patients, additional factors are suspected in the background. This fact suggested that, compared with the general population with HNSCC, the young group might show a different pattern. The importance of our examination is that the majority of HNSCC studies did not handle young patients separately. The proportions of smokers and alcohol consumers, as well as the gender distribution and the proportions of certain primary tumor locations in our control HNSCC patient group were practically identical with large-scale international hypothesis-free epidemiological HNSCC studies (15, 16). We found that, in contrast to the general HNSCC populations, the oral cavity proved to be the most common tumor site in young patients. In addition, the majority of patients were diagnosed in an early tumor stage. In parallel with previous works, among our examined patients an advanced T and N status were associated with significantly worse prognosis, which underlines the relevance of early recognition and treatment (15). This also corroborates with our findings that young age was associated to relatively better outcome. The location-based 5-year survival analysis showed significantly worse survival in the hypopharynx subgroup than in the other subgroups in young patients. However, the comparability of tumor site specific survival data was limited due to the small number of the subgroups. The low prevalence of p16 positivity suggested that HPV infection is unlikely to play a relevant role in our patient groups.

There is also an unanswered question of whether young HNSCC patients form a distinct disease entity (17). A recent report by Pickering et al. suggested, that oral tongue SCCs from younger and older patients are genomically similar (18). This might indicate, that the younger and older patients might rather differ in their susceptibility to carcinogenesis than the characteristics of the tumors. Intrinsic (mainly genetic) and environmental factors might act synergically. Tobacco use and

alcohol consumption are well-known causative factors. Although the duration of the exposure is necessarily shorter (by decades) among young patients, prevalence of tobacco and alcohol consumption in our study population was significantly higher compared to the >15 years old regional general population (30.6% (19); 32.3% (20) respectively. A recent Hungarian report of oral squamous cell cancer cases has also stated that the number of smokers was high in both the older and younger oral cancer patient groups (21) however, the definition of drinkers is often used inconsistently, which makes the comparisons less exact between various studies. We hypothesize that the sufficiency of lower cumulative doses of these harmful agents suggests an increased vulnerability of this population to lifestyle-related risks, which might originate from a diminished damage control on the cellular level, or a weaker capacity to eliminate tumor cells by the innate immune responses. This concept is suggested by Wang et al. who linked reduced DNA repair capacity with tobacco -related carcinogenesis and also Kostrzewska-Poczekaj et al. who identified polimorphisms of DNA repair genes in young HNSCC patients (22, 23). Our hypothesis might be in line with previous reports regarding other malignancies associated with extrinsic factors: candidate genes involved in the regulation of cellular proliferation and the prevention of DNA damage have already been identified in association with early onset lung cancer (24, 25), and a distinct immune signature of early and late onset colorectal cancer has also been described (26). On the other hand, the higher proportions of non-smoking and abstinent patients among young patients are unexplained by the traditional carcinogenic theories. Thus, the young HNSCC population might not be homogenous (10). For instance, Lee et al. suggested that young patients with HNSCCs linked primarily to extrinsic risks (smoking and alcohol) might carry a more favorable prognosis than less heavily exposed individuals (27). However, the latter group seems to remain a minority in our study population. Additionally, in Hungary all the three major risk factors are endemic, which does not allow to determine strict risk groups (28). The age distribution of our patients is heavily distorted towards the cut-off value of 39 years, which might indicate that the majority of them might represent an extreme value of the general patient population. Of note, five of the sixteen young patients (31.2%) who lacked any traditional cancer risk factors (tobacco and/or alcohol use and also p16 positivity) were immunocompromised (three after bone marrow transplantation, one with Crohn's disease, one during pregnancy) however their number was insufficient for a subgroup analysis. Previous studies also found that chronic immunodeficiency (such as immunosuppression following organ transplantation or HIV) is associated with a higher incidence of oral squamous cancer in young patients; however, the available results are contradictory (4). Additionally, the metaanalysis of van Monsjou et al. identified different hereditary syndromes, such as Fanconi anemia and Bloom's syndrome as causative factors in a subgroup of young-onset HNSCC, but our examinatory sample was not able to reflect to this question (6).

In summary, in our study we found that young patients with HNSCC might represent an extreme value within the spectrum of the general HNSCC patient population. This is suggested by their age distribution and the high prevalence, but necessarily lower cumulative doses of traditional risks. Thus HNSCC in young adults is unlikely to be based on endogenous risks directly for carcinogenesis (i.e., tumor predisposition syndromes) but they might rather show an exceeded susceptibility to classical risk factors.

Although the etiological factors might be similar, young patients do have a better prognosis according to our results. Given that the most common tumor site was the oral cavity in young patients we should highlight the importance and feasibility of screening.

Data availability statement

The raw data supporting the conclusion of this article will be made available by the authors, without undue reservation.

Ethics statement

The studies involving human participants were reviewed and approved by Scientific and Research Ethics Committee of the Medical Research Council (approval number: BMEÜ/3719-1 2022/EKU). Written informed consent for participation was not required for this study in accordance with the national legislation and the institutional requirements. Written informed consent was not obtained from the individual(s) for the publication of any potentially identifiable images or data included in this article.

Author contributions

Study concepts: ZT-N. Data acquisition: MR, ÖF, and AS. Data analysis and interpretation: MR Statistical analysis: IK and MR. Manuscript preparation: MR. Manuscript review: IK, ZT-N, and FO.

Funding

The project was implemented with the support from the National Research, Development and Innovation Fund of the Ministry of Culture and Innovation under the National

Laboratories Program (National Tumor Biology Laboratory (2022-2.1.1-NL-2022-00010)) and the Hungarian Thematic Excellence Program (under project TKP2021-EGA-44) Grant Agreements with the National Research, Development and Innovation Office.

Conflict of interest

The authors declare that the research was conducted in the absence of any commercial or financial relationships that could be construed as a potential conflict of interest.

References

1. Sung H, Ferlay J, Siegel RL, Laversanne M, Soerjomataram I, Jemal A, et al. Global cancer statistics 2020: GLOBOCAN estimates of incidence and mortality worldwide for 36 cancers in 185 countries. *CA Cancer J Clin* (2021) 71:209–49. doi:10.3322/caac.21660

2. World Health Organization. *Cancer today* (2022). Available at: http://gco.iarc.fr/today/home (Accessed December 15, 2022).

3. Mafi N, Kadivar M, Hosseini N, Ahmadi S, Zare-Mirzaie A. Head and neck squamous cell carcinoma in Iranian patients and risk factors in young adults: A fifteen-year study. *Asian Pac J Cancer Prev* (2012) 13:3373–8. doi:10.7314/apjcp.2012.13.7.3373

4. Llewellyn CD, Johnson NW, Warnakulasuriya KA. Risk factors for squamous cell carcinoma of the oral cavity in young people--a comprehensive literature review. *Oral Oncol* (2001) 37:401–18. doi:10.1016/s1368-8375(00)00135-4

5. Gamez ME, Kraus R, Hinni ML, Moore EJ, Ma DJ, Ko SJ, et al. Treatment outcomes of squamous cell carcinoma of the oral cavity in young adults. *Oral Oncol* (2018) 87:43–8. doi:10.1016/j.oraloncology.2018.10.014

6. van Monsjou HS, Wreesmann VB, van den Brekel MWM, Balm AJM. Head and neck squamous cell carcinoma in young patients. *Oral Oncol* (2013) 49:1097–102. doi:10.1016/j.oraloncology.2013.09.001

7. Túri K, Barabás P, Csurgay K, Léhner GY, Lőrincz A, Németh ZS. An analysis of the epidemiological and etiological factors of oral tumors of young adults in a Central-Eastern European population. *Pathol Oncol Res* (2013) 19:353–63. doi:10.1007/s12253-013-9628-y

8. Majchrzak E, Szybiak B, Wegner A, Pienkowski P, Pazdrowski J, Luczewski L, et al. Oral cavity and oropharyngeal squamous cell carcinoma in young adults: A review of the literature. *Radiol Oncol* (2014) 48:1–10. doi:10.2478/raon-2013-0057

9. Lacy PD, Piccirillo JF, Merritt MG, Zequeira MR. Head and neck squamous cell carcinoma: Better to be young. *Otolaryngol–head Neck Surg Off J Am Acad Otolaryngol-head Neck Surg* (2000) 122:253–8. doi:10.1016/S0194-5998(00)70249-X

10. Németh Z, Turi K, Léhner G, Veres SD, Csurgay K. The prognostic role of age in oral cancer. A clinical study. *Magy Onkol* (2013) 57:166–72.

11. Coccia PF, Pappo AS, Beaupin L, Borges VF, Borinstein SC, Chugh R, et al. Adolescent and young adult oncology, version 2.2018, NCCN clinical practice guidelines in oncology. *JNCCN* (2018) 16:66–97.

12. Allen PW. ICDO—international classification of diseases for Oncology. *Pathology (Phila)* (1991) 23:280. doi:10.1016/S0031-3025(16)36112-8

13. World Health Organization. *International guide for monitoring alcohol consumption and related harm* (2000). Available at: https://apps.who.int/iris/handle/10665/66529 (Accessed June 17, 2012).

14. Sobin LH, Gospodarowicz MK, Wittekind C. *TNM classification of malignant tumours*. 7th ed. Wiley-Blackwell (2010).

15. Du E, Mazul AL, Farquhar D, Brennan P, Anantharaman D, Abedi-Ardekani B, et al. Long-term survival in head and neck cancer: Impact of site, stage, smoking, and human papillomavirus status. *The Laryngoscope* (2019) 129:2506–13. doi:10.1002/lary.27807

16. Cadoni G, Giraldi L, Petrelli L, Pandolfini M, Giuliani M, Paludetti G, et al. Prognostic factors in head and neck cancer: A 10-year retrospective analysis in a single-institution in Italy. *Acta Otorhinolaryngol Ital Organo Uff Della Soc Ital Otorinolaringol E Chir Cerv-facc* (2017) 37:458–66. doi:10.14639/0392-100X-1246

17. Toner M, O'Regan EM. Head and neck squamous cell carcinoma in the young: A spectrum or a distinct group? Part 1. *Head Neck Pathol* (2009) 3:246–8. doi:10.1007/s12105-009-0135-0

18. Pickering CR, Zhang J, Neskey DM, Zhao M, Jasser SA, Wang J, et al. Squamous cell carcinoma of the oral tongue in young non-smokers is genomically similar to tumors in older smokers. *Clin Cancer Res* (2014) 20:3842–8. doi:10.1158/1078-0432.CCR-14-0565

19. Ritchie H, Roser M. *Smoking. Our World data* (2013). Available at: https://ourworldindata.org/smoking (Accessed August 5, 2021).

20. Ritchie H, Roser M. *Alcohol consumption*. Our World Data (2018). Available at: https://ourworldindata.org/alcohol-consumption (Accessed August 5, 2021).

21. Csurgay K, Zalatnai A, Benczik M, Csomó BK, Horváth F, Lőrincz Á, et al. A study of prognostic factors in young patients with non-HPV oral cancer in central Europe. *Pathol Oncol Res* (2021) 27:1609991. doi:10.3389/pore.2021.1609991

22. Wang L-E, Hu Z, Sturgis EM, Spitz MR, Strom SS, Amos CI, et al. Reduced DNA repair capacity for removing tobacco carcinogen-induced DNA adducts contributes to risk of head and neck cancer but not tumor characteristics. *Clin Cancer Res* (2010) 16:764–74. doi:10.1158/1078-0432.ccr-09-2156

23. Kostrzewska-Poczekaj M, Gawęcki W, Illmer J, Rydzanicz M, Gajecka M, Szyfter W, et al. Polymorphisms of DNA repair genes and risk of squamous cell carcinoma of the head and neck in young adults. *Eur Arch Oto-Rhino-Laryngol Off J Eur Fed Oto-Rhino-Laryngol Soc EUFOS Affil Ger Soc Oto-Rhino-Laryngol - Head Neck Surg* (2013) 270:271–6. doi:10.1007/s00405-012-1993-8

24. Wei Q, Cheng L, Amos CI, Wang LE, Guo Z, Hong WK, et al. Repair of tobacco carcinogen-induced DNA adducts and lung cancer risk: A molecular epidemiologic study. *J Natl Cancer Inst* (2000) 92:1764–72. doi:10.1093/jnci/92.21.1764

25. Landi S, Gemignani F, Canzian F, Gaborieau V, Barale R, Landi D, et al. DNA repair and cell cycle control genes and the risk of young-onset lung cancer. *Cancer Res* (2006) 66:11062–9. doi:10.1158/0008-5472.CAN-06-1039

26. Gardner IH, Siddharthan R, Watson K, Dewey E, Ruhl R, Khou S, et al. A distinct innate immune signature of early onset colorectal cancer. *ImmunoHorizons* (2021) 5:489–99. doi:10.4049/immunohorizons.2000092

27. Lee SU, Moon SH, Choi SW, Cho KH, Park JY, Jung Y-S, et al. Prognostic significance of smoking and alcohol history in young age oral cavity cancer. *Oral Dis* (2020) 26:1440–8. doi:10.1111/odi.13432

28. Vánkos JB, Piurkó V, Suba Z, Németh Z, Tímár J, Kenessey I. The prognostic role of expression of p16 tumor suppressor gene in Hungarian patients with oral squamous cell carcinoma. *Magy Onkol* (2015) 59:352–9.

Pathology & Oncology Research | frontiers

TYPE Brief Research Report
PUBLISHED 10 November 2023
DOI 10.3389/pore.2023.1611375

Check for updates

OPEN ACCESS

EDITED BY
Agota Szepesi,
Semmelweis University, Hungary

*CORRESPONDENCE
Gábor Mikala,
gmikala@dpckorhaz.hu

RECEIVED 28 June 2023
ACCEPTED 31 October 2023
PUBLISHED 10 November 2023

CITATION
Ceglédi A, Csukly Z, Fekete M, Kozma A, Szemlaky Z, Andrikovics H and Mikala G (2023), Effective venetoclax-based treatment in relapsed/refractory multiple myeloma patients with translocation t(6;14).
Pathol. Oncol. Res. 29:1611375.
doi: 10.3389/pore.2023.1611375

COPYRIGHT
© 2023 Ceglédi, Csukly, Fekete, Kozma, Szemlaky, Andrikovics and Mikala. This is an open-access article distributed under the terms of the Creative Commons Attribution License (CC BY). The use, distribution or reproduction in other forums is permitted, provided the original author(s) and the copyright owner(s) are credited and that the original publication in this journal is cited, in accordance with accepted academic practice. No use, distribution or reproduction is permitted which does not comply with these terms.

Effective venetoclax-based treatment in relapsed/refractory multiple myeloma patients with translocation t(6;14)

Andrea Ceglédi[1], Zoltán Csukly[1], Mónika Fekete[2], András Kozma[3], Zsuzsanna Szemlaky[1], Hajnalka Andrikovics[3] and Gábor Mikala[1]*

[1]Department of Hematology and Stem Cell Transplantation, Central Hospital of Southern Pest, National Institute for Hematology and Infectious Diseases, Budapest, Hungary, [2]Department of Public Health, Semmelweis University, Budapest, Hungary, [3]Laboratory of Molecular Genetics, Central Hospital of Southern Pest, National Institute for Hematology and Infectious Diseases, Budapest, Hungary

Introduction: The selective Bcl-2 inhibitor venetoclax has shown promising therapeutic potential in multiple myeloma, particularly in cases associated with t(11;14) *IGH::CCND1* translocation. However, the efficacy of venetoclax in myeloma patients with the t(6;14) *IGH::CCND3* translocation remains less investigated.

Methods: In this study, we conducted a retrospective analysis to investigate the efficacy of venetoclax-based therapy in relapsed/refractory myeloma patients with t(6;14) translocation. The treatment courses of three patients, that included previous therapies and responses to venetoclax, were assessed. Clinical data, laboratory results, and adverse events were analyzed to evaluate treatment outcomes.

Results: Our findings demonstrated remarkable therapeutic responses in three consecutive patients with t(6;14) translocation-associated myeloma who received venetoclax-based therapy. Patient 1, a lenalidomide-bortezomib-daratumumab and alkylator treatment refractory patient, achieved sustained stringent complete remission (sCR) after combining carfilzomib-dexamethasone with venetoclax, which was his best response ever. Similarly, Patient 2, refractory to frontline bortezomib-thalidomide-dexamethasone therapy, attained CR following a transition to bortezomib-dexamethason-venetoclax treatment. Patient 3, who was immunomodulatory (IMID)-intolerant, showed a highly favorable response to venetoclax-dexamethasone therapy after his first relapse following autologous stem cell transplantation. No significant adverse effects were observed in any of the patients.

Discussion: Our study provides compelling preliminary evidence for the efficacy of venetoclax in t(6;14) translocation-associated myeloma. The outcomes observed in our patients suggest that venetoclax-based therapy holds substantial promise as an effective treatment option for this specific genetic subgroup. Furthermore, the similarities in treatment response between

t(11;14) and t(6;14) translocation subgroups highlight the importance of personalized approaches targeting specific genetic abnormalities to optimize therapeutic outcomes.

KEYWORDS

multiple myeloma, venetoclax, translocation t(6;14), IGH::CCND3, personalized therapy

Introduction

Multiple myeloma is a complex hematological malignancy characterized by the clonal proliferation of plasma cells in the bone marrow. It is considered a quintessential disease of aging, as it is typically diagnosed at an average age of 70 years [1]. The incidence of multiple myeloma significantly increases with advancing age, making it more prevalent in older individuals [1]. Despite the challenges associated with an aging population, advancements in treatment options have significantly improved outcomes for patients with multiple myeloma. Among these therapeutic advancements, the selective Bcl-2 inhibitor venetoclax has emerged as a promising avenue, demonstrating notable efficacy in multiple myeloma patients. This efficacy has been highlighted by the landmark BELLINI study, which investigated the use of venetoclax-based therapy for multiple myeloma [2]. It revealed encouraging results, demonstrating favorable response rates and improved progression-free survival in patients receiving venetoclax in combination with standard treatment regimens [2]. This promising efficacy has positioned venetoclax as an attractive addition to the therapeutic armamentarium against multiple myeloma.

Despite the therapeutic benefits observed with venetoclax [2–18], concerns have emerged regarding its safety profile, particularly in relation to infectious complications [19–21]. Subsequent investigations have indicated a higher incidence of infectious mortality within the venetoclax treatment groups, raising important questions regarding patient selection and risk management strategies. As such, there is an urgent need to identify and carefully select patients who are most likely to derive substantial benefits from venetoclax therapy while minimizing the potential risks associated with infectious complications.

The expression of Bcl-2, a key anti-apoptotic protein and the molecular target of venetoclax, has emerged as an important predictor of therapeutic response to venetoclax in myeloma patients. Multiple myeloma is characterized by significant genomic heterogeneity [22]. Expression profiles of Bcl-2 family members can vary significantly across multiple myeloma patients with different genetic backgrounds, emphasizing the distinct genetic subtypes that exist. Notably, the t(11;14) translocation has been commonly associated with elevated Bcl-2 expression, serving as a potential genetic marker for identifying patients who may particularly benefit from venetoclax treatment [2–4]. However, routine diagnostic measurement of Bcl-2 expression levels remains a challenge, hindering its widespread use in clinical practice. Further investigation into the relationship between genetic subtypes and Bcl-2 expression patterns holds great promise for refining patient selection strategies and optimizing the efficacy of venetoclax in the management of multiple myeloma.

Recognizing the striking similarity in gene expression profiles between patients with t(11;14) and t(6;14) translocations [23–25], our recent endeavors have focused on implementing venetoclax-based therapy specifically for patients harboring the t(6; 14) translocation. This decision finds support in studies, which extensively compared the transcriptomes of multiple myeloma cells across diverse genetic backgrounds [25]. Analysis of the molecular landscape of various genetic subtypes underscores the noteworthy presence of elevated Bcl-2 expression and thus the potential effectiveness of venetoclax in t(6;14) translocation-associated multiple myeloma. By leveraging this knowledge, our objective is to broaden treatment options for patients with the t(6;14) translocation, fostering personalized approaches that specifically target genetic abnormalities to optimize therapeutic outcomes.

Within this context, our present pilot study aims to investigate the safety and efficacy of venetoclax in a distinct subset of multiple myeloma patients. By analyzing the clinical data of a meticulously selected relapsed/refractory patient cohort exhibiting the t(6;14) translocation, our study seeks to elucidate the therapeutic potential of venetoclax for this particular genetic subtype. Furthermore, our research endeavors to provide valuable insights into the identification and selection of patients who are most suited to receive venetoclax-based therapy, thus maximizing therapeutic outcomes while ensuring that their safety remains paramount.

Methods

We conducted a retrospective analysis of the medical records of three patients diagnosed with multiple myeloma characterized by the presence of the t(6;14) founding translocation, who received treatment that included venetoclax. The publication of this report was approved by the ethics committee of Central Hospital of South Pest/National Institute of Hematology and Infectious Diseases, and written informed consent was obtained from the patients. Each individual therapy was a preapproved “off-label” therapy authorized by

10.3389/pore.2023.1611375

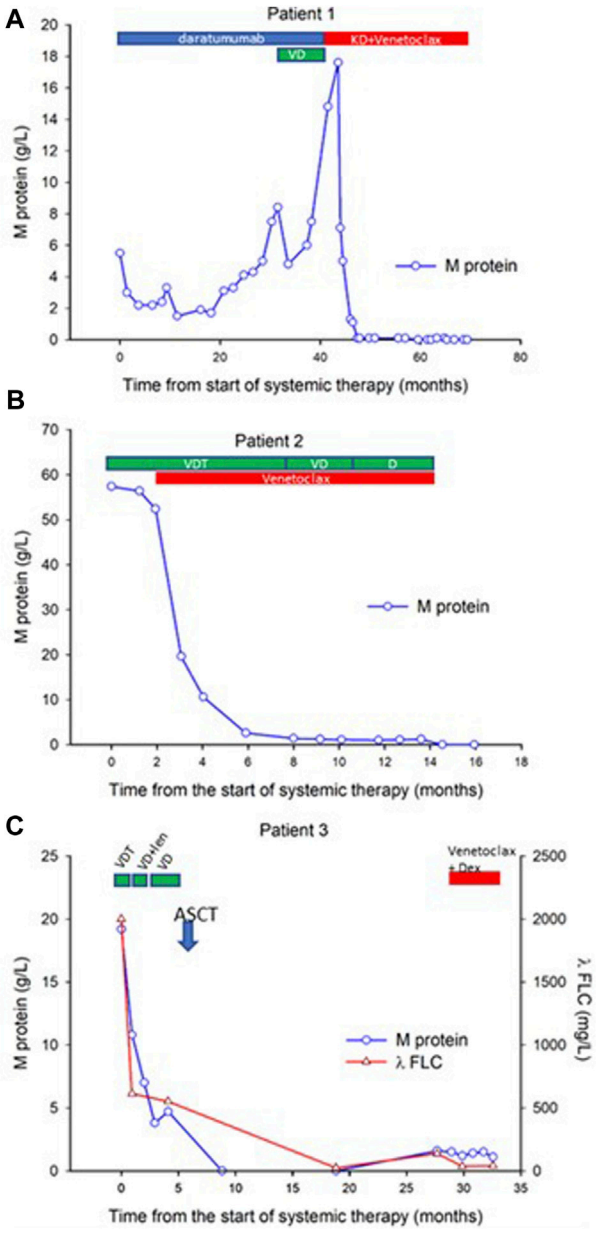

FIGURE 1
Time course of venetoclax therapy-induced changes in M protein in three myeloma patients. Sequential serum concentrations of M protein throughout the disease course are presented for three patients. Panels **(A–C)** depict the individual patients (patients 1, 2, and 3, respectively), showcasing the treatment type and duration (Patient #1 is treated for 24 months, patient #2 is treated for 12 months, patient #3 is treated for 6 months, therapies for patients #2 and #3 are currently ongoing, patient #1 is in treatment-free remission). Patient 3 results also include serial measurements of λ FLC to further demonstrate treatment response. VDT: Bortezomib, Dexamethasone, and Thalidomide; VD, Bortezomib, Dexamethasone; D, Dexamathasone; ASCT, Autologous Stem Cell Transplantation; Len, Lenalidomide; KD, Carfilzomib and Dexamethasone.

the Hungarian National Institute for Pharmacy and Public Health (OGYÉI/22147-2/2021).

Data were collected from the patient's medical records, which included comprehensive information such as laboratory test results, imaging studies, surgical reports, and medication administration records. The patients' clinical courses were meticulously tracked from their initial admission to our department up to the present day. Descriptive statistics were employed to analyze the patient's clinical data, including laboratory test results and medication regimens. The changes in M protein and λFLC (free light chain) over time were graphically depicted to illustrate the treatment response. Assessment of therapy response additionally encompassed monitoring clinical symptoms, laboratory test results, and the occurrence of adverse events.

Results

Case report: patient #1

Patient Information: A 56 year-old male was diagnosed with IgG kappa myeloma in June 2013. He presented with an International Staging System (ISS) score of III and demonstrated the *IGH::CCND3* translocation and monosomy 13 based on fluorescence *in situ* hybridization (FISH) analysis.

Treatment History: The patient underwent multiple treatment lines over the course of his disease. From 06/14/2013 he received 5 cycles of VDT (combination therapy with bortezomib, dexamethasone, and thalidomide), followed by high-dose cyclophosphamide (HDCy priming; 6,000 mg) mobilization and autologous stem cell transplantation (ASCT; in 05/20/2015; 400 mg Melphalan). In subsequent treatment lines, the patient received 4 cycles of Len-Dex (lenalidomide and dexamethasone). The 5th and 6th cycles of Len-Dex were unsuccessfully combined with *per os* Melphalan treatment. In 2017, he was administered daratumumab monotherapy, followed by daratumumab, bortezomib, and dexamethasone triplet treatment in 2020. Despite the various treatment approaches, the patient's myeloma remained refractory to available therapies, as evidenced by the serial measurements of the M protein, a key marker of myeloma (Figure 1A). He also developed a paramedullary plasmacytoma in the cervical spine, further complicating his medical condition. The clinical situation became increasingly desperate, prompting a thorough evaluation. Genetic analysis from $CD138^{+}$ sorted plasma cells confirmed the presence of the t(6; 14) translocation, further contributing to the complexity of the case.

KD-Venetoclax Treatment: Given the patient's refractory myeloma, the presence of a plasmacytoma, and the identification of t(6;14) translocation, a decision was made to

initiate KD (carfilzomib plus dexamethasone)-Venetoclax (400 mg) therapy in 2021. This therapeutic approach aimed to target the identified genetic abnormality and overcome the patient's refractoriness to previous treatments. Regular monitoring of treatment response, disease progression, and potential adverse effects was carried out to assess the efficacy and safety of the KD-Venetoclax regimen.

Best Response Ever: Stringent Complete Remission: Remarkably, the patient demonstrated an unprecedented response to the KD-Venetoclax treatment. Serial measurements of the M protein revealed a complete remission, indicating the absence of detectable levels (Figure 1A) and normal free light-chain ratio. This profound response to the KD-Venetoclax regimen represents the best response achieved thus far in the patient's treatment history. Furthermore, the patient now enjoys ongoing CR for a year without any maintenance therapy, reflecting a very low disease burden achieved with venetoclax-based therapy Such positive outcome offers hope for improved long-term outcomes and underscores the potential effectiveness of targeted therapies tailored to specific genetic abnormalities.

Conclusion: Patient #1, a 56 year-old male with IgG kappa myeloma, faced multiple treatment lines with limited success. The presence of cervical spine plasmacytoma and the identification of t(6;14) translocation posed significant challenges in managing his refractory disease. The initiation of KD-Venetoclax therapy aimed to address these complexities, providing a targeted approach against the identified genetic abnormality. The remarkable sustained complete remission observed following KD-Venetoclax treatment represents a significant milestone in the patient's journey and highlights the potential of tailored therapies in improving treatment outcomes. Continuous monitoring and further investigation are required to assess the durability and long-term benefits of this exceptional treatment response.

Case report: patient #2

Patient Information: A 78 year-old male was diagnosed with IgG kappa myeloma in January 2022. The ISS score was determined as I, and FISH analysis from $CD138^+$ selected plasma cells revealed an atypical *IGH::CCND3* fusion with the absence of *CCND3::IGH* on the derivative chromosome 6. Notably, three intact *FGFR3* genes (possible trisomy 4) and three intact *CCND1* genes (possible trisomy 11) were also detected by interphase FISH.

Treatment History: The patient initially received VDT (bortezomib-thalidomide-dexamethason) treatment, but not even minimal response (MR) was observed. The patient's condition and the refractoriness to VDT treatment necessitated salvage treatment. Due to the presence of t(6;14) translocation, the treatment was switched to a combination of VDT with Venetoclax (400 mg) in March 2022 and to a combination of VD (bortezomib and dexamethasone) with Venetoclax (400 mg) from September 2022 to March 2023. Notably, the patient achieved a rapid VGPR concluding into complete immunohematological response following the treatment combination with Venetoclax/dexamethasone (bortezomib was stopped at month 7 of therapy). Serial measurements of the M protein indicating complete remission are shown in Figure 1B.

Case report: patient #3

Patient Information: A 73 year-old male was diagnosed with IgA lambda myeloma in September 2020, accompanied by significant light chain excretion. The ISS score was determined as II, and FISH analysis revealed the presence of a t(6;14) translocation, as well as gains of chromosomes 1q21, 11, and 17.

Treatment History: The patient initially received VDT. However, due to intolerance to thalidomide (adverse skin reaction), the treatment line was discontinued. From November VD treatment was combined with lenalidomide, however, due to again adverse skin reactions, this treatment line had to be discontinued. From the end of November, VD treatment (bortezomib and dexamethasone) was administered until February. At the end of February 2021, the patient received high-dose cyclophosphamide (HDCy) priming treatment for peripheral stem cell mobilization, and in March 2021 autologous stem cell transplantation (ASCT) was performed with standard melphalan conditioning. The patient achieved a complete immunohematological response following this treatment combination. Serial measurements of the M protein and λFLC indicating a temporal complete remission are shown in Figure 1C. Unfortunately, due to IMID intolerance, the patient was unable to receive lenalidomide maintenance. After a remission period of 10 months, in December 2022 the disease presented with its first relapse (Figure 1C). As a salvage therapy, Venetoclax (400 mg) plus dexamethasone treatment was initiated on January 20, 2022. Partial remission was achieved as indicated by the serial measurements of the M protein and λFLC shown in Figure 1C.

Discussion

The three cases presented in this report underscore the potential efficacy of venetoclax treatment in myeloma patients with the t(6;14) translocation. These findings further extend the initial observations from the BELLINI study, emphasizing the importance of targeted therapies in specific genetic subtypes of multiple myeloma. Importantly, our study contributes novelty by specifically evaluating the response to

venetoclax in patients with the t(6;14) translocation, a relatively understudied area.

The t(6;14) translocation is rarely seen in multiple myeloma, accounting for approximately 1%–3% of cases. This translocation leads to distinct alterations in gene expression profiles. One of the notable consequences of the t(6;14) translocation is the dysregulation of the *CCND3* (Cyclin D3) gene, which is involved in cell cycle regulation. This dysregulation results in increased expression of Cyclin D3, leading to uncontrolled cell proliferation and contributing to the pathogenesis of myeloma with t(6;14) translocation. Prognostically, myeloma patients with t(6;14) translocation tend to exhibit distinct molecular patterns, clinical features, and outcomes compared to those without this translocation. Studies with limited power have suggested that myeloma cases with t(6;14) translocation may be associated with a higher risk of disease progression, shorter survival times, and poorer responses to conventional treatments. The presence of this translocation may correlate with a more aggressive disease course and with a more challenging clinical scenario. Given the unique gene expression profile and uncertain prognosis associated with myeloma harboring t(6;14) translocation, there is a need for targeted therapeutic approaches.

The BELLINI study provided valuable insights into the therapeutic potential of venetoclax in multiple myeloma. It demonstrated promising efficacy and improved progression-free survival in patients receiving venetoclax in combination with standard treatment regimens [2]. However, in multiple myeloma BCL-2 expression is varied significantly across molecular and cytogenetic subgroups in multiple myeloma [26, 27]. As a result, the efficacy of venetoclax is also likely to differ accordingly. Previous studies reported the highest expression of BCL-2 among patients with t(11;14) molecular subtypes (CD1, CD2, ie Cyclin D1 high expressor subgroups 1 and 2). Myeloma patients with translocation t(6;14) also characteristically belong either to the CD1 or CD2 subgroups of the TC (Translocation/Cyclin expression) classification system. There is compelling evidence that venetoclax is unusually effective in patients with the t(11;14) translocation [26–29]. However, neither the BELLINI study nor subsequent similar studies focused specifically on the effects of venetoclax in rare patients with the t(6;14) translocation. The unique aspect of our study lies in its dedicated evaluation of venetoclax treatment in this specific genetic subgroup.

The treatment outcomes observed in our three patients with t(6;14) translocation-associated myeloma provide compelling evidence of the rapid and deep therapeutic responses achieved with venetoclax-based therapies. Patient 1, who had been battling myeloma for nearly a decade and experienced partial responses alternating with relapses during previous treatments, achieved sustained complete remission (CR) when carfilzomib-dexamethasone treatment was combined with venetoclax. Similarly, Patient 2, who exhibited complete refractoriness to frontline VDT therapy, attained CR after transitioning to VD-venetoclax treatment. Patient 3, an IMID-intolerant individual with the t(6;14) translocation, demonstrated a highly favorable response to Venetoclax-Dexamethasone therapy in his first relapse after ASCT. These outcomes highlight the efficacy of venetoclax in this specific genetic subgroup and reinforce its potential as a valuable therapeutic option. Notably, no significant adverse effects were observed in any of the patients.

The collective evidence derived from these cases strongly suggests that venetoclax holds substantial promise as an effective treatment option for myeloma patients harboring the t(6;14) translocation. The notable efficacy of venetoclax in both t(11;14) and t(6;14) translocation subgroups can be attributed to the striking similarity in gene expression profiles observed between these two subgroups. Recent studies suggest that venetoclax-sensitive myeloma cell lines retain a B cell–like pattern of gene expression and chromatin accessibility [26]. It is also likely that gene expression signatures that determine venetoclax sensitivity in myeloma cells are linked to the expression/activity of components of the electron transport chain [28]. The observed treatment responses, such as complete remission and immunohematological response, underscore the potential of venetoclax to overcome refractoriness to prior therapies and deliver significant clinical benefits within these specific genetic subgroups. These patients did not receive CYP3A4 inhibitors to enhance venetoclax blood levels and activity, indicating that in this subgroup of patients the 400 mg daily dose may be sufficient to induce remission. These findings emphasize the critical significance of personalized therapeutic strategies that effectively target specific genetic abnormalities, including the t(6;14) translocation, to optimize treatment outcomes and enhance the overall prognosis for affected patients.

In addition to the treatment outcomes observed in our three patients, our study plays a pivotal role in addressing a significant gap in the existing literature by specifically investigating the efficacy of venetoclax in the context of t(6;14) translocation-associated myeloma. By focusing on this specific genetic abnormality, we provide novel insights into the management of a subgroup that has historically faced limited treatment options. Through our ongoing research, we aim to contribute to the growing body of knowledge surrounding this specific genetic alteration, ultimately advancing the understanding and therapeutic management of t(6;14) translocation-associated myeloma. A comprehensive investigation of venetoclax's efficacy in t(6;14) translocation-associated myeloma will provide valuable information for clinicians and researchers, offering potential new avenues for improving patient outcomes.

It is important to acknowledge certain limitations associated with this retrospective analysis. These include the potential for missing or incomplete data within the medical records and the lack of Bcl-2 expression analysis, which would have provided valuable insight into the relationship between Bcl-2 expression levels and treatment response. Additionally, these case reports represent the experiences of a limited number of patients and

may not be entirely generalizable to other individuals with similar conditions. Further studies involving larger patient cohorts and prospective designs are required to confirm and expand upon our findings.

In conclusion, our findings provide preliminary evidence supporting the targeted efficacy of venetoclax in t(6;14) *IGH::CCND3* translocation-associated myeloma, thus extending the existing evidence from the BELLINI study. However, further research and larger studies are necessary to validate these findings and optimize treatment strategies specifically tailored to this genetic subtype. The exploration of personalized approaches targeting specific genetic abnormalities, including the t(6;14) translocation, holds great potential for improving outcomes in patients with multiple myeloma [30–33]. Therefore, when we encounter myeloma patients with an IgH-related translocation lacking an identified partner, pursuing further genetic investigations is of utmost importance. This diligent approach allows us to identify the rare occurrences of t(6;14) translocation, which may constitute only 3% of cases. Nevertheless, such identification presents a valuable opportunity for these individuals to receive highly effective therapies. It is crucial to note that the random application of venetoclax-based therapeutic regimens in other cytogenetic contexts is not recommended in the absence of Bcl-2 expression measurement.

Data availability statement

The raw data supporting the conclusion of this article will be made available by the authors, without undue reservation.

Ethics statement

The studies involving humans were approved by Országos Gyógyszerészeti és Élelmezés-egészségügyi Intézet. The studies were conducted in accordance with the local legislation and institutional requirements. The participants provided their written informed consent to participate in this study.

Author contributions

GM, AC, ZC, and ZS: treated the patients. AC and MF wrote the initial manuscript. AC, AK, HA, and GM: analyzed the data, all authors contributed the revised versions of the manuscript. GM conceptualized the study, obtained the necessary permission and treatment funding coverage and supervised the entire study.

Conflict of interest

GM received research funding and honoraria from AbbVie.

The remaining authors declare that the research was conducted in the absence of any commercial or financial relationships that could be construed as a potential conflict of interest.

Acknowledgments

We gratefully acknowledge the patients for allowing us to publish their case reports.

References

1. Urban VS, Cegledi A, Mikala G. Multiple myeloma, a quintessential malignant disease of aging: a geroscience perspective on pathogenesis and treatment. *Geroscience* (2023) 45:727–46. doi:10.1007/s11357-022-00698-x

2. Kumar SK, Harrison SJ, Cavo M, de la Rubia J, Popat R, Gasparetto C, et al. Venetoclax or placebo in combination with bortezomib and dexamethasone in patients with relapsed or refractory multiple myeloma (BELLINI): a randomised, double-blind, multicentre, phase 3 trial. *Lancet Oncol* (2020) 21:1630–42. doi:10.1016/S1470-2045(20)30525-8

3. Bahlis NJ, Baz R, Harrison SJ, Quach H, Ho SJ, Vangsted AJ, et al. Phase I study of venetoclax plus daratumumab and dexamethasone, with or without bortezomib, in patients with relapsed or refractory multiple myeloma with and without t(11;14). *J Clin Oncol* (2021) 39:3602–12. doi:10.1200/JCO.21.00443

4. Kaufman JL, Gasparetto C, Schjesvold FH, Moreau P, Touzeau C, Facon T, et al. Targeting BCL-2 with venetoclax and dexamethasone in patients with relapsed/refractory t(11;14) multiple myeloma. *Am J Hematol* (2021) 96:418–27. doi:10.1002/ajh.26083

5. Regidor B, Goldwater MS, Wang J, Bujarski S, Swift R, Eades B, et al. Low dose venetoclax in combination with bortezomib, daratumumab, and dexamethasone for the treatment of relapsed/refractory multiple myeloma patients-a single-center retrospective study. *Ann Hematol* (2021) 100:2061–70. doi:10.1007/s00277-021-04555-3

6. Nguyen N, Chaudhry S, Totiger TM, Diaz R, Roberts E, Montoya S, et al. Combination venetoclax and selinexor effective in relapsed refractory multiple myeloma with translocation t(11;14). *NPJ Precis Oncol* (2022) 6:73. doi:10.1038/s41698-022-00315-2

7. Abuelgasim KA, Alherz N, Alhejazi A, Damlaj M. Venetoclax in combination with carfilzomib and dexamethasone in relapsed/refractory multiple myeloma harboring t(11,14)(q13;q32): two case reports and a review of the literature. *J Med Case Rep* (2020) 14:54. doi:10.1186/s13256-020-02376-y

8. Basali D, Chakraborty R, Rybicki L, Rosko N, Reed J, Karam M, et al. Real-world data on safety and efficacy of venetoclax-based regimens in relapsed/refractory t(11;14) multiple myeloma. *Br J Haematol* (2020) 189:1136–40. doi:10.1111/bjh.16454

9. Boccon-Gibod C, Talbot A, Le Bras F, Frenzel L, Royer B, Harel S, et al. Carfilzomib, venetoclax and dexamethasone for relapsed/refractory multiple myeloma. *Br J Haematol* (2020) 189:e73–6. doi:10.1111/bjh.16483

10. Costa LJ, Davies FE, Monohan GP, Kovacsovics T, Burwick N, Jakubowiak A, et al. Phase 2 study of venetoclax plus carfilzomib and dexamethasone in patients with relapsed/refractory multiple myeloma. *Blood Adv* (2021) 5:3748–59. doi:10.1182/bloodadvances.2020004146

11. Gasparetto C, Bowles KM, Abdallah AO, Morris L, Mander G, Coppola S, et al. A phase II study of venetoclax in combination with pomalidomide and dexamethasone in relapsed/refractory multiple myeloma. *Clin Lymphoma Myeloma Leuk* (2021) 21:775–84. doi:10.1016/j.clml.2021.07.029

12. He W, He F, Hu H. Efficacy and safety of Venetoclax-based regimens in relapsed or refractory multiple myeloma: a systematic review and meta-analysis of prospective clinical trials. *Ann Med* (2023) 55:1029–36. doi:10.1080/07853890.2023.2186480

13. Kovacs SB, Luan J, Dold SM, Weis A, Pantic M, Duyster J, et al. Venetoclax in combination with carfilzomib, doxorubicin and dexamethasone restores responsiveness in an otherwise treatment-refractory multiple myeloma patient. *Haematologica* (2020) 105:e138–40. doi:10.3324/haematol.2019.232330

14. Kumar S, Kaufman JL, Gasparetto C, Mikhael J, Vij R, Pegourie B, et al. Efficacy of venetoclax as targeted therapy for relapsed/refractory t(11;14)

multiple myeloma. *Blood* (2017) 130:2401–9. doi:10.1182/blood-2017-06-788786

15. Sidiqi MH, Al Saleh AS, Kumar SK, Leung N, Jevremovic D, Muchtar E, et al. Venetoclax for the treatment of multiple myeloma: outcomes outside of clinical trials. *Am J Hematol* (2021) 96:1131–6. doi:10.1002/ajh.26269

16. Swan D, Delaney C, Natoni A, O'Dwyer M, Krawczyk J. Successful venetoclax salvage in the setting of refractory, dialysis-dependent multiple myeloma with t(11;14). *Haematologica* (2020) 105:e141–3. doi:10.3324/haematol.2019.228338

17. Szita VR, Mikala G, Kozma A, Fabian J, Hardi A, Alizadeh H, et al. Targeted venetoclax therapy in t(11;14) multiple myeloma: real world data from seven hungarian centers. *Pathol Oncol Res* (2022) 28:1610276. doi:10.3389/pore.2022.1610276

18. Touzeau C, Le Gouill S, Mahe B, Boudreault JS, Gastinne T, Blin N, et al. Deep and sustained response after venetoclax therapy in a patient with very advanced refractory myeloma with translocation t(11;14). *Haematologica* (2017) 102:e112–4. doi:10.3324/haematol.2016.160408

19. Lee R, Cho SY, Lee DG, Choi H, Park S, Cho BS, et al. Infections of venetoclax-based chemotherapy in acute myeloid leukemia: rationale for proper antimicrobial prophylaxis. *Cancers (Basel)* (2021) 13:6285. doi:10.3390/cancers13246285

20. Papayannidis C, Nanni J, Cristiano G, Marconi G, Sartor C, Parisi S, et al. Impact of infectious comorbidity and overall time of hospitalization in total outpatient management of acute myeloid leukemia patients following venetoclax and hypomethylating agents. *Eur J Haematol* (2022) 108:449–59. doi:10.1111/ejh.13753

21. Zhu LX, Chen RR, Wang LL, Sun JN, Zhou D, Li L, et al. A real-world study of infectious complications of venetoclax combined with decitabine or azacitidine in adult acute myeloid leukemia. *Support Care Cancer* (2022) 30:7031–8. doi:10.1007/s00520-022-07126-y

22. Bhalla S, Melnekoff DT, Aleman A, Leshchenko V, Restrepo P, Keats J, et al. Patient similarity network of newly diagnosed multiple myeloma identifies patient subgroups with distinct genetic features and clinical implications. *Sci Adv* (2021) 7:eabg9551. doi:10.1126/sciadv.abg9551

23. Shaughnessy JD, Jr, Barlogie B. Using genomics to identify high-risk myeloma after autologous stem cell transplantation. *Biol Blood Marrow Transpl* (2006) 12:77–80. doi:10.1016/j.bbmt.2005.10.002

24. Sarin V, Yu K, Ferguson ID, Gugliemini O, Nix MA, Hann B, et al. Evaluating the efficacy of multiple myeloma cell lines as models for patient tumors via transcriptomic correlation analysis. *Leukemia* (2020) 34:2754–65. doi:10.1038/s41375-020-0785-1

25. Szalat R, Avet-Loiseau H, Munshi NC. Gene expression profiles in myeloma: ready for the real world? *Clin Cancer Res* (2016) 22:5434–42. doi:10.1158/1078-0432.CCR-16-0867

26. Gupta VA, Barwick BG, Matulis SM, Shirasaki R, Jaye DL, Keats JJ, et al. Venetoclax sensitivity in multiple myeloma is associated with B-cell gene expression. *Blood* (2021) 137:3604–15. doi:10.1182/blood.2020007899

27. Todoerti K, Taiana E, Puccio N, Favasuli V, Lionetti M, Silvestris I, et al. Transcriptomic analysis in multiple myeloma and primary plasma cell leukemia with t(11;14) reveals different expression patterns with biological implications in venetoclax sensitivity. *Cancers (Basel)* (2021) 13:4898. doi:10.3390/cancers13194898

28. Bajpai R, Sharma A, Achreja A, Edgar CL, Wei C, Siddiqa AA, et al. Electron transport chain activity is a predictor and target for venetoclax sensitivity in multiple myeloma. *Nat Commun* (2020) 11:1228. doi:10.1038/s41467-020-15051-z

29. Matulis SM, Gupta VA, Neri P, Bahlis NJ, Maciag P, Leverson JD, et al. Functional profiling of venetoclax sensitivity can predict clinical response in multiple myeloma. *Leukemia* (2019) 33:1291–6. doi:10.1038/s41375-018-0374-8

30. van Laar R, Flinchum R, Brown N, Ramsey J, Riccitelli S, Heuck C, et al. Translating a gene expression signature for multiple myeloma prognosis into a robust high-throughput assay for clinical use. *BMC Med Genomics* (2014) 7:25. doi:10.1186/1755-8794-7-25

31. Zhan F, Barlogie B, Mulligan G, Shaughnessy JD, Jr, Bryant B. High-risk myeloma: a gene expression based risk-stratification model for newly diagnosed multiple myeloma treated with high-dose therapy is predictive of outcome in relapsed disease treated with single-agent bortezomib or high-dose dexamethasone. *Blood* (2008) 111:968–9. doi:10.1182/blood-2007-10-119321

32. Shaughnessy JD, Jr, Zhan F, Burington BE, Huang Y, Colla S, Hanamura I, et al. A validated gene expression model of high-risk multiple myeloma is defined by deregulated expression of genes mapping to chromosome 1. *Blood* (2007) 109:2276–84. doi:10.1182/blood-2006-07-038430

33. Shaughnessy J, Jr, Zhan F, Barlogie B, Stewart AK. Gene expression profiling and multiple myeloma. *Best Pract Res Clin Haematol* (2005) 18:537–52. doi:10.1016/j.beha.2005.02.003

Pathology & Oncology Research | frontiers

TYPE Review
PUBLISHED 10 August 2023
DOI 10.3389/pore.2023.1611338

Check for updates

OPEN ACCESS

EDITED BY
Anna Sebestyén,
Semmelweis University, Hungary

*CORRESPONDENCE
Lijuan Li,
lijuan@sina.com
Liansheng Zhang,
doctorzhanglsh@sina.com

RECEIVED 05 June 2023
ACCEPTED 01 August 2023
PUBLISHED 10 August 2023

CITATION
Tie W, Ma T, Yi Z, Liu J, Li Y, Bai J, Li L and Zhang L (2023), Obesity as a risk factor for multiple myeloma: insight on the role of adipokines.
Pathol. Oncol. Res. 29:1611338.
doi: 10.3389/pore.2023.1611338

COPYRIGHT
© 2023 Tie, Ma, Yi, Liu, Li, Bai, Li and Zhang. This is an open-access article distributed under the terms of the Creative Commons Attribution License (CC BY). The use, distribution or reproduction in other forums is permitted, provided the original author(s) and the copyright owner(s) are credited and that the original publication in this journal is cited, in accordance with accepted academic practice. No use, distribution or reproduction is permitted which does not comply with these terms.

Obesity as a risk factor for multiple myeloma: insight on the role of adipokines

Wenting Tie[1,2], Tao Ma[3], Zhigang Yi[1], Jia Liu[1], Yanhong Li[1], Jun Bai[1], Lijuan Li[1]* and Liansheng Zhang[1]*

[1]Department of Hematology, Lanzhou University Second Hospital, Lanzhou, China, [2]Department of Endocrinology, Lanzhou University Second Hospital, Lanzhou, China, [3]Department of Hematology, The Affiliated Hospital of Southwest Medical University, Luzhou, China

Multiple myeloma (MM) is a hematologic disorder characterized by the accumulation of malignant plasma cells in the bone marrow. Genetic and environmental factors are contributed to the etiology of MM. Notably, studies have shown that obesity increases the risk of MM and worsens outcomes for MM patients. Adipokines play an important role in mediating the close association between MM and metabolic derangements. In this review, we summarize the epidemiologic studies to show that the risk of MM is increased in obese. Accumulating clinical evidence suggests that adipokines could display a correlation with MM. *In vitro* and *in vivo* studies have shown that adipokines are linked to MM, including roles in the biological behavior of MM cells, cancer-associated bone loss, the progression of MM, and drug resistance. Current and potential therapeutic strategies targeted to adipokines are discussed, proposing that adipokines can guide early patient diagnosis and treatment.

KEYWORDS

multiple myeloma, adipokine, obesity, adiponectin, leptin

Introduction

Multiple myeloma (MM) is a blood cancer of abnormal clonal plasma cells in the bone marrow. MM accounts for 1% of neoplastic diseases and is the second most common hematological malignancy that commonly affects older adults (median age at diagnosis is 69 years) [1, 2]. Patients often suffer from anemia, kidney injury, bone destruction, and hypercalcemia. MM develops from the premalignant state monoclonal gammopathy of undetermined significance (MGUS) and smoldering multiple myeloma (SMM). To diagnose MM, clinical symptoms are used, and the monoclonal proteins in blood and urine need to be detected. Clinical symptoms are used to diagnose MM, and the monoclonal proteins in blood and urine must be detected. Autologous stem-cell transplantation (ASCT), proteasome inhibitors, immunomodulatory drugs, and monoclonal antibodies have improved outcomes with MM. Although therapeutic advances made in the past few years have led to improved outcomes and longer survival, MM remains incurable. Therefore, it is of great significance to study the

etiology and pathogenesis of myeloma to find new therapeutic targets and improve the survival rate of patients.

Although little is known about the etiology of MM, genetic, antigenic stimulation, and environmental factors are believed to contribute to MM onset and progression [3]. Some risk factors are associated with MM, such as obesity, male sex, age, chronic inflammation, and dioxin exposure [2]. Accumulating evidence suggests that obesity plays a critical role in the risk of developing MM, and the increased body mass index (BMI) has been linked to the progression and higher mortality [4–6]. The bone marrow microenvironment plays a vital role in the proliferation, survival, progression, and drug resistance of MM cells [2]. The bone marrow microenvironment is composed of cellular and non-cellular compartments. The cellular compartment comprises MM cells, lymphocytes, natural killer cells, macrophages, monocytes, dendritic cells, osteoclasts, osteoblasts, and adipocytes. And the non-cellular compartment is made up of extracellular matrix proteins, adhesion molecules, cytokines, and growth factors. Bone marrow adipocytes are the main component of the bone marrow microenvironment [7]. Bone marrow adipocytes in close contact with bone cells, hematopoietic cells, and immune cells are considered within bone metabolism, hematopoiesis, cancer, and systemic energy metabolism. Adipocytes found in bone marrow have important connections with bone cells, hematopoietic cells, and immune cells. These connections play significant roles in bone metabolism, hematopoiesis, cancer, and systemic energy metabolism. Using the C57BL/KaLwRij murine model of myeloma, mice were inoculated with 5TGM1-GFP cells or PBS control by intravenous injection. Bone marrow adipocytes were found to be increased in early-stage myeloma [8]. MM cell lines (RPMI-8226 and NCI-H929) were cocultured with adipocytes and showed greater capabilities of proliferation and adhesion [9]. These findings indicate that bone marrow adipocytes promote the proliferation of MM cells.

Obesity is closely related to the onset of many types of malignancies [10]. The mechanisms linking obesity to cancer involve insulin resistance, abnormalities of the IGF-1 axis, inappropriate sex hormone secretion, inflammation and oxidative stress, adipokines action, microenvironment perturbations, and the altered intestinal microbiome [11]. In obesity, adipose tissue hypoxia triggers alternations of adipokines levels altering adipokines levels, may be associated with the progression of various cancers [12–14]. This review critically summarizes the rapidly expanding field of bone marrow adipocytes as an endocrine organ and how they communicate with MM cells through the secretion of adipokines. First, we will briefly address the changes in adipokines discuss the changes in adipokines of MM. Second, we will present the biological effect of adipokines. Finally, we will elaborate on the adipokines associated with MM progression as growth, proliferation, and drug resistance, including findings from *in vitro*, *in vivo*, and human studies, and therapeutic strategy target to adipokines.

Adipokines in MM: friend or foe?

Adipose tissue was initially thought of as a fat depot but is now widely recognized as an endocrine organ that secretes numerous peptide factors called adipokines. They play an essential role in metabolic diseases and neoplasms in paracrine and endocrine. They can regulate glucose and lipid metabolism, inflammation, and immune response [15]. After the first adipokine leptin was discovered, over 600 adipokines have been discovered and studied [16]. Some adipokines stimulate cancer progression through oncogenic signaling or indirect mechanisms, such as angiogenesis and immunomodulation [17], while others with oncogenic effects have their expression suppressed in malignancies. Therefore, alterations in adipokines may affect the processes and the immune responses of cancers. The role of adipokines in MM is comparatively less known. A selected group of adipokines with demonstrated roles in MM are reviewed below (Figure 1).

Adiponectin

Adiponectin is a 28 KDa protein secreted by adipose tissue, which is one of the most widely studied adipokines [18]. Besides the adipose tissue, adiponectin is also produced to some extent by bone marrow [19]. Adiponectin has two major receptors, AdipoR1 and AdipoR2. A third receptor had been isolated, identical to a unique cadherin molecule [20, 21]. Adiponectin binds to receptors to participate in insulin-sensitizing, lipid metabolism, energy regulation, inflammation, and cancer development [22]. Circulating levels of adiponectin show an inverse correlation with multiple diseases, such as obesity, type 2 diabetes, atherosclerosis, hypertension, dyslipidemia, and nonalcoholic fatty liver disease [23–27]. It also negatively correlates with several cancers, one of which is MM [28, 29]. Thus adiponectin has generally been considered a beneficial adipokine.

In a pooled investigation of 624 MM patients and 1,246 controls from seven cohorts, Hofmann et al. revealed that serum adiponectin levels were lower among the patients than controls (medians of 11.5 and 12.8 μg/mL, respectively; $p = 0.001$). Furthermore, they stratified the samples according to BMI and observed an inverse association between adiponectin levels and MM risk among overweight (OR = 0.41, CI = 0.26–0.65, $p < 0.001$) or obese subjects (OR = 0.41, CI = 0.17–0.98, $p \leq 0.039$) [30]. Hofmann et al. investigated the levels of adiponectin in serum samples from 213 patients (84 with MGUS, 104 with SMM, and 25 with MM). They found total adiponectin levels were 16% lower among SMM patients (CI = −31% to 2%) and 20% lower among MM patients (CI = −40% to 7%) compared to patients with MGUS [29]. Furthermore, another study showed decreased levels of high molecular weight adiponectin in MGUS patients who progressed to MM (4.5 ± 0.5 μg/mL) compared to MGUS who did not progress to MM (6.4 ± 1.6 μg/mL). The studies

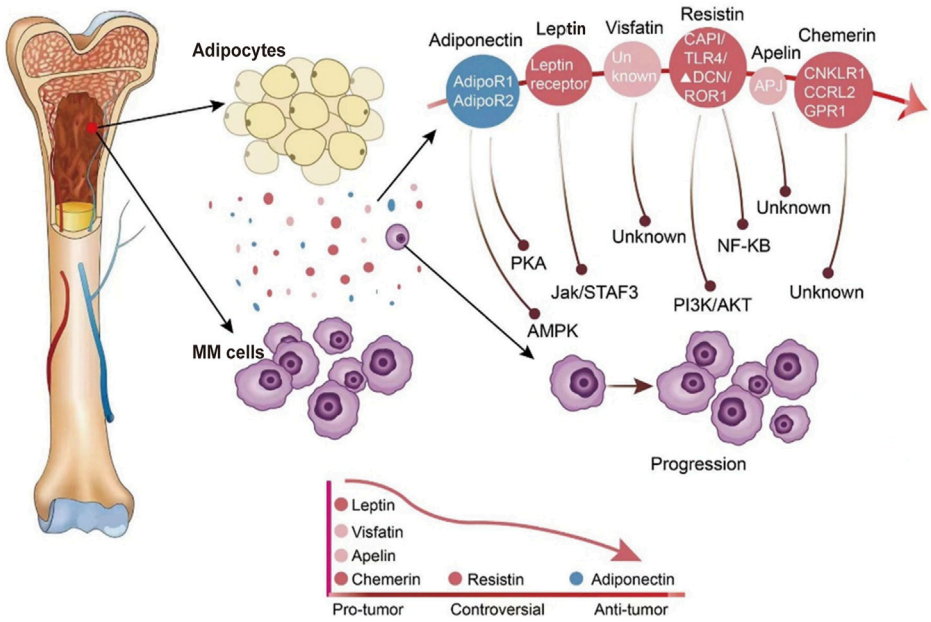

FIGURE 1
The expression of adipokines in the bone marrow environment and adipokines modify the behavior of MM cells. Adipocytes in the bone marrow secrete a variety of different adipokines. The expression of adipokines in the bone marrow microenvironment of MM patients is indicated by different colors, with blue indicating reduced secretion and red indicating increased secretion.

used gene array analysis of bone marrow between KaLwRij mice that permit murine 5T myeloma cells compared to nonpermissive mice. Adiponectin was decreased in the bone marrow of KaLwRij mice [31]. These studies suggested low adiponectin levels may associate with MM, particularly among overweight and obese individuals. And adiponectin may play a protective role in the development of MGUS to SMM/MM. This suggests that adiponectin may have a protective effect in the development of MGUS to SMM/MM. Lower blood levels of adiponectin in MM patients before the start of any treatment suggest that adiponectin represents a potential biomarker at the onset of disease to predict progression.

The mechanisms behind the association between adiponectin and MM are still unclear. Some studies provide insights into the mechanisms of adiponectin in MM. Adiponectin induces the apoptosis and cell cycle arrest of MM cells via activation of protein kinase A (PKA) and increased AMP-activated protein kinase (AMPK) activation [32]. Furthermore, $CD169^+$ radiation-resistant tissue-resident macrophages regulate MM cells in the bone marrow via interleukin-6(IL-6) and tumor necrosis factor α (TNF-α) pathway [33]. And adiponectin Adiponectin receptor signaling suppresses TNF-α expression by T cells or myeloid cells [34]. Therefore, we can speculate whether adiponectin changes the biological effect of MM cells by affecting the inflammatory factors. The correlation between the effects of adiponectin receptors and MM progression remains to be studied. Interestingly, adiponectin was found to be downregulated by MM cells themselves via the blockade of TNF-α [8]. It is suggested that adiponectin interacts with myeloma cells to alter the microenvironment of the disease. In addition, it is well known that MM cells enhance the process of osteoclastogenesis and bone resorption while suppressing osteoblast cells differentiation, leading to systemic bone destruction with rapid bone loss [35]. Some studies have paid attention to the association between adiponectin and bone disease. Serum level of adiponectin correlated with markers of bone disease, such as OCN, CTX, and PINP. *In vitro* study, the anti-osteolysis effects of adiponectin may be explained by the inhibition of osteoclasts via the mTOR signaling pathway [36]. In murine models of MM, adiponectin suppressed nerve growth factor, which is thought to be associated with bone pain [37]. Adiponectin may have a positive effect on myeloma bone disease. In summary, adiponectin exerts its antitumor effects in MM by promoting cell apoptosis, causing cell cycle arrest, inhibiting osteolysis, and possibly modulating cytokines in the bone marrow microenvironment (Table 1).

These beneficial effects of adiponectin have promoted research on adjuvants that mimic adiponectin or the adiponectin receptor agonist to treat MM. L-4F is an apolipoprotein mimetic peptide that can upregulate the adiponectin level [38]. Moreover, L-4F affected inhibiting the progression of MGUS to MM [31]. In addition, L-4F,

TABLE 1 Adipokines and their molecular pathways and functions in MM.

Adipokine	Receptors	Signaling pathways	Functions in MM	References
Adiponectin	AdipoR1 and AdipoR2	PKA (+), AMPK(+)	Promote apoptosis of MM cells	[27]
			Induce cell cycle arrest of MM cells	
			Inhibit the differentiation of osteoclasts	[30, 31]
Leptin	Leptin receptor	STAT-3 (+) Jak/Stat3	Promote proliferation of MM cells	[9, 32]
			Inhibit apoptosis of MM cells	[32, 33]
			Regulate anti-tumor immunity	[34–36]
Visfatin	Insulin receptor	Jak/Stat3	Promote MM cells proliferation	[37]
			Inhibit apoptosis of MM cells	[38, 39]
			Downregulate drug sensitivity of MM cells	[40]
Resistin	CAP1, TLR4, ΔDCN, ROR1	NF-κB, PI3K/Akt	Inhibit apoptosis of MM cells	[41]
			Promote drug resistance	
Apelin	APJ	Unknown	Elevated in patients with MM	[42]
Chemerin	CMKLR1, CCRL2, GPR1	Unknown	Elevated in patients with MM	[43]

CAP1, Adenylyl cyclase-associated protein 1; TLR4, Toll-like receptor 4; ΔDCN, An isoform of decorin; ROR1, Receptor tyrosine kinase-like orphan receptor 1; APJ, apelin-angiotensin receptor-like 1; GPR1, G Protein Receptor 1; CMKLR1, chemerin chemokine-like receptor 1.

downregulating the expression of nerve growth factor (NGF) and IL-6, has a positive effect on destructive osteolytic bone disease [37]. The adiponectin receptor agonist adipoRon can inhibit MM by reversing the effect of TNF-α and IL-6 [37]. Since it was found that adiponectin-induced apoptosis in MM cells may be achieved by downregulating acetyl-CoA-carboxylase. 5-(tetradecyloxy)-2-furan carboxylic acid (TOFA), an acetyl-CoA-carboxylase inhibitor, was found to inhibit fatty acid synthesis and also can inhibit MM cell proliferation [32]. Taken together, the anti-myeloma effect of adiponectin may be a promising target candidate to start with the new area of MM.

Leptin

Leptin was the first adipokine to be identified in 1994 and was shown to be expressed in adipose tissue as a secreted 16 kDa polypeptide [39]. Leptin binds to the leptin receptor to exert pleiotropic effects, such as energy homeostasis, metabolism, hematopoiesis, and immunomodulation [40, 41]. A clinical study conducted by Considine et al. showed that serum leptin concentrations in obese subjects were higher than the normal weight subjects [42]. Emerging findings have demonstrated leptin levels in serum samples related to various cancers. Serum leptin level was higher in colorectal cancer patients than in healthy controls [43]. Similar results were found in breast cancer, prostate cancer, non-small cell lung cancer, and bladder cancer [44–47].

The assays of leptin levels in MM patients presented contradictory results. A study including 14 MM patients and 25 healthy controls demonstrated that the serum level of leptin was upregulated in the MM group (22.6 ± 14.7 ng/mL) compared to the healthy control (10.3 ± 7.6 ng/mL) [48]. Similarly, another research between newly diagnosed MM and healthy controls revealed higher serum leptin levels in MM patients [49]. A meta-analysis was conducted by Liu et al. in 2021 to analyze seven studies with 406 MM patients and 530 controls. They demonstrated higher leptin concentrations in MM patients than in controls (SMD = 0.87, CI = 0.33–1.41, z = 3.14, p = 0.002) [50]. Alexandrakis et al. examine examined leptin levels in the serum of 62 MM patients, according to the established Durie and Salmon criteria, they divided patients into stage I (n = 13), stage II (n = 22), stage III (n = 27). There was no significance according to each group. The increased leptin levels were not associated with the progression of MM [51]. These results indicate that leptin levels are increased in MM patients. However, Hofmann et al. investigated the serum levels of leptin in 174 patients (10.01 ± 2.64 ng/mL) and 348 controls (9.6 ± 2.71 ng/mL) between 1993 and 2001 in the US and found no significant difference (p = 0.78) [52].

The potential mechanisms of leptin on the development of MM could be largely as follows:The potential mechanisms of leptin in the development of MM could be as follows: (1) The pronounced proliferative response induced by leptin. Researchers cocultured MM cell line (RPMI-8226) with adipocytes, MM cells proliferated faster and displayed increased leptin protein level via pSTAT3/STAT-3 signaling [9]. Whether leptin promotes proliferation-mediated STAT3 signaling in RPMI-8226 must be verified by knockdown or by inhibiting leptin expression. Using the cell lines U266 and H929, researchers observed that leptin could promote proliferation, and they also found phosphorylated AKT and STAT3 proteins were increased when upregulated leptin [53]. (2) Leptin may promote MM development by inhibiting apoptosis. Leptin was shown to induce an upregulation of BCL-2 expression and the inhibition of caspase-3 activation [53]. It also can promote the expression of autophagic proteins via Jak/Stat3 pathway and then play an anti-apoptosis anti-apoptotic

role in MM cells [54]. (3) Leptin as a regulator of anti-tumor immunity, may contribute to MM oncogenesis. Based on previous studies, we have known that invariant natural killer T (iNKT) cells with the effect of anti-tumor immunity were decreased in MM [55, 56]. Favreau et al. used the murine 5T33MM model, a pre-clinical immunocompetent model mimicking human MM disease, to investigate the leptin levels and expression of the leptin receptor. They found that the leptin level and expression of leptin receptors on iNKT cells were increased obviously. Similar results were obtained in the MM patients. *In vitro*, they coculture the MM cells with iNKT cells and found the IFN-γ production was inhibited. This effect can be reversed by leptin receptor antagonism [57]. Using a leptin-deficient mice model, Wang et al. found leptin increased CD8+T cell exhaustion and upregulated PD-1 expression, which impairs anti-tumor immunity [58] (Table 1).

The results of studies conducted to explore the associations between MM and leptin have been inconsistent and limited. Taken together, the vast majority of the above studies have concluded that leptin is highly expressed in MM. Myeloma types, different stages, risk stratification, and tumor heterogeneity may be responsible for the inconsistent results. Additionally, sex hormone secretion and sleep time could also affect leptin changes [59, 60]. Lastly, leptin levels are more influenced by the amount of subcutaneous fat than BMI [61]. Future clinical studies and additional mechanism studies of leptin in MM are needed further to clarify leptin's alteration of the bone marrow microenvironment.

Visfatin

Visfatin, also known as nicotinamide phosphoribosyltransferase (NAMPT), was initially discovered as a protein for the differentiation of B cells. Named for pre-B-cell colony-enhancing factor (PBEF) [62]. In the intracellular, its function is mainly as the rate-limiting enzyme in NAD^+ biosynthesis [63]. In the extracellular environment, it was thought to be an adipokine secreted by adipose tissue [64]. Visfatin is highly enriched in visceral fat and found in bone marrow, liver, kidney, and other tissues [62]. The main physiological functions are regulating metabolism, pro-inflammatory, and immune modulation [64]. Serum concentrations of visfatin were significantly higher in overweight and obedity obesity subjects when compared to normal weight controls [65]. Multiple studies conducted in the past decades investigated that visfatin was involved in the progression of different cancer types [66–69].

In MM, visfatin was shown to be elevated in 39 patients when compared with age-matched 20 healthy controls (102.76 ± 90.41 ng/mL vs. 22.55 ± 21.41 ng/mL; $p < 0.001$) [36]. Among some *in vitro* experiments, studies have tried to explore the mechanism of visfatin in MM researchers have attempted to investigate the mechanism of visfatin in MM. In one study, researchers using small interfering RNA (si-RNA) silenced the expression of visfatin then the growth and proliferation of MM cells were inhibited [70]. It was suggested that visfatin might upregulate NAD^+ to supply energy for MM cells' growth and survival. Apart from that, researchers also found that visfatin suppress apoptosis of MM cell depending on autophagy [71, 72]. Furthermore, visfatin can downregulate the sensibility of MM cells to bortezomib [73] and reduce the efficacy of anti-CD38 immunotherapies in MM [74]. Finally, in the SCID-rab model, inhibiting the expression of visfatin can suppress osteoclast formation and activity [75]. These studies suggest that visfatin regulates MM cells' proliferation, apoptosis, drug sensitivity, and bone metastasis.

The research on visfatin as a promising target for treatment has yielded some results. FK866, an inhibitor of visfatin, enhanced the effect of bortezomib and reduced drug resistance. The mechanism of FK866 included activation of pro-apoptosis proteins, reduction of intracellular NAD^+, and inhibition of angiogenesis [73].

Resistin

Resistin was discovered in 2001 and named for its function in promoting insulin resistance and glucose intolerance [76]. Resistin is secreted from white adipose adipose tissue in mice, whereas synthesized from monocytes and macrophages in humans. It is highly expressed in bone marrow [77]. Resistin is involved in insulin resistance, inflammation, immunoregulation, and cancer development [78]. Several studies have demonstrated that resistin can promote proliferation, associate with angiogenesis, regulate the epithelial to mesenchymal transition, and stimulate metastasis in various solid tumors [79–83]. Studies have yielded a positive correlations between serum levels of resistin and BMI [84]. Resistin has been shown to improve the survival and stemness of human breast cancer cells by activating STAT3 signaling [85]. At the neuronal levels, resistin bind to TLR4 receptors inducing the activation of AKT, NF-κB, and MAPK pathway and promoting insulin resistance [86].

Regarding its role in multiple myeloma, one case-control study showed that serum resistin was lower in MM patients (n = 73, 9.4 ± 5.0 ng/mL) compared to gender and age-matched healthy controls (n = 73, 15.9 ± 6.8 ng/mL, $p < 0.001$) [87]. A nested case-control study involving 178 MM patients and 358 controls showed lower resistin levels in male MM patients (5.2 (3.93–6.46) ng/mL) than controls (5.82 (4.44–7.33) ng/mL, $p = 0.006$) [88]. In contrast, using the primary myeloma cells and myeloma cell lines, Pang et al. have found that resistin suppressed caspase cleavage to promote drug resistance through the NF-κB and PI3K/Akt pathways. Besides, they demonstrated that resistin increased the expression of ATP-binding cassette (ABC) transporters and induced the ATP-driven efflux of chemotherapy drugs. *In vivo* mice model, they validated that resistin plays an anti-apoptosis anti-apoptotic role by annexin V binding assay and *in situ* TUNEL assay [89]. Interestingly

Reseland et al. showed that the level of resistin had no significant difference between the newly diagnosed MM patients and controls [49]. Pooled analysis of 367 MM patients and 524 controls showed no significant difference in circulating resistin levels (SMD = −0.08, 95%CI = −0.55 to 0.39, p = 0.73) [50].

Above all, the role of resistin in MM is polarized. Some studies demonstrated it is a protective adipokine; Pang et al. considered resistin is bad for MM through promoting drug resistance. More studies have shown no discrepancy in the level of resistin between MM patients and controls. The discrepancy in the role of resistin in MM could be explained as follows: First, the secretion of resistin is associated with the dietary approaches, BMI, and the level of glucose [90]. *In vitro* experiments were not affected by the above factors. Second, the different types, stages, and risk stratification may be responsible. However, the exact relationship between resistin and MM warrants further investigation.

Apelin

There are two ligands of apelin-angiotensin receptor-like1 (APJ). One is elabela/toddler (ELA), the other is apelin [91, 92]. Apelin also is an adipokine with several functions in many physiological and pathological processes, such as angiogenesis, fluid homeostasis, food intake, and metabolic regulation [93, 94]. The obese subjects presented a higher serum concentration of apelin than controls. The obese subjects (BMI ranged from 31 to 34 kg/m^2) presented a higher serum concentration of apelin than age-matched controls (BMI ranged from 23 to 24 kg/m^2) [95]. It was demonstrated that apelin had important effects on malignant diseases. The apelin and apelin receptor systems regulate autophagy and apoptosis [96–98]. Apelin was shown to be elevated (1.99 ± 1.1 ng/mL vs. 0.42 ± 0.16 ng/mL) in patients with MM (n = 29) when compared with healthy controls (n = 19). Furthermore, the level of apelin may associate with angiogenesis [99]. Some gains have been made in the mechanism of the affection of apelin in several cancers. The exact relationship between apelin and MM warrants further investigation. However, clinical studies with larger sample sizes are needed to support the correlation between MM and apelin.

Chemerin

Chemerin was first described as a chemoattractant agent, promoting the chemotaxis of leukocyte populations [100]. The highest expression of chemerin has been detected in white adipose tissue, liver, and lung [101]. Then chemerin is considered an adipokine involved in inflammation, adipogenesis, immunity, and energy metabolism [102]. A growing body of human experimental data indicated that serum chenerin chemerin levels are elevated in obese patients [103]. Increased chemerin levels have been found in gastric, colorectal, and pancreatic cancer [104–106]. The pro-tumor mechanism of chemerin is to promote the proliferation and migration of tumor cells [107, 108]. Westhrin et al. determined the serum levels of chemerin between MM patients (n = 122) and healthy controls (n = 58). They found chemerin serum levels of MM patients was higher than healthy controls (199.2 ± 88.2 ng/mL vs. 156.5 ± 52.5 ng/mL, $p < 0.001$). It was also shown that the levels of chemerin were associated with the stage of MM [109]. A study has shown that chemerin suppressed the differentiation of osteoblast [110]. It is not known whether chemerin can also play similar roles in myeloma bone disease. As a relatively new adipokine, data on chemerin involvement in MM are sparse. Nonetheless, the clinical evidence demonstrated that chemerin is increased in MM patients, which indicated that possibilities for chemerin as a biomarker should be further explored [109].

TABLE 2 Clinical studies of adipokines in MM.

Author, year	Sample source	Study design	Case			Control			*p*
			Mean	SD	N	Mean	SD	N	
Adiponectin(ug/mL)									
[30]	Serum	Pooled investigation	11.5	No value	624	12.8	No value	1,246	0.001
Leptin(ng/mL)									
[48]	Serum	Case-control Study	22.6	14.7	14	10.3	7.6	25	<0.01
[52]	Serum	Case-control Study	10.01	2.64	174	9.6	2.71	348	0.78
Visfatin(ng/mL)									
[36]	Serum	Case-control Study	102.76	90.41	39	22.55	21.41	20	<0.01
Resistin(ng/mL)									
[87]	Serum	Case-control Study	9.4	5.0	73	15.9	6.8	73	<0.001
Apelin(ng/mL)									
[99]	Serum	Case-control Study	1.99	1.1	29	0.42	0.16	19	<0.001
Chemerin(ng/mL)									
[109]	Serum	Case-control Study	199.2	88.2	122	156.5	52.5	58	<0.001

Conclusion

As MM is the second most common form of hematological malignancy and the incidence of obesity is increasing, the need for awareness of the association between obesity and MM development and progression is evident. The correlation between obesity and MM has gained significant attention in recent times. Emma V. Morris and Claire M. Edwards have discussed the association between adiposity, adipokines, and MM [111]. Our review includes new publications from the last 5 years that explore the relationship between MM and new adipokines, including apelin and chemerin. Furthermore, we have also included recent clinical studies that examine the levels of specific adipokines in MM patients, such as leptin. Additionally, we have delved into more in-depth investigations of the roles that visfatin and resistin play in MM. Lastly, the effect of adipokines on the immune microenvironment of MM is a new research highlight.

In this review, we have briefly summarized recent work on representative adipokines linked to MM initiation and progression (Table 2). First, the circulating levels of adipokines showed discrepancies when compared with control groups. Adipokines may be helpful as a biomarker for MM. In addition, adipokines such as adiponectin, leptin, and visfatin can regulate several aspects of myelosis, including promoting MM cell survival and creating a pro-tumorigenic environment for MM. Lastly, there is emerging evidence from *in vitro* studies that showed adipokines interventions could positively affect disease course.

However, steps forward are hampered by the variation in study outcomes, such as resistin hindered by the inconsistencies in study outcomes, such as resistin. The large heterogeneity partly explains such a phenomenon in MM patients. Based on these achievements, future work should better address as follows: (1) Conducting more clinical and cohorts researches on circulating adipokine levels and the correlation with known biomarkers of immunotypes, bone destruction, and progression. (2) The mechanisms of adipokines affect myelosis and elucidate the pathways of adipokines effects and underlying mechanism in the development of MM. (3) Find potential therapeutic implications target adipokines to halt MM. Taken together, adipokines are promising candidates both for novel pharmacological treatment strategies and as diagnostic tools, provided that we can develop a better understanding of the function and molecular targets of the more recently discovered adipokines.

Author contributions

WT: Writing-Original draft. LZ and LL: Funding acquisition. TM and ZY: Writing-Review and editing. JL: Visualization. YL and JB: Supervision. All authors contributed to the article and approved the submitted version.

Funding

This review was funded by National Clinical Medicine Research Center for Hematological System Diseases, grant number "2021WWA01," the Talent Innovation and Entrepreneurshio Project of Lanzhou, grant number "2020-RC-48" and the Cuiying Scientific and Technological Innovation Program of Lanzhou University Second Hospital, grant number "CY2017-ZD04, CY2019-MS14."

Conflict of interest

The authors declare that the research was conducted in the absence of any commercial or financial relationships that could be construed as a potential conflict of interest.

References

1. Cowan AJ, Green DJ, Kwok M, Lee S, Coffey DG, Holmberg LA, et al. Diagnosis and management of multiple myeloma: A review. *JAMA* (2022) 327:464–77. doi:10.1001/jama.2022.0003

2. van de Donk NWCJ, Pawlyn C, Yong KL. Multiple myeloma. *Lancet* (2021) 397:410–27. doi:10.1016/S0140-6736(21)00135-5

3. Podar K, Richardson PG, Hideshima T, Chauhan D, Anderson KC. The malignant clone and the bone-marrow environment. *Best Pract Res Clin Haematol* (2007) 20:597–612. doi:10.1016/j.beha.2007.08.002

4. Teras LR, Kitahara CM, Birmann BM, Hartge PA, Wang SS, Robien K, et al. Body size and multiple myeloma mortality: A pooled analysis of 20 prospective studies. *Br J Haematol* (2014) 166:667–76. doi:10.1111/bjh.12935

5. Kleinstern G, Larson DR, Allmer C, Norman AD, Muntifering G, Sinnwell J, et al. Body mass index associated with monoclonal gammopathy of undetermined significance (MGUS) progression in Olmsted County, Minnesota. *Blood Cancer J* (2022) 12:67. doi:10.1038/s41408-022-00659-9

6. Went M, Cornish AJ, Law PJ, Kinnersley B, van Duin M, Weinhold N, et al. Search for multiple myeloma risk factors using Mendelian randomization. *Blood Adv* (2020) 4:2172–9. doi:10.1182/bloodadvances.2020001502

7. Veldhuis-Vlug AG, Rosen CJ. Clinical implications of bone marrow adiposity. *J Intern Med* (2018) 283:121–39. doi:10.1111/joim.12718

8. Morris EV, Suchacki KJ, Hocking J, Cartwright R, Sowman A, Gamez B, et al. Myeloma cells down-regulate adiponectin in bone marrow adipocytes via TNF-alpha. *J Bone Mineral Res* (2020) 35:942–55. doi:10.1002/jbmr.3951

9. Bullwinkle EM, Parker MD, Bonan NF, Falkenberg LG, Davison SP, DeCicco-Skinner KL. Adipocytes contribute to the growth and progression of multiple myeloma: Unraveling obesity related differences in adipocyte signaling. *Cancer Lett* (2016) 380:114–21. doi:10.1016/j.canlet.2016.06.010

10. Lauby-Secretan B, Scoccianti C, Loomis D, Grosse Y, Bianchini F, Straif K, et al. Body fatness and cancer--viewpoint of the IARC working group. *N Engl J Med* (2016) 375:794–8. doi:10.1056/NEJMsr1606602

11. Avgerinos KI, Spyrou N, Mantzoros CS, Dalamaga M. Obesity and cancer risk: Emerging biological mechanisms and perspectives. *Metabolism* (2019) 92: 121–35. doi:10.1016/j.metabol.2018.11.001

12. Tarasiuk A, Mosińska P, Fichna J. The mechanisms linking obesity to colon cancer: An overview. *Obes Res Clin Pract* (2018) 12:251–9. doi:10.1016/j.orcp.2018.01.005

13. Divella R, De Luca R, Abbate I, Naglieri E, Daniele A. Obesity and cancer: The role of adipose tissue and adipo-cytokines-induced chronic inflammation. *J Cancer* (2016) 7:2346–59. doi:10.7150/jca.16884

14. Diedrich J, Gusky HC, Podgorski I. Adipose tissue dysfunction and its effects on tumor metabolism. *Horm Mol Biol Clin Investig* (2015) 21:17–41. doi:10.1515/hmbci-2014-0045

15. Vegiopoulos A, Rohm M, Herzig S. Adipose tissue: Between the extremes. *EMBO J* (2017) 36:1999–2017. doi:10.15252/embj.201696206

16. Fasshauer M, Blüher M. Adipokines in health and disease. *Trends Pharmacol Sci* (2015) 36:461–70. doi:10.1016/j.tips.2015.04.014

17. Khandekar MJ, Cohen P, Spiegelman BM. Molecular mechanisms of cancer development in obesity. *Nat Rev Cancer* (2011) 11:886–95. doi:10.1038/nrc3174

18. Khoramipour K, Chamari K, Hekmatikar AA, Ziyaiyan A, Taherkhani S, Elguindy NM, et al. Adiponectin: Structure, physiological functions, role in diseases, and effects of nutrition. *Nutrients* (2021) 13:1180. doi:10.3390/nu13041180

19. Cawthorn WP, Scheller EL, Learman BS, Parlee SD, Simon BR, Mori H, et al. Bone marrow adipose tissue is an endocrine organ that contributes to increased circulating adiponectin during caloric restriction. *Cell Metab* (2014) 20:368–75. doi:10.1016/j.cmet.2014.06.003

20. Yamauchi T, Iwabu M, Okada-Iwabu M, Kadowaki T. Adiponectin receptors: A review of their structure, function and how they work. *Best Pract Res Clin Endocrinol Metab* (2014) 28:15–23. doi:10.1016/j.beem.2013.09.003

21. Hug C, Wang J, Ahmad NS, Bogan JS, Tsao T-S, Lodish HF. T-cadherin is a receptor for hexameric and high-molecular-weight forms of Acrp30/adiponectin. *Proc Natl Acad Sci U. S. A.* (2004) 101:10308–13. doi:10.1073/pnas.0403382101

22. Fang H, Judd RL. Adiponectin regulation and function. *Compr Physiol* (2018) 8:1031–63. doi:10.1002/cphy.c170046

23. Lindberg S, Jensen JS, Pedersen SH, Galatius S, Frystyk J, Flyvbjerg A, et al. Low adiponectin levels and increased risk of type 2 diabetes in patients with myocardial infarction. *Diabetes Care* (2014) 37:3003–8. doi:10.2337/dc14-0932

24. Liu L, Shi Z, Ji X, Zhang W, Luan J, Zahr T, et al. Adipokines, adiposity, and atherosclerosis. *Cell Mol Life Sci* (2022) 79:272. doi:10.1007/s00018-022-04286-2

25. Yanai H, Yoshida H. Beneficial effects of adiponectin on glucose and lipid metabolism and atherosclerotic progression: Mechanisms and perspectives. *Int J Mol Sci* (2019) 20:1190. doi:10.3390/ijms20051190

26. Ma W, Zhang S, Li Y, Chen T, Yang Q, Feng X. Adiponectin alleviates nonalcoholic fatty liver injury via regulating oxidative stress in liver cells. *Minerva Med* (2020) 113:990–9. doi:10.23736/S0026-4806.20.06734-8

27. Tilg H, Moschen AR. Adipocytokines: Mediators linking adipose tissue, inflammation and immunity. *Nat Rev Immunol* (2006) 6:772–83. doi:10.1038/nri1937

28. Di Zazzo E, Polito R, Bartollino S, Nigro E, Porcile C, Bianco A, et al. Adiponectin as link factor between adipose tissue and cancer. *Int J Mol Sci* (2019) 20:839. doi:10.3390/ijms20040839

29. Hofmann JN, Mailankody S, Korde N, Wang Y, Tageja N, Costello R, et al. Circulating adiponectin levels differ between patients with multiple myeloma and its precursor disease. *Obesity (Silver Spring)* (2017) 25:1317–20. doi:10.1002/oby.21894

30. Hofmann JN, Birmann BM, Teras LR, Pfeiffer RM, Wang Y, Albanes D, et al. Low levels of circulating adiponectin are associated with multiple myeloma risk in overweight and obese individuals. *Cancer Res* (2016) 76:1935–41. doi:10.1158/0008-5472.CAN-15-2406

31. Fowler JA, Lwin ST, Drake MT, Edwards JR, Kyle RA, Mundy GR, et al. Host-derived adiponectin is tumor-suppressive and a novel therapeutic target for multiple myeloma and the associated bone disease. *Blood* (2011) 118:5872–82. doi:10.1182/blood-2011-01-330407

32. Medina EA, Oberheu K, Polusani SR, Ortega V, Velagaleti GVN, Oyajobi BO. PKA/AMPK signaling in relation to adiponectin's antiproliferative effect on multiple myeloma cells. *Leukemia* (2014) 28:2080–9. doi:10.1038/leu.2014.112

33. Akhmetzyanova I, Aaron T, Galbo P, Tikhonova A, Dolgalev I, Tanaka M, et al. Tissue-resident macrophages promote early dissemination of multiple myeloma via IL-6 and TNFα. *Blood Adv* (2021) 5:3592–608. doi:10.1182/bloodadvances.2021005327

34. Meacham CE, Jeffery EC, Burgess RJ, Sivakumar CD, Arora MA, Stanley AM, et al. Adiponectin receptors sustain haematopoietic stem cells throughout adulthood by protecting them from inflammation. *Nat Cell Biol* (2022) 24: 697–707. doi:10.1038/s41556-022-00909-9

35. Bernstein ZS, Kim EB, Raje N. Bone disease in multiple myeloma: Biologic and clinical implications. *Cells* (2022) 11:2308. doi:10.3390/cells11152308

36. Liu Z, Liu H, Li Y, Wang Y, Xing R, Mi F, et al. Adiponectin inhibits the differentiation and maturation of osteoclasts via the mTOR pathway in multiple myeloma. *Int J Mol Med* (2020) 45:1112–20. doi:10.3892/ijmm.2020.4475

37. Olechnowicz SWZ, Weivoda MM, Lwin ST, Leung SK, Gooding S, Nador G, et al. Multiple myeloma increases nerve growth factor and other pain-related markers through interactions with the bone microenvironment. *Scientific Rep* (2019) 9:14189. doi:10.1038/s41598-019-50591-5

38. Peterson SJ, Drummond G, Kim DH, Li M, Kruger AL, Ikehara S, et al. L-4F treatment reduces adiposity, increases adiponectin levels, and improves insulin sensitivity in obese mice. *J Lipid Res* (2008) 49:1658–69. doi:10.1194/jlr.M800046-JLR200

39. Zhang Y, Proenca R, Maffei M, Barone M, Leopold L, Friedman JM. Positional cloning of the mouse obese gene and its human homologue. *Nature* (1994) 372: 425–32. doi:10.1038/372425a0

40. Trinh T, Broxmeyer HE. Role for leptin and leptin receptors in stem cells during health and diseases. *Stem Cell Rev Rep* (2021) 17:511–22. doi:10.1007/s12015-021-10132-y

41. Obradovic M, Sudar-Milovanovic E, Soskic S, Essack M, Arya S, Stewart AJ, et al. Leptin and obesity: Role and clinical implication. *Front Endocrinol* (2021) 12: 585887. doi:10.3389/fendo.2021.585887

42. Considine RV, Sinha MK, Heiman ML, Kriauciunas A, Stephens TW, Nyce MR, et al. Serum immunoreactive-leptin concentrations in normal-weight and obese humans. *N Engl J Med* (1996) 334:292–5. doi:10.1056/NEJM199602013340503

43. Mhaidat NM, Alzoubi KH, Kubas MA, Banihani MN, Hamdan N, Al-Jaberi TM. High levels of leptin and non-high molecular weight-adiponectin in patients with colorectal cancer: Association with chemotherapy and common genetic polymorphisms. *Biomed Rep* (2021) 14:13. doi:10.3892/br.2020.1389

44. García-Estevez L, González-Martínez S, Moreno-Bueno G. The leptin Axis and its association with the adaptive immune system in breast cancer. *Front Immunol* (2021) 12:784823. doi:10.3389/fimmu.2021.784823

45. Xu CJ, Dong LL, Kang XL, Li ZM, Zhang HY. Leptin promotes proliferation and inhibits apoptosis of prostate cancer cells by regulating ERK1/2 signaling pathway. *Eur Rev Med Pharmacol Sci* (2020) 24:8341–8. doi:10.26355/eurrev_202008_22630

46. Wang J, Zhou F, Li F, Wang B, Hu Y, Li X. Autocrined leptin promotes proliferation of non-small cell lung cancer (NSCLC) via *PI3K/AKT* and *p53* pathways. *Ann Transl Med* (2021) 9:568. doi:10.21037/atm-20-7482

47. Kashiwagi E, Abe T, Kinoshita F, Ushijima M, Masaoka H, Shiota M, et al. The role of adipocytokines and their receptors in bladder cancer: Expression of adiponectin or leptin is an independent prognosticator. *Am J Transl Res* (2020) 12:e195–45. doi:10.1016/s2666-1683(20)32677-x

48. Pamuk GE, Demir M, Harmandar F, Yesil Y, Turgut B, Vural O. Leptin and resistin levels in serum of patients with hematologic malignancies: Correlation with clinical characteristics. *Exp Oncol* (2006) 28:241–4.

49. Reseland JE, Reppe S, Olstad OK, Hjorth-Hansen H, Brenne AT, Syversen U, et al. Abnormal adipokine levels and leptin-induced changes in gene expression profiles in multiple myeloma. *Eur J Haematol* (2009) 83:460–70. doi:10.1111/j.1600-0609.2009.01311.x

50. Liu R, Gao D, Lv Y, Zhai M, He A. Importance of circulating adipocytokines in multiple myeloma: A systematic review and meta-analysis based on case-control studies. *BMC Endocr Disord* (2022) 22:29. doi:10.1186/s12902-022-00939-2

51. Alexandrakis MG, Passam FH, Sfiridaki A, Pappa CA, Moschandrea JA, Kandidakis E, et al. Serum levels of leptin in multiple myeloma patients and its relation to angiogenic and inflammatory cytokines. *The Int J Biol Markers* (2004) 19:52–7. doi:10.5301/jbm.2008.510

52. Hofmann JN, Liao LM, Pollak MN, Wang Y, Pfeiffer RM, Baris D, et al. A prospective study of circulating adipokine levels and risk of multiple myeloma. *Blood* (2012) 120:4418–20. doi:10.1182/blood-2012-06-438606

53. Yu W, Cao D-D, Li Q-B, Mei H-L, Hu Y, Guo T. Adipocytes secreted leptin is a pro-tumor factor for survival of multiple myeloma under chemotherapy. *Oncotarget* (2016) 7:86075–86. doi:10.18632/oncotarget.13342

54. Liu Z, Xu J, He J, Liu H, Lin P, Wan X, et al. Mature adipocytes in bone marrow protect myeloma cells against chemotherapy through autophagy activation. *Oncotarget* (2015) 6:34329–41. doi:10.18632/oncotarget.6020

55. Chan AC, Neeson P, Leeansyah E, Tainton K, Quach H, Prince HM, et al. Natural killer T cell defects in multiple myeloma and the impact of lenalidomide therapy. *Clin Exp Immunol* (2014) 175:49–58. doi:10.1111/cei.12196

56. Dhodapkar MV, Richter J. Harnessing natural killer T (NKT) cells in human myeloma: Progress and challenges. *Clin Immunol (Orlando, Fla* (2011) 140:160–6. doi:10.1016/j.clim.2010.12.010

57. Favreau M, Menu E, Gaublomme D, Vanderkerken K, Faict S, Maes K, et al. Leptin receptor antagonism of iNKT cell function: A novel strategy to combat multiple myeloma. *Leukemia* (2017) 31:2678–85. doi:10.1038/leu.2017.146

58. Wang Z, Aguilar EG, Luna JI, Dunai C, Khuat LT, Le CT, et al. Paradoxical effects of obesity on T cell function during tumor progression and PD-1 checkpoint blockade. *Nat Med* (2019) 25:141–51. doi:10.1038/s41591-018-0221-5

59. Sih R, Morley JE, Kaiser FE, Perry HM, Patrick P, Ross C. Testosterone replacement in older hypogonadal men: A 12-month randomized controlled trial. *J Clin Endocrinol Metab* (1997) 82:1661–7. doi:10.1210/jcem.82.6.3988

60. Simon C, Gronfier C, Schlienger JL, Brandenberger G. Circadian and ultradian variations of leptin in normal man under continuous enteral nutrition: Relationship to sleep and body temperature. *J Clin Endocrinol Metab* (1998) 83: 1893–9. doi:10.1210/jcem.83.6.4864

61. Montague CT, Prins JB, Sanders L, Digby JE, O'Rahilly S. Depot- and sex-specific differences in human leptin mRNA expression: Implications for the control of regional fat distribution. *Diabetes* (1997) 46:342–7. doi:10.2337/diab.46.3.342

62. Samal B, Sun Y, Stearns G, Xie C, Suggs S, McNiece I. Cloning and characterization of the cDNA encoding a novel human pre-B-cell colony-enhancing factor. *Mol Cell Biol* (1994) 14:1431–7. doi:10.1128/mcb.14.2.1431

63. Zhai RG, Rizzi M, Garavaglia S. Nicotinamide/nicotinic acid mononucleotide adenylyltransferase, new insights into an ancient enzyme. *Cell Mol Life Sci* (2009) 66:2805–18. doi:10.1007/s00018-009-0047-x

64. Fukuhara A, Matsuda M, Nishizawa M, Segawa K, Tanaka M, Kishimoto K, et al. Visfatin: A protein secreted by visceral fat that mimics the effects of insulin. *Science (New York, N.Y.)* (2005) 307:426–30. doi:10.1126/science.1097243

65. Chang Y-H, Chang D-M, Lin K-C, Shin S-J, Lee Y-J. Visfatin in overweight/obesity, type 2 diabetes mellitus, insulin resistance, metabolic syndrome and cardiovascular diseases: A meta-analysis and systemic review. *Diabetes Metab Res Rev* (2011) 27:515–27. doi:10.1002/dmrr.1201

66. Fazeli MS, Dashti H, Akbarzadeh S, Assadi M, Aminian A, Keramati MR, et al. Circulating levels of novel adipocytokines in patients with colorectal cancer. *Cytokine* (2013) 62:81–5. doi:10.1016/j.cyto.2013.02.012

67. Nakajima TE, Yamada Y, Hamano T, Furuta K, Gotoda T, Katai H, et al. Adipocytokine levels in gastric cancer patients: Resistin and visfatin as biomarkers of gastric cancer. *J Gastroenterol* (2009) 44:685–90. doi:10.1007/s00535-009-0063-5

68. Reddy PS, Umesh S, Thota B, Tandon A, Pandey P, Hegde AS, et al. PBEF1/NAmPRTase/Visfatin: A potential malignant astrocytoma/glioblastoma serum marker with prognostic value. *Cancer Biol Ther* (2008) 7:663–8. doi:10.4161/cbt.7.5.5663

69. Lu Z, Fang Z, Guo Y, Liu X, Chen S. Cisplatin resistance of NSCLC cells involves upregulation of visfatin through activation of its transcription and stabilization of mRNA. *Chem Biol Interact* (2022) 351:109705:109705. doi:10.1016/j.cbi.2021.109705

70. Bong IPN, Ng CC, Fakiruddin SK, Lim MN, Zakaria Z. Small interfering RNA-mediated silencing of nicotinamide phosphoribosyltransferase (NAMPT) and lysosomal trafficking regulator (lyst) induce growth inhibition and apoptosis in human multiple myeloma cells: A preliminary study. *Bosnian J Basic Med Sci* (2016) 16:268–75. doi:10.17305/bjbms.2016.1568

71. Cea M, Cagnetta A, Patrone F, Nencioni A, Gobbi M, Anderson KC. Intracellular NAD(+) depletion induces autophagic death in multiple myeloma cells. *Autophagy* (2013) 9:410–2. doi:10.4161/auto.22866

72. Cea M, Cagnetta A, Fulciniti M, Tai Y-T, Hideshima T, Chauhan D, et al. Targeting NAD+ salvage pathway induces autophagy in multiple myeloma cells via mTORC1 and extracellular signal-regulated kinase (ERK1/2) inhibition. *Blood* (2012) 120:3519–29. doi:10.1182/blood-2012-03-416776

73. Cagnetta A, Cea M, Calimeri T, Acharya C, Fulciniti M, Tai Y-T, et al. Intracellular NAD^+ depletion enhances bortezomib-induced anti-myeloma activity. *Blood* (2013) 122:1243–55. doi:10.1182/blood-2013-02-483511

74. Kennedy BE, Sadek M, Elnenaei MO, Reiman A, Gujar SA. Targeting NAD+ synthesis to potentiate CD38-based immunotherapy of multiple myeloma. *Trends Cancer* (2020) 6:9–12. doi:10.1016/j.trecan.2019.11.005

75. Venkateshaiah SU, Khan S, Ling W, Bam R, Li X, van Rhee F, et al. NAMPT/PBEF1 enzymatic activity is indispensable for myeloma cell growth and osteoclast activity. *Exp Hematol* (2013) 41:547–57. doi:10.1016/j.exphem.2013.02.008

76. Steppan CM, Bailey ST, Bhat S, Brown EJ, Banerjee RR, Wright CM, et al. The hormone resistin links obesity to diabetes. *Nature* (2001) 409:307–12. doi:10.1038/35053000

77. Patel L, Buckels AC, Kinghorn IJ, Murdock PR, Holbrook JD, Plumpton C, et al. Resistin is expressed in human macrophages and directly regulated by PPAR gamma activators. *Biochem Biophys Res Commun* (2003) 300:472–6. doi:10.1016/s0006-291x(02)02841-3

78. Deb A, Deshmukh B, Ramteke P, Bhati FK, Bhat MK. Resistin: A journey from metabolism to cancer. *Transl Oncol* (2021) 14:101178. doi:10.1016/j.tranon.2021.101178

79. Qiu L, Zhang G-F, Yu L, Wang H-Y, Jia X-J, Wang T-J. Novel oncogenic and chemoresistance-inducing functions of resistin in ovarian cancer cells require miRNAs-mediated induction of epithelial-to-mesenchymal transition. *Scientific Rep* (2018) 8:12522. doi:10.1038/s41598-018-30978-6

80. Lee JO, Kim N, Lee HJ, Lee YW, Kim SJ, Park SH, et al. Resistin, a fat-derived secretory factor, promotes metastasis of MDA-MB-231 human breast cancer cells through ERM activation. *Scientific Rep* (2016) 6:18923. doi:10.1038/srep18923

81. Pang L, Zhang Y, Yu Y, Zhang S. Resistin promotes the expression of vascular endothelial growth factor in ovary carcinoma cells. *Int J Mol Sci* (2013) 14:9751–66. doi:10.3390/ijms14059751

82. Rak A, Drwal E, Wróbel A, Gregoraszczuk EŁ. Resistin is a survival factor for porcine ovarian follicular cells. *Reproduction (Cambridge, England)* (2015) 150: 343–55. doi:10.1530/REP-15-0255

83. Mu H, Ohashi R, Yan S, Chai H, Yang H, Lin P, et al. Adipokine resistin promotes *in vitro* angiogenesis of human endothelial cells. *Cardiovasc Res* (2006) 70:146–57. doi:10.1016/j.cardiores.2006.01.015

84. Owecki M, Miczke A, Nikisch E, Pupek-Musialik D, Sowiński J. Serum resistin concentrations are higher in human obesity but independent from insulin resistance. *Exp Clin Endocrinol Diabetes* (2011) 119:117–21. doi:10.1055/s-0030-1263111

85. Deshmukh SK, Srivastava SK, Zubair H, Bhardwaj A, Tyagi N, Al-Ghadhban A, et al. Resistin potentiates chemoresistance and stemness of breast cancer cells: Implications for racially disparate therapeutic outcomes. *Cancer Lett* (2017) 396: 21–9. doi:10.1016/j.canlet.2017.03.010

86. Benomar Y, Gertler A, De Lacy P, Crépin D, Ould Hamouda H, Riffault L, et al. Central resistin overexposure induces insulin resistance through Toll-like receptor 4. *Diabetes* (2013) 62:102–14. doi:10.2337/db12-0237

87. Dalamaga M, Karmaniolas K, Panagiotou A, Hsi A, Chamberland J, Dimas C, et al. Low circulating adiponectin and resistin, but not leptin, levels are associated with multiple myeloma risk: A case-control study. *Cancer Causes Control* (2009) 20: 193–9. doi:10.1007/s10552-008-9233-7

88. Santo L, Teras LR, Giles GG, Weinstein SJ, Albanes D, Wang Y, et al. Circulating resistin levels and risk of multiple myeloma in three prospective cohorts. *Br J Cancer* (2017) 117:1241–5. doi:10.1038/bjc.2017.282

89. Pang J, Shi Q, Liu Z, He J, Liu H, Lin P, et al. Resistin induces multidrug resistance in myeloma by inhibiting cell death and upregulating ABC transporter expression. *Haematologica* (2017) 102:1273–80. doi:10.3324/haematol.2016.154062

90. Millar SR, Navarro P, Harrington JM, Shivappa N, Hébert JR, Perry IJ, et al. Dietary score associations with markers of chronic low-grade inflammation: A cross-sectional comparative analysis of a middle-to older-aged population. *Eur J Nutr* (2022) 61:3377–90. doi:10.1007/s00394-022-02892-1

91. Tatemoto K, Hosoya M, Habata Y, Fujii R, Kakegawa T, Zou MX, et al. Isolation and characterization of a novel endogenous peptide ligand for the human APJ receptor. *Biochem Biophys Res Commun* (1998) 251:471–6. doi:10.1006/bbrc.1998.9489

92. Charo DN, Ho M, Fajardo G, Kawana M, Kundu RK, Sheikh AY, et al. Endogenous regulation of cardiovascular function by apelin-APJ. *Am J Physiol Heart Circulatory Physiol* (2009) 297:H1904–13. doi:10.1152/ajpheart.00686.2009

93. Kershaw EE, Flier JS. Adipose tissue as an endocrine organ. *J Clin Endocrinol Metab* (2004) 89:2548–56. doi:10.1210/jc.2004-0395

94. Dawid M, Mlyczyńska E, Jurek M, Respekta N, Pich K, Kurowska P, et al. Apelin, APJ, and ELABELA: Role in placental function, pregnancy, and foetal development-an overview. *Cells* (2021) 11:99. doi:10.3390/cells11010099

95. Boucher J, Masri B, Daviaud D, Gesta S, Guigné C, Mazzucotelli A, et al. Apelin, a newly identified adipokine up-regulated by insulin and obesity. *Endocrinology* (2005) 146:1764–71. doi:10.1210/en.2004-1427

96. Picault F-X, Chaves-Almagro C, Projetti F, Prats H, Masri B, Audigier Y. Tumour co-expression of apelin and its receptor is the basis of an autocrine loop involved in the growth of colon adenocarcinomas. *Eur J Cancer* (2014) 50:663–74. doi:10.1016/j.ejca.2013.11.017

97. Sorli SC, Le Gonidec S, Knibiehler B, Audigier Y. Apelin is a potent activator of tumour neoangiogenesis. *Oncogene* (2007) 26:7692–9. doi:10.1038/sj.onc.1210573

98. Kälin RE, Glass R. APLN/APLNR signaling controls key pathological parameters of glioblastoma. *Cancers* (2021) 13:3899. doi:10.3390/cancers13153899

99. Maden M, Pamuk ON, Pamuk GE. High apelin levels could be used as a diagnostic marker in multiple myeloma: A comparative study. *Cancer Biomark* (2016) 17:391–6. doi:10.3233/CBM-160654

100. Fischer TF, Beck-Sickinger AG. Chemerin - exploring a versatile adipokine. *Biol Chem* (2022) 403:625–42. doi:10.1515/hsz-2021-0409

101. Helfer G, Wu Q-F. Chemerin: A multifaceted adipokine involved in metabolic disorders. *J Endocrinol* (2018) 238:R79–R94. doi:10.1530/JOE-18-0174

102. Bozaoglu K, Curran JE, Stocker CJ, Zaibi MS, Segal D, Konstantopoulos N, et al. Chemerin, a novel adipokine in the regulation of angiogenesis. *J Clin Endocrinol Metab* (2010) 95:2476–85. doi:10.1210/jc.2010-0042

103. Rourke JL, Dranse HJ, Sinal CJ. Towards an integrative approach to understanding the role of chemerin in human health and disease. *Obes Rev* (2013) 14:245–62. doi:10.1111/obr.12009

104. Wang C, Wu WKK, Liu X, To K-F, Chen GG, Yu J, et al. Increased serum chemerin level promotes cellular invasiveness in gastric cancer: A clinical and experimental study. *Peptides* (2014) 51:131–8. doi:10.1016/j.peptides.2013.10.009

105. Erdogan S, Yilmaz FM, Yazici O, Yozgat A, Sezer S, Ozdemir N, et al. Inflammation and chemerin in colorectal cancer. *Tumour Biol* (2016) 37:6337–42. doi:10.1007/s13277-015-4483-y

106. Wang Q, Wang H, Ding Y, Wan M, Xu M. The role of adipokines in pancreatic cancer. *Front Oncol* (2022) 12:926230. doi:10.3389/fonc.2022.926230

107. Gao C, Shi J, Zhang J, Li Y, Zhang Y. Chemerin promotes proliferation and migration of ovarian cancer cells by upregulating expression of PD-L1. *J Zhejiang Univ Sci B* (2022) 23:164–70. doi:10.1631/jzus.B2100392

108. Friebus-Kardash J, Schulz P, Reinicke S, Karthaus C, Schefer Q, Bandholtz S, et al. A chemerin peptide analog stimulates tumor growth in two xenograft mouse models of human colorectal carcinoma. *Cancers* (2021) 14:125. doi:10.3390/cancers14010125

109. Westhrin M, Moen SH, Kristensen IB, Buene G, Mylin AK, Turesson I, et al. Chemerin is elevated in multiple myeloma patients and is expressed by stromal cells and pre-adipocytes. *Biomark Res* (2018) 6:21. doi:10.1186/s40364-018-0134-y

110. Muruganandan S, Roman AA, Sinal CJ. Role of chemerin/CMKLR1 signaling in adipogenesis and osteoblastogenesis of bone marrow stem cells. *J Bone Mineral Res* (2010) 25:222–34. doi:10.1359/jbmr.091106

111. Morris EV, Edwards CM. Adipokines, adiposity, and bone marrow adipocytes: Dangerous accomplices in multiple myeloma. *J Cel Physiol* (2018) 233:9159–66. doi:10.1002/jcp.26884

Pathology & Oncology Research | frontiers

TYPE Original Research
PUBLISHED 22 December 2023
DOI 10.3389/pore.2023.1611518

Check for updates

OPEN ACCESS

EDITED BY
Agota Szepesi,
Semmelweis University, Hungary

*CORRESPONDENCE
Gunay Aliyeva,
galiyeva@rocketmail.com

RECEIVED 27 September 2023
ACCEPTED 07 December 2023
PUBLISHED 22 December 2023

CITATION
Hasanova A, Asadov C, Karimova N, Shirinova A, Aliyeva G and Alimirzoyeva Z (2023), Spectrum of BCR-ABL mutations in Azerbaijanian imatinib-resistant patients with chronic myeloid leukemia.
Pathol. Oncol. Res. 29:1611518.
doi: 10.3389/pore.2023.1611518

COPYRIGHT
© 2023 Hasanova, Asadov, Karimova, Shirinova, Aliyeva and Alimirzoyeva. This is an open-access article distributed under the terms of the Creative Commons Attribution License (CC BY). The use, distribution or reproduction in other forums is permitted, provided the original author(s) and the copyright owner(s) are credited and that the original publication in this journal is cited, in accordance with accepted academic practice. No use, distribution or reproduction is permitted which does not comply with these terms.

Spectrum of BCR-ABL mutations in Azerbaijanian imatinib-resistant patients with chronic myeloid leukemia

Aypara Hasanova[1], Chingiz Asadov[2], Nigar Karimova[3], Aytan Shirinova[4], Gunay Aliyeva[2]* and Zohra Alimirzoyeva[4]

[1]Leukemogenesis Laboratory, Institute of Hematology and Transfusiology, Baku, Azerbaijan, [2]Hematopoiesis Department, Institute of Hematology and Transfusiology, Baku, Azerbaijan, [3]Human Genetics Laboratory, Biotechnology Department, Institute of Genetic Resources, Baku, Azerbaijan, [4]Hematology Department, Institute of Hematology and Transfusiology, Baku, Azerbaijan

Objective: BCR-ABL1 kinase domain (KD) mutations can lead to resistance to first- and second-generation tyrosine kinase inhibitors (TKIs) in chronic myeloid leukemia (CML). Here, we present the first report of the spectrum of mutations in the BCR-ABL1 KD of CML patients from Azerbaijan.

Materials and methods: Samples for mutation screening were obtained from patients experiencing resistance to first line TKIs or from patients in acceleration phase (AP) or blast crisis (BC) at the time of diagnosis. The cDNA region corresponding to BCR-ABL1 KD was sequenced by pyrosequencing method. The χ^2 test was used to assess the association of categorical variables between mutation-positive and -negative groups. In addition, the Kaplan-Meier method was applied to generate survival curves.

Results: Eight different point mutations were identified in 22 (13.4%) out of 163 CML patients experiencing resistance to TKIs. The types of mutations detected were as follows: Contact binding site mutations 50% (11), SH2 domain mutations 27.4% (six), P-loop mutations 18.1% (four), and SH3 domain mutations accounting for 4.5% (one). The most common mutation was T315I, accounting for 5% (n = 8) of all patients. Significant association was identified between BCR-ABL1 mutations and additional chromosomal aberrations as well as between the mutations and disease phases ($p < 0.05$). Twelve out of 22 patients with BCR-ABL1 mutations and seven out of eight with T315I were in BC. Overall survival (OS) of the patients with BCR-ABL1 mutations was significantly lower comparing to the patients with no mutation ($p < 0.05$) and 8 patients with T315I mutation presented OS of 0%.

Conclusion: T315I was the most commonly identified BCR-ABL1 mutation in TKI-resistant CML patients of Azerbaijani origin, being associated with disease progression and poor OS.

KEYWORDS

chronic myeloid leukemia, mutation, tyrosine kinase inhibitor resistance, kinase domain, BCR-ABL

Introduction

Rearrangements involving the ABL1 gene at chromosome 9q and the BCR gene at 22q result in formation of the Philadelphia (Ph) chromosome, t(9; 22)(q34; q11), and are present in all cases of chronic myeloid leukemia (CML) and in some cases of acute lymphoblastic leukemia (Ph+ ALL). The BCR-ABL1 fusion gene, characteristic for these patients, encodes an oncoprotein that has an activated tyrosine kinase domain in the ABL region. This infamous protein promotes cell proliferation leading to loss of stromal adhesion and inhibits apoptosis by activating downstream pathways, including Janus kinase-signal transducer and activator of transcription (Jak-Stat) and Myc [1, 2].

Introduction and widespread clinical use of the tyrosine kinase inhibitor (TKI), imatinib in CML patients, has resulted in much better overall survival compared to interferon [3]. Furthermore, imatinib has reduced the need for allogeneic stem cell transplantation in these patients [4]. Despite the extraordinary success of imatinib for the treatment of CML, up to 40% of patients experience intolerance or resistance. The most common reason for treatment failure is the acquisition of mutations within the kinase domain (KD) of BCR-ABL1 that impair drug binding. Although more developed second-generation TKIs were designed to target most imatinib-resistant mutations, some mutations show resistance even to these new generation drugs (T315I) [5, 6]. Almost 25% of imatinib-resistant patients were reported to have more than one BCR-ABL1 KD mutation, and the presence of multiple mutations defines a poor-risk subgroup of chronic phase (CP) CML patients [7]. These patients have a higher likelihood of acquiring new resistant mutations and poor response to treatment with second-generation TKIs, irrespective of the resistance profile of the mutations [7].

Currently, TKIs applied to treat CML strongly improve the overall survival (OS) of patients [2, 8]. The majority of patients achieve a life expectancy close to that of the general population [9]. However, there are still some treatment-related problems present: 1) The disease still progresses to an acceleration phase (AP) or blast crisis (BC) following treatment with TKIs; 2) a number of patients are resistant to TKIs; and 3) patients cannot endure the side effects of TKIs [10].

Patients frequently develop primary or secondary resistance to TKIs, despite the high response rates (primary or intrinsic resistance is a lack of initial response, whereas secondary or acquired resistance (relapse) is a loss of an established response) [11]. According to the European LeukemiaNet (ELN) criteria, resistance is defined as failure of first-line TKI therapy: less than a complete hematologic response and/or no cytogenetic response (CyR; defined as Ph+ bone marrow metaphases >95%) at 3 months, BCR-ABL1 transcript levels above 10% and/or less than a partial CyR (PcyR; defined as ≤35% Ph+ metaphases) at 6 months, BCR-ABL1 transcript levels above 1% and/or less than a complete CyR (CCyR; defined as no Ph+ metaphases) at 12 months, or loss of a complete hematologic response or complete CyR or confirmed loss of MMR, mutations, or clonal chromosome abnormalities in Ph− cells at any subsequent time during therapy [1, 12]. According to the National Comprehensive Cancer Network (NCCN) guidelines, on the other hand, resistance is defined as the detection of BCR-ABL1/ABL1 transcript levels above 10% on the International Scale or failure to achieve PCyR at 3 months, or failure to achieve CCyR at 12 months or 18 months [13]. Several mechanisms have been associated with resistance, including BCR-ABL1-dependent and BCR-ABL1-independent mechanisms [14]. BCR-ABL1 KD mutations and BCR-ABL1 genomic amplification are well-known mechanisms of resistance to TKI therapy [15].

Mutation analysis is usually performed after patients experience TKI treatment resistance; the results of mutation analysis may guide the selection of subsequent TKIs [1, 12, 13, 16]. Imatinib resistance, regardless of aetiology, necessitates a change in treatment strategy. However, the choice of second-generation TKI should take into account ABL1 KD mutation status to ensure optimum efficiency of TKI. Imatinib resistance often results from ABL1 mutations in the P-loop (G250E or E255K/V) and in the ATP-binding site (F317L) or from the panresistant mutation T315I [17–20]. Only few mutations are known to cause clinical resistance to nilotinib (Y253H, E255K/V, and F359V/C/I) [21, 22] or dasatinib (V299L, T315A, F317L/I/V/C) [22–25] or both (T315I). Patients already having mutations have higher likelihood of developing new mutations [15, 22] and multiple mutations can be associated with poor prognosis [24, 26, 27]. BCR-ABL1 KD mutation analysis can be done either by direct Sanger sequencing or Pyrosequencing which has been largely used to-date [1, 16]. Although newer technologies with greater sensitivity are available, most of them are limited by their specificity and limited spectrum of mutations, next-generation sequencing (NGS), nevertheless, is an exception.

The aim of this study is thus to analyse the association of identified BCR-ABL1 KD mutations with resistance to first-line TKI imatinib.

Methods

Patients

In this study, 163 CML patients treated in the clinical department of the Scientific Research Institute of Hematology and Transfusion were analyzed retrospectively. At the time of the analysis, 119 patients were in the CP, 26 were in the AP, and 18 were in the BC phase. Phases of the disease were determined according to ELN recommendations [1]. Mutation screening for BCR-ABL1 KD was performed in CML patients who showed resistance to imatinib treatment and failed to achieve MMR after

12, 18, and 24 months. Data was collected from patients undergoing mutation screening during imatinib treatment. Mutation screening was performed in patients who showed resistance to the drug or progressed to AP or BC phase of the disease, as required. Patients were grouped according to BCR-ABL1 mutational status. The relationship between the clinical data of the patients and the mutation status was analyzed. The study was approved by institutional review board and consent was obtained from all patients included in the study.

Real-time polymerase chain reaction (RT PCR)

Evaluation of p210 BCR/ABL1 chimeric oncogene expression was implemented in several steps: RNA isolation; Obtaining cDNA by reverse transcriptase reaction; Real-time PCR. RNA isolation was performed using QIAamp® RNA Blood Mini Kit (QiaGen, Germany), Reverse Transcriptase RT® Kit (QiaGen, Germany). Quantification of BCR-ABL1 p210, b2a2 or b3a2 transcripts in bone marrow or peripheral blood samples of CML patients was carried out by RT PCR on Rotor-Gene Q (QiaGen, Germany) device and BCR-ABL1 Mbcr IS-MMR Kit (QiaGen, Germany). The background level (LoB) equal to 0.0022 BCR-ABL Mbcr NCN. The limit of detection (LoD or analytical sensitivity) equal to 0.0069 BCR-ABL Mbcr NCN.

Fluorescence *in situ* hybridization (FISH) method

FISH analysis was performed using the BCR/ABL(ABL1) Translocation, Dual Fusion DNA probe (Cytocell, United Kingdom) on metaphase chromosomes or interphase nuclei obtained by short-term culture. The cut-off value was 2.39% for bone marrow and 2.55% for peripheral blood. Preparations were examined using an Imager A2 microscope (Carl Zeiss), Isis software (Metasystems) and DAPI/TexasRed/FITC filters.

Cytogenetic method

Metaphases obtained after culturing bone marrow (24 h) or peripheral blood samples (72 h) were stained by GTL-banding. Karyotyping of metaphases was performed using an Axio Imager A2 microscope (Carl Zeiss) and Ikaros software (Metasystems).

BCR-ABL1 mutation analysis

These examinations were carried out with the support of ATQ Biotechnology Laboratory operating in Ankara, Türkiye. Pyrosequencing analysis is based on the principle of sequencing by synthesis. This method is a real-time quantitative sequence analysis based on the detection of pyrophosphates released during DNA synthesis. All tests were performed in peripheral blood. First, RNA was isolated from peripheral blood samples with the QIAamp® RNA Blood Mini Kit (QiaGen, Germany). In the next step, RNA to cDNA was converted using RT® Kit (QiaGen, Germany) to obtain cDNA. Then, two rounds of PCR were performed using the Pyromark PCR kit (QiaGen, Germany). After the PCR step, pyrosequencing analysis was performed on a Pyromark Q24 (QiaGen, Germany) device. The investigation of mutations resulting from single nucleotide variants (SNVs) was carried out through BCR-ABL1 pyrosequencing analysis, as outlined in Table 1.

Statistical analyses

To assess the associations between two groups of categorical variables, χ^2 test was used. OS was calculated from the identification of the mutation until the last follow-up, death or the censor date. To generate survival curves, the Kaplan-Meier method was applied. $p < 0.05$ was considered to indicate a statistically significant difference.

Results

Patient characteristics

The clinical, hematologic, and epidemiologic characteristics were analyzed altogether during the diagnosis and mutation screening of the 163 patients included in this study (Table 2). Patients were stratified by BCR-ABL1 mutation status. No significant difference was observed between clinical characteristics of the two groups, except for gender and mean age: male were more likely to have BCR-ABL1 mutations compared to female patients, and the mean age was higher in patients with mutations ($p < 0.05$). There was a significant correlation between ABL KD mutations and gender ($p = 0.004$).

Mutation analysis

During a 5.5 years Pyrosequencing-based analysis (January 2014 to May 2019) of BCR-ABL1 kinase domain mutations, at least one point mutation was identified in 22 of 163 patients (13.4%). Figure 1 shows the frequency of the mutations, as well as mutations leading to high levels of resistance to second-line TKIs [28]. A total of 8 different point mutations were identified. Table 3 shows the frequency of identified mutations and their distribution by the disease phases. The most frequently identified

TABLE 1 Mutations determined by BCR-ABL1 pyrosequencing analysis.

No	Sequencing primer	Amino acid change	Point mutation	Sequence
1	BCR-ABL 253 Forward	Y253H	(TAC>CAC)	1: T/CACGGGG/AAGGTGTACGA
2		Y253F	(TAC>TTC)	
3		E255K	(GAG>AAG)	2: TA/TCGGGGA/TGGTGTACGA
4		E255V	(GAG>GTG)	
5	BCR-ABL 299 Reverse	V299L	(GTG>CTG)	AC/G/ACAGGTTAGGGTGTTT
6		V299L	(GTG>TTG)	
7	BCR-ABL 315 Forward	T315A	(ACT>GCT)	A/GC/TTGAGT/C/GTC/A/GATGACCT
8		T315I	(ACT>ATT)	
9		F317L	(TTC>TTA)	
10		F317L	(TTC>TTG)	
11		F317L	(TTC>CTC)	
12		F317V	(TTC>GTC)	
13	BCR-ABL 359 Forward	F359V	(TTC>GTC)	1: CT/GTCATCCACA
14		F359C	(TTC>TGC)	2: CTT/GCATCCACA

mutation was T315I and mutations were mostly observed in patients in the BC or AP.

Additionally, only 1 mutation was identified in 18 (11%) patients, 2 mutations in 4 (2.4%) patients, and no mutation in 141 (86.6%) patients. Thus, 8 of 14 mutations were identified in 22 patients (13.4%) out of 163. The frequencies of the 8 mutations identified in our patient group were as follows: T315I—8 (36.4%), F359V—3 (13.7%), F359C—3 (13.7%), F317L (TTG)—2 (9.0%), F317V (CTC)—1 (4.5%), Y253H—3 (13.7%), E255K—1 (4.5%), V299L (CTG)—1 (4, 5%). The most common mutation appeared to be the T315I mutation followed by F359V, F359C, and Y253H (Table 3).

Mutations occurring in different regions of the ABL KD are presented in Table 4. Mutations occurring in the contact binding site region included T315I, F317L (TTA), F317L (TTG), F317L (CTC), F317V, T315A, which accounted for 50% of the mutations identified in the current study. The proportion of mutations identified in P-loop, SH2 domain and SH3 domain are presented in Table 4. Four patients had more than one mutation: F359V/F359C (3 patients), T315I/Y253H (1 patient). Figure 2 depicts the T315I mutation identified in the Contact binding site region of the ABL-kinase domain in patient 22 by Pyrosequencing method.

Karyotyping

Karyotype analysis was performed in 163 patients. It was not possible to identify the karyotype in 7 patients due the inability to obtain mitosis. Specimens for cytogenetic analysis were obtained during mutation screening of patients. Molecular cytogenetic (FISH) examination was performed in some samples in addition to cytogenetic analysis (Figure 3).

During the analysis, a duplication of the Philadelphia chromosome (+Ph), additional chromosomal aberrations and some structural aberrations were found in metaphases: (+8), (−7), (+19), (+21), i(17)(q10). Various chromosomal abnormalities were identified in 31 patients. ABL KD mutations were present in 9 out of 31 patients. Additional chromosomal aberrations were detected in 5 out of 8 patients with T315I mutations. Duplication of the Philadelphia chromosome (+Ph) was identified in 2 of them. We found an association between ABL KD mutations and additional chromosomal aberrations in CML patients ($p = 0.006$).

Survival analysis

The median follow-up for all patients was 22 months (range, 2–89 months). The OS rates of patients in the BCR-ABL1 mutation-positive (B) and negative (A) groups were 50% and 93%, respectively ($p < 0.00001$) (Figure 4). Following 43 months, the OS indicators of the patient groups with T315I mutation (BX) and without (A) were 0% and 92%, respectively ($p < 0.00001$) (Figure 5). Estimated median overall survival for BX group was 26. However, for group A median overall survival was not reached at the time of analysis. These results indicated that the OS rate of patients with the T315I mutation was notably decreased.

TABLE 2 Clinical, hematological and epidemiological characteristics of the patients at the time of diagnosis.

	Total (n = 163)	BCR-ABL mutation positive (n = 22)	p-value
Sex			
Male	80	17	<0.004[a]
Female	83	5	Chi = 8.08
Age, years			
Mean, 43 (range, 12–79)	163	53 (24–79)	0.231
≤49	86	9	Chi = 1.43
≥50	77	13	
Disease phase at screening			
CP	119	5	0.00001
AP	26	5	Chi = 53.12
BC	18	12	
Risk group			
Low	48	3	0.126
Mean	94	17	Chi = 4.13
High	21	2	
Spleen			
Normal	10	1	0.811
Medium (growth up to 8 cm)	118	17	Chi = 0.41
Massive (>8 cm)	35	4	
Hb			
Normal (120–160 g/L)	13	3	<0.480
Mild anemia (100–119 g/L)	49	4	Chi = 2.47
Mean anemia (80–99 g/L)	57	9	
Severe anemia (65–79 g/L)	42	6	
WBC			
Normal 3.9–9 (10^9/L)	2	0	0.843
Leukopenia <3.9 (10^9/L)	0	0	Chi = 0.34
Leukocytosis >9 (10^9/L)	161	22	
PLT			
Normal 180–400 (10^9/L)	92	12	0.920
Thrombocytopenia <180 (10^9/L)	23	3	Chi = 0.16
Thrombocytosis >400 (10^9/L)	46	7	
Blast cell (peripheral blood)			
0	62	3	0.017
1–10	99	18	Chi = 8.12
>10	2	1	
Eosinophil Basophil Association			
Eosinophils superiority	118	16	0.187
Basophilic superiority	20	4	Chi = 4.79
Without superiority	23	1	
No Association	2	1	
Additional chromosome			
Present	31	9	0.006
Absent	125	11	Chi = 10.13
Missing	7	2	

(Continued on following page)

TABLE 2 (*Continued*) Clinical, hematological and epidemiological characteristics of the patients at the time of diagnosis.

	Total (n = 163)	BCR-ABL mutation positive (n = 22)	p-value
Blood group			
O (I)	49	6	0.645
A (II)	76	10	Chi = 1.66
B (III)	24	5	
AB (IV)	14	1	
Rh-factor			
Rh+	155	21	0.932
Rh−	8	1	Chi = 0.007
Seasons			
Spring	38	3	0.394
Summer	50	10	Chi = 2.98
Autumn	16	2	
Winter	57	6	
Missing	2	1	

CP, chronic phase; AP, acceleration phase; BC, blast crisis.
[a]p < 0,05.

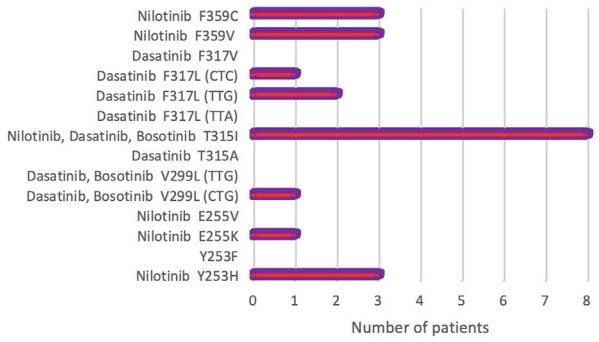

FIGURE 1
Frequency of rare BCR-ABL1 kinase domain mutations detected by Pyrosequencing in 163 CML patients. Mutations causing high-level resistance to second-line TKIs have been presented (NCCN, Version 2.2021) [28].

Discussion

Data from a cohort of 163 CML patients, subjected to mutation screening, were rigorously examined, revealing that 119 individuals (73%) were classified as being in the CP, 26 individuals (15.9%) in the AP, and 18 individuals (11.1%) in the BC. Remarkably, we identified 5 mutations in CP, 5 in AP, and 12 in BC. Our statistical analysis unveiled a pronounced association between mutations in the ABL kinase domain (ABL KD) and the respective disease phases, with a statistically significant p-value of <0.05.

Notably, the T315I mutation emerged as the predominant genetic aberration and exhibited a significant correlation with overall survival (OS). Patients afflicted with the T315I mutation (n = 7), T315I/Y253H (n = 1), Y253H (n = 2), and E255K (n = 1) mutations faced adverse clinical outcomes, culminating in mortality. By the end of the study, the majority of patients with T315I, Y253H and E255K mutations had progressed to the BC phase and they failed to respond to combination chemotherapy and second-line TKIs.

Our investigation conclusively established that these mutations were significantly associated with resistance to both first- and second-line TKIs. Within the cohort of patients in whom mutations were identified, four individuals demonstrated the presence of multiple mutations. Three patients exhibited co-occurrence of F359V/F359C mutations, while one patient manifested both T315I/Y253H mutations. However, due to the retrospective design of the study, it was not possible to confirm whether these mutations were complex or polyclonal. Furthermore, the limited representation of such patients in our study impeded the assessment of the potential impact of compound mutations on overall survival.

43-month survival was noted in 92% (142) of resistant patients without the T315I mutations. 30 (21%) out of 142 patients were treated with imatinib dose escalation, and the rest 112 (79%) patients received second-line TKIs. At the culmination of a 24 month interval, 48 patients (43%) subjected to second-line TKI therapy manifested MMR, while 64 individuals (57%) exhibited concurrent hematological response and achieved CCyR.

Subsequently, the cohort was stratified into low-, medium-, and high-risk groups based on their clinical characteristics at the time of initial CML diagnosis, revealing no significant associations between risk stratification, patients' blood groups, Rh-factor, seasonality of morbidity, and ABL KD mutations. Additionally, the analysis failed to reveal any significant correlations between initial HB, WBC, PLT, eosinophil count, basophil count, spleen

TABLE 3 Frequency of identified mutations and their distrubition according to the disease phases.

Mutations	CP	AP	BC	Total
T315I	—	1 (0.6%)	7 (4.4%)	8 (5.0%)
F359V	1 (0.6%)	1 (0.6%)	1 (0.6%)	3 (1.8%)
F359C	1 (0.6%)	1 (0.6%)	1 (0.6%)	3 (1.8%)
F317L (TTG)	1 (0.6%)	1 (0.6%)	—	2 (1.2%)
F317V (CTC)	1 (0.6%)	—	—	1 (0.6%)
Y253H	—	—	3 (1.8%)	3 (1.8%)
E255K	—	1 (0.6%)	—	1 (0.6%)
V299L (CTG)	1 (0.6%)	—	—	1 (0.6%)
Total	5 (3.0%)	5 (3.0%)	12 (7.4%)	22 (13.4%)
Total patient[a]	119 (73%)	26 (16%)	18 (11%)	163 (100%)

CP, chronic phase; AP, acceleration phase; BC, blast crisis.
More than 1 mutation was identified in 4 patients.
[a]Total number of patients with and without mutations detected.

TABLE 4 The proportion of mutations occurring in distinct regions.

Region	Mutation	Proportion%
P-loop	E255K	18.1%
	E255V	
	Y253H Y253F	
Contact binding site	T315I	50%
	F317L (TTA) F317L (TTG) F317L (CTC) F317V	
	T315A	
SH2 domain	F359V	27.4%
	F359C	
SH3 domain	V299L (CTG) V299L (TTG)	4.5%

size at the time of diagnosis, and the presence of mutations. Nevertheless, a substantial association was observed between baseline blast cell count and the occurrence of ABL KD mutations, with a statistically significant p-value of <0.05.

The emergence of resistance to tyrosine kinase inhibitors (TKIs) can be dichotomized into BCR-ABL-dependent and BCR-ABL-independent processes. BCR-ABL-dependent mechanisms encompass BCR-ABL kinase overexpression and mutations within the BCR-ABL domain, while BCR-ABL-independent processes involve the activation of alternative signaling pathways, such as JAK/STAT, as well as the upregulation of efflux transporters or downregulation of influx transporters, resulting in reduced intracellular TKI levels [29]. Among these mechanisms, mutations in the BCR/ABL KD are of paramount importance. Intriguingly, our study affirmed that mutations in the KD, which confer resistance to TKI therapy, exhibit a markedly higher incidence in patients in the BC phase compared to those in the CP. Furthermore, patients with

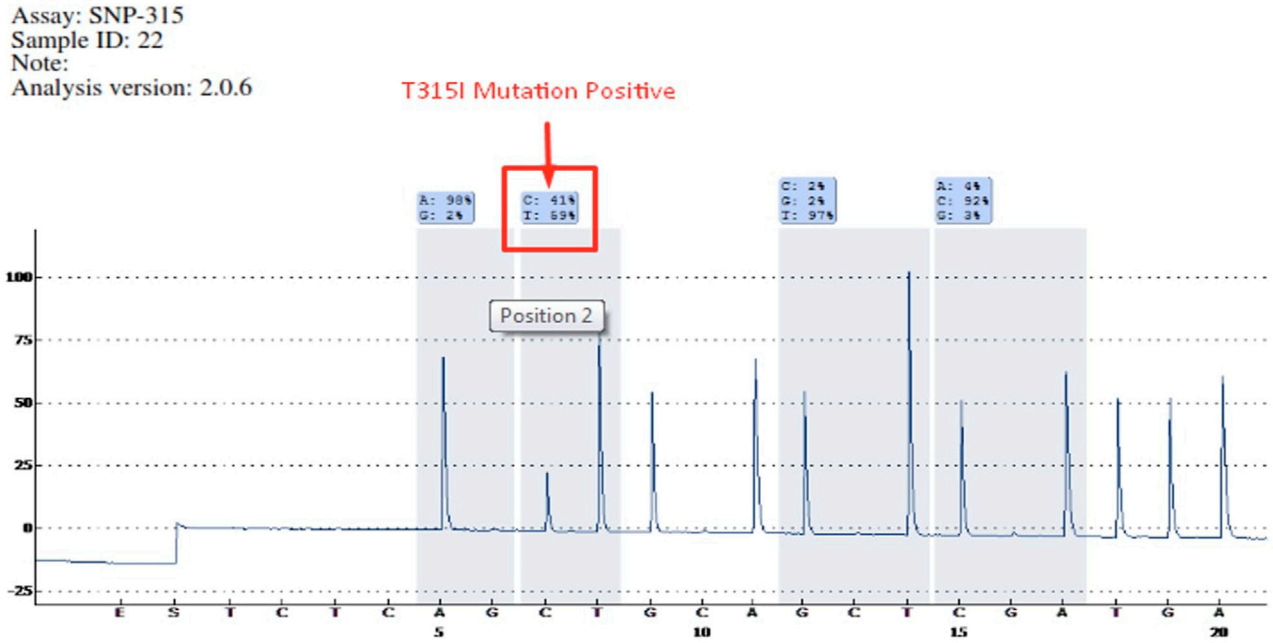

Sequence to analyze:
A/GC/TTGAGT/C/GTC/A/GATGACCTACGGGAACCT

Position	1	2	3	4
Quality	Passed	Passed	Passed	Passed
A (%)	98	-	-	4
C (%)	-	41	2	92
G (%)	2	-	2	3
T (%)	-	59	97	-

FIGURE 2
Determination of T315I mutation by Pyrosequencing method in patient 22 (C = 41%—T = 59%).

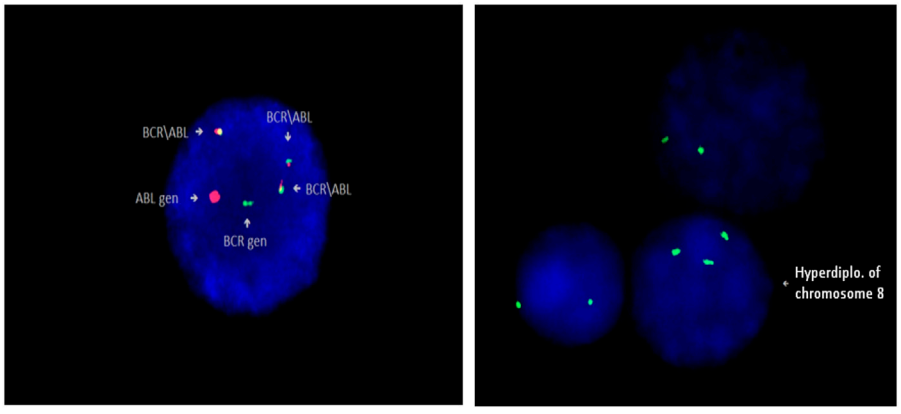

FIGURE 3
Identification of Philadelphia chromosome (Ph+) in patient 5, and trisomy 8 (+8) in patient 94 by FISH method (Cytocell).

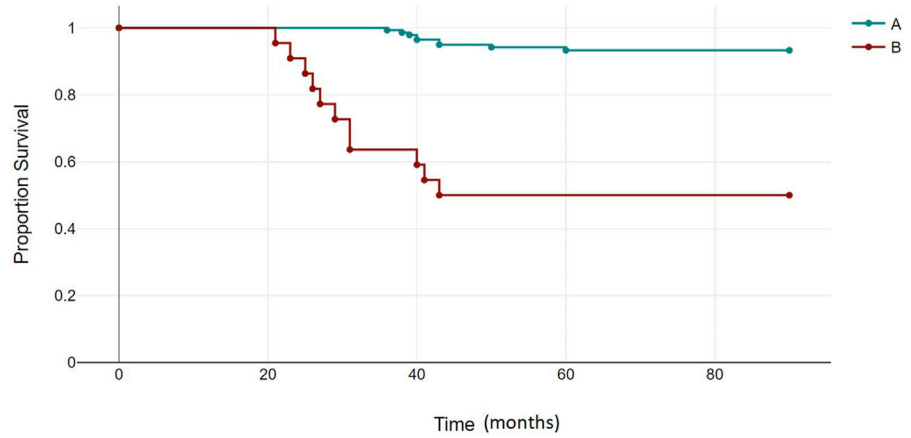

FIGURE 4
BCR-ABL1 negative (A) and BCR-ABL1 positive (B) OS based on mutational status of 163 CML patients. $p < 0.00001$.

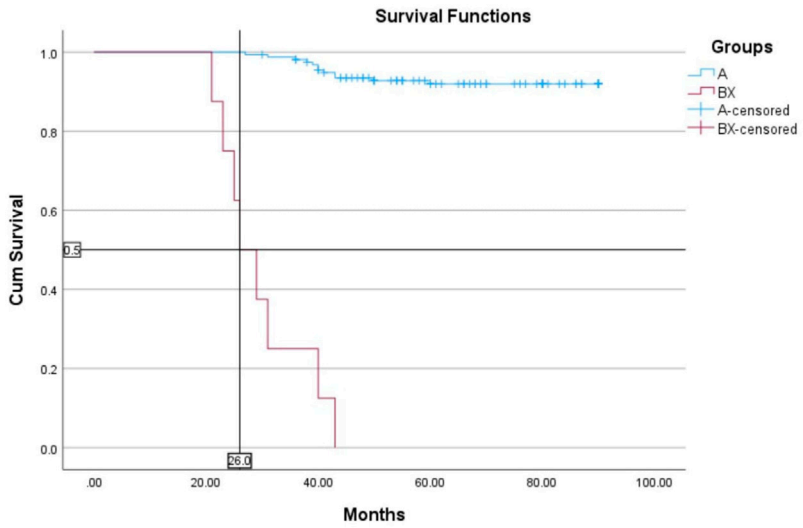

FIGURE 5
T315I negative (A) and T315I positive (BX) OS based on mutational status of 163 CML patients. $p < 0.00001$.

mutations in the CP category demonstrated an elevated propensity for progressing to AP or BC. Consequently, these mutations bear clinical significance by providing insights into patients who fail to achieve optimal responses to TKIs [30, 31]. Notably, the current therapeutic landscape offers a plethora of alternative options for TKI treatment contingent upon the specific mutations associated with TKI resistance [32, 33]. Acquired mutations, in particular, interfere with TKI binding or result in diminished TKI sensitivity [34]. Notably, distinct mutations display varying degrees of sensitivity to TKIs, underscoring the importance of mutation detection in guiding TKI selection and influencing patient prognosis. These principles align with recommendations from both the European LeukemiaNet (ELN) and the National Comprehensive Cancer Network (NCCN), advocating the consideration of mutational profiles in the determination of subsequent therapy [13, 35].

It is noteworthy that, owing to the contribution of TKIs and an enhanced understanding of the influence of the BCR-ABL mutational profile on drug efficacy, CML is presently recognized as a chronic ailment. However, it remains pertinent to acknowledge that a subset of patients continues to experience disease progression. Consequently, there is an imperative need for further investigations elucidating the intricate interplay between genes and drugs, with the aim of achieving optimal coverage in the treatment of CML.

Data availability statement

The raw data supporting the conclusions of this article will be made available by the authors, without undue reservation.

Ethics statement

The studies involving humans were approved by the National Hematology and Transfusion Center Review Board. The studies were conducted in accordance with the local legislation and institutional requirements. The participants provided their written informed consent to participate in this study.

Author contributions

Collection of biospecimens, conducting laboratory work and completion of the project were carried out by AH. CA and AS played an important role in data analysis and selection of statistical methodology. NK, GA, and ZA made significant contributions to the conception and design of the study. The manuscript was written by AH and edited by GA. All authors contributed to the article and approved the submitted version.

Conflict of interest

The authors declare that the research was conducted in the absence of any commercial or financial relationships that could be construed as a potential conflict of interest.

Acknowledgments

We are thankful to the patients who participated in this study and provided samples. The study was supported by the Scientific Research Institute of Hematology and Transfusion. Also, we express our deep gratitude to the employees of ATQ Biotechnology Laboratory operating in Ankara, Türkiye, for their support.

References

1. Baccarani W, Deininger MW, Rosti G, Hochhaus A, Soverini S, Apperley JF, et al. European leukemianet recommendations for the management of chronic myeloid leukemia. *Blood* (2013) 122(6):872–84. doi:10.1182/blood-2013-05-501569

2. Apperley JF. Chronic myeloid leukaemia. *Lancet* (2015) 385:1447–59. doi:10.1016/S0140-6736(13)62120-0

3. O'Brien SG, Guilhot F, Larson RA, Gathmann I, Baccarani M, Cervantes F, et al. Imatinib compared with interferon and low-dose cytarabine for newly diagnosed chronic-phase chronic myeloid leukemia. *N Engl J Med* (2003) 348: 994–1004. doi:10.1056/nejmoa022457

4. Gratwohl A, Brand R, Apperley J, Ruutu T, Corradini P, Carreras E, et al. Allogeneic hematopoietic stem cell transplantation for chronic myeloid leukemia in Europe 2006: transplant activity, long-term data and current results. An analysis by the chronic leukemia working party of the european group for blood and marrow transplantation (EBMT). *Haematologica* (2006) 91:513e21.

5. Hughes T, Saglio G, Branford S, Soverini S, Kim DW, Müller MC, et al. Impact of baseline BCR-ABL mutations on response to nilotinib in patients with chronic myeloid leukemia in chronic phase. *J Clin Oncol* (2009) 27(25):4204–10. doi:10.1200/JCO.2009.21.8230

6. Müller MC, Cortes JE, Kim DW, Druker BJ, Erben P, Pasquini R, et al. Dasatinib treatment of chronic-phase chronic myeloid leukemia: analysis of responses according to preexisting BCR-ABL mutations. *Blood* (2009) 114(24): 4944–53. doi:10.1182/blood-2009-04-214221

7. Parker WT, Yeung DTO, Yeoman AL, Altamura HK, Jamison BA, Field CR, et al. The impact of multiple low-level BCR-ABL1 mutations on response to ponatinib. *Blood* (2016) 127(15):1870–80. doi:10.1182/blood-2015-09-666214

8. Pasic I, Lipton JH. Current approach to the treatment of chronic myeloid leukaemia. *Leuk Res* (2017) 55:65–78. doi:10.1016/j.leukres.2017.01.005

9. Loscocco F, Visani G, Galimberti S, Curti A, Isidori A. BCR-ABL independent mechanisms of resistance in chronic myeloid leukemia. *Front Oncol* (2019) 9:939. doi:10.3389/fonc.2019.00939

10. Eide CA, O'Hare T. Chronic myeloid leukemia: advances in understanding disease biology and mechanisms of resistance to tyrosine kinase inhibitors. *Curr Hematol Malig Rep* (2015) 10:158–66. doi:10.1007/s11899-015-0248-3

11. Hochhaus A. Chronic myelogenous leukemia (CML): resistance to tyrosine kinase inhibitors. *Ann Oncol* (2006) 17(Suppl. 10):x274–9. doi:10.1093/annonc/mdl273

12. Baccarani M, Cortes J, Pane F, Niederwieser D, Saglio G, Apperley J, et al. Chronicmyeloid leukemia: an update of concepts and management recommendations of European LeukemiaNet. *J Clin Oncol* (2009) 27:6041–51. doi:10.1200/JCO.2009.25.0779

13. O'Brien S, Radich JP, Abboud CN, Akhtari M, Altman JK, Berman E, et al. Chronic myelogenous leukemia, version 1.2014. *J Natl Compr Canc Netw* (2013) 11(11):1327–1340. doi:10.6004/jnccn.2013.0157

14. Apperley JF. Part I: mechanisms of resistance to imatinib in chronic myeloid leukaemia. *Lancet Oncol* (2007) 8:1018–29. doi:10.1016/S1470-2045(07)70342-X

15. Khorashad JS, Kelley TW, Szankasi P, Mason CC, Soverini S, Adrian LT, et al. BCR-ABL1 compound mutations in tyrosine kinase inhibitor-resistant CML: frequency and clonal relationships. *Blood* (2013) 121:489–98. doi:10.1182/blood-2012-05-431379

16. Soverini S, Hochhaus A, Nicolini FE, Gruber F, Lange T, Saglio G, et al. BCR-ABL kinase domain mutation analysis in chronic myeloid leukemia patients treated with tyrosine kinase inhibitors: recommendations from an expert panel on behalf of European LeukemiaNet. *Blood* (2011) 118:1208–15. doi:10.1182/blood-2010-12-326405

17. Shiotsu Y, Kiyoi H, Ishikawa Y, Tanizaki R, Shimizu M, Umehara H, et al. KW-2449, a novel multikinase inhibitor, suppresses the growth of leukemia cells with FLT3 mutations or T315I-mutated BCR/ABL translocation. *Blood* (2009) 114: 1607–17. doi:10.1182/blood-2009-01-199307

18. Moore AS, Blagg J, Linardopoulos S, Pearson ADJ. Aurora kinase inhibitors: novel small molecules with promising activity in acute myeloid and Philadelphia-positive leukemias. *Leukemia* (2010) 24:671–8. doi:10.1038/leu.2010.15

19. Giles FJ, Cortes J, Jones D, Bergstrom D, Kantarjian H, Freedman SJ. MK-0457, a novel kinase inhibitor, is active in patients with chronic myeloid leukemia or acute lymphocytic leukemia with the T315I BCR-ABL mutation. *Blood* (2007) 109: 500–2. doi:10.1182/blood-2006-05-025049

20. Modugno M, Casale E, Soncini C, Rosettani P, Colombo R, Lupi R, et al. Crystal structure of the T315I Abl mutant in complex with the aurora kinases inhibitor PHA-739358. *Cancer Res* (2007) 67:7987–90. doi:10.1158/0008-5472.CAN-07-1825

21. Hughes T, Saglio G, Branford S, Soverini S, Kim DW, Muller MC, et al. Impact of baseline BCR-ABL mutations on response to nilotinib in patients with chronic myeloid leukemia in chronic phase. *J Clin Oncol* (2009) 27:4204–10. doi:10.1200/JCO.2009.21.8230

22. Soverini S, Gnani A, Colarossi S, Castagnetti F, Abruzzese E, Paolini S, et al. Philadelphia-positive patients who already harbor imatinib-resistant Bcr-Abl kinase domain mutations have a higher likelihood of developing additional

mutations associated with resistance to second- or third-line tyrosine kinase inhibitors. *Blood* (2009) 114:2168–71. doi:10.1182/blood-2009-01-197186

23. Muller MC, Cortes JE, Kim DW, Druker BJ, Erben P, Pasquini R, et al. Dasatinib treatment of chronic-phase chronic myeloid leukemia: analysis of responses according to preexisting BCR-ABL mutations. *Blood* (2009) 114: 4944–53. doi:10.1182/blood-2009-04-214221

24. Shah NP, Skaggs BJ, Branford S, Hughes TP, Nicoll JM, Paquette RL, et al. Sequential ABL kinase inhibitor therapy selects for compound drug-resistant BCR-ABL mutations with altered oncogenic potency. *J Clin Invest* (2007) 117:2562–9. doi:10.1172/JCI30890

25. Soverini S, Colarossi S, Gnani A, Castagnetti F, Rosti G, Bosi C, et al. Resistance to dasatinib in Philadelphia-positive leukemia patients and the presence or the selection of mutations at residues 315 and 317 in the BCR-ABL kinase domain. *Haematological* (2007) 92:401–4. doi:10.3324/haematol.10822

26. Parker WT, Ho M, Scott HS, Hughes TP, Branford S. Poor response to second-line kinase inhibitors in chronic myeloid leukemia patients with multiple low-level mutations, irrespective of their resistance profile. *Blood* (2012) 119: 2234–8. doi:10.1182/blood-2011-08-375535

27. Parker WT, Lawrence RM, Ho M, Irwin DL, Scott HS, Hughes TP, et al. Sensitive detection of BCR-ABL1 mutations in patients with chronic myeloid leukemia after imatinib resistance is predictive of outcome during subsequent therapy. *J Clin Oncol* (2011) 29:4250–9. doi:10.1200/JCO.2011.35.0934

28. Deininger MW, Shah NP, Altman JK, Berman E, Bhatia R, Bhatnagar B, et al. Chronic myeloid leukemia, version 2.2021, NCCN clinical practice guidelines in oncology. *NCCN Clinical Practice Guidelines Oncology* (2020) 18:1385–415. doi:10.6004/jnccn.2020.0047

29. Apperley JF. Part I: mechanisms of resistance to imatinib in chronic myeloid leukaemia. *Lancet Oncol* (2007) 8:1018–29. doi:10.1016/S1470-2045(07)70342-X

30. Baccarani M, Castagnetti F, Gugliotta G, Rosti G. A review of the European LeukemiaNet recommendations for the management of CML. *Ann Hematol* (2015) 94(Suppl. 2):S141–7. doi:10.1007/s00277-015-2322-2

31. Soverini S, De Benedittis C, Mancini M, Martinelli G. Present and future of molecular monitoring in chronic myeloid leukaemia. *Br J Haematol* (2016) 173: 337–49. doi:10.1111/bjh.13966

32. Corbin AS, La Rosée P, Stoffregen EP, Druker BJ, Deininger MW. Several BCR-ABL kinase domain mutants associated with imatinib mesylate resistance remain sensitive to imatinib. *Blood* (2003) 101:4611–4. doi:10.1182/blood-2002-12-3659

33. Hochhaus A, Schenk T, Erben P, Ernst T, La Rosée P, Müller MC. Cause and management of therapy resistance. *Best Pract Res Clin Haematol* (2009) 22:367–79. doi:10.1016/j.beha.2009.05.004

34. Soverini S, de Benedittis C, Mancini M, Martinelli G. Mutations in the BCR-ABL1 kinase domain and elsewhere in chronic myeloid leukemia. *Clin Lymphoma Myeloma Leuk* (2015) S1(Suppl. l):S120–S128. doi:10.1016/j.clml.2015.02.035

35. Hochhaus A, Baccarani M, Silver RT, Schiffer C, Apperley JF, Cervantes F, et al. European LeukemiaNet 2020 recommendations for treating chronic myeloid leukemia. *Leukemia* (2020) 34:966–84. doi:10.1038/s41375-020-0776-2

Pathology & Oncology Research | frontiers

TYPE Brief Research Report
PUBLISHED 24 January 2023
DOI 10.3389/pore.2023.1610844

Check for updates

OPEN ACCESS

EDITED BY
Edit Bardi,
St.Anna Kinderspital, Austria

*CORRESPONDENCE
Mutita Junking,
mutita.jun@mahidol.ac.th
Pa-Thai Yenchitsomanus,
ptyench@gmail.com

RECEIVED 26 September 2022
ACCEPTED 11 January 2023
PUBLISHED 24 January 2023

CITATION
Phikulsod P, Sukpanichnant S, Kunacheewa C, Chieochansin T, Junking M and Yenchitsomanus P-T (2023), High prevalence of Wilms tumor 1 expression in multiple myeloma and plasmacytoma: A cohort of 142 Asian patients' samples.
Pathol. Oncol. Res. 29:1610844.
doi: 10.3389/pore.2023.1610844

COPYRIGHT
© 2023 Phikulsod, Sukpanichnant, Kunacheewa, Chieochansin, Junking and Yenchitsomanus. This is an open-access article distributed under the terms of the Creative Commons Attribution License (CC BY). The use, distribution or reproduction in other forums is permitted, provided the original author(s) and the copyright owner(s) are credited and that the original publication in this journal is cited, in accordance with accepted academic practice. No use, distribution or reproduction is permitted which does not comply with these terms.

High prevalence of Wilms tumor 1 expression in multiple myeloma and plasmacytoma: A cohort of 142 Asian patients' samples

Ployploen Phikulsod[1,2,3], Sanya Sukpanichnant[4], Chutima Kunacheewa[3], Thaweesak Chieochansin[1], Mutita Junking[1]* and Pa-Thai Yenchitsomanus[1]*

[1]Siriraj Center of Research Excellence for Cancer Immunotherapy (SiCORE-CIT), Division of Molecular Medicine, Research Department, Faculty of Medicine Siriraj Hospital, Mahidol University, Bangkok, Thailand, [2]International Graduate Program in Immunology, Department of Immunology, Faculty of Medicine Siriraj Hospital, Mahidol University, Bangkok, Thailand, [3]Division of Hematology, Department of Medicine, Faculty of Medicine Siriraj Hospital, Mahidol University, Bangkok, Thailand, [4]Department of Pathology, Faculty of Medicine Siriraj Hospital, Mahidol University, Bangkok, Thailand

Wilms tumor 1 (WT1) is a promising target antigen for cancer immunotherapy. However, WT1 protein expression and its clinical correlation in multiple myeloma (MM) patients are still limited. We, therefore, investigated WT1 expression in 142 bone marrow and plasmacytoma samples of MM patients at different stages of the disease by immunohistochemistry. The correlations between WT1 expression and clinical parameters or treatment outcomes were evaluated. The overall positive rate of WT1 expression was 91.5%; this high prevalence was found in both bone marrow and plasmacytoma samples, regardless of the disease status. Cytoplasmic WT1 expression was correlated with high serum free light chain ratio at presentation. However, no significant association between WT1 expression and treatment outcome was observed. This study confirms the high prevalence of WT1 expression in an Asian cohort of MM, encouraging the development of immunotherapy targeting WT1 in MM patients, particularly in those with extramedullary plasmacytoma or relapsed disease.

KEYWORDS

multiple myeloma, immunohistochemistry (IHC), plasmacytoma, WT1 protein, cohort study Thailand, Asian cohort, treatment outcome, clinical relevance

Introduction

Wilms tumor 1 (WT1) is a zinc-finger transcription factor encoded by *WT1* gene on human chromosome 11p13 (1). WT1 is overexpressed in many cancers and is correlated with poor prognosis in some types of cancers (2–6). WT1 was ranked as the most promising target antigen for cancer immunotherapy in 2009 by the US National Cancer Institute (7). Since then, immunotherapy targeting WT1 has been studied and clinical efficacies were shown in various cancer models (6).

10.3389/pore.2023.1610844

TABLE 1 Clinicopathological features of multiple myeloma patients.

Clinical factors	Overall (n = 142)	WT+ (n = 130, 91.5%)	WT- (n = 12, 8.5%)	p-value
Age (years)	62 ± 10	62.4 ± 10.6	61.4 ± 9.3	0.760
Gender, % (n)				1.000
Female	50% (71)	50% (65)	50% (6)	
Subtype of MM, % (n)				0.914
IgG	54.8%	54.6%	75%	
IgD	1.4%	0.8%	0.8%	
IgA	13.9%	14.6%	8.3%	
Light chain	25%	26.2%	16.7%	
Heavy chain	0.7%	0.8%	0%	
Isolated plasmacytoma	2.1%	1.5%	0%	
NA	1.4%	1.5%	0%	
ISS staging, % (n)				0.778
Stage I	7.2% (5)	7.8% (5)	0% (0)	
Stage II	31.9% (22)	31.3% (20)	40% (2)	
Stage III	60.9% (42)	60.9% (39)	60% (3)	
Clinical manifestation				
Hemoglobin (g/dL)	8.8 ± 2.1	8.8 ± 2.2	8.6 ± 2	0.815
Platelets (10^3cells/uL)	182 (32–561)	178 (32–561)	224 (73–366)	0.783
Creatinine (mg/dL)	1.2 (0.4–15.4)	1.2 (0.4–15.4)	1.2 (0.5–2.3)	0.513
Corrected Ca^{2+} (mg/dL)	10.4 ± 1.7	10.4 ± 1.7	10.6 ± 1.2	0.788
Beta-2-microglobulin (mg/dL)	6.6 (1.8–69.1)	6.7 (1.8–69.1)	6.3 (2.9–12.5)	0.438
M protein (g/dL)	4.04 ± 1.98	4.01 ± 2.01	4.41 ± 1.67	0.704
Serum free light chain ratio	94.2 (1.1–5,537.9)	108.5 (1.1–5,537.9)	8.02 (5.6–241.7)	0.084
Bone fracture, % (n)	43.2% (41/95)	41.6% (37/89)	66.7% (4/6)	0.230
Status of disease, % (n)				1.000
First diagnosis	64.8% (92)	64.6% (84)	66.7% (8)	
Relapse	35.2% (50)	35.4% (46)	33.3% (4)	
Tissues, % (n)				0.704
Bone marrow	80.3% (114)	80.8% (105)	75% (9)	
Plasmacytoma	19.7% (28)	19.2% (25)	25% (3)	
Complete remission rate, % (n)	45.8% (27/59)	49.2% (29/54)	40% (2/5)	1.000
Novel therapy, % (n)	69% (49/71)	68.2% (45/66)	80% (4/5)	1.000
Transplantation rate, % (n)	17.7% (14/79)	17.6% (13/74)	20% (1/5)	1.000

Multiple myeloma (MM) is the second most common hematologic malignancy worldwide (8). The median age at the diagnosis is 66–70 years of age. Even though the treatment of MM has been improved and able to increase the overall survival of the patients, MM is still considered incurable (9). Targeted therapy and immunotherapies have been developed and approved for the treatment of MM (9). A cancer vaccine is an alternative method that could deepen disease responses after the failure of conventional treatment in patients with relapsed disease. Many target antigens, including WT1, have been studied in MM patients (10). At an early stage of the studies, WT1 seemed not to be a potential target for MM because of its low RNA expression in bone marrow samples (2,11). Despite that, myeloma cells were found to be highly sensitive to lysis by WT1-specific cytotoxic T lymphocytes (12). WT1-specific T cells were also found in the MM patients and their increment correlated with disease control after donor lymphocyte infusions (13). Moreover, clinical efficacies of WT1 vaccine in MM were shown in clinical trials (14,15). This led to the fast-track approval of WT1 peptide vaccine as maintenance for high-risk MM by US FDA in 2018.

Previously, WT1 protein was found to be expressed in all 15 MM patients in the western population using immunohistochemistry (IHC) method (13). Therefore, instead

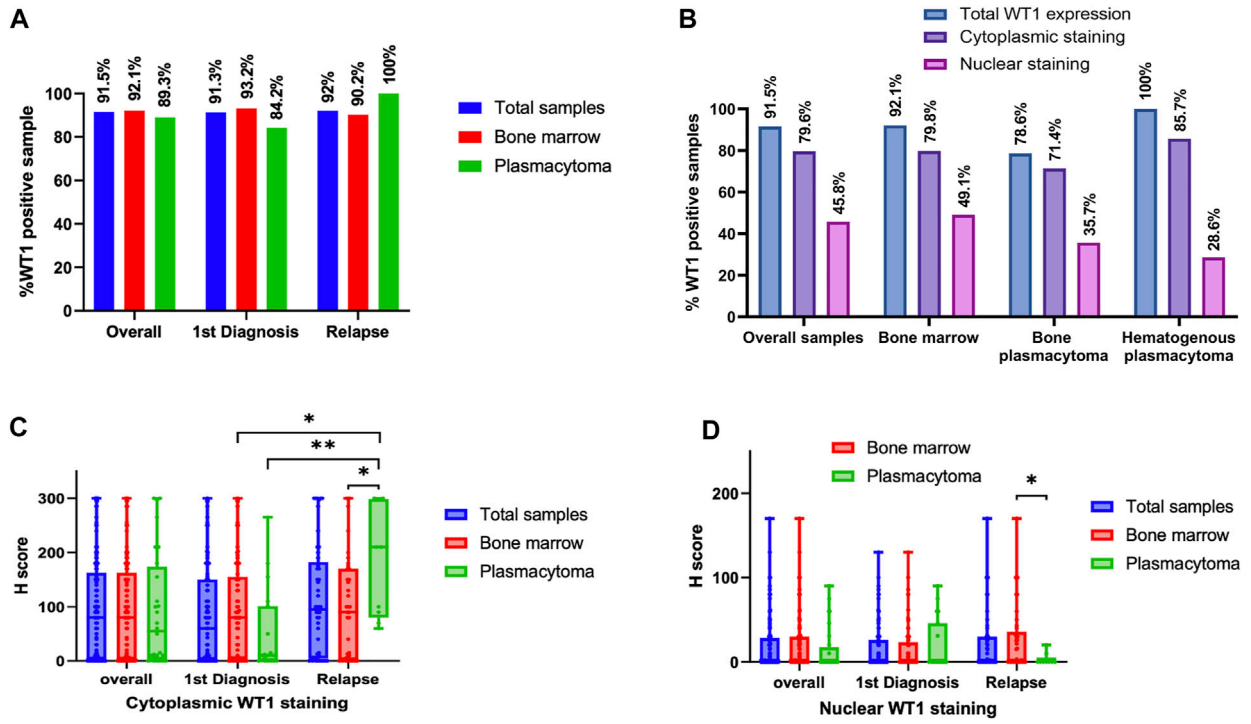

FIGURE 1
WT1 protein expression in tissues at different stages of multiple myeloma (MM): Rates of WT1 protein expression in MM tissues at different clinical settings **(A)**, Rates of cytoplasmic and nuclear WT1 staining in different tissue samples **(B)**, Histology score (H-score) of WT1 cytoplasmic staining **(C)**, and nuclear staining **(D)** in different myeloma samples at first diagnosis or relapse stage (*$p < 0.05$, **$p < 0.01$).

of detection of mRNA expression, WT1 immunostaining could be more useful as a marker for immunotherapy targeting WT1 in MM. However, the data on WT1 protein expression in MM is still limited and controversial. Another study from China showed that WT1 IHC staining was positive only in 30% of MM samples ($n = 62$) (16). To study the prevalence of WT1 protein expression in MM, we used IHC method to detect WT1 protein expression in a larger and more variety of MM samples in Thai patients as a representative of the Asian cohort.

Materials and methods

Tissue samples and associated clinical data

Samples from patients who has been diagnosed with MM at Siriraj Hospital between January 2014 and December 2016 were included. To verify the diagnosis, diagnostic reports along with hematoxylin and eosin slides were reviewed. Cases with inadequate paraffin-embedded samples and less than 20% of myeloma cell involvement were excluded. Associated clinical data were retrieved from electronic medical records. Detailed baseline clinical characteristics were listed in Table 1.

Immunohistochemistry

Tissue sections of 3 μm thickness were prepared. The tissue sections were retrieved at 95°C, pH 8.5, for 64 min in CC1 solution (Ventana). Non-specific activities were blocked with 3% H_2O_2 and antibody diluent (Ventana). Prediluted 1: 500 mouse anti-WT1 antibody (clone 6F-H2; Cell Marque) was incubated for 1 h at 36°C. A positive signal was detected using the amplification and UltraView Universal DAB detection kit (Roche). Sections from Wilms tumor, kidney, tonsil, and samples with omission of the primary antibody as positive and negative controls.

Evaluation method

The proportion of positive myeloma cells and reaction strength for WT1 protein expression were determined. The level and distribution of expression were reviewed and estimated in agreement by three investigators. The positive reaction strength was described as −, +, + and +++. To assess the extent of immunoreactivity, H-score was calculated by the formula: (3 x % strongly staining cells) + (2 x % moderately staining cells) + % weakly staining cells.

Statistical analysis

Statistical analyses were carried out using SPSS 13.0 for Windows (SPSS, USA). Categorical data are given as numbers and percentages, and continuous data are reported as either mean ± standard deviation (SD) (normal distribution) or median and range (non-normal distribution). In the univariate analysis of the independent samples, *t*-test was used for normally distributed variables, and the Mann-Whitney U test was used for non-normally distributed variables. Pearson's X^2 or Fisher's exact test was used to examine the association between categorical variables. Correlation among the factors was calculated using Spearman/Pearson correlation coefficient test. Patient survival was analyzed using the Kaplan-Meier method and a log-rank test. A two-sided *p*-value of less than 0.05 was considered statistically significant.

Results

Baseline patient characteristics and specimens

A total of 142 specimens from 95 MM patients were studied. The average age of the patients was 62 years. Half of them were females. The majority of patients had IgG subtype. Ninety-two samples (65%) were collected at diagnosis whereas 50 samples (35%) were collected at the time of relapse. One hundred and fourteen samples (80%) were bone marrow tissues and twenty-eight (20%) were plasmacytoma tissues. For the plasmacytoma specimens ($n = 28$), half of them arose from bone and the other half were hematogenous spreading of plasma cells. The clinical characteristics and laboratory findings of the patients are summarized in Table 1. There were no significant differences in baseline characteristics between the cases with positive WT1 staining and those with negative WT1 staining.

WT1 protein expression

WT1 protein expression was found in 91.5% of total samples. The rates of WT1 expressions were 91.3%, 92.0%, 92.1%, and 89.3% in samples at the diagnosis, at relapse, bone marrow, and plasmacytoma, respectively (Figure 1A). In the plasmacytoma samples ($n = 28$), soft-tissue plasmacytoma ($n = 14$) and relapsed plasmacytoma ($n = 9$) had an exceptional high rate of WT1 protein expression (100%) as compared to bone plasmacytoma (78.6%, $n = 11/14$) ($p = 0.067$) (Figure 1B). Both cytoplasmic staining and nuclear staining of WT1 were observed (Figure 2). WT1 cytoplasmic staining was detected in 79.6% (114/142) of samples with an H-score ranging from 0 to 300, and a median score of 80, whereas nuclear staining was detected in 45.8% (65/142) of samples and H score ranged from 0 to 170, with a median score of 0 (Figure 1B; Table 2). WT1 positive cells per sample in the samples at a relapse stage were higher than that of the samples at the first diagnosis (50% vs. 30%) but without a statistical significance ($p = 0.222$). There was no difference in the overall rate and intensity of WT1 positivity between myeloma cells in the bone marrow and extramedullary samples. However, in a subgroup analysis, the highest cytoplasmic WT1 expression was found in relapsed plasmacytoma samples (Figure 1C). A median WT1 cytoplasmic H score in relapsed plasmacytomas was 210 (60–300) in comparison to 10 (0–265) ($p = 0.002$), 80 (0–300) ($p = 0.011$), and 90 (0–300) ($p = 0.031$) in plasmacytoma samples at first diagnosis, bone marrow samples at first diagnosis, and bone marrow samples at relapse, respectively (Figure 1C; table 2). The median percentage of cytoplasmic positive cells per sample was 99% (30–100) in the relapsed plasmacytoma compared to 5% (0–100) ($p = 0.004$), 30% (0–100) ($p = 0.016$), and 40% (0–100) ($p = 0.023$) in plasmacytoma samples at first diagnosis, bone marrow samples at first diagnosis, and bone marrow samples at relapse, respectively. The comprehensive data of WT1 staining was shown in Figure 1 and Table 2.

WT1 staining pattern in paired samples

There were 13 cases of bone marrow and plasmacytoma tissues obtained in the same clinical setting. WT1 staining results were concordant in both positivity and staining patterns in most cases, except in two cases with WT1 positivity only in bone marrow samples but negativity in bone plasmacytoma.

There were 22 cases containing sequential samples from the diagnosis and during relapses. Two cases (9%) had no WT1 expression on the diagnosis, then later expressed WT1 at relapse (1 with cytoplasmic staining and 1 with nuclear and cytoplasmic staining). Of 20 cases with WT1 expression at the diagnosis, 17 (85%) cases remained the expression throughout clinical courses. The pattern of WT1 staining was consistent in 11 cases, whereas changes in the staining pattern were found in 6 cases. There were 3 cases with WT1 expression at the diagnosis which turned to be negative at a relapse stage. Interestingly, two of these cases relapsed more than once and became WT1 positive during a later relapse.

WT1 expression and clinical correlation

To explore the relationship of WT1 expression with clinical characteristics, we analyzed the correlation between WT1 expressions and patients' clinical parameters. Patients with ISS stage III tended to have a higher percentage of cells with cytoplasmic positivity [10% (0%–100%) vs. 50% (0%–100%), $p = 0.087$] and cytoplasmic H score than those of

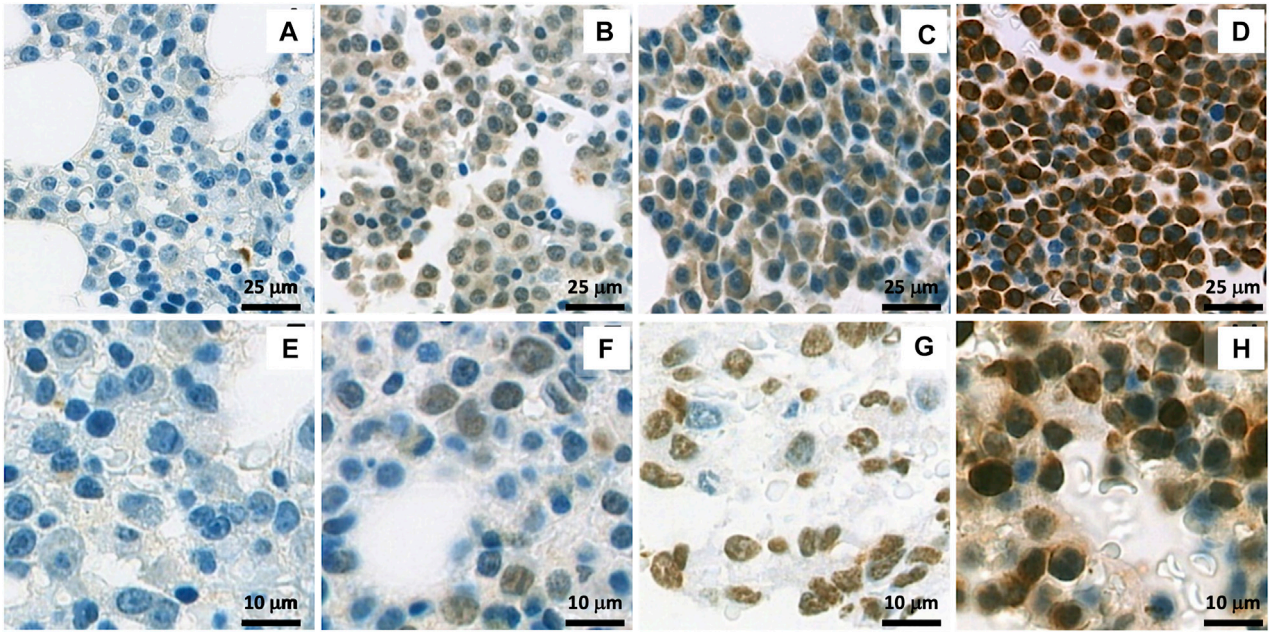

FIGURE 2
Immunohistochemistry (IHC) staining of WT1 protein: **(A–D)** show a representative cytoplasmic staining with different intensities in samples: Negative staining **(A)**, + **(B)**, ++ **(C)** and +++ **(D)**; **(E–H)** show a representative nuclear staining with different intensities in samples: Negative staining **(E)**, + **(F)**, ++ **(G)** and +++ **(H)**.

patients with other stages [11 (0–300) vs. 90 (0–300), $p = 0.127$]. However, the differences were not statistically significant. Other clinical factors, including M protein levels, serum free light chain ratio, hemoglobin, and calcium level, were not statistically different between cases with WT1+ and WT- or cases with different WT1 staining patterns. The summary of clinical parameters in different groups were shown in Table 2 and Supplementary Table S1.

In the patients with positive WT1 staining, the proportion of cells and H-score of cytoplasmic WT1 staining were correlated to high serum free light chain ratio (% positive cells; $p = 0.011$ with a correlation coefficient of 0.284, H score; $p = 0.039$ with correlation coefficient 0.233). No other clinical characteristics (e.g., creatinine, β-2-mg, platelets, ISS staging, etc.) were associated with WT1 expression. The median survival of the patients in this cohort was 45 months. There was no significant association between WT1 expression and treatment response or survival.

Discussion

In this study, the WT1 expression was investigated by IHC in 142 bone marrow and plasmacytoma samples from a cohort of 95 Thai patients, which is the largest cohort to date. The expression of WT1 in extramedullary MM was first reported in this study. We found that 91.5% of total samples from Thai patients had WT1 expression (Figure 1). High prevalence of WT1 expression was found across all types of tissue samples; bone marrow (92.1%), bone plasmacytoma (78.5%), and hematogenous plasmacytoma (100%). Moreover, a high rate of WT1 expression was still consistent in the samples at the relapse stage (92%; overall relapsed samples, 100%; relapsed plasmacytoma vs. 91.3% in samples at diagnosis). This finding highlights the potential use of WT1 as a target antigen of immunotherapy, particularly in relapsing patients with extramedullary disease that usually respond poorly to currently approved drugs (17). Moreover, the use of WT vaccine to enhance the deeper response during the remission period to control the disease and prevent extramedullary disease is also of interest.

Our results correspond to the high prevalence of WT1 protein expression in MM found in a previous study by Tyler EM et al. (13) despite the different ethnicities of patients. However, this was in contrast to a study from China by Li GJ et al. (16), which showed WT1 expression only in 30% of the patients. In a literature review and our own experience, it has been shown that different WT1 antibody clones and antigen retrieving protocols could offer different staining patterns and positivity rates (4,5,18,19). In our study, similar to Tyler EM et al. (13), the

TABLE 2 Characteristics of WT1 positivity in samples.

Samples	Cytoplasmic staining			Nuclear staining		
	% Positive samples (n)	% Positive cells, median (range)	IHC score median (range)	% Positive samples (n)	% Positive cells, median (range)	IHC score median (range)
Overall	79.6 (113)	30 (0–100)	80 (0–300)	45.8 (65)	0 (0–100)	0 (0–170)
1st Dx	78.3 (72)	30 (0–100)	60 (0–300)	41.3 (38)	0 (0–70)	0 (0–130)
Relapse	82 (41)	50 (0–100)	95 (0–300)	54 (27)	1 (0–100)	1.75 (0–170)
Bone marrow	79.8 (91)	35 (0–100)	80 (0–300)	49.1 (56)	0 (0–100)	0 (0–170)
1st Dx	80.8 (59)	30 (0–100)	80 (0–300)	42.5 (31)	0 (0–70)	0 (0–130)
Relapse	78 (32)	40 (0–100)	90 (0–300)	61 (25)	1 (0–100)	2 (0–170)
Bone plasmacytoma	71.4 (10)	30 (0–100)	65 (0–300)	35.7 (5)	0 (0–70)	0 (0–90)
1st Dx	60 (6)	7.5 (0–100)	10 (0–265)	30 (3)	0 (0–70)	0 (0–90)
Relapse	100 (4)	65 (30–100)	185 (60–300)	50 (2)	5 (0–10)	5 (0–20)
Hematogenous plasmacytoma	85.7 (12)	20 (0–100)	32.5 (0–297)	28.6 (4)	0 (0–55)	0 (0–75)
1st Dx	77.8 (7)	5 (0–100)	10 (0–101)	44.4 (4)	0 (0–55)	0 (0–75)
Relapse	100 (5)	99 (30–100)	210 (90–297)	0	0	0
ISS stage						
I	90 (9)	7.5 (0–100)	8.5 (0–180)	60 (6)	3.5 (0–70)	4.6 (0–90)
II	73.3 (22)	22.5 (0–100)	40 (0–300)	40 (12)	0 (0–85)	0 (0–130)
III	84.5 (60)	50 (0–100)	90 (0–300)	39.4 (28)	0 (0–100)	0 (0–170)
Ig subtype						
IgG	72.5 (58)	30 (0–100)	70 (0–300)	48.8 (39)	0 (0–100)	0 (0–130)
IgA	95 (19)	50 (0–100)	105 (0–300)	35 (7)	0 (0–20)	0 (0–40)
IgD	100 (1)	100	295	100 (1)	20.5	26.5
Light chain	83.3 (30)	20.5 (0–100)	41.5 (0–300)	50 (18)	3 (0–90)	4 (0–170)
Heavy chain	100 (1)	70	190	0	0	0
Isolated plasmacytoma	100 (2)	72.5 (50–95)	157.5 (50–265)	0	0	0
NA	100 (2)	80 (60–100)	190 (130–250)	0	0	0

most frequently reported WT1 antibody; clone 6FH7 was used. Unfortunately, we could not access the IHC protocol used by Li GJ et al. (17).

Apart from cytoplasmic WT1 staining reported by Tyler EM et al. (13), which we found in the majority of cases, we also observed nuclear staining of WT1 in a significant number of cases (45.7%). Differences in staining pattern and intensity could be found between sample groups (Figure 2). Extramedullary tissue samples at relapse had a low rate of nuclear WT1 staining, but had a high rate and H-score of cytoplasmic WT1 staining. The cytoplasmic expression of WT1 is more prominent in extramedullary samples compared to in any other tissues analyzed (Figures 2B,C). However, only cytoplasmic WT1 expression has some associations with clinical factors.

The percentage of cells with cytoplasmic WT1 expression and cytoplasmic H-score in samples had positive correlations with a serum free light chain ratio, which could represent a high disease burden and may increase the risk for renal injury (20). However, there was no correlation between WT1 expression and serum creatinine level, rate of kidney dialysis, or treatment outcomes. A further study in a population with more homogenous treatment is needed to clarify the significance of WT1 staining pattern and clinical outcomes.

WT1 gene located on chromosome 11 (Chr 11p13) and transcribed to zinc finger transcription factor that regulates many gene in proliferation and oncogenesis (1). WT1 importance in MM pathogenesis has not been studied. Although chromosome 11 trisomy has been reported in 32.9% of cases in MM genomic landscape study (21), WT1 mRNA overexpression has not been found by gene expression profiling, next generation sequencing or RQ-PCR study (2,11,21,22,23,24). Moreover, WT1 mutation was found only in 0%–0.41% in MM patients (22,23). All these findings

suggested that WT1 protein expression found in our study may be correlated with protein translation or post translational regulation of WT1.

WT1 protein is known to have two different functions. Its cellular localization affects the function of the protein (25,26). In the nucleus, WT1 binds to DNA and acts as a transcription factor. It can shuttle to cytoplasm and interact with mRNA, ribonucleoprotein particles (RNPs), and functional polysomes to act as translational regulator (25). Both functions of WT1 as a transcription regulator and a translation regulator may contribute to the pathogenesis of cancer. WT1 has been reported to associate with many oncogenic pathways known in MM pathogenesis. NFκB is one of the main dysregulated pathways in MM pathogenesis (24). The overactivation of NFκB/Rel family members is important for activating the expression of WT1 (27). WT1 expression in the nucleus found in our study may have a transcriptional regulator role, which is known to involve many oncogenic pathways found in MM, e.g., KRAS, MYC, and BCL2 (21,28–31). Interestingly, we found WT1 cytoplasmic expression in the majority of cases. It has been previously shown that WT1 accumulates in the cytoplasm in tumors of different tissue origins (5,32–34). A potential oncogenic role of cytoplasmic WT1 could be the regulation of protein translation. It has been reported that phosphorylation of WT1 by protein kinase A or C causes cytoplasmic retention of WT1 and may decrease the transcription function of WT1 (35). Protein kinase C (PKC) is overexpressed in MM and is important for MM pathogenesis, e.g., cell apoptosis and cell migration (36,37). It is interesting to examine whether PKC activity in MM cells causes WT1 cytoplasmic retention. In our study, extramedullary tissue expressed higher cytoplasmic WT1, especially at relapse in hematogenous plasmacytoma and plasmacytoma. There is evidence that WT1 transcription increases the adhesion molecule and decreases inhibitory chemokine during development (38,39). A further study to clarify whether cytoplasmic retention of WT1 could lead to a decrease in adhesion molecule on MM cells and promote plasmacytoma growth would be of interest.

Conclusion

Despite low mRNA expression reported in previous studies, we confirmed that the high prevalence of WT1 protein expression detected by IHC could be found in the MM samples. We have shown for the first time that WT1 has high expression rates in both medullary myeloma and plasmacytoma regardless of disease status. There was an exceptionally high rate of WT1 expression in the cases with hematogenous plasmacytoma and plasmacytoma at the relapse stage, which were difficult to treat. Our findings support the use of WT1 as a target antigen for immunotherapy in MM and plasmacytoma irrespective of disease status. WT1 expression detected by IHC could be a potential marker for WT1 immunotherapy; however, antibody and IHC protocol might affect WT1 positive rate and staining pattern. WT1 correlated with a high-risk clinical feature but it did not correlate with poor outcome.

Data availability statement

The original contributions presented in the study are included in the article/Supplementary Material, further inquiries can be directed to the corresponding authors.

Ethics statement

The studies involving tissues from human participants were reviewed and approved by Siriraj hospital Institutional Review Board (Certificate of Approval no. Si 203/2022). All data had been retrieved from the hospital medical archive and deidentified before collection; this retrospective study had no traceable personal data.

Author contributions

PP, MJ, P-TY, CK, and TC planned and designed experiments. SS, MJ, and PP reviewed and graded IHC staining results. PP conducted the experiments, acquired, analyzed, interpreted the data and was a major contributor in writing the manuscript. All authors read and approved the final manuscript.

Funding

SS, MJ, and CK, are supported by Chalermphrakiat Grant, Faculty of Medicine Siriraj Hospital, Mahidol University. This research project was supported by the Faculty of Medicine Siriraj Hospital (R016333039), the International Research Network (grant numbers IRN58W0001) and (IRN5801PHDW06). Mahidol University (Basic Research Fund: Fiscal Year 2022, grant number BRF1-029/2565).

Conflict of interest

The authors declare that the research was conducted in the absence of any commercial or financial relationships that could be construed as a potential conflict of interest.

Supplementary material

The Supplementary Material for this article can be found online at: https://www.por-journal.com/articles/10.3389/pore.2023.1610844/full#supplementary-material

References

1. Call KM, Glaser T, Ito CY, Buckler AJ, Pelletier J, Haber DA, et al. Isolation and characterization of a zinc finger polypeptide gene at the human chromosome 11 Wilms' tumor locus. *Cell* (1990) 60(3):509–20. doi:10.1016/0092-8674(90)90601-a

2. Liu HS, Zhu MS, Zhang HL, Wei SY, Wang XN, Xi XP, et al. WT1 gene expression difference in leukemia and non-leukemia and its clinical significance. *Zhongguo Shi Yan Xue Ye Xue Za Zhi* (2014) 22(5):1217–21. doi:10.7534/j.issn.1009-2137.2014.05.005

3. Qiwei X, Zhang F, Wu H, Liu JL, Zongge B, Xu C, et al. Wilms' tumor 1 (WT1) expression and prognosis in solid cancer patients: a systematic review and meta-analysis. *Sci Rep* (2015) 5:8924. doi:10.1038/srep08924

4. Parenti R, Perris R, Vecchio GM, Salvatorelli L, Torrisi A, Gravina L, et al. Immunohistochemical expression of Wilms' tumor protein (WT1) in developing human epithelial and mesenchymal tissues. *Acta Histochem* (2013) 115(1):70–5. doi:10.1016/j.acthis.2012.04.006

5. Nakatsuka S-I, Oji Y, Horiuchi T, Kanda T, Kitagawa M, Takeuchi T, et al. Immunohistochemical detection of WT1 protein in a variety of cancer cells. *Mod Pathol Off J U S Can Acad Pathol Inc* (2006) 19(6):804–14. doi:10.1038/modpathol.3800588

6. Hein KZ, Yao S, Fu S. Wilms' tumor 1 (WT1): The vaccine for cancer. *J Immunother Precis Oncol* (2020) 3(4):165–71. doi:10.36401/JIPO-20-12

7. Cheever MA, Allison JP, Ferris AS, Finn OJ, Hastings BM, Hecht TT, et al. The prioritization of cancer antigens: a national cancer institute pilot project for the acceleration of translational research. *Clin Cancer Res Off J Am Assoc Cancer Res* (2009) 15(17):5323–37. doi:10.1158/1078-0432.CCR-09-0737

8. Sung H, Ferlay J, Siegel RL, Laversanne M, Soerjomataram I, Jemal A, et al. Global cancer statistics 2020: GLOBOCAN estimates of incidence and mortality worldwide for 36 cancers in 185 countries. *CA Cancer J Clin* (2021) 71(3):209–49. doi:10.3322/caac.21660

9. Mateos MV, Martínez BP, González-Calle V. High-risk multiple myeloma: how to treat at diagnosis and relapse? *Hematology* (2021) 2021(1):30–6. doi:10.1182/hematology.2021000229

10. Verheye E, Bravo Melgar J, Deschoemaeker S, Raes G, Maes A, De Bruyne E, et al. Dendritic cell-based immunotherapy in multiple myeloma: Challenges, opportunities, and future directions. *Int J Mol Sci* (2022) 23(2):904. doi:10.3390/ijms23020904

11. Saatci C, Caglayan AO, Kocyigit I, Akalin H, Kaynar LG, Altuntas F, et al. Expression of WT1 gene in multiple myeloma patients at diagnosis: Is WT1 gene expression a useful marker in multiple myeloma? *Hematol Amst Neth* (2010) 15(1):39–42. doi:10.1179/102453310X12583347009496

12. Azuma T, Otsuki T, Kuzushima K, Froelich CJ, Fujita S, Yasukawa M. Myeloma cells are highly sensitive to the granule exocytosis pathway mediated by WT1-specific cytotoxic T lymphocytes. *Clin Cancer Res Off J Am Assoc Cancer Res* (2004) 10(21):7402–12. doi:10.1158/1078-0432.CCR-04-0825

13. Tyler EM, Jungbluth AA, O'Reilly RJ, Koehne G. WT1-specific T-cell responses in high-risk multiple myeloma patients undergoing allogeneic T cell-depleted hematopoietic stem cell transplantation and donor lymphocyte infusions. *Blood* (2013) 121(2):308–17. doi:10.1182/blood-2012-06-435040

14. Koehne G, Devlin S, Korde N, Mailankody S, Heather L, Hassoun H, et al. Galinpepimut-S, a WT1-targeting immuno-oncology treatment, induces specific, robust and durable immune responses (IRs) in patients (pts) with high-risk (HR) multiple myeloma (MM). *Clin Lymphoma Myeloma Leuk* (2017) 17:S343–4. doi:10.1016/j.clml.2017.07.164

15. Tsuboi A, Oka Y, Nakajima H, Fukuda Y, Elisseeva OA, Yoshihara S, et al. Wilms tumor gene WT1 peptide-based immunotherapy induced a minimal response in a patient with advanced therapy-resistant multiple myeloma. *Int J Hematol* (2007) 86(5):414–7. doi:10.1007/BF02983998

16. Li GJ, Ding H, Yang L. Correlation of WT1 and VEGF expression with angiogenesis in bone marrow biopsies of multiple myeloma patients. *Zhongguo Shi Yan Xue Ye Xue Za Zhi* (2015) 23(3):733–6. doi:10.7534/j.issn.1009-2137.2015.03.026

17. Avivi I, Cohen YC, Suska A, Shragai T, Mikala G, Garderet L, et al. Hematogenous extramedullary relapse in multiple myeloma - a multicenter retrospective study in 127 patients. *Am J Hematol* (2019) 94(10):1132–40. doi:10.1002/ajh.25579

18. Tsuta K, Kato Y, Tochigi N, Hoshino T, Takeda Y, Hosako M, et al. Comparison of different clones (WT49 versus 6F-H2) of WT-1 antibodies for immunohistochemical diagnosis of malignant pleural mesothelioma. *Appl Immunohistochem Mol Morphol AIMM* (2009) 17(2):126–30. doi:10.1097/PAI.0b013e318187dd26

19. Novacescu D, Cut TG, Cumpanas AA, Latcu SC, Bardan R, Ferician O, et al. Evaluating established roles, future perspectives and methodological heterogeneity for Wilms' tumor 1 (WT1) antigen detection in adult renal cell carcinoma, using a novel N-terminus targeted antibody (clone WT49). *Biomedicines* (2022) 10(4):912. doi:10.3390/biomedicines10040912

20. Yadav P, Cockwell P, Cook M, Pinney J, Giles H, Aung YS, et al. Serum free light chain levels and renal function at diagnosis in patients with multiple myeloma. *BMC Nephrol* (2018) 19(1):178. doi:10.1186/s12882-018-0962-x

21. Walker BA, Mavrommatis K, Wardell CP, Ashby TC, Bauer M, Davies FE, et al. Identification of novel mutational drivers reveals oncogene dependencies in multiple myeloma. *Blood* (2018) 132(6):587–97. doi:10.1182/blood-2018-03-840132

22. Bolli N, Biancon G, Moarii M, Gimondi S, Li Y, de Philippis C, et al. Analysis of the genomic landscape of multiple myeloma highlights novel prognostic markers and disease subgroups. *Leukemia* (2018) 32(12):2604–16. doi:10.1038/s41375-018-0037-9

23. AACR Project GENIE Consortium. AACR project GENIE: Powering precision medicine through an international consortium. *Cancer Discov* (2017) 7(8):818–31. doi:10.1158/2159-8290.CD-17-0151

24. Broyl A, Hose D, Lokhorst H, de Knegt Y, Peeters J, Jauch A, et al. Gene expression profiling for molecular classification of multiple myeloma in newly diagnosed patients. *Blood* (2010) 116(14):2543–53. doi:10.1182/blood-2009-12-261032

25. Niksic M, Slight J, Sanford JR, Caceres JF, Hastie ND. The Wilms' tumour protein (WT1) shuttles between nucleus and cytoplasm and is present in functional polysomes. *Hum Mol Genet* (2004) 13(4):463–71. doi:10.1093/hmg/ddh040

26. Toska E, Roberts SGE. Mechanisms of transcriptional regulation by WT1 (Wilms' tumour 1). *Biochem J* (2014) 461(1):15–32. doi:10.1042/BJ20131587

27. Dehbi M, Hiscott J, Pelletier J. Activation of the wt1 Wilms' tumor suppressor gene by NF-kappaB. *Oncogene* (1998) 16(16):2033–9. doi:10.1038/sj.onc.1201747

28. Chesi M, Bergsagel PL. Molecular pathogenesis of multiple myeloma: Basic and clinical updates. *Int J Hematol* (2013) 97(3):313–23. doi:10.1007/s12185-013-1291-2

29. Vicent S, Chen R, Sayles LC, Lin C, Walker RG, Gillespie AK, et al. Wilms tumor 1 (WT1) regulates KRAS-driven oncogenesis and senescence in mouse and human models. *J Clin Invest* (2010) 120(11):3940–52. doi:10.1172/JCI44165

30. Zhou B, Jin X, Jin W, Huang X, Wu Y, Li H, et al. WT1 facilitates the self-renewal of leukemia-initiating cells through the upregulation of BCL2L2: WT1-BCL2L2 axis as a new acute myeloid leukemia therapy target. *J Transl Med* (2020) 18(1):254. doi:10.1186/s12967-020-02384-y

31. Han Y, San-Marina S, Liu J, Minden MD. Transcriptional activation of c-myc proto-oncogene by WT1 protein. *Oncogene* (2004) 23:6933–41. doi:10.1038/sj.onc.1207609

32. Silberstein GB, Van Horn K, Strickland P, Roberts CT, Daniel CW. Altered expression of the WT1 Wilms tumor suppressor gene in human breast cancer. *Proc Natl Acad Sci* (1997) 94(15):8132–7. doi:10.1073/pnas.94.15.8132

33. Ohno S, Dohi S, Ohno Y, Kyo S, Sugiyama H, Suzuki N, et al. Immunohistochemical detection of WT1 protein in endometrial cancer. *Anticancer Res* (2009) 29(5):1691–5.

34. Carpentieri DF, Nichols K, Chou PM, Matthews M, Pawel B, Huff D. The expression of WT1 in the differentiation of rhabdomyosarcoma from other pediatric small round blue cell tumors. *Mod Pathol Off J U S Can Acad Pathol Inc* (2002) 15(10):1080–6. doi:10.1097/01.MP.0000028646.03760.6B

35. Ye Y, Raychaudhuri B, Gurney A, Campbell CE, Williams BR. Regulation of WT1 by phosphorylation: Inhibition of DNA binding, alteration of transcriptional activity and cellular translocation. *EMBO J* (1996) 15(20):5606–15. doi:10.1002/j.1460-2075.1996.tb00945.x

36. Podar K, Raab MS, Zhang J, McMillin D, Breitkreutz I, Tai YT, et al. Targeting PKC in multiple myeloma: *In vitro* and *in vivo* effects of the novel, orally available small-molecule inhibitor enzastaurin (LY317615.HCl). *Blood* (2007) 109:1669–77. Available from: https://ashpublications.org/blood/article/109/4/1669/23434/Targeting-PKC-in-multiple-myeloma-in-vitro-and-in. doi:10.1182/blood-2006-08-042747

37. Ni H, Ergin M, Tibudan SS, Denning MF, Izban KF, Alkan S. Protein kinase C-delta is commonly expressed in multiple myeloma cells and its downregulation by rottlerin causes apoptosis. *Br J Haematol* (2003) 121(6):849–56. doi:10.1046/j.1365-2141.2003.04368.x

38. Kirschner KM, Wagner N, Wagner KD, Wellmann S, Scholz H. The Wilms tumor suppressor Wt1 promotes cell adhesion through transcriptional activation of the alpha4integrin gene. *J Biol Chem* (2006) 281(42):31930–9. doi:10.1074/jbc.M602668200

39. Velecela V, Lettice LA, Chau YY, Slight J, Berry RL, Thornburn A, et al. WT1 regulates the expression of inhibitory chemokines during heart development. *Hum Mol Genet* (2013) 22(25):5083–95. doi:10.1093/hmg/ddt358

Pathology & Oncology Research | frontiers

TYPE Original Research
PUBLISHED 16 July 2024
DOI 10.3389/pore.2024.1611851

Check for updates

OPEN ACCESS

EDITED BY
Gabor Mikala,
Central Hospital of Southern Pest, Hungary

*CORRESPONDENCE
Reka Rahel Bicsko,
bicskorekaa@gmail.com

RECEIVED 27 May 2024
ACCEPTED 02 July 2024
PUBLISHED 16 July 2024

CITATION
Bicsko RR, Nyilas R, Szasz R, Varoczy L, Kiss A, Udvardy M, Illes A and Gergely L (2024), The efficacy and safety of second salvage autologous transplantation in myeloma patients. *Pathol. Oncol. Res.* 30:1611851. doi: 10.3389/pore.2024.1611851

COPYRIGHT
© 2024 Bicsko, Nyilas, Szasz, Varoczy, Kiss, Udvardy, Illes and Gergely. This is an open-access article distributed under the terms of the Creative Commons Attribution License (CC BY). The use, distribution or reproduction in other forums is permitted, provided the original author(s) and the copyright owner(s) are credited and that the original publication in this journal is cited, in accordance with accepted academic practice. No use, distribution or reproduction is permitted which does not comply with these terms.

The efficacy and safety of second salvage autologous transplantation in myeloma patients

Reka Rahel Bicsko*, Renata Nyilas, Robert Szasz, Laszlo Varoczy, Attila Kiss, Miklos Udvardy, Arpad Illes and Lajos Gergely

Department of Hematology, Faculty of Medicine, Doctoral School of Clinical Sciences, Institute of Internal Medicine, University of Debrecen, Debrecen, Hungary

Despite the availability of many novel therapies for multiple myeloma, it remains an incurable disease with relapse fated in almost all patients. In the era of modern agents, second autologous stem cell transplantation still holds its role in patients relapsing after first-line autologous transplant. The authors reviewed a single-center experience with a second auto-SCT for relapsed multiple myeloma. Thirty patients had received a salvage auto-SCT at the institution. The median follow-up after diagnosis was 86 months, and the median time between transplants was 59.1 months. Response before second ASCT was the following: CR – 11 cases, VGPR – 9 cases, PR – 10 cases. Most patients received reduced dose (140 mg/m2) of melphalan as a conditioning regimen for the second auto-SCT. Treatment-related mortality was 3%. With a median follow-up time of 34 months after the second transplant, median progression-free survival was 24 months. The median PFS in the patients achieving CR or VGPR at day 100 after the second transplantation was 32 months. By 15 months, all patients achieved only partial remission progressed, with a median PFS of 8.5 months. During the follow-up period, no MDS or AML developed, and the frequency of second malignancy was also low, 3%. In conclusion, second autologous stem cell transplantation is a well-tolerated and effective treatment option for relapsed multiple myeloma in selected patients, though with a shorter PFS than in first remission.

KEYWORDS

multiple myeloma, salvage therapy, salvage transplantation, second autologous stem cell transplantation, survival

Introduction

The survival of myeloma patients has drastically improved during the last two decades, with the introduction of new drugs like proteasome inhibitors and imids. The first improvement in survival was demonstrated by high-dose melphalan therapy with autologous transplantation after first-line induction. In the early 1990s, it was

documented that adding autologous transplantation to the front-line chemotherapy increases the progression-free survival (PFS) and overall survival (OS) of myeloma patients, and an 80% estimated 3-year OS could be achieved [1]. Since then, for more than three decades, the role of autologous transplantation still holds its place after first-line induction therapy despite the introduction of newer drugs into induction therapy. It was demonstrated that the deeper remission the patient achieves before the transplantation, the better the PFS after the transplantation. The mortality rate from this procedure has drastically decreased from 10% to less than 1%. In the early 2000s, it was shown that second autologous transplantation may increase the 10-year OS from 20.4% to 35.2%, highlighting the importance of this therapy [2]. Upfront tandem transplantation could achieve a 55% chance of 5-year OS, and the essential survival predictor was the response quality after either transplantation [3]. These results showed that chemotherapy with melphalan adds a survival benefit for myeloma patients. The concept of second autologous transplantation as a consolidation of salvage modality for relapsed myeloma patients was established in that era, with a mortality of 3%. The median event-free survival (EFS) after the first transplant was 15.7 months and 12.9 months after the second transplantation [4].

The long-term results of the Total Therapy III trial have recently been published. The data demonstrates that adding melphalan to myeloma therapy increases survival of patients. The median PFS was 5.6 years, and the 15-year PFS was still 27.9% with an OS of 35.9% [5].

The treatment of relapsed/refractory myeloma has drastically changed during the last 10 years. New proteasome inhibitors, immunomodulators, monoclonal antibodies, bispecific antibodies, and CAR-T cells became available, giving clinicians several choices to treat the patients. All these drugs achieve better PFS for patients, but the price of these therapies is markedly increasing. Also, by utilizing these drugs, we are facing new problems, like the so-called "penta-refractory" myeloma patients, where most of the novel drugs failed. The use of second autologous transplantation to consolidate a remission is still a viable option in selected cases, however there is a big debate whether this modalitiy should still be used. There are several results of using high-dose melphalan with second autologous transplantation. In 2006, the MD. Anderson Cancer Center reported a retrospective analysis with a median PFS of 6.9 months and a median OS of 29 months in a relatively young patient population, with a median age of 52 years [6]. In another report, the median PFS was 8.5 months, and the median OS was 20.7 months after the second autologous transplantation, with a median of 37 months after the first transplantation [7]. Another retrospective study showed that patients who achieve at least 24 months of PFS after the first transplantation do better with a second autograft. The median PFS was 19 months, but patients who relapsed within 24 months after the first transplantation had a median PFS of 9.83 months compared to 17.3 months for later relapsing patients. This was also reflected in the OS as early relapsing patients had a median OS of 28.47 months compared to 71.3 months in the other group [8]. This publication highlighted the importance of selecting patients based on their response to first high-dose melphalan therapy. Another retrospective multivariate analysis also confirmed that the time to progression after the first transplantation and the quality of response before the second transplantation impact the outcome of the salvage transplantation. Patients with at least a PR had a 2-year OS of 85.9% compared to the other patients, whose 2-year OS was 51.3% [9]. In a retrospective study by the Karolinska Institute, the authors compared the results of a second autograft with the results of novel drugs in relapsed patients. They confirmed the superiority of the second autograft as the median OS was 4 years, compared to 3.3 years in the novel drug group [10]. It has also been reported that the timing of a second autologous transplantation is optimal after the first relapse compared to later, as both PFS and OS were significantly better in the first group [11].

These data highlight that autologous transplantation may still hold its place in myeloma therapy and that second transplantation as a salvage option is still a possible option for selected patients.

Second transplantation as a salvage option is not widely used; there are only a few reports on this approach. The authors report their findings on myeloma patients who underwent a second ASCT to provide data on the validity of second salvage autologous transplantation in the era of novel therapies. Authors demonstrate that the survival results are still comparable to what is achievable with novel therapies, with minimal toxicity.

Study design

This is a retrospective single-center cohort analysis of multiple myeloma patients undergoing second autologous transplantation at the University of Debrecen. All patients were included who underwent a second autologous transplantation with the diagnosis of multiple myeloma between 1 January 2008 and 31 December 2023. The patient's clinical data was retrospectively collected from the hospital's medical records. The data was also cross-checked with the data reported towards the European Bone Marrow Transplantation Society (EBMT). All patients agreed on the data collection in a consent form at the time of both transplantations. A second transplant was considered if the patient had received a prior autologous stem cell transplantation, after which they required subsequent treatment due to disease progression. A relapse was defined as a reappearance of serum or urine M-protein by immunofixation or electrophoresis, development of ≥5%

plasma cells in the bone marrow or appearance of any other sign of progression based on IMWG criteria [12]. No planned tandem transplantation case was included. Response to transplantation was assigned as the change of burden of myeloma plasma cells in the bone marrow and the amount of circulating monoclonal protein in the sera. May-Grünwald-Giemsa-stained smears and flow cytometric assay was performed to examine the number of plasma cells in the bone marrow. Day 100 after the transplant was used as a landmark point to analyze the response to auto-SCT. Complete response was defined in case of negative immunofixation in the serum and urine, and disappearance of any soft tissue plasmacytomas and 5% or fewer plasma cells in bone marrow aspiration. A very good partial response was stated when at least a 90% reduction of serum M-protein plus urine M-protein level <100 mg per 24 h was confirmed. Partial response was described as ≥50% reduction of serum monoclonal protein level plus reduction in 24 h urinary M-protein >90% or to <200 mg per 24 h. The upper age limit for a second autologous transplant was 75 years with adequate physiological function, according to Karnofsky status scale and Eastern Cooperative Oncology Group performance status, and a life expectancy longer than 6 months.

Heart failure, reduced pulmonary function, chronic respiratory diseases and liver failure were exclusion factors. Renal failure due to cast nephropathy, even hemodialysis dependency, was not an exclusion criterion. The conditioning regimen was full-dose (200 mg/m^2) or reduced dose (140 mg/m^2) of melphalan. As per local guidelines, most patients were given a reduced dose of melphalan (140 mg/m^2) for the second transplantation due to age and previous exposure to this drug. A single intravenous dose of conditioning was given on day −2, followed by peripheral stem cell administration 48 h later. All patients received antiviral prophylaxis with acyclovir, Pneumocystis jirovecii prophylaxis during the peritransplant period with trimethoprim/sulfamethoxazole and antifungal prophylaxis with fluconazole. Filtered, irradiated red blood cells and platelet suspensions were givenif needed. Survival times were calculated on the one hand from the time of diagnosis and on the other hand from the time of the second transplant. OS was defined as the time from diagnosis and time from the second ASCT to death from any cause and PFS was defined as the time from auto-SCT to relapse or progressive disease or death from any cause, whichever came first. PFS from the second transplant was also calculated. Transplant-related mortality was defined as mortality from any cause other than disease progression within 100 days from the date of transplantation.

Statistical analysis was performed using GraphPad Prism 10.1 software. The survival times were calculated using the Kaplan-Meier method. The difference between survival times was compared using the Log-Rank test. Statistical significance was stated if the p-value was less than 0.05. The data collection protocol has been approved by the authors' respective Institutional Review Board for human subjects (IRB reference number: 6739/2024). This study was managed according to the Declaration of Helsinki.

Results

Thirty multiple myeloma patients underwent two autologous hematopoietic stem cell transplantations (auto-SCT) in the defined time interval in a single institution. Clinical characteristics at diagnosis and at the time of initial auto-SCT are summarized in Table 1. The median age at diagnosis was 53.5 years (range 37–68). The proportion of men and women was the same (15:15, 50%–50%). M protein was IgG in most cases (50%), IgA in 23.3%, and light chain only disease occurred in 13.3%. The cytogenetic profile of some patients is not available as at the time of these treatments the test was not routinely used. All patients received bortezomib-based induction therapy and a median of 1 (range 1–4) line of treatment before the first transplant. The median time interval between diagnosis and first transplant was 49 months (range 5–129). Almost all patients (29, 97%) received full-dose (200 mg/m^2) intravenous melphalan conditioning. Complete remission was developed in two-thirds (66.6%) of patients after the initial auto-SCT. Median follow-up after diagnosis was 86 months, while median overall survival was 118 months in the defined population (Figure 1). Median progression-free survival was 39 months after the first autologous transplant.

Patients' clinical characteristics at the time of the second transplantation are shown in Table 2. The median follow-up after the second transplantation was 34 months (range 11–110). The selection criteria for the second autologous transplantation was no progression within 24 months after the first transplant and inability to continue bortezomib due to toxicity. In one case, the second autologous transplant was performed within 24 months of the first transplant, in the best-achieved response status, because innovative drugs were not available at the time. Median age at second transplantation was 59 years (range 43–73). The median time from diagnosis to second auto-SCT was 94 months (range 27–305), and the median interval between the two transplantations was 59.1 months (range 19–138). Patients received a median of 2 (range 2–6) lines of salvage therapy after the first transplantation. The most commonly used salvage regimens were VRD (bortezomib, lenalidomide, dexamethasone) in 11 cases, CRD (carfilzomib, lenalidomide, dexamethasone) in 7 cases, VTD-PACE (bortezomib, thalidomide, dexamethasone, cisplatin, doxorubicin, cyclophosphamide, etoposide) in 6 cases, Vel-Dex (bortezomib-dexamethasone) in 6 cases, and daratumumab-based therapy in 4 cases (2 DRD–daratumumab, lenalidomide, dexamethasone, 2 DPD–daratumumab, pomalidomide, dexamethasone). There was no difference in PFS between patients who received 1 line of therapy or more than 1 line of

TABLE 1 Patients' characteristics at the diagnosis and first autologous stem cell transplantation.

Variable	*Value*
Gender	15 male, 15 female
Age at diagnosis (years)	53.5 years (37–68)
Multiple myeloma disease types	
IgG IgA kappa light chain lambda light chain	15 (50%) 7 (23.3%) 4 (13.3%) 4 (13.3%)
ISS stage at diagnosis	
No data Stage I Stage II Stage III	5 9 10 6
Interval between diagnosis and first auto-SCT	49 months (5–129)
Status of disease before first auto-SCT	
complete response very good partial response partial response	11 (37%) 12 (40%) 7 (23%)
Conditioning regimen	
Full dose melphalan (200mg/m2) Reduced dose melphalan (140mg/m2)	29 (97%) 1 (3%)
Response 100 days after first auto-SCT	
complete response very good partial response partial response	20 (66.7%) 8 (26.7%) 2 (6.6%)

The table lists patients' data at the time of diagnosis and at the time of first stem cell transplantation. SCT, stem cell transplantation.

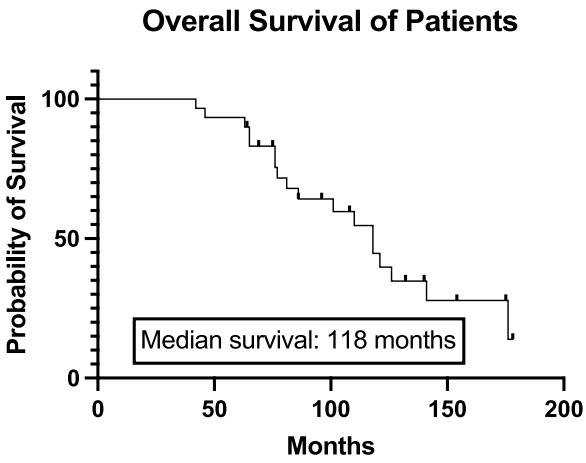

FIGURE 1
Overall survival of the total study population from the diagnosis. The Kaplan-Meier curve represents the overall survival of all patients from the diagnosis. The median overall survival was 118 months.

therapy before the second transplantation (median PFS 32 months vs. 24 months p = 0.469). All second transplantations were performed using peripherally collected stem cells. In 17 cases, the stored frozen stem cells from the collection before the first transplant were used, and the other 13 patients were re-mobilized with G-CSF, and stem cells were collected and were frozen. There was no difference in progression-free survival between the two groups. The median engraftment was 9 days in the stored PBSC group compared to 10 days in the second mobilization and collection group, but the results were not statistically significant (data not shown). 11 patients entered the transplant in CR, 9 patients in VGPR, while 10 patients achieved only a partial response.

The conditioning regimen was full-dose melphalan (200 mg/m^2) in 8 patients, while a reduced dose (140 mg/m^2) was used in 22 cases. The two different conditioning regimens did not statistically influence the PFS (p = 0.4732, data not shown). The median time to neutrophil engraftment after stem cell infusion was 9 (8–13) days. PFS was not statistically significant based on the engraftment days (cut-off: 9 days, p = 0.822, data not shown). Transplant-related mortality was 3%, as one patient died during the first 100 days due to nosocomial pneumonia at day 32. 60% of the patients (18) achieved complete remission evaluated 100 days after salvage transplantation. Of the 10 patients in PR entering the second transplantation, 3 were converted to VGPR and 3 to CR. Only 4 patients remained in PR. Fourteen (46.7%) patients received maintenance therapy after the second transplantation, of which the most common was lenalidomide monotherapy. There was no significant difference between PFS (p = 0.836) and OS (p = 0.773) based on the use of any maintenance therapy or not (data not shown). Median progression-free survival after the second auto-SCT (PFS-ASCT2) was 24 months, while median overall survival (OS-ASCT2) was 48 months (Figure 2). The median PFS in patients entering the second transplant in CR or VGPR was 32 months, compared to 14 months in the PR patients (p = 0.182, NS). The median PFS (PFS-ASCT2) in the patients achieving CR or VGPR at day 100 after the second transplantation was significantly higher at 32 months, compared to 8.5 months in the PR group (p = 0.0006) (Figures 3, 4). During the follow-up period, a second malignancy developed in the form of lung cancer in one case. There were no cases of myelodysplastic syndrome (MDS) or acute myeloid leukemia (AML) during the follow-up.

Discussion

The authors conducted a single-center retrospective review of all multiple myeloma patients who received a second autologous stem cell transplantation between 2008 and 2023 to report the efficacy and safety of this therapy. In the analysis, second autologous stem cell transplantation appears to be a well-

TABLE 2 Patients' characteristics at the time of second autologous stem cell transplantation.

Variable	*Value*
Age at salvage transplantation	59 years (43–73)
Interval between diagnosis and salvage auto-SCT	94 months (27–305)
Lines of therapy before salvage auto-SCT	
2 3 4 5 6	17 (56.7%) 4 (13.3%) 4 (13.3%) 3 (10%) 2 (6.7%)
Status of disease before salvage auto-SCT	
complete response very good partial response partial response	11 (36.7%) 9 (30%) 10 (33.3%)
Conditioning regimen	
Full dose melphalan 200 mg/m2 Reduced dose melphalan (140 mg/m2)	8 (26.7%) 22 (73.3%)
Treatment related mortality	1 (3%)
Response 100 days after salvage auto-SCT	
complete response very good partial response partial response	18 (60%) 8 (26.7%) 4 (13.3%)
Maintenance therapy lenalidomide ixazomib lenalidomide + bortezomib + dexamethasone	n = 14 11 2 1

The table lists the patients' detailed data at the time of the second autologous stem cell transplantation. SCT, stem cell transplantation.

tolerated and effective treatment option for relapsed multiple myeloma, even in a heavily pretreated cohort. Most patients (22, 73%) received a reduced dose of melphalan at 140 mg/m^2 for the second ASCT. There was no significant difference in PFS or OS between patients who received reduced or full-dose melphalan. This suggests that salvage autologous stem cell transplant may still be effective in advanced age, renal insufficiency, or other comorbidities. Merely one patient suffered a treatment-related mortality.In agreement with the literature, the authors state that CR or VGPR is the optimal pre-transplant condition for better survival [13, 14], but patients entering the transplant in PR may also benefit from the transplant. In the reported case series, of the 10 patients proceeding to the second auto-SCT in PR, 6 (60%) converted to VGPR or CR. Based on the author's limited case series, the post-transplant PR is not an acceptable result. These patients require additional active anti-myeloma therapy to improve survival.

As reported in other analyses, the response to the second transplant appears to be shorter than the first autologous-SCT, with a median PFS of 39 vs. 24 months in our study. The median PFS achieved after the second transplantation is slightly better than reported in other cohorts, in which the median PFS was 20.4 months [15, 16]. Another large CIBMTR study analyzed the role of maintenance therapy after the second auto-SCT in myeloma in 522 patients treated in 92 centers [17]. They reported that maintenance significantly improved PFS (27.8%) and OS (9.8%) at 5 years, compared to no maintenance. This was not reflected in this cohort; the PFS at 5 years was 17% for the whole group, and no difference was found between the subgroups, possibly due to a much smaller sample size. The frequency of second malignancy was lower in this cohort (3%) compared to the reported incidence of 5%–7%, possibly because of the small sample size and shorter follow-up period.

The use and timing of second autologous stem cell transplantation for multiple myeloma have been published by several authors with different outcomes. In the early 2000s, Quazilbash et al. reported that both auto-and allografting is feasible in case of relapsing after the first transplant. Olin et al. concluded that patients who received more than five

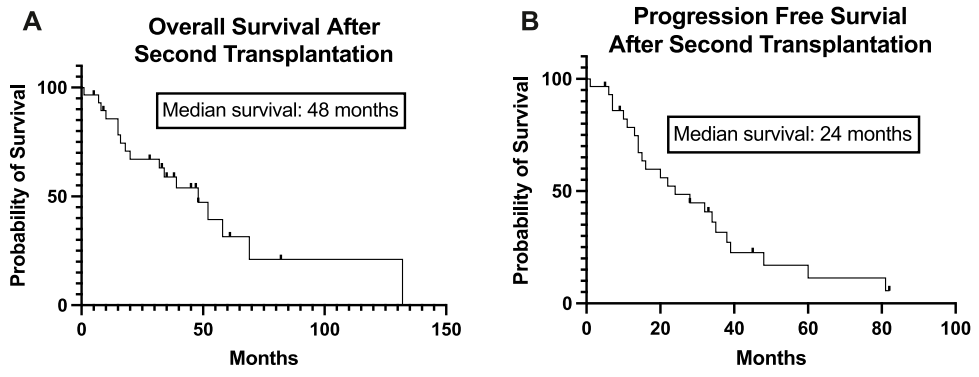

FIGURE 2
Overall and Progression-Free Survival of the patients from the time of the second stem cell transplantation. The Kaplan-Meier estimated overall survival **(A)** and progression-free survival **(B)** of the study population from the time of the second stem cell transplantation is presented. The median overall survival was 48 months, and the median progression-free survival was 24 months.

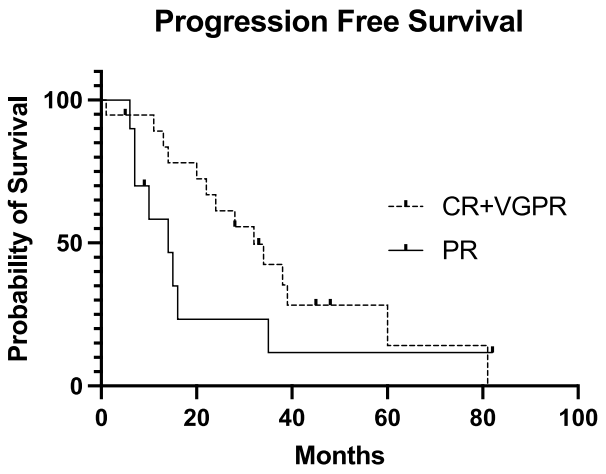

FIGURE 3
Progression-free Survival of the patients after the second stem cell transplantation based on pretransplant disease status. The Kaplan-Meier estimated progression-free survival (PFS) presented after the second stem cell transplantation based on the pretransplant disease status. The median PFS in the CR + VGPR pretransplant group was 32 months, while the median PFS in the PR pretransplant group was 14 months (p = 0.182). CR, complete remission; VGPR, very good partial remission; PR, partial remission.

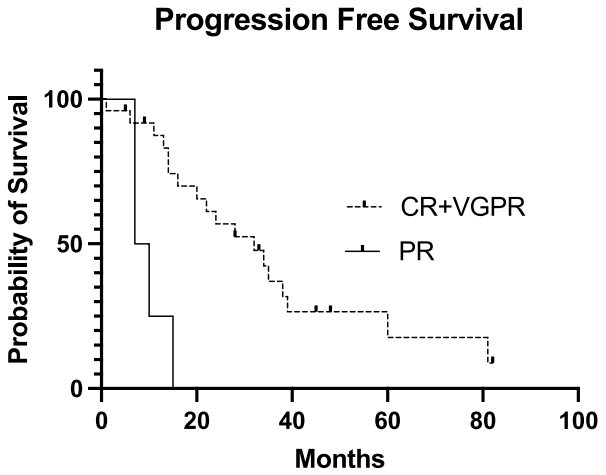

FIGURE 4
Progression-free Survival of the patients after the second stem cell transplantation based on the day 100 post-transplant disease status. The Kaplan-Meier estimated Progression-Free Survival (PFS) presented after the second stem cell transplantation based on the day 100 post-transplant disease status. The median PFS in the CR + VGPR post-transplant group was 32 months, and the median PFS in the PR post-transplant group was only 8.5 months (p = 0.0006). CR, complete remission; VGPR, very good partial remission; PR, partial remission.

lines of prior treatment are unlikely to benefit significantly from a second transplant [7]. Fermand et al. did not provide evidence of second auto-SCT's superiority over conventional chemotherapy [18]. Another Italian cohort demonstrated that two autografts are superior to one auto-transplant [19]. One Tunisian study showed that a single auto-SCT followed by 6 months of thalidomide maintenance therapy was significantly superior to two autologous stem cell transplants without maintenance therapy in OS and EFS [20]. For these reasons, the reported data validates that the second autologous transplantation may be a rational therapeutic option for selected myeloma patients. The results presented are comparable to salvage treatment with bispecific antibodies. The use of CAR-T cells in refractory myeloma may result better survival, but a French real-world analysis of ide-cel in refractory myeloma resulted in a median PFS of 12.5 months and median OS of 20.8 months, which is comparable to our results [21].

Several limitations must be considered in the interpretation of the results. First, the retrospective design is subject to inherent selection bias of non-randomized retrospective data. Second, the study needs to provide evidence on the timing of the second auto-transplant. Also, the patients selected for a second auto-SCT did have a minimum of 24 months response after the first transplantation, which is an obvious selection bias of patients. Bigger sample size and complete data on known prognostic factors and cytogenetics were needed, as FISH testing was not commonly available for the earlier cohort years. Furthermore, long study periods with different eras of diagnostic criteria, as well as therapy with potentially different management approaches, are involved. The results of this study are also limited by the relatively small cohort of heterogeneous patients and the heterogeneity of the prior treatments.

However, the reported study's real-life results are significant in the novel agent era and the context of CAR-T therapy, as the decision-making for heavily pretreated patients or patients with advanced disease is complicated, considering the efficacy, toxicity, and cost of available treatments. The authors conclude that second salvage autologous stem cell transplantation has a favorable risk/benefit profile in relapsed multiple myeloma and can be considered a viable treatment option for appropriate patients.

Data availability statement

The original contributions presented in the study are included in the article/supplementary material, further inquiries can be directed to the corresponding author.

Ethics statement

The studies involving humans were approved by the Regional Research Ethics Committee of the University of Debrecen, Code: DE RKEB/IKEB 6739/2024, Date: 01/01/2024. The studies were conducted in accordance with the local legislation and institutional requirements. Written informed consent for participation was not required from the participants or the

participants' legal guardians/next of kin in accordance with the national legislation and institutional requirements.

Author contributions

Conceptualization, RB and LG; methodology, LG; validation, RB; formal analysis, LG; investigation, RB, RN, and LG; resources, LG; data curation, RB; writing–original draft preparation, RB; writing–review and editing, LG, LV, and RS; visualization LG and RB; supervision, LG, AI, AK, and MU; project administration, RB, RN, and LG. All authors contributed to the article and approved the submitted version.

Funding

The author(s) declare financial support was received for the research, authorship, and/or publication of this article. The publication costs are covered by a grant from the Hungarian Society of Hematology and Transfusiology.

Conflict of interest

The authors declare that the research was conducted in the absence of any commercial or financial relationships that could be construed as a potential conflict of interest.

References

1. Barlogie B, Gahrton G. Bone marrow transplantation in multiple myeloma. *Bone Marrow Transpl* (1991) 7:71–9.

2. Moreau P, Misbahi R, Milpied N, Morineau N, Mahé B, Vigier M, et al. Long-term results (12 years) of high-dose therapy in 127 patients with *de novo* multiple myeloma. *Leukemia* (2002) 16:1838–43. doi:10.1038/sj.leu.2402613

3. Lahuerta JJ, Grande C, Martínez-Lopez J, De La Serna J, Toscano R, Ortiz MC, et al. Tandem transplants with different high-dose regimens improve the complete remission rates in multiple myeloma. Results of a Grupo Español de Síndromes Linfoproliferativos/Trasplante Autólogo de Médula Osea phase II trial. *Br J Haematol* (2003) 120:296–303. doi:10.1046/j.1365-2141.2003.04067.x

4. Krivanová A, Hájek R, Krejcí M, Scudla V, Indrák K, Bacovský J, et al. Second autologous transplantation for multiple myeloma patients relapsing after the first autograft - a pilot study for the evaluation of experimental maintenance therapies. Report of the prospective non-randomized pilot study of the Czech Myeloma Group. *Onkologie* (2004) 27:275–9. doi:10.1159/000077977

5. Al Hadidi S, Ababneh O, Schinke C, Thanendrarajan S, Bailey C, Smith RT, et al. Three years maintenance with VRD in multiple myeloma: results of total therapy IIIB with a 15-year follow up. *Blood Adv* (2023) 8:703–7. doi:10.1182/bloodadvances.2023011601

6. Qazilbash MH, Saliba R, De Lima M, Hosing C, Couriel D, Aleman A, et al. Second autologous or allogeneic transplantation after the failure of first autograft in patients with multiple myeloma. *Cancer* (2006) 106:1084–9. doi:10.1002/cncr.21700

7. Olin RL, Vogl DT, Porter DL, Luger SM, Schuster SJ, Tsai DE, et al. Second auto-SCT is safe and effective salvage therapy for relapsed multiple myeloma. *Bone Marrow Transpl* (2009) 43:417–22. doi:10.1038/bmt.2008.334

8. Jimenez-Zepeda VH, Mikhael J, Winter A, Franke N, Masih-Khan E, Trudel S, et al. Second autologous stem cell transplantation as salvage therapy for multiple myeloma: impact on progression-free and overall survival. *Biol Blood Marrow Transpl* (2012) 18:773–9. doi:10.1016/j.bbmt.2011.10.044

9. Auner HW, Szydlo R, Rone A, Chaidos A, Giles C, Kanfer E, et al. Salvage autologous stem cell transplantation for multiple myeloma relapsing or progressing after up-front autologous transplantation. *Leuk Lymphoma* (2013) 54:2200–4. doi:10.3109/10428194.2013.773998

10. Grövdal M, Nahi H, Gahrton G, Liwing J, Waage A, Abildgaard N, et al. Autologous stem cell transplantation versus novel drugs or conventional chemotherapy for patients with relapsed multiple myeloma after previous ASCT. *Bone Marrow Transpl* (2015) 50:808–12. doi:10.1038/bmt.2015.39

11. Lemieux C, Muffly LS, Iberri DJ, Craig JK, Johnston LJ, Lowsky R, et al. Outcomes after delayed and second autologous stem cell transplant in patients with relapsed multiple myeloma. *Bone Marrow Transpl* (2021) 56:2664–71. doi:10.1038/s41409-021-01371-1

12. Kumar S, Paiva B, Anderson KC, Durie B, Landgren O, Moreau P, et al. International Myeloma Working Group consensus criteria for response and minimal residual disease assessment in multiple myeloma. *Lancet Oncol* (2016) 17:e328–46. doi:10.1016/S1470-2045(16)30206-6

13. Cook G, Liakopoulou E, Pearce R, Cavet J, Morgan GJ, Kirkland K, et al. Factors influencing the outcome of a second autologous stem cell transplant (ASCT) in relapsed multiple myeloma: a study from the British Society of Blood and Marrow Transplantation Registry. *Biol Blood Marrow Transpl* (2011) 17:1638–45. doi:10.1016/j.bbmt.2011.04.005

14. Hagen PA, Stiff P. The role of salvage second autologous hematopoietic cell transplantation in relapsed multiple myeloma. *Biol Blood Marrow Transpl* (2019) 25:e98–e107. doi:10.1016/j.bbmt.2018.12.002

15. Dhakal B, D'Souza A, Kleman A, Chhabra S, Mohan M, Hari P. Salvage second transplantation in relapsed multiple myeloma. *Leukemia* (2021) 35(4): 1214–7. doi:10.1038/s41375-020-1005-8

16. Galligan D, Williamson S, Myers J, Silbermann R, Medvedova E, Nagle S, et al. Second autologous stem cell transplant as salvage in multiple myeloma - the Oregon health and science university experience. *Clin Lymphoma Myeloma Leuk* (2022) 22: 105–12. doi:10.1016/j.clml.2021.08.008

17. Pasvolsky O, Yeshurun M, Fraser R, Estrada-Merly N, Rozovski U, Shargian-Alon L, et al. Maintenance therapy after second autologous hematopoietic cell transplantation for multiple myeloma. A CIBMTR analysis. *Bone Marrow Transpl* (2022) 57:31–7. doi:10.1038/s41409-021-01455-y

18. Fermand JP, Katsahian S, Divine M, Leblond V, Dreyfus F, Macro M, et al. High-dose therapy and autologous blood stem-cell transplantation compared with conventional treatment in myeloma patients aged 55 to 65 years: long-term results of a randomized control trial from the Group Myelome-Autogreffe. *J Clin Oncol* (2005) 23:9227–33. doi:10.1200/JCO.2005.03.0551

19. Cavo M, Tosi P, Zamagni E, Cellini C, Tacchetti P, Patriarca F, et al. Prospective, randomized study of single compared with double autologous stem-cell transplantation for multiple myeloma: bologna 96 clinical study. *J Clin Oncol* (2007) 25:2434–41. doi:10.1200/JCO.2006.10.2509

20. Mehta J. One or two autografts for myeloma. *Blood* (2008) 111(7):3899–900. doi:10.1182/blood-2007-12-127704

21. Ferment B, Lambert J, Caillot D, Lafon I, Karlin L, Lazareth A, et al. French early nationwide idecabtagene vicleucel chimeric antigen receptor T-cell therapy experience in patients with relapsed/refractory multiple myeloma (FENIX): a real-world IFM study from the DESCAR-T registry. *Br J Haematol* (2024). doi:10.1111/bjh.19505

Pathology & Oncology Research | frontiers

TYPE Original Research
PUBLISHED 08 July 2024
DOI 10.3389/pore.2024.1611811

Check for updates

OPEN ACCESS

EDITED BY
Gábor Barna,
Semmelweis University, Hungary

*CORRESPONDENCE
Márk Plander,
planderm@yahoo.com

†These authors have contributed equally to this work

RECEIVED 29 April 2024
ACCEPTED 26 June 2024
PUBLISHED 08 July 2024

CITATION
Plander M, Kányási M, Szendrei T, Skrapits J and Timár B (2024), Flow cytometry in the differential diagnosis of myelodysplastic neoplasm with low blasts and cytopenia of other causes. *Pathol. Oncol. Res.* 30:1611811. doi: 10.3389/pore.2024.1611811

COPYRIGHT
© 2024 Plander, Kányási, Szendrei, Skrapits and Timár. This is an open-access article distributed under the terms of the Creative Commons Attribution License (CC BY). The use, distribution or reproduction in other forums is permitted, provided the original author(s) and the copyright owner(s) are credited and that the original publication in this journal is cited, in accordance with accepted academic practice. No use, distribution or reproduction is permitted which does not comply with these terms.

Flow cytometry in the differential diagnosis of myelodysplastic neoplasm with low blasts and cytopenia of other causes

Márk Plander[1,2*†], Mária Kányási[2†], Tamás Szendrei[1], Judit Skrapits[2] and Botond Timár[3]

[1]Department of Hematology, Markusovszky University Teaching Hospital, Szombathely, Hungary, [2]Central Laboratory, Markusovszky University Teaching Hospital, Szombathely, Hungary, [3]Department of Pathology and Experimental Cancer Research, Semmelweis University, Budapest, Hungary

Background: Myelodysplastic neoplasms (MDS) are characterized by cytopenia, morphologic dysplasia, and genetic abnormalities. Multiparameter flow cytometry (FCM) is recommended in the diagnostic work-up of suspected MDS, but alone is not sufficient to establish the diagnosis. Our aim was to investigate the diagnostic power of FCM in a heterogeneous population of patients with cytopenia, excluding cases with increased blast count.

Methods: We analyzed bone marrow samples from 179 patients with cytopenia (58 MDS, 121 non-MDS) using a standardized 8-color FCM method. We evaluated the sensitivity, specificity, and accuracy of several simple diagnostic approaches, including Ogata score, extended Ogata score, the WHO and ELN iMDSFlow recommended "3 aberrations in two cell compartments method," and the combination of the Ogata score and "3 aberrations in two cell compartments method." The patients were followed until the diagnosis was confirmed, with a median follow-up of 2 months (range 0.2–27).

Results: The combination of Ogata score and "3 aberrations in two cell compartments method" achieved the highest diagnostic accuracy (78%) with sensitivity and specificity 61% and 86%, respectively. When using only the "3 aberrations in two cell compartments method," the accuracy was 77% with a sensitivity of 72% and a specificity of 79%. The most frequently observed etiologies among the false positive cases were substrate deficiencies, inflammation/infection, or toxic effects. MDS can be excluded in all these cases after a thorough clinical evaluation and a relatively short follow-up.

Conclusion: FCM remains an important but supplementary part in an integrated diagnostic process of MDS with low blasts. The combination of the Ogata score and the "3 aberrations in two cell compartments method" slightly improves accuracy compared to the detection of "3 aberrations in two cell compartments method" alone.

KEYWORDS

flow cytometry, myelodysplastic neoplasms, low blasts, differential diagnosis, accuracy

Introduction

Myelodysplastic neoplasms (MDS) are a group of clonal haematopoietic neoplasms defined by cytopenias and morphological dysplasia [1]. Based on recurrent chromosomal abnormalities MDS can also be confirmed in a cytopenic patient, even in the absence of diagnostic morphological dysplasia [2]. The recommended threshold for dysplasia is set at 10% for all lineages [1, 2]. The MDS entities are grouped in the new World Health Organization (WHO) Classification according to genetic events and morphological aberrancies [1]. The morphologically defined categories are based on the blast count with the longstanding cut-off of 5% in the bone marrow (BM) distinguishing cases with low or high blasts. The myeloblast percentage should be determined by counting well-prepared, cellular BM aspirate smears and/or touch preparations and a peripheral blood (PB) smear [2]. To discriminate MDS cases with low blasts from reactive cytopenia is frequently a diagnostic challenge for more reasons: dysplasia over 10% of cells may occur in nonneoplastic causes of cytopenia [3, 4]; dysplasia is often subtle and not recognizable necessitating a repeated bone marrow examination [2]; identification of dysplasia is not always reproducible even among experienced hematopathologists [4–6] and cytogenetic abnormalities specific for MDS are present only in about 50% of cases [7]. Because of these difficulties other approaches such as molecular genetics and immunophenotyping can assist in the diagnosis of MDS, although neither flow cytometry nor somatic mutations alone are considered diagnostic for MDS by the WHO Classification. Recently, a prospective study identified 17 immunophenotypic aberrations that were independently associated with MDS/CMML [8]. However, it is not a single immunophenotypic aberration but a combination of different parameters that is indicative of MDS [9]. Therefore, both the WHO and the ELN iMDSFlow recommend that aberrant findings in at least three tested features affecting at least two cell compartments are highly associated with MDS [2, 10]. In addition to this recommendation, many diagnostic MDS FCM-scores such as Ogata-score [11], extended Ogata-score [12], RED-score [13], ELN-NEC [14], FCSS [15], integrated flow-score (iFS) [16] have been developed to differentiate MDS from other cytopenias. The Ogata-score with four parameters including the percentage of myeloblasts and B-progenitors, the ratio of the lymphocyte to myeloblast CD45 MFI and the granulocyte to lymphocyte SSC mode is recommended by the iMDSFlow for screening purposes [10]. Most of the FCM scores focus on only a part of hematopoiesis, except iFS, which analyzes 44 parameters including all four cell compartments [16].

Our aim was to investigate the diagnostic power of a standardized 8-color FCM method in a heterogeneous population of patients with cytopenia, excluding cases with increased blast count (myeloid progenitors≥5%).

Materials and methods

Patients

Bone marrow samples sent for routine immunophenotyping from cytopenic patients with suspected MDS between 01-Nov-2019 and 01-Sep-2022 were included in the study. The definition of cytopenia was at least one of the following: absolute neutrophil count $<1.8 \times 10^9$/L, platelet count $<100 \times 10^9$/L, hemoglobin concentration <100 g/L. None of the patients had received vitamin supplementation or growth factors prior to the diagnostic bone marrow aspiration, and none had received therapy for MDS during the follow-up. In all cases, bone marrow smear was evaluated in parallel with FCM, and in most cases, cytogenetics and trephine biopsy were also performed. Flow cytometry and cytomorphology were analyzed independently. Cases with myeloid progenitors ≥5% detected by either bone marrow smear or flow cytometry (FCM) and with inadequate material for cytomorphological analysis were excluded. The patients were followed until the diagnosis of MDS was confirmed. This was based on the following criteria: 1. the presence of cytogenetic aberration except for loss of chromosome Y; 2. ≥5% myeloblast in the trephine biopsy; 3. no improvement in the blood counts during the follow-up, and MDS diagnosis confirmed by a second bone marrow examination or no other etiology was found.

All patients provided informed consent for the diagnostic analysis and for the follow-up. The study was conducted in accordance with the Declaration of Helsinki and was approved by the institutional Review Board of Markusovszky University Teaching Hospital.

Multiparameter flow cytometry

The monoclonal antibody (mAb) panel consisted of three 8-color tubes (Table 1) designed according to the iMDSFlow guidelines [10, 17]. EDTA was used as an anticoagulant in all samples. Samples were processed within 24 h after the bone marrow aspiration. For labeling, the samples were incubated with mAbs for 15 min at room temperature in the dark according to the manufacturers' data sheets. Red blood cells were lysed using FACS lysing solution containing 1.5% formaldehyde (BD Biosciences). After washing twice in PBS, the cells were resuspended in 500 μL of PBS and measured within one hour. Samples were measured on FACSCanto II cytometer (BD Biosciences), with 50000 events acquired. Data acquisition and analysis were performed using FACSDiva software (BD Biosciences). A hierarchical gating strategy was employed for data analysis. Initially, doublets were excluded based on forward scatter area (FSC-A) versus forward scatter width (FSC-W). Subsequently, debris were excluded based on forward scatter versus side scatter (FSC vs. SSC). Finally, the main bone marrow cell lineages were gated. Monocytopoesis was

TABLE 1 Monoclonal antibody panel.

	FITC	PE	PerCP-Cy5.5/PC5.5	PC7	APC	APC-H7	Pacific Blue	Pacific Orange
Monocyte	CD14	CD11b	CD33	CD56	CD300e	CD64	HLADR	CD45
Granulocyte	CD15	CD11b	CD34	CD13	CD10	CD16	CD7	CD45
Eryhtroid	CD71	CD117	CD33	CD105	CD36	CD235a	HLADR	CD45

identified by $CD33^{int}$ $CD64^{int}$, granulopoesis by $CD15^{+}$, nucleated erythropoetic cells by $CD45^{dim/neg}SSC^{low/int}CD33^{-}CD235a^{+}CD71^{+}$. The ratio of myeloid progenitors was enumerated by gating the $CD45^{dim}SSC^{low/int}CD34^{+}CD13^{+}$ and $CD45^{dim}SSC^{low/int}CD117^{+}CD33^{+}$ populations using the total number of nucleated cells as the denominator. In instances where the ratios differed between the two gating strategies, the higher ratio of myeloid progenitors was utilized.

Diagnostic MDS FCM-scores and thresholds

The Ogata score [11] and extended Ogata score [12] were counted and the thresholds of MDS were set to ≥2 for both scores. For Ogata score, four parameters were analyzed (1 point each): the percentage of myeloblasts in all nucleated cells (cut-off ≥2%), the percentage of B-progenitors in all $CD34^{+}$ cells (cut-off ≤5%), the lymphocyte to myeloblast CD45 MFI ratio (≤4 or ≥7.5), and the granulocyte to lymphocyte SSC mode ratio (cut-off ≤6). In the case of extended Ogata score, one extra point was added for the expression of CD7 on myeloid progenitors with a threshold of 20% or of CD56 on monocytes, with a threshold of 30% positive cells.

In addition to these scores, the presence of at least three aberrations in at least two cell compartments was considered indicative of MDS. During the data analysis predefined templates and gates were applied in the FACSDiva software to assess the distinction from the normal pattern. The sensitivity, specificity, and accuracy of Ogata score, extended Ogata score, "3 aberrations in two cell compartments method" and the combination of the Ogata score and "3 aberrations in two cell compartments method" were evaluated.

Results

Description of the study population

A total of 179 patients with cytopenia were included in the study. The median age was 72 years (range 28–90). Of these patients, 95 were female. A total of 58 cases were diagnosed as MDS. In the majority of MDS cases the mean corpuscular volume (MCV) was increased or normal in 28 and 27 cases, respectively. In 15 cases, cytogenetic aberrancies in addition to morphological dysplasia were observed. The detected chromosomal abnormalities were complex in 7 cases, del (5q) alone in 4 cases, del (20q) in 2 cases, trisomy 8 (+8) in 1 case, del (9q) in 1 case. In five cases, a ≥5% myeloblast count was found in the trephine biopsy. In 38 cases with morphological dysplasia, there was no improvement in the blood counts during the follow-up period and the diagnosis was confirmed by a second bone marrow examination and/or by excluding other etiologies. Of these 38 patients, ring sideroblasts in 7 cases, increasing ratio of myeloblasts in 3 cases or progression of cytopenia during follow-up in 4 cases, clonal chromosomal (not MDS defining) abnormality in 2 cases, abnormal monocytosis and granulocytosis in 1-1 cases, and dysplasia in more than one lineage in 12 cases were indicative of MDS. The median follow-up period was 2 months (range 0.2–27). MDS was classified according to the 2016 WHO classification: MDS with isolated del (5q) 4 (7%), MDS with single lineage dysplasia (SLD) 5 (9%), MDS with multilineage dysplasia (MLD) 34 (57%), MDS with ring sideroblasts and single lineage dysplasia (RS-SLD) 3 (5%), MDS with ring sideroblasts and with multilineage dysplasia (RS-MLD) 5 (9%), MDS with excess blasts (EB1) 5 (9%), chronic myelomonocytic leukaemia (CMML) 1, myelodysplastic/myeloproliferative neoplasm, unclassifiable (MDS/MPN-U) 1.

The etiology of non-MDS cytopenias is listed in Table 2. The most common causes are vitamin B12 deficiency, toxic effects of drugs, inflammation, and chronic myeloproliferative neoplasia, with primary myelofibrosis being the most prevalent. In many cases, a combination of different causes was diagnosed. In non-MDS cases, a normal MCV was observed most frequently then increased and decreased in 59, 52, and 10 cases, respectively.

Myeloid progenitors

The ratio of myeloid progenitor cells (MPCs) was determined by gating the $CD45^{dim}SSC^{low/int}CD34^{+}CD13^{+}$ or $CD45^{dim}SSC^{low/int}CD117^{+}CD33^{+}$ populations, which correlated in most of the cases well (Figure 1). In MDS cases, the mean ratio of MPCs with the two different gating strategies was 1.6% (range 0%–4.7%) and 1.6% (range 0.1–4.6%), respectively. A difference in the MPCs exceeding 1% between the two gating strategies was observed in only 2 cases (3.4%) due to loss of either CD34 or CD33.

TABLE 2 Etiology of non-MDS cytopenia.

Etiology	Number of cases (n = 121)
Chronic kidney disease	9
Inflammatory	12
Vitamin B12 deficiency	16
Toxic (drugs, alcohol)	16
ITP	6
Aplastic anaemia	6
Iron deficiency, bleeding	6
Myeloproliferativ neoplasms	12
Autoimmune (SLE, PRCA, CIN)	7
Liver cirrhosis, hypersplenism	3
Solid tumor, T-LGL	3
Combined	19
Unknown	6

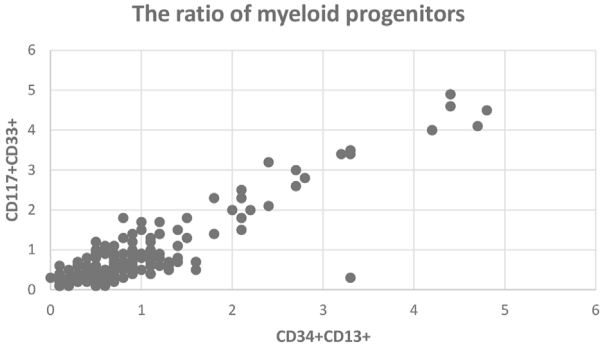

FIGURE 1
The ratio of myeloid progenitors by two different gating strategy.

In non-MDS cases, the ratio of MPCs by the two different gating approaches was 0.8% (range 0.1–2.7%) and 0.7% (range 0.1%–3%), respectively. Myeloid progenitors over 2% were detected in five patients: 2 cases with pancytopenia due to methotrexate, 2 cases with myeloproliferative neoplasia (MPN), and one case with infection.

Sensitivity of FCM approaches

The sensitivity, specificity, and accuracy of the Ogata score, the extended Ogata score, the "3 aberrations in two cell compartments method" and the combination of the Ogata score with the "3 aberrations in two cell compartments method" were calculated.

The Ogata score was not applicable in only one MDS case due to the loss of CD34 expression on myeloid progenitors. The sensitivity of the Ogata score proved to be 75%. Regarding the 14 false negative cases, 12 of them belonged to the low or very low risk group by R-IPSS, with normal karyotype and myeloid progenitors ≤2% by either method (BM smear, trephine biopsy or FCM). One of the remaining two cases was MDS with fibrosis and complex cytogenetics, while the other was an MDS/MPN with 4% myeloblast in the trephine biopsy. The sensitivity of the extended Ogata score was improved to 81% by identifying an additional 3 MDS cases.

The "3 aberrations in two cell compartments method" yielded a sensitivity of 72%. Sixteen cases were identified as false negatives. Eight of these cases were classified as low or very low risk according to the R-IPSS, while three were placed in the intermediate risk group. In five cases, the R-IPSS could not be calculated due to unsuccessful karyotyping. Two of these cases were classified as MDS-EB1 based on the increased blasts observed in the trephine biopsy.

The sensitivity decreased to 61% when the Ogata score and the "3 aberrations in two cell compartments method" were combined, classifying the cases as MDS if both turned out to be suggestive of MDS (Table 3).

Specificity and accuracy of FCM approaches

In patients with non-MDS cytopenia all four FCM approaches showed a specificity of at least 62%. The Ogata score and the extended Ogata score exhibited the same specificity. Regarding the Ogata score, score 2 was observed with high frequency in 36 false positive cases. Scores 3 and 4 were more specific and were found in only 10 of non-MDS cases. The decreased B-progenitor cluster size and reduced granulocyte/lymphocyte SSC ratio were detected in 43 (93%) and 33 (72%) of the false positive non-MDS cases, respectively. These two aberrations were observed in cases of any etiology. The decreased B-progenitor cluster size occurred most often in elderly (>70 years), in autoimmune cytopenia and in inflammatory diseases, while reduced granulocyte/lymphocyte SSC ratio was most often found in cytopenia due to toxic effects and inflammation. Abnormal lymphocyte to myeloblast CD45 ratio and increased myeloblast ratio were shown in 15 (32%) and 4 (9%) false positive non-MDS cases, respectively. The most common etiology for the high (3 and 4 points) Ogata scores was pancytopenia due to toxic effects from methotrexate (4 cases). The specificity of the "3 aberrations in two cell compartments method" was 79%. The majority of the false positive cases were attributed to substrate deficiencies, inflammation/infection, and toxic effects. The combination of the Ogata score with the "3 aberrations in two cell compartments method" allowed the exclusion of the majority of non-MDS cases with a specificity of 86% (Table 4). The reasons for false positivity with the combination approach were variable.

TABLE 3 The sensitivity for different FCM approaches in MDS. Ogata score and extended Ogata score are not applicable in one case.

	MDS Sensitivity	
	Number of patients (n = 58)	Percentage of patients (%)
Ogata-score	43	75
Extended Ogata-score	46	81
ELN	42	72
Ogata-score + ELN	35	61

TABLE 4 The specificity for different FCM approaches in non-MDS cases.

	Non-MDS Specificity	
	Number of patients (n = 121)	Percentage of patients (%)
Ogata-score	75	62
Extended Ogata-score	75	62
ELN	96	79
Ogata-score + ELN	104	86

These included vitamin B12 deficiency (4 cases), inflammation/infection (3 cases), toxic effects (3 cases), combination of different causes (4 cases) (Table 5).

Interestingly, in 12 cases, dysplastic changes in the bone marrow smear were observed without an increase in blasts or cytogenetic aberrancies. These cases demonstrated improvement in blood counts during the follow-up period, which led to the exclusion of MDS. In half of these cases, FCM demonstrated the absence of signs of MDS using any method, while in only three cases, MDS was identified based on the combination of the Ogata score and the "3 aberrations in two cell compartments" method.

The highest accuracy (78%) was achieved by the combination of the Ogata score and the "3 aberrations in two cell compartments method." The application of the "3 aberrations in two cell compartments method" resulted in almost the same accuracy (77%) (Table 6).

Results of the repeated bone marrow examination

In 9 cases the bone marrow examination was repeated after a median of 11 months (range 7–24). In 3 cases, an increasing ratio of myeloblasts was detected in the second bone marrow sample (2 MDS-EB2 and 1 AML). In 2 cases, both the Ogata and the ELN scores were already abnormal in the first bone marrow sample and the myeloblast ratio did not increase in the second sample. In 3 cases, the Ogata score and in one case the ELN score became abnormal in the second sample. As a result of these changes, both scores became abnormal in two patients.

Discussion

The differential diagnosis of myelodysplastic neoplasms with low blasts represents a diagnostic challenge in patients presenting with cytopenia. The gold standard in the diagnosis is the evaluation of bone marrow smears for dysplastic features. Even in the absence of morphological dysplasia, several chromosomal abnormalities and two mutations—biallelic TP53 and SF3B1 mutations—are considered MDS defining as per the WHO 5th edition (WHO5ED) criteria [1]. An abnormal immunophenotype alone is only a co-criterion for the diagnosis of MDS [18]. FCM, however, is widely available and provides results in a relatively short time frame, typically within 24 h. Despite the efforts of iMDSFlow in the standardization of flow cytometry in MDS there are difficulties in the application due to the large number of proposed markers (20 antigens). Furthermore, none of the markers are specific to MDS, and there are no clear cut-off values for most of these markers [10, 17]. A number of FCM scoring systems have been published and validated for the analysis of MDS [11–16, 19]. The goal of these scoring systems was to determine the most relevant markers for the evaluation and to establish cut-offs that best discriminate between MDS and non-MDS cases. Recently, two studies compared the most important scoring systems and not surprisingly, the most comprehensive one, iFS, proved to be the most useful [20, 21]. iFS combines a modified FCSS, Ogata-score and ELN-NEC requiring the analysis of 44 markers and calculation of 3 scores [16]. Therefore, the application of iFS is labor-intensive and time-consuming. A survey evaluating the current FCM practice for the diagnosis of MDS in 229 laboratories worldwide showed that the usage of any FCM scoring system was very limited [22]. This result reflects that calculating the scores is hardly compatible with the routine clinical practice. In the present work, we tested the simplest FCM approaches for the diagnosis of MDS such as the Ogata score, the extended Ogata score, and the ELN and the WHO recommended "3 aberrations in two cell compartments method." An important feature of the Ogata score is its lower sensitivity in low-risk MDS patients. Therefore, we investigated whether the combination of the Ogata score with the "3 aberrations in two cell compartments method" improves this sensitivity.

Furthermore, we focused on the most problematic group of MDS (MDS with low blasts), excluding cases with myeloid progenitors≥5% detected by either bone marrow smear analysis or FCM. Follow-up of these patients, even with morphologic dysplasia allowed confirmation of the diagnosis in all cases. The follow-up seemed necessary because in 12 cases

TABLE 5 Diseases resulted in false positivity with the different FCM approaches.

Etiology	Ogata score	ELN	Ogata score + ELN
Substrate deficiency	9	8	4
Inflammatory	9	4	3
Toxic	6	3	3
Autoimmune	6	3	1
Myeloproliferative neoplasms	3	2	1
T-LGL	1	1	1
Chronic kidney disease	2	0	0
Chronic liver disease	2	0	0
Combined	8	4	4

TABLE 6 The accuracy of different FCM approaches in patients with cytopenia. Ogata score and extended Ogata score are not applicable in one case.

	MDS and non-MDS Accuracy	
	Number of patients (n = 179)	Percentage of patients (%)
Ogata-score	118	66
Extended Ogata-score	121	68
ELN	138	77
Ogata-score + ELN	139	78

the bone marrow smear showed dysplastic changes, but the blood counts normalized suggesting reactive causes in the background. This finding confirms that dysplastic changes are not specific for MDS [3, 4] and the need for follow-up.

The identification of myeloid progenitor cells (MPCs) represents a pivotal aspect in the diagnosis and prognostication of MDS. An aberrantly low expression of CD34 on MPCs may occur in MDS [23], therefore two distinct gating strategies for MPCs were employed: one based on CD34 expression and the other on CD117 and CD33 expression. Using this approach, we were able to identify MPCs even in cases with loss of CD34 or CD33, otherwise the results correlated perfectly. In cytomorphology, a cut-off of 5% blasts is used for diagnosis and classification. However, there are striking differences in overall survival and AML evolution depending on blast counts even under 5% [24]. A lower cut-off of myeloid progenitors is recommended for FCM in MDS diagnosis. In the Ogata-score, a 2% cut-off is applied for myeloblast-related cluster size in all nucleated cells [11]. In a prospective FCM study, MPCs over 3% among the $CD45^+$ cells were associated with the diagnosis of MDS [8]. We confirmed these findings because in all non-MDS cases the ratio of MPCs was at a maximum of 3%, although it should be noted that the results are not completely comparable due to the use of all nucleated cells as a denominator. MPCs above 2% were found in some patients with regenerating myelopoiesis after drug-induced pancytopenia or in MPNs.

One of the diagnostic tools we selected was the Ogata score, which was chosen for its simplicity. This score eliminates errors deriving from the inter-observer variability. The sensitivity of the Ogata score was found to be slightly higher (75%) in our hands than in the previous studies [11, 12, 21]. The sensitivity of the Ogata score is the lowest in low risk cases [12, 21], as evidenced by the fact that almost all false negative cases in our patient group were classified as IPSS-R low or very low risk. CD5 was excluded from the extended Ogata score due to its low sensitivity. The addition of CD56 and CD7 allowed the identification of 3 more MDS patients, thereby improving the sensitivity of the Ogata score in a manner similar to that reported in the original publication [12].

The sensitivity of the "3 aberrations in two cell compartments method" was somewhat lower than that of the Ogata-score, missing 16 cases, including 5 with either intermediate risk category or higher blast counts. These higher risk cases were correctly diagnosed with the Ogata-score, suggesting that these two methods are to some extent complimentary. When both a positive Ogata-score and a "3 aberrations in two cell compartments method" were required for MDS diagnosis, the sensitivity decreased to 61%.

The most surprising finding of our analysis is the low specificity of the Ogata score. In previously published studies, this score demonstrated at least 80% specificity making it an effective tool for excluding the majority of non-MDS cases [11, 12, 19–21]. However, in our analysis, even score 4 was not entirely specific for MDS, in contrast to the findings of previous studies [11, 25]. The most common parameter in non-MDS cases was the decreased B-progenitor cluster size, as previously described in the literature [11, 25]. The older age of our patient population [26], the high frequency of inflammation [27], autoimmunity and its treatment by drugs such as metothrexate [28] may explain the high prevalence of low numbers in B-progenitors. The reduced granulocyte/lymphocyte SSC ratio was the second most common parameter in our non-MDS cohort, although this is considered to be MDS specific and is associated with the defective maturation of myeloid precursors [29]. Our methodology may contribute to the high rate of reduced granulocyte/lymphocyte SSC ratio, because FACS Lysing solution (BD) was used to lyse the non-nucleated red blood cells. ELN iMDSFlow recommends ammonium chloride [17], and it was also used in the original publication of the Ogata score [30]. FACS Lysing Solution and a stain-lyse-wash protocol, which we used, significantly reduce the light scatter CV for the different leukocyte populations compared to ammonium chloride [31], and may therefore influence the granulocyte/lymphocyte SSC ratio. However, this staining procedure did not decrease the sensitivity of the Ogata score in our cohort, and Matzen et al also used FACS Lysing solution with high specificity in their MDS analysis [32], so the

FACS Lysing solution is unlikely to have a significant effect on the SSC ratio. The specificity of the "3 aberrations in two cell compartments method" was found to be higher (79%), although this figure is still far from 100%. This result confirms that the altered patterns of antigen expression observed in MDS are not specific for this disease and are susceptible to misinterpretation.

The combination of the Ogata score and the "3 aberrations in two cell compartments method" yielded the highest accuracy, correctly identifying 79% of the cases. The application of the "3 aberrations in two cell compartments method" resulted in an almost identical accuracy.

In conclusion, this study confirms that the diagnosis of MDS with low blasts should be an integrated approach that includes morphology, cytogenetics, immunophenotyping and molecular genetics. Flow cytometry can support the diagnosis of MDS, but it does not provide a definitive diagnosis or exclude the possibility of MDS. This work emphasizes the importance of patient follow-up, as even dysplastic morphology and indicative FCM results can be misleading.

Data availability statement

The datasets presented in this article are not readily available because the dataset is anonymized and not available for the public. Requests to access the datasets should be directed to planderm@yahoo.com.

Ethics statement

The studies involving humans were approved by the Review Board of Markusovszky University Teaching Hospital. The studies were conducted in accordance with the local legislation and institutional requirements. The participants provided their written informed consent to participate in this study.

Author contributions

MP and MK designed the work, analysed the samples and wrote the manuscript. MP and TS provided the samples and collected the clinical data. JS and BT supervised the project. BT reviewed the paper. All authors contributed to the article and approved the submitted version.

Funding

The author(s) declare that financial support was received for the research, authorship, and/or publication of this article. The Hungarian Society of Hematology and Transfusiology supported the publication fee of this article.

Conflict of interest

The authors declare that the research was conducted in the absence of any commercial or financial relationships that could be construed as a potential conflict of interest.

Acknowledgments

The authors would like to thank Éva Kiss, Éva Szanyiné Bejczi, Ákosné Guzmics for their excellent technical assistance and for the physicians for providing samples and caring the patients.

Supplementary material

The Supplementary Material for this article can be found online at: https://www.por-journal.com/articles/10.3389/pore.2024.1611811/full#supplementary-material

References

1. Khoury JD, Solary E, Abla O, Akkari Y, Alaggio R, Apperley JF, et al. The 5th edition of the world Health organization classification of haematolymphoid tumours: myeloid and histiocytic/Dendritic Neoplasms. *Leukemia* (2022) 36: 1703–19. doi:10.1038/s41375-022-01613-1

2. Arber DA, Orazi A, Hasserjian R, Thiele J, Borowitz MJ, Le Beau MM, et al. The 2016 revision to the World Health Organization classification of myeloid neoplasms and acute leukemia. *Blood* (2016) 127(20):2391–405. doi:10.1182/blood-2016-03-643544

3. Senent L, Arenillas L, Luño E, Ruiz JC, Sanz G, Florensa L. Reproducibility of the world Health organization 2008 criteria for myelodysplastic syndromes. *Haematologica* (2013) 984:568–75. doi:10.3324/haematol.2012.071449

4. Font P, Loscertales J, Benavente C, Bermejo A, Callejas M, Garcia-Alonso L, et al. Inter-observer variance with the diagnosis of myelodysplastic syndromes (MDS) following the 2008 WHO classification. *Ann Hematol* (2013) 921:19–24. doi:10.1007/s00277-012-1565-4

5. Font P, Loscertales J, Soto C, Ricard P, Novas CM, Martín-Clavero E, et al. Interobserver variance in myelodysplastic syndromes with less than 5 % bone marrow blasts: unilineage vs. multilineage dysplasia and reproducibility of the threshold of 2 % blasts. *Ann Hematol* (2015) 94(4):565–73. doi:10.1007/s00277-014-2252-4

6. Della Porta MG, Travaglino E, Boveri E, Ponzoni M, Malcovati L, Papaemmanuil E, et al. Rete Ematologica Lombarda (REL) Clinical Network Minimal morphological criteria for defining bone marrow dysplasia: basis for clinical implementation of WHO classification of myelodysplastic syndromes. *Leukemia* (2015) 291:66–75. doi:10.1038/leu.2014.161

7. Haase D, Germing U, Schanz J, Pfeilstöcker M, Nösslinger T, Hildebrandt B, et al. New insights into the prognostic impact of the karyotype in MDS and correlation with subtypes: evidence from a core dataset of 2124 patients. *Blood* (2007) 110(13):4385–95. doi:10.1182/blood-2007-03-082404

8. Kern W, Westers TM, Bellos F, Bene MC, Bettelheim P, Brodersen LE, et al. Multicenter prospective evaluation of diagnostic potential of flow cytometric aberrancies in myelodysplastic syndromes by the ELN iMDS flow working group. *Cytometry B Clin Cytom* (2023) 104(1):51–65. doi:10.1002/cyto.b.22105

9. Malcovati L, Hellström-Lindberg E, Bowen D, Adès L, Cermak J, del Cañizo C, et al. Diagnosis and treatment of primary myelodysplastic syndromes in adults:

recommendations from the European LeukemiaNet. *Blood* (2013) 122(17): 2943–64. doi:10.1182/blood-2013-03-492884

10. Porwit A, van de Loosdrecht AA, Bettelheim P, Eidenschink Brodersen L, Burbury K, Cremers E, et al. Revisiting guidelines for integration of flow cytometry results in the WHO classification of myelodysplastic syndromes—proposal from the International/European LeukemiaNet Working Group for Flow Cytometry in MDS. *Leukemia* (2014) 28:1793–8. doi:10.1038/leu.2014.191

11. Della Porta MG, Picone C, Pascutto C, Malcovati L, Tamura H, Handa H, et al. Multicenter validation of a reproducible flow cytometric score for the diagnosis of low-grade myelodysplastic syndromes: results of a European LeukemiaNET study. *Haematologica* (2012) 97(8):1209–17. doi:10.3324/haematol.2011.048421

12. Bardet V, Wagner-Ballon O, Guy J, Morvan C, Debord C, Trimoreau F, et al. Multicentric study underlining the interest of adding CD5, CD7 and CD56 expression assessment to the flow cytometric Ogata score in myelodysplastic syndromes and myelodysplastic/myeloproliferative neoplasms. *Haematologica* (2015) 100(4):472–8. doi:10.3324/haematol.2014.112755

13. Mathis S, Chapuis N, Debord C, Rouquette A, Radford-Weiss I, Park S, et al. Flow cytometric detection of dyserythropoiesis: a sensitive and powerful diagnostic tool for myelodysplastic syndromes. *Leukemia* (2013) 27:1981–7. doi:10.1038/leu.2013.178

14. Westers TM, Cremers EMP, Oelschlaegel U, Johansson U, Bettelheim P, Matarraz S, et al. Immunophenotypic analysis of erythroid dysplasia in myelodysplastic syndromes. A report from the IMDSFlow working group. *Haematologica* (2017) 102:308–19. doi:10.3324/haematol.2016.147835

15. Wells DA, Benesch M, Loken MR, Vallejo C, Myerson D, Leisenring WM, et al. Myeloid and monocytic dyspoiesis as determined by flow cytometric scoring in myelodysplastic syndrome correlates with the IPSS and with outcome after hematopoietic stem cell transplantation. *Blood* (2003) 102:394–403. doi:10.1182/blood-2002-09-2768

16. Cremers EMP, Westers TM, Alhan C, Cali C, Visser-Wisselaar HA, Chitu DA, et al. Implementation of erythroid lineage analysis by flow cytometry in diagnostic models for myelodysplastic syndromes. *Haematologica* (2017) 102:320–6. doi:10.3324/haematol.2016.147843

17. Westers TM, Ireland R, Kern W, Alhan C, Balleisen JS, Bettelheim P, et al. Standardization of flow cytometry in myelodysplastic syndromes: a report from an international consortium and the European LeukemiaNet Working Group. *Leukemia* (2012) 26(7):1730–41. doi:10.1038/leu.2012.30

18. Valent P, Orazi A, Steensma DP, Ebert BL, Haase D, Malcovati L, et al. Proposed minimal diagnostic criteria for myelodysplastic syndromes (MDS) and potential pre-MDS conditions. *Oncotarget* (2017) 8(43):73483–500. doi:10.18632/oncotarget.19008

19. Kárai B, Bedekovics J, Miltényi Z, Gergely L, Szerafin L, Ujfalusi A, et al. A single-tube flow cytometric procedure for enhancing the diagnosis and prognostic classification of patients with myelodysplastic syndromes. *Int J Lab Hematol* (2017) 39(6):577–84. doi:10.1111/ijlh.12700

20. Davydova YO, Parovichnikova EN, Galtseva IV, Kokhno AV, Dvirnyk VN, Kovrigina AM, et al. Diagnostic significance of flow cytometry scales in diagnostics of myelodysplastic syndromes. *Cytometry B Clin Cytom* (2021) 100(3):312–21. doi:10.1002/cyto.b.21965

21. Oelschlaegel U, Oelschlaeger L, von Bonin M, Kramer M, Sockel K, Mohr B, et al. Comparison of five diagnostic flow cytometry scores in patients with myelodysplastic syndromes: diagnostic power and prognostic impact. *Cytometry B Clin Cytom* (2023) 104:141–50. doi:10.1002/cyto.b.22030

22. Grille E, Iastrebner M, Lorand-Metze I, van der Veldene VHJ, Ikoma MRV, Vidal-Senmache G, et al. Flow cytometry diagnosis in myelodysplastic syndrome: current practice in Latin America and comparison with other regions of the world. *Leuk Res* (2019) 79:69–74. doi:10.1016/j.leukres.2019.01.009

23. Matarraz S, López A, Barrena S, Fernandez C, Jensen E, Flores-Montero J, et al. Bone marrow cells from myelodysplastic syndromes show altered immunophenotypic profiles that may contribute to the diagnosis and prognostic stratification of the disease: a pilot study on a series of 56 patients. *Cytometry* (2010) 78B:154–68. doi:10.1002/cyto.b.20513

24. Greenberg PL, Tuechler H, Schanz J, Sanz G, Garcia-Manero G, Solé F, et al. Revised international prognostic scoring system for myelodysplastic syndromes. *Blood* (2012) 120(12):2454–65. doi:10.1182/blood-2012-03-420489

25. Rajab A, Porwit A Screening bone marrow samples for abnormal lymphoid populations and myelodysplasia-related features with one 10-color 14-antibody screening tube. *Cytometry* (2015) 88(4):253–60. doi:10.1002/cyto.b.21233

26. Valiathan R, Ashman M, Asthana D. Effects of ageing on the immune system: infants to elderly. *Scand J Immunol* (2016) 83(4):255–66. doi:10.1111/sji.12413

27. Cain D, Kondo M, Chen H, Kelsoe G. Effects of acute and chronic inflammation on B-cell development and differentiation. *J Invest Dermatol* (2009) 129(2):266–77. doi:10.1038/jid.2008.286

28. Wascher TC, Hermann J, Brezinschek HP, Brezinschek R, Wilders-Truschnig M, Rainer F, et al. Cell-type specific response of peripheral blood lymphocytes to methotrexate in the treatment of rheumatoid arthritis. *Clin Investig* (1994) 72(7): 535–40. doi:10.1007/BF00207484

29. Stetler-Stevenson M, Arthur DC, Jabbour N, Xie XY, Molldrem J, Barrett AJ, et al. Diagnostic utility of flow cytometric immunophenotyping in myelodysplastic syndrome. *Blood* (2001) 98(4):979–87. doi:10.1182/blood.v98.4.979

30. Ogata K, Della Porta MG, Malcovati L, Picone C, Yokose N, Matsuda A, et al. Diagnostic utility of flow cytometry in low-grade myelodysplastic syndromes: a prospective validation study. *Haematologica* (2009) 94(8):1066–74. doi:10.3324/haematol.2009.008532

31. Kalina T, Flores-Montero J, van der Velden VHJ, Martin-Ayuso M, Böttcher S, Ritgen M, et al. EuroFlow standardization of flow cytometer instrument settings and immunophenotyping protocols. *Leukemia* (2012) 26(9):1986–2010. doi:10.1038/leu.2012.122

32. Matzen S, Raaschou-Jensen KK, Kallenbach K Implementation of the Ogata flow cytometric scoring system in routine diagnostics of myelodysplastic syndrome. *Health Sci Rep* (2018) 1(11):e90. doi:10.1002/hsr2.90

Pathology & Oncology Research | frontiers

TYPE Hypothesis & Theory
PUBLISHED 02 February 2023
DOI 10.3389/pore.2023.1610819

Check for updates

OPEN ACCESS

EDITED BY
Andrea Ladányi,
National Institute of Oncology (NIO), Hungary

*CORRESPONDENCE
Yang Liu,
liuyanglyon@uestc.edu.cn,
liuyang@scszlyy.org.cn

†These authors share first authorship

RECEIVED 08 September 2022
ACCEPTED 16 January 2023
PUBLISHED 02 February 2023

CITATION
Hou J, Guo P, Lu Y, Jin X, Liang K, Zhao N, Xue S, Zhou C, Wang G, Zhu X, Hong H, Chen Y, Lu H, Wang W, Xu C, Han Y, Cai S and Liu Y (2023), A prognostic 15-gene model based on differentially expressed genes among metabolic subtypes in diffuse large B-cell lymphoma.
Pathol. Oncol. Res. 29:1610819.
doi: 10.3389/pore.2023.1610819

COPYRIGHT
© 2023 Hou, Guo, Lu, Jin, Liang, Zhao, Xue, Zhou, Wang, Zhu, Hong, Chen, Lu, Wang, Xu, Han, Cai and Liu. This is an open-access article distributed under the terms of the Creative Commons Attribution License (CC BY). The use, distribution or reproduction in other forums is permitted, provided the original author(s) and the copyright owner(s) are credited and that the original publication in this journal is cited, in accordance with accepted academic practice. No use, distribution or reproduction is permitted which does not comply with these terms.

A prognostic 15-gene model based on differentially expressed genes among metabolic subtypes in diffuse large B-cell lymphoma

Jun Hou[1†], Peng Guo[1†], Yujiao Lu[2†], Xiaokang Jin[2], Ke Liang[2], Na Zhao[1], Shunxu Xue[1], Chengmin Zhou[1], Guoqiang Wang[2], Xin Zhu[2], Huangming Hong[3], Yungchang Chen[3], Huafei Lu[2], Wenxian Wang[4], Chunwei Xu[5], Yusheng Han[2], Shangli Cai[2] and Yang Liu[1*]

[1]Department of Pathology, Sichuan Cancer Hospital and Institute, Sichuan Cancer Center, School of Medicine, University of Electronic Science and Technology of China, Chengdu, China, [2]Burning Rock Biotech, Guangzhou, China, [3]Medical Oncology, Sichuan Cancer Hospital and Institute, Sichuan Cancer Center, School of Medicine, University of Electronic Science and Technology of China, Chengdu, China, [4]Department of Clinical Trial, The Cancer Hospital of the University of Chinese Academy of Sciences (Zhejiang Cancer Hospital), Hangzhou, China, [5]Institute of Basic Medicine and Cancer (IBMC), Chinese Academy of Sciences, Hangzhou, China

The outcomes of patients with diffuse large B-cell lymphoma (DLBCL) vary widely, and about 40% of them could not be cured by the standard first-line treatment, R-CHOP, which could be due to the high heterogeneity of DLBCL. Here, we aim to construct a prognostic model based on the genetic signature of metabolic heterogeneity of DLBCL to explore therapeutic strategies for DLBCL patients. Clinical and transcriptomic data of one training and four validation cohorts of DLBCL were obtained from the GEO database. Metabolic subtypes were identified by PAM clustering of 1,916 metabolic genes in the 7 major metabolic pathways in the training cohort. DEGs among the metabolic clusters were then analyzed. In total, 108 prognosis-related DEGs were identified. Through univariable Cox and LASSO regression analyses, 15 DEGs were used to construct a risk score model. The overall survival (OS) and progression-free survival (PFS) of patients with high risk were significantly worse than those with low risk (OS: HR 2.86, 95%CI 2.04–4.01, $p < 0.001$; PFS: HR 2.42, 95% CI 1.77–3.31, $p < 0.001$). This model was also associated with OS in the four independent validation datasets (GSE10846: HR 1.65, $p = 0.002$; GSE53786: HR 2.05, $p = 0.02$; GSE87371: HR 1.85, $p = 0.027$; GSE23051: HR 6.16, $p = 0.007$) and PFS in the two validation datasets (GSE87371: HR 1.67, $p = 0.033$; GSE23051: HR 2.74, $p = 0.049$). Multivariable Cox analysis showed that in all datasets, the risk model could predict OS independent of clinical prognosis factors ($p < 0.05$). Compared with the high-risk group, patients in the low-risk group predictively respond to R-CHOP ($p = 0.0042$), PI3K inhibitor ($p < 0.05$), and proteasome inhibitor ($p < 0.05$). Therefore, in this study, we developed a signature model of 15 DEGs among 3 metabolic subtypes, which could predict survival and drug sensitivity in DLBCL patients.

KEYWORDS

prognosis, risk score, drug sensitivity, DEGs, diffuse large B-cell lymphoma (DLBCL), metabolic subtypes

Introduction

Diffuse large B-cell lymphoma (DLBCL), a type of highly heterogeneous cancer, accounts for 30%–40% of non-Hodgkin lymphoma (1). The prognosis of DLBCL varies due to its distinct characteristics such as clinical factors, recurring mutations, cell of origin (COO) (2), etc. Currently, while approximately 60% of DLBCL patients could be cured by R-CHOP (a combined therapy of rituximab, cyclophosphamide, doxorubicin, vincristine, and prednisone), the rest still suffer from a poor prognosis with fatal recurrent or progressive disease (3). Hence, effective prognostic stratification systems for DLBCL could benefit these patients in clinical decision-making and treatment.

At present, there are several commonly used prognosis-related classification systems for DLBCL in clinical practice, especially International Prognostic Index (IPI) (4) and COO (5, 6). Although IPI is convenient for application, its limitations are also obverse, in which only clinical factors are used and heterogeneous features of DLBCL, such as intrinsic genes and other biomarkers, are not considered. In the COO classification system, DLBCL is divided into germinal center B-cell-like (GCB) and non-GCB including activated B-cell-like (ABC) and type-III DLBCL based on immunohistochemistry algorithms (5) or gene expression profiling (GEP) analysis (6). Patients with GCB-DLBCL have better outcomes than those with non-GCB (6). However, the COO classification is mainly based on the B cell receptor (BCR) signaling pathway (7), and the isotype of BCR alone can predict the prognosis similar to COO (8). In addition, neither IPI nor COO classification can predict the efficacy of most drugs, although BTK inhibitor (BTKi)' ibrutinib, was reported more effective in ABC than GCB DLBCL in a phase 1/2 clinical trial (9). Therefore, prognostic models of novel biomarkers are needed to assist the therapeutic drug selection in DLBCL.

Cancer cells autonomously alter their metabolic flux to meet the demands for rapid growth and survival, including increased bioenergetic and biosynthetic, mitigating oxidative stress, and immune evasion, etc. (10). For instance, the Warburg effect is a classic alteration in carbohydrate metabolism in tumors (11). Conversely, aberrantly accumulated metabolites also promote tumorigenesis (12). Targeting metabolic alterations has been considered a promising therapeutic strategy in some cancer types (13, 14). Meanwhile, there is a great interest in exploiting the relationship between metabolic gene expression and cancer prognosis stratification both in pan-cancer (15, 16, 17) and single solid tumors (18, 19, 20). In DLBCL, metabolism heterogeneity was reported a long time ago (21). However, just limited attention has been paid to correlating risk signatures to metabolic alterations. Therefore, the heterogeneity of metabolic expression profiles could be a novel perspective on prognosis stratification for DLBCL patients.

In this study, we identified three subtypes of DLBCL based on expression levels of genes in metabolism pathways. With the selected DEGs among these subtypes, we developed a risk score model to help stratify the survival of DLBCL patients and analyzed the relationships between the risk score and clinicopathological characteristics, drug sensitivity, and immune cell infiltrations. Our research provided a new prognosis model for DLBCL patients, rendering novel insights into the individual management of DLBCL.

Methods

Data obtaining

Microarray gene expression profiles and corresponding clinical-related information of the training dataset (GSE31312) and four validation datasets (GSE10846, GSE53786, GSE87371, and GSE23501) were downloaded from the NCBI Gene Expression Omnibus (GEO) database (https://www.ncbi.nlm.nih.gov/geo/). Excluding 0-month survival samples, 470, 412, 119, 221, and 69 DLBCL patients were respectively included in GSE31312, GSE10846, GSE53786, GSE87371, and GSE23501. For genes with multiple probes, the median value of gene expression was used in the following analyses. The clinicopathological data of the patients in each dataset were summarized in Supplementary Table S1.

Metabolic subtype classification

Overall, 1,916 metabolic genes of 7 major metabolic processes from Peng et al. (16) were initially studied and listed in Supplementary Table S2. The expression profiles of these 1,916 metabolic genes in GSE31312 were employed to perform Partitioning Around Medoids (PAM) clustering by the "ConsensusClusterPlus (v1.50.0)" R package with Euclidean distance. The distribution of clinical characteristics of patients was analyzed among subtypes. The "survival" and "survminer" R packages were used to analyze survival differences among subtypes, and the result was shown by the Kaplan-Meier survival curve.

ssGSEA

Single sample gene set enrichment analysis (ssGSEA) was applied by the "GSVA" R package using the 50 hallmark gene sets from the Molecular Signatures Database (MSigDB, http://www.gsea-msigdb.org/gsea/index.jsp). The result was shown as a heatmap by the "ComplexHeatmap" R package.

Differentially expressed gene (DEG) analysis

Fold change (FC) was calculated by dividing the mean value of gene expression in one subtype group by that in the other subtype group. Wilcoxon signed-rank test was employed to calculate p value. The genes with $|\log_2 FC| > 0.585$ and Benjamini-Hochberg-adjusted $p < 0.05$ were identified as DEGs. For DEGs in these subtype groups, KEGG and GO enrichment analyses were performed independently using "clusterProfiler" R package.

Construction and validation of the risk score model

First, the p value of <0.01 was used as the threshold to select DEGs with prognostic significance in univariable Cox regression analysis. Then, the selected DEGs were analyzed by least absolute shrinkage and selection operator (LASSO)-Cox regression analysis through the "glmnet" and "survival" packages. Ten-fold cross-validation was employed to determine the penalty parameter (λ) of the prognostic model and followed minimum criteria. The formula below was to calculate the risk score based on the expression level of each gene and its corresponding regression coefficient:

$$\text{Risk Score} = \sum_{i=0}^{n} \beta_i * \chi_i$$

β_i: weight coefficient of each gene; χ_i: expression quantity of each gene.

The high- and low-risk groups were divided according to the median value. Overall survival (OS) and progression-free survival (PFS) of patients between the two groups were compared by the Kaplan-Meier survival curves using the "survminer" package. Then, the signature was validated in four external datasets (GSE10846, GSE53786, GSE87371, and GSE23051).

Univariable and multivariable Cox analyses were conducted to determine whether the risk score was an independent prediction factor of OS and PFS in the training and four validation cohorts. Meanwhile, receiver operating characteristic (ROC) curves in the above datasets were constructed and determined the AUC values through the "timeROC" package.

Association analysis between clinicopathological characteristics and risk score

The risk scores were compared in different groups of age, sex, stage, extranodal sites, ECOG score, IPI, and GEP subtype, separately.

Drug sensitivity analysis

The drug sensitivity of different risk groups was predicted by the data from The Genomics of Drug Sensitivity in Cancer (GDSC) database (https://www.cancerrxgene.org/) (22). The half maximal inhibitory concentration (IC50) was analyzed using "pRRophic" R package (23).

Immune cell infiltration analysis

According to the LM22 gene signature of tumor-infiltrating immune cells (TIICs) pattern for distinguishing human immune cell phenotypes (24), the fraction of TIICs was analyzed by CIBERSORT (the Cell-type Identification by Estimating Relative Subsets of RNA Transcripts, http://cibersort.stanford.edu/).

Statistical analysis

Statistical analyses and mapping of data were performed by the R software (version 4.1.2; https://www.R-project.org). Continuous variables were compared by Mann-Whitney U test or Kruskal-Wallis test. Categorical variables were compared by Fisher's exact test. A two-tailed p value <0.05 indicated statistical significance.

Results

Classification of metabolic subtypes and their prognostic differences

The overall study plan was depicted in Supplementary Figure S1. To characterize the metabolic heterogeneity of DLBCL patients, we analyzed 1,916 genes in 7 metabolic pathways (16) in the GSE31312 cohort, including 766 genes in the lipid metabolism pathway, 286 genes in the carbohydrate metabolism pathway, 348 genes in the amino acid metabolism pathway, 110 genes in the integration of energy pathway, 90 genes in the nucleotide metabolism pathway, 168 genes in the vitamin cofactor metabolism pathway, and 148 genes in the tricarboxylic acid cycle (TCA cycle) pathway. Using an unsupervised consensus algorithm, 470 patients were divided into 3 metabolic subtypes (clusters A, B, and C with 227, 170, and 73 patients, respectively) in the training cohort (Figure 1A). The respective median OS of clusters A, B, and C was 87.3 months, 73.5 months, and 47.7 months (Log-rank $p < 0.001$; Figure 1B). Notably, the median OS of cluster C was significantly shorter than those of clusters A and B.

We further investigated the differences in pathway enrichment among the three metabolic subtypes. We found

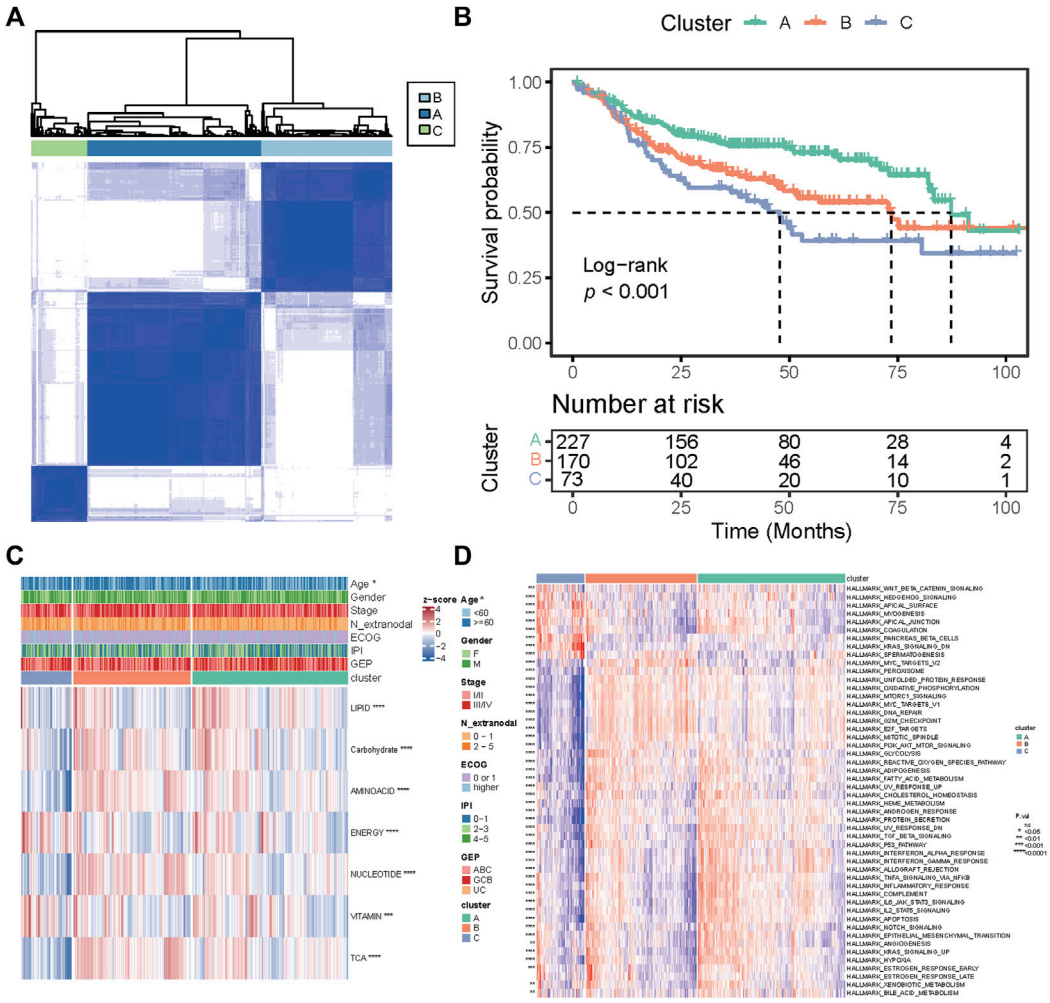

FIGURE 1
Classification of metabolic subtypes and their prognostic difference in the GSE31312 dataset. **(A)** Consensus matrix heatmap of three metabolic expression clusters. **(B)** Kaplan–Meier curves of OS among the three clusters. **(C)** Heatmap of seven metabolic pathway expression patterns of the three clusters. *$p < 0.05$; **$p < 0.01$; ***$p < 0.001$; ****$p < 0.0001$. **(D)** Heatmap of expression patterns of 50 hallmark gene sets of the three clusters. *p* value was measured by the log-rank test.

that compared with clusters A and B, cluster C had lower expression of genes in the nucleotide metabolism, TCA cycle, and amino acid metabolism and higher expression of genes in the integration of energy and vitamin cofactor metabolism (Figure 1C). The clinical variable analyses showed that patients in cluster C were older ($p = 0.044$) than those in other clusters (Figure 1C). Then, we conducted ssGSEA to assess the differential expression levels of 50 biological hallmarks in the three groups. The expression pattern of those hallmarks in cluster C was different from that in other clusters (Figure 1D). These results indicate that the differences in the expression of genes in seven major metabolic pathways could stratify the prognosis of DLBCL.

Identification of DEGs and functional annotation

To select the metabolic genetic signature, DEG analysis was conducted and identified 1,854 DEGs. There were 43, 21, and 102 downregulated genes and 1, 1, 1,743 upregulated genes in clusters A, B, and C, respectively (Figures 2A–C, Supplementary Table S3). Functional analyses of those DEGs *via* KEGG pathway and GO analyses were not able to provide any results for clusters A and B, probably due to the small sizes of DEGs sets (44 vs. 22). DEGs in cluster C were more related to neuroactive ligand-receptor interaction, cytokine-cytokine receptor interaction, and calcium signaling pathway (Figure 2D). Biological processes associated with the regulation of membrane potential, organic

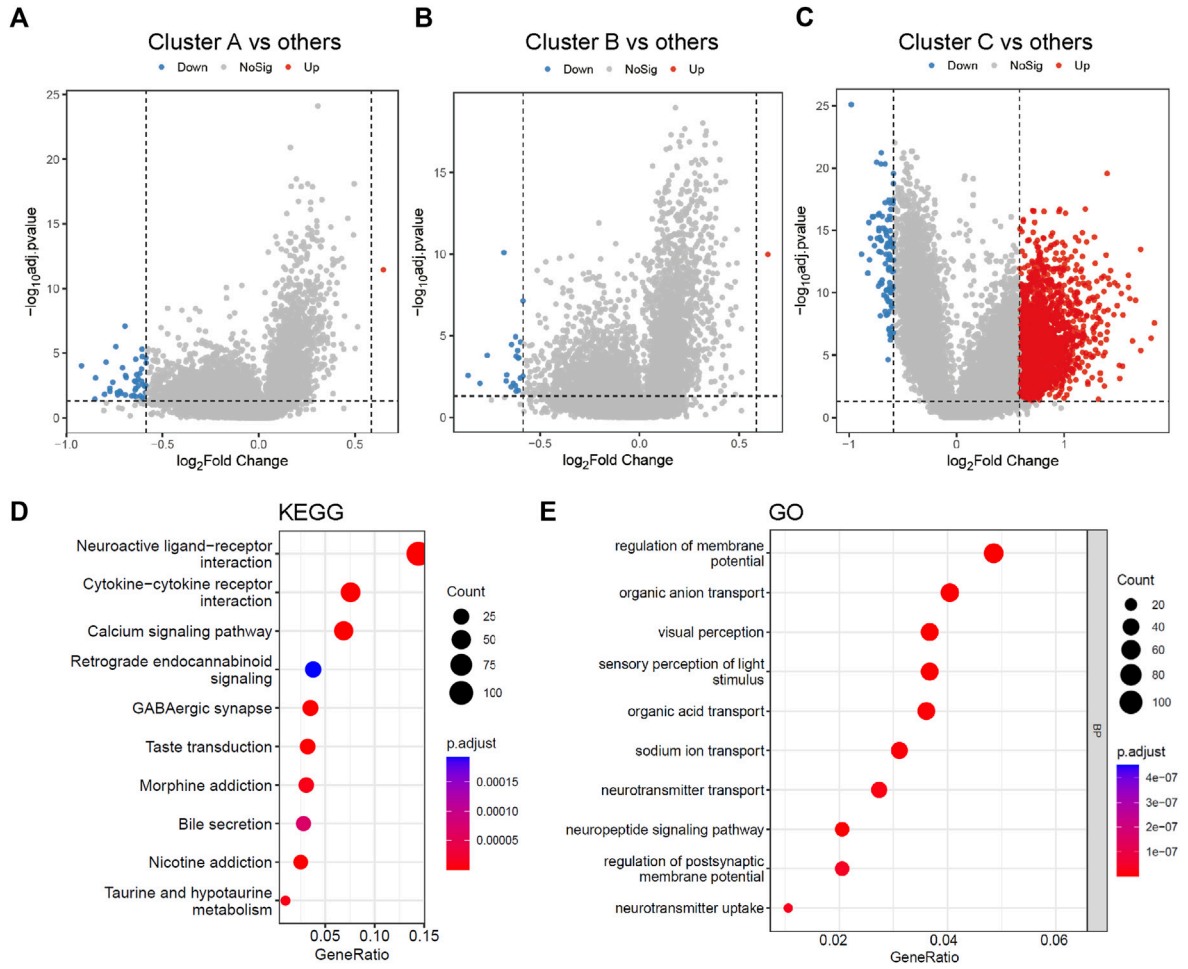

FIGURE 2
Differentially expressed genes among three metabolic subtypes and gene function enrichment analysis. **(A–C)** Volcano plots of the DEGs between cluster A and the other two clusters, cluster B and the other two clusters, cluster C and the other two clusters, separately. **(D,E)** KEGG and GO analysis of DEGs between cluster C and the other two clusters. The size of the bubbles denotes the number of genes enriched in the corresponding pathways, and the difference in color represents distinct significance. KEGG, Kyoto Encyclopedia of Genes and Genomes; GO, Gene Ontology; BP, biological process.

anion transport, organic acid transport, and sodium ion transport were also enriched in cluster C (Figure 2E).

Construction of the risk score model

To construct a risk score model, we analyzed 1,854 DEGs identified above using univariable Cox regression. The threshold of $p < 0.01$ were used to screen genes that were most related to the prognosis of DLBCL patients. A total of 108 prognosis-associated genes were selected in the training set (Supplementary Table S4). The top-20 prognosis-associated genes, according to the significance level (p value), are listed in Figure 3A. Then, we performed LASSO penalty regression to construct the prognostic model in the training set (Figure 3B). A subset of 15 genes and their weighting coefficients were finally identified (Figure 3C; Supplementary Table S5). Furthermore, the risk score of individual patients was calculated, and all patients were dichotomized into high- or low-risk groups according to the median value of the risk score.

In the training dataset, patients in the high-risk group had both shorter OS (HR 2.86, 95% CI 2.04–4.01; $p < 0.001$; Figure 3D) and PFS (HR 2.42, 95% CI 1.77–3.31; $p < 0.001$; Figure 3E) than those in the low-risk group. The areas under the receiver operating characteristic curve (AUCs) for 1-, 3-, and 5- years OS were 0.701, 0.703, and 0.724, respectively (Supplementary Figure S2A). For 1-, 3-, and 5-years PFS, the AUCs were 0.667, 0.699, and 0.685, respectively (Supplementary Figure S2B). Moreover, the

10.3389/pore.2023.1610819

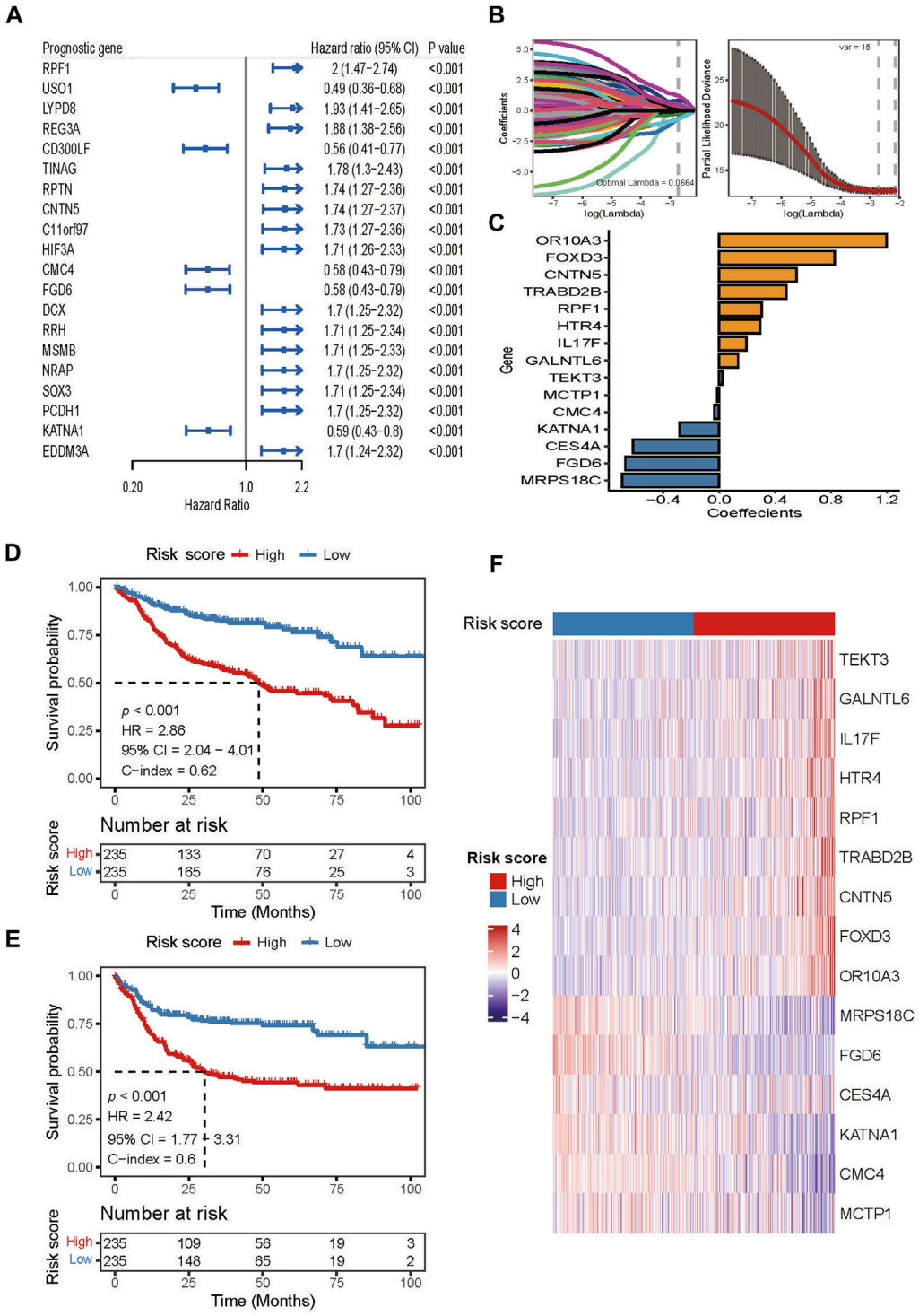

FIGURE 3
Construction of the risk score model in the training dataset. **(A)** Top 20 of the 108 prognosis-related DEGs identified by univariable Cox regression analysis. **(B)** LASSO regression analysis of the 108 prognosis-related DEGs. **(C)** Fifteen DEGs and their coefficients used for constructing the risk score. **(D,E)** Kaplan-Meier curves of OS and PFS of patients in the training dataset assigned to high and low-risk groups. **(F)** Heatmap of gene expression patterns of the 15 model-used genes in patients assigned to high- and low-risk groups.

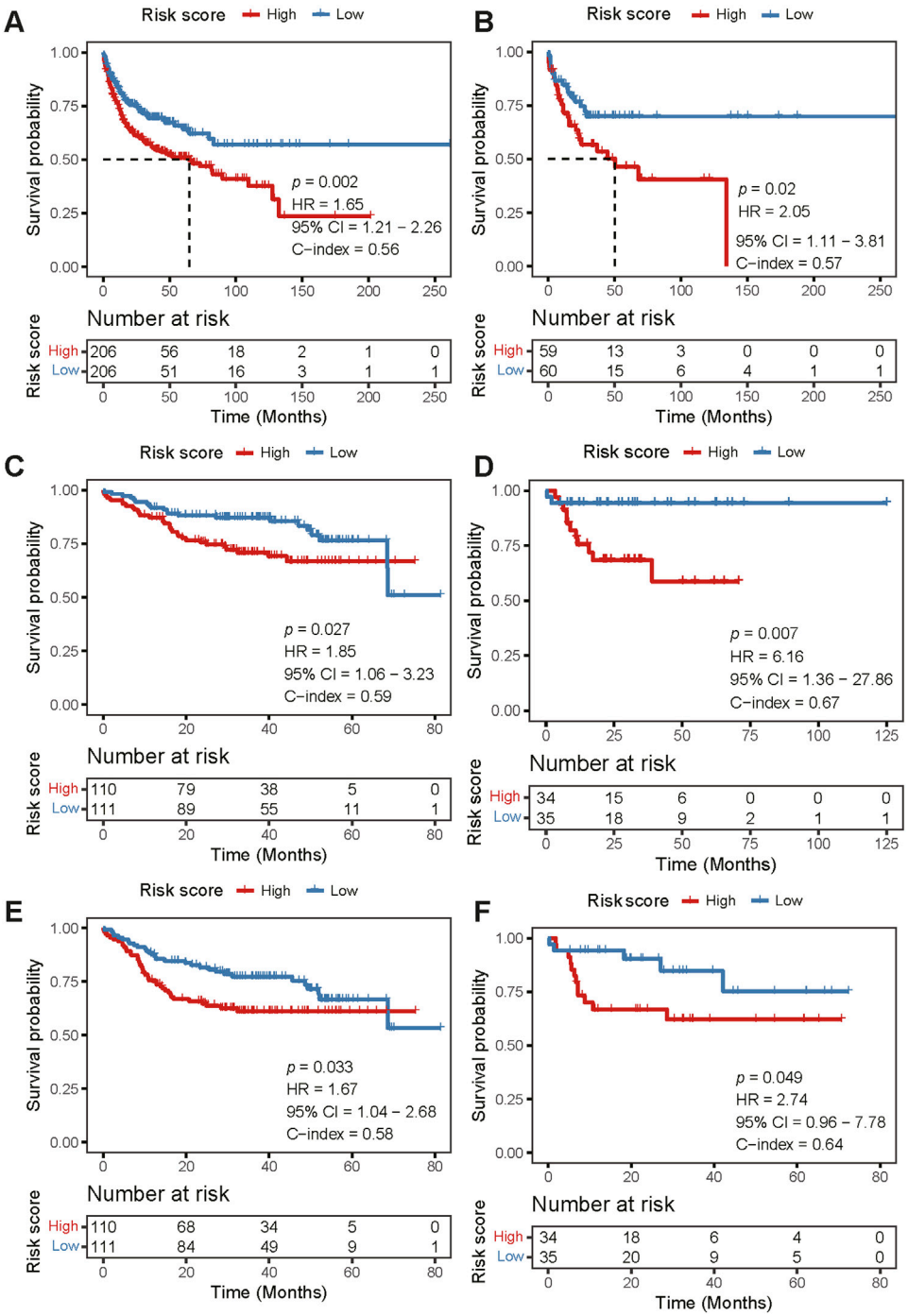

FIGURE 4
External validation of the risk score model. **(A–D)** Kaplan-Meier curve analysis of OS between the high- and low-risk groups in four independent validation cohorts [GSE10846 **(A)**, GSE53786 **(B)**, GSE87371 **(C)**, and GSE23501 **(D)**, respectively]. **(E,F)** Kaplan-Meier curve analysis of PFS between the high- and low-risk groups in two independent cohorts [GSE87371 **(E)** and GSE23501 **(F)**, respectively]. There was no PFS information in GSE10846 and GSE53786. OS, overall survival; PFS, progression-free survival.

gene expression heatmap revealed that the high expressions of genes, *OR10A3*, *FOXD3*, *CNTN5*, *TRABD2B*, *RPF1*, *HTR4*, *IL17F*, *GALNTL6*, and *TEKT3* were observed in the high-risk group, while in the low-risk group, *MCTP1*, *CMC4*, *KATNA1*, *CES4A*, *FGD6*, and *MRPS18C* were highly expressed (Figure 3F).

Validation of risk score model in the independent validation cohorts

We further validated the risk score model in four external cohorts, the robustness of the prognostic model was supported by significant prognostic values for OS in GSE10846 (HR 1.65, 95% CI 1.21–2.26; $p = 0.002$; Figure 4A), GSE53786 (HR 2.05, 95% CI 1.11–3.81; $p = 0.02$; Figure 4B), GSE87371 (HR 1.85, 95% CI 1.06–3.23; $p = 0.027$; Figure 4C), and GSE23051 (HR 6.16, 95% CI 1.36–27.86; $p = 0.007$; Figure 4D). For PFS validation, the results showed the same trend with statistical significance (GSE87371: HR 1.67, 95% CI 1.04–2.68; $p = 0.033$; Figure 4E; GSE23051: HR 2.74, 95% CI 0.96–7.78; $p = 0.049$; Figure 4F). In the validation datasets, the AUCs of the model were higher in GSE23501 for both OS (Supplementary Figures S2C–F) and PFS (Supplementary Figures S2G, H) for 1-, 3-, and 5- years. Therefore, compared with the high-risk group, patients in the low-risk group had better outcomes, indicating the predictive potential of our model.

Independent prognostic role of the risk score model

The independent prognostic value of the model was further studied, taking into consideration of age, sex, stage, ECOG, and IPI. The risk score was verified to be an independent prognostic factor of OS in all cohorts in both univariable and multivariable Cox regression analyses ($p < 0.05$; Supplementary Figures S3A–E) and an independent prognostic factor of PFS in GSE31312 ($p < 0.001$; Supplementary Figure S3F) and GSE87371 ($p = 0.015$; Supplementary Figure S3G). As expected, IPI was also an independent factor to predict PFS and OS (Supplementary Figure S3).

Association between clinicopathological characteristics and risk score

Further analysis of clinical characteristics showed that the risk score was higher in patients with the following characteristics: age >60 years ($p = 0.0018$), stage III/IV disease ($p = 0.029$), >1 extranodal sites ($p = 0.024$), higher IPI scores ($p = 0.00017$), or cluster C ($p < 0.01$) (Supplementary Figure S4).

Association between drug sensitivity and risk score

All patients in the training cohort were treated with the R-CHOP regimen, the first-line standard-of-care treatment for DLBCL (25). We studied the response rates to the R-CHOP in the high- and low-risk groups. We found that the complete response (CR) rate was higher in the low-risk group (82.1% vs. 68.5%, $p = 0.0042$; Figure 5A). Then, we used the data from the GDSC database to predict the response to targeted agents in the two risk groups (Figure 5B). The estimated IC50s for BCL2i (ABT.263) and BTKi (LFM.A13) were lower in the high-risk group ($p < 0.05$), while estimated IC50s for PI3K inhibitor (PI3Ki and AZD6482) and proteasome inhibitors (Bortezomib) were lower in the low-risk group ($p < 0.05$).

Characteristics of immune cell infiltration of the two risk score groups

Tumor-infiltrating immune cells (TIICs), a component of the tumor microenvironment (TME), have been found to be associated with prognosis and treatment response. To explore the relationship between the risk score and TIICs, we analyzed the discrepancy of immune cell infiltration between two risk groups according to the LM22 gene signature[24] (Figure 6A). The proportion of naïve B cells, eosinophils, M1 Macrophages, activated CD4 memory T cells, resting CD4 memory T cells, follicular helper T cells, M0 Macrophages, and gamma delta (γδ) T cells were significantly higher in the low-risk group ($p < 0.05$). By contrast, neutrophils, resting NK cells, naïve CD4 T cells, and regulatory T cells (T-regs) were notably higher in the high-risk group ($p < 0.05$). In the training cohort, M1 macrophages, memory B cells, γδ T cells, activated CD4 memory T cells, neutrophils, and CD8 T cells were found at the core of the correlation network (Figure 6B). The correlation heatmap showed that activated CD4 memory T cells correlated positively with γδ T cells and negatively with T-regs (Figure 6C, Supplementary Figure S5). Altogether, these results suggest a remarkable discrepancy in immune cell infiltration between the high- and low-risk groups while the potential mechanism may be complex.

Discussion

DLBCL is a challenge in individualized treatments due to its significant heterogeneity. Although R-CHOP can cure over 60% of patients (2, 3) using traditional stratification systems like IPI (26) and COO (5, 6), a limitation of these systems is evident, either neglect biological factors (26) or only focus on the BCR signal (7, 8). Importantly, none of them can predict drug response. Metabolic signatures have been proposed for prognosis in many other neoplasms (18, 19, 27, 28) but not in DLBCL yet. Therefore, we distinguished three metabolic subtypes with different prognoses in DLBCL. Among them, 108 prognosis-associated DEGs were identified, of which

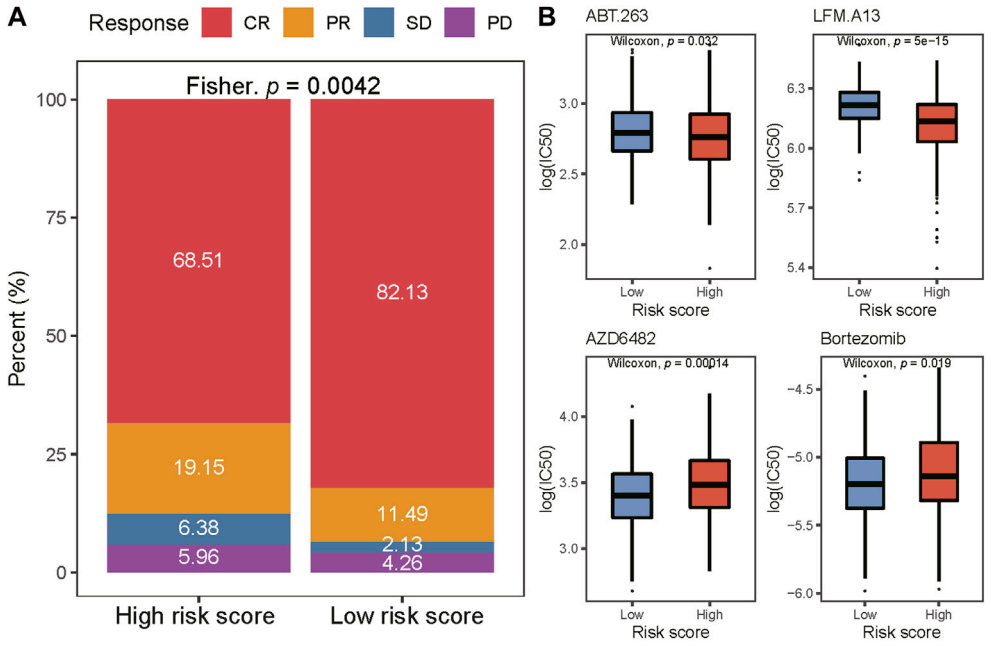

FIGURE 5
Comparison of drug sensitivity between two risk groups. **(A)** Distribution of CR, PR, SD, and PD in two risk groups. CR complete response; PR partial response; SD stable disease; PD progressive disease. **(B)** The IC50 of ABT263., LFM. A13, AZD6482, and Bortezomib in low-and high-risk groups. IC50, the half maximal-inhibitory concentration.

15 genes were used to construct a risk score model of DLBCL. The model showed a robust ability to predict the outcomes of DLBCL independently. As expected, there were distinctly different immune cell infiltration and clinicopathological characteristics between the high- and low-risk groups. The results also imply that patients in the high-risk group predictively respond to BCL2 and BTK inhibitors, while patients in the low-risk group might consider PI3Ki and proteasome inhibitors.

In this study, we explored the metabolic genetic features in DLBCL and identified three subtypes of patients with distinct survival. The most distinct differences were in cluster C, which had the shortest OS with lower expression of genes in nucleotide metabolism, TCA cycle, or amino acid metabolism and higher expression of genes in the integration of energy and vitamin cofactor metabolism. Interestingly, another metabolic expression subtype of 32 cancers also showed the clinical outcomes of subtypes with upregulated vitamin/cofactor metabolism were worse, while subtypes with upregulated nucleotide metabolism had a better prognosis (16). However, there were some inconsistent results. For instance, increased expressions of numerous nucleotide metabolism genes were associated with worse outcomes in breast cancer patients (29). The inconsistency may attribute to the following reasons: 1) previous studies merely focused on one or several metabolites and genes of an individual metabolic pathway (29,30,31), 2) signaling pathways may interact with each other (20, 32), and 3) the same signaling could play distinct roles in different diseases. In summary, the results suggest metabolic heterogeneity in DLBCL can be used for prognostic stratification though it needs more validation.

Based on DEGs among the three metabolic subtypes, a risk score model of 15 genes was developed. Among the 15 genes, *OR10A3*, *FOXD3*, *CNTN5*, *TRABD2B*, *RPF1*, *HTR4*, *IL17F*, *GALNTL6*, and *TEKT3* were highly expressed in the high-risk group, which was associated with poor prognosis, while the high expression of *MRPS18C*, *FGD6*, *CES4A*, *KATNA1*, *CMC4*, and *MCTP1* were characterized in the low-risk group and related to favorable prognosis. Among the poor prognosis-related genes, *TRABD2B* (also known as *TIKI2*), *IL17F*, and *GALNTL6* were reported to be related to the oncogenesis of renal cell carcinoma (33), cutaneous T-cell lymphoma (34), and thyroid carcinoma (35), respectively. Moreover, the mutations in *CNTN5* were reported to contribute to the metastatic process of pancreatic cancer (36), *HTR4* was found predominantly in only high-grade prostate cancer (37, 38), and the high expression of *TEKT3* could be influenced by HBV integration events in liver cancer (39). Therefore, these genes promoting pathogenesis or progression in several cancers may also lead to poor survival in DLBCL. However, *FOXD3*, a poor prognosis gene in our model, was reported as a suppressor factor of *H pylori* infection-induced gastric carcinoma (40) and melanoma (41). One possible

10.3389/pore.2023.1610819

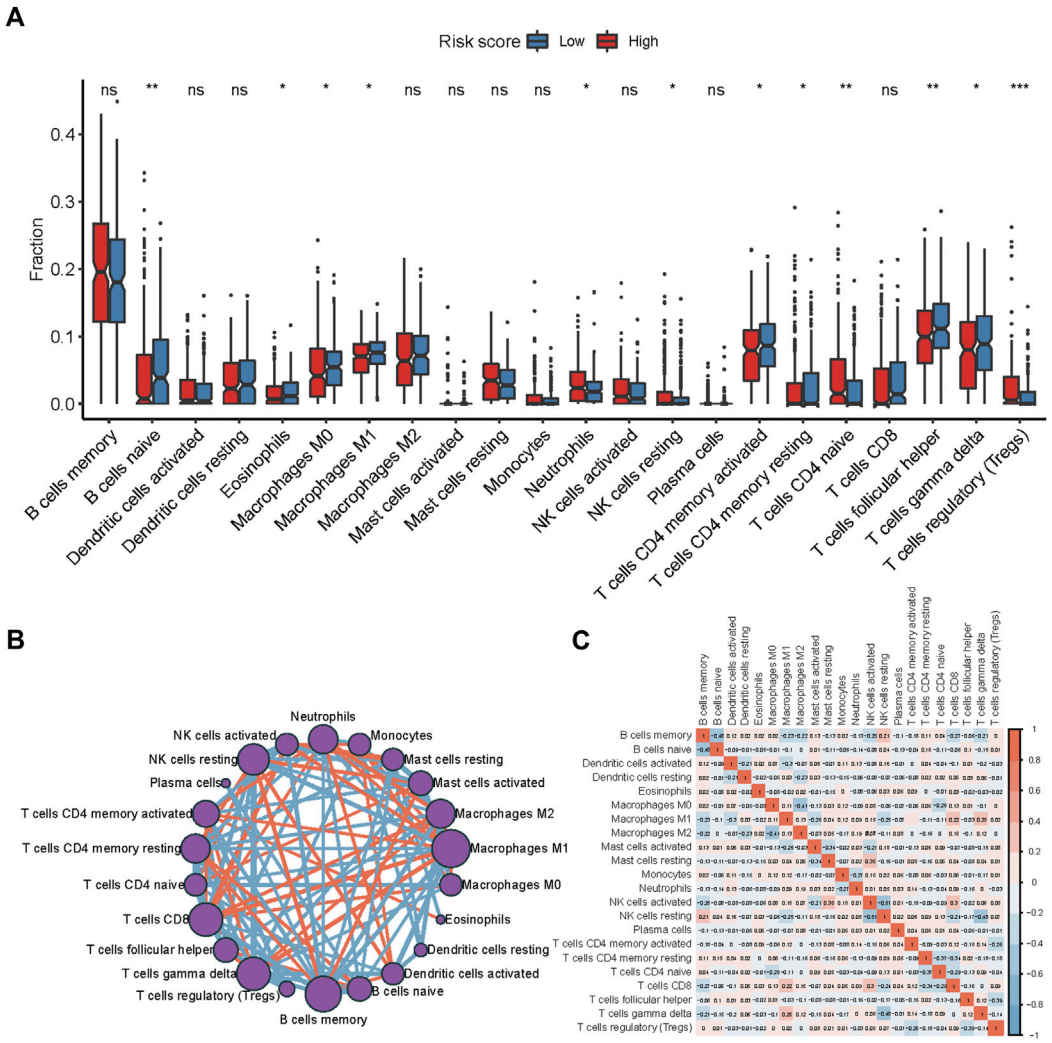

FIGURE 6
Immune cell infiltration discrepancy between two risk groups. **(A)** Comparison of the infiltration of 22 types of immune cells in the low- and high-risk groups. *$p < 0.05$; **$p < 0.01$; ***$p < 0.001$ by the Wilcoxon test. **(B)** Chord diagram of the correlation among 22 leukocyte subtypes in patients from the GSE31312 cohort. **(C)** The correlation diagram of the immune cells from the GSE31312 cohort.

explanation for this difference is the dual role of forkhead Box D3 encoded by *FOXD3*. Forkhead Box D3, a member of the forkhead family of transcription factors, can function as both a transcriptional repressor and activator. Of the favorable prognosis-related genes, previous studies have reported that the downregulated *MCTP1* was related to drug-resistance of esophageal cancer (42), and *MRPS18C* was the least expressed MRPS18 family member in malignantly transformed B-cells (43). Thus, the higher expression of these genes may be associated with favorable prognosis. The expression of *FGD* genes, a gene family comprising *FGD6*, were analyzed to predict the OS of head and neck squamous cell carcinoma (HNSC) (44), in which the OS was positively related to high expression of *FGD2* and *FGD3* but not *FGD6*. The favorable effect of *FGD6* on prognosis in DLBCL needs further investigation. In addition, the over-expression of *CMC4* (also known as *MTCP1*), as a favorable prognosis gene in our model, was discordantly reported to produce clonal $CD5^+/CD19^+$ leukemia in mice (45), which was thought to be a chronic lymphocytic leukemia driving gene. For the remaining genes, *OR10A3*, *RPF1*, *KATNA1*, and *CES4A*, in our risk score model, no specific relationship to cancer had been reported yet, further exploration should be carried out for their roles in the prognosis in DLBCL patients.

The relationship of risk score with clinical characteristics and treatment response was explored in our study. Patients with an age older than 60 years, advanced stage (stage III/IV), and high

IPI scores had higher risk scores. Older than 60 years, LDH (lactate dehydrogenase) greater than normal, PS score of 2–4 points, stage III/IV, and more than 1 extranodal sites are well-known high-risk factors in DLBCL (4), which is consistent with our results. Meanwhile, a greater proportion of patients in the cluster C subtype was observed in the high-risk group, which is also consistent with our result that cluster C was a poor prognosis factor in our research. In addition, our results showed that low-risk patients had a significantly higher CR rate than high-risk patients after R-CHOP treatment. Previous studies have confirmed that the higher CR/CRu rate of DLBCL patients after chemotherapy would improve the overall survival (46, 47), suggesting that the higher sensitivity to the R-CHOP regimen in the low-risk group may be another reason for its favorable prognosis.

DLBCL is a heterogeneous lymphoma (48). In this study, we observed immune cell infiltration discrepancy in two risk groups. A higher proportion of activated CD4 memory T cells, M1 macrophages, and γδ T cells were in the low-risk group relevant to better prognosis. These results were consistent with previous studies. Chen et al. reported that when patients had a higher proportion of CD4 memory T cells and γδ T cells, they were more sensitive to R-CHOP regimen so that more patients achieved CR/PR (49). Another study also showed that activated CD4 memory T cell was an independent factor of favorable prognosis in DLBCL patients (50). The reason may be that after chemotherapy, $CD4^+$ T cells can produce multiple proinflammatory cytokines including IFNγ, TNFα, and IL2 (51). These factors may allow patients to achieve durable remissions through $CD8^+$ effector cell-mediated antitumor immunity (51). For γδ T cells, their cytotoxic effect and ability to secrete IFN can generate antitumor effects (52). Its subgroup, Vγ9Vδ2T cells, can increase antibody dependent cellular cytotoxicity (ADCC) of rituximab and further enhance the efficacy of the R-CHOP regimen (53). Meanwhile, Yan et al. (54) found that M1 macrophage infiltration was related to a lower risk of progression and improved overall survival, as FCγR-dependent stimulation of M1 macrophage mediated ADCP (antibody-dependent cellular phagocytosis) maintained anti-lymphoma activity. In addition, T-regs were highly expressed in the high-risk group, suggesting that T-regs are relevant to poor prognosis. The prognostic role of T-regs is now a matter of debate. Autio et al. (55) found in the Nordic Lymphoma Group trial cohort (NCT01325194), a higher proportion of T-regs was associated with worse prognosis, but this could not be repeated in the Helsinki study cohort (NCT01502982). These controversial results may be caused by the heterogeneity of DLBCL. Interestingly, in this study, we found that CD4 memory-activated T cells were positively related to γδ T cells but negatively correlated with T-regs. This mechanism of the correlation between those immune cells is needed in the future.

In our study, we also explored the potential response of the high- and low-risk groups to targeted drugs, in which BCL2 inhibitor and PI3K inhibitor were suggested for the high- and low-risk groups, respectively. Interestingly, in the previous classification based on genetic heterogeneity (3), the BCL2 SVs were associated with poor outcomes of GCB-DLBCLs and PI3K with good-risk GCB-DLBCLs, while BCL2 was considered in the EZB subtype of DLBCL with favorable outcomes in another genetic classification (56). A therapeutic classification of DLBCL was constructed based on the responses to drugs targeted at genetic alteration (57) and both BCL2 inhibitor and PI3K inhibitor were suggested for the MCD subgroup with poor survival and EZB subgroup with good survival. Hopefully, combining the study of Chapuy et al. (3), our results would provide more clues to make the decision of treatment for DLBCL.

Some limitations are in our study. Although we included a total of 1,291 patients and 4 independent validation sets, which suggests that the results may be highly reliable, the risk score model should be further verified through a prospective study. Second, our study was based on bioinformatic analyses of public data, while validations by clinical specimens are needed to be studied. Last, the mechanism of how the 15 genes in the risk score model affect prognosis in DLBCL needs to be further explored.

Conclusion

Overall, we identified three metabolic subtypes in DLBCL patients with different clinical outcomes and further constructed a prognostic 15-gene model based on DEGs among the three subtypes, which indicates that the differentially expressed gene profile of metabolic heterogeneity may provide a new strategy for prognosis stratification in DLBCL patients. Additionally, the risk score model demonstrated a remarkable predictive value of survival and drug sensitivity, which may benefit individualized prognosis management and personalized therapeutic intervention in DLBCL.

Data availability statement

The datasets generated and analyzed in the present study are available in the public data repository, GEO: https://www.ncbi.nlm.nih.gov/geo/.

Author contributions

JH, PG, YuL, XJ, and KL: processing data and conducting bioinformatic analysis. NZ, SX, CZ, and GW: writing original draft of the manuscript. XZ, HH, YC, HL, WW, CX, and YH:

reviewing and editing the manuscript. SC: final review of the manuscript. YaL: conception, design, supervision, and funding acquisition. All authors contributed to the article and approved the submitted version.

Funding

This study was supported by 2018 Entrepreneurial Leading Talent of Guangzhou Huangpu District and Guangzhou Development District (No. 2022-L023).

Conflict of interest

Authors YuL, XJ, KL, GW, XZ, HL, YH, and SC were employed by the company Burning Rock Biotech.

The remaining authors declare that the research was conducted in the absence of any commercial or financial relationships that could be construed as a potential conflict of interest.

Acknowledgments

We thank Wenchuan Xie, Jing Zhao and Leo Li for their useful discussion and suggestions.

Supplementary material

The Supplementary Material for this article can be found online at: https://www.por-journal.com/articles/10.3389/pore.2023.1610819/full#supplementary-material

References

1. Susanibar-Adaniya S, Barta SK. 2021 update on diffuse large B cell lymphoma: A review of current data and potential applications on risk stratification and management. *Am J Hematol* (2021) 96(5):617–29. doi:10.1002/ajh.26151

2. Liu Y, Barta SK. Diffuse large B-cell lymphoma: 2019 update on diagnosis, risk stratification, and treatment. *Am J Hematol* (2019) 94(5):604–16. doi:10.1002/ajh.25460

3. Chapuy B, Stewart C, Dunford AJ, Kim J, Kamburov A, Redd RA, et al. Molecular subtypes of diffuse large B cell lymphoma are associated with distinct pathogenic mechanisms and outcomes. *Nat Med* (2018) 24(5):679–90. doi:10.1038/s41591-018-0016-8

4. International Non-Hodgkin's Lymphoma Prognostic Factors Project. A predictive model for aggressive non-Hodgkin's lymphoma. *New Engl J Med* (1993) 329(14):987–94. doi:10.1056/NEJM199309303291402

5. Hans CP, Weisenburger DD, Greiner TC, Gascoyne RD, Delabie J, Ott G, et al. Confirmation of the molecular classification of diffuse large B-cell lymphoma by immunohistochemistry using a tissue microarray. *Blood* (2004) 103(1):275–82. doi:10.1182/blood-2003-05-1545

6. Rosenwald A, Wright G, Chan WC, Connors JM, Campo E, Fisher RI, et al. The use of molecular profiling to predict survival after chemotherapy for diffuse large-B-cell lymphoma. *New Engl J Med* (2002) 346(25):1937–47. doi:10.1056/NEJMoa012914

7. Miao Y, Medeiros LJ, Xu-Monette ZY, Li J, Young KH. Dysregulation of cell survival in diffuse large B cell lymphoma: Mechanisms and therapeutic targets. *Front Oncol* (2019) 9:107. doi:10.3389/fonc.2019.00107

8. Ruminy P, Etancelin P, Couronné L, Parmentier F, Rainville V, Mareschal S, et al. The isotype of the BCR as a surrogate for the GCB and ABC molecular subtypes in diffuse large B-cell lymphoma. *Leukemia* (2011) 25(4):681–8. doi:10.1038/leu.2010.302

9. Wilson WH, Young RM, Schmitz R, Yang Y, Pittaluga S, Wright G, et al. Targeting B cell receptor signaling with ibrutinib in diffuse large B cell lymphoma. *Nat Med* (2015) 21(8):922–6. doi:10.1038/nm.3884

10. Hanahan D, Weinberg RA. Hallmarks of cancer: The next generation. *Cell* (2011) 144(5):646–74. doi:10.1016/j.cell.2011.02.013

11. Vander Heiden MG, Cantley LC, Thompson CB. Understanding the Warburg effect: The metabolic requirements of cell proliferation. *Science (New York, NY)* (2009) 324(5930):1029–33. doi:10.1126/science.1160809

12. Martinez-Reyes I, Chandel NS. Cancer metabolism: Looking forward. *Nat Rev Cancer* (2021) 21(10):669–80. doi:10.1038/s41568-021-00378-6

13. Fendt SM, Frezza C, Erez A. Targeting metabolic plasticity and flexibility dynamics for cancer therapy. *Cancer Discov* (2020) 10(12):1797–807. doi:10.1158/2159-8290.CD-20-0844

14. Ricci JE, Chiche J. Metabolic reprogramming of non-hodgkin's B-cell lymphomas and potential therapeutic strategies. *Front Oncol* (2018) 8:556. doi:10.3389/fonc.2018.00556

15. Gaude E, Frezza C. Tissue-specific and convergent metabolic transformation of cancer correlates with metastatic potential and patient survival. *Nat Commun* (2016) 7:13041. doi:10.1038/ncomms13041

16. Peng X, Chen Z, Farshidfar F, Xu X, Lorenzi PL, Wang Y, et al. Molecular characterization and clinical relevance of metabolic expression subtypes in human cancers. *Cell Rep* (2018) 23(1):255–69.e4. doi:10.1016/j.celrep.2018.03.077

17. Sung JY, Cheong JH. Pan-cancer analysis reveals distinct metabolic reprogramming in different epithelial-mesenchymal transition activity states. *Cancers (Basel)* (2021) 13(8):1778. doi:10.3390/cancers13081778

18. Cui L, Xue H, Wen Z, Lu Z, Liu Y, Zhang Y. Prognostic roles of metabolic reprogramming-associated genes in patients with hepatocellular carcinoma. *Aging (Albany NY)* (2020) 12(21):22199–219. doi:10.18632/aging.104122

19. Tan Z, Lei Y, Xu J, Shi S, Hua J, Zhang B, et al. The value of a metabolic reprogramming-related gene signature for pancreatic adenocarcinoma prognosis prediction. *Aging (Albany NY)* (2020) 12(23):24228–41. doi:10.18632/aging.104134

20. Zhang Z, Zhu H, Li Q, Gao W, Zang D, Su W, et al. Gene expression profiling of tricarboxylic acid cycle and one carbon metabolism related genes for prognostic risk signature of colon carcinoma. *Front Genet* (2021) 12:647152. doi:10.3389/fgene.2021.647152

21. Caro P, Kishan AU, Norberg E, Stanley IA, Chapuy B, Ficarro SB, et al. Metabolic signatures uncover distinct targets in molecular subsets of diffuse large B cell lymphoma. *Cancer cell* (2012) 22(4):547–60. doi:10.1016/j.ccr.2012.08.014

22. Cokelaer T, Chen E, Iorio F, Menden MP, Lightfoot H, Saez-Rodriguez J, et al. GDSCTools for mining pharmacogenomic interactions in cancer. *Bioinformatics* (2018) 34(7):1226–8. doi:10.1093/bioinformatics/btx744

23. Geeleher P, Cox N, Huang RS. pRRophetic: an R package for prediction of clinical chemotherapeutic response from tumor gene expression levels. *PLoS One* (2014) 9(9):e107468. doi:10.1371/journal.pone.0107468

24. Newman AM, Liu CL, Green MR, Gentles AJ, Feng W, Xu Y, et al. Robust enumeration of cell subsets from tissue expression profiles. *Nat Methods* (2015) 12(5):453–7. doi:10.1038/nmeth.3337

25. Visco C, Li Y, Xu-Monette ZY, Miranda RN, Green TM, Li Y, et al. Comprehensive gene expression profiling and immunohistochemical studies support application of immunophenotypic algorithm for molecular subtype classification in diffuse large B-cell lymphoma: A report from the international DLBCL rituximab-CHOP consortium program study. *Leukemia* (2012) 26(9):2103–13. doi:10.1038/leu.2012.83

26. Ruppert AS, Dixon JG, Salles G, Wall A, Cunningham D, Poeschel V, et al. International prognostic indices in diffuse large B-cell lymphoma: A comparison of IPI, R-IPI, and NCCN-IPI. *Blood* (2020) 135(23):2041–8. doi:10.1182/blood.2019002729

27. Nie Y, Liu L, Liu Q, Zhu X. Identification of a metabolic-related gene signature predicting the overall survival for patients with stomach adenocarcinoma. *PeerJ* (2021) 9:e10908. doi:10.7717/peerj.10908

28. Zhang ZY, Yao QZ, Liu HY, Guo QN, Qiu PJ, Chen JP, et al. Metabolic reprogramming-associated genes predict overall survival for rectal cancer. *J Cel Mol Med* (2020) 24(10):5842–9. doi:10.1111/jcmm.15254

29. Kollareddy M, Dimitrova E, Vallabhaneni KC, Chan A, Le T, Chauhan KM, et al. Regulation of nucleotide metabolism by mutant p53 contributes to its gain-of-function activities. *Nat Commun* (2015) 6:7389. doi:10.1038/ncomms8389

30. Cao Y, Chen P, Cai M, Shi Q, Xu P, Wang L, et al. Prognostic impact of B-vitamins involved in one-carbon metabolism in patients with diffuse large B-cell lymphoma. *Hematol Oncol* (2020) 38(4):456–66. doi:10.1002/hon.2752

31. Shen N, Korm S, Karantanos T, Li D, Zhang X, Ritou E, et al. DLST-dependence dictates metabolic heterogeneity in TCA-cycle usage among triple-negative breast cancer. *Commun Biol* (2021) 4(1):1289. doi:10.1038/s42003-021-02805-8

32. Vacanti NM, Divakaruni AS, Green CR, Parker SJ, Henry RR, Ciaraldi TP, et al. Regulation of substrate utilization by the mitochondrial pyruvate carrier. *Mol Cel* (2014) 56(3):425–35. doi:10.1016/j.molcel.2014.09.024

33. Yuan X, Dong B, Xu Y, Dong L, Huang J, Zhang J, et al. TIKI2 is upregulated and plays an oncogenic role in renal cell carcinoma. *Oncotarget* (2016) 7(13): 17212–9. doi:10.18632/oncotarget.7873

34. Krejsgaard T, Litvinov IV, Wang Y, Xia L, Willerslev-Olsen A, Koralov SB, et al. Elucidating the role of interleukin-17F in cutaneous T-cell lymphoma. *Blood* (2013) 122(6):943–50. doi:10.1182/blood-2013-01-480889

35. Iqbal MA, Li M, Lin J, Zhang G, Chen M, Moazzam NF, et al. Preliminary study on the sequencing of whole genomic methylation and transcriptome-related genes in thyroid carcinoma. *Cancers (Basel)* (2022) 14(5):1163. doi:10.3390/cancers14051163

36. Yachida S, Jones S, Bozic I, Antal T, Leary R, Fu B, et al. Distant metastasis occurs late during the genetic evolution of pancreatic cancer. *Nature* (2010) 467(7319):1114–7. doi:10.1038/nature09515

37. Dizeyi N, Bjartell A, Hedlund P, Taskén KA, Gadaleanu V, Abrahamsson PA. Expression of serotonin receptors 2B and 4 in human prostate cancer tissue and effects of their antagonists on prostate cancer cell lines. *Eur Urol* (2005) 47(6): 895–900. doi:10.1016/j.eururo.2005.02.006

38. Nakamura Y, Ise K, Yamazaki Y, Fujishima F, McNamara KM, Sasano H. Serotonin receptor 4 (5-hydroxytryptamine receptor Type 4) regulates expression of estrogen receptor beta and cell migration in hormone-naive prostate cancer. *Indian J Pathol Microbiol* (2017) 60(1):33–7. doi:10.4103/0377-4929.200022

39. Zapatka M, Borozan I, Brewer DS, Iskar M, Grundhoff A, Alawi M, et al. The landscape of viral associations in human cancers. *Nat Genet* (2020) 52(3):320–30. doi:10.1038/s41588-019-0558-9

40. Cheng AS, Li MS, Kang W, Cheng VY, Chou JL, Lau SS, et al. *Helicobacter pylori* causes epigenetic dysregulation of FOXD3 to promote gastric carcinogenesis. *Gastroenterology* (2013) 144(1):122–33. doi:10.1053/j.gastro.2012.10.002

41. Rosenbaum SR, Knecht M, Mollaee M, Zhong Z, Erkes DA, McCue PA, et al. FOXD3 regulates VISTA expression in melanoma. *Cel Rep* (2020) 30(2):510–24. doi:10.1016/j.celrep.2019.12.036

42. Kong L, Yang W, Chen L, Qian L. The DNA methylation-regulated MCTP1 activates the drug-resistance of esophageal cancer cells. *Aging (Albany NY)* (2021) 13(3):3342–52. doi:10.18632/aging.104173

43. Kovalevska L, Kashuba E. Expression pattern of MRPS18 family genes in malignantly transformed b-cells. *Exp Oncol* (2020) 42(4):295–9. doi:10.32471/exp-oncology.2312-8852.vol-42-no-4.15366

44. Ma C, Li H, Li X, Lu S, He J. The prognostic value of faciogenital dysplasias as biomarkers in head and neck squamous cell carcinoma. *Biomarkers Med* (2019) 13(16):1399–415. doi:10.2217/bmm-2019-0273

45. Walker JS, Hing ZA, Sher S, Cronin J, Williams K, Harrington B, et al. Rare t(X;14)(q28;q32) translocation reveals link between MTCP1 and chronic lymphocytic leukemia. *Nat Commun* (2021) 12(1):6338. doi:10.1038/s41467-021-26400-x

46. Pfreundschuh M, Kuhnt E, Trumper L, Osterborg A, Trneny M, Shepherd L, et al. CHOP-Like chemotherapy with or without rituximab in young patients with good-prognosis diffuse large-B-cell lymphoma: 6-year results of an open-label randomised study of the MabThera international trial (MInT) group. *Lancet Oncol* (2011) 12(11):1013–22. doi:10.1016/S1470-2045(11)70235-2

47. Pfreundschuh M, Trumper L, Osterborg A, Pettengell R, Trneny M, Imrie K, et al. CHOP-Like chemotherapy plus rituximab versus CHOP-like chemotherapy alone in young patients with good-prognosis diffuse large-B-cell lymphoma: A randomised controlled trial by the MabThera international trial (MInT) group. *Lancet Oncol* (2006) 7(5):379–91. doi:10.1016/S1470-2045(06)70664-7

48. Lang R, Gill MJ. Diffuse large B-cell lymphoma. *New Engl J Med* (2021) 384(23):2261–2. doi:10.1056/NEJMc2105452

49. Chen W, Liang W, He Y, Liu C, Chen H, Lv P, et al. Immune microenvironment-related gene mapping predicts immunochemotherapy response and prognosis in diffuse large B-cell lymphoma. *Med Oncol* (2022) 39(4):44. doi:10.1007/s12032-021-01642-3

50. Keane C, Gill D, Vari F, Cross D, Griffiths L, Gandhi M. CD4(+) tumor infiltrating lymphocytes are prognostic and independent of R-IPI in patients with DLBCL receiving R-CHOP chemo-immunotherapy. *Am J Hematol* (2013) 88(4): 273–6. doi:10.1002/ajh.23398

51. Emens LA. Chemoimmunotherapy. *Cancer J* (2010) 16(4):295–303. doi:10.1097/PPO.0b013e3181eb5066

52. Zhao Y, Niu C, Cui J. Gamma-delta (γδ) T cells: Friend or foe in cancer development? *J translational Med* (2018) 16(1):3. doi:10.1186/s12967-017-1378-2

53. Tokuyama H, Hagi T, Mattarollo SR, Morley J, Wang Q, So HF, et al. V gamma 9 V delta 2 T cell cytotoxicity against tumor cells is enhanced by monoclonal antibody drugs-rituximab and trastuzumab. *Int J Cancer* (2008) 122(11):2526–34. doi:10.1002/ijc.23365

54. Yan M, Chang YM, Raghavan V, Dong E, Klein C, Nielsen TG, et al. Lymphoma microenvironment deconvolution links M1 macrophage infiltration to clinical outcome in diffuse large B-cell lymphoma. *Blood* (2020) 136(1):29–30. doi:10.1182/blood-2020-134867

55. Autio M, Leivonen SK, Bruck O, Mustjoki S, Meszaros Jorgensen J, Karjalainen-Lindsberg ML, et al. Immune cell constitution in the tumor microenvironment predicts the outcome in diffuse large B-cell lymphoma. *Haematologica* (2021) 106(3):718–29. doi:10.3324/haematol.2019.243626

56. Schmitz R, Wright GW, Huang DW, Johnson CA, Phelan JD, Wang JQ, et al. Genetics and pathogenesis of diffuse large B-cell lymphoma. *New Engl J Med* (2018) 378(15):1396–407. doi:10.1056/NEJMoa1801445

57. Wright GW, Huang DW, Phelan JD, Coulibaly ZA, Roulland S, Young RM, et al. A probabilistic classification tool for genetic subtypes of diffuse large B cell lymphoma with therapeutic implications. *Cancer cell* (2020) 37(4):551–68. doi:10.1016/j.ccell.2020.03.015

Pathology & Oncology Research | frontiers

TYPE Original Research
PUBLISHED 05 July 2024
DOI 10.3389/pore.2024.1611747

Check for updates

OPEN ACCESS

EDITED BY
Anna Sebestyén,
Semmelweis University, Hungary

*CORRESPONDENCE
Adrienn Márton,
martonadika@gmail.com

RECEIVED 26 February 2024
ACCEPTED 12 June 2024
PUBLISHED 05 July 2024

CITATION
Márton A, Veres KB, Erdődi F, Udvardy M, Illés Á and Rejtő L (2024), The roles of phosphorylation of signaling proteins in the prognosis of acute myeloid leukemia.
Pathol. Oncol. Res. 30:1611747.
doi: 10.3389/pore.2024.1611747

COPYRIGHT
© 2024 Márton, Veres, Erdődi, Udvardy, Illés and Rejtő. This is an open-access article distributed under the terms of the Creative Commons Attribution License (CC BY). The use, distribution or reproduction in other forums is permitted, provided the original author(s) and the copyright owner(s) are credited and that the original publication in this journal is cited, in accordance with accepted academic practice. No use, distribution or reproduction is permitted which does not comply with these terms.

The roles of phosphorylation of signaling proteins in the prognosis of acute myeloid leukemia

Adrienn Márton[1,2]*, Katalin Beáta Veres[3], Ferenc Erdődi[4], Miklós Udvardy[1], Árpád Illés[1] and László Rejtő[5]

[1]Division of Hematology, Department of Internal Medicine, Faculty of Medicine, University of Debrecen, Debrecen, Hungary, [2]Kálmán Laki Doctoral School, University of Debrecen, Debrecen, Hungary, [3]Laboratory of Cellular Therapy, MEDYAG Kft, Debrecen, Hungary, [4]Department of Medical Chemistry, Faculty of Medicine, University of Debrecen, Debrecen, Hungary, [5]Department of Hematology, Szabolcs-Szatmár-Bereg County Teaching Hospital, Nyíregyháza, Hungary

Signaling pathways of Retinoblastoma (Rb) protein, Akt-kinase, and Erk-kinase (extracellular signal-regulated kinase) have an important role in the pathogenesis of acute myeloid leukemia. Constitutive activation of these proteins by phosphorylation contributes to cell survival by regulation of cell cycle, proliferation and proapoptotic signaling processes. According to previous data phosphorylated forms of these proteins represent a worse outcome for cancer patients. We investigated the presence of phosphorylated Rb (P-Rb), Akt (P-Akt) and Erk (P-Erk) proteins by Western blot technique using phospho-specific antibodies in bone marrow or peripheral blood samples of 69 AML patients, 36 patients with myelodysplastic syndrome (MDS) and 10 healthy volunteers. Expression level of PTEN (Phosphatase and tensin homolog) and PHLPP (PH domain and leucine-rich repeat Protein Phosphatase) phosphatases, the negative regulators of Akt kinase pathway were also examined. We tested the effect of these proteins on survival and on the correlation with known prognostic features in AML. We found 46.3% of AML patients had detectable P-Rb, 34.7% had P-Akt and 28.9% had P-Erk protein. 66.1% of patients expressing PTEN, 38.9% PHLPP, 37.2% both PTEN and PHLPP and 32.2% neither PTEN nor PHLPP phosphatases. Compared to nucleophosmin mutation (NPMc) negative samples P-Erk was significantly less in nucleophosmin mutated patients, P-Rb was significantly less in patients' group with more than 30 G/L peripheral leukocyte count by diagnosis. PHLPP was significantly present in FAB type M5. The expression of P-Rb represented significant better overall survival (OS), while P-Akt represented significantly worse event-free survival (EFS) in unfavorable cytogenetics patients. The presence of both PHLPP and PTEN phosphatases contributes to better OS and EFS, although the differences were not statistically significant. We confirmed significant positive correlation between P-Akt and PHLPP. Assessing the phosphorylation of Rb, Akt and Erk may define a subgroup of

AML patients who would benefit especially from new targeted treatment options complemented the standard chemotherapy, and it may contribute to monitoring remission, relapse or progression of AML.

KEYWORDS

acute myeloid leukemia, retinoblastoma, AKT, ERK, protein phosphorylation

Introduction

Acute myeloid leukemia (AML) is characterized by clonal malignant proliferation of immature myeloid blast cells. AML may develop by dysregulation of signaling pathways that enhance the proliferation and survival of hematopoietic progenitor cells. Among others, these may include altered activation of oncogenic protein kinase pathways such as mitogen-activated protein kinases (Raf/MEK/Erk or p44/p42) [1], Akt kinase (also termed as protein kinase B, PKB) [2] and dysfunction of tumor suppressor proteins such as retinoblastoma protein (Rb) [3]. These changes may lead to uncontrolled cell growth and attenuate the efficacy of chemotherapeutic treatments contributing to poor prognosis of leukemia patients. The reversible phosphorylation of proteins balanced by protein kinases and protein phosphatases plays a crucial role in the regulation of the above processes [4, 5], therefore selective targeting of these interconverting enzymes in the signaling pathways might represent novel therapeutic possibilities in AML treatment.

Flt3 (Fms-like tyrosine kinase 3) is the most frequently mutated genes in AML [6, 7]. In normal cells, FL-mediated triggering of Flt3 affect the activation of downstream phosphatidylinositol-3-kinase (PI3K)/Akt and Ras/Raf/MEK/Erk pathways [8]. Flt3-internal tandem duplication (ITD) and tyrosine kinase domain (TKD) mutations result in the constitutive activation of Flt3 kinase and its downstream proliferative signaling pathways including the Mitogen-activated protein kinases (MAPKs) and Akt pathway in leukemic blast cells [9–11].

Mitogen-activated protein kinases are members of the serine/threonine specific protein kinase family. MAPKs play an important role in cell proliferation, differentiation, motility and cell death [12, 13]. The MAPK signaling pathways can be activated by several extracellular stimuli including mitogens, growth factors and cytokines [14, 15]. After stimulation, a sequential protein kinase cascade is initiated. In general, the ligand such as epidermal growth factor (EGF) or platelet-derived growth factor (PDGF) binds to their receptor tyrosine kinase that leads to GTP loading and Ras-GTPase activation [16], which recruits Raf to the membrane and results in its activation. Then Raf phosphorylates, thereby activates MEK1/2 which activates Erk1/2 or p44/p42 by phosphorylation of residues Thr202/Tyr204 (Erk1) and Thr185/Tyr187 (Erk2) in the activation loop. The active Erk1/2 translocates to the nucleus [17] and activates various downstream targets including several transcription factors such as Elk-1 [18], c-Fos [19], c-Myc [20]. Inactivation of MAPKs occurs through dephosphorylation by a family of dual-specificity (phospho-Ser/Thr and -Tyr) phosphatases known as mitogen-activated protein kinase phosphatases (MKPs) [21]. Previous data suggest that protein phosphatase-2A (PP2A), one major type of the phospho-Ser/Thr specific protein phosphatase may also take part in the dephosphorylation of Erk1/2 [22, 23].

Akt serine/threonine kinase or PKB plays a crucial role in cell survival by inhibiting apoptosis. Akt phosphorylates and inactivates several proapoptotic proteins, a few examples are Bax, Bad [24] caspase-9 [25], FOXO tumor suppressors [26]. Akt diminishes the cellular level of p53 through Mdm2 activation [27], activates NFκB [28] and CREB [29] transcription factors, thereby increases the transcription of several anti-apoptotic proteins. Akt upregulates the anti-apoptotic Bcl-2 expression through cAMP-response element-binding protein [30]. Akt also plays a role in cell cycle regulation due to preventing glycogen synthase kinase-3beta (GSK-3β) mediated degradation of cyclin D1 [31]. Akt is activated by various growth factors and survival signals that induce the production of phosphatidylinositol (3,4,5)-triphosphate (PIP3) generated by PI3 kinase. PIP3 recruits phosphoinositide-dependent protein kinase 1 (PDK1) and Akt to the plasma membrane, where PDK1 phosphorylates Akt in the activation loop of the kinase domain at Thr308 [32]. Full activation of Akt requires phosphorylation on the regulatory tail at Ser473 by phosphoinositide-dependent protein kinase 2 (PDK2) or mTORC2 [33], which regulates the degree of activation. PTEN phosphatase is a major negative regulator of the PIP3K/Akt pathway [34]. PTEN limits the production of PIP3 by its dephosphorylation. Genetic inactivation of PTEN leads to constitutive activation of the PI3K/Akt pathway [35]. The PH domain and leucine-rich repeat Protein Phosphatase (PHLPP) dephosphorylates Akt directly on Ser473 [36]. Phosphorylation of Akt is also negatively regulated by PP2A [22, 23].

Retinoblastoma protein is the product of a tumor suppressor gene that plays a crucial role in the regulation of differentiation, apoptosis and cell cycle by coordinating the checkpoint in G1/S transition. Loss of Rb function results in cell cycle progression and enhanced proliferation, which has been shown in a variety of human malignancies [37]. The activity of Rb protein is regulated by reversible phosphorylation and dephosphorylation through

protein kinases and protein phosphatases. Hypophosphorylated Rb binds the transcription factor E2F, thereby suppresses the transcription of genes controlling cell cycle such as DNA polymerase alpha [38] and cyclin [39] genes. Rb can interact with chromatin remodeling enzymes, such as histone deacetylase (HDAC) through LXCXE amino acid binding motif [40]. Some studies demonstrated that interaction of Rb with HDAC is required for Rb to inhibit E2F [41]. During the cell cycle, Rb is phosphorylated in a sequential manner by distinct cyclin/cyclin dependent kinase (CDK) complexes [42], thereby Rb is converted to a functionally inactive, phosphorylated state which leads to the release of sequestered E2F [43] inducing G1/S transition and the synthesis of genes in S phase [44]. Rb is phosphorylated up to 16 Ser/Thr residues including Ser249/Thr252, Thr356, Thr373, Ser608, Ser612, Ser780, Ser807/Ser811, Thr821 and Thr826. Phosphorylation at these sites may induce structural changes in Rb protein, which leads to the E2F dissociation. Among these sites, Thr821 and Thr826 have special importance because phosphorylation of either residue may result in disjunction of pRb from LXCXE motif-containing interacting partners, like HDAC and viral oncoproteins like T-Ag, Elf-1 and E7 [45]. It suggests that LXCXE binding site is regulated by phosphorylation of Thr 821/826, but not obligatory to inhibit E2F binding [45]. Functional inactivation of Rb can occur from increased phosphorylation resulting from overexpression of cyclins, mutation of CDKs or loss of function of CDK inhibitors [46]. The dephosphorylation process of phospho-Ser/Thr residue of Rb is regulated by protein phosphatase-1 (PP1) and PP2A. Previous data suggest that PP1 is the major Rb phosphatase involved in the direct dephosphorylation of Rb, while PP2A may influence Rb dephosphorylation via an indirect way by regulating the PP1 catalytic subunit (PP1c) [23, 47].

Epigenetic modifications, especially DNA methylation and posttranslational histone modification (methylation and acetylation) represent key mechanisms in regulating gene expression and the pathogenesis of MDS and AML [48, 49]. Increasing evidence has demonstrated that critical epigenetic modifiers, such as DNA methyltransferase enzymes (DNMTs) and chromatin-modifying enzymes - (lysine acetyltransferases (KATs) and histone deacetylases (HDACs), lysine methyltransferases (KMTs) and protein arginine methyltransferases (PRMTs) - are directly or indirectly modulated by PI3K/Akt [50, 51], MEK/Erk [52, 53] and Rb [54] signaling in malignant cells. Following with this several genes with role in PIP3/Akt or Raf/MEK/Erk pathways show altered DNA methylation status in AML [55].

In the present study, we investigated the presence of phosphorylated forms of MAPK, Akt kinase and Rb proteins using phospho-specific antibodies in leukemic blast cells separated from AML patients. The phosphorylated forms of the above-mentioned proteins may be accompanied by increased leukemic cell proliferation and drug resistance with poor prognosis of survival in AML patients. PTEN and PHLPP phosphatases, negative regulators of the Akt kinase, were investigated, too.

Materials and methods

Reagents and antibodies

The following reagents and antibodies were used with the provider indicated in brackets:

Ficoll-Paque PLUS (GE Healthcare), MACS human CD34 MicroBead kit (Miltenyi Biotec), protease inhibitor mix (Roche); rabbit anti-human Akt, rabbit anti-human phospho-Ser473-Akt, rabbit anti-human phosphatase and tensin homolog (PTEN), rabbit anti-human Erk, rabbit anti-human phospho-Thr202/Tyr404-Erk antibodies (Cell Signaling Technology); rabbit anti-human PH domain and Leucine rich repeat Protein Phosphatases (PHLPP) antibody (Abcam); mouse anti-human Retinoblastoma (Rb), goat anti-human phospho-Thr821/826-Rb, goat anti-human glyceraldehyde-3-phosphate-dehydrogenase (GAPDH) antibodies (Santa Cruz Biotechnology); horseradish peroxidase-conjugated secondary rabbit antibody (in cases of Akt, phospho-Ser473-Akt, PTEN, Erk, phospho-Thr202/Tyr404-Erk and PHLPP primary antibodies), horseradish peroxidase-conjugated secondary mouse antibody (in case of Rb primary antibody) and horseradish peroxidase-conjugated secondary goat antibody (in cases of phospho-Thr821/826-Rb and GAPDH primary antibodies) (Sigma Aldrich), enhanced chemiluminescence (ECL) reagents, BCA protein assay (Thermo Scientific), NPM1 12th exon (NPM1 F02: 5'-GTT-TCT-TTT-TTT-TTT-TTT-TTT-CCA-GGC-TAT-TCA-AG-3') (NPM1 R02: 5'-CA-(C/T)-GGT-AGG-GAA-AGT-TCT-CAC-TCT-GC-3') primers (BioScience Kft), Flt3 ITD 1 (Flt3 14F: 5'-GCA-ATT-TAG-GTA-TGA-AAG-CCA-GC-3') and 2 (Flt3 15R: 5'-CTT-TCA-GCA-TTT-TGA-CGG-CAA-CC-3'), Flt3 TKD (Flt3 20F: 5'-CCG-CCA-GGA-ACG-TGC-TTG-3') and (Flt3 20R: 5'-GCA-GCC-TCA-CAT-TGC-CCC-3')primers (Merc Kft), AmpliTaq Gold buffer 1 and 2, AmpliTaq Gold polymerase enzyme, $MgCl_2$ solution (Applied Biosystems), dNTP (Roche), Betaine solution (Sigma Aldrich), QIAmp kit (Qiagen).

Patient samples

A total of 69 AML patients were examined, including 57 newly diagnosed, 3 relapsed and 9 refractory AML patients (29 males and 40 females). The median age was 61 years, with a range from 19 to 89 years of age. According to World Health Organization (WHO) classification [56] 29 patients with AML with recurrent genetic abnormalities, 25 patients with AML with myelodysplasia-related changes (MRC), 2 patients with AML related to previous

10.3389/pore.2024.1611747

TABLE 1 Characteristics of AML patients with respect to age, ECOG status, WHO classification, French-American-British (FAB) classification, cytogenetics and type of collected sample.

		Number of patients (69)
AML patients	Newly diagnosed	57
	Relapsed	3
	Refractory	9
Age	Under 60 years	33
	Over 60 years	36
ECOG	0–1	38
	2–3	27
	4–5	4
WHO classification	AML with recurrent genetic abnormalities	29
	AML with myelodysplasia-related changes	25
	AML related to previous chemotherapy	2
	AML with myeloid sarcoma	2
	Mixed phenotype acute leukemia	6
	AML not otherwise classified	5
FAB classification	M0	5
	M1	9
	M2	15
	M3	3
	M4	21
	M5	5
	M6	4
	M7	0
	No appraisable result	2
Cytogenetics	Favorable	7
	Intermediate	33
	Unfavorable	20
	No appraisable cytogenetic result	9
Origine of samples	Bone marrow	60
	Peripheral blood	6
	both	3

chemotherapy because of preceding malignancies, 2 patients with myeloid sarcoma concurrently with AML were diagnosed. Six examined patients were diagnosed with acute leukemia of ambiguous lineage or mixed phenotype acute leukemia (MPAL). The other patients were not otherwise classified. According to 2017 ELN risk stratification by genetics [57] 7 patients with favorable, 20 patients with unfavorable and 33 patients with intermediate abnormalities were examined. The others (9 patients) had no appraisable cytogenetic result. There were patients in all French-American-British (FAB) classification categories except M7. The majority of patients belong to the M2 (15) or M4 (21) FAB group.

Bone marrow samples from 60 patients, peripheral blood samples from 6 patients were collected. From 3 patients both

bone marrow and peripheral blood samples were taken simultaneously. In case of 34 patients, consecutive samples were collected after the induction treatment. Samples were obtained between May 2012 and April 2015. The median follow-up of AML survivors is 48 months (31–56 months) and all but 2 surviving patients have more than 3 years of follow-up from the time of diagnosis. Follow up is failed in case of one patient. The characteristics of AML patients with respect to age, ECOG performance status, WHO classification, French-American-British classification and type of sample collected are shown in Table 1.

In addition, 10 healthy volunteers and 36 myelodysplastic syndrome (MDS) patients were investigated: 19 males and 17 females, the median age was 73 years, with a range from 23 to 86 years of age. According to Revised International Prognostic Scoring System (R-IPSS) score [58] 8 patients with very low, 12 patients with low, 7 patients with intermedier, another 7 patients with high, 2 patients with very high risk categories were diagnosed. Samples were collected with informed consent from patients during the regularly scheduled diagnostic protocol. The procedure of this study meets the directive of The Declaration of Helsinki [59] and is based on the approval of the Research Ethics Committee ETT-TUKEB (file number: RKEB.5824).

Young patients with good clinical performance received "3 + 7" induction therapy. It consisted of ara-C combined with anthracycline daunorubicin or idarubicin according to standard protocol [60]. We administred 45, 60 or 90 mg/m2 daunorubicin [61] depending on the patient's age and performance according to literature recommendations [62, 63]. Two patients who were not suitable for intensive chemotherapy got hypomethylating agents with nucleoside analog as initial treatment as study participants. High-dose ara-C was administered as consolidation therapy. Acute promyelocytic leukemia (APL) patients received their chemotherapy according to AIDA protocol [64]. Flag-Ida [65] (fludarabine + high-dose ara-C with idarubicin) induction therapy was given the good clinical performance mixed phenotype acute leukemia patients. Flag-Ida, Flag (fludarabine + high-dose ara-C with or without idarubicin), HAM [66] (high-dose ara-C + mitoxantrone) MEC [67] (mitoxantrone + etoposide + ara-C), FLAMSA [68] (fludarabine + amsacrine + ara-C), CLAG-M [69] (cladribine, ara-C, filgastrim, mitoxantrone) or clofarabine was used as salvage protocol. 16 patients underwent an allogeneic transplant. Patients with poor clinical performance got reduced dose ara-C combined with reduced dose daunorubicin or ara-C alone or Hydroxyurea monotherapy. 4 patients got only supportive treatment. Applied treatment regimens are shown in Supplementary Table S1.

Isolation of primary blasts

Mononuclear cells enriched in leukemic blasts were separated by Ficoll-Paque PLUS density-gradient centrifugation. The samples were heparin-treated and diluted with physiological saline. First 2–3 mL Ficoll-Paque PLUS was added to the centrifuge tube, then 4–6 mL diluted sample was layered carefully on it. This sample was centrifuged at 400 *g* for 20 min at 20 °C. The mononuclear layer was drawn and cells were washed twice with physiological saline by centrifugation at 100 *g* for 5 min at 20 °C. In some cases, $CD34^+$ cells were selected by using MACS human CD34 MicroBead kit. After counting, cells were centrifuged at 300 *g* for 10 min. Then cells were suspended in 300 µL phosphate-buffered saline (PBS) and 100 µL of CD34 MicroBeads were added. The cell suspension was incubated for 30 min in the refrigerator (2°C–8 °C). Then cells were washed with 5–10 mL PBS and centrifuged at 300 *g* for 10 min. After aspirating supernatant, cells were resuspended in 500 µL of PBS. Magnetic separation was carried out using MS MACS column placed in the magnetic field of the MiniMACS Separator. The column was rinsed with 500 µL PBS. Then the cell suspension was applied onto the column and flow-through containing unlabeled cells were collected. The column was washed 3 times with 500 µL PBS buffer. Then the column was removed from the separator and placed on a collection tube. After 1 mL of PBS was added onto the column, magnetically labelled cells were flushed out by flatly pushing the plunger into the column.

Western blotting

Separated mononuclear cells were counted in the Bürker chamber and 5×10^6 cells were collected by centrifugation at 800 *g*. Then cells were washed with PBS and lysed in 150 µL RIPA lysis buffer (50 mM Tris-HCl, 10 g/L Nonident P-40, 10 g/L Na-deoxycholate, 1 g/L Na-dodecyl sulfate (SDS), 0.15 M NaCl, 2 mM EDTA), containing 1 mM DTT, 0.5% protease inhibitor mix and 0.1 µM microcystin-LR. Cell lysis was accelerated by ultrasonic treatment; cell debris was removed by centrifugation (4°C, 16,000 x *g*, 10 min). Lysates were boiled at 100 °C for 10 min with 5x SDS sample buffer (320 mM Tris-Cl pH 6.8, 10% SDS, 50% glycerol, 25% β-mercaptoethanol, 0.01% bromophenol blue). The protein concentration of the lysates was measured by BCA protein assay at 540 nm in an ELISA Reader (Labsystem Multiscan MS). Equal amounts of cell lysates (100 µg) were loaded onto 10% SDS-polyacrylamide gel and subjected to SDS-PAGE, then transferred to nitrocellulose membrane. Nonspecific binding sites were blocked by room temperature (24 °C) for 1 hour with 5% nonfat dried milk in Tris-Buffered Saline (TBS) containing 0.5% Tween-20 (TBST). Membranes were incubated by 4 °C overnight with primary antibodies (1:1000). The membranes were washed three times with TBST for 10 min, then were incubated by room temperature (24 °C) for 1 hour with

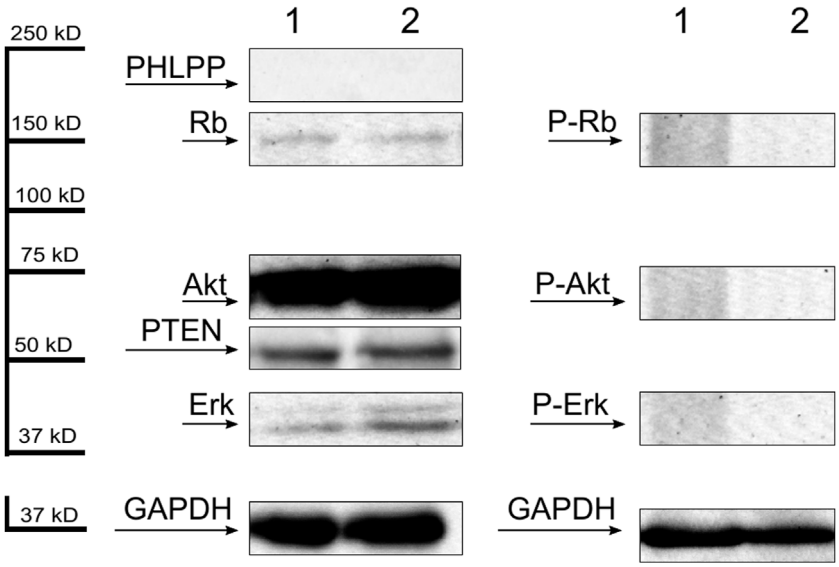

FIGURE 1
Representative Western blots of dephosphorylated (first panel) and phosphorylated (second panel) forms of Rb, Akt and Erk proteins and PHLPP and PTEN phosphatases (first panel) of mononuclear cells separated from 2 healthy volunteers. GAPDH was used as an internal control.

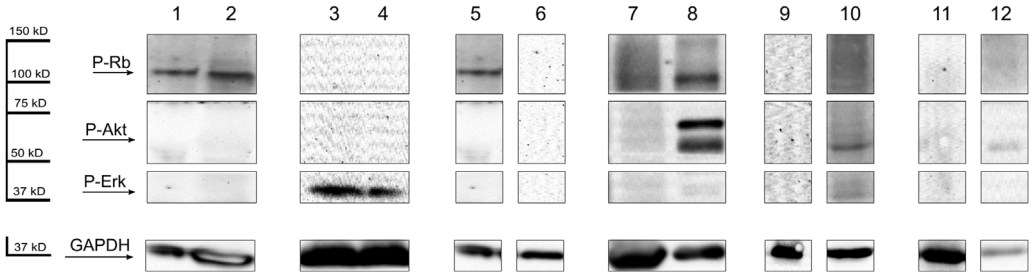

FIGURE 2
Lane 1, magnetic separated CD34$^+$ blast cells, and whole mononuclear cells **(lane 2)** after density-gradient separation from bone marrow of the same AML patient. GAPDH was used as an internal control. **Lane 3**, representative Western blots of phospho-Erk of mononuclear cells separated from peripheral blood, and from bone marrow **(lane 4)** of the same AML patient. GAPDH was used as an internal control. **Lane 5**, representative Western blots of P-Rb of mononuclear cells separated from an AML patient at the time of diagnosis, and after chemotherapy treatment **(lane 6)**. GAPDH was used as an internal control. **Lane 7**, Western blots of P-Rb, P-Akt and P-Erk in mononuclear cells separated from an AML patient at the time of diagnosis, and by progression (**lane 8**). GAPDH was used as an internal control. **Lane 9**, Western blots of P-Rb, P-Akt and P-Erk of mononuclear cells separated from a bone marrow of an MDS patient, samples without the presence of AML in the bone marrow. **Lane 10**, samples after the patients progress to AML. GAPDH was used as an internal control. **Lane 11,** Western blots of P-Rb, P-Akt and P-Erk of mononuclear cells separated from a bone marrow of a PNH patient, samples without the presence of AML in the bone marrow. **Lane 12**, samples after the patients progress to AML. GAPDH was used as an internal control.

horseradish peroxidase-conjugated secondary antibody (1: 9000). Then membranes were washed two times with TBST and once with TBS for 10 min. The immunoreactive bands were detected by ECL reagents and imaged with FluorChem FC2 Imager (Alpha Innotech). GAPDH identified with anti-GAPDH (1:9000) was used as a loading control after membrane stripping procedures. Due to the limited amount of samples, each experiment could be repeated two times.

Membrane stripping

Membranes were washed three times with TBST for 5 min. Then membranes were incubated with stripping buffer (0.5 M Tris-HCl pH 6.8, 10% SDS, 8% β-mercaptoethanol) at 50 °C and shaking at 200 rpm for 30 min. Membranes were washed three times with TBST for 5 min, then membranes were ready for the next cycle of antigen identification.

TABLE 2 Comparison of clinical features–World Health Organization (WHO) classification, French-American-British (FAB) classification, cytogenetics, Fms Related Receptor Tyrosine Kinase 3 (FLT-3) and nucleophosmin (NPMc) mutation status, leukocyte count and percentage of bone marrow blasts at diagnosis - known as prognostic in AML for each phosphorylated protein group.

Characteristic		Total number of patients	Phosphorylated proteins			*p*-value
			P-Rb$^{(Thr826)}$	P-Akt$^{(Ser473)}$	P-Erk$^{(Thr202/Tyr404)}$	
			32/69	24/69	20/69	
WHO classification	AML with recurrent genetic abnormalities	29	15/29 (51.7)	8/29 (27.5)	5/29 (17.2)	P = NS
	AML with myelodysplasia-related changes	25	13/25 (52)	11/25 (44)	7/25 (28)	P = NS
	AML related to previous chemotherapy	2	0	1/2 (50)	2/2 (100)	P = NS
	Myeloid sarcoma	2	1/2 (50)	1/2 (50)	1/2 (50)	P = NS
	MPAL	6	3/6 (50)	3/6 (50)	2/6 (33)	P = NS
FAB classification	M0	5	2/5 (40)	2/5 (40)	1/5 (20)	P = NS
	M1	9	2/9 (22.2)	2/9 (22.2)	4/9 (44.4)	P = NS
	M2	15	8/15 (53.3)	5/15 (33.3)	2/15 (13.3)	P = NS
	M3	3	1/3 (33.3)	2/3 (66.6)	0	P = NS
	M4	21	11/21 (52.3)	5/21 (23.8)	8/21 (38)	P = NS
	M5	5	3/5 (60)	1/5 (20)	0	P = NS
	M6	4	2/4 (50)	2/4 (50)	1/4 (25)	P = NS
	M7	0	0	0	0	P = NS
Cytogenetics	favorable cytogenetics	7	1/7 (14.2)	1/7 (14.2)	2/7 (28.5)	P = NS
	Intermediate cytogenetics	33	16/33 (48.4)	11/33 (33.3)	7/33 (21.2)	P = NS
	unfavorable cytogenetics	20	10/20 (50)	9/20 (45)	9/20 (45)	P = NS
FLT-3	wild type	33	18/33 (54.5)	13/33 (39.3)	11/33 (33.3)	P = NS
	ITD-heterozygous	5	3/5 (60)	2/5 (40)	1/5 (20)	P = NS
	TKD- heterozygous	6	1/6 (16.6)	2/6 (33.3)	3/6 (50)	P = NS
	ITD/TKD	1	0	0	0	P = NS
NPMc	mutated	17	11/17 (64.7)	5/17 (29.4)	1/17 (5.8)*	*p = 0.009
	not mutated	31	13/31 (41.9)	12/31 (38.7)	13/31 (41.9)*	*p = 0.009
% blast cells in bone marrow at diagnosis	>30%	56	26/56 (46)	18/56 (32)	17/56 (30)	P = NS
leukocyte count at diagnosis	>30 G/L	27	8/27 (29.6)*	7/27 (25.9)	6/27 (22.2)	*p = 0.029

The cells show the number of cases and percentage in parentheses. Pearson Chi-Square test or in case of sample size under 5 Fisher's Exact Test was used by analysis of distribution of each prognostic features between each phosphorylated protein group.

Densitometry

For densitometry analysis of the Western blot images, ImageJ 1.47v software was used. The densitometric results of Western blots of p-Rb, p-Akt, p-Erk, PHLPP and PTEN proteins were normalized to the internal control GAPDH. The averages of the expression levels were calculated based on the densitometric analysis of two Western blots for each patient. Relative

10.3389/pore.2024.1611747

TABLE 3 Comparison of clinical features–World Health Organization (WHO) classification, French-American-British (FAB) classification, cytogenetics, Fms Related Receptor Tyrosine Kinase 3 (FLT-3) internal tandem duplication (ITD) or tyrosine kinase domain (TKD) and nucleophosmin (NPMc) mutation status, leukocyte count and percentage of bone marrow blasts at diagnosis - known as prognostic in AML for each phosphatase group.

Characteristic		Total number of patients	Phosphatases				*p*-Value
			PTEN	PHLPP	Both PTEN and PHLPP	None of phosphatase	
			39/59	23/59	22/59	19/59	
WHO classification	AML with recurrent genetic abnormalities	27	20/27 (74)	14/27 (51.8)	13/27 (48.1)	6/27 (22.2)	P = NS
	AML with myelodysplasia-related changes	19	11/19 (57.8)	4/19 (21)	4/19 (21)	8/19 (42.1)	P = NS
	AML related to previous chemotherapy	2	2/2 (100)	1/2 (50)	1/2 (50)	0	P = NS
	Myeloid sarcoma	2	2/2 (100)	1/2 (50)	1/2 (50)	0	P = NS
	MPAL	5	3/5 (60)	3/5 (60)	3/5 (60)	2/5 (40)	P = NS
FAB classification	M0	5	4/5 (80)	1/5 (20)	1/5 (20)	1/5 (20)	P = NS
	M1	9	7/9 (77.7)	2/9 (22.2)	2/9 (22.2)	2/9 (22.2)	P = NS
	M2	12	7/12 (58.3)	4/12 (33.3)	4/12 (33.3)	5/12 (41.6)	P = NS
	M3	3	2/3 (66.6)	2/3 (66.6)	2/3 (66.6)	1/3 (33.3)	P = NS
	M4	18	11/18 (61.1)	8/18 (44.4)	7/18 (38.8)	6/18 (33.3)	P = NS
	M5	3	3/3 (100)	3/3 (100)*	3/3 (100) **	0	*p = 0.05 **p = 0.043
	M6	4	2/4 (50)	0	0	2/4 (50)	P = NS
	M7	0	0	0	0	0	P = NS
Cytogenetics	favorable cytogenetics	5	4/5 (80)	2/5 (40)	2/5 (40)	1/5 (20)	P = NS
	Intermediate cytogenetics	30	21/30 (70)	15/30 (50)	14/30 (46.6)	8/30 (26.6)	P = NS
	unfavorable cytogenetics	17	9/17 (52.9)	5/17 (29.4)	5/17 (29.4)	8/17 (47)	P = NS
FLT-3	wild type	30	20/30 (66.7)	11/30 (36.6)	11/30 (36.6)	10/30 (33.3)	P = NS
	ITD-heterozygous	5	3/5 (60)	4/5 (80)	3/5 (60)	1/5 (20)	P = NS
	TKD- heterozygous	6	4/6 (66.6)	2/6 (33.3)	2/6 (33.3)	2/6 (33.3)	P = NS
	ITD/TKD	1	0	0	0	1/1 (100)	P = NS
NPMc	mutated	17	12/17 (70.5)	9/17 (52.9)	8/17 (47)	4/17 (23.5)	P = NS
	not mutated	27	17/27 (62.9)	10/27 (37)	10/27 (37)	10/27 (37)	P = NS
% blast cells in bone marrow at diagnosis	>30%	50	32/50 (64)	20/50 (40)	20/50 (40)	17/50 (34)	P = NS
leukocyte count at diagnosis	>30 G/L	25	17/25 (68)	11/25 (44)	10/25 (40)	7/25 (28)	P = NS

The cells show the number of cases and percentage in parentheses. Pearson Chi-Square test or in case of sample size under 5 Fisher's Exact Test was used by analysis of distribution of each prognostic features between each phosphatase group.

expression levels of each investigated proteins were considered as relatively high or low depending on their relationship to the median expression level of the full cohort of positive samples for the given protein in order to determine subgroups of patients, in which the relative expression levels are high or low. In the case of PTEN protein a third subgroup of patients considered too, in which the relative expression level of PTEN was lower than the median relative expression level of PTEN in healthy individuals. We also paid special attention if the expression level of protein normalized to GAPDH was above 1 (highest relaively expression level).

PCR

PCR was used to investigate possible mutations in NPM1 genes, FLT-3 ITD and TKD mutation. The examination was done in central laboratory as part of routine investigation protocol. The results are available in the institutional computer system. The Total DNA for PCR was isolated by QIAmp kit reagent according to the manufacturer's protocol. The investigated region of the NPM1, and FLT-3 genes was amplified by PCR using specific primers. In case of TKD mutation the PCR product was digested by *Eco* RV enzyme. Nuclease free water was used as a template negative control, DNA isolated from healthy volunteer was used as a negative control. DNA isolated from cancerous or leukemic patients in our institute verified positive for NPM1, and FLT-3 mutation was used as a positive control. Plasmid DNA was used as positive control of digestion. Veriti (Applied Biosystems) PCR machine was used. PCR products were loaded onto 3% agarose gel and subjected to electrophoresis.

Statistical analysis

Statistical analysis was carried out using SPSS Statistics 26 and Graphpad Prism 9.0.2 software. The distribution of prognostic features between the protein groups were compared by Pearson Chi-Square test or Fisher's Exact Test. Independent Samples *t*-test were used by comparisation the median expression level of each proteins between different groups of patients. Overall (OS) and event-free survival (EFS) was examined, and survival distributions were estimated by Kaplan-Meier's method, and comparisons were based on Log Rank (Mantel-Cox) tests. OS was measured in all patients from the time of diagnosis until death. EFS was estimated from the date of diagnosis until failure to achieve CR or disease progression after CR or death from any cause [70]. Spearman correlation tests were used by the correlation examination. Cox proportional hazard model was used to test the impact of the different proteins on survival simultaneously with other prognostic factors. Rb category (phosphorylated or unphosphorylated), and other prognostic features: ECOG performance status (0–1 or 4–5), age at diagnosis over 60 years (yes or no), AML with MRC (yes or no) and underwent an allogenic bone marrow transplantation (ABMT) (yes or no) categories were added to the first model (Supplementary Table S2). PTEN, PHLPP and both phosphatase (yes or no), ECOG performance status (0–1 or 4–5), age at diagnosis over 60 years (yes or no), AML with MRC (yes or no), unfavorable cytogenetics (yes or no) and underwent an ABMT (yes or no) categories were added to the another model (Supplementary Table S3.).

Results

Phosphoprotein levels and phosphatases in AML patients

Thirty-two AML patients (46.3%) had detectable phosphorylated Rb protein level. Akt protein phosphorylation was observed in 24 patients (34.7%). Phospho-Erk protein was detectable in 20 cases (28.9%). Phosphorylation was not detected in mononuclear cells of the 10 healthy individuals, but each showed nonphosphorylated bands of the examined proteins (Figure 1.). Consequently, the observed phosphorylated protein signals must have been attributed to the leukemic cells. The presence of PTEN and PHLPP phosphatases were examined in 59 patients. There were 22 patients (37.2%) expressing both PTEN and PHLPP phosphatases and 19 patients (32.2%) with neither PTEN nor PHLPP expression. Overall, there were 39 patients with detectable PTEN (66.1%) and 23 patients (38.9%) with PHLPP protein. In healthy volunteers, PTEN was detectable in all cases, but PHLPP was not present (Figure 1.). There were no differences in Western blotting results between the magnetic separated $CD34^+$ cells and whole mononuclear cells (Figure 2 lane 1 and 2). Therefore, we found the density-gradient separation sufficient for isolating the samples for the assays. There were no differences between results if the samples were collected from blood or bone marrow or obtained simultaneously from 3 patients (Figure 2 lane 3 and 4). Therefore, blood samples may be used in that case if leukemic blasts are detectable in peripheral blood. The presented patient has about 90% blast infiltration in bone marrow and 67% blast cells in peripheral blood.

Distribution of phosphoproteins and phosphatases among patients grouped by World Health Organization (WHO) classification groups, FAB type, cytogenetic, FLT3-and nucleophosmin mutation status, leukocyte count and percentage of bone marrow blasts at diagnosis

The distribution of phosphoproteins and phosphatases among patients grouped by World Health Organization (WHO) classification, French-American-British (FAB)

classification, cytogenetics, Fms Related Receptor Tyrosine Kinase 3 (FLT-3) internal tandem duplication (ITD) or tyrosine kinase domain (TKD) and nucleophosmin (NPMc) mutation status, leukocyte count and percentage of bone marrow blasts at diagnosis is shown in Tables 2, 3.

According to WHO classification we found no significant correlation between groups and the presence of phosphorylated protein or phosphatases.

We found no significant correlation between FAB subtypes and the presence of phosphorylated protein or PTEN phosphatase alone. In FAB5 patients both PHLPP and PTEN, and PHLPP alone was significantly more often present (Table 3).

There was no significant correlation between cytogenetics and presence of phosphorylated proteins or phosphatases.

FLT3 mutation status was identified in case of 45 patients. Internal tandem duplication (ITD) was seen in 5 patients, tyrosine kinase domain mutations (TKD) were present in 6 patients. One patient was found to have both ITD and TKD mutation. These differences were not statistically significant, as the number of cases were not sufficient.

Nucleophosmin mutations were identified in 17 patients, while in 31 patients nucleophosmin were not mutated, but 21 patients had no accessible result. Nucleophosmin mutations were significantly less frequently seen in patients with phosphorylated Erk protein (Table 2).

The percentage of bone marrow blasts (>30%) did not correlate with the presence of phosphorylated proteins or phosphatases. The white blood cell (WBC) counts over 30 G/L at diagnosis were seen significantly less frequently in patients with phosphorylated Rb protein (Table 2).

The occurrence of phosphoproteins or phosphatases showed no correlation with the patients' age, sex and ECOG performance status.

In summary, the distribution of clinical features was generally similar among the groups. There were no significant differences in age, sex, performance status, presence or absence of preceding MDS, cytogenetics, FLT-3 mutation status or FAB type expect for the presence of both PHLPP and PTEN, and PHLPP in the FAB5 group. Regarding leukocyte count at diagnosis in phosphorylated Rb group and nucleophosmin mutation status in phosphorylated Erk group were significant differences found, but among the other patients' group the distribution of these prognostic features were similar. The distribution of phosphoproteins and phosphatases between the distinct categories were demonstrated in Tables 2, 3.

Comparison of the expression levels between different groups of patients

In the subgroup of patients with recurrent genetic abnormalities according to WHO classification, most patients have relative expression level of PTEN higher than the median relative expression level of PTEN in health individuals (N = 27/16 Pearson Chi-Square test $p = 0.029$). Phosphorylated Akt had a significantly higher median expression level in AML with recurrent genetic abnormalities compared to the others (N = 29, Independent Samples t-test $p = 0.044$), in concordance with this, only one patient had low phospho-Akt level in this subgroup (N = 29/1 Pearson Chi-Square test $p = 0.026$).

In mixed phenotype acute leukemia patients a significantly higher median expression level of phospho-Rb protein was found (N = 6, Independent Samples t-test $p = 0.044$).

Among the different FAB subtypes of AML, heterogeneous expression levels have been detected. In FAB0 subgroup, most patients have relative expression level of PTEN lower than the median relative expression level of PTEN in healthy individuals (N = 5/3, Pearson Chi-Square test $p = 0.042$). In FAB1 subgroup, relatively low phospho Akt level was present and no patients have relatively high expression level (N = 9/0, Pearson Chi-Square test $p = 0.018$). In contrast, in FAB2 relatively high expression level was found and no patients had relatively low phospho-Akt level (N = 15/0, Pearson Chi-Square test $p = 0.039$). In FAB4 relatively high PTEN level was detectable in the majority of PTEN-positive patients (N = 11/9, Pearson Chi-Square test $p = 0.048$) In FAB5 relatively high PHLPP expression was found in every PHLPP positive patients (N = 3/3 Pearson Chi-Square test $p = 0.006$) Among FAB6 patients relatively low phospho-Retinoblastoma level was found and only one patient had relatively high phospho-Retinoblastoma level (N = 4/1 Pearson Chi-Square test $p = 0.026$) There was no significant correlation between the expression level of the other proteins and FAB groups.

There was no significant correlation between cytogenetics, FLT3 and Nucleophosmin mutation status, and the expression level of proteins.

A significantly higher median expression level of phospho-Rb protein was found in the patient's subgroup in which the percentage of bone marrow blasts was above 30% at diagnosis (N = 56, Independent Samples t-test $p = 0.033$). In concordance with this, only minority of patients had low phospho-Retinoblastoma level (N = 56/8 Pearson Chi-Square test $p = 0.031$).

In the subgroup of patients with white blood cell (WBC) counts over 30 G/L at diagnosis relatively low phospho-Erk expression level was detected in the majority of patients. Only two patients presented relatively high phospho-Erk expression level (N = 27/2 Pearson Chi-Square test $p = 0.047$). The white blood cell (WBC) counts over 100 G/L at diagnosis show a significant correlation with lower median phospho-Akt expression level (N = 11 Independent Samples t-test $p = 0.033$), in accordance with this, no relatively high phospho-Akt level was detected in this subgroup (N = 11/0 Pearson Chi-Square test $p = 0.019$).

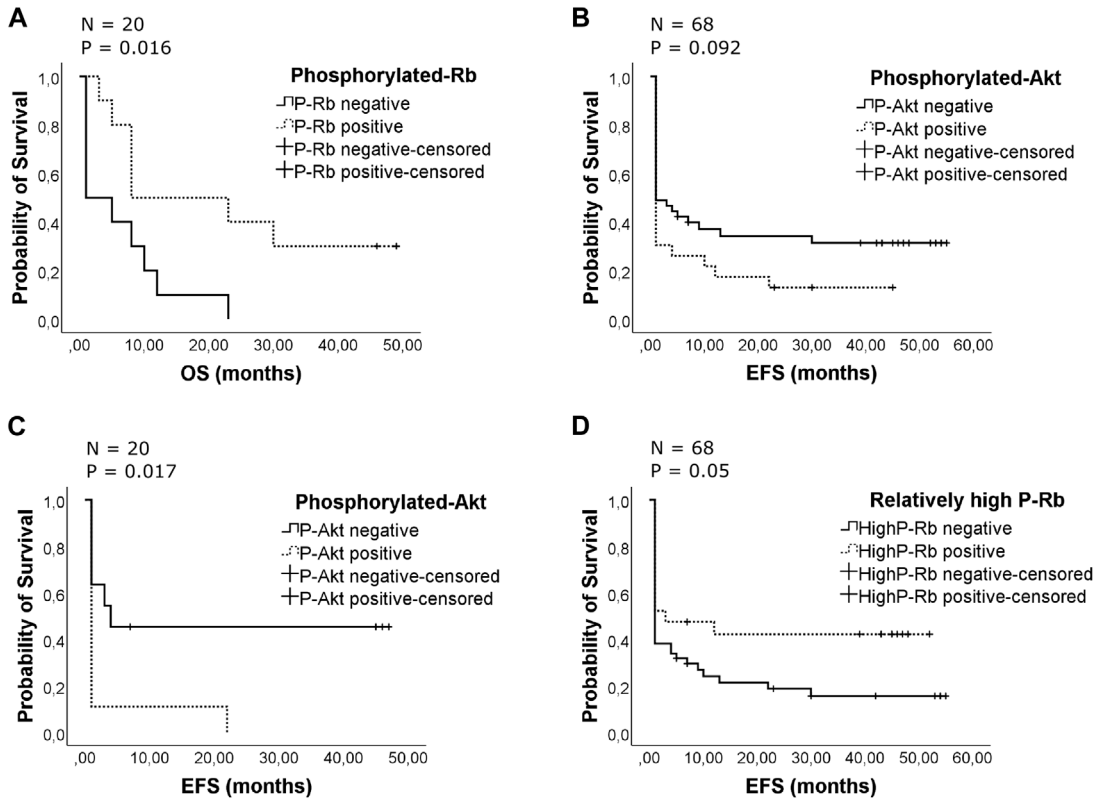

FIGURE 3
(A) Effect of the presence of phosphorylated retinoblastoma protein on patients' overall survival with unfavorable cytogenetics. The Kaplan-Meier curves compare phosphorylated and unphosphorylated Rb groups for overall survival. The patients were censored at the time of death. Overall, there were 17 deaths, 7 from 10 P-Rb patients and 10 from 10 unphosphorylated patients. The median survival was 1 month in patients' group with unphosphorylated Rb protein, while the median survival was 8 months in patients' group with phosphorylated Rb (p = 0.016). **(B)** Effect of the presence of phosphorylated Akt on duration of event-free survival. The Kaplan-Meier curves compare phosphorylated and unphosphorylated Akt groups for event-free survival. The patients were censored at time of relapse or death or finding of failure to achieve CR. The survival for the whole studied patient population is shown. Overall, there were 50 events occurring in 20 from 23 P-Akt patients and 30 from 45 unphosphorylated ones. The mean survival was 8 months in patients' group with phosphorylated Akt protein, while the mean survival was 19 months in patients' group with unphosphorylated Akt (p = 0.092). **(C)** Effect of the presence of phosphorylated Akt on duration of event-free survival with unfavorable cytogenetics. The Kaplan-Meier curves compare phosphorylated and unphosphorylated Akt groups for event-free survival. The patients were censored at time of relapse or death or finding of failure to achieve CR. Overall, there were 15 events occurring in 9 from 9 P-Akt patients and 6 from 11 unphosphorylated patients. The mean survival was 3 months in patients' group with phosphorylated Akt protein, while the mean survival was 22 months in patients' group with unphosphorylated Akt (p = 0.017). **(D)** Effect of the presence of relatively high phosphorylated retinoblastoma protein on patients' event-free survival. The Kaplan-Meier curves compare relatively high phosphorylated Rb groups with the others for event-free survival. The patients were censored at the time of relapse or death or finding of failure to achieve CR. Overall, there were 50 events, 12 from 21 relatively high P-Rb expression level patients and 38 from 47 patients with relatively low P-Rb or unphosphorylated Rb. The mean event-free survival was 23 months in patients' group with relatively high phosphorylated Rb protein, while the mean event-free survival was 12 months in the other patients' group (p = 0.05).

Relationship between PTEN, PHLPP and AKT

We hypothesized that loss of PTEN or PHLPP, or their decreased expression would lead to high Akt phosphorylation in phospho-Akt positive cases. However, the Spearman correlation test showed significant positive correlation between the presence of phosphorylated Akt and PHLPP (r = 0.318, p = 0.014). These data suggest that Akt phosphorylation results in consequent elevation of PHLPP expression in leukemic patients, while PHLPP is not detected in healthy patients. We did not find significant correlation between the presence of PTEN and P-Akt, but if the relative expression level of the proteins considered too, highest PTEN level and highest phosphorylated Akt level showed a significant positive correlation (r = 0.26, p = 0.047). The exact molecular mechanisms which lead to constitutive Akt phosphorylation in AML are subject of further investigation.

Relationship of phosphoprotein level to clinical outcome

The patients studied had a median overall survival (OS) of 8 months with complete remission (CR) rates of 38% after first

or second induction therapy (29% after first induction). The mean duration of event-free survival was 16 months. No statistically significant differences were found between the phosphorylated protein groups compared with their nonphosphorylated ones regarding median survival for all of the examined patients. No major differences in the cause of death were noted between the distinct groups. Surprisingly, we found phosphorylated Rb improve OS among patients with unfavorable cytogenetics (median 1 vs. 8 months, $p = 0.016$) (Figure 3A). Among patients with unfavorable cytogenetics phosphorylated-Rb represent a significant predictor of outcome examined by univariate (B = - 1.116; Exp(B) = 0.328; 95% CI for Exp(B) = 0.116–0.929; $p = 0.036$) and multivariate (B = - 1.465; Exp(B) = 0.231; 95% CI for Exp(B) = 0.06–0.885; $p = 0.032$) Cox proportional hazard regression analysis (data are not shown). Although the patients received a variety of therapeutic regimens, the type of chemotherapy was not a predictor of outcome among patients with unfavorable cytogenetics. Only the allogenic bone marrow transplantation (ABMT) represents a significant predictor of outcome (B = - 1.427; Exp(B) = 0.24; 95% CI for Exp(B) = 0.076–0.763; $p = 0.016$, data are not shown). Phospho-Rb remained a statistically significant independent predictor when ABMT category (yes or no) was added to the model (B = −1.645; Exp(B) = 0.193; 95% CI for Exp(B) = 0.053–0.707; $p = 0.013$). The summaries of multivariate regression analysis are shown in Supplementary Table S2.

The differences between groups in duration of event-free survival and the percentage of patients who achieved a complete remission were not statistically significant, although the phospho-Akt group showed inferior event-free survival compared to the others (mean 8 versus 19 months) but the difference was not significant (Figure 3B). Among patients with unfavorable cytogenetics presence of phosphorylated Akt represent significant worse EFS (mean 3 versus 22 months, $p = 0.017$) (Figure 3C). When CR status was analyzed, only 21% of the P-Akt positive patients achieved CR after the first induction, while it was only 11% among unfavorable cytogenetics patients (P = NS). The presence of phosphorylated Rb has a positive impact on event-free survival in unfavorable patients' group (mean 5.5 vs. 16.6 months, results are not shown), but the differences were not statistically significant. When relative expression level was analyzed, relatively high phospho-Rb level provided a significant better EFS in full cohort of AML patients (mean 12 vs. 23 months, $p = 0.05$) (Figure 3D).

The presence of either phosphatase does not cause statistically significant difference in OS or in EFS, but we found the highest expression level of PHLPP provided significantly worse OS (median 1 vs. 10 months, $p = 0.033$) among full cohort of AML patients. If only PHLPP positive patients were analyzed, the highest PHLPP expression level worsenedoverall survival even more compared to others (median 1 vs. 23 months, 0.021). When overall survival time was analyzed among patients with Cox proportional hazard regression model, groups with both PTEN and PHLPP phosphatases represented significant predictors of outcome (B = −2.502; Exp(B) = 0.082; 95% CI for Exp(B) = 0.007–0.939; $p = 0.044$, data are not shown). It remained statistically significant predictor when ABMT category (yes or no) was added to the model (B = −2.939; Exp(B) = 0.053; 95% CI for Exp(B) = 0.004–0.636; $p = 0.021$). The summaries of the analysis are shown in Supplementary Table S3. When remission duration was analyzed only by age over 60 years at diagnosis it was an independent predictor (B = 1.174; Exp(B) = 3.234; 95% CI for Exp(B) = 1.371–7.628; $p = 0.007$, data are not shown).

The phosphoproteins detected at diagnosis usually disappear when the patient achieves complete remission with negative minimal residual disease. As an example, Western blot analysis of mononuclear cells separated from an AML patient the phosphorylated Rb detected at the time of diagnosis disappeared after induction treatment. The patient achieved minimal residual disease negative complete remission and proved to be a long-term survivor. The patient is still alive 10 years and 5 months after diagnosis (Figure 2 lane 5 and 6).

In some cases, phosphorylated proteins were not detectable at diagnosis but appeared after progression of disease. For example, Western blot analysis of mononuclear cells separated from an AML patient showed no phosphorylated protein at the time of diagnosis, but phosphorylated Rb and Akt protein appeared after progression of leukemia. There were 28% blast cells in the bone marrow at the diagnosis, and the patient achieved partial remission after induction treatment. There were 10% blast cells in the bone marrow by progression. The patient died in 3 months after the diagnosis due to septicemia and pneumonia (Figure 2 lane 7 and 8).

There was one MDS patient and one patient with paroxysmal nocturnal hemoglobinuria (PNH) whose first sample was taken before the appearance of AML and phosphorylated proteins were not detectable at that time. The second sample was taken when the MDS or PNH progressed to AML and phosphorylated Akt and Erk proteins were appeared in MDS patient (Figure 2 lane 9 and 10) and phosphorylated Akt were developed by PNH patient (Figure 2 lane 11 and 12) at the time of AML transformation. It suggests the pathogenic role of phosphoproteins in the development of AML.

Phosphoprotein levels in MDS patients

Nine MDS patients (25%) had detectable phosphorylated Rb protein level. Akt and Erk protein phosphorylation was observed in five patients (15%). Nine from the 36 patients progressed to acute leukemia, and six from these patients showed at least one phosphorylated protein. For example, Western blot analysis of

mononuclear cells separated from an MDS patient detected phosphorylated Rb and Akt protein. There were 1.6% blast cells in the bone marrow at the time of diagnosis. The patient progresses to AML in 11 months after diagnosis (Supplementary Figure S1.). There was no correlation between the Revised International Prognostic Scoring System (R-IPSS) score [58] and protein phosphorylation. Median survival was similar in the phosphorylated and unphosphorylated groups of patients. The median expression level of p-RB was significantly lower in MDS patients compared to AML patients (Independent Samples *t*-test, $p = 0.045$). Regarding the other proteins, there was no difference in the median expression levels between the MDS and AML patient groups.

Discussion

Our present study shows that hyperphosphorylation of Rb, Akt or Erk proteins is a common event in the development of acute myeloid leukemia. Other research groups have also analyzed the occurrence of phosphoproteins in myeloid blast cells and concluded that hyperphosphorylation of signaling proteins affect negatively the clinical outcome of AML [46, 71, 72]. We have demonstrated that 69% of AML patients show at least one constitutive phosphorylated form of the above (Rb, Akt and Erk) examined proteins. The appearance of phosphoproteins simultaneously with the development or progression of AML confirm the key role of protein phosphorylation in the pathogenesis of leukemia and the progression from MDS to AML. The clonal evolution may explain the development of phosphorylation of proteins in leukemic blast cells during the course of disease. This process can select one or more phosphorylated proteins in blasts, which seems to provide survival advantage against cells negative for phosphorylated proteins. The existence of two or three phosphorylated protein at the same time represent worse event-free survival. The presence of phosphorylated Akt protein alone reduces the EFS among AML patients. The difference is significant in patients with unfavorable cytogenetics. Overall, the vast majority of patients with phosphorylated Akt relapsed or died (91.3%, P = NS). Phospho-Akt protein was detectable in 34.7% of AML patients. Min et al. demonstrated constitutive phosphorylation of Akt on Ser473 residue in more than 70% of blast cells separated from AML patients with significantly shorter overall survival compared to patients without phosphorylated Akt. Similar to our findings, there were no significant differences in Akt phosphorylation regarding FAB subtype, cytogenetic abnormalities or white blood cell counts [71].

PTEN and PHLPP phosphatases, the negative regulators of the PIP3K/Akt pathway, have also been investigated. Previous reports indicated significantly better outcome in PHLPP expressing solid tumors [73, 74]. In contrast, Ono et al. found that high PHLPP expression in AML blast cells is associated with poor prognosis [75]. Several investigators presented lower PTEN mRNA and protein level in AML patients compared with healthy people, and it correlates positively with poor prognostic factors [76, 77]. Huang et al. demonstrated that PTEN positive elderly patients with refractory AML tended to have an improved prognosis compared to PTEN negative patients [78]. In our study, the presence of either phosphatase did not show a significant impact on survival in our AML patients.

We found a significant correlation between the FAB5 subtype and the presence of both PHLPP and PTEN and PHLPP alone. Although the number of patients in the FAB5 group is small, these data suggest a possible link between the PHLPP and PTEN pathway and myeloid development or monocytic differentiation, respectively. This is supported by the well-known role of the PI3K/Akt pathway in monocyte differentiation [79, 80]. FAB5 maturation state in AML is of particular interest because in a recent publication Pei S et al demonstrated that the monocyte morphology was found highly significant to be associated with a disease that was refractory to the combination treatment of hypomethylating agent Azacitidine and the highly specific Bcl-2 inhibitor Venetoclax [81]. The investigators proved that monocytic leukemia blasts lose expression of the Venetoclax target Bcl-2 while Myeloid cell leukemia-1 (MCL-1) protein, an antiapoptotic member of the Bcl-2 family [82] expression is significantly higher in FAB-M5 patients. The exact role of the PTEN and PHLPP in the emergence of Venetoclax resistance requires further investigation. Nevertheless, the role of the Akt signaling pathway possibly by upregulation of non-Bcl-2 antiapoptotic proteins such as MCL-1 and Bcl-XL in the development of venetoclax resistance has been confirmed in hematologic malignancies [83–85]. In addition, treatment with inhibitors acting on the Akt signaling pathway helps restore Venetoclax sensitivity in leukemic cells [86]. Clarifying the role of PTEN and PHLPP protein in Venetoclax resistance and monocyte differentiation may be of great importance even in terms of therapeutic decisions. This subgroup of AML patients benefits from MLC-1 inhibitors in addition to chemotherapy treatment compared to Venetoclax [81,83].

We observed Erk phosphorylation in 26% of samples from our patients. Authors from MD Anderson Cancer Centre demonstrated elevated phospho-Erk level via a flow cytometric technique in more than 80% of AML patients. The authors found no correlation between constitutive Erk phosphorylation and the course of disease [72]. The higher occurrence rate of phospho-Erk protein demonstrated by these authors compared with our result (26%) might be explained with better sensitivity of flow cytometric technique compared with Western blots.

Contradictory data exist about the impact of retinoblastoma protein on survival. For example, Kornblau et al. found phosphorylated Rb protein in 15% of blast cells from AML patients with significant shorter survival compared with patients without hyperphosphorylated Rb [46]. The difference

between this previous study and our data (15% versus 46.3%) may be due to the fact that our group studied Rb protein phosphorylated on Thr821/826 sites, while Kornblau et al. investigated maximally phosphorylated Rb. Also, Kornblau et al. found low retinoblastoma protein level associated with a significantly worse outcome among AML patients [3]. In contrast, more and more data suggest that loss of Rb function increases chemosensitivity in different type of cancer. For example, Zagorski et al. presented this finding in lung cancer cell lines [87]. Derenzini et al. demonstrated superior disease-free survival in human breast cancer cells with lack of retinoblastoma protein expression [88]. In accordance with those findings, Treré et al. found better outcome among triple-negative breast cancer patients with retinoblastoma protein negative compared to retinoblastoma positive patients [89]. Presumably, loss of retinoblastoma protein or functionally inactivated phosphorylated form may provide greater chemosensitivity and consequently better outcome among treated patients. Greater chemosensitivity may explain better OS among our AML patients with unfavorable cytogenetics, but establishing an exact mechanism requires further investigation. These conflicting data highlight the complexity concerning the regulation of the process of leukemogenesis by protein phosphorylation and the impacts on survival. Another explanation for better outcome with P-Rb is the lower leukocyte count at the time of diagnosis in patients with phosphorylated Rb. 90% of the P-Rb positive patients had less than 30 G/L leukocyte count by diagnosis in patients' group with unfavorable cytogenetics (P = NS).

The phosphorylated form of the investigated proteins is present in mononuclear cells separated from MDS patients. Our results suggest that constitutive phosphorylation can be responsible for progression from MDS to AML. In accordance with our finding a recent publication by Zheng Z et al. [90] demonstrated patients with MDS or MDS-AML presented elevated levels of phosphorylated Erk and phosphorylated Akt proteins. The authors confirmed the role of the MEK/Erk and PI3K/Akt signaling pathway in the transformation of MDS to AML by modulating histone methylation via the trimethylation of H3 on lysine 27 (H3K27me3) methylase and demethylase pathways and by regulating distal-less homeobox 5 (DLX5) gene transcription which gene has previously determined to have an anti-tumor effect in AML an MDS [91, 92]. Another investigator examined phosphoproteins in MDS patients too. For example, Nyakern et al. observed high levels of phospho-Ser473-Akt in 90% of mononuclear cells separated from patients diagnosed with high-risk MDS. In contrast, low-risk MDS patients exhibited low level or absence of phosphorylated Akt protein [93]. In our study, we did not find correlation between the MDS risk score and presence of phosphorylated proteins.

Most patients with acute myeloid leukemia, especially patients with complex cytogenetics develop refractory or relapsed disease even in the presence of novel therapeutic agents and combined chemotherapy. For this reason, it is particularly important to develop new agents that target different mechanisms of leukemogenesis - specific genetic abnormalities or mutant proteins - and their personalized application can improve long-term remission. Numerous kinase inhibitors against constitutively activated cell signaling pathways have been developed. The agents listed below targeting the Akt or Erk signaling pathways are currently in various phases of active clinical trials or have been available in recently completed studies. The Raf inhibitor Sorafenib [94], the MEK inhibitor GDC-0973 (Cobimetinib) [95], the ERK1/2 inhibitor LY3214996 (Temuterkib) [96], a pan-class I PI3K inhibitor Rigosertib [97], Akt inhibitor MK2206 [98] and Akt/Erk inhibitor ONC201 [99] may be accessible for AML patients within the framework of clinical trials alone or in combination with other chemotherapeutic agents. Several clinical trials have been reported that the combination of hypomethylating agents (HMAs) Azacitidine or Decitabine and Venetoclax can increase the response rates and the overall survival for older or unfit newly diagnosed AML patients who are not suitable for intensive chemotherapy [100, 101]. These findings resulted in the United States Food and Drug Administration's (FDA) approval of this combination as a standard of care for this population. In addition, azacitidine has a place in the maintenance treatment [102] and in the treatment of relapsed or refractory AML in combination with Venetoclax or as a supplement to salvage chemotherapy [103, 104]. According to a recently published recommendation, venetoclax-based regimen is preferable in young adult leukemia patients too [105]. Patients with adverse genetic abnormalities (especially abnormalities of chromosome 5, 7, or 17 [106, 107], and mutated TP53 [108]) may benefit mostly from HMA treatment, and supplementing the therapy with Venetoclax is particularly recommended [109], although the treatment of patients with TP53 mutation remains a major challenge. The addition of Venetoclax to the therapeutic regimens may be of particular interest in p-Akt positive patients because it is known that Akt upregulates Bcl-2 expression [30] Beside the Venetoclax [110], BP1002, a liposomal Bcl-2 antisense oligodeoxynucleotide [111] is still available now in a clinical trial for AML patients. Furthermore, Akt activates Mdm2 [27], therefore Mdm2 antagonists, for example, Milademetan [100] and AMG-232 (Navtemadlin) [112] in the case of AML patients expressing phosphorylated Akt may be especially reasonable choices.

The role of DNA methylation [113, 114] and activation of the Akt and Erk signaling pathways [115, 116] in the development of chemoresistance is widely investigated. There is considerable evidence that both processes contribute to reduced sensitivity to chemotherapy agents. Thus, by attacking the leukemic cells at two points, therapeutic response can be improved in p-Akt and p-Erk

positive patients with a combination of HMAs and kinase inhibitors acting on the Akt and Erk signaling pathway.

Limitations of our study are the low number of cases, in some patients missing FLT3, nucleophosmin, and cytogenetics data, and the limited amount of samples. Resulting from this, each experiment could be repeated only a few times.

In summary, we identified subgroups of AML patients with hyperphosphorylated proteins with Western blot technique. Akt phosphorylation seems to have a negative impact on event-free survival, especially in patients with unfavorable cytogenetics. The presence of phosphorylated retinoblastoma improves the overall survival in the patients' group with unfavorable cytogenetics. The exact molecular mechanisms how these phosphorylated proteins influence survival is not clear, but presumably, patients with phosphorylated proteins may profit from targeted treatments especially kinase inhibitors supplemented with the standard therapy. Although our results need to be confirmed on a larger number of patients, it appears that in P-Akt positive patients more emphasis should be placed on targeted therapy and chemotherapy supplemented with HMA or Venetoclax respectively and they may be candidates for an early bone marrow transplantation because of unfavorable outcome and frequent relapse rate. The preference for the method applied here is that in the case of measurable peripheral leukemic blasts, it can be useful to specify the phosphorylated proteins without unpleasant bone marrow aspiration. In selected cases, it could be suitable for monitoring remission, relapse, or progression of disease.

Data availability statement

The original contributions presented in the study are included in the article/Supplementary Material, further inquiries can be directed to the corresponding author.

Ethics statement

The studies involving humans were approved by the Regional and Institutional Research Ethics Committee University of Debrecen. The studies were conducted in accordance with the local legislation and institutional requirements. The participants provided their written informed consent to participate in this study.

Author contributions

AM: design of research, experimental procedures, data analysis, writing the manuscript. KV: experimental procedures, data analysis. FE: design of research, providing laboratory background, supervision of experimental procedures, analyzing results, correction of the manuscript. MU: design of research, supervision of experimental procedures, correction of the manuscript. ÁI, correction of the manuscript. LR: design of research, collection of bone marrow specimens, supervision of experimental procedures, correction of the manuscript. All authors contributed to the article and approved the submitted version.

Funding

The authors declare financial support was received for the research, authorship, and/or publication of this article. The work was carried out at the Kálmán Laki Doctoral School, University of Debrecen. Funding is provided by the University of Debrecen and the Foundation "Harc Az Életért" of Szabolcs-Szatmár-Bereg County Teaching Hospital.

Acknowledgments

The authors are grateful to Andrea Kiss, Dóra Dedinszki and Zoltán Kónya (Department of Medical Chemistry, Faculty of Medicine, University of Debrecen, Debrecen, Hungary) for their help in Western blot experiments and Mrs. Ágnes Németh, Andrea Docsa (Department of Medical Chemistry, Faculty of Medicine, University of Debrecen, Debrecen, Hungary), Zsuzsanna Kiss, Mrs. Éva Baráth (Department of Internal Medicine, Faculty of Medicine, University of Debrecen, Debrecen, Hungary) for their technical assistance. The authors would like to acknowledge the support of Katalin Hodosi in respect of statistical analysis (Department of Internal Medicine, Faculty of Medicine, University of Debrecen, Debrecen, Hungary). A part of the content of the manuscript have previously appeared online as KV's dissertation [117].

Conflict of interest

The authors declare that the research was conducted in the absence of any commercial or financial relationships that could be construed as a potential conflict of interest.

Supplementary material

The Supplementary Material for this article can be found online at: https://www.por-journal.com/articles/10.3389/pore.2024.1611747/full#supplementary-material

References

1. Steelman LS, Franklin RA, Abrams SL, Chappell W, Kempf CR, Bäsecke J, et al. Roles of the Ras/Raf/MEK/ERK pathway in leukemia therapy. *Leukemia* (2011) 25: 1080–94. doi:10.1038/leu.2011.66

2. Martelli AM, Evangelisti C, Chappell W, Abrams SL, Bäsecke J, Stivala F, et al. Targeting the translational apparatus to improve leukemia therapy: roles of the PI3K/PTEN/Akt/mTOR pathway. *Leukemia* (2011) 25:1064–79. doi:10.1038/leu.2011.46

3. Kornblau SM, Xu HJ, Zhang W, Hu SX, Beran M, Smith TL, et al. Levels of retinoblastoma protein expression in newly diagnosed acute myelogenous leukemia. *Blood* (1994) 84:256–61. doi:10.1182/blood.v84.1.256.bloodjournal841256

4. Cheng X, Bennett RL, Liu X, Byrne M, Stratford May W. PKR negatively regulates leukemia progression in association with PP2A activation, Bcl-2 inhibition and increased apoptosis. *Blood Cancer J* (2013) 3:e144. doi:10.1038/bcj.2013.42

5. Grethe S, Pörn-Ares MI. p38 MAPK regulates phosphorylation of Bad via PP2A-dependent suppression of the MEK1/2-ERK1/2 survival pathway in TNF-alpha induced endothelial apoptosis. *Cell. Signal.* (2006) 18:531–40. doi:10.1016/j.cellsig.2005.05.023

6. Nakao M, Yokota S, Iwai T, Kaneko H, Horiike S, Kashima K, et al. Internal tandem duplication of the flt3 gene found in acute myeloid leukemia. *Leuk Off J Leuk Soc Am Leuk Res Fund, U.K* (1996) 10:1911–8.

7. Stirewalt DL, Radich JP. The role of FLT3 in haematopoietic malignancies. *Nat Rev Cancer* (2003) 3:650–65. doi:10.1038/nrc1169

8. Takahashi S. Downstream molecular pathways of FLT3 in the pathogenesis of acute myeloid leukemia: biology and therapeutic implications. *J Hematol Oncol* (2011) 4:13. doi:10.1186/1756-8722-4-13

9. Gary Gilliland D, Griffin JD. The roles of FLT3 in hematopoiesis and leukemia. *Blood* (2002) 100:1532–42. doi:10.1182/blood-2002-02-0492

10. Mizuki M, Fenski R, Halfter H, Matsumura I, Schmidt R, Müller C, et al. Flt3 mutations from patients with acute myeloid leukemia induce transformation of 32D cells mediated by the Ras and STAT5 pathways. *Blood* (2000) 96:3907–14. doi:10.1182/blood.v96.12.3907.h8003907_3907_3914

11. Zheng R, Friedman AD, Levis M, Li L, Weir EG, Small D, et al. Internal tandem duplication mutation of FLT3 blocks myeloid differentiation through suppression of C/EBPα expression. *Blood* (2004) 103:1883–90. doi:10.1182/blood-2003-06-1978

12. Pearson G, Robinson F, Beers Gibson T, Xu BE, Karandikar M, Berman K, et al. Mitogen-activated protein (MAP) kinase pathways: regulation and physiological functions. *Endocr Rev* (2001) 22:153–83. doi:10.1210/edrv.22.2.0428

13. Roux PP, Blenis J. ERK and p38 MAPK-activated protein kinases: a family of protein kinases with diverse biological functions. *Microbiol Mol Biol Rev* (2004) 68: 320–44. doi:10.1128/MMBR.68.2.320-344.2004

14. Ramos JW. The regulation of extracellular signal-regulated kinase (ERK) in mammalian cells. *Int J Biochem Cel Biol.* (2008) 40:2707–19. doi:10.1016/j.biocel.2008.04.009

15. Cargnello M, Roux PP. Activation and function of the MAPKs and their substrates, the MAPK-activated protein kinases. *Microbiol Mol Biol Rev* (2011) 75: 50–83. doi:10.1128/MMBR.00031-10

16. Omerovic J, Laude AJ, Prior IA. Ras proteins: paradigms for compartmentalised and isoform-specific signalling. *Cell. Mol. Life Sci.* (2007) 64: 2575–89. doi:10.1007/s00018-007-7133-8

17. Fukuda M, Gotoh Y, Nishida E. Interaction of MAP kinase with MAP kinase kinase: its possible role in the control of nucleocytoplasmic transport of MAP kinase. *EMBO J* (1997) 16:1901–8. doi:10.1093/emboj/16.8.1901

18. Marais R, Wynne J, Treisman R. The SRF accessory protein Elk-1 contains a growth factor-regulated transcriptional activation domain. *Cell* (1993) 73:381–93. doi:10.1016/0092-8674(93)90237-k

19. Kortenjann M, Thomae O, Shaw PE. Inhibition of v-raf-dependent c-fos expression and transformation by a kinase-defective mutant of the mitogen-activated protein kinase Erk2. *Mol Cel Biol.* (1994) 14:4815–24. doi:10.1128/mcb.14.7.4815

20. Sears R, Nuckolls F, Haura E, Taya Y, Tamai K, Nevins JR. Multiple Ras-dependent phosphorylation pathways regulate Myc protein stability. *Genes Dev* (2000) 14:2501–14. doi:10.1101/gad.836800

21. Owens DM, Keyse SM. Differential regulation of MAP kinase signalling by dual-specificity protein phosphatases. *Oncogene* (2007) 26:3203–13. doi:10.1038/sj.onc.1210412

22. Van Kanegan MJ, Adams DG, Wadzinski BE, Strack S. Distinct protein phosphatase 2A heterotrimers modulate growth factor signaling to extracellular signal-regulated kinases and Akt. *J Biol Chem* (2005) 280:36029–36. doi:10.1074/jbc.M506986200

23. Dedinszki D, Kiss A, Márkász L, Márton A, Tóth E, Székely L, et al. Inhibition of protein phosphatase-1 and -2A decreases the chemosensitivity of leukemic cells to chemotherapeutic drugs. *Cel Signal.* (2015) 27:363–72. doi:10.1016/j.cellsig.2014.11.021

24. Datta SR, Dudek H, Tao X, Masters S, Fu H, Gotoh Y, et al. Akt phosphorylation of BAD couples survival signals to the cell-intrinsic death machinery. *Cell* (1997) 91:231–41. doi:10.1016/s0092-8674(00)80405-5

25. Cardone MH, Roy N, Stennicke HR, Salvesen GS, Franke TF, Stanbridge E, et al. Regulation of cell death protease caspase-9 by phosphorylation. *Science* (1998) 282:1318–21. doi:10.1126/science.282.5392.1318

26. Brunet A, Bonni A, Zigmond MJ, Lin MZ, Juo P, Hu LS, et al. Akt promotes cell survival by phosphorylating and inhibiting a Forkhead transcription factor. *Cell* (1999) 96:857–68. doi:10.1016/s0092-8674(00)80595-4

27. Mayo LD, Donner DB. A phosphatidylinositol 3-kinase/Akt pathway promotes translocation of Mdm2 from the cytoplasm to the nucleus. *Proc Natl Acad Sci U S A* (2001) 98:11598–603. doi:10.1073/pnas.181181198

28. Kane LP, Shapiro VS, Stokoe D, Weiss A. Induction of NF-kappaB by the Akt/PKB kinase. *Curr Biol* (1999) 9:601–4. doi:10.1016/s0960-9822(99)80265-6

29. Du K, Montminy M. CREB is a regulatory target for the protein kinase Akt/PKB. *J Biol Chem* (1998) 273:32377–9. doi:10.1074/jbc.273.49.32377

30. Pugazhenthit S, Nesterova A, Sable C, Heidenreich KA, Boxer LM, Heasley LE, et al. Akt/protein kinase B up-regulates Bcl-2 expression through cAMP-response element-binding protein. *J Biol Chem* (2000) 275:10761–6. doi:10.1074/jbc.275.15.10761

31. Diehl JA, Cheng M, Roussel MF, Sherr CJ. Glycogen synthase kinase-3beta regulates cyclin D1 proteolysis and subcellular localization. *Genes Dev* (1998) 12: 3499–511. doi:10.1101/gad.12.22.3499

32. Alessi DR, Andjelkovic M, Caudwell B, Cron P, Morrice N, Cohen P, et al. Mechanism of activation of protein kinase B by insulin and IGF-1. *EMBO J* (1996) 15:6541–51. doi:10.1002/j.1460-2075.1996.tb01045.x

33. Sarbassov DD, Guertin D. a, Ali, S. M. and Sabatini, D. M. Phosphorylation and regulation of Akt/PKB by the rictor-mTOR complex. *Science* (2005) 307: 1098–101. doi:10.1126/science.1106148

34. Wu X, Senechal K, Neshat MS, Whang YE, Sawyers CL. The PTEN/MMAC1 tumor suppressor phosphatase functions as a negative regulator of the phosphoinositide 3-kinase/Akt pathway. *Proc Natl Acad Sci U S A* (1998) 95: 15587–91. doi:10.1073/pnas.95.26.15587

35. Stambolic V, Suzuki A, de la Pompa JL, Brothers GM, Mirtsos C, Sasaki T, et al. Negative regulation of PKB/Akt-dependent cell survival by the tumor suppressor PTEN. *Cell* (1998) 95:29–39. doi:10.1016/s0092-8674(00)81780-8

36. Gao T, Furnari F, Newton AC. PHLPP: a phosphatase that directly dephosphorylates Akt, promotes apoptosis, and suppresses tumor growth. *Mol Cel* (2005) 18:13–24. doi:10.1016/j.molcel.2005.03.008

37. Weinberg RA. The retinoblastoma protein and cell cycle control. *Cell* (1995) 81:323–30. doi:10.1016/0092-8674(95)90385-2

38. Pearson BE, Nasheuer HP, Wang TS. Human DNA polymerase alpha gene: sequences controlling expression in cycling and serum-stimulated cells. *Mol Cel Biol* (1991) 11:2081–95. doi:10.1128/mcb.11.4.2081

39. Ohtani K, DeGregori J, Nevins JR. Regulation of the cyclin E gene by transcription factor E2F1. *Proc Natl Acad Sci U S A* (1995) 92:12146–50. doi:10.1073/pnas.92.26.12146

40. Morris EJ, Dyson NJ. Retinoblastoma protein partners. *Adv Cancer Res* (2001) 82:1–54. doi:10.1016/S0065-230X(01)82001-7

41. Brehms A, Miska EA, McCance DJ, Reid JL, Bannister AJ, Kouzarides T. Retinoblastoma protein recruits histone deacetylase to repress transcription. *Nature* (1998) 391:597–601. doi:10.1038/35404

42. Lukas J, Bartkova J, Bartek J. Convergence of mitogenic signalling cascades from diverse classes of receptors at the cyclin D-cyclin-dependent kinase-pRb-controlled G1 checkpoint. *Mol Cel Biol.* (1996) 16:6917–25. doi:10.1128/mcb.16.12.6917

43. Chellappan SP, Hiebert S, Mudryj M, Horowitz JM, Nevins JR. The E2F transcription factor is a cellular target for the RB protein. *Cell* (1991) 65:1053–61. doi:10.1016/0092-8674(91)90557-f

44. La Thangue NB. DRTF1/E2F: an expanding family of heterodimeric transcription factors implicated in cell-cycle control. *Trends Biochem Sci* (1994) 19:108–14. doi:10.1016/0968-0004(94)90202-x

45. Knudsen ES, Wang JYJ. Differential regulation of retinoblastoma protein function by specific Cdk phosphorylation sites. *J Biol Chem* (1996) 271:8313–20. doi:10.1074/jbc.271.14.8313

46. Kornblau SM, Andreeff M, Hu SX, Xu HJ, Patel S, Theriault A, et al. Low and maximally phosphorylated levels of the retinoblastoma protein confer poor prognosis in newly diagnosed acute myelogenous leukemia: a prospective study. *Clin Cancer Res* (1998) 4:1955–63.

47. Kolupaeva V, Janssens V. PP1 and PP2A phosphatases - cooperating partners in modulating retinoblastoma protein activation. *FEBS J* (2013) 280:627–43. doi:10.1111/j.1742-4658.2012.08511.x

48. Venney D, Mohd-Sarip A, Mills KI. The impact of epigenetic modifications in myeloid malignancies. *Int J Mol Sci* (2021) 22(9):5013. doi:10.3390/ijms22095013

49. Fong CY, Morison J, Dawson MA. Epigenetics in the hematologic malignancies. *Haematologica* (2014) 99:1772–83. doi:10.3324/haematol.2013.092007

50. Yang Q, Jiang W, Hou P. Emerging role of PI3K/AKT in tumor-related epigenetic regulation. *Semin Cancer Biol* (2019) 59:112–24. doi:10.1016/j.semcancer.2019.04.001

51. Spangle JM, Roberts TM, Zhao JJ. The emerging role of PI3K/AKT-mediated epigenetic regulation in cancer. *Biochim Biophys Acta - Rev Cancer* (2017) 1868:123–31. doi:10.1016/j.bbcan.2017.03.002

52. Li J, Wang R, Hu X, Gao Y, Wang Z, Li J, et al. Activated MEK/ERK pathway drives widespread and coordinated overexpression of UHRF1 and DNMT1 in cancer cells. *Sci Rep* (2019) 9:907. doi:10.1038/s41598-018-37258-3

53. Suganuma T, Workman JL. MAP kinases and histone modification. *J Mol Cel Biol.* (2012) 4:348–50. doi:10.1093/jmcb/mjs043

54. Guzman F, Fazeli Y, Khuu M, Salcido K, Singh S, Benavente CA. Retinoblastoma tumor suppressor protein roles in epigenetic regulation. *Cancers (Basel).* (2020) 12:2807. doi:10.3390/cancers12102807

55. Lamba JK, Cao X, Raimondi S, Downing J, Ribeiro R, Gruber TA, et al. Dna methylation clusters and their relation to cytogenetic features in pediatric aml. *Cancers (Basel).* (2020) 12:3024. doi:10.3390/cancers12103024

56. Arber DA, Orazi A, Hasserjian R, Thiele J, Borowitz MJ, Le Beau MM, et al. The 2016 revision to the World Health Organization classification of myeloid neoplasms and acute leukemia. *Blood* (2016) 127:2391–405. doi:10.1182/blood-2016-03-643544

57. Döhner H, Estey E, Grimwade D, Amadori S, Appelbaum FR, Büchner T, et al. Diagnosis and management of AML in adults: 2017 ELN recommendations from an international expert panel. *Blood* (2017) 129:424–47. doi:10.1182/blood-2016-08-733196

58. Greenberg PL, Tuechler H, Schanz J, Sanz G, Garcia-Manero G, Solé F, et al. Revised international prognostic scoring system for myelodysplastic syndromes. *Blood* (2012) 120:2454–65. doi:10.1182/blood-2012-03-420489

59. Gandevia B, Tovell A. Australia's first medical library. *Med J Aust* (1964) 2:91–2. doi:10.5694/j.1326-5377.1973.tb128668.x

60. Cheson BD, Bennett JM, Kopecky KJ, Büchner T, Willman CL, Estey EH, et al. Revised Recommendations of the International Working Group for diagnosis, standardization of response criteria, treatment outcomes, and reporting standards for therapeutic trials in acute myeloid leukemia. *J Clin Oncol* (2003) 21:4642–9. doi:10.1200/JCO.2003.04.036

61. Selmeczi A, Udvardy M, Illés A, Telek B, Kiss A, Batár P, et al. Treatment of acute myeloid leukemia -- a single center experience (2007-2013). *Orv Hetil* (2014) 155:653–8. doi:10.1556/oh.2014.29884

62. Schiller G, Lee M. Long-term outcome of high-dose cytarabine-based consolidation chemotherapy for older patients with acute myelogenous leukemia. *Lymphoma* (1997) 25:111–9. doi:10.3109/10428199709042501

63. Fernandez HF, Sun Z, Yao X, Litzow MR, Luger SM, Paietta EM, et al. Anthracycline dose intensification in acute myeloid leukemia. *N Engl J Med* (2009) 361:1249–59. doi:10.1056/nejmoa0904544

64. Sanz MA, Martín G, Rayón C, Esteve J, González M, Díaz-Mediavilla J, et al. A modified AIDA protocol with anthracycline-based consolidation results in high antileukemic efficacy and reduced toxicity in newly diagnosed PML/RARalpha-positive acute promyelocytic leukemia. PETHEMA group. *Blood* (1999) 94:3015–21.

65. Parker JE, Pagliuca A, Mijovic A, Cullis JO, Czepulkowski B, Rassam SM, et al. Fludarabine, cytarabine, G-CSF and idarubicin (FLAG-IDA) for the treatment of poor-risk myelodysplastic syndromes and acute myeloid leukaemia. *Br J Haematol* (1997) 99:939–44. doi:10.1046/j.1365–2141.1997.4763281.x

66. Hiddemann W, Kreutzmann H, Straif K, Ludwig WD, Mertelsmann R, Donhuijsen-Ant R, et al. High-dose cytosine arabinoside and mitoxantrone: a highly effective regimen in refractory acute myeloid leukemia. *Blood* (1987) 69:744–9. doi:10.1182/blood.v69.3.744.bloodjournal693744

67. Amadori S, Arcese W, Isacchi G, Meloni G, Petti MC, Monarca B, et al. Mitoxantrone, etoposide, and intermediate-dose cytarabine: an effective and tolerable regimen for the treatment of refractory acute myeloid leukemia. *J Clin Oncol* (1991) 9:1210–4. doi:10.1200/JCO.1991.9.7.1210

68. Schmid C, Schleuning M, Ledderose G, Tischer J, Kolb HJ. Sequential regimen of chemotherapy, reduced-intensity conditioning for allogeneic stem-cell transplantation, and prophylactic donor lymphocyte transfusion in high-risk acute myeloid leukemia and myelodysplastic syndrome. *J Clin Oncol* (2005) 23:5675–87. doi:10.1200/JCO.2005.07.061

69. Wierzbowska A, Robak T, Pluta A, Wawrzyniak E, Cebula B, Hołowiecki J, et al. Cladribine combined with high doses of arabinoside cytosine, mitoxantrone, and G-CSF (CLAG-M) is a highly effective salvage regimen in patients with refractory and relapsed acute myeloid leukemia of the poor risk: a final report of the Polish Adult Leukemia Group. *Eur J Haematol* (2008) 80:115–26. doi:10.1111/j.1600–0609.2007.00988.x

70. ScienceDirect. *Event free survival - an overview* (2022). Available from: https://www.sciencedirect.com/topics/medicine-and-dentistry/event-free-survival Accessed 2019.

71. Min YH, Eom JI, Cheong JW, Maeng HO, Kim JY, Jeung HK, et al. Constitutive phosphorylation of Akt/PKB protein in acute myeloid leukemia: its significance as a prognostic variable. *Leukemia* (2003) 17:995–7. doi:10.1038/sj.leu.2402874

72. Ricciardi MR, McQueen T, Chism D, Milella M, Estey E, Kaldjian E, et al. Quantitative single cell determination of ERK phosphorylation and regulation in relapsed and refractory primary acute myeloid leukemia. *Leukemia* (2005) 19:1543–9. doi:10.1038/sj.leu.2403859

73. Lv D, Yang H, Wang W, Xie Y, Hu W, Ye M, et al. High PHLPP expression is associated with better prognosis in patients with resected lung adenocarcinoma. *BMC Cancer* (2015) 15:687. doi:10.1186/s12885-015-1711-1

74. Wang Z, Shu H, Wang Z, Li G, Cui J, Wu H, et al. Loss expression of PHLPP1 correlates with lymph node metastasis and exhibits a poor prognosis in patients with gastric cancer. *J Surg Oncol* (2013) 108:427–32. doi:10.1002/jso.23419

75. Ono T, Nakamura S, Kazuyuki S, Takeshita K, Keiji O, Hirano I, et al. Expression analysis and prognostic significance of the PHLPP gene in acute leukemias and myelodysplastic syndromes. *Blood* (2007) 110:4234. doi:10.1182/blood.v110.11.4234.4234

76. Zou XL, Liu T, Meng WT, Huang XO. Expression of tumor suppressor gene pten in patients with myelodysplastic syndrome and acute myeloid leukemia. *Zhongguo Shi Yan Xue Ye Xue Za Zhi* (2008) 16:1086–90.

77. Shen Q, Chen Z, Liu XP, Xing HY, Wang M, Wang JX. Expression of PTEN mRNA in acute leukemia and its clinical significance. *Zhonghua Xue Ye Xue Za Zhi* (2005) 26:493–6.

78. Huang X, Li D, Li T, Zhao B, Chen X. Prognostic value of the expression of phosphatase and tensin homolog and CD44 in elderly patients with refractory acute myeloid leukemia. *Oncol Lett* (2015) 10:103–10. doi:10.3892/ol.2015.3189

79. Xie J, Qian J, Yang J, Wang S, Freeman ME, Yi Q. Critical roles of Raf/MEK/ERK and PI3K/AKT signaling and inactivation of p38 MAP kinase in the differentiation and survival of monocyte-derived immature dendritic cells. *Exp Hematol* (2005) 33:564–72. doi:10.1016/j.exphem.2005.03.001

80. Miranda MB, Johnson DE. Signal transduction pathways that contribute to myeloid differentiation. *Leukemia* (2007) 21:1363–77. doi:10.1038/sj.leu.2404690

81. Pei S, Pollyea DA, Gustafson A, Stevens BM, Minhajuddin M, Fu R, et al. Monocytic subclones confer resistance to venetoclax-based therapy in patients with acute myeloid leukemia. *Cancer Discov* (2020) 10:536–51. doi:10.1158/2159-8290.CD-19-0710

82. Sancho M, Leiva D, Lucendo E, Orzáez M. Understanding MCL1: from cellular function and regulation to pharmacological inhibition. *FEBS J* (2022) 289:6209–34. doi:10.1111/febs.16136

83. Liu J, Chen Y, Yu L, Yang L. Mechanisms of venetoclax resistance and solutions. *Front Oncol* (2022) 12:1005659. doi:10.3389/fonc.2022.1005659

84. Huang S, Jiang C, Guo H, Wang J, Liu Y, Li C, et al. Resistance mechanisms underlying venetoclax resistance in mantle cell lymphoma. *Blood* (2017) 130:2749.

85. Alkhatabi HA, Zohny SF, Shait Mohammed MR, Choudhry H, Rehan M, Ahmad A, et al. Venetoclax-resistant MV4-11 leukemic cells activate PI3K/AKT pathway for metabolic reprogramming and redox adaptation for survival. *Antioxidants* (2022) 11:461. doi:10.3390/antiox11030461

86. Li X, Su Y, Hege K, Madlambayan G, Edwards H, Knight T, et al. The HDAC and PI3K dual inhibitor CUDC-907 synergistically enhances the antileukemic activity of venetoclax in preclinical models of acute myeloid leukemia. *Haematologica* (2020) 106:1262–77. doi:10.3324/haematol.2019.233445

87. Zagorski WA, Knudsen ES, Reed MF. Retinoblastoma deficiency increases chemosensitivity in lung cancer. *Cancer Res* (2007) 67:8264–73. doi:10.1158/0008–5472.CAN-06-4753

88. Derenzini M, Donati G, Mazzini G, Montanaro L, Vici M, Ceccarelli C, et al. Loss of retinoblastoma tumor suppressor protein makes human breast cancer cells more sensitive to antimetabolite exposure. *Clin Cancer Res* (2008) 14:2199–209. doi:10.1158/1078–0432.CCR-07-2065

89. Treré D, Brighenti E, Donati G, Ceccarelli C, Santini D, Taffurelli M, et al. High prevalence of retinoblastoma protein loss in triple-negative breast cancers and its association with a good prognosis in patients treated with adjuvant chemotherapy. *Ann Oncol* (2009) 20:1818–23. doi:10.1093/annonc/mdp209

90. Zheng Z, Chen X, Zhang Y, Ren F, Ma Y. MEK/ERK and PI3K/AKT pathway inhibitors affect the transformation of myelodysplastic syndrome into acute myeloid leukemia via H3K27me3 methylases and de-methylases. *Int J Oncol* (2023) 63:140. doi:10.3892/ijo.2023.5588

91. Zhang T, Xu ZJ, Gu Y, Wen XM, Ma JC, Zhang W, et al. Identification and validation of prognosis-related *DLX5* methylation as an epigenetic driver in myeloid neoplasms. *Clin Transl Med* (2020) 10:e29. doi:10.1002/ctm2.29

92. Zheng Z, Li L, Li G, Zhang Y, Dong C, Ren F, et al. EZH2/EHMT2 histone methyltransferases inhibit the transcription of DLX5 and promote the transformation of myelodysplastic syndrome to acute myeloid leukemia. *Front Cel Dev. Biol.* (2021) 9:619795. doi:10.3389/fcell.2021.619795

93. Nyåkern M, Tazzari PL, Finelli C, Bosi C, Follo MY, Grafone T, et al. Frequent elevation of Akt kinase phosphorylation in blood marrow and peripheral blood mononuclear cells from high-risk myelodysplastic syndrome patients. *Leukemia* (2006) 20:230–8. doi:10.1038/sj.leu.2404057

94. Zhang W, Konopleva M, Shi Y, McQueen T, Harris D, Ling X, et al. Mutant FLT3: a direct target of sorafenib in acute myelogenous leukemia. *J Natl Cancer Inst* (2008) 100:184–98. doi:10.1093/jnci/djm328

95. Konopleva MY, Dail M, Daver NG, Garcia JS, Jonas BA, Yee KWL, et al. Venetoclax and cobimetinib in relapsed/refractory AML: a phase 1b trial. *Clin Lymphoma Myeloma Leuk* (2024) 24:364–74. doi:10.1016/j.clml.2024.01.007

96. Weisberg E, Meng C, Case A, Sattler M, Tiv HL, Gokhale PC, et al. Evaluation of ERK as a therapeutic target in acute myelogenous leukemia. *Leukemia* (2020) 34:625–9. doi:10.1038/s41375-019-0552-3

97. Navada SC, Garcia-Manero G, OdchimarReissig R, Pemmaraju N, Alvarado Y, Ohanian MN, et al. Rigosertib in combination with azacitidine in patients with myelodysplastic syndromes or acute myeloid leukemia: results of a phase 1 study. *Leuk Res* (2020) 94:106369. doi:10.1016/j.leukres.2020.106369

98. Konopleva MY, Walter RB, Faderl SH, Jabbour EJ, Zeng Z, Borthakur G, et al. Preclinical and early clinical evaluation of the oral AKT inhibitor, MK-2206, for the treatment of acute myelogenous leukemia. *Clin Cancer Res* (2014) 20:2226–35. doi:10.1158/1078–0432.CCR-13-1978

99. Bhatt VR, Wichman C, Bouska AC, Maness L, Al-Kadhimi ZS, Iqbal J, et al. Novel first-in-class drug ONC201 as a post-transplant maintenance for AML and MDS: a phase I trial in progress. *Blood* (2022) 140:12918–9. doi:10.1182/blood-2022-156316

100. DiNardo CD, Pratz K, Pullarkat V, Jonas BA, Arellano M, Becker PS, et al. Venetoclax combined with decitabine or azacitidine in treatment-naive, elderly patients with acute myeloid leukemia. *Blood* (2019) 133:7–17. doi:10.1182/blood-2018-08-868752

101. DiNardo CD, Pratz KW, Letai A, Jonas BA, Wei AH, Thirman M, et al. Safety and preliminary efficacy of venetoclax with decitabine or azacitidine in elderly patients with previously untreated acute myeloid leukaemia: a non-randomised, open-label, phase 1b study. *Lancet Oncol* (2018) 19:216–28. doi:10.1016/S1470-2045(18)30010-X

102. Döhner H, Wei AH, Appelbaum FR, Craddock C, DiNardo CD, Dombret H, et al. Diagnosis and management of AML in adults: 2022 recommendations from an international expert panel on behalf of the ELN. *Blood* (2022) 140:1345–77. doi:10.1182/blood.2022016867

103. Kantarjian H, Kadia T, DiNardo C, Daver N, Borthakur G, Jabbour E, et al. Acute myeloid leukemia: current progress and future directions. *Blood Cancer J* (2021) 11:41. doi:10.1038/s41408-021-00425-3

104. Premnath N, Madanat YF. Paradigm shift in the management of acute myeloid leukemia—approved options in 2023. *Cancers (Basel).* (2023) 15:3002. doi:10.3390/cancers15113002

105. Chatzikalil E, Roka K, Diamantopoulos PT, Rigatou E, Avgerinou G, Kattamis A, et al. Venetoclax combination treatment of acute myeloid leukemia in adolescents and young adult patients. *J Clin Med* (2024) 13:2046. doi:10.3390/jcm13072046

106. Raj K, John A, Ho A, Chronis C, Khan S, Samuel J, et al. CDKN2B methylation status and isolated chromosome 7 abnormalities predict responses to treatment with 5-azacytidine. *Leukemia* (2007) 21:1937–44. doi:10.1038/sj.leu.2404796

107. Greve G, Schüler J, Grüning BA, Berberich B, Stomper J, Zimmer D, et al. Decitabine induces gene derepression on monosomic chromosomes: *in vitro* and *in vivo* effects in adverse-risk cytogenetics AML. *Cancer Res* (2021) 81:834–46. doi:10.1158/0008-5472.CAN-20-1430

108. Welch JS, Petti AA, Miller CA, Fronick CC, O'Laughlin M, Fulton RS, et al. *TP53* and decitabine in acute myeloid leukemia and myelodysplastic syndromes. *N Engl J Med* (2016) 375:2023–36. doi:10.1056/NEJMoa1605949

109. Pollyea DA, Pratz KW, Wei AH, Pullarkat V, Jonas BA, Recher C, et al. Outcomes in patients with poor-risk cytogenetics with or without *TP53* mutations treated with venetoclax and azacitidine. *Clin Cancer Res* (2022) 28:5272–9. doi:10.1158/1078-0432.CCR-22-1183

110. Pollyea DA, Amaya M, Strati P, Konopleva MY. Venetoclax for AML: changing the treatment paradigm. *Blood Adv* (2019) 3:4326–35. doi:10.1182/bloodadvances.2019000937

111. Konopleva M, Tari AM, Estrov Z, Harris D, Xie Z, Zhao S, et al. Liposomal Bcl-2 antisense oligonucleotides enhance proliferation, sensitize acute myeloid leukemia to cytosine-arabinoside, and induce apoptosis independent of other antiapoptotic proteins. *Blood* (2000) 95:3929–38. doi:10.1182/blood.v95.12.3929.012k01_3929_3938

112. Erba HP, Becker PS, Shami PJ, Grunwald MR, Flesher DL, Zhu M, et al. Phase 1b study of the MDM2 inhibitor AMG 232 with or without trametinib in relapsed/refractory acute myeloid leukemia. *Blood Adv* (2019) 3:1939–49. doi:10.1182/bloodadvances.2019030916

113. Kantharidis P, El-Osta A, deSilva M, Wall DM, Hu XF, Slater A, et al. Altered methylation of the human MDR1 promoter is associated with acquired multidrug resistance. *Clin Cancer Res* (1997) 3:2025–32.

114. Baker EK, El-Osta A. The rise of DNA methylation and the importance of chromatin on multidrug resistance in cancer. *Exp Cel Res.* (2003) 290:177–94. doi:10.1016/s0014-4827(03)00342-2

115. Lee S, Rauch J, Kolch W. Targeting MAPK signaling in cancer: mechanisms of drug resistance and sensitivity. *Int J Mol Sci* (2020) 21:1102. doi:10.3390/ijms21031102

116. Zhang J, Gu Y, Chen B. Mechanisms of drug resistance in acute myeloid leukemia. *Onco Targets Ther* (2019) 12:1937–45. doi:10.2147/OTT.S191621

117. Veres KB. *A retinoblasztoma fehérje (Rb), az Akt-kináz, Erk-kináz és a Bcl-2 fehérje foszforiláltsági állapotának vizsgálata akut myeloid leukémiás és mielodiszpláziás szindrómás betegekben*. Dissertation. Debrecen: University of Debrecen (2014).

Glossary

ABMT	Allogenic bone marrow transplantation
AML	Acute myeloid leukemia
APL	Acute promyelocytic leukemia
Ara-C	Cytosine arabinoside
Bad	Bcl-2 Associated Agonist Of Cell Death
Bax	Bcl-2-associated X protein
BCA	Bicinchoninic acid
Bcl-2	B-cell lymphoma 2
cAMP	Cyclic Adenosine Monophosphate
CDK	Cyclin dependent kinase
CR	Complete remission
CREB	cAMP response element-binding protein
ECL	Enhanced chemiluminescence
EFS	Event free survival
Erk	extracellular signal-regulated kinases
FAB	French-American-British classification
FLT-3	Fms-like tyrosine kinase 3
FOXO	Forkhead box O
GAPDH	Glyceraldehyde-3-phosphate-dehydrogenase
GSK-3β	glycogen synthase kinase-3beta
HDAC	Histone deacetylase
HMAs	Hypomethylating agents
ITD	Internal tandem duplication
MAPKs	Mitogen-activated protein kinases
MCL-1	Myeloid cell leukemia-1
Mdm2	Mouse double minute 2
MDS	Myelodysplastic syndrome
MKPs	Mitogen-activated protein kinase phosphatases
MPAL	Mixed phenotype acute leukemia
MRC	Myelodysplasia-related changes
mTOR	Mammalian target of rapamycin
NFκB	Nuclear factor kappa-light-chain-enhancer of activated B cells
NMPc	Cytoplasmic nucleophosmin
OS	Overall survival
P-Akt	Phosphorylated-Akt
PBS	Phosphate-buffered saline
PDK1/2	Phosphoinositide-dependent protein kinase 1/2
P-Erk	Phosphorylated- extracellular signal-regulated kinases
PHLPP	PH domain and leucine-rich repeat Protein Phosphatase
PIP3	Phosphatidylinositol (3,4,5)-triphosphate
PIP3K	Phosphoinositide 3-kinases
PKB	Protein kinase B
PNH	Paroxysmal nocturnal hemoglobinuria
PP1	Protein phosphatase-1
PP2A	Protein phosphatase-2A
P-Rb	Phosphorylated-retinoblastoma
PTEN	Phosphatase and tensin homolog
Rb	Retinoblastoma
R-IPSS	Revised International Prognostic Scoring System
SDS	Na-dodecyl sulfate
TBS	Tris-Buffered Saline
TKD	Tyrosine kinase domain mutations
WBC	White blood cell
WHO	World Health Organization

Pathology & Oncology Research | frontiers

TYPE Original Research
PUBLISHED 18 October 2024
DOI 10.3389/pore.2024.1611882

Check for updates

OPEN ACCESS

EDITED BY
Jozsef Dudas,
Innsbruck Medical University, Austria

*CORRESPONDENCE
Gábor Barna,
barna.gabor@semmelweis.hu
Ágnes Márk,
kovacsne.mark.agnes@semmelweis.hu

‡These authors have contributed equally to this work

RECEIVED 18 June 2024
ACCEPTED 01 October 2024
PUBLISHED 18 October 2024

CITATION
Czeti Á, Sashalmi S, Takács F, Szalóki G, Kriston C, Varga G, Farkas P, Hamed A, Márk Á and Barna G (2024) Investigating the effect of immunomagnetic separation on the immunophenotype and viability of plasma cells in plasma cell disorders.
Pathol. Oncol. Res. 30:1611882.
doi: 10.3389/pore.2024.1611882

COPYRIGHT
© 2024 Czeti, Sashalmi, Takács, Szalóki, Kriston, Varga, Farkas, Hamed, Márk and Barna. This is an open-access article distributed under the terms of the Creative Commons Attribution License (CC BY). The use, distribution or reproduction in other forums is permitted, provided the original author(s) and the copyright owner(s) are credited and that the original publication in this journal is cited, in accordance with accepted academic practice. No use, distribution or reproduction is permitted which does not comply with these terms.

Investigating the effect of immunomagnetic separation on the immunophenotype and viability of plasma cells in plasma cell disorders

Ágnes Czeti [1], Soma Sashalmi[1], Ferenc Takács [1], Gábor Szalóki [1], Csilla Kriston [1], Gergely Varga[2], Péter Farkas[2], Aryan Hamed[3], Ágnes Márk [1*‡] and Gábor Barna [1*‡]

[1]Department of Pathology and Experimental Cancer Research, Semmelweis University, Faculty of Medicine, Budapest, Hungary, [2]Department of Internal Medicine and Haematology, Semmelweis University, Faculty of Medicine, Budapest, Hungary, [3]Department of Haematology, Aladar Petz County Teaching Hospital, Győr, Hungary

Plasma cell enrichment plays a pivotal role in the accurate prognosis and molecular characterization of multiple myeloma. The separation is commonly carried out by positive cell selection using CD138 monoclonal antibody conjugated to magnetic beads. Optimally, during the separation procedure, the cells should neither be damaged, nor should their phenotype be significantly altered, as these changes would falsify the results if the isolated cells were subsequently used. For this reason, we investigated the expression patterns of different surface markers by flow cytometry before and after magnetic isolation using bone marrow or peripheral blood samples from 12 patients with plasma cell disorders. The selected markers are not only used as backbone markers in routine diagnostics (CD19, CD38, CD45, CD117, and CD138), but they also play an important role in cell adhesion and connection with microenvironment (CD44, CD49d, CD56, and CD81) or possibly drug resistance (CD69, CD86, and CD184), making them promising targets for myeloma research. Moreover, we examined the effects of separation on cell viability in 8 cases. The intensities of 8 out of the 12 investigated markers were slightly influenced, while CD138, CD38, CD56, and CD184 were changed significantly, however the immunophenotype of the cells was not changed. Positive markers remained positive and negative ones remained negative after the separation procedure. In addition, the number of apoptotic plasma cells was significantly reduced during separation, facilitating further examination of the cells. Our results showed that magnetic isolation can be considered as a reliable

option but the immunophenotype of plasma cells should be validated after the separation if the intensities of the markers are important for further experiments.

KEYWORDS

multiple myeloma, flow cytometry, immunomagnetic separation, immunophenotype, positive selection

Introduction

Multiple myeloma (MM) is a currently incurable malignant disease of plasma cells. It is the second most common hematologic malignancy, accounting for more than 15% of all hematologic tumors in the United States [1]. In this disease, myeloma cells can be present in various proportions in both bone marrow (BM) and peripheral blood (PB) [2].

Low percentage of tumor cells and the presence of other, non-malignant cells in the samples may make the diagnostic procedures (e.g., fluorescence *in situ* hybridization) or the research of the molecular mechanisms of the disease (e.g., gene expression profiling) more challenging [3–6]. Therefore, the enrichment of the plasma cells is crucial to detect chromosomal aberrations or studying myeloma cells at the molecular or protein level.

One of the most commonly used methods is immunomagnetic isolation, which can be used to produce a highly pure, homogeneous cell population quickly and in a relatively cost-efficient way. This technique is based on antibodies conjugated to magnetic beads that bind a marker on the surface of the target cells we aim to enrich. Then, by placing the sample in a magnetic field, the magnetically labeled cells are separated from the other cells (positive selection). Purification of myeloma cells is often performed by this method using anti-CD138 monoclonal antibodies conjugated to magnetic beads, since plasma cells, in contrast to other cells in the bone marrow, express high levels of the proteoglycan CD138 (syndecan-1) [7–9].

It is crucial to maintain the phenotype of the cells unaltered throughout the separation procedure, as any modification could significantly skew the results. This is particularly important in experiments assessing the presence of surface markers.

Despite the potentially serious consequences, we have only found limited studies from a single research group in the literature [10, 11] that investigated the effects of magnetic separation on the immunophenotype of myeloma cells. In their most recent research, Bansal et al. reported a significant decrease in several surface markers (e.g., CD138, CD11a, CD49e, and CD69) as a result of separation.

Therefore, in this paper, we aimed to study and validate whether CD138-based immunomagnetic separation affects the phenotype or viability of myeloma cells. We examined the protein expression patterns of various surface markers by flow cytometry before and after isolation. The studied markers are of great importance in clinical research as they are either used as backbone markers in routine diagnostics (CD19, CD38, CD45, CD117, and CD138) [12], involved in cell adhesion and connection with microenvironment (CD44, CD49d, CD56, and CD81) [13–15], or possibly in drug resistance (CD69, CD86, and CD184) [16–19].

For this reason, it is crucial to investigate whether and how the expression of these markers changes during immunomagnetic separation.

Materials and methods

Patient samples

We analyzed 12 samples (11 BM from myeloma and 1 PB from plasma cell leukemia patients) by flow cytometry. The samples were collected in EDTA (ethylenediamine tetraacetic acid) tubes. A total of seven women [median age: 64 years (50–79)] and five men (median age: 69 years [53–86]) were enrolled in the study. The clinical parameters of the samples are summarized in Supplementary Table S1. The diagnoses were made according to the recommendations of the World Health Organization [20] and the International Myeloma Working Group (IMWG) [21]. Following the recommendations of J. Cumova et al. [7], all of our samples contained at least 5% plasma cells (PC) among all BM or PB cells. The mean percentage of malignant plasma cells was 26.6% [9.3%–56.3%] relative to all cells in the samples. All samples were processed within 1 day of collection. The study was conducted in accordance with the Declaration of Helsinki and approved by the local ethics committee (ethical approval number: SE RKEB: 214/2020).

Immunomagnetic separation of CD138+ cells

Plasma cells were enriched from samples using the EasySep™ Human Whole Blood and Bone Marrow CD138 Positive Selection Kit II (StemCell Technologies, Vancouver, BC, Canada). First, samples (at least 1 mL of bone marrow or peripheral blood), were filtered through a 40 μm filter, then red blood cells were lysed without fixation (BD Pharm Lyse™,

TABLE 1 Overview table of antibodies used in our experiments.

Laser	*Violet* 405nm, 40 mW			*Blue* 488nm, 40 mW				*Red* 640nm, 40 mW
Fluorescent channels	FL1	FL2	FL3	FL4	FL5	FL6	FL7	FL8
Filters	448/45	528/45	606/36	527/32	586/42	700/54	783/56	660/10
Panel 1	Syto40	CD138 BV510 (MI15, Sony)	CD45 BV605 (HI30, Sony)	CD81 FITC (JS-81, BD)	CD56 PE (C5.9, Dako)	CD19 PERCP-Cy5.5 (HIB19, Sony)	CD117 PC7 (104D2D1, BC)	CD38 APC (LS198-4–3, BC)
Panel 2	Syto40	CD138 BV510 (MI15, Sony)	CD45 BV605 (HI30, Sony)	CD69 FITC (FN50, BD)	CD38 PE (AT13/5, Dako)	CD44 PERCP-Cy5.5 (IM7, Sony)		CD86 APC (2331-(FUN-1), BD)
Panel 3	Syto40	CD138 BV510 (MI15, Sony)	CD45 BV605 (HI30, Sony)	CD38 FITC (AT13/5, Dako)	CD184 PE (12G5, BD)			CD49d APC (9F10, Sony)

Summary of the antibodies used in our experiment to investigate cell phenotypes before and after immunomagnetic separation, using a 10-color BD FACSLyric™ flow cytometer. (BC, beckman coulter; BD, becton dickinson; APC, allophycocyanin; BV, Brilliant Violet™; FITC, fluorescein isothiocyanate; PC7, Phycocyanin-7; PE, phycoerythrin; PERCP-Cy5.5, Peridinin-chlorophyll-Cyanine5.5).

Becton Dickinson (BD) Bioscience, New Jersey, United States), as it is crucial to maintain the integrity of the cells and the right conformation of surface proteins. After removing the lysing solution and washing with phosphate-buffered saline (PBS) (pH = 7.4, 300 g, 10 min with the brake off), EasySep Buffer was added to the pellets. Then, following the manufacturer's protocol [22], cells were mixed with the positive selection cocktail containing anti-CD138 antibodies. After incubation, magnetic particles were added to the samples. Finally, the separation tubes were placed in the EasySep™ magnet for 10 min. After the purification steps, isolated plasma cells were obtained. The purity of the homogeneous plasma cell population was confirmed by flow cytometry where plasma cells were identified by CD45/CD38 and CD138 markers (for details, see Cell surface staining protocol section). The gating strategy used to verify the purity of the separated samples is described in detail in Supplementary Figure S1.

Flow cytometry analysis before and after magnetic cell separation

Cell surface staining protocol

The myeloma cell ratio (%) was determined by flow cytometry in a preceding measurement, wherein 10^6 cells were stained by the Panel 1 (Table 1) in 50 μL total volume and plasma cell ratio were assessed. The plasma cell concentrations of samples were set to 0.25×10^6/samples for immunophenotype determination before and after separation. Samples were stained with fluorochrome-conjugated monoclonal antibodies against the following surface antigens: CD19, CD38, CD44, CD45, CD49d, CD56, CD69, CD81, CD86, CD117, CD138, and CD184 (see Table 1 for details). The samples were incubated with the antibodies for 13 min at 4°C. After incubation, we lysed the red blood cells with FACSLysing solution (BD Bioscience), containing fixation agent (paraformaldehyde). This lysis step was applied both on the separated and unseparated plasma cells to keep the experimental conditions identical. The lysing solution was removed by centrifugation (400 g, 10 min, room temperature (RT)). Then, we washed the cells with PBS using the same settings (400 g, 10 min, RT). Afterwards, the fluorescent nucleic acid dye SYTO-40 (Invitrogen, Waltham, United States) was added to the collected cells. 10,000–150,000 events were measured per sample using a 10-color BD FACSLyric™ flow cytometer (BD Bioscience). The cytometer was regularly calibrated with CS&T Beads (BD Bioscience). Myeloma cells were identified by their high CD38/CD138 expression and low CD45 levels.

In this experiment, the immunophenotype of 12 samples was examined. Due to the large number of antibodies involved, we used three panels during the procedure (Panel 1, Panel 2, Panel 3). Each panel contained conventional myeloma backbone markers (Table 1). Panel 2 and Panel 3 were applied on all 12 samples, while Panel 1 was used on 8 of them.

All antibodies were pre-titrated and isotype controls were used for most antibodies to exclude non-specific binding. The relative median fluorescence intensity (rMFI) values were calculated by subtracting the MFI of the isotype controls from the MFI values associated with the markers. The gating strategy is described in detail in Supplementary Figure S2.

Measurement of viability with propidium-iodide

In 8 cases we also investigated the effect of separation on the viability of plasma cells. For this purpose, we compared the

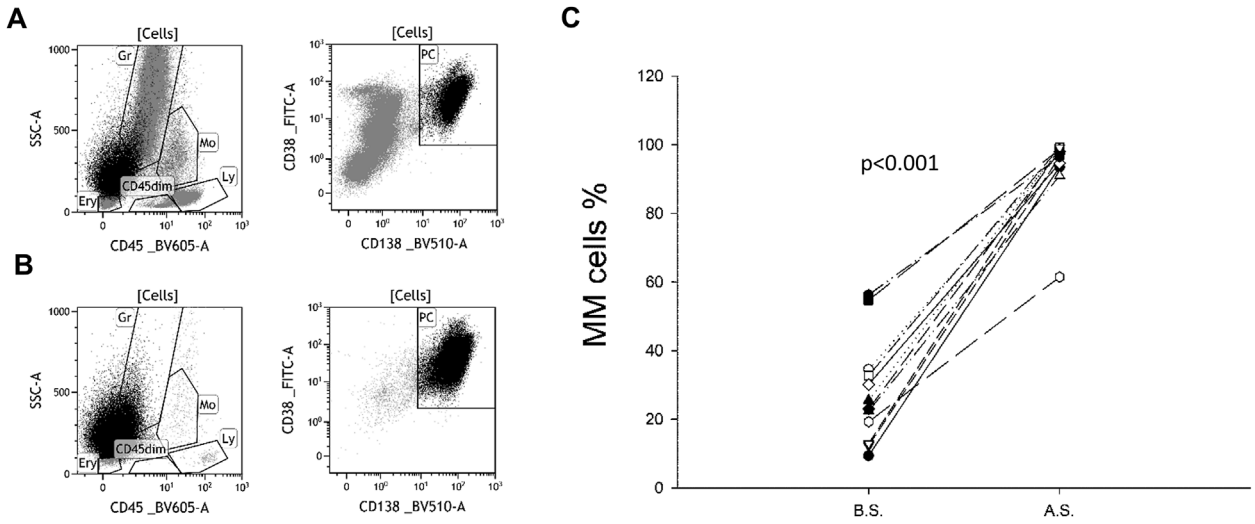

FIGURE 1
Plasma cell ratio before and after separation. CD138-CD38 dot plots of a representative sample before **(A)** and after **(B)** separation. Originally, plasma cells (PC) accounted for 23.4% of all cells. As a result of magnetic separation, the vast majority of non-plasma cells (grey) were removed, increasing the percentage of PC to 95.2%. A similar trend was observed in all 12 samples **(C)**. B.S. means before separation, A.S. means after separation.

proportion of propidium-iodide-positive cells (PI+) among all plasma cells before and after separation. In this experiment, CD38-FITC (DAKO, Agilent, Santa Clara, United States) antibody was used to identify the plasma cells. After cell surface labeling (13 min, 4°C), the samples were gently lysed with an ammonium chloride-based lysing reagent (BD Pharm Lyse™). The lysing solution was removed by centrifugation (400 g, 10 min, RT) and the samples were washed with PBS (400 g, 10 min, RT). Cells were then stained with propidium-iodide (2 μg/10^5 cells) (PI, Sigma). Samples were measured on an 8-color Navios flow cytometer (Beckman Coulter (BC), Brea, California, United States) after the final washing step. The cytometer is regularly calibrated with Flow-Check Pro and Flow-Set Pro QC beads (BC). The gating strategy is described in detail in Supplementary Figure S3.

Data analysis and statistics

Flow cytometric data were analyzed with the Kaluza 2.1.1 software (Beckman Coulter, Brea, CA, United States). The values used in our statistics are either MFI, or the percentage of PI-positive cells compared to all plasma cells in the sample. We used SigmaPlot 12.5 (Systat Software Inc., San Jose, California) for plotting and statistical analysis. Normality (Shapiro-Wilk) and equal variance tests were performed in each case, followed by paired t-test and the Wilcoxon signed-rank test to determine statistical significance with $p < 0.05$.

Results

Purity of plasma cell isolation

In this study, we investigated the effect of CD138 antibody-based immunomagnetic separation on plasma cells in 12 samples from patients with plasma cell disorder.

The purity of the plasma cell population after isolation ranged from 61.46% to 99.22% with a mean of 93.74% and a standard deviation (SD) of 10.48 (Figure 1).

Examination of changes in cell surface markers

The immunophenotypes of 12 samples were studied. In eight of these, we examined 12 surface markers commonly used in myeloma research, while in four cases we studied only a subset of them (CD38, CD44, CD45, CD49d, CD69, CD86, CD138, and CD184).

In our experiments, we compared the median fluorescence intensities (MFI) of the malignant plasma cell population before and after magnetic separation in the samples in which the myeloma cells formed a homogeneous population. In a few samples for certain surface markers, multiple subpopulations of myeloma cells with different expression levels were observed, see Table 2. The results of these samples were evaluated separetly from those with homogeneous populations.

10.3389/pore.2024.1611882

TABLE 2 Overview of cases with distinct subpopulations. Changes in the MFI values of the subpopulations and in their relative ratio before (B.S.) and after the separation (A.S.) are shown. Relative MFI values are marked with *italic*. Results with significant changes are marked with bold.

Cell surface marker	*Patient Sample*	*Dimmer subpopulation B.S.*		*Dimmer subpopulation A.S.*		*Brighter subpopulation B.S.*		*Brighter subpopulation A.S.*	
		%	MFI	%	MFI	%	MFI	%	MFI
CD38	***Sample 4***	43.87	75.88	50.59	82.17	56.13	199.26	49.41	237.22
CD44	***Sample 4***	**10.22**	*−0.54*	**12.97**	*−6.06*	**89.78**	*111.01*	**87.03**	*128.51*
	Sample 10	**58.03**	*0.56*	**63.28**	*−3.58*	**41.97**	*59.93*	**36.72**	*64.54*
	Sample 11	**35.05**	*2.67*	**40.31**	*−2.91*	**64.95**	*35.12*	**59.69**	*41.57*
	Sample 12	**21.67**	*0.12*	**26.02**	*0.67*	**78.33**	*115.74*	**73.98**	*149.46*
CD45	***Sample 4***	40.64	1.21	44.4	0.99	59.36	7.53	55.6	7.01
	Sample 10	26.13	1.64	22.45	2.25	73.87	10.98	77.55	17.09
	Sample 11	89.1	1.23	83.87	1.14	10.9	9.89	16.13	1.34
CD69	***Sample 8***	28.51	*0.18*	25.75	*0.23*	71.49	*3.35*	74.25	*3.09*
CD86	***Sample 5***	14.15	*0.17*	12.93	*0.08*	85.85	*3.53*	87.07	*2.88*
CD138	***Sample 2***	0	0	41.34	7.3	100	19.51	58.66	45.59
	Sample 8	45.28	24.7	23.68	13.71	54.72	89.95	76.32	61.42
CD81	***Sample 10***	96.94	1.56	95.32	2.07	3.06	12.68	3.01	12.64
	Sample 12	8.98	1.44	5.22	1.09	91.02	7.98	94.78	11.94
CD184	***Sample 2***	79.91	*0.58*	69.82	*1.79*	20.09	*4.87*	30.18	*10.05*
CD56	***Sample 11***	73.96	3.3	71.42	2.53	26.04	31.66	28.58	44.85
CD19	***Sample 11***	74.53	1.6	74.02	1,91	25.47	21.38	25.98	19.61

10.3389/pore.2024.1611882

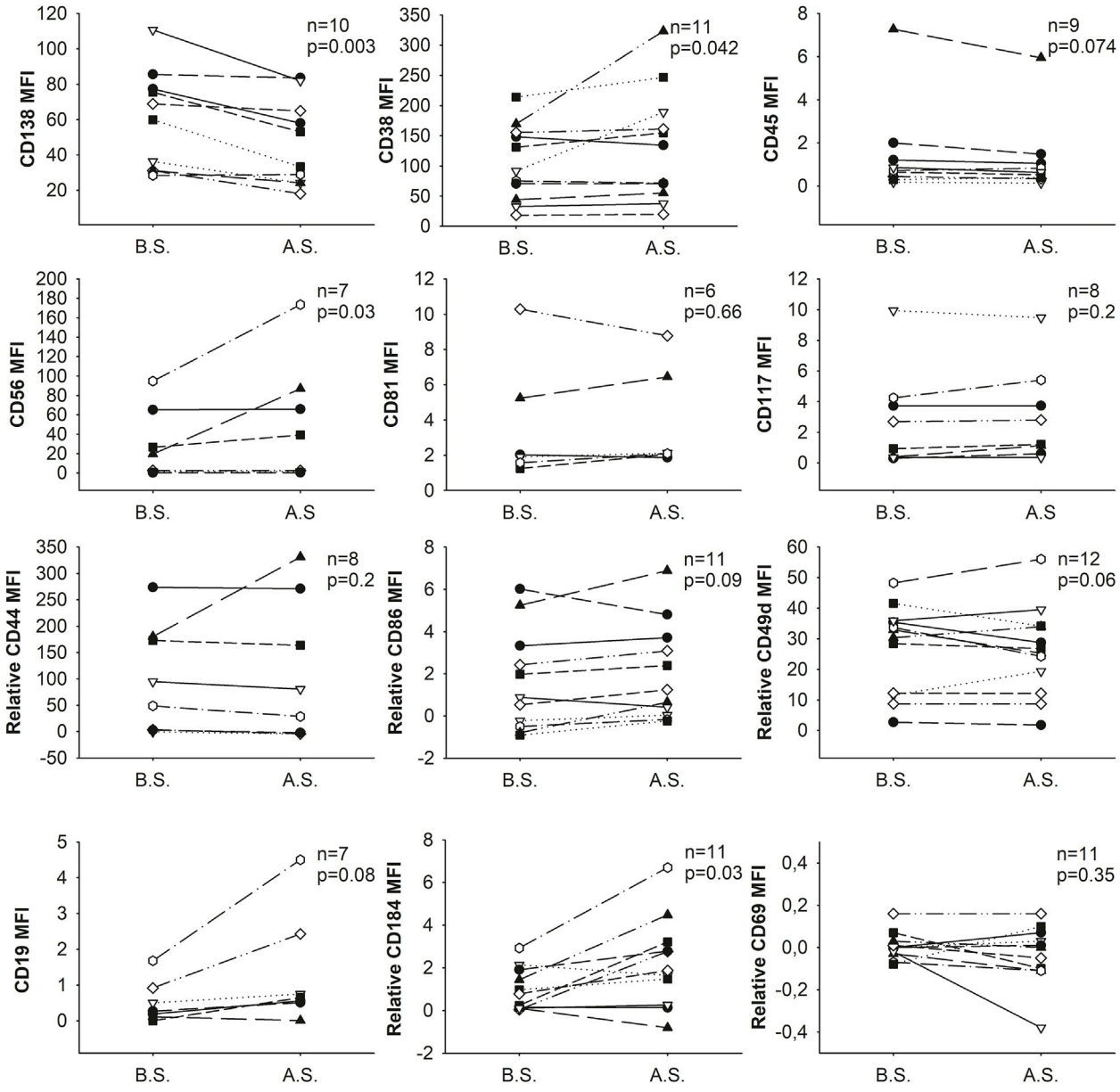

FIGURE 2
Changes in the expression (MFI: median fluorescence intensity) of cell surface markers as a result of separation. B.S. means before separation, A.S. stands for after separation.

The intensity changes of tested markers varied among different donors. In samples with homogeneously stained populations, the intensity of most tested markers (8/12) did not change significantly, and any changes observed were not consistently in one direction. Nevertheless, the intensity of CD38 (8/11 samples), CD56 (4/7 samples), and CD184 (6/11 samples) were increased, while the intensity of CD138 (9/10 samples) was decreased significantly (Figure 2).

In the case of CD38, CD56 and CD138 the change of intensity was remarkable (mean of the MFI±SD before vs. after separation, CD38: 104.7 ± 63.2 vs. 133.2 ± 94.5, $p = 0.042$; CD56: 30.1 ± 36.5 vs. 52.9 ± 63.2, $p = 0.03$; CD138: 60.5 ± 28.0 vs. 47.0 ± 24.6, $p = 0.003$, respectively) while in the case of CD184 the change was minor (mean of the relative MFI±SD of CD184 before vs. after separation: 0.8 ± 1.3 vs. 2.0 ± 2.3; $p = 0.029$).

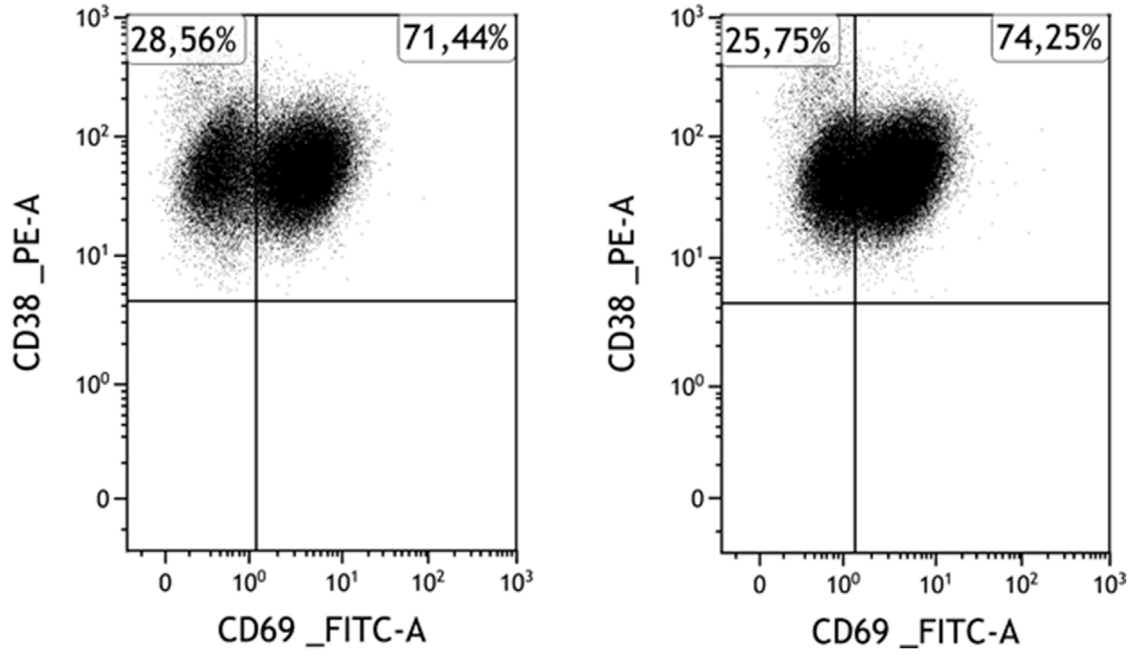

FIGURE 3
A representative case for marker expression stability: Expression of CD69 of myeloma cells before (left) and after (right) separation in a CD69-positive case. Among myeloma cells, the CD69-positive subpopulation is clearly distinguishable and intact both before and after the separation.

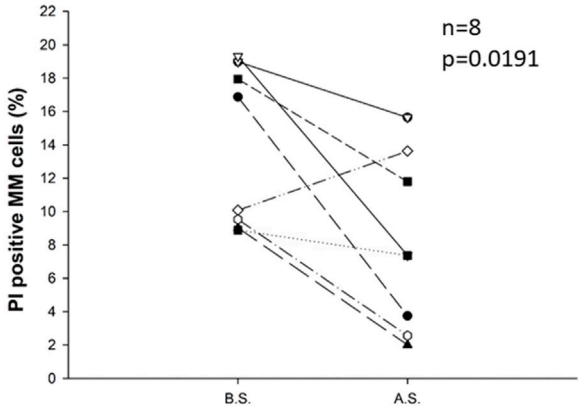

FIGURE 4
Change in the percentage of propidium-iodide-positive cells compared with all plasma cells before (B.S.) and after the separation procedure (A.S.) for eight samples. Immunomagnetic cell separation significantly decreased the percentage of PI-positive apoptotic cells in the plasma cell population ($p = 0.0191$). Statistical significance was set at $p < 0.05$.

Nevertheless, these changes did not affect the abnormal plasma cells' phenotype, i.e., positive/negative cells remained positive/negative, respectively, when compared to isotype controls or unstained cells for CD38, CD56, CD138, and CD184 markers (Supplementary Figure S2).

To examine the effects of isolation on samples with distinct subpopulations, we measured the change in MFI values of their dimmer and brighter subpopulations separately. In addition, we also examined whether the relative ratio of these subsets has changed. Samples involved and their corresponding results are shown in Table 2. Distinct populations within samples were rare, but when present, their findings mirrored those from samples with single populations. In these rare cases involving distinct populations, neither the MFI values of the subpopulations nor their relative ratios changed significantly (see Figure 3), except in the case of CD44 (mean ratio of subpopulations relative to all myeloma cells before vs. after separation, dimmer: 31.2% ± 20.5% vs. 35.6% ± 21.5, $p = 0.005$, brighter: 68.8% ± 20.5% vs. 64.4% ± 21.5, $p = 0.0049$).

In an effort to identify potential relationships between changes in intensity of tested markers and factors such as myeloma cell ratio, age or chromosomal alterations, we conducted comparisons across the examined samples. However, our analysis did not reveal any significant correlations (see Supplementary Table S1).

Viability of plasma cells before and after separation

We examined the percentage of propidium-iodide-positive cells compared with all plasma cells before and after separation in

8 cases. The results show that the ratio of dead cells in the plasma cell population was significantly reduced (from an average of 13.8% to 8.0%) during the separation procedure ($p = 0.0191$). Consequently, the percentage of viable plasma cells in the plasma cell population was significantly increased, see Figure 4.

Discussion

Enrichment and purification of the malignant population is a critical step to perform molecular experiments and for the clinical research of multiple myeloma. One of the most suitable methods for this purpose is the positive immunomagnetic cell separation based on the CD138 positivity of myeloma cells. However, procedural conditions and environmental changes can lead to cell damage, molecule shedding, or the expression of previously unexpressed proteins [10, 23], potentially altering the phenotype of the cells and significantly affecting the outcomes of *ex vivo* or *in vitro* experiments.

In our study, we observed slight changes in the intensity of most tested markers following magnetic separation, but significant differences in the expression patterns of the majority of proteins (CD44, CD45, CD49d, CD69, CD81, CD86, CD117, and CD19) were not detected. Notably, only the intensities of CD38, CD56, and CD184 were significantly increased, whereas the intensity of CD138 significantly decreased during the separation process. Contrary to the findings of Bansal et al. [10], who observed significant reductions in the expression levels of various cell surface markers (including CD11a, CD11b, CD49e, CD69, CD71, and CD138) following magnetic separation with the same kit, our results do not align, especially regarding CD69 and CD138. In our study, CD69 expression remained consistent, showing no significant change (Figures 2, 3). While CD138 (syndecan-1) was basically absent from the cell surface after Bansal's isolation procedure, we observed only a slight decrease in the fluorescence intensity of CD138.

This slight decrease could be attributed to technical factors, such as the blockage caused by residual attached antibodies following the separation process. The reason can also be biological, including shedding, potentially triggered by various conditions like cellular activation or stress (e.g., hyperosmolarity) experienced during the isolation process [24].

In addition to shedding, the observed reduction in CD138 expression might be explained by an increase of apoptotic cells, as it is established that dead cells exhibit diminished levels of CD138 [25]. To test whether an elevated proportion of apoptotic cells during the separation process contributed to the reduced CD138 expression, we assessed the ratio of apoptotic and necrotic (propidium-iodide, or PI-positive) cells before and after isolation. As expected and previously demonstrated in the literature [26], the ratio of dead cells decreased following the separation process, likely because apoptotic cells, which have lower CD138 levels, are washed away. Thus, we can conclusively state that apoptotic or necrotic cells were not responsible for the decrease in CD138 levels observed.

In our samples, we observed increased staining of CD38, CD56, and CD184. However, only the CD38 levels were systematically elevated in most of the samples.

The observed phenomenon might be due to the samples being predominantly composed of myeloma cells, thereby attracting more antibodies, even though the antibodies for CD38 detection were carefully titrated before use. Since CD38 expression is easily inducible on immun cells [27], an increase in their levels may also be caused by changes in the cytokine environment during isolation.

Providing a clear explanation for the changes in intensity of the other two molecules proves challenging. The intensity of CD56 significantly increased in only half of the samples, demonstrating inconsistency. In the case of CD184, while the intensity changing were statistically significant, the absolute values changed minimally in the samples.

In a few cases, multiple subpopulations of the myeloma cells occurred during our experiments for some of the surface markers. For these samples, we measured the change in MFI values of these dimmer and brighter subpopulations separately and found that they did not change notably, similar to samples with a single population. To further study the potential changes in heterogenous samples, we also examined whether their relative ratio compared to all myeloma cells changed (see Table 2). However, except for the case of CD44, no significant change occurred.

Additionally, we have explored the possibility that changes in marker intensity post-separation could be linked to factors such as cytogenetic abnormalities, age, or myeloma cell ratio. However, our investigations revealed no association between these factors and the alterations in marker expression observed after the separation process.

The limitations of our study may arise from using only 12 samples, which could narrow the scope of our conclusions. To address this concern, we standardized the staining procedures across all samples, ensuring each was analyzed with an identical number of plasma cells.

Conclusion

In this study we examined the expression pattern of several cell surface markers that are important for the diagnosis and progression of multiple myeloma before and after magnetic isolation. We found in our experiments that in the vast majority of cases, immunomagnetic separation may slightly change the intensity of tested markers of plasma cells but

does not change the immunophenotype of the cells. Positive markers remained positive and negative ones remained negative after the separation procedure. Still, it is recommended to validate the immunophenotype of the isolated cells after magnetic separation in experiments where the marker intensity of the cells or the amount of cell surface proteins are particularly important.

Data availability statement

The raw data supporting the conclusions of this article will be made available by the authors, without undue reservation.

Ethics statement

The studies involving humans were approved by the Semmelweis Egyetem Regionális Kutatásetikai Bizottság. The studies were conducted in accordance with the local legislation and institutional requirements. The participants provided their written informed consent to participate in this study.

Author contributions

ÁC: data curation; investigation; software; validation; visualization; writing-original draft; SS: Investigation; methodology; FT: writing-review and editing; GS: visualization; methodology; validation; writing-review and editing; CK: writing-review and editing; GV: resources; writing-review and editing; PF: resources; writing-review and editing; AH: resources; writing-review and editing; ÁM: data curation; investigation; methodology; supervision; validation; writing-review and editing; GB: conceptualization; formal analysis; funding acquisition; methodology; project administration; resources; supervision; validation; writing-review and editing. All authors contributed to the article and approved the submitted version.

Funding

The author(s) declare that financial support was received for the research, authorship, and/or publication of this article. This work was supported by research grants from the Hungarian National Research, Development and Innovation Office (NFKIH) Development of scientific workshops of medical, health sciences and pharmaceutical educations under Grant [EFOP-3.6.3-VEKOP-16-2017-00009]; and the EU's Horizon 2020 research and innovation program under grant agreement No. 739593.

Conflict of interest

The authors declare that the research was conducted in the absence of any commercial or financial relationships that could be construed as a potential conflict of interest.

Supplementary material

The Supplementary Material for this article can be found online at: https://www.por-journal.com/articles/10.3389/pore.2024.1611882/full#supplementary-material

References

1. Siegel RL, Miller KD, Jemal A. Cancer statistics, 2019. *CA Cancer J Clin* (2019) 69:7–34. doi:10.3322/caac.21551

2. Tai Y, Teoh G, Shima Y, Chauhan D, Treon SP, Raje N, et al. Isolation and characterization of human multiple myeloma cell enriched populations. *J Immunol Methods* (2000) 235:11–9. doi:10.1016/s0022-1759(99)00199-4

3. Shin SY, Jang S, Park C, Chi H, Lee J, Lee JH, et al. Application of an immune-magnetic cell sorting method for CD138-positive plasma cells in FISH analysis of multiple myeloma. *Int J Lab Hematol* (2012) 34:541–6. doi:10.1111/j.1751-553X.2012.01433.x

4. Kishimoto RK, de Freitas SLVV, Ratis CA, Borri D, Sitnik R, Edrp V. Validation of interphase fluorescence *in situ* hybridization (iFISH) for multiple myeloma using CD138 positive cells. *Rev Bras Hematol Hemoter* (2016) 38:113–20. doi:10.1016/j.bjhh.2016.01.005

5. Zhan F, Huang Y, Colla S, Stewart JP, Hanamura I, Gupta S, et al. The molecular classification of multiple myeloma. *Blood* (2006) 108:2020–8. doi:10.1182/blood-2005-11-013458

6. Mattioli M, Agnelli L, Fabris S, Baldini L, Morabito F, Bicciato S, et al. Gene expression profiling of plasma cell dyscrasias reveals molecular patterns associated with distinct IGH translocations in multiple myeloma. *Oncogene* (2005) 24:2461–73. doi:10.1038/sj.onc.1208447

7. Cumova J, Kovarova L, Potacova A, Buresova I, Kryukov F, Penka M, et al. Optimization of immunomagnetic selection of myeloma cells from bone marrow using magnetic activated cell sorting. *Int J Hematol* (2010) 92:314–9. doi:10.1007/s12185-010-0651-4

8. Wijdenes J, Vooijs WC, Clément C, Post J, Morard F, Vita N, et al. A plasmocyte selective monoclonal antibody (B-B4) recognizes syndecan-1. *Br J Haematol* (1996) 94:318–23. doi:10.1046/j.1365-2141.1996.d01-1811.x

9. Potéčová A, Štossová J, Burešová I, Kovářová L, Almáši M, Penka M, et al. Sample processing and methodological pitfalls in multiple myeloma research. *Klin Onkol* (2011) 24:18–23.

10. Bansal R, Kimlinger T, Gyotoku KA, Smith M, Rajkumar V, Kumar S. Impact of CD138 magnetic bead-based positive selection on bone marrow plasma cell surface markers. *Clin Lymphoma Myeloma Leuk* (2021) 21:e48–e51. doi:10.1016/j.clml.2020.08.003

11. Kimlinger TK, Rajkumar SV, Kline MP, Haug JL, Timm MM, Witzig TE, et al. Changes in bone marrow plasma cell surface markers following cd138-magnetic bead based positive selection. *Blood* (2006) 108:3516. doi:10.1182/blood.v108.11.3516.3516

12. Flores-Montero J, de Tute R, Paiva B, Juan Perez J, Wind H, Sanoja L, et al. Immunophenotype of normal vs. myeloma plasma cells: toward antibody panel specifications for MRD detection in multiple myeloma. *Euroflow Cytom B Clin Cytom* (2016) 90:61–72. doi:10.1002/cyto.b.21265

13. Tatsumi T, Shimazaki C, Goto H, Araki SI, Sudo Y, Yamagata N, et al. Expression of adhesion molecules on myeloma cells. *Jpn J. Cancer Res* (1996) 87:837–42. doi:10.1111/j.1349-7006.1996.tb02108.x

14. Bjorklund CC, Baladandayuthapani V, Lin HY, Jones RJ, Kuiatse I, Wang H, et al. Evidence of a role for CD44 and cell adhesion in mediating resistance to lenalidomide in multiple myeloma: therapeutic implications. *Leukemia* (2014) 28: 373–83. doi:10.1038/leu.2013.174

15. Márk Á, Varga G, Timár B, Kriston C, Szabó O, Deák L, et al. The effect of microenvironmental factors on the development of myeloma cells. *Hematol Oncol* (2017) 35:741–5. doi:10.1002/hon.2354

16. Buda G, Carulli G, Orciuolo E, Sammuri P, Galimberti S, Rousseau M, et al. CD69 expression predicts favorable outcome in multiple myeloma patients treated with VTD. *Blood* (2015) 126:1768. doi:10.1182/blood.v126.23.1768.1768

17. Stessman HAF, Mansoor A, Zhan F, Linden MA, Van Ness B, Baughn LB. Bortezomib resistance can be reversed by induced expression of plasma cell maturation markers in a mouse *in vitro* model of multiple myeloma. *PLoS One* (2013) 8:e77608. doi:10.1371/journal.pone.0077608

18. Moser-Katz T, Gavile CM, Barwick BG, Lee KP, Boise LH. PDZ proteins SCRIB and DLG1 regulate myeloma cell surface CD86 expression, growth, and survival. *Mol Cancer Res* (2022) 20:1122–36. doi:10.1158/1541-7786.MCR-21-0681

19. Ullah TR. The role of CXCR4 in multiple myeloma: cells' journey from bone marrow to beyond. *J Bone Oncol* (2019) 17:100253. doi:10.1016/j.jbo.2019.100253

20. McKenna RW, Kyle RA, Kuehl WM, Harris NL, Coupland RWFF. Plasm cell neoplasms. In: Swerdlow SH, Campo NLH E, editors. *WHO Classif. tumors Haematop. lymphoid tissues*. 4th ed. Lyon (2017). p. 241–58.

21. Rajkumar SV, Dimopoulos MA, Palumbo A, Blade J, Merlini G, Mateos MV, et al. International Myeloma Working Group updated criteria for the diagnosis of multiple myeloma. *Lancet Oncol* (2014) 15:e538–48. doi:10.1016/S1470-2045(14)70442-5

22. Anon. *EasySepTM human WB and BM CD138 positive selection kit II | STEMCELL technologies* (2022). Available from: https://www.stemcell.com/easysep-human-whole-blood-and-bone-marrow-cd138-positive-selection-kit-ii.html#section-data-and-publications (Accessed August 21, 2022).

23. Hayashida K, Bartlett AH, Chen Y, Park PW. Molecular and cellular mechanisms of ectodomain shedding. *Anat Rec* (2010) 293:925–37. doi:10.1002/ar.20757

24. Fitzgerald ML, Wang Z, Park PW, Murphy G, Bernfield M. *Shedding of syndecan-1 and-4 ectodomains is regulated by multiple signaling pathways and mediated by a TIMP-3-sensitive metalloproteinase* (2000). 811–24.

25. Jourdan M, Ferlin M, Legouffe E, Horvathova M, Liautard J, Rossi JF, et al. The myeloma cell antigen syndecan-1 is lost by apoptotic myeloma cells. *Br J Haematol* (1998) 100:637–46. doi:10.1046/j.1365-2141.1998.00623.x

26. Kimlinger TK, Rajkumar SV, Kline M, Timm MM, Haug JL, Witzig TE, et al. Apoptosis rates in myeloma cells can Be significantly affected by CD138 sorting and by the specific method used to detect apoptotic cells. *Blood* (2006) 108:3442. doi:10.1182/blood.v108.11.3442.3442

27. Piedra-Quintero ZL, Wilson Z, Nava P, Guerau-de-Arellano M. CD38: an immunomodulatory molecule in inflammation and autoimmunity. *Front Immunol* (2020) 11:3–6. doi:10.3389/fimmu.2020.597959

Pathology & Oncology Research | frontiers

TYPE Original Research
PUBLISHED 28 April 2023
DOI 10.3389/pore.2023.1611171

Check for updates

OPEN ACCESS

EDITED BY
Anna Sebestyén,
Semmelweis University, Hungary

*CORRESPONDENCE
Gergely Varga,
vargager@gmail.com

RECEIVED 09 March 2023
ACCEPTED 18 April 2023
PUBLISHED 28 April 2023

CITATION
Wiedemann Á, Szita VR, Horváth R, Szederjesi A, Sebő A, Tóth AD, Masszi T and Varga G (2023), Soluble B-cell maturation antigen as a monitoring marker for multiple myeloma. *Pathol. Oncol. Res.* 29:1611171. doi: 10.3389/pore.2023.1611171

COPYRIGHT
© 2023 Wiedemann, Szita, Horváth, Szederjesi, Sebő, Tóth, Masszi and Varga. This is an open-access article distributed under the terms of the Creative Commons Attribution License (CC BY). The use, distribution or reproduction in other forums is permitted, provided the original author(s) and the copyright owner(s) are credited and that the original publication in this journal is cited, in accordance with accepted academic practice. No use, distribution or reproduction is permitted which does not comply with these terms.

Soluble B-cell maturation antigen as a monitoring marker for multiple myeloma

Ádám Wiedemann, Virág Réka Szita, Róbert Horváth, Attila Szederjesi, Attila Sebő, András Dávid Tóth, Tamás Masszi and Gergely Varga*

Department of Internal Medicine and Haematology, Semmelweis University, Budapest, Hungary

Objective: Response to treatment in multiple myeloma (MM) is routinely measured by serum and urine M-protein and free light chain (FLC), as described by the International Myeloma Working Group (IMWG) consensus statement. A non-negligible subgroup of patients however present without measurable biomarkers, others become oligo or non-secretory during recurrent relapses. The aim of our research was to evaluate soluble B-cell maturation antigen (sBCMA) as a monitoring marker measured concurrent with the standard monitoring in MM patients at diagnosis, at relapse and during follow up, in order to establish its potential usefulness in oligo and non-secretory disease.

Method: sBCMA levels were measured in 149 patients treated for plasma cell dyscrasia (3 monoclonal gammopathy of unknown significance, 5 smoldering myeloma, 7 plasmacytoma, 8 AL amyloidosis and 126 MM) and 16 control subjects using a commercial ELISA kit. In 43 newly diagnosed patients sBCMA levels were measured at multiple timepoints during treatment, and compared to conventional IMWG response and progression free survival (PFS).

Results: sBCMA levels among control subjects were significantly lower than among newly diagnosed or relapsed MM patients [20.8 (14.7–38.7) ng/mL vs. 676 (89.5–1,650) and 264 (20.7–1,603) ng/mL, respectively]. Significant correlations were found between sBCMA and the degree of bone marrow plasma cell infiltration. Out of the 37 newly diagnosed patients who have reached partial response or better per IMWG criteria, 33 (89%) have had at least a 50% drop in sBCMA level by therapy week 4. Cohorts made similarly to IMWG response criteria—achieving a 50% or 90% drop in sBCMA levels compared to level at diagnosis—had statistically significant differences in PFS.

Conclusion: Our results confirmed that sBCMA levels are prognostic at important decision points in myeloma, and the percentage of BCMA change is predictive for PFS. This highlights the great potential use of sBCMA in oligo- and non-secretory myeloma.

KEYWORDS

multiple myeloma, monitoring, monoclonal gammopathie, soluble B-cell maturation antigen, BCMA

Introduction

At first glance, the monitoring of multiple myeloma (MM) seems straightforward compared to other types of cancers. The tumor cells usually keep the innate ability of normal plasma cells (PC) to synthetize large quantities of monoclonal immunoglobulins and/or produce free immunoglobulin light chains (FLC), which are present in the serum of patients and can then be utilized to define the well-established International Myeloma Working Group (IMWG) response criteria (1, 2). However, approximately 3% of MM patients present without conventionally measurable serum markers. Several different etiologies can account for this occurrence. Defects in the immunoglobulin synthesis result in non-producer patients, in whom even the use of free light chain assay will not reveal measurable disease (3–7). Another subgroup of patients has defects in the secretion of immunoglobulins, leading to oligosecretory multiple myeloma. The defining criteria for these patients (serum M-protein of <10.0 g/L, urine M-protein of <200 mg/24 h, and free light chain of <100 mg/L) can make reliable measurements and therefore the monitoring of disease activity challenging. This is a particularly common problem in AL amyloidosis. The exact frequency of non- and oligosecretory myeloma is difficult to quantify, as with each subsequent relapse the tendency of clonal evolution into FLC only or true non-secretory myeloma increases. This often goes parallel with the development of other high risk features, such as genomic instability, extramedullary disease manifestations and drug resistance (8).

Oligo- and non-secretory myeloma patients present a problematic subgroup. Their diagnosis is frequently delayed; they do not meet the inclusion criteria of most clinical trials. To objectively measure response to treatment, FDG PET-CT and bone marrow biopsy are the only techniques currently being used, making the evaluation of the optimal timing to end or restart active therapy a challenge. The nature of these modalities also prevent them from being repeated on any regular basis.

B-cell maturation antigen (BCMA) is a member of the tumor necrosis factor receptor superfamily, present almost exclusively on the surface of mature B-cells and plasma cells. Recently it became a popular target for the development of cellular and non-cellular immunotherapies in MM, several of which are now licensed for treatment, such as belantamab mafodotin (9), ciltacabtagene autoleucel (10), idecabtagene vicleucel (11), and teclistamab (12).

BCMA is actively cleaved from the plasma cell surface by the ubiquitous multisubunit gamma-secretase complex, which then releases a soluble BCMA fragment (sBCMA) into the serum (13). Soluble BCMA was evaluated at first from the viewpoint of BCMA-targeted therapies: cleavage not only leads to the reduction of ligand density on tumor cells, sBCMA is capable of inhibiting CAR-T-cell function as well. Decreasing sBCMA levels can be a sign of biallelic loss of the BCMA target (14), whereas the reappearance of sBCMA can indicate the elimination of the anti-BCMA CAR-T-cell clone (15). The use of sBCMA as a prognostic and/or monitoring tool was suggested in non-BCMA targeted therapies as well. The levels of sBCMA not only positively correlate with disease stage, its increase was also reported through the progression from monoclonal gammopathy of unknown significance (MGUS) to active MM (16, 17). In another study, sBCMA levels were shown to correlate with the proportion of plasma cells found in bone marrow biopsies, the quality of response to therapy, and were prognostic towards progression free survival (PFS) and overall survival (OS) as well (18). Importantly, serum B-cell maturation antigen levels do not show any dependence on renal function, like free light chains do. Compared to M-protein, sBCMA has a drastically shorter plasma half-life (24–36 h), permitting rapid changes in measurable serum values, which could in turn reflect the ongoing changes in plasma cell burden, making it a potentially great monitoring tool (18).

The aim of our research was to evaluate sBCMA as a monitoring marker measured concurrent with the standard monitoring in MM patients at diagnosis, at relapse and during follow up, in order to establish its potential usefulness in oligo and non-secretory disease.

Materials and methods

Patients

Peripheral blood samples were obtained from patients with MM at their standard clinic visits parallel with the conventional monitoring strategy, and were kept frozen at −95°C until evaluation. Standard monitoring included routine full blood count and chemistry, serum and urine electrophoresis (SPEP and UPEP), serum FLC, and in addition immunofixation (IFX) when needed. These assays were performed in the hospital's routine laboratory and served as benchmark values for the study. Newly diagnosed and relapsed patients had follow up tests 1 week after treatment initiation (±3 days) and then monthly (±7 days).

Samples were collected after written consent from 3 MGUS, 5 smoldering MM, 7 plasmacytoma, 8 AL amyloidosis and 126 MM patients, as well as 16 normal controls, who were included in our research (Table 1.). Out of the 126 MM patients, 90 had multiple measurements evaluated. 43 out of

TABLE 1 Subjects included in the analysis.

Category	Number of subjects
Healthy control	16
MGUS	3
Smouldering myeloma	5
Amyloidosis	8
Plasmacytoma	7
MM	126
Newly diagnosed	56
Relapsed	19
Follow up	51

these were newly diagnosed, being treated with bortezomib-thalidomide-dexamethasone (VTD) protocol, which was the standard approach in Hungary at the time.

ELISA assay

Frozen serum samples were thawed and diluted 1:500. An enzyme-linked immunosorbent assay with a polyclonal anti-BCMA antibody (Human BCMA/TNFRSF17 DuoSet ELISA DY193—R&D Systems, Minneapolis, MN, United States) was used to measure the sBCMA levels, as previously published (19). The ELISA plates were read by IL Biokit ELx800 ELISA Reader (Werfen Company, Barcelona, Spain) plate reader at 450 nm using Biotek Gen5 1.11 software.

Response categories and statistics

Soluble BCMA levels were then analyzed both as absolute values and also as percentage of the original reading to indicate response. We followed the way IMWG defined response categories based on the change from initial M-protein and FLC, i.e., as 50% and 90% drop from the original level to define sBCMA response categories sBCMA-SD, PR and VGPR.

The overall response rate was defined as the collective proportion of patients with complete response (CR), very good partial remission (VGPR), partial remission (PR), or stable disease (SD) as their best response (1). The primary endpoint for outcome was PFS which was measured from start of treatment to disease progression or death. Comparisons of dichotomous variables were performed by Fisher's exact test. Continuous variables were compared using Mann-Whitney U test and Spearmann correlation analysis. PFS and OS were estimated by Kaplan–Meier analysis. The analyses were carried out using the SPSS (version 20.0; SPSS, Chicago, IL) software package.

The study was approved by the Institutional Review Board and informed consent was obtained in accordance with the Declaration of Helsinki.

Results

Soluble BCMA levels correlated with disease stage

The median sBCMA level among the normal controls was 20.8 (14.7–38.7) ng/mL, in the MGUS cases 18.1 (12.0–20.5) ng/mL. In newly diagnosed, as well as relapsed patients the sBCMA levels were significantly higher: median 676.0 (89.5–1650.0) and 264 (20.7–1603.0) ng/mL respectively. In responding patients, the median sBCMA levels were significantly lower: patients in CR had 9.5 (0.0–55.0) ng/mL, VGPR 19.3 (4.0–57.0) ng/mL, PR 59.5 (0.0–1160.0) ng/mL, SD 104.5 (13.5–1660.0) ng/mL. There were more outliers in the more broadly defined IMWG response categories (i.e., PR and SD). Importantly, in paired analysis using Mann-Whitney U test, there were statistically significant differences between all categories of active disease and response, as well as between normal or MGUS and active myeloma (Figures 1A–C).

We found significant correlations between sBCMA level and bone marrow PC infiltration (BM biopsy PC% and sBCMA Spearman $r = 0.6376$; $p = 0.0044$, BM aspiration PC% and sBCMA Spearman $r = 0.5203$; $p = 0.0054$) and sBCMA and B2MG levels (Spearman $r = 0.3643$; $p = 0.01$). Lactate dehydrogenase levels were unfortunately not collected systematically in all cases, so we did not have the power to analyze its connection with sBCMA.

Changes in BCMA levels during treatment in responding patients

37 newly diagnosed patients were treated with VTD protocol and reached at least partial response according to IMWG criteria, as well as had BCMA levels measured at least twice following treatment initiation. At week one, 30 of these patients had a sBCMA measurement, 19 of whom had an at least 50% drop by this time compared to the initial result. All 37 patients had a repeat BCMA level measurement by week 4 (done either on week 1 or week 4), and only 4 of them failed to show more than 50% drop. For a graphic illustration of these responses see Figures 2A, B. The difference between week 0 measurements and any other timepoints was statistically significant.

sBCMA levels correlated with changes in M-protein and serum FLC levels measured at the same timepoints in individual patients. See Figures 3A–G for eight examples.

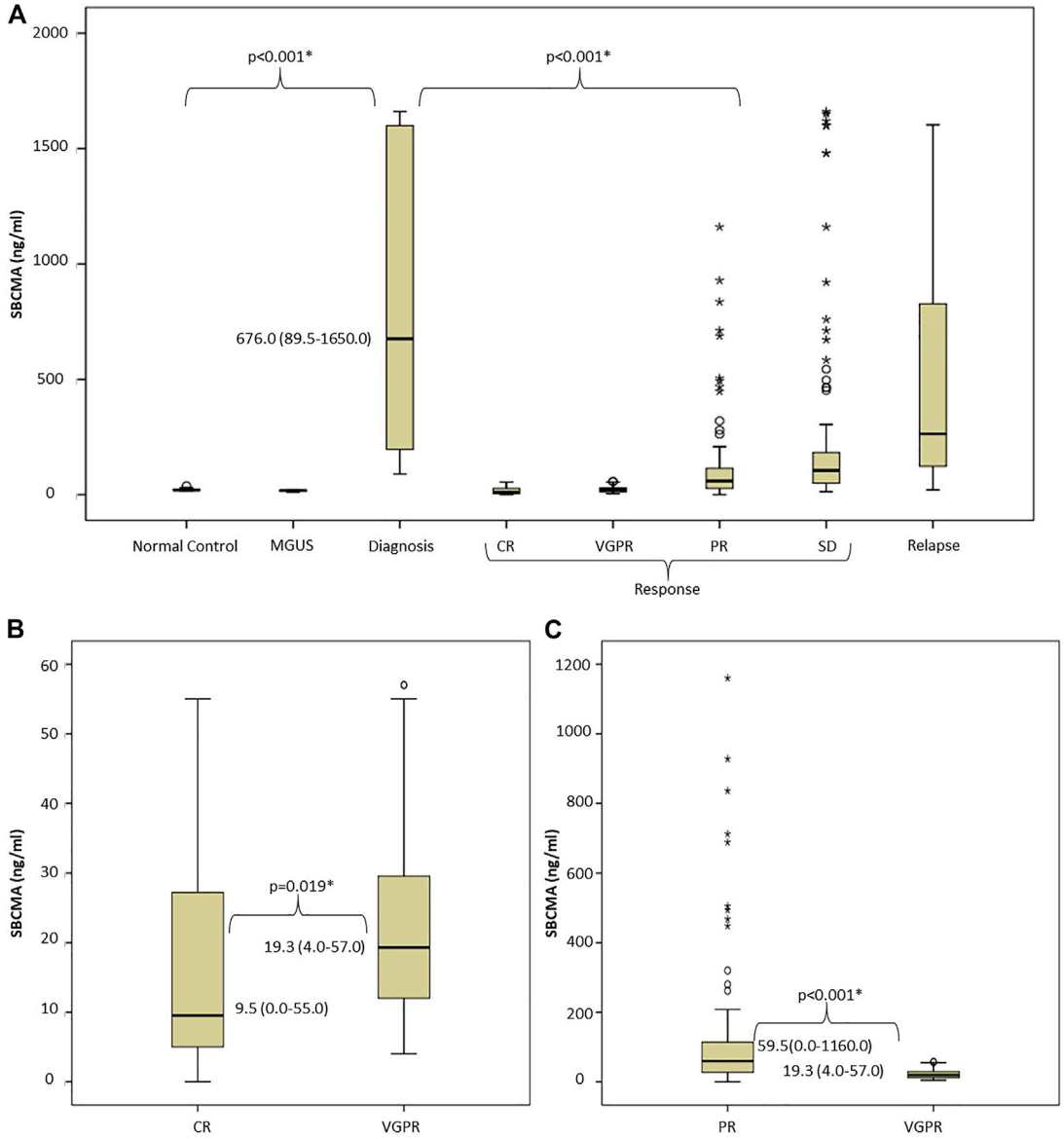

FIGURE 1
Evaluation of soluble BCMA levels: **(A)** There was significant difference between normal controls, MGUS cases, and MM patients with active disease or in remission, **(B,C)** Paired analysis of sBCMA levels using Mann-Whitney U test shows significant difference between IMWG response groups Abbreviations: sBCMA, soluble B-cell maturation antigen; MGUS, monoclonal gammopathy of undetermined significance; DG, diagnosis; CR, complete remission; VGPR, very good partial response; PR, partial response; SD, stable disease; PD, progressive disease; IMWG, International Myeloma Working Group.

Changes in BCMA levels in patients requiring salvage treatment and in relapse

There were 6 newly diagnosed patients who failed to reach PR or progressed on VTD treatment, requiring a change to salvage therapy (to daratumumab-bortezomib-dexamethasone in 3, bortezomib-lenalidomide-dexamethasone in 1, carfilzomib-lenalidomide-dexamethasone in 1 and carfilzomib-venetoclax-dexamethasone in 1 case). Figures 2C, D shows sBCMA levels before and after these treatment changes demonstrating that all of them reached at least sBCMA-PR after switch.

During the follow up, 6 further patients relapsed biochemically based on M-protein and/or sFLC measurements, according to IMWG criteria. Parallel with this, each of these cases showed a marked rise in their sBCMA, with at minimum a doubling of their initial value.

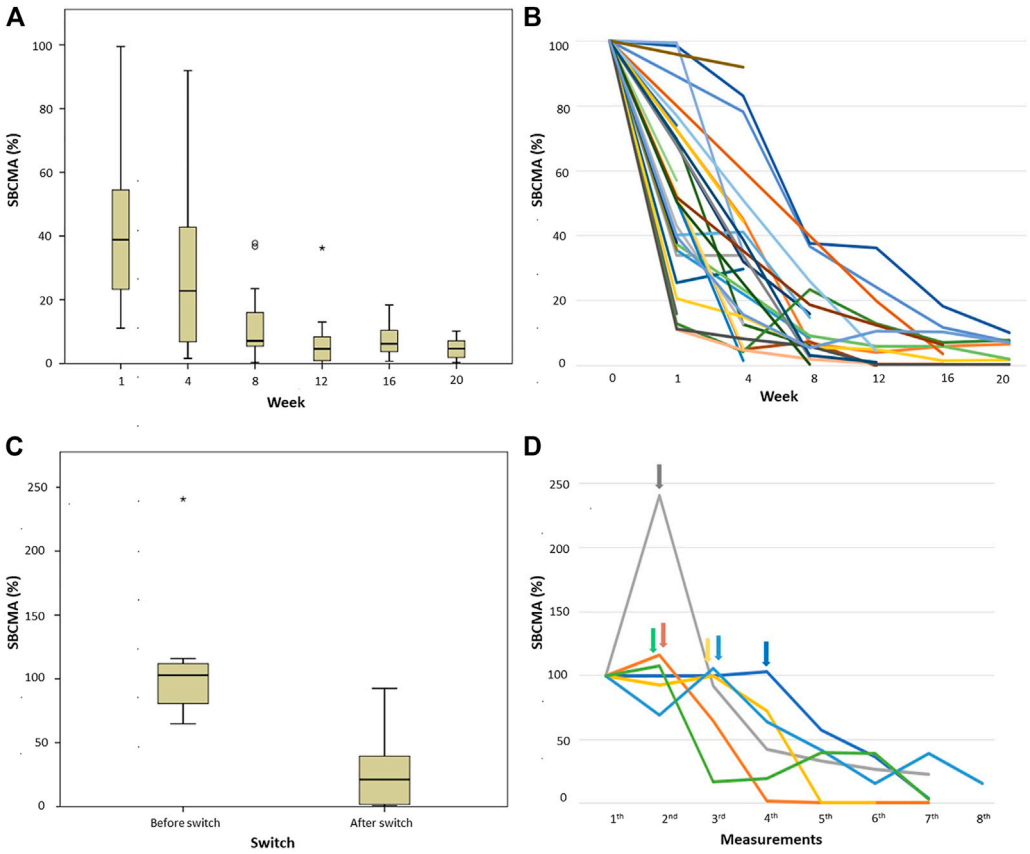

FIGURE 2
sBCMA levels measured in patients who had induction treatment with VTD protocol. **(A,B)** percentage of sBCMA drop in patient achieved IMWG-PR or better response compared to day 0 (100%), **(A)** box and whisker plot and **(B)** graphic representation of individual cases; and **(C,D)** patients not achieving PR after first line treatment and therefor having salvage treatment, **(C)** box and whisker plot of percentage of sBCMA change before and after switch to salvage treatment compared to presentation (100%), **(D)** graphic representation of the individual cases, arrows indicating the time of treatment change. Abbreviations: sBCMA, soluble B-cell maturation antigen; PR, partial response.

Month 1 sBCMA level changes define cohorts of patients with distinct survival probabilities

All patients who had week 0 and week 4 (±7 days) sBCMA measurements were included in this part of the analysis. We followed the IMWG standard for the analysis of M-protein and sFLC changes, and used the 50% and 10% sBCMA change thresholds to define response categories of sBCMA-SD, sBCMA-PR and sBCMA-VGPR. Following this, we analyzed PFS in these subgroups, and found marked differences (PFS not reached in responding patients and only 5 months in those not reaching sBCMA-PR, $p < 0.001$, Figure 4).

Non-secretory patients, localized relapse and amyloidosis

Only two of the follow up patients were true non-secretory, and one had oligosecretory disease, none of them showed signs of relapse. We had limited experience with only plasmocytic relapse which was observed in 6 patients. All 6 had at least doubling of the sBCMA level, compared to nadir exceeding the 95% confidence interval of CR and VGPR patients, but the absolute rise was small (<100 ng/mL). The number of patients with amyloidosis was also two small to draw any conclusions, but BCMA levels were lower in this group (<100 ng/mL in all but one case).

Discussion

Our results indicate the feasibility of using sBCMA for the monitoring of MM in conjunction with or—in the case of nonsecretory MM—instead of standard SPEP, UPEP and FLC measurements.

We successfully used the conventional 50% and 10% thresholds when segregating sBCMA response into SD, PR

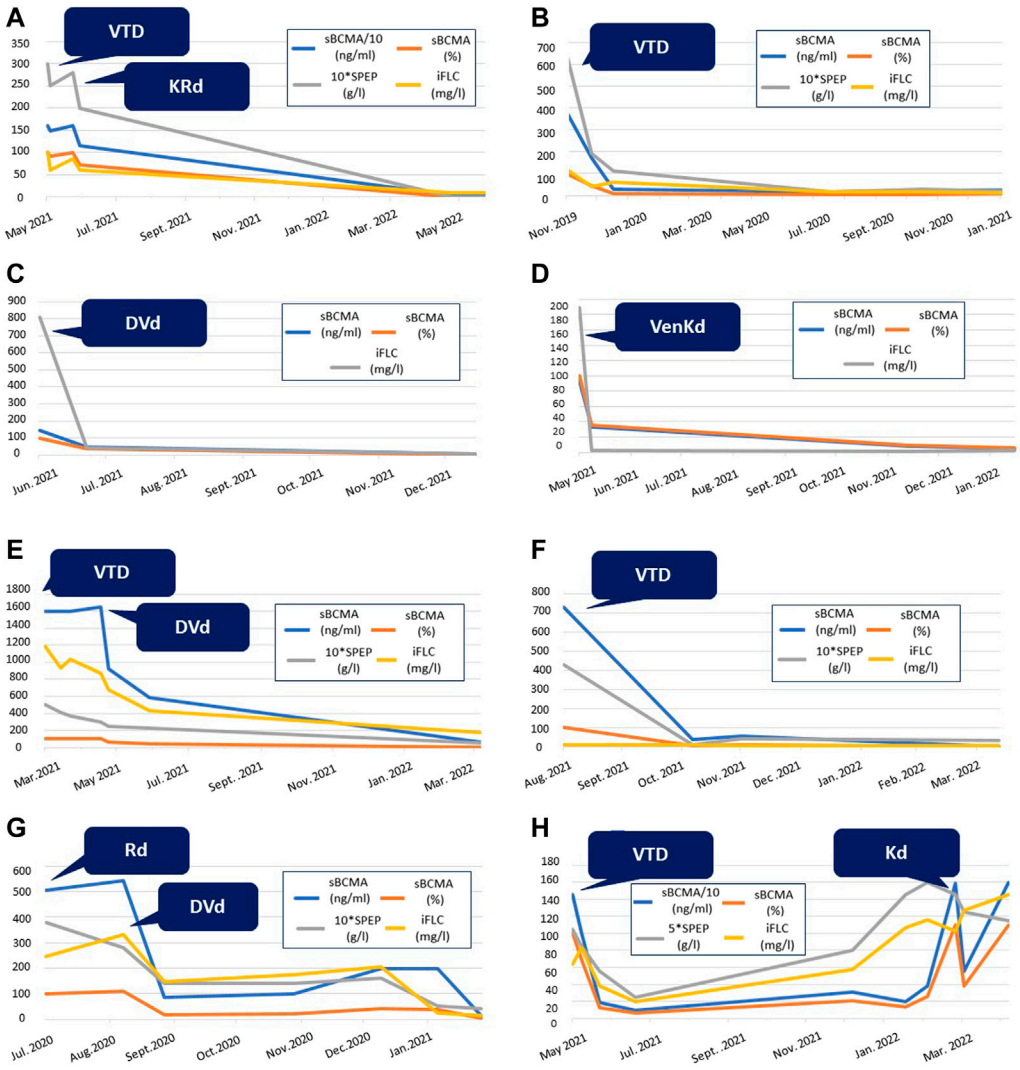

FIGURE 3
Graphic comparison of the changes in conventional myeloma biomarkers and sBCMA levels during the treatment of eight different patients from our cohort. SPEP is multiplied by 10 in selected diagrams for easier representation. Abbreviations: sBCMA, soluble B-cell maturation antigen; SPEP, serum protein electrophoresis; iFLC, involved free light chain; VTD, bortezomib-thalidomide-dexamethason; VenKD, venetoclax-carfilzomib-dexamethason; KRd, carfilzomib-lenalidomid-dexamethason; DVd, daratumumab-bortezomib-dexamethason; KD, carfilzomib-dexamethason; Rd, lenalidomid-dexamethason.

and VGPR groups, and found at least 100% rise from baseline in all cases of relapse. We think that sBCMA used this way could be a valuable addition to standard monitoring, especially in non- and oligosecretory disease. The problem with cases relapsing as oligo- or non-secretory is that lacking early biochemical warning signs, we are forced to wait until patients become outright symptomatic—often suffering serious consequences, such as skeletal fractures—until we may know they are truly relapsing. This is in part because mild variations in the M-protein and FLC levels are not uncommon, and moderate relapse symptoms such as anaemia, renal failure and bone pain may be related to other diseases or pre-existing conditions. In such situations, another layer of information could prove invaluable, giving a warning signal to prompt more frequent monitoring, bone marrow analysis or PET-CT.

Mass spectrometry was recently used in some of the leading laboratories to replace gel electrophoretic techniques (20, 21). Matrix-assisted laser desorption/ionization time of flight (MALDI TOF) mass spectrometry

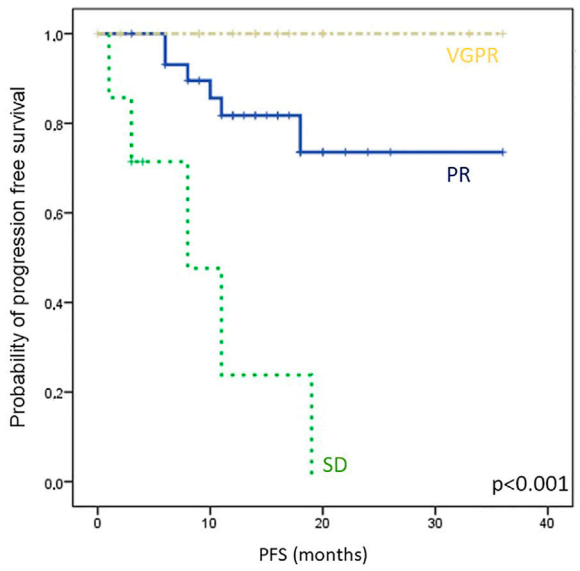

FIGURE 4
Kaplan-Meier analysis of progression free survival (PFS) in different sBCMA response groups, classified by sBCMA levels after 4 weeks of treatment. Abbreviations: sBCMA, soluble B-cell maturation antigen; VGPR, very good partial response; PR, partial response; SD, stable disease.

is several magnitudes more sensitive compared to the standard monitoring (i.e., SPEP, IFX, UPEP and FLC used together), reaching sensitivity similar to bone marrow based MRD techniques (22). Still, these promising techniques are only available in a handful of outstanding laboratories, and this situation is not expected to change in the near future. Possible limitations are the large initial cost of the installation of a mass spectrometer, and the lack of sufficient expertise in most laboratories. In addition to these, the current IMWG categories are established using gel techniques, and replacing them with mass spectrometry based measurements would require standardization as well as large scale validation.

Another potential candidate to improve myeloma monitoring is the Hevylite assay, developed by Binding Site, the same company that produced Freelite. For obvious reasons Hevylite will not be of help with light chain only oligosecretory disease, but can increase the sensitivity of monoclonal IgA and IgG detection at the point when SPEP and IFX cannot give a numerical value any longer due to the presence of polyclonal immunoglobulins (23). As a result Hevylite was included in the IMWG monitoring guideline in 2016, but so far did not get accepted generally in the routine clinical practice (24).

One important issue with FLC as a monitoring tool is that what we actually measure is the total FLC level and not the monoclonal fraction, and both kappa and lambda FLC levels are affected by renal clearance as well as immune activation. As renal failure is one of the important hallmarks of multiple myeloma, the abnormally elevated polyclonal FLC background very frequently makes FLC interpretation difficult, if not impossible. As Ghermezi et al. demonstrated, sBCMA levels are not dependent on renal function, and therefore can eliminate this important complication.

Another protein expressed on the surface of plasmacells similarly to BCMA is CD-138 (Syndecan) which is also shed into serum. This marker was suggested as independent prognostic parameter in multiple myeloma (25, 26), and the drop of serum level correlated with outcome in a cohort of patients (26, 27).

We did not include oligo and non-secretory patients in this analysis, and the benchmark we compared sBCMA response to, were the standard biomarkers IMWG suggests to use. We believe that our findings can still be generalized and utilized in oligo and non-secretory MM. Further studies enrolling oligo and non-secretory MM patients are warranted.

In conclusion, sBCMA is a cheap, noninvasive and easy to utilize ELISA measurement to monitor myeloma suggested to be used when the current monitoring strategy cannot give a reliable result.

Data availability statement

The raw data supporting the conclusion of this article will be made available by the authors, without undue reservation.

Ethics statement

The studies involving human participants were reviewed and approved by SE RKEB 12/2023. The patients/participants provided their written informed consent to participate in this study.

Author contributions

AW, VS, and GV treated the patients and collected the clinical information. RH, AW, and AS performed the laboratory analysis. AW, VS, AT, TM, and GV wrote the paper. All authors read and approved the final manuscript.

Conflict of interest

The authors declare that the research was conducted in the absence of any commercial or financial relationships that could be construed as a potential conflict of interest.

References

1. Durie BGM, Harousseau J-L, Miguel JS, Bladé J, Barlogie B, Anderson K, et al. International uniform response criteria for multiple myeloma. *Leukemia* (2006) 20: 1467–73. doi:10.1038/sj.leu.2404284

2. Kyle RA, Rajkumar SV. Criteria for diagnosis, staging, risk stratification and response assessment of multiple myeloma. *Leukemia* (2009) 23:3–9. doi:10.1038/leu.2008.291

3. Blade J, Kyle RA. Nonsecretory myeloma, immunoglobulin D myeloma, and plasma cell leukemia. *Hematol/oncol Clin North Am* (1999) 13:1259–72. doi:10.1016/S0889-8588(05)70125-8

4. Smith DB, Harris M, Gowland E, Chang J, Scarffe JH. Non-secretory multiple myeloma: A report of 13 cases with a review of the literature. *Hematol Oncol* (1986) 4(4):307–13. doi:10.1002/hon.2900040407

5. Ma ES, Shek TW, Ma SY. Non-secretory plasma cell myeloma of the true non-producer type. *Br J Haematol* (2007) 138(5):561. doi:10.1111/j.1365-2141.2007.06691.x

6. Decourt C, Galea HR, Sirac C, Cogné M. Immunologic basis for the rare occurrence of true nonsecretory plasma cell dyscrasias. *J Leukoc Biol* (2004) 76(3): 528–36. doi:10.1189/jlb.0803382

7. Coriu D, Weaver K, Schell M, Eulitz M, Murphy CL, Weiss DT, et al. A molecular basis for nonsecretory myeloma. *Blood* (2004) 104(3):829–31. doi:10.1182/blood-2004-02-0477

8. Meister S, Schubert U, Neubert K, Herrmann K, Burger R, Gramatzki M, et al. Extensive immunoglobulin production sensitizes myeloma cells for proteasome inhibition. *Cancer Res* (2007) 67(4):1783–92. doi:10.1158/0008-5472.CAN-06-2258

9. Trudel S, Lendvai N, Popat R, Voorhees PM, Reeves B, Libby EN, et al. Targeting B-cell maturation antigen with GSK2857916 antibody-drug conjugate in relapsed or refractory multiple myeloma (BMA117159): A dose escalation and expansion phase 1 trial. *Lancet Oncol* (2018) 19(12):1641–53. doi:10.1016/S1470-2045(18)30576-X

10. Berdeja JG, Madduri D, Usmani SZ, Jakubowiak A, Agha M, Cohen AD, et al. Ciltacabtagene autoleucel, a B-cell maturation antigen-directed chimeric antigen receptor T-cell therapy in patients with relapsed or refractory multiple myeloma (CARTITUDE-1): A phase 1b/2 open-label study. *Lancet* (2021) 398(10297): 314–24. doi:10.1016/S0140-6736(21)00933-8

11. Raje N, Berdeja J, Lin Y, Siegel D, Jagannath S, Madduri D, et al. Anti-BCMA CAR T-cell therapy bb2121 in relapsed or refractory multiple myeloma. *N Engl J Med* (2019) 380(18):1726–37. doi:10.1056/NEJMoa1817226

12. Moreau P, Garfall AL, van de Donk NWCJ, Nahi H, San-Miguel JF, Oriol A, et al. Teclistamab in relapsed or refractory multiple myeloma. *N Engl J Med* (2022) 387(6):495–505. doi:10.1056/NEJMoa2203478

13. Laurent SA, Hoffmann FS, Kuhn PH, Cheng Q, Chu Y, Schmidt-Supprian M, et al. γ-Secretase directly sheds the survival receptor BCMA from plasma cells. *Nat Commun* (2015) 6:7333. doi:10.1038/ncomms8333

14. Samur MK, Fulciniti M, Aktas Samur A, Bazarbachi AH, Tai YT, Prabhala R, et al. Biallelic loss of BCMA as a resistance mechanism to CAR T cell therapy in a patient with multiple myeloma. *Nat Commun* (2021) 12(1):868. doi:10.1038/s41467-021-21177-5

15. Seipel K, Porret N, Wiedemann G, Jeker B, Bacher VU, Pabst T. sBCMA plasma level dynamics and anti-BCMA CAR-T-cell treatment in relapsed multiple myeloma. *Curr Issues Mol Biol* (2022) 44(4):1463–71. doi:10.3390/cimb44040098

16. Sanchez E, Li M, Kitto A, Li J, Wang CS, Kirk DT, et al. Serum B-cell maturation antigen is elevated in multiple myeloma and correlates with disease status and survival. *Br J Haematol* (2012) 158(6):727–38. doi:10.1111/j.1365-2141.2012.09241.x

17. Visram A, Soof C, Rajkumar SV, Kumar SK, Bujarski S, Spektor TM, et al. Serum BCMA levels predict outcomes in MGUS and smoldering myeloma patients. *Blood Cancer J* (2021) 11(6):120. doi:10.1038/s41408-021-00505-4

18. Ghermezi M, Li M, Vardanyan S, Harutyunyan NM, Gottlieb J, Berenson A, et al. Serum B-cell maturation antigen: A novel biomarker to predict outcomes for multiple myeloma patients. *Haematologica* (2017) 102(4):785–95. doi:10.3324/haematol.2016.150896

19. Ghermezi M, Vardanyan S, Harutyunyan NM, Gottlieb J, Berenson A, Andreu-Vieyra C, et al. Serum B-cell maturation antigen is a novel prognostic indicator for multiple myeloma patients and correlates with clinical status and survival. *Blood* (2014) 124(21):3405. doi:10.1182/blood.V124.21.3405.3405

20. Puig N, Contreras MT, Agulló C, Martínez-López J, Oriol A, Blanchard MJ, et al. Mass spectrometry vs immunofixation for treatment monitoring in multiple myeloma. *Blood Adv* (2022) 6(11):3234–9. doi:10.1182/bloodadvances.2021006762

21. Dasari S, Kohlhagen MC, Dispenzieri A, Willrich MAV, Snyder MR, Kourelis TV, et al. Detection of plasma cell disorders by mass spectrometry: A comprehensive review of 19,523 cases. *Mayo Clin Proc* (2022) 97(2):294–307. doi:10.1016/j.mayocp.2021.07.024

22. Dispenzieri A, Arendt B, Dasari S, Kohlhagen M, Kourelis T, Kumar SK, et al. Blood mass spectrometry detects residual disease better than standard techniques in light-chain amyloidosis. *Blood Cancer J* (2020) 10(2):20. doi:10.1038/s41408-020-0291-8

23. Tovar N, Fernández de Larrea C, Elena M, Cibeira MT, Aróstegui JI, Rosiñol L, et al. Prognostic impact of serum immunoglobulin heavy/light chain ratio in patients with multiple myeloma in complete remission after autologous stem cell transplantation. *Biol Blood Marrow Transpl* (2012) 18(7):1076–9. doi:10.1016/j.bbmt.2012.03.004

24. Kumar S, Paiva B, Anderson KC, Durie B, Landgren O, Moreau P, et al. International Myeloma Working Group consensus criteria for response and minimal residual disease assessment in multiple myeloma. *Lancet Oncol* (2016) 17(8):e328–46. doi:10.1016/s1470-2045(16)30206-6

25. Seidel C, Sundan A, Hjorth M, Turesson I, Dahl IM, Abildgaard N, et al. Serum syndecan-1: A new independent prognostic marker in multiple myeloma. *Blood* (2000) 95(2):388–92. doi:10.1182/blood.v95.2.388

26. Richard L, Janet AD, Gulnaz B, Nicola JB, Tim P, Paul AM, et al. Soluble syndecan-1 level at diagnosis is an independent prognostic factor in multiple myeloma and the extent of fall from diagnosis to plateau predicts for overall survival. *B J Haem* (2005) 130:542–8. doi:10.1111/j.1365-2141.2005.05647.x

27. Janosi J, Sebestyen A, Mikala G, Nemeth J, Kiss Z, Valyi-Nagy I. Soluble syndecan-1 levels in different plasma cell dyscrasias and in different stages of multiple myeloma. *Haematologica* (2004) 89:370–1.

Pathology & Oncology Research | frontiers

TYPE Original Research
PUBLISHED 26 August 2024
DOI 10.3389/pore.2024.1611785

Check for updates

OPEN ACCESS

EDITED BY
Anna Sebestyén,
Semmelweis University, Hungary

*CORRESPONDENCE
Boglárka Brúgós,
brugosb@med.unideb.hu

RECEIVED 28 March 2024
ACCEPTED 13 August 2024
PUBLISHED 26 August 2024

CITATION
Brúgós B, Simon Z, Méhes G, Illés Á and Pfliegler G (2024) Diagnostic challenges in patients with Castleman disease, a single center experience from Hungary. *Pathol. Oncol. Res.* 30:1611785. doi: 10.3389/pore.2024.1611785

COPYRIGHT
© 2024 Brúgós, Simon, Méhes, Illés and Pfliegler. This is an open-access article distributed under the terms of the Creative Commons Attribution License (CC BY). The use, distribution or reproduction in other forums is permitted, provided the original author(s) and the copyright owner(s) are credited and that the original publication in this journal is cited, in accordance with accepted academic practice. No use, distribution or reproduction is permitted which does not comply with these terms.

Diagnostic challenges in patients with Castleman disease, a single center experience from Hungary

Boglárka Brúgós [1,2]*, Zsófia Simon[1], Gábor Méhes[3], Árpád Illés[1] and György Pfliegler[1,2]

[1]Division of Hematology, Department of Internal Medicine, University of Debrecen, Debrecen, Hungary, [2]Center of Expertise of Rare Diseases, University of Debrecen, Debrecen, Hungary, [3]Department of Pathology, University of Debrecen, Debrecen, Hungary

Castleman disease is a rare and atypical lymphoproliferative disorder characterized by diverse clinical manifestations. It has both unicentric and multicentric forms, the latter with further subdivisions, i.e., human herpesvirus 8-associated and idiopathic forms. The diagnosis of Castleman disease is often delayed, as it is rare, and because it shares clinical features with different autoimmune, inflammatory, and malignant lymphoproliferative disorders. The first-line treatment in unicentric form is mainly surgical, while in idiopathic Castleman disease, anti-interleukin-6 treatment is the therapy of choice. In virus-associated diseases, antiretroviral therapy and rituximab are recommended. In Hungary, only a few cases of Castleman disease have been published. This report presents our two decades of experience in the challenging diagnosis and management of this rare disorder, most properly underdiagnosed in Hungary. We provide insights into seven unicentric and five idiopathic multicentric Castleman disease cases, the latter ones especially highlighting the diagnostic and therapeutic challenges due to the variable and unique clinical features both of patients and diseases, e.g., bronchiolitis obliterans, stage IV diabetic renal failure, anti-HBc positivity, siltuximab treatment period, respectively.

KEYWORDS

unicentric Castleman disease, multicentric Castleman disease, interleukin-6, siltuximab, rituximab

Introduction

Castleman disease (CD) is a rare lymphoproliferative disorder with several names, the most widely used "angiofollicular lymph node hyperplasia" [1, 2]. The exact annual incidence remains uncertain. In the United States, idiopathic multicentric Castleman disease (iMCD) incidence and prevalence were reported to be 3.4 and 6.9 per million in 2017–2018 [3]. To our present knowledge, CD has no ethnical or race preferences, which means that, when compared to the populations of the two countries, in Hungary, the annual incidence should be around 50 new cases. However, only 4–6 cases per year are reported, suggesting that it is underdiagnosed.

CD is classified into two main types: unicentric (UCD) and multicentric (MCD) Castleman disease. The latter is further subdivided by the Castleman Disease Collaborative Network (CDCN) based on etiology and includes human herpesvirus 8/

TABLE 1 B-cell lymphoid proliferations and lymphomas [7].

WHO classification 5th edition	WHO classification 4th edition
Tumor-like lesions with B-cell predominance	
Reactive B-cell-rich lymphoid proliferations that can mimic lymphoma	Not previously included
IgG4-related disease	Not previously included
Unicentric Castleman disease	Not previously included
Idiopathic multicentric Castleman disease	Not previously included
KSHV/HHV8-associated multicentric Castleman disease	Multicentric Castleman disease

Kaposi sarcoma-associated herpesvirus (HHV8/KSHV-associated) and idiopathic MCD (iMCD) [1].

In HHV-8-associated disease, the uncontrolled viral signal, infecting B-cells, and plasmablasts are responsible for cytokine overproduction and systemic symptoms [4]. In these cases, both the human interleukin-6 (IL-6) and viral IL-6 play an important role in B-cell proliferation, mainly because the viral IL-6 binds directly to the IL-6 receptor without its coreceptor (gp80) [5, 6].

Idiopathic MCD has at least four clinical subgroups: POEMS (polyneuropathy, organomegaly, endocrinopathy, monoclonal plasma cell disorder, skin changes) associated MCD, iMCD-TAFRO (thrombocytopenia, ascites, reticulin fibrosis, renal dysfunction, organomegaly), iMCD-IPL (iMCD idiopathic plasmacytic lymphadenopathy), and iMCD-not otherwise specified (iMCD-NOS) [2]. The latest 2022 WHO-HAEM5 classification characterizes CD as a tumor-like lesion with B-cell predominance (Table 1.) [7]. POEMS-associated MCD is caused by the cytokine production from the affected monoclonal plasma cells, which have undergone genomic events [4]. The assumed cytokines in the pathogenesis are vascular endothelial growth factor (VEGF), IL-6, IL-12, transforming-growth factor-1β, and tumor necrosis factor-α.

The pathogenesis of idiopathic MCD is multifactorial [8]. One proposed mechanism is autoimmunity; auto-reactive antibodies stimulate the synthesis and release of cytokines since the histology of CD lymph nodes is 15%–30% similar to lymph nodes found in patients with rheumatoid arthritis (RA) and systemic lupus erythematosus (SLE) [9, 10]. Autoinflammatory syndromes also could share similarities with some iMCD cases. French authors have found an association between the mutation in the Mediterranean fever gene and CD [11]. Moreover, Stone et al. have shown a polymorphism in the IL-6 receptor of iMCD patients, leading to increased levels of IL-6 receptor, thereby IL-6 activity [12]. The fourth proposed mechanism is the neoplastic, which assumes that the development of iMCD is due to acquired oncogenic mutation in lymph nodes [13]. The role of viral infection beyond HHV-8 infection was also proposed as a driving mechanism in iMCD patients (Epstein-Barr virus, HHV-6, hepatitis B virus, Cytomegalovirus, Toxoplasma, etc.) [4].

Clinical manifestations of MCD are systemic inflammation, flu-like symptoms, night sweats, fever, skin rash, edema, and pleural effusions, along with other common symptoms (hepato-splenomegaly) and laboratory abnormalities (high sedimentation rate, increased C-reactive protein, hypoalbuminemia, thrombocytopenia or thrombocytosis). The time to diagnosis of patients with MCD is long not only because of its rarity but the broad spectrum of symptoms mimicking systemic autoimmune diseases, infections, or malignancies. The diagnosis beyond clinical symptoms is based on imaging and histological examination of the lymph nodes, thus the role of the pathologist is decisive.

The 5-year survival of patients with MCD is around 50%–77% [14], while for those with UCD is 100%.

If MCD is suspected, HHV-8 serology is recommended, but it is most commonly developing in immunocompromised patients (also HIV-associated) [1]. Specific biomarkers are not known in iMCD patients, and despite the important role of interleukin-6 (IL-6), it is not necessarily elevated [1].

Fajgenbaum et al. formulated the consensus criteria for iMCD in 2017 [1]. Based on their study *major criteria* of the disease are enlarged lymph nodes and histopathologic lymph node features such as atrophic germinative centers, vascularity, "lollipop" appearance, plasmacytosis, etc. *Minor criteria* are divided into clinical and laboratory criteria. Clinical criteria include "1" constitutional symptoms (fever, night sweats, weight loss, fatigue), "2" large spleen and/or liver, "3" fluid accumulation (edema, anasarca, ascites, pleural fluid), "4" eruptive cherry hemangiomatosis, "5" lymphocytic interstitial pneumonitis. The laboratory criteria include: "1" increased CRP and high sedimentation rate, "2" anemia, "3" thrombocytopenia or thrombocytosis, "4" hypoalbuminemia, "5" renal dysfunction or proteinuria, "6" polyclonal hypergammaglobulinemia [1]. Moreover, infections (HHV-8, HIV, EBV, CMV, toxoplasmosis, tuberculosis), autoimmune and autoinflammatory diseases (systemic lupus erythematosus, rheumatoid arthritis, adult-onset Still disease, autoimmune lymphoproliferative disease) and lymphoproliferative disease (lymphoma, multiple myeloma, plasmacytoma) should be excluded (*exclusion criteria*) [1].

The UCD forms are mainly hyaline vascular type on histology; only a minority of cases are plasmacytic. The lymphoid follicles are abnormal, and the mantle cell lymphocytes surrounding the follicle give the typical onion-skin-like appearance with radially penetrating blood vessels (lollipop appearance). The lymph nodes from MCD patients have three main histological types: hypervascularized, plasmacytic, and mixed type [15].

Surgery is the first-line treatment in UCD. However, there are cases where surgical removal is not feasible because of location or size, and these forms are called unresectable UCD [16]. The latter is further divided into asymptomatic and symptomatic forms. The asymptomatic unresectable UCD must be regularly followed, while in symptomatic forms, debulking, embolization, radiotherapy, or even systemic treatment are recommended [16] using corticosteroids, rituximab, or anti-IL-6 treatment.

Idiopathic MCD and intermediate forms (clinical picture falling between UCD and iMCD) are treated with anti-IL-6 treatment, siltuximab (monoclonal antibody against IL-6) or tocilizumab (monoclonal antibody inhibiting IL-6-receptor). The effectiveness of siltuximab was established in different clinical trials; in an open-label extension analysis of two trials, the patients received 11 mg/kg siltuximab every 3 weeks for up to 6 years [17], and the treatment was well tolerated. The half-life of siltuximab is 20.6 days. In some cases, administration may be extended to 6 weeks. Common side effects were nausea, vomiting, respiratory tract infection, hypertriglyceridemia, arthralgia, and headache; no serious adverse event occurred [18].

Rituximab also can be used in patients with mild symptoms. Siltuximab is recommended to be used continuously, while in non-responders, other immunosuppressive treatments (thalidomide, cyclosporine A, sirolimus, anakinra, bortezomib) are optional. In severe cases combined chemotherapy is appropriate: R-CHOP (rituximab, cyclophosphamide, doxorubicin, vincristine, prednisone, R-VDT-PACE (rituximab, bortezomib, dexamethasone, thalidomide, cisplatin, doxorubicin, cyclophosphamide, etoposide), or etoposide/cyclophosphamide/rituximab [19].

Rituximab and antiretroviral therapy should be used in HHV8/HIV-associated MCD [20] since siltuximab does not bind to viral IL-6 formed in these patients [18].

UCD could be associated with bronchiolitis obliterans and paraneoplastic pemphigus (PNP) which can occur if the treatment is delayed. MCD could increase the risk of thromboembolic complications and could progress into non-Hodgkin lymphomas. In the 2008 WHO classification, a new entity was proposed, the large-B-cell associated HHV-8 positive multicentric Castleman disease which is an aggressive disease caused by the proliferation of HHV-8 infected plasmablasts [21].

Response criteria of CD were defined by the CDCN based on laboratory, lymph node, and clinical response. Complete response (CR) means that there is a recovery in all three above-mentioned parameters. Partial response (PR) by definition is improvement in all four symptom categories (anorexia, fever, weight change, fatigue) and improvement in more than 50% of laboratory tests, stable disease is defined as <50% improvement in laboratory tests, and improvement in at least one of each symptom. Progressive disease is more than 25% worsening in laboratory tests and any symptoms [19].

At present, we aim to review the data and clinical characteristics of patients treated for Castleman disease at a Hungarian rare disease and hematology center.

Material and methods

We performed a retrospective analysis in the Department of Internal Medicine Division of Hematology and Rare Disease Center of University of Debrecen (UD) over 20 years, from 2002 to 2022. Patient records were thoroughly reviewed using the electronic registries (Medsolution and UDMed) of the University of Debrecen. We evaluated demographic information, clinical presentations, histopathologic findings, treatment approaches, and patient outcomes. Histopathologic examinations were primarily performed by the Department of Pathology at UD, and in some cases, a second opinion was sought.

The data analyzed in this study were obtained with the approval of the Regional and Institutional Ethics Committee (RKEB.6437-2023).

Results

The mean age of all patients was 41.5 ± 18.1 years. We diagnosed and followed seven patients with UCD and five patients with MCD, all of them fulfilled the diagnosis of iMCD. Demographic data are listed in Table 2.

UCD patients

The mean age of UCD patients was 32.28 ± 13.47 years. The mean time to diagnosis was 5.57 ± 3.4 months. UCD was defined as the involvement of a single lymph node or extranodal site, diagnosed by physical examination, computed tomography (CT), magnetic resonance imaging (MRI), or positron emission tomography (PET/CT).

Most of the patients with UCD had normal inflammatory parameters and complete blood cell counts (CBC) on admission, and all cases were HHV8 negative. Surgical procedures to remove pathological lymph nodes were performed in six patients, with five patients undergoing lymphadenectomy by mediastinoscopy and one patient having right lobectomy as a complication of CD. Histologic examination revealed the hyaline vascular type in most patients (n = 6) (Figure 1) and the plasmacytic type in one patient. In addition to surgery, two patients received thalidomide at doses of 50 and 100 mg for 3 years each. Patients with plasmacytic histology (in 2002) received the CAD protocol (cyclophosphamide 600 mg iv, 10 mg adriamycin, and 40 mg dexamethasone) for four cycles. One patient with mediastinal lymphadenopathy who underwent surgery with hyaline vascular histology (most of the lymphocytes were CD20 positive) received 700 mg rituximab for six cycles, because of unresectable UCD and an increase in inflammatory parameters. At the end of the treatment, PET/CT or chest CT scans showed complete remission in all UCD cases, with a median disease-free remission of 6.83 ± 6.17 years.

iMCD patients

The mean age of iMCD patients was 54.4 ± 16.68 years. The mean time to diagnosis was 13.6 ± 3.56 months. We diagnosed

TABLE 2 Demographic data of CD (UCD and iMCD) patients.

	UCD (n = 7)	iMCD (n = 5)
Age (years) Gender (M/F)	32.28 ± 13.47 4/3	54.4 ± 16.68 3/2
Localization	Mediastinum (n = 5) Cervical lymph node (n = 2)	Multicentric
Histology	Hyaline vascular n = 6 Plasmacytic (n = 1)	Hyaline vascular n = 4 Plasmacytic n = 1
Surgery	Lymphadenectomy by mediastinoscopy n = 5 Lobectomy = 1	—
Therapy	Chemoimmunotherapy n = 4	Chemoimmunotherapy n = 5

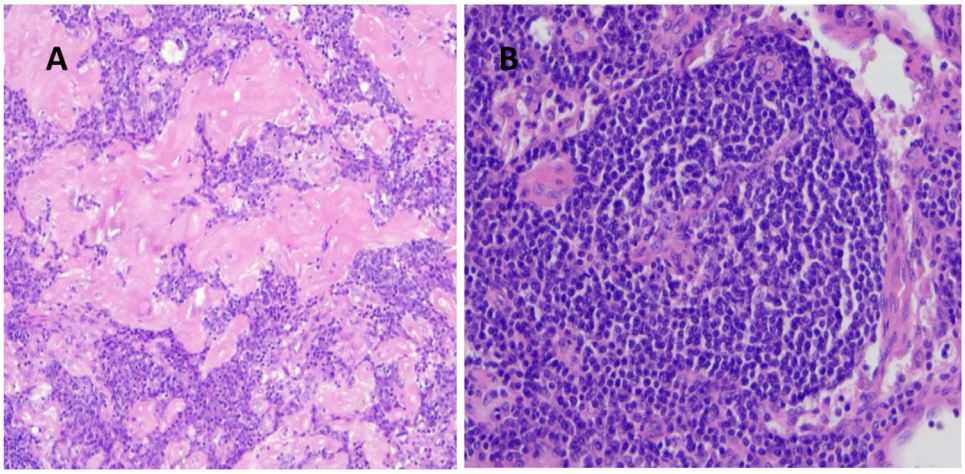

FIGURE 1
(A) Hyalin vascular type histology of a UCD patient (regressed germinal centers, interfollicular vascular proliferation, hyalin deposition, H&E staining magnification ×10), **(B)** umbilical-cord like central vascular pattern (H&E staining magnification ×20).

and followed three male and two female patients with iMCD. The diagnosis of MCD was based on general symptoms, physical examination, CT, MRI, or PET/CT. HHV8 serology was performed in all patients with negative results.

Case 1

A 46-year-old woman had a previous history of immune thrombocytopenia that responded well to prednisolone treatment. In 2019, she presented with severe leg edema, livedo reticularis, Raynaud's phenomenon, vasculitis on the lower leg, hyperpigmentation of the neck, and enlarged axillary lymph nodes. Laboratory tests revealed reduced complement levels and the presence of giant platelets. Tumor markers were negative. Trephine biopsy was performed because prolonged thrombocytopenia showing bone marrow hyperplasia, while information content of axillar and inguinal lymph node core biopsy seemed to be questionable. The renal function was normal, but because of severe leg edema and microscopic hematuria, renal biopsy was performed, showing diffuse mesangial IgM deposition. A skin punch biopsy suggested lupus erythematosus with a positive antinuclear factor (mitotic spindle, titer 1:160). Antibodies to double-stranded deoxyribonucleic acid (DNA), anti-neutrophil cytoplasmic antibody (ANCA), and antiphospholipid antibodies were all negative. Low complement levels were detected (C3 0.38 g/L, C4 0.03 g/L, CH50 < 10). The antiplatelet antibody was positive. Capillary microscopy showed bushy capillaries. In 2022, immunologist excluded systemic autoimmune disease. Therefore, because ultrasonography and CT imaging detected hepatomegaly, enlarged lymph nodes,we decided to get a lymph node biopsy by laparoscopic technique. Based on the clinical symptoms, lymphadenomegaly, laboratory criteria and histology of the lymph node (hyalin vascular CD), we were able to diagnose iMCD (Figure 2), unfortunately with a significant delay. The serum IL-6 concentration was mildly increased, 20 ng/L (N < 7 ng/L). We started the first infusion of siltuximab (11 mg/kg) in

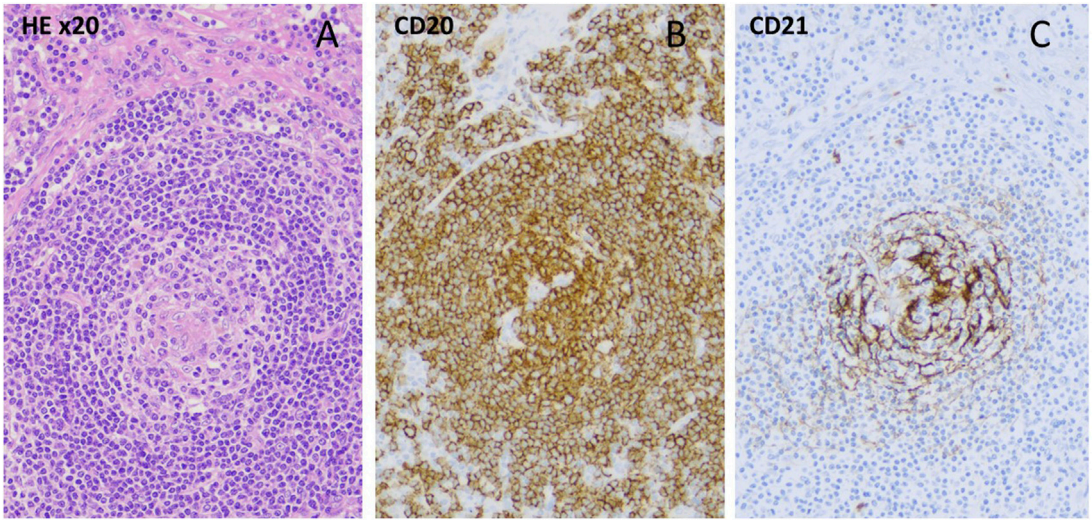

FIGURE 2
(A) Hyalinized centrum germinativum, target plate-like mantle zone/HE ×10, **(B)**-CD20 staining/, **(C)**-loose circular follicular dendritic cell network (CD21 staining).

January 2023. After the first dose, the blood cell count result showed a marked polycythemia (Hgb 182 g/L, before the infusion it was 165 g/L), which is not a common side effect of siltuximab. Since the possibility of the myeloproliferative disease could not be completely ruled out analysis of Janus kinase-2 (JAK-2) gene-(V617F mutation), JAK2 exon 12-, calreticulin (CALR)-, and myeloproliferative leukemia virus oncogene (MPL) mutations were done with negative results, erythropoietin level was decreased. Phlebotomy was performed twice. After improvement of hemoglobin level, three additional infusions of siltuximab were given without complications. However, after the last infusion, a new enlarged lymph node appeared in the right supraclavicular region, which was removed and histopathology showed CD of the same type. Six weeks after surgery, we restarted siltuximab therapy, which is still ongoing.

Case 2

The 32-year-old woman presented with painful cervical lymphadenopathy, skin lesions diagnosed as paraneoplastic pemphigus based on positive indirect immunofluorescence staining of mouse bladder epithelium, and B symptoms in 2012. AntiBP-180 and antiBP-230 antibodies were also positive, while other tumor markers were negative. Chest and abdominal CT scans showed mediastinal and retroperitoneal lymphadenomegaly, pulmonary nodules, and emphysema. In April 2013, a laparoscopic biopsy confirmed plasmacytic Castleman disease with elevated IgG4 levels (Figure 3). The retroperitoneal mass was removed surgically. The patient also had dyspnea, and spirometry showed severe irreversible central and peripheral airway obstruction (alpha-1-antitrypsin deficiency was excluded). Transbronchial biopsy showed occlusion of small bronchioles, and FEV1 was significantly decreased (17%). Our diagnosis was plasmacytic Castleman disease associated with bronchiolitis obliterans ("popcorn lung") requiring lung transplantation.

The patient received oral methylprednisolone at a dose of 0.5 mg/kg, budesonide, and tiotropium, as well as six cycles of rituximab (600 mg) for CD. Subsequent PET/CT scans showed metabolic remission, so maintenance rituximab (600 mg) was continued every other month for 1 year. Unfortunately, before the final rituximab infusion, the patient developed an acute respiratory failure and required ventilatory support. No infection was found. Given the known CD, we initiated siltuximab infusion (11 mg/kg), which improved the patient's clinical condition and allowed the discontinuation of respiratory support. She subsequently received siltuximab infusions every 3 weeks for a total of 16 infusions. Tragically, after the last treatment, she experienced sudden respiratory failure and died at the age of 35.

Case 3

A 56-year-old male patient with a history of type 1 diabetes and hypertension presented in 2015 with dizziness, weight loss, and generalized symptoms. Laboratory tests revealed grade 3 anemia and an elevated erythrocyte sedimentation rate (>100 mm/h). Multiple myeloma, systemic vasculitis, and bone marrow involvement were excluded. Abdominal CT revealed retroperitoneal lymphadenopathy and supraclavicular lymphadenomegaly, and a lymph node biopsy was made. The diagnosis was hyaline vascular iMCD since he was

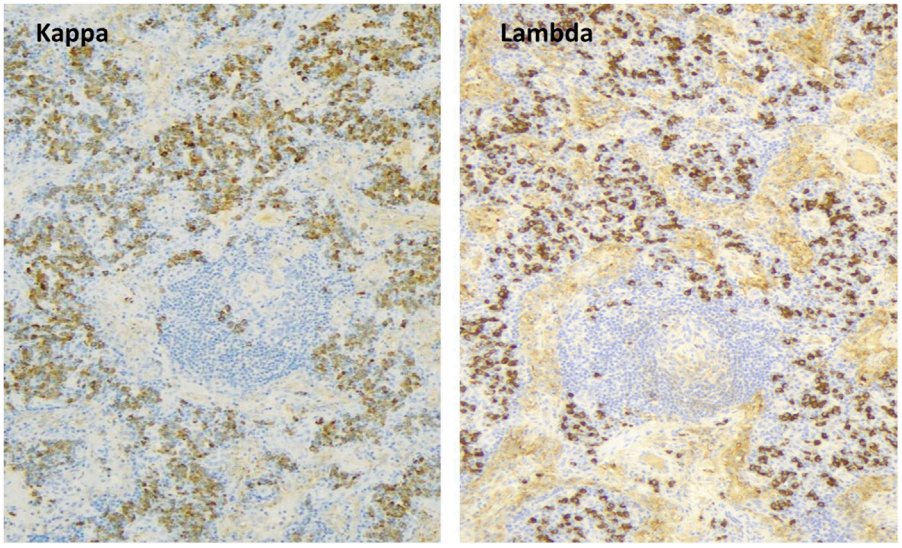

FIGURE 3
Plasmacytic Castleman disease (degenerative germinal center, plasmocytes, kappa/lambda light chain 2:1).

HHV8 negative. Methylprednisolone was started in a 1 mg/kg dose, and he received 10 mg of vinblastine every 2 weeks, five times until permission was received for anti-Il-6 treatment, siltuximab. Then siltuximab in a dose of 11 mg/kg was planned; however, due to anti-HBc positivity, antiviral (entecavir) protection (0.5 mg) was required before initiation. Approval was granted to administer 10 cycles of siltuximab (September 2016 to June 2017), during which time the patient remained symptom-free for 3 years and follow-up CT scans showed no lymphadenomegaly.

In 2020, anemia-related symptoms recurred, accompanied by lymphadenomegaly and hepatosplenomegaly on abdominal CT. Siltuximab treatment was restarted and continued for seven cycles (Figure 4). The patient experienced a third relapse in November 2022, characterized by lymphadenomegaly and nephrotic proteinuria, along with declining renal function (serum creatinine 229 umol/L, GFR 25 mL/min). However, a renal biopsy confirmed diabetic nephropathy as the cause of renal failure, unrelated to CD. The patient was subsequently treated with six cycles of siltuximab for CD activity. While imaging showed complete remission, there was no improvement in renal function.

Case 4

A 76-year-old man with a history of type 2 diabetes, hypertension, and chronic stage IV renal failure (GFR 12 mL/min) presented in January 2022 with anasarca and grade 2 anemia. Chest and abdominal CT revealed generalized lymphadenomegaly (>1 cm), prompting biopsy of an enlarged inguinal lymph node. Histologic analysis confirmed the diagnosis of hyaline vascular CD (iMCD). He was treated with siltuximab for six cycles with no deterioration in renal function. Follow-up imaging showed complete remission.

Case 5

A 60-year-old patient with a history of hypertension presented for evaluation of dyspnea and constitutional symptoms in 2015. CT and PET/CT scans revealed generalized lymphadenomegaly and a right lung tumor in the fourth lobe. Lobectomy was performed and histology confirmed HHV8-negative hyaline vascular CD. Treatment with siltuximab was initiated, and of note, the patient has received continuous infusions since 24 September 2015 to date, for a total of 114 siltuximab infusions. Currently, the patient remains in stable disease and no side effects from the infusions have been observed.

Discussion

Castleman's disease is a rare lymphoproliferative disorder classified as a tumor-like lesion with B-cell predominance in the new 2022 WHO-HAEM5 classification [7]. The etiology is unknown but is assumed to be related to viral infection (HHV-8), especially in immunocompromised patients, somatic mutations in clonal cells, and autoinflammation [1]. The hypercytokinaemia, the dysregulated cytokine profile, and increased IL-6 level lead to systemic, constitutional symptoms [4].

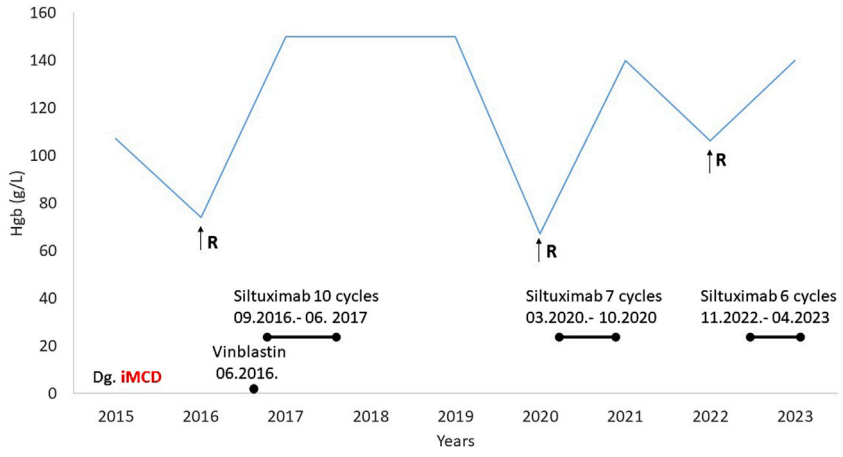

FIGURE 4
Medical history of Case 3 (R-relapse, Hgb-hemoglobin, MCD-multicentric Castleman disease).

The unicentric form (UCD) is typically localized to one lymph node region and is often diagnosed incidentally in the absence of general symptoms and normal laboratory tests. Most of the cases could be treated by the surgical removal of the lymph nodes, but in unresectable UCD, especially in those with symptomatic cases systemic treatment is recommended [16]. In our study, five patients had mediastinal and two patients had cervical lymph node enlargement, all malignancies were excluded, and laboratory tests were normal. Surgery was performed in six patients, four of whom received maintenance therapy such as thalidomide, rituximab, prednisolone, or other cytostatic therapy (cyclophosphamide, vinblastine) because of constitutive symptoms despite the lack of morphological signs of lymph node enlargement in other regions. Our median follow-up was 5 years, and the longest disease-free survival was 17 years. Our UCD patients who need systemic treatment may have oligocentric or intermediate CD which is a form between UCD and iMCD [16, 22]. Oligocentric CD is a recently defined type of the disease group which is characterized by regional or neighboring lymph node involvement, which may be asymptomatic, or cause only mild systemic symptoms compared to multicentric form, but sometimes needs further systemic therapy beyond the surgical removal [23]. Based on Turkish observations of a multicentric case series (n = 140), UCD patients received rituximab, radiotherapy, or in a few cases, chemotherapy after surgical removement of the lymph nodes [24].

The diversity of the idiopathic multicentric Castleman disease (iMCD) patients in our study is noteworthy. A unique and fatal combination of plasmacytic CD, bronchiolitis obliterans, severe pulmonary emphysema, and progressive dyspnea occurred in our 32-years-old iMCD patient. Only a few similar cases have been reported in the literature in which the lung disease was complicated by CD-type vascular hyalinosis. The dyspnea improved significantly after removing pathological lymph nodes [25, 26]. This patient needed long in-hospital treatment, similar to the observation of the ACCELERATE study, a longitudinal natural history study of CD. The authors of the mentioned study concluded that iMCD-TAFRO patients needed longer hospitalization than those with iMCD-NOS. Moreover, mechanical ventilation or hemodialysis often became necessary for these patients [27]. The patients under 30 years were more likely to present with severe symptoms [27]. Severe respiratory symptoms were also associated with iMCD in our patient, with the initial symptoms being paraneoplastic pemphigus. Cutaneous manifestations are common in CD as lichenoid eruptions, paraneoplastic pemphigus, maculopapular eruptions, Kaposi sarcoma, cutaneous necrotizing vasculitis, autoimmune bleeding disorders [28, 29]. These cutaneous symptoms occur in 55% of CD patients. The symptoms could be treated with systemic or topical corticosteroids or even with other immunomodulatory treatments.

Our working grouppreviously presented the case of a 30-year-old woman presenting with PNP, the investigation revealed a retroperitoneal mass, and the histology verified the diagnosis of hyalin vascular CD. Considering her young, fertile age, only immunomodulatory treatment with corticosteroid, thalidomide, and cyclosporine-A was started, which led to remission of both the tumor and PNP [30].

Livedo reticularis, Raynaud phenomenon, and lower limb vasculitis in case 2 raised the possibility of antiphospholipid syndrome or systemic lupus erythematosus since the skin biopsy suggested it, but the clinical symptoms did not fulfill the

diagnostic criteria of SLE. Nishimura et al. suggested that some patients with iMCD could have undiagnosed autoimmune diseases [31]. They examined retrospectively 63 patients with iMCD, 19 patients had at least one positive autoantibody, and five patients had positive antiphospholipid antibodies. In such patients, immunosuppressive treatment is also recommended, in our iMCD patient we also observed some symptoms suggesting autoimmune disease.

The association of systemic autoimmune disease and CD is rare, but it was shown previously that 30% of iMCD patients in case reports have autoantibodies [4, 31]. In one case report, UCD was associated with mixed connective tissue disease, and in another one TAFRO syndrome (histology was mixed type) was developed in a patient with Sjögren syndrome [32, 33]. Our previously mentioned patient (case 2) had Raynaud-phenomenon, livedo reticularis, low complement level, and antibody against antinuclear factor on skin biopsy, although negative lupus-specific antibodies are also unique symptoms in patients with CD. Association of systemic lupus erythematosus with CD was reported in only three pediatric cases [34].

In most of our cases, no side effects of siltuximab were observed, except in case 2, where the first siltuximab infusion resulted in significant polycythemia (Hgb 181 g/L, Htc 0.55). Therefore, we delayed the next infusion until a mild reduction in hemoglobin level (Hgb 167 g/L)and exclusion of any genetic mutation behind her polycythemia. In her case, secondary polycythemia seemed to be more likely while she has been a 1 pack/day smoker for more than 20 years, which was deteriorated by the use of siltuximab. In a 2018 systemic review that included 171 cases of MCD patients, polycythemia was reported as a side effect of siltuximab treatment in only one case [17, 35].

In case 3, the patient's disease course included remissions and relapses [36], but siltuximab was effective in each relapse and at least stabilized the disease course. Siltuximab treatment was effective without serious side effects even in cases with stage IV renal failure, as observed in cases 3 and 4. Renal involvement is uncommon in CD. Karoui et al. published a case series with histology-approved renal involvement with CD. 19 CD patients were included, mostly iMCD patients and four cases were HIV-positive. The HIV-negative iMCD patients have mostly small-vessel lesions with endotheliosis and in some cases AA amyloidosis [37]. 50% of patients with TAFRO syndrome have renal dysfunction, and most of the kidney histology shows thrombotic microangiopathy-like pathology and mesangioproliferative-like glomerulonephritis [38]. In case 3 the patient's renal dysfunction was thought to be caused by a relapse in his Castleman disease, but a renal biopsy revealed diabetic nephropathy behind his nephrotic proteinuria and stage IV renal failure. In case 4 the stage IV renal failure was diagnosed 2 years before the occurrence of CD and was due to his 10-year history of type 2 diabetes mellitus. A remarkable observation in case 5 iMCD patients is the continuous administration of siltuximab for almost 8 years, significantly longer than reported in an extension analysis study with an average duration of 5.5 years [17]. The maximum duration of the use of siltuximab is not established. In a previous case report, Lang et al. have been using siltuximab for 15 years as a maintenance therapy [39], and they found it to be safe in such long-term treatment.

The median survival of our iMCD patients was 4 years which is comparable to the average survival of the patients published previously, 25%–45% of them die within the first 5 years, and patients often relapse within 1–2 years [19]. In a phase II clinical trial siltuximab had a 34% overall response rate [40].

The diagnosis and treatment of iMCD are challenging [41] since it shares symptoms similar to different chronic inflammatory diseases. In milder cases, glucocorticoids might be enough, but in severe cases targeted therapy as anti-IL-6 treatment, or the use of combined chemotherapy could be optional.

Considering the high mortality rates of the iMCD patients new, targeted therapies are needed to improve the survival rate.

We recognize our study's limitations, this was a retrospective single-center review of a rare disease with a limited sample size. The small sample size and the incomplete, reliable data were not sufficient to make a serious statistical analysis. Multicenter data with long-term follow-up can improve our results.

Conclusion

Castleman disease is a rare and atypical lymphoproliferative disorder that often presents with symptoms similar to other malignant lymphoproliferative and autoimmune or inflammatory disorders. As a result, an accurate diagnosis might be delayed, sometimes for several months or years. A key feature of the disease is lymphadenomegaly, making lymph node biopsy and histologic examination essential for accurate diagnosis. The unicentric form typically follows a benign course and usually requires no systemic treatment beyond lymph node sampling. In contrast, the multicentric variants of Castleman disease both the HHV8-positive cases and iMCD are associated with generalized symptoms and laboratory abnormalities which require systemic treatment, primarily anti-IL-6 therapy. Given the rarity of the disease, the diagnosis is challenging and the role of histological diagnosis cannot be questioned.

Data availability statement

The raw data supporting the conclusions of this article will be made available by the authors, without undue reservation.

Ethics statement

The studies involving humans were approved by Regional and Institutional Ethics Committee RKEB.6437-2023. The studies were conducted in accordance with the local legislation and institutional requirements. The participants provided their written informed consent to participate in this study. Written informed consent was obtained from the individual(s) for the publication of any potentially identifiable images or data included in this article.

Author contributions

BB, GP, and ZS were treating and following the patients, GM performed the histological examinations, BB wrote the manuscript. Manuscript review and editing for important intellectual content: ZS, GM, GP, and ÁI. All authors contributed to the article and approved the submitted version.

Funding

The authors declare that no financial support was received for the research, authorship, and/or publication of this article.

Acknowledgments

The authors express their special thanks to Professor David Fajgenbaum (University of Pennsylvania) for his extremely useful advice and suggestions while preparing this manuscript.

Conflict of interest

The authors declare that the research was conducted in the absence of any commercial or financial relationships that could be construed as a potential conflict of interest.

References

1. Fajgenbaum DC, Uldrick TS, Bagg A, Frank D, Wu D, Srkalovic G, et al. International, evidence-based consensus diagnostic criteria for HHV-8-negative/idiopathic multicentric Castleman disease. *Blood* (2017) 129(12):1646–57. doi:10.1182/blood-2016-10-746933

2. Dispenzieri A, Fajgenbaum DC. Overview of castleman disease. *Blood* (2020) 135(16):1353–64. doi:10.1182/blood.2019000931

3. Mukherjee S, Martin R, Sande B, Paige JS, Fajgenbaum DC. Epidemiology and treatment patterns of idiopathic multicentric Castleman disease in the era of IL-6–directed therapy. *Blood Adv* (2022) 6(2):359–67. doi:10.1182/bloodadvances.2021004441

4. Fajgenbaum DC, Shilling D. Castleman disease pathogenesis. *Hematol Oncol Clin N Am* (2018) 32(1):11–21. doi:10.1016/j.hoc.2017.09.002

5. Amy YL, Nabel CS, Finkelman BS, Ruth JR, Kurzrock R, vanRhee F, et al. Idiopathic multicentric Castleman's disease: a systemic literature review. *Lancet Hematol* (2016) 3(4):e163–75. doi:10.1016/S2352-3026(16)00006-5

6. Uldrick TS, Polizzotto MN, Yarchoan R. Recent advances in Kaposi sarcoma herpesvirus-associated multicentric Castleman disease. *Curr Opin Oncol* (2012) 24(5):495–505. doi:10.1097/CCO.0b013e328355e0f3

7. Alaggio R, Amador C, Anagnostopoulos I, Attygalle AD, Araujo IBO, Berti E, et al. The 5th edition of the world health organization classification of haematolymphoid tumours: lymphoid neoplasms. *Leukemia* 2022; 36: 1720–48. doi:10.1038/s41375-022-01620-2

8. Fajgenbaum DC, van Rhee F, Nabel CS. HHV-8 negative, idiopathic multicentric Castleman disease: novel insights into biology, pathogenesis, and therapy. *Blood* (2014) 123(19):2924–33. doi:10.1182/blood-2013-12-545087

9. Kojima M, Motoori T, Asano S, Nakamura S. Histological diversity of reactive and atypical proliferative lymph node lesions in systemic lupus erythematosus patients. *Pathol Res Pract* (2007) 203(6):423–31. doi:10.1016/j.prp.2007.03.002

10. Kojima M, Motoori T, Nakamura S. Benign, atypical and malignant lymphoproliferative disorders in rheumatoid arthritis patients. *Biomed Pharmacother* (2006) 60(10):663–72. doi:10.1016/j.biopha.2006.09.004

11. Kone-Paut I, Hentgen V, Guillaume-Czitrom S, Trau T-A, Touitou I. The clinical spectrum of 94 patients carrying a single mutated MEFV gene allele. *Rheumatology (Oxford)* (2009) 48(7):840–2. doi:10.1093/rheumatology/kep121

12. Stone K, Woods E, Szmania SM, Stephens OW, Garg TK, Barlogie B, et al. Interleukin-6 receptor polymorphism is prevalent in HIV-negative Castleman disease and is associated with increased soluble interleukin-6 receptor levels. *PLos One* (2013) 8(1):E54610. doi:10.1371/journal.pone.0054610

13. Al-Maghrabi J, Kamel-Reid S, Bailey D. Immunglobulin and T-cell receptor gene rearrangement in Castleman's disease: molecular genetic analysis. *Histopathology* (2006) 48(3):233–8. doi:10.1111/j.1365-2559.2005.02319.x

14. Pierson SK, Kanhai K, Bagg A, Alapat D, Lim MS, Lechowicz MJ, et al. Characterizing mortality associated with idiopathic multicentric Castleman disease. *Blood* (2021) 138(Suppl. 1):1623. doi:10.1182/blood-2021-153397

15. Wu D, Lim MS, Jaffe ES. Pathology of Castleman disease. *Hematol Oncol Clin N Am* (2018) 32:37–52. doi:10.1016/j.hoc.2017.09.004

16. van Rhee F, Oksenhendler E, Srkalovic G, Voorhees P, Lim M, Dispenzieri A, et al. International, evidence-based consensus diagnostic and treatment guidelines for unicentric Castleman disease. *Blood Adv* (2020) 4(23):6039–50. doi:10.1182/bloodadvances.2020003334

17. van Rhee F, Casper C, Voorhees PM, Fayad LE, Gibson D, Kanhai K, et al. Long-term safety of siltuximab in patients with idiopathic Castleman disease: a prespecified, open-label, extension analysis of two trials. *Lancet Haematol* (2020) 7(3):e209–e217. doi:10.1016/S2352-3026(19)30257-1

18. Sarosiek S, Shah R, Munshi NC. Review of siltuximab in the treatment of multicentric Castleman's disease. *Ther Adv Hematol* (2016) 7(6):360–6. doi:10.1177/2040620716653745

19. van Rhee F, Voorhees P, Dispenzieri A, Fossa A, Srkalovic G, Ide M, et al. International, evidence-based consensus treatment guidelines for idiopathic multicentric Castleman disease. *Blood* (2018) 132(20):2115–24. doi:10.1182/blood-2018-07-862334

20. Guayboon T, Chinthammitr Y, Sukpanichnant HN, Angkasekwinai N. Human herpesvirus 8-associated multicentric Castleman disease in a patient with advanced HIV infection. *Medicine* (2021) 100:49. doi:10.1097/MD.0000000000028077

21. Payer E, Miltenyi Z, Simon Z, Magyari F, Barna S, Méhes G, et al. Idiopathic multicentric Castleman disease with positive diffuse large B-cell lymphoma arising from HHV-8 positive Castleman disease. *J Hematol* (2012) 1(2-3):65–9. doi:10.4021/jh27w

22. Brandstadter JD, Fajgenbaum DC. How we manage idiopathic multicentric Castleman Disease. *Clin Adv Hematol Oncol* (2022) 20(9):564–71.

23. Beckham TH, Yang JC, Chau KW, Noy A, Yahalom J. Excellent outcome with surgery or radiotherapy in the management of Castleman disease including a case of oligocentric disease. *Clin Lymph Myeloma Leuk* (2020) 20(10):685–9. doi:10.1016/j.clml.2020.05.002

24. Gündüz E, Kirkizlar HO, Ümit EG, Gülsaran SK, Özkocaman V, Özkalemkas F, et al. Castleman disease: a multicenter case series from Turkey. *Turk J Hematol* (2022) 39:130–5. doi:10.4274/tjh.galenos.2022.2021.0670

25. Kondo M, Matsuda N, Chiyotani A, Kawakami M, Konno K, Takizawa T, et al. A case of bronchobronchiolitis obliterans with Castleman's lymphoma. *Nihon Kyobu Shikkan Gakkai Zasshi* (1989) 27(6):735–41.

26. Radzikowska E, Pawlowski J, Chabowski M, Langfort R. Constrictive bronchiolitis obliterans in patients with Castleman's disease. *Monaldi Arch Chest Di* (2005) 63(4):226–9. doi:10.4081/monaldi.2005.624

27. Bustamante MS, Pierson SK, Ren Y, Bagg A, Brandstadter JD, Skralovic G, et al. Longitudinal, natural history study reveals the disease burden of idiopathic multicentric Castleman disease. *Haematologica* (2024) 109(7): 2196–206. doi:10.3324/haematol.2023.283603

28. Kim HJ, Han JH, Bang CH, Park KS, Cho S-G, Yoo DS, et al. Cutaneous disorders associated with Castleman's disease. *Acta Derm Venereol* (2019) 99:984–9. doi:10.2340/00015555-3253

29. Fujimoto W, Kanehiro A, Kuwamoto-Hara K, Saitoh M, Nakakita T, Amagai M, et al. Paraneoplastic pemphigus associated with Castleman's disease and asymptomatic bronchiolitis obliterans. *Eur J Dermatol* (2002) 12(4):355–9.

30. Miltenyi Z, Toth J, Gonda A, Tar I, Remenyik E, Illes A. Successful immunomodulatory therapy in Castleman disease with paraneoplastic pemphigus vulgaris. *Pathol Oncol Res* (2009) 15(3):375–81. doi:10.1007/s12253-008-9133-x

31. Nishimura Y, Nishikori A, Sawada H, Czech T, Otsuka Y, Nishimura MF, et al. Idiopathic multicentric Castleman disease with positive antiphospholipid antibody: atypical or undiagnosed autoimmune disease. *J Clin Exp Hematop* (2022) 62(2):99–105. doi:10.3960/jslrt.21038

32. Chrispal A, Vasuki Z, Thomas EM, Boorugu HK. Mixed connective tissue disorder and Castleman's disease. *J Assoc Physicians India* (2010) 58:515–7.

33. Fujimoto S, Kawabata H, Kurose N, Kawanami-Iwao H, Sakai T, Kawanami T, et al. Sjögren's syndrome manifesting as clinicopathological features of TAFRO syndrome: a case report. *Medicine (Baltimore)* (2017) 96(5):e9220. doi:10.1097/MD.0000000000009220

34. Demirkan FG, Dogan S, Ucar AK, Sönmez HE, Ayaz NA. Systemic lupus erythematosus complicated with Castleman disease: a case-based review. *Rheumatol Int* (2021) 41(2):475–9. doi:10.1007/s00296-020-04684-4

35. Sitenga J, Aird G, Ahmed A, Silberstein PT. Impact of siltuximab on patient-related outcomes in multicentric Castleman's disease. *Patients Relat Outcome Meas* (2018) 9:35–41. doi:10.2147/PROM.S140011

36. Carbone A, Borok M, Damania B, Gloghini A, Polizzotto MN, Jayanthan RK, et al. Castleman disease. *Nat Rev Dis Primers* (2021) 7(1):84. doi:10.1038/s41572-021-00317-7

37. Karoui AE, Vuiblet V, Dion D, Izzedine H, Guitard J, Frimat L, et al. Renal involvement in Castleman disease. *Nephrol Dial Transpl* (2011) 26:599–609. doi:10.1093/ndt/gfq427

38. Leurs A, Gnemmi V, Lionet A, Renaud L, Gibier J-B, Copin M-C, et al. Renal pathologic findings in TAFRO syndrome: is there a continuum between thrombotic microangiopathy and membranoproliferative glomerulonephritis? A case report and literature review. *Front Immunol* (2019) 10:1489. doi:10.3389/fimmu.2019.01489

39. Lang E, Sande B, Brodkin S, vanRhee F. Idiopathic multicentric Castleman disease treated with siltuximab for 15 years: a case report. *Ther Adv Hematol* (2022) 13:20406207221082552–6. doi:10.1177/20406207221082552

40. van Rhee F, Wong RS, Munshi N, Rossi J-F, Ke X-Y, Fossa A, et al. Siltuximab for multicentric Castleman's disease: a randomised, double-blind, placebo-controlled trial. *Lancet Oncol* (2014) 15:966–74. doi:10.1016/S1470-2045(14)70319-5

41. Müzes G, Sipos F, Csomor J, Sréter L. Multicentric Castleman's disease: a challenging diagnosis. *Pathol Oncol Res* (2013) 19:345–51. doi:10.1007/s12253-013-9619-z

Pathology & Oncology Research | frontiers

TYPE Brief Research Report
PUBLISHED 08 November 2023
DOI 10.3389/pore.2023.1611378

Check for updates

OPEN ACCESS

EDITED BY
Gábor Méhes,
University of Debrecen, Hungary

*CORRESPONDENCE
Botond Timár,
timar.botond@semmelweis.hu

†These authors have contributed equally to this work

RECEIVED 29 June 2023
ACCEPTED 27 October 2023
PUBLISHED 08 November 2023

CITATION
Ferenczi K, Nagy ZF, Istenes I, Eid H, Bödör C, Timár B and Demeter J (2023), Long term follow-up of refractory/relapsed hairy cell leukaemia patients treated with low-dose vemurafenib between 2013 and 2022 at the Department of Internal Medicine and Oncology, Semmelweis University. *Pathol. Oncol. Res.* 29:1611378. doi: 10.3389/pore.2023.1611378

COPYRIGHT
© 2023 Ferenczi, Nagy, Istenes, Eid, Bödör, Timár and Demeter. This is an open-access article distributed under the terms of the Creative Commons Attribution License (CC BY). The use, distribution or reproduction in other forums is permitted, provided the original author(s) and the copyright owner(s) are credited and that the original publication in this journal is cited, in accordance with accepted academic practice. No use, distribution or reproduction is permitted which does not comply with these terms.

Long term follow-up of refractory/relapsed hairy cell leukaemia patients treated with low-dose vemurafenib between 2013 and 2022 at the Department of Internal Medicine and Oncology, Semmelweis University

Kata Ferenczi[1], Zsófia Flóra Nagy[1], Ildikó Istenes[1], Hanna Eid[1], Csaba Bödör[2], Botond Timár[2*†] and Judit Demeter[1†]

[1]Department of Internal Medicine and Oncology, Semmelweis University, Budapest, Hungary, [2]1st Department of Pathology and Experimental Cancer Research, Semmelweis University, Budapest, Hungary

Introduction: Hairy cell leukemia (HCL) is an indolent B-cell lymphoproliferative disease. *BRAF* V600E mutation is detected in nearly all classical HCL cases which offers the possibility of targeted therapy.

Objective: The aim of our study was to assess the efficacy of low-dose vemurafenib as well as to assess the long term outcome of HCL patients treated with this drug at the Department of Internal Medicine and Oncology at Semmelweis University.

Methods: We report on 10 patients with classical HCL treated with low-dose vemurafenib at our Department between 2013 and 2022.

Results: As a result of fixed time low-dose vemurafenib treatment, 5 of 10 patients (5/10) achieved partial remission, 4 (4/10) had stable disease, and 1 (1/10) had MRD positivity. No patients achieved complete remission. The median progression-free survival was 28.5 months while the overall survival was 82 months.

Conclusion: We confirm that low dose of vemurafenib is effective and safe in the vast majority of patients with HCL. This small-molecule oral treatment allows to gain valuable time—months or even years—before further, usually parenteral treatment options have to be given or before previous treatment has

to be repeated. There are also promising data supporting the combination of vemurafenib with other drugs for the treatment of HCL patients which could provide even further possibility to bridge treatment.

KEYWORDS

relapsed/refractory, infection, hairy cell leukemia, BRAF inhibitors, vemurafenib

Introduction

Hairy cell leukemia (HCL) is an indolent B-cell lymphoproliferative disease characterized by pancytopenia, splenomegaly, and infiltration of bone marrow, liver, and spleen with mature B cells. HCL as a well-defined entity was recognized in 1958 by [1].

It is a rare neoplasm representing 2% of lymphoid leukemias [2]. Affected patients often have non-specific symptoms including weakness and fatigue, as well as symptoms related to cytopenias and splenomegaly. Infectious complications are common, due to both the underlying immunosuppression from cytopenias and myelosuppressive therapy. In peripheral smear, the hairy cells present as characteristic-appearing mononuclear cells which are typically large with circumferential hair-like cytoplasmic projections and a round nucleus [3].

Diagnosis of HCL is based on the presence of hairy cells in the blood or bone marrow (BM). Hairy cells express the following markers: CD11c, CD19, CD20, CD22, CD103, CD123, and CD25. Histological examination of a bone marrow biopsy specimen is used to assess bone marrow infiltration. This highlights the clinical importance of immunophenotypic analysis. A wide range of antibodies have been reported as useful markers including annexin-A1, DBA.44 (mouse monoclonal HSL antibody), TRAP (tartrate-resistant acid phosphatase), Tbet, HBME1 (Hector Battifora) and BRAF V600E mutation specific mouse monoclonal antibodies [4].

The V600E mutation of the *BRAF* gene was identified in 2011 by using whole exome sequencing of genomic DNA from purified leukemic cells of a HCL patient by [5]. The mutation replaces thymine with adenine in exon 15 of *BRAF* at the 1799th nucleotide position of the coding sequence. This results in an amino acid change from valine to glutamate at the 600th amino acid position of the protein sequence and leads to aberrant activation of the MEK-ERK pathway, resulting in increased cell proliferation and survival. *BRAF* V600E mutation is detected in nearly all classical HCL cases and offers the possibility of targeted therapy [5]. The diagnostic toolkit has been expanded since 2011 (and is increasingly important) to detect the presence of the *BRAF* V600E mutation. *BRAF* gene mutation is detected by sequence analysis or using the monoclonal mouse antibody VE1 [6].

The current gold standard first-line treatment of hairy cell leukemia is the administration of purine nucleoside analogs (cladribine or pentostatin) [7]. Thanks to purine nucleoside analogue (PNA) treatment, the life expectancy of patients today does not differ from the life expectancy of the average healthy population, but 40% still have a relapse [8, 9]. Treatment with anti-CD20 monoclonal antibody, rituximab, is used with high efficacy not only in refractory cases but also in low tumor burden patients unsuitable for purine nucleoside analogue therapy [10–12]. Since the vast majority of HCL patients carry the *BRAF* p.V600E mutation the use of vemurafenib, a *BRAF* inhibitor, that shows an unusual specificity for the p.V600E mutation has been suggested in individual patients as early as 2012. By now it is an accepted treatment modality in relapsed/refractory hairy cell leukaemia patients. Moreover, in clinical studies the first line use of rituximab combined with vemurafenib is under evaluation.

Methods and patients

We report the treatment characteristics and long-term outcomes of 10 classical HCL patients treated with vemurafenib between January of 2013 and December of 2022 at the 1st Department of Internal Medicine and Oncology, Semmelweis University. In our institution HCL patients were diagnosed and treated within the addressed 10 years. Early results of our vemurafenib treated patients have been published in our 2013 (these patients are marked as No. 1,2,3 in the current paper—same as in the 2013 publication) [3]. Over the past four decades in our center the majority of HCL patients have received first-line treatment with alfa interferon. If there were no contraindications to PNA treatment and after the improvement of the blood counts subcutaneous cladribine treatment followed. Since 2013 those elderly and frail patients who progressed despite treatment with alfa interferon have received second-line vemurafenib (Patients No. 7, 8 and 10 in the present paper). All the patients underwent dermatologic examination at baseline.

Clinical data and follow-up information were collected by regular follow-ups and chart review. Follow-ups and control visits were carried out during an active treatment biweekly, after the active treatment period monthly, and after 6 months of stable disease every 3 months. Responses were evaluated based on blood counts, bone marrow findings, and peripheral blood hairy cell count using standard criteria (Table 1).

TABLE 1 Criteria for response to treatment.

Response	Criteria
CR	ANC> 1.5 G/L, Hgb> 11 g/L, Thr> 100 G/L, no organomegaly by physical examination, no hairy cells in peripheral blood and bone marrow
MRD negative CR	ANC> 1.5 G/L, Hgb> 11 g/L, Thr> 100 G/L, no organomegaly, no hairy cell detected in bone marrow by immunohistochemistry
PR	ANC> 1.5 G/L, Hgb> 11 g/L, Thr> 100 G/L, organomegaly decreases by> 50%, hairy cell in peripheral blood <5%, bone marrow infiltration decreases by <50%
SD	CR and PR criteria are not met.
PD	Decrease in cell numbers> 25%, increase in organomegaly by> 25%
Relapse	Morphological relapse: recurrence of hairy cells in peripheral blood and/or bone marrow
	Haematological relapse: development of cytopenia involving at least one cell line

Patient characteristics are summarized in Table 2. Median age at diagnosis was 50 years (range, 35–68), at initiation of vemurafenib treatment was 73 years (range, 41–87). Patients were heavily pretreated (median of 2 prior treatment lines; range, 1–4 lines; n = 10). All consecutive treatments were administered due to progression.

Descriptive and comparative statistical methods were used to analyze the clinical data.

BRAF V600E mutation–specific immunohistochemistry

Immunohistochemistry was performed on formalin-fixed, paraffin-embedded (FFPE) tissue using a mutation-specific antibody to BRAF V600E protein (VE1 clone; ready-to-use dilution; Ventana Medical System, Tucson, AZ) in a Leica Bond-Max automated immunostainer (Leica Biosystems, Deer Park, IL). Three-μm thick sections mounted on adhesive glass slides were deparaffinized and subjected to heat-induced epitope retrieval (HIER) at pH 9 (using Bond ER Solution 2) for 30 min before incubation with pre-diluted BRAF V600E mutation-specific primary antibody for 40 min. The Bond Polymer Refine Detection Kit (DS9800 Leica Biosystems, Deer Park, IL) was used to visualize reactivity. Immunoreactions were completed by nuclear counterstaining with hematoxylin.

Molecular analysis for BRAF mutations

The mononuclear cell fraction of peripheral blood or bone marrow samples collected in EDTA containing collection tubes was separated by Ficoll gradient centrifugation. Cellular DNA was extracted using the MagCore Plus II Automated Nucleic Acid Extractor (RBC Bioscience Corporation, Taiwan). Isolated DNA samples were quantified using a Qubit 4 Fluorometer (Thermo Fisher Scientific, USA) and stored at 4°C. The extracted DNA was subjected to PCR amplification of a 91 bp region of the BRAF gene harboring codon V600 with a forward (TGAAGACCTCACAGT AAAAATAGG) and a biotin-conjugated reverse primer (TCCAGA CAACTGTTCAAACTGAT) using the ABI-Veriti 96 Well Thermal Cycler (Thermo Fisher Scientific, Waltham, MA). The amplified sequence was subjected to pyrosequencing of codons 599 to 601 using PyroMark Q24 (Quiagen). Briefly, single-stranded DNA templates for were obtained with the assistance of the PyroMark Q24 Vacuum Prep Workstation (Qiagen) according to manufacturer's instructions. The DNA template was incubated with the sequencing primer (5′-TGATTTTGGTCTAGCTACA-3′) on the PyroMark Q24 heat-block at 80°C–85°C for 2 min. Pyrosequencing was performed using the following dispensation order (CGATGATC) on the PyroMark Q24 system following the manufacturer's guidelines. All sequencing results were confirmed by pathologist review.

Results

Median time from diagnosis to treatment was 90 months (range, 2–228 months). Vemurafenib dose of 240 mg twice daily was used in 8 patients. Further patients received 480 mg twice daily (n = 2). Nine patients continued at this dose, whereas dose was escalated in 1 patient number 9. In patient number 9 we tried to deepen the remission by escalating the dose of vemurafenib. Dose and duration of the vemurafenib treatment was escalated in patient number 10 due to concomitant *M. tuberculosis* infection which was diagnosed before starting vemurafenib treatment. Median duration of vemurafenib treatment in the whole patient cohort was 56 days (range, 14–180 days).

Tables 3, 4 contains data on organ involvement, bone marrow infiltration and blood counts before initiating and after completion of vemurafenib treatment in all of our patients. As a result of vemurafenib treatment, 5 of 10 patients (5/10) achieved partial remission. 4 (4/10) had stable disease, and 1 (1/10) had MRD positivity. Patient number 1 achieved MRD positive CR after 180 days of vemurafenib treatment, at his 6 months bone marrow biopsy histology 2.4% residual hairy cells were found. MRD negative complete remission was not achieved in any of the patients. Median progression-free survival (PFS; from start of vemurafenib treatment to retreatment or death) was 28.5 months. Median overall survival (OS; from start of vemurafenib treatment to the end of our retrospective analysis or death) was 82 months. Median overall survival from the diagnosis to the end of the study or death was 164.5 months. During this long follow-up time 7 of 10 patients are still alive.

Figure 1 shows the effectivity of vemurafenib exemplified by a patient's control bone marrow biopsy.

To treat relapse following vemurafenib, 4 of 10 (4/10) patients received alpha interferon, 2 of 10 (2/10) patients received cladribine and rituximab, 1 of 10 patient (1/10)

TABLE 2 Data from our patients treated with vemurafenib.

Patient	Age at dg	Prior treatment lines	Time until treatment(month)	Duration of vemurfenib treatment (day)	Dose of vemurafenib (mg/day)	Response	PFS(month)	OS(month)	Side effect	Treatment after vemurafenib
1.	40	2 (caldribine, interferon)	12	58	2 × 240	PR	37	115	—	Rituximab, Cladribine
2.	45	3 (interferon, cladribine, rituximab)	180	14	2 × 240	SD	2	89	arthralgia hyperbilirubinaemia	Pentostatin
3.	65	3 (interferon, cladribine, rituximab)	96	110	2 × 240	SD	32	72	toxicoderma, arthralgia	IFN
4.	72	1 (interferon)	56	56	2 × 240	PR	32	32	photosensitivity	IFN
5.	64	2 (interferon, rituximab)	228	14	2 × 240	PR	49	49	tumorlysis sy (grade 2)	-
6.	48	3 (interferon, cladribine, rituximab)	72	91	2 × 240	SD	14	89	photosensitivity, arthralgia	IFN
7.	80	1 (interferon)	84	14	2 × 240	SD	25	24	toxicoderma	IFN
8.	69	1 (interferon)	96	56	2 × 240	PR	8	78	atrophy of skin	Rituximab
9.	35	4 (interferon, cladribine, interferon, rituximab)	216	47	2 × 480 for 28 days 2 × 720 until day 47	PR	5	86	keratoacanthoma	Rituximab mono 4x
10.	72	1 (interferon)	2	180	2 × 480	MRD	97	97	hyperkeratosis	—

10.3389/pore.2023.1611378

TABLE 3 Data about the blood counts, bone marrow- and organ involvement in our patients before vemurafenib treatment.

Patients	Before vemurafenib treatment				
-	-	-	Blood cell counts		
-	Bone marrow infiltration	Organ involvement	White blood cell (G/L)	Hemoglobin (g/L)	Platelet count (G/L)
1.	30% hairy cell	Hepatosplenomegaly	0.8	110	109
2.	80% hairy cell	Splenomegaly	0.8	100	49
3.	30%–40% hairy cell	—	1.1	110	107
4.	90% hairy cell	—	2.82	105	191
5.	diffuse infiltration	—	1.11	63	23
6.	80% hairy cell	Splenomegaly	2	147	71
7.	60%–70% hairy cell	—	11	75	44
8.	80% hairy cell	Splenomegaly	3.58	131	54
9.	40% hairy cell	—	2.47	129	90
10.	40% hairy cell	—	2.66	156	94

TABLE 4 Data about the blood counts, bone marrow- and organ involvement in our patients after vemurafenib treatment.

Patients	After vemurafenib treatment				
-	-	-	Blood cell counts		
-	Bone marrow infiltration	Organ involvement	White blood cell (G/L)	Hemoglobin (g/L)	Platelet count (G/L)
1.	<10% hairy cell	Splenomegaly	4	155	98
2.	no data	Splenomegaly	1.21	111	77
3.	40% hairy cell	—	2.3	141	118
4.	70% hairy cell	—	4.38	126	172
5.	there is no data	—	2.56	78	89
6.	40% hairy cell	—	3	159	112
7.	no data	—	2.77	104	72
8.	60% hairy cell	Splenomegaly	4.37	150	65
9.	20% hairy cell	—	3	111	162
10.	24% hairy cell	—	2.61	151	132

10.3389/pore.2023.1611378

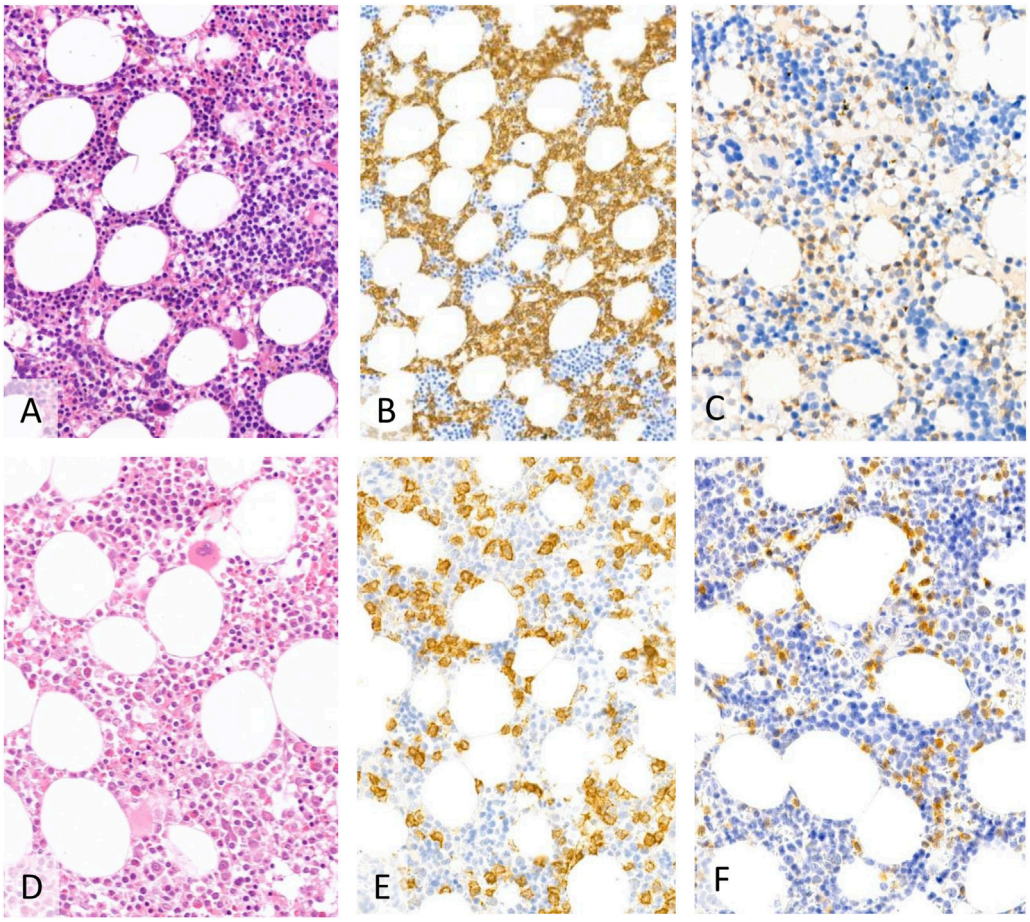

FIGURE 1
The first biopsy showed a more extensive infiltration (40%–50%) of hairy cell leukaemia (**(A)**–H&E, **(B)**–CD20, **(C)**–BRAF, 20X). After treatment the bone marrow was normocellular with maturing hematopoesis with residual patchy, interstitial lymphocytic aggregates (**(D)**–H&E) of CD20 positive **(E)** B-cells and with characteristic BRAF VE1 expression **(F)** accounting for ~15%–20% of the cellularity.

received rituximab, and 1 of 10 (1/10) received pentostatin. 2 patients did not receive treatment, because it was not necessary.

The side-effects of vemurafenib included photosensitivity (n = 2), toxicoderma (n = 2), keratoacanthoma (n = 1), hyperkeratosis (n = 1), arthralgia (n = 3), and elevation of bilirubin level (n = 1). In patient No. 5 grade 2 tumorlysis syndrome occurred as a side effect of the vemurafenib treatment within a few days. In patients with toxicoderma the skin symptoms disappeared after topical steroid treatment. Arthralgia was tolerable with non-steroidal agents. All patients were advised to stay out of the Sun. Side effects did not necessitate lowering of the dose or stopping the administration of vemurafenib.

Discussion

The discovery of the activating mutation *BRAF* V600E in 2011 has provided novel insights into the pathogenesis and had implications for the diagnosis and targeted therapy of HCL. This disease-defining genetic mutation, detected in nearly 100% of HCL patients, has opened the opportunity to investigate new targeted agents for the treatment of HCL [5]. The first reports documented in HCL patients treated with vemurafenib, a BRAF inhibitor approved for first-line treatment of unresectable or metastatic melanoma, been published in 2012 [13]. BRAF inhibitors such as vemurafenib are currently not approved in HCL and are used "off-label" in patients with refractory/relapsed HCL [14] In two phase 2 studies in 2015, that enrolled 54 BRAF-mutated HCL patients relapsed/refractory to purine analogue-based treatments, vemurafenib was administered at the standard melanoma dose of 960 mg twice daily for 16–18 weeks, respectively [15]. In comparison, patients in our study only received vemurafenib for an average of only 8 weeks. The ORR was 100% in the US study, 96% in the Italian study and the CR rate was 42% and 35%, respectively. MRD was detectable in all CR patients and relapses occurred soon after treatment. In

our study no patient achieved complete remission with the shorter and lower dosing schedule. However, the median PFS in the Italian study was 9 months, which is significantly lower than the PFS we reported in the current analysis [15].

Dietrich et al. published a retrospective analysis of 21 refractory/relapsed HCL patients treated with vemurafenib at a lower dose (240 mg/day) with a median follow-up time of 17 months. The median duration of treatment was 90 days. The CR rate was 40%. Interestingly the median PFS (17 months) of these 21 R/R HCL patients is very similar to that found in our retrospective analysis (28.5 months), although our patients did not achieve complete remission [16].

Tiacci et al published the highly efficient and well-tolerated combination of vemurafenib + rituximab in refractory/relapsed HCL. Thus, new potential chemotherapy-free agents, the combination of BRAF inhibitors and anti-CD20 monoclonal antibodies may improve the duration of response and may add to the therapeutic armamentarium [17]. However, compared to this combination treatment, the advantage of vemurafenib monotherapy is that it can be used orally, requires less monitoring and adverse events are low-grade and manageable. Combined inhibition of BRAF and MEK represents another promising chemotherapy-free regimen that avoids infusion-related reactions, and infections potentially associated with rituximab treatment. There are also promising preclinical data with B cell lymphoma 2 (Bcl 2) inhibitor venetoclax, which support combinations with other drugs for the treatment of HCL patients [18].

Our results show that low dose of vemurafenib is effective and safe in the vast majority of HCL patients. Although none of our HCL patients achieved CR, still the overall survival of our R/R HCL patients is excellent. This indicates the very good therapeutic potential of vemurafenib to bridge the time between more aggressive therapies. Thanks to the lack of myelosuppressive and immunosuppressive effects, unlike PNA, vemurafenib is a chemotherapy-free option to treat HCL patients who have an active infection and who cannot wait for the infection to clear before starting treatment for HCL [19]. Thus, it could be administered even during the COVID-19 pandemic or in the event of an impending pandemic, either in the first-line setting or as a bridge to PNA until the resolution of the infection [20].

Data availability statement

The original contributions presented in the study are included in the article/supplementary material, further inquiries can be directed to the corresponding author.

Ethics statement

The studies involving humans were approved by TUKEB Semmelweis University, Hungary. The studies were conducted in accordance with the local legislation and institutional requirements. The participants provided their written informed consent to participate in this study.

Author contributions

Conceptualization: CB, BT, and JD. Methodology: KF, BT, and JD. Resources, Clinical Care: KF, ZN, II, HE, and JD. Data Curation: KF and JD. Writing–Original Draft: KF. Writing–Review and Editing: ZN, II, BT, and JD. Visualization: CB and BT. Supervision: JD.

Conflict of interest

The authors declare that the research was conducted in the absence of any commercial or financial relationships that could be construed as a potential conflict of interest.

Acknowledgments

We thank the patients and their physicians for their participation in this research project.

References

1. Bouroncle BA, Wiseman BK, Doan CA. Leukemic reticuloendotheliosis. *Blood* (1958) 13:164 609–30. doi:10.1182/blood.v13.7.609.609

2. Sári E, Rajnai H, Dénes K, Bödör C, Csomor J, Körösmezey G, et al. Novelties in the diagnostics and therapy of hairy cell leukemia. Új utak a hajas sejtes leukémia és a rokon kórképek diagnosztikájában és kezelésében. *Magy Onkol* (2016) 60:137–44. [Hungarian].

3. Sári E, Nagy ZG, Baghy K, Rajnai H, Bödör C, Csomor J, et al. Treatment of refractory hairy cell leukemia with a BRAF-inhibitor: lessons to be learnt. *Pathol Oncol Res* (2014) 20(4):973–80. doi:10.1007/s12253-014-9783-9

4. Tóth-Lipták J, Piukovics K, Borbényi Z, Demeter J, Bagdi E, Krenács L. A comprehensive immunophenotypic marker analysis of hairy cell leukemia in paraffin-embedded bone marrow trephine biopsies-a tissue microarray study. *Pathol Oncol Res* (2015) 21:203–11. doi:10.1007/s12253-014-9807-5

5. Tiacci E, Trifonov V, Schiavoni G, Holmes A, Kern W, Martelli MP, et al. BRAF mutations in hairy-cell leukemia. *New Engl J Med* (2011) 364(24):2305–15. doi:10.1056/NEJMoa1014209

6. Andrulis M, Penzel R, Weichert W, von Deimling A, Capper D. Application of a BRAF V600E mutation-specific antibody for the diagnosis of hairy cell leukemia. *Am J Surg Pathol* (2012) 36(12):1796–800. doi:10.1097/PAS.0b013e3182549b50

7. Maitre E, Cornet E, Troussard X. Hairy cell leukemia. 2020 update on diagnosis, risk stratification and treatment. *Am J Hematol* (2019) 94:1413–22. doi:10.1002/ajh.25653

8. Saven A, Burian C, Koziol JA, Piro LD. Long-term follow-up of patients with hairy cell leukemia after cladribine treatment. *Blood* (1998) 92:1918–26. doi:10.1182/blood.v92.6.1918.418k33_1918_1926

9. Dinmohamed AG, Posthuma EFM, Visser O, Kater AP, Raymakers A, Doorduijn JK, et al. Relative survival reaches a plateau in HCL. *Blood* (2018) 131:1380–8. doi:10.1182/blood-2017-12-820381

10. Thomas Da O, Brian S, Bueso-Ramos C, Fader S, Michael J, Francis J, et al. Rituximab in relapsed or refractory hairy cell leukemia. *Blood* (2003) 102:3906–11. doi:10.1182/blood-2003-02-0630

11. Ravandi F O, Brian S, Jorgenden J, Pierce S, Faderl S, Ferrajoli A, et al. Phase 2 study of cladribine followed by rituximab in patients with hairy cell leukemia. *Blood* (2011) 118:3818–23. doi:10.1182/blood-2011-04-351502

12. Robak T, Matutes E, Catovsky D ESMO Guidelines Committee. Hairy cell leukaemia: ESMO Clinical Practice Guidelines for diagnosis, treatment and follow-up. *Ann Oncol* (2015) 5:100–7. doi:10.1093/annonc/mdv200

13. Dietrich S, Glimm H, Andrulis M, von Kalle C, Ho AD, Zenz T. BRAF inhibition in refractory hairy-cell leukemia. *N Engl J Med* (2012) 366:2038–40. doi:10.1056/NEJMc1202124

14. Bohn JP, Wanner D, Steurer M. Ibrutinib for relapsed/refractory hairy cell leukemia variant. *Leuk Lymphoma* (2017) 58(5):1224–6. doi:10.1080/10428194.2016.1239262

15. Tiacci E, Park J, De Carolis L, Chung SS, Broccoli A, Scott S, et al. Targeting mutant BRAF in relapsed or refractory hairy-cell leukemia. *N Engl J Med* (2015) 373:1733–47. doi:10.1056/NEJMoa1506583

16. Dietrich S, Pircher A, Endris V, Peyrade F, Wendtner CM, Follows GA, et al. BRAF inhibition in hairy cell leukemia with low-dose vemurafenib. *Blood* (2016) 127(23):2847–55. doi:10.1182/blood-2015-11-680074

17. Tiacci E, De Carolis L, Simonetti E, Capponi M, Ambrosetti A, Lucia E, et al. Vemurafenib plus rituximab in refractory or relapsed hairy-cell leukemia. *New Engl J Med* (2021) 384(19):1810–23. doi:10.1056/NEJMoa2031298

18. Vereertbrugghen A, Colado A, Gargiulo E, Bezares RF, Fernández Grecco H, Cordini G, et al. *In vitro* sensitivity to venetoclax and microenvironment protection in hairy cell leukemia. *Front Oncol* (2021) 11(11):2595. doi:10.3389/fonc.2021.598319

19. Bohn JP, Pircher A, Wanner D, Vill D, Foeger B, Wolf D, et al. Low-dose vemurafenib in hairy cell leukemia patients with active infection. *Am J Hematol* (2019) 6:E180–2. doi:10.1002/ajh.25474

20. Grever M, Andritsos L, Banerji V, Barrientos JC, Bhat S, Blachly JS, et al. Hairy cell leukemia and COVID-19 adaptation of treatment guidelines. *Leukemia* (2021) 35(7):1864–72. doi:10.1038/s41375-021-01257-7

Pathology & Oncology Research | frontiers

TYPE Original Research
PUBLISHED 20 February 2024
DOI 10.3389/pore.2024.1611497

Check for updates

OPEN ACCESS

EDITED BY
Agota Szepesi,
Semmelweis University, Hungary

*CORRESPONDENCE
Peter Batar,
pbatar@med.unideb.hu

RECEIVED 15 September 2023
ACCEPTED 07 February 2024
PUBLISHED 20 February 2024

CITATION
Batar P, Alizadeh H, Rokszin G, Abonyi-Toth Z and Demeter J (2024), Comorbidities and outcomes of patients with chronic myeloid leukemia treated with tyrosine kinase inhibitors: a real-world, nationwide, retrospective study from Hungary.
Pathol. Oncol. Res. 30:1611497.
doi: 10.3389/pore.2024.1611497

COPYRIGHT
© 2024 Batar, Alizadeh, Rokszin, Abonyi-Toth and Demeter. This is an open-access article distributed under the terms of the Creative Commons Attribution License (CC BY). The use, distribution or reproduction in other forums is permitted, provided the original author(s) and the copyright owner(s) are credited and that the original publication in this journal is cited, in accordance with accepted academic practice. No use, distribution or reproduction is permitted which does not comply with these terms.

Comorbidities and outcomes of patients with chronic myeloid leukemia treated with tyrosine kinase inhibitors: a real-world, nationwide, retrospective study from Hungary

Peter Batar[1]*, Hussain Alizadeh[2], Gyorgy Rokszin[3], Zsolt Abonyi-Toth[3,4] and Judit Demeter[5]

[1]Department of Hematology, Faculty of Medicine, University of Debrecen, Debrecen, Hungary, [2]1st Department of Medicine, Division of Haematology, Clinical Center, Medical School, University of Pecs, Pecs, Hungary, [3]RxTarget Ltd., Szolnok, Hungary, [4]Department of Biostatistics, University of Veterinary Medicine, Budapest, Hungary, [5]Department of Internal Medicine and Oncology, Faculty of Medicine, Semmelweis University, Budapest, Hungary

Purpose: This study aimed to provide real-world evidence on the characteristics, treatment patterns, and outcomes of patients with chronic myeloid leukemia (CML) receiving tyrosine kinase inhibitor (TKI) treatment in Hungary between 2011 and 2019.

Patients and methods: This nationwide, retrospective study included patients who were newly diagnosed with CML in Hungarian clinical practice between January 2011 and December 2019. The analysis was based on the reimbursed prescription claims for imatinib, bosutinib, dasatinib, nilotinib, or ponatinib with the ICD-10 code C9210 in a public pharmacy between January 2009 and December 2019 using data from the National Health Insurance Fund (NHIF) of Hungary. CML incidence and prevalence, TKI treatment patterns, comorbidities, and overall survival (OS) were examined.

Results: Between 2011 and 2019, altogether 1,407 patients were diagnosed with CML, with an annual average of 156 patients. The number of patients newly initiating first-line TKI therapy for CML significantly increased between 2011 and 2019 (2011: n = 136 vs. 2019: n = 191; p = 0.0043). Nilotinib was typically prescribed for younger patients (≤64 years), while older patients (≥65 years) mostly received imatinib. The most common comorbidity of CML patients was hypertension, and the proportion of patients with other malignancies was relatively high in all treatment groups. 5-year OS was 77.1% during the whole study period. Patients initiating first-line TKI treatment for CML in 2015 had significantly better 4-year OS compared to those starting treatment in 2011 (82.4% vs. 73.5%, respectively, (HR 0.53 (95%CI 0.32–0.87) p = 0.0118).

Conclusion: This study is the first to provide insights into the characteristics, treatment patterns, and outcomes of CML patients treated with TKIs in Hungarian clinical practice between 2011 and 2019. We found slightly lower

OS rates compared to other European countries, however, there was a statistically significant improvement in 4-year OS during the study period. The management of CML was in line with international guidelines and recommendations.

KEYWORDS

chronic myeloid leukemia, real-word evidence, tyrosine kinase inhibitors, treatment outcome, overall survival

Introduction

Chronic myeloid leukemia (CML) accounts for 10%–15% of all leukemia cases, with an estimated incidence of 0.7–1.8/100,000 persons worldwide [1]. The course of CML can be divided into chronic, accelerated and blastic phases, and most patients are diagnosed during the chronic phase when the disease is often asymptomatic or very few symptoms are present [2].

The prognosis of CML has dramatically improved over the past two decades, due to the introduction of tyrosine kinase inhibitors (TKI) [2]. The development of imatinib, a first-generation TKI, represented the first real breakthrough in the treatment of CML [3]. Since then, four further TKIs have been added to the therapeutic armamentarium: the second-generation TKIs dasatinib, nilotinib, bosutinib, and the third-generation TKI ponatinib [4]. As a result of targeted therapy, in developed countries, the life expectancy of CML patients diagnosed in the chronic phase and receiving TKI therapy is very close to that of the age-matched general population, with 5-year survival rates of around 90% [5–7].

The 2020 guidelines of the European LeukemiaNet (ELN) recommend TKI for the first-line treatment of CML [5]. Imatinib is approved by the United States (U.S.) Food and Drug Administration (FDA) and the European Medicines Agency (EMA) for first line treatment while dasatinib, nilotinib, and bosutinib are registered in the first-, second- and further-line settings, and the third-generation TKI ponatinib is recommended for treatment beyond second-line. The treatment of CML requires close monitoring to allow for the timely detection of relapses or intolerable toxicities. In these cases, the ELN 2020 recommends the continuation of therapy with another TKI for up to four lines, with the careful consideration of patient-related factors including age, comorbidities, and previous TKI-related toxicities. As TKIs have different contraindications, early and late toxicity profiles, appropriate patient selection is of utmost importance to ensure good tolerability and optimize treatment outcomes.

The first registered TKI for treatment of CML was imatinib which was approved in 2001. In Hungary, nilotinib was approved for the first-line treatment of CML in 2014, which was soon followed by the approval of dasatinib in 2015. Bosutinib gained approval for second and subsequent lines of therapy in 2013 and for first line treatment of CML in 2018, while ponatinib is currently the only effective option in the case of T315L resistance mutations, approved for second- and subsequent treatment lines since 2013. The reimbursement of the TKIs may influence the application of treatment options.

Although clinical trials have consistently demonstrated the survival benefits and good tolerability of TKIs among patients with CML, there is a need for real-world evidence to gain more insights into the performance of these drugs in unselected patient populations encountered in routine clinical practice [8]. Several studies have reported real-world evidence on the characteristics, treatment patterns, and outcomes of CML patients treated with TKIs [9–19], however, no nationwide data have been published so far from Hungary in this regard.

Therefore, the aim of the current study was to examine the characteristics, outcomes, and survival of CML patients receiving TKI treatment in real-world Hungarian clinical practice between 2011 and 2019, focusing on treatment patterns, comorbidity profiles, and overall survival (OS).

Material and methods

This was a nationwide, retrospective study which included patients newly diagnosed with CML in Hungarian clinical practice between January 2011 and July 2020 who had at least one reimbursed prescription claim for imatinib, bosutinib, dasatinib, nilotinib, or ponatinib with the ICD-10 code C9210 in a public pharmacy between January 2009 and June 2020 based on the database of the National Health Insurance Fund of Hungary (NHIF). The NHIF contains patient ID and ICD-10 code information about all in- and out-patient visits as well as prescriptions of reimbursed drugs in Hungary. The NHIF covers the whole Hungarian population, therefore it served as a comprehensive data source for our nationwide study. Of note, the diagnosis of CML was established merely in a deductive way based on prescription claims for TKIs; no information on cytogenetics or molecular genetics were available. The requested data from NHIF covered the patient data from January 2011 and July 2020 however to be able to demonstrate whole year analyses this work includes data from the period of January 2011 and December 2019.

The incidence and prevalence of CML were examined between January 2011 and December 2019. The 2009-2010 period served as a screening period for the identification

of newly diagnosed CML patients and was not included in the analysis. Incidence and prevalence were examined in the whole patient population as well as according to age (0–64 vs. >65 years), sex, and line of therapy.

Treatment decisions regarding the choice of first-line TKI and change of therapy were at the discretion of the treating physician and were carried out according to EMA label recommendations. Patients already receiving ongoing imatinib therapy in 2009 were considered first-line. A new line of therapy was recorded if one of the following two scenarios occurred: i) a new TKI was initiated at least 60 days after the first TKI initiation; ii) a new TKI was initiated which was not claimed within 30 days prior to the previous TKI. Therefore, if a patient was switched from one TKI to another within 60 days, both TKIs were registered as first-line therapy (e.g., in the case of an imatinib-nilotinib-nilotinib-nilotinib sequence if nilotinib was initiated within 60 days after imatinib), and the recurrence of a TKI after a previous change of treatment line was not regarded as a new change of line (e.g., in the case of an imatinib-imatinib-imatinib-nilotinib-imatinib-imatinib-imatinib sequence). In summary, patients may have appeared with two different TKIs within the same treatment line. As a result of this methodology, the sum of annual patient numbers for a given TKI may have exceeded the total number of CML patients in the same year.

Comorbidities were examined 365 days prior to the initiation of therapy and were defined based on conditions included in the Charlson Comorbidity Index (CCI) [20] for the period between January 2011 to June 2020. The observation period for the analysis of comorbidities was extended until June 2020 to ensure that comorbidities affecting a low number of patients were also included in the analysis as the NHIF does not provide data with patient numbers below 10. Patients were classified as having a comorbidity based on one ICD-10 code record in in-patient care or an ICD-10 code record in out-patient care and at least one record of the same ICD-10 code in in- or out-patient care within more than 30 but fewer than 360 days following the first record. Of note, the identification of comorbidities was solely based on ICD-10 code records, and not on clinical findings or cardiology registries (Supplementary Table S1). Comorbidities were examined in the whole patient population and according to type of TKI and line of therapy.

For patients eligible for inclusion, all types of care recorded in the NHIF were queried including in- and out-patient visits, prescription claims, CT or MRI, and hemodialysis irrespective of their association with CML.

Statistics

Overall survival (OS), defined as the period between the initiation of TKI therapy for CML and death, was estimated using the Kaplan-Meier method between 1 January 2011 and 31 December 2019. 4-year OS rates were calculated separately for patients initiating first-line TKI therapy in 2011 and 2015.

We used Cox regression to analyse the change of the survival in time. We corrected for the differences in the baseline hazard by gender and age group (0–64, 65-).

We analysed the chage of age group distribution in time using binomial logistic regression. We used linear regression to calculate the annual trend for the number of new cases/100.000 patient years.

The study protocol was approved by Hungarian National Institute of Pharmacy and Nutrition, and by Medical Research Council Ethical Committee (IV/5969-1/2020/EKU, IV/210-1/2021/EKU) and was carried out in accordance with the 1975 Declaration of Helsinki, as revised in 2000, and Good Clinical Practice guidelines. Data collection and analysis was performed on anonymized and aggregated data.

Results

Between 2011 and 2019, altogether 1,407 patients were newly initiated on TKI therapy for CML, with an annual average of 156 patients (mean age: 56 years, 52% male). The incidence of CML varied between 1.16/100,000 in 2012 and 1.96/100,000 in 2019. There was a statistically significant increase in the number of patients newly initiating first-line therapy for CML between 2011 and 2019 (2011: n = 136 vs. 2019: n = 191; p = 0.0043) (Table 1). The number of patients initiating second-line therapy for CML remained constant during the observation period (2011: n = 79 vs. 2019: n = 73; p = 0.9875), with an annual average of 74.

Figure 1 shows the distribution of patients according to the type of TKI in the first-line setting between 2011 and 2019. Between 2011 and 2013, all patients newly diagnosed with CML received imatinib as first-line treatment. Nilotinib and dasatinib were registered for first-line treatment in Hungary in 2014 and 2015, respectively. Therefore, since 2015, three TKIs have been available as first-line treatment options in Hungary (imatinib, nilotinib, and dasatinib). The proportion of patients receiving dasatinib remained constant between 2015 and 2019, the proportion of those treated with imatinib increased from 43% to 53%, and the proportion of patients receiving nilotinib decreased from 44% to 28%.

In 2011 and 2019, 29% and 41% of patients newly initiating first-line therapy for CML were 65 years or older, respectively (Figure 2). Among patients treated with imatinib, the proportion of patients aged 65 years or older significantly increased from 30% in 2011 to 50% in 2019 (p = 0.0035). The same trend was observed with dasatinib between

TABLE 1 Incidence and number of patients initiating first-line treatment for CML according to age and sex between 2011 and 2019 in Hungary.

	2011–2019	2011	2012	2013	2014	2015	2016	2017	2018	2019
new 1L incidence/ 100,000		1.36	1.16	1.46	1.72	1.55	1.71	1.66	1.70	1.96
new 1L (n)	1,407	136	116	144	170	153	168	163	166	191
male	52%	54%	49%	53%	51%	52%	48%	58%	59%	46%
female	48%	46%	51%	47%	49%	48%	52%	42%	41%	54%
mean age (years) (SD, years)	56.13 (±17.15)	55.35 (±16.42)	55.15 (±16.69)	56.25 (±17.28)	55.83 (±16.87)	56.02 (±18.63)	56.46 (±16.35)	57.19 (±17.07)	55.40 (±18.41)	57.57 (±16.67)

CML, chronic myeloid leukemia; SD, standard deviation; 1L, first line.



FIGURE 1
Distribution of patients newly receiving first-line treatment for CML between 2011 and 2019 according to type of TKI. CML, chronic myeloid leukemia; TKI, tyrosine kinase inhibitor. N/A, not applicable (NHIF does not provide data with patient numbers below 10).

2015 and 2019 (10% vs. 39%; $p = 0.0165$). In contrast, the proportion of patients aged 65 years or older remained constant among those treated with nilotinib between 2014 and 2019 (Supplementary Figure S1). Among patients aged 65 years or older, the proportion of those receiving nilotinib decreased from 35% to 17% between 2015 and 2019, while the proportion of patients treated with imatinib increased from 32% to 65% (Supplementary Figure S2).

Comorbidities of CML patients

In our study, 53.5% of all CML patients had at least one comorbidity at treatment initiation. In all treatment lines combined, the most common comorbidity of CML patients was hypertension. The proportion of patients with comorbidities was the highest among those receiving bosutinib (60.5%), and the lowest among patients treated with nilotinib (46.5%) (Supplementary Table S2).

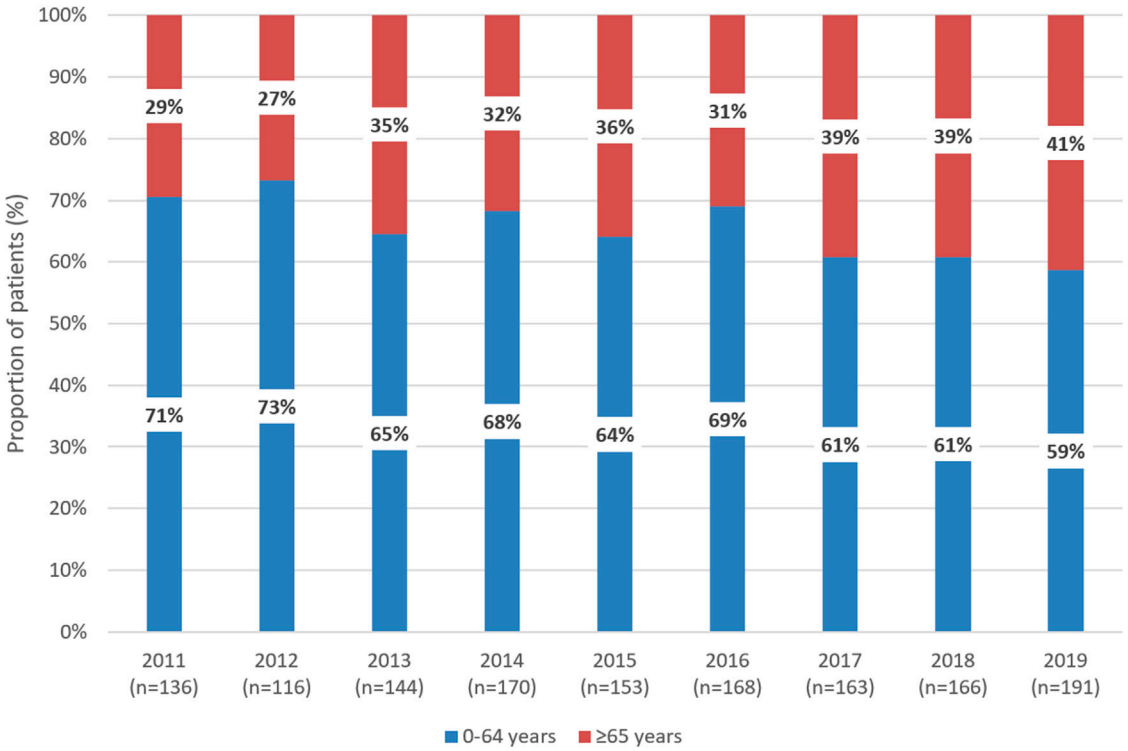

FIGURE 2
Distribution of patients receiving first-line TKI treatment for CML according to age 0–64 years vs. 65 years between 2011 and 2019 in Hungary. TKI, tyrosine kinase inhibitor; CML, chronic myeloid leukemia.

TABLE 2 Comorbidities among patients receiving dasatinib, imatinib, or nilotinib for CML in the first-line setting between 2011 and 2019.

	All TKI (n = 1403)	dasatinib (n = 161)	imatinib (n = 865)	nilotinib (n = 377)
Hypertension	511 (36.4%)	57 (35.4%)	345 (39.9%)	109 (28.9%)
Metabolic disorders	267 (19.0%)	34 (21.1%)	179 (20.7%)	54 (14.3%)
Diabetes mellitus	208 (14.8%)	31 (19.3%)	138 (16.0%)	39 (10.3%)
Ischemic heart disease	187 (13.3%)	17 (10.6%)	130 (15.0%)	40 (10.6%)
Other cancer	159 (11.3%)	20 (12.4%)	108 (12.5%)	31 (8.2%)
Pulmonary disease (lower tract)	120 (8.6%)	14 (8.7%)	86 (9.9%)	20 (5.3%)
Cerebral vascular accident	105 (7.5%)	10 (6.2%)	73 (8.4%)	22 (5.8%)
Arrythmiac condition (including AF)	94 (6.7%)	13 (8.1%)	60 (6.9%)	21 (5.6%)
Peripheral vascular disease	82 (5.8%)	10 (6.2%)	55 (6.4%)	17 (4.5%)
Congestive heart failure	70 (5.0%)	N/A[a]	49 (5.7%)	12 (3.2%)
TOTAL WITH COMORBIDITIES	**750 (53.5%)**	**86 (53.4%)**	**507 (58.6%)**	**157 (41.6%)**

CML: chronic myeloid leukemia, AF: atrial fibrillation.
[a]Groups fewer than 10 are automatically cancelled by the National Health Insurance Fund (NHIF) due to data protection reasons.

At first-line treatment initiation, patients treated with nilotinib had the lowest number of comorbidities (41.6%), while those receiving imatinib (58.6%) had the highest. The proportion of patients with "Other malignancies" was relatively high in all treatment groups: in total, 159 patients had "Other malignancies," of whom 108 were treated with imatinib, 31 received nilotinib, and 20 received dasatinib treatment (Table 2).

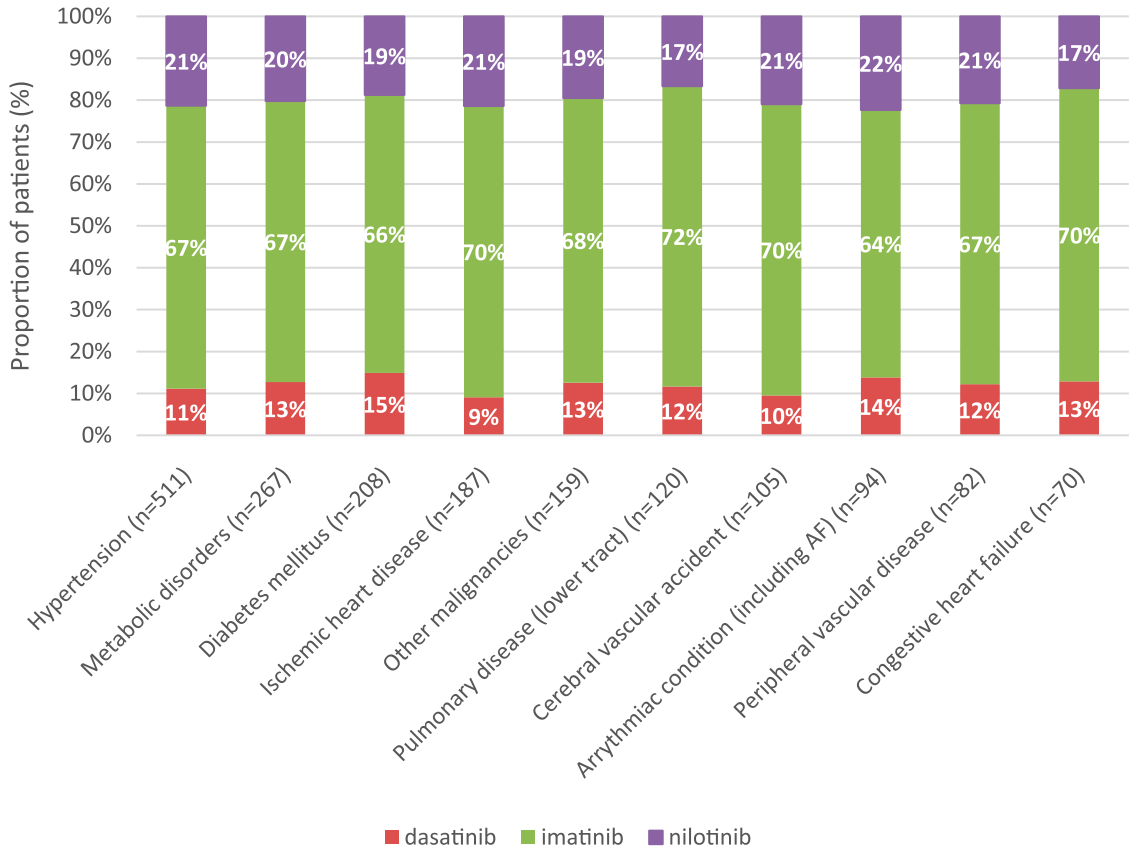

FIGURE 3
Distribution of TKIs according to the 10 most common comorbidities in first-line treatment of CML between 2011 and 2019. CML, chronic myeloid leukemia.

In all comorbidity groups, the majority of patients (67%–72%) received imatinib as first-line TKI treatment for CML. The second most common TKI was nilotinib (17%–22%), followed by dasatinib (9%–15%) (Figure 3).

Overall survival of patients with CML

Five-year OS was 77.1% among patients initiating first-line therapy for CML. (Figure 4). Four-year OS was 73.5% and 82.4% in patients initiating first-line TKI treatment in 2011 and 2015, respectively (Figure 5, HR: 0.53 (95% CI: 0.32–0.87); $p = 0.0118$).

Discussion

This nationwide, retrospective, longitudinal study examined comorbidities and treatment outcomes in an unselected real-world population of 1,407 patients with CML treated with TKIs over a 9-year period in Hungary. The number of patients initiating first-line TKI treatment for CML significantly increased between 2011 and 2019, with an annual average of 156 patients. The most common comorbidity was hypertension, and the proportion of patients with comorbidities was the lowest in the nilotinib and ponatinib treatment groups. Overall survival at 5 years was 77.1% among patients initiating first-line treatment for CML. 4-year OS was higher in those initiating TKI treatment in 2015 compared to patients starting TKI therapy in 2011 (82.4% and 73.5%, respectively).

Before the development of TKIs, CML was a fatal disease with a median OS of 5–7 years [21]. Treatment options for patients with CML included cytoreductive agents, interferon alpha (INF-α) and allogeneic stem cell transplantation (SCT) [22]. Imatinib, the first TKI to be approved in this setting in 2001, revolutionized the treatment landscape for CML and dramatically improved outcomes, transforming CML to a chronic disease with a close to normal expected life span. The pivotal International Randomized Study of Interferon and STI571 (IRIS) study compared imatinib 400 mg daily with IFN-alpha plus low-dose cytarabine in patients with newly diagnosed chronic-phase CML, and demonstrated the long-term, sustained efficacy and tolerability of imatinib with estimated 5-year and 10-year OS rates of 89% and 83.3%,

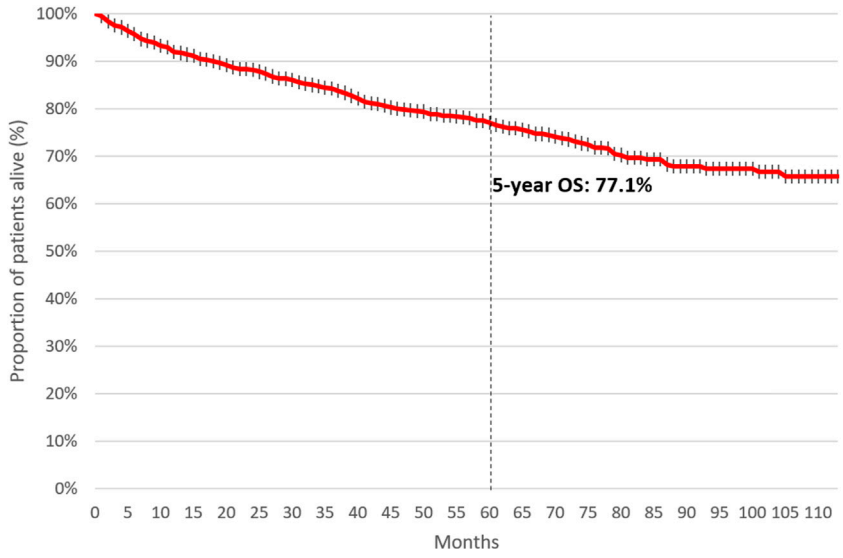

FIGURE 4
5-year overall survival of patients initiating first-line TKI treatment for CML between 2011 and June 2020. CML, chronic myeloid leukemia; TKI, tyrosine kinase inhibitor.

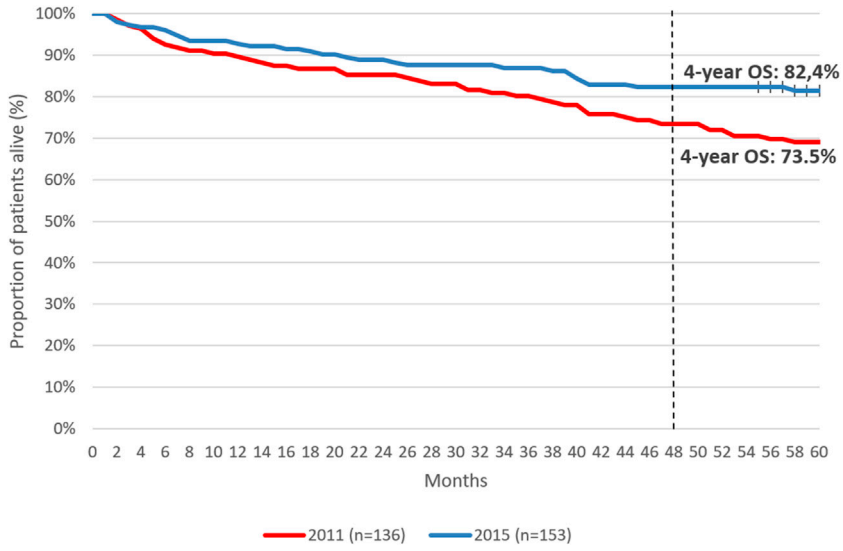

FIGURE 5
4-year overall survival of patients initiating first-line TKI therapy for the treatment of CML in 2011 vs. 2015. CML, chronic myeloid leukemia; OS, overall survival.

respectively [23–25]. Further studies with CML patients under imatinib treatment reported 10-year relative survival rate of 92% [26].

However, approximately 30% of patients receiving imatinib as first-line treatment in the chronic phase might experience treatment failure either due to TKI resistance (primary or secondary) [27] or intolerance [28]. Inadequate treatment response due to imatinib resistance or treatment-related toxicities requires the change of TKI treatment [5]. These limitations of imatinib therapy initiated the development of the second- (dasatinib, nilotinib, bosutinib) and third-generation (ponatinib) TKIs which provide enhanced efficacy and activity against several imatinib-resistant BCR-ABL1 mutants [29–32].

The phase 3 DASISION trial demonstrated the safety and efficacy of dasatinib as first-line treatment in patients with CML in the chronic

phase, with an estimated 5-year OS rate of 91% [29]. Frontline nilotinib 300 mg BID and 400 mg BID were associated with estimated 5-year OS rates of 93.7% and 96.2%, respectively, in the phase 3 ENESTnd study [30]. In the phase 3 BFORE trial comparing the efficacy and safety of bosutinib vs. imatinib in patients newly diagnosed with CP-CML, bosutinib was associated with a 5-year OS rate of 94.5% and showed superior efficacy vs. imatinib in terms of earlier and deeper molecular response [33]. Ponatinib was developed with the highest potency among all TKIs, and subsequently approved for the treatment of patients with CML who are resistant or intolerant to prior TKI therapies and in particular, in the presence of T315I mutation. In the international, randomized, phase 2 PACE study, evaluating patients resistant or intolerant to dasatinib or nilotinib, or who had the BCR-ABL1 T315I mutation regardless of prior TKI use, estimated 5-year OS was 73% in patients with chronic-phase CML [32].

Randomized controlled clinical trials almost never reliably represent everyday clinical practice. Patient selection often excludes elderly and frail patients with multiple comorbidities as well as patients with inappropriate ECOG (Eastern Cooperative Oncology Group) performance status. Despite the well-known limitations of real-world analyses, they can help to better understand the aspects of disease management that could be properly optimized to improve patient care. Real-world data may also help to guide the development of improved health plan operations, health system administration, cost management, epidemiologic research and can potentially contribute to the understanding and optimization of real-life treatment patterns and patient outcomes.

Since the advent of TKIs, the prognosis of CML is rather driven by coexisting comorbidities, than by CML itself [20]. Several studies have demonstrated the high prevalence of comorbidities among patients with CML treated with TKIs, and the strong association between comorbidities and outcomes [11, 34–36]. Specifically, in the randomized, 5-arm CML IV study of first-line imatinib therapy in patients with CML, higher Charlson Comorbidity Index (CCI) scores were significantly associated with lower OS, with an 8-year survival of 93.6% in patients with CCI = 2 and only 46.4% in patients with a score of >7 [20]. Of note, comorbidities had no negative impact on the success of imatinib therapy in terms of remission rates and disease progression, suggesting that patients with multiple comorbidities benefit from treatment with imatinib. Apart from overall survival, several studies suggest that comorbidities may also influence the risk of drug-related adverse events. A retrospective analysis of 125 chronic-phase CML patients treated with dasatinib at 21 Italian centers demonstrated a significant association between a higher comorbidity score and drug-related side effects [37]. Furthermore, pre-existing cardiovascular conditions have been shown to increase the risk of developing cardiovascular and arterio-occlusive events among CML patients treated with TKIs, especially in the case of newer agents [13, 38–40].

In this study, 53.5% of patients had at least one comorbidity at treatment initiation. The most common comorbidity of patients receiving any type of TKI in any treatment line was hypertension, which is in line with observations from other studies examining comorbidities among CML patients treated with TKIs in routine clinical practice. The ongoing, observational SIMPLICITY study is exploring the real-world use and management patterns of TKI in patients with chronic-phase CML receiving first-line imatinib, dasatinib or nilotinib in the United States and 6 European countries [41]. Of 1,242 prospective patients enrolled between October 2010 and September 2015, 81% had baseline comorbidities, including hypertension (all TKIs: 36%; imatinib: 41%, dasatinib: 36%, nilotinib: 31%) [9]. In the EUTOS population-based registry of newly diagnosed CML patients in 20 countries, 55.5% of patients had baseline comorbidities, among which the most frequent was hypertension in 25.7% [11]. Age-standardized prevalence of hypertension among adults aged 30–79 years in 2019 was 48% (male: 56%, female: 41%) in Hungary [42] which is in line with our finding of 53,3% cases of hypertension, as the most common comorbidity among CML patients in Hungary.

Given the overlapping indications of approved TKIs and their different toxicity profiles, there is a need for guidance on the appropriate use of TKIs. While disease state, BCR/ABL1 TKD mutational status, additional chromosomal abnormalities and line of treatment are key considerations for the selection of TKI, patient comorbidities and differences in TKI safety profiles should also be taken into consideration. Nilotinib and ponatinib treatments are not recommended in patients with previous or concomitant cardiovascular disease due to the increased risk of cardiovascular complications [5, 43]. Dasatinib should be avoided among patients with respiratory failure and previous or concomitant pleuro-pulmonary disease [5]. Imatinib should be avoided in patients with significant renal impairment [5]. Nilotinib treatment may also be an increased risk in the presence of diabetes mellitus, hypertension, hyperlipidemia, and it is not recommended in case of previous pancreatitis [5]. Furthermore, patients treated with bosutinib may develop diarrhea, and treatment with bosutinib and nilotinib requires caution among patients with hepatic conditions [5]. Our findings regarding the selection of TKI for patients with patient profiles and comorbidities are in line with label recommendations. Dasatinib and nilotinib were typically prescribed for younger patients compared to imatinib, which is consistent with previous real-world observations showing that imatinib is predominantly prescribed for older patients [44]. An increasing proportion of elderly patients (65 years or older) was prescribed imatinib during the study period, which is likely to reflect the favorable tolerability of imatinib.

In this study, the 5-year OS of patients receiving first-line TKI treatment for CML was 77.1%, which is lower than OS rates reported by randomized trials and real-world publications. This may be attributed to the comorbidity profile of the Hungarian CML patient population. On the other hand, 4-year OS rates showed clinically relevant improvements during our study period: patients initiating first-line TKI therapy for CML in 2015 had a 4-year OS of 82.4%, compared to the 4-year OS of 73.4% in those initiating treatment in 2011. The improvement in OS rates may explained

by the increasing knowledge and learning curve of hematologists on individual TKIs as well as the accumulation of real-world experience with TKIs and their adverse event profiles in patient populations with various comorbidities over time. As a growing body of evidence became available on TKIs over the past decade, hematologists were becoming more and more confident in the selection of individual agents while closely monitoring patient compliance. The OS improvement found in our study is a promising sign of improving patient management in real-world clinical practice and warrants further investigations to explore future trends in outcomes.

To our knowledge, our study is the first to describe the epidemiology, treatment patterns, and outcomes of patients with CML treated with TKIs in Hungarian clinical practice. However, it has certain limitations which need to be taken into consideration when interpreting the results. First, the NHIF database does not contain any information on non-reimbursed claims, laboratory data, patient parameters, symptoms, vital signs, adverse events, or the pathological and molecular features of CML. Furthermore, the database does not contain any data regarding the reason for a treatment switching, therefore, it did not allow for the evaluation of progression-free survival. Of note, overall survival was examined in our whole patient population and not separately for patients receiving different TKIs, therefore, conclusions regarding OS associated with individual TKIs cannot be drawn from this analysis.

Conclusion

This study provides insights into the characteristics, treatment patterns, and outcomes of the Hungarian CML patient population treated with TKIs. The results show that the management of CML patients in Hungarian clinical practice is in line with international guidelines. The lower OS observed in this study compared to findings from other developed countries reflect the overall worse health status and comorbidity profile of the Hungarian patient population. Treatment patterns observed in routine clinical practice show that Hungarian caretaking hematologists adequately consider age, comorbidities, and other patient-related risk factors when selecting the proper TKI treatment for patients with CML.

Data availability statement

The original contributions presented in the study are included in the article/Supplementary Material, further inquiries can be directed to the corresponding author.

Ethics statement

The studies involving humans were approved by the Scientific and Research Committee of the National Medical Research Council, Hungary. The studies were conducted in accordance with the local legislation and institutional requirements. Written informed consent for participation was not required from the participants or the participants' legal guardians/next of kin in accordance with the national legislation and institutional requirements.

Author contributions

PB, HA, and JD designed the analysis and wrote the paper, GR and ZA-T collected the data, performed the analysis and contributed to writing the paper. All authors contributed to the article and approved the submitted version.

Conflict of interest

GR and ZA-T are employees of RxTarget Ltd., which was a paid contractor to Pfizer in connection with the development of this manuscript and was responsible for data curation and statistical analysis. This study was sponsored by Pfizer. Medical writing support was provided by Zsófia Barcza at Syntesia Medical Communications Ltd. and was funded by Pfizer. The funder had the following involvement in the study: administrative support and review regarding study design, statistical analysis, and manuscript development.

The remaining authors declare that the research was conducted in the absence of any commercial or financial relationships that could be construed as a potential conflict of interest.

Acknowledgments

Medical writer Zsófia Barcza at Syntesia Medical Communications Ltd.

Supplementary material

The Supplementary Material for this article can be found online at: https://www.por-journal.com/articles/10.3389/pore.2024.1611497/full#supplementary-material

References

1. Thielen N, Visser O, Ossenkoppele G, Janssen J. Chronic myeloid leukemia in The Netherlands: a population-based study on incidence, treatment, and survival in 3585 patients from 1989 to 2012. *Eur J Haematol* (2016) 97(2):145–54. doi:10.1111/ejh.12695

2. Jabbour E, Kantarjian H. Chronic myeloid leukemia: 2018 update on diagnosis, therapy and monitoring. *Am J Hematol* (2018) 93(3):442–59. doi:10.1002/ajh.25011

3. Iqbal N, Iqbal N. Imatinib: a breakthrough of targeted therapy in cancer. *Chemother Res Pract* (2014) 2014:357027. doi:10.1155/2014/357027

4. Pan P, Wang L, Wang Y, Shen L, Zheng P, Bi C, et al. Systematic review and meta-analysis of -New-Generation tyrosine kinase inhibitors versus imatinib for newly diagnosed chronic myeloid leukemia. *Acta Haematol* (2020) 143(3):204–16. doi:10.1159/000501537

5. Hochhaus A, Baccarani M, Silver RT, Schiffer C, Apperley JF, Cervantes F, et al. European LeukemiaNet 2020 recommendations for treating chronic myeloid leukemia. *Leukemia* (2020) 34(4):966–84. doi:10.1038/s41375-020-0776-2

6. Hehlmann R, Müller MC, Lauseker M, Hanfstein B, Fabarius A, Schreiber A, et al. Deep molecular response is reached by the majority of patients treated with imatinib, predicts survival, and is achieved more quickly by optimized high-dose imatinib: results from the randomized CML-study IV. *J Clin Oncol* (2014) 32(5):415–23. doi:10.1200/JCO.2013.49.9020

7. Sasaki K, Strom SS, O'Brien S, Jabbour E, Ravandi F, Konopleva M, et al. Relative survival in patients with chronic-phase chronic myeloid leukaemia in the tyrosine-kinase inhibitor era: analysis of patient data from six prospective clinical trials. *Lancet Haematol* (2015) 2(5):e186–93. doi:10.1016/S2352-3026(15)00048-4

8. Webster J, Smith BD. The case for real-world evidence in the future of clinical research on chronic myeloid leukemia. *Clin Ther* (2019) 41(2):336–49. doi:10.1016/j.clinthera.2018.12.013

9. Goldberg SL, Cortes JE, Gambacorti-Passerini C, Hehlmann R, Khoury HJ, Michallet M, et al. First-line treatment selection and early monitoring patterns in chronic phase-chronic myeloid leukemia in routine clinical practice: SIMPLICITY. *Am J Hematol* (2017) 92(11):1214–23. doi:10.1002/ajh.24887

10. Hoffmann VS, Baccarani M, Lindoerfer D, Castagnetti F, Turkina A, Zaritsky A, et al. The EUTOS prognostic score: review and validation in 1288 patients with CML treated frontline with imatinib. *Leukemia* (2013) 27(10):2016–22. doi:10.1038/leu.2013.171

11. Hoffmann VS, Baccarani M, Hasford J, Lindoerfer D, Burgstaller S, Sertic D, et al. The EUTOS population-based registry: incidence and clinical characteristics of 2904 CML patients in 20 European Countries. *Leukemia* (2015) 29(6):1336–43. doi:10.1038/leu.2015.73

12. Hasford J, Baccarani M, Hoffmann V, Guilhot J, Saussele S, Rosti G, et al. Predicting complete cytogenetic response and subsequent progression-free survival in 2060 patients with CML on imatinib treatment: the EUTOS score. *Blood* (2011) 118(3):686–92. doi:10.1182/blood-2010-12-319038

13. Dahlén T, Edgren G, Lambe M, Höglund M, Björkholm M, Sandin F, et al. Cardiovascular events associated with use of tyrosine kinase inhibitors in chronic myeloid leukemia: a population-based cohort study. *Ann Intern Med* (2016) 165(3):161–6. doi:10.7326/M15-2306

14. Smith BD, Liu J, Latremouille-Viau D, Guerin A, Fernandez D, Chen L. Treatment patterns, overall survival, healthcare resource use and costs in elderly Medicare beneficiaries with chronic myeloid leukemia using second-generation tyrosine kinase inhibitors as second-line therapy. *Curr Med Res Opin* (2016) 32(5):817–27. doi:10.1185/03007995.2016.1140030

15. Geelen IGP, Thielen N, Janssen JJWM, Hoogendoorn M, Roosma TJA, Willemsen SP, et al. Treatment outcome in a population-based, 'real-world' cohort of patients with chronic myeloid leukemia. *Haematologica* (2017) 102(11):1842–9. doi:10.3324/haematol.2017.174953

16. Höglund M, Sandin F, Hellström K, Björeman M, Björkholm M, Brune M, et al. Tyrosine kinase inhibitor usage, treatment outcome, and prognostic scores in CML: report from the population-based Swedish CML registry. *Blood* (2013) 122(7):1284–92. doi:10.1182/blood-2013-04-495598

17. Gunnarsson N, Sandin F, Höglund M, Stenke L, Björkholm M, Lambe M, et al. Population-based assessment of chronic myeloid leukemia in Sweden: striking increase in survival and prevalence. *Eur J Haematol* (2016) 97(4):387–92. doi:10.1111/ejh.12743

18. Beinortas T, Tavorienė I, Žvirblis T, Gerbutavičius R, Jurgutis M, Griškevičius L. Chronic myeloid leukemia incidence, survival and accessibility of tyrosine kinase inhibitors: a report from population-based Lithuanian haematological disease registry 2000-2013. *BMC Cancer* (2016) 16:198. doi:10.1186/s12885-016-2238-9

19. Castagnetti F, Di Raimondo F, De Vivo A, Spitaleri A, Gugliotta G, Fabbiano F, et al. A population-based study of chronic myeloid leukemia patients treated with imatinib in first line. *Am J Hematol* (2017) 92(1):82–7. doi:10.1002/ajh.24591

20. Saussele S, Krauss MP, Hehlmann R, Lauseker M, Proetel U, Kalmanti L, et al. Impact of comorbidities on overall survival in patients with chronic myeloid leukemia: results of the randomized CML study IV. *Blood* (2015) 126(1):42–9. doi:10.1182/blood-2015-01-617993

21. Apperley JF. Chronic myeloid leukaemia. *Lancet* (2015) 385(9976):1447–59. doi:10.1016/S0140-6736(13)62120-0

22. Goldman JM. Chronic myeloid leukemia: a historical perspective. *Semin Hematol* (2010) 47(4):302–11. doi:10.1053/j.seminhematol.2010.07.001

23. O'Brien SG, Guilhot F, Larson RA, Gathmann I, Baccarani M, Cervantes F, et al. Imatinib compared with interferon and low-dose cytarabine for newly diagnosed chronic-phase chronic myeloid leukemia. *N Engl J Med* (2003) 348(11):994–1004. doi:10.1056/NEJMoa022457

24. Druker BJ, Guilhot F, O'Brien SG, Gathmann I, Kantarjian H, Gattermann N, et al. Five-year follow-up of patients receiving imatinib for chronic myeloid leukemia. *N Engl J Med* (2006) 355(23):2408–17. doi:10.1056/NEJMoa062867

25. Hochhaus A, Larson RA, Guilhot F, Radich JP, Branford S, Hughes TP, et al. Long-term outcomes of imatinib treatment for chronic myeloid leukemia. *N Engl J Med* (2017) 376(10):917–27. doi:10.1056/NEJMoa1609324

26. Hehlmann R, Lauseker M, Saußele S, Pfirrmann M, Krause S, Kolb HJ, et al. Assessment of imatinib as first-line treatment of chronic myeloid leukemia: 10-year survival results of the randomized CML study IV and impact of non-CML determinants. *Leukemia* (2017) 31(11):2398–406. doi:10.1038/leu.2017.253

27. Bixby D, Talpaz M. Mechanisms of resistance to tyrosine kinase inhibitors in chronic myeloid leukemia and recent therapeutic strategies to overcome resistance. *Hematol Am Soc Hematol Educ Program* (2009) 2009:461–76. doi:10.1182/asheducation-2009.1.461

28. Molica M, Scalzulli E, Colafigli G, Foà R, Breccia M. Insights into the optimal use of ponatinib in patients with chronic phase chronic myeloid leukaemia. *Ther Adv Hematol* (2019) 10:2040620719826444. doi:10.1177/2040620719826444

29. Cortes JE, Saglio G, Kantarjian HM, Baccarani M, Mayer J, Boqué C, et al. Final 5-year study results of DASISION: the dasatinib versus imatinib study in treatment-naïve chronic myeloid leukemia patients trial. *J Clin Oncol* (2016) 34(20):2333–40. doi:10.1200/JCO.2015.64.8899

30. Hochhaus A, Saglio G, Hughes TP, Larson RA, Kim DW, Issaragrisil S, et al. Long-term benefits and risks of frontline nilotinib vs imatinib for chronic myeloid leukemia in chronic phase: 5-year update of the randomized ENESTnd trial. *Leukemia* (2016) 30(5):1044–54. doi:10.1038/leu.2016.5

31. Cortes JE, Gambacorti-Passerini C, Deininger MW, Mauro MJ, Chuah C, Kim DW, et al. Bosutinib versus imatinib for newly diagnosed chronic myeloid leukemia: results from the randomized BFORE trial. *J Clin Oncol* (2018) 36(3):231–7. doi:10.1200/JCO.2017.74.7162

32. Cortes JE, Kim DW, Pinilla-Ibarz J, le Coutre PD, Paquette R, Chuah C, et al. Ponatinib efficacy and safety in Philadelphia chromosome-positive leukemia: final 5-year results of the phase 2 PACE trial. *Blood* (2018) 132(4):393–404. doi:10.1182/blood-2016-09-739086

33. Brümmendorf TH, Cortes JE, Milojkovic D, Gambacorti-Passerini C, Clark RE, le Coutre PD, et al. Bosutinib (BOS) versus imatinib for newly diagnosed chronic phase (CP) chronic myeloid leukemia (CML): final 5-year results from the bfore trial. In: Presented at the 62nd ASH Annual Meeting and Exposition; December 5, 2020. Washington, DC: American Society of Hematology (2020). Available from: https://ash.confex.com/ash/2020/webprogram/Paper137393.html (Accessed November 24, 2021).

34. Ono T, Takahashi N, Kizaki M, Kawaguchi T, Suzuki R, Yamamoto K, et al. Prognostic effect of comorbidities in patients with chronic myeloid leukemia treated with a tyrosine kinase inhibitor. *Cancer Sci* (2020) 111(10):3714–25. doi:10.1111/cas.14580

35. Jabbour E, Makenbaeva D, Lingohr-Smith M, Lin J. Use of real-world claim databases to assess prevalence of comorbid conditions relevant to the treatment of chronic myelogenous leukemia based on national comprehensive network treatment guidelines. *Clin Lymphoma Myeloma Leuk* (2015) 15(12):797–802. doi:10.1016/j.clml.2015.09.008

36. Cortes J. How to manage CML patients with comorbidities. *Hematol Am Soc Hematol Educ Program* (2020) 2020(1):237–42. doi:10.1182/hematology.2020006911

37. Breccia M, Latagliata R, Stagno F, Luciano L, Gozzini A, Castagnetti F, et al. Charlson comorbidity index and adult comorbidity evaluation-27 scores might predict treatment compliance and development of pleural effusions in elderly patients with chronic myeloid leukemia treated with second-line dasatinib. *Haematologica* (2011) 96(10):1457–61. doi:10.3324/haematol.2011.041251

38. Jain P, Kantarjian H, Boddu PC, Nogueras-González GM, Verstovsek S, Garcia-Manero G, et al. Analysis of cardiovascular and arteriothrombotic adverse events in chronic-phase CML patients after frontline TKIs. *Blood Adv* (2019) 3(6): 851–61. doi:10.1182/bloodadvances.2018025874

39. Douxfils J, Haguet H, Mullier F, Chatelain C, Graux C, Dogné JM. Association between BCR-ABL tyrosine kinase inhibitors for chronic myeloid leukemia and cardiovascular events, major molecular response, and overall survival: a systematic review and meta-analysis. *JAMA Oncol* (2016) 2(5):625–32. doi:10.1001/jamaoncol.2015.5932

40. Assunção PM, Lana TP, Delamain MT, Duarte GO, Zulli R, Lorand-Metze I, et al. Cardiovascular risk and cardiovascular events in patients with chronic myeloid leukemia treated with tyrosine kinase inhibitors. *Clin Lymphoma Myeloma Leuk* (2019) 19(3):162–6. doi:10.1016/j.clml.2018.12.004

41. ICON Clinical Research. *Studying first line treatment of chronic myeloid leukemia (CML) in a real-world setting (SIMPLICITY)* (2022). Available from: https://clinicaltrials.gov/ct2/show/NCT01244750 (Accessed January 10, 2024).

42. World Health Organization. *Global report on hypertension: the race against a silent killer* (2023). p. 152. Available from: https://www.who.int/publications/i/item/9789240081062 (Accessed January 10, 2024).

43. Quintás-Cardama A, Kantarjian H, Cortes J. Nilotinib-associated vascular events. *Clin Lymphoma Myeloma Leuk* (2012) 12(5):337–40. doi:10.1016/j.clml.2012.04.005

44. Specchia G, Pregno P, Breccia M, Castagnetti F, Monagheddu C, Bonifacio M, et al. Prognostic factors for overall survival in chronic myeloid leukemia patients: a multicentric cohort study by the Italian CML GIMEMA network. *Front Oncol* (2021) 11:739171. doi:10.3389/fonc.2021.739171

Pathology & Oncology Research | frontiers

TYPE Original Research
PUBLISHED 09 February 2023
DOI 10.3389/pore.2023.1610996

Check for updates

OPEN ACCESS

EDITED BY
József Tímár,
Semmelweis University, Hungary

*CORRESPONDENCE
Anna Sebestyén,
hsebanna@gmail.com,
sebestyen.anna@med.semmelweis-univ.hu

†These authors have contributed equally to this work

RECEIVED 06 December 2022
ACCEPTED 16 January 2023
PUBLISHED 09 February 2023

CITATION
Sztankovics D, Moldvai D, Petővári G, Gelencsér R, Krencz I, Raffay R, Dankó T and Sebestyén A (2023), 3D bioprinting and the revolution in experimental cancer model systems—A review of developing new models and experiences with *in vitro* 3D bioprinted breast cancer tissue-mimetic structures.
Pathol. Oncol. Res. 29:1610996.
doi: 10.3389/pore.2023.1610996

COPYRIGHT
© 2023 Sztankovics, Moldvai, Petővári, Gelencsér, Krencz, Raffay, Dankó and Sebestyén. This is an open-access article distributed under the terms of the Creative Commons Attribution License (CC BY). The use, distribution or reproduction in other forums is permitted, provided the original author(s) and the copyright owner(s) are credited and that the original publication in this journal is cited, in accordance with accepted academic practice. No use, distribution or reproduction is permitted which does not comply with these terms.

3D bioprinting and the revolution in experimental cancer model systems—A review of developing new models and experiences with *in vitro* 3D bioprinted breast cancer tissue-mimetic structures

Dániel Sztankovics†, Dorottya Moldvai†, Gábor Petővári, Rebeka Gelencsér, Ildikó Krencz, Regina Raffay, Titanilla Dankó and Anna Sebestyén*

Department of Pathology and Experimental Cancer Research, Semmelweis University, Budapest, Hungary

Growing evidence propagates those alternative technologies (relevant human cell-based—e.g., organ-on-chips or biofabricated models—or artificial intelligence-combined technologies) that could help *in vitro* test and predict human response and toxicity in medical research more accurately. *In vitro* disease model developments have great efforts to create and serve the need of reducing and replacing animal experiments and establishing human cell-based *in vitro* test systems for research use, innovations, and drug tests. We need human cell-based test systems for disease models and experimental cancer research; therefore, *in vitro* three-dimensional (3D) models have a renaissance, and the rediscovery and development of these technologies are growing ever faster. This recent paper summarises the early history of cell biology/cellular pathology, cell-, tissue culturing, and cancer research models. In addition, we highlight the results of the increasing use of 3D model systems and the 3D bioprinted/biofabricated model developments. Moreover, we present our newly established 3D bioprinted luminal B type breast cancer model system, and the advantages of *in vitro* 3D models, especially the bioprinted ones. Based on our results and the reviewed developments of *in vitro* breast cancer models, the heterogeneity and the real *in vivo* situation of cancer tissues can be represented better by using 3D bioprinted, biofabricated models. However, standardising the 3D bioprinting methods is necessary for future applications in different high-throughput drug tests and patient-derived tumour models. Applying these standardised new models can lead to the point that cancer drug developments will be more successful, efficient, and consequently cost-effective in the near future.

KEYWORDS

cancer, breast cancer, 3D bioprinting, disease models, biofabrication

Introduction

"ALL models are wrong but some are useful."

This April, the European Union (EU) prohibited selling new cosmetic products tested on animals without any exemptions (1). Accordingly, it is forbidden to place a new product on the market that contains even one new ingredient tested on animals in or out of the EU, even if the final product was not tested on animals (2). It is also well-known that pharmaceutical drug development is extremely time-consuming and expensive; moreover, about 90% of drugs fail after preclinical animal testing in human safety and efficacy trials. Additionally, in patients, ~1/6 newly marketed drugs are withdrawn or discontinued due to serious adverse effects (e.g., hepatic, cardiovascular, hematologic, neurologic, and carcinogenic) (3). Potentially beneficial drugs can also fail and never be placed on the market if these are categorised as toxic or ineffective during preselection based on animal tests (e.g., in recent conditions, aspirin could fail regarding its toxicity test results on rats and rhesus monkey embryos). Thus, certain patients could not benefit or even be omitted due to the limitations of animal models (4). Both U.S. Food and Drug Administration (FDA) and European Medicine Agency (EMA) modernisation acts aim to replace and decrease animal testing. Therefore, the bioengineering research area has rapidly improved in the last decade. Moreover, *in vitro* human model systems have undergone enormous developments nowadays. In the last pandemic situation, the development of COVID vaccines showed that faster and more efficient technologies are necessary for crisis and medical developments, and we have to leap over animal experiments and use clinical tests as fast as possible (5). Growing evidence propagates those alternative technologies (relevant human cell-based—e.g., organ-on-chips or biofabricated models—or artificial intelligence-combined technologies) could help test and predict human response and toxicity in medical research more accurately (6, 7).

In vitro disease model developments have great efforts to create and serve the need of reducing, and replacing animal experiments and establishing human cell-based *in vitro* test systems for research use, innovations, and drug tests. We know and accept the quote: "ALL models are wrong but some are useful"—(George E.O. Box, one of the greatest statisticians of the 20th century). We need human cell-based test systems for disease models and experimental cancer research; therefore, *in vitro* three-dimensional (3D) models have a renaissance, and the development of these technologies is growing ever faster.

The early history of cell biology/cellular pathology, cell-, tissue culturing, and cancer research models

Aristotelian doctrine about spontaneous generation describes those non-living substances (water, stones, and salts) that have some additional potential to spontaneously create complex systems and organisms. Regarding these explanations, insects, and flies are developed from mud and inorganic matter (8). The revolution of cell biology and the birth of cellular biology would not have been possible without one great invention—the microscope, after the invention of convex lenses by *Janssen* and the telescopes created by *Galilei*. Among many other early medical descriptions (9) *Hook* and *van Leeuwenhoek* made their unusual discovery of the invisible microscopic world (life) at the beginning of the 17th century (10). *van Leeuwenhoek* handcrafted lenses and constructed microscopes. In 1665, *Hook* published his outstanding findings in *Micrographia*; he described and illustrated many biological entities as well as defined microscopic units (e.g., "cells" or "pores"). The term "cell" directly comes from this work. The spontaneous generation doctrine was experimentally disproved and laid by *Pasteur* proving that life arises from pre-existing living organisms (it was demonstrated that microorganisms are present even in the air) (11). The developments in microscopic technologies helped to improve and even carry out more detailed studies. *Virchow*, *Schwann,* and *Kölliker* examined cells and tissues and also observed that "the elementary parts of all tissues are formed from cells" and suggested that "there is one universal principle of development for the elementary parts of organisms. . .and this principle is in the formation of cells" (12). Schwann and his colleagues described that the "cells arise inside and near other cells by differentiation of a homogenous primary substance" (13). *Virchow* and other scientists presented the view that cells are formed *via* the scission of pre-existing cells. Finally, in 1858, *Virchow* defined the *cell* as the fundamental unit of life, and he also created a pathogenic concept—accordingly, diseases are the results of changes in normal cells ("cells with bad behaviour") (14). In addition, he was the one who laid the base of cellular pathology in 1863 (15) (Figure 1).

The first registered successful *in vitro* cultures were performed by *Roux*. He could maintain living cells (from chick embryos) outside the body for a few days (16). In parallel, *Loeb* could culture skin fragments from guinea pigs in agar culture (17). Then, *Harrison* developed the first, later termed hanging drop technology from small pieces of frog embryonic tissues, as well as described and introduced the aseptic method which could maintain sterile cell specimens *in vitro* for weeks (18). In New York, *Carrel* and his co-workers established cell cultures *in vitro* using embryonic and adult tissues of many species maintained in special culture media; they were able to culture their cells and tissues for several months (19). They started to work with cancer tissues and also introduced the term "tissue culture." In 1912, the first "cell line" derived from an explanted chicken embryo heart was also established by *Carrel*. In 1938, based on his observations and studies, he published a book entitled "The Culture of Organs". In the 1920s, the introduction of the tissue

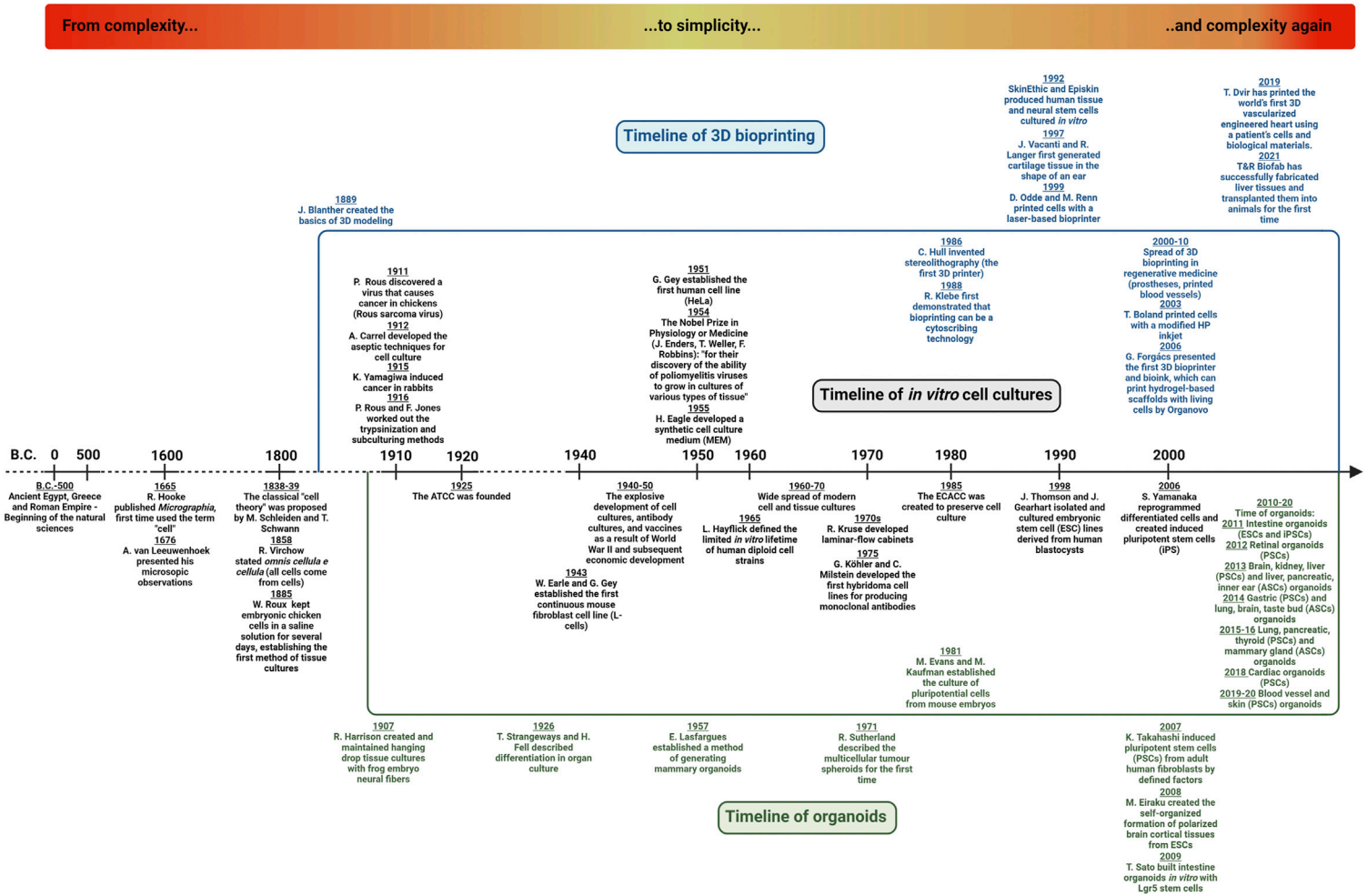

FIGURE 1
Timeline of cell biology and experimental cancer models—From complexity. . .to simplicity. . .and complexity again. The three research areas—*in vitro* cell- and tissue-culturing, organoid technology and 3D bioprinting—are developing, and their co-evolution with cancer research supports the establishment of new cancer models. A detailed explanation can be found in the text.

Published by Frontiers

10.3389/pore.2023.1610996

trypsinization method had a significant impact on cell culture development (20). *Rous* and his colleague were able to produce single-cell suspension from tissues, detach and subculture adherent cells obtaining homogenous cell strains which were successfully performed with this innovation.

After establishing some animal cell lines, the first human cell line (HeLa derived from cervix cancer) was established by *Gey* in 1951. In 1961, *Hayflick* inspired by *Carrel's* observations expected that cancer cells have special cancer-like properties (immortalised and gain limitless proliferation potential), but normal human fibroblasts have restricted growth potential (limited division capacity), and some other normal cells did not grow any longer (21). In parallel, cancer research development, tumorigenesis theories, and developing knowledge about spontaneous or induced transformation allowed viral and cell fusions, to immortalise isolated normal cells, and produce antibodies or recombinant proteins using hybridoma, selection, and molecular biology technologies (22).

In 2006, after the development and isolation of stem cells, *Yamanaka* and his colleagues described that mouse tail-tip adult fibroblasts can be reprogramed to stem cells by the simultaneous induction of four transcription factors—Oct3/4, Sox2, Klf4, and c-Myc. These and the developed induced pluripotent stem cell (iPSC) technologies provide the capacity to form tissues of all three germ layers for tissue cultures (23). Additionally, *Takahashi's* pioneer works contributed to the establishment of pluripotent stem cell culturing technologies in many laboratories in the last decades. These results have great importance in medical science, transplantation, oncology, and regenerative medicine, as well.

The history of cancer model system development started at the beginning of the last century in spite of the fact that human tumours are as "old" as human life. There were several prehistorical findings, and the first written documents can be found on *Imhotep's* papyrus with 48 described surgical cases, including some breast and other cancers (24). In the ancient ages, *Hippocrates* had many observations about malignant tumours which reminded him of the moving crabs, therefore, he named the disease *cancer*. *Celsus* highlighted the tumours' invasive behaviour, and in the Middle Ages, *Fallopius* distinguished benign and malignant tumours, as well. Cancer epidemiology studies were started by *Ramazzini* and *Hill* (breast cancers in nuns and testicular cancers in chimney sweeps) in the 17th–18th centuries (25). However, the first Cancer Hospital was established in Reims (France) in 1779, and there were many described and treated cases, the first experimental models on tumours were performed only at the beginning of the last century with chickens and rabbits (*Rous*, *Yamagiwa,* and *Ichikawa*) (26). After these first models, the number of cancer research experiments increased and the fast development of cell culturing technologies began. The American Type Cell Collection (ATCC) was founded in 1925 and 60 years later, the European one (European Collection of Authenticated Cell Cultures - ECACC) was also established. These developments contributed to the discovery of the first oncogene related to the first viral carcinogenesis experiments with *Rous* sarcomas in chicken (27). Carcinogenesis-related experiments and implantation of human tumours in immunosuppressed animals were developed, however, all these models have some limitations which need to be considered (28,29,30).

For decades, researchers' studies relied on a combination of cell culture and animal models for studying cellular mechanisms that lead to human diseases. These models have limited ability to recapitulate the complex tissue microenvironment, organ and body structures. The recognition of the cellular properties and role of tissue microenvironment have motivated the development and use of new techniques/3D cell culturing technologies/biofabrication in more complex *in vitro* models (31). However, the clinical translation ability of animal models to human disease has been questioned, in correlation with low success rates of clinical phase trials after many promising animal experiments (32). Furthermore, the high cost, the strict ethical regulations and concerns in animal testing are initiated to find less expensive, more predictive and human cell- and extracellular matrix (ECM)-based alternatives. 3D *in vitro* models are proposed to be bridges between cell cultures and *in vivo* animal models and even human trials. Early 3D culturing studies involved explanted host tissue, slice cultures and different spheroid cultures using hanging drop cultures, ultra-low attachment plates (ULA), and natural biopolymers (e.g., collagen, cell-extracted native extracellular matrix, matrigels, or polyacrylamide, agarose gels).

Regarding the increasingly well-known and renewed characteristics of various tumour tissues (33), as well as the enormously intensive therapeutic developments, their cost/benefit ratio, and many unsatisfactory clinical test results clear that new models switch to 3D technological platforms are necessary to better understand the background of the resistance mechanisms and tumour evolution. Mimicking the native cellular environment as precisely as possible is the first fundamental step to developing 3D human disease model systems (34). Recent newly developed 3D cell culturing methods (even combined with organoid or stem cell technologies) could be better and hopefully help more in drug screening in the preclinical phase and personalised treatments, as well (35).

Going beyond standard 3D models—3D bioprinting as a new technology for disease modelling

The organoid cultures re-appeared in the late 1950s (e.g., *Lasfargues* established mammary organoids), and after the emerging technologies, they have been widely applied to support pluripotent stem cell culturing and differentiation studies since the late 2010s. Regarding the results of many 3D

Cancer Models	Advantages	Disadvantages
2D cell culture 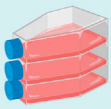	-fast, simple, and low maintenance costs -various, well-characterised cell types -cell processes can be well-studied -can be high-throughput -standardised, high reproducibility -high sample number for statistical analysis -easy to interpret -materials commercially available -ethically favored (3Rs)	-homogeneous, not represent the heterogeneous cell-cell, cell-extracellular environment interactions -altered cell morphology -unlimited nutrients, no concentration gradient, no drug penetration -short lifespan
3D cell culture (e.g. spheroid, organoid) 	-low maintenance cost (e.g. spheroid) or higher (e.g. organoid) -cell-cell, cell-ECM interactions -can be co-cultured and heterogeneous -the oxygen, nutrients gradients, and drug penetration can be modeled -materials commercially available -ethically favored (3Rs)	-lack of complexity, no immune system, and vascularisation -low repeatability, difficult to reproduce the spatial organisation -difficult to maintain -difficult to interpret -not very suitable for high-throughput -limited cell types suitable for the spheroid culture -limited in size -short lifespan
3D bioprinted 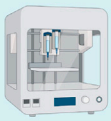	-cell-cell, cell-ECM interactions -high resolution, repeatability -the model can be large, with high cell density and complexity -the model can be vascularised -the oxygen, nutrients gradients, and drug penetration can be modeled -different printing strategies available -materials commercially available, a wide-range of material choice -long lifespan -ethically favored (3Rs)	-expensive maintenance and materials -high-throughput is limited -printing process can decrease the cell viability -time-consuming -the large model needs extra perfusion
Xenograft 	-the process of metastasis can be studied -mimic tumour evolution -the safety, toxicity, and efficacy of a drug candidate can evaluate -whole organism interaction -long lifespan	-high cost and time-consuming model -cannot model the human physiology -high variability of tumour size, cannot be suitable for large-scale screening -engraftment failures -not ethically favored (3Rs)

FIGURE 2
"All models are wrong but some are useful"—Advantages and disadvantages of different cancer models.

culturing systems, the tissue-like structures of 3D cell cultures except organoids are far from *in vivo* or *in situ* environment. Additionally, there are certain *in vivo* models in which human tumours such as xenografts in SCID (severe combined immunodeficiency) mice or initiated tumorigenesis could also be investigated. Although it is getting more and more challenging to get permission to perform animal experiments; moreover, there is a need to make efforts to apply the 3R rules (replacement, reduction, refinement) as a consequence, *in vivo* studies are more and more difficult to perform. Besides, interpreting the observations made in animal experiments also poses a challenge since animal model systems could neither represent the human cellular microenvironment nor the ECM (35, 36). Comparing different options for 3D culturing and even the *in vivo* models, the advantages and disadvantages of the given experimental system have to be taken into account (Figure 2). Accordingly, the limitations of model systems have to be considered during data evaluation. 3D models are more applicable for reproducing the mechanical and biochemical characteristics, e.g., cell-cell/matrix connections, tissue stiffness, and the gradient distribution of certain factors in tumour tissues (37–39).

Among the new cutting-edge solutions, 3D bioprinted models and the continuous technological developments of tumour models could make novel opportunities for more effective pharmaceutical tests and even for the testing of personalised therapeutic alternatives (35). Combining new cell culturing technologies with applying more complex organoid cultures is expected to result in significantly better disease models. In 1992, the Episkin technique initiated the use of synthetic tissue-like cultures with the application of different cell layers mimicking the epidermis-like structures.

A further breakthrough in tissue engineering and biofabrication is the establishment of 3D bioprinting - Following the first stereolithographic (SLA) printer designed by *Hull* in the 1980s, the initial developmental steps of bioprinting were formed rapidly, and these coincided with the advancement of 3D printing. The primary bioprinting process, only in two-dimensional (2D), can be attributed to the research group of *Thomas Boland* (2003) (40). Soon after that, the first 3D bioprinter was also completed, which was able to print more complex multi-layered structures. It is well-known that the Hungarian-born *Gábor Forgács* and the company named Organovo had a significant role in the development of the 3D bioprinting platform (41). Furthermore, the various bioprinters

that have been widespread since 2010 have established the conditions for the creation of 3D printed mini-organs, or even complete organs, with which the printing of "beating hearts", future transplantable hearts, or other replaceable tissues can be started (42–44). In parallel with these developments, various living tissues, prostheses, and other bioprinted structures and devices have appeared. Such devices are not only being developed, but are already in use in regenerative medicine and dentistry (45, 46), and there are also considerable efforts in the development of testing active drug ingredients (organ-on-chip technology for drug toxicity tests) or drug formulation (e.g., 3D bioprinted pills) and the improvement of various disease models. Additive manufacturing (47), 3D printing and thus 3D bioprinting technology can enable the designed structure to be generated rapidly layer-by-layer by applying computer-aided design (CAD).

Several methods - Have been developed which can be classified based on the printing technology with cell-contained bioinks: 1) drop-based (inkjet- or laser-based bioprinting), 2) extrusion-based, and 3) digital light processing (DLP) or SLA printing. In contrast with other printing methods, the benefits of the most common extrusion-based printing technology are the choice of resolution (fibre thickness)—which of course depends on the material –, fast execution, and relative cost-effectiveness (48). Traditionally, the materials used in 3D printing for medical purposes were inert and cell-free, like plastic (49). As a result of the developments, other types of materials are now also used during 3D bioprinting as biocompatible or biodegradable materials for creating implants or soft tissue reconstruction (e.g., bone replacements, reconstructive plastic surgery) (50, 51). One of the newest areas that have developed from 3D printing is 3D bioprinting with live cells, during which so-called bioinks consisting of cells mixed in a matrix material are used for printing. Applying these, we can create a living tissue-like structure in the course of their long-term *in vitro* culturing (52). The requirements for bioinks were summarised by Groll et al. as follows: bioink is a cellular preparation that contains biologically active components and biomaterials and can be used in automated production technology (53). The primary criteria for an ideal scaffold or bioink are to provide a suitable environment for cell adhesion, proliferation, differentiation, and migration, as well as cell-matrix interactions. Tumour cells form and develop in a rather complex, multicellular-originated, heterogeneous environment which is made up of various cell types and extracellular matrix components.

Different bioinks - Used in the field of tumour modelling are biomaterials that consist of mixtures of hydrogels and primarily tumour cells and tumour-associated normal cells. Numerous bioinks are biomaterials that are combinations of hydrogels and cells. Bioinks can be made from naturally occurring ingredients, but synthetic versions are also available (54). It is required that the substances of bioinks have appropriate mechanical and biodegradable characteristics. For example, printability and later shape retention are important, so the bioink must meet certain mechanical conditions, e.g., easy application and a high degree of shape fidelity. It is not negligible that the materials used for printing are not allowed to cause cell death, thus these have to be biocompatible or biodegradable even after the printing process (55, 56). The most frequently used components of bioinks are the hydrogels, of which the main ingredient is water, imitating the natural cellular environment (57).

Natural hydrogels differ from synthetic ones; bioinks belonging to the former type have a limited mechanical force, however, these degrade rapidly. In contrast, non-natural bioinks have less biocompatibility, but these can be characterised by great printability and appropriate mechanical properties. Consequently, certain researchers apply a mixture of natural and synthetic gels, a so-called hybrid bioink exploiting their advantageous features. Bioink-selection depends on multiple factors: 1) the type of bioprinting technology, 2) the characteristics of the model tissue (e.g., stiffness, elements in the microenvironment), 3) the necessity of shape-preserving, and 4) the appropriate crosslinking process and application, the influencing effects on cell proliferation, differentiation, and survival. Crosslinking stabilises the 3D bioprinted structure, preserving the viability of the cellular elements of the bioink. This causes physical and chemical modifications in the bioink which ensures that the printed layers remain together. There are several options for crosslinking: e.g., enzymatic (fibrinogen + thrombin = fibrin); ionic (alginate—$CaCl_2$); chemical (alginate—horseradish peroxidase); physical (gelatine-methacrylate—UV), or thermal (gelatine—high temperature) which can be performed either before or during or even after the printing process is finished (58). 3D bioprinting is a very effective tool, however, the standardisation of 3D bioprinting protocols is essential, and additionally, multi-faceted improvements are also required: 1) developing printing protocols, 2) standardising the materials used as bioinks, 3) creating novel biomaterials which have more sophisticated physical and biological properties, 4) improving the usability of 3D printed structures, as well as establishing test systems required for these (59, 60).

3D bioprinted and biofabricated cancer models

Living cell 3D bioprinting technologies require some major tools - An appropriate number of cells, bioinks, bioprinters, the specific printing design, and pre/post-processing before and after bioprinting. Additionally, biological tests and other biochemical, molecular biology or morphology studies also need special handling with the printed 3D materials. The development of this technology has required newly printable and biocompatible (adequate cell-compatible) materials. 3D bioprinting is easier with cancer

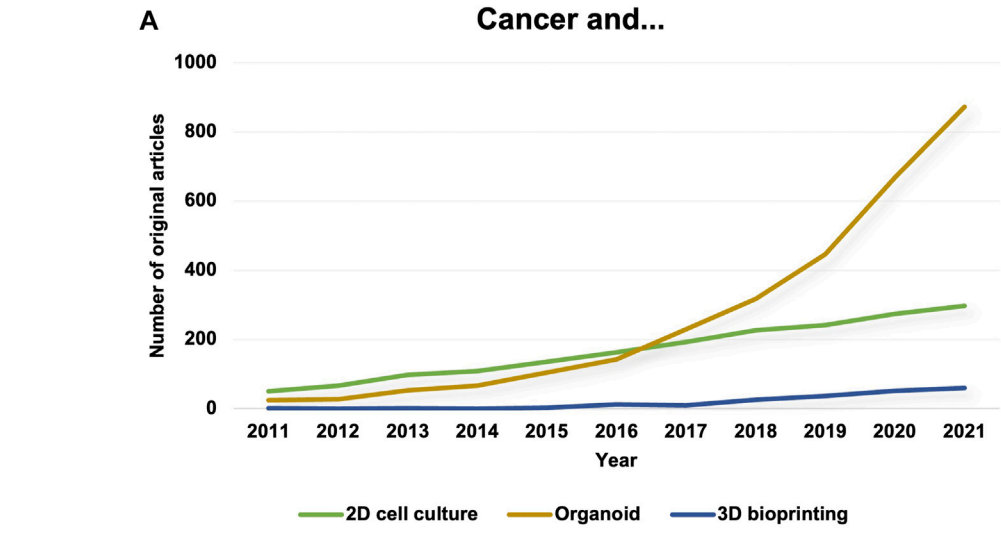

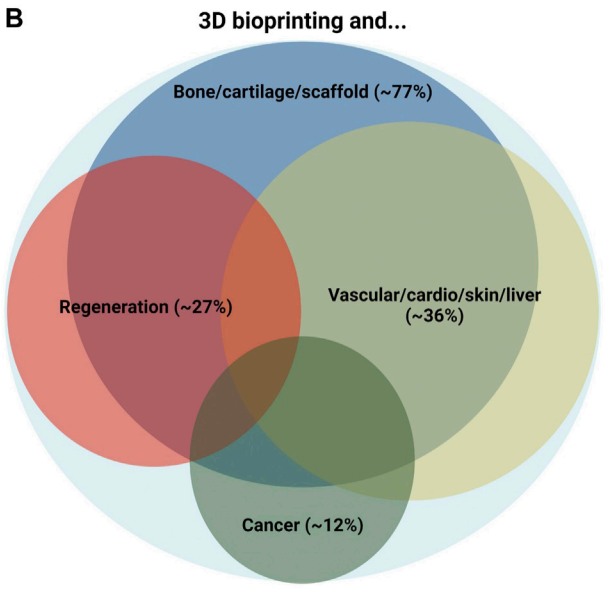

C

Type of Cancer	Percentage of Articles
Breast	17%
Bone	9%
Brain	8%
Liver	7%
Skin	7%
Lung	6%
Pancreatic	5%
Kidney	3%
Colorectal	2%
Head and Neck	2%
Prostate	2%
Bladder	1%
Sarcoma	1%
Other (less than 1%)	30%
Total	**100%**

FIGURE 3
The number and distribution of cancer research papers regarding 3D bioprinting. **(A)** The number of research papers between 2011 and 2021 mentioning cancer models combined with 2D cell culture/organoid/3D bioprinting. The data show that the number of publications using 2D cell culture models is stagnating. Additionally, the organoid research area has increased faster for the last years and 3D bioprinted model systems have just been developing, but the application of 3D bioprinting technologies would also be increased rapidly in the future. **(B)** Original research papers which mention 3D bioprinting in relation with different scientific disciplines (>2260) mainly focused on 1. creating bone/cartilage and scaffold, 2. regeneration, 3. applications in the creation of vascular/cardio/skin/liver tissues/mini-organs and 4. cancer research. The distribution and the areas of the frontiers are also shown by Venn-diagram, the size of different circles represents the percentages of publications excluding review papers. **(C)** The distribution of cancer types among cancer research-related non-review and experimental papers (we excluded the papers where cancer research was only mentioned as a potential other research area or where 3D bioprinting was highlighted among technologies that are spreading or could help develop). Tumour types where the percentages of publications could not be higher than 1% merged into other studied malignancies groups.

cells in correlation with their unlimited cell growth supporting the production of a huge number of cells for bioinks. Additionally, we could combine cancer cell bioinks with cancer-associated and/or "normal" cells, and finally, the layer-by-layer bioprinted materials can form living cancer tissues during longer *in vitro* culturing.

Applying traditional 3D culturing so-called spheroid cultures, e.g., where cells are maintained in non-adherent plates or hanging

drops (without applying matrix-embedded technology, only with the cells' own matrix production) created by manual seeding of the cells, results in non-uniform cell distribution. Spheroids developed in these types of culturing methods could have various shapes, moreover, final analyses show high statistical deviation in the experimental datasets. For modelling the heterogeneity and the real *in vivo* situation of cancer tissues, new biofabricated models are required considering to achieve better complexity and standardisation. New approaches—forming small concave wells using a bioprinter, casting forms (grids) for cells or printing similar drops with bioinks (with homogenous cell concentration)—were started to be used in several tumour types (e.g., glioma, sarcoma, breast or cervical cancer cells) (61). The widespread extrusion-based and droplet bioprinting technologies provide more homogenous, controllable size, cell number and shape distributions, as well as potentially "real" tissue formations for tumour biology studies. One of the first layer-by-layer cell printing applications described better cell seeding uniformity and long-term viability (>90%, 14 days) of the printed primary cells (62). Additionally, after 2010, in some studies, magnetic levitation of the tumour cells and fibroblasts was applied aiding the formation of tumour spheres (breast cancer) with defined cellular composition and density by *Leonard's* method (63). Others started to print 3D printed and *in vitro* cultured models with different cancer cell lines (64). In this decade, several functional tests were reconsidered, e.g., bioengineered 3D bone-mimetic structures have been started to be used for bone metastasis models (65), as well. These bone-mimetic and osteogenic niches are developing and are useful to test the effects of new compounds *in vitro* with potential inhibitory effects in breast tumour cell colonisation in the bone (66). In 2017, researchers started to fabricate multi-cellular bioprinted models for drug penetration and toxicity tests to investigate tumour tissue-like and liver tissue models (67, 68). Organovo and some other companies developed new 3D bioprinted liver tissues for drug tests (69). Several tissue-mimetic structures have been developed combining stem cells with organoid, spheroid cultures or 3D bioprinting in biofabrication. Organoid technologies have recently been exponentially developing; however, these technologies are very expensive and need a special supplement and careful handling. These technologies and different types of cancer cells (e.g., glioma, neuroblastoma, breast, kidney, colorectal, and lung cancer models) have been applied. Furthermore, rare tumours have to also be represented in these innovative approaches (e.g., chondrosarcoma, pelvic carcinomas) (70).

Analysing the increasing number of 3D bioprinting-related publications - About 500 publications are available regarding cancer research and 3D bioprinting shows that about 1/3 of the publications are reviews or not cancer-specific papers (only mention cancer research as a potential another research area where 3D bioprinting technologies are spreading or could help develop new cancer models). Among these ~500 publications, there are about 180 original experimental papers mentioning cancer models and 3D bioprinting. In these studies, breast- and lung cancer, and brain tumours are represented in higher numbers (~40 breast cancers or ~20 each of lung cancers and central nervous system malignancies), but in these studies mainly only one tumour type was used in correlation with the presented research projects until the end of 2021 (Figure 3).

After several pioneer 3D cell culture studies, the development of new breast cancer models - Was started to be tested, therefore, we summarise the recent history of breast cancer model development. Different 3D cultures, 3D basement membranes, and 3D hydrogel scaffolds with breast cancer cells highlighted the importance and alterations of many different behaviours (metabolic alterations, adherence, migration, sensitivity etc.) and the role of cancer microenvironments *in vitro* models and suggested engineering for 3D tumour models (71, 72). After creating manually prepared breast tumoroids in matrigel, *Swaminathan* and colleagues investigated directly bioprinted breast epithelial spheroids with different bioinks and combined these spheroids with HUVEC cells as co-cultures. They validated the remaining viability and analysed the morphology of these spheroids (73). Reid et al. described and demonstrated that using a small number (defined concentration) of tumour cells in bioprinted collagen gels, forms tumoroids and could mimic lumen formation when cancer cells are co-printed with "normal breast epithelial cells" (74). In further works, Mollica et al. tested different hydrogels and decellularised breast tissues with human breast cancer cells using 3D bioprinting and showed that using these technologies they could maintain and culture large 3D bioprinted organoids and tumoroids (75). They described the direct bioprinting technology of 3D multi-cellular breast spheroids with endothelial cells (76). In another breast cancer model work, tumour cells and adipocytes were used and monitored the viability of cells after printing in a 10-day culturing course. They described that direct printing of these co-cultures resulted in morphology, localisation, and distribution changes of cells in the printed tissue-mimetic structures (77). An important topic of the bioprinting technique is the vascularised structure development which could increase the complexity of the generated models. There are many attempts with magnetic-ring and coaxial bioprinting to build some tubular structures between spheroids covered with endothelial cells, *in vitro* forming tissues (78,79,80,81). Cancer-associated adipocytes have a special role in the tumour microenvironment, these cells are involved in some new models using co-printed, co-cultured breast cancer cells with adipocytes to increase the similarity to real tissue environment (82). Besides, there are efforts to build more complex tissue-mimetic structures with stromal cells (fibroblasts), breast cancer cells, and endothelial cells to increase the phenotypic similarities *in vitro* in 3D bioprinting protocols (83).

The central nerve system (CNS)-derived 3D models - Have also been developed regarding the need for new and more

effective targets and therapeutic treatments. These models require the reconstitution of the complexity and heterogeneity of glioblastoma and neuroblastoma tissues, and additionally, the special tumour-stroma interactions and blood-brain barriers for accelerating potential therapeutic interventions (84). These models represent scaffold-free 3D bioprinted spheroid cultures or co-printed, co-cultured glioblastoma or other CNS malignancy-derived tumour cells (e.g., neuroblastoma) cells with the associated macrophages, stromal cells to build the special microenvironment (85,86,87,88). To develop more reliable models in these diseases, patient-derived newly isolated glioma cells are preferred instead of traditional glioma cell lines which were long cultured in 2D cultures (89), and another research direction is to combine these with 3D bioprinted blood-brain barrier models (90, 91).

There are new efforts to validate bioprinted organoids/spheroids in 96-well plates drug screening with several cancer cell lines and patient-derived tumour cells including carcinomas, glioblastomas, sarcomas, and melanomas, respectively (92, 93). Additionally, many new bone metastatic behaviour tests or cancer tissue-associated tumour antigenicity tests have been developed using 3D bioprinters and breast cancer models (94–96). These models and their applications combined with microfluidics and chips, such as tumour-on-chip, will revolutionise both drug and patient-derived tests in the near future (34,97–99).

Overall, the feasibility and complexity of biofabricating multi-cellular, cell-laden bioprinted tissue-mimetic models with the real human microenvironment of breast tumours have started to be developed in many laboratories, however, standardising these is necessary for future applications in different high-throughput drug tests and patient-derived tumour model developments (100, 101).

To complete this short review about the developing 3D bioprinted cancer models, we show our new 3D bioprinted breast cancer model and some new experiences with its establishment and suggestions for others who start applying this cutting-edge technology shortly. In our previous work, we described the metabolic characteristics and differences of the already used breast cancer models and highlighted that 3D bioprinted models are closer to the *in vivo* situation than the others. In this review, we supplement these data with the already followed long-term growing capacity and the *in situ* expression patterns and differences of some previously not studied proteins and their heterogeneity in the 3D bioprinted breast cancer model. Additionally, differences in doxorubicin and rapamycin sensitivity among 3D bioprinted, traditional 2D cell culture systems and *in vivo* xenograft models using luminal B subtype human breast cancer cells could also be highlighted.

Materials and methods

Cell culturing and reagents

ZR75.1 (ATCC-CRL1500), luminal B subtype human breast cancer cell line was used in our experiments. Cells were grown in 10% foetal bovine serum (FBS, Biosera), glutamine (2 mM) and gentamycin-contained RPMI-1640 media (Biosera—Nuaille, France) at standard cell culture conditions. Different treatments were applied in 96-well plates, tissue culture flasks, and 3D bioprinted tissue-mimetic scaffolds. Before the treatments, the bioprinted scaffolds were maintained for 7 days, while the cells in 2D cell cultures were incubated for 24 h. After media refreshment, the 72-h treatments were carried out in 96-well plates, tissue culture flasks, and on scaffolds (minimum 6 parallels maintained in every well of 6-well plates) for sensitivity tests. mTORC1 inhibitor rapamycin (Rapa; 50 ng/mL; Focus Biomolecules, Plymouth Meeting, PA, United States), the natural anthracycline antibiotic and chemotherapeutic agent doxorubicin (Doxo; 50 ng/mL; TEVA, Debrecen, Hungary) and their combinations were applied regarding our previous mTOR inhibitor combination sensitivity studies (102).

3D bioprinting

For printing, two types of bioinks were used: a. cell-containing-gel: 3% alginate and 1% gelatine (Merck-Sigma-Aldrich, Darmstadt, Germany) bioinks were mixed with cells (1×10^7/mL) immediately before printing; b. cell-free-gel, more rigid gel, 6% alginate and 11% methylcellulose (Merck-Sigma-Aldrich). The scaffold layout (6 layers alternately) was designed with GeSiM Robotics software and performed by an extrusion-based bioprinter (Bioscaffolder 3.2, GeSiM, Radeberg, Germany). The printing conditions were the following: radius and height (2.5–5 mm, 0.5–1 mm); interlayer angle (90°); the distance of infill (1.5 μm); printing speed (10 mm/s); needle diameter and height (110 μm for cell-free-gel and 50–50 μm for cell-gel); pressure (400 kPa for cell-free-gel and 20 kPa for cell-gel). The scaffolds were post-processed by $CaCl_2$ crosslinking (200 mM, 2 min) and washed twice then maintained in culture media (103).

Cell viability assays

For quantitative analysis of cell viability and proliferation, Alamar Blue (AB) and Sulforhodamine B (SRB) assays were used regarding mainly to standard protocols—the 3D scaffolds were transferred into new 96-well plates (1 scaffold/well/100 μL media) directly before the measurements. The fluorescence (change) of AB (Thermo Fisher Scientific) was measured after a 4-h incubation, the detected signs were evaluated as relative fluorescence units (RFU) using a fluorimeter (570–590 nm; Labsystems International; Ascent software v. 2.6—Vantaa,

Finland) culture system independently. In SRB assays, 10% trichloroacetic acid (60 min; 4°C; Merck-Sigma-Aldrich) fixation, washing steps, and overnight drying were applied before SRB (Merck-Sigma-Aldrich, 0.4 m/V % diluted in 1% acetic acid; 50 µL/well; 15 min for 2D and 1 h for 3D plate; RT) staining. The washing steps were performed carefully with 1% acetic acid then plates were left to dry overnight again (the overnight drying has special importance in the case of scaffolds). The bound SRB was re-dissolved in Tris base solution (10 mM; 150 µL/well, Merck-Sigma-Aldrich) and measured by LabSystems Multiskan RC/MS/EX Microplate Reader (570 nm; Labsystems International; Transmit Software Version 4.5—Vantaa, Finland). Relative cell proliferation was calculated in the percentage of control cells. The proliferation assays were performed with six parallels in three independent experiments.

In vivo experiments

The *in vivo* experiments were performed in the Animal Care Facility unit located at the Department of Pathology and Experimental Cancer Research Institute (permission—No# PEI/001/1733-2/2015), the experimental protocols were approved by the Institutional Ethical Review Board (permission—No# PE/EA/801-7/2020). To create ZR75.1 human xenograft mouse models, 2.5×10^6 cells in 100 µL RPMI-1640 media were implanted subcutaneously into the breast region of 8-week-old female SCID mice. The size of the tumours and the body weight were registered in a 3-week treatment course. Afterwards, the mice were sacrificed and tumours were removed, formalin-fixed, paraffin-embedded (FFPE) and sectioned or freshly frozen and lysed for further analyses. Tumour volume calculation was performed using the following equitation: $\pi/6 \times (2\times\text{shorter diameter} + \text{longer diameter}^3)^3$.

Protein analysis (immunohistochemistry and WES™ simple)

Immunohistochemistry was carried out using FFPE scaffolds, xenografts, and 2D cell culture slides (gel-embedded spheroids—10^5 cells/mL) or cytospins. After deparaffinization, antigen retrieval was applied on FFPE materials (citric acid, pH 6, 30 min, pressure cooker). The fresh culture slides and cytospins were fixed in ethanol. After endogenous peroxidases and aspecific immunoreactions blocking, the used primary antibodies were the following: anti-ALDH1 (Cell Signaling; #54135; 1:200), anti-cleaved-caspase-3 (Cell Signaling; #9661; 1:1000), anti-COXIV (Cell Signaling; #4850; 1:2000), anti-LDHA (Cell Signaling; #3582; 1:400), anti-phospho-histone-H3 (Cell Signaling; #9701; 1:100). To visualize the reaction, Novolink™ Polymer Detection Systems (Leica Biosystems, Wetzlar, Germany) were used with 3,3′-diaminobenzidine (Dako, Carpinteria, CA, United States) and haematoxylin counterstaining. The stained slides were evaluated using Pannoramic Viewer Software (3D Histech). Quantitative protein expression from the cell, tissue, and scaffold lysates was investigated with WES™ Simple (ProteinSimple 004-600; Minneapolis, MN, United States) a fully-automated Western blot system regarding the instructions of manufacturer using Anti-Rabbit or Anti-Mouse Detection Kits (ProteinSimple DM-001, DM-002). The samples were processed in a 12–230-kDa Separation Module (ProteinSimple SM-W004). To dissolve the 3D bioprinted scaffolds, sodium citrate was added to each sample (0.1 M, 30 min, RT), then the samples were centrifuged and lysis buffer (Tris—50 mM, pH 7.5, glycerol 10%, NaCl 150 mM, Nonidet-P40 1%, NaF 10 mM, phenylmethylsulfonyl fluoride 1 mM, Na_3VO_4 0.5 mM) was added to the pellet. To evaluate protein content, Bradford reagent was used (Bio-Rad, Hercules, CA, United States). The primary antibody dilutions were 1:50 (applied primary antibodies: anti-COXIV, anti-LDHA, anti-Rictor (Cell Signaling; 2140)) and β-actin (Cell Signaling; #4970) was the normalisation control in our measurements. The electropherograms were analysed with Compass software 6.1.0 (San Jose, CA, United States). The original WES™ Simple graphs were attached to Supplementary Documentation.

Statistics

To calculate standard deviations (SD) and mean values, the results of three independent experiments with three or more parallels were evaluated. Statistical analysis was performed using PAST (version 3.24) software. Data evaluation of *in vitro* experiments was performed using Student's t (two-tailed) test. Statistical significance was defined as $p < 0.05$.

The included figures (Figures 1–3.) were created with BioRender (https://biorender.com) covered by the Department of Pathology and Experimental Cancer Research, Semmelweis University, institutional license.

Results and discussion

At Semmelweis University, in the Tumour biology – Tumour metabolism laboratory, different breast cancer cells (the well-known triple-negative MDA-MB-231, MDA-MB-468, luminal A—T47D or luminal B—ZR75.1 etc.) were used to construct 3D bioprinted models for performing a metabolic comparison with the same cell lines maintained in different culture systems. As we previously described, ZR75.1 luminal B breast cancer cells formed lumens after bioprinting and some-day maintenance (103). In this presented brief study, the continuous and significant growth activity of 3D bioprinted tissue-mimetic

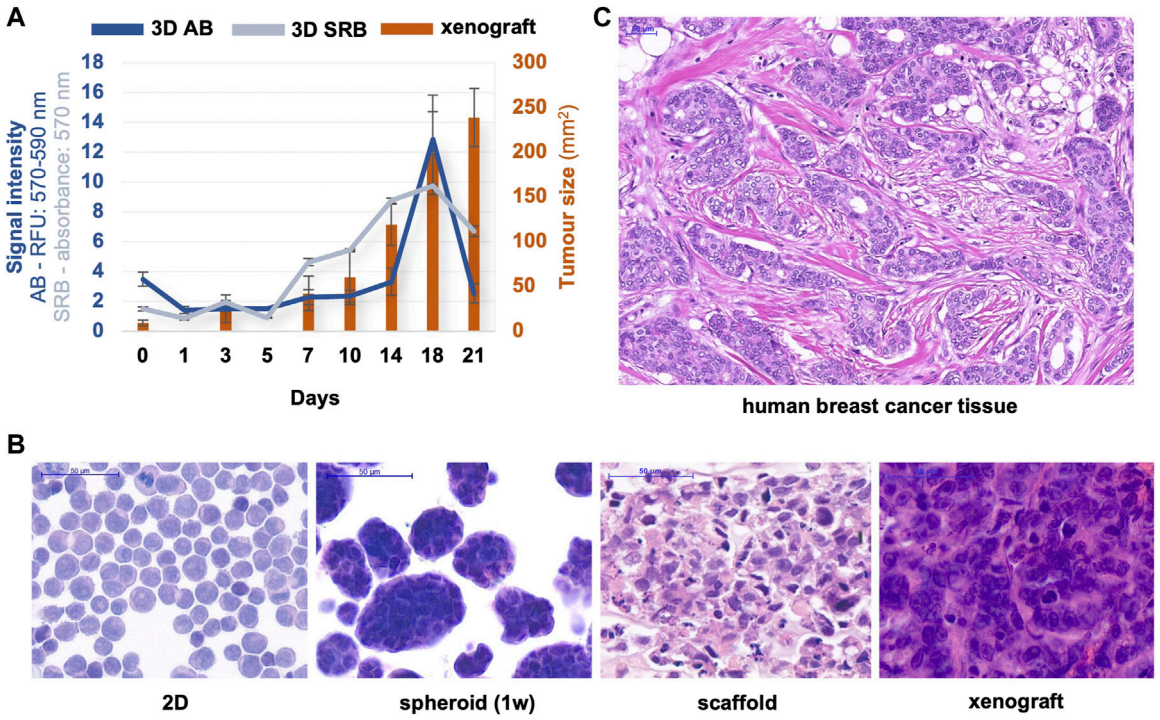

FIGURE 4
Proliferation/tumour growth and morphological characteristics of different *in vitro/in vivo* models of ZR75.1. **(A)** The growth of *in vivo* xenotransplanted and 3D bioprinted scaffold of ZR75.1 tumour. Tumour growth was indicated by the calculated tumour volume of the xenograft (right scale), while the increase in cell amount in 3D scaffolds was estimated by both Alamar Blue (AB) and Sulforhodamine B (SRB) proliferation tests (left scale). **(B,C)** Microscope images of haematoxylin-eosin-stained slides from the human xenograft mouse model, 3D bioprinted scaffold (1-week maintaining), spheroid cell culture (1-week maintaining), 2D cell culture (prepared with cytospin) of ZR75.1 cells **(B)**, human luminal B type breast cancer tissue section **(C)**. (scale bar: 50 μm).

structures was detected by different proliferation tests or cell number analyses from 3 to 5 days after bioprinting to ~3 weeks. Both the AB and SRB tests showed a fine growth curve, but around the 21st day of culturing, the detected metabolic activity and the protein content were not increased further, suggesting that the cell growth stopped. The metabolic activity changes can be followed immediately by monitoring the alterations of the pyridine nucleotide pool (nicotinamide-adenine-dinucleotides); however, the cellular protein content alters slower. Therefore, a higher amount of proteins could be detected in an extended time frame. This could be an explanation for the observed higher alteration in metabolic activity. Additionally, in the detected 21-day time period, the tumour growth of these 3D bioprinted materials was comparable with the xenotransplanted cells, where the tumour growth monitoring could be started after the tumours became palpable (1 week after inoculation) and continued for additional 3 weeks. The tumour size during this period reaches an intolerable level in SCID mice, therefore, the treatments usually need to be discontinued. These growth curves and their comparisons show that the optimal time range to perform drug tests (toxicity or proliferation tests) falls between 10 and 18days *in vitro* model systems using either 3D bioprinted materials at standard conditions or insert cultures. In *vitro* studies, we usually analyse the effects of 72-h treatments (this period is drug-dependent), which allows faster sensitivity tests than the xenograft experiments. In the 3D bioprinted *in vitro* models, we can apply these 72-h treatments after maintaining the bioprinted scaffolds for 3–10 days, but treating and culturing these printed cells can be continued even longer.

The morphological characteristics of haematoxylin-eosin stained samples of different cell cultures, 3D printed materials, and *in vivo* xenotransplanted ZR75.1 cells were shown in Figure 4. The characteristics, the cell-cell contacts, and the lumen formation could be recognised both in xenografts and in 3D bioprinted scaffolds, and these were even more comparable with the real morphology of luminal-type breast tumours as we show in a representative human case. The heterogeneous size and shape of monomorphic cells and the cells in monolayer 2D cell cultures are much more similar to each other than to the printed and *in vivo* growing breast cancer cells (Figure 4).

The 7/10/14/18-day cultured printed scaffolds form tissue-like structures in which the cells have a distinguished morphology compared with the 2D cultured, single cells, and even in the

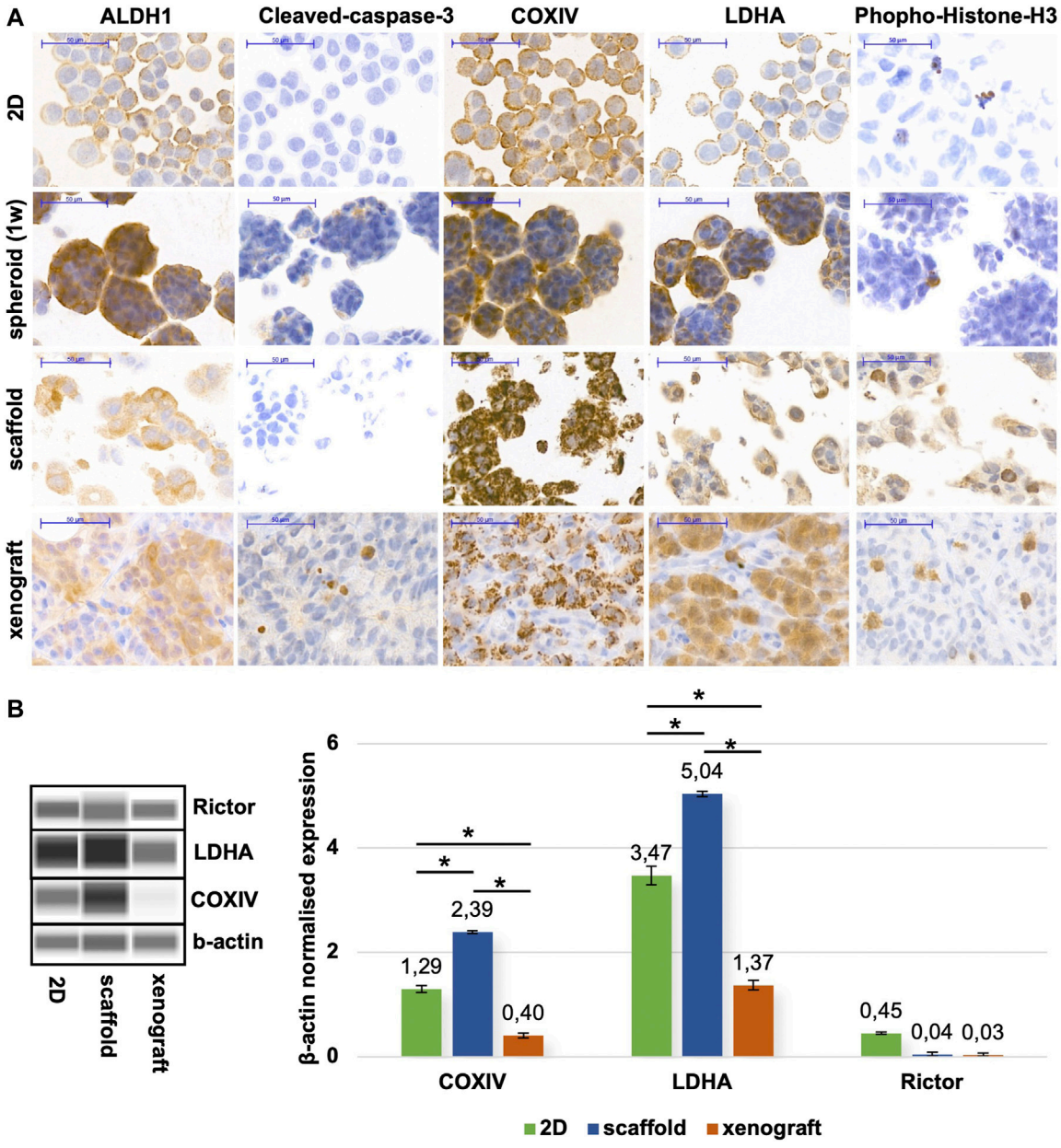

FIGURE 5
Metabolic alterations of different *in vitro/in vivo* models of ZR75.1. **(A)** Immunostainings of 2D cell cultures (prepared with cytospin technique), spheroid cell culture (maintained for 1 week), *in vivo* xenotransplanted ZR75.1 tumour, and 3D bioprinted scaffold (maintained for 1 week). The expression of ALDH1 (aldehyde dehydrogenase 1), Cleaved-caspase-3 (apoptosis marker), COXIV (Cytochrome c oxidase complex IV), LDHA (lactate dehydrogenase A), Phoshpo-Histone-H3 (mitotic marker). Immunohistochemistry was accomplished with brown (DAB, diaminobenzidine) substrate and haematoxylin counterstaining (scale bar: 50 μm). **(B)** Different maintaining condition (2D; scaffold; xenograft) affects protein expression pattern in ZR75.1 cells and xenograft tumour. WES™ Simple was used to detecting metabolic enzymes (LDHA—lactate dehydrogenase A, COXIV—cytochrome c oxidase subunit 4) and Rictor expressions (left panel). Densitometric analysis was performed to present the normalised protein expression differences and was used β-actin as a loading control (right panel). *$p < 0.05$.

confluent cell cultures. To further analyse the characteristics of different model systems, immunohistochemistry stainings were performed on FFPE xenograft specimens, scaffold tissues and cytospin slides (Figure 5A). As we detected metabolic processes with COXIV, ALDH1 (oxidative phosphorylation markers) and LDHA (glycolysis marker) stainings, the tissue heterogeneity can also be represented in a 3D bioprinted scaffold as it can be in tumour xenografts and human tumours. The observed differences

in heterogeneity can support the understanding of the possible adaptation mechanisms, especially in the case of altered metabolic pathway activities in tissue masses *in situ* (104). The heterogeneity of ALDH1 and COXIV stainings was increased, especially in 3D structures, which could correlate with potential metabolic rewiring processes. These findings are in association with site-dependent nutrient and oxygen distribution changes regarding the *in situ* heterogeneity in highly or less proliferative cell groups depending on the vascularisation of tumours (105). There are several publications which suggest that in starving conditions, breast cancer cells alter their glycolytic phenotype, and start to oxidase glucose on one side, if there is enough oxygen, however, use the Warburg glycolysis in oxygen-depleted or pseudo-hypoxic regions (106, 107). These heterogeneous staining patterns were detected in xenografts and 3D bioprinted materials based on the expression patterns of ALDH1, COXIV, and LDHA. In correlation with these, significantly higher growth capacity (increased proportion of phospho-histone-H3 positive cells) was also detected in these tissue-like cells and xenograft tumours vs. spheroid and 2D cell cultures. The active-caspase 3 positive apoptotic cells can also be found in the inner part of spheroids and xenografted cells. These apoptotic cells were represented at a very low level as usual (108) in 2D cell cultures (especially with a slower proliferation rate close to reaching total confluence) and in the 7-day maintained 3D bioprinted scaffolds since these "cultures" survive and proliferate at these time points. In nearly confluent 2D cell and spheroid cultures, more homogenous metabolic enzyme expressions were found, additionally, these cultures contain more uniform cell shapes and homogenous stainings. In our 3D bioprinted models, we could detect the developing resistance against many mono-treatments as we described in our previous paper (103). Formerly, we studied the *in situ* heterogeneously stained mTOR activity markers. In that study, we could compare and perform quantitative analyses including the expression differences of the above-described COXIV, LDHA, and the mTORC2 complex-specific Rictor scaffold protein expressions. These quantitative evaluations made with the use of WES^{TM} Simple and tissue lysates could not show the heterogeneity but highlighted that the 3D bioprinted models are closer to the xenograft model regarding metabolic aspects based on the expression patterns of the few studied enzymes. These confirm many previous hypotheses and findings described by other tumour models (Figure 5B).

Future perspectives

There are several studies about the applications of 3D models in breast cancer research including 3D spheroids (hanging drops and ULA) and only a few biofabricated 3D models. In most of these studies, mainly the less aggressive MCF7 (luminal A) or the more aggressive triple-negative (MDA-MB-231) breast cancer cell lines were used. Only a few papers describe multi-cellular models, 3D models combined with vessels, adipocytes, fibroblasts or 3D bioprinted tissue mimetic *in vitro* structures in the field of breast cancer research (82, 83, 109). We also have experience printing triple-negative breast cancers using MDA-MB-23 and MDA-MD-468 cell lines. To describe and present breast cancer bioprinting in our practice, we show some new results with another breast cancer cell line, the luminal B type ZR75.1 cells. The already published printed breast cancer models have almost similar characteristics, however, different research groups use various bioinks as we analysed and referred 30 research papers. Furthermore, the bioink composition and the type of printing technologies (e.g., inkjet, extrusion-based printing) vary in these publications (Table 1).

Bioinks can be divided into two groups: bioinks containing only one component (natural or synthetic biomaterial) or bioinks formulated with different combinations of biomaterials. Usually, they have several components to achieve appropriate printing and cell- or biocompatibility, therefore, bioinks have several components with different features (Table 2). Alginate-based bioinks stabilised and $CaCl_2$ stabilised preferably avoiding mutagenic UV for human cell printing (e.g., in the case of GELMA) (155). In the other part of these works, matrigels decellularized ECM with additional collagen or other gradients, GELMA, fibrinogen or hyaluronic acid (HA), and PEG- (polyethylene glycol) based materials are also used (82, 109, 124). The main problem with the published descriptions and protocols is that the used biomaterials are different and not fully characterised or specified in most of the papers. To start bioprinting and select the optimal conditions and bioinks is not an easy task, however, many companies provide different bioinks. Based on these, the first step, which is one of the most important ones, is the pre-processing to select the optimal bioink for the cells. Every laboratory has its way and strategy, therefore, there are no same and comparable results regarding the last few years. Hopefully, in the next years, some protocols will be cleared and standardised in 3D bioprinted cancer and breast cancer models depending on the applications (e.g., drug test, migration/metastasis/tumour progression models).

Due to the exponential developments and cutting-edge technological solutions, it is expected that several biological mechanisms would be characterised better and model systems would become more standardised in the case of tumours and other disease models. This improvement is greatly supported by the fact that not only the EU, EMA, and FDA but several other authorities also urge the implementation of the 3R strategy in various investigational studies including the basic and applied research areas, respectively. This initiates the replacement of animal models with *in vitro* ones, of which industrial application could only be realised if standardised models would be used or available in the future.

TABLE 1 3D bioprinting technology application in breast cancer studies.

		Bioink	3D technique	Cell lines	Novelty	References		
		Group	Composition					
Manually Prepared 3D Model		N + S	Matrigel + synthetic sheets	Cells were seeded on preformed multi-layered mesh sheets	MDA-MB-231	Could create different levels of hypoxia in tissue mimetic structure	Karen A. Simon et al.	2014 (110)
		N	Chitosan + hydroxyapatite	Cells were seeded on the preformed bone biomimetic scaffold	MDA-MB-231, MCF-7	A novel biomimetic engineered nano-bone model for bone metastatic studies	Wei Zhu et al.	2015 (65)
		N	Collagen-I + hyaluronan + laminin + fibronectin	Manually prepared 3D model	patient-derived breast tissue	Growing patient-derived breast cancer cells in ECM matrix	Ethan S. Sokol et al.	2016 (72)
		S	GelMa	Manually prepared microengineered tumour model	MDA-MB-231, MCF-7, MCF10A	Modelling two distinct regions of the tumour microenvironment with differential stiffness	Nitish Peela et al.	2016 (111)
		N + S	Alginate-gelatin blend, HA-PEGDA blend	Cell-containing hydrogel beads formed manually	MDA-MB-231, MCF-7	Cellular responses depend on different hydrogel properties	Rafael Schmid et al.	2020 (112)
		N	Fibrin-based	Manually prepared gel-embedded spheroids	MDA-MB-231	Vascularised metastatic breast tumour model	Madhuri Dey et al.	2021 (79)
Pre – printed cell – free mold/matrix		S	PEG-based + hydroxyapatite	3D bioprinted bone matrices, then cells were seeded on the bioprinted scaffold	MDA-MB-231, FOB	Fabricating artificial bone matrices then hosting breast cancer cells and osteoblasts for bone metastatic studies	Wei Zhu et al.	2016 (113)
		N	Porcine skin + human decellularised adipose tissue	3D preprinted mold, then cells were seeded on the bioprinted scaffold	MCF-7	Characterisation of the photothermal properties of gold nanorods with bioprinted 3D complex tissue constructs	Ki-Hwan Nam et al.	2021 (114)
		S	PEOT/PBT	3D bioprinted scaffold, then cells were seeded on the bioprinted scaffold	MDA-MB-231	Cells are more dormant in this 3D model	Afroditi Nanou et al.	2022 (115)
Live – cell 3D bioprinting	Bioprinted droplets	S	GelMa	3D bioprinted droplets	MDA-MB-231	3D tumour model chip with "layer cake" structure as an innovative 3D drug screening system	Mingjun Xie et al.	2020 (116)
		S	PEG-4MAL (+- RGD)	3D bioprinted droplets	MCF-7, MDA-MB-231	3D bioprinted model for *in situ* and real-time measurement of cell movement, migration and invasion	MoonSun Jung et al.	2022 (117)
		S	PEG-based	3D bioprinted droplets	MCF-7, MDA-MB-231, fibroblast	These 3D tissue cultures can readily be used with standard 2D high throughput assays	Martin Engel et al.	2022 (118)
	Bioprinted mono – culture scaffolds	N	Human and rat-derived hydrogels, rat-tail collagen	3D bioprinted scaffolds	MCF-7, MDA-MB-468	Generate large organoids/ tumoroids for studying cell and native ECM interactions	Peter A. Mollica et al.	2019 (75)
		N	TIB - PBS used as bioink	3D bioprinted scaffolds	MCF-7	Bioprinting activates key pathways implicated in drug resistance, cell motility, proliferation, survival, and differentiation	Aleli Campbell et al.	2020 (119)
		N	Polypeptide-based	3D bioprinted scaffolds	MDA-MB-231	Breast cancer (cell line) and lung (PDX) cancer models for drug sensitivity tests	A. Gebeyehu et al.	2021 (93)
		N	alginate-gelatine, alginate-gelatine-matrigel blend	3D bioprinted scaffolds, then continuous passaging	MDA-MB-231	Harvested cells are used for continuous passaging and reprinting in 3D bioprintable alginate–gelatine systems (up to three rounds)	S. Flores-Torres et al.	2021 (120)

(Continued on following page)

TABLE 1 (*Continued*) 3D bioprinting technology application in breast cancer studies.

	Bioink		3D technique	Cell lines	Novelty	References		
	Group	Composition						
	N	TIB - PBS used as bioink	3D bioprinted scaffolds	MCF7, MDA-MB-231	Higher resistance in bioprinted structures	Aleli Campbell et al.	2021	(121)
	N	Tissue derived matrix, gelma, alginate, collagen-I	3D bioprinted with 3D bioplotter	MCF-7	Recreate the complex composition of breast tumours	B. Blanco-Fernandez et al.	2022	(122)
	N	Alginate-gelatine blend	3D bioprinted scaffolds	MCF-7, $CD44^+$ MCF-7	Drug-resistant spheroids were able to maintain their drug-resistant phenotype during 3D culturing	Sera Hong et al.	2022	(123)
	N + S	Decellularised porcine fat + gelma	3D printed construct	MCF-7	New ECM-like hybrid bioinks were developed	You Chen et al.	2022	(124)
	N	Alginate-based	3D bioprinted scaffolds	ZR75.1	3D bioprinted cultures represent higher similarity to the *in vivo* situation	Titanilla Dankó et al.	2022	(103)
Bioprinted complex structures, co — cultures	N	Rat-tail collagen gels	3D bioprinted tumoroids	MCF-7, MDA-MB-468, MCF-12A	Bioprinted multicellular organoids to generate tumoroid arrays for assay standardisation	John A. Reid et al.	2019	(74)
	N	Alginate-gelatine blend	3D bioprinted complex tumour model	MCF-7, SKBR3, HCC1143, MDA-MB-231, HUVEC, patient-derived tissue	Generating complex tumour models - investigating cells' maturing, self-organisation, heterogeneity, migration, therapeutic response, signalling	Ellen M. Langer et al.	2019	(83)
	N	Alginate-gelatine blend	3D bioprinted scaffolds	MCF-7, stromal cells	Modelling the breast cancer tumour environment with adipocytes and breast cancer cells	Sarah Chaji et al.	2020	(77)
	N	Matrigel, gelatine-alginate, collagen-alginate	3D bioprinted scaffolds	MDA-MB-231, MCF-7, MCF10A	Bioprinting multicellular breast tumour spheroids	Swathi Swaminathan et al.	2020	(76)
	N	Thiol-modified HA-based	3D bioprinted constructs (mono- and co-cultures)	MDA-MB-231	Generating a more complex bioprinted breast cancer model (3D adipose tissue model + 3D breast cancer model)	Hannes Horder et al.	2021	(82)
	N	Sodium-alginate	3D bioprinted droplets on mesometrium tissue	4T1	A tumour microvasculature model with cancer cells	Ariana D. Suarez-Martinez et al.	2021	(80)
	N	Matrigel	3D bioprinting with pre-formed 3D breast-epithelial spheroids and HUVEC networks	MDA-MB-231, MCF10A	Direct bioprinting of breast epithelial spheroids on pre-formed HUVEC networks to create a 3D multicellular co-culture tumour model	Swathi Swaminathan et al.	2021	(76)
	N	Collagen-based, fibrin-based	3D bioprinted complex immune-cancer model	MDA-MB-231	3D tumour models were fabricated with increased complexity to study immune-cancer interactions	Madhuri Dey et al.	2022	(109)

N, natural; S, synthetic; GelMa, gelatin methacrylate; HA, hyaluronic acid; PEGDA, poly(ethyleneglycol)diacrylate; PEOT, poly(ethyleneoxide-terephthalate); PBT, poly(butylene-terephthalate); PEG-4MAL, polyethylene-glycol-4-maleimide; RGD, arginylglycylaspartic-acid; TIB, thermal inkjet bioprinting.

The wide variety of bioinks, bioink protocols as well as innovative bioprinters and technologies point out that various factors have to be taken into account during project planning, not even mentioning the measurements and settings required in certain experiments, the design and usability of assays suitable for monitoring growth and proliferation changes, or other biological and molecular processes (56). As we described earlier, the gel composition is diverging nearly in all laboratories (or within the same research group based on the researcher's choice). Based on our previous experiments, which are not presented here, and others' results, it can be stated that the composition of bioinks and gels used for printing can significantly change not only the growth and survival of cells but also the morphological features of cells that form the spheroids and tissue-like structures. Thus, the printing conditions and the exact composition of materials have special importance so that the published results could be reproduced, at least in case of using the same cell lines.

TABLE 2 Bioinks in cancer research.

	Base	Examples of cancer model application	Advantages	Disadvantages	Crosslinking	Examples of "ready-to-use" bioinks at companies	Ref.
Derived from natural sources	Alginate	Drug delivery model	Low cost	Poor cell adhesion	Ionic	Cellink - PhotoAlginate®-INK, CELLINK Bioink, GelMA A	(125–127)
		Cancer stem cell	Good printability	Poor stability			
		Breast cancer	High biocompatibility	Immunogenicity			
		Melanoma	Mild crosslinking conditions (Ca2+)	Non-biomimetic ECM		Growdex - GrowInk™-ALG, PhotoAlginate®	
		Tumour spheroids	Rapid gelation				
	Gelatine	Cholangiocarcinoma	Excellent biocompatibility	Low viscosity at rt or higher	Chemical		(128–130)
		Bladder cancer	Low cost	Needs temperature control	Thermal	Cellink - PhotoGel®, GelMA	
		Tumour spheroids	High cellular adhesion	Low mechanical strength (higher if blended with other bioinks)	UV	Advanced Biomatrix - GelMA, PhotoGel®, BioInx - GelMa, EASYGEL INX	
			High solubility in water		Covalent		
			Gelation is thermally reversible		Enzymatic		
	Cellulose, nanocellulose	Drug delivery model	Ecm-similarity	Low viscosity (cellulose nanocrystals)	Enzymatic	Cellink - CELLINK Bioink, GelMa C	(131–133)
		Gastric cancer	Excellent biocompatibility	Needs to be mixed with other natural biomaterials	UV	Growdex - GrowInk™-N, GrowInk™-T, GrowInk™-ALG	
		Cervical cancer					
		Pancreatic cancer					
	Matrigel	Tumour spheroids	Most used material in cancer research	Cannot be used alone (complex rheological behaviour, low mechanical properties)	Thermal		(134–136)
		Many types of cancer	Excellent biocompatibility	Limited use in vivo			
			Very well characterised for organoid/spheroid formation	Expensive High batch variability			
	Collagen-I	Tumour spheroids	Excellent biocompatibility	Low shape fidelity	pH	Cellink - Lifeink® Collagen Bioink, Advanced Biomatrix - PureCol® EZ Gel, RatCol®, Lifeink®, PhotoCol®, CollPlant - Collink.3D	(137–139)
		Neuroblastoma	High cellular adhesion		Thermal		
		Breast cancer	Low immunogenicity				
			Excellent printability				
			Enzymatically degradable				
			Mechanical and structural properties close to native tissue				
	Hyaluronic – acid	Tumour spheroids	Excellent biocompatibility	Poor mechanical strength	Physical or covalent	Cellink - PhotoHA®, Advanced Biomatrix - PhotoHA®	(140, 141)
		Melanoma	Highly tunable (wide variety and high degree of potential chemical modifications)	Mainly used as a mixture			
		Breast cancer	Interact with cell receptors				
			Fast gelation				
			Promotes cell proliferation				

(Continued on following page)

TABLE 2 (*Continued*) Bioinks in cancer research.

	Base	Examples of cancer model application	Advantages	Disadvantages	Crosslinking	Examples of "ready-to-use" bioinks at companies	Ref.
Derived from synthetic sources	Agarose	Leukaemia	Good biocompatibility	Poor cell viability if not blended with another biomaterial	Thermal		(142)
			High ECM-similarity	Poor printability (needs high temperature for dispensing - 70°C)	Ionic		
			Thermo reversible (non-toxic) gelling	Poor cell adhesion			
			High stability	Not degradable			
	Fibrin	Drug release model	High shape fidelity (depending on fibrinogen-thrombin concentration)	Medium cell adhesion	Enzymatic (fibrinogen - thrombin)	Cellink - CELLINK FIBRIN	(143, 144)
		Glioblastoma	Excellent biocompatibility	Low mechanical properties and limited printability			
			Enzymatically degradable				
			Rapid gelation				
	Polypeptides	Ovarian cancer	Self-assembly	Low cell viability (low ph)	Ionic-complementary	Manchester Biogel TheWell Bioscience - VitroINK	(145, 146)
			Adapted for soft-tissue applications and in conjunction with other materials				
	Decellularised matrix (dECM)	Many tumour models depending on dECM	Renders natural ECM	Low stability	Depends on chemical modifications		(147–149)
			Tissue specific	Protein denaturation during fabrication processes			
			High biological relevance	Poor printability if not mixed with another biomaterial			
			High cell survival	Long procedure			
				Undefined and inconsistent			
				Loss of native ECM			
	Acrylamide	Melanoma	Wide-range of elasticity and flexibility	Needs other supportive material for cell proliferation (alginate, gelatine, etc)	UV	Cellink - PhotoAlginate®, PhotoGel®, PhotoHA®, GelMA	(150–152)
		Breast cancer	Most standardised protocol			Advanced Biomatrix - Mebiol®, PhotoGel®, PhotoHA®, PhotoCol®, PhotoAlginate®, PhotoDextran®, BioInx - GelMa	
	PCL		Good mechanical strength and rigidity	Not compatible with live-cell bioprinting (mainly used as a preprinted frame or mold)	Depends on the natural biomaterial used	Cellink - CELLINK PCL	(153)
			Controllable degradation	Needs other supportive material for cell proliferation (alginate, gelatine, etc)			
	Pluronic	Vascularised tissues, complicated tissue constructs	High shape fidelity	Short of cell-binding domains	Covalent	Cellink - Pluronics 40%, Advanced Biomatrix - Pluronics 40%	(154)
		Drug release model	Good printability	Low cell viability			
				Poor mechanical strength			

Potentially, the most important point will be to examine how drug preselection tests performed with specific 3D bioprinted model systems show and predict the results previously obtained in the phase trials and the future outcomes. If it can be proved that with the use of these 3D bioprinted or the developing organoid models and their combination such *in vitro* tissue, organ models could be created which would be more appropriate for performing more efficient drug screening tests than in animal models *in vivo*. Then,

there would be the time for tightening the regulations. Accordingly, most of the studies would be carried out with human cell-based *in vitro* tests to replace several animal experiments. All of these can lead to the point that the pharmaceutical developments mentioned in the introduction will be more successful, efficient, and consequently cost-effective in the near future.

Data availability statement

The original contributions presented in the study are included in the article/Supplementary Material, further inquiries can be directed to the corresponding author.

Ethics statement

The studies involving human participants were reviewed and approved by Hungarian Scientific Council National Ethics Committee for Scientific Research (SE-KREB 216/2020). Written informed consent for participation was not required for this study in accordance with the national legislation and the institutional requirements. The animal study was reviewed and approved by Institutional Animal Care Facility and the Institutional Ethical Review Board (PEI/001/1733-2/2015, PE/EA/801-7/2020).

Author contributions

AS designed the study, and supervised the reviewing of literature and the manuscript preparation; DS and DM contributed equally to reviewing the literature, performing all experiments and writing the manuscript; TD, RG, RR, and GP, assisted in 3D bioprinting and maintaining cell cultures; RR and IK helped in immunostainings; GP supervised the animal experiments and WES™ analyses performed by DS, DM, TD, and RG; TD carefully revised the final version of the manuscript.

Funding

Recent research works at the Department of Pathology and Experimental Cancer Research was funded by the National Bionics Program (Project No. ED_17-1-2017-0009) from the National Research part of the Hungarian National Research, Development and Innovation Office (NKFIH) and TKP2021-EGA-24. Our research was supported by NKFI-FK-128404, NKFI-K-142799 and NFKI-PD-142418 (National Research, Development and Innovation Office—AS and GP), EFOP-3.6.3-VEKOP-16-2017-00009 (TD, DM, and DS), Hungarian Society of Senology (GP), ÚNKP-22-4-II-SE-9 (GP), ÚNKP-22-4-I-SE-12 (TD), and the Stephen W. Kuffler Research Grant (TD).

Conflict of Interest

The authors declare that the research was conducted in the absence of any commercial or financial relationships that could be construed as a potential conflict of interest.

Acknowledgments

The authors thank András Rókusz and Csilla Kurucz for their excellent technical assistance in the Department of Pathology and Experimental Cancer Research, Semmelweis University. We are also grateful to András Sztodola for helping with animal experiments.

Supplementary material

The Supplementary Material for this article can be found online at: https://www.por-journal.com/articles/10.3389/pore.2023.1610996/full#supplementary-material

SUPPLEMENTARY FIGURE S1
The original and unadjusted images of WES™ Simple electropherograms.

References

1. *Regulation of the European parliament and of the Council on cosmetic products*, No 1223/2009 (2009). Available at: https://eur-lex.europa.eu/legal-content/EN/ALL/?uri=celex%3A32009R1223 (Accessed November 03, 2022).

2. Swaters D, van Veen A, van Meurs W, Turner JE, Ritskes-Hoitinga M. A history of regulatory animal testing: What can we learn? *Alternatives Lab Anim* (2022) 50(5):322–9. doi:10.1177/02611929221118001

3. Van Norman GA. Limitations of animal studies for predicting toxicity in clinical trials: Is it time to rethink our current approach? *JACC Basic Transl Sci* (2019) 4(7):845–54. doi:10.1016/j.jacbts.2019.10.008

4. Wilson JG, Ritter EJ, Scott WJ, Fradkin R. Comparative distribution and embryotoxicity of acetylsalicylic acid in pregnant rats and rhesus monkeys. *Toxicol Appl Pharmacol* (1977) 41(1):67–78. doi:10.1016/0041-008x(77)90054-0

5. Ritskes-Hoitinga M. Medical regulators: Look beyond animal tests. *Nature* (2022) 604(7907):599. doi:10.1038/d41586-022-01110-6

6. Sandeep Ganesh G, Kolusu AS, Prasad K, Samudrala PK, Nemmani KVS. Advancing health care via artificial intelligence: From concept to clinic. *Eur J Pharmacol* (2022) 934:175320. doi:10.1016/j.ejphar.2022.175320

7. Jahagirdar D, Bangde P, Jain R, Dandekar P. Degenerative disease-on-a-chip: Developing microfluidic models for rapid availability of newer therapies. *Biotechnol J* (2021) 16(10):e2100154. doi:10.1002/biot.202100154

8. Parke EC. Flies from meat and wasps from trees: Reevaluating Francesco Redi's spontaneous generation experiments. *Stud Hist Philos Biol Biomed Sci* (2014) 45:34–42. doi:10.1016/j.shpsc.2013.12.005

9. Hajdu SI. The first use of the microscope in medicine. *Ann Clin Lab Sci* (2002) 32(3):309–10.

10. Mazzarello P. A unifying concept: The history of cell theory. *Nat Cel Biol* (1999) 1(1):E13–5. doi:10.1038/8964

11. Louis P. On spontaneous generation. *Revue de Cours Scientifics* (1864)(1) 257–64.

12. Schwann T, Smith H, Schleiden MJ. *Microscopical researches into the accordance in the structure and growth of animals and plants*. London: Sydenham Society (1847).

13. Hall TS. *Ideas of life and matter; studies in the history of general physiology, 600 B.C.-1900 A.D.* Chicago: Thomas S. HallUniversity of Chicago Press (1969).

14. Schultz MG. Rudolf Virchow. *Emerging Infect Dis* (2008) 14(9):1480–1. doi:10.3201/eid1409.086672

15. Wagner RP. Anecdotal, historical and critical commentaries on genetics. Rudolph Virchow and the genetic basis of somatic ecology. *Genetics* (1999) 151(3): 917–20. doi:10.1093/genetics/151.3.917

16. Roux W. *Gesammelte Abhandlungen über Entwickelungsmechanik der Organismen*. Leipzig: Wilhelm Engelmann (1895).

17. Blumenthal HT, Loeb L. Leo Loeb, experimental pathologist and humanitarian. *Science* (1960) 131(3404):907–8. doi:10.1126/science.131.3404.907

18. Harrison RG. Observations on the living developing nerve fiber. *Proc Soc Exp Biol Med* (1906) 4(1):140–3. doi:10.3181/00379727-4-98

19. Carrel A, Burrows MT. An addition to the technique of the cultivation of tissues *in vitro*. *J Exp Med* (1911) 14(3):244–7. doi:10.1084/jem.14.3.244

20. Rous P, Jones FS. A method for obtaining suspensions of living cells from the fixed tissues, and for the plating out of individual cells. *J Exp Med* (1916) 23(4): 549–55. doi:10.1084/jem.23.4.549

21. Hayflick L, Moorhead PS. The serial cultivation of human diploid cell strains. *Exp Cel Res* (1961) 25:585–621. doi:10.1016/0014-4827(61)90192-6

22. Hahn WC. Immortalization and transformation of human cells. *Mol Cell* (2002) 13(3):351–61.

23. Yamanaka S. Induced pluripotent stem cells: Past, present, and future. *Cell Stem Cell* (2012) 10(6):678–84. doi:10.1016/j.stem.2012.05.005

24. Hajdu SI. Pathfinders in oncology from ancient times to the end of the Middle Ages. *Cancer* (2016) 122(11):1638–46. doi:10.1002/cncr.29955

25. Waldron HA. A brief history of scrotal cancer. *Br J Ind Med* (1983) 40(4): 390–401. doi:10.1136/oem.40.4.390

26. Rous P. A transmissible avian neoplasm. sarcoma of the common fowl. *J Exp Med* (1910) 12(5):696–705. doi:10.1084/jem.12.5.696

27. Stehelin D, Varmus HE, Bishop JM, Vogt PK. DNA related to the transforming gene(s) of avian sarcoma viruses is present in normal avian DNA. *Nature* (1976) 260(5547):170–3. doi:10.1038/260170a0

28. Rygaard J, Povlsen CO. Heterotransplantation of a human malignant tumour to "Nude" mice. *Acta Pathol Microbiol Scand* (1969) 77(4):758–60. doi:10.1111/j.1699-0463.1969.tb04520.x

29. Stanbridge EJ, Perkins FT, Hayflick L. Cell tumourigenicity detected by heterotransplantation into mice immunosuppressed with anti-lymphocytic serum. *Prog Immunobiol Stand* (1971) 5:243–51.

30. Kopper L, Steel GG. The therapeutic response of three human tumor lines maintained in immune-suppressed mice. *Cancer Res* (1975) 35(10):2704–13.

31. Justice BA, Badr NA, Felder RA. 3D cell culture opens new dimensions in cell-based assays. *Drug Discov Today* (2009) 14(1-2):102–7. doi:10.1016/j.drudis.2008.11.006

32. Knight A. Systematic reviews of animal experiments demonstrate poor human clinical and toxicological utility. *Altern Lab Anim* (2007) 35(6):641–59. doi:10.1177/026119290703500610

33. Hanahan D. Hallmarks of cancer: New dimensions. *Cancer Discov* (2022) 12(1):31–46. doi:10.1158/2159-8290.Cd-21-1059

34. Rodrigues J, Heinrich MA, Teixeira LM, Prakash J. 3D *in vitro* model (R) evolution: Unveiling tumor-stroma interactions. *Trends Cancer* (2021) 7(3):249–64. doi:10.1016/j.trecan.2020.10.009

35. Asghar W, El Assal R, Shafiee H, Pitteri S, Paulmurugan R, Demirci U. Engineering cancer microenvironments for *in vitro* 3-D tumor models. *Mater Today (Kidlington)* (2015) 18(10):539–53. doi:10.1016/j.mattod.2015.05.002

36. Sung KE, Beebe DJ. Microfluidic 3D models of cancer. *Adv Drug Deliv Rev* (2014) 79-80:68–78. doi:10.1016/j.addr.2014.07.002

37. Langhans SA. Three-dimensional *in vitro* cell culture models in drug discovery and drug repositioning. *Front Pharmacol* (2018) 9:6. doi:10.3389/fphar.2018.00006

38. Duval K, Grover H, Han LH, Mou Y, Pegoraro AF, Fredberg J, et al. Modeling physiological events in 2D vs. 3D cell culture. *Physiology (Bethesda)* (2017) 32(4): 266–77. doi:10.1152/physiol.00036.2016

39. Jensen C, Teng Y. Is it time to start transitioning from 2D to 3D cell culture? *Front Mol Biosci* (2020) 7:33. doi:10.3389/fmolb.2020.00033

40. Boland T, Mironov V, Gutowska A, Roth EA, Markwald RR. Cell and organ printing 2: Fusion of cell aggregates in three-dimensional gels. *Anat Rec A Discov Mol Cel Evol Biol* (2003) 272(2):497–502. doi:10.1002/ar.a.10059

41. Jakab K, Damon B, Neagu A, Kachurin A, Forgacs G. Three-dimensional tissue constructs built by bioprinting. *Biorheology* (2006) 43(34):509–13.

42. Asulin M, Michael I, Shapira A, Dvir T. One-step 3D printing of heart patches with built-in electronics for performance regulation. *Adv Sci (Weinh)* (2021) 8(9): 2004205. doi:10.1002/advs.202004205

43. Shah AM, Han JJ. First successful porcine to human heart transplantation performed in the United States. *Artif Organs* (2022) 46(4):543–5. doi:10.1111/aor.14203

44. Yang H, Sun L, Pang Y, Hu D, Xu H, Mao S, et al. Three-dimensional bioprinted hepatorganoids prolong survival of mice with liver failure. *Gut* (2021) 70(3):567–74. doi:10.1136/gutjnl-2019-319960

45. Ho CMB, Ng SH, Yoon Y-J. A review on 3D printed bioimplants. *Int J Precision Eng Manufacturing* (2015) 16(5):1035–46. doi:10.1007/s12541-015-0134-x

46. Diment LE, Thompson MS, Bergmann JHM. Clinical efficacy and effectiveness of 3D printing: A systematic review. *BMJ Open* (2017) 7(12): e016891. doi:10.1136/bmjopen-2017-016891

47. Huang SH, Liu P, Mokasdar A, Hou L. Additive manufacturing and its societal impact: A literature review. *Int J Adv Manufacturing Technology* (2013) 67(5): 1191–203. doi:10.1007/s00170-012-4558-5

48. Ramesh S, Harrysson OLA, Rao PK, Tamayol A, Cormier D, Zhang Y, et al. Extrusion bioprinting: Recent progress, challenges, and future opportunities. *Bioprinting* (2021) 21:e00116. doi:10.1016/j.bprint.2020.e00116

49. Yan Q, Dong H, Su J, Han J, Song B, Wei Q, et al. A review of 3D printing technology for medical applications. *Engineering* (2018) 4(5):729–42. doi:10.1016/j.eng.2018.07.021

50. Nuseir A, Hatamleh MM, Alnazzawi A, Al-Rabab'ah M, Kamel B, Jaradat E. Direct 3D printing of flexible nasal prosthesis: Optimized digital workflow from scan to fit. *J Prosthodont* (2019) 28(1):10–4. doi:10.1111/jopr.13001

51. Faglin P, Gradwohl M, Depoortere C, Germain N, Drucbert A-S, Brun S, et al. Rationale for the design of 3D-printable bioresorbable tissue-engineering chambers to promote the growth of adipose tissue. *Scientific Rep* (2020) 10(1):11779. doi:10.1038/s41598-020-68776-8

52. Wang X, Ao Q, Tian X, Fan J, Wei Y, Hou W, et al. 3D bioprinting technologies for hard tissue and organ engineering. *Materials (Basel)* (2016) 9(10):802. doi:10.3390/ma9100802

53. Groll J, Burdick JA, Cho DW, Derby B, Gelinsky M, Heilshorn SC, et al. A definition of bioinks and their distinction from biomaterial inks. *Biofabrication* (2018) 11(1):013001. doi:10.1088/1758-5090/aaec52

54. Panwar A, Tan LP. Current status of bioinks for micro-extrusion-based 3D bioprinting. *Molecules* (2016) 21(6):685. doi:10.3390/molecules21060685

55. Gopinathan J, Noh I. Recent trends in bioinks for 3D printing. *Biomater Res* (2018) 22:11. doi:10.1186/s40824-018-0122-1

56. Gungor-Ozkerim PS, Inci I, Zhang YS, Khademhosseini A, Dokmeci MR. Bioinks for 3D bioprinting: An overview. *Biomater Sci* (2018) 6(5):915–46. doi:10.1039/c7bm00765e

57. Das S, Basu B. An overview of hydrogel-based bioinks for 3D bioprinting of soft tissues. *J Indian Inst Sci* (2019) 99:405–28. doi:10.1007/s41745-019-00129-5

58. GhavamiNejad A, Ashammakhi N, Wu XY, Khademhosseini A. Crosslinking strategies for 3D bioprinting of polymeric hydrogels. *Small* (2020) 16(35):2002931. doi:10.1002/smll.202002931

59. Germain N, Dhayer M, Dekiouk S, Marchetti P. Current advances in 3D bioprinting for cancer modeling and personalized medicine. *Int J Mol Sci* (2022) 23(7):3432. doi:10.3390/ijms23073432

60. Augustine R, Kalva SN, Ahmad R, Zahid AA, Hasan S, Nayeem A, et al. 3D Bioprinted cancer models: Revolutionizing personalized cancer therapy. *Transl Oncol* (2021) 14(4):101015. doi:10.1016/j.tranon.2021.101015

61. Schueler J, Borenstein J, Buti L, Dong M, Masmoudi F, Hribar K, et al. How to build a tumor: An industry perspective. *Drug Discov Today* (2022) 27(10):103329. doi:10.1016/j.drudis.2022.07.014

62. Moon S, Hasan SK, Song YS, Xu F, Keles HO, Manzur F, et al. Layer by layer three-dimensional tissue epitaxy by cell-laden hydrogel droplets. *Tissue Eng C Methods* (2010) 16(1):157–66. doi:10.1089/ten.TEC.2009.0179

63. Leonard F, Godin B. 3D *in vitro* model for breast cancer research using magnetic levitation and bioprinting method. *Methods Mol Biol* (2016) 1406:239–51. doi:10.1007/978-1-4939-3444-7_21

64. Zhao Y, Yao R, Ouyang L, Ding H, Zhang T, Zhang K, et al. Three-dimensional printing of Hela cells for cervical tumor model *in vitro*. *Biofabrication* (2014) 6(3):035001. doi:10.1088/1758-5082/6/3/035001

65. Zhu W, Wang M, Fu Y, Castro NJ, Fu SW, Zhang LG. Engineering a biomimetic three-dimensional nanostructured bone model for breast cancer bone metastasis study. *Acta Biomater* (2015) 14:164–74. doi:10.1016/j.actbio.2014.12.008

66. Liu C, Hu A, Chen H, Liang J, Gu M, Xiong Y, et al. The osteogenic niche-targeted arsenic nanoparticles prevent colonization of disseminated breast tumor cells in the bone. *Acta Pharm Sin B* (2022) 12(1):364–77. doi:10.1016/j.apsb.2021.06.012

67. Kolesky DB, Truby RL, Gladman AS, Busbee TA, Homan KA, Lewis JA. 3D bioprinting of vascularized, heterogeneous cell-laden tissue constructs. *Adv Mater* (2014) 26(19):3124–30. doi:10.1002/adma.201305506

68. Neiman JA, Raman R, Chan V, Rhoads MG, Raredon MS, Velazquez JJ, et al. Photopatterning of hydrogel scaffolds coupled to filter materials using stereolithography for perfused 3D culture of hepatocytes. *Biotechnol Bioeng* (2015) 112(4):777–87. doi:10.1002/bit.25494

69. Nguyen DG, Funk J, Robbins JB, Crogan-Grundy C, Presnell SC, Singer T, et al. Bioprinted 3D primary liver tissues allow assessment of organ-level response to clinical drug induced toxicity *in vitro*. *PLoS One* (2016) 11(7):e0158674. doi:10.1371/journal.pone.0158674

70. Li R, Ting Y-H, Youssef SH, Song Y, Garg S. Three-dimensional printing for cancer applications: Research landscape and technologies. *Pharmaceuticals* (2021) 14(8):787. doi:10.3390/ph14080787

71. Petersen OW, Rønnov-Jessen L, Howlett AR, Bissell MJ. Interaction with basement membrane serves to rapidly distinguish growth and differentiation pattern of normal and malignant human breast epithelial cells. *Proc Natl Acad Sci U S A* (1992) 89(19):9064–8. doi:10.1073/pnas.89.19.9064

72. Sokol ES, Miller DH, Breggia A, Spencer KC, Arendt LM, Gupta PB. Growth of human breast tissues from patient cells in 3D hydrogel scaffolds. *Breast Cancer Res* (2016) 18(1):19. doi:10.1186/s13058-016-0677-5

73. Swaminathan S, Hamid Q, Sun W, Clyne AM. Bioprinting of 3D breast epithelial spheroids for human cancer models. *Biofabrication* (2019) 11(2):025003. doi:10.1088/1758-5090/aafc49

74. Reid JA, Palmer XL, Mollica PA, Northam N, Sachs PC, Bruno RD. A 3D bioprinter platform for mechanistic analysis of tumoroids and chimeric mammary organoids. *Sci Rep* (2019) 9(1):7466. doi:10.1038/s41598-019-43922-z

75. Mollica PA, Booth-Creech EN, Reid JA, Zamponi M, Sullivan SM, Palmer XL, et al. 3D bioprinted mammary organoids and tumoroids in human mammary derived ECM hydrogels. *Acta Biomater* (2019) 95:201–13. doi:10.1016/j.actbio.2019.06.017

76. Swaminathan S, Clyne AM. Direct bioprinting of 3D multicellular breast spheroids onto endothelial networks. *J Vis Exp* (2020) 165. doi:10.3791/61791

77. Chaji S, Al-Saleh J, Gomillion CT. Bioprinted three-dimensional cell-laden hydrogels to evaluate adipocyte-breast cancer cell interactions. *Gels* (2020) 6(1):10. doi:10.3390/gels6010010

78. Shao L, Gao Q, Xie C, Fu J, Xiang M, He Y. Directly coaxial 3D bioprinting of large-scale vascularized tissue constructs. *Biofabrication* (2020) 12(3):035014. doi:10.1088/1758-5090/ab7e76

79. Dey M, Ayan B, Yurieva M, Unutmaz D, Ozbolat IT. Studying tumor angiogenesis and cancer invasion in a three-dimensional vascularized breast cancer micro-environment. *Adv Biol (Weinh)* (2021) 5(7):e2100090. doi:10.1002/adbi.202100090

80. Suarez-Martinez AD, Sole-Gras M, Dykes SS, Wakefield ZR, Bauer K, Majbour D, et al. Bioprinting on live tissue for investigating cancer cell dynamics. *Tissue Eng A* (2021) 27(7-8):438–53. doi:10.1089/ten.TEA.2020.0190

81. Zhu W, Qu X, Zhu J, Ma X, Patel S, Liu J, et al. Direct 3D bioprinting of prevascularized tissue constructs with complex microarchitecture. *Biomaterials* (2017) 124:106–15. doi:10.1016/j.biomaterials.2017.01.042

82. Horder H, Guaza Lasheras M, Grummel N, Nadernezhad A, Herbig J, Ergün S, et al. Bioprinting and differentiation of adipose-derived stromal cell spheroids for a 3D breast cancer-adipose tissue model. *Cells* (2021) 10(4):803. doi:10.3390/cells10040803

83. Langer EM, Allen-Petersen BL, King SM, Kendsersky ND, Turnidge MA, Kuziel GM, et al. Modeling tumor phenotypes *in vitro* with three-dimensional bioprinting. *Cell Rep* (2019) 26(3):608–23. doi:10.1016/j.celrep.2018.12.090

84. Tang M, Rich JN, Chen S. Biomaterials and 3D bioprinting strategies to model glioblastoma and the blood-brain barrier. *Adv Mater* (2021) 33(5):e2004776. doi:10.1002/adma.202004776

85. van Pel DM, Harada K, Song D, Naus CC, Sin WC. Modelling glioma invasion using 3D bioprinting and scaffold-free 3D culture. *J Cel Commun Signal* (2018) 12(4):723–30. doi:10.1007/s12079-018-0469-z

86. Heinrich MA, Bansal R, Lammers T, Zhang YS, Michel Schiffelers R, Prakash J. 3D-Bioprinted mini-brain: A glioblastoma model to study cellular interactions and therapeutics. *Adv Mater* (2019) 31(14):e1806590. doi:10.1002/adma.201806590

87. Nothdurfter D, Ploner C, Coraça-Huber DC, Wilflingseder D, Müller T, Hermann M, et al. 3D bioprinted, vascularized neuroblastoma tumor environment in fluidic chip devices for precision medicine drug testing. *Biofabrication* (2022) 14(3):035002. doi:10.1088/1758-5090/ac5fb7

88. Neufeld L, Yeini E, Reisman N, Shtilerman Y, Ben-Shushan D, Pozzi S, et al. Microengineered perfusable 3D-bioprinted glioblastoma model for *in vivo* mimicry of tumor microenvironment. *Sci Adv* (2021) 7(34):eabi9119. doi:10.1126/sciadv.abi9119

89. Hermida MA, Kumar JD, Schwarz D, Laverty KG, Di Bartolo A, Ardron M, et al. Three dimensional *in vitro* models of cancer: Bioprinting multilineage glioblastoma models. *Adv Biol Regul* (2020) 75:100658. doi:10.1016/j.jbior.2019.100658

90. Sivandzade F, Cucullo L. *In-vitro* blood-brain barrier modeling: A review of modern and fast-advancing technologies. *J Cereb Blood Flow Metab* (2018) 38(10):1667–81. doi:10.1177/0271678x18788769

91. Marino A, Tricinci O, Battaglini M, Filippeschi C, Mattoli V, Sinibaldi E, et al. A 3D real-scale, biomimetic, and biohybrid model of the blood-brain barrier fabricated through two-photon lithography. *Small* (2018) 14(6):1702959. doi:10.1002/smll.201702959

92. Maloney E, Clark C, Sivakumar H, Yoo K, Aleman J, Rajan SAP, et al. Immersion bioprinting of tumor organoids in multi-well plates for increasing chemotherapy screening throughput. *Micromachines (Basel)* (2020) 11(2):208. doi:10.3390/mi11020208

93. Gebeyehu A, Surapaneni SK, Huang J, Mondal A, Wang VZ, Haruna NF, et al. Polysaccharide hydrogel based 3D printed tumor models for chemotherapeutic drug screening. *Scientific Rep* (2021) 11(1):372. doi:10.1038/s41598-020-79325-8

94. Hughes AM, Kolb AD, Shupp AB, Shine KM, Bussard KM. Printing the pathway forward in bone metastatic cancer research: Applications of 3D engineered models and bioprinted scaffolds to recapitulate the bone-tumor niche. *Cancers (Basel)* (2021) 13(3):507. doi:10.3390/cancers13030507

95. Grunewald L, Lam T, Andersch L, Klaus A, Schwiebert S, Winkler A, et al. A reproducible bioprinted 3D tumor model serves as a preselection tool for CAR T cell therapy optimization. *Front Immunol* (2021) 12:689697. doi:10.3389/fimmu.2021.689697

96. Meng F, Meyer CM, Joung D, Vallera DA, McAlpine MC, Panoskaltsis-Mortari A. 3D bioprinted *in vitro* metastatic models via reconstruction of tumor microenvironments. *Adv Mater* (2019) 31(10):e1806899. doi:10.1002/adma.201806899

97. Quinn CH, Beierle AM, Hutchins SC, Marayati R, Bownes LV, Stewart JE, et al. Targeting high-risk neuroblastoma patient-derived xenografts with oncolytic virotherapy. *Cancers (Basel)* (2022) 14(3):762. doi:10.3390/cancers14030762

98. Lopez J, Ruiz-Toranzo M, Antich C, Chocarro-Wrona C, López-Ruiz E, Jiménez G, et al. Biofabrication of a tri-layered 3D-bioprinted CSC-based malignant melanoma model for personalized cancer treatment. *Biofabrication* (2022). doi:10.1088/1758-5090/ac8dc6

99. Trujillo-de Santiago G, Flores-Garza BG, Tavares-Negrete JA, Lara-Mayorga IM, González-Gamboa I, Zhang YS, et al. The tumor-on-chip: Recent advances in the development of microfluidic systems to recapitulate the physiology of solid tumors. *Materials (Basel)* (2019) 12(18):2945. doi:10.3390/ma12182945

100. Ma X, Liu J, Zhu W, Tang M, Lawrence N, Yu C, et al. 3D bioprinting of functional tissue models for personalized drug screening and *in vitro* disease modeling. *Adv Drug Deliv Rev* (2018) 132:235–51. doi:10.1016/j.addr.2018.06.011

101. Neufeld L, Yeini E, Pozzi S, Satchi-Fainaro R. 3D bioprinted cancer models: From basic biology to drug development. *Nat Rev Cancer* (2022) 22(12):679–92. doi:10.1038/s41568-022-00514-w

102. Dankó T, Petővári G, Sztankovics D, Moldvai D, Raffay R, Lőrincz P, et al. Rapamycin plus doxycycline combination affects growth arrest and selective autophagy-dependent cell death in breast cancer cells. *Int J Mol Sci* (2021) 22(15):8019. doi:10.3390/ijms22158019

103. Dankó T, Petővári G, Raffay R, Sztankovics D, Moldvai D, Vetlényi E, et al. Characterisation of 3D bioprinted human breast cancer model for *in vitro* drug and metabolic targeting. *Int J Mol Sci* (2022) 23(13):7444. doi:10.3390/ijms23137444

104. Petővári G, Dankó T, Tőkés AM, Vetlényi E, Krencz I, Raffay R, et al. *In situ* metabolic characterisation of breast cancer and its potential impact on therapy. *Cancers (Basel)* (2020) 12(9):2492. doi:10.3390/cancers12092492

105. Vasan N, Baselga J, Hyman DM. A view on drug resistance in cancer. *Nature* (2019) 575(7782):299–309. doi:10.1038/s41586-019-1730-1

106. Fiorillo M, Sotgia F, Lisanti MP. Energetic" cancer stem cells (e-CSCs): A new hyper-metabolic and proliferative tumor cell phenotype, driven by mitochondrial energy. *Front Oncol* (2018) 8:677. doi:10.3389/fonc.2018.00677

107. Witkiewicz AK, Whitaker-Menezes D, Dasgupta A, Philp NJ, Lin Z, Gandara R, et al. Using the "reverse Warburg effect" to identify high-risk breast cancer patients: Stromal MCT4 predicts poor clinical outcome in triple-negative breast cancers. *Cell Cycle* (2012) 11(6):1108–17. doi:10.4161/cc.11.6.19530

108. Riedl A, Schlederer M, Pudelko K, Stadler M, Walter S, Unterleuthner D, et al. Comparison of cancer cells in 2D vs 3D culture reveals differences in AKT-mTOR-S6K signaling and drug responses. *J Cel Sci* (2017) 130(1):203–18. doi:10.1242/jcs.188102

109. Dey M, Kim MH, Nagamine M, Karhan E, Kozhaya L, Dogan M, et al. Biofabrication of 3D breast cancer models for dissecting the cytotoxic response of human T cells expressing engineered MAIT cell receptors. *Biofabrication* (2022) 14(4):044105. doi:10.1088/1758-5090/ac925a

110. Simon KA, Park KM, Mosadegh B, Subramaniam AB, Mazzeo AD, Ngo PM, et al. Polymer-based mesh as supports for multi-layered 3D cell culture and assays. *Biomaterials* (2014) 35(1):259–68. doi:10.1016/j.biomaterials.2013.09.049

111. Peela N, Sam FS, Christenson W, Truong D, Watson AW, Mouneimne G, et al. A three dimensional micropatterned tumor model for breast cancer cell migration studies. *Biomaterials* (2016) 81:72–83. doi:10.1016/j.biomaterials.2015.11.039

112. Schmid R, Schmidt SK, Hazur J, Detsch R, Maurer E, Boccaccini AR, et al. Comparison of hydrogels for the development of well-defined 3D cancer models of breast cancer and melanoma. *Cancers (Basel)* (2020) 12(8):2320. doi:10.3390/cancers12082320

113. Zhu W, Castro NJ, Cui H, Zhou X, Boualam B, McGrane R, et al. A 3D printed nano bone matrix for characterization of breast cancer cell and osteoblast interactions. *Nanotechnology* (2016) 27(31):315103. doi:10.1088/0957-4484/27/31/315103

114. Nam KH, Jeong CB, Kim H, Ahn M, Ahn SJ, Hur H, et al. Quantitative photothermal characterization with bioprinted 3D complex tissue constructs for early-stage breast cancer therapy using gold nanorods. *Adv Healthc Mater* (2021) 10(18):e2100636. doi:10.1002/adhm.202100636

115. Nanou A, Lorenzo-Moldero I, Gazouleas KD, Cortese B, Moroni L. 3D culture modeling of metastatic breast cancer cells in additive manufactured scaffolds. *ACS Appl Mater Inter* (2022) 14(24):28389–402. doi:10.1021/acsami.2c07492

116. Xie M, Gao Q, Fu J, Chen Z, He Y. Bioprinting of novel 3D tumor array chip for drug screening. *Bio-Design and Manufacturing* (2020) 3(3):175–88. doi:10.1007/s42242-020-00078-4

117. Jung M, Skhinas JN, Du EY, Tolentino MAK, Utama RH, Engel M, et al. A high-throughput 3D bioprinted cancer cell migration and invasion model with versatile and broad biological applicability. *Biomater Sci* (2022) 10(20):5876–87. doi:10.1039/D2BM00651K

118. Engel M, Belfiore L, Aghaei B, Sutija M. Enabling high throughput drug discovery in 3D cell cultures through a novel bioprinting workflow. *SLAS Technology* (2022) 27(1):32–8. doi:10.1016/j.slast.2021.10.002

119. Campbell A, Mohl JE, Gutierrez DA, Varela-Ramirez A, Boland T. Thermal bioprinting causes ample alterations of expression of LUCAT1, IL6, CCL26, and NRN1L genes and massive phosphorylation of critical oncogenic drug resistance pathways in breast cancer cells. *Front Bioeng Biotechnol* (2020) 8:82. doi:10.3389/fbioe.2020.00082

120. Flores-Torres S, Peza-Chavez O, Kuasne H, Munguia-Lopez JG, Kort-Mascort J, Ferri L, et al. Alginate-gelatin-Matrigel hydrogels enable the development and multigenerational passaging of patient-derived 3D bioprinted cancer spheroid models. *Biofabrication* (2021) 13(2):025001. doi:10.1088/1758-5090/abdb87

121. Campbell A, Gutierrez DA, Knight C, Vines CM, Heydarian R, Philipovskiy A, et al. Novel combinatorial strategy using thermal inkjet bioprinting, chemotherapy, and radiation on human breast cancer cells; an *in-vitro* cell viability assessment. *Materials (Basel)* (2021) 14(24):7864. doi:10.3390/ma14247864

122. Blanco-Fernandez B, Rey-Vinolas S, Bağcı G, Rubi-Sans G, Otero J, Navajas D, et al. Bioprinting decellularized breast tissue for the development of three-dimensional breast cancer models. *ACS Appl Mater Inter* (2022) 14(26):29467–82. doi:10.1021/acsami.2c00920

123. Hong S, Song JM. 3D bioprinted drug-resistant breast cancer spheroids for quantitative *in situ* evaluation of drug resistance. *Acta Biomater* (2022) 138:228–39. doi:10.1016/j.actbio.2021.10.031

124. Chen Y, Xu L, Li W, Chen W, He Q, Zhang X, et al. 3D bioprinted tumor model with extracellular matrix enhanced bioinks for nanoparticle evaluation. *Biofabrication* (2022) 14(2):025002. doi:10.1088/1758-5090/ac48e4

125. Axpe E, Oyen ML. Applications of alginate-based bioinks in 3D bioprinting. *Int J Mol Sci* (2016) 17(12):1976. doi:10.3390/ijms17121976

126. Qiao SP, Zhao YF, Li CF, Yin YB, Meng QY, Lin FH, et al. An alginate-based platform for cancer stem cell research. *Acta Biomater* (2016) 37:83–92. doi:10.1016/j.actbio.2016.04.032

127. Reig-Vano B, Tylkowski B, Montané X, Giamberini M. Alginate-based hydrogels for cancer therapy and research. *Int J Biol Macromol* (2021) 170:424–36. doi:10.1016/j.ijbiomac.2020.12.161

128. Jiang T, Munguia-Lopez JG, Gu K, Bavoux MM, Flores-Torres S, Kort-Mascort J, et al. Engineering bioprintable alginate/gelatin composite hydrogels with tunable mechanical and cell adhesive properties to modulate tumor spheroid growth kinetics. *Biofabrication* (2019) 12(1):015024. doi:10.1088/1758-5090/ab3a5c

129. He H, Li D, Lin Z, Peng L, Yang J, Wu M, et al. Temperature-programmable and enzymatically solidifiable gelatin-based bioinks enable facile extrusion bioprinting. *Biofabrication* (2020) 12(4):045003. doi:10.1088/1758-5090/ab9906

130. Dai X, Ma C, Lan Q, Xu T. 3D bioprinted glioma stem cells for brain tumor model and applications of drug susceptibility. *Biofabrication* (2016) 8(4):045005. doi:10.1088/1758-5090/8/4/045005

131. Piras CC, Fernández-Prieto S, De Borggraeve WM. Nanocellulosic materials as bioinks for 3D bioprinting. *Biomater Sci* (2017) 5(10):1988–92. doi:10.1039/c7bm00510e

132. Wang X, Wang Q, Xu C. Nanocellulose-based inks for 3D bioprinting: Key aspects in research development and challenging perspectives in applications-A mini review. *Bioengineering (Basel)* (2020) 7(2):40. doi:10.3390/bioengineering7020040

133. Kim J, Jang J, Cho DW. Controlling cancer cell behavior by improving the stiffness of gastric tissue-decellularized ECM bioink with cellulose nanoparticles. *Front Bioeng Biotechnol* (2021) 9:605819. doi:10.3389/fbioe.2021.605819

134. De Stefano P, Briatico-Vangosa F, Bianchi E, Pellegata AF, Hartung de Hartungen A, Corti P, et al. Bioprinting of matrigel scaffolds for cancer research. *Polymers (Basel)* (2021) 13(12):2026. doi:10.3390/polym13122026

135. Fan R, Piou M, Darling E, Cormier D, Sun J, Wan J. Bio-printing cell-laden Matrigel-agarose constructs. *J Biomater Appl* (2016) 31(5):684–92. doi:10.1177/0885328216669238

136. Snyder JE, Hamid Q, Wang C, Chang R, Emami K, Wu H, et al. Bioprinting cell-laden matrigel for radioprotection study of liver by pro-drug conversion in a dual-tissue microfluidic chip. *Biofabrication* (2011) 3(3):034112. doi:10.1088/1758-5082/3/3/034112

137. Osidak EO, Kozhukhov VI, Osidak MS, Domogatsky SP. Collagen as bioink for bioprinting: A comprehensive review. *Int J Bioprint* (2020) 6(3):270. doi:10.18063/ijb.v6i3.270

138. Marques CF, Diogo GS, Pina S, Oliveira JM, Silva TH, Reis RL. Collagen-based bioinks for hard tissue engineering applications: A comprehensive review. *J Mater Sci Mater Med* (2019) 30(3):32. doi:10.1007/s10856-019-6234-x

139. Duarte Campos DF, Bonnin Marquez A, O'Seanain C, Fischer H, Blaeser A, Vogt M, et al. Exploring cancer cell behavior *in vitro* in three-dimensional multicellular bioprintable collagen-based hydrogels. *Cancers (Basel)* (2019) 11(2):180. doi:10.3390/cancers11020180

140. Noh I, Kim N, Tran HN, Lee J, Lee C. 3D printable hyaluronic acid-based hydrogel for its potential application as a bioink in tissue engineering. *Biomater Res* (2019) 23:3. doi:10.1186/s40824-018-0152-8

141. Petta D, D'Amora U, Ambrosio L, Grijpma DW, Eglin D, D'Este M. Hyaluronic acid as a bioink for extrusion-based 3D printing. *Biofabrication* (2020) 12(3):032001. doi:10.1088/1758-5090/ab8752

142. López-Marcial GR, Zeng AY, Osuna C, Dennis J, García JM, O'Connell GD. Agarose-based hydrogels as suitable bioprinting materials for tissue engineering. *ACS Biomater Sci Eng* (2018) 4(10):3610–6. doi:10.1021/acsbiomaterials.8b00903

143. Abelseth E, Abelseth L, De la Vega L, Beyer ST, Wadsworth SJ, Willerth SM. 3D printing of neural tissues derived from human induced pluripotent stem cells using a fibrin-based bioink. *ACS Biomater Sci Eng* (2019) 5(1):234–43. doi:10.1021/acsbiomaterials.8b01235

144. Sharma R, Smits IPM, De La Vega L, Lee C, Willerth SM. 3D bioprinting pluripotent stem cell derived neural tissues using a novel fibrin bioink containing drug releasing microspheres. *Front Bioeng Biotechnol* (2020) 8:57. doi:10.3389/fbioe.2020.00057

145. Roth AD, Lama P, Dunn S, Hong S, Lee MY. Polymer coating on a micropillar chip for robust attachment of PuraMatrix peptide hydrogel for 3D hepatic cell culture. *Mater Sci Eng C Mater Biol Appl* (2018) 90:634–44. doi:10.1016/j.msec.2018.04.092

146. Yang Z, Xu H, Zhao X. Designer self-assembling peptide hydrogels to engineer 3D cell microenvironments for cell constructs formation and precise oncology remodeling in ovarian cancer. *Adv Sci (Weinh)* (2020) 7(9):1903718. doi:10.1002/advs.201903718

147. Pati F, Jang J, Ha DH, Won Kim S, Rhie JW, Shim JH, et al. Printing three-dimensional tissue analogues with decellularized extracellular matrix bioink. *Nat Commun* (2014) 5:3935. doi:10.1038/ncomms4935

148. Ferreira LP, Gaspar VM, Mano JF. Decellularized extracellular matrix for bioengineering physiomimetic 3D *in vitro* tumor models. *Trends Biotechnol* (2020) 38(12):1397–414. doi:10.1016/j.tibtech.2020.04.006

149. Jang J, Park HJ, Kim SW, Kim H, Park JY, Na SJ, et al. 3D printed complex tissue construct using stem cell-laden decellularized extracellular matrix bioinks for cardiac repair. *Biomaterials* (2017) 112:264–74. doi:10.1016/j.biomaterials.2016.10.026

150. Yue K, Trujillo-de Santiago G, Alvarez MM, Tamayol A, Annabi N, Khademhosseini A. Synthesis, properties, and biomedical applications of gelatin methacryloyl (GelMA) hydrogels. *Biomaterials* (2015) 73:254–71. doi:10.1016/j.biomaterials.2015.08.045

151. Ying G, Jiang N, Yu C, Zhang YS. Three-dimensional bioprinting of gelatin methacryloyl (GelMA). *Bio-Design and Manufacturing* (2018) 1(4):215–24. doi:10.1007/s42242-018-0028-8

152. Rajabi N, Rezaei A, Kharaziha M, Bakhsheshi-Rad HR, Luo H, RamaKrishna S, et al. Recent advances on bioprinted gelatin methacrylate-based hydrogels for tissue repair. *Tissue Eng Part A* (2021) 27(11-12):679–702. doi:10.1089/ten.TEA.2020.0350

153. Yang X, Wang Y, Zhou Y, Chen J, Wan Q. The application of polycaprolactone in three-dimensional printing scaffolds for bone tissue engineering. *Polymers (Basel)* (2021) 13(16):2754. doi:10.3390/polym13162754

154. Gori M, Giannitelli SM, Torre M, Mozetic P, Abbruzzese F, Trombetta M, et al. Biofabrication of hepatic constructs by 3D bioprinting of a cell-laden thermogel: An effective tool to assess drug-induced hepatotoxic response. *Adv Healthc Mater* (2020) 9(21):e2001163. doi:10.1002/adhm.202001163

155. Klak M, Gomółka M, Dobrzański T, Tymicki G, Cywoniuk P, Kowalska P, et al. Irradiation with 365 nm and 405 nm wavelength shows differences in DNA damage of swine pancreatic islets. *PLoS One* (2020) 15(6):e0235052. doi:10.1371/journal.pone.0235052

Pathology & Oncology Research | frontiers

TYPE Original Research
PUBLISHED 16 April 2024
DOI 10.3389/pore.2024.1611586

Check for updates

OPEN ACCESS

EDITED BY
József Tóvári,
National Institute of Oncology (NIO), Hungary

*CORRESPONDENCE
Michael R. King,
mike.king@rice.edu

RECEIVED 11 November 2023
ACCEPTED 03 April 2024
PUBLISHED 16 April 2024

CITATION
Grayson KA, Greenlee JD, Himmel LE, Hapach LA, Reinhart-King CA and King MR (2024), Spatial distribution of tumor-associated macrophages in an orthotopic prostate cancer mouse model.
Pathol. Oncol. Res. 30:1611586.
doi: 10.3389/pore.2024.1611586

COPYRIGHT
© 2024 Grayson, Greenlee, Himmel, Hapach, Reinhart-King and King. This is an open-access article distributed under the terms of the Creative Commons Attribution License (CC BY). The use, distribution or reproduction in other forums is permitted, provided the original author(s) and the copyright owner(s) are credited and that the original publication in this journal is cited, in accordance with accepted academic practice. No use, distribution or reproduction is permitted which does not comply with these terms.

Spatial distribution of tumor-associated macrophages in an orthotopic prostate cancer mouse model

Korie A. Grayson[1,2], Joshua D. Greenlee[1], Lauren E. Himmel[3], Lauren A. Hapach[1,2], Cynthia A. Reinhart-King[1] and Michael R. King[1]*

[1]Department of Biomedical Engineering, Vanderbilt University, Nashville, TN, United States, [2]Meinig School of Biomedical Engineering, Cornell University, Ithaca, NY, United States, [3]Department of Pathology, Microbiology and Immunology, Translational Pathology Shared Resource, Vanderbilt University Medical Center, Nashville, TN, United States

Mounting evidence suggests that the immune landscape within prostate tumors influences progression, metastasis, treatment response, and patient outcomes. In this study, we investigated the spatial density of innate immune cell populations within NOD.SCID orthotopic prostate cancer xenografts following microinjection of human DU145 prostate cancer cells. Our laboratory has previously developed nanoscale liposomes that attach to leukocytes via conjugated E-selectin (ES) and kill cancer cells via TNF-related apoptosis inducing ligand (TRAIL). Immunohistochemistry (IHC) staining was performed on tumor samples to identify and quantify leukocyte infiltration for different periods of tumor growth and E-selectin/TRAIL (EST) liposome treatments. We examined the spatial-temporal dynamics of three different immune cell types infiltrating tumors using QuPath image analysis software. IHC staining revealed that F4/80+ tumor-associated macrophages (TAMs) were the most abundant immune cells in all groups, irrespective of time or treatment. The density of TAMs decreased over the course of tumor growth and decreased in response to EST liposome treatments. Intratumoral versus marginal analysis showed a greater presence of TAMs in the marginal regions at 3 weeks of tumor growth which became more evenly distributed over time and in tumors treated with EST liposomes. TUNEL staining indicated that EST liposomes significantly increased cell apoptosis in treated tumors. Additionally, confocal microscopy identified liposome-coated TAMs in both the core and periphery of tumors, highlighting the ability of liposomes to infiltrate tumors by "piggybacking" on macrophages. The results of this study indicate that TAMs represent the majority of innate immune cells within NOD.SCID orthotopic prostate tumors, and spatial density varies widely as a function of tumor size, duration of tumor growth, and treatment of EST liposomes.

KEYWORDS

tumor-associated macrophages, TRAIL, liposomes, prostate cancer, pathologic analysis

Introduction

Prostate cancer (PCa) is the most common malignancy in men and the second leading cause of cancer-related death in American men [1]. Surgery, radiation, chemotherapy, and androgen-deprivation therapy (ADT) are the standard treatments administered at local or regional stages of disease [2]. Once the cancer has reached an advanced or metastatic stage that no longer responds to ADT, a stage known as castration-resistant prostate cancer (CRPC), treatment options become limited [3]. Due to the lack of curative therapies for advanced and metastatic disease, new anticancer therapeutics are needed to treat life-threatening metastases without the side effects of ADT, chemotherapy, and surgery.

It is widely accepted that inflammation is a hallmark of cancer [4, 5]. There is epidemiological and pathological evidence linking chronic inflammation with the etiology of PCa and the course of tumor progression [6–8]. Studies have demonstrated the importance of immune-tumor interactions along with the role of immune cell infiltration in tumor recurrence and overall survival in patients [9, 10]. Leukocytes are key components of tumorigenesis and are known to infiltrate tumors and drive cancer development via multiple signaling pathways. Many studies have connected prostatitis and PCa due to the frequent observation of inflammatory infiltrates in PCa lesions, although the source of intraprostatic inflammation remains unclear [11, 12]. The most well studied infiltrating immune cells in PCa to date have been T cells ($CD4^+$, $CD8^+$, Th17), B cells, macrophages, mast cells, immunosuppressive cells (Tregs, MDSCs), neutrophils, and natural killer cells [13, 14]. Studies on biopsy tissues from PCa patients across different stages have correlated pro-tumorigenic or anti-tumorigenic inflammatory responses with overall survival. One study showed that very low or very high $CD3^+$ T cell infiltration correlated with PSA recurrence-free survival in prostate cancer patients [15]. In other studies, patients treated with androgen deprivation therapy had higher densities of $CD3^+$ and $CD8^+$ lymphocytes with no correlation to biochemical occurrence [16]. The highlighted role of T lymphocytes associated with PCa and its progression has led to two FDA-approved immunotherapies, Sipuleucel-T and pembrolizumab, along with many others in preclinical studies [17, 18]. Most immunotherapies are T cell focused and do not take advantage of innate immune cells in treating prostate cancer. However, recent preclinical studies and early clinical trials suggest that myeloid cells such as macrophages are an emerging target of novel anticancer therapies [19].

Macrophages are one of the most abundant immune cells in PCa tumors [20, 21]. When infiltrating tumors, macrophages are termed tumor-associating macrophages (TAMs). TAMs are traditionally classified into two types based on different activation pathways: classically activated (M1) and alternatively activated (M2) macrophages which possess anti-tumor or pro-tumor functionality, respectively [22]. Accumulating evidence suggests an oversimplification of binary M1/M2 labeling for macrophages, and that they more accurately exist on a spectrum between pro-inflammatory (M1) and wound healing (M2) [23]. TAM ontology and regional associations within tumors are areas currently being explored to explain their role in tumor immunity and progression. Additionally, the phenotypic heterogeneity of TAMs has spurred research into therapeutic agents to control macrophage polarization for therapeutic benefit [24]. For example, CSF1R blockade via small molecule agonists or monoclonal antibodies have been shown to reprogram TAMs toward an antitumor phenotype in preclinical studies [25, 26].

Tumor necrosis factor-related apoptosis inducing ligand (TRAIL) is a type II transmembrane protein that can be cleaved from the cell surface to produce its soluble form. TRAIL selectively induces apoptosis in cancer cells via binding to transmembrane death receptors (DR4, DR5) [27]. Death receptors cluster and then recruit Fas-associated death domain (FADD), which in turn activates caspase-8. Caspase-8 activates two pathways, one through the mitochondria causing cytosolic release of cytochrome c, and a more direct route which signals directly to the executioner caspase-3 [27]. TRAIL is expressed in a variety of immune cells, such as natural killer cells, and has shown therapeutic utility *in vitro* and *in vivo* [28, 29]. However, TRAIL's clinical implementation has been confounded by a lack of bioavailability, and mechanisms of tumor cell resistance [30, 31].

Our lab has previously designed and tested a liposomal formulation designed to target circulating tumor cells (CTCs) via conjugation of E-selectin, an adhesion molecule expressed by activated endothelium and involved in metastasis and inflammation, and TRAIL [32]. These E-selectin/TRAIL (EST) liposomes have been shown to kill a variety cancer cells in the circulation by functionalizing leukocytes with TRAIL via E-selectin receptor adhesion [32–34]. These EST liposomes have also been tested in orthotopic xenograft tumor models of the prostate and breast [35, 36]. Orthotopic injection of cancer cells into the prostate has become a commonly used method to understand tumor progression and treatment efficacy over the past decade [37, 38]. These models are advantageous as they have been shown to metastasize to clinically relevant foci and better recapitulate the tumor microenvironment compared to subcutaneous tumors [39]. TRAIL-coated leukocytes were found to block widespread metastasis and increase survival in NOD.SCID orthotopic models of prostate and breast cancer [35, 36]. While these studies demonstrated that EST liposomes bind to leukocytes in the circulation, it remains to be determined how these liposomes affect immune cell infiltration into orthotopic tumors.

The aim of the present study was to investigate both the type and distribution of different innate immune cell subsets within NOD.SCID orthotopic PCa tumors in response to EST liposome

treatment. An additional aim was to identify how the spatial distribution of immune cells, specifically macrophages, changes between early and late-stage tumors. Some prior studies have examined the location and distribution of specific leukocytes in human and mouse prostate tumors [40–42]. However, this is the first study to examine the spatial distribution of immune cells within a NOD.SCID orthotopic PCa mouse model and investigate innate immune cell infiltration in response to liposome treatments.

Materials and methods

Transduction of DU145 human prostate cancer cells

DU145 human prostate cancer cells (ATCC #HTB-81) were obtained from American Type Culture Collection (Manassas, VA, United States). The cells were maintained in Eagle's Minimum Essential Medium (EMEM) (Corning, Corning, NY, United States). Media was supplemented with 10% fetal bovine serum and 1% penicillin (Gibco, ThermoFisher, Waltham, MA, United States). DU145 cells were transfected with a pCMV lentivirus containing mCherry and D-luciferase (LP466-025) markers along with a puromycin gene (GeneCopoeia, Rockville, MD, United States). Infected cells were selected with puromycin (P8833, Sigma Aldrich, St. Louis, MO, United States) for puromycin resistance and were cultured according to ATCC guidelines. To confirm the stability of transduction, cells were imaged using an Olympus IX81 epifluorescence microscope to detect mCherry expression/fluorescence. Bioluminescence imaging (BLI) using a Xenogen IVIS 200 Imaging System was used to confirm luciferase expression.

Prostate orthotopic implantation

All experimental procedures were approved by the Vanderbilt University Institutional Animal Care and Use Committee and were conducted in an AAALAC-accredited facility in accordance with the Guide for the Care and Use of Laboratory Animals and the Public Health Service Policy on Humane Care and Use of Laboratory Animals. Male NOD.CB17-Prkdc^{scid}/J mice 6–8 weeks old (#001303, Jackson Laboratory, Bar Harbor, ME, United States) were placed under anesthesia using 5% isoflurane and then reduced to 2% after animals were completely anesthetized. Mice were dehaired using a depilatory cream and a sterile cotton swab. The area was cleaned with 70% ethanol. After removing the hair, the area was cleaned using iodine and 70% ethanol swabs 3 times each. A low midline abdominal incision about 1–3 mm long was made through the skin and muscle layer using a sterile scalpel. The bladder was exteriorized from the body and the ventral lobes of the prostate were located. Using a 30G needle, 1 million D-luciferase:mCherry labeled DU145 cells suspended in 30 μL PBS were injected into the ventral prostate. The muscle layer was closed with 4–0 absorbable sutures. The skin layer was closed with 5–0 non-absorbable sutures. Animals were monitored every 24 h and given analgesic medication for 2 days post-surgery.

Preparation and injection of EST liposomes

Multilamellar liposomes, composed of egg L-α-lysophosphatidylcholine (Egg PC, #840051C), egg sphingomyelin (Egg SM, #86001C), ovine wool cholesterol (Chol, #700000P), and 1,2-dioleoyl-sn-glyc- ero-3- [(N-(5-amino-1-carboxypentyl) iminodiacetic acid) succinyl] (nickel salt) (DOGS NTA-Ni, #790404C) at weight ratios 50%:30%:10%:10% (Egg PC/Egg SM/Chol/DOGS NTA-Ni), were prepared using a thin lipid film method (Avanti Polar Lipids, Alabaster, AL). DOGS-NTA-Ni is a lipid conjugated to nickel-nitrilotriacetic acid (Ni-NTA) that allows for attachment to histidine-tagged proteins. Briefly, stock solutions of all of the lipids were prepared by dissolving powdered lipids in chloroform to produce a final concentration of 5 mg/mL Egg PC, 20 mg/mL Egg SM, 5 mg/mL Chol, and 20 mg/mL DOGS-NTA-Ni in glass containers and stored at −20°C. Appropriate volumes of the lipids were taken from the stock solution to prepare the lipids in a glass tube. TopFluor® Cholesterol was also added to the lipid mix to fluorescently label liposomes. Lipids were gently dried under vacuum for 12 h to remove chloroform. The lipid film was hydrated with a liposome buffer composed of 150 mM NaCl, 10 mM Hepes, and 1 mM $MgCl_2$ dissolved in nuclease-free water to create multilamellar liposomes. The resulting multilamellar liposomes were resized by repeated thawing and freezing, and then subjected to 10 extrusion cycles at 55°C through two different pore size (200 and 100 nm, #WHA800281 and #WHA800309) polycarbonate membranes (Sigma Aldrich, St. Louis, MO, United States) to produce unilamellar nanoscale liposomes. Liposomes were conjugated with E-selectin and TRAIL for 30 min at 37°C and then stored overnight at 4°C. Soluble histidine-tagged TNF-related apoptosis-inducing ligand (TRAIL) (BML-SE721-0100) was purchased from Enzo Life Sciences (Farmingdale, NY, United States). Histidine-tagged recombinant human E-selectin (724-ES) was purchased from R&D Systems (Minneapolis, MN, United States). Mice in the 3 weeks (treated) group received one tail-vein injection of EST liposomes (0.002 mg/kg) occurring at three-weeks post tumor implantation. Mice in the 6 weeks (treated) group received liposome injections once every 3 days in alternating veins occurring at three-weeks post tumor implantation until week 6 (6 doses total). Mice were humanely sacrificed via CO_2 asphyxiation 2 days following the last injection of liposomes.

Bioluminescence imaging

Post tumor implantation, animals were monitored weekly for bioluminescent activity. Luciferin was administered at 150 mg/kg via intraperitoneal injection using a 30G insulin syringe needle. Animals were placed under anesthesia using 2% isoflurane and imaged 5 min post injection for maximum bioluminescence signal. Images were taken at 1 s exposure time using a Xenogen IVIS 200 Imaging System. For the quantitative measurements of average radiance, the area of the orthotopic prostate xenograft BLI signal was constant throughout all time points for each animal.

Histology

Pathology endpoints were carried out in the Vanderbilt Translational Pathology Shared Resource (TPSR). Mice were euthanized by CO_2 asphyxiation, in accordance with AVMA Guidelines for the Euthanasia of Animals. Complete necropsy was performed, and body weights and organ weights were recorded. Prostatic xenograft length and width were measured with calipers, and volume was calculated using the equation $V = (L \times W^2)/2$. Tissues were fixed in 10% neutral buffered formalin for 72 h. Fixed tissues were routinely processed using a standard 8-h processing cycle of graded alcohols, xylenes, and paraffin wax, embedded and sectioned at 4–5 microns, floated on a water bath, and mounted on adhesive glass slides. Hematoxylin and eosin (H&E) staining was performed on a Gemini AS Automated Slide Stainer (ThermoFisher Scientific, Waltham, MA).

Immunohistochemistry

Immunohistochemical (IHC) staining for innate immune cell infiltrates was performed using macrophage (F4/80), monocyte and granulocyte (CD11b), neutrophil and monocyte (MPO), eosinophil (MBP), and neutrophil (Neutro) antibodies on a Leica Bond-Max automated stainer (Leica Biosystems Inc., Buffalo Grove, IL, United States). All five antibodies used for immunophenotyping in this study are validated, on-demand stains maintained in the Translational Pathology Shared Resource (TPSR) by regular quality assurance. All steps besides dehydration, clearing, and cover slipping were performed on the Bond-Max. Immunolabeling was conducted using antibodies listed in Supplementary Table S1. The Bond Polymer Refine Detection system was used for visualization. Where a rat primary antibody was used, a rabbit anti-rat secondary antibody was substituted in the Bond Polymer Refine Detection kit, and the rest was used as specified by the manufacturer. Slides were then dehydrated, cleared, and cover slipped. All histopathologic interpretation was conducted by a board-certified veterinary pathologist under masked conditions. Slide scanning was performed on the Pannoramic 250 Flash III digital scanner (3DHISTECH Ltd., Budapest, Hungary). Quantification of immunolabeled cells in the tumors was performed using manual region of interest (ROI) delineation of the tumor and a single-threshold positive cell detection feature. Orthotopic prostate xenografts were manually outlined and then a margins script was applied to distinguish between ROIs. A smoothing feature was applied to create a heatmap visualization of leukocyte density in terms of these ROIs for each leukocyte marker. The distribution of immune cell infiltrates in the periphery vs. the inner portions of the tumors was assessed. The periphery was defined as the outer ¼ of the radius of a mass; the inner region was denoted as the remaining ¾ of the radius of a mass. Data were collected per tumor section and then group-wide means of percentage of positively stained cells were calculated.

To identify apoptotic cells in tumor sections, terminal deoxynucleotidyl transferase dUTP nick end labeling (TUNEL) staining was performed. Slides were placed on a Leica Bond RX IHC stainer (Leica Biosystems Inc.). All steps besides dehydration, clearing, and cover slipping were performed on the Bond RX. Slides were deparaffinized. Antigen retrieval was performed on the Bond RX using Triton X-100 (Cat#T9284, Sigma-Aldrich, St. Louis, MO) for 5 min. Slides were incubated with Equilibration Buffer (#G7130, Promega, Madison, WI, United States) for 5 min, followed with the TdT reaction mix (#G7130, Promega) for 10 min and SSC-x20 (#G7130, Promega) for 10 min. The slides were incubated with streptavidin-HRP (#RE7104, Novocastra, Newcastle Upon Tyne, United Kingdom) for 5 min, and the Bond polymer refine detection system (#DS9800, Leica Biosystems Inc.) was used for visualization. Slides were then dehydrated, cleared, and cover slipped. Slide scanning was performed on a Pannoramic 250 Flash III digital scanner. Quantification of immunolabeled cells in the tumors was performed by a board-certified veterinary anatomic pathologist in QuPath (Supplementary Figures S5, S6), an open source software for digital pathology image analysis, using a script for manual region of interest delineation of the tumor and a single-threshold positive cell detection feature [43, 44]. Data were collected per tumor section and then group-wide means of the percentage of TUNEL-positive cells were calculated.

Confocal microscopy

For liposome and leukocyte infiltration imaging, orthotopic prostate xenografts were removed from all animals after sacrifice. Xenografts were embedded in OCT compound on dry ice and sectioned at 4–5 microns, and then mounted on adhesive glass slides. Samples were fixed with 4% paraformaldehyde (PFA) in PBS for 10 min at room temperature (RT). Slides were subsequently washed with wash buffer (PBS + 0.02% Tween 20) three times for 5 min each at RT. Samples were then permeabilized using PBS + 1% Triton for 5 min at RT. Slides

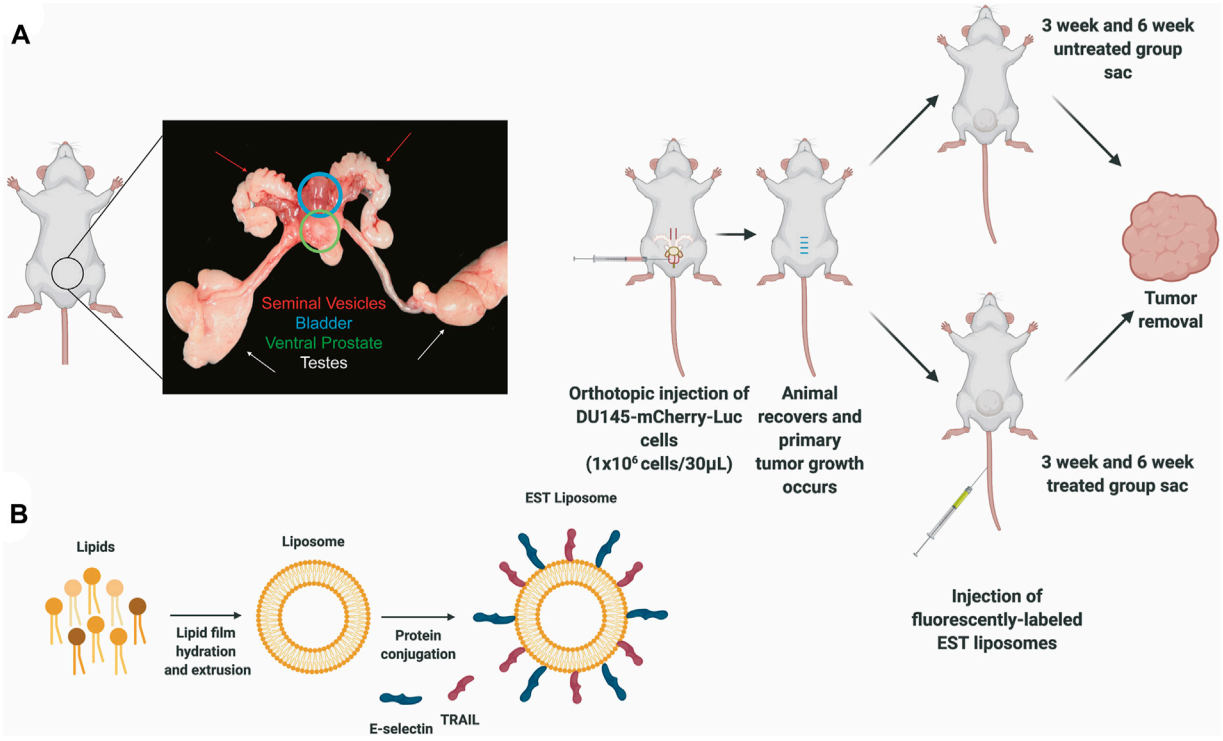

FIGURE 1
Protocols for inoculating orthotopic prostate xenografts and preparing E-selectin/TRAIL (EST) liposomes. **(A)** Schematic of orthotopic xenograft model for whole tumor analysis depicting an anatomical picture of the male mouse reproductive system to denote location of ventral prostate with tumor. **(B)** Preparation of E-selectin/TRAIL liposomes.

were washed 3X. Slides were blocked with blocking buffer (PBS + 10% FBS + 5% donkey serum 5% goat serum) for 2 h at RT. Rat mAb F4/80 primary antibody (#NB600-404, Novus Biologicals, Littleton, CO, United States) was diluted 1:500 into blocking solution. Slides were incubated with primary antibody solution overnight at 4°C in a humidified chamber. After primary antibody staining, samples were washed 3X on the following day. Anti-rat Alexa Fluor® 647 Conjugate secondary antibody (#4418S, Cell Signaling Technology, Danvers, MA, United States) was diluted 1:500 into blocking solution and all samples were stained with secondary antibody for 2 h at RT in the dark. Slides were washed 3X. Samples were then stained with DAPI for 30 min followed by washing 3X at RT in the absence of light. Mounting medium (#H-1000, Vector Labs, Burlingame, CA, United States) was added followed by a coverslip, then the edges were sealed with nail polish. Confocal z-stacks of immunofluorescence-stained histology samples were obtained using a Zeiss LSM 800 inverted confocal microscope equipped with a 40X/1.1 N.A. long working distance water-immersion objective and a 100X/1.46 N.A oil immersion objective using 405, 488, 561, and 640 laser lines and operated by Zen 2.3 software. Maximum z-projections were used to assess liposome tumor infiltration and macrophage localization. Photomicrographs were processed in ImageJ.

Statistical analysis

GraphPad Prism 8 software (San Diego, CA, United States) was used to plot and analyze data sets. Two-tailed unpaired *t*-test was used for comparisons between two groups, with $p < 0.05$ considered significant. ANOVA with Tukey post-test was used for comparing multiple groups with $p < 0.05$ considered significant. Shapiro-Wilk test was used to test normality. Data are presented as mean ± SD with at least three independent replicates used for each experiment. A minimum sample size of n = 3 mice per group was calculated using mean and standard deviation data from our previous TRAIL liposome treatment study, assuming $\alpha = 0.05$ and power = 80% [35].

Results

Total leukocytes in prostate tumors decrease over time and in response to TRAIL liposomes

To identify and quantify the types of mouse leukocytes that infiltrate orthotopic prostate xenografts, dual labeled DU145-mCherry-Luc human prostate cells were orthotopically injected

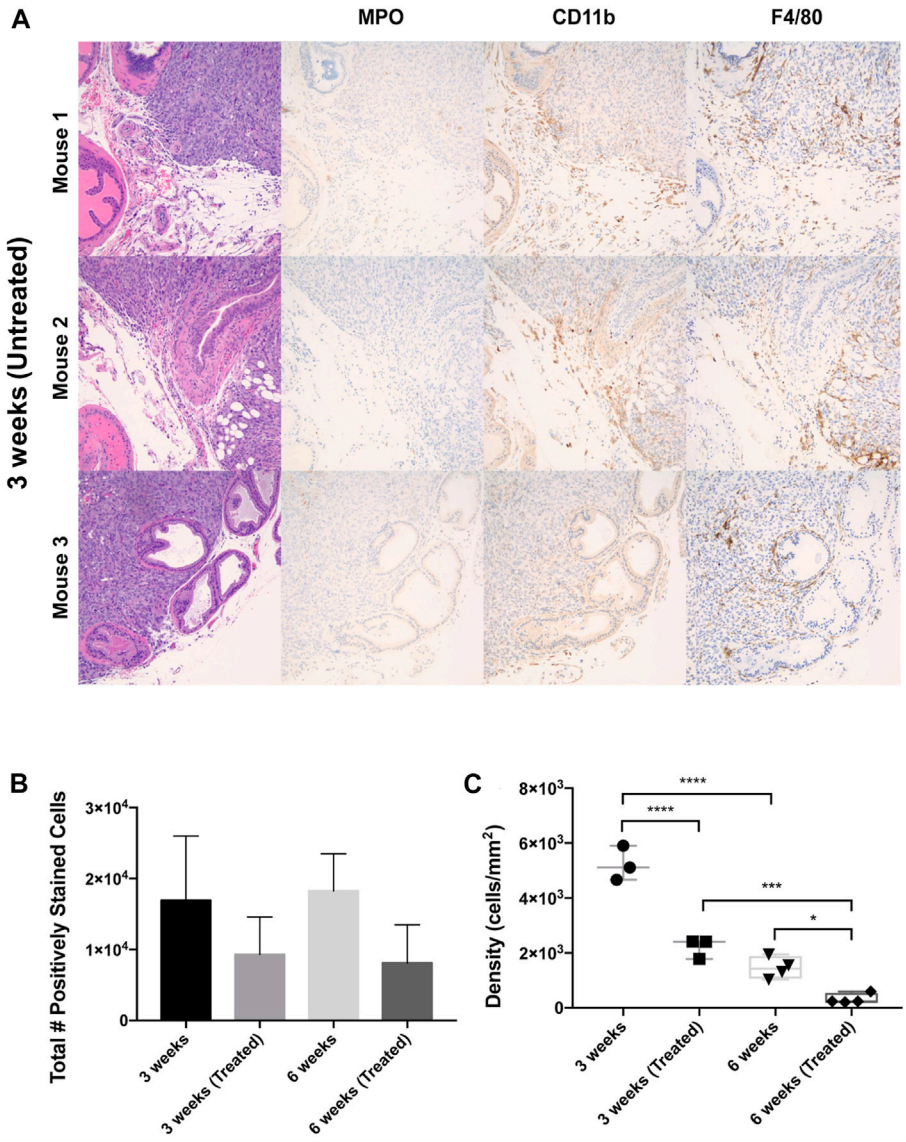

FIGURE 2
Leukocyte populations within orthotopic prostate tumors across liposome treatments and endpoints. **(A)** IHC staining of mouse ventral prostate tissue subjected to orthotopic tumor engraftment. MPO = myeloperoxidase/neutrophil granulocyte marker, CD11b = myeloid marker, F4/80 = macrophage marker. Images show the interface of the ventral prostatic xenograft with adjacent normal prostate and adipose tissue in three mice from the 3 weeks untreated group. All photomicrographs taken at ×200 magnification. **(B)** Total number of F4/80+, CD11b+, MPO + cells in whole tumor section for each treatment cohort. **(C)** Overall leukocyte density across treatment groups. The values represent the mean ± SD (n = 3 or 4). *$p < 0.05$, ***$p < 0.001$, ****$p \leq 0.0001$.

into the ventral prostate of NOD.SCID mice (Figure 1A). Mice were sorted by primary tumor size, as measured by BLI, at week two and size-matched into four groups: 3 weeks (Untreated) (n = 4), 3 weeks (Treated) (n = 3, 1 injection of EST liposomes), 6 weeks (Untreated) (n = 4), and 6 weeks (Treated) (n = 4, 6 injections of EST liposomes) (Figures 1A, B). Interestingly, EST liposome treatments had no significant effect on terminal tumor volume or tumor burden measured through bioluminescence imaging (Supplementary Figure S1). Terminal body weight, and relative organ weights of the liver, heart, spleen, and kidneys showed no significant difference among cohorts (Supplementary Figure S2). Metastasis was not observed in any group, and all subsequent analysis was completed using orthotopic xenograft tumors of the prostate.

Immunophenotyping of tumoral leukocytes was accomplished via immunohistochemical staining with F4/80, CD11b, and MPO markers (Figure 2A). F4/80 is a well-characterized and highly cited mouse macrophage marker

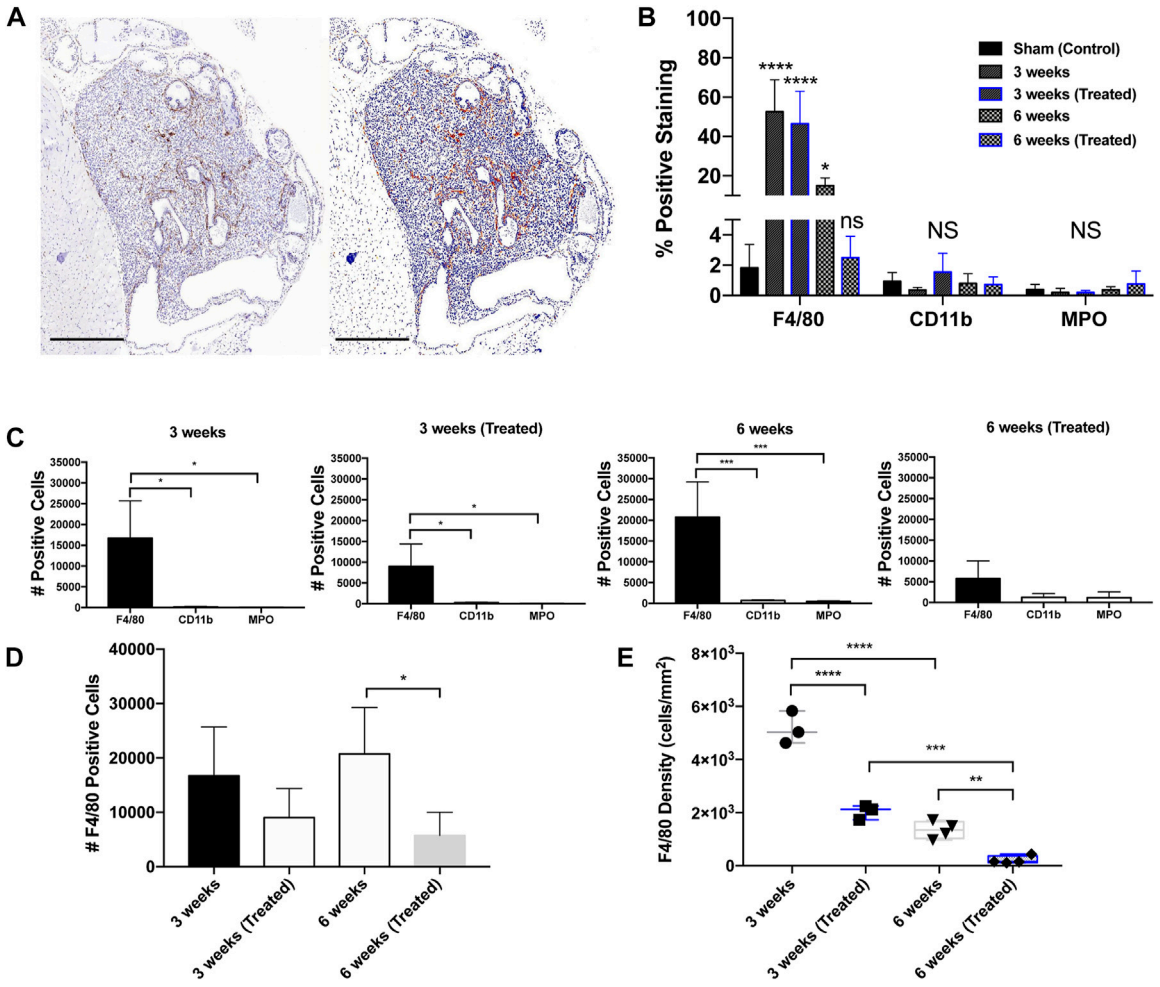

FIGURE 3
Immunohistochemical staining in orthotopic mouse prostate tumors. **(A)** Prostatic xenograft tumor from a 3-week untreated mouse (40X). The left panel shows a digital photomicrograph of F4/80 IHC. The right panel demonstrates a positive pixel count image analysis mock-up that enables quantitative analysis of DAB immunohistochemical staining. Scale bar = 500 μm. **(B)** Positive staining expression in all groups including control (n = 3). **(C)** Positive staining for leukocyte markers in different treatment groups: 3 weeks untreated (n = 3), 3 weeks treated (n = 3), 6 weeks untreated (n = 4), and 6 weeks treated (n = 4). **(D)** F4/80+ TAM positive cell counts across groups. **(E)** F4/80+ TAM density across groups. The values represent the mean ± SD (n = 3 or 4). *$p < 0.05$, **$p < 0.01$, ***$p < 0.001$, ****$p \leq 0.0001$.

expressed at high levels in various tissues [45]. CD11b is a common myeloid marker for monocytes and granulocytes [46], and myeloperoxidase (MPO) is a marker for neutrophil granulocytes [47]. Tumors were also stained for eosinophils (MBP) and an additional marker for neutrophils (Neutro) but only exhibited < 1% positively stained cells, so these markers were not studied further. To establish a baseline of leukocyte infiltration caused by surgery alone, a control group of mice was subjected to sham surgery involving an injection of PBS administered to the ventral prostate. These non-tumor bearing mice displayed infrequent prostatic inflammatory infiltrates with F4/80, CD11b, and MPO positive staining of less than 2% each (Supplementary Figure S3). Interestingly, the total number of leukocytes (total F4/80, CD11b, and MPO cells combined) detected in orthotopic prostate xenografts decreased in EST liposome-treated animals by 46% at the 3-week timepoint and by 55% at 6 weeks (Figure 2B). This observation suggests that EST liposomes have a measurable effect on the degree of leukocyte infiltration within these orthotopic prostate tumors. Additionally, total leukocyte density in xenografts showed not only a decrease in EST liposome-treated animals, but also decreased over time from 3-week to 6-week tumors (Figure 2C). In untreated tumors, leukocyte density decreased significantly from ~5200 cells per mm^2 at 3 weeks to ~1,400 cells per mm^2 after 6 weeks. A significant decrease in leukocyte density was also observed in EST liposome-treated tumors between 3-week and 6-week timepoints. Similar to treatment trends observed from total leukocyte counts, leukocyte density

significantly decreased in response to liposome treatments. The discrepancies between total positive staining and density can be attributed to the difference in tumor sizes seen in each group (Supplementary Figure S1).

Macrophages are the most abundant infiltrating immune cell type within orthotopic PCa tumors

IHC analysis on whole tumor sections revealed that macrophages were the most abundant infiltrating immune cell type in all groups. The predominant immune infiltrates were mature macrophages, indicated by significant F4/80-positive staining (Figures 3A, B). When compared to the sham control (1.8%), tumors showed a significant increase in F4/80+ cells in the 3 weeks (Untreated) (52.6%), 3 weeks (Treated) (46.5%), and 6 weeks (Untreated) (15.0%) groups. Infiltration of CD11b+ and MPO+ cells was negligible in all treatment groups compared to the tumor-free control prostate tissue (Figures 3B, C). Based on these findings, all subsequent analysis was done solely for F4/80+ staining to measure differences across timepoints and EST liposome treatments. F4/80+ cell counts and density measurements followed similar trends to total leukocytes since macrophages were found to make up the majority of tumor immune cells. The number of F4/80+ cells decreased in EST liposome-treated animals by 46% at 3 weeks and 72% at 6 weeks (Figure 3D). Macrophage density decreased significantly with time and in tumors from animals administered EST liposomes: 3 weeks (~5100 cells/mm^2), 3 weeks (Treated) (~2000 cells/mm^2), 6 weeks (~1,300 cells/mm^2), 6 weeks (Treated) (~210 cells/mm^2) (Figure 3E). There was a significant decrease in the abundance of macrophages in the 6 weeks (Treated) group (receiving 6 liposome injections) compared to the 3 weeks (Treated) group (only one liposome injection), suggesting that sustained EST liposome injections decrease the number of TAMs within these prostate tumors.

Spatial distribution of TAMs changes according to tumor progression and EST liposome treatments

To interrogate the spatial distribution of TAMs in orthotopic prostate xenografts, two regions of interest (ROIs) were annotated to denote the marginal and intratumoral regions. F4/80 detection in each group displayed greater density compared to CD11b and MPO, which were both primarily located at the tumor margin (Figure 4A). In all four groups, macrophages were widely distributed throughout both tumor ROIs but were more densely concentrated near the tumor margin than intratumorally at 3 weeks of tumor growth (Figure 4B). After 6 weeks, there was a significant decrease in the number of marginal macrophages, but interestingly this did not coincide with an increase in intratumoral macrophages. When comparing the effects of treatment at the 3-week timepoint, the number of marginal macrophages decreased but intratumoral macrophages increased (Figure 4C).

The marginal and intratumoral spatial densities of macrophages in each treatment group were also explored. In early untreated tumors, TAM density was most concentrated at the tumor margins (Figure 4D). However, the ratio of marginal-to-intratumoral macrophages decreased in response to liposome treatment and time. TAM densities also differed in the untreated and treated groups at 3 and 6 weeks, demonstrating a significant decrease in macrophage quantity over time of tumor growth. These findings suggest that the spatial infiltration of macrophages is dependent on time, tumor growth, and EST liposome treatments. This is supported by macrophage density measurements in the 6 weeks treatment group, which showed the lowest density in both ROIs and compared to all other groups.

EST liposomes functionalized to TAMs induce apoptosis in orthotopic PCa tumors

To determine whether this liposomal delivery method of TRAIL was inducing cellular apoptosis in orthotopic prostate xenografts, TUNEL staining was performed on tumor sections from each treatment group (Figure 5A). This assay detects DNA fragmentation that occurs in late-stage apoptosis. Mice treated with EST liposomes saw a significant increase in apoptotic cells compared to untreated mice (Figure 5B). Notably, just one injection of liposomes at 3 weeks increased apoptotic cells by over two-fold. Mice treated with six injections in the 6 weeks treated group saw an even greater effect with an over four-fold increase in apoptotic cells compared to untreated tumors.

To evaluate whether EST liposomes adhere to TAM populations in solid tumors, we used confocal microscopy to examine TRAIL-coated TAM presence in xenografts. The periphery and center of 3 weeks treated tumors were imaged to visualize EST liposome and F4/80+ cell interactions (Figure 5C). Tumors from the 6-week timepoint were too large to conduct whole tumor fluorescence confocal microscopy in this manner. Negative control confocal micrographs for 3 weeks untreated tumors with F4/80+ TAMs were also taken to confirm positive identification of liposomes (Supplementary Figure S4). In treated tumors, the majority of TAMs were located at the tumor margins, and EST liposomes were positively identified on the surface of these macrophages (Figure 5D). Intratumorally, fewer F4/80+ cells were present, however liposome-coated TAMs and free EST liposomes were also identified within the core of the tumor (Figure 5D). Collectively, these findings demonstrate that EST liposomes are capable of attaching to TAMs, infiltrating orthotopic prostate tumors, and increasing apoptosis of tumor cells.

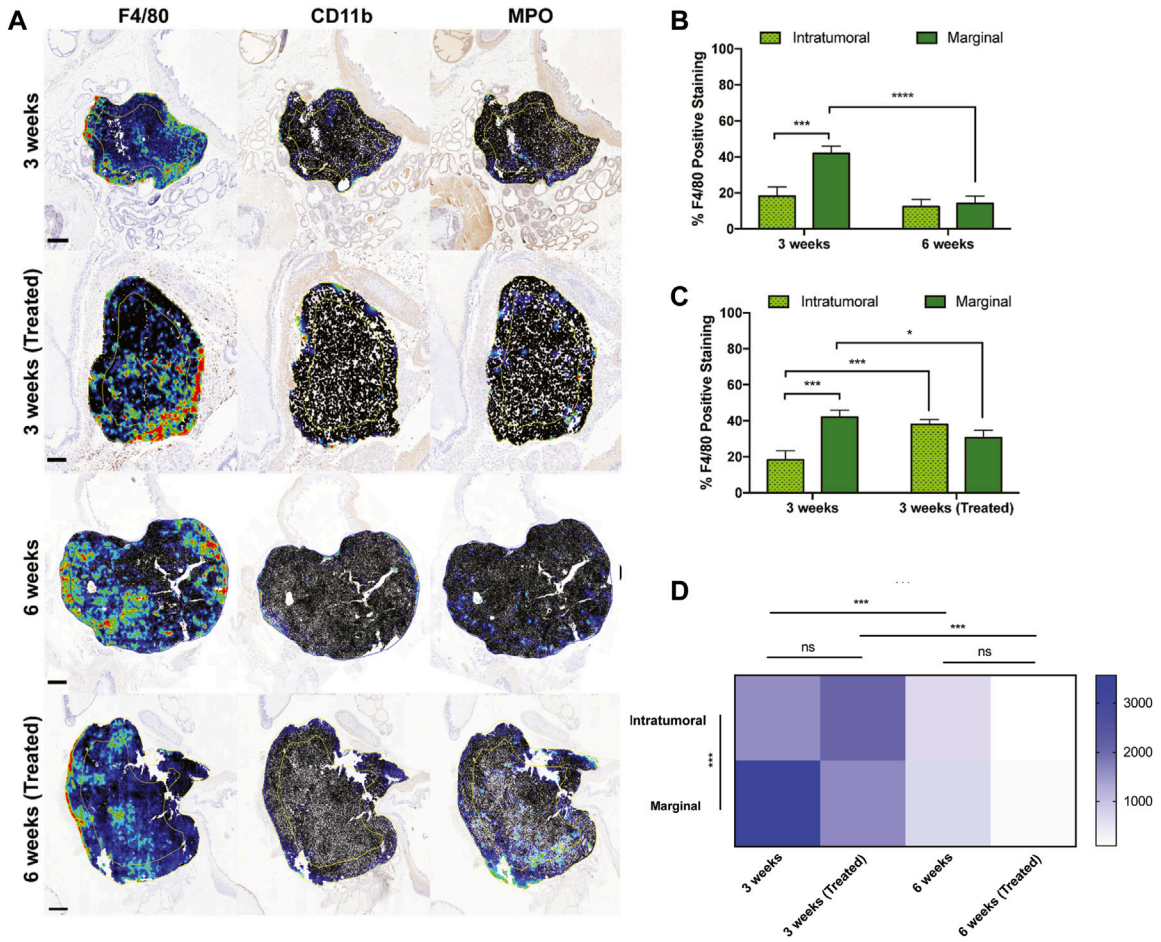

FIGURE 4
Intratumoral versus marginal distribution of F4/80+ cells in each treatment group. **(A)** Digital micrographs of F4/80, CD11b, and MPO IHC stain depicting two regions of interest to define the "intratumoral" versus "marginal" tumor microenvironments. Heatmaps were generated from positive cell detection image analysis of IHC stains for immune cell markers. Yellow/blue lines within each tumor recapitulate the perimetric shape and demarcates the "margin" area from the "center." Scale bars = 500 μm, 1 mm, 2 mm, respectively. **(B,C)** Percent positively stained F4/80+ cells represented intratumorally and marginally at different time points and treatments. **(D)** TAM density among ROIs and treatment cohorts. *Y*-axis is cells/mm^2. The values represent the mean ± SD (n = 3 or 4). NS = non-significant difference, *$p < 0.05$, ***$p < 0.001$, ****$p \leq 0.0001$.

Discussion

Here, we report the distribution of infiltrating leukocytes in an orthotopic prostate cancer model while demonstrating a nanoscale immunotherapy approach to create TRAIL-coated leukocytes that can induce apoptosis in solid tumors. Similar to our 2016 study, we used an orthotopic prostate cancer model to study how immune cells infiltrate orthotopic prostate xenografts with EST liposomes as surface-tethered cargo [35]. We have previously demonstrated that E-selectin/TRAIL conjugated liposomes bind to leukocytes in the blood circulation and bombard circulating tumor cells (CTCs) to induce programmed cell death [32–34]. We hypothesized that these same TRAIL-coated leukocytes not only kill CTCs in the circulation, but can also hitchhike on the surface of immune cells to increase apoptosis in solid tumors. Encouragingly, we have demonstrated that this approach is effective in a variety of animal models with no off target toxicity to the liver or other organs [32, 35, 36, 48].

We first identified different populations of immune cells within orthotopic xenografts in an immunodeficient mouse model. Because NOD.SCID mice lack functional T cells, B cells, and natural killer cells, we focused on leukocytes in the innate immune arm, of which macrophages were found to be the most prevalent. Neutrophils were found in very low quantities within tumors despite accounting for approximately 50% of the white blood cell count in NOD.SCID mice [49]. However, neutrophils have the shortest half-life of all immune

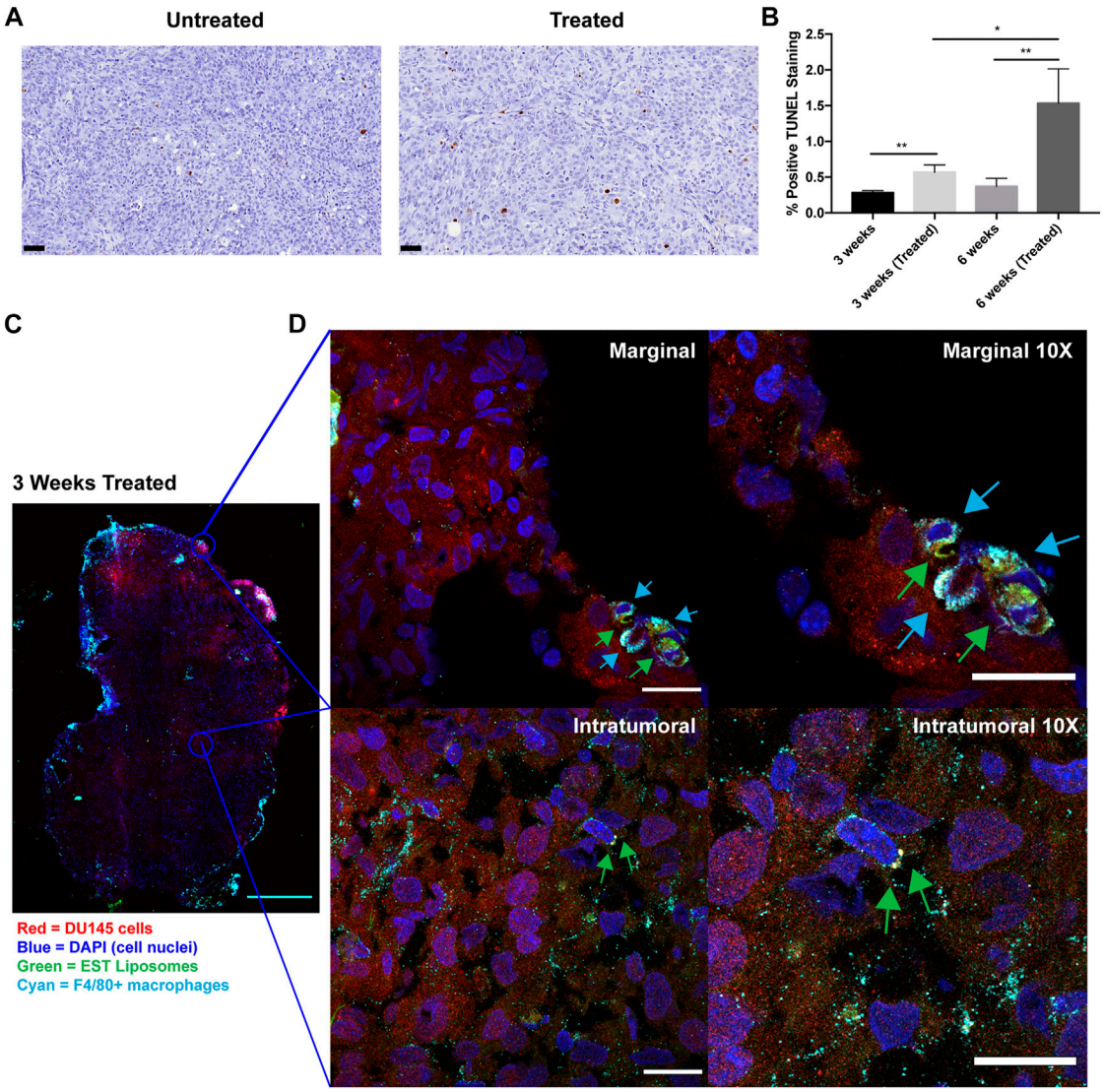

FIGURE 5
TRAIL-coated leukocytes bind to macrophages and increase apoptosis in treated tumors. **(A)** Representative annotated prostatic xenografts from 3 weeks (Untreated) and 3 weeks (Treated) animals with TUNEL IHC stain. Scale bar = 50 μm. **(B)** Percent positive TUNEL cells in each treatment group. **(C)** Confocal immunofluorescence analysis of intratumoral and marginal TRAIL-coated TAMs in the 3 weeks treated group. Cancer cells were labeled with mCherry (red), macrophages were labeled with F4/80 Alexa Fluor® 647 Conjugate (cyan), cell nuclei were labeled with DAPI (blue), EST liposomes were labeled with TopFluor (green). Scale bar = 2 mm. **(D)** Representative images of TRAIL-coated TAMs (×1 and ×10 magnification) at the periphery and center of an orthotopic prostate xenograft. Blue arrows represent F4/80+ macrophages and green arrows represent EST liposomes. Scale bars = 200 μm and 20 μm, respectively. The values represent the mean ± SD (n = 3 or 4). *$p < 0.05$, **$p < 0.005$.

cells, 6–11 h, which may account for why their presence is minimal within these tumors [50–52]. Macrophages are a diverse population of cells, making characterization difficult using one broad marker. Macrophages can either be derived from monocytes originating from hematopoietic stem cells, or can be embryonic, characteristic of quiescent tissue-resident macrophages. Some studies have shown that F4/80^{high} macrophages are derived from the yolk sac, while F4/80^{low} macrophages derive from hematopoietic stem cells [53]. We used the F4/80 marker because it is a widely accepted mature macrophage marker; however, future studies should include a multiplicity of markers using flow cytometry and/or immunofluorescence to denote ontogeny of macrophage populations, as well as M1/M2-like characteristics across tumor microenvironments and treatments. In this study, it is possible that pro-tumor polarization of macrophages towards an

M2 phenotype is occurring. An indicator could be the large increase in tumor volume from 3 weeks to 6 weeks. We also demonstrate throughout this study that macrophage infiltration decreases with time and increasing tumor size, which supports previous work that demonstrated the extent to which infiltration of TAMs was inversely associated with clinical stage [54]. Future studies should further investigate M1/M2 polarization within early and late-stage tumors to identify mechanisms that drive hot versus cold prostate tumors.

Tumors treated with E-selectin/TRAIL liposomes consistently saw decreased macrophage counts compared to untreated tumors. Treated tumors also demonstrated increased apoptosis as verified by TUNEL staining. This indicates that EST liposomes may be inducing TRAIL-mediated apoptosis in TAMs in addition to tumor cells. There is increasing evidence that macrophages, similar to tumor cells, express functional death receptors and are sensitive to TRAIL-induced apoptosis [55, 56]. Macrophages display particularly high death receptor expression and TRAIL sensitivity compared to other immune cells such as lymphocytes and neutrophils. The increase in TUNEL staining in treated mice may be explained by apoptotic macrophages present in these xenografts. This also correlates with the decrease in macrophage numbers seen in treated groups. Additionally, macrophage infiltration density decreased as a response to tumor progression and liposome treatment which might also be explained by TAMs displaying some sensitivity to TRAIL liposomes. Future studies should investigate mechanisms of TRAIL-mediated apoptosis in tumor-associated macrophages, especially between M1 and M2 phenotypes.

In contrast to our 2016 orthotopic prostate tumor study, TRAIL liposomes were unable to reduce primary tumor volume [35]. Recent data suggests DU145 cells are TRAIL resistant and show very minimal apoptosis in 2D and 3D cultures when treated with TRAIL alone [57, 58]. Tumor cells can also develop mechanisms to avoid TRAIL cytotoxicity [55]. Additionally, we hypothesize that minimal treatment effects were observed due to subtherapeutic liposome dosing as a consequence of changing TRAIL manufacturers over the years. In future studies, we anticipate a higher dosage of TRAIL with minimal injections will yield more significant results, as evidenced by our 2019 study using TRAIL-resistant mouse breast cancer cells (2.5 mg/kg TRAIL per injection) [36]. Future studies should investigate dosing with different concentrations of TRAIL liposomes to establish a dose response and maximum tolerated dose in mice. If necessary, EST liposomes can be combined with known TRAIL sensitizers such as taxanes [57, 58] curcumin [59], piperlongamine [60], or Yoda1 [61, 62].

Although NOD.SCID mouse models are acceptable for representing prostate cancer progression, the lack of a fully functioning immune system minimizes important cross-talk between innate and adaptive immune cells. Additionally, macrophages in this model may also be hypofunctional and other antigen presenting cells not fully mature or differentiated which may have affected their localization of the chosen markers. Future studies should explore leukocyte infiltration using a syngeneic prostate cancer mouse model, such as engrafting B6CaP cells in C57BL/6 mice [63]. Alternatively, and perhaps most translationally relevant, these human prostate tumors can be inoculated in mice with humanized immune systems [64]. While our study provides new understanding of the spatial distribution of the predominant innate inflammatory cell types in these types of xenografts, inclusion of adaptive immune cells will allow for a greater understanding of T cell, B cell, and NK cell infiltration and treatment interactions within these cell types.

Conclusion

Prostate tumors contain multiple infiltrating leukocytes that subdue or aid tumor progression in response to local inflammation. There have been extensive studies examining the immune profile of prostatic tumors. However, no study has investigated immune cell spatial organization with nanoscale cargo in a NOD.SCID orthotopic prostate cancer model. For the first time, we demonstrated here that tumor-associated macrophages are the most abundant immune cell group in orthotopic prostate xenografts with a spatial distribution that evolves according to tumor growth time, size, and EST liposome treatment. We were able to identify TAMs coated with EST liposomes in solid orthotopic prostate xenografts, demonstrating that these liposomes are capable of infiltrating and inducing apoptosis within the tumor microenvironment. This work provides an important proof-of-concept for harnessing innate immune cells for the liposomal delivery of TRAIL to prostate tumors. Furthermore, macrophage infiltration seen in these orthotopic prostate xenografts provides a groundwork for understanding immune landscapes within this NOD.SCID model and beyond.

Data availability statement

The raw data supporting the conclusion of this article will be made available by the authors, without undue reservation.

Ethics statement

Ethical approval was not required for the studies on humans in accordance with the local legislation and institutional requirements because only commercially available established cell lines were used. The animal study was approved by the Vanderbilt University Institutional Animal Care and Use

Committee. The study was conducted in accordance with the local legislation and institutional requirements.

Author contributions

KG: investigation, writing, conceived of study. JG: writing, data analysis. LEH: methods, data analysis. LAH: methods. CR-K: methods. MK: editing, supervision, conceived of study. All authors contributed to the article and approved the submitted version.

Funding

The author(s) declare(s) financial support was received for the research, authorship, and/or publication of this article. The Translational Pathology Shared Resource is supported by NCI/NIH Cancer Center Support Grant 5P30 CA68485-19 and the Vanderbilt Mouse Metabolic Phenotyping Center Grant 2 U24 DK059637-16. This work was funded by NIH Grant No. R01CA203991 to MK, NSF GRFP Grant Numbers 1650441 to KG and 1445197 to JG, and Alfred P. Sloan Fellowship to KG.

Conflict of interest

The authors declare that the research was conducted in the absence of any commercial or financial relationships that could be construed as a potential conflict of interest.

Acknowledgments

We thank the staff at the Vanderbilt Translational Pathology Shared Resource (TPSR) for processing samples.

Supplementary material

The Supplementary Material for this article can be found online at: https://www.por-journal.com/articles/10.3389/pore.2024.1611586/full#supplementary-material

References

1. Siegel RL, Miller KD, Jemal A. Cancer statistics, 2020. *CA A Cancer J Clin* (2020) 70:7–30. doi:10.3322/caac.21590

2. Denmeade SR, Isaacs JT. A history of prostate cancer treatment. *Nat Rev Cancer* (2002) 2:389–96. doi:10.1038/nrc801

3. Nuhn P, De Bono JS, Fizazi K, Freedland SJ, Grilli M, Kantoff PW, et al. Update on systemic prostate cancer therapies: management of metastatic castration-resistant prostate cancer in the era of precision Oncology. *Eur Urol* (2019) 75:88–99. doi:10.1016/j.eururo.2018.03.028

4. Mantovani A, Allavena P, Sica A, Balkwill F. Cancer-related inflammation. *Nature* (2008) 454:436–44. doi:10.1038/nature07205

5. Balkwill F, Mantovani A. Inflammation and cancer: back to Virchow? *The Lancet* (2001) 357:539–45. doi:10.1016/S0140-6736(00)04046-0

6. Jiang J, Li J, Zhang Y, Zhu H, Liu J, Pumill C. The role of prostatitis in prostate cancer: meta-analysis. *PLoS One* (2013) 8:e85179. doi:10.1371/journal.pone.0085179

7. Nakai Y, Nonomura N. Inflammation and prostate carcinogenesis. *Int J Urol* (2013) 20:150–60. doi:10.1111/j.1442-2042.2012.03101.x

8. Bardan R, Dumache R, Dema A, Cumpanas A, Bucuras V. The role of prostatic inflammation biomarkers in the diagnosis of prostate diseases. *Clin Biochem* (2014) 47:909–15. doi:10.1016/j.clinbiochem.2014.02.008

9. Lança T, Silva-Santos B. The split nature of tumor-infiltrating leukocytes: implications for cancer surveillance and immunotherapy. *OncoImmunology* (2012) 1:717–25. doi:10.4161/onci.20068

10. Gajewski TF, Schreiber H, Fu Y-X. Innate and adaptive immune cells in the tumor microenvironment. *Nat Immunol* (2013) 14:1014–22. doi:10.1038/ni.2703

11. Sutcliffe S, Platz EA. Inflammation in the etiology of prostate cancer: an epidemiologic perspective. *Urol Oncol Semin Original Invest* (2007) 25:242–9. doi:10.1016/j.urolonc.2006.09.014

12. Dennis LK, Lynch CF, Torner JC. Epidemiologic association between prostatitis and prostate cancer. *Urology* (2002) 60:78–83. doi:10.1016/s0090-4295(02)01637-0

13. Solinas C, Chanzá NM, Awada A, Scartozzi M. The immune infiltrate in prostate, bladder and testicular tumors: an old friend for new challenges. *Cancer Treat Rev* (2017) 53:138–45. doi:10.1016/j.ctrv.2016.12.004

14. Strasner A, Karin M. Immune infiltration and prostate cancer. *Front Oncol* (2015) 5:128. doi:10.3389/fonc.2015.00128

15. Flammiger A, Bayer F, Cirugeda-Kühnert A, Huland H, Tennstedt P, Simon R, et al. Intratumoral T but not B lymphocytes are related to clinical outcome in prostate cancer. *APMIS* (2012) 120:901–8. doi:10.1111/j.1600-0463.2012.02924.x

16. Gannon PO, Poisson AO, Delvoye N, Lapointe R, Mes-Masson A-M, Saad F. Characterization of the intra-prostatic immune cell infiltration in androgen-deprived prostate cancer patients. *J Immunological Methods* (2009) 348:9–17. doi:10.1016/j.jim.2009.06.004

17. Antonarakis ES, Piulats JM, Gross-Goupil M, Goh J, Ojamaa K, Hoimes CJ, et al. Pembrolizumab for treatment-refractory metastatic castration-resistant prostate cancer: multicohort, open-label phase II KEYNOTE-199 study. *J Clin Oncol* (2020) 38:395–405. doi:10.1200/JCO.19.01638

18. Kantoff PW, Higano CS, Shore ND, Berger ER, Small EJ, Penson DF, et al. Sipuleucel-T immunotherapy for castration-resistant prostate cancer. *New Engl J Med* (2010) 363:411–22. doi:10.1056/NEJMoa1001294

19. Mantovani A, Allavena P, Marchesi F, Garlanda C. Macrophages as tools and targets in cancer therapy. *Nat Rev Drug Discov* (2022) 21:799–820. doi:10.1038/s41573-022-00520-5

20. Lo CH, Lynch CC. Multifaceted roles for macrophages in prostate cancer skeletal metastasis. *Front Endocrinol (Lausanne)* (2018) 9:247. doi:10.3389/fendo.2018.00247

21. Pollard JW. Tumour-educated macrophages promote tumour progression and metastasis. *Nat Rev Cancer* (2004) 4:71–8. doi:10.1038/nrc1256

22. Lanciotti M, Masieri L, Raspollini MR, Minervini A, Mari A, Comito G, et al. The role of M1 and M2 macrophages in prostate cancer in relation to extracapsular tumor extension and biochemical recurrence after radical prostatectomy. *Biomed Res Int* (2014) 2014:e486798. doi:10.1155/2014/486798

23. Laviron M, Boissonnas A. Ontogeny of tumor-associated macrophages. *Front Immunol* (2019) 10:1799. doi:10.3389/fimmu.2019.01799

24. Duan Z, Luo Y. Targeting macrophages in cancer immunotherapy. *Sig Transduct Target Ther* (2021) 6:127–1. doi:10.1038/s41392-021-00506-6

25. Pyonteck SM, Akkari L, Schuhmacher AJ, Bowman RL, Sevenich L, Quail DF, et al. CSF-1R inhibition alters macrophage polarization and blocks glioma progression. *Nat Med* (2013) 19:1264–72. doi:10.1038/nm.3337

26. Pfirschke C, Zilionis R, Engblom C, Messemaker M, Zou AE, Rickelt S, et al. Macrophage-targeted therapy unlocks antitumoral cross-talk between ifnγ-secreting lymphocytes and IL12-producing dendritic cells. *Cancer Immunol Res* (2022) 10:40–55. doi:10.1158/2326-6066.CIR-21-0326

27. Wang S, El-Deiry WS. TRAIL and apoptosis induction by TNF-family death receptors. *Oncogene* (2003) 22:8628–33. doi:10.1038/sj.onc.1207232

28. Ashkenazi A, Pai RC, Fong S, Leung S, Lawrence DA, Marsters SA, et al. Safety and antitumor activity of recombinant soluble Apo2 ligand. *J Clin Invest* (1999) 104: 155–62. doi:10.1172/JCI6926

29. von Karstedt S, Montinaro A, Walczak H. Exploring the TRAILs less travelled: TRAIL in cancer biology and therapy. *Nat Rev Cancer* (2017) 17:352–66. doi:10.1038/nrc.2017.28

30. Snajdauf M, Havlova K, Vachtenheim J, Ozaniak A, Lischke R, Bartunkova J, et al. The TRAIL in the treatment of human cancer: an update on clinical trials. *Front Mol Biosciences* (2021) 8:628332. doi:10.3389/fmolb.2021.628332

31. Stuckey DW, Shah K. TRAIL on trial: preclinical advances in cancer therapy. *Trends Molecular Medicine* (2013) 19:685–94. doi:10.1016/j.molmed.2013.08.007

32. Mitchell MJ, Wayne E, Rana K, Schaffer CB, King MR. TRAIL-coated leukocytes that kill cancer cells in the circulation. *Proc Natl Acad Sci* (2014) 111:930–5. doi:10.1073/pnas.1316312111

33. Greenlee JD, Lopez-Cavestany M, Ortiz-Otero N, Liu K, Subramanian T, Cagir B, et al. Oxaliplatin resistance in colorectal cancer enhances TRAIL sensitivity via death receptor 4 upregulation and lipid raft localization. *eLife* (2021) 10:e67750. doi:10.7554/eLife.67750

34. Ortiz-Otero N, Marshall JR, Lash B, King MR. Chemotherapy-induced release of circulating-tumor cells into the bloodstream in collective migration units with cancer-associated fibroblasts in metastatic cancer patients. *BMC Cancer* (2020) 20: 873. doi:10.1186/s12885-020-07376-1

35. Wayne EC, Chandrasekaran S, Mitchell MJ, Chan MF, Lee RE, Schaffer CB, et al. TRAIL-coated leukocytes that prevent the bloodborne metastasis of prostate cancer. *J Control Release* (2016) 223:215–23. doi:10.1016/j.jconrel.2015.12.048

36. Jyotsana N, Zhang Z, Himmel LE, Yu F, King MR. Minimal dosing of leukocyte targeting TRAIL decreases triple-negative breast cancer metastasis following tumor resection. *Sci Adv* (2019) 5:eaaw4197. doi:10.1126/sciadv.aaw4197

37. Pavese J, Ogden IM, Bergan RC. An orthotopic murine model of human prostate cancer metastasis. *J Vis Exp* (2013) 2013:50873. doi:10.3791/50873

38. Somers KD, Brown RR, Holterman DA, Yousefieh N, Glass WF, Wright GL, et al. Orthotopic treatment model of prostate cancer and metastasis in the immunocompetent mouse: efficacy of flt3 ligand immunotherapy. *Int J Cancer* (2003) 107:773–80. doi:10.1002/ijc.11464

39. Shahryari V, Nip H, Saini S, Dar AA, Yamamura S, Mitsui Y, et al. Pre-clinical orthotopic murine model of human prostate cancer. *J Vis Exp* (2016):54125. doi:10.3791/54125

40. Copeland BT, Shallal H, Shen C, Pienta KJ, Foss CA, Pomper MG. Imaging and characterization of macrophage distribution in mouse models of human prostate cancer. *Mol Imaging Biol* (2019) 21:1054–63. doi:10.1007/s11307-019-01318-5

41. Halin Bergström S, Nilsson M, Adamo H, Thysell E, Jernberg E, Stattin P, et al. Extratumoral heme oxygenase-1 (HO-1) expressing macrophages likely promote primary and metastatic prostate tumor growth. *PLoS One* (2016) 11:e0157280. doi:10.1371/journal.pone.0157280

42. Saltz J, Gupta R, Hou L, Kurc T, Singh P, Nguyen V, et al. Spatial organization and molecular correlation of tumor-infiltrating lymphocytes using deep learning on pathology images. *Cell Rep* (2018) 23:181–93.e7. doi:10.1016/j.celrep.2018.03.086

43. Bankhead P, Loughrey MB, Fernández JA, Dombrowski Y, McArt DG, Dunne PD, et al. QuPath: open source software for digital pathology image analysis. *Sci Rep* (2017) 7:16878. doi:10.1038/s41598-017-17204-5

44. Bankhead P. *Creating annotations around the tumor*. Pete's blog (2018). Available from: https://petebankhead.github.io/qupath/scripts/2018/08/08/three-regions.html (Accessed March 17, 2024).

45. Waddell LA, Lefevre L, Bush SJ, Raper A, Young R, Lisowski ZM, et al. ADGRE1 (EMR1, F4/80) is a rapidly-evolving gene expressed in mammalian monocyte-macrophages. *Front Immunol* (2018) 9:2246. doi:10.3389/fimmu.2018.02246

46. Schmid MC, Khan SQ, Kaneda MM, Pathria P, Shepard R, Louis TL, et al. Integrin CD11b activation drives anti-tumor innate immunity. *Nat Commun* (2018) 9:5379. doi:10.1038/s41467-018-07387-4

47. Odobasic D, Kitching AR, Holdsworth SR. Neutrophil-mediated regulation of innate and adaptive immunity: the role of myeloperoxidase. *J Immunol Res* (2016) 2016:2349817. doi:10.1155/2016/2349817

48. Chandrasekaran S, Chan MF, Li J, King MR. Super natural killer cells that target metastases in the tumor draining lymph nodes. *Biomaterials* (2016) 77:66–76. doi:10.1016/j.biomaterials.2015.11.001

49. Jackson Laboratory. *Physiological data summary – NOD.CB17-prkdcscid/J (001303)* (2007). Available from: http://jackson.jax.org/rs/444-BUH-304/images/physiological_data_001303.pdf (Accessed May 13, 2020).

50. O'Connell KE, Mikkola AM, Stepanek AM, Vernet A, Hall CD, Sun CC, et al. Practical murine hematopathology: a comparative review and implications for research. *Comp Med* (2015) 65:96–113.

51. Gabelloni ML, Trevani AS, Sabatté J, Geffner J. Mechanisms regulating neutrophil survival and cell death. *Semin Immunopathol* (2013) 35:423–37. doi:10.1007/s00281-013-0364-x

52. Wu L, Zhang XH-F. Tumor-associated neutrophils and macrophages—heterogenous but not chaotic. *Front Immunol* (2020) 11:553967. doi:10.3389/fimmu.2020.553967

53. Hashimoto D, Chow A, Noizat C, Teo P, Beasley MB, Leboeuf M, et al. Tissue resident macrophages self-maintain locally throughout adult life with minimal contribution from circulating monocytes. *Immunity* (2013) 38:792–804. doi:10.1016/j.immuni.2013.04.004

54. Shimura S, Yang G, Ebara S, Wheeler TM, Frolov A, Thompson TC. Reduced infiltration of tumor-associated macrophages in human prostate cancer: association with cancer progression. *Cancer Res* (2000) 60:5857–61.

55. Sag D, Ayyildiz ZO, Gunalp S, Wingender G. The role of TRAIL/DRs in the modulation of immune cells and responses. *Cancers (Basel)* (2019) 11:1469. doi:10.3390/cancers11101469

56. Liguori M, Buracchi C, Pasqualini F, Bergomas F, Pesce S, Sironi M, et al. Functional TRAIL receptors in monocytes and tumor-associated macrophages: a possible targeting pathway in the tumor microenvironment. *Oncotarget* (2016) 7: 41662–76. doi:10.18632/oncotarget.9340

57. Grayson KA, Jyotsana N, Ortiz-Otero N, King MR. Overcoming TRAIL-resistance by sensitizing prostate cancer 3D spheroids with taxanes. *PLoS One* (2021) 16:e0246733. doi:10.1371/journal.pone.0246733

58. Grayson KA, Hope JM, Wang W, Reinhart-King CA, King MR. Taxanes sensitize prostate cancer cells to TRAIL-induced apoptotic synergy via endoplasmic reticulum stress. *Mol Cancer Ther* (2021) 20:833–45. doi:10.1158/1535-7163.MCT-20-0495

59. Park S, Cho DH, Andera L, Suh N, Kim I. Curcumin enhances TRAIL-induced apoptosis of breast cancer cells by regulating apoptosis-related proteins. *Mol Cell Biochem* (2013) 383:39–48. doi:10.1007/s11010-013-1752-1

60. Sharkey CC, Li J, Roy S, Wu Q, King MR. Two-stage nanoparticle delivery of piperlongumine and tumor necrosis factor-related apoptosis-inducing ligand (TRAIL) anti-cancer therapy. *Technology (Singap World Sci).* (2016) 4:60–9. doi:10.1142/S2339547816500011

61. Hope JM, Lopez-Cavestany M, Wang W, Reinhart-King CA, King MR. Activation of Piezo1 sensitizes cells to TRAIL-mediated apoptosis through mitochondrial outer membrane permeability. *Cell Death Dis* (2019) 10:837–15. doi:10.1038/s41419-019-2063-6

62. Greenlee JD, Liu K, Lopez-Cavestany M, King MR. Piezo1 mechano-activation is augmented by resveratrol and differs between colorectal cancer cells of primary and metastatic origin. *Molecules* (2022) 27:5430. doi:10.3390/molecules27175430

63. Simons BW, Kothari V, Benzon B, Ghabili K, Hughes R, Zarif JC, et al. A mouse model of prostate cancer bone metastasis in a syngeneic immunocompetent host. *Oncotarget* (2019) 10:6845–54. doi:10.18632/oncotarget.27317

64. Allen TM, Brehm MA, Bridges S, Ferguson S, Kumar P, Mirochnitchenko O, et al. Humanized immune system mouse models: progress, challenges and opportunities. *Nat Immunol* (2019) 20:770–4. doi:10.1038/s41590-019-0416-z

Pathology & Oncology Research | frontiers

TYPE Original Research
PUBLISHED 27 January 2023
DOI 10.3389/pore.2023.1610867

Check for updates

OPEN ACCESS

EDITED BY
József Tímár,
Semmelweis University, Hungary

*CORRESPONDENCE
Nobuyuki Takakura,
ntakaku@biken.osaka-u.ac.jp

RECEIVED 06 October 2022
ACCEPTED 16 January 2023
PUBLISHED 27 January 2023

CITATION
Inukai K, Kise K, Hayashi Y, Jia W, Muramatsu F, Okamoto N, Konishi H, Akuta K, Kidoya H and Takakura N (2023), Cancer apelin receptor suppresses vascular mimicry in malignant melanoma.
Pathol. Oncol. Res. 29:1610867.
doi: 10.3389/pore.2023.1610867

COPYRIGHT
© 2023 Inukai, Kise, Hayashi, Jia, Muramatsu, Okamoto, Konishi, Akuta, Kidoya and Takakura. This is an open-access article distributed under the terms of the Creative Commons Attribution License (CC BY). The use, distribution or reproduction in other forums is permitted, provided the original author(s) and the copyright owner(s) are credited and that the original publication in this journal is cited, in accordance with accepted academic practice. No use, distribution or reproduction is permitted which does not comply with these terms.

Cancer apelin receptor suppresses vascular mimicry in malignant melanoma

Koichi Inukai[1], Kazuyoshi Kise[1], Yumiko Hayashi[2], Weizhen Jia[1], Fumitaka Muramatsu[1], Naoki Okamoto[1], Hirotaka Konishi[1], Keigo Akuta[1], Hiroyasu Kidoya[2] and Nobuyuki Takakura[1,3,4,5]*

[1]Department of Signal Transduction, Research Institute for Microbial Diseases, Osaka University, Suita, Japan, [2]Department of Integrative Vascular Biology, Faculty of Medical Sciences, University of Fukui, Fukui, Japan, [3]World Premier Institute Immunology Frontier Research Center, Integrated Frontier Research for Medical Science Division, Osaka University, Suita, Japan, [4]Institute for Open and Transdisciplinary Research Initiatives (OTRI), Osaka University, Suita, Japan, [5]Center for Infectious Disease Education and Research, Osaka University, Suita, Japan

Several reports indicate that apelin is often over-expressed in tumors, and therefore it has been suggested that the apelin–apelin receptor (APJ) system may induce tumor progression. In contrast, our previous research revealed high expression of the apelin–APJ system in tumor blood vessels, suggesting its involvement in the regulation of tumor vessel formation and normalization, resulting in the suppression of tumor growth by promoting the infiltration of T cells. Thus, the effect of the apelin–APJ system on tumors remains controversial. In this report, to clarify the effect of apelin in tumor cells, we analyzed the function of APJ in tumor cells using APJ knock out (KO) mice. In APJ-KO mice, Apelin overexpression in B16/BL6 (B16) melanoma cells induced greater tumor growth than controls. In an APJ-KO melanoma inoculation model, although angiogenesis is suppressed compared to wild type, no difference is evident in tumor growth. We found that APJ deficiency promoted vascular mimicry in tumors. *In vitro*, cultured APJ-KO B16 cells demonstrated a spindle-like shape. This phenotypic change was thought to be induced by epithelial–mesenchymal transition (EMT) based on evidence that APJ-KO B16 cells show persistently high levels of the mesenchymal maker, Zeb1; however, we found that EMT did not correlate with the transforming growth factor-β/smad signaling pathway in our model. We propose that apelin-APJ system in cancer cells induces tumor growth but negatively regulates EMT and tumor malignancy.

KEYWORDS

epithelial-mesenchymal transition, melanoma, apelin, apelin receptor, neovascularization

Introduction

Apelin is a bioactive oligopeptide identified as a ligand for the G-protein coupled receptor (GPCR), APJ. Apelin is expressed in various tissues and is involved in a variety of physiological functions, from organogenesis to homeostasis. In addition to apelin, a new ligand for APJ, apelin early ligand A (APELA), also known as Elabela (ELA) or Toddler, has been identified and was shown to be important in angiogenesis and embryonic development [1,2,3]. Moreover, gene and protein expression of apelin and APJ are modulated by fluid flow depending on the magnitude of shear stress [4], and it is possible that APJ activation is induced by such mechanical stress.

We previously described the function of the apelin–APJ system in physiological and pathological vascular development [5, 6]. In a physiological setting, we found that apelin is involved in regulating the caliber size of blood vessels, inducing the formation of larger caliber-sized capillaries by exerting cell–cell aggregation of endothelial cells (ECs). Moreover, we found that apelin suppressed vascular permeability by stabilizing the membrane expression of vascular endothelial (VE)-cadherin [7]. Furthermore, we identified the function of apelin/APJ in the juxtapositional alignment of arteries and veins by mainly regulating the movement of veins to arteries [8].

Recently, apart from cardiovascular development, high expression of apelin and APJ has also been observed in tumor tissue compared to normal tissue, suggesting their involvement in the regulation of tumor vessel formation and normalization [9,10,11]. We also found that apelin was involved in the formation of a vascular system in tumors, showing a variety of effects. For example, Colon 26 tumors showing apelin overexpression in mice after subcutaneous implantation inhibited tumor growth. Tumor growth by LLC or MC38 cells was enhanced significantly in apelin-knockout (KO) mice [12, 13]. However, in other reports, apelin induces the growth of tumors by enhancing the tumor vasculature [14, 15]. These findings suggested that apelin might have diverse functions in tumor formation depending on the tumor microenvironment.

In our previous study, APJ activation by apelin induced the morphological and functional maturation of blood vessels in tumors, resulting in the suppression of tumor growth by promoting the infiltration of T cells into the central region of the tumor and thereby robustly inducing apoptosis in tumor cells [12, 13]. However, several lines of evidence indicate that apelin is often over-expressed in tumors, suggesting that this factor may induce tumor growth because its expression correlates with tumor malignancy [10].

Discrepancies in tumor growth affected by apelin may due to the expression of its receptor, APJ, in the tumor microenvironment. Usually, APJ is expressed on vascular ECs during embryogenesis and is weakly expressed in ECs after birth. When angiogenesis is induced, ECs may re-express APJ; however, tumor cells themselves are suggested to express APJ with a wide range of expression. This may affect complicity in the tumor growth affected by apelin. To elucidate the effect of apelin on tumor cells, the elimination of APJ expression in host cells (mainly ECs) is required. In the present study, therefore, we analyzed the function of APJ in tumor cells by using APJ-KO mice and observed the role of APJ in cancer cells.

Methods

Mice and cell lines

Wild-type C57BL/6 mice were purchased from Japan SLC (Shizuoka, Japan). APJ-KO mice were gifts from Prof. Fukamizu [16]. All mice were used between 8 and 11 weeks of age. Animals were housed in environmentally-controlled rooms in an animal experimentation facility at Osaka University. All mouse experiments were performed under the guidelines of the Osaka University Committee for Animal and Recombinant DNA Experiments (Approval number 4784).

B16/BL6, a murine melanoma cell line, was purchased from the Riken Cell Bank (Tsukuba, Japan) and maintained in DMEM (Sigma–Aldrich, St. Louis, MO, United States) supplemented with 10% fetal bovine serum (FBS, Sigma–Aldrich) and 1% penicillin/streptomycin (Life Technologies, Tokyo, Japan). B16/BL6 cells were starved and then stimulated with LY364947 (10 μM; Selleck Biotech, Huston, TX, United States) or dimethyl sulfoxide (Nacalai Tesque, Inc., Kyoto, Japan) for 24 h. Methods for the generation of apelin-overexpressing cancer cells were previously described [12].

CRISPR-Cas9 method for APJ-KO tumor cells

To establish APJ-KO cells using a CRISPR/Cas9 genome editing system, single-guide RNAs were designed using a CRISPRdirect Web application (https://crispr.dbcls.jp) for the mAPLNR first exon using pSpCas9(BB)-2A-Puro (PX459) V2.0 (plasmid number 62988; Addgene, Watertown, MA, United States). The two-pair gene-specific single-guide RNA sequences were 5′-CAC CGA GGC CAG TCA AAC TCC CGG T - 3′(sense), 5′- AAA CAC CGG GAG TTT GAC TGG CCT C -3′ (antisense), 5′-CAC CGA GGT GCA GGC TTG GCG AAA T′ (sense), and 5′- AAA CAT TTC GCC AAG CCT GCA CCT C-3′ (antisense). The oligos were ligated into a BbsI site of PX459. The constructed targeting vector was transfected into a B16/BL6 cell line. Clones were selected, and elimination of APJ expression at mRNA and protein levels was detected through real-time quantitative PCR (RT–qPCR) and western blot analysis, respectively (as described below).

In vivo tumor subcutaneous inoculation

B16/BL6 cells (1×10^7 cells/mL per mouse in 150 μL PBS) were inoculated subcutaneously into WT C57BL/6 or APJ-KO mice (8–11 weeks of age). Tumors were dissected 14 days after implantation. Tumor volumes were measured with calipers every 5–7 days and calculated as follows: width × width × length × 0.5.

Western blot analysis

In APJ western blot analysis, cell extracts were prepared with GPCR extraction and stabilization reagent (Thermo Fisher Scientific, Waltham, MA, United States) for APJ or with radioimmunoprecipitation assay buffer (Thermo Fisher Scientific) according to the manufacturer's protocol. Proteins were separated by sodium dodecyl sulfate–polyacrylamide gel electrophoresis, transferred to polyvinylidene difluoride membranes, and blocked with 5% skimmed milk in 0.1% Tris-buffered saline and Tween 20. Membranes were subsequently incubated with antibodies against APJ (5H5L9; Thermo Fisher Scientific), p-Smad2, Smad2, p-Smad3, Smad3 (Cell Signaling Technology, Danvers, MA, United States), or glyceraldehyde-3-phosphate dehydrogenase (Millipore, Temecula, CA, United States), and then developed with horseradish peroxidase–conjugated secondary antibodies (Jackson ImmunoResearch Laboratories, West Grove, PA, United States). Antibody binding was visualized using electrochemiluminescence reagents (GE Healthcare, Milwaukee, WI, United States).

Transwell assay

Cell migration was evaluated using a transwell assay. For the analysis of cell migration, cells were suspended in DMEM at a density of 1×10^6 cells/mL and added to the upper chamber (200 μL/chamber); 750 μL of medium (DMEM containing 10% FBS) was added to the lower chamber. After 14 h, cells on the top membrane surface of the upper chamber were removed using a cotton swab, and the infiltrating cells on the bottom surface were fixed in 4% paraformaldehyde for 1 min, stained with hematoxylin and eosin, and visualized and counted using a microscope.

Tube formation assay

Each well of a 96-well plate was coated with 60 μL of growth factor–reduced UltiMatrix (R&D Systems, Inc., Minneapolis, MN, United States) for 30–60 min at 37°C. Melanoma cells were seeded onto the gel surface at a density of 4.0×10^4 cells per well in a volume of 200 μL medium. Network formation was analyzed after a 15-h incubation. Images were analyzed with ImageJ and Angiogenesis analyzer software [17].

Immunostaining

Tumor sections were rehydrated in PBS and blocked with normal goat serum in PBS for 20 min at room temperature. Primary antibodies used were: rabbit anti-APJ (5H5L9; Thermo Fisher Scientific; 1:200), hamster anti-CD31 (Millipore; 1:200), and rat anti-GFP (BioLegend, San Diego, CA, United States; 1:200) with overnight incubation. Following three washes with PBS, sections were incubated with Alexa Fluor-conjugated secondary antibody (Thermo Fisher Scientific) and diluted 1:200 in blocking solution for 60 min. After three washing steps with PBS, sections were mounted using Vectashield (Vector Laboratories, Burlingame, CA, United States) under coverslips. Stained sections were examined using confocal microscopy (TCS/SP8 or TCS/SP5; Leica Microsystems, Wetzlar, Germany).

Angiogenesis analysis

To quantify the length and density of blood vessels, CD31-positive immunofluorescence images were analyzed with the computational analysis tool, Angiotool (version 0.6; National Institutes of Health, National Cancer Institute, Bethesda, MD, United States) [18]. It performs the analysis of vascular morphometric parameters like vessel length and density. Tumor sections were scanned under low-power magnification (×200) to identify areas of highest CD31-positive vessel density. All images shown are representative of more than five independent experiments.

qRT–PCR analysis

Briefly, total RNA was extracted from cells using RNeasy-plus mini kits (Qiagen, Hilden, Germany) and reverse-transcribed using a PrimeScript RT reagent kit (Takara, Shiga, Japan) according to the manufacturer's protocol. Quantitative real-time PCR analysis was performed with TB Green Premix Ex Taq II (Takara) using a LightCycler 96 System (Roche Diagnostics GmbH, Penzberg, Germany). Primers are described in Supplementary Table S1. Results were normalized to GAPDH using a comparative threshold cycle method.

Results

APJ is expressed in malignant melanoma cells

We examined melanoma cells for the expression of APJ protein. We found that B16/BL6 (B16) melanoma cells strongly expressed this compared with murine ECs (MS-1), which were previously reported to express APJ (Figure 1A). As observed in cultured cells, immunohistochemical staining in tumor tissues of C57/BL6 wild-

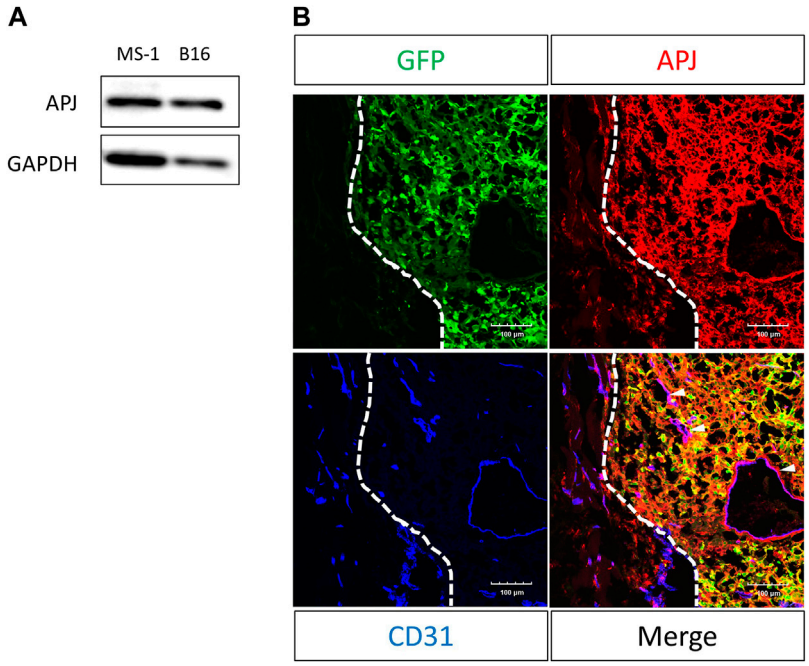

FIGURE 1
APJ is expressed in B16/BL6 malignant melanoma cells. **(A)** Western blot analysis with anti-APJ and anti–glyceraldehyde-3-phosphate dehydrogenase (GAPDH) antibodies in whole cell lysates, as indicated. **(B)** Representative image of a B16/BL6 tumor from a mouse (n = 4). Tumor sections were stained with anti-green fluorescent protein (GFP) (green), -APJ (red), and -CD31 (blue) antibodies. Dashed lines indicate the tumor edge. White arrowheads indicate APJ-positive blood vessels. Scale bars = 100 μm.

type mice subcutaneously inoculated with B16 cells overexpressing green fluorescent protein (GFP) revealed that B16 melanoma cells (GFP positive) expressed APJ protein (Figure 1B); APJ expression was equivalently observed in tumor ECs.

APJ expressed in B16 melanoma cells induces tumor growth by apelin

To analyze the effect of apelin on APJ in cancer cells, we overexpressed apelin in B16 cells (B16/apelin; Figure 2A; $p < 0.01$). When cell proliferation was compared in mock-transfected B16 cells and those transfected with apelin, we found that apelin significantly promoted the proliferation of apelin-overexpressing B16 cancer cells (Figure 2B; $p < 0.05$). Next, to evaluate whether or not cell proliferation by apelin reflects *in vivo* tumor growth, we transplanted cancer cells into APJ-KO mice to eliminate the effect of apelin on cells other than cancer cells, especially ECs. We subcutaneously inoculated B16/apelin or mock-transfected control cells into APJ-KO mice and found that B16/apelin mice showed significantly higher tumor growth than B16/mock-transfected control mice (Figures 2C, D; $p < 0.05$). In this tumor model, the density of blood vessels in B16/apelin tumors did not significantly differ from that in B16/mock-transfected control tumors (Figure 2E). Taken together, these data suggested that APJ deficiency in the tumor host microenvironment does not affect tumor angiogenesis when B16 cells were used as tumor models. An excess amount of apelin induced the growth of B16 melanoma cells by affecting APJ in tumor cells.

Lack of APJ in B16 melanoma cells attenuates angiogenesis but does not affect tumor growth

We found that overexpression of apelin in B16 melanoma cells induced the growth of tumors. Therefore, we next observed whether or not a lack of APJ in B16 cells would affect tumor growth. To assess this, we knocked out the *APJ* gene in B16 cells by a clustered regularly interspaced short palindromic repeats/CRISPR-associated protein (CRISPR/Cas9) method and established two sublines (B16/APJ-KO#1, 2). The mRNA (Figure 3A) and protein (Figure 3B) levels of APJ in cell lines were analyzed. When cells were cultured, we found no significant difference in cell growth between wild-type (WT) and APJ-KO B16 cell lines (Figure 3C).

Next, these cancer cell lines were subcutaneously inoculated into C57/BL6 WT mice and the growth of tumors was evaluated. All three tumors (B16/WT, B16/APJ-KO#1, 2) showed similar tumor growth. We calculated the tumor volume on day 14 after the inoculation of tumor cells. Unexpectedly, we found that the elimination of APJ from B16 cells did not affect the growth of tumors (Figure 3D). Tumor

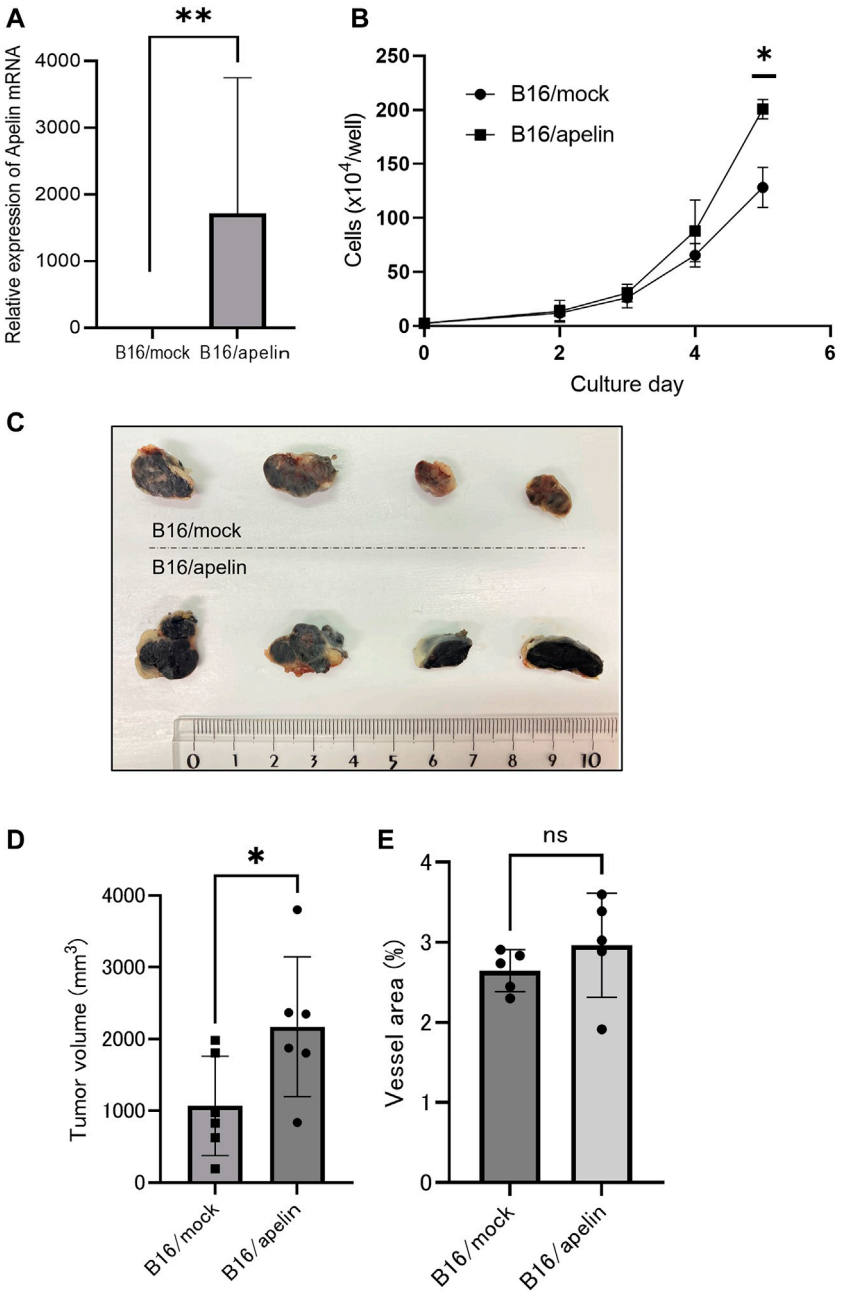

FIGURE 2
APJ induces cell proliferation and tumor growth by apelin. **(A)** Quantitative evaluation of apelin mRNA expression in B16 cells transfected with an apelin expression plasmid ($n = 3$). **(B)** *In vitro* growth of apelin-overexpressing B16 (B16/apelin) and control B16 (B16/mock-transfected) cells ($n = 3$). **(C, D)** Comparison of tumor growth by control B16/mock-transfected cells with B16/apelin cells. **(C)** Representative gross appearance ($n = 4$). **(D)** Quantification of tumor sizes ($n = 6$). **(E)** Quantification of blood vessel areas in B16/mock-transfected and B16/apelin tumors on day 14 after B16 cell inoculation of APJ-knockout (KO) mice ($n = 6$). Data are expressed as mean ± SD, $*p < 0.05$, $**p < 0.01$, ns: not significant.

vascular development is a major factor in regulating tumor growth in the tumor microenvironment and therefore we next evaluated the vascular density of each tumor. Initially, we suspected that APJ deficiency induced tumor angiogenesis and compensated tumor proliferation that should be observed in the presence of an apelin/APJ system on B16 cells. However, unexpectedly, tumors generated by B16/WT cells showed a higher vascular density than tumors by B16/APJ-KO cells (Figures 3E, F; $p < 0.01$). This suggested that progression of tumor growth by B16/APJ-KO is induced by factors other than angiogenesis factors.

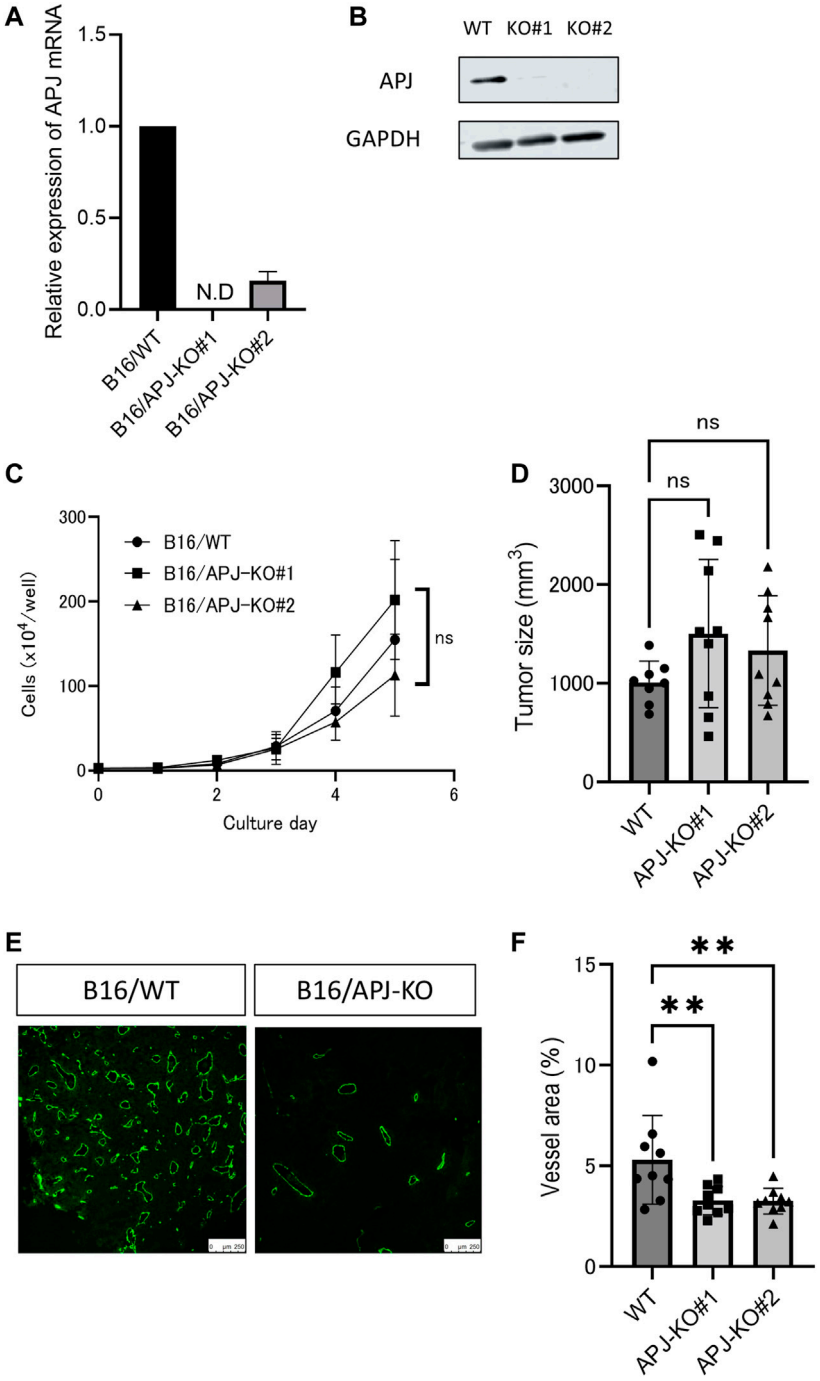

FIGURE 3
APJ knockout in melanoma retains tumor growth without angiogenesis. **(A)** Real-time quantitative PCR of APJ mRNA expression in B16/wild-type (WT) and APJ knock-out (KO) B16 clones (#1, 2) (n = 3). **(B)** Western blot analysis of cell lysates from B16/WT, B16/APJ-KO clones. Glyceraldehyde-3-phosphate dehydrogenase (GAPDH) protein was used as a loading control. **(C)** *In vitro* growth of B16/WT and B16/APJ-KO cells (n = 3). **(D)** The sizes of tumors derived from B16/WT and B16/APJ cell lines subcutaneously inoculated into WT mice on day 14 (n = 8/WT vs. n = 9/APJ-KO). **(E)** Representative immunofluorescence staining for CD31 in B16/WT and B16/APJ-KO tumors (n = 8/WT vs. n = 9/APJ-KO). Scale bars = 250 μm. **(F)** Quantitative evaluation of vessel areas in tumors derived from B16/WT and B16/APJ-KO (#1, 2) cell lines (n = 8/WT vs. n = 9/APJ-KO). Data are expressed as mean ± SD, KO, knockout; N.D, not detected; WT, wild type; $^{**}p < 0.01$; ns, not significant.

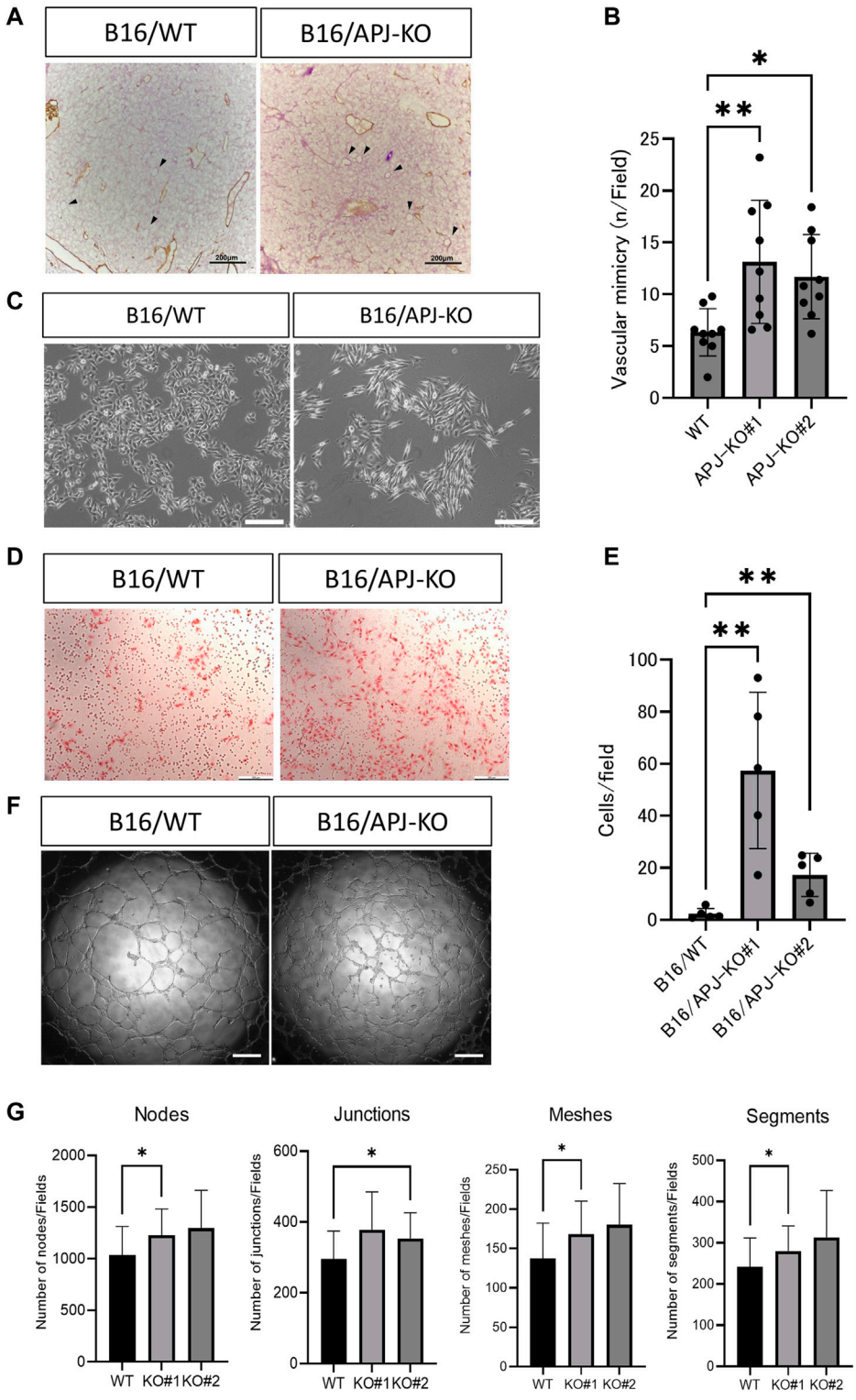

FIGURE 4
APJ knock out in B16 cells promotes vascular mimicry *in vivo* and *in vitro*. **(A)** Representative microscopic images of B16/wild-type (WT) and B16/APJ-knockout (KO) cells with double staining of CD31 (DAB; brown) and PAS (pink). Arrowheads indicates vessel-like structures induced by vascular mimicry (CD31 negative and PAS positive). Scale bars = 200 μm. **(B)** Quantitative evaluation of the vessel number induced by vascular mimicry in B16/WT and B16/APJ-KO (#1, 2) (n = 9) cells. **(C)** Phase contrast light microscopic images of cultured cells. Scale bars = 500 μm. **(D)** Microscopic images of cells that migrated through the transwell membrane in the migration assay (hematoxylin and eosin stain, scale bars = 200 μm. (E) The quantitation of cells that migrated through the transwell membrane in the migration assay (n = 5). **(F)** Microscopic images of a tube formation assay (B16/WT vs. B16/APJ-KO). Scale bars = 500 μm. **(G)** Quantitative analysis of several parameters of tube-like structures observed in a tube formation assay using ImageJ software (n = 9). Data are expressed as mean ± SD, *p < 0.05, **p < 0.01.

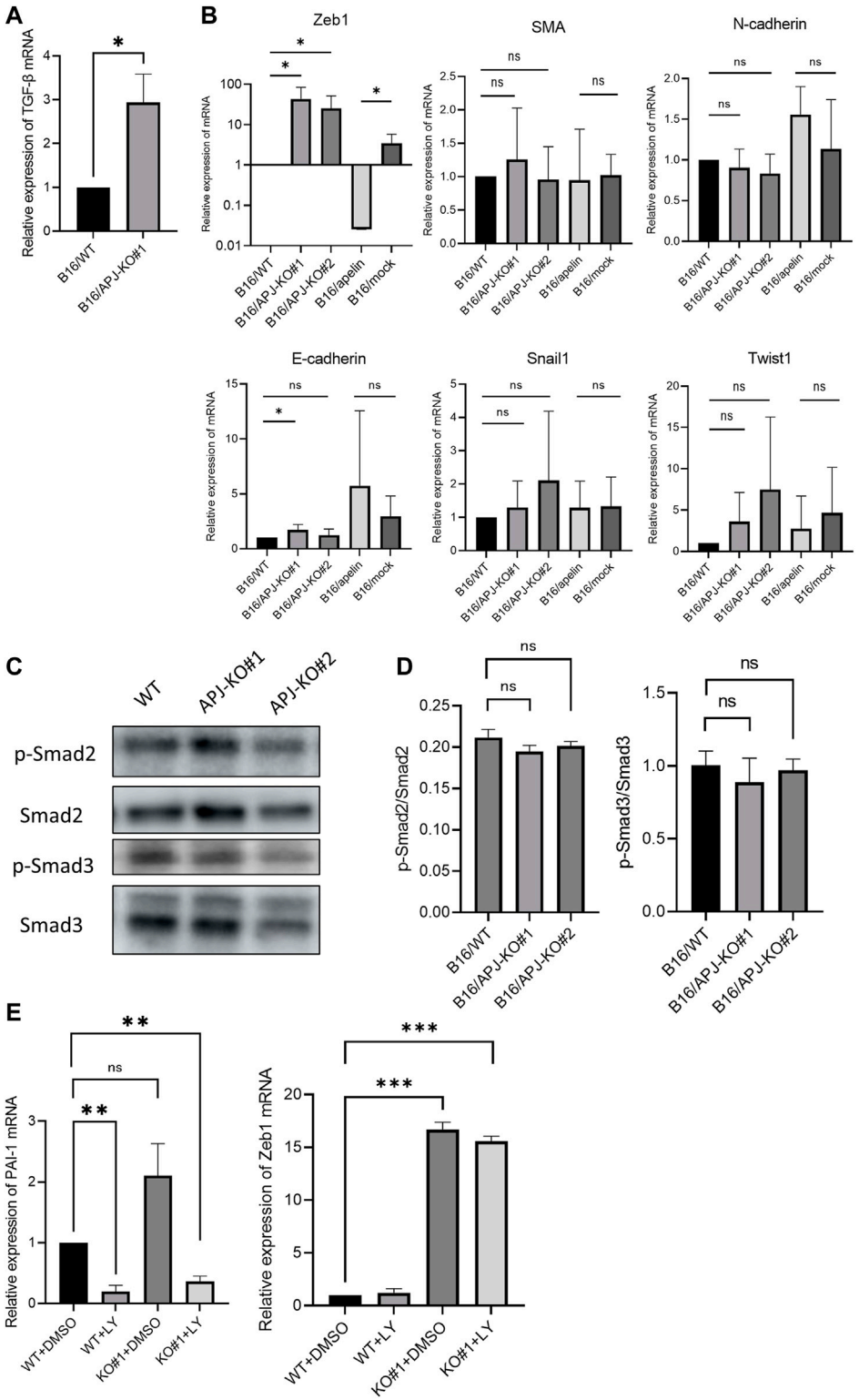

FIGURE 5
APJ knock out in B16 cells shows persistently high Zeb1 expression uncorrelated with TGF-β/smad signaling. **(A)** Quantitative evaluation of transforming growth factor (TGF)-β mRNA expression in B16/WT and B16/APJ-KO#1 cells (n = 3). **(B)** Quantitative evaluation of epithelial–mesenchymal (EMT) markers (Zeb1, smooth muscle actin [SMA], N-cadherin, E-cadherin, Snail, Twist1) mRNA expression in B16/wild-type (WT), B16/APJ-knockout (KO) (#1, 2), and B16/apelin and B16/mock-transfected cells (n = 4). **(C)** Western blot analysis of phosphorylated Smad2 (p-Smad), Smad2, phosphorylated Smad3 (p-Smad3), and Smad3 protein levels in cell lysates of B16/WT (WT) and B16/APJ-KO#1,2 (APJ-KO#1, 2) cells. **(D)** Quantitative evaluation of the p-Smad2/Smad protein ratio and p-Smad3/Smad3 protein ratio in B16/WT and B16/APJ-KO cells (n = 4). **(E)** Quantitative evaluation of plasminogen activator inhibitor-1 (PAI-1) and Zeb1 mRNA expression in WT and APJ-KO cells after treatment with dimethyl sulfoxide (DMSO) (control) or LY364947 (n = 3). Data are expressed as mean ± SD, *$p < 0.05$, **$p < 0.01$. ***$p < 0.001$. ns, not significant.

APJ deficiency in B16 cells promotes vascular mimicry

In order to maintain the same volume between B16/WT and B16/APJ-KO tumors, we postulated that blood supply other than through tumor vessels is required. Therefore, we speculated that vascular mimicry (VM) may be induced in B16/APJ-KO tumors and indeed we detected abundant periodic acid Schiff (PAS)-positive, but CD31-negative, vascular-like structures in tumors generated by B16/APJ-KO cells compared to those of B16/WT cells (Figures 4A, B).

It is widely accepted that a change in cell shape is involved in vascular mimicry by tumor cells [19]. We found that APJ-KO B16 cells showed a more spindle-like shape compared to WT cells (Figure 4C). Several studies suggested that VM by B16 cells requires cancer cell migration. We therefore compared the migration of B16/WT and B16/APJ-KO cell lines using transwell assays. We found that B16/APJ-KO (#1 and 2) cells showed more transmigration than B16/WT cells (Figures 4D, E). Moreover, an *in vitro* tube formation assay that mimics vascular formation indicated that the lack of APJ more effectively generated tube-like structures in B16 cells (Figures 4F, G).

Lack of APJ in B16 cells induces high Zeb1 expression by not correlating with TGF-β/smad signaling pathways

Thus far, we found that a lack of APJ in B16 cells meant that these showed a spindle-like phenotype with high migrating potency. We hypothesized that this phenotypic change may be induced by mechanisms involved in epithelial–mesenchymal Transition (EMT). Signaling affected by transforming growth factor (TGF)-β is a key factor for EMT. Therefore, we examined the expression of TGF-β and transcription factors associated with EMT. We found that TGF-β mRNA was expressed in B16/APJ-KO cells at a higher level than in B16/WT cells (Figure 5A). Correlating with this expression, expression of the mesenchymal maker, Zeb1, was also higher in APJ-KO melanoma and B16/apelin cells than in B16/WT cells (Figure 5B). By contrast, when smooth muscle actin (SMA) mRNA expression was observed, a slightly higher level was detected in B16/apelin compared to B16/mock-transfected cells; however, an increase in SMA mRNA was not detected in B16/APJ-KO cells. Since the expression of another EMT-related molecule was not altered in B16/apelin or B16/APJ-KO cells, as far as we could determine, this phenotypic change by APJ or apelin may have been induced by partial EMT. Recently, it has been reported that partial EMT status prior to the acquisition of full mesenchymal phenotype provides maximal stemness, tumor initiation capacity, and the ability to adapt to environmental changes [20].

Next, we investigated the relationship of TGF-β/Smad signaling with Zeb1 expression. At first, phosphorylated Smad2 and Smad3 (pSmad2 and pSmad3) proteins were measured by western blotting in B16 cells. However, we found that the ratio of pSmad2/Smad2 and pSmad3/Smad3 proteins were not altered by the absence of APJ (Figures 5C, D). Next, we further observed the relationship between Zeb1 and TGF-β/Smad signaling by using an inhibitor of TGF-β/Smad signaling pathways. We showed that an inhibitor of the TGF-β1 receptor (LY364947) affected B16/WT and B16/APJ-KO cells since the mRNA level of plasminogen activator inhibitor-1, which is an end-product of the Smad signaling pathway, was inhibited. In this setting, however, Zeb1 expression was not suppressed by LY364947 in the B16/APJ-KO group (Figure 5E). Therefore, we concluded that APJ negatively regulated Zeb1 expression in B16 cells and therefore attenuation of APJ in B16 cells promoted Zeb1 expression to induce EMT; however, this APJ signaling is independent of TGF-β/Smad signaling pathways.

Discussion

In subcutaneous inoculation of tumor cell mouse models, we previously reported that overexpression of apelin in colon 26 tumor cells significantly inhibited tumor growth by promoting penetration of natural killer T cells into the tumor. Additionally, [Pyr1] apelin-13 infusion induced $CD8^+$ T-cell infiltration into tumors, resulting in inhibition of tumor growth through C-C Motif Chemokine Ligand 8 expression [13]. In contrast to our previous findings, several studies have shown that the apelin/APJ axis plays a role in the development of tumors. In many types of tumors, it has been shown that apelin and APJ expression levels are significantly increased. For example, in the lung adenocarcinoma cell line A549, apelin increases cyclin D1 expression and induces cell proliferation through enhancement of extracellular signal–regulated kinase (ERK)1/2 phosphorylation [21]. In the case of colon cancer, apelin and APJ expression is elevated in tissues of colon adenocarcinoma and the human colon carcinoma cell line LS180 [22]. Apelin induces the proliferation of LS180 cells *via* upregulation of Notch3 resulting in the activation of JAG1/Notch3 signaling. Also, in the human oral cancer cell line, HSC-3, apelin promotes cell proliferation through phosphorylation of ERK1/2 [23]. Thus, the effect of apelin on the cancer cell itself is thought to be involved in tumor growth. In the present study, to clarify the effect of apelin in cancer cells, we used APJ-KO mice as a host in subcutaneous tumor cell inoculation models. Based on our present studies, we showed that apelin has a role in tumor progression, affecting tumor cells directly. Taken together with our previous reports, it was elucidated that apelin has dual roles in tumor growth, i.e., cancer cell proliferation directly affecting APJ in cancer cells and a cancer-suppressive effect by enhancing tumor immunity through the tumor vasculature.

To date, reports that highlight the relationship between APJ and VM are non-existent. Vascular mimicry, in which cancer cells themselves display vascular-like structures to maintain blood flow in the absence of blood vessels covered with vascular ECs, supports tumor growth. The mechanism of VM has not been well elucidated compared with tumor blood vessels regulated by angiogenesis mainly induced by VEGF. The process of VM is induced by signaling pathways associated with hypoxia, cancer stemness, and

angiogenesis [24]. Of these pathways, hypoxia is associated with VM in melanoma [25]. Hypoxia induces VM formation by upregulating VE-cadherin expression. Hypoxia-inducible factor 1, a key effector of this pathway, increases the stemness and differentiation potential of highly plastic cells in highly malignant tumor cell populations (especially cancer stem cells) in the tumor microenvironment. Such tumor cells transform into more mobile cells through hypoxia-induced phenotype change. Then, as the cells expand and contract, the expression of related transcription factors, such as Twist and Snail, in cells increases, the expression of E-cadherin decreases, and the expression of angiogenesis-related molecules such as fibronectin increases [26]. These cancer stem cells subsequently show characteristics of endothelial-like cells [27].

Like hypoxia, VEGF is an important factor in angiogenesis. Vascular endothelial growth factor expression in melanomas promotes VM development through activation of the PI3K/AKT pathway in the tumor microenvironment [28]. Phosphoinositide 3-kinase elevates the level of matrix metalloproteinase-14 (MMP-14) in aggressive cells; MMP-14 in turn activates MMP-2, which in turn activates the secretion of γ2′ and γ2x pro-migratory fragments leading to VM in melanomas [29]. It restructures the extracellular matrix, facilitates tumor cell migration and conversion to a malignant phenotype, and provides the stretch space and environment for VM network formation [30].

Several VM inhibitors to suppress these pathways have been identified in previous studies. For example, molecules suppressing VEGF/VEGF receptor pathways, such as thalidomide, efficiently inhibit VM [31,32]. However, the other angiogenesis-related ligand/receptor pair associated with VM has not been well documented. Here, we revealed that APJ expression in cancer cells negatively correlated with the formation of VM. In brief, the lack of APJ benefits B16 cells in promoting VM.

Several studies have reported that increased expression of Zeb1 in melanoma is involved in phenotype change into an invasive one [33]. In our study, we also detected that a high migration state in APJ-KO B16 cells is accompanied by high Zeb1 expression. Epithelial–mesenchymal-like phenotypic change is also associated with VM formation [26, 34]. Interestingly, in glioblastoma, a representative tumor that shows VM, a reduction in apelin expression led to accelerated glioblastoma cell invasion [35]. Taken together with our present data, more tumor cell types are likely to exist that show an aggressive migration phenotype due to a lack of apelin/APJ expression.

In summary, depending on tumor cell types, apelin may act as a promotor of tumor proliferation. However, apelin is a regulator of mature blood vessel formation in both physiological and pathological settings. Based on the analysis shown in this report, we interpret that specific regulation of APJ expression in tumor cells is required to control tumor growth by affecting cancer cells themselves. The regulation of APJ expression in cancer cells is currently unknown. We need to analyze the regulation of APJ expression in tumor cells, including epigenetic regulation. In the present study, we did not specifically elucidate how an EMT-like phenotype or VM was induced by a lack of APJ in B16 melanoma cells, although Zeb1 expression was apparently induced. Further analysis to determine molecular insights of how Zeb1 is negatively regulated by APJ in cancer is required.

Data availability statement

The original contributions presented in the study are included in the article/Supplementary Material, further inquiries can be directed to the corresponding author.

Ethics statement

The animal study was reviewed and approved by the Osaka University Committee for Animal and Recombinant DNA Experiments (Approval number 4784).

Author contributions

All authors contributed to the study conception and design. KI conducted the experiments and analyzed the data. KI and KK wrote the paper; NT supervised the study, interpreted the data and reviewed the manuscript; YH, WJ, FM, NO, HKo, KA, and HKi discussed and revised the paper. All of the authors approved this paper.

Funding

This work was supported by a Japan Society for the Promotion of Science (JSPS) Grant-in-Aid for JSPS Fellows (JP21J14797) to KI, Grants-in-Aid for Scientific Research (S) (20H05698) to NT, and the Japan Agency for Medical Research and Development (AMED) under Grant number (22ck0106727h0001) to NT.

Conflict of interest

The authors declare that the research was conducted in the absence of any commercial or financial relationships that could be construed as a potential conflict of interest.

Acknowledgments

We thank Y. Morimoto, Y. Mori, and N. Aikawa for excellent technical assistance.

Supplementary material

The Supplementary Material for this article can be found online at: https://www.por-journal.com/articles/10.3389/pore.2023.1610867/full#supplementary-material

References

1. Serene HL, Tian J, Reversade B. Elabela: A hormone essential for heart development signals via the apelin receptor. *Dev Cel* (2013) 27(6):672–80. doi:10.1016/j.devcel.2013.11.002

2. Perjés Á, Kilpiö T, Ulvila J, Magga J, Alakoski T, Szabó Z, et al. Characterization of apela, a novel endogenous ligand of apelin receptor, in the adult heart. *Basic Res Cardiol* (2016) 111(1):2. doi:10.1007/s00395-015-0521-6

3. Kuba K, Sato T, Imai Y, Yamaguchi T. Apelin and Elabela/Toddler; double ligands for APJ/Apelin receptor in heart development, physiology, and pathology. *Peptides* (2019) 111:62–70. doi:10.1016/j.peptides.2018.04.011

4. Busch R, Strohbach A, Pennewitz M, Lorenz F, Bahls M, Busch MC, et al. Regulation of the endothelial apelin/APJ system by hemodynamic fluid flow. *Cell Signal* (2015) 27(7):1286–96. doi:10.1016/j.cellsig.2015.03.011

5. Kidoya H, Ueno M, Yamada Y, Mochizuki N, Nakata M, Yano T, et al. Spatial and temporal role of the apelin/APJ system in the caliber size regulation of blood vessels during angiogenesis. *EMBO J* (2008) 27(3):522–34. doi:10.1038/sj.emboj.7601982

6. Kidoya H, Takakura N. Maturation of blood vessels by haematopoietic stem cells and progenitor cells: Involvement of apelin/APJ and angiopoietin/Tie2 interactions in vessel caliber size regulation. *Thromb Haemost* (2009) 101(06):999–1005. doi:10.1160/th08-06-0358

7. Kidoya H, Naito H, Takakura N. Apelin induces enlarged and nonleaky blood vessels for functional recovery from ischemia. *Blood* (2010) 115(15):3166–74. doi:10.1182/blood-2009-07-232306

8. Kidoya H, Naito H, Muramatsu F, Yamakawa D, Jia W, Ikawa M, et al. APJ regulates parallel alignment of arteries and veins in the skin. *Dev Cel* (2015) 33(3):247–59. doi:10.1016/j.devcel.2015.02.024

9. Frisch A, Kälin S, Monk R, Radke J, Heppner FL, Kälin RE. Apelin controls angiogenesis-dependent glioblastoma growth. *Int J Mol Sci* (2020) 21(11):4179. doi:10.3390/ijms21114179

10. Masoumi J, Jafarzadeh A, Khorramdelazad H, Abbasloui M, Abdolalizadeh J, Jamali N. Role of Apelin/APJ axis in cancer development and progression. *Adv Med Sci* (2020) 65(1):202–13. doi:10.1016/j.advms.2020.02.002

11. Zhang L, Takara K, Yamakawa D, Kidoya H, Takakura N. Apelin as a marker for monitoring the tumor vessel normalization window during antiangiogenic therapy. *Cancer Sci* (2016) 107(1):36–44. doi:10.1111/cas.12836

12. Kidoya H, Kunii N, Naito H, Muramatsu F, Okamoto Y, Nakayama T, et al. The apelin/APJ system induces maturation of the tumor vasculature and improves the efficiency of immune therapy. *Oncogene* (2012) 31(27):3254–64. doi:10.1038/onc.2011.489

13. Hu L, Hayashi Y, Kidoya H, Takakura N. Endothelial cell-derived Apelin inhibits tumor growth by altering immune cell localization. *Sci Rep* (2021) 11(1):14047. doi:10.1038/s41598-021-93619-5

14. Berta J, Török S, Tárnoki-Zách J, Drozdovszky O, Tóvári J, Paku S, et al. Apelin promotes blood and lymph vessel formation and the growth of melanoma lung metastasis. *Sci Rep* (2021) 11(1):5798. doi:10.1038/s41598-021-85162-0

15. Berta J, Kenessey I, Dobos J, Tovari J, Klepetko W, Jan Ankersmit H, et al. Apelin expression in human non-small cell lung cancer: Role in angiogenesis and prognosis. *J Thorac Oncol* (2010) 5(8):1120–9. doi:10.1097/jto.0b013e3181e2c1ff

16. Ishida J, Hashimoto T, Hashimoto Y, Nishiwaki S, Iguchi T, Harada S, et al. Regulatory roles for APJ, a seven-transmembrane receptor related to angiotensin-type 1 receptor in blood pressure *in vivo*. *J Biol Chem* (2004) 279(25):26274–9. doi:10.1074/jbc.m404149200

17. Carpentier G, Berndt S, Ferratge S, Rasband W, Cuendet M, Uzan G, et al. Angiogenesis analyzer for ImageJ — a comparative morphometric analysis of "endothelial tube formation assay" and "fibrin bead assay". *Sci Rep* (2020) 10(1):11568. doi:10.1038/s41598-020-67289-8

18. Zudaire E, Gambardella L, Kurcz C, Vermeren S. A computational tool for quantitative analysis of vascular networks. *PLoS One* (2011) 6(11):e27385. doi:10.1371/journal.pone.0027385

19. Morales-Guadarrama G, Garcia-Becerra R, Mendez-Perez EA, Garcia-Quiroz J, Avila E, Diaz L. Vasculogenic mimicry in breast cancer: Clinical relevance and drivers. *Cells* (2021) 10(7):1758. doi:10.3390/cells10071758

20. Brabletz S, Schuhwerk H, Brabletz T, Stemmler MP. Dynamic EMT: A multi-tool for tumor progression. *EMBO J* (2021) 40(18):e108647. doi:10.15252/embj.2021108647

21. Yang L, Su T, Lv D, Xie F, Liu W, Cao J, et al. ERK1/2 mediates lung adenocarcinoma cell proliferation and autophagy induced by apelin-13. *Acta Biochim Biophys Sinica* (2014) 46(2):100–11. doi:10.1093/abbs/gmt140

22. Chen T, Liu N, Xu GM, Liu TJ, Liu Y, Zhou Y, et al. Apelin13/APJ promotes proliferation of colon carcinoma by activating Notch3 signaling pathway. *Oncotarget* (2017) 8(60):101697–706. doi:10.18632/oncotarget.21904

23. Heo K, Kim YH, Sung HJ, Li HY, Yoo CW, Kim JY, et al. Hypoxia-induced up-regulation of apelin is associated with a poor prognosis in oral squamous cell carcinoma patients. *Oral Oncol* (2012) 48(6):500–6. doi:10.1016/j.oraloncology.2011.12.015

24. Wechman SL, Emdad L, Sarkar D, Das SK, Fisher PB. Vascular mimicry: Triggers, molecular interactions and *in vivo* models. *Adv Cancer Res* (2020) 148:27–67. doi:10.1016/bs.acr.2020.06.001

25. Zhao N, Sun B-C, Sun T, Ma Y-M, Zhao X-L, Liu Z-Y, et al. Hypoxia-induced vasculogenic mimicry formation via VE-cadherin regulation by Bcl-2. *Med Oncol* (2012) 29(5):3599–607. doi:10.1007/s12032-012-0245-5

26. Liu Q, Qiao L, Liang N, Xie J, Zhang J, Deng G, et al. The relationship between vasculogenic mimicry and epithelial-mesenchymal transitions. *J Cel Mol Med* (2016) 20(9):1761–9. doi:10.1111/jcmm.12851

27. Bussolati B, Grange C, Sapino A, Camussi G. Endothelial cell differentiation of human breast tumour stem/progenitor cells. *J Cel Mol Med* (2009) 13(2):309–19. doi:10.1111/j.1582-4934.2008.00338.x

28. Xu X, Zong Y, Gao Y, Sun X, Zhao H, Luo W, et al. VEGF induce vasculogenic mimicry of choroidal melanoma through the PI3k signal pathway. *Biomed Res Int* (2019) 2019:3909102–13. doi:10.1155/2019/3909102

29. Seftor RE, Seftor EA, Koshikawa N, Meltzer PS, Gardner LM, Bilban M, et al. Cooperative interactions of laminin 5 gamma2 chain, matrix metalloproteinase-2, and membrane type-1-matrix/metalloproteinase are required for mimicry of embryonic vasculogenesis by aggressive melanoma. *Cancer Res* (2001) 61(17):6322–7.

30. Hendrix MJ, Seftor RE, Seftor EA, Gruman LM, Lee LM, Nickoloff BJ, et al. Transendothelial function of human metastatic melanoma cells: Role of the microenvironment in cell-fate determination. *Cancer Res* (2002) 62(3):665–8.

31. Zhang S, Li M, Gu Y, Liu Z, Xu S, Cui Y, et al. Thalidomide influences growth and vasculogenic mimicry channel formation in melanoma. *J Exp Clin Cancer Res* (2008) 27:60. doi:10.1186/1756-9966-27-60

32. Zhang X, Luo H. Effects of thalidomide on growth and VEGF-A expression in SW480 colon cancer cells. *Oncol Lett* (2018) 15(3):3313–20. doi:10.3892/ol.2017.7645

33. Wels C, Joshi S, Koefinger P, Bergler H, Schaider H. Transcriptional activation of ZEB1 by slug leads to cooperative regulation of the epithelial–mesenchymal transition-like phenotype in melanoma. *J Invest Dermatol* (2011) 131(9):1877–85. doi:10.1038/jid.2011.142

34. Wei X, Chen Y, Jiang X, Peng M, Liu Y, Mo Y, et al. Mechanisms of vasculogenic mimicry in hypoxic tumor microenvironments. *Mol Cancer* (2021) 20(1):7. doi:10.1186/s12943-020-01288-1

35. Mastrella G, Hou M, Li M, Stoecklein VM, Zdouc N, Volmar MNM, et al. Targeting APLN/APLNR improves antiangiogenic efficiency and blunts proinvasive side effects of VEGFA/VEGFR2 blockade in glioblastoma. *Cancer Res* (2019) 79(9):2298–313. doi:10.1158/0008-5472.CAN-18-0881

Pathology & Oncology Research | frontiers

TYPE Original Research
PUBLISHED 07 June 2023
DOI 10.3389/pore.2023.1611038

Check for updates

OPEN ACCESS

EDITED BY
József Tímár,
Semmelweis University, Hungary

*CORRESPONDENCE
Yi-Wen Chu,
yiwen@trx.com.tw

RECEIVED 27 December 2022
ACCEPTED 19 May 2023
PUBLISHED 07 June 2023

CITATION
Shen L, Chen Y-L, Huang C-C, Shyu Y-C, Seftor REB, Seftor EA, Hendrix MJC, Chien D-S and Chu Y-W (2023), CVM-1118 (foslinanib), a 2-phenyl-4-quinolone derivative, promotes apoptosis and inhibits vasculogenic mimicry via targeting TRAP1.
Pathol. Oncol. Res. 29:1611038.
doi: 10.3389/pore.2023.1611038

COPYRIGHT
© 2023 Shen, Chen, Huang, Shyu, Seftor, Seftor, Hendrix, Chien and Chu. This is an open-access article distributed under the terms of the Creative Commons Attribution License (CC BY). The use, distribution or reproduction in other forums is permitted, provided the original author(s) and the copyright owner(s) are credited and that the original publication in this journal is cited, in accordance with accepted academic practice. No use, distribution or reproduction is permitted which does not comply with these terms.

CVM-1118 (foslinanib), a 2-phenyl-4-quinolone derivative, promotes apoptosis and inhibits vasculogenic mimicry via targeting TRAP1

Lifen Shen[1], Yen-Ling Chen[1], Chu-Chun Huang[1], Yu-Chiau Shyu[2,3], Richard E. B. Seftor[4], Elisabeth A. Seftor[4], Mary J. C. Hendrix[4], Du-Shieng Chien[1] and Yi-Wen Chu[1]*

[1]TaiRx, Inc., Taipei, Taiwan, [2]Community Medicine Research Center, Chang Gung Memorial Hospital Keelung Branch, Keelung, Taiwan, [3]Department of Nursing, Chang Gung University of Science and Technology, Taoyuan, Taiwan, [4]Department of Biology, Shepherd University, Shepherdstown, WV, United States

CVM-1118 (foslinanib) is a phosphoric ester compound selected from 2-phenyl-4-quinolone derivatives. The NCI 60 cancer panel screening showed CVM-1125, the major active metabolite of CVM-1118, to exhibit growth inhibitory and cytotoxic effects at nanomolar range. CVM-1118 possesses multiple bioactivities, including inducing cellular apoptosis, cell cycle arrest at G_2/M, as well as inhibiting vasculogenic mimicry (VM) formation. The TNF receptor associated protein 1 (TRAP1) was identified as the binding target of CVM-1125 using nematic protein organization technique (NPOT) interactome analysis. Further studies demonstrated CVM-1125 reduced the protein level of TRAP1 and impeded its downstream signaling by reduction of cellular succinate levels and destabilization of HIF-1α. The pharmacogenomic biomarkers associated with CVM-1118 were also examined by Whole Genome CRISPR Knock-Out Screening. Two hits (*STK11* and *NF2*) were confirmed with higher sensitivity to the drug in cell knock-down experiments. Biological assays indicate that the mechanism of action of CVM-1118 is via targeting TRAP1 to induce mitochondrial apoptosis, suppress tumor cell growth, and inhibit vasculogenic mimicry formation. Most importantly, the loss-of-function mutations of *STK11* and *NF2* are potential biomarkers of CVM-1118 which can be applied in the selection of cancer patients for CVM-1118 treatment. CVM-1118 is currently in its Phase 2a clinical development.

KEYWORDS

TRAP1, vasculogenic mimicry, CVM-1118, foslinanib, Hsp75, *STK11*, *NF2*

Introduction

CVM-1118 (generic name: foslinanib) is a phosphoric ester selected from a series of synthetic 2-phenyl-4-quinolone analogues which contain phenol-quinoline chemophore as the core structure required to exhibit anti-neoplastic and anti-mutagenic properties [1–9]. In humans and animal species (e.g., mouse, rat, dog, monkey), CVM-1118 is rapidly and completely metabolized via dephosphorylation to form CVM-1125 following either intravenous or oral administration. Their anti-cancer activities have been tested using a panel of 60 human cancer cell lines (NCI 60 screen). The results showed that 87% cell lines tested had an average GI_{50} value < 100 nM. CVM-1125 inhibits cell proliferation, while induces apoptosis in human melanoma cells. In addition, CVM-1118 exhibits potent inhibition of vasculogenic mimicry (VM) [10]. Currently, this novel chemical entity (NCE) is being developed as an oral anti-cancer drug.

VM describes the plasticity of aggressive cancer cells forming *de novo* vascular perfusion networks, which is distinct from traditional endothelial tumor angiogenesis [11, 12]. The VM phenotype is known to correlate with malignant characteristics, invasion, tumor progression, metastasis, and worse survival outcome in cancer patients [13]. Angiogenesis inhibitors, such as bevacizumab, a monoclonal antibody against vascular endothelial growth factor A (VEGF-A), are ineffective in reducing VM, which may contribute to drug resistance in cancer cells [14, 15]. Until now, there are no inhibitors targeting VM on the drug market; therefore, development of anti-VM compounds is considered a novel approach for next-generation cancer treatment.

Tumor necrosis factor receptor associated protein 1 (TRAP1), also known as Hsp75, is a molecular chaperon localized in the mitochondria and is a member of the heat shock protein family [16, 17]. It has been reported that TRAP1 has multiple cellular functions, e.g., antagonizing mitochondrial apoptosis by regulating mitochondrial permeability transition pores, antagonizing mitochondrial oxidative stress, and promoting drug resistance [18–21]. Recently, the role of TRAP1 has also been linked to reprogramming metabolism by inhibiting oxidative phosphorylation and switching to aerobic glycolysis [22]. TRAP1 is highly expressed in many types of human tumors, including breast cancer, hepatocellular carcinoma (HCC), and glioblastoma [23–25]. Its expression is correlated with tumor stage, and high expression of TRAP1 correlates with poor survival in colon cancer and NSCLC [26, 27].

In this report, we present experimental evidence demonstrating the mechanism of action of CVM-1118 as a novel anti-cancer drug. The results show that CVM-1118 targets multiple cellular processes, including induction of cell apoptosis and cell cycle arrest. In addition, CVM-1118 inhibits the formation of VM *in vitro* and *in vivo*. Moreover, through nematic protein organization technique (NPOT) and further analysis by surface plasmon resonance (SPR), TRAP1 was identified as one of the cellular binding targets of CVM-1118. Translating the discovery of the binding between CVM-1118 and TRAP1 into a functional cellular activity, it was found that one of the impacts of CVM-1118 on TRAP1 was affecting its protein level by lysosomal degradation. These results demonstrate CVM-1118 as a potential novel anti-cancer drug, which functions to inhibit tumor growth and VM formation and induce cancer cell apoptosis via targeting TRAP1. The potential pharmacogenomic biomarkers for CVM-1118 were further identified which may be applied in cancer patient selection for future clinical investigation of CVM-1118.

Materials and methods

Cell culture

For cytotoxicity and cell cycle analysis, the following cell lines were used, and their culture conditions were as described: for A549, DU-145, HT-29, MDA-MB-231, Mia PaCa-2, and U118MG, cells were cultured in DMEM containing 10% FCS; for MDA- MB-435 and NCI-ADR-RES, cells were cultured in RPMI-1640 containing 10% FCS, and for SK-N-MC, cells were cultured in MEM containing 10% FCS. For the animal pharmacology study, HCT-116, a colon cancer cell line was tested. Cells were cultured in McCoy's 5a medium supplemented with 10% heat inactivated fetal bovine serum. For the cell lines used in VM analysis and target identification, C8161 and COLO205 cells were maintained in RPMI-1640 containing 10% FBS and 0.1% gentamycin sulfate. The SKOV3 line was cultured in RPMI-1640 supplemented with 15% FBS and 0.1% gentamycin sulfate. For the SK-MEL28 and MCF-7, cells were maintained in MEM/Earles Salts supplemented with 10% FBS and 0.1% gentamycin sulfate.

Cytotoxicity assays

This assay was conducted in ProQinase GmbH (Freiburg, Germany). Nine cancer cell lines (A549, DU-145, HT-29, MDA-MB-231, MDA-MB-435, Mia PaCa-2, NCI-ADR-RES, SK-N-MC, and U118MG) were seeded at 5,000 cells/well in 96-well cell culture plates in 150 μL of complete medium for 24 h prior to treatment. The test compounds CVM-1118 and CVM-1125 were synthesized by China Medical University, Chengdu Chempartner Co., Ltd., and Formosa Laboratories, Inc. To prepare the assay, the compounds were dissolved in 100% DMSO at a concentration of 10 μM. Cells were then treated with vehicle, CVM-1118 or CVM-1125 at various concentrations for 72 h. Cell viability was determined by the fluorescent quantification of Alamar Blue (Invitrogen, Thermo Fisher

Scientific). By the end of incubation, Alamar Blue reagent was added to the well for 4 h and the fluorescence was measured at 590 nm. The amount of fluorescence produced is proportional to the number of metabolically active cells. IC_{50} determination was performed using a variable slope sigmoidal response fitting model with 0% cell growth as a bottom constraint and 100% cell growth as a top constraint (GraphPad Prism, United States).

Flow cytometry analysis

This assay was conducted by ProQinase GmbH (Freiburg, Germany). HT-29 colorectal adenocarcinoma cells were seeded at 150,000 cells/well in 6-well cell culture plates in 5 mL complete medium and incubated at 37°C overnight. On the day of the assay, CVM-1118 at various concentrations or 0.1% DMSO were added to the cells. After 48 h incubation, cells were harvested including the supernatant, fixed in 80% methanol, and stored at −20°C overnight. The next day, cells were rehydrated in PBS for 30 min and treated with RNAse A (100 µg/mL) and propidium iodide (PI) (25 µg/mL). Cell cycle distribution was analyzed by flow cytometry (FACSCalibur, BD Biosciences), assessing approximately 10,000 events. Detection of DNA intercalated with PI was done by fluorescence detector FL3, in which amplification was set in such a manner that the first amplitude peak of the FL3 signal (FL3-A) in untreated cells (corresponding to the G_1 cell population) was found at approximately 200 units. For analysis, events were plotted as histogram. The peak at ~200 units was defined as cells in G_1, events below the G_1-peak were considered apoptotic cells (sub-G_1), and events at ~400 units as G_2/M cells. All signals in between 200 and 400 units were defined as cells in S-Phase, and those beyond 400 units as endoreduplicated cells (endoR).

In vitro VM assay

Aggressive human melanoma (C8161) cells were seeded at 1.0×10^5 onto 3D polymerized LDEV-free Matrigel (75 µL; 14 mg/ml; Corning Cat. No. 356232) for VM analysis in 12-well dishes containing no drug or various concentrations of CVM-1118. Matrigel-coated dishes were photographed for tubular network formation after 24 h.

Orthotopic HCT-116 mouse xenograft study and *in vivo* vasculogenic mimicry

This animal study was contracted to CrownBio International R&D Center (Beijing, China) and was conducted under the approval of the Animal Ethics Committee at CrownBio in compliance with institutional and national guidelines. Seven- to eight-week-old female BALB/c nude mice were obtained from HFK Bio-Technology Co., Ltd. (Beijing, China). HCT-116 cells (2×10^6) were suspended in 20 µL PBS and then injected into the cecal wall. Treatment began on day 14 after cell inoculation when tumor reached ~100 mm^3 measured in a satellite group of three mice. Treatment groups include vehicle control [PEG400: pH 10 carbonate buffer (40:60)], CVM-1118 at 20, 50, and 100 mg/kg given orally daily for 28 days, and CVM-1118 at 20 mg/kg given as intravenous injection once every 2 days for 7 times. Tumor volumes were measured at the end of in-life study on day 43. At the end of *in vivo* study, tumor tissues from selected groups were excised, collected, and subjected to standard immunohistochemical procedures to visualize the effect of CVM-1118 on VM network formation. Briefly, rabbit anti-human CD31 antibody (Abcam) was used as the primary Ab for the staining and the number of channels with CD31+/red blood cell (RBC)+, or CD31−/RBC+ were counted based on five light fields (×200) on the whole section of each sample in each group under microscope. Analysis of difference in tumor volume for drug-treated group against vehicle control group was conducted using one-way ANOVA followed by least significant difference (LSD) test (equal variance tested and confirmed by Brown-Forsythe test). Statistical analysis for VM formation was evaluated using Mann-Whitney test. All data were analyzed using GraphPad Prism 9.5.

Nematic protein organization technique (NPOT) and *in silico* target interaction studies

This assay was contracted to Inoviem Scientific (Strasbourg, France). The NPOT proprietary technology is based on the Kirkwood-Buff molecular crowding and aggregation theory [28, 29]. COLO205 and MCF7 cell lines as well as human primary colorectal cancer tissues and human melanoma cancer tissues were used for the study. The colorectal cancer tissues were obtained from the tumor bank of the Mannheim Medical Faculty, University of Heidelberg, Germany. The biobank was approved by the Ethical Committee of this institution. The melanoma tissues were obtained from Strasbourg University Hospital, France. The sample collection was approved by the Commission Nationale Informatique et Liberté and the Institutional Board of Strasbourg University Hospital. All the enrolled subjects provided written informed consent and were collected through protocols conforming to ethical requirements. Cell or tissue lysates were prepared under low temperature (4°C) in the absence of any detergents, reducing agents and protease or phosphatase inhibitors. All dilutions and washes were performed in standard 4- (2-hydroxyethyl)-1-piperazine ethanesulfonic acid (HEPES)-buffered saline solution (HBSS) unless otherwise indicated. NPOT was performed as described elsewhere [30–32]. Briefly, under sterile conditions at 4°C, 1 µM of CVM-1125 was mixed

separately with 1 μg of COLO205 and MCF7 cell lysates, or human colorectal and melanoma tumor homogenates which contain both cytoplasmic and membrane proteins, and then subjected to NPOT isolation. Experiments were performed three times independently. After NPOT isolation, the heteroassemblies were allowed to form overnight, and captured in 96-well plates in the form of a droplet on the surface of mineral oil, and then isolated by microdissection under a microscope. Isolated heteroassemblies were washed in acetone, solubilized in HBSS, then filtered through a 10% sodium dodecyl sulfate polyacrylamide gel electrophoresis (SDS-PAGE) gel composed of 5 mm stacking and 5 mm running gels. Heteroassemblies after SDS-PAGE isolation were solubilized in 10 μL of 2D buffer (7 M urea, 2 M thiourea, 4% CHAPS, 20 mM DTT, 1 mM PMSF). Proteins were precipitated in acetate buffer by centrifugation for 20 min at 7500xg. Thereafter, pellets were digested for 1 h with trypsin Gold (Promega) at 37°C. The samples were resuspended at 1 μg/μL in 50 mM acetic acid, and then diluted in 40 mM NH_4HCO_3 to 20 μg/mL. The samples were then dried in SpeedVac® at room temperature and subsequently purified and concentrated using ZipTip® pipette tips (Millipore Corporation) before being subjected to LC-MS/MS using ESI-QUAD-TOF machine. Proteins were identified using Mascot software.

To confirm the molecular binding of the targeted protein, Surface Plasmon Resonance (SPR) was performed with a Biacore 3000. TRAP1 recombinant protein (Abcam, ab123775) or human Hsp90 recombinant protein (HSP90AB1, Abcam, ab131923) were immobilized on a CM5 sensor chip surface using the amine coupling method according to the manufacturer's instruction (Biacore, GE Healthcare). CVM-1125 was dissolved in sodium carbonate buffer (pH 9) and then diluted in HBS-EDTA-P20 buffer to desired concentrations (five serial dilutions from 1×10^{-5} to 1×10^{-8} M) and injected at flow 30 μL/min with KINJET 60/180 %pos, analyte position, volume, and dissociation time. Specific binding was calculated using BiaEval 3 software.

In silico exploration was performed using Accelrys Discovery Studio 2.1 software. A Protein Data Bank (PDB) format of CVM-1125 was generated using the same program. PDB for TRAP1 (PDB 4Z1G) and CVM-1125 were subjected to CHARM force filed before using Libdock module to look for eventual binding sites. Proteins were thereafter subjected to dynamic stimulation cascade before calculating the binding energy between CVM-1125 and the target.

Succinate level

Succinate levels in the cells were assessed using the Abcam assay kit (ab204718). Cells were grown under hypoxic conditions (1% O_2) at 37°C using a ProOx P110 Oxygen Controller (BioSpherix) and hypoxia chamber to establish a consistent and steady expression of HIF-1α in these cells for the experiments. At 80% confluence, cells were rinsed with phosphate buffered saline (PBS; 137 mM NaCl/2.7 mM KCl/10 mM Na_2HPO_4/1.8 mM KH_2PO_4, pH 7.4), then harvested by scrapping into a modified radio-immunoprecipitation assay (RIPA) buffer (100 mM Tris-HCl, 150 mM NaCl, 1% deoxycholate, 1% Triton X-100, 0.1% SDS, pH 7.4) plus protease inhibitor cocktail (Complete Mini; Roche) using 100 μL buffer per 1×10^6 cells. After sonication using a Fisher sonic dismembrator with microprobe (Fisher Scientific; five pulses at 2 s intervals) and centrifugation at 13,000 rpm for 30 min, the protein lysates (supernatants) were recovered, and protein concentrations determined using a bicinchoninic acid (BCA) assay (Bio-Rad). The samples were then deproteinated using Abcam 10 kDa Spin Columns (ab93349; which reduced the protein concentration by about 90%) and the samples were standardized at <10 μg of protein per sample per 50 μL of assay volume (as directed by the Abcam technical response team for working with these samples). The concentration of succinate (nmol/μL or μmol/mL or nM) for each sample was calculated after subtracting a background control (which was the sample run with assay buffer in place of the succinate converter component to account for and subtract any contaminating signal generated by NADH), as follows: Succinate = (A/B) × D; where: A = Amount of succinate (succinic acid) from the Standard Curve; B = Sample volume added into the reaction well (μL); D = Sample dilution factor. Two separate experiments were performed for each cell line.

Western blotting

The methods for detecting Nodal (in its more stable ProNodal form) and Smad2/P-Smad2 proteins were as follows: 5.0×10^6 human melanoma cells (C8161) were seeded into T175 culture flasks in the presence of 10 nM CVM-1118 and samples recovered for analysis at 1, 4, 8, and 24 h. Cells at 80% confluence were rinsed with PBS, harvested by scrapping into a modified RIPA buffer plus protease inhibitor cocktail using 100 μL buffer per 1×10^6 cells. After sonication and centrifugation, the protein concentrations in the supernatants were determined using a BCA assay (Thermo Fisher Scientific). After addition of lithium dodecyl sulfate sample buffer (NuPage 4X LDS sample buffer; Invitrogen) and heating at 95°C for 5 min, 40 μg (for Nodal detection) or 25 μg (for Smad2/P-Smad2 detection) of protein were loaded per lane of 4%–12% Bis/Tris polyacrylamide electrophoresis gel (NuPAGE; Invitrogen) run with a MES running buffer (Invitrogen) and after separation of the proteins, the proteins electroblotted onto Immobilon-P membranes (Millipore). The blots were then blocked at 37°C with 5% bovine serum albumin (BSA) and then washed. Nodal was detected using a mouse monoclonal anti-Nodal antibody (sc-373910; Santa Cruz; 1 μg/ml in 20 mM

Tris/150 mM NaCl/0.1% [w/v] Tween 20, pH 7.4 [TBST] plus 5% BSA) followed by an anti-mouse plus horseradish peroxidase (HRP) secondary antibody (NXA931; GE Healthcare; 1 μg/ml in TBST plus 5% BSA) and enhanced chemiluminescence (ECL; GE Healthcare). Smad2 was detected using a rabbit polyclonal anti-Smad2/3 antibody (07-408; Millipore; 1 μg/ml in TBST plus 5% BSA) followed by an anti-rabbit plus HRP secondary antibody (NA934V; GE Healthcare; 1 μg/ml in TBST plus 5% BSA) and ECL. The Smad2 blot was then stripped (100 mM 2-mercaptoethanol, 2% [w/v] SDS, 62.5 mM Tris-HCl, pH 6.7 at 50°C for 30 min), washed and re-probed for P-Smad2 using a polyclonal antibody (44–244G; Invitrogen; 1 μg/ml in TBST plus 5% BSA) followed by an anti-rabbit plus HRP secondary antibody (NA934V; 1 μg/ml in TBST plus 5% BSA) and ECL (IT's Science Corporation Ltd., IT96-K004M). The Nodal and Smad2/P-Smad2 blots where then stripped and re-probed with a monoclonal mouse anti-β-actin antibody (MAB1501; Millipore; 0.5 μg/ml in TBST plus 5% BSA) followed by an anti-mouse plus HRP secondary antibody (NXA931; 0.5 μg/ml in TBST plus 5% BSA) and ECL. To assess relative changes in protein expression, the exposed films were digitized using a ChemiDoc XRS imager (Bio-Rad Laboratories) and the relative amount of protein determined against the untreated control cells normalized to a value of 1.0 using the imager's Quantity One software package (Bio-Rad Laboratories) and corrected for loading of protein into each lane against the β-actin protein measured in the control lane.

Changes in the expression HIF-1α protein in SK-MEL28, SK-OV3, MDA-MB-231 and COLO205 cells in response to treatment with CVM-1125 was performed as follows: 5.0×10^6 cells were grown under hypoxic conditions (as previously described) for 72 h, with or without 100 nM CVM-1125 in T175 culture flasks, then sub-confluent cultures harvested and whole cell protein lysates prepared and analyzed by Western blot (as above). Thirty micrograms of protein was loaded per lane of the gel for each sample followed by detection of HIF-1α protein on the final blot using a polyclonal rabbit anti- HIF-1α antibody (#3716; Cell Signaling Technologies), secondary antibody plus HRP (NA934V), then ECL. The blots were then stripped and re-probed for β-actin protein as a control (as above).

The methods for detecting TRAP1 proteins were as follows: 4×10^5 SKOV-3 cells and 8×10^5 COLO-205 cells were seeded onto 6-well plates. After 18 h, the culture medium was changed to contain 50, 100, 200, and 400 nM CVM-1125, and samples were recovered for analysis at 24 or 48 h. To explore the pathway of CVM-1125 degradation of TRAP1 protein, the experimental design was as follows: 1×10^6 COLO-205 cells were seeded onto 6-well plates. After 18 h, the culture medium was changed to contain 200 nM CVM-1125, 25 μM chloroquine (CQ), and 2.5 μM MG132, and samples were recovered for analysis at 24 h. Cells at 80% confluence were collected with trypsin, centrifuged, and harvested by PBS into a sample buffer (1M Tris pH 6.8, 50% Glycerol, 10% SDS, 1% bromophenol blue, and 2-mercaptoethanol). Cell lysates were heated at 95°C for 10 min and loaded onto 10% SDS-PAGE. Proteins separated on the gel were transferred to a 0.45 μM PVDF membrane (Merk Milipore, IPVH00010) at 4°C overnight and was then blocked at room temperature with 5% skim milk for 30 min. The primary antibodies were diluted with 5% skim milk in PBS for β-actin (Sigma, A5441, 1:20,000) and TRAP1 (Santa Cruz, sc-13557, 1:100) and incubated for 2 h at room temperature. The PVDF membranes were then washed and incubated with an anti-mouse-IgG secondary antibody (Sigma, A9044, diluted at 1:3,000 for TRAP1, and 1: 10,000 for β-actin with 5% skim milk) followed by the incubation with ECL. To assess relative changes in protein expression, the exposed films were digitized using a UVP BioSpectrum 500 Imaging System, and the Image J system was used to measure the protein expression. In cells treated with different concentrations of CVM-1125, statistical difference in relative protein expression levels was tested using Kruskal-Wallis test in COLO205 and using one-way ANOVA followed by Dunnett's multiple comparisons test in SKOV3 cells. In COLO205 cells treated with inhibitors in addition to CVM-1125, statistical analysis was conducted using one-way ANOVA followed by Dunnett's multiple comparisons test.

Quantitative polymerase chain reaction (qPCR) analysis

For the qPCR analysis of Nodal and Notch expression, total RNA was isolated from cells using the PerfectPure RNA Cell Isolation kit (5Prime) and then reverse-transcribed using 1 μg RNA, RT master mix cocktail and MMLV reverse transcriptase. qPCR was performed on a 7500 Real-Time PCR System (Life Technologies) using manufacturer recommended protocol. TaqMan gene expression human primer/probe sets (Applied Biosystems) utilized were Nodal (Hs00250630_s1) and Notch4 (Hs00270200_m1). Target gene expression was normalized to appropriate house-keeping genes (e.g., RPLP0 or GAPDH). Data was analyzed using Life Technologies Sequence Detection Software.

For the expression analysis of *STK11* and *NF2* genes, total RNA was isolated from cells using QIAGEN® RNeasy Plus kit and quantified using QuantStudio 3 Real-Time PCR machine. All RT-qPCR reactions were performed in a 20 μL mixture containing 100 ng of RNA template, 1X One-Step RT-qPCR Master Mix (PrimeTime®), and 1X qPCR Assay reagent (premixed primers and probe) (PrimeTime®). Target gene expression was normalized to *ACTB* and the relative RNA fold change between knockdown cell and scramble control cell was analyzed by comparative CT (ΔΔCT) analysis.

Statistical significance between groups was tested using one-way ANOVA followed by Dunnett's multiple comparisons test.

Primers and probes used are as follows:

(1) *NF2*

Probe 5′-/56-FAM/AGCAACCCA/ZEN/AGACGTTCACCGT/3IABkFQ/-3′

Primer 1 5′-TTCCCGCATGAGCTTCAG-3′

Primer 2 5′-GGAGGGCAGTAGATCTTTTCATC-3′

(2) *STK11*

Probe 5′-/56-FAM/TTGTGCCGT/ZEN/AACCTCCTCAGTAGTTG/3IABkFQ/-3′

Primer 1 5′-GCCGTCAAGATCCTCAAGAAG-3′

Primer 2 5′-TCGTTGTATAACACATCCACCAG-3′

(3) *ACTB*

Probe 5′-/5SUN/TCATCCATG/ZEN/GTGAGCTGGCGG/3IABkFQ/-3′

Primer 1 5′-ACAGAGCCTCGCCTTTG-3′

Primer 2 5′-CCTTGCACATGCCGGAG-3

Whole genome CRISPR knock-out screening and validation

This study was conducted by Horizon Discovery (Cambridge, United Kingdom). COLO205 cells were transduced with whole-genome All-In-One high complexity CRISPRko library, containing eight guides per gene, at ×300 coverage. The edited population was selected with puromycin at 0.5 μg/mL for 10 days to remove any non-transduced cells ahead of screening. The screen treatment was conducted with or without 30 nM of CVM-1125, in duplicate, and maintained at 300X coverage for approximately 12 population doublings of the vehicle control condition. At screen endpoint, cell pellets were collected and gDNA was extracted using the QIAamp DNA Blood Maxi kit (Qiagen #51194). A two-step PCR protocol was used to prepare amplicons with Herculase II fusion DNA polymerase (Agilent) using custom primers based on the Illumina system followed by Kapa HiFi HotStart DNA Polymerase (Roche #KK2502) using primers from Nextera XT Index Kit v2; the amplicons were then sequenced by Next-Generation Sequencing (NGS) on an Illumina NextSeq platform. FASTQ files were evaluated for sequencing quality using the Phred scoring system for base-calling accuracy, biological quality control analysis was performed by assessing log2 fold changes of controls including non-targeting control guides, positive/essential genes control guides, and non-essential genes control guides, and then data was deconvoluted and quantified using Horizon Discovery's proprietary mapping scripts based on published analysis tools MAGeCK robust rank aggregation (RRA) (v0.5.9.2) [33] and DrugZ (v.1.1.0.2) [34]. Unbiased hit calling was conducted by comparing samples collected from vehicle control versus drug-treated samples. The gene hits selected from CRISPR knock-out screening were analyzed with DAVID Functional Annotation Bioinformatics Microarray Analysis (ncifcrf.gov) to identify significantly enriched Kyoto Encyclopedia of Genes and Genomes (KEGG) pathways at $p < 0.05$.

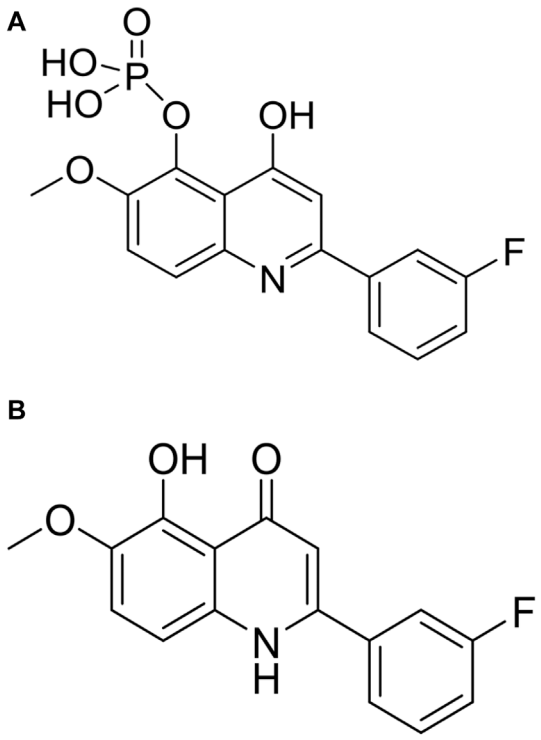

FIGURE 1
The chemical structure of CVM-1118 **(A)** with the molecular formula as $C_{16}H_{13}FNO_6P$, and CVM-1125 **(B)** with the molecular formula as $C_{16}H_{12}FNO_3$.

Further validation of *STK11* and *NF2* by shRNA knockdown system were performed. The lentivirus containing *STK11* or *NF2*-targeting small hairpin RNA (shRNA) was prepared by the National RNAi Core Facility, Academia Sinica (Taipei, Taiwan). The shRNAs targeting *STK11*#sh1 were 5′-GCCAACGTGAAGAAGGAAATT-3′; *STK11*#sh2 was: 5′-CATCTACACTCAGGACTTCAC-3′; *NF2*#sh1 was 5′- TAGTTCTCTGACCTGAGTCTT-3′; *NF2*#sh2 was 5′-GCTCTGGATATTCTGCACAAT-3′. One shRNA was used as the scramble control: 5′-CCTAAGGTTAAGTCGCCCTCG-3′. COLO205 and HCT-116 were transfected with shRNA lentivirus and the knockdown efficiency were evaluated by q-PCR. The viability of the knockdown cells after treatment with CVM-1125 compared to the respective scramble control was evaluated using one-way ANOVA followed by Dunnett's multiple comparisons test.

TABLE 1 Potency of CVM-1118 and its active metabolite, CVM-1125, in human cancer cell lines.

Cell lines	Cancer type	IC_{50} (nM)	
		CVM-1118	CVM-1125
A549	Lung	26	29
DU-145	Prostate	21	27
HT-29	Colon	15	17
MDA-MB-231	Breast	18	14
MDA-MB-435[a]	Melanoma	4	5
Mia PaCa-2	Pancreatic	11	7
NCI-ADR-RES	Ovarian	14	14
SK-N-MC	Neuroblastoma	9	8
U118MG	Glioma	10	8

Cytotoxicity assays performed in nine human cancer cell lines using both CVM-1118 and CVM-1125.
[a]MDA-MB-435 cells are now confirmed of melanoma origin and are derived from M14 melanoma cell line.

Results

CVM-1118 and its active metabolite, CVM-1125, have potent anticancer activity in various cancer cell lines

CVM-1118 (Figure 1A) is currently under development as an oral anti-cancer drug. The pharmacokinetic studies of CVM-1118 in mice, Sprague-Dawley rat and beagle dog indicated that CVM-1118 converted to CVM-1125 (Figure 1B) very rapidly following oral administration (Supplementary Figure S1; Supplementary Table S1). CVM-1125 showed growth inhibitory activity against a panel of 60 human cancer cell lines (NCI 60 screen) with over 80% of cell lines tested had $GI_{50} < 100$ nM. The most sensitive cell lines with $GI_{50} < 50$ nM were listed in Supplementary Table S2. A panel of nine selected human cancer cell lines was further used to compare the anti-proliferative activity of CVM-1118 and CVM-1125. Both compounds showed comparable potent cytotoxicity, with IC_{50} values below 50 nM, in all cell lines (Table 1). The results confirmed the potency of CVM-1118 and its active metabolite, CVM-1125, in growth inhibition and cytotoxicity for further evaluation of its potential use in cancer treatment.

CVM-1118 induces apoptosis and G_2/M arrest *in vitro*

To further elucidate the function of CVM-1118 in cytotoxicity, cell cycle profile analysis with FACS was performed in one of the above tested cell lines, HT-29. The results showed that after 48-h treatment of CVM-1118 in HT-29 cells, there was an accumulation of cells arresting at G_2/M phase, accompanied by a reduction of cells in G_1 phase in a dose-dependent manner (Figure 2). The percentages of G_1 population in 100 nM and 300 nM CVM-1118 treated cells were 16.27% and 1.58%, respectively, compared to 51.93% cells in G_1 phase in control group (Table 2). In addition, 100 nM and 300 nM CVM-1118 treatment increased the population of HT-29 cells in sub-G_1 phase to 26.96% and 22.46%, respectively, compared to control group (1.06%). The endoreduplicated cells (EndoR) were also increased to 2.84% after 100 nM treatment of CVM-1118 compared to the 1.36% in the vehicle control group. These results suggested a dose-dependent effect of CVM-1118 on HT-29 in the inhibition of tumor cell proliferation with a cell cycle arrest at G_2/M phase. Apoptotic cell death indicated by the sub-G_1 peak after treatment also occurred. Similar results in G_2/M arrest and increased sub-G_1 were also observed with the treatment of CVM-1125 in HCT-116 colon cancer cell line (Supplementary Figure S2).

CVM-1118 inhibits human melanoma vasculogenic mimicry signaling molecules

Similar to the results reported previously [10], human melanoma cells VM (*in vitro*) was disrupted beginning with 5 nM of CVM-1118 treatment, and was significantly inhibited by 10 and 50 nM of CVM-1118 treatment at 24 h (Figure 3A). At the CVM-1118 concentration of 10 nM, most of the cells remained viable with the percentage of viable cells to be more than 90%. Thus, the reduction and inhibition of VM formation were the direct result of reduced capability of cells to form VM tubular networks. To understand how CVM-1118 was involved in the inhibition of VM formation mechanically, we analyzed the effect of CVM-1118 on the mRNA levels of two critical signaling proteins, Notch4 ICD and Nodal, in VM formation. The expression of Notch4 ICD and Nodal was decreased in C8161 cells treated with 10 nM of CVM-1118 for 8–72 h (Figures 3B, C). The effect of CVM-1118 on Nodal signaling was also confirmed by a 63% reduction on its protein levels after incubation with CVM-1118 for 24 h (Figure 3D). In addition, 10 nM of CVM-1118 for 24 h also resulted in 76% reduction in the ratio of phosphorylated Smad2 (P-Smad2) to Smad2 protein level (relative to β-actin) against the ratio in control (Figure 3E). Thus, CVM-1118 inhibits VM formation possibly by interfering with the Nodal signaling pathway.

CVM-1118 inhibits formation of vasculogenic mimicry *in vivo*

VM inhibition by CVM-1118 was further assessed in an orthotopic mouse xenograft model using the human HCT-116 colorectal cancer cell line. HCT-116 is one of the sensitive cell

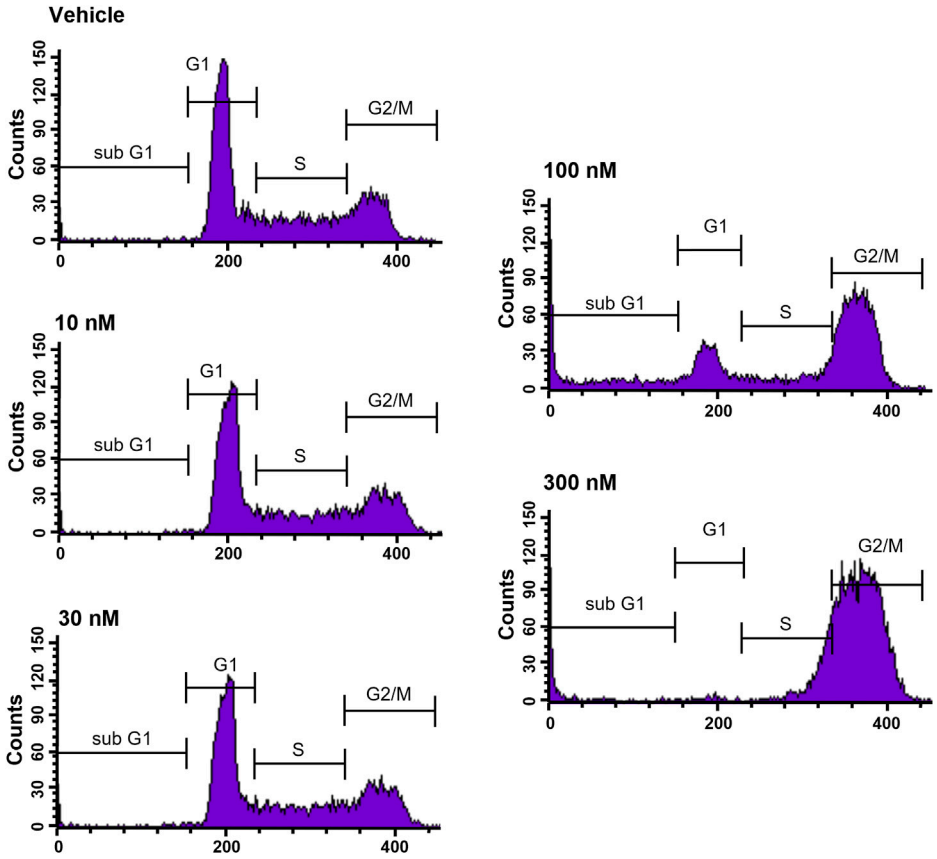

FIGURE 2
CVM-1118 induced cell cycle arrest at G_2/M in HT29 cells. Dose-response of CVM-1118 in HT-29 cell cycle profile after 48 h treatment. Fluorescence signals of propidium iodide (FL3-A) of single cells were attributed to cell cycle phases and converted into percentage of the whole population of single cells (100%).

TABLE 2 Effect of CVM-1118 on cell cycle distribution in HT-29 cells after CVM-1118 treatment for 48 h.

		Cell cycle profile (%)				
Test article		**Sub-G_1**	**G_1 phase**	**S phase**	**G_2/M phase**	**EndoR**
Vehicle Control		1.06	51.93	22.17	23.91	1.36
CVM-1118	10 nM	1.24	49.34	23.02	25.66	1.28
	30 nM	1.44	50.63	23.30	23.71	1.23
	100 nM	26.96	16.27	10.90	43.42	2.84
	300 nM	22.46	1.58	23.63	50.77	2.45

lines with IC_{50} at 33 nM to CVM-1125 (Supplementary Table S2). The animals were treated with CVM-1118 orally or intravenously (i.v.). Body weight loss was observed in all the tested groups, including the vehicle control, which might be caused by the tumor development. One mouse in the 50 mg/kg treatment group, and two mice in the 20 mg/kg i.v. treatment group were found dead prior to the termination of the study which may be due to the above reason. The results showed that tumor volume of vehicle group was 1,139 ± 580 mm^3 on day 43 post tumor inoculation. The tumor volumes were 1,591 ± 747 mm^3, 722 ± 595 mm^3, 475 ± 415 mm^3, and 670 ± 447 mm^3 for the orally 20, 50, and 100 mg/kg treatment groups, and 20 mg/kg i.v. group, respectively. CVM-1118 treatment resulted in inhibition of tumor growth, which appeared to be in a dose-dependent manner (Figure 4A). Further analysis for the numbers of VM channels revealed that CVM-1118 significantly

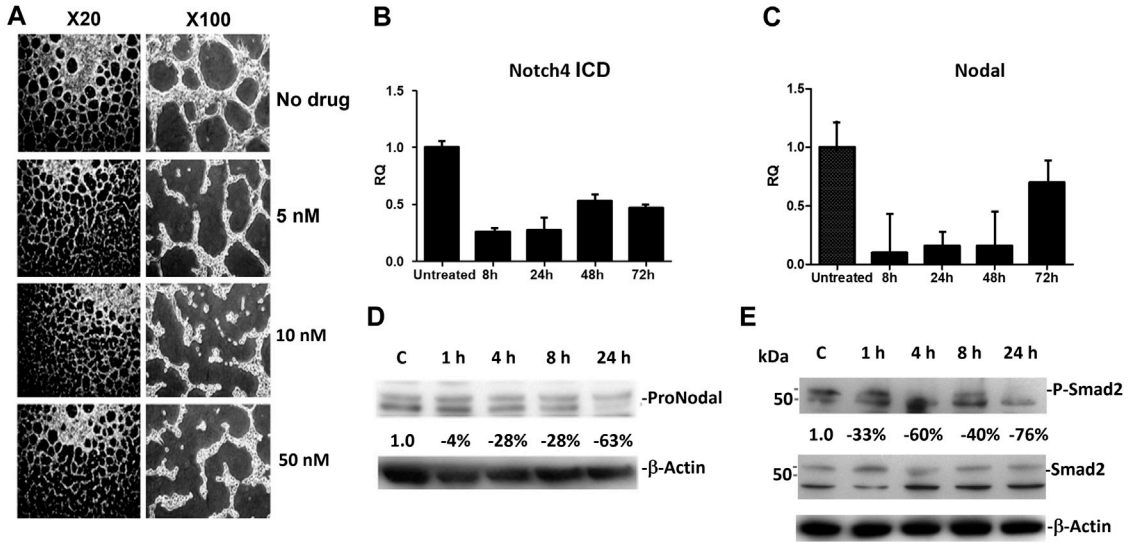

FIGURE 3
Effect of CVM-1118 on vasculogenic mimicry signaling molecules **(A)** *In vitro* standard VM assay in C8161 cells after treatment with CVM-1118 using various concentrations. ×20: 20-fold magnification. ×100: 100-fold magnification. **(B,C)** Quantitative Real Time PCR analysis of Notch4 ICD and Nodal after 10 nM of CVM-1118 treatment for 8, 24, 48, and 72 h in C8161 cells. RQ: Relative quantification of RNA expression level. **(D)** Protein level of ProNodal was determined by Western blot analysis after treatment with 10 nM CVM-1118 for 1, 4, 8, and 24 h. The percentage changes were corrected for protein loading using β-actin. **(E)** Cells were untreated (Control) or treated with 10 nM CVM-1118 for 1, 4, 8, and 24 h. The changes in the expression of Smad2 and phosphorylated Smad2 (P-Smad2) proteins (relative to β-actin) were determined by Western blot analysis. The percentage change is the reduction of protein expression ratio of P-Smad2 to Smad2 protein level relative to β-actin against the ratio in the Control cells.

reduced VM network formation by 85% in excised colon tumor tissues compared with that in vehicle-treated control (Figure 4B). The result further confirmed the role of CVM-1118 in reducing VM formation *in vivo*.

TRAP1 is a direct binding target of CVM-1125—a major metabolite of CVM-1118

To identify direct targets of CVM-1125, NPOT interactome analysis technology was applied to find the direct binding targets of the compound. CVM-1125 was tested in COLO205 and MCF7 cell lines and tissues of human colorectal cancer and melanoma patients (Figure 5A). Mass spectrometry analysis using human proteome database identified 52 different proteins: 30 of which were shared among the four samples (Supplementary Table S3), whereas 22 of which were specific for colorectal cancer clinical tissues (Supplementary Table S4). Eleven proteins which were functionally related to cancer were chosen to confirm the binding via SPR, including: 1) Carcinoembryonic antigen-related cell adhesion molecule 5 (CEACAM5); 2) Transforming growth factor-beta-induced protein ig-h3 (TGFβig-h3); 3) Integrin beta-4; 4) Catenin alpha-2; 5) Integrin beta-2 (CD18); 6) Transforming growth factor beta-1 induced transcript 1 protein (TGFβ1/1) (HIC5); 7) Growth arrest and DNA damage-inducible proteins-interacting protein1 (GADD45GIP1); 8) Catenin beta-1; 9) Nucleolin; 10) TNF receptor associated protein 1 (TRAP1); and 11) Renin receptor (ATP6IP2).

SPR experiments revealed that a dose-dependent interaction exists between immobilized recombinant human TRAP1 protein (Abcam, ab123775) and CVM-1125. The dissociation constant (K_D) between TRAP1 protein and CVM-1125 was estimated to be 6.7×10^{-8} M (Figure 5B), which was the strongest binding affinity of the 11 selected candidates (Table 3). Moreover, *in silico* analysis demonstrated that CVM-1125 interacts with TRAP1 at the N-terminal domain. The interaction pocket is comprised of 11 amino acids all in 10 Å distance from CVM-1125. These amino acids are Phe90, Asn119, Met163, Ser170, Phe205, Tyr206, Val217, Trp231, Phe239, Thr251, and Ile253. *In silico* docking analysis showed at the flourophenyl ring of CVM-1125, it interacts with Trp231 through a hydrogen bond. The hydrogen from CVM-1125 within quinolin forms electrostatic interaction with Val217 (Figure 5C). Since CVM-1125 was shown to bind to the ATP binding pocket of TRAP1, it is speculated that CVM-1125 also binds to other proteins within the Hsp90 family. Thus, SPR analysis using recombinant human Hsp90 beta protein (Abcam, P08238) was performed; however, no specific interaction to CVM-1125 was observed (Figure 5B). This result indicates that CVM-1125 binds to TRAP1 specifically, but not universally to any other heat-shock proteins.

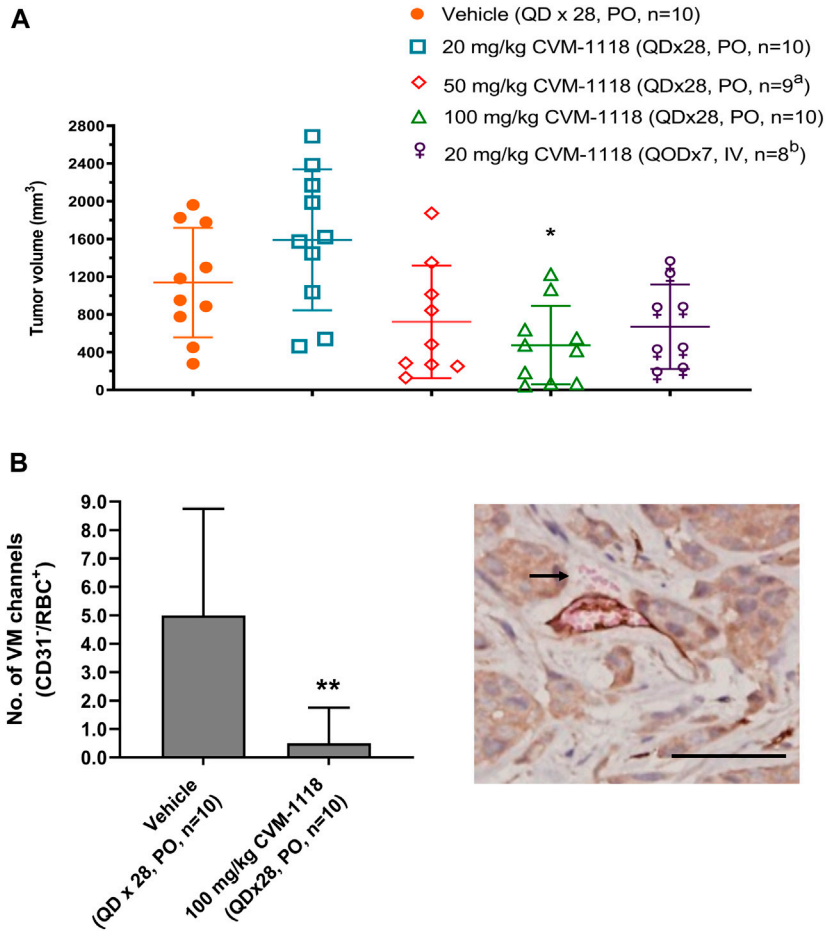

FIGURE 4
Orthotopic HCT-116 mouse xenograft model and *in vivo* vasculogenic mimicry analysis **(A)** Tumor volumes in different groups of orthotopic HCT-116 mouse xenografts on Day 43 after cell inoculation. The bars indicated the mean ± SD. **(B)** Numbers of VM ($CD31^-/RBC^+$) channels of the tumor tissues from two groups of orthotopic HCT-116 mouse xenografts treated with vehicle or 100 mg/kg of CVM-1118. Data indicate median ± interquartile range. Representative photograph shows VM presence with $CD31^-/RBC^+$ staining as indicated by arrow (×400 magnification, scale bar 20 μm). a: one animal was found dead prior to study termination. b: two animals were found dead prior to study termination. *$p < 0.05$, **$p < 0.01$ vs. vehicle.

CVM-1125 reduces TRAP1 protein level *in vitro*

To further investigate the impact of CVM-1125 on TRAP1, the protein level of TRAP1 was analyzed in COLO205, as well as in an ovarian cancer cell line SKOV3 after CVM-1125 treatment. TRAP1 protein levels were reduced with increasing concentrations of CVM-1125 in both COLO205 and SKOV3 cells (Figure 6A). To further clarify how CVM-1125 affects TRAP1 protein, COLO205 cells were co-treated with CVM-1125 and either the lysosomal inhibitor, chloroquine, or the proteasome inhibitor, MG132. The results show that treatment with CVM-1125 alone inhibited the expression of TRAP1 and this effect was abrogated to the same level of vehicle control only in cells co-treated with chloroquine but not with MG132 (Figure 6B). This data demonstrated that the decrease of TRAP1 protein level by CVM-1125 was mediated by the lysosomal degradation system. We further investigated the downstream effect of TRAP1 inhibition. The levels of succinate with or without CVM-1125 treatment in COLO205 and other cell lines were measured. The reduction of succinate levels was observed after treatment with 100 nM CVM-1125 for 72 h–by 18%, 35%, 23%, and 20% in COLO205, SKOV3, SK-MEL28, and MDA-MB-231 cells, respectively, compared to the respective vehicle control (Figure 6C). Consistently, the reduction of HIF-1α protein levels was also observed after treatment with 100 nM CVM-1125—by 9%, 25%, 28%, and 17% in COLO205, SKOV3, SK-MEL28, and MDA-MB-231 cells, respectively (Figure 6D). These results, along with the concurrent observation of a reduction in the accumulation of cellular succinate levels after treating the cells with CVM-1125, suggest that a reduction in accumulated cellular succinate levels may, in part, contribute to the destabilization of HIF-1α.

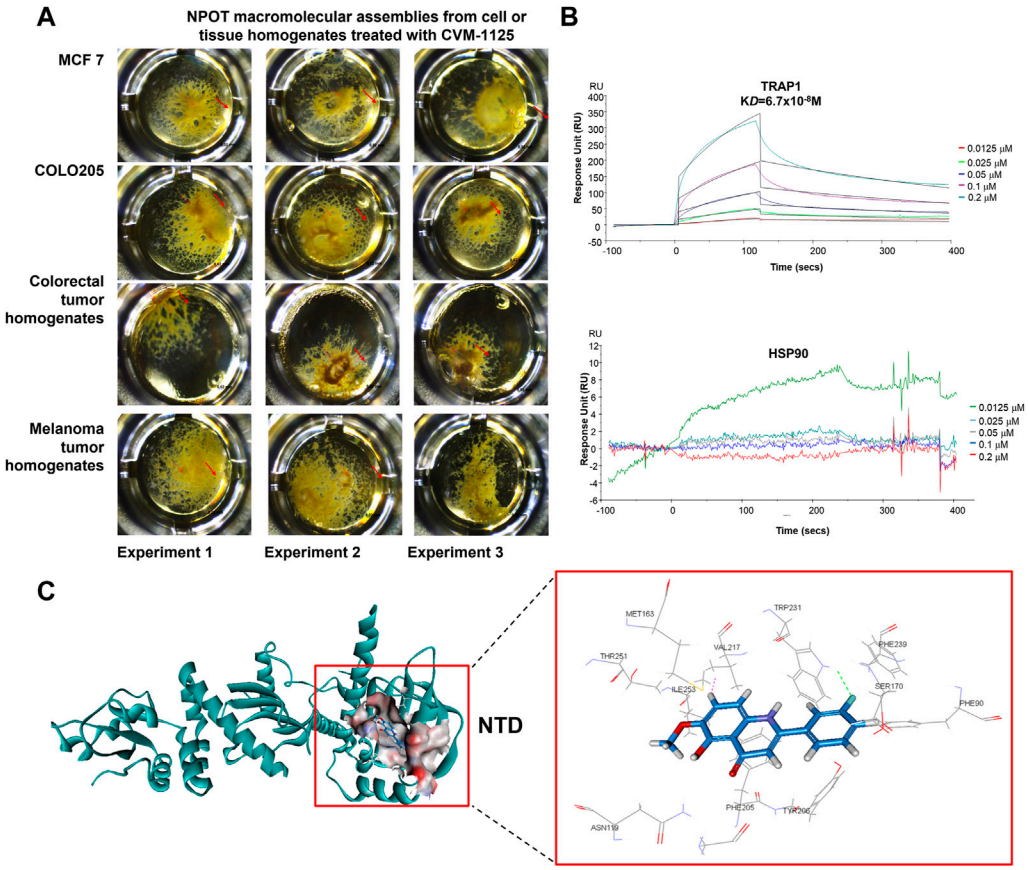

FIGURE 5
CVM-1125 binds strongly to TRAP1 **(A)** To identify CVM-1125 binding target, the NPOT assay was performed on CVM-1125 treated MCF7 and COLO205 cells, as well as the colorectal and melanoma tumor homogenates. The experiments were performed three times independently. Arrows point at the isolated drug specific macromolecular assemblies. **(B)** The binding between TRAP1 and CVM-1125 was confirmed using SPR. There is a dose-dependent interaction between CVM-1125 and the immobilized TRAP1 with K_D of 6.7 × 10^{-8} M. However, no specific interaction of Hsp90 to CVM-1125 was observed. **(C)** *In silico* interaction analysis of CVM-1125 with TRAP1 at the N-terminal domain (NTD).

TABLE 3 Kinetic and affinity constants (*ka*, *kd*, and K_D) to CVM-1125 determined by SPR.

No.	Protein	Association (*ka*) $M^{-1}s^{-1}$	Dissociation (*kd*) s^{-1}	K_D (*kd*/*ka*) M
1	TRAP1	3.02×10^4	2.2×10^{-3}	6.68×10^{-8}
2	ATP6IP2	1.22×10^5	2.1×10^{-2}	1.73×10^{-7}
3	CD18	14.4	1.08×10^{-5}	7.48×10^{-7}
4	Nucleolin	1.35×10^4	1.22×10^{-2}	9.06×10^{-7}
5	Catenin α2	No dose dependent interaction		
6	Integrin β4	No dose dependent interaction		
7	CEACAM5	No interaction		
8	TGFβ1/1	No dose dependent interaction		
9	GADD45GIP1	No interaction		
10	Catenin β-1	No interaction		
11	TGFβig-h3	No interaction		

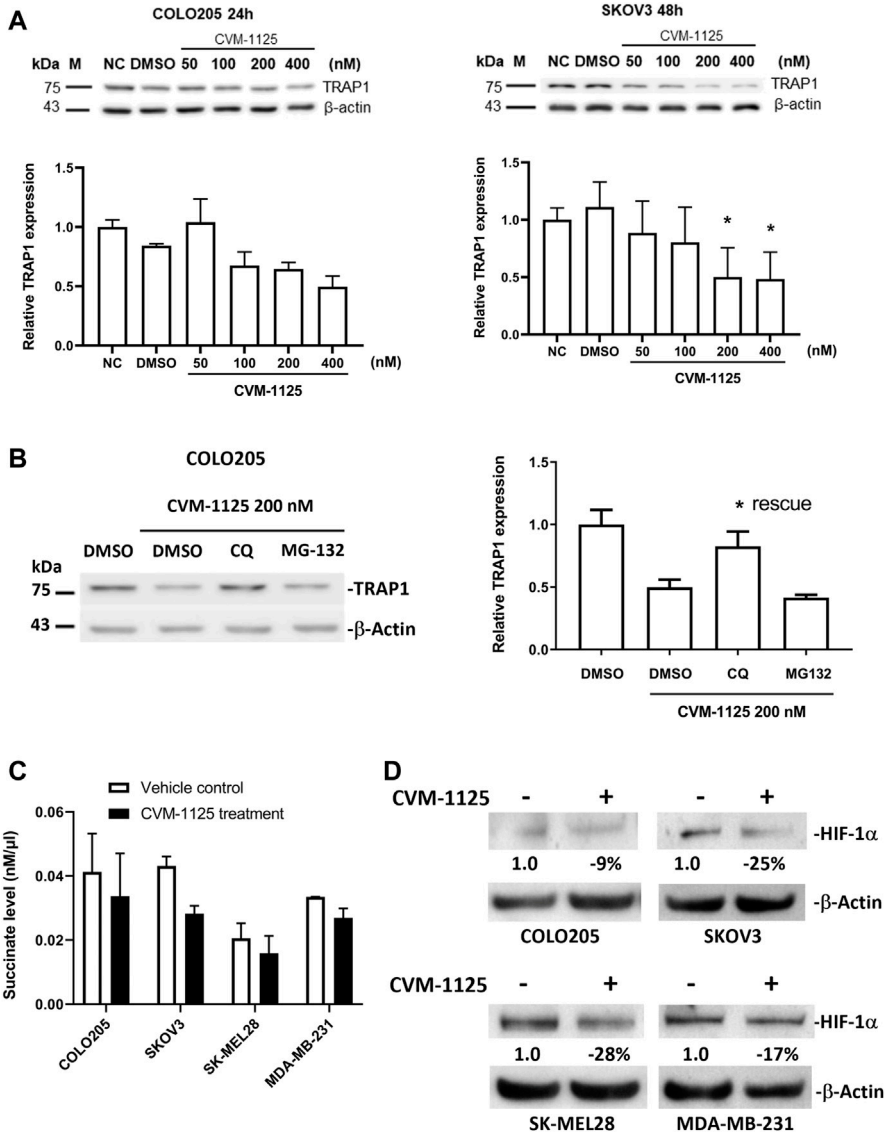

FIGURE 6
Changes of TRAP1, HIF-1α and succinate levels after CVM-1125 treatment **(A)** TRAP1 protein levels, with or without CVM-1125 treatment, in COLO205 and SKOV3 cell lines. The protein level of TRAP1 was examined by Western blot and the relative expression at different treatment concentration was calculated by normalization to β-actin and normal control (NC) set as 1.0. Data represent median ± interquartile range for not normally distributed data in COLO205 cells and mean ± SD for normally distributed data in SKOV3 cells. **(B)** TRAP1 protein levels after treatment with CVM-1125 and chloroquine (CQ) lysosome inhibitor or proteasome inhibitor (MG132) in COLO205 cell line. Relative TRAP1 protein level was calculated by normalization to β-actin and DMSO vehicle control set as 1.0 and is shown in right. Significant difference (* = $p < 0.05$) is shown in the CQ treatment group that rescues the inhibition of TRAP1 expression by CVM-1125 treatment alone ($n = 3$). **(C)** Succinate levels without (Vehicle control) or with CVM-1125 treatment in SK-MEL28, MDA-MB-231, COLO205, and SKOV3 cell lines. **(D)** HIF-1α protein levels without or with CVM-1125 treatment in SK-MEL28, MDA-MB-231, COLO205, and SKOV3 cell lines. The relative amount of HIF-1α protein level was calculated against the untreated control cells normalized to a value of 1.0 after correcting for loading of β-actin protein measured in the control lane.

Identification of pharmacogenomic biomarkers of CVM-1125

To identify pharmacogenomic biomarkers of CVM-1125, a whole genome CRISPR knockout screening was performed in COLO205 cells to identify loss of function perturbations that enhance sensitivity of cancer cells to CVM-1125. The result showed that several hits significantly enhanced the cellular sensitivity to CVM-1125 (Figure 7A). There are 86 common gene hits from the top 100 sensitive and resistance genes obtained by DrugZ and RRA analysis (Supplementary Table S5). We thus further performed KEGG pathway enrichment analysis with

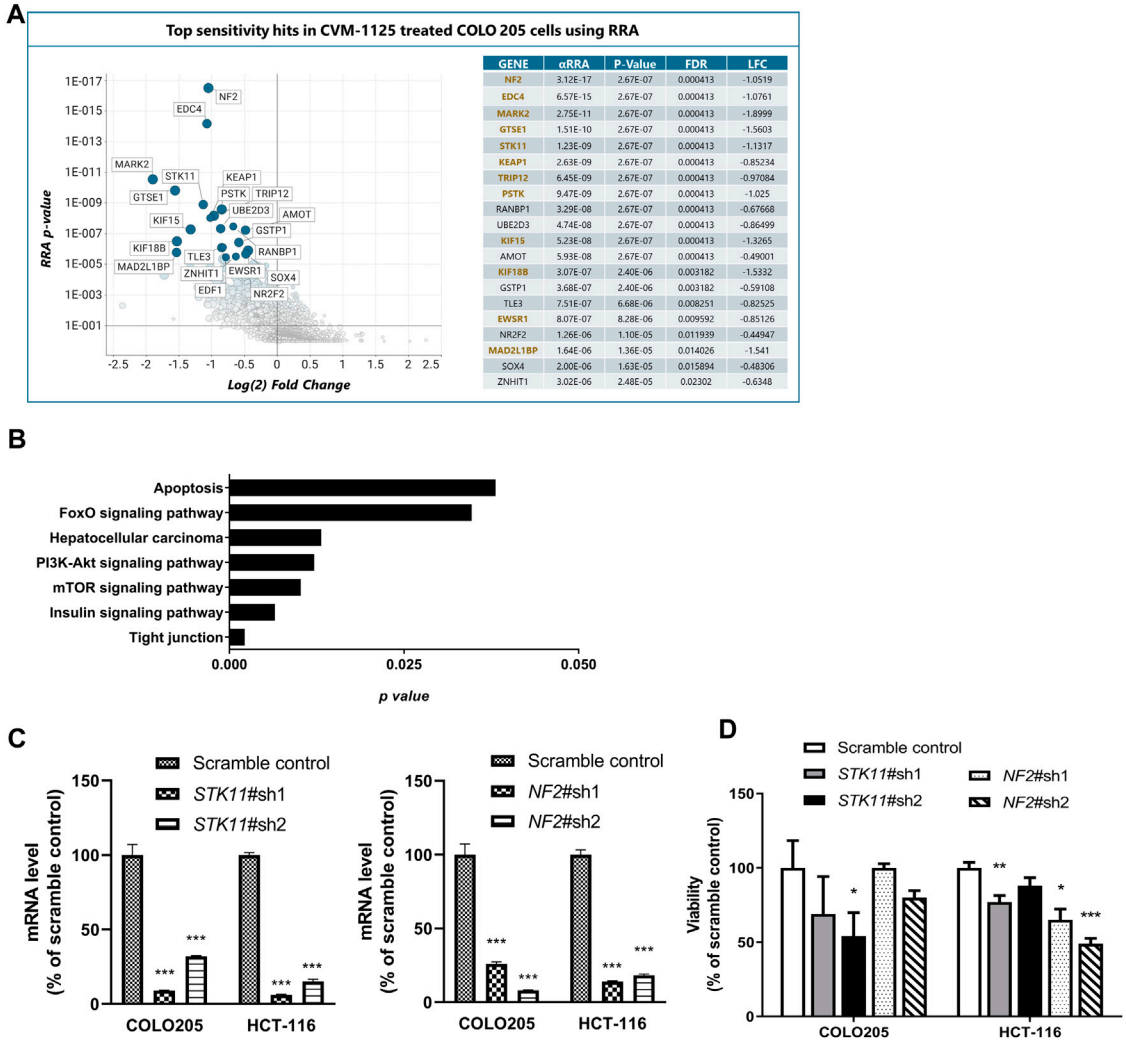

GENE	αRRA	P-Value	FDR	LFC
NF2	3.12E-17	2.67E-07	0.000413	-1.0519
EDC4	6.57E-15	2.67E-07	0.000413	-1.0761
MARK2	2.75E-11	2.67E-07	0.000413	-1.8999
GTSE1	1.51E-10	2.67E-07	0.000413	-1.5603
STK11	1.23E-09	2.67E-07	0.000413	-1.1317
KEAP1	2.63E-09	2.67E-07	0.000413	-0.85234
TRIP12	6.45E-09	2.67E-07	0.000413	-0.97084
PSTK	9.47E-09	2.67E-07	0.000413	-1.025
RANBP1	3.29E-08	2.67E-07	0.000413	-0.67668
UBE2D3	4.74E-08	2.67E-07	0.000413	-0.86499
KIF15	5.23E-08	2.67E-07	0.000413	-1.3265
AMOT	5.93E-08	2.67E-07	0.000413	-0.49001
KIF18B	3.07E-07	2.40E-06	0.003182	-1.5332
GSTP1	3.68E-07	2.40E-06	0.003182	-0.59108
TLE3	7.51E-07	6.68E-06	0.008251	-0.82525
EWSR1	8.07E-07	8.28E-06	0.009592	-0.85126
NR2F2	1.26E-06	1.10E-05	0.011939	-0.44947
MAD2L1BP	1.64E-06	1.36E-05	0.014026	-1.541
SOX4	2.00E-06	1.63E-05	0.015894	-0.48306
ZNHIT1	3.02E-06	2.48E-05	0.02302	-0.6348

FIGURE 7
Identification of Pharmacogenomic Biomarkers of CVM-1125 **(A)** Top sensitivity hits to CVM-1125 (ranked by RRA adjusted *p*-value) are labelled by gene name in the graph on the left and individual metrics are listed in the table on the right. Hit overlap with DrugZ analysis is indicated by gene names in gold. (αRRA: a modified robust rank aggregation algorithm; FDR: false discovery rate; LFC: Log2 of fold change) **(B)** KEGG pathway enrichment was carried out with the top hits. The *p*-value (bar) for each pathway was shown. **(C)** Quantitative PCR analysis of *STK11* or *NF2* mRNA expression in scramble control or shRNA knockdown of COLO205 and HCT-116 cells after approximately 48 h transfection. **(D)** Cell viability was determined by Alamar Blue assay in COLO205 and HCT-116 cells treated with 50 nM CVM-1125 for 72 h. For each bar, the fluorescence of CVM-1125-treated cells was first normalized to the respective vehicle control, then normalized to the scramble control of COLO205 or HCT-116, respectively and presented as percentage viability as shown. Bars indicate the mean ± SD of triplicate analyses. *$p < 0.05$, ***$p < 0.001$ vs. scramble control.

these hits. The results indicated that tight junction, mTOR, insulin, PI3k-AKT, hepatocellular carcinoma, FoxO, and apoptosis pathways ($p < 0.05$) were the possible druggable signaling pathways of CVM-1125 (Figure 7B). From these hits, we further validated two tumor suppressor genes, *STK11* and *NF2*, using shRNA knockdown in COLO205 and HCT-116. The data show that even in these highly CVM-1125-sensitive cancer cell lines, silencing of *STK11* or *NF2* (Figure 7C) was able to induce further reduction in cell viability compared with scramble control (Figure 7D). These results indicate that *STK11* and *NF2* are likely major pharmacogenomic biomarkers of CVM-1118.

Discussion

CVM-1118 is a novel small-molecule drug, currently under Phase 2a clinical development for cancer treatment. Our investigation focused on assessing the effects of CVM-1118 in inhibiting cancer growth and tumor cell vasculogenic mimicry. It

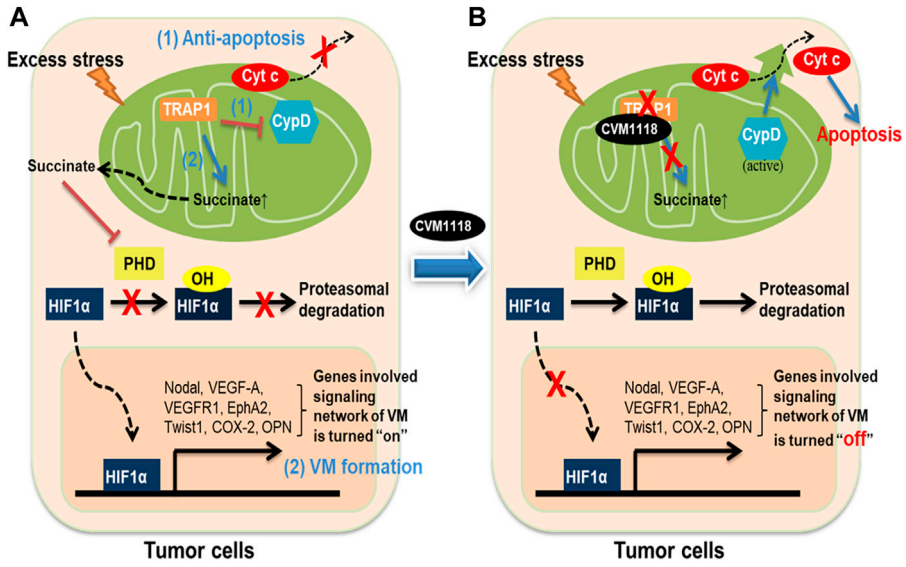

FIGURE 8
Schematic diagram showing the anti-tumor mechanisms of CVM-1118 via targeting TRAP1. Molecular mechanisms in tumor cells to show how TRAP1 mediates anti-apoptosis and promotes VM formation **(A)** and the effects of CVM-1118 treatment **(B)**.

was important to use various cell lines to determine if the mechanistic targets we observed were cell line specific or universal in nature. Since CVM-1118 has been shown to be rapidly and completely metabolized to form active CVM-1125 following administration in animals, further biological tests were conducted using CVM-1125. The cytotoxicity related studies using various cell lines was to demonstrate the ability of CVM-1118/1125 in treating different cancer types. Overall, our study results show that CVM-1118 at low concentrations exhibited not only anti-proliferation and pro-apoptosis activities but also prominent activity in the inhibition of VM formation and VM signaling molecules critical for network tubulogenesis. To further elucidate the molecular mechanism of CVM-1118 as a novel anti-cancer agent, the potential binding targets of CVM-1118 were identified by the NPOT method. Further validation with SPR showed that TRAP1, also named as Hsp75, has the strongest binding affinity to CVM-1125. The binding of CVM-1125 to TRAP1 was also confirmed in a dose-dependent manner.

The mechanism of action of CVM-1125 targeting TRAP1 was examined. A previous report indicated that TRAP1 promotes tumorigenesis by binding to and inhibiting succinate dehydrogenase (SDH), the complex II of the respiratory chain, which subsequently elicits the stabilization of the proneoplastic transcription factor HIF-1α, as a result of succinate accumulation [35]. It was found that CVM-1125 reduced TRAP1 protein level by the lysosomal degradation system and suppressed the downstream signaling of TRAP1 by inhibiting SDH activity to reduce succinate levels, which then increased prolyl hydroxylase activity leading to destabilization of HIF-1α, an important regulator for neoplastic growth and VM formation. Recent studies have demonstrated that a high level of succinate in the tumor microenvironment is an active factor promoting tumorigenesis [36] and cancer metastasis [37]. Thus, developing compounds such as CVM-1118 by targeting the binding to TRAP1 will help reduce the succinate accumulation and prevent tumor progression. It is known that overexpression of TRAP1 exerts its protective function in cancer cells by inhibiting the activation of CypD [38]. Blocking the function of TRAP1 may lead to opening of the mitochondrial permeability transition pore (mPTP) and release cytochrome c from mitochondria into the cytosol and activate the caspase kinase cascade which then leads to cell apoptosis [39]. Previous study showed that using Human Apoptosis Array Kit to measure the expression level of 35 apoptosis-related proteins in CVM-1118 treated cells, the expression levels of eight proteins were elevated with the largest changes in cleaved caspase-3, p27, p21, and phosphorylated p53 [10]. This study further provides the evidence that CVM-1125 binds to TRAP1, which may interfere the interaction of TRAP1 with CypD to negate its protective function, and subsequently induce mitochondrial apoptosis in cancer cells. Therefore, the reduction of TRAP1 protein levels by CVM-1125 may act to obstruct the downstream signaling axis, which contributes to the inhibition of tumor growth and the induction of apoptosis via caspase-3.

Additionally, our previous data showed that CVM-1118 exhibited a distinct ability to reduce VM tubular and branching structures in cancer cells [10]. Here, the *in vivo* data confirmed that CVM-1118 significantly inhibited VM formation in a mouse orthotopic xenograft model of human colon cancer. TRAP1 is known to engage in hypoxia-associated signaling pathways, particularly affecting HIF-1α, a critical transcription

factor responsible for turning on the expression of genes regulating VM formation, e.g., Nodal, VEGF-A, VEGFR1, EphA2, and Twist1. Thus, hyper-expression of TRAP1 facilitates the formation of VM. HIF-1α also stabilizes the Notch intracellular domain (NICD) protein and subsequently activates genes with Notch-responsive promoters, including Nodal. Notch4 and Nodal have been identified as two critical signaling proteins in metastatic melanoma which contribute to VM formation [40]. By inhibition of the Nodal expression, the phosphorylation of Smad2 is decreased and the Smad2-mediated downstream pathway can be inhibited [41]. Here, we confirmed that treating tumor cells with CVM-1125 reduced the downstream factors of TRAP1 including HIF-1α, Nodal, and Notch. In summary, current data support the actions of CVM-1125 on reduction of VM formation via downregulating HIF-1α by targeting TRAP1.

TRAP1 has been regarded as a potential therapeutic target for cancer treatment. Several active compounds were developed as inhibitors for blocking TRAP1's chaperon activity by targeting the ATP binding pocket, such as 17-AAG, Gamitrinib, SMTIN-P01 and DN401 [42–44]. However, proteins within the heat shock protein family share the same protein domain structure, including the ATP binding pocket at the N-terminal domain [45]. These investigational compounds share the same inhibitory activity on Hsp90 due to targeting the highly conserved domain among the HSP family members. Although the *in silico* analysis indicated that CVM-1125 bound to the ATP binding pocket of TRAP1, SPR analysis demonstrated CVM-1125 was not interacting with Hsp90, and the *in vitro* ATPase assay showed no influence on the ATPase activity of TRAP1 (data not shown). Therefore, CVM-1118 is expected to cause fewer off-target effects in clinical applications compared with other TRAP1 inhibitors.

To further explore the usage of CVM-1118 in precision medicine, we performed whole genome CRISPR knockout screen to identify potential pharmacogenomic biomarkers. Several genes were found to be associated with significant improvement of the drug sensitivity in relevant knockout cells. Further analysis of these potential biomarkers by KEGG showed two signaling pathways, mTOR and PI3K-AKT, which were also identified as CVM-1118 druggable signaling pathways in previous work [10]. Here, we validated the two tumor suppressor genes, *STK11* and *NF2*, involved in the mTOR signaling pathway which have been suggested as promising oncogenic therapeutic targets in recent studies [46, 47]. *STK11*, also named *LKB1*, controls the activity of AMP-activated protein kinase (AMPK) by phosphorylation and downregulates mTOR signaling, thereby inhibiting cancer cell proliferation and protein synthesis [48]. *STK11* is also a central regulator of tumor metabolism through the regulation of HIF-1α-dependent metabolic reprogramming [49]. In NSCLC, S*TK11* is the third commonly mutated gene (16% in the Caucasian population) and found to co-mutate with KRAS in 12% of patients [50]. Patients with *STK11*/*KRAS* co-mutation are more resistant to conventional therapies and immunotherapy. Thus, new drug treatment for these patients is needed [51]. Interestingly, in the NCI 60 assay, CVM-1125 exhibited high cytotoxicity in the two NSCLC cancer cell lines (A549 and H460) carrying *STK11* loss-of-function mutation [10, 52]. Similarly, another tumor suppressor gene, *NF2*, was validated as a potential biomarker of CVM-1118. In human schwannomas and meningiomas, loss of *NF2* leads to activation of PI3K/AKT/mTOR and thereby inhibits cancer cell proliferation [53]. It is known that TRAP1 can overcome metabolic stress and promote tumor cell metastasis by inhibiting the activation of AMPK and then activate mTOR signaling [54]. This suggests CVM-1118 may have the potential to treat cancer patients carrying *STK11*- or *NF2*-deficient mutation–via targeting TRAP1 and inhibiting the activation of mTOR/AKT signaling pathways.

In conclusion, these data allow us to propose a mechanism of action for CVM-1118 in the suppression of tumor growth, induction of cell apoptosis, and inhibition of VM formation–via targeting TRAP1 (Figure 8). Here, we found that the action of CVM-1125 on inhibiting TRAP1 protein level impeded succinate accumulation and led to destabilization of HIF-1α. These findings clearly support CVM-1118 as a novel TRAP1 inhibitor with distinctive activity in inhibiting VM formation and is thus considered a promising anti-cancer therapeutic. In addition, from the identified pharmacogenomic biomarkers of CVM-1118, treating cancer patients carrying specific mutations that activate signaling pathways downstream of TRAP1, such as mTOR and AKT, is expected to have a greater drug response that can be further tested in future clinical trials.

Data availability statement

The original contributions presented in the study are included in the article/Supplementary Material, further inquiries can be directed to the corresponding author.

Ethics statement

The animal study was reviewed and approved by Institutional Animal Care and Use Committee (IACUC) of CrownBio International R&D Center, Beijing, China.

Author contributions

LS and C-CH designed study, analyzed data, and drafted the manuscript. Y-CS supervised the studies on TRAP1. RS and ES performed studies on the mechanism of vasculogenic mimicry. MH, Y-LC, D-SC, and Y-WC supervised the studies and edited

the manuscript. All authors contributed to the article and approved the submitted version.

Funding

The authors declare that this study received funding from TaiRx, Inc.. Five employees of this company were involved in the study design, collection, analysis, interpretation of data, and the writing of this article, in collaboration with several scientists from other institutions, but the funder was not involved in the study design, collection, analysis, interpretation of data, the writing of this article, or the decision to publish.

Conflict of interest

Authors LS, Y-LC, C-CH, D-SC, and Y-WC were employed by the company TaiRx, Inc.

The remaining authors declare that the research was conducted in the absence of any commercial or financial relationships that could be construed as a potential conflict of interest.

The authors declare Inoviem Scientific performed the target identification using their own proprietary technology NPOT, and provided valuable discussion on the evaluation and confirmation of the identified target.

Acknowledgments

We acknowledge Inoviem Scientific (Strasbourg, France) to conduct the study of NPOT and *In silico* Target Interaction Studies. We acknowledge National RNAi Core Facility, Academia Sinica (Taipei, Taiwan) for preparation of the lentivirus containing *STK11* and *NF2*-targeting small hairpin RNA (shRNA). Special thanks to Dr. Tiffany Chao, Research Scientist of TaiRx, Inc. in preparing the figures and editing the manuscript.

Supplementary material

The Supplementary Material for this article can be found online at: https://www.por-journal.com/articles/10.3389/pore.2023.1611038/full#supplementary-material

References

1. Chou L-C, Yang J-S, Huang L-J, Wu H-C, Lu C-C, Chiang J-H, et al. The synthesized 2-(2-fluorophenyl)-6,7-methylenedioxyquinolin-4-one (CHM-1) promoted G2/M arrest through inhibition of CDK1 and induced apoptosis through the mitochondrial-dependent pathway in CT-26 murine colorectal adenocarcinoma cells. *J Gastroenterol* (2009) 44:1055–63. doi:10.1007/s00535-009-0111-1

2. Chou LC, Chen CT, Lee JC, Way TD, Huang CH, Huang SM, et al. Synthesis and preclinical evaluations of 2-(2-fluorophenyl)-6,7- methylenedioxyquinolln-4-one monosodium phosphate (CHM-I-P-Na) as a potent antitumor agent. *J Med Chem* (2010) 53:1616–26. doi:10.1021/jm901292j

3. Chou LC, Tsai MT, Hsu MH, Wang SH, Way TD, Huang CH, et al. Design, synthesis, and preclinical evaluation of new 5,6- (or 6,7-) disubstituted-2-(fluorophenyl)quinolin-4-one derivatives as potent antitumor agents. *J Med Chem* (2010) 53:8047–58. doi:10.1021/jm100780c

4. Hour MJ, Huang LJ, Kuo SC, Xia Y, Bastow K, Nakanishi Y, et al. 6-Alkylamino- and 2,3-dihydro-3'-methoxy-2-phenyl-4-quinazolinones and related compounds: Their synthesis, cytotoxicity, and inhibition of tubulin polymerization. *J Med Chem* (2000) 43:4479–87. doi:10.1021/jm000151c

5. Kuo S-C, Lee H-Z, Juang J, Lin Y-T, Wu T-S, Chang J-J, et al. Synthesis and cytotoxicity of 1,6,7,8-substit uted 2-(4'-S ubstit uted phenyl)-4-quinolones and related compounds: Identification as antimitotic agents interacting with tubulin. *J Med Chem* (1993) 39:1146–56. doi:10.1021/jm00061a005

6. Li L, Wang HK, Kuo SC, Wu TS, Mauger A, Lin CM, et al. Antitumor agents 155. Synthesis and biological evaluation of 3',6,7-substituted 2-phenyl-4-quinolones as antimicrotubule agents. *J Med Chem* (1994) 37:3400–7. doi:10.1021/jm00046a025

7. Li L, Wang HK, Kuo SC, Wu TS, Lednicer D, Lin CM, et al. Antitumor agents 150. 2',3',4',5',5,6,7-substituted 2-phenyl-4-quinolones and related compounds: Their synthesis, cytotoxicity, and inhibition of tubulin polymerization. *J Med Chem* (1994) 37:1126–35. doi:10.1021/jm00034a010

8. Xia Y, Yang ZY, Xia P, Bastow KF, Tachibana Y, Kuo SC, et al. Antitumor agents 181. Synthesis and biological evaluation of 6,7,2',3',4'-substituted-1,2,3,4-tetrahydro-2-phenyl-4-quinolones as a new class of antimitotic antitumor agents. *J Med Chem* (1998) 41:1155–62. doi:10.1021/jm9707479

9. Xia Y, Yang ZY, Xia P, Hackl T, Hamel E, Mauger A, et al. Antitumor Agents 211. Fluorinated 2-phenyl-4-quinolone derivatives as antimitotic antitumor agents. *J Med Chem* (2001) 44:3932–6. doi:10.1021/jm0101085

10. Hendrix MJC, Seftor EA, Seftor REB, Chao JT, Chien DS, Chu YW. Tumor cell vascular mimicry: Novel targeting opportunity in melanoma. *Pharmacol Ther* (2016) 159:83–92. doi:10.1016/j.pharmthera.2016.01.006

11. Maniotis AJ, Folberg R, Hess A, Seftor EA, Gardner LM, Pe'er J, et al. Vascular channel formation by human melanoma cells *in vivo* and *in vitro*: Vasculogenic mimicry. *Am J Pathol* (1999) 155:739–52. doi:10.1016/S0002-9440(10)65173-5

12. Wagenblast E, Soto M, Gutiérrez-Ángel S, Hartl CA, Gable AL, Maceli AR, et al. A model of breast cancer heterogeneity reveals vascular mimicry as a driver of metastasis. *Nature* (2015) 520:358–62. doi:10.1038/nature14403

13. Luo Q, Wang J, Zhao W, Peng Z, Liu X, Li B, et al. Vasculogenic mimicry in carcinogenesis and clinical applications. *J Hematol Oncol* (2020) 13:19. doi:10.1186/s13045-020-00858-6

14. Dey N, De P, Brian L-J. Evading anti-angiogenic therapy: Resistance to anti-angiogenic therapy in solid tumors. *Am J Transl Res* (2015) 7:1675–98.

15. Pinto MP, Sotomayor P, Carrasco-Avino G, Corvalan AH, Owen GI. Escaping antiangiogenic therapy: Strategies employed by cancer cells. *Int J Mol Sci* (2016) 17. doi:10.3390/ijms17091489

16. Altieri DC, Stein GS, Lian JB, Languino LR. TRAP-1, the mitochondrial Hsp90. *Biochim Biophys Acta Mol Cel Res* (2012) 1823:767–73. doi:10.1016/j.bbamcr.2011.08.007

17. Song HY, Dunbar JD, Zhang YX, Guo D, Donner DB. Identification of a protein with homology to hsp90 that binds the type 1 tumor necrosis factor receptor. *J Biol Chem* (1995) 270:3574–81. doi:10.1074/jbc.270.8.3574

18. Costantino E, Maddalena F, Calise S, Piscazzi A, Tirino V, Fersini A, et al. TRAP1, a novel mitochondrial chaperone responsible for multi-drug resistance and protection from apoptotis in human colorectal carcinoma cells. *Cancer Lett* (2009) 279:39–46. doi:10.1016/j.canlet.2009.01.018

19. Im CN. Past, present, and emerging roles of mitochondrial heat shock protein TRAP1 in the metabolism and regulation of cancer stem cells. *Cell Stress Chaperones* (2016) 21:553–62. doi:10.1007/s12192-016-0687-3

20. Gesualdi NM, Chirico G, Pirozzi G, Costantino E, Landriscina M, Esposito F. Tumor necrosis factor-associated protein 1 (TRAP-1) protects cells from oxidative stress and apoptosis. *Stress* (2007) 10:342–50. doi:10.1080/10253890701314863

21. Sisinni L, Maddalena F, Lettini G, Condelli V, Matassa DS, Esposito F, et al. TRAP1 role in endoplasmic reticulum stress protection favors resistance to

anthracyclins in breast carcinoma cells. *Int J Oncol* (2014) 44:573–82. doi:10.3892/ijo.2013.2199

22. Yoshida S, Tsutsumi S, Muhlebach G, Sourbier C, Lee MJ, Lee S, et al. Molecular chaperone TRAP1 regulates a metabolic switch between mitochondrial respiration and aerobic glycolysis. *Proc Natl Acad Sci U S A* (2013) 110:E1604–12. doi:10.1073/pnas.1220659110

23. Zhang B, Wang J, Huang Z, Wei P, Liu Y, Hao J, et al. Aberrantly upregulated TRAP1 is required for tumorigenesis of breast cancer. *Oncotarget* (2015) 6: 44495–508. doi:10.18632/oncotarget.6252

24. Megger DA, Bracht T, Kohl M, Ahrens M, Naboulsi W, Weber F, et al. Proteomic differences between hepatocellular carcinoma and nontumorous liver tissue investigated by a combined gel-based and label-free quantitative proteomics study. *Mol Cell Proteomics* (2013) 12:2006–20. doi:10.1074/mcp.M113.028027

25. Li S, Lv Q, Sun H, Xue Y, Wang P, Liu L, et al. Expression of TRAP1 predicts poor survival of malignant glioma patients. *J Mol Neurosci* (2015) 55:62–8. doi:10.1007/s12031-014-0413-5

26. Pak MG, Koh HJ, Roh MS. Clinicopathologic significance of TRAP1 expression in colorectal cancer: A large scale study of human colorectal adenocarcinoma tissues. *Diagn Pathol* (2017) 12:6. doi:10.1186/s13000-017-0598-3

27. Agorreta J, Hu J, Liu D, Delia D, Turley H, Ferguson DJP, et al. TRAP1 regulates proliferation, mitochondrial function, and has prognostic significance in NSCLC. *Mol Cancer Res* (2014) 12:660–9. doi:10.1158/1541-7786.MCR-13-0481

28. Gee MB, Smith PE. Kirkwood-Buff theory of molecular and protein association, aggregation, and cellular crowding. *J Chem Phys* (2009) 131:165101. doi:10.1063/1.3253299

29. Shimizu S, Boon CL. The Kirkwood-Buff theory and the effect of cosolvents on biochemical reactions. *J Chem Phys* (2004) 121:9147–55. doi:10.1063/1.1806402

30. Beyrath J, Pellegrini M, Renkema H, Houben L, Pecheritsyna S, van Zandvoort P, et al. KH176 safeguards mitochondrial diseased cells from redox stress-induced cell death by interacting with the thioredoxin system/peroxiredoxin enzyme machinery. *Sci Rep* (2018) 8:6577. doi:10.1038/s41598-018-24900-3

31. Walf-Vorderwülbecke V, Pearce K, Brooks T, Hubank M, van den Heuvel-Eibrink MM, Zwaan CM, et al. Targeting acute myeloid leukemia by drug-induced c-MYB degradation. *Leukemia* (2018) 32:882–9. doi:10.1038/leu.2017.317

32. Wang L, Eftekhari P, Schachner D, Ignatova ID, Palme V, Schilcher N, et al. Novel interactomics approach identifies ABCA1 as direct target of evodiamine, which increases macrophage cholesterol efflux. *Sci Rep* (2018) 8:11061. doi:10.1038/s41598-018-29281-1

33. Li W, Xu H, Xiao T, Cong L, Love MI, Zhang F, et al. MAGeCK enables robust identification of essential genes from genome-scale CRISPR/Cas9 knockout screens. *Genome Biol* (2014) 15:554. doi:10.1186/s13059-014-0554-4

34. Colic M, Wang G, Zimmermann M, Mascall K, McLaughlin M, Bertolet L, et al. Identifying chemogenetic interactions from CRISPR screens with drugZ. *Genome Med* (2019) 11:52. doi:10.1186/s13073-019-0665-3

35. Sciacovelli M, Guzzo G, Morello V, Frezza C, Zheng L, Nannini N, et al. The mitochondrial chaperone TRAP1 promotes neoplastic growth by inhibiting succinate dehydrogenase. *Cell Metab* (2013) 17:988–99. doi:10.1016/j.cmet.2013.04.019

36. Zhao T, Mu X, You Q. Succinate: An initiator in tumorigenesis and progression. *Oncotarget* (2017) 8:53819. doi:10.18632/ONCOTARGET.17734

37. Wu JY, Huang TW, Hsieh YT, Wang YF, Yen CC, Lee GL, et al. Cancer-derived succinate promotes macrophage polarization and cancer metastasis via succinate receptor. *Mol Cel* (2020) 77:213–27.e5. doi:10.1016/J.MOLCEL.2019.10.023

38. Kang BH. TRAP1 regulation of mitochondrial life or death decision in cancer cells and mitochondria-targeted TRAP1 inhibitors. *BMB Rep* (2012) 45:1–6. doi:10.5483/BMBRep.2012.45.1.1

39. Xie S, Wang X, Gan S, Tang X, Kang X, Zhu S. The mitochondrial chaperone TRAP1 as a candidate target of oncotherapy. *Front Oncol* (2021) 10:585047. doi:10.3389/fonc.2020.585047

40. Hardy KM, Kirschmann DA, Seftor EA, Margaryan NV, Postovit LM, Strizzi L, et al. Regulation of the embryonic morphogen nodal by Notch4 facilitates manifestation of the aggressive melanoma phenotype. *Cancer Res* (2010) 70: 10340–50. doi:10.1158/0008-5472.CAN-10-0705

41. Schier AF. Nodal signaling in vertebrate development. *Annu Rev Cel Dev Biol* (2003) 19:589–621. doi:10.1146/annurev.cellbio.19.041603.094522

42. Kang BH, Plescia J, Dohi T, Rosa J, Doxsey SJ, Altieri DC. Regulation of tumor cell mitochondrial homeostasis by an organelle-specific Hsp90 chaperone network. *Cell* (2007) 131:257–70. doi:10.1016/j.cell.2007.08.028

43. Masgras I, Sanchez-Martin C, Colombo G, Rasola A. The chaperone TRAP1 as a modulator of the mitochondrial adaptations in cancer cells. *Front Oncol* (2017) 7:58. doi:10.3389/fonc.2017.00058

44. Park H-K, Yoon NG, Lee J-E, Hu S, Yoon S, Kim SY, et al. Unleashing the full potential of Hsp90 inhibitors as cancer therapeutics through simultaneous inactivation of Hsp90, Grp94, and TRAP1. *Exp Mol Med* (2020) 52:79–91. doi:10.1038/s12276-019-0360-x

45. Hoter A, El-Sabban ME, Naim HY. The HSP90 family: Structure, regulation, function, and implications in health and disease. *Int J Mol Sci* (2018) 19. doi:10.3390/ijms19092560

46. Mograbi B, Heeke S, Hofman P. The importance of stk11/lkb1 assessment in non-small cell lung carcinomas. *Diagnostics* (2021) 11:196. doi:10.3390/diagnostics11020196

47. Petrilli AM, Fernández-Valle C. Role of Merlin/NF2 inactivation in tumor biology. *Oncogene* (2016) 35:537–48. doi:10.1038/onc.2015.125

48. Shackelford DB, Shaw RJ. The LKB1-AMPK pathway: Metabolism and growth control in tumour suppression. *Nat Rev Cancer* (2009) 9:563–75. doi:10.1038/nrc2676

49. Faubert B, Vincent EE, Griss T, Samborska B, Izreig S, Svensson RU, et al. Loss of the tumor suppressor LKB1 promotes metabolic reprogramming of cancer cells via HIF-1α. *Proc Natl Acad Sci U S A* (2014) 111:2554–9. doi:10.1073/pnas.1312570111

50. Shen H, Zhu M, Wang C. Precision oncology of lung cancer: Genetic and genomic differences in Chinese population. *NPJ Precis Oncol* (2019) 3:14. doi:10.1038/s41698-019-0086-1

51. Wang H, Guo J, Shang X, Wang Z. Less immune cell infiltration and worse prognosis after immunotherapy for patients with lung adenocarcinoma who harbored STK11 mutation. *Int Immunopharmacol* (2020) 84:106574. doi:10.1016/j.intimp.2020.106574

52. Ikediobi ON, Davies H, Bignell G, Edkins S, Stevens C, O'Meara S, et al. Mutation analysis of 24 known cancer genes in the NCI-60 cell line set. *Mol Cancer Ther* (2006) 5:2606–12. doi:10.1158/1535-7163.MCT-06-0433

53. Agnihotri S, Gugel I, Remke M, Bornemann A, Pantazis G, Mack SC, et al. Gene-expression profiling elucidates molecular signaling networks that can be therapeutically targeted in vestibular schwannoma. *J Neurosurg* (2014) 121: 1434–45. doi:10.3171/2014.6.JNS131433

54. Caino MC, Chae YC, Vaira V, Ferrero S, Nosotti M, Martin NM, et al. Metabolic stress regulates cytoskeletal dynamics and metastasis of cancer cells. *J Clin Invest* (2013) 123:2907–20. doi:10.1172/JCI67841

Pathology & Oncology Research | frontiers

TYPE Original Research
PUBLISHED 18 January 2024
DOI 10.3389/pore.2024.1611571

Check for updates

OPEN ACCESS

EDITED BY
Anna Sebestyén,
Semmelweis University, Hungary

*CORRESPONDENCE
Yasutaka Hayashido,
ishidayas@hiroshima-u.ac.jp
Yasutaka Ishida,
hayashiy@hiroshima-u.ac.jp

RECEIVED 31 October 2023
ACCEPTED 09 January 2024
PUBLISHED 18 January 2024

CITATION
Sakurai S, Ishida Y, Shintani T, Yamasaki S, Matsui K, Hamana T, Nobumoto T, Yanamoto S and Hayashido Y (2024), Clinical significance of integrin αV and β superfamily members and focal adhesion kinase activity in oral squamous cell carcinoma: a retrospective observational study.
Pathol. Oncol. Res. 30:1611571.
doi: 10.3389/pore.2024.1611571

COPYRIGHT
© 2024 Sakurai, Ishida, Shintani, Yamasaki, Matsui, Hamana, Nobumoto, Yanamoto and Hayashido. This is an open-access article distributed under the terms of the Creative Commons Attribution License (CC BY). The use, distribution or reproduction in other forums is permitted, provided the original author(s) and the copyright owner(s) are credited and that the original publication in this journal is cited, in accordance with accepted academic practice. No use, distribution or reproduction is permitted which does not comply with these terms.

Clinical significance of integrin αV and β superfamily members and focal adhesion kinase activity in oral squamous cell carcinoma: a retrospective observational study

Shigeru Sakurai[1], Yasutaka Ishida[1]*, Tomoaki Shintani[2], Sachiko Yamasaki[1], Kensaku Matsui[1], Tomoaki Hamana[1], Tadayoshi Nobumoto[1], Souichi Yanamoto[1] and Yasutaka Hayashido[1]*

[1]Department of Oral Oncology, Graduate School of Biomedical and Health Science, Hiroshima University, Hiroshima, Japan, [2]Center of Oral Clinical Examination, Hiroshima University Hospital, Hiroshima, Japan

Objectives: Integrins are heterodimeric transmembrane plasma membrane proteins composed of α- and β-chains. They bind to extracellular matrix (ECM) and cytoskeletal proteins as ECM protein receptors. Upon ECM protein binding, integrins activate focal adhesion kinase (FAK) and transduce various signals. Despite their importance, integrin and FAK expression in oral squamous cell carcinoma (OSCC) tissue and the prognosis of patients with OSCC remains elusive.

Methods: In a retrospective observational study, we immunohistochemically evaluated integrin αV, β1, β3, β5, β6, FAK, and phosphorylated-FAK (pFAK) expressions as prognostic predictors in 96 patients with OSCC. Patients were classified as positive or negative based on staining intensity, and clinicopathologic characteristics and survival rates of the two groups were compared. The association between above integrin-related proteins and PD-1 or PD-L1 in OSCC tissues was investigated.

Results: We observed immunohistochemical integrin αV, β1, β6, β8, and FAK expressions in the cell membrane and cytoplasm but not integrin β3 and β5 in the OSCC tissues. pFAK was expressed in the cytoplasm of OSCC cells. The overall survival rate significantly decreased in pFAK-positive OSCC patients compared to the negative group, and cervical lymph node metastasis significantly increased in integrin β8-positive patients with OSCC ($p < 0.05$). No association between integrin-related proteins and PD-1 or PD-L1 in OSCC tissues was observed.

Conclusion: Our results indicate that pFAK and integrin β8 are prognostic factors for OSCC. Therefore, pFAK- and integrin β8-targeting new oral cancer diagnostic and therapeutic methods hold a promising potential.

KEYWORDS

prognosis, oral squamous cell carcinoma, integrin β superfamily members, FAK signaling pathway, integrin αv

Introduction

Cancer invasion and metastasis are regulated by both the cancer cell characteristics and their interactions with the host, including surrounding stromal cells and components [1–6]. Extracellular matrix (ECM) proteins, major stromal components, are responsible for maintaining tissue and organ architecture and, like humoral factors such as growth factors and cytokines, they exert various biological activities. These activities occur upon integrin binding on the cell membrane and are crucial for cancer invasion and metastasis as regulators of cancer cell growth, proteolytic enzyme production, cell adhesion, and motility [7–11].

Integrins are α and β chain-containing heterodimeric transmembrane proteins with 18 and 8 reported α and β chain types, respectively, forming 24 types of heterodimers [12–14]. The extracellular integrin domain bind ECM proteins while the intracellular binds various cytoskeletal proteins (e.g., talin, α-actinin, and actin filaments) as ECM protein receptors [15–17]. Furthermore, integrins activate focal adhesion kinase (FAK) bound to their intracellular domain β-chain by binding extracellular substrate proteins, thereby transducing various signals [18–22]. Therefore, integrins are not only adhesion molecules between cellular and ECM proteins but also pivotal for organogenesis and tissue differentiation by regulating cell morphology, motility, proliferation, differentiation, and other signal transduction processes [23–27].

The expression of various integrin molecules reportedly correlates with tumor invasion, metastasis, and prognosis in various malignant tumors [8, 10, 28–30]. In particular, the integrin αV family is closely associated with malignant tumor growth and progression [31–35]. We have previously described that integrin αV-high expressing oral squamous cell carcinoma (OSCC) cell proliferation and invasive potential is promoted by type I collagen [36]. Integrin αVβ6 has been studied in more detail in OSCC. Ramos et al. reported that αVβ6 integrin is upregulated in oral cancer, being central to cancer cell migration as well as to reduced fibronectin matrix deposition and assembly [37]. The authors also demonstrated that integrin

TABLE 1 OSCC patients and tumor characteristics.

Characteristics	*N*	%
OSCC patients	96	
Age (Mean ± SD)	66.2 ± 12.9	
Sex		
Male	56	58.3
Female	40	41.7
Localization		
Tongue	31	32.3
Maxillary gingiva	15	15.6
Mandibular gingiva	36	37.5
Buccal mucosa	4	4.2
Plantar of the mouth	10	10.4
UICC stage		
I	10	10.4
II	31	42.4
III	16	9.1
IV	39	30.3
Cervical lymph node metastasis		
Negative	51	53.1
Positive	45	46.9

OSCC, oral squamous cell carcinoma; SD, standard deviation; UICC, international union for cancer control.

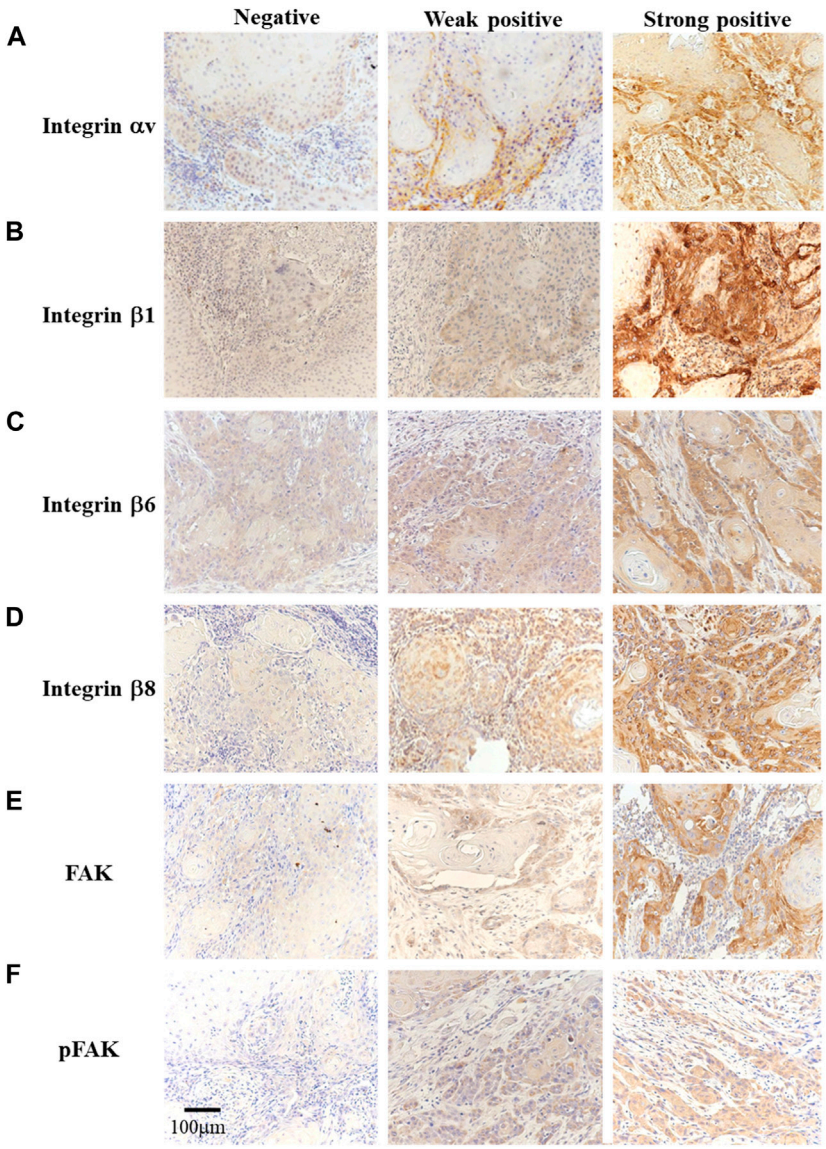

FIGURE 1
Immunohistochemistry for integrin αV, β1, β6, β8, FAK, and pFAK identification [**(A–F)**, original magnification ×200]. The participants were divided into three groups based on the immunostaining results: negative (left), weak positive (center), and strong positive (right).

αVβ6 regulates epithelial-to-mesenchymal transition in oral cancer [38]. Increased αVβ6 integrin and metalloproteinase-3 expression-related alterations in collagen fibers are associated with unfavorable clinical prognostic factors and reduced survival in OSCC [39]. However, integrin β chain expression, function, or prognostic impact in OSCC remain less understood apart from the β6 chain-related aspects [40, 41].

This study aimed at clarifying the relationship between the expression of integrin αV and its counterparts β1, β3, β5, β6, and β8 in OSCC tissues and OSCC progression and prognosis. In addition, we also performed the immunohistochemical assessment of FAK and phosphorylated-FAK (pFAK) expression, closely involved in integrin-mediated signal transduction. Finally, we investigated the relationship between the expression of the abovementioned molecules and that of PD-1 or PD-L1.

Materials and methods

Patients and specimens

Of the 210 patients with OSCC treated by surgical procedures at the Department of Oral and Maxillofacial Surgery, Hiroshima University Hospital between January 2001 and September 2013,

TABLE 2 Comparison of clinical variables between positive and negative groups for integrin or FAK expression.

Characteristics	Integrin αv			Integrin β1			Integrin β6			Integrin β8		
	Negative	Positive	*p*-value	Negative	Positive	*p*-value	Negative	Positive	*p*-value	Negative	Positive	*p*-value
Age (mean ± SD)[a]	66.8 ± 11.1	65.2 ± 13.0	0.55	66.7 ± 13.3	64.1 ± 11.9	0.34	67.4 ± 11.4	64.8 ± 13.7	0.34	67.7 ± 13.5	64.4 ± 12.2	0.22
Sex (male/female)[b]	24/17	32/23	0.97	34/30	22/10	0.14	21/18	35/22	0.46	20/22	36/18	0.06
Localization[b]												
Tongue	12	19	0.59	17	14	0.27	9	22	0.11	15	16	0.46
Maxillary gingiva	8	7		13	2		7	8		7	8	
Mandibular gingiva	13	23		24	12		20	16		17	19	
Buccal mucosa	2	2		3	1		1	3		1	3	
Plantar of the mouth	6	4		7	3		2	8		2	8	
UICC stage[b]												
I	3	7	0.31	8	2	0 65	6	4	0.28	6	4	0.34
II	10	21		21	10		9	22		16	15	
III	8	8		9	7		6	10		5	11	
IV	20	19		26	13		18	21		15	24	

OSCC, oral squamous cell carcinoma; UICC, international union for cancer control; FAK, focal adhesion kinase; pFAK, phosphorylated FAK.

[a]Student's t-test.

[b]Chi-squared test.

10.3389/pore.2024.1611571

TABLE 3 Univariate analysis to determine associations with lymph node metastasis.

Category		Lymphonode metastases		*p*-value[a]
		No	Yes	
Age	<65/65≤	19/32	26/19	0.04*
Integrin αv	Negative/Positive	19/32	22/23	0.25
Integrin β1	Negative/Positive	36/15	28/17	0.39
Integrin β6	Negative/Positive	22/29	17/28	0.59
Integrin β8	Negative/Positive	29/22	13/32	0.01*
FAK	Negative/Positive	24/29	19/28	0.04*
pFAK	Negative/Positive	25/29	20/28	0.59

*$p < 0.05$ (statically significant).
FAK, focal adhesion kinase; pFAK, phosphorylated FAK.
[a]Chi-squared test.

we enrolled in this study with 96 available biopsy specimens for immunohistochemical stainings. The inclusion criteria were as follows: archived prior-to-treatment biopsy sample availability, clinical data, and OSCC pathological diagnosis. Living patients underwent at least 6 months of follow-up care. The exclusion criteria included a history of surgery on the primary tumor, chemotherapy, and radiotherapy. We obtained formalin-fixed and paraffin-embedded (FFPE) tissue samples prior to the treatments. The data collected from the medical chart of the patients included age, sex, site of lesion, treatment details, and disease classification on the TNM classification of the International Union for Cancer Control (UICC), 8th Ed [42]. T and N statuses were assessed using depth of invasion (DOI) and extra nodal extension (ENE) based on histopathological examination of specimens. DOI was microscopically measured by an oral surgeon, whereas ENE was classified as ENE (+) in the presence of soft tissue invasion with strong adherence to underlying muscle/adjacent tissue or clinical signs of nerve invasion. Stages 3 and 4 were defined as advanced.

Immunohistochemical staining

The specific immunohistochemical staining methods we applied in this study have been described previously [43–45]. Supplementary Table S1 summarizes the list of primary and secondary antibodies used in this study.

For staining evaluation, we divided the specimens into three groups according to the staining intensity as follows: 1) no staining at all, 2) weak staining, and 3) strong staining, with group 1 being considered negative while 2 and 3 being judged positive.

Ethical considerations

This retrospective observational study was approved by the Research Ethics Board of Hiroshima University (Approval no. epidemiology 2023-0025). The study protocol was posted on websites. Participants could opt out of the study if they did not wish to provide consent. The need for informed consent was waived.

Statistical analysis

We analyzed the correlations between integrin family, FAK, or pFAK expression and each clinicopathological factor using Chi-squared or Student's t-test. We calculated the survival curves using the Kaplan-Meier method and the log-rank test to assess significant differences in overall survival (OS) rates between integrin family, FAK, and pFAK-negative and positive groups. We analyzed the relation between the expression of the abovementioned integrin-related proteins and that of PD-1 or PD-L1 using chi-square

TABLE 4 Multivariate analysis to determine associations with lymph node metastasis.

Category		Reference	Odd ratio	95% CI		*p*-value[a]
				Lower	Upper	
Age	<65/65≤	65≤	2.24	0.95	5.41	0.06
Integrin αv	Negative/Positive					
Integrin β1	Negative/Positive					
Integrin β6	Negative/Positive					
Integrin β8	Negative/Positive	Positive	0.33	0.13	0.79	0.01*
FAK	Negative/Positive	Positive	0.47	0.17	1.19	0.11
pFAK	Negative/Positive					

*$p < 0.05$ (statically significant).
CI, confidence of interval; FAK, focal adhesion kinase; pFAK, phosphorylated FAK.
[a]Logistic multivariate analysis.

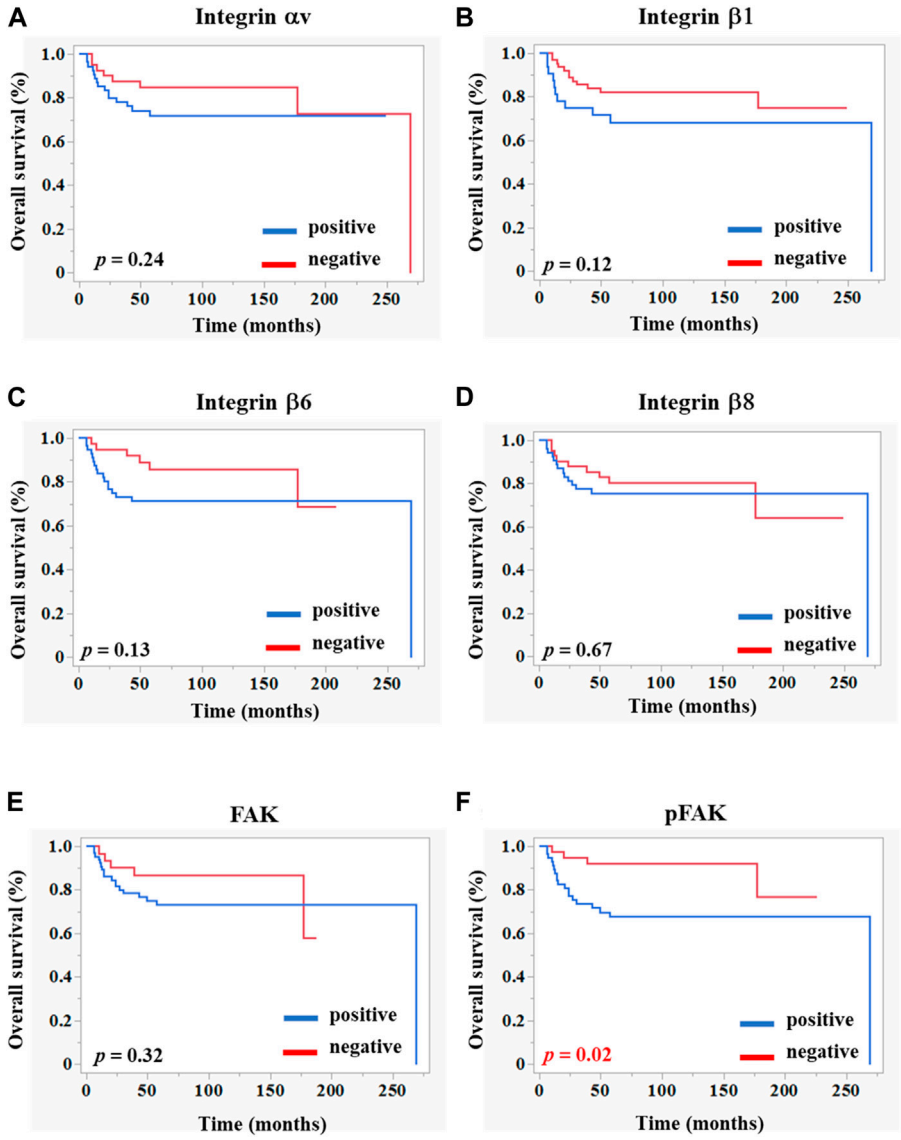

FIGURE 2
Kaplan–Meier curves of overall survivals according to the integrin-related protein expression in OSCC tissues. Each graph indicates the overall survival of patients with OSCC comprising positive (blue line) and negative (red line) groups of integrins **(A–D)**, FAK **(E)**, and pFAK **(F)**. The statistical differences were determined using the log-rank test. $p < 0.05$ (statically significant).

tests. Univariate analysis using the chi-square test was performed to compare clinicopathological variables between groups with and without lymph node metastases. Next, we applied a logistic regression analysis to estimate the odds ratio and 95% confidence interval (CI) of lymph node metastasis that could serve as a risk factor, including age, the positive expressions of integrin β8, or FAK. We evaluated the associations between the examined integrin, FAK, and pFAK expressions as well as the OS rate using the Cox proportional hazards model-estimated hazard ratios with a 95% CI. We performed Cox regression analyses incorporating an interaction term between pFAK and selected patient characteristics (age and stage) to determine if these variables impeded the effect of pFAK expression on the OS rate. We considered differences significant at risk rates of <5% and performed all statistical analyses using the JMP 17 statistical software (SAS Institute Inc., Cary, NC, United States).

Results

Baseline characteristics

Of the 96 patients, 56 and 40 were males and females, respectively, with a mean age of 66 years. By site of onset, 10,

TABLE 5 Univariate and multivariate Cox regression analyses to determine associations with OS.

Category	Univariate analysis					Multivariate analysis				
	Reference	HR	95% CI		*p*-value[a]	Reference	HR	95% CI		*p*-value[a]
			Lower	Upper				Lower	Upper	
Age	65≤	1.1	0.51	2.32	0.82	65≤	0.77	0.36	1.66	0.5
Stage	Advance	0.24	0.09	0.64	0.004*	Advance	0.22	0.08	0.61	0.003*
Integrin α-V	Positive	0.84	0.39	1.83	0.67					
Integrin β1	Positive	0.57	0.27	1.21	0.14					
Integrin β6	Positive	0.48	0.2	1.14	0.1					
Integrin β8	Positive	0.75	0.34	1.65	0.48					
FAK	Positive	0.72	0.31	1.71	0.46					
pFAK	Positive	0.37	0.15	0.92	0.03*	Positive	0.35	0.14	0.87	0.02*

*$p < 0.05$ (statically significant).
[a]Cox proportional hazards model.
HR, hazard ratio; CI, confidence of interval; FAK, focal adhesion kinase; pFAK, phosphorylated FAK.

TABLE 6 Comparison of PD-1 or PD-L1 expression between positive and negative groups for integrin or FAK expression.

Category	PD-L1			PD-1		
	Positive	Negative	*p*-value[a]	Positive	Negative	*p*-value[a]
Integrin αv (positive/negative)	6/9	22/20	0.41	12/9	17/21	0.42
Integrin β1 (positive/negative)	3/12	11/31	0.63	3/18	11/27	0.19
Integrin β6 (positive/negative)	8/7	26/16	0.56	15/6	20/18	0.15
Integrin β8 (positive/negative)	9/6	23/19	0.73	13/8	21/17	0.62
FAK (positive/negative)	9/6	27/15	0.77	16/5	22/16	0.15
pFAK (positive/negative)	8/7	21/21	0.82	11/10	18/20	0.71

FAK, focal adhesion kinase; pFAK, phosphorylated FAK; PD-1, programmed cell death 1, PD-L1 PD-ligand 1.
[a]Chi-squared test.

15, 36, 4, and 31 patients had carcinoma of the floor of the mouth, maxillary gingival carcinoma, mandibular gingival carcinoma, buccal mucosa carcinoma, and tongue carcinoma, respectively. N0–3 cervical lymph node metastases could be observed in 51, 17, 28, and 45 patients, respectively. Finally, 10, 31, 16, and 39 patients were in Stages I–IV, respectively (Table 1).

Expression of integrins, FAK, and pFAK in OSCC

First, we immunohistochemically investigated integrin αV and β superfamily member expressions and FAK activity in OSCC. Integrin αV, β1, β6, and β8 expressions localized in the cell membrane and cytoplasm of OSCC cells in the weak- and strong-positive groups, but not in the negative group (Figure 1) while no expression of integrin β3 and β5 was found in FFPE tissue from OSCC patients in this study. FAK was expressed in the OSCC cell membrane and cytoplasm while pFAK in the cytoplasm in the weak- and strong-positive groups, but not in the negative group (Figure 1).

Comparison of clinicopathological variables between integrin-, FAK-, and pFAK-negative and positive groups

Next, we compared the clinical variables between the positive and negative groups for each integrin-related proteins. The FAK-positive group exhibited significantly more advanced stages than the negative group (Table 2, $p < 0.05$). We observed no significant differences in other clinical variables between the integrin αV, β1, β6, FAK, and pFAK-positive and negative groups.

Prognosis comparison between integrin-, FAK-, and pFAK-positive and negative groups

We compared cervical lymph node metastasis and OS rate between the positive and negative groups for each integrin-related molecule. Our univariate analysis indicated significantly more subjects with lymph node metastasis at the baseline in the integrin β8-positive compared to the negative group (Table 3, $p < 0.05$). We changed the applied variables for our multivariate logistic regression analysis (Table 4) and observed that the integrin β8 expression was independently associated with cervical lymph node metastasis (odds ratio 0.33, 95% CI 0.13–0.79, $p < 0.05$).

The OS rate was significantly lower in the pFAK expression–positive group than in the–negative group (Figure 2). We conducted Cox regression analyses incorporating an interaction term between age, stage, and immunostaining expression of each molecule and demonstrated a significant correlation between the hazard ratio of the pFAK-positive group (hazard ratio 0.35, 95% CI 0.14–0.87, $p < 0.05$) and the OS rate in our multivariate analysis (Table 5).

Relation between the expression of integrin family members, FAK and pFAK, and that of PD-1 and PD-L1 in OSCC

We examined the relation between the expression of integrin family members, FAK and pFAK, and that of PD-1 and PD-L1 in OSCC using immunostaining for PD-1 and PD-L1 (Supplementary Figure S1). However, no significant relationship was found between the expression levels of these molecules (Table 6). We also evaluated the OS rates based on PD-1 or PD-L1 expression in groups with or without the expressions of each inregrin-related molecule in OSCC; however, no significant differences were observed (Supplementary Figures S2, S3).

Discussion

Integrins are heterodimeric plasma membrane proteins consisting of two transmembrane subunits (α- and β-chain). As ECM protein receptors, integrins regulate cell adhesion to the ECM and also transmit signals that regulate cell growth, differentiation, and motility [11–13]. Integrins are central to cancer invasion and metastasis as tumorigenesis, cancer cell motility, and proteolytic enzyme production regulators [46–48]. Therefore, we investigated whether integrins, FAK, or pFAK expression could serve as prognostic biomarkers for OSCC.

Multiple studies documented that integrin αV family members are closely associated with malignant tumor growth and progression [31–35]. Among them, integrin αVβ3 reportedly regulates proteolytic activity on cancer cell membranes as a plasma membrane receptor for active matrix metalloproteinase-2 (MMP-2), beyond acting as a cancer cell motility and promoter of angiogenic factor [49]. We have previously demonstrated that integrin αV is a plasma membrane receptor for active MMP-2 and that type I collagen activates FAK and MEK/ERK in OSCC cells via integrin αV, thereby increasing their proliferation [36, 50]. In this study, we examined the immunohistochemical expression of integrin αV and its counterpart integrins β1, β3, β5, β6, and β8 in resected tissue before treatment, then analyzed their association with clinicopathological factors, stage classification, and the OS rate. In addition, we examined FAK and pFAK expressions, involved in integrin-mediated signal transduction as well as malignant tumor growth and prognosis, in OSCC tissues and their association with the abovementioned clinical variables. Our results showed that integrin αV, β1, β6, and β8 were expressed in OSCC cells, but integrin β3 and β5 were not. To date, no studies reported integrin β3 or β5 protein expression in OSCC tissue. Kurokawa et al. reported that the integrin β5 mRNA is expressed in OSCC tissues [51]. Furthermore, it has been reported that the integrin β5 mRNA is also expressed in OSCC-derived cultured cells [52]. These discrepancies need to be examined in the future. We observed no statistically significant differences in gender, age, stage classification, or tissue differentiation between the integrin αV, β1, β6, and β8 positive and negative groups. Metastasis to the regional lymph nodes was significantly higher in the integrin β8-positive than that in the negative group, confirming our previous findings [36]. However, our comparison of the OS rate between the positive and negative groups for each integrin expression indicated no significant difference between the two groups.

Integrins bind to ECM proteins such as laminin and fibronectin in the extracellular domain, whereas the intracellular domain binds various signaling factors and actin-binding proteins directly or indirectly [15–17]. Integrins themselves do not exert any kinase activity, but when cells bind extracellular matrix proteins via integrins, FAK, an intracellular domain-binding protein of integrins, is activated, leading to mitogen- (MAP) kinase activation, thereby regulating cell proliferation as well as PI3-Akt pathway and Rho family small G protein activation, which regulate cell survival and cell motility and intracellular skeletal reorganization, respectively [18–22, 53]. We previously described that culturing integrin αV-overexpressing SCCKN cells transfected with the αV gene on type I collagen induced rapid FAK, MEK, and ERK1/2 phosphorylation compared to the control [36]. The OS rate in patients with OSCC was significantly lower in the pFAK-positive than in the negative group. No previous studies reported that integrin β8 or pFAK expression would play any role in the prognosis of patients with OSCC. To assess the predictive

potential of integrins in immunotherapy, some studies have examined their association with immunological markers, including PD1, PD-L1, and TILs [54–57]. In gastric cancer, high expression levels of integrin β5 have been linked to poor prognosis and have been identified as an independent prognostic factor. Moreover, integrin β5 expression was positively correlated with the infiltration levels of $CD4^+$ T cells, macrophages, and dendritic cells, particularly where lower macrophage infiltration led to improved prognosis in gastric cancer [54]. In patients with gastric cancer, integrin β1 and PD-L1 expression levels were correlated, as confirmed at the protein level via immunohistochemical analysis [57]. Subgroups with higher expression levels of integrin β4/PD-L1 and CD8/PD-1 in oral cancer exhibited a relatively better prognosis than other subgroups [56]. Therefore, we conducted IHC analysis to explore the correlation of integrin, FAK, and pFAK expression levels with PD-1 or PD-L1 expression. Although there was a trend toward a higher survival rate in the integrin- or FAK-negative group/PD-1- or PD-L1-positive group, this difference was not statistically significant.

This study has some limitations that must be considered. First, as it is a single-center, retrospective case-controlled study with a small sample size, regional bias might occur. Second, intratumor heterogeneity could affect integrin, FAK, and pFAK expression assessment. Third, basic factors such as smoking history, alcohol consumption history, and systemic diseases were not considered. Finally, because this was a retrospective study, the assessment of DOI for TNM classification (UICC 8th edition) at baseline was performed using histopathological specimens, which may differ from the assessment based on clinical findings.

Our results indicated significantly lower OS rates in pFAK-positive patients with OSCC compared to their negative counterparts, and cervical lymph node metastasis significantly increased in integrin β8-expressing patients with OSCC. Our results indicate that pFAK could be used as a potent prognostic factor for the OS rate and integrin β8 as a predictor of regional lymph node metastasis in patients with OSCC. We believe there is future potential for the development of new diagnostic and therapeutic methods for oral cancer targeting integrin β8 and pFAK.

Data availability statement

The original contributions presented in the study are included in the article/Supplementary Material, further inquiries can be directed to the corresponding authors.

Ethics statement

The studies involving humans were approved by Research Ethics Board of Hiroshima University. The studies were conducted in accordance with the local legislation and institutional requirements. The ethics committee/institutional review board waived the requirement of written informed consent for participation from the participants or the participants' legal guardians/next of kin because This is the retrospective study. Written informed consent was not obtained from the individual(s) for the publication of any potentially identifiable images or data included in this article because This was a retrospective study.

Author contributions

SS and YH designed the experiments. SS, YH, KM, YI, TH, TN, and SaY performed the experiments. SS, YI, TS, SoY, and YH wrote and reviewed the manuscript. All authors contributed to the article and approved the submitted version.

Conflict of interest

The authors declare that the research was conducted in the absence of any commercial or financial relationships that could be construed as a potential conflict of interest.

Supplementary material

The Supplementary Material for this article can be found online at: https://www.por-journal.com/articles/10.3389/pore.2024.1611571/full#supplementary-material

References

1. Chrenek MA, Wong P, Weaver VM. Tumour-stromal interactions. Integrins and cell adhesions as modulators of mammary cell survival and transformation. *Breast Cancer Res* (2001) 3:224–9. doi:10.1186/bcr300

2. He Y, Liu XD, Chen ZY, Zhu J, Xiong Y, Li K, et al. Interaction between cancer cells and stromal fibroblasts is required for activation of the uPAR-uPA-MMP-2 cascade in pancreatic cancer metastasis. *Clin Cancer Res* (2007) 13:3115–24. doi:10.1158/1078-0432.Ccr-06-2088

3. Ingber DE. Cancer as a disease of epithelial-mesenchymal interactions and extracellular matrix regulation. *Differentiation* (2002) 70:547–60. doi:10.1046/j.1432-0436.2002.700908.x

4. Mahadevan D, Von Hoff DD. Tumor-stroma interactions in pancreatic ductal adenocarcinoma. *Mol Cancer Ther* (2007) 6:1186–97. doi:10.1158/1535-7163.Mct-06-0686

5. Shekhar MP, Pauley R, Heppner G. Host microenvironment in breast cancer development: extracellular matrix-stromal cell contribution to neoplastic phenotype of epithelial cells in the breast. *Breast Cancer Res* (2003) 5:130–5. doi:10.1186/bcr580

6. Smillie CS, Biton M, Ordovas-Montanes J, Sullivan KM, Burgin G, Graham DB, et al. Intra- and inter-cellular rewiring of the human colon during ulcerative colitis. *Cell* (2019) 178:714–30. doi:10.1016/j.cell.2019.06.029

7. Ahmad K, Lee EJ, Shaikh S, Kumar A, Rao KM, Park SY, et al. Targeting integrins for cancer management using nanotherapeutic approaches: recent advances and challenges. *Semin Cancer Biol* (2021) 69:325–36. doi:10.1016/j.semcancer.2019.08.030

8. Kechagia JZ, Ivaska J, Roca-Cusachs P. Integrins as biomechanical sensors of the microenvironment. *Nat Rev Mol Cel Biol* (2019) 20:457–73. doi:10.1038/s41580-019-0134-2

9. Lewczuk Ł, Pryczynicz A, Guzińska-Ustymowicz K. Cell adhesion molecules in endometrial cancer - a systematic review. *Adv Med Sci* (2019) 64:423–9. doi:10.1016/j.advms.2019.08.003

10. Bair EL, Massey CP, Tran NL, Borchers AH, Heimark RL, Cress AE, et al. Integrin- and cadherin-mediated induction of the matrix metalloprotease matrilysin in cocultures of malignant oral squamous cell carcinoma cells and dermal fibroblasts. *Exp Cel Res* (2001) 270:259–67. doi:10.1006/excr.2001.5347

11. Berry MG, Gui GP, Wells CA, Carpenter R. Integrin expression and survival in human breast cancer. *Eur J Surg Oncol* (2004) 30:484–9. doi:10.1016/j.ejso.2004.01.016

12. Takada Y, Ye X, Simon S. The integrins. *Genome Biol* (2007) 8:215. doi:10.1186/gb-2007-8-5-215

13. Barczyk M, Carracedo S, Gullberg D. Integrins. *Cell Tissue Res.* (2010) 339:269–80. doi:10.1007/s00441-009-0834-6

14. Fu G, Wang W, Luo BH. Overview: structural biology of integrins. *Methods Mol Biol* (2012) 757:81–99. doi:10.1007/978-1-61779-166-6_7

15. Zhang P, Azizi L, Kukkurainen S, Gao T, Baikoghli M, Jacquier MC, et al. Crystal structure of the FERM-folded talin head reveals the determinants for integrin binding. *Proc Natl Acad Sci U S A* (2020) 117:32402–12. doi:10.1073/pnas.2014583117

16. Ziegler WH, Gingras AR, Critchley DR, Emsley J. Integrin connections to the cytoskeleton through talin and vinculin. *Biochem Soc Trans* (2008) 36:235–9. doi:10.1042/bst0360235

17. Svitkina T. The actin cytoskeleton and actin-based motility. *Cold Spring Harb Perspect Biol* (2018) 10:a018267. doi:10.1101/cshperspect.a018267

18. Huang Y, Liao J, Vlashi R, Chen G. Focal adhesion kinase (FAK): its structure, characteristics, and signaling in skeletal system. *Cell Signal* (2023) 111:110852. doi:10.1016/j.cellsig.2023.110852

19. Peterman E, Gibieža P, Schafer J, Skeberdis VA, Kaupinis A, Valius M, et al. The post-abscission midbody is an intracellular signaling organelle that regulates cell proliferation. *Nat Commun* (2019) 10:3181. doi:10.1038/s41467-019-10871-0

20. Mitra SK, Schlaepfer DD. Integrin-regulated FAK-Src signaling in normal and cancer cells. *Curr Opin Cel Biol* (2006) 18:516–23. doi:10.1016/j.ceb.2006.08.011

21. Hehlgans S, Haase M, Cordes N. Signalling via integrins: implications for cell survival and anticancer strategies. *Biochim Biophys Acta* (2007) 1775:163–80. doi:10.1016/j.bbcan.2006.09.001

22. Wang S, Basson MD. Integrin-linked kinase: a multi-functional regulator modulating extracellular pressure-stimulated cancer cell adhesion through focal adhesion kinase and AKT. *Cell Oncol* (2009) 31:273–89. doi:10.3233/clo-2009-0469

23. Cavallaro U, Dejana E. Adhesion molecule signalling: not always a sticky business. *Nat Rev Mol Cel Biol* (2011) 12:189–97. doi:10.1038/nrm3068

24. Mobley AK, McCarty JH. Use of cre-lox technology to analyze integrin functions in astrocytes. *Methods Mol Biol* (2012) 814:555–70. doi:10.1007/978-1-61779-452-0_37

25. Bökel C, Brown NH. Integrins in development: moving on, responding to, and sticking to the extracellular matrix. *Dev Cel* (2002) 3:311–21. doi:10.1016/s1534-5807(02)00265-4

26. Juliano RL, Reddig P, Alahari S, Edin M, Howe A, Aplin A. Integrin regulation of cell signalling and motility. *Biochem Soc Trans* (2004) 32:443–6. doi:10.1042/bst0320443

27. Raymond K, Faraldo MM, Deugnier MA, Glukhova MA. Integrins in mammary development. *Semin Cel Dev Biol* (2012) 23:599–605. doi:10.1016/j.semcdb.2012.03.008

28. Kelly AJ, Long A. Targeting T-cell integrins in autoimmune and inflammatory diseases. *Clin Exp Immunol* (2023) 215:15–26. doi:10.1093/cei/uxad093

29. Vay C, Hosch SB, Stoecklein NH, Klein CA, Vallböhmer D, Link BC, et al. Integrin expression in esophageal squamous cell carcinoma: loss of the physiological integrin expression pattern correlates with disease progression. *PLoS One* (2014) 9:e109026. doi:10.1371/journal.pone.0109026

30. Zhang PF, Zeng GQ, Yi LZ, Liu JP, Wan XX, Qu JQ, et al. Identification of integrin β1 as a prognostic biomarker for human lung adenocarcinoma using 2D-LC-MS/MS combined with iTRAQ technology. *Oncol Rep* (2013) 30:341–9. doi:10.3892/or.2013.2477

31. Khan S, Qadir M, Khalid A, Ashraf S, Ahmad I. Characterization of cervical tissue using mueller matrix polarimetry. *Lasers Med Sci* (2023) 38:46. doi:10.1007/s10103-023-03712-6

32. Fukumoto T, Sakaguchi M, Oka M, Nishimura M, Mukohara T, Nishigori C. Malignant melanoma with bone marrow involvement diagnosed from hypercalcemia: development of a neural cell adhesion molecule stain. *J Dermatol* (2017) 44:e105–6. doi:10.1111/1346-8138.13718

33. Koistinen P, Ahonen M, Kähäri VM, Heino J. AlphaV integrin promotes *in vitro* and *in vivo* survival of cells in metastatic melanoma. *Int J Cancer* (2004) 112:61–70. doi:10.1002/ijc.20377

34. Lu JG, Sun YN, Wang C, Jin DJ, Liu M. Role of the alpha v-integrin subunit in cell proliferation, apoptosis and tumor metastasis of laryngeal and hypopharyngeal squamous cell carcinomas: a clinical and *in vitro* investigation. *Eur Arch Otorhinolaryngol* (2009) 266:89–96. doi:10.1007/s00405-008-0675-z

35. Dingemans AM, van den Boogaart V, Vosse BA, van Suylen RJ, Griffioen AW, Thijssen VL. Integrin expression profiling identifies integrin alpha5 and beta1 as prognostic factors in early stage non-small cell lung cancer. *Mol Cancer* (2010) 9:152. doi:10.1186/1476-4598-9-152

36. Hayashido Y, Kitano H, Sakaue T, Fujii T, Suematsu M, Sakurai S, et al. Overexpression of integrin αv facilitates proliferation and invasion of oral squamous cell carcinoma cells via MEK/ERK signaling pathway that is activated by interaction of integrin αvβ8 with type I collagen. *Int J Oncol* (2014) 45:1875–82. doi:10.3892/ijo.2014.2642

37. Ramos DM, But M, Regezi J, Schmidt BL, Atakilit A, Dang D, et al. Expression of integrin beta 6 enhances invasive behavior in oral squamous cell carcinoma. *Matrix Biol* (2002) 21:297–307. doi:10.1016/s0945-053x(02)00002-1

38. Ramos DM, Dang D, Sadler S. The role of the integrin alpha v beta6 in regulating the epithelial to mesenchymal transition in oral cancer. *Anticancer Res* (2009) 29:125–30.

39. Li HX, Zheng JH, Fan HX, Li HP, Gao ZX, Chen D. Expression of αvβ6 integrin and collagen fibre in oral squamous cell carcinoma: association with clinical outcomes and prognostic implications. *J Oral Pathol Med* (2013) 42:547–56. doi:10.1111/jop.12044

40. Eke I, Dickreuter E, Cordes N. Enhanced radiosensitivity of head and neck squamous cell carcinoma cells by β1 integrin inhibition. *Radiother Oncol* (2012) 104:235–42. doi:10.1016/j.radonc.2012.05.009

41. Eriksen JG, Steiniche T, Søgaard H, Overgaard J. Expression of integrins and E-cadherin in squamous cell carcinomas of the head and neck. *Apmis* (2004) 112:560–8. doi:10.1111/j.1600-0463.2004.apm1120902.x

42. Lydiatt WM, Patel SG, O'Sullivan B, Brandwein MS, Ridge JA, Migliacci JC, et al. Head and neck cancers-major changes in the American Joint Committee on cancer eighth edition cancer staging manual. *CA Cancer J Clin* (2017) 67:122–37. doi:10.3322/caac.21389

43. Ito N, Yamasaki S, Shintani T, Matsui K, Obayashi F, Koizumi K, et al. Tumor-infiltrating CD45RO(+) memory cells are associated with favorable prognosis in oral squamous cell carcinoma patients. *Cancers (Basel)* (2023) 15:2221. doi:10.3390/cancers15082221

44. Shintani T, Higaki M, Okamoto T. Heparin-binding protein 17/fibroblast growth factor-binding protein-1 knockout inhibits proliferation and induces differentiation of squamous cell carcinoma cells. *Cancers (Basel)* (2021) 13:2684. doi:10.3390/cancers13112684

45. Higaki M, Shintani T, Hamada A, Rosli SNZ, Okamoto T. Eldecalcitol (ED-71)-induced exosomal miR-6887-5p suppresses squamous cell carcinoma cell growth by targeting heparin-binding protein 17/fibroblast growth factor-binding protein-1 (HBp17/FGFBP-1). *Vitro Cel Dev Biol Anim* (2020) 56:222–33. doi:10.1007/s11626-020-00440-x

46. Liu J, Cheng S, Zhang Y, Li H, Huang J, Zhang P. Association between polymorphisms in the integrin gene predicted microRNA binding sites and bladder cancer risk. *Int J Clin Exp Med* (2014) 7:4398–405.

47. Samanna V, Wei H, Ego-Osuala D, Chellaiah MA. Alpha-V-dependent outside-in signaling is required for the regulation of CD44 surface expression, MMP-2 secretion, and cell migration by osteopontin in human melanoma cells. *Exp Cel Res* (2006) 312:2214–30. doi:10.1016/j.yexcr.2006.03.022

48. Pavlakis E, Neumann M, Merle N, Wieboldt R, Wanzel M, Ponath V, et al. Mutant p53-ENTPD5 control of the calnexin/calreticulin cycle: a druggable target for inhibiting integrin-α5-driven metastasis. *J Exp Clin Cancer Res* (2023) 42:203. doi:10.1186/s13046-023-02785-z

49. Sabeh F, Ota I, Holmbeck K, Birkedal-Hansen H, Soloway P, Balbin M, et al. Tumor cell traffic through the extracellular matrix is controlled by the membrane-anchored collagenase MT1-MMP. *J Cel Biol* (2004) 167:769–81. doi:10.1083/jcb.200408028

50. Hayashido Y, Urabe K, Yoshioka Y, Kitano H, Okamoto T, Matsuya T. Participation of fibroblasts in MMP-2 binding and activation on the surface of oral squamous cell carcinoma cells. *Int J Oncol* (2003) 22:657–62.

51. Kurokawa A, Nagata M, Kitamura N, Noman AA, Ohnishi M, Ohyama T, et al. Diagnostic value of integrin alpha3, beta4, and beta5 gene expression levels for the clinical outcome of tongue squamous cell carcinoma. *Cancer* (2008) 112: 1272–81. doi:10.1002/cncr.23295

52. Fan QC, Tian H, Wang Y, Liu XB. Integrin-α5 promoted the progression of oral squamous cell carcinoma and modulated PI3K/AKT signaling pathway. *Arch Oral Biol* (2019) 101:85–91. doi:10.1016/j.archoralbio.2019.03.007

53. Schäringer K, Maxeiner S, Schalla C, Rütten S, Zenke M, Sechi A. LSP1-myosin1e bimolecular complex regulates focal adhesion dynamics and cell migration. *Faseb J* (2021) 35:e21268. doi:10.1096/fj.202000740RR

54. Liu D, Liu S, Fang Y, Liu L, Hu K. Comprehensive analysis of the expression and prognosis for ITGBs: identification of ITGB5 as a biomarker of poor prognosis and correlated with immune infiltrates in gastric cancer. *Front Cel Dev Biol* (2021) 9: 816230. doi:10.3389/fcell.2021.816230

55. Zhang J, Wang H, Yuan C, Wu J, Xu J, Chen S, et al. ITGAL as a prognostic biomarker correlated with immune infiltrates in gastric cancer. *Front Cel Dev Biol* (2022) 10:808212. doi:10.3389/fcell.2022.808212

56. Ma SR, Liu JF, Jia R, Deng WW, Jia J. Identification of a favorable prognostic subgroup in oral squamous cell carcinoma: characterization of ITGB4/PD-L1(high) with CD8/PD-1(high). *Biomolecules* (2023) 13:1014. doi:10.3390/biom13061014

57. Xu C, Xie XL, Kang N, Jiang HQ. Evaluation of ITGB1 expression as a predictor of the therapeutic effects of immune checkpoint inhibitors in gastric cancer. *BMC Gastroenterol* (2023) 23:298. doi:10.1186/s12876-023-02930-0

Pathology & Oncology Research | frontiers

TYPE Review
PUBLISHED 19 January 2023
DOI 10.3389/pore.2023.1610884

Check for updates

OPEN ACCESS

EDITED BY
Andrea Ladányi,
National Institute of Oncology (NIO), Hungary

*CORRESPONDENCE
Jun Huang,
Huangjun0727@163.com

RECEIVED 15 October 2022
ACCEPTED 06 January 2023
PUBLISHED 19 January 2023

CITATION
Zhao S, Zhang D, Liu S and Huang J (2023), The roles of NOP56 in cancer and SCA36.
Pathol. Oncol. Res. 29:1610884.
doi: 10.3389/pore.2023.1610884

COPYRIGHT
© 2023 Zhao, Zhang, Liu and Huang. This is an open-access article distributed under the terms of the Creative Commons Attribution License (CC BY). The use, distribution or reproduction in other forums is permitted, provided the original author(s) and the copyright owner(s) are credited and that the original publication in this journal is cited, in accordance with accepted academic practice. No use, distribution or reproduction is permitted which does not comply with these terms.

The roles of NOP56 in cancer and SCA36

Shimin Zhao[1,2], Dongdong Zhang[1,2], Sicheng Liu[1,2] and Jun Huang[1]*

[1]Department of General Surgery, The Second Affiliated Hospital of Nanchang University, Nanchang, China, [2]Jiangxi Province Key Laboratory of Molecular Medicine, The Second Affiliated Hospital of Nanchang University, Nanchang, China

NOP56 is a highly conserved nucleolar protein. Amplification of the intron GGCCTG hexanucleotide repeat sequence of the *NOP56* gene results in spinal cerebellar ataxia type 36 (SCA36). NOP56 contains an N-terminal domain, a coiled-coil domain, and a C-terminal domain. Nucleolar protein NOP56 is significantly abnormally expressed in a number of malignant tumors, and its mechanism is different in different tumors, but its regulatory mechanism in most tumors has not been fully explored. NOP56 promotes tumorigenesis in some cancers and inhibits tumorigenesis in others. In addition, NOP56 is associated with methylation in some tumors, suggesting that NOP56 has the potential to become a tumor-specific marker. This review focuses on the structure, function, related signaling pathways, and role of NOP56 in the progression of various malignancies, and discusses the progression of NOP56 in neurodegenerative and other diseases.

KEYWORDS

methylation, NOP56, malignant tumor, box C/D RNP, SCA36

Introduction

NOP56 is an essential nucleolar protein with a molecular mass of 66 KDa. NOP56 and NOP58 are highly homologous throughout the sequence, with a KKE/D repeat at the carboxyl terminus, and like NOP58, NOP56 is highly conserved from yeast to human (1, 2). NOP56, NOP58, fibrillarin (FBL), SNU13, and more than a dozen small nucleolar RNAs (snoRNAs) are involved in ribosome production in eukaryotes (3). The snoRNAs are divided into three categories: two main categories of snoRNAs are C/D box snoRNAs and H/ACA box RNAs, respectively, and the third category of snoRNAs are small Cajal body specific RNAs (scaRNAs), which have the complex functions of the first two snoRNAs (4). C/D box snoRNA exists in the nucleolus as a stable form of small nucleolar ribonucleoprotein complex (snoRNP) (5). NOP56 has an N-terminal domain (NTD), a coiled-coil domain (CC), and a C-terminal domain (CTD) (6).

In recent years, more and more studies have demonstrated that dysregulation of NOP56 is closely related to the occurrence and development of various malignant tumors. The expression of NOP56 is significantly upregulated in acute myeloid leukemia, diffuse large B-cell lymphoma, and Myc-mutant Burkitt's lymphoma, and may also be associated with poorer prognosis (7–9). Downregulation of NOP56 expression significantly

inhibited the proliferation of KRAS mutant lung, pancreatic and colorectal cancer cells, and NOP56 mRNA levels have been suggested to be a predictive marker of rapamycin sensitivity (IC50) in KRAS mutant cancers (10). The study found that the expansion of the intron GGCCTG hexanucleotide repeat of NOP56 gene will lead to a new phenotype of spinocerebellar ataxias (SCAs), SCA36, in patients with advanced limb ataxia, dystonia and dysarthria (11–15). However, the biological functions and molecular mechanisms of NOP56 in cancer remain largely unexplored. Therefore, in this review, we discuss the structure, function, and knowledge of the NOP56 related signaling pathway, and emphasize the expression and role of NOP56 in various diseases.

Overview of NOP56

NOP56 gene and NOP56 protein functional characteristics

The gene encoding NOP56 is located on human chromosome 20p13 and contains 13 exons (16). NOP56 can participate in the processing of rRNA precursors, promote the synthesis of mature rRNA, and impair rRNA biosynthesis when NOP56 is underexpressed (1). snoRD86 in box C/D snoRNA plays a key role in restrictively controlling the level of box C/D snoRNP core protein NOP56, which is very important for ribosome biosynthesis. Alternative splicing on both sides of snoRD86 provides different donors. The donor provided upstream of snoRD86 is spliced to form mRNA encoding NOP56, and the donor provided downstream of snoRD86 is spliced to form the substrate mRNA of the NMD pathway, which is mediated by SMG6 to generate snoRD86-cSPA, which is a lncRNA. The study found that when NOP58 and FBL are depleted, positive feedback promotes NOP56 production and leads to changes in the nucleolar organization. Conversely, when NOP56 and FBL are depleted, there is positive feedback to promote NOP58 production (17). NOP56 appears to be the last core protein to enter the snoRNP complex and this could be decisive for activation of the complex. Moreover, its level of expression plays a key role in the assembly of 60S ribosomal subunit (18). SUMOylation is a post-translational modification of proteins by small ubiquitin analogs (SUMO), and SUMOylation is crucial in ribosome biogenesis. SUMOylation plays a key role in regulating the interaction of NOP58 with snoRNAs, SUMOylated NOP58 has a higher affinity for snoRNAs, and, SUMOylated NOP58 is essential for the localization of C/D box snoRNAs in nucleolus (19). The deubiquitinase USP36 promotes SUMOylation of NOP56 and NOP58 and promotes binding of NOP58 to snoRNA, and knockout of deubiquitinase USP36 significantly inhibits rRNA processing (20). Myc directly impacts RNA Pol I transcription, and it also affects expression of many nucleolar proteins, which include NOP56 (21). Myc has been shown to participate in ribosome biogenesis and protein synthesis by controlling the expression of the target gene NOP56 (22).

Box C/D snoRNP structural features

Box C/D snoRNA forms stable RNA-protein complexes (RNPs) with various proteins, which catalyze the site-specific 2′-O-methylation of rRNA, snRNA, and tRNA in an RNA-guided manner (23–26). The box C/D snoRNP in yeast consists of a box C/D snoRNA with NOP56, NOP58, NOP1, and SNU13. The box C/D snoRNP in eukaryotes consists of a box C/D snoRNA with NOP56, NOP58, fibrillarin (FBL, NOP1 in Saccharomyces cerevisiae), and SNU13 (15.5K in Homo sapiens). Box C/D snoRNP in Archaea consists of a box C/D snoRNA with Nop5, fibrillarin, and L7Ae. Fibrillarin contains the well-conserved S-adeninosine-L-methionine (SAM) binding motif and is thus the center of methyltransferase. Fibrillarin has a common structural domain consisting of a mixture of seven central β-sheets and α-sheets (23–25). NOP56 and NOP58 are a pair of homologous proteins, which are also homologous to Nop5 in Archaea, and target the C'/D′ motif inside the box C/D snoRNA and the C/D motif at the end, respectively (26,27). Nop5/56/58 contains three domains, an N-terminal domain (NTD), a coiled-coil domain (CC), and a C-terminal domain (CTD). NOP56 and NOP58 are the core proteins of two of the box C/D snoRNP complexes that interact through the coiled-coil structural domain (28). The C-terminal domain is highly charged and conserved in evolution. In yeast, the CTD is formed by repeated KKD/E sequences and can directly interact with Tgs1p. In mammalian cells, the CTD contains the nucleolar localization signal (NoLS) of box C/D snoRNP, and the CTD of NOP58 can directly bind to TGS1. TGS1-LF (full-length form of the protein, see below) can mask these nucleolar localization signals (1, 29). The two long coils of the coiled-coil domain can take either parallel or intersecting positions. The NTD and the coiled-coil domain form a hinge N, and the CTD and the coiled-coil domain form a hinge C, around which the NTD and CTD can rotate. The box C/D snoRNA has a symmetrical stem-loop structure, including a C-box (RUGAUGA) and a D-box (CUGA) at the end of the snoRNA, and the related C'box and D'box inside (26). After binding to SNU13/L7Ae protein, the C/D or C′/D′ motif forms an acute bend (K-turn or K-loop) structure (30). There are two spacer RNA sequences between the C/D and C'/D′ motifs. The average length of Archaeal spacers is 12–13 nt, and the length of eukaryotic spacers ranges from a few bases to hundreds of bases. The spacer region contains a guide region, which forms a 10 bp double-stranded RNA with the substrate through the principle of complementary base pairing, and the substrate base corresponding to the fifth base upstream of the D/D′ motif is methylated modification (Figure 1). In Archaea, spacers that are too long (more than 14 nt) or too short (less than

10.3389/pore.2023.1610884

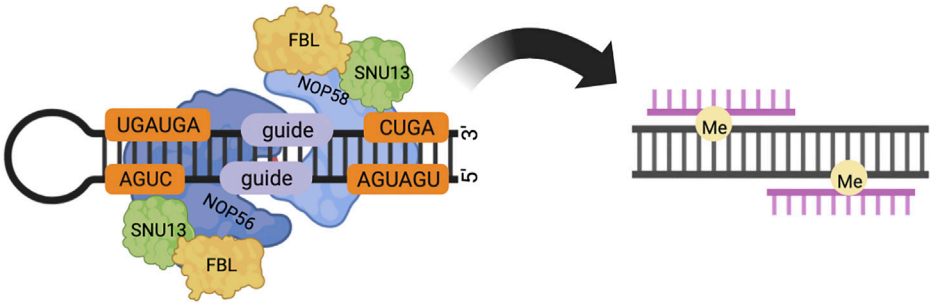

FIGURE 1
In eukaryotes, box C/D snoRNP consists of core proteins NOP58, NOP56, FBL, SNU13 and box C/D snoRNA. NOP56 and NOP58 bind to C′/D′ and C/D motifs respectively through the C-terminal structural domain. The spacer region between the C/D and C′/D′ motifs contains a guide region, which forms a 10 bp double-stranded RNA with the substrate, and modifies the substrate base corresponding to the fifth base upstream of the D/D′ motif by methylation.

12 nt) do not affect box C/D and C'/D′ RNP assembly, but do affect the activity of the target RNA methylation modification of the box C/D and C'/D′ RNP lineage (3, 31, 32).

In Archaea, L7Ae first recognizes box C/D snoRNA, assembles to form L7Ae-C/D RNA complex, and then recruits fibrillarin by binding Nop5 to form L7Ae- C/D RNP complex in which L7Ae recognizes the CTD domain of Nop5 (33–37). In eukaryotes, assembly of the box C/D snoRNP requires the HSP90/R2TP system, and the R2TP complex consists of PIH1D1, RPAP3, and RUVBL1 and RUVBL2. RUVBL1 and RUVBL2 are two highly conserved AAA + ATPases that form a heterohexamer complex. ATP binds to the R2TP complex to release RUVBL1 and RUVBL2 from the R2TP complex and load them onto SNU13 and NOP58. The assembly factors NUFIP, ZNHIT3 and ZNHIT6 bind to it to form a pure protein complex. The complex binds to box C/D snoRNA, recruits FBL and NOP56 and removes NUFIP, ZNHIT3, ZNHIT6, RUVBL1, and RUVBL2, forming box C/D snoRNP particles (18, 38). Box C/D snoRNA has a long GU repeat sequence, and TCAB1 (also known as WRAP53/WDR79) recognizes the long GU repeat sequence. TCAB1 sends a translocation signal to transport box C/D snoRNP particles to Cajal bodies (CBs) (39). TGS1 has two isoforms: a full-length protein called TGS1 long type (TGS1-LF), which is mainly localized in the cytoplasm and CBs. The other is the short type (TGS1-SF), produced by proteolytic cleavage of its N-terminal structural domain, is mainly localized in the CBs and nucleoplasm (40). TGS1-LF binds to the C-terminal structural domains of NOP56 and NOP58, and CRM1 reduces the affinity of TGS1-LF for NOP58. The reduced affinity of TGS1- LF for NOP58 may activate the nucleolus localization signal (NoLS) of NOP58 to facilitate translocation of box C/D snoRNP particles from CBs to the nucleolus (29).

NOP56 and signaling pathways

NOP56 is located at the key crossroads of many signaling pathways and plays an important role in tumorigenesis and development. Exploring the role of NOP56 in these signaling pathways will help us further understand the mechanism of tumorigenesis and development. The p38 pathway is one of the major mitogen-activated protein kinase (MAPK) signaling pathways and plays an important role in many cellular processes, including inflammation, cell differentiation, cell growth, and cell death (41). In KRAS-mutant NSCLC, inhibition of NOP56 expression resulted in a significant increase in IRE1α, and NOP56 mediated UPR activation of mTOR signaling *via* p38/MAPK (10). NF-κB is a transcription factor in the TLR signaling pathway and plays a key role in the innate immune response. The NF-κB family includes p65 (RelA), NF-εB1 (p50/p105), NF-κB2 (p52/p100), RelB and c-Rel (42). Studies in teleosts reported that overexpression of NOP56 significantly inhibited MyD88-mediated NF-κB signaling pathway and suppressed IL-1β and IL-8 transcription. And the NOSIC domain of NOP56 is critical for the inhibition of MyD88-mediated NF-κB signaling pathway by NOP56 (43). The JAK/STAT signaling pathway is highly conserved from invertebrates to vertebrates and plays an important role in many growth and developmental processes. Studies have shown that dysregulation of the JAK/STAT signaling pathway leads to the development and progression of a variety of malignancies and autoimmune diseases (44). In Drosophila studies, NOP56 has been found to be a functional target of the JAK/STAT signaling pathway, and the JAK/STAT signaling pathway promotes Drosophila neuroepithelial growth through activation of NOP56 (45).

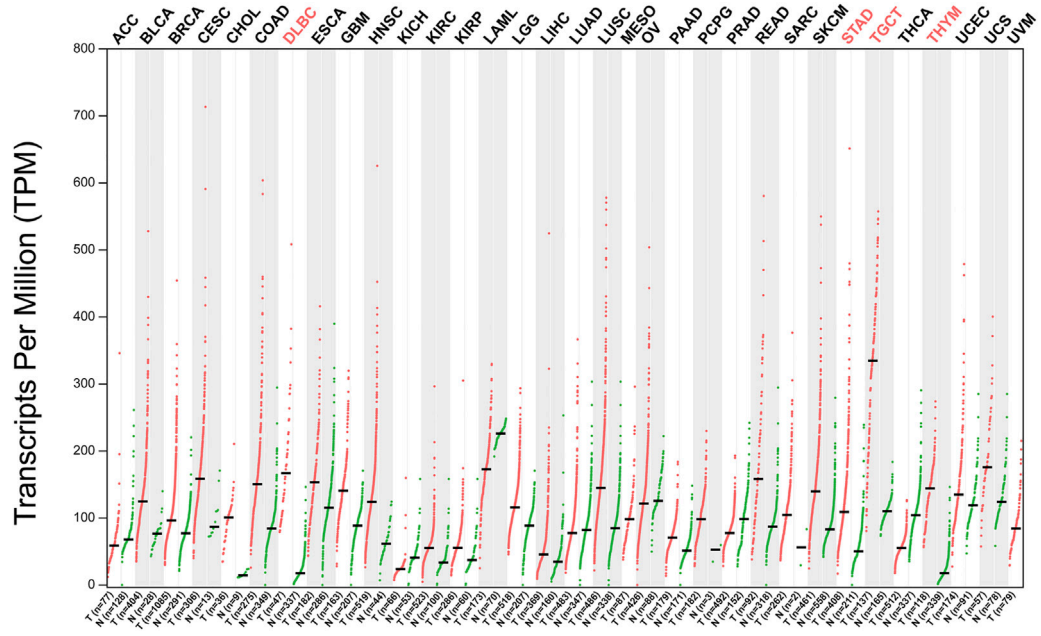

FIGURE 2
NOP56 expression in cancer. Expression level of NOP56 across 33 TCGA tumors compared to TCGA normal using GEPIA. For each TCGA tumor (red), its matched normal (green) are given; T: tumor; N: normal; Y axis: transcript per million. X axis: number of tumor and normal samples. Acronyms of cancers with statistically significant differences are shown in red. ACC, adrenocortical carcinoma; BLCA, bladder urothelial carcinoma; BRCA, breast invasive carcinoma; CESC, cervical squamous cell carcinoma and endocervical adenocarcinoma; CHOL, cholangiocarcinoma; COAD, colon adenocarcinoma; DLBC, lymphoid neoplasm diffuse large B-cell lymphoma; ESCA, esophageal carcinoma; GBM, glioblastoma multiforme; HNSC, head and neck squamous cell carcinoma; KICH, kidney chromophobe; KIRC, kidney renal clear cell carcinoma; KIRP, kidney renal papillary cell carcinoma; LAML, acute myeloid leukemia; LGG, brain lower grade glioma; LIHC, liver hepatocellular carcinoma; LUAD, lung adenocarcinoma; LUSC, lung squamous cell carcinoma; MESO, mesothelioma; OV, ovarian serous cystadenocarcinoma; PAAD, pancreatic adenocarcinoma; PCPG, pheochromocytoma and paraganglioma; PRAD, prostate adenocarcinoma; READ, rectum adenocarcinoma; SARC, Sarcoma; SKCM, skin cutaneous melanoma; STAD, stomach adenocarcinoma; TGCT, testicular germ cell tumors; THCA, thyroid carcinoma; THYM, thymoma; UCEC, uterine corpus endometrial carcinoma; UCS, uterine carcinosarcoma; UVM, uveal melanoma. Data was downloaded from GEPIA database (http://gepia2.cancer-pku.cn/#analysis).

The expression of NOP56 in cancer

An increasing number of studies have proved that abnormal expression of NOP56 is closely related to the occurrence and development of various tumors (Figure 2). NOP56 is significantly increased in KRAS-mutant non-small cell lung cancer, KRAS-mutant pancreatic cancer, KRAS-mutant colorectal cancer, Wilms tumor, diffuse large B-cell lymphoma, Myc-mutant Burkitt's lymphoma, breast cancer, prostate cancer, and acute lymphoblastic leukemia (8, 9, 46–51). Hypermethylation in the NOP56 promoter region in HPV+ cervical cancer leads to downregulation of NOP56 (52). NOP56 promotes the occurrence and development of tumor cells by activating signaling pathways, inhibition of reactive oxygen species production, regulation of tumor-like stem cell pluripotency, and DNA hypermethylation. DNA methylation is the most common epigenetic modification in human tumors, and hypermethylation of gene promoter CpG islands has been associated with inactivation of tumor suppressor genes in tumor cells, particularly in colorectal cancer (53, 54). Therefore, hypermethylation of NOP56 gene has the potential to become a tumor-specific marker in the future. These findings indicate that NOP56 plays diverse roles in tumor progression and the details are specifically summarized in Table 1. NOP56 is one of many methylated genes, and examining the methylation status of genes can help identify tumor-specific markers and therapeutic targets for cancer patients. There are three main methods for genome-wide DNA methylation analysis commonly used today: the first is restriction enzyme-based techniques, the second is affinity enrichment-based techniques, and the third is bisulfite conversion-based methods (55).

NOP56 and non-small cell lung cancer

KRAS is the most frequently mutated oncogene in non-small cell lung cancer (NSCLC) (46). Recent studies have found that the expression of NOP56 in KRAS mutant non-small cell lung cancer cell lines is significantly higher than that in KRAS wild-type non-small cell lung cancer cell lines. In addition, the disease-

TABLE 1 The expression and roles of NOP56 in different human cancers.

Cancer type	Levels of NOP56	Function	Relevant targets/mechanisms/ signaling pathways	Types of references	Reference:
Non-small cell lung cancer (NSCLC)	Up	Inhibit ROS and reduce sensitivity to chemotherapy drugs	IRE1α, UPR, p38/MAPK/mTOR	Cell culture	(10)
Wilms tumor(WT)	Up	Inhibit tumor cell proliferation, invasion and migration, and promote tumor cell apoptosis	CD24, CD133, KLF4 and SOX2	Cell culture	(47, 48)
Diffuse large B-cell lymphoma (DLBCL)	Up	-	-	Cell culture	(8)
Myc-mutant Burkitt's lymphoma (BL)	Up	Promote tumor cell proliferation, promote Myc wild-type tumor cell differentiation, and increase tumor volume	-	Cell culture	(9)
Cervical cancer (CCA)	Up	-	E7 protein binds to DNMT1 to enhance the methylation of NOP56 gene promoter, resulting in a decrease in NOP56 expression level	Cell culture	(52)
Hepatocellular carcinoma (HCC)	Up	Significantly correlated with survival prognosis, pathological stage, immune infiltration and tumor progression	NOP56 promoter hypomethylation leads to NOP56 overexpression	Bioinformatics	(66–68)
Acute lymphoblastic leukemia (ALL)	Up	Delayed remission	-	whole body	(7)
Breast cancer	Up	Promotes colony formation and cell growth	-	Cell culture	(49)

free survival (DFS) and overall survival (OS) of tumor patients in the NOP56 high expression group were significantly shortened. Knockdown of NOP56 in KRAS-mutant lung cancer cell lines significantly increased reactive oxygen species (ROS) in KRAS-mutant cell lines, resulting in significantly higher levels of apoptosis in KRAS-mutant cell lines than in controls. Inhibition of NOP56 increases IRE1α-mediated UPR activation of mTOR signaling through p38/MAPK, thereby reducing oxidative stress. NOP56 knockdown significantly increases resistance of KRAS mutant cell lines to PI3K/AKT inhibitors (LY294002, AZD5363), anti-mTOR drugs (rapamycin, everolimus), and ER stress inducers (bortezomib and HA15) sensitivity (10). Targeted inhibition of NOP56 expression combined with rapamycin treatment significantly inhibited the growth of KRAS-mutant non-small cell lung cancer (10). Thus, the development of specific NOP56 inhibitors in combination with mTOR inhibitor therapy may be an effective strategy for the treatment of KRAS-mutant lung cancer in the future. In the study of papillary lung adenocarcinoma (PLACs), NOP56 was shown to be a Myc-induced oncogene and NOP56 was significantly upregulated in papillary lung adenocarcinomas (56).

NOP56 and Wilms tumor

PIWI-interacting RNA (piRNA) is a small non-coding RNA of 24–31 nucleotides (nt) in length found in germ cells and somatic cells (57). Recently, an increasing number of studies have shown that piRNA and PIWI proteins are abnormally expressed in a variety of tumors and can be used as biomarkers for tumor diagnosis and treatment (58). The research shows that NOP56 is highly expressed in Wilms tumor, while the expression level of piRNA NU13 in Wilms tumor (G401) is significantly lower than that in renal tubular epithelial cells (HK2). piRNA NU13 indirectly regulates NOP56, thereby inhibiting the proliferation, invasion, and migration of tumor cells and promoting tumor cell apoptosis (47). Both piRNA MW557525 and NOP56 were significantly highly expressed in piwil2-induced tumor-like stem cells (Piwil2-iCSCs), while inhibition of piRNA MW557525 could increase the expression level of NOP56, and knockdown of NOP56 upregulated the pluripotency markers CD24, CD133, and KLF4 of tumor stem cells and SOX2 expression, and the proliferation ability of tumor-like stem cells in NOP56 silencing group was significantly higher than that in the control group, suggesting that NOP56 inhibits Piwil2-iCSCs proliferation, invasion, migration and stem cell pluripotency, and promotes their apoptosis (48).

NOP56 and non-Hodgkin lymphoma

Diffuse large B-cell lymphoma (DLBCL) is the most common non-Hodgkin's lymphoma with high aggressiveness and heterogeneity. The mRNA and protein expression levels of NOP56 are significantly higher in diffuse large B-cell lymphoma than in normal lymphoid tissue. Interestingly, NOP56 expression was significantly downregulated in diffuse large B-cell lymphoma cell lines resistant to adriamycin (Pfeiffer/ADM) compared with diffuse large B-cell lymphoma cell lines (Pfeiffer). However, treatment of

adriamycin-resistant diffuse large B-cell lymphoma with paclitaxel was able to significantly reverse this downregulation trend. It indicates that NOP56 and ribosome biosynthesis play a key role in paclitaxel treatment of adriamycin-resistant diffuse large B-cell lymphoma (8). Previous studies have shown that Myc-mutant Burkitt's lymphoma cells express significantly higher levels of NOP56 compared with Myc wild-type cells. And compared with Myc wild-type cells, the degree of histone acetylation in Myc mutant cells was positively correlated with NOP56 levels. Reduced expression of NOP56 will severely inhibit tumor cell proliferation and promote tumor cell death. Moreover, upregulation of NOP56 expression in Myc wild-type tumor cells promotes Myc wild-type tumor cell differentiation and significantly increases tumor volume (9). This study suggests that NOP56-targeted therapy may be a method to improve treatment efficiency in the molecular targeted therapy of Burkitt's lymphoma.

NOP56 and cervical cancer

DNA methylation modification is an epigenetic event that does not lead to permanent changes in DNA sequence. DNA methylation is involved in regulating gene transcription and cell differentiation. DNA hypermethylation is usually associated with gene silencing. DNA demethylation often promotes gene transcription (59). More and more studies have proved that dysregulation of DNA methylation leads to the occurrence and progression of various diseases. Methylation of specific genes will help in the early detection, diagnosis, treatment, and monitoring of the prognosis of cervical cancer patients (60). Cervical cancer is the second leading cause of cancer death in women aged 20–39 years, and HPV is recognized as an important risk factor for cervical cancer, especially HPV16 and HPV18 (61). The E7 protein translated from the HPV16 E7 gene can bind to DNA methyltransferase 1 (DNMT1) to induce methylation of tumor suppressor genes, leading to inactivation of tumor suppressor genes and promoting tumor progression (62–64). The expression of NOP56 in HPV+ cervical cancer cell lines is lower than that in HPV- cervical cancer cell lines. The methylation level of NOP56 in HPV+ cervical cancer cell lines is higher than that in HPV- cervical cancer cell lines. The E7 protein can interact with DNA methyltransferase 1 (DNMT1) and significantly increase the methylation level of the NOP56 gene promoter, which in turn leads to a significant decrease in the expression of the NOP56 gene. Furthermore, treatment of cervical cancer cells with 5′-azacytidine (5-aza), a DNA methyltransferase inhibitor, can significantly reverse the methylation of NOP56 gene promoter, thereby increasing the expression level of NOP56 (52). These further suggest that the NOP56 promoter methylation site may be a therapeutic target for cervical cancer. Currently, there are no studies reporting methods to detect methylation of the NOP56 promoter. However, there are recent studies using liquid biopsy and quantitative methylation-specific PCR analysis to detect circulating tumor DNA and methylation markers (65).

NOP56 and hepatocellular carcinoma

Based on bioinformatics analysis of gene expression and GCNA-Kpca algorithm analysis, NOP56 and NOP58 are key genes in hepatocellular carcinoma. Moreover, NOP56 is significantly correlated with the survival prognosis, pathological stage, immune infiltration, and tumor progression of patients with hepatocellular carcinoma, and may be used as a target for the diagnosis and treatment of hepatocellular carcinoma in the future. The methylation analysis indicated that the hypomethylation of the NOP56 promoter may lead to the overexpression of NOP56, which proved that expression of NOP56 may be a potential biomarker of hepatocellular carcinoma (66, 67). In hepatocellular carcinoma, NOP56 is considered as a potential immune marker associated with HBV virus, which can be processed and presented by antigen-presenting cells (APCs) to induce immune responses. Moreover, NOP56 is considered as a potential antigen of HBV-related mRNA vaccine for hepatocellular carcinoma (68).

NOP56 and other tumors

Acute lymphoblastic leukemia (ALL) is the most common malignancy in childhood, accounting for approximately 25% of cancers in children under the age of 15. The most common subtype is B-cell precursor acute lymphoblastic leukemia, with 20% of patients dying of drug resistance or relapse (69). Recent studies have shown that NOP56 and FBL are significantly upregulated in relapsed patients. Even if drug resistance does not occur, high expression of NOP56 will significantly delay the remission of patients (7). Breast cancer is the most common malignant tumor in women, and breast cancer accounts for 30% of female cancers (61). NOP56 significantly promotes colony formation and cell growth in breast cancer tumor cells (49). At the late stage of prostate cancer progression, NOP56 was significantly elevated in both prostate cancer tissue and metastatic tissue (50). The expression of NOP56 in KRAS mutant pancreatic cancer cell lines (MIAPaCa, HPAF-II) and colon cancer cell lines (HCT-116, DLD-1) is significantly higher than that in KRAS wild-type tumor cell lines (46). Studies in endometrial cancer have found that NOP56 correlates with patient survival, suggesting prognostic relevance. However, the difference in NOP56 expression between endometrial cancer and healthy endometrial epithelium was not statistically significant. Using statistical methods, NOP56 was found to be significantly and positively correlated with telomere-associated protein TERF2 (70). In the whole blood mRNA gene expression of metastatic renal cell carcinoma, the increase of NOP56 was statistically significant (71). The mRNA level of NOP56 was significantly upregulated in glioblastoma by bioinformatics analysis in the TCGA-GBM database and Oncomine database (72).

NOP56 and spinocerebellar ataxia type 36

Spinocerebellar ataxias type 36 (SCA36) is an autosomal dominant heterogenous neurodegenerative disorder with cerebellar ataxia. Patients with cerebellar Purkinje cells and sublingual nucleus motor neurons Absence, resulting in overt ataxia symptoms characterized by loss of balance and rhythm, progressive gait, and limb ataxia (12–14, 73). Expansion of the GGCCTG hexanucleotide repeat in the NOP56 intron results in spinocerebellar ataxia type 36 (SCA36), with marked motor nerve involvement in late stages of SCA36, and a typically suppressed tongue in all affected individuals Atrophy with fascicular contractions results in dysarthria, but the severity varies (13). SCA36 is very rare in mainland China. SCA36 studies in mainland China show that patients in mainland China have a late onset and slow progression, and the main symptoms and signs are ataxia, dysarthria, and hyperreflexia. Most affected patients present with neuropathic hearing loss (74). Today, zebrafish have become an important model for studying neurological diseases, which are highly homologous to human genes, and show a variety of molecules and structures that are homologous to human diseases in the zebrafish central nervous system (75). A study in zebrafish found that NOP56 heterozygous mutants exhibited severe neurodegenerative phenotypes, including cerebellar loss, reduced number of spinal neurons, and motor impairment. NOP56 homozygous mutants show increased apoptosis and early death in zebrafish (76). The study found that the mRNA expression of the ZPLD1 gene was reduced in NOP56 homozygous mutants, and the reduced expression of ZPLD1 was associated with balance dysfunction (77).

NOP56 and other diseases

Compared with age-matched wild-type mice, transgenic mice of the amyotrophic lateral sclerosis (ALS) model showed a progressive decrease in NOP56 expression levels early in the disease, especially in the large motor neurons of the lumbar and cervical spine (78). Studies have found that hypermethylation in the NOP56 promoter region is not only associated with cancer, but may also be associated with age-related macular degeneration (AMD). Collecting blood samples from AMD patients, the NOP56 promoter region is hypermethylated in AMD, resulting in low expression of NOP56. It is suggested that hypermethylation of NOP56 promoter region may serve as a biomarker for future diagnosis and treatment of age-related macular degeneration (79). NOP56 has also been studied in degenerative disc disease (DDD), through single-cell RNA sequencing (scRNA-seq) reporting and weighted gene co-expression network analysis (WGCNA), found in the cartilage plate, NOP56 is one of the core therapeutic genes in degenerative disc disease (80).

Conclusion and prospects

In this review, we elucidate the structure and function of NOP56 and box C/D snoRNPs. Studies in various organisms have found that NOP56 affects a variety of signaling pathways and targets, and leads to a variety of epigenetic changes, thereby affecting the biological function of the organism. In recent years, more and more studies have demonstrated that NOP56 is associated with the occurrence and progression of malignant tumors and the treatment of cancer patients. Today, biomarker-based personalized or precision therapy will be a promising approach to improve patient care and prognosis, not only significantly improving patient health, but also reducing treatment-related harm and treatment costs. Although the role and mechanism of NOP56 in the occurrence and development of tumors are still unclear, NOP56 provides a direction for the development and treatment of tumors in the future. Given the previous studies, we have good reasons to believe that NOP56 is a promising therapeutic and prognostic biomarker for future tumor therapy.

Author contributions

DZ and SL collected the related paper. SZ drafted and revised the manuscript. DZ designed the review. SL provided direction and guidance throughout the preparation of this manuscript. JH participated in the design of the review and helped to draft and revise the manuscript. All authors read and approved the final manuscript.

Funding

The study was supported by the Key Research and Development Program of Jiangxi Province Grant/Award number: 20181BBG70019 and the National Natural Science Foundation of JH Grant/Award number: 82060445.

Conflict of interest

The authors declare that the research was conducted in the absence of any commercial or financial relationships that could be construed as a potential conflict of interest.

Acknowledgments

Figure 1 was created with BioRender software (http://borender.com/ (accessed on 12 September 2022).

References

1. Gautier T, Bergès T, Tollervey D, Hurt E. Nucleolar KKE/D repeat proteins Nop56p and Nop58p interact with Nop1p and are required for ribosome biogenesis. *Mol Cell Biol* (1997) 17:7088–98. doi:10.1128/mcb.17.12.7088

2. GeneCards NOP56. GeneCards NOP56 (2022). Available at: https://www.genecards.org/Search/Keyword?queryString=NOP56 (Accessed October 10, 2022).

3. Omer AD, Lowe TM, Russell AG, Ebhardt H, Eddy SR, Dennis PP. Homologs of small nucleolar RNAs in Archaea. *Science* (2000) 288:517–22. doi:10.1126/science.288.5465.517

4. Wajahat M, Bracken CP, Orang A. Emerging functions for snoRNAs and snoRNA-derived fragments. *Int J Mol Sci* (2021) 22:10193. doi:10.3390/ijms221910193

5. Newman DR, Kuhn JF, Shanab GM, Maxwell ES. Box C/D snoRNA-associated proteins: Two pairs of evolutionarily ancient proteins and possible links to replication and transcription. *RNA* (2000) 6:861–79. doi:10.1017/s1355838200992446

6. Yi Y, Li Y, Meng Q, Li Q, Li F, Lu B, et al. A PRC2-independent function for EZH2 in regulating rRNA 2′-O methylation and IRES-dependent translation. *Nat Cell Biol* (2021) 23:341–54. doi:10.1038/s41556-021-00653-6

7. Marcel V, Catez F, Berger CM, Perrial E, Plesa A, Thomas X, et al. Expression profiling of ribosome biogenesis factors reveals nucleolin as a novel potential marker to predict outcome in AML patients. *PLoS One* (2017) 12:e0170160. doi:10.1371/journal.pone.0170160

8. Hong H, Luo B, Qin Y, Li S, Peng Z. RNA-seq and integrated network analysis reveals the hub genes and key pathway of paclitaxel inhibition on Adriamycin resistant diffuse large B cell lymphoma cells. *Bioengineered* (2022) 13:7607–21. doi:10.1080/21655979.2022.2048772

9. Cowling VH, Turner SA, Cole MD. Burkitt's lymphoma-associated c-Myc mutations converge on a dramatically altered target gene response and implicate Nol5a/Nop56 in oncogenesis. *Oncogene* (2014) 33:3519–27. doi:10.1038/onc.2013.338

10. Yang Z, Liang S-Q, Zhao L, Yang H, Marti TM, Hegedüs B, et al. Metabolic synthetic lethality by targeting NOP56 and mTOR in KRAS-mutant lung cancer. *J Exp Clin Cancer Res* (2022) 41:25. doi:10.1186/s13046-022-02240-5

11. Kobayashi H, Abe K, Matsuura T, Ikeda Y, Hitomi T, Akechi Y, et al. Expansion of intronic GGCCTG hexanucleotide repeat in NOP56 causes SCA36, a type of spinocerebellar ataxia accompanied by motor neuron involvement. *Am J Hum Genet* (2011) 89:121–30. doi:10.1016/j.ajhg.2011.05.015

12. Schöls L, Bauer P, Schmidt T, Schulte T, Riess O. Autosomal dominant cerebellar ataxias: Clinical features, genetics, and pathogenesis. *Lancet Neurol* (2004) 3:291–304. doi:10.1016/S1474-4422(04)00737-9

13. Ikeda Y, Ohta Y, Kobayashi H, Okamoto M, Takamatsu K, Ota T, et al. Clinical features of SCA36: A novel spinocerebellar ataxia with motor neuron involvement (asidan). *Neurology* (2012) 79:333–41. doi:10.1212/WNL.0b013e318260436f

14. García-Murias M, Quintáns B, Arias M, Seixas AI, Cacheiro P, Tarrío R, et al. Costa da morte" ataxia is spinocerebellar ataxia 36: Clinical and genetic characterization. *Brain* (2012) 135:1423–35. doi:10.1093/brain/aws069

15. Arias M, García-Murias M, Sobrido MJ. Spinocerebellar ataxia 36 (SCA36): «Costa da morte ataxia. *Neurologia* (2017) 32:386–93. doi:10.1016/j.nrl.2014.11.005

16. NOP56. National Center for Biotechnology information (2022). Available at: https://www.ncbi.nlm.nih.gov/gene/10528 (Accessed September 11, 2022).

17. Lykke-Andersen S, Ardal BK, Hollensen AK, Damgaard CK, Jensen TH. Box C/D snoRNP Autoregulation by a cis-Acting snoRNA in the NOP56 Pre-mRNA. *Mol Cell* (2018) 72:99–111. e5. doi:10.1016/j.molcel.2018.08.017

18. Bizarro J, Charron C, Boulon S, Westman B, Pradet-Balade B, Vandermoere F, et al. Proteomic and 3D structure analyses highlight the C/D box snoRNP assembly mechanism and its control. *J Cell Biol* (2014) 207:463–80. doi:10.1083/jcb.201404160

19. Westman BJ, Verheggen C, Hutten S, Lam YW, Bertrand E, Lamond AI. A proteomic screen for nucleolar SUMO targets shows SUMOylation modulates the function of Nop5/Nop58. *Mol Cell* (2010) 39:618–31. doi:10.1016/j.molcel.2010.07.025

20. Ryu H, Sun X, Chen Y, Li Y, Wang X, Dai RS, et al. The deubiquitinase USP36 promotes snoRNP group SUMOylation and is essential for ribosome biogenesis. *EMBO Rep* (2021) 22:e50684. doi:10.15252/embr.202050684

21. Schlosser I, Hölzel M, Mürnseer M, Burtscher H, Weidle UH, Eick D. A role for c-Myc in the regulation of ribosomal RNA processing. *Nucleic Acids Res* (2003) 31:6148–56. doi:10.1093/nar/gkg794

22. Ruggero D. The role of myc-induced protein synthesis in cancer. *Cancer Res* (2009) 69:8839–43. doi:10.1158/0008-5472.CAN-09-1970

23. Cheng X, Roberts RJ. AdoMet-dependent methylation, DNA methyltransferases and base flipping. *Nucleic Acids Res* (2001) 29:3784–95. doi:10.1093/nar/29.18.3784

24. Martin JL, McMillan FM. SAM (dependent) I AM: The S-adenosylmethionine-dependent methyltransferase fold. *Curr Opin Struct Biol* (2002) 12:783–93. doi:10.1016/s0959-440x(02)00391-3

25. Feric M, Vaidya N, Harmon TS, Mitrea DM, Zhu L, Richardson TM, et al. Coexisting liquid phases underlie nucleolar subcompartments. *Cell* (2016) 165:1686–97. doi:10.1016/j.cell.2016.04.047

26. Yu G, Zhao Y, Li H. The multistructural forms of box C/D ribonucleoprotein particles. *RNA* (2018) 24:1625–33. doi:10.1261/rna.068312.118

27. Yang Z, Wang J, Huang L, Lilley DMJ, Ye K. Functional organization of box C/D RNA-guided RNA methyltransferase. *Nucleic Acids Res* (2020) 48:5094–105. doi:10.1093/nar/gkaa247

28. Höfler S, Lukat P, Blankenfeldt W, Carlomagno T. High-resolution structure of eukaryotic Fibrillarin interacting with Nop56 amino-terminal domain. *RNA* (2021) 27:496–512. doi:10.1261/rna.077396.120

29. Pradet-Balade B, Girard C, Boulon S, Paul C, Azzag K, Bordonné R, et al. CRM1 controls the composition of nucleoplasmic pre-snoRNA complexes to licence them for nucleolar transport: CRM1 controls transport and assembly of snoRNPs. *EMBO J* (2011) 30:2205–18. doi:10.1038/emboj.2011.128

30. Shi X, Huang L, Lilley DMJ, Harbury PB, Herschlag D. The solution structural ensembles of RNA kink-turn motifs and their protein complexes. *Nat Chem Biol* (2016) 12:146–52. doi:10.1038/nchembio.1997

31. Omer AD, Ziesche S, Ebhardt H, Dennis PP. *In vitro* reconstitution and activity of a C/D box methylation guide ribonucleoprotein complex. *Proc Natl Acad Sci U S A* (2002) 99:5289–94. doi:10.1073/pnas.082101999

32. Tran E, Zhang X, Lackey L, Maxwell ES. Conserved spacing between the box C/D and C′/D′ RNPs of the archaeal box C/D sRNP complex is required for efficient 2′-O-methylation of target RNAs. *RNA* (2005) 11:285–93. doi:10.1261/rna.7223405

33. Ye K, Jia R, Lin J, Ju M, Peng J, Xu A, et al. Structural organization of box C/D RNA-guided RNA methyltransferase. *Proc Natl Acad Sci USA* (2009) 106:13808–13. doi:10.1073/pnas.0905128106

34. Gagnon KT, Biswas S, Zhang X, Brown BA, Wollenzien P, Mattos C, et al. Structurally conserved Nop56/58 N-terminal domain facilitates archaeal box C/D ribonucleoprotein-guided methyltransferase activity. *J Biol Chem* (2012) 287:19418–28. doi:10.1074/jbc.M111.323253

35. Lin J, Lai S, Jia R, Xu A, Zhang L, Lu J, et al. Structural basis for site-specific ribose methylation by box C/D RNA protein complexes. *Nature* (2011) 469:559–63. doi:10.1038/nature09688

36. Tran EJ, Zhang X, Maxwell ES. Efficient RNA 2'-O-methylation requires juxtaposed and symmetrically assembled archaeal box C/D and C'/D' RNPs. *EMBO J* (2003) 22:3930–40. doi:10.1093/emboj/cdg368

37. Gagnon KT, Zhang X, Agris PF, Maxwell ES. Assembly of the archaeal box C/D sRNP can occur via alternative pathways and requires temperature-facilitated sRNA remodeling. *J Mol Biol* (2006) 362:1025–42. doi:10.1016/j.jmb.2006.07.091

38. Massenet S, Bertrand E, Verheggen C. Assembly and trafficking of box C/D and H/ACA snoRNPs. *RNA Biol* (2017) 14:680–92. doi:10.1080/15476286.2016.1243646

39. Jorjani H, Kehr S, Jedlinski DJ, Gumienny R, Hertel J, Stadler PF, et al. An updated human snoRNAome. *Nucleic Acids Res* (2016) 44:5068–82. doi:10.1093/nar/gkw386

40. Girard C, Verheggen C, Neel H, Cammas A, Vagner S, Soret J, et al. Characterization of a short isoform of human Tgs1 hypermethylase associating with small nucleolar ribonucleoprotein core proteins and produced by limited proteolytic processing. *J Biol Chem* (2008) 283:2060–9. doi:10.1074/jbc.M704209200

41. Ono K, Han J. The p38 signal transduction pathway: Activation and function. *Cell Signal* (2000) 12:1–13. doi:10.1016/s0898-6568(99)00071-6

42. Verma IM, Stevenson JK, Schwarz EM, Van Antwerp D, Miyamoto S. Rel/NF-kappa B/I kappa B family: Intimate tales of association and dissociation. *Genes Dev* (1995) 9:2723–35. doi:10.1101/gad.9.22.2723

43. Ren X, Zhang H, Yan X, Sun Y, Xu T. NOP56 negatively regulates MyD88-mediated NF-κB signaling in miiuy croaker, Miichthys miiuy. *Fish Shellfish Immunol* (2022) 120:75–81. doi:10.1016/j.fsi.2021.11.011

44. Hu X, li J, Fu M, Zhao X, Wang W. The JAK/STAT signaling pathway: From bench to clinic. *Signal Transduct Target Ther* (2021) 6:402. doi:10.1038/s41392-021-00791-1

45. Wang H, Chen X, He T, Zhou Y, Luo H. Evidence for tissue-specific JAK/STAT target genes in *Drosophila* optic lobe development. *Genetics* (2013) 195: 1291–306. doi:10.1534/genetics.113.155945

46. Judd J, Abdel Karim N, Khan H, Naqash AR, Baca Y, Xiu J, et al. Characterization of KRAS mutation subtypes in non–small cell lung cancer. *Mol Cancer Ther* (2021) 20:2577–84. doi:10.1158/1535-7163.MCT-21-0201

47. Zhang Z, Wang Z, Jin L, Tan X, Shen L, Wei G, et al. Effect of piRNA NU13 in regulating biological behaviors of human Wilms tumor cells *in vitro*. *Nan Fang Yi Ke Da Xue Xue Bao* (2021) 41:184–92. doi:10.12122/j.issn.1673-4254.2021.02.04

48. Zhang Z, Wang Z, Tan X, Jin L, Wang Z, Shen L, et al. PiRNA MW557525 promotes the vitality and pluripotency of piwil2-iCSCs by regulating NOP56. (2021). doi:10.21203/rs.3.rs-439016/v1

49. Su H, Xu T, Ganapathy S, Shadfan M, Long M, Huang TH-M, et al. Elevated snoRNA biogenesis is essential in breast cancer. *Oncogene* (2014) 33:1348–58. doi:10.1038/onc.2013.89

50. Vellky JE, Ricke EA, Huang W, Ricke WA. Expression, localization, and function of the nucleolar protein BOP1 in prostate cancer progression. *Am J Pathol* (2021) 191:168–79. doi:10.1016/j.ajpath.2020.09.010

51. Ussowicz M, Marcel V, Nguyen Van Long F, Kazanowska B, Diaz J-J, Wołowiec D. Analysis of the rRNA methylation complex components in pediatric B-cell precursor acute lymphoblastic leukemia: A pilot study. *Adv Clin Exp Med* (2020) 29:107–13. doi:10.17219/acem/112608

52. Singh P, Chalertpet K, Sukbhattee J, Wongmanee N, Suwannakart P, Yanatatsaneejit P. Association between promoter methylation and gene expression of CGB3 and NOP56 in HPV-infected cervical cancer cells. *Biomed Rep* (2022) 16:1. doi:10.3892/br.2021.1484

53. Ng JM-K, Yu J. Promoter hypermethylation of tumour suppressor genes as potential biomarkers in colorectal cancer. *Int J Mol Sci* (2015) 16:2472–96. doi:10.3390/ijms16022472

54. Jung G, Hernández-Illán E, Moreira L, Balaguer F, Goel A. Epigenetics of colorectal cancer: Biomarker and therapeutic potential. *Nat Rev Gastroenterol Hepatol* (2020) 17:111–30. doi:10.1038/s41575-019-0230-y

55. Soozangar N, Sadeghi MR, Jeddi F, Somi MH, Shirmohamadi M, Samadi N. Comparison of genome-wide analysis techniques to DNA methylation analysis in human cancer. *J Cell Physiol* (2018) 233:3968–81. doi:10.1002/jcp.26176

56. Ciribilli Y, Singh P, Inga A, Borlak J. c-Myc targeted regulators of cell metabolism in a transgenic mouse model of papillary lung adenocarcinoma. *Oncotarget* (2016) 7:65514–39. doi:10.18632/oncotarget.11804

57. Liu P, Dong Y, Gu J, Puthiyakunnon S, Wu Y, Chen X-G. Developmental piRNA profiles of the invasive vector mosquito *Aedes albopictus*. *Parasit Vectors* (2016) 9:524. doi:10.1186/s13071-016-1815-8

58. Liu Y, Dou M, Song X, Dong Y, Liu S, Liu H, et al. The emerging role of the piRNA/piwi complex in cancer. *Mol Cancer* (2019) 18:123. doi:10.1186/s12943-019-1052-9

59. Pan Y, Liu G, Zhou F, Su B, Li Y. DNA methylation profiles in cancer diagnosis and therapeutics. *Clin Exp Med* (2018) 18:1–14. doi:10.1007/s10238-017-0467-0

60. Zhu H, Zhu H, Tian M, Wang D, He J, Xu T. DNA methylation and hydroxymethylation in cervical cancer: Diagnosis, prognosis and treatment. *Front Genet* (2020) 11:347. doi:10.3389/fgene.2020.00347

61. Siegel RL, Miller KD, Fuchs HE, Jemal A. Cancer statistics, 2017. *CA Cancer J Clin* (2021) 71:7–30. doi:10.3322/caac.21387

62. Rosendo-Chalma P, Antonio-Vejar V, Bigoni-Ordóñez GD, Patiño-Morales CC, Cano-García A, García-Carrancá A. CDH1 and SNAI1 are regulated by E7 from human papillomavirus types 16 and 18. *Int J Oncol* (2020) 57:301–13. doi:10.3892/ijo.2020.5039

63. Chalertpet K, Pakdeechaidan W, Patel V, Mutirangura A, Yanatatsaneejit P. Human papillomavirus type 16 E7 oncoprotein mediates CCNA1 promoter methylation. *Cancer Sci* (2015) 106:1333–40. doi:10.1111/cas.12761

64. Cao J, Dong J, Wang Y, Chen Y. The expressions of DNA methyltransferase 1 (DNMT1) and cyclin A1 (CCNA1) in cervical carcinogenesis. *Int J Clin Exp Pathol* (2019) 12:40–9.

65. Herbst J, Pantel K, Effenberger K, Wikman H. Clinical applications and utility of cell-free DNA-based liquid biopsy analyses in cervical cancer and its precursor lesions. *Br J Cancer* (2022) 127:1403–10. doi:10.1038/s41416-022-01868-6

66. Zhang Y, Lin Z, Lin X, Zhang X, Zhao Q, Sun Y. A gene module identification algorithm and its applications to identify gene modules and key genes of hepatocellular carcinoma. *Sci Rep* (2021) 11:5517. doi:10.1038/s41598-021-84837-y

67. Zhou W, Chen Y, Luo R, Li Z, Jiang G, Ou X. Identification of biomarkers related to immune cell infiltration in hepatocellular carcinoma using gene Co-expression network. *Pathol Oncol Res* (2021) 27:601693. doi:10.3389/pore.2021.601693

68. Li A, Ye B, Lin F, Zhou P, Wang Y, Miao X, et al. Dissecting novel tumor antigens and immune subtypes guided mRNA vaccine development for HBV related-hepatocellular carcinoma. [preprint]. In Review (2022). doi:10.21203/rs.3.rs-1962830/v1

69. Coccaro N, Anelli L, Zagaria A, Specchia G, Albano F. Next-generation sequencing in acute lymphoblastic leukemia. *Int J Mol Sci* (2019) 20:2929. doi:10.3390/ijms20122929

70. Button L, Rogers B, Thomas E, Bradfield A, Alnafakh R, Drury J, et al. Telomere and telomerase-associated proteins in endometrial carcinogenesis and cancer-associated survival. *Int J Mol Sci* (2022) 23:626. doi:10.3390/ijms23020626

71. Giridhar KV, Sosa CP, Hillman DW, Sanhueza C, Dalpiaz CL, Costello BA, et al. Whole blood mRNA expression-based prognosis of metastatic renal cell carcinoma. *Int J Mol Sci* (2017) 18:2326. doi:10.3390/ijms18112326

72. Bhushan A, Kumari R, Srivastava T. Scouting for common genes in the heterogenous hypoxic tumor microenvironment and their validation in glioblastoma. *3 Biotech* (2021) 11:451. doi:10.1007/s13205-021-02987-2

73. Expansion of intronic. Expansion of intronic GGCCTG hexanucleotide repeat in NOP56 causes SCA36, a type of spinocerebellar ataxia accompanied by motor neuron involvement - PubMed (2022). Available at: https://pubmed.ncbi.nlm.nih.gov/21683323/(Accessed August 18, 2022).

74. Zeng S, Zeng J, He M, Zeng X, Zhou Y, Liu Z, et al. Genetic and clinical analysis of spinocerebellar ataxia type 36 in Mainland China. *Clin Genet* (2016) 90: 141–8. doi:10.1111/cge.12706

75. Kozol RA, Abrams AJ, James DM, Buglo E, Yan Q, Dallman JE. Function over form: Modeling groups of inherited neurological conditions in zebrafish. *Front Mol Neurosci* (2016) 9:55. doi:10.3389/fnmol.2016.00055

76. Quelle-Regaldie A, Folgueira M, Yáñez J, Sobrido-Cameán D, Alba-González A, Barreiro-Iglesias A, et al. A nop56 zebrafish loss-of-function model exhibits a severe neurodegenerative phenotype. *Biomedicines* (2022) 10:1814. doi:10.3390/biomedicines10081814

77. Vijayakumar S, Jones S, Jones T, Tian C, Johnson K. Spontaneous mutations of the Zpld1 gene in mice cause semicircular canal dysfunction but do not impair gravity receptor or hearing functions. *Scientific Rep* (2019) 9:12430. doi:10.1038/s41598-019-48835-5

78. Miyazaki K, Yamashita T, Morimoto N, Sato K, Mimoto T, Kurata T, et al. Early and selective reduction of NOP56 (Asidan) and RNA processing proteins in the motor neuron of ALS model mice. *Neurol Res* (2013) 35:744–54. doi:10.1179/1743132813Y.0000000196

79. Xu Z, Ruan Z, Huang X, Liu Q, Li Z, Zhou X, et al. Identification of aberrantly methylated differentially expressed genes in age-related macular degeneration. *Medicine* (2019) 98:e15083. doi:10.1097/MD.0000000000015083

80. Li W, Zhang S, Zhao Y, Wang D, Shi Q, Ding Z, et al. Revealing the key MSCs niches and pathogenic genes in influencing cep homeostasis: A conjoint analysis of single-cell and WGCNA. *Front Immunol* (2022) 13:933721. doi:10.3389/fimmu.2022.933721

Pathology & Oncology Research | frontiers

TYPE Brief Research Report
PUBLISHED 11 January 2024
DOI 10.3389/pore.2023.1611444

Check for updates

OPEN ACCESS

EDITED BY
Anna Sebestyén,
Semmelweis University, Hungary

*CORRESPONDENCE
Daniela Vargova,
vargova238@uniba.sk

RECEIVED 08 August 2023
ACCEPTED 05 December 2023
PUBLISHED 11 January 2024

CITATION
Vargova D, Kolková Z, Dargaj J, Bris L, Luptak J, Dankova Z, Franova S, Svihra J, Slávik P and Sutovska M (2024), Analysis of HIF-1α expression and genetic polymorphisms in human clear cell renal cell carcinoma.
Pathol. Oncol. Res. 29:1611444.
doi: 10.3389/pore.2023.1611444

COPYRIGHT
© 2024 Vargova, Kolková, Dargaj, Bris, Luptak, Dankova, Franova, Svihra, Slávik and Sutovska. This is an open-access article distributed under the terms of the Creative Commons Attribution License (CC BY). The use, distribution or reproduction in other forums is permitted, provided the original author(s) and the copyright owner(s) are credited and that the original publication in this journal is cited, in accordance with accepted academic practice. No use, distribution or reproduction is permitted which does not comply with these terms.

Analysis of HIF-1α expression and genetic polymorphisms in human clear cell renal cell carcinoma

Daniela Vargova[1]*, Zuzana Kolková[2], Jan Dargaj[3], Lukas Bris[3], Jan Luptak[3], Zuzana Dankova[2], Sona Franova[1], Jan Svihra[3], Pavol Slávik[4] and Martina Sutovska[1]

[1]Department of Pharmacology, Jessenius Faculty of Medicine in Martin, Comenius University in Bratislava, Martin, Slovakia, [2]Biomedical Center Martin, Jessenius Faculty of Medicine in Martin, Comenius University in Bratislava, Martin, Slovakia, [3]Department of Urology, Jessenius Faculty of Medicine in Martin, Comenius University in Bratislava, and University Hospital Martin, Martin, Slovakia, [4]Department of Pathological Anatomy, Jessenius Faculty of Medicine in Martin, Comenius University in Bratislava, and University Hospital Martin, Martin, Slovakia

Introduction: Clear cell renal cell carcinoma (ccRCC) is mostly diagnosed incidentally and has relatively high recurrence rates. Alterations in VHL/HIF and mTOR pathways are commonly present in ccRCC. The present study attempted to identify potential diagnostic markers at the biochemical and molecular level.

Methods: In total, 54 subjects (36 patients with ccRCC and 18 cancer-free controls) were enrolled. ELISA was used to measure the levels of HIF-1α in the tumor and healthy kidney tissue. The association between five selected SNPs (rs779805, rs11549465, rs2057482, rs2295080 and rs701848) located in genes of pathologically relevant pathways (VHL/HIF and mTOR) and the risk of ccRCC in the Slovak cohort was studied using real-time PCR.

Results: Significant differences in HIF-1α tissue levels were observed between the tumor and healthy kidney tissue ($p < 0.001$). In the majority (69%) of cases, the levels of HIF-1α were higher in the kidney than in the tumor. Furthermore, the concentration of HIF-1α in the tumor showed a significant positive correlation with CCL3 and IL-1β (p (R2) 0.007 (0.47); p (R2) 0.011 (0.38). No relationship between intratumoral levels of HIF-1α and clinical tumor characteristics was observed. Rs11549465, rs2057482 in the *HIF1A* gene did not correlate with the expression of HIF-1α either in the tumor or in the normal kidney. None of the selected SNPs has influenced the susceptibility to ccRCC.

Conclusion: More research is neccesary to elucidate the role of HIF-1α in the pathogenesis of ccRCC and the association between selected SNPs and susceptibility to this cancer.

KEYWORDS

HIF-1α, SNP, RCC, tumor, kidney

Introduction

Renal cell carcinoma (RCC) is the most common type of primary kidney cancer with a clear cell variant (ccRCC) representing the majority of cases (70%–90%) [1]. The highest incidences of this cancer were recorded in North America and the Czech Republic [2]. RCC is mostly (60%) diagnosed incidentally and around 30% of patients have metastatic disease at the time of the diagnosis [3,4]. Five-year cancer specific survival (CSS) rates for patients with high grade (grades 3 and 4) tumors is significantly worse than for patients with low grade (grades 1 and 2) masses [5]. Furthermore, despite conventional therapy, a relatively high number of patients (20%–40%) experience recurrence [6]. Biological markers that would enable earlier diagnosis are therefore indispensable.

Various molecular mechanisms are involved in the pathogenesis of ccRCC. The most common alterations in this cancer are observed in the VHL/HIF pathway. Approximately 50%–60% of patients with sporadic ccRCC have some abnormality in the *VHL* gene [7]. Loss of the function of tumor suppressor protein VHL (pVHL) leads to accumulation and constitutive activation of hypoxia inducible factor 1α (HIF-1α) in cancer cells [8]. This transcription factor is responsible for the metabolic switch that allows survival of cells in the hypoxic environment. It induces the expression of genes involved in the Warburg effect (e.g., pyruvate dehydrogenase kinase) and angiogenesis (*VEGF, PDGF-BB*) [9–11]. Increased levels of HIF-1α are usually associated with a worse prognosis [12,13]. Additionally, HIF-1α is believed to play an important role in tumor-associated inflammatory signaling [14].

The mammalian target of rapamycin (mTOR) is a protein kinase that regulates cell growth and proliferation. Inappropriate activation of mTOR has been reported in RCC and in a variety of other cancers as well [15–17]. Once activated, mTOR affects the translation of oncogenic and angiogenic proteins (including HIF-1α), thus supporting cancer progression [7,18]. Aberrant mTOR signaling can result from genetic alterations in various components of the pathway (e.g., mTOR complexes or its upstream regulators PI3K and PTEN) [18].

Several single nucleotide polymorphisms (SNPs) were previously identified in the genes of the VHL/HIF and mTOR pathways. Among them, rs779805, rs11549465, rs2057482, rs2295080 and rs701848 were proposed to be potentially functional and responsible for the increased risk of various malignancies, including RCC [19–30].

The current study attempted to fulfill several objectives: 1.) analyze differences between the expression of HIF-1α in tumor and healthy renal tissue from patients diagnosed with ccRCC, 2.) analyze changes of HIF-1α tissue amount with respect to tumor nuclear grade (G) and tumor-node-metastasis (TNM) stage, 3.) determine the relationship between HIF-1α and cytokines in tumor tissue, and 4.) investigate whether any of the selected SNPs (rs779805, rs11549465, rs2057482, rs2295080 and rs701848) may serve as a potential diagnostic marker of ccRCC in Slovak cohort, by determining their association with the susceptibility to this cancer.

Patients and methods

Patients

In total, 54 subjects of Slovakian nationality participated in this study: 36 patients (28 men of 62.4 ± 8.3 years and 8 women of 63.6 ± 8.9 years) and 18 cancer-free controls (12 men of 65.1 ± 9.8 years and 6 women of 67 ± 5.9 years) aged 63.0 ± 8.4 and 66.0 ± 7.2 years, respectively. Both study groups were age-matched, as it is proved by statistically nonsignificant age difference between the two groups [*p* (t) 0.152 (1.45)]. Six female and 15 male patients had tumors of low grade (LG; grades 1 and 2). The other 15 subjects (3 women and 12 men) had high grade (HG; grades 3 and 4) tumors. Seven women and 19 men had the organ-confined (OC; pT1 and 2), while the other 2 females and 8 males had locally advanced (LA; pT3 and 4) tumors. The clinicopathological characteristics of patients study group is summarized in Supplementary Table S1. The inclusion criterium for the patients was histologically verified ccRCC that meets the criteria for surgical treatment. Any individual suffering from chronic disease of the urogenital system or any systemic diseases such as autoimmune, rheumatologic, endocrinne or severe cardiovascular disease were excluded from the study by taking a thorough medical history. The stage of the cancer was determined by computed tomography according to the World Health Organization 2016 classification criteria [31]. Tumor grade was determined by histopathological examination according to the WHO/ISUP (International Society of Urological Pathology) classification system [31]. Control subjects were recruited from individuals who underwent medical examination for non-malignant urological disease. They were not related to patients and had no history of any oncological disease. Both the healthy subjects and the patients provided 6 mL of peripheral venous blood. The blood was collected into EDTA tubes, promptly transported to the lab, and centrifuged at 3,000 rpm for 10 min. The buffy coat was then separated and stored at −80°C until further analysis. Tissue specimens (tumor- T and macroscopically normal kidney tissue- N) were obtained from patients during tumor removal performed at the Department of Urology of the Jessenius Faculty of Medicine in Martin and University Hospital Martin, Slovakia. Both ccRCC and healthy renal samples were removed from the same kidney, placed in sterile polypropylene tubes, and stored at −80°C until further analysis.

DNA isolation and SNP genotyping

Genomic DNA was extracted from white blood cells using the DNeasy Blood & Tissue Kit (Qiagen). This simple and time-

efficient procedure enables DNA isolation from fresh or frozen anticoagulated blood. First, blood samples were lysed with proteinase K in AL buffer (provided by the kit) during 10 min of incubation at 56°C. Ethanol (99.6%) was then added to the lysates and the mixture was loaded onto the DNeasy membrane in a mini spin column placed in a 2 mL collection tube and centrifugated at 8,000 rpm for 1 min. During this step, DNA bound to the DNeasy membrane, and excess fluid was removed. Subsequently, two additional centrifugation cycles were performed using AW1 and AW2 buffers (provided by the kit) to ensure the elimination of residual contaminants and increase the purity of the DNA. Finally, DNA was eluted in AE buffer (provided by the kit) and its concentration was evaluated using a NanoDropTM spectrophotometer (Thermo Scientific, USA) at 260 nm.

The extracted DNA was analyzed for individual genotypes using the TaqMan allelic discrimination method based on conventional real-time PCR. The genotyping reaction mixture consisted of genotyping TaqMan Master Mix, RNase-free water, and pre-designed Applied BiosystemsTM TaqMan® SNP genotyping assays. Genotypic detection was performed in the 7,500 Fast Real-Time PCR instrument (Applied BiosystemsTM, Thermofisher Scientific, USA). Characteristics of the selected SNPs are shown in Supplementary Table S2.

Assessment of HIF-1α protein

HIF1α tissue levels were measured in the healthy kidney and ccRCC from 26 patients with the use of sandwich ELISA (LS-F4224). Clinical characteristics of these patients and all the raw data are described in the Supplementary Table S3. Supernatants used for the ELISA reaction were prepared according to the kit protocol as follows: 100 mg of tissue was washed with 0.02 M PBS (7.0–7.2 pH) to remove excess blood tissue and minced on ice. The samples were then placed into a tube containing 500 µL of 0.02 M PBS and homogenized on ice at 4,000 rpm (Homogenizer Stuart SHM2/Euro, Bibby Scientific, UK). The homogenates were subsequently subjected to a 3 freeze/thaw cycle and centrifuged at 7,170 rpm for 5 min at 4°C. Finally, the supernatant was collected, aliquoted, and frozen at −80°C until further analysis.

Assessment of cytokine tissue levels

Cell cytokine tissue levels were determined using a commercially available kit Bio-PlexTM Human Cytokine Standard 27-Plex assay (Bio-Rad, Hercules, California, USA). This assay allowed us to detect 27 biologically relevant cell signaling molecules that are significantly involved in cancer biology: basic fibroblast growth factor (bFGF), CXCL11 (eotaxin), granulocyte macrophage colony stimulating factor (GM-CSF), granulocyte colony stimulating factor (G-CSF); interferon gamma (IFN-γ); interleukins 1β, 1Ra, 2, 4, 5, 6, 7, 8 (CXCL8), 9, 10, 12p70, 13, 15 and 17A; interferon gamma-induced protein 10 (IP-10 also known as CXCL10); monocyte chemoattractant protein 1 (MCP-1 also known as CCL2); macrophage inflammatory proteins 1 α and β (MIP-1α and MIP-1β also known as CCL3 and CCL4); platelet-derived growth factor-BB (PDGF-BB); RANTES (CCL5); tumor necrosis factor α (TNF-α), and vascular endothelial growth factor (VEGF). The biomarkers of interest were measured in each sample simultaneously during one reaction. This method combines two detection approaches: sandwich ELISA and flow cytometry. First, the target molecule reacts with the capture antibody coupled to magnetic beads, and then the unbound proteins are removed in series of washes. Next, biotinylated antibody is added, and a sandwich complex is formed. The streptavidin-phycoerythrin (SA-PE) conjugate is used to visualize the created complex. Identification and quantification of analytes are performed by two laser lights with different wavelengths (635 nm and 532) built in the Bio-Plex® 200 System reader. The final concentration of cytokines is proportional to the mean fluorescence intensity (MFI) and is expressed in pg/mL. To acquire standardized values, the tissue concentrations of HIF-1α and cytokines were divided by total tissue protein levels (mg/mL) measured by Bicinchoninic acid assay (BCA) kit (Thermofisher Scientific).

Statistical analysis

A two-sample paired t-test was used to estimate the difference between HIF-1α expression in tumor (HIF-1α_{TU}) and normal kidney tissue (HIF-1α_{N}). Since the data were not trivial, the logarithmically transformed ratios of HIF-1α_{TU} and HIF-1α_{N} (log-T/N) of the patient samples were subjected to exploratory data analysis (EDA) and each observation was assigned to one of the two groups (Group 1 and Group 2) according to a higher posterior probability. The logarithmic ratios in each group were normally distributed. Group 1 was further analyzed using parametric unpaired t-tests (with Welch correction if necessary). The relationship between HIF-1α_{TU} and cytokines in tumor tissue was determined by a Pearson correlation coefficient. The final results were visualized using boxplots and scatter plots.

The null hypothesis of no association between SNP and ccRCC was tested by Fisher exacts test in general, dominant, recessive, and multiplicative models. Odds ratio (OR) with 95% confidence interval (95% CI) was computed for each model. Chi-square test was performed as well. The Hardy-Weinberg equilibrium test was tested in both patients and controls.

The data were explored and analyzed in R [1], ver. 4.0.5 and in GraphPad, ver. 8.0.1 software. The precision of the estimates was quantified by the 95% confidence limits. Dichotomization was performed using the cutoff *p*-value of 0.05.

TABLE 1 The frequency of genotypes and alleles of selected gene polymorphisms in patients with ccRCC and controls.

Model	Genotype	Patients (N = 37)	Controls (N = 18)	OR	95% CI	*P*	χ^2 (*P*)
			rs779805 (*VHL*) A > G				
G	AA	19 (53%)	9 (50%)				0.27 (0.87)
	AG	16 (44%)	8 (44.4%)	0.95	0.29–3.03	>0.99	
	GG	1 (3%)	1 (5.6%)	0.47	0.03–8.46	>0.99	
D	AA	19	9				
	AG + GG	17	9	0.90	0.29–2.78	>0.99	
R	AA + AG	35	17				
	GG	1	1	0.48	0.03–8.25	>0.99	
M	A	54	26				
	G	18	10	0.87	0.35–2.14	0.82	
			rs2057482 (*HIF1A*) C > T				
G	CC	27 (75%)	16 (88.9%)				
	CT	9 (25%)	1 (5.6%)	-	-	-	-
	TT	0 (0%)	1 (5.6%)				
D	CC	27	16				
	CT + TT	9	2	2.67	0.51–13.92	0.30	
R	CC + CT	36	17				
	TT	0	1	-	-	-	
M	C	63	33				
	T	9	3	1.57	0.39–6.20	0.75	
			rs11549465 (*HIF1A*) C > T				
G	CC	27 (75%)	14 (77.8%)				
	CT	9 (25%)	3 (16.7%)	-	-	-	-
	TT	0 (0%)	1 (5.6%)				
D	CC	27	14				
	CT + TT	9	4	1.17	0.31–4.47	>0.99	
R	CC + CT	36	17				
	TT	0	1	-	-	-	
M	C	63	31				
	T	9	5	0.89	0.27–2.87	>0.99	
			rs2295080 (*MTOR*) T > G				
G	TT	14 (39%)	7 (38.9%)				0.33 (0.85)
	TG	16 (44%)	9 (50.0%)	0.89	0.26–3.01	>0.99	
	GG	6 (17%)	2 (11.1%)	1.50	0.24–9.44	>0.99	
D	TT	14	7				
	TG + GG	22	11	1.00	0.31–3.19	>0.99	
R	TT +TG	30	16				
	GG	6	2	1.60	0.29–8.86	0.70	
M	T	44	23				
	G	28	13	1.13	0.49–2.58	0.84	
			rs701848 (*PTEN*) T > C				
G	TT	13 (36%)	3 (16.7%)				3.13 (0.21)
	TC	17 (47%)	13 (72.2%)	0.30	0.07–1.28	0.12	
	CC	6 (17%)	2 (11.1%)	0.69	0.09–5.29	>0.99	

(Continued on following page)

TABLE 1 (*Continued*) The frequency of genotypes and alleles of selected gene polymorphisms in patients with ccRCC and controls.

Model	Genotype	Patients (N = 37)	Controls (N = 18)	OR	95% CI	*P*	χ^2 (*P*)
D	TT	13	3				
	TC + CC	23	15	0.35	0.09–1.45	0.21	
R	TT + TC	30	16				
	CC	6	2	1.60	0.29–8.86	0.70	
M	T	43	19				
	C	29	17	0.75	0.34–1.69	0.54	

The table shows a summary of the results of genetic association analysis for five selected SNPs in patients with clear cell renal cell carcinoma (ccRCC) and control subjects. The association was tested in four different genetic models: dominant (D), general (G), recessive (R) and multiplicative (M). The cut off value for the level of significance was 0.05. 95% CI, 95% confidence interval; OR, odds ratio; P, *p*-value of Fisher's exact test; χ (P), Chi-squared test with *p*-value.

Results

Genetic association study

We have performed a genetic association study (GAS) in five selected SNPs (rs779805 (*VHL*), rs2057482 (*HIF1A*), rs11549465 (*HIF1A*), rs2295080 (*MTOR*) and rs701848 (*PTEN*)) using various models (general, dominant, recessive, and multiplicative). Wild-type genotypes/alleles were used as reference. Genotype frequencies of all the SNPs were consistent with the Hardy-Weinberg equilibrium in both the patient and control group (at a level of significance 0.05). Interestingly, the distribution genotypes for rs2057482 and for rs11549465 in *HIF1A* were the same in all patients, but not in controls. We were unable to evaluate these two SNPs in a general or recessive model as the minor polymorphic genotype was present only in the control group. The results of GAS are summarized in Table 1. The raw data from this analysis are shown in Supplementary Tables S5, S6.

In all cases *p* values have reached extremely high levels. Therefore, it is not possible to draw any explicit conclusions from these results at the moment and further investigations are warranted. However, according to the odds ratios (ORs) of general and dominant models, we can hypothesize that one or two recessive alleles at rs779805 may possibly have protective character with regard to the risk of ccRCC [GG vs. AA: OR (95% CI) = 0.47 (0.03–8.46), $p > 0.99$; AG vs. AA: OR (95% CI) = 0.95 (0.29–3.03), $p > 0.99$; GG/AG vs. AA: OR (95% CI) = 0.90 (0.29–2.78), $p > 0.99$]. The results of recessive and multiplicative models appear to be in line with this hypothesis [GG vs. AA/AG: OR (95% CI) = 0.48 (0.03–8.25), $p > 0.99$; G vs. A: OR (95% CI) = 0.87 (0.35–2.14), $p = 0.82$]. The general and recessive models for rs2295080 suggest that individuals with two minor alleles could have one and a half times higher odds ratio of developing ccRCC than subjects with one or two major alleles [GG vs. TT: OR (95% CI) = 1.50 (0.24–9.44), $p > 0.99$; GG vs. TG/TT: OR (95% CI) = 1.60 (0.29–8.86), $p = 0.70$]. In other words, based on the OR values in general model, we can hypothesize that one minor allele probably may not be sufficient to increase the susceptibility to ccRCC [TG vs. TT: OR (95% CI) = 0.89 (0.26–3.01), $p > 0.99$]. As for rs701848, the results of individual models are contradictory. While recessive model indicates that individuals with two minor alleles have higher odds ratio of developing ccRCC [CC vs. TC/TT: OR (95% CI) = 1.60 (0.29–8.86), $p = 0.70$], neither general [CC vs. TT: OR (95% CI) = 0.69 (0.09–5.29), $p > 0.99$] nor multiplicative model agree with this [C vs. T: OR (95% CI) = 0.75 (0.34–1.69), $p = 0.54$].

HIF-1α expression in ccRCC and kidney tissue

The results of our analysis have shown that two different groups of patients were present in our data set according to the means of log-HIF-1α_{TU} and HIF-1α_N. Group 1 consisted of 18 patients (69% of all cases) and Group 2 comprised 8 patients (31%). The samples were further classified according to clinical characteristics of the tumor as LG or HG and OC or LA. In Group 2 there were 87.5% patients with HG tumors, while in Group 1 the majority (72%) of subjects had LG tumors. In Group 2, 37.5% of the patients had LA disease, while in Group 1 it was 28%.

The means of log-HIF-1α_{TU} and HIF-1α_N values were compared between both groups using the unpaired t-test. The results have shown that the patients in Group 1 had higher levels of HIF-1α in normal tissue than in the tumor, while the individuals in Group 2 had exactly the opposite profile. The difference between the means of log-HIF-1α_{TU} and log-HIF-1α_N was statistically significant in both groups [p (t) < 0.0001 (5.82); p (t) = 0.0005 (5.28) respectively] (Table 2; Figure 1A). Furthermore, the tumor amount of HIF-1α in Group 1 was significantly lower compared to Group 2 [p (t) < 0.0001

TABLE 2 Differences in HIF-1α concentration between two groups of patients and with regard to clinical and genetic parameters.

	Group 1	Group 2	T1 vs. T2	N1 vs. N2	LG vs. HG	OC vs. LA	CT vs. CC in tumor	CT vs. CC in normal tissue
N	(18, 18)	(8, 7)	(18, 7)	(18, 8)	(13, 5)	(13, 5)	(5, 13)	(5, 13)
p-value	<0.0001	0.0005	<0.0001	0.64	0.44	0.17	0.44	0.9
	****	***	****	*ns*	*ns*	*ns*	*ns*	*ns*
t statistics	5.82	5.28	14.74	0.49	0.78	1.42	0.79	0.13
Diff. of means (±SEM)	−0.81 (±0.14)	2.17 (±0.41)	2.78 (±0.19)	−0.19 (±0.39)	−0.18 (±0.23)	−0.31 (±0.22)	−0.18 (±0.23)	−0.03 (±0.22)
95% CI	−1.09 to −0.52	1.25 to 3.09	2.39 to 3.17	−1.09 to 0.71	−0.66 to 0.30	−0.77 to 0.15	−0.66 to 0.30	−0.49 to 0.44
R2	0.5	0.75	0.90	0.03	0.04	0.11	0.04	0.001

The Table shows a summary of unpaired t-test results comparing the means of logarithmically transformed HIF-1α concentration between different subpopulations: tumor vs. normal tissue in Group 1 and Group 2, tumor tissue of Group 1 (T1) vs. tumor tissue of Group 2 (T2), normal tissue of Group 1 (N1) vs. normal tissue of Group 2 (N2), Group 1 tumors of low grade (LG) vs. Group 1 tumors of high grade (HG), organ-confined tumors of Group 1 (OC) vs. locally advanced tumors of Group 1 (LA), Group 1 tumors with heterozygous genotype for rs11549465/rs2057482 vs. Group 1 tumors with homozygous genotype for rs11549465/rs2057482 (CT vs. CC in tumor) and finally Group 1 normal tissues with heterozygous genotype for rs11549465/rs2057482 vs. Group 1 normal tissues with homozygous genotype for rs11549465/rs2057482 (CT vs. CC in normal tissue); CI, confidence interval; diff, difference; N, number of data analyzed without outliers; ns, not significant; R2, R squared; SEM, standard error of the mean.

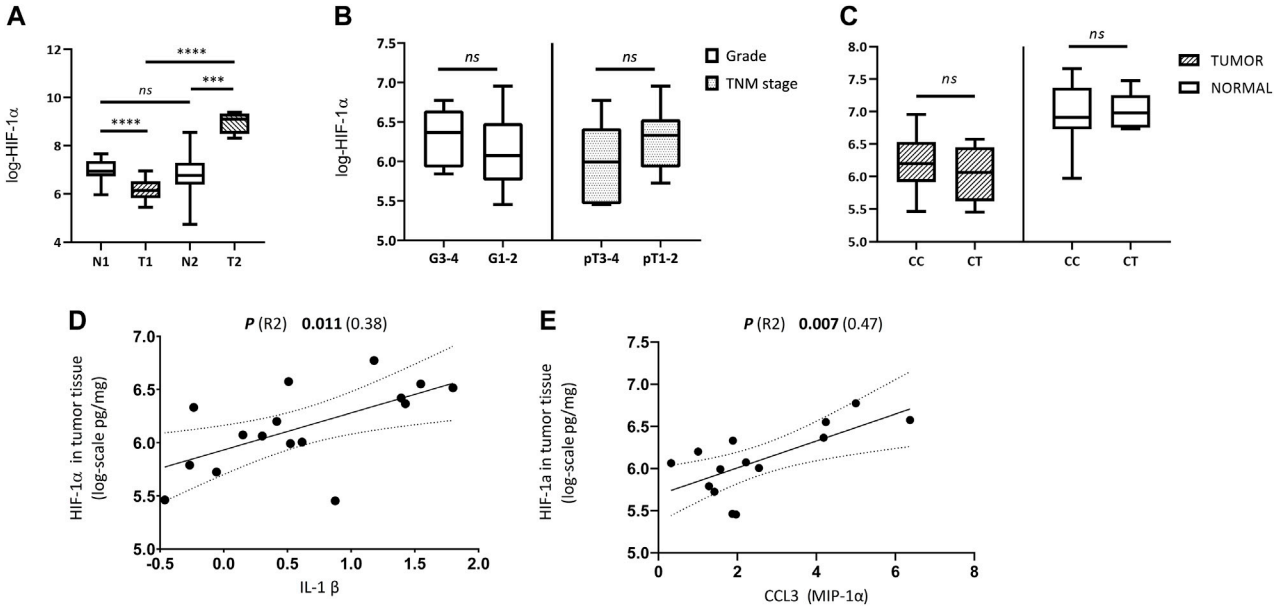

FIGURE 1
Comparison of HIF-1α tissue levels with regard to histological, clinical, genetic and immunological parameters. **(A)** Differences between HIF-1α expression in tumor and normal kidney tissue samples from patients with ccRCC in Group 1 (T1, N1) and Group 2 (T2, N2); **(B)** Differences in tumor tissue HIF-1α levels between high grade vs. low grade tumors (G3-4 vs. G1-2), and between locally advanced (LA) vs. organ-confined (OC) tumors (pT3 and 4 vs. pT1 and 2) of Group 1; **(C)** Difference in HIF-1α expression between tumor and normal kidney tissue of Group 1 according to genotypes (CC vs. CT) of rs2057482/rs11549465 in *HIF1A* gene; **(D)** Relationship between the amounts of HIF-1α and IL-1β in tumor tissue; **(E)** Relationship between the amounts of HIF-1α and CCL3 (MIP-1α) in tumor tissue. Concentration values of HIF-1α and cytokines used in the analyses were logarithmically transformed.

(14.74)]. On the other hand, HIF-1α in normal tissue reached similar levels in both groups [*p* (t) = 0.64 (0.49)] (Table 2; Figure 1A). Since Group 1 was more numerous as to the samples, subsequent analyzes were performed only on this data set.

Expression of HIF-1α and clinical tumor characteristics

We have examined tumor tissue expression of HIF-1α in the Group 1 according to clinical tumor characteristics using unpaired

TABLE 3 Association between HIF-1a and cytokines.

	Pearson r	95% CI	R2	*p*	Signif.
HIF-1α- IL-1β	0.62	0.18 to 0.85	0.38	0.011	*
HIF-1α-CCL3	0.69	0.24 to 0.89	0.47	0.007	**

The table shows the results of correlation analysis between HIF-1a and two cytokines (IL-1β and CCL3/MIP-1α). The data used in the analysis were logarithmically transformed. CI, confidence interval; R2, R squared; p, wo-tailed *p*-value; signif., significance with 0.05 cut-off.

t-test. No significant differences in HIF-1α tumor tissue levels were observed between LG and HG [*p* (t) = 0.44 (0.78)] nor between OC and LA [p (t) = 0.17 (1.42)] (Table 2; Figure 1B).

Effect of *HIF1A* polymorphisms on HIF-1α tumor and kidney expression

Next, we have analyzed whether the genetic status (genotype for rs2057482/rs11549465 in *HIF1A*) influences HIF-1α expression in either normal or tumor tissue. The mean value of log-HIF-1α in samples with the CC genotype was compared to log-HIF-1α in samples with the CT genotype. This was performed on tumor and normal tissue separately. No significant differences were detected in either case [*p* (t) = 0.44 (0.79); *p* (t) = 0.9 (0.13)] (Table 2; Figure 1C).

Association between HIF-1α expression and cytokine amounts in ccRCC

Finally, the levels of 27 biologically relevant cytokines (listed in Materials and methods) were measured in tumor tissue of Group 1 and correlated with HIF-1α tumor tissue levels. CCL3 (MIP-1α) and IL-1β have shown a significant positive correlation with HIF-1α_{TU} [*p* (R-squared -R2) = 0.007 (0.47); *p* (R2) = 0.011 (0.38) respectively] (Table 3; Figures 1D, E). The raw data on cytokines used for this analysis are described in Supplementary Table S4 and were studied in more detail in our previous work [32].

Discussion

HIF-1 is a ubiquitously expressed protein consisting of α and β subunits. Under normoxia, HIF-1α is hydroxylated and undergoes proteasomal degradation. Oxygen deficiency typical for solid tumors or abnormalities in the *VHL* gene that are often present in ccRCC, disrupt this process and lead to the accumulation of α subunit in the cytoplasm which is then translocated to the nucleus and initiates the transcription of its target genes. Increased expression of crucial proteins for angiogenesis, glucose metabolism, tumor growth and progression (VEGF, PDGF, EGFR, IGF, GLUT-1, CXCR, CAIX and XII), can contribute markedly to the tumorigenesis of RCC [11, 12]. The expression of HIF-1α was shown to correlate with the clear cell phenotype of RCC [10, 33]. The percentage of ccRCC specimens positive for high levels of HIF-1α reported in previous studies ranged from 17% to 97% [10]. The results of the present study have shown that the majority (69%) of the patients with ccRCC had significantly higher levels of HIF-1α in kidney than in tumor tissue. A possible explanation for these low HIF-1α levels in our ccRCC samples may be a deletion of 14q or alternative mRNA splicing leading to production aberrant HIF-1α isoforms [11, 34]. Alternatively, this observation may be related to the clinicopathological tumor profile of the samples. Tumors in which HIF-1α was significantly lower than in healthy adjacent kidney tissue were mostly (72%) organ-confined and low grade. Thus, we can hypothesize that HIF-1α levels depend on the disease stage. This, indeed, was confirmed in the study by Chen et al. (2020). These authors observed a positive correlation between *HIF1A* overexpression and the more aggressive tumor phenotype of various human cancers [35]. However, another study reported significantly lower HIF-1α levels in locally aggressive ccRCC tumors than in localized tumors [36]. Hoefflin et al. (2020) also suggested that the loss of *HIF1A,* which is supposed to cause a decrease in HIF-1α protein levels, is more frequent in high-grade and high-stage ccRCC tumors [9]. When we compared the HIF-1α tissue levels between LG and HG tumors, and between OC and LA tumors from patients with a low HIF-1α log-T/N ratio (Group 1), no significant differences were observed in either case. This corresponds to the study by Klatte et al. (2007) [12]. Neither these authors did find any association between HIF-1α tumor expression and clinicopathological tumor characteristics. Clearly, more research is necessary to explain these discrepancies and elucidate the role of HIF-1α in ccRCC pathogenesis and its relationship with disease progression. However, its involvement in the pathological processes of this tumor is supported by the fact that the normal kidney tissue of both groups we studied contained significantly different amounts of HIF-1α than tumor tissue.

HIF-1α is not only a master regulator of hypoxia, but it also participates in the regulation of innate and adaptive immune responses [37–40]. Inflammation is one of the prominent features of the tumor microenvironment (TME) [41]. The presence of highly complex crosstalk between the inflammatory and hypoxia pathways is supported by the fact that many of the key signaling molecules (cytokines and chemokines) are induced by low oxygen levels [42–44]. For example, in the context of rheumatoid arthritis, HIF-1α was shown to directly interfere with the production of TNF-α, IL-1β, IL-6 and IL-8 [45]. The role of HIF factors in sterile inflammation was also demonstrated in epithelial and fibroblast cancer cell lines [46]. In the present study, we found a statistically significant positive correlation between HIF-1α and CCL3, and between HIF-1α and IL-1β. Both CCL3 and IL-1β are known to

participate in cancer pathogenesis [47,48]. Although data on the association between HIF-1α and these cytokines in the available literature are scarce, similar observations but in different circumstances have been reported. For example, inhibition of HIF-1α in multiple myeloma cells was shown to decrease CCL3 secretion [49]. In contrast, IL-1β appears to be rather upstream than downstream component of HIF-1α pathway. Jung et al., 2003 suggested that this interleukin may indirectly (through NF-κB and COX-2) mediate HIF-1α upregulation [50]. Clearly, further investigation is needed to determine the direction, character and consequences of the complex interaction between HIF-1α and these cytokines.

Rs11549465 (Pro582Ser/C1772T) and rs2057482 (C191T) are supposed to be functional polymorphisms. The former is found in the exon 12 of *HIF1A* and codes for the oxygen-dependent degradation domain of HIF-1α protein. The C > T substitution in rs11549465 is supposed to give rise to a molecule resistant to degradation which leads to increased transcriptional activity of HIF1 complex [19]. Rs2057482 is located in 3′UTR of *HIF1A*. There are several reports that hypothesized that the minor T allele in this polymorphism may decrease the *HIF1A* expression by creating a new microRNA binding site [22,51–54]. However, according to our data, neither the tumor nor the normal kidney HIF-1α tissue levels did not appear to be influenced by any of these two polymorphisms in *HIF1A*.

Regarding the results of our GAS, we could not interpret the association between the *HIF1A* genotypes (rs1149465, rs2057482) and the risk of developing ccRCC since no recessive homozygotes were present in the group of patients. The results of other studies on this SNP are inconsistent. The possible importance of variant alleles in rs11549465 with respect to RCC susceptibility was proposed in European patients [21]. Additionally, the meta-analysis by Wu et al. (2019) performed on Asian population revealed that the polymorphism rs2057482 was associated with decreased overall cancer risk [55]. On the other hand, no significant differences between RCC cases and controls in genotype frequencies for rs11549465 and rs2057482 were observed in the Chinese population [22]. These discrepancies may be ascribed to different ethnicities.

Polymorphism rs779805 is located within the *VHL* gene promoter, which is abundant in CpG islands and prone to methylation [56]. Therefore, we can hypothesize that A > G substitution may increase the probability of silencing of the *VHL* gene and subsequently increase the risk of developing ccRCC. Our results do not appear to support this assumption. Although the level of significance for either general or recessive model was far above the cut-off *p*-value, OR indicate that individuals carrying either one or two risk alleles could probably have lower risk of developing ccRCC. No significant differences in rs779805 genotypes between RCC cases and controls were reported also by Bensouilah et al. (2020) and Qin et al. (2012) [22, 29]. On the other hand, several other studies demonstrated a positive association between G allele at rs779805 and RCC risk [26–28].

The importance of mTOR pathway-related genes in RCC pathogenesis is well established [57–59]. Dysregulation of this pathway is usually associated with an aggressive tumor behavior [57]. Transcriptional activity of the *MTOR* gene can be altered in different ways. For example, a minor G allele at rs2295080 in the promoter region of *MTOR* was shown to be significantly associated with decreased mRNA levels of *MTOR* [23]. Consequently, several studies reported that Asian people carrying TG and TG/GG genotypes have a lower risk of urinary cancers (including RCC) than carriers of two dominant alleles [23,24,30]. Contrary to these, are the results of the present study. The relationship between this polymorphism and ccRCC risk was not significant, but the general and recessive models indicate that two minor alleles in this polymorphism could potentially increase the risk of ccRCC development.

Another frequently mutated gene in solid tumors, including RCC, is *PTEN* [60,61]. Loss of activity of this tumor suppressor gene is responsible for upregulation of the PI3K-Akt-mTOR pathway and eventually leads to enhanced cell growth and proliferation [62]. Rs701848 polymorphism located in 3′UTR of the PTEN gene is supposed to alter the binding affinity of miRNAs to this region and thus interfere with the process of gene splicing and protein expression [63,64]. Therefore, it is possible that the variant allele in rs701848 may influence cancer susceptibility. Indeed, a meta-analysis performed in Asian individuals showed that the recessive homozygous genotype (CC) at rs701848 is significantly associated with an increased risk of overall and urinary system cancer [25]. Regarding RCC, only a marginal association of rs701848 with this malignancy was reported in subjects from China [23]. We did not confirm any significant relationship between the minor allele or minor genotype in rs7018484 and the risk of ccRCC but there is an indication that minor allele could possibly have a protective character. However, more research is undoubtedly necessary to verify this.

To conclude, our study has shown significant differences in HIF-1α tissue expression levels between ccRCC and healthy kidney, with most cases having a significantly higher amount of HIF-1α in normal than in tumor tissue. Tumor tissue levels of CCL3 (MIP-1α) and IL-1β displayed significant positive correlation with the amount of HIF-1α in the tumor. None of the selected SNPs (rs779805, rs11549465, rs2057482, rs2295080 and rs701848) were associated with increased susceptibility to ccRCC. One of the major limitations of the study is a small data set. Therefore, the presented results should be considered as preliminary only.

Data availability statement

All relevant data is contained within the article and supplementary materials. Any further inquiries can be directed to corresponding authors.

Ethics statement

The studies involving humans were approved by Committee of Jessenius Faculty of Medicine in Martin Comenius University in Bratislava (protocol code No. 53/2020, date of approval). The studies were conducted in accordance with the local legislation and institutional requirements. The participants provided their written informed consent to participate in this study.

Author contributions

Conceptualization, DV, ZK, MS, and ZD; methodology DV, ZK, JD, and LB; validation and formal analysis, DV and ZK; resources, JD, LB, and JL; data curation DV; writing original draft preparation, DV; writing–review and editing, MS, SF, and ZK; visualization, DV; supervision, MS; project administration, DV and ZK; funding acquisition, MS, SF, JS, and DV. All authors contributed to the article and approved the submitted version.

Funding

This publication has been produced with the support of grants VEGA 1/0428/21; VEGA 1/0072/23, APVV-19-0033, GUK 6/2021, GUK 132/2023 and the Operational Program Integrated Infrastructure for the project New Possibilities for the Management of Serious Diseases in Medical and Preventive Care with Regard to the Safety of Healthy Professionals, ITMS: 313011AUA5, co-financed by the European Regional Development Fund.

Conflict of interest

The authors declare that the research was conducted in the absence of any commercial or financial relationships that could be construed as a potential conflict of interest.

Acknowledgments

We wish to thank assoc. prof. Zora Lasabova and the Department of molecular biology and genomics JFM CU and Katarína Jesenská for technical support.

Supplementary material

The Supplementary Material for this article can be found online at: https://www.por-journal.com/articles/10.3389/pore.2023.1611444/full#supplementary-material

References

1. Warren AY, Harrison D. WHO/ISUP classification, grading and pathological staging of renal cell carcinoma: standards and controversies. *World J Urol* (2018) 36: 1913–26. doi:10.1007/s00345-018-2447-8

2. Chow W-H, Dong LM, Devesa SS. Epidemiology and risk factors for kidney cancer. *Nat Rev Urol* (2010) 7:245–57. doi:10.1038/nrurol.2010.46

3. Vasudev NS, Wilson M, Stewart GD, Adeyoju A, Cartledge J, Kimuli M, et al. Challenges of early renal cancer detection: symptom patterns and incidental diagnosis rate in a multicentre prospective UK cohort of patients presenting with suspected renal cancer. *BMJ Open* (2020) 10:e035938. doi:10.1136/bmjopen-2019-035938

4. Makhov P, Joshi S, Ghatalia P, Kutikov A, Uzzo RG, Kolenko VM. Resistance to systemic therapies in clear cell renal cell carcinoma: mechanisms and management strategies. *Mol Cancer Ther* (2018) 17:1355–64. doi:10.1158/1535-7163.MCT-17-1299

5. Kuthi L, Jenei A, Hajdu A, Németh I, Varga Z, Bajory Z, et al. Prognostic factors for renal cell carcinoma subtypes diagnosed according to the 2016 WHO renal tumor classification: a study involving 928 patients. *Pathol Oncol Res* (2017) 23: 689–98. doi:10.1007/s12253-016-0179-x

6. Kim SH, Park B, Hwang EC, Hong S-H, Jeong CW, Kwak C, et al. Retrospective multicenter long-term follow-up analysis of prognostic risk factors for recurrence-free, metastasis-free, cancer-specific, and overall survival after curative nephrectomy in non-metastatic renal cell carcinoma. *Front Oncol* (2019) 9:859. doi:10.3389/fonc.2019.00859

7. Nabi S, Kessler ER, Bernard B, Flaig TW, Lam ET. Renal cell carcinoma: a review of biology and pathophysiology. *F1000Res* (2018) 7:307. doi:10.12688/f1000research.13179.1

8. Sato Y, Yoshizato T, Shiraishi Y, Maekawa S, Okuno Y, Kamura T, et al. Integrated molecular analysis of clear-cell renal cell carcinoma. *Nat Genet* (2013) 45: 860–7. doi:10.1038/ng.2699

9. Hoefflin R, Harlander S, Schäfer S, Metzger P, Kuo F, Schönenberger D, et al. HIF-1α and HIF-2α differently regulate tumour development and inflammation of clear cell renal cell carcinoma in mice. *Nat Commun* (2020) 11:4111. doi:10.1038/s41467-020-17873-3

10. Gudas LJ, Fu L, Minton DR, Mongan NP, Nanus DM. The role of HIF1α in renal cell carcinoma tumorigenesis. *J Mol Med* (2014) 92:825–36. doi:10.1007/s00109-014-1180-z

11. Shen C, Kaelin WG. The VHL/HIF axis in clear cell renal carcinoma. *Semin Cancer Biol* (2013) 23:18–25. doi:10.1016/j.semcancer.2012.06.001

12. Klatte T, Seligson DB, Riggs SB, Leppert JT, Berkman MK, Kleid MD, et al. Hypoxia-inducible factor 1 alpha in clear cell renal cell carcinoma. *Clin Cancer Res* (2007) 13:7388–93. doi:10.1158/1078-0432.CCR-07-0411

13. Fan Y, Li H, Ma X, Gao Y, Chen L, Li X, et al. Prognostic significance of hypoxia-inducible factor expression in renal cell carcinoma: a PRISMA-compliant systematic review and meta-analysis. *Medicine* (2015) 94:e1646. doi:10.1097/MD.0000000000001646

14. Balamurugan K. HIF-1 at the crossroads of hypoxia, inflammation, and cancer. *Int J Cancer* (2016) 138:1058–66. doi:10.1002/ijc.29519

15. Alayev A, Holz MK. mTOR signaling for biological control and cancer. *J Cel Physiol* (2013) 228:1658–64. doi:10.1002/jcp.24351

16. Cargnello M, Tcherkezian J, Roux PP. The expanding role of mTOR in cancer cell growth and proliferation. *Mutagenesis* (2015) 30:169–76. doi:10.1093/mutage/geu045

17. Pezzicoli G, Filoni E, Gernone A, Cosmai L, Rizzo M, Porta C. Playing the devil's advocate: should we give a second chance to mTOR inhibition in renal clear cell carcinoma? – ie strategies to revert resistance to mTOR inhibitors. *Cancer Manag Res* (2021) 13:7623–36. doi:10.2147/CMAR.S267220

18. Tian T, Li X, Zhang J. mTOR signaling in cancer and mtor inhibitors in solid tumor targeting therapy. *Int J Mol Sci* (2019) 20:755. doi:10.3390/ijms20030755

19. Enedina J-C, Maria del Pilar C-V, VictorAlberto M-A, Patricia M-B, Javier F-T, Alberto L-R, et al. Hypoxia inducible factor-1α gene rs11549465 might be protective factor for the development of type 1 diabetes mellitus. *Endocrinol Diabetes Res* (2018) 04. doi:10.4172/2470-7570.1000131

20. Tanimoto K, Yoshiga K, Eguchi H, Kaneyasu M, Ukon K, Kumazaki T, et al. Hypoxia-inducible factor-1alpha polymorphisms associated with enhanced

transactivation capacity, implying clinical significance. *Carcinogenesis* (2003) 24: 1779–83. doi:10.1093/carcin/bgg132

21. Ollerenshaw M, Page T, Hammonds J, Demaine A. Polymorphisms in the hypoxia inducible factor-1alpha gene (HIF1A) are associated with the renal cell carcinoma phenotype. *Cancer Genet Cytogenet* (2004) 153:122–6. doi:10.1016/j.cancergencyto.2004.01.014

22. Qin C, Cao Q, Ju X, Wang M, Meng X, Zhu J, et al. The polymorphisms in the VHL and HIF1A genes are associated with the prognosis but not the development of renal cell carcinoma. *Ann Oncol* (2012) 23:981–9. doi:10.1093/annonc/mdr325

23. Cao Q, Ju X, Li P, Meng X, Shao P, Cai H, et al. A functional variant in the MTOR promoter modulates its expression and is associated with renal cell cancer risk. *PLoS One* (2012) 7:e50302. doi:10.1371/journal.pone.0050302

24. Qi G-H, Wang C-H, Zhang H-G, Yu J-G, Ding F, Song Z-C, et al. Comprehensive analysis of the effect of rs2295080 and rs2536 polymorphisms within the *mTOR* gene on cancer risk. *Biosci Rep* (2020) 40. doi:10.1042/BSR20191825

25. Zhang Z, Chen Q, Zhang J, Wang Y, Hu X, Yin S, et al. Associations of genetic polymorphisms in pTEN/AKT/mTOR signaling pathway genes with cancer risk: a meta-analysis in Asian population. *Sci Rep* (2017) 7:17844. doi:10.1038/s41598-017-17250-z

26. Lv C, Bai Z, Liu Z, Luo P, Zhang J. Renal cell carcinoma risk is associated with the interactions of APOE, VHL and MTHFR gene polymorphisms. *Int J Clin Exp Pathol* (2015) 8:5781–6.

27. van de Pol JAA, van den Brandt PA, van Engeland M, Godschalk RWL, van Schooten FJ, Hogervorst JGF, et al. Germline polymorphisms in the Von Hippel-Lindau and Hypoxia-inducible factor 1-alpha genes, gene-environment and gene-gene interactions and renal cell cancer. *Sci Rep* (2020) 10:137. doi:10.1038/s41598-019-56980-0

28. Wang W-C, Tsou M-H, Chen H-J, Hsu W-F, Lai Y-C. Two single nucleotide polymorphisms in the von Hippel-Lindau tumor suppressor gene in Taiwanese with renal cell carcinoma. *BMC Res Notes* (2014) 7:638. doi:10.1186/1756-0500-7-638

29. Bensouilah FZ, Chellat-Rezgoune D, Garcia-Gonzalez MA, Carrera N, Abadi N, Dahdouh A, et al. Association of single nucleotide polymorphisms with renal cell carcinoma in Algerian population. *Afr J Urol* (2020) 26:48. doi:10.1186/s12301-020-00055-4

30. Min Z, Mi Y, Lv Z, Sun Y, Tang B, Wu H, et al. Associations of genetic polymorphisms of mTOR rs2295080 T/G and rs1883965 G/A with susceptibility of urinary system cancers. *Dis Markers* (2022) 2022:1720851–16. doi:10.1155/2022/1720851

31. Moch H, Cubilla AL, Humphrey PA, Reuter VE, Ulbright TM. The 2016 WHO classification of tumours of the urinary system and male genital organs—Part A: renal, penile, and testicular tumours. *Eur Urol* (2016) 70: 93–105. doi:10.1016/j.eururo.2016.02.029

32. Vargová D, Dargaj J, Fraňová S, Dohál M, Ľupták J, Švihra J, et al. Immunobiochemical profile of clear cell renal cell carcinoma (ccRCC): a preliminary study. *Gen Biophys Physiol* (2023) 42:387–401. doi:10.4149/gpb_2023015

33. Medina Villaamil V, Aparicio Gallego G, Santamarina Caínzos I, Valladares-Ayerbes M, Antón Aparicio LM. Searching for Hif1-α interacting proteins in renal cell carcinoma. *Clin Translational Oncol* (2012) 14:698–708. doi:10.1007/s12094-012-0857-4

34. Monzon FA, Alvarez K, Peterson L, Truong L, Amato RJ, Hernandez-McClain J, et al. Chromosome 14q loss defines a molecular subtype of clear-cell renal cell carcinoma associated with poor prognosis. *Mod Pathol* (2011) 24:1470–9. doi:10.1038/modpathol.2011.107

35. Chen B, Li L, Li M, Wang X. HIF1A expression correlates with increased tumor immune and stromal signatures and aggressive phenotypes in human cancers. *Cell Oncol* (2020) 43:877–88. doi:10.1007/s13402-020-00534-4

36. Lidgren A, Hedberg Y, Grankvist K, Rasmuson T, Bergh A, Ljungberg B. Hypoxia-inducible factor 1alpha expression in renal cell carcinoma analyzed by tissue microarray. *Eur Urol* (2006) 50:1272–7. doi:10.1016/j.eururo.2006.05.043

37. Kojima H, Gu H, Nomura S, Caldwell CC, Kobata T, Carmeliet P, et al. Abnormal B lymphocyte development and autoimmunity in hypoxia-inducible factor 1alpha -deficient chimeric mice. *Proc Natl Acad Sci* (2002) 99:2170–4. doi:10.1073/pnas.052706699

38. Lukashev D, Caldwell C, Ohta A, Chen P, Sitkovsky M. Differential regulation of two alternatively spliced isoforms of hypoxia-inducible factor-1 alpha in activated T lymphocytes. *J Biol Chem* (2001) 276:48754–63. doi:10.1074/jbc.M104782200

39. Cramer T, Yamanishi Y, Clausen BE, Förster I, Pawlinski R, Mackman N, et al. HIF-1alpha is essential for myeloid cell-mediated inflammation. *Cell* (2003) 112: 645–57. doi:10.1016/S0092-8674(03)00154-5

40. Islam SMT, Won J, Khan M, Mannie MD, Singh I. Hypoxia-inducible factor-1 drives divergent immunomodulatory functions in the pathogenesis of autoimmune diseases. *Immunology* (2021) 164:31–42. doi:10.1111/imm.13335

41. Greten FR, Grivennikov SI. Inflammation and cancer: triggers, mechanisms, and consequences. *Immunity* (2019) 51:27–41. doi:10.1016/j.immuni.2019.06.025

42. Malkov MI, Lee CT, Taylor CT. Regulation of the hypoxia-inducible factor (HIF) by pro-inflammatory cytokines. *Cells* (2021) 10:2340. doi:10.3390/cells10092340

43. Singh N, Baby D, Rajguru J, Patil P, Thakkannavar S, Pujari V. Inflammation and cancer. *Ann Afr Med* (2019) 18:121–6. doi:10.4103/aam.aam_56_18

44. Balkwill F, Mantovani A. Inflammation and cancer: back to Virchow? *The Lancet* (2001) 357:539–45. doi:10.1016/S0140-6736(00)04046-0

45. Hu F, Liu H, Xu L, Li Y, Liu X, Shi L, et al. Hypoxia-inducible factor-1α perpetuates synovial fibroblast interactions with T cells and B cells in rheumatoid arthritis. *Eur J Immunol* (2016) 46:742–51. doi:10.1002/eji.201545784

46. Rider P, Kaplanov I, Romzova M, Braiman L, Braiman A, Voronov E, et al. The transcription of the alarmin cytokine interleukin-1 alpha is controlled by hypoxia inducible factors 1 and 2 alpha in hypoxic cells. *Front Immunol* (2012) 3: 290. doi:10.3389/fimmu.2012.00290

47. Bhavsar I, Miller CS, Al-Sabbagh M. Macrophage inflammatory protein-1 alpha (MIP-1 alpha)/CCL3: as a biomarker. *Gen Methods Biomarker Res their Appl* (2015) 2015:223–49. doi:10.1007/978-94-007-7696-8_27

48. Rébé C, Ghiringhelli F. Interleukin-1β and cancer. *Cancers (Basel)* (2020) 12: 1791. doi:10.3390/cancers12071791

49. Storti P, Bolzoni M, Donofrio G, Airoldi I, Guasco D, Toscani D, et al. Hypoxia-inducible factor (HIF)-1α suppression in myeloma cells blocks tumoral growth *in vivo* inhibiting angiogenesis and bone destruction. *Leukemia* (2013) 27: 1697–706. doi:10.1038/leu.2013.24

50. Jung Y-J, Isaacs JS, Lee S, Trepel J, Neckers L. IL-1β mediated up-regulation of HIF-lα via an NFkB/COX-2 pathway identifies HIF-1 as a critical link between inflammation and oncogenesis. *FASEB J* (2003) 17:1–22. doi:10.1096/fj.03-0329fje

51. Wang X, Ren H, Zhao T, Ma W, Dong J, Zhang S, et al. Single nucleotide polymorphism in the microRNA-199a binding site of HIF1A gene is associated with pancreatic ductal adenocarcinoma risk and worse clinical outcomes. *Oncotarget* (2016) 7:13717–29. doi:10.18632/oncotarget.7263

52. Yamamoto Y, Kiyohara C, Ogata-Suetsugu S, Hamada N, Nakanishi Y. Association between genetic polymorphisms involved in the hypoxia-inducible factor pathway and lung cancer risk: a case-control study in Japan. *Asia Pac J Clin Oncol* (2017) 13:234–42. doi:10.1111/ajco.12640

53. Peckham-Gregory EC, Thapa DR, Martinson J, Duggal P, Penugonda S, Bream JH, et al. MicroRNA-related polymorphisms and non-Hodgkin lymphoma susceptibility in the Multicenter AIDS Cohort Study. *Cancer Epidemiol* (2016) 45: 47–57. doi:10.1016/j.canep.2016.09.007

54. Almáši M, Besse L, Brožová L, Jarkovský J, Bezděková R, Pour L, et al. Selected genetic polymorphisms associated with hypoxia and multidrug resistance in monoclonal gammopathies patients. *Klinicka Onkologie* (2018) 31:213–29. doi:10.14735/amko2018213

55. Wu L-F, Xu G-P, Zhao Q, Zhou L-J, Wang D, Chen W-X. The association between hypoxia inducible factor 1 subunit alpha gene rs2057482 polymorphism and cancer risk: a meta-analysis. *BMC Cancer* (2019) 19:1123. doi:10.1186/s12885-019-6329-2

56. Moore LE, Nickerson ML, Brennan P, Toro JR, Jaeger E, Rinsky J, et al. Von hippel-lindau (VHL) inactivation in sporadic clear cell renal cancer: associations with germline VHL polymorphisms and etiologic risk factors. *Plos Genet* (2011) 7: e1002312. doi:10.1371/journal.pgen.1002312

57. Miricescu D, Balan D, Tulin A, Stiru O, Vacaroiu I, Mihai D, et al. PI3K/AKT/mTOR signalling pathway involvement in renal cell carcinoma pathogenesis (Review). *Exp Ther Med* (2021) 21:540. doi:10.3892/etm.2021.9972

58. The Cancer Genome Atlas Research Network. Comprehensive molecular characterization of clear cell renal cell carcinoma. *Nature* (2013) 499:43–9. doi:10.1038/nature12222

59. Pantuck AJ, Seligson DB, Klatte T, Yu H, Leppert JT, Moore L, et al. Prognostic relevance of the mTOR pathway in renal cell carcinoma: implications for molecular patient selection for targeted therapy. *Cancer* (2007) 109:2257–67. doi:10.1002/cncr.22677

60. Fusco N, Sajjadi E, Venetis K, Gaudioso G, Lopez G, Corti C, et al. PTEN alterations and their role in cancer management: are we making headway on precision medicine? *Genes (Basel)* (2020) 11:719. doi:10.3390/genes11070719

61. Fan C, Zhao C, Wang F, Li S, Wang J. Significance of PTEN mutation in cellular process, prognosis, and drug selection in clear cell renal cell carcinoma. *Front Oncol* (2019) 9:357. doi:10.3389/fonc.2019.00357

62. Song MS, Salmena L, Pandolfi PP. The functions and regulation of the PTEN tumour suppressor. *Nat Rev Mol Cel Biol* (2012) 13:283–96. doi:10.1038/nrm3330

63. Lin L, Zhang Z, Zhang W, Wang L, Wang J. Roles of genetic variants in the PI3K/PTEN pathways in susceptibility to colorectal carcinoma and clinical outcomes treated with FOLFOX regimen. *Int J Clin Exp Pathol* (2015) 8:13314–22.

64. Ding J, Gao Y, Liu R, Xu F, Liu H. Association of PTEN polymorphisms with susceptibility to hepatocellular carcinoma in a Han Chinese population. *DNA Cel Biol* (2011) 30:229–34. doi:10.1089/dna.2010.1126

Pathology & Oncology Research | frontiers

TYPE Original Research
PUBLISHED 05 January 2023
DOI 10.3389/pore.2022.1610598

Check for updates

OPEN ACCESS

EDITED BY
Janina Kulka,
Semmelweis University, Hungary

*CORRESPONDENCE
Andras Voros,
andrasvoros@libero.it

RECEIVED 16 May 2022
ACCEPTED 16 December 2022
PUBLISHED 05 January 2023

CITATION
Olah O, Majlat E, Koszo R, Vereb Z and Voros A (2023), Predictive role of neostromal CD10 expression in breast cancer patients treated with neoadjuvant chemotherapy. *Pathol. Oncol. Res.* 28:1610598. doi: 10.3389/pore.2022.1610598

COPYRIGHT
© 2023 Olah, Majlat, Koszo, Vereb and Voros. This is an open-access article distributed under the terms of the Creative Commons Attribution License (CC BY). The use, distribution or reproduction in other forums is permitted, provided the original author(s) and the copyright owner(s) are credited and that the original publication in this journal is cited, in accordance with accepted academic practice. No use, distribution or reproduction is permitted which does not comply with these terms.

Predictive role of neostromal CD10 expression in breast cancer patients treated with neoadjuvant chemotherapy

Orsolya Olah[1], Edit Majlat[1], Renata Koszo[2], Zoltan Vereb[3] and Andras Voros[1]*

[1]Department of Pathology, School of Medicine, University of Szeged, Szeged, Hungary, [2]Department of Oncotherapy, School of Medicine, University of Szeged, Szeged, Hungary, [3]Department of Dermatology and Allergology, School of Medicine, University of Szeged, Szeged, Hungary

Background: The therapeutic strategy of invasive breast cancer is based on routine histopathological markers (estrogen-, progesterone receptor, HER2, Ki67) routinely evaluated in tumor cells. However, the assessment of cancer stroma could influence therapeutic strategies. Studies have shown that stromal expression of CD10, a zinc-dependent metalloproteinase, is associated with biological aggressiveness of the tumor. In the present retrospective study, we aimed to evaluate stromal CD10 expression and association between CD10 expression and response to neoadjuvant chemotherapy in invasive breast cancer.

Methods: CD10 immunohistochemistry was performed on core biopsies taken before the neoadjuvant therapy. Stromal CD10 expression was determined and compared with well-known predictive and prognostic tissue markers as well as with the following groups defined according to the degree of tumor response: no regression, partial regression, and complete regression.

Results: A total of 60 locally advanced invasive breast carcinomas of "no special type" were included. The proportion of CD10 positive tumors was significantly higher in the "no regression" group compared to "complete regression" group (p = 0.000). Stromal CD10 expression was found to be significantly associated with decrease in response to neoadjuvant chemotherapy. According to CD10 expression we did not find any difference in hormone receptor status, Ki67, tumor grade or neostromal area.

Conclusion: Our data suggest that CD10 expression can serve as a predictive marker of the effect of neoadjuvant chemotherapy in breast cancer patients. Therefore, its inclusion into the routine assessment of biopsies to tailor tumor-specific therapeutic strategies merits consideration.

KEYWORDS

advanced breast cancer, predictive factors, CD10, neoadjuvant therapy, neostroma

Introduction

Although early breast cancer detection programs are well organized in developed countries, a number of patients remain hidden until developing late-stage disease. In locally advanced cases, primary systemic chemotherapy is often indicated, and the choice of treatment is influenced by the evaluation of routine prognostic and predictive factors. Unfortunately, proper quantification of estrogen- and progesterone receptors (ER and PR), human epidermal growth factor receptor-2 (HER2/Neu) and proliferation markers are insufficient to predict chemosensitivity of some breast tumors. In these cases, despite the high proliferation and receptor statuses, chemotherapy remains unsuccessful, and the fast progression is associated with recurrence and high mortality. The identification of these cases during routine pathological examination of biopsy specimens could be especially useful in planning the oncotherapeutic strategy for proper patient management.

Recently, not only the epithelial component of breast cancers, but also their microenvironment, particularly the neostroma with immune cells came into focus. Tissue microenvironment has a vital role in promoting and controlling the development and dissemination of malignant tumors (1, 2). Particularly, tumor-infiltrating lymphocytes are of therapeutic relevance, in case of high PD-L1 expression.

Carcinoma-associated fibroblasts (CAFs) are a major constituent of the tumor stroma and represent a heterogenous population of activated fibroblasts (3). CAFs play a crucial role in tumor development through promotion of tumor progression and maintenance of chemoresistance (4). Special subtypes of CAFs with different biologic role are identified *in vitro* and *ex vivo*, and this is based on their intracellular cytokine expression. There are also attempts to identify and characterize CAFs on routine samples, as this may clarify their role in tumor development (5).

CD10 is a 90–110-kDa cell surface zinc-dependent metalloprotease that is normally expressed by the epithelial cells of diverse tissues, including prostate, colon, liver, stomach and apocrine breast lesions, but is also present in endometrial stroma (6–9). The detection of CD10 is a useful tool in numerous pathological entities, such as acute lymphomas and non-malignant tumors of the breast (10). As many of the matrix metalloproteinases (MMPs), CD10 is accountable for degradation of extracellular matrix components. It also regulates the biological activities of various peptide substrates by lowering the local concentrations available for receptor binding (11). It has also been proposed that CD10 overproduction appears in tumor neostroma, and this may contribute to tumor development and progression by degrading extracellular matrix and giving way to local invasion (3). Studies have also shown that in other types of tumors the expression of CD10 in stromal cells is associated with higher grade and agressive biological behavior (12, 13).

According to recent studies, CD10 has a possible role in the progression of breast cancer, too, since this marker is found to be expressed by CAFs in tumors with faster progression (5). It is also reported, that tumors with higher number of CD10 positive CAFs are less chemosensitive *in vitro* (5). Since neoadjuvant chemotherapy is the most used therapy in locally advanced breast cancer (LABC), patients with chemoresistance or only with minor chemosensitivity can have an extended time to curative surgery.

We aimed to examine CD10 expression on initial routine diagnostic core biopsies from patients with newly discovered LABC, and correlate this with tumor regression achieved during neoadjuvant chemotherapy.

Materials and methods

This retrospective study was conducted in the Department of Pathology of the University of Szeged. It was approved by the Ethical Committee of University of Szeged (265/18-SZTE).

Study population and samples

The retrospective cohort included cases of LABC diagnosed at the University of Szeged between 2010 and 2018 and treated with neoadjuvant chemotherapy. For inclusion, the tumor had to fulfill the criteria of LABC defined by the 4th Hungarian Breast Cancer Consensus Conference; the tumor had to be locally advanced, primary, with or without multifocality and/or lymph node metastasis without distant metastasis (Stage IIb to Stage III) (14). All patients received anthracycline based chemotherapy followed by surgical treatment.

The initial core needle biopsy sample and the surgically removed tissue sample with the related histologic reports were provided by the Department of Pathology. The predictive and prognostic markers were obtained during the routine histopathologic examination according to international guidelines and the 4th Hungarian Breast Cancer Consensus Conference, and included the ER-, PR status and Ki67 proliferation fraction (labelling index). HER2 protein expression was determined *via* immunohistochemistry, in the case of equivocal expression *in situ* hybridization was also performed. Tumor-infiltrating lymphocytes (TIL) was defined according to the protocol established in 2014 by an International TILs Working Group and cases exceeding 5% were considered positive (15). The evaluation of these assays followed internationally accepted recommendations (16, 17) in keeping with national guidelines (18). All core biopsy samples contained more than 70% neoplastic area.

The initial tumor size was determined according to the radiologic finding made at the time of core biopsy or staging examination prior to the neoadjuvant treatment.

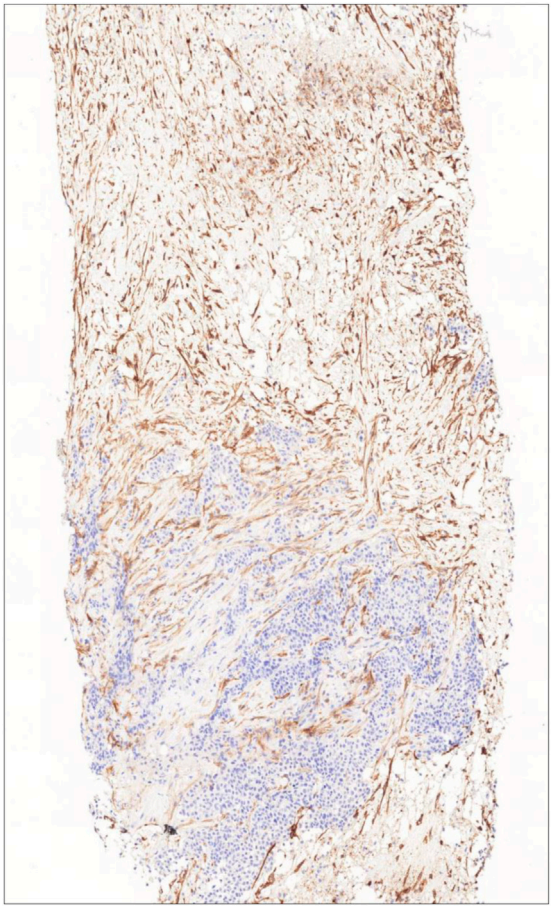

FIGURE 1
Intensive CD10 expression of stromal cells representing the whole stromal area (CD10 immunohistochemistry, 10X).

The experimental groups were determined according to the regression grade assessed on surgical specimens following neoadjuvant chemotherapy. The regression grade was also retrieved from the pathological reports and was reported according to the Hungarian Breast Cancer Diagnostic guidelines (18) based on the European guidelines (19). According to regression grades, three groups were defined: 1) no regression (TR3), 2) partial regression (TR2), and 3) complete regression (TR1).

Immunohistochemistry and evaluation

CD10 immunohistochemistry was performed on 4 μm thick sections of the core needle biopsy samples with an automated method (Leica Bond autostainer, Wetzlar, Germany). The primary monoclonal antibody (CellMarque, Rocklin, California, United States) was used with a dilution of 1:50 (incubation time 20 min) and was applied after antigen retrieval in ER2 (pH9).

CD10 expression in the tumor stroma (both cellular elements and extracellular matrix) was assessed qualitatively and quantitatively. Qualitative analysis was conducted by two independent pathologists (OO and VA) who were unaware of the response of the tumors to primary systemic therapy. The samples showing stromal expression greater than 10% were considered positive, following the methodology of Iwaya et al (20) (Figure 1). In case of disagreement the case was reviewed by both investigators and consensus was made.

Quantitative analysis was performed on digitalized slides (Pannoramic Midi slide scanner, 3DHistech, Budapest, Hungary). Overwiev pictures were made on ×10 magnification. The digital evaluation program was treated to recognize and distinguish the epithelial component from the stroma by labelling different components. The process was controlled by pathologist (OO). In the analysis phase the automatic area selection was continuously monitored and, if necessary, corrected it manually to avoid epithelial expression involvement. The pixels representing neostroma were conwerted to black and white pixels according to brown color density reflecting the diaminobenzidine chromogen of the immunohistochemistry, also normalized to background brown staining. Black represented the immunostained areas, while white the unstained areas. The proportion of the stained (black) area was derived from the area stained and its relation to the total neostromal area (Pannoramic QuantCenter modules, 3DHistech, Budapest, Hungary).

High content imaging system and image analysis

The Olympus IX83 microscope based high content screening platform (Olympus, Tokyo, Japan) was used for image acquisition and fully automated analysis of all images taken from all specimens. To get a higher X/Y resolution than would be possible with a single field of view, stitched images of the full tissue specimens were made. Automated stitching alignment was carried out with meander scanpath and alpha (linear) blending.

Super resolution images were analyzed with the automated method of the CellSense software (Olympus, Tokyo, Japan).

Statistical analysis

Statistical analyses were performed using the SigmaPlot 12.0 software (Systat Software Inc., San Jose, CA, United States). Data were expressed as mean ± standard error of the mean (SEM) derived from at least three independent measurements. The clinical data were analyzed with chi-square test. The stromal area as a proportion of total tumor area and both qualitative and quantitative measurement of CD10 expression were examined using the t test for independent samples (two groups) or ANOVA (more than two groups); $p < 0.05$ was considered statistically

TABLE 1 Distribution of clinical data among groups.

		Complete regression	Partial regression	No regression	*p* value
Molecular type	Luminal B	9	9	10	0.9965
	HER2	4	4	4	
	TNBC	7	7	6	
Stage	II	8	9	10	0.8170
	III	12	11	10	
Grade	II	2	4	3	0.6756
	III	18	16	17	
Tumor size	Mean	45.18	38.33	29.58	**0.0448**
	SD	18.40	26.25	9.51	
	n	20	20	20	

The bold value means that the value is significant.

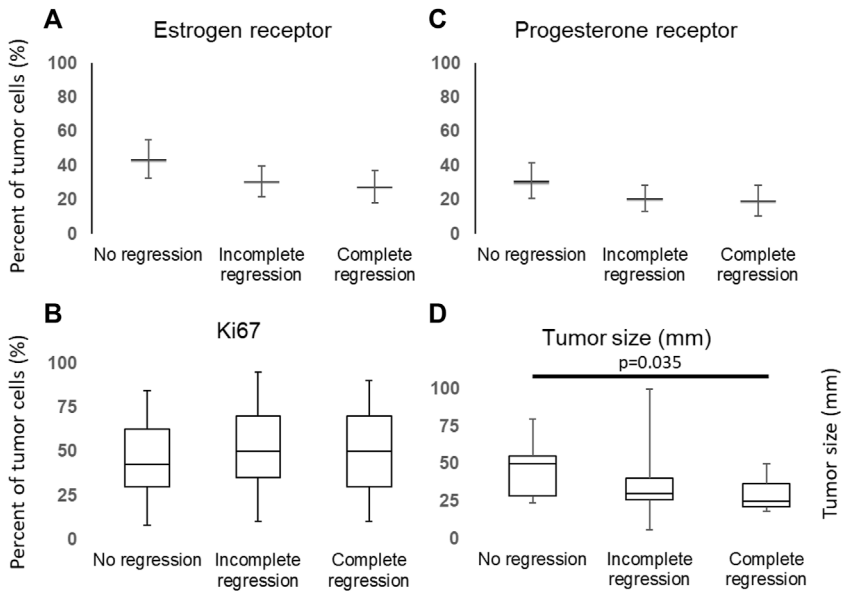

FIGURE 2
Distribution of ER **(A)**, PR **(C)**, Ki67 **(B)** and tumor size **(D)** among cases and groups.

significant. In cases ANOVA showed significance Bonferroni *post hoc* test was used to compare groups.

Results

Qualitative CD10 expression

A total of 60 patients were included with 20 cases in each group. Their mean (±standard deviation, SD) age was 53.5 ± 8.6 years. The remarkable clinical data distribution among groups is listed in Table 1 and the protocol of neoadjuvant oncotherapy in detail is listed in the Supplementary Table S1.

There were no statistical differences between the regression groups in terms of mean proportion of ER positive tumor cells (43.75 ± 11.18, 30.55 ± 9.09, and 27.56 ± 9.54, respectively), PR positive tumor cells (31.25 ± 10.28, 20.83 ± 7.73, and 19.4 ± 8.80, respectively) and expression of Ki67 (50.63 ± 5.95, 54.69 ± 5.64, and 53.21 ± 7.33, respectively) (Figure 2).

TABLE 2 Distribution of HER2 and TIL positive (>5%) and negative (<5%) cases among groups.

Group		TIL	HER2
No regression	Positive	2	5
	Negative	18	14
Partial regression	Positive	3	4
	Negative	17	16
Complete regression	Positive	4	6
	Negative	16	15

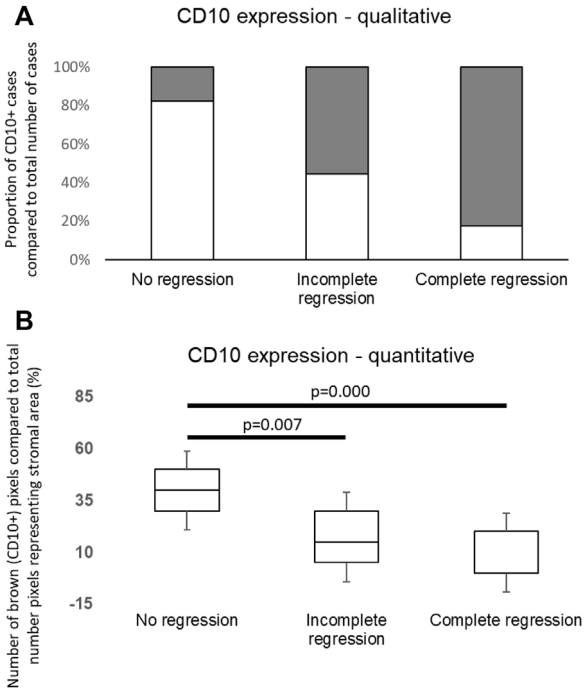

FIGURE 3
(A) Distribution of CD10 positive and negative cases in groups. The white columns are indicating positive (>10% stromal CD10 immunolabeling) cases. The number of CD10 positive cases was significantly higher in the non-responding group to neoadjuvant chemotherapy (p = 0.006). **(B)** Quantitative evaluation of CD10 expression showed significant differences among distinct groups similarly to qualitative data.

We also have found significant differences between initial tumor sizes (p = 0.0448), the median of initial tumor size was significantly lower in the complete regression group than in the group showed no regression (pairvise comparison: p = 0.035, Figure 2D), although the tumor size did not differ regarding CD10 expression (Supplementary Figure S1).

There were also no significant differences in the proportion of HER2 positive cases (Table 2). The ratio of (stromal) tumor

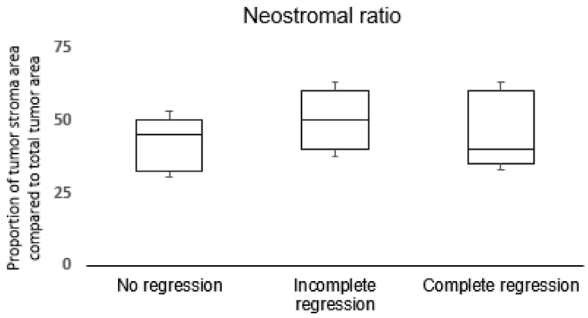

FIGURE 4
Distribution of neostromal area in proportion of the total tumor area among groups.

infiltrating lymphocytes (TILs) was lower than 5% in majority of cases; furthermore, there was no difference in the mean proportion of TILs among the groups (Table 2).

CD10 signals were found in both the epithelial and stromal components, nevertheless only neostromal expression was considered. In order to determine applicability of CD10 immunohistochemistry in routine histopathologic work, a qualitative "eye-balling" evaluation with a 10% cut-off value was made. The investigators gave concordant results except one case in the complete regression group that was later considered positive according to their consensus. This qualitative evaluation of CD10 expression suggested significantly less CD10 positive cases among tumors showing complete regression. In parallel, approximately half of the cases in the partial regression group and most of the cases in the no regression group were CD10 positive (Figure 3A).

To determine the expression of CD10 in neostroma more precisely, quantitative measurements were made. Our quantitative evaluation with both evaluation methods (Panoramic Quant Centre and Olympus CellSense) showed similar results to those of the qualitative estimations; the ratio of area showing immunopositivity for CD10 was significantly different in the defined subgroups (p = 0.019) with significant difference between the "no regression" and "incomplete regression," also "no regression" and "complete regression" groups (p = 0.007 and p = 0.000, respectively, Figure 3B).

According to our measurements the specificity of CD10 immunohistochemistry was 82%, while sensitivity was 83%.

To exclude the variability in desmoplastic reaction, we evaluated the proportion of neostroma and total tumor area, and this showed no differences among the three groups (Figure 4).

We evaluated the routine predictive and prognostic parameters according to CD10 positivity. Although the number of cases was not sufficient for proper correlation studies there were no significant differences in estrogen-, progesterone receptor, Ki67 expression and HER2 status, histologic grade and neostromal ratio between CD10 positive and negative cases (Table 3). Since we did not notice differences in these parameters depending on the CD10 status we considered CD10 expression independent.

TABLE 3 Expression of routine prognostic markers depending on CD10 positivity.

			CD10 negative	CD10 positive	*p*
Estrogen receptor	Mean		32.92	24.83	0.424
	SD		38.73	39.04	
	n		29	31	
Progesterone receptor	Mean		13.33	23.74	0.231
	SD		29.14	36.72	
	n		29	31	
Ki67	Mean		49.68	47.72	0.772
	SD		30.46	21.09	
	n		29	31	
HER2	n		7	8	0.881
Grade	II	n	4	5	0.800
	III	n	25	26	
Neostromal ratio	Mean		46.11	40.83	0.148
	SD		15.03	12.81	
	n		29	31	

Discussion

Although breast cancer is an epithelial malignancy originating from cells of the terminal ductal lobular unit, it is well documented that tumor microenvironment has also significant role in its biological behavior. It has been proved that tissue microenvironment as well as the tumor neostroma play a key role in controlling cell survival, proliferation, migration, and differentiation (1, 2, 21). CAFs as a special cell type of the neostroma, can promote cancer progression by regulating cancer stem cells and chemoresistance (22).

The close bilateral molecular cooperation between the epithelial and stromal cells is disrupted by several factors/expressed proteins that are secreted by either the tumor cells or the stromal cells modulated by the epithelial component of cancer (23, 24). Members of the MMP group are examples of these factors and play a key role in tumor progression, invasion and metastasis (25, 26). Up-regulation of extracellular matrix gene expression and elevated MMP activities correlate with poor patient prognosis (26). High expression of estrogen receptors is also associated with enhanced activity of MMP-2, while high expression of progesterone receptor is correlated with low TIMP-1 protein (tissue inhibitor of MMPs) levels that promotes matrix destruction (25). The MMP expression also plays an important role in the production of TGF-β (tissue growth factor-β) secreted by the CAFs and this promotes tumorigenesis, angiogenesis, immunosuppression and tumor progression (26). The breakdown products of the matrix components produced by MMP activity together with growth factors (insulin like growth factors) have chemotactic activity thus help in tumor cell migration through the extracellular matrix (27).

CD10 is a membrane-bound zinc-dependent metalloproteinase with endopeptidase activity, which regulates the physiological action of various peptides by lowering their extracellular concentration available for receptor binding (10, 28). CD10 has widespread functions in maintaining early progenitor population in the human mammary lineage thus preventing the unchecked proliferation in mammary stem cells under physiologic conditions (29).

CD10 has also roles in breast cancer formation. Maguer-Satta et al have shown that an early oncogenic event in stem cells modulates the expression of the CD10enzyme in the altered cells or even in the neighboring cellular environment resulting in a decrease of CD10 function and a commitment in neoplastic lineage (10). It has also been shown that upregulation of mutated CD10 enzymatic activity could lead to accumulation of cleaved peptides that inhibit cell differentiation and maintain the state of cancer stemness (28).

There are some previous studies concluding that stromal expression of CD10 is an obvious negative prognostic factor of breast cancer. It is correlated with higher grade, node positivity, increased Ki67 index, positive HER2 status and poorer prognosis supplemented with the antiapoptotic effect that plays role in

reduced chemosensitivity (12, 20, 30-34). Diem Vo et al. concluded that CD10 expression in stroma may function as a powerful prognostic factor for invasive breast cancer disease-free survival rates, and in predicting potential recurrence (35). Desmedt at al. Highlighted the importance of $CD10^+$ cells in breast cancer prognosis and efficacy of chemotherapy. This was principally seen when they characterized $CD10^+$ cells isolated from tumor vs. normal breast containing cell cultures (36).

Our retrospective study has shown that the presence of CD10 in the neostromal component of breast cancer is commonly associated with resistance to neoadjuvant treatment in LABC. These findings are in partial concordance with preliminary findings of Thomas et al. They have found that stromal CD10 expression in breast cancer is not static and changes over time in breast cancers treated with neoadjuvant anthracycline based chemotherapy. Stability or decrease in CD10 expression correlates with complete or partial clinical response, while an increase in CD10 expression appears to correlate with poor clinical response. They also mentioned that stromal CD10 expression and its changes with chemotherapy may have a prognostic significance, they should be documented in breast cancer patients before and after chemotherapy (30). Jana SH and al reported poorer prognosis associated with CD10 expression although they have not assessed chemoresistance separately (31).

We have also shown that a qualitative analysis of CD10 expression with a 10% cut-off gives similar results to the quantitative analysis, and this facilitates its application in a routine histopathological diagnostic setting. Although the qualitative analysis of CD10 immunohistochemistry is easy to implement there are several limitations. The qualitative analysis of any staining shows variable reproducibility; thus, the evaluation guidelines have to be clearly defined. Therapeutic strategies are limited to neoadjuvant therapies or extended surgical removal in LABC. The most preferred strategy is neoadjuvant chemotherapy with or without targeted treatment, which is planned according to routine predictive and prognostic markers tested during histopathologic examination. Despite onco-radio-pathologic correlation and precise therapeutic planning, chemotherapy fails in a number of cases, and this results in a delay in surgical treatment. Prediction of chemosensitivity could be an effective method to refine oncotherapeutic strategy allowing personalized breast cancer patient management. The $CD10^+$ CAF type described by Su S et al. also gives the opportunity for targeting neostromal background of cancer in cases non-responding to conventional chemotherapeutic agents (5).

Albeit there are studies showing correlation between histology subgroups and CD10 expression our study focused on mixed population of LABC to investigate the theoretical usability of CD10 immunohistochemistry in predicton of chemosensitivity. For precise determination of LABC subgroup suitable for chemosensitivity prediction with CD10 immunohistochemisty further studies have to be made.

Despite limitations of the study our results show correlation between CD10 expression and chemosensitivity. This emphasizes the potential of CD10 immunohistochemistry in routine histologic examination as a predictive marker. CD10 did not show unequivocal concordance with the well-known predictive and prognostic markers (ER, PR, HER2 and Ki67). CD10 expression was independent from tumor size, too, although tumors showing complete remission following neoadjuvant chemotherapy had significantly smaller initial tumor sizes. These findings suggest that stromal CD10 could be a predictive marker of treatment efficacy and chemosensitivity that warrants further studies.

Conclusion

In conclusion, we analyzed the expression of CD10 in a series of pre-treatment core biopsies taken from advanced breast cancer patients candidate for neoadjuvant chemotherapy. Our results indicate that the higher the stromal CD10 expression on pre-treatment core biopsies, the worse the regression after neoadjuvant chemotherapy. We also found stromal CD10 to be independent from other well-known prognostic and/or predictive markers like ER, PR, HER2 and Ki67 in the neoadjuvant setting. These findings highlight a role of CD10, as a possible independent predictive marker of the possible efficacy of neoadjuvant chemotherapy in case of breast cancer. We also propose that CD10, despite some technical limitations mentioned above, could implement the conventional immunohistochemistry in the course of planning neoadjuvant chemotherapy. and requires further investigation.

Data availability statement

The original contributions presented in the study are included in the article/Supplementary Material, further inquiries can be directed to the corresponding author.

Ethics statement

The studies involving human participants were reviewed and approved by the ethical committee of University of Szeged. Written informed consent for participation was not required for this study in accordance with the national legislation and the institutional requirements.

Author contributions

AV was the supervisor of the study and dreamed up this research. OO wrote the article and analysed the data. RK provided the relevant data about the oncologic treatment. EM collected the data and prepared the tables. ZV worked on the digital data analysis in case of quantitative data collection.

Conflict of interest

The authors declare that the research was conducted in the absence of any commercial or financial relationships that could be construed as a potential conflict of interest.

Supplementary material

The Supplementary Material for this article can be found online at: https://www.por-journal.com/articles/10.3389/pore.2022.1610598/full#supplementary-material

References

1. De Wever O, Mareel M. Role of tissue stroma in cancer cell invasion. *J Pathol* (2003) 200(4):429–47. doi:10.1002/path.1398

2. Bremnes RM, Dønnem T, Al-Saad S, Al-Shibli K, Andersen S, Sirera R, et al. The role of tumor stroma in cancer progression and prognosis: Emphasis on carcinoma-associated fibroblasts and non-small cell lung cancer. *J Thorac Oncol* (2011) 6(1):209–17. doi:10.1097/JTO.0b013e3181f8a1bd

3. Orimo A, Weinberg RA. Stromal fibroblasts in cancer: A novel tumor-promoting cell type. *Cell Cycle* (2006) 5(15):1597–601. doi:10.4161/cc.5.15.3112

4. Paulsson J, Micke P. Prognostic relevance of cancer-associated fibroblasts in human cancer. *Semin Cancer Biol* (2014) 25:61–8. doi:10.1016/j.semcancer.2014.02.006

5. Su S, Chen J, Yao H, Liu J, Yu S, Lao L, et al. CD10+GPR77+ cancer-associated fibroblasts promote cancer formation and chemoresistance by sustaining cancer stemness. *Cell* (2018) 172(4):841–56. e16. doi:10.1016/j.cell.2018.01.009

6. Song J, Aumüller G, Xiao F, Wilhelm B, Albrecht M. Cell specific expression of CD10/neutral endopeptidase 24.11 gene in human prostatic tissue and cells. *Prostate* (2004) 58(4):394–405. doi:10.1002/pros.10345

7. Sato Y, Itoh F, Hinoda Y, Ohe Y, Nakagawa N, Ueda R, et al. Expression of CD10/neutral endopeptidase in normal and malignant tissues of the human stomach and colon. *J Gastroenterol* (1996) 31(1):12–7. doi:10.1007/BF01211181

8. Loke SL, Leung CY, Chiu KY, Yau WL, Cheung KN, Ma L. Localisation of CD10 to biliary canaliculi by immunoelectron microscopical examination. *J Clin Pathol* (1990) 43(8):654–6. doi:10.1136/jcp.43.8.654

9. Kővári B, Báthori Á, Cserni G. CD10 immunohistochemical expression in apocrine lesions of the breast. *Pathobiology* (2015) 82(6):259–63. doi:10.1159/000440664

10. Maguer-Satta V, Chapellier M, Delay E, Bachelard-Cascales E. CD10: A tool to crack the role of stem cells in breast cancer. *Proc Natl Acad Sci U S A* (2011) 108(49):E1264; author reply E1265. ; author reply E1265 (2011). doi:10.1073/pnas.1116567108

11. Shipp MA, Look AT. Hematopoietic differentiation antigens that are membrane-associated enzymes: Cutting is the key. *Blood* (1993) 82(4):1052–70. doi:10.1182/blood.v82.4.1052.1052

12. Makretsov NA, Hayes M, Carter BA, Dabiri S, Gilks CB, Huntsman DG. Stromal CD10 expression in invasive breast carcinoma correlates with poor prognosis, estrogen receptor negativity, and high grade. *Mod Pathol* (2007) 20(1):84–9. doi:10.1038/modpathol.3800713

13. Voutsadakis IA, Vlachostergios PJ, Daliani DD, Karasavvidou F, Kakkas G, Moutzouris G, et al. CD10 is inversely associated with nuclear factor-kappa B and predicts biochemical recurrence after radical prostatectomy. *Urol Int* (2012) 88(2):158–64. doi:10.1159/000335299

14. Horváth Z, Boér K, Dank M, Kahán Z, Kocsis J, Kövér E, et al. Systemic treatment of breast cancer: Professional guideline]. *Magy Onkol* (2020) 64(4):348–68.

15. Salgado R, Denkert C, Demaria S, Sirtaine N, Klauschen F, Pruneri G, et al. The evaluation of tumor-infiltrating lymphocytes (TILs) in breast cancer: Recommendations by an international TILs working group 2014. *Ann Oncol* (2014) 26(2):259–71. doi:10.1093/annonc/mdu450

16. Wolff AC, Hammond MEH, Allison KH, Harvey BE, Mangu PB, Bartlett JMS, et al. Human epidermal growth factor receptor 2 testing in breast cancer: American society of clinical oncology/college of American pathologists clinical practice guideline focused update. *J Clin Oncol* (2018) 36(20):2105–22. doi:10.1200/jco.2018.77.8738

17. Allison KH, Hammond MEH, Dowsett M, McKernin SE, Carey LA, Fitzgibbons PL, et al. Estrogen and progesterone receptor testing in breast cancer: ASCO/CAP guideline update. *J Clin Oncol* (2020) 38(12):1346–66. doi:10.1200/jco.19.02309

18. Cserni G, Kulka J, Francz M, Járay B, Kálmán E, Kovács I, et al. Pathological diagnosis, work-up and reporting of breast cancer. Recommendations of the 3rd Hungarian Consensus Conference on Breast Cancer]. *Magy Onkol* (2016) 60(3):209

19. Amendoeira I, et al. *European guidelines for quality assurance in breast cancer screening and diagnosis*. In: Ed N Perry, M Broeders, C de Wolf, S Törnberg, R Holland&L. von Karsa. European Commission, Belgium (2013)

20. Iwaya K, Ogawa H, Izumi M, Kuroda M, Mukai K. Stromal expression of CD10 in invasive breast carcinoma: A new predictor of clinical outcome. *Virchows Arch* (2002) 440(6):589–93. doi:10.1007/s00428-002-0639-4

21. Mott JD, Werb Z. Regulation of matrix biology by matrix metalloproteinases. *Curr Opin Cel Biol* (2004) 16(5):558–64. doi:10.1016/j.ceb.2004.07.010

22. Vermeulen L, De Sousa E Melo F, van der Heijden M, Cameron K, de Jong JH, Borovski T, et al. Wnt activity defines colon cancer stem cells and is regulated by the microenvironment. *Nat Cel Biol* (2010) 12(5):468–76. doi:10.1038/ncb2048

23. Lin EY, Pollard JW. Macrophages: Modulators of breast cancer progression. *Novartis Found Symp* (2004) 256:158–68. ; discussion 168-72, 259-69 (2004).

24. Pollard JW. Tumour-educated macrophages promote tumour progression and metastasis. *Nat Rev Cancer* (2004) 4(1):71–8. doi:10.1038/nrc1256

25. Jinga DC, Blidaru A, Condrea I, Ardeleanu C, Dragomir C, Szegli G, et al. MMP-9 and MMP-2 gelatinases and TIMP-1 and TIMP-2 inhibitors in breast cancer: Correlations with prognostic factors. *J Cel Mol Med* (2006) 10(2):499–510. doi:10.1111/j.1582-4934.2006.tb00415.x

26. Curran CS, Keely PJ. Breast tumor and stromal cell responses to TGF-β and hypoxia in matrix deposition. *Matrix Biol* (2013) 32(2):95–105. doi:10.1016/j.matbio.2012.11.016

27. Kass L, Erler JT, Dembo M, Weaver VM. Mammary epithelial cell: Influence of extracellular matrix composition and organization during development and tumorigenesis. *Int J Biochem Cel Biol* (2007) 39(11):1987–94. doi:10.1016/j.biocel.2007.06.025

28. Maguer-Satta V, Besançon R, Bachelard-Cascales E. Concise review: Neutral endopeptidase (CD10): A multifaceted environment actor in stem cells, physiological mechanisms, and cancer. *Stem Cells* (2011) 29(3):389–96. doi:10.1002/stem.592

29. Smollich M, Götte M, Yip GW, Yong ES, Kersting C, Fischgräbe J, et al. On the role of endothelin-converting enzyme-1 (ECE-1) and neprilysin in human breast cancer. *Breast Cancer Res Treat* (2007) 106(3):361–9. doi:10.1007/s10549-007-9516-9

30. Thomas S, Babu RJ, Agarwal K, Puri V, Jain M, Andley M, et al. Effect of neoadjuvant chemotherapy on stromal CD10 antigens in breast cancer - a preliminary study. *Indian J Cancer* (2013) 50(1):46–51. doi:10.4103/0019-509X.112299

31. Jana S, Jha B, Patel C, Jana D, Agarwal A. CD10-A new prognostic stromal marker in breast carcinoma, its utility, limitations and role in breast cancer pathogenesis. *Indian J Pathol Microbiol* (2014) 57(4):530–6. doi:10.4103/0377-4929.142639

32. Goodman OB, Febbraio M, Simantov R, Zheng R, Shen R, Silverstein RL, et al. Neprilysin inhibits angiogenesis via proteolysis of fibroblast growth factor-2. *J Biol Chem* (2006) 281(44):33597–605. doi:10.1074/jbc.M602490200

33. Puri V, Jain M, Mahajan G, Pujani M. Critical appraisal of stromal CD10 staining in fibroepithelial lesions of breast with a special emphasis on expression patterns and correlation with WHO grading. *J Cancer Res Ther* (2016) 12(2):667–70. doi:10.4103/0973-1482.177215

34. Dhande AN, Sinai Khandeparkar SG, Joshi AR, Kulkarni MM, Pandya N, Mohanapure N, et al. Stromal expression of CD10 in breast carcinoma and its correlation with clinicopathological parameters. *South Asian J Cancer* (2019) 8(1):18–21. doi:10.4103/sajc.sajc_56_18

35. Vo TN, Mekata E, Umeda T, Abe H, Kawai Y, Mori T, et al. Prognostic impact of CD10 expression in clinical outcome of invasive breast carcinoma. *Breast Cancer* (2015) 22(2):117–28. doi:10.1007/s12282-013-0459-1

36. Desmedt C, Majjaj S, Kheddoumi N, Singhal SK, Haibe-Kains B, El Ouriaghli F, et al. Characterization and clinical evaluation of CD10+ stroma cells in the breast cancer microenvironment. *Clin Cancer Res* (2012) 18(4):1004–14. doi:10.1158/1078-0432.CCR-11-0383

Pathology & Oncology Research | frontiers

TYPE Hypothesis & Theory
PUBLISHED 09 June 2023
DOI 10.3389/pore.2023.1610980

Check for updates

OPEN ACCESS

EDITED BY
József Tímár,
Semmelweis University, Hungary

*CORRESPONDENCE
Hong Fei Liao,
lhfzf@126.com
Yue Li,
yuepang92@qq.com

RECEIVED 29 November 2022
ACCEPTED 26 May 2023
PUBLISHED 09 June 2023

CITATION
Li Y, Xiong C, Wu LL, Zhang BY, Wu S, Chen YF, Xu QH and Liao HF (2023), Tumor subtypes and signature model construction based on chromatin regulators for better prediction of prognosis in uveal melanoma. *Pathol. Oncol. Res.* 29:1610980. doi: 10.3389/pore.2023.1610980

COPYRIGHT
© 2023 Li, Xiong, Wu, Zhang, Wu, Chen, Xu and Liao. This is an open-access article distributed under the terms of the Creative Commons Attribution License (CC BY). The use, distribution or reproduction in other forums is permitted, provided the original author(s) and the copyright owner(s) are credited and that the original publication in this journal is cited, in accordance with accepted academic practice. No use, distribution or reproduction is permitted which does not comply with these terms.

Tumor subtypes and signature model construction based on chromatin regulators for better prediction of prognosis in uveal melanoma

Yue Li[1,2,3,4]*, Chao Xiong[1,2,3,4], Li Li Wu[1,2,3,4], Bo Yuan Zhang[1,2,3,4], Sha Wu[1,2,3,4], Yu Fen Chen[1,2,3,4], Qi Hua Xu[1,2,3,4] and Hong Fei Liao[1,2,3,4]*

[1]School of Ophthalmology and Optometry, Nanchang University, Nanchang, Jiangxi, China, [2]Affiliated Eye Hospital of Nanchang University, Nanchang, Jiangxi, China, [3]National Clinical Research Center for Ocular Diseases Jiangxi Province Division, Nanchang, Jiangxi, China, [4]Jiangxi Clinical Research Center for Ophthalmic Disease, Nanchang, Jiangxi, China

Background: Uveal Melanoma (UM) is the most prevalent primary intraocular malignancy in adults. This study assessed the importance of chromatin regulators (CRs) in UM and developed a model to predict UM prognosis.

Methods: Gene expression data and clinical information for UM were obtained from public databases. Samples were typed according to the gene expression of CRs associated with UM prognosis. The prognostic key genes were further screened by the protein interaction network, and the risk model was to predict UM prognosis using the least absolute shrinkage and selection operator (LASSO) regression analysis and performed a test of the risk mode. In addition, we performed gene set variation analysis, tumor microenvironment, and tumor immune analysis between subtypes and risk groups to explore the mechanisms influencing the development of UM.

Results: We constructed a signature model consisting of three CRs (RUVBL1, SIRT3, and SMARCD3), which was shown to be accurate, and valid for predicting prognostic outcomes in UM. Higher immune cell infiltration in poor prognostic subtypes and risk groups. The Tumor immune analysis and Tumor Immune Dysfunction and Exclusion (TIDE) score provided a basis for clinical immunotherapy in UM.

Conclusion: The risk model has prognostic value for UM survival and provides new insights into the treatment of UM.

KEYWORDS

prognosis, uveal melanoma, TCGA, chromatin regulators, tumor subtypes

Introduction

Uveal melanoma (UM) is the most prevalent primary intraocular malignancy in adults [1, 2]. Primary UM is usually well controlled by surgery or radiotherapy, but metastases still occur in more than half of UM patients [3, 4]. UM most often metastasizes to the liver, and has a median survival of less than 1 year after metastasis [5–7]. Over the years, there has been an evolution in prognostic assessment (metastatic risk) of UM, from clinical and histological features to the analysis of genetic mutations and chromosomal abnormalities. These included clinical and histological features (patient age, tumor size, ciliary body involvement, extraocular extension, and so on), the genetic mutations [G protein subunit alpha q (GNAQ), G protein subunit alpha 11 (GNA11), Splicing Factor 3b Subunit 1(SF3B1), BRCA1 associated protein 1(BAP1), and Eukaryotic Translation Initiation Factor 1A X-Linked (EIF1AX)], and the composition of chromosomal anomalies of chromosome 3, 6 and 8 [8]. Some studies classify tumors and assess prognosis based on gene expression and chromosomal data [9, 10]. Despite extensive studies, the prognosis of UM has not significantly improved and there are no efficient therapies for metastatic UM, and treatments for metastatic UM such as immune checkpoint inhibitors (ICI), vaccination and t-cell therapy are much less effective than for other tumors [11–15]. Therefore, selecting key genomes for the stratification of UM patients and construction of tumor prediction models could provide new strategies for more precise molecular subtyping, screening of prognostic markers and potential therapeutic targets, and corresponding personalized treatment. At present, the rapid development of bioinformatics analysis is conducive to the screening of prognostic markers related to UM [16–18].

Epigenetic alterations can lead to aberrant gene regulation, which plays an important role in tumorigenesis by silencing tumor suppressor genes or activating oncogenes. These epigenetic changes include DNA methylation, histone modifications, and small non-coding RNA, many of which are associated with the initiation and progression of UM [19]. It has been found that mutations in BAP1, SF3B1, and EIF1AX in UM with different prognoses exhibit different types of methylation cluster status, and hypermethylation of chromosome 3 in UM is also associated with downregulation of BAP1 gene expression, which was further confirmed *in vitro* experiments that knockdown of BAP1 gene or deletion of the protein induces effects on methylation status in UM cells, causing UM cells to exhibit a low metastatic risk phenotype [20–22]. Histone modifications have also been associated with UM metastasis and proliferation [23–25]. MicroRNAs, the most widely studied small non-coding RNAs, have been shown to have dysregulated anti-apoptotic effects, accelerated cell cycle progression, and enhanced invasion and metastasis of many cancers [26]. Epigenetic mechanisms have been found to regulate the expression and activation of miRNAs in UM, which in turn regulate the progression of UM [27, 28]. These studies suggest that epigenetic alterations are closely associated with the onset and progression of UM and that epigenetic mechanisms play an important role in the development of UM.

Chromatin regulators (CRs) are drivers of epigenetic alterations and are classified by function as DNA methylators, histone modifiers, and chromatin remodelers [29–31]. In recent years, abnormal expression of CRs is closely associated with the development of several diseases, including several cancers [32–35]. Aberrant expression of CRs CHD8 and CTCF led to abnormal chromatin structure and epigenetic changes in many cancer-associated genes, ultimately leading to tumor progression and metastasis in prostate cancer patients [36]. Several CRs associated with cancer subtypes and prognosis have been identified as potential drivers of carcinogenesis [37]. There were very few studies on the role of CRs in UM, so a comprehensive analysis of CRs may make a theoretical contribution to the diagnosis, classification, prognostic assessment, and other features of UM. The simultaneous screening of key genes for the stratification of UM patients and the construction of tumor prediction models may provide new strategies for more precise molecular typing and corresponding personalized treatment.

In this study, we applied bioinformatics analysis to identify the key regulators and prognostic genes of CRs in UM. We applied the Non-negative Matrix Factorization (NMF) to cluster The Cancer Genome Atlas (TCGA) dataset based on the expression levels of prognostic-related CRs genes in UM, and the differences in patient prognosis and clinical traits between subtypes were also studied. We also screened core genes using protein interaction networks and constructed prognostic risk models using univariate Cox regression, least absolute shrinkage and selection operator (LASSO) regression, and multivariate Cox regression analysis. Then the accuracy, independence, and validity of the risk model were assessed in the training cohort and validation cohort. In addition, the relationship of the risk model with the tumor microenvironment, immune infiltration and immune checkpoints, and drug sensitivity was investigated, thereby expanding the risk model prognostic values for patients with UM. In summary, our work constructs a new risk model based on CRs gene expression levels associated with UM prognosis, which may have implications for the development of diagnosis and treatment of UM.

Materials and methods

Data download and collation

A list of CRs (870 genes) was collected from previous research [37], and the list of the CRs gene name was shown in Supplementary Table S1. The mRNA data and clinical and pathological characteristics were obtained from three datasets,

including the TCGA-UM downloaded from the public dataset TCGA (The Cancer Genome Atlas, https://portal.gdc.cancer.gov/) and the UCSC Xena website (https://xena.ucsc.edu/), the GEO database (Gene Expression Omnibus, https://www.ncbi.nlm.nih.gov/geo/) datasets GSE22138and GSE84976 [38, 39]. All data were normalized using R software, and the ComBat method from the "SVA" R package was used to remove the batch effects among three datasets [40]. The Principal Component Analysis (PCA) showed the batch correction of three datasets.

Classification validation and variance analysis of TCGA data sets

First, CRs genes significantly associated with UM prognosis were screened by univariate Cox analysis, and prognosis-related CRs genes were treated with the R package "survival" with selection $p < 0.01$. Unsupervised subgroups of TCGA-UM datasets were identified using the R package "NMF" [41], based on these prognosis-related CRs genes. The subtypes were verified by PCA using the R package "ggplot2." The Kaplan–Meier survival curves of the different subgroups were analyzed and plotted using the R packages "survival" and "survminer" [including overall survival (OS) and progression-free survival (PFS)].

To explore the differences in clinical and pathological traits, tumor microenvironment, and tumor immunity between the two subgroups. The gene expression of prognosis-related CRs genes and clinical traits in different subtypes were visualized using the R package "Heatmap" and "ggplot2," respectively. The KEGG pathway was analyzed to explore the differences in the biological processes between the different subgroups using the R package "GSVA." The ESTIMATE algorithm calculated immune, stromal, and ESTIMATE scores in different subtypes by using the R package "estimate." A ssGSEA algorithm was used to investigate the immune cell infiltration relationships between the different subgroups using the R package "GSVA" and "GSEABase," R package "reshape2," "ggpubr," and "pheatmap" was used to draw a heatmap and differential boxplot.

Screening for key genes

To further screen the key CRs genes, the protein regulatory networks of the prognosis-related CRs genes were analyzed using the STRING online database, and only interactions that enjoyed a minimum required combined score >0.4 were set as significant, and visualized the results by Cytoscape software. Furthermore, the key genes were identified based on the PPI network by using cytoHubba, which is another plug-in of Cytoscape. We defined the genes with node (degree > 9) as key genes and used them for subsequent study analysis.

Risk model construction

Based on key CRs genes expression profiles and survival data were combined for further analysis, and to further minimize the dimensionality and build the risk signature, The R package "glmnet" and "survminer" were used to perform the least absolute shrinkage and selection operator (LASSO) regression analysis to determine the minimum lambda value of the lasso model, and further reduce the number of genes by multivariate Cox analysis to determine the final genes and coefficients that constitute the risk model. The patients' risk scores were then determined. Before that, the TCGA dataset was randomly grouped to obtain the TCGA training group ($N = 56$) and testing group ($N = 28$). The risk score formula for the sample is as follows:

Risk score = (Coef1 *mRNA1 expression) + (Coef2 * mRNA2 expression) +. . .+ (Coef n *mRNA n expression).

The verification datasets GSE22138 and GSE84976 were categorized into high- and low-risk groups based on the risk score's median value in the TCGA training group.

Risk model validation

To assess the prognostic value of the risk model, we used the following approaches. First, the predictive ability of the risk model was assessed by using the R package "survminer" and "timeROC," and the Kaplan-Meier curves, with $p < 0.05$ between the two groups indicating a significant difference in overall or progression-free survival. ROC curves at 1, 3, and 5 years were used to measure the accuracy of the predictive ability of the risk model, with AUC (Area Under ROC Curve) value > 0.7 as a valid criterion. Then, the risk model was compared with other clinical characteristics. Finally, the "rms" R package plotted the clinical nomogram. The performance of the nomogram in predicting the overall survival (OS) of UM patients was evaluated using factors such as sex, age, stage, TNM staging of the tumor, and risk score. The calibration curve then proved the nomogram's efficacy.

Gene set variation analysis

To explore the potential molecular mechanisms affecting prognosis, we performed functional enrichment analysis of genes in high- and low-risk groups. The KEGG pathway was analyzed to explore the differences in the biological processes between the high and low-risk group using the R packages "GSVA."

Tumor microenvironment and immune landscape analysis

To confirm whether the CRs characteristics of the risk model were correlated with the tumor microenvironment and tumor

immunity, we assessed the differences in ESTIMATE scoring and immune cell infiltration between the two groups. The ESTIMATE algorithm calculated immune, stromal, and ESTIMATE scores in different subtypes by using the R package "estimate." Correlation tests were used to calculate the correlation between the three signature genes and risk scores and the expression of immune checkpoint-associated genes. The TIDE algorithm was applied to predict the response to immunotherapy in both high and low-risk groups.

Analysis of signature genes in the risk model

To observe the distribution of TCGA samples in terms of subtyping and risk grouping, we performed an analysis using R packages "ggalluvial" and "ggplot2," and presented the results with a Sankey diagram. The distribution of 80 TCGA UM patients in subtypes and risk subgroups was statistically and consistently analyzed, and the results were presented in a 2 × 2 contingency table, while SPSS software was applied to calculate the kappa coefficient to verify the consistency of the two classifications. In addition, we compared whether risk scores differed between subtypes, and the expression and survival analysis of signature genes in risk models between risk subgroups was done by R packages "limma" and "survminer." Dividing the dataset samples into high and low gene expression groups by the median value of characteristic gene expression (which varies across datasets).

Statistics analysis

All statistical analyses were performed in R software (version 4.2.0). $p < 0.05$ was considered statistically significant unless otherwise stated. The consistency test was calculated by SPSS software, and a kappa coefficient (κ) greater than 0.61 indicated a good agreement [42, 43].

Results

Detailed clinical data from three study cohorts

A total of three cohorts were used in this study: 80 UM samples that came from TCGA-UM. The datasets GSE22138 with 63 samples and GSE84976 with 28 samples. The detailed baseline data, clinical and pathological characteristics, and survival time of the three cohorts were presented in Table 1. Three data sets were calibrated by combat functions, and PCA showed successful correction of batch effects (Supplementary Figure S1).

Typing and analysis of CRs-based subtypes

First, the univariate Cox regression analysis identified 111 CRs genes that were significantly associated with UM prognosis, and the results of the analysis are shown in Supplementary Table S2. Then, based on the expression of these 111 genes, the TCGA samples were divided into two subtypes (namely C1, $n = 41$, and C2 $n = 39$) by NMF analysis according to the results of the heatmap of subtypes (Figure 1A). As shown by the results of PCA analysis (Figure 1B), 80 patients were well grouped into two distinct subtypes. The Kaplan-Meier (KM) curve results showed that the C2 subtype was the high-risk group with significantly shorter OS and PFS ($p < 0.001$) (Figures 1C, D). These results indicated that TCGA-UM can be classified based on prognosis-related CRs genes.

To further explore the differences between these two subgroups, we analyzed the distribution of prognosis-related CRs genes and clinical traits among different subtypes. As the results in Figure 2A showed that the expression of prognosis-related CRs genes showed a difference between the two subgroups, with differences in tumor stage and tumor diameter among clinical traits ($p < 0.05$) (Figure 2B). The results indicated that subgroup C2 had a distinct pattern of immune infiltration compared to subgroup C1 (Figure 2C), and the results of the analysis of tumor microenvironment and immune infiltration levels between the two subtypes are shown in Figure 2D, the stromal, immune, and estimate scores of the C2 subgroup were higher than those of the C1 subgroup, and the differences were statistically significant ($p < 0.05$). The results of the different KEGG pathways within the two subtypes showed that subgroup C1 was highly enriched in substance metabolism (including pyrimidine metabolism, amino sugar and nucleotide sugar metabolism, and sulfur metabolism), and in addition, the C2 subgroup was also highly enriched in apoptosis, P53 signaling pathway, and O-glycan biosynthesis (Figure 2E), all of which KEGG pathways are closely associated with tumors. Furthermore, subgroup C2 had a significantly higher abundance of immune cells—including CD8 T cells, activated memory CD4 T cells, follicular helper T cells, and Macrophages M1, while the abundance of immune cells (including resting memory CD4 T cells and resting Mast cells) was significantly higher in subgroup C1 than in subgroup C2 (Figure 2F). These results suggest that the two subgroups have different characteristics in terms of the KEGG pathway, tumor microenvironment, and immune infiltration level.

Selection of key CRs genes

The PPI network of prognostic-related CRs genes were shown in Figure 3A, with the help of the String database analysis and Cytoscape software, direct or indirect functional

10.3389/pore.2023.1610980

TABLE 1 The detailed baseline data and clinical characteristics of the three cohorts.

Characteristics	Training cohort	Validation cohort	
	(TCGA-UM, *n* = 80)	GSE22138 (N = 63)	GSE84976 (N = 28)
Age at diagnosis, years			
≤65	46	36	13
>65	34	27	15
Gender			
Female	35	24	—
Male	45	39	—
Stage			
Stage I	0	—	—
Stage II	36	—	—
Stage III	40	—	—
Stage IV	4	—	—
T			
T1	0	—	—
T2	5	—	—
T3	36	—	—
T4	39	—	—
N			
N0	76	—	—
Unknown	4	—	—
M			
M0	73	—	—
M1	4	—	—
Unknown	3	—	—
Tumor location			
Posterior to equator	67	54	—
Anterior to equator	5	3	—
All over the eye	8	1	—
Unknown	0	5	—
Tumor diameter			
≤15 mm	24	27	—
>15 mm	55	26	—
unknown	1	10	—
Tumor thickness			
≤10 mm	37	12	—
>10 mm	43	51	—
Extrascleral extension			
Yes	7	5	—
No	68	48	—
Unknown	5	10	—
Person neoplasm cancer status			
Tumor free	56	—	28
With tumor	9	—	0
Unknown	15	—	0
OS(years)	0.01~7.12	—	1.17~13
PFS(years)	0.01~6.84	0.01~10.05	—

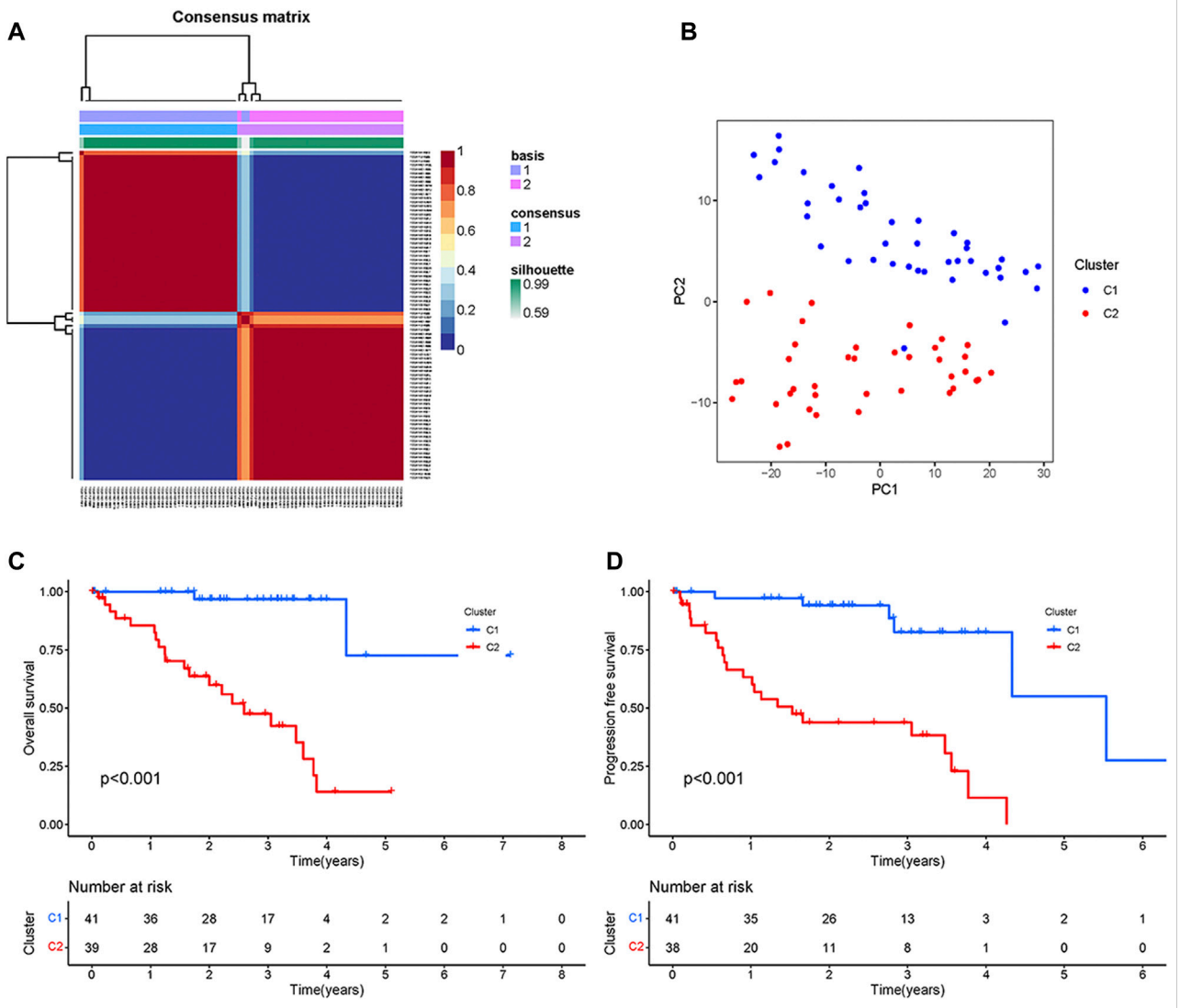

FIGURE 1
Typing and Identification of CRs-based Subtypes: **(A)** The cluster heatmap of tumor subtypes. **(B)** PCA showed a significant difference between the two subtypes. **(C)** Survival curves of overall survival for patients with two subtypes. **(D)** Survival curves of progression-free survival for patients with two subtypes.

interactions of proteins were visualized, and core genes were specifically marked (the darker the red color, the higher the number of nodes). The names and number of nodes of the key genes are shown in Figure 3B, and these 40 genes were defined as key CRs genes for subsequent study analysis.

Establishment and validation of CRs-based signature risk model

First, the random grouping of the TCGA training and test groups was reasonable, with no bias in the selection of clinical traits ($p > 0.05$). Statistical data of each group are shown in Table 2. Then, LASSO regression analysis successfully screened out 5 CRs including CDK2, CUL1, RUVBL1, SIRT3, SMARCD3, and multifactorial Cox analysis was performed on these 5 genes (Figures 3C, D), and finally, a risk model consisting of 3 genes (RUVBL1, SIRT3, and SMARCD3) were successfully constructed (Table 3).

Risk score = (−0.52462896083222 × RUVBL1 expression) + (−1.12003130376948 × SIRT3 expression) + (0.837694828472529 × SMARCD3 expression).

The median risk score (1.324375242) of the TCGA training group was used as the threshold to distinguish the high-risk group from the low-risk group. Based on the grouping, a total of five cohorts were available for assessing and validating the

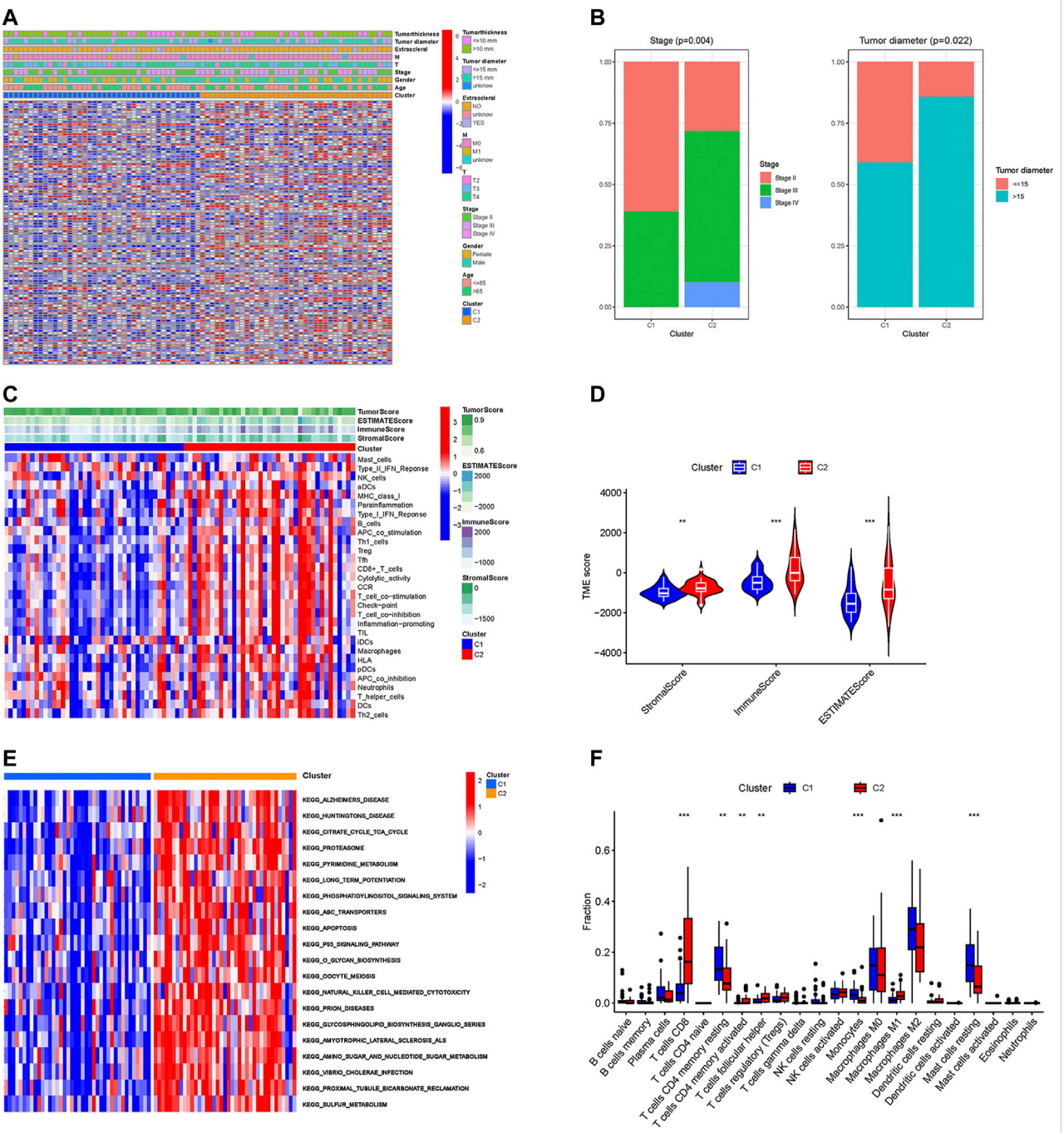

FIGURE 2
Different characteristics between two subtypes. **(A)** The heatmap of expression levels of prognosis-related CRs genes and clinical traits in the two subgroups. **(B)** Percentage distribution of clinical traits with significant differences between the two subtypes. **(C)** The ssGSEA analysis of the immune cell infiltration level in the two subgroups. **(D)** Difference analysis of TME scores. **(E)** KEGG pathway analyses of GSVA in the two subgroups. **(F)** Boxplot of the abundance of immune cells in the two subgroups. $^{**}p < 0.01$, $^{***}p < 0.001$.

prognostic value of the model in this study, including the TCGA training group ($N = 56$), the TCGA testing group ($N = 24$), the TCGA all group ($N = 80$) and two independent datasets GSE22138 ($N = 63$) and GSE84976 ($N = 28$).

Validation of the risk model

The results of Kaplan-Meier survival curves for all datasets are shown in Figures 4A–F, patients with a high-risk score tended

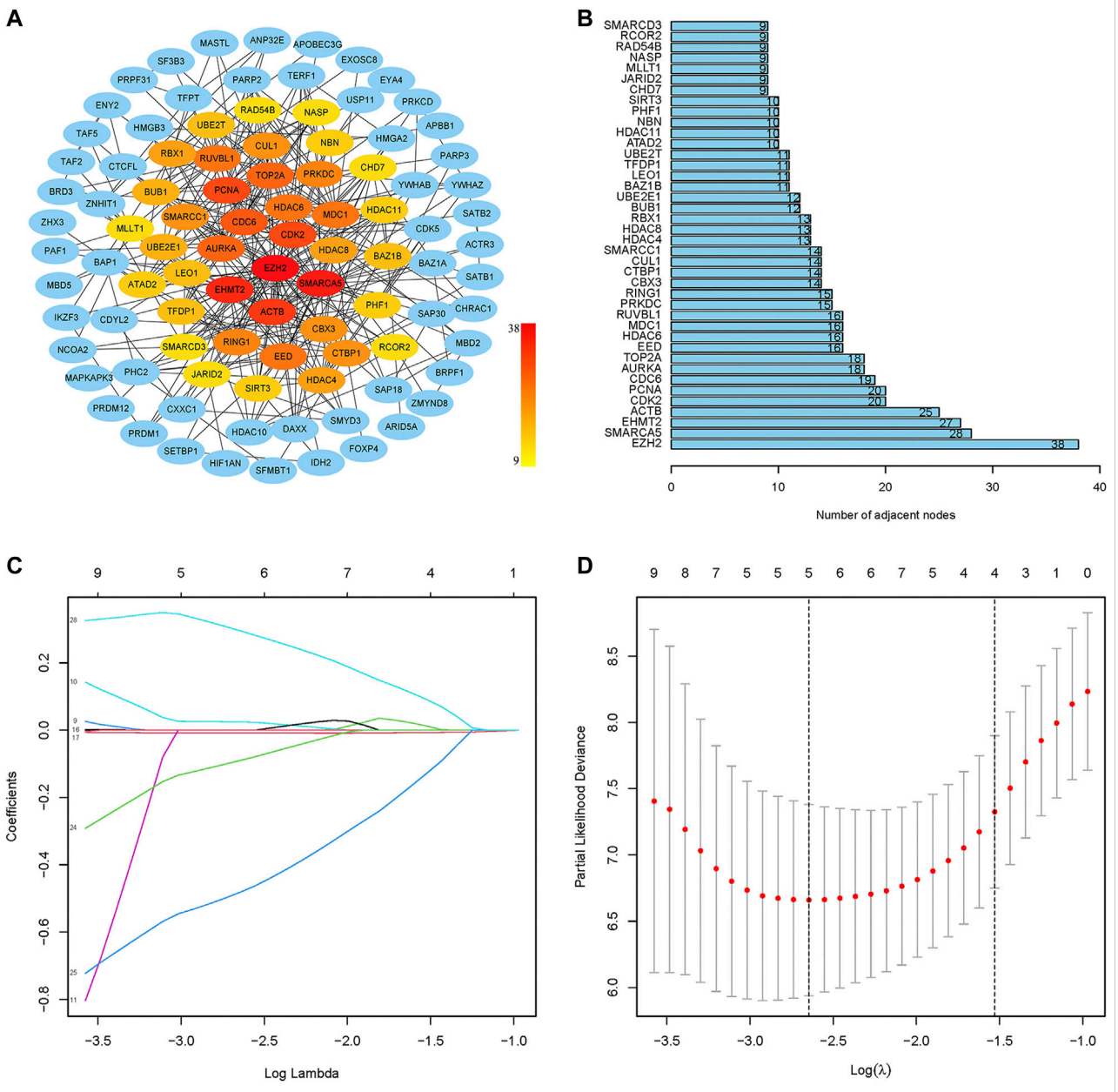

FIGURE 3
Screening of key CRs genes and construction of risk model. **(A)** The PPI network of prognostic CRs genes. **(B)** The names and number of nodes of the top 40 genes in the PPI network. **(C)** Coefficient curve. Different colors represent different genes. **(D)** The minimum lambda value of the lasso model, λ = 5, was determined at the minimum deviation from the partial likelihood, and five genes were available for the analysis.

to have a lower survival probability and die (or metastasis) earlier than those with a low-risk score. The AUC values for the rest of the dataset exceeded 0.7, except for the 1-year and 5-year AUC values of 0.655 for GSE22138. The results suggest that our risk model has a good predictive effect on the prognosis of UM patients.

In the 3-year ROC curves, the AUC values for risk scores were greater than those for other clinical traits, suggesting that the use of risk scores predicted the survival of UM patients better than other clinical traits (Figure 5A). Furthermore, we developed a prognostic nomogram for estimating the UM patients' survival likelihood (Figure 5B). This prognostic nomogram could systematically anticipate the 1-, 2-, and 3-year OS of UM patients. The calibration curve showed that actual results were consistent with predicted results (Figure 5C).

TABLE 2 Statistical analysis of clinical features of a randomized grouping of TCGA dataset.

Covariates	Type	Training group	Testing group	Total group	*p*-value
Age	≤65	33 (58.93%)	13 (54.17%)	46 (57.5%)	0.8823
	>65	23 (41.07%)	11 (45.83%)	34 (42.5%)	
Gender	Female	23 (41.07%)	12 (50%)	35 (43.75%)	0.6229
	Male	33 (58.93%)	12 (50%)	45 (56.25%)	
Stage	Stage II	28 (50%)	8 (33.33%)	36 (45%)	0.0975
	Stage III	24 (42.86%)	16 (66.67%)	40 (50%)	
	Stage IV	4 (7.14%)	0 (0%)	4 (5%)	
M	M0	50 (89.29%)	23 (95.83%)	73 (91.25%)	0.4047
	M1	4 (7.14%)	0 (0%)	4 (5%)	
	Unknown	2 (3.57%)	1 (4.17%)	3 (3.75%)	
N	N0	53 (94.64%)	23 (95.83%)	76 (95%)	1
	Unknown	3 (5.36%)	1 (4.17%)	4 (5%)	
T	T2	5 (8.93%)	0 (0%)	5 (6.25%)	0.3081
	T3	25 (44.64%)	11 (45.83%)	36 (45%)	
	T4	26 (46.43%)	13 (54.17%)	39 (48.75%)	

TABLE 3 Genes in the prognostic signatures of the risk model.

Gene symbol	Full name	Risk coefficient
RUVBL1	RuvB-like AAA ATPase 1	−0.52462896083222
SIRT3	Sirt3, Silent Mating Type Information Regulation 2 Homolog 3	−1.12003130376948
SMARCD3	BAF60C/SWI-SNF related, matrix associated, actin dependent regulator of chromatin, subfamily d, member 3 protein	0.837694828472529

Gene set variation analysis

The GSVA results displayed in Figure 6A, the high-risk group genes are enriched in ABC transporters, apoptosis, RIG-I-like receptor signaling pathway, cell-cytokine receptor interaction, glucose metabolism, pyrimidine metabolism, and sulfur metabolism pathways. These pathways are closely associated with tumor development, and the ABC transporters were closely related to the multidrug resistance (MDR) of the tumor.

Tumor microenvironment and immune-correlation analysis of the model

For confirming if the risk model was associated with tumor microenvironment and tumor immunity, we analyzed the differences in TME scoring, immune cells, and immune checkpoint gene expression between the two groups. As shown in Figure 6B, the results of the ESTIMATE analysis showed that the TME-related scores of the high-risk group were higher than those of the low-risk group. Moreover, we used the ssGSEA method for evaluating differences in immune cell infiltration between the two groups. The heatmap of immune cell expression is shown in Figure 6C, and the different analysis results are shown in Figure 6D. As Figure 6D indicates, the expression of T cells CD8, T cells CD4 memory resting, T cells CD4 memory activated, T cells follicular helper, NK cells resting, Monocytes, Macrophages M1, Macrophages M2 and Mast cells resting had significant differences between the two groups. Among them, within the high-risk group, T cells CD8, T cells CD4 memory activated, T cells follicular helper, and Macrophages M1 proportion were significantly increased, while the opposite results occurred in T cells CD4 memory resting, NK cells resting, Monocytes, Macrophages M2, and Mast cells resting proportions. Additionally, the results of correlation analysis demonstrated that the risk score and the expression of SMARCD3 were positively correlated with the expression of many immune checkpoints (Figure 6E), and as Figure 6F indicates, significant differences were found in immune checkpoint expression. Many immune checkpoints were upregulated in high-risk subgroups, such as PDCD1/PD-

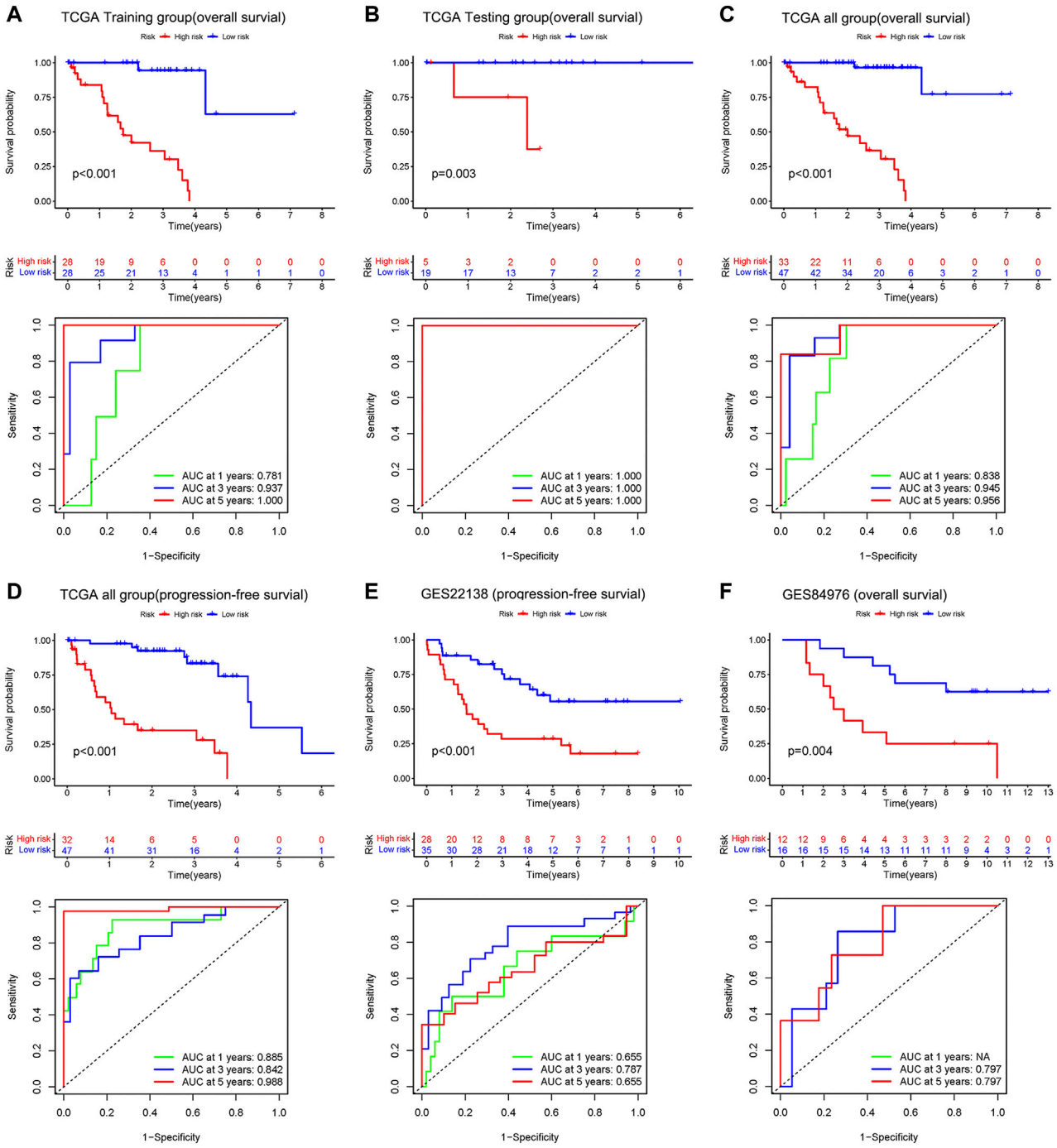

FIGURE 4
Upper: Kaplan–Meier survival analyses based on the risk model. Bottom: 1 -, 3-, and 5-year ROC analyses based on the risk model. Overall survival of patients in the TCGA training group **(A)**, the internal validation group of the TCGA testing group **(B)**, the entire TCGA dataset **(C)**, and the independent dataset GSE84976 **(F)**. Progression-free survival of patients in TCGA dataset **(D)** and the independent dataset GSE22138 **(E)**.

L1, BLTA, CTLA4, LAG3, CD276, TNFRSF25, IDO1, SIGLEC7, TIGIT, LILRB2, and so on. Moreover, the TIDE score of the high-risk group was significantly lower than that of the low-risk group ($p < 0.01$) (Figure 6G), which suggested that patients in the high-risk group may have a better response to immune checkpoint blockade (ICB) treatment.

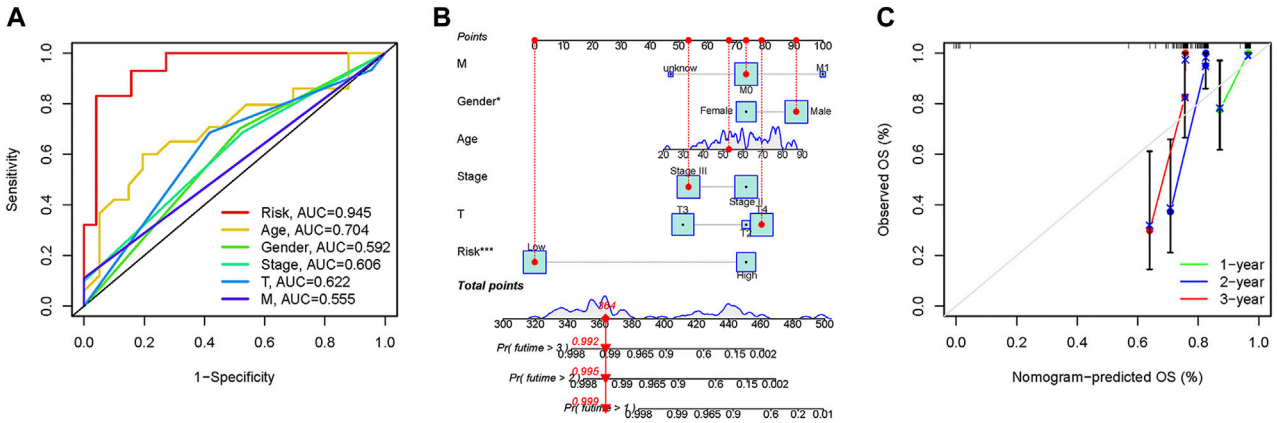

FIGURE 5
Prognostic assessment efficiency comparison of the ROC curve and construction of the nomogram based on risk score and clinical factors. **(A)** ROC curve analysis at 3 years. **(B)** The nomogram to predict the 1-, 2- and 3-year survival risk of UM patients. **(C)** Calibration curve for the 1-, 2-, and 3-year predicted survival nomogram. *$p < 0.05$, ***$p < 0.001$.

Analysis of signature genes in the risk model

First, we found the distribution and relationship of two subgroups, two risk groups, and two clinical outcomes (Figure 7A). And statistical and consistency analysis was performed on 80 UM patients in TCGA for subtypes and risk groupings, and the results were presented as a 2 × 2 contingency table (Supplementary Table S3), and the result of the consistency test Kappa coefficient (κ = 0.691) showed a substantial consistency in the classification of UM samples by tumor subtypes and risk groupings. We found a significant difference between the two subgroups in risk score (Figure 7B). Additionally, the relative expression of the signature gene SMARCD3 was higher in the poor prognosis group (C2 and high-risk group), and RUVBL1 expression in the better prognosis group (C1 and low-risk group) in the three datasets, but the SIRT3 expression was higher in the TCGA subtype and the group with good prognosis in the dataset GSE22138, while no difference was found in the risk group of the dataset GSE84976 (Figures 7C–E). Interestingly, the difference analysis results of the three signature genes between the group's metastasis and non-metastasis in data set GSE22138 are shown in Figure 7F, the SMARCD3 expression is different, and the expression is higher in the group with metastasis. Moreover, the lower RUVBL1 and SIRT3 expressions were significantly correlated with poor survival probability (Figures 8A–C, E–G), and the higher expression of SMARCD3 was significantly correlated with poor survival probability (Figures 8I–L). Notably, RUVBL1 and SIRT3 expressions were not associated with progression-free survival in dataset 22138 (Figures 8D, H). These results suggest that the SMARCD3 gene may be closely associated with the progression of UM.

Discussion

UM is the most common primary malignant intraocular tumor in adults and is characterized by high mortality (>95%), high metastasis (>50%), and poor prognosis within 5 years, making the search for effective biomarkers for accurate diagnosis, assessing prognosis and guiding treatment crucial [44]. CRs play various roles in tumorigenesis. It is a diagnostic and prognostic marker for many cancers [45–50].

In this study, we synthesized and analyzed the UM dataset collected from TCGA and GEO and developed a risk model for UM prognosis consisting of 3 CRs. Unlike other tumors, the UM dataset lacks normal tissue, and we used the NMF method to classify UM patients into two subtypes. The results of the survival analysis showed significant differences in overall survival and progression-free survival between the two subtypes. The results confirm that the expression of prognosis-related CRs based on the prognosis helps to identify UM subtypes. We obtained a risk model by the LASSO Cox regression model before which we improved the generalization ability of the model by preventing "overfitting" by randomly grouping the TCGA dataset. The survival analysis of the model was statistically significant in both the training and validation cohorts. The results of ROC curves comparing risk scores with other clinical traits for prognosis prediction of UM also confirmed the better prediction accuracy of the risk model, while the nomogram constructed based on clinical characteristics and risk scores could systematically predict OS of UM patients.

We further analyzed the TME and immune cell infiltration differences in subtypes and risk subgroups. Immune cells and stromal cells are the two major non-tumor components of the TME, and the ratio of these two cells has an important impact on tumor prognosis. ESTIMATE (Estimation of STromal and

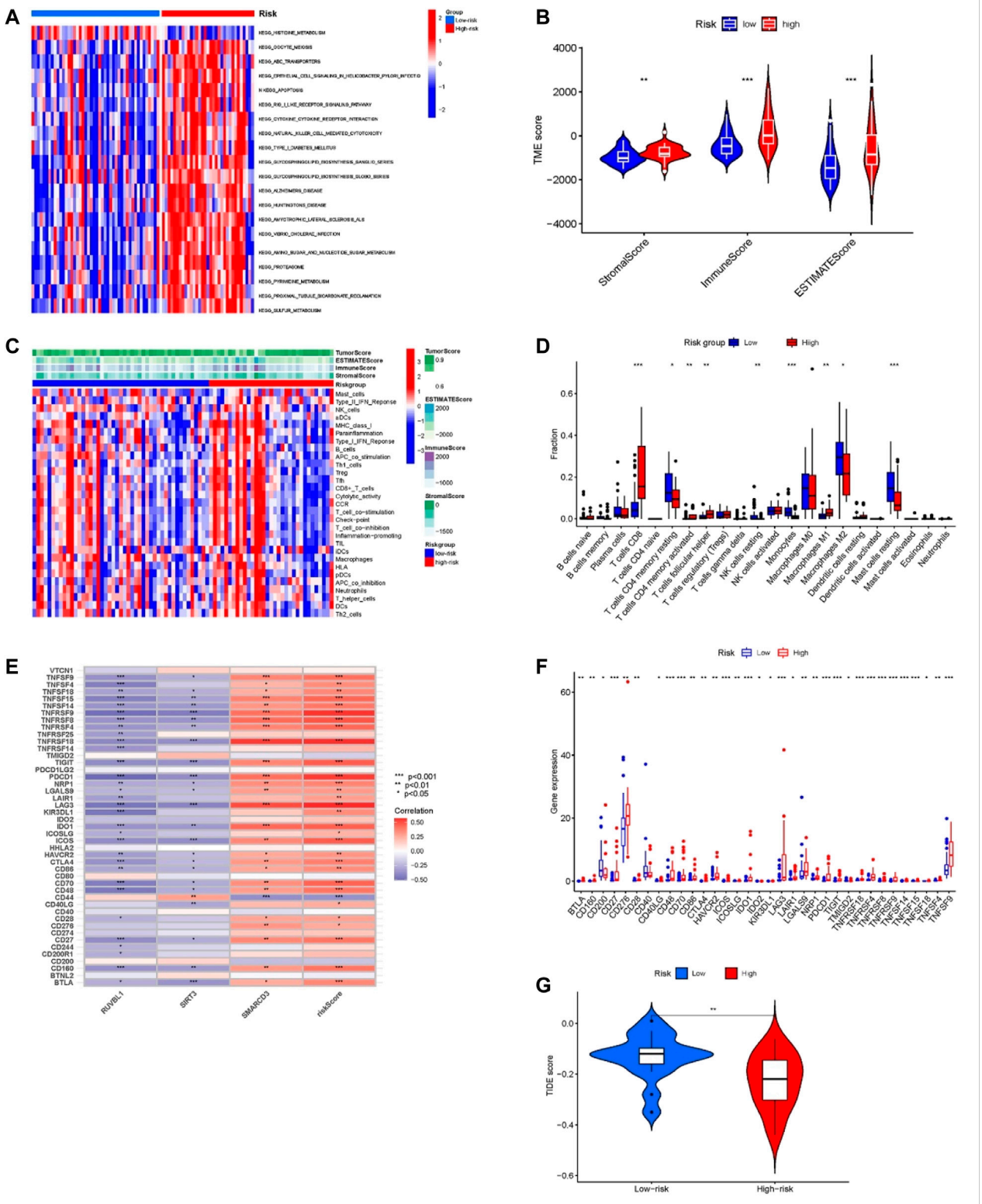

FIGURE 6
Tumor microenvironment and immune-related analysis in two groups. **(A)** KEGG pathway analyses of GSVA in the two groups. **(B)** Difference analysis of TME scores in two groups. **(C)** The ssGSEA analysis of the immune cell infiltration level in the two subgroups. **(D)** Comparison of immune cell infiltration in two groups. **(E)** Correlation of risk score and 3 risk model-related genes with the expression of immune checkpoints. **(F)** Comparison of the expression of immune checkpoints in two groups. **(G)** Difference analysis of TIDE score in two groups. $*p < 0.05$, $**p < 0.01$, $***p < 0.001$.

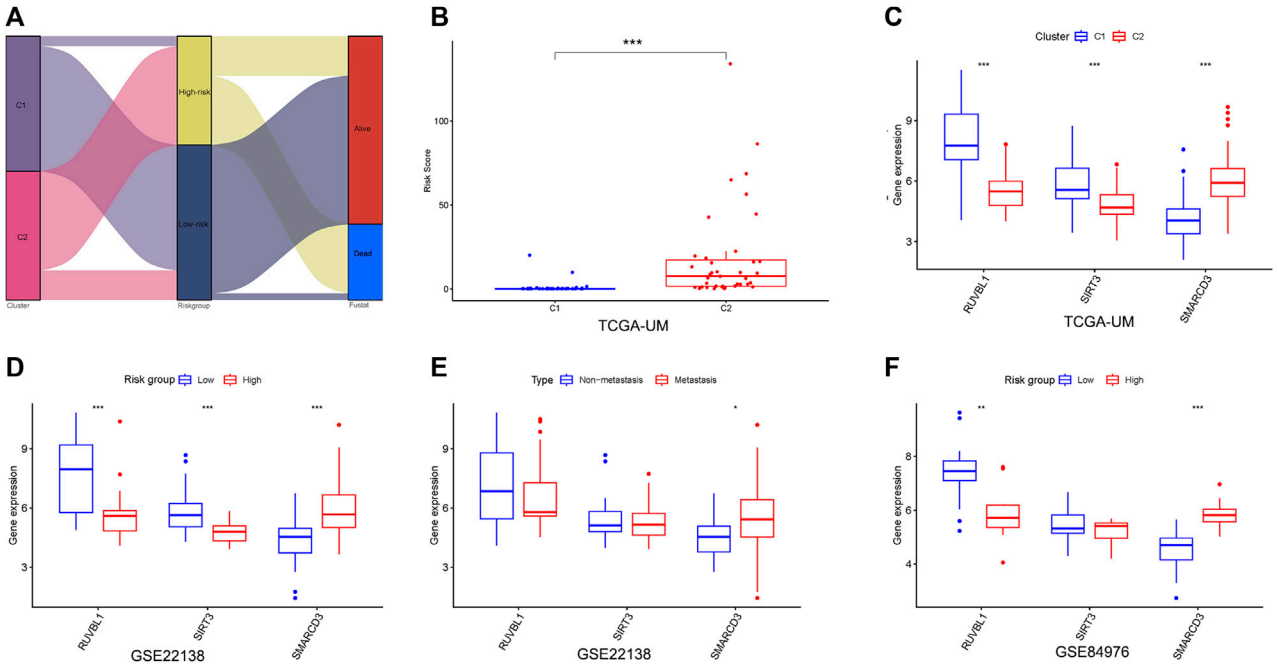

FIGURE 7
Analysis of signature genes in the risk model. **(A)** Sankey diagram of the two subgroups, two risk groups, and two clinical outcomes. **(B)** Differences in the risk scores between the two subgroups. **(C)** Differential expression of three signature genes in subtypes. **(D,E)** Differential expression of three signature genes in risk groupings for datasets GSE22138 and GSE84976. **(F)** Differential expression of three signature genes in the metastasis subgroup of GSE22138. $*p < 0.05$, $**p < 0.01$, $***p < 0.001$.

Immune cells in MAlignant Tumour tissues using Expression data) was calculated by analyzing transcriptional data from cancer samples to calculate the proportion of relevant immune, stromal, and tumor cells in the TME [51]. In our study, stromal score, immune score, and ESTIMATE score were significantly higher in the poor prognosis groups than in the better prognosis groups, suggesting that the prognosis of UM was associated with non-tumor cell infiltration. It has been demonstrated that the poor prognosis of UM is positively correlated with immune cell infiltration [52], so we further analyzed the differences in immune cell infiltration. The infiltration of T-cell CD8, T-cell CD4 memory activation, T-cell follicular helper cells, and macrophages was higher in the poorer prognosis group (C2 and high-risk group) than in the better prognosis group (C1 and low-risk group). These types of immune cells were also closely associated with tumor development. For example, $CD8^+$ T cells themselves can selectively detect and eradicate cancer cells, but tumors continue to develop when they coexist with tumor cells, which is associated with dysfunctional tumor-responsive $CD8^+$ T cells [53]. Accumulation of T follicular helper (Tfh) cells has positive or negative prognostic effects in different human cancers. In melanoma, Tfh cells exert an immunosuppressive function and suppress the function of $CD8^+$ T cells. Additional studies have shown that high Tfh levels are associated with an increase in $CD8^+$ T cells and that CD8+/Tfh crosstalk plays an important role in shaping the antitumor immune response generated by immunotherapy [54–56]. Infiltration of CD4 memory-activated T cells may be a poor prognostic factor in many cancers [57–60]. In cutaneous melanoma, high infiltration of CD4 memory-activated T cells promotes melanoma metastasis [61]. Macrophages play an important role in tumorigenesis and metastasis [62, 63]. In uveal melanoma, macrophages are a negative prognostic factor for it [64]. The mechanisms by which they influence the progression and prognosis of UM need further investigation. In addition, we performed a TIDE analysis between the high- and low-risk groups. Tumor immune dysfunction and rejection (TIDE) is a computational framework for identifying factors underlying both mechanisms of tumor immune escape, which include, in some tumors, high levels of cytotoxic T-cell infiltration but dysfunction of these T cells, and in other tumors, immunosuppressive factors that may preclude T-cell infiltration of the tumor [65–67]. The TIDE score can predict the immune checkpoint suppression efficacy, and the results of the TIDE score will better help physicians to select patients more suitable for immune checkpoint blockade (ICB) therapy [68]. Our study showed that the TIDE score was significantly lower in the high-risk group than in the low-risk

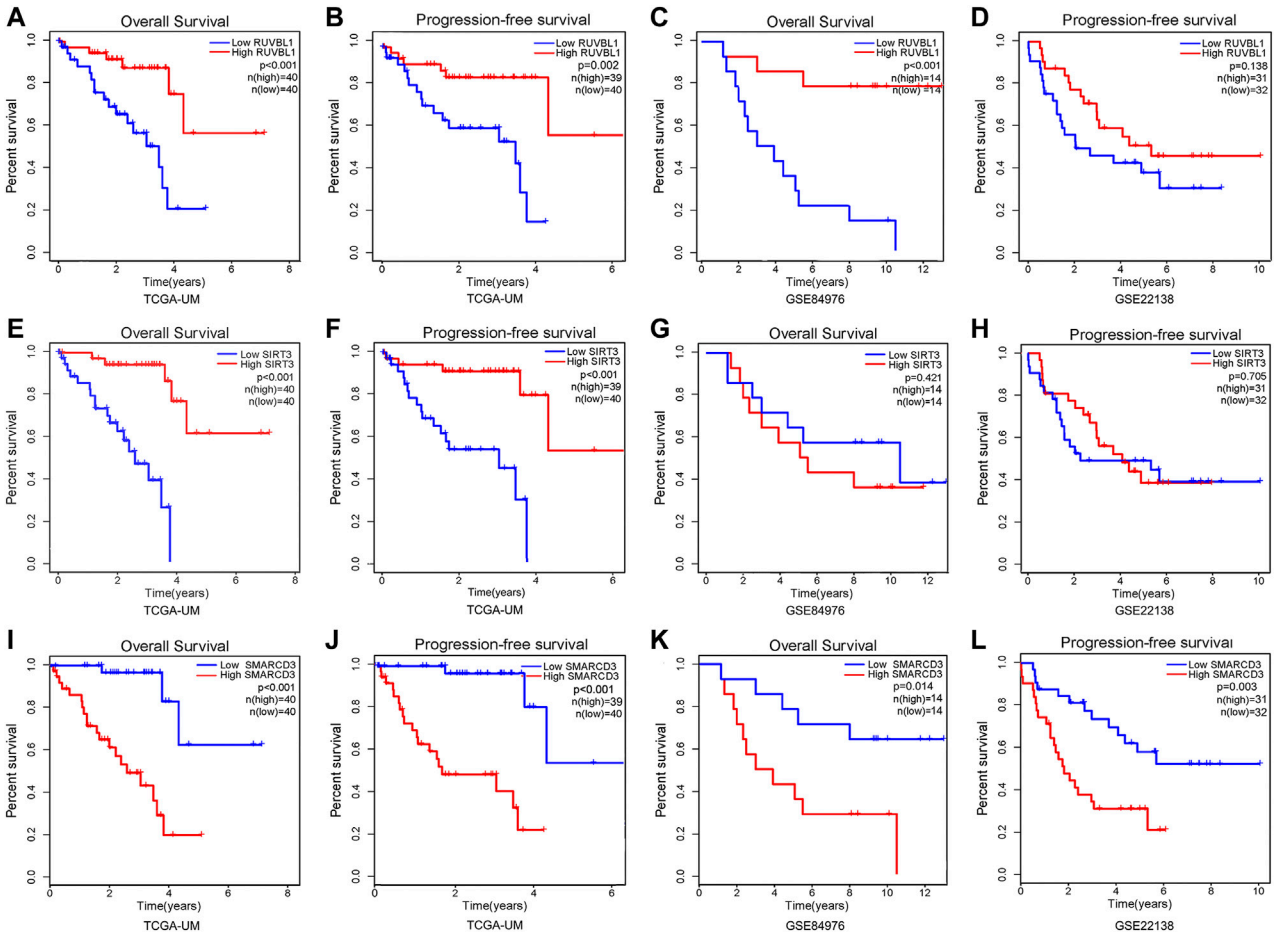

FIGURE 8
Survival analysis of signature genes in the risk model. Red represents patients in the high gene expression group and blue represents patients in the low-risk group. The x-axis represents the survival time and the y-axis represents the survival rate. **(A–D)** Survival analysis of OS and PFS in the RUVBL1 expression subgroup. **(E–H)** Survival analysis of OS and PFS in the SIRT3 expression subgroup. **(I–L)** Survival analysis of OS and PFS in the SMARCD3 expression subgroup.

group, which also suggests that patients in the high-risk group may be more effective when receiving ICB therapy. Many immune checkpoint genes expression was higher in the high-risk group with a poorer prognosis, and we showed significant correlations between risk model scores and three signature genes and many immune checkpoint genes expression, which also suggests that patients in the high-risk group may be more effective when treated with immune checkpoint blockade.

Our risk model consisted of RUVBL1, SIRT3, and SMARCD3. These three genes have also been reported several times in previous studies to play a role in the development of tumors. Sirtuin 3(SIRT3)is the most talked about Sirtuin family member in recent times (a family of NAD+-dependent deacetylases that regulate signaling pathways involved in cellular proliferation and differentiation, metabolism, response to stress, and cancer. Recent studies have pointed out that SIRT3 is a critical regulator of cell metabolism and played a dual role in cancer, as it can act as a suppressor or promoter in a variety of tumors [69], such as breast cancer, colon cancer, and prostate cancer [70–76]. Our findings suggest that SIRT3 may act as a protective factor in the development of uveal melanoma, which is similar to previous findings [77]. However, the specific role and molecular mechanisms of SIRT3 in UM have not been reported. SMARCD3 (SWI-SNF-associated, matrix-associated, actin-dependent regulator of chromatin, subfamily d, member 3 protein) is an important member of the SWI/SNF chromatin remodeling complex, has a role in regulating gene expression [78, 79]. Previous studies have confirmed that SMARCD3 has a cancer-promoting effect in ER+ breast cancer [80, 81]. The results of the related bioinformatic analysis also suggested that SMARCD3 was a prognostic and potential treatment target maker for colorectal cancer, neuroblastoma, hematologic malignancy, and uveal melanoma [82–85]. RUVBL1 belongs to the AAA+ superfamily of ATPases and plays an important

role in many cellular activities [86]. It has been widely reported as an oncogenic factor. For example, it can accelerate the progression of lung cancer by activating the RAF/MEK/ERK pathway, and the high expression of RUVBL1 in mammary carcinoma suggests a worse prognosis [87, 88]. However, a recent study found that a decrease in RUVBL1 promoted the progression of hepatocellular carcinoma [89]. In our study, SMARCD3 expression was negatively correlated with prognosis. OS and PFS were significantly different between high and low expression groups, while SMARCD3 expression levels differed both between subtypes and between risk subgroups, with higher SMARCD3 expression levels in the poorer prognosis group and higher SMARCD3 expression levels in the metastatic group in dataset GSE22138. The expression of SIRT3 and RUVBL1 was positively correlated with prognosis, with differential and survival analyses showing opposite trends to SMARCD3. These results also suggest that SMARCD3 may play a facilitating role in UM progression, while SIRT3 and RUVBL1 play a protective role. This of course requires further experiments to verify.

Notably, we pioneered the construction of a risk model consisting of three CRs genes that can predict the prognosis of UM. Our risk model consists of only three genes, which reduces the cost of clinical testing and improves the possibility of clinical application. Our research offers new insight into the projection of UM but still has some limitations. First, the sample data in this study were from predominantly white Western countries, and there may be genetic inheritance differences. Second, the lack of normal or paracancerous tissues compared with tumor tissues made it impossible to observe the expression of the three characteristic genes in normal and tumor tissues, which needs to be demonstrated with more samples. In addition, all three genes included in our risk model are involved in tumor biological processes. However, the mechanism of how these CRs regulate the biological behavior of UM cells needs to be validated experimentally.

Conclusion

In conclusion, we successfully constructed a risk model consisting of only three signature chromatin regulators that are valuable in predicting the prognosis of uveal melanoma patients. In addition, the model interacts closely with the tumor immune environment and TIDE score results, which may facilitate the development of new therapies for uveal melanoma treatment.

Data availability statement

The data in this study are publicly available, and readers can request them by contacting the corresponding author's email address.

Author contributions

YL: as the first author of the study, performed all the data analysis and wrote the manuscript. CX, LW, BZ, SW, YC, and QX: responsible for collating research results and editing pictures. HL: as the instructor of this study, participated in the whole process of the study. All authors contributed to the article and approved the submitted version.

Funding

This work was supported by grants from the General Project of the Education Department of Jiangxi Province, China (No. GJJ210201).

Conflict of interest

The authors declare that the research was conducted in the absence of any commercial or financial relationships that could be construed as a potential conflict of interest.

Supplementary material

The Supplementary Material for this article can be found online at: https://www.por-journal.com/articles/10.3389/pore.2023.1610980/full#supplementary-material

References

1. Kaur J, Malik MA, Gulati R, Azad SV, Goswami S. Genetic determinants of uveal melanoma. *Tumour Biol* (2014) 35:11711–7. doi:10.1007/s13277-014-2681-7

2. Kaliki S, Shields CL. Uveal melanoma: Relatively rare but deadly cancer. *Eye* (2016) 31(2):241–57. doi:10.1038/eye.2016.275

3. Hoiom V, Helgadottir H. The genetics of uveal melanoma: Current insights. *Appl Clin Genet* (2016) 9:147–55. doi:10.2147/tacg.s69210

4. Augsburger JJ, Corrêa ZM, Shaikh AH. Effectiveness of treatments for metastatic uveal melanoma. *Am J Ophthalmol* (2009) 148(1):119–27. doi:10.1016/j.ajo.2009.01.023

5. Rietschel P, Panageas KS, Hanlon C, Patel A, Abramson DH, Chapman PB. Variates of survival in metastatic uveal melanoma. *J Clin Oncol* (2005) 23(31):8076–80. doi:10.1200/jco.2005.02.6534

6. Patrone S, Maric I, Rutigliani M, Lanza F, Puntoni M, Banelli B, et al. Prognostic value of chromosomal imbalances, gene mutations, and BAP1 expression in uveal melanoma. *Genes, Chromosomes, and Cancer* (2018) 57(8):387–400. doi:10.1002/gcc.22541

7. Damato B. Ocular treatment of choroidal melanoma in relation to the prevention of metastatic death – a personal view. *Prog Retin Eye Res* (2018) 66:187–99. doi:10.1016/j.preteyeres.2018.03.004

8. Smit KN, Jager MJ, de Klein A, Kiliç E. Uveal melanoma: Towards a molecular understanding. *Prog Retin Eye Res* (2020) 75:100800. doi:10.1016/j.preteyeres.2019.100800

9. Onken MD, Worley LA, Ehlers JP, Harbour JW. Gene expression profiling in uveal melanoma reveals two molecular classes and predicts metastatic death. *Cancer Res* (2004) 64(20):7205–9. doi:10.1158/0008-5472.CAN-04-1750

10. Jager MJ, Brouwer NJ, Esmaeli B. The cancer genome Atlas Project: An integrated molecular view of uveal melanoma. *Ophthalmology* (2018) 125(8):1139–42. doi:10.1016/j.ophtha.2018.03.011

11. Bol KF, van den Bosch T, Schreibelt G, Mensink HW, Keunen JEE, Kiliç E, et al. Adjuvant dendritic cell vaccination in high-risk uveal melanoma. *Ophthalmology* (2016) 123(10):2265–7. doi:10.1016/j.ophtha.2016.06.027

12. Verdegaal EM. Adoptive cell therapy: A highly successful individualized therapy for melanoma with great potential for other malignancies. *Curr Opin Immunol* (2016) 39:90–5. doi:10.1016/j.coi.2016.01.004

13. Larkin J, Chiarion-Sileni V, Gonzalez R, Grob JJ, Cowey CL, Lao CD, et al. Combined nivolumab and ipilimumab or monotherapy in untreated melanoma. *New Engl J Med* (2015) 373(1):23–34. doi:10.1056/nejmoa1504030

14. Weber JS, D'Angelo SP, Minor D, Hodi FS, Gutzmer R, Neyns B, et al. Nivolumab versus chemotherapy in patients with advanced melanoma who progressed after anti-CTLA-4 treatment (CheckMate 037): A randomised, controlled, open-label, phase 3 trial. *Lancet Oncol* (2015) 16(4):375–84. doi:10.1016/s1470-2045(15)70076-8

15. Hodi FS, O'Day SJ, McDermott DF, Weber RW, Sosman JA, Haanen JB, et al. Improved survival with ipilimumab in patients with metastatic melanoma. *New Engl J Med* (2010) 363(8):711–23. doi:10.1056/nejmoa1003466

16. Xue M, Shang J, Chen B, Yang Z, Song Q, Sun X, et al. Identification of prognostic signatures for predicting the overall survival of uveal melanoma patients. *J Cancer* (2019) 10(20):4921–31. doi:10.7150/jca.30618

17. Wan Q, Tang J, Lu J, Jin L, Su Y, Wang S, et al. Six-gene-based prognostic model predicts overall survival in patients with uveal melanoma. *Cancer Biomarkers* (2020) 27(3):343–56. doi:10.3233/cbm-190825

18. Li Y, Yang X, Yang J, Wang H, Wei W. An 11-gene-based prognostic signature for uveal melanoma metastasis based on gene expression and DNA methylation profile. *J Cell Biochem* (2018) 120(5):8630–9. doi:10.1002/jcb.28151

19. Sharma A, Stei MM, Fröhlich H, Holz FG, Loeffler KU, Herwig-Carl MC. Genetic and epigenetic insights into uveal melanoma. *Clin Genet* (2018) 93(5):952–61. doi:10.1111/cge.13136

20. Robertson AG, Shih J, Yau C, Gibb EA, Oba J, Mungall KL, et al. Integrative analysis identifies four molecular and clinical subsets in uveal melanoma. *Cancer cell* (2017) 32(2):204–20.e15. doi:10.1016/j.ccell.2017.07.003

21. Herlihy N, Dogrusöz M, van Essen TH, Harbour JW, van der Velden PA, van Eggermond MC, et al. Skewed expression of the genes encoding epigenetic modifiers in high-risk uveal melanoma. *Invest Ophthalmol Vis Sci* (2015) 56(3):1447–58. doi:10.1167/iovs.14-15250

22. Field MG, Kuznetsov JN, Bussies PL, Cai LZ, Alawa KA, Decatur CL, et al. BAP1 loss is associated with DNA methylomic repatterning in highly aggressive Class 2 uveal melanomas. *Clin Cancer Res* (2019) 25:5663–73. doi:10.1158/1078-0432.CCR-19-0366

23. Landreville S, Agapova OA, Matatall KA, Kneass ZT, Onken MD, Lee RS, et al. Histone deacetylase inhibitors induce growth arrest and differentiation in uveal melanoma. *Clin Cancer Res* (2012) 18:408–16. doi:10.1158/1078-0432.CCR-11-0946

24. Matatall KA, Agapova OA, Onken MD, Worley LA, Bowcock AM, Harbour JW. BAP1 deficiency causes loss of melanocytic cell identity in uveal melanoma. *BMC Cancer* (2013) 13:371. doi:10.1186/1471-2407-13-371

25. Kuznetsov JN, Aguero TH, Owens DA, Kurtenbach S, Field MG, Durante MA, et al. BAP1 regulates epigenetic switch from pluripotency to differentiation in developmental lineages giving rise to BAP1-mutant cancers. *Sci Adv* (2019) 5:eaax1738. doi:10.1126/sciadv.aax1738

26. Deng S, Calin GA, Croce CM, Coukos G, Zhang L. Mechanisms of microRNA deregulation in human cancer. *Cell Cycle* (2008) 7:2643–6. doi:10.4161/cc.7.17.6597

27. Chen X, He D, Da Dong X, Dong F, Wang J, Wang L, et al. MicroRNA-124a is epigenetically regulated and acts as a tumor suppressor by controlling multiple targets in uveal melanoma. *Investig Ophthalmol Vis Sci* (2013) 54:2248–56. doi:10.1167/iovs.12-10977

28. Chen X, Wang J, Shen H, Lu J, Li C, Hu D-N, et al. Epigenetics, microRNAs, and carcinogenesis: Functional role of microRNA-137 in uveal melanoma. *Investig Ophthalmol Vis Sci* (2011) 52:1193–9. doi:10.1167/iovs.10-5272

29. Plass C, Pfister SM, Lindroth AM, Bogatyrova O, Claus R, Lichter P. Mutations in regulators of the epigenome and their connections to global chromatin patterns in cancer. *Nat Rev Genet* (2013) 14(11):765–80. doi:10.1038/nrg3554

30. Gonzalez-Perez A, Jene-Sanz A, Lopez-Bigas N. The mutational landscape of chromatin regulatory factors across 4,623 tumor samples. *Genome Biol* (2013) 14(9):r106. doi:10.1186/gb-2013-14-9-r106

31. Medvedeva YA, Lennartsson A, Ehsani R, Kulakovskiy IV, Vorontsov IE, Panahandeh P, et al. EpiFactors: A comprehensive database of human epigenetic factors and complexes. *Database* (2015) 2015:bav067. doi:10.1093/database/bav067

32. Marazzi I, Greenbaum BD, Low DHP, Guccione E. Chromatin dependencies in cancer and inflammation. *Nat Rev Mol Cel Biol* (2017) 19(4):245–61. doi:10.1038/nrm.2017.113

33. Li T, Yang J, Yang B, Zhao G, Lin H, Liu Q, et al. Ketamine inhibits ovarian cancer cell growth by regulating the lncRNA-PVT1/EZH2/p57 Axis. *Front Genet* (2021) 11:597467. doi:10.3389/fgene.2020.597467

34. Chu Y, Chen W, Peng W, Liu Y, Xu L, Zuo J, et al. Amnion-derived mesenchymal stem cell exosomes-mediated autophagy promotes the survival of trophoblasts under hypoxia through mTOR pathway by the downregulation of EZH2. *Front Cel Develop Biol* (2020) 8:545852. doi:10.3389/fcell.2020.545852

35. Chen J, Wang F, Xu H, Xu L, Chen D, Wang J, et al. Long non-coding RNA SNHG1 regulates the wnt/β-catenin and PI3K/AKT/mTOR signaling pathways via EZH2 to affect the proliferation, apoptosis, and autophagy of prostate cancer cell. *Front Oncol* (2020) 10:552907. doi:10.3389/fonc.2020.552907

36. Damaschke NA, Yang B, Blute ML, Lin CP, Huang W, Jarrard DF. Frequent disruption of chromodomain helicase DNA-binding protein 8 (CHD8) and functionally associated chromatin regulators in prostate cancer. *Neoplasia* (2014) 16(12):1018–27. doi:10.1016/j.neo.2014.10.003

37. Lu J, Xu J, Li J, Pan T, Bai J, Wang L, et al. Facer: Comprehensive molecular and functional characterization of epigenetic chromatin regulators. *Nucleic Acids Res* (2018) 46(19):10019–33. doi:10.1093/nar/gky679

38. Laurent C, Valet F, Planque N, Silveri L, Maacha S, Anezo O, et al. High PTP4A3 phosphatase expression correlates with metastatic risk in uveal melanoma patients. *Cancer Res* (2011) 71(3):666–74. doi:10.1158/0008-5472.can-10-0605

39. van Essen TH, van Pelt SI, Bronkhorst IHG, Versluis M, Némati F, Laurent C, et al. Upregulation of HLA expression in primary uveal melanoma by infiltrating leukocytes. *PLOS ONE* (2016) 11(10):e0164292. doi:10.1371/journal.pone.0164292

40. Dai W, Li Y, Mo S, Feng Y, Zhang L, Xu Y, et al. A robust gene signature for the prediction of early relapse in stage I-III colon cancer. *Mol Oncol* (2018) 12(4):463–75. doi:10.1002/1878-0261.12175

41. Gaujoux R, Seoighe C. A flexible R package for nonnegative matrix factorization. *BMC Bioinformatics* (2010) 11(1):367. doi:10.1186/1471-2105-11-367

42. Tang W, Hu J, Zhang H, Wu P, He H. Kappa coefficient: A popular measure of rater agreement. *Shanghai Arch Psychiatry* (2015) 27(1):62–7. doi:10.11919/j.issn.1002-0829.215010

43. McHugh ML. Interrater reliability: The kappa statistic. *Biochemia Med* (2012) 22(3):276–82. doi:10.11613/bm.2012.031

44. Marseglia M, Amaro A, Solari N, Gangemi R, Croce E, Tanda ET, et al. How to make immunotherapy an effective therapeutic choice for uveal melanoma. *Cancers* (2021) 13(9):2043. doi:10.3390/cancers13092043

45. Zhu K, Liu X, Deng W, Wang G, Fu B. Identification of a chromatin regulator signature and potential candidate drugs for bladder cancer. *Hereditas* (2022) 159(1):13. doi:10.1186/s41065-021-00212-x

46. Mardinian K, Adashek JJ, Botta GP, Kato S, Kurzrock R. SMARCA4: Implications of an altered chromatin-remodeling gene for cancer development and therapy. *Mol Cancer Ther* (2021) 20(12):2341–51. doi:10.1158/1535-7163.mct-21-0433

47. Shu X-S, Li L, Tao Q. Chromatin regulators with tumor suppressor properties and their alterations in human cancers. *Epigenomics* (2012) 4(5):537–49. doi:10.2217/epi.12.50

48. Gurard-Levin ZA, Wilson LOW, Pancaldi V, Postel-Vinay S, Sousa FG, Reyes C, et al. Chromatin regulators as a guide for cancer treatment choice. *Mol Cancer Ther* (2016) 15(7):1768–77. doi:10.1158/1535-7163.mct-15-1008

49. Debaugny RE, Skok JA. CTCF and CTCFL in cancer. *Curr Opin Genet Develop* (2020) 61:44–52. doi:10.1016/j.gde.2020.02.021

50. Jiang Y, Liu S, Chen X, Cao Y, Tao Y. Genome-wide distribution of DNA methylation and DNA demethylation and related chromatin regulators in cancer. *Biochim Biophys Acta (Bba) - Rev Cancer* (2013) 1835(2):155–63. doi:10.1016/j.bbcan.2012.12.003

51. Becht E, Giraldo NA, Lacroix L, Buttard B, Elarouci N, Petitprez F, et al. Estimating the population abundance of tissue-infiltrating immune and stromal cell populations using gene expression. *Genome Biol* (2016) 17(1):218. doi:10.1186/s13059-016-1070-5

52. Zhao H, Chen Y, Shen P, Gong L. Identification of immune cell infiltration landscape and their prognostic significance in uveal melanoma. *Front Cel Dev Biol* (2021) 9:713569. doi:10.3389/fcell.2021.713569

53. Hellstrom KE, Hellstrom I. From the Hellstrom paradox toward cancer cure. *Prog Mol Biol translational Sci* (2019) 164:1–24. doi:10.1016/bs.pmbts.2018.11.002

54. Ma QY, Huang DY, Zhang HJ, Chen J, Miller W, Chen XF. Function of follicular helper T cell is impaired and correlates with survival time in non-small cell lung cancer. *Int immunopharmacology* (2016) 41:1–7. doi:10.1016/j.intimp.2016.10.014

55. Zappasodi R, Budhu S, Hellmann MD, Postow MA, Senbabaoglu Y, Manne S, et al. Non-conventional inhibitory CD4+Foxp3-PD-1hi T cells as a biomarker of immune checkpoint blockade activity. *Cancer cell* (2018) 33(6):1017–32. doi:10.1016/j.ccell.2018.05.009

56. Niogret J, Berger H, Rebe C, Mary R, Ballot E, Truntzer C, et al. Follicular helper-T cells restore CD8+-dependent antitumor immunity and anti-PD-L1/PD-1 efficacy. *J Immunother Cancer* (2021) 9(6):e002157. doi:10.1136/jitc-2020-002157

57. Bromwich EJ, McArdle PA, Canna K, McMillan DC, McNicol AM, Brown M, et al. The relationship between T-lymphocyte infiltration, stage, tumour grade and survival in patients undergoing curative surgery for renal cell cancer. *Br J Cancer* (2003) 89(10):1906–8. doi:10.1038/sj.bjc.6601400

58. Kinoshita T, Muramatsu R, Fujita T, Nagumo H, Sakurai T, Noji S, et al. Prognostic value of tumor-infiltrating lymphocytes differs depending on histological type and smoking habit in completely resected non-small-cell lung cancer. *Ann Oncol : official J Eur Soc Med Oncol* (2016) 27(11):2117–23. doi:10.1093/annonc/mdw319

59. McArdle PA, Canna K, McMillan DC, McNicol AM, Campbell R, Underwood MA. The relationship between T-lymphocyte subset infiltration and survival in patients with prostate cancer. *Br J Cancer* (2004) 91(3):541–3. doi:10.1038/sj.bjc.6601943

60. Droeser R, Zlobec I, Kilic E, Güth U, Heberer M, Spagnoli G, et al. Differential pattern and prognostic significance of CD4+, FOXP3+ and IL-17+ tumor infiltrating lymphocytes in ductal and lobular breast cancers. *BMC cancer* (2012) 12:134. doi:10.1186/1471-2407-12-134

61. Li M, Zhao J, Yang R, Cai R, Liu X, Xie J, et al. CENPF as an independent prognostic and metastasis biomarker corresponding to CD4+ memory T cells in cutaneous melanoma. *Cancer Sci* (2022) 113(4):1220–34. doi:10.1111/cas.15303

62. Mantovani A, Marchesi F, Malesci A, Laghi L, Allavena P. Tumour-associated macrophages as treatment targets in oncology. *Nat Rev Clin Oncol* (2017) 14(7):399–416. doi:10.1038/nrclinonc.2016.217

63. Cassetta L, Pollard JW. Targeting macrophages: Therapeutic approaches in cancer. *Nat Rev Drug Discov* (2018) 17(12):887–904. doi:10.1038/nrd.2018.169

64. Herwig MC, Bergstrom C, Wells JR, Höller T, Grossniklaus HE. M2/M1 ratio of tumor associated macrophages and PPAR-gamma expression in uveal melanomas with class 1 and class 2 molecular profiles. *Exp Eye Res* (2013) 107:52–8. doi:10.1016/j.exer.2012.11.012

65. Gajewski TF, Schreiber H, Fu YX. Innate and adaptive immune cells in the tumor microenvironment. *Nat Immunol* (2013) 14(10):1014–22. doi:10.1038/ni.2703

66. Joyce JA, Fearon DT. T cell exclusion, immune privilege, and the tumor microenvironment. *Science (New York, N.Y.)* (2015) 348(6230):74–80. doi:10.1126/science.aaa6204

67. Spranger S, Gajewski TF. Tumor-intrinsic oncogene pathways mediating immune avoidance. *Oncoimmunology* (2015) 5(3):e1086862. doi:10.1080/2162402X.2015.1086862

68. Jiang P, Gu S, Pan D, Fu J, Sahu A, Hu X, et al. Signatures of T cell dysfunction and exclusion predict cancer immunotherapy response. *Nat Med* (2018) 24(10):1550–8. doi:10.1038/s41591-018-0136-1

69. Torrens-Mas M, Oliver J, Roca P, Sastre-Serra J. SIRT3: Oncogene and tumor suppressor in cancer. *Cancers* (2017) 9(7):90. doi:10.3390/cancers9070090

70. Kenny TC, Craig AJ, Villanueva A, Germain D. Mitohormesis primes tumor invasion and metastasis. *Cel Rep* (2019) 27(8):2292–303. doi:10.1016/j.celrep.2019.04.095

71. Kenny TC, Hart P, Ragazzi M, Sersinghe M, Chipuk J, Sagar MAK, et al. Selected mitochondrial DNA landscapes activate the SIRT3 axis of the UPRmt to promote metastasis. *Oncogene* (2017) 36(31):4393–404. doi:10.1038/onc.2017.52

72. Lee JJ, van de Ven RAH, Zaganjor E, Ng MR, Barakat A, Demmers JJPG, et al. Inhibition of epithelial cell migration and Src/FAK signaling by SIRT3. *Proc Natl Acad Sci United States America* (2018) 115(27):7057–62. doi:10.1073/pnas.1800440115

73. Wei Z, Song J, Wang G, Cui X, Zheng J, Tang Y, et al. Deacetylation of serine hydroxymethyl-transferase 2 by SIRT3 promotes colorectal carcinogenesis. *Nat Commun* (2018) 9(1):4468. doi:10.1038/s41467-018-06812-y

74. Liang L, Li Q, Huang L, Li D, Li X. Sirt3 binds to and deacetylates mitochondrial pyruvate carrier 1 to enhance its activity. *Biochem biophysical Res Commun* (2015) 468(4):807–12. doi:10.1016/j.bbrc.2015.11.036

75. Fu W, Li H, Fu H, Zhao S, Shi W, Sun M, et al. The SIRT3 and SIRT6 promote prostate cancer progression by inhibiting necroptosis-mediated innate immune response. *J Immunol Res* (2020) 2020:8820355. doi:10.1155/2020/8820355

76. Li R, Quan Y, Xia W. SIRT3 inhibits prostate cancer metastasis through regulation of FOXO3A by suppressing Wnt/β-catenin pathway. *Exp Cel Res* (2018) 364(2):143–51. doi:10.1016/j.yexcr.2018.01.036

77. Luo H, Ma C, Shao J, Cao J. Prognostic implications of novel ten-gene signature in uveal melanoma. *Front Oncol* (2020) 10:567512. doi:10.3389/fonc.2020.567512

78. Ho L, Crabtree GR. Chromatin remodelling during development. *Nature* (2010) 463(7280):474–84. doi:10.1038/nature08911

79. Lickert H, Takeuchi JK, von Both I, Walls JR, McAuliffe F, Lee Adamson S, et al. Baf60c is essential for function of BAF chromatin remodelling complexes in heart development. *Nature* (2004) 432(7013):107–12. doi:10.1038/nature03071

80. Tropée R, de la Peña Avalos B, Gough M, Snell C, Duijf PHG, Dray E. The SWI/SNF subunit SMARCD3 regulates cell cycle progression and predicts survival outcome in ER+ breast cancer. *Breast Cancer Res Treat* (2020) 185(3):601–14. doi:10.1007/s10549-020-05997-5

81. Jordan NV, Prat A, Abell AN, Zawistowski JS, Sciaky N, Karginova OA, et al. SWI/SNF chromatin-remodeling factor smarcd3/baf60c controls epithelial-mesenchymal transition by inducing Wnt5a signaling. *Mol Cell Biol* (2013) 33(15):3011–25. doi:10.1128/mcb.01443-12

82. Jiang M, Wang H, Chen H, Han Y. SMARCD3 is a potential prognostic marker and therapeutic target in CAFs. *Aging* (2020) 12(20):20835–61. doi:10.18632/aging.104102

83. Takita J, Ishii M, Tsutsumi S, Tanaka Y, Kato K, Toyoda Y, et al. Gene expression profiling and identification of novel prognostic marker genes in neuroblastoma. *Genes, Chromosomes and Cancer* (2004) 40(2):120–32. doi:10.1002/gcc.20021

84. Ajore R, Niroula A, Pertesi M, Cafaro C, Thodberg M, Went M, et al. Functional dissection of inherited non-coding variation influencing multiple myeloma risk. *Nat Commun* (2022) 13(1):151. doi:10.1038/s41467-021-27666-x

85. Zhao D-D, Zhao X, Li WT. Identification of differentially expressed metastatic genes and their signatures to predict the overall survival of uveal melanoma patients by bioinformatics analysis. *Int J Ophthalmol* (2020) 13(7):1046–53. doi:10.18240/ijo.2020.07.05

86. Matias PM, Gorynia S, Donner P, Carrondo MA. Crystal structure of the human AAA+ protein RuvBL1. *J Biol Chem* (2006) 281(50):38918–29. doi:10.1074/jbc.m605625200

87. Guo H, Zhang X-Y, Peng J, Huang Y, Yang Y, Liu Y, et al. RUVBL1, a novel C-RAF-binding protein, activates the RAF/MEK/ERK pathway to promote lung cancer tumorigenesis. *Biochem Biophysical Res Commun* (2018) 498(4):932–9. doi:10.1016/j.bbrc.2018.03.084

88. Fan W, Xie J, Xia J, Zhang Y, Yang M, Wang H, et al. RUVBL1-ITFG1 interaction is required for collective invasion in breast cancer. *Biochim Biophys Acta (Bba) - Gen Subjects* (2017) 1861(7):1788–800. doi:10.1016/j.bbagen.2017.03.016

89. Mello T, Materozzi M, Zanieri F, Simeone I, Ceni E, Bereshchenko O, et al. Liver haploinsufficiency of RuvBL1 causes hepatic insulin resistance and enhances hepatocellular carcinoma progression. *Int J Cancer* (2019) 146(12):3410–22. doi:10.1002/ijc.32787

Pathology & Oncology Research | frontiers

TYPE Review
PUBLISHED 09 April 2024
DOI 10.3389/pore.2024.1611719

Check for updates

OPEN ACCESS

EDITED BY
Andrea Ladányi,
National Institute of Oncology (NIO), Hungary

*CORRESPONDENCE
József Tímár,
jtimar@gmail.com

RECEIVED 05 February 2024
ACCEPTED 27 March 2024
PUBLISHED 09 April 2024

CITATION
Nádorvári ML, Lotz G, Kulka J, Kiss A and Tímár J (2024), Microsatellite instability and mismatch repair protein deficiency: equal predictive markers?
Pathol. Oncol. Res. 30:1611719.
doi: 10.3389/pore.2024.1611719

COPYRIGHT
© 2024 Nádorvári, Lotz, Kulka, Kiss and Tímár. This is an open-access article distributed under the terms of the Creative Commons Attribution License (CC BY). The use, distribution or reproduction in other forums is permitted, provided the original author(s) and the copyright owner(s) are credited and that the original publication in this journal is cited, in accordance with accepted academic practice. No use, distribution or reproduction is permitted which does not comply with these terms.

Microsatellite instability and mismatch repair protein deficiency: equal predictive markers?

Maja L. Nádorvári, Gábor Lotz, Janina Kulka, András Kiss and József Tímár*

Department of Pathology, Forensic and Insurance Medicine, Semmelweis University, Budapest, Hungary

Current clinical guidelines recommend mismatch repair (MMR) protein immunohistochemistry (IHC) or molecular microsatellite instability (MSI) tests as predictive markers of immunotherapies. Most of the pathological guidelines consider MMR protein IHC as the gold standard test to identify cancers with MMR deficiency and recommend molecular MSI tests only in special circumstances or to screen for Lynch syndrome. However, there are data in the literature which suggest that the two test types may not be equal. For example, molecular epidemiology studies reported different rates of deficient MMR (dMMR) and MSI in various cancer types. Additionally, direct comparisons of the two tests revealed relatively frequent discrepancies between MMR IHC and MSI tests, especially in non-colorectal and non-endometrial cancers and in cases with unusual dMMR phenotypes. There are also scattered clinical data showing that the efficacy of immune checkpoint inhibitors is different if the patient selection was based on dMMR versus MSI status of the cancers. All these observations question the current dogma that dMMR phenotype and genetic MSI status are equal predictive markers of the immunotherapies.

KEYWORDS

mismatch repair deficiency, microsatellite instability, immunohistochemistry, molecular testing, cancer

Introduction

MMR deficiency (dMMR), and the resultant microsatellite instability (MSI), is one of the most frequent genetic alterations of the DNA repair systems of cancer. It is most prevalent in the gastrointestinal (GI) tract (colorectal, gastric, and esophageal) and endometrial cancers but can occur at a much lower frequency in any other cancer types. Initially, they served only as a genetic marker for the hereditary cancer disease Lynch syndrome [1, 2], but now most tests for microsatellite instability are performed as predictive marker tests of immune checkpoint inhibitor (ICI) therapies [3–7]. Currently, the two main diagnostic methods of microsatellite instability are testing the expression of MMR proteins with immunohistochemistry (IHC) and molecular diagnostics of MSI

mostly by polymerase chain reaction (PCR)-based techniques. Next-generation sequencing (NGS)-based detection has also become a tool to determine MSI status, as it can analyze more microsatellite markers and MMR gene mutations simultaneously, which can help in therapeutic decisions [8]. Immunohistochemistry can only reveal the absence of MMR proteins, which is excellent for Lynch syndrome. However, IHC cannot test the mismatch repair system from a functional aspect, which is a crucial factor in immune checkpoint inhibitor therapies, since this defect increases the mutational burden and the amount of neoantigens. In routine diagnostics, MMR IHC and MSI PCR are the most frequently used techniques, and their predictive values are equivalent according to the international guidelines. Molecular epidemiology data of dMMR and MSI demonstrated different incidences in various cancer types, suggesting that the two markers may not be equivalent. On the other hand, there are several smaller or larger studies that directly compared various testing methods of dMMR and MSI and indicated smaller or larger differences in sensitivities, specificities, and predictive values. Since the breakthrough investigation of immunotherapies, the diagnostic aim of MSI/MMR status have overgrown Lynch syndrome. It is important to consider that most diagnostic tools on the market now are optimized for colorectal carcinomas (CRCs), so they are not necessarily equally sensitive in other cancer types. The goal of this review is to analyze the prevalence of MSI-high/dMMR status in various cancer types, the current detection strategies, and their discrepancies and validity in the light of prognostic value for immunotherapies.

Mismatch repair deficiency and resultant microsatellite instability

DNA repair deficiency is a hallmark of cancer and may involve all the possible forms, namely homologous recombination repair (HRR), mismatch repair (MMR), nucleotide excision repair (NEJR), and base excision repair (BER), but current clinical attention is on MMR and HR deficiencies [9]. There are ~2×10^7 microsatellites present in the whole genome, including exomes (~5×10^5), the non-coding regions, and the introns which make up 3% of the genome [10, 11]. Every microsatellite consists of repetitive sequences in which the aberrant shift in the length of the microsatellites usually occur during replication [12]. Microsatellites are highly conservative parts of the genome, and they are exceptionally prone to mismatched base pairing and frameshift mutation. Accumulation of them leads to increased tumor mutational burden (TMB), an increased neoantigen load and, as a consequence, stronger antitumoral immune responses [13]. All these consequences of microsatellite instability make it an excellent predictive biomarker for immune checkpoint inhibitor therapies [14]. It is of note that cancers share the most frequently involved microsatellite markers, but they are also characterized by their own unique sets involved in MSI [11] (Table 1).

The MMR system corrects spontaneously arising somatic mutations and is indispensable for the reduction of mutational rate. Its impaired function results in the loss of the integrity of the genome and promotes malignant transformation, which is even more accentuated in the germline mutations of the MMR system. The main MMR proteins are MLH1, MSH2, MSH6, and PMS2, but MSH3, MLH3, and PMS1 can also be important in special circumstances [9, 15]. The MMR proteins repair the incorrectly paired bases, thus the ones which did not form cytosine-guanine or thymidine-adenine pairs. These mismatches are mostly caused by replicational errors but also by oxidative stress, lipid peroxidation, or methylation and alkylation [16]. The MMR proteins function as heterodimers: MLH1 and PMS2 form MutLalpha while MSH2 and MSH6 form MutSalpha. The activation of MutSalpha complex is dependent on ATPase activity, which is crucial for the connection with the mismatched DNA and the initiation of the reparation. A flawed DNA string is bound to MSH6 by the mismatched base pair as a part of MutSalpha. There is an alternative complex, MutSbeta, consisting of MSH2 and MSH3 in a 1: 10 ratio to MutSalpha and it usually binds larger defects [16, 17]. The binding of MutSalpha stimulates ATP hydrolysis and facilitates the binding of MutLalpha, thus the tetramer of the four mismatch-correcting protein can evolve. The MMR pathway is bidirectional. The 5′-end binds the newly synthetized strand, allowing exonuclease 1 (EXO1) and ATP binding with MutSalpha and MutLalpha to carry out conformational changes on DNA. The MutSalpha/MutLaplha/EXO1 complex facilitates the function of RPA (replication protein) and PCNA (proliferating cell nuclear antigen) so these enzymes can repair the mutations. 3′-5′ repair also exists, but our knowledge on it is limited. Alternatively, MLH1 can form dimer with MLH3 (resulting in MutLγ complex), which has a role in meiotic recombination [17]. MLH1 can also form another alternative dimer, MLH1/PMS1, resulting in the MutLβ complex. The MMR system arrests cell cycle when it detects any defect. It is possible that, after revealing the error in the freshly synthetized strand, the mismatch repair system tries to cut them out and, if it fails, the original strand will break as well, inducing the ATM/ATR/p53 cell death pathway. Alternatively, it is possible that MutSalpha and MutLalpha signal the cell death pathway directly after the detection of mismatches [18, 19]. The mutation rate of MMR genes is different by cancer types and include not only the common MMR genes (MLH1, MSH2, MSH6, and PMS2) but also the minor ones (MSH3, MLH3, and PMS1). Analysis of the TCGA database indicates that one-third of MMR gene mutations affect these minor MMR genes. MMR gene mutation frequency is the highest in endometrial adenocarcinoma (>50%), followed by gastric (>30%), colorectal, and ovarian cancers (>20%) (Table 2).

TABLE 1 Most frequently involved microsatellite markers in various cancer types [11].

COAD	READ	STAD	UCEC
ACVR2A	ACVR2A	ACVR2A	
ATPEV0A2	ATPEV0A2	ATPEV0A2	
DEFB105A/B		DEFB105A/B	DEFB105A/B
NOMO1		NOMO1	
AP4S1		AP4S1	
TIAL1		TIAL1	
UBR5		UBR5	
TM2D1		TM2D1	
BRAF	BRAF	PIP5K1A	PIP5K1A
		TAF2	TAF2
		PDE4DIP	PDE4DIP
CRP2	AHCYL2	MACF1	
BMPR2	PLCB4	DOCK10	
	IQGAP1	KNOP1	
	SCLT1	GTF2H2B	
	EFCAB5	NMS	
	ARHGEF15	UTP20	
	ABLIM1	HMCN1	
	APH1B	NLN	
		CACNA1D	

COAD, colon adenocarcinoma; READ, rectal adenocarcinoma; STAD, stomach adenocarcinoma; UCEC, uterine endometrial adenocarcinoma (bold: cancer-specific patterns).

TABLE 2 Incidence of MMR gene mutations in various cancer types in TCGA database.

MMR gene	Endometrial adenocarcinoma	Gastric adenocarcinoma	Colon adenocarcinoma	Rectal adenocarcinoma	Ovarian carcinoma
MLH1	7	3	4	1	2
MSH2	9	3	4	2	3
MSH6	12	3	5	2	3
PMS2	8	5	3	1	3
mutation rate	36	14	16	6	11
MSH3	10	4	2	3	5
MLH3	2	4	4	0	1
PMS1	6	3	3	1	5
total MMR mutation rate	54	35	25	10	22

Data are expressed in %. MMR, mismatch repair.

MMR deficiency during tumor progression

A large cohort of 100,000 colorectal cancer patients in the US was analyzed for MSI/dMMR prevalence according to stages and demonstrated a gradual decrease of incidence from stage I to stage IV [20]. A large meta-analysis of MSI/dMMR literature also indicated that the MSI prevalence in colorectal cancers decreased significantly from Stage I/II to Stage III/IV in Japan and South Korea while no such changes were reported in endometrial or ovarian cancers [21]. Contrary to what would be expected if we consider MMR deficiency as a founder genetic alteration during CRC progression, data may suggest that, during tumor progression, MMR deficiency is lost in a significant number of cases. To test this directly, the MSI/dMMR genetic status was compared in a ~100 patient cohort in primary tumor and their metastases. This analysis found the loss of MSI/dMMR in CRC metastases was a rare event (3.4%) [22]. An analysis of a small number of MSI-high cancers (six different types) directly evaluated the clonal development during tumor progression by using multiregional tumor sequencing. This analysis did not find loss of MSI clones in various types of metastases but rather detected progressive changes in the forms of MSI paralleled with an increase in TMB and the emergence of new driver mutations in various clones. These data seem to be contradictory unless the biology of MSI/dMMR colorectal cancers is different [23]. A study of a large cohort of CRC patients analyzed the survival after recurrence (SAR) of >2,500 patients and found that MSI/dMMR patients have a significantly longer survival compared to MSS/pMMR ones [24]. Biologically, MSI/dMMR colorectal cancers tend to be less metastatic, although they are resistant to 5-FU-based chemotherapies [15].

Diagnostic techniques of dMMR/MSI

Immunohistochemical diagnosis of MMR deficiency

Loss of expression of mismatch repair proteins can be detected by immunohistochemistry. The currently recommended method applies detection of four MMR proteins, which is an excellent tool for the original aim of MMR testing: detecting Lynch syndrome [17, 25]. These proteins work in heterodimers, so in the majority of dMMR cases, double loss of MLH1 and PMS2 or MSH2 and MSH6 is present, which is called the classical dMMR [26]. When MLH1 or MSH2 is mutated or degraded, it will cause the loss of PMS2 or MSH6 as well, thus the isolated loss is more frequent in the last two proteins [27, 28]. This is due to the compensatory function of other MMR proteins such as MSH3 for MLH1 and MSH2 or PMS1 for MLH3. MLH1 promoter hypermethylation can also cause dMMR phenotype [15]. Immunohistochemistry of the MMR proteins is performed on FFPE blocks by using the CE-marked kit Ventana-MMR-RxDx[1] or Dako/Agilent-set [29] containing antibodies to MLH1, MSH2, PMS2, and MSH6. Two types of positive controls have to be used: a positive control sample is necessary while tumor stromal fibroblasts and lymphoid cells serve as internal controls. These latter cells are extremely important since their positivity indicates that the sample is correctly preserved while weak or lost nuclear staining of normal cells indicates severe preanalytical problems such as over- or underfixation or long hypoxia times that will lead to equivocal interpretation [30–33] (Table 3).

dMMR can be diagnosed as classical two-protein losses (MLH1/PMS2, Figures 1A, B, or MSH2/MSH6 losses), non-classical single or multiple losses in >90% of tumor cells, or as unusual (focal/subclonal or heterogenous losses of >10% of tumor cells in the background of positive stromal cells [10, 15, 34–36] (Table 3; Figures 1C, D). In some previous reports, abnormal IHC staining was divided into three intensity categories: strong, intermediate/equivocal/unusual, and complete loss/negativity. An indeterminate IHC phenotype was found to occur at a low rate of ~3–6% [2, 37, 38], but in one study the incidence was reported to occur at 15% [26]. In case of negativity of the normal stromal cells, the test must be repeated and, if still negative, the case must be considered equivocal, irrespective of the tumor cell nuclear staining [30, 34] (Table 3). It seems that the most challenging situation is when there are differences in the staining intensities of control stromal cells and tumor cells, since in those cases the diagnosis is equivocal but can easily be considered unusual. Although the MMR IHC is considered to be a four-protein detection, in certain analyses five- or six-MMR-protein detections were performed by IHC using anti-MSH3 and anti-MLH3 antibodies [39]. On the other hand, there are several reports which follow a two-antibody staining protocol of using MSH6 and PMS2 as an initial method and determinations of MSH2 and MLH1 are performed only in cases of loss or abnormality [40].

Sequencing of MMR genes

Loss-of-function mutations of MMR genes can be detected by classical Sanger sequencing but is done more frequently by NGS using focus panels which contain all six MMR genes as well as BRAF and EpCAM. The advantage of NGS is that it can detect loss of heterozygosity (LOH) of an MMR gene as well. It can be performed using tumor tissue, but in cases of mutations with high variant allele frequency, germline testing must be done to identify Lynch syndrome patients. However, in cases of

1 www.diagnostics.roche.com

TABLE 3 Four-protein MMR IHC evaluation protocol [**www.nice.org.uk/guidance/dg42**, [**34**]].

Inner control nuclear	Positive	Positive	Positive	Positive	Negative	Negative
tumor nuclear	+>90%	−>90%	Unusual >10%	T+ weaker than IC+	negative	Positive any type
variants	–	A/B/C	A/B/C	A/B/C		
interpretation	pMMR	dMMR	dMMR	equivocal	equivocal	equivocal

A: classical ML1/PMS2 or MSH2/MSH6 double loss, B: single MMR protein loss, C: multiple (>2) MMR protein losses, IC, inner control cells; dMMR, mismatch repair deficient; pMMR, mismatch repair proficient; T, tumor cells; unusual, clonal loss; heterogeneity etc.

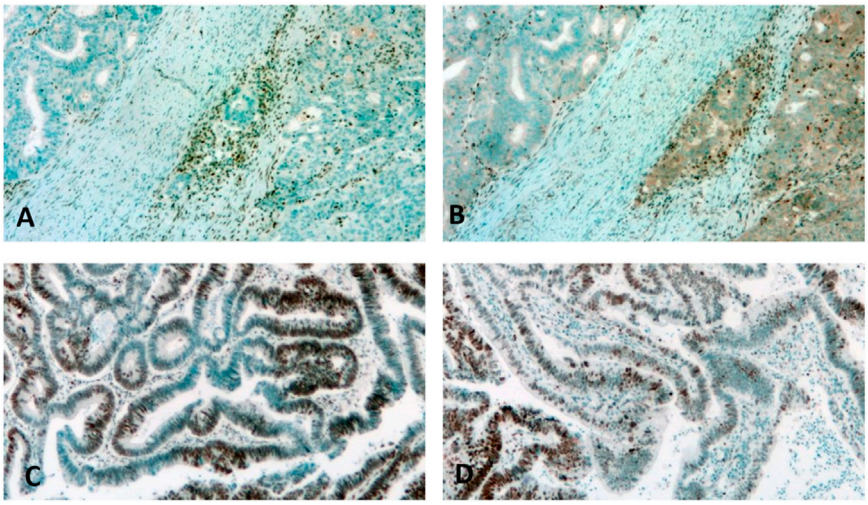

FIGURE 1
Detection of dMMR by immunohistochemistry. **(A,B)**: Classic two-protein loss in colon cancer. Note the intense labeling of stromal cells. **(A)**: MLH1, **(B)**: PMS2. **(C)**: Focal loss of MSH2 in a colon cancer case. Note the intense staining of stromal normal cells adjacent to the negative tumor cells. **(D)**: Heterogenous loss of MSH6 in a rectal cancer case. Note the intense staining of the stromal cells adjacent to the negative tumor cells.

mutations of VUS (variant of uncertain significance) category, further analysis of the functional consequence must be carried out to detect microsatellite instability.

Methylation analysis of MMR gene

In cases of MLH1/PMS2 protein losses in tested cancers, beside the loss-of-function mutation of MLH1, promoter methylation may also be the genetic cause; therefore, a methylation analysis can be performed with in-house PCR protocols or using commercial kits such as SALSA MS-MLPA [41].

Diagnosis of microsatellite instability (MSI)

PCR-based techniques

The gold-standard test for microsatellite instability is fluorescent polymerase chain reaction which detects the instability (variability of length) of the tested microsatellite markers with a technical sensitivity of ~10%. The most frequently used MSI-PCR kits apply five microsatellite markers (Promega Pentaplex). One is the Bethesda panel (Table 4) with three dinucleotides and two mononucleotides designed to test Lynch syndrome [2, 17, 43]. The improved version of this Pentaplex panel uses five mononucleotide markers (Table 4). The tumor cell/normal cell (T/N) ratio is critical for assay performance, since 20% can be used as a cut-off. In case of low T/N ratio, a microdissection can be used to improve it. DNA is isolated from tumor tissue and from normal tissue; an MSS cell line can also be used. After PCR reaction, the fragment length analysis can be performed. According to international recommendations, samples are defined as MSI-high if two or more markers are unstable (≥40%); MSI-indeterminate (MSI-low) is diagnosed if one marker is unstable (20%) [2, 15, 34].

Idylla™ MSI is another PCR test, which is an automated analysis system. It also works from FFPE blocks and there is no need for control tissue. The Idylla™ system uses seven microsatellite loci (Table 4). At least five markers must be

TABLE 4 Microsatellite markers used in MSI diagnostics.

TCGA [11]	TCGA [42]	Bethesda [43]	Pentaplex [43]	Idylla [41]	Easy PGX [44]	MSI-Titano [45]	NGS-10 [46]
DEFB105A/B	ACVR2A	BAT25 (KIT)	BAT25 (KIT)	ACVR2	BAT25	BAT25	KDM6A
ACVR2A	TGFBR2	BAT26 (MSH2)	BAT26 (MSH2)	BTBD7	BAT26	BAT26	SMARCB1
RNF43	RNF43	D5S346	NR21 (SLC7A8)	DIDO1	NR21	BAT40	GRIN2A
DOCK3	RPL22	D2S123	NR24	MRE11	NR22	NR21	FLT1
GTF2IP1	MLL3	D17S250	MONO27 (BIRC3)	RYR3	NR24	NR24	CDK4
ARHGEF12	PRDM2			SEC31A	NR27	D2S123	KTM2A
NOMO1	JAK1			SULF2	MONO27	D17S250	KIF5B
PIP5K1A	APC				CAT25	D5S346	BCL2L11
KIF14						D18S58	MSH6
DDX59						TGFBR2	EML4
		MSI-H cut-off	MSI-H cut-off	MSI-H cut-off	MSI-H cut-off	MSI-H cut-off	MSI-H cut-off
top MS markers	top MS markers	2 (40%)	2 (40%)	2 (28.6%)	2 (25%)	4 (40%)	3 (30%)

MS, microsatellite; MSI-H, microsatellite instability-high.

detectable to be able to evaluate the case and MSI-H is defined if a minimum of two unstable markers (28.6%) are detected [41, 47]. Another assay uses eight microsatellite markers, again a combination of the two Pentaplex systems (EasyPGX) [44]. Another automatic PCR test system is the Titano MSI, which uses 10 microsatellite markers, a kind of combination of the Bethesda and Pentaplex marker systems with similar evaluation criteria for MSI-H (≥40% [45] (Table 4). Last but not least, NGS-based MSI tests have also been developed using the Pentaplex markers or 10 different microsatellite markers (Table 4) and various MSI-H diagnostic algorithms, mostly using 30% as an MSI-H cut-off value [46].

Large gene panel-based MSI determinations

There are several FDA-approved CAP-accredited large gene panel-based NGS tests available to assess MSI. The F1Dx assay is based on 1,880 mononucleotide homopolymers and allelic length variability can be computed, with the assessment performed by principal component analysis using a 30% cut-off value for MSI [48]. The MSK-Impact assay applies 1,581 MS loci to assess variability in length and the sequencing data are analyzed by MSI sensor where the % of unstable loci is provided as a score, with the cut-off for MSI at 20% [37, 49]. The Illumina TruSight Oncology 500 system evaluates 1.24 Mb genome and is based on 130 MS marker sites evaluated by Dragon-MSI, where the cut-off is set at 20% [50]. A similar NGS-based MSI test is also available from Thermo Fisher Scientific: Oncomine Comprehensive Assay Plus-MSI, where 76 microsatellite markers can be tested, including the Bethesda and Pentaplex ones. Sequencing data are analyzed by MSICall software. In this system, a tumor-type specific score was applied with cut-off ranges of 19.7%–32.9% [51]. Furthermore, MSI analyses based on whole genome sequencing (WGS) or whole exome sequencing (WES) are also possible using many different bioinformatic tools, extensively reviewed in [32].

dMMR/MSI as predictive markers for immune checkpoint inhibitors and the Lynch syndrome: recommendations

According to the recommendations of ESMO for MMR/MSI testing as a predictive marker for immunotherapy, IHC is the first test of choice, using four antibodies for MMR proteins (MLH1, PMS2, MSH2, and MSH6). It is important to keep in mind that these proteins form heterodimers and the most trustworthy pattern is when the protein expression is lost in pairs of MLH1/PMS2 or MSH2/MSH6 (called the classical pattern). ESMO recommends PCR testing in case of any doubt in IHC or confirmatory analysis. The Bethesda panel of two mononucleotides (BAT-25 and BAT-26) and three dinucleotides (D5S346, D2S123, and D17S250) and the Pentaplex panel of five mononucleotides (BAT-25, BAT-26, NR-21, NR-24, and MONO-27) can be used to determine MSI status. However, the Pentaplex panel is recommended since it is characterized by higher sensitivity and specificity. In cases of colorectal cancer, IHC and PCR tests are both recommended but for non-Lynch syndrome cancers data are limited for reliability; therefore, NGS-based techniques are recommended [52].

The College of American Pathologists (CAP) separates testing methods by cancer types. In colorectal carcinoma, IHC and PCR are considered equivalent for MSI/dMMR testing. NGS can also be used. For gastroesophageal and small bowel cancers, pathologists can use MSI PCR, MMR IHC, or NGS for diagnosis. In cases of endometrial cancer, MMR IHC test is the first choice. For cancer types other than those mentioned above, MMR proteins should be tested, but the optimal approach has not yet been established. TMB should not be used as a surrogate for DNA MMR defects; MMR IHC or MSI PCR must be performed to determine whether the TMB-high status is secondary to MMR deficiency [34]. The recent ASCO guideline for immunotherapy diagnostics suggested MMR-IHC, MSI-PCR, and NGS for colorectal cancer, MMR-IHC and MSI-PCR for other GI tract cancers, and only MMR-IHC for endometrial cancer. In case of any other type of non-GI tract cancers, no particular test method was recommended when testing for MMR deficiency/MSI [53].

German pathologists also created a guideline for MMR/MSI testing. They emphasized dMMR phenotypes and the importance of their interpretation. Their suggestion is that complete expression of all four proteins is normal, dMMR is the classical dual loss of MMR proteins MLH1/PMS2 and MSH2/MSH6, any other type of MMR losses should be considered abnormal, and it is advised to perform alternative diagnostic tests. If in doubt, it is important to check all preanalytical factors and the test should be repeated or the protocol be adjusted. According to them, MMR protein IHC outperforms MSI-PCR for non-CRC tumors. Supplementary molecular testing should be performed for further clarification of MMR-IHC if it is ambiguous or unusual. MLH1 methylation and mutation testing and NGS should be performed to determine MMR gene mutation status. NGS can be used only if it is validated against PCR or IHC. IHC is superior to PCR in non-colorectal cancer samples because PCR tests are mostly optimized for CRC [54].

The Colorectal Pathway Group (UK) also created a diagnostic approach for MSI/dMMR colorectal cancers. They divided CRC cases into two groups. Group 1 is all colorectal cancer patients aged under 50 years old. Group 2 A) consists of cancers with histologic features suspicious of Lynch syndrome and patients with family history of CRC, group 2 B) is cases with an oncologist's request. The pathway for MMR testing starts with any group 1 tumors or requested referral from a molecular team, where a consultant surgeon or oncologist should be responsible for the patient and a clear referral must be made. A tumor block must be provided, preferably in continuity with normal tissue as well as a separate block of normal tissue, along with sufficient demographic data and the copy of the original histopathologic report. Tumor materials are assessed for loss of MLH1, PMS2, MSH2, and MSH6 proteins. Samples demonstrating MLH1 with or without PMS2 loss by IHC must be sent for genetic analysis for MLH1 promoter methylation, MLH1, and BRAF mutation statuses. The report of MMR-IHC or MSI-PCR must be a clear statement and will be sent for referral to a histopathologic department. Patients with loss of MSH2 and/or MSH6 or with loss of PMS2 alone are at high-risk of Lynch syndrome and should be referred and tested for the appropriate MMR gene mutation[2].

Molecular epidemiology of dMMR and MSI: discrepancies

The incidence of MSI in human cancers can be defined best on the basis of data available from the TCGA where 2×10^7 microsatellite markers can be analyzed genomically. There are several major analyses performed using different bioinformatic tools to define MSI frequency. The common theme of these studies is that all of them used MSI-H defined by multiplex PCR as a reference (Bethesda and/or Pentaplex [11, 42, 48, 55–57]. All these studies found that endometrial cancer has the highest incidence of MSI (three studies: 28.3%–31.4%, one at a significantly higher rate) (Table 5). Gastric cancer is in the second highest (MSI 18%–20%), closely followed by colon cancer (16.6%–19%). In fourth place we find rectal cancer, where the incidence rates are spread from 3% to 9.2%. A large study corrected these figures to 2.7% based on dMMR [58]. In fifth place of the MSI list is ovarian cancer, with a lower frequency of 2%–5%. It is of note that adrenocortical, esophageal, liver, and cervical cancers are also found to have a relatively high incidence of MSI in TCGA (3%–5%). It is equally important that in melanoma, thyroid, and pancreatic cancers MSI is extremely rare [11, 42]. An analysis of a very large patient cohort using the FDA-approved F1Dx MSI test found significantly lower incidences of MSI in cancers of the highest frequencies, where the reference was MSI-PCR or MMR protein IHC [48] (Table 5). Meanwhile, if we compare the MSI frequency in various cancer types to the incidence of the MMR mutations we can see that the mutation rate of MMR genes in endometrial, gastric, colorectal, or ovarian cancers is significantly higher than the incidence of MSI determined by NGS, which is interesting since MMR genes can be turned off not only by mutations but also by methylation, which would result in a higher MSI rate than MMR gene mutation (Table 5). This discrepancy deserves further attention, since it seems that MMR gene mutation does not automatically lead to MSI at genome level.

Two major meta-analyses have been performed on the frequency of MSI (and dMMR) in various cancer types [21,59], Which indicate that, as compared to TCGA analyses, the incidence of MSI-H (as defined by PCR) in the top cancer types are under-reported by a factor of 30%–50%. It is of note that in these analyses the dMMR incidences (detected by IHC)

2 https//mft.nhs.uk.app.uploads2018/09

TABLE 5 Molecular epidemiology of MSI as determined by NGS in TCGA using various bioinformatic tools.

Cancer	Mozaik [11]	Sputnik [42]	Mantis [55]	mSINGS [56]	F1Dx [48]	MMR mutation rate
UCEC	29.5	28.3	31.4	40	16.5	54
COAD	18.5	16.6	19.7	19	4.4	25
STAD	18	21.9	19.1	20	3.4	35
READ	3	9.2	5.7	5		10
OVCAR	2	3.2	1.4	5	0.7	22
reference	multiplex PCR	multiplex PCR	multiplex PCR	multiplex PCR	dMMR/MSI-H	

Data are expressed in % of MSI tumors. MMR genes: MLH1, MSH2, MSH6, PMS2, MSH3, MLH3, and PMS1.
dMMR, mismatch repair deficient; MSI-H, microsatellite instability-high; COAD, colon adenocarcinoma; OVCAR, ovarian carcinoma; STAD, stomach adenocarcinoma; READ, rectal adenocarcinoma; UCEC, uterine endometrial carcinoma.

frequently differ from MSI by a factor of 16%–40%. Another meta-analysis of the incidence of MSI/dMMR was performed in ovarian cancer, where the MSI incidence is low in TCGA [60]. This analysis found that the MSI incidence (determined by PCR) was in the range of that in TCGA (6%) but, disturbingly, the incidence of dMMR was twice as high as that of MSI [60]. These data are suggestive but are not based on the direct comparison of PCR and IHC tests on the same patient population and on the same cancer type.

Direct comparison of various diagnostic techniques

Diagnostics of Lynch syndrome was developed well before the widespread use of MMR/MSI marker testing for therapeutic purposes. It was based on MMR immunohistochemistry followed by functional tests for MSI and, ultimately, sequencing germline MMR genes. This led to the generally accepted perception of MMR IHC as the gold standard of dMMR testing, supported by various pathological guidelines in which molecular techniques for MSI are recommended mainly in so-called equivocal cases. Meanwhile, MSI incidence in various cancers was defined by WGS or WES technologies by analyzing TCGA or other databases where the reference tests were Bethesda or Pentaplex PCRs [11, 42, 48, 55, 56]. Various analyses suggested a 5%–10% error rate of MMR protein IHC and MSI PCR, resulting potentially in 10%–20% discordance rates [13, 32]. Earlier studies demonstrated that a relatively high proportion (~30%) of equivocal dMMR cases are MSI-high by PCR and have Lynch syndrome [2], while 6% of MSI-H cancers retain the expression of MMR proteins studied by IHC [37], suggesting a more complex relation between dMMR and MSI. A large study of colorectal cancers identified a very low discrepancy rate (1.6%) of MMR IHC and MSI PCR where both the MMR test and MSI PCR were not homogenous; it used non-standard approaches and was corrected post-diagnosis [61] (Table 6). In a smaller colorectal cancer cohort, four-protein MMR IHC and Pentaplex MSI PCR results were compared, with a similarly low discrepancy rate (1.2%) [62] (Table 6). A comparative analysis of the four-protein MMR IHC to Bethesda MSI PCR in a large colorectal cancer cohort, however, found low correlation (~0.5) and low sensitivity (81.1%) due to low correlation of MSI-H with dMMR [63]. A recent analysis of the four-protein IHC and the Pentaplex PCR tests, performed on a large series of colorectal cancers, found a high discrepancy rate of ~18%, mostly in case of the non-classical and especially of the unusual immunophenotypes [64] (Table 6).

A large study on gastric cancer reported a very low discrepancy rate of four-protein MMR IHC with Pentaplex PCR [65].

Analysis of a large cohort of endometrial cancers by MMR IHC and a variant of MSI PCR (a combination of Bethesda and Pentaplex panel) found 4.6% discordance, which was higher in MSS-MSI-L cases but was very low for MSI-H [66]. Other studies on endometrial cancer compared various MSI test types to IHC. Interestingly, the sensitivity of PCR, Idylla, or NGS tests was relatively low (58%–75%) [41, 46] (Table 6).

A large NGS-based analysis of tumors associated with Lynch syndrome found that non-colorectal/non-endometrial cancers were characterized in ~30% by MSI-low status (determined by NGS) and were all dMMR by IHC [67]. In other study on non-colorectal cancers, the Pentaplex PCR exhibited a low sensitivity but high specificity using IHC as gold standard [64].

The comparison of Bethesda PCR and Idylla tests to IHC in another pan-cancer non-colorectal cohort found the MSI tests to have high specificities but much lower sensitivities [45] (Table 6).

All these data point to the fact that MMR IHC and MSI PCR-based techniques are not as equal as once thought. Even a relatively high concordance rate is not necessarily sufficient in daily routine diagnostics if the sensitivity or specificity are not high. Potential factors affecting these discordances are technical and preclinical factors (mostly hypoxia time and fixation issues) [31] and the low T/N cell ratios of the tumor sample [32], but it is now evident that there must be other, yet unidentified genetic/biological factors as well behind those differences. One of those

TABLE 6 Comparison of various MSI test types to MMR IHC.

Comparison	N of patients	Discordance (%)	Sensitivity (%)	Specificity (%)	Reference
colorectal cancer					
PCR to IHC4	3,228	1.6	NA	NA	61
Pentaplex to IHC4	593	1.2	NA	NA	62
Bethesda to IHC4	569	8.1	81.1	92.7	63
Pentaplex to IHC4	543	18.0	41.4	98.5	64
PCR8	28	NA	100	100	42
Idylla		NA	100	100	
NGS to IHC4		NA	100	100	
gastric cancer					
PCR7 to IHC4	488	0.8	100	92.9	65
endometrial cancer					
PCR to IHC4	696	4.6	NA	NA	66
PCR8	21	NA	58	100	42
Idylla		NA	67	100	
NGS to IHC4		NA	75	100	
Idylla to IHC4	100	13.3	80.4	100	47
pan-cancer non-colorectal					
Bethesda	185	NA	77.3	94.5	46
Idylla to IHC4		NA	68.2	91.4	
Pentaplex to IHC4	160	23.8	32.0	96.4	64

IHC4, four-protein immunohistochemistry; PCR7, seven MS marker PCR; PCR8, eight MS marker PCR.

factors could well be the genetic differences between Lynch-associated cancers and non-Lynch cancers.

Clinical observations

Immune checkpoint inhibitor trials followed a three-way protocol by design according to predictive biomarkers in case of colorectal cancer. Usually in phase II trials patient selection was based on MSI-H (pembrolizumab: NCT01876511, nivolumab + ipilimumab: NCT03026140, durvalumab: NCT02227667, avelumab: NCT03186326). In the majority of the phase III trials patient selection was extended to dMMR/MSI-H (pembrolizumab: NCT02563002, nivolumab + ipilimumab: NCT04008030) or restricted to dMMR (atezolizumab: NCT02997228). In some trials, MSI-H-based selection was completed with TMB (BAT1306:NCT03638297) or POLE mutation (durvalumab: NCT13435107). However, the registration trials of pembrolizumab and nivolumab in colorectal cancer paved the way for dMMR/MSI-H biomarker pairs, which was followed by the tumor-agnostic indications [3–8]. None of these later trials have separately compared the dMMR and MSI-H biomarkers for therapy efficacy. Later analysis of trial data revealed that dMMR patients can be divided by MSI levels into a broad spectrum (MSIsensor NGS-based MSI analysis) and higher MSI levels were associated with higher response rates while progressing disease patients had significantly lower MSI levels in CRC patients (n = 36) [68]. In a different GI-tract cancer cohort (n = 6) of ICI-treated dMMR patients, survival upon treatment was significantly associated with the level of MSI [68]. In another small cohort of colorectal cancer patients (n = 33) treated with anti-PD-1 antibodies, treatment efficacy (ORR and PFS) was assessed according to the level of MSI determined by the Bethesda panel (patient selection was based on either dMMR or MSI-H). In this analysis no response was detected in MSS and MSI-L tumors and a significantly longer PFS was observed in patients with tumors of MSI≥3/5 marker positivity. It is of note that the three dMMR/MSS cases showed no response to immunotherapy [69]. Actually, this is the only study that suggested that MSI PCR could be a better predictor than MMR IHC.

A retrospective analysis of metastatic colorectal patients treated with immune checkpoint inhibitors evaluated dMMR and MSI-H (as determined by NGS) for efficacy. In this analysis

both dMMR and MSI-H were positive predictors of PFS and OS in addition to TMB-high status. However, when MSI was added to dMMR, the predictive power increased for PFS and OS but dMMR addition to MSI did not influence the predictive power of MSI [70]. In a similar analysis on endometrial cancers, statistical evaluation of the superiority of MSI (as determined by NGS) vs. MMR for immune checkpoint inhibitor efficacy (time to treatment discontinuation, time to next treatment, and OS) was observed, whereas a superiority analysis for MMR vs. MSI was negative [71]. In this study, the concordance of IHC with NGS was found to be 91%, however, in the discordant cases NGS results better predicted therapy efficacy than IHC results.

There are data to support the value of MSI level as a predictor of immune checkpoint inhibitor therapy efficacy. A large cohort of MSI-H colorectal patients treated with ICIs was tested for TMB and a possible association with therapy efficacy. In this large analysis, it was found that MSI-H tumors of high TMB level (>37/Mb) were exclusively responders with longer PFS than the non-responder low-TMB patients [72]. A similar association of better survival and MSI-H and high TMB (>10 m/Mb) was observed in a large cohort of gastroesophageal cancer patients treated with immune checkpoint inhibitors [73]. According to these data, dMMR tumors can be subclassified by the level of MSI. Secondly, publications so far suggest that MSI is a stronger predictor of ICI therapy efficacy than dMMR.

Conclusion

MMR deficiency is one form of the oncogenic alterations of the DNA repair systems. MMR deficiency is the cause of the inheritable Lynch syndrome, which leads to accelerated development of colorectal, endometrial, and other cancer types. On the other hand, MMR deficiency is used nowadays to identify patients eligible for immunotherapies due to the tumor agnostic indications of several immune checkpoint inhibitors. Current clinical guidelines recommend MMR protein IHC or the molecular MSI tests as predictive markers of immunotherapies. Most of the pathological guidelines consider MMR protein IHC as the gold standard test to identify cancers with MMR deficiency and recommend molecular MSI tests only in special circumstances and to screen for Lynch syndrome. However, there are data in the literature which suggest that the two test types may not be equal. Molecular epidemiology studies reported different rates of dMMR and MSI in various cancer types. In addition, direct comparisons of the two tests revealed relatively frequent discrepancies between MMR IHC and MSI tests, especially in non-colorectal and non-endometrial cancers and in cases with the unusual dMMR phenotype. Further, there are scattered clinical data showing that the clinical efficacy of immune checkpoint inhibitors is different if the patient selection was based on dMMR versus MSI status of the cancers. All these observations question the current dogma that dMMR phenotype and genetic MSI status are equal predictive markers of immunotherapies. It is time to consider international efforts to answer these questions and correct clinical and/or pathological guidelines if necessary.

Author contributions

MN: concept, writing. GL: reviewing. JK: reviewing and writing. AK: reviewing. JT: concept, writing, finalization. All authors contributed to the article and approved the submitted version.

Funding

The author(s) declare that no financial support was received for the research, authorship, and/or publication of this article.

Conflict of interest

The authors declare that the research was conducted in the absence of any commercial or financial relationships that could be construed as a potential conflict of interest.

References

1. Sepulveda AR, Hamilton SR, Allegra CJ, Grody W, Cushman-Vokoun AM, Funkhouser WK, et al. Molecular biomarkers for the evaluation of colorectal cancer: guideline from the American society for clinical pathology, College of American pathologists, association for molecular pathology, and the American society of clinical oncology. *J Clin Oncol* (2017) 35:1453–86. doi:10.1200/JCO.2016.71.9807

2. Sarode VR, Robinson L. Screening for Lynch syndrome by immunohistochemistry of mismatch repair proteins: significance of indeterminate result and correlation with mutational studies. *Arch Pathol Lab Med* (2019) 143:1225–33. doi:10.5858/arpa.2018-0201-OA

3. Le DT, Uram JN, Wang H, Barlett BR, Kemberling H, Eyring AD, et al. PD-1 blockade in tumors with mismatch-repair deficiency. *N Engl J Med* (2015) 372: 2509–20. doi:10.1056/NEJMoa1500596

4. Marabelle A, Le DT, Ascierto PA, Di Giacomo AM, De Jesus-Acosta AD, Delord JP, et al. Efficacy of pembrolizumab in patients with noncolorectal high microsatellite instability/mismatch repair-deficient cancer: results from the phase II KEYNOTE-158 study. *J Clin Oncol* (2019) 38:1–10. doi:10.1200/JCO.19.02105

5. Le DT, Kim WT, Van Cutsem E, Geva R, Jäger D, Hara H, et al. Phase-II open label study of pembrolizumab in treatment refractory, microsatellite instability-high/mismatch repair deficient metastatic colorectal cancer. KEYNOTE-164. *J Clin Oncol* (2020) 38:11–9. doi:10.1200/JCO.19.02107

6. Overman MJ, McDermott R, Leach JL, Lonardi S, Lenz H-J, Morse M. A., et al. Nivolumab in patients with metastatic DNA mismatch repair deficient/ microsatellite instability-high colorectal cancer (CheckMate 142). *Lancet Oncol* (2017) 18:1182–91. doi:10.1016/S1470-2045(17)30422-9

7. Lenz H-J, van Cutsem E, Limon M, Wong KYM, Hendlis A, Aglietta M, et al. First-line nivolumab plus low-dose ipilimumab for microsatellite instability-high/ mismatch repair-deficient metastatic colorectal cancer: the phase II Checkmate 142 study. *J Clin Oncol* (2021) 40:161–70. doi:10.1200/JCO.21.01015

8. Palmeri M, Mehnert J, Silk AW, Jabbour SK, Ganesan S, Popli P, et al. Real-world application of tumor mutational burden-high (TMB-high) and microsatellite instability (MSI) confirms their utility as immunotherapy biomarkers. *ESMO Open* (2022) 7:100336. doi:10.1016/j.esmoop.2021.100336

9. Hopkins JL, Lan L, Zou L. DNA repair defects in cancer and therapeutic opportunities. *Genes Dev* (2022) 36:278–93. doi:10.1101/gad.349431.122

10. Bellizzi AM, Frankel WL. Colorectal cancer due to deficiency in DNA mismatch repair function: a review. *Adv Anat Pathol* (2009) 16:405–17. doi:10.1097/PAP.0b013e3181bb6bdc

11. Hause RJ, Pritchard CC, Shendure J, Salipante SJ. Classification and characterization of microsatellite instability across 18 cancer types. *Nat Med* (2016) 22:1342–50. doi:10.1038/nm.4191

12. Loewer SS, McGurk MP, Clark AG, Barbash DA. Satellite DNA evolution: old ideas, new approaches. *Curr Opin Genet Dev* (2018) 49:70–8. doi:10.1016/j.gde.2018.03.003

13. Evrard C, Tachon G, Randrian V, Karayan-Tapon L, Tougeron D. Microsatellite instability: diagnosis, heterogeneity, discordance and clinical impact in colorectal cancer. *Cancers* (2019) 11:1567. doi:10.3390/cancers11101567

14. Campbell BB, light N, Fabrizio D, Zatzman M, Fuligni F, de Borja R, et al. Comprehensive analysis of hypermutation in human cancer. *Cell* (2017) 171:1042–56. doi:10.1016/j.cell.2017.09.048

15. Chen W, Swanson BJ, Frankel WL. Molecular genetics of microsatellite-unstable colorectal cancer for pathologists. *Diagn Pathol* (2017) 12:24. doi:10.1186/s13000-017-0613-8

16. Modrich P, Lahue R. Mismatch repair in replication fidelity, genetic recombination and cancer biology. *Ann Rev Biochem* (1996) 65:101–33. doi:10.1146/annurev.bi.65.070196.000533

17. Abildgaard AB, Nielsen SV, Bernstein I, Stein A, Lindorff-Larsen K, Hartmann-Petersen R. Lynch syndrome, molecular mechanisms and variant classification. *Br J Cancer* (2022) 128:726–34. doi:10.1038/s41416-022-02059-z

18. Peltomaki P. Update on Lynch syndrome genomics. *Fam Cancer* (2016) 15:385–93. doi:10.1007/s10689-016-9882-8

19. Li K, Luo H, Huang L, Luo H, Zhu X. Microsatellite instability: a review of what the oncologist should know. *Cancer Cel Int* (2020) 20:16. doi:10.1186/s12935-019-1091-8

20. Gutierrez C, Ogino S, Meyerhardt JA, Iorgulescu B. The prevalence and prognosis of microsatellite instability-high/mismatch repair deficient colorectal adenocarcinomas in the United States. *JCO Precis Oncol* (2023) 7:e2200179. doi:10.1200/PO.22.00179

21. Lorenzi M, Amonkar M, Zhang J, Mehta S, Liaw K-L. Epidemiology of microsatellite instability high (MSI-H) and deficient mismatch repair (dMMR) in solid tumors: a structured literature review. *J Oncol* (2020) 2020:1–17. doi:10.1155/2020/1807929

22. Evrard C, Messina S, Sefrioui D, Frouin E, Auriault M-L, Chautard R, et al. Heterogeneity of mismatch repair status and microsatellite instability between primary tumour and metastasis and its implications for immunotherapy in colorectal cancers. *Int J Mol Sci* (2022) 23:4427. doi:10.3390/ijms23084427

23. Bonneville R, Paruchuri A, Wing MR, Krook MA, Reeser JW, Chen HZ, et al. Characterization of clonal evolution in microsatellite unstable metastatic cancers through multiregional tumor sequencing. *Mol Cancer Res* (2021) 19:465–74. doi:10.1158/1541-7786.MCR-19-0955

24. Toieb J, Shi O, Pederson L, Alberts S, Wolmark N, Van Cutsem E, de Gramont A, et al. Prognosis of microsatellite instability and/or mismatch repair deficiency stage III colon cancer patients after disease recurrence following adjuvant treatments: results of an ACCENT pooled analysis of seven studies. *Ann Oncol* (2019) 30:1466–71. doi:10.1093/annonc/mdz208

25. Cohen SA, Pritchard CC, Jarvik GP. Lynch syndrome: from screening to diagnosis to treatment in the era of modern molecular oncology. *Ann Rev Genomics Hum Genet* (2019) 20:293–307. doi:10.1146/annurev-genom-083118-015406

26. Jaffrelot M, Fares N, Brunac AC, Laurenty AP, Danjoux M, Grand D, et al. An unusual phenotype occurs in 15% of mismatch repair-deficient tumors and is associated with non-colorectal cancers and genetic syndromes. *Mod Pathol* (2022) 35:427–37. doi:10.1038/s41379-021-00918-3

27. Cerretelli G, Ager A, Arends MJ, Frayling IM. Molecular pathology of Lynch syndrome. *J Pathol* (2020) 250:518–31. doi:10.1002/path.5422

28. Williams MH, Hadjinicolaou AV, Norton BC, Kader R, Lovat LB. Lynch syndrome: from detection to treatment. *Front Oncol* (2023) 13:1166238. doi:10.3389/fonc.2023.1166238

29. Yoshida H, Takigawa W, Kobayashi-Kato M, Nishikawa T, Shiraishi K, Ishikawa M. Mismatch repair protein expression in endometrial cancer: assessing concordance and unveiling pitfalls in two different immunohistochemistry assays. *J Pers Med* (2023) 13:1260. doi:10.3390/jpm13081260

30. Sari A, Pollett A, Eriksson LR, Lumsden-Johanson B, van de Laar E, Kazerouni H, et al. Interobserver agreement for mismatch repair protein immunohistochemistry in endometrial and nonserous, nonmucinous ovarian carcinomas. *Am J Surg Path* (2019) 43:591–600. doi:10.1097/PAS.0000000000001220

31. Malapelle U, Parente P, Pepe F, de Luca C, Cerino P, Covelli C, et al. Impact of pre-analytical factors on MSI test accuracy in mucinous colorectal adenocarcinoma: a multi-assay concordance study. *Cells* (2020) 9:9092019. doi:10.3390/cells9092019

32. Wang C, Zhang L, Vakiani E, Shia J. Detecting mismatch repair deficiency in solid neoplasms: immunohistochemistry, microsatellite instability or both? *Mod Pathol* (2022) 35:1515–28. doi:10.1038/s41379-022-01109-4

33. Reidinger CJ, Esnakula A, Haight PJ, Suarez AA, Chen W, Gillespie J, et al. Characterization of mismatch-repair (MMR)/microsatellite instability (MSI)-discordant endometrial cancers. *Cancer* (2023) 2023:35030. doi:10.1002/cncr.35030

34. Bartley AN, Mills AM, Konnick E, Overman M, Ventura CB, Souter L, et al. Mismatch repair and microsatellite instability testing for immune checkpoint inhibitor therapy: guideline from the College of American pathologists in collaboration with the association for molecular pathology and fight colorectal cancer. *Arch Pathol Lab Med* (2022) 146:1194–210. doi:10.5858/arpa.2021-0632-CP

35. McCarthy AJ, Capo-Chichi J-M, Spence T, Grenier S, Stockley T, Kamel-Reid S, et al. Heterogenous loss of mismatch repair (MMR) protein expression: a challenge for immunohistochemical interpretation and microsatellite instability (MSI) evaluation. *J Pathol Clin Res* (2019) 5:115–29. doi:10.1002/cjp2.120

36. Amato M, Franco R, Facchini G, Addeo R, Ciardiello F, Berretta M, et al. Microsatellite instability: from the implementation of the detection to a prognostic and predictive role in cancers. *Int J Mol Sci* (2022) 23:8726. doi:10.3390/ijms23158726

37. Hechtman JF, Rana S, Middha S, Stadler Z, Latham A, Benayed R, et al. Retained mismatch repair protein expression occurs in approximately 6% of microsatellite instability-high cancers and is associated with missense mutations in mismatch repair genes. *Mod Pathol* (2020) 33:871–9. doi:10.1038/s41379-019-0414-6

38. Watkins JC, Nucci MR, Ritterhause LL, Howitz BE, Sholl LM. Unusual mismatch repair immunohistochemical patterns in endometrial carcinoma. *Am J Surg Pathol* (2016) 40:909–16. doi:10.1097/PAS.0000000000000663

39. Quaas A, Rehkaemper J, Rueschoff J, Pamuk A, Zander T, Hillmer A, et al. Occurrence of high microsatellite-instability/mismatch repair deficiency in nearly 2,000 human adenocarcinomas of the gastrointestinal tract, pancreas, and bile ducts: a study from a large German comprehensive cancer center. *Front Oncol* (2021) 11:569–475. doi:10.3389/fonc.2021.569475

40. Aiyer KTS, Doeleman T, Ryan NA, Nielsen M, Crosbie EJ, Smit VTHBM, et al. Validity of a two-antibody resting algorithm for mismatch repair deficiency testing in cancer: a systematic literature review and meta-analysis. *Mod Pathol* (2022) 35:1775–83. doi:10.1038/s41379-022-01149-w

41. Dedeurwaerdere F, Claes KBM, Van Dorpe J, Rottiers I, Van der Meulen J, Breyne J, et al. Comparison of microsatellite instability detection by immunohistochemistry and molecular techniques in colorectal and endometrial cancer. *Sci Rep* (2021) 11:12880. doi:10.1038/s41598-021-91974-x

42. Cortez-Ciriano I, Lee S, Park W-Y, Kim T-M, Park PJ. A molecular portrait of microsatellite instability across multiple cancers. *Nat Commun* (2017) 8:15180. doi:10.1038/ncomms15180

43. Murphy KM, Zhang S, Geiger T, Hafez MJ, Bacher J, Berg KD, et al. Comparison of the microsatellite instability analysis system and the Bethesda panel for determination of microsatellite instability in colorectal cancers. *J Mol Diagn* (2006) 8:305–11. doi:10.2353/jmoldx.2006.050092

44. Libera L, Sahnane N, Pepe F, Pisapia P, De Luca C, Russo G, et al. Critical aspects of microsatellite instability testing in endometrial cancer: a comparison study. *Hum Pathol* (2022) 128:134–40. doi:10.1016/j.humpath.2022.07.014

45. Malapelle U, Parente P, Pepe P, Pepe F, De Luca C, Sgariglia R, et al. Evaluation of microsatellite instability and mismatch repair status in different solid tumors: a multicenter analysis in a real world setting. *Cells* (2021) 10:1878. doi:10.3390/cells10081878

46. Siemanowski J, Schöming-Markiefka B, Buhl T, Haak A, Siebolts U, Dietmaier W, et al. Managing difficulties of microsatellite instability testing in endometrial cancer. Limitations and advantages of four different PCR-based approaches. *Cancers* (2021) 13:1268. doi:10.3390/cancers13061268

47. Zwaenepoel K, Holmgaard Duelund J, de Winne K, Maes V, Weyn C, Lambin S, et al. Clinical performance of the Idylla MSI test for a rapid assessment of the DNA microsatellite status in human colorectal cancer. *J Mol Diagn* (2020) 22:386–95. doi:10.1016/j.jmoldx.2019.12.002

48. Trabucco SE, Gowen K, Maund SL, Sanford E, Fabrizio DA, Hall MJ, et al. A novel next generation sequencing approach to detecting microsatellite instability and pan-tumor characterization of 1000 microsatellite instability-high cases in

67,000 patient samples. *J Mol Diagn* (2019) 21:1053–66. doi:10.1016/j.jmoldx.2019.06.011

49. Middha S, Zhang L, Nafa K, Jayakumaran G, Wong D, Kim HR, et al. Reliable pan-cancer microsatellite instability assessment by using targeted next generation sequencing data. *JCO Precis Oncol* (2017) 2017:1–17. doi:10.1200/PO.17.00084

50. VanderWalde A, Spetzler D, Xiao N, Gatalica Z, Marshall J. Microsatellite instability status determined by next generation sequencing and compared with PD-L1 and tumor mutational burden in 11,348 patients. *Cancer Med* (2018) 7:746–56. doi:10.1002/cam4.1372

51. Bartels S, Grote I, Wagner M, Boog J, Schipper E, Reineke-Plaass T, et al. Concordance in detection of microsatellite instability by PCR and NGS in routinely processed tumor specimens of several cancer types. *Cancer Med* (2023) 12:16707–15. doi:10.1002/cam4.6293

52. Luchini C, Bibeau F, Ligtenberg MJL, Singh N, Nottegar A, Bosse T, et al. ESMO recommendations on microsatellite instability testing for immunotherapy in cancer and its relationship with PD-1/PD-L1 expression and tumor mutational burden. *Ann Oncol* (2019) 30:1232–43. doi:10.1093/annonc/mdz116

53. Vikas P, Messersmith H, Compton C, Sholl L, Bradduss RR, Davis A, et al. Mismatch repair and microsatellite instability testing for immune checkpoint inhibitor therapy. ASCO endorsement of College of American Pathologists guideline. *J Clin Oncol* (2023) 41:1943–8. doi:10.1200/JCO.22.02462

54. Rüschoff J, Schildhaus H-U, Rüschoff JH, Jöhrens K, Edmonston TB, Dietmaier W, et al. Testing for deficient mismatch repair and microsatellite instability: A focused update. *Die Pathologie* (2023) 44:61–70. doi:10.1007/s00292-023-01208-2

55. Bonneville R, Krook MA, Kautto EA, Miya J, Wing MR, Chen HZ, et al. Landscape of microsatellite instability across 39 cancer types. *JCO Precis Oncol* (2017) 1:1–15. doi:10.1200/PO.17.00073

56. Long DR, Waalkes A, Panicker VP, Hause RJ, Salipante SJ. Identifying optimal loci for the molecular diagnosis of microsatellite instability. *Clin Chem* (2020) 66:1310–8. doi:10.1093/clinchem/hvaa177

57. Salipante SJ, Scroggins SM, Hampel HL, Turner EH, Pritchard CC. Microsatellite instability testing in endometrial cancer. Limitations and advantages of four different PCR based approaches. *Clin Chem* (2014) 60:1192–9. doi:10.1373/clinchem.2014.223677

58. Papke D, Yurgelun MB, Noffsinger AE, Redston M, Genta RM. Prevalence of mismatch repair deficiency in rectal adenocarcinomas. *N Engl J Med* (2022) 387:1714–6. doi:10.1056/NEJMc2210175

59. Kang Y-J, O'Hare S, Franchini F, Uzerman M, Zalcberg J, Macrae F, et al. A scoping review and meta-analysis on the prevalence of pan-tumour biomarkers (dMMR, MSI, high TMB) in different solid tumours. *Sci Rep* (2022) 12:20495. doi:10.1038/s41598-022-23319-1

60. Mitric C, Salman L, Abrahamyan L, Kim SR, Pechlivanoglou P, Chan KKW, et al. Mismatch repair deficiency, microsatellite instability and Lynch syndrome in ovarian cancer: a systematic review and meta-analysis. *Gynecol Oncol* (2023) 170:133–42. doi:10.1016/j.ygyno.2022.12.008

61. De Salins AGD, Tachon G, Cohen R, Karayan-Tapon L, Junca A, Frouin E, et al. Discordance between immunohistochemistry of mismatch repair proteins and molecular testing of microsatellite instability in colorectal cancer. *ESMO Open* (2021) 3:100120. doi:10.1016/jesmoop.2021.100120

62. Loughrey MB, McGrath J, Coleman HG, Bankhead P, Maxwell P, McGready C, et al. Identifying mismatch repair-deficient colon cancer: near-perfect concordance between immunohistochemistry and microsatellite instability testing in a large, population-based series. *Histopathology* (2021) 78:401–13. doi:10.1111/his.14233

63. Chen M-L, Chen J-Y, Hu J, Chen Q, Liu B-R, Qian X-P, et al. Comparison of microsatellite status detection methods in colorectal carcinoma. *Int J Exp Pathol* (2018) 11:1431–8.

64. Nádorvári ML, Kenessey I, Kiss A, Barbai T, Kulka J, Rásó E, et al. Comparison of standard mismatch repair deficiency and microsatellite instability tests in a large cancer series. *J Transl Med* (2024) 22:150. doi:10.1186/s12967-024-04960-y

65. Yamamoto G, Ito T, Suzuki O, Kamae N, Kakuta M, Takahashi A, et al. Concordance between microsatellite instability testing and immunohistochemistry for mismatch repair proteins and efficient screening of mismatch repair deficient gastric cancer. *Oncol Lett* (2023) 26:494. doi:10.3892/ol.2023.14081

66. Stelloo E, Jansen AML, Osse EM, nout RA, Creutzberg CL, Ruano D, et al. Practical guidance for mismatch repair-deficiency testing in endometrial cancer. *Ann Oncol* (2017) 28:96–102. doi:10.1093/annonc/mdw542

67. Latham A, Srinivasan P, Kemel Y, Shia J, Bandlamudi C, Mandelker D, et al. Microsatellite instability is associated with the presence of Lynch syndrome pan-cancer. *J Clin Oncol* (2018) 37:286–95. doi:10.1200/JCO.18.00283

68. Mandal R, Samstein RM, Lee K-W, Havel JJ, Wang H, Krishna C, et al. Genetic diversity of tumors with mismatch repair deficiency influences anti-PD1 immunotherapy response. *Science* (2019) 364:485–91. doi:10.1126/science.aau0447

69. Wang Q-X, Qu C-H, Gao Y-H, Ding P-R, Yun J-P, Xie D, et al. The degree of microsatellite instability predicts response to PD-1 blockade immunotherapy in mismatch repair deficient/microsatellite instability-high colorectal cancers. *Exp Hematol Oncol* (2021) 10:2. doi:10.1186/s40164-020-00193-z

70. Quintanilha JCF, Graf RP, Fisher VA, Oxnard GR, Ellis H, Panarelli N, et al. Comparative effectiveness of immune checkpoint inhibitors vs chemotherapy in patients with metastatic colorectal cancer with measures of microsatellite instability, mismatch repair or tumor mutational burden. *JAMA Netw Open* (2023) 6:e2252244. doi:10.1001/jamanetworkopen.2022.52244

71. Hill BL, Graf RP, Shah K, Danziger N, Lin D, Quintanilha J, et al. Mismatch repair deficiency, next generation sequencing-based microsatellite instability and tumor mutational burden as predictive biomarkers for immune checkpoint inhibitor effectiveness in frontline treatment of advanced stage endometrial cancer. *Int J Gynecol Cancer* (2023) 33:504–13. doi:10.1136/ijgc-2022-004026

72. Schrock AB, Ouyang C, Sandhu J, Sokol E, Jin D, Ross JS, et al. Tumor mutational burden is predictive of response to immune checkpoint inhibitors in MSI-high metastatic colorectal cancer. *Ann Oncol* (2019) 30:1096–103. doi:10.1093/annonc/mdz134

73. Graf RP, Fisher V, Creeden J, Schrock AB, Ross JS, Nimeiri H, et al. Real-world validation of TMB and microsatellite instability as predictive biomarkers of immune checkpoint inhibitor effectiveness in advanced gastroesophageal cancer. *Cancer Res Commun* (2022) 2:1037–48. doi:10.1158/2767-9764.CRC-22-0161

Pathology & Oncology Research | frontiers

TYPE Original Research
PUBLISHED 26 August 2024
DOI 10.3389/pore.2024.1611809

Check for updates

OPEN ACCESS

EDITED BY
Anna Sebestyén,
Semmelweis University, Hungary

*CORRESPONDENCE
Uğur Çakır,
cakir.ugur@semmelweis.hu

RECEIVED 28 April 2024
ACCEPTED 14 August 2024
PUBLISHED 26 August 2024

CITATION
Çakır U, Balogh P, Ferenczik A, Brodszky V, Krenács T, Kárpáti S, Sárdy M, Holló P and Fábián M (2024) G protein-coupled estrogen receptor 1 and collagen XVII endodomain expression in human cutaneous melanomas: can they serve as prognostic factors?
Pathol. Oncol. Res. 30:1611809.
doi: 10.3389/pore.2024.1611809

COPYRIGHT
© 2024 Çakır, Balogh, Ferenczik, Brodszky, Krenács, Kárpáti, Sárdy, Holló and Fábián. This is an open-access article distributed under the terms of the Creative Commons Attribution License (CC BY). The use, distribution or reproduction in other forums is permitted, provided the original author(s) and the copyright owner(s) are credited and that the original publication in this journal is cited, in accordance with accepted academic practice. No use, distribution or reproduction is permitted which does not comply with these terms.

G protein-coupled estrogen receptor 1 and collagen XVII endodomain expression in human cutaneous melanomas: can they serve as prognostic factors?

Uğur Çakır[1]*, Petra Balogh[2], Anikó Ferenczik[3,4], Valentin Brodszky[4], Tibor Krenács[5], Sarolta Kárpáti[1], Miklós Sárdy[1], Péter Holló[1] and Melinda Fábián[1]

[1]Department of Dermatology, Venereology and Dermatooncology, Semmelweis University, Budapest, Hungary, [2]Queen Elizabeth Hospital, Cellular Pathology Department, University Hospitals Birmingham, Birmingham, United Kingdom, [3]Doctoral School of Economics, Business and Informatics, Corvinus University of Budapest, Budapest, Hungary, [4]Department of Health Policy, Institute of Social and Political Sciences, Corvinus University of Budapest, Budapest, Hungary, [5]1st Department of Pathology and Experimental Cancer Research, Semmelweis University, Budapest, Hungary

Melanoma incidence is increasing globally. Although novel therapies have improved the survival of primary melanoma patients over the past decade, the overall survival rate for metastatic melanoma remains low. In addition to traditional prognostic factors such as Breslow thickness, ulceration, and mitotic rate, novel genetic and molecular markers have been investigated. In our study, we analyzed the expression of G-protein coupled estrogen receptor 1 (GPER1) and the endodomain of collagen XVII (COL17) in relation to clinicopathological factors in primary cutaneous melanomas with known lymph node status in both sexes, using immunohistochemistry. We found, that GPER1 expression correlated with favorable clinicopathological factors, including lower Breslow thickness, lower mitotic rate and absence of ulceration. In contrast, COL17 expression was associated with poor prognostic features, such as higher tumor thickness, higher mitotic rate, presence of ulceration and presence of regression. Melanomas positive for both GPER1 and COL17 had significantly lower mean Breslow thickness and mitotic rate compared to cases positive for COL17 only. Our data indicate that GPER1 and COL17 proteins may be of potential prognostic value in primary cutaneous melanomas.

KEYWORDS

estrogen receptor, collagen xvii, prognostic factors, immunohistochemistry, prognosis

Introduction

Melanoma is a life-threatening type of cancer that has shown a rising incidence worldwide over the past few decades [1, 2]. Major histopathological features predicting the prognosis of melanoma include Breslow thickness, ulceration, and mitotic rate [3]. In addition, age, gender, anatomical site, Clark level, lymphovascular and perineural invasion, regression, and tumor-infiltrating lymphocytes are important prognostic indicators and predictors of survival [3].

It has been observed that women exhibit a somewhat lower incidence and mortality rate of cutaneous melanoma, suggesting the role of sex hormones in tumorigenesis [4–6]. Consequently, estrogen receptors have been extensively investigated over the past decades in various malignancies, including melanoma [7–22]. Estrogen signaling and its effects are mediated through distinct receptor subtypes: ERα and ERβ, which are considered the classical estrogen receptors and function as ligand-activated transcription factors [23, 24]. Immunohistochemical and molecular studies have suggested that the downregulation of ERβ may serve as an indicator of metastatic potential in melanoma [25, 26]. Besides the classical estrogen receptors, estrogen signaling can also be mediated through the seven-transmembrane receptor, G-protein coupled estrogen receptor 1 (GPER1), which is expressed in various tissues under physiological conditions, including the nervous, reproductive, musculoskeletal systems, and gastrointestinal tract [27–30]. In tumor biology, GPER1 has been shown to facilitate cancer progression and migration, serving as a poor prognostic factor in ER-negative and human epidermal growth factor receptor 2 (HER2)-overexpressed breast and lung cancer cell lines [12–14, 19, 31, 32]. Conversely, it has also been associated with better overall survival in ER-positive and HER2-negative breast cancer [20, 32]. Furthermore, GPER1 has been reported to inhibit tumor proliferation in colorectal, prostate, and adrenocortical carcinomas, and GPER agonists have demonstrated growth inhibition in ovarian cancer [15–18, 22]. In the skin, GPER1 protein is thought to be essential for estrogen-mediated melanogenesis and is linked to hyperpigmentation during pregnancy through activation of the cAMP/pCREB/MITF signaling pathway, leading to melasma formation [33–35]. GPER1 activation inhibits melanoma proliferation in both human and murine melanoma cell lines and induces c-Myc depletion, which is associated with reduced PD-L1 expression, potentially enhancing the response to immune checkpoint inhibitor therapies [36, 37]. GPER1 knockdown has been shown to negate the effects of G-1 and tamoxifen, indicating a GPER1-dependent pathway and suggesting that GPER1 activation exerts anti-proliferative effects in melanoma [30].

In contrast to GPER1, which is associated with better outcome and mortality rates of cutaneous melanoma in women [4, 6], collagen XVII (COL17) appears to be implicated in skin cancer development [38, 39]. COL17 is a transmembrane glycoprotein of the hemidesmosome [40]. The intracellular domain of COL17 interacts with the intermediate filament network, while its extracellular domain anchors into the basement membrane zone, engaging with extracellular matrix proteins [41]. Beyond its structural role in the hemidesmosome complex, overexpression of COL17 is presumed to play a role in cancer development, tumor invasion, and decreased survival rates in squamous cell carcinoma, as well as colorectal, lung and pancreatic cancer [39, 42–47]. Contrarily, in human breast cancer, COL17 expression has been found to be decreased [48]. Krenács et al. showed that the cell-residual 60 kDa endodomain of COL17 (but not the shedding ectodomain) can be detected in primary and metastatic human melanoma as well as melanoma cell lines, but not in resting melanocytes and nevi [49].

As stated above, the existing literature has reported on the expression of GPER1 and COL17 in various tumors, including melanoma, using immunohistochemistry and mRNA levels, yet without specific emphasis on lymph node metastatic status. In our retrospective study, we aimed to investigate the expression of GPER1 and the cell-residual endodomain of COL17 proteins in primary melanoma samples with known lymph node status in relation to the major clinicopathological factors.

Materials and methods

Study population

Ethics approval was obtained from the Semmelweis University Institutional Review Board (32-4/2007). The database of the Department of Dermatology, Venereology and Dermatooncology of Semmelweis University was reviewed for melanoma patients who were diagnosed between 1st of January 2000, and 31st of December 2010, and completed a 10-year follow-up period. The total number of patients (n = 94) had an equal distribution of males (n = 47) and females (n = 47, respectively). The female patients were further subcategorized as premenopausal (<45 years old) and postmenopausal (≥45 years old) [50]. The registered clinicopathological characteristics are listed in Table 1. All examined melanoma samples were grouped according to the Breslow thickness categories reported in the 2018 American Joint Committee on Cancer (AJCC) melanoma staging system [51].

Immunohistochemistry

The protein expressions of GPER1 and COL17 were evaluated in archived, formalin-fixed, paraffin-embedded melanoma tissue samples from primary melanomas of the 94 patients. Three μm thick sections were cut, dewaxed in xylene and rehydrated in decreasing concentrations of

TABLE 1 Clinicopathological characteristics of the study population.

	Female	Male	Total
Total number of patients	47	47	94
Premenopausal	19 (40.42%)		
Postmenopausal	28 (59.58%)		
Anatomical site			
Trunk	16 (34.04%)	37 (78.72%)	53 (56.38%)
Upper extremities	7 (14.89%)	6 (12.77%)	13 (12.83%)
Lower extremities	24 (51.07%)	4 (8.51%)	28 (29.79%)
Melanoma subtype			
SSM	42 (89.36%)	41 (87.23%)	83 (88.30%)
NM	1 (2.13%)	4 (8.51%)	5 (5.32%)
LMM	1 (2.13%)	0 (0%)	1 (1.06%)
Unclassifiable	3 (6.38%)	2 (4.26%)	5 (5.32%)
Breslow thickness[a]			
≤1 mm	15 (31.91%)	18 (38.30%)	33 (35.11%)
>1, ≤2 mm	14 (29.79%)	8 (17.02%)	22 (23.40%)
>2, ≤4 mm	10 (21.28%)	10 (21.28%)	20 (21.28%)
>4 mm	8 (17.02%)	11 (23.40%)	19 (20.21%)
Mean mitotic rate/HPF	7.239 (±6.647)	6.851 (±6.438)	7.045 (±6.543)
Ulceration			
Present	14 (29.79%)	15 (31.91%)	29 (30.85%)
Absent	31 (65.96%)	29 (61.70%)	60 (63.83%)
No information	2 (4.25%)	3 (6.39%)	5 (5.32%)
Regression			
Present	11 (23.4%)	13 (27.66%)	19 (20.21%)
Absent	36 (76.60%)	34 (72.34%)	70 (74.47%)
Peritumoral lymphocytic infiltrate			
Present	28 (59.57%)	31 (65.96%)	59 (62.77%)
Absent	19 (40.43%)	15 (31.91%)	34 (36.17%)
No information	0 (0%)	1 (2.13%)	1 (1.06%)
***De-novo* melanoma**	40 (85.10%)	41 (87.23%)	81 (86.17%)
Nevus-associated melanoma	7 (14.89%)	6 (12.77%)	13 (13.83%)
Sentinel lymph node			
Positive	13 (27.66%)	13 (27.66%)	26 (27.66%)
Negative	34 (72.34%)	32 (68.09%)	66 (70.21%)
No information	0 (0%)	2[b] (4.25%)	2[b] (2.13%)
Distant lymph node metastasis			
Positive	4 (8.51%)	2 (4.26%)	6 (6.38%)
Negative	43 (91.49%)	45 (95.74%)	88 (93.62%)
Distant visceral/cutaneous metastasis (during the 10-year follow-up period)			
Detected	9 (19.15%)	4 (8.51%)	13 (13.83%)
Not detected	38 (80.85%)	43 (91.49%)	81 (86.17%)
5-year survival	45 (95.74%)	45 (95.74%)	90 (95.74%)

(Continued on following page)

TABLE 1 (*Continued*) Clinicopathological characteristics of the study population.

	Female	Male	Total
10-year survival	41 (87.23%)	44 (93.62%)	85 (90.43%)
Mean follow-up time (months)	139.545 (±33.879)	139.313 (±30.33)	139.429 (±32.105)

HPF, high-power field; LMM, lentigo maligna melanoma; NM, nodular melanoma; PLI, peritumoral lymphocytic infiltrate; SLNB, sentinel lymph node biopsy; SSM, superficial spreading melanoma.

[a]Breslow thickness was categorized according to the 2018 American Joint Committee on Cancer (AJCC) melanoma staging system for all patients.

[b]Instead of sentınel lymph node biopsy a block dissection was performed.

ethanol. Heat-induced epitope retrieval was done by boiling slides for 20 min in 500 mL of 0.1 M Tris-buffered-saline (TBS) containing 0.01 M ethylenediamine-tetraacetic acid (Tris-EDTA), pH 9.0, followed by 20 min cooling with open lid. The blocking of endogenous peroxidases was completed in 3% hydrogen peroxide (H_2O_2) diluted in methanol for 20 min, followed by blocking of non-specific antigen binding in TBS, pH 7.4, for 30 min containing 3% bovine serum albumin (BSA, #82-100-6, Millipore, Kankakee, Illinois, United States). For the detection of target proteins, rabbit polyclonal GPER1 (#NLS4271, 1:100; GPER/GPR30, Bio-Techne, Abingdon, United Kingdom) and mouse monoclonal anti-COL17 antibody clone 9G2, recognizing the aa507–529 uppermost extracellular part of COL17a endodomain region, as produced, validated and described by Stelkovics et al. [42, 49] antibodies were applied overnight in a humidified chamber. Tissue-bound antibody detection was performed with MACH4 Universal HRP-polymer, biotin-free detection (Biocare Medical, Concord, MA, United States). Aminoethyl-carbazole (AEC) H_2O_2 chromogen-substrate system dissolved in 0.1 M acetate buffer, pH 4.6, was used for revealing the peroxidase activity under microscopic control followed by nuclear staining using hematoxylin. After mounting, stained slides were digitalized using Panoramic Scan (3DHISTECH, Budapest, Hungary).

Assessment of immunostaining

Single immunolabeling for GPER1 and COL17 was completed on serial sections from each sample. Immunohistochemical scoring for both proteins was completed using the Histo-score (H-score), incorporating both the staining intensity and a percentage of stained tumor cells at each intensity level. The staining intensity values were indicated as 0 (absent), 1 (mild staining), 2 (moderate staining), and 3 (intensive staining) (Figure 1), which were then multiplied with the percentage of stained cells in the sample (ranging from 0% to 100%). The final H-score is derived from the sum of staining intensity values multiplied by percentage of stained cells as the equation shown. This score, therefore, is in the range of 0–300 (H-score = [0 × (% cells 0) + 1 × (% cells 1+) + 2 × (% cells 2+) + 3 × (% cells 3+)]) [52–55].

In order to minimize potential bias, the scoring was independently performed by four investigators (referred to as UC, MF, PB, TK). Disagreements in scoring were resolved through discussion and mutual consensus. Breast cancer tissue microarray (TMA) samples served as positive external controls for GPER1. As internal positive control of GPER1 staining, keratinocytes as well as sebaceous and sweat gland epithelia were used. For COL17, the surrounding healthy skin in each sample was deemed as positive control. Omitting the primary antibodies in each run served as negative controls.

Statistical analysis

First, descriptive statistics were calculated for all variables. Then bivariate analyses were conducted, non-parametric Mann-Whitney U test was performed between groups and Pearson correlation analysis was used to determine the strength of the association between continuous variables, while cross tabulation analysis with Spearman's chi-squared tests was performed between categorical variables. Statistical analyses were carried out by IBM SPSS Statistics for Windows, Version 25.0. Armonk, NY: IBM Corp.

Results

GPER1 protein expression and clinicopathological factors of melanoma

GPER1 expression was detected in over half of the melanoma samples (n = 54/94, 57.45%). The majority of thinner melanomas [Breslow thickness ≤2 mm (n = 40/57, 70.18%)] were positive for GPER1.

GPER1 positive melanoma samples had significantly lower Breslow thickness ($p = 0.01$) and mitotic rate ($p = 0.007$) when compared to GPER1 negative cases (Figure 2). Mean H-score of GPER1 positive cases with Breslow thickness of more than 2 mm (H-score: 47.69) was significantly lower when compared with melanoma samples with Breslow thickness of 2 mm and less (H-score: 94.90) ($p < 0.005$). Furthermore, the presence of GPER1 receptor positivity showed inverse correlation with the

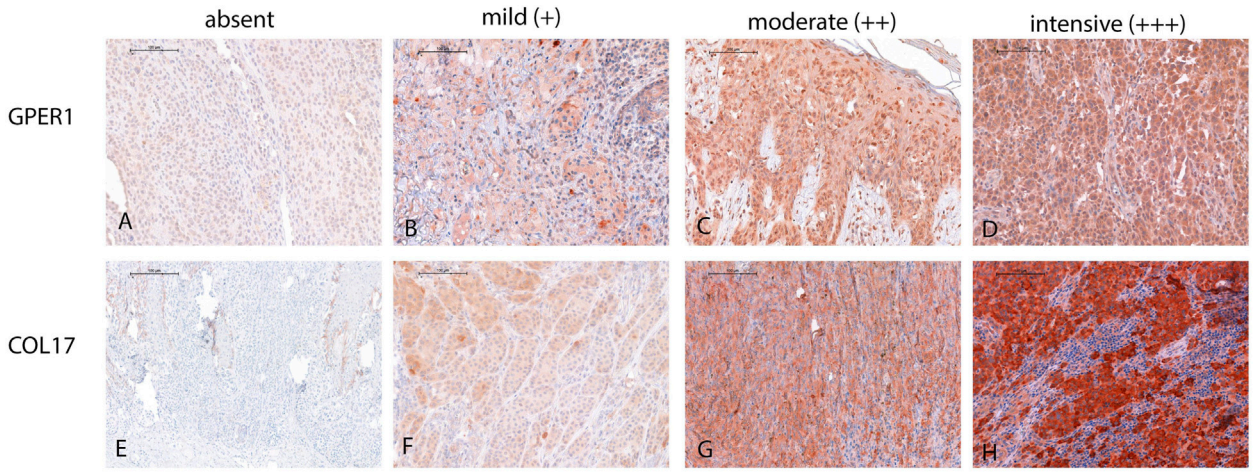

FIGURE 1
Illustration of GPER1 and COL17 protein expression intensity in the four-tier system in melanoma. **(A)** Representative image demonstrating the absence of GPER1 labelling. **(B–D)** Intensity differences between GPER1 positive tumor cells. **(E)** Absence of COL17 labelling of the tumor cells, only healthy keratinocytes at the basal layer showed positivity for COL17. **(F–H)** Intensity differences between COL17 positive tumor cells (for all images: original magnification ×40, scale bar: 100 μm).

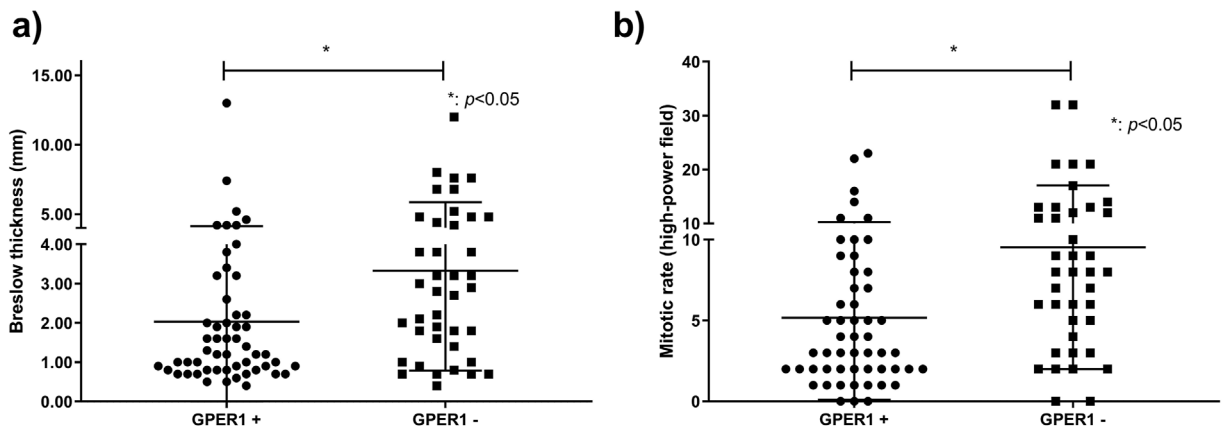

FIGURE 2
Association of Breslow thickness and mitotic rate with GPER1 protein expression. Dots and squares represent Breslow thickness (n = 94) **(A)** and mitotic rate (n = 93) **(B)** of individual primary melanomas.

presence of ulceration and sentinel lymph node (SLN) positivity based on cross-tabulation analyses (Table 2).

With regards to the different subtypes of melanoma, GPER1 protein was expressed in the majority of superficial spreading melanomas (SSM, n = 50/83, 60.20%), while it was only seen in one case out of the five nodular melanomas (NM) (Supplementary Table S1).

Considering the gender difference, GPER1 protein expression was more frequently detected in females compared to males (n = 31/47 versus n = 23/47, p = 0.095) (Supplementary Table S1).

GPER1 expression showed no statistically significant relationship with peritumoral lymphocytic infiltrate (PLI), lymph node or distant metastases, patient's age or between pre- and postmenopausal women group (Supplementary Table S1).

COL17 endodomain expression and clinicopathological factors of melanoma

COL17 endodomain expression was found in nearly two-third of the melanoma samples (n = 62/94, 65.96%), and was

TABLE 2 Association of GPER1 protein expression with clinicopathological factors.

		GPER1		
		Negative	Positive	*p*-value
Ulceration	Absent	20	40	0.004
	Present	19	10	
Sentinel lymph node	Negative	25	41	0.084
	Positive	15	11	
Regression	Absent	31	39	0.562
	Present	9	15	

Numbers represent case counts.

predominantly present along the growing tumor front (Figure 3). The majority of thicker melanomas [Breslow thickness >2 mm (n = 32/37, 86.48%)] were positive for COL17 endodomain.

COL17 endodomain expression showed positive correlation with increased Breslow thickness ($p = 0.004$) and mitotic rate ($p = 0.0009$) (Figure 4). Mean H-score of COL17 endodomain positive cases with Breslow thickness of more than 2 mm (H-score: 77.44) was significantly higher than cases with Breslow thickness of 2 mm and less (H-score: 29.81) ($p < 0.001$). Furthermore, COL17 endodomain-expressing tumors exhibited more frequently unfavorable characteristics such as ulceration, regression, and SLN positivity (Table 3).

The presence of distant lymph node and cutaneous/visceral metastases was more commonly seen in samples with

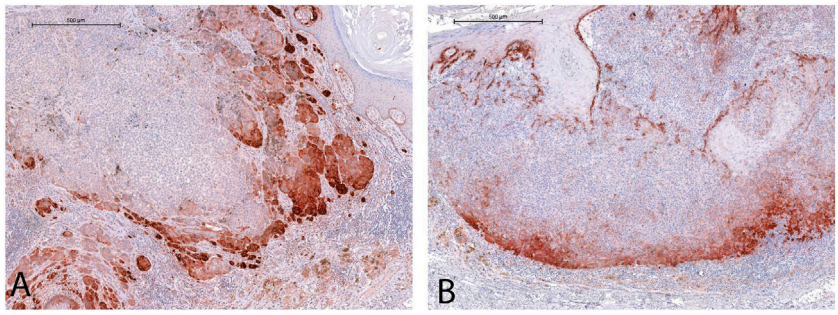

FIGURE 3
Cytoplasmic COL17 protein expression was mostly observed along the lateral **(A)** and deep **(B)**, growing fronts of the tumors. [See endogenous positive control reaction in the basal epidermal layer in **(B)**] (For both images: original magnification ×5, scale bar: 500 μm).

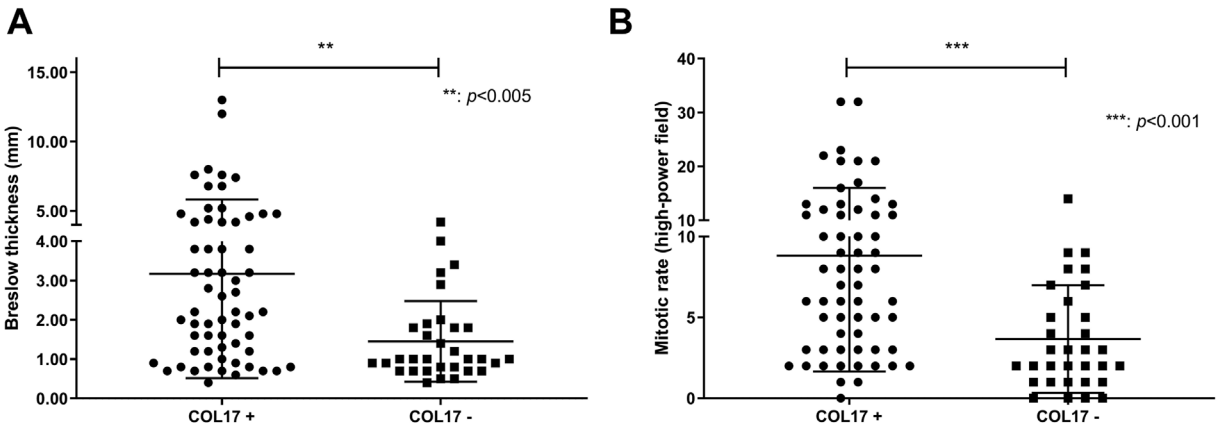

FIGURE 4
Association of Breslow thickness and mitotic rate with COL17 protein expression. Dots and squares represent Breslow thickness (n = 94) **(A)** and mitotic rate (n = 93) **(B)** of individual primary melanomas.

TABLE 3 Association of COL17 protein expression with clinicopathological factors.

		COL17		
		Negative	Positive	*p*-value
Ulceration	Absent	28	30	<0.0001
	Present	3	26	
Sentinel lymph node	Negative	27	38	0.056
	Positive	5	20	
Regression	Absent	28	41	0.043
	Present	4	19	

Numbers represent case counts.

COL17 endodomain expression, compared to COL17 negative tumors (Supplementary Table S2). The expression of the protein was observed more frequently in melanomas located on the trunk (n = 37/53, 69.81%) and upper extremities (n = 10/13, 76.92%) than in those with localization along the lower extremities (n = 13/28, 46.43%) (Supplementary Table S2).

Considering the histological subtypes, almost all nodular melanoma cases (n = 4/5, 80.00%) showed COL17 endodomain expression, and a subset of superficial spreading melanomas were also positive for COL17 endodomain (54/83, 65.00%) (Supplementary Table S2).

COL17 endodomain expression showed no significant association with gender, age, or presence of PLI (Supplementary Table S2).

GPER1 and COL17 double expression

Nearly one-third (n = 32/94, 34.04%) of the cases exhibited simultaneous positivity for GPER1 and COL17 proteins. Melanomas positive for both markers had significantly lower mean Breslow thickness (2.425 mm vs. 3.957 mm, $p = 0.004$) and mitotic rate (6.61/HPF vs. 11.1/HPF, $p = 0.008$) compared to cases positive for COL17 only (Table 4). Conversely, double-positive cases had higher mean Breslow thickness (2.425 mm vs. 1.464 mm, $p = 0.056$) and mitotic rate (6.61/HPF vs. 3.14/HPF, $p = 0.003$) compared to cases positive for GPER1 only (Table 4).

Discussion

In this retrospective study, we aimed to explore the expression patterns of GPER1 and the COL17 endodomain proteins in primary cutaneous melanoma tissue samples from patients with known sentinel lymph node status and correlated this with the common clinicopathological features of melanoma.

GPER1 protein expression has been described in various tissues under physiological conditions including the nervous-, reproductive-, musculoskeletal system, and gastrointestinal tract [27–29]. Human and animal studies both revealed the role of GPER1 in the regulation of physiological responses involving mammary gland development [56], oocyte maturation [57, 58], endometrial cell growth [59], cardiomyocyte growth [60], vasodilation [61, 62], T-cell differentiation [63], inhibition of inflammation [64, 65], insulin secretion [61, 62], and chondrocyte differentiation [66]. In the murine skin, GPER1 mediates melanocyte differentiation and melanin pigment production; and it has also been shown to decreases expression of the oncodriver c-Myc, as described by Natale et al. using murine melanoma xenograft models [37].

Besides its expression in normal tissues, GPER1 has also been found in many types of cancers/cancer cell lines. Its role has been most intensively studied in breast cancer, where it appears to contribute to cancer cell proliferation, migration and invasion through its ability to transactivate epidermal growth factor receptors (EGFRs) [14, 67]. However, it was also shown to be a predictor of better overall survival (OS) in ER-positive breast cancer [20]. In ovarian cancer cells, GPER1 can be detected both within the nucleus and the cytoplasm, and the nuclear GPER1 is a potential predictive factor of poor survival [68]. Similar to its effect in breast cancer, GPER1 promotes cell proliferation, migration, lymph node metastasis and invasion in ER-negative ovarian cancer, and its overexpression correlates with tumor size and stage [69–71]. Cytoplasmic GPER1 overexpression was also found in high-grade estrogen receptor- and progesterone receptor-negative endometrial adenocarcinomas in association with myometrial invasion and poor survival [72]. Furthermore, GPER1 agonists enhance tumor growth of endometrial cancer cell line xenografts [73]. Similar to gynecological cancers, GPER1 (over) expression in lung cancer is also associated with high TNM stage and lymph node metastasis [13, 15, 74]. In human

TABLE 4 Comparison of mean Breslow thickness and mean mitotic rate of GPER1/COL17 double positive cases (n = 32) with GPER1 (n = 22) or COL17 (n = 30) positive cases.

	Mean Breslow thickness	Mean mitotic rate		Mean Breslow thickness	Mean mitotic rate
GPER1 positive	1.464 mm	3.14/HPF	COL17 positive	3.957 mm	11.1/HPF
GPER1/COL17 double positive	2.425 mm	6.61/HPF	GPER1/COL17 double positive	2.425 mm	6.61/HPF
	$p = 0.056$	$p = 0.003$		$p = 0.004$	$p = 0.008$

HPF, high-power field.

non-small-cell lung cancer cell lines, the expression of cytoplasmic GPER1 was high [13] and treatment of non-small-cell lung cancer cell lines with GPER1 antagonists impaired tumor growth [75]. In colorectal cancer, on the other hand, GPER1 appears to act as a tumor suppressor and its expression is negatively correlated with increased tumor stage and lymph node metastasis [16]. Moreover, higher GPER1 expression meant survival benefit for colorectal cancer patients [16]. In adrenocortical cancer, GPER1 presented tumor suppressive properties as GPER1 agonists suppressed adrenocortical carcinoma proliferation via cell cycle arrest, DNA damage, and apoptosis via ERK1/2 activation [18].

In our previous study [6], we found that GPER1 expression in pregnancy-related melanoma samples was associated with lower Breslow thickness, lower mitotic rate, lower hazard of local or distant metastases, and the protein expression was inversely associated with the presence of ulceration [6].

Our current study cohort, which included both genders and known sentinel lymph node status for all patients, showed similar results. GPER1 protein expression was correlated with lower Breslow thickness and mitotic rate. The presence of ulceration and sentinel lymph node metastases were found less frequently in GPER1-positive cases, suggesting that GPER1 may serve as a favorable prognostic marker.

Considering the role of GPER1 in cancer pathophysiology, it has been suggested as a potential target for cancer therapy [30]. *In vivo* and *in vitro* studies using GPER1 agonists such as G-1 demonstrated beneficial effects for cancer prognosis; these involved the inhibition of proliferation and the promotion of apoptosis in leukemia cell lines of T lineage [76], as well as the inhibition of growth in both mantle cell lymphoma [77] and pancreatic ductal adenocarcinoma [78]. Furthermore, G-1 assisted temozolamide to impair glioblastoma proliferation [79], and inhibited the growth of ovarian cancer cells [80] and gastric cancer [81]. In melanoma, the activation of GPER1 by its specific agonist G-1, inhibited the proliferation of mouse melanoma cell lines by decreasing cell division and blocking cell cycle progression in the G2 phase [36]. In a murine model, co-treatment with PD-1 inhibitor and GPER1 agonist G-1 resulted in reduced cell proliferation and tumor volume along with better survival [37]. *In vitro* treatment of uveal melanoma cell lines with GPER1 agonist induced mitotic arrest and apoptosis of tumor cells [82]. Based on these observations, an ongoing phase I clinical trial has been initiated using pembrolizumab and a selective agonist of GPER1 for treatment of melanoma [83].

After establishing the favorable prognostic aspects of GPER1, we sought to identify a marker that could potentially have reverse effects in our cohort. Based on our research group's previous findings, namely, that uppermost extracellular part (aa507-529) of COL17a endodomain (but not the shedding ectodomain) is expressed in proliferating melanocytes and melanomas but not in benign melanocytic lesions [49], we aimed to examine COL17 expression in our current primary cutaneous melanoma cohort. The overexpression of COL17 coding mRNA and protein levels in colorectal carcinoma was associated with higher TNM staging, infiltrative growth, metastases, and decreased survival rates [45]. In lung cancer, elevated expression of COL17 was seen in the stromal environment and was associated with increased metastatic potential [47]. Furthermore, COL17 may contribute to the epithelial-to-mesenchymal transition and poor disease prognosis [84]. Overexpression of COL17 in cervix carcinoma exhibited a relation to increased local dissemination and metastasis [85, 86]. In contrast, COL17 showed reduced expression in advanced breast cancer [48] in correlation with higher TNM staging, increased invasion, postmenopausal status and poorer prognosis [48]. The antagonistic expression of COL17 in breast cancer is suggested to be due to hypermethylation of the COL17 coding gene promoter [86]. The role of COL17 was widely studied in both normal skin and cutaneous malignancies [39, 42, 43], also in head and neck squamous cell carcinoma (SCC) [87, 88]. SCC demonstrated COL17 overexpression promoting tumor invasion [42, 89]. Krenács et al. found that the cell residual endodomain, COL17, but not the ectodomain, was expressed in melanoma, but not in normal melanocytic and dysplastic nevi. It was also shown that immunological targeting of this protein sequence of COL17 with a specific antibody lead to apoptosis in melanoma cell lines [49]. Another study using murine melanoma models demonstrated that dysfunction of COL17 in keratinocytes promoted melanoma progression [90]. A recent publication demonstrated that in mucosal melanoma, the COL17 coding gene has a variant (p.Ser1029Ala) in the ectodomain, which may be less efficiently shed compared to the wild-type, thereby assisting melanoma progression [91]. All these previous data suggested the dysfunction of COL17 and its potential role in melanoma development and progression.

The current study shows that in primary melanoma samples, the expression of COL17 endodomain had an inverse relationship when compared to GPER1 expression by showing positive association with poor prognostic factors including increased Breslow thickness, higher mitotic rate and presence of ulceration. COL17 endodomain expression was more frequently seen in sentinel lymph node positive melanomas. Furthermore, the overexpression of COL17 along the invasive tumor front was suggestive of its potential role in tumor invasion in line with some earlier results: for example, COL17 was found to be at the invasive tumor fronts in squamous cell carcinoma of the tongue [89].

While there has been no direct interactions described so far between GPER1 and COL17 at a molecular level, COL17 protein has already been shown to inhibit breast cancer cell proliferation and growth via decreasing the phosphorylation of key proteins in the AKT/mTOR pathway [92], which is known to be one of the major downstream signaling target of the GPER1 pathway as well [93–96]. GPER1, in reverse, is found to enhance the

phosphorylation of AKT/mTOR pathway leading to its activation in breast, ovarian and lung cancer resulting in increased cell proliferation in these types of cancers [93–95].

The rationale for investigating both GPER1 and COL17 concurrently was to determine whether their co-expression shows any correlation with the major clinicopathological factors of melanoma. Co-expression of both proteins in our study was observed in nearly one-third of the cases. Melanomas positive for both GPER1 and COL17 exhibited lower mean Breslow thickness and mitotic rates compared to cases positive for COL17 alone. Conversely, double-positive cases demonstrated higher mean Breslow thickness and mitotic rates than cases positive for GPER1 alone. Theoretically, while GPER1 expression decreases with increasing tumor size, COL17 expression emerges in high-risk, thicker melanomas, particularly at deeper invasive fronts. Our current results suggest that double positivity for GPER1 and COL17 may indicate an intermediate phase in tumor progression, however, future studies with larger cohorts and detailed molecular analyses are necessary to study any potential link between the two proteins and their potential interactions.

Although the association of GPER1 with favorable prognostic clinicopathological features suggests a trend towards better overall survival (OS), and COL17 endodomain is anticipated to correlate with poorer OS, a larger cohort of patients will be necessary in future studies to substantiate these findings.

In summary, our study demonstrated that GPER1 expression is associated with lower Breslow thickness, lower mitotic rate, absence of ulceration, and absence of sentinel lymph node metastasis in both genders, all of which are predictive clinicopathological factors for better survival outcomes. In contrast, COL17 endodomain expression in human melanoma, when present along the growing tumor front, suggests its involvement in melanoma invasion. COL17 endodomain expression was proven to be associated with poor prognostic features such as greater tumor thickness, higher mitotic rate, presence of regression, and sentinel lymph node positivity, indicating worse survival outcomes. Our findings suggest that the immunohistochemical detection of GPER1 and COL17 proteins in melanoma may serve as valuable prognostic markers.

Limitations of our study include the relatively small patient cohort, the retrospective study design, and the exclusive use of immunohistochemistry for biomarker detection. Further investigations with larger patient cohorts, supplemented by functional experiments, are necessary to corroborate our findings and elucidate the potential role of GPER1 and COL17 protein expression in melanoma.

Data availability statement

The raw data supporting the conclusions of this article will be made available by the authors, without undue reservation.

Ethics statement

The studies involving humans were approved by the Semmelweis University Institutional Review Board. The studies were conducted in accordance with the local legislation and institutional requirements. Written informed consent for participation was not required from the participants or the participants' legal guardians/next of kin in accordance with the national legislation and institutional requirements.

Author contributions

UC, MF, PB, and TK planned the experiments, UC conducted the experiments. UC, MF, PB, and TK scored the immunohistochemistry stainings. AF and VB conducted the statistical analysis. All authors contributed to the article and approved the submitted version.

Funding

The authors declare that financial support was received for the research, authorship, and/or publication of this article. This work was supported by the Nékám Foundation and by the Hungarian Scientific Research Fund (OTKA NN 114460).

Acknowledgments

The authors are grateful to Krisztián Németh for his help in editing the manuscript. We are thankful to Judit Hársing and Enikő Kuroli for their help with gathering paraffin-based melanoma tissue sections from the histopathology archive of the Department of Dermatology, Venereology and Dermatooncology, as well as for their help with hematoxylin-eosin staining of the tissue samples. We thank to Lajos Vince Kemény, Zsófia Csábi and Benedek Nagy for their help with literature analysis.

Conflict of interest

The authors declare that the research was conducted in the absence of any commercial or financial relationships that could be construed as a potential conflict of interest.

Supplementary material

The Supplementary Material for this article can be found online at: https://www.por-journal.com/articles/10.3389/pore.2024.1611809/full#supplementary-material

References

1. Erdmann F, Lortet-Tieulent J, Schüz J, Zeeb H, Greinert R, Breitbart EW, et al. International trends in the incidence of malignant melanoma 1953–2008--are recent generations at higher or lower risk? *Int J Cancer* (2013) 132:385–400. doi:10.1002/ijc.27616

2. Sacchetto L, Zanetti R, Comber H, Bouchardy C, Brewster DH, Broganelli P, et al. Trends in incidence of thick, thin and *in situ* melanoma in Europe. *Eur J Cancer Oxf Engl* (2018) 92:108–18. doi:10.1016/j.ejca.2017.12.024

3. Current Staging. Prognostic factors in melanoma- ClinicalKey. Available from: https://www.clinicalkey.com/#!/content/playContent/1-s2.0-S1055320714001240?returnurl=https:%2F%2Flinkinghub.elsevier.com%2Fretrieve%2Fpii%2FS1055320714001240%3Fshowall%3Dtrue&referrer=https:%2F%2Fpubmed.ncbi.nlm.nih.gov%2F (Accessed March 9, 2021).

4. Bellenghi M, Puglisi R, Pontecorvi G, De Feo A, Carè A, Mattia G. Sex and gender disparities in melanoma. *Cancers* (2020) 12:1819. doi:10.3390/cancers12071819

5. Smalley KS. Why do women with melanoma do better than men? *eLife* (2018) 7:e33511. doi:10.7554/eLife.33511

6. Fábián M, Rencz F, Krenács T, Brodszky V, Hársing J, Németh K, et al. Expression of G protein-coupled oestrogen receptor in melanoma and in pregnancy-associated melanoma. *J Eur Acad Dermatol Venereol JEADV* (2017) 31:1453–61. doi:10.1111/jdv.14304

7. Dika E, Patrizi A, Lambertini M, Manuelpillai N, Fiorentino M, Altimari A, et al. Estrogen receptors and melanoma: a Review. *Cells* (2019) 8:1463. doi:10.3390/cells8111463

8. Zhou JH, Kim KB, Myers JN, Fox PS, Ning J, Bassett RL, et al. Immunohistochemical expression of hormone receptors in melanoma of pregnant women, nonpregnant women, and men. *Am J Dermatopathol* (2014) 36:74–9. doi:10.1097/DAD.0b013e3182914c64

9. Dika E, Fanti PA, Vaccari S, Capizzi E, Degiovanni A, Gobbi A, et al. Oestrogen and progesterone receptors in melanoma and nevi: an immunohistochemical study. *Eur J Dermatol EJD* (2017) 27:254–9. doi:10.1684/ejd.2017.3019

10. de Giorgi V, Mavilia C, Massi D, Sestini S, Grazzini M, Brandi ML, et al. The role of estrogens in melanoma and skin cancer. *Carcinogenesis* (2009) 30:720. doi:10.1093/carcin/bgp025

11. Lee HJ, Wall B, Chen S. G-protein-coupled receptors and melanoma. *Pigment Cell Melanoma Res* (2008) 21:415–28. doi:10.1111/j.1755-148X.2008.00478.x

12. Gründker C, Emons G. The role of gonadotropin-releasing hormone in cancer cell proliferation and metastasis. *Front Endocrinol* (2017) 8:187. doi:10.3389/fendo.2017.00187

13. Jala VR, Radde BN, Haribabu B, Klinge CM. Enhanced expression of G-protein coupled estrogen receptor (GPER/GPR30) in lung cancer. *BMC Cancer* (2012) 12:624. doi:10.1186/1471-2407-12-624

14. Meng R, Qin Q, Xiong Y, Wang Y, Zheng J, Zhao Y, et al. NHERF1, a novel GPER associated protein, increases stability and activation of GPER in ER-positive breast cancer. *Oncotarget* (2016) 7:54983–97. doi:10.18632/oncotarget.10713

15. Jacenik D, Cygankiewicz AI, Krajewska WM. The G protein-coupled estrogen receptor as a modulator of neoplastic transformation. *Mol Cell Endocrinol* (2016) 429:10–8. doi:10.1016/j.mce.2016.04.011

16. Liu Q, Chen Z, Jiang G, Zhou Y, Yang X, Huang H, et al. Epigenetic down regulation of G protein-coupled estrogen receptor (GPER) functions as a tumor suppressor in colorectal cancer. *Mol Cancer* (2017) 16:87. doi:10.1186/s12943-017-0654-3

17. Lau K-M, Ma FM-T, Xia JT, Chan QKY, Ng CF, To KF. Activation of GPR30 stimulates GTP-binding of Gαi1 protein to sustain activation of Erk1/2 in inhibition of prostate cancer cell growth and modulates metastatic properties. *Exp Cell Res* (2017) 350:199–209. doi:10.1016/j.yexcr.2016.11.022

18. Chimento A, Sirianni R, Casaburi I, Zolea F, Rizza P, Avena P, et al. GPER agonist G-1 decreases adrenocortical carcinoma (ACC) cell growth *in vitro* and *in vivo*. *Oncotarget* (2015) 6:19190–203. doi:10.18632/oncotarget.4241

19. Talia M, De Francesco EM, Rigiracciolo DC, Muoio MG, Muglia L, Belfiore A, et al. The G protein-coupled estrogen receptor (GPER) expression correlates with pro-metastatic pathways in ER-negative breast cancer: a bioinformatics analysis. *Cells* (2020) 9:622. doi:10.3390/cells9030622

20. Zhang D, Wang J, Chen H, Yan S. Cytoplasmic G protein-coupled estrogen receptor 1 as a prognostic indicator of breast cancer: a meta-analysis. *Technol Cancer Res Treat* (2022) 21:15330338221131664. doi:10.1177/15330338221131664

21. Martin SG, Lebot MN, Sukkarn B, Ball G, Green AR, Rakha EA, et al. Low expression of G protein-coupled oestrogen receptor 1 (GPER) is associated with adverse survival of breast cancer patients. *Oncotarget* (2018) 9:25946–56. doi:10.18632/oncotarget.25408

22. Lv X, Hua G, He C, Davis JS, Wang C. Abstract B82: G-protein coupled estrogen receptor (GPER) agonist G-1 inhibits growth of human granulosa cell tumor cells via blocking microtubule assembly. *Clin Cancer Res* (2014) 19:B82. doi:10.1158/1078-0432.OVCA13-B82

23. Glatthaar H, Katto J, Vogt T, Mahlknecht U. Estrogen receptor alpha (ESR1) single-nucleotide polymorphisms (SNPs) affect malignant melanoma susceptibility and disease course. *Genet Epigenetics* (2016) 8:1–6. doi:10.4137/GEG.S31264

24. Fuentes N, Silveyra P. Estrogen receptor signaling mechanisms. *Adv Protein Chem Struct Biol* (2019) 116:135–70. doi:10.1016/bs.apcsb.2019.01.001

25. de Giorgi V, Mavilia C, Massi D, Gozzini A, Aragona P, Tanini A, et al. Estrogen receptor expression in cutaneous melanoma: a real-time reverse transcriptase-polymerase chain reaction and immunohistochemical study. *Arch Dermatol* (2009) 145:30–6. doi:10.1001/archdermatol.2008.537

26. Marzagalli M, Montagnani Marelli M, Casati L, Fontana F, Moretti RM, Limonta P. Estrogen receptor β in melanoma: from molecular insights to potential clinical utility. *Front Endocrinol* (2016) 7:140. doi:10.3389/fendo.2016.00140

27. Xu S, Yu S, Dong D, Lee LTO. G protein-coupled estrogen receptor: a potential therapeutic target in cancer. *Front Endocrinol* (2019) 10:725. doi:10.3389/fendo.2019.00725

28. Kvingedal AM, Smeland EB. A novel putative G-protein-coupled receptor expressed in lung, heart and lymphoid tissue. *FEBS Lett* (1997) 407:59–62. doi:10.1016/s0014-5793(97)00278-0

29. Feng Y, Gregor P. Cloning of a novel member of the G protein-coupled receptor family related to peptide receptors. *Biochem Biophys Res Commun* (1997) 231:651–4. doi:10.1006/bbrc.1997.6161

30. Pepermans RA, Sharma G, Prossnitz ER. G protein-coupled estrogen receptor in cancer and stromal cells: functions and novel therapeutic perspectives. *Cells* (2021) 10:672. doi:10.3390/cells10030672

31. Sjöström M, Hartman L, Fornander T, Grabau D, Malmström P, Nordenskjöld B, et al. Abstract P1-08-12: G protein-coupled estrogen receptor in the plasma membrane is prognostic in early breast cancer. *Cancer Res* (2013) 73:P1–08-12-P1-08-12. doi:10.1158/0008-5472.SABCS13-P1-08-12

32. Yang F, Shao Z-M. Double-edged role of G protein-coupled estrogen receptor 1 in breast cancer prognosis: an analysis of 167 breast cancer samples and online data sets. *Oncotargets Ther* (2016) 9:6407–15. doi:10.2147/OTT.S111846

33. Natale CA, Duperret EK, Zhang J, Sadeghi R, Dahal A, O'Brien KT, et al. Sex steroids regulate skin pigmentation through nonclassical membrane-bound receptors. *eLife* (2016) 5:e15104. doi:10.7554/eLife.15104

34. Nicolaidou E, Katsambas AD. Pigmentation disorders: hyperpigmentation and hypopigmentation. *Clin Dermatol* (2014) 32:66–72. doi:10.1016/j.clindermatol.2013.05.026

35. Sun M, Xie H-F, Tang Y, Lin SQ, Li JM, Sun SN, et al. G protein-coupled estrogen receptor enhances melanogenesis via cAMP-protein kinase (PKA) by upregulating microphthalmia-related transcription factor-tyrosinase in melanoma. *J Steroid Biochem Mol Biol* (2017) 165:236–46. doi:10.1016/j.jsbmb.2016.06.012

36. Ribeiro MPC, Santos AE, Custódio JBA. The activation of the G protein-coupled estrogen receptor (GPER) inhibits the proliferation of mouse melanoma K1735-M2 cells. *Chem Biol Interact* (2017) 277:176–84. doi:10.1016/j.cbi.2017.09.017

37. Natale CA, Li J, Zhang J, Dahal A, Dentchev T, Stanger BZ, et al. Activation of G protein-coupled estrogen receptor signaling inhibits melanoma and improves response to immune checkpoint blockade. *eLife* (2018) 7:e31770. doi:10.7554/eLife.31770

38. Mallipeddi R, Keane FM, McGrath JA, Mayou BJ, Eady RAJ. Increased risk of squamous cell carcinoma in junctional epidermolysis bullosa. *J Eur Acad Dermatol Venereol JEADV* (2004) 18:521–6. doi:10.1111/j.1468-3083.2004.00968.x

39. Jones VA, Patel PM, Gibson FT, Cordova A, Amber KT. The role of collagen XVII in cancer: squamous cell carcinoma and beyond. *Front Oncol* (2020) 10:352. doi:10.3389/fonc.2020.00352

40. Hammers CM, Stanley JR. Mechanisms of disease: pemphigus and bullous pemphigoid. *Annu Rev Pathol* (2016) 11:175–97. doi:10.1146/annurev-pathol-012615-044313

41. Koster J, Geerts D, Favre B, Borradori L, Sonnenberg A. Analysis of the interactions between BP180, BP230, plectin and the integrin alpha6beta4 important for hemidesmosome assembly. *J Cell Sci* (2003) 116:387–99. doi:10.1242/jcs.00241

42. Stelkovics E, Korom I, Marczinovits I, Molnar J, Rasky K, Raso E, et al. Collagen XVII/BP180 protein expression in squamous cell carcinoma of the skin detected with novel monoclonal antibodies in archived tissues using tissue

microarrays and digital microscopy. *Appl Immunohistochem Mol Morphol AIMM* (2008) 16:433–41. doi:10.1097/PAI.0b013e318162f8aa

43. Moilanen JM, Löffek S, Kokkonen N, Salo S, Väyrynen JP, Hurskainen T, et al. Significant role of collagen XVII and integrin β4 in migration and invasion of the less aggressive squamous cell carcinoma cells. *Sci Rep* (2017) 7:45057. doi:10.1038/srep45057

44. Meng X, Matsumoto F, Mori T, Miura N, Ino Y, Onidani K, et al. BP180 is a prognostic factor in head and neck squamous cell carcinoma. *Anticancer Res* (2021) 41:1089–99. doi:10.21873/anticanres.14867

45. Moilanen JM, Kokkonen N, Löffek S, Väyrynen JP, Syväniemi E, Hurskainen T, et al. Collagen XVII expression correlates with the invasion and metastasis of colorectal cancer. *Hum Pathol* (2015) 46:434–42. doi:10.1016/j.humpath.2014.11.020

46. Laval S, Laklai H, Fanjul M, Pucelle M, Laurell H, Billon-Galés A, et al. Dual roles of hemidesmosomal proteins in the pancreatic epithelium: the phosphoinositide 3-kinase decides. *Oncogene* (2014) 33:1934–44. doi:10.1038/onc.2013.146

47. Papay J, Krenacs T, Moldvay J, Stelkovics E, Furak J, Molnar B, et al. Immunophenotypic profiling of nonsmall cell lung cancer progression using the tissue microarray approach. *Appl Immunohistochem Mol Morphol AIMM* (2007) 15:19–30. doi:10.1097/01.pai.0000213143.32030.f5

48. Bergstraesser LM, Srinivasan G, Jones JC, Stahl S, Weitzman SA. Expression of hemidesmosomes and component proteins is lost by invasive breast cancer cells. *Am J Pathol* (1995) 147:1823–39.

49. Krenacs T, Kiszner G, Stelkovics E, Balla P, Teleki I, Nemeth I, et al. Collagen XVII is expressed in malignant but not in benign melanocytic tumors and it can mediate antibody induced melanoma apoptosis. *Histochem Cell Biol* (2012) 138:653–67. doi:10.1007/s00418-012-0981-9

50. Blondeaux E, Massarotti C, Fontana V, Poggio F, Arecco L, Fregatti P, et al. The PREgnancy and FERtility (PREFER) study investigating the need for ovarian function and/or fertility preservation strategies in premenopausal women with early breast cancer. *Front Oncol* (2021) 11:690320. doi:10.3389/fonc.2021.690320

51. Keung EZ, Gershenwald JE. The eighth edition American Joint Committee on Cancer (AJCC) melanoma staging system: implications for melanoma treatment and care. *Expert Rev Anticancer Ther* (2018) 18:775–84. doi:10.1080/14737140.2018.1489246

52. Hirsch FR, Varella-Garcia M, Bunn PA, Di Maria MV, Veve R, Bremmes RM, et al. Epidermal growth factor receptor in non-small-cell lung carcinomas: correlation between gene copy number and protein expression and impact on prognosis. *J Clin Oncol Off J Am Soc Clin Oncol* (2003) 21:3798–807. doi:10.1200/JCO.2003.11.069

53. McCarty KS, Miller LS, Cox EB, Konrath J. Estrogen receptor analyses. Correlation of biochemical and immunohistochemical methods using monoclonal antireceptor antibodies. *Arch Pathol Lab Med* (1985) 109:716–21.

54. McCarty KS, Szabo E, Flowers JL, Cox EB, Leight GS, Miller L, et al. Use of a monoclonal anti-estrogen receptor antibody in the immunohistochemical evaluation of human tumors. *Cancer Res* (1986) 46:4244s–8s.

55. Ruengwanichayakun P. Histochemical scoring assessment (H-score). *Asian Arch Pathol* (2021). Available from: https://www.asianarchpath.com/view/152 (Accessed July 20, 2024).

56. Dennis MK, Burai R, Ramesh C, Petrie WK, Alcon SN, Nayak TK, et al. *In vivo* effects of a GPR30 antagonist. *Nat Chem Biol* (2009) 5:421–7. doi:10.1038/nchembio.168

57. Wang C, Prossnitz ER, Roy SK. Expression of G protein-coupled receptor 30 in the hamster ovary: differential regulation by gonadotropins and steroid hormones. *Endocrinology* (2007) 148:4853–64. doi:10.1210/en.2007-0727

58. Peyton C, Thomas P. Involvement of epidermal growth factor receptor signaling in estrogen inhibition of oocyte maturation mediated through the G protein-coupled estrogen receptor (Gper) in zebrafish (*Danio rerio*). *Biol Reprod* (2011) 85:42–50. doi:10.1095/biolreprod.110.088765

59. Gao F, Ma X, Ostmann AB, Das SK. GPR30 activation opposes estrogen-dependent uterine growth via inhibition of stromal ERK1/2 and estrogen receptor alpha (ERα) phosphorylation signals. *Endocrinology* (2011) 152:1434–47. doi:10.1210/en.2010-1368

60. Patel VH, Chen J, Ramanjaneya M, Karteris E, Zachariades E, Thomas P, et al. G-protein coupled estrogen receptor 1 expression in rat and human heart: protective role during ischaemic stress. *Int J Mol Med* (2010) 26:193–9. doi:10.3892/ijmm_00000452

61. Uea M, Salehi SA, Windahl S, Gomez MF, Swärd K, Daszkiewicz-Nilsson J, et al. Deletion of the G protein-coupled receptor 30 impairs glucose tolerance, reduces bone growth, increases blood pressure, and eliminates estradiol-stimulated insulin release in female mice. *Endocrinology* (2009) 150:687–98. doi:10.1210/en.2008-0623

62. Haas E, Bhattacharya I, Brailoiu E, Damjanović M, Brailoiu GC, Gao X, et al. Regulatory role of G protein-coupled estrogen receptor for vascular function and obesity. *Circ Res* (2009) 104:288–91. doi:10.1161/CIRCRESAHA.108.190892

63. Wang C, Dehghani B, Magrisso IJ, Rick EA, Bonhomme E, Cody DB, et al. GPR30 contributes to estrogen-induced thymic atrophy. *Mol Endocrinol Baltim Md* (2008) 22:636–48. doi:10.1210/me.2007-0359

64. Brunsing RL, Prossnitz ER. Induction of interleukin-10 in the T helper type 17 effector population by the G protein coupled estrogen receptor (GPER) agonist G-1. *Immunology* (2011) 134:93–106. doi:10.1111/j.1365-2567.2011.03471.x

65. Yates MA, Li Y, Chlebeck PJ, Offner H. GPR30, but not estrogen receptor-alpha, is crucial in the treatment of experimental autoimmune encephalomyelitis by oral ethinyl estradiol. *BMC Immunol* (2010) 11:20. doi:10.1186/1471-2172-11-20

66. Jenei-Lanzl Z, Straub RH, Dienstknecht T, Huber M, Hager M, Grässel S, et al. Estradiol inhibits chondrogenic differentiation of mesenchymal stem cells via nonclassic signaling. *Arthritis Rheum* (2010) 62:1088–96. doi:10.1002/art.27328

67. Filardo EJ, Graeber CT, Quinn JA, Resnick MB, Giri D, DeLellis RA, et al. Distribution of GPR30, a seven membrane–spanning estrogen receptor, in primary breast cancer and its association with clinicopathologic determinants of tumor progression. *Clin Cancer Res* (2006) 12:6359–66. doi:10.1158/1078-0432.CCR-06-0860

68. Smith HO, Arias-Pulido H, Kuo DY, Howard T, Qualls CR, Lee SJ, et al. GPR30 predicts poor survival for ovarian cancer. *Gynecol Oncol* (2009) 114:465–71. doi:10.1016/j.ygyno.2009.05.015

69. Jung J. Role of G Protein-Coupled estrogen receptor in cancer progression. *Toxicol Res* (2019) 35:209–14. doi:10.5487/TR.2019.35.3.209

70. Liu H, Yan Y, Wen H, Jiang X, Cao X, Zhang G, et al. A novel estrogen receptor GPER mediates proliferation induced by 17β-estradiol and selective GPER agonist G-1 in estrogen receptor α (ERα)-negative ovarian cancer cells. *Cell Biol Int* (2014) 38:631–8. doi:10.1002/cbin.10243

71. Yan Y, Liu H, Wen H, Jiang X, Cao X, Zhang G, et al. The novel estrogen receptor GPER regulates the migration and invasion of ovarian cancer cells. *Mol Cell Biochem* (2013) 378:1–7. doi:10.1007/s11010-013-1579-9

72. Smith HO, Leslie KK, Singh M, Qualls CR, Revankar CM, Joste NE, et al. GPR30: a novel indicator of poor survival for endometrial carcinoma. *Am J Obstet Gynecol* (2007) 196:386.e1–9. discussion 386.e9-11. doi:10.1016/j.ajog.2007.01.004

73. Petrie WK, Dennis MK, Hu C, Dai D, Arterburn JB, Smith HO, et al. G protein-coupled estrogen receptor-selective ligands modulate endometrial tumor growth. *Obstet Gynecol Int* (2013) 2013:472720. doi:10.1155/2013/472720

74. Avino S, De Marco P, Cirillo F, Santolla MF, De Francesco EM, Perri MG, et al. Stimulatory actions of IGF-I are mediated by IGF-IR cross-talk with GPER and DDR1 in mesothelioma and lung cancer cells. *Oncotarget* (2016) 7:52710–28. doi:10.18632/oncotarget.10348

75. Liu C, Liao Y, Fan S, Fu X, Xiong J, Zhou S, et al. G-Protein-Coupled estrogen receptor antagonist G15 decreases estrogen-induced development of non-small cell lung cancer. *Oncol Res* (2019) 27:283–92. doi:10.3727/096504017X15035795904677

76. Torres-López L, Olivas-Aguirre M, Villatoro-Gómez K, Dobrovinskaya O. The G-protein-coupled estrogen receptor agonist G-1 inhibits proliferation and causes apoptosis in leukemia cell lines of T lineage. *Front Cell Dev Biol* (2022) 10:811479. doi:10.3389/fcell.2022.811479

77. Zhou L, Yu T, Yang F, Han J, Zuo B, Huang L, et al. G protein-coupled estrogen receptor agonist G-1 inhibits mantle cell lymphoma growth in preclinical models. *Front Oncol* (2021) 11:668617. doi:10.3389/fonc.2021.668617

78. Natale CA, Li J, Pitarresi JR, Norgard RJ, Dentchev T, Capell BC, et al. Pharmacologic activation of the G protein-coupled estrogen receptor inhibits pancreatic ductal adenocarcinoma. *Cell Mol Gastroenterol Hepatol* (2020) 10:868–80. doi:10.1016/j.jcmgh.2020.04.016

79. Hirtz A, Lebourdais N, Rech F, Bailly Y, Vaginay A, Smaïl-Tabbone M, et al. GPER agonist G-1 disrupts tubulin dynamics and potentiates temozolomide to impair glioblastoma cell proliferation. *Cells* (2021) 10:3438. doi:10.3390/cells10123438

80. Schüler-Toprak S, Skrzypczak M, Ignatov T, Ortmann O, Treeck O. G protein-coupled estrogen receptor 1 (GPER-1) and agonist G-1 inhibit growth of ovarian cancer cells by activation of anti-tumoral transcriptome responses: impact of GPER-1 mRNA on survival. *J Cancer Res Clin Oncol* (2020) 146:3175–88. doi:10.1007/s00432-020-03333-4

81. Lee S-J, Kim TW, Park GL, Hwang YS, Cho HJ, Kim J-T, et al. G protein-coupled estrogen receptor-1 agonist induces chemotherapeutic effect via ER stress signaling in gastric cancer. *BMB Rep* (2019) 52:647–52. doi:10.5483/BMBRep.2019.52.11.007

82. Ambrosini G, Natale CA, Musi E, Garyantes T, Schwartz GK. The GPER agonist LNS8801 induces mitotic arrest and apoptosis in uveal melanoma cells. *Cancer Res Commun* (2023) 3:540–7. doi:10.1158/2767-9764.CRC-22-0399

83. Linnaeus Therapeutics, Inc. *Study assessing MTD, safety, tolerability, PK and anti-tumor effects of LNS8801alone and with pembrolizumab*. clinicaltrials.gov (2022). Available from: https://clinicaltrials.gov/study/NCT04130516?intr=LNS8801&rank=1 (Accessed August 18, 2022).

84. Liu C-C, Lin J-H, Hsu T-W, Hsu JW, Chang JW, Su K, et al. Collagen XVII/laminin-5 activates epithelial-to-mesenchymal transition and is associated with poor prognosis in lung cancer. *Oncotarget* (2018) 9:1656–72. doi:10.18632/oncotarget.11208

85. Yamada T, Endo R, Tsukagoshi K, Fujita S, Honda K, Kinoshita M, et al. Aberrant expression of a hemidesmosomal protein, bullous pemphigoid antigen 2, in human squamous cell carcinoma. *Lab Investig J Tech Methods Pathol* (1996) 75: 589–600.

86. Thangavelu PU, Krenács T, Dray E, Duijf PHG. In epithelial cancers, aberrant COL17A1 promoter methylation predicts its misexpression and increased invasion. *Clin Epigenetics* (2016) 8:120. doi:10.1186/s13148-016-0290-6

87. Tamás L, Szentkúti G, Eros M, Dános K, Brauswetter D, Szende B, et al. Differential biomarker expression in head and neck cancer correlates with anatomical localization. *Pathol Oncol Res POR* (2011) 17:721–7. doi:10.1007/s12253-011-9376-9

88. Parikka M, Kainulainen T, Tasanen K, Väänänen A, Bruckner-Tuderman L, Salo T. Alterations of collagen XVII expression during transformation of oral epithelium to dysplasia and carcinoma. *J Histochem Cytochem Off J Histochem Soc* (2003) 51:921–9. doi:10.1177/002215540305100707

89. Parikka M, Nissinen L, Kainulainen T, Bruckner-Tuderman L, Salo T, Heino J, et al. Collagen XVII promotes integrin-mediated squamous cell carcinoma transmigration--a novel role for alphaIIb integrin and tirofiban. *Exp Cell Res* (2006) 312:1431–8. doi:10.1016/j.yexcr.2006.01.015

90. Hwang B-J, Zhang Y, Brozowski JM, Liu Z, Burette S, Lough K, et al. The dysfunction of BP180/collagen XVII in keratinocytes promotes melanoma progression. *Oncogene* (2019) 38:7491–503. doi:10.1038/s41388-019-0961-9

91. Tong D, Tanaka M, Eguchi H, Okazaki Y, Muramatsu M, Arai T. COL17A1 germline variant p.Ser1029Ala and mucosal malignant melanoma: an autopsy study. *Mol Clin Oncol* (2022) 16:32. doi:10.3892/mco.2021.2465

92. Lothong M, Sakares W, Rojsitthisak P, Tanikawa C, Matsuda K, Yodsurang V. Collagen XVII inhibits breast cancer cell proliferation and growth through deactivation of the AKT/mTOR signaling pathway. *PLoS One* (2021) 16: e0255179. doi:10.1371/journal.pone.0255179

93. Fujiwara S, Terai Y, Kawaguchi H, Takai M, Yoo S, Tanaka Y, et al. GPR30 regulates the EGFR-Akt cascade and predicts lower survival in patients with ovarian cancer. *J Ovarian Res* (2012) 5:35. doi:10.1186/1757-2215-5-35

94. Chen J, Zhao R, Wang Y, Xiao H, Lin W, Diao M, et al. G protein-coupled estrogen receptor activates PI3K/AKT/mTOR signaling to suppress ferroptosis via SREBP1/SCD1-mediated lipogenesis. *Mol Med* (2024) 30:28. doi:10.1186/s10020-023-00763-x

95. Wang Y, Peng Z, Meng R, Tao T, Wang Q, Zhao C, et al. NHERF1 inhibits proliferation of triple-negative breast cancer cells by suppressing GPER signaling. *Oncol Rep* (2017) 38:221–8. doi:10.3892/or.2017.5649

96. Hou X, Zhao M, Wang T, Zhang G. Upregulation of estrogen receptor mediates migration, invasion and proliferation of endometrial carcinoma cells by regulating the PI3K/AKT/mTOR pathway. *Oncol Rep* (2014) 31:1175–82. doi:10.3892/or.2013.2944

Pathology & Oncology Research | frontiers

TYPE Original Research
PUBLISHED 05 April 2024
DOI 10.3389/pore.2024.1611574

Check for updates

OPEN ACCESS

EDITED BY
Andrea Ladányi,
National Institute of Oncology (NIO), Hungary

*CORRESPONDENCE
Anna Jakab,
jakab.anna@semmelweis.hu,
annajakab272@gmail.com

RECEIVED 04 November 2023
ACCEPTED 12 March 2024
PUBLISHED 05 April 2024

CITATION
Jakab A, Patai ÁV, Darvas M, Tormássi-Bély K and Micsik T (2024), Microenvironment, systemic inflammatory response and tumor markers considering consensus molecular subtypes of colorectal cancer.
Pathol. Oncol. Res. 30:1611574.
doi: 10.3389/pore.2024.1611574

COPYRIGHT
© 2024 Jakab, Patai, Darvas, Tormássi-Bély and Micsik. This is an open-access article distributed under the terms of the Creative Commons Attribution License (CC BY). The use, distribution or reproduction in other forums is permitted, provided the original author(s) and the copyright owner(s) are credited and that the original publication in this journal is cited, in accordance with accepted academic practice. No use, distribution or reproduction is permitted which does not comply with these terms.

Microenvironment, systemic inflammatory response and tumor markers considering consensus molecular subtypes of colorectal cancer

Anna Jakab[1,2]*, Árpád V. Patai[2,3], Mónika Darvas[2,3], Karolina Tormássi-Bély[1,2] and Tamás Micsik[1,2,4]

[1]Department of Pathology and Experimental Cancer Research, Semmelweis University, Budapest, Hungary, [2]Interdisciplinary Gastroenterology Working Group, Semmelweis University, Budapest, Hungary, [3]Department of Surgery, Transplantation and Gastroenterology, Semmelweis University, Budapest, Hungary, [4]Saint George University Teaching Hospital of Fejér County, Székesfehérvár, Hungary

Introduction: Colorectal carcinomas (CRC) are one of the most frequent malignancies worldwide. Based on gene expression profile analysis, CRCs can be classified into four distinct subtypes also known as the consensus molecular subtypes (CMS), which predict biological behaviour. Besides CMS, several other aspects of tumor microenvironment (TME) and systemic inflammatory response (SIR) influence the outcome of CRC patients. TME and inflammation have important role in the immune (CMS1) and mesenchymal (CMS4) subtypes, however, the relationship between these and systemic inflammation has not been assessed yet. Our objective was to evaluate the connection between CMS, TME and SIR, and to analyze the correlation between these markers and routinely used tumor markers, such as CEA (Carcinoembryonic Antigen) and CA19-9 (Carbohydrate Antigen 19-9).

Methods: FFPE (Formalin Fixed Paraffin Embedded) samples of 185 CRC patients were collected. TME was described using tumor-stroma ratio (TSR), Klintrup-Makinen (KM) grade, and Glasgow Microenvironment Score (GMS). CMS classification was performed on tissue microarray using MLH1, PMS2, MSH2 and MSH6, and pan-cytokeratin, CDX2, FRMD6, HTR2B and ZEB1 immunohistochemical stains. Pre-operative tumor marker levels and

Abbreviations: ALC, absolute lymphocyte count; ANC, absolute neutrophil count; APC, absolute platelet count; CA19-9, Carbohydrate antigen; CEA, Carcinoembryonic antigen; CK, Cytokeratin; CMS, Consensus molecular subtype; CRC, colorectal cancer; CRP, C reactive protein; dMMR, mismatch repair deficient; EMT, Epithelial-mesenchymal transition; FFPE, formalin fixed paraffin embedded; GMS, Glasgow microenvironment score; HE, hematoxylin-eosin; KM score, Klintrup-Makinen score; M, distant metastasis; mGPS, modified Glasgow prognostic score; MSI, microsatellite instability or instable; NLR, neutrophil—lymphocyte ratio; NPS, Neutrophil—platelet score; OS, overall survival; PLR, platelet—lymphocyte ratio; pMMR, proficient MMR; pN, pathological, regional lymph node metastasis; pT, pathological, extent of primary tumor; SIR, systemic inflammatory response; STM, Stroma-tumor marker; TMA, Tissue Microarray; TME, Tumor microenvironment; TSR, Tumor-stroma ratio.

inflammatory markers [C-reactive protein - CRP, albumin, absolute neutrophil count (ANC), absolute lymphocyte count (ALC), absolute platelet count (APC)] and patient history were retrieved using MedSolution database.

Results: Amongst TME-markers, TSR correlated most consistently with adverse clinicopathological features ($p < 0.001$) and overall survival ($p < 0.001$). Elevated CRP and modified Glasgow Prognostic Score (mGPS) were associated with worse outcome and aggressive phenotype, similarly to tumor markers CEA and CA19-9. Stroma–Tumor Marker score (STM score), a new combined score of CA19-9 and TSR delivered the second best prognostication after mGPS. Furthermore, CMS4 showed association with TSR and several laboratory markers (albumin and platelet derived factors), but not with other SIR descriptors. CMS did not show any association with CEA and CA19-9 tumor markers.

Conclusion: More routinely available TME, SIR and tumor markers alone and in combination deliver reliable prognostic data for choosing the patients with higher risk for propagation. CMS4 is linked with high TSR and poor prognosis, but in overall, CMS-classification showed only limited effect on SIR- and tumor-markers.

KEYWORDS

colorectal cancer, consensus molecular subtypes, tumor microenvironment (TME), tumor-stroma ratio, systemic inflammation

Introduction

Colorectal cancer (CRC) is amongst the most frequent malignancies worldwide, and the second most common cause of death in cancer patients [1]. Despite advancements in targeted therapy, a large subset of CRC patients is not eligible for specialized treatment or often presents resistance [2].

The tumor microenvironment (TME) is an inseparable element of malignancies, providing comprehensive understanding to cancer biology and presenting strong prognosticators of patient outcome and therapy response [3–5]. There are several aspects of the TME in CRC, that provide clinically relevant information on tumor biology and patient outcome, moreover, some of these can be assessed conveniently by hematoxylin-eosin (HE) slides. Such markers may focus on the inflammatory infiltrate, like the Klintrup-Makinen (KM) score, that describes the inflammatory infiltrate at the invasive front without subtle measurements and is reported to be positively linked with favorable prognosis [6, 7]. Another set of TME markers is based on the assessment of stromal matrix and its components, like the tumor-stroma ratio (TSR) [8]. The TSR provides information on the amount of stromal content at the invasive front of the tumor [9]. Stroma-high (or TSR–high) tumors are linked to a more aggressive phenotype with notably poor prognosis and potential resistance to standard chemotherapy [10, 11]. Furthermore, utilizing the combination of these two, a novel grading system, the so-called Glasgow Microenvironment Score (GMS), was introduced [12]. The GMS, a combined assessment of stromal and inflammatory infiltrate in CRC, further improves the risk stratification of CRC patients and is also a strong independent prognostic factor [13].

To further understand the complex biological behavior of CRC, the consensus molecular subtyping consortium identified four distinct subclasses of CRC with the help of transcriptome-based gene expression pattern analysis, the consensus molecular subtypes (CMS) [14]. The TME has particular role in the CMS1 (also known as "immune") and the CMS4 (a.k.a. "mesenchymal") subtype [15]. CMS1 tumors exhibit abundant antitumoral inflammatory infiltrate and overexpression of genes associated with $CD8^+$, T helper1 cell activation and T cell attracting chemokines [15], and are enriched in mismatch repair deficient (dMMR) tumors, while the mesenchymal subtype displays pronounced stromal infiltration and TGFβ signaling [14, 16]. Although currently present in the research field only, CMS classification seems a promising risk stratification method and soon might play an important role in both predicting response to traditional agents and personalized therapy as well, since the usual targeted agents may be particularly ineffective in CMS4 tumors [17, 18].

Markers of systemic inflammatory reaction (SIR), like C reactive protein (CRP), absolute neutrophil count (ANC) or lymphocyte count (ALC), or platelet count (APC), are often associated with poor prognosis in many cancer types, including CRC [19, 20]. Several inflammation-related markers might be associated with TME, however, their relationship to CMS, or more specifically, CMS4, is yet to be explored [21]. Some components of the SIR can be examined in combination,

which might be utilized using composite ratios or cumulative scores. The modified Glasgow Prognostic Score (mGPS), comprising of serum albumin and CRP, is an approved indicator of systemic inflammatory processes, as well as cachexia [22, 23]. In patients with CRC, mGPS accurately predicts outcomes, with a high score associated with worse overall survival (OS) [22]. Neutrophil-lymphocyte ratio (NLR) and platelet-lymphocyte ratio (PLR), and neutrophil-platelet score (NPS) are also robust inflammation-related prognosticators in many cancers, including CRC [21, 23, 24].

Besides the TME, and the SIR, other readily available blood markers may also reflect tumor aggressiveness and predict patient outcome. Carcinoembryonic antigen (CEA) and carbohydrate antigen 19-9 (CA19-9) are frequently used tumor markers in CRC follow-up, and while these might not have the same efficacy in monitoring recurrence [25], they might be useful in certain subgroups of CRC patients [26, 27]. Even though these markers are not suited for screening purposes, their elevated levels are associated with advanced stages and therefore worse outcomes, or even therapy resistance [28–30]. Currently it is unclear, how these tumor markers are associated with the tumor microenvironment, SIR or CMS.

The aim of our study was to investigate the relation between microenvironment, systemic inflammation, CMS and tumor markers, as well as to explore and compare their prognostic significance. We investigated a few markers of systemic inflammation, including ANC, ALC, APC, CRP, albumin, and derived scores, like mGPS, NLR and to examine their relation to TME markers, tumor markers and CMS.

Methods

Patients and clinical data collection

185 stage I-IV patients, who underwent surgery due to colorectal cancer between 2009–2017, were selected retrospectively and their slides and formaline fixed paraffin embedded (FFPE) blocks were retrieved from the archives of the Department of Pathology and Experimental Cancer Research, Semmelweis University, Budapest, Hungary. Patients who received neoadjuvant treatment, died within 30 days of surgery, had other synchronous or metachronous primary colorectal cancer, or another malignancy requiring systemic treatment in their history, were excluded from the study. Patient history and laboratory results were collected using the medical database of Semmelweis University (MedSolution, T-Systems, Budapest, Hungary). Preoperative serum CA19-9 and CEA levels were measured routinely using Abbott Architect CA 19-9 XR immunoassay (Chicago, IL, United States of America) and Abbott Architect CEA immunoassay (Chicago, IL, United States of America). Pathological characterization of surgically resected primary tumors was performed according to the UICC TNM classification, 8th edition.

Assessment of tumor microenvironment

TSR was evaluated on HE-stained slides in accordance with recommendations [8]: stromal content was estimated visually per 10% increments at ×10 magnification field of the invasive front of the tumor (containing the stromal hotspot). If stromal content exceeded 50% of the examined area, patients were classified as TSR-high, if not, they were categorized as TSR-low (Figure 1).

KM grade was estimated according to the criteria established by Klintrup et al [6]. Briefly, inflammatory reaction was graded as KM-low when there was no or only mild increase in inflammatory cells at the invasive front, and a KM-high score was given when there was a band- or cup-like infiltrate of inflammatory cells at the margin with destruction of cancer cells (Figure 1). The GMS is a combination of KM score and TSR. Briefly, when there was extensive inflammatory reaction (KM-high), a score of GMS0 was given. In case of stroma-low and KM-low tumors, a score of GMS1, and in case of stroma-high and KM-low tumors a score of GMS2 was given (Supplementary Table S1), as described previously [12, 13]. All parameters were graded by two independent observers (AJ and TSM) blinded to clinicopathological data and disease outcome.

Assessment of SIR and tumor markers

All blood samples were obtained from patients within 30 days before surgery. Cutoff values and scoring of SIR markers are included in Supplementary Table S1.

Microarray construction and immunohistochemistry

Tissue microarray (TMA) blocks containing 6 × 9 cores (core diameter: 2 mm) selected from surgically derived FFPE blocks of 167 patients were created using TMA Master1000 (3DHistech, Budapest, Hungary). At least two representative cores were selected per case. Non-neoplastic kidney samples were used as normal tissues and stain controls in each block.

Immunohistochemistry was performed on 4 um thick sections of TMAs. For mismatch repair status (MMR) assessment, anti-MLH1, anti-PMS2, anti-MSH2, and anti-MSH6 primary stains were used and graded as recommended [31]. CMS classification was carried out on proficient MMR (pMMR) samples using anti-cytokeratin (CK), anti-CDX2, anti-FRMD6, and anti-ZEB1 immunhistochemistry as described by Ten Hoorn et al [32]. For further details of

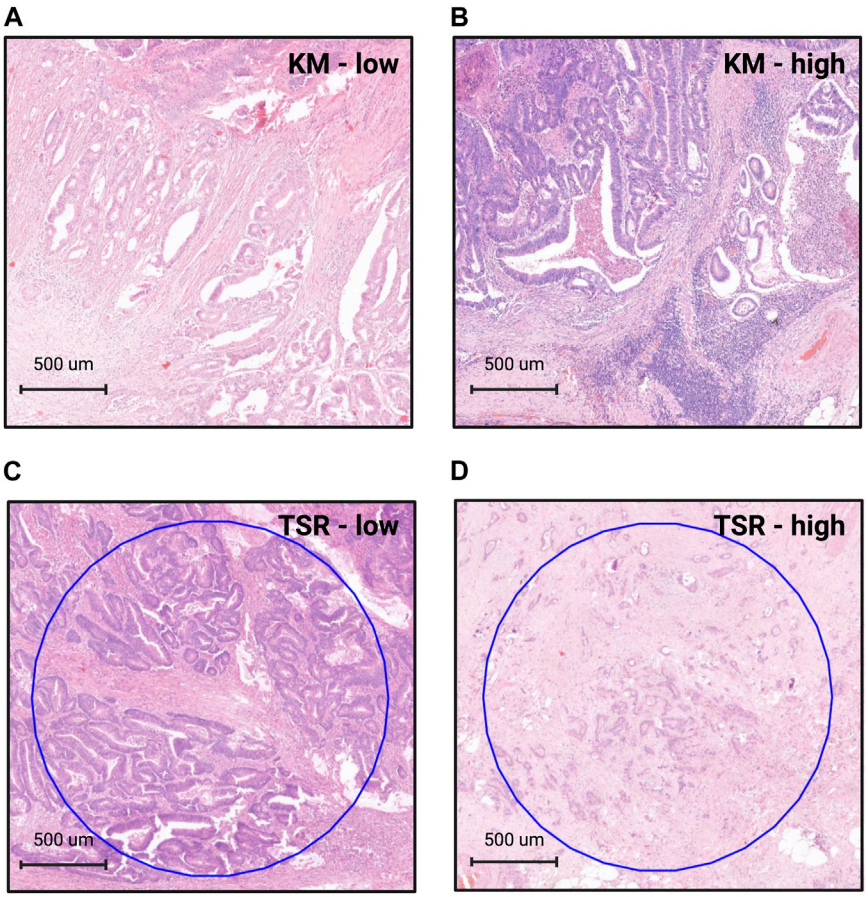

FIGURE 1
Grading the tumor microenvironment on HE-slides. For assessing Klintrup-Makinen grade, the inflammatory infiltrate has to be examined at the invasive front of the tumor. In case there is none or only patchy, mild inflammation, cases are classified as KM-low **(A)**. If there is a band- or cup-like, florid inflammatory infiltrate with destruction of tumor cells, cases are graded as KM-high **(B)**. When assessing the tumor-stroma ratio (TSR), the stromal hotspot has to be evaluated at the invasive front using a ×10 objective. Tumor cells must be present at all four poles of the field of view. If stromal content is less than 50% of the examined area, cases are graded as TSR-low **(C)**. If stromal content equals or exceeds 50% of this area, cases are graded as TSR-high **(D)**. List of abbreviations: HE, hematoxylin-eosin; KM, Klintrup-Makinen grade; TSR, tumor-stroma ratio. Figure was created using https://www.biorender.com/.

immunohistochemistry, please see Supplementary Table S2. Cytoplasmic CK and FRMD6, nuclear CDX2, as well as membrane and cytoplasmic HTR2B were graded as low, moderate or high. In case of ZEB1, the presence of nuclear staining was scored as either present or absent. All CMS stains were graded both in accordance with Ten Hoorn et al's recommendations, and, apart from ZEB1, using H-score as well [33].

All immunohistochemical reactions were assessed by two observers (AJ and TSM).

CMS classification

Cases with deficient MMR-status (dMMR) were classified as CMS1. For proficient MMR tumors, CMS classification was performed using an online, TMA-based and validated, robust and reliable random forest classifier[1] as described previously [32, 33]. Briefly, four immunostains (ZEB1, HTRB2, FRMD6 and CDX2) were selected based on distinct gene expression profile differences in CMS2/3 and CMS4 tumors. In pMMR tumors, the stain intensity and content of these four stains in tumor epithelium correlates with their CMSs [32]. Typically, low FRMD6 and HTR2B staining intensities, lack of nuclear ZEB1 expression and strong CDX2 stain correlate with epithelial subtypes (CMS2/3); while strong positive FRMD6 and HTR2B, loss of CDX2 and positive nuclear ZEB1 reaction is expected in mesenchymal CRCs (CMS4)

1 https://crcclassifier.shinyapps.io/appTesting/

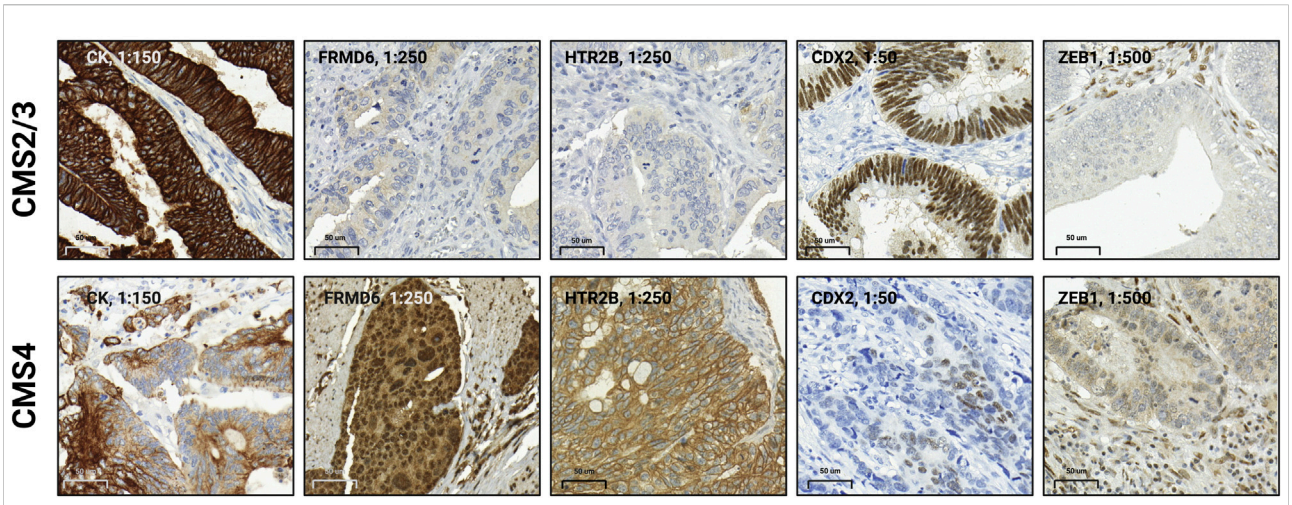

FIGURE 2
Immunohistochemistry-based phenotype of epithelial and mesenchymal subtypes of colorectal cancer (CRC). In CMS2/3 or epithelial CRCs, predominantly strong positive CK reaction, negative or weak positive FRMD6 and HTR2B stains, prominent CDX2 nuclear reaction and lack of nuclear ZEB1 expression can be observed. In CMS4 or mesenchymal tumors, usually a somewhat weaker or less intense CK reaction, strong positive FRMD6 and HTR2B reaction, loss of CDX2 stain, and presence of nuclear ZEB1 expression can be detected. CMS classification was carried out using an online, validated CMS-classifier at https://crcclassifier.shinyapps.io/appTesting/. Figure was created using https://www.biorender.com/.

(Figure 2) [33]. In case the probability of a CMS was estimated higher than 0.6, we automatically labeled the case in concordance with the software. Where the probability of estimated CMS was between 0.5 and. 0.6, the case was automatically excluded from our analysis. In total, 12 cases were excluded due to uncertain subtyping.

Establishing a novel scoring system: stroma-tumor marker (STM) score

To reflect the biological behaviour of certain cancer subtypes classified by TSR and CA19-9, a novel scoring system was established by combining CA19-9 and TSR into stroma-tumor marker (STM) score. In case of TSR-low and CA 19-9 low cases, STM 0 score was given. If either CA19-9 or TSR was classified as high, but the other marker as low, an STM 1 score was given. When both markers were classified as "high," STM 2 score was given (Supplementary Table S1).

Statistical analysis

Shapiro-Wilks test of normality was performed on the continuous variables. In order to determine the relationship between clinicopathological features and categorical variables, Chi-squared test was performed. Mann-Whitney *U*-test or Kruskal-Wallis H-test was performed to examine the correlation between clinicopathological features and continuous variables. Spearman's rank order correlation coefficent was calculated to investigate the correlation between certain systemic inflammation-related and tumor markers. The relationship between TME, systemic and tumor markers and survival was carried out using Kaplan-Meier log-rank survival analysis. To assess how certain variables affect the overall survival (OS), uni- and multivariate Cox regression analysis was performed. All variables that reached $p < 0.1$ in the univariate analysis were included for the multivariate analysis. The complete statistical analysis was performed using SPSS version 28.0.1.0 (IBM, Armonk, NY, United States).

Results

Patient characteristics

Altogether, 185 patients were included in our cohort, 155 patients had available CEA, and 135 patients had available CA19-9 results. CMS classification was carried out in 155 patients. Further information can be found in Tables 1–3 and Supplementary Table S1.

TME characteristics

Patients with TSR-high tumors were significantly associated with higher pT ($p = 0.043$), pN ($p < 0.001$) and M ($p < 0.001$) descriptors (Table 1). Also, lymphatic and perineural invasion was significantly higher amongst TSR-high patients ($p < 0.001$ and $p = 0.002$) (Table 1). TSR correlated with age, CEA

TABLE 1 The relationship between tumor-stroma ratio (TSR), Klintrup-Makinen (KM) grade and clinicopathological parameters.

	All patients (n = 185*)	TSR (n = 185)			KM grade (n = 185)		
		TSR-low (n = 121)	TSR-high (n = 64)	*p*-value	KM-low (n = 123)	KM-high (n = 62)	*p*-value
Age (n = 185)				**$p = 0.022$**			$p = 0.237$
<65	65 (35%)	**34 (28%)**	**31 (48%)**		45 (37%)	20 (32%)	
65-74	77 (42%)	**56 (46%)**	**21 (33%)**		54 (44%)	23 (37%)	
75<	43 (23%)	**31 (26%)**	**12 (19%)**		24 (20%)	19 (31%)	
Sex (n = 185)				$p = 0.353$			$p = 0.434$
Female	97 (52%)	60 (50%)	37 (58%)		67 (55%)	30 (48%)	
Male	88 (48%)	61 (50%)	27 (42%)		56 (46%)	32 (52%)	
Location (n = 185)				$p = 0.350$			$p = 0.488$
Right colon	75 (41%)	53 (44%)	22 (34%)		47 (38%)	28 (45%)	
Left colon	58 (31%)	34 (28%)	24 (37.5%)		42 (34%)	16 (26%)	
Rectum	52 (28%)	34 (28%)	18 (28%)		35 (28%)	18 (29%)	
pT (n = 185)				**$p = 0.043$**			**$p = 0.029$**
pT1	2 (1%)	**2 (2%)**	**0 (0%)**		**0 (0%)**	**2 (3%)**	
pT2	34 (18%)	**28 (23%)**	**6 (9%)**		**22 (18%)**	**12 (19%)**	
pT3	134 (72%)	**84 (69%)**	**50 (78%)**		**87 (71%)**	**47 (76%)**	
pT4	15 (8%)	**7 (6%)**	**8 (13%)**		**14 (11%)**	**1 (2%)**	
pN (n = 184)				**$p < 0.001$**			**$p = 0.024$**
pN0	82 (45%)	**66 (55%)**	**16 (25%)**		**47 (39%)**	**35 (57%)**	
pN1	67 (36%)	**37 (31%)**	**30 (47%)**		**46 (38%)**	**21 (34%)**	
pN2	35 (19%)	**17 (14%)**	**18 (28%)**		**29 (24%)**	**6 (10%)**	
M (n = 185)				**$p < 0.001$**			**$p = 0.009$**
M0	143 (77%)	**104 (86%)**	**39 (61%)**		**88 (72%)**	**55 (89%)**	
M1	42 (23%)	**17 (14%)**	**25 (39%)**		**35 (29%)**	**7 (11%)**	
Stage (n = 185)				**$p < 0.001$**			**$p = 0.017$**
I	26 (14%)	**23 (19%)**	**3 (5%)**		**16 (13%)**	**10 (16%)**	
II	48 (26%)	**37 (31%)**	**11 (17%)**		**25 (20%)**	**23 (37%)**	
III	69 (37%)	**44 (36%)**	**25 (39%)**		**47 (38%)**	**22 (36%)**	
IV	42 (23%)	**17 (14%)**	**25 (39%)**		**35 (29%)**	**7 (11%)**	
Grade (n = 185)				$p = 0.108$			$p = 0.629$
Low/moderate	161 (87%)	109 (90%)	52 (81%)		106 (86%)	55 (89%)	
High	24 (13%)	12 (10%)	12 (19%)		17 (14%)	7 (11%)	
Lymphatic invasion (n = 185)				**$p < 0.001$**			*$p = 0.093$*
Not present	122 (66%)	**94 (78%)**	**28 (44%)**		*76 (62%)*	*46 (74%)*	
Present	63 (34%)	**27 (22%)**	**36 (56%)**		*47 (38%)*	*16 (26%)*	

(Continued on following page)

TABLE 1 (*Continued*) The relationship between tumor-stroma ratio (TSR), Klintrup-Makinen (KM) grade and clinicopathological parameters.

	All patients (n = 185*)	TSR (n = 185)			KM grade (n = 185)		
		TSR-low (n = 121)	TSR-high (n = 64)	*p*-value	KM-low (n = 123)	KM-high (n = 62)	*p*-value
Perineural invasion (n = 185)				**$p = 0.002$**			$p = 0.247$
Not present	170 (92%)	**117 (97%)**	**53 (83%)**		111 (90%)	59 (95%)	
Present	15 (8%)	**4 (3%)**	**11 (17%)**		12 (10%)	3 (5%)	
mGPS (n = 96)				$p = 0.395$			$p = 0.680$
mGPS 0	39 (41%)	28 (44%)	11 (34%)		27 (40%)	14 (50%)	
mGPS 1	36 (38%)	24 (38%)	12 (38%)		25 (37%)	9 (32%)	
mGPS 2	21 (22%)	12 (20%)	9 (28%)		15 (22%)	5 (18%)	
CMS (n = 155)				*$p = 0.054$*			$p = 0.354$
CMS1	16 (10%)	*12 (12%)*	*4 (7%)*		8 (8%)	8 (15%)	
CMS2/3	109 (70%)	*75 (74%)*	*34 (63%)*		73 (72%)	36 (68%)	
CMS4	30 (19%)	*14 (14%)*	*16 (30%)*		21 (21%)	9 (17%)	
CEA (n = 155)				**$p = 0.029$**			$p = 0.919$
CEA-low	101 (65%)	**72 (71%)**	**29 (54%)**		70 (65%)	31 (65%)	
CEA-high	54 (35%)	**29 (29%)**	**25 (46%)**		37 (35%)	17 (35%)	
CA19-9 (n = 135)				**$p = 0.035$**			$p = 0.584$
CA19-9-low	111 (82%)	**80 (87%)**	**31 (72%)**		77 (81%)	34 (85%)	
CA19-9-high	24 (18%)	**31 (13%)**	**28 (28%)**		19 (19%)	6 (15%)	

The relationship between TSR, KM, grade and clinicopathological features was assessed using Chi-squared test. Significant correlations were marked with bold font, while tendencies where $p < 0.1$ were marked with italic font. In some cases, percentages do not add up to 100% precisely due to rounding. Abbreviations: TSR, tumor-stroma ratio; KM, grade, Klintrup Makinen grade; mGPS, modified Glasgow Prognostic Score; CMS, consensus molecular subtypes; CEA, carcinoembryonic antigen; CA 19-9, Carbohydrate antigen 19-9.

and CA19-9, using Chi-squared test ($p = 0.022$, $p = 0.029$, $p = 0.035$). Similarly, KM-low correlated with advanced pT, pN, stage and M-status ($p = 0.029$, $p = 0.024$, $p = 0.017$ and $p = 0.009$) and also, a tendency towards lymphatic invasion ($p = 0.093$) was found (Table 1). As expected based on TSR and KM grading results, GMS was also associated with more advanced pT, pN and M descriptors and stage ($p = 0.015$, $p = 0.001$, $p < 0.001$ and $p < 0.001$) and lymphatic and perineural invasion ($p < 0.001$, $p = 0.010$), and there was a tendency towards vascular invasion ($p = 0.065$) (Table 2). KM, TSR or GMS were not associated with any SIR markers (Supplementary Tables S3, S4).

Pre-operative SIR assessment

Elevation of serum CRP was associated with increasing stage ($p = 0.002$), pT ($p < 0.001$), distant metastasis ($p = 0.007$), higher grade ($p = 0.027$), vascular invasion ($p = 0.026$), lymphatic invasion ($p = 0.032$) and there was a trend towards perineural invasion ($p = 0.063$) (Supplementary Table S3). There was a significant correlation between ANC and higher pT ($p = 0.011$) and a trend towards advanced pN ($p = 0.058$) (Supplementary Table S3). ALC did not correlate with any of the examined features, but with younger age ($p = 0.007$). APC was significantly elevated in males ($p = 0.003$), associated with right-sidedness ($p = 0.013$), CMS1 ($p < 0.001$), showed significant association with lymphatic invasion ($p = 0.045$) and there was a tendency towards distant metastasis ($p = 0.068$) and vascular invasion ($p = 0.077$) (Supplementary Table S3, Figure 3).

NLR did not show any correlation with tumor descriptors, but PLR showed significant association with higher age ($p = 0.046$), right sidedness ($p = 0.022$) and CMS1 ($p = 0.005$) using nonparametric Kruskal-Wallis H-test (Supplementary Table S3). The mGPS showed significant association with higher grade ($p = 0.042$) and a tendency towards elevated pT ($p = 0.057$) (Supplementary Table S4). NLR and PLR did not show any correlation with clinicopathological descriptors, whereas NPS was significantly associated with male gender ($p = 0.003$), higher pT and pN stages ($p = 0.043$ and $p = 0.032$) and was inversely associated with the frequency of epithelial phenotype using Chi-squared test ($p = 0.034$) (Supplementary Table S4).

TABLE 2 The relationship between Glasgow microenvironment score (GMS) and clinicopathological parameters.

Clinico-pathological features	All patients (n = 185*)	GMS (n = 185)			
		GMS0 (n = 102)	GMS1 (n = 42)	GMS2 (n = 41)	*p*-value
Age (n = 185)					**$p = 0.008$**
<65	65 (35%)	**26 (26%)**	**16 (38%)**	**23 (56%)**	
65-74	77 (42%)	**50 (49%)**	**14 (33%)**	**13 (32%)**	
75<	43 (23%)	**26 (26%)**	**12 (29%)**	**5 (12%)**	
Sex (n = 185)					$p = 0.904$
Female	97 (52%)	52 (51%)	23 (55%)	22 (54%)	
Male	88 (48%)	50 (49%)	19 (45%)	19 (46%)	
Location (n = 185)					$p = 0.158$
Right colon	75 (41%)	49 (48%)	13 (31%)	13 (32%)	
Left colon	58 (31%)	25 (25%)	17 (41%)	16 (39%)	
Rectum	52 (28%)	28 (28%)	12 (29%)	12 (29%)	
pT (n = 185)					**$p = 0.015$**
pT1	2 (1%)	**2 (2%)**	**0 (0%)**	**0 (0%)**	
pT2	34 (18%)	**26 (26%)**	**6 (14%)**	**2 (5%)**	
pT3	134 (72%)	**70 (69%)**	**32 (76%)**	**32 (78%)**	
pT4	15 (8%)	**4 (4%)**	**4 (10%)**	**7 (17%)**	
pN (n = 184)					**$p = 0.001$**
pN0	82 (45%)	**56 (55%)**	**19 (46%)**	**7 (17%)**	
pN1	67 (36%)	**32 (31%)**	**14 (34%)**	**21 (51%)**	
pN2	35 (19%)	**14 (14%)**	**8 (20%)**	**13 (32%)**	
M (n = 185)					**$p < 0.001$**
M0	143 (77%)	**89 (87%)**	**32 (76%)**	**22 (54%)**	
M1	42 (23%)	**13 (13%)**	**10 (24%)**	**19 (46%)**	
Stage (n = 185)					**$p < 0.001$**
I	26 (14%)	**21 (21%)**	**4 (10%)**	**1 (2%)**	
II	48 (26%)	**30 (29%)**	**13 (31%)**	**5 (12%)**	
III	69 (37%)	**38 (37%)**	**15 (36%)**	**16 (39%)**	
IV	42 (23%)	**13 (13%)**	**10 (24%)**	**19 (46%)**	
Grade (n = 185)					$p = 0.718$
Low/moderate	161 (87%)	90 (88%)	35 (83%)	36 (88%)	
High	24 (13%)	12 (12%)	7 (17%)	5 (12%)	
Lymphatic invasion (n = 185)					**$p < 0.001$**
Not present	122 (66%)	**74 (73%)**	**32 (76%)**	**16 (39%)**	
Present	63 (34%)	**28 (28%)**	**10 (24%)**	**25 (61%)**	

(Continued on following page)

TABLE 2 (*Continued*) The relationship between Glasgow microenvironment score (GMS) and clinicopathological parameters.

Clinico-pathological features	All patients (n = 185*)	GMS (n = 185)			
		GMS0 (n = 102)	GMS1 (n = 42)	GMS2 (n = 41)	*p*-value
Perineural invasion (n = 185)					***p* = 0.010**
Not present	170 (92%)	**97 (95%)**	**40 (95%)**	**33 (81%)**	
Present	15 (8%)	**5 (5%)**	**2 (5%)**	**8 (20%)**	
mGPS (n = 96)					*p* = 0.316
mGPS 0	39 (41%)	25 (52%)	7 (33%)	9 (35%)	
mGPS 1	36 (38%)	16 (33%)	7 (33%)	11 (42%)	
mGPS 2	21 (22%)	7 (15%)	7 (33%)	6 (23%)	
CMS (n = 155)					*p* = 0.119
CMS1	16 (10%)	12 (14%)	1 (3%)	3 (8%)	
CMS2/3	109 (70%)	59 (69%)	28 (82%)	22 (61%)	
CMS4	30 (19%)	14 (17%)	5 (15%)	11 (37%)	
CEA (n = 155)					*p* = 0.215
CEA-low	101 (65%)	55 (68%)	25 (71%)	21 (54%)	
CEA-high	54 (35%)	26 (32%)	10 (29%)	18 (46%)	
CA19-9 (n = 135)					***p* = 0.011**
CA19-9-low	111 (82%)	**62 (86%)**	**29 (91%)**	**20 (65%)**	
CA19-9-high	24 (18%)	**10 (14%)**	**3 (9%)**	**11 (36%)**	

The relationship between the Glasgow microenvironment score and clinicopathological features was assessed using Chi-squared test. Significant correlations were marked with bold font, while tendencies where $p < 0.1$ were marked with italic font. In some cases, percentages do not add up to 100% precisely due to rounding. Abbreviations: GMS, Glasgow microenvironment score; mGPS, modified Glasgow Prognostic Score; CMS, consensus molecular subtypes; CEA, carcinoembryonic antigen; CA 19-9, Carbohydrate antigen 19-9.

Pre-operative serum CEA and CA19-9

CEA was significantly lower in left sided tumors ($p = 0.033$). Elevated CEA levels were associated with stage ($p < 0.001$), pT ($p = 0.044$) and distant metastasis ($p < 0.001$) and also showed a tendency towards higher pN ($p = 0.062$) stage, besides, using Chi-squared test, TSR-high tumors were associated with higher CEA levels ($p = 0.029$) (Supplementary Table S3, Table 1 and Figure 4).

CA19-9 was also associated with stage ($p < 0.001$), pT ($p = 0.002$), distant metastasis ($p < 0.001$), lymphatic invasion ($p = 0.015$), and GMS ($p = 0.027$). There was a tendency towards vascular ($p = 0.065$) and perineural ($p = 0.081$) invasion, and with Chi-squared test there was significant association between TSR-high status and elevated CA19-9 ($p = 0.035$) (Supplementary Table S3, Table 1 and Figure 4).

CMS immunohistochemistry and classification

Low CK expression was associated with higher age, and TSR-low ($p = 0.012$, $p = 0.003$), and inversely associated with presence of lymphatic invasion ($p = 0.020$) (Supplementary Table S5). Low FRMD6 expression was positively associated with TSR-low ($p = 0.041$), elevated serum CEA ($p = 0.008$) and albumin concentration ($p = 0.026$). Loss of CDX2 expression positively correlated with lymphatic and perineural invasion ($p = 0.026$ and $p = 0.037$), with NLR-high ($p = 0.023$) and showed tendency towards higher pT ($p = 0.087$) and increased serum albumin concentration ($p = 0.081$). The expression of ZEB1 was observed in only 14% of CMS classified cases. Interestingly, ZEB1 positive cases had lower CRP-levels ($p = 0.039$) and showed tendency towards lower mGPS ($p = 0.074$). No significant associations were revealed regarding HTR2B expression, only a tendency towards higher pN ($p = 0.092$) and M ($p = 0.075$) and higher PLR ($p = 0.083$) (Supplementary Table S5).

CMS1 was significantly associated with right colonic localization ($p = 0.006$) and higher histological grades ($p < 0.001$). CMS4 was associated with higher stage ($p = 0.006$), lymphatic and perineural invasion ($p < 0.001$ and $p = 0.006$, respectively) pN ($p = 0.001$) and M ($p = 0.022$) descriptors, and there was a tendency towards high TSR just failing to be

TABLE 3 The relationship between consensus molceular subtypes and clinicopathological parameters.

Clinico-pathological features	All patients (n = 185*)	CMS (n = 155)			
		CMS1 (n = 16)	CMS2/3 (n = 109)	CMS4 (n = 30)	*p*-value
Age (n = 185)					$p = 0.883$
<65	65 (35%)	4 (25%)	35 (32%)	12 (40%)	
65-74	77 (42%)	8 (50%)	49 (45%)	12 (40%)	
75<	43 (23%)	4 (25%)	25 (23%)	6 (20%)	
Sex (n = 185)					$p = 0.337$
Female	97 (52%)	6 (38%)	59 (54%)	18 (60%)	
Male	88 (48%)	10 (63%)	50 (46%)	12 (40%)	
Location (n = 185)					**$p = 0.006$**
Right colon	75 (41%)	**13 (81%)**	**37 (34%)**	**13 (43%)**	
Left colon	58 (31%)	**2 (13%)**	**36 (33%)**	**11 (37%)**	
Rectum	52 (28%)	**1 (6%)**	**36 (33%)**	**6 (20%)**	
pT (n = 185)					*$p = 0.062$*
pT1	2 (1%)	0 (0%)	2 (2%)	0 (0%)	
pT2	34 (18%)	3 (19%)	22 (20%)	1 (3%)	
pT3	134 (72%)	11 (69%)	80 (73%)	23 (77%)	
pT4	15 (8%)	2 (13%)	5 (5%)	6 (20%)	
pN (n = 184)					**$p = 0.001$**
pN0	82 (45%)	**6 (38%)**	**62 (57%)**	**6 (20%)**	
pN1	67 (36%)	**4 (25%)**	**32 (30%)**	**13 (43%)**	
pN2	35 (19%)	**6 (38%)**	**14 (13%)**	**11 (37%)**	
M (n = 185)					**$p = 0.022$**
M0	143 (77%)	**15 (94%)**	**86 (79%)**	**18 (60%)**	
M1	42 (23%)	**1 (6%)**	**23 (21%)**	**12 (40%)**	
Stage (n = 185)					**$p = 0.006$**
I	26 (14%)	**2 (13%)**	**9 (17%)**	**0 (0%)**	
II	48 (26%)	**4 (25%)**	**37 (34%)**	**5 (17%)**	
III	69 (37%)	**9 (56%)**	**30 (28%)**	**13 (43%)**	
IV	42 (23%)	**1 (6%)**	**23 (21%)**	**12 (40%)**	
Grade (n = 185)					**$p < 0.001$**
Low/moderate	161 (87%)	**9 (56%)**	**100 (92%)**	**24 (80%)**	
High	24 (13%)	**7 (44%)**	**9 (8%)**	**6 (20%)**	
Lymphatic invasion (n = 185)					**$p < 0.001$**
Not present	122 (66%)	**9 (56%)**	**83 (86%)**	**12 (40%)**	
Present	63 (34%)	**7 (44%)**	**26 (24%)**	**18 (60%)**	

(Continued on following page)

TABLE 3 (*Continued*) The relationship between consensus molceular subtypes and clinicopathological parameters.

Clinico-pathological features	All patients (n = 185*)	CMS (n = 155)			
		CMS1 (n = 16)	CMS2/3 (n = 109)	CMS4 (n = 30)	*p*-value
Perineural invasion (n = 185)					**$p = 0.006$**
Not present	170 (92%)	**14 (88%)**	**104 (95%)**	**26 (77%)**	
Present	15 (8%)	**2 (13%)**	**5 (5%)**	**7 (23%)**	
mGPS (n = 96)					$p = 0.486$
mGPS 0	39 (41%)	2 (40%)	24 (44%)	10 (56%)	
mGPS 1	36 (38%)	3 (60%)	17 (31%)	5 (28%)	
mGPS 2	21 (22%)	0 (0%)	14 (26%)	3 (17%)	
CEA (n = 155)					$p = 0.439$
CEA-low	101 (65%)	7 (58%)	62 (70%)	15 (58%)	
CEA-high	54 (35%)	4 (42%)	27 (30%)	11 (42%)	
CA19-9 (n = 135)					$p = 0.215$
CA19-9-low	111 (82%)	12 (100%)	63 (84%)	17 (77%)	
CA19-9-high	24 (18%)	0 (0%)	12 (16%)	5 (23%)	

The relationship between the consensus molecular subtypes and clinicopathological features was assessed using Chi-squared test. Significant correlations were marked with bold font, while tendencies where $p < 0.1$ were marked with italic font. In some cases, percentages do not add up to 100% precisely due to rounding. Abbreviations: CMS, consensus molecular subtypes; mGPS, modified Glasgow Prognostic Score; CEA, carcinoembryonic antigen; CA 19-9, Carbohydrate antigen 19-9.

significant ($p = 0.054$) as well (Tables 1, 3; Figure 3). We did not find significant correlation between the examined tumor markers (CEA and CA19-9) and CMS ($p = 0.439$ and $p = 0.215$) (Figure 3; Table 3).

Survival analysis

With Kaplan-Meier survival analysis we found that some microenvironmental and systemic markers of CRC were associated with OS (Supplementary Table S6). Patients with high stromal content ($p < 0.001$), high GMS ($p = 0.003$), high ANC ($p = 0.007$), low albumin ($p = 0.027$), elevated CRP ($p = 0.006$), elevated CEA ($p < 0.001$) and CA19-9 ($p < 0.001$) as well as higher mGPS ($p = 0.002$) and mesenchymal subtype ($p = 0.049$) had shorter overall survival (Supplementary Table S6, Figure 5).

As for local relapse free survival, CEA was the only variable that stratified survival significantly ($p = 0.009$), and also a tendency for high PLR ($p = 0.087$) was observed (Supplementary Table S6). For distant metastasis free survival, TSR ($p = 0.017$) and serum albumin ($p = 0.031$) were associated with survival, while there was a tendency towards poor survival with GMS ($p = 0.057$), CEA ($p = 0.066$) and CRP ($p = 0.092$). Figure 6.

In the univariate Cox regression analysis TSR, GMS, mGPS, ANC, CRP, Albumin, CEA and CA19-9 were significantly associated with OS; CMS presented a tendency (with a $p = 0.055$, just failing to be significant) towards increased risk of death in CMS4 patients and NLR and NPS also showed tendency for poorer OS (Supplementary Table S7).

In the multivariate analysis, TSR ($p = 0.029$), NPS ($p = 0.033$), mGPS ($p = 0.003$), Albumin ($p = 0.003$), CRP ($p = 0.018$), CA19-9 ($p = 0.013$), and STM-score ($p \leq 0.001$) were significant predictors of OS (independently of sex, grade, stage and vascular invasion) (Supplementary Table S7).

STM score

Scoring systems comprising of semi-quantitative aspects of certain TME or systemic inflammation-based markers are no novelty in oncology. A combination of strong prognostic factors have the ability to further identify a subset of patients with particularly poor outcome.

In our research the strongest independent TME-based marker was the TSR (Supplementary Table S7). Also, CA19-9, a tumor marker, often, though not routinely used in colorectal cancer follow up, came out as a predictor of overall survival in our analysis (Supplementary Table S7). Incorporating these two, STM was created. The assessment of STM is described in Methods previously.

Cases classified as STM2 were associated with younger age ($p = 0.014$), higher pN ($p = 0.033$) and M ($p < 0.001$), as well as

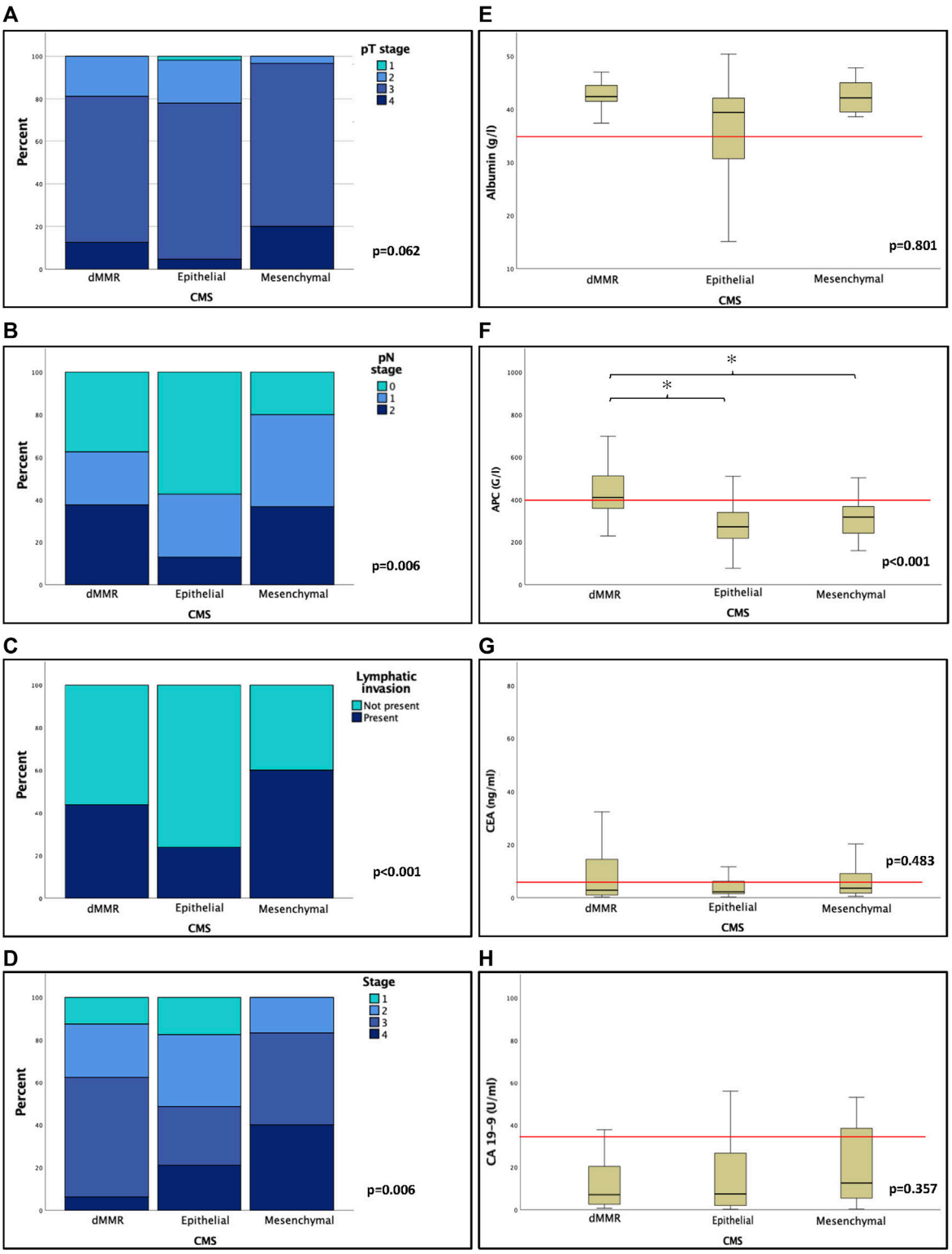

FIGURE 3
The relationship of CMS and clinicopathological features was analysed using Chi-square test **(A–D)**. Generally, mesenchymal subtype was associated with higher T, N, and TNM status and presence of lymphatic invasion. Markers of systemic inflammation and tumor markers as well as their association with CMS were also examined using non-parametric Kruskal-Wallis tests. Preoperative absolute platelet count was significantly elevated in dMMR tumors compared to both epithelial and mesenchymal subtypes. The relationship of CMS and SIR and tumor markers was assessed

(*Continued*)

FIGURE 3 (Continued)
using non-parametric Mann-Whitney and Kruskal-Wallis test **(E–H)**. There was a significant association towards elevated APC in dMMR tumors. Tumor markers were not significantly associated with CMS. Abbreviations: dMMR, Mismatch repair deficient/deficiency; CMS, consensus molecular subtypes; APC, absolute platelet count; CEA, carcinoembryonic antigen; CA 19-9, carbohydrate antigen 19-9. Asterisks (*) mark significant associations $p < 0.05$.

higher TNM stage ($p < 0.001$), and presence of lymphatic ($p < 0.001$) and perineural invasion ($p < 0.001$), and also with elevated CEA-levels ($p = 0.002$) (Table 4). The mesenchymal subtype of CMS was also more prevalent in STM1 and STM2 groups ($p = 0.048$) (Table 4). There was a tendency towards higher pT ($p = 0.071$), also, preoperative serum CRP and CEA levels correlated with STM1 and STM2 ($p = 0.017$ and $p < 0.001$) (Table 4 and Supplementary Table S8).

The STM score significantly stratified 5-year overall survival (86% versus 54% versus 42%) with Kaplan-Meier analysis (Supplementary Table S6). Also in stage I-III patients there was significant difference between the distant metastasis free survival of STM0, 1 and 2 patients ($p = 0.005$) (Supplementary Table S6). In the univariate Cox-regression analysis STM was significantly associated with OS (HR: 7.4 (3-18), $p < 0.001$), and in the multivariate Cox-regression analysis STM was found to be an independent prognosticator of OS independently of sex, grade, stage and vascular invasion ($p < 0.001$, HR: 4.3 (1.5-12) (Supplementary Table S7).

Discussion

In our study we characterized TME with TSR, KM-grade and their combination, the GMS grading system, which are all convenient descriptors to use and present good reproducibility. Similarly to previous studies [10, 12, 34], stroma-high tumors represented an aggressive phenotype with poor prognosis and inferior survival in this cohort. According to literature data, higher KM grade is associated with favorable clinicopathological features [6, 34], which was the case in our study as well, though a significant association with OS could not be presented. Although KM grade was described to be related to systemic inflammation [35], this finding was not observed in our study. Similarly to TSR, GMS also successfully stratified patients' characteristics and survival, in agreement with preceding results [36]. In conclusion, the aformentioned and easily assessible descriptors, TSR, KM-grade and GMS, can guide us in CRC-prognostication.

The pre-operative systemic inflammation can be described using a variety of SIR markers. As described in previous reports [23, 37], some of the SIR markers were associated with poor patient outcomes in our cohort as well. Four of them (CRP, albumin, mGPS and NPS) even came out as independent factors of overall survival. Amongst these markers CRP not only delivered robust prognostic power, but was also associated with adverse histological features and advanced stages. These results suggest that CRP represented the effect of inflammatory response on clinical outcome the most, which is not surprising, as CRP is a key acute phase protein of inflammatory processes [38].

Another substantial finding regarding SIR markers was that APC elevation correlated with male sex and right sidedness. Interestingly, women generally tend to have higher APC than men [39]. It is also understood that higher APC is associated with poorer survival in CRC patients [40]. In our study, men also had worse OS, than women ($p = 0.039$ using log-rank test, mean OS (men): 6.3 years, OS (women): 8.3 years). We believe, elevated APC possibly indicated the poorer outcome of men in our cohort. Another observation that might explain our findings is that APC is significantly higher in dMMR CRC than in proficient MMR tumors [35], and dMMR CRCs are associated with right sidedness [35].

Tumor markers CEA and CA19-9 and their relationship with TME and SIR was also assessed. In concordance with previous articles [41, 42], our study also showed that both CEA and CA19-9 were linked to advanced stages of CRC and CA19-9 even emerged as an independent factor of OS.

Surprisingly, both CEA and CA19-9 showed a statistically significant association with TSR, but not with KM grade and CMS, which were not yet reported elsewhere. The connection between TSR-high tumors and elevated tumor markers could be attributed to the higher presence of distant metastasis or locally advanced disease indicated by both markers.

Important to point out, that both TSR and CA19-9 delivered strong prognostic value, whichproposed a possible combined score, the STM, that bears similar or even stronger prognostic power than these two variables separately. STM was strongly associated with dismal clinicopathological parameters and proved to be the second best prognosticator of OS. In conclusion, combined scores based on histopathological features and routine laboratory tests, like mGPS or STM, could help to identify a subset of CRC patients with higher risk of death or recurrence in a cost-effective and time sparing manner.

Reportedly, our study is the first one to assess the connection between CMS and SIR markers. CMS1 displays a characteristic inflammatory infiltrate that could lead to systemic inflammation which may be reflected in elevated SIR markers [35]. In our analysis, CMS1 was associated with right-sidedness and elevated APC, similarly to previous findings [21], and it correlated with NPS and PLR as well.

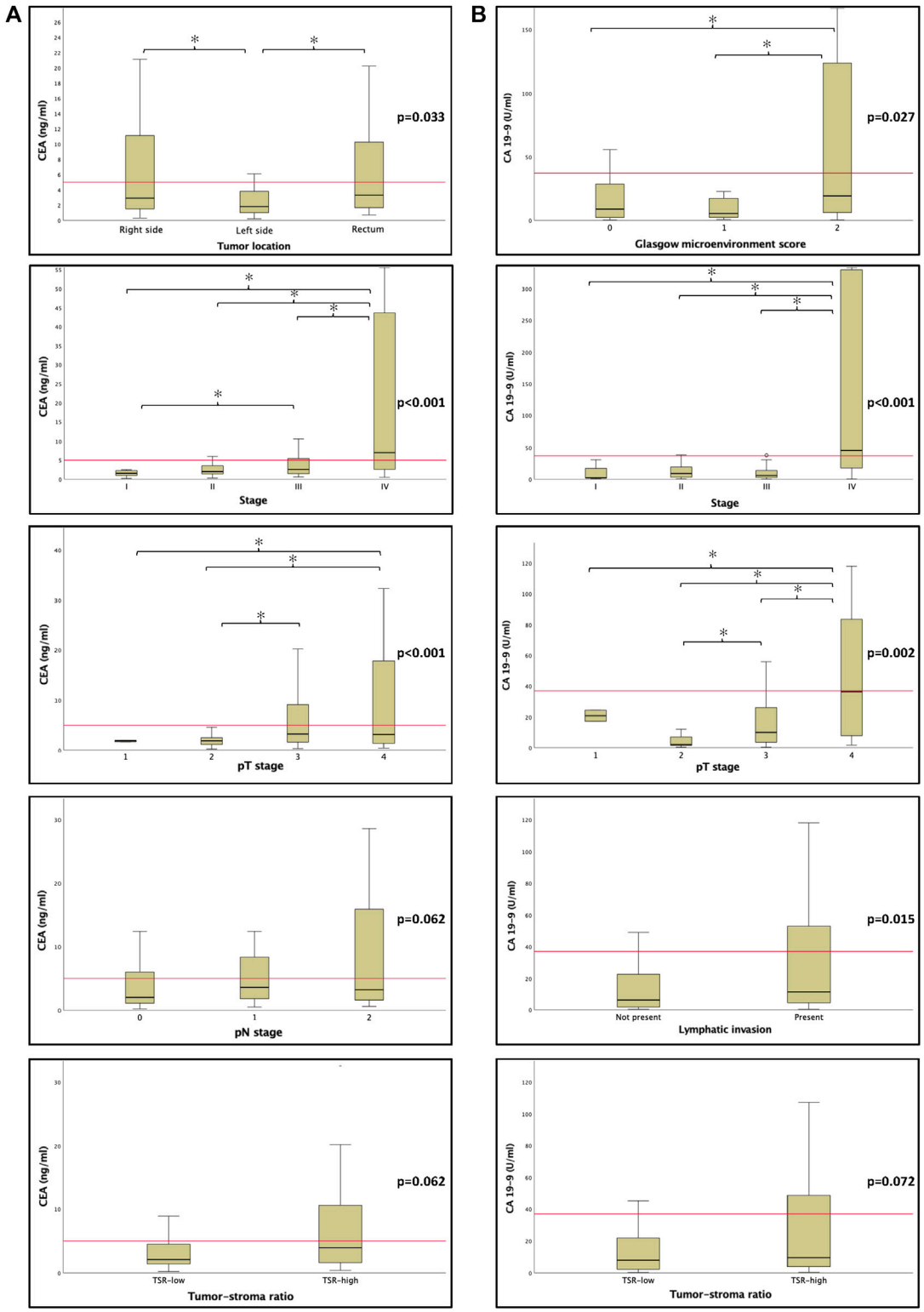

FIGURE 4
The relationship between canonical tumor markers CEA **(A)** and CA 19-9 **(B)** and clinicopathological features. Unsuprisingly, elevated tumor marker levels were mostly associated with adverse features. There was a tendency between tumor markers and high tumor-stroma ratio (TSR). The horizontal red line represents clinically relevant cut off values mentioned in Supplementary Table S1. Abbreviations: CEA, carcinoembryonic antigen; CA 19-9, carbohydrate antigen 19-9; TSR, tumor-stroma ratio. Asterisks (*) mark significant associations $p < 0.05$.

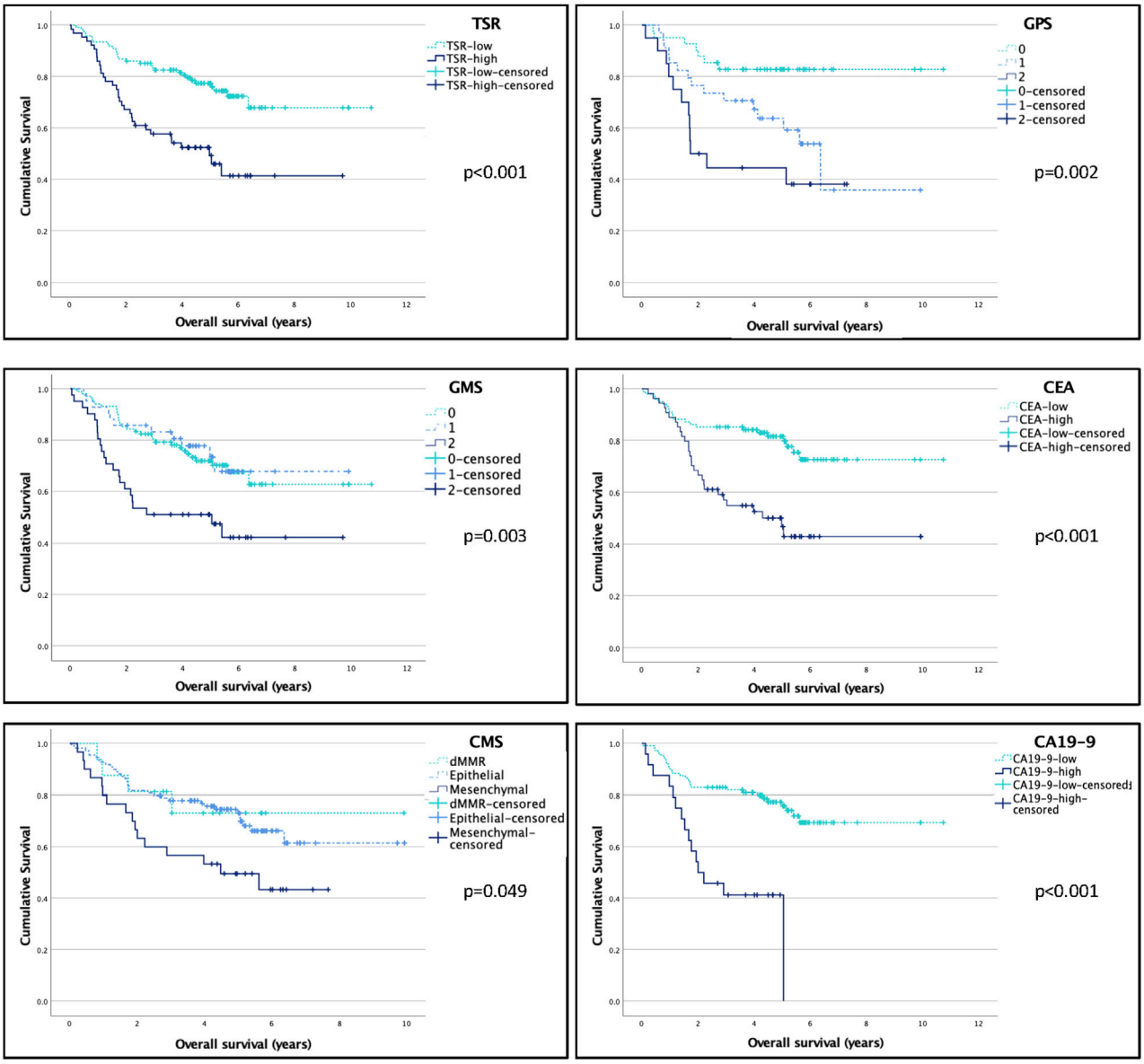

FIGURE 5
The effect of microenviromental and systemic markers on overall survival (OS). Log-rank test was used to compare the OS of certain subgroups. Bold font denotes significant correlations in the multivariate model, italic font denotes tendencies with $p < 0.1$ in the multivariate model. For further information on multivariate analysis, see Table 2. Abbreviations: TSR, tumor stroma ratio; STM score, Stroma-Tumor Marker Score; CMS, consensus molecular subtype; mGPS, modified Glasgow Prognostic Score; CEA, carcinoembryonic antigen; CA19-9, carbohydrate antigen 19-9.

It is understood that CMS4 is associated with EMT-like gene expression profile and stromal infiltration signature [14], complement components and immunosuppressive chemokines [15]. This signature is similar to wound healing responses or chronic tumor-supportive inflammation, where platelets are the first responders and several mediators present in CMS4 tumors are associated with to platelet activation [43], hence an elevated APC was expected amongst mesenchymal CRCs. Interestingly, CMS4 tumors did not exhibit elevation of any platelet-related, nor any other SIR markers in our cohort. In conclusion, no significant association between CMS and inflammation was found. A recent paper emphasizes the diversity of immunological subtypes and their distribution within CMS, that might provide an explanation as to why there is a lack of distinct SIR-related characteristic of each molecular subtype [44]. Surprisingly, this research associates CMS2 (also, most epithelial-like CRCs) with a dominant wound healing-like immune response, while in CMS4 tumors such an

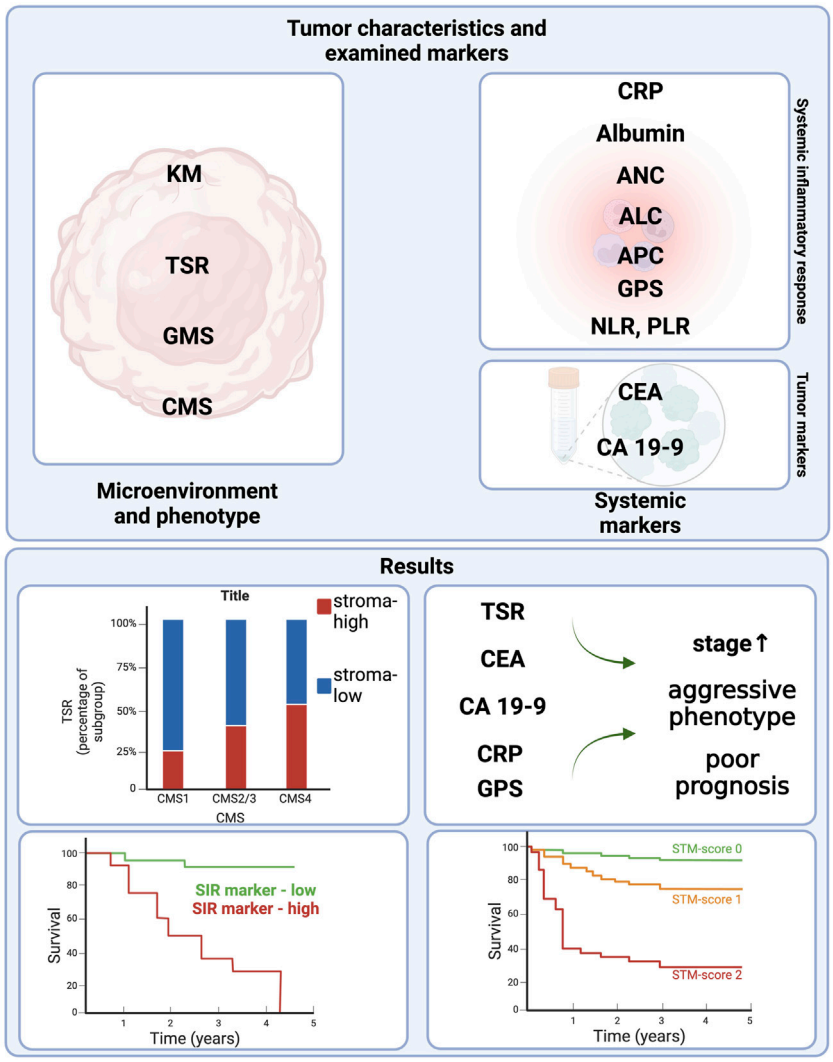

FIGURE 6
Study design and results. Figure was created using https://www.biorender.com/. Abbreviations: KM, Klintrup-Makinen grade; TSR, tumor-stroma ratio; GMS, Glasgow microenvironment score; CMS, consensus molecular subtype; CRP, C reactive protein; ANC, absolute neutrophil count; ALC, absolute lymphocyte count; APC, absolute platelet count; GPS, (modified) Glasgow Prognostic Score; CEA, Carcinoembryonic antigen; CA19-9 carbohydrate antigen 19-9; SIR, systemic inflammatory response; STM score, Stroma-Tumor Marker Score.

immunological profile is less frequent [44], which is contradictory with the previously mentioned report [43]. Apparently, the rationale and exact mechanisms behind the resemblance of SIR-profiles of CMS-classified tumors are to be further examined.

Also, our study assigned poorer survival and higher TNM-stages to CMS4-tumors, which is similar to literature data showing that advanced CRCs are enriched in CMS4 [14, 45]. A possible pitfall of CMS classification could be the intratumoral heterogeneity and EMT, especially if samples derive from the invasive front of the tumor, which can lead to misclassifying cases as CMS4 [46]. To avoid sampling bias, our TMA cores were selected from the tumor centre. As of now, it is still difficult to answer whether CMS4 is the cause or the consequence of advanced CRCs. A study on exploring the relationship between interval CRC and CMS or more precise studies dealing with heterogeneity within tumor areas (e.g.,: multiple sampling from more tumor areas) could answer these questions.

No significant association between traditional tumor markers and CMS was found in our research. Another article found that in stage III CMS4 CRCs, elevated CEA was associated with exceptionally poor prognosis, and suppressed tumor immunity was also observed in this subgroup [47]. Similar analysis could not be performed in our database, as there were only 11 stage III CMS4 cases.

TABLE 4 The relationship between stroma-tumor marker (STM) score and clinicopathological features.

Clinico-pathological features	All patients (n = 135)	STM score (n = 135)			
		STM 0 (n = 80)	STM 1 (n = 43)	STM 2 (n = 12)	*p*-value
Age					**0.014**
<65	46 (34%)	21 (26%)	16 (37%)	9 (75%)	
65-74	60 (44%)	42 (53%)	16 (37%)	2 (17%)	
75<	29 (22%)	17 (21%)	11 (26%)	1 (8%)	
Sex					0.877
Female	73 (54%)	44 (55%)	22 (51%)	7 (58%)	
Male	62 (46%)	36 (45%)	21 (49%)	5 (42%)	
Location					0.288
Right colon	57 (42%)	36 (45%)	16 (37%)	5 (42%)	
Left colon	44 (33%)	26 (33%)	12 (28%)	6 (50%)	
Rectum	34 (25%)	18 (23%)	15 (35%)	1 (8%)	
pT					*0.071*
pT1	2 (1.5%)	2 (3%)	0 (0%)	0 (0%)	
pT2	25 (19%)	20 (25%)	5 (12%)	0 (0%)	
pT3	97 (72%)	55 (69%)	32 (74%)	10 (83%)	
pT4	11 (8%)	3 (4%)	6 (14%)	2 (17%)	
pN					**0.033**
pN0	58 (43%)	41 (52%)	16 (37%)	1 (8%)	
pN1	51 (38%)	27 (34%)	18 (42%)	6 (50%)	
pN2	25 (19%)	11 (14%)	9 (21%)	5 (42%)	
M					**<0.001**
M0	104 (77%)	73 (91%)	28 (65%)	3 (25%)	
M1	31 (23%)	7 (9%)	15 (35%)	9 (75%)	
Stage					**<0.001**
I	21 (16%)	17 (23%)	4 (9%)	0 (0%)	
II	30 (22%)	22 (28%)	8 (19%)	0 (0%)	
III	53 (39%)	34 (43%)	16 (37%)	3 (25%)	
IV	31 (23%)	7 (9%)	15 (35%)	9 (75%)	
Grade					0.916
Low/moderate	119 (88%)	70 (88%)	38 (88%)	11 (92%)	
High	19 (12%)	10 (13%)	5 (12%)	1 (8%)	
Lymphatic invasion					**<0.001**
Not present	89 (64%)	62 (78%)	20 (47%)	4 (33%)	
Present	49 (36%)	18 (23%)	23 (54%)	8 (67%)	

(Continued on following page)

TABLE 4 (*Continued*) The relationship between stroma-tumor marker (STM) score and clinicopathological features.

Clinico-pathological features	All patients (n = 135)	STM score (n = 135)			
		STM 0 (n = 80)	STM 1 (n = 43)	STM 2 (n = 12)	*p*-value
Perineural invasion					**0.001**
Not present	121 (90%)	78 (98%)	34 (79%)	9 (75%)	
Present	14 (10%)	2 (3%)	9 (21%)	3 (25%)	
Vascular invasion					0.440
Not present	103 (76%)	64 (80%)	31 (72%)	8 (67%)	
Present	32 (24%)	16 (20%)	12 (28%)	4 (33%)	
CMS dMMR	12 (11%)	10 (15%)	2 (6%)	0 (0%)	**0.048**
Epithelial	75 (69%)	48 (73%)	20 (59%)	7 (78%)	
Mesenchymal	22 (20%)	8 (12%)	12 (25%)	2 (22%)	
mGPS					0.414
mGPS 0	37 (50%)	24 (60%)	9 (39%)	4 (36%)	
mGPS 1	26 (35%)	12 (30%)	9 (39%)	5 (46%)	
mGPS 2	11 (15%)	4 (10%)	5 (22%)	2 (18%)	
CEA (n = 152)					**0.002**
CEA-low	90 (67%)	62 (78%)	24 (56%)	4 (33%)	
CEA-high	45 (33%)	18 (23%)	19 (44%)	8 (67%)	

The relationship between stroma-tumor marker (STM) score and clinicopathological features was assessed using Chi-squared test. Significant correlations were marked with bold font, while tendencies where $p < 0.1$ were marked with italic font. In some cases, percentages do not add up to 100% precisely due to rounding. Abbreviations: STM, stroma-tumor marker score; CMS, consensus molecular subtype; dMMR, mismatch repair deficient; mGPS, modified Glasgow prognostic score; CEA, carcinoembryonic antigen.

A probable limitation of our study was the relatively small cohort size sometimes resulting few cases in the subclasses (especially for CMS4) and weak to moderate statistical power, as well as the retrospective nature of inclusion of stage IV patients. In addition, the immunohistochemistry-based approach was used for CMS classification, which is simple and cost-effective, presenting 87% of concordance with the gold-standard gene-expression based profiling, and CMS2 and CMS3 cannot be distingiushed [32, 33].

Conclusion

In conclusion, our results are in line with the literature data claiming that most TME, SIR markers and elevated CEA or CA19-9 are associated with adverse histological features and patient outcome. The authors' work further broadens the potential options of cost-effective, evidence based prognostic tools. Assessing and combining routine histopathology (TSR) with laboratory findings (CA19-9) resulted in a novel, robust prognostic score, the STM score, which could be a simple and easily accessible risk stratificator. The authors believe this could be useful in identifying subsets of CRC patients who benefit from more intensive therapy to prevent recurrence or progression.

As in previous studies, CMS4 tumors represented an aggressive phenotype of CRC with adverse histological features and poor patient outcome, which was also reflected by its association with higher TSR. This further confirms the versatility of TSR assessment and its potential role in identifying patients at risk or cases with high probability of CMS4.

Up to now only very few studies investigated the connection between CMS and TME, SIR and tumor markers. Contrary to the authors' expectations, CMS4 and CMS2/3 were not associated with any SIR nor tumor markers, only dMMR (CMS1) tumors correlated with plateled derived SIR markers, as described previously. This underlines the complexity of tumor-host response and proposes possible future investigations of this field.

Data availability statement

The raw data supporting the conclusion of this article will be made available by the authors, without undue reservation.

Ethics statement

The studies involving humans were approved by the Hungarian Scientific Council National Ethics Committee for Scientific Research (no. 216/2020, President: Prof. Péter Sótonyi, MD, PhD). The studies were conducted in accordance with the local legislation and institutional requirements. Written informed consent for participation was not required from the participants or the participants' legal guardians/next of kin because in accordance with the Hungarian Law, the ethical guidelines of the country and the Helsinki Declaration, no formal consent was required to this retrospective study from our patients. Written informed consent was not obtained from the individual(s) for the publication of any potentially identifiable images or data included in this article because in accordance with the Hungarian Law, the ethical guidelines of the country and the Helsinki Declaration, no formal consent was required to this retrospective study from our patients.

Author contributions

AJ: study design, tissue microarray construction and immunohistochemistry reactions, assessment of immunohistochemistry, histopathological evaluation, statistics, figures, tables, construction of original manuscript. ÁVP: study design, clinical data analysis, review of original manuscript MD: data collection, statistics, review of original manuscript KT-B: data collection, statistics, review of original manuscript TM: study design, assessment of immunohistochemistry, histopathological evaluation of slides, figures, tables, review of original manuscript. All authors contributed to the article and approved the submitted version.

Conflict of interest

The authors declare that the research was conducted in the absence of any commercial or financial relationships that could be construed as a potential conflict of interest.

Supplementary material

The Supplementary Material for this article can be found online at: https://www.por-journal.com/articles/10.3389/pore.2024.1611574/full#supplementary-material

References

1. WHO. *Colorectal cancer* (2023). Available at: https://www.who.int/news-room/fact-sheets/detail/colorectal-cancer?gad_source=1&gclid=CjwKCAjwzN-vBhAkEiwAYiO7oDbqYfWJo7SRc4nbrjuz_2OyLP0z0d5Z9bu-ez8ShQKny8ZkUyhi4xoCBucQAvD_BwE.

2. Di Nicolantonio F, Vitiello PP, Marsoni S, Siena S, Tabernero J, Trusolino L, et al. Precision oncology in metastatic colorectal cancer — from biology to medicine. *Nat Rev Clin Oncol* (2021) 18(8):506–25. doi:10.1038/s41571-021-00495-z

3. Kobayashi H, Enomoto A, Woods SL, Burt AD, Takahashi M, Worthley DL. Cancer-associated fibroblasts in gastrointestinal cancer. *Nat Rev Gastroenterol Hepatol* (2019) 16(5):282–95. doi:10.1038/s41575-019-0115-0

4. Schürch CM, Bhate SS, Barlow GL, Phillips DJ, Noti L, Zlobec I, et al. Coordinated cellular neighborhoods orchestrate antitumoral immunity at the colorectal cancer invasive front. *Cell* (2020) 182(5):1341–59. doi:10.1016/j.cell.2020.07.005

5. Wilkinson K, Ng W, Roberts TL, Becker TM, Lim SHS, Chua W, et al. Tumour immune microenvironment biomarkers predicting cytotoxic chemotherapy efficacy in colorectal cancer. *J Clin Pathol* (2021) 74(10):625–34. doi:10.1136/jclinpath-2020-207309

6. Klintrup K, Mäkinen JM, Kauppila S, Väre PO, Melkko J, Tuominen H, et al. Inflammation and prognosis in colorectal cancer. *Eur J Cancer* (2005) 41(17):2645–54. doi:10.1016/j.ejca.2005.07.017

7. Jakubowska K, Kisielewski W, Kańczuga-Koda L, Koda M, Famulski W. Diagnostic value of inflammatory cell infiltrates, tumor stroma percentage and disease-free survival in patients with colorectal cancer. *Oncol Lett* (2017) 14(3):3869–77. doi:10.3892/ol.2017.6639

8. van Pelt GW, Kjær-Frifeldt S, van Krieken JHJM, Al Dieri R, Morreau H, Tollenaar RAEM, et al. Scoring the tumor-stroma ratio in colon cancer: procedure and recommendations. *Virchows Arch* (2018) 473(4):405–12. doi:10.1007/s00428-018-2408-z

9. Mesker WE, Junggeburt JMC, Szuhai K, de Heer P, Morreau H, Tanke HJ, et al. The carcinoma-stromal ratio of colon carcinoma is an independent factor for survival compared to lymph node status and tumor stage. *Cell Oncol* (2007) 29(5):387–98. doi:10.1155/2007/175276

10. Huijbers A, Tollenaar RAEM, v Pelt GW, Zeestraten ECM, Dutton S, McConkey CC, et al. The proportion of tumor-stroma as a strong prognosticator for stage II and III colon cancer patients: validation in the VICTOR trial. *Ann Oncol* (2013) 24(1):179–85. doi:10.1093/annonc/mds246

11. Hansen TF, Kjær-Frifeldt S, Lindebjerg J, Rafaelsen SR, Jensen LH, Jakobsen A, et al. Tumor-stroma ratio predicts recurrence in patients with colon cancer treated with neoadjuvant chemotherapy. *Acta Oncol* (2018) 57(4):528–33. doi:10.1080/0284186x.2017.1385841

12. Park JH, McMillan DC, Edwards J, Horgan PG, Roxburgh CSD. Comparison of the prognostic value of measures of the tumor inflammatory cell infiltrate and tumor-associated stroma in patients with primary operable colorectal cancer. *Oncoimmunology* (2016) 5(3):e1098801. doi:10.1080/2162402x.2015.1098801

13. Alexander PG, Roseweir AK, Pennel KAF, van Wyk HC, Powell AGMT, McMillan DC, et al. The Glasgow Microenvironment Score associates with prognosis and adjuvant chemotherapy response in colorectal cancer. *Br J Cancer* (2021) 124(4):786–96. doi:10.1038/s41416-020-01168-x

14. Guinney J, Dienstmann R, Wang X, de Reyniès A, Schlicker A, Soneson C, et al. The consensus molecular subtypes of colorectal cancer. *Nat Med* (2015) 21(11):1350–6. doi:10.1038/nm.3967

15. Becht E, de Reyniès A, Giraldo NA, Pilati C, Buttard B, Lacroix L, et al. Immune and stromal classification of colorectal cancer is associated with molecular subtypes and relevant for precision immunotherapy. *Clin Cancer Res* (2016) 22(16):4057–66. doi:10.1158/1078-0432.ccr-15-2879

16. Dienstmann R, Vermeulen L, Guinney J, Kopetz S, Tejpar S, Tabernero J. Consensus molecular subtypes and the evolution of precision medicine in colorectal cancer. *Nat Rev Cancer* (2017) 17(2):79–92. doi:10.1038/nrc.2016.126

17. Roepman P, Schlicker A, Tabernero J, Majewski I, Tian S, Moreno V, et al. Colorectal cancer intrinsic subtypes predict chemotherapy benefit, deficient mismatch repair and epithelial-to-mesenchymal transition. *Int J Cancer* (2014) 134(3):552–62. doi:10.1002/ijc.28387

18. De Sousa E Melo F, Wang X, Jansen M, Fessler E, Trinh A, de Rooij LPMH, et al. Poor-prognosis colon cancer is defined by a molecularly distinct subtype and develops from serrated precursor lesions. *Nat Med* (2013) 19(5):614–8. doi:10.1038/nm.3174

19. Golder AM, McMillan DC, Park JH, Mansouri D, Horgan PG, Roxburgh CS. The prognostic value of combined measures of the systemic inflammatory response in patients with colon cancer: an analysis of 1700 patients. *Br J Cancer* (2021) 124(11):1828–35. doi:10.1038/s41416-021-01308-x

20. Park JH, Fuglestad AJ, Køstner AH, Oliwa A, Graham J, Horgan PG, et al. Systemic inflammation and outcome in 2295 patients with stage I–III colorectal cancer from scotland and Norway: first results from the ScotScan colorectal cancer group. *Ann Surg Oncol* (2020) 27(8):2784–94. doi:10.1245/s10434-020-08268-1

21. Climent M, Ryan ÉJ, Stakelum Á, Khaw YL, Creavin B, Lloyd A, et al. Systemic inflammatory response predicts oncological outcomes in patients undergoing elective surgery for mismatch repair-deficient colorectal cancer. *Int J Colorectal Dis* (2019) 34(6):1069–78. doi:10.1007/s00384-019-03274-6

22. Park JH, Watt G, Roxburgh CSD, Horgan PG, McMillan DC Colorectal cancer, systemic inflammation, and outcome. *Ann Surg* (2016) 263(2):326–36. doi:10.1097/sla.0000000000001122

23. Yamamoto T, Kawada K, Obama K. Inflammation-related biomarkers for the prediction of prognosis in colorectal cancer patients. *Int J Mol Sci* (2021) 22(15): 8002. doi:10.3390/ijms22158002

24. Watt DG, Proctor MJ, Park JH, Horgan PG, McMillan DC. The neutrophil-platelet score (NPS) predicts survival in primary operable colorectal cancer and a variety of common cancers. *PLOS ONE* (2015) 10(11):e0142159. doi:10.1371/journal.pone.0142159

25. Yakabe T, Nakafusa Y, Sumi K, Miyoshi A, Kitajima Y, Sato S, et al. Clinical significance of CEA and CA19-9 in postoperative follow-up of colorectal cancer. *Ann Surg Oncol* (2010) 17(9):2349–56. doi:10.1245/s10434-010-1004-5

26. Liu J-M, Wang YY, Liu W, Xu D, Wang K, Xing BC. Preoperative CA19-9: a competitive predictor of recurrence in patients with colorectal cancer liver metastases after hepatectomy. *Int J Colorectal Dis* (2021) 36(4):767–78. doi:10.1007/s00384-020-03828-z

27. Yang SH, Jiang JK, Chang SC, Juang CJ, Lin JK. Clinical significance of CA19-9 in the follow-up of colorectal cancer patients with elevated preoperative serum CA19-9. *Hepatogastroenterology* (2013) 60(125):1021–7. doi:10.5754/hge121151

28. Zhang SY, Lin M, Zhang HB. Diagnostic value of carcinoembryonic antigen and carcinoma antigen 19-9 for colorectal carcinoma. *Int J Clin Exp Pathol* (2015) 8(8):9404–9.

29. Baqar AR, Wilkins S, Staples M, Angus Lee CH, Oliva K, McMurrick P. The role of preoperative CEA in the management of colorectal cancer: a cohort study from two cancer centres. *Int J Surg* (2019) 64:10–5. doi:10.1016/j.ijsu.2019.02.014

30. Jia J, Zhang P, Gou M, Yang F, Qian N, Dai G. The role of serum CEA and CA19-9 in efficacy evaluations and progression-free survival predictions for patients treated with cetuximab combined with FOLFOX4 or FOLFIRI as a first-line treatment for advanced colorectal cancer. *Dis markers* (2019) 2019: 6812045. doi:10.1155/2019/6812045

31. Nowak JA, Hornick JL. Molecular evaluation of colorectal adenocarcinoma: current practice and emerging concepts. *Surg Pathol Clin* (2016) 9(3):427–39. doi:10.1016/j.path.2016.04.007

32. Ten Hoorn S, Trinh A, de Jong J, Koens L, Vermeulen L. Classification of colorectal cancer in molecular subtypes by immunohistochemistry. *Methods Mol Biol* (2018) 1765:179–91. doi:10.1007/978-1-4939-7765-9_11

33. Trinh A, Trumpi K, De Sousa E Melo F, Wang X, de Jong JH, Fessler E, et al. Practical and robust identification of molecular subtypes in colorectal cancer by immunohistochemistry. *Clin Cancer Res* (2017) 23(2):387–98. doi:10.1158/1078-0432.Ccr-16-0680

34. Park JH, Richards CH, McMillan DC, Horgan PG, Roxburgh CSD. The relationship between tumour stroma percentage, the tumour microenvironment and survival in patients with primary operable colorectal cancer. *Ann Oncol* (2014) 25(3):644–51. doi:10.1093/annonc/mdt593

35. Park JH, Powell AG, Roxburgh CSD, Horgan PG, McMillan DC, Edwards J. Mismatch repair status in patients with primary operable colorectal cancer: associations with the local and systemic tumour environment. *Br J Cancer* (2016) 114(5):562–70. doi:10.1038/bjc.2016.17

36. Park JH, McMillan DC, Powell AG, Richards CH, Horgan PG, Edwards J, et al. Evaluation of a tumor microenvironment–based prognostic score in primary operable colorectal cancer. *Clin Cancer Res* (2015) 21(4):882–8. doi:10.1158/1078-0432.ccr-14-1686

37. Park JH, Ishizuka M, McSorley ST, Kubota K, Roxburgh CSD, Nagata H, et al. Staging the tumor and staging the host: a two centre, two country comparison of systemic inflammatory responses of patients undergoing resection of primary operable colorectal cancer. *Am J Surg* (2018) 216(3):458–64. doi:10.1016/j.amjsurg.2017.08.044

38. Black S, Kushner I, Samols D. C-Reactive protein. *J Biol Chem* (2004) 279(47): 48487–90. doi:10.1074/jbc.R400025200

39. Butkiewicz AM, Kemona H, Dymicka-Piekarska V, Matowicka-Karna J, Radziwon P, Lipska A. Platelet count, mean platelet volume and thrombocytopoietic indices in healthy women and men. *Thromb Res* (2006) 118(2):199–204. doi:10.1016/j.thromres.2005.06.021

40. Long Y, Wang T, Gao Q, Zhou C. Prognostic significance of pretreatment elevated platelet count in patients with colorectal cancer: a meta-analysis. *Oncotarget* (2016) 7(49):81849–61. doi:10.18632/oncotarget.13248

41. Wu T, Mo Y, Wu C. Prognostic values of CEA, CA19-9, and CA72-4 in patients with stages I-III colorectal cancer. *Int J Clin Exp Pathol* (2020) 13(7):1608–14.

42. Rao H, Wu H, Huang Q, Yu Z, Zhong Z. Clinical value of serum CEA, CA24-2 and CA19-9 in patients with colorectal cancer. *Clin Lab* (2021) 67(4). doi:10.7754/Clin.Lab.2020.200828

43. Lam M, Roszik J, Kanikarla-Marie P, Davis JS, Morris J, Kopetz S, et al. The potential role of platelets in the consensus molecular subtypes of colorectal cancer. *Cancer Metastasis Rev* (2017) 36(2):273–88. doi:10.1007/s10555-017-9678-9

44. Soldevilla B, Carretero-Puche C, Gomez-Lopez G, Al-Shahrour F, Riesco MC, Gil-Calderon B, et al. The correlation between immune subtypes and consensus molecular subtypes in colorectal cancer identifies novel tumour microenvironment profiles, with prognostic and therapeutic implications. *Eur J Cancer* (2019) 123: 118–29. doi:10.1016/j.ejca.2019.09.008

45. Fontana E, Eason K, Cervantes A, Salazar R, Sadanandam A. Context matters-consensus molecular subtypes of colorectal cancer as biomarkers for clinical trials. *Ann Oncol* (2019) 30(4):520–7. doi:10.1093/annonc/mdz052

46. Dunne PD, McArt DG, Bradley CA, O'Reilly PG, Barrett HL, Cummins R, et al. Challenging the cancer molecular stratification dogma: intratumoral heterogeneity undermines consensus molecular subtypes and potential diagnostic value in colorectal cancer. *Clin Cancer Res* (2016) 22(16):4095–104. doi:10.1158/1078-0432.ccr-16-0032

47. Kagawa H, Hatakeyama K, Shiomi A, Hino H, Manabe S, Yamaoka Y, et al. Consensus molecular subtyping improves the clinical usefulness of canonical tumor markers for colorectal cancer. *Biomed Res* (2022) 43(6):201–9. doi:10.2220/biomedres.43.201

Pathology & Oncology Research | frontiers

TYPE Original Research
PUBLISHED 22 December 2023
DOI 10.3389/pore.2023.1611365

Check for updates

OPEN ACCESS

EDITED BY
Janina Kulka,
Semmelweis University, Hungary

*CORRESPONDENCE
Szintia Almási,
szinti951023@gmail.com

RECEIVED 22 June 2023
ACCEPTED 07 December 2023
PUBLISHED 22 December 2023

CITATION
Almási S, Nagy Á, Krenács T, Lantos T, Zombori T and Cserni G (2023), The prognostic value of stem cell markers in triple-negative breast cancer. *Pathol. Oncol. Res.* 29:1611365. doi: 10.3389/pore.2023.1611365

COPYRIGHT
© 2023 Almási, Nagy, Krenács, Lantos, Zombori and Cserni. This is an open-access article distributed under the terms of the Creative Commons Attribution License (CC BY). The use, distribution or reproduction in other forums is permitted, provided the original author(s) and the copyright owner(s) are credited and that the original publication in this journal is cited, in accordance with accepted academic practice. No use, distribution or reproduction is permitted which does not comply with these terms.

The prognostic value of stem cell markers in triple-negative breast cancer

Szintia Almási [1]*, Ágnes Nagy[2], Tibor Krenács [2], Tamás Lantos [3], Tamás Zombori [1] and Gábor Cserni [1,4]

[1]Department of Pathology, Albert Szent-Györgyi Medical Centre, University of Szeged, Szeged, Hungary, [2]Department of Pathology and Experimental Cancer Research, Faculty of Medicine, Semmelweis University, Budapest, Hungary, [3]Department of Medical Physics and Informatics, University of Szeged, Szeged, Hungary, [4]Department of Pathology, Bács-Kiskun County Teaching Hospital, Kecskemét, Hungary

Among the many consecutive theories of cancer, the stem cell theory is currently the most accepted one. Cancer stem cells are located in small niches with specific environment, renew themselves and are believed to be responsible for many recurrences. They can be highlighted with stem cell markers, but often these markers also label tumor cells, and this may represent a phenotypical change associated with prognosis. In this study, we attempted to match tumor outcomes with the expression of the following stem cell markers: ALDH1, AnnexinA1, CD44, CD117, CD166, Nanog and oct-4. Tissue microarray blocks from triple-negative breast cancers were immunostained for the listed markers, and their expression by the majority of tumor cells (diffuse positivity) was correlated with prognosis. Of the 106 tumors investigated, diffuse positivity was seen in 7 (ALDH1), 33 (AnnexinA1), 53 (CD44), 44 (CD117 membranous only), 49 (CD117), 72 (CD166), 19 (Nanog), and 11 (oct-4) cases. With a median follow-up of 83 months, ALDH1 and CD117 expression was associated with DFS, whereas CD44, CD117 and CD166 were associated with OS estimates, based on Kaplan-Meier analyses. In the multivariate Cox proportional hazard models (including the examined markers and clinicopathological data which had a statistical impact in the univariate analysis), the pN category and the lack of ALDH1 expression were independent prognosticators for DFS, and the pN category and diffuse CD44 staining were independent prognosticators for OS. In the multivariate analysis including all of the examined clinicopathological data and markers, only CD117 showed a statistical impact on OS. We failed to demonstrate a prognostic impact for most stem cell markers tested in triple-negative breast cancer, but lack of ALDH1 staining and CD44 expression appears as of prognostic value, requiring further examination in independent studies.

KEYWORDS

immunohistochemistry, prognosis, CD44, ALDH1, stem cell markers, triple-negative breast cancer

Introduction

Among the many consecutive theories of cancer, the stem cell theory is currently the most accepted one. Carcinomas harbor a set of stem cells from which the tumor originates; these are located in small niches with a specific environment, renew themselves and are believed to be responsible for many recurrences [1], whereas the major part of the tumor bulk is composed of more differentiated tumor cells [1]. Tumor stem cells can be highlighted by stem cell markers, but the antibodies used to highlight these markers are not specific for stem cells and often highlight other cell populations along with them [1]. Immunostaining with stem cell marker antibodies may represent a phenotypical change associated with prognosis [1]. In this study, we attempted to match tumor outcomes with stem cell marker expression by the majority of tumor cells. The following markers were assessed.

Aldehyde dehydrogenase-1 (ALDH1) is a member of the aldehyde dehydrogenase enzyme superfamily [2]. ALDH enzymes are localized in the cytosol, nucleus, endoplasmic reticulum and also in the mitochondria [2]. These enzymes are involved in the metabolism of aldehyde, which can be exogenous or can be produced inside the body, for example, by lipid peroxidation or amino acid catabolism. ALDHs can protect the cells from the toxicity of active aldehydes by catalyzing their oxidation [2]. ALDH1 can be used to identify not just normal stem cells, but also cancer stem cells, and it is also a dependable marker of cancer stem cells in a variety of solid tumors, including cancers of the breast, head and neck, liver, pancreas, colon, lung, cervix, ovary, prostate and bladder [2, 3]. Additionally, ALDH1 can be used as a marker for normal and malignant stem cells both in the mammary gland and the colon [2]. ALDH1 is expressed in normal colonic and gastric epithelium, cells of the liver and pancreas cells and can also be expressed in lung tissue [2]. ALDH1A1 and ALDH32, both play an important role in cell self-protection, cellular expansion and differentiation. In breast cancer, ALDH1 staining would highlight both normal and malignant stem cells [2, 3]. This marker can be used efficiently to identify cancer stem cells in tissues which do not express ALDH1 at high levels under normal circumstances, for example, in the breast [2, 3].

AnnexinA1 is a calcium-dependent phospholipid-binding protein, and also known as lipocortin 1, the first member of the Annexin superfamily [4]. AnnexinA1 is located in the cytoplasm, or it can bind to cytoskeletal proteins and then it can control the communication between the cell and the extracellular matrix, alternately it can be located in the nucleus, and when the cell is finally activated, it will be moved to the cell surface [4]. AnnexinA1 has an important role in pro-inflammatory and anti-inflammatory response, cell proliferation, differentiation, metastasis formation and also in the apoptotic process [4]. This marker is expressed in gastrointestinal tissues, and a wide range of malignancies, like esophageal, gastric, colorectal, biliary, pancreatic cancers, lung adenocarcinomas and also gliomas [4]. AnnexinA1 expression in cancers is not just tissue-specific but can be different in different types of cancers of the same tissue, for example, it is differently expressed in primary invasive breast cancer, *in situ* breast carcinoma and metastatic breast cancer. In the first two, the expression is generally reduced, but in the latter, it is significantly increased. In benign breast epithelium, AnnexinA1 expression can be variable [4]. AnnexinA1 can promote the invasiveness of tumor cells by activating the Transforming Growth Factor-β (TGFβ) and Nuclear factor kappa B (NF-κB) pathways. The activation of the TGFβ pathway will lead to epithelial-to-mesenchymal transition in cancer cells. Both AnnexinA1 and A2 are mediators of the endocytosis of epidermal growth factor receptor (EGFR), and it is known that EGFR activity is related to breast cancer progression. Of note, EGFR expression is also a marker of the basal-like phenotype in triple-negative breast cancers [4–6].

Cluster of differentiation 44 (CD44) is considered a cell surface glycoprotein receptor, which mainly binds hyaluronic acid, and this linkage takes part in cell invasiveness [7]. CD44 can also be connected with a cell adhesion molecule, an integrin which takes part in signaling between cells, cell proliferation and cell differentiation [7]. It has a short standard form (CD44s) and several isoforms as a result of alternative splicing (CD44v) [8]. CD44 has an important role in cell-cell and cell-matrix communication [7]. This receptor is expressed in a wide range of cell types, for example, in leukocytes, epithelial cells, mesodermal cells and also in numerous cancer stem cells [7]. Cancer stem cells produce hyaluronic acid to invoke tumor-associated macrophages [7]. Both cells can synthesize platelet-derived growth factor (PDGF), which keeps the tumor cells in a constant proliferative phase, this collaboration leads to stromal cells gathering into the cancer stem cell niche, and the stromal cells produce growth factors which coordinate stem cell activity and reproduction [7]. CD44 expression on breast cancer cell surface is increased compared to normal breast epithelial cells [9].

Cluster of differentiation 117 (CD117) also known as c-Kit, is a proto-oncogene or stem cell factor receptor; it is a transmembrane receptor tyrosine kinase, and as a ligand, stem cell factor (SCF) can bind to it [10]. CD117 is expressed in progenitor cells, for example, in the breast, in the hemopoietic system, in the myocardium, in the lung, in the testis and it is also expressed in luminal epithelial cells in adult normal breast tissue [10]. CD117 can become oncogenic either by being overactivated or by constitutive mutations leading to CD117 being activated without a ligand, and as a consequence, cell proliferation, differentiation and migration will be upregulated [11]. The inactive c-Kit is located on the cell surface, and when SCF binds to the receptor, autophosphorylation occurs [11]. This process will promote signal transduction pathways, for example, in the Janus kinase/signal transducer and activator of

transcription (JAK/STAT), rat sarcoma virus/mitogen-activated protein (RAS/MAP) kinase pathways [11]. By triggering these pathways, CD117 has an important role in cell proliferation, differentiation, apoptosis and motility [11]. CD117 can be used as a marker to detect hemopoietic stem cells and cancer stem cells by immunohistochemistry, and the staining is positive when seen on the cell membrane, but also if present in the cytoplasm [10–12]. CD117 expression has also been linked to the basal-like phenotype in a study searching for immunohistochemistry (IHC) based surrogate markers of this intrinsic subtype, but cytokeratin 5 (CK5) and EGFR were found superior [5].

Cluster of differentiation 166 (CD166), also known as activated leukocyte cell adhesion molecule (ALCAM), was identified as a cell surface glycoprotein on the surface of activated leukocytes [13]. It is a prognostic marker for various tumors and correlates with poor outcome [13]. CD166 can be found in epithelial cells, myeloid progenitor cells, vascular endothelial cells, and also a variety of stem cells, including cancer stem cells [13]. CD166 can be expressed in invasive cancers, such as breast, lung, bladder, prostate, liver, pancreas, head and neck cancers, as well as epithelial ovarian carcinomas, [13]. CD166 has a role in interaction between cells, like epithelial or endothelial cells and lymphocytes, and in angiogenesis [13]. CD6, CD9, S100B and galectin-8 are ligands for CD166 in breast tumors and endothelial tumor cells. The localization of CD166 is different in normal breast epithelial cells and breast tumor cells [13]. In normal cells, CD166 expression is increased on the cell surface, and the expression is decreased in the cytoplasm [13].

Nanog is a stem cell transcription factor, which has a role in cell differentiation, the apoptotic process and cell fate determination [14]. It is involved in the preservation of pluripotency in embryonic stem cells [14]. Under physiological circumstances, during life, Nanog expression is at a low level in a wide range of tissues, in contrast to cancer stem cells, where Nanog expression can be increased [15]. Nanog can be expressed in the ovaries, the testis, the small intestines, the thyroid gland and also in the glandular cells of the uterine cervix [15]. Despite this fact, Nanog is not expressed in most of the normal tissues [15]. The expression of this marker can be seen as nuclear and cytoplasmic positivity in different types of precancerous lesions and invasive cancers, for example, in head and neck squamous cell dysplasias and carcinomas, salivary gland mucoepidermoid carcinomas, gliomas, lung, colorectal, gastric, esophageal, renal cell and urothelial carcinomas, furthermore in testicular germ cell tumors and ovarian cancers [15]. In breast cancer, it shows rather nuclear than cytoplasmic positivity [15]. Nanog expression positively correlates with proliferation, and also with higher stage, worse patient outcome, poor differentiation, and according to some studies, the expression correlates with therapy resistance [16].

Octamer binding transcription factor 4 (oct-4) is a homeodomain transcription factor of the Pit-Oct-Unc (POU) family, and it has an important role in the regulation of pluripotency in somatic cells, embryonic stem cells and in cancer stem cells [17]. A wide range of adult stem cells, such as breast epithelial, kidney-, mesenchymal, liver- and pancreatic stem cells express oct-4 [18]. Oct-4 expression can be found in bladder, ovarian, prostate, rectal cancers, gliomas, medulloblastoma, melanoma, hepatocellular carcinoma, esophageal squamous cell carcinoma and acute myeloid leukemia [18]. When breast epithelial stem cells start their differentiation, oct-4 expression decreases [18]. In normal breast tissue, and also in breast carcinoma, IHC demonstrates nuclear and cytoplasmic staining [18].

Materials and methods

We examined triple-negative breast cancers (TNBCs) surgically treated at the Bács-Kiskun County Teaching Hospital between 2005 and 2017. By definition, all the tumors lacked estrogen (ER) and progesterone receptor (PR) and human epidermal growth factor receptor 2 (HER2) expression. From the selected formalin-fixed, paraffin-embedded tumor samples, tissue microarray (TMA) cores were taken. In each case, two, three or four cores were taken from the donor blocks. One TMA contained 7 rows, and 10 columns, therefore, on a single TMA slide, we could examine 70 TNBC core samples.

Four-μm-thick TMA serial sections of the TNBC series were immunostained using either the Roche-Ventana BenchMark (Tucson, AZ, USA) automated instrument with high pH antigen retrieval (in CC1 buffer) for 60 min and the Ultraview detection system for 20 min; or using a manual procedure at room temperature, including routine dewaxing and rehydration, antigen retrieval in pH 9.0 Tris (0.1 M)-EDTA (0.01 M) buffer using an electric pressure cooker (Avair, Biofa, Veszprém, Hungary) for 20 min. and incubations using the primary antibodies overnight followed by a micropolymer detection system (Histols, Histopathology Ltd. Pecs, Hungary) for 60 min. Finally, both types of reactions were developed using DAB-hydrogen peroxide, resulting in a brown staining. The following human antigen-specific antibodies were used: mouse monoclonal anti-ALDH1 (1:75; clone 44, CellMarque, Merck, Darmstadt, Germany); anti-Annexin1 (1: 200, clone MRQ-3), anti-CD44 (1:50; clone MRQ13), anti-oct-4 (1:20-35; clone MRQ-10; all three CellMarque, Rocklin, CA, USA); and anti-CD166 (1:100, clone MOG/07, Novocastra, Newcastle upon Tyne, UK); rabbit monoclonal anti-Nanog (1: 35, clone EP225, CellMarque); as well as rabbit polyclonal anti-CD117 (manual 1:100 or Ventana 1:700, RB-9038, Thermo Fisher, LabVision, Fremont, CA, USA). Immunostained TMA slides were digitalized using a Pannoramic 1000 whole slide scanner (3DHistech Ltd. Budapest, Hungary) and analyzed using a visual scoring system.

The scanned slides were evaluated by two observers, SzA and GC. For each marker, the proper localization of the staining (e.g., nuclear,

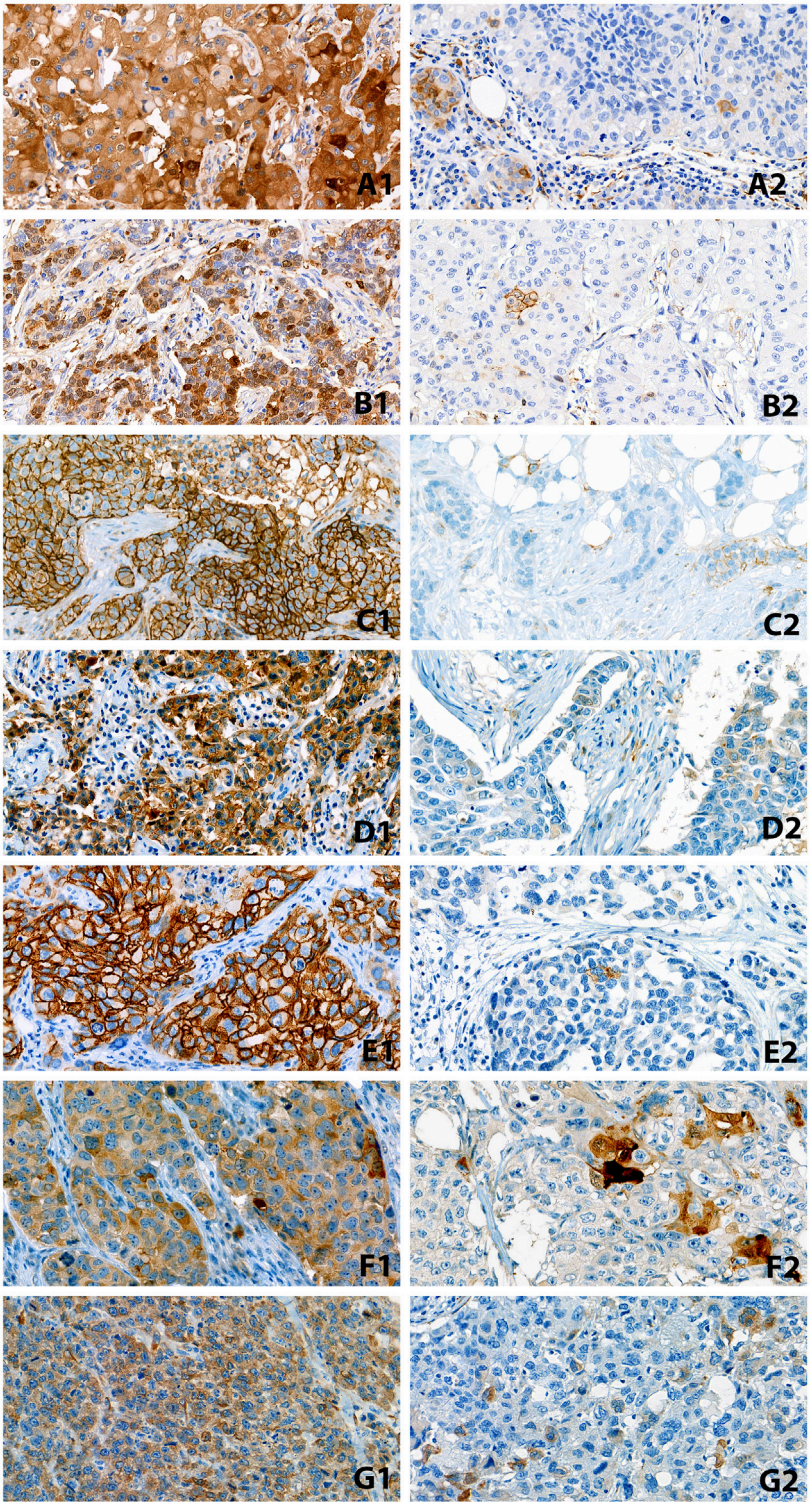

FIGURE 1
Examples of diffusely (1) and focally (2) positive staining with the studied markers. **(A)**: ALDH1, **(B)**: AnnexinA1, **(C)**: CD44, **(D)**: CD117, **(E)**: CD166, **(F)**: Nanog, **(G)**: oct-4 (All ×40 magnification).

TABLE 1 Clinicopathological parameters of the studied cases.

		Value (range)
Median age (years)		59 (29–81)
Median tumor size (mm)		20 (7–107)
Histological type		
	NST	98
	Mixed micropapillary	3
	Metaplastic	5
pT category		
	pT1	55
	pT2	43
	pT3	4
	pT4	4
pN category		
	pN0	57
	pN1	37
	pN2	10
	pN3	2
Grade		
	1	0
	2	5
	3	101
Surgery type		
	Breast-conservative	80
	Mastectomy	26
	SNB	56
	SNB and ALND	24
	ALND	25
	No axillary surgery	1
Chemo and Radiotherapy		
	Taxane containing therapy	67
	Anthracyclin containing therapy	12
	CMF	4
	RT	83
	Only RT without Chemotherapy	9
	Neither chemotherapy nor RT	14

NST: no special type breast cancer, SNB: sentinel lymph node biopsy, ALND: Level I-II axillary lymph node dissection, CMF: cyclophosphamide, methotrexate, and fluorouracil, RT: radiotherapy

cytoplasmic or membranous) of any intensity in at least 50% of the tumor cells was interpreted as diffusely positive, labelling between 1% and 50% was considered focally positive, and cases with no staining at all or false staining with non-proper localization were interpreted as negative. Accordingly, we distinguished between 3 rough patterns of staining: negative, focal and diffuse. For AnnexinA1, CD44, CD117 and CD166, cytoplasmic and membranous expression, while for ALDH1, Nanog and oct-4 IHC, nuclear and/or cytoplasmic stainings were considered positive. CD117 was also evaluated as a membranous staining only (CD117*). Examples of positive stainings are depicted in Figure 1.

The Spearman rank correlation test was used for the analysis of marker expression and different clinicopathological variables. After the evaluation, we compared the different marker expressions for overall survival (OS) and disease-free survival (DFS). Treatment and follow-up-related data were taken from the patients' digital charts. For the statistical analyses, and generation of the Kaplan-Meier curves, the SPSS (IBM, SPSS 23.0, Armonk, NY, USA) package was used. The log-rank test was utilized when comparing survival curves. The level of significance was set at $p < 0.05$. Patients lost to follow-up or alive at the last follow-up were censored at the time of the last visit. Stem cell markers with a statistical impact on survival were entered into a multivariate model including known prognosticators of breast cancer, such as tumor size, nodal status and histological grade, and the Cox proportional hazard model was applied to check whether any had an independent effect on the outcome. For the evaluation of the differences between the marker expression and OS, DFS we performed the chi-square (Fisher's exact) test with Bonferroni-Holm correction. This correction compensates for repetitive multiple pairwise tests and leads to the modification of the original $p < 0.05$ threshold for significance. As most events with high-grade TNBCs occur within 5 years, 5 year survival estimates have been chosen to reflect the outcome of subgroups according to stem cell marker expression.

Results

Study population

Altogether TMAs from 106 female TNBCs were selected. The clinicopathological characteristics of the examined cases are presented in Table 1. The median age of the patients was 59 years. The majority of the cases included were invasive breast carcinomas of no special type, with the addition of 5 metaplastic and 3 mixed micropapillary carcinomas. None of the tumors was well differentiated. Most tumors were of the pT1 and pN0 categories and were treated by breast conservation and sentinel lymph node biopsy. The majority of the patients received adjuvant chemotherapy and radiotherapy as summarized in Table 1. Most of the patients got chemotherapy in the adjuvant setting, while 7 patients had neoadjuvant chemotherapy (these latter were included in the series as no substantial regression occurred in their disease). Altogether, 14 patients did not receive any treatment besides surgery, either based on their known comorbidities and relative contraindications or the rare refusal to all forms of further therapy.

The median follow-up of the cases was 83 months (range: 5–209), with median DFS and OS of 62 (range: 1–203) and 83 (range: 5–209) months, respectively. There were 36 deaths (21 due to breast cancer) during the follow-up period, in

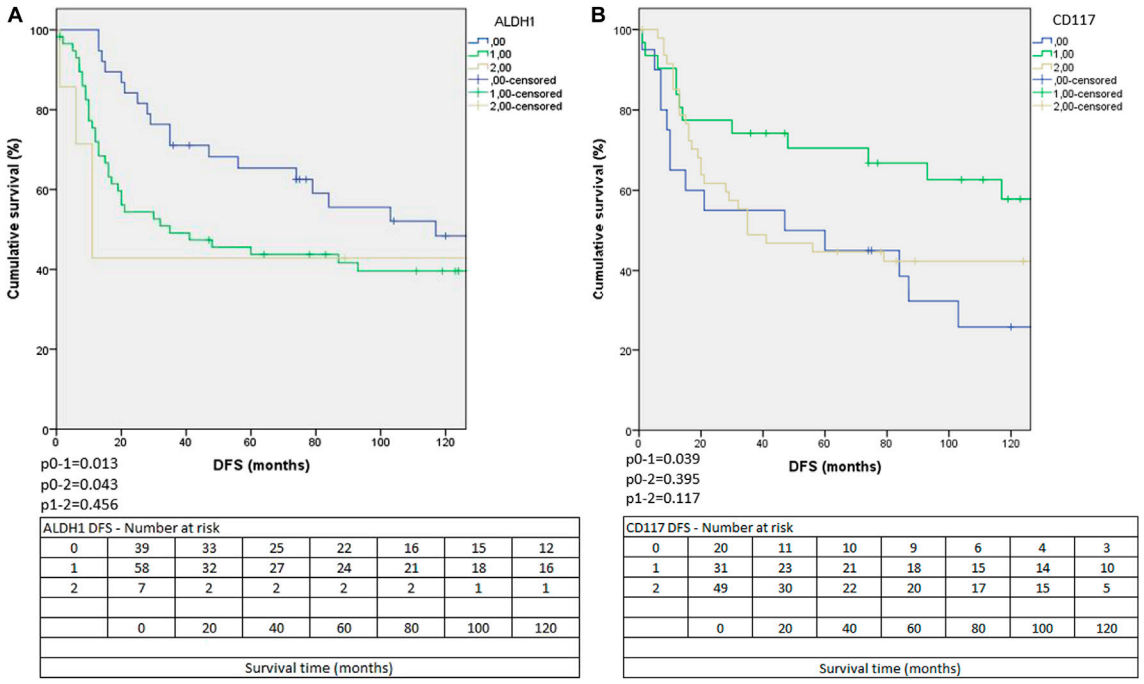

FIGURE 2
The Kaplan-Meier curves of ALDH1 **(A)** and CD117 membranous and/or cytoplasmic expressions **(B)** according to DFS. (0: negative, 1: focally positive, 2 diffusely positive staining).

addition, 20 patients had recurrent disease, whereas 50 were with no evidence of disease at the last follow-up.

Stem cell marker expression

The stem cell marker expression showed no correlation with clinicopathological variables (patient age, tumor size and grade, pT or pN categories) except for three (Supplementary Table S1). A positive correlation was found between ALDH1 expression and pT categories (p = 0.024). CD166 expression showed a positive correlation with tumor grade (p = 0.045), and patient age (p = 0.044). The Fisher's exact test showed an association between CD166 expression and tumor grade (p = 0.038) (Supplementary Table S2). Of the 98 cases with evaluable CD166 staining, 95 were of Grade 3 and 71, 16, and 8 showed diffuse, focal, and no CD166 staining, respectively. Two grade 2 TNBCs showed no staining, and one was diffusely positive for this marker. The proportion of cases staining with each stem cell marker and the associated 5 year survival estimates are reported in Supplementary Table S3. Based on the results there were no significant differences in survivals according to stem cell marker expression; focal or diffuse cytoplasmic and membranous CD117 expressing cases showed marginally significant differences in DFS: 22/49 with a diffuse staining pattern and 22/31 with a focal staining pattern were with no evidence of disease after 5 years (Supplementary Table S3).

For DFS, only ALDH1 and CD117 (with either membranous or cytoplasmic staining) had different survivals according to their staining patterns based on the Kaplan-Meier analysis (Figures 2A, B), whereas for OS, we noted differences in survival according to the stainings of CD44, CD117 (with either membranous or cytoplasmic staining) and CD166 (Figures 3A–C).

In ALDH1-negative tumors, a significantly better DFS was seen compared to the cases with focal, (p = 0.013) or diffuse positivity (p = 0.043). In the focally or diffusely positive cases, the DFS was similar (p = 0.456) (Figure 2A). The OS was the highest in ALDH1 negative cases, and the diffuse positive cases had the shortest OS, but the differences were not significant (p = 0.208). ALDH1 positivity showed a negative prognostic effect.

For CD117, only combined membranous and/or cytoplasmic staining categories showed differences in survival according to the Kaplan-Meier analysis. For DFS, cases with focal staining had better survival than negative cases (p = 0.039), but cases with diffuse staining did not differ significantly from the other two groups (negative cases compared to diffusely positive cases: p = 0.395, focally positive cases compared to diffusely positive cases p = 0.117) (Figure 2B). For OS, cases with no staining had worse survival than cases with either focal (p = 0.016) or diffuse

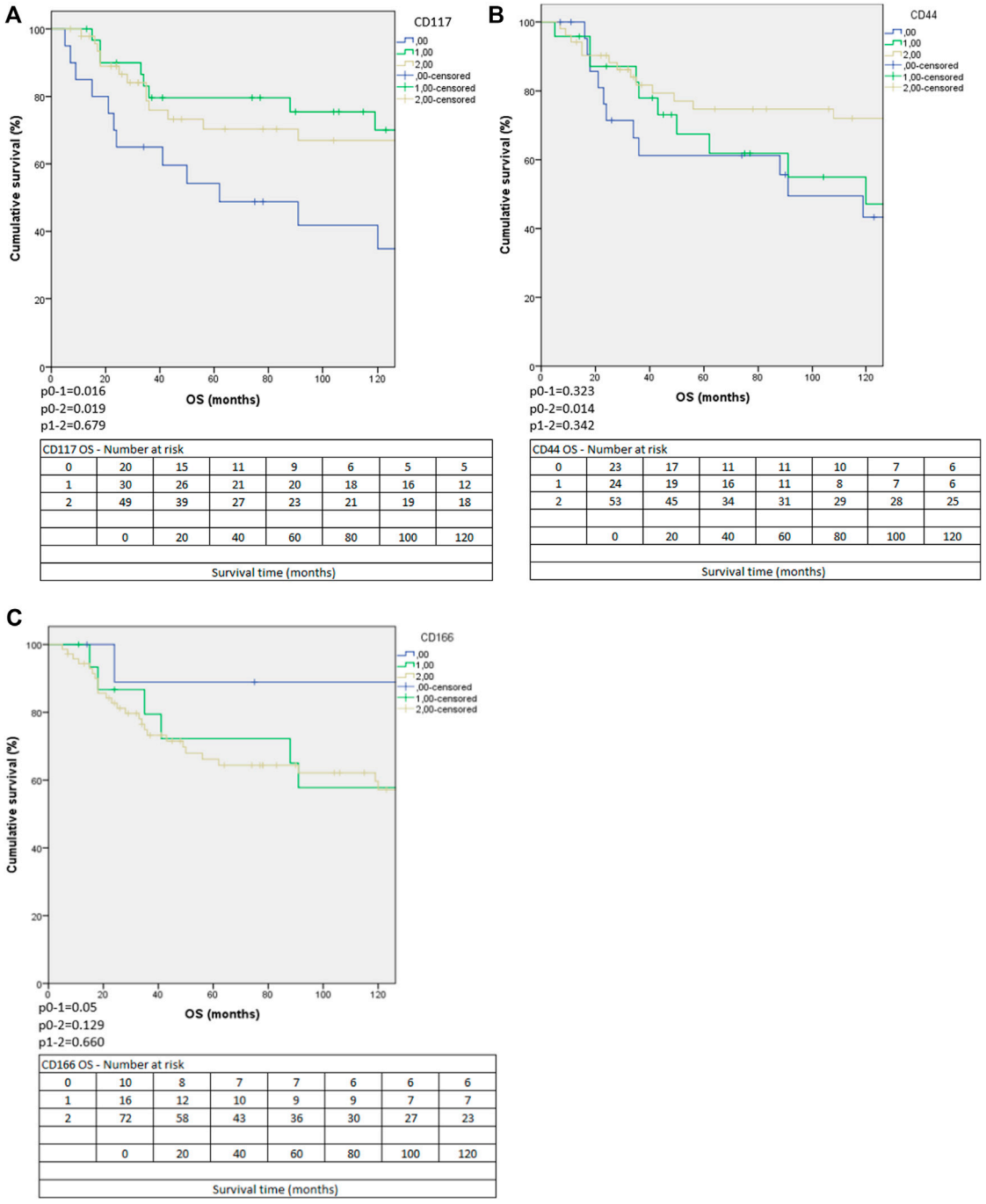

FIGURE 3
The Kaplan-Meier curves of membranous and/or cytoplasmic expression of CD117 **(A)**, CD44 **(B)** and CD166 **(C)** expressions according to OS. (0: negative, 1: focally positive, 2 diffusely positive staining).

(p = 0.019) staining. Cases with focal or diffuse staining had similar OS (Figure 3A). According to these results, CD117 might have prognostic value.

Concerning CD44, a significant difference was seen between the OS of negative and diffusely positive cases (p = 0.014) with better survival for the latter group. Interestingly the OS of focally positive cases was nearly the same as that of the negative cases (Figure 3B). We found no significant difference according to the OS between the focally and diffusely positive cases (p = 0.342).

TABLE 2 The results of the univariate and multivariate Cox regression analysis for OS.

	Univariate analysis			Multivariate analysis		
	HR	**95% CI**	***p***	**HR**	**95% CI**	***p***
pT						
1	reference			reference		
2	1.103	0.581–2.092	0.763	0.836	0.348–2.008	0.689
3	4.027	0.890–18.219	0.070	1.228	0.062–24.257	0.892
4	**6.398**	**1.406–29.106**	**0.016**	0.795	0.092–6.836	0.835
pN						
0	reference			reference		
1	0.918	0.445–1.894	0.817	1.336	0.463–3.854	0.591
2	**3.607**	**1.512–8.603**	**0.004**	1.592	0.348–7.268	0.548
3	7.211	0.919–12.583	0.060	9.289	0.840–102.707	0.069
Grade						
2	reference			reference		
3	1.308	0.315–5.429	0.700	0.317	0.010–10.001	0.514
ALDH1						
Negative	reference			reference		
Focal	1.591	0.813–3.114	0.175	2.602	0.773–8.754	0.122
Diffuse	2.187	0.621–7.708	0.223	1.845	0.254–13.381	0.544
AnnexinA1						
Negative	reference			reference		
Focal	1.943	0.584–6.463	0.278	1.914	0.433–8.459	0.391
Diffuse	1.693	0.481–5.952	0.411	2.080	0.452–9.566	0.346
CD44						
Negative	reference			reference		
Focal	0.636	0.277–1.459	0.285	0.669	0.210–2.134	0.497
Diffuse	**0.428**	**0.206–0.888**	**0.022**	0.460	0.154–1.373	0.164
CD117*						
Negative	reference			reference		
Focal	0.577	0.246–1.350	0.205	0.225	0.028–1.776	0.157
Diffuse	0.764	0.377–1.551	0.457	2.025	0.186–21.978	0.561
CD117**						
Negative	reference			reference		
Focal	0.377	0.165–1.345	0.078	0.615	0.082–4.589	0.635
Diffuse	0.441	0.212–1.331	0.104	**0.076**	**0.006–0.929**	**0.043**
CD166						
Negative	reference			reference		
Focal	3.699	0.794–17.226	0.095	9.020	0.313–259.600	0.199
Diffuse	3.131	0.740–13.244	0.120	11.974	0.472–303.720	0.132
Nanog						
Negative	reference			reference		
Focal	0.907	0.384–2.140	0.823	0.404	0.112–1.447	0.164
Diffuse	1.414	0.647–3.092	0.384	1.491	0.542–4.099	0.438
oct-4						
Negative	reference			reference		
Focal	0.866	0.425–1.764	0.692	0.873	0.309–2.464	0.798
Diffuse	1.672	0.652–4.287	0.283	2.904	0.680–12.388	0.149

Membranous (*); membranous and/or cytoplasmic (**) immunostaining.
Significant variables are highlighted in bold.

TABLE 3 The results of the univariate and multivariate Cox regression analysis for DFS.

	Univariate analysis			Multivariate analysis		
	HR	**95%CI**	***p***	**HR**	**95%CI**	***p***
pT						
1	reference			reference		
2	1.029	0.595–1.781	0.915	0.839	0.411–1.711	0.629
3	**6.008**	**1.749–20.635**	**0.004**	**16.835**	**1.539–184.083**	**0.020**
4	**5.497**	**1.881–16.058**	**0.001**	2.200	0.402–12.027	0.362
pN						
0	reference			reference		
1	1.249	0.702–2.220	0.448	1.007	0.448–2.262	0.986
2	**2.708**	**1.224–5.991**	**0.013**	1.045	0.265–4.111	0.949
3	**19.754**	**4.031–96.790**	**<0.001**	**11.365**	**1.290–100.067**	**0.028**
Grade						
2	reference			reference		
3	1.037	0.324–3.318	0.950	4.273	0.359–50.843	0.250
ALDH1						
Negative	reference			reference		
Focal	**1.889**	**1.052–3.077**	**0.044**	2.539	1.032–6.245	0.042
Diffuse	1.775	0.602–5.230	0.297	2.858	0.633–12.894	0.171
AnnexinA1						
Negative	reference			reference		
Focal	0.931	0.425–2.037	0.858	0.665	0.245–1.804	0.424
Diffuse	1.063	0.467–2.420	0.884	0.828	0.282–2.427	0.731
CD44						
Negative	reference			reference		
Focal	0.637	0.306–1.326	0.227	0.626	0.233–1.676	0.351
Diffuse	0.625	0.337–1.162	0.137	0.582	0.237–1.431	0.238
CD117*						
Negative	reference			reference		
Focal	0.668	0.315–1.415	0.292	0.859	0.136–5.408	0.872
Diffuse	1.136	0.624–2.066	0.675	0.730	0.129–4.118	0.722
CD117**						
Negative	reference			reference		
Focal	0.453	0.212–1.101	0.061	0.472	0.081–2.737	0.403
Diffuse	0.758	0.400–1.438	0.397	0.524	0.080–3.425	0.500
CD166						
negative	reference			reference		
Focal	1.670	0.594–4.696	0.330	1.390	0.329–5.863	0.653
Diffuse	1.221	0.479–3.111	0.674	0.743	0.201–2.746	0.656
Nanog						
Negative	reference			reference		
Focal	0.959	0.481–1.910	0.906	0.701	0.268–1.829	0.468
Diffuse	1.092	0.548–2.174	0.801	1.650	0.714–3.811	0.240
oct-4						
Negative	reference			reference		
Focal	0.624	0.347–1.123	0.115	0.802	0.358–1.798	0.592
Diffuse	0.911	0.397–2.091	0.827	0.684	0.208–2.254	0.533

Membranous (*); membranous and/or cytoplasmic (**) immunostaining.
Significant variables are highlighted in bold.

TABLE 4 The results of the multivariate Cox regression analysis for OS and DFS, including the markers which showed statistical impact on survival in the univariate Cox regression analysis.

	OS			DFS		
	HR	**95%CI**	***p***	**HR**	**95%CI**	***p***
pT						
1	reference			reference		
2	0.894	0.460–1.737	0.741	0.877	0.500–1.538	0.647
3	1.369	0.150–12.426	0.779	2.768	0.454–16.868	0.269
4	1.155	0.190–7.006	0.875	2.167	0.505–9.298	0.297
pN						
0	reference			reference		
1	0.953	0.4462.036	0.901	1.140	0.634–2.053	0.659
2	3.367	1.210–9.371	0.020	1.895	0.614–5.848	0.266
3	**10.179**	**1.143–90.640**	**0.037**	**12.041**	**2.036–71.210**	**0.006**
ALDH1						
Negative				reference		
Focal				**1.832**	**1.014–3.410**	**0.048**
Diffuse				2.029	0.655–6.288	0.219
CD44						
Negative	reference					
Focal	0.665	0.279–1.582	0.356			
Diffuse	**0.386**	**0.172–0.862**	**0.020**			

Significant variables are highlighted in bold.

Regarding CD166 staining, a marginally significantly worse OS was identified for cases with focal staining, when compared to the negative cases ($p = 0.05$). Interestingly, the cases with diffuse marker expression showed no statistical significance from negative cases, which can probably be explained by the low case number in the negative group (Figure 3C).

According to the univariate Cox regression analysis for OS (Table 2) the pT category (HR: 6.398), the pN category (HR: 3.607) and the diffuse CD44 expression (HR: 0.428) had a statistical impact. For DFS (Table 3) the pT category (pT3: HR: 6.008; pT4: HR: 5.497), the pN category (pN2: HR: 2.708; pN3: HR: 19.754) and the focal ALDH1 expression (HR: 1.889) had statistical impact. Based on the multivariate Cox regression analysis including those clinicopathological data and marker expressions which had a statistical impact in the univariate analysis (Table 4), for OS, only CD44 staining (HR: 0.386) and the pN category (HR: 10.179) had an independent impact on prognosis. For DFS, only the pN category (HR: 12.041) and among the stem cell markers ALDH1 (HR: 1.832) were found to be of independent prognostic impact. In addition, in the multivariate Cox regression analysis for both DFS and OS including all the examined markers and clinicopathological data, we found that pT and pN categories had a statistical impact on DFS (pT3: HR: 16.835; pN3: HR: 11.365) (Table 3). Interestingly, based on this analysis only CD117 diffuse positivity showed statistical impact on OS (HR: 0.076) (Table 2).

Discussion

Of the 7 examined stem cell markers in TNBCs, the Kaplan-Meier analyses suggested a prognostic value only for ALDH1, CD117, CD44 and CD166, whereas the multivariate analysis reduced this to ALDH1 (for DFS) and CD44 (for OS). Although not numerous, several previous studies have examined the prognostic impact of stem cell marker expression in breast cancers.

We experienced no prognostic associations with AnnexinA1, Nanog and oct-4, but there are some publications with opposite results. Wang et al. analyzed the prognostic value of AnnexinA1 expression in TMAs of 135 invasive breast carcinomas; lack of AnnexinA1 expression (0 to <5% staining) correlated with pathological TNM stage and especially with lymph node metastases [19]. AnnexinA1 expression correlated with better OS estimates, but such an association was not seen with DFS estimates [19].

Nagata et al. examined the correlation between pluripotent stem cell-inducing factor expression and the prognosis of breast cancer in 100 cases [20]. Among the cases examined, there were ER-positive and HER2-negative, ER-negative and HER2-positive and also triple-negative (TN) cases [20]. They found a significant association between high Nanog expression and worse OS and DFS ($p = 0.033$, $p = 0.004$), but 8 of the 9 high Nanog-expressing tumors were ER-positive [20]. No significant differences in DFS

or OS were found according to oct-4 expression [20]. Another study also found that in ER+ tumors, oct-4 expression was related to a worse outcome and resistance to tamoxifen [17], but the lack of ER expression in the present series does not make the results comparable.

According to Wang et al., Nanog and oct-4 are associated with poor prognosis among breast cancer patients [21]. They examined 126 breast cancers inclusive of 19 with basal-like phenotype. 52 cases (15 basal-like tumors) were positive for oct-4 and 47 (14 basal-like carcinomas) for Nanog with 26 cases (12 basal-like cancers) co-expressing the two markers [21]. (Their definition of IHC positivity, ≥1%, corresponds to a category inclusive of our focally and diffusely staining categories.) With multivariate analysis, there was an association between oct-4 or Nanog expression and the presence of lymph node metastasis (p = 0.003], and the molecular type of breast cancer (p = 0.001) [21]. Cumulative survival was shorter in all cases expressing either of the markers than in patients with dual negative tumors [21].

In our study, the CD117 negative cases had significantly shorter OS than the positive ones, but the multivariate analysis did not find this to be of independent effect. A similar effect was noted for DFS, too, but again, this did not turn out to be of significance in the multivariable analysis. Luo et al examined the cytoplasmic or membranous CD117 expression in 58 TNBC and 48 non-TNBC, of which the first set showed a significantly greater percentage of staining (48% vs. 29%) [22]. CD117 positivity was associated with tumor recurrence and some markers of poor prognosis (vascular invasion, proliferation) [22]. Tsutsui et al. also examined the association between CD117 expression and prognosis [23]. They investigated 217 no special type invasive breast cancers: 59 cases (27%) were positive, and the remaining 158 (73%) were negative [23]. They found a significant correlation between the lack of CD117 expression and lymph node metastasis ($p < 0.0001$), but not with tumor size or grade [23]. In keeping with our Kaplan-Meier analyses, they found a significant association in univariate analysis between the lack of CD117 expression and a worse DFS ($p = 0.0041$), but with multivariate analysis, the CD117 expression lost its significance (p = 0.31) [23]. CD117 has been found to be associated with the basal-like phenotype, but had no additive value in identifying these tumors by immunohistochemistry when EGFR or CK5 expression was present [5]; as this phenotype has great overlap with TNBCs, CD117 expression is likely to reflect the basal-like nature of the tumor, and this may also explain the lack of significance in multivariate analysis.

With CD166 staining, marginally significantly worse OS was identified for cases with focal staining, when compared to the negative cases (p = 0.05). Interestingly, the survival of cases with diffuse labeling with the antibody showed no statistical significance from negative cases, which can probably be explained by the low case number in the negative group. In TNBCs, the intensity of CD166 staining is lower than in other subtypes, and lower CD166 membranous labelling has been correlated with aggressive behavior [13]. Hein et al. examined 347 breast cancer patients' TMA with IHC [24]. These cases contained no special type carcinomas, lobular carcinomas, "ductulolobular" carcinomas and others, and also included ER/PR-positive and -negative cases [24]. In 74 cases, the staining was negative, 136 cases had weak staining, 95 cases were moderately positive (these latter 2 categories were then combined into one as there was no significant difference between them), and finally 42 cases were strongly positive [24]. With Kaplan-Meier analysis, compared to the OS estimates of the weak/moderate category, they found an association between high ALCAM expression and a worse prognosis (p = 0.021) [24]. The differences in RFS were not significant (p = 0.279) [24]. The prognostic impact of this marker expression was higher in invasive ductal carcinomas (no special type) than in the other subtypes (OS p = 0.003; RFS p = 0.048) [24]. With univariate Cox regression analysis, in no special type carcinomas, ALCAM overexpression was associated with worse prognosis (OS: HR = 4.32, 95% CI: 1.61–11.56, p = 0.004, and the RFS: HR = 2.47, 95% CI: 1.17–5.22, p = 0.018), while in the multivariate analysis, with stage, nodal status, grade, ER status, the prognostic value of ALCAM expression was borderline, p = 0.050 [24].

In our study, ALDH1 expression was associated with shorter DFS, but not with shorter OS. Both cases with focal, ($p = 0.013$) and diffuse positivity ($p = 0.043$) had significantly worse DFS than cases without expression. The prognostic relevance of ALDH1 expression is supported by several literature data. Ginestier et al. examined the ALDH1 staining in TMAs of 481 breast cancers of different phenotypes from two different centers [25]. ALDH1 staining correlated with basal cytokeratin expression which is a common feature in TNBCs [25]. Like in our series, only a minority of the cases showed diffuse staining, the average labelling was 5%. The relative risk of death because of cancer in ALDH1-expressing and ALDH1-negative tumor cases was 1.76 ($p < 0.028$) [25]. ALDH1-positive cases had worse 5-year-OS (20% and 70% in the two centers, respectively) than ALDH1-negative ones (59% and 85%, respectively) [25]. Although our OS analysis did not show a prognostic effect, this was observed with the DFS analysis, the worse 5 year-DFS seen with ALDH1 staining was intermediate between the OS values of the two centers reported by Ginestier et al. [25]. Zhou et al examined different marker expressions, including ALDH1 expression by IHC in 31 TNBC and 89 non-TNBC cases [26]. The ALDH1 expression rate was significantly higher in TNBCs than in non-TNBCs ($p = 0.015$) and was associated with OS in both subsets; it turned out to be an independent prognostic factor reflecting poor prognosis [26]. Kida et al found 21% of 653 invasive BC core needle biopsy samples to be positive for ALDH1 by IHC, whereas the rate in TNBCs was somewhat higher (30%) [27]. Expression was correlated with larger tumor size ($p < 0.001$) (like in our study), clinical node metastasis ($p = 0.004$), higher clinical stage ($p < 0.001$), higher nuclear grade ($p = 0.005$), hormone receptor positivity ($p < 0.001$), and HER2 negativity ($p < 0.001$) [27]. ALDH1-expressing tumors had significantly shorter DFS ($p < 0.001$) and OS (p = 0.044), and ALDH1 proved to be an independent

predictor for DFS (p = 0.033), but not OS [27]. Taking into consideration the subtypes of BCs, ALDH1 expression was associated with poor prognosis in luminal-type cancers, but not in TNBCs or HER2-positive tumors [27]. Ma F. et al examined ALDH1 expression by IHC in 158 TNBCs. Similarly to our results, somewhat more than half of the cases were positive, and expression was associated with tumor size (p = 0.02) and stage (p = 0.04). ALDH1-positive cases had shorter relapse-free survival (RFS) and OS [28]. The multivariate Cox regression showed that ALDH1 expression was an independent prognostic indicator for both RFS and OS in TNBCs [28].

With the evaluation of CD44 expression, we found a significant difference between the OS of negative and diffusely positive cases (p = 0.014). Interestingly, in the focally positive cases, the OS was 62% which is close to the OS of negative cases. Kim et al., in 2010, investigated the prognostic significance of CD24 and CD44 expression in breast cancer [29]. In their study, the 10-year-DFS was 62% for the cases lacking CD44 expression, and it was 73% for CD44-positive patients (p = 0.012) [29]. The 10 year-OS of CD44-negative cases was 68%, and that of CD44-positive cases was 78% (p = 0.013) [29]. In contrast, Collina F et al examined 160 TNBCs with IHC for several marker expressions, including CD44, and reported that the rare cytoplasmic staining was associated with metastasis and DFS [30]. Shadbad et al. made a systematic review to determine the prognostic value of CD44 expression in TNBCs [31]. Based on the 9 studies included, CD44 and CD44+/CD24-/low phenotype is associated with poor OS and DFS estimates [31]. The two above-quoted results [30, 31] are in contrast with ours, and this might be explained by the dual nature of the CD44 function detailed below [32].

Louderbough et al. evaluated 15 studies which were examining the correlation between CD44 expression and prognosis [32]. Based on their summary, in 4 studies, CD44 expression was associated with an unfavorable prognosis, in 6 studies the expression was related to a favorable prognosis, while in 2 studies it was neutral [32]. In 2 studies, the association between CD44 expression and prognosis was dependent on the variant expression [32]. The remaining 1 study did not evaluate the clinical outcome [32]. Based on their research, CD44 has a connection with both cancer progression inhibition and promotion [32]. The metastasis-suppressing activity of CD44 is increased by high molecular weight hyaluronan, while low molecular weight hyaluronan acts antagonistically [32]. Another important feature is that CD44 has differently spliced isoforms, and this can also explain how $CD44^+$ tumor cells differently mediate biology; e.g., CD44v3 isoform is associated with increased cell migration and invasion [32]. The variants' expression could also be a reason behind the differences in the favorable and unfavorable prognosis [32].

The present study has several limitations. Some marker expression subgroups were small (Supplementary Table S3), as discussed in connection with CD166 expression. The patients received different adjuvant therapies. Although most systemic treatments were acceptable according to guidelines at their time, including the denial of adjuvant treatment in some patients, this may have influenced survivals. Seven patients with neoadjuvant treatment without treatment effect on the tumor were also included, and this ineffective treatment might have also affected the outcome.

We attempted to compare the stem cell marker expression and the clinical outcome in TNBCs. With CD44-, CD117-and CD166-positive cancers, we found a significant effect of the expression of these markers on OS. In ALDH1- and CD117-positive cases, the staining differences showed a correlation with DFS. In all the other IHC markers, we could not identify significant correlations. CD117 was the only marker for which we found a correlation with both OS and DFS. According to the multivariate Cox-regression analysis, CD44, ALDH1 and the lymph node status showed a significant effect on prognosis. Owing to the controversial nature of the interpretation of the results, the role of CD44 expression in TNBC requires further investigation.

Data availability statement

The original contributions presented in the study are included in the article/Supplementary Material, further inquiries can be directed to the corresponding author.

Ethics statement

This study was approved by the Human Investigation Review Board, University of Szeged (approval number 133/2019-SZTE) The approval included an exemption from informed consent due to retrospective nature of the study.

Author contributions

GC selected the cases for tissue microarrays. TK was responsible for making tissue microarrays and the immunostains. ÁN and GC collected outcome data. SA and GC evaluated the immunohistochemistry and drafted the manuscript. TZ and TL gave statistical advice, performed statistical tests, interpreted and worded the results, edited the manuscript. All authors have approved the final submitted version of the manuscript.

Funding

This research was partly funded by a grant from the Hungarian Society of Senology.

Conflict of interest

The authors declare that the research was conducted in the absence of any commercial or financial relationships that could be construed as a potential conflict of interest.

Supplementary material

The Supplementary Material for this article can be found online at: https://www.por-journal.com/articles/10.3389/pore.2023.1611365/full#supplementary-material

References

1. Alvarez-Elizondo MB, Weihs D. Breast cancer stem cells: mechanobiology reveals highly invasive cancer cell subpopulations. *Cell Mol Life Sci* (2022) 79(3): 134. doi:10.1007/s00018-022-04181-w

2. Ma I, Allan AL. The role of human aldehyde dehydrogenase in normal and cancer stem cells. *Stem Cel Rev Rep* (2011) 7(2):292–306. doi:10.1007/s12015-010-9208-4

3. Demir H, Dulgar O, Gulle BT, Turna H, Ilvan S. Prognostic value of aldehyde dehydrogenase 1 (ALDH1) in invasive breast carcinomas. *Bosn J Basic Med Sci* (2018) 18(4):313–9. doi:10.17305/bjbms.2018.3094

4. Shao G, Zhou H, Zhang Q, Jin Y, Fu C. Advancements of Annexin A1 in inflammation and tumorigenesis. *OncoTargets Ther* (2019) 12:3245–54. doi:10.2147/ott.s202271

5. Nielsen TO, Hsu FD, Jensen K, Cheang M, Karaca G, Hu Z, et al. Immunohistochemical and clinical characterization of the basal-like subtype of invasive breast carcinoma. *Clin Cancer Res* (2004) 10(16):5367–74. doi:10.1158/1078-0432.CCR-04-0220

6. Cheang MC, Voduc D, Bajdik C, Leung S, McKinney S, Chia SK, et al. Basal-like breast cancer defined by five biomarkers has superior prognostic value than triple-negative phenotype. *Clin Cancer Res* (2008) 14(5):1368–76. doi:10.1158/1078-0432.CCR-07-1658

7. Basakran NS. CD44 as a potential diagnostic tumor marker. *Saudi Med J* (2015) 36(3):273–9. doi:10.15537/smj.2015.3.9622

8. Xu H, Niu M, Yuan X, Wu K, Liu A. CD44 as a tumor biomarker and therapeutic target. *Exp Hematol Oncol* (2020) 9(1):36. doi:10.1186/s40164-020-00192-0

9. Shan NL, Shin Y, Yang G, Furmanski P, Suh N. Breast cancer stem cells: a review of their characteristics and the agents that affect them. *Mol Carcinog* (2021) 60(2):73–100. doi:10.1002/mc.23277

10. Kim J, Villadsen R. Expression of luminal progenitor marker CD117 in the human breast gland. *J Histochem Cytochem* (2018) 66(12):879–88. doi:10.1369/0022155418788845

11. Foster BM, Zaidi D, Young TR, Mobley ME, Kerr BA. CD117/c-kit in cancer stem cell-mediated progression and therapeutic resistance. *Biomedicines* (2018) 6(1):31. doi:10.3390/biomedicines6010031

12. Huang R, Wu D, Yuan Y, Li X, Holm R, Trope CG, et al. CD117 expression in fibroblasts-like stromal cells indicates unfavorable clinical outcomes in ovarian carcinoma patients. *PLoS One* (2014) 9(11):e112209. doi:10.1371/journal.pone.0112209

13. Ferragut F, Vachetta VS, Troncoso MF, Rabinovich GA, Elola MT. ALCAM/CD166: a pleiotropic mediator of cell adhesion, stemness and cancer progression. *Cytokine Growth Factor Rev* (2021) 61:27–37. doi:10.1016/j.cytogfr.2021.07.001

14. Jeter CR, Yang T, Wang J, Chao HP, Tang DG. Concise review: NANOG in cancer stem cells and tumor development: an update and outstanding questions. *Stem Cells* (2015) 33(8):2381–90. doi:10.1002/stem.2007

15. Grubelnik G, Boštjančič E, Pavlič A, Kos M, Zidar N. NANOG expression in human development and cancerogenesis. *Exp Biol Med (Maywood)* (2020) 245(5): 456–64. doi:10.1177/1535370220905560

16. Vasefifar P, Motafakkerazad R, Maleki LA, Najafi S, Ghrobaninezhad F, Najafzadeh B, et al. Nanog, as a key cancer stem cell marker in tumor progression. *Gene* (2022) 15:146448. doi:10.1016/j.gene.2022.146448

17. Mohiuddin IS, Wei SJ, Kang MH. Role of OCT4 in cancer stem-like cells and chemotherapy resistance. *Biochim Biophys Acta Mol Basis Dis* (2020) 1866(4): 165432. doi:10.1016/j.bbadis.2019.03.005

18. Tai MH, Chang CC, Kiupel M, Webster JD, Olson LK, Trosko JE. Oct4 expression in adult human stem cells: evidence in support of the stem cell theory of carcinogenesis. *Carcinogenesis* (2005) 26(2):495–502. doi:10.1093/carcin/bgh321

19. Wang LP, Bi J, Yao C, Xu XD, Li XX, Wang SM, et al. Annexin A1 expression and its prognostic significance in human breast cancer. *Neoplasma* (2010) 57(3): 253–9. doi:10.4149/neo_2010_03_253

20. Nagata T, Shimada Y, Sekine S, Hori R, Matsui K, Okumura T, et al. Prognostic significance of NANOG and KLF4 for breast cancer. *Breast Cancer* (2014) 21(1):96–101. doi:10.1007/s12282-012-0357-y

21. Wang D, Lu P, Zhang H, Luo M, Zhang X, Wei X, et al. Oct-4 and Nanog promote the epithelial-mesenchymal transition of breast cancer stem cells and are associated with poor prognosis in breast cancer patients. *Oncotarget* (2014) 5(21): 10803–15. doi:10.18632/oncotarget.2506

22. Luo Y, Huang W, Zhang H, Liu G. Prognostic significance of CD117 expression and TP53 missense mutations in triple-negative breast cancer. *Oncol Lett* (2018) 15(5):6161–70. doi:10.3892/ol.2018.8104

23. Tsutsui S, Yasuda K, Suzuki K, Takeuchi H, Nishizaki T, Higashi H, et al. A loss of c-kit expression is associated with an advanced stage and poor prognosis in breast cancer. *Br J Cancer* (2006) 94(12):1874–8. doi:10.1038/sj.bjc.6603183

24. Hein S, Müller V, Wikman H, Krenkel S, Streichert T, Schweizer M, et al. Biologic role of activated leukocyte cell adhesion molecule overexpression in breast cancer cell lines and clinical tumor tissue. *Breast Cancer Res Treat* (2011) 129: 347–60. doi:10.1007/s10549-010-1219-y

25. Ginestier C, Hur MH, Charafe-Jauffret E, Monville F, Dutcher J, Brown M, et al. ALDH1 is a marker of normal and malignant human mammary stem cells and a predictor of poor clinical outcome. *Cell Stem Cell* (2007) 1(5):555–67. doi:10.1016/j.stem.2007.08.014

26. Zhou L, Li K, Luo Y, Tian L, Wang M, Li C, et al. Novel prognostic markers for patients with triple-negative breast cancer. *Hum Pathol* (2013) 44(10):2180–7. doi:10.1016/j.humpath.2013.03.021

27. Kida K, Ishikawa T, Yamada A, Shimada K, Narui K, Sugae S, et al. Effect of ALDH1 on prognosis and chemoresistance by breast cancer subtype. *Breast Cancer Res Treat* (2016) 156(2):261–9. doi:10.1007/s10549-016-3738-7

28. Ma F, Li H, Li Y, Ding X, Wang H, Fan Y, et al. Aldehyde dehydrogenase 1 (ALDH1) expression is an independent prognostic factor in triple negative breast cancer (TNBC). *Medicine (Baltimore)* (2017) 96(14):6561. doi:10.1097/MD.0000000000006561

29. Kim HJ, Kim MJ, Ahn SH, Son BH, Kim SB, Ahn JH, et al. Different prognostic significance of CD24 and CD44 expression in breast cancer according to hormone receptor status. *Breast* (2011) 20(1):78–85. doi:10.1016/j.breast.2010.08.001

30. Collina F, Di Bonito M, Li Bergolis V, De Laurentiis M, Vitagliano C, Cerrone M, et al. Prognostic value of cancer stem cells markers in triple-negative breast cancer. *Biomed Res Int* (2015) 2015:158682. doi:10.1155/2015/158682

31. Abdoli Shadbad M, Hosseinkhani N, Asadzadeh Z, Derakhshani A, Karim Ahangar N, Hemmat N, et al. A systematic review to clarify the prognostic values of CD44 and CD44+CD24- phenotype in triple-negative breast cancer patients: lessons learned and the road ahead. *Front Oncol* (2021) 11:689839. doi:10.3389/fonc.2021.689839

32. Louderbough JM, Schroeder JA. Understanding the dual nature of CD44 in breast cancer progression. *Mol Cancer Res* (2011) 9(12):1573–86. doi:10.1158/1541-7786.MCR-11-0156

Pathology & Oncology Research | frontiers

TYPE Original Research
PUBLISHED 04 January 2023
DOI 10.3389/pore.2022.1610808

Check for updates

OPEN ACCESS

EDITED BY
Andrea Ladányi,
National Institute of Oncology (NIO), Hungary

*CORRESPONDENCE
Wenfeng Huang,
dove-wenfeng@163.com
Weimin Xie,
xieweimin@gxmu.edu.cn

†These authors have contributed equally to this work

RECEIVED 02 September 2022
ACCEPTED 16 December 2022
PUBLISHED 04 January 2023

CITATION
Liao X, Chen J, Luo D, Luo B, Huang W and Xie W (2023), Prognostic value of long non-coding RNA *MALAT1* in hepatocellular carcinoma: A study based on multi-omics analysis and RT-PCR validation.
Pathol. Oncol. Res. 28:1610808.
doi: 10.3389/pore.2022.1610808

COPYRIGHT
© 2023 Liao, Chen, Luo, Luo, Huang and Xie. This is an open-access article distributed under the terms of the Creative Commons Attribution License (CC BY). The use, distribution or reproduction in other forums is permitted, provided the original author(s) and the copyright owner(s) are credited and that the original publication in this journal is cited, in accordance with accepted academic practice. No use, distribution or reproduction is permitted which does not comply with these terms.

Prognostic value of long non-coding RNA *MALAT1* in hepatocellular carcinoma: A study based on multi-omics analysis and RT-PCR validation

Xiaoli Liao[1†], Junming Chen[2†], DongCheng Luo[1†], Baohua Luo[3], Wenfeng Huang[4*] and Weimin Xie[1*]

[1]Department of Chemotherapy, Guangxi Medical University Cancer Hospital, Nanning, China, [2]Department of Medical Oncology, Fujian Medical University Union Hospital, Fuzhou, China, [3]Department of Gastroenterology, Jiangbin Hospital, Nanning, China, [4]Department of Medical Oncology, Second Affiliated Hospital of Guangxi Medical University, Nanning, China

Background: This study aimed to explore the relationship between *MALAT1* and the prognosis of patients with hepatocellular carcinoma (HCC).

Methods: We constructed a *MALAT1* protein-protein interaction network using the STRING database and a network of competing endogenous RNAs (ceRNAs) using the StarBase database. Using data from the GEPIA2 database, we studied the association between genes in these networks and survival of patients with HCC. The potential mechanisms underlying the relationship between *MALAT1* and HCC prognosis were studied using combined data from RNA sequencing, DNA methylation, and somatic mutation data from The Cancer Genome Atlas (TCGA) liver cancer cohort. Tumor tissues and 19 paired adjacent non-tumor tissues (PANTs) from HCC patients who underwent radical resection were analyzed for *MALAT1* mRNA levels using real-time PCR, and associations of *MALAT1* expression with clinicopathological features or prognosis of patients were analyzed using log-rank test and Gehan-Breslow-Wilcoxon test.

Results: Five interacting proteins and five target genes of *MALAT1* in the ceRNA network significantly correlated with poor survival of patients with HCC ($p < 0.05$). High *MALAT1* expression was associated with mutations in two genes leading to poor prognosis and may upregulate some prognostic risk genes through methylation. *MALAT1* was significantly co-expressed with various signatures of genes involved in HCC progression, including the cell cycle, DNA damage repair, mismatch repair, homologous recombination, molecular cancer m6A, exosome, ferroptosis, infiltration of lymphocyte ($p < 0.05$). The expression of *MALAT1* was markedly upregulated in HCC tissues compared with PANTs. In Kaplan-Meier analysis, patients with high *MALAT1* expression had significantly shorter progression-free survival (PFS) ($p = 0.033$) and overall survival (OS) ($p = 0.023$) than those with low *MALAT1* expression. Median PFS was 19.2 months for patients with high *MALAT1* expression and 52.8 months for patients with low expression, while the corresponding median OS was 40.5 and 78.3 months. In subgroup analysis of patients with vascular invasion, cirrhosis, and HBsAg positive or AFP positive, MALAT1 overexpression

was significantly associated with shorter PFS and OS. Models for predicting PFS and OS constructed based on *MALAT1* expression and clinicopathological features had moderate predictive power, with areas under the receiver operating characteristic curves of 0.661–0.731. Additionally, *MALAT1* expression level was significantly associated with liver cirrhosis, vascular invasion, and tumor capsular infiltration ($p < 0.05$ for all).

Conclusion: *MALAT1* is overexpressed in HCC, and higher expression is associated with worse prognosis. *MALAT1* mRNA level may serve as a prognostic marker for patients with HCC after hepatectomy.

KEYWORDS

prognosis, hepatocellular carcinoma, mutation, DNA methylation, metastasis associated lung adenocarcinoma transcript 1 (*MALAT1*), interacting proteins, competing endogenous RNAs (ceRNAs), multi-omics

Introduction

Hepatocellular carcinoma (HCC) is the most frequent subtype of primary liver cancer and a common malignancy. HCC has been rising in incidence in the last decades and is a major cancer-related cause of death among men in China (1, 2). Non-curative therapies such as transcatheter arterial chemoembolization (TACE) and stereotactic radiotherapy (SBRT) can prolong the survival of patients with advanced HCC by slowing tumor progression (3, 4), while the combination of angiogenesis and immune checkpoint inhibitors can prolong progression-free survival (PFS) (5, 6).

Patients with early disease can benefit from curative treatments such as radical resection, liver transplantation (LT), and ablative techniques (7–9), but 5-year recurrence rates after such procedures are 40%–70% (8). A growing body of studies has focused on screening and clinical application of biomarkers for prognostic monitoring, but the sensitivity and specificity of traditional prognostic indicators such as alpha-fetoprotein (AFP) are inadequate on their own to guide clinical decisions (9). Emerging markers based on histology and genomics may more comprehensively reflect the biological characteristics of cancer cells and therefore support individualized diagnosis and treatment of HCC (10).

Genomic and transcriptomic sequencing studies suggest that long non-coding RNAs (lncRNAs) regulate many of the characteristics of HCC, including proliferation, invasion, metastasis, and immunosuppression (11, 12). These RNAs more than 200 nucleotides long are not translated into proteins but can regulate gene expression at the levels of transcription, post-transcriptional processing, and translation (13). In addition, lncRNAs may compete with microRNAs (miRNAs) to bind to the same target mRNA in order to regulate its translation (14). In this case, the lncRNA is referred to as a competing endogenous RNA (ceRNA). LncRNAs can also regulate DNA methylation to influence cancer (15, 16).

Recently, studies have shown that the 8-kb lncRNA *MALAT1* could be linked to other cancers, including breast cancer, prostate cancer, pancreatic cancer, glioma, and leukemia. (17). Therefore, *MALAT1* may be a biomarker for early diagnosis, severity assessment, or prognostic evaluation in HCC (18). In this study, we analyzed *MALAT1* expression at the multi-omics level and identified associations of its expression with gene transcription, DNA methylation, and gene mutations, and we explored the potential influence of these associations on prognosis. Second, we investigated the relationships of *MALAT1* expression with clinicopathological features and prognosis of HCC patients after hepatectomy.

Methods

Public data preparation and preprocessing

RNA-sequencing (RNA-seq) counts and tumor data for 368 patients in The Cancer Genome Atlas liver hepatocellular carcinoma (TCGA-LIHC) cohort were downloaded using UCSCXenaTools (19). Counts were normalized using the transcript per million (TPM) method, and genes with expression levels below the lower end of the interquartile range (IQR) of expression across all genes in the sample were excluded. Samples with low-frequency counts (the number of occasions of "count-per-million values > 0.5" in the sample less than 2) were excluded.

We also downloaded somatic mutation and DNA methylation profiling data for 364 and 430 patients, respectively, in the TCGA-LIHC cohort using UCSCXenaTools.

Interacting protein analysis

We constructed the network of *MALAT1* with interacting proteins using text mining in the STRING database. A first shell

was created with no more than 10 interactors, and a second shell with no more than 20 interactors. Enrichment of terms from the Kyoto Encyclopedia of Genes and Genomes (KEGG) in the network were visualized using the GOplot package in R. Genes encoding first-shell proteins were analyzed for potential assocations with HCC patient survival using the GEPIA2 database (http://gepia2.cancer-pku.cn/).

Construction of ceRNA network

StarBase is an online database that can build ceRNA networks based on thousands of interactions between miRNAs and their target genes in a CLIP-seq (Crosslinking or RNA immunoprecipitation followed by sequencing) database (https://starbase.sysu.edu.cn/). We obtained potential *MALAT1* target miRNAs and genes that may compete with *MALAT1* for binding miRNAs through StarBase (screening by miRNA number ≥ 30 and *p*-value ≤ 1.0e-5). In this way, a network of ceRNAs was constructed and visualized by Cytoscape. Genes regulated by *MALAT1* and miRNAs were analyzed for their potential associations with survival of HCC patients using the GEPIA2 database.

Somatic mutation data analysis

Somatic mutations were analyzed using the maftools package in R (4.1.0). We selected samples tested for both expression and mutation, then selected 84 samples whose *MALAT1* expression was below the lower end of the IQR and 85 samples whose *MALAT1* expression exceeded the upper end of the IQR. We summarized the overall mutation profiles of samples expressing low or high *MALAT1,* then we compared the prevalences of differentially mutated genes between the two groups using Fisher's exact test and enrichment analysis. Differences associated with $p < 0.05$ were considered significant. Samples were categorized as wild-type or mutant depending on the presence or absence of somatic mutations. Survival of patients in the wild-type or mutant groups was compared using the Kaplan-Meier method and log-rank test.

DNA methylation data analysis

After being loaded, methylation data were filtered, quality-controlled, and normalized using the ChAMP package in R. Beta values were the quantification values of methylation levels. The singular value decomposition method (SVD) calculated the correlation between biological factors (*MALAT1* and other clinical features) and the variation of beta values. Differentially methylated positions (DMPs) were identified by comparing samples expressing high or low *MALAT1*. We considered that the following DMPs could upregulate target genes of *MALAT1*: hypermethylated DMPs in the coding sequence of the gene, or hypomethylated DMPs in the promoter or transcriptional start site (TSS). Conversely, we considered that the following DMPs could downregulate target genes of *MALAT1:* hypomethylated DMPs in the coding sequence of the gene, or hypermethylated DMPs in the promoter or TSS. We then calculated correlation coefficients between *MALAT1* and target genes to identify genes regulated by *MALAT1*-associated methylation. Results associated with $p < 0.05$ were considered significant. Cox regression was performed on the beta values of each DMP. DMPs that emerged as significant ($p < 0.05$) were shown as forest plots. Enrichment of Molecular Signatures Database's terms or pathways in DMPs was assessed using gene set enrichment analysis (GSEA) using the "champ.GSEA()" function.

Analysis of tumor-associated signatures and patient survival

We used the Immuno-Oncology-Biological-Research (IOBR) package in R integrating six commonly used algorithms (MCPcounter, TIMER, xCell, CIBERSORT, EPIC, and quanTiseq), to calculate scores for tumor-infiltrating lymphocytes (TILs) and tumor-associated signatures. Scores that reached statistical significance were determined for 92 samples whose *MALAT1* expression was below the lower end of the IQR and 92 samples whose *MALAT1* expression exceeded the upper end of the IQR. Kaplan-Meier analysis was used to compare survival of patients whose *MALAT1* expression was above or below the median, based on data for the TCGA-LIHC cohort. Differences between the two groups were compared using the log-rank test.

Collection of clinical data and survival information

We analyzed samples from 179 HCC patients who underwent radical resection in the Affiliated Tumor Hospital of Guangxi Medical University between April 2004 and December 2012. None of the patients received TACE, radiotherapy, chemotherapy, or other anti-tumor treatments before surgery. Tumor tissues from all patients, as well as paired adjacent non-tumor tissues (PANTs) from 19 patients, were frozen in liquid nitrogen immediately after surgery and stored at −80°C until RNA extraction. Two pathologists participated in the diagnosis of histopathology of resected tumor samples. One of these two pathologists is responsible for routine pathological diagnosis in the clinical practice, while the other is responsible for routine quality control in the clinical study. This work was approved by the Institutional Ethics Committee of the Affiliated Tumor Hospital of Guangxi

Medical University (Nanning, China, Approval Number: LW2022145), which waived the requirement for informed consent because patients, at the time of treatment, consented for their anonymized data to be analyzed and published for research purposes.

Clinicopathological data on all patients were collected, including age, sex, Child-Pugh classification, tumor size, tumor numbers, clinical TNM stage, the presence or absence of vascular invasion, capsular infiltration, and cirrhosis. Laboratory results were also collected, such as serum levels of alpha-fetoprotein (AFP) and hepatitis B surface antigen (HBsAg).

Follow-up information of patients was collected for survival analysis. Patients were followed up every 3 months during the first 2 years, and thereafter every 6 months, for 2–10 years. Tumor recurrence was detected based on radiology and serum AFP examination. Relationships of *MALAT1* expression with PFS and overall survival (OS) were explored.

Detection of *MALAT1* expression

Total RNA was extracted from HCC tumors and PANTs using TRIzol (Invitrogen, Carlsbad, CA, United States) and stored at −80°C. RNA (1 μg) was reverse-transcribed into complementary DNA (cDNA) using the PrimeScriptTM RT Reagent Kit (Takara Bio, Kusatsu, Japan) in reactions with a total volume of 20 μl. Real-time PCR (RT-PCR) was performed in 10-μl reactions on a LightCycler® 480 II Real-time PCR system (Roche, Basel, Switzerland) using GAPDH as an internal reference. Reactions were performed in a microassay plate (Roche) at 95°C for 10 min, followed by 40 cycles at 95°C for 10 s and 60°C for 30 s. Primer sequences were: *MALAT1* forward, 5′-CAGGCGTTGTGCGTAGAGGA-3′; *MALAT1* reverse, 5′-TGCCGACCTCACGGATTTT-3′; GAPDH forward, 5′-GTCAGCCGCATCTTCTTT-3′; and GAPDH reverse, 5′-CGCCCAATACGACCAAAT-3′. All samples were tested in triplicate. Expression levels of *MALAT1* were normalized to those of GAPDH and were calculated using the $2^{-\Delta\Delta CT}$ method (20).

Statistical analysis

All statistical analyses were performed using SPSS 22.0 (IBM, Chicago, IL, United States) and R version 4.1.0. Differences in continuous variables were compared using Student's t-test for normally distributed data or Mann-Whitney *U*-test for skewed data. Patients' survival was analyzed by the Kaplan-Meier method, and differences were assessed for significance using the log-rank test. Univariate analysis was performed to identify clinicopathological features associated with survival, and results were assessed for significance using the Gehan-Breslow-Wilcoxon test.

Covariates that were associated with $p < 0.05$ in univariate analysis were included in multivariate Cox analysis, which was

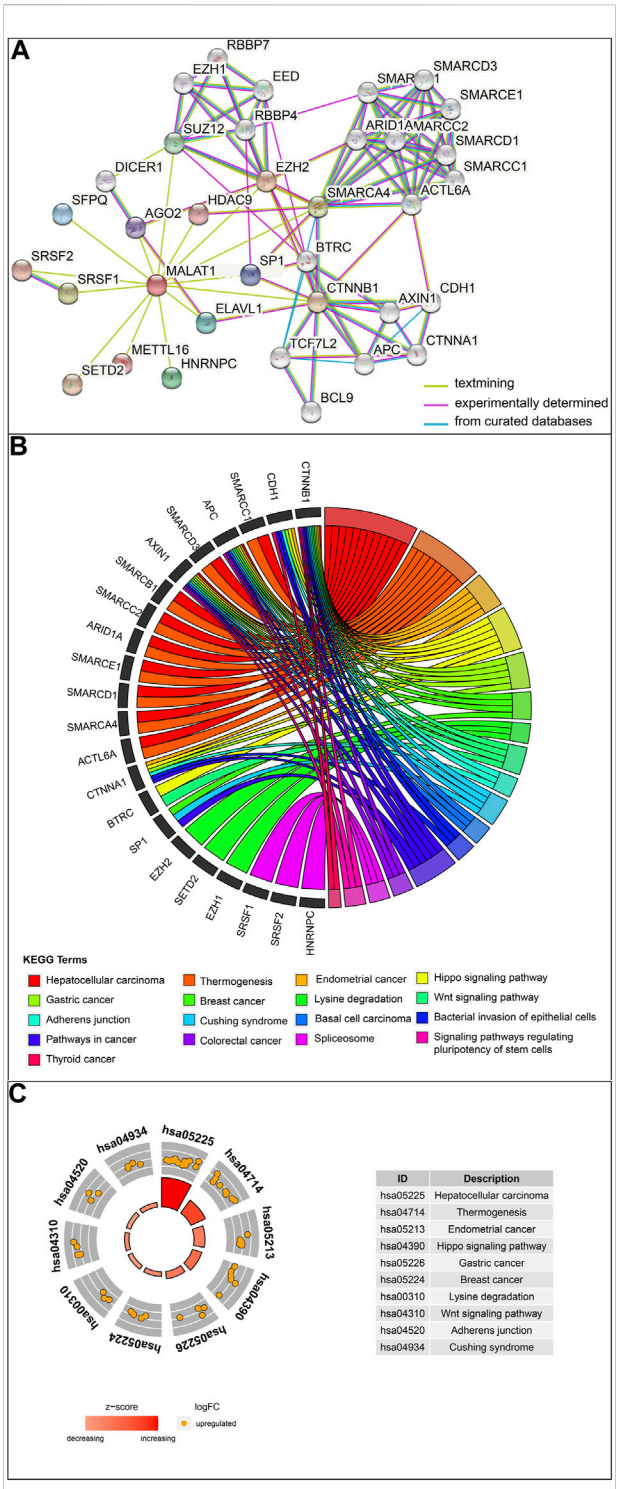

FIGURE 1
Analysis of *MALAT1*-interacting proteins. **(A)** The protein–protein interaction network of *MALAT1* was analyzed using the STRING tool. **(B)** Chord plot displaying the relationship between MALAT1-interacting proteins and Kyoto Encyclopedia of Genes and Genomes (KEGG) terms. **(C)** The outer circle shows a scatter plot for each term of the log (fold change) of the assigned genes. Orange circles indicate upregulation. The z-score is a crude measure of significance of enrichment.

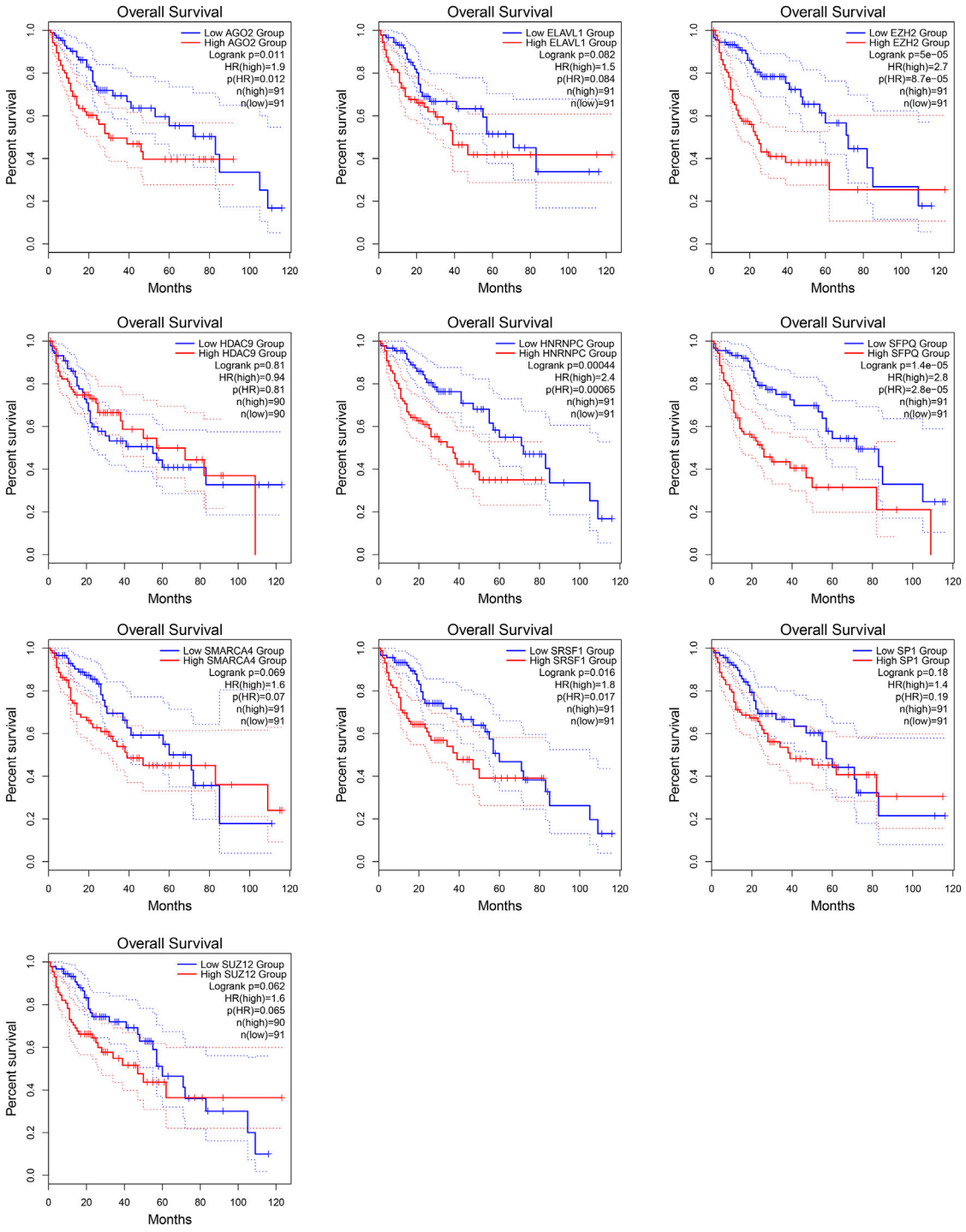

FIGURE 2
Kaplan-Meier survival curves for patients showing high or low expression of genes encoding *MALAT1*-interacting proteins.

used to select features for constructing Cox proportional hazard models to predict survival. Models for predicting PFS and OS were assessed using the area under time-dependent receiver operating characteristic curves (AUC), as calculated with the timeROC package in R. Net benefits of models was assessed using decision curves, plotted with the ggDCA package in R. The ability of *MALAT1* expression to diagnose clinicopathological features of HCC patients was assessed using AUCs. All hypothesis testing was two-sided, with $p < 0.05$ considered statistically significant.

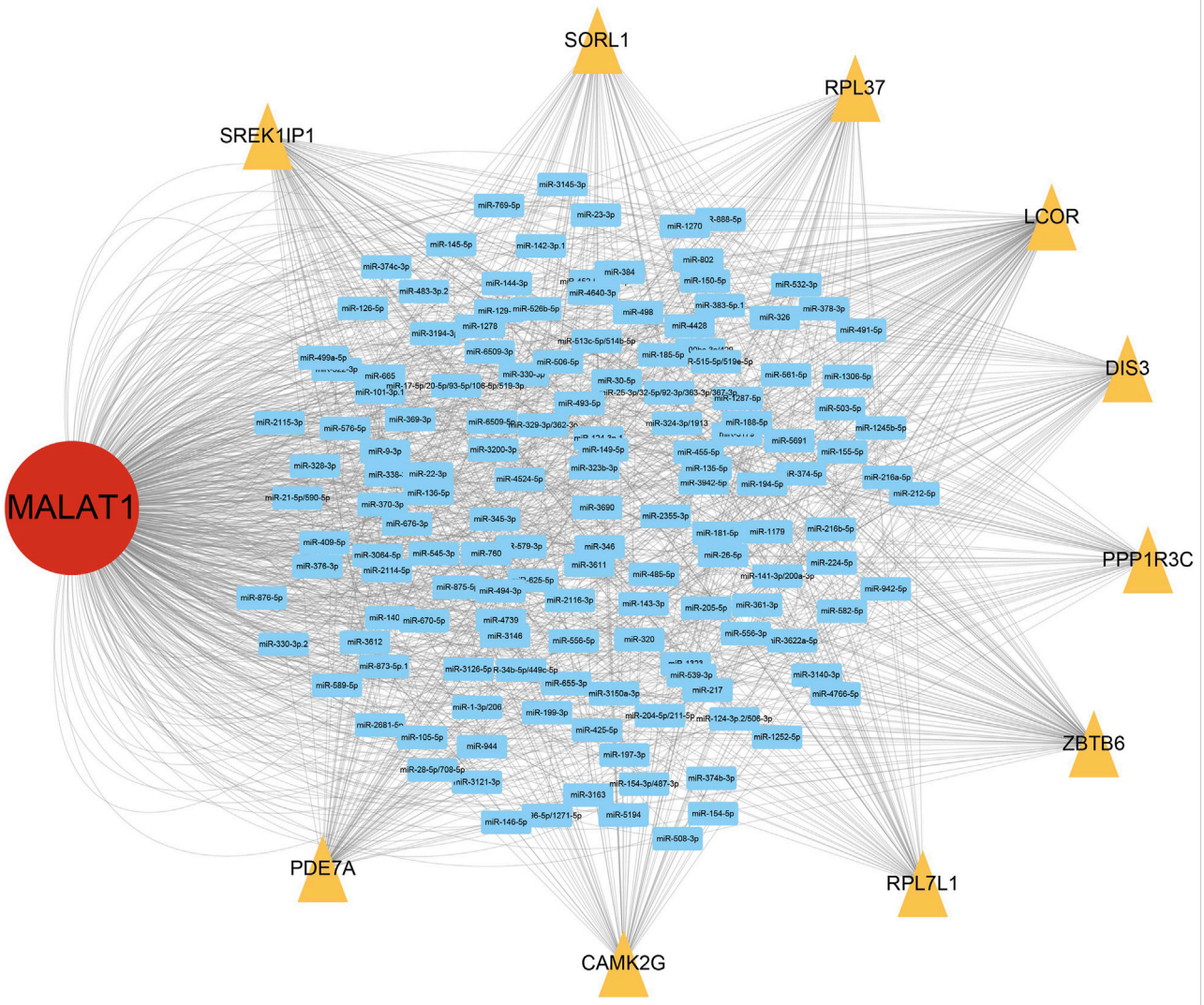

FIGURE 3
MALAT1-associated network of competing endogenous RNAs (ceRNAs). Blue rectangles represent microRNAs (miRNAs) that can bind to *MALAT1*; yellow triangles represent target genes that compete with *MALAT1* for binding to miRNAs.

Results

MALAT1-associated interacting proteins are associated with HCC and prognosis

The protein interaction network related to *MALAT1* was obtained using the text mining algorithm in *STRING* (Figure 1A). The text mining identified 10 proteins interacting with *MALAT1* as *EZH2, SRSF1, SMARCA4, HNRNPC, SUZ12, ELAVL1, SFPQ, SP1, AGO2, HDAC9*. The proteins in the network were most enriched in KEGG terms associated with cancer (Figure 1B). Among these terms, HCC had the highest z-score, indicating that the proteins in this network were most closely related to HCC (Figure 1C). Five protein-coding genes in the first shell of the network were significantly associated with worse survival when highly expressed: *AGO2, HNRNPC, EZH2, SFPQ,* and *SRSF1* (Figure 2; log-rank $p < 0.05$).

Target genes of *MALAT1* in the ceRNA network are associated with prognosis

From the ceRNA network for *MALAT1*, we obtained 10 target genes: *ZBTB6, LCOR, PDE7A, SORL1, RPL37, RPL7L1, SREK1IP1, DIS3, PPP1R3C, CAMK2G*. All these genes may competitively bind to the same miRNAs as *MALAT1* (Figure 3). Higher expression of *LCOR, PDE7A, RPL7L1, RPL37,* and *SREK1IP1* was associated with worse survival of HCC patients (log-rank $p < 0.05$; Figure 4).

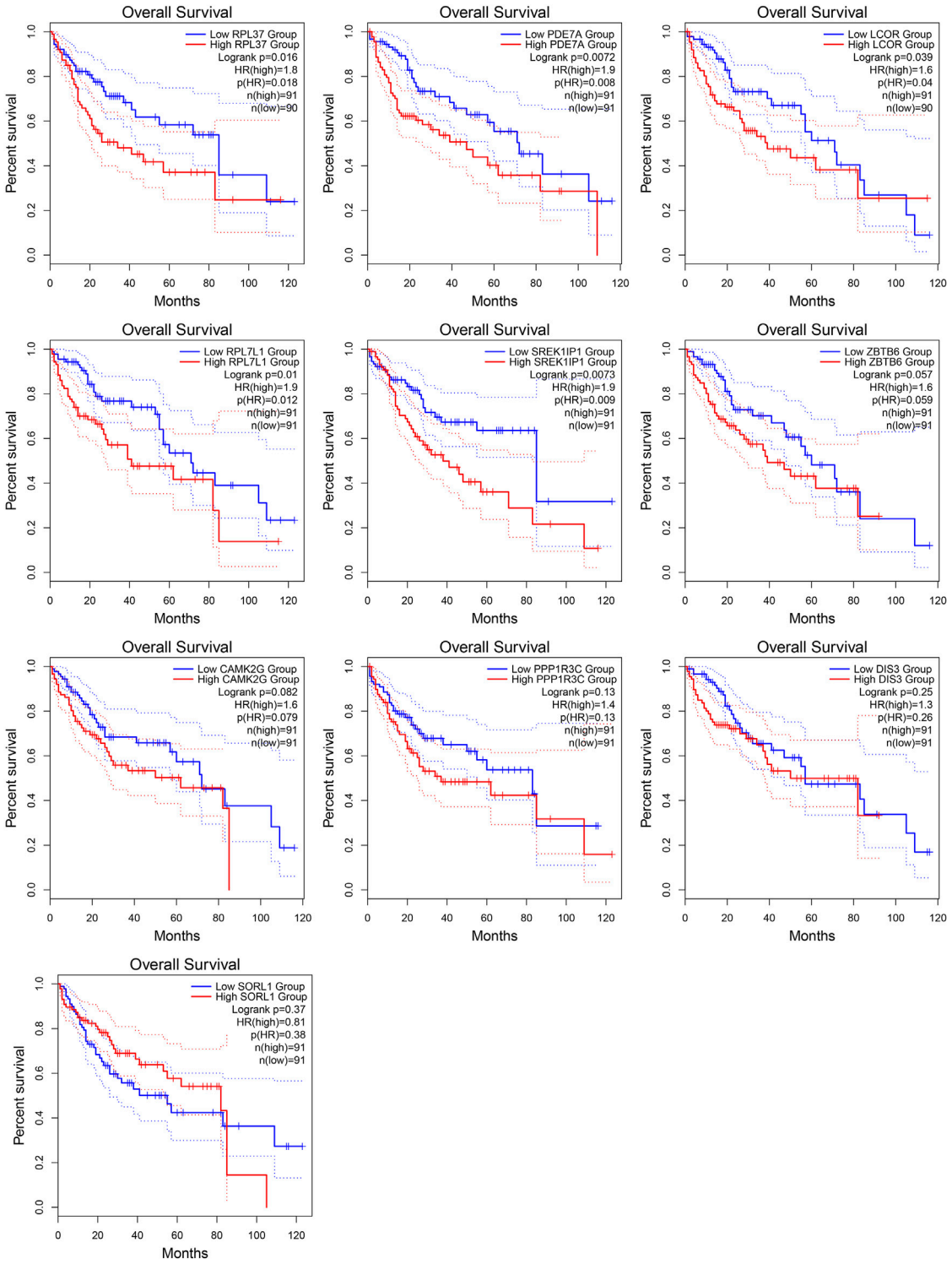

FIGURE 4
Kaplan-Meier survival curves for patients showing high or low expression of *MALAT1* target genes.

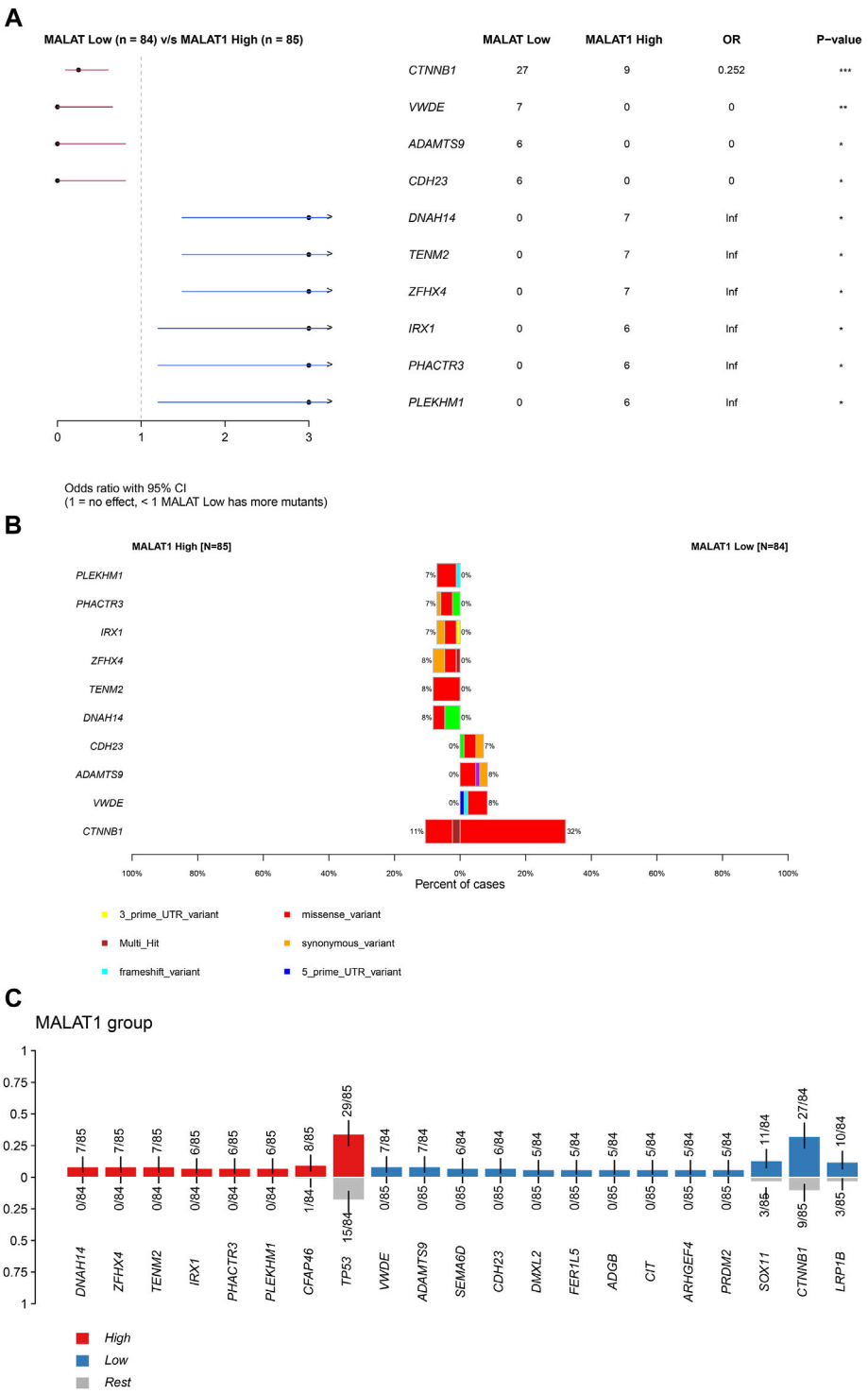

FIGURE 5
Differentially mutated genes. **(A)** Forest plot of Fisher testing to identify differentially mutated genes. **(B)** Proportion of each type of mutation and the overall mutation percentage of differentially mutated genes. The left half of the graph shows samples expressing high MALAT1 and the right half shows samples expressing low MALAT1. **(C)** Red represents mutated genes enriched in samples expressing high *MALAT1*. Blue represents mutated genes enriched in samples expressing low *MALAT1*.

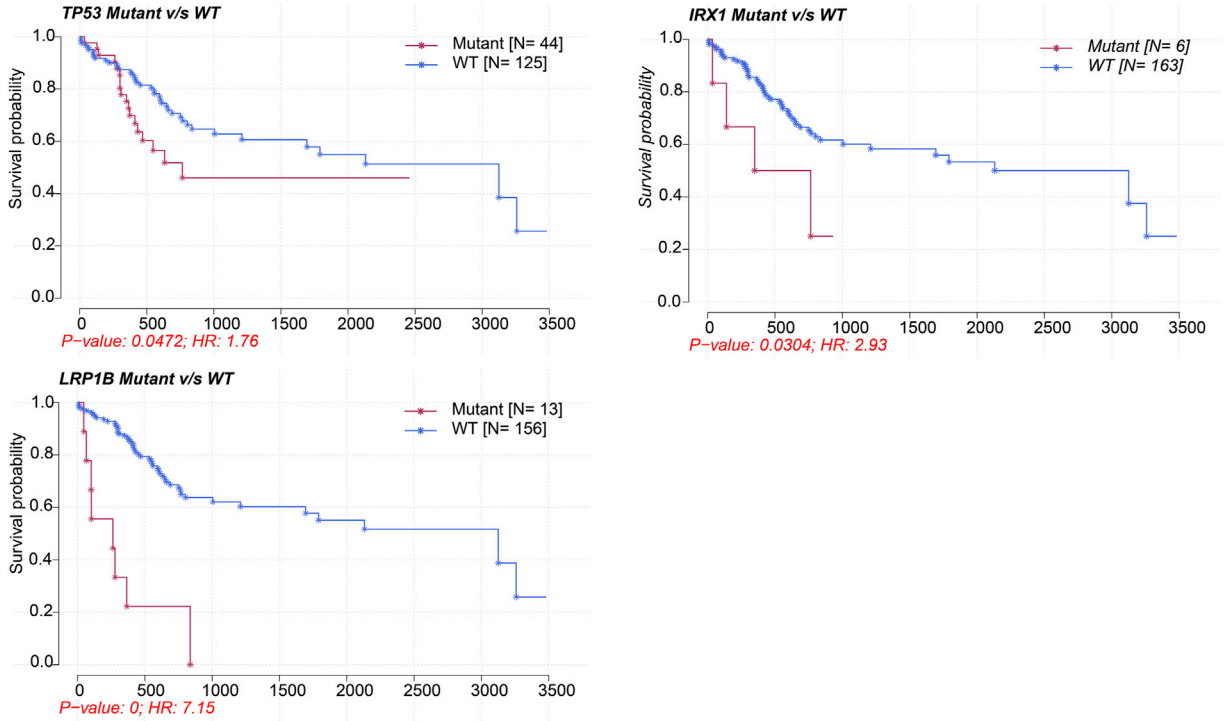

FIGURE 6
Kaplan-Meier survival curves comparing patients carrying mutant or wild-type versions of *TP53, IRX1,* and *LRP1B*.

MALAT1 expression is associated with genetic mutations in HCC

Supplementary Figure S1 showed the mutation profiles of the samples. Samples expressing high or low *MALAT1* were compared using Fisher's exact test to identify 10 differentially mutated genes (Figures 5A, B). Eight mutated genes were enriched in samples expressing high *MALAT1* and 13 mutated genes were enriched in samples expressing low *MALAT1* (Figure 5C). Patients with higher *MALAT1* expression showed more mutations in *IRX1* or *TP53* and mutations in IRX1 and TP53 indicated worse survival than those with the corresponding wild-type alleles (log-rank $p < 0.05$; Figure 6). Patients with lower *MALAT1* expression were associated with more *LRP1B* mutations and *LRP1B* mutations indicated worse survival (log-rank $p < 0.05$; Figure 6). Mutations in the 10 differentially mutated genes altered the protein sequences (Supplementary Figure S2).

MALAT1 expression is a correlate of DNA methylation in HCC

After normalizing the methylation signal value matrix, samples expressing high or low *MALAT1* were analyzed by multidimensional scaling (Supplementary Figure S3A). The beta distributions for each sample showed that most probes were completely unmethylated (beta value ≤ 0.2), and a smaller number of probes were partially methylated (0.4 < beta value < 0.6) or completely methylated (beta value ≥ 0.8) (Supplementary Figure S3B). Sample clustering showed no outliers (Supplementary Figure S3C). The SVD plot showed that several principal components that best explained the methylation variation significantly correlated with *MALAT1* (Figure 7). More principal components significantly correlated with *MALAT1* than the clinical features of tumor stage and tumor grade, indicating that *MALAT1* correlated with methylation variants more strongly than stage or grading did (Figure 7). In samples expressing high *MALAT1,* hypomethylation occurred in 88 positions and hypermethylation in 250 positions (Figure 8A).

Beta values of DMPs were visualized using a clustering heatmap (Figure 8B). In the case of high *MALAT1* expression, 157 DMPs were hypermethylated and located in coding regions of genes, while 28 DMPs were hypomethylated and located in promoters and TSS. These DMPs may positively correlated with gene expression. Conversely, 60 DMPs were hypomethylated and located in coding regions of genes, while 93 DMPs were hypermethylated and

10.3389/pore.2022.1610808

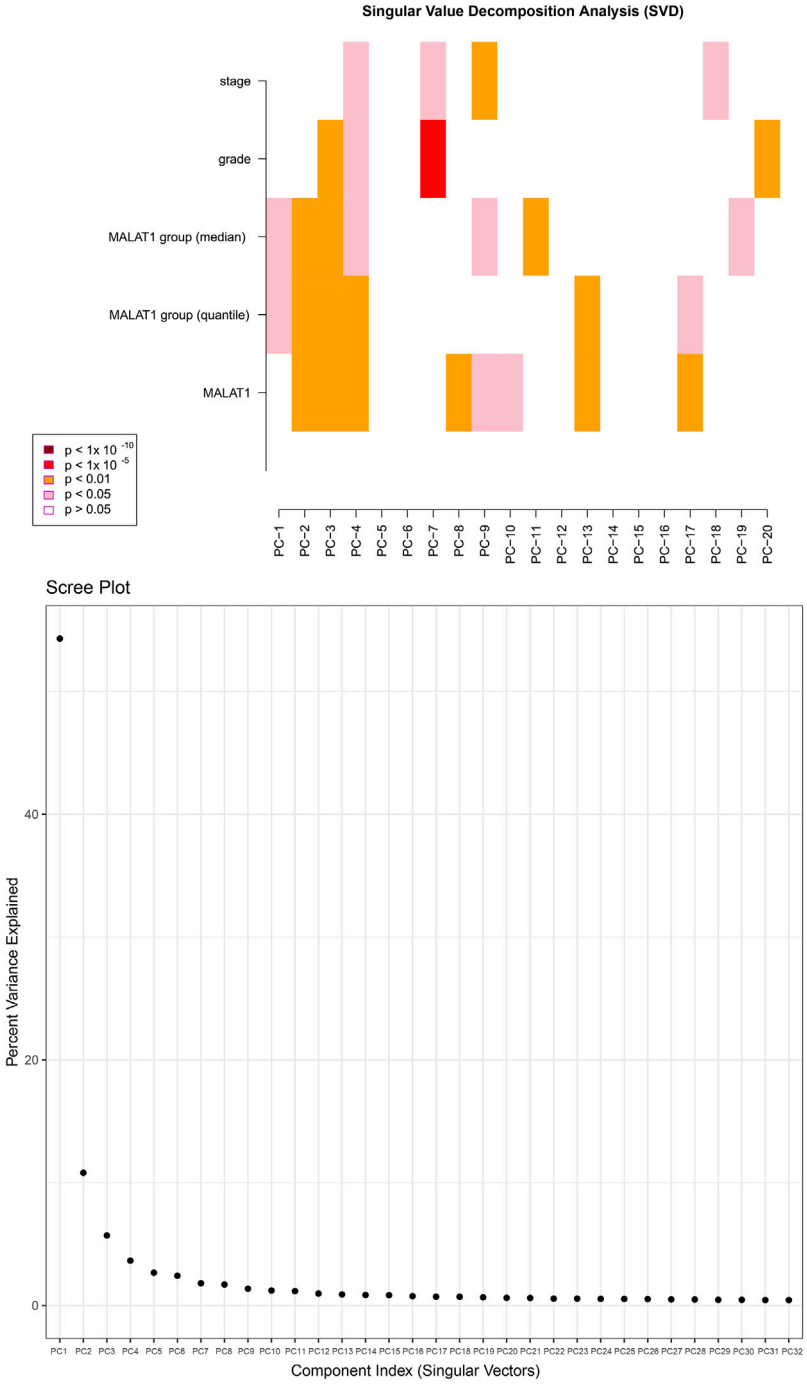

FIGURE 7
The upper plot is a heatmap of the top principal components correlating with *MALAT1*, tumor stage and tumor grade. "*MALAT1*" represents continuous variables, while "*MALAT1* group (median)" and "*MALAT1* group (quantile)" represent categorical variables grouped by median and quartiles. The color represents the degree of significance. The lower plot shows how much of the observed methylation variation was explained by the principal components.

located in promoters and TSS. These DMPs therefore may negatively correlated with gene expression (Supplementary Figure S4).

We further analyzed the correlation of these genes with *MALAT1* expression at the transcriptome level. We assumed that 87 genes were upregulated by *MALAT1* through

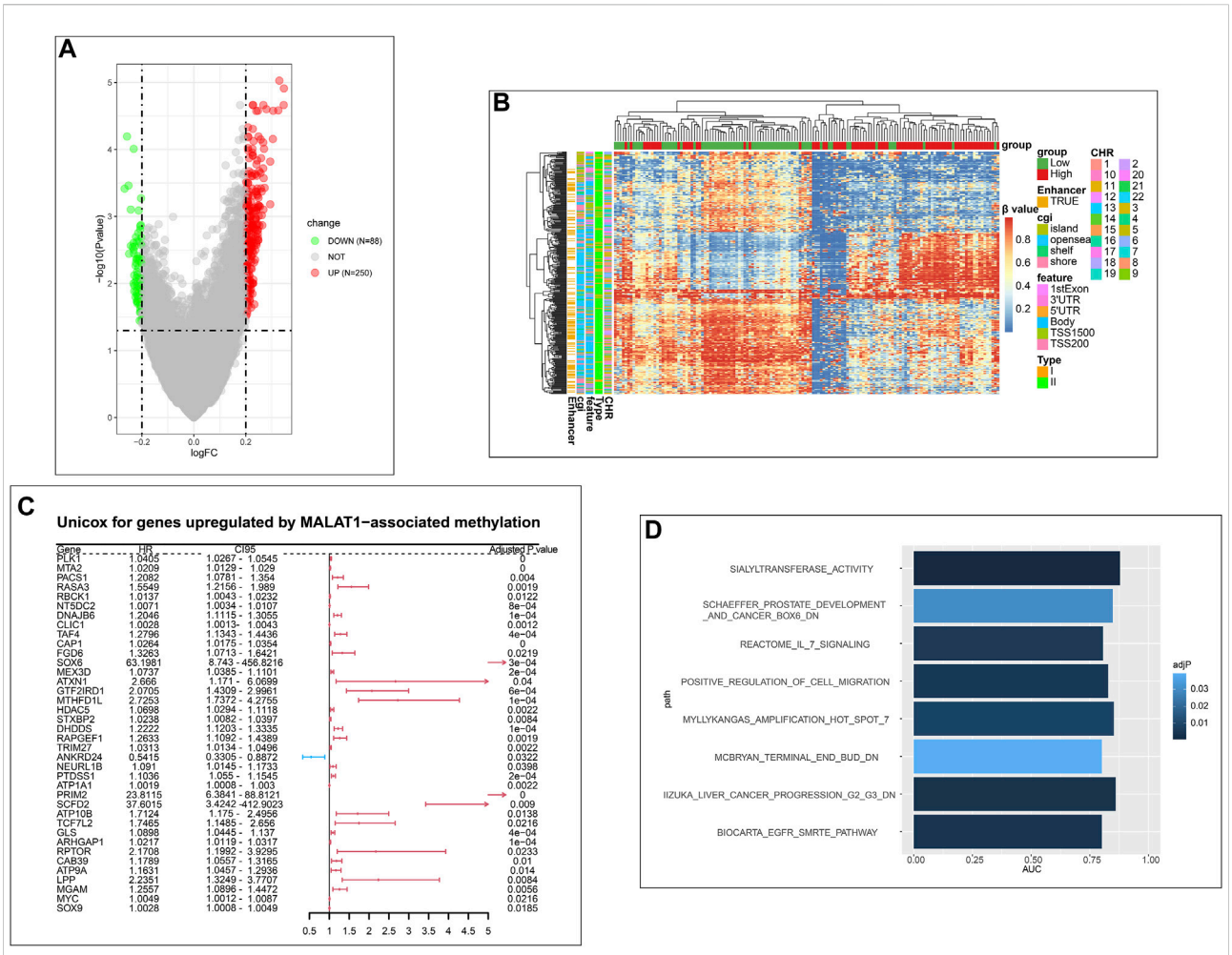

FIGURE 8
Analysis of differentially methylated positions (DMPs). **(A)** Volcano plot of DMPs. Green dots represent the positions that are hypomethylated. Red dots represent the positions that are hypermethylated. **(B)** Clustering heatmap of DMPs. Column annotations provide information about samples expressing high or low MALAT1. Row annotations provide information about DMPs. **(C)** Forest plot showing genes upregulated by MALAT1-associated methylation that were significant in Cox univariate analysis. **(D)**: Bar plot of pathways with areas under curves (AUCs) > 0.75 in the Gene Set Enrichment Analysis (GSEA).

methylation, and confirmed that their expression positively correlated with that of *MALAT1*. Conversely, three genes were assumed down-regulated by *MALAT1* through methylation, and their expression negatively were confirmed correlated with that of *MALAT1* (Supplementary Figure S5).

Univariate Cox regression was performed for 87 up-regulated genes and 3 down-regulated genes, of which 38 were significantly upregulated; all genes emerged as risk factors for poor survival except *ANKRD24,* which was a protective factor (Figure 8C). Eight terms with AUCs > 0.75 in GSEA were associated with tumors. One of the terms "IIZUKA_LIVER_CANCER_PROGRESSION_G2_G3_DN" was directly related to liver cancer progression (Figure 8D). Therefore, the *MALAT1*-related methylation probes were associated with HCC progression and survival of patients.

MALAT1 expression is associated with tumor signatures and TILs

In tumor signatures and TIL analysis, we found significant enrichment in some tumor-related signatures scores in samples expressing high *MALAT1*. These signatures included genes involved in the cell cycle, DNA damage repair (DDR), mismatch repair, homologous recombination, molecular cancer m6A, exosome, and positive regulation of exosomal secretion (Figure 9). In contrast, ferroptosis scores were significantly lower in samples expressing high *MALAT1*.

We used six algorithms to estimate TILs in HCC. Several algorithms showed consistent results for the analysis of macrophages and fibroblasts. Macrophage scores were significantly higher in samples expressing low *MALAT1*, whereas fibroblasts scores

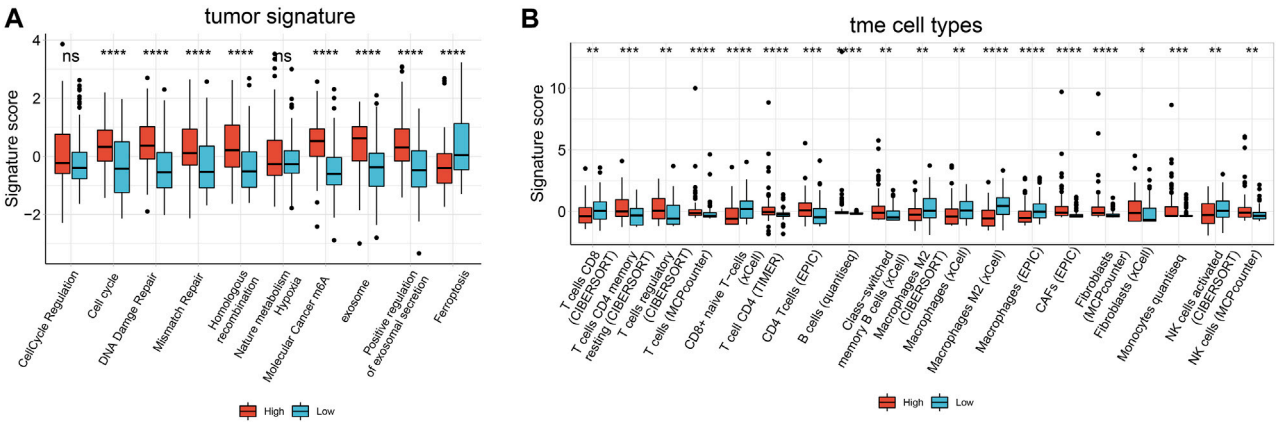

FIGURE 9
Boxplot of the results of Immuno-Oncology-Biological-Research (IOBR) analysis comparing samples expressing high or low *MALAT1* in terms of **(A)** tumor-associated signatures and **(B)** cells within the tumor microenvironment. *$p < 0.05$, **$p < 0.01$, *** < 0.001, ****$p < 0.0001$.

were significantly higher in samples expressing high *MALAT1* ($p < 0.05$; Figure 9). In analyses of other cell types, there were few significant results or different algorithms were inconsistent in predicting the trends (Figure 9).

MALAT1 is associated with HCC progression

Among HCC patients in the TCGA-LIHC cohort, there was no significant difference in OS between those with high or low *MALAT1* expression (Figure 10A). PFS was significantly shorter in patients with high *MALAT1* expression than in those with low expression (Figure 10B; $p = 0.014$). In a multivariate Cox regression model for *MALAT1* expression and baseline clinical information (age, gender, tumor stage, and tumor grade), *MALAT1* independently predicted shorter PFS (Figure 10C; $p = 0.023$).

General characteristics of study subjects

The median age of the 179 HCC patients was 51 years (19–77 years). There were 160 males and 19 females. The median diameter of tumors was 5.5 cm (range, 2–19 cm). The proportion of patients positive for HBsAg was 86.6%, and the proportion with serum AFP was 65.4%. The baseline features of the cases are shown in Table 1.

MALAT1 expression in HCC tumors and PANTs

Median relative expression of *MALAT1* was significantly higher in cancer tissues than in PANTs (5.42 ± 3.84 vs. 0.048 ± 0.032, $p < 0.001$), confirming that *MALAT1* was markedly upregulated in HCC (Figure 11A).

Correlation between *MALAT1* expression and clinicopathological features of HCC patients

Subgroup analysis showed that patients with a history of liver cirrhosis, patients who were positive for HBsAg, patients who were positive for AFP, patients with vascular invasion and patients with tumor capsule infiltration had significantly higher *MALAT1* expression than the corresponding patient subgroups without these characteristics (all $p < 0.05$). Nevertheless, there was no significant correlation between *MALAT1* expression and age, sex, tumor diameter or number, Child-Pugh classification, clinical TNM stage, serum level of transaminase, total bilirubin, or albumin (all $p \geq 0.05$; Table 1).

Correlation between *MALAT1* expression and prognosis of HCC patients

Across all 179 patients, the median follow-up duration was 41 months (range, 23–59 months) for PFS and 70 months (range, 55–85 months) for OS. Patients were divided based on the mean value of *MALAT1* relative expression level of 38.76 into a high expression group ($n = 63$) and low expression group ($n = 116$).

Patients with high *MALAT1* expression were with 19.2 months mPFS and 40.5 months mOS and patients with low *MALAT1* expression were with 52.8 months mPFS and 78.3 months mOS. Patients with high *MALAT1* expression showed significantly shorter PFS than those with a low

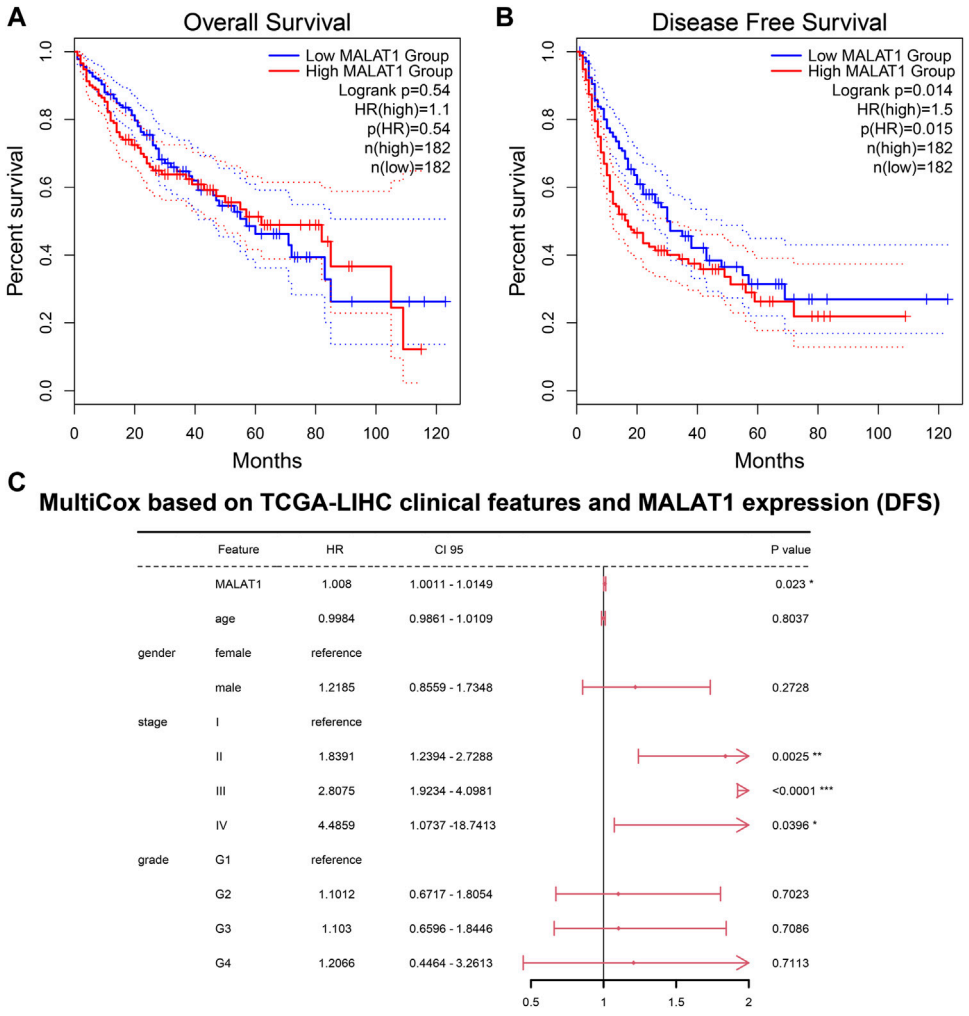

FIGURE 10
Prognosis analysis based on the TCGA LIHC cohort. **(A)** Overall survival and **(B)** Disease-free survival. Survival curves of patients with MALAT1 high expression or low expression were compared using the log-rank test. **(C)** A multivariate Cox regression model for disease-free survival containing MALAT1 and baseline clinical information. *$p < 0.05$; **$p < 0.01$; ***$p < 0.001$.

MALAT1 expression ($p = 0.033$, Figure 11B). Similarly, they showed significantly shorter OS ($p = 0.023$, Figure 11C).

In 59 patients with vascular invasion, the mPFS of patients with *MALAT1* overexpression and low expression were 14 months and 49 months, and PFS was significantly shorter among those with high *MALAT1* expression than among those with low expression (HR 2.63, 95% CI 1.294–5.346; $p = 0.008$, Figure 11D). Similarly, the mOS of patients with *MALAT1* overexpression and low expression were 58 and 72 months, and OS was significantly shorter among those with high *MALAT1* expression (HR 2.416, 95% CI 1.160–5.031; $p = 0.018$, Figure 11E).

MALAT1 overexpression was associated with shorter PFS and OS in subgroups who were positive for HBsAg or AFP (Table 2). Among 130 patients with liver cirrhosis, high *MALAT1* expression was associated with significantly shorter OS than low expression ($p = 0.018$) and with a tendency toward shorter PFS ($p = 0.0566$; Table 2). In contrast, the expression level of *MALAT1* was not significantly associated with PFS or OS among patients without vascular invasion, without cirrhosis, who were negative for HBsAg or who were negative for AFP (Table 2).

Prognostic factors in patients with HCC after hepatectomy

Univariate analysis showed that sex, HBsAg, tumor number, tumor diameter, TNM stage, and *MALAT1* expression were significantly associated with OS and PFS (Table 3).

Variables with $p < 0.05$ in the univariate analysis were included in the multivariate Cox analysis. Furthermore, the

10.3389/pore.2022.1610808

TABLE 1 Association between *MALAT1* expression and clinicopathological variables in 179 HCC patients.

Variable	n	Relative *MALAT1* expression	|Z/F|	*P*
		Median (Q_L-Q_U)		
Age (years)				
≥50	95	15.86 (5.12–55.29)	0.893	0.372
<50	84	18.50 (7.08–52.25)		
Sex				
Male	160	18.00 (6.55–51.53)	0.782	0.434
Female	19	9.51 (3.34–60.36)		
Family history of HCC				
yes	48	16.12 (5.74–65.23)	0.147	0.884
no	131	17.40 (6.07–49.58)		
Alcohol consumption				
Yes	56	18.50 (6.80–58.95)	0.495	0.621
No	123	16.14 (5.83–49.58)		
Liver cirrhosis				
Yes	130	23.79 (7.03–60.27)	2.701	0.007*
No	49	12.27 (3.27–31.13)		
HBsAg				
(+)	154	18.00 (6.70–56.52)	2.093	0.036*
(−)	25	9.11 (3.02–31.13)		
AFP				
(+)	115	24.03 (6.77–60.36)	2.068	0.039*
(−)	64	13.70 (3.73–45.08)		
ALT (μ/L)				
<1 ULN	92	15.35 (5.85–53.32)	0.185	0.911
1–2 ULN	65	16.23 (6.34–57.00)		
>2 ULN	22	21.93 (7.43–41.14)		
AST (μ/L)				
<1 ULN	91	15.36 (5.61–54.04)	1.925	0.382
1–2 ULN	67	22.58 (9.31–59.23)		
>2 ULN	21	11.97 (3.96–41.89)		
TBIL (μmol/L)				
<21	152	15.15 (5.74–51.53)	1.761	0.078
≥21	27	31.13 (15.27–66.53)		
PT (Sec)[a]				
<11	18	33.57 (21.89–67.92)	5.980	0.05
11–16	156	14.87 (5.62–47.45)		
≥17	3	23.55 (13.75–80.10)		

(Continued on following page)

TABLE 1 (*Continued*) Association between *MALAT1* expression and clinicopathological variables in 179 HCC patients.

Variable	n	Relative *MALAT1* expression	|Z/F|	*P*
		Median (Q_L-Q_U)		
ALB (g/L)				
<35	21	28.94 (3.96–54.52)	0.211	0.833
≥35	158	16.19 (6.13–54.76)		
Tumor number (tumor nodes)				
1	146	16.91 (5.8–52.24)	0.517	0.605
≥2	33	16.14 (8.70–68.61)		
Vaso-invasion (vascular invasion)				
Yes	59	45.82 (8.65–98.93)	3.82	<0.001*
No	120	14.87 (5.81–36.42)		
Tumor capsular infiltration				
No capsule or infiltration	53	44.84 (5.77–86.76)	2.205	0.027*
Complete capsule	126	15.46 (6.06–41.38)		
Child-Pugh classification[a]				
A	163	15.86 (5.95–51.89)	0.647	0.518
B	14	27.88 (9.18–52.89)		
Tumor diameter (size, cm)				
≤5	79	16.39 (4.54–56.84)	0.084	0.933
>5	100	16.33 (6.97–45.99)		
Clinical TNM stage				
I	137	16.42 (5.60–51.17)	0.773	0.440
II–III	42	15.75 (8.20–68.82)		

[a]2 cases absent.

*$p < 0.05$. AFP, alpha-fetoprotein; ALB, albumin; ALT, alanine aminotransferase; AST, aspartate aminotransferase; HBsAg, hepatitis B surface antigen; HCC, hepatocellular carcinoma; MALAT1, metastasis-associated lung adenocarcinoma transcript 1; PT, prothrombin time; Q_L-Q_U, quartile range; TBIL, total bilirubin.

results showed that the independent risk factors for OS included sex, HBsAg, and clinical TNM stage ($p < 0.05$; Figure 12). At the same time, HBsAg and clinical TNM stage were independent risk factors for PFS ($p < 0.05$; Figure 12). The *p*-values of tumor size from OS and PFS multivariate Cox analysis was less than 0.1, and the *p*-value of *MALAT1* expression from PFS multivariate Cox analysis was less than 0.1 (Figure 12).

A prognostic model based on *MALAT1* in combination with other prognostic indicators has moderate predictive power

The multivariate Cox analysis showed that there was strong collinearity between the variable "tumor number" and "clinical TNM stage" and the prognostic value of "sex" was not clear. Therefore, we constructed prediction models based on four promising variables: "*MALAT1*," "size," "clinical TNM stage," and "HBsAg" (Figures 13A, B). The calibration curves showed that the progression prediction model fit the data well at 1, 2 and 3 years (Figure 13C), while the survival prediction model fit the data moderately well at 1, 3, and 5 years (Figure 13D). Using the progression prediction model, we obtained AUCs of 0.683 for 1-year progression rate, 0.692 for 2-year progression rate, and 0.661 for 3-year progression rate (Figure 14A). Using the survival prediction model, we obtained AUCs of 0.731 for 1-year survival rate, 0.703 for 3-year survival rate, and 0.699 for 5-year survival rate (Figure 14B). Time-dependent AUCs showed that the prediction models outperformed the predictions of individual indicators. Predictive models constructed with other indicators

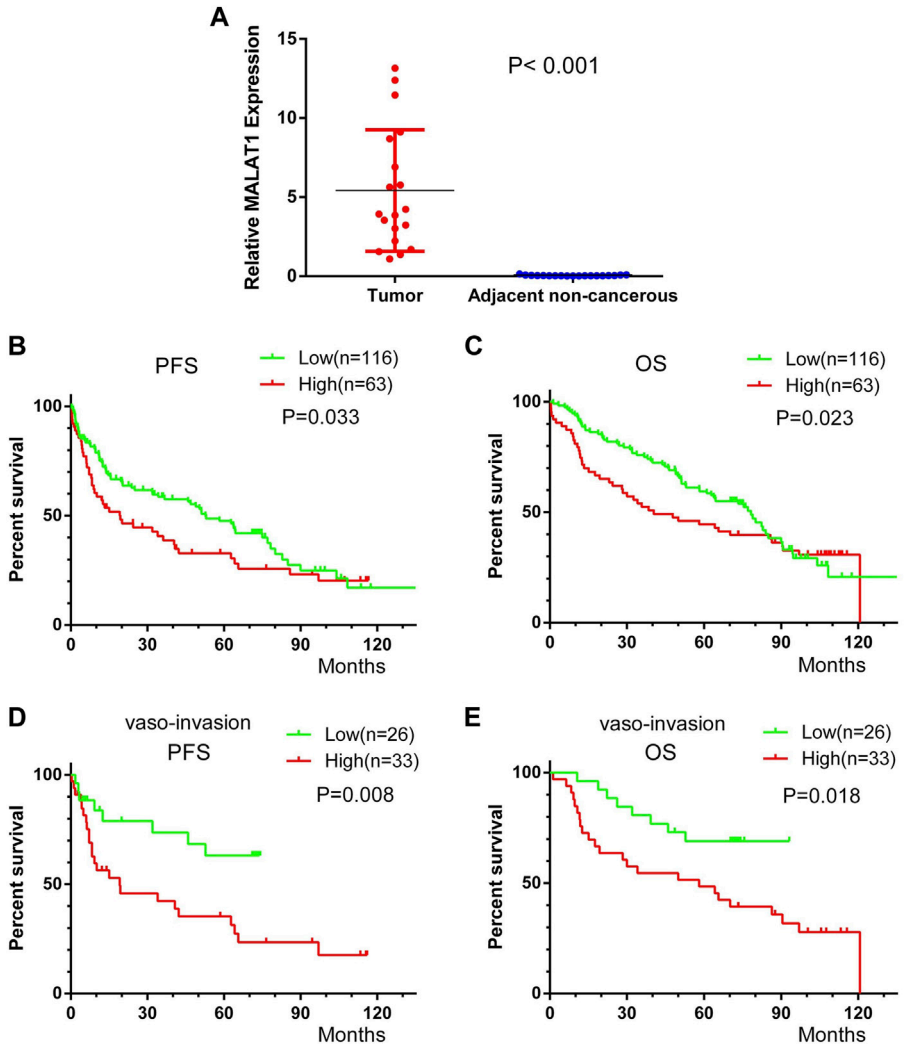

FIGURE 11
Kaplan-Meier survival curves of HCC patients after radical resection, stratified by low or high *MALAT1* expression. **(A)** MALAT1 expression in 19 paired HCC and adjacent non-cancerous tissues from patients who underwent curative resection. **(B,C)** Progression-free survival (PFS) and overall survival (OS) of all patients. **(D,E)** PFS and OS of 59 patients with vascular invasion. Curves were compared using the log-rank test.

excluding *MALAT1* were slightly inferior to *MALAT1*-based predictive models, for both PFS and OS. The performance of *MALAT1* alone was not inferior to that of clinical stage and HBsAg in the prediction of progression, or from that of tumor size and HBsAg in the prediction of survival when data were censored at > 40 months (Figures 14C, D). Decision curves were plotted by depicting the net benefit ratio along the vertical axis and the risk threshold along the horizontal axis (Figures 14E, F). The results showed that the smaller the risk threshold value, the greater the net benefit. Over most threshold intervals, the progression and survival prediction models led to greater net benefit than models based on other independent indicators.

Diagnostic value of *MALAT1* for clinicopathological features

Using an appropriate cut-off value, the AUC of *MALAT1* expression level used to distinguish patients with or without liver cirrhosis was 0.631 (cut-off value 3.86, $p = 0.006$; Table 4; Figure 15A), 0.676 for patients with or without vascular invasion (cut-off value 54.52, $p < 0.001$; Figure 15B), 0.605 for patients with or without tumor capsule infiltration (cut-off value 54.52, $p = 0.039$; Figure 15C), and 0.593 for patients positive or negative for AFP (cut-off value 4.23, $p = 0.037$; Figure 15D).

TABLE 2 Univariate analysis to identify factors associated with PFS or OS in different subgroups of HCC patients.

Clinical variable	n	*MALAT1* expression		PFS		OS	
		Low	High	|F|	P	|F|	P
Vaso-invasion							
Yes	59	26 (44.07%)	33 (55.93%)	5.623	0.0177*	5.797	0.0161*
No	120	90 (75%)	30 (25%)	2.621	0.1055	2.772	0.0959
Tumor capsular infiltration							
No capsule or infiltration	53	25 (47.17%)	28 (52.83%)	2.236	0.1348	3.005	0.0830
Complete capsule	126	91 (72.22%)	35 (27.78%)	3.515	0.0608	2.476	0.1156
HBsAg							
(+)	154	96 (62.34%)	58 (37.66%)	4.230	0.0397*	5.675	0.0172*
(−)	25	20 (80%)	5 (20%)	0.166	0.6834	0.108	0.7425
AFP							
(+)	115	71 (61.74%)	44 (38.26%)	4.249	0.0393*	3.875	0.0490*
(−)	64	45 (70.31%)	19 (29.69%)	1.814	0.1780	2.173	0.1405
Liver cirrhosis							
Yes	130	76 (58.46%)	54 (41.54%)	3.635	0.0566	5.597	0.0180*
No	49	40 (81.63%)	9 (18.37%)	3.729	0.0535	0.750	0.2865

Test, Gehan-Breslow-Wilcoxon test. |F|, Effect size generated in the Gehan-Breslow-Wilcoxon test, which showed a chi-squared distribution. *$p < 0.05$. AFP, alpha-fetoprotein; HBsAg, hepatitis B surface antigen.

Discussion

MALAT1 was initially reported as a biomarker of metastasis in the early lung adenocarcinoma (21). Increasingly investigations showed that *MALAT1* was not only a reliable metastasis-related biomarker but also a vital regulator involved in occurrence, invasiveness, drug resistance, and metastasis of various cancers such as HCC and lung cancer. Studies have revealed that *MALAT1* overexpression is significantly related to patient outcomes. For example, upregulated *MALAT1* is associated with poor disease-free survival and OS in patients with middle thoracic esophageal squamous cell carcinoma (22) and osteosarcoma (23). Recently, several studies have been conducted to investigate the prognostic value of *MALAT1* in HCC, but the results have been inconsistent. Lai et al. (24) found that *MALAT1* was overexpressed in 9 liver cancer cell lines and 112 HCC tissues, and survival analysis showed that patients with high level of *MALAT1* had a significantly increased risk of recurrence after liver transplantation. Multivariate analysis confirmed that *MALAT1* was an independent prognostic factor for predicting the recurrence of HCC (HR 3.280, $p = 0.003$). However, another study obtained quite different results: Sonohara et al. found increased expression of *MALAT1* in HCC and that *MALAT1* expression in HCC was associated with better survival (25). Therefore, the prognostic value of *MALAT1* in HCC needs to be investigated by a broader range of research methods.

Since *MALAT1* is a lncRNA, it is not directly involved in protein coding but instead it regulates the expression of coding genes through mechanisms such as ceRNA (14) and perhaps also methylation and mutation (15, 26). In this study, we investigated the relationships of *MALAT1* with protein-coding genes, ceRNAs, methylation profiles, and mutation profiles, thus identifying various ways in which *MALAT1* affects the survival of HCC patients. First, we used text mining to find *MALAT1*-interacting proteins, half of whose coding genes were significantly associated with the poor survival of HCC. Enrichment analysis suggested a high correlation between *MALAT1*-interacting proteins and HCC. These analyses suggest that *MALAT1*-interacting proteins may mediate the observed association of *MALAT1* with prognosis of HCC patients. The high correlation between *MALAT1*-interacting proteins and HCC also suggests that *MALAT1* has a vital role in the pathogenesis underlying HCC. Indeed, five prognosis-related *MALAT1*-interacting proteins, *AGO2, HNRNPC, EZH2, SFPQ,* and *SRSF1*, have previously been linked to

TABLE 3 Comparison of PFS and OS between HCC patients expressing low or high *MALAT1* levels, stratified by clinicodemographic variables.

Variable	*MALAT1* expression		PFS		OS	
	Low	High	|F|	P	|F|	P
Age (years)						
≥50	64 (67.37%)	31 (32.63%)	2.497	0.114	0.887	0.346
<50	52 (61.9%)	32 (38.1%)				
Sex						
Male	104 (65%)	56 (35%)	4.908	0.027*	5.953	0.015*
Female	12 (63.16%)	7 (36.84%)				
Family history of HCC						
Yes	31 (64.58%)	17 (35.42%)	0.831	0.362	0.594	0.441
No	85 (64.89%)	46 (35.11%)				
Alcohol consumption						
Yes	34 (60.71%)	22 (39.29%)	0.073	0.788	0.055	0.815
No	82 (66.67%)	41 (33.33%)				
Liver cirrhosis						
Yes	76 (58.46%)	54 (41.54%)	0.701	0.402	0.981	0.321
No	40 (81.63%)	9 (18.37%)				
HBsAg						
(+)	96 (62.34%)	58 (37.66%)	7.714	0.005*	6.435	0.011*
(−)	20 (80%)	5 (20%)				
AFP						
(+)	71 (61.74%)	44 (38.26%)	2.452	0.117	0.926	0.336
(−)	45 (70.31%)	19 (29.69%)				
Tumor number						
Single	96 (65.75%)	50 (34.25%)	8.429	0.004*	8.057	0.005*
≥2	20 (60.61%)	13 (39.39%)				
Vaso-invasion						
Yes	26 (44.07%)	33 (55.93%)	0.573	0.449	0.530	0.466
No	90 (75%)	30 (25%)				
Tumor capsular infiltration						
Yes	25 (47.17%)	28 (52.83%)	0.000	1.00	0.089	0.766
No	91 (72.22%)	35 (27.78%)				
Child-Pugh classification						
A	107 (65.64%)	56 (34.36%)	0.126	0.723	0.064	0.801
B	9 (64.29%)	5 (35.71%)				

(Continued on following page)

TABLE 3 (*Continued*) Comparison of PFS and OS between HCC patients expressing low or high *MALAT1* levels, stratified by clinicodemographic variables.

Variable	*MALAT1* expression		PFS		OS	
	Low	High	|F|	P	|F|	P
Tumor size (cm)						
≤5	49 (62.03%)	30 (37.97%)	4.654	0.031*	3.940	0.047*
>5	67 (67%)	33 (33%)				
Clinical TNM stage						
I	90 (65.69%)	47 (34.31%)	6.132	0.013*	5.110	0.024*
II–III	26 (61.9%)	16 (38.1%)				

Test, Gehan-Breslow-Wilcoxon test. |F|, effect size from the Gehan-Breslow-Wilcoxon test, which showed a chi-squared distribution. *$p < 0.05$. AFP, alpha-fetoprotein; HBsAg, hepatitis B surface antigen.

hepatotumorigenesis. *AGO* promotes cell proliferation and angiogenesis in HCC (27, 28); silencing *HNRNPC* inhibits proliferation, migration, and invasion of HCC cells (29); *EZH2* enhances protein kinase B activation to promote HCC progression (30); *SFPQ* plays an important role in the enhancement of fatty acid biosynthesis by NONO to promote HCC progression (31); and *SRSF1* promotes HCC development, which can be regulated by *MALAT1* (32, 33).

The most important link between *MALAT1* and HCC pathogenesis appears to be mediated by *MALAT1* acting as a ceRNA to affect the target pathways FOXA1/CD24/Src and PI3K/Akt/mTOR, as well as the target genes *IAP, ZEB1,* and *FOXM1*. Through these targets, *MALAT1* promotes HCC proliferation and angiogenesis, inhibiting apoptosis, and promoting the progression of HCC (34–38). To identify more potential target genes, we constructed a network of *MALAT1*-related ceRNAs using CLIP-seq data. Interestingly, the predicted target gene *CAMK2G* has been linked to the proto-oncogene tyrosine-protein kinase Src family, which was previously confirmed by others an *MALAT1* target (34). CAMK2G is a subunit of calcium/calmodulin-dependent protein kinase II (CaMKII). The reactome database showed that CaMKII and Src participate together in several serine threonine kinase (RAF)-related pathways or complexes (39), and that both CAMK2G and Src are targets of tyrosine kinase inhibitors (40). These predicted target genes may be linked to confirmed target genes or new, yet-to-explored mechanisms.

Half of the target genes regulated by *MALAT1* as a ceRNA were significantly associated with poor survival, suggesting that *MALAT1* may influence both HCC pathogenesis and patient prognosis. Among these, *LCOR* and *PDE7A* have been shown to play roles in other types of cancer. *LCOR* activates transcription and can promote the development of breast cancer (41) and the low differentiation of cervical intraepithelial neoplasia (42). Inhibition of *PDE7A* expression inhibits cancer cell proliferation, migration and invasion in endometrial cancer, while overexpression of *PDE7A* has the opposite effects (43). The effects of *MALAT1* regulation of its target genes and the effect of those genes on HCC should be explored.

MALAT1 expression was also associated with mutational events in our study. Lv et al. found that *MALAT1* expression could be used as a marker of *EGFR* mutation status (44). Badalamenti et al. discovered that *MALAT1* expression was associated with *c-KIT* mutation status (26). Ak et al. revealed that the *C228T* mutation in the *TERT* gene was associated *MALAT1* expression and with worse prognosis in glioblastoma patients (45). The present study identified a correlation between *MALAT1* and more than 20 mutational events in HCC by somatic mutation data analysis. Mutational events associated with high or low *MALAT1* expression may explain the poor prognosis in HCC. In addition, we found that mutations in *IRX1* and *TP53* were more likely to occur when *MALAT1* was highly expressed and were associated with worse survival. *TP53* mutation, the most well-known cause of cancer, has been associated with adverse outcomes in HCC patients (46). Mutation in *LRP1B*, which was associated with low *MALAT1* expression in HCC, also emerged as a prognostic indicator of worse survival. Therefore, *MALAT1*-associated mutations may be one of the reasons why dysregulation of *MALAT1* expression is accompanied by poor prognosis.

In addition to genetic mutation, epigenetic modification of methylation in the promoter region has been suggested as an important alternative mechanism of tumorigenesis. Methylation of promoter regions of several genes has been associated with the development of HCC (47), and methylation features detected in tissues and serum have been used as biomarkers to predict the prognosis of patients with HCC (48). In our analysis of DNA methylation profiling data, *MALAT1* expression significantly correlated with methylation variations, suggesting that *MALAT1* as lncRNA may also have been associated with the up-or down-regulation of methylation signals at many methylation positions. Subsequently, we found that *MALAT1*-associated methylation was associated with poor survival of HCC patients and was enriched for

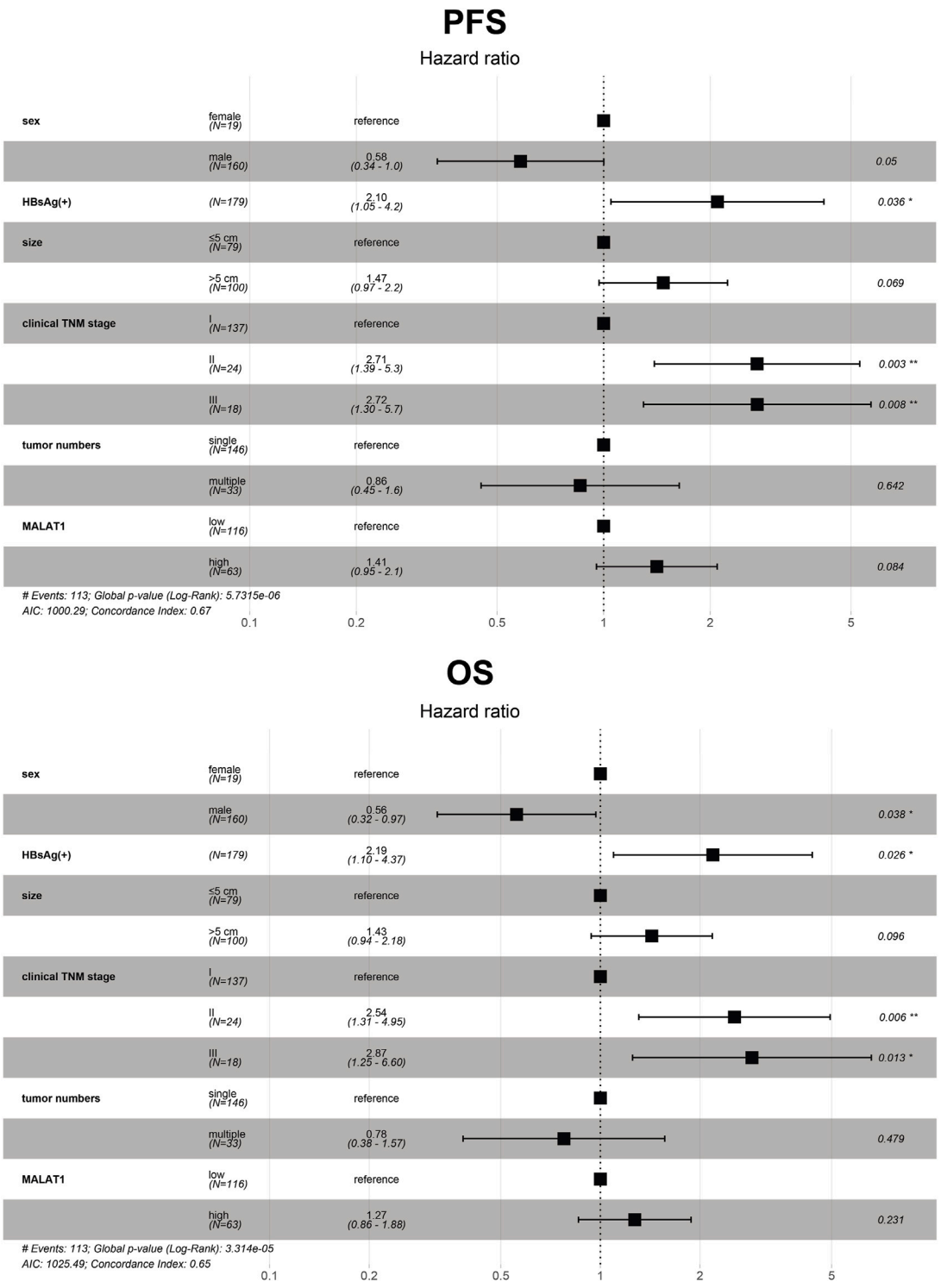

FIGURE 12
Multivariate analysis of 179 HCC patients to identify independent risk factors of progression-free survival and overall survival. The dots and bars represent the HR and 95% CI, respectively. CI, confidence interval; HR, hazard ratio; *MALAT1*, metastasis-associated lung adenocarcinoma transcript 1; OS, overall survival; PFS, progression-free survival.

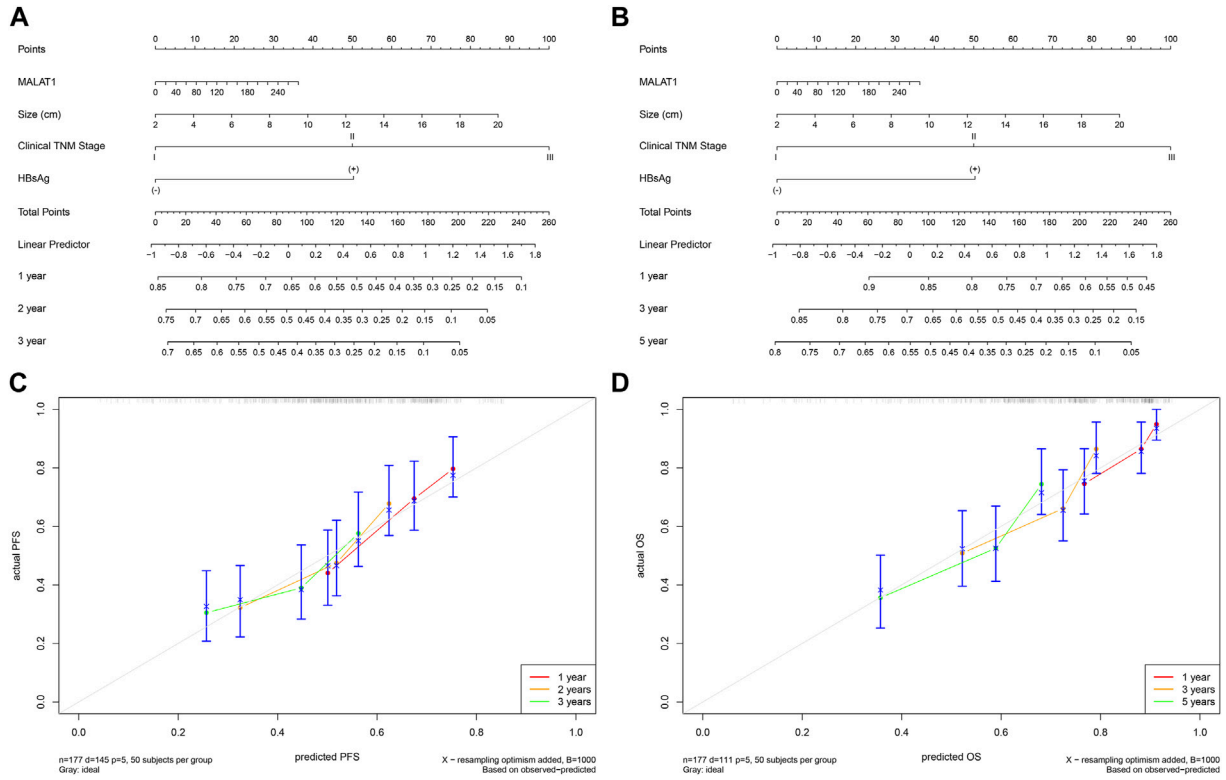

FIGURE 13
Progression and survival prediction models. **(A)**: Nomogram of the progression prediction model. **(B)**: Nomogram of the survival prediction model. **(C)**: Calibration curve for the progression prediction model. **(D)**: Calibration curve for the survival prediction model.

terms associated with liver cancer progression. These findings suggest that *MALAT1* may be involved in the progression and prognosis of HCC through its association with DNA methylation. Further work is needed to elucidate the molecular pathways linking *MALAT1* expression and DNA methylation.

Based on RNA sequencing data, we transformed the gene expression profile into multiple tumor-associated signatures. *MALAT1* is co-expressed with multiple signatures that can promote HCC progression. We were able to observe that high *MALAT1* expression was accompanied by high expression of cell cycle-related genes, which is consistent with the finding of several studies that *MALAT1* overexpression promotes the cell cycle and inhibits apoptosis (49–51). Similarly, high *MALAT1* expression is accompanied by high expression of DNA repair-related genes, and studies have successfully induced DNA damage by targeting *MALAT1* (52, 53). We found *MALAT1* was positively associated with exosome characteristics, and others found that exosome-mediated intercellular communication allowed the transfer of *MALAT1* as a lncRNA to play a regulatory role (54, 55). In contrast, *MALAT1* was negatively associated with ferroptosis signature, and one study reported that silencing *MALAT1* induced ferroptosis (56), reflecting the possibility that *MALAT1* may also contribute to the development of HCC by inhibiting ferroptosis. TIL prediction analysis showed that high *MALAT1* expression was associated with several immunosuppressive signatures, such as reduced macrophage infiltration and increased fibroblast infiltration. Wang et al. found that *MALAT1* could induce fibroblast activation leading to gastric cancer progression (57). Hou et al. also found that *MALAT1* was associated with macrophage differentiation in HCC. They found that *MALAT1* negatively correlated with miR-140 and that inhibition of miR-140 polarized macrophages toward the M2 subtype and away from the M1 subtype (58). Further work is needed to clarify how *MALAT1* functions in the tumor microenvironment.

We have discussed the multiple potential ways in which *MALAT1* may be involved in the progression of HCC and the poor outcomes of HCC patients. To directly confirm the relationship between *MALAT1* and the prognosis of HCC patients, we collected tissue samples from patients and conducted RT-PCR assays. The results showed that *MALAT1* was significantly upregulated in HCC tissues relative to PANTs. Moreover, *MALAT1* overexpression was closely related to the shorter PFS and OS in HCC patients after hepatectomy, especially in patients who were positive with HBsAg, who had a tumor diameter ≥ 5.0 cm, or who had tumor number ≥ 2. Thus, *MALAT1*

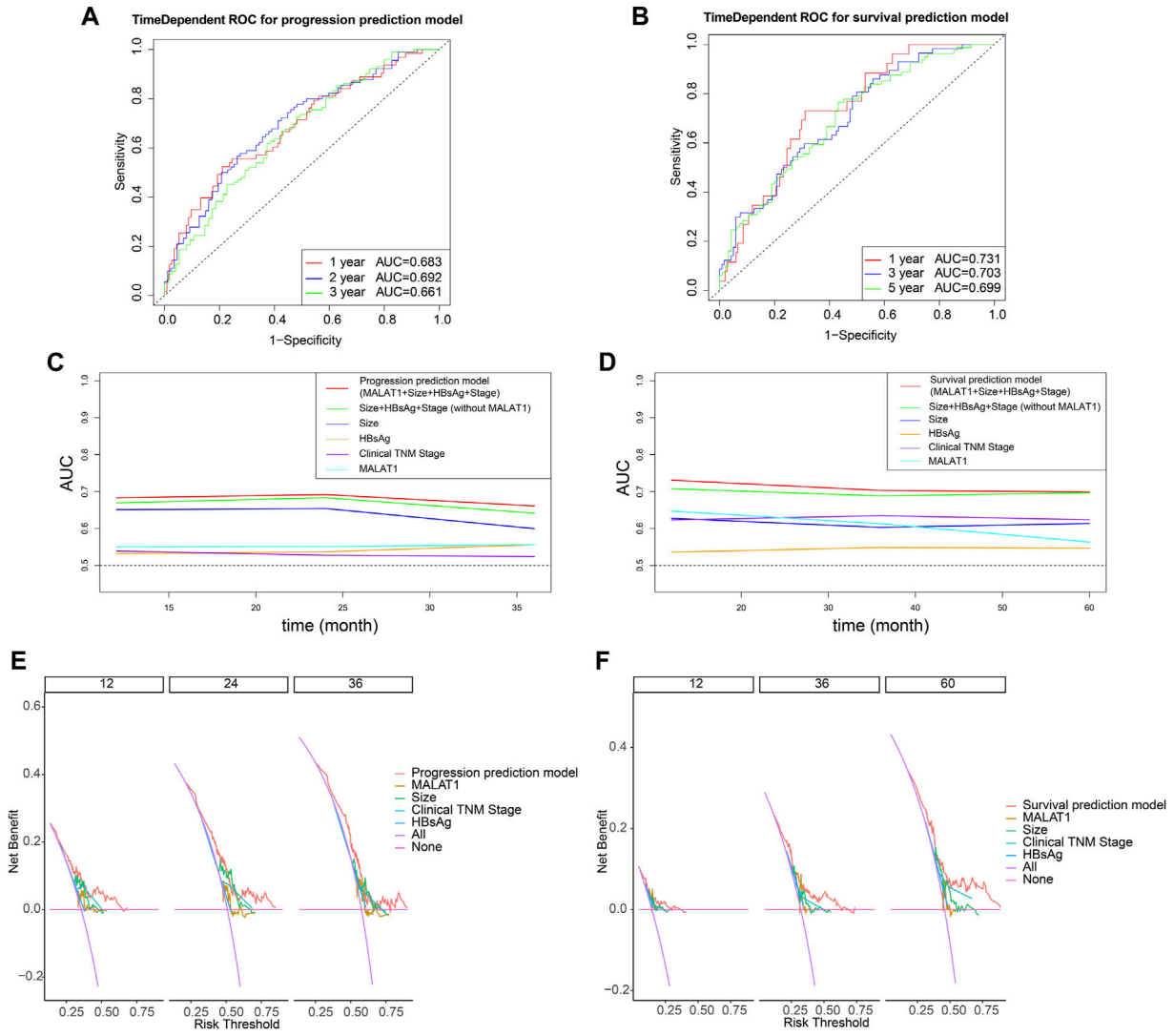

FIGURE 14
Evaluation of model performance using time-dependent receiver operating characteristic curves. **(A)** Predictive power of the progression prediction model. **(B)** Predictive power of the survival prediction model. **(C)** Comparisons of areas under curves (AUCs) for progression prediction model, other prognostic parameters and MALAT1 alone. **(D)** Comparisons of areas under curves (AUCs) for survival prediction model, other prognostic parameters and MALAT1 alone. **(E)**: Decision curves for the progression prediction model, other prognostic parameters and MALAT1 alone. **(F)**: Decision curves for the survival prediction model, other prognostic parameters and MALAT1 alone.

TABLE 4 Assessment of the ability of *MALAT1* to diagnose clinicopathological characteristics in HCC patients undergoing radical resection.

Characteristic	Cut-off *MALAT1* expression level	Se (%)	Sp (%)	AUC	P	HR 95% *CI*	
						Low	High
Liver cirrhosis	3.86	89.2	34.7	0.631	0.006	0.556	0.702
Vaso-invasion	54.52	49.2	86.7	0.676	<0.001	0.602	0.744
Tumor capsular infiltration	54.52	47.2	84.1	0.605	0.039	0.529	0.677
AFP	4.23	86.1	31.2	0.593	0.037	0.518	0.666

AFP, alpha-fetoprotein; AUC, area under the receiver operating characteristic curve; CI, confidence interval; HR, hazard ratio; Se: sensitivity; Sp: specificity.

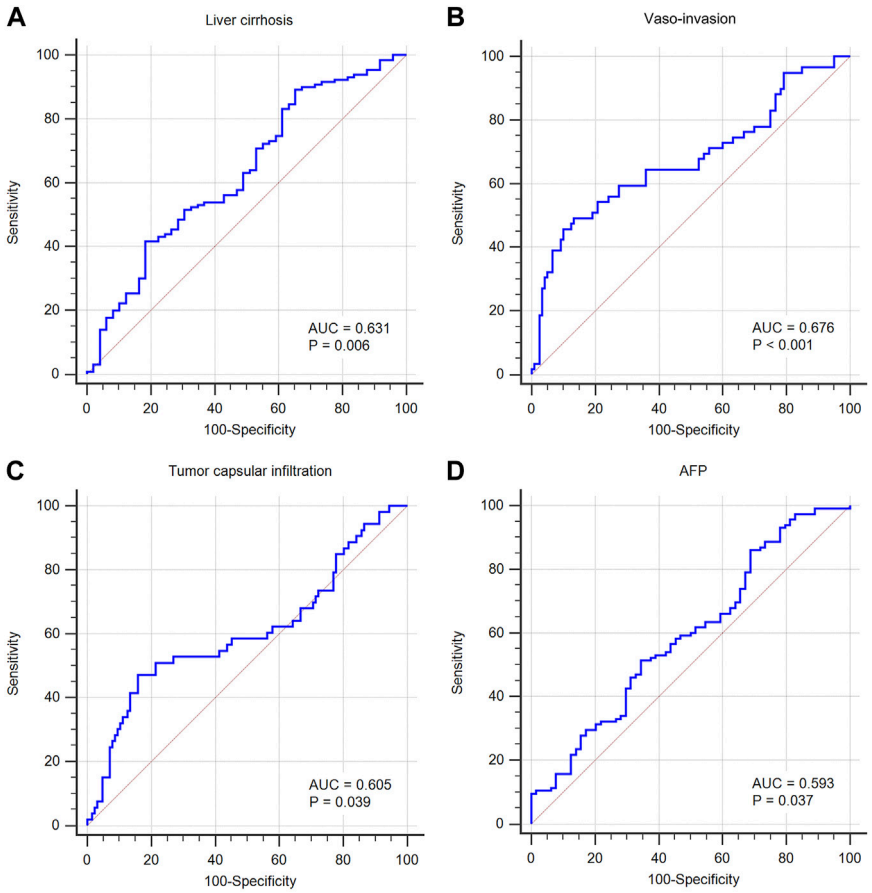

FIGURE 15
Predictive value of *MALAT1* for diagnosing clinicopathological characteristics, based on the area under the time-dependent receiver operating characteristic curve (AUC). **(A)** AUC was 0.631 for cirrhosis (95% CI: 55.6%–70.2%, $p = 0.006$). **(B)** AUC was 0.676 for vascular invasion (95% CI: 60.2%–74.4%, $p < 0.001$). **(C)** AUC was 0.605 for tumor capsular infiltration (95% CI: 52.9%–67.7%, $p = 0.039$). **(D)** AUC was 0.593 for AFP positive (95% CI: 51.8%–66.6%, $p = 0.037$).

is associated with poor outcomes in HCC. However, different from previous results (24), the present study found that *MALAT1* overexpression was not an independent risk factor for the prognosis of HCC patients after Cox multivariate analysis. The reason for this disrepancy may be that the patients in that previous study underwent liver transplantation, whereas our patients underwent radical resection, such that variation in regenerative capacity of residual liver tissue and liver function may have confounded the effects of *MALAT1* overexpression on survival.

Molecular mechanisms of signaling pathways have shown that the upregulation of *MALAT1* expression significantly promotes the malignant phenotype of HCC cells. By promoting β-catenin expression, *MALAT1* activates the canonical Wnt signaling pathway and contributes to the formation of HCC tumor sphere, as well as the increase in CD133+ and CD90+ HCC cell populations (59). *MALAT1* is involved in HCC cellular glucose metabolism: it enhances *TCF7L2* translation and activates the mTORC1-4EBP1 axis (60). Other researchers found that the interaction of *MALAT1* and miR-124 promotes HBx-induced stem cell characteristics in HepG2 cells by regulating PI3K/Akt signaling (61). By cooperating with enhancer of zeste homolog 2 (*EZH2*), *MALAT1* promotes Snail family transcriptional repressor 1 (*SNAI1*) expression by sponging miR-22 and suppressing E-cadherin expression, ultimately promoting the epithelial-mesenchymal transition in HCC (62). The miR-3064-5p plays an anti-angiogenic role by inhibiting the FOXA1/CD24/Src pathway, and *MALAT1* sponges this miRNA to weaken its suppressive effect (34). Overexpression of *MALAT1* inhibits Mir-140, leading to overexpression of vascular endothelial growth factor A (VEGF-A) and promoting angiogenesis in human umbilical vein endothelial cells (HUVECs) (58).

Through the analysis of the relationship between *MALAT1* and other HCC-associated clinical features, we also revealed that overexpression of *MALAT1* was closely associated with clinical features such as liver cirrhosis, vascular invasion, tumor capsular infiltration, AFP positivity, and HBsAg positivity. Further analysis of the AUC curve confirmed that *MALAT1* expression was helpful

in the differentiation of patients with cirrhosis, vascular invasion, capsule infiltration, and AFP positivity.

In China, chronic infection with hepatitis B virus (HBV) is one of the key risk factors for HCC, and 80% of HCC cases are complicated with liver cirrhosis caused by hepatitis (63). Yuan et al. found that *MALAT1* expression level was progressively unregulated as HCC advanced from normal liver to dysplastic liver to cirrhotic liver and finally to HCC (64). These results demonstrate an association between *MALAT1* and HCC occurrence. In addition, *MALAT1* overexpression induced proliferation and metastasis of cancer cells associated with vascular and capsular invasion in HCC (34, 58–62). The overexpression of *MALAT1* was significantly correlated with serum indicators (65). Unlike previous research (65), we found here that the expression of *MALAT1* did not significantly correlate with liver function indicators, such as alanine aminotransferase (ALT), aspartate aminotransferase (AST), or total bilirubin. The reason might be related to the differences in the types of the samples analyzed (e.g., tissue or plasma), and the clinicopathological features of the patients enrolled (e.g., type of viral hepatitis, presence or absence of liver cirrhosis). Since *MALAT1* did not have covariance with significant prognostic factors including size of tumor, number of tumors, tumor stage, and gender, we constructed prediction models for progression rate and survival rate based on *MALAT1* and those factors. The prognostic models showed moderate performance in predicting progression and survival, and the models outperformed individual indicators. These models may be a new method in the clinic to predict the outcome of HCC patients.

The main limitation of this study was also its strength: we investigated aspects of interacting proteins, ceRNAs, somatic mutations, methylation, and tumor-related features based on multi-omics data. While our analyses had a broad reach, they were difficult to integrate together in order to identify deep relationships. Future research should focus on the more promising findings to follow up in mechanistic studies. Secondly, there were some discrepancies between the results of the survival analysis based on TCGA-LIHC in this study and the analysis based on the samples we collected. These could be due to the fact that the patients in our collected sample underwent radical resection, whereas those in the TCGA-LIHC may have undergone a variety of radical or partial surgeries. The two cohorts may also have differed in additional treatments. The discrepancies may also be due to ethnic, environmental, and socioeconomic differences.

Conclusion

MALAT1 expression was significantly higher in hepatocellular carcinoma, and patients with a high expression level had a worse prognosis than those with a low expression level. *MALAT1* could serve as a prognostic marker for patients with hepatocellular carcinoma who have undergone liver resection.

Data availability statement

The raw data supporting the conclusion of this article will be made available by the authors, without undue reservation.

Ethics statement

The studies involving human participants were reviewed and approved by the ethics committee at the Affiliated Tumor Hospital of Guangxi Medical University, and verbal informed consent was obtained from all the patients.

Author contributions

Conception/design: WH and WX. Provision of study materials: BL and JC. Collection and/or assembly of data: XL and DL. Analysis: XL, JC, and DL. Manuscript writing: XL, JC, and DL. Supervision and project administration: WH and WX. All authors contributed to the article and approved the submitted version.

Funding

This research was supported by the National Natural Science Foundation of China (Grant Number: 81060169), Guangxi Natural Science Foundation (Grant Number: 2017GXNSFBA198041), Guangxi Science and Technology Research Project (Grant Number: GUIKEGONG 16380215). The Guangxi Medical and Health Appropriate Technology Development and Application Project (Grant No. S2020100). The Self-Raised Funds of Guangxi Health Department (Grant No. Z20210852). The Guangxi Natural Science Foundation (Grant No. 2017GXNSFAA198103).

Conflict of interest

The authors declare that the research was conducted in the absence of any commercial or financial relationships that could be construed as a potential conflict of interest.

Supplementary material

The Supplementary Material for this article can be found online at: https://www.por-journal.com/articles/10.3389/pore.2022.1610808/full#supplementary-material

References

1. Bray F, Ferlay J, Soerjomataram I, Siegel RL, Torre LA, Jemal A. Global cancer statistics 2018: GLOBOCAN estimates of incidence and mortality worldwide for 36 cancers in 185 countries. *CA Cancer J Clin* (2018) 68(6):394–424. doi:10.3322/caac.21492

2. Sun D, Cao M, Li H, He S, Chen W. Cancer burden and trends in China: A review and comparison with Japan and South Korea. *Chin J Cancer Res* (2020) 32(2):129–39. doi:10.21147/j.issn.1000-9604.2020.02.01

3. Chen LT, Martinelli E, Cheng AL, Pentheroudakis G, Qin S, Bhattacharyya GS, et al. Pan-asian adapted ESMO clinical practice guidelines for the management of patients with intermediate and advanced/relapsed hepatocellular carcinoma: A TOS-ESMO initiative endorsed by CSCO, ISMPO, JSMO, KSMO, MOS and SSO. *Ann Oncol* (2020) 31(3):334–51. doi:10.1016/j.annonc.2019.12.001

4. Marrero JA, Kulik LM, Sirlin CB, Zhu AX, Finn RS, Abecassis MM, et al. Diagnosis, staging, and management of hepatocellular carcinoma: 2018 practice guidance by the American association for the study of liver diseases. *Hepatology* (2018) 68(2):723–50. doi:10.1002/hep.29913

5. Hilmi M, Neuzillet C, Calderaro J, Lafdil F, Pawlotsky JM, Rousseau B. Angiogenesis and immune checkpoint inhibitors as therapies for hepatocellular carcinoma: Current knowledge and future research directions. *J Immunother Cancer* (2019) 7(1):333. doi:10.1186/s40425-019-0824-5

6. Pinter M, Scheiner B, Peck-Radosavljevic M. Immunotherapy for advanced hepatocellular carcinoma: A focus on special subgroups. *Gut* (2021) 70(1):204–14. doi:10.1136/gutjnl-2020-321702

7. Makary MS, Khandpur U, Cloyd JM, Mumtaz K, Dowell JD. Locoregional therapy approaches for hepatocellular carcinoma: Recent advances and management strategies. *Cancers (Basel)* (2020) 12(7):1914. doi:10.3390/cancers12071914

8. Yarchoan M, Agarwal P, Villanueva A, Rao S, Dawson LA, Llovet JM, et al. Recent developments and therapeutic strategies against hepatocellular carcinoma. *Cancer Res* (2019) 79(17):4326–30. doi:10.1158/0008-5472.Can-19-0803

9. Vogel A, Cervantes A, Chau I, Meyer T, Llovet JM, Ricke J, et al. Correction to: "Hepatocellular carcinoma: ESMO clinical practice guidelines for diagnosis, treatment and follow-up". *Ann Oncol* (2019) 30(5):871–3. doi:10.1093/annonc/mdy510

10. Piñero F, Dirchwolf M, Pessôa MG. Biomarkers in hepatocellular carcinoma: Diagnosis, prognosis and treatment response assessment. *Cells* (2020) 9(6):1370. doi:10.3390/cells9061370

11. Huang Z, Zhou JK, Peng Y, He W, Huang C. The role of long noncoding RNAs in hepatocellular carcinoma. *Mol Cancer* (2020) 19(1):77. doi:10.1186/s12943-020-01188-4

12. Forrest ME, Khalil AM. Review: Regulation of the cancer epigenome by long non-coding RNAs. *Cancer Lett* (2017) 407:106–12. doi:10.1016/j.canlet.2017.03.040

13. Lee JT. Epigenetic regulation by long noncoding RNAs. *Science* (2012) 338(6113):1435–9. doi:10.1126/science.1231776

14. Salmena L, Poliseno L, Tay Y, Kats L, Pandolfi PP. A ceRNA hypothesis: The rosetta stone of a hidden RNA language? *Cell* (2011) 146(3):353–8. doi:10.1016/j.cell.2011.07.014

15. Huang W, Li H, Yu Q, Xiao W, Wang DO. LncRNA-mediated DNA methylation: An emerging mechanism in cancer and beyond. *J Exp Clin Cancer Res* (2022) 41(1):100. doi:10.1186/s13046-022-02319-z

16. He S, Chen J, Gao H, Yang G, Zhang F, Ding Y, et al. Extended transcriptome analysis reveals genome-wide lncRNA-mediated epigenetic dysregulation in colorectal cancer. *Comput Struct Biotechnol J* (2020) 18:3507–17. doi:10.1016/j.csbj.2020.11.004

17. Sun Y, Ma L. New insights into long non-coding RNA MALAT1 in cancer and metastasis. *Cancers (Basel)* (2019) 11(2):216. doi:10.3390/cancers11020216

18. Lei L, Chen J, Huang J, Lu J, Pei S, Ding S, et al. Functions and regulatory mechanisms of metastasis-associated lung adenocarcinoma transcript 1. *J Cel Physiol* (2018) 234(1):134–51. doi:10.1002/jcp.26759

19. Wang S, Liu X. The UCSCXenaTools R package: A toolkit for accessing genomics data from UCSC xena platform, from cancer multi-omics to single-cell RNA-seq. *J Open Source Softw* (2019) 4(40):1627. doi:10.21105/joss.01627

20. Schmittgen TD, Livak KJ. Analyzing real-time PCR data by the comparative C(T) method. *Nat Protoc* (2008) 3(6):1101–8. doi:10.1038/nprot.2008.73

21. Ji P, Diederichs S, Wang W, Boing S, Metzger R, Schneider PM, et al. MALAT-1, a novel noncoding RNA, and thymosin beta4 predict metastasis and survival in early-stage non-small cell lung cancer. *Oncogene* (2003) 22(39):8031–41. doi:10.1038/sj.onc.1206928

22. Cao X, Zhao R, Chen Q, Zhao Y, Zhang B, Zhang Y, et al. MALAT1 might be a predictive marker of poor prognosis in patients who underwent radical resection of middle thoracic esophageal squamous cell carcinoma. *Cancer Biomark* (2015) 15(6):717–23. doi:10.3233/cbm-150513

23. Liu M, Yang P, Mao G, Deng J, Peng G, Ning X, et al. Long non-coding RNA MALAT1 as a valuable biomarker for prognosis in osteosarcoma: A systematic review and meta-analysis. *Int J Surg* (2019) 72:206–13. doi:10.1016/j.ijsu.2019.11.004

24. Lai MC, Yang Z, Zhou L, Zhu Q, Xie H, Zhang F, et al. Long non-coding RNA MALAT-1 overexpression predicts tumor recurrence of hepatocellular carcinoma after liver transplantation. *Med Oncol* (2012) 29(3):1810–6. doi:10.1007/s12032-011-0004-z

25. Sonohara F, Inokawa Y, Hayashi M, Yamada S, Sugimoto H, Fujii T, et al. Prognostic value of long non-coding RNA HULC and MALAT1 following the curative resection of hepatocellular carcinoma. *Sci Rep* (2017) 237(1):16142. doi:10.1038/s41598-017-16260-1

26. Badalamenti G, Barraco N, Incorvaia L, Galvano A, Fanale D, Cabibi D, et al. Are long noncoding RNAs new potential biomarkers in gastrointestinal stromal tumors (GISTs)? The role of H19 and MALAT1. *J Oncol* (2019) 2019:5458717. doi:10.1155/2019/5458717

27. Ye ZL, Huang Y, Li LF, Zhu H, Gao H, Liu H, et al. Argonaute 2 promotes angiogenesis via the PTEN/VEGF signaling pathway in human hepatocellular carcinoma. *Acta Pharmacol Sin* (2015) 36(10):1237–45. doi:10.1038/aps.2015.18

28. Yang Y, Mei Q. Accumulation of AGO2 facilitates tumorigenesis of human hepatocellular carcinoma. *Biomed Res Int* (2020) 2020:1631843. doi:10.1155/2020/1631843

29. Hu J, Cai D, Zhao Z, Zhong GC, Gong J. Suppression of heterogeneous nuclear ribonucleoprotein C inhibit hepatocellular carcinoma proliferation, migration, and invasion via ras/MAPK signaling pathway. *Front Oncol* (2021) 11:659676. doi:10.3389/fonc.2021.659676

30. Zhou J, Che J, Xu L, Yang W, Li Y, Zhou W, et al. Enhancer of zeste homolog 2 promotes hepatocellular cancer progression and chemoresistance by enhancing protein kinase B activation through microRNA-381-mediated SET domain bifurcated 1. *Bioengineered* (2022) 13(3):5737–55. doi:10.1080/21655979.2021.2023792

31. Ding H, Liu J, Wang C, Su Y. NONO promotes hepatocellular carcinoma progression by enhancing fatty acids biosynthesis through interacting with ACLY mRNA. *Cancer Cel Int* (2020) 20:425. doi:10.1186/s12935-020-01520-4

32. Lei S, Zhang B, Huang L, Zheng Z, Xie S, Shen L, et al. SRSF1 promotes the inclusion of exon 3 of SRA1 and the invasion of hepatocellular carcinoma cells by interacting with exon 3 of SRA1pre-mRNA. *Cell Death Discov* (2021) 7(1):117. doi:10.1038/s41420-021-00498-w

33. Malakar P, Shilo A, Mogilevsky A, Stein I, Pikarsky E, Nevo Y, et al. Long noncoding RNA MALAT1 promotes hepatocellular carcinoma development by SRSF1 upregulation and mTOR activation. *Cancer Res* (2017) 77(5):1155–67. doi:10.1158/0008-5472.Can-16-1508

34. Zhang P, Ha M, Li L, Huang X, Liu C. MicroRNA-3064-5p sponged by MALAT1 suppresses angiogenesis in human hepatocellular carcinoma by targeting the FOXA1/CD24/Src pathway. *Faseb j.* (2020) 34(1):66–81. doi:10.1096/fj.201901834R

35. Peng N, He J, Li J, Huang H, Huang W, Liao Y, et al. Long noncoding RNA MALAT1 inhibits the apoptosis and autophagy of hepatocellular carcinoma cell by targeting the microRNA-146a/PI3K/Akt/mTOR axis. *Cancer Cel Int* (2020) 20:165. doi:10.1186/s12935-020-01231-w

36. Chen F, Zhong Z, Tan HY, Guo W, Zhang C, Cheng CS, et al. Suppression of lncRNA MALAT1 by betulinic acid inhibits hepatocellular carcinoma progression by targeting IAPs via miR-22-3p. *Clin Transl Med* (2020) 10(6):e190. doi:10.1002/ctm2.190

37. Chen L, Yao H, Wang K, Liu X. Long non-coding RNA MALAT1 regulates ZEB1 expression by sponging miR-143-3p and promotes hepatocellular carcinoma progression. *J Cel Biochem.* (2017) 118(12):4836–43. doi:10.1002/jcb.26158

38. Liu S, Qiu J, He G, Liang Y, Wang L, Liu C, et al. LncRNA MALAT1 acts as a miR-125a-3p sponge to regulate FOXM1 expression and promote hepatocellular carcinoma progression. *J Cancer* (2019) 10(26):6649–59. doi:10.7150/jca.29213

39. Gillespie M, Jassal B, Stephan R, Milacic M, Rothfels K, Senff-Ribeiro A, et al. The reactome pathway knowledgebase 2022. *Nucleic Acids Res* (2022) 50(D1):D687–D692. doi:10.1093/nar/gkab1028

40. Varallo-Rodriguez C, Freyer CW, Jr, Ontiveros EP, Griffiths EA, Wang ES, Wetzler M. Bosutinib for the treatment of philadelphia chromosome-positive

leukemias. *Expert Opin Orphan Drugs* (2015) 3(5):599–608. doi:10.1517/21678707.2015.1036027

41. Celià-Terrassa T, Liu DD, Choudhury A, Hang X, Wei Y, Zamalloa J, et al. Normal and cancerous mammary stem cells evade interferon-induced constraint through the miR-199a-LCOR axis. *Nat Cel Biol.* (2017) 19(6):711–23. doi:10.1038/ncb3533

42. Vogelsang TLR, Schmoeckel E, Kuhn C, Blankenstein T, Temelkov M, Heidegger H, et al. Regulation of LCoR and RIP140 expression in cervical intraepithelial neoplasia and correlation with CIN progression and dedifferentiation. *J Cancer Res Clin Oncol* (2020) 146(7):1847–55. doi:10.1007/s00432-020-03178-x

43. Yamamoto N, Nishikawa R, Chiyomaru T, Goto Y, Fukumoto I, Usui H, et al. The tumor-suppressive microRNA-1/133a cluster targets PDE7A and inhibits cancer cell migration and invasion in endometrial cancer. *Int J Oncol* (2015) 47(1):325–34. doi:10.3892/ijo.2015.2986

44. Lv P, Yang S, Liu W, Qin H, Tang X, Wu F, et al. Circulating plasma lncRNAs as novel markers of EGFR mutation status and monitors of epidermal growth factor receptor-tyrosine kinase inhibitor therapy. *Thorac Cancer* (2020) 11(1):29–40. doi:10.1111/1759-7714.13216

45. Ak Aksoy S, Mutlu M, Tunca B, Kocaeli H, Taskapilioglu MO, Bekar A, et al. Coexistence of TERT C228T mutation and MALAT1 dysregulation in primary glioblastoma: New prognostic and therapeutic targets. *Neurol Res* (2021) 43(11):916–25. doi:10.1080/01616412.2021.1948738

46. Zhan P, Ji YN, Yu LK. TP53 mutation is associated with a poor outcome for patients with hepatocellular carcinoma: Evidence from a meta-analysis. *Hepatobiliary Surg Nutr* (2013) 2(5):260–5. doi:10.3978/j.issn.2304-3881.2013.07.06

47. Tischoff I, Tannapfe A. DNA methylation in hepatocellular carcinoma. *World J Gastroenterol* (2008) 14(11):1741–8. doi:10.3748/wjg.14.1741

48. Liu A, Wu Q, Peng D, Ares I, Anadon A, Lopez-Torres B, et al. A novel strategy for the diagnosis, prognosis, treatment, and chemoresistance of hepatocellular carcinoma: DNA methylation. *Med Res Rev* (2020) 40(5):1973–2018. doi:10.1002/med.21696

49. Dai X, Liu L, Liang Z, Guo K, Xu S, Wang H. Silencing of lncRNA MALAT1 inhibits cell cycle progression via androgen receptor signaling in prostate cancer cells. *Pathol Res Pract* (2019) 215(4):712–21. doi:10.1016/j.prp.2019.01.011

50. Tripathi V, Shen Z, Chakraborty A, Giri S, Freier SM, Wu X, et al. Long noncoding RNA MALAT1 controls cell cycle progression by regulating the expression of oncogenic transcription factor B-MYB. *Plos Genet* (2013) 9(3):e1003368. doi:10.1371/journal.pgen.1003368

51. Samimi H, Haghpanah V, Irani S, Arefian E, Sohi AN, Fallah P, et al. Transcript-level regulation of MALAT1-mediated cell cycle and apoptosis genes using dual MEK/Aurora kinase inhibitor "BI-847325" on anaplastic thyroid carcinoma. *Daru.* (2019) 27(1):1–7. doi:10.1007/s40199-018-0231-3

52. Huang J, Lin C, Dong H, Piao Z, Jin C, Han H, et al. Targeting MALAT1 induces DNA damage and sensitize non-small cell lung cancer cells to cisplatin by repressing BRCA1. *Cancer Chemother Pharmacol* (2020) 86(5):663–72. doi:10.1007/s00280-020-04152-7

53. Hu Y, Lin J, Fang J, Fang H, Li C, Chen W, et al. Targeting the MALAT1/PARP1/LIG3 complex induces DNA damage and apoptosis in multiple myeloma. *Leukemia* (2018) 32(10):2250–62. doi:10.1038/s41375-018-0104-2

54. Hardin H, Helein H, Meyer K, Robertson S, Zhang R, Zhong W, et al. Thyroid cancer stem-like cell exosomes: Regulation of EMT via transfer of lncRNAs. *Lab Invest* (2018) 98(9):1133–42. doi:10.1038/s41374-018-0065-0

55. Klinge CM. Non-coding RNAs in breast cancer: Intracellular and intercellular communication. *Noncoding RNA* (2018) 4(4):40. doi:10.3390/ncrna4040040

56. Liang Z, Wu Q, Wang H, Tan J, Gou Y, Cao Y, et al. Silencing of lncRNA MALAT1 facilitates erastin-induced ferroptosis in endometriosis through miR-145-5p/MUC1 signaling. *Cel Death Discov* (2022) 8(1):190. doi:10.1038/s41420-022-00975-w

57. Wang Z, Wang X, Zhang T, Su L, Liu B, Zhu Z, et al. LncRNA MALAT1 promotes gastric cancer progression via inhibiting autophagic flux and inducing fibroblast activation. *Cell Death Dis* (2021) 12(4):368. doi:10.1038/s41419-021-03645-4

58. Hou ZH, Xu XW, Fu XY, Zhou LD, Liu SP, Tan DM. Long non-coding RNA MALAT1 promotes angiogenesis and immunosuppressive properties of HCC cells by sponging miR-140. *Am J Physiol Cel Physiol.* (2020) 318(3):C649–c663. doi:10.1152/ajpcell.00510.2018

59. Chang HL, Bamodu OA, Ong JR, Lee WH, Yeh CT, Tsai JT. Targeting the epigenetic non-coding RNA MALAT1/wnt signaling Axis as a therapeutic approach to suppress stemness and metastasis in hepatocellular carcinoma. *Cells* (2020) 9(4):1020. doi:10.3390/cells9041020

60. Malakar P, Stein I, Saragovi A, Winkler R, Stern-Ginossar N, Berger M, et al. Long noncoding RNA MALAT1 regulates cancer glucose metabolism by enhancing mTOR-mediated translation of TCF7L2. *Cancer Res* (2019) 79(10):2480–93. doi:10.1158/0008-5472.Can-18-1432

61. He B, Peng F, Li W, Jiang Y. Interaction of lncRNA-MALAT1 and miR-124 regulates HBx-induced cancer stem cell properties in HepG2 through PI3K/Akt signaling. *J Cel Biochem.* (2019) 120(3):2908–18. doi:10.1002/jcb.26823

62. Chen S, Wang G, Tao K, Cai K, Wu K, Ye L, et al. Long noncoding RNA metastasis-associated lung adenocarcinoma transcript 1 cooperates with enhancer of zeste homolog 2 to promote hepatocellular carcinoma development by modulating the microRNA-22/Snail family transcriptional repressor 1 axis. *Cancer Sci* (2020) 111(5):1582–95. doi:10.1111/cas.14372

63. Fattovich G, Stroffolini T, Zagni I, Donato F. Hepatocellular carcinoma in cirrhosis: Incidence and risk factors. *Gastroenterology* (2004) 127(5):S35–50. doi:10.1053/j.gastro.2004.09.014

64. Yuan LT, Chang JH, Lee HL, Yang YC, Su SC, Lin CL, et al. Genetic variants of lncRNA MALAT1 exert diverse impacts on the risk and clinicopathologic characteristics of patients with hepatocellular carcinoma. *J Clin Med* (2019) 8(9):1406. doi:10.3390/jcm8091406

65. Toraih EA, Ellawindy A, Fala SY, Al Ageeli E, Gouda NS, Fawzy MS, et al. Oncogenic long noncoding RNA MALAT1 and HCV-related hepatocellular carcinoma. *Biomed Pharmacother* (2018) 102:653–69. doi:10.1016/j.biopha.2018.03.105

Pathology & Oncology Research | frontiers

TYPE Original Research
PUBLISHED 16 August 2024
DOI 10.3389/pore.2024.1611835

Check for updates

OPEN ACCESS

EDITED BY
Anna Sebestyén,
Semmelweis University, Hungary

*CORRESPONDENCE
Jorge Lima,
jorgeramoslima@sapo.pt

RECEIVED 14 May 2024
ACCEPTED 31 July 2024
PUBLISHED 16 August 2024

CITATION
Casanova J, da Costa AG, Lopes AP, Catarino A, Nave M, Sousa AC and Lima J (2024) Molecular classification of endometrial cancer: preliminary experience from a single Portuguese academic center.
Pathol. Oncol. Res. 30:1611835.
doi: 10.3389/pore.2024.1611835

COPYRIGHT
© 2024 Casanova, da Costa, Lopes, Catarino, Nave, Sousa and Lima. This is an open-access article distributed under the terms of the Creative Commons Attribution License (CC BY). The use, distribution or reproduction in other forums is permitted, provided the original author(s) and the copyright owner(s) are credited and that the original publication in this journal is cited, in accordance with accepted academic practice. No use, distribution or reproduction is permitted which does not comply with these terms.

Molecular classification of endometrial cancer: preliminary experience from a single Portuguese academic center

João Casanova[1], Ana G. da Costa[1], Ana Pestana Lopes[2], Ana Catarino[2], Mónica Nave[3], Ana Carla Sousa[4] and Jorge Lima[5,6]*

[1]Gynecologic Oncology Unit, Obstetrics and Gynecology Service, Department of Surgery, Hospital da Luz Lisboa, Lisbon, Portugal, [2]Gynecologic Oncology Unit, Department of Pathology, Hospital da Luz Lisboa, Lisbon, Portugal, [3]Gynecologic Oncology Unit, Department of Oncology, Hospital da Luz Lisboa, Lisbon, Portugal, [4]GenoMed—Diagnósticos de Medicina Molecular, Lisbon, Portugal, [5]Obstetrics and Gynecology Service, Department of Surgery, Hospital da Luz Lisboa, Lisbon, Portugal, [6]Comprehensive Health Research Center (CHRC), NOVA Medical School|Faculdade de Ciências Médicas, NMS|FCM, Universidade Nova De Lisboa, Lisbon, Portugal

Background: Since the seminal publication of the TCGA consortium in 2013, the molecular classification of endometrial cancer has been widely accepted as a new and powerful tool to better understand the natural history of this malignancy. Adoption of routine molecular classification around the world has been limited. We sought to demonstrate our initial experience in incorporating the four molecular subtypes for endometrioid carcinomas.

Methods: This was a retrospective analysis at a single center in Portugal. Molecular classification was determined using immunohistochemical staining for MMR and p53 and *Sanger Sequencing* to determine *POLE* mutation status as per published PROMISE method. Descriptive statistics were reported.

Results: 20 patients with endometrioid histology were included. Median age of the cohort was 64 years (range 45–76). Median Body Mass Index (kg/m^2) was 29.81 (range 21.3–43.1). In terms of tumor grading, 16 (80%) of the endometrial carcinomas of the cohort were low-grade (either grade 1 or grade 2). 16 (80%) of the cases were FIGO stage I. Regarding the molecular classification the tumors were classified as: MMRd [n = 6 (30%)]; p53 abn [n = 2 (10%)]; NSMP (n = 10 (50%)), *POLE* ultramut [n = 2 (10%)].

Conclusion: Despite the small sample size, we were able to show that molecular classification is feasible. To our knowledge this is the first cohort of endometroid endometrial carcinomas fully characterized according to the TCGA classification in Portugal, from one single center.

KEYWORDS

endometrial cancer, molecular subtypes, molecular profiling, POLE mutation, DNA sequencing

Introduction

As obesity continues to increase all over the world, so is the incidence of endometrial cancer (EC). Besides obesity playing a major role in the development of endometrial cancer, other risk factors such as diabetes, polycystic ovarian syndrome, estrogen-secreting tumors, unopposed estrogen replacing hormone therapy and tamoxifen use, they all predispose women to endometrial cancer [1]. Historically endometrial carcinomas have been classified using a two-tier classification, type I usually comprising estrogen related tumors and type II non-estrogen/hormone related tumors. Pathologically, type I comprises endometrioid histology and affects roughly 80% of the patients; and type II comprises non-endometrioid histology and it affects the remaining 20% of patients [2]. As previously noted, hormonal factors, namely estrogen excess plays a major role in the etiopathogenesis of endometrioid-type endometrial carcinomas [1]. Focusing more on this subtype, according to the International Federation of Gynecology and Obstetrics (FIGO), endometrioid endometrial carcinomas are graded in a three-tier system, noting the relative proportion of glandular and solid-tumor components [3]. Grade 1 and 2 endometrioid endometrial carcinomas are usually called "low-grade" tumors and are associated with a favorable prognosis. Grade 3 tumors are also called "high-grade" tumors and are usually associated with and intermediate/poor prognosis [1].

In 2013, The Cancer Genome Atlas (TCGA) research network performed and integrated genomic and transcriptomic analysis of 373 endometrial cancers [4]. These findings translated into a proposed molecular classification for EC, comprising four molecular subtypes: DNA Polymerase epsilon (*POLEmut*) ultramutated, microsatellite instability (MSI) hypermutated, copy number high and copy number low [4]. To simplify all these new findings the Proactive Molecular Risk Classifier for Endometrial Cancer (ProMisE) guidelines were established and distinguished the following subtypes of EC: mismatch repair deficiency (MMRd), p53 abnormal (p53abn), non-specified molecular profile (NSMP) and *POLE* ultramutated [5]. These new guidelines are currently more widespread, as the complex and expensive genetic sequencing used by the TCGA consortium can be replaced by immunohistochemistry surrogates to determine most of these profiles [6]. Currently only the *POLE* status needs to be determined by DNA sequencing. For the five most common *POLE* mutations (P286R, V411L, S297F, A456P and S459F), pathogenicity (causing tumor ultramutation) has been confirmed [7].

The firm establishment of these new molecular categories of EC has had a significant impact and interest in a more tailored adjuvant therapy, particularly since the PORTEC-3 trial showed a strong prognostic value of the molecular classification in high risk EC [8]. Interestingly, robust data in the literature has been consistent in demonstrating that *POLE* ultramutated tumors have an incredible favorable prognosis [1, 4, 8–10]. More recently,

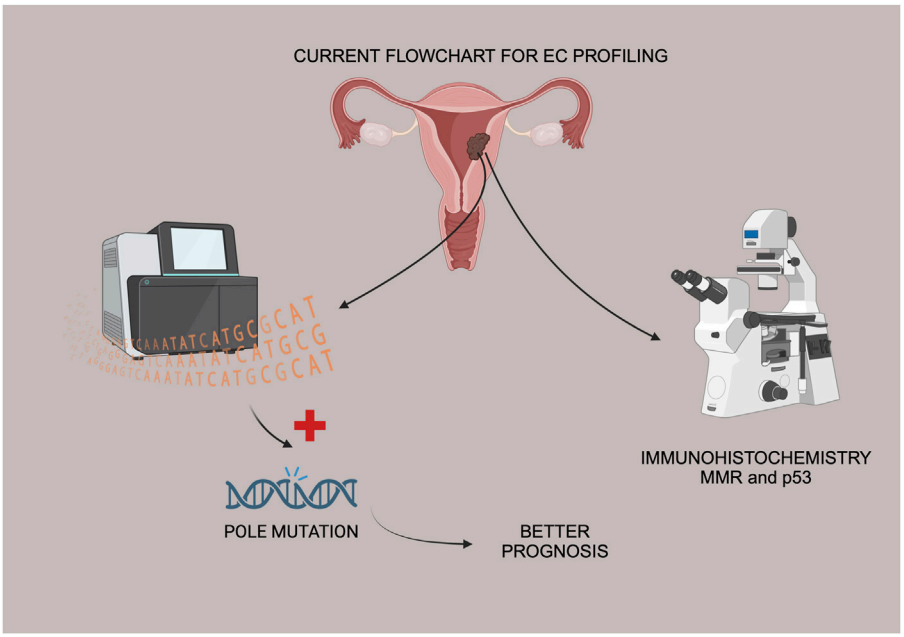

FIGURE 1
Flowchart of EC tissue samples, IHC and Sanger sequencing for *POLE* mutation status.

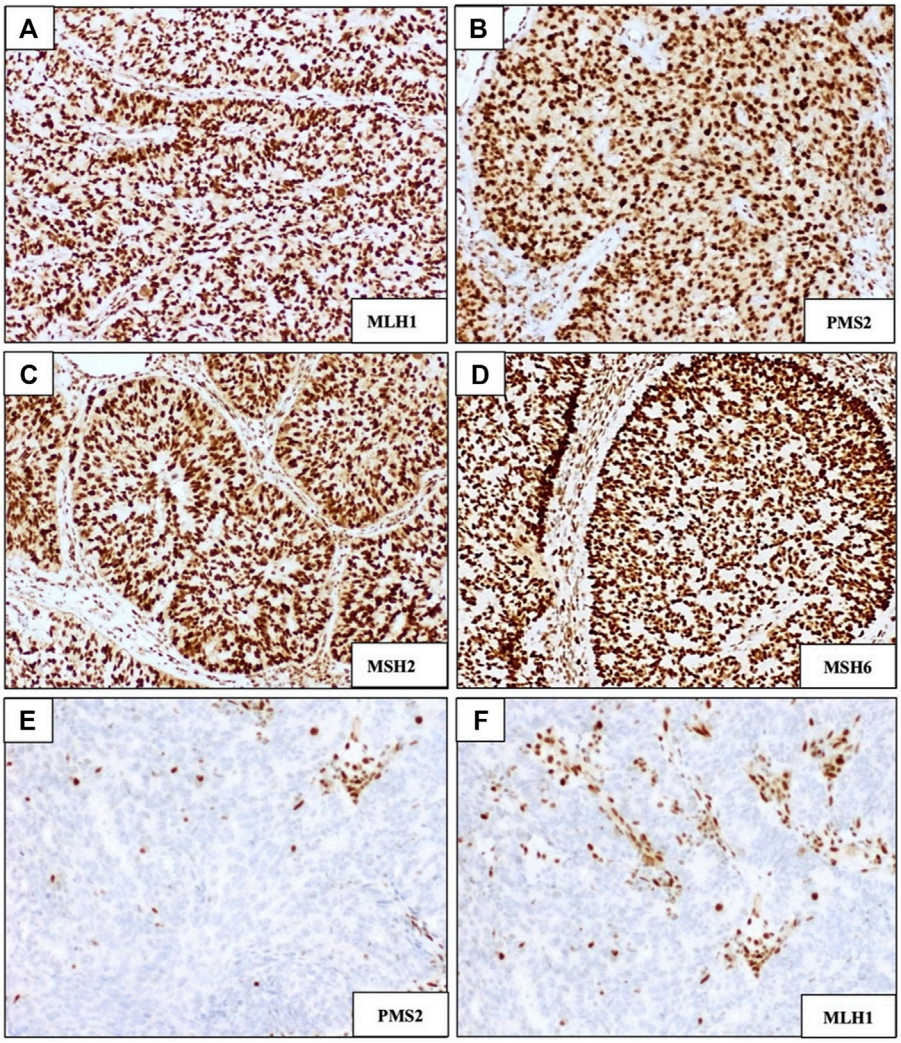

FIGURE 2
Immunohistochemical staining of DNA mismatch repair (MMR) markers MLH1, PMS2, MSH2, and MSH6. **(A–D)** Examples of DNA MMR-proficient staining patterns showing intact/retained nuclear staining. **(E,F)** Examples of MMR-deficient staining patterns showing loss of expression of PMS2 and MLH1, respectively; (magnification ×100).

the new FIGO guidelines for EC staging include the new molecular profiling highlighting that this is the new standard of care [9].

Despite all data available, to the authors knowledge, *POLE* testing has not been widely used in Portugal. The authors would argue that this is mainly due to the absence of available surrogates for *POLE* sequencing. Other factor would be related to health cost, namely DNA sequencing.

According to the landmark paper by the TCGA group, *POLE* ultramutated endometrial carcinomas are a subgroup of endometrioid EC, representing roughly 10% of the endometrioid histology [4]. Data from the literature supports this finding and this was why the authors decided to focus this preliminary analysis only in endometrioid EC (Figure 1).

Materials and methods

Cohort

This retrospective study was approved by the local Ethics Committee. Formalin-fixed paraffin-embedded tissue blocks of 20 patients diagnosed between January of 2022 and February of 2024 with endometrioid EC at a tertiary/academic hospital were retrieved. Informed consent was obtained from all patients. The inclusion criterion was endometrioid histology. Biopsy samples were prioritized due to more potential tumor cells (either from hysteroscopy, curettage and Pipelle biopsy). If these tissue samples were not available, tissue from the surgical specimen containing the primary tumor was used.

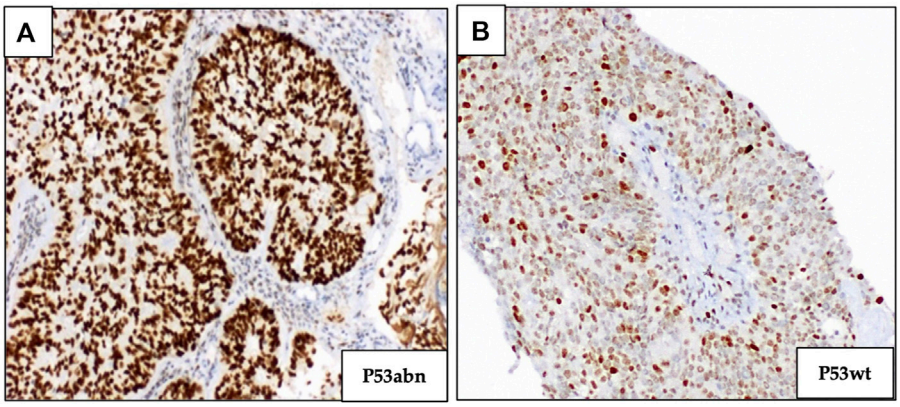

FIGURE 3
Immunohistochemical staining of p53 marker. **(A)** p53 overexpression (abnormal p53). **(B)** Normal expression of p53 (p53 wild type); (magnification ×100).

DNA sequencing

The detection of POLE somatic mutations was performed at an external certified laboratory using Sanger Sequencing. Mutation screening of exons 9, 11, 13, and 14 of the *POLE* gene (12q24.33, OMIM#174762, NM_006231.3, and LRG_789t1) was conducted in samples with tumor content higher than 20% and subsequently analysed by Sanger sequencing. Exonic regions of interest were amplified by polymerase-chain-reaction (PCR) with flanking intronic primers and sequenced by an automatic sequencer (ABI Prism 3100-Avant Capillary Array, 36 cm, Applied Biosystems). Data was evaluated using the DNA Sequencing Analysis Software 6™ Version 6.0 (Applied Biosystems).

Immunohistochemistry

MMR status was investigated by immunohistochemistry (IHC), evaluating the presence or absence of four proteins involved in the mismatch repair pathway: MLH1, PMS2, MSH2, and MSH6. p53 abnormalities were also analysed using IHC. A representative slide of each sample was selected, and then three-micron-thick serial paraffin sections were processed by IHC using an automated immunostainer (Ventana BenchMark Ultra). Each IHC marker was examined under light microscopy by two pathologists. Regarding to MMR enzyme immunohistochemistry, cases were scored as "retained" if uniform intact nuclear staining for the protein was observed, whereas MMRd tumors were characterized by a complete absence of intact nuclear staining (Figure 2). The specifications of the antibodies used for MSI staining were as follow: Ventana anti-MSH2 (G219-1129), mouse monoclonal primary antibody, 5 mL (~20 µg/mL); Ventana anti-PMS2 (A16-4), mouse monoclonal antibody, 5 mL (~1 µg/mL); Ventana anti-MLH1 (M1) mouse monoclonal primary antibody, 5 mL (~1 µg/mL); Ventana anti-MSH6 (SP93) rabbit monoclonal primary antibody, 5 mL (~1 µg/mL).

Abnormal p53 (p53abn) staining was recognized either by overexpression (diffuse strong staining of >75% tumor cell nuclei) or a complete absence of staining of tumor cell nuclei, in the presence of an intact internal control. p53 wild-type (p53wt) tumors were characterized by scattered nuclear staining with a mixture of negative, weak, and strong staining of tumor cell nuclei (Figure 3). Ventana CONFIRM anti p53 (DO-7) primary antibody, 5 mL (~0.5 µg/mL) was used for p53 staining.

Results

DNA sequencing to determine *POLE* status was successful in all cases. IHC was performed in all samples. The clinicopathologic characteristics of the cohort are listed in Table 1. The 2009 FIGO Staging System of endometrial cancer was used.

Afterwards, the EC samples were classified into one of the four molecular subgroups:

- MMR*d* – 6 (30%)
- p53*abn* – 2 (10%)
- NSMP – 10 (50%)
- POLE ultramutated – 2 (10%)

Regarding the specific location of the POLE mutations, one case had the mutation (c1366G>C p (Ala456Pro) in exon 14. The other patient with a POLE ultramutated tumor had the mutation (c.857C>G p.(Pro286Arg) in exon 9.

TABLE 1 Clinicopathologic characteristics of the EC cohort.

Clinicopathologic characteristics	N = 20[a]
Age (years) Median (range)	64 (45–76)
BMI (kg/m^2) Mean (range)	29.57 (21.3–43.15)
Tumor Grade	
Low Grade (G1&2)	16 (80%)
High Grade (G3)	4 (20%)
Lymphovascular Invasion	
Yes	4 (20%)
No	15 (75%)
FIGO Stage[b]	
IA	12 (63%)
IB	4 (21%)
II	0
III	2 (10%)
IV	1 (5%)
Adjuvant Therapy	
None	11 (58%)
Radiotherapy	4 (21%)
Chemotherapy	1 (5%)
Chemo-Radiation Therapy	3 (16%)
SLN	
Yes	16 (84%)
No	3 (16%)
MIS	
Yes	18 (95%)
No	1 (5%)

SLN, Sentinel Lymph Node Dissection; MIS, Minimally invasive Surgery (robotic surgery or laparoscopic surgery).
[a]One patient pursued treatment at other medical institution.
[b]2009 FIGO, staging system of Endometrial Cancer.

One *POLE* ultramutated tumor was identified in a patient included in the multiple classifiers group (this patient had a tumor with both p53*abn* and MMR*d*). The other POLE ultramutated tumor was an early stage (FIGO IB) low-grade tumor. Regarding MMRd tumors, four cases had MLH1 and PSM2 deficiency, one case had MSH6 and MSH2 deficiency and one case had MSH6 and PSM2 deficiency. Both p53*abn* tumors were high-grade tumors, but interestingly both were FIGO Stage I. Regarding the six MMR*d* tumors, five tumors were low-grade (either grade 1 or grade 2) and one was high-grade. Among the MMR*d* tumors, four cases presented as FIGO Stage I, one as FIGO Stage IIIC1 and another one as FIGO stage IVB. Regarding the surgical approach, the majority of patients (95%) underwent MIS and one patient underwent a primary cytoreductive surgery, via laparotomy. SLN biopsy was performed in 84% of the cases. Table 2 shows every patient classified according to the molecular subtype. FIGO stage, tumor grading and adjuvant therapy are also described.

Discussion

As previously discussed, EC is one of the most common gynecologic malignancies and its incidence is rising [11]. The advances catalyzed by the TCGA consortium, have now set molecular profiling of endometrial cancer as an extremely useful tool, with major impacts in refining adjuvant therapy and with prognostic implications. Of note, the *POLE* ultramutated subgroup of EC seems to carry an excellent prognosis [12–14]. Regarding MSI EC (or MMR*d*) data in the literature found that these tumors were more likely to present with poor prognostic factors, such as higher grading and frequent lympho-vascular space invasion [15]. Interestingly, the clinical outcome of these patients seems to be more on the favorable side [15–18]. Regarding p53*abn* EC, they carry the worst prognosis and most likely benefit from aggressive adjuvant therapy [19]. Lastly the NSMP endometrial carcinomas have been mostly classified as intermediate risk, but further refining is necessary to have a more tailored approach to these tumors [20]. To our knowledge, this is the first cohort of Portuguese patients, from one single center, with endometrioid EC to be fully classified according to the molecular profile. In all twenty patients of the cohort, the IHC studies were performed, and *POLE* sequencing was successful. As expected, most of the patients had low grade and early-stage tumors. Two *POLE* ultramutated tumors were identified in our cohort. According to the literature, *POLE* ultramutated tumors are approximately 10% of all endometrioid EC so the authors expect that as the sample size will grow, the corresponding *POLE* mutations will be identified. We would also mention that one of the POLE mutated patient was not submitted to adjuvant brachytherapy. This decision was taken after discussion in our tumor board meeting and there is robust data supporting this, including the new FIGO staging system for EC [9]. The authors would like to highlight that both p53*abn* EC were early stage (FIGO Stage IA), and underwent adjuvant therapy, after discussion in a multidisciplinary decision management meeting. In Portugal, due to limited resources specifically in genetic sequencing facilities, to our knowledge, the "new" molecular EC classification has not been fully embraced by most healthcare institutions, either in the public and private sector. As previously mentioned, the molecular profiling of EC has major prognostic implications, and as data in the literature matures, significant changes in the management of EC are underway [9]. For instance, PORTEC4a, will be addressing the risk of vaginal recurrence in women with high-intermediate risk EC treated after

TABLE 2 Molecular classification of the EC cohort.

Patient	Grade	FIGO Stage	Subtype	Adjuvant therapy
A	2	IA	NSMP	None
B	2	IIIC1	NSMP	Chemo-Radiation
C	1	IA	MMR*d*	None
D	3	IVB	MMR*d*	Chemotherapy
E	2	IIIC1	MMR*d*	Chemo-Radiation
F	1	IA	NSMP	None
G	3	IA	p53*abn*	Radiation
H	1	IA	NSMP	None
I	3	IB	MMR*d*	Chemo-Radiation
J	3	IA	p53*abn*	Radiation
K	1	IA	NSMP	None
L	1	IA	MMR*d*	None
M	1	IA	*POLEult*	None
N	1	IA	MMR*d*	None
O	1	IA	NSMP	None
P	1	IA	NSMP	None
Q	2	N/A	NSMP	N/A
R	1	IB	NSMP	Radiation
S	2	IB	NSMP	Radiation
T	2	IB	*POLEult*	None

N/A, data not available.

surgery with molecular-integrated risk profile-based recommendations (observation, vaginal brachytherapy or external pelvic beam radiotherapy versus standard adjuvant vaginal brachytherapy) [21]. Recently, the ESGO/ESTRO/ESP published in 2021, encourage molecular profiling of all EC, especially high-grade tumors [22]. Regarding high-grade tumors, specifically high-grade EC, having a full molecular-integrated risk profile can be extremely useful in "de-escalating" adjuvant therapy if certain conditions apply. As an example, studies have shown that *POLE* mutations are common in high-grade endometrioid EC, and that these tumors, G3 *POLEmut* have favorable oncologic outcomes and possibly a more conservative adjuvant approach can be recommended in a near future [23–27]. Our group recently published a systematic review and meta-analysis supporting these findings [10]. Bearing all the above, our objective with this preliminary study was to investigate if it would be possible with appropriate funding, to cooperate with a genetic testing certified laboratory and address the lack of data in Portugal regarding the molecular profile of endometrioid EC.

As for the main limitations of this study, the small number of patients enrolled is the most important one. However, being this a preliminary experience, we feel that it would be important to "start small and then go big" as it was necessary to establish new protocols with a certified laboratory regarding *POLE* sequencing and internally validate the data, before setting molecular profiling of EC as the standard of care in our institution. Despite that the literature has robust data regarding the importance of having a full molecular profile for EC, the authors feel that having data of a very small cohort of Portuguese patients can help to disseminate the clinical relevance of this fact. Other limitation that the authors would like to point out is related with the necessity of sequencing the *POLE* in all EC. The group that developed The Proactive Molecular Risk Classifier for EC (ProMiSe) has published several studies, mentioning that POLE sequencing may be omitted in low-risk EC, with low risk histologies [6, 28]. To this fact the we would like to point out that routine IHC (p53, MMR) was already being routinely performed at our institution, however, all genetic sequencing had to be done at an outside laboratory so the authors felt that it would be important to establish routines, and again to internally validate the data. We also expect that by leading this initiative in our country more collaboration will be established and we can

move forward in offering a comprehensive histologic and molecular profile to all patients with EC.

Data availability statement

The original contributions presented in the study are included in the article/supplementary material, further inquiries can be directed to the corresponding author.

Ethics statement

The studies involving humans were approved by the Comissão de Ética, Hospital da Luz Lisboa. The studies were conducted in accordance with the local legislation and institutional requirements. The participants provided their written informed consent to participate in this study.

Author contributions

Conceptualization, JC and JL; methodology, AL, AC, and AS; validation, JC, AdC, AL, MN, AS, and JL; formal analysis, JC and JL; investigation, JC, AL, and AS; data curation, JC, AL, and AC; writing–original draft preparation, JC; writing–review and editing, JC, AdC, AL; AC, MN, AS, and JL; supervision, JL; project administration, JL; funding acquisition, JL. All authors contributed to the article and approved the submitted version.

Funding

The author(s) declare that financial support was received for the research, authorship, and/or publication of this article. This research in the context of the "Women's Health and Maternal and Fetal Research Group" was partially co-financed by Hospital da Luz Lisboa under the initiative "Luz Investigação".

Acknowledgments

The authors acknowledge the contribution of GenoMed and their staff. The authors would also like to acknowledge the extremely important contribution from the administrative staff, from the Pathology, Oncology and Gynecology Departments at Hospital da Luz Lisboa.

Conflict of interest

The authors declare that the research was conducted in the absence of any commercial or financial relationships that could be construed as a potential conflict of interest.

References

1. Lu KH, Broaddus RR. Endometrial cancer. *N Engl J Med* (2020) 383(21): 2053–64. From NLM Medline. doi:10.1056/NEJMra1514010

2. Bokhman JV. Two pathogenetic types of endometrial carcinoma. *Gynecol Oncol* (1983) 15(1):10–7. From NLM. doi:10.1016/0090-8258(83)90111-7

3. Hanby AM, walker C, Tavassoli FA, Devilee P. Tavassoli FA, devilee P: Pathology and genetics: tumours of the breast and female genital organs. WHO classification of tumours series - volume IV. Lyon, France: IARC press: 2003. 250pp. ISBN 92 832 2412 4. *Breast Cancer Res* (2004) 6(3):133. doi:10.1186/bcr788

4. Cancer Genome Atlas Research N, Kandoth C, Schultz N, Cherniack AD, Akbani R, Liu Y, et al. Integrated genomic characterization of endometrial carcinoma. *Nature* (2013) 497(7447):67–73. From NLM Medline. doi:10.1038/nature12113

5. Henry CE, Phan K, Orsman EJ, Kenwright D, Thunders MC, Filoche SK. Molecular profiling of endometrial cancer: an exploratory study in aotearoa, New Zealand. *Cancers (Basel)* (2021) 13(22):5641. From NLM PubMed-not-MEDLINE. doi:10.3390/cancers13225641

6. Kommoss S, McConechy MK, Kommoss F, Leung S, Bunz A, Magrill J, et al. Final validation of the ProMisE molecular classifier for endometrial carcinoma in a large population-based case series. *Ann Oncol* (2018) 29(5):1180–8. From NLM Medline. doi:10.1093/annonc/mdy058

7. León-Castillo A, Britton H, McConechy MK, McAlpine JN, Nout R, Kommoss S, et al. Interpretation of somatic POLE mutations in endometrial carcinoma. *J Pathol* (2020) 250(3):323–35. From NLM. doi:10.1002/path.5372

8. Leon-Castillo A, de Boer SM, Powell ME, Mileshkin LR, Mackay HJ, Leary A, et al. Molecular classification of the PORTEC-3 trial for high-risk endometrial cancer: impact on prognosis and benefit from adjuvant therapy. *J Clin Oncol* (2020) 38(29):3388–97. From NLM Medline. doi:10.1200/JCO.20.00549

9. Berek JS, Matias-Guiu X, Creutzberg C, Fotopoulou C, Gaffney D, Kehoe S, et al. FIGO staging of endometrial cancer: 2023. *Int J Gynaecol Obstet* (2023) 162(2): 383–94. From NLM Medline. doi:10.1002/ijgo.14923

10. Casanova J, Duarte GS, da Costa AG, Catarino A, Nave M, Antunes T, et al. Prognosis of polymerase epsilon (POLE) mutation in high-grade endometrioid endometrial cancer: systematic review and meta-analysis. *Gynecol Oncol* (2024) 182: 99–107. From NLM Publisher. doi:10.1016/j.ygyno.2024.01.018

11. Imboden S, Nastic D, Ghaderi M, Rydberg F, Rau TT, Mueller MD, et al. Phenotype of POLE-mutated endometrial cancer. *PLoS One* (2019) 14(3):e0214318. From NLM Medline. doi:10.1371/journal.pone.0214318

12. Church DN, Stelloo E, Nout RA, Valtcheva N, Depreeuw J, ter Haar N, et al. Prognostic significance of POLE proofreading mutations in endometrial cancer. *J Natl Cancer Inst* (2015) 107(1):402. From NLM Medline. doi:10.1093/jnci/dju402

13. Stelloo E, Bosse T, Nout RA, MacKay HJ, Church DN, Nijman HW, et al. Refining prognosis and identifying targetable pathways for high-risk endometrial cancer; a TransPORTEC initiative. *Mod Pathol* (2015) 28(6):836–44. From NLM Medline. doi:10.1038/modpathol.2015.43

14. Stelloo E, Nout RA, Osse EM, Jurgenliemk-Schulz IJ, Jobsen JJ, Lutgens LC, et al. Improved risk assessment by integrating molecular and clinicopathological factors in early-stage endometrial cancer-combined analysis of the PORTEC cohorts. *Clin Cancer Res* (2016) 22(16):4215–24. From NLM Medline. doi:10.1158/1078-0432.CCR-15-2878

15. McMeekin DS, Tritchler DL, Cohn DE, Mutch DG, Lankes HA, Geller MA, et al. Clinicopathologic significance of mismatch repair defects in endometrial cancer: an NRG oncology/gynecologic oncology group study. *J Clin Oncol* (2016) 34(25):3062–8. From NLM Medline. doi:10.1200/JCO.2016.67.8722

16. Black D, Soslow RA, Levine DA, Tornos C, Chen SC, Hummer AJ, et al. Clinicopathologic significance of defective DNA mismatch repair in endometrial carcinoma. *J Clin Oncol* (2006) 24(11):1745–53. From NLM Medline. doi:10.1200/JCO.2005.04.1574

17. Zighelboim I, Goodfellow PJ, Gao F, Gibb RK, Powell MA, Rader JS, et al. Microsatellite instability and epigenetic inactivation of MLH1 and outcome of

patients with endometrial carcinomas of the endometrioid type. *J Clin Oncol* (2007) 25(15):2042–8. From NLM Medline. doi:10.1200/JCO.2006.08.2107

18. Kato M, Takano M, Miyamoto M, Sasaki N, Goto T, Tsuda H, et al. DNA mismatch repair-related protein loss as a prognostic factor in endometrial cancers. *J Gynecol Oncol* (2015) 26(1):40–5. From NLM Medline. doi:10.3802/jgo.2015.26.1.40

19. Vermij L, Leon-Castillo A, Singh N, Powell ME, Edmondson RJ, Genestie C, et al. p53 immunohistochemistry in endometrial cancer: clinical and molecular correlates in the PORTEC-3 trial. *Mod Pathol* (2022) 35(10):1475–83. From NLM Medline. doi:10.1038/s41379-022-01102-x

20. Kasius JC, Pijnenborg JMA, Lindemann K, Forsse D, van Zwol J, Kristensen GB, et al. Risk stratification of endometrial cancer patients: FIGO stage, biomarkers and molecular classification. *Cancers (Basel)* (2021) 13(22):5848. From NLM PubMed-not-MEDLINE. doi:10.3390/cancers13225848

21. van den Heerik A, Horeweg N, Nout RA, Lutgens L, van der Steen-Banasik EM, Westerveld GH, et al. PORTEC-4a: international randomized trial of molecular profile-based adjuvant treatment for women with high-intermediate risk endometrial cancer. *Int J Gynecol Cancer* (2020) 30(12):2002–7. From NLM. doi:10.1136/ijgc-2020-001929

22. Concin N, Matias-Guiu X, Vergote I, Cibula D, Mirza MR, Marnitz S, et al. ESGO/ESTRO/ESP guidelines for the management of patients with endometrial carcinoma. *Int J Gynecol Cancer* (2021) 31(1):12–39. From NLM Medline. doi:10.1136/ijgc-2020-002230

23. Billingsley CC, Cohn DE, Mutch DG, Hade EM, Goodfellow PJ. Prognostic significance of POLE exonuclease domain mutations in high-grade endometrioid endometrial cancer on survival and recurrence: a subanalysis. *Int J Gynecol Cancer* (2016) 26(5):933–8. From NLM Medline. doi:10.1097/IGC.0000000000000681

24. Bosse T, Nout RA, McAlpine JN, McConechy MK, Britton H, Hussein YR, et al. Molecular classification of grade 3 endometrioid endometrial cancers identifies distinct prognostic subgroups. *Am J Surg Pathol* (2018) 42(5):561–8. From NLM Medline. doi:10.1097/PAS.0000000000001020

25. Meng B, Hoang LN, McIntyre JB, Duggan MA, Nelson GS, Lee CH, et al. POLE exonuclease domain mutation predicts long progression-free survival in grade 3 endometrioid carcinoma of the endometrium. *Gynecol Oncol* (2014) 134(1):15–9. From NLM Medline. doi:10.1016/j.ygyno.2014.05.006

26. Yu S, Sun Z, Zong L, Yan J, Yu M, Chen J, et al. Clinicopathological and molecular characterization of high-grade endometrial carcinoma with POLE mutation: a single center study. *J Gynecol Oncol* (2022) 33(3):e38. From NLM Medline. doi:10.3802/jgo.2022.33.e38

27. Zong L, Mo S, Sun Z, Lu Z, Chen J, Yu S, et al. Incorporating molecular classification when stratifying the survival risk of patients with high-grade endometrial carcinomas. *J Clin Med* (2023) 12(2):530. From NLM PubMed-not-MEDLINE. doi:10.3390/jcm12020530

28. Talhouk A, McConechy MK, Leung S, Yang W, Lum A, Senz J, et al. Confirmation of ProMisE: a simple, genomics-based clinical classifier for endometrial cancer. *Cancer* (2017) 123(5):802–13. From NLM Medline. doi:10.1002/cncr.30496

Pathology & Oncology Research | frontiers

TYPE Original Research
PUBLISHED 19 May 2023
DOI 10.3389/pore.2023.1611162

Check for updates

OPEN ACCESS

EDITED BY
Andrea Ladányi,
National Institute of Oncology (NIO), Hungary

*CORRESPONDENCE
Paramee Thongsuksai,
tparamee@gmail.com

RECEIVED 05 March 2023
ACCEPTED 11 May 2023
PUBLISHED 19 May 2023

CITATION
Leeha M, Kanokwiroon K, Laohawiriyakamol S and Thongsuksai P (2023), Immunohistochemistry-based molecular subtyping of triple-negative breast cancer and its prognostic significance.
Pathol. Oncol. Res. 29:1611162.
doi: 10.3389/pore.2023.1611162

COPYRIGHT
© 2023 Leeha, Kanokwiroon, Laohawiriyakamol and Thongsuksai. This is an open-access article distributed under the terms of the Creative Commons Attribution License (CC BY). The use, distribution or reproduction in other forums is permitted, provided the original author(s) and the copyright owner(s) are credited and that the original publication in this journal is cited, in accordance with accepted academic practice. No use, distribution or reproduction is permitted which does not comply with these terms.

Immunohistochemistry-based molecular subtyping of triple-negative breast cancer and its prognostic significance

Marisa Leeha[1], Kanyanatt Kanokwiroon[1], Suphawat Laohawiriyakamol[2] and Paramee Thongsuksai[3]*

[1]Department of Biomedical Sciences and Biomedical Engineering, Faculty of Medicine, Prince of Songkla University, Hat Yai, Songkhla, Thailand, [2]Department of Surgery, Faculty of Medicine, Prince of Songkla University, Hat Yai, Songkhla, Thailand, [3]Department of Pathology, Faculty of Medicine, Prince of Songkla University, Hat Yai, Songkhla, Thailand

Background: Immunohistochemistry (IHC)-based protein markers representing molecular subtypes are of great value for routine use. This study aimed to evaluate the frequency distributions of the molecular subtypes of triple-negative breast cancer (TNBC) using IHC-based surrogate markers and examined their prognostic value.

Methods: Patients with TNBC treated at a university hospital in Southern Thailand were included in this study. Expression levels of androgen receptor, CD8, Forkhead box transcription factor C1, and Doublecortin-like kinase 1 were detected in tumor tissue to classify them into luminal androgen receptor (LAR), immunomodulatory (IM), basal-like immunosuppressed (BLIS), mesenchymal-like (MES), and unclassifiable (UC) subtypes. The association between variables and disease-free survival (DFS) and overall survival (OS) was analyzed using Cox proportional hazards regression.

Results: Among the 195 cases of TNBC, the frequency distribution of the IHC-based subtype was as follows: BLIS, 52.8%; LAR, 19.0%; IM, 17.4%; MES, 0.5%; and un-classifiable, 10.3%. BLIS subtype was significantly found in younger ages (mean: 49.6 years) than other subtypes (mean: 51–57.7 years). LAR and BLIS subtypes were significantly associated with poorer OS compared to the IM subtype in univariate analysis, however, only BLIS was significant in multivariate analysis (HR: 3.29, 95% CI: 1.01–10.72). IHC-based subtype was not found to be associated with DFS.

Conclusion: This study revealed the differences in the proportion frequency of IHC-based TNBC subtypes in Thai patients compared to other populations. IHC-based molecular subtyping may be beneficial for prognosis. However further refinement of the molecular classification of TNBC is needed for better clinical relevance.

KEYWORDS

immunohistochemistry, breast cancer, prognosis, triple-negative breast cancer, molecular subtype

Introduction

Female breast cancer is the most commonly diagnosed cancer (11.7%) worldwide, with an estimated 2.3 million new cases in 2020. It is also the leading cause of cancer-related death (15.5%) in women [1]. Triple-negative breast cancer (TNBC) is characterized by the lack of estrogen receptor (ER), progesterone receptor (PR), and human epidermal growth factor receptor 2 (HER2), accounting for approximately 15%–20% of all breast cancers [2]. Studies have discovered ethnic variations in TNBC prevalence and clinical behavior, possibly owing to disease heterogeneity and genetic variations among races [3, 4]. Patients with TNBC are younger and have a worse prognosis with a higher relapse rate than non-TNBC [5]. Currently, there is no targeted therapy against TNBC, leaving chemotherapy as the primary treatment option. Hence, there is a need to discover targeted therapies for TNBC to improve the survival rate of patients and enhance their quality of life.

TNBC subtyping based on molecular and clinical features may help to identify potential therapeutic targets and predict prognosis. The most commonly recognized studies on TNBC molecular subtypes include those by Lehmann et al. [6, 7], Burstein et al. [8], and Jiang et al. [9]. Jiang et al. [9] performed multi-omic profiling of 465 Chinese TNBC patients at Fudan University Shanghai Cancer Center (FUSCC) and classified TNBCs into four subtypes: luminal androgen receptor (LAR), mesenchymal-like (MES), basal-like immunosuppressed (BLIS), and immunomodulatory (IM) subtypes. However, using gene expression profiling for molecular subtypes is not practical for routine use because it is time-consuming and expensive and requires fresh frozen tissue. Subsequently, they selected protein markers from each molecular subtype and evaluated their potential use in routine practice by immunohistochemistry (IHC) [10]. They demonstrated that each IHC-based subtype showed substantial differences in clinicopathological features and survival outcomes. However, external validation studies of this IHC-based TNBC subtyping have not yet been reported.

A recent study regarding mutational profiles revealed differences in many frequently mutated TBNC genes in Thai patients compared to that in patients from Western countries [11]. However, there have been no studies on the molecular subtypes of TNBC in Thai patients. In this study, we sought to evaluate the frequency distribution and prognostic significance of the IHC-based molecular subtypes of TNBC in a cohort of Thai patients treated in a university hospital in Southern Thailand. We used IHC-based subtyping proposed by Zhao et al. [10] as it was developed from Chinese patients [9]. This would be the first external validation study of this subtyping algorithm.

Materials and methods

Patients and clinical data

This was a retrospective cohort study. The study protocol was approved by the Ethics Committee on Human Research, Faculty of Medicine, Prince of Songkla University (REC. 64-037-4-2). Patients who were diagnosed with TNBC between 2011 and 2019 at Songklanakarind Hospital, a university hospital in Southern Thailand, were included. The inclusion criteria were patients with primary TNBC whose tissue samples before adjuvant chemotherapy and/or radiation therapy were available in our institute. TNBC was identified when ER, PR, and HER2 staining was negative in the tissues using IHC and fluorescence/dual *in situ* hybridization assays. Evaluation of immunoreactivity of ER, PR, and HER2 followed the guidelines of the American Society of Clinical Oncology and College of American Pathologists (ASCO/CAP) [12–14].

Patient data, including age, clinical characteristics, pathological features, treatment, and follow-up information for recurrence, were retrieved from the electronic medical records of the hospital. The first episode of locoregional recurrence or distant metastasis was defined as a recurrence. Locoregional recurrence was defined as tumor recurrence in the chest wall/breast (ipsilateral or contralateral) and four lymphatic drainage regions of the breast (axillary, supraclavicular, subclavian, and internal mammary). Information regarding death was obtained from the Cancer Registry Unit of the faculty, which was updated biannually from the national death registration data.

Tissue microarray (TMA)

Formalin-fixed, paraffin-embedded (FFPE) tissue samples and hematoxylin and eosin-stained histological slides were retrieved from the archives of the Department of Pathology. A Quick Ray® manual tissue microarray (Unitma, Seoul, Korea) was used for TMA construction. Histological slides were reviewed, and two foci of the representative areas with viable and abundant tumor cells were selected and marked for each case. Then, the corresponding point in the respective FFPE block was marked and cut out using a 2-mm core needle and embedded within the recipient paraffin block. The recipient blocks were then heated at 40°C in a hot-air oven for 15 min. TMA was performed only for excisional biopsied tissue, whereas whole tissue sections were used for core needle biopsy specimens.

Immunohistochemistry (IHC)

IHC was performed using an automated immunostaining system (BONDMAX; Leica Biosystems, Melbourne, Australia).

Briefly, to begin with, the samples were rinsed with xylene for deparaffinization. The slides were rehydrated using increasing concentrations of alcohol and washed with phosphate-buffered saline. Antigens were retrieved and incubated with a bond peroxidase-blocking reagent, followed by primary antibodies against AR (1:200 dilution, Cell Signaling), CD8 (1:500, Cell Signaling), FOXC1 (1:200, Abcam), and DCLK1 (1:100, Cell Signaling Technology). A Bond Polymer Refining Detection Kit (Leica) was used for detection, and 3,3′-diaminobenzidine was used for immunodetection, followed by Mayer's hematoxylin for counterstaining. We used prostate tissue and tonsil as positive controls for AR and CD8 expression, respectively. TNBC tissues which were tested strongly positive were used as positive control for DCLK1 and FOXC1 expression. The positive control tissues were put simultaneously on all of the examined slides.

Immunostaining evaluation

Immunostaining was evaluated independently by two authors (M.L and P.T.) who were blinded from clinical data as the percentage of positive cells, irrespective of the signal intensity. For any discordant interpretation, the two authors would study the immunostaining slides together and discuss. Agreement on the positive or negative results of each stain was obtained.

For AR, FOXC1, and DCLK1 expression, the percentage of positive tumor cells over the total number of tumor cells on the slides was estimated. For CD8, stromal $CD8^+$ tumor-infiltrating lymphocytes (TILs) were detected in five randomly selected fields (×200 magnification) using digitalized images of full tissue sections. The percentage of stromal $CD8^+$ TILs was obtained based on the recommendation of the International TILs Working Group 2014 [15]; that is, the percentage of CD8+TILs was semi-quantitatively estimated over the area of stromal tissue within the borders of the invasive tumor, excluding the TILs outside the tumor boundary, such as tertiary lymphoid aggregation and tumor area with artifacts or necrosis.

For the TMA slides, the average percentage of the two cores was used for further analysis. The cutoff value of positive versus negative protein expression, according to Zhao et al. [10] was used. Tumors positive for AR, DCLK1, and FOXC1 were defined as tumors with ≥ 10% positive cells, whereas CD8-positive tumors were defined as ≥ 20% $CD8^+$ TILs.

Assigning IHC-based molecular subtype

The classification method proposed by Zhao et al. [10] was used (Figure 1). Tumor with AR-positive (+) irrespective of other protein positivity was defined as LAR subtype, AR-negative (−)/CD8+ as IM subtype, AR-/CD8-/FOXC1+ as BLIS subtype, and AR-/CD8-/FOXC-/DCLK1+ as MES subtype. Tumors that could not be classified into any of these subtypes were designated as unclassifiable (UC).

Statistical analysis

Statistical analysis was performed using R program version 4.0.3 (R Foundation for Statistical Computing, Vienna, Austria). Categorical variables were described by the number of observations and percentages. Continuous variables are represented as mean ± standard deviation (SD). The correlation between clinicopathological characteristics and the TNBC subtypes was calculated using the Fisher exact or Pearson's chi-square test, as appropriate. Disease-free survival (DFS) was defined as the time interval from the date of diagnosis to the date of first recurrence (local or distant), the date of last known follow-up, or the date of death for those who had no recurrence (censored data). Overall survival (OS) was defined as the time interval from the date of diagnosis to the date of death or the date of the last follow-up if the patients were alive (censored data). OS and DFS were determined using Kaplan-Meier analysis. The Cox proportional hazard regression model was used to determine the prognostic significance of variables. For this analysis, the missing values of clinical stage, chemotherapy and radiotherapy were imputed and replaced by random sampling imputation. IHC-based TNBC subtype and significant variables from univariate analysis were selected for multivariate analysis. Statistical significance was set at a two-sided p-value < 0.05.

Results

Patient characteristics

During the study period, 198 patients with primary TNBC for whom tissue blocks were available, from the Department of Pathology, Songklanagarind Hospital, between 2011 and 2019 were involved. Three patients had no follow-up information, and a total of 195 TNBC patients were included in the analysis. The mean age of the patients in the cohort was 52.3 years (range: 25–92 years). The patients were grouped into two categories, based on their ages, namely, <50 and ≥50 years, for further analysis. Pathologically, most tumors were invasive ductal carcinomas (invasive breast carcinoma of no special type) (93.3%) and histologic grade 3 (81.5%). At the time of diagnosis, approximately half of the patients were in stage II (47.4%), followed by stage III (27.3%) of the disease. Majority of patients had received mastectomy (61%). Surgery was not performed in 8 patients as they died shortly after biopsy or unfit for surgery. Seventeen patients did not receive chemotherapy due to various reasons including death before treatment (8), denied treatment (3), clinically unfit (3), and non-

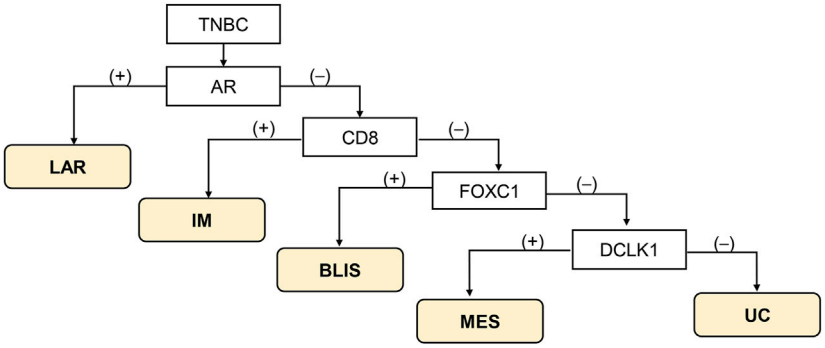

FIGURE 1
Immunohistochemistry-based classification scheme according to Zhao et al. [10]. Abbreviations: BLIS, basal-like immunosuppressed; IM, immunomodulatory; LAR, luminal androgen receptor; MES, mesenchymal-like; TNBC, triple-negative breast cancer; UC, unclassifiable.

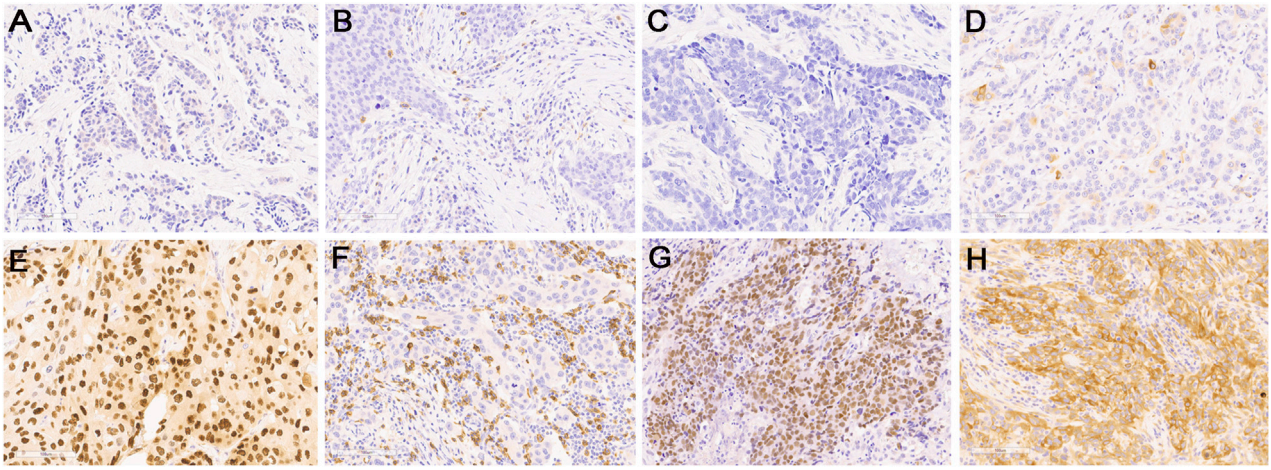

FIGURE 2
Representative images of immunohistochemical staining for low expression (upper panel) and high expression (lower panel) of protein markers: **(A,E)** AR, **(B,F)** CD8, **(C,G)** FOXC1, and **(D,H)** DCKL1. Original magnification, ×200.

chemotherapy option for stage I disease (2 patients). Data on treatments were missing in some patients as they transferred to receive treatments at other hospitals.

IHC-based TNBC subtypes and their clinicopathological characteristics

Representative IHC for all proteins is shown in Figure 2. According to IHC-based subtypes, BLIS was the most common subtype (103 cases, 52.82%), followed by LAR (37 cases, 18.97%), IM (34 cases, 17.44%), and MES (1 case, 0.51%). Twenty patients (10.26%) could not be classified and were categorized as UC. The clinicopathological characteristics of the patients according to TNBC subtypes are presented in Table 1. No characteristics, except age, were significantly varied between the subtypes. The BLIS subtype was found majorly in younger patients (mean: 49.6 years) as opposed to the other subtypes (mean: 51–57.7 years). The only one patient with MES subtype was 30 years old with clinical stage III and histologic type of invasive ductal carcinoma, grade 2. The patient received chemo-radiation therapy.

Disease-free survival and overall survival of the patients

The median follow-up time was 40.95 months (interquartile range (IQR): 23.48–89.22 months). By the end of the study

TABLE 1 Clinicopathological characteristics of the IHC-based TNBC subtypes.

Variables	LAR	IM	BLIS	MES	UC	*p*-value
	(*n* = 37)	(*n* = 34)	(*n* = 103)	(*n* = 1)	(*n* = 20)	
Age, years						<0.001
Mean (SD)	57.7 (11.7)	55.7 (10.6)	49.6 (12.5)	30	51.0 (10.3)	
<50 years	6 (16.2)	11 (32.4)	61 (59.2)	1 (100)	9 (45)	
≥50 years	31 (83.8)	23 (67.6)	42 (40.8)	0 (0)	11 (55)	
Clinical stage[a]						0.542
I	5 (13.5)	10 (29.4)	22 (21.6)	0 (0)	2 (10)	
II	18 (48.6)	17 (50)	47 (46.1)	0 (0)	10 (50)	
III	11 (29.7)	7 (20.6)	28 (27.5)	1 (100)	6 (30)	
IV	3 (8.1)	0 (0)	5 (4.9)	0 (0)	2 (10)	
Histologic type						
Invasive ductal carcinoma	34 (91.9)	32 (94.1)	97 (94.2)	1 (100)	18 (90)	0.362
Invasive lobular carcinoma	2 (5.4)	0 (0)	1 (1)	0 (0)	2 (10)	
Metaplastic carcinoma	1 (2.7)	1 (2.9)	2 (1.9)	0 (0)	0 (0)	
Other	0 (0)	1 (2.9)	3 (2.9)	0 (0)	0 (0)	
Histologic grade						0.231
1	1 (2.7)	0 (0)	1 (1)	0 (0)	1 (5)	
2	11 (29.7)	5 (14.7)	14 (13.6)	0 (0)	3 (15)	
3	25 (67.6)	29 (85.3)	88 (85.4)	1 (100)	16 (80)	
Lymphovascular invasion						0.419
No	22 (59.5)	27 (79.4)	68 (66)	1 (100)	13 (65)	
Yes	15 (40.5)	7 (20.6)	35 (34)	0 (0)	7 (35)	
Type of surgery[a]						0.245
Conservative surgery	9 (27.3)	13 (40.6)	31 (32)	0 (0)	3 (15)	
Mastectomy	24 (72.7)	19 (59.4)	60 (61.9)	1 (100)	15 (75)	
No surgery	0 (0)	0 (0)	6 (6.2)	0 (0)	2 (10)	
Chemotherapy[a]						0.503
No	4 (11.1)	1 (3.1)	9 (9.1)	0 (0)	3 (15)	
Yes	32 (88.9)	31 (96.9)	90 (90.9)	1 (100)	17 (85)	
Radiotherapy[a]						0.922
No	17 (47.2)	14 (43.8)	44 (44.4)	0 (0)	9 (45)	
Yes	19 (52.8)	18 (56.2)	55 (55.6)	1 (100)	11 (55)	

BLIS, basal-like immunosuppressed; IM, immunomodulatory; LAR, luminal androgen receptor; MES, mesenchymal-like; UC, unclassifiable; SD, standard deviation.
[a]Number of missing data: clinical stage (1); chemotherapy (7); radiotherapy (7), type of surgery (12).

(December 2021), 63 patients had experienced at least one episode of recurrence, and 66 patients died. The 5-year rate of DFS was 64.7% (95% CI: 0.576–0.726), and OS was 65.0% (95% CI: 0.581–0.728). The Kaplan–Meier estimates of DFS between different IHC-based subtypes did not show any variation ($p = 0.28$), but the OS was significantly different ($p = 0.034$) (Figure 3). MES subtype was not included in the Kaplan-Meier curves because there was only one case. Patients with the IM subtype had a better OS than those with other subtypes, while the survival curves of the patients with other subtypes overlapped. The patient with MES experienced no recurrence and remained alive until the end of the study.

Prognostic significance of IHC-based TNBC subtypes

Tables 2, 3 present univariate and multivariate Cox regression analyses of DFS and OS, respectively. Age, clinical stage, histologic type, lymphovascular invasion, and radiotherapy were significant factors in the univariate analysis of DFS. However, only age and clinical stage remained significant in the multivariate model.

In the Cox regression analysis for OS, clinical stage, chemotherapy, and IHC-based subtype were significant factors. Specifically, compared to IM, LAR (HR: 5.05, 95% CI: 1.46–17.4) and BLIS (HR: 4.72, 95% CI: 1.46–15.24) were

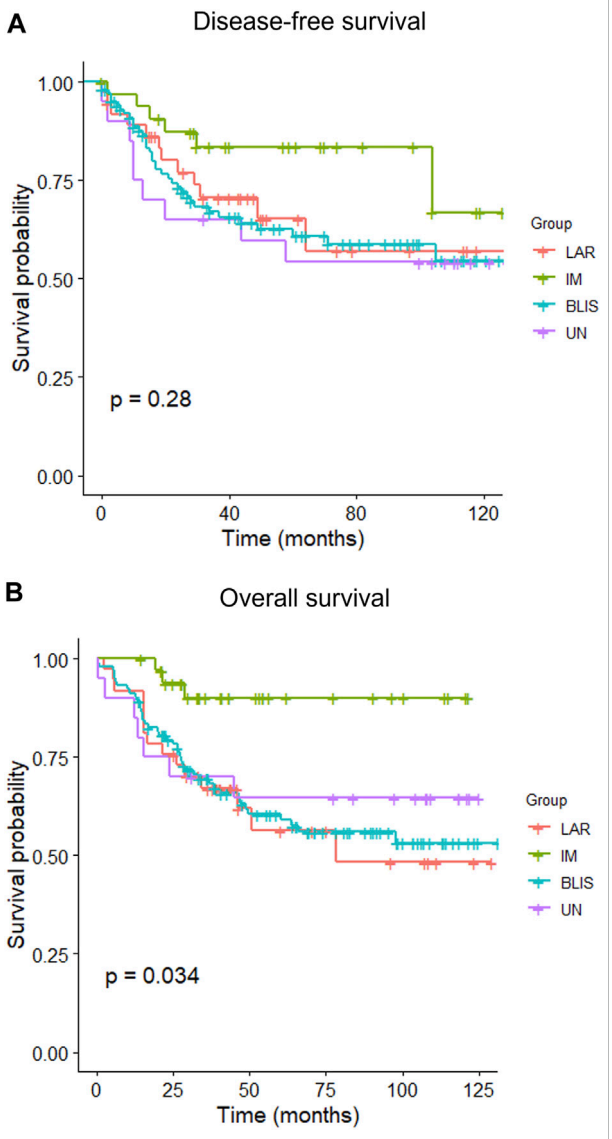

FIGURE 3
Kaplan–Meier curves of disease-free survival **(A)** and overall survival **(B)** of patients with different IHC-based molecular subtypes of triple-negative breast cancer. BLIS, basal-like immunosuppressed; IM, immunomodulatory; LAR, luminal androgen receptor; UC, unclassifiable.

significantly associated with poorer OS in univariate analysis. However, only BLIS remained significant in the multivariate model (HR: 3.29, 95% CI: 1.01–10.72).

Discussion

TNBC subtyping based on relevant biological characteristics may help to guide treatment and predict prognosis. In this study, we evaluated IHC-based TNBC subtypes based on studies conducted in a Chinese cohort [9, 10]. We found that BLIS was the most frequent subtype (52.82%), followed by LAR (18.97%), IM (17.4%), and the very rare MES subtype (0.5%). IHC-based subtype was significantly associated with OS but not DFS. Patients with BLIS had significant unfavorable OS compared to patients with IM subtype.

In 2020, Zhao et al. [10] selected four top proteins from a list of differentially expressed genes that helped classify TNBC into four molecular subtypes from a transcriptomic subtyping study of a Chinese cohort [9]. We assessed the IHC-based TNBC subtypes based on the study by Zhao et al. [10], as the population in this study was also Asian. We used the same IHC markers and immunostaining criteria for comparison. Here, we found a difference in IHC-based subtypes. Our TNBC cohort had a considerably higher percentage of patients with BLIS (52.82%) but a lower percentage of patients with LAR (18.97%) than those reported by Zhao et al. (38.1% for BLIS and 28.6% for LAR) [10]. Different proportions of TNBC molecular subtypes among different populations have also been reported. Jiang et al. [9] applied and compared their mRNA-based TNBC subtypes based on 360 Chinese patients to different populations (Caucasian and African-American) in the Cancer Genome Atlas (TCGA) database. They found BLIS (39%–42%) and IM (24%–32%), and MES (15%–20%) had comparable distribution, while LAR was higher in the Chinese cohort (23%) compared to Caucasian (12%) and African-American (9%). Therefore, a higher proportion of Thai patients with TNBC in the current study had the BLIS subtype and a remarkably lower proportion had the MES subtype than both Western and Chinese populations. A high proportion of Hispanic patients (53.2%) with the BLIS subtype has also been found in a US cohort [16]. This evidence suggests that the differences in the distribution of TNBC subtypes may reflect different genetic backgrounds across races or ethnic groups.

Based on molecular subtyping of the Chinese cohort, CD8 was found to be the top-ranked gene with a high area under the ROC curve (AUC) and a good correlation between mRNA and protein expression [10]. CD8 is a marker for cytotoxic T-cells, an essential component of TILs and tumor immune microenvironment [17]. Our study found that the IM subtype, represented by the presence of stromal $CD8^+$ TILs, had a favorable prognosis, and this finding is consistent with other studies [10, 18]. The IM subtype has been shown to have higher expression of genes involved in immune pathways, such as cytokine signaling, immune cell signaling, antigen processing as well as presentation, chemokine signaling pathway, immune signal transduction pathway, and immune response process [6–9]. Immunotherapy with immune checkpoint inhibitors, such as PD-L1 inhibitors, has been used to treat TNBC [19]. Previous studies have shown that PD-L1 expression is associated with high levels of $CD8^+$ T cell infiltration in TNBC [20, 21]. Therefore, the evaluation of CD8 expression by IHC in TNBC

TABLE 2 Univariate and multivariate Cox regression analysis for disease-free survival.

Variables	Univariate analysis		Multivariate analysis	
	HR (95% CI)	*p*-value	HR (95% CI)	*p*-value
Age, years				
<50	1			
≥50	0.55 (0.33–0.9)	0.018	0.45 (0.25–0.81)	0.008
Clinical stage				
I	1			
II	1.26 (0.55–2.86)	0.586	0.98 (0.42–2.27)	0.957
III	5.09 (2.29–11.31)	<0.001	3.83 (1.58–9.3)	0.003
IV	129.75 (40.19–418.89)	<0.001	157.17 (43.63–566.12)	<0.001
Histologic type				
Invasive ductal carcinoma	1		1	
Invasive lobular carcinoma	3.52 (1.27–9.72)	0.015	1.54 (0.51–4.61)	0.441
Metaplastic carcinoma	0 (0– Inf)	0.997	0 (0–Inf)	0.998
Other	0 (0– Inf)	0.996	0 (0–Inf)	0.997
Histologic grade				
1–2	1			
3	0.95 (0.51–1.78)	0.874		
Lymphovascular invasion				
No	1		1	
Yes	1.69 (1.03–2.78)	0.039	1.65 (0.97–2.79)	0.066
Chemotherapy				
No	1			
Yes	0.67 (0.27–1.68)	0.396		
Radiotherapy				
No	1			
Yes	1.88 (1.09–3.22)	0.022	0.97 (0.51–1.83)	0.915
IHC-based molecular subtype				
IM	1		1	
LAR	1.97 (0.74–5.26)	0.174	1.27 (0.46–3.49)	0.642
BLIS	2.21 (0.93–5.25)	0.072	1.28 (0.52–3.13)	0.596
MES	0 (0– Inf)	0.997	0 (0–Inf)	0.996
UC	2.5 (0.89–7.05)	0.083	1.5 (0.51–4.43)	0.467

HR, hazard ratio; IHC, immunohistochemistry; BLIS, basal-like immunosuppressed; IM, immunomodulatory; LAR, luminal androgen receptor; MES, mesenchymal-like; UC, unclassifiable.

has an implication in predicting prognosis and guiding treatment strategies.

BLIS was the most frequent subtype in our cohort. It was found in younger women, while the LAR and IM subtypes were found in older women. We did not find significant differences of clinical stage and histologic grade among different subtypes which is consistent to previous studies [10, 16]. However, Kim et al. [22] found that histologic grade 3 was most frequently observed in Basal-like type. This subtype is characterized by the upregulation of cell cycle regulators, activation of DNA repair, and downregulation of immune response genes [8, 9]. These biological mechanisms may explain the proliferated phenotypic features of the BLIS subtype which leads to poor survival outcome.

In this study, patients with the LAR subtype were the oldest compared to those with other subtypes, which is consistent with the previous studies [10, 22, 23]. These studies also found that the patients with the LAR subtype had a lower histological grade, and apocrine morphology; however, we did not find these patterns. In addition, they found that the LAR subtype is associated with a favorable prognosis compared to MES subtype while in our study, the LAR subtype was associated with poorer survival compared to the IM subtype, although it was not statistically significant in multivariate analysis. We did have only one patient with MES subtype, therefore, the results would not be explicitly compared. Consistent with other studies, survival patterns among some different subtypes were overlapped [7, 10]. In

TABLE 3 Univariate and multivariate Cox regression analysis for overall survival.

Variables	Univariate analysis		Multivariate analysis	
	HR (95% CI)	*p*-value	HR (95% CI)	*p*-value
Age, years				
<50	1			
≥50	0.7 (0.43–1.14)	0.131		
Clinical stage				
I	1		1	
II	6.17 (1.46–26.14)	0.013	9.05 (2.08–39.35)	0.003
III	17.62 (4.2–73.93)	<0.001	26.33 (6–115.51)	<0.001
IV	81.82 (17.69–378.37)	<0.001	105.62 (21.69–514.23)	<0.001
Histologic type				
Invasive ductal carcinoma	1			
Invasive lobular carcinoma	2.6 (0.94–7.17)	0.064		
Metaplastic carcinoma	0 (0–Inf)	0.996		
Other	0 (0– Inf)	0.996		
Histologic grade				
1–2	1			
3	1.09 (0.7–1.97)	0.777		
Lymphovascular invasion				
No	1			
Yes	1.27 (0.77–2.09)	0.34		
Chemotherapy				
No	1		1	
Yes	0.27 (0.14–0.53)	0.001	0.14 (0.07–0.29)	<0.001
Radiotherapy				
No	1			
Yes	1.3 (0.78–2.18)	0.307		
IHC-based molecular subtype				
IM	1		1	
LAR	5.04 (1.46–17.4)	0.011	2.86 (0.81–10.04)	0.101
BLIS	4.72 (1.46–15.24)	0.01	3.29 (1.01–10.72)	0.048
MES	0 (0–Inf)		0 (0–Inf)	0.996
UC	3.83 (0.99–14.86)	0.052	3.08 (0.79–12.04)	0.106

HR, hazard ratio; IHC, immunohistochemistry; BLIS, basal-like immunosuppressed; IM, immunomodulatory; LAR, luminal androgen receptor; MES, mesenchymal-like; UC, unclassifiable.

our study, the survival pattern of LAR, BLIS, and UC overlapped and in the study by Zhao et al, BLIS, LAR, IM, and UC did not differ [10]. These results indicate that the current surrogate molecular subtyping needs further refinement to improve clinical relevance.

Our study had some limitations. First, we used long-term stored FFPE tissue blocks, which might have affected IHC staining results. Second, we evaluated immunostaining in TMA tissues, which was used as a substitute for the entire tumor. Third, the number of cases, especially for some subtypes, was low and may be insufficient to determine the association of subtypes with clinicopathological characteristics and survival outcomes. Fourth, it is known that gene expressions from transcriptomic data are the gold standard of molecular subtyping, however, we did not have our transcriptomic data to validate the results. Therefore, the findings in this study should be interpreted with caution. Lastly, even though IHC markers have more clinical implications in routine practice than mRNA expression profiles, a unified method of immunostaining evaluation is needed before their usage. In particular, protein markers with cytoplasmic staining, like DCLK1, may pose some challenges than those with nuclear reactivity as staining evaluation is more difficult to quantify.

In conclusion, our study, which is based on the IHC of surrogate markers, revealed certain differences in the distribution of TNBC subtypes in Thai patients compared to that in the

Chinese and Western populations. The BLIS subtype accounted for half of the cases, whereas the MES subtype was rare. This evidence suggests that molecular TNBC subtypes may reflect different genetic backgrounds across races or ethnic groups. However, refinement of molecular subtyping of TNBC needs further refinement to improve clinical relevance.

Data availability statement

The raw data supporting the conclusion of this article will be made available by the authors, without undue reservation.

Ethics statement

The study protocol was approved by the Ethics Committee on Human Research, Faculty of Medicine, Prince of Songkla University (REC. 64-037-4-2).

Author contributions

ML, KK, and SL designed the study. ML and PT interpreted the laboratory results and performed statistical analysis. ML and PT wrote the manuscript. All authors contributed to the article and approved the submitted version.

Funding

This research was funded by the Research Fund of the Faculty of Medicine, Prince of Songkla University, and the Health Systems Research Institute, Thailand (grant number HSRI 63-107).

Conflict of interest

The authors declare that the research was conducted in the absence of any commercial or financial relationships that could be construed as a potential conflict of interest.

Acknowledgments

We thank the Cancer Registry Unit of the Faculty of Medicine, Prince of Sonkla University, for allowing the use of their follow-up data. We thank Onpawee Phanthuvet, Sirinat Nakmont and Kanda Tongmit for the laboratory procedures.

References

1. Sung H, Ferlay J, Siegel RL, Laversanne M, Soerjomataram I, Jemal A, et al. Global cancer statistics 2020: GLOBOCAN estimates of incidence and mortality worldwide for 36 cancers in 185 countries. *CA Cancer J Clin* (2021) 71:209–49. doi:10.3322/caac.21660

2. Morris GJ, Naidu S, Topham AK, Guiles F, Xu Y, McCue P, et al. Differences in breast carcinoma characteristics in newly diagnosed african-American and caucasian patients: A single-institution compilation compared with the national cancer institute's surveillance, epidemiology, and end results database. *Cancer* (2007) 110:876–84. doi:10.1002/cncr.22836

3. Hines LM, Risendal B, Byers T, Mengshol S, Lowery J, Singh M. Ethnic disparities in breast tumor phenotypic subtypes in Hispanic and non-Hispanic white women. *J Womens Health (Larchmt)* (2011) 20:1543–50. doi:10.1089/jwh.2010.2558

4. Zhang W, Bai Y, Sun C, Lv Z, Wang S. Racial and regional disparities of triple negative breast cancer incidence rates in the United States: An analysis of 2011-2019 NPCR and SEER incidence data. *Front Public Health* (2022) 10:1058722. doi:10.3389/fpubh.2022.1058722

5. Dent R, Trudeau M, Pritchard KI, Hanna WM, Kahn HK, Sawka CA, et al. Triple-negative breast cancer: Clinical features and patterns of recurrence. *Clin Cancer Res* (2007) 13:4429–34. doi:10.1158/1078-0432.CCR-06-3045

6. Lehmann BD, Bauer JA, Chen X, Sanders ME, Chakravarthy AB, Shyr Y, et al. Identification of human triple-negative breast cancer subtypes and preclinical models for selection of targeted therapies. *Clin Invest* (2011) 121:2750–67. doi:10.1172/JCI45014

7. Lehmann BD, Jovanović B, Chen X, Estrada MV, Johnson KN, Shyr Y, et al. Refinement of triple-negative breast cancer molecular subtypes: Implications for neoadjuvant chemotherapy selection. *PLoS One* (2016) 11:e0157368. doi:10.1371/journal.pone.0157368

8. Burstein MD, Tsimelzon A, Poage GM, Covington KR, Contreras A, Fuqua SA, et al. Comprehensive genomic analysis identifies novel subtypes and targets of triple-negative breast cancer. *Clin Cancer Res* (2015) 21:1688–98. doi:10.1158/1078-0432.CCR-14-0432

9. Jiang YZ, Ma D, Suo C, Shi J, Xue M, Hu X, et al. Genomic and transcriptomic landscape of triple-negative breast cancers: Subtypes and treatment strategies. *Cancer Cell* (2019) 35:428–40. doi:10.1016/j.ccell.2019.02.001

10. Zhao S, Ma D, Xiao Y, Li XM, Ma JL, Zhang H, et al. Molecular subtyping of triple-negative breast cancers by immunohistochemistry: Molecular basis and clinical relevance. *Oncologist* (2020) 25:e1481–e1491. doi:10.1634/theoncologist.2019-0982

11. Niyomnaitham S, Parinyanitikul N, Roothumnong E, Jinda W, Samarnthai N, Atikankul T, et al. Tumor mutational profile of triple negative breast cancer patients in Thailand revealed distinctive genetic alteration in chromatin remodeling gene. *PeerJ* (2019) 7:e6501. doi:10.7717/peerj.6501

12. Hammond ME, Hayes DF, Dowsett M, Allred DC, Hagerty KL, Badve S, et al. American society of clinical oncology/college of American Pathologists guideline recommendations for immunohistochemical testing of estrogen and progesterone receptors in breast cancer. *Arch Pathol Lab Med* (2010) 134:907–22. doi:10.1043/1543-2165-134.6.907

13. Wolff AC, Hammond ME, Hicks DG, Dowsett M, McShane LM, Allison KH, et al. Recommendations for human epidermal growth factor receptor 2 testing in breast cancer: American society of clinical oncology/college of American Pathologists clinical practice guideline update. *J Clin Oncol* (2013) 31:3997–4013. doi:10.1200/JCO.2013.50.9984

14. Wolff AC, Hammond MEH, Allison KH, Harvey BE, Mangu PB, Bartlett JMS, et al. Human epidermal growth factor receptor 2 testing in breast cancer: American society of clinical oncology/college of American Pathologists clinical practice

guideline focused update. *Arch Pathol Lab Med* (2018) 142:1364–82. doi:10.5858/arpa.2018-0902-SA

15. Salgado R, Denkert C, Demaria S, Sirtaine N, Klauschen F, Pruneri G, et al. The evaluation of tumor-infiltrating lymphocytes (TILs) in breast cancer: Recommendations by an international TILs working group 2014. *Ann Oncol* (2015) 26:259–71. doi:10.1093/annonc/mdu450

16. Ding YC, Steele L, Warden C, Wilczynski S, Mortimer J, Yuan Y, et al. Molecular subtypes of tri-ple-negative breast cancer in women of different race and ethnicity. *Oncotarget* (2019) 10:198–208. doi:10.18632/oncotarget.26559

17. Goff SL, Danforth DN. The role of immune cells in breast tissue and immunotherapy for the treatment of breast cancer. *Clin Breast Cancer* (2021) 21:e63–e73. doi:10.1016/j.clbc.2020.06.011

18. Katsuta E, Yan L, Opyrchal M, Kalinski P, Takabe K. Cytotoxic T-lymphocyte infiltration and chemokine predict long-term patient survival independently of tumor mutational burden in triple-negative breast cancer. *Ther Adv Med Oncol* (2021) 13:17588359211006680. doi:10.1177/17588359211006680

19. Chen F, Chen N, Gao Y, Jia L, Lyu Z, Cui J. Clinical progress of PD-1/L1 inhibitors in breast cancer immunotherapy. *Front Oncol* (2022) 11:724424. doi:10.3389/fonc.2021.724424

20. Lian J, Ma HX, Xu EW, Bu P, Yun KM, Xi YF. Subclassifying triple-negative breast cancers and its potential clinical utility. *Virchows Arch* (2022) 481:13–21. doi:10.1007/s00428-022-03329-0

21. Salisbury T, Abozina A, Zhang C, Mao E, Banyi N, Leo J, et al. Histological subtype is associated with PD-L1 expression and CD8+ T-cell infiltrates in triple-negative breast carcinoma. *Ann Diagn Pathol* (2022) 57:151901. doi:10.1016/j.anndiagpath.2022.151901

22. Kim S, Moon BI, Lim W, Park S, Cho MS, Sung SH. Feasibility of classification of triple negative breast cancer by immunohistochemical surrogate markers. *Clin Breast Cancer* (2018) 18:e1123–e1132. doi:10.1016/j.clbc.2018.03.012

23. Kumar S, Bal A, Das A, Bhattacharyya S, Laroiya I, Khare S, et al. Molecular subtyping of triple negative breast cancer by surrogate immunohistochemistry markers. *Appl Immunohistochem Mol Morphol* (2021) 29:251–7. doi:10.1097/PAI.0000000000000897

Pathology & Oncology Research | frontiers

TYPE Original Research
PUBLISHED 03 July 2023
DOI 10.3389/pore.2023.1611224

Check for updates

OPEN ACCESS

EDITED BY
Anna Sebestyén,
Semmelweis University, Hungary

*CORRESPONDENCE
Chunfang Wang,
asangna009@163.com

RECEIVED 04 April 2023
ACCEPTED 14 June 2023
PUBLISHED 03 July 2023

CITATION
Chai J, Liu X, Hu X and Wang C (2023), Correlation analysis of circulating tumor cells and Claudin-4 in breast cancer. *Pathol. Oncol. Res.* 29:1611224. doi: 10.3389/pore.2023.1611224

COPYRIGHT
© 2023 Chai, Liu, Hu and Wang. This is an open-access article distributed under the terms of the Creative Commons Attribution License (CC BY). The use, distribution or reproduction in other forums is permitted, provided the original author(s) and the copyright owner(s) are credited and that the original publication in this journal is cited, in accordance with accepted academic practice. No use, distribution or reproduction is permitted which does not comply with these terms.

Correlation analysis of circulating tumor cells and Claudin-4 in breast cancer

Jie Chai[1], Xiangli Liu[1], Xinju Hu[1] and Chunfang Wang[2]*

[1]Pathology Department, The First Affiliated Hospital of Henan University of Traditional Chinese Medicine, Zhengzhou, China, [2]Breast Surgery, The First Affiliated Hospital of Henan University of Traditional Chinese Medicine, Zhengzhou, China

Objective: We aimed to explore the relationship between peripheral blood circulating tumor cells (CTCs) and the expression of Claudin-4 in patients with breast cancer, and further explore the potential impact on clinical prognosis and risk assessment.

Methods: We classified and enumerated circulating tumor cells in the blood of breast cancer patients by CTC-enriched *in situ* hybridization and the detection of Claudin-4 expression by immunohistochemistry. We carried out an analysis of the correlation between the two and the comparison of their impact on clinical parameters and prognosis.

Results: There were 38 patients with a low expression of Claudin-4 and 27 patients with a high expression of Claudin-4. Compared with Claudin-4 low-expression patients, the number of CTCs was higher in patients with high Claudin-4 expression (11.7 vs. 7.4, $p < 0.001$). High Claudin-4 expression was associated with a lower count of epithelial CTCs (E-CTCs) (3.4 vs. 5.0, $p = 0.033$), higher counts of mesenchymal CTCs (M-CTC) (4.4 vs. 1.1, $p < 0.001$), and epithelial/mesenchymal CTCs (E/M-CTCs) (4.0 vs. 3.5, $p = 0.021$). The intensity of Claudin-4 was positively correlated with CTC ($r_s = 0.43$, $p = 0.001$). Multivariate COX regression analysis showed that CTC counts (HR = 1.3, $p < 0.001$), Claudin-4 (HR = 4.6, $p = 0.008$), and Lymphatic metastasis (HR = 12.9, $p = 0.001$) were independent factors for poor prognosis. COX regression of CTC classification showed that epithelial/mesenchymal CTCs (E/M-CTC) (HR = 1.9, $p = 0.001$) and mesenchymal CTCs (M-CTC) (HR = 1.5, $p = 0.001$) were independent influencing factors of adverse reactions in breast cancer patients.

Conclusion: The number of CTC in breast cancer is positively correlated with the expression of Claudin-4. High CTC counts and a high proportion of M-CTCs correlated with Claudin-4 expression. CTC counts and Claudin-4 expression were independent predictors of poor prognosis in breast cancer patients.

KEYWORDS

breast cancer, circulating tumor cells, tight junction protein, claudin-4, molecular subtype

Introduction

Breast cancer is the most common malignant tumor in women [1, 2]. In 2020, there were an estimated 2,261,419 new breast cancer cases, accounting for 11.7% of the total cancer incidence, surpassing lung cancer and becoming the leading cause of cancer death among women [2]. Early (or operable) and non-inflammatory locally advanced inoperable breast cancers are considered potentially curable, but the prognosis is better with lower stages [3–6], emphasizing the need for screening and early detection [7, 8].

Several countries have breast cancer screening programs based on mammography, and these programs are associated with a 15%–30% decrease in breast cancer-related mortality but not in overall mortality [8–10]. Breast cancer screening programs are mainly based on mammography, and their sensitivity and specificity remain relatively low, leading to several false-positive and false-negative results [8–11]. Therefore, it is particularly important to find highly sensitive indicators of prognosis and recurrent risks of breast cancer [12].

A small amount of circulating tumor cells (CTCs) in peripheral blood can escape the tumor after the epithelial-mesenchymal transition [13]. In addition, monitoring peripheral blood CTCs could fill the diagnostic gap in tumors <5 mm [14]. The monitoring of CTCs is convenient and conducive to the early diagnosis and prognosis evaluation of breast cancer [15, 16]. They act as seeds for metastases and can be classified as epithelial type (E-CTC), mesenchymal type (M-CTC), or intermediate (E/M-CTC) with a transition from epithelial to mesenchymal phenotype. These subtypes can be distinguished based on the expression of surface markers. Claudin-4 is a tight junction protein family member and mainly regulates tight junctions [17]. Therefore, Claudin-4 plays an important role in the occurrence and metastasis of cancer cells [18]. Studies have shown that Claudin-4 is highly expressed in various malignant tumors [19], suggesting that Claudin-4 may become a tumor marker and an emerging target for treatment [20–22]. Claudin-4 has been reported to regulate EMT through p21-activated kinase 4 (PAK4) expression in human breast cancer cells [23]. However, the relationship between CTCs and Claudin-4 in breast cancer is unclear.

Therefore, we speculate that Claudin-4 may be involved in the EMT process by altering CTC numbers and typing. This study aimed to explore the relationship between peripheral blood CTCs and the expression of Claudin-4 in patients with breast cancer and their relationship with the survival and prognosis of breast cancer patients.

Methods

Study design and patients

This cross-sectional study included patients who underwent routine surgical resection and were pathologically confirmed as having breast cancer at the First Affiliated Hospital of Henan University of Traditional Chinese Medicine between January 2018 and December 2020. This study was approved by the ethics committee of the First Affiliated Hospital of Henan University of Traditional Chinese Medicine. The requirement for informed consent was waived due to the retrospective nature of the study. The inclusion criteria were: 1) available clinical data, 2) diagnosis of breast cancer and available tissue specimens, and 3) available peripheral blood samples. The exclusion criteria were: 1) incomplete clinical data or 2) recipient of neoadjuvant treatments.

Data collection

The demographic and clinical data of the patients were collected, including age, sex, lymph node metastasis, carcinogenic molecular detection, pathological type, tumor size, and Ki-67 expression. Molecular subtypes included Luminal A, Luminal B, human epidermal growth factor receptor-2 (HER-2) amplification, and basal-like. Luminal A type showed estrogen-receptor (ER) positive or progesterone-receptor (PR) positive and PR high expression (≥20%), HER2 negative, or Ki-67 low expression (<14%). Luminal (luminal or hormone receptor-positive) type B was divided into two subtypes, Luminal B (HER-2 negative) and Luminal B (HER-2 positive): Luminal B (HER-2 negative): ER and/or PR positive, HER-2 negative, and high expression of Ki-67 (greater than or equal to 14%). Luminal B (HER-2 positive): ER and/or PR positive, HER- 2 overexpression or proliferation, and any level of Ki-67. HER-2 amplification type, also known as HER2 positive (non-Luminal) type, showed ER and PR deletion, HER-2 overexpression or proliferation, and any level of Ki-67. Basal-like breast cancers have low expressions of ER, PR, and HER2 and high expressions of markers of breast basal or myoepithelial cells, such as caveolin-1, p63.

CTC detection

Peripheral venous blood (5 mL) was collected from an antecubital vein using a vacuum EDTA anticoagulant tube and transferred to a sample storage tube. The tube was inverted >10 times and incubated at 15°C–30°C for 30 min to lyse the cells. The blood was centrifuged at 1850 rpm for 5 min. The supernatant was discarded, and 4 mL of PBS and 1 mL of RI fixative solution were added, vortexed, and let to stand for 8 min at room temperature. The liquid was poured into the filter connected to a vacuum pump with a negative pressure of −0.06 MPa. The fixative (1 mL) was added for 1 h. The membrane was dehydrated with gradient alcohol to capture the cells. Labels for EP-CAM, CK8, and CK8/18 (as epithelial

markers) and Vimentin (as mesenchymal markers) produced by CanPatrol Biotechnology Co., Ltd. were used for mRNA fluorescence *in situ* hybridization. Fluorescence from any of the epithelial/mesenchymal makers are indicative of epithelial/mesenchymal-type circulating tumor cells. The membrane was scanned, and the count of each type of cell was analyzed using Isis5 and Metafer3 fluorescence analysis software produced by German Midas. Red fluorescence represented epithelial-type CTCs (E-CTC), green fluorescence represented mesenchymal-type CTCs (M-CTC), and both red and green represented mixed-type CTCs (E/M-CTC).

Immunohistochemistry

The postoperative specimens were fixed in 10% formalin, dehydrated, paraffin-embedded, and serially cut into 4-μm sections. After dewaxing and rehydrating, the sections were put into ethylenediaminetetraacetic acid (EDTA) solution (pH 8.0) produced by Beijing Soleibao Technology Co., Ltd. at 100°C for 20 min. The endogenous peroxidase activity was blocked with 3% H_2O_2 for 10 min. After rinsing with phosphate buffer solution (PBS), the sections were incubated with an anti-rabbit primary antibody for Claudin-4 (Shanghai Jiehao Biotechnology Technology Co., Ltd., CRM-1251) at 37°C for 1 h. After washing with PBS, the sections were incubated with the secondary antibody (Roche Shanghai Co., Ltd., J19565) and rinsed**.** The sections were revealed with diaminobenzidine (DAB), stained with hematoxylin, dehydrated, and mounted. The cells were counted in 10 randomly selected visual fields at ×400 magnification. For number scoring, <5% of positive cells were scored zero, 5%–25% was one, 26%–50% was two, and >50% was three. For intensity scoring, no staining was zero, light yellow was one, brown was two, and tan was three. The number and intensity scores were multiplied; zero points were negative, one to two represented 1+, three to four represented 2+, and five to six represented 3+. Claudin-4 negative and Claudin-4 1+ were considered low expressions. Claudin-4 2+ and 3+ were considered high expressions. The scores were determined by two pathologists with 10 years of experience, and the average value was taken as the final result.

Follow-up

The patients were followed up every 2 months by telephone contact after enrollment. Patients' vital signs and disease progression were recorded. If necessary, the patients were admitted to the hospital to evaluate their progress. The expected follow-up time was 24 months. The follow-up endpoint was all-cause death. The follow-up deadline was 30 October 2020.

TABLE 1 Characteristics of the patients and CTC counts.

Pathological parameters	Number of cases (%) n = 65
Age (years)	
<50	34 (52.3)
≥50	31 (47.7)
Lymph node metastasis	
No	44 (67.7)
Yes	21 (32.3)
Molecular subtype	
Luminal A	7 (10.8)
Luminal B	42 (64.6)
Her-2 amplification	12 (18.5)
Basal-like	4 (6.2)
Pathological type	
Invasive cancer	51 (78.5)
Ductal carcinoma *in situ*	14 (21.5)
Size (cm)	
<5	48 (73.9)
≥5	17 (26.2)
Ki-67 (%)	
<14	12 (18.5)
≥14	53 (81.5)

CTC, circulating tumor cells; SD, standard deviation.

Statistical analysis

All data were analyzed using SPSS 20.0 (IBM, Armonk, NY, United States). Continuous data were expressed as means ± standard deviation and analyzed using Student's t-test. Categorical data were presented as n (%) and analyzed using the chi-square test. The relationship between CTCs and Claudin-4 expression was analyzed using Spearman rank correlation and the Kaplan-Meier method was used to draw the survival curve. Log-rank test was used to compare the differences. A Multivariate COX risk regression model was established to analyze the independent adverse factors of prognosis. The statistical analysis of the data from two groups was performed using a t-test. The comparisons of multiple groups were performed by one-way ANOVA and then an LSD-t test. $p < 0.05$ was considered to be significant. Two-sided p-values < 0.05 were considered statistically significant.

Results

Characteristics of the patients

Sixty-five breast cancer patients, 39 to 61 (median, 49) years of age, were included. All patients were women, including 51 with

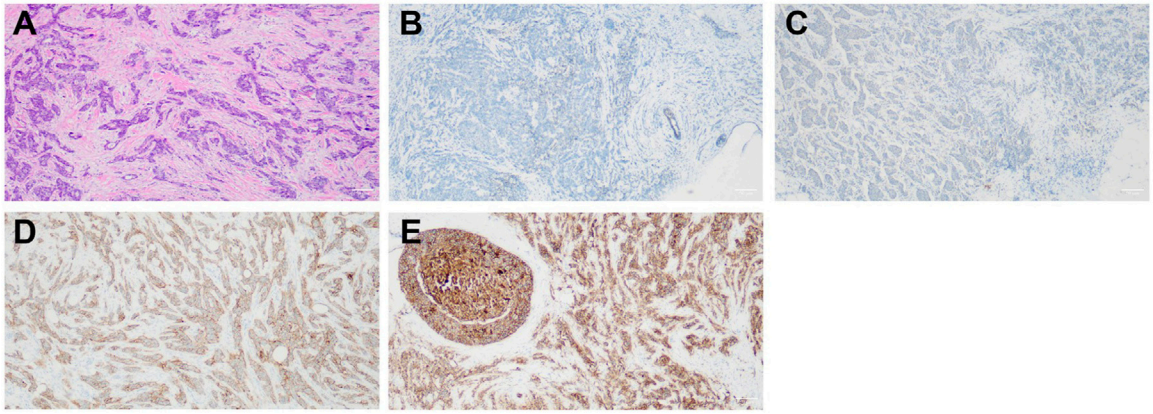

FIGURE 1
(A) Non-specific invasive carcinoma with HE staining (×100). **(B)** Non-specific invasive carcinoma with negative claudin-4 (SP ×100). **(C)** Non-specific invasive carcinoma claudin-4 (+, SP ×100). **(D)** Non-specific invasive carcinoma claudin-4 (2+, SP ×100). **(E)** Non-specific invasive carcinoma claudin-4 (3+, SP ×100).

TABLE 2 Comparison of Claudin-4 in patients' age, lymph node metastasis, and molecular classification.

Pathological parameters	Claudin-4 low n = 38	Claudin-4 high n = 27	p
Age (years)			
<50	19 (50.0)	15 (55.55)	0.659
≥50	19 (50.0)	12 (44.44)	
Lymph node metastasis			
No	32 (84.2)	12 (44.4)	<0.001
Yes	6 (15.8)	15 (55.6)	
Molecular			
Luminal A	3 (7.9)	4 (14.8)	0.760
Luminal B	25 (65.8)	17 (63.0)	
Her-2 amplification	8 (21.1)	4 (14.8)	
Basal-like	2 (5.3)	2 (7.4)	
Pathological type			
Invasive cancer	32 (84.2)	19 (70.4)	0.181
Ductal carcinoma *in situ*	6 (15.8)	8 (29.6)	
Size (cm)			
<5	35 (92.1)	13 (48.1)	<0.001
≥5	3 (7.9)	14 (51.9)	
Ki-67 (%)			
<14	6 (15.8)	6 (22.2)	0.510
≥14	32 (84.2)	21 (77.8)	

invasive carcinoma and 14 cases of ductal carcinoma *in situ*. There were 48 patients with a tumor <5 cm and 17 with a tumor >5 cm. There were 21 patients with lymph node metastasis and 44 without. There were 12 patients with Ki-67 < 14% and 53 with Ki-67 ≥ 14% (Table 1).

Claudin-4

Among the 65 patients, there were 11 Claudin-4-negative tumors, 27 with Claudin-4 +, 22 with Claudin-4 2+, and five with Claudin-4 3+ (Figure 1). Most patients with high Claudin-4

TABLE 3 Relationship between CTCS and pathological parameters in patients with breast cancer.

Pathological parameters	Number of cases (%) $n = 65$	CTC count ($x \pm s$)	p
Age (years)			
<50	34 (52.4)	9.08 ± 2.63	<0.001
≥50	31 (47.6)	11.77 ± 2.31	
Lymph node metastasis			
No	44 (67.7)	6.59 ± 2.28	<0.001
Yes	21 (32.3)	11.23 ± 1.54	
Molecular			
Luminal A	7 (10.7)	10.14 ± 2.11	<0.001
Luminal B	42 (64.6)	11.33 ± 2.56	
Her-2 amplification	12 (18.5)	8.58 ± 2.07	
Basal-like	4 (6.1)	6.08 ± 1.82	
Pathological type			
Invasive cancer	51 (78.5)	11.8 ± 2.82	0.334
Ductal carcinoma *in situ*	14 (21.5)	10.71 ± 2.52	
Size (cm)			
<5	48 (73.8)	11.41 ± 2.92	0.755
≥5	17 (26.2)	11.10 ± 2.18	
Ki-67 (%)			
<14	12 (18.5)	11.67 ± 2.49	0.694
≥14	53 (81.5)	11.31 ± 2.89	

expression had lymph node metastasis (55.6% vs. 15.8%, $p < 0.001$ vs. without low Claudin-4 expression). Most patients with high Claudin-4 expression had a tumor >5 cm (51.9% vs. 7.9%, $p < 0.001$ vs. low Claudin-4 expression) (Table 2).

Circulating tumor cells

CanPatrol CTC enrichment and *in situ* hybridization were used to monitor the number and classification of CTC in the blood of 65 patients. Red fluorescence was used to represent epithelial CTC, and green fluorescence was used to represent interstitial CTC. CTC was divided into epithelial type (E-CTC), mixed type (E/M-CTC), and interstitial type (M-CTC). The number of CTCs in patients aged ≥50 was significantly high (11.8 vs. 9.1, $p < 0.001$ vs. Age < 50). The number of CTCs in patients with lymph node metastasis was high (11.2 vs. 6.5, $p < 0.001$ vs. without lymph node metastasis). There are significant differences in the number of CTCs in different molecular types of breast cancer ($p < 0.001$) (Table 3).

Circulating tumor cells and Claudin-4

The number of CTCs was higher in patients with high Claudin-4 expression (11.7 vs. 7.4, $p < 0.001$). A more detailed analysis revealed that a high Claudin-4 expression was associated with a lower count of E-CTCs (3.4 vs. 5.0, $p = 0.033$) but high counts of E/M-CTCs (5.0 vs. 3.5, $p = 0.021$) and M-CTCs (4.4 vs. 1.1, $p < 0.001$) (Table 4 and Figure 2). Spearman correlation analysis showed that the intensity of Claudin-4 was positively correlated with CTC ($r_s = 0.43$, $p = 0.001$) (Figure 3).

Correlation analysis between CTC classification and lymph node metastasis

E-CTC in breast cancer patients with lymph node metastasis was significantly higher than that in the lymph node metastasis group (3.4 vs. 1.4, $p < 0.001$). E/M-CTC was significantly lower than that in the lymph node metastasis group (1.5 vs. 4.3, $p = 0.002$), and the M-CTC count was lower than that in the lymph node metastasis group (1.6 vs. 6.4, $p < 0.001$) (Table 5).

Survival analysis of Claudin-4 expression level cancer

By the last follow-up, the average survival time of 65 patients with high expressions of Claudin-4 ($n = 27$) was 18.22 months, and the average survival time of the low-expression group ($n =$

TABLE 4 Comparison of Claudin-4 in patient CTC types.

CTC types (/mL)	Claudin-4 low (n = 38)	Claudin-4 high (n = 27)	p
Total CTC	7.42 ± 2.23	11.70 ± 2.35	<0.001
E-CTC	4.97 ± 3.04	3.41 ± 2.57	0.033
E/M-CTC	3.50 ± 2.83	4.04 ± 2.17	0.021
M-CTC	1.12 ± 1.94	4.41 ± 2.11	<0.001

CTC, circulating tumor cells; E, epithelial; M, mesenchymal.

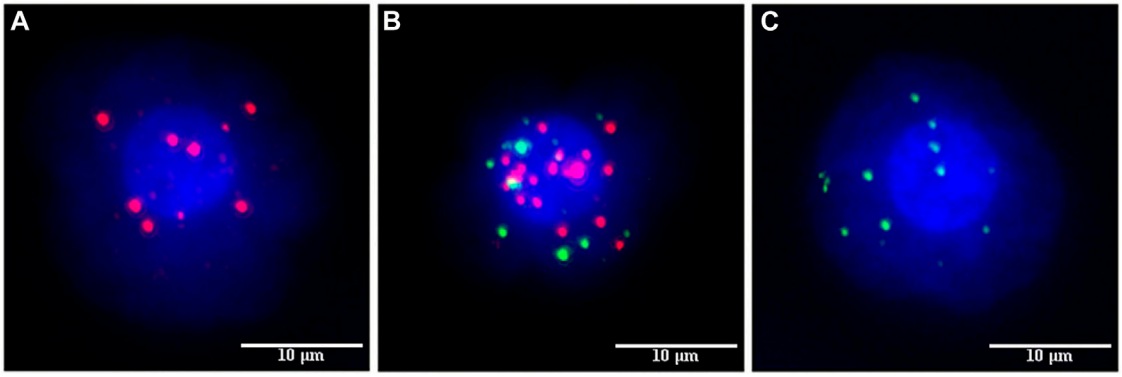

FIGURE 2
Fluorescence marking different types of circulating tumor cells (CTCs). **(A)** EPCAM, CK8, and cK8/18 epithelial fluorescent markers emit red fluorescence to label epithelial circulating tumor cells. **(B)** Hybrid circulating tumor cells were labeled with both red and green fluorescence. **(C)** Vimentin mesenchymal fluorescent marker emits green fluorescence to label mesenchymal circulating tumor cells.

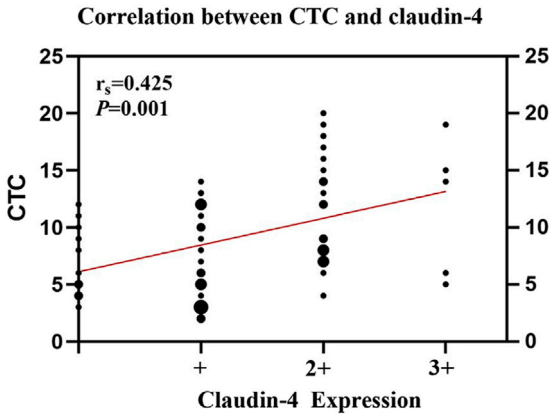

FIGURE 3
Spearman rank correlation analysis between circulating tumor cells (CTCs) and Claudin-4 expression.

38) was 21.81 months. The survival rate of the high-expression group was significantly lower than that of the low-expression group (Log Rank X^2 = 4.71, p = 0.030) (Figure 4).

A multivariate COX regression analysis model was constructed

The results showed that CTC counts (HR = 1.3, p < 0.001), Claudin-4 (HR = 4.6, p = 0.008), and lymph node metastasis (HR = 12.9, p = 0.001) were independent prognostic factors for poor prognosis (Table 6).

The COX risk regression model of CTC classification and prognosis of breast cancer patients was constructed

Our analysis showed that E/M-CTC (HR = 1.9, p = 0.001) and M-CTC (HR = 1.5, p = 0.001) were independent influencing factors of poor prognosis in breast cancer patients (Table 7).

Discussion

Breast cancer with metastases can reduce survival rates, so markers for early diagnosis and prognostic monitoring are urgently needed for breast cancer patients. Based on this

TABLE 5 The relationship between the type of CTC and Lymph node metastasis.

CTC types (/mL)	No lymph node metastasis (n = 44)	Lymph node metastasis (n = 21)	p
E-CTC	3.37 ± 1.67	1.41 ± 1.01	<0.001
E/M-CTC	1.58 ± 1.40	4.33 ± 1.71	0.002
M-CTC	1.62 ± 2.61	6.45 ± 2.44	<0.001

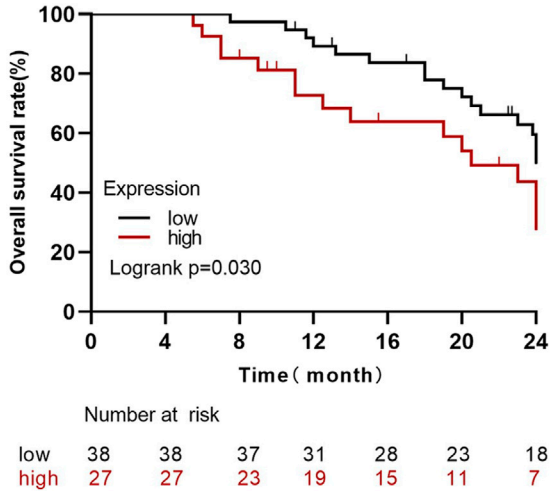

FIGURE 4
Survival analysis of Claudin-4 expression level and prognosis of breast cancer.

study, we can explore the prognosis of patients by assessing the expression of Claudin-4 and circulating tumor cells in peripheral blood.

The results showed that the CTC count and classification in breast cancer are associated with the expression of Claudin-4. The results may help define novel molecular targets for the early diagnosis and prognosis of breast cancer. Future studies should examine the diagnostic and prognostic values of CTCs and Claudin-4 in breast cancer patients.

Claudins are the most important structural and functional component of tight junction transmembrane proteins and can maintain cell-to-cell molecular flow and cell polarity [24]. Claudins are overexpressed or silenced in pancreatic cancer, colon cancer, ovarian cancer, breast cancer, and other solid tumors [25]. In particular, Claudin-4 can directly or indirectly promote tumor metastasis through the second extracellular loop structure [26]. The changes in the expression of Claudin-4 can modify the structure of the tight junctions and adhesion between cells, leading to tumor metastasis and spread [27]. Claudin-4 is overexpressed in ovarian and breast cancers [28]. Kolokytha et al. [29] showed that the positive expression of Claudin-4 in triple-negative breast cancer might be a marker of good prognosis. Radi et al. [30] showed that Claudin-4 was related to the expression of D240 (a lymphatic vessel marker) in prostate cancer, and Claudin-4 is associated with lymph node metastasis and a marker of poor prognosis. Moreover, the present study also confirmed that the expression level of Claudin-4 was associated with lymph node metastasis and tumors ≥5 cm, suggesting that higher Claudin-4 expression may be associated with a poor prognosis in breast cancer. In our study, Claudin-4 was poorly significantly associated with molecular subtypes of breast cancer, and Sara Ricardo's study showed that a single IHC for Claudin-4 is not sufficient to assess and identify molecular subtypes of breast cancer and that additional markers, such as CSC (cancer stem cell) markers, are needed to improve subgroup identification [31]. The survival time of the Claudin-4 high-expression group was significantly lower than that of the low-expression group, and a multivariate COX regression model was established to find that high expression of Claudin-4 was an independent factor affecting the poor prognosis of breast cancer.

The present study showed that the number of E/M-CTC and M-CTC in the lymph node metastasis group was higher than that in the lymph node non-metastasis group and the numbers of CTCs in the high Claudin-4 group were higher than in the low expression level group, mainly due to the E/M- and M-CTCs since the E-CTCs were lower in the high Claudin-4 group. These results suggest that Claudin-4 is involved in EMT

TABLE 6 Multivariate COX regression risk model.

Factors	B	SE	Wald	P	HR (95% CI)
Total CTC	0.25	0.06	18.13	<0.001	1.29 (1.147–1.450)
Claudin-4 (low vs. high)	1.53	0.57	7.14	0.008	4.6 (1.504–14.248)
Lymphatic metastasis (-vs +)	2.55	0.49	27.44	0.001	12.86 (4.945–33.431)

TABLE 7 Multivariate COX regression model of CTC typing.

Factors	*B*	SE	Wald	*P*	HR (95% CI)
E-CTC	0.19	0.24	0.71	0.400	1.22 (0.768–1.936)
E/M-CTC	0.66	0.19	11.46	0.001	1.93 (1.319–2.827)
M-CTC	0.40	0.12	11.62	0.001	1.49 (1.186–1.883)

and tumor metastasis and recurrence. The Spearman correlation analysis also showed that CTCs in peripheral blood were positively correlated with the expression level of Claudin-4. The Multivariate COX regression model showed that Claudin-4, lymph node metastasis, and CTC classification E/M-CTC and M-CTC were adverse factors for the prognosis of breast cancer patients. Therefore, both Claudin-4 and CTC might be used to evaluate the prognosis and recurrence risk of patients with breast cancer. Meanwhile, the high expression of Claudin-4 might regulate or be regulated by the tumor EMT process, but the present study could not determine cause-to-effect relationships.

This study has limitations. It was a single-center study with a small sample size. Only CTCs and Claudin-4 were examined. Future studies should look at the correlations of multiple biomarkers and in-depth mechanism research to help personalize the prognosis of breast cancer. It was a cross-sectional study, and cause-to-effect relationships could not be determined.

In conclusion, CTC count and classification in breast cancer are associated with the expression of Claudin-4. CTC count and classification and the expression level of Claudin-4 may be used for the early diagnosis and prognosis of breast cancer. Future large studies should attempt to investigate the diagnostic and prognostic value of CTCs and claudin-4 in breast cancer patients.

Data availability statement

The original contributions presented in the study are included in the article/supplementary material, further inquiries can be directed to the corresponding author.

Ethics statement

This study was approved by the ethics committee of the First Affiliated Hospital of Henan University of Traditional Chinese Medicine. The requirement for informed consent was waived due to the retrospective nature of the study.

Author contributions

Material preparation, data collection, and analysis were performed by JC, XL, and XH. The first draft of the manuscript was written by CW. All authors contributed to the article and approved the submitted version.

Conflict of interest

The authors declare that the research was conducted in the absence of any commercial or financial relationships that could be construed as a potential conflict of interest.

Acknowledgments

The authors acknowledge the help of the breast surgery department of our hospital.

References

1. Siegel RL, Miller KD, Fuchs HE, Jemal A. Cancer statistics, 2022. *Ca: A Cancer J Clin* (2022) 72(1):7–33. doi:10.3322/caac.21708

2. Sung H, Ferlay J, Siegel RL, Laversanne M, Soerjomataram I, Jemal A, et al. Global cancer statistics 2020: Globocan estimates of incidence and mortality worldwide for 36 cancers in 185 countries. *Ca: A Cancer J Clin* (2021) 71(3): 209–49. doi:10.3322/caac.21660

3. Harbeck N, Gnant M. Breast cancer. *Lancet* (2017) 389(10074):1134–50. doi:10.1016/s0140-6736(16)31891-8

4. Senkus E, Kyriakides S, Ohno S, Penault-Llorca F, Poortmans P, Rutgers E, et al. Primary breast cancer: Esmo clinical practice guidelines for diagnosis, treatment and follow-up. *Ann Oncol* (2015) 26(5):v8–30. doi:10.1093/annonc/mdv298

5. Cardoso F, Costa A, Senkus E, Aapro M, André F, Barrios CH, et al. 3rd ESO-ESMO international consensus guidelines for advanced breast cancer (ABC 3). *Ann Oncol* (2017) 28(1):16–33. doi:10.1093/annonc/mdw544

6. Nccn Clinical Practice Guidelines in Oncology (Nccn Guidelines). *Breast cancer*. Version 2.2022. Fort Washington: National Comprehensive Cancer Network (2021).

7. Nccn Clinical Practice Guidelines in Oncology (Nccn Guidelines). *Breast cancer risk reduction*. Version 1.2022. Fort Washington: National Comprehensive Cancer Network (2022).

8. Nccn Clinical Practice Guidelines in Oncology (Nccn Guidelines). *Breast cancer screening and diagnosis*. Version 1.2021. Fort Washington: National Comprehensive Cancer Network (2021).

9. Gøtzsche PC, Jørgensen KJ. Screening for breast cancer with mammography. *Cochrane Database Syst Rev* (2013) 2013(6):Cd001877. doi:10.1002/14651858

10. Myers ER, Moorman P, Gierisch JM, Havrilesky LJ, Grimm LJ, Ghate S, et al. Benefits and harms of breast cancer screening: A systematic review. *Jama* (2015) 314(15):1615–34. doi:10.1001/jama.2015.13183

11. Nelson HD, Fu R, Cantor A, Pappas M, Daeges M, Humphrey L. Effectiveness of breast cancer screening: Systematic review and meta-analysis to update the 2009 U.S. Preventive services task force recommendation. *Ann Intern Med* (2016) 164(4):244–55. doi:10.7326/m15-0969

12. Liu X, Tang JH, Wang MS. Expression of claudin-4 in human breast cancer tissue and clinical significance. *J Jainan Med Coll* (2014) 20(12):1607–13. doi:10.13210/j.cnki.jhmu.20140926.005

13. Li R, Gong Z, Liu Y, Zhao X, Guo SJNF. Detection of circulating tumor cells and single cell extraction Technology: Principle, effect and application prospect. *Futures* (2021) 5(3):032002. doi:10.1088/2399-1984/ac1325

14. Wu F, Zhao J, Zhang X. Comparison of value of circulating tumor cells and tumor markers in lung cancer diagnosis. *Int J Inspection Med* (2020) 41(5):527–31. doi:10.3969/j.issn.1673-4130.2020.05.004

15. Thery L, Meddis A, Cabel L, Proudhon C, Latouche A, Pierga JY, et al. Circulating tumor cells in early breast cancer. *JNCI Cancer Spectr* (2019) 3(2): pkz026. doi:10.1093/jncics/pkz026

16. Zhang H, Lin X, Huang Y, Wang M, Cen C, Tang S, et al. Detection methods and clinical applications of circulating tumor cells in breast cancer. *Front Oncol* (2021) 11:652253. doi:10.3389/fonc.2021.652253

17. Luo L, Ma GR, Liu FG. Expression and clinical significance of tight junction proteins 1,3 and 4 in breast cancer patients. *J Difficult Dis* (2017) 16(06):610. doi:10.3969/j.issn.1671-6450.2017.06.017

18. Lee KW, Lee NK, Kim JH, Kang MS, Yoo HY, Kim HH, et al. Twist1 causes the transcriptional repression of claudin-4 with prognostic significance in esophageal cancer. *Biochem Biophys Res Commun* (2012) 423(3):454–60. doi:10.1016/j.bbrc.2012.05.140

19. Xiang RL, Su YC, Pei XQ. Progress in functions of tight junction protein claudin-4. *Sheng Li Ke Xue Jin Zhan [Progress Physiol]* (2012) 43(4):310–4. doi:10.3969/j.issn.0559-7765

20. Abd-Elazeem MA, Abd-Elazeem MA. Claudin 4 expression in triple-negative breast cancer: Correlation with androgen receptors and ki-67 expression. *Ann Diagn Pathol* (2015) 19(1):37–42. doi:10.1016/j.anndiagpath.2014.10.003

21. Luo Y, Kishi S, Sasaki T, Ohmori H, Fujiwara-Tani R, Mori S, et al. Targeting claudin-4 enhances chemosensitivity in breast cancer. *Cancer Sci* (2020) 111(5): 1840–50. doi:10.1111/cas.14361

22. Duarte GM, Almeida NR, Tocchet F, Espinola J, Barreto CTR, Pinto GA, et al. Claudin-4 expression is associated with disease-free survival in breast carcinoma-*in-situ*: Mean follow-up of 8.2 years. *Clin Breast Cancer* (2018) 18(5):e1111–6. doi:10.1016/j.clbc.2018.06.005

23. Wang F, Gao Y, Tang L, Ning K, Geng N, Zhang H, et al. A novel pak4-cebpb-cldn4 Axis involving in breast cancer cell migration and invasion. *Biochem Biophys Res Commun* (2019) 511(2):404–8. doi:10.1016/j.bbrc.2019.02.070

24. Singh AB, Dhawan P. Claudins and cancer: Fall of the soldiers entrusted to protect the gate and keep the barrier intact. *Semin Cel Dev Biol* (2015) 42:58–65. doi:10.1016/j.semcdb.2015.05.001

25. Tabariès S, Siegel PM. The role of claudins in cancer metastasis. *Oncogene* (2017) 36:1176–90. doi:10.1038/onc.2016.289

26. Webb PG, Spillman MA, Baumgartner HK. Claudins play a role in normal and tumor cell motility. *BMC Cel Biol* (2013) 14:19. doi:10.1186/1471-2121-14-19

27. Escudero-Esparza A, Jiang WG, Martin TA. The claudin family and its role in cancer and metastasis. *Front Biosci (Landmark Edition)* (2011) 16(3):1069–83. doi:10.2741/3736

28. Fabisiewicz A, Szostakowska-Rodzos M, Zaczek AJ, Grzybowska EA. Circulating tumor cells in early and advanced breast cancer; biology and prognostic value. *Int J Mol Sci* (2020) 21(5):1671. doi:10.3390/ijms21051671

29. Kolokytha P, Yiannou P, Keramopoulos D, Kolokythas A, Nonni A, Patsouris E, et al. Claudin-3 and claudin-4: Distinct prognostic significance in triple-negative and luminal breast cancer. *Appl Immunohistochem Mol Morphol* (2014) 22(2): 125–31. doi:10.1097/PAI.0b013e31828d9d62

30. Radi DA, Abd-Elazeem MA. Prognostic significance of lymphatic vessel density detected by D2-40 and its relation to claudin-4 expression in prostatic adenocarcinoma. *Int J Surg Pathol* (2016) 24(3):219–26. doi:10.1177/1066896915611488

31. Ricardo S, Gerhard R, Cameselle-Teijeiro JF, Schmitt F, Paredes J. Claudin expression in breast cancer: High or low, what to expect? *Histol Histopathol* (2012) 27(10):1283–95. doi:10.14670/hh-27.1283

Pathology & Oncology Research | frontiers

TYPE Review
PUBLISHED 06 February 2024
DOI 10.3389/pore.2024.1611549

Check for updates

OPEN ACCESS

EDITED BY
Hajnalka Rajnai,
Semmelweis University, Hungary

*CORRESPONDENCE
Yue Chen,
chenyue@bjsjth.cn,
chenyue8249@163.com

RECEIVED 13 October 2023
ACCEPTED 16 January 2024
PUBLISHED 06 February 2024

CITATION
Dai J, Jiang Y, Hu H, Zhang S and Chen Y (2024), Extracellular vesicles as modulators of glioblastoma progression and tumor microenvironment. *Pathol. Oncol. Res.* 30:1611549. doi: 10.3389/pore.2024.1611549

COPYRIGHT
© 2024 Dai, Jiang, Hu, Zhang and Chen. This is an open-access article distributed under the terms of the Creative Commons Attribution License (CC BY). The use, distribution or reproduction in other forums is permitted, provided the original author(s) and the copyright owner(s) are credited and that the original publication in this journal is cited, in accordance with accepted academic practice. No use, distribution or reproduction is permitted which does not comply with these terms.

Extracellular vesicles as modulators of glioblastoma progression and tumor microenvironment

Jie Dai[1], Yong Jiang[2], Haoyue Hu[3], Shuang Zhang[4] and Yue Chen[4]*

[1]Department of Pathology, Sichuan Clinical Research Center for Cancer, Sichuan Cancer Hospital & Institute, Sichuan Cancer Center, Affiliated Cancer Hospital of University of Electronic Science and Technology of China, Chengdu, China, [2]Department of Neurosurgery, Sichuan Clinical Research Center for Cancer, Sichuan Cancer Hospital & Institute, Sichuan Cancer Center, Affiliated Cancer Hospital of University of Electronic Science and Technology of China, Chengdu, China, [3]Department of Medical Oncology, Sichuan Clinical Research Center for Cancer, Sichuan Cancer Hospital & Institute, Sichuan Cancer Center, Affiliated Cancer Hospital of University of Electronic Science and Technology of China, Chengdu, China, [4]Department of Pathology, Beijing Shijitan Hospital, Capital Medical University, Beijing, China

Glioblastoma is the most aggressive brain tumor with extremely poor prognosis in adults. Routine treatments include surgery, chemotherapy, and radiotherapy; however, these may lead to rapid relapse and development of therapy-resistant tumor. Glioblastoma cells are known to communicate with macrophages, microglia, endothelial cells, astrocytes, and immune cells in the tumor microenvironment (TME) to promote tumor preservation. It was recently demonstrated that Glioblastoma-derived extracellular vesicles (EVs) participate in bidirectional intercellular communication in the TME. Apart from promoting glioblastoma cell proliferation, migration, and angiogenesis, EVs and their cargos (primarily proteins and miRNAs) can act as biomarkers for tumor diagnosis and prognosis. Furthermore, they can be used as therapeutic tools. In this review, the mechanisms of Glioblastoma-EVs biogenesis and intercellular communication with TME have been summarized. Moreover, there is discussion surrounding EVs as novel diagnostic structures and therapeutic tools for glioblastoma. Finally, unclear questions that require future investigation have been reviewed.

KEYWORDS

extracellular vesicles, tumor microenvironment, glioblastoma, exosomes, microvesicles

Introduction

Gliomas are common central nervous system (CNS) tumors that are classified according to morphology and molecular characteristics, graded according to malignancy. The World Health Organization (WHO) has classified gliomas into the four subtypes of grades I-IV as per histopathological standards [1]. Glioblastoma is the

most malignant form of glioma, with an incidence of 0.59–3.69 per 100,000 people per year worldwide. Glioblastoma is considered the most fatal brain tumor in adults owing to its poor prognosis, with a median survival of 14–16 months after diagnosis despite receiving standard therapy and care [2]. With the development of the CNS 5th WHO standard, molecular tests have been included the classification criteria [3]. In the latest 5th WHO brain tumor classification, the previous use of the term primary glioblastoma was re-characterized as grade IV astrocytoma (IDH-wildtype), whereas secondary glioblastoma was re-characterized as grade IV astrocytoma (IDH-mutant) [4].

At present, many therapies for glioblastoma have failed to improve outcomes, including surgical tumor resection, temozolomide (TMZ) chemotherapy and radiation therapy, and immunotherapeutic approaches, with <5% patients surviving past 5 years [5, 6]. Glioblastoma heterogeneity (intra- and intertumoral), resistance, and insufficient tumor microenvironment (TME) understanding are critical challenges influencing effective therapy development [7–9]. Therefore, specific mechanisms that affect treatment and prognosis as well as new therapies need to be identified and investigated.

The TME includes components from the tumor niche and extracellular components surrounding tumor cells. The TME generally comprises tumor cells, extracellular matrix (ECM), blood vessels, and tumor-infiltrating immune cells (monocytes, macrophages, neutrophils, T cells, and others) [10]. However, the glioblastoma TME displays particular heterogeneity and complexity, and, in addition to the abovementioned components, contains resident microglia (constituting 30%–50% of the cellular content), neurons, astrocytes, oligodendrocytes, Glioblastoma stem cells (GSCs), and endothelial and vascular pericytes [11].

The TME favors tumor growth, invasion, angiogenesis, and immunosuppression in glioblastoma, which benefits from the communication between glioblastoma cells and the surrounding non-tumor cells [12]. This process involves multiple modes of communication, including direct cell-to-cell contact, soluble factors (chemokines, cytokines, and growth factors), and extracellular vesicles (EVs) [13]. EVs are different cell-derived membranous structures surrounded by a phospholipid bilayer membrane that encapsulates various signaling molecules, such as dsDNA fragments, RNA variants, proteins, lipids, and metabolites [14]. EVs have been detected in different human CNS diseases, including Alzheimer's disease, Parkinson's disease, and brain tumors, making them an area of interest and ongoing field of research during the last few years [15]. Glioma derived-EVs have a profound effect on the activity and synchrony of neuronal networks, though the specific mechanism has not been addressed sufficiently [16]. Moreover, brain metastases-derived EVs (Br-EVs) trigger low-density lipoprotein aggregation, which accelerates Br-EVs uptake by monocytes (key components in the brain metastatic niche) [17]. Several studies have shown that EVs are a potential source of new biomarkers, relevant to novel targeted therapeutics, or drug delivery materials for many tumors [18].

This review explores the biological functions of EVs and the mechanistic interactions between glioblastoma cells and TME via EVs. In addition, the potential role of EVs in the antitumor effects against glioblastoma has been discussed and explored.

Biogenesis and isolation methods of EVs

EVs can be classified into three subclasses based on their origin and/or size: exosomes (50–90 nm in diameter), microvesicles (100–1,000 nm in diameter), and apoptotic bodies (100–5,000 nm in diameter) [19, 20]. Exosomes, small vesicles of endocytic origin, were first proposed in 2012 as a protective envelope for viable blood microRNAs (miRNAs) [21]. By contrast, microvesicles, also known as ectosomes, are larger molecules that are produced from a cell via direct external budding, whereas apoptotic bodies are produced in the form of blebs during programmed cell death [21, 22]. The specific biogenesis mechanisms of these EVs, which are still being investigated, are different.

Biogenesis of exosomes

Exosomes are formed via an invagination of the endosomal plasma membrane and first divided into three compartments: early, recycling, and late endosomes [23]. Late endosomes subsequently accumulate to form intraluminal vesicles (ILVs) contained in multivesicular bodies (MVBs), which are then secreted during the fusion of MVBs with the cell membrane of various cell types [24]. There are at least two known mechanisms involved in ILV and exosome production: the endosomal sorting complexes required for transport (ESCRT)-dependent and ESCRT-independent pathways [25]. The ESCRT-dependent machinery comprises the significant functions for MVBs biogenesis. The ESCRT pathway consists of five components: ESCRT-0, ESCRT-I, ESCRT-II, ESCRT-III, accessory protein ATPases, and vacuolar protein sorting-associated protein 4 (VSP4). Among these, ESCRT-0 is involved in ubiquitin-dependent clustering and ESCRT-I/II and ESCRT-III induce bud formation and vesicle abscission, respectively. ATPases and VSP4 regulate the dissociation and recycling of the ESCRT subunit [26]. In particular, ESCRT-0 binds to ILVs/MVBs, which are enriched in lipids (cholesterol and lysobisphosphatidic acid), and gathers ubiquitinated membrane proteins into these areas. Then, lipid-ubiquitinated domains begin to deform and invaginate, followed by the recruitment of ESCRT-I and ESCRT-II to stabilize and

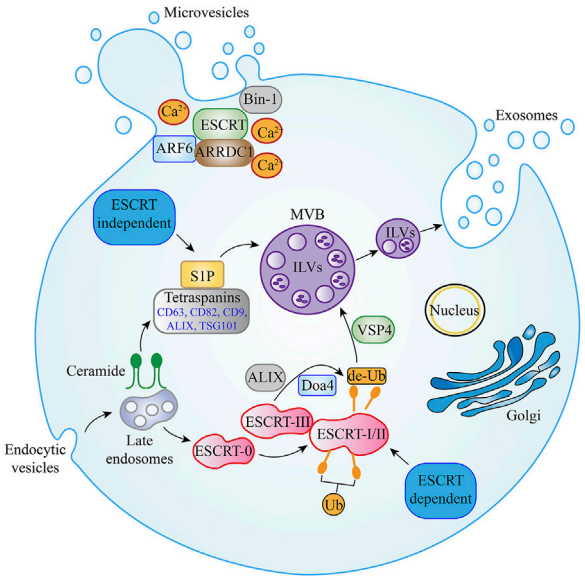

FIGURE 1
Biogenesis pathways of EVs. Multiple EV secretion mechanisms have been described. MVBs contain ILVs, which are formed during endosomal maturation. In ESCRT-dependent secretion, ESCRT-0, ESCRT-I, ESCRT-II, ESCRT-III, VSP4, Doa4, and ALIX proteins have been shown to promote exosome secretion. In exosome secretion via the ESCRT-independent pathway, ceramide, S1P, and tetraspanin family members such as CD63, CD82, CD9, ALIX, and TSG101 are essential. For plasma membrane-derived microvesicles, ARRDC1, ARF6, Bin-1, and Ca^{2+} in addition to some components of the ESCRT family (including ALIX and TSG101) have been shown to regulate outward budding. Abbreviation: EVs, Extracellular Vesicle; MVBs, Multivesicular bodies; ILVs, Intraluminal vesicles; ESCRT, endosomal sorting complexes required for transport; VSP4, Vacuolar protein sorting-associated protein 4; ALIX, Apoptosis-linked gene 2 interacting protein X; S1P, Sphingosine-1-phosphate; TSG101, Tumor susceptibility gene-101; ARRDC1, Arrestin domain-containing protein 1; ARF6, ADP-ribosylation factor 6.

maintain the membrane status and prevent deformation. Subsequently, Vps20 and Snf7 (ESCRT-III subunits) are recruited into the invaginated lipid-ubiquitinated domain, which is deubiquitinated via polymerization to recruit Doa4. Finally, with the help of VSP4, vesicles are released from the limiting cell membrane along with the disassembling and recycling of the ESCRT-III complex [27]. Previous studies have shown that depletion of the ESCRT-0 proteins [Hrs, Tumor susceptibility 1 (TSG1)] and the ESCRT-l protein [Signal transducing adapter molecule 1 (STAM1)] reduced the secretion of exosomes [28]. However, one recent study suggested that the silencing of apoptosis-linked gene 2 interacting protein X (ALIX) could modify the protein composition of exosomes and reduce the release of exosomes, thereby demonstrating the significance of ALIX for exosome biogenesis [29].

Studies have found that some mammalian cells can form ILVs without abundant ESCRT components. With a deeper understanding, this approach is called the ESCRT-independent pathway, which operates to form MVBs and promote exosomal biogenesis through ceramide production. In this mechanism, ceramide can directly promote the membrane budding of ILVs or activate sphingosine-1-phosphate (S1P), subsequently binding to the MVB membrane receptors [30, 31]. By contrast, the tetraspanin family [such as CD63, CD82, CD9, ALIX, and the tumor susceptibility gene-101 (TSG101)] were consistently observed on the surface of exosomes, suggesting that these proteins constitute a separate mechanism for MVB and exosome biogenesis (Figure 1) [32].

Biogenesis of microvesicles

In the past, it was difficult to distinguish microvesicles and exosomes because of their similar function. However, with the discovery of their biogenesis mechanisms, the two molecules were clearly differentiable owing to fundamental differences in their biogenesis mechanisms [33]. Microvesicles are produced directly from the outward budding of the plasma membrane where multiple mechanisms appear to be at play, although specific mechanisms are still being explored [34]. At present, the biogenesis pathway of arrestin domain-containing protein 1 (ARRDC1)-mediated microvesicles is one of the more recognized mechanisms. ARRDC1 is recruited to the plasma membrane along with elements of the ESCRT pathway generating microvesicles. This approach requires the involvement of VPS4 ATPase (an ESCRT pathway component), which participates in the ubiquitination of ARRDC1 [35]. In addition, ADP-ribosylation factor 6 and other ESCRT pathway components (including ALIX and TSG101) have recently been implicated in the regulation of the outward budding of microvesicles. Other microvesicles have been reported to utilize Bin-1 (ampiphysin) or Ca^{2+} to promote physical tension and molecular curvatures on the plasma membrane, thereby favoring microvesicle budding (Figure 1) [36, 37].

Isolation methods of EVs

In order for microvesicles and exosomes to serve as viable tumor biomarkers, the EVs need to be isolated from the liquid biopsies. Traditional methods for exosome isolation are differential ultracentrifugation, density gradient centrifugation, ultrafiltration, immunoaffinity, polymer precipitation and size exclusion chromatography (SEC) [38]. Each method has advantages and disadvantages, of which ultracentrifugation has the advantages of being relatively cheap and mature, but it is time-consuming and is not convenient to operate, and may also damage exosomes [39]. Although density gradient

TABLE 1 List of RNAs isolated from Glioblastoma-EVs.

RNA type	Key findings	Reference
mRNAs	Glioblastoma-EVs mRNAs stimulate glioma cells proliferation and initiate angiogenesis in brain endothelial cells	[47]
miR-9-5p	Higher expressions of miR-9-5p and miR-138-5p are correlated to the shorter survival in astrocytoma grade IV, not in glioblastoma	[48]
miR-138-5p		
miR-25-3p	Glioblastoma-EVs microRNA miR-25-3p facilitates tumor proliferation and TMZ resistance by promoting C-MYC and cyclin E expression via FBXW7 downregulation	[49]
miR-27a-3p	Glioblastoma-EVs microRNA miR-27a-3p promotes cell proliferation and motility and promotes M2 macrophage polarization via the EZH1/KDM3A/CTGF axis	[50]
miR-30b-3p	Glioblastoma-EVs microRNA miR-30b-3p decreases cell apoptosis and increases proliferation by directly targeting RHOB	[51]
miR-182-5p	Glioblastoma-EVs microRNA miR-182-5p promotes tumor angiogenesis and proliferation via the targeting of KLF2 and KLF4	[52]
miR-1238	Glioblastoma-EVs microRNA miR-1238 facilitates TMZ resistance by directly targeting the CAV1/EGFR pathway	[53]
miR-1246	Glioblastoma-EVs microRNA miR-1246 accelerates cell proliferation and invasion and promotes M2 macrophage polarization by directly targeting the TERF2IP pathway	[54]
miR-124	Glioblastoma-EVs microRNA miR-124 suppresses the cell growth and inhibits M2 microglial polarization by regulating STAT3 signaling	[55]
miR-504	Glioblastoma-EVs microRNA miR-504 decreases tumor aggressiveness and inhibits M2 macrophage polarization by targeting Grb10 expression	[56]
miR-512-5p	Glioblastoma-EVs microRNA miR-512-5p promotes tumor progression and proliferation by targeting JAG1	[57]
lncRNA HOTAIR	Glioblastoma-EVs lncRNA HOTAIR promotes angiogenesis by induction of VEGFA expression	[58]
lncRNA SBF2-AS1	Glioblastoma-EVs lncRNA SBF2-AS1 is regulated by transcription factor ZEB1 and promotes TMZ resistance	[59]
lncRNA ROR1-AS1	Glioblastoma-EVs lncRNA ROR1-AS1 facilitates tumor progression via miR-4686 regulation	[60]
circKIF18A	Glioblastoma-EVs circKIF18A enhances the FOXC2 transcription factor activity, leading to increased angiogenesis	[61]
circSMARCA5	CircSMARCA5 and circHIPK3 were significantly less abundant in EVs from glioblastoma patients compared with unaffected controls, which suggests that these molecules can act as glioblastoma diagnostic biomarkers	[62]
circHIPK3		

Abbreviation: EVs, Extracellular Vesicle; miRNA, microRNA; lncRNA, long non-coding RNAs; TMZ, temozolomide; EZH1, Enhancer zeste homologue 1; KLF2/4, Kruppel-like factor 2/4; EGFR, epidermal growth factor receptor; TERF2IP, Telomeric repeat binding factor 2 interacting protein; STAT3, Signal transducer and activator of transcription 3; JAG1, Jagged 1; ZEB1, Zinc finger E-box binding homeobox 1.

centrifugation can obtain high purity EVs and avoid exosome damage, the operation is very complicated. In contrast, ultrafiltration is easy to operate, but may result in loss of exosomes of a small particle diameter [40]. The SEC method can balance the advantages of simple operation, economy, and maintaining biological function and structure, but it may lead to lipoprotein contamination [41]. Immunoaffinity has high specificity for exosome subtype isolation, but it is expensive. Polymer precipitation is a simple operation and suitable for large-volume samples, but there are potential contaminants [42]. The most widely used technique for microvesicle isolation is specific anticoagulants coupled with high-speed ultra-centrifugation. The use of particular anticoagulants is essential, which can preserve microvesicles counts (such as protease inhibitor anticoagulants) rather than diminish microvesicles counts (such as citrate and EDTA anticoagulants) [43]. Different methods should be used for EV isolation according to their physical properties or the surface

protein types. In addition to the choice of isolation technology, it is also necessary to consider which liquids (serum, plasma, CSF) from which EVs are extracted, as well as considering the transportation, storage temperature, and storage time. Refer to the guidelines published by the International Society for Extracellular Vesicles for specific options [44].

Glioblastoma-derived EVs specific cargos

EV biological functions are complex and diverse, and many pathways have not yet been completely understood. However, the key role of EVs is in cellular intercommunication, as mentioned earlier [45]. EVs can be released and used by normal and tumor cells, although the molecular composition of the two is different. Regardless of the physiological or pathophysiological state, the diverse cargo composition of EVs determines their function in various cellular processes. Tumor cells are known to produce more EVs compared with non-tumor cells and carry specific bioactive molecules (proteins and RNAs) [46]. Glioblastoma cells also release EVs, and the major cargos are presented in Table 1.

Proteins from Glioblastoma-EVs

There are many common EV surface protein biomarkers, including CD9, CD63, CD81, ALIX, TSG101, ESCRT proteins (Rab27a, Rab27b, and Rab11), and RNA-binding proteins. Likewise, there are many specific protein markers in Glioblastoma-EVs, including the anti-inflammatory enzymes CD39 and CD73 and the anti-inflammatory molecules programmed death ligand-1 (PD-L1) and indoleamine-2,3-dioxygenase 1, which are all involved in tumor progression [63]. Vascular endothelial growth factor (VEGF), matrix metalloproteinase 9 (MMP9), epidermal growth factor receptor (EGFR), and platelet-derived growth factor receptor, genes related to angiogenesis, are overexpressed in glioblastoma and presented on Glioblastoma-EVs surface [64]. Proteomic studies identified HSP27 and CD44, which participate in apoptosis inhibition and cell adhesion, respectively, as surface protein cargos in Glioblastoma-EVs [65].

RNA types from Glioblastoma-EVs

Many key RNA types contained in Glioblastoma-EVs have been identified, including mRNAs, miRNAs, long non-coding RNAs (lncRNAs), and other rare RNAs. Indeed, >27,000 mRNA species have been identified in the serum of patients with glioblastoma, and 4700 of these mRNAs are specific to Glioblastoma-EVs. The biological processes of the 500 most abundant mRNA species in Glioblastoma-EVs are mainly distributed in the cellular process (27%), metabolic process (21%), biological regulation (10%), and developmental process (8%). Moreover, mRNAs belonging to angiogenesis, cell proliferation and migration, immune response, and histone modification functions have been identified [47]. In this study, the authors also found that the U87 glioma cells had increased 5-fold (incubated in normal growth medium) and 8-fold (incubated in medium with microvesicles) after 3 days of cultivation. And *in vitro* angiogenesis assay, there was a doubling of tubule length by the human brain microvascular endothelial cells within 16 h with the presence of microvesicles. These results revealed that glioblastoma-EVs can stimulate proliferation of the glioma cells and initiate angiogenesis in brain endothelial cells [47].

miR-9-5p, overexpressed in GSC-EVs, probably plays a distinct and complementary role to its angiogenic effects in endothelial cells (ECs) [66]. Higher expression levels of miR-9-5p and miR-138-5p are correlated to the shorter survival in glioblastoma patients carrying IDH mutation (now called astrocytoma grade IV), not in IDH wild type patients (glioblastoma) [48]. Moreover, the exosomal transfer of overexpressed miR-25-3p facilitated the proliferation and TMZ resistance of sensitive glioblastoma cells by promoting C-MYC and cyclin E expression via FBXW7 downregulation [49]. Glioblastoma-EV-packaged miR-27a-3p could promote M2 macrophage polarization via the EZH1/KDM3A/CTGF axis, and contribute to glioblastoma cell proliferation and motility, thereby increasing GSC tumorigenicity *in vivo* [50]. Glioblastoma-EV-delivered miR-30b-3p has been shown both *in vitro* and *in vivo* to decrease apoptosis and increase proliferation by directly targeting RHOB, offering a potential treatment strategy for glioblastoma [51]. Under hypoxic stress conditions, miR-182-5p was significantly upregulated in Glioblastoma-EVs, resulting in the promotion of tumor angiogenesis and tumor proliferation via the targeting of kruppel-like factor (KLF) 2 and KLF4(52). It was shown that high exosome-transferred miR-1238 level in TMZ-resistant glioblastoma cells could confer TMZ resistance by directly targeting the CAV1/EGFR pathway [53]. Qian et al. confirmed that exosomal miR-1246 in glioblastoma may play a role in M2 macrophage polarization to accelerate glioblastoma cell proliferation and invasion by directly targeting the telomeric repeat binding factor 2 interacting protein (TERF2IP) signaling pathway [54]. In addition, a set of underrepresented miRNAs have been identified in Glioblastoma-EVs. For example, a study demonstrated that miR-124 obtained from the U373MG glioblastoma cell line, in which an oncosuppressor is highly downregulated, exerted an antitumor effect by suppressing glioblastoma cell growth and inhibiting M2 microglial polarization by regulating the signal transducer and activator of transcription 3 (STAT3) signaling [55]. Moreover, miR-504 was identified as one of the most downregulated miRNAs in GSC-EVs that acted as a negative regulator of GSC migration,

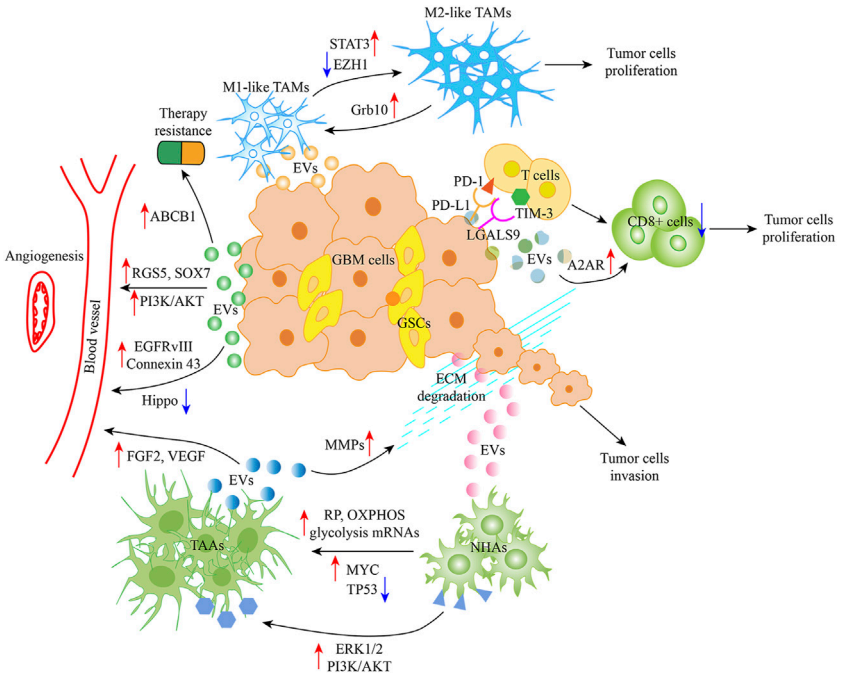

FIGURE 2
Glioblastoma-EVs and TME. Glioblastoma-EVs can induce TAMs with the M1 (antitumor) phenotype to the M2 (protumor) phenotype by activating the STAT3 signaling and targeting Grb10 as well as inhibiting EZH1. Glioblastoma-EVs can also increase PD-L1 and LGALS9 expression by interacting with the ligand PD-1 and TIM-3 present on activated T cell surface, thereby inhibiting T cell-associated immune response. Moreover, A2AR in T cells is involved in inhibiting T cell clonal proliferation. Meanwhile, Glioblastoma-EVs target ECs, which activate angiogenic mechanisms by regulating RGS5, SOX7, EGFRvIII, connexin 43, PI3K/AKT, and Hippo signaling. Moreover, ABCB1 appears to play a role in cancer therapy resistance, and Glioblastoma-EV uptake by NHAs leads to their conversion to TAAs, thereby favoring angiogenesis and tumor invasion by regulating FGF2 and VEGF and degrading ECM, respectively. Abbreviation: EVs, Extracellular Vesicle; TME, Tumor microenvironment; TAMs, Tumor-associated macrophages; STAT3, Signal transducer and activator of transcription 3; EZH1, Enhancer zeste homologue 1; PD-L1, Programmed death ligand-1; PD-1, Programmed cell death 1; TIM-3, T cell immunoglobulin domain and mucin domain-3; A2AR, Adenosine receptor 2A; RGS5, G protein signaling 5; EGFRvIII, EGFR mutant/variant III; ECs, endothelial cells; NHAs, Normal human astrocytes; TAAs, Tumor associated astrocytes; FGF2, Fibroblast growth factor 2; VEGF, Vascular endothelial growth factor; ECM, Extracellular matrix.

and miR-504 overexpression decreased tumorigenicity and induced microglia M1 phenotypes by targeting Grb10 expression, resulting in increased tumor aggressiveness and poor prognosis [56]. Besides the effect of miR-504, exosomal miR-512-5p, previously reported as an anti-oncogene in multiple solid tumors, was downregulated in glioblastoma. Furthermore, a reduction in miR-512-5p in glioblastoma played an important role in glioblastoma progression and proliferation by targeting Jagged 1 (JAG1) [57].

Aside from mRNAs and miRNAs, various specific lncRNAs have been identified in Glioblastoma-EVs. The lncRNA HOTAIR, an oncogene identified in gliomas, was involved in angiogenesis via its transmission into ECs through Glioblastoma-EVs, a process that requires VEGFA induction [58]. Zhang et al. found that high exosomal lncRNA SBF2-AS1 levels isolated from TMZ-resistant glioblastoma cells promoted TMZ resistance and were associated with poor prognosis. The SBF2-AS1 level was regulated by transcription factor zinc finger E-box binding homeobox 1 (ZEB1) and affected TMZ resistance in GBM cells [59]. Moreover, the exosome-packaged lncRNA ROR1-AS1 facilitated glioma progression via miR-4686 regulation, which was confirmed using a xenograft nude mice model [60].

Uncharacterized EV-isolated RNAs < 500 nucleotides were detected in circulating peripheral blood; however, their function could not be identified [67]. These RNAs, mapped in the intronic and intergenic regions, are also known as short non-coding RNAs and include piRNA, rRNA, snoRNA, snRNA, and yRNA [68]. Recently, circular RNAs (belonging to short non-coding RNAs) were considered a part of the specific RNA cargos of Glioblastoma-EVs. CircKIF18A can bind to the transcription factor FOXC2 to promote angiogenesis in glioblastoma by activating the PI3K/AKT signaling pathway [61]. CircSMARCA5 and circHIPK3 were significantly less abundant in Glioblastoma-EVs compared with unaffected controls, which suggests that these molecules can act as good glioblastoma diagnostic biomarkers when combined with the preoperative inflammatory markers of neutrophil to lymphocyte, platelet to lymphocyte, and lymphocyte to monocyte ratios [62]. Information concerning the major RNA cargos of Glioblastoma-EVs is summarized in Table 1.

Glioblastoma-EVs and TME

As discussed earlier, tumor cells, ECM, blood vessels, monocytes, macrophages, T cells, neurons, astrocytes, oligodendrocytes, ependymocytes, microglia, ECs, and pericytes are part of the glioblastoma TME. Important findings regarding the effect of Glioblastoma-EVs on different TME components, specifically on macrophages, microglia, vasculature, T cells, astrocytes, and glioblastoma cells, are discussed in this section (Figure 2).

Effect on tumor-associated macrophages (TAMs)

Microglia, the resident brain innate immune cells previously called TAMs, together with monocytes and macrophages, play a key role in pathogen infection [69]. Macrophages are converted to either M1 (proinflammatory) or M2 (anti-inflammatory; promoting tumor progression) phenotype depending on TME cytokines and signaling molecules. Recent evidence has revealed that glioblastoma tissue supports the induction of such tumor-supportive phenotype modulation of TAMs through various EV-dependent mechanisms, as detailed below [70]. As noted above, several miRNAs (miR-27a-3p, miR-1246, miR-124, and miR-504) participate in microglial phenotype transformation. A 2022 study revealed that Glioblastoma-EV-derived miR-27a-3p could modify TAM phenotype *in vitro*, changing it to an M2 anti-inflammatory phenotype and promoting tumor progression by inhibiting enhancer zeste homologue 1 [50]. Qian et al. (2020) demonstrated that miRNA-1246 contained in Glioblastoma-EVs was transferred to recipient TAMs, resulting in an M2-like anti-inflammatory phenotype polarization of the macrophages. One of these targets is the TERF2IP, a transcription factor and regulator of telomere function, which activates the signal transducer and activator of transcription 3 signaling pathway and inhibits the NF-κB signaling pathway [54]. miRNA-124, which acts as an oncosuppressor, reduces cell growth and inhibits glycolytic pathways in colorectal cancer and breast cancer [71]. miR-124 present in microglia-derived small EVs was one of the most downregulated miRNAs in glioblastoma and may be associated with significantly reduced glioblastoma aggressiveness. However, macrophage-produced EVs could modify the macrophage antitumor phenotype to tumor-supportive phenotype when exposed to Glioblastoma-EVs. Moreover, the expression level of the M1 microglial polarization marker interleukin-6 was upregulated, whereas those of the M2 microglial polarization markers transforming growth factor-β and arginase 1 were significantly downregulated [55, 72]. Bier et al. showed that miR-504 contained in GSC-secreted EVs was transferred from GSCs to the surrounding neighboring cells such as microglia, subsequently promoting oncogenic functions. However, miR-504 was downregulated in glioblastoma cells and GSCs, suggesting that miR-504 is a negative regulator of glioblastoma tumorigenicity. Moreover, the overexpression of miR-504 in microglial cells upregulated the level of M1 phenotypic markers CD86 and tumor necrosis factor-α, indicating an increase in M1-like TAMs. These phenomena suggest that GSC-EVs induce microglial phenotype change. It has been speculated that the mechanism of this induction is related to Grb10 targeting [56]. In addition, Glioblastoma-EVs could promote tumor migration and invasion by accelerating ECM degradation in TME through macrophage phagocytic activity enhancement [73].

Effect on ECs

The modification of angiogenesis in TME is a key mechanism that promotes glioblastoma growth via Glioblastoma-EVs. One mechanism through which glioblastoma cells accomplish this is through the transfer of miR-9-5p from GSC-EVs to brain ECs, which is associated with angiogenesis via the regulation of downstream G protein signaling 5 (RGS5), SOX7, and ABCB1(66). RGS5 and SOX7 have been identified to play critical roles in vascular growth by recruiting host pericytes and acting as the positive feedback regulators of VEGF signaling, respectively, thereby promoting physiological angiogenesis [74, 75]. Meanwhile, ABCB1 appears to play a role in cancer therapy resistance [76]. Ma et al. demonstrated that lncRNA HOTAIR delivered via the glioblastoma cell line A172 cell-derived EVs are involved in the promotion of angiogenesis via the upregulation of the expression of VEGFA, a well-known proangiogenic factor [58]. Another type of circular RNA, the microglia-derived exosomal circKIF18A, plays a role in proangiogenic effects, contributing in the RNA-aided nuclear entry of FOXC2, leading to its direct binding to the promoter of ITGB3 (C-X-C chemokine receptor type 4 and DLL4, and activating the PI3K/AKT signaling axis [61]. VEGF-C, a specific 120-kDa isoform of VEGF, transported via Glioblastoma-EVs (exosomes) have been identified in the promotion of EC viability, migration, and tubulation. The proangiogenic effects of VEGF-C have been attributed to inhibiting Hippo signaling to stimulate tafazzin expression in ECs by binding to VEGF receptor 2 [77]. The Glioblastoma-EV-mediated release of EGFR mutant/variant III (EGFRvIII) in the context of CD9 tetraspanin may enhance glioblastoma progression, including cell invasion and angiogenesis. Research has shown that EGFRvIII expression resulted in the downregulation of EV markers, notably including CD81 and CD82 [78]. Under 3% oxygen (hypoxia), the level of connexin 43 (Cx43) in exosomes secreted in the glioblastoma cell line U251 cells was elevated. However, compared with PBS (control), exosomal Cx43 remarkably promoted tube

formation in human umbilical vein endothelial cells, thereby contributing to angiogenesis in hypoxic glioblastoma TME [79].

Effect on T cells

Infiltrating T cells in the TME can be the target of Glioblastoma-EV-released cargos, various T cell types and mechanisms are involved in their interaction with the cargos [80]. Some findings have demonstrated that Glioblastoma-derived EVs can induce the formation of immunosuppressive monocytes such as non-classical monocytes (NCMs) and myeloid-derived suppressor cells (MDSCs) as well as increase PD-L1 expression [by binding with programmed cell death 1 (PD-1) located on the surface of activated T cells]. The formation of NCMs was PD-L1 dependent and that of MDSCs was PD-L1 independent. Further experiments revealed that PD-1 was present on NCM surfaces. NCMs and MDSCs interacted with T cells via PD-L1/PD-1 and inhibited T cell proliferation *in vitro*, thereby accelerating tumor formation and progression [81]. In low oxygen conditions (hypoxia), CD73 can be induced by the enzyme ecto-5′-nucleotidase, playing a crucial role in suppressing the systemic immune system and supporting tumor progression [82]. A recent study has suggested that CD73 is highly expressed in T cells and that this expression originates from Glioblastoma-EVs. Researchers also observed that elevated CD73 blocked the clonal proliferation of T cells by increasing adenosine concentration around T cells *in vitro*. This may be attributed to the production of adenosine requiring AMP degradation and aerobic glycolysis inhibition by activating adenosine receptor 2A in T cells, thereby starving the energy needed for T cell clonal proliferation [83]. LGALS9 (galectin-9) acts as the ligand for the T cell immunoglobulin domain and mucin domain-3 on $CD4^+$ T cell surface, thereby leading to T cell apoptosis and poor prognosis in glioblastoma [84]. In other work, the percentages of neutrophils and CD8 + T cells in the cerebrospinal fluid (CSF) of patients with glioblastoma were reduced compared with that of healthy controls. LGALS9, a specific protein cargo contained in Glioblastoma-CSF-EVs, was shown to inhibit the antigen presentation of dendritic cells and cytotoxic T cell ($CD8^+$) immunity, promoting tumor progression [85].

Effect on astrocytes

Among the cell types associated with glioblastoma TME, astrocytes are the most likely to establish direct contact with glioblastoma cells. Astrocytes are directly involved in the formation of the primary blood–brain barrier (BBB) structure by closely associating with ECs and pericytes. In addition, astrocytes participate in modulating the diffusion of neurotransmitters across brain EVs [86]. A group of activated astrocytes, known as tumor-associated astrocytes, has been shown to be directly regulated by glioblastoma cells to enhance tumor growth and invasion and chemotherapy resistance. Some contents of astrocyte-derived EVs, such as HSP70, fibroblast growth factor 2, VEGF, and MMPs, have all been shown to be involved in neuroprotection, ECM remodeling, and angiogenesis, thereby supporting tumor processes [87]. Glioblastoma-EVs can regulate TME to benefit tumor survival by driving astrocytes toward a tumorigenic phenotype. In a study, normal human astrocyte molecules were modified to resemble known tumor signaling pathways (ERK1/2, PI3K, and AKT) to enhance their growth and migratory capacity in a semisolid matrix [88]. In a later study, Zeng et al. reported increased mitochondrial respiration and glycolysis in pretransformed astrocytes cultured with Glioblastoma-derived EVs owing to the direct transfer of ribosomal protein, OXPHOS, and glycolysis mRNAs. Indeed, patients with glioblastoma and high glycolysis enrichment scores had worse overall survival [89]. Results from a previous study suggest that reduced TP53 levels are related to an ECM modulation composition that favors tumor malignancy [90]. MYC, a proto-oncogene, is involved in cell cycle regulation, apoptosis, and GSC acquisition and maintenance [91]. Of note, MYC induction and decreased TP53 levels in Glioblastoma-EVs stimulated normal astrocytes to shift to a senescence-associated secretory phenotype (a tumor-supportive phenotype) to induce a favorable TME for tumorigenic abilities (growth and invasion) [92]. These findings suggest that Glioblastoma-derived EVs stimulate astrocytes to promote glioblastoma progression and invasion.

Clinical applications of Glioblastoma-EVs

The diagnosis or post-treatment monitoring of glioblastoma is heavily dependent on imaging (e.g., magnetic resonance imaging [MRI]) and tissue biopsies. However, because the tumor mass can only be detected in MRI when it is sufficiently large, it is easy to miss the correct diagnosis and delay disease treatment. By contrast, it is impossible to obtain a real map of intratumoral heterogeneity using imaging, which limits the ability to predict and monitor treatment response. Tumor biopsies, particularly of brain tissues, are likewise not an ideal option owing to their invasiveness, which can cause brain swelling and hemorrhage [93]. In recent years, in an effort to improve the diagnostic sensitivity and outcome of glioblastoma, several non-invasive or minimally invasive strategies have been explored to optimize its diagnosis and monitoring including speed, cost, and patient acceptability. One of these strategies is the analysis of non-invasive liquid biopsy using Glioblastoma-derived EVs from breast milk, plasma, CSF, urine, and saliva, among other physiological fluids [94]. This new strategy showed significant advantages in terms of precise personalized diagnosis

[95]. Glioblastoma-EVs carry numerous specific molecules that may be associated with oncogenesis and are released outside the cells. These circulating EVs are considered significant biomarker sources that may help improve diagnosis, monitoring, and follow-up [96]. The term "vesiclemia" defines EV concentration in the plasma, which can change according to the state of the patient. For example, vesiclemia is higher in patients with glioblastoma than in healthy donors. Moreover, vesiclemia is increased after recurrence. However, it has been shown to decrease after resective surgery therapy [97]. In line with this idea, several mRNAs, miRNAs, lncRNAs, circular RNAs, and proteins in plasmatic EVs have been shown to be upregulated or downregulated in patients with glioblastoma patients compared with healthy donors, as described above. Johan et al. found that 14 of the 30 tumor samples (47%) contained the EGFRvIII transcript, however, EGFRvIII was not found in serum exosomes of 30 normal control individuals, which indicated that EV RNA could be used as biomarkers for glioblastoma [47]. In addition, Johnny et al. found that the level of CSF EV miR-21 was higher than that in non-oncologic patients. Interestingly, only CSF EV miR-21 was suitable for disease diagnosis while no significant difference in miR-21 level was found in serum, suggesting that CSF EV miR-21 could be a feasible biomarker for the presence of glioblastoma [98]. These results suggest that EVs are a promising source of biomarkers during early diagnosis [95]. TMZ chemotherapy is commonly administered together with radiation therapy offered in glioblastoma treatment after surgical resection. As described earlier, some EV-derived proteins and RNA types confer radiotherapy or chemotherapy resistance and promote tumor recurrence. MiR-25-3p is overexpressed in EVs of TMZ resistant glioma cells and high miR-25-3p level in the serum of a glioblastoma patient is relevant to TMZ resistance and greater tumor size [49]. MiR-1238 level was significantly higher in serum exosomes of patients with recurrent glioblastoma compared to patients with primary glioblastoma [53]. Furthermore, a high level of lncRNA SBF2-AS1 in serum exosomes was associated with poor response to TMZ treatment in glioblastoma patients [59]. Therefore, the analysis of different cargos as well as the concentration of EVs isolated from liquid biopsy (plasma and CSF) are believed to represent predictive and prognostic biomarkers for glioblastoma therapy and recurrence [99].

EVs are a potential therapeutic tool for glioblastoma. EV formation promotes tumorigenesis and progression. Therefore, some researchers have expressed interest in exploring strategies to block EV formation, thereby inhibiting tumor development. Microvesicle biogenesis is modulated by lipid composition, cytoskeleton proteins, and Ca^{2+}, all of which can alter membrane fluidity and deformability. Calpain comprises a family of cysteine proteases whose regulatory subunits contain a calcium-binding site. This cysteine protease family can apparently promote microvesicle shedding by remodeling the cytoskeleton. It has been reported that calpain inhibitors can reduce microvesicle production [100]. A low concentration (10–20 μg/mL) of calpeptin, the most widely used calpain inhibitor, has been reported to reduce microvesicle shedding from activated platelets [101]. In a subsequent study, Atanassoff et al. showed that 60 μM calpeptin reduced microvesicle release from human embryonic kidney 293 cells [102]. Researchers have also focused on the therapeutic effect of calpeptin on solid tumors. Experiments in a prostate cancer cell line (PC3) model and preclinical mouse model have demonstrated that calpeptin combined with docetaxel or methotrexate decreased intratumoral vascularisation and tumor proliferation [103]. However, a recent study found that calpeptin treatment increased the resistance of glioblastoma cells to TMZ chemotherapy, contradicting previous research [104]. Thus, the therapeutic effect of calpeptin in glioblastoma needs further exploration. Stillger et al. revealed that the overexpression of calpain-2 (member of calpain) and the calpain small subunit in glioblastoma contributed to TMZ resistance. A combination of the synthetic calpain inhibitor PD150606 and TMZ led to a decreased viability of U251N cells compared with TMZ treatment alone [105].

Exosome biogenesis is modulated by the ESCRT-dependent or -independent pathway. Manumycin A was identified as an inhibitor of exosome biogenesis in prostate cancer cells via the attenuation of the ESCRT-0 protein Hrs and ESCRT-accessory protein ALIX by Ras signaling inhibition [106]. An early report on the small molecule imipramine, an inhibitor of exosome biogenesis and secretion, highlighted the ability of combination chemotherapy (imipramine plus liposomal doxorubicin) to prolong the survival of patients with glioblastoma. This mechanism may be related to the inhibition of NADPH reactive oxygen species generation and conditional actin regulatory elements [107]. Neutral sphingomyelinase (nSMase) generates the bioactive lipid ceramide, which plays a key role in ESCRT-independent exosome generation. GW4869 has been identified as a specific non-competitive inhibitor of nSMase that reduced exosome release. Xu et al. performed animal experiments along with primary glioma cells G15-Luc-mimic cells. GW4869-treated mice displayed significantly reduced tumor size and exhibited better survival than controls (Figure 3) [108]. EVs are less immunogenic than standard transfection agents and can pass through BBB to a certain degree, suggesting that they offer an effective mode of drug delivery to the target site. Some research groups have evaluated the role of anti-miR-9 in reversing multidrug resistance to TMZ and suppressing glioblastoma malignant phenotypes [109, 110].

Conclusion and future perspectives

Glioblastoma is a devastating disease with a high mortality rate. Thus, new therapies are required to improve its prognosis.

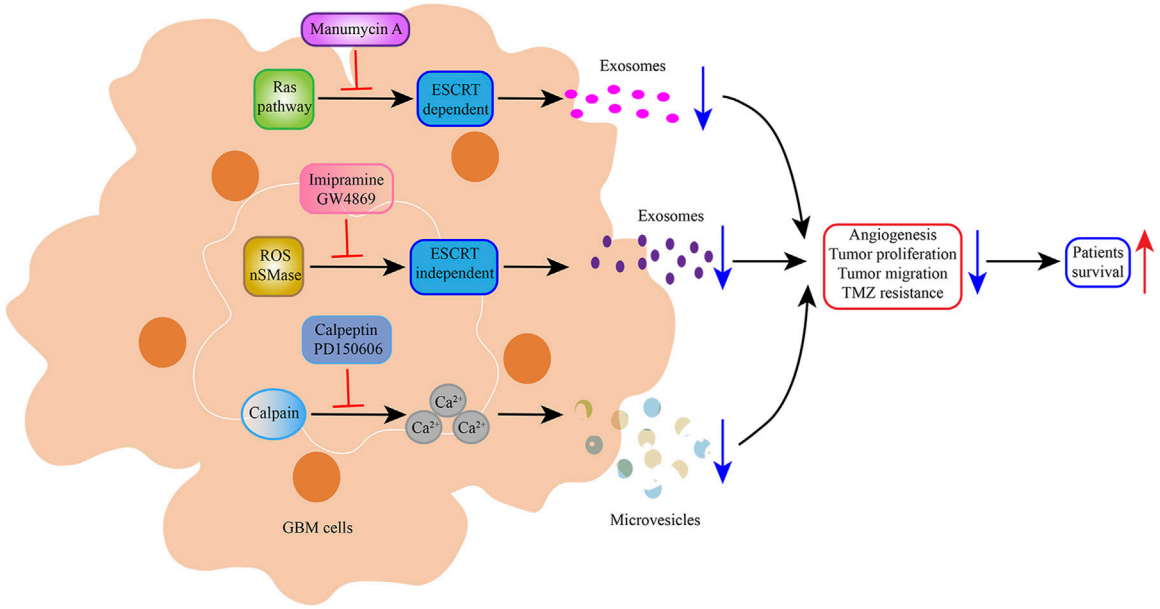

FIGURE 3
Schematic representation of the inhibition of Glioblastoma-EVs biogenesis and secretion. Manumycin A, imipramine, and GW4869 reduced exosome biogenesis and secretion, thereby prolonging the survival of patients with glioblastoma. Calpeptin and PD150606, potent calpain inhibitors, prevented the formation and budding of microvesicles, which decreased glioblastoma cell viability.

The chemotherapy resistance of tumor cells is a frequent obstacle to therapy. The deepening of knowledge about intercellular communication, discovery of EVs, and new biomarkers have enhanced the efficacy of therapies [111]. The discovery of EV structure, specific cargo components, and their potential clinical applications in various tumors are topics that are currently the focus of many studies. The study of the role of EVs in the glioblastoma TME has also emerged in the last few decades. EVs are involved in different ways in glioblastoma tumor cell proliferation, migration, and drug resistance. This review summarized the current understanding on Glioblastoma-EVs and their potential as diagnostic, prognostic, and therapeutic tools.

Various EV-derived cargos (proteins, mRNAs, miRNAs, lncRNAs, and circular RNAs) act in glioblastoma target cells via intercellular communication and their ability to cross BBB. These findings suggest that they can be used as diagnostic and therapeutic tools [112].

However, many challenges regarding EV utilization in glioblastoma remain, including reaching a consensus regarding protocols for EV purification and criteria for characterization [113]. Thus, it is necessary to optimize EV isolation protocols before clinical translation can be considered. Moreover, the obtention and storage of EVs, especially exosomes, are challenging [112]. The use of innovative strategies to enhance exosome storage and long-term stability are emerging to preserve the physicochemical and biological properties of EVs, which may be crucial for clinical application. Taken together, although huge advances have been made in understanding the roles of EVs in glioblastoma, overcoming the aforementioned barriers may help EVs become essential components in the routine treatment of glioblastoma in the future.

Author contributions

YC contributed to the conception of the study. JD and YJ were responsible for the draft of the manuscript and the data collection. HH, YC, and SZ worked on the figures and Table. All authors contributed to the article and approved the submitted version.

Conflict of interest

The authors declare that the research was conducted in the absence of any commercial or financial relationships that could be construed as a potential conflict of interest.

References

1. Nabors LB, Portnow J, Ahluwalia M, Baehring J, Brem H, Brem S, et al. Central nervous system cancers, version 3.2020, nccn clinical practice guidelines in oncology. *J Natl Compr Canc Netw* (2020) 18(11):1537–70. doi:10.6004/jnccn.2020.0052

2. Molinaro AM, Taylor JW, Wiencke JK, Wrensch MR. Genetic and molecular epidemiology of adult diffuse glioma. *Nat Rev Neurol* (2019) 15(7):405–17. doi:10.1038/s41582-019-0220-2

3. Whitfield BT, Huse JT. Classification of adult-type diffuse gliomas: impact of the world Health organization 2021 update. *Brain Pathol* (2022) 32(4):e13062. doi:10.1111/bpa.13062

4. Louis DN, Perry A, Wesseling P, Brat DJ, Cree IA, Figarella-Branger D, et al. The 2021 who classification of tumors of the central nervous system: a summary. *Neuro Oncol* (2021) 23(8):1231–51. doi:10.1093/neuonc/noab106

5. Stupp R, Mason WP, van den Bent MJ, Weller M, Fisher B, Taphoorn MJ, et al. Radiotherapy plus concomitant and adjuvant temozolomide for glioblastoma. *N Engl J Med* (2005) 352(10):987–96. doi:10.1056/NEJMoa043330

6. Burster T, Traut R, Yermekkyzy Z, Mayer K, Westhoff MA, Bischof J, et al. Critical view of novel treatment strategies for glioblastoma: failure and success of resistance mechanisms by glioblastoma cells. *Front Cell Dev Biol* (2021) 9:695325. doi:10.3389/fcell.2021.695325

7. Kopper TJ, Yu X, Graner MW. Immunopathology of extracellular vesicles in macrophage and glioma cross-talk. *J Clin Med* (2023) 12(10):3430. doi:10.3390/jcm12103430

8. Patel AP, Tirosh I, Trombetta JJ, Shalek AK, Gillespie SM, Wakimoto H, et al. Single-cell rna-seq highlights intratumoral heterogeneity in primary glioblastoma. *Science* (2014) 344(6190):1396–401. doi:10.1126/science.1254257

9. Burko P, D'Amico G, Miltykh I, Scalia F, Conway de Macario E, Macario AJL, et al. Molecular pathways implicated in radioresistance of glioblastoma multiforme: what is the role of extracellular vesicles? *Int J Mol Sci* (2023) 24(5):4883. doi:10.3390/ijms24054883

10. Perus LJM, Walsh LA. Microenvironmental heterogeneity in brain malignancies. *Front Immunol* (2019) 10:2294. doi:10.3389/fimmu.2019.02294

11. Broekman ML, Maas SLN, Abels ER, Mempel TR, Krichevsky AM, Breakefield XO. Multidimensional communication in the microenvirons of glioblastoma. *Nat Rev Neurol* (2018) 14(8):482–95. doi:10.1038/s41582-018-0025-8

12. Matarredona ER, Pastor AM. Extracellular vesicle-mediated communication between the glioblastoma and its microenvironment. *Cells* (2019) 9(1):96. doi:10.3390/cells9010096

13. van Niel G, D'Angelo G, Raposo G. Shedding light on the cell biology of extracellular vesicles. *Nat Rev Mol Cell Biol* (2018) 19(4):213–28. doi:10.1038/nrm.2017.125

14. Cano A, Ettcheto M, Bernuz M, Puerta R, Esteban de Antonio E, Sanchez-Lopez E, et al. Extracellular vesicles, the emerging mirrors of brain physiopathology. *Int J Biol Sci* (2023) 19(3):721–43. doi:10.7150/ijbs.79063

15. Colombo M, Raposo G, Thery C. Biogenesis, secretion, and intercellular interactions of exosomes and other extracellular vesicles. *Annu Rev Cell Dev Biol* (2014) 30:255–89. doi:10.1146/annurev-cellbio-101512-122326

16. Spelat R, Jihua N, Sanchez Trivino CA, Pifferi S, Pozzi D, Manzati M, et al. The dual action of glioma-derived exosomes on neuronal activity: synchronization and disruption of synchrony. *Cell Death Dis* (2022) 13(8):705. doi:10.1038/s41419-022-05144-6

17. Busatto S, Yang Y, Walker SA, Davidovich I, Lin WH, Lewis-Tuffin L, et al. Brain metastases-derived extracellular vesicles induce binding and aggregation of low-density lipoprotein. *J Nanobiotechnology* (2020) 18(1):162. doi:10.1186/s12951-020-00722-2

18. Barile L, Vassalli G. Exosomes: therapy delivery tools and biomarkers of diseases. *Pharmacol Ther* (2017) 174:63–78. doi:10.1016/j.pharmthera.2017.02.020

19. Virgintino D, Rizzi M, Errede M, Strippoli M, Girolamo F, Bertossi M, et al. Plasma membrane-derived microvesicles released from tip endothelial cells during vascular sprouting. *Angiogenesis* (2012) 15(4):761–9. doi:10.1007/s10456-012-9292-y

20. Ban LA, Shackel NA, McLennan SV. Extracellular vesicles: a new frontier in biomarker discovery for non-alcoholic fatty liver disease. *Int J Mol Sci* (2016) 17(3):376. doi:10.3390/ijms17030376

21. Vlassov AV, Magdaleno S, Setterquist R, Conrad R. Exosomes: current knowledge of their composition, biological functions, and diagnostic and therapeutic potentials. *Biochim Biophys Acta* (2012) 1820(7):940–8. doi:10.1016/j.bbagen.2012.03.017

22. Azam Z, Quillien V, Wang G, To ST. The potential diagnostic and prognostic role of extracellular vesicles in glioma: current status and future perspectives. *Acta Oncol* (2019) 58(3):353–62. doi:10.1080/0284186X.2018.1551621

23. Grant BD, Donaldson JG. Pathways and mechanisms of endocytic recycling. *Nat Rev Mol Cell Biol* (2009) 10(9):597–608. doi:10.1038/nrm2755

24. Xu M, Ji J, Jin D, Wu Y, Wu T, Lin R, et al. The biogenesis and secretion of exosomes and multivesicular bodies (mvbs): intercellular shuttles and implications in human diseases. *Genes Dis* (2022) 10(5):1894–907. doi:10.1016/j.gendis.2022.03.021

25. Tschuschke M, Kocherova I, Bryja A, Mozdziak P, Angelova Volponi A, Janowicz K, et al. Inclusion biogenesis, methods of isolation and clinical application of human cellular exosomes. *J Clin Med* (2020) 9(2):436. doi:10.3390/jcm9020436

26. Juan T, Furthauer M. Biogenesis and function of escrt-dependent extracellular vesicles. *Semin Cell Dev Biol* (2018) 74:66–77. doi:10.1016/j.semcdb.2017.08.022

27. Babst M. Mvb vesicle formation: escrt-dependent, escrt-independent and everything in between. *Curr Opin Cell Biol* (2011) 23(4):452–7. doi:10.1016/j.ceb.2011.04.008

28. Xie S, Zhang Q, Jiang L. Current knowledge on exosome biogenesis, cargo-sorting mechanism and therapeutic implications. *Membranes (Basel)* (2022) 12(5):498. doi:10.3390/membranes12050498

29. Hessvik NP, Llorente A. Current knowledge on exosome biogenesis and release. *Cell Mol Life Sci* (2018) 75(2):193–208. doi:10.1007/s00018-017-2595-9

30. Jin Y, Ma L, Zhang W, Yang W, Feng Q, Wang H. Extracellular signals regulate the biogenesis of extracellular vesicles. *Biol Res* (2022) 55(1):35. doi:10.1186/s40659-022-00405-2

31. Pavlic A, Poelman H, Wasilewski G, Wichapong K, Lux P, Maassen C, et al. Inhibition of neutral sphingomyelinase 2 by novel small molecule inhibitors results in decreased release of extracellular vesicles by vascular smooth muscle cells and attenuated calcification. *Int J Mol Sci* (2023) 24(3):2027. doi:10.3390/ijms24032027

32. Hurwitz SN, Cheerathodi MR, Nkosi D, York SB, Meckes DG. Tetraspanin Cd63 bridges autophagic and endosomal processes to regulate exosomal secretion and intracellular signaling of epstein-barr virus Lmp1. *J Virol* (2018) 92(5):e01969. doi:10.1128/JVI.01969-17

33. Al-Nedawi K, Meehan B, Rak J. Microvesicles: messengers and mediators of tumor progression. *Cell Cycle* (2009) 8(13):2014–8. doi:10.4161/cc.8.13.8988

34. Stahl PD, Raposo G. Extracellular vesicles: exosomes and microvesicles, integrators of homeostasis. *Physiology (Bethesda)* (2019) 34(3):169–77. doi:10.1152/physiol.00045.2018

35. Nabhan JF, Hu R, Oh RS, Cohen SN, Lu Q. Formation and release of arrestin domain-containing protein 1-mediated microvesicles (armms) at plasma membrane by recruitment of Tsg101 protein. *Proc Natl Acad Sci U S A* (2012) 109(11):4146–51. doi:10.1073/pnas.1200448109

36. Russo MN, Whaley LA, Norton ES, Zarco N, Guerrero-Cazares H. Extracellular vesicles in the glioblastoma microenvironment: a diagnostic and therapeutic perspective. *Mol Aspects Med* (2023) 91:101167. doi:10.1016/j.mam.2022.101167

37. Minciacchi VR, You S, Spinelli C, Morley S, Zandian M, Aspuria PJ, et al. Large oncosomes contain distinct protein cargo and represent a separate functional class of tumor-derived extracellular vesicles. *Oncotarget* (2015) 6(13):11327–41. doi:10.18632/oncotarget.3598

38. Chen J, Li P, Zhang T, Xu Z, Huang X, Wang R, et al. Review on strategies and technologies for exosome isolation and purification. *Front Bioeng Biotechnol* (2021) 9:811971. doi:10.3389/fbioe.2021.811971

39. Lin S, Yu Z, Chen D, Wang Z, Miao J, Li Q, et al. Progress in microfluidics-based exosome separation and detection technologies for diagnostic applications. *Small* (2020) 16(9):e1903916. doi:10.1002/smll.201903916

40. Ding L, Yang X, Gao Z, Effah CY, Zhang X, Wu Y, et al. A holistic review of the state-of-the-art microfluidics for exosome separation: an overview of the current status, existing obstacles, and future outlook. *Small* (2021) 17(29):e2007174. doi:10.1002/smll.202007174

41. Mohammadi M, Zargartalebi H, Salahandish R, Aburashed R, Wey Yong K, Sanati-Nezhad A. Emerging technologies and commercial products in exosome-based cancer diagnosis and prognosis. *Biosens Bioelectron* (2021) 183:113176. doi:10.1016/j.bios.2021.113176

42. Coumans FAW, Brisson AR, Buzas EI, Dignat-George F, Drees EEE, El-Andaloussi S, et al. Methodological guidelines to study extracellular vesicles. *Circ Res* (2017) 120(10):1632–48. doi:10.1161/CIRCRESAHA.117.309417

43. Jayachandran M, Miller VM, Heit JA, Owen WG. Methodology for isolation, identification and characterization of microvesicles in peripheral blood. *J Immunol Methods* (2012) 375(1-2):207–14. doi:10.1016/j.jim.2011.10.012

44. Thery C, Witwer KW, Aikawa E, Alcaraz MJ, Anderson JD, Andriantsitohaina R, et al. Minimal information for studies of extracellular vesicles 2018 (Misev2018): a position statement of the international society for extracellular vesicles and update of the Misev2014 guidelines. *J Extracell Vesicles* (2018) 7(1):1535750. doi:10.1080/20013078.2018.1535750

45. Iraci N, Leonardi T, Gessler F, Vega B, Pluchino S. Focus on extracellular vesicles: physiological role and signalling properties of extracellular membrane vesicles. *Int J Mol Sci* (2016) 17(2):171. doi:10.3390/ijms17020171

46. Pancholi S, Tripathi A, Bhan A, Acharya MM, Pillai P. Emerging concepts on the role of extracellular vesicles and its cargo contents in glioblastoma-microglial crosstalk. *Mol Neurobiol* (2022) 59(5):2822–37. doi:10.1007/s12035-022-02752-3

47. Skog J, Wurdinger T, van Rijn S, Meijer DH, Gainche L, Sena-Esteves M, et al. Glioblastoma microvesicles transport rna and proteins that promote tumour growth and provide diagnostic biomarkers. *Nat Cell Biol* (2008) 10(12):1470–6. doi:10.1038/ncb1800

48. Zottel A, Samec N, Kump A, Raspor Dall'Olio LR, Puzar Dominkus P, Romih R, et al. Analysis of mir-9-5p, mir-124-3p, mir-21-5p, mir-138-5p, and mir-1-3p in glioblastoma cell lines and extracellular vesicles. *Int J Mol Sci* (2020) 21(22):8491. doi:10.3390/ijms21228491

49. Wang J, Li T, Wang B. Exosomal transfer of mir-25-3p promotes the proliferation and temozolomide resistance of glioblastoma cells by targeting Fbxw7. *Int J Oncol* (2021) 59(2):64. doi:10.3892/ijo.2021.5244

50. Zhao G, Yu H, Ding L, Wang W, Wang H, Hu Y, et al. Microrna-27a-3p delivered by extracellular vesicles from glioblastoma cells induces M2 macrophage polarization via the ezh1/kdm3a/ctgf Axis. *Cell Death Discov* (2022) 8(1):260. doi:10.1038/s41420-022-01035-z

51. Yin J, Ge X, Shi Z, Yu C, Lu C, Wei Y, et al. Extracellular vesicles derived from hypoxic glioma stem-like cells confer temozolomide resistance on glioblastoma by delivering mir-30b-3p. *Theranostics* (2021) 11(4):1763–79. doi:10.7150/thno.47057

52. Li J, Yuan H, Xu H, Zhao H, Xiong N. Hypoxic cancer-secreted exosomal mir-182-5p promotes glioblastoma angiogenesis by targeting kruppel-like factor 2 and 4. *Mol Cancer Res* (2020) 18(8):1218–31. doi:10.1158/1541-7786.MCR-19-0725

53. Yin J, Zeng A, Zhang Z, Shi Z, Yan W, You Y. Exosomal transfer of mir-1238 contributes to temozolomide-resistance in glioblastoma. *EBioMedicine* (2019) 42:238–51. doi:10.1016/j.ebiom.2019.03.016

54. Qian M, Wang S, Guo X, Wang J, Zhang Z, Qiu W, et al. Hypoxic glioma-derived exosomes deliver microRNA-1246 to induce M2 macrophage polarization by targeting TERF2IP via the STAT3 and NF-κB pathways. *Oncogene* (2020) 39(2):428–42. doi:10.1038/s41388-019-0996-y

55. Hong S, You JY, Paek K, Park J, Kang SJ, Han EH, et al. Inhibition of tumor progression and M2 microglial polarization by extracellular vesicle-mediated microrna-124 in a 3d microfluidic glioblastoma microenvironment. *Theranostics* (2021) 11(19):9687–704. doi:10.7150/thno.60851

56. Bier A, Hong X, Cazacu S, Goldstein H, Rand D, Xiang C, et al. Mir-504 modulates the stemness and mesenchymal transition of glioma stem cells and their interaction with microglia via delivery by extracellular vesicles. *Cell Death Dis* (2020) 11(10):899. doi:10.1038/s41419-020-03088-3

57. Yan T, Wu M, Lv S, Hu Q, Xu W, Zeng A, et al. Exosomes derived from microrna-512-5p-transfected bone mesenchymal stem cells inhibit glioblastoma progression by targeting Jag1. *Aging (Albany NY)* (2021) 13(7):9911–26. doi:10.18632/aging.202747

58. Ma X, Li Z, Li T, Zhu L, Li Z, Tian N. Long non-coding rna hotair enhances angiogenesis by induction of vegfa expression in glioma cells and transmission to endothelial cells via glioma cell derived-extracellular vesicles. *Am J Transl Res* (2017) 9(11):5012–21.

59. Zhang Z, Yin J, Lu C, Wei Y, Zeng A, You Y. Exosomal transfer of long non-coding rna sbf2-as1 enhances chemoresistance to temozolomide in glioblastoma. *J Exp Clin Cancer Res* (2019) 38(1):166. doi:10.1186/s13046-019-1139-6

60. Chai Y, Wu HT, Liang CD, You CY, Xie MX, Xiao SW. Exosomal lncrna ror1-as1 derived from tumor cells promotes glioma progression via regulating mir-4686. *Int J Nanomedicine* (2020) 15:8863–72. doi:10.2147/IJN.S271795

61. Jiang Y, Zhao J, Xu J, Zhang H, Zhou J, Li H, et al. Glioblastoma-associated microglia-derived exosomal Circkif18a promotes angiogenesis by targeting Foxc2. *Oncogene* (2022) 41(26):3461–73. doi:10.1038/s41388-022-02360-4

62. Stella M, Falzone L, Caponnetto A, Gattuso G, Barbagallo C, Battaglia R, et al. Serum extracellular vesicle-derived Circhipk3 and Circsmarca5 are two novel diagnostic biomarkers for glioblastoma multiforme. *Pharmaceuticals (Basel)* (2021) 14(7):618. doi:10.3390/ph14070618

63. Scholl JN, de Fraga Dias A, Pizzato PR, Lopes DV, Moritz CEJ, Jandrey EHF, et al. Characterization and antiproliferative activity of glioma-derived extracellular vesicles. *Nanomedicine (Lond)* (2020) 15(10):1001–18. doi:10.2217/nnm-2019-0431

64. Ngo MT, Harley BAC. Perivascular signals alter global gene expression profile of glioblastoma and response to temozolomide in a gelatin hydrogel. *Biomaterials* (2019) 198:122–34. doi:10.1016/j.biomaterials.2018.06.013

65. Szatanek R, Baj-Krzyworzeka M. Cd44 and tumor-derived extracellular vesicles (tevs). Possible gateway to cancer metastasis. *Int J Mol Sci* (2021) 22(3):1463. doi:10.3390/ijms22031463

66. Lucero R, Zappulli V, Sammarco A, Murillo OD, Cheah PS, Srinivasan S, et al. Glioma-derived mirna-containing extracellular vesicles induce angiogenesis by reprogramming brain endothelial cells. *Cell Rep* (2020) 30(7):2065–74. doi:10.1016/j.celrep.2020.01.073

67. Musatova OE, Rubtsov YP. Effects of glioblastoma-derived extracellular vesicles on the functions of immune cells. *Front Cell Dev Biol* (2023) 11:1060000. doi:10.3389/fcell.2023.1060000

68. de Mooij T, Peterson TE, Evans J, McCutcheon B, Parney IF. Short non-coding rna sequencing of glioblastoma extracellular vesicles. *J Neurooncol* (2020) 146(2):253–63. doi:10.1007/s11060-019-03384-9

69. Li Q, Barres BA. Microglia and macrophages in brain homeostasis and disease. *Nat Rev Immunol* (2018) 18(4):225–42. doi:10.1038/nri.2017.125

70. Hambardzumyan D, Gutmann DH, Kettenmann H. The role of microglia and macrophages in glioma maintenance and progression. *Nat Neurosci* (2016) 19(1):20–7. doi:10.1038/nn.4185

71. Hou L, Zhao Y, Song GQ, Ma YH, Jin XH, Jin SL, et al. Interfering cellular lactate homeostasis overcomes taxol resistance of breast cancer cells through the microrna-124-mediated lactate transporter (Mct1) inhibition. *Cancer Cell Int* (2019) 19:193. doi:10.1186/s12935-019-0904-0

72. Serpe C, Monaco L, Relucenti M, Iovino L, Familiari P, Scavizzi F, et al. Microglia-derived small extracellular vesicles reduce glioma growth by modifying tumor cell metabolism and enhancing glutamate clearance through mir-124. *Cells* (2021) 10(8):2066. doi:10.3390/cells10082066

73. Kiyokawa J, Kawamura Y, Ghouse SM, Acar S, Barcin E, Martinez-Quintanilla J, et al. Modification of extracellular matrix enhances oncolytic adenovirus immunotherapy in glioblastoma. *Clin Cancer Res* (2021) 27(3):889–902. doi:10.1158/1078-0432.CCR-20-2400

74. Kim K, Kim IK, Yang JM, Lee E, Koh BI, Song S, et al. Soxf transcription factors are positive feedback regulators of vegf signaling. *Circ Res* (2016) 119(7):839–52. doi:10.1161/CIRCRESAHA.116.308483

75. Svensson A, Ozen I, Genove G, Paul G, Bengzon J. Endogenous brain pericytes are widely activated and contribute to mouse glioma microvasculature. *PLoS One* (2015) 10(4):e0123553. doi:10.1371/journal.pone.0123553

76. de Gooijer MC, de Vries NA, Buckle T, Buil LCM, Beijnen JH, Boogerd W, et al. Improved brain penetration and antitumor efficacy of temozolomide by inhibition of Abcb1 and Abcg2. *Neoplasia* (2018) 20(7):710–20. doi:10.1016/j.neo.2018.05.001

77. Wang Z, Yuan Y, Ji X, Xiao X, Li Z, Yi X, et al. The hippo-taz Axis mediates vascular endothelial growth factor C in glioblastoma-derived exosomes to promote angiogenesis. *Cancer Lett* (2021) 513:1–13. doi:10.1016/j.canlet.2021.05.002

78. Choi D, Montermini L, Kim DK, Meehan B, Roth FP, Rak J. The impact of oncogenic egfrviii on the proteome of extracellular vesicles released from glioblastoma cells. *Mol Cell Proteomics* (2018) 17(10):1948–64. doi:10.1074/mcp.RA118.000644

79. Yang ZJ, Bi QC, Gan LJ, Zhang LL, Wei MJ, Hong T, et al. Exosomes derived from glioma cells under hypoxia promote angiogenesis through up-regulated exosomal connexin 43. *Int J Med Sci* (2022) 19(7):1205–15. doi:10.7150/ijms.71912

80. Wang M, Pan W, Xu Y, Zhang J, Wan J, Jiang H. Microglia-mediated neuroinflammation: a potential target for the treatment of cardiovascular diseases. *J Inflamm Res* (2022) 15:3083–94. doi:10.2147/JIR.S350109

81. Himes BT, Peterson TE, de Mooij T, Garcia LMC, Jung MY, Uhm S, et al. The role of extracellular vesicles and Pd-L1 in glioblastoma-mediated immunosuppressive monocyte induction. *Neuro Oncol* (2020) 22(7):967–78. doi:10.1093/neuonc/noaa029

82. Thompson LF, Eltzschig HK, Ibla JC, Van De Wiele CJ, Resta R, Morote-Garcia JC, et al. Crucial role for ecto-5'-nucleotidase (Cd73) in vascular leakage during hypoxia. *J Exp Med* (2004) 200(11):1395–405. doi:10.1084/jem.20040915

83. Wang M, Jia J, Cui Y, Peng Y, Jiang Y. Cd73-Positive extracellular vesicles promote glioblastoma immunosuppression by inhibiting T-cell clonal expansion. *Cell Death Dis* (2021) 12(11):1065. doi:10.1038/s41419-021-04359-3

84. Liang T, Wang X, Wang F, Feng E, You G. Galectin-9: a predictive biomarker negatively regulating immune response in glioma patients. *World Neurosurg* (2019) 132:e455–e62. doi:10.1016/j.wneu.2019.08.117

85. Wang M, Cai Y, Peng Y, Xu B, Hui W, Jiang Y. Exosomal Lgals9 in the cerebrospinal fluid of glioblastoma patients suppressed dendritic cell antigen presentation and cytotoxic T-cell immunity. *Cell Death Dis* (2020) 11(10):896. doi:10.1038/s41419-020-03042-3

86. Vargova L, Sykova E. Astrocytes and extracellular matrix in extrasynaptic volume transmission. *Philos Trans R Soc Lond B Biol Sci* (2014) 369(1654): 20130608. doi:10.1098/rstb.2013.0608

87. Brandao M, Simon T, Critchley G, Giamas G. Astrocytes, the rising stars of the glioblastoma microenvironment. *Glia* (2019) 67(5):779–90. doi:10.1002/glia.23520

88. Oushy S, Hellwinkel JE, Wang M, Nguyen GJ, Gunaydin D, Harland TA, et al. Glioblastoma multiforme-derived extracellular vesicles drive normal astrocytes towards a tumour-enhancing phenotype. *Philos Trans R Soc Lond B Biol Sci* (2018) 373(1737):20160477. doi:10.1098/rstb.2016.0477

89. Zeng A, Wei Z, Rabinovsky R, Jun HJ, El Fatimy R, Deforzh E, et al. Glioblastoma-derived extracellular vesicles facilitate transformation of astrocytes via reprogramming oncogenic metabolism. *iScience* (2020) 23(8):101420. doi:10.1016/j.isci.2020.101420

90. Biasoli D, Sobrinho MF, da Fonseca AC, de Matos DG, Romao L, de Moraes Maciel R, et al. Glioblastoma cells inhibit astrocytic P53-expression favoring cancer malignancy. *Oncogenesis* (2014) 3(10):e123. doi:10.1038/oncsis.2014.36

91. Laurenti E, Wilson A, Trumpp A. Myc's other life: stem cells and beyond. *Curr Opin Cell Biol* (2009) 21(6):844–54. doi:10.1016/j.ceb.2009.09.006

92. Hallal S, Mallawaaratchy DM, Wei H, Ebrahimkhani S, Stringer BW, Day BW, et al. Extracellular vesicles released by glioblastoma cells stimulate normal astrocytes to acquire a tumor-supportive phenotype via P53 and myc signaling pathways. *Mol Neurobiol* (2019) 56(6):4566–81. doi:10.1007/s12035-018-1385-1

93. Neagu MR, Huang RY, Reardon DA, Wen PY. How treatment monitoring is influencing treatment decisions in glioblastomas. *Curr Treat Options Neurol* (2015) 17(4):343. doi:10.1007/s11940-015-0343-8

94. Marei HE, Althani A, Afifi N, Hasan A, Caceci T, Cifola I, et al. Glioma extracellular vesicles for precision medicine: prognostic and theragnostic application. *Discov Oncol* (2022) 13(1):49. doi:10.1007/s12672-022-00514-0

95. Zhou B, Xu K, Zheng X, Chen T, Wang J, Song Y, et al. Application of exosomes as liquid biopsy in clinical diagnosis. *Signal Transduct Target Ther* (2020) 5(1):144. doi:10.1038/s41392-020-00258-9

96. Macedo-Pereira A, Martins C, Lima J, Sarmento B. Digging the intercellular crosstalk via extracellular vesicles: may exosomes Be the drug delivery solution for target glioblastoma? *J Control Release* (2023) 358:98–115. doi:10.1016/j.jconrel.2023.04.038

97. Osti D, Del Bene M, Rappa G, Santos M, Matafora V, Richichi C, et al. Clinical significance of extracellular vesicles in plasma from glioblastoma patients. *Clin Cancer Res* (2019) 25(1):266–76. doi:10.1158/1078-0432.CCR-18-1941

98. Akers JC, Ramakrishnan V, Kim R, Skog J, Nakano I, Pingle S, et al. Mir-21 in the extracellular vesicles (evs) of cerebrospinal fluid (csf): a platform for glioblastoma biomarker development. *PLoS One* (2013) 8(10):e78115. doi:10.1371/journal.pone.0078115

99. Sabbagh Q, Andre-Gregoire G, Guevel L, Vesiclemia GJ. Vesiclemia: counting on extracellular vesicles for glioblastoma patients. *Oncogene* (2020) 39(38):6043–52. doi:10.1038/s41388-020-01420-x

100. Catalano M, O'Driscoll L. Inhibiting extracellular vesicles formation and release: a review of ev inhibitors. *J Extracell Vesicles* (2020) 9(1):1703244. doi:10.1080/20013078.2019.1703244

101. Fox JE, Austin CD, Reynolds CC, Steffen PK. Evidence that agonist-induced activation of calpain causes the shedding of procoagulant-containing microvesicles from the membrane of aggregating platelets. *J Biol Chem* (1991) 266(20):13289–95. doi:10.1016/s0021-9258(18)98837-x

102. Atanassoff AP, Wolfmeier H, Schoenauer R, Hostettler A, Ring A, Draeger A, et al. Microvesicle shedding and lysosomal repair fulfill divergent cellular needs during the repair of streptolysin O-induced plasmalemmal damage. *PLoS One* (2014) 9(2):e89743. doi:10.1371/journal.pone.0089743

103. Jorfi S, Ansa-Addo EA, Kholia S, Stratton D, Valley S, Lange S, et al. Inhibition of microvesiculation sensitizes prostate cancer cells to chemotherapy and reduces docetaxel dose required to limit tumor growth *in vivo*. *Sci Rep* (2015) 5: 13006. doi:10.1038/srep13006

104. Cai L, Li Q, Li W, Wang C, Tu M, Zhu Z, et al. Calpain suppresses cell growth and invasion of glioblastoma multiforme by producing the cleavage of filamin A. *Int J Clin Oncol* (2020) 25(6):1055–66. doi:10.1007/s10147-020-01636-7

105. Stillger MN, Chen CY, Lai ZW, Li M, Schafer A, Pagenstecher A, et al. Changes in calpain-2 expression during glioblastoma progression predisposes tumor cells to temozolomide resistance by minimizing DNA damage and P53-dependent apoptosis. *Cancer Cell Int* (2023) 23(1):49. doi:10.1186/s12935-023-02889-8

106. Datta A, Kim H, Lal M, McGee L, Johnson A, Moustafa AA, et al. Manumycin a suppresses exosome biogenesis and secretion via targeted inhibition of ras/raf/erk1/2 signaling and hnrnp H1 in castration-resistant prostate cancer cells. *Cancer Lett* (2017) 408:73–81. doi:10.1016/j.canlet.2017.08.020

107. Munson JM, Fried L, Rowson SA, Bonner MY, Karumbaiah L, Diaz B, et al. Anti-invasive adjuvant therapy with imipramine blue enhances chemotherapeutic efficacy against glioma. *Sci Transl Med* (2012) 4(127):127ra36. doi:10.1126/scitranslmed.3003016

108. Xu X, Liu Y, Li Y, Chen H, Zhang Y, Liu J, et al. Selective exosome exclusion of mir-375 by glioma cells promotes glioma progression by activating the ctgf-egfr pathway. *J Exp Clin Cancer Res* (2021) 40(1):16. doi:10.1186/s13046-020-01810-9

109. Munoz JL, Bliss SA, Greco SJ, Ramkissoon SH, Ligon KL, Rameshwar P. Delivery of functional anti-mir-9 by mesenchymal stem cell-derived exosomes to glioblastoma multiforme cells conferred chemosensitivity. *Mol Ther Nucleic Acids* (2013) 2(10):e126. doi:10.1038/mtna.2013.60

110. Geng L, Xu J, Zhu Y, Hu X, Liu Y, Yang K, et al. Targeting mir-9 in glioma stem cell-derived extracellular vesicles: a novel diagnostic and therapeutic biomarker. *Transl Oncol* (2022) 22:101451. doi:10.1016/j.tranon.2022.101451

111. Gabizon AA, de Rosales RTM, La-Beck NM. Translational considerations in nanomedicine: the oncology perspective. *Adv Drug Deliv Rev* (2020) 158:140–57. doi:10.1016/j.addr.2020.05.012

112. Benecke L, Coray M, Umbricht S, Chiang D, Figueiro F, Muller L. Exosomes: small evs with large immunomodulatory effect in glioblastoma. *Int J Mol Sci* (2021) 22(7):3600. doi:10.3390/ijms22073600

113. Simon T, Kumaran A, Veselu DF, Giamas G. Three method-combination protocol for improving purity of extracellular vesicles. *Int J Mol Sci* (2020) 21(9): 3071. doi:10.3390/ijms21093071

Glossary

ALIX	Apoptosis-linked gene 2 interacting protein X
ARRDC1	Arrestin domain-containing protein 1
ARF6	ADP-ribosylation factor 6
ARG1	Arginase 1
A2AR	Adenosine receptor 2A
BBB	Brain blood barrier
CSF	Cerebrospinal fluid
CXCR4	C-X-C chemokine receptor type 4
Cx43	Connexin 43
CNS	Central nervous system
DCs	Dendritic cells
EVs	Extracellular vesicles
ECM	Extracellular matrix
ECs	Endothelial cells
EZH1	Enhancer zeste homologue 1
ESCRT	Endosomal sorting complexes required for transport
EGFR	Epidermal growth factor receptor
EGFRvIII	EGFR mutant/variant III
GSCs	Glioblastoma stem cells
ILVs	Intraluminal vesicles
IL-6	Interleukin-6
IDO1	Indoleamine-2,3-dioxygenase 1
JAG1	Jagged 1
KLF2/4	Kruppel-like factor 2/4
LBPA	Lysobisphosphatidic acid
LMR	Lymphocyte to monocyte
lncRNAs	Long non-coding RNAs
MVBs	Multivesicular bodies
MMP9	Matrix metalloproteinase 9
MA	Manumycin A
MDSCs	Myeloid-derived suppressor cells
miRNAs	microRNAs
NLR	Neutrophil to lymphocyte
NT5E	Enzyme ecto-5′-nucleotidase
NHAs	Normal human astrocytes
nSMase	Neutral sphingomyelinase
NCMs	Nonclassical monocytes
PDGFR	Platelet derived growth factor receptor
PD-L1	Programmed death ligand-1
PD-1	Programmed cell death 1
PM	Plasma membrane
PLR	Platelet to lymphocyte
ROS	Reactive oxygen species
RBPs	RNA binding proteins
RGS5	G protein signaling 5
RP	Ribosomal protein
SASP	Senescence-associated secretory phenotype
S1P	Sphingosine-1-phosphate
STAT3	Signal transducer and activator of transcription 3
TME	Tumor microenvironment
TSG101	Tumor susceptibility gene-101
TMZ	Temozolomide
TC	Tumor cells
TAMs	Tumor-associated macrophages
TGF-β	Transforming growth factor-β
TNF-α	Tumor necrosis factor-α
TERF2IP	Telomeric repeat binding factor 2 interacting protein
TIM-3	T cell immunoglobulin domain and mucin domain-3
TAAs	Tumor associated astrocytes
VEGF	Vascular endothelial growth factor
VSP4	Vacuolar protein sorting-associated protein 4
WHO	World Health Organization
ZEB1	Zinc finger E-box binding homeobox 1

Pathology & Oncology Research | frontiers

TYPE Original Research
PUBLISHED 26 September 2023
DOI 10.3389/pore.2023.1611391

Check for updates

OPEN ACCESS

EDITED BY
Andrea Ladányi,
National Institute of Oncology (NIO), Hungary

*CORRESPONDENCE
Hao Pan,
Panhao_nz@163.com

RECEIVED 06 July 2023
ACCEPTED 12 September 2023
PUBLISHED 26 September 2023

CITATION
Wang Q, Liang Q, Wei W, Niu W, Liang C, Wang X, Wang X and Pan H (2023), Concordance analysis of cerebrospinal fluid with the tumor tissue for integrated diagnosis in gliomas based on next-generation sequencing.
Pathol. Oncol. Res. 29:1611391.
doi: 10.3389/pore.2023.1611391

COPYRIGHT
© 2023 Wang, Liang, Wei, Niu, Liang, Wang, Wang and Pan. This is an open-access article distributed under the terms of the Creative Commons Attribution License (CC BY). The use, distribution or reproduction in other forums is permitted, provided the original author(s) and the copyright owner(s) are credited and that the original publication in this journal is cited, in accordance with accepted academic practice. No use, distribution or reproduction is permitted which does not comply with these terms.

Concordance analysis of cerebrospinal fluid with the tumor tissue for integrated diagnosis in gliomas based on next-generation sequencing

Qiang Wang[1], Qiujin Liang[2], Wuting Wei[1], Wenhao Niu[1], Chong Liang[1], Xiaoliang Wang[1], Xiaoxuan Wang[2] and Hao Pan[1]*

[1]Department of Neurosurgery, Jinling Hospital, Nanjing, China, [2]State Key Laboratory of Neurology and Oncology Drug Development, Jiangsu Simcere Diagnostics Co., Ltd., Nanjing, China

Purpose: The driver mutations of gliomas have been identified in cerebrospinal fluid (CSF). Here we compared the concordance between CSF and tumor tissue for integrated diagnosis in gliomas using next-generation sequencing (NGS) to evaluate the feasibility of CSF detection in gliomas.

Patients and methods: 27 paired CSF/tumor tissues of glioma patients were sequenced by a customized gene panel based on NGS. All CSF samples were collected through lumbar puncture before surgery. Integrated diagnosis was made by analysis of histology and tumor DNA molecular pathology according to the 2021 WHO classification of the central nervous system tumors.

Results: A total of 24 patients had detectable circulating tumor DNA (ctDNA) and 22 had at least one somatic mutation or chromosome alteration in CSF. The ctDNA levels varied significantly across different ages, Ki-67 index, magnetic resonance imaging signal and glioma subtypes ($p < 0.05$). The concordance between integrated ctDNA diagnosis and the final diagnosis came up to 91.6% (Kappa, 0.800). We reclassified the clinical diagnosis of 3 patients based on the results of CSF ctDNA sequencing, and 4 patients were reassessed depending on tumor DNA. Interestingly, a rare *IDH1* R132C was identified in CSF ctDNA, but not in the corresponding tumor sample.

Conclusion: This study demonstrates a high concordance between integrated ctDNA diagnosis and the final diagnosis of gliomas, highlighting the practicability of NGS based detection of mutations of CSF in assisting integrated diagnosis of gliomas, especially glioblastoma.

KEYWORDS

cerebrospinal fluid, glioma, circulating tumor DNA, integrated diagnosis, IDH1 R132C

Introduction

Central nervous system (CNS) tumors present survival challenges for people because of high incidence and high mortality. Glioma is the most common primary CNS tumor, accounting for 80.8% of the malignant CNS tumors in adults [1]. Integrated diagnosis of the CNS tumors has been updated and highlighted by the World Health Organization (WHO) since the discovery of novel molecular markers in recent years [2]. A comprehensive molecular profiling of glioma can provide more detailed information on biological classifications.

The method of integrating histological and molecular characteristics heightens the objectivity of CNS tumor diagnosis and prompts the precision treatment for the CNS tumors. Mutations including IDH (*IDH1* and *IDH2*), 1p/19q codeletion, *EGFR* amplification, amplification of chromosome 7 and loss of chromosome 10 (+7/−10), *TERT* promoter alteration, *ATRX* deletion, *TP53* positive, and *CDKN2A/B* deletion are usually used for molecular diagnosis and stratification of most patients with gliomas [2]. Identification of such biomarkers in brain tumors is critical for the diagnosis, treatment, and prognosis of patients. The tumor tissue obtained from surgery has been widely used for clinical diagnosis and personalized medicine decision-making [3]. However, tumor tissue sampling in gliomas is affected by invasive craniotomy. The randomness of sampling means that it cannot completely represent the whole tumor feature. Liquid biopsy, a new cancer diagnostic technique, is minimally invasive and able to monitor potential dynamic changes in the tumors [4].

Cell-free circulating tumor DNA (ctDNA) is shed by tumor cells, and can be found in circulating blood, along with normal cells [5]. The clinical use of ctDNA has been evaluated in a variety of fields, including cancers [6]. Obviously, the amount of ctDNA in peripheral circulation is low by virtue of the low permeability of blood-brain barrier in gliomas [6, 7]. Cerebrospinal fluid (CSF) as an important source of potential molecular biomarkers contains various biomarkers, such as ctDNA, circulating tumor cells, miRNA, and extracellular vesicles, which are usually derived from brain tumor cells [8]. Previous studies showed that CSF was more sensitive than peripheral blood in the detection of DNA mutations, epigenetic alterations, and copy number variations, indicating the possibility of CSF ctDNA for precise diagnosis [9–11].

In this study, we performed a comprehensive genomic analysis based on targeted next-generation sequencing (NGS) of DNA from the tumor tissue and CSF ctDNA of 27 glioma patients, aiming at determining the feasibility of ctDNA from CSF in Chinese population. We compared the mutational and diagnostic concordance between the tumor tissue and CSF and revealed the utility of CSF ctDNA for advancing and complementing the diagnosis of gliomas.

Materials and methods

Patients and samples

We prospectively collected the clinical data of 27 glioma patients admitted to Nanjing Jinling Hospital (Nanjing, China) from December 2020 to July 2021. All patients were confirmed with glioma by magnetic resonance imaging (MRI). CSF samples (4–8 mL) were collected from the lumbar puncture before surgery. Tumor tissue samples were collected from surgical specimens, and part of removed tumor tissue was used for histopathologic diagnosis. 4 CSF samples were collected from patients with encephalitis as normal controls. In accordance with the Declaration of Helsinki, written informed consent was obtained from all individuals or guardians, and the study was approved by the Institutional Review Board of Nanjing Jinling Hospital (2022DZKY-093-01) and local regulations.

DNA extraction and quantification

Cell-free DNA (cfDNA) was extracted using an Apostle MiniMax High Efficiency cfDNA Isolation Kit (APOSTLE) according to the manufacturer's instructions. Fresh tissue DNA was extracted using a QIAamp DNA Tissue & Blood Kit (Qiagen) according to the manufacture's recommendations. Extracted cfDNA and DNA were quantified by Qubit4.0 (Life Technologies) according to the manufacturer's protocols. Quantitative levels of CSF cfDNA were measured in haploid genome equivalents per milliliter (hGE/mL), which was calculated as the result of total cfDNA concentration and the mean allele fraction of somatic mutations.

NGS library establishment and sequencing

NGS libraries of tumor tissue DNA were prepared with KAPA HyperPlus Kit (Roche). cfDNA libraries were established with the xGenTM Prism DNA Library Prep Kit (IDT). After hybridization of DNA and cfDNA libraries, the captured libraries were amplified by polymerase chain reaction (PCR) according to the manufacturer's protocols. As described previously, we performed the targeted sequencing by NGS with the panel containing 131 genes and 4 chromosomes (131 + 4 panel) related to brain tumors (see Supplementary Table S1 for gene list) [12]. Sequencing was carried out using NovaSeq 6000 system in this study.

Bioinformatics analysis

All CSF and tumor samples were measured for single nucleotide variants (SNVs), copy number variants (CNVs),

and chromosomal variations. Initial sequencing reads were trimmed and filtered with fastp (v.2.20.0) and then aligned against the human reference genome (hg19) using BWA-mem (v.0.7.17). The realignment of local regions was performed to improve the accuracy of variant detection around Indels using ABRA2.

We used VarDict (v.1.5.7) for variant detection. The results of variant detection were annotated to multiple databases using SnpEff and ANNOVAR software, including dbNSFP (v.4.2a), COSMIC (v.9.6), gnomAD (v.3.11), ClinVar and more. According to annotation results, the filtration was further conducted, and the background baseline was used to filter systematic false positive results. In combination of Intervar results and pathogenic interpretation from databases including ClinVar, somatic and germline mutations were finally identified. Threshold for mutation calling is ≥0.5% variant allele frequency (VAF) in CSF and ≥1.0% VAF in tumor tissue.

The original sequencing depth was counted, which was standardized to exclude the influence of the amount of sequencing data. The CNVkit algorithm was used to construct the background distribution model of the copy number with normal genomic sequencing. CNVs were determined based on the difference between the copy number in each region of the sample and the background model. The structural variations of chromosomes were determined according to the copy number distribution of the whole chromosome arm. CNVs were analyzed by CNVkit (dx1.1). We used CSF from the patients with non-tumor diseases as the baseline, and mutations that were identified as false positive were excluded.

Immunohistochemical staining detection

Hematoxylin and eosin staining and immunohistochemistry (IHC) were performed on 4 μm-thick sections using standard protocols. IHC stains contains Ki-67 (Roche), and IDH1 R132H (Agilent).

Integrated diagnosis

All cases were comprehensively diagnosed and reviewed by the two pathologists (NYL and NW) using histology, as well as molecular features of tumor DNA according to the 2021 WHO CNS classification criteria and the Consortium to Inform Molecular and Practical Approaches to CNS Tumour Taxonomy group in 2018–2020 [2, 13–16].

Statistical analysis

Statistical analysis and plots were conducted by Graphpad Prism 5 and IBM SPSS statistics software version 19. Quantitative ctDNA differences across different characteristics of patients were assessed using Mann-Whitney U test. Spearman's rank correlation coefficient test was used to evaluate the association between the tissue DNA and CSF ctDNA with SNVs and CNVs. *p*-values lower than 0.05 were considered as statistically significant. To assess the possibility of CSF ctDNA test for glioma diagnosis, we performed a receiver operating characteristic (ROC) curve analysis. Consistency of diagnosis was examined by Kappa measure of agreement. The Kappa values were categorized as "almost perfect" (0.8–1.0), "fair to good" (0.4–0.8), or "poor" (below 0.2) [17].

Results

Clinicopathological characteristics and detection of ctDNA levels

Twenty-seven gliomas were recruited for the CSF and tumor biopsy tissue collection. Histopathological subtypes included glioblastoma (GBM, n = 13), astrocytoma (n = 6), pilocytic astrocytoma (n = 2), pleomorphic xanthoastrocytoma (n = 2), oligodendroglioma (n = 1), ganglioglioma (n = 1), glioneuronal tumor (n = 1), and gliosarcoma (n = 1). The median age of the participants was 54 years (range 15–78 years) and 66.7% (n = 18) were male. These patients were confirmed pathologically and classified into histological grade I (n = 3), grade II (n = 6), grade III (n = 4), grade IV (n = 14). After surgery, 63.0% (n = 19) patients received standard Stupp treatments, including adjuvant radiotherapy and temozolomide (TMZ) chemotherapy, 11.1% (n = 3) patients received adjuvant radiotherapy. The characteristics of these patients were presented in Table 1.

We measured the ctDNA level among 27 CSF samples and found the ctDNA level showed significant differences across age (p = 0.025, Figure 1A), Ki-67 index (p = 0.013, Figure 1B), MRI signal (p = 0.004, Figure 1C), and tumor subtypes (p = 0.001, Figure 1D). There was no significant association of ctDNA levels with other clinical characteristics, including tumor size (p = 0.064), ventricular involvement (p = 0.303), tumor number (p = 0.644) and location (p = 0.762), as well as involvement of cerebral cortex (p = 0.769) (Figures 1E–I).

Genomic profiling of gliomas from CSF ctDNA and tumor tissue DNA

Twenty-seven patients were all detected using 131 + 4 panel, and 3 of them were excluded on the grounds of their undetectable ctDNA concentration. We identified at least 1 tumor-related gene mutation or chromosome variant from CSF ctDNA of 22 patients, consistent with the number of tumor tissue DNA

TABLE 1 Patient characteristics, n(%).

Total		n = 27		
Age, years		54.1 ± 16.6		
Gender	Male		Female	
	18 (66.7)		9 (33.3)	
Histologic grade	I	II	III	IV
	3 (11.1)	6 (22.2)	4 (14.8)	14 (51.9)
Recurrence		1 (3.7)		
Post-Treatment	Treatment Naïve	RT	TMZ	TTField
	3 (11.1)	21 (77.9)	19 (70.4)	1 (3.7)
Tumor size	<57 mm	≥57 mm		Missing
	15 (55.6)	9 (33.3)		3 (11.1)
Tumor location	Supratentorial	Infratentorial		Missing
	23 (85.2)	3 (11.1)		1 (3.7)
MRI signal	Enhancement	Non-enhancement		Missing
	15 (55.6)	8 (29.6)		4 (14.8)
Characteristics	Multi lesions	Non-multi lesions		Missing
	8 (29.6)	18 (66.7)		1 (3.7)
	Involving ventricle	Not-involving ventricle		Missing
	20 (74.1)	5 (18.5)		2 (7.4)
	Involving cerebral cortex	Not-involving cerebral cortex		Missing
	14 (51.9)	10 (37.0)		3 (11.1)
	Ki 67 <20%	Ki 67 ≥20%		Missing
	8 (29.6)	14 (51.9)		5 (18.5)

Abbreviations: MRI, magnetic resonance imaging; RT, radiotherapy; TMZ, temozolomide; TTField, tumor-treating field.

samples (Figure 2). In contrast, we did not detect any oncogenic alterations in four individuals with encephalitis. Based on the cancer targeted panel, 32 mutant genes were detected in 24 gliomas. Of them, *TERT* was the most prevalent gene. *TERT* promoter mutations were detected in 12 (50%) of patients via CSF, while were identified in 16 (66.7%) of patients though tumor tissue. The concordance with the *TERT* mutation status between CSF and tumor tissue yielded 83.3%. The mutations were detected both in tumor tissue and CSF samples, apart from *FLT4* and *CIC* mutations. Abnormal gene copy number was found in 10 patients for CSF ctDNA. The coincidence between CSF and tumor tissue for *CDKN2A/B* deletion was 87.5%. However, 8 patients presented with *PTEN* deletion in tumor DNA but not detected in CSF ctDNA. Alterations of chromosome chr 1p, chr 19q, chr 7, or chr 10 were detected in 11 CSF samples.

Concordance of SNVs and CNVs in matched tumor/CSF pairs

We examined the concordance between SNVs and CNVs detected in tumor/CSF pairs. Comparison of CSF ctDNA and tumor DNA showed a moderately preferential correlation in the variant allele frequency (r = 0.64, p < 0.0001; Figure 3A) and a high correlation in the copy number (r = 0.86; p < 0.0001; Figure 3B). The most mutated genes in tumor samples and CSF ctDNA were *TERT*, *TP53*, *EGFR*, *PTEN*, *PIK3CA*, and *PDGFRA* (Figure 3C), which were completely shared in 18 patients, yielding an overall concordance rate of 81.8% between tumor and CSF ctDNA samples (Figure 3D). In addition, 5 out of 24 patients showed a gene concordance of less than 50%. Interestingly, the sensitivity of CSF in glioma was less than the tumor tissue in the detection of +7/−10 and *TERT* mutations, but presented a superior detection ability for *TP53* mutations and *EGFR* amplification (Figure 3E).

Performance of CSF ctDNA in diagnosis of glioma

To further explore the performance of CSF ctDNA test, ROC curves for integrated diagnosis of all gliomas were generated (Figure 4). CSF ctDNA performed well in diagnosis of GBMs with the area under the curve (AUC) of 1 (95% CI: 1–1; Figure 4A). We also tested the possibility of CSF ctDNA as a strong classifier of non-GBM diagnosis (AUC = 0.82, 95% CI: 0.65–0.99, Figure 4B). When

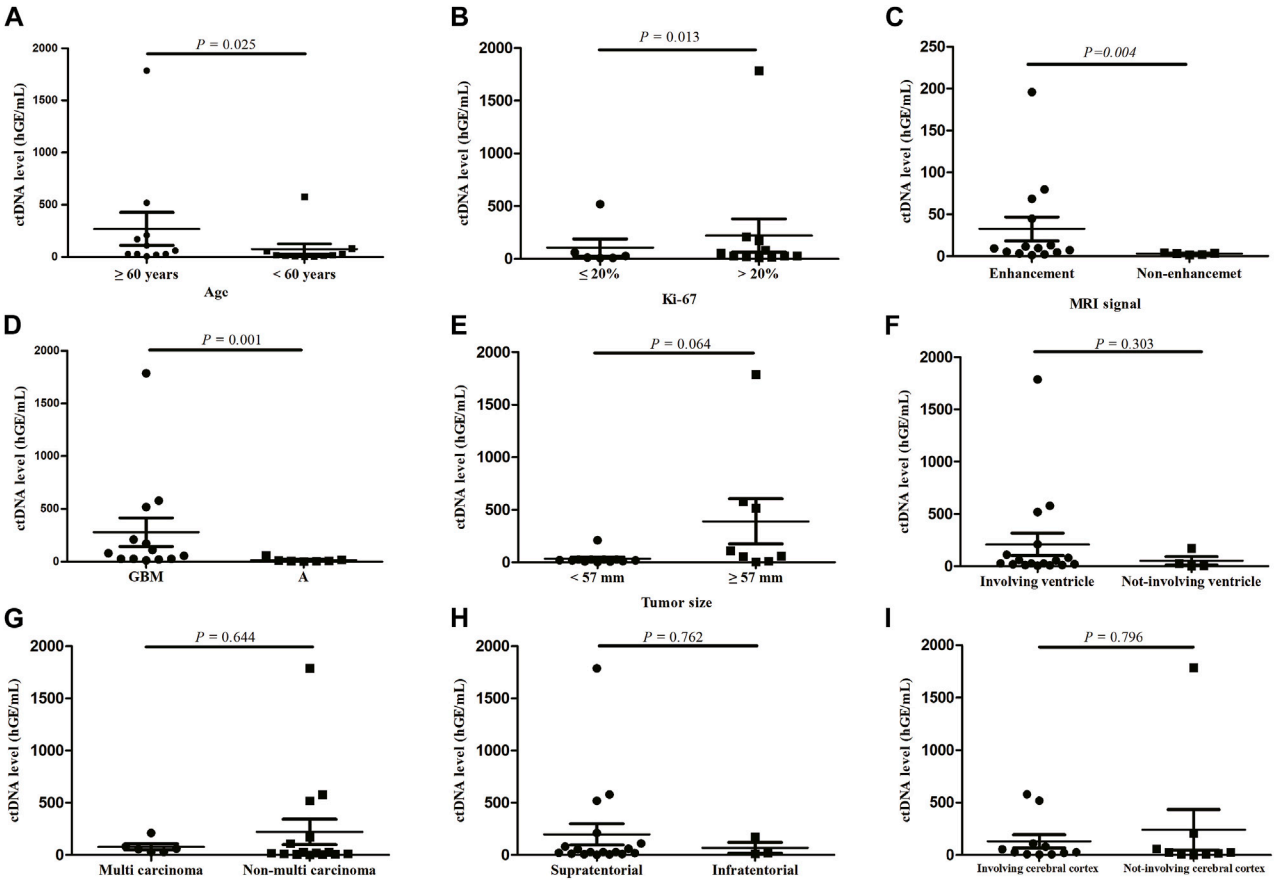

FIGURE 1
ctDNA levels according to patient characteristics, **(A)** age, **(B)** Ki-67, **(C)** MRI signal, **(D)** tumor subtypes, **(E)** tumor size, **(F)** ventricular involvement, **(G)** tumor number, **(H)** location, **(I)** involvement of cerebral cortex. Quantitative ctDNA levels were compared by Mann-Whitney U test. GBM, glioblastoma; A, astrocytoma.

3 cases with low ctDNA concentration was excluded, an AUC of 0.91 (95% CI: 0.77–1, Supplementary Figure S1A) was reached. Additionally, for patients with enhanced MRI signal, the AUC value was 1 (95% CI: 1–1; Supplementary Figure S1B).

We established a new integrated diagnostic method by combining histology with tumor DNA and CFS ctDNA as the final diagnosis, which was used as the positive control. The diagnostic diagram of histology, and histology combined with CSF ctDNA and tumor DNA molecular features was revealed in Figure 5. The diagnosis of 5 patients were amended based on the integrated histological and molecular criteria, including 1 GBM and 4 astrocytomas. Among these, the diagnosis of 4 patients was rectified based upon histology and tumor DNA. In addition, there were 3 patients whose diagnosis was corrected depending on the histological and CSF ctDNA data. Kappa measure of agreement was used to determine whether the diagnosis was consistent and found the agreement between CSF and positive control was better. The agreement between CSF ctDNA and positive control was 91.6% (Kappa, 0.800), indicating a high concordance. Meanwhile, the conformity between histology and positive control was 79.1% (Kappa, 0.565), and the consistency in diagnosis between tumor DNA and positive control was 95.8% (Kappa, 0.895). The genotyping consistency of GBM was completely matched for CSF.

Glioma subtyping and risk stratification based on CSF ctDNA

We found that CSF ctDNA sequencing could identify the glioma subtyping and determine the patient risk level. *IDH1/2* mutation was highly associated with the prolonged overall survival (OS).17 Case 11, a 59 year-old woman, was diagnosed as anaplastic pleomorphic xanthoastrocytoma, WHO Ⅲ, in September 2019, and recurred in March 2021 with histologically confirmed as GBM, WHO IV (Figure 6A). *IDH1* was positive at the time of initial diagnosis but negative at the

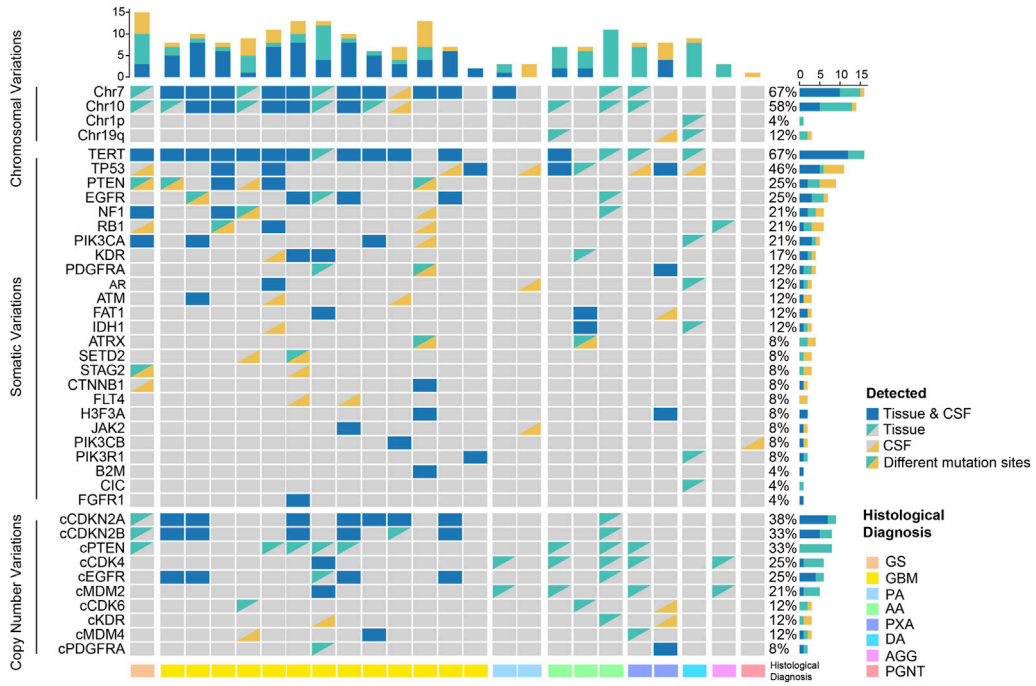

FIGURE 2
Genomic profiling in the spectra of CSF ctDNA and tumor DNA. GS, gliosarcoma; GBM, glioblastoma; PA, pilocytic astrocytoma; AA, anaplastic astrocytoma; PXA, pleomorphic xanthoastrocytoma; DA, diffuse astrocytoma; AGG, anaplastic ganglioglioma; PGNT, papillary glioneuronal tumor.

time of recurrence according to immunohistochemical results. Next, tumor DNA sequencing failed to capture the mutation in *IDH1*, however, CSF ctDNA sequencing showed a rare mutation of R132C in IDH1, and corrected the tumor diagnosis into IDH1-mutated astrocytoma, WHO IV, according to CSF test. This patient experienced recurrence in the left temporal-occipital lobe, with greater possibilities of secondary GBM with IDH1 mutation. The remaining 4 genes were found as the shared alterations.

We also found different mutations between tumor DNA and CSF ctDNA sequencing. Case 13, a 78 year-old man with GBM, +7/−10 and *ATM* mutation were found in the CSF ctDNA but not in the tumor DNA, at the same time, loss of *CDKN2B* was only found in tumor DNA (Figure 6B). Three shared somatic mutation genes were identified between the tumor and the CSF, namely *TERT*, *PI3KCB*, and *CDKN2A* (Figure 6C). Importantly, these results suggested that the CSF ctDNA analysis can be invoked as an appropriate diagnostic tool to classify and stratify for some cases.

Discussion

The 5 years survival rate of malignant CNS tumors was only 23.5%, which creates a great challenge for human health [1]. The publishing of the fourth and fifth edition of the WHO classification of tumors of the CNS underlined the importance of molecular diagnosis [2, 18]. Previous studies indicated that CSF could be used as an effective source of ctDNA for genotyping gliomas and monitoring tumor evolution [10, 19, 20], but the consistency of paired CSF and tumor of gliomas remains unclear. We prospectively collected 27 paired CSF and tumor tissue from surgical patients with gliomas and compared multiple gene mutations by using an NGS-based customized panel.

Currently, there are various methods for glioma liquid biopsy in CSF, such as Sanger sequencing, droplet digital (dd) PCR, and next-generation sequencing [21]. Sanger sequencing can detect gene variations with high precision. Since the ctDNA from CSF is limited, sequencing technologies should be improved [21]. Although ddRCR has satisfactory sensitivity for CSF ctDNA analysis, the throughput on variant analysis is still low and only can discover the known mutations [22]. NGS significantly compensates for Sanger sequencing and ddPCR deficiencies with improving the throughput of detection. Moreover, NGS can simultaneously capture known or unknown genetic mutations, cover the mutation types that cannot be detected by ddPCR or Sanger sequencing, and identify the chromosomal abnormalities [23]. Piccioni et al. found 55% of GBMs in blood ctDNA had at least one somatic alteration by a ctDNA NGS panel [24]. Miller et al. used NGS to analyze CSF samples and identified at least one tumor-derived

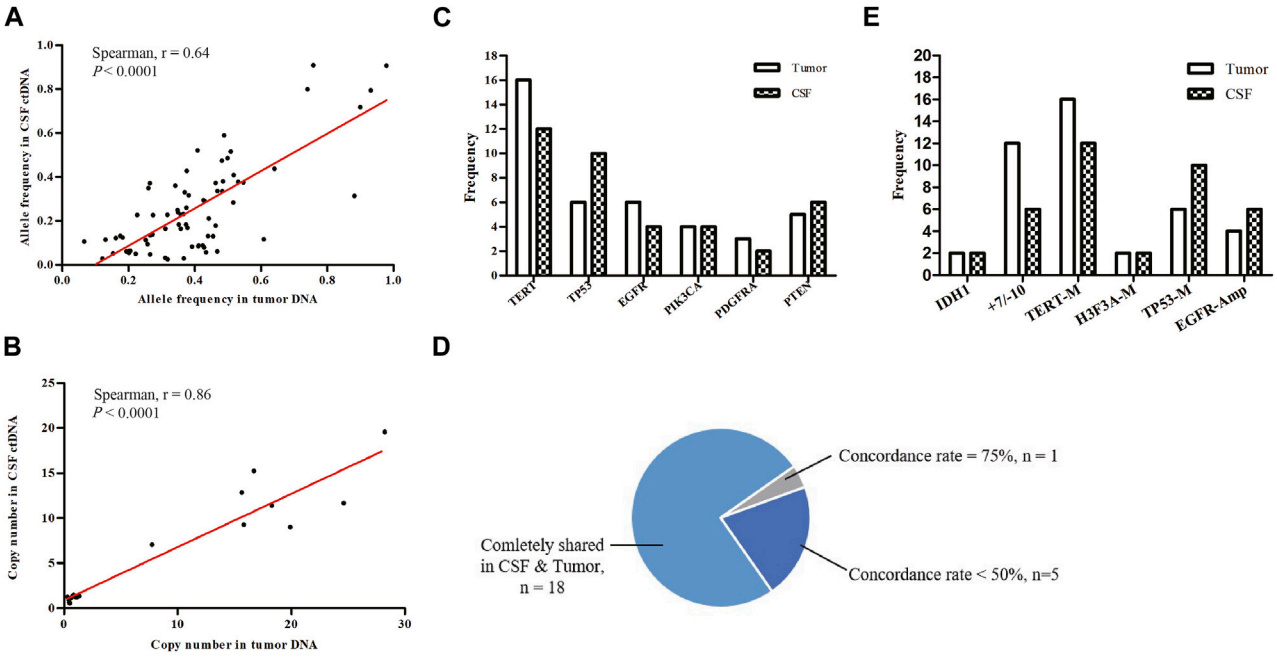

FIGURE 3
Mutational concordance between CSF ctDNA and tumor DNA. **(A)** Scatter plots of variant allele frequencies for all SNVs in CSF ctDNA and tumor DNA. **(B)** Scatter plots of copy number for all CNVs in CSF ctDNA and tumor DNA. Linear regression was calculated by Spearman correlation. Tumor and CSF profiles of high-frequency mutant genes **(C)** and key prognosis-related genes **(E)**. **(D)** Proportions of consistency between CSF and tumor high-frequency mutant genes were presented as a fan diagram.

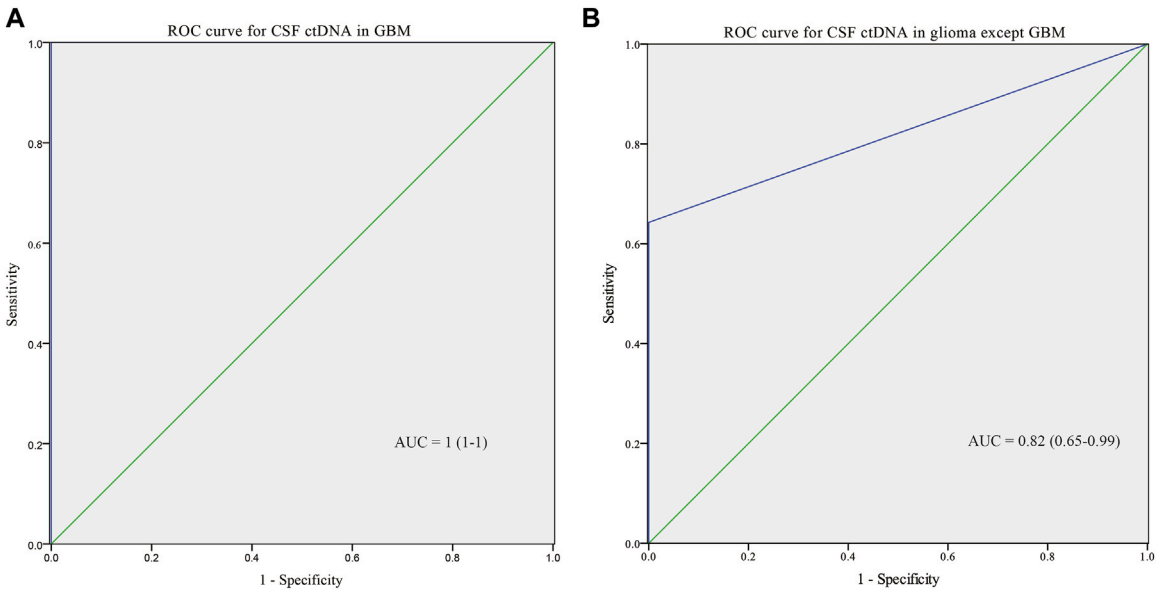

FIGURE 4
ROC curve for CSF ctDNA in GBM **(A)** and non-GBM **(B)**.

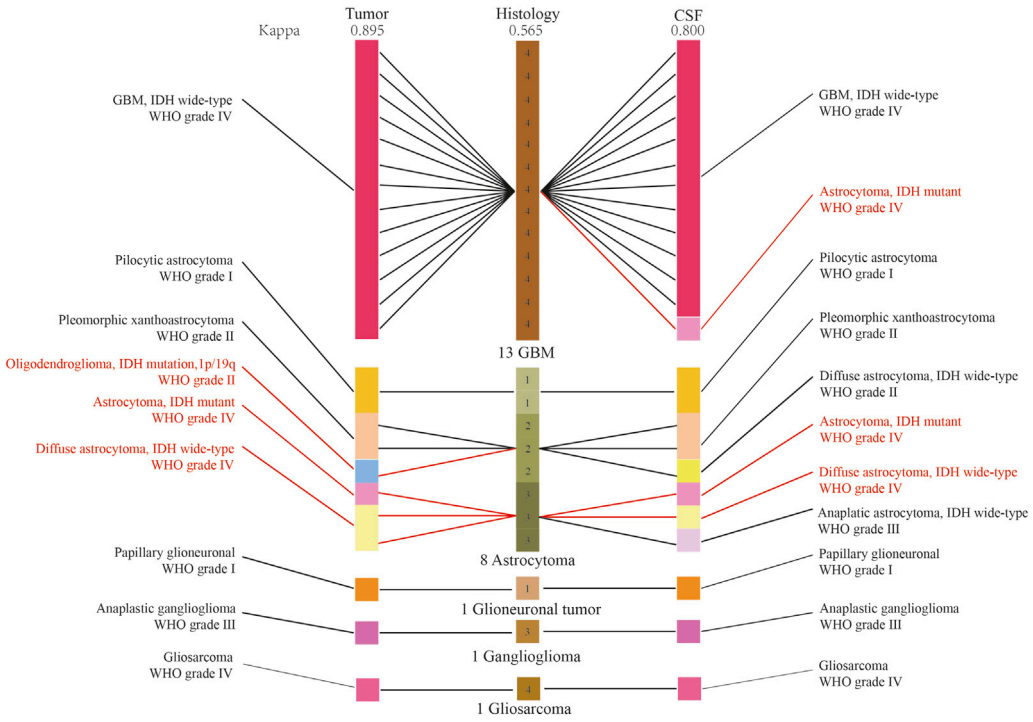

FIGURE 5
The diagnostic diagram of histology, and histology combined with CSF ctDNA and tumor DNA molecular features. The red character indicated the diagnoses were reclassified. Kappa measure of agreement was used to determine whether the diagnosis was consistent.

DNA alteration in 42/85 patients with diffuse glioma [10]. We utilized a 131 + 4 gene panel based on NGS and demonstrated that 87.5% of gliomas harbored at least one somatic variation in CSF. Among the 24 patients with positive CSF cfDNA, we identified 18 cases with at least one mutation shared in tumor tissue and CSF. A prior study found that there was a shared somatic mutation between the tumor and CSF in pediatric, adolescent, and young adult brain tumors using MSK-IMPACT panel [20]. All CSF samples were obtained before surgery, aiming at aiding in integrated diagnosis. The sensitivity and specificity of our NGS-based method for CSF ctDNA detection was both better in GBM diagnosis, indicating that this detection technique may be appropriate for diagnosing higher-grade gliomas.

In our study, 3 patients (2 astrocytoma, 1 oligodendroglioma) with grade II diagnosed by histology showed ctDNA concentration below the detection limit. In general, people with CNS tumors harbored a very low ctDNA level in CSF, although it was much higher in CSF than in blood [6, 25]. Furthermore, the ctDNA level is also related to tumor stage. Lower-grade tumors usually have lower ctDNA levels, whereas higher-grade or metastatic tumors have higher levels [26, 27].

Tumor cell turnover is accelerated as tumor size and degree of malignancy, resulting in release of apoptotic and necrotic tumor cells into the circulation [26–28]. We discovered that patients with a high fraction of Ki-67 (>20%) had higher ctDNA levels, and that the ctDNA levels in GBM were much higher, but the difference in tumor size was not significant. Human Ki-67 expression was highly associated with the cell proliferation, indicating the association of Ki-67 index with the tumor progression [29]. GBM is the most malignant and aggressive glioma, accounting for 48.6% of all malignant CNS tumors [1]. Xu et al. considered that ctDNA for the diagnosis of advanced gastrointestinal stromal tumors was possible, and the Ki-67 affected the levels of ctDNA significantly [30]. We also found tumor DNA is not affected by the tumor location or number. The tumor DNA that invades the liquoral spaces can circulate throughout the entire CSF, causing to be collected from lumbar puncture in this study.

In our cohort, the hotspot aberrations detected involved *TERT* mutation, *TP53* mutation, *PTEN* mutation, *EGFR* mutation, and *CDKN2A/2B* loss. The molecular features were consistent with those of an adult glioma cohort previously reported [31]. *TERT* mutation is recognized as the most prevalent molecular marker for GBMs [32]. *H3F3A* G35R and K28M variants had been found in two gliomas separately, but no *IDH* mutations were detected in these two patients. It has been reported that mutations in *H3F3A* and *IDH1* were mutually exclusive [33]. The diagnostic accuracy rate of GBM by CSF ctDNA was higher compare of astrocytoma according to ROC

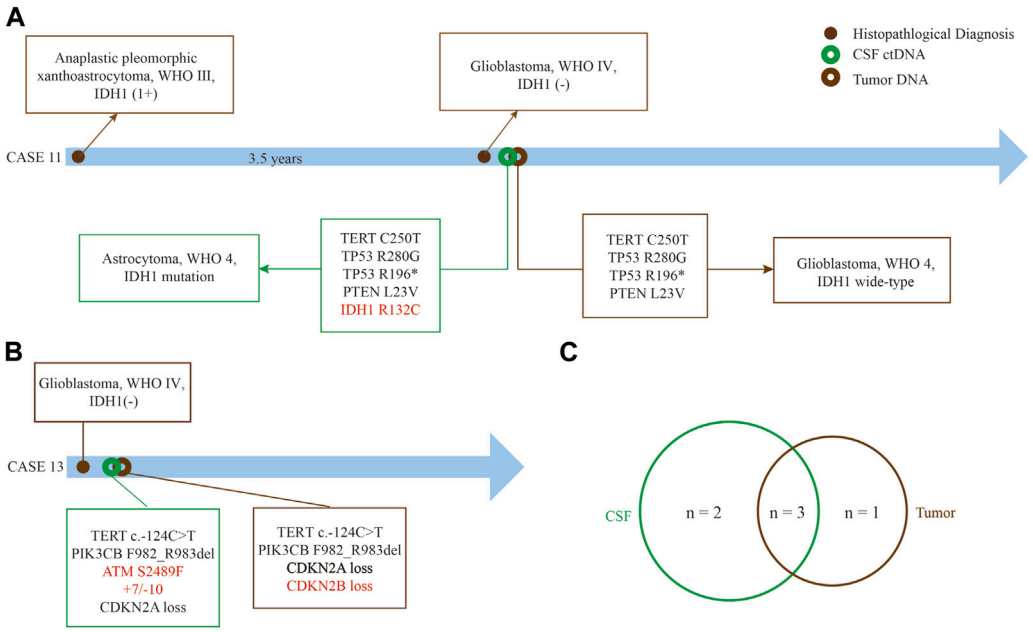

FIGURE 6
Superiority of CSF ctDNA detection in gliomas. **(A)** Case 11 who was diagnosed as recurrent GBM without *IDH1* mutation by tumor tissue but a rare IDH1 (R132C) mutation by CSF ctDNA sequencing. **(B)** Amplification of chromosome 7 and loss of chromosome 10 can be detected in case 13 by CSF ctDNA sequencing. **(C)** The common genes between CSF ctDNA and tumor tissue. The red font represents differential genes detected between CSF ctDNA and tumor tissue.

analysis. A similar finding has also been described in a meta-analysis [34]. Generally, high-grade tumors contain more ctDNA to circulate. The concordance between diagnosis by CSF ctDNA and the final diagnosis was 91.6%. Compared with the tumor DNA, we found the existence of false negatives in some cases. The false negatives may be caused by the limited amount of ctDNA extracted, which limited the detection of variants with low allele frequency [35]. Low sensitivity in catching the variation of chromosome would limit the application of CSF ctDNA in low-grade gliomas.

CSF ctDNA detection exhibited some attractive features in help to observe the molecular biomarkers. We found a rare *IDH1* mutation in CSF ctDNA from case 11, whereas a negative result was found in tumor DNA. The samples we collected were prospectively obtained by removing a small section of the tumor. Intratumor heterogeneity may explain why sampling bias leads to a difference in biomarker discovery and not every driver or passenger mutation will be discovered in each cancer cell [36, 37]. CSF ctDNA can reflect the whole genetic heterogeneity and make longitudinal assessments possible [38]. IDH1/2 are enzymes that play critical roles in a variety of cellular functions such as carbohydrate metabolism, differentiation, DNA repair and redox state regulation [39, 40]. Arginine 132 is the hotspot of *IDH1* in gliomas and *IDH1* R132H mutations are the most predominant mutation which indicates a better prognosis and may be effective for inhibitor treatment [41]. In our study the *IDH1* mutation with R132C was found. Previous studies showed that R132C had a more favorable prognosis than R132H for gliomas with a much higher enzymatic metabolism efficiency [40, 42]. *EGFR* amplification, +7/−10, and *TERT* promoter mutation are alterations frequently observed in adult *IDH*-wildtype GBM [43]. Notably, a case of GBM was identified to harbor +7/−10 and *TERT* promoter mutations in CSF ctDNA. Weller *et al.* found *TERT* promoter mutations combined with +7/−10 had the worst progression-free survival and OS compared with those having TERT promoter mutation alone [44]. Importantly, CSF can be collected before tumor tissue, which means earlier diagnosis and timely treatment for the patients.

Precise tumor subtyping and grading are essential for prognosis and treatment of patients. Our present study demonstrated that CSF ctDNA may be a reliable alternate tumor source for integrated molecular diagnosis of gliomas, especially for GBMs, supported by previous studies [45, 46]. In lower-grade gliomas, both CSF and tumors showed unique mutant genes, indicating that CSF may act as a potential supplementary tool for tumor biopsy to improve the molecular diagnosis. Collectively, this novel integrated diagnosis based on histology, tumor DNA and CSF ctDNA molecular pathology revealed a powerful clinical diagnostic value. Due to the limitations of CSF sources, we did not conduct any further

validation tests. To further confirm the utilization of CSF, larger cohorts and validation testing should be used.

In conclusion, CSF ctDNA detection for integrated molecular diagnosis of gliomas especially GBMs is feasible. NGS-based detection of CSF ctDNA could be used as a supplement for integrated diagnosis of gliomas. In the future, CSF ctDNA sequencing will form genetic profiling for each patient, assisting in targeted therapy and enhancing the therapeutic effect.

Data availability statement

The raw data supporting the conclusion of this article will be made available by the authors, without undue reservation.

Ethics statement

In accordance with the Declaration of Helsinki, written informed consent was obtained from all individuals or guardians and the study was approved by the Institutional Review Board of Nanjing Jinling Hospital (2022DZKY-093-01) and local regulations.

Author contributions

HP: Conception and design of the research, funding acquisition; WTW, WHN, and CL: Acquisition of data; QW and HP: Analysis and interpretation of data, Revision of manuscript for important intellectual content; XLW: Statistical analysis; QW: Drafting the manuscript; QL and XXW: testing of specimens. All authors contributed to the article and approved the submitted version.

Funding

This work is supported by the National Natural Science Foundation of China (Grant No. 81402072, 81672503, and 81772689), and the Young Medical Talents in Jiangsu Province (QNRC2016898).

Conflict of interest

Authors QL and XXW were employed by the company Jiangsu Simcere Diagnostics Co., Ltd.

The remaining authors declare that the research was conducted in the absence of any commercial or financial relationships that could be construed as a potential conflict of interest.

Acknowledgments

We would like to thank Dr. Xing Zhang, Yanda Zeng and Xueyu Yang at Jiangsu Simcere Diagnostics Co., Ltd. for processing the CSF samples. We gratefully acknowledge Nanyun Li and Nan Wu in the Department of Pathology.

Supplementary material

The Supplementary Material for this article can be found online at: https://www.por-journal.com/articles/10.3389/pore.2023.1611391/full#supplementary-material

SUPPLEMENTARY FIGURE S1
ROC curve for CSF ctDNA in non-GBM. **(A)** and glioma with enhanced MRI signal. **(B)** mergeindicator:supplemental_dummy:start.

References

1. Ostrom QT, Patil N, Cioffi G, Waite K, Kruchko C, Barnholtz-Sloan JS. CBTRUS statistical report: primary brain and other central nervous system tumors diagnosed in the United States in 2013-2017. *Neuro Oncol* (2020) 22:iv1–iv96. doi:10.1093/neuonc/noaa200

2. Louis DN, Perry A, Reifenberger G, von Deimling A, Figarella-Branger D, Cavenee WK, et al. The 2016 World health organization classification of tumors of the central nervous system: a summary. *Acta Neuropathol* (2016) 131:803–20. doi:10.1007/s00401-016-1545-1

3. Stupp R, Brada M, van den Bent MJ, Tonn JC, Pentheroudakis G, ESMO Guidelines Working Group. High-grade glioma: ESMO clinical practice guidelines for diagnosis, treatment and follow-up. *Ann Oncol* (2014) 25(3):iii93–101. doi:10.1093/annonc/mdu050

4. Alix-Panabières C, Pantel K. Liquid biopsy: from discovery to clinical application. *Cancer Discov* (2021) 11:858–73. doi:10.1158/2159-8290.CD-20-1311

5. Heitzer E, Ulz P, Geigl JB. Circulating tumor DNA as a liquid biopsy for cancer. *Clin Chem* (2015) 61:112–23. doi:10.1373/clinchem.2014.222679

6. Keller L, Belloum Y, Wikman H, Pantel K. Clinical relevance of blood-based ctDNA analysis: mutation detection and beyond. *Br J Cancer* (2021) 124:345–58. doi:10.1038/s41416-020-01047-5

7. Daneman R, Prat A. The blood-brain barrier. *Cold Spring Harb Perspect Biol* (2015) 7:a020412. doi:10.1101/cshperspect.a020412

8. Rincon-Torroella J, Khela H, Bettegowda A, Bettegowda C. Biomarkers and focused ultrasound: the future of liquid biopsy for brain tumor patients. *J Neurooncol* (2022) 156:33–48. doi:10.1007/s11060-021-03837-0

9. De Mattos-Arruda L, Mayor R, Ng CKY, Weigelt B, Martínez-Ricarte F, Torrejon D, et al. Cerebrospinal fluid-derived circulating tumour DNA better represents the genomic alterations of brain tumours than plasma. *Nat Commun* (2015) 6:8839. doi:10.1038/ncomms9839

10. Miller AM, Shah RH, Pentsova EI, Pourmaleki M, Briggs S, Distefano N, et al. Tracking tumour evolution in glioma through liquid biopsies of cerebrospinal fluid. *Nature* (2019) 565:654–8. doi:10.1038/s41586-019-0882-3

11. Wang Y, Springer S, Zhang M, McMahon KW, Kinde I, Dobbyn L, et al. Detection of tumor-derived DNA in cerebrospinal fluid of patients with primary tumors of the brain and spinal cord. *Proc Natl Acad Sci U S A* (2015) 112:9704–9. doi:10.1073/pnas.1511694112

12. Wang Y, Wang L, Blümcke I, Zhang W, Fu Y, Shan Y, et al. Integrated genotype-phenotype analysis of long-term epilepsy-associated ganglioglioma. *Brain Pathol* (2022) 32(1):e13011. doi:10.1111/bpa.13011

13. Brat DJ, Aldape K, Colman H, Holland EC, Louis DN, Jenkins RB, et al. cIMPACT-NOW update 3: recommended diagnostic criteria for "Diffuse astrocytic glioma, IDH-wildtype, with molecular features of glioblastoma, WHO grade IV". *Acta Neuropathol* (2018) 136:805–10. doi:10.1007/s00401-018-1913-0

14. Brat DJ, Aldape K, Colman H, Figrarella-Branger D, Fuller GN, Giannini C, et al. cIMPACT-NOW update 5: recommended grading criteria and terminologies for IDH-mutant astrocytomas. *Acta Neuropathol* (2020) 139:603–8. doi:10.1007/s00401-020-02127-9

15. Louis DN, Wesseling P, Aldape K, Brat DJ, Capper D, Cree IA, et al. cIMPACT-NOW update 6: new entity and diagnostic principle recommendations of the cIMPACT-Utrecht meeting on future CNS tumor classification and grading. *Brain Pathol* (2020) 30:844–56. doi:10.1111/bpa.12832

16. Parsons DW, Jones S, Zhang X, Lin JC, Leary RJ, Angenendt P, et al. An integrated genomic analysis of human glioblastoma multiforme. *Science* (2008) 321:1807–12. doi:10.1126/science.1164382

17. Landis JR, Koch GG. The measurement of observer agreement for categorical data. *Biometrics* (1977) 33:159–74. doi:10.2307/2529310

18. Louis DN, Perry A, Wesseling P, Brat DJ, Cree IA, Figarella-Branger D, et al. The 2021 WHO classification of tumors of the central nervous system: a summary. *Neuro Oncol* (2021) 23:1231–51. doi:10.1093/neuonc/noab106

19. Pentsova EI, Shah RH, Tang J, Boire A, You D, Briggs S, et al. Evaluating cancer of the central nervous system through next-generation sequencing of cerebrospinal fluid. *J Clin Oncol* (2016) 34:2404–15. doi:10.1200/JCO.2016.66.6487

20. Miller AM, Szalontay L, Bouvier N, Hill K, Ahmad H, Rafailov J, et al. Next-generation sequencing of cerebrospinal fluid for clinical molecular diagnostics in pediatric, adolescent and young adult brain tumor patients. *Neuro Oncol* (2022) 24:1763–72. doi:10.1093/neuonc/noac035

21. Saenz-Antoñanzas A, Auzmendi-Iriarte J, Carrasco-Garcia E, Moreno-Cugnon L, Ruiz I, Villanua J, et al. Liquid biopsy in glioblastoma: opportunities, applications and challenges. *Cancers (Basel)* (2019) 11(7):950. doi:10.3390/cancers11070950

22. Fujioka Y, Hata N, Akagi Y, Kuga D, Hatae R, Sangatsuda Y, et al. Molecular diagnosis of diffuse glioma using a chip-based digital PCR system to analyze IDH, TERT, and H3 mutations in the cerebrospinal fluid. *J Neurooncol* (2021) 152:47–54. doi:10.1007/s11060-020-03682-7

23. Guan YF, Li GR, Wang RJ, Yi YT, Yang L, Jiang D, et al. Application of next-generation sequencing in clinical oncology to advance personalized treatment of cancer. *Chin J Cancer* (2012) 31(10):463–70. doi:10.5732/cjc.012.10216

24. Piccioni DE, Achrol AS, Kiedrowski LA, Banks KC, Boucher N, Barkhoudarian G, et al. Analysis of cell-free circulating tumor DNA in 419 patients with glioblastoma and other primary brain tumors. *CNS Oncol* (2019) 8:CNS34. doi:10.2217/cns-2018-0015

25. Bettegowda C, Sausen M, Leary RJ, Kinde I, Wang Y, Agrawal N, et al. Detection of circulating tumor DNA in early- and late-stage human malignancies. *Sci Transl Med* (2014) 6:224ra24. doi:10.1126/scitranslmed.3007094

26. Diaz LA, Jr, Bardelli A. Liquid biopsies: genotyping circulating tumor DNA. *J Clin Oncol* (2014) 32:579–86. doi:10.1200/JCO.2012.45.2011

27. Bryzgunova OE, Konoshenko MY, Laktionov PP. Concentration of cell-free DNA in different tumor types. *Expert Rev Mol Diagn* (2021) 21:63–75. doi:10.1080/14737159.2020.1860021

28. Gao Y, Zhang K, Xi H, Cai A, Wu X, Cui J, et al. Diagnostic and prognostic value of circulating tumor DNA in gastric cancer: a meta-analysis. *Oncotarget* (2017) 8:6330–40. doi:10.18632/oncotarget.14064

29. Scholzen T, Gerdes J. The ki-67 protein: from the known and the unknown. *J Cell Physiol* (2000) 182:311–22. doi:10.1002/(SICI)1097-4652(200003)182:3<311:AID-JCP1>3.0.CO;2-9

30. Xu H, Chen L, Shao Y, Zhu D, Zhi X, Zhang Q, et al. Clinical application of circulating tumor DNA in the genetic analysis of patients with advanced GIST. *Mol Cancer Ther* (2018) 17:290–6. doi:10.1158/1535-7163.MCT-17-0436

31. Torre M, Vasudevaraja V, Serrano J, DeLorenzo M, Malinowski S, Blandin AF, et al. Molecular and clinicopathologic features of gliomas harboring NTRK fusions. *Acta Neuropathol Commun* (2020) 8:107. doi:10.1186/s40478-020-00980-z

32. Pekmezci M, Rice T, Molinaro AM, Walsh KM, Decker PA, Hansen H, et al. Adult infiltrating gliomas with WHO 2016 integrated diagnosis: additional prognostic roles of ATRX and TERT. *Acta Neuropathol* (2017) 133:1001–16. doi:10.1007/s00401-017-1690-1

33. Sturm D, Witt H, Hovestadt V, Khuong-Quang DA, Jones DT, Konermann C, et al. Hotspot mutations in H3F3A and IDH1 define distinct epigenetic and biological subgroups of glioblastoma. *Cancer Cell* (2012) 22:425–37. doi:10.1016/j.ccr.2012.08.024

34. Kang Y, Lin X, Kang D. Diagnostic value of circulating tumor DNA in molecular characterization of glioma: a meta-analysis. *Medicine (Baltimore)* (2020) 99:e21196. doi:10.1097/MD.0000000000021196

35. Weber S, Spiegl B, Perakis SO, Ulz CM, Abuja PM, Kashofer K, et al. Technical evaluation of commercial mutation analysis platforms and reference materials for liquid biopsy profiling. *Cancers (Basel)* (2020) 12:1588. doi:10.3390/cancers12061588

36. Gerlinger M, Rowan AJ, Horswell S, Math M, Larkin J, Endesfelder D, et al. Intratumor heterogeneity and branched evolution revealed by multiregion sequencing. *N Engl J Med* (2012) 366:883–92. doi:10.1056/NEJMoa1113205

37. McGranahan N, Swanton C. Biological and therapeutic impact of intratumor heterogeneity in cancer evolution. *Cancer Cell* (2015) 27:15–26. doi:10.1016/j.ccell.2014.12.001

38. Peng M, Chen C, Hulbert A, Brock MV, Yu F. Non-blood circulating tumor DNA detection in cancer. *Oncotarget* (2017) 8:69162–73. doi:10.18632/oncotarget.19942

39. Molenaar RJ, Wilmink JW. IDH1/2 mutations in cancer stem cells and their implications for differentiation therapy. *J Histochem Cytochem* (2022) 70:83–97. doi:10.1369/00221554211062499

40. Tesileanu CMS, Vallentgoed WR, Sanson M, Taal W, Clement PM, Wick W, et al. Non-IDH1-R132H IDH1/2 mutations are associated with increased DNA methylation and improved survival in astrocytomas, compared to IDH1-R132H mutations. *Acta Neuropathol* (2021) 141:945–57. doi:10.1007/s00401-021-02291-6

41. Rohle D, Popovici-Muller J, Palaskas N, Turcan S, Grommes C, Campos C, et al. An inhibitor of mutant IDH1 delays growth and promotes differentiation of glioma cells. *Science* (2013) 340:626–30. doi:10.1126/science.1236062

42. Avellaneda Matteo D, Grunseth AJ, Gonzalez ER, Anselmo SL, Kennedy MA, Moman P, et al. Molecular mechanisms of isocitrate dehydrogenase 1 (IDH1) mutations identified in tumors: the role of size and hydrophobicity at residue 132 on catalytic efficiency. *J Biol Chem* (2017) 292:7971–83. doi:10.1074/jbc.M117.776179

43. Stichel D, Ebrahimi A, Reuss D, Schrimpf D, Ono T, Shirahata M, et al. Distribution of EGFR amplification, combined chromosome 7 gain and chromosome 10 loss, and TERT promoter mutation in brain tumors and their potential for the reclassification of IDHwt astrocytoma to glioblastoma. *Acta Neuropathol* (2018) 136:793–803. doi:10.1007/s00401-018-1905-0

44. Weller M, Weber RG, Willscher E, Riehmer V, Hentschel B, Kreuz M, et al. Molecular classification of diffuse cerebral WHO grade II/III gliomas using genome- and transcriptome-wide profiling improves stratification of prognostically distinct patient groups. *Acta Neuropathol* (2015) 129:679–93. doi:10.1007/s00401-015-1409-0

45. Zhao Z, Zhang C, Li M, Shen Y, Feng S, Liu J, et al. Applications of cerebrospinal fluid circulating tumor DNA in the diagnosis of gliomas. *Jpn J Clin Oncol* (2020) 50(3):325–32. doi:10.1093/jjco/hyz156

46. Martínez-Ricarte F, Mayor R, Martínez-Sáez E, Rubio-Pérez C, Pineda E, Cordero E, et al. Molecular diagnosis of diffuse gliomas through sequencing of cell-free circulating tumor DNA from cerebrospinal fluid. *Clin Cancer Res* (2018) 24(12):2812–9. doi:10.1158/1078-0432.CCR-17-3800

Pathology & Oncology Research | frontiers

TYPE Mini Review
PUBLISHED 14 May 2024
DOI 10.3389/pore.2024.1611693

Check for updates

OPEN ACCESS

EDITED BY
Gabriella Galffy,
Törökbálint Pulmonology Hospital, Hungary

*CORRESPONDENCE
Zesen Han,
hanzesen908@163.com
Fenglei Li,
lflhuayi@126.com

RECEIVED 19 January 2024
ACCEPTED 29 April 2024
PUBLISHED 14 May 2024

CITATION
Han Z, Yang F, Wang F, Zheng H, Chen X, Meng H and Li F (2024), Advances in combined neuroendocrine carcinoma of lung cancer.
Pathol. Oncol. Res. 30:1611693.
doi: 10.3389/pore.2024.1611693

COPYRIGHT
© 2024 Han, Yang, Wang, Zheng, Chen, Meng and Li. This is an open-access article distributed under the terms of the Creative Commons Attribution License (CC BY). The use, distribution or reproduction in other forums is permitted, provided the original author(s) and the copyright owner(s) are credited and that the original publication in this journal is cited, in accordance with accepted academic practice. No use, distribution or reproduction is permitted which does not comply with these terms.

Advances in combined neuroendocrine carcinoma of lung cancer

Zesen Han[1]*, Fujun Yang[2], Fang Wang[1], Huayu Zheng[1], Xiujian Chen[1], Hongyu Meng[1] and Fenglei Li[1]*

[1]Hua Country People's Hospital, Anyang, Henan, China, [2]Department of Medical Oncology, Sanmenxia Central Hospital, Henan University of Science and Technology, Sanmenxia, China

Lung cancer incidence and mortality rates are increasing worldwide, posing a significant public health challenge and an immense burden to affected families. Lung cancer encompasses distinct subtypes, namely, non-small-cell lung cancer (NSCLC) and small-cell lung cancer (SCLC). In clinical investigations, researchers have observed that neuroendocrine tumors can be classified into four types: typical carcinoid, atypical carcinoid, small-cell carcinoma, and large-cell neuroendocrine carcinoma based on their unique features. However, there exist combined forms of neuroendocrine cancer. This study focuses specifically on combined pulmonary carcinomas with a neuroendocrine component. In this comprehensive review article, the authors provide an overview of combined lung cancers and present two pathological images to visually depict these distinctive subtypes.

KEYWORDS

small cell neuroendocrine carcinoma, large cell neuroendocrine carcinoma, adenocarcinoma, squamous cell carcinoma, lung cancer

Introduction

Globally, the morbidity and mortality rates of lung cancer are increasing [1], making it a significant public health concern and burden for families [2]. Approximately 75% of the 2.20 million newly diagnosed lung cancer patients will succumb to the disease within 5 years [3–5]. Lung cancer comprises distinct subtypes, such as non-small-cell lung cancer (NSCLC) and small-cell lung cancer (SCLC). The mortality rate of NSCLC has been shown to improve from 2013 to 2016 following diagnosis [6], due to advances in screening, early patient management, immunotherapy, and other interventions [7]. However, SCLC remains challenging due to its propensity for relapse and higher mortality rates accounting for up to 15% of all lung cancers [8]. Despite decades of research focused on targeted treatments based on biomarker selection and immunotherapy, SCLC continues to be one of the most difficult-to-treat tumorigenic diseases [9].

In 2021, the WHO classified the lung tumors since 2015 [10] into five categories: 1) Small cell carcinoma, 2) Large cell neuroendocrine carcinoma, 3) Adenosquamous carcinoma (if both components ≥10%), 4) Adenocarcinoma, squamous cell

carcinoma, adenosquamous carcinoma, or large cell carcinoma with unclear immunohistochemical features, 5) Pleomorphic, spindle cell, and/or giant cell carcinoma for the resection specimens. However, in clinical work, researchers have observed an additional subtype. In pathology studies, neuroendocrine tumors can be further divided into four types: typical carcinoid tumor, atypical carcinoid tumor, small cell carcinoma, and large cell neuroendocrine carcinoma based on their combined features [11]. This study focuses specifically on combined pulmonary carcinoma with a neuroendocrine component.

Combined small cell neuroendocrine carcinoma with adenocarcinoma

The current consensus is that small-cell lung cancer is transferred from adenocarcinoma following treatment with EGFR tyrosine kinase inhibitors [12]. This phenomenon was initially reported in a female patient diagnosed with adenocarcinoma who received erlotinib in 2007. After prolonged treatment, a biopsy of the same site revealed SCLC based on the exon 19 mutation of the epidermal growth factor receptor (EGFR), which was consistent with primary NSCLC [13]. Another case involved a 38-year-old patient with EGFR exon 21 L8585R lung adenocarcinoma who developed SCLC transformation after receiving regular erlotinib treatment for 18 months [14]. Two hypotheses have been proposed to elucidate the pathogenesis of SCLC transformation [15]. The majority of researchers posit that this transformation arises from resistance to tyrosine kinase inhibitors (TKIs) [16] targeting EGFR, ALK, and ROS1, or immunotherapies [17]. Five resistant tumors were found to harbor mechanisms such as the EGFR T790M mutation, MET gene amplification, EGFR amplification, mutations in the PIK3CA gene and others associated with the epithelial-to-mesenchymal transition. These transformed tumors from NSCLC to SCLC showed sensitivity to standard SCLC treatments. However, due to significant heterogeneity in resistance mechanisms and different prognoses among cases [18, 19], individualized therapeutic strategies are required. The transformation can be detected by mutations in biomarkers such as EGFR, tumor protein p53 (TP53), RB transcriptional corepressor 1 (RB1), and SRY-box transcription factor 2 (SOX2) before and after transformation [20].

However, it should be noted that this transformation may also be pseudo. In a study conducted by Rui Li et al. in 2021 involving 11 cases previously diagnosed as SCLC, only one sample did not exhibit any SCLC elements within the primary adenocarcinoma sections. This case was defined as true small-cell transformation (SCT) [21]. In other words, there were instances where SCLC components coexisted within the adenocarcinoma but were considered pseudo-SCT. The observation of RB1 deletion and mutant TP53 overexpression in either pseudo-SCT or true SCT cannot exclude the possibility of combined SCLC with adenocarcinoma.

Meanwhile, 34 cases of combined high-grade neuroendocrine carcinoma (HGNEC) were reported with 48% of subjects with combined HGNEC and adenocarcinoma having a lepidic adenocarcinoma component suggesting that HGNEC can develop in association with pre-existing adenocarcinoma which is often retained [22]. In the same year, a case based on combined SCLC with non-small cell carcinoma component was reported, in which two distinct neoplastic components were found. One consisted of small-sized cells without giant cell carcinoma shown in the biopsy specimen while the other was verified as combined SCLC with a giant cell carcinoma through histopathological examination of the lobectomy specimen [23]. These findings indicated that SCLC and adenocarcinoma can coexist in the same patients. The results cannot be solely attributed to the transformation from adenocarcinoma, and it is imperative not to overlook the significance of combined SCLC.

The origin of two different tumor components may be from the same pluripotent epithelial precursor cell due to loss of heterozygosity (LOH) in the different tumor areas [24]. Additionally, IL-16 rs859 was found to have a statistically significant susceptibility to lung small-cell carcinoma and adenocarcinoma [25].

Expression of stem cell transcription factors (scTF) has been detected in both small cell carcinoma and non-adenocarcinoma in prostate cancer, influencing the transformation from adenocarcinoma [26]. Inhibition of exportin 1 has been suggested as a potential therapeutic target for the prevention or treatment of neuroendocrine transformation of lung and prostate adenocarcinomas [27]. Nowadays, a platinum plus etoposide chemotherapy regimen is preferred to treat patients with SCLC transformation based on EGFR mutation. However, new strategies, such as immune checkpoint inhibitors are being explored [28]. The DLL3-directed antibody-drug conjugate rovalpituzumab tesirine [29] and its application have been considered for the unique EGFR mutant SCLC transformation cancer [30]. Serum neuron-specific enolase (NSE) may serve as a novel marker for predicting neuroendocrine tumor transformation [31].

Combined large cell neuroendocrine carcinoma with adenocarcinoma

The incidence of large cell neuroendocrine carcinoma (LCNC) in lung cancer is only 3% [32], and it has a poor prognosis due to its rarity, aggressiveness, and distinct treatment approach [33]. In 2009, E Cakir et al. identified different combinations of histological subtypes in lung cancer, such as adenosquamous carcinoma, combined neuroendocrine tumors, and biphasic tumors. Combined neuroendocrine carcinoma consists of SCLC + nonneuroendocrine carcinoma (NNEC), SCLC + LCNC, and LCNC + NNEC, it has been revealed that patients with

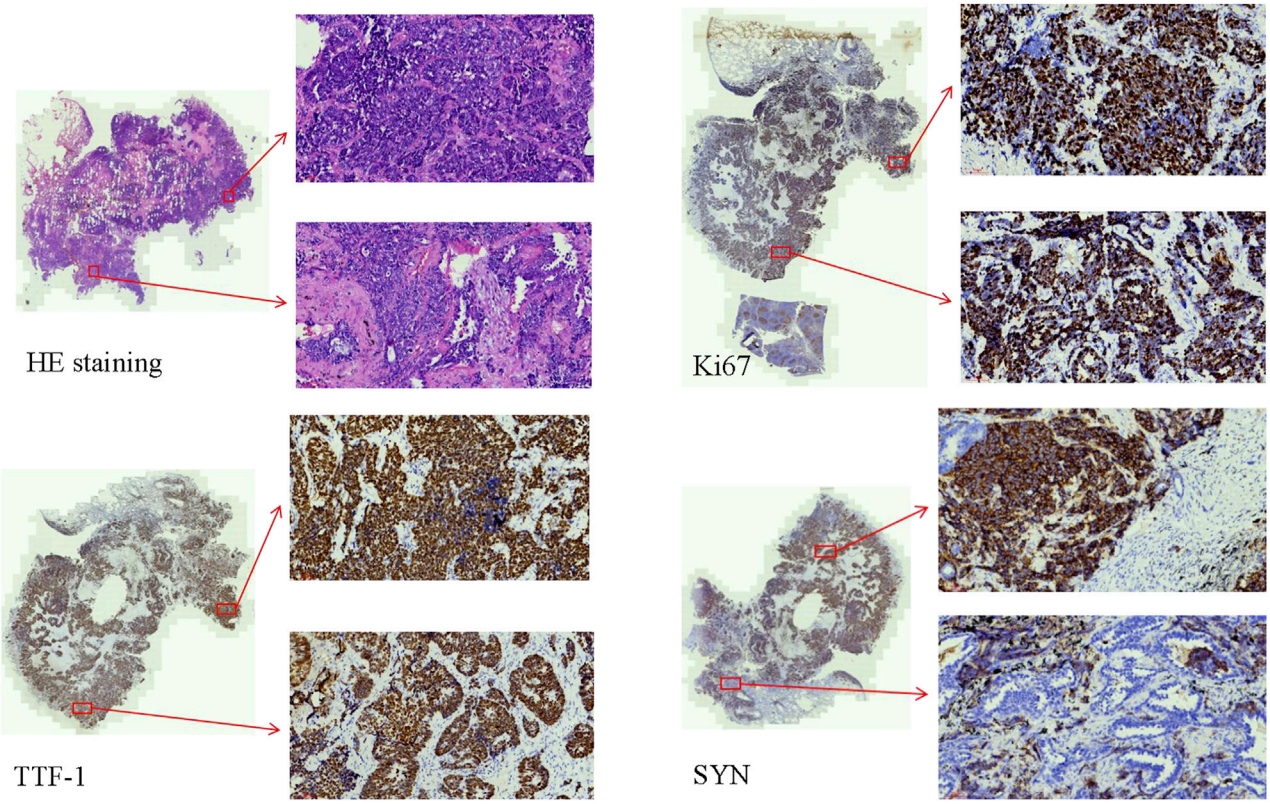

FIGURE 1
The HE staining and IHC of the combined LCNC with adenocarcinoma (x20). The Ki67 index was approximately 85%. TTF-1 and SYN were positive.

combined neuroendocrine tumors had more advanced stages and vascular invasion compared to those with single histology types, their 2-year survival rate was only 25% [34]. Moreover, accurate differentiation of LCNC from atypical carcinoids is challenging with the limited tissue samples obtained through lung biopsy [35].

These findings highlight the existence of evidence of combined large-cell neuroendocrine carcinoma. The diagnosis of LCNC relies on histopathological examination while immunohistochemical (IHC) features provide precise and accurate identification. Neuroendocrine components strongly express markers such as Chromogranin A (CgA), Synaptophysin (Syn), and neural cell adhesion molecule 56 (CD56). On the other hand, thyroid transcription factor 1 (TTF-1) is associated with EGFR mutations, while NapsinA is highly specific for lung adenocarcinoma [36]. P40 serves as an excellent marker for distinguishing between squamous cell carcinoma and lung adenocarcinoma [37], similar to P63. Among combined LCNC cases, adenocarcinoma is the most common combination, accounting for approximately 70% of cases [38]. A retrospective study of surgical resection of combined LCNC included 96 patients, 71 of whom were diagnosed as having LCNC combined with adenocarcinoma.

During clinical work, the authors encountered a case of LCNC combined with adenocarcinoma that could be diagnosed by IHC. This is a resection specimen. In this particular case, positive markers for TTF-1, SYN, CD56, CK, and P63 were observed, along with partial positivity for NapsinA. However, CgA and P40 showed negative results. The Ki67 index was approximately 85% (Figure 1). Metastasis was observed in 22 of 33 lymphatic nodes.

Adjuvant chemotherapy, particularly etoposide-based chemotherapy, proved to be a beneficial option [39]. Furthermore, it is crucial to confirm the importance of adjuvant chemotherapy (especially using the small cell carcinoma regimen) to improve patients' outcomes [40]. Nevertheless, immunotherapy rarely provides benefits when combined with LCNC treatment. Further research should be done [41].

Combined large cell neuroendocrine carcinoma with squamous cell carcinoma

Squamous cell carcinoma is a subtype of non-small cell carcinoma, which also constitutes the composition in

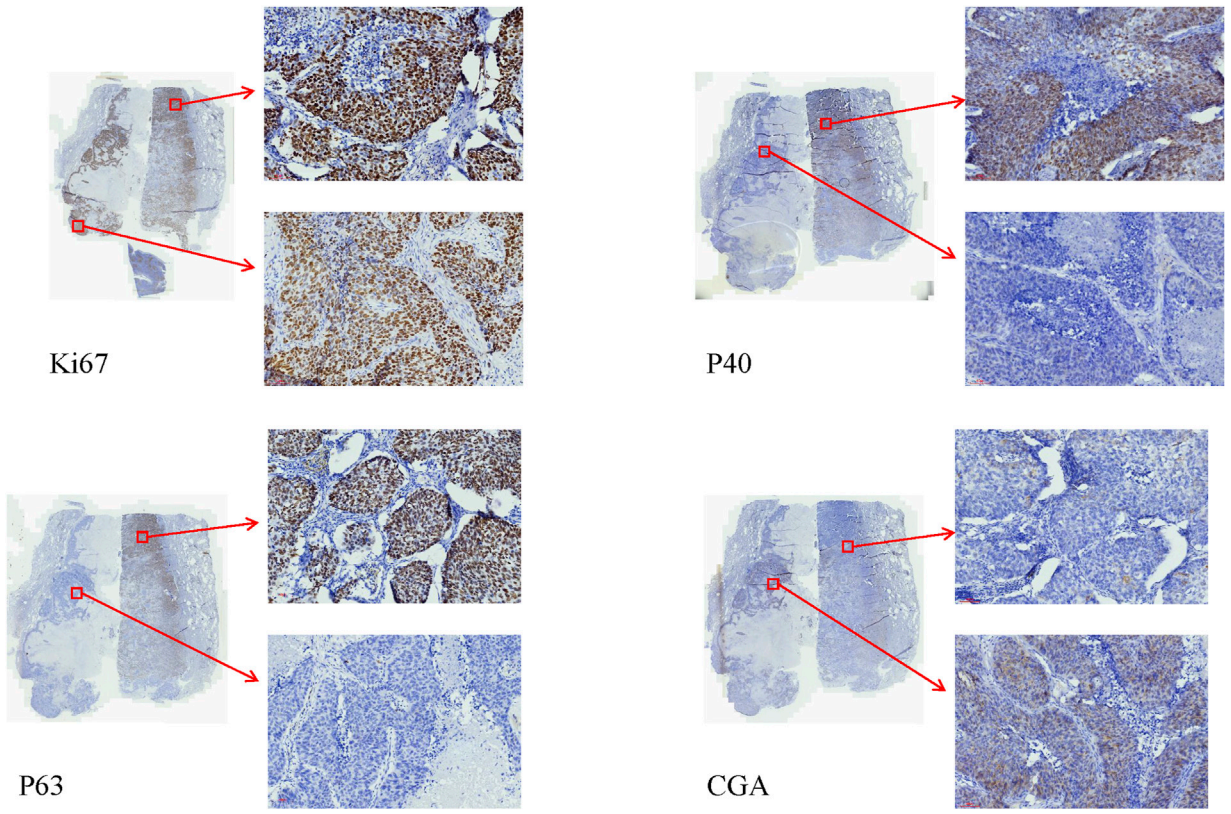

FIGURE 2
The IHC of the combined LCNC with squamous cell carcinoma (×20). The Ki67 index was approximately 80%. The sections of the P40, and P63 of squamous cell carcinoma were positive. The sections of the P40, and P63 of LCNC were negative. The sections of CgA of LCNC were positive. The sections of CgA of the squamous cell carcinoma were negative.

combined LCNC. A case of LCNC of the lung with carcinoid syndrome was reported involving a 76-year-old woman who underwent computed tomography that revealed a liver mass originating from the lung as diagnosed by biopsy. The pathology analysis of the lung biopsy demonstrated combined LCNC and squamous cell carcinoma. The tumor area tested negative for TTF-1 but positive for cytokeratin14 (CK14) and P40 [42]. Despite receiving chemotherapy following the diagnosis, the patient died 50 days after hospital admission due to her deteriorating physical condition. In 2004, another case was reported in which a patient diagnosed with combined LCNC as part of squamous cell carcinoma [pT4 (pm) N2M0] on postoperative histological tissue remained in good health for 9 months until the article was published [43]. In addition, other similar cases have been documented [44].

The authors encountered a case of combined LCNC with squamous cell carcinoma that was diagnosed using IHC and pathological features. In this particular case, the IHC markers: CK, and CK17 were found to be positive. Additionally, the tumor sections were positive for CgA, P40, and P63. However, the markers CK7, TTF-1, NapsinA, SYN, CD56, and CD117 were negative. The Ki67 index was approximately 80%. Notably, organoid and palisading patterns were observed in the majority of the lung tumor cells within the tumor areas. Furthermore, another section revealed a prominent presence of atypical cells exhibiting keratinization (Figure 2). Importantly, no lymphatic node metastasis was detected.

According to the IHC, the patient was diagnosed with combined LCNC and squamous cell carcinoma due to the presence of two distinct elements. Additionally, molecular testing could be used to satisfy the criteria of precision medicine [45].

Conversely, miR-31 is found to be upregulated in adenocarcinoma, squamous cell carcinoma, and large-cell neuroendocrine carcinoma of the lung, while it is not overexpressed in small-cell carcinoma or carcinoids. MiR-31 has been identified as a potential therapeutic target that promotes tumor growth in mice of xenografted human adenocarcinoma and squamous cell carcinoma cell lines but not in large- or small-cell carcinoma lines [46]. The Ki-67 proliferation index cutoff of 55% could predict the prognosis of LCNC and combined LCNC, with combined LCNC patients

having longer overall survival (OS) when diagnosed with adenocarcinoma compared to those diagnosed with squamous cell carcinoma [47].

Notably, there was a case report demonstrating the coexistence of LCNC with adenocarcinoma, and squamous cell carcinoma. Hematoxylin—Eosin staining revealed that the tumor consisted of 40% acinar adenocarcinoma, 10% mucous adenocarcinoma, 40% LCNC, and 10% poorly differentiated squamous cell carcinoma. The markers TTF-1, SYN, and P40 exhibited positive expression in the correlative tumor [48]. The researcher indicated that surgical resection along with adjuvant chemotherapy using SCLC regimen may improve Disease Free Survival (DFS) and OS.

Treatment of combined LCNC with squamous cell carcinoma could include immune checkpoint inhibitors after multimodality therapy incorporating cytotoxic anticancer drugs and radiotherapy. A 60-year-old man diagnosed with LCNEC combined with squamous cell carcinoma and staged as T2aN0M0 stage IB through histopathology showed a favorable response to treatment and achieved a survival period exceeding 5 years [49].

The identical phenomenon of merging two or more compounds has also been observed in other parts of the body, such as the head and neck region [50] and the uterine cervix [51].

In this comprehensive review, the authors meticulously summarize the various types of combined lung cancers, including the concurrence of combined small cell neuroendocrine carcinoma with adenocarcinoma, combined LCNC with adenocarcinoma, and combined LCNC with squamous cell carcinoma.

Interestingly, there seems to be no literature available on the coexistence of small-cell neuroendocrine carcinoma and squamous cell carcinoma in the lung. This particular type of lung cancer has a significantly poorer prognosis, and thus, research concerning its treatment is currently underway. The review also highlights the importance of understanding the different combinations of lung cancer subtypes, as this knowledge can greatly contribute to more tailored and effective treatment strategies.

Author contributions

HZ, HM, XC, and FL conducted the experiments, FW supplied critical pathologic immunohistochemical markers, ZH and FY wrote the manuscript. All authors contributed to the article and approved the submitted version.

Funding

The authors declare that no financial support was received for the research, authorship, and/or publication of this article.

Conflict of interest

The authors declare that the research was conducted in the absence of any commercial or financial relationships that could be construed as a potential conflict of interest.

References

1. Bade BC, Dela Cruz CS. Lung cancer 2020: epidemiology, etiology, and prevention. *Clin Chest Med* (2020) 41(1):1–24. doi:10.1016/j.ccm.2019.10.001

2. Wu F, Wang L, Zhou C. Lung cancer in China: current and prospect. *Curr Opin Oncol* (2021) 33(1):40–6. doi:10.1097/CCO.0000000000000703

3. Thai AA, Solomon BJ, Sequist LV, Gainor JF, Heist RS. Lung cancer. *Lancet* (2021) 398(10299):535–54. doi:10.1016/S0140-6736(21)00312-3

4. Svoboda E. Artificial intelligence is improving the detection of lung cancer. *Nature* (2020) 587(7834):S20–S22. doi:10.1038/d41586-020-03157-9

5. Li Y, Wu X, Yang P, Jiang G, Luo Y. Machine learning for lung cancer diagnosis, treatment, and prognosis. *Genomics Proteomics Bioinformatics* (2022) 20(5): 850–66. doi:10.1016/j.gpb.2022.11.003

6. Howlader N, Forjaz G, Mooradian MJ, Meza R, Kong CY, Cronin KA, et al. The effect of advances in lung-cancer treatment on population mortality. *N Engl J Med* (2020) 383(7):640–9. doi:10.1056/NEJMoa1916623

7. Mithoowani H, Febbraro M. Non-small-cell lung cancer in 2022: a review for general practitioners in oncology. *Curr Oncol* (2022) 29(3):1828–39. doi:10.3390/curroncol29030150

8. Wang Y, Zou S, Zhao Z, Liu P, Ke C, Xu S. New insights into small-cell lung cancer development and therapy. *Cell Biol Int* (2020) 44(8):1564–76. doi:10.1002/cbin.11359

9. Meijer JJ, Leonetti A, Airò G, Tiseo M, Rolfo C, Giovannetti E, et al. Small cell lung cancer: novel treatments beyond immunotherapy. *Semin Cancer Biol* (2022) 86(Pt 2):376–85. doi:10.1016/j.semcancer.2022.05.004

10. Nicholson AG, Tsao MS, Beasley MB, Borczuk AC, Brambilla E, Cooper WA, et al. The 2021 WHO classification of lung tumors: impact of advances since 2015. *J Thorac Oncol* (2022) 17(3):362–87. doi:10.1016/j.jtho.2021.11.003

11. Zheng M. Classification and pathology of lung cancer. *Surg Oncol Clin N Am* (2016) 25(3):447–68. doi:10.1016/j.soc.2016.02.003

12. Wang W, Xu C, Chen H, Jia J, Wang L, Feng H, et al. Genomic alterations and clinical outcomes in patients with lung adenocarcinoma with transformation to small cell lung cancer after treatment with EGFR tyrosine kinase inhibitors: a multicenter retrospective study. *Lung Cancer* (2021) 155:20–7. doi:10.1016/j.lungcan.2021.03.006

13. Morinaga R, Okamoto I, Furuta K, Kawano Y, Sekijima M, Dote K, et al. Sequential occurrence of non-small cell and small cell lung cancer with the same EGFR mutation. *Lung Cancer* (2007) 58(3):411–3. doi:10.1016/j.lungcan.2007.05.014

14. Liu Y. Small cell lung cancer transformation from EGFR-mutated lung adenocarcinoma: a case report and literature review. *Cancer Biol Ther* (2018) 19(6):445–9. doi:10.1080/15384047.2018.1435222

15. Yin X, Li Y, Wang H, Jia T, Wang E, Luo Y, et al. Small cell lung cancer transformation: from pathogenesis to treatment. *Semin Cancer Biol* (2022) 86(Pt 2): 595–606. doi:10.1016/j.semcancer.2022.03.006

16. Norkowski E, Ghigna MR, Lacroix L, Le Chevalier T, Fadel É, Dartevelle P, et al. Small-cell carcinoma in the setting of pulmonary adenocarcinoma: new insights in the era of molecular pathology. *J Thorac Oncol* (2013) 8(10):1265–71. doi:10.1097/JTO.0b013e3182a407fa

17. Giaccone G, He Y. Current knowledge of small cell lung cancer transformation from non-small cell lung cancer. *Semin Cancer Biol* (2023) 94: 1–10. doi:10.1016/j.semcancer.2023.05.006

18. Sequist LV, Waltman BA, Dias-Santagata D, Digumarthy S, Turke AB, Fidias P, et al. Genotypic and histological evolution of lung cancers acquiring resistance to EGFR inhibitors. *Sci Transl Med* (2011) 3(75):75ra26. doi:10.1126/scitranslmed.3002003

19. Oxnard GR, Arcila ME, Sima CS, Riely GJ, Chmielecki J, Kris MG, et al. Acquired resistance to EGFR tyrosine kinase inhibitors in EGFR-mutant lung cancer: distinct natural history of patients with tumors harboring the T790M mutation. *Clin Cancer Res* (2011) 17(6):1616–22. doi:10.1158/1078-0432.CCR-10-2692

20. Hao L, Chen H, Wang L, Zhou H, Zhang Z, Han J, et al. Transformation or tumor heterogeneity: mutations in EGFR, SOX2, TP53, and RB1 persist in the histological rapid conversion from lung adenocarcinoma to small-cell lung cancer. *Thorac Cancer* (2023) 14(11):1036–41. doi:10.1111/1759-7714.14832

21. Li R, Jiang L, Zhou X, Lu Y, Zhang Y. Pseudo-small cell transformation in EGFR-mutant adenocarcinoma. *Lung Cancer* (2021) 153:120–5. doi:10.1016/j.lungcan.2020.12.036

22. Yamada K, Maeshima AM, Tsuta K, Tsuda H. Combined high-grade neuroendocrine carcinoma of the lung: clinicopathological and immunohistochemical study of 34 surgically resected cases. *Pathol Int* (2014) 64(1):28–33. doi:10.1111/pin.12127

23. Ebisu Y, Ishida M, Saito T, Murakawa T, Uemura Y, Tsuta K. Combined small cell carcinoma with giant cell carcinoma component of the lung: a case successfully diagnosed by computed tomography-guided fine-needle aspiration cytology. *Oncol Lett* (2018) 15(2):1907–11. doi:10.3892/ol.2017.7448

24. Fellegara G, D'adda T, Pilato FP, Froio E, Ampollini L, Rusca M, et al. Genetics of a combined lung small cell carcinoma and large cell neuroendocrine carcinoma with adenocarcinoma. *Virchows Arch* (2008) 453(1):107–15. doi:10.1007/s00428-008-0620-y

25. Zhuo M, Zhuang X, Tang W, Xu J, Zhang C, Qian X, et al. The impact of IL-16 3'UTR polymorphism rs859 on lung carcinoma susceptibility among Chinese han individuals. *Biomed Res Int* (2018) 2018:8305745. doi:10.1155/2018/8305745

26. Kanan AD, Corey E, Vêncio RZN, Ishwar A, Liu AY. Lineage relationship between prostate adenocarcinoma and small cell carcinoma. *BMC Cancer* (2019) 19(1):518. doi:10.1186/s12885-019-5680-7

27. Quintanal-Villalonga A, Durani V, Sabet A, Redin E, Kawasaki K, Shafer M, et al. Exportin 1 inhibition prevents neuroendocrine transformation through SOX2 down-regulation in lung and prostate cancers. *Sci Transl Med* (2023) 15(707):eadf7006. doi:10.1126/scitranslmed.adf7006

28. Antonia SJ, López-Martin JA, Bendell J, Ott PA, Taylor M, Eder JP, et al. Nivolumab alone and nivolumab plus ipilimumab in recurrent small-cell lung cancer (CheckMate 032): a multicentre, open-label, phase 1/2 trial. *Lancet Oncol* (2016) 17(7):883–95. doi:10.1016/S1470-2045(16)30098-5

29. Rudin CM, Pietanza MC, Bauer TM, Ready N, Morgensztern D, Glisson BS, et al. Rovalpituzumab tesirine, a DLL3-targeted antibody-drug conjugate, in recurrent small-cell lung cancer: a first-in-human, first-in-class, open-label, phase 1 study. *Lancet Oncol* (2017) 18(1):42–51. doi:10.1016/S1470-2045(16)30565-4

30. Farago AF, Piotrowska Z, Sequist LV. Unlocking the mystery of small-cell lung cancer transformations in EGFR mutant adenocarcinoma. *J Clin Oncol* (2017) 35(26):2987–8. doi:10.1200/JCO.2017.73.5696

31. Mao X, Liu J, Hu F, Niu Y, Pan F, Fu X, et al. Serum NSE is early marker of transformed neuroendocrine tumor after EGFR-TKI treatment of lung adenocarcinoma. *Cancer Manag Res* (2022) 14:1293–302. doi:10.2147/CMAR.S349082

32. Hendifar AE, Marchevsky AM, Tuli R. Neuroendocrine tumors of the lung: current challenges and advances in the diagnosis and management of well-differentiated disease. *J Thorac Oncol* (2017) 12(3):425–36. doi:10.1016/j.jtho.2016.11.2222

33. Lo RG, Pusceddu S, Proto C, Macerelli M, Signorelli D, Vitali M, et al. Treatment of lung large cell neuroendocrine carcinoma. *Tumour Biol* (2016) 37(6): 7047–57. doi:10.1007/s13277-016-5003-4

34. Cakir E, Demirag E, Aydin M, Unsal E. Clinicopathologic features and prognostic significance of lung tumours with mixed histologic patterns. *Acta Chir Belg* (2009) 109(4):489–93. doi:10.1080/00015458.2009.11680466

35. Filosso PL. Large-cell neuroendocrine carcinoma (LCNC) of the lung: a dilemma. *Eur J Cardio-Thoracic Surg* (2003) 24(4):671–2. doi:10.1016/s1010-7940(03)00467-6

36. Ortega MA, Navarro F, Pekarek L, Fraile-Martínez O, García-Montero C, Saez MA, et al. Exploring histopathological and serum biomarkers in lung adenocarcinoma: clinical applications and translational opportunities (Review). *Int J Oncol* (2022) 61(6):154. doi:10.3892/ijo.2022.5444

37. Affandi KA, Tizen NMS, Mustangin M, Zin RRMRM. p40 immunohistochemistry is an excellent marker in primary lung squamous cell carcinoma. *J Pathol Transl Med* (2018) 52(5):283–9. doi:10.4132/jptm.2018.08.14

38. Wang Y, Qian F, Chen Y, Yang Z, Hu M, Lu J, et al. Comparative study of pulmonary combined large-cell neuroendocrine carcinoma and combined small-cell carcinoma in surgically resected high-grade neuroendocrine tumors of the lung. *Front Oncol* (2021) 11:714549. doi:10.3389/fonc.2021.714549

39. Yang Z, Wang Y, Chen Y, Qian F, Zhang Y, Hu M, et al. Combined large cell neuroendocrine carcinoma: clinical characteristics, prognosis and postoperative management. *Eur J Cardiothorac Surg* (2022) 62(2):ezac069. doi:10.1093/ejcts/ezac069

40. Filosso PL, Fontana EC, Ruffini E. Large-cell neuroendocrine carcinoma and combined large-cell neuroendocrine carcinoma: 2 characters in search of an author. *Eur J Cardiothorac Surg* (2022) 62(2):ezac176. doi:10.1093/ejcts/ezac176

41. Li M, Yang L, Lu H. Pulmonary combined large cell neuroendocrine carcinoma. *Pathol Oncol Res* (2022) 28:1610747. doi:10.3389/pore.2022.1610747

42. Yamamoto M, Ito R, Tsujibata A, Morita H, Yoneda T, Matano Y, et al. Large-cell neuroendocrine carcinoma of the lung with carcinoid syndrome. *Intern Med* (2023) 62(10):1557–63. doi:10.2169/internalmedicine.0099-22

43. Bessho T, Yokochi K, Sakurai T. Combined large cell neuroendocrine carcinoma. *Jpn J Thorac Cardiovasc Surg* (2004) 52(9):426–8. doi:10.1007/s11748-004-0037-8

44. Masuya D, Gotoh M, Nakashima T, Liu D, Ishikawa S, Yamamoto Y, et al. Combined large cell neuroendocrine carcinoma and squamous cell carcinoma of the lung; report of a case. *Kyobu Geka* (2006) 59(6):491–5.

45. Pelosi G, Barbareschi M, Cavazza A, Graziano P, Rossi G, Papotti M. Large cell carcinoma of the lung: a tumor in search of an author. A clinically oriented critical reappraisal. *Lung Cancer* (2015) 87(3):226–31. doi:10.1016/j.lungcan.2015.01.008

46. Davenport ML, Echols JB, Silva AD, Anderson JC, Owens P, Yates C, et al. miR-31 displays subtype specificity in lung cancer. *Cancer Res* (2021) 81(8): 1942–53. doi:10.1158/0008-5472.CAN-20-2769

47. Milione M, Maisonneuve P, Grillo F, Mangogna A, Centonze G, Prinzi N, et al. Ki-67 index of 55% distinguishes two groups of bronchopulmonary pure and composite large cell neuroendocrine carcinomas with distinct prognosis. *Neuroendocrinology* (2021) 111(5):475–89. doi:10.1159/000508376

48. Zhu Z, Liu Y, Xu H, Ning H, Xia Y, Shen L. Combined large cell neuroendocrine carcinoma, lung adenocarcinoma, and squamous cell carcinoma: a case report and review of the literature. *J Cardiothorac Surg* (2023) 18(1):254. doi:10.1186/s13019-023-02349-4

49. Oda R, Okuda K, Yamashita Y, Sakane T, Tatematsu T, Yokota K, et al. Long-term survivor of pulmonary combined large cell neuroendocrine carcinoma treated with nivolumab. *Thorac Cancer* (2020) 11(7):2036–9. doi:10.1111/1759-7714.13471

50. Archibald H, Keel S, Becker E. Large cell neuroendocrine carcinoma of the floor of mouth and retromolar trigone in association with basaloid squamous cell carcinoma. *Int J Oral Maxillofac Surg* (2022) 51(12):1520–4. doi:10.1016/j.ijom.2022.01.020

51. Le DT, Do KH, Do TA, Bui HTT, Nguyen CV. Combined large-cell neuroendocrine and squamous cell carcinoma of the uterine cervix with a personal history of the primary breast duct carcinoma *in situ*: a clinicopathological characteristic and outcome. *Case Rep Oncol* (2022) 15(2): 770–5. doi:10.1159/000526337

Pathology & Oncology Research | frontiers

TYPE Review
PUBLISHED 22 April 2024
DOI 10.3389/pore.2024.1611743

Check for updates

OPEN ACCESS

EDITED BY
Nora Bittner,
National Koranyi Institute of TB and Pulmonology, Hungary

*CORRESPONDENCE
Lőrinc S. Pongor,
lorinc.pongor@hcemm.eu

RECEIVED 23 February 2024
ACCEPTED 03 April 2024
PUBLISHED 22 April 2024

CITATION
Für GM, Nemes K, Magó É, Benő AÁ, Topolcsányi P, Moldvay J and Pongor LS (2024), Applied models and molecular characteristics of small cell lung cancer. *Pathol. Oncol. Res.* 30:1611743. doi: 10.3389/pore.2024.1611743

COPYRIGHT
© 2024 Für, Nemes, Magó, Benő, Topolcsányi, Moldvay and Pongor. This is an open-access article distributed under the terms of the Creative Commons Attribution License (CC BY). The use, distribution or reproduction in other forums is permitted, provided the original author(s) and the copyright owner(s) are credited and that the original publication in this journal is cited, in accordance with accepted academic practice. No use, distribution or reproduction is permitted which does not comply with these terms.

Applied models and molecular characteristics of small cell lung cancer

Gabriella Mihalekné Für[1], Kolos Nemes[1], Éva Magó[1,2], Alexandra Á. Benő[1], Petronella Topolcsányi[1], Judit Moldvay[3,4] and Lőrinc S. Pongor[1]*

[1]Cancer Genomics and Epigenetics Core Group, Hungarian Centre of Excellence for Molecular Medicine (HCEMM), Szeged, Hungary, [2]Genome Integrity and DNA Repair Core Group, Hungarian Centre of Excellence for Molecular Medicine (HCEMM), Szeged, Hungary, [3]Department of Pulmonology, Szeged University Szent-Gyorgyi Albert Medical School, Szeged, Hungary, [4]1st Department of Pulmonology, National Koranyi Institute of Pulmonology, Budapest, Hungary

Small cell lung cancer (SCLC) is a highly aggressive type of cancer frequently diagnosed with metastatic spread, rendering it surgically unresectable for the majority of patients. Although initial responses to platinum-based therapies are often observed, SCLC invariably relapses within months, frequently developing drug-resistance ultimately contributing to short overall survival rates. Recently, SCLC research aimed to elucidate the dynamic changes in the genetic and epigenetic landscape. These have revealed distinct subtypes of SCLC, each characterized by unique molecular signatures. The recent understanding of the molecular heterogeneity of SCLC has opened up potential avenues for precision medicine, enabling the development of targeted therapeutic strategies. In this review, we delve into the applied models and computational approaches that have been instrumental in the identification of promising drug candidates. We also explore the emerging molecular diagnostic tools that hold the potential to transform clinical practice and patient care.

KEYWORDS

SCLC, drug response, ctDNA, liquid biopsy, databases

Introduction

Small Cell Lung Cancer (SCLC) is an extremely aggressive form of cancer, accounting for about 15% of all lung cancer cases. Due to its aggressive nature, over 60% of SCLC cases already show metastasis at the time of diagnosis, despite regular imaging [1]. Consequently, surgical resection is rarely an option, leaving chemotherapy, radiation, and in some instances, immunotherapy, as the main treatment methods. This situation adversely affects SCLC research and the development of new molecular diagnostic tools as well, as tumor samples are rarely available. Since no major improvements have been achieved in SCLC treatment in over three decades, which is paired with short life expectancy, the National Cancer Institute to categorizes this disease as a "recalcitrant" cancer. Therefore, there is an urgent need for a more profound understanding of SCLC's

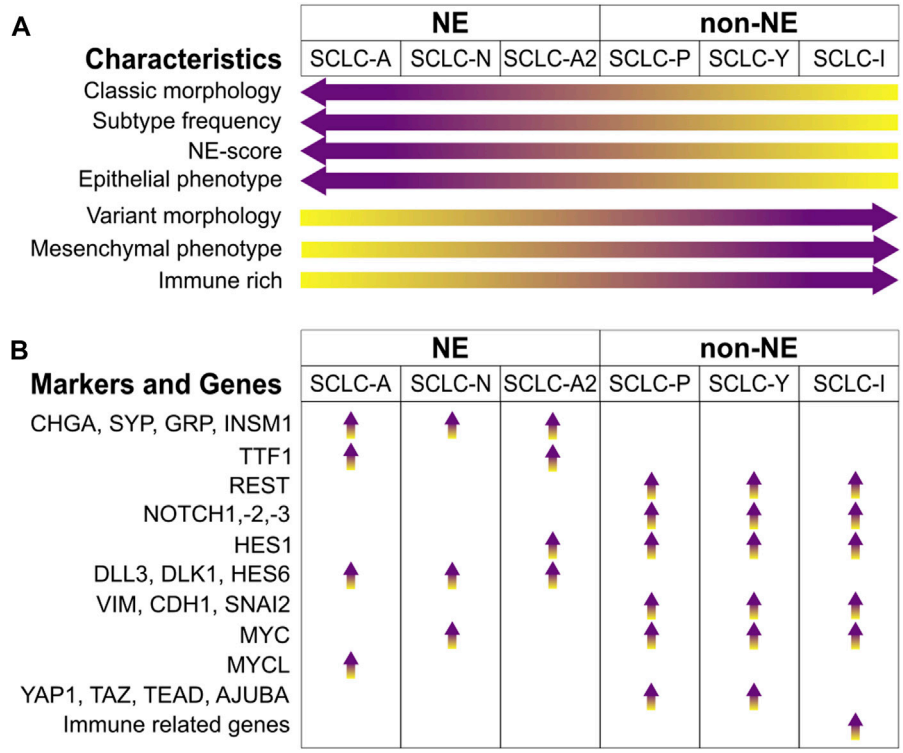

FIGURE 1
SCLC subtypes. **(A)** Signature enrichment of subtypes. **(B)** Key markers and genes enriched in the different SCLC subtypes. Abbreviations: CHGA, Chromogranin A; SYP, Synaptophysin; GRP, Gastrin-Releasing Peptide; INSM1, Insulinoma-Associated Protein 1; TTF1, Thyroid-Transcription Factor 1; REST, RE1-Silencing Transcription Factor; NOTCH1,-2,-3, Neurogenic Locus Notch Homolog Protein 1, -2, -3; HES1, Hes Family BHLH Transcription Factor 1; DLL3, Delta Like Canonical Notch Ligand 3; DLK1, Protein Delta Homologue 1; HES6, Hes Family BHLH Transcription Factor 6; VIM, Vimentin; CDH1, Cadherin 1; SNAI2, Snail Family Transcriptional Repressor 2; MYC, MYC Proto-Oncogene, BHLH Transcription Factor; MYCL, MYCL Proto-Oncogene, BHLH Transcription Factor; YAP1, Yes1 Associated Transcriptional Regulator; TAZ, Transcriptional Coactivator With A PDZ-Binding Domain; TEAD, TEA Domain Transcription Factors; AJUBA, LIM Domain-Containing Protein Ajuba.

development and progression, the creation of more accurate models, and the development of new molecular diagnostic tools that can overcome the challenges presented by this complex disease.

Subtypes of SCLC

A decade ago, SCLC was predominantly viewed as a uniform type of pulmonary neuroendocrine cancer. The World Health Organization (WHO) and the National Comprehensive Cancer Network (NCCN) still classify SCLC into two subtypes: small cell carcinoma (previously known as oat cell carcinoma) and combined-SCLC, characterized by features of both small and non-small cell carcinoma [2].[1] When SCLC cell lines were first developed approximately 30 years ago, they revealed two distinct morphological subtypes: classic and variant subtypes. Classic cell lines formed non-adherent aggregates or spheroid cells, while variant cell lines exhibited either loosely adhering aggregates or formed tightly adhering monolayers [3].

The homogeneity of SCLC is exhausted by the prevalent TP53 and RB1 inactivation [4–7], from which new characterizations have been developed over the years. A critical finding was that SCLCs could be categorized based on their neuroendocrine (NE) characteristics, into NE (with high NE scores) and non-NE (with low NE scores) types by IHC staining for neuroendocrine markers such as SYP (Synaptophysin) or CHGA (Chromogranin A) [8]. Transcriptomic profiling of these cell lines has led to the identification of further subtypes based on the expression of transcription factors, a classification also supported by tumor sample analysis [7, 9–11], which we summarized in Figure 1.

The most prevalent subtype is characterized by elevated expression of Achaete-scute homologue 1 (ASCL1), termed SCLC-A, which is crucial in regulating neuroendocrine differentiation [12–14]. NEUROD1 (Neuronal Differentiation

1 https://www.nccn.org/

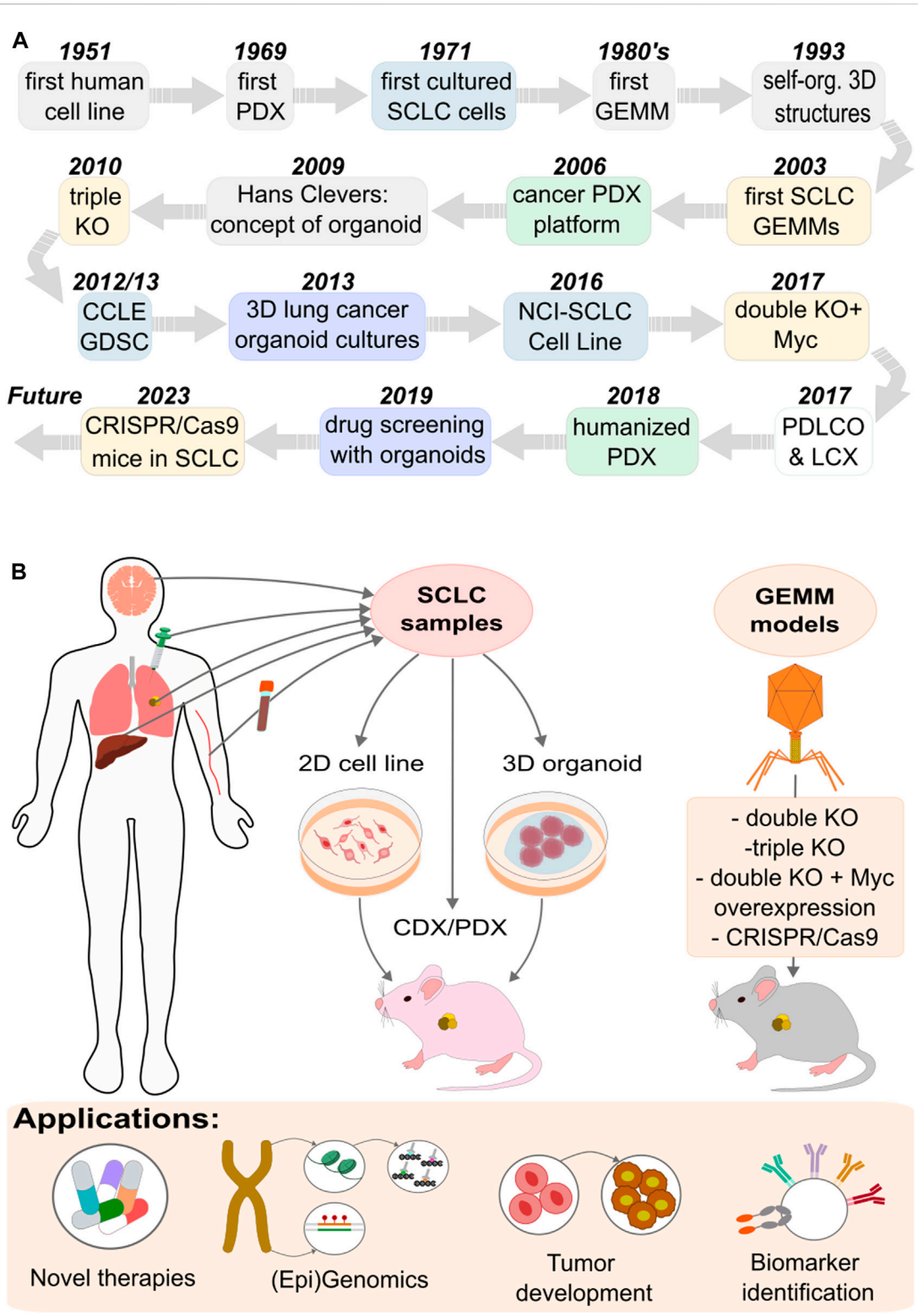

FIGURE 2
Experimental model systems used to explore SCLC. **(A)** Timeline of the developed models. **(B)** Approaches and applications of the different models.

1), another marker for the NE subtype, often co-exists with ASCL1. NEUROD1, enriched in the SCLC-N subtype, also influences NE differentiation and contributes to the progression of cancer, [14]. A less common group, which is negative for both ASCL1 and NEUROD1, falls into the non-NE category. These tumors and cell lines sometimes express ASCL2, suggesting its role as an alternative transcription driver [12]. The main non-NE subtypes are distinguished by the expression of POU2F3 (SCLC-P) and YAP1 (SCLC-Y). POU2F3 (POU Class 2 Homeobox 3), a key transcription factor in chemosensory tuft cells, is expressed in SCLC variants that share a similar expression profile with these cells, indicating a possible origin from this cell lineage [15]. YAP1 (Yes1 Associated Transcriptional Regulator) and TAZ (Transcriptional Coactivator with a PDZ-Binding Domain) are involved in the Hippo pathway as transcriptional coactivators and effector proteins, leading to tissue overgrowth and oncogenesis [16]. SCLCs expressing YAP1 represent a relatively rare subgroup [7, 11, 17].

The (NE) and non-NE subtypes of SCLC show distinct transcriptional signatures. Zhang et al. identified a set of 50 genes that are differentially expressed in SCLC tumors, cell lines, and genetically engineered mouse models (GEMMs) [12]. This set includes 25 genes closely associated with NE SCLCs and another 25 linked with non-NE SCLCs. These genes were used to generate an NE scoring system to help patient stratification. An ASCL1 subset that expresses HES1 (Hes Family BHLH Transcription Factor 1) was also identified and was termed as SCLC-A2 or NEv2 [18–20], which was often associated to liver metastases [19].

The CHGA and SYP genes are widely recognized NE markers, showing high expression levels in both SCLC-A and SCLC-N subtypes [9, 12]. Insulinoma-Associated Protein 1 (INSM1), a zinc-finger transcription factor found in developing neuroendocrine tissues [21], is indicative of SCLC and associated with NE characteristics [22, 23]. Additional genes linked with NE subtypes include Gastrin-Releasing Peptide (GRP) [7], Protein Delta Homologue 1 (DLK1) [24], and BEX1 (Brain Expressed, X-Linked 1) [25]. NKX2-1, the gene for Thyroid-Transcription Factor 1 (TTF1), is a transcriptional target of ASCL1, making its expression specific to the SCLC-A subtype [9, 26].

Notch signaling is known to facilitate a transition from NE to a chemoresistant non-NE phenotype in SCLC [20]. It activates the expression of REST (RE1-Silencing Transcription Factor), which suppresses the expression of NE markers such as ASCL1, SYP, or CHGA. Similarly, YAP1 has been found to support this Notch-induced shift to a non-NE phenotype [27]. Additionally, HES1 (Hes Family BHLH Transcription Factor 1) has a negative correlation with NE scoring [12], as its expression is governed by NOTCH1, which hinders the transcription of REST and YAP1 [27, 28]. While Notch signaling fosters non-NE differentiation, some genes, such as DLL3, DLK1 and HES6, which activate this pathway, have been found to correlate with the NE subtype, thereby acting in a pro-tumorigenic manner towards NE cells [12, 19, 29, 30].

Genes in the TGFβ pathway have been found to be expressed in non-NE cases of SCLC, acting as suppressors of ASCL1 [12, 19]. There is a crosstalk between the Notch and the Hippo pathway [31, 32]. YAP1 and TAZ are overexpressed in SCLC-Y, as well as the TEAD genes (TEAD2 and TEAD3) and AJUBA (Ajuba LIM Protein), negative regulators of the pathway [12, 19]. Additionally, the transition from NE to non-NE phenotype can be influenced by Notch and TGFβ signaling, which is linked with the process of epithelial to mesenchymal transition (EMT). EMT is known to promote metastasis and resistance to treatment in cancer cells [33]. The expression of the intermediate filament vimentin (VIM), and SNAI2 (Snail Family Transcriptional Repressor 2), a repressor of E-cadherin (CDH1), has been observed to negatively correlate with the NE state of SCLC [12, 20]. The MYC proto-oncogene paralogues (BHLH Transcription Factors), are differentially expressed in SCLC. MYCL being the target of ASCL1 is expressed in SCLC-A [19], while MYC, a target of NEUROD1, which drives to a non-NE phenotype is elevated in SCLC-N [34, 35] and in non-NE SCLC-Y [7] subtypes.

DNA replication stress is a key biological feature of SCLC [36]. The near universal loss of p53 and RB1 tumor suppressors is one reason of replication stress as they play roles in cell cycle progression [37]. Another reason could be the overexpression of MYC family of oncogenes, which promote heightened replication initiation, which lead to defects in replication [38, 39]. Replication stress is higher in NE tumors, presenting a specific gene expression pattern with genes to deal with the elevated replication rates, to hinder the DNA damage, DNA repair, and cell cycle related genes [19, 40]. The elevated replication stress observed in NE tumors may be a reason why many tumors have exceptional initial response [36].

A new subtype of small cell lung cancer (SCLC) has been recently identified, which does not fully align with the previous four subtypes based on transcription factor expression, although SCLC-Y is commonly found. Instead, this subtype, termed SCLC-inflamed or SCLC-I, is characterized by the expression of immune-related genes. SCLC-I tumors exhibit the highest levels of $CD8^+$ T-cell and overall immune infiltration among all the subtypes. Additionally, SCLC-I is marked by high levels of immune checkpoint molecules (such as PD-L1, PDCD1, CTLA4, CD38, IDO1, TIGIT, VISTA, ICOS, LAG3), T cell attractant chemokines (CCL5, CXCL10), and MHC genes (HLA-DRB1, HLA-DQA1, MICA). This suggests they may be more responsive to checkpoint inhibitors compared to other subtypes. Gay et al., in a reanalysis of the *IMpower133* data, noted that SCLC-I tumors tend to respond favorably to carboplatin/etoposide/atezolizumab treatment [9, 41].

This highlights the heterogeneity of SCLC and underscores the importance of adopting these proposed subtype classifications. Continued subtype-specific research is essential

TABLE 1 Summary of advantages and disadvantages of each model.

Characteristics	SCLC models			
	Cell line	CDX/ PDX	PDO	GEMM
Cost	–	+	+	+
Time consuming	–	+	·	+
Difficult to generate	–	+	·	+
Rapid expansion	+	–	+	–
Reproducibility	+	–	–	·
Tumor heterogenity	–	+	+	·
Original tumor biology	·	·	+	+
Primary disease	+	·	+	+
Metastasis	·	+	+	·
Biomarker discovery	·	+	+	·
Drugscreening	+	+	+	+
Translational research	–	+	+	·

to understand their distinct pathophysiologies and to identify optimal treatment strategies.

Experimental models of SCLC

There are several model systems used to examine cancer and SCLC (Figure 2). Each system has advantages and disadvantages, covering a wide range of application, such as drug testing, performing omics studies, or to characterize SCLC development (Table 1).

Patient derived cell lines (PDC)

The basic growth properties of SCLC were first defined using panels of cell lines developed from 1971 through the early 1990s [42–45] (Figure 2A). Primarily derived from metastatic SCLC tumors, these cell lines have been instrumental models for understanding gene functions and testing potential drug candidates.

During the early 1990s, the National Cancer Institute (NCI, Bethesda, MD), pioneered a new method for drug screening focused on specific diseases. This method involved using a collection of 60 human cancer cell lines from nine different cancer types [46, 47]. Originally, SCLC was not part of the NCI-60, which made drug predictions for this cancer type unfeasible. However, the advent of high-throughput technologies and improvements in characterizing cell lines have led to the development of more extensive cell line collections that now include SCLC. These databases contain detailed information on gene mutations, structural alterations, and changes in copy numbers, as well as mRNA expression profiles. This allows for comparative analyses across different cell lines and cancer types. For example, the Cancer Cell Line Encyclopedia (CCLE) [48] resource utilized data from massively parallel sequencing and microarray expression profiles from 947 human cancer cell lines, alongside the responses to 24 anticancer drugs in 479 of these lines. Additionally, the Genomics of Drug Sensitivity in Cancer (GDSC) has become a major public source for data on cancer cell drug sensitivity and molecular indicators of drug response [49]. The GDSC database includes information from nearly 75,000 experiments, covering responses to 138 anticancer drugs across approximately 700 cancer cell lines. Recent studies enable the exploration of the role of microRNAs as potential biomarkers in SCLC. By the early 1990s, investigations had already been conducted on 126 SCLC cell lines, providing insights into the response of these cell lines to anticancer drugs, and a library of investigational agents complemented by exon and microRNA arrays [50].

Despite their affordability and suitability for high throughput screening, these cells do not fully capture the complex nature of the tumor environment [51]. For this reason, such cancer models have roughly a 10% success rate in advancing anti-cancer drugs to clinical trial stages [52]. In addition, even the promising drug candidates usually failed at preventing recurrence in pre-clinical and clinical trials [52]. Nonetheless, they are still useful model organisms that can be used to better characterize and study what genetic and epigenetic factors affect SCLC growth and development, providing quick and easy tools for drug and CRISPR based screens.

Patient derived organoids (PDO)

In 2009, Hans Clevers laid the foundation for organoid research, demonstrating new methods for organoid culture [53, 54] (Figure 2A), significantly boosting the development of patient-derived organoids (PDOs). The first lung cancer PDOs were generated by Inoue and coworkers [55, 56]. Compared to traditional cancer cell lines and patient-derived xenograft (PDX) models, lung cancer PDOs offer several advantages [57, 58]. PDO is a 3D structure culture formed from enriched patient cancer cells. It exhibits genetic stability, self-renewal capabilities, drug sensitivity, and high degrees of similarity to human organs in both structure and function [59].

A key attribute of PDOs is their faithful retention of the parental tumor's genomic changes, yet they allow for faster modeling and some degree of gene editing [57, 60–62]. Through whole-exome sequencing, whole-genome sequencing, and RNA-seq Kim and their colleagues found that short-term cultured lung organoids retained 92.7% and 77% of the driver mutations found in the primary tissue, respectively [63, 64]. They developed 80 lung cancer organoid lines, including five from SCLC. These SCLC organoids accurately reproduced the tissue structure of the original tumors and maintained key SCLC diagnostic markers such as CD56, SYP, and TTF-1. It was

also noted that the culture conditions for non-small cell lung cancer (NSCLC) PDOs and SCLC PDOs differed, with R-spondin1 and Wnt3a being crucial for the long-term culture of SCLC tumor organoids [57, 65]. In addition, Zhang et al. were able to establish 3D co-culture models to expand circulating tumor cells (CTCs) *ex vivo* from early-stage SCLC patients [66, 67].

Recent studies using engineered mouse lung cancer organoids (LCOs) have shed light on SCLC metastasis mechanisms, showing that KMT2C deficiency leads to extensive metastasis [68, 69]. This particular SCLC model, driven by Trp53 and Rb1 (mouse homologs of human TP53 and RB1, respectively) deficiencies and Myc overexpression, displayed multiple diagnostic markers of SCLC and developed significant distal metastases in multiple organs [68]. In SCLC research, brain organoids can be propagated on a large scale, facilitating the testing of various cell subtype combinations [70]. However, creating a PDO model is time-intensive, costly, and technically challenging, necessitating further research into PDOs [54].

Patient and circulating tumor cell xenografts (PDX/CDX)

The *in vivo* preclinical methods of SCLC research include the application of mouse xenograft models. These models are either cell line-derived xenografts, created from SCLC cell lines, or PDX models, which involve directly implanting tumor material into immunocompromised mice like NOD/SCID or NSG [45, 71] (Figure 2B). The advantage of these models can be seen in the example of BH3 mimetics (BCL2/BCLxL inhibitors), where significant effectiveness in SCLC cell line models has been observed [45, 72, 73], with limited sensitivity in SCLC PDX models [74]. The discrepancy between PDX models and cell-line models in drug sensitivity underscores the potential impact of *in vitro* selection artifacts on clinical outcomes, suggesting that PDX models may better reflect the expression profiles and drug sensitivities of SCLC patient tumors [75, 76].

Obtaining SCLC samples is unfortunately very challenging as it is rarely surgically removed, and invasive tumor sampling is typically unnecessary after diagnosis [45]. To bridge this gap CTCs from the blood of cancer patients can be sampled noninvasively and are highly abundant in SCLC patients [77, 78]. In the CDX technique, changes in CTC numbers are closely aligned with chemotherapy responses, indicating that CTCs may reflect the biology of SCLC tumors. Both PDX and CDX techniques maintain the original human tumor's histopathological and genetic characteristics, preserving its heterogeneity and complexity [45, 79]. This significantly improves the ability to identify and test biomarkers for treatment and prognosis [64].

PDX models are thought to preserve the tumor microenvironment and epigenetic features, which are crucial for tumorigenesis, invasion, metastasis, and the effectiveness of anticancer therapies [60]. However, PDX has several limitations, including chances of tumor tissue engraftment failure, a long tumor development timeline, dissimilarity of the tumor microenvironment between human and murine models, and low throughput for drug screening [80]. Furthermore, the requirement for immunocompromised hosts limits their use in studying cancer-immunity interactions. Advances in humanized mice and mice with reconstituted human immune systems offer potential solutions [54]. Sequencing studies using next-generation sequencing on SCLC PDX models have proven valuable for unraveling the molecular landscape of this disease [78], and also reported the presence of a concordant somatic TP53 mutation in all CTCs [77].

Genetically engineered mouse models (GEMM)

Research in lung cancer has progressed significantly due to studies using genetically engineered mouse models (GEMMs), which facilitate the examination of tumor biology and environmental interactions *in vivo* conditions [78]. The first SCLC GEMM model was developed in the laboratory of Anton Bern in 2003 [10]. It incorporated loss-of-function mutations in the Rb1 and Trp53 tumor suppressor genes (double knockout), mirroring mutations found in over 90% of SCLC patients [81] (Figure 2A). These mutations were believed to exhibit significant histological and molecular biological similarities to the human disease, though the rate of tumor development in the model was slower than typically observed in human cases [82].

GEMMs laid the groundwork for numerous subsequent studies, which explored the roles of various potential tumor suppressors and oncogenes in SCLC [83]. A notable study within this framework examined P130, also known as Rbl2 (RB Transcriptional Corepressor Like 2), a member of the retinoblastoma (Rb) family (Figure 2B). The deletion of the P130 gene in mice already having Rb1 and Trp53 gene knockouts led to faster tumor growth, thereby affirming P130's tumor suppressor function in SCLC (triple knockout) [81, 84]. Similar methods were used to demonstrate the importance of PTEN and NOTCH tumor suppressors [7, 85].

Conditional Trp53/Rb1 (double knockout) and Trp53/Rb1/Rbl2 (triple knockout) knockout mouse models displayed traits typical of the ASCL1-high/NEUROD1-low subtype of human SCLC [35]. The double knockout model was further developed by introducing a CRE-activated Myc-T58A mutation. The stabilization of MYC in this model hastened tumor development and growth processes, and the resulting invasive tumors were representative of the high NEUROD1 subtype [35, 82].

Since the 2010s, CRISPR/Cas9 GEMMs have been applied in cancer research [86, 87], and significant breakthroughs occurred in 2023. These innovations include the development of mice

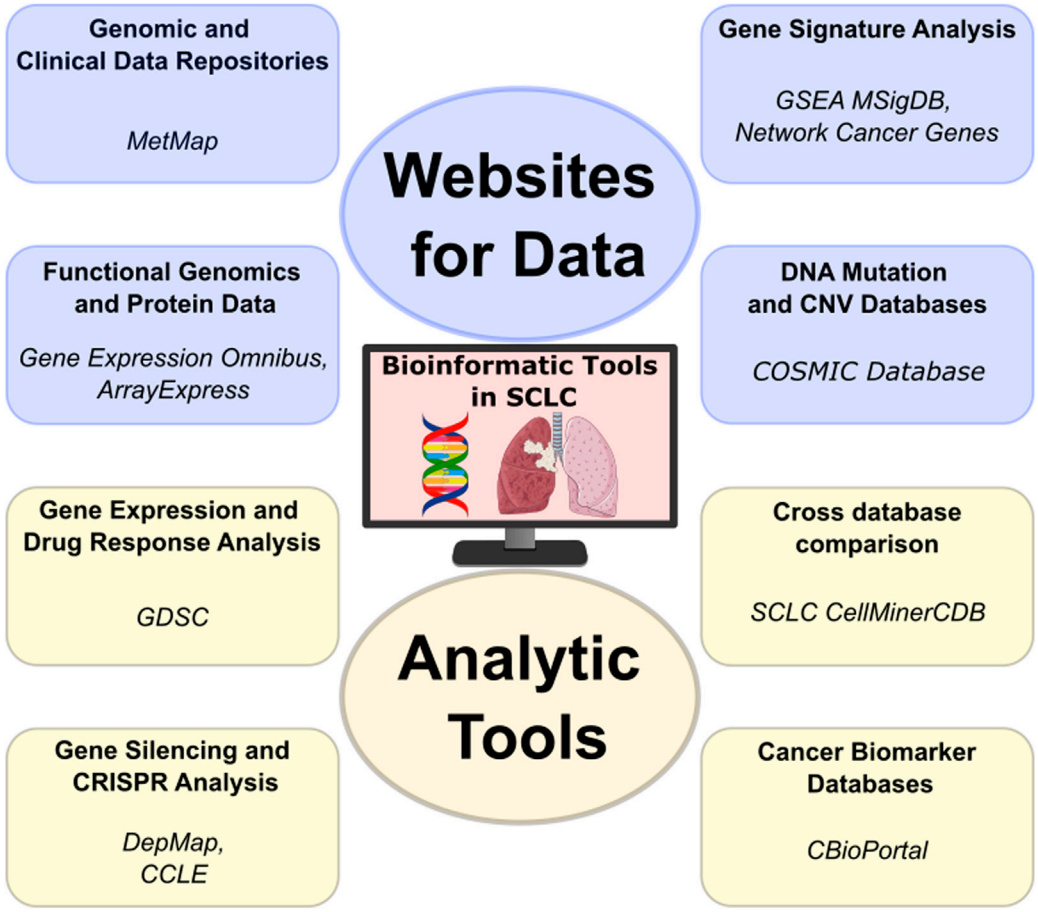

FIGURE 3
The analytic tools used in SCLC research are pivotal not only for their analytical capabilities but also for the downloadable databases they offer. This feature allows for versatile data manipulation, enabling researchers to conduct customized analyses that can lead to novel insights into SCLC's molecular intricacies and potential treatments. (Lung—lung-cancer icon by Servier https://smart.servier.com/ is licensed under CC-BY 3.0 Unported https://creativecommons.org/licenses/by/3.0/, DNA—dna-nucleotides-ribbon icon by Servier https://smart.servier.com/ is licensed under CC-BY 3.0 Unported https://creativecommons.org/licenses/by/3.0/.

capable of CRISPR/Cas9 base editing [88] and prime editing [89]. Prime editing, which employs Cas9 with a reverse transcriptase, allows for precise and efficient mutation engineering, as demonstrated in a proof-of-principle study introducing hotspot mutations for Kras and Trp53 in the lung and pancreas [90].

Databases and tools to mine SCLC

Research on SCLC is guided by a wealth of data from specialized websites, analyzed using integrative approaches. This combination of resources is not only changing the paradigm of the disease but also improving its treatment. The scientific progress is centered around data repositories that provide raw genomic, proteomic, and clinical data, as well as analytical tools that interpret this data to derive meaningful disease insights.

Websites for data in SCLC research

Data repositories have become indispensable in SCLC research (Figure 3). They serve not only as collections of genomic and clinical data but also as platforms that enable intricate comparative studies and groundbreaking translational research. Data can be directly accessed through different sites, such as the SRA (Sequence Read Archive) [91] and ENA (European Nucleotide Archive) [92] in case of experimental models, or European Genome-phenome Archive (EGA) [93] and dbGAP [94] for protected patient data that requires access. These allow researchers to process and analyze data in any preferred way. In many cases, processed data is also made available, such as at the GEO or ArrayExpress, which allows users to directly access results without having to reprocess large data amounts. Recent studies leveraging published data have revealed novel gene signatures that are correlated with SCLC

progression [95–97]. Overall, these databases play a crucial role in discovering biomarkers, which aid in developing new diagnostic and prognostic tools. This, in turn, helps personalize patient care for SCLC.

Mutation databases such as Catalogue Of Somatic Mutations In Cancer (COSMIC) [98] offer a comprehensive record of genomic aberrations discovered in cancer, including SCLC. COSMIC documents genetic alterations, such as mutations and copy number variations (CNVs), which can be used to find recurrent alterations and hotspots through interactive plots. It is an essential resource for identifying genetic alterations in cancer, including SCLC, and for the continuous search for targeted therapies. In addition, the MetMap [99] provides a detailed profiling of metastatic potential of cell lines including SCLC, aiding in the identification of potential therapeutic targets.

Gene signature analysis, facilitated by platforms such as GSEA's [100] MSigDB [101], and Network Cancer Genes [102], enables the identification of predictive gene patterns [103]. This approach is essential for developing targeted and personalized therapies for SCLC, tailoring treatments to individual genetic profiles [104].

Analytic tools facilitating SCLC research

The analytical tools utilized in research on SCLC are crucial not only for their capabilities but also for the provided easy data access (Figure 3). This feature allows for versatile data manipulation, enabling researchers to conduct customized analyses that can lead to novel insights into SCLC's molecular intricacies and potential treatments.

The Genomics of Drug Sensitivity in Cancer (GDSC) [49] offers a vast repository of data specifically focused on drug response in cancer, providing insights into how various cancer cells react to different treatments. Using the GDSC portal, users can compare drug sensitivity across cell lines and tissue types, compare drug response based on mutational status and correlate compound response.

The Cancer Cell Line Encyclopedia (CCLE) [48] provides another critical piece in cancer research, offering detailed genetic and molecular information on a wide range of cancer cell lines [49, 105, 106]. Building upon this, the DepMap portal [107] presents as a precious tool for functional genomics. DepMap utilizes the data from CCLE to identify essential genes for cancer cell survival, employing cutting-edge CRISPR technology. This integration allows researchers to perform in-depth analysis of CCLE data within the DepMap framework, enhancing our understanding of cancer dependencies and paving the way for new therapeutic approaches targeting these vulnerabilities in cancer cells.

The SCLC-CellMinerCDB tool at the National Cancer Institute (NCI) stands out for its integration of diverse databases, including GDSC, CCLE, UT Southwestern (UTSW) Medical Center [108] and NCI-SCLC [17, 109]. This integration not only consolidates a wealth of data but also facilitates advanced analysis capabilities. Researchers can seamlessly explore and compare data from multiple sources, encompassing diverse omics datasets such as gene mutation/copy-number data, expression data, epigenetics data (DNA methylation and enhancer signal, [97, 110]) and gene signature enrichment, which can be compared to each other or to drug response data.

The cBioPortal [111] for Cancer Genomics is an excellent example of the power of integrative data analysis. It provides researchers with a multifaceted view of molecular data sets alongside clinical attributes. This tool is particularly adept at uncovering biomarkers for SCLC and for cancer in general. With cBioPortal, we can interrogate and visualize mutation distribution in patient cohorts, identify co-expressing or anti-expressing genes, or even compare survival between patient groups based on mutational status of selected genes. In addition, processed data and clinical information can be easily obtained, helping researcher create custom analyses from a curated set.

The integration of data repositories and analytical tools is crucial in navigating the complex molecular landscape of SCLC, representing the forefront of precision oncology. The future of SCLC research and treatment depends on the continued fusion of data acquisition with analytical sophistication, which holds the key to unlocking new realms in cancer therapy.

Developing non-invasive diagnostics

SCLC is histologically characterized as a malignant epithelial tumor composed of small cells that feature minimal cytoplasm, indistinct cell borders, finely granular nuclear chromatin, and either absent or barely noticeable nucleoli. The majority of SCLC cases, roughly 90%, fall into the category of typical SCLC, which exclusively comprises these small cells. The rest are identified as combined SCLC, where the tumor also includes elements of large cell carcinoma [112]. SCLC can be classified into two stages: limited disease (LD-SCLC), when it is limited to the hemithorax, where radiochemotherapy is effective; or extensive disease (ED-SCLC), where metastatic disease can be found outside of the hemithorax at diagnosis [113].

The diagnostic process for SCLC typically includes a physical examination, an assessment of the patient's performance status, laboratory tests, and various imaging techniques. These imaging techniques often comprise contrast-enhanced CT scans of the chest and abdomen, brain imaging through MRI or CT, and potentially FDG PET/CT for cases of limited-stage disease [114]. Prior to initiating treatment, a definitive tissue diagnosis of SCLC is necessary. The choice of sampling method for diagnosis largely depends on the anatomical location of the tumor [115].

10.3389/pore.2024.1611743

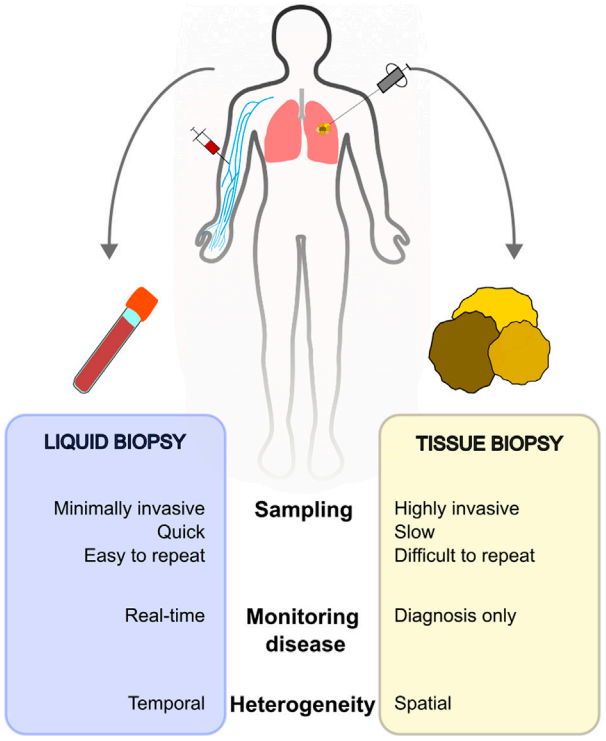

FIGURE 4
Comparison of liquid biopsy and tissue biopsy sampling.

Depending on the tumor's position in the chest, biopsies can be performed using bronchoscopy, mediastinoscopy, endobronchial ultrasound (EBUS), transthoracic needle aspiration, or thoracoscopy, if required. Obtaining biopsy samples of distant metastases is often recommended as it not only aids in diagnosing the tumor but also confirms the advanced stage of the disease [112].

Nonetheless, obtaining a tissue biopsy involves invasive methods and is not always feasible or repeatable. Moreover, the quality and quantity of the samples are frequently inadequate [116]. This underscores the necessity for investigating new diagnostic techniques.

Presently, new methods are emerging that address the limitations of traditional biopsies, such as liquid biopsy. Liquid biopsy involves analyzing biomarkers present in non-solid biological tissues, mainly blood. This technique offers significant benefits compared to conventional methods (Figure 4). The most extensively researched non-invasive cancer biomarkers include CTCs [117, 118], circulating tumor DNA (ctDNA) [119, 120], and circulating cell-free DNA (cfDNA) [96, 121, 122]. These circulating biomarkers are crucial for early cancer detection and can help determine the tissue of origin and prognosis. Additionally, they are useful in monitoring treatment responses, assessing potential resistance to therapies, and detecting minimal residual disease.

Although CTCs and ctDNAs often provide a more precise indication of tumor burden, the concentration of cfDNA still holds relevance in cancer management. Measuring total cfDNA concentration is more cost-effective than analyzing ctDNA or CTCs, which necessitate the use of expensive assays [123, 124]. While cfDNA can be increased in healthy patients for various reasons, ctDNA detection is more specific to tumors. Mutations identified in ctDNA samples are highly similar to those identified in the matched tumor tissues [125].

Due to the rapid growth and highly metastatic capacity of SCLC tumors, ctDNA levels can be valuable markers. Among others, TP53 and RB1 alterations play an important role in SCLC tumorigenesis, and can be used for monitoring of relapse through ctDNA sequencing [121, 125–127]. Fernandez-Cuesta et al. studied the possibility of detecting TP53 mutations from ctDNA. They were able to detect TP53 mutations in 35.7% of early-stage SCLC patients and 54.1% of late-stage SCLC patients [128]. Herbreteau et al. extracted circulating DNA from plasma and detected mutations in the TP53, RB1, NOTCH1, NOTCH2 and NOTCH3 genes using targeted next-generation sequencing [126]. Circulating tumor DNA was detectable if at least one somatic mutation was identified. Overall, mutations in TP53, RB1, and NOTCH1–3 genes were identified in 49 of 68 patients (70.6%), where the most frequently identified mutations affected TP53 (32/49; 65.3%) and RB1 (25/49; 51.0%) genes. Interestingly, almost a quarter of the patients harbored at least one mutation in one of the NOTCH genes (12/49; 24.5%), consistent with results seen in tumor samples [7].

In order to understand the subclonal architecture of SCLC, Nong et al. analyzed the cfDNA samples of 22 SCLC patients before and at different points in therapy using a panel of 430 genes [125]. All patients had a somatic mutation at baseline, the most common being the TP53 mutation, which was observed in 91% (20/22) of patients, and the RB1 mutation, which was observed in 64% (14/22) of patients. Overall, over 90% of patients had mutations in TP53, RB1, or both genes, and 27.3% had NOTCH1–3 mutations. In addition, plasma and tissue samples from eight patients were analyzed, showing a 94% concordance for mutations, indicating that cfDNA sequencing is a sensitive tool for detecting somatic mutations in SCLC patients. Despite the high concordance in the patient cohort, in one case none of the 26 mutations detected in tumor tissue were found the matched cfDNA sample. Also, two of the discordant cases became positive after increasing the sequencing depth. Importantly, in some patients a subset of mutations was detected exclusively in cfDNA, which may be a cause of tumor heterogeneity. Overall, a similar subclonal architecture was revealed between tissue and cfDNA, supporting the use of cfDNA to detect somatic mutations and study molecular heterogeneity in SCLC.

Serial plasma samples from 27 SCLC patients were analyzed by Almodovar et al., where disease-related mutations were detected in 85% of patients. TP53 and RB1 were the most frequently altered genes, and 10 additional genes (PTEN, NOTCH1–4, MYC, MYCL1, PIK3CA, KIT and BRAF) were detected in 52% of patients. In nine patients, cfDNA changes preceded radiological evidence of relapse [127]. Consistent with other studies, ctDNA monitoring has also been shown to identify disease recurrence prior to disease progression seen on imaging or in cases where imaging is equivocal [121, 122, 127]. Similar results were found in other studies, where cfDNA levels were found to be associated with disease outcome, as patients with high levels had a worse prognosis [129].

Conclusion

The fight against SCLC has been a path filled with both obstacles and progress. The disease's rapid spread, limited treatment choices, and the typically brief survival periods of patients have highlighted the urgent need for ongoing improvement and innovation in treatment methods and diagnostics. Our growing knowledge of SCLC is being fueled by the use of cell lines, patient-derived organoids, and mouse models, coupled with the rise of multi-omics studies and cutting-edge computational techniques. These help us better understand genetic and epigenetic changes that regulate SCLC, which may be exploited as potential therapeutic vulnerabilities. In addition, the field of diagnostics has undergone significant transformation. The limitations of traditional, more invasive biopsy methods and the scarcity of surgical specimens have given rise to advanced techniques such as liquid biopsies. These modern approaches, which analyze biomarkers like circulating tumor cells, circulating tumor DNA, and circulating cell free DNA, provide a less invasive and more dynamic perspective on the genetic makeup of the tumor and its response to treatments. As this journey progresses, each new breakthrough offers renewed hope and enhances our understanding of this complex and formidable disease.

Author contributions

All authors listed have made a substantial, direct, and intellectual contribution to the work and approved it for publication. All authors contributed in writing the manuscript and preparing the figures.

Funding

The authors declare that financial support was received for the research, authorship, and/or publication of this article. This research was funded by the János Bolyai Research Scholarship of the Hungarian Academy of Sciences BO/00697/23 (LP). The project received funding from the EU's Horizon 2020 Research and Innovation Program with grant agreement No. 739593. Project nos TKP-2021-EGA-05 and 2022-2.1.1-NL-2022-00005 has been implemented with the support provided by the Ministry of Culture and Innovation of Hungary from the National Research, Development and Innovation Fund, funded by the TKP2021-EGA and National Laboratories grant program. The funders had no role in the study design, data collection and analysis, decision to publish, or preparation of the manuscript.

Conflict of interest

The authors declare that the research was conducted in the absence of any commercial or financial relationships that could be construed as a potential conflict of interest.

References

1. Thomas A, Pattanayak P, Szabo E, Pinsky P. Characteristics and outcomes of small cell lung cancer detected by CT screening. *Chest* (2018) 154(6):1284–90. doi:10.1016/j.chest.2018.07.029

2. Travis WD, Brambilla E, Nicholson AG, Yatabe Y, Austin JHM, Beasley MB, et al. The 2015 world health organization classification of lung tumors: impact of genetic, clinical and radiologic advances since the 2004 classification. *J Thorac Oncol* (2015) 10(9):1243–60. doi:10.1097/JTO.0000000000000630

3. Carney DN, Gazdar AF, Bepler G, Guccion JG, Marangos PJ, Moody TW, et al. Establishment and identification of small cell lung cancer cell lines having classic and variant features. *Cancer Res* (1985) 45(6):2913–23.

4. Takahashi T, Nau MM, Chiba I, Birrer MJ, Rosenberg RK, Vinocour M, et al. p53: a frequent target for genetic abnormalities in lung cancer. *Science* (1989) 246(4929):491–4. doi:10.1126/science.2554494

5. Rudin CM, Durinck S, Stawiski EW, Poirier JT, Modrusan Z, Shames DS, et al. Comprehensive genomic analysis identifies SOX2 as a frequently amplified gene in small-cell lung cancer. *Nat Genet* (2012) 44(10):1111–6. doi:10.1038/ng.2405

6. Peifer M, Fernández-Cuesta L, Sos ML, George J, Seidel D, Kasper LH, et al. Integrative genome analyses identify key somatic driver mutations of small-cell lung cancer. *Nat Genet* (2012) 44(10):1104–10. doi:10.1038/ng.2396

7. George J, Lim JS, Jang SJ, Cun Y, Ozretić L, Kong G, et al. Comprehensive genomic profiles of small cell lung cancer. *Nature* (2015) 524(7563):47–53. doi:10.1038/nature14664

8. Guinee DG, Fishback NF, Koss MN, Abbondanzo SL, Travis WD. The spectrum of immunohistochemical staining of small-cell lung carcinoma in specimens from transbronchial and open-lung biopsies. *Am J Clin Pathol* (1994) 102(4):406–14. doi:10.1093/ajcp/102.4.406

9. Gay CM, Stewart CA, Park EM, Diao L, Groves SM, Heeke S, et al. Patterns of transcription factor programs and immune pathway activation define four major subtypes of SCLC with distinct therapeutic vulnerabilities. *Cancer Cell* (2021) 39(3):346–60.e7. doi:10.1016/j.ccell.2020.12.014

10. Rudin CM, Poirier JT, Byers LA, Dive C, Dowlati A, George J, et al. Molecular subtypes of small cell lung cancer: a synthesis of human and mouse

model data. *Nat Rev Cancer* (2019) 19(5):289–97. doi:10.1038/s41568-019-0133-9

11. Qu S, Fetsch P, Thomas A, Pommier Y, Schrump DS, Miettinen MM, et al. Molecular subtypes of primary SCLC tumors and their associations with neuroendocrine and therapeutic markers. *J Thorac Oncol* (2022) 17(1):141–53. doi:10.1016/j.jtho.2021.08.763

12. Zhang W, Girard L, Zhang YA, Haruki T, Papari-Zareei M, Stastny V, et al. Small cell lung cancer tumors and preclinical models display heterogeneity of neuroendocrine phenotypes. *Transl Lung Cancer Res* (2018) 7(1):32–49. doi:10.21037/tlcr.2018.02.02

13. Borges M, Linnoila RI, van de Velde HJ, Chen H, Nelkin BD, Mabry M, et al. An achaete-scute homologue essential for neuroendocrine differentiation in the lung. *Nature* (1997) 386(6627):852–5. doi:10.1038/386852a0

14. Borromeo MD, Savage TK, Kollipara RK, He M, Augustyn A, Osborne JK, et al. ASCL1 and NEUROD1 reveal heterogeneity in pulmonary neuroendocrine tumors and regulate distinct genetic programs. *Cell Rep* (2016) 16(5):1259–72. doi:10.1016/j.celrep.2016.06.081

15. Huang YH, Klingbeil O, He XY, Wu XS, Arun G, Lu B, et al. POU2F3 is a master regulator of a tuft cell-like variant of small cell lung cancer. *Genes Dev* (2018) 32(13–14):915–28. doi:10.1101/gad.314815.118

16. Werneburg N, Gores GJ, Smoot RL. The Hippo pathway and YAP signaling: emerging concepts in regulation, signaling, and experimental targeting strategies with implications for hepatobiliary malignancies. *Gene Expr* (2020) 20(1):67–74. doi:10.3727/105221619X15617324583639

17. Tlemsani C, Pongor L, Elloumi F, Girard L, Huffman KE, Roper N, et al. SCLC-CellMiner: a resource for small cell lung cancer cell line genomics and pharmacology based on genomic signatures. *Cel Rep* (2020) 33(3):108296. doi:10.1016/j.celrep.2020.108296

18. Wooten DJ, Groves SM, Tyson DR, Liu Q, Lim JS, Albert R, et al. Systems-level network modeling of small cell lung cancer subtypes identifies master regulators and destabilizers. *Plos Comput Biol* (2019) 15(10):e1007343. doi:10.1371/journal.pcbi.1007343

19. Lissa D, Takahashi N, Desai P, Manukyan I, Schultz CW, Rajapakse V, et al. Heterogeneity of neuroendocrine transcriptional states in metastatic small cell lung cancers and patient-derived models. *Nat Commun* (2022) 13(1):2023. doi:10.1038/s41467-022-29517-9

20. Lim JS, Ibaseta A, Fischer MM, Cancilla B, O'Young G, Cristea S, et al. Intratumoural heterogeneity generated by Notch signalling promotes small-cell lung cancer. *Nature* (2017) 545(7654):360–4. doi:10.1038/nature22323

21. Fujino K, Motooka Y, Hassan WA, Ali Abdalla MO, Sato Y, Kudoh S, et al. Insulinoma-associated protein 1 is a crucial regulator of neuroendocrine differentiation in lung cancer. *Am J Pathol* (2015) 185(12):3164–77. doi:10.1016/j.ajpath.2015.08.018

22. Pedersen N, Pedersen MW, Lan MS, Breslin MB, Poulsen HS. The insulinoma-associated 1: a novel promoter for targeted cancer gene therapy for small-cell lung cancer. *Cancer Gene Ther* (2006) 13(4):375–84. doi:10.1038/sj.cgt.7700887

23. Christensen CL, Gjetting T, Poulsen TT, Cramer F, Roth JA, Poulsen HS. Targeted cytosine deaminase-uracil phosphoribosyl transferase suicide gene therapy induces small cell lung cancer-specific cytotoxicity and tumor growth delay. *Clin Cancer Res* (2010) 16(8):2308–19. doi:10.1158/1078-0432.CCR-09-3057

24. Takagi H, Zhao S, Muto S, Yokouchi H, Nishihara H, Harada T, et al. Delta-like 1 homolog (DLK1) as a possible therapeutic target and its application to radioimmunotherapy using 125I-labelled anti-DLK1 antibody in lung cancer models (HOT1801 and FIGHT004). *Lung Cancer* (2021) 153:134–42. doi:10.1016/j.lungcan.2021.01.014

25. Hofsli E, Wheeler TE, Langaas M, Laegreid A, Thommesen L. Identification of novel neuroendocrine-specific tumour genes. *Br J Cancer* (2008) 99(8):1330–9. doi:10.1038/sj.bjc.6604565

26. Cardnell RJ, Li L, Sen T, Bara R, Tong P, Fujimoto J, et al. Protein expression of TTF1 and cMYC define distinct molecular subgroups of small cell lung cancer with unique vulnerabilities to aurora kinase inhibition, DLL3 targeting, and other targeted therapies. *Oncotarget* (2017) 8(43):73419–32. doi:10.18632/oncotarget.20621

27. Shue YT, Drainas AP, Li NY, Pearsall SM, Morgan D, Sinnott-Armstrong N, et al. A conserved YAP/Notch/REST network controls the neuroendocrine cell fate in the lungs. *Nat Commun* (2022) 13(1):2690. doi:10.1038/s41467-022-30416-2

28. Ito T, Kudoh S, Ichimura T, Fujino K, Hassan WAMA, Udaka N. Small cell lung cancer, an epithelial to mesenchymal transition (EMT)-like cancer: significance of inactive Notch signaling and expression of achaete-scute complex homologue 1. *Hum Cel* (2017) 30(1):1–10. doi:10.1007/s13577-016-0149-3

29. Gratton MO, Torban E, Jasmin SB, Theriault FM, German MS, Stifani S. Hes6 promotes cortical neurogenesis and inhibits Hes1 transcription repression activity by multiple mechanisms. *Mol Cel Biol* (2003) 23(19):6922–35. doi:10.1128/mcb.23.19.6922-6935.2003

30. Owen DH, Giffin MJ, Bailis JM, Smit MAD, Carbone DP, He K. DLL3: an emerging target in small cell lung cancer. *J Hematol Oncol* (2019) 12(1):61. doi:10.1186/s13045-019-0745-2

31. Totaro A, Castellan M, Di Biagio D, Piccolo S. Crosstalk between YAP/TAZ and Notch signaling. *Trends Cel Biol* (2018) 28(7):560–73. doi:10.1016/j.tcb.2018.03.001

32. Sutherland KD, Ireland AS, Oliver TG. Killing SCLC: insights into how to target a shapeshifting tumor. *Genes Dev* (2022) 36(5–6):241–58. doi:10.1101/gad.349359.122

33. Thiery JP, Acloque H, Huang RYJ, Nieto MA. Epithelial-mesenchymal transitions in development and disease. *Cell* (2009) 139(5):871–90. doi:10.1016/j.cell.2009.11.007

34. Ireland AS, Micinski AM, Kastner DW, Guo B, Wait SJ, Spainhower KB, et al. MYC drives temporal evolution of small cell lung cancer subtypes by reprogramming neuroendocrine fate. *Cancer Cell* (2020) 38(1):60–78. doi:10.1016/j.ccell.2020.05.001

35. Mollaoglu G, Guthrie MR, Böhm S, Brägelmann J, Can I, Ballieu PM, et al. MYC drives progression of small cell lung cancer to a variant neuroendocrine subtype with vulnerability to aurora kinase inhibition. *Cancer Cell* (2017) 31(2):270–85. doi:10.1016/j.ccell.2016.12.005

36. Thomas A, Pommier Y. Small cell lung cancer: time to revisit DNA-damaging chemotherapy. *Sci Transl Med* (2016) 8(346):346fs12. doi:10.1126/scitranslmed.aaf6282

37. Macheret M, Halazonetis TD. Intragenic origins due to short G1 phases underlie oncogene-induced DNA replication stress. *Nature* (2018) 555(7694):112–6. doi:10.1038/nature25507

38. Dominguez-Sola D, Gautier J. MYC and the control of DNA replication. *Cold Spring Harb Perspect Med* (2014) 4(6):a014423. doi:10.1101/cshperspect.a014423

39. Bian X, Lin W. Targeting DNA replication stress and DNA double-strand break repair for optimizing SCLC treatment. *Cancers (Basel)* (2019) 11(9):1289. doi:10.3390/cancers11091289

40. Takahashi N, Kim S, Schultz CW, Rajapakse VN, Zhang Y, Redon CE, et al. Replication stress defines distinct molecular subtypes across cancers. *Cancer Res Commun* (2022) 2(6):503–17. doi:10.1158/2767-9764.crc-22-0168

41. Horn L, Mansfield AS, Szczęsna A, Havel L, Krzakowski M, Hochmair MJ, et al. First-line atezolizumab plus chemotherapy in extensive-stage small-cell lung cancer. *N Engl J Med* (2018) 379(23):2220–9. doi:10.1056/NEJMoa1809064

42. Oboshi S, Tsugawa S, Seido T, Shimosato Y, Koide T. A new floating cell line derived from human pulmonary carcinoma of oat cell type. *Gan* (1971) 62(6):505–14.

43. Carney DN, Gazdar AF, Minna JD. Positive correlation between histological tumor involvement and generation of tumor cell colonies in agarose in specimens taken directly from patients with small-cell carcinoma of the lung. *Cancer Res* (1980) 40(6):1820–3.

44. Pettengill OS, Sorenson GD, Wurster-Hill DH, Curphey TJ, Noll WW, Cate CC, et al. Isolation and growth characteristics of continuous cell lines from small-cell carcinoma of the lung. *Cancer* (1980) 45(5):906–18. doi:10.1002/1097-0142(19800301)45:5<906::aid-cncr2820450513>3.0.co;2-h

45. Drapkin BJ, Rudin CM. Advances in small-cell lung cancer (SCLC) translational research. *Cold Spring Harb Perspect Med* (2021) 11(4):a038240. doi:10.1101/cshperspect.a038240

46. Monks A, Scudiero D, Skehan P, Shoemaker R, Paull K, Vistica D, et al. Feasibility of a high-flux anticancer drug screen using a diverse panel of cultured human tumor cell lines. *J Natl Cancer Inst* (1991) 83(11):757–66. doi:10.1093/jnci/83.11.757

47. Wilding JL, Bodmer WF. Cancer cell lines for drug discovery and development. *Cancer Res* (2014) 74(9):2377–84. doi:10.1158/0008-5472.CAN-13-2971

48. Barretina J, Caponigro G, Stransky N, Venkatesan K, Margolin AA, Kim S, et al. The cancer cell line encyclopedia enables predictive modelling of anticancer drug sensitivity. *Nature* (2012) 483(7391):603–7. doi:10.1038/nature11003

49. Yang W, Soares J, Greninger P, Edelman EJ, Lightfoot H, Forbes S, et al. Genomics of drug sensitivity in cancer (GDSC): a resource for therapeutic biomarker discovery in cancer cells. *Nucleic Acids Res* (2013) 41(Database issue):D955–61. doi:10.1093/nar/gks1111

50. Polley E, Kunkel M, Evans D, Silvers T, Delosh R, Laudeman J, et al. Small cell lung cancer screen of oncology drugs, investigational agents, and gene and

microRNA expression. *J Natl Cancer Inst* (2016) 108(10):djw122. doi:10.1093/jnci/djw122

51. Sen C, Freund D, Gomperts BN. Three-dimensional models of the lung: past, present and future: a mini review. *Biochem Soc Trans* (2022) 50(2):1045–56. doi:10.1042/BST20190569

52. Martinez-Pacheco S, O'Driscoll L. Pre-clinical *in vitro* models used in cancer research: results of a worldwide survey. *Cancers (Basel)* (2021) 13(23):6033. doi:10.3390/cancers13236033

53. Sato T, Vries RG, Snippert HJ, van de Wetering M, Barker N, Stange DE, et al. Single Lgr5 stem cells build crypt-villus structures *in vitro* without a mesenchymal niche. *Nature* (2009) 459(7244):262–5. doi:10.1038/nature07935

54. Hou X, Du C, Lu L, Yuan S, Zhan M, You P, et al. Opportunities and challenges of patient-derived models in cancer research: patient-derived xenografts, patient-derived organoid and patient-derived cells. *World J Surg Oncol* (2022) 20(1):37. doi:10.1186/s12957-022-02510-8

55. Endo H, Okami J, Okuyama H, Kumagai T, Uchida J, Kondo J, et al. Spheroid culture of primary lung cancer cells with neuregulin 1/HER3 pathway activation. *J Thorac Oncol* (2013) 8(2):131–9. doi:10.1097/JTO.0b013e3182779ccf

56. Yokota E, Iwai M, Yukawa T, Yoshida M, Naomoto Y, Haisa M, et al. Clinical application of a lung cancer organoid (tumoroid) culture system. *NPJ Precis Oncol* (2021) 5(1):29. doi:10.1038/s41698-021-00166-3

57. Li Y, Gao X, Ni C, Zhao B, Cheng X. The application of patient-derived organoid in the research of lung cancer. *Cel Oncol (Dordr)* (2023) 46(3):503–19. doi:10.1007/s13402-023-00771-3

58. Kunz-Schughart LA, Groebe K, Mueller-Klieser W. Three-dimensional cell culture induces novel proliferative and metabolic alterations associated with oncogenic transformation. *Int J Cancer* (1996) 66(4):578–86. doi:10.1002/(SICI)1097-0215(19960516)66:4<578::AID-IJC25>3.0.CO;2-2

59. Phan N, Hong JJ, Tofig B, Mapua M, Elashoff D, Moatamed NA, et al. A simple high-throughput approach identifies actionable drug sensitivities in patient-derived tumor organoids. *Commun Biol* (2019) 2:78. doi:10.1038/s42003-019-0305-x

60. Song Y, Wang Y, Guan A, Xue J, Li B, Huang Z, et al. Footprints: stamping hallmarks of lung cancer with patient-derived models, from molecular mechanisms to clinical translation. *Front Bioeng Biotechnol* (2023) 11:1132940. doi:10.3389/fbioe.2023.1132940

61. Hutmacher DW. Biomaterials offer cancer research the third dimension. *Nat Mater* (2010) 9(2):90–3. doi:10.1038/nmat2619

62. Shi R, Radulovich N, Ng C, Liu N, Notsuda H, Cabanero M, et al. Organoid cultures as preclinical models of non-small cell lung cancer. *Clin Cancer Res* (2020) 26(5):1162–74. doi:10.1158/1078-0432.CCR-19-1376

63. Kim SY, Kim SM, Lim S, Lee JY, Choi SJ, Yang SD, et al. Modeling clinical responses to targeted therapies by patient-derived organoids of advanced lung adenocarcinoma. *Clin Cancer Res* (2021) 27(15):4397–409. doi:10.1158/1078-0432.CCR-20-5026

64. Kim M, Mun H, Sung CO, Cho EJ, Jeon HJ, Chun SM, et al. Patient-derived lung cancer organoids as *in vitro* cancer models for therapeutic screening. *Nat Commun* (2019) 10(1):3991. doi:10.1038/s41467-019-11867-6

65. Choi SY, Cho YH, Kim DS, Ji W, Choi CM, Lee JC, et al. Establishment and long-term expansion of small cell lung cancer patient-derived tumor organoids. *Int J Mol Sci* (2021) 22(3):1349. doi:10.3390/ijms22031349

66. Zhang Z, Shiratsuchi H, Lin J, Chen G, Reddy RM, Azizi E, et al. Expansion of CTCs from early stage lung cancer patients using a microfluidic co-culture model. *Oncotarget* (2014) 5(23):12383–97. doi:10.18632/oncotarget.2592

67. Zhu Z, Hu E, Shen H, Tan J, Zeng S. The functional and clinical roles of liquid biopsy in patient-derived models. *J Hematol Oncol* (2023) 16(1):36. doi:10.1186/s13045-023-01433-5

68. Na F, Pan X, Chen J, Chen X, Wang M, Chi P, et al. KMT2C deficiency promotes small cell lung cancer metastasis through DNMT3A-mediated epigenetic reprogramming. *Nat Cancer* (2022) 3(6):753–67. doi:10.1038/s43018-022-00361-6

69. Rossi R, De Angelis ML, Xhelili E, Sette G, Eramo A, De Maria R, et al. Lung cancer organoids: the rough path to personalized medicine. *Cancers (Basel).* (2022) 14(15):3703. doi:10.3390/cancers14153703

70. Quaranta V, Linkous A. Organoids as a systems platform for SCLC brain metastasis. *Front Oncol* (2022) 12:881989. doi:10.3389/fonc.2022.881989

71. Hidalgo M, Amant F, Biankin AV, Budinská E, Byrne AT, Caldas C, et al. Patient-derived xenograft models: an emerging platform for translational cancer research. *Cancer Discov* (2014) 4(9):998–1013. doi:10.1158/2159-8290.CD-14-0001

72. Shoemaker AR, Mitten MJ, Adickes J, Ackler S, Refici M, Ferguson D, et al. Activity of the Bcl-2 family inhibitor ABT-263 in a panel of small cell lung cancer xenograft models. *Clin Cancer Res* (2008) 14(11):3268–77. doi:10.1158/1078-0432.CCR-07-4622

73. Oltersdorf T, Elmore SW, Shoemaker AR, Armstrong RC, Augeri DJ, Belli BA, et al. An inhibitor of Bcl-2 family proteins induces regression of solid tumours. *Nature* (2005) 435(7042):677–81. doi:10.1038/nature03579

74. Hann CL, Daniel VC, Sugar EA, Dobromilskaya I, Murphy SC, Cope L, et al. Therapeutic efficacy of ABT-737, a selective inhibitor of BCL-2, in small cell lung cancer. *Cancer Res* (2008) 68(7):2321–8. doi:10.1158/0008-5472.CAN-07-5031

75. Daniel VC, Marchionni L, Hierman JS, Rhodes JT, Devereux WL, Rudin CM, et al. A primary xenograft model of small-cell lung cancer reveals irreversible changes in gene expression imposed by culture *in vitro*. *Cancer Res* (2009) 69(8):3364–73. doi:10.1158/0008-5472.CAN-08-4210

76. Drapkin BJ, George J, Christensen CL, Mino-Kenudson M, Dries R, Sundaresan T, et al. Genomic and functional fidelity of small cell lung cancer patient-derived xenografts. *Cancer Discov* (2018) 8(5):600–15. doi:10.1158/2159-8290.CD-17-0935

77. Hodgkinson CL, Morrow CJ, Li Y, Metcalf RL, Rothwell DG, Trapani F, et al. Tumorigenicity and genetic profiling of circulating tumor cells in small-cell lung cancer. *Nat Med* (2014) 20(8):897–903. doi:10.1038/nm.3600

78. Lallo A, Schenk MW, Frese KK, Blackhall F, Dive C. Circulating tumor cells and CDX models as a tool for preclinical drug development. *Transl Lung Cancer Res* (2017) 6(4):397–408. doi:10.21037/tlcr.2017.08.01

79. Guo S, Qian W, Cai J, Zhang L, Wery JP, Li QX. Molecular pathology of patient tumors, patient-derived xenografts, and cancer cell lines. *Cancer Res* (2016) 76(16):4619–26. doi:10.1158/0008-5472.CAN-15-3245

80. Jung J, Seol HS, Chang S. The generation and application of patient-derived xenograft model for cancer research. *Cancer Res Treat* (2018) 50(1):1–10. doi:10.4143/crt.2017.307

81. Kim KB. The new way to define key oncogenic drivers of small cell lung cancer. *Dev Reprod* (2023) 27(1):1–7. doi:10.12717/DR.2023.27.1.1

82. Brägelmann J, Böhm S, Guthrie MR, Mollaoglu G, Oliver TG, Sos ML. Family matters: how MYC family oncogenes impact small cell lung cancer. *Cell Cycle* (2017) 16(16):1489–98. doi:10.1080/15384101.2017.1339849

83. Semenova EA, Nagel R, Berns A. Origins, genetic landscape, and emerging therapies of small cell lung cancer. *Genes Dev* (2015) 29(14):1447–62. doi:10.1101/gad.263145.115

84. Schaffer BE, Park KS, Yiu G, Conklin JF, Lin C, Burkhart DL, et al. Loss of p130 accelerates tumor development in a mouse model for human small-cell lung carcinoma. *Cancer Res* (2010) 70(10):3877–83. doi:10.1158/0008-5472.CAN-09-4228

85. Sault C, Auger C, Roux B, Corvee N, Monier JC. Monoclonal antibodies against an epitope common to desmin and some keratins. *Immunol Lett* (1987) 16(2):151–5. doi:10.1016/0165-2478(87)90123-4

86. Nishida K, Arazoe T, Yachie N, Banno S, Kakimoto M, Tabata M, et al. Targeted nucleotide editing using hybrid prokaryotic and vertebrate adaptive immune systems. *Science* (2016) 353(6305):aaf8729. doi:10.1126/science.aaf8729

87. Komor AC, Badran AH, Liu DR. CRISPR-based technologies for the manipulation of eukaryotic genomes. *Cell* (2017) 169(3):559. doi:10.1016/j.cell.2017.04.005

88. Katti A, Vega-Pérez A, Foronda M, Zimmerman J, Zafra MP, Granowsky E, et al. Generation of precision preclinical cancer models using regulated *in vivo* base editing. *Nat Biotechnol* (2023) 42:437–47. doi:10.1038/s41587-023-01900-x

89. Ely ZA, Mathey-Andrews N, Naranjo S, Gould SI, Mercer KL, Newby GA, et al. A prime editor mouse to model a broad spectrum of somatic mutations *in vivo*. *Nat Biotechnol* (2023) 42:424–36. doi:10.1038/s41587-023-01783-y

90. Oser MG, MacPherson D, Oliver TG, Sage J, Park KS. Genetically-engineered mouse models of small cell lung cancer: the next generation. *Oncogene* (2024) 43:457–69. doi:10.1038/s41388-023-02929-7

91. Leinonen R, Sugawara H, Shumway M, International Nucleotide Sequence Database Collaboration. The sequence read archive. *Nucleic Acids Res* (2011) 39(Database issue):D19–21. doi:10.1093/nar/gkq1019

92. Burgin J, Ahamed A, Cummins C, Devraj R, Gueye K, Gupta D, et al. The European nucleotide archive in 2022. *Nucleic Acids Res* (2023) 51(D1):D121–5. doi:10.1093/nar/gkac1051

93. Lappalainen I, Almeida-King J, Kumanduri V, Senf A, Spalding JD, Ur-Rehman S, et al. The European Genome-phenome Archive of human data consented for biomedical research. *Nat Genet* (2015) 47(7):692–5. doi:10.1038/ng.3312

94. Mailman MD, Feolo M, Jin Y, Kimura M, Tryka K, Bagoutdinov R, et al. The NCBI dbGaP database of genotypes and phenotypes. *Nat Genet* (2007) 39(10):1181–6. doi:10.1038/ng1007-1181

95. Feng S, Zhang X, Gu X, Zhou M, Chen Y, Wang C. Identification of six novel prognostic gene signatures as potential biomarkers in small cell lung cancer. *Comb Chem High Throughput Screen* (2023) 26(5):938–49. doi:10.2174/1386207325666220427121619

96. Pongor LS, Schultz CW, Rinaldi L, Wangsa D, Redon CE, Takahashi N, et al. Extrachromosomal DNA amplification contributes to small cell lung cancer heterogeneity and is associated with worse outcomes. *Cancer Discov* (2023) 13(4):928–49. doi:10.1158/2159-8290.CD-22-0796

97. Pongor LS, Tlemsani C, Elloumi F, Arakawa Y, Jo U, Gross JM, et al. Integrative epigenomic analyses of small cell lung cancer cells demonstrates the clinical translational relevance of gene body methylation. *iScience* (2022) 25(11): 105338. doi:10.1016/j.isci.2022.105338

98. Tate JG, Bamford S, Jubb HC, Sondka Z, Beare DM, Bindal N, et al. COSMIC: the catalogue of somatic mutations in cancer. *Nucleic Acids Res* (2019) 47(D1): D941–7. doi:10.1093/nar/gky1015

99. Jin X, Demere Z, Nair K, Ali A, Ferraro GB, Natoli T, et al. A metastasis map of human cancer cell lines. *Nature* (2020) 588(7837):331–6. doi:10.1038/s41586-020-2969-2

100. Subramanian A, Tamayo P, Mootha VK, Mukherjee S, Ebert BL, Gillette MA, et al. Gene set enrichment analysis: a knowledge-based approach for interpreting genome-wide expression profiles. *Proc Natl Acad Sci U S A* (2005) 102(43): 15545–50. doi:10.1073/pnas.0506580102

101. Liberzon A, Birger C, Thorvaldsdóttir H, Ghandi M, Mesirov JP, Tamayo P. The molecular signatures database (MSigDB) hallmark gene set collection. *Cell Syst.* (2015) 1(6):417–25. doi:10.1016/j.cels.2015.12.004

102. Dressler L, Bortolomeazzi M, Keddar MR, Misetic H, Sartini G, Acha-Sagredo A, et al. Comparative assessment of genes driving cancer and somatic evolution in non-cancer tissues: an update of the network of cancer genes (NCG) resource. *Genome Biol* (2022) 23(1):35. doi:10.1186/s13059-022-02607-z

103. Nemes K, Benő A, Topolcsányi P, Magó É, Für GM, Pongor LS. Predicting drug response of small cell lung cancer cell lines based on enrichment analysis of complex gene signatures. *J Biotechnol* (2024) 383:86–93. doi:10.1016/j.jbiotec.2024.01.010

104. Sampson ER, McMurray HR, Hassane DC, Newman L, Salzman P, Jordan CT, et al. Gene signature critical to cancer phenotype as a paradigm for anticancer drug discovery. *Oncogene* (2013) 32(33):3809–18. doi:10.1038/onc.2012.389

105. Garnett MJ, Edelman EJ, Heidorn SJ, Greenman CD, Dastur A, Lau KW, et al. Systematic identification of genomic markers of drug sensitivity in cancer cells. *Nature* (2012) 483(7391):570–5. doi:10.1038/nature11005

106. Iorio F, Knijnenburg TA, Vis DJ, Bignell GR, Menden MP, Schubert M, et al. A landscape of pharmacogenomic interactions in cancer. *Cell* (2016) 166(3):740–54. doi:10.1016/j.cell.2016.06.017

107. Tsherniak A, Vazquez F, Montgomery PG, Weir BA, Kryukov G, Cowley GS, et al. Defining a cancer dependency map. *Cell* (2017) 170(3):564–76. doi:10.1016/j.cell.2017.06.010

108. McMillan EA, Ryu MJ, Diep CH, Mendiratta S, Clemenceau JR, Vaden RM, et al. Chemistry-first approach for nomination of personalized treatment in lung cancer. *Cell* (2018) 173(4):864–78. doi:10.1016/j.cell.2018.03.028

109. Rajapakse VN, Luna A, Yamade M, Loman L, Varma S, Sunshine M, et al. CellMinerCDB for integrative cross-database genomics and pharmacogenomics analyses of cancer cell lines. *iScience* (2018) 10:247–64. doi:10.1016/j.isci.2018.11.029

110. Krushkal J, Silvers T, Reinhold WC, Sonkin D, Vural S, Connelly J, et al. Epigenome-wide DNA methylation analysis of small cell lung cancer cell lines suggests potential chemotherapy targets. *Clin Epigenetics* (2020) 12(1):93. doi:10.1186/s13148-020-00876-8

111. Cerami E, Gao J, Dogrusoz U, Gross BE, Sumer SO, Aksoy BA, et al. The cBio cancer genomics portal: an open platform for exploring multidimensional cancer genomics data. *Cancer Discov* (2012) 2(5):401–4. doi:10.1158/2159-8290.CD-12-0095

112. Früh M, De Ruysscher D, Popat S, Crinò L, Peters S, Felip E, et al. Small-cell lung cancer (SCLC): ESMO clinical practice guidelines for diagnosis, treatment and follow-up. *Ann Oncol* (2013) 24(Suppl. 6):vi99–105. doi:10.1093/annonc/mdt178

113. Micke P, Faldum A, Metz T, Beeh KM, Bittinger F, Hengstler JG, et al. Staging small cell lung cancer: veterans administration lung study group versus international association for the study of lung cancer--what limits limited disease? *Lung Cancer* (2002) 37(3):271–6. doi:10.1016/s0169-5002(02)00072-7

114. Krpina K, Vranić S, Tomić K, Samaržija M, Batičić L. Small cell lung carcinoma: current diagnosis, biomarkers, and treatment options with future perspectives. *Biomedicines* (2023) 11(7):1982. doi:10.3390/biomedicines11071982

115. Megyesfalvi Z, Gay CM, Popper H, Pirker R, Ostoros G, Heeke S, et al. Clinical insights into small cell lung cancer: tumor heterogeneity, diagnosis, therapy, and future directions. *CA Cancer J Clin* (2023) 73(6):620–52. doi:10.3322/caac.21785

116. Siravegna G, Mussolin B, Venesio T, Marsoni S, Seoane J, Dive C, et al. How liquid biopsies can change clinical practice in oncology. *Ann Oncol* (2019) 30(10): 1580–90. doi:10.1093/annonc/mdz227

117. Su Z, Wang Z, Ni X, Duan J, Gao Y, Zhuo M, et al. Inferring the evolution and progression of small-cell lung cancer by single-cell sequencing of circulating tumor cells. *Clin Cancer Res* (2019) 25(16):5049–60. doi:10.1158/1078-0432.CCR-18-3571

118. Aggarwal C, Wang X, Ranganathan A, Torigian D, Troxel A, Evans T, et al. Circulating tumor cells as a predictive biomarker in patients with small cell lung cancer undergoing chemotherapy. *Lung Cancer* (2017) 112:118–25. doi:10.1016/j.lungcan.2017.08.008

119. Iams WT, Kopparapu PR, Yan Y, Muterspaugh A, Zhao Z, Chen H, et al. Blood-based surveillance monitoring of circulating tumor DNA from patients with SCLC detects disease relapse and predicts death in patients with limited-stage disease. *JTO Clin Res Rep* (2020) 1(2):100024. doi:10.1016/j.jtocrr.2020.100024

120. Devarakonda S, Sankararaman S, Herzog BH, Gold KA, Waqar SN, Ward JP, et al. Circulating tumor DNA profiling in small-cell lung cancer identifies potentially targetable alterations. *Clin Cancer Res* (2019) 25(20):6119–26. doi:10.1158/1078-0432.CCR-19-0879

121. Mohan S, Foy V, Ayub M, Leong HS, Schofield P, Sahoo S, et al. Profiling of circulating free DNA using targeted and genome-wide sequencing in patients with SCLC. *J Thorac Oncol* (2020) 15(2):216–30. doi:10.1016/j.jtho.2019.10.007

122. Sivapalan L, Iams WT, Belcaid Z, Scott SC, Niknafs N, Balan A, et al. Dynamics of sequence and structural cell-free DNA landscapes in small-cell lung cancer. *Clin Cancer Res* (2023) 29(12):2310–23. doi:10.1158/1078-0432.CCR-22-2242

123. Fernandez-Garcia D, Hills A, Page K, Hastings RK, Toghill B, Goddard KS, et al. Plasma cell-free DNA (cfDNA) as a predictive and prognostic marker in patients with metastatic breast cancer. *Breast Cancer Res* (2019) 21(1):149. doi:10.1186/s13058-019-1235-8

124. Gristina V, Barraco N, La Mantia M, Castellana L, Insalaco L, Bono M, et al. Clinical potential of circulating cell-free DNA (cfDNA) for longitudinally monitoring clinical outcomes in the first-line setting of non-small-cell lung cancer (NSCLC): a real-world prospective study. *Cancers (Basel)* (2022) 14(23): 6013. doi:10.3390/cancers14236013

125. Nong J, Gong Y, Guan Y, Yi X, Yi Y, Chang L, et al. Circulating tumor DNA analysis depicts subclonal architecture and genomic evolution of small cell lung cancer. *Nat Commun* (2018) 9(1):3114. doi:10.1038/s41467-018-05327-w

126. Herbreteau G, Langlais A, Greillier L, Audigier-Valette C, Uwer L, Hureaux J, et al. Circulating tumor DNA as a prognostic determinant in small cell lung cancer patients receiving atezolizumab. *J Clin Med* (2020) 9(12):3861. doi:10.3390/jcm9123861

127. Almodovar K, Iams WT, Meador CB, Zhao Z, York S, Horn L, et al. Longitudinal cell-free DNA analysis in patients with small cell lung cancer reveals dynamic insights into treatment efficacy and disease relapse. *J Thorac Oncol* (2018) 13(1):112–23. doi:10.1016/j.jtho.2017.09.1951

128. Fernandez-Cuesta L, Perdomo S, Avogbe PH, Leblay N, Delhomme TM, Gaborieau V, et al. Identification of circulating tumor DNA for the early detection of small-cell lung cancer. *EBioMedicine* (2016) 10:117–23. doi:10.1016/j.ebiom.2016.06.032

129. Mondelo-Macía P, García-González J, Abalo A, Mosquera-Presedo M, Aguín S, Mateos M, et al. Plasma cell-free DNA and circulating tumor cells as prognostic biomarkers in small cell lung cancer patients. *Transl Lung Cancer Res* (2022) 11(10):1995–2009. doi:10.21037/tlcr-22-273

Pathology & Oncology Research | frontiers

TYPE Review
PUBLISHED 28 March 2024
DOI 10.3389/pore.2024.1611715

Check for updates

OPEN ACCESS

EDITED BY
Maximilian Hochmair,
Klinik Floridsdorf, Austria

*CORRESPONDENCE
Zoltán Lohinai,
LOHINAI.ZOLTAN@SEMMELWEIS.HU

RECEIVED 31 January 2024
ACCEPTED 21 February 2024
PUBLISHED 28 March 2024

CITATION
Gálffy G, Morócz É, Korompay R, Hécz R, Bujdosó R, Puskás R, Lovas T, Gáspár E, Yahya K, Király P and Lohinai Z (2024), Targeted therapeutic options in early and metastatic NSCLC-overview. *Pathol. Oncol. Res.* 30:1611715. doi: 10.3389/pore.2024.1611715

COPYRIGHT
© 2024 Gálffy, Morócz, Korompay, Hécz, Bujdosó, Puskás, Lovas, Gáspár, Yahya, Király and Lohinai. This is an open-access article distributed under the terms of the Creative Commons Attribution License (CC BY). The use, distribution or reproduction in other forums is permitted, provided the original author(s) and the copyright owner(s) are credited and that the original publication in this journal is cited, in accordance with accepted academic practice. No use, distribution or reproduction is permitted which does not comply with these terms.

Targeted therapeutic options in early and metastatic NSCLC-overview

Gabriella Gálffy, Éva Morócz, Réka Korompay, Réka Hécz, Réka Bujdosó, Rita Puskás, Tímea Lovas, Eszter Gáspár, Kamel Yahya, Péter Király and Zoltán Lohinai*

Pulmonology Hospital Törökbálint, Törökbálint, Hungary

The complex therapeutic strategy of non-small cell lung cancer (NSCLC) has changed significantly in recent years. Disease-free survival increased significantly with immunotherapy and chemotherapy registered in perioperative treatments, as well as adjuvant registered immunotherapy and targeted therapy (osimertinib) in case of EGFR mutation. In oncogenic-addictive metastatic NSCLC, primarily in adenocarcinoma, the range of targeted therapies is expanding, with which the expected overall survival increases significantly, measured in years. By 2021, the FDA and EMA have approved targeted agents to inhibit EGFR activating mutations, T790 M resistance mutation, BRAF V600E mutation, ALK, ROS1, NTRK and RET fusion. In 2022, the range of authorized target therapies was expanded. With therapies that inhibit KRASG12C, EGFR exon 20, HER2 and MET. Until now, there was no registered targeted therapy for the KRAS mutations, which affect 30% of adenocarcinomas. Thus, the greatest expectation surrounded the inhibition of the KRAS G12C mutation, which occurs in ~15% of NSCLC, mainly in smokers and is characterized by a poor prognosis. Sotorasib and adagrasib are approved as second-line agents after at least one prior course of chemotherapy and/or immunotherapy. Adagrasib in first-line combination with pembrolizumab immunotherapy proved more beneficial, especially in patients with high expression of PD-L1. In EGFR exon 20 insertion mutation of lung adenocarcinoma, amivantanab was registered for progression after platinum-based chemotherapy. Lung adenocarcinoma carries an EGFR exon 20, HER2 insertion mutation in 2%, for which the first targeted therapy is trastuzumab deruxtecan, in patients already treated with platinum-based chemotherapy. Two orally administered selective c-MET inhibitors, capmatinib and tepotinib, were also approved after chemotherapy in adenocarcinoma carrying MET exon 14 skipping mutations of about 3%. Incorporating reflex testing with next-generation sequencing (NGS) expands personalized therapies by identifying guideline-recommended molecular alterations.

KEYWORDS

NSCLC, driver oncogenes, targeted therapy, central nervous system efficacy, molecular testing

Introduction

In recent years, there has been an expansion in the treatment options of non-small cell lung cancer (NSCLC) with the advent of targeted therapies and immuno-oncology therapies [1, 2]. Lung tumors are heterogeneous, with distinct oncogenic drivers and tumor microenvironments. Tumor evolution results in distinct organ site metastases representing intratumor heterogeneity and the ongoing development of resistance mutations [3]. Recent advancements in cost-effective parallel high-throughput molecular diagnostics might drive personalized therapy beyond adenocarcinoma subtypes associated with the most targetable genetic alterations [3]. Prior to precision medicine, patients were treated uniformly without considering the differences in clinicopathological characteristics and genetic backgrounds of different patients. The careful selection for upfront treatments of brain metastases (BM) might be detrimental to outcomes [1, 2]. Now, it is clear that patients with oncogenic driver alteration-positive NSCLC are associated with better outcomes treated with frontline targeted therapy compared to chemotherapy and anti-Programmed death (anti-PD) immunotherapy [1, 2]. Today, the right choice of molecular diagnostics is increasingly important, following the careful classification of pathological diagnostics. While stand-alone single gene assays remain valid, increasing requirements for synchronous testing for multiple targets make massive parallel sequencing technology the preferred option [2]. DNA sequencing is the standard for mutation detection, and RNA sequencing is an emerging option for fusion gene detection. EGFR, ALK, and ROS1 alterations are common for young female non-smokers with adenocarcinoma [4]. While ALK and ROS1 mutations do not show ethnic prevalence, one can observe a four times elevated EGFR prevalence in the Asian population compared to the Western population [4]. KRAS and MET mutations occur in older age populations with smoker status and adenocarcinoma. There is no clear gender preference, but a distinct excess of KRAS mutations in the Caucasian population is observable. It is widely accepted that KRAS mutation in lung cancer is smoking-associated, but it is only proven for G12C [5, 6]. BRAF mutations occur in smokers without age or ethical tendencies. The BRAF V600 mutations are detected with a higher incidence for females; other BRAF mutations have a higher incidence for the opposite sex. HER2 mutations have a higher likelihood for female and never-smoker patients [4]. In contrast to the known associations of genetic alteration with clinicopathological characteristics, according to the latest guidelines, molecular testing is now the standard for advanced-stage adenoma-carcinoma-containing cancers independent of sex, ethnicity, or smoking [2]. Therefore, histology assessments are key in clinical practice, with a cautious interpretation of mixed histology specimens and NSCLC not otherwise specified (NSCLC NOS) because molecular testing is recommended for non-squamous NSCLC cases. Testing is also recommended for NSCLC cases below 50 years of age and all kinds of tobacco in patients who quit smoking more than 15 years ago, or in never (<100 cigarettes overall) or former light (≤15 6 pack-years) or long-time ex-smokers (quit >15 years ago). Importantly, the presence of any adenocarcinoma component in a biopsy specimen that is otherwise squamous should trigger molecular testing. Accordingly, cautious minimization of tissue slides used for immunohistochemistry (IHC) stainings and preserving material for molecular testing is critical. Oncogenic driver tests usually follow the Programmed death-ligand 1 (PD-L1) IHC testing for non-squamous cases. The present review summarizes the available data on targeted therapy strategies in treating NSCLC (Figure 1). A particular focus is given to central nervous system (CNS) activity that is detrimental in the era of better control of oligoprogressive disease. Additionally, for optimal treatment outcomes, we highlight the role of distinct molecular analyses based on accurate guideline-based histology classifications to avoid excluding patients from therapy. Nevertheless, the emergence of early-stage targeted therapies extends molecular testing beyond advanced-stage disease.

Adjuvant osimertinib therapy in the treatment of NSCLC

As adjuvant treatment in NSCLC, osimertinib is the first targeted therapy approved based on the ADAURA trial. The ADAURA trial enrolled stage I/B -III/A patients with classical epidermal EGFR mutations (ex19del/L858R) who underwent complete tumor resection [7]. Patients were allowed to receive adjuvant chemotherapy before osimertinib, and optionally, they were allowed to start osimertinib therapy after surgery. According to the 1:1 randomization, the study group received osimertinib, and the other group received a placebo at a planned interval of 3 years. The primary endpoint was disease-free survival (DFS) in stage II/IIIA patients. DFS in the osimertinib group compared to placebo showed a significant benefit (hazard ratio (HR): 0.23, 95% CI 0.18–0.30) median DFS was 65.8 months for the osimertinib compared to 21.9 months for the placebo arm [8]. Subgroup analysis (gender, age, race, stage, mutation type) revealed significant benefits in DFS. Adjuvant osimertinib also showed efficacy without cytotoxic chemotherapy, with a significant benefit in DFS (HR: 0.23), and osimertinib given followed by adjuvant chemotherapy showed a similar significant benefit in DFS (HR: 0.16) [8].

NSCLC with actionable EGFR mutations

The HER/Erb family epidermal growth factor receptor (EGFR) is a transmembrane tyrosine kinase (TK) receptor

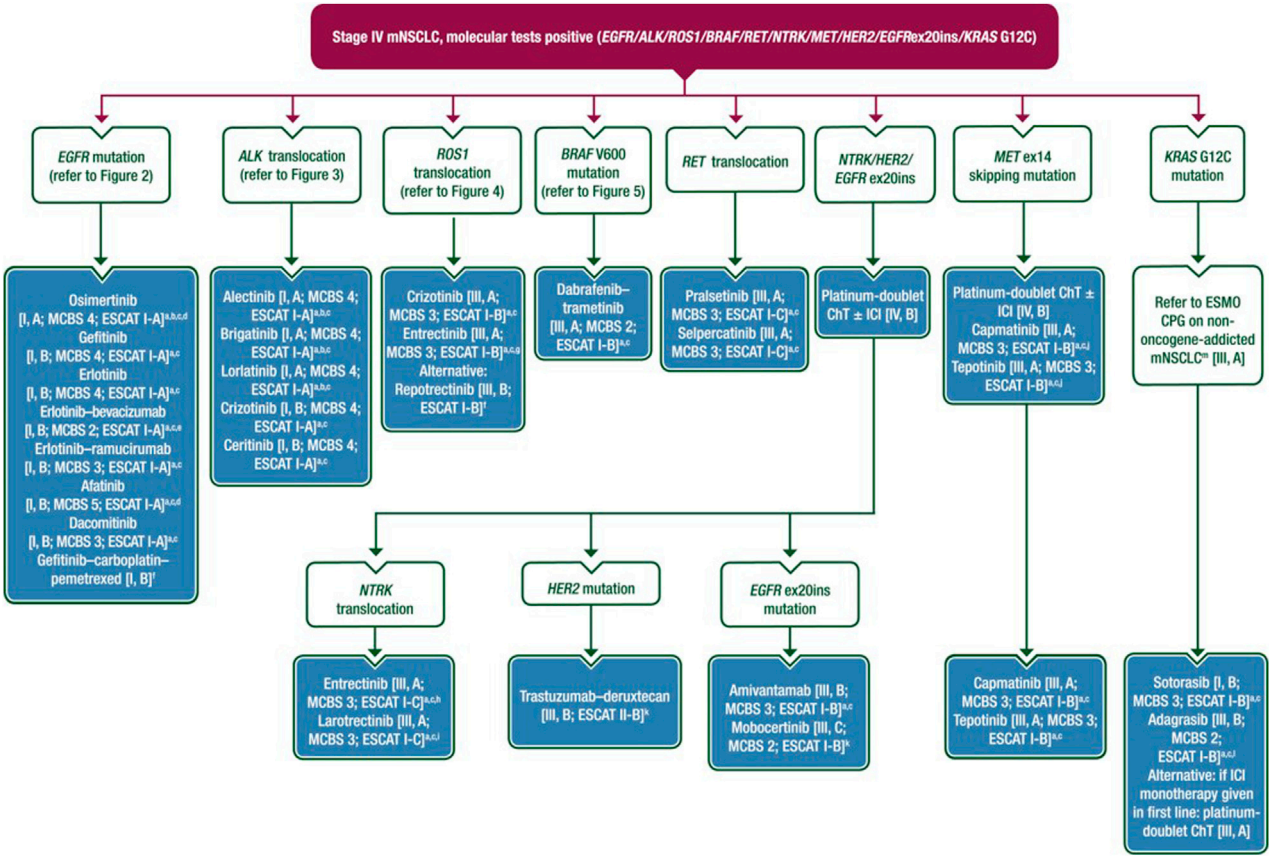

FIGURE 1
Treatment recommendation for stage IV mNSCLC based on the ESMO 2023 guideline [1].

that stimulates cell proliferation, differentiation, survival, and motility through MAP kinase and PI3K signaling pathways [9]. Overexpression and increased activity of EGFR tyrosine kinase in non-small cell lung tumors were first described in 2004, which may result from mutation, deletion, or amplification of the tyrosine kinase coding region [10].

The mutation most commonly affects exons 18–21 and occurs in 10%–20% of the Caucasian population, predominantly in young, never-smoker women. In almost 90% of cases, a so-called "classical mutation" is encountered, a deletion of exon 19 or a point mutation of exon 21 (L858R). The exon 20 insertion is the third most common EGFR mutation, accounting for 4%–12% of all EGFR mutations, it is more common in women, non-smokers, and Asians and is associated with a worse prognosis. In addition to the exon 20 insertion mutation, the most common rare mutations include exon 18 G719X, exon 20 S768I and exon 21 L861Q, which occur in 1%–3% of cases and smoking history [11].

In locally advanced or metastatic non-small cell lung cancer, EGFR tyrosine kinase inhibitor (TKI) treatment is the recommended first-line therapy with confirmed actionable EGFR mutations. EGFR tyrosine kinase inhibitors are classified into three generations based on their appearance in chronological order. The first-generation includes the reversible binding agents gefitinib and erlotinib, the second-generation includes the irreversible ErbB/HER2 inhibitor afatinib and the EGFR/pan-HER inhibitor dacomitinib, while the third-generation is osimertinib. Since then, several studies have demonstrated the benefit of EGFR tyrosine kinase inhibitors in terms of tumor response, safety, quality of life, and progression-free survival (PFS) compared with conventional chemotherapy regimens [12].

First-generation reversible EGFR inhibitors

Pioneering in the treatment of adenocarcinoma patients, gefitinib, in its pivotal phase 3 IPASS trial, showed a significant benefit in progression-free survival [median PFS (mPFS) gefitinib 9.5 months vs. chemotherapy 6.3 months; HR 0.48, 95% confidence interval (CI) 0.36–0.64 $p < 0.001$] and

tumor response [objective response rate (ORR) 71.2% v 47.3%, $p = 0.0001$], with good quality of life maintained [13].

The efficacy of erlotinib was analyzed in the OPTIMAL trial in Asia and the EURTAC trials in Europe [14, 15]. A significant difference was demonstrated in favor of erlotinib in terms of overall survival (OS) and tumor response compared to the standard platinum-based chemotherapy regimens (EURTAC mPFS erlotinib 9.7 months vs. chemotherapy 5.2 months; $p < 0.0001$; ORR 64% vs. 18%; $p < 0.0001$) (OPTIMAL mPFS erlotinib 13.1 months vs. chemotherapy 4.6 months; $p < 0.0001$; ORR 83% vs. 36%; $p < 0.0001$) (5,6). Although no benefit in overall survival was demonstrated, following these trials, both products were registered in the first-line setting for treating EGFR mutation-positive stage IIIB/IV non-small cell lung cancer.

It is now well known that the first-generation drugs are most commonly associated with skin side effects (rash, xeroderma, pruritus, and paronychia), diarrhea, fatigue, and elevation of liver function, typically AST/ALT. The most common cutaneous side effects are acneiform rash, dry skin, itching, and nail bed lesions, which are well controlled by topical or systemic antibiotic treatment (doxycycline). Diarrhea can be reduced by per os medication (appropriate dose of loperamide), with drug dose reduction if necessary. Once the side effects are resolved, the original dose is often restored. Compared with chemotherapy regimens, first-generation regimens have shown a much better side-effect profile and fewer serious (grade 3–4) adverse events [13, 15–18].

A vascular endothelial growth factor (VEGF) inhibitor, Ramucirumab plus erlotinib, showed increased PFS compared to placebo plus erlotinib arm in patients with untreated EGFR-mutated metastatic NSCLC (mNSCLC) [19]. Safety was consistent with the safety profiles of the individual compounds in advanced lung cancer.

Second-generation EGFR inhibitors

The second-generation EGFR tyrosine kinase inhibitors (afatinib and dacomitinib) are more potent EGFR and HER2 inhibitors, forming irreversible binding. The efficacy of afatinib was analyzed in LUX-lung studies. In the phase 2 LUX-lung 3 and LUX-lung 6 trials, afatinib showed significantly better tumor response and progression-free survival than platinum-based chemotherapy combinations (LUX-lung 3, mPFS for afatinib vs. chemotherapy, 13.6 months vs. 6.9 months; respectively, $p = 0.0004$; ORR, 56% vs. 23%; $p = 0.001$; respectively; LUX-lung 6, mPFS for afatinib vs. chemotherapy 11.0 months vs. 5.6 months; $p < 0.0001$; respectively, ORR 66.9% vs. 23%; $p < 0.0001$). [20, 21]. It should be noted that afatinib did not provide a benefit in OS in the overall patient group; however, in subgroup analyses, targeted therapy in patients with exon 19 deletion showed a significant benefit in overall survival (LUX-lung 3, OS for afatinib vs. chemotherapy 33.3 months 21.1 months respectively; LUX-lung 6, OS for afatinib vs. chemotherapy 31.4 months vs. 18.4 months, respectively). This benefit was not confirmed for point mutations [22]. Based on these studies, afatinib was registered as a first-line treatment for non-small cell lung tumors carrying EGFR mutations.

The LUX-lung 7 phase 2 trial comparing first- and second-generation EGFR tyrosine kinase inhibitors compared afatinib with gefitinib, where afatinib was shown to be superior in terms of progression-free survival (mPFS for afatinib vs. gefitinib, 11.0 months vs. 10.9 months; respectively, $p = 0.017$), however, the study did not show a significant benefit in terms of overall survival and more toxicity leading to dose reduction was observed when using the second-generation drugs [23]. A higher rate of G3-severe skin rash (9.4% vs. 3.1%) and G3 diarrhea (12.5% vs. 1.3%) was also observed in the afatinib group. Dacomtinib, also a second-generation irreversible EGFR and panHER inhibitor, was superior to gefitinib in first-line use in the ARCHER1050 phase 3 trial in terms of both PFS and OS [PFS for dacomitinib vs. gefitinib, 14.7 months vs. 9.2 months, respectively, $p < 0.0001$; median OS (mOS) dacomitinib vs. gefitinib, 34.1 months vs. 26.8 months, respectively], but again a less favorable side effect profile was observed with dacomitinib [24, 25].

Third-generation EGFR inhibitors and T790 resistance mutation

Acquired resistance to first- and second-generation drugs develops after 9–13 months, with a T790 resistance mutation affecting exon 20 being confirmed in 50%–60% of cases [26]. This has led to the development of third-generation therapies [26]. Osimertinib is a third-generation irreversible EGFR TKI that is also effective in the presence of T790 resistance mutations. The efficacy of the first mutation selective TKI was analyzed in AURA trials. In the AURA 3 phase 3 trial, compared with platinum-based chemotherapy, osimertinib showed a significant PFS benefit in T790 resistance mutation-positive, locally advanced or metastatic NSCLC (mPFS osimertinib vs. chemotherapy, 10.1 month vs. 4.4 months, respectively, $p < 0.001$) [27]. This was followed by the phase 3 FLAURA trial, which compared the efficacy of osimertinib with first-generation agents; osimertinib achieved a significant benefit in both progression-free and overall survival, with osimertinib providing an 8.8 months OS benefit, reducing the risk of death by 20% (mOS osimertinib vs. first-generation EGFR inhibitor, 38.6 months vs. 31.8 months; respectively, HR 0.80; 95% CI, 0.6410 .997; $p = 0.046$). The side effect profile was similar, but G3 side effects were less frequent with osimertinib [28]. The most common osimertinib-induced adverse events were acneiform rash, diarrhea, and paronychia, and a small percentage of cardiomyopathy (~1.4%–2.4%), QT prolongation (2.7%), and interstitial lung disease (ILD) (3.3%) were also described [29]. After 3 years of follow-up, 28% of patients received osimertinib, compared with only 9% in the

comparator group. Notably, first-line osimertinib reduced the risk of CNS progression by 52% (HR, 0.48; 95% CI, 0.260.86; $p = 0.014$) and fewer *de novo* CNS metastases were recorded [30]. The importance of these results is demonstrated by the fact that 10%–30% of patients with NSCLC develop CNS metastases, which are associated with a worse prognosis and worse survival. EGFR mutations are present in 40%–60% of non-small cell lung tumors affecting the central nervous system, and the risk of central nervous system metastasis is higher in the presence of EGFR mutations, making the concentration of each drug in cerebrospinal fluid a key determinant. First- and second-generation drugs have limited brain penetration, while osimertinib rapidly crosses the blood-brain barrier (BBB) and reaches higher concentrations. Osimertinib, which has the best efficacy and most favorable side-effect profile of all EGFR inhibitors, is currently the drug for first-line treatment of EGFR mutant NSCLC, particularly in patients with BM [31]. If not available in the first line, first or second-generation agents should be administered, and in case of progression, efforts should be made to confirm T790 resistance mutation from liquid biopsy or repeated histological sampling. In the presence of a T790 resistance mutation, osimertinib is preferred while platinum-based chemotherapy is recommended in case of negative resistance mutation status. With the widespread use of osimertinib, the development of new resistance mutations is expected. Most commonly, mutation of exon 20 C797X, MET amplification, and HER 2 amplification have been described in addition to aberrations of other non-EGFR mediated pathways [1].

Immunotherapy and targeted treatment options

The IMpower 150 phase 3 three-arm trial compared the combination of chemotherapeutic doublet immunotherapy and VEGF inhibitor with VEGF inhibitor-chemotherapeutic doublet and chemo-immunotherapy. EGFR mutant patients were also eligible for inclusion in the study. Subgroup analyses showed that a significant OS benefit was achieved with the combination of four regimens vs. VEGF inhibitor-chemotherapy doublet, regardless of the presence of EGFR mutations (EGFR positive subgroup mOS 26.1 months vs. 20.3 months; respectively), making the combination of four regimens an additional option after exhaustion of targeted therapies [32].

NSCLC harboring a rare EGFR mutation

Approximately 10%–20% of non-small cell lung tumors carrying EGFR mutations carry rare EGFR mutations [33]. While the presence of classical activating mutations is a strong predictor of favorable tumor response to EGFR tyrosine kinase inhibitors, rare EGFR mutations, such as the exon 20 insertion mutation, are heterogeneous, largely resistant to first- and second-generation drugs, and the efficacy of third-generation osimertinib is limited. In recent years, several new products have been developed for this patient group. Mobocertinib is an irreversible EGFR and HER inhibitor targeting exon 20 alterations. In the phase 1/2 EXCLAIM trial, mobocertinib in the multilineage setting resulted in a 32% tumor response and a median progression-free survival of 7.3 months. Based on the phase 1/2 results, mobocertinib received Food and Drug Administration (FDA) approval. Amivantamab is a bispecific monoclonal antibody that prevents tumor growth and progression by blocking EGFR and c-MET pathways and stimulates immune-mediated destruction of EGFR and cMET-expressing cells. In the CHRYSALIS phase 1 study, patients with exon20 insertion mutations received multiple lines of amivantamab treatment, with an mPFS of 8.3 months and an ORR of 40%. Based on this study, the FDA approved amivantamab for the treatment of patients progressing on platinum-based chemotherapy. Although the use of amivantamab and mobocertinib has improved the tumor response and progression-free survival of this poor prognosis patient group, the presence of EGFR exon 20 insertions is still associated with poor prognosis and unfavorable survival, and further studies on drug development are needed [33].

In addition to the exon 20 insertion mutation, the most common rare mutations include exon 18 G719X, exon 20 S768I, and exon 21 L861Q, often in associated with other mutations [2]. Most clinical trials conducted to date have recruited patients with classical EGFR exon 19 deletion and exon 21 point mutations. An exception was the LUX-lung 2,3,6 trial (afatinib vs. chemotherapy), which included patients with rare EGFR mutations. Following a detailed, retrospective analysis of the trials, the benefit of afatinib in this patient group in terms of tumor response and PFS was published, leading to the registration of afatinib for the treatment of NSCLs with rare EGFR mutations. In the FLAURA 3 study comparing osimertinib and first-generation EGFR TKIs, rare EGFR mutation was an exclusion criterion, but in phase 2 Korean study (KCSG-LU15-09), patients with rare mutations showed a better tumor response and progression-free survival with osimertinib treatment, which was confirmed in some small patient studies. First-generation formulations have shown little activity in rare mutations. Although data are scarce, real-world studies to date suggest the use of second or third-generation drugs, afatinib or osimertinib, in the presence of a major EGFR rare mutation. The choice is a clinical decision, which is best made based on the side effects encountered, the patient's general condition, and the products' availability [34].

Summary of EGFR targeted therapy

Treatment recommendation for EGFR mutant metastatic NSCLC based on the ESMO 2023 guideline is shown in Figure 2. In all patients with advanced/metastatic lung tumors, molecular profiling is recommended after histological diagnosis. If an EGFR mutation is confirmed, first-line EGFR tyrosine kinase inhibitor therapy is recommended (I,A). When exon

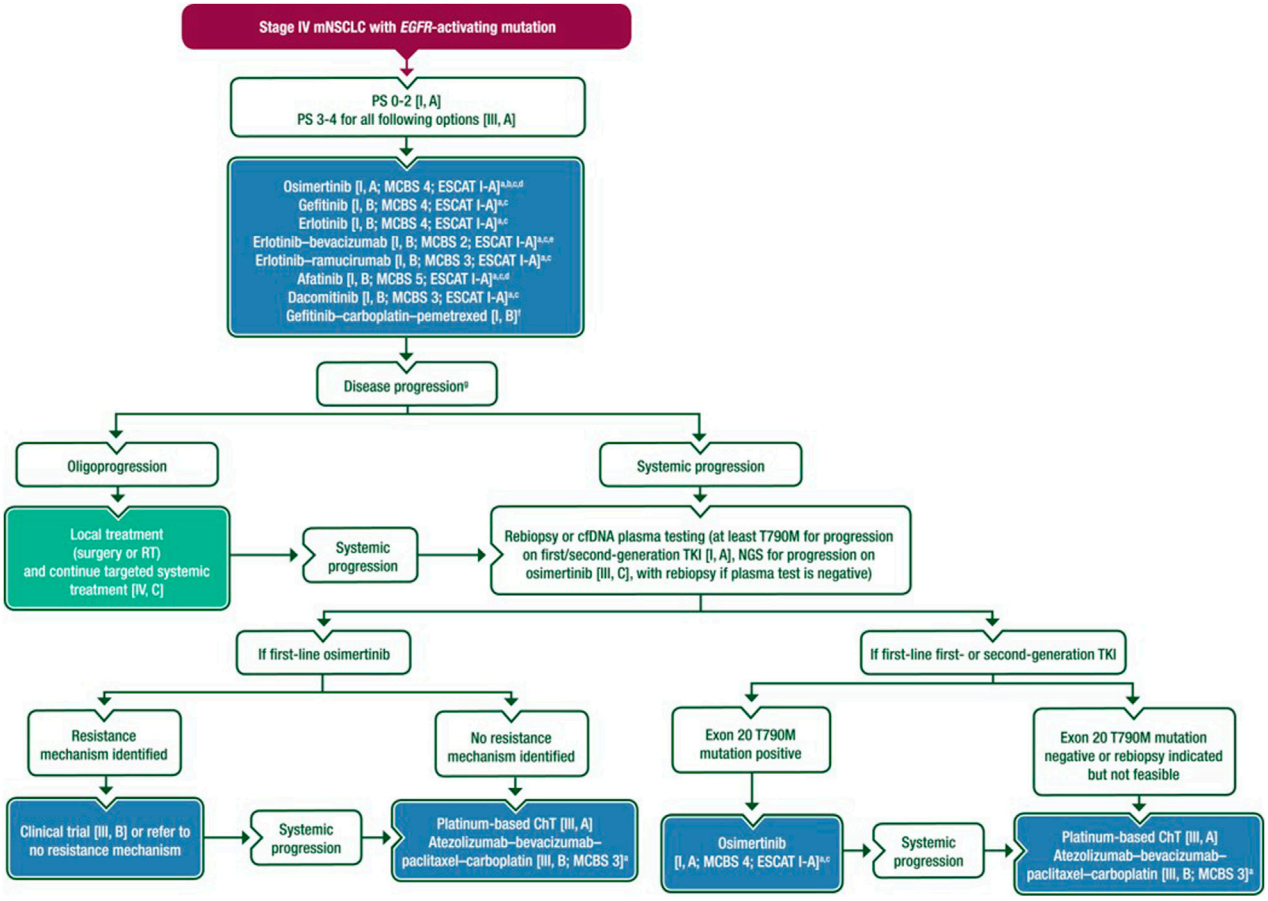

FIGURE 2
Treatment recommendation for EGFR mutant metastatic NSCLC based on the ESMO 2023 guideline [1].

19 del or exon 21 L858R EGFR mutation confirmed, osimertinib is the first choice, especially in the presence of BM (I, A). As first-line therapy, gefitinib chemotherapy and erlotinib-VEGF inhibitor therapy are also considered (I, B), but due to side effects and higher costs, EGFR TKI therapy alone is the preferred option (I, A). If osimertinib is not available, first-generation (gefitinib, erlotinib) or second-generation (afatnib, dacomitinib) agents are preferred (I, A). In case of progression, liquid biopsy or repeated tissue sampling is recommended to confirm T790 resistance mutation (I, A). In the case of a resistance mutation is present, second-line osimertinib is recommended (I, A), while platinum-based chemotherapy is the treatment of choice in case of negative results (III, A). In the case of osimertinib resistance, next-generation sequencing (NGS) is recommended to detect resistance genes (III, C). Enrolling in a clinical trial is a preferred option if available (III, B) (III, B). Otherwise, platinum-based chemotherapy is administered (III, A). After exhaustion of TKIs, chemotherapy doublet-immunotherapy-VEGF-quadruplet combination may be considered in patients with good overall Eastern Cooperative Oncology Group (ECOG PS) 0–1, if immunotherapy is not contraindicated (III, B) [1]. If oligoprogression is confirmed during EGFR tyrosine kinase inhibitor therapy, local metastasis treatment is recommended, while targeted therapy should be continued (III, A) [1]. In the presence of a rare mutation, non-exon 20 insertion, osimertinib, or afatinib is recommended (III, B). In the presence of exon20 insertion mutations, amivantamab can be given as second-line therapy in the case of progression after first-line therapy (III, B), while mobocertinib EMA approval is pending in these clinical settings (III, C) [1].

Treatment of NSCLC with anaplastic lymphoma kinase (ALK) genetical alterations

ALK fusion genes are potent, albeit uncommon, driver oncogenes of non-small cell lung cancer. Notably, the detection of ALK fusion oncogene is of great importance

because ALK-positive tumors are highly sensitive to ALK inhibitors, which significantly improves the life expectancy of patients.

Diagnosis

Molecular testing for ALK fusion can be performed as part of standard clinical care in non-small cell lung cancer, primarily adenocarcinoma, from both tumor tissue and plasma samples [35]. Methods for detecting ALK translocation include NGS, IHC, Fluorescence *in situ* hybridization (FISH), RT-PCR. The standard methodology is FISH, but immunohistochemistry with monoclonal antibodies of high sensitivity and specificity and a validated method is an equivalent method for detecting ALK fusion oncoprotein. RNA-based multigene NGS assays are also suitable instead of IHC or FISH, with the advantage of simultaneous testing for other fusion oncogenes [36, 37].

Epidemiology

The ALK fusion oncogene is present in 3%–5% of non-small cell lung cancers, with the majority of lung cancers carrying the gene being adenocarcinoma (97%). It is a disease of non-smokers or light smokers (<10 pack-years). Relative younger age at onset, with a median age of 52 years. The incidence of ALK molecular alteration in squamous cell carcinoma is limited. Cerebral metastasis is common, approximately 30% at the time of disease discovery [38, 39].

First-line treatment of ALK-positive lung cancer with ALK tyrosine kinase inhibitor (ALK-TKI)

Crizotinib is a multitarget TKI, the first ALK inhibitor to improve the life expectancy of ALK-positive patients compared to chemotherapy in both first-line and subsequent-line settings.

In the phase 3 PROFILE 1014 trial, therapy-naive patients were included, and first-generation ALK inhibitor, crizotinib, was compared with pemetrexed and platinum doublet chemotherapy, and crossover was allowed [40]. At a median follow-up of 17 months, the primary endpoint, progression-free survival, was longer with crizotinib than with chemotherapy (median 10.9 vs. 7 months; HR 0.45, 95% CI 0.35–0.60). Objective tumor response was also increased (74% vs. 45%). At 46 months follow-up, there was no significant difference in overall survival (HR 0.76, 95% CI 0.55–1.05). However, after crossover adjustment, crizotinib also improved overall survival compared with chemotherapy (HR 0.35, 95% CI 0.08–0.72). The median overall survival of more than 4 years was reported in the crizotinib arm [40].

Ceritinib, a second-generation ALK inhibitor, has also been shown to be superior to chemotherapy when administered as first-line therapy [41].

The second-and third-generation ALK inhibitors are more effective than crizotinib in metastatic disease, including BM based on phase 1 randomized controlled trials, and are considered the preferred first-line agents. Second-generation ALK-TKIs are alectinib, brigatinib, and ensartinib (not approved by the European Medicines Agency (EMA)), and third-generation agents are lorlatinib [42–45].

Alectinib indicated for therapy naïve patients in first-line or previously treated with crizotinib in locally advanced or metastatic ALK-positive non-small cell lung cancer. In the phase 3 ALEX randomized controlled trial (N = 303), the median progression-free survival (mPFS) in the first-line setting compared with alectinib plus crizotinib was 35 months for alectinib and 11 months for crizotinib (HR 0.43, 95% CI 0.32–0.58). The results are not yet mature; the median overall survival (mOS) for the alectinib arm was not yet reached, and for the crizotinib arm, it was 57 months (HR 0.67 95% CI 0.46–0.98). Immature data showed a 5-year OS rate of 63% (alectinib) and 46% (crizotinib). Time to CNS progression was longer for alectinib than crizotinib (HR 0.16, 95% CI 0.10–0.28) in the overall population. The rates of grade 3–5 toxicity were similar for alectinib and crizotinib (52% vs. 56%). In the Alectinib arm, there was a higher incidence of anemia, myalgia, se bilirubin elevation, weight gain, and photosensitivity. Nausea, vomiting, and diarrhea were more frequent on the crizotinib arm [42, 46].

Brigatinib is currently approved for use in ALK-positive non-small cell lung cancer in locally advanced or metastatic ALK-positive patients previously treated with crizotinib or not previously treated with an ALK inhibitor. Brigatinib shows efficacy in a broad spectrum of ALK mutations. The phase 3 ALTA-1L randomized controlled trial (N = 275) compared brigatinib with crizotinib in ALK-TKI naive patients. Chemotherapy administration prior to randomization was not an exclusion criterion in the trial. In ALK inhibitor naïve ALK-positive patients at 3-year follow-up, the PFS was 43% vs. 19% for crizotinib vs. crizotinib arm, respectively, according to a standardized independent evaluation. mPFS at 9–11 months follow-up was 24 months versus 11 months (HR 0.48, 95% CI 0.35–0.66). The therapeutic benefit was observed in all subgroups and was prominent in patients with BM. The brain metastasis-related tumor response was significantly higher with brigatinib compared with crizotinib (78% versus 26%). mOS has not yet been reached by either group.

There was ILD/pneumonitis occurred in 4% of patients on brigatinib and 2% on crizotinib. The incidence of grade 3–4 ILD/pneumonitis was 3% versus 0.7%. The risk decreased by gradually increasing the dose of brigatinib (90 mg once daily for 7 days, then increased to 180 mg/day if tolerated). Symptoms associated with elevated creatine kinase (myalgia, muscle pain) did not differ significantly between the two agents. Nausea, diarrhea,

constipation, peripheral edema, elevated liver function (GPT), and visual disturbances were more frequent with crizotinib. Grade ≥3 adverse events occurred in 61% with brigatinib and 55% with crizotinib [43].

Lorlatinib is recommended as monotherapy for adult patients with advanced ALK-positive non-small cell lung cancer who have not been previously treated with an ALK inhibitor. It is also for patients with advanced-stage ALK-positive NSCLC whose disease has progressed on first-line treatment with alectinib ceritinib or crizotinib.

In the phase 3 CROWN randomized controlled trial (N = 296), patients with the locally advanced or metastatic stage-naive disease were randomized to the lorlatinib or crizotinib arm. The mPFS was significantly better with lorlatinib than with crizotinib. In the first interim analysis, mPFS at 18 months of follow-up was not yet reached with lorlatinib versus 9.3 months with crizotinib (HR 0.28 95% CI 0.19–0.41). Lorlatinib showed robust CNS efficacy. Grade 3–4 adverse events occurred in 72% of patients treated with lorlatinib and 56% with crizotinib. Hypercholesterolaemia and hypertriglyceridemia occurred in >70% of patients on lorlatinib and neurocognitive side effects may affect the first-line use of lorlatinib [45, 47, 48].

Duration of treatment

Treatment with ALK inhibitors is continued until disease progression. In the case of oligoprogression, local intervention is recommended in addition to the continuation of ALK-TKI. A more potent next-generation ALK inhibitor or standard chemotherapy is indicated for extensive progressive disease.

Treatment for progression on crizotinib

For progression following crizotinib, alectinib or brigatinib is recommended, given their systemic and CNS efficacy and good tolerability.

Alectinib—In the phase 3 ALUR study (N = 107), patients with advanced ALK-positive disease pretreated with platinum-based chemotherapy and crizotinib were randomized to alectinib or mono-chemotherapy (pemetrexed or docetaxel). PFS was longer with alectinib, 7.1 months vs. 1.6 months (HR 0.32, 95% CI 0.17–0.59), and the number of grades ≥3 adverse events was lower with alectinib (27% versus 41%). CNS efficacy was also better with alectinib [49].

Brigatinib—In the phase 2 ALTA study (N = 222), patients refractory to crizotinib at 1 × 90 mg/day (arm A) or 1 × 180 mg/day (arm B) after a seven-day 1 × 90 mg/day lead-in period with brigatinib had an mPFS of 9.2 months versus 16.7 months at lower and higher doses of the agent, respectively. The median overall survival (OS) was 29.5 months versus 34.1 months. In patients with baseline BM, the independently assessed CNS objective tumor response was 50% versus 67%. Both arms had low rates of grade ≥3 toxicity [50].

Ceritinib is not preferable because it is less effective than the former in cross-trial comparisons. In the open-label ASCEND-5 study, 231 patients were randomized to ceritinib 750 mg/day or chemotherapy arm after crizotinib treatment, with ceritinib having better PFS (5.4 versus 1.6 months; HR 0.49) and ORR (39.1% versus 6.9%), both statistically significant. Nevertheless, OS analysis is still immature. Due to crossover, the OS advantage is expected to be decreased in the ceritinib arm. While initial studies used a ceritinib dose of 750 mg/day with fasting intake, a randomized open-label trial found an equivalent dose of 450 mg/day with meals was associated with lower gastrointestinal toxicity [51].

Although a phase 2 trial has shown lorlatinib to be effective in progression on crizotinib (ORR 69%, intracranial ORR 68%, mPFS not yet achieved), the EMA prescribing after crizotinib requires the prior use of a second-generation TKI [48, 52].

Treatment for progression on second-generation ALK TKI

Lorlatinib is a third generation ALK-TKI. Lorlatinib is effective against acquired resistance mutations in most ALK kinase domains, including G1202R and other ALK kinase domain mutations. Lorlatinib is the preferred agent for alectinib-induced resistance [53]. This is probably also true for other second-generation ALK inhibitors [52]. Lorlatinib is also characterized by high CNS penetration.

In a phase 2 trial, lorlatinib in patients previously treated with one or more ALK inhibitors resulted in high objective tumor response (47%), complete remission (2%) and partial tumor response (45%). Following crizotinib, treatments with lorlatinib, the ORR was 73%, and mPFS was 11.1 months. After one or more second-generation ALK inhibitors, ORR was 40% and mPFS was 6.9 months. At >30 months median follow-up, mOS was 21 months. The most common adverse events in this study were hypercholesterolemia (81%), hypertriglyceridemia (61%), edema (43%) and peripheral neuropathy (30%). Serious treatment-related adverse events developed in 7% of patients, the most common being cognitive impairment (1%). In patients who progressed with second generation ALK-TKI, the ORR for lorlatinib was higher when an ALK mutation was present in addition to the ALK fusion oncogene, suggesting that second generation ALK mutations may be associated with the development of a new oncogene. Therefore, genotyping ALK mutations after progression on second generation ALK inhibitors may identify patients more likely to benefit from lorlatinib treatment [52].

Although lorlatinib has not been studied in comparison with chemotherapy in alectinib-resistant disease, lorlatinib after

alectinib is recommended because chemotherapy can only achieve poorer survival after progression from ALK-TKI.

Alternative target therapies -ceritinib and brigatinib also show activity in progression after alectinib based on small observational studies [54, 55].

Treatment options for subsequent lines in ALK-positive NSCLC

The IMpower 150 trial suggests chemo-immunotherapy + VEGF inhibitor, the median PFS in patients with EGFR activating mutation + ALK-positive subgroup in TKI pretreated patients were 9.7 vs. 6.1 months; respectively, (HR 0.59, 95% CI 0.37–0.94). Nevertheless, there is no evidence on the efficacy of mono-immunotherapy in the presence of ALK-positivity. Chemotherapy alone is an acceptable additional option with moderate activity in this patient population. Some experts recommend a standard combination of pemetrexed, carboplatin, and pembrolizumab combinations for lung adenocarcinoma, although clinical trials demonstrating the efficacy of this combination have excluded ALK-positive patients [56, 57].

Treatment of brain metastases in ALK-positive NSCLC

In cases of BM, both for symptomatic or asymptomatic cases, second or third generation ALK-TKI is recommended, as these agents have good blood barrier penetration and CNS efficacy. The majority of patients with BM, whether TKI naïve or treated with crizotinib, are likely to respond to these agents and may be able to defer surgical intervention or radiotherapy, thereby reducing morbidity associated with local care. However, surgical treatment may be considered as initial therapy in cases of spatial disproportionation or risk of herniation due to massive BM [58].

Summary of ALK targeted therapy

Treatment recommendation for ALK translocated metastatic NSCLC based on the ESMO 2023 guideline is shown in Figure 3. NSCLC with ALK rearrangements is a subtype of lung cancer with specific clinical and pathological features. Due to the availability of effective therapies, all lung adenocarcinomas should be investigated for ALK fusion oncogenicity. In locally-advanced or metastatic stage ALK-positive NSCLC, a second or third-generation ALK inhibitor is recommended in the frontline setting. Treatment should be continued until progression or intolerable toxicity. In case of oligoprogression in mildly symptomatic or asymptomatic patients, local ablative therapy for the progressive formulation is recommended with continuation of the ALK inhibitor. For progression on a second-generation ALK inhibitor, lorlatinib is recommended over chemotherapy or other ALK inhibitors. Following the exhaustion of TKIs, platinum doublet CHT or in CHT combination with bevacizumab and/or anti-PD immunotherapy can be administered if the patient is still fit for further treatment.

Further studies are needed for TKI-treated ALK-positive cases to determine whether identifying specific tyrosine kinase domain mutation can identify appropriate next steps in therapy. Nevertheless, some preliminary data suggest that specific kinase domain mutations may impact the following line of therapy [2]. Broad genomic profiling may be the most informative approach to examining potential resistance mechanisms, which may require repeated sampling during treatments. Assay methodology selection can impact the ability to identify subclonal events in this setting.

KRAS mutant NSCLC treatment

KRAS mutations activate several additional signaling pathways, occur in about 20%–25% of lung adenocarcinomas and are usually associated with lung cancer in smokers [59]. G12G KRAS mutation subtype is associated with smoking status [6].

The presence of the KRAS mutation in early lung cancer does not seem to affect overall survival, however others have shown that it is associated with a poor prognosis [60]. The focus of targeted therapy for KRAS mutant lung cancer is on irreversible inhibitors of KRAS G12C. KRAS G12C mutations account for nearly 50% of all KRAS mutations [60].

Treatment of non-small cell lung cancer with KRAS G12C mutation

First line treatment

First-line therapy regimens are recommended similarly to non-oncogene-dependent, non-squamous NSCLC [1].

Second-line treatment

Targeted treatment for KRAS G12C mutant tumors after first-line platinum-based chemotherapy and/or anti-PD immunotherapy is considered.

Sotorasib is the first target agent to receive regulatory approval for KRAS G12C mutant locally advanced or metastatic adenocarcinoma in patients who have received at least one prior systemic therapy [61].

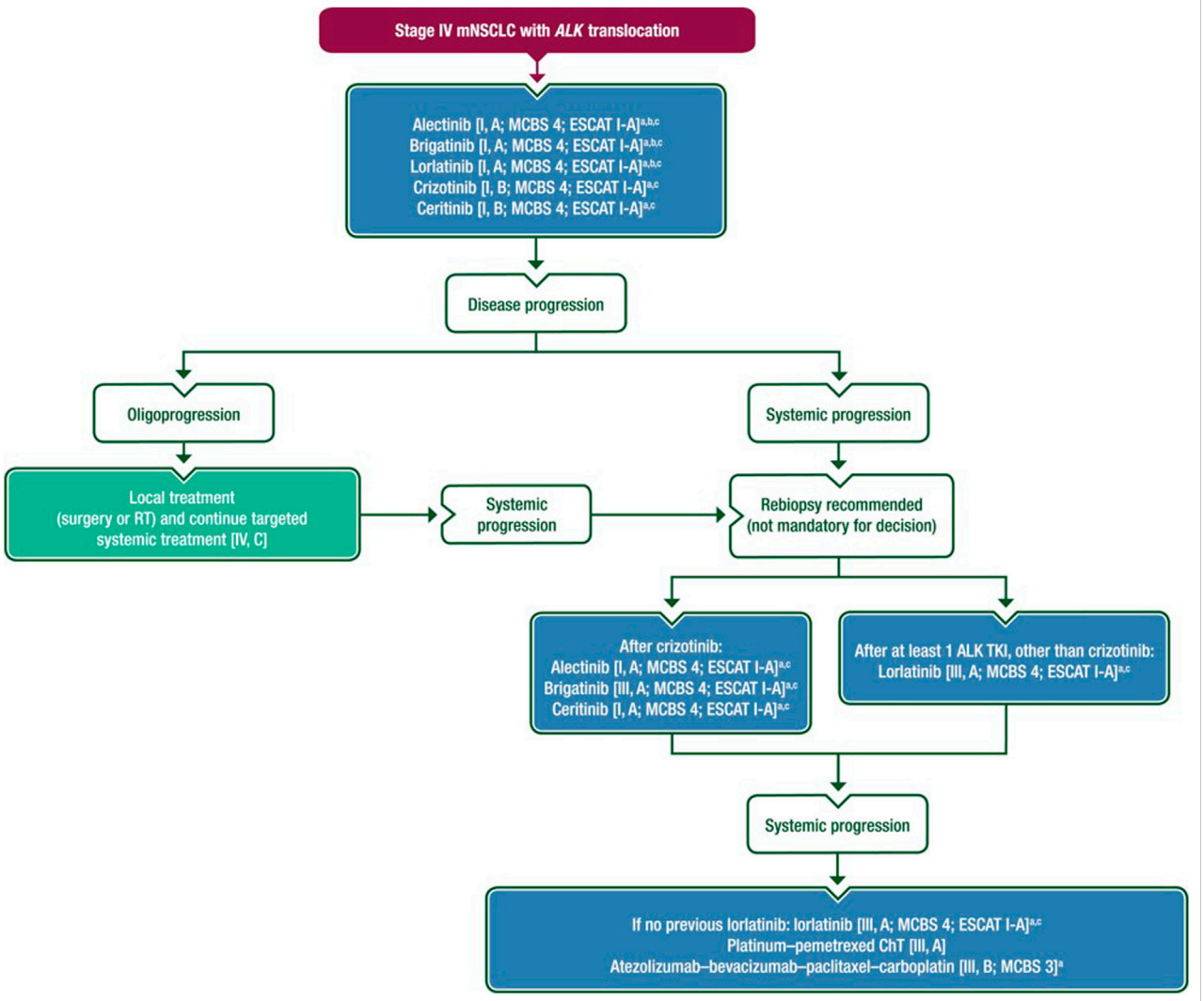

FIGURE 3
Treatment recommendation for ALK translocated metastatic NSCLC based on the ESMO 2023 guideline [1].

In the randomized, open-label, phase 3 CodeBreak 200 trial (N = 345), patients with KRAS G12C mutations were randomized to sotorasib or docetaxel after progression on platinum-based chemotherapy and anti-PD immunotherapy treatment. Better PFS was achieved with sotorasib than docetaxel based on independent unblinded assessment (5.6 versus 4.5 months HR 0.66, 95% CI 0.51–0.86), with fewer grade ≥3 toxicities (33 versus 40%) and fewer serious adverse events (11 versus 23%). Overall survival was similar in the two groups (10.6 months with sotorasib and 11.3 months with docetaxel, HR 1.0). The most common grade ≥3 treatment-related adverse events were diarrhea (12%) and elevated transaminase levels (5%–8%) [62].

In the phase 1 CodeBreak 100 trial, sotorasib achieved an objective tumor response of 41%, mPFS of 6.3 months, OS of 12.5 months, and a two-year survival rate of 33% [63].

Several drug interactions are known to occur with sotorasib. It is not recommended for co-administration with antacids such as proton pump inhibitors, H2 receptor blockers, potent cytochrome P450 3A4 (CYP3A4) inducers, and certain CYP3A4 and P-gp substrates [61].

Adagrasib has been granted conditional marketing authorization by the EMA to treat advanced non-small cell lung cancer with KRAS G12C mutation and progression on at least one prior systemic therapy [64].

In the Krystal-1 single-arm, phase 1–2 study (N = 116), KRAS G12C mutant patients received 2 × 600 mg of adjuvant adagrasib daily after prophylactic chemotherapy and PDL1 inhibitor immunotherapy. The mPFS was 6.5 months, objective tumor response was 43%, the median duration of response was 8.5 months, and OS was 12.6 months. In

33 patients with previously treated stable BM, the intracranial confirmed objective response was 33%. Grade ≥3 treatment-related adverse events occurred in 45% of patients, the most common being fatigue, nausea and elevated liver function tests. Two grade 5 events occurred: heart failure in a patient previously known to have pericardial effusion and one pulmonary hemorrhage [65].

Summary of targeted therapy in KRAS mutant NSCLC

For patients with KRAS G12C mutant NSCLC progressed after a prior line of therapy, second-line sotorasib or adagrasib may be recommended over subsequent chemo and/or immunotherapy.

Treatment of NSCLC with ROS1 genetical alterations

The ROS1 proto-oncogene encodes a tyrosine kinase of the insulin receptor family, which is structurally similar to ALK. ROS1 gene fusion was first identified in 1987 in the glioblastoma cell line U118MG [66]. Since then, ROS1 gene rearrangements have been observed in 22 adult and pediatric malignancies [67]. It is detectable in 1%–2% of NSCLC, with a higher prevalence in non-smoking, younger women. ROS1 mutations do not co-occur with other driver mutations, with rare exceptions including in *EGFR* (1/166) and *KRAS* (3/166) and no co-occurring *ROS1* and *ALK* alterations [68]. They are almost exclusively detected in adenocarcinoma, but rare cases are also found in squamous cell, pleiomorphic, and large cell lung carcinoma [69]. FISH is the gold standard method for the detection of ROS1 gene rearrangements. IHC has high sensitivity but low specificity and is not recommended as a primary determinant for treatment. In the case of a positive or inconclusive ROS1 IHC result, confirmatory FISH, NGS, and RT-qPCR should be performed [69, 70]. Treatment recommendation for ROS1 translocated metastatic NSCLC based on the ESMO 2023 guideline is shown in Figure 4.

Crizotinib was the first TKI inhibitor to be approved by both the EMA and the FDA for the treatment of ROS1 mutant non-small cell lung cancer based on the results of the phase 1 PROFILE 1001 clinical trial [71]. The study cohort included 53 patients with ROS1-positive NSCLC, most of whom (87%) had previously received first-line platinum-based chemotherapy. The ORR for crizotinib was 72%, associated with a disease control rate (DCR) of 90%. The mPFS and mOS were 19.3 and 51.4 months, respectively. The median duration of therapy with treatment was 22.4 months (15.0–35.9 months) [71]. Subsequently, several retrospective and prospective phase 2 studies have demonstrated the efficacy of crizotinib [69]. However, it is important to emphasize that the drug has a low BBB penetration and, due to the poor brain penetration with crizotinib, the primary site of progression is the central nervous system [72].

Entrectinib is a new generation TKI that inhibits tropomyosin-related kinases in addition to its anti-ROS1 activity. Based on the results of an analysis of data from three prospective phase 1 and 2 clinical trials (ALKA-372–001, STARTRK-1, STARTRK-2), the ORR with entrectinib was 67% and mPFS was 15.7 months. A significant proportion of the 161 patients included in the study (62.7%) had received prior systemic therapy and 34.8% had BM at baseline. The 24 patients who had measurable BM at diagnosis had an intracranial ORR of 79%, mPFS of 12 months and mOS of 26.3 months. The majority of adverse events associated with entrectinib were grade 1 and 2, and overall, the tolerability and safety profile of the agent was similar to other ROS1 inhibitors [73, 74]. Based on these results, entrectinib was granted a marketing authorization by the FDA in 2019 and by the EMA in 2020. Entrectinib is the first line drug for known BM based on the ESMO 2023 recommendation [1].

Ceritinib is a second-generation ALK/ROS1 TKI with significant central nervous system activity. In a phase 2 clinical trial in Korea, 32 patients with advanced ROS1-positive disease, mostly crizotinib-naive (n = 30), were treated with ceritinib. In the whole cohort, ORR was 62%, mPFS was 9.3 months, and DCR was 81%. Among patients who had not received crizotinib treatment, ORR reached 67% and mPFS 18.3 months. Of note, no treatment response was observed in the two patients previously treated with crizotinib while on ceritinib [75]. Based on these results, ceritinib may be considered for crizotinib treatment in patients with ROS1-positive NSCLC who have not previously received crizotinib; however, currently, the agent is neither FDA nor EMA-approved.

Lorlatinib is a third-generation ALK/ROS1 TKI that penetrates the brain and has been effective in a phase 1 and phase 2 single-arm clinical trial that enrolled 69 ROS1-positive patients [52, 76]. The ORR in the TKI-naïve cohort (n = 21) was 62%, mPFS 21 months, and intracranial ORR 64%, compared to a group of previously crizotinib-treated patients (n = 40), where ORR was only 35%, mPFS 8.5 months, and intracranial ORR 50%. There was also a significant difference in the median duration of response (mDOR) (25.3 months vs. 13.8 months). Along with ceritinib, lorlatinib does not have FDA or EMA approval.

Repotrectinib is a new generation ROS1/TRK/ALK tyrosine kinase inhibitor. In the phase 1/2 TRIDENT-1 clinical trial in the ROS1 TKI-naïve group (n = 71), ORR was 79% and mDOR was 34.1 months [77, 78]. In patients who had previously received ROS1 TKI therapy but did not receive chemotherapy/immunotherapy (n = 56), ORR was 38% and mDOR was 14.8 months. Based on these results, in November 2023, the FDA approved repotrectinib to treat ROS1-positive NSCLC [79].

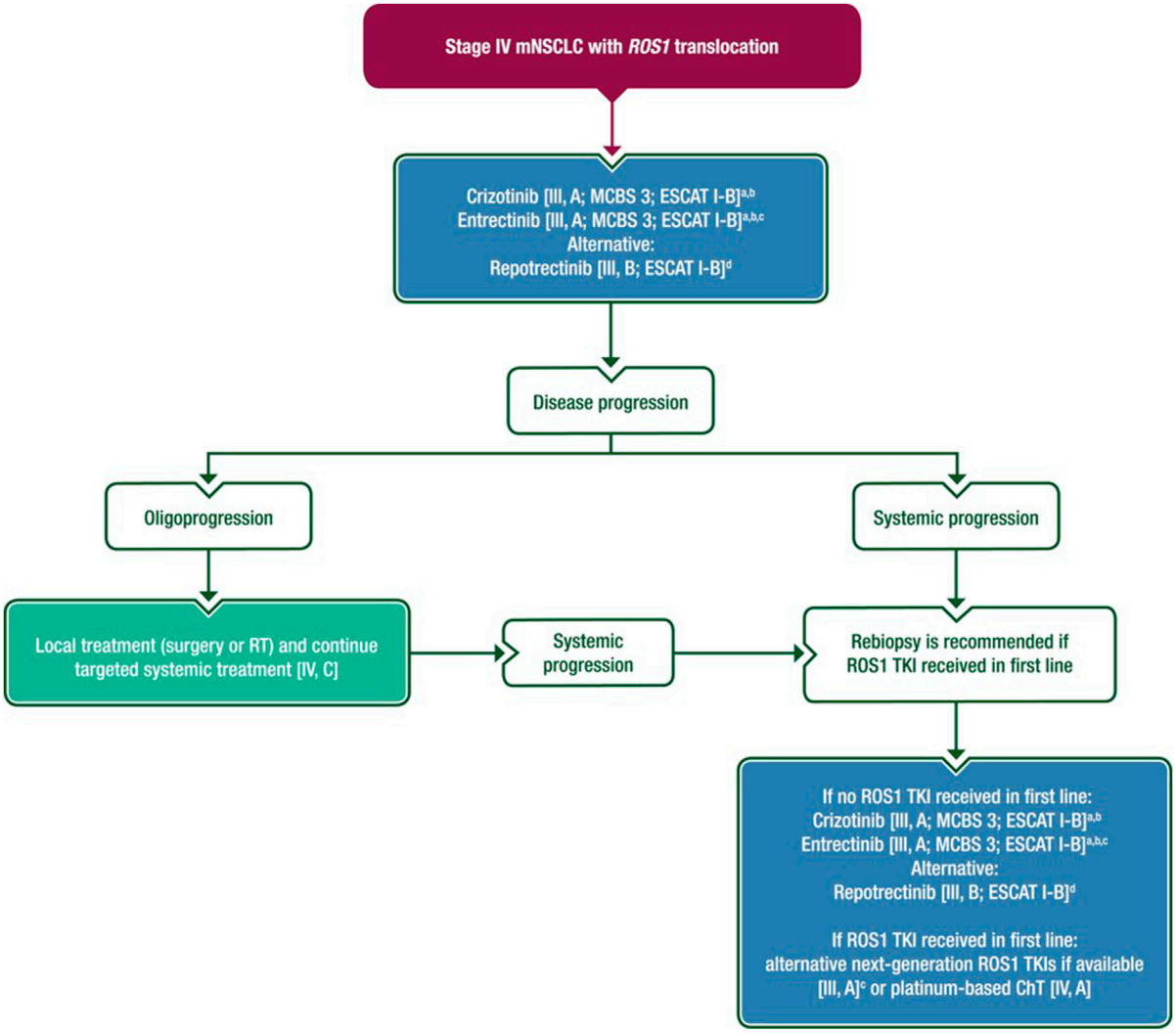

FIGURE 4
Treatment recommendation for ROS1 translocated metastatic NSCLCbased on the ESMO 2023 guideline [1].

Brigatinib, cabozantinib, thaletrectinib, and ensartinib also have ROS1 inhibitory effects based on preclinical and phase 1/2 studies [80–83].

RET-positive NSCLC treatment

The RET gene encodes a tyrosine kinase-activated membrane receptor protein, primarily involved in the differentiation of the enteric nervous system and urogenital tract [84]. Oncogenic RET alterations can be detected in several solid tumor types [85], such as thyroid cancers, NSCLCs, pancreatic, colorectal, and breast tumors, and are involved in, among others, multiple endocrine neoplasia type 2 [86], and Hirschprung's disease [87]. RET gene rearrangement is detected in 1%–2% of NSCLCs; these tumors are typically found in non-smoking, younger patients and are associated with an increased risk of BM [88]. Histologically, they are almost exclusively of the adenocarcinoma subtype; others showed 92.3% non-squamous histology [89]. Several fusion partners of RET are known, the most common being KIF5B and CCD6C [90]. IHC and RT-PCR have proven to be unreliable methods for diagnosing RET-positive NSCLCs due to their low sensitivity and variable specificity and are replaced by FISH and NGS [85, 90].

Selpercatinib is a low molecular weight drug that can penetrate the BBB and is a highly selective RET tyrosine kinase inhibitor (TKI) that has demonstrated efficacy in RET translocation-positive NSCLC in the LIBRETTO-001 phase 1/2 clinical trial [91]. The trial enrolled 105 patients previously treated with platinum-based chemotherapy and 39 therapy-naive

patients. For pretreated patients, the ORR was 64% (95% CI, 54%–73%) and the mDOR was 17.5 months. In the therapy-naïve group, the ORR was 85% (95% CI, 70%–94%). Of note, 91% of the n = 11 patients with BM observed an intracranial clinical response. The most common grade 3 or more severe adverse events were hypertension (14%), elevated alanine aminotransferase (12%) and aspartate aminotransferase (10%) levels, hyponatremia (6%) and lymphopenia (6%). Based on these results, both FDA (2020) and EMA (2021) have approved selpercatinib for the treatment of locally advanced and metastatic NSCLC [92]. The randomized phase 3 multicentre trial (LIBRETTO-431) compared the efficacy of first-line selpercatinib with or without chemotherapy (carboplatin/cisplatin + pemetrexed) with or without pembrolizumab [93]. The results of the study were presented at the ESMO Congress 2023 [94, 95]. The selpercatinib group had a significantly higher mPFS compared to the chemotherapy ± immunotherapy group (24.8 months vs. 11.2 months; HR:0.465, CI: 0.309–0.699; $p < 0.001$) [95].

Pralsetinib is the other selective RET inhibitor that will be registered by the FDA in 2020 and by the EMA in 2021, based on the results of the ARROW clinical trial. However, while the EMA approval (for both selprecatinib and pralsetinib) is only valid for patients who have not previously received RET TKI therapy, the FDA approval does not include such a restriction [96–99]. The ORR was 72% in the treatment-naïve (n = 75) and 59% in the group of patients (n = 136) who had received prior platinum-based chemotherapy. The mDOR was not reached in the therapy-naïve group and 22.3 months in the pretreated group. As with selpercatinib, pralsetinib has significant intracranial activity, with an intracranial ORR of 70% (95% CI, 35%–93%) in the group of patients with BM (n = 10, all of whom had received prior chemotherapy) in the study. The agent's tolerability and side effect profile were similar to the other TKIs [100]. In the ongoing AcceleRET phase 3 clinical trial, similar to the LIBRETTO-431 trial, first-line pralsetinib therapy is being compared with platinum-based chemotherapy ± pembrolizumab [101, 102]. Results of the trial are expected in 2024.

BRAF mutant NSCLC treatment

Mutations in BRAF (V-raf murine sarcoma viral oncogene homolog B) are mutations in the MAPK mitogen-activated protein kinase pathway, which affects downstream signaling proteins. BRAF mutations are alternative oncogenic drivers in NSCLC, which mutually exclude EGFR mutations and ALK and ROS1 rearrangements. The incidence of lung adenocarcinoma is 4.5% [103]. BRAF mutations in the serine/threonine kinase domain most commonly affect V600 [104]. Kinase inhibitors are now available for BRAF V600E mutations. These include dabrafenib, a serine/threonine kinase inhibitor, and trametinib, which has both serine/threonine and tyrosine kinase inhibitory activity [105].

The registration of the drugs was based on a prospective, multicentre, multicohort phase 2 study (BRF113928). The study enrolled 171 patients with metastatic NSCLC with BRAF-V600E mutations, of whom 78 patients received dabrafenib monotherapy (Cohort A), 57 patients received the MEK inhibitor trametinib in combination in multiple lines (Cohort B) and 36 patients received first-line combination therapy (Cohort C). The dose of dabrafenib was 2 × 150 mg/day in both monotherapy and combination therapy, while trametinib treatment was administered at 1 × 2 mg/day. With dabrafenib monotherapy, the response rate (ORR) was 33%, the mPFS was 5.5 months, and the mDOR was 9.6 months. In pretreated patients with the dabrafenib-trametinib combination, the ORR was 68%, mPFS was 10.2 months, and mDOR was 9.8 months. In previously untreated patients on dabrafenib-trametinib combination therapy, the ORR was 64%, mPFS was 10.8 months, and mDOR was 10.2 months. In patients receiving pretreated combination therapy (Cohort B), a median overall survival (OS) of 18.2 months was observed, with 4-year and 5-year survival rates of 34% and 22%, respectively, representing a significant improvement compared to both dabrafenib monotherapy and conventional chemotherapy. The combination of dabrafenib and trametinib is indicated for the treatment of patients with advanced metastatic-stage NSCLC with BRAF V600E mutations (the study on which the registry was based included only BRAF V600 mutation-positive patients, so its efficacy in wild-type BRAF mutant NSCLC has not been proven) [106].

NSCLC with distant metastases should be tested for BRAF V600 mutation status [ESMO II, A]. For NSCLC with BRAF V600E mutation in metastatic stage, first-line treatment with dabrafenib + trametinib is recommended [ESMO III, A; ESCAT: I-B]. If patients have received first-line BRAF and MEK inhibition, platinum-based chemotherapy with or without immunotherapy may be recommended as second-line treatment [ESMO IV, B] [106].

MET exon 14 skipping mutation and MET amplification in NSCLC

Oncogenic activation of the MET (mesenchymal-epithelial transition) signaling pathway can be caused by overexpression, gene amplification, gene rearrangements, and various mutations [1].

MET exon 14 skipping mutations are found in about 3%–4% of younger/smoker/gender patients with NSCLC, mostly in cases where no other driver mutation can be identified, and more often in elderly and smoker patients. In addition to adenocarcinoma, its occurrence has also been observed in sarcomatoid carcinoma. It is considered an unfavorable prognostic marker. The skipping

mutation can be detected by DNA- or RNA-based NGS (ESMO IB), while MET amplification can be detected by immunohistochemistry or *in situ* hybridization (ESMO IIB) [107–109].

Detection of MET overexpression is not associated with effective target therapy, but MET exon 14 skipping mutations or MET amplification is associated with the efficacy of MET inhibitors. MET amplification occurs in 1%–6% of NSCLC cases and may be a cause of acquired resistance to EGFR and ALK inhibitors. For MET amplification, the method of detection and the definition of high gene copy numberstill need to be standardized, while for high gene amplification the MET inhibitor capmatinib has been shown to be effective, but the FDA and EMA have not yet approved its use in this indication. In the case of MET exon 14 skipping mutations, registered targeted treatment options are available. Detection of MET exon 14 skipping mutation and MET amplification is recommended in the initial evaluation of patients diagnosed with non-squamous NSCLC (ESMO IIA).

The FDA has approved capmatinib and tepotinib for the first-line treatment of NSCLC with MET exon 14 skipping mutations, but the EMA has not approved it for first-line, only second- and multiline therapy at present. Thus, first-line platinum-based chemotherapy ± immunotherapy is recommended in these cases.

For patients with MET-amplification, platinum-based chemotherapy with/without immunotherapy is recommended as first-line treatment (ESMO IVB). Following first-line treatment, treatment with capmatinib or tepotinib monotherapy is recommended for patients with MET exon 14 skipping mutation-positive NSCLC (ESMO III A). For tumors carrying less frequent driver mutations, there is little data on the efficacy of immunotherapy, and in these cases, platinum-based chemotherapy or chemotherapy + immunotherapy is recommended if targeted therapy is not an option, while monotherapy immunotherapy is not recommended [108].

Capmatinib

Capmatinib is a potent, selective MET receptor inhibitor and has been shown to be effective in various types of MET activation *in vitro* and *in vivo* tumor models [110]. Capmatinib can cross the BBB.

The registration of the medicine was based on the results of the GEOMETRY mono-1 study [110, 111]. The phase 2, open-label, multi-arm study enrolled 364 patients with advanced (stage IIIB or IV) NSCLC who were found to have MET amplification or MET exon 14 skipping mutations. Patients who had received prior chemotherapy and subjects who had not yet received treatment were also included. Patients received capmatinib therapy in the form of 2 × 1,400 mg tablets daily.

In patients with MET exon 14 skipping mutations, the ORR was 41% in previously treated patients and 68% in previously untreated patients. The mPFS was 5.4 months in previously treated subjects and 12.4 months in patients who received first-line treatment. The effect of capmatinib treatment was typically rapid, with the vast majority of patients showing a response (82% of the previously treated patients and 68% of those who had not received treatment previously) having a tumor response at the first tumor evaluation [110]. Of the patients studied, 14 had BM, 12 of whom showed intracranial tumor control, 7 had reduced BM and 4 patients had complete remission.

Among patients, 98% reported some adverse effects, with 67% reporting grade 3–4 adverse effects. The most common symptom was peripheral edema, followed by nausea, vomiting and elevated serum creatinine. The incidence of serious treatment-related adverse events was 13%, with 11% of patients having to stop treatment. Dose reduction was required in 23% of subjects included. In one patient, pneumonitis leading directly to death may likely have been related to capmatinib treatment.

Tepotinib

Tepotinib is also a selective MET tyrosine kinase inhibitor, capable of penetrating the BBB [112]. It has demonstrated efficacy in advanced NSCLC with MET exon 14 skipping mutations in the phase 2 VISION clinical trial [113–115]. Patients with MET amplification were not included in this study. The skipping mutation was detected by histology or liquid biopsy. Patients received the investigational agent in a once-daily oral dose of 500 mg.

In the study, the ORR was 44.7% and the median PFS was 8.9 months. The median overall survival was 17.6 months. Response rates and PFS showed no difference whether the patient received first-line or multi-line treatment with tepotinib. The investigational drug also showed efficacy in elderly patients over 80 (ORR: 35.1%, PFS: 8.6 months). Intracranial tumor control was achieved in the majority of subjects with BM.

Treatment-related adverse events occurred in 86.3% of patients on tepotinib, 24.3% experienced grade 3–4 adverse events, and 12.2% experienced serious adverse events. Three cases were fatal, with death resulting from ILD-related respiratory failure or liver failure. The most common adverse events were peripheral edema, followed by nausea, diarrhea, serum creatinine elevation, and hypoalbuminemia.

HER2 mutant NSCLC treatment

HER2 is a human epidermal growth factor receptor (EGFR/ERBB2) family and is encoded by the ERBB2 gene. The

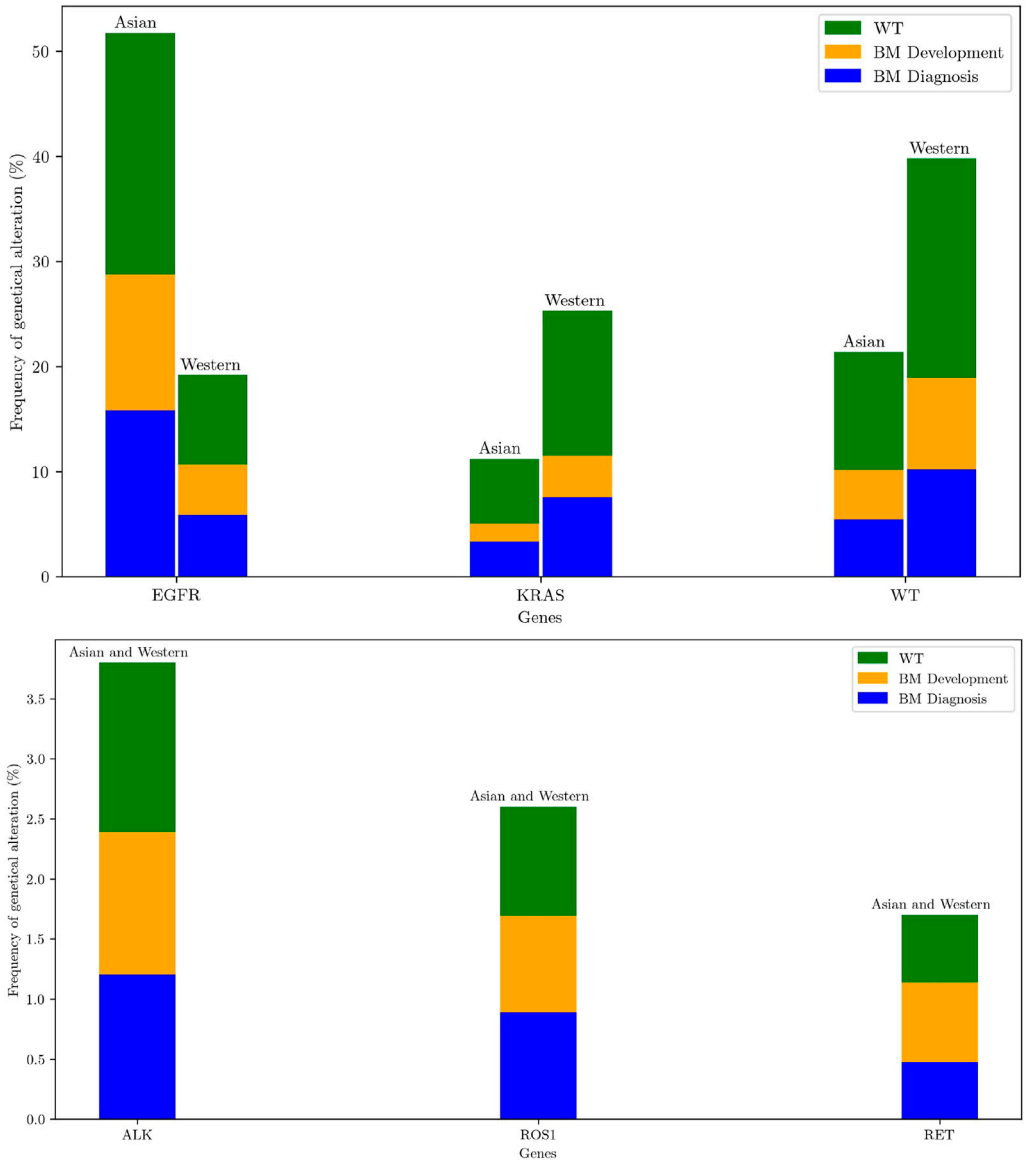

FIGURE 5
Frequency of oncogenic drivers for East-Asian and Western populations [134]. Bars are stratified according to proportions of brain metastases (BM) at diagnosis (blue) and BM development after diagnosis (orange) and pan-wild-type for all genetic alterations reported including rare ones (WT, green) [131]. For visual enhancement low frequencies of ALK, ROS1, RET genetical alterations are presented in a separate figure.

prevalence of HER2 mutations in patients with non-small cell carcinoma is between 1%–4%. HER2 lesions can develop by three mechanisms: HER2 protein overexpression, HER2 amplification and HER2 gene mutation. IHC, FISC and NGS can be used to detect these lesions. Double platinum-based chemotherapy is the first-line treatment of choice and can be complemented with immunotherapy (ESMO IV.B) [116].

In the DESTINY LUNG01 clinical trial, the HER2 antibody-drug conjugate, trastuzumab-deruxtecan treatment efficacy was investigated. In the study, 91 patients with metastatic HER2 mutant NSCLC received second-line trastuzumab-deruxtecan treatment following standard therapy. In the study, PF was 8.2 months (95% CI, 6.0–11.9), while median OS was 17.8 months (95% CI, 13.8–22.1). Treatment-related adverse events included neutropenia and drug-induced ILD, the latter resulting in 2 deaths identified in the study [117].

The DESTINY LUNG02 phase 2 randomized trial also investigated the efficacy and safety of trastuzumab-deruxtecan following platinum-based treatment in the second line, also at two different doses. At both doses (5.4 mg/kg or 6.4 mg/kg every

TABLE 1 Intracranial objective response rate in patients with BM according to the presence of drive oncogenes and targeted therapy administration [135].

Study	Year/Trial ID	Driver oncogene	Targeted therapy	Intracranial efficacy (%)
FLAURA	2014 NCT02296125	EGFR Ex19del, Ex21 L858R	osimertinib	91
ALEX	2014 NCT02075840	ALK	alectinib	81
ALTA-1L	2016 NCT02737501	ALK	brigatinib	78
CROWN	2017 NCT03052608	ALK	lorlatinib	82
STARTRK2	2015 NCT02568267	ROS1	entrectinib	79
Geometry Mono-1	2015 NCT02414139	MET exon 14 skipping mutation, MET amplification	capmatinib	54
VISION	2016 NCT02864992	MET exon 14 skipping mutation, MET amplification	tepotinib	55
LIBRETTO-001	2017 NCT03157128	RET	selpercatinib	82
ARROW	2017 NCT03037385	RET	pralsetinib	78
CodeBreaK 100	2018 NCT03600883	*KRAS* G12C	sotorasib	25

3 weeks), a significant and sustained antitumor effect with an acceptable safety profile was observed, but the lower dose had a lower rate of drug-induced ILD [118]. The study's results led to EMA approval of second-line trastuzumab-deruxtecan treatment for NSCLC with metastatic or unresectable HER2 mutations. First line trial phase 3 is recruiting [119].

Treatment of NTRK gene fusion-positive NSCLC

Neurotrophic tyrosine receptor kinase (NTRK) gene fusions initiate downstream signaling pathways, such as the AKT and MEK pathways, and are present at a very low frequency (<1) in solid tumors [1].

Entrectinib is an NTRK and ROS1 inhibitor that can penetrate the central nervous system. In a clinical study of the efficacy of entrectinib in a total of 22 NSCLC patients, the mPFS was 14.9 months (95% Cl, 6.5–30.4), median OS results are not yet available [120].

Larotrectinib is a sensitive tropomyosin receptor kinase inhibitor. In two multicentre clinical trials, a total of 20 NRTK gene fusion-positive patients were tested for the efficacy of larotrectinib. Median PFS outcome was 35.4 months (95% CI, 5.3–35.4), and the median OS was 40.7 months [121].

Discussion

Patients with guideline-recommended molecular alteration-based therapies have better outcomes with first-line targeted therapy for advanced-stage NSCLC [1]. In a retrospective study, others showed a significant increase in OS in patients with non-squamous NSCLC with molecular testing available compared to non-tested patients [122]. Importantly, comprehensive NGS vs. incomplete or no testing before initiating first-line therapy impacts the OS (22.1 vs. 11.6 months, $p = 0.017$) respectively [123]. Nevertheless, a multidisciplinary approach is essential in finding the proper diagnostic procedures and treatments to personalize NSCLC therapy. There is a broad repertoire of targeted therapies in the standard of care settings. However, there is a need for improvements; therefore, participation in clinical trials is especially encouraged [2]. Accurate imaging-based clinical staging and tissue availability influence subsequent molecular assay-based personalized therapeutic decisions in multidisciplinary teams (MDT) before first line therapy administration. The gold standard for molecular testing in NSCLC is tissue-based testing. Liquid biopsy-based ctDNA detection can guide therapy; however, it should not be used instead of tissue samples. However, the plasma-first approach is recommended if tissue is unavailable [124]. Molecular testing for stage IV NSCLC with reflex testing is associated with shorter turnaround times. There is an emerging requirement for testing in early-stage disease. Formalin-fixed paraffin-embedded (FFPE) material suits for most molecular analyses and non-acid decalcification approaches on bone biopsies. Molecular assays, such as cell blocks, direct smears, or touch preparations, are recommended in order not to miss a targetable genetic alteration. Nevertheless, adequate biopsy sampling should ensure that the sample is suitable for molecular analysis, and in small specimens, minimal IHC should be used to preserve the tissue for molecular studies [2]. Accordingly, the acceptable terms NSCLC favor adenocarcinoma or favor squamous cell carcinoma is recommended with any extent of adenocarcinoma component in a biopsy specimen that is otherwise squamous should trigger molecular testing [2]. At a minimum, EGFR and ALK testing is

recommended before initiating immunotherapy because rapid and sensitive tests are available [2, 124]. MDT is best assisted by complete-scale molecular testing for a first-line treatment decision that includes NGS and PDL1 expression [123]. DNA-based NGS oncology panels are recommended to detect EGFR, KRAS, MET, RET, HER2, and BRAF. ALK, ROS1, and NTRK1/2/3 alterations can be identified with FISH. IHC, for screening purposes with low specificity, can also be applied. Therefore, validation with NGS DNA panels with reasonable specificity may detect ALK, RET, and NTRK2 but may underdetect ROS1, NTRK1, and NTRK3 fusions. In the case of RET and METex14, skipping events, RNA-based NGS is preferable to DNA-based NGS or fusion detection [2].

Following the expansion in molecular alteration-based targeted therapy in advanced stages, recently, attention has turned to early-stage cases and resection specimens. Recent advancements in the NSCLC adjuvant treatment setting, the molecular diagnostics for EGFR and ALK in the early stage, indeed necessary to exclude targetable alterations to pave the way to proceed with immunotherapy based on PD-L1 expressors. Accordingly, molecular testing of early-stage resectable NSCLC before neoadjuvant nivolumab plus chemotherapy was performed in CheckMate 816 [125]. Additionally, molecular testing was performed to exclude driver oncogenes in the perioperative early-stage setting in the AEGEAN study on durvalumab plus neoadjuvant chemotherapy [126].

Osimertinib is the first approved targeted therapy based on the ADAURA trial that enrolled patients with classical EGFR mutant (ex19del/L858R) after complete resection, stage I/B -III/A [127, 128]. Adjuvant ALK therapy is currently in a clinical trial [129]. According to an interim analysis of the ALINA trial, adjuvant targeted treatment with alectinib was associated with significant disease-free survival (DFS) benefits compared with platinum-based chemotherapy, with favorable results for alectinib seen in both the stage II–IIIA population (n = 231; hazard ratio [HR] 0.24; 95% confidence interval [CI] 0.13–0.45; $p < 0.0001$) and the intention-to-treat (ITT) (stage IB–IIIA) population (n = 257; HR 0.24; 95% CI 0.13–0.43; $p < 0.0001$) [129, 130].

A key factor with targeted therapies includes the control rate of BM; however, there is a significant difference between targeted therapies regarding brain efficacy. New-generation targeted therapies with blood barrier penetration increased the prognosis of brain metastatic NSCLC patients [58]. 20%–30% with advanced NSCLC were found to have BM at diagnosis [131, 132]. Figure 5 shows the distribution of BM according to genetical alterations. A recent meta-analysis suggests that patients with ALK-positive and EGFR-positive NSCLC had higher rates of BM development than other genomic alterations and wild-type tumors [131]. Others showed an association with metastasis development in tumors with ROS1, MET, and RET alterations [131]. However, a meta-analysis does not support a higher rate of BM in these cases compared with wild-type cohorts [131]. BM are frequent in advanced EGFR-mutated or ALK-rearranged NSCLCs, with an estimated >45% of patients with CNS involvement by 3 years of survival with targeted therapies [133].

The intracranial tumor response to TKIs is shown in Table 1 [135]. Patients with EGFR, ALK, and ROS1 positive tumors with oligo- or asymptomatic BM should be treated by upfront systemic targeted therapy [ESMO: III, B] [136]. Of note close MRI surveillance is strongly recommended [1]. The upfront use of radiotherapy might be considered upon BM progression [137]. However, there is no available data on trials comparing the two strategies to assess the impact of delayed radiation in terms of survival or neurologic deficit [138]. ALK inhibitors with CNS activity include Brigatinib, Lorlatinib, and Alectinib [43, 45, 46]. ROS1: Entrectinib is recommended in patients with BM [ESCAT: I-B]. Compared with earlier-generation drugs, CNS activity of the EGFR TKI, osimertinib showed better intracranial response rates, including stable CNS metastatic cases, in 60% [23, 139].

Conclusion

Recent expansion in the targeted treatment options into the adjuvant setting of non-small cell lung cancer using accurate pathology diagnostics can minimize the number of excluded patients from molecular diagnostics. Accordingly, careful planning of subsequent hierarchical steps of diagnostic and therapeutic aspects can lead to improved outcomes without excluding patients from best-match targeted therapy. The selection of biopsy procedures and sites, tissue processing, and interpretation, followed by accurate molecular testing-based biomarker identification, is critical. Accordingly, the complexity of theranostics and possible resistance mechanisms can lead to better quality of life and outcomes in special populations, in patients with BM. Future trials should address drug properties such as CNS activity and other special populations, including oligometastatic disease and the emergence of resistance genes to maximize patient survival. Despite the novel standard of care therapies, clinical trials are guideline-recommended options to improve patient outcomes. Accordingly, the therapeutic options are expanding based on the innovative and positive trial results.

Author contributions

GG, ÉM, RK, RH, RB, RP, TL, EG, KY, PK, and ZL: writing, original structure and validation. All authors contributed to the article and approved the submitted version.

Conflict of interest

The authors declare that the research was conducted in the absence of any commercial or financial relationships that could be construed as a potential conflict of interest.

References

1. Hendriks LE, Kerr KM, Menis J, Mok TS, Nestle U, Passaro A, et al. Oncogene-addicted metastatic non-small-cell lung cancer: ESMO Clinical Practice Guideline for diagnosis, treatment and follow-up. *Ann Oncol* (2023) 34:339–57. doi:10.1016/j.annonc.2022.12.009

2. NCCN. *NCCN guidelines non-small cell lung cancer version 1* (2024). Available from: https://www.nccn.org/professionals/physician_gls/pdf/nscl.pdf (Accessed January 30, 2024).

3. Ahn M, Arcila M, Bazhenova L, Beasley M, Berezowska S, Bubendorf L, et al. *IASLC atlas of molecular testing for targeted therapy in lung cancer*. Denver: International Association for the Study of Lung Cancer (2023).

4. Fois SS, Paliogiannis P, Zinellu A, Fois AG, Cossu A, Palmieri G Molecular epidemiology of the main druggable genetic alterations in non-small cell lung cancer. *Int J Mol Sci* (2021) 22:612. doi:10.3390/ijms22020612

5. Westcott PMK, Halliwill KD, To MD, Rashid M, Rust AG, Keane TM, et al. The mutational landscapes of genetic and chemical models of Kras-driven lung cancer. *Nature* (2015) 517:489–92. doi:10.1038/nature13898

6. Cserepes M, Ostoros G, Lohinai Z, Raso E, Barbai T, Timar J, et al. Subtype-specific KRAS mutations in advanced lung adenocarcinoma: a retrospective study of patients treated with platinum-based chemotherapy. *Eur J Cancer Oxf Engl* (2014) 50:1819–28. doi:10.1016/j.ejca.2014.04.001

7. Wu YL, John T, Grohe C, Majem M, Goldman JW, Kim SW, et al. Postoperative chemotherapy use and outcomes from ADAURA: osimertinib as adjuvant therapy for resected EGFR-mutated NSCLC. *J Thorac Oncol* (2022) 17:423–33. doi:10.1016/j.jtho.2021.10.014

8. Herbst RS, Wu Y-L, John T, Grohe C, Majem M, Wang J, et al. Adjuvant osimertinib for resected EGFR-mutated stage IB-IIIA non-small-cell lung cancer: updated results from the phase III randomized ADAURA trial. *J Clin Oncol* (2023) 41:1830–40. doi:10.1200/JCO.22.02186

9. Kohno T, Matsui T, Enatsu S Differences between EGFR exon 19 deletion and exon 21 L858R point mutation, frequently detected EGFR mutations in patients with non-small cell lung cancer, from a molecular biology viewpoint. *Gan To Kagaku Ryoho* (2021) 48:1463–7.

10. Karachaliou N, Fernandez-Bruno M, Bracht JWP, Rosell R EGFR first- and second-generation TKIs—there is still place for them in EGFR-mutant NSCLC patients. *Transl Cancer Res* (2019) 8:S23–47. doi:10.21037/tcr.2018.10.06

11. Ko HW, Shie SS, Wang CW, Chiu CT, Wang CL, Yang TY, et al. Association of smoking status with non-small cell lung cancer patients harboring uncommon epidermal growth factor receptor mutation. *Front Immunol* (2022) 13:1011092. doi:10.3389/fimmu.2022.1011092

12. Malapelle U, Pilotto S, Passiglia F, Pepe F, Pisapia P, Righi L, et al. Dealing with NSCLC EGFR mutation testing and treatment: a comprehensive review with an Italian real-world perspective. *Crit Rev Oncol Hematol* (2021) 160:103300. doi:10.1016/j.critrevonc.2021.103300

13. Fukuoka M, Wu Y-L, Thongprasert S, Sunpaweravong P, Leong S-S, Sriuranpong V, et al. Biomarker analyses and final overall survival results from a phase III, randomized, open-label, first-line study of gefitinib versus carboplatin/paclitaxel in clinically selected patients with advanced non-small-cell lung cancer in Asia (IPASS). *J Clin Oncol* (2011) 29:2866–74. doi:10.1200/JCO.2010.33.4235

14. Zhou C, Wu YL, Chen G, Feng J, Liu XQ, Wang C, et al. Erlotinib versus chemotherapy as first-line treatment for patients with advanced EGFR mutation-positive non-small-cell lung cancer (OPTIMAL, CTONG-0802): a multicentre, open-label, randomised, phase 3 study. *Lancet Oncol* (2011) 12:735–42. doi:10.1016/S1470-2045(11)70184-X

15. Rosell R, Carcereny E, Gervais R, Vergnenegre A, Massuti B, Felip E, et al. Erlotinib versus standard chemotherapy as first-line treatment for European patients with advanced EGFR mutation-positive non-small-cell lung cancer (EURTAC): a multicentre, open-label, randomised phase 3 trial. *Lancet Oncol* (2012) 13:239–46. doi:10.1016/S1470-2045(11)70393-X

16. Zhou C, Wu Y-L, Chen G, Feng J, Liu X, Wang C, et al. Efficacy results from the randomised phase III OPTIMAL (CTONG 0802) study comparing first-line erlotinib versus carboplatin (CBDCA) plus gemcitabine (GEM) in Chinese advanced non small cell lung cancer (NSCLC) patients (PTS) with EGFR activating mutations. *Ann Oncol* (2010) 21(supp.8):LBA13. doi:10.1093/annonc/mdq601

17. Chen KL, Lin CC, Cho YT, Yang CW, Sheen YS, Tsai HE, et al. Comparison of skin toxic effects associated with gefitinib, erlotinib, or afatinib treatment for non-small cell lung cancer. *JAMA Dermatol* (2016) 152:340–2. doi:10.1001/jamadermatol.2015.4448

18. Cárdenas-Fernández D, Soberanis Pina P, Turcott JG, Chávez-Tapia N, Conde-Flores E, Cardona AF, et al. Management of diarrhea induced by EGFR-TKIs in advanced lung adenocarcinoma. *Ther Adv Med Oncol* (2023) 15:17588359231192396. doi:10.1177/17588359231192396

19. Nakagawa K, Garon EB, Seto T, Nishio M, Ponce Aix S, Paz-Ares L, et al. Ramucirumab plus erlotinib in patients with untreated, EGFR-mutated, advanced non-small-cell lung cancer (RELAY): a randomised, double-blind, placebo-controlled, phase 3 trial. *Lancet Oncol* (2019) 20:1655–69. doi:10.1016/S1470-2045(19)30634-5

20. Sequist LV, Yang JC-H, Yamamoto N, O'Byrne K, Hirsh V, Mok T, et al. Phase III study of afatinib or cisplatin plus pemetrexed in patients with metastatic lung adenocarcinoma with EGFR mutations. *J Clin Oncol* (2013) 31:3327–34. doi:10.1200/JCO.2012.44.2806

21. Wu Y-L, Zhou C, Hu C-P, Feng J, Lu S, Huang Y, et al. Afatinib versus cisplatin plus gemcitabine for first-line treatment of Asian patients with advanced non-small-cell lung cancer harbouring EGFR mutations (LUX-Lung 6): an open-label, randomised phase 3 trial. *Lancet Oncol* (2014) 15:213–22. doi:10.1016/S1470-2045(13)70604-1

22. Yang JC-H, Wu Y-L, Schuler M, Sebastian M, Popat S, Yamamoto N, et al. Afatinib versus cisplatin-based chemotherapy for EGFR mutation-positive lung adenocarcinoma (LUX-Lung 3 and LUX-Lung 6): analysis of overall survival data from two randomised, phase 3 trials. *Lancet Oncol* (2015) 16:141–51. doi:10.1016/S1470-2045(14)71173-8

23. Park K, Tan E-H, O'Byrne K, Zhang L, Boyer M, Mok T, et al. Afatinib versus gefitinib as first-line treatment of patients with EGFR mutation-positive non-small-cell lung cancer (LUX-Lung 7): a phase 2B, open-label, randomised controlled trial. *Lancet Oncol* (2016) 17:577–89. doi:10.1016/S1470-2045(16)30033-X

24. Wu Y-L, Cheng Y, Zhou X, Lee KH, Nakagawa K, Niho S, et al. Dacomitinib versus gefitinib as first-line treatment for patients with EGFR-mutation-positive non-small-cell lung cancer (ARCHER 1050): a randomised, open-label, phase 3 trial. *Lancet Oncol* (2017) 18:1454–66. doi:10.1016/S1470-2045(17)30608-3

25. Mok TS, Cheng Y, Zhou X, Lee KH, Nakagawa K, Niho S, et al. Improvement in overall survival in a randomized study that compared dacomitinib with gefitinib in patients with advanced non-small-cell lung cancer and EGFR-activating mutations. *J Clin Oncol* (2018) 36:2244–50. doi:10.1200/JCO.2018.78.7994

26. He J, Huang Z, Han L, Gong Y, Xie C Mechanisms and management of 3rd-generation EGFR-TKI resistance in advanced non-small cell lung cancer (Review). *Int J Oncol* (2021) 59:90. doi:10.3892/ijo.2021.5270

27. Papadimitrakopoulou VA, Mok TS, Han J-Y, Ahn M-J, Delmonte A, Ramalingam SS, et al. Osimertinib versus platinum-pemetrexed for patients with EGFR T790M advanced NSCLC and progression on a prior EGFR-tyrosine kinase inhibitor: AURA3 overall survival analysis. *Ann Oncol* (2020) 31:1536–44. doi:10.1016/j.annonc.2020.08.2100

28. Ramalingam SS, Vansteenkiste J, Planchard D, Cho BC, Gray JE, Ohe Y, et al. Overall survival with osimertinib in untreated, EGFR-mutated advanced NSCLC. *N Engl J Med* (2020) 382:41–50. doi:10.1056/NEJMoa1913662

29. Belani N, Liang K, Fradley M, Judd J, Borghaei H How to treat EGFR-mutated non–small cell lung cancer. *JACC CardioOncology* (2023) 5:542–5. doi:10.1016/j.jaccao.2023.04.005

30. Vaid AK, Gupta A, Momi G Overall survival in stage IV EGFR mutation-positive NSCLC: comparing first-second- and third-generation EGFR-TKIs (Review). *Int J Oncol* (2021) 58:171–84. doi:10.3892/ijo.2021.5168

31. Tatineni V, O'Shea PJ, Ozair A, Khosla AA, Saxena S, Rauf Y, et al. First- versus third-generation EGFR tyrosine kinase inhibitors in EGFR-mutated non-small cell lung cancer patients with brain metastases. *Cancers* (2023) 15:2382. doi:10.3390/cancers15082382

32. Nogami N, Barlesi F, Socinski MA, Reck M, Thomas CA, Cappuzzo F, et al. IMpower150 final exploratory analyses for atezolizumab plus bevacizumab and chemotherapy in key NSCLC patient subgroups with EGFR mutations or metastases in the liver or brain. *J Thorac Oncol* (2022) 17:309–23. doi:10.1016/j.jtho.2021.09.014

33. Bai Q, Wang J, Zhou X EGFR exon20 insertion mutations in non-small cell lung cancer: clinical implications and recent advances in targeted therapies. *Cancer Treat Rev* (2023) 120:102605. doi:10.1016/j.ctrv.2023.102605

34. Passaro A, Mok T, Peters S, Popat S, Ahn M-J, de Marinis F Recent advances on the role of EGFR tyrosine kinase inhibitors in the management of NSCLC with uncommon, non exon 20 insertions, EGFR mutations. *J Thorac Oncol* (2021) 16:764–73. doi:10.1016/j.jtho.2020.12.002

35. Zugazagoitia J, Ramos I, Trigo JM, Palka M, Gómez-Rueda A, Jantus-Lewintre E, et al. Clinical utility of plasma-based digital next-generation sequencing in patients with advance-stage lung adenocarcinomas with insufficient tumor samples for tissue genotyping. *Ann Oncol* (2019) 30:290–6. doi:10.1093/annonc/mdy512

36. Weickhardt AJ, Aisner DL, Franklin WA, Varella-Garcia M, Doebele RC, Camidge DR Diagnostic assays for identification of anaplastic lymphoma kinase-positive non-small cell lung cancer. *Cancer* (2013) 119:1467–77. doi:10.1002/cncr.27913

37. Li W, Zhang J, Guo L, Chuai S, Shan L, Ying J Combinational analysis of FISH and immunohistochemistry reveals rare genomic events in ALK fusion patterns in NSCLC that responds to crizotinib treatment. *J Thorac Oncol* (2017) 12:94–101. doi:10.1016/j.jtho.2016.08.145

38. Shaw AT, Yeap BY, Mino-Kenudson M, Digumarthy SR, Costa DB, Heist RS, et al. Clinical features and outcome of patients with non-small-cell lung cancer who harbor EML4-ALK. *J Clin Oncol* (2009) 27:4247–53. doi:10.1200/JCO.2009.22.6993

39. National Institutes of Health. *Cancer of the lung and bronchus - cancer stat facts* (2024). Available from: https://seer.cancer.gov/statfacts/html/lungb.html (Accessed January 24, 2024).

40. Solomon BJ, Mok T, Kim D-W, Wu Y-L, Nakagawa K, Mekhail T, et al. First-line crizotinib versus chemotherapy in ALK-positive lung cancer. *N Engl J Med* (2014) 371:2167–77. doi:10.1056/NEJMoa1408440

41. Soria J-C, Tan DSW, Chiari R, Wu Y-L, Paz-Ares L, Wolf J, et al. First-line ceritinib versus platinum-based chemotherapy in advanced ALK-rearranged non-small-cell lung cancer (ASCEND-4): a randomised, open-label, phase 3 study. *Lancet Lond Engl* (2017) 389:917–29. doi:10.1016/S0140-6736(17)30123-X

42. Camidge DR, Dziadziuszko R, Peters S, Mok T, Noe J, Nowicka M, et al. Updated efficacy and safety data and impact of the EML4-ALK fusion variant on the efficacy of alectinib in untreated ALK-positive advanced non-small cell lung cancer in the global phase III ALEX study. *J Thorac Oncol* (2019) 14:1233–43. doi:10.1016/j.jtho.2019.03.007

43. Camidge DR, Kim HR, Ahn M-J, Yang JCH, Han J-Y, Hochmair MJ, et al. Brigatinib versus crizotinib in ALK inhibitor-naive advanced ALK-positive NSCLC: final results of phase 3 ALTA-1L trial. *J Thorac Oncol* (2021) 16:2091–108. doi:10.1016/j.jtho.2021.07.035

44. Horn L, Wang Z, Wu G, Poddubskaya E, Mok T, Reck M, et al. Ensartinib vs crizotinib for patients with anaplastic lymphoma kinase-positive non-small cell lung cancer: a randomized clinical trial. *JAMA Oncol* (2021) 7:1617–25. doi:10.1001/jamaoncol.2021.3523

45. Shaw AT, Bauer TM, de Marinis F, Felip E, Goto Y, Liu G, et al. First-line lorlatinib or crizotinib in advanced ALK-positive lung cancer. *N Engl J Med* (2020) 383:2018–29. doi:10.1056/NEJMoa2027187

46. Mok T, Camidge DR, Gadgeel SM, Rosell R, Dziadziuszko R, Kim D-W, et al. Updated overall survival and final progression-free survival data for patients with treatment-naive advanced ALK-positive non-small-cell lung cancer in the ALEX study. *Ann Oncol* (2020) 31:1056–64. doi:10.1016/j.annonc.2020.04.478

47. Solomon BJ, Bauer TM, Ignatius Ou S-H, Liu G, Hayashi H, Bearz A, et al. *Post hoc* analysis of lorlatinib intracranial efficacy and safety in patients with ALK-positive advanced non-small-cell lung cancer from the phase III CROWN study. *J Clin Oncol* (2022) 40:3593–602. doi:10.1200/JCO.21.02278

48. EMA. *Summary of the risk management plan for Lorviqua (lorlatinib)* (2024). Available from: https://www.ema.europa.eu/en/documents/rmp-summary/lorviqua-epar-risk-management-plan-summary_en.pdf (Accessed January 31, 2024).

49. Novello S, Mazières J, Oh I-J, de Castro J, Migliorino MR, Helland Å, et al. Alectinib versus chemotherapy in crizotinib-pretreated anaplastic lymphoma kinase (ALK)-positive non-small-cell lung cancer: results from the phase III ALUR study. *Ann Oncol* (2018) 29:1409–16. doi:10.1093/annonc/mdy121

50. Huber RM, Hansen KH, Paz-Ares Rodríguez L, West HL, Reckamp KL, Leighl NB, et al. Brigatinib in crizotinib-refractory ALK+ NSCLC: 2-year follow-up on systemic and intracranial outcomes in the phase 2 ALTA trial. *J Thorac Oncol* (2020) 15:404–15. doi:10.1016/j.jtho.2019.11.004

51. Shaw AT, Kim TM, Crinò L, Gridelli C, Kiura K, Liu G, et al. Ceritinib versus chemotherapy in patients with ALK-rearranged non-small-cell lung cancer previously given chemotherapy and crizotinib (ASCEND-5): a randomised, controlled, open-label, phase 3 trial. *Lancet Oncol* (2017) 18:874–86. doi:10.1016/S1470-2045(17)30339-X

52. Solomon BJ, Besse B, Bauer TM, Felip E, Soo RA, Camidge DR, et al. Lorlatinib in patients with ALK-positive non-small-cell lung cancer: results from a global phase 2 study. *Lancet Oncol* (2018) 19:1654–67. doi:10.1016/S1470-2045(18)30649-1

53. Shaw AT, Solomon BJ, Besse B, Bauer TM, Lin CC, Soo RA, et al. ALK resistance mutations and efficacy of lorlatinib in advanced anaplastic lymphoma kinase-positive non-small-cell lung cancer. *J Clin Oncol* (2019) 37:1370–9. doi:10.1200/JCO.18.02236

54. Lin JJ, Zhu VW, Schoenfeld AJ, Yeap BY, Saxena A, Ferris LA, et al. Brigatinib in patients with alectinib-refractory ALK-positive NSCLC. *J Thorac Oncol* (2018) 13:1530–8. doi:10.1016/j.jtho.2018.06.005

55. Yoshida H, Kim YH, Ozasa H, Sakamori Y, Tsuji T, Nomizo T, et al. Efficacy of ceritinib after alectinib for ALK-positive non-small cell lung cancer. *Vivo* (2018) 32:1587–90. doi:10.21873/invivo.11418

56. Lin JJ, Schoenfeld AJ, Zhu VW, Yeap BY, Chin E, Rooney M, et al. Efficacy of platinum/pemetrexed combination chemotherapy in ALK-positive NSCLC refractory to second-generation ALK inhibitors. *J Thorac Oncol* (2020) 15:258–65. doi:10.1016/j.jtho.2019.10.014

57. Socinski MA, Jotte RM, Cappuzzo F, Orlandi FJ, Stroyakovskiy D, Nogami N, et al. Overall survival (OS) analysis of IMpower150, a randomized Ph 3 study of atezolizumab (atezo) + chemotherapy (chemo) ± bevacizumab (bev) vs chemo + bev in 1L nonsquamous (NSQ) NSCLC. *J Clin Oncol* (2018) 36:9002. doi:10.1200/JCO.2018.36.15_suppl.9002

58. Singh K, Saxena S, Khosla AA, McDermott MW, Kotecha RR, Ahluwalia MS Update on the management of brain metastasis. *Neurotherapeutics* (2022) 19:1772–81. doi:10.1007/s13311-022-01312-w

59. Moldvay J, Tímár J KRASG12C mutant lung adenocarcinoma: unique biology, novel therapies and new challenges. *Pathol Oncol Res* (2024) 29:1611580. doi:10.3389/pore.2023.1611580

60. Shepherd FA, Domerg C, Hainaut P, Jänne PA, Pignon J-P, Graziano S, et al. Pooled analysis of the prognostic and predictive effects of KRAS mutation status and KRAS mutation subtype in early-stage resected non-small-cell lung cancer in four trials of adjuvant chemotherapy. *J Clin Oncol* (2013) 31:2173–81. doi:10.1200/JCO.2012.48.1390

61. Nakajima EC, Drezner N, Li X, Mishra-Kalyani PS, Liu Y, Zhao H, et al. FDA approval summary: sotorasib for KRAS G12C-Mutated metastatic NSCLC. *Clin Cancer Res* (2022) 28(8):1482–1486. doi:10.1158/1078-0432.CCR-21-3074

62. de Langen AJ, Johnson ML, Mazieres J, Dingemans A-MC, Mountzios G, Pless M, et al. Sotorasib versus docetaxel for previously treated non-small-cell lung cancer with KRASG12C mutation: a randomised, open-label, phase 3 trial. *Lancet Lond Engl* (2023) 401:733–46. doi:10.1016/S0140-6736(23)00221-0

63. Dy GK, Govindan R, Velcheti V, Falchook GS, Italiano A, Wolf J, et al. Long-term outcomes and molecular correlates of sotorasib efficacy in patients with pretreated KRAS G12C-mutated non-small-cell lung cancer: 2-year analysis of CodeBreaK 100. *J Clin Oncol* (2023) 41:3311–7. doi:10.1200/JCO.22.02524

64. ESMO. *EMA recommends granting a conditional marketing authorisation for adagrasib following a Re-examination procedure* (2023). Available from: https://www.esmo.org/oncology-news/ema-recommends-granting-a-conditional-marketing-authorisation-for-adagrasib-following-a-re-examination-procedure (Accessed January 24, 2024).

65. Jänne PA, Riely GJ, Gadgeel SM, Heist RS, Ou S-HI, Pacheco JM, et al. Adagrasib in non-small-cell lung cancer harboring a $KRAS^{G12C}$ mutation. *N Engl J Med* (2022) 387:120–31. doi:10.1056/NEJMoa2204619

66. Birchmeier C, Sharma S, Wigler M Expression and rearrangement of the ROS1 gene in human glioblastoma cells. *Proc Natl Acad Sci U S A* (1987) 84:9270–4. doi:10.1073/pnas.84.24.9270

67. Drilon A, Jenkins C, Iyer S, Schoenfeld A, Keddy C, Davare MA ROS1-dependent cancers - biology, diagnostics and therapeutics. *Nat Rev Clin Oncol* (2021) 18:35–55. doi:10.1038/s41571-020-0408-9

68. Lin JJ, Ritterhouse LL, Ali SM, Bailey M, Schrock AB, Gainor JF, et al. ROS1 fusions rarely overlap with other oncogenic drivers in non-small cell lung cancer. *J Thorac Oncol* (2017) 12:872–7. doi:10.1016/j.jtho.2017.01.004

69. Gendarme S, Bylicki O, Chouaid C, Guisier F ROS-1 fusions in non-small-cell lung cancer: evidence to date. *Curr Oncol Tor Ont* (2022) 29:641–58. doi:10.3390/curroncol29020057

70. Lindeman NI, Cagle PT, Aisner DL, Arcila ME, Beasley MB, Bernicker EH, et al. Updated molecular testing guideline for the selection of lung cancer patients for treatment with targeted tyrosine kinase inhibitors: guideline from the college of American pathologists, the international association for the study of lung cancer, and the association for molecular pathology. *Arch Pathol Lab Med* (2018) 142:321–46. doi:10.5858/arpa.2017-0388-CP

71. Shaw AT, Riely GJ, Bang YJ, Kim DW, Camidge DR, Solomon BJ, et al. Crizotinib in ROS1-rearranged advanced non-small-cell lung cancer (NSCLC): updated results, including overall survival, from PROFILE 1001. *Ann Oncol* (2019) 30:1121–6. doi:10.1093/annonc/mdz131

72. Fischer H, Ullah M, de la Cruz CC, Hunsaker T, Senn C, Wirz T, et al. Entrectinib, a TRK/ROS1 inhibitor with anti-CNS tumor activity: differentiation from other inhibitors in its class due to weak interaction with P-glycoprotein. *Neuro-Oncol* (2020) 22:819–29. doi:10.1093/neuonc/noaa052

73. Drilon A, Siena S, Dziadziuszko R, Barlesi F, Krebs MG, Shaw AT, et al. Entrectinib in ROS1 fusion-positive non-small-cell lung cancer: integrated analysis of three phase 1-2 trials. *Lancet Oncol* (2020) 21:261–70. doi:10.1016/S1470-2045(19)30690-4

74. Dziadziuszko R, Krebs MG, De Braud F, Siena S, Drilon A, Doebele RC, et al. Updated integrated analysis of the efficacy and safety of entrectinib in locally advanced or metastatic ROS1 fusion-positive non-small-cell lung cancer. *J Clin Oncol* (2021) 39:1253–63. doi:10.1200/JCO.20.03025

75. Lim SM, Kim HR, Lee J-S, Lee KH, Lee Y-G, Min YJ, et al. Open-label, multicenter, phase II study of ceritinib in patients with non-small-cell lung cancer harboring ROS1 rearrangement. *J Clin Oncol* (2017) 35:2613–8. doi:10.1200/JCO.2016.71.3701

76. Shaw AT, Solomon BJ, Chiari R, Riely GJ, Besse B, Soo RA, et al. Lorlatinib in advanced ROS1-positive non-small-cell lung cancer: a multicentre, open-label, single-arm, phase 1-2 trial. *Lancet Oncol* (2019) 20:1691–701. doi:10.1016/S1470-2045(19)30655-2

77. Lin JJ, Drilon AE, Cho BC, Felip E, De Langen A, Yang N, et al. Intracranial and systemic efficacy of repotrectinib in advanced ROS1 fusion-positive (ROS1+) non-small cell lung cancer (NSCLC) and central nervous system metastases (CNS mets) in the phase 1/2 TRIDENT-1. *J Clin Oncol* (2023) 41:9017. doi:10.1200/JCO.2023.41.16_suppl.9017

78. Yun MR, Kim DH, Kim SY, Joo HS, Lee YW, Choi HM, et al. Repotrectinib exhibits potent antitumor activity in treatment-naïve and solvent-front-mutant ROS1-rearranged non-small cell lung cancer. *Clin Cancer Res* (2020) 26:3287–95. doi:10.1158/1078-0432.CCR-19-2777

79. FDA. *FDA approves repotrectinib for ROS1-positive non-small cell lung cancer* (2023). Available from: https://www.fda.gov/drugs/resources-information-approved-drugs/fda-approves-repotrectinib-ros1-positive-non-small-cell-lung-cancer (Accessed January 24, 2024).

80. Dudnik E, Agbarya A, Grinberg R, Cyjon A, Bar J, Moskovitz M, et al. Clinical activity of brigatinib in ROS1-rearranged non-small cell lung cancer. *Clin Transl Oncol* (2020) 22:2303–11. doi:10.1007/s12094-020-02376-w

81. Katayama R, Gong B, Togashi N, Miyamoto M, Kiga M, Iwasaki S, et al. The new-generation selective ROS1/NTRK inhibitor DS-6051b overcomes crizotinib resistant ROS1-G2032R mutation in preclinical models. *Nat Commun* (2019) 10:3604. doi:10.1038/s41467-019-11496-z

82. Papadopoulos KP, Borazanci E, Shaw AT, Katayama R, Shimizu Y, Zhu VW, et al. U.S. Phase I first-in-human study of taletrectinib (DS-6051b/AB-106), a ROS1/TRK inhibitor, in patients with advanced solid tumors. *Clin Cancer Res* (2020) 26:4785–94. doi:10.1158/1078-0432.CCR-20-1630

83. Ai X, Wang Q, Cheng Y, Liu X, Cao L, Chen J, et al. Safety but limited efficacy of ensartinib in ROS1-positive NSCLC: a single-arm, multicenter phase 2 study. *J Thorac Oncol* (2021) 16:1959–63. doi:10.1016/j.jtho.2021.06.023

84. Mulligan LM RET revisited: expanding the oncogenic portfolio. *Nat Rev Cancer* (2014) 14:173–86. doi:10.1038/nrc3680

85. Ferrara R, Auger N, Auclin E, Besse B Clinical and translational implications of RET rearrangements in non-small cell lung cancer. *J Thorac Oncol* (2018) 13:27–45. doi:10.1016/j.jtho.2017.10.021

86. Mulligan LM, Kwok JB, Healey CS, Elsdon MJ, Eng C, Gardner E, et al. Germline mutations of the RET proto-oncogene in multiple endocrine neoplasia type 2A. *Nature* (1993) 363:458–60. doi:10.1038/363458a0

87. Romeo G, Ronchetto P, Luo Y, Barone V, Seri M, Ceccherini I, et al. Point mutations affecting the tyrosine kinase domain of the RET proto-oncogene in Hirschsprung's disease. *Nature* (1994) 367:377–8. doi:10.1038/367377a0

88. Drilon A, Lin JJ, Filleron T, Ni A, Milia J, Bergagnini I, et al. Frequency of brain metastases and multikinase inhibitor outcomes in patients with RET-rearranged lung cancers. *J Thorac Oncol* (2018) 13:1595–601. doi:10.1016/j.jtho.2018.07.004

89. Feng J, Li Y, Wei B, Guo L, Li W, Xia Q, et al. Clinicopathologic characteristics and diagnostic methods of RET rearrangement in Chinese non-small cell lung cancer patients. *Transl Lung Cancer Res* (2022) 11:617–31. doi:10.21037/tlcr-22-202

90. Andrini E, Mosca M, Galvani L, Sperandi F, Ricciuti B, Metro G, et al. Non-small-cell lung cancer: how to manage RET-positive disease. *Drugs Context* (2022) 11:1–12. doi:10.7573/dic.2022-1-5

91. Drilon A, Oxnard GR, Tan DSW, Loong HHF, Johnson M, Gainor J, et al. Efficacy of selpercatinib in RET fusion-positive non-small-cell lung cancer. *N Engl J Med* (2020) 383:813–24. doi:10.1056/NEJMoa2005653

92. Duke ES, Bradford D, Marcovitz M, Amatya AK, Mishra-Kalyani PS, Nguyen E, et al. FDA approval summary: selpercatinib for the treatment of advanced RET fusion-positive solid tumors. *Clin Cancer Res* (2023) 29:3573–8. doi:10.1158/1078-0432.CCR-23-0459

93. Solomon BJ, Zhou CC, Drilon A, Park K, Wolf J, Elamin Y, et al. Phase III study of selpercatinib versus chemotherapy ± pembrolizumab in untreated *RET* positive non-small-cell lung cancer. *Future Oncol Lond Engl* (2021) 17:763–73. doi:10.2217/fon-2020-0935

94. Loong HHF, Goto K, Solomon BJ, Park K, Pérol M, Arriola E, et al. LBA4 Randomized phase III study of first-line selpercatinib versus chemotherapy and pembrolizumab in RET fusion-positive NSCLC. *Ann Oncol* (2023) 34:S1303. doi:10.1016/j.annonc.2023.10.059

95. Zhou C, Solomon B, Loong HH, Park K, Pérol M, Arriola E, et al. First-line selpercatinib or chemotherapy and pembrolizumab in RET fusion-positive NSCLC. *N Engl J Med* (2023) 389:1839–50. doi:10.1056/NEJMoa2309457

96. FDA. *FDA approves selpercatinib for lung and thyroid cancers with RET gene mutations or fusions* (2021). Available from: https://www.fda.gov/drugs/resources-information-approved-drugs/fda-approves-selpercatinib-lung-and-thyroid-cancers-ret-gene-mutations-or-fusions (Accessed January 24, 2024).

97. FDA. *FDA approves pralsetinib for lung cancer with RET gene fusions* (2020). Available from: https://www.fda.gov/drugs/resources-information-approved-drugs/fda-approves-pralsetinib-lung-cancer-ret-gene-fusions (Accessed January 24, 2024).

98. EMA. *Selpercatinib - summary of opinion (post authorisation)* (2022). Available from: https://www.ema.europa.eu/en/documents/smop/chmp-post-authorisation-summary-positive-opinion-retsevmo-ii-0014-g_en.pdf (Accessed January 31, 2024).

99. EMA. *Pralsetinib - summary of product characteristics* (2024). Available from: https://www.ema.europa.eu/en/documents/product-information/gavreto-epar-product-information_en.pdf (Accessed January 31, 2024).

100. Griesinger F, Curigliano G, Thomas M, Subbiah V, Baik CS, Tan DSW, et al. Safety and efficacy of pralsetinib in RET fusion-positive non-small-cell lung cancer including as first-line therapy: update from the ARROW trial. *Ann Oncol* (2022) 33:1168–78. doi:10.1016/j.annonc.2022.08.002

101. Besse B, Felip E, Kim ES, Clifford C, Louie-Gao M, Yagui-Beltran A, et al. P87.02 AcceleRET lung: a phase 3 study of first-line pralsetinib in patients with RET-fusion+ advanced/metastatic NSCLC. *J Thorac Oncol* (2021) 16:S684. doi:10.1016/j.jtho.2021.01.1257

102. Chevallier M, Borgeaud M, Addeo A, Friedlaender A Oncogenic driver mutations in non-small cell lung cancer: past, present and future. *World J Clin Oncol* (2021) 12:217–37. doi:10.5306/wjco.v12.i4.217

103. Abdayem P, Planchard D Ongoing progress in BRAF-mutated non-small cell lung cancer. *Clin Adv Hematol Oncol HO* (2022) 20(1):662–672.

104. O'Leary CG, Andelkovic V, Ladwa R, Pavlakis N, Zhou C, Hirsch F, et al. Targeting BRAF mutations in non-small cell lung cancer. *Transl Lung Cancer Res* (2019) 8:1119–24. doi:10.21037/tlcr.2019.10.22

105. Harada G, Yang S-R, Cocco E, Drilon A Rare molecular subtypes of lung cancer. *Nat Rev Clin Oncol* (2023) 20:229–49. doi:10.1038/s41571-023-00733-6

106. Hendriks LE, Kerr KM, Menis J, Mok TS, Nestle U, Passaro A, et al. Non-oncogene-addicted metastatic non-small-cell lung cancer: ESMO Clinical Practice Guideline for diagnosis, treatment and follow-up. *Ann Oncol Off J Eur Soc Med Oncol* (2023) 34:358–76. doi:10.1016/j.annonc.2022.12.013

107. Davies KD, Lomboy A, Lawrence CA, Yourshaw M, Bocsi GT, Camidge DR, et al. DNA-based versus RNA-based detection of MET exon 14 skipping events in lung cancer. *J Thorac Oncol* (2019) 14:737–41. doi:10.1016/j.jtho.2018.12.020

108. Socinski MA, Pennell NA, Davies KD MET exon 14 skipping mutations in non-small-cell lung cancer: an overview of biology, clinical outcomes, and testing considerations. *JCO Precis Oncol* (2021) 5:653–63. doi:10.1200/PO.20.00516

109. FDA. *List of cleared or approved companion diagnostic devices (*in vitro *and imaging tools)* (2024). Available from: https://www.fda.gov/medical-devices/in-vitro-diagnostics/list-cleared-or-approved-companion-diagnostic-devices-in-vitro-and-imaging-tools (Accessed January 31, 2024).

110. Wolf J, Seto T, Han J-Y, Reguart N, Garon EB, Groen HJM, et al. Capmatinib in MET exon 14-mutated or MET-amplified non-small-cell lung cancer. *N Engl J Med* (2020) 383:944–57. doi:10.1056/NEJMoa2002787

111. ClinicalTrials.gov. *Clinical study of oral cMET inhibitor INC280 in adult patients with EGFR wild-type advanced non-small cell lung cancer (geometry mono-1)* (2023). Available from: https://clinicaltrials.gov/study/NCT02414139 (Accessed January 31, 2024).

112. Le X, Sakai H, Felip E, Veillon R, Garassino MC, Raskin J, et al. Tepotinib efficacy and safety in patients with MET exon 14 skipping NSCLC: outcomes in patient subgroups from the VISION study with relevance for clinical practice. *Clin Cancer Res* (2022) 28:1117–26. doi:10.1158/1078-0432.CCR-21-2733

113. ClinicalTrials.gov. *Tepotinib phase II in NSCLC harboring MET alterations (VISION)* (2023). Available from: https://clinicaltrials.gov/study/NCT02864992 (Accessed January 31, 2024).

114. Paik PK, Felip E, Veillon R, Sakai H, Cortot AB, Garassino MC, et al. Tepotinib in non-small-cell lung cancer with MET exon 14 skipping mutations. *N Engl J Med* (2020) 383:931–43. doi:10.1056/NEJMoa2004407

115. Xiong W, Papasouliotis O, Jonsson EN, Strotmann R, Girard P Population pharmacokinetic analysis of tepotinib, an oral MET kinase inhibitor, including data from the VISION study. *Cancer Chemother Pharmacol* (2022) 89:655–69. doi:10.1007/s00280-022-04423-5

116. Jebbink M, de Langen AJ, Boelens MC, Monkhorst K, Smit EF The force of HER2 - a druggable target in NSCLC? *Cancer Treat Rev* (2020) 86:101996. doi:10.1016/j.ctrv.2020.101996

117. Li BT, Smit EF, Goto Y, Nakagawa K, Udagawa H, Mazières J, et al. Trastuzumab deruxtecan in HER2-mutant non-small-cell lung cancer. *N Engl J Med* (2022) 386:241–51. doi:10.1056/NEJMoa2112431

118. Goto K, Goto Y, Kubo T, Ninomiya K, Kim S-W, Planchard D, et al. Trastuzumab deruxtecan in patients with HER2-mutant metastatic non-small-cell lung cancer: primary results from the randomized, phase II DESTINY-lung02 trial. *J Clin Oncol* (2023) 41:4852–63. doi:10.1200/JCO.23.01361

119. ClinicalTrials.gov. *A study to investigate the efficacy and safety of trastuzumab deruxtecan as the first treatment option for unresectable, locally advanced/metastatic non-small cell lung cancer with HER2 mutations* (2023). Available from: https://clinicaltrials.gov/study/NCT05048797 (Accessed January 31, 2024).

120. Demetri GD, De Braud F, Drilon A, Siena S, Patel MR, Cho BC, et al. Updated integrated analysis of the efficacy and safety of entrectinib in patients with NTRK fusion-positive solid tumors. *Clin Cancer Res* (2022) 28:1302–12. doi:10.1158/1078-0432.CCR-21-3597

121. Drilon A, Tan DSW, Lassen UN, Leyvraz S, Liu Y, Patel JD, et al. Efficacy and safety of larotrectinib in patients with tropomyosin receptor kinase fusion-positive lung cancers. *JCO Precis Oncol* (2022) 6:e2100418. doi:10.1200/PO.21.00418

122. Aggarwal C, Marmarelis ME, Hwang W-T, Scholes DG, McWilliams TL, Singh AP, et al. Association between availability of molecular genotyping results and overall survival in patients with advanced nonsquamous non-small-cell lung cancer. *JCO Precis Oncol* (2023) 7:e2300191. doi:10.1200/PO.23.00191

123. Aggarwal C, Marmarelis ME, Hwang W-T, Scholes DG, McWilliams T, Singh AP, et al. Association of comprehensive molecular genotyping and overall survival in patients with advanced non-squamous non-small cell lung cancer. *J Clin Oncol* (2022) 40:9022. doi:10.1200/JCO.2022.40.16_suppl.9022

124. Sequist LV, Neal JV, Jett JR, Ross ME Personalized, genotype-directed therapy for advanced non-small cell lung cancer. UpToDate (2016).

125. Forde PM, Spicer J, Lu S, Provencio M, Mitsudomi T, Awad MM, et al. Neoadjuvant nivolumab plus chemotherapy in resectable lung cancer. *N Engl J Med* (2022) 386:1973–85. doi:10.1056/NEJMoa2202170

126. Heymach JV, Harpole D, Mitsudomi T, Taube JM, Galffy G, Hochmair M, et al. Perioperative durvalumab for resectable non-small-cell lung cancer. *N Engl J Med* (2023) 389:1672–84. doi:10.1056/NEJMoa2304875

127. Wu Y-L, Tsuboi M, He J, John T, Grohe C, Majem M, et al. Osimertinib in resected EGFR-mutated non-small-cell lung cancer. *N Engl J Med* (2020) 383:1711–23. doi:10.1056/NEJMoa2027071

128. Tsuboi M, Herbst RS, John T, Kato T, Majem M, Grohé C, et al. Overall survival with osimertinib in resected EGFR-mutated NSCLC. *N Engl J Med* (2023) 389:137–47. doi:10.1056/NEJMoa2304594

129. Solomon BJ, Ahn JS, Dziadziuszko R, Barlesi F, Nishio M, Lee DH, et al. LBA2 ALINA: efficacy and safety of adjuvant alectinib versus chemotherapy in patients with early-stage ALK+ non-small cell lung cancer (NSCLC). *Ann Oncol* (2023) 34:S1295–6. doi:10.1016/j.annonc.2023.10.051

130. Solomon BJ, Ahn JS, Barlesi F, Dziadziuszko R, Nishio M, Shaw AT, et al. ALINA: a phase III study of alectinib versus chemotherapy as adjuvant therapy in patients with stage IB–IIIA anaplastic lymphoma kinase-positive (ALK+) non-small cell lung cancer (NSCLC). *J Clin Oncol* (2019) 37:TPS8569. doi:10.1200/JCO.2019.37.15_suppl.TPS8569

131. Gillespie CS, Mustafa MA, Richardson GE, Alam AM, Lee KS, Hughes DM, et al. Genomic alterations and the incidence of brain metastases in advanced and metastatic NSCLC: a systematic review and meta-analysis. *J Thorac Oncol* (2023) 18:1703–13. doi:10.1016/j.jtho.2023.06.017

132. Nishino M, Soejima K, Mitsudomi T Brain metastases in oncogene-driven non-small cell lung cancer. *Transl Lung Cancer Res* (2019) 8:S298–S307. doi:10.21037/tlcr.2019.05.15

133. Rangachari D, Yamaguchi N, VanderLaan PA, Folch E, Mahadevan A, Floyd SR, et al. Brain metastases in patients with EGFR-mutated or ALK-rearranged non-small-cell lung cancers. *Lung Cancer Amst Neth* (2015) 88:108–11. doi:10.1016/j.lungcan.2015.01.020

134. Tan AC, Tan DSW Targeted therapies for lung cancer patients with oncogenic driver molecular alterations. *JCO* (2022) 40:611–625. doi:10.1200/JCO.21.01626

135. De Carlo E, Bertoli E, Del Conte A, Stanzione B, Berto E, Revelant A, et al. Brain metastases management in oncogene-addicted non-small cell lung cancer in the targeted therapies era. *Int J Mol Sci* (2022) 23:6477. doi:10.3390/ijms23126477

136. Le Rhun E, Guckenberger M, Smits M, Dummer R, Bachelot T, Sahm F, et al. EANO-ESMO Clinical Practice Guidelines for diagnosis, treatment and follow-up of patients with brain metastasis from solid tumours. *Ann Oncol* (2021) 32:1332–47. doi:10.1016/j.annonc.2021.07.016

137. Thomas NJ, Myall NJ, Sun F, Patil T, Mushtaq R, Yu C, et al. Brain metastases in EGFR- and ALK-positive NSCLC: outcomes of central nervous system-penetrant tyrosine kinase inhibitors alone versus in combination with radiation. *J Thorac Oncol* (2022) 17:116–29. doi:10.1016/j.jtho.2021.08.009

138. NCCN. *NCCN guidelines brain metastases version 1* (2023). Available from: https://www.nccn.org/professionals/physician_gls/pdf/cns.pdf (Accessed January 30, 2024).

139. Soria J-C, Ohe Y, Vansteenkiste J, Reungwetwattana T, Chewaskulyong B, Lee KH, et al. Osimertinib in untreated EGFR-mutated advanced non-small-cell lung cancer. *N Engl J Med* (2018) 378:113–25. doi:10.1056/NEJMoa1713137

Pathology & Oncology Research | frontiers

TYPE Mini Review
PUBLISHED 19 April 2024
DOI 10.3389/pore.2024.1611716

Check for updates

OPEN ACCESS

EDITED BY
Nora Bittner,
National Koranyi Institute of TB and Pulmonology, Hungary

*CORRESPONDENCE
Zsuzsanna Orosz,
zsuzsa.orosz@gmail.com

RECEIVED 31 January 2024
ACCEPTED 08 April 2024
PUBLISHED 19 April 2024

CITATION
Orosz Z and Kovács Á (2024), The role of chemoradiotherapy and immunotherapy in stage III NSCLC. *Pathol. Oncol. Res.* 30:1611716. doi: 10.3389/pore.2024.1611716

COPYRIGHT
© 2024 Orosz and Kovács. This is an open-access article distributed under the terms of the Creative Commons Attribution License (CC BY). The use, distribution or reproduction in other forums is permitted, provided the original author(s) and the copyright owner(s) are credited and that the original publication in this journal is cited, in accordance with accepted academic practice. No use, distribution or reproduction is permitted which does not comply with these terms.

The role of chemoradiotherapy and immunotherapy in stage III NSCLC

Zsuzsanna Orosz[1]* and Árpád Kovács[2]

[1]Department of Pulmonology, Faculty of Medicine, University of Debrecen, Debrecen, Hungary, [2]Department of Oncoradiology, Faculty of Medicine, University of Debrecen, Debrecen, Hungary

Locally advanced non-small lung cancer encompasses a diverse range of tumors. In the last few years, the treatment of stage III unresectable non-small lung cancer has evolved significantly. The PACIFIC trial opened a new therapeutic era in the treatment of locally advanced NSCLC, establishing durvalumab consolidation therapy as the new standard of care worldwide. A careful evaluation of this type of lung cancer and a discussion of the management of these patients within a multidisciplinary team represents a crucial step in defining the best treatment strategy for each patient. For unresectable stage III NSCLC, definitive concurrent chemoradiotherapy (CCRT) was historically recommended as a treatment with a 5-year survival rate ranging from 20% to 30%. The PACIFIC study conducted in 2017 compared the use of chemoradiotherapy and maintenance therapy with the anti-PD-L1 monoclonal antibody durvalumab to a placebo in patients with locally advanced NSCLC who had not experienced disease progression. The study was prospective, randomized, and phase III. The administration of this medication in patients with locally advanced non-small cell lung cancer (NSCLC) has demonstrated a notable improvement in overall survival. Multiple clinical trials are currently exploring various immune checkpoint inhibition regimens to enhance the treatment efficacy in patients with stage III cancer. Our goal is to offer an up-to-date summary of the planned clinical trials for treatment options, focusing on the significant obstacles and prospects in the post-PACIFIC era.

KEYWORDS

locally advanced, NSCLC, chemoradiotherapy, immunotherapy, durvalumab

Abbreviations: ICIs, Immune checkpoint inhibitors; RT, Radiotherapy; LA-NSCLC, locally advanced non-small cell lung cancer; NSCLC, Non-small cell lung cancer; LA, Locally Advanced; SoC, Standard of care; OS, Overall survival; ORR, Objective Response Rate; TME, tumor microenvironment; PD-1, Programmed cell death 1; PD-L1, Programmed cell death-ligand 1; CTLA-4, Cytotoxic T-lymphocyte associated antigen 4; PFS, Progression-free survival; CRT, Chemoradiotherapy; AEs, Adverse events; PR, Partial response.

Introduction

Many diseases became more common as a result of the altered smoking habits that emerged in the first half of the 20th century and the air pollution that was seen to coincide with industrial development. Lung cancer is currently the most common cause of cancer-related mortality in developed nations [1]. The 5-year survival rates are 15%–40% in stage IIIA and 5%–10% in stage IIIB lung cancer, respectively [2]. Three subgroups exist for locally advanced stage III non-small-cell lung cancer (NSCLC) according to the 8th edition of the TNM classification: stage IIIA, IIIB, and IIIC tumors [2, 3]. However, in clinical practice, we can also identify stage lung cancer that is resectable, potentially resectable, and unresectable [4]. Lung cancer requires meticulous examination and staging [3]. The imaging and diagnostic methods include bronchoscopy, endobronchial ultrasound (EBUS), cryobiopsy, liquid biopsy, computed tomography (CT), FDG positron emission tomography (PET), magnetic resonance imaging (MRI), and in some cases it is necessary to perform video-assisted thoracoscopic surgery (VATS) [5]. After cytological or histological confirmation of non-small cell lung cancer, especially of adenocarcinomas, it is essential to determine the status of EGFR, ALK, and PDL1 is essential [5]. Therapy of stage III non-small cell lung cancer (NSCLC) needs a multimodal approach that involves chemotherapy, radiotherapy, surgical treatment, and in special cases targeted therapy and immunotherapy [2, 3].

Tumor location, volume, histology, immunohistochemical and molecular pathological features, patient age, performance level, and comorbidities are some of the variables that affect the treatment plan [1–3].

Before 2018, the standard of care therapy of locally advanced non-small cell lung cancer was definitive chemoradiotherapy, that contains platinum-based doublet chemotherapy regimen combined with either concurrent or sequential radiation therapy (RT) [6, 7]. The progression-free survival (PFS) was 8 months, and the 5-year survival was less than 20% in these patient population [8, 9].

A phase III clinical trial conducted in 2002 by Albain et al. showed that concomitant cisplatin, etoposide chemotherapy, and thoracic radiation improved the median overall survival (OS) to 15 months, with 3- and 5-year survival rates of 17% and 15%, respectively [10].

Subsequently, Govindan et al. reported that combination chemoradiotherapy using pemetrexed and carboplatin demonstrated fewer adverse effects while still demonstrating the same efficacy as cisplatin and etoposide [11].

Chemoradiotherapy and immunotherapy for stage III unresectable NSCLC

The introduction of immune checkpoint inhibitors (ICI) opened a new era in the treatment of lung cancer 8 years ago [8, 12]. Previous studies showed the efficacy of immunotherapy after definitive chemoradiotherapy for stage III unresectable NSCLC. CRT is administered to reduce local recurrence and prevent the onset of distant metastases and is administered during or after the completion of chemoradiotherapy [12, 13].

The efficacy of durvalumab as maintenance therapy and the completion of concurrent chemoradiotherapy in locally advanced non-small cell lung cancer was assessed in 2017 by the phase III PACIFIC trial [12]. In the PACIFIC study, durvalumab (a human IgG1 monoclonal antibody against PD-L1) was added to concurrent chemoradiotherapy for stage III non-small cell lung cancer after a year of maintenance. 713 patients with stage III (TNM 7th edition) who had not received prior anticancer treatment were enrolled in the PACIFIC trial and were randomized to receive durvalumab or placebo beginning 1–42 days after combination chemoradiotherapy [5]. Concurrent radiotherapy (54–66 Gy) and platinum doublet chemotherapy (cisplatin or carboplatin plus paclitaxel, docetaxel, vinblastine, vinorelbine, etoposide, or pemetrexed) were administered to the patients [12]. Patients who did not progress after chemoradiotherapy were randomly assigned to receive durvalumab or placebo [12, 14]. Durvalumab was administered intravenously every 2 weeks at a dose of 10 mg/kg [12]. Durvalumab maintenance therapy for a year resulted in increases in overall survival (47.5 vs. 42.9 months) and progression-free survival (PFS; 11.2 vs. 10.9 months), with about one-third of patients continuing to live without distant metastases or local recurrence. Better 5-year OS (42.9% vs. 33.4%) and median OS (47.5 months vs. 29.1 months) were reported in the updated analysis for 2022 [13, 15].

In addition, patients treated with consolidation durvalumab had a longer median time to death or distant metastases (28.3 months against 16.2 months) and a lower incidence of brain metastases (6.3% vs. 11.8%) compared to placebo [13, 14, 16]. The efficacy of durvalumab in combination with concurrent or sequential radiation therapy in patients engaged in an early access program is being investigated in real-world data by an international retrospective trial known as PACIFIC-R [17]. Compared to PD-L1 negative patients, PD-L1 positive patients had a longer PFS (22.4 vs. 15.6 months) [13]. concurrent chemoradiotherapy with durvalumab is the current standard of care [5, 12, 18].

The optimal sequence of chemoradiotherapy and immunotherapy

Sequential radiochemotherapy is less effective than concurrent platinum-based chemoradiotherapy (CRT) [6, 10, 19, 20]. However, the patient's age, overall health, comorbidities, financial situation, and logistical challenges all affect the availability of competing radiation therapies [20].

The timing of immunotherapy is under investigation. Sequential immunotherapy is preferable because it has fewer side effects, can enhance treatment outcomes, and prevents resistance to immunotherapy through the immune system's interaction with radiation [12]. According to the PACIFIC study's subgroup analysis, patients who started their ICI earlier, in 30 days had a greater OS rate at 30 months compared to patients who received durvalumab after 1 months following chemoradiotherapy (90% vs. 44%) [7, 10].

In the LUN 14-179 [21], GEMSTONE-301 [22, 23], PACIFIC-6 [24], DETERRED [25, 26], and KEYNOTE 799 [26, 27] trials, immunotherapy was administered as a maintenance therapy after concurrent chemoradiotherapy.

In phase II DETERRED trial, chemoradiotherapy with concurrent and consolidative atezolizumab led to an efficacy similar to consolidative durvalumab in the PACIFIC trial [25, 26]. The patients received in part 1 chemoradiotherapy and consolidation of atezolizumab treatment, in part 2 they took concurrent maintenance atezolizumab. An updated analysis of this trial showed that the median progression-free survival for concurrent vs sequential atezolizumab was 15.1 vs. 18.9 months [25, 28].

The phase III KEYNOTE 799 study is similar to the PACIFIC trial. The KEYNOTE 799 trial evaluated the safety and efficacy of pembrolizumab and concurrent chemoradiotherapy in stage III non-small cell lung cancer. KEYNOTE 799 demonstrated an increase in ORR and an accelerated effect in establishing the antitumor immune response [27].

Phase III GEMSTONE 301 compared the efficacy of sugemalimab after chemoradiotherapy in patients with stage III unresectable driver mutation negative stage III NSCLC in China [22, 23]. PFS was significantly longer with sugemalimab than with placebo (median 10.5 vs. 6.2 months), but OS in the sugemalimab and placebo groups was inconclusive [29].

Phase II trial LUN 14–179 evaluates the efficacy and safety of pembrolizumab as consolidation therapy after concurrent chemoradiotherapy [21]. Consolidation with pembrolizumab after chemoradiotherapy prolonged PFS and OS compared to chemoradiotherapy (CRT) alone and did not increase the rates of grade 3–5 pneumonitis [21].

The single-arm phase II NICOLAS trial demonstrated the safety of nivolumab combined with radiation therapy in stage IIIA and IIIB disease. Significant overall survival differences were observed between patients with stage IIIA vs IIIB disease (2-year OS 81% vs. 56%) [30].

Novel agents

The ongoing phase III PACIFIC-8 study investigates the efficacy and safety of domvanalimab and durvalumab compared to durvalumab. The phase III PACIFIC-9 trial compares durvalumab + chemotherapy treatment with the combination of oleclumab (CD73 inhibitor) or added monalizumab (NKG2 inhibitor). The SKYSCRAPER-03 study investigates consolidation therapy with atezolizumab and the TIGIT inhibitor tiragolumab after chemoradiotherapy. CHORUS is a phase III study that compares canakinumab combined with chemoradiotherapy and durvalumab. The KEYVIBE-006 study evaluated pembrolizumab/vibostolimab (TIGIT inhibitor) in combination with concurrent chemoradiotherapy followed by pembrolizumab/vibostolimab versus cCRT followed by durvalumab. The KEYLYNK-012 study assesses pembrolizumab in combination with concurrent chemoradiotherapy followed by pembrolizumab with olaparib placebo or olaparib compared to concurrent chemoradiotherapy followed by durvalumab.

Next step: immunoradiotherapy, treatment without chemotherapy

In an attempt to avoid overtreating patients while dealing with the side effects of chemotherapy, a novel strategy known as radiation therapy with immunotherapy has been developed. The ongoing SPRINT study aims to evaluate the efficacy of a shortened 4-week radiation therapy course for high-grade PD-L1 patients with locally advanced non-small cell lung disease [31, 32]. The DUART trial, a phase II single-arm study, was finished to evaluate durvalumab's clinical efficacy in patients with non-small cell lung cancer (NSCLC) that is incurable and not amenable to treatment [31]. In the finished PARTICLE-D trial, durvalumab, the study drug, and proton beam therapy were combined [32]. The active phase I NRG-LU004 trial examines durvalumab in combination with conventionally fractionated radiation therapy or accelerated hypofractionated radiation therapy (ACRT) in patients with locally advanced non-small cell lung cancer. It also investigate the safety of combining durvalumab with conventional radiation therapy in addition to monalizumab or oleclumab [33]. CHECKMATE 73L is a trial that is currently in progress. The main objective of the study is to examine the effectiveness of nivolumab plus concurrent chemoradiotherapy (CCRT) followed by nivolumab plus ipilimumab against CCRT followed by durvalumab in patients with untreated stage III unresectable non-small cell lung cancer [34].

Driver mutations and advanced non-small lung cancer treatment

The therapy of non-small cell lung cancer with driver mutations in stage III disease raises many questions [35]. Targeted therapies especially tyrosine kinase inhibitors are

evaluated in unresectable stage III NSCLC with actionable genomic alterations.

Unfortunately, there is no optimal treatment strategy for patients with driver mutation in locally advanced NSCLC. The PACIFIC trial enrolled patients with the EGFR mutation. Antonia et al. presented their exploratory subgroup analysis, showing that PFS and OS with durvalumab were similar to placebo in patients with EGFR mutation [15, 36, 37]. Hellyer et al. found that patients with LA- NSCLC mutations of the human epidermal growth factor receptor 2 (HER2) or EGFR had shorter PFS than those with wild-type genes (7.5 months vs. not reached) [35, 38]. We must use these data with caution due to the small number and characteristics of the patients (male, smokers, squamous cell carcinoma). The safety profile was the same in the durvalumab arm as in the overall population [15, 30]. The DETERRED trial examined individuals with specific oncogene mutations that can be targeted, which resulted in a poorer progression-free survival (PFS) [25]. The LAURA (phase III) trial enrolled patients with locally advanced, unresectable epidermal growth factor receptor mutation-positive stage III NSCLC. Patients received at least two cycles of concurrent/sequential platinum-based cCRT and were randomly assigned 2:1–80 mg or placebo once a day [39]. Currently, the effectiveness of osimertinib treatment is under investigation. The latest consensus of ESMO guideline does not recommend using ICI consolidation therapy after curative intention chemoradiotherapy in EGFR-positive NSCLC [3, 5, 40]. Patients with a KRAS mutation profit from durvalumab maintenance therapy [38, 41, 42].

Toxicity and safety

Immunotherapy can affect multiple organ systems, 50% of patients treated with ICI are estimated to experience some form of irAE. AE of any grade of those who receive ICI treatment is fatigue, gastrointestinal (colitis, diarrhoea, abdominal pain, hepatitis), endocrine (alteration of thyroid function, hypocalcemia), myocarditis, renal, peripheral neuropathy, and dermatological side effects (i.e., rash). Respiratory complications, pneumonitis, and respiratory failure are the most common cause of immune-related deaths [12–14, 43–47].

Treatment-related pneumonitis with immune checkpoint inhibitors is a challenging side effect. The spectrum of symptoms moves on a wide range from the asymptomatic case to acute respiratory failure [48]. The diagnosis of ICI pneumonitis confirms the symptoms (developing dry cough, dyspnea, and other respiratory symptoms), laboratory test (inflammatory markers, i.e., neutrophil lymphocyte ratio), lung function test, microbial culture, the presence of new infiltrates on chest imaging without new infections [14, 43, 49]. Chest CT should be combined with other diagnostic tools. However, differential diagnosis is complicated and it is difficult to distinguish between radiotherapy-related pneumonitis, new-onset interstitial lung disease, tumour progression, or pulmonary infection (i.e., Covid infection) [48, 49].

Treatment-related adverse events of grade 3–4 were 29.9% in the PACIFIC trial. The most common AE was pneumonitis, with an incidence of 4.4%, and 15.4% of these patients discontinued durvalumab because of AEs [13, 14, 50].

With respect to adverse events, pneumonitis was reported to be more severe in patients who received durvalumab. However, grade 3 or 4 pneumonitis was similar in both groups: 1.9% in the durvalumab arm and 1.7% in the control group. Furthermore, radiation-related pneumonitis contributed to the discontinuation of durvalumab in 1.3% of patients, as in the placebo arm [12–15].

The novel combinations of immunochemoradiotherapy show similar data compared to those of the PACIFIC trial. In the GEMSTONE-301 trial, grade 3 or 4 pneumonitis occurred in 3% of patients in the sugemalimab group compared to 6% in the placebo group [22]. The grade 2 or higher pneumonitis rate was around 10% in the DETERRED trial [25].

Treatment of immune-related pneumonitis depends on the severity of the disease [51]. Grade 1 pneumonitis does not need special treatment. Grade 2 pneumonitis requires ICI withdrawal therapy and administration of corticosteroid treatment administration. Grade 3 and 4 pneumonitis requires discontinuation of immunotherapy, corticosteroid treatment, hospitalization, empiric broad-spectrum antibiotic therapy, oxygen administration, and mechanical ventilation in severe cases. Guidelines recommend other immunosuppressive agents: TNFα inhibitor - infliximab, intravenous immunoglobulins, and mycophenolat mofetil [51].

Progression during and after ICI consolidation therapy

Regular chest CT or PET CT controls the efficacy of disease treatment and follow-up. PET-CT scan is recommended to evaluate tumor metabolic activity if it suggests progression of the disease [12]. Changes in F-18 fluorodeoxyglucose uptake occur commonly between 8 and 12 weeks after radiation therapy on PET CT [52]. Furthermore, several conditions (such as atelectasis, consolidation, infection, granulomatous pulmonary disease, and radiation fibrosis) are challenging to differentiate from neoplasm because areas previously treated with radiation therapy can remain avid 18F-FDG for up to 2 years.

More than half patients with stage III disease will progress within 2 years of the start of treatment. Updated data from the PACIFIC trial showed that 49.0% of patients completed 12 months of durvalumab therapy, and 31.3% discontinued due to disease progression [13]. In the PACIFIC trial, 7.1% of the patients in the ICI arm received durvalumab retreatment and

completed the first year of consolidation immunotherapy, and the median time to second progression was 48 months [13, 24].

We must distinguish between oligo- and systemic progression. If primary resistance is confirmed (progression observed during durvalumab treatment), therapeutic strategies depend on the type of progression. Oligometastasis is treatable (e.g., bone, brain) with surgery or stereotaxic ablation; a tight follow-up is recommended. In systemic progression, the rechallenge of immunotherapy is doubtful and participation in clinical trials, including a PDL-1 inhibitor, can be recommended. Delasos et al. in their retrospective examination investigated pembrolizumab treatment after chemoradiotherapy and maintenance immunotherapy (durvalumab) [53]. Patients with refractory or recurrent NSCLC require more attention, their survival is worse (median OS 10.6 months, median PFS 6.1 months) than patients with metastatic NSCLC diagnosed *de novo* and treated with chemotherapy (median OS 12.9 months) [53].

Conclusion

Treatments for locally advanced, incurable NSCLC have been evolving quickly in the field of lung cancer therapy in recent years. When treating unresectable stage III non-small lung cancer, chemotherapy plus immunotherapy have demonstrated a synergistic effect on both local and distant tumor control. The current therapeutic recommendations for unresectable stage III NSCLC include chemotherapy and 1 year of ICI consolidation therapy; however, there are a number of unanswered problems and potential techniques. We are currently awaiting the results to establish the best time to administer chemotherapy, radiation, and ICI as well as the function of targeted therapy. One major clinical barrier to improving the prognosis of patients with advanced lung cancer is resistance to immune checkpoint inhibitors.

Author contributions

ZO and AK participated in the design and review of the manuscript. ZO wrote the manuscript. All authors contributed to the article and approved the submitted version.

Funding

The authors declare that no financial support was received for the research, authorship, and/or publication of this article.

Conflict of interest

The authors declare that the research was conducted in the absence of any commercial or financial relationships that could be construed as a potential conflict of interest.

References

1. Siegel RL, Miller KD, Wagle NS, Jemal A. Cancer statistics, 2023. *CA Cancer J Clin* (2023) 73(1):17–48. doi:10.3322/caac.21763

2. Detterbeck FC, Boffa DJ, Kim AW, Tanoue LT. The eighth edition lung cancer stage classification. *Chest* (2017) 151(1):193–203. doi:10.1016/j.chest.2016.10.010

3. Aredo JV, Mambetsariev I, Hellyer JA, Amini A, Neal JW, Padda SK, et al. Durvalumab for stage III EGFR-mutated NSCLC after definitive chemoradiotherapy. *J Thorac Oncol* (2021) 16(6):1030–41. doi:10.1016/j.jtho.2021.01.1628

4. Passiglia F, Leone G, Olmetto E, Delcuratolo MD, Tabbò F, Reale ML, et al. Immune-checkpoint inhibition in stage III unresectable NSCLC: challenges and opportunities in the post-PACIFIC era. *Lung Cancer* (2021) 157:85–91. doi:10.1016/j.lungcan.2021.05.009

5. Remon J, Soria JC, Peters S, ESMO Guidelines Committee. Electronic address: clinicalguidelines@esmo.org. Early and locally advanced non-small-cell lung cancer: an update of the ESMO clinical practice guidelines focusing on diagnosis, staging, systemic and local therapy. *Ann Oncol* (2021) 32(12):1637–42. doi:10.1016/j.annonc.2021.08.1994

6. Curran WJ, Paulus R, Langer CJ, Komaki R, Lee JS, Hauser S, et al. Sequential vs. concurrent chemoradiation for stage III non-small cell lung cancer: randomized phase III trial RTOG 9410. *J Natl Cancer Inst* (2011) 103(19):1452–60. doi:10.1093/jnci/djr325

7. Auperin A, Le Péchoux C, Pignon JP, Koning C, Jeremic B, Clamon G, et al. Concomitant radio-chemotherapy based on platin compounds in patients with locally advanced non-small cell lung cancer (NSCLC): a meta-analysis of individual data from 1764 patients. *Ann Oncol* (2006) 17(3):473–83. doi:10.1093/annonc/mdj117

8. Duma N, Santana-Davila R, Molina JR Non-small cell lung cancer: epidemiology, screening, diagnosis, and treatment. *Mayo Clin Proc* (2019) 94(8):1623–40. doi:10.1016/j.mayocp.2019.01.013

9. Cheema PK, Rothenstein J, Melosky B, Brade A, Hirsh V. Perspectives on treatment advances for stage III locally advanced unresectable non-small-cell lung cancer. *Curr Oncol* (2019) 26(1):37–42. doi:10.3747/co.25.4096

10. Albain KS, Crowley JJ, Turrisi AT, Gandara DR, Farrar WB, Clark JI, et al. Concurrent cisplatin, etoposide, and chest radiotherapy in pathologic stage IIIB non-small-cell lung cancer: a Southwest Oncology Group phase II study, SWOG 9019. *J Clin Oncol* (2002) 20(16):3454–60. doi:10.1200/JCO.2002.03.055

11. Govindan R, Bogart J, Stinchcombe T, Wang X, Hodgson L, Kratzke R, et al. Randomized phase II study of pemetrexed, carboplatin, and thoracic radiation with or without cetuximab in patients with locally advanced unresectable non-small-cell lung cancer: cancer and Leukemia Group B trial 30407. *J Clin Oncol* (2011) 29(23):3120–5. doi:10.1200/JCO.2010.33.4979

12. Antonia SJ, Villegas A, Daniel D, Vicente D, Murakami S, Hui R, et al. Durvalumab after chemoradiotherapy in stage III non-small-cell lung cancer. *N Engl J Med* (2017) 377(20):1919–29. doi:10.1056/NEJMoa1709937

13. Spigel DR, Faivre-Finn C, Gray JE, Vicente D, Planchard D, Paz-Ares L, et al. Five-year survival outcomes from the PACIFIC trial: durvalumab after chemoradiotherapy in stage III non-small-cell lung cancer. *J Clin Oncol* (2022) 40(12):1301–11. doi:10.1200/JCO.21.01308

14. Antonia SJ, Ozguroglu M, Durvalumab in stage III non-small-cell lung cancer. *N Engl J Med* (2018) 378(9):869–70. doi:10.1056/NEJMc1716426

15. Naidoo J, Antonia S, Wu YL, Cho BC, Thiyagarajah P, Mann H, et al. Brief report: durvalumab after chemoradiotherapy in unresectable stage III EGFR-mutant NSCLC: a *post hoc* subgroup analysis from PACIFIC. *J Thorac Oncol* (2023) 18(5):657–63. doi:10.1016/j.jtho.2023.02.009

16. Faivre-Finn C, Vicente D, Kurata T, Planchard D, Paz-Ares L, Vansteenkiste JF, et al. Four-year survival with durvalumab after chemoradiotherapy in stage III NSCLC-an update from the PACIFIC trial. *J Thorac Oncol* (2021) 16(5):860–7. doi:10.1016/j.jtho.2020.12.015

17. Girard N, Bar J, Garrido P, Garassino MC, McDonald F, Mornex F, et al. Treatment characteristics and real-world progression-free survival in patients with unresectable stage III NSCLC who received durvalumab after chemoradiotherapy: findings from the PACIFIC-R study. *J Thorac Oncol* (2023) 18(2):181–93. doi:10.1016/j.jtho.2022.10.003

18. Hendriks LE, Kerr KM, Menis J, Mok TS, Nestle U, Passaro A, et al. Non-oncogene-addicted metastatic non-small-cell lung cancer: ESMO clinical practice guideline for diagnosis, treatment and follow-up. *Ann Oncol* (2023) 34(4):358–76. doi:10.1016/j.annonc.2022.12.013

19. O'Rourke N, Roqué I Figuls M, Farré Bernadó N, Macbeth F. Concurrent chemoradiotherapy in non-small cell lung cancer. *Cochrane Database Syst Rev* (2010) 16(6):CD002140. doi:10.1002/14651858.CD002140.pub3

20. Wu L, Zhang Z, Bai M, Yan Y, Yu J, Xu Y. Radiation combined with immune checkpoint inhibitors for unresectable locally advanced non-small cell lung cancer: synergistic mechanisms, current state, challenges, and orientations. *Cell Commun Signal* (2023) 21(1):119. doi:10.1186/s12964-023-01139-8

21. Durm GA, Jabbour SK, Althouse SK, Liu Z, Sadiq AA, Zon RT, et al. A phase 2 trial of consolidation pembrolizumab following concurrent chemoradiation for patients with unresectable stage III non-small cell lung cancer: hoosier Cancer Research Network LUN 14-179. *Cancer* (2020) 126(19):4353–61. doi:10.1002/cncr.33083

22. Zhou Q, Chen M, Jiang O, Pan Y, Hu D, Lin Q, et al. Sugemalimab versus placebo after concurrent or sequential chemoradiotherapy in patients with locally advanced, unresectable, stage III non-small-cell lung cancer in China (GEMSTONE-301): interim results of a randomised, double-blind, multicentre, phase 3 trial. *Lancet Oncol* (2022) 23(2):209–19. doi:10.1016/S1470-2045(21)00630-6

23. Wu YL Sequential chemoradiotherapy followed by sugemalimab for locally advanced NSCLC - author's reply. *Lancet Oncol* (2022) 23(4):e159. doi:10.1016/S1470-2045(22)00144-9

24. Garassino MC, Mazieres J, Reck M, Chouaid C, Bischoff H, Reinmuth N, et al. Durvalumab after sequential chemoradiotherapy in stage III, unresectable NSCLC: the phase 2 PACIFIC-6 trial. *J Thorac Oncol* (2022) 17(12):1415–27. doi:10.1016/j.jtho.2022.07.1148

25. Liu Y, Yao L, Kalhor N, Carter BW, Altan M, Blumenschein G, et al. Final efficacy outcomes of atezolizumab with chemoradiation for unresectable NSCLC: the phase II DETERRED trial. *Lung Cancer* (2022) 174:112–7. doi:10.1016/j.lungcan.2022.10.006

26. Manapov F, Kenndoff S, Kasmann L NICOLAS, DETERRED and KEYNOTE 799: focus on escalation of conventionally fractionated chemoradiotherapy by immune checkpoint inhibition in unresectable stage III non-small cell lung cancer. *Transl Lung Cancer Res* (2022) 11(4):702–5. doi:10.21037/tlcr-21-950

27. Jabbour SK, Lee KH, Frost N, Breder V, Kowalski DM, Pollock T, et al. Pembrolizumab plus concurrent chemoradiation therapy in patients with unresectable, locally advanced, stage III non-small cell lung cancer: the phase 2 KEYNOTE-799 nonrandomized trial. *JAMA Oncol* (2021) 7(9):1–9. doi:10.1001/jamaoncol.2021.2301

28. Carter L, Apte V, Shukla A, Ghose A, Mamidi R, Petohazi A, et al. Stage 3 N2 lung cancer: a multidisciplinary therapeutic conundrum. *Curr Oncol Rep* (2024) 26(1):65–79. doi:10.1007/s11912-023-01486-2

29. Wu YL, Zhou Q, Chen M, Pan Y, Jian O, Hu D, et al. OA02.05 sugemalimab vs placebo after cCRT or sCRT in pts with unresectable stage III NSCLC: final PFS analysis of a phase 3 study. *J Thorac Oncol* (2022) 17(9):S7–S8. doi:10.1016/j.jtho.2022.07.021

30. Peters S, Felip E, Dafni U, Tufman A, Guckenberger M, Álvarez R, et al. Progression-free and overall survival for concurrent nivolumab with standard concurrent chemoradiotherapy in locally advanced stage IIIA-B NSCLC: results from the European thoracic oncology platform NICOLAS phase II trial (European thoracic oncology platform 6-14). *J Thorac Oncol* (2021) 16(2):278–88. doi:10.1016/j.jtho.2020.10.129

31. Filippi AR, Dziadziuszko R, García Campelo MR, Paoli JB, Sawyer W, Díaz Pérez IE. DUART: durvalumab after radiotherapy in patients with unresectable, stage III NSCLC who are ineligible for chemotherapy. *Future Oncol* (2021) 17(34):4657–63. doi:10.2217/fon-2021-0952

32. Ma L, Deng L, Peng J, Yu J, Meng X. Chemotherapy-free radiotherapy combined with immune checkpoint inhibitors: a new regimen for locally advanced non-small cell lung cancer? *Cancer Biol Med* (2024) 20(12):1035–46. doi:10.20892/j.issn.2095-3941.2023.0402

33. Lin SH, Pugh SL, Tsao AS, Edelman MJ, Doemer A, Simone CB, et al. Safety results of NRG-LU004: phase I trial of accelerated or conventionally fractionated radiotherapy combined with durvalumab in PD-L1–high locally advanced non-small cell lung cancer. *J Clin Oncol* (2022) 40(16_Suppl. l):8513. doi:10.1200/jco.2022.40.16_suppl.8513

34. De Ruysscher D, Ramalingam S, Urbanic J, Gerber DE, Tan DSW, Cai J, et al. CheckMate 73L: a phase 3 study comparing nivolumab plus concurrent chemoradiotherapy followed by nivolumab with or without ipilimumab versus concurrent chemoradiotherapy followed by durvalumab for previously untreated, locally advanced stage III non-small-cell lung cancer. *Clin Lung Cancer* (2022) 23(3):e264–e268. doi:10.1016/j.cllc.2021.07.005

35. Mazieres J, Drilon A, Lusque A, Mhanna L, Cortot AB, Mezquita L, et al. Immune checkpoint inhibitors for patients with advanced lung cancer and oncogenic driver alterations: results from the IMMUNOTARGET registry. *Ann Oncol* (2019) 30(8):1321–8. doi:10.1093/annonc/mdz167

36. Passiglia F, Bironzo P, Bertaglia V, Listì A, Garbo E, Scagliotti GV. Optimizing the clinical management of EGFR-mutant advanced non-small cell lung cancer: a literature review. *Transl Lung Cancer Res* (2022) 11(5):935–49. doi:10.21037/tlcr-22-1

37. Loh J, Low JL, Sachdeva M, Low PQ, Wong RSJ, Huang Y, et al. Management of oncogene driven locally advanced unresectable non-small cell lung cancer. *Expert Rev Anticancer Ther* (2023) 23(9):913–26. doi:10.1080/14737140.2023.2245140

38. Hellyer JA, Aredo JV, Das M, Ramchandran K, Padda SK, Neal JW, et al. Role of consolidation durvalumab in patients with EGFR- and HER2-mutant unresectable stage III NSCLC. *J Thorac Oncol* (2021) 16(5):868–72. doi:10.1016/j.jtho.2020.12.020

39. Lu S, Casarini I, Kato T, Cobo M, Özgüroğlu M, Hodge R, et al. Osimertinib maintenance after definitive chemoradiation in patients with unresectable EGFR mutation positive stage III non-small-cell lung cancer: LAURA trial in progress. *Clin Lung Cancer* (2021) 22(4):371–5. doi:10.1016/j.cllc.2020.11.004

40. Passaro A, Leighl N, Blackhall F, Popat S, Kerr K, Ahn MJ, et al. ESMO expert consensus statements on the management of EGFR mutant non-small-cell lung cancer. *Ann Oncol* (2022) 33(5):466–87. doi:10.1016/j.annonc.2022.02.003

41. Addeo A, Passaro A, Malapelle U, Banna GL, Subbiah V, Friedlaender A. Immunotherapy in non-small cell lung cancer harbouring driver mutations. *Cancer Treat Rev* (2021) 96:102179. doi:10.1016/j.ctrv.2021.102179

42. Attili I, Passaro A, Corvaja C, Trillo Aliaga P, Del Signore E, Spitaleri G, et al. Immune checkpoint inhibitors in EGFR-mutant non-small cell lung cancer: a systematic review. *Cancer Treat Rev* (2023) 119:102602. doi:10.1016/j.ctrv.2023.102602

43. Senan S, Bahce I Pulmonary toxicity in patients treated with immune checkpoint inhibitors and radiation. *Ann Oncol* (2020) 31(12):1597–8. doi:10.1016/j.annonc.2020.10.476

44. Suresh K, Naidoo J Lower survival in patients who develop pneumonitis following immunotherapy for lung cancer. *Clin Lung Cancer* (2020) 21(3):e169–70. doi:10.1016/j.cllc.2019.10.009

45. Berner F, Bomze D, Diem S, Ali OH, Fässler M, Ring S, et al. Association of checkpoint inhibitor-induced toxic effects with shared cancer and tissue antigens in non-small cell lung cancer. *JAMA Oncol* (2019) 5(7):1043–7. doi:10.1001/jamaoncol.2019.0402

46. Fukihara J, Sakamoto K, Koyama J, Ito T, Iwano S, Morise M, et al. Prognostic impact and risk factors of immune-related pneumonitis in patients with non-small-cell lung cancer who received programmed death 1 inhibitors. *Clin Lung Cancer* (2019) 20(6):442–50. doi:10.1016/j.cllc.2019.07.006

47. Fukihara J, Sakamoto K, Koyama J, Ito T, Iwano S, Morise M, et al. Reply to "prognostic impact and risk factors of immune-related pneumonitis in patients with non-small-cell lung cancer who received programmed death-1 inhibitors. *Clin Lung Cancer* (2020) 21(3):e205. doi:10.1016/j.cllc.2019.11.013

48. Akkad N, Thomas TS, Luo S, Knoche E, Sanfilippo KM, Keller JW. A real-world study of pneumonitis in non-small cell lung cancer patients receiving durvalumab following concurrent chemoradiation. *J Thorac Dis* (2023) 15(12):6427–35. doi:10.21037/jtd-22-1604

49. Delaunay M, Cadranel J, Lusque A, Meyer N, Gounant V, Moro-Sibilot D, et al. Immune-checkpoint inhibitors associated with interstitial lung disease in cancer patients. *Eur Respir J* (2017) 50(2):1700050. doi:10.1183/13993003.00050-2017

50. Naidoo J, Vansteenkiste JF, Faivre-Finn C, Özgüroğlu M, Murakami S, Hui R, et al. Characterizing immune-mediated adverse events with durvalumab in patients with unresectable stage III NSCLC: a post-hoc analysis of the PACIFIC trial. *Lung Cancer* (2022) 166:84–93. doi:10.1016/j.lungcan.2022.02.003

51. Haanen J, Obeid M, Spain L, Carbonnel F, Wang Y, Robert C, et al. Management of toxicities from immunotherapy: ESMO Clinical Practice Guideline for diagnosis, treatment and follow-up. *Ann Oncol* (2022) 33(12):1217–38. doi:10.1016/j.annonc.2022.10.001

52. Massaccesi M, Calcagni ML, Spitilli MG, Cocciolillo F, Pelligrò F, Bonomo L, et al. ^{18}F-FDG PET-CT during chemo-radiotherapy in patients with non-small cell lung cancer: the early metabolic response correlates with the delivered radiation dose. *Radiat Oncol* (2012) 7:106. doi:10.1186/1748-717X-7-106

53. Delasos L, Wei W, Hassan KA, Pennell NA, Patil P, Stevenson J. Clinical outcomes with pembrolizumab-based therapies in recurrent/refractory NSCLC after chemoradiation and consolidative durvalumab. *Clin Lung Cancer* (2023) 24(6):e205–e213. doi:10.1016/j.cllc.2023.04.008

Pathology & Oncology Research | frontiers

TYPE Systematic Review
PUBLISHED 20 June 2024
DOI 10.3389/pore.2024.1611773

Check for updates

OPEN ACCESS

EDITED BY
Nora Bittner,
National Koranyi Institute of TB and Pulmonology, Hungary

*CORRESPONDENCE
Xiaoyang Xie,
13990559066@163.com

RECEIVED 21 March 2024
ACCEPTED 11 June 2024
PUBLISHED 20 June 2024

CITATION
Wang Y, Lei Y, Zheng D, Yang Y, Luo L, Li J and Xie X (2024), Prognostic value of lung immune prognostic index in non-small cell lung cancer patients receiving immune checkpoint inhibitors: a meta-analysis.
Pathol. Oncol. Res. 30:1611773.
doi: 10.3389/pore.2024.1611773

COPYRIGHT
© 2024 Wang, Lei, Zheng, Yang, Luo, Li and Xie. This is an open-access article distributed under the terms of the Creative Commons Attribution License (CC BY). The use, distribution or reproduction in other forums is permitted, provided the original author(s) and the copyright owner(s) are credited and that the original publication in this journal is cited, in accordance with accepted academic practice. No use, distribution or reproduction is permitted which does not comply with these terms.

Prognostic value of lung immune prognostic index in non-small cell lung cancer patients receiving immune checkpoint inhibitors: a meta-analysis

Yi Wang, Yu Lei, Delai Zheng, Yanhui Yang, Lei Luo, Ji Li and Xiaoyang Xie*

Department of Thoracic Surgery, The First People's Hospital of Neijiang, Neijiang Affiliated Hospital of Chongqing Medical University, Neijiang, Sichuan, China

Background and Purpose: Until now, it has been difficult to accurately predict the efficacy of immunotherapy in patients with non-small cell lung cancer (NSCLC). A novel indicator, the lung immune prognostic index (LIPI), has shown relatively high prognostic value in patients with solid cancer. Therefore, this study aimed to further identify the association between LIPI and the survival of patients with NSCLC who receive immune checkpoint inhibitors (ICIs).

Methods: Several electronic databases were searched for available publications up to April 23, 2023. Immunotherapy outcomes included overall survival (OS), progression-free survival (PFS), and hazard ratios (HRs) with 95% confidence intervals (CIs). Subgroup analysis based on the study design and comparison of the LIPI was conducted.

Results: In this meta-analysis, 21 studies with 9,010 patients were included in this meta-analysis. The pooled results demonstrated that elevated LIPI was significantly associated with poor OS (HR = 2.50, 95% CI:2.09–2.99, $p < 0.001$) and PFS (HR = 1.77, 95% CI:1.64–1.91, $p < 0.001$). Subgroup analyses stratified by study design (retrospective vs. prospective) and comparison of LIPI (1 vs. 0, 2 vs. 0, 1–2 vs. 0, 2 vs. 1 vs. 0, 2 vs. 0–1 and 2 vs. 1) showed similar results.

Conclusion: LIPI could serve as a novel and reliable prognostic factor in NSCLC treated with ICIs, and elevated LIPI predicts worse prognosis.

KEYWORDS

lung immune prognostic index, non-small cell lung cancer, immune checkpoint inhibitor, prognosis, meta-analysis

Introduction

Lung cancer remains the most common malignancy and leading cause of tumor-related deaths worldwide [1, 2]. Non-small cell lung cancer (NSCLC) accounts for approximately 85% of all lung cancer cases [3]. Despite great advances in early screening, surgical techniques, and adjuvant therapies for NSCLC, the overall prognosis remains poor, representing a relatively high risk of recurrence and therapeutic resistance [4, 5]. In the last few years, immunotherapy has become an important treatment option for NSCLC, especially for patients with advanced-stage and metastatic NSCLC. Unfortunately, less than 20% of patients could benefit from immunotherapy [6].

In clinics, immune checkpoint inhibitors (ICIs), particularly anti-programmed death ligand 1 (PD-L1)/programmed death 1 (PD-1) antibodies, are widely used as first- or second-line treatments for metastatic/advanced NSCLC alone or in combination with chemotherapy. However, as mentioned above, the number of patients who benefit from ICIs is fairly limited [6]. Thus, accurate and effective indicators to predict the efficacy of ICIs are urgently needed to help select potential beneficiaries of ICIs. Overall, PD-L1 expression and tumor mutation burden (TMB) are the most commonly used biomarkers to select ICI-advantaged populations and predict prognosis. Nevertheless, the predictive effect of these two biomarkers on ICI efficacy is not satisfactory in clinical practice [7, 8]. Patients with high PD-L1 expression are more likely to experience better survival, but a subset of patients do not benefit from immunotherapy [9, 10]. Therefore, further exploration of effective predictive indicators for the prognosis of ICIs treated NSCLC is required.

Since the immune checkpoint pathway includes an important circulatory phase, changes in some parameters based on peripheral blood may be associated with the response to immunotherapy. Increasing evidence suggests that inflammatory responses play an essential role in the development and progression of cancers [11, 12]. The inflammatory process in the body is considered to be the immune resistance mechanism in cancer patients, which promotes the growth and spread of tumor cells and activates the carcinogenic signaling pathway [11, 12]. Some biomarkers, such as the neutrophil-to-lymphocyte ratio (NLR), derived neutrophil-to-lymphocyte ratio (dNLR), and platelet-to-lymphocyte ratio (PLR) have been used to detect inflammatory status and predict prognosis in various cancers, including NSCLC [11–14]. The lung immune prognostic index (LIPI) is a novel indicator based on a dNLR >3 and lactate dehydrogenase (LDH) > upper limit of normal range (ULN), which was first reported by Mezquita et al. [15]. Patients were divided into three groups based on the number of risk factors from the LIPI: low-risk, intermediate-risk, and high-risk groups with 0, 1, and 2 risk factors, respectively. Previous studies have revealed that pretreatment LIPI play a role in predicting the therapeutic outcomes of ICIs in patients with solid cancers. However, whether it can predict the prognosis of ICIs ICI-treated NSCLC remains unclear.

Therefore, this meta-analysis aimed to further identify the association between LIPI and survival of NSCLC patients receiving ICIs, which might contribute to the selection of an advantaged population and improvement of the therapeutic efficacy of immunotherapy among NSCLC patients.

Materials and methods

The current meta-analysis was performed according to the Preferred Reporting Items for Systematic Reviews and Meta-Analyses 2020 [16].

Literature search

The PubMed, EMBASE, Web of Science, and CNKI databases were searched from inception to April 23, 2023. The following terms were used for the search: PD-1, PD-L1, CTLA-4, ICIs, immune checkpoint inhibitor, lung, pulmonary, cancer, tumor, carcinoma, neoplasm, LIPI, lung immune prognostic index, survival, prognosis, and prognostic. The detailed search strategies were as follows: (PD-1 OR PD-L1 OR CTLA-4 OR ICIs OR immune checkpoint inhibitor) AND (lung OR pulmonary) AND (cancer OR tumor OR carcinoma OR neoplasm) AND (LIPI OR lung immune prognostic index) AND (survival OR prognosis OR prognostic). Free text and Medical Subject Headings terms were also applied. All the references cited in the included studies were reviewed.

Inclusion criteria

Studies that met the following criteria were included:1) patients were pathologically diagnosed with primary NSCLC; 2) patients who received ICIs with or without other combined therapies such as chemotherapy; 3) LIPI score was assessed according to the dNLR values and LDH level before immunotherapy, and the association between LIPI and efficacy of immunotherapy was evaluated; 4) the overall survival (OS) and (or) progression-free survival (PFS) were defined as outcomes of immunotherapy; 5) hazard ratios (HRs) with 95% confidence intervals (CIs) for OS and PFS were directly reported in articles.

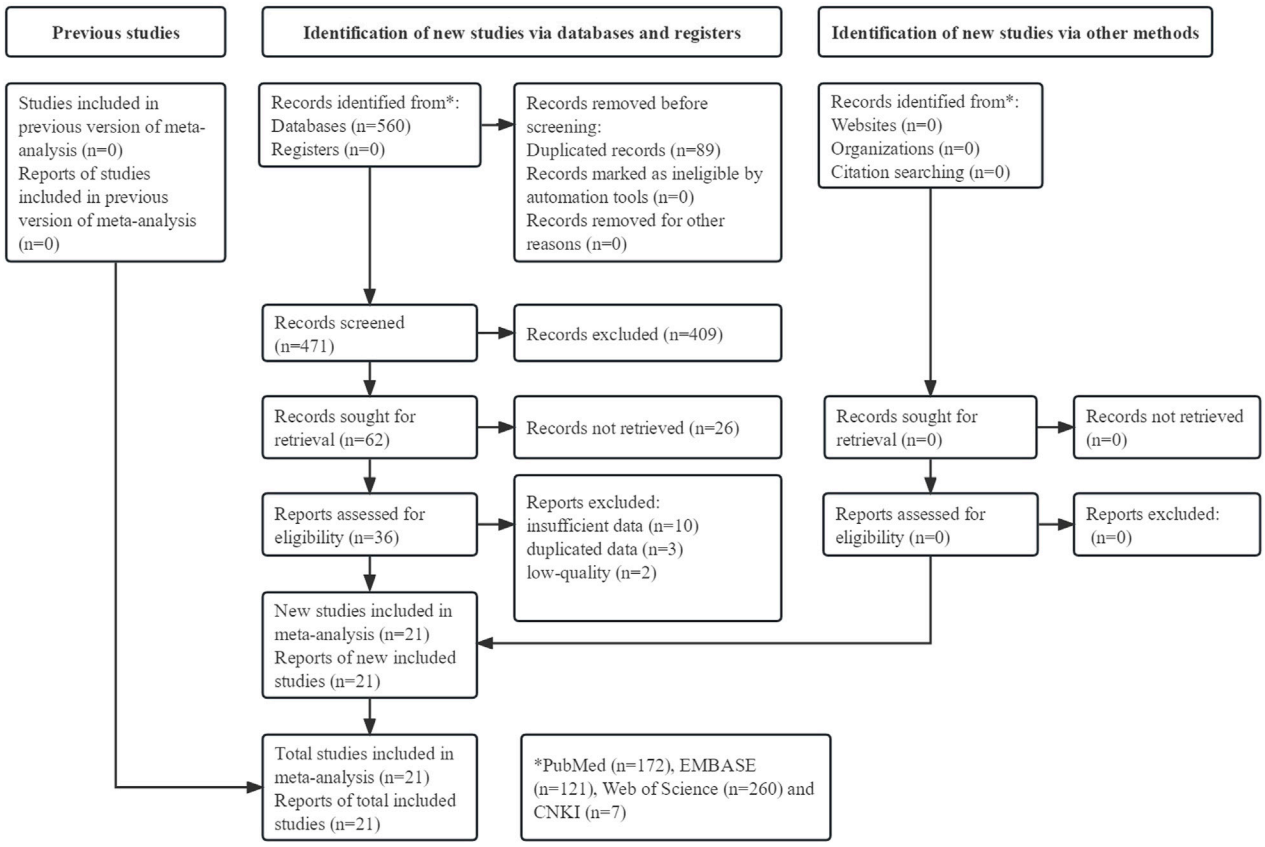

FIGURE 1
Prisma flow diagram of this meta-analysis.

Exclusion criteria

Studies that met any of the following criteria were excluded:1) low-quality studies; 2) letters, editorials, reviews, case reports, or animal trials; and 3) studies with insufficient or duplicated data.

Data extraction

The following information was collected from the included studies: name of first author, publication year, country, study design (retrospective or prospective), sample size, TNM stage, pathological type, detailed drugs of ICIs, threshold and comparison of LIPI, endpoint, HR, and 95% CI.

Quality assessment

Owing to the nature of the included studies, the Newcastle-Ottawa Scale (NOS) score system was used to evaluate the quality of the included studies. As mentioned above, only high-quality studies with an NOS score ≥6 were included.

The literature search, selection, information collection, and quality assessment were conducted by two authors independently and any disagreement was resolved by team discussion.

Statistical analysis

All statistical analyses were performed using STATA 12.0. Heterogeneity between studies was evaluated using I^2 statistics and Q test. If significant heterogeneity was observed ($I^2 > 50\%$ and/or $p < 0.1$), the random-effects model was applied; otherwise, the fixed-effects model was used. HRs and 95% CIs were combined to evaluate the association between the LIPI, OS, and PFS. Subgroup analysis based on study design (retrospective vs. prospective) and comparison of LIPI (1 vs. 0, 2 vs. 0, 1–2 vs. 0, 2 vs. 1 vs. 0, 2 vs. 0–1 and 2 vs. 1) were conducted. Sensitivity analysis was conducted to detect the sources of heterogeneity and assess the stability of the overall results. Furthermore, Begg's funnel plot and Egger's test were conducted to detect publication bias, and significant publication bias was defined as $p < 0.05$ [17–19].

TABLE 1 Basic characteristics of included studies.

Author	Year	Country	Study design	Sample size	TNM stage	Pathological type	ICIs	Threshold and comparison of LIPI	Endpoint	NOS
Mezquita [15]	2018	France	R	466	IIIB-IV	Mixed	Nivolumab, pembrolizumab, atezolizumab, durvalumab, and durvalumab-ipilimumab	0: dNLR≤3 and LDH ≤ ULN; 1: dNLR >3 or LDH > ULN; 2: dNLR >3 and LDH > ULN; 0 vs. 1 and 0 vs. 2	OS, PFS	7
Kazandjian [20]	2019	United States	P	1,368	IV	Mixed	NR	0: dNLR≤3 and LDH ≤ ULN; 1: dNLR >3 or LDH > ULN; 2: dNLR >3 and LDH > ULN; 0 vs. 2 and 1 vs. 2	OS, PFS	8
Ruiz-Bañobre [21]	2019	Spain	R	188	IIIB-IV	Mixed	Nivolumab	0: dNLR≤3 and LDH ≤ ULN; 1: dNLR >3 or LDH > ULN; 2: dNLR >3 and LDH > ULN; 0 vs. 1 vs. 2	OS, PFS	8
Sorich [22]	2019	Australia	P	1,489	Advanced	Mixed	Atezolizumab	0: dNLR≤3 and LDH ≤ ULN; 1: dNLR >3 or LDH > ULN; 2: dNLR >3 and LDH > ULN; 0 vs. 1 and 0 vs. 2	OS, PFS	7
Mazzaschi [23]	2020	Italy	P	109	IV	Mixed	NR	0: dNLR≤3 and LDH ≤ ULN; 1: dNLR >3 or LDH > ULN; 2: dNLR >3 and LDH > ULN; 0 vs. 1 vs. 2	OS, PFS	8
Wang [24]	2020	China	R	330	IIIB-IV	Mixed	Nivolumab, pembrolizumab, atezolizumab, and other PD-1/PD-L1 inhibitors	0: dNLR≤3 and LDH ≤ ULN; 1: dNLR >3 or LDH > ULN; 2: dNLR >3 and LDH > ULN; 0vs 1 and 0 vs. 2	OS, PFS	8
Ali [25]	2021	China	R	73	IV	Mixed	Pembrolizumab, nivolumab, camrelizumab and atezolizumab	0: dNLR≤3 and LDH ≤ ULN; 1: dNLR >3 or LDH > ULN; 2: dNLR >3 and LDH > ULN; 0 vs. 1–2	OS, PFS	6
Galland [27]	2021	France	R	231	NR	Adenocarcinoma	PD-1/PD-L1 inhibitors	0: dNLR≤3 and LDH ≤ ULN; 1: dNLR >3 or LDH > ULN; 2: dNLR >3 and LDH > ULN; 0 vs. 1–2	OS, PFS	6

(Continued on following page)

TABLE 1 (*Continued*) Basic characteristics of included studies.

Author	Year	Country	Study design	Sample size	TNM stage	Pathological type	ICIs	Threshold and comparison of LIPI	Endpoint	NOS
Grosjean [28]	2021	Canada	R	327	I-IV	Mixed	Pembrolizumab	0: dNLR≤3 and LDH ≤ ULN; 1: dNLR >3 or LDH > ULN; 2: dNLR >3 and LDH > ULN; 0 vs. 1–2	OS	6
Hopkins [29]	2021	Australia	P	1,148	Advanced	Mixed	Atezolizumab	0: dNLR≤3 and LDH ≤ ULN; 1: dNLR >3 or LDH > ULN; 2: dNLR >3 and LDH > ULN; 0 vs. 1 and 0 vs. 2	OS, PFS	6
Mountzios [30]	2021	Greece	R	672	IV	Mixed	PD-L1 inhibitors	0: dNLR≤3 and LDH ≤ ULN; 1: dNLR >3 or LDH > ULN; 2: dNLR >3 and LDH > ULN; 0 vs. 1–2	OS, PFS	6
Chen [26]	2021	China	R	84	IIIB-IV	Mixed	PD-1/PD-L1 inhibitors	0: dNLR≤3 and LDH ≤ ULN; 1: dNLR >3 or LDH > ULN; 2: dNLR >3 and LDH > ULN; 0 vs. 1–2	OS, PFS	6
Chen [31]	2022	China	R	85	IV	Mixed	PD-1 inhibitors	0: dNLR≤3 and LDH ≤ ULN; 1: dNLR >3 or LDH > ULN; 2: dNLR >3 and LDH > ULN; 0 vs. 1–2	OS, PFS	6
De Giglio [32]	2022	Italy	R	182	IV	Mixed	NR	0: dNLR≤3 and LDH ≤ ULN; 1: dNLR >3 or LDH > ULN; 2: dNLR >3 and LDH > ULN; 0 vs. 1–2	OS	6
Holtzman [33]	2022	Israel	R	423	III-IV	Mixed	Pembrolizumab	0: dNLR≤3 and LDH ≤ ULN; 1: dNLR >3 or LDH > ULN; 2: dNLR >3 and LDH > ULN; 0 vs. 1–2	OS	6
Ortega-Franco [34]	2022	United Kingdom	R	113	III-IV	Mixed	Pembrolizumab	0: dNLR≤3 and LDH ≤ ULN; 1: dNLR >3 or LDH > ULN; 2: dNLR >3 and LDH > ULN; 0 vs. 1	OS, PFS	6

(Continued on following page)

TABLE 1 (*Continued*) Basic characteristics of included studies.

Author	Year	Country	Study design	Sample size	TNM stage	Pathological type	ICIs	Threshold and comparison of LIPI	Endpoint	NOS
Tanaka [35]	2022	Japan	R	237	I-IV	Mixed	NR	0: dNLR≤3 and LDH ≤ ULN; 1: dNLR >3 or LDH > ULN; 2: dNLR >3 and LDH > ULN; 0–1 vs. 2	OS, PFS	6
Zhou J [36]	2022	China	R	51	IIIB-IV	Mixed	PD-1 inhibitors	0: dNLR≤3 and LDH ≤ ULN; 1: dNLR >3 or LDH > ULN; 2: dNLR >3 and LDH > ULN; 0 vs. 1–2	PFS	6
Zhou S [37]	2022	China	R	53	IV	Mixed	Pembrolizumab, nivolumab, sintilimab, camrelizumab, tislelizumab, and atezolizumab	0: dNLR≤3 and LDH ≤ ULN; 1: dNLR >3 or LDH > ULN; 2: dNLR >3 and LDH > ULN; 0–1 vs. 2	PFS	6
Zhou Y [38]	2022	China	R	86	I-IV	Mixed	Pembrolizumab, nivolumab and sindillimab	0: dNLR≤3 and LDH ≤ ULN; 1: dNLR >3 or LDH > ULN; 2: dNLR >3 and LDH > ULN; 0 vs. 1 and 0 vs. 2	PFS	7
Huang [39]	2023	China	R	147	IIIB-IV	Mixed	Nivolumab, pembrolizumab, atezolizumab, durvalumab, treprizumab, carrelizumab, sintilimab and tislelizumab	0: dNLR≤3 and LDH ≤ ULN; 1: dNLR >3 or LDH > ULN; 2: dNLR >3 and LDH > ULN; 0 vs. 2 and 1 vs. 2	PFS	7

ICIs: immune checkpoint inhibitors; LIPI: lung immune prognostic index; NOS: Newcastle-Ottawa Scale; R: retrospective; P: prospective; NR: not reported; PD-1: programmed death-1; PD-L1: programmed cell death 1 ligand 1; dNLR: derived neutrophil-to-lymphocyte ratio; ULN: upper limit of normal level; LDH: lactate dehydrogenase; OS: overall survival; PFS: progression-free survival.

Results

Literature search and selection

The detailed process is illustrated in Figure 1. Initially, 560 records were searched from four databases and a total of 21 studies were included [15, 20–39].

Basic characteristics of included studies

A total of 9,010 participants were enrolled in 21 studies published between 2018 and 2023. Most of the included studies were retrospective and focused on patients with advanced NSCLC. The sample size ranged from 51 to 1,489, and all studies applied the same definition of LIPI risk grading: LIPI 0, dNLR≤3 and LDH ≤ ULN; LIPI 1, dNLR >3 or LDH > ULN; and LIPI 2, dNLR >3 and LDH > ULN. Specific data are presented in Table 1.

Association between LIPI and OS and PFS

Seventeen studies explored the relationship between LIPI and OS in NSCLC patients receiving ICIs. The pooled results showed that elevated LIPI predicted poorer OS (HR = 2.50, 95% CI: 2.09–2.99, $p < 0.001$; $I^2 = 68.6\%$, $p < 0.001$), and subgroup analysis based on the study design showed the same results (Figure 2A).

Eighteen studies identified a relationship between LIPI and PFS in immunotherapy-treated NSLC. The pooled results demonstrated

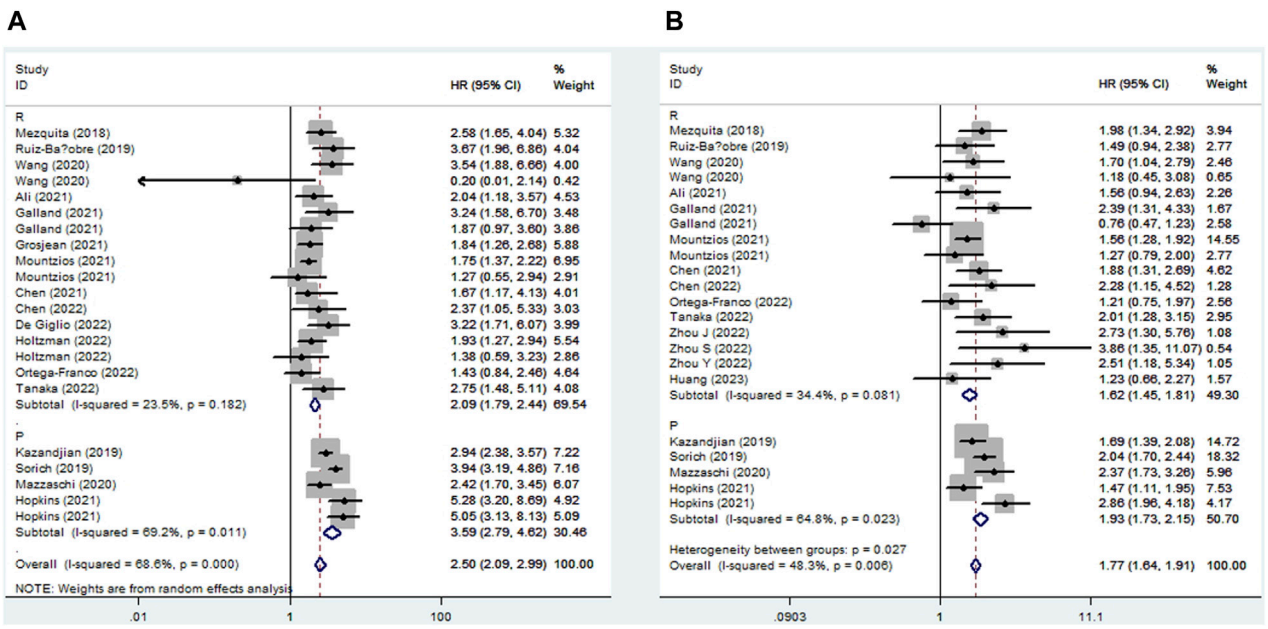

FIGURE 2
Subgroup analysis based on study design for the association between LIPI and overall survival **(A)** and progression-free survival **(B)** of non-small cell lung cancer patients receiving immune checkpoint inhibitors.

that elevated LIPI was obviously associated with poor PFS (HR = 1.77, 95% CI:1.64–1.91, $p < 0.001$; $I^2 = 48.3\%$, $p = 0.006$), and subgroup analysis stratified by study design further verified the significant relationship between LIPI and PFS (Figure 2B).

Subgroup analysis for OS

In this meta-analysis, we conducted a subgroup analysis based on a comparison of the LIPI and study design. The pooled results further demonstrated that elevated LIPI was significantly related to worse OS (LIPI 1 vs. 0: HR = 1.72, 95% CI: 1.52–1.94, $p < 0.001$; LIPI 2 vs. 0: HR = 3.81, 95% CI: 2.84–5.10, $p < 0.001$; LIPI 1–2 vs. 0: HR = 1.90, 95% CI: 1.64–2.20, $p < 0.001$; LIPI 2 vs. 1 vs. 0: HR = 2.68, 95% CI: 1.97–3.64, $p < 0.001$; LIPI 2 vs. 0–1: HR = 2.75, 95% CI: 1.48–5.11, $p < 0.001$; LIPI 2 vs. 1: HR = 1.69, 95% CI: 1.37–2.08, $p < 0.001$). In addition, a more specific subgroup analysis based on study design for the comparison of LIPI 1 vs. 0 (Figure 3A), LIPI 2 vs. 0 (Figure 3B), LIPI 1–2 vs. 0 (Figure 3C), and LIPI 2 vs. 1 vs. 0 (Figure 3D) further identified the above findings. Detailed results are presented in Table 2.

Subgroup analysis for PFS

Similarly, subgroup analysis for PFS based on the comparison of LIPI and the study design was performed. Pooled results revealed that elevated LIPI was obviously associated with poorer PFS (LIPI 1 vs. 0: HR = 1.44, 95% CI: 1.31–1.57, $p < 0.001$; LIPI 2 vs. 0: HR = 1.91, 95% CI: 1.69–2.16, $p < 0.001$; LIPI 1–2 vs. 0: HR = 1.60, 95% CI: 1.26–2.04, $p < 0.001$; LIPI 2 vs. 1 vs. 0: HR = 1.94, 95% CI: 1.24–3.05, $p = 0.004$; LIPI 2 vs. 0–1: HR = 2.22, 95% CI: 1.47–3.36, $p < 0.001$; LIPI 2 vs. 1: HR = 1.25, 95% CI: 1.02–1.53, $p = 0.030$). Furthermore, specific subgroup analysis based on study design for the comparison of LIPI 1 vs. 0 (Figure 4A), LIPI 2 vs. 0 (Figure 4B), LIPI 1–2 vs. 0 (Figure 4C), and LIPI 2 vs. 1 vs. 0 (Figure 4D) further confirmed the above findings. The detailed results are presented in Table 2.

Sensitivity analysis

Sensitivity analysis for the association between LIPI and OS and PFS was performed, which demonstrated that the pooled results of this meta-analysis were stable, and none of the included studies had an obvious impact on the relationship between LIPI and OS (Figure 5A) and PFS (Figure 5B) among immunotherapy-treated NSCLC patients.

Publication bias

The Begg's funnel plots for OS (Figure 6A) and PFS (Figure 6B) were both symmetrical, and the *p*-values of

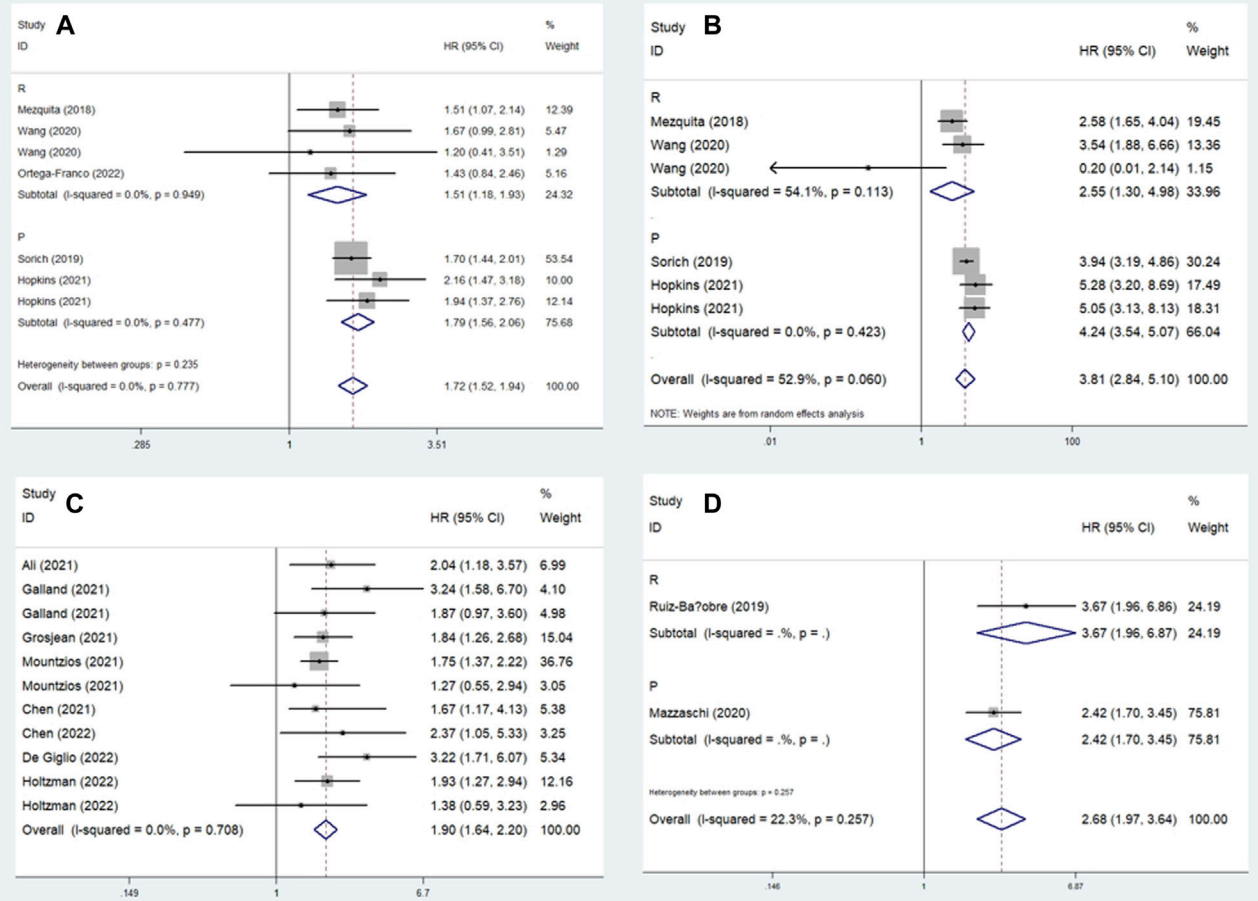

FIGURE 3
Subgroup analysis based on study design for the association between LIPI and overall survival of non-small cell lung cancer patients receiving immune checkpoint inhibitors. **(A)** LIPI 1 vs. 0; **(B)** LIPI 2 vs. 0; **(C)** LIPI 1–2 vs. 0; **(D)** LIPI 2 vs. 1 vs. 0.

Egger's test for OS and PFS were 0.208 and 0.992, respectively. Thus, no significant publication bias was observed in this meta-analysis.

Discussion

This meta-analysis explored the predictive role of LIPI for the long-term survival of NSCLC patients who received ICIs based on current evidence, and the pooled results showed that LIPI was significantly associated with OS and PFS in this group of patients. Patients with elevated LIPIs were more likely to have a worse prognosis than patients with good LIPIs. Therefore, the LIPI could serve as a novel and reliable prognostic indicator in patients with NSCLC receiving ICIs.

The invasiveness of malignant tumors depends on the nature of tumor cells and their microenvironment. Previous studies have indicated that inflammation is a recognized feature of cancer, and inflammatory reactions play a crucial role in the process of carcinogenesis [40]. On the one hand, in malignant solid tumors, inflammatory stimulation leads to immune cell infiltration, angiogenesis, and fibroblast proliferation [41, 42]. In contrast, it is one of the mechanisms of immune tolerance, promoting tumor growth and dissemination, and activating oncogenic signaling pathways in cancer patients [43]. The dNLR was calculated using the neutrophil and lymphocyte counts. Neutrophils are key participants in tumor inflammation and immunity, and participate in tumor progression. Studies have found that neutrophils can produce vascular endothelial growth factor (VEGF), which plays an important role in mediating tumor angiogenesis and is a powerful immunosuppressive factor of natural and adaptive anti-tumor immunity [44]. In addition, neutrophil-derived proteases can degrade cytokines and chemokines and reshape the extracellular matrix, and neutrophil elastase in tumor cells can overactivate the PI3K pathway, further accelerating uncontrolled tumor proliferation [45]. It has been reported

TABLE 2 Results of meta-analysis.

	No. of studies	Hazard ratio	95% confidence interval	*p*-Value	I^2 (%)	*p*-Value
Overall survival						
Overall	17	2.50	2.09–2.99	<0.001	68.6	<0.001
Retrospective	13	2.09	1.79–2.44	<0.001	23.5	0.182
Prospective	4	3.59	2.79–4.62	<0.001	69.2	0.011
LIPI 1 vs. 0	5	1.72	1.52–1.94	<0.001	0.0	0.777
Retrospective	3	1.51	1.18–1.93	0.001	0.0	0.949
Prospective	2	1.79	1.56–2.06	<0.001	0.0	0.477
LIPI 2 vs. 0	4	3.81	2.84–5.10	<0.001	52.9	0.423
Retrospective	2	2.55	1.30–4.98	0.006	54.1	0.113
Prospective	2	4.24	3.54–5.07	<0.001	0.0	0.423
LIPI 1–2 vs. 0	8	1.90	1.64–2.20	<0.001	0.0	0.708
Retrospective	8	1.90	1.64–2.20	<0.001	0.0	0.708
LIPI 2 vs. 1 vs. 0	2	2.68	1.97–3.64	<0.001	22.3	0.257
Retrospective	1	3.67	1.96–6.87	<0.001	—	—
Prospective	1	2.42	1.70–3.45	<0.001	—	—
LIPI 2 vs. 0–1	1	2.75	1.48–5.11	<0.001	—	—
Retrospective	1	2.75	1.48–5.11	<0.001	—	—
LIPI 2 vs. 1	1	1.69	1.37–2.08	<0.001	—	—
Prospective	1	1.69	1.37–2.08	<0.001	—	—
Progression-free survival						
Overall	18	1.77	1.64–1.91	<0.001	48.3	0.006
Retrospective	14	1.62	1.45–1.81	<0.001	34.4	0.081
Prospective	4	1.93	1.73–2.15	<0.001	64.8	0.023
LIPI 1 vs. 0	6	1.44	1.31–1.57	<0.001	0.0	0.979
Retrospective	4	1.35	1.13–1.61	0.001	0.0	0.927
Prospective	2	1.47	1.32–1.63	<0.001	0.0	0.982
LIPI 2 vs. 0	6	1.91	1.69–2.16	<0.001	41.0	0.105
Retrospective	4	1.75	1.36–2.24	<0.001	0.0	0.529
Prospective	2	1.97	1.71–2.27	<0.001	75.0	0.018
LIPI 1–2 vs. 0	6	1.60	1.26–2.04	<0.001	55.3	0.028
Retrospective	6	1.60	1.26–2.04	<0.001	55.3	0.028
LIPI 2 vs. 1 vs. 0	2	1.94	1.24–3.05	0.004	61.8	0.106
Retrospective	1	1.49	0.94–2.37	0.092	—	—
Prospective	1	2.37	1.73–3.25	<0.001	—	—
LIPI 2 vs. 0–1	2	2.22	1.47–3.36	<0.001	19.9	0.264
Retrospective	2	2.22	1.47–3.36	<0.001	19.9	0.264
LIPI 2 vs. 1	2	1.25	1.02–1.53		0.0	0.652
Retrospective	1	1.09	0.58–2.04	0.788	—	—
Prospective	1	1.27	1.03–1.57	0.027	—	—

LIPI: lung immune prognostic index.

that T cells producing interleukin (IL)-17 can release CXC chemokines to supplement neutrophils, and IL17a is involved in resistance to ICIs [46]. Therefore, higher dNLR levels may reflect negative inflammation and contribute to resistance to ICIs. Peripheral blood lymphocyte count is considered a predictive factor for the prognosis of various cancers [47]. Lymphocytes play an important role in tumor-related immunity, have potential anti-tumor immune functions to inhibit tumor development, participate in cytotoxic cell death and cytokine production, and inhibit tumor cell proliferation and metastasis through the immune response to cancer [48].

LDH is widely distributed in major human organs and catalyzes the conversion of lactate and pyruvate. It is an indicator of tumor burden, cell damage, and necrosis. Studies have shown that elevated LDH levels are an adverse prognostic factor for tumors [49, 50]. Elevated LDH levels are a product of enhanced tumor glycolysis and hypoxia-induced tumor necrosis [51]. On one hand, in tumors with increased glycolytic activity, both aerobic and anaerobic glycolysis under hypoxia can affect immune cell function due to glucose deficiency or tumor acidity [52]. Furthermore, hypoxia itself or the excessive expression of hypoxia-

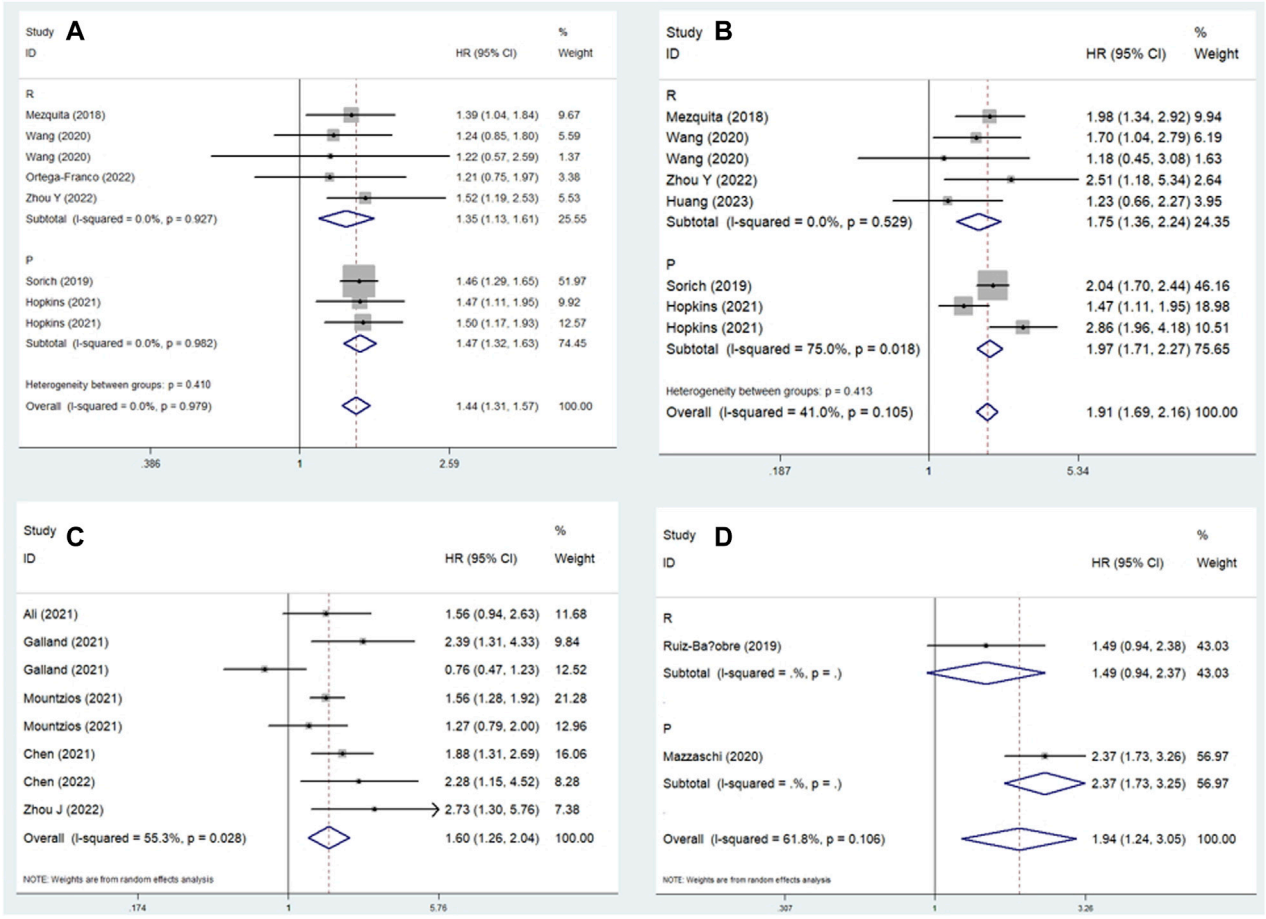

FIGURE 4
Subgroup analysis based on study design for the association between LIPI and progression-free survival of non-small cell lung cancer patients receiving immune checkpoint inhibitors. **(A)** LIPI 1 vs. 0; **(B)** LIPI 2 vs. 0; **(C)** LIPI 1–2 vs. 0; **(D)** LIPI 2 vs. 1 vs. 0.

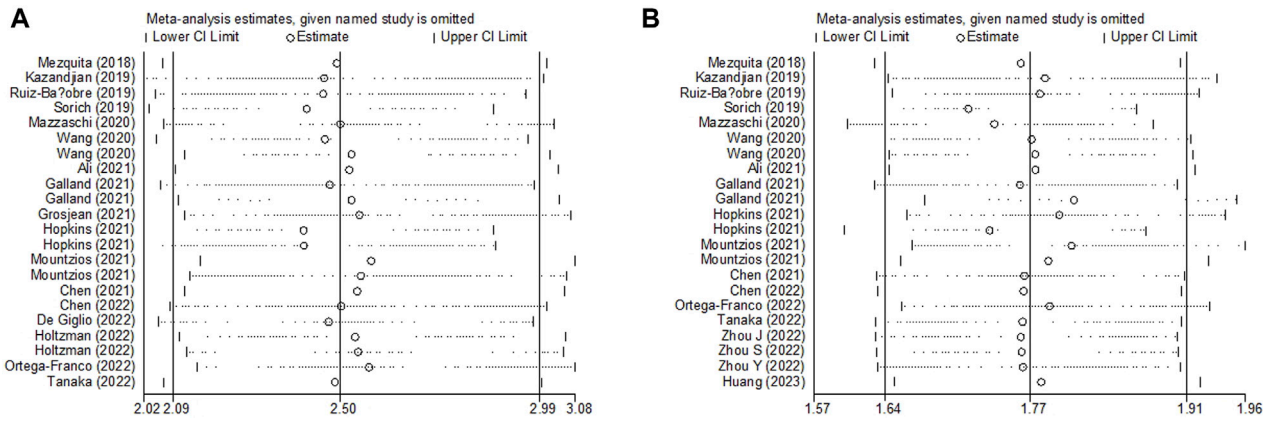

FIGURE 5
Sensitivity analysis about the association between LIPI and overall survival **(A)** and progression-free survival **(B)** of non-small cell lung cancer patients receiving immune checkpoint inhibitors.

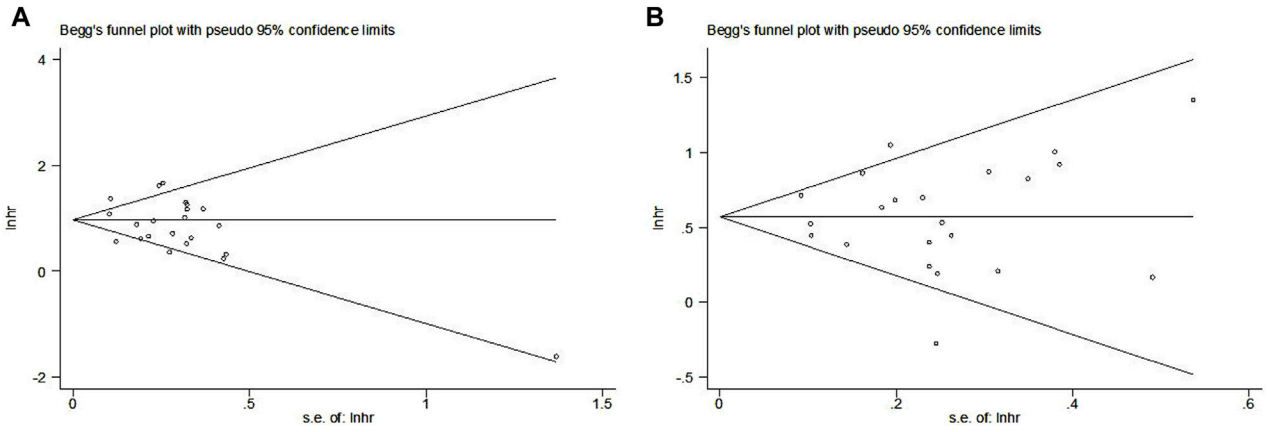

FIGURE 6
Begg's funnel plots for the association between LIPI and overall survival **(A)** and progression-free survival **(B)** of non-small cell lung cancer patients receiving immune checkpoint inhibitors.

regulated factors in highly glycolytic tumors may affect antitumor immunity [53]. In addition, the main switch for hypoxia-induced angiogenesis, hypoxia-inducible factor-1 (HIF-1), is activated by hypoxia and upregulates VEGF in tumors [54]. VEGF promotes tumor angiogenesis by inducing the proliferation and survival of endothelial cells, forming a large number of malformed and dysfunctional neovasculatures in the tumor [55]. These tumor blood vessels interfere with the active anticancer immune system and inhibit the therapeutic effect of ICI treatment. Therefore, LDH levels can affect the efficacy of ICIs.

Liu et al. included 12 studies with 4,883 solid cancer patients who received ICIs treatment and demonstrated that elevated pretreatment LIPI was significantly associated with worse OS (HR = 3.33, 95% CI:2.64–4.21, $p < 0.001$; HR = 1.71, 95%CI 1.43–2.04, $p < 0.001$) and PFS (HR = 2.73, 95% CI: 2.00–3.73, $p < 0.001$; HR = 1.43, 95%CI 1.28–1.61, $p < 0.001$) [56]. However, only six studies explored the relationship between pretreatment LIPI and survival, and five studies were included in the pooled analysis [56]. In another meta-analysis by Xie et al., four studies involving 7,373 advanced NSCLC patients receiving ICIs, targeted therapy, or chemotherapy and their results revealed that intermediate and poor LIPI predicted worse OS (HR = 1.61, 95% CI: 1.48–1.75, $p < 0.01$; HR = 2.74; 95% CI:2.26–3.33, $p < 0.01$) [57]. However, only three of the included studies identified the predictive role of pretreatment LIPI for OS in immunotherapy-treated NSCLC patients. Therefore, we performed this meta-analysis to determine the predictive value of LIPI for prognosis among patients with NSCLC receiving ICIs, and the pooled results indicated that LIPI could serve as a reliable prognostic factor in this group of patients.

This meta-analysis had several limitations that should be noted. First, all included studies were observational, and most of them were retrospectively conducted. Second, some of the included studies had relatively small sample sizes, which might have caused bias. Third, we were unable to conduct more subgroup analyses based on other parameters such as the pathological subtype, drugs of ICIs, and combinations of other therapies due to the lack of original data and sufficient information reported in the included studies.

Conclusion

Overall, LIPI could serve as a novel and reliable prognostic factor in NSCLC treated with ICIs, and intermediate LIPIs predict a worse prognosis. However, further high-quality studies are required to verify our findings.

Data availability statement

The original contributions presented in the study are included in the article/supplementary material, further inquiries can be directed to the corresponding author.

Author contributions

XX designed the study. YW, YL, and DZ performed the literature search and selection, collected the data, and wrote the paper. YY, LL, and JL performed statistical analysis and revised the manuscript. All authors contributed to the article and approved the submitted version.

Funding

The author(s) declare that no financial support was received for the research, authorship, and/or publication of this article.

Conflict of interest

The authors declare that the research was conducted in the absence of any commercial or financial relationships that could be construed as a potential conflict of interest.

References

1. Torre LA, Siegel RL, Jemal A. Lung cancer statistics. *Adv Exp Med Biol* (2016) 893:1–19. doi:10.1007/978-3-319-24223-1_1

2. Jenkins R, Walker J. 2022 cancer statistics: focus on lung cancer. *Future Oncol (London, England)* (2023) 1–11. doi:10.2217/fon-2022-1214

3. Siegel RL, Miller KD, Fuchs HE, Jemal A. Cancer statistics, 2021. *CA: a Cancer J clinicians* (2021) 71(1):7–33. doi:10.3322/caac.21654

4. Ju W, Zheng R, Zhang S, Zeng H, Sun K, Wang S, et al. Cancer statistics in Chinese older people, 2022: current burden, time trends, and comparisons with the US, Japan, and the Republic of Korea. *Sci China Life Sci* (2022) 66:1079–91. doi:10.1007/s11427-022-2218-x

5. Siegel RL, Miller KD, Wagle NS, Jemal A. Cancer statistics. *CA: a Cancer J clinicians* (2023) 73(1):17–30. doi:10.3322/caac.21332

6. Garon EB, Rizvi NA, Hui R, Leighl N, Balmanoukian AS, Eder JP, et al. Pembrolizumab for the treatment of non-small-cell lung cancer. *New Engl J Med* (2015) 372(21):2018–28. doi:10.1056/NEJMoa1501824

7. Adam T, Becker TM, Chua W, Bray V, Roberts TL. The multiple potential biomarkers for predicting immunotherapy response-finding the needle in the haystack. *Cancers* (2021) 13(2):277. doi:10.3390/cancers13020277

8. Dong A, Zhao Y, Li Z, Hu H. PD-L1 versus tumor mutation burden: which is the better immunotherapy biomarker in advanced non-small cell lung cancer? *J Gene Med* (2021) 23(2):e3294. doi:10.1002/jgm.3294

9. Herbst RS, Baas P, Kim DW, Felip E, Pérez-Gracia JL, Han JY, et al. Pembrolizumab versus docetaxel for previously treated, PD-L1-positive, advanced non-small-cell lung cancer (KEYNOTE-010): a randomised controlled trial. *Lancet (London, England)* (2016) 387(10027):1540–50. doi:10.1016/S0140-6736(15)01281-7

10. Reck M, Rodríguez-Abreu D, Robinson AG, Hui R, Csőszi T, Fülöp A, et al. Pembrolizumab versus chemotherapy for PD-L1-positive non-small-cell lung cancer. *New Engl J Med* (2016) 375(19):1823–33. doi:10.1056/NEJMoa1606774

11. Wang Y, Hu X, Xu W, Wang H, Huang Y, Che G. Prognostic value of a novel scoring system using inflammatory response biomarkers in non-small cell lung cancer: a retrospective study. *Thorac Cancer* (2019) 10(6):1402–11. doi:10.1111/1759-7714.13085

12. Tian L, Wang Y, Tian J, Song W, Li L, Che G. Prognostic value and genome signature of m6A/m5C regulated genes in early-stage lung adenocarcinoma. *Int J Mol Sci* (2023) 24(7):6520. doi:10.3390/ijms24076520

13. Yang T, Hao L, Yang X, Luo C, Wang G, Lin CC, et al. Prognostic value of derived neutrophil-to-lymphocyte ratio (dNLR) in patients with non-small cell lung cancer receiving immune checkpoint inhibitors: a meta-analysis. *BMJ Open* (2021) 11(9):e049123. doi:10.1136/bmjopen-2021-049123

14. Platini H, Ferdinand E, Kohar K, Prayogo SA, Amirah S, Komariah M, et al. Neutrophil-to-Lymphocyte ratio and platelet-to-lymphocyte ratio as prognostic markers for advanced non-small-cell lung cancer treated with immunotherapy: a systematic review and meta-analysis. *Medicina (Kaunas, Lithuania)* (2022) 58(8):1069. doi:10.3390/medicina58081069

15. Mezquita L, Auclin E, Ferrara R, Charrier M, Remon J, Planchard D, et al. Association of the lung immune prognostic index with immune checkpoint inhibitor outcomes in patients with advanced non-small cell lung cancer. *JAMA Oncol* (2018) 4(3):351–7. doi:10.1001/jamaoncol.2017.4771

16. Page MJ, McKenzie JE, Bossuyt PM, Boutron I, Hoffmann TC, Mulrow CD, et al. The PRISMA 2020 statement: an updated guideline for reporting systematic reviews. *BMJ (Clinical research ed)* (2021) 372:n71. doi:10.1136/bmj.n71

17. Begg CB, Mazumdar M. Operating characteristics of a rank correlation test for publication bias. *Biometrics* (1994) 50(4):1088–101. doi:10.2307/2533446

18. Egger M, Davey Smith G, Schneider M, Minder C. Bias in meta-analysis detected by a simple, graphical test. *BMJ (Clinical research ed)* (1997) 315(7109):629–34. doi:10.1136/bmj.315.7109.629

19. Zeng X, Ye L, Luo M, Zeng D, Chen Y. Prognostic value of pretreatment systemic immune-inflammation index in Chinese esophageal squamous cell carcinoma patients receiving radical radiotherapy: a meta-analysis. *Medicine* (2023) 102(25):e34117. doi:10.1097/MD.0000000000034117

20. Kazandjian D, Gong Y, Keegan P, Pazdur R, Blumenthal GM. Prognostic value of the lung immune prognostic index for patients treated for metastatic non-small cell lung cancer. *JAMA Oncol* (2019) 5(10):1481–5. doi:10.1001/jamaoncol.2019.1747

21. Ruiz-Banobre J, Areses-Manrique MC, Mosquera-Martinez J, Cortego A, Afonso-Afonso FJ, de Dios-Alvarez N, et al. Evaluation of the lung immune prognostic index in advanced non-small cell lung cancer patients under nivolumab monotherapy. *Translational Lung Cancer Res* (2019) 8(6):1078–85. doi:10.21037/tlcr.2019.11.07

22. Sorich MJ, Rowland A, Karapetis CS, Hopkins AM. Evaluation of the lung immune prognostic index for prediction of survival and response in patients treated with atezolizumab for non-small cell lung cancer: pooled analysis of clinical trials. *J Thorac Oncol : official Publ Int Assoc Study Lung Cancer* (2019) 15. doi:10.1016/j.jtho.2019.04.006

23. Mazzaschi G, Minari R, Zecca A, Cavazzoni A, Ferri V, Mori C, et al. Soluble PD-L1 and circulating cd8+pd-1+ and NK cells enclose a prognostic and predictive immune effector score in immunotherapy treated NSCLC patients. *Lung Cancer (Amsterdam, Netherlands)* (2020) 148:1–11. doi:10.1016/j.lungcan.2020.07.028

24. Wang W, Huang Z, Yu Z, Zhuang W, Zheng W, Cai Z, et al. Prognostic value of the lung immune prognostic index may differ in patients treated with immune checkpoint inhibitor monotherapy or combined with chemotherapy for non-small cell lung cancer. *Front Oncol* (2020) 10:572853. doi:10.3389/fonc.2020.572853

25. Ali WAS, Hui P, Ma Y, Wu Y, Zhang Y, Chen Y, et al. Determinants of survival in advanced non-small cell lung cancer patients treated with anti-PD-1/PD-L1 therapy. *Ann translational Med* (2021) 9(22):1639. doi:10.21037/atm-21-1702

26. Chen P. Clinical study on prognostic factors of immunotherapy for non-small cell lung cancer. Taiyuan, China: Shanxi Medical University (2021). Master.

27. Galland L, Le Page AL, Lecuelle J, Bibeau F, Oulkhouir Y, Derangere V, et al. Prognostic value of Thyroid Transcription Factor-1 expression in lung adenocarcinoma in patients treated with anti PD-1/PD-L1. *Oncoimmunology* (2021) 10(1):1957603. doi:10.1080/2162402X.2021.1957603

28. Grosjean HAI, Dolter S, Meyers DE, Ding PQ, Stukalin I, Goutam S, et al. Effectiveness and safety of first-line pembrolizumab in older adults with PD-L1 positive non-small cell lung cancer: a retrospective cohort study of the Alberta immunotherapy database. *Curr Oncol* (2021) 28(5):4213–22. doi:10.3390/curroncol28050357

29. Hopkins AM, Kichenadasse G, Abuhelwa AY, McKinnon RA, Rowland A, Sorich MJ. Value of the lung immune prognostic index in patients with non-small cell lung cancer initiating first-line atezolizumab combination therapy: subgroup analysis of the impower150 trial. *Cancers* (2021) 13(5):1176–9. doi:10.3390/cancers13051176

30. Mountzios G, Samantas E, Senghas K, Zervas E, Krisam J, Samitas K, et al. Association of the advanced lung cancer inflammation index (ALI) with immune checkpoint inhibitor efficacy in patients with advanced non-small-cell lung cancer. *ESMO open* (2021) 6(5):100254. doi:10.1016/j.esmoop.2021.100254

31. Chen J, Wei S, Zhao T, Wang Y, Zhang X. Clinical significance of serum biomarkers in stage IV non-small-cell lung cancer treated with PD-1 inhibitors: LIPI score, NLR, dNLR, LMR, and PAB. *Dis markers* (2022) 2022:7137357. doi:10.1155/2022/7137357

32. De Giglio A, Tassinari E, Zappi A, Di Federico A, Lenzi B, Sperandi F, et al. The palliative prognostic (PaP) score without clinical evaluation predicts early mortality among advanced NSCLC patients treated with immunotherapy. *Cancers* (2022) 14(5845):5845. doi:10.3390/cancers14235845

33. Holtzman L, Moskovitz M, Urban D, Nechushtan H, Keren S, Reinhorn D, et al. dNLR-based score predicting overall survival benefit for the addition of platinum-based chemotherapy to pembrolizumab in advanced NSCLC with PD-L1 tumor proportion score ≥50. *Clin Lung Cancer* (2022) 23(2):122–34. doi:10.1016/j.cllc.2021.12.006

34. Ortega-Franco A, Hodgson C, Raja H, Carter M, Lindsay C, Hughes S, et al. Real-world data on pembrolizumab for pretreated non-small-cell lung cancer: clinical outcome and relevance of the lung immune prognostic index. *Targeted Oncol* (2022) 17(4):453–65. doi:10.1007/s11523-022-00889-8

35. Tanaka S, Uchino J, Yokoi T, Kijima T, Goto Y, Suga Y, et al. Prognostic nutritional index and lung immune prognostic index as prognostic predictors for combination therapies of immune checkpoint inhibitors and cytotoxic anticancer chemotherapy for patients with advanced non-small cell lung cancer. *Diagnostics* (2022) 12(2):423. doi:10.3390/diagnostics12020423

36. Zhou J, Bao M, Gao G, Cai Y, Wu L, Lei L, et al. Increased blood-based intratumor heterogeneity (bITH) is associated with unfavorable outcomes of immune checkpoint inhibitors plus chemotherapy in non-small cell lung cancer. *BMC Med* (2022) 20(256):256. doi:10.1186/s12916-022-02444-8

37. Zhou S, Ren F, Meng X. Efficacy of immune checkpoint inhibitor therapy in EGFR mutation-positive patients with NSCLC and brain metastases who have failed EGFR-TKI therapy. *Front Immunol* (2022) 13:955944. doi:10.3389/fimmu.2022.955944

38. Zhou Y, Wu L, Xu T, Ma C, Song L, Zhang J. Predictive value of lung immune prognostic index scoring system for patients treated with immunotherapy in non-small cell lung cancer. *Clin J Med Offic* (2022) 50(03):237–41. doi:10.16680/j.1671-3826.2022.03.05

39. Huang J, Pu H, He J, Tang X. Prognostic value of the lung immune prognostic index for metastatic non-small cell lung cancer patients: a Chinese cohort study. *Int J Gen Med* (2023) 16:881–93. doi:10.2147/IJGM.S393263

40. Shah SC, Itzkowitz SH. Colorectal cancer in inflammatory bowel disease: mechanisms and management. *Gastroenterology* (2022) 162(3):715–30.e3. doi:10.1053/j.gastro.2021.10.035

41. Kolb M. Inflammation and dysregulated fibroblast proliferation--new mechanisms? *Sarcoidosis, vasculitis, diffuse Lung Dis : official J WASOG* (2013) 30(Suppl. 1):21–6.

42. Yu K, Li D, Xu F, Guo H, Feng F, Ding Y, et al. Ido1 as a new immune biomarker for diabetic nephropathy and its correlation with immune cell infiltration. *Int immunopharmacology* (2021) 94:107446. doi:10.1016/j.intimp.2021.107446

43. Ai L, Xu A, Xu J. Roles of PD-1/PD-L1 pathway: signaling, cancer, and beyond. *Adv Exp Med Biol* (2020) 1248:33–59. doi:10.1007/978-981-15-3266-5_3

44. Mizuno R, Kawada K, Itatani Y, Ogawa R, Kiyasu Y, Sakai Y. The role of tumor-associated neutrophils in colorectal cancer. *Int J Mol Sci* (2019) 20(3):529. doi:10.3390/ijms20030529

45. Yang R, Zhong L, Yang XQ, Jiang KL, Li L, Song H, et al. Neutrophil elastase enhances the proliferation and decreases apoptosis of leukemia cells via activation of PI3K/Akt signaling. *Mol Med Rep* (2016) 13(5):4175–82. doi:10.3892/mmr.2016.5051

46. Liu C, Liu R, Wang B, Lian J, Yao Y, Sun H, et al. Blocking IL-17A enhances tumor response to anti-PD-1 immunotherapy in microsatellite stable colorectal cancer. *J Immunother Cancer* (2021) 9(1):e001895. doi:10.1136/jitc-2020-001895

47. Huang H, Liu Q, Zhu L, Zhang Y, Lu X, Wu Y, et al. Prognostic value of preoperative systemic immune-inflammation index in patients with cervical cancer. *Scientific Rep* (2019) 9(1):3284. doi:10.1038/s41598-019-39150-0

48. Takada K, Kashiwagi S, Asano Y, Goto W, Morisaki T, Shibutani M, et al. Differences in tumor-infiltrating lymphocyte density and prognostic factors for breast cancer by patient age. *World J Surg Oncol* (2022) 20(1):38. doi:10.1186/s12957-022-02513-5

49. Comandatore A, Franczak M, Smolenski RT, Morelli L, Peters GJ, Giovannetti E. Lactate Dehydrogenase and its clinical significance in pancreatic and thoracic cancers. *Semin Cancer Biol* (2022) 86(Pt 2):93–100. doi:10.1016/j.semcancer.2022.09.001

50. Dang C, Deng YH, Qin RY. Prognostic value of ALP and LDH in periampullary carcinoma patients undergoing surgery. *Curr Med Sci* (2022) 42(1):150–8. doi:10.1007/s11596-021-2452-9

51. Ye Y, Chen M, Chen X, Xiao J, Liao L, Lin F. Clinical significance and prognostic value of lactate dehydrogenase expression in cervical cancer. *Genet Test Mol biomarkers* (2022) 26(3):107–17. doi:10.1089/gtmb.2021.0006

52. Paredes F, Williams HC, San Martin A. Metabolic adaptation in hypoxia and cancer. *Cancer Lett* (2021) 502:133–42. doi:10.1016/j.canlet.2020.12.020

53. Shao X, Hua S, Feng T, Ocansey DKW, Yin L. Hypoxia-regulated tumor-derived exosomes and tumor progression: a focus on immune evasion. *Int J Mol Sci* (2022) 23(19):11789. doi:10.3390/ijms231911789

54. Korbecki J, Simińska D, Gąssowska-Dobrowolska M, Listos J, Gutowska I, Chlubek D, et al. Chronic and cycling hypoxia: drivers of cancer chronic inflammation through HIF-1 and NF-κB activation: a review of the molecular mechanisms. *Int J Mol Sci* (2021) 22(19):10701. doi:10.3390/ijms221910701

55. Melincovici CS, Boşca AB, Şuşman S, Mărginean M, Mihu C, Istrate M, et al. Vascular endothelial growth factor (VEGF) - key factor in normal and pathological angiogenesis. *Rom J Morphol Embryol = Revue roumaine de morphologie embryologie* (2018) 59(2):455–67.

56. Liu H, Yang XL, Yang XY, Dong ZR, Chen ZQ, Hong JG, et al. The prediction potential of the pretreatment lung immune prognostic index for the therapeutic outcomes of immune checkpoint inhibitors in patients with solid cancer: a systematic review and meta-analysis. *Front Oncol* (2021) 11:691002. doi:10.3389/fonc.2021.691002

57. Xie J, Zang Y, Liu M, Peng L, Zhang H. The lung immune prognostic index may predict the efficacy of different treatments in patients with advanced NSCLC: a meta-analysis. *Oncol Res Treat* (2021) 44(4):164–75. doi:10.1159/000514443

Pathology & Oncology Research | frontiers

TYPE Original Research
PUBLISHED 03 June 2024
DOI 10.3389/pore.2024.1611754

Check for updates

OPEN ACCESS

EDITED BY
Nora Bittner,
National Koranyi Institute of TB and Pulmonology, Hungary

*CORRESPONDENCE
Zoltán Kiss,
zoltan_kiss2@merck.com

†These authors have contributed equally to this work

RECEIVED 29 February 2024
ACCEPTED 17 May 2024
PUBLISHED 03 June 2024

CITATION
Gálffy G, Szabó GT, Tamási L, Müller V, Moldvay J, Sárosi V, Kerpel-Fronius A, Kardos T, Csada E, Pápai-Székely Z, Szász Z, Király Z, Hódi G, Kovács Z, Balogh É, Kovács KA, Darida M, Buga V, Rokszin G, Abonyi-Tóth Z, Kiss Z, Vokó Z and Bogos K (2024), Decreasing incidence and mortality of lung cancer in Hungary between 2011 and 2021 revealed by robust estimates reconciling multiple data sources. *Pathol. Oncol. Res.* 30:1611754. doi: 10.3389/pore.2024.1611754

COPYRIGHT
© 2024 Gálffy, Szabó, Tamási, Müller, Moldvay, Sárosi, Kerpel-Fronius, Kardos, Csada, Pápai-Székely, Szász, Király, Hódi, Kovács, Balogh, Kovács, Darida, Buga, Rokszin, Abonyi-Tóth, Kiss, Vokó and Bogos. This is an open-access article distributed under the terms of the Creative Commons Attribution License (CC BY). The use, distribution or reproduction in other forums is permitted, provided the original author(s) and the copyright owner(s) are credited and that the original publication in this journal is cited, in accordance with accepted academic practice. No use, distribution or reproduction is permitted which does not comply with these terms.

Decreasing incidence and mortality of lung cancer in Hungary between 2011 and 2021 revealed by robust estimates reconciling multiple data sources

Gabriella Gálffy[1†], Géza Tamás Szabó[2†], Lilla Tamási[3], Veronika Müller[3], Judit Moldvay[4,5], Veronika Sárosi[6], Anna Kerpel-Fronius[7], Tamás Kardos[8], Edit Csada[5], Zsolt Pápai-Székely[9], Zoltán Szász[10], Zsolt Király[11], Gábor Hódi[2], Zsuzsanna Kovács[2], Éva Balogh[2], Krisztina Andrea Kovács[2], Miklós Darida[2], Viktória Buga[2], György Rokszin[12], Zsolt Abonyi-Tóth[12,13], Zoltán Kiss[2,14*†], Zoltán Vokó[15,16†] and Krisztina Bogos[17†]

[1]Department of Pulmonology, Pulmonology Center of the Reformed Church in Hungary, Törökbálint, Hungary, [2]MSD Pharma Hungary Ltd., Budapest, Hungary, [3]Department of Pulmonology, Semmelweis University, Budapest, Hungary, [4]Department of Pulmonology, National Korányi Institute of Pulmonology, Budapest, Hungary, [5]Department of Pulmonology, University of Szeged Albert Szent-Györgyi Medical School, Szeged, Hungary, [6]Faculty of Medicine, University of Pécs, Pécs, Hungary, [7]National Korányi Institute of Pulmonology, Department of Radiology, Budapest, Hungary, [8]Department of Pulmonology, University of Debrecen, Debrecen, Hungary, [9]Fejér County Szent György, University Teaching Hospital, Székesfehérvár, Hungary, [10]Department of Pulmonology, Petz Aladár University Teaching Hospital, Győr, Hungary, [11]Veszprém County Pulmonary Hospital Farkasgyepű, Farkasgyepű, Hungary, [12]RxTarget Ltd Szolnok, Szolnok, Hungary, [13]Department of Biostatistics, University of Veterinary Medicine, Budapest, Hungary, [14]2nd Department of Medicine and Nephrology-Diabetes Center, University of Pécs Medical School, Pécs, Hungary, [15]Center for Health Technology Assessment, Semmelweis University, Budapest, Hungary, [16]Syreon Research Institute, Budapest, Hungary, [17]National Korányi Institute of Pulmonology, Budapest, Hungary

Objective: Hungary has repeatedly been shown to have the highest cancer-related mortality and incidence in Europe. Despite lung cancer being the most abundant malignant diagnosis in Hungary, numerous concerns have been raised recently regarding the bias inherent to reported incidence estimates. Re-analysis of reimbursement claims has been suggested previously by our group as an alternative approach, offering revised figures of lung cancer incidence between 2011 and 2016. Leveraging on this methodology, we aimed at updating Hungarian lung cancer incidence estimates with an additional 5 years (2017–2021), including years affected by the COVID-19 pandemic. Additionally, we also attempted to improve the robustness of estimates by taking additional characteristics of the patient pathway into account.

Methods: Lung cancer patients between 2011 and 2021 were identified based on reimbursement-associated ICD-10 codes, histology codes and time patterns.

Multiple query architectures were tested for sensitivity and compared to official estimates of the Hungarian National Cancer Registry (HNCR). Epidemiological trends were estimated by Poisson-regression, corrected for age and sex.

Results: A total of 89,948 lung cancer patients diagnosed in Hungary between 2011 and 2021 have been identified by our study. In 2019 alone, 7,887 patients were diagnosed according to our optimized query. ESP2013 standardized rate was estimated between 92.5/100,000 (2011) and 78.4/100,000 (2019). In 2019, standardized incidence was 106.8/100,000 for men and 59.7/100,000 for women. Up until the COVID-19 pandemic, lung cancer incidence was decreasing by 3.18% (2.1%–4.3%) yearly in men, while there was no significant decrease in women. Young age groups (40–49 and 50–59) featured the largest improvement, but women aged 60–79 are at an increasing risk for developing lung cancer. The COVID-19 pandemic resulted in a statistically significant decrease in lung cancer incidence, especially in the 50–59 age group (both sexes).

Conclusion: Our results show that using an optimized approach, re-analysis of reimbursement claims yields robust estimates of lung cancer incidence. According to this approach, the incidence rate of male lung cancer is declining in Hungary, in concordance with the trend observed for lung cancer mortality. Among women aged 60–79, the incidence of lung cancer has risen, requiring more attention in the near future.

KEYWORDS

lung cancer, incidence, mortality, COVID-19, Hungary

Introduction

Current understanding of lung cancer epidemiology in Hungary

It is widely accepted that compared to most European countries, Hungary suffers from a relatively high malignant disease incidence and mortality. This has been shown for example by a series of papers comparing 40 European countries [1–3], for both overall cancer epidemiology and individual tumor types. It is important to stress that for Hungary, these epidemiological studies estimate cancer incidence indirectly, based on statistical models relying on reported deaths and incidence in neighboring countries [4]. This indirect approach might already add some uncertainty to the estimates, while other reports have suggested mortality reported for Hungary to be exaggerated recently [5].

Furthermore, the reliability of tumor classification in reports has also been questioned by a recent amendment [6, 7] of the Hungarian National Cancer Registry (HNCR). One of the tumor types most frequently misclassified was lung cancer, possibly since lung is also a common site of metastases. Lung cancer on the other hand, is the most abundant cancer type in men, accounting for more than 20% of all cases and the top cause of cancer mortality in both sexes. Given its share, an inflated number of reported lung cancer cases can already impact the assessment of the total number of cancer patients, while the described bias might also affect other cancer types (common metastatic sites, for example), adding further uncertainty to epidemiological observations. A potential solution would be manual curation of individual records before reporting case numbers, as it was done by the HNCR with the amendment of lung cancer cases for 2018. This was found to be extremely demanding and not routinely feasible for each tumor type and year given the current resources.

Approaches to refine incidence estimates

An alternative approach to manual curation of hospital records for the estimation of cancer incidence could be the utilization of alternative sources of information. The National Health Insurance Fund of Hungary (NHIF) is a valuable resource capturing detailed information on patient pathways via reimbursement claims. Previous publications from our research group [4, 8] have already demonstrated that epidemiological indicators can be estimated efficiently using this data source. Additionally, patient-level details captured in reimbursement claims have also provided valuable insights on the high number of *post mortem* diagnosed lung cancer cases as a potential confounder of reported case numbers [7].

Even if incidence estimated by any of the above described methods cannot be 100% accurate, reproducibility of querying the NHIF database and the possibility to finetune stringency of the query provides information on the range where the actual value lies and what biases one should look out for. This deeper understanding of epidemiological indicators is essential in the timely allocation of

resources to meet emerging challenges as well as in the assessment of updates to healthcare policies. Lung cancer being the most frequent malignant disease in Hungary, it is the first choice of cancer type for modelling the robustness of epidemiological indicators and trends.

Aims

The present research was carried out as part of the Hungarian Evaluation of Lung cancer Patient Pathway Project (HELP3) research project describing lung cancer epidemiology and patient pathways in Hungary. The primary aim of the current study is to update lung cancer incidence and mortality figures in Hungary. Recent advances uncovering potential confounders offer an excellent opportunity to refine epidemiological trends incorporating data based on the NHIF, using an improved query structure. The impact of query parameter optimization is assessed based on the robustness of trends calculated from results yielded by these queries. The impact of the COVID-19 pandemic, caused by the SARS-CoV-2 virus, on lung cancer epidemiology in Hungary can be traced in the risk ratio of pre-COVID and COVID years 2019 and 2020.

Materials and methods

Data sources

Yearly incidence of lung cancer was estimated based on healthcare reimbursement claims in the NHIF database, as described by our group previously [4, 8, 9]. Briefly, patients named in claims with the ICD-10 code of C34 were regarded as lung cancer patients. The year of the first occurrence of C34 was accepted as the year of diagnosis. Patients newly diagnosed between the 1st of January 2011 and the 31st of December 2021 were studied, with an additional screening period of 2009-2010 to account for patients already diagnosed outside the study period.

To further improve the specificity of our definitions, additional constraints were added to the query, specifying the number of C34 codes in an individual's history and the minimum (30 days) as well as the maximum (180 or 365 days) amount of time accepted between two C34 codes. Patients who have died within 60 days of the first diagnosis were not required to feature multiple C34 codes in their history. This multi-tier, optimized query is referred to as "Optimized," in sensitivity analyses (Supplementary Figure S1). When comparing the optimized query, the alternative requiring only one single mention of C33 or C34 will be referred to as *1.1*, while the query requiring 2 mentions is *1.2A*. A minimum of two mentions within a year is referred to as *1.2B*, while 2 mentions within 180 days is *1.2C*. Three mentions within 180 days is *1.3*. Estimates provided by the HNCR (stat.nrr.hu, accessed 20/10/23) were used as a reference. Please note that the optimized query is very similar to the 1.2B alternative, with the additional constraint of at least 30 days between the two claims and a small relaxation regarding patients deceased within 60 days.

Number of deaths associated with lung cancer are based on reports of the Hungarian Central Statistical Office (HCSO). Both incidence and mortality were standardized using the European Standard Population (ESP) of 2013 and standardized rates are given using that reference, unless otherwise indicated. For the sake of comparison with estimates of Ferlay's workgroup, rates standardized to the ESP 1976 population are also shown in this context. To facilitate reproducibility of our results, patient numbers yielded by NHIF queries, retrieved from the HNCR or the HCSO are provided in a tidy long format as Supplementary Table S1, as well as mid-year population retrieved from the HCSO (Supplementary Table S2)

Statistical analysis

All calculations were carried out in the open source software environment for statistical computing R (v4.2.1). Average Yearly Change was estimated by Poisson-regression, correcting the model for population size, age, and sex. The logarithmic value of the number of individuals in a given age group was used as offset, while age, sex and year were explanatory variables. Statistical significance was inferred from the *p*-values of Wald-tests implemented by the *Testing Linear Regression Models* (lmtest v0.9) package and considered significant in case it was $p \leq 0.05$. Confidence intervals (95% CI) were estimated using the packages lmtest and *Robust Covariance Matrix Estimators* (sandwich v3.1) variance estimation [10] to correct for non-independent nature of the data. A normal distribution was assumed when assigning (95% CI) of direct standardized rates. Risk ratio was calculated using the *Epidemiology Tools* (epitools v0.5) package.

Results

Annual number of patients

The number of yearly diagnosed lung cancer patients in Hungary ranged between 8,752 and 7,003. For 2019, the last year before the COVID-19 pandemic, our query after optimizations has identified 7,887 new lung cancer patients (Supplementary Figure S1). As a comparison, the least stringent case definition 1.1 returned 9,600 hits, while changing the stringency by requiring multiple visits in the patient history (filters 1.2A, 1.2B, 1.2C) increased the number of candidates to 8,498, 8,144 and 8,240, respectively. Requiring 3 visits, without further restrictions (filter 1.3C) picked up only 7,121 potential lung cancer cases.

The highest number following each approach was observed for 2011 and a steady decrease in patient numbers could be observed until 2020, featuring the lowest number of new patients during the studied period. For each year, a male predominance in the number of patients could be observed. For the initial year 2011, 5,517 men and 3,235 women were found to be diagnosed with lung cancer. By

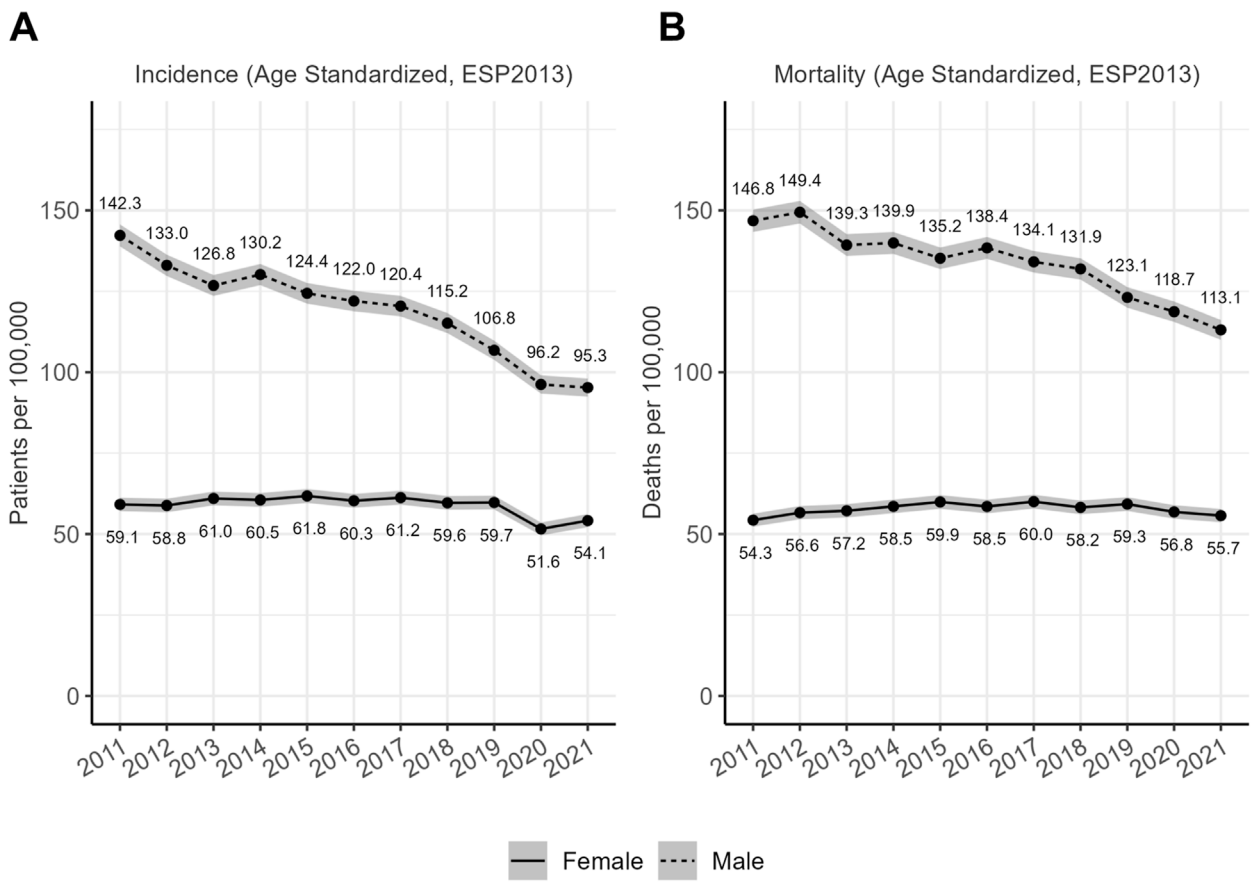

FIGURE 1
(A) Standardized incidence rates of lung cancer in Hungary between 2011 and 2021. Direct standardized rates using the ESP2013 population weights. Grey ribbon around the lines represents the 95% confidence interval. **(B)** Standardized mortality rates of lung cancer in Hungary between 2011 and 2021 (ESP2013 standardized rates). Direct standardized rates using the ESP2013 population weights. Grey ribbon around the lines represents the 95% confidence interval.

the end of the study period, this difference was smaller (4,424 and 3,436, respectively, in 2019), but still visible.

Age standardized rates

In 2011, according to the results of the optimized, consensus query, there were 142.3/100,000 (ESP2013) new male lung cancer patients identified, while only 59.1/100,000 (ESP2013) female patients (Figure 1A). Standardized incidence has decreased to 106.8/100,000 in men by 2019, while it remained at the same level with 59.7/100,000 for women. As a comparison, standardized mortality due to lung cancer was reported to be 146.8/100,000 in men and 54.3/100,000 for women (Figure 1B) in 2011, which has changed to 123.1 in men and 59.3 in women. A detailed report of standardized incidence (Supplementary Table S3) and mortality (Supplementary Table S4) rates for all studied years and both sexes can be found in the Supplementary Material.

Lung cancer had the highest incidence in the 60–69 (women) and 70–79 (men) age groups (Figure 2). Age distribution of lung cancer patients has been shifting towards stronger representation of older age groups, especially in women. Age distribution of patients died of lung cancer shows a similar pattern, with an even more pronounced decrease in the share of the 40–49 age group in both sexes.

Observed trends

Lung cancer incidence in the general population was found to decrease between 2011 and 2019 by 1.76% on an annual basis (95% CI: 0.5%–3%). For men only, the decrease was 3.18% (95% CI: 2.1%–4.3%), while for women, the estimated 0.33% increase (95% CI: −0.1%–1.6%) did not indicate a significant change (Figure 3; Supplementary Table S7). Young age groups (40–49 ad 50–59) featured the largest decrease in lung cancer incidence for both women and men. Conversely, the incidence was less likely to decrease in the 60–69 and the 70–79 age

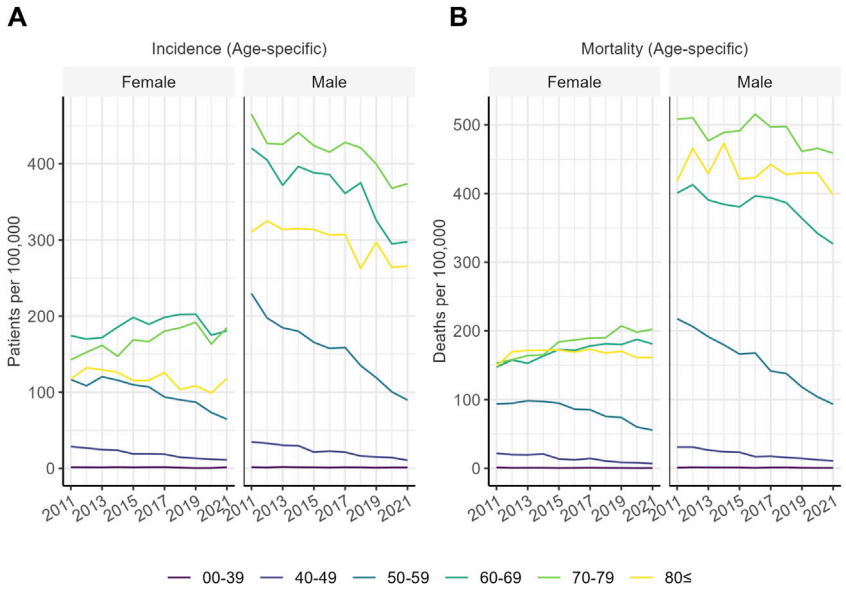

FIGURE 2
(A) Age-specific incidence of lung cancer in Hungary in the studied age groups. Values indicate the number of patients diagnosed in a given year out of 100,000 individuals of the age group. **(B)** Age-specific mortality of lung cancer in Hungary in the studied age groups. Values indicate the number of patients deceased in a given year out of 100,000 individuals of the age group.

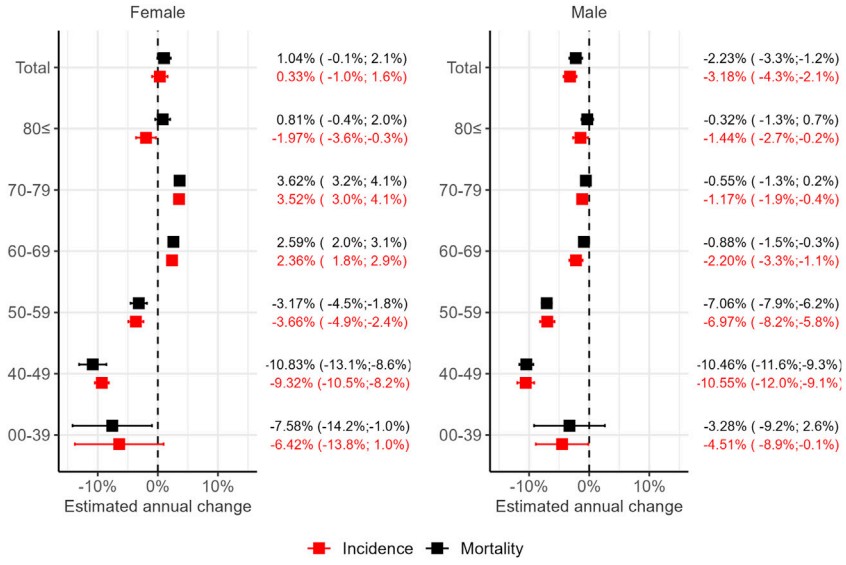

FIGURE 3
The average annual change in lung cancer incidence and mortality in Hungary between 2011 and 2019 for the total population, as well as by age groups. Estimated using Poisson regression and robust confidence intervals (95% CI) with the sandwich method.

groups. Lung cancer incidence in elderly women has even increased slightly during the study period.

A similar pattern of lung cancer mortality (Figure 3; Supplementary Table S8) could be observed between 2011 and 2019, with an overall decrease of 0.99% (95% CI: −2.0%–0.1% change). While the overall trend was not found to be statistically significant, there was a significant, 2.23% decrease (95% CI: −1.2%–3.3%) change when taking only men into account. The 1.04% yearly increase (95% CI: −0.1%–2.1%) estimated for women was not statistically significant either. An improvement in

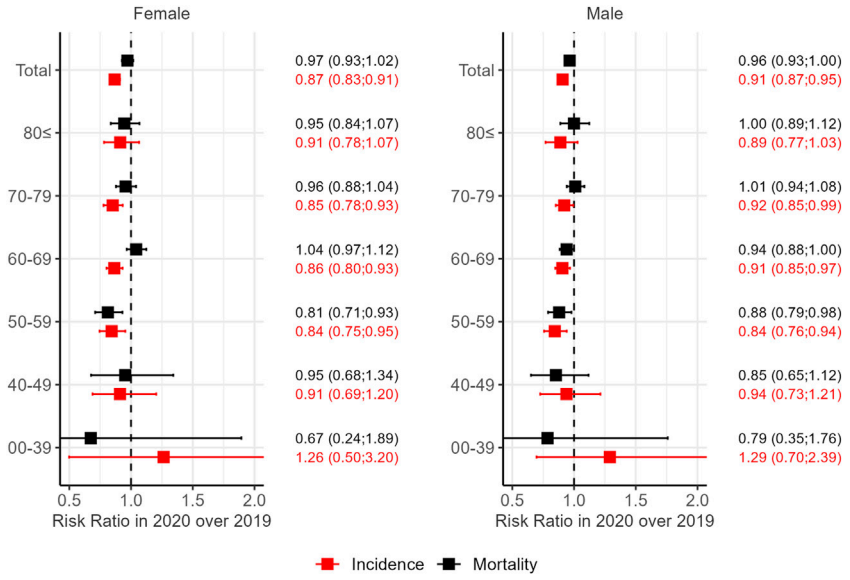

FIGURE 4
Change in lung cancer incidence and mortality in Hungary during the COVID year 2020 expressed as the risk ratio (RR) of 2020 vs. 2019. Confidence intervals (95% CI) of RR are given in brackets.

mortality could be confirmed in the 40–49 and 50–59 age groups of both sexes, while mortality has increased among women aged 60–69 and 70–79.

COVID-19 impact

To assess the impact of the COVID-19 pandemic on lung cancer incidence and mortality in Hungary, the pandemic year 2020 was compared to the previous year, 2019 (Figure 4). The risk of lung cancer diagnosis was significantly lower for both women and men in 2020 than in 2019 (Risk Ratio (RR) = 0.87 and 0.91, respectively), while the risk of lung cancer specific death did not decrease significantly (RR = 0.97 and RR = 0.96, respectively). The difference in terms of patient numbers means that 891 less patients were diagnosed with lung cancer in 2020 than in 2019 (6,970 and 7,861, respectively). The decrease in incidence compared to 2019 was driven mainly by the 50–59, 60–69, and 70–79 age groups in both sexes. Lung cancer mortality, however, showed a similar decrease only in the 50–59 age group (RR = 0.81, women; RR = 0.88, men). The calculated RR values for incidence (Supplementary Table S9) and mortality (Supplementary Table S10) are also available in the Supplementary Material.

Sensitivity analysis

Standardized lung cancer incidence estimated using different case definitions resulted in a range around 133–179/100,000 for men and a narrower range of 55–79/100,000 for women in 2011 (Supplementary Figure S2). Estimate using the less stringent query (1.1) was close to the number reported by the HNCR and restricting the definition by requiring more than one record featuring the ICD-10 code of lung cancer (1.2A) already yielded results similar to the final estimate. Restrictions regarding the minimum or maximum amount of time between visits (1.2B or 1.2C) had a much smaller impact on the results. Capturing the raw numbers behind these rates, a total of 8,191 to 11,261 new lung cancer patients were found for the reference year 2012 (Supplementary Figure S1). The least stringent case definition aligns well with the 11,000 patients reported by the HNCR. Using different case definitions had hardly any effect on the time trend analysis (Supplementary Figure S3).

European context

Comparison of previously reported standardized incidence rates of Hungary to neighboring countries also suggests a possible bias, resulting in the overestimation of Hungarian lung cancer incidence. In a comprehensive study including 40 European countries, Ferlay's workgroup has reported a 109.3/100,000 male lung cancer incidence rate (ESP1976) for Hungary in 2012 [3] and 111.6/100,000 in 2018 [2]. These rates would be extremely high in Europe and this extent of outlying alone would be alarming. On the other hand, the 133 per 100,000 Person Years estimated based on the ESP2013 standards for 2012 and reported above (Figure 1.), is equivalent to 95.2/100,000 calculated using the ESP1976 weights. Similarly, the ESP1976-eqivalent incidence rate for 2018 was 80.5/100,

000 based on our data. These estimates are much closer to the (Central) European average (Supplementary Figures S4, S5) than the ones reported previously for Hungary. The ESP1976 standardized rates for all studied years are provided for multiple incidence estimates (Supplementary Table S5) as well as for mortality reported by the HCSO (Supplementary Table S6) in the Supplementary Material.

Discussion

Updated lung cancer incidence in Hungary

By extending the studied period to more than 10 years, the current study provides updates to epidemiological indicators of lung cancer in Hungary with an even more refined approach, but also largely building on our previous reports [4, 7, 9]. This update confirms the inconsistency between lung cancer incidence rates reported previously for Hungary and the rates estimated by our approach. Differences in the numerical values of lung cancer estimates reported for Hungary are partially due to differences in standardization methods as they have been evolving through time. Values given relative to the ESP2013 population can be converted to reflect the rate in the ESP1976 population, as also done in this study to compare with historical data. Even after conversion, however, conflicting rates have been for Hungary [2, 3]. We claim that this remaining difference originates at least partially from differences between statistical models used to estimate incidence. One can even trace the changes that occur to the model used by one single research group over time, changing the input slightly to rely on different countries [2, 3], to improve confidence of the estimate.

Appreciating that the increasing weight of input from the national cancer registry of the Czech Republic in the reported Hungarian estimate is in agreement with our observations regarding the similarity of healthcare indicators in Hungary to other Eastern European countries [7], we would like to advocate for granting greater importance to local datasets, when developing these models. Since the availability of observational data for Hungary is limited currently, we would like to provide such empirical data, hoping to contribute to closing the gap between lung cancer incidence estimates in the literature.

While a critical revision of standard incidence contributes to a realistic assessment of current disease burden, the trends described by these figures are even more crucial when planning future preventive actions. Acknowledging that limitations to our approach prevent us from identifying some patients, thus our data can be regarded as close estimates only, we argue that the trends identified in these figures are robust enough to identify emerging needs or give positive feedback on improvement. Differences in the dynamics of the epidemiology of lung cancer between women and men has been shown multiple times, including our publications [4], and our current results recapitulate this pattern nicely. Furthermore, an increasing lung cancer incidence among women between 60 and 79 already points out a population that needs more attention regarding prevention, early detection, or care.

Improving trend in 2011–2019

Our data suggests that lung cancer incidence has started to decline during the last decade (2011–2019) in men, similar to observations for Germany [11]. This observation is in line with our previous reports on lung cancer, describing improvements over previous periods [4, 8], in contrast to interpretations forecasting an alarming number of new lung cancer cases [12]. As smoking contributes to about 85%–90% of lung cancers [13], based on the slowly decreasing smoking prevalence in almost every European country [14], a consequent decrease in lung cancer suggested by our results seems logical.

An increase in lung cancer incidence within the population would only be expected if other risk factors were emerging, or in certain subpopulations. While air pollution could be such an emerging risk factor, showing a well-established association with lung cancer etiology [15], no major rise in Particulate Matter <2.5 μm (PM2.5) or PM10 levels has been reported for Hungary during the study period. Nevertheless, PM2.5 levels, a recently re-confirmed etiological factor in the pathogenesis of adenocarcinoma [16], have been constantly high in Hungary for decades [17]. This prolonged exposition might contribute to the increased risk among women. Occupational risk factors, such as asbestos have been shown to contribute little to population-level lung cancer risk in Central Eastern Europe [18]. Inherited genetic variations generally contribute to lung cancer etiology indirectly via susceptibility to environmental exposure [13]. Even though positive family history of lung cancer has been shown to increase lung cancer risk in the Eastern European population [19], contribution of genetic causes can still be considered minor compared to the risk of smoking in patients above 50.

While the observed improvement at the population level is logical considering the decrease in smoking prevalence, the lack of improvement among women is in certain age groups is somewhat surprising. As described in our previous revision of lung cancer epidemiology in Hungary [4], however, smoking prevalence is not homogenous in the population and even gender imbalance has dynamically changed over time. In contrast to men, where the number of ever-smokers has decreased steadily in every birth cohort, an increase in smoking prevalence has preceded the recent decrease in women. This difference in smoking patterns has already been shown to affect lung cancer incidence in European populations [20] and explains the heterogenous trends observed in our data stratified by age groups.

It is also important to note that our study focuses on changes regarding the risk of an individual, captured in standardized

incidence and mortality rates. Standardization is carried out precisely to compensate for the confounding effect of the population's aging. The increasing number of elderly people in a population inevitably leads to an increase in age-related diseases, like lung cancer. This might lead to a paradoxical observation of increasing patient numbers (and burden on the healthcare system) even when the individual's risk is decreasing. Although both indicators (patient numbers and risk) carry important information, we decided to focus on risk as this better describes the effect of preventive measures or the improvement in quality of care. Nonetheless, this is the measure that can be compared among countries or regions.

The impact of COVID-19

The COVID-19 pandemic declared by the World Health Organization (WHO) in 2020 has resulted in a sudden, dramatic change in accessibility. The impact of these restrictions on lung cancer detection has been shown for example by a direct comparison of the number of lung cancer cases in the UK during lockdowns in 2020 and the same period of 2019 [21], reporting a 26% decrease during the pandemic. A 14.4% decrease in lung cancer incidence has also been observed for Hungary, together with decrease in breast and colorectal cancer patient numbers [22]. Thus, the incidence during the COVID-19 pandemic was not specific to lung cancer, only the extent of the decrease varied between tumor types. In addition to confirming the decreased breast cancer incidence [23], we have also described that breast cancer mortality did not increase significantly. This suggests that care of patients already diagnosed was not affected by restrictions or bottlenecks in resources, but rather the detection of cancer cases was delayed. Screening program participation, for example, has also reduced dramatically due to the pandemic: 25.8% less centrally organized mammography examinations were conducted in 2020 than in the previous year [24]. The reduction in diagnostic capacities was probably even greater in the case of cancer types where an organized screening program is not available, like lung cancer.

Reduced incidence was not associated with a change in mortality in our study population of Hungarian lung cancer patients, similarly to what has been described for breast cancer earlier [23]. Delayed diagnosis is, however, expected to cause an increase in lung cancer mortality of around 4.8%–5.3% during the next years, as suggested by a modeling study based on the UK population [25]. Another model based on the Australian population warns about a potential mid-term reversal of positive epidemiological trends (decreasing cancer incidence and mortality) caused by the aftermath of the restrictions in 2020 [26].

Patients not identified in 2020 are also likely to increase lung cancer incidence or at least mortality in the post-pandemic era. According to our data, as many as 891 lung cancer patients might have been missed in 2020. Even if the decreasing trend is considered, ~800 lung cancer patients will receive a delayed diagnosis due to the COVID-19 pandemic. These patients are expected to either show up in the healthcare system as an excess number of new patients in 2021, 2022 or might never actually be identified if they also suffered from COVID and the outcome was fatal. It is not yet clear from currently available data, which scenario is true, but these considerations should be taken into account, when assessing lung cancer epidemiology of post-pandemic years.

Lung cancer incidence has decreased during the COVID-19 pandemic primarily in the 50–59, 60–69, and 70–79 age groups, both sexes. The sex-related pattern of lung cancer epidemiology is not reflected in the changes attributable to the COVID-19 pandemic. Interestingly, no decrease was seen among elderly patients, above 80. This might be due to the simultaneous prevalence of multiple diseases in this age group and consequently, frequent hospitalizations. There are sporadic reports on incidental findings on chest CTs requested to confirm COVID turned out to be early lung cancer [27] and these non-targeted diagnostic procedures might have been carried out at a higher rate in elderly, multimorbid patients presenting with symptoms suggestive of COVID. Even if part of the population at risk for lung cancer might have profited from the preventive measures during the pandemic, the chance of recognizing lung cancer was hindered in the general population.

The only age group featuring a significant change in mortality is patients between 50 and 59. Our data is not sufficient yet to decide if this age group profited from the alertness of the healthcare system during the pandemic or this decrease is independent of the COVID-19 pandemic. The strongly decreasing trend in both incidence and mortality of lung cancer in this age group already before the COVID-19 pandemic suggests an idiosyncratic effect.

Robustness of data and limitations

A major limitation to our claims-data-based approach is that detailed clinical history is not available in this database, thus it is not possible to medically validate the records. In fact, this confirmation would also not be feasible at this scale even if all health records were available and accessible. In a similar attempt, the HNCR carried out manual validation of the diagnoses associated with every individual reported as lung cancer patients in 2018 [28]. Reviewing the patients from one single year has already proven to be a tremendous effort, far beyond resources available for epidemiological studies. The amended patient number (9,541 patients), however, is an important reference to benchmark any alternative approach, such as the one followed in this study.

The present approach has identified 8,252 patients in 2018 that is lower than the reference reported by the HNCR. Identifying this subset of claimed patients with a high probability of a valid disease classification might offer an opportunity on the other hand to associate a confidence level to patients registered by the HNCR. Despite still not being able to identify some lung cancer patients, performance of the current approach features remarkable improvements even over the method used in a previous study based on the same source [4]. This improvement was enabled by a combinatorial optimization of the query parameters, better adapting to common patient pathway scenarios. One such scenario would be the common case, when a late-stage patient is not able to go through the diagnostic procedure to arrive at a definite diagnosis. By requiring less stringent conditions for patients deceased within 60 days of the first claim featuring a lung cancer related ICD-10 code, reduces the risk of missing these patients. Using patient pathway-related criteria to exclude patients coded as lung cancer by mistake is a reproducible, high-throughput approach that is feasible to be carried out even in case of large patient cohorts. Thereby we suggest that, while not being able to achieve data quality offered by manual curation, it is able to flag potentially miscoded patients; the error type identified most frequently during manual curation [28].

Another potential issue identified by researchers at the HNCR, could be the inconsistent reporting of lung metastases from other sites [5] and this is related to a third source of uncertainty, identified by our research group recently: the considerable number of lung cancer patients diagnosed *post mortem* only [7]. As a comparison, ~10% of lung cancer cases in Germany are recognized only during autopsy [11]. Patients presenting at a very advanced stage might be in such a severe condition already that diagnostic procedures cannot be carried out and a definite diagnosis will never be made. Although some of these patients might appear in the claims dataset under ICD-10 codes D38 or R91H0, it is very hard to assess the number of the patients recognized at this stage and we cannot describe the change in this patient segment over the studied period using our method. A change in coding preference of the hospitals during the period might also confound our observations. Both lung metastases and *post mortem* diagnosed patients add a further level of complexity to obtaining a realistic estimate of lung cancer incidence, but a consistent, reproducible methodology described here can still provide valuable insights on epidemiological indicators.

Bias related to *post mortem* diagnosis, or even unspecified metastases could also impact on cause-specific mortality reported by the HCSO. It has already been proposed by studies conducted within the HNCR that a slight overestimation of patient numbers is inherent to many cancer registries [5] and perhaps, even mortality reports. According to our previous observations described in the HULC study [7], the number of *post mortem* diagnosed lung cancer cases is comparable to the total number of lung cancer patients. Based on the proportion of these cases, it seems logical that individuals never diagnosed with lung cancer, but reported after an autopsy to have died of the disease, contribute to an overestimation of lung cancer mortality, as suggested also by the HNCR. A further argument supporting this possibility is that the mortality-to-incidence ratio (MIR) calculated from our revised incidence rates is close to 1, while globally it has been around 0.7 [29, 30]. This problem does not affect every cancer type equally. Lung cancer is likely among the sites more severely impacted by this bias due to the high probability of metastases from other sites developing in the lung. Similarly, not every country is affected equally, possibly due to the disparate autopsy rates among countries, as discussed earlier [7]. While revising the accuracy of diagnosis for patients registered in the HNCR has been carried out recently [28], such a revision regarding cause-specific mortality reported by the HCSO was not in the scope of the current study.

Regardless of the number of lung cancer patients missed by our approach, it is important that the error rate is constant across years, rendering trend estimations based on our data robust and reproducible. As shown in Supplementary Figure S3, the stringency of our case definition did not significantly change the trend estimated by our models. As an alternative validation approach, incidence trends estimated by our approach were also compared to mortality trends. Only one age group (women above 80) featured a significant difference that confirms the expected parallel change of incidence and mortality in most age groups. Notably, trend estimated based of HNCR data is also not parallel with mortality in this single age group. These observations support the validity of epidemiological trends calculated using our approach and corroborates evidence supporting recent improvements in Hungarian lung cancer epidemiology.

Conclusion

Our results provide further evidence challenging currently reported case numbers and offers an alternative approach to estimate lung cancer incidence, yielding more robust estimates. Better alignment of the resulting figures with numbers reported from neighboring countries, as well as with the dynamics of cause-specific mortality suggest that the more conservative estimates are closer to the actual number of new patients. Without denying the burden imposed by lung cancer on Hungary, we would like to advocate for a more realistic picture, where the dynamics of lung cancer in Hungary is very similar to other Central European countries.

A more realistic assessment of lung cancer epidemiology in Hungary offers a better opportunity to identify emerging challenges, allocate resources and confirm success. Furthermore, our data suggests that the described trends are

even more robust than the individual yearly estimates. Identifying differences in the dynamics of the epidemiology between women and men offers opportunities for intervention. One such emerging challenge identified by our study is the increasing risk of lung cancer in women between 60 and 79 despite improvements in the general population. Robust estimation of lung cancer incidence also contributes to a more precise assessment of the impact of the COVID-19 pandemic on delaying lung cancer diagnosis and highlight potential consequences.

Data availability statement

The original contributions presented in the study are included in the article/Supplementary Material, further inquiries can be directed to the corresponding author.

Ethics statement

The studies involving humans were approved by the Central Ethical Committee of Hungary (IV/3940-3/2021/EKU). The studies were conducted in accordance with the local legislation and institutional requirements. Written informed consent for participation was not required from the participants or the participants' legal guardians/next of kin in accordance with the national legislation and institutional requirements.

Author contributions

GG: conceptualization, methodology, writing–original draft, GS: data analysis, visualization, writing–original draft, LT: supervision, writing–review editing, VM: conceptualization, supervision, writing–review editing, JM: conceptualization, supervision, writing–review editing, VS: supervision, AK-F: supervision, writing–review editing, TK: supervision, validation, EC: supervision, validation, ZP-S: supervision, validation, ZS: supervision, validation, ZtK: supervision, validation, GH: methodology, supervision, validation, ZaK: validation, ÉB: validation, KK: supervision, validation, MD: methodology, writing–review editing, data curation, VB: methodology, writing–review editing, data curation, GR: methodology, writing–review editing, data curation, data acquisition, supervision, ZA-T: data analysis, data acquisition, visualization, validation, ZnK: conceptualization, methodology, investigation, visualization, supervision, writing–original draft, ZV: conceptualization, methodology, writing–original draft, KB: conceptualization, methodology, supervision, validation, writing–original draft. All authors contributed to the article and approved the submitted version.

Funding

The author(s) declare that financial support was received for the research, authorship, and/or publication of this article. The authors declare that this study received funding from MSD Pharma Hungary Ltd. The funder was consulted on the study design and approved on submitting the results for publication.

Acknowledgments

We would like to thank the NHIF for supporting data acquisition by enabling running custom-tailored queries on the reimbursement database. We would also like to thank Dr. István Kenessey, head of the HNCR for his valuable suggestions and critical review of our approach.

Conflict of interest

GS, GH, ÉB, and KK are employees of MSD Pharma Hungary Ltd. ZV is an employee of Semmelweis University where his contribution to this project was financially compensated. ZKis is also an employee of MSD Pharma Hungary Ltd. and has an affiliation at the Second Department of Medicine and Nephrology-Diabetes Center, University of Pécs Medical School, Pécs, Hungary. GR and ZA-T are employees of RxTarget Ltd. where their contribution to this project was financially compensated. The project was financed by MSD Pharma Hungary Ltd. VM has received consultation fees from AstraZeneca, Boehringer Ingelheim, Roche, Berlin-Chemie, Chiesi, BMS, Novartis, Actelion, Gilead, Pfizer, Richter, Lilly, Orion Pharma and Ipsen and served as PI for over 10 LC studies. LT is an employee of Semmelweis University.

The remaining authors declare that the research was conducted in the absence of any commercial or financial relationships that could be construed as a potential conflict of interest.

Supplementary material

The Supplementary Material for this article can be found online at: https://www.por-journal.com/articles/10.3389/pore.2024.1611754/full#supplementary-material

SUPPLEMENTARY FIGURE S1
Comparison of patient numbers estimated via different approaches. The consensus estimate of the present study is compared to the raw number of incident patients reported by the National Cancer Registry (NCR) as well as to query variations (1.1–1.3C, see methods for detailed definition) featuring different levels of stringency.

SUPPLEMENTARY FIGURE S2
Sensitivity analysis of incidence estimates based on different approaches. Direct standardized rates are calculated for the ESP2013 population standard. The consensus estimate of the present study is compared to

the incidence reported by the National Cancer Registry (NCR) as well as to query variations (1.1–1.3C, see methods for detailed definition) featuring different levels of stringency.

SUPPLEMENTARY FIGURE S3
Sensitivity analysis of trend estimations. Epidemiological trends estimated based on officially reported mortality, reported new patients in the National Cancer Registry (NCR) and queries of different stringency (1.1–1.3C, see methods for detailed definition) are compared to the consensus estimated by the present study. Annual change estimated using Poisson regression; 95% confidence intervals calculated via the sandwich method. Young age cohorts with small numbers of reported cases not shown for the sake of clarity.

SUPPLEMENTARY FIGURE S4
Hungarian lung cancer incidence (women) in the European context. Female Lung cancer incidence rates standardized to the ESP1976 population by our approach for 2012 and 2018 (Hungary*) are compared to numbers reported by Ferlay et al. for Hungary, as well as other European countries.

SUPPLEMENTARY FIGURE S5
Hungarian lung cancer incidence (men) in the European context. Male Lung cancer incidence rates standardized to the ESP1976 population by our approach for 2012 and 2018 (Hungary*) are compared to numbers reported by Ferlay et al. for Hungary, as well as other European countries.

References

1. Dyba T, Randi G, Bray F, Martos C, Giusti F, Nicholson N, et al. The European cancer burden in 2020: incidence and mortality estimates for 40 countries and 25 major cancers. *Eur J Cancer* (2021) 157:308–47. doi:10.1016/j.ejca.2021.07.039

2. Ferlay J, Colombet M, Soerjomataram I, Dyba T, Randi G, Bettio M, et al. Cancer incidence and mortality patterns in Europe: estimates for 40 countries and 25 major cancers in 2018. *Eur J Cancer* (2018) 103:356–87. doi:10.1016/j.ejca.2018.07.005

3. Ferlay J, Steliarova-Foucher E, Lortet-Tieulent J, Rosso S, Coebergh JW, Comber H, et al. Cancer incidence and mortality patterns in Europe: estimates for 40 countries in 2012. *Eur J Cancer* (2013) 49(6):1374–403. doi:10.1016/j.ejca.2012.12.027

4. Bogos K, Kiss Z, Galffy G, Tamasi L, Ostoros G, Muller V, et al. Revising incidence and mortality of lung cancer in central Europe: an epidemiology review from Hungary. *Front Oncol* (2019) 9:1051. doi:10.3389/fonc.2019.01051

5. Weber A, Szatmari I, Dobozi M, Hilbert L, Branyiczkine Geczy G, Nagy P, et al. Comparison of Hungarian central statistical office's causes of death data with the database of the Hungarian national cancer registry. *Orv Hetil* (2022) 163(37): 1481–9. doi:10.1556/650.2022.32573

6. Weber A, Mery L, Nagy P, Polgar C, Bray F, Kenessey I. Evaluation of data quality at the Hungarian national cancer registry, 2000-2019. *Cancer Epidemiol* (2023) 82:102306. doi:10.1016/j.canep.2022.102306

7. Kiss ZN, Bogos K, Tamasi L, Ostoros G, Muller V, Bittner N, et al. Underlying reasons for post-mortem diagnosed lung cancer cases - a robust retrospective comparative study from Hungary (HULC study). *Front Oncol* (2022) 12:1032366. doi:10.3389/fonc.2022.1032366

8. Galffy G, Vastag A, Bogos K, Kiss Z, Ostoros G, Muller V, et al. Significant regional differences in lung cancer incidence in Hungary: epidemiological study between 2011 and 2016. *Pathol Oncol Res* (2021) 27:1609916. doi:10.3389/pore.2021.1609916

9. Kiss Z, Galffy G, Muller V, Moldvay J, Sarosi V, Papai-Szekely Z, et al. Significant changes in advanced lung cancer survival during the past decade in Hungary: impact of modern immunotherapy and the COVID-19 pandemic. *Front Oncol* (2023) 13:1207295. doi:10.3389/fonc.2023.1207295

10. Zeileis A. Object-oriented computation of sandwich Estimators. *J Stat Softw* (2006) 16:9. doi:10.18637/jss.v016.i09

11. Zentrum für Krebsregisterdaten. *Krebs in Deutschland für 2019/2020* (2023). Available from: https://www.krebsdaten.de/Krebs/DE/Content/Publikationen/Krebs_in_Deutschland/kid_2023/kid_2023_c33_c34_lunge.pdf (Accessed January 12, 2024).

12. Menyhart O, Fekete JT, Gyorffy B. Demographic shift disproportionately increases cancer burden in an aging nation: current and expected incidence and mortality in Hungary up to 2030. *Clin Epidemiol* (2018) 10:1093–108. doi:10.2147/CLEP.S155063

13. Li X, Hemminki K. Inherited predisposition to early onset lung cancer according to histological type. *Int J Cancer* (2004) 112(3):451–7. doi:10.1002/ijc.20436

14. Gallus S, Lugo A, Liu X, Behrakis P, Boffi R, Bosetti C, et al. Who smokes in Europe? Data from 12 European countries in the TackSHS survey (2017-2018). *J Epidemiol* (2021) 31(2):145–51. doi:10.2188/jea.JE20190344

15. Raaschou-Nielsen O, Andersen ZJ, Beelen R, Samoli E, Stafoggia M, Weinmayr G, et al. Air pollution and lung cancer incidence in 17 European cohorts: prospective analyses from the European Study of Cohorts for Air Pollution Effects (ESCAPE). *Lancet Oncol* (2013) 14(9):813–22. doi:10.1016/S1470-2045(13)70279-1

16. Hill W, Lim EL, Weeden CE, Lee C, Augustine M, Chen K, et al. Lung adenocarcinoma promotion by air pollutants. *Nature* (2023) 616(7955):159–67. doi:10.1038/s41586-023-05874-3

17. European Environment Agency. *European air quality index* (2023). Available from: https://airindex.eea.europa.eu/Map/AQI/Viewer/ (Accessed January 12, 2024).

18. Carel R, Olsson AC, Zaridze D, Szeszenia-Dabrowska N, Rudnai P, Lissowska J, et al. Occupational exposure to asbestos and man-made vitreous fibres and risk of lung cancer: a multicentre case-control study in Europe. *Occup Environ Med* (2007) 64(8):502–8. doi:10.1136/oem.2006.027748

19. Lissowska J, Foretova L, Dabek J, Zaridze D, Szeszenia-Dabrowska N, Rudnai P, et al. Family history and lung cancer risk: international multicentre case-control study in Eastern and Central Europe and meta-analyses. *Cancer Causes Control* (2010) 21(7):1091–104. doi:10.1007/s10552-010-9537-2

20. Guarga L, Ameijide A, Marcos-Gragera R, Carulla M, Delgadillo J, Borras JM, et al. Trends in lung cancer incidence by age, sex and histology from 2012 to 2025 in Catalonia (Spain). *Sci Rep* (2021) 11:23274. doi:10.1038/s41598-021-02582-8

21. Gysling S, Morgan H, Ifesemen O, West D, Conibear J, Navani N, et al. The impact of COVID-19 on lung cancer incidence in england: analysis of the national lung cancer audit 2019 and 2020 rapid cancer registration datasets. *Chest* (2023) 163:1599–607. doi:10.1016/j.chest.2023.01.008

22. Elek P, Csanadi M, Fadgyas-Freyler P, Gervai N, Oross-Becsi R, Szecsenyi-Nagy B, et al. Heterogeneous impact of the COVID-19 pandemic on lung, colorectal and breast cancer incidence in Hungary: results from time series and panel data models. *BMJ Open* (2022) 12(8):e061941. doi:10.1136/bmjopen-2022-061941

23. Kiss Z, Kocsis J, Nikolenyi A, Horvath Z, Knollmajer K, Benedek A, et al. Opposite trends in incidence of breast cancer in young and old female cohorts in Hungary and the impact of the Covid-19 pandemic: a nationwide study between 2011-2020. *Front Oncol* (2023) 13:1182170. doi:10.3389/fonc.2023.1182170

24. Laczo A, Bodis J, Bogner P, Molnar K, Vajda R, Ponusz-Kovacs D, et al. Participation indicators of organized mammography screening in Hungary between 2012-2021. *Magy Onkol* (2022) 66(3):195–200.

25. Maringe C, Spicer J, Morris M, Purushotham A, Nolte E, Sullivan R, et al. The impact of the COVID-19 pandemic on cancer deaths due to delays in diagnosis in England, UK: a national, population-based, modelling study. *Lancet Oncol* (2020) 21(8):1023–34. doi:10.1016/S1470-2045(20)30388-0

26. Luo Q, O'Connell DL, Yu XQ, Kahn C, Caruana M, Pesola F, et al. Cancer incidence and mortality in Australia from 2020 to 2044 and an exploratory analysis of the potential effect of treatment delays during the COVID-19 pandemic: a statistical modelling study. *Lancet Public Health* (2022) 7(6):e537–e548. doi:10.1016/S2468-2667(22)00090-1

27. Valluri S, Lakshmi HN, Sunkavalli C. Incidental findings in CT scans on screening for COVID-19. *Indian J Surg Oncol* (2023) 14(2):318–23. doi:10.1007/s13193-022-01669-6

28. Kenessey I, Nagy P, Polgar C. The Hungarian situation of cancer epidemiology in the second decade of the 21st century. *Magy Onkol* (2022) 66(3):175–84.

29. Global Burden of Disease Cancer Collaboration. Fitzmaurice C, Akinyemiju TF, Al Lami FH, Alam T, Alizadeh-Navaei R, et al. Global, regional, and national cancer incidence, mortality, years of life lost, years lived with disability, and disability-adjusted life-years for 29 cancer groups, 1990 to 2016: a systematic analysis for the global burden of disease study. *JAMA Oncol* (2018) 4(11): 1553–68. doi:10.1001/jamaoncol.2018.2706

30. Global Burden of Disease 2019 Cancer Collaboration. Kocarnik JM, Compton K, Dean FE, Fu W, Gaw BL, et al. Cancer incidence, mortality, years of life lost, years lived with disability, and disability-adjusted life years for 29 cancer groups from 2010 to 2019: a systematic analysis for the global burden of disease study 2019. *JAMA Oncol* (2022) 8(3):420–44. doi:10.1001/jamaoncol.2021.6987

Pathology & Oncology Research | frontiers

TYPE Original Research
PUBLISHED 09 August 2023
DOI 10.3389/pore.2023.1611328

Check for updates

OPEN ACCESS

EDITED BY
Anna Sebestyén,
Semmelweis University, Hungary

*CORRESPONDENCE
Judit Moldvay,
drmoldvay@hotmail.com

RECEIVED 29 May 2023
ACCEPTED 27 July 2023
PUBLISHED 09 August 2023

CITATION
Gyulai M, Harko T, Fabian K, Karsko L, Agocs L, Szigeti B, Fillinger J, Szallasi Z, Pipek O and Moldvay J (2023), Claudin expression in pulmonary adenoid cystic carcinoma and mucoepidermoid carcinoma.
Pathol. Oncol. Res. 29:1611328.
doi: 10.3389/pore.2023.1611328

COPYRIGHT
© 2023 Gyulai, Harko, Fabian, Karsko, Agocs, Szigeti, Fillinger, Szallasi, Pipek and Moldvay. This is an open-access article distributed under the terms of the Creative Commons Attribution License (CC BY). The use, distribution or reproduction in other forums is permitted, provided the original author(s) and the copyright owner(s) are credited and that the original publication in this journal is cited, in accordance with accepted academic practice. No use, distribution or reproduction is permitted which does not comply with these terms.

Claudin expression in pulmonary adenoid cystic carcinoma and mucoepidermoid carcinoma

Marton Gyulai[1,2], Tunde Harko[3], Katalin Fabian[4], Luca Karsko[5], Laszlo Agocs[5,6], Balazs Szigeti[3], Janos Fillinger[3], Zoltan Szallasi[7,8,9,10], Orsolya Pipek[11] and Judit Moldvay[12]*

[1]County Institute of Pulmonology, Torokbalint, Hungary, [2]Karoly Racz Doctoral School of Clinical Medicine, Semmelweis University, Budapest, Hungary, [3]Department of Pathology, National Koranyi Institute of Pulmonology, Budapest, Hungary, [4]Department of Pathology, South-Buda Center Hospital St. Imre University Teaching Hospital, Budapest, Hungary, [5]Department of Thoracic Surgery, National Koranyi Institute of Pulmonology, Budapest, Hungary, [6]Department of Thoracic Surgery, National Institute of Oncology, Semmelweis University, Budapest, Hungary, [7]National Koranyi Institute of Pulmonology, Budapest, Hungary, [8]Department of Bioinformatics, Semmelweis University, Budapest, Hungary, [9]Computational Health Informatics Program, Boston Children's Hospital, Harvard Medical School, Boston, MA, United States, [10]Danish Cancer Society Research Center, Copenhagen, Denmark, [11]Department of Physics of Complex Systems, ELTE Eotvos Lorand University, Budapest, Hungary, [12]1st Department of Pulmonology, National Koranyi Institute of Pulmonology, Budapest, Hungary

Background: Although the expression of tight junction protein claudins (CLDNs) is well known in common histological subtypes of lung cancer, it has not been investigated in rare lung cancers. The aim of our study was to examine the expression of different CLDNs in pulmonary salivary gland tumors.

Methods: 35 rare lung cancers including pathologically confirmed 12 adenoid cystic carcinomas (ACCs) and 23 mucoepidermoid carcinomas (MECs) were collected retrospectively. Immunohistochemical (IHC) staining was performed on formalin fixed paraffin embedded (FFPE) tumor tissues, and CLDN1, -2, -3, -4, -5, -7, and -18 protein expressions were analyzed. The levels of immunopositivity were determined with H-score. Certain pathological characteristics of ACC and MEC samples (tumor grade, presence of necrosis, presence of blood vessel infiltration, and degree of lymphoid infiltration) were also analyzed.

Results: CLDN overexpression was observed in both tumor types, especially in CLDN2, -7, and -18 IHC. Markedly different patterns of CLDN expression were found for ACC and MEC tumors, especially for CLDN1, -2, -4, and -7, although none of these trends remained significant after correction for multiple testing. Positive correlations between expressions of CLDN2 and -5, CLDN3 and -4, and CLDN5 and -18 were also demonstrated. Tumors of never-smokers presented lower levels of CLDN18 than tumors of current smokers (p-value: 0.003).

Conclusion: This is the first study to comprehensively describe the expression of different CLDNs in lung ACC and MEC. Overexpression of certain CLDNs may

Abbreviations: ACC, adenoid cystic carcinoma; CLDN, claudin; IHC, immunohistochemistry; MEC, mucoepidermoid carcinoma; NSCLC, non-small cell lung cancer; SCLC, small cell lung cancer.

pave the way for targeted anti-claudin therapy in these rare histological subtypes of lung cancer.

KEYWORDS

adenoid cystic carcinoma, mucoepidermoid carcinoma, rare lung tumors, claudin expression, immunohistochemistry

Introduction

Adenoid cystic carcinoma (ACC) and mucoepidermoid carcinoma (MEC) belong to the group of rare lung cancers. They originate from the salivary glands of the tracheobronchial tree and represent 0.1%–0.2% of all lung cancer cases [1]. In low-grade and early-stage tumors complete bronchoscopic excision or surgical resection result in long term survival [2]. In high-grade tumors and in metastatic cases, however, the therapeutic options are often limited and combination of radiotherapy and chemotherapy yields only modest survival [3].

Claudins (CLDNs) are important constituents of tight junctions, and play key role in cell proliferation, glandular differentiation, cellular adhesion, and metastasis formation [4]. They serve as a barrier regulating the passage of ions, water and different macromolecules to maintain homeostasis, and work as a fence to keep cell polarity by regulating the separate passages of molecules in the apical and basolateral membrane. At least 27 different CLDN members are known today, all of which are thought to vary in expression depending on location and cell type [5, 6]. Altered expression of different CLDNs was found in a wide variety of human malignancies, and in many tumor types it had prognostic significance [7, 8]. In 2007, our research group was the first to demonstrate that CLDN1, -2, -3, -4, and -7 proteins are expressed in normal bronchial epithelial cells as well as in different histologic subtypes of lung cancer [9]. We observed distinct CLDN mRNA and protein expression profile within the non-small cell lung cancer (NSCLC) group and marked differences between small cell lung cancers (SCLCs) and carcinoids that may have differential diagnostic impact. In our other work, we showed that CLDN expression differences can also be observed between the histological subtypes of lung adenocarcinomas, namely, between tumors with lepidic spread and non-lepidic spread [8]. We also demonstrated the overexpression of different CLDNs, especially CLDN2, -3 and -4, and -7 as has already been described in other tumor types, which might serve as a therapeutic target [10, 11].

Since there is only very little data available on CLDN protein expression in primary bronchial ACC and MEC, the aim of our present work was to comprehensively investigate the CLDN expression in these rare pulmonary cancers in order to determine the potential role of anti-CLDN treatment.

Patients and methods

Patients

In our retrospective study, we included 35 pathologically confirmed rare lung tumors including 12 adenoid cystic carcinomas, and 23 mucoepidermoid carcinomas. These patients were diagnosed and treated in the National Koranyi Institute of Pulmonology in Budapest between 1987 and 2023. In 27 cases surgical resection was performed, and eight patients had bronchoscopic tumor excision with rigid bronchoscope under general anesthesia. In the cases of surgical resection pathologic TNM (pTNM), while in the cases of bronchoscopic excision clinical TNM (cTNM) was applied.

The clinicopathological characteristics of patients including age, gender, smoking history, histology, stage, and the type of biopsy material are summarized in Table 1.

Histology and TMA construction

Since the vast majority of biopsy tissue samples were obtained before 2020, therefore, all tumor samples were re-examined. The ACC and MEC diagnoses were confirmed with the following immunohistochemical (IHC) markers: pancytokeratin, actin, S100, and p63. Tissue characteristics, such as tumor grade [1–3], presence of necrosis (yes/no), presence of blood vessel infiltration (yes/no), and degree of lymphoid infiltration (slight/moderate) were determined on hematoxylin-eosin stained sections.

In the case of surgical specimens IHC staining was performed on tissue microarrays (TMAs) (5 × 6; diameter, 2 mm) with one or two cores per patient, prepared from selected areas of formalin fixed paraffin embedded (FFPE) tissue samples (TMA Master; 3DHistech, Budapest, Hungary). In the case of bronchoscopic excisions 3-μm-thick sections were prepared for IHC without TMA construction.

Immunohistochemistry

For immunoreactions, the following antibodies and dilutions were used: CLDN1 mAb (Invitrogen, 1:200), CLDN2 mAb (Invitrogen, 1:300), CLDN3 pAb (Invitrogen, 1:200), CLDN4 mAb (Invitrogen, 1:200), CLDN5 mAb (Invitrogen, 1:20), CLDN7 mAb (Invitrogen, 1:200), and CLDN18 mAb (Invitrogen, 1:200). All primary antibodies were incubated at

TABLE 1 Major characteristics of 35 patients diagnosed and treated with adenoid cystic carcinoma and mucoepidermoid carcinoma between 1987 and 2023.

	ACC	MEC	*p*-value
	N = 12	*N = 23*	
Gender			1.000[a]
Female	5 (41.7%)	10 (43.5%)	
Male	7 (58.3%)	13 (56.5%)	
Age, years—median (range)	64 (32–81)	48 (19–67)	**0.014**[b]
Smoking			0.175[a]
Never	4 (33.3%)	11 (47.8%)	
Ex	2 (16.7%)	0 (0.00%)	
Current	4 (33.3%)	7 (30.4%)	
nd	2 (16.7%)	5 (21.7%)	
Grade			**0.010**[a]
1	0 (0.00%)	11 (47.8%)	
2	10 (83.3%)	9 (39.1%)	
3	2 (16.7%)	3 (13.0%)	
Vascular involvement			0.594[a]
No	10 (83.3%)	21 (91.3%)	
Yes	2 (16.7%)	2 (8.70%)	
Lymphoid infiltration			0.709[a]
Slight	9 (75.0%)	15 (65.2%)	
Moderate	3 (25.0%)	8 (34.8%)	
Necrosis			0.725[a]
No	7 (58.3%)	11 (47.8%)	
Yes	5 (41.7%)	12 (52.2%)	
Stage category			**0.016**[a]
I	3 (25.0%)	16 (69.6%)	
II	2 (16.7%)	4 (17.4%)	
III	5 (41.7%)	3 (13.0%)	
IV	2 (16.7%)	0 (0.00%)	
Sample type			
Bronchoscopic excision	7 (58.3%)	1 (4.3%)	
Surgical material	5 (41.7%)	22 (95.7%)	

ACC, adenoid cystic carcinoma; MEC, mucoepidermoid carcinoma; nd, no data.
p-values are non-adjusted ones, but bold lettering mark those associations that remained significant after correction as well. Adjustment for multiple testing was performed with the Benjamini-Hochberg method.
[a]Fisher's exact test.
[b]Kruskal-Wallis test.

42°C for 32 min. IHC staining was performed using the Roche Ventana Benchmark ULTRA automated slide stainer (Ventana Medical Systems, Roche Diagnostics, France) with the UltraView universal DAB IHC Detection Kit (Roche, France). After antibody visualization the slides were counterstained with hematoxylin. As a positive control, CLDN positive lung cancer tissues were used for CLDN1, -2, -3, -4, -5, -7, and -18 reactions.

All sections were examined and evaluated by two experienced pathologists at ×400 magnification. The levels of immunopositivity were determined with H-score, which was calculated by a semi-quantitative assessment of both the intensity of staining (graded as: 0 = non-staining; 1 = weak; 2 = median; or 3 = strong) and the percentage of positive cells (H-score: 0–300). In heterogeneous tumor samples we analyzed the H-score in different regions, and the final score was determined by taking into account the proportion of heterogeneous areas.

Statistical analysis

All statistical analyses were performed using R version 4.2.1 (R Foundation for Statistical Computing, Vienna, Austria). Categorical and ordinal parameters were statistically analyzed by Fisher's exact tests. Continuous variables were compared with Mann-Whitney test or Kruskal-Wallis tests. Hierarchical clustering of samples based on the measured expression levels was performed with the ComplexHeatmap R package (v.2.10.0; URL)[1]. The distance matrix was calculated using Euclidean distance measure and the dendrograms were created using the ward.D clustering method. Correlations of expression levels were calculated in a pairwise manner using Pearson correlation. The value of linear correlation coefficient (R) varies from −1 to 1 both values inclusive. Throughout the analyses, the Benjamini–Hochberg correction was used to adjust for multiple testing.

Results

Comparison of clinicopathological characteristics of ACC and MEC samples

We observed that ACC tumors tended to have both significantly higher grades (adjusted *p*-value = 0.044, Table 1) and higher stages (adjusted *p*-value = 0.044, Table 1) than MEC tumors. Patients with ACC tumors were also generally older than patients with MEC tumors (medians: 64 vs. 48 years, adjusted *p*-value = 0.044, Table 1). No other significant tendencies could be detected when comparing tumors of the two subtypes regarding either gender, smoking, vascular involvement, lymphoid infiltration or necrosis.

CLDN immunohistochemistry

The majority of CLDN IHC positive tumors showed strong and homogenous staining. In certain cases of CLDN IHC

1 https://jokergoo.github.io/ComplexHeatmap-reference/book/; date last accessed: 5/10/2021.

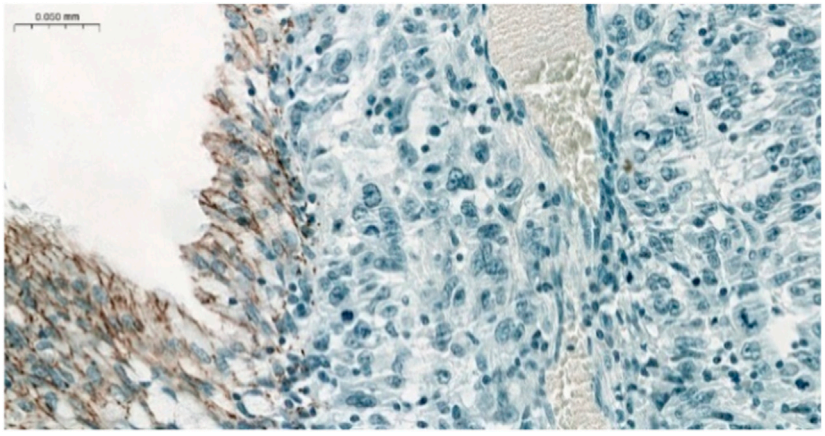

FIGURE 1
Negative CLDN4 IHC in MEC. Note the positive normal bronchial cells serving as a positive endogenous control (×200).

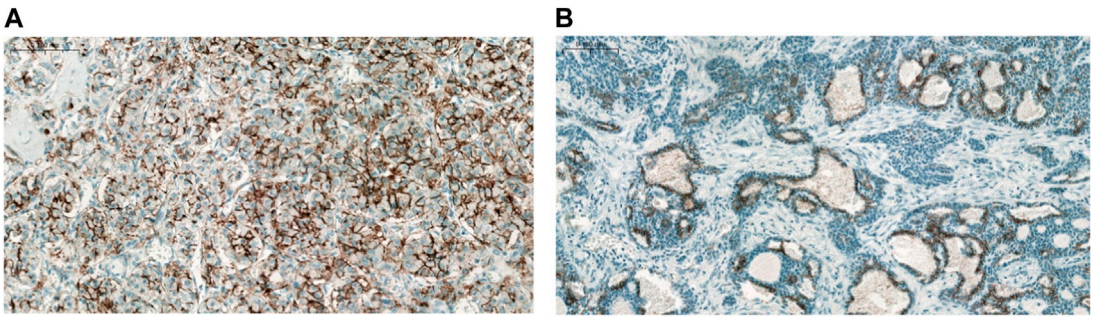

FIGURE 2
CLDN7 expression in ACC. **(A)** No major intratumoral heterogeneity (×200), **(B)** Marked intratumoral heterogeneity (×100).

negative tumors, non-tumorous tissue serving as an endogenous positive control helped the correct scoring (Figure 1). Membranous CLDN immunopositivity could be observed in CLDN1, -3, -4, and -7 IHC, while cytoplasmic staining was found in CLDN2, -5, and -18 IHC. Generally, all positive tumors stained diffusely and in fairly uniform manner (Figure 2A). The intensity of immunostaining was usually similar to—or even stronger than—the adjacent normal bronchial epithelium. Heterogeneity of expression in different areas within the same tumor was observed only in very few cases (Figures 2B, 3J). Representative pictures of CLDN IHC in ACC and MEC cases are demonstrated in Figures 3A–J.

Associations between CLDN expression and clinicopathological characteristics

Given the low number of available cases, relationships between expression levels and other clinicopathological features were investigated on all data, disregarding tumor subtype.

Out of all measured CLDN expression levels, CLDN4 seemed to be most influenced by different factors. We found that grade 2 tumors expressed higher levels of CLDN4 than grade 1 tumors (median H-scores: 60 vs. 1; Mann-Whitney test p-value: 0.045), and a positive correlation could be observed between stage category and CLDN4 expression (R = 0.5, p-value: 0.003). CLDN4 levels also seemed to be positively correlated with age (R = 0.49, p-value: 0.004).

Additionally, we found that tumors with signs of necrosis expressed higher levels of CLDN5 than tumors without (median H-scores: 60 vs. 0; Mann-Whitney test p-value: 0.009).

The most compelling relationship was observed between CLDN18 expression and smoking: tumors of never-smokers presented lower levels of CLDN18 than tumors of current smokers (median H-scores: 70 vs. 190, Mann-Whitney test p-value: 0.003).

Out of all these associations, only the latter one remained significant when correcting for multiple testing.

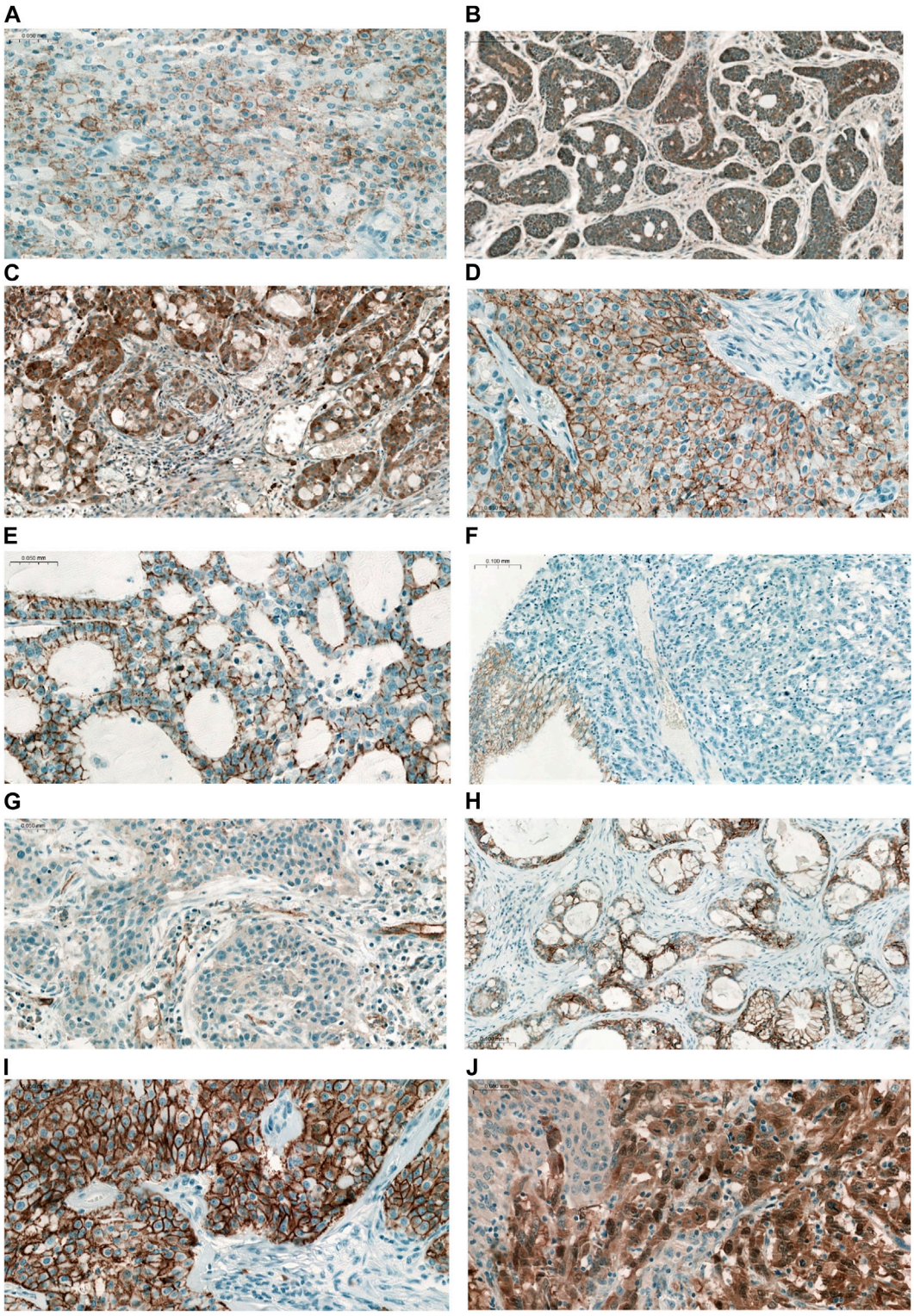

FIGURE 3
Representative IHC reactions of different CLDNs in pulmonary ACC and MEC. **(A)** CLDN1 MEC (×200), **(B)** CLDN2 ACC (×100), **(C)** CLDN2 MEC (×100), **(D)** CLDN3 MEC (×200), **(E)** CLDN4 ACC (×200), **(F)** CLDN4 MEC (×100). Note the negative tumor cells and the positive normal bronchial cells serving as a positive endogenous control, **(G)** CLDN5 MEC (×200). Weak positive staining in tumor cells, and vessels served as positive endogenous control, **(H)** CLDN7 ACC (×100), **(I)** CLDN7 MEC (×200), **(J)** CLDN18 MEC (×200). Note the heterogeneity of IHC staining.

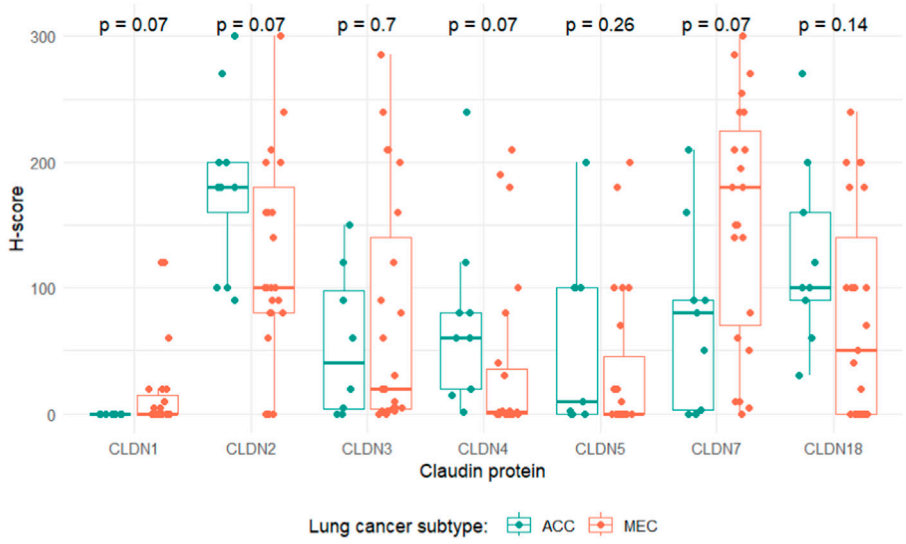

FIGURE 4
Distributions of claudin expression levels grouped by lung cancer subtype. *p*-values indicate adjusted *p*-values, corrected for multiple testing with the Benjamini-Hochberg method.

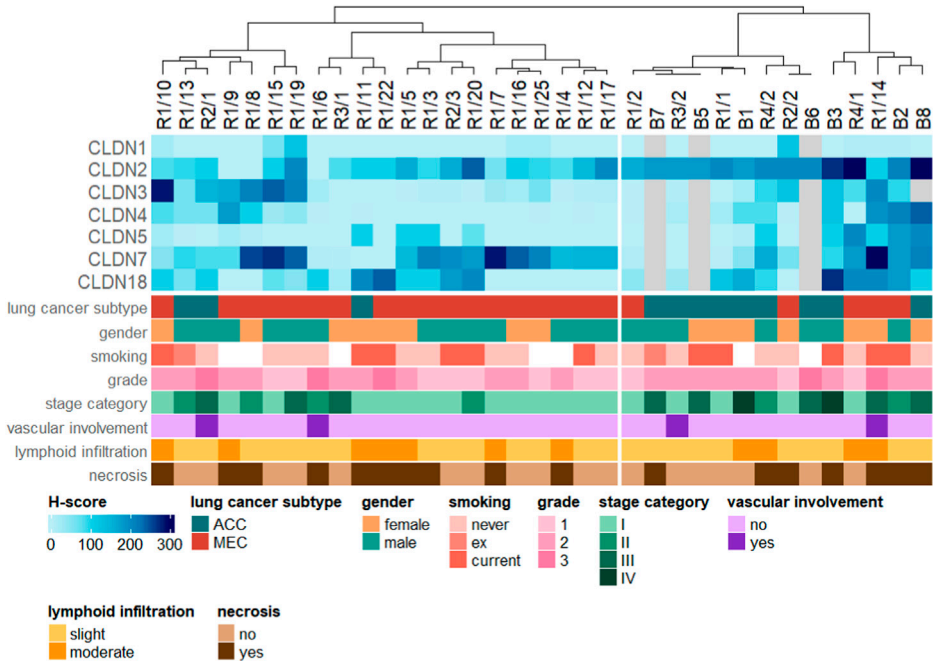

FIGURE 5
Hierarchical clustering of the samples based on CLDN expression levels. Clinicopathological parameters are shown as column annotations at the bottom.

Differences in CLDN expression profiles between ACC and MEC

Expression levels of CLDN1, -2, -4 and -7 showed markedly different distributions for ACC and MEC tumors. Specifically, ACC samples exhibited a propensity for heightened CLDN2 and -4 expression, whereas MEC cases displayed elevated levels of CLDN1 and -7. However, none of these tendencies remained significant when correcting for multiple testing (Figure 4). In

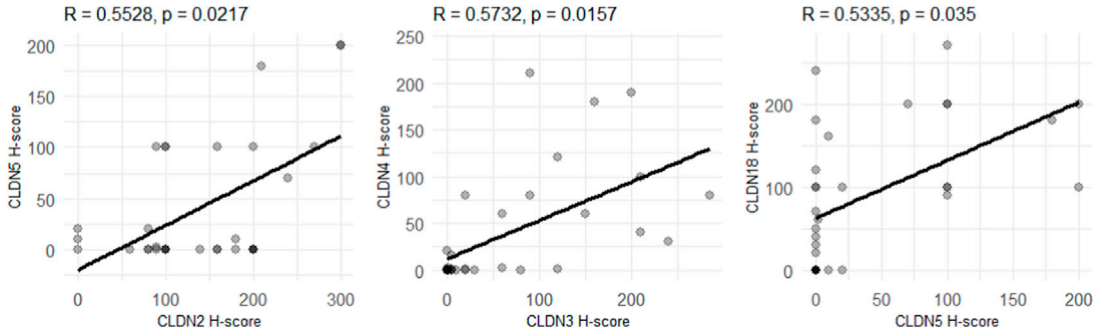

FIGURE 6
Correlations between CLDN expression levels in the whole dataset. *p*-values indicate adjusted *p*-values, corrected for multiple testing with the Benjamini-Hochberg method. R-values correspond to the Pearson correlation-coefficient.

ACC CLDN1 was the only marker that was negative in all tumor tissues, whereas in MEC there was no such a marker that was negative in all samples.

As an additional insight, a simple unsupervised hierarchical clustering of the samples was performed based on the measured expression levels (Figure 5). The resulting dendrogram of the cases was split to obtain two groups. Column annotations at the bottom of the figure show that lung cancer subtypes within the two groups (with a few exceptions) are fairly uniform, suggesting that patterns of CLDN expression inherently differentiate between ACC and MEC tumors (adjusted *p*-value = 0.032). On the other hand, remaining clinicopathological parameters are relatively well-mixed in the two groups (adjusted *p*-values: 1.0, 1.0, 1.0, 0.468, 1.0, 1.0, 1.0 for gender, smoking, grade, stage category, vascular involvement, lymphoid infiltration and necrosis, respectively), indicating that the main factor influencing the separation based on CLDN expression levels is indeed cancer subtype.

Correlations of different CLDN expression levels

Due to the low number of cases, correlations between CLDN expressions were assessed on the whole dataset, regardless of tumor subtype.

We identified positive correlations between the expression levels of CLDN5 and -2 (R = 0.55, adjusted *p*-value = 0.02), CLDN3 and -4 (R = 0.57, adjusted *p*-value = 0.02) and CLDN5 and -18 (R = 0.53, adjusted *p*-value = 0.04) (Figure 6). All of these associations remain significant when corrected for multiple testing.

FFPE block age-related artifacts

Given the well-known degradation of FFPE blocks over time, we reanalyzed older and newer samples separately to validate the above observed trends. Samples were classified into "old" and "new" cohorts based on the year of FFPE block creation: blocks prepared before 2009 were designated as "old," while those created thereafter as "new." The threshold for this categorization was chosen as the median of the FFPE block creation years in our dataset.

Generally, as expected, regarding all CLDN expression levels, old cases were lower expressors than new ones, although in most cases not to a significant extent. Exceptions for this trend were CLDN1 and -4, with very low median H-scores in both sample groups. (Medians and multiple testing-adjusted Kruskal-Wallis test *p*-values for old vs. new cases: 0 vs. 0, $p = 0.76$ (CLDN1), 100 vs. 200, $p = 0.003$ (CLDN2), 20 vs. 50, $p = 0.90$ (CLDN3), 2 vs. 1, $p = 0.95$ (CLDN4), 0 vs. 10, $p = 0.56$ (CLDN5), 140 vs. 150, $p = 0.76$ (CLDN7), 50 vs. 160, $p = 0.11$ (CLDN18).) However, despite these general trends, the results discussed above remain valid for both new and old samples when analyzed separately, albeit in some cases with slightly diminished statistical power.

Regarding the expression patterns of ACC and MEC tumors, the elevated CLDN1 and -7 levels of MEC cases could be observed in both old and new samples. ACC samples were verified to express higher levels of CLDN4 in both cohorts, and CLDN2 in old samples.

Discussion

The CLDN expression in MEC and ACC is poorly investigated, and the results published so far only refer to head and neck salivary gland tumors [12].

Maria et al. examined CLDN1, - 2, -3, -4, and -5 expression in 10 salivary gland tumor samples (1 parotid and 9 submandibular without further histologic specification) and found that all CLDNs were expressed, except CLDN5 [13]. Aoyama et al. examined CLDN1, -4, and -7 expression in 2 parotid and 2 submandibular salivary gland tumors and described membranous immunopositivity for all studied IHC markers [14]. In our present work we observed CLDN IHC immunopositivity for all studied IHC markers, including

CLDN5, however, we found a significant difference in the localization of their immunopositivity and the degree of their expression, as detailed in the description of the results. The observed intertumoral heterogeneity in CLDN expression in ACC seems to be confirmed by recent molecular genetic studies on salivary gland ACC, when molecular genetic differences were described and potentially actionable molecular alterations were found in 28 of 135 studied patients (21%) [15].

If we compare the CLDN expression pattern of ACC with our previously described results in histological subtypes of lung cancer, we find that ACC shows lower expression of CLDN1, -3, and -4, and higher expression of CLDN2 than NSCLC tumors [9]. The CLDN expression pattern of ACC–regarding CLDN1, -2, -3, -4, and -7—is most similar to that of lung adenocarcinoma with lepidic spread [8]. It is worth emphasizing that significant CLDN2 expression was observed in ACC, which is contrary to what we previously observed in SCLC, where there was no CLDN2 IHC positive tumor. Both CLDN5 and CLDN18 were described for the first time in pulmonary ACC. Half of the cases showed moderate CLDN5 immunostaining, while one-third of the tumors showed particularly strong CLDN18 staining.

Regarding CLDN expression in MEC, Aoyama et al. examined CLDN1, -4, and -7 expression in six parotid and three submandibular salivary gland MEC tumors and observed membranous immunostaining in all markers, which is similar to our observations [14]. Aro et al. analyzed CLDN1, -3, -4, and -7 expression in salivary gland MEC [16]. They found that high expression of CLDN1 was seen in low-grade MEC, and it appeared to be a marker of good prognosis. High CLDN3 expression was seen in intermediate- and high-grade MEC, while it was low in low-grade MEC. In our work grading was only observed to have an association with the expression of CLDN4 (with grade 2 tumors expressing higher levels than grade 1 tumors), but this trend was neither specific to MEC cases, nor remained significant after multiple testing correction.

In our own study, the most prominent CLDN positivity in MEC was observed for CLDN2 and CLDN7, although IHC negative tumors were also found for both markers.

If we compare the CLDN expression pattern of MEC with our previously described results in histological subtypes of lung cancer, we could observe high CLDN2 and CLDN7 expression, as well as low CLDN3 expression, which was most characteristic of squamous cell carcinoma among lung cancers [9].

It is undeniable that our results might suffer from the limitations of having a relatively small number of cases. Undoubtedly, a significantly larger cohort would give more reliable insights into the expression of different CLDNs in pulmonary ACC and MEC, however, in rare tumors, usually it takes many years to collect the number of cases suitable for such examinations. Furthermore, it will be necessary to expand the range of tested anti-CLDN antibodies (e.g., CLDN6 and -18.2) and a wider clinical data analysis. Other limitation might be the age of FFPE tissue samples, which may affect IHC reactions. In order to investigate this, we compared the IHC results of old and new tissue samples and observed that, as expected, measured H-scores are generally lower for old cases. However, we also validated our results obtained on the whole dataset separately on old and new samples and found that the previously established associations between various parameters hold true for both cohorts, although naturally with lower statistical power. Notwithstanding this encouraging outcome, the possibility of age-related FFPE block artifacts highlights the necessity of international, multi-center studies that could provide an increased sample size even for rare malignancies with a focus on analyzing relatively recent tissue samples.

In rare pulmonary tumors, there is unmet need to develop more efficient therapeutic modalities, especially for patients with advanced-stage disease [17–22].

In a recent study of Roehlen et al. targeting non-junctional CLDN1 (on the basolateral membrane of the human hepatocyte) markedly suppressed tumor growth and invasion in cell line-based models of hepatocellular carcinoma and patient-derived 3D *ex vivo* models. Moreover, the robust effect on tumor growth was confirmed *in vivo* in a large series of cell line-derived xenograft and patient-derived xenograft mouse models [23]. In our work ACC did not express CLDN1, and MEC showed only mild expression, therefore targeting CLDN1 is not a promising therapeutic strategy.

On the contrary, CLDN2 expression was very characteristic for both ACC and MEC. Wei et al. demonstrated in colorectal cancer that CLDN2 is upregulated and associated with poor survival, and CLDN2 depletion significantly promoted N-myc downstream-regulated gene 1 (NDRG1) transcription, leading to termination of the cancer cell growth and metastasis *in vitro* and *in vivo* [24]. Thus, this study suggested that CLDN2 may serve as a promising target for colorectal cancer treatment.

Clostridium perfringens enterotoxin (CPE) triggers lysis of epithelial cells through binding to tight-junction proteins CLDN3 and CLDN4, therefore, high expression of these proteins might facilitate CLDN-targeted therapy using CPE. Maeda et al. investigated the therapeutic effect of CPE in prostate cancer xenografts in athymic mice [25]. Reduced expression of CLDN4, but not CLDN3, led to remarkable decreases of cytotoxicity, and the injection of CPE around PC3 xenografts significantly suppressed tumor growth. It has been published by Luo et al. that targeting CLDN-4 enhances chemosensitivity in breast cancer [26]. In our study, both ACC and MEC showed CLDN3 and -4 IHC positivity, but only to a moderate extent on average. Certain tumor samples, however, especially in the MEC group showed high expression of CLDN3 and -4.

Until now, no therapeutic approach against CLDN5 has been described. In our work the IHC scores of CLDN5 both in ACC

and MEC varied from 0-200, therefore, in the case of some highly expressing tumors, anti-CLDN5 treatment can theoretically be considered.

CLDN7 is highly expressed both in the lung cancers we previously investigated as well as in the ACC and MEC cases we studied now, especially in half of the MEC tumors. The role of CLDN7 in carcinogenesis is somewhat controversial. In 2018, Li et al. demonstrated a previously undescribed role of CLDN7 as a clear cell renal cell carcinoma suppressor and suggested that loss of CLDN7 potentiates epithelial-mesenchymal transition and tumor progression [27]. On the contrary, Philip et al. reported that CLDN7 promotes the epithelial-mesenchymal transition in human colorectal cancer cell lines [28]. In an interesting study by Hoggard et al. CLDN7 was found to increase chemosensitivity to cisplatin through the upregulation of caspase pathway in human NCI-H522 lung cancer cells [29].

Overexpression of CLDN18 paves the way for anti-CLDN18 antibody therapy. Xu et al. published the results of the application of a novel anti-CLDN18.2/anti-CD3 bispecific antibody, which exhibited low affinity for anti-CD3, highly specific binding, potent cytotoxicity, and anti-tumor activity [30]. Recently, Wang et al. reported that CLDN18 isoform 2 (CLDN18.2) is highly expressed in primary ovarian mucinous carcinomas and metastatic gastrointestinal mucinous carcinomas derived from upper gastrointestinal tract primary tumors [31]. They concluded that CLDN18.2-targeted therapy might serve as a potential therapeutic strategy for primary ovarian mucinous carcinomas and metastatic gastrointestinal mucinous carcinomas from the upper gastrointestinal tract. Very recently, in a multicenter, randomized, double-blind, phase 3 trial (SPOTLIGHT), zolbetuximab, a monoclonal antibody targeting CLDN18.2 was found to significantly prolong progression-free survival and overall survival when combined with mFOLFOX6 versus placebo plus mFOLFOX6 in patients with CLDN18.2-positive, HER2-negative, locally advanced unresectable or metastatic gastric or gastro-oesophageal junction adenocarcinoma [32]. The results of this clinical trial may bring a paradigm shift in the treatment of malignant tumors that overexpress CLDN proteins. In our cohort CLDN18 overexpression was pronounced in 2/3 of the ACC and in half of the MEC cases. The planned CLDN18.2 immunostainings could not be performed due to technical reasons.

In summary, this is the first study which comprehensively describes the CLDN expression pattern in pulmonary ACC and MEC. The overexpression of certain CLDNs both in ACC and MEC opens the door to anti-claudin treatment in these rare lung cancer subtypes. Based on the results of our present study, in the case of pulmonary ACC and MEC, oncotherapies against CLDN-2, -7, and -18 arise mostly, but in some cases CLDN-3 and -4 overexpression might also serve as a target.

Data availability statement

The original contributions presented in the study are included in the article/supplementary material, further inquiries can be directed to the corresponding author.

Ethics statement

The present study was conducted in accordance with the guidelines of the Helsinki Declaration of the World Medical Association. The study was approved by the national ethics committees (Hungarian Scientific and Research Ethics Committee of the Medical Research Council, ETT TUKEB 7214-1/2016/EKU [0109/16], ÁNTSZ IF-77-3/2016, SE IKEB 241/2016). The need for individual informed consent for this retrospective study was waived. After the collection of clinical information, patient identifiers were removed, and subsequently, patients could not be directly or indirectly identified.

Author contributions

MG: Conceptualization, methodology, bronchoscopic sampling, investigation, writing—original draft. TH: TMA construction, investigation. KF: Immunohistochemical investigations. LK: Development of clinical database. LA: Providing surgical materials. BS: Immunohistochemical investigations. JF: Methodology, supervision. ZS: Supervision, writing—review editing. OP: Statistical analysis, writing—original draft. JM: Conceptualization, validation, supervision, writing—original draft. All authors contributed to the article and approved the submitted version.

Funding

This work was supported by the Research and Technology Innovation Fund (KTIA_NAP_13-2014-0021 and 2017-1.2.1-NKP-2017-00002 to ZS), Breast Cancer Research Foundation (BCRF-21-159 to ZS), Kræftens Bekæmpelse (R281-A16566 and to ZS), Det Frie Forskningsråd Sundhed og Sygdom (7016-00345B to ZS). JM was supported by the Hungarian National Research, Development and Innovation Office (K129065) and by the Hungarian Brain research Program (grant 2017-1.2.1-NKP-2017-00002).

Conflict of Interest

The authors declare that the research was conducted in the absence of any commercial or financial relationships that could be construed as a potential conflict of interest.

References

1. Pisano C, Witel G, De Filippis M, Listi A, Napoli F, Righi L, et al. Moving through rare lung cancer histologies: A narrative review on diagnosis and treatment of selected infrequent entities. *Precision Cancer Med* (2022) 5:27. doi:10.21037/pcm-22-4

2. Qin BD, Jiao XD, Liu K, Wu Y, He X, Liu J, et al. Clinical, pathological and treatment factors associated with the survival of patients with primary pulmonary salivary gland-type tumors. *Lung Cancer (Amsterdam, Netherlands)* (2018) 126: 174–81. doi:10.1016/j.lungcan.2018.11.010

3. Lee RH, Wai KC, Chan JW, Ha PK, Kang H. Approaches to the management of metastatic adenoid cystic carcinoma. *Cancers* (2022) 14(22):5698. doi:10.3390/cancers14225698

4. Wang DW, Zhang WH, Danil G, Yang K, Hu JK. The role and mechanism of claudins in cancer. *Front Oncol* (2022) 12:1051497. doi:10.3389/fonc.2022.1051497

5. Mineta K, Yamamoto Y, Yamazaki Y, Tanaka H, Tada Y, Saito K, et al. Predicted expansion of the claudin multigene family. *FEBS Lett* (2011) 585(4): 606–12. doi:10.1016/j.febslet.2011.01.028

6. Osanai M, Takasawa A, Murata M, Sawada N. Claudins in cancer: Bench to bedside. *Pflugers Archiv Eur J Physiol* (2017) 469(1):55–67. doi:10.1007/s00424-016-1877-7

7. Popova OP, Kuznetsova AV, Bogomazova SY, Ivanov AA. Claudins as biomarkers of differential diagnosis and prognosis of tumors. *J Cancer Res Clin Oncol* (2021) 147(10):2803–17. doi:10.1007/s00432-021-03725-0

8. Moldvay J, Fábián K, Jäckel M, Németh Z, Bogos K, Furák J, et al. Claudin-1 protein expression is a good prognostic factor in non-small cell lung cancer, but only in squamous cell carcinoma cases. *Pathol Oncol Res* (2017) 23(1):151–6. doi:10.1007/s12253-016-0115-0

9. Moldvay J, Jäckel M, Páska C, Soltész I, Schaff Z, Kiss A. Distinct claudin expression profile in histologic subtypes of lung cancer. *Lung Cancer* (2007) 57(2):159–67. Amsterdam, Netherlands. doi:10.1016/j.lungcan.2007.02.018

10. Wang YB, Shi Q, Li G, Zheng JH, Lin J, Qiu W. MicroRNA-488 inhibits progression of colorectal cancer via inhibition of the mitogen-activated protein kinase pathway by targeting claudin-2. *Am J Physiol Cel Physiol* (2019) 316(1): C33–C47. doi:10.1152/ajpcell.00047.2018

11. Beier LS, Piontek J, Piontek A, Protze J, Kobelt D, Walther W. Claudin-targeted suicide gene therapy for claudin-overexpressing tumor cells by using modified *Clostridium perfringens* enterotoxin (CPE). *Methods Mol Biol (Clifton, NJ)* (2022) 2521:173–88. doi:10.1007/978-1-0716-2441-8_9

12. Arrojo ML, Oliveira KK, Bettim BB, Kowalski LP, Carraro DM, Meira I, et al. Tight junction gene expression in salivary gland tumors. *Pathol Res Pract* (2022) 238:154113. doi:10.1016/j.prp.2022.154113

13. Maria OM, Kim JW, Gerstenhaber JA, Baum BJ, Tran SD. Distribution of tight junction proteins in adult human salivary glands. *J Histochem Cytochem official J Histochem Soc* (2008) 56(12):1093–8. doi:10.1369/jhc.2008.951780

14. Aoyama T, Takasawa A, Murata M, Osanai M, Takano K, Hasagawa T, et al. Immunoreactivity patterns of tight junction proteins are useful for differential diagnosis of human salivary gland tumors. *Med Mol Morphol* (2019) 52(1):23–35. doi:10.1007/s00795-018-0199-6

15. Morris LGT, Chandramohan R, West L, Zehir A, Chakravarty D, Pfister DG, et al. The molecular landscape of recurrent and metastatic head and neck cancers: Insights from a precision oncology sequencing platform. *JAMA Oncol* (2017) 3(2): 244–55. doi:10.1001/jamaoncol.2016.1790

16. Aro K, Rosa LE, Bello IO, Soini Y, Mäkitie AA, Salo T, et al. Expression pattern of claudins 1 and 3-an auxiliary tool in predicting behavior of mucoepidermoid carcinoma of salivary gland origin. *Virchows Archiv : Int J Pathol* (2011) 458(3): 341–8. doi:10.1007/s00428-010-1026-1

17. Garg PK, Sharma G, Rai S, Jakhetiya A. Primary salivary gland-type tumors of the lung: A systematic review and pooled analysis. *Lung India* (2019) 36(2):118–22. doi:10.4103/lungindia.lungindia_284_18

18. Li D, Pang X, Zhu X, Shanzhou Q, Wen G, Ma D. Low-dose radiotherapy combined with immunotherapy for suboral adenoid cystic carcinoma with bilateral lung metastasis: A case report and literature review. *Oncol Lett* (2022) 24(2):279. doi:10.3892/ol.2022.13399

19. Mueller SK, Haderlein M, Lettmaier S, Agaimy A, Haller F, Hecht M, et al. Targeted therapy, chemotherapy, immunotherapy and novel treatment options for different subtypes of salivary gland cancer. *J Clin Med* (2022) 11(3):720. doi:10.3390/jcm11030720

20. Hu S, Gong J, Zhu X, Lu H. Pulmonary salivary gland tumor, mucoepidermoid carcinoma: A literature review. *J Oncol* (2022) 2022:9742091. doi:10.1155/2022/9742091

21. de Sousa LG, Jovanovic K, Ferrarotto R. Metastatic adenoid cystic carcinoma: Genomic landscape and emerging treatments. *Curr Treat Options Oncol* (2022) 23(8):1135–50. doi:10.1007/s11864-022-01001-y

22. de Sousa LG, Neto FL, Lin J, Ferrarotto R. Treatment of recurrent or metastatic adenoid cystic carcinoma. *Curr Oncol Rep* (2022) 24(5):621–31. doi:10.1007/s11912-022-01233-z

23. Roehlen N, Muller M, Nehme Z, Crouchet E, Jühling F, Del Zompo F, et al. Treatment of HCC with claudin-1-specific antibodies suppresses carcinogenic signaling and reprograms the tumor microenvironment. *J Hepatol* (2023) 78(2): 343–55. doi:10.1016/j.jhep.2022.10.011

24. Wei M, Zhang Y, Yang X, Ma P, Li Y, Wu Y, et al. Claudin-2 promotes colorectal cancer growth and metastasis by suppressing NDRG1 transcription. *Clin translational Med* (2021) 11(12):e667. doi:10.1002/ctm2.667

25. Maeda T, Murata M, Chiba H, Takasawa A, Tanaka S, Kojima T, et al. Claudin-4-targeted therapy using *Clostridium perfringens* enterotoxin for prostate cancer. *The Prostate* (2012) 72(4):351–60. doi:10.1002/pros.21436

26. Luo Y, Kishi S, Sasaki T, Ohmori H, Fujiwara-Tani R, Mori S, et al. Targeting claudin-4 enhances chemosensitivity in breast cancer. *Cancer Sci* (2020) 111(5): 1840–50. doi:10.1111/cas.14361

27. Li Y, Gong Y, Ning X, Peng D, Liu L, He S, et al. Downregulation of CLDN7 due to promoter hypermethylation is associated with human clear cell renal cell carcinoma progression and poor prognosis. *J Exp Clin Cancer Res : CR* (2018) 37(1):276. doi:10.1186/s13046-018-0924-y

28. Philip R, Heiler S, Mu W, Büchler MW, Zöller M, Thuma F. Claudin-7 promotes the epithelial-mesenchymal transition in human colorectal cancer. *Oncotarget* (2015) 6(4):2046–63. doi:10.18632/oncotarget.2858

29. Hoggard J, Fan J, Lu Z, Lu Q, Sutton L, Chen YH. Claudin-7 increases chemosensitivity to cisplatin through the upregulation of caspase pathway in human NCI-H522 lung cancer cells. *Cancer Sci* (2013) 104(5):611–8. doi:10.1111/cas.12135

30. Xu G, Qian N, Liu Y, Li H, Yang C, Wang J, et al. Preclinical characterization of a Fab-like CD3/CLDN18.2 XFab® bispecific antibody against solid tumors. *Immunobiology* (2022) 227(6):152283. doi:10.1016/j.imbio.2022.152283

31. Wang F, Yang Y, Du X, Zhu X, Hu Y, Lu C, et al. Claudin18.2 as a potential therapeutic target for primary ovarian mucinous carcinomas and metastatic ovarian mucinous carcinomas from upper gastrointestinal primary tumours. *BMC cancer* (2023) 23(1):44. doi:10.1186/s12885-023-10533-x

32. Shitara K, Lordick F, Bang YJ, Enzinger P, Ilson D, Shah MA, et al. Zolbetuximab plus mFOLFOX6 in patients with cldn18.2-positive, HER2-negative, untreated, locally advanced unresectable or metastatic gastric or gastro-oesophageal junction adenocarcinoma (SPOTLIGHT): A multicentre, randomised, double-blind, phase 3 trial. *Lancet* (2023) 401(10389):1655–68. London, England. doi:10.1016/s0140-6736(23)00620-7

Pathology & Oncology Research | frontiers

TYPE Review
PUBLISHED 04 January 2024
DOI 10.3389/pore.2023.1611580

Check for updates

OPEN ACCESS

EDITED BY
Anna Sebestyén,
Semmelweis University, Hungary

*CORRESPONDENCE
József Tímár,
jtimar@gmail.com

RECEIVED 07 November 2023
ACCEPTED 18 December 2023
PUBLISHED 04 January 2024

CITATION
Moldvay J and Tímár J (2024), KRASG12C mutant lung adenocarcinoma: unique biology, novel therapies and new challenges. *Pathol. Oncol. Res.* 29:1611580. doi: 10.3389/pore.2023.1611580

COPYRIGHT
© 2024 Moldvay and Tímár. This is an open-access article distributed under the terms of the Creative Commons Attribution License (CC BY). The use, distribution or reproduction in other forums is permitted, provided the original author(s) and the copyright owner(s) are credited and that the original publication in this journal is cited, in accordance with accepted academic practice. No use, distribution or reproduction is permitted which does not comply with these terms.

KRASG12C mutant lung adenocarcinoma: unique biology, novel therapies and new challenges

Judit Moldvay[1,2] and József Tímár[3]*

[1]National Institute of Pulmonology, Budapest, Hungary, [2]Pulmonology Clinic, Szentgyörgyi A. University, Szeged, Hungary, [3]Department of Pathology, Forensic and Insurance Medicine, Semmelweis University, Budapest, Hungary

KRAS mutant lung cancer is the most prevalent molecular subclass of adenocarcinoma (LUAD), which is a heterogenous group depending on the mutation-type which affects not only the function of the oncogene but affects the biological behavior of the cancer as well. Furthermore, KRAS mutation affects radiation sensitivity but leads also to bevacizumab and bisphosphonate resistance as well. It was highly significant that allele specific irreversible inhibitors have been developed for the smoking associated G12C mutant KRAS (sotorasib and adagrasib). Based on trial data both sotorasib and adagrasib obtained conditional approval by FDA for the treatment of previously treated advanced LUAD. Similar to other target therapies, clinical administration of KRASG12C inhibitors (sotorasib and adagrasib) resulted in acquired resistance due to various genetic changes not only in KRAS but in other oncogenes as well. Recent clinical studies are aiming to increase the efficacy of G12C inhibitors by novel combination strategies.

KEYWORDS

KRAS, lung adenocarcinoma, G12C mutation, sotorasib, adagrasib

Introduction

The most frequent histological type of lung cancer is adenocarcinoma (LUAD) comprising half of the cases and the vast majority of the non-small cell lung cancers (NSCLC). The molecular classification of adenocarcinoma subgroup is established and is well known, where the most frequent genetic alteration among non-Asian patients is KRAS mutation (1/3) followed by EGFR (5%–15%) while in Asian patients EGFR mutation is the most frequent followed by KRAS mutation [1, 2]. Other relatively frequent mutations affecting BRAF and MET and by incidence followed by so called

Abbreviations: CI, confidence interval; CNS, central nervous system; DCR, disease control rate; GFR, growth factor receptor; HR, hazard ratio; HRD, homologous recombination repair deficiency; HRR, homologous recombination repair; LUAD, lung adenocarcinoma; NSCLC, non-small cell lung cancer; ORR, overall response rate; OS, overall survival; PD, progressive disease; PFS, progression-free survival; TMB, tumor mutational burden.

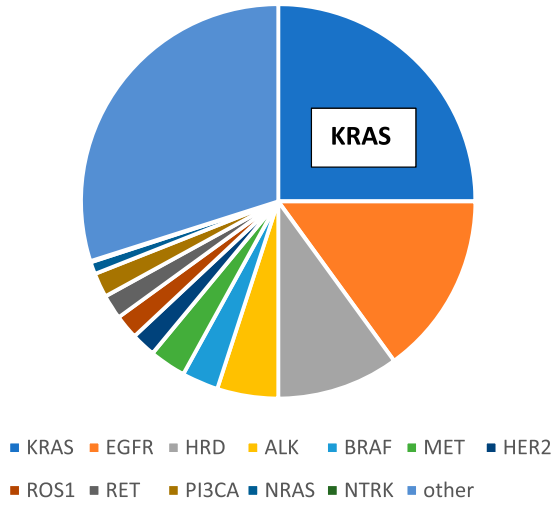

FIGURE 1
Molecular classification of lung adenocarcinoma.

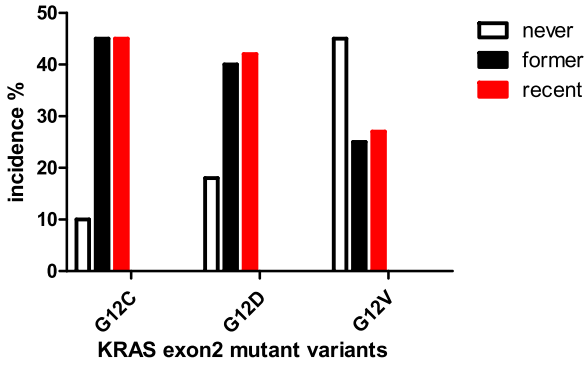

FIGURE 2
Connection between smoking history and KRAS mutant types in lung adenocarcinoma [10].

translocation cancers involving ALK/ROS1 less frequently RET or NTRK. At the same incidence levels, MET and HER2 amplifications also occur in this histological type [3]. It is of note that HRR mutations are also relatively frequent though less appreciated [4] (Figure 1). In the past decade target therapy changed the treatment of lung adenocarcinoma which left KRAS mutant lung cancer in an orphan status which changed recently significantly [5].

Molecular epidemiology of KRASG12C mutant lung cancer

KRAS mutant lung cancer has three variants: type-1 is a characterized by mucinous histology with TTF1 expression, type-2 is characterized by high TMB and PDL1 expression while type-3 group contains KEAP mutation [6]. Other studies performed subclassification based on gene expression signatures and defined a p16 mutant, a p53 mutant and a STK11 mutant forms all having different expression profiles [7].

KRAS mutation in lung cancer has three predominant forms: the most frequent is G12C (~40%) followed by ~20–20%, G12D and G12V, respectively [1, 2, 8]. It is widely accepted that KRAS mutation in lung cancer is smoking associated but it is only proven for G12C while the G12D and G12V are associated with chromosomal instability and/or mismatch repair deficiency [9]. There is a clear association between smoking and allelic variants of mutant KRAS: among recent smokers far the most frequent is G12C mutation while among non-smokers G12V is the predominant (Figure 2). The presence of G12C mutation among non-smokers (~10%) indicates the effect of passive smoking [10].

Various KRAS mutants are differ in biochemical and signaling functions: in G12C mutant the mitogenic RAS-RAF-MEK pathway is the most active, while in others the AKT signaling seems to be equally active, most probably due to changes in RAF affinity of the protein (Table 1, Ref [11]). Furthermore, individual mutants are characterized by differential alterations in GTP-ase activity or to sensitivity toward GAP proteins. Furthermore, the GDP/GTP exchange potential of the individual mutants seems also be different in various variants. There are other data supporting different lung carcinogenesis behind mutant KRAS variants: G12C mutation is associated with EGFR4 mutation, G12D mutations tend to have PDGRA mutation while G12V mutation containing tumor used to have PTEN mutation [1, 7]. Allelic imbalance of KRAS genes may also affect its function. In KRAS mutant lung adenocarcinoma heterozygous loss of the wild type allele is very frequent (~75%) leaving the mutant allele the only functioning KRAS (a kind of homozygosity), whereas the copy gains of the mutant allele is much less frequent [12]. Other analyses defined the oncogenic driver roles of various KRAS mutant forms and found that G12C is a real major driver oncogene in lung cancer, unlike G12D/V which are only "mini-drivers," cooperating with other mutant oncogens [13].

Biology and therapeutic sensitivity of KRASG12C mutant lung cancer

Analysis of a large KRAS mutant LUAD database indicated that this type of lung cancer has increased potency to metastatize to the lung but decreased one to the liver and to invade the pleural surface [14]. Furthermore, it was shown that in case of bone metastases KRAS mutant status is an independent negative prognostic factor [14]. As far as the chemotherapeutic sensitivity concerns, most of the KRAS mutant variant

TABLE 1 Biochemical characteristics of KRAS mutant proteins [11].

KRAS	Wild type (G12)	G12C	G12D	G12V
GTP affinity	High	High	High	High
GDP/GTP exchange	Fast	Medium	Slow	Slow
GTP-ase activity	High	High	Decreased	Lost
GAP sensitivity	High	Lost	Lost	Lost
(B)RAF affinity	High	High	Decreased	Decreased

GAP, GTP-ase activating protein.

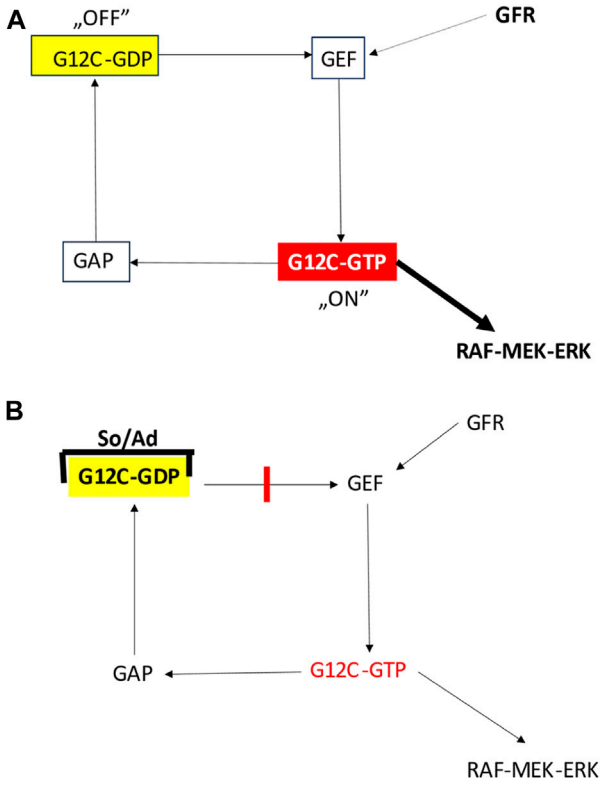

FIGURE 3
Effect of G12C inhibitors on the function of mutant KRAS protein [11]. **(A)** Function of the G12C mutated KRAS protein. **(B)** Function of the G12C mutated KRAS protein bound to inhibitors. Ad, adagrasib; GAP, GTP-ase activating protein; GEF, guanin nucleotide exchange factor; GFR, growth factor receptor; So, sotorasib.

containing tumors are equally sensitive toward platinum-based therapies, except the G12V mutant which seems to be more sensitive to this chemotherapy than others [10]. Another retrospective analysis tested the efficacy of bevacizumab in combination with chemotherapy and demonstrated that it is more efficient in KRAS wild-type tumors which was due to the resistance of the G12D mutant form [15]. Analysis of the treatment outcome of bone metastatic lung carcinoma patients indicated that the KRAS mutant tumors seems to be resistant to radiation therapy and to bisphosphonates [16] as it was predicted by the preclinical models [17]. A recent analysis of the G12D mutant lung cancers demonstrated that the density of $CD8^+$ T cells, the TMB and the tumor cell expression level of PDL1 are lower as compared to other KRAS mutants including G12C [18]. More importantly, the efficacy of immune checkpoint inhibitors turned out to be poorer in G12D mutant lung cancers.

Novel drugs to target mutant KRAS

The race for the G12C mutant KRAS inhibitor

Although it was considered undruggable, development of mutant KRAS inhibitors lastly became successful [19]. By the development of KRASG12C inhibitors. The challenge was here that—on the contrary to the various oncogenic tyrosine kinases where the increase kinase activity is the target—here in case of a GTP-ase the lost function is the target so a direct enzyme inhibitor is not an option. On the other hand, since the wild type KRAS is a critical signaling component of most of the normal cells, the inhibitor must be highly selective for the mutant isoform. As a result, a new class of inhibitors have been designed: the allele-specific (i.e., mutation specific) irreversible inhibitors. The idea was that since the KRAS is active in the GTP-bound state the novels drugs accumulate it in the off-state which is the GDP-bound KRAS (Figure 3).

The first in class of such KRASG12C inhibitor was published in 2013 [20] and a drug was approved for lung cancer in 2021 [20] which was a very rapid developmental process. The race was won by Amgen by a novel drug which is not only allele-specific (G12C) but also bind to a novel pocket (c95-99) critical in GTP-binding (ref [21], AMG-510, sotorasib). Preclinical data indicated that this novel inhibitor, not only blocks the mitogenic signaling (RAS-RAF-MEK) but is synergistic with platinum-based chemotherapy, with MEK inhibitors or with immune checkpoint inhibitors [21]. For the second place of this race arrived Mirati with a chemically distinct but functionally similar compound MRTX849/adagrasib which is characterized by very good pharmacological characteristics and which has a very good

penetrance of the blood-brain barrier, forecasting its use for brain metastases [22]. It is of note that the half -life in the circulation of AMG510 is 5 h as compared to adagrasib's 23 h. Meanwhile there are several other G12C inhibitors developed [23], some even reached clinical testing but only GDC-6036 exhibited early clinical efficacy [24].

Other mutant KRAS inhibitors

Developments in this filed continued by the G12D inhibitors which is far more frequent in other cancers but much less in lung adenocarcinoma. Unfortunately, irreversible inhibitors are nonexistent but a G12D selective inhibitor was developed: MRTX1133 which locks KRAS protein in the GTP-bound state which is in clinical development right now [25]. Furthermore, there are other novel inhibitors such as KRAS12D1-3 and RAS(ON)G12D [26].

Pan-RAS inhibitors

Other directions are the development of so-called pan-RAS inhibitors. BI-2852 induces homodimers of KRAS and turned out to be a KRASG12D selective inhibitor [27]. A real pan-KRAS inhibitor which even reached successful clinical testing is RMC-6236, a powerful RAS(ON) inhibitor which showed activity in G12V and other rare mutant forms [28].

Indirect RAS inhibitors

One of the main GTP-exchange protein of RAS is SOS1 and it serves as drug development target: there are several new molecules are on the market and some of them entered the clinic [29]. It would be interesting to see the side effect profile since these inhibitors are equally effective against all RAS isoforms and all variants, wild type or mutant. RAS proteins are phosphorylated at C32 of the exon2 by SRC and SHP2 phosphatase acting at this site. There are several SHP2 blockers in development and some of them entered clinical phase [30].

Novel treatment options for KRASG12C mutant lung adenocarcinoma

In the past nearly 20 years, treatments targeting EGFR and ALK have already become part of everyday patient care, but at the same time, the use of targeted therapy against the driver mutation present in the largest proportion, the KRAS mutation, has only become a realistic possibility in recent years. We currently have the most experience with two KRAS inhibitors; these are sotorasib and adagrasib. The phase II trial for sotorasib was the Code-BreaK100, while that for adagarasib was the Krystal-1 clinical trial [31, 32].

The Code-BreaK100 trial investigated the activity of once-daily oral sotorasib 960 mg in patients with KRASG12C mutation-positive advanced NSCLC previously treated with platinum-based chemotherapy [31]. The primary endpoint was objective response (complete or partial) based on independent central review. Key secondary endpoints included duration of response, disease control (complete response, partial response, or stable disease), progression-free survival, overall survival, and patient safety. The predictive value of some biomarkers was also analyzed. Among the 126 enrolled patients, the majority (81.0%) had previously received platinum-based chemotherapy and PD-1 or PD-L1 inhibitors. According to the central review, 124 patients had measurable disease at baseline and the therapeutic response could be evaluated. An objective response was observed in 46 patients [37.1%; 95% confidence interval (CI), 28.6–46.2], including 4 (3.2%) complete responses and 42 (33.9%) partial responses shown. The median duration of therapeutic response was 11.1 months (95% CI, 6.9-not evaluable). Disease control occurred in 100 patients (80.6%; 95% CI, 72.6–87.2). Median progression-free survival was 6.8 months (95% CI, 5.1–8.2), and median overall survival was 12.5 months (95% CI, 10.0-not evaluable). Treatment-related adverse events occurred in 88 of 126 patients (69.8%), including a grade 3 event in 25 patients (19.8%) and a grade 4 event in 1 patient (0.8%). Therapeutic responses were also analyzed in subgroups defined by PD-L1 expression, tumor mutational burden (TMB), and concurrent STK11, KEAP1, or TP53 mutations. Based on all of this, in this phase II study, sotorasib therapy showed clinical benefit in patients with previously treated KRASG12C-mutated NSCLC without new patient safety signals [31].

The Krystal-1 study evaluated adagrasib (600 mg orally twice daily) in patients with KRASG12C-mutated NSCLC who had received prior platinum-based chemotherapy and anti-PD1 or anti-PD-L1 immunotherapy [32]. The primary endpoint was objective therapeutic response (ORR), assessed by an independent central review. Secondary endpoints included duration of response, progression-free survival, overall survival, and patient safety. A total of 116 patients with KRASG12C mutation-positive NSCLC were treated until October 15, 2021 (mean follow-up: 12.9 months); 98.3% had previously received both chemotherapy and immunotherapy. Of the 112 patients with measurable disease at baseline, 48 (42.9%) had a confirmed objective response with a median duration of 8.5 months [95% confidence interval (CI), 6.2–13.8], and the median progression-free survival was 6.5 months (95% CI, 4.7–8.4). As of January 15, 2022 (median follow-up, 15.6 months), the median overall survival was 12.6 months (95% CI, 9.2–19.2). In 33 patients with previously treated stable CNS metastases, the intracranial objective response rate was 33.3% (95% CI, 18.0–51.8). Treatment-related adverse events occurred in 97.4% of patients; grade 1 or 2 in 52.6%, grade 3 or higher in 44.8% (including two grade 5 events), and it became necessary to suspend medication in 6.9% of patients. Overall, in previously treated patients with KRASG12C-

TABLE 2 Summary of the clinical efficacies of sotorasib and adagrasib.

	Sotorasib	Adagrasib
	CodeBreaK100	KRYSTAL-1
N of patients	126	116
Primary endpoint	ORR	ORR
ORR (95% CI) (%)	37.1 (28.6–46.2)	43 (33.5–52.6)
DOR (95% CI) (month)	11.1 (6.9–NE)	8.5 (6.2–13.8)
DCR (95% CI) (%)	80.6 (72.6–87.2)	80 (70.8–86.5)
PFS (95% CI) (month)	6.6 (5.1–8.2)	6.5 (4.7–8.4)
OS (95% CI) (month)	12.5 (10.0–NE)	12.6 (9.2–19.2)
Follow-up (month)	15.3	12.9
Brain metastasis, n (%)	26 (20.6)	24 (21)
Intracranial ORR, DCR (%)	33, 85	12.5, 88
PD rate (%)	16.1	5
Dose reduction/suspension (%)	22.3	Reduction: 52; suspension: 61

ORR, objective response rate; DOR, duration of response; DCR, disease control rate; PFS, progression-free survival; OS, overall survival; CI, confidence interval; NE, not evaluated; PD, progressive disease.

mutated NSCLC, adagrasib demonstrated clinical efficacy with no new patient safety alerts [32].

Below, we will review what differences can be verified between the two agents based on the results of these trials (Table 2). In phase II trials, the ORR was higher with adagrasib (43%) than with sotorasib (37%), and the rate of progressive disease (PD) was lower with adagrasib (16% for sotorasib vs. 5% for adagrasib), as shown in Table 2. However, in the absence of a head-to-head comparison, the results of such comparisons should be evaluated with caution [33]. Median PFS was similar between the two drugs (sotorasib, 6.6 months and adagrasib, 6.5 months). Drug-related adverse events were more common with adagrasib than with sotorasib, and, as a result, treatment interruption or dose reduction is more common with adagrasib (sotorasib, 22% and adagrasib, 52%). The confirmatory phase III trial for sotorasib was the Code-BreaK200 [34], while for adagrasib it was the Krystal-12 study.

In the Code-BreaK200 trial, between 4 June 2020 and 26 April 2021, 345 patients were randomized in a 1:1 ratio to the sotorasib (n = 171) or docetaxel (n = 174) arm. In the sotorasib group 169 (99%), and in the docetaxel group 151 (87%) patients received at least one course of treatment. After a median follow-up of 17.7 months, the study reached its primary endpoint, a statistically significant increase in PFS for sotorasib compared with docetaxel [median PFS 5.6 months (95% CI 4, 3–7.8) vs 4.5 months (3.0–5.7); HR: 0.66 (0.51–0.86) p = 0.0017]. Sotorasib was well tolerated, fewer grades 3 or worse [n = 56 (33%) vs n = 61 (40%)] and serious treatment-related adverse events compared with docetaxel [n = 18 (11%) vs n = 34 (23%)].

For sotorasib, the most common treatment-related adverse events of grade 3 or worse were diarrhoea [n = 20 (12%)], alanine aminotransferase increase [n = 13 (8%)], and aspartate aminotransferase increase [n = 9 (5%)]. For docetaxel, treatment-related adverse reactions of grade 3 or worse were neutropenia [n = 13 (9%)], fatigue [n = 9 (6%)], and febrile neutropenia [n = 8 (5%)]. In conclusion, sotorasib significantly increased progression-free survival and showed a more favorable safety profile compared to docetaxel in patients with advanced stage (IIIB/IV), good performance status (ECOG 0-1), KRASG12C-mutated LUAD who had already received platinum-based chemotherapy and immune checkpoint inhibitor therapy as first-line treatment and had no symptomatic brain metastases [34].

In the Krystal-12 trial, docetaxel was also the comparator agent and the inclusion criteria were the same as in the CodeBreak200 study, however, the randomization ratio was 2: 1 in favor of adagrasib. Patients received 600 mg of adagrasib twice daily, and 75 mg/body surface area of docetaxel every 3 weeks. Adagrasib produced an ORR of 42.9% and a PFS of 6.5 months. Both drugs showed the already known side effect profile, the most common toxicities were diarrhea, musculoskeletal pain, fatigue and hepatotoxicity [35].

In NSCLC approximately 30%–40% of patients develop brain metastases during the course of the disease. In 2022, brain metastasis specific activity of adagrasib has been reported by Sabari et al. [36] Retrospectively, 374 NSCLC patients with KRAS mutations (149 with G12C mutation and 225 with non-G12C mutation) were analyzed for brain metastases. Overall, 40% of patients with KRASG12C or non-G12C mutations developed

brain metastases during the follow-up period. 77% of patients had a diagnosis of synchronous brain metastases detected within 3 months of initial diagnosis. Brain metastasis occurred less frequently in NSCLC patients with KRAS mutations than in NSCLC patients with other oncogenic driver mutations [30]. In a retrospective review of 579 patients with metastatic NSCLC, the incidence of brain metastasis was highest in NSCLC patients with ROS1 (36%) and ALK (34%) mutations/fusions, followed by EGFR (28%) and KRAS (28%). In NSCLC without a driver oncogene, brain metastasis occurred in only 21% of patients [37]. The response of brain metastases to radiation therapy may vary depending on the driver oncogene. In an analysis by Arrieta et al., the response rate to radiotherapy was higher in NSCLC patients with EGFR (64.5%) or ALK (54.5%) mutations than in those without driver mutations (35%). However, in NSCLC patients with KRAS mutations, this rate is only 20%, which further emphasizes the need for effective treatments in this group [38].

Only limited data are available on the CNS activity of sotorasib in metastatic NSCLC. Although patients with active, untreated brain metastases were excluded from the CodeBreaK100 study, 2 of 16 patients with stable brain metastases had a complete response to therapy, and 12 achieved stable disease with sotorasib therapy, representing 88% of the patients with intracranial disease control [39]. In addition, several case studies have been published of patients with brain metastases in whom radiological regression was confirmed and symptoms resolved with sotorasib treatment [40, 41]. Yeh et al. reported a patient with NSCLC harboring a KRASG12C mutation with symptomatic leptomeningeal involvement and multiple brain metastases treated with sotorasib monotherapy [41]. The patient showed clinical improvement 2 weeks after the start of sotorasib treatment, and brain MRI showed clear radiological improvement in several metastatic foci and meningeal involvement. In this case, sotorasib was effective against untreated, symptomatic metastases. However, severe hepatotoxicity necessitated discontinuation of sotorasib, leading to disease progression. Therefore, although sotorasib is also effective in metastases affecting the central nervous system, further prospective studies are needed.

Negrao et al. studied the intracranial efficacy of adagrasib in KRASG12C-mutated NSCLC patients with untreated CNS metastases enrolled in the KRYSTAL-1 study [42]. 25 patients were enrolled and evaluated (mean follow-up, 13.7 months), and 19 patients had radiologically evaluable intracranial activity. Safety was consistent with previous reports for adagrasib: treatment-related grade 3 adverse events occurred in 10 patients (40%), grade 4 in 1 patient (4%), and there was no grade 5 adverse events. The most common CNS-specific adverse reactions were dysgeusia (24%) and dizziness (20%). Adagrasib showed an intracranial ORR of 42% and a DCR of 90%, as well as a PFS of 5.4 months and an OS of 11.4 months, which is promising for the treatment of patients with untreated CNS metastases.

The clinical trial results of the KRAS inhibitors sotorasib and adagrasib are promising, however, currently they are inferior to EGFR inhibitors or ALK inhibitors in terms of both therapeutic duration (PFS, OS) and side effect profile. Further extensive studies—mainly targeting predictive markers and resistance mechanisms—are necessary in order to be able to treat permanently and effectively this large group of patients with a good quality of life.

Primary and acquired resistance mechanisms

Primary resistance

There are characteristic co-occurring mutations in KRAS mutant lung cancer such as STK11 and KEAP1. STK11 mutation was shown to be associated with resistance to immunotherapy [43]. In the CodeBreak100 study the association of STK11 and KEAP1 mutations have been evaluated in relation to the efficacy of sotorasib and found that the lowest response rate was found in tumors having KEAP1 mutation/STK11 wild type genotype while the highest was seen in tumors with STK11mutant/KEAP1 wild type genotype [44]. A recent genomic analysis of a large G12C mutant lung cancer cohort treated with G12C inhibitors revealed that co-occurring mutations of KEAP1, SMARC4 and CDKN2A were independent negative predictive factors of inhibitor efficacy while mutations in the DDR genes were positive predictive ones [45].

Acquired resistance

Acquired resistance to sotorasib treatment of lung cancer patients had various pathomechanisms At the first place it was found the disappearance of G12C mutation from cancer cells or the amplification of the wild type KRAS gene. Other KRAS-related genetic alterations were the acquired novel mutation types (G13V, G12D, G12V, V8L, V141I) or the novel mutations affecting NRAS. Furthermore, mutations of the EGFR signaling pathway members such as EGFR or BRAF are also occurred [46]. Although at not high frequency, but amplifications of MET or HER2 have also been reported [47, 48].

Upon adagrasib resistance it was described histological transformation from adenocarcinoma to squamous [49] a bit similar to what was seen in case of EGFR inhibitor resistance. It can occur most probably in those cases where the original tumor is a combined adenosquamous variant since KRAS mutation is adenocarcinoma specific genetic alterations. In case of acquired resistance to adagrasib at first place also novel KRAS mutations have been identified (G12D/R/W, G13D, Q61H, R68S, H95D/Q/R, Y96C). The resistance mechanism does not involve the EGFR signaling instead the RET signaling with mutations affecting RET, BRAF and MAP2K1. Furthermore, gene amplification here also involved MET but interestingly there were several gene fusions in the resistant tumors involving, ALK, RET, FGFR3 and BRAF [49].

TABLE 3 Clinical developments of G12C inhibitor combinations [51].

G12C inhibitor	Partner	Function	NCT	Clinical phase	Cancer
sotorasib	AMG404	PD-1 inhibitor	03600883	I/II	NSCLC
	carboplatin/pemetrexed	chemotherapy	(Japan)	II	NSCLC
	palbociclib	CDK4/6 inhibitor	05178888	I/Ib	solid tumor
	afatinib	EGFR-inhibitor	04185883	Ib/II	NSCLC
	panitumumab	anti-EGFR	05198934	III	CRC
	everolimus	mTOR inhibitor	04185883	Ib/II	solid tumor
	RMC-4630	SHP2 inhibitor	04185883	Ib/II	solid tumor
	bevacizumab	anti-VEGF	05180422	I/II	NSCLC
adagrasib	pembrolizumab	anti-PD1	046113596	II	NSCLC
	cetuximab	anti-EGFR	04793958	III	CRC
	TNO-155	SHP2 inhibitor	04330664	I/II	solid tumor
	BI-17011963	SOS1 inhibitor	04975256	I/Ib	solid tumor

CRC, colorectal cancer; NSCLC, non-small cell lung cancer.

The resistance mutations of KRAS can be classified into three main categories. Mutations in the codon12 or codon61 decrease the potential of the KRAS protein to hydrolyze GTP. Mutations at codon 13 increase the GDP-GTP exchange, while mutations at R68, H95, Y96 and Q99 decreases the affinity of the inhibitors.

It is interesting that various mutational profiles of the KRAS mutant lung cancers affect the development of resistance to sotorasib or adagrasib [49] The H95 mutations may confer resistance to adagrasib but does not affect the activity of sotorasib. On the other hand, G13D, R68M, A59S/T mutations confer sotorasib resistance but retain adagrasib sensitivity [48]. Finally, m72 or Q99 mutations cause adagrasib resistance but do not affect sotorasib sensitivity [50]. Based on these data it can be hypothesized that the development of acquired resistance could be treated by sequential use of the other G12C inhibitor.

Developing combinational approaches

The observed clinical efficacy and the developing resistances both stimulated novel clinical approaches to improve the efficacy of G12C inhibitors sotorasib and adagrasib (Table 3) [51]. Since G12C mutant lung cancer is an immunologically hot tumor it was evident to start combinations with PD1/PDL1 inhibitors: in case of sotorasib the combination partner is AKG404 (a PD1 inhibitor) in case of adagrasib the partner is Pembrolizumab (also a PD1 inhibitor). Since one of the resistance mechanisms of G12C inhibitors involves the reactivation of EGFR signaling pathway, sotorasib is now clinically tested in combination with afatinib (an EGFR tirozin kinase inhibitor). In case of both G12C inhibitors the efficacy against colorectal cancer is a significant problem therefore combinational trials using anti-EGFR antibodies. Other interesting novel combination involves bevacizumab (anti-VEGF) since this therapy was shown to be inactive in KRAS mutant lung cancer [15]. Furthermore, combinational trials of G12C inhibitors are already initiated with traditional chemotherapies such as carboplatin/pemetrexed. Since acquired resistance to G12C inhibitors may involve reactivation of alternative signaling pathways such as PI3KCA (sotorasib) combination with mTOR inhibitor seems to be a rational approach. It is a completely different approach to increase the KRAS inhibitory efficacy of G12C inhibitors by either SOS1 inhibitors (to block GEF protein activation) or with SHP2 inhibitors (to block reactivation mechanisms) [51]. Since these approaches are pan-RAS targeted, it will be an interesting issue to see that for the prize of increased G12C inhibition what kind of prize can be paid in terms of side effects.

Conclusion

KRAS mutant lung adenocarcinoma is the most frequent molecular subtype of lung cancer but it is still a heterogenous entity since the individual allelic variants are biologically heterogenous. The most frequent allelic variant of KRAS mutant lung cancer is the smoking related G12C which became the focus of the development of mutant-specific irreversible KRAS inhibitors. More importantly, two of the

G12C inhibitors, sotorasib and adagrasib were effective clinically in advanced G12C mutant lung adenocarcinoma patients resulting in conditional approval (linked to annual reporting of the expected clinical efficacy). Meanwhile, similar to other target therapies, upon administration of G12C inhibitors clinical resistance develops which is due to various biological processes predominated by secondary mutations of the KRAS gene. Since the clinical efficacy of G12C inhibitors is not overwhelming, there is a room for improvement which is the bases of development of various combination approaches of G12C inhibitors including immunotherapeutic agents, EGFR inhibitors or RAS signaling modulators. Since mutant KRAS was long considered undruggable, the development and the clinical success of G12C inhibitors pave the way for the development of non-G12C mutant KRAS inhibitors, opening the door for a new era of target therapies aiming at the most frequently mutated human oncogene in various cancers including the lung adenocarcinoma.

Author contributions

JT: writing, original structure, validation. JM: writing, clinical data, validation. All authors contributed to the article and approved the submitted version.

Funding

This work was supported by the Hungarian National Research, Development and Innovation Office (JT: 2020-1.1.6-JÖVŐ-2021-00004; JM: K129065).

Conflict of interest

The authors declare that the research was conducted in the absence of any commercial or financial relationships that could be construed as a potential conflict of interest.

References

1. Tímár J, Kashofer K. Molecular epidemiology and diagnostics of KRAS mutations in human cancer. *Cancer Metast Rev* (2020) 39:1029–38. doi:10.1007/s10555-020-09915-5

2. Ceddia S, Landi L, Cappuzzo F. KRAS-mutant non-small cell lung cancer: from past efforts to future challenges. *Int J Mol Sci* (2022) 23:9391. doi:10.3390/ijms23169391

3. Nicholson AG, Tsao MS, Beasley MB, Borczuk AC, Brambilla E, Cooper WA, et al. The 2021 WHO classification of lung tumors: impact of advances since 2015. *J Thorac Oncol* (2021) 17:362–87. doi:10.1016/j.jtho.2021.11.003

4. Hathaway F, Martins R, Sorcher S, Bzura A, Dudbridge F, Fenell DA. Family matters: germline testing in thoracic cancer. *ASCO EDBK* (2023) 389956:2023.

5. Moore AR, Rosenberg SC, McCormick F, Malek S. RAS-targeted therapies: is the undruggable drugged? *Nat Rev Drug Discov* (2020) 19:533–52. doi:10.1038/s41573-020-0068-6

6. Tímár J. The clinical relevance of KRAS gene mutation in non-small-cell lung cancer. *Curr Opin Oncol* (2014) 26:138–44. doi:10.1097/CCO.0000000000000051

7. Skoulidis F, Byers LA, Diao L, Papadimitrakopoulou VA, Tong P, Izzo J, et al. Co-occurring genomic alterations define major subsets of KRAS mutant lung adenocarcinoma with distinct biology, immune profiles and therapeutic vulnerabilities. *Cancer Discov* (2015) 5:860–77. doi:10.1158/2159-8290.CD-14-1236

8. Lim TLH, Skoulidis F, Kerr KM, Ahn M-I, Kapp JR, Soares FA, et al. KRAS G12C in advanced NSCLC: prevalence, co-mutations and testing. *Lung Cancer* (2023) 184:107293. doi:10.1016/j.lungcan.2023.107293

9. Estcott PM, Hallwill KD, To MD, Rashid M, Rust AG, Keane TM, et al. The mutational landscapes of genetic and chemical models of Kras-driven lung cancer. *Nature* (2015) 517:489–92. doi:10.1038/nature13898

10. Cserepes M, Ostoros G, Lohinai Z, Rásó E, Barbai T, Tímár J, et al. Subtype-specific KRAS mutations in advanced lung adenocarcinoma: a retrospective study of patients treated with platinum-based chemotherapy. *Eur J Cancer* (2014) 50:1819–28. doi:10.1016/j.ejca.2014.04.001

11. Hunter JC, Manandhar A, Carrasco MA, Gurbani D, Gondi S, Westover KD. Biochemical and structural analysis of common cancer-associated KRAS mutations. *Mol Cancer Res* (2015) 13:1325–35. doi:10.1158/1541-7786.MCR-15-0203

12. Burgess MR, Hwang E, mrou R, Bielski CM, Wandler A, Huang BJ, et al. KRAS allelic imbalance enhances fitness and modulates MAP kinase dependence in cancer. *Cell* (2017) 168:817–29.e15. doi:10.1016/j.cell.2017.01.020

13. Temko D, Tomlison JPM, Severini S, Schuster-Böckler B, Graham TA. The effects of mutational processes and selection on driver mutations across cancer types. *Nat Comm* (2018) 9:1857. doi:10.1038/s41467-018-04208-6

14. Lohinai Z, Klikovits T, Moldvay J, Ostoros G, Raso E, Timar J, et al. KRAS-mutation incidence and prognostic value are metastatic site-specific in lung adenocarcinoma: poor prognosis in patients with KRAS mutation and bone metastasis. *Sci Rep* (2017) 7:39721. doi:10.1038/srep39721

15. Ghimessy AK, Gellert A, Schleghl E, Hegedűs B, Raso E, Barbai T, et al. KRAS mutations predict response and outcome in advanced lung adenocarcinoma patients receiving first-line bevacizumab and platinum-based chemotherapy. *Cancers* (2019) 11:1514. doi:10.3390/cancers11101514

16. Radeczky P, Medgyesfalvi Z, László V, Fillinger J, Moldvay J, Raso E, et al. The effects of bisphosphonate and radiation therapy in bone-metastatic lung adenocarcinoma: the impact of KRAS mutation. *Transl Lung Cancer Res* (2021) 10:675–84. doi:10.21037/tlcr-20-754

17. Kenessey I, Koi K, Horváth O, Cserepes M, Molnár D, Izsák V, et al. KRAS-mutation status dependent effect of zoledronic acid in human non-small cell cancer preclinical models. *Oncotarget* (2016) 7:79503–14. doi:10.18632/oncotarget.12806

18. Ricciuti B, Alessi JV, Elkrief A, Wang X, cortellini A, Li YY, et al. Dissecting the clinicopathologic, genomic and immunophenotypic correlates of KRASG12D-mutated non-small-cell lung cancer. *Ann Oncol* (2022) 33:1029–40. doi:10.1016/j.annonc.2022.07.005

19. Rathod LS, Dabhade PS, Mokale SN. Recent progress in targeting KRAS mutant cancers with covalent G12C-specific inhibitors. *Drug Discov Today* (2023) 28:103557. doi:10.1016/j.drudis.2023.103557

20. Osrem JM, Peters U, sos ML, Wells JA, Shokat KM. K-Ras(G12C) inhibitors allosterically control GTP affinity and effector interactions. *Nature* (2013) 503:548–51.

21. Canon J, Rex K, Saiki A, Mohr C, Cooke K, Bagal D, et al. The clinical KRAS(G12C) inhibitor AMG 510 drives anti-tumour immunity. *Nature* (2019) 575:217–23. doi:10.1038/s41586-019-1694-1

22. Fell JB, Fischer JP, Baer BR, Blake JF, Bouhana K, Briere DM, et al. Identification of the clinical development candidate MRTX849, a covalent KRASG12C inhibitor for the treatment of cancer. *J Med Chem* (2020) 63:6679–93. doi:10.1021/acs.jmedchem.9b02052

23. Kwan AK, Piazza GA, Keeton AB, leite CA. The path to the clinic: a comprehensive review on direct KRASG12C inhibitors. *J Exp Clin Cancer Res* (2022) 41:27. doi:10.1186/s13046-021-02225-w

24. Sacher A, LoRusso P, Patel MR, Miller W, Garralda E, Forster MD, et al. Single-agent divarasib (GDC-6036) in solid tumors with a KRAS G12C mutation. *N Engl J Med* (2023) 389:710–21. doi:10.1056/NEJMoa2303810

25. Wang X, Allen S, Blake JF, Browcut V, Briene DM, Calinisan A, et al. Identification of MRTX1133, a noncovalent, potent, and selective KRAS(G12D) inhibitor. *J Med Chem* (2022) 65:3123–33. doi:10.1021/acs.jmedchem.1c01688

26. Mullard A. The KRAS crowd targets its next cancer mutations. *Nat Drug Discov* (2023) 22:167–71. doi:10.1038/d41573-023-00015-x

27. Tran TH, Alexander P, Dharmaiah S, Agamasu C, Nissley DV, McCormick F, et al. The small molecule BI-2852 induces a nonfunctional dimer of KRAS. *PNAS* (2020) 117:3363–4. doi:10.1073/pnas.1918164117

28. Poh A. Drugging RAS: moving beyond KRASG12C. *Cancer Discov* (2023). doi:10.1158/2159-8290.CD.ND2023-0010

29. Hillig RC, Sautier B, Schroeder J, Moosmayer D, Hilpmann A, Stegmann CM, et al. Discovery of potent SOS1 inhibitors that block RAS activation via disruption of the RAS-SOS1 interaction. *PNAS* (2019) 116:2551–60. doi:10.1073/pnas.1812963116

30. Drilon A, Sharma MR, Johnson ML, Yap TA, Gadgeel S, Nepert D, et al. SHP2 inhibition sensitizes diverse oncogene-addicted solid tumors to Re-treatment with targeted therapy. *Cancer Discov* (2023) 13:1789–801. doi:10.1158/2159-8290.CD-23-0361

31. Skoulidis F, Li BT, Dy GK, Price TJ, Falchook GS, Wolf J, et al. Sotorasib for lung cancers with KRAS p.G12C mutation. *N Engl J Med* (2021) 384:2371–81. doi:10.1056/NEJMoa2103695

32. Jänne PA, Riely GJ, Gadgeel SM, Heist RS, Ou SHI, Pacheco JM, et al. Adagrasib in non-small-cell lung cancer harboring a *KRAS^{G12C}* mutation. *N Engl J Med* (2022) 387:120–31. doi:10.1056/NEJMoa2204619

33. Oya Y, Mitsudomi T. Is adagrasib just another sotorasib?or, should we differentiate their usage according to patients' clinical presentation? *Transl Lung Cancer Res* (2023) 12:940–3. doi:10.21037/tlcr-23-97

34. de Langen AJ, Johnson ML, Mazieres J, Dingemans A-M, Mountzios G, Pless M, et al. Sotorasib versus docetaxel for previously treated non-small-cell lung cancer with KRAS^{G12C} mutation: a randomised, open-label, phase 3 trial. *Lancet* (2023) 401:733–46. doi:10.1016/S0140-6736(23)00221-0

35. Mok TSK, Lawler WE, Shum MK, Dakhil SR, Spira AI, Barlesi F, et al. KRYSTAL-12: a randomized phase 3 study of adagrasib (MRTX849) versus docetaxel in patients (pts) with previously treated non-small-cell lung cancer (NSCLC) with KRAS^{G12C} mutation. *J Clin Oncol* (2021) 39:TPS9129. doi:10.1200/jco.2021.39.15_suppl.tps9129

36. Sabari JK, Velcheti V, Shimizu K, Strickland MR, Heist RS, Singh M, et al. Activity of adagrasib (MRTX849) in brain metastases: preclinical models and clinical data from patients with KRASG12C-mutant non-small cell lung cancer. *Clin Cancer Res Í* (2022) 28:3318–28. doi:10.1158/1078-0432.CCR-22-0383

37. Patil T, Smith DE, Bunn PA, Aisner DL, Le AT, Hancock M, et al. The incidence of brain metastases in stage IV ROS1-rearranged non-small cell lung cancer and rate of central nervous system progression on crizotinib. *J Thorac Oncol* (2018) 13:1717–26. doi:10.1016/j.jtho.2018.07.001

38. Arrieta O, Ramírez-Tirado LA, Caballé-Perez E, Mejia-Perez A, Zatarain-Barrón ZL, Cardona AF, et al. Response rate of patients with baseline brain metastases from recently diagnosed non-small cell lung cancer receiving radiotherapy according to EGFR, ALK and KRAS mutation status. *Thorac Cancer* (2020) 11:1026–37. doi:10.1111/1759-7714.13359

39. Ramalingam S, Skoulidis F, Govindan R, Velcheti V, Li B, Besse B, et al. P52.03 efficacy of sotorasib in KRAS p.G12C-mutated NSCLC with stable brain metastases: a post-hoc analysis of CodeBreaK 100. *J Thorac Oncol* (2021) 16:S1123. doi:10.1016/j.jtho.2021.08.547

40. Koster KL, Appenzeller C, Lauber A, Früh M, Schmid S. Sotorasib shows intracranial activity in patients with KRAS G12C-mutated adenocarcinoma of the lung and untreated active brain metastases. *Case Rep Oncol* (2022) 15:720–5. doi:10.1159/000525341

41. Yeh J, Marks JA, Alzeer AH, Sloan EA, Varghese R, Paudel N, et al. Remarkable intracranial response to sotorasib in a patient with KRAS (G12C)-Mutated lung adenocarcinoma and untreated brain metastases: a case report. *JTO Clin Res Rep* (2022) 3:100428. doi:10.1016/j.jtocrr.2022.100428

42. Negrao MV, Spira AI, Heist RS, Janne PA, Pacheco JM, Weiss J, et al. Intracranial efficacy of adagrasib in patients from the KRYSTAL-1 trial with *KRAS^{G12C}*-Mutated non-small-cell lung cancer who have untreated CNS metastases. *J Clin Oncol* (2023) 41:4472–7. doi:10.1200/JCO.23.00046

43. Arbour KC, Jordan E, Kim HR, Dienstag J, Yu HA, Sanchez-Vega F, et al. Effects of Co-occurring genomic alterations on outcomes in patients with KRAS-mutant non-small cell lung cancer. *Clin Cancer Res* (2018) 24:334–40. doi:10.1158/1078-0432.CCR-17-1841

44. Luo J, Osrem J, Pellini B, Imbody D, Stern Y, Solanki HS, et al. Overcoming KRAS-mutant lung cancer. *Am Soc Clin Oncol Educ Book* (2022) 10:700–10. doi:10.1200/edbk_360354

45. Negrao MV, Araujo HA, Lamberti G, Cooper AJ, Akhave NS, Zhou T, et al. Comutations and KRASG12C inhibitor efficacy in advanced NSCLC. *Cancer Discov* (2023) 13:1556–71. doi:10.1158/2159-8290.CD-22-1420

46. Zhao Y, Murciano-Goroff YR, Xue JY, Ang A, Lucas J, Mai TT, et al. Diverse alterations associated with resistance to KRASG12C inhibition. *Nature* (2021) 599:679–83. doi:10.1038/s41586-021-04065-2

47. Tanaka N, Lin JJ, Li C, Ryan MB, Zhang J, Kiedrowski LA, et al. Clinical acquired resistance to KRASG12C inhibition through a novel KRAS switch-II pocket mutation and polyclonal alterations converging on RAS-MAPK reactivation. *Cancer Discov* (2021) 11:1913–22. doi:10.1158/2159-8290.CD-21-0365

48. Ho CSL, Tüns AI, Schildhaus H-U, Wiesweg M, Grüner BM, Hegedus B, et al. HER2 mediates clinical resistance to the KRASG12C inhibitor sotorasib, which is overcome by co-targeting SHP2. *Eur J Cancer* (2021) 159:16–23. doi:10.1016/j.ejca.2021.10.003

49. Awad MM, Liu S, Rybkin II, Arbour KC, Dilly J, Zhu VW, et al. Acquired resistance to KRASG12C inhibition in cancer. *N Engl J Med* (2021) 384:2382–93. doi:10.1056/NEJMoa2105281

50. Koga T, Suda K, Fujino T, Ohara S, Hamada A, Nishino M, et al. KRAS secondary mutations that confer acquired resistance to KRAS G12C inhibitors, sotorasib and adagrasib, and overcoming strategies: insights from *in vitro* experiments. *J Thorac Oncol* (2021) 16:1321–32. doi:10.1016/j.jtho.2021.04.015

51. Lietman CD, Johnson ML, McCormick F, Lindsay CR. More to the RAS story: KRASG12C inhibition, resistance mechanisms and moving beyond KRAS^{G12C}. *Am Soc Clin Oncol Educ Book* (2022) 42:1–13. doi:10.1200/EDBK_351333

Pathology & Oncology Research | frontiers

TYPE Hypothesis & Theory
PUBLISHED 18 April 2023
DOI 10.3389/pore.2023.1610899

Check for updates

OPEN ACCESS

EDITED BY
Anna Sebestyén,
Semmelweis University, Hungary

*CORRESPONDENCE
Ping Leng,
18661808926@163.com

RECEIVED 24 October 2022
ACCEPTED 27 March 2023
PUBLISHED 18 April 2023

CITATION
Zuo Y, Leng G and Leng P (2023), Identification and validation of molecular subtype and prognostic signature for lung adenocarcinoma based on neutrophil extracellular traps. *Pathol. Oncol. Res.* 29:1610899. doi: 10.3389/pore.2023.1610899

COPYRIGHT
© 2023 Zuo, Leng and Leng. This is an open-access article distributed under the terms of the Creative Commons Attribution License (CC BY). The use, distribution or reproduction in other forums is permitted, provided the original author(s) and the copyright owner(s) are credited and that the original publication in this journal is cited, in accordance with accepted academic practice. No use, distribution or reproduction is permitted which does not comply with these terms.

Identification and validation of molecular subtype and prognostic signature for lung adenocarcinoma based on neutrophil extracellular traps

Yanhua Zuo[1], Guangyi Leng[2] and Ping Leng[1]*

[1]Department of Pharmacy, The Affiliated Hospital of Qingdao University, Qingdao, China, [2]Laboratory of Drug Metabolism and Pharmacokinetics, Shenyang Pharmaceutical University, Shenyang, China

Background: Neutrophil Extracellular Traps (NETs) are fibrous networks made of DNA-histone complexes and proteins protruded from activated neutrophils. Accumulating evidences have highlighted the vital role of NETs in tumor progression and diffusion. However, limited systematic studies regarding the role of NETs in LUAD have been performed.

Methods: Differentially expressed NETs-related genes and their mutation landscape were identified with TCGA database. Consensus clustering analysis was performed to determine the NETs-related subtypes of LUAD. LASSO algorithm was employed to construct a prognostic signature. Moreover, GSE30219 and GSE31210 were used as independent validation. We also constructed a lncRNA-miRNA-mRNA regulatory axis with several miRNA and lncRNA databases.

Results: Consensus clustering identified two NETs-related clusters in LUAD. High NETs score was correlated with a favorable overall survival, abundant immune cell infiltration, and high activity of immune response signal pathways. Six NET-related genes (G0S2, KCNJ15, S100A12, AKT2, CTSG, and HMGB1) with significant prognostic value were screened to develop a prognostic signature. LUAD patients with low-risk had a significantly favorable overall survival both in the training set and validation set. Moreover, NETs-related risk score and clinical stage could act as an independent prognostic factor for LUAD patients. Significant correlation was obtained between risk score and tumor immune microenvironment. We also identified lncRNA BCYRN1/miR-3664-5p/CTSG regulatory axis that may be involved in the progression of LUAD.

Conclusion: We developed two molecular subtypes and a prognostic signature for LUAD based on NETs-related genes. This stratification could provide more evidences for estimating the prognosis and immunotherapy of LAUD patients.

KEYWORDS

immunotherapy, lung adenocarcinoma, tumor microenvironment, prognostic signature, neutrophil extracellular traps

Introduction

Lung cancer is second most common malignancy following by breast cancer, with an estimated 228,820 new cases globally (1). Moreover, lung cancer ranks the leading cause of cancer related deaths globally, claiming about 2 million lives in 2019 (2). Lung cancer has a high aggression and recurrence rate, resulting in a poor prognosis, and the 5-year overall survival of lung cancer is only about 20% (2, 3). Without typical clinical symptoms in early stages, lung cancer patients are usually in the advanced stages when initially diagnosed with disease. Among all cases of lung cancer, lung adenocarcinoma (LUAD) is the most common pathological subtype (4). Despite some mutated genes related to the progression of LUAD, including EGFR and ALK, have been identified, the mechanism of its occurrence and development has not been fully elucidated (5, 6). At present, there is no ideal marker for predicting the prognosis of LUAD patients.

Neutrophils, the most abundant endogenous immune effector cells, are referred as a prognosis biomarker and therapeutic strategy for cancer (7). Neutrophil Extracellular Traps (NETs) are fibrous networks made of DNA-histone complexes and proteins protruded from activated neutrophils (8). NETs contain histone and decondensed DNA chromatin from dying neutrophils, which could respond to specific stimuli by a cell death process named NETosis (9, 10). Accumulating evidences have highlighted the vital role of the disorder and dysregulation of NETosis in many diseases, including rheumatoid arthritis, cardiovascular diseases and cancer (11–13). However, there is no systematic study regarding NETs-related genes in the molecular mechanisms and prognosis of LUAD.

With the development of the second-generation gene sequencing technology, many landmark cancer genomics databases were developed, including the Cancer Genome Atlas (TCGA, https://portal.gdc.cancer.gov/) and Gene Expression Omnibus (GEO, https://www.ncbi.nlm.nih.gov/geo/). More and more prognostic signatures had been constructed by big data mining. Herein, we identified two NETs-related molecular subtypes and a prognostic signature for LUAD by mining database. Our result may provide more evidences about the vital role of NETs in the prognosis of LUAD.

Materials and methods

Datasets

The collection of 69 NETs-related genes were conducted from previous studies (Supplementary Table S1) (9, 13, 14). The gene expression profile (Level 3 data, RPKM values), single nucleotide variants (SNV) data and matching clinical data of LUAD patients were downloaded from TCGA database. Two GEO datasets (GSE30219 and GSE31210) were retrieved for validation set. Copy number variation (CNV) data of LUAD were isolated from UCSC Xena (https://xena.ucsc.edu/). The mRNA expression data of TCGA, GSE30219 and GSE31210 were standardized and normalized using "sva" package before analysis.

Identification of expression and mutation atlas

Using the "limma" and "pheatmap" package, we identified the differentially expressed NETs-related genes in LUAD and "$p < 0.05$ and Log^2 |(Fold Change)| >2" were set as the threshold. The SNV and CNV atlas of NETs-related genes in LUAD were drawn with "maftools" and "RCircos" package, respectively.

Consensus clustering

In order to identify NETs-related molecular subtypes in LUAD, we conducted consensus clustering analysis with the ConcensusClusterPlus tool in R. In this analysis, cluster numbers were set from 2 to 6 and replicated process repeated 1,000 times. "Survminer" tool in R was used to generate the survival curve of each cluster of LUAD patients. Cluster map was drawn with "pheatmap" package.

Functional enrichment analysis and gene set enrichment analysis (GSEA)

After obtaining the differentially expressed genes (DEGs) between low NETs-score cohort and high NETs-score cohort, we employed Gene Ontology (GO) and Kyoto Encyclopedia of Genes and Genomes (KEGG) analyses with "clusterProfiler" package to explore the difference of these two cohorts in signal pathway and biological effects. GSEA was also performed to identify the difference of the signal pathway and biological effects between low NETs-score cohort and high NETs-score cohort with "org.Hs.eg.db," "clusterProfiler" and "enrichplot" package in R.

Characterization of immune landscape between two NETs-score cohorts

ESTIMATE algorithm was employed to calculate the immunoscore, stromascore, ESTIMATEScore, tumorPurity of each LUAD case. The difference of these scores between low NETs-score cohort and high NETs-score cohort were evaluated with Student's t-test with "ggpubr" package. To identify immune characteristics of LUAD cases, expression data were submitted into CIBERSORT (https://cibersort.stanford.edu/) and repeated

1,000 times, which could calculate the relative percentage of 22 immune cell types. The difference of 22 immune cell types between low NETs-score cohort and high NETs-score cohort were analyzed with Student's t-test and the results were visualized with "vioplot" package. Moreover, we also evaluated the difference in the expression of human leukocyte antigen (HLA)-related genes and immune checkpoints using "reshape2," "ggplot2" and "ggpubr" packages in R.

Development of prognostic signature based on NETs-related genes

After identifying the significantly prognostic NETs-related genes with univariate Cox regression analysis, we then performed LASSO cox regression analysis, which could compute the exact coefficient values of each identified association. The risk score of each LUAD case was calculated by a computational equation (sum of coefficient value x gene expression). We then separated LUAD patients into low- and high-risk subgroups with the median riskscore value as the cut-off. The overall survival curve of low- and high-risk subgroups were generated with Kaplan-Meier method. C-index and time ROC analysis were performed with "survminer" package to evaluate the performance of this signature in the prognosis prediction.

lncRNA-miRNA-mRNA regulatory axis

To identify the NETs-related prognostic signature genes (hub gene) possibly associated with the progression of LUAD, we then employed Wilcox-test to evaluate the expression difference in different TNM stage of LUAD patients. The miRNA targets of hub gene were predicted with miRDB (http://mirdb.org/), miRWalk (http://mirwalk.umm.uni-heidelberg.de/) and Targetscan (https://www.targetscan.org/). LncRNA targets of miRNA were predicted with LncBase (https://carolina.imis.athena-innovation.gr/) and RNAInter (http://www.rna-society.org/).

Validation of the expression of prognostic signature in LUAD cell lines

Human bronchial epithelial cell lines (HBE) and human lung cancer cell lines (A549, H1299, H1650, HCC827, and PC9) were provided by the Core Facility of Sichuan University west China Hospital (Sichuan, China). These cells were cultured in BEGM™ Bronchial Epithelial Cell Growth Medium (BEGM medium, Lonza, United States) or Roswell Park Memorial Institute 1640 (RPMI1640 medium, Gibco, Waltham, MA, United States). All cell lines were cultured at 37°C in a humidified atmosphere of 5% carbon dioxide (CO_2). Total RNA of cell lines were extracted using a TRIzol kit (Vazyme, Nanjing, China). RT-q PCR experiments were used to verify the expression of the prognostic signature in LUAD cell lines. The human 18 Svedberg Ribosomal RNA (18S rRNA) was used as the endogenous control for quantifying the expression of selected genes. The relative gene expression levels were calculated by using the comparative 2–DeltaDelta Cycle threshold ($2^{-\Delta\Delta CT}$) method.

Statistical analysis

All statistical analyses were performed with R software (version 4.2.1). Shapiro-Wilk normality test is used to test the normality distribution of samples. The difference in mRNA levels between two groups with Wilcoxon rank sum test. Kruskal-Wallis Test was performed to evaluate the difference among three groups and Bonferroni method was chosen for the correction of *p*-value. Pearson's or Spearman's rank correlation analysis was performed to evaluate the correlations between two continuous variables.

Results

Defining of the expression and genetic mutation landscape of NETs-related gene in LUAD

Heatmap of Figure 1A showed differentially expressed NETs-related genes in LUAD. Among 69 NETs-related genes, a total of 64 genes were differentially expressed in LUAD versus normal lung tissues, including 11 upregulated genes and 53 downregulated genes (Figure 1A, Supplementary Table S2). CNV atlas in Figure 1B revealed that half of NETs-related genes had copy number (CNV) amplification while another half of NETs-related genes had a widespread CNV deletion. The location of CNV alteration of NETs-related genes on chromosomes were showed in Figure 1C. Supplementary Figure S1A showed the SNV landscape of NETs-related genes in LUAD, which revealed that TLR4 has a highest frequency of SNV, followed by MGAM and DYSF. We then constructed a protein-protein interaction (PPI) network to further clarify the connections between these NETs-related genes (Supplementary Figure S1B).

Consensus clustering identified two subtypes in LUAD based on NETs-related genes

We next determined the numbers of subtype of LUAD based on NETs-related genes using consensus clustering. As a result, two subtypes of LUAD were identified with distinct the genes expression

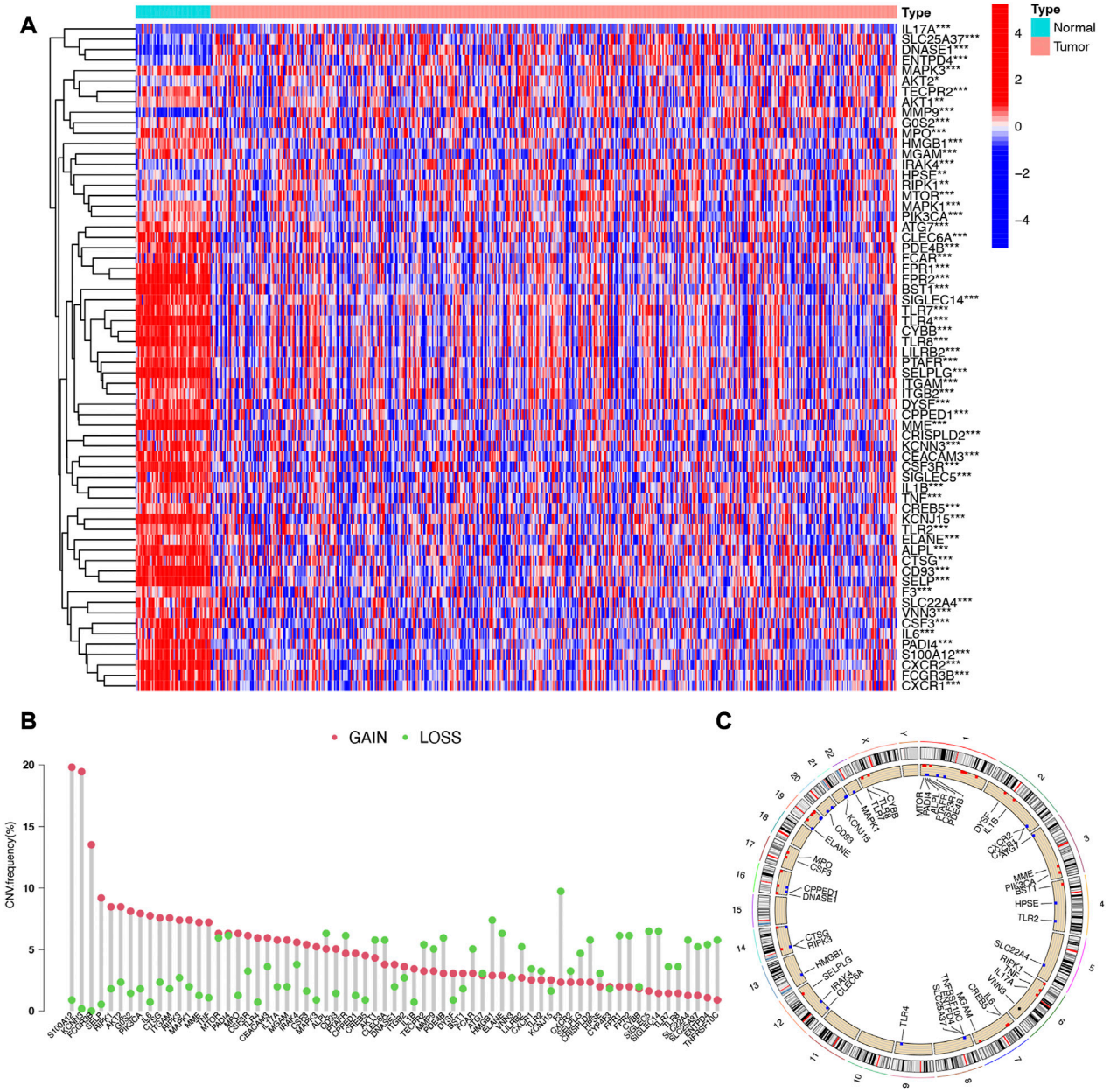

FIGURE 1
Expression and somatic mutation landscape of NETs-related genes in LUAD. **(A)** Heatmap reveals differentially expressed NETs-related genes in LUAD. **(B,C)** The copy number variation landscape of NETs-related genes in LUAD and their location on chromosomes.

patterns of NETs-related genes after k-means (Figure 2A). Subtype C2 showed overall high NETs-related genes expression pattern was defined as a high NETs score cluster, while Subtype C1 presented low expression pattern was defined as a low NETs score cluster (Figure 2B). Further prognostic analysis revealed that LUAD patients with high NETs score presented a dismal clinical outcome while low NETs score was correlated with a favorable overall survival in LUAD (Figure 2C).

Identification of signal pathways and biological effects in different NETs score cluster

Since significantly different clinical outcome were obtained in different NETs score cluster, we then explore the key DEGs, signal pathways and biological effects in each cluster, which may clarify molecular mechanism modulating patients' prognosis. As

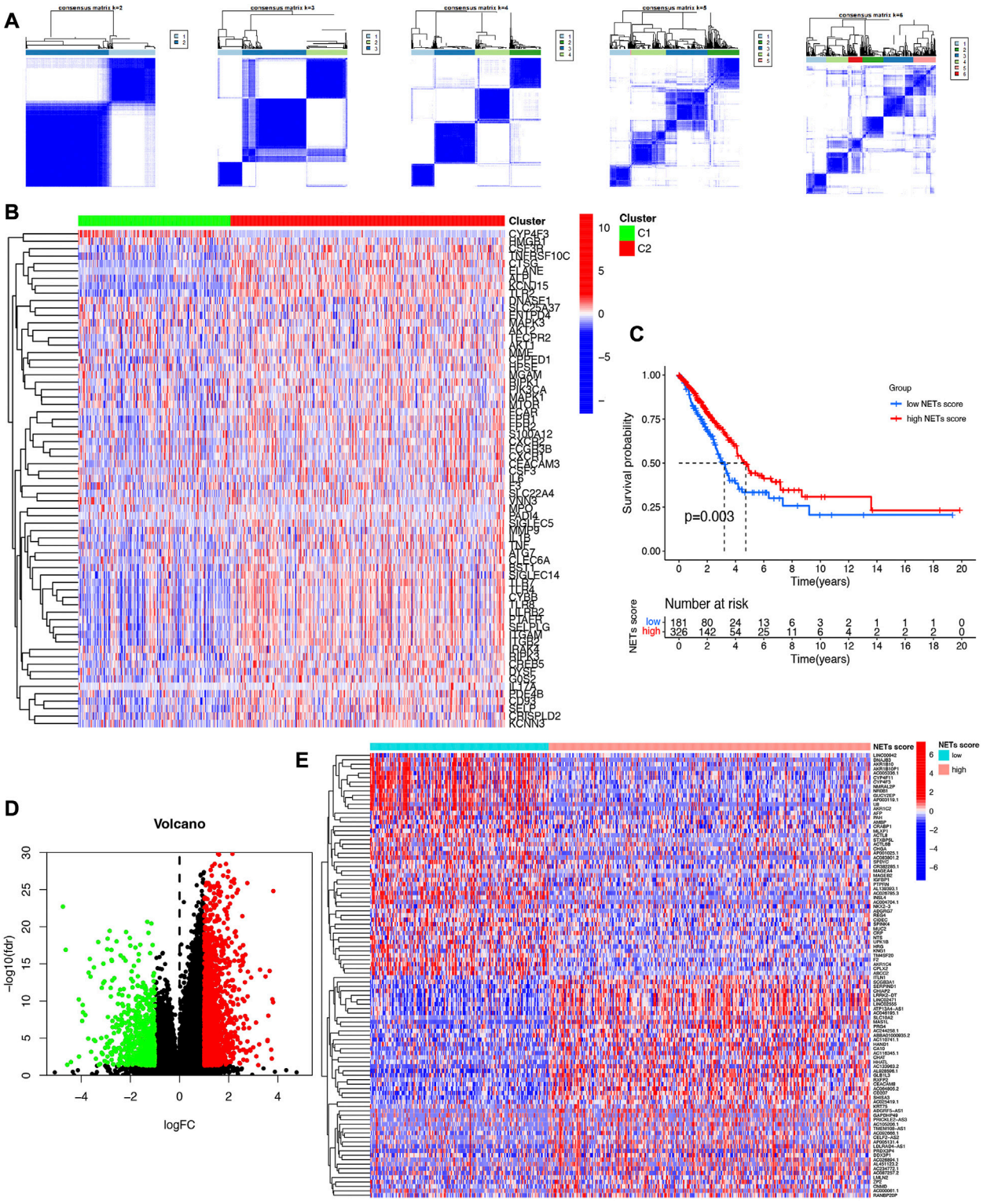

FIGURE 2
Identification of NETs-related clusters by consensus clustering. **(A)** Consensus clustering matrix about the number of clusters of LUAD. **(B)** Heatmap reveals NETs-related gene expression pattern in different NETs score cluster. **(C)** Overall survival curve of different NETs score cluster. **(D,E)** Volcano plot and heatmap reveal the differentially expressed genes between high NETs score and low NETs score subtypes.

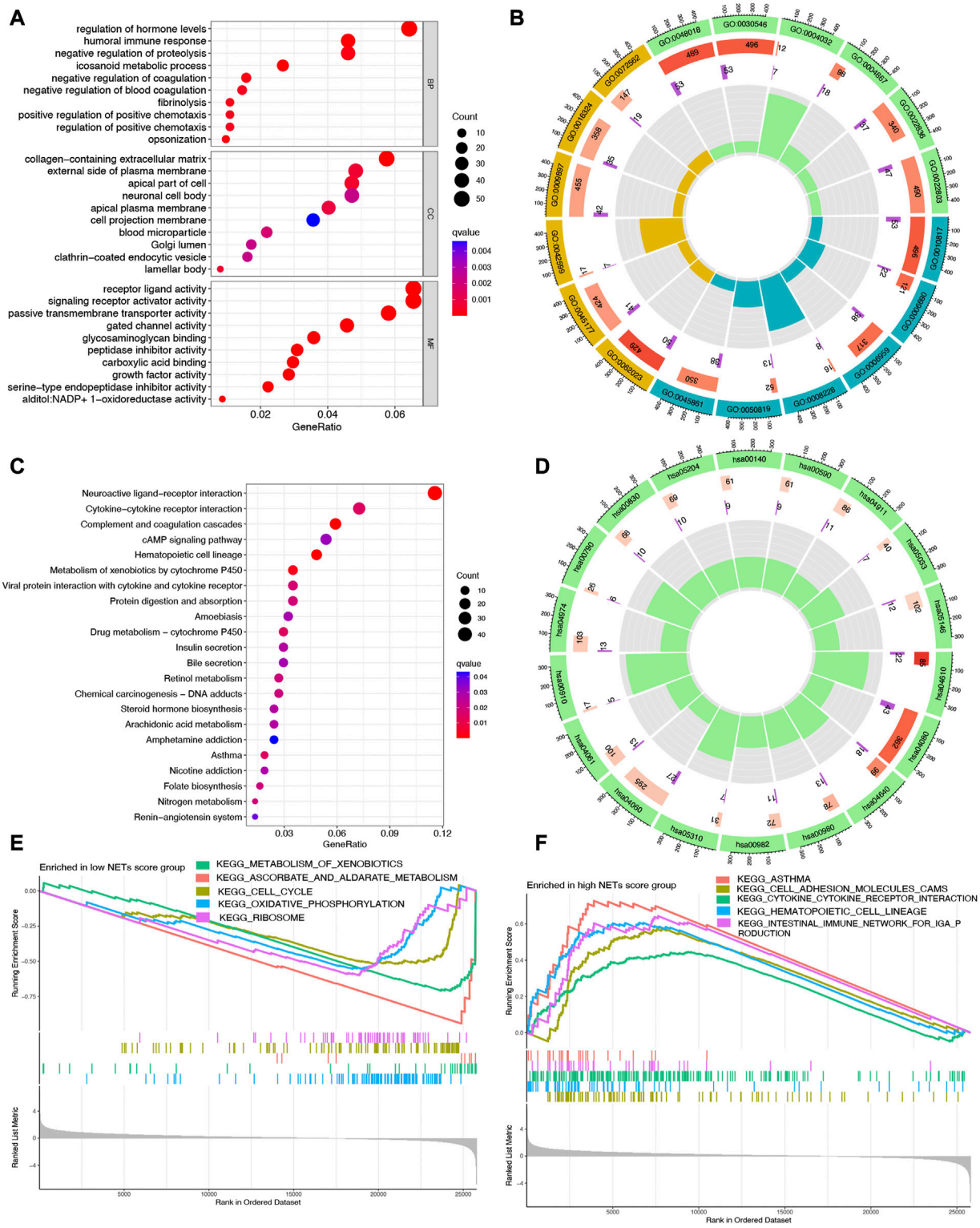

FIGURE 3
Functional enrichment and GSEA analysis in different cluster. **(A,B)** The enriched items in GO analysis. **(C,D)** The enriched items in KEGG analysis. **(E,F)** The enriched items in low and high NETs score clusters based on GSEA analysis.

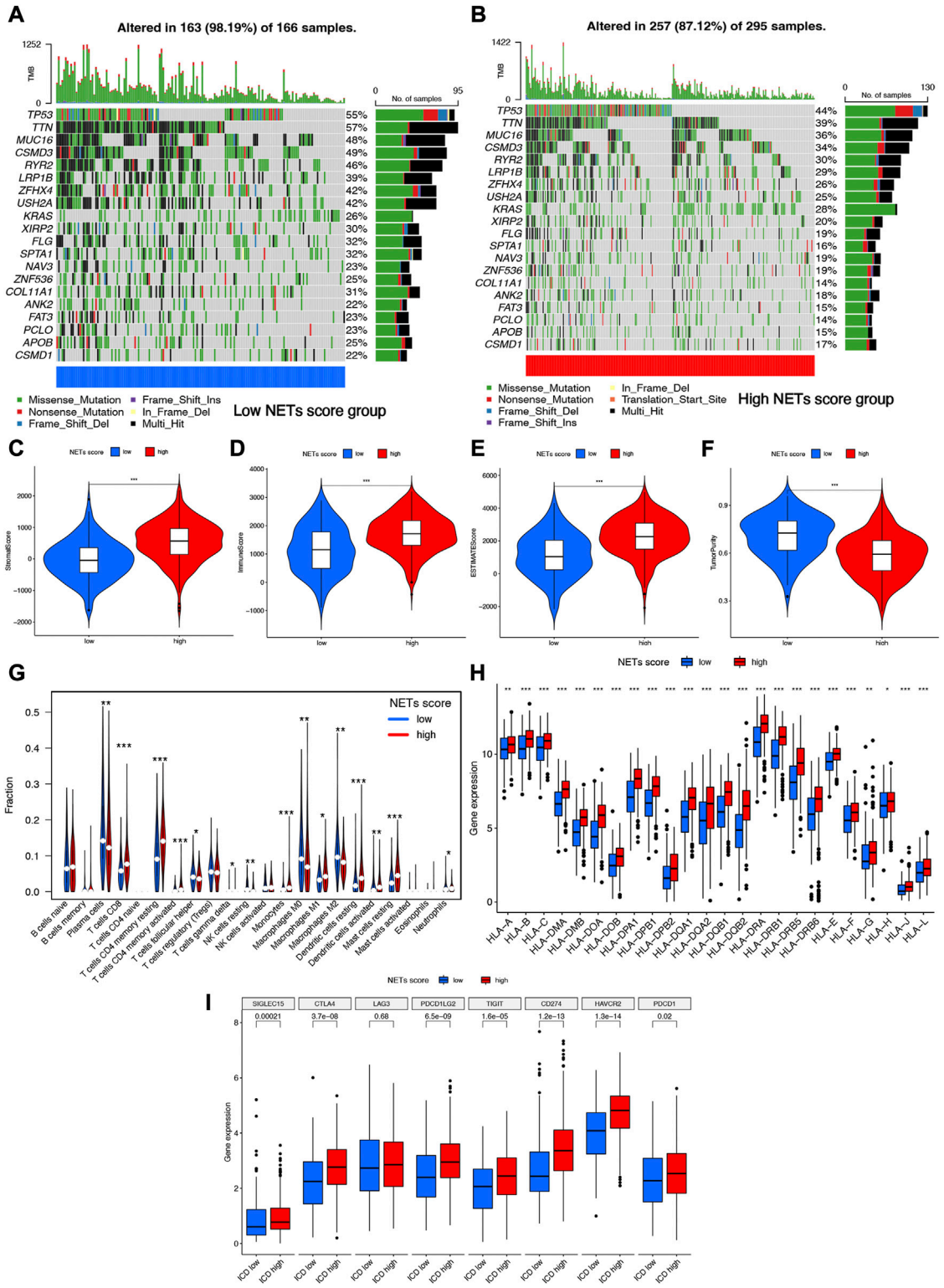

FIGURE 4
Somatic mutations and tumor microenvironment landscape in different cluster. **(A,B)** The somatic mutation profiles in high and low NETs score cluster. **(C–F)** High NETs score cluster had a higher stromal score, immune score, ESTIMAE score and tumor purity than low NETs score cluster. **(G–I)** The level of immune cells, human leukocyte antigen genes and common immune checkpoints in high and low NETs score cluster.

a result, a total of 2,120 DEGs were obtained between two different NETs score clusters (Figure 2D). Among these DEGs, the top 50 upregulated genes in two different NETs score clusters were showed in Figure 2E. Interestingly, the result of GO and KEGG pathways revealed that the dysregulated genes of NETs score cluster were mainly correlated with in immunity-related activities, including humoral immune response, regulation of positive chemotaxis, cytokine and cytokine receptor interaction, asthma, complement and coagulation cascades (Figures 3A–D). These data demonstrated a significant correlation between high NETs score cluster and immune active microenvironment. In order to further confirm the difference of signal pathways between high and low NETs score cluster, we performed GSEA analysis. Here, gene sets enriched in low NETs score cluster were correlated with oxidative phosphorylation, metabolism of xenobiotica by cytochrome, cell cycle and ribosome (Figure 3E). On the contrary, gene sets enriched in high NETs score cluster were correlated with cytokine and cytokine receptor interaction, cell adhesion molecules cams, asthma, and intestinal immune network for IgA production (Figure 3F).

Somatic mutations and tumor microenvironment landscape in different NETs score cluster

The somatic mutation profiles in high and low NETs score cluster were summarized in Figures 4A, B. Among them, TP53 (55% vs. 44%), TTN (57% vs. 39%), MUC16 (48% vs. 36%), GSMD3(49% vs. 34%), and RYR2 (39% vs. 30%) ranked the top fine the most frequency gens, exerting a greater somatic mutation frequency in low NETs score cluster than in the high NETs score cluster (Figures 4A, B). Accumulating evidences revealed that NETs played a vital role in innate immune response (12). The current study also clarified analyzed the composition of tumor microenvironment in different NETs score clusters. Overall, high NETs score cluster had a higher stromal score (Figure 4C), immune score (Figure 4D), ESTIMAE score (Figure 4E) and lower tumor purity (Figure 4F) than low NETs score cluster (all $p < 0.001$). The relative percentage of 22 immune cell types in each TCGA LUAD sample was summarized in Supplementary Figure S2A. And the correlation heatmap of each immune cell type was shown in Supplementary Figure S2B. To be more specific, LUAD patients with low NETs score cluster had a higher abundance of plasma cell, follicular helper T cell, NK resting cell, macrophage M0, macrophage M2. However, low NETs score cluster had a lower abundance of CD8 T cell, activated CD4 T cell, memory resting CD4 T cell, activated NK cell, Monocyte, macrophage M1, resting dendritic cell, active dendritic cell, resting mast cell and neutrophils (Figure 4G). Further analysis revealed that the expression of most of the human leukocyte antigen (HLA) genes and common immune checkpoints were higher in LUAD patients with high NETs score cluster (Figures 4H, I).

Construction and validation of prognostic signature based on NET-related genes

Cox univariate analysis indicated that 6 NET-related genes (G0S2, KCNJ15, S100A12, AKT2, CTSG, and HMGB1) were significantly correlated with the prognosis of LUAD patients (Figure 5A). These 6 genes were submitted for LASSO regression analysis and, as a result, all of them were selected in the prediction model (Figures 5B, C). The risk score of LUAD cases were calculated with the algorithm below: Risk score = (0.100)*G0S2 + (−0.079)*KCNJ15 + (0.088)*S100A12 + (0.238) AKT2 + (−0.156)*CTSG + (0.314)*HMGB1. We further investigated the correlation between clinical outcome and risk score. As expected, LUAD patients with high risk score were associated with a poor overall survival in TCGA cohort (Figure 5D, $p < 0.001$). The number of dead statuses in high risk group was more than that in low risk group (Figure 5E). We also obtained the similar results in GSE30219 cohort (Figures 5F, G) and GSE31210 cohort (Figures 5H, I). Further ROC curve indicated that the AUC value in 1-year, 3-year, and 5-year overall survival were 0.671, 0.674, and 0.592, respectively (Figure 6A). Diagnostic ROC curve and C-index revealed that risk score and clinal stage was relatively good predictors for the clinical outcome of LUAD patients (Figures 6B, C). Moreover, univariate and multivariate analysis revealed that NETs-related risk score and clinical stage could act independent prognostic factors for LUAD patients (Figures 6D, E).

NETs-risk score was significantly correlated with immune cell infiltration in LUAD

Since NETs played a vital role in the progression of cancer and immunological responses, it was necessary to clarify the correlation between NETs-risk score and tumor microenvironment. As shown in Figures 7A–F, the abundance of Macrophages M0, Macrophages M1, NK cells resting, T cells CD4 memory activated, T cells CD8, and T cells follicular helper was positively correlated with NETs-risk score in LUAD. As NETs-risk score increased, the abundance of B cells memory, Dendritic cells activated, Dendritic cells resting, Mast cells resting, Monocytes, Plasma cells, and T cells CD4 memory resting decreased (Figures 7G–M). Moreover, TIDE was used to assess the predictive value of NETs-risk score in the potential clinical efficacy of immunotherapy. Interestingly, immunotherapy non-response group had a higher risk score than that in immunotherapy response group (Figure 7N, $p = 0.0067$), demonstrating that LUAD patients with low NETs-risk

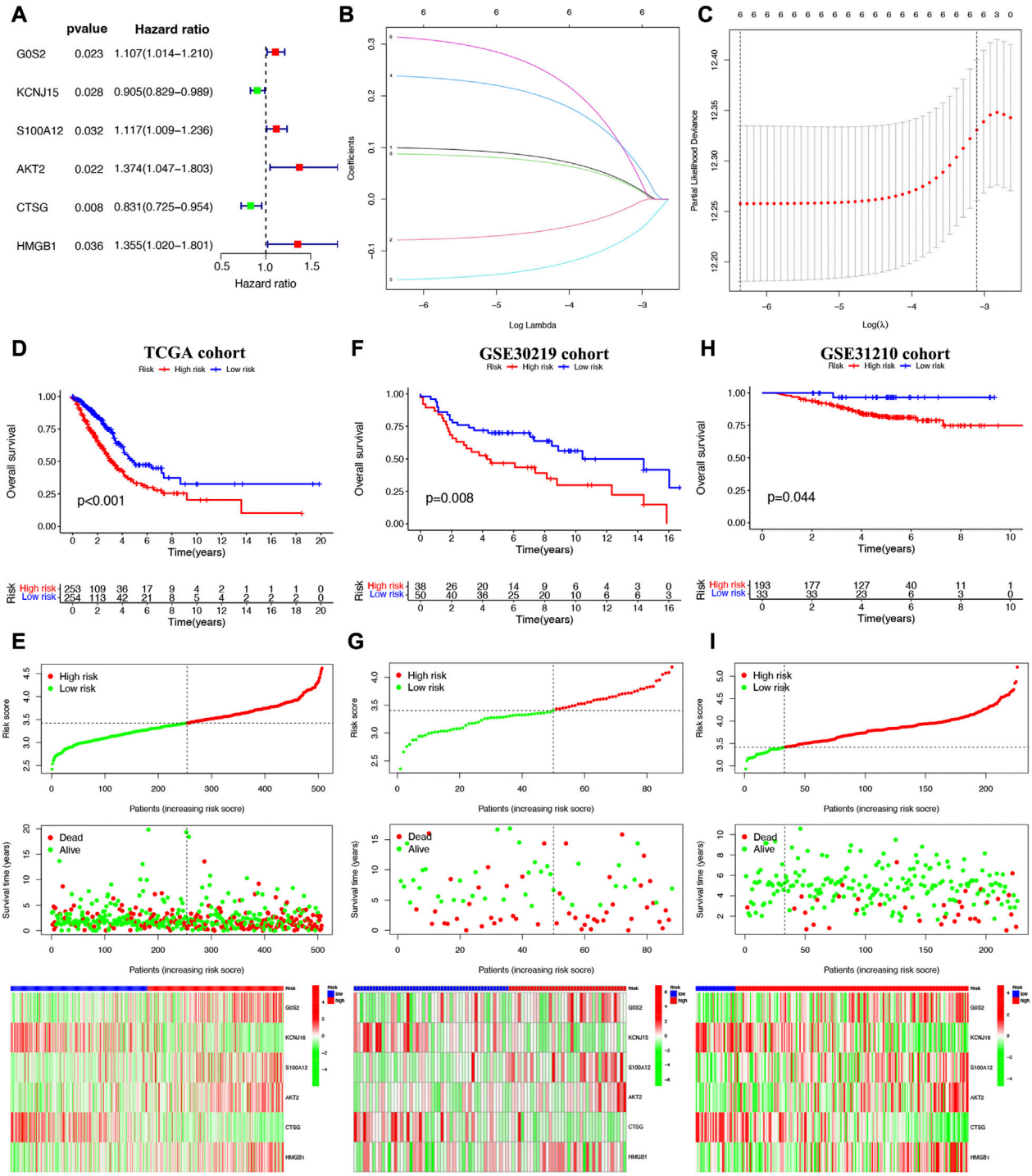

FIGURE 5
Construction of a NETs-related prognostic signature. **(A)** NETs-related genes with significant prognostic value based on univariate cox regression analysis. **(B,C)** The coefficient and partial likelihood deviance of prognostic signature. Overall survival curve, risk scores distribution, patients' survival status, gene expression heatmap of NETs-related prognostic signature in TCGA cohort **(D,E)**, GSE30219 cohort **(F,G)** and GSE31210 cohort **(H,I)**.

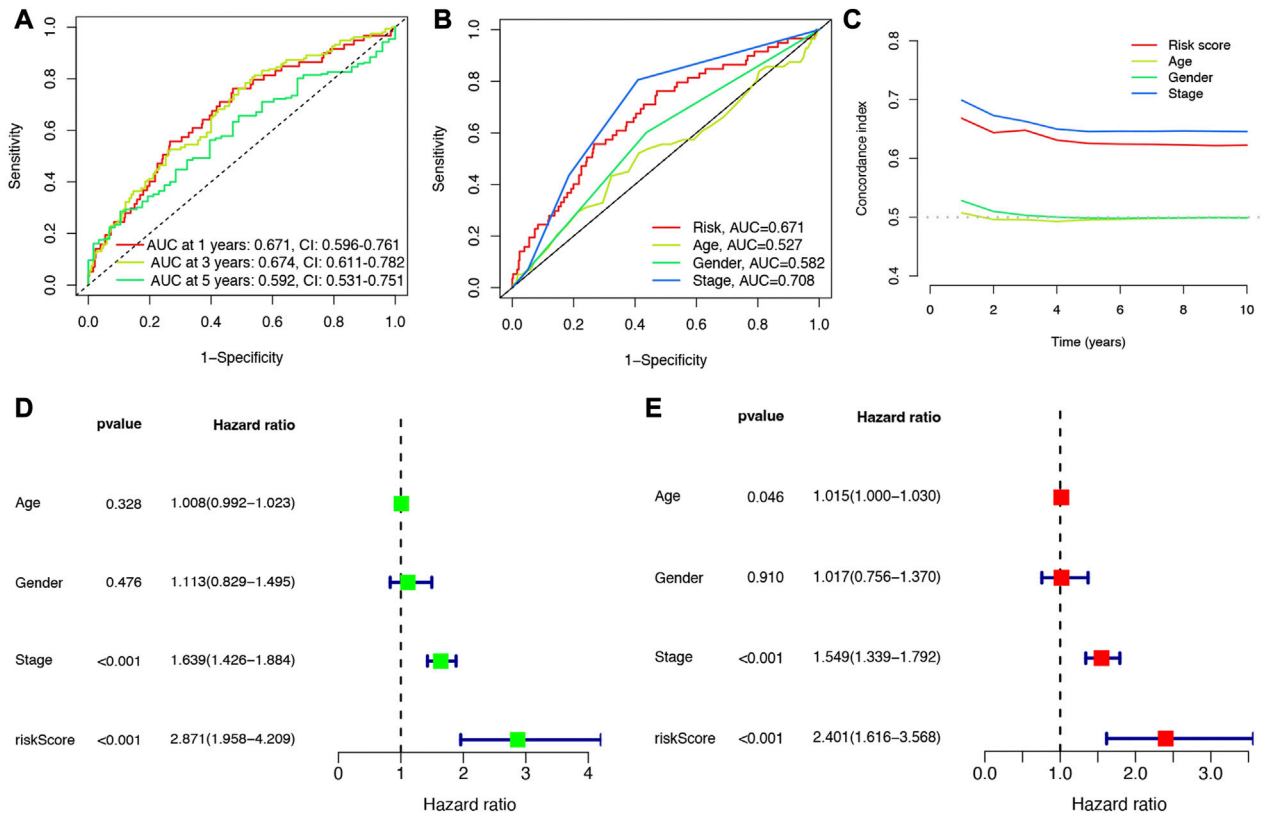

FIGURE 6
Evaluation of the performance of NETs-related prognostic signature. **(A)** The AUCs under ROC curves for 1-, 3-, and 5-year overall survival. **(B,C)** ROC and C-index compared the diagnosed performance of risk scores with clinical characters. **(D,E)** Univariate and multivariate cox regression considering clinical parameters and NETs-risk score.

score would be more possibly benefited more from immunotherapy.

Construction of lncRNA-miRNA-mRNA regulatory axis

The expression of G0S2, HMGB1, S100A12, AKT2 were upregulated (Supplementary Figures S3A–D) while the expression of CTSG and KCNJ15 were decreased in most of LUAD cell lines compared with human bronchial epithelioid cells (HBE) (Supplementary Figures S3E, F). We then analyzed the correlation between the expression of NETs-prognostic signature genes and clinical stage. Here, only CTSG expression was significantly correlated clinical stage in LUAD (Figure 8A). Thus, we selected CTSG for further analysis. In order to further clarified the mechanism of CTSG in the progression of LUAD, we then constructed a lncRNA-miRNA-mRNA regulatory axis. Using miRDB, miRWalk and TargetScan, we identified miR-7114-5p, miR-487a-5p, miR-3664-5p and miR-487b-5p as the miRNA targets of CTSG (Figure 8B). Among these four miRNA targets, only miR-3664-5p was significantly dysregulated in LUAD (Figure 8C, $p < 0.001$) and correlated with clinical outcome though the p-value was 0.063 (Figure 8D). Thus, miR-3664-5p was the most promising miRNA target of CTSG. We then used RNAInter and lncBase to further explore its upstream lncRNA targets. As shown in Figure 8E, lncRNA BCYRN1 and RP11-805I24.1 were suggested as the targets of miR-3664-5p. However, only BCYRN1 was significantly dysregulated in LUAD (Figure 8F, $p < 0.001$) and correlated with clinical outcome in LUAD (Figure 8G), indicating BCYRN1 as the most promising lncRNA target. All in all, we identified lncRNA BCYRN1/miR-3664-5p/CTSG regulatory axis in the progression in LUAD. Further study would be performed to confirm the results.

Discussion

NETs are decondensed extracellular chromatin filaments and play a vital role in innate immune response (15). Accumulating evidences have shown that NETs are involved in many biological processes of cancer, including

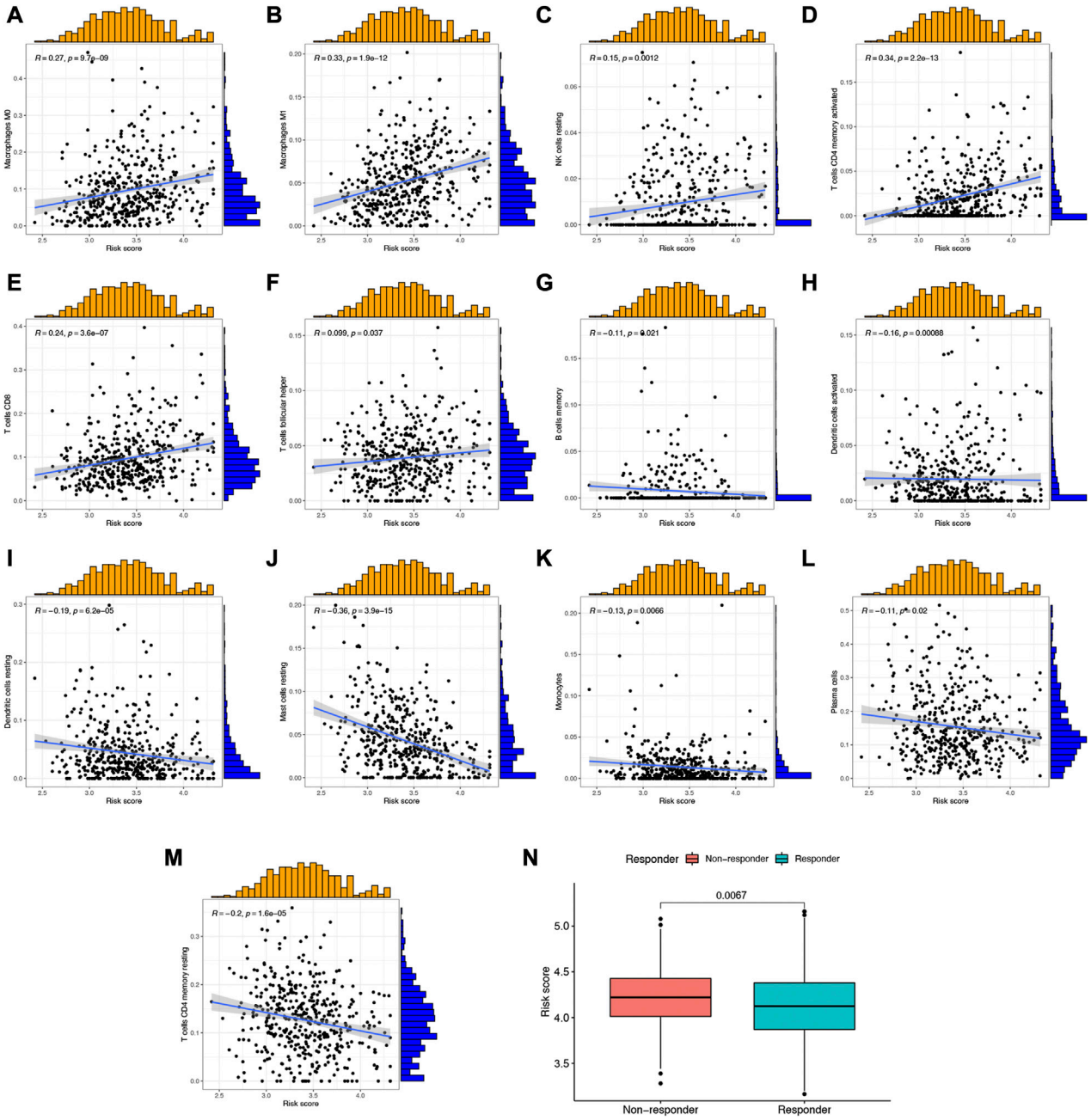

FIGURE 7
The correlation between NETs-related risk score and immune cell level as well as TIDE score. **(A–M)** Scatter plots revealed the correlation of risk score and the abundance of different immune cells. **(N)** The risk score in immunotherapy response and immunotherapy non-response group.

invasion and evasion (16). Moreover, NETs could also catch circulating cancer cells and facilitate metastasis (12). Interestingly, NETs could serve as therapeutic target and associate with clinical outcome in cancer (9, 17). In the current study, we performed a systematic study regarding NETs-related genes in the molecular mechanisms and prognosis of LUAD.

Based on the expression pattern of NETs-related genes, we conducted consensus clustering analysis and two NETs-related clusters of LUAD were obtained. High NETs score cluster was correlated with a favorable overall survival rate, abundant immune cell infiltration, high immuneScore, high sromaScore and high ESTIMATEScore, and high activity of immune response signal pathways, referring to “hot tumor” (18). Further analysis revealed

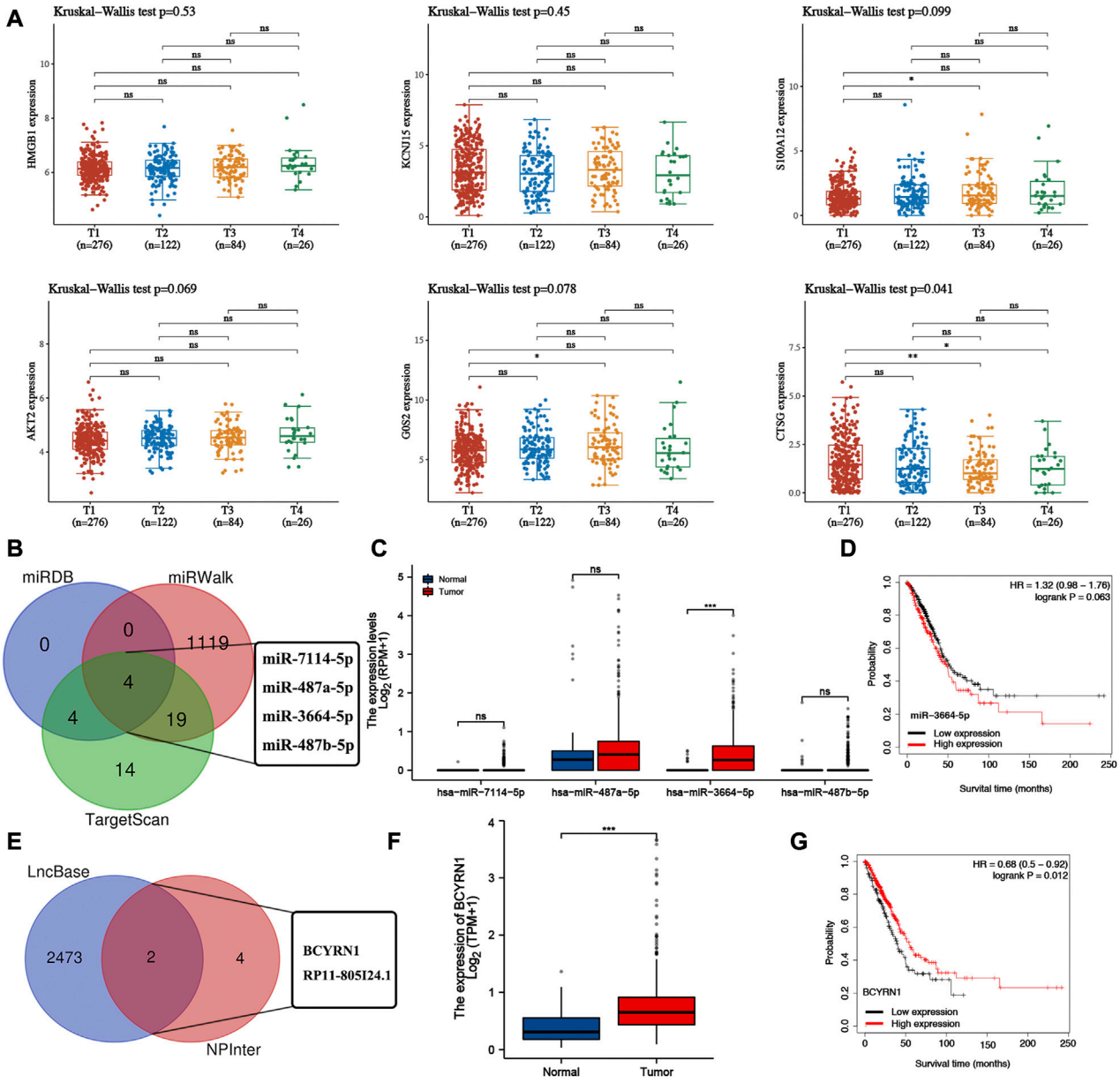

FIGURE 8
Construction of lncRNA-miRNA-mRNA regulatory axis. **(A)** The expression of NETs-related prognostic signature genes in different clinical stage group of LUAD patients. **(B)** miRNA targets of CTSG predicted by miRDB, miRWalk and TargetScan. **(C,D)** The expression and prognostic value of miRNA targets in LUAD. **(E)** LncRNA targets of miR-3664-5p predicted by lncBase and RNAIter. **(F,G)** The expression and prognostic value of lncRNA targets in LUAD. *$p < 0.05$, **$p < 0.01$, ***$p < 0.001$.

that high NETs score cluster was correlated with active immune activities, including cytokine and cytokine receptor interaction, cell adhesion molecules cams, asthma, and intestinal immune network for IgA production. "Hot tumors" with significant T-cell infiltration are linked to better immune therapy efficacy (19). Cancer patients with "Hot tumors" phenotype was associated with favorable clinical outcome (20). Actually, previous study also demonstrated that LUAD patients with high immuneScore, sromaScore and ESTIMATEScore were associated with better clinical outcome (18). Low NETs score cluster had a higher abundance of plasma cell, follicular helper T cell, NK resting cell, macrophage M0, macrophage M2. However, high NETs score indicated a lower abundance of CD8 T cell, activated CD4 T cell, memory resting CD4 T cell, activated NK cell, Monocyte, macrophage M1, resting dendritic cell, active dendritic cell, resting mast cell and neutrophils. Higher level of CD8 T cell, activated CD4 T cell, memory resting

CD4 T cell, activated NK cell and macrophage M1 were associated with better immune response. While macrophage M2 could promote the progression of many types of cancer, including LUAD (21–23). Without immune checkpoints expression, those patients would not benefit from immunotherapy. And the patients with high immune checkpoints expression would benefit from immunotherapy such as anti-PD1 or anti-CTLA4 drug. Tumor cell HLA expression helps antitumor immune response (24). This may be one of the reasons why LUAD patients in High NETs score cluster was correlated with the favorable overall survival.

Six NET-related genes (G0S2, KCNJ15, S100A12, AKT2, CTSG and HMGB1) with significant prognostic value were screened to develop a prognostic signature. We found that LUAD patients with low-risk score had a favorable overall survival rate both in the training set and validation set. Moreover, NETs-related risk score and clinical stage could act as independent prognostic factors for LUAD patients. These data suggested that this NETs-related prognostic signature had a good performance in the prognosis prediction of LUAD patients. As far as we known, only two NETs-related prognostic signatures had been constructed in cancers. Chen et al. constructed a lncRNA signature based on NETs-related gene in non-small-cell lung cancer, which had good performance in predicting survival (10). Another bioinformatics analysis also developed a NETs-related prognostic signature for pan-cancer (9).

Some of six NET-related prognostic biomarkers (G0S2, KCNJ15, S100A12, AKT2, CTSG and HMGB1) also played a vital role in LUAD. High AKT2 drives cancer progression in lung adenocarcinoma (25). Moreover, silencing of AKT2 could reduce cellular motility and invasion in LUAD (26). Another study revealed that high HMGB1 may induce tumorigenesis, metastasis and chemotherapy resistance in lung cancer (27).

We also identified lncRNA BCYRN1/miR-3664-5p/CTSG regulatory axis that may be involved in the progression of LUAD. BCYRN1 was suggested as an oncogenic lncRNA in diverse cancers (28). Moreover, BCYRN1 could accelerate glycolysis and tumor progression *via* miR-149/PKM2 axis in lung cancer (29). Moreover, BCYRN1 could also regulate cell metastasis in lung cancer (30). miR-3664-5p also exert vital functions in certain types of cancer. miR-3664-5P could inhibit the proliferation and metastasis of gastric cancer *via* NF-κB signaling pathway (31). CTSG was suggested as a prognostic biomarker in certain types of cancer including bladder cancer, LUAD, oral squamous cell carcinoma (32–34). In our further study, we would focus on the verification of the vital of BCYRN1/miR-3664-5p/CTSG regulatory axis in the progression of LUAD *via in vitro* and *in vivo* analysis.

There are some limitations of our study. The 5-year survival in high and low risk score of TCGA cohort was only about 10% difference and the clinical relevance is questionable. It would be better to verify our prognostic signature using another dataset. Moreover, the expression and prognostic role of prognostic signature genes should be verified using clinical tissues.

Conclusion

In conclusion, we identified two new molecular subtypes and a prognostic signature for lung adenocarcinoma based on NETs-related genes. This stratification could provide more evidence for estimating prognosis and immunotherapy of LAUD patients.

Data availability statement

The original contributions presented in the study are included in the article/Supplementary Material, further inquiries can be directed to the corresponding author.

Author contributions

YZ performed data analysis work and aided in writing the manuscript. PL designed the study, assisted in writing the manuscript. GL edit the manuscript. All authors read and approved the final manuscript.

Funding

This work was supported by the Natural Science Foundation of Shandong Province (grant no. ZR2020MH418).

Conflict of interest

The authors declare that the research was conducted in the absence of any commercial or financial relationships that could be construed as a potential conflict of interest.

Supplementary material

The Supplementary Material for this article can be found online at: https://www.por-journal.com/articles/10.3389/pore.2023.1610899/full#supplementary-material

SUPPLEMENTARY FIGURE S1
The mutation landscape and interaction network of NETs-related gens. **(A)** Oncoprint visualization of the mutation of NETs-related gens in LUAD. **(B)** Protein-protein interactions among NETs-related gens.

SUPPLEMENTARY FIGURE S2
Immune landscape of high and low NETs score cluster. **(A)** Relative proportion of immune infiltration in high and low NETs score cluster. **(B)** Correlation heatmap among 22 immune cell types.

SUPPLEMENTARY FIGURE S3
The expression of prognostic signature in LUAD cell lines. The expression of G0S2 , **(A)** HMGB1 **(B)**, S100A12 **(C)**, AKT2 **(D)**, CTSG **(E)** and KCNJ15 **(F)** in LUAD cell lines and human bronchial epithelioid cells (HBE).

References

1. Siegel RL, Miller KD, Jemal A. Cancer statistics, 2020. *CA Cancer J Clin* (2020) 70(1):7–30. doi:10.3322/caac.21590

2. Brody H. Lung cancer. *Nature* (2020) 587(7834):S7. doi:10.1038/d41586-020-03152-0

3. Slim A, Kamoun H, Hadidene Y, Smadhi H, Meddeb A, Megdiche ML. Postoperative recurrence of primary lung cancer: Anatomo-clinical and therapeutic study. *Tunis Med* (2021) 99(5):560–8.

4. Denisenko TV, Budkevich IN, Zhivotovsky B. Cell death-based treatment of lung adenocarcinoma. *Cell Death Dis* (2018) 9(2):117. doi:10.1038/s41419-017-0063-y

5. Cui Y, Fang W, Li C, Tang K, Zhang J, Lei Y, et al. Development and validation of a novel signature to predict overall survival in "driver gene-negative" lung adenocarcinoma (LUAD): Results of a multicenter study. *Clin Cancer Res* (2019) 25(5):1546–56. doi:10.1158/1078-0432.CCR-18-2545

6. Lee KC, Koh J, Chung DH, Jeon YK. A case of concomitant EGFR/ALK alteration against a mutated EGFR background in early-stage lung adenocarcinoma. *J Pathol Transl Med* (2021) 55(2):139–44. doi:10.4132/jptm.2020.12.16

7. Ocana A, Nieto-Jiménez C, Pandiella A, Templeton AJ. Neutrophils in cancer: Prognostic role and therapeutic strategies. *Mol Cancer* (2017) 16(1):137. doi:10.1186/s12943-017-0707-7

8. Rada B. Neutrophil extracellular traps. *Methods Mol Biol* (2019) 1982:517–28. doi:10.1007/978-1-4939-9424-3_31

9. Zhang Y, Guo L, Dai Q, Shang B, Xiao T, Di X, et al. A signature for pan-cancer prognosis based on neutrophil extracellular traps. *J Immunother Cancer* (2022) 10(6):e004210. doi:10.1136/jitc-2021-004210

10. Fang C, Liu F, Wang Y, Yuan S, Chen R, Qiu X, et al. A innovative prognostic symbol based on neutrophil extracellular traps (NETs)-related lncRNA signature in non-small-cell lung cancer. *Aging (Albany NY)* (2021) 13(13):17864–79. doi:10.18632/aging.203289

11. Klopf J, Brostjan C, Eilenberg W, Neumayer C. Neutrophil extracellular traps and their implications in cardiovascular and inflammatory disease. *Int J Mol Sci* (2021) 22(2):559. doi:10.3390/ijms22020559

12. Masucci MT, Minopoli M, Del Vecchio S, Carriero MV. The emerging role of neutrophil extracellular traps (NETs) in tumor progression and metastasis. *Front Immunol* (2020) 11:1749. doi:10.3389/fimmu.2020.01749

13. Papayannopoulos V. Neutrophil extracellular traps in immunity and disease. *Nat Rev Immunol* (2018) 18(2):134–47. doi:10.1038/nri.2017.105

14. Şenbabaoğlu Y, Gejman RS, Winer AG, Liu M, Van Allen EM, de Velasco G, et al. Tumor immune microenvironment characterization in clear cell renal cell carcinoma identifies prognostic and immunotherapeutically relevant messenger RNA signatures. *Genome Biol* (2016) 17(1):231. doi:10.1186/s13059-016-1092-z

15. Khan U, Chowdhury S, Billah MM, Islam KMD, Thorlacius H, Rahman M. Neutrophil extracellular traps in colorectal cancer progression and metastasis. *Int J Mol Sci* (2021) 22(14):7260. doi:10.3390/ijms22147260

16. Demkow U. Neutrophil extracellular traps (NETs) in cancer invasion, evasion and metastasis. *Cancers (Basel)* (2021) 13(17):4495. doi:10.3390/cancers13174495

17. Yang D, Liu J. Neutrophil extracellular traps: A new player in cancer metastasis and therapeutic target. *J Exp Clin Cancer Res* (2021) 40(1):233. doi:10.1186/s13046-021-02013-6

18. Sun S, Guo W, Wang Z, Wang X, Zhang G, Zhang H, et al. Development and validation of an immune-related prognostic signature in lung adenocarcinoma. *Cancer Med* (2020) 9(16):5960–75. doi:10.1002/cam4.3240

19. Liu YT, Sun ZJ. Turning cold tumors into hot tumors by improving T-cell infiltration. *Theranostics* (2021) 11(11):5365–86. doi:10.7150/thno.58390

20. Li B, Cui Y, Nambiar DK, Sunwoo JB, Li R. The immune subtypes and landscape of squamous cell carcinoma. *Clin Cancer Res* (2019) 25(12):3528–37. doi:10.1158/1078-0432.CCR-18-4085

21. Wei K, Ma Z, Yang F, Zhao X, Jiang W, Pan C, et al. M2 macrophage-derived exosomes promote lung adenocarcinoma progression by delivering miR-942. *Cancer Lett* (2022) 526:205–16. doi:10.1016/j.canlet.2021.10.045

22. Lan J, Sun L, Xu F, Liu L, Hu F, Song D, et al. M2 macrophage-derived exosomes promote cell migration and invasion in colon cancer. *Cancer Res* (2019) 79(1):146–58. doi:10.1158/0008-5472.CAN-18-0014

23. Chen J, Zhang K, Zhi Y, Wu Y, Chen B, Bai J, et al. Tumor-derived exosomal miR-19b-3p facilitates M2 macrophage polarization and exosomal LINC00273 secretion to promote lung adenocarcinoma metastasis via Hippo pathway. *Clin Transl Med* (2021) 11(9):e478. doi:10.1002/ctm2.478

24. Morandi F, Airoldi I. HLA-G and other immune checkpoint molecules as targets for novel combined immunotherapies. *Int J Mol Sci* (2022) 23(6):2925. doi:10.3390/ijms23062925

25. Liu T, Zhu J, Du W, Ning W, Zhang Y, Zeng Y, et al. AKT2 drives cancer progression and is negatively modulated by miR-124 in human lung adenocarcinoma. *Respir Res* (2020) 21(1):227. doi:10.1186/s12931-020-01491-0

26. Attoub S, Arafat K, Kamel Hammadi N, Mester J, Gaben AM. Akt2 knock-down reveals its contribution to human lung cancer cell proliferation, growth, motility, invasion and endothelial cell tube formation. *Sci Rep* (2015) 5:12759. doi:10.1038/srep12759

27. Wu L, Yang L. The function and mechanism of HMGB1 in lung cancer and its potential therapeutic implications. *Oncol Lett* (2018) 15(5):6799–805. doi:10.3892/ol.2018.8215

28. Ghafouri-Fard S, Dashti S, Hussen BM, Farsi M, Taheri M. BCYRN1: An oncogenic lncRNA in diverse cancers. *Pathol Res Pract* (2021) 220:153385. doi:10.1016/j.prp.2021.153385

29. Lang N, Wang C, Zhao J, Shi F, Wu T, Cao H. Long non-coding RNA BCYRN1 promotes glycolysis and tumor progression by regulating the miR-149/PKM2 axis in non-small-cell lung cancer. *Mol Med Rep* (2020) 21(3):1509–16. doi:10.3892/mmr.2020.10944

30. Hu T, Lu YR. BCYRN1, a c-MYC-activated long non-coding RNA, regulates cell metastasis of non-small-cell lung cancer. *Cancer Cel Int* (2015) 15:36. doi:10.1186/s12935-015-0183-3

31. Jiao Y, Yang H, Qian J, Gong Y, Liu H, Wu S, et al. miR-3664-5P suppresses the proliferation and metastasis of gastric cancer by attenuating the NF-κB signaling pathway through targeting MTDH. *Int J Oncol* (2019) 54(3):845–58. doi:10.3892/ijo.2019.4680

32. Huang GZ, Wu QQ, Zheng ZN, Shao TR, Li F, Lu XY, et al. Bioinformatics analyses indicate that cathepsin G (CTSG) is a potential immune-related biomarker in oral squamous cell carcinoma (OSCC). *Onco Targets Ther* (2021) 14:1275–89. doi:10.2147/OTT.S293148

33. Li N, Li Y, Zheng P, Zhan X. Cancer stemness-based prognostic immune-related gene signatures in lung adenocarcinoma and lung squamous cell carcinoma. *Front Endocrinol (Lausanne)* (2021) 12:755805. doi:10.3389/fendo.2021.755805

34. Song Y, Jin D, Chen J, Luo Z, Chen G, Yang Y, et al. Identification of an immune-related long non-coding RNA signature and nomogram as prognostic target for muscle-invasive bladder cancer. *Aging (Albany NY)* (2020) 12(12):12051–73. doi:10.18632/aging.103369

Pathology & Oncology Research | frontiers

TYPE Review
PUBLISHED 17 June 2024
DOI 10.3389/pore.2024.1611733

Check for updates

OPEN ACCESS

EDITED BY
Nora Bittner,
National Koranyi Institute of TB and Pulmonology, Hungary

*CORRESPONDENCE
László József Tóth,
tothlasz@med.unideb.hu

RECEIVED 18 February 2024
ACCEPTED 04 June 2024
PUBLISHED 17 June 2024

CITATION
Tóth LJ, Mokánszki A and Méhes G (2024), The rapidly changing field of predictive biomarkers of non-small cell lung cancer.
Pathol. Oncol. Res. 30:1611733.
doi: 10.3389/pore.2024.1611733

COPYRIGHT
© 2024 Tóth, Mokánszki and Méhes. This is an open-access article distributed under the terms of the Creative Commons Attribution License (CC BY). The use, distribution or reproduction in other forums is permitted, provided the original author(s) and the copyright owner(s) are credited and that the original publication in this journal is cited, in accordance with accepted academic practice. No use, distribution or reproduction is permitted which does not comply with these terms.

The rapidly changing field of predictive biomarkers of non-small cell lung cancer

László József Tóth*, Attila Mokánszki and Gábor Méhes

Department of Pathology, Faculty of Medicine, University of Debrecen, Debrecen, Hungary

Lung cancer is a leading cause of cancer-related death worldwide in both men and women, however mortality in the US and EU are recently declining in parallel with the gradual cut of smoking prevalence. Consequently, the relative frequency of adenocarcinoma increased while that of squamous and small cell carcinomas declined. During the last two decades a plethora of targeted drug therapies have appeared for the treatment of metastasizing non-small cell lung carcinomas (NSCLC). Personalized oncology aims to precisely match patients to treatments with the highest potential of success. Extensive research is done to introduce biomarkers which can predict the effectiveness of a specific targeted therapeutic approach. The EGFR signaling pathway includes several sufficient targets for the treatment of human cancers including NSCLC. Lung adenocarcinoma may harbor both activating and resistance mutations of the EGFR gene, and further, mutations of KRAS and BRAF oncogenes. Less frequent but targetable genetic alterations include ALK, ROS1, RET gene rearrangements, and various alterations of MET proto-oncogene. In addition, the importance of anti-tumor immunity and of tumor microenvironment has become evident recently. Accumulation of mutations generally trigger tumor specific immune defense, but immune protection may be upregulated as an aggressive feature. The blockade of immune checkpoints results in potential reactivation of tumor cell killing and induces significant tumor regression in various tumor types, such as lung carcinoma. Therapeutic responses to anti PD1-PD-L1 treatment may correlate with the expression of PD-L1 by tumor cells. Due to the wide range of diagnostic and predictive features in lung cancer a plenty of tests are required from a single small biopsy or cytology specimen, which is challenged by major issues of sample quantity and quality. Thus, the efficacy of biomarker testing should be warranted by standardized policy and optimal material usage. In this review we aim to discuss major targeted therapy-related biomarkers in NSCLC and testing possibilities comprehensively.

KEYWORDS

NSCLC, driver oncogenes, immune checkpoint inhibitor, gene fusion, biomarker

Introduction

Primary lung cancer used to be a rare tumor in the past, however today it is the most common cause of cancer mortality worldwide. In 2020, lung carcinoma was the second most common malignancy, with around 2.2 million newly diagnosed cases. Moreover, with 1.796 million cases, it was the number one cause of cancer deaths [1]. The incidence in both of US and EU is now declining, that follows the trend of shrinking smoking prevalence [2]. The incidence rate in male patients increased from 1973 to 1984 (83.5 and 97.9/100,000 person-years, respectively) followed by a gradual decrease till 2015 (55.3/100,000 person-years), while in female patients the incidence increased in a more extended period from 1973 to 2007 (20.2–51.3/100,000 person-years) and then subsequently decreased to 2015 (44.2/100,000 person-years). The trend in the incidence of lung carcinoma in men in Central Europe is similar to that seen in Western countries, but with a slight delay. Unfortunately, according to the latest data, the incidence of lung cancer is still rising in women [3].

About 85% of lung cancer cases are non-small cell carcinoma, the remaining 15% belong to the clinically separate category of small cell carcinoma. The group of non-small cell carcinomas is further subdivided as adenocarcinoma, squamous cell carcinoma, large cell carcinoma, and several other relatively rare histological types [4]. The relative frequency of histological types of lung carcinoma has also changed significantly in recent decades. In the past the squamous cell carcinoma was the most common type of lung cancer but their relative frequency declined and the general occurrence of adenocarcinoma increased. Today, adenocarcinoma is the most common type, accounting for about 50%–56% of all lung cancer cases and is the most frequent histological subtype in never-smokers [5]. Increased risk of adenocarcinoma in smokers is a result of changes in design and composition of tobacco products. The introduction of ventillated filters in cigarettes and the increased levels of tobacco-specific nitrosamines both have played a role [6–10]. The decline of squamous cell carcinoma follows the trend of declining smoking prevalence in industrialized countries [2].

As incidence and mortality data indicate, lung cancer is one of the most aggressive cancers and has an unfavorable outcome. Classical treatment options for lung cancer include surgical resection or chemo- and radiotherapy, depending on clinic-pathological variables. For patients with early-stage lung cancer, surgical resection is the optimal treatment option, while patients with locally advanced or metastatic NSCLC and most SCLC patients are treated with chemo-radiotherapy. However, in the last decades, significant progress has been made in understanding the molecular pathogenesis of lung tumours, both NSCLC and SCLC groups. Even SCLC, which was previously thought to be uniform, has been shown by recent data to be divided into at least 4 distinct molecular subgroups [11].

Thanks to the massive increase in genetic and immunological knowledge the variety of treatment methods has also shifted over the decades. Therapeutic targeting of the EGF-receptor introduced the era of biological therapies, and a growing list of specifically acting agents is now effectively used in selected cancer patients. So-called oncogene-addicted NSCLC is a molecular genetically distinct group of lung cancers in which well-defined driver mutations direct the pathogenesis, and pharmacological blockade of this target is expected to result in a significant therapeutic response. These patients also form a clinically well-defined group, mostly non-smokers, female predominance, and a relatively younger age are the main characteristics.

The frequency of currently known clinically significant driver gene defects is shown in Figure 1.

In addition, another group of lung tumours is also emerging, lacking targetable driver mutations to our present knowledge. However, due to marked immunogenicity, these patients may well benefit from immune checkpoint inhibitor therapies [12].

The introduction of molecularly targeted therapies promise a major advance, however lung cancer still has a poor prognosis and the 5-year survival rate remains at a very low level, the 5-year OS was 10.7 in 1973 for all lung cancer patients, which increased to 19.8% in 2010 [13, 14]. As seen in Western countries, survival rates for lung cancer patients in Central Europe have improved over the past decade, particularly after the introduction of immunotherapy. For non-squamous NSCLC, the 3-year survival in 2019 was 28.7% compared to 14.5% in 2011, and for squamous cell carcinoma 22.3% versus 13.37%. Unfortunately, for SCLC, there was no significant improvement over the study period [15].

The emergence of new molecular targets has also challenged diagnostic pathology by requiring the identification of appropriate predictive biomarkers and by the development of reliable, cost-effective testing options.

In this study, we aim to review the main events in the molecular pathogenesis of NSCLC also serving as therapeutic targets. Furthermore, we aim to present the status of biomarker testing options.

Gene mutations and copy number changes

EGFR mutations

Adenocarcinomas harbor mutations of genes of EGFR signaling pathway. EGFR belongs to the epidermal growth factor RTK (receptor tyrosine kinase) family. The EGF receptor has an extracellular ligand-binding, a transmembrane and an intracellular domain, the latter having tyrosine kinase

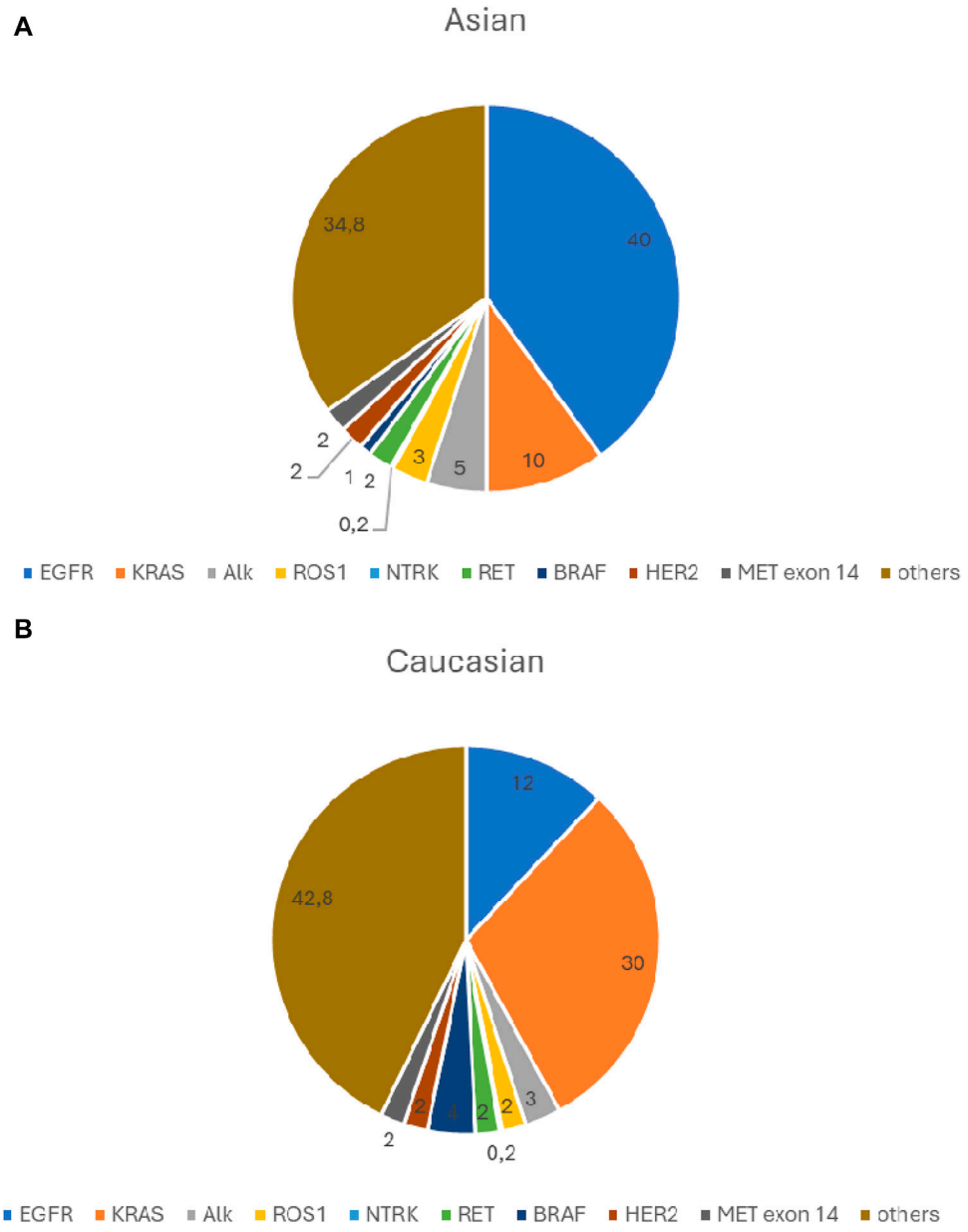

FIGURE 1
(A) Significant driver gene defects frequency- Asian population. **(B)** Significant driver gene defects frequency- Caucasian population.

activity. The intracellular protein kinase domain contains a small N-terminal lobe and a larger C-terminal lobe. The two parts form the active site cleft that serves as a binding site for ATP. In physiological conditions the extracellular ligand binding (EGF) activates the receptor and the downstream signaling results in cellular transactivation, cell proliferation and survival.

The use of the EGFR receptor as a potential therapeutic target was already suggested in the 1980s by Mendelshon and colleagues [16, 17]. As in many other tumors, EGFR expression has been shown to be increased in lung adenocarcinomas, an early event in carcinogenesis [18]. In 2002, the first data on an EGFR inhibitor treatment in NSCLC were published [19, 20]. The first clinical results showed considerable variability in the response rate [21, 22]. Benefits were mostly observed in non-smokers, women and in the Far Eastern population. The level of EGFR expression detected by immunohistochemistry has not been shown to be of predictive value [23, 24]. Mutations in EGFR were first identified in 2004 and have also been associated with response to therapy [25–27]. All the detected genetic abnormalities were

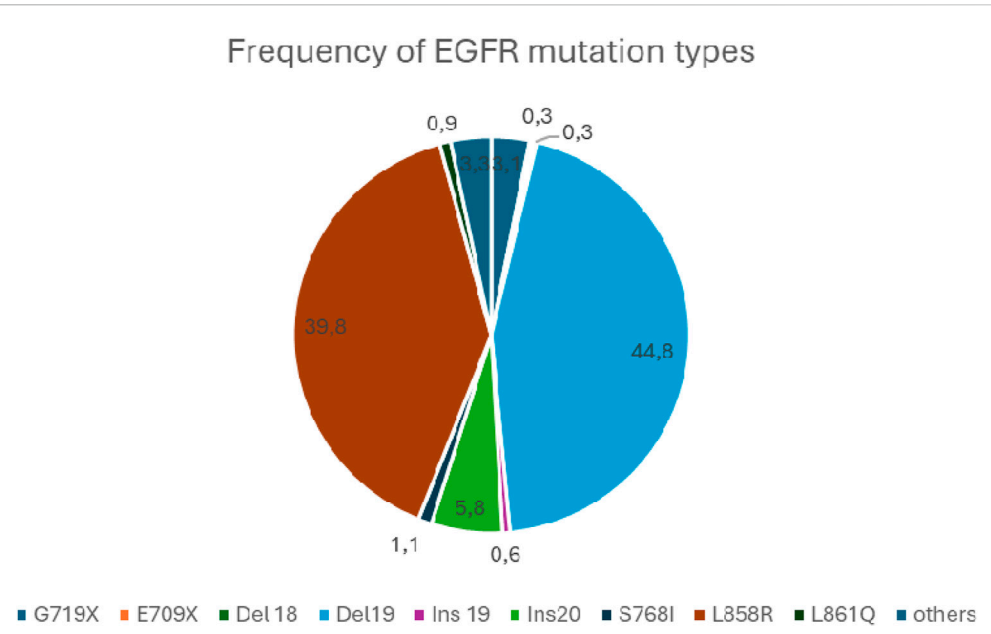

FIGURE 2
The relative frequency of EGFR mutations.

heterozygous, and wild-type EGFR was found in normal lung tissue adjacent to the tumor, suggesting that these mutations are somatic [25]. The EGFR mutation could also be detected in the benign epithelium surrounding the tumor, demonstrating that it is an early event in carcinogenesis [28]. Mutations were demonstrated to affect the kinase domain of the receptor protein causing constitutive activation and downstream signaling in the absence of the receptor ligand. Women and never-smokers were preferentially involved. EGFR mutations show ethnic differences, prevalence ranges 10%–15% in Caucasians and 30%–40% in Asians [29]. Genetic alterations of other major oncogenes, such as KRAS, ALK, ROS1 are mutually exclusive with EGFR mutations. Among adenocarcinomas EGFR mutations are frequently detected in cases with lepidic and papillary growth patterns. The two most common mutations, the so called classical EGFR mutations are i) mutation at codon 858, replacing leucine 858 with arginine (L858R) and ii) the in-frame deletion in exon 19 causing removal of amino-acid residues 746–750 of the expressed protein [30]. These two mutations account for 85%–90% of all EGFR mutations.

Both classical EGFR mutations affect the kinase domain. In the inactive form of the wild-type EGFR molecule an outward rotation of the alphaC helix in the N lobe is provided, which is stabilized by the helical turn of the A-loop. This conformation inhibits the association of amino acids K745 with E762 and the consecutive binding and orientation of ATP. The L858R mutation occurs in the C lobe N-terminal portion of the activation loop resulting the destabilization of the inactive state thereby promoting the conversion in a more active state [31, 32]. The deletion in exon 19 (746ELREA750) occurs immediately before the αC-helix in the N lobe and desrupts the inactive conformation through the shortening of the alpha C loop. The L858R mutant is approximately 50-fold more active than the wild-type enzyme, and the G719S mutant shows about ten times more activity over the wild-type.

In addition to the classic mutations mentioned above (L858R and del19), about 600 other rare EGFR mutations have been described, accounting for about 10%–15% of all EGFR mutations [33]. These include exon 18 E709x, del18, G719x, exon19 insertion, exon20 insertion, and S768I, as well as L861Q affecting exon21. Of these, exon 20 insertions are the most common (4%–10% of all EGFR mutations).

The relative frequency of EGFR mutations based on the COSMIC database is shown in Figure 2 [34].

EGFR mutations show variable sensitivity to EGFR tyrosine kinase inhibition. The specific genotype obtained by DNA sequencing gains special importance as the type of mutation carries the basic potential of resistance to given inhibitor agents. It is of note that resistance or low response to TKI today indicates the consideration of an alternative inhibitor. No response to EGFR TKI treatment has been observed in case of exon 20 insertions [35] except A763-Y764insFQEA [36–38]. For others, the therapeutic effect is less than observed for the classical mutations, e.g., G719x, exon 19 insertions, S768I, L861Q. For these mutations 2nd generation TKI treatment may show improved results.

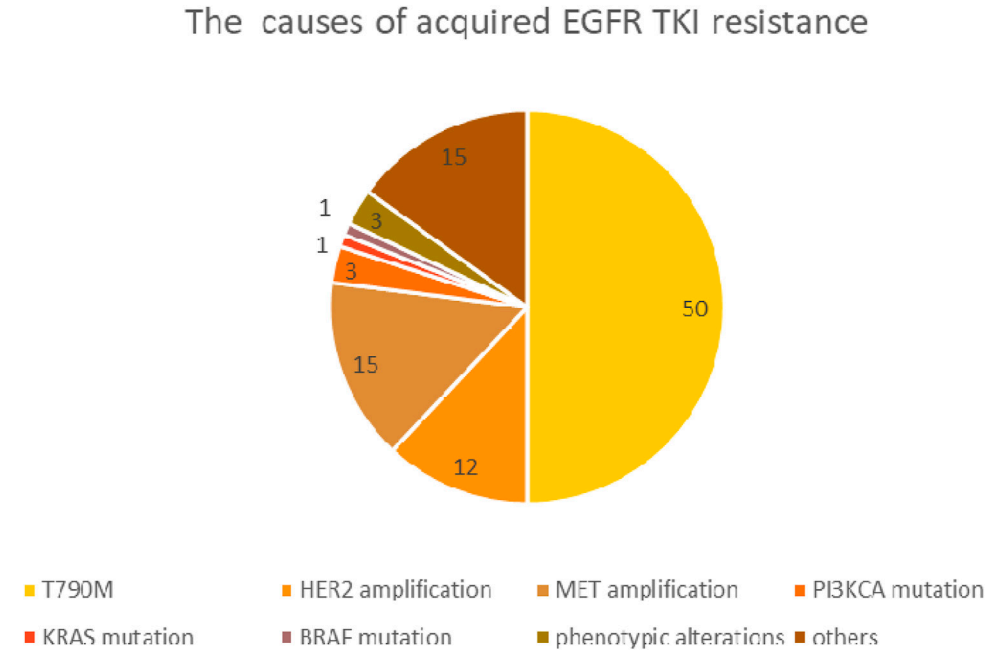

FIGURE 3
The most common causes of acquired EGFR TKI resistance.

Germline mutations of the EGFR gene were also described [39], which, if present, increase the incidence of adenocarcinoma, mostly in the presence of additional somatic mutations. The 4 most common germline mutations are T790M (which is one of the most important causes of acquired TKI resistance), V843I, R776H, P848L, all point mutations.

An EGFR activating mutation is a prognostic factor indicating unfavorable outcome. On the other hand, it is a factor predicting the response to tyrosin kinase inhibitor treatment. T790M mutations and mutations in exon 20 are associated with resistance to tyrosin kinase inhibitors.

Although EGFR-TKI treatment has been shown to be effective in most patients with EGFR mutant lung adenocarcinomas, no response is observed in 5%–25% of patients due to intrinsic resistance to these drugs. In addition to the pharmacokinetic complications of the drug, intrinsic resistance is frequently due to some genetic variation. These include most of the exon20 insertions, with the exception of A763-Y764insFQEA- [36–38], T790M, exon 2-7 variant III(vIII) in frame deletion [40] and some other secondary genetic events.

Patients with an initially good therapeutic response may show unfortunate disease progression after 9–19 months of treatment initialization due to acquired resistance (first line TKI: 9–12 months, 19 months first line third generation TKI) [41, 42]. Acquired resistance is often the result of a secondary EGFR mutation, while in many cases it occurs due to activation of an alternative signaling pathway. The most common (49%–63%) acquired mutation is T790M, which results in a threonine-methionine substitution at position 790, the ATP binding site of the receptor protein. This amino acid exchange prevents EGFR-TKI from binding to the kinase domain and results in increased ATP affinity. Further to *de novo* mutagenesis it is assumed, that a co-existing, drug-resistant EGFR T790M positive subclone has been selected by TKI treatment. In addition to the T790M mutation, EGFR gene amplification and several rare second/third EGFR mutations are considered as resistance mechanisms, including the C797S, L792, L718Q, SV768IL genotypes. The activation of alternative signaling pathways may also occur through a gene amplification, such as MET, HER2 or other rare gene mutations. Resistance may also result from tumor phenotypic alterations, such as transformation towards squamous or small cell carcinoma and epithelial-mesenchymal transition [43, 44]. The most common causes of acquired EGFR TKI resistance and their relative frequency are shown in Figure 3.

It is surprising that, despite the wealth of data that has been accumulated on the incidence and therapeutic significance of EGFR mutations, very little is known about the origin and causes of EGFR mutations. Few publications correlate different etiological factors and EGFR mutations. It appears that air pollution, including exposure to microparticles, can induce EGFR mutations [45]. In addition, exposure to radon in the residential environment may also have a potential EGFR mutation-inducing effect [46].

EGFR genotyping is generally based on sequence analysis of tumor DNA isolated from biopsy samples. As a fast alternative approach to predict the efficacy of EGFR inhibitory treatment, the expression of total EGFR protein was first attempted for immunohistochemistry, but as already mentioned, this remained inconclusive [23, 47] Mutation-specific monoclonal antibodies against exon 19 E746-A750del and exon 21 L858R mutations are available, which represent approx. 90% of all EGFR mutations (clone 6B6 for exon19 deletions; and clone 43B2 against point mutation of exon21 L858R, Cell Signaling Technology) [48]. Tests with these antibodies have shown relatively high sensitivity and specificity for the two mutations indicated, especially for L858R. The lower sensitivity for exon19 deletions is mostly explained by the fact that the exon19 antibody only detects the most common deletion of exon19 (deletion E746-A750). This deletion is of 15 base pairs and represents 50%–65% of all exon19 deletions. However, a variety of deletions, including 9, 12, 16, 18, and 24base-pairs variants have been identified, each producing slightly different protein and antigen epitope structure not detectable by the commercial exon19 antibody [49]. According to the literature the EGFR mutation-specific antibodies have a fair sensitivity and high specificity in identifying lung adenocarcinomas with classic EGFR mutations, while they do not recognise uncommon EGFR mutations. They did not provide sufficient sensitivity (about 40%–60%) or specificity (70%) for the detection of all EGFR mutations, compared to gold standard sequencing methods [50–53]. Sanger DNA sequencing has been widely used, but its disadvantages, primarily its low sensitivity (requirement of 40%–50% mutant DNA in samples) [54], has before led to the development of more sensitive detecting methods including real-time quantitative PCR (RT-PCR). However, this method is relatively expensive, time consuming, and not incorporated in routine diagnostic procedures in many departments of pathology. In contrast, immunohistochemistry has lower costs, shorter turnaround time, and is available in the majority of laboratories. IHC is a rapid, cheap and well-known assay that does not require huge tumor cell content and performs quite well even in degraded tissue (e.g., decalcified bone tissue) or cytology samples. EGFR-mutant-specific antibodies cannot replace conventional molecular methodologies, but they could be very helpful in small tumor samples with poor material [53].

KRAS mutations

KRAS is one of the longest known oncogenes and activating mutations play a crucial role in the early oncogenesis of several types of tumors, such as pancreatic ductal adenocarcinoma, colon cancer and lung cancer [55]. HRAS and NRAS are the other two members of the RAS gene family with clinical impact [56]. The human homologue of the RAS gene, HRAS, located on the short arm of chromosome 11 at position 11p15.1-11p15.3, was first described in the early 1980s in a human bladder cancer cell line. A short time later KRAS, a gene showing homologue features was detected in lung adenocarcinoma, located on the short arm of chromosome 12 at position 12p11.1-12p12.1. The NRAS gene is located on chromosome 1 [57]. All three RAS genes have 4 exons and broadly similar structures [58]. The KRAS gene encodes two protein isoforms composed of 188 and 189 amino acids (KRAS-4B and 4A), the single amino acid difference is a result of alternative splicing [59]. The KRAS protein is a cell membrane-associated G protein with GTP-ase activity [60,61], coupling cell surface growth factor receptors such as EGFR to various intracellular (mitogenic) signaling pathways. The most common signaling pathways involved are the mitogen activated protein kinase (MAPK) [62, 63] and phosphatidylinositol 3-kinase (PI3K) pathways [64]. The active RAS protein binds GTP, in which guanine nucleotide exchange factors (GEFs) participate through GTP-GDP exchange. GTPase activating proteins (GAPs) inactivate RAS by enhancing the GTPase activity of the RAS [60, 61, 65]. RAS gene mutations at specific sites result in spontaneous activation of the RAS protein without mitogen signaling, leading to uncontrolled cell proliferation and cell survival. As these play an important role from the earliest phase of carcinogenesis they are called oncogenic, or hot-spot mutations [55, 66] In the case of KRAS G12C or G12V mutations, intracellular levels of RAS-related proteins (RALs) are elevated and AKT phosphorylation is reduced [67].

The earliest and most frequent mutations in lung adenocarcinoma occurs in the KRAS gene and affects the EGFR/RAS/RAF signaling pathway [68–70]. The prevalence of the KRAS mutation is around 30% in the Western population, compared to around 10% in the Far East. In lung cancer, mutations in NRAS or HRAS are rare, with a prevalence of less than 1% each. The vast majority of KRAS mutations (about 80%) affect codon 12 within exon 2 of the gene and is close to the section encoding the nucleotide binding site of the KRAS protein. The most common change of codon 12 mutations is a G>T transversion, which results in a glycine-cysteine (G12C) or glycine-valine (G12V) substitution at the protein level. Another type of codon 12 mutation is G>A transition, replacing amino acid glycine by aspartic acid (G12D). Less frequent codon 12 mutations are also known: G12A, G12S, G12R, G12F. Occasionally, mutations can be detected in codon 13 (G13C) or codon 61 (Q61H) [71].

Mutations generally inhibit the interaction of KRAS with GAPs and the hydrolysis of GTP bound by KRAS, thereby keeping the KRAS protein in an active conformation [72]. Different mutations activate different intracellular signaling pathways to different degrees. In KRAS G12C mutant tumors, the classical mitogenic signaling pathway (RAS-RAF-MEK-ERK) is activated, whereas the PI3K-AKT-mTOR pathway is dominant for the other mutant genotypes. This may be due to a different RAF affinity in each mutation type [73] The G>T transversions

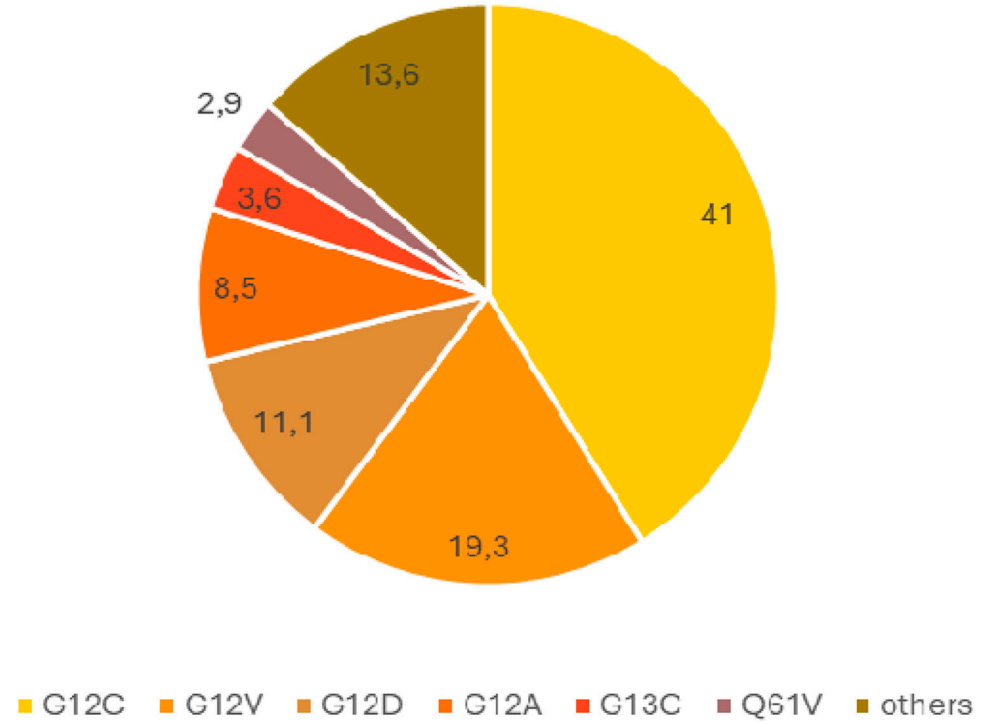

FIGURE 4
Average relative frequency of the most common KRAS mutation types.

resulting in G12C exchange are supposedly associated with polycyclic aromatic hydrocarbons (PAH) exposure in tobacco smoke. On the other hand, G>A mutations resulting in KRAS G12D are more common in non-smokers. The prevalence of KRAS mutations is 40% in heavy smokers, 30% in former current non-smokers and 20% in never-smokers [74]. The most common type is G12C, which accounts for 40% of all KRAS mutations, while G12V and G12D account for 19% and 11%, respectively. The average relative frequency of KRAS mutation types, based on large databases, is shown in Figure 4.

There are also significant geographical and social differences in the prevalence of KRAS G12C, with a higher prevalence in Western countries and a lower prevalence in the Far East (8.9%–19.5% and 1.4%–3%, respectively), which may be related to smoking habits. Our own observation also suggests this, as KRAS G12C is more common in Eastern Hungary, the care area of our centre, than in the better developed western part of the country, which may be explained by the smoking habits of the population here (unpublished data). Although KRAS mutations, especially G12C, are strongly associated with smoking, KRAS mutations are surprisingly unfrequent in small cell lung cancer, which occurs almost exclusively in heavy smokers [74, 75]. In squamous cell carcinomas, which are also strongly associated with smoking, the occurrence of KRAS mutations is rare or only occurs in mixed tumors, such as adenosquamous carcinoma [71]. The frequency of KRAS mutations also varies in the histological subtypes of adenocarcinoma. KRAS mutations are most often detected with mucinous morphology, but different genotypes show variable frequencies (G12C rarely, whereas G12V and G12D more often) [76]. Among mucinous tumors, KRAS mutations are almost exclusively found in invasive mucinous adenocarcinomas (69%), with no KRAS mutations detected in adenocarcinoma *in situ* and colloid carcinoma. However, mucinous carcinomas do not harbour EGFR mutations [77]. Interestingly, the KRAS mutation is more common in women [78]. The metastatic pattern of the tumor also differs with the mutant genotype, with G12C tumors having a higher incidence of intrapulmonary metastasis (38% vs. 21%) and a lower incidence of pleural metastasis (4% vs. 39%). It was also observed that brain metastasis is less frequent in KRAS mutations (33% vs. 40%), but the frequency of brain metastasis is similar for each KRAS mutation type [79, 80].

The presence of EGFR and KRAS mutations are mutually exclusive. In theory they affect the same signaling pathway and the presence of one mutation is sufficient for tumourigenesis. Despite this generally accepted view, KRAS and EGFR mutations can rarely occur within the same tumor [76, 81]. A recent large retrospective study of data from 3,774 patients found the concomitant presence of two or three driver mutations in 1.7% of cases, most commonly EGFR/KRAS mutations (in 0.53% of cases). It should be noted that this study examined a patient population from the Far East, where the prevalence of EGFR mutations is inherently high, 43% in this study [82].

The particular role of KRAS in tumorigenesis is also suggested by the observation that in one of the most common congenital pulmonary malformations, congenital pulmonary airway malformation type I (CPAM), KRAS mutations (G12V or G12D) are often detected, predominantly in intracystic mucinous cell clusters. In fact, these mutations can be identified in nonmucinous cystic regions as well, but not in healthy lung tissue. In these patients, KRAS mutant adenocarcinoma of mucinous character frequently appears later, indicating to the oncogenic nature of the mutation [83–85].

The prognostic role of KRAS mutations in lung adenocarcinoma has long been the subject of intensive studies. Although many data have been published on this issue, its prognostic significance is still not clearly understood. Investigations of prognostic significance are complicated by the fact that the term "KRAS mutation" itself is not uniform, mutation types, ethnic, gender and histological differences as well as treatment mode should also be considered. In addition, other genetic abnormalities, such as EGFR mutations, modify the behavior of KRAS wild-type cases and affect prognosis [86]. However, most of the large case-control studies published in recent years support the hypothesis that the presence of KRAS mutations, particularly KRAS G12C mutations, has a negative prognostic significance, and reduce both OS and PFS [87–90]. There is also evidence that increased mutated KRAS levels in circulating tumour DNA also have a negative prognostic significance [91].

The predictive significance of the KRAS mutation has also been extensively studied. Many reports suggest that mutant KRAS is not a negative predictor of conventional chemotherapy [92] However, as with prognostic significance, the question is more nuanced, with many factors to consider, such as the type of KRAS mutation, the patient population studied and treatment characteristics. In early-stage resected NSCLC patients, no significant predictive value of KRAS mutation status was found for adjuvant treatment [93], and similar results were obtained in the neoadjuvant setting [94]. A more recent study showed that KRAS mutation is a negative predictor of cytotoxic chemotherapy in advanced NSCLC [95].

Another important question is the impact of KRAS mutations on targeted therapies, especially EGFR targeting. Many conflicting observations have been reported on this topic, too. Most studies have shown that the presence of a KRAS mutation has a negative predictive effect in this respect, EGFR TKI treatment in these patients having a worse objective response rate. However, no difference in survival has been found between KRAS mutant/EGFR wild-type and KRAS wild-type/EGFR wild-type patients, therefore, the significance of KRAS mutation to select patients for EGFR TKI treatment appeared to be limited [96]. The results of individual studies are significantly affected by the type of KRAS mutation present: while poor treatment efficacy is seen with G12C and G12V, better response rates are seen with G12D and G12S [97].

Testing for KRAS mutations is possible from tumor DNA isolated from tumor tissue, bronchial brush smears, plasma or pleural fluid (cfDNA analysis), using either a single-gene PCR-based approaches, classical or a next-generation sequencing [98, 99].

BRAF mutations

BRAF is a member of the rapidly accelerated fibrosarcoma (RAF) kinase family. Its role is signal transduction from the RAS protein to the mitogen-activated protein kinase cascade (MAPK) [100]. The RAF protein is composed of three main domains: CR1, CR2, CR3. CR1 functions as an auto-inhibitor of the kinase CR3 domain and is also responsible for RAS-GTP binding. The CR2 region forms a flexible link between the CR1 and CR3 domains. Upon activation the RAS-GTP binds to the RAS-GTP binding site (RBD) of the CR1 domain. BRAF is then phosphorylated on amino acids T599 and S602, which results in a protein conformational change. This active form homo- or heterodimerizes with other RAF family proteins, also contributing to the stabilization of the active conformation. The results is the activated BRAF kinase domain, which phosphorylates MEK1, the downstream member of the MAPK signaling pathway [101].

BRAF is one of the most frequently mutated genes in human tumors. Mutations are most frequently detected in melanoma (40%–50% of cases), but are also common in papillary thyroid cancer, colorectal cancer and NSCLC [102–105].

(It is interesting to note that Davies [102] was the first to report the BRAF mutation, but in her publication she uses a different nomenclature, V599E, to refer to the mutation he detected - now called V600E-because the sequence of the protein had previously been misinterpreted, A31 G32 A33 was mistaken for R31 P32. Because A33 was missing from earlier sequences, some studies incorrectly assigned wrong numbers to coding mutations and amino acids.)

BRAF mutations most commonly occur at codon 600 in exon 15 of the gene, resulting in the exchange of amino acid valine to glutamate (V600E) of the protein. Other substitutions, such as V600D/K/R, can be also rarely seen at this site. These mutations are also known as class I mutations [106]. The V600E mutation

results in a marked increase in BRAF kinase activity (up to 500-700-fold compared to wild-type BRAF), with a consequent stimulation of the MAPK signaling pathway. The V600E mutation results in the conformational change of the monomer BRAF protein already possessing with an active kinase function that would otherwise gain through dimerization of the wild-type conformation [107]. In melanoma, V600E is the most common BRAF mutation, whereas in NSCLC only half of the mutations affecting BRAF belong to this group. NonV600E mutations form a heterogeneous group and can be further classified into class II and class III [101].

BRAF mutations play an important role in lung carcinogenesis, as also demonstrated experimentally *in vivo* [108]. Data from large case-control studies suggest that BRAF mutations occur in 2.2%–4.9% of NSCLC. Owsley found 772 BRAF mutations (4.1%) out of 18,944 NSCLC cases, of which 30.7% (237 cases) were V600E mutations [103]. In Villaruz's study, 21 cases (2.2%) of 951 adenocarcinomas proved to be BRAF mutant, 81% of which were V600E [109]. V600E mutations occur mainly in women, non-smokers, are associated with micropapillary morphology and have a worse prognosis than wild type [110]. Non-V600E mutations are exclusively detected in smokers, in equal proportions in men and women, and are not associated with a prognosis worse than the wild type (Marchetti, 36 BRAF mutations detected in 739 adenocarcinomas- 4.9%- of which 56.8% were V600E) [111]. The results of individual studies are contradictory regarding the prognostic role. Villaruz et al. observed a better outcome for V600E, while others did not observe any difference in prognosis [109, 112] The contradictory results are likely explained by the fact that BRAF mutations are relatively rare and only small cohorts of patients could be examined despite extended studies. Co-mutations are relatively common, mainly mutations in KRAS and PI3K, while in nonV600E, mutations in p53 and STK11 are common [106].

The conformational change through the mutation enables the differentiation of the BRAF protein from the wild-type form. Thus, the BRAF status can also be assessed by immunohistochemistry for V600E mutations. The commercially available monoclonal diagnostic antibody was raised against a synthetic version of the V600E-encoded protein fragment located around the amino acid affected by the mutation [113]. This antibody detects the BRAF V600E mutant epitope with sufficient sensitivity and specificity, as has been demonstrated in several tumor types such as colorectal carcinoma, papillary thyroid cancer and melanoma [114–118] However, it is not applicable to V600D/K/R or class II and III non-V600E mutations. Since almost half of the BRAF mutations in NSCLC are nonV600E, the IHC test is of limited use to identify tumors harbouring BRAF mutations. However, according to current NCCN recommendations, specific TKI inhibitor treatment should be used for V600E mutation positive tumors [119]. Thus, the IHC methodology may be considered as a screening test for the identification of these patients in histological conditions. In addition, the same guidelines (and updated version also) recommend an NGS-based methodology to determine a comprehensive BRAF status [120].

Gene fusions with clinical relevance

In addition to the now "classic" MAP-kinase pathway mutations, several clinically relevant chromosomal rearrangements have also been identified in NSCLC. It has long been known that specific gene fusions determine the development of several haematological malignancies and sarcomas. The earliest such gene fusion identified was bcr-abl characteristic for chronic myeloid leukaemia, discovery finally leading to the pioneering concept of tyrosine kinase inhibitor therapies [121]. Oncogenic gene translocations play a special role in NSCLC carcinogenesis, especially if their functionality can be therapeutically blocked. The most important ones are ALK, ROS1 and RET rearrangements and the significantly less frequent NTRK gene fusions, with prevalence rates of 4%–6%, 2%, 1%–2% and 0.1%–0.23%, respectively. These fusions occur in a patient population clinically distinct from classical NSCLC (predominantly younger, non-demented patients with adenocarcinoma histology).

Due to the availability of effective targeted TKI drugs with FDA or EMA approval it is particularly important to identify these patients within the confines of predictive molecular testing. The selection of sufficiently effective and validated, yet rapid and not least relatively inexpensive methodology is a major challenge for pathology laboratories and molecular geneticists. In addition to the "big four," additional gene fusions have recently become known, such as those involving NRG1, SMARCA4, BRAF, FGFR1 and EGFR, further complicating the everyday molecular diagnostic practice of NSCLC.

ALK rearrangements

The ALK gene (anaplastic lymphoma kinase) was discovered as a result of genetic studies in anaplastic large cell lymphoma. The gene is located on the short arm of chromosome 2, in the 2p23 region. As a member of the insulin receptor superfamily, ALK encodes a tyrosine kinase-activated transmembrane receptor protein whose function is only partially understood. In humans, ALK expression is detected intermittently during neural development, with a decline in expression during postnatal life. In adults, it is expressed only scattered in some neurons, endothelium and in pericytes of the brain. The ALK protein contains an extracellular ligand-binding, a transmembrane, and a cytoplasmic kinase domain [122]. The

ligand(s) for the ALK receptor have not been unequivocally identified. The role of pleiotrophin, midkine was hypothesized [123], followed by other candidates, including heparin, FAM150A and FAM150B [124].

The main types of ALK gene alterations include rearrangements (fusions), gene amplification, and point mutations [125].

Fusions of the ALK gene, like the amplification of the gene leads to constitutive activation. Amplification of ALK has been detected in neuroblastoma [126] breast cancer, anaplastic large cell lymphoma and pulmonary sarcomatoid carcinoma [127]. On the contrary, point mutations are the most common causes of resistance to ALK TKI treatment. Known resistance mutations are G1269A, C1156Y, L1196M and several other point mutations [128, 129].

The 2p chromosomal region is sensitive to genotoxic effects, favoring the breakage of the ALK gene, with the result of gene fusions and increased expression of the kinase domain of the ALK protein. In 1994, a t [2, 5] translocation was first described in anaplastic large cell lymphoma, resulting in an NPM (nucleophosmin)-ALK fusion gene, an event that is detected in 60%–80% of ALCL [130]. It has subsequently been described in additional tumors: e.g., inflammatory myofibroblastic tumor [131], colorectal and breast cancer, and esophageal squamous cell carcinoma [132]. Further fusion partners were later identified. The setup of the rearrangements is common in that the breakpoint leaves the entire ALK tyrosine kinase domain intact, while the promoter region always comes from the fusion partner. The fusion partner also contains an oligomerization domain, the presence of which allows ligand-independent constitutive activation of the receptor protein.

In 2007, Soda and colleagues detected the EML4 (echinoderm microtubule associated protein-like 4)-ALK gene rearrangement in NSCLC. This gene rearrangement is caused by an inversion of the chromosome region 2p21-23. The extracellular and transmembrane regions of ALK are replaced by EML4. There are various EML4 breakpoints and therefore, several variants of the fusion gene are known [133]. The EML4-ALK gene rearrangement results in constitutive activation of ALK RTK, an oncogenic pathway in NSCLC. The resulting EML4-ALK fusion gene product represents a novel molecular target for the treatment of non-small cell lung cancer. ALK gene rearrangement occurs in 3%–6% of all NSCLC. It is typically associated with adenocarcinoma morphology (including papillary, mucinous, and squamous cell variants) [134]. Detected mainly in non-smokers or light smokers and typically in young patients. ALK gene rearrangement, EGFR and KRAS mutation are mutually exclusive events [135].

The demonstration of EML4-ALK gene rearrangements was challenging due different variants of the fusion, requiring multiplex testing in the PCR era. FISH-based detection could be adopted with satisfying efficacy since the 3′and 5′ends of the ALK gene get separated due to the rearrangement, and their labelling with separate fluorescent probes result in the characteristic split signal. Currently, the FISH test is the gold standard for the detection of ALK rearrangements in clinical samples, requiring specific probes, fluorescence equipment and properly experienced pathologist.

Because of the above drawbacks, an immunohistochemical alternative for the detection of ALK gene involvement has been attempted. This assumes that ALK protein is not expressed in normal lung tissue, but gene fusion and ALK gene activation result in moderately increased expression of ALK protein. However, the detection of the protein underwent an evolution. A “traditional” diagnostic antibody (ALK1) previously used for anaplastic lymphoma was not sufficiently sensitive (sensitivity 67%, specificity 97%). However, the release of new antibody clones promptly followed [5A4, D5F3, anti-ALK (1A4)] and the use of highly sensitive amplification systems allowed to achieve adequate sensitivity and specificity. The advantage of IHC testing is its low cost, wide availability and rapid turnaround time. In immunohistochemistry, the ALK fusion protein shows granular cytoplasmic staining. In signet ring cells (a morphology often seen in ALK-positive adenocarcinoma), staining is present along the membrane in a thin rim that can be difficult to distinguish from background staining. Several studies have demonstrated that the use of properly validated antibody and immunohistochemical platform, together with an external control (e.g., appendix with intense ALK positivity in the ganglion cells of the wall), provides a highly reproducible result. The study of Mino-Kenudson et al. in 2010 (n = 153, sensitivity 100%, specificity 99.0%) using clone D5F3 [136] and that of Paik et al. in 2011 (n = 735, sensitivity 100%, specificity 96.2%) using clone 5A4 both showed high concordance between Ventana IHC and FISH results [137].

The high sensitivity of IHC to detect ALK aberrations is today generally accepted. Despite the rare IHC negative but FISH positive cases published in the literature, the current recommendations accept the use of IHC methodology without FISH confirmatory testing in histological specimens [138] as well as in cell block specimens prepared from malignant pleural effusions [139]. However, the IHC methodology is neither perfectly applicable nor validated in large series on bronchoscopic brush cytology specimens. For cytology preparations the FISH break apart test should primarily be chosen.

ROS1 rearrangements

The ROS1 gene is located on chromosome 6 in the 6q22 region. The gene was originally discovered in the 1980s during the study of avian sarcoma viruses. The human ROS gene is homologous to the v-ros proto-oncogene of the UR2 sarcoma virus [140, 141]. The protein contains an extracellular and an intracellular domain, the latter having tyrosine kinase activity

with structural similarity to the ALK protein. The physiological role of the ROS1 gene and protein is poorly understood, but it is thought to be involved in differentiation signaling pathways of various epithelial tissues during embryonic development [142]. ROS1 protein expression is observed in the kidney, the cerebellum, the peripheral nerves, various parts of the alimentary canal, but is not expressed in lung tissue under normal conditions [143]. The physiological ligand of the receptor is still debated. The structure of the extracellular domain suggests that cell adhesion plays a role in its activation [142] The intracellular signaling pathways activated by ROS1 are also not well understood, but induction of MAPK and PI3K pathways is hypothesized [144]. Its oncogenic relevance was first demonstrated in the early 2000s in glioblastoma [145]. In lung tumors, rearrangements affecting ROS1 gene were first described in 2007 [146]. ROS1 involvement was observed in 1%–2% of NSCLC [147]. As a result of the rearrangement, various breakpoints in the ROS1 gene may evolve, including exons 32, 34-36, or introns 31 or 33. The fusion gene commonly contains the tyrosine kinase domain of ROS. There are 9 different fusion partners known in lung cancer, such as FIG, CD74, SLC34A2 and SDC4, EZR and the list is growing [148, 149]. The oncogenic mechanism of gene rearrangement is not understood. ROS1 rearrangements typically occur in lung adenocarcinomas, rarely in adenosquamous carcinoma. These adenocarcinomas generally show a solid pattern, frequently of signet ring cell type. Younger patients and non-smokers are more frequently affected [150]. It is often detected at an advanced stage and brain metastasis is common [151]. Interestingly, lung carcinoma patients with ROS1 gene rearrangements have a higher incidence of paraneoplastic thromboembolic events [152].

Due to the larger set of fusion variants the ROS1 rearrangement can be most effectively demonstrated by FISH analysis, using ROS1 specific DNA-probes and the detection strategy of the ALK testing. Sequencing by different NGS platforms is also applicable if tumor tissue and appropriate amounts of DNA or RNA are provided. Rearrangement of the gene is associated with overexpression of the ROS-protein, allowing the use of ROS1-specific antibodies. For IHC-based diagnostic testing, the use of the D4D6 ROS1 antibody clones is recommended. In positive cases, fine granular cytoplasmic staining is observed. Fusion variants show a different staining pattern, which may be the result of the intracellular function and localization of the fusion partner. For CD74-ROS1, a globular pattern with randomly arranged cytoplasmic granules of 6–8 mm diameter and weaker background cytoplasmic staining was described, explained by the fact that CD74 is associated with intracellular membrane systems. Membranous staining was seen in the presence of EZR-ROS1 fusion, presumably due to the ezrin protein binding to plasma membrane and actin cytoskeleton [153] A uniform scoring system for the ROS1 IHC reaction is still missing, most studies use the H-score calculated from the staining intensity and the proportion of positive tumor cells. With appropriate preanalytical and analytical standards, this antibody can achieve high sensitivity (95%–100%) but relatively poor specificity (63%–90%) [154–157]. The low specificity may potentially originate from a moderate ROS1 expression by macrophages, reactive alveolar epithelium, or even by tumors without ROS rearrangement. A higher cut-off value results in a higher specificity. Overall, the IHC test has a high negative predictive value and is therefore suitable as a screening test, with a negative IHC result virtually ruling out the presence of ROS1 fusion. A positive IHC result requires confirmation by genetic means, such as FISH or NGS technology [158, 159]. Since ROS1 rearrangements are rare, the relatively simple IHC staining is highly effective and avoids the mass need for expensive molecular testing [138, 160].

RET rearrangements

The RET oncogene was identified in the 1980s by transfection of DNA extracted from a human T-cell lymphoma cell line [161]. The RET gene is located on chromosome 10 at position 10q11.22 [162] and encodes a transmembrane tyrosine kinase growth factor receptor. Its extracellular domain contains 4 cadherin-like structures [163]. Its ligand is glial cell line-derived neurotrophic factor [164, 165]. Ligand binding results in dimerization and activation of the receptor, which then activates several intracellular signaling pathways such as PI3K/AKT, RAS/RAF/MEK/ERK or JAK2/STAT3. RET activity is important for kidney and nervous system development, gene expression is precisely regulated in space and time during embryogenesis [165]. RET is required for the proper development of the enteric nervous system, in particular for the migration of neural crest cells and enteric neurons into the wall of the alimentary canal. The absence of RET expression or activity is associated with the development of Hirschsprung disease (segmental aganglionosis of the colon) [166].

Various genetic defects within the RET gene are also related with carcinogenesis. CCDC6-RET fusions have been detected in thyroid cancer as early as in 1990 [167]. Further to oncogenic fusions, activating point mutations of the RET gene are also known. They are involved in the development of medullary thyroid carcinoma and MEN2A syndrome, among others [168, 169]. In NSCLC, RET gene rearrangement was first reported in a Korean non-smoking male patient in 2012 [170–173]. Several large studies have reported that RET rearrangement is present in 1%–2% of NSCLC (Takeuchi 0.9% in 1482 NSCLC, Qiu 1.4% in 1587 NSCLC) [149, 173]. Following the summary of data from 4857 NSCLC patients from previous studies, the prevalence of RET rearrangement proved to be 1.4%, while in the adenocarcinoma group of 3,576 patients 1.8% had RET fusions [174]. KIF5B-RET fusion was observed with the highest prevalence (52%), this type was typical for women, while

CCDC6-RET was mostly observed in men with a prevalence of 26% in total. In addition, several rare fusion partners have been described (MIR392, ZBTB41, ITGA8, SLC39A8 [149]. Along with the RET rearrangements, several other genetic events may be detected; [175]. It is known that RET fusions are responsible for acquired therapy resistance during EGFR TKI inhibitor treatment in 1%–2% of the cases, mainly involving CCDC6 as the fusion partner; [176]. In most RET rearrangements, the transmembrane domain is lost, resulting in a chimeric cytosolic protein that exerts its oncogenic effect through constitutive activation of the kinase domain [161] The majority of RET rearrangements, like ALK and ROS1 fusions, occur in young, non-smoker or mild smoker women with lung adenocarcinoma diagnosis; [173, 177]. This patient group has a significantly higher incidence of brain metastases both at diagnosis (27%) and overall during the course of the disease than the RET wild-type group [178].

The demonstration of RET gene fusions in clinical samples is of great importance, as there are several FDA-approved small-molecule inhibitors promising effective treatment. Initially, non-specific multikinase inhibitors were used, more recently followed by RET-selective inhibitors [179–182].

RET rearrangements can be demonstrated by several alternative methodologies. Although immunohistochemistry is a widely available method and has proven useful in detecting ALK and ROS1 rearrangements, its value in detecting RET fusions is unfortunately limited. The IHC methodology using RET specific antibodies had low sensitivity and specificity, with a false positive rate of 62% and a false negative rate of 46%, in other words, RET rearranged samples could not be equivocally identified. These results have been unanimously confirmed by several studies, and therefore the use of IHC is not recommended for the diagnosis of RET gene rearrangement [183, 184].

On the contrary, the FISH methodology has been shown to be successful in detecting a substantial amount of gene rearrangements. Using RET gene region specific probes FISH had a high sensitivity of 100% for the chimeric proteins KIF5B and CCDC6 but less than 100% for the other partners. On the other hand, a surprisingly poor specificity of 45%–60% was measured, therefore, the currently available DNA probes have not been recommended for routine diagnostics of RET gene fusions [184, 185]. Considering all these issues NGS remains the optimal tool for general RET testing. DNA-based NGS showed a sensitivity of 87.2%–100% for detecting RET fusions, while its specificity was also highly satisfying (98.1%–100%) [186].

NTRK fusions

In humans, three neurotrophic tyrosine receptor kinase (NTRK) genes are known, encoding the transmembrane neurotrophin receptors TrkA, TrkB and TrkC. These Trk receptors are involved in embryonic development of the central and peripheral nervous system [187]. In adults, they are expressed only in neural tissue and skeletal muscle [188]. Ligand-dependent activation of Trk receptors activate several biochemical pathways, including MAPK and PI3K signaling [189]. Chromosomal rearrangements of NTRK genes result in increased expression and/or activation of Trk receptors [190]. The occurrence of NTRK gene fusions is characteristic for some rare tumor types, such as mammary analogue secretory carcinoma of the salivary gland or congenital infantile fibrosarcoma. ETV6-NTRK3 rearrangements are detected in 90% of these cases [191, 192]. Although NTRK gene rearrangements are generally rare, they have been detected in a broad range of common solid tumor types. NSCLC, colorectal carcinoma, GIST, papillary thyroid carcinoma, melanoma, pancreatic adenocarcinoma and gliomas were reported with very rare NTRK involvement of less than 1% of cases [193]. In NSCLC, the incidence rate was only 0.1%–0.3%, an order of magnitude lower than the frequency of ALK or ROS1 gene rearrangements [194]. In two very large NSCLC case-control studies, the rates of NTrk fusions were 0.1% (Gatalica, 4,073 lung adenocarcinomas [195]) and 0.23% (Solomon, 3,993 lung adenocarcinomas [196]). NTRK1 fusion could be demonstrated most (68%), followed by NTRK3 (24%) and NTRK3 fusion as the least common change. Because of the rarity of occurrence, even the largest studies had limitations defining detailed clinical characteristics of patients with NTRK fusions. They suggest equal distribution in both women and men, with a wide age range. The majority of those carrying the fusion are non-smokers, but heavy smokers were not excluded. Most NTRK-positive tumors proved to be adenocarcinomas with mucinous or poorly differentiated morphology, but fusions have also been detected in neuroendocrine carcinoma and even squamous cell carcinoma [197].

Although rare, the identifications of these tumors opens the way for NTRK-targeted TKI therapy, that is available in the last couple of years promising a favorable therapeutic response in patients with NTRK gene fusion [198, 199]. In a 2023 study, 51 patients with advanced NSCLC harboring an NTRK fusion had an ORR of 62.7% following entrectinib treatment, while the PFS and OS was 28.0 and 41.5 months, respectively [200]. Predictive testing of NTRK gene fusion-due to the altogether 3 TrK genes and numerous fusion partner genes-is quite cumbersome, even by the classic FISH arrangement. Due to the 3 independent NTRK gene regions potentially involved, three FISH assays and tests would be required. However, while the detection of fusions involving the NTRK3 gene by FISH had good sensitivity, too many false negative cases were reported for NTRK1 fusion detection. This may be due to intrachromosomal rearrangements involving a short segment, allowing only limited signal separation in the break-apart probe assay, causing interpretation difficulties. Another problem appeared as FISH probes could not detect rearrangements with some fusion partners. Because of these drawbacks, NTRK

FISH were not recommended for routine diagnostics [201]. As an alternative, RNA-based massively parallel sequencing (MPS) is considered as a favorable methodology. However, this technique is not widely available, not mentioning the turnaround time and costs of the test.

Taking everything together, immunohistochemical detection of Trk proteins as a screening test should be considered. Immunohistochemistry is available in virtually all pathology departments, is relatively rapid and inexpensive and sufficiently works with small amounts of tumor tissue. Commercially available diagnostic antibodies detect all Trk proteins. The staining pattern is variable: membrane, cytoplasmic and nuclear positivity can all be present. Unfortunately, a validated scoring system is not available at this time. A positive tumor is defined as one with at least 1% of tumor cell positivity, any kind of positivity more intense than background should be satisfactory, regardless of the staining pattern. Confirmatory testing of positive cases by MPS seems to be necessary for proper interpretation.

According to the literature the sensitivity of the IHC method ranges from 75% to 97% and the specificity is remarkably high, reaching 98%–100% [202–204]. Previous large studies have shown that the sensitivity of IHC is not uniform for the three NTRK gene fusions, 96.2%, 100% and 79.4% sensitivity rates were measured for NTRK1, -2, and -3, respectively, while the specificity was 81.1%. More specifically for the lung adenocarcinoma patient group, IHC sensitivity was 87.5% and specificity 100% [196]. The above large studies all used the Abcam EPR17341 antibody clone. However, in a more recent study, 133 (14.8%) out of 1068 NSCLC cases were panTrk IHC positive, but only 2 cases could be confirmed by RNA-based testing, resulting a positive predictive value of 1.5% for the IHC test applied [205]. Unlike in previous studies, in this work the C17F1 antibody clone was used and any staining was accepted as positive. In conclusion, predictive IHC testing of NTRK involvement also should be performed with care. Sensitivity and specificity rates may be strongly influenced by the type of the diagnostic antibody used. However, sensitivity of IHC supposed to be relatively lower for NTRK3 fusions, the reason of which is not known in detail. If uncovered, low sensitivity of the IHC screening could drop out patients of an effective treatment opportunity.

Novel driver gene defects in NSCLC

MET alterations. Met exon 14 skipping mutations

The mesenchymal epithelial transition (MET) proto-oncogene is located in t4.1he chromosomal region 7q21-q31 and encodes a transmembrane receptor tyrosine kinase protein [206, 207]. The MET protein is expressed in diverse cells of epithelial origin, and is further expressed in liver cells, endothelial cells and neurons. The ligand for this receptor is hepatocyte growth factor (HGF), which is mainly produced by mesenchymal cells, such as fibroblasts [208]. The extracellular part of the receptor protein is responsible for ligand binding and includes domains like the semaphoring and the immunoglobulin-plexin transcription factor domain. The intracellular part is composed of the juxtamembrane domain and the catalytic domain [209, 210]. Ligand binding activates the protein by causing homodimerization, which then leads to autophosphorylation of tyrosine residues in the catalytic domain. Activated MET induces several intracellular activation pathways through MAPK, PI3K, Nf-kB and signal transducer and activator of transcription3 (STAT) signaling. HGF/MET activation plays a key role in epithelial-to-mesenchymal transitions (EMT) by regulating extracellular matrix adhesion and cytoskeletal changes [211, 212]. The deactivation mechanism of the activated signaling pathway deserves attention, as changes in this process play a key role in the carcinogenic effect of MET [213]. After ligand binding, homodimerisation and intracellular signaling the active receptor protein is internalized by clathrin-mediated endocytosis, it is partially degraded but recycling and return to the cell membrane is possible. This process is controlled by ubiquitin ligase casitas B-lineage lymphoma (CBL), which recognizes the Tyr1003 residue encoded in exon 14 of the MET gene and the ubiquitinated MET is degraded by the endosome system [214, 215].

Genetic events may affect MET protein function resulting in oncogenic effects. MET gene amplification results in increased expression and constitutive activation of the kinase protein. This mechanism is supposed to be responsible for acquired resistance during EGFR TKI treatment in 3%–4% of [42, 216, 217]. Various point mutations have also been detected in several tumours, including lung carcinoma, but their oncogenic role remains unclear [218]. Moreover, some gene fusions have also been described, such as KIF5B-MET, which have potential oncogenic effects and serving as therapeutic targets [219].

Exon 14 mutations are the best known MET alterations with pathogenetic and apparently, clinical significance. This specific mutation type is a result of a two base pair insertion in intron 13. The insertion represents an alternative mRNA splicing site with the consequence of the “skipping” of the entire exon 14 during translation for protein synthesis. Therefore, the functional molecule lacks the juxtamembrane segment containing the Tyr1003 residue responsible for the internalisation of the activated receptor. Thus, the exon 14 skipping mutation enhances the stability of activated MET on the surface of the cell, resulting in a prolonged activity of the receptor signaling [220, 221]. According to one of the first large case-control studies, this mutation is present in about 3% (131/4,402) of NSCLC cases [222]. According to a recent large meta-analysis, exon14 skipping mutations can be detected at a rate of 2% in NSCLC, no significant geographical differences are reported. The

prevalence proved to be 12% in non-smokers and 2% in smokers, with a similar overall prevalence of MET14 skipping mutation positive patients with a history of smoking and non-smoking. It is more common in women and at older age (average is 73 years). It is noteworthy that while the histological type of adenocarcinoma has a prevalence of 2.4%, it is detected in 12% of sarcomatoid carcinomas [223]. Association with major driver mutations (EGFR, KRAS, BRAF and ALK, ROS1 gene fusions) appears to be rare, but some other genetic events, such as MET, EGFR amplification, or PI3K mutations may co-occur [222]. Data to date suggest that MET exon 14 mutations in NSCLC are associated with a poor prognosis.

The therapeutic targeting of MET kinase is relevant with multiple TKI drugs (e.g., tepotinib, capmatinib, savolitinib) resulting in good therapeutic response [224, 225]. This is true for the exon-skipping alteration but also for the Y1003N mutation of the juxtamembrane domain, which also inhibits CBL-mediated degradation [222].

Due to the heterogeneity of Met exon 14 aberrations, their detection is another challenge for diagnostic pathology laboratories. Attempts have also been made to detect MET alterations by immunohistochemistry. While overexpression of MET protein can be detected in many tumor types in many cases, MET overexpression can be detected in 35%–72% of NSCLC by immunohistochemistry [226, 227]. Unfortunately, in the majority of IHC positive cases, there is no Met exon 14 skipping or MET amplification. As shown in a recent study, 71 tumors in 181 NSCLC cases had MET overexpression detectable, but only 1% of IHC positive cases had amplification and 3% had Met exon 14 skipping. These results also show that IHC-based detection is not a suitable screening test for MET alterations [228]. RNA-based assays have the highest sensitivity and can detect exon 14 skipping independent of the underlying diverse genetic alterations by detecting fusions of exons 13 and 15 following mRNA transcription. The disadvantage of the RNA-based methodology is its sensitivity to RNA degradation [229]. Unfortunately, amplicon-based DNA NGS tests have a detection rate of only 63% [230], whereas hybrid-capture NGS methodology can achieve better results, but requires larger amounts of sample DNA, which is frequently not provided from small biopsy samples [231]. To overcome this issue circulating free DNA (liquid biopsy) should have lower sensitivity but a high positive predictive value [232].

HER2 alterations

HER2 (ERBB2) is a member of the HER growth factor receptor family. This family also includes EGFR, EGFR3 and EGFR4. The HER2 gene is located in the 17q11.2-q12 region. The encoded receptor protein has an extracellular ligand-binding, a transmembrane and an intracellular tyrosine kinase domain, like other growth factor receptors of the family [233]. It is unique compared to other members of the HER family in that it has no known ligand but has an intrinsic tyrosine kinase activity and is specifically prone to homo- or heterodimerization, which results in its activation. A frequent heterodimerization partner is HER3. Activated HER2 can activate several intracellular signaling pathways such as MAPK, PI3K, and STAT [234].

Several alterations may occur in the HER2 gene, which have oncogenic effects. Gene amplification of HER2 is well known in breast cancer, one of the oldest known therapeutic targets [235], but is also common in gastric [236] and ovarian cancer. HER2 alterations can also occur in lung carcinoma, but gene amplification is relatively rare. However, HER2 amplification in NSCLC may be a potential cause of acquired resistance during EGFR TKI treatment [42]. HER2 amplification is most easily detected by FISH, which is analogous to the common testing practice in breast carcinoma, with a HER2/CEP17 hybridization signal ratio greater than 2. Importantly, HER2 overexpression is often detected by immunohistochemistry, which is usually due to a balanced increase of copy number (polysomy). In this case the HER2/CEP17 ratio does not exceed 2 determined the FISH analysis [237]. Various mutations in the HER2 gene may also occur in the coding regions of all three domains with a rate of 2%–4% of NSCLC. In the first study, published in 2004, HER2 mutations were presented in 10% of the lung adenocarcinomas [238] Subsequently, several studies have reported higher case numbers, with lower frequencies (1.6% testing 671 NSCLC cases) [239]. The most common types of mutations proved to be in-frame insertions in the kinase domain coding region in exon 20. These mutations change the protein conformation and increase kinase activity, thereby activating intracellular signaling [240]. HER2 exon 20 insertions are like exon 20 insertions detected in the EGFR gene [241]. Many of these insertions have been described, the most common being the YVMA insertion, which was detected in 68% of the 98 HER2 mutant tumors detected in a study of altogether 2,788 patients [242]. HER2 mutations occur mainly in women, non-smokers, are associated with adenocarcinoma histology and brain metastasis is common in these patients [243]. Another large study reported HER2 mutations in 24 of 920 patients (3%), 71% non-smokers, 58% women, mean age was 62 years [244]. The co-occurrence of HER2 mutations with other classical driver mutations is virtually excluded [239, 245]. However, some HER2 mutations develop in about 1% of cases of acquired resistance to EGFR TKI treatment [246]. Neither immunohistochemistry nor FISH is suitable for HER2 mutation detection. Since many types of these mutations are known, NGS sequencing methodology is the only effective way of testing [247].

Immune-checkpoint alterations

Modulation of the anti-tumor immune response as another option of anti-tumor therapy becoming part of everyday oncological care. Tumor-related antigens can be recognised by immune cells through the complex process of antigen-presentation and T-cell activation. Ideally, T-cells migrate to the tumor, where they recognise and destroy tumor cells, the efficacy of which is regulated by several receptors and ligands triggering co-stimulatory and inhibitory signals (immune checkpoints). Tumour neoantigens play an important role in the activation of the immune response enabling the separation of tumor from normal cells. The accumulation of mutations in genomically instable cancers is associated with the generation of neo-antigens showing marked immunogenicity. More specifically, the mutational burden is higher in cancers associated with prolonged exposure to environmental carcinogens. Examples include UV radiation in melanoma development, and respiratory carcinogens, primarily polycyclic aromatic compounds in the tobacco smoke, in relation with lung cancer, both small cell and non-small cell type. Increased mutation frequency is a result of insufficient DNA repair mechanisms, e.g., the loss of mismatch repair (MMR) gene functions [248].

The immune checkpoint regulation can be modified by tumor cells, an important immune resistance mechanism. Programmed cell death protein 1 (PD1) is a cell surface immune checkpoint receptor in activated T- and B-lymphocytes, with inhibitory impact on effector cell functions [249]. The PD1 gene is located on chromosome 2 and belongs to the immunoglobulin gene family [250]. The PD1 protein has an extracellular domain consistent with immunoglobulin variable IgV domain, and is featured with an intracellular segment including the immunoreceptor inhibitory tyrosine-based switching motif (ITSM), responsible for inhibition of T-cell activation. The ligand for the PD1 receptor is PD-L1, a cell surface protein containing IgV and IgC domains [251]. PD-L1 can be expressed by T and B cells, macrophages, dendritic cells, and many non-haemopoietic cells. Cells expressing PD-L1 are tolerated by the immune system. Antigen-presenting cells expressing PD-L1 can inhibit T lymphocytes. Thus, the physiological function of PD-L1 is to provide immune-tolerance by inhibiting the adaptive immune response [252]. Unfortunately, tumor cells may also acquire PD-L1 expression in an adaptive or constitutional manner. Adaptive PD-L1 expression occurs in response to interferon-gamma, secreted by T-cells activated by tumor antigens and is mainly observed in the tumor-immune contact zone. Constitutive expression results from activation of various signaling pathways and is uniformly distributed throughout the tumor. Upregulation of PD-L1 ligand by tumor cells inhibits the antitumor immune response in the tumor microenvironment. In many tumor types, including NSCLC, PD-L1 expression is observed in tumor cells, especially in poorly differentiated tumors, and several large meta-analyses have shown that increased PD-L1 expression has a negative prognostic impact [253, 254].

Consequently, the therapeutic blockade of the PD1-PD-L1 relationship represents a promising therapeutic modality in oncology which was outlined by a surprising response in several tumor types from the earliest stage of clinical studies [255]. By now, therapeutic monoclonal antibodies with immune checkpoint inhibitory effect have been introduced for the treatment of a variety of tumor types. However, only about 20% of patients developed an objective response, the rest either having no meaningful effect or developing resistance to treatment. Although ICI treatment does not have serious side effects compared to chemotherapy, characteristic adverse effects may occur, which are often also serious. Therefore, predictive biomarkers for patient selection of PD-L1-PD1 inhibitor treatment would be of particular importance [256]. Unfortunately, there is currently no really good universal predictive biomarker to select patients who could potentially benefit from ICI treatment. In theory, the potential predictive role of factors influencing the tumor-host immune system relationship could be all be considered, including the tumor mutational burden (TMB), the tumor infiltrating lymphocyte (TIL) count, DNA repair systems, in particular mismatch repair and finally the expression of PD-L1. Unfortunately, the predictive clinical value of these factors varies significantly between tumor types.

In NSCLC, the assessment of PD-L1 expression in tumor tissue has been shown to have the strongest predictive value. Early studies have already indicated that the efficacy of PD1 blockade is highly dependent on PD-L1 expression in tumor cells. However, a confusing situation has developed in the field of predictive PD-L1 testing. In a short period of time, four PD1-PD-L1 inhibitor drugs (nivolumab, pembrolizumab, atezolizumab, durvalumab and more recently cemiplimab) have been launched. In parallel, several diagnostic antibodies have been released for the detection of PD-L1 expression. Large clinical studies to test the therapeutic efficacy of their agents applied different antibodies and used different immunohistochemistry platforms. Currently, there are four FDA-approved PD-L1 diagnostic antibodies run on two different IHC platforms: clones 22C3 and 28-8 are determined for the Dako link48 platform (Agilent), and clones SP263 and SP142 for the Ventana (Roche) platform. In addition, various scoring systems for PD-L1 expression have been established. Briefly, the tumor proportion score (TPS) gives the proportion of tumor cells with membrane expression, the combined proportion score (CPS) to assesses the expression of immune cells in the surrounding area in addition to tumor cells, and the IC score to determine the expression of immune cells. Moreover, different cut-off values have been set for the same active substance, depending on whether it is defined for a first-line or a multi-

line treatment. For some of the drugs, national medicines authorities insist on the use of companion testing, e.g., the 22C3 antibody Dako link48 for pembrolizumab or SP263 for durvalumab treatment. In other indications the use of PD-L1 testing is complementary, helping to select patients for a more pronounced therapeutic response, thus providing a more accurate assessment of the risk/benefit ratio. Such a complementary test should be used, for example, for atezolizumab with SP142 or for nivolumab with 28-8 antibody clones. There are some indications and drugs where predictive marker testing is not justified under the current pharmacopoeian standards [257]. The results of the KEYNOTE-001 clinical drug trial have shown a strong correlation between the efficacy of pembrolizumab and the level of PD-L1 expression as determined by the 22C3 antibody [256, 258]. The results suggested the utility of 50% TPS as a cut-off, a value which was confirmed by subsequent studies (Keynote-010 and 024). Interestingly, PD-L1 expression as determined by 28-8 antibodies in the Checkmate 017 study was not found to be predictive for nivolumab response. However, the Checkmate 057 study concluded, that PD-L1 expression and clinical response significantly correlate, although only a modest ORR increase was observed as expression increased. Thus, the FDA has accepted PD-L1 detection for this drug as a complementary test [259]. PD-L1 detection for atezolizumab has also been accepted as a complementary test, based on data from the POPLAR and OAK studies [260]. Most recently, cemiplimab has received FDA approval for use, based on the results of the EMPOWER-lung-1 study, and the use of this drug was also linked to greater than 50% PD-L1 expression, determined by SP263 and the Ventana platform as a companion test [261, 262]. The alternatives of specific ICI therapies and PD-L1 predictive testing techniques resulted in differences in the current NCCN and ESMO recommendations, and these are also reflected in the various national medicines regulatory specifications [120, 263].

Taken together the above, a never seen complexity of a biomarker determination can be stated. The variety of different diagnostic PD-L1 antibodies and development platforms and different evaluation systems as well as the growing number of ICI drugs and relevant national recommendations required the comparison of PD-L1 detection methodologies. The results of PD-L1 determination with four commonly available anti-PD-L1 antibodies (22C3, 28-8, SP142 and EIL3N) were compared in a multi-institutional study [264]. In addition to IASCL, the relevant pharmaceutical and diagnostic companies were also involved in the design and conduction of the Blueprint 1 and 2 studies. The very detailed results indicated that the evaluated tests were not always interchangeable. The 22C3, 28-8 and SP263 antibodies and their elicitation systems have been shown to be highly concordant, in terms of sensitivity and specificity, for the determination of TPS. In contrast, SP142 showed a consistently lower TPS value, while 73-10, tested in the Blueprint 2 study, showed a much more intense staining reaction [265, 266].

A major limitation in PD-L1 testing is that it can only be reliably done on embedded tissue samples. Although some studies have reported results of PD-L1 detection on cytological smears (bronchial brush smear, lymph node EBUS guided FNA smear) [267], IHC on this sample type is difficult to standardize and results show a large variability. The large variability of preanalytical characteristics in cytology samples is well known. As indicated in previous studies, fixation is a key pre-analytical factor, e.g., alcohol-based fixatives strongly reduce the feasibility of IHC reactions. Thus, the PD-L1 IHC reaction on smears should be validated in every laboratory. The determination of IC and CPS in cytology is also problematic as the assessment of tumor cell-immune cell relations in direct smears is almost impossible. Larger cell clusters, 3-dimensional clusters, blood contamination hamper the evaluation. In addition, instead of the membranous staining seen in tissue sections, there may be diffuse surface staining on direct smears, mimicking a cytoplasmic reaction [268–270]. As a result, there is a high interpretation and interobserver variability in the assessment of PD-L1 detection when cytology smears are used [268]. For these reasons, the manufacturers of FDA-approved diagnostic antibodies do not recommend the use of cytology smears and users are advised to favor cell blocks. Cytology samples processed in cell block format have been shown to be suitable for PD-L1 detection. This methodology is optimized for and is analytically similar to IHC and allows standardization criteria of the IHC reaction. Several studies have shown satisfactory concordance between the results of PD-L1 detection on cell blocks and tissue samples [271]. In special cases, when the sampling from the tumor tissue (both histology or cytology) fails, it is possible to determine PD-L1 expression from cell blocks of malignant pleural effusion (MPE) samples. Relatively few studies have been performed on this sample type, with small case numbers. The results to date have shown good concordance (85.1%, kappa 0.774) with PD-L1 expression detected in paired primary tumor tissue samples, using three TPS cut-off values. Interestingly, MPE cells appeared to show significantly higher PD-L1 expression (p = 0.005) [272]. Our own institute has also had positive experience, successfully using MPE cell blocks in the absence of tissue samples to assess tumor PD-L1 status (data not published) In conclusion, the formalin-fixed paraffin-embedded cell block preparation technology is the ideal alternative to test PD-L1 in cytology specimen [272–274].

The development of pioneering assays to make PD-L1 determination is highly progressive. A new potential tool to assess PD-L1 expression following immunohistochemistry is digital image analysis, with or without the support of artificial intelligence. One such system is the Aitrox AI Model [275]. These digital systems provide powerful assistance in exact

quantification and scoring of PD-L1 expression in classic histological conditions.

Determination of soluble PD-1 or PD-L1 in plasma by enzyme-linked immunosorbent assay (ELISA) is another new approach to investigate PD-L1 status. High soluble PD-L1 detected before treatment indicates unfavorable prognosis in ICI-treated lung carcinomas patients, with both PFS and OS being shorter. Changes is sPD-L1 levels after therapy could not be associated with disease outcome. A predictive role of sPD-L1 has not been confirmed to date.

A further promising blood-based assay evaluates exosomal PD-L1 and PD-L1 in circulating tumor cells. In the first series of studies there was no significant correlation between circulating tumor cell PD-L1 expression (neither pre- nor post-treatment) and OS following ICI treatment. However, the dynamic interaction between tumor and immune system was suggested as significantly shorter PFS was observed with high exoPD-L1 levels before ICI treatment, whereas longer PFS was observed with higher exoPD-L1 after treatment.

These plasma-derived PD-L1-associated assays, in addition to simple and non-invasive sampling promise the potential of PD-L1 monitoring to reflect the dynamic, temporal relationship between tumor and immune system. The actual prognostic and predictive role of these biomarkers for ICI treatment is not yet clear [276].

There is generally a negative correlation between tumor PD-L1 expression and response to immunotherapy and the presence of oncogene driver mutations, except for KRAS and partially BRAF and met exon 14 skipping mutations [277]. This correlation has been confirmed in several studies [278, 279]. Since oncogene addicted NSCLC is a rather heterogeneous group both genetically and biologically, there are differences in response to ICI therapy between tumors defined by individual gene defects [280]. Classical EGFR mutations and exon 20 insertions usually show moderate PD-L1 expression and low TMB, and are generally unresponsive to ICI treatment [281]. ALK and ROS1 gene rearrangements often show high PD-L1 expression but low TMB, and these tumours are not responsive to ICI treatment [282, 283]. So strong is this negative correlation that the presence of EGFR and ALK mutations is a treatment exclusion in most ICI recommendations. HER2 mutations are also associated with moderate levels of PD-L1 expression and low TMB detection, and ICI treatments are not effective [284]. RET rearrangements also show low TMB, variable levels of PD-L1 expression and, although there are few and conflicting data, they do not suggest that ICI treatment is effective [285]. The tumours defined by the gene defects listed so far, as previously detailed, are predominantly located in the periphery of the lung and occur mostly in never-smokers or light smokers. Driver mutations play a key role in the formation of these tumours, with escape from immune mechanisms playing a minor role, so that ICI treatment is usually ineffective or results in a modest response [12]. EGFR mutations and driver gene fusions are rare in lung tumors that develop with prolonged exposure to carcinogen tobacco smoke, but KRAS mutations are common [286, 287]. In addition, the tumour mutational burden of these tumours is high. These smoking-associated tumours are markedly immunogenic, and thus tumour formation is influenced by immune escape mechanisms, such as high expression of PD-L1 by tumour cells. Not surprisingly, these smoking-associated tumours with high PD-L1 expression and high TMB generally respond well to ICI treatment [12]. However, due to genetic heterogeneity, there are also significant differences within these tumour groups. In the case of KRAS mutation, good results with ICI treatment are seen in the presence of p53 mutation [288]. Such good results are not observed for STK11 or KEAP co-mutations (KRAS mut/STK11 mut: ORR11.6%, PFS: 2.0 months, OS: 6.2 months, KRAS mut/STK11 wild type: ORR: 32.4%, PFS: 4.8 months, OS: 17.3 months, KRASmut/KEAP mut: ORR: 17.8%, PFS: 1.8 months, OS: 4.8 months, KRAS mut/KEAP wild type: ORR 29.3%, PFS: 4.6 months, OS: 18.4 months) [289]. Among BRAF mutations, a relatively good therapeutic response to ICI treatment is expected in the presence of smoking-associated class II-III non-V600E mutations. In the presence of V600e mutations, only moderate results are observed with ICI treatment [290, 291]. For tumours carrying Met exon 14 mutations, moderate therapeutic response with ICI treatment has been observed [292].

The everyday challenges of biomarker testing

There has been an explosion of knowledge on the oncogenic mechanisms of NSCLC drivers in recent years. Consequently, molecular biomarkers have become known, which are in use for predictive testing to optimize treatment of patients with advanced lung cancer. The conventional approach to biomarker testing is based on the analysis of tumour tissue samples. The extended needs on different testing platforms require increased amounts of tissue and DNA or RNA extracted. Unfortunately, only about 20% of patients are resectable, and in about 80% of cases the diagnosis is based on small biopsy and/or cytological sample [293]. Previous reports (before 2010) suggested that in up to 70% of all lung tumours, diagnosis was made on cytological specimen alone [294]. In the past decades, the differentiation of SCLC and NSCLC was sufficient, but today the accurate subtyping of NSCLC is required as the effect of targeted treatments is mostly expected in adenocarcinomas [295]. NSCLC subtyping is most reliable when tumor specimens are used but cytology smears are principally useless in specific cases, e.g., PD-L1 determination.

The predictive molecular testing recommendations for lung cancer therapy are constantly changing and in the light of new scientific findings and evolving technologies. Further, there are significant differences between the current NCCN, CAP, ESMO

TABLE 1 Most common diagnostic antibodies used to test for driver gene alterations or PD-L1 expression.

Driver gene alteration	Antibody clone	Vendor
EGFR L858R [48–52]	43B2 SP125	Cell Signaling Ventana
EGFR del 19 (E746-A750) [48–52]	6B6 SP111	Cell Signaling Ventana
Alk [136, 137]	D5F3 5A4	Cell Signaling Novocastra
ROS1 [153, 155]	D4D6	Cell Signaling
RET [185]	EPR2871	Abcam
NTRK [196, 204, 205]	EPR17341 C17F1	Abcam Cell Signaling
BRAF [115, 117]	VE1	SpringBio
MET [228, 231]	SP44	Ventana
PD-L1 [265, 266]	22C3 28-8 SP142 SP263 73-10	Dako Dako Ventana Ventana Dako

and Pan-Asian NSCLC recommendations [120, 263, 296, 297]. At the beginning of the era only one or two biomarkers needed to be tested, starting with the EGFR mutational status. According to 2023 ESMO recommendations, all advanced non-squamous NSCLC cases should be tested for ALK, ROS1, NTRK, RET fusions, MET exon14 skipping mutations, BRAF, KRAS G12C and HER2 mutations in addition to EGFR mutations. Molecular testing is only justified for squamous cell carcinoma in special circumstances: young age (below 50 years), non-smoker, ex-moderate smoker or long-time non-smoker status. At this complexity the use an NGS testing platform is recommended, if available. Due to the expansion of gene fusions of interest, RNA-based NGS appears to be the best option. In addition, liquid-based cfDNA testing is also acceptable, but in case of negative results, tissue sampling is required [297]. It is reasonable to determine PD-L1 expression by IHC testing for both advanced squamous and non-squamous NSCLC cases [263]. As already detailed above, the available diagnostic platforms and scoring should be carefully applied: testing with 22C3, 28-8, and SP263 antibody clones show a high concordance, whereas the clone SP142 results in a lower TPS [265, 266]. All these factors require a carefully standardized planning of the daily diagnostic practice.

National guidelines based on international recommendations tend to develop, tailored to the national healthcare system and financial resources. Accordingly, there might be significant differences in the national recommendations. While the reflex testing of biopsy specimens from all patients with advanced NSCLC is generally recommended, on-demand testing is preferred in some countries to save costs. Unfortunately, according to a 2018 study, access to molecular testing is more limited in several Central European countries due to limited resources, and in many countries, on-demand testing is preferred to reflex testing [298]. Since the publication of the aforementioned study, there have been several encouraging developments in these countries [299]. The question arises if it is worth to expend resources on quasi-useless testing for patients with poor performance status, ECOG4, who are not suitable for active oncological care. The hierarchy of testing methods should also be considered for the routine detection of rare genetic events. As an example, it is cost-effective to screen for rare NTRK rearrangements by immunohistochemistry and then to confirm only positive cases by sequencing. The most commonly used diagnostic antibodies currently commercially available are summarised in Table 1.

Individual tests, like series of immunohistochemistry, FISH, and PCR can lead to sample exhaustion, and thus, inconclusive, or false negative results in small biopsies and/or samples with low tumour cell counts by providing insufficient amounts of extracted nucleic acid [300]. Thus, biomarker testing practice is increasingly moving towards multigene technologies, such as the NGS [301].

Based on cost-effectiveness calculations, NGS is already preferable to single-gene tests when testing more than 4 targets simultaneously. In addition, this approach also realizes life-year gains, as calculated in several states [302, 303].

A not negligible aspect of predictive biomarker testing for NSCLC is turnaround time (TAT). Time consuming testing will result in delays in patient treatment, which may even fail due to patient deterioration. International recommendations suggest a TAT of 10 days from receipt of the sample to the communication of the result. The molecular test optimally should be performed in nearby laboratory. However, molecular testing is frequently centralized, which may prolong the TAT for logistical reasons (sample transport). Reflex testing also shortens the TAT, and supports optimal sample usage. In contrast, on-demand testing is more appropriate to avoid unnecessary tests, at the expense of the TAT [304]. It is important mentioning that the 10-day TAT recommendations is difficult to achieve with NGS in general. The sequencing approach is usually designed for 8 samples run simultaneously and the biochemistry is followed by a bioinformatic session of various complexity [304]. Any molecular techniques have their pros and cons laboratories should consider for their specific aims and needs. The choice of sequencing chemistry, device and software solutions also defines the acquisition of specific targets, the reagent requirements, the rate of the testing and turnaround times.

In lung cancer patients the tumour is frequently irresectable and/or the patient, or the tumor is unsuitable for bronchoscopic and/or transthoracic sampling. Small biopsy samples may often be not representative. In many of these cases, malignant pleural fluid is an alternative diagnostic specimen. MPE is present in about 15%–25% of lung tumours at diagnosis and occurs in 50%–

60% of lung cancer patients overall during the disease [305–307]. However, the fluid cytology samples are sometimes also difficult to evaluate. It is recommended to prepare a cell block from the MPE specimen instead of the conventional cytospin smear. In general, cell blocks offer several advantages: the sample specimen can be examined as a tissue sample, it allows safe separation of activated mesothelial and tumour cells, and it provides accurate tumour typing. The cell block has higher diagnostic specificity and sensitivity than the cytospin smear, depending on tumor type (25, 53, 78% and 95% for squamous cell carcinoma, SCLC, adenocarcinoma and ovarian carcinoma, respectively [306, 308]. As a major benefit, cell blocks are suitable for immunohistochemical and molecular studies, including the investigation of all common predictive biomarkers for NSCLC therapy (EGFR, KRAS and ALK, ROS1, PD-L1 state).

Conclusion

As described in our study, over the last 20 years, the increasing understanding of the molecular background of NSCLC has led to the identification of new therapeutic targets. Year after year, molecularly targeted treatment options are giving a growing group of patients with advanced NSCLC longer survival and better quality of life, without the life-threatening serious side effects of cytotoxic treatments. At the same time, patient selection has created unprecedented challenges for the diagnostic professions, particularly pathology departments. Further persistent work is needed to identify new molecular aberrations in addition to the current therapeutic targets, which will allow the use of more effective treatments for patients without the already identified driver mutation.

Author contributions

LT: conceptualization, methodology, data curation, writing-original draft, visualisation. AM: writing-review and editing, supervision. GM: writing-reviewing and editing, project administration. All authors contributed to the article and approved the submitted version.

Funding

The author(s) declare that no financial support was received for the research, authorship, and/or publication of this article.

Conflict of interest

The authors declare that the research was conducted in the absence of any commercial or financial relationships that could be construed as a potential conflict of interest.

References

1. Sung H, Ferlay J, Siegel RL, Laversanne M, Soerjomataram I, Jemal A, et al. Global cancer statistics 2020: GLOBOCAN estimates of incidence and mortality worldwide for 36 cancers in 185 countries. *CA Cancer J Clin* (2021) 71:209–49. doi:10.3322/caac.21660

2. Islami F, Torre LA, Jemal A. Global trends of lung cancer mortality and smoking prevalence. *Transl Lung Cancer Res* (2015) 4:327–38. doi:10.3978/j.issn.2218-6751.2015.08.04

3. Bogos K, Kiss Z, Gálffy G, Tamási L, Ostoros G, Müller V, et al. Revising incidence and mortality of lung cancer in central Europe: an epidemiology review from Hungary. *Front Oncol* (2019) 9:1051. doi:10.3389/fonc.2019.01051

4. Tsao MS, Asamura H, Borczuk AC, Dacic S, Devesa SS, Kerr KM, et al. Tumours of the lung. Introduction. In WHO classification of tumours editorial board. In: *Thoracic tumours*. In: *WHO classification of tumours series*. 5th ed., 5. Lyon: IASCL Press (2021). p. 20–8.

5. Zhang Y, Vaccarella S, Morgan E, Li M, Etxeberria J, Chokunonga E, et al. Global variations in lung cancer incidence by histological subtype in 2020: a population-based study. *Lancet Oncol* (2023) 24:1206–18. doi:10.1016/S1470-2045(23)00444-8

6. Brooks DR, Austin JH, Heelan RT, Ginsberg MS, Shin V, Olson SH, et al. Influence of type of cigarette on peripheral versus central lung cancer. *Cancer Epidemiol Biomarkers Prev* (2005) 14:576–81. doi:10.1158/1055-9965.EPI-04-0468

7. Ito H, Matsuo K, Tanaka H, Koestler DC, Ombao H, Fulton J, et al. Nonfilter and filter cigarette consumption and the incidence of lung cancer by histological type in Japan and the United States: analysis of 30-year data from population-based cancer registries. *Int J Cancer* (2011) 128:1918–28. doi:10.1002/ijc.25531

8. Stellman SD, Muscat JE, Hoffmann D, Wynder EL. Impact of filter cigarette smoking on lung cancer histology. *Prev Med* (1997) 26:451–6. doi:10.1006/pmed.1997.0212

9. Hoffmann D, Hoffmann I. The changing cigarette, 1950-1995. *J Toxicol Environ Health* (1997) 50:307–64. doi:10.1080/009841097160393

10. Everaert S, Schoeters G, Lardon F, Janssens A, Van Larebeke N, Raquez JM, et al. Protecting public health and the environment: towards a general ban on cellulose acetate cigarette filters in the European Union. *Front Public Health* (2023) 11:1282655. doi:10.3389/fpubh.2023.1282655

11. Rudin CM, Poirier JT, Byers LA, Dive C, Dowlati A, George J, et al. Molecular subtypes of small cell lung cancer: a synthesis of human and mouse model data. *Nat Rev Cancer* (2019) 19:289–97. doi:10.1038/s41568-019-0133-9

12. Yatabe Y. Molecular pathology of non-small cell carcinoma. *Histopathology*. (2024) 84:50–66. doi:10.1111/his.15080

13. Lu T, Yang X, Huang Y, Zhao M, Li M, Ma K, et al. Trends in the incidence, treatment, and survival of patients with lung cancer in the last four decades. *Cancer Manag Res* (2019) 11:943–53. doi:10.2147/CMAR.S187317

14. Löfling L, Bahmanyar S, Kieler H, Lambe M, Wagenius G. Temporal trends in lung cancer survival: a population-based study. *Acta Oncologica* (2022) 61:625–31. doi:10.1080/0284186X.2021.2013529

15. Kiss Z, Gálffy G, Müller V, Moldvay J, Sárosi V, Pápai-Székely Z, et al. Significant changes in advanced lung cancer survival during the past decade in Hungary: impact of modern immunotherapy and the COVID-19 pandemic. *Front Oncol* (2023) 13:1207295. doi:10.3389/fonc.2023.1207295

16. Mendelsohn J. The epidermal growth factor receptor as a target for cancer therapy. *Endocr Relat Cancer* (2001) 8:3–9. doi:10.1677/erc.0.0080003

17. Baselga J, Albanell J. Targeting epidermal growth factor receptor in lung cancer. *Curr Oncol Rep* (2002) 4:317–24. doi:10.1007/s11912-002-0007-1

18. Rusch V, Klimstra D, Venkatraman E, Pisters PW, Langenfeld J, Dmitrovsky E. Overexpression of the epidermal growth factor receptor and its ligand transforming growth factor alpha is frequent in resectable non-small cell lung

cancer but does not predict tumor progression. *Clin Cancer Res* (1997) 3:515–22. PMID: 9815714.

19. Ciardiello F, De Vita F, Orditura M, Tortora G. The role of EGFR inhibitors in nonsmall cell lung cancer. *Curr Opin Oncol* (2004) 16:130–5. doi:10.1097/00001622-200403000-00008

20. Herbst RS, Maddox AM, Rothenberg ML, Small EJ, Rubin EH, Baselga J, et al. Selective oral epidermal growth factor receptor tyrosine kinase inhibitor ZD1839 is generally well-tolerated and has activity in non-small-cell lung cancer and other solid tumors: results of a phase I trial. *J Clin Oncol* (2002) 20:3815–25. doi:10.1200/JCO.2002.03.038

21. Fukuoka M, Yano S, Giaccone G, Tamura T, Nakagawa K, Douillard JY, et al. Multi-institutional randomized phase II trial of gefitinib for previously treated patients with advanced non–small-cell lung cancer. *J Clin Oncol* (2023) 41:1162–71. doi:10.1200/JCO.22.02499

22. Jänne PA, Gurubhagavatula S, Yeap BY, Lucca J, Ostler P, Skarin AT, et al. Outcomes of patients with advanced non-small cell lung cancer treated with gefitinib (ZD1839, "Iressa") on an expanded access study. *Lung Cancer* (2004) 44:221–30. doi:10.1016/j.lungcan.2003.12.014

23. Bailey R, Kris M, Wolf M, Kay A, Averbuch S, Askaa J, et al. Gefitinib ('Iressa', ZD1839) monotherapy for pretreated advanced non-small-cell lung cancer in IDEAL 1 and 2: tumor response is not clinically relevantly predictable from tumor EGFR membrane staining alone. *Lung Cancer* (2003) 41:S2–S71. doi:10.1016/S0169-5002(03)91900-3

24. Parra HS, Cavina R, Latteri F, Zucali PA, Campagnoli E, Morenghi E, et al. Analysis of epidermal growth factor receptor expression as a predictive factor for response to gefitinib ('Iressa', ZD1839) in non-small-cell lung cancer. *Br J Cancer* (2004) 91:208–12. doi:10.1038/sj.bjc.6601923

25. Paez JG, Jänne PA, Lee JC, Tracy S, Greulich H, Gabriel S, et al. EGFR mutations in lung cancer: correlation with clinical response to gefitinib therapy. *Science* (2004) 304:1497–500. doi:10.1126/science.1099314

26. Lynch TJ, Bell DW, Sordella R, Gurubhagavatula S, Okimoto RA, Brannigan BW, et al. Activating mutations in the epidermal growth factor receptor underlying responsiveness of non-small-cell lung cancer to gefitinib. *N Engl J Med* (2004) 350:2129–39. doi:10.1056/NEJMoa040938

27. Pao W, Miller V, Zakowski M, Doherty J, Politi K, Sarkaria I, et al. EGF receptor gene mutations are common in lung cancers from "never smokers" and are associated with sensitivity of tumors to gefitinib and erlotinib. *Proc Natl Acad Sci USA* (2004) 101:13306–11. doi:10.1073/pnas.0405220101

28. Tang X, Shigematsu H, Bekele BN, Roth JA, Minna JD, Hong WK, et al. EGFR tyrosine kinase domain mutations are detected in histologically normal respiratory epithelium in lung cancer patients. *Cancer Res* (2005) 65(17):7568–72. doi:10.1158/0008-5472.CAN-05-1705

29. Graham RP, Treece AL, Lindeman NI, Vasalos P, Shan M, Jennings LJ, et al. Worldwide frequency of commonly detected EGFR mutations. *Arch Pathol Lab Med* (2018) 142:163–7. doi:10.5858/arpa.2016-0579-CP

30. Sharma M, Basu DA, Nathany S, Amrith BP, Batra U. A narrative review of the role of common EGFR mutations in pathogenesis and treatment of non-small-cell lung carcinoma. *Cancer Res Stat Treat* (2022) 5:507–18. doi:10.4103/crst.crst_222_22

31. Yun CH, Boggon TJ, Li Y, Woo MS, Greulich H, Meyerson M, et al. Structures of lung cancer-derived EGFR mutants and inhibitor complexes: mechanism of activation and insights into differential inhibitor sensitivity. *Cancer Cell* (2007) 11:217–27. doi:10.1016/j.ccr.2006.12.017

32. Shan Y, Eastwood MP, Zhang X, Kim ET, Arkhipov A, Dror RO, et al. Oncogenic mutations counteract intrinsic disorder in the EGFR kinase and promote receptor dimerization. *Cell* (2012) 149(4):860–70. doi:10.1016/j.cell.2012.02.063

33. Harrison PT, Vyse S, Huang PH. Rare epidermal growth factor receptor (EGFR) mutations in non-small cell lung cancer. *Semin Cancer Biol* (2020) 61:167–79. doi:10.1016/j.semcancer.2019.09.015

34. Kobayashi Y, Mitsudomi T. Not all epidermal growth factor receptor mutations in lung cancer are created equal: perspectives for individualized treatment strategy. *Cancer Sci* (2016) 107:1179–86. doi:10.1111/cas.12996

35. Yasuda H, Park E, Yun CH, Sng NJ, Lucena-Araujo AR, Yeo WL, et al. Structural, biochemical, and clinical characterization of epidermal growth factor receptor (EGFR) exon 20 insertion mutations in lung cancer. *Sci Transl Med* (2013) 5(216):216ra177. doi:10.1126/scitranslmed.3007205

36. Voon PJ, Tsui DW, Rosenfeld N, Chin TM. EGFR exon 20 insertion A763-Y764insFQEA and response to erlotinib--Letter. *Mol Cancer Ther* (2013) 12:2614–5. doi:10.1158/1535-7163.MCT-13-0192

37. Bai Q, Wang J, Zhou X. EGFR exon20 insertion mutations in non-small cell lung cancer: clinical implications and recent advances in targeted therapies. *Cancer Treat Rev* (2023) 120:102605. doi:10.1016/j.ctrv.2023.102605

38. Yang G, Yang Y, Hu J, Xu H, Zhang S, Wang Y. EGFR exon 20 insertion variants A763_Y764insFQEA and D770delinsGY confer favorable sensitivity to currently approved EGFR-specific tyrosine kinase inhibitors. *Front Pharmacol* (2022) 13:984503. doi:10.3389/fphar.2022.984503

39. Liu M, Niu X, Liu H, Chen J. Germline EGFR mutations in lung cancer (Review). *Oncol Lett* (2023) 26:282. doi:10.3892/ol.2023.13868

40. Ji H, Zhao X, Yuza Y, Shimamura T, Li D, Protopopov A, et al. Epidermal growth factor receptor variant III mutations in lung tumorigenesis and sensitivity to tyrosine kinase inhibitors. *Proc Natl Acad Sci USA* (2006) 103:7817–22. doi:10.1073/pnas.0510284103

41. Maemondo M, Inoue A, Kobayashi K, Sugawara S, Oizumi S, Isobe H, et al. Gefitinib or chemotherapy for non–small-cell lung cancer with mutated EGFR. *N Engl J Med* (2010) 362:2380–8. doi:10.1056/NEJMoa0909530

42. Laface C, Maselli FM, Santoro AN, Iaia ML, Ambrogio F, Laterza M, et al. The resistance to EGFR-TKIs in non-small cell lung cancer: from molecular mechanisms to clinical application of new therapeutic strategies. *Pharmaceutics* (2023) 15:1604. doi:10.3390/pharmaceutics15061604

43. Sequist LV, Waltman BA, Dias-Santagata D, Digumarthy S, Turke AB, Fidias P, et al. Genotypic and histological evolution of lung cancers acquiring resistance to EGFR inhibitors. *Sci Transl Med* (2011) 3:75ra26. doi:10.1126/scitranslmed.3002003

44. Yu L, Bazhenova L, Gold K, Tran L, Hilburn V, Vu P, et al. Clinicopathologic and molecular characteristics of EGFR-mutant lung adenocarcinomas that transform to small cell lung cancer after TKI therapy. *Transl Lung Cancer Res* (2022) 11:452–61. doi:10.21037/tlcr-21-665

45. Hill W, Lim EL, Weeden CE, Lee CL, Augustine M, Chen K, et al. Lung adenocarcinoma promotion by air pollutants. *Nature* (2023) 616:159–67. doi:10.1038/s41586-023-05874-3

46. Ruano-Ravina A, Torres-Durán M, Kelsey KT, Parente-Lamelas I, Leiro-Fernández V, Abdulkader I, et al. Residential radon, EGFR mutations and ALK alterations in never-smoking lung cancer cases. *Eur Respir J* (2016) 48:1462–70. doi:10.1183/13993003.00407-2016

47. Sholl LM, Xiao Y, Joshi V, Yeap BY, Cioffredi LA, Jackman DM, et al. EGFR mutation is a better predictor of response to tyrosine kinase inhibitors in non-small cell lung carcinoma than FISH, CISH, and immunohistochemistry. *Am J Clin Pathol* (2010) 133:922–34. doi:10.1309/AJCPST1CTHZS3PSZ

48. Yu J, Kane S, Wu J, Benedettini E, Li D, Reeves C, et al. Mutation-specific antibodies for the detection of EGFR mutations in non-small-cell lung cancer. *Clin Cancer Res* (2009) 15:3023–8. doi:10.1158/1078-0432.CCR-08-2739

49. Bondgaard AL, Høgdall E, Mellemgaard A, Skov BG. High specificity but low sensitivity of mutation-specific antibodies against EGFR mutations in non-small-cell lung cancer. *Mod Pathol* (2014) 27:1590–8. doi:10.1038/modpathol.2014.67

50. Kato Y, Peled N, Wynes MW, Yoshida K, Pardo M, Mascaux C, et al. Novel epidermal growth factor receptor mutation-specific antibodies for non-small cell lung cancer: immunohistochemistry as a possible screening method for epidermal growth factor receptor mutations. *J Thorac Oncol* (2010) 5:1551–8. doi:10.1097/JTO.0b013e3181e9da60

51. Brevet M, Arcila M, Ladanyi M. Assessment of EGFR mutation status in lung adenocarcinoma by immunohistochemistry using antibodies specific to the two major forms of mutant EGFR. *J Mol Diagn* (2010) 12:169–76. doi:10.2353/jmoldx.2010.090140

52. Seo AN, Park TI, Jin Y, Sun PL, Kim H, Chang H, et al. Novel EGFR mutation-specific antibodies for lung adenocarcinoma: highly specific but not sensitive detection of an E746_A750 deletion in exon 19 and an L858R mutation in exon 21 by immunohistochemistry. *Lung Cancer* (2014) 83:316–23. doi:10.1016/j.lungcan.2013.12.008

53. Ragazzi M, Tamagnini I, Bisagni A, Cavazza A, Pagano M, Baldi L, et al. Diamond: immunohistochemistry versus sequencing in EGFR analysis of lung adenocarcinomas. *J Clin Pathol* (2016) 69:440–7. doi:10.1136/jclinpath-2015-203348

54. Warth A, Penzel R, Brandt R, Sers C, Fischer JR, Thomas M, et al. Optimized algorithm for Sanger sequencing-based EGFR mutation analyses in NSCLC biopsies. *Virchows Arch* (2012) 460:407–14. doi:10.1007/s00428-012-1219-x

55. Bos JL. Ras oncogenes in human cancer: a review. *Cancer Res* (1989) 49:4682–9. Erratum in: Cancer Res (1990) 50: 1352. PMID: 2547513.

56. Chang EH, Gonda MA, Ellis RW, Scolnick EM, Lowy DR. Human genome contains four genes homologous to transforming genes of Harvey and Kirsten murine sarcoma viruses. *Proc Natl Acad Sci U S A.* (1982) 79:4848–52. doi:10.1073/pnas.79.16.4848

57. McBride OW, Swan DC, Tronick SR, Gol R, Klimanis D, Moore DE, et al. Regional chromosomal localization of N-ras, K-ras-1, K-ras-2 and myb oncogenes in human cells. *Nucleic Acids Res* (1983) 11:8221–36. doi:10.1093/nar/11.23.8221

58. Barbacid M. Ras genes. *Annu Rev Biochem* (1987) 56:779–827. doi:10.1146/annurev.bi.56.070187.004023

59. Karnoub AE, Weinberg RA. Ras oncogenes: split personalities. *Nat Rev Mol Cell Biol* (2008) 9:517–31. doi:10.1038/nrm2438

60. Pantsar T. The current understanding of KRAS protein structure and dynamics. *Comput Struct Biotechnol J* (2019) 18:189–98. doi:10.1016/j.csbj.2019.12.004

61. Simanshu DK, Nissley DV, McCormick F. RAS proteins and their regulators in human disease. *Cell* (2017) 170:17–33. doi:10.1016/j.cell.2017.06.009

62. Bahar ME, Kim HJ, Kim DR. Targeting the RAS/RAF/MAPK pathway for cancer therapy: from mechanism to clinical studies. *Signal Transduct Target Ther* (2023) 8:455. doi:10.1038/s41392-023-01705-z

63. Molina JR, Adjei AA. The Ras/Raf/MAPK pathway. *J Thorac Oncol* (2006) 1:7–9. PMID: 17409820. doi:10.1016/s1556-0864(15)31506-9

64. Fruman DA, Chiu H, Hopkins BD, Bagrodia S, Cantley LC, Abraham RT. The PI3K pathway in human disease. *Cell* (2017) 170:605–35. doi:10.1016/j.cell.2017.07.029

65. Mo SP, Coulson JM, Prior IA. RAS variant signalling. *Biochem Soc Trans.* (2018) 46:1325–32. doi:10.1042/BST20180173

66. Prior IA, Hood FE, Hartley JL. The frequency of ras mutations in cancer. *Cancer Res* (2020) 80:2969–74. doi:10.1158/0008-5472.CAN-19-3682

67. Ihle NT, Byers LA, Kim ES, Saintigny P, Lee JJ, Blumenschein GR, et al. Effect of KRAS oncogene substitutions on protein behavior: implications for signaling and clinical outcome. *J Natl Cancer Inst* (2012) 104:228–39. doi:10.1093/jnci/djr523

68. Rodenhuis S, Slebos RJ, Boot AJ, Evers SG, Mooi WJ, Wagenaar SS, et al. Incidence and possible clinical significance of K-ras oncogene activation in adenocarcinoma of the human lung. *Cancer Res* (1988) 48:5738–41. PMID: 3048648.

69. Suzuki Y, Orita M, Shiraishi M, Hayashi K, Sekiya T. Detection of ras gene mutations in human lung cancers by single-strand conformation polymorphism analysis of polymerase chain reaction products. *Oncogene* (1990) 5:1037–43. PMID: 2197591.

70. Dearden S, Stevens J, Wu YL, Blowers D. Mutation incidence and coincidence in non small-cell lung cancer: meta-analyses by ethnicity and histology (mutMap). *Ann Oncol* (2013) 24:2371–6. doi:10.1093/annonc/mdt205

71. Dogan S, Shen R, Ang DC, Johnson ML, D'Angelo SP, Paik PK, et al. Molecular epidemiology of EGFR and KRAS mutations in 3,026 lung adenocarcinomas: higher susceptibility of women to smoking-related KRAS-mutant cancers. *Clin Cancer Res* (2012) 18:6169–77. doi:10.1158/1078-0432.CCR-11-3265

72. Hunter JC, Manandhar A, Carrasco MA, Gurbani D, Gondi S, Westover KD. Biochemical and structural analysis of common cancer-associated KRAS mutations. *Mol Cancer Res* (2015) 13:1325–35. doi:10.1158/1541-7786.MCR-15-0203

73. Zafra MP, Parsons MJ, Kim J, Alonso-Curbelo D, Goswami S, Schatoff EM, et al. An *in vivo* kras allelic series reveals distinct phenotypes of common oncogenic variants. *Cancer Discov.* (2020) 10:1654–71. doi:10.1158/2159-8290.CD-20-0442

74. Timar J, Kashofer K. Molecular epidemiology and diagnostics of KRAS mutations in human cancer. *Cancer Metastasis Rev.* (2020) 39:1029–38. doi:10.1007/s10555-020-09915-5

75. Wang WZ, Shulman A, Amann JM, Carbone DP, Tsichlis PN. Small cell lung cancer: subtypes and therapeutic implications. *Semin Cancer Biol* (2022) 86(Pt 2):543–54. doi:10.1016/j.semcancer.2022.04.001

76. Lee B, Lee T, Lee SH, Choi YL, Han J. Clinicopathologic characteristics of EGFR, KRAS, and ALK alterations in 6,595 lung cancers. *Oncotarget* (2016) 7:23874–84. doi:10.18632/oncotarget.8074

77. Kadota K, Yeh YC, D'Angelo SP, Moreira AL, Kuk D, Sima CS, et al. Associations between mutations and histologic patterns of mucin in lung adenocarcinoma: invasive mucinous pattern and extracellular mucin are associated with KRAS mutation. *Am J Surg Pathol* (2014) 38:1118–27. doi:10.1097/PAS.0000000000000246

78. Judd J, Abdel KN, Khan H, Naqash AR, Baca Y, Xiu J, et al. Characterization of KRAS mutation subtypes in non-small cell lung cancer. *Mol Cancer Ther* (2021) 20:2577–84. doi:10.1158/1535-7163.MCT-21-0201

79. Wu MY, Zhang EW, Strickland MR, Mendoza DP, Lipkin L, Lennerz JK, et al. Clinical and imaging features of non-small cell lung cancer with G12C KRAS mutation. *Cancers (Basel)* (2021) 13:3572. doi:10.3390/cancers13143572

80. Cui W, Franchini F, Alexander M, Officer A, Wong HL, Ijzerman M, et al. Real world outcomes in KRAS G12C mutation positive non-small cell lung cancer. *Lung Cancer* (2020) 146:310–7. doi:10.1016/j.lungcan.2020.06.030

81. Gainor JF, Varghese AM, Ou SH, Kabraji S, Awad MM, Katayama R, et al. ALK rearrangements are mutually exclusive with mutations in EGFR or KRAS: an analysis of 1,683 patients with non-small cell lung cancer. *Clin Cancer Res* (2013) 19:4273–81. doi:10.1158/1078-0432.CCR-13-0318

82. Zhuang X, Zhao C, Li J, Su C, Chen X, Ren S, et al. Clinical features and therapeutic options in non-small cell lung cancer patients with concomitant mutations of EGFR, ALK, ROS1, KRAS or BRAF. *Cancer Med* (2019) 8:2858–66. doi:10.1002/cam4.2183

83. Lantuejoul S, Nicholson AG, Sartori G, Piolat C, Danel C, Brabencova E, et al. Mucinous cells in type 1 pulmonary congenital cystic adenomatoid malformation as mucinous bronchioloalveolar carcinoma precursors. *Am J Surg Pathol* (2007) 31:961–9. doi:10.1097/01.pas.0000249444.90594.27

84. Hermelijn SM, Wolf JL, Dorine den Toom T, Wijnen RMH, Rottier RJ, Schnater JM, et al. Early KRAS oncogenic driver mutations in nonmucinous tissue of congenital pulmonary airway malformations as an indicator of potential malignant behavior. *Hum Pathol* (2020) 103:95–106. doi:10.1016/j.humpath.2020.07.015

85. Garinet S, Rahshenas M, Galmiche-Rolland L, Abbo O, Bonnard A, Hameury F, et al. Cancer-associated mutations in congenital pulmonary malformations: a prospective cohort. *Am J Respir Crit Care Med* (2023) 207:615–9. doi:10.1164/rccm.202208-1573LE

86. Ghimessy A, Radeczky P, Laszlo V, Hegedus B, Renyi-Vamos F, Fillinger J, et al. Current therapy of KRAS-mutant lung cancer. *Cancer Metastasis Rev.* (2020) 39:1159–77. doi:10.1007/s10555-020-09903-9

87. Mascaux C, Iannino N, Martin B, Paesmans M, Berghmans T, Dusart M, et al. The role of RAS oncogene in survival of patients with lung cancer: a systematic review of the literature with meta-analysis. *Br J Cancer* (2005) 92:131–9. doi:10.1038/sj.bjc.6602258

88. Guan JL, Zhong WZ, An SJ, Yang JJ, Su J, Chen ZH, et al. KRAS mutation in patients with lung cancer: a predictor for poor prognosis but not for EGFR-TKIs or chemotherapy. *Ann Surg Oncol* (2013) 20:1381–8. doi:10.1245/s10434-012-2754-z

89. Cao H, Ma Z, Li Y, Zhang Y, Chen H. Prognostic value of KRAS G12C mutation in lung adenocarcinoma stratified by stages and radiological features. *J Thorac Cardiovasc Surg* (2023) 166:e479–e499. doi:10.1016/j.jtcvs.2023.04.037

90. Finn SP, Addeo A, Dafni U, Thunnissen E, Bubendorf L, Madsen LB, et al. Prognostic impact of KRAS G12C mutation in patients with NSCLC: results from the European thoracic oncology platform lungscape project. *J Thorac Oncol* (2021) 16:990–1002. doi:10.1016/j.jtho.2021.02.016

91. Wahl SGF, Dai HY, Emdal EF, Ottestad AL, Dale VG, Richardsen E, et al. Prognostic value of absolute quantification of mutated KRAS in circulating tumour DNA in lung adenocarcinoma patients prior to therapy. *J Pathol Clin Res* (2021) 7:209–19. doi:10.1002/cjp2.200

92. Eberhard DA, Johnson BE, Amler LC, Goddard AD, Heldens SL, Herbst RS, et al. Mutations in the epidermal growth factor receptor and in KRAS are predictive and prognostic indicators in patients with non-small-cell lung cancer treated with chemotherapy alone and in combination with erlotinib. *J Clin Oncol* (2005) 23:5900–9. doi:10.1200/JCO.2005.02.857

93. Tsao MS, Aviel-Ronen S, Ding K, Lau D, Liu N, Sakurada A, et al. Prognostic and predictive importance of p53 and RAS for adjuvant chemotherapy in non small-cell lung cancer. *J Clin Oncol* (2007) 25:5240–7. doi:10.1200/JCO.2007.12.6953

94. Zalcman G, Beau-Faller M, Creveuil C, de Fraipont F, Mounawar M, Richard N, et al. Use of Ras effector RASSF1A promoter gene methylation and chromosome 9p loss of heterozygosity (LOH) to predict progression-free survival (PFS) in perioperative chemotherapy (CT) phase III trial IFCT- 0002 in resectable non-small cell lung cancer. *J Clin Oncol* (2008) 26(15_Suppl. l):7500. doi:10.1200/jco.2008.26.15_suppl.7500

95. Hames ML, Chen H, Iams W, Aston J, Lovly CM, Horn L. Correlation between KRAS mutation status and response to chemotherapy in patients with advanced non-small cell lung cancer. *Lung Cancer* (2016) 92:29–34. doi:10.1016/j.lungcan.2015.11.004

96. Mao C, Qiu LX, Liao RY, Du FB, Ding H, Yang WC, et al. KRAS mutations and resistance to EGFR-TKIs treatment in patients with non-small cell lung cancer: a meta-analysis of 22 studies. *Lung Cancer* (2010) 69:272–8. doi:10.1016/j.lungcan.2009.11.020

97. Zer A, Ding K, Lee SM, Goss GD, Seymour L, Ellis PM, et al. Pooled analysis of the prognostic and predictive value of KRAS mutation status and mutation subtype in patients with non-small cell lung cancer treated with epidermal growth factor receptor tyrosine kinase inhibitors. *J Thorac Oncol* (2016) 11:312–23. doi:10.1016/j.jtho.2015.11.010

98. Roberts PJ, Stinchcombe TE. KRAS mutation: should we test for it, and does it matter? *J Clin Oncol* (2013) 31:1112–21. doi:10.1200/JCO.2012.43.0454

99. Palmieri M, Zulato E, Wahl SGF, Guibert N, Frullanti E. Diagnostic accuracy of circulating free DNA testing for the detection of KRAS mutations in non-small

cell lung cancer: a systematic review and meta-analysis. *Front. Genet.* (2022) 13: 1015161. doi:10.3389/fgene.2022.1015161

100. Malumbres M, Barbacid M. RAS oncogenes: the first 30 years. *Nat Rev Cancer* (2003) 3:459–65. doi:10.1038/nrc1097

101. Dankner M, Rose AAN, Rajkumar S, Siegel PM, Watson IR. Classifying BRAF alterations in cancer: new rational therapeutic strategies for actionable mutations. *Oncogene* (2018) 37:3183–99. doi:10.1038/s41388-018-0171-x

102. Davies H, Bignell GR, Cox C, Stephens P, Edkins S, Clegg S, et al. Mutations of the BRAF gene in human cancer. *Nature* (2002) 417:949–54. doi:10.1038/nature00766

103. Owsley J, Stein MK, Porter J, In GK, Salem M, O'Day S, et al. Prevalence of class I-III BRAF mutations among 114,662 cancer patients in a large genomic database. *Exp Biol Med (Maywood)* (2021) 246:31–9. doi:10.1177/1535370220959657

104. Namba H, Nakashima M, Hayashi T, Hayashida N, Maeda S, Rogounovitch TI, et al. Clinical implication of hot spot BRAF mutation, V599E, in papillary thyroid cancers. *J Clin Endocrinol Metab* (2003) 88:4393–7. doi:10.1210/jc.2003-030305

105. Jones JC, Renfro LA, Al-Shamsi HO, Schrock AB, Rankin A, Zhang BY, et al. Non-V600 BRAF mutations define a clinically distinct molecular subtype of metastatic colorectal cancer. *J Clin Oncol* (2017) 35:2624–30. doi:10.1200/JCO.2016.71.4394

106. Ambrosini-Spaltro A, Rengucci C, Capelli L, Chiadini E, Calistri D, Bennati C, et al. Clinicopathological features of non-small cell lung carcinoma with BRAF mutation. *Curr Oncol* (2023) 30:10019–32. doi:10.3390/curroncol30110728

107. Wan PT, Garnett MJ, Roe SM, Lee S, Niculescu-Duvaz D, Good VM, et al. Mechanism of activation of the RAF-ERK signaling pathway by oncogenic mutations of B-RAF. *Cell* (2004) 116:855–67. doi:10.1016/s0092-8674(04)00215-6

108. Dankort D, Filenova E, Collado M, Serrano M, Jones K, McMahon M. A new mouse model to explore the initiation, progression, and therapy of BRAFV600E-induced lung tumors. *Genes Dev* (2007) 21:379–84. doi:10.1101/gad.1516407

109. Villaruz LC, Socinski MA, Abberbock S, Berry LD, Johnson BE, Kwiatkowski DJ, et al. Clinicopathologic features and outcomes of patients with lung adenocarcinomas harboring BRAF mutations in the Lung Cancer Mutation Consortium. *Cancer* (2015) 121:448–56. doi:10.1002/cncr.29042

110. Paik PK, Arcila ME, Fara M, Sima CS, Miller VA, Kris MG, et al. Clinical characteristics of patients with lung adenocarcinomas harboring BRAF mutations. *J Clin Oncol* (2011) 29:2046–51. doi:10.1200/JCO.2010.33.1280

111. Marchetti A, Felicioni L, Malatesta S, Grazia Sciarrotta M, Guetti L, Chella A, et al. Clinical features and outcome of patients with non-small-cell lung cancer harboring BRAF mutations. *J Clin Oncol* (2011) 29:3574–9. doi:10.1200/JCO.2011.35.9638

112. Cardarella S, Ogino A, Nishino M, Butaney M, Shen J, Lydon C, et al. Clinical, pathologic, and biologic features associated with BRAF mutations in non-small cell lung cancer. *Clin Cancer Res* (2013) 19:4532–40. doi:10.1158/1078-0432.CCR-13-0657

113. Capper D, Preusser M, Habel A, Sahm F, Ackermann U, Schindler G, et al. Assessment of BRAF V600E mutation status by immunohistochemistry with a mutation-specific monoclonal antibody. *Acta Neuropathol* (2011) 122:11–9. doi:10.1007/s00401-011-0841-z

114. Dvorak K, Higgins A, Palting J, Cohen M, Brunhoeber P. Immunohistochemistry with anti-BRAF V600E (VE1) mouse monoclonal antibody is a sensitive method for detection of the BRAF V600E mutation in colon cancer: evaluation of 120 cases with and without KRAS mutation and literature review. *Pathol Oncol Res* (2019) 25:349–59. doi:10.1007/s12253-017-0344-x

115. Ritterhouse LL, Barletta JA. BRAF V600E mutation-specific antibody: a review. *Semin Diagn Pathol* (2015) 32:400–8. doi:10.1053/j.semdp.2015.02.010

116. Rössle M, Sigg M, Rüschoff JH, Wild PJ, Moch H, Weber A, et al. Ultra-deep sequencing confirms immunohistochemistry as a highly sensitive and specific method for detecting BRAF V600E mutations in colorectal carcinoma. *Virchows Arch* (2013) 463:623–31. doi:10.1007/s00428-013-1492-3

117. Routhier CA, Mochel MC, Lynch K, Dias-Santagata D, Louis DN, Hoang MP. Comparison of 2 monoclonal antibodies for immunohistochemical detection of BRAF V600E mutation in malignant melanoma, pulmonary carcinoma, gastrointestinal carcinoma, thyroid carcinoma, and gliomas. *Hum Pathol.* (2013) 44:2563–70. doi:10.1016/j.humpath.2013.06.018

118. Qiu T, Lu H, Guo L, Huang W, Ling Y, Shan L, et al. Detection of BRAF mutation in Chinese tumor patients using a highly sensitive antibody immunohistochemistry assay. *Sci Rep* (2015) 5:9211. doi:10.1038/srep09211

119. Hwang I, Choi YL, Lee H, Hwang S, Lee B, Yang H, et al. Selection strategies and practical application of BRAF V600e-mutated non-small cell lung carcinoma. *Cancer Res Treat* (2022) 54:782–92. doi:10.4143/crt.2021.843

120. Ettinger DS, Wood DE, Riely GJ, Aisner DL, Akerley W, Bauman JR, et al. NCCN guidelines insights: non-small cell lung cancer, version 2.2021. *J Natl Compr Canc Netw* (2021) 19:254–66. doi:10.6004/jnccn.2021.0013

121. Bartram CR, de Klein A, Hagemeijer A, van Agthoven T, Geurts van Kessel A, Bootsma D, et al. Translocation of c-ab1 oncogene correlates with the presence of a Philadelphia chromosome in chronic myelocytic leukaemia. *Nature* (1983) 306: 277–80. doi:10.1038/306277a0

122. Iwahara T, Fujimoto J, Wen D, Cupples R, Bucay N, Arakawa T, et al. Molecular characterization of ALK, a receptor tyrosine kinase expressed specifically in the nervous system. *Oncogene* (1997) 14:439–49. doi:10.1038/sj.onc.1200849

123. Stoica GE, Kuo A, Aigner A, Sunitha I, Souttou B, Malerczyk C, et al. Identification of anaplastic lymphoma kinase as a receptor for the growth factor pleiotrophin. *J Biol Chem* (2001) 276:16772–9. doi:10.1074/jbc.M010660200

124. De Munck S, Provost M, Kurikawa M, Omori I, Mukohyama J, Felix J, et al. Structural basis of cytokine-mediated activation of ALK family receptors. *Nature* (2021) 600:143–7. doi:10.1038/s41586-021-03959-5

125. Barreca A, Lasorsa E, Riera L, Machiorlatti R, Piva R, Ponzoni M, et al. Anaplastic lymphoma kinase in human cancer. *J Mol Endocrinol* (2011) 47:R11–23. doi:10.1530/JME-11-0004

126. Carén H, Abel F, Kogner P, Martinsson T. High incidence of DNA mutations and gene amplifications of the ALK gene in advanced sporadic neuroblastoma tumours. *Biochem J* (2008) 416:153–9. doi:10.1042/bj20081834

127. Zito Marino F, Rocco G, Morabito A, Mignogna C, Intartaglia M, Liguori G, et al. A new look at the ALK gene in cancer: copy number gain and amplification. *Expert Rev Anticancer Ther* (2016) 16:493–502. doi:10.1586/14737140.2016.1162098

128. Smolle E, Taucher V, Lindenmann J, Jost PJ, Pichler M. Current knowledge about mechanisms of drug resistance against ALK inhibitors in non-small cell lung cancer. *Cancers (Basel)* (2021) 13:699. doi:10.3390/cancers13040699

129. Elshatlawy M, Sampson J, Clarke K, Bayliss R. EML4-ALK biology and drug resistance in non-small cell lung cancer: a new phase of discoveries. *Mol Oncol* (2023) 17:950–63. doi:10.1002/1878-0261.13446

130. Morris SW, Kirstein MN, Valentine MB, Dittmer KG, Shapiro DN, Saltman DL, et al. Fusion of a kinase gene, ALK, to a nucleolar protein gene, NPM, in non-Hodgkin's lymphoma. *Science* (1994) 263:1281–4. doi:10.1126/science.8122112

131. Griffin CA, Hawkins AL, Dvorak C, Henkle C, Ellingham T, Perlman EJ. Recurrent involvement of 2p23 in inflammatory myofibroblastic tumors. *Cancer Res* (1999) 59:2776–80. PMID: 10383129.

132. Lin E, Li L, Guan Y, Soriano R, Rivers CS, Mohan S, et al. Exon array profiling detects EML4-ALK fusion in breast, colorectal, and non-small cell lung cancers. *Mol Cancer Res* (2009) 7:1466–76. doi:10.1158/1541-7786.MCR-08-0522

133. Soda M, Choi YL, Enomoto M, Takada S, Yamashita Y, Ishikawa S, et al. Identification of the transforming EML4-ALK fusion gene in non-small-cell lung cancer. *Nature* (2007) 448:561–6. doi:10.1038/nature05945

134. Inamura K, Takeuchi K, Togashi Y, Nomura K, Ninomiya H, Okui M, et al. EML4-ALK fusion is linked to histological characteristics in a subset of lung cancers. *J Thorac Oncol* (2008) 3:13–7. doi:10.1097/JTO.0b013e31815e8b60

135. Takahashi T, Sonobe M, Kobayashi M, Yoshizawa A, Menju T, Nakayama E, et al. Clinicopathologic features of non-small-cell lung cancer with EML4-ALK fusion gene. *Ann Surg Oncol* (2010) 17:889–97. doi:10.1245/s10434-009-0808-7

136. Mino-Kenudson M, Chirieac LR, Law K, Hornick JL, Lindeman N, Mark EJ, et al. A novel, highly sensitive antibody allows for the routine detection of ALK-rearranged lung adenocarcinomas by standard immunohistochemistry. *Clin Cancer Res* (2010) 16:1561–71. doi:10.1158/1078-0432.CCR-09-2845

137. Paik JH, Choi CM, Kim H, Jang SJ, Choe G, Kim DK, et al. Clinicopathologic implication of ALK rearrangement in surgically resected lung cancer: a proposal of diagnostic algorithm for ALK-rearranged adenocarcinoma. *Lung Cancer* (2012) 76: 403–9. doi:10.1016/j.lungcan.2011.11.008

138. Conde E, Rojo F, Gómez J, Enguita AB, Abdulkader I, González A, et al. Molecular diagnosis in non-small-cell lung cancer: expert opinion on ALK and ROS1 testing. *J Clin Pathol* (2022) 75:145–53. doi:10.1136/jclinpath-2021-207490

139. Zhou J, Yao H, Zhao J, Zhang S, You Q, Sun K, et al. Cell block samples from malignant pleural effusion might be valid alternative samples for anaplastic lymphoma kinase detection in patients with advanced non-small-cell lung cancer. *Histopathology.* (2015) 66:949–54. doi:10.1111/his.12560

140. Matsushime H, Wang LH, Shibuya M. Human c-ros-1 gene homologous to the v-ros sequence of UR2 sarcoma virus encodes for a transmembrane receptorlike molecule. *Mol Cell Biol* (1986) 6:3000–4. doi:10.1128/mcb.6.8.3000

141. Balduzzi PC, Notter MF, Morgan HR, Shibuya M. Some biological properties of two new avian sarcoma viruses. *J Virol* (1981) 40:268–75. doi:10.1128/JVI.40.1.268-275.1981

142. Acquaviva J, Wong R, Charest A. The multifaceted roles of the receptor tyrosine kinase ROS in development and cancer. *Biochim Biophys Acta* (2009) 1795:37–52. doi:10.1016/j.bbcan.2008.07.006

143. Rimkunas VM, Crosby KE, Li D, Hu Y, Kelly ME, Gu TL, et al. Analysis of receptor tyrosine kinase ROS1-positive tumors in non-small cell lung cancer: identification of a FIG-ROS1 fusion. *Clin Cancer Res* (2012) 18:4449–57. doi:10.1158/1078-0432.CCR-11-3351

144. Nguyen KT, Zong CS, Uttamsingh S, Sachdev P, Bhanot M, Le MT, et al. The role of phosphatidylinositol 3-kinase, rho family GTPases, and STAT3 in Ros-induced cell transformation. *J Biol Chem* (2002) 277:11107–15. doi:10.1074/jbc.M108166200

145. Charest A, Lane K, McMahon K, Park J, Preisinger E, Conroy H, et al. Fusion of FIG to the receptor tyrosine kinase ROS in a glioblastoma with an interstitial del(6)(q21q21). *Genes Chromosomes Cancer* (2003) 37:58–71. doi:10.1002/gcc.10207

146. Rikova K, Guo A, Zeng Q, Possemato A, Yu J, Haack H, et al. Global survey of phosphotyrosine signaling identifies oncogenic kinases in lung cancer. *Cell* (2007) 131:1190–203. doi:10.1016/j.cell.2007.11.025

147. Zhang Q, Wu C, Ding W, Zhang Z, Qiu X, Mu D, et al. Prevalence of ROS1 fusion in Chinese patients with non-small cell lung cancer. *Thorac Cancer* (2019) 10:47–53. doi:10.1111/1759-7714.12899

148. Cui M, Han Y, Li P, Zhang J, Ou Q, Tong X, et al. Molecular and clinicopathological characteristics of ROS1-rearranged non-small-cell lung cancers identified by next-generation sequencing. *Mol Oncol* (2020) 14:2787–95. doi:10.1002/1878-0261.12789

149. Qiu Z, Ye B, Wang K, Zhou P, Zhao S, Li W, et al. Unique genetic characteristics and clinical prognosis of female patients with lung cancer harboring RET fusion gene. *Sci Rep* (2020) 10:10387. doi:10.1038/s41598-020-66883-0

150. Bergethon K, Shaw AT, Ou SH, Katayama R, Lovly CM, McDonald NT, et al. ROS1 rearrangements define a unique molecular class of lung cancers. *J Clin Oncol* (2012) 30:863–70. doi:10.1200/JCO.2011.35.6345

151. Zhu Q, Zhan P, Zhang X, Lv T, Song Y. Clinicopathologic characteristics of patients with ROS1 fusion gene in non-small cell lung cancer: a meta-analysis. *Transl Lung Cancer Res* (2015) 4:300–9. doi:10.3978/j.issn.2218-6751.2015.05.01

152. Zhu VW, Zhao JJ, Gao Y, Syn NL, Zhang SS, Ou SI, et al. Thromboembolism in ALK+ and ROS1+ NSCLC patients: a systematic review and meta-analysis. *Lung Cancer* (2021) 157:147–55. doi:10.1016/j.lungcan.2021.05.019

153. Yoshida A, Tsuta K, Wakai S, Arai Y, Asamura H, Shibata T, et al. Immunohistochemical detection of ROS1 is useful for identifying ROS1 rearrangements in lung cancers. *Mod Pathol.* (2014) 27:711–20. doi:10.1038/modpathol.2013.192

154. Selinger CI, Li BT, Pavlakis N, Links M, Gill AJ, Lee A, et al. Screening for ROS1 gene rearrangements in non-small-cell lung cancers using immunohistochemistry with FISH confirmation is an effective method to identify this rare target. *Histopathology* (2017) 70:402–11. doi:10.1111/his.13076

155. Su Y, Goncalves T, Dias-Santagata D, Hoang MP. Immunohistochemical detection of ROS1 fusion. *Am J Clin Pathol* (2017) 147:77–82. doi:10.1093/ajcp/aqw201

156. Zhao J, Chen X, Zheng J, Kong M, Wang B, Ding W. A genomic and clinicopathological study of non-small-cell lung cancers with discordant ROS1 gene status by fluorescence *in-situ* hybridisation and immunohistochemical analysis. *Histopathology.* (2018) 73:19–28. doi:10.1111/his.13492

157. Sharma S, Mishra SK, Bhardwaj M, Jha S, Geller M, Dewan A, et al. Correlation of ROS1 (D4D6) immunohistochemistry with ROS1 fluorescence *in situ* hybridization assay in a contemporary cohort of pulmonary adenocarcinomas. *South Asian J Cancer* (2022) 11:249–55. doi:10.1055/s-0042-1750187

158. Hung YP, Sholl LM. Diagnostic and predictive immunohistochemistry for non-small cell lung carcinomas. *Adv Anat Pathol* (2018) 25:374–86. doi:10.1097/PAP.0000000000000206

159. Bubendorf L, Büttner R, Al-Dayel F, Dietel M, Elmberger G, Kerr K, et al. Testing for ROS1 in non-small cell lung cancer: a review with recommendations. *Virchows Arch* (2016) 469:489–503. doi:10.1007/s00428-016-2000-3

160. Hofman V, Goffinet S, Bontoux C, Long-Mira E, Lassalle S, Ilié M, et al. A real-world experience from a single center (LPCE, nice, France) highlights the urgent need to abandon immunohistochemistry for ROS1 rearrangement screening of advanced non-squamous non-small cell lung cancer. *J Pers Med* (2023) 13:810. doi:10.3390/jpm13050810

161. Takahashi M, Ritz J, Cooper GM. Activation of a novel human transforming gene, ret, by DNA rearrangement. *Cell* (1985) 42:581–8. doi:10.1016/0092-8674(85)90115-1

162. Ishizaka Y, Itoh F, Tahira T, Ikeda I, Sugimura T, Tucker J, et al. Human ret proto-oncogene mapped to chromosome 10q11.2. *Oncogene* (1989) 4:1519–21. PMID: 2687772.

163. Kjaer S, Ibáñez CF. Identification of a surface for binding to the GDNF-GFR alpha 1 complex in the first cadherin-like domain of RET. *J Biol Chem* (2003) 278:47898–904. doi:10.1074/jbc.M309772200

164. Regua AT, Najjar M, Lo HW. RET signaling pathway and RET inhibitors in human cancer. *Front Oncol* (2022) 12:932353. doi:10.3389/fonc.2022.932353

165. Ibanez CF. Structure and physiology of the ret receptor tyrosine kinase. *Cold Spring Harb Perspect Biol* (2013) 5:a009134–10. doi:10.1101/cshperspect.a009134

166. Tomuschat C, Puri P. Ret gene is a major risk factor for Hirschsprung's disease: a meta-analysis. *Pediatr Surg Int* (2015) 31:701–10. doi:10.1007/s00383-015-3731-y

167. Grieco M, Santoro M, Berlingieri MT, Melillo RM, Donghi R, Bongarzone I, et al. PTC is a novel rearranged form of the ret proto-oncogene and is frequently detected *in vivo* in human thyroid papillary carcinomas. *Cell* (1990) 60:557–63. doi:10.1016/0092-8674(90)90659-3

168. Donis-Keller H, Dou S, Chi D, Carlson KM, Toshima K, Lairmore TC, et al. Mutations in the RET proto-oncogene are associated with MEN 2A and FMTC. *Hum Mol Genet* (1993) 2:851–6. doi:10.1093/hmg/2.7.851

169. Mulligan LM, Kwok JB, Healey CS, Elsdon MJ, Eng C, Gardner E, et al. Germ-line mutations of the RET proto-oncogene in multiple endocrine neoplasia type 2A. *Nature* (1993) 363:458–60. doi:10.1038/363458a0

170. Ju YS, Lee WC, Shin JY, Lee S, Bleazard T, Won JK, et al. A transforming KIF5B and RET gene fusion in lung adenocarcinoma revealed from whole-genome and transcriptome sequencing. *Genome Res* (2012) 22:436–45. doi:10.1101/gr.133645.111

171. Lipson D, Capelletti M, Yelensky R, Otto G, Parker A, Jarosz M, et al. Identification of new ALK and RET gene fusions from colorectal and lung cancer biopsies. *Nat Med* (2012) 18:382–4. doi:10.1038/nm.2673

172. Kohno T, Ichikawa H, Totoki Y, Yasuda K, Hiramoto M, Nammo T, et al. KIF5B-RET fusions in lung adenocarcinoma. *Nat. Med.* (2012) 18:375–7. doi:10.1038/nm.2644

173. Takeuchi K, Soda M, Togashi Y, Suzuki R, Sakata S, Hatano S, et al. RET, ROS1 and ALK fusions in lung cancer. *Nat. Med.* (2012) 18:378–81. doi:10.1038/nm.2658

174. Kohno T, Tsuta K, Tsuchihara K, Nakaoku T, Yoh K, Goto K. RET fusion gene: translation to personalized lung cancer therapy. *Cancer Sci* (2013) 104:1396–400. doi:10.1111/cas.12275

175. Kato S, Subbiah V, Marchlik E, Elkin SK, Carter JL, Kurzrock R. Ret aberrations in diverse cancers: next-generation sequencing of 4,871 patients. *Clin Cancer Res* (2017) 23:1988–97. doi:10.1158/1078-0432.CCR-16-1679

176. Piotrowska Z, Isozaki H, Lennerz JK, Gainor JF, Lennes IT, Zhu VW, et al. Landscape of acquired resistance to osimertinib in EGFR-mutant NSCLC and clinical validation of combined EGFR and RET inhibition with osimertinib and BLU-667 for acquired RET fusion. *Cancer Discov.* (2018) 8:1529–39. doi:10.1158/2159-8290.CD-18-1022

177. Wang R, Hu H, Pan Y, Li Y, Ye T, Li C, et al. RET fusions define a unique molecular and clinicopathologic subtype of non-small-cell lung cancer. *J Clin Oncol* (2012) 30:4352–9. doi:10.1200/JCO.2012.44.1477

178. Drilon A, Lin JJ, Filleron T, Ni A, Milia J, Bergagnini I, et al. Frequency of brain metastases and multikinase inhibitor outcomes in patients with RET-rearranged lung cancers. *J Thorac Oncol* (2018) 13:1595–601. doi:10.1016/j.jtho.2018.07.004

179. Drilon A, Wang L, Hasanovic A, Suehara Y, Lipson D, Stephens P, et al. Response to Cabozantinib in patients with RET fusion-positive lung adenocarcinomas. *Cancer Discov* (2013) 3:630–5. doi:10.1158/2159-8290.CD-13-0035

180. Subbiah V, Velcheti V, Tuch BB, Ebata K, Busaidy NL, Cabanillas ME, et al. Selective RET kinase inhibition for patients with RET-altered cancers. *Ann Oncol* (2018) 29:1869–76. doi:10.1093/annonc/mdy137

181. Mulligan L. Selective RET kinase inhibitors and lung cancer. *N Engl J Med* (2023) 389:1913–6. doi:10.1056/NEJMe2311295

182. Zhou C, Solomon B, Loong HH, Park K, Pérol M, Arriola E, et al. First-line selpercatinib or chemotherapy and pembrolizumab in RET fusion-positive NSCLC. *N Engl J Med* (2023) 389:1839–50. doi:10.1056/NEJMoa2309457

183. Go H, Jung YJ, Kang HW, Park IK, Kang CH, Lee JW, et al. Diagnostic method for the detection of KIF5B-RET transformation in lung adenocarcinoma. *Lung Cancer* (2013) 82:44–50. doi:10.1016/j.lungcan.2013.07.009

184. Feng J, Li Y, Wei B, Guo L, Li W, Xia Q, et al. Clinicopathologic characteristics and diagnostic methods of RET rearrangement in Chinese non-small cell lung cancer patients. *Transl Lung Cancer Res* (2022) 11:617–31. doi:10.21037/tlcr-22-202

185. Yang SR, Aypar U, Rosen EY, Mata DA, Benayed R, Mullaney K, et al. A performance comparison of commonly used assays to detect RET fusions. *Clin Cancer Res* (2021) 27:1316–28. doi:10.1158/1078-0432.CCR-20-3208

186. Pu X, Xu C, Wang Q, Wang W, Wu F, Cai X, et al. Expert consensus on the diagnosis and treatment of RET gene fusion non-small cell lung cancer in China. *Thorac Cancer* (2023) 14:3166–77. doi:10.1111/1759-7714.15105

187. Huang EJ, Reichardt LF. Trk receptors: roles in neuronal signal transduction. *Annu Rev Biochem* (2003) 72:609–42. doi:10.1146/annurev.biochem.72.121801.161629

188. Donovan MJ, Miranda RC, Kraemer R, McCaffrey TA, Tessarollo L, Mahadeo D, et al. Neurotrophin and neurotrophin receptors in vascular smooth muscle cells. Regulation of expression in response to injury. *Am J Pathol* (1995) 147:309–24. PMID: 7639328.

189. Arévalo JC, Wu SH. Neurotrophin signaling: many exciting surprises. *Cell Mol Life Sci* (2006) 63:1523–37. doi:10.1007/s00018-006-6010-1

190. Martin-Zanca D, Hughes SH, Barbacid M. A human oncogene formed by the fusion of truncated tropomyosin and protein tyrosine kinase sequences. *Nature* (1986) 319(6056):743–8. doi:10.1038/319743a0

191. Knezevich SR, McFadden DE, Tao W, Lim JF, Sorensen PH. A novel ETV6-NTRK3 gene fusion in congenital fibrosarcoma. *Nat Genet* (1998) 18:184–7. doi:10.1038/ng0298-184

192. Tognon C, Knezevich SR, Huntsman D, Roskelley CD, Melnyk N, Mathers JA, et al. Expression of the ETV6-NTRK3 gene fusion as a primary event in human secretory breast carcinoma. *Cancer Cell* (2002) 2:367–76. doi:10.1016/s1535-6108(02)00180-0

193. Westphalen CB, Krebs MG, Le Tourneau C, Sokol ES, Maund SL, Wilson TR, et al. Genomic context of NTRK1/2/3 fusion-positive tumours from a large real-world population. *NPJ Precis Oncol* (2021) 5:69. doi:10.1038/s41698-021-00206-y

194. Vaishnavi A, Capelletti M, Le AT, Kako S, Butaney M, Ercan D, et al. Oncogenic and drug-sensitive NTRK1 rearrangements in lung cancer. *Nat Med* (2013) 19:1469–72. doi:10.1038/nm.3352

195. Gatalica Z, Xiu J, Swensen J, Vranic S. Molecular characterization of cancers with NTRK gene fusions. *Mod Pathol.* (2019) 32:147–53. doi:10.1038/s41379-018-0118-3

196. Solomon JP, Linkov I, Rosado A, Mullaney K, Rosen EY, Frosina D, et al. NTRK fusion detection across multiple assays and 33,997 cases: diagnostic implications and pitfalls. *Mod Pathol* (2020) 33:38–46. doi:10.1038/s41379-019-0324-7

197. Farago AF, Taylor MS, Doebele RC, Zhu VW, Kummar S, Spira AI, et al. Clinicopathologic features of non-small-cell lung cancer harboring an NTRK gene fusion. *JCO Precis Oncol* (2018) 2018:1–12. PO.18.00037. doi:10.1200/PO.18.00037

198. Harada G, Santini FC, Wilhelm C, Drilon A. NTRK fusions in lung cancer: from biology to therapy. *Lung Cancer* (2021) 161:108–13. doi:10.1016/j.lungcan.2021.09.005

199. Delgado J, Pean E, Melchiorri D, Migali C, Josephson F, Enzmann H, et al. The European Medicines Agency review of entrectinib for the treatment of adult or paediatric patients with solid tumours who have a neurotrophic tyrosine receptor kinase gene fusions and adult patients with non-small-cell lung cancer harbouring ROS1 rearrangements. *ESMO Open* (2021) 6:100087. doi:10.1016/j.esmoop.2021.100087

200. Cho BC, Chiu CH, Massarelli E, Buchschacher GL, Goto K, Overbeck TR, et al. Updated efficacy and safety of entrectinib in NTRK fusion-positive non-small cell lung cancer. *Lung Cancer* (2023) 188:107442. doi:10.1016/j.lungcan.2023.107442

201. Liu F, Wei Y, Zhang H, Jiang J, Zhang P, Chu Q. NTRK fusion in non-small cell lung cancer: diagnosis, therapy, and TRK inhibitor resistance. *Front Oncol* (2022) 12:864666. doi:10.3389/fonc.2022.864666

202. Strohmeier S, Brcic I, Popper H, Liegl-Atzwanger B, Lindenmann J, Brcic L. Applicability of pan-TRK immunohistochemistry for identification of NTRK fusions in lung carcinoma. *Sci Rep* (2021) 11:9785. doi:10.1038/s41598-021-89373-3

203. Vingiani A, Lorenzini D, Conca E, Volpi CC, Trupia DV, Gloghini A, et al. Pan-TRK immunohistochemistry as screening tool for NTRK fusions: a diagnostic workflow for the identification of positive patients in clinical practice. *Cancer Biomark* (2023) 38:301–9. doi:10.3233/CBM-220357

204. Hechtman JF, Benayed R, Hyman DM, Drilon A, Zehir A, Frosina D, et al. Pan-trk immunohistochemistry is an efficient and reliable screen for the detection of NTRK fusions. *Am J Surg Pathol.* (2017) 41:1547–51. doi:10.1097/PAS.0000000000000911

205. Overbeck TR, Reiffert A, Schmitz K, Rittmeyer A, Körber W, Hugo S, et al. NTRK gene fusions in non-small-cell lung cancer: real-world screening data of 1068 unselected patients. *Cancers (Basel)* (2023) 15:2966. doi:10.3390/cancers15112966

206. Cooper CS, Park M, Blair DG, Tainsky MA, Huebner K, Croce CM, et al. Molecular cloning of a new transforming gene from a chemically transformed human cell line. *Nature* (1984) 311:29–33. doi:10.1038/311029a0

207. Dean M, Park M, Le Beau MM, Robins TS, Diaz MO, Rowley JD, et al. The human met oncogene is related to the tyrosine kinase oncogenes. *Nature* (1985) 318:385–8. doi:10.1038/318385a0

208. Naldini L, Weidner KM, Vigna E, Gaudino G, Bardelli A, Ponzetto C, et al. Scatter factor and hepatocyte growth factor are indistinguishable ligands for the MET receptor. *EMBO J.* (1991) 10:2867–78. doi:10.1002/j.1460-2075.1991.tb07836.x

209. Giordano S, Di Renzo MF, Narsimhan RP, Cooper CS, Rosa C, Comoglio PM. Biosynthesis of the protein encoded by the c-met proto-oncogene. *Oncogene* (1989) 4:1383–8. PMID: 2554238.

210. Gherardi E, Youles ME, Miguel RN, Blundell TL, Iamele L, Gough J, et al. Functional map and domain structure of MET, the product of the c-met protooncogene and receptor for hepatocyte growth factor/scatter factor. *Proc Natl Acad Sci U S A* (2003) 100:12039–44. doi:10.1073/pnas.2034936100

211. Lamorte L, Royal I, Naujokas M, Park M. Crk adapter proteins promote an epithelial-mesenchymal-like transition and are required for HGF-mediated cell spreading and breakdown of epithelial adherens junctions. *Mol Biol Cell* (2002) 13:1449–61. doi:10.1091/mbc.01-10-0477

212. Organ SL, Tsao MS. An overview of the c-MET signaling pathway. *Ther Adv Med Oncol* (2011) 3:S7–S19. doi:10.1177/1758834011422556

213. Gherardi E, Birchmeier W, Birchmeier C, Vande Woude G. Targeting MET in cancer: rationale and progress. *Nat Rev Cancer* (2012) 12:89–103. doi:10.1038/nrc3205

214. Petrelli A, Gilestro GF, Lanzardo S, Comoglio PM, Migone N, Giordano S. The endophilin-CIN85-Cbl complex mediates ligand-dependent downregulation of c-Met. *Nature* (2002) 416:187–90. doi:10.1038/416187a

215. Joffre C, Barrow R, Ménard L, Calleja V, Hart IR, Kermorgant S. A direct role for Met endocytosis in tumorigenesis. *Nat Cell Biol* (2011) 13:827–37. doi:10.1038/ncb2257

216. Engelman JA, Zejnullahu K, Mitsudomi T, Song Y, Hyland C, Park JO, et al. MET amplification leads to gefitinib resistance in lung cancer by activating ERBB3 signaling. *Science* (2007) 316:1039–43. doi:10.1126/science.1141478

217. Bean J, Brennan C, Shih JY, Riely G, Viale A, Wang L, et al. MET amplification occurs with or without T790M mutations in EGFR mutant lung tumors with acquired resistance to gefitinib or erlotinib. *Proc Natl Acad Sci U S A* (2007) 104:20932–7. doi:10.1073/pnas.0710370104

218. Schmidt L, Duh FM, Chen F, Kishida T, Glenn G, Choyke P, et al. Germline and somatic mutations in the tyrosine kinase domain of the MET proto-oncogene in papillary renal carcinomas. *Nat Genet* (1997) 16:68–73. doi:10.1038/ng0597-68

219. Gow CH, Liu YN, Li HY, Hsieh MS, Chang SH, Luo SC, et al. Oncogenic function of a KIF5B-met fusion variant in non-small cell lung cancer. *Neoplasia* (2018) 20:838–47. doi:10.1016/j.neo.2018.06.007

220. Kong-Beltran M, Seshagiri S, Zha J, Zhu W, Bhawe K, Mendoza N, et al. Somatic mutations lead to an oncogenic deletion of met in lung cancer. *Cancer Res* (2006) 66:283–9. doi:10.1158/0008-5472.CAN-05-2749

221. Lee JH, Gao CF, Lee CC, Kim MD, Vande Woude GF. An alternatively spliced form of Met receptor is tumorigenic. *Exp Mol Med* (2006) 38:565–73. doi:10.1038/emm.2006.66

222. Frampton GM, Ali SM, Rosenzweig M, Chmielecki J, Lu X, Bauer TM, et al. Activation of MET via diverse exon 14 splicing alterations occurs in multiple tumor types and confers clinical sensitivity to MET inhibitors. *Cancer Discov* (2015) 5:850–9. doi:10.1158/2159-8290.CD-15-0285

223. Mazieres J, Vioix H, Pfeiffer BM, Campden RI, Chen Z, Heeg B, et al. MET exon 14 skipping in NSCLC: a systematic literature review of epidemiology, clinical characteristics, and outcomes. *Clin Lung Cancer* (2023) 24:483–97. doi:10.1016/j.cllc.2023.06.008

224. Markham A. Savolitinib: first approval. *Drugs* (2021) 81:1665–70. doi:10.1007/s40265-021-01584-0

225. Cortot AB, Kherrouche Z, Descarpentries C, Wislez M, Baldacci S, Furlan A, et al. Exon 14 deleted MET receptor as a new biomarker and target in cancers. *J Natl Cancer Inst* (2017) 109. doi:10.1093/jnci/djw262

226. Ma PC, Tretiakova MS, MacKinnon AC, Ramnath N, Johnson C, Dietrich S, et al. Expression and mutational analysis of MET in human solid cancers. *Genes Chromosomes Cancer* (2008) 47:1025–37. doi:10.1002/gcc.20604

227. Salgia R. MET in lung cancer: biomarker selection based on scientific rationale. *Mol Cancer Ther* (2017) 16:555–65. doi:10.1158/1535-7163.MCT-16-0472

228. Guo R, Berry LD, Aisner DL, Sheren J, Boyle T, Bunn PA, Jr, et al. MET IHC is a poor screen for MET amplification or MET exon 14 mutations in lung adenocarcinomas: data from a tri-institutional cohort of the lung cancer mutation consortium. *J Thorac Oncol* (2019) 14:1666–71. doi:10.1016/j.jtho.2019.06.009

229. Davies KD, Lomboy A, Lawrence CA, Yourshaw M, Bocsi GT, Camidge DR, et al. DNA-based versus RNA-based detection of MET exon 14 skipping events in lung cancer. *J Thorac Oncol* (2019) 14:737–41. doi:10.1016/j.jtho.2018.12.020

230. Poirot B, Doucet L, Benhenda S, Champ J, Meignin V, Lehmann-Che J. MET exon 14 alterations and new resistance mutations to tyrosine kinase inhibitors: risk of inadequate detection with current amplicon-based NGS panels. *J Thorac Oncol* (2017) 12:1582–7. doi:10.1016/j.jtho.2017.07.026

231. Heydt C, Ihle MA, Merkelbach-Bruse S. Overview of molecular detection technologies for MET in lung cancer. *Cancers (Basel)* (2023) 15:2932. doi:10.3390/cancers15112932

232. Lee JK, Madison R, Classon A, Gjoerup O, Rosenzweig M, Frampton GM, et al. Characterization of non-small-cell lung cancers with MET exon 14 skipping alterations detected in tissue or liquid: clinicogenomics and real-world treatment patterns. *JCO Precis Oncol* (2021) 5:1354–76. PO.21.00122. doi:10.1200/PO.21.00122

233. Bargmann CI, Hung MC, Weinberg RA. The neu oncogene encodes an epidermal growth factor receptor-related protein. *Nature* (1986) 319:226–30. doi:10.1038/319226a0

234. Gutierrez C, Schiff R. HER2: biology, detection, and clinical implications. *Arch Pathol Lab Med* (2011) 135:55–62. doi:10.1043/2010-0454-RAR.1

235. Goldenberg MM. Trastuzumab, a recombinant DNA-derived humanized monoclonal antibody, a novel agent for the treatment of metastatic breast cancer. *Clin Ther* (1999) 21:309–18. doi:10.1016/S0149-2918(00)88288-0

236. Hechtman JF, Polydorides AD. HER2/neu gene amplification and protein overexpression in gastric and gastroesophageal junction adenocarcinoma: a review of histopathology, diagnostic testing, and clinical implications. *Arch Pathol Lab Med.* (2012) 136:691–7. doi:10.5858/arpa.2011-0168-RS

237. Hirsch FR, Varella-Garcia M, Franklin WA, Veve R, Chen L, Helfrich B, et al. Evaluation of HER-2/neu gene amplification and protein expression in non-small cell lung carcinomas. *Br J Cancer* (2002) 86:1449–56. doi:10.1038/sj.bjc.6600286

238. Stephens P, Hunter C, Bignell G, Edkins S, Davies H, Teague J, et al. Lung cancer: intragenic ERBB2 kinase mutations in tumours. *Nature* (2004) 431:525–6. doi:10.1038/431525b

239. Shigematsu H, Takahashi T, Nomura M, Majmudar K, Suzuki M, Lee H, et al. Somatic mutations of the HER2 kinase domain in lung adenocarcinomas. *Cancer Res* (2005) 65:1642–6. doi:10.1158/0008-5472.CAN-04-4235

240. Wang SE, Narasanna A, Perez-Torres M, Xiang B, Wu FY, Yang S, et al. HER2 kinase domain mutation results in constitutive phosphorylation and activation of HER2 and EGFR and resistance to EGFR tyrosine kinase inhibitors. *Cancer Cell* (2006) 10:25–38. doi:10.1016/j.ccr.2006.05.023

241. Sentana-Lledo D, Academia E, Viray H, Rangachari D, Kobayashi SS, VanderLaan PA, et al. EGFR exon 20 insertion mutations and ERBB2 mutations in lung cancer: a narrative review on approved targeted therapies from oral kinase inhibitors to antibody-drug conjugates. *Transl Lung Cancer Res* (2023) 12:1590–610. doi:10.21037/tlcr-23-98

242. Yang S, Wang Y, Zhao C, Li X, Liu Q, Mao S, et al. Exon 20 YVMA insertion is associated with high incidence of brain metastasis and inferior outcome of chemotherapy in advanced non-small cell lung cancer patients with HER2 kinase domain mutations. *Transl Lung Cancer Res* (2021) 10:753–65. doi:10.21037/tlcr-20-559

243. Offin M, Feldman D, Ni A, Myers ML, Lai WV, Pentsova E, et al. Frequency and outcomes of brain metastases in patients with HER2-mutant lung cancers. *Cancer* (2019) 125:4380–7. doi:10.1002/cncr.32461

244. Pillai RN, Behera M, Berry LD, Rossi MR, Kris MG, Johnson BE, et al. HER2 mutations in lung adenocarcinomas: a report from the Lung Cancer Mutation Consortium. *Cancer* (2017) 123:4099–105. doi:10.1002/cncr.30869

245. Arcila ME, Chaft JE, Nafa K, Roy-Chowdhuri S, Lau C, Zaidinski M, et al. Prevalence, clinicopathologic associations, and molecular spectrum of ERBB2 (HER2) tyrosine kinase mutations in lung adenocarcinomas. *Clin Cancer Res* (2012) 18:4910–8. doi:10.1158/1078-0432.CCR-12-0912

246. Ramalingam SS, Yang JC, Lee CK, Kurata T, Kim DW, John T, et al. Osimertinib as first-line treatment of EGFR mutation-positive advanced non-small-cell lung cancer. *J Clin Oncol* (2018) 36:841–9. doi:10.1200/JCO.2017.74.7576

247. Ren S, Wang J, Ying J, Mitsudomi T, Lee DH, Wang Z, et al. Consensus for HER2 alterations testing in non-small-cell lung cancer. *ESMO Open* (2022) 7:100395. doi:10.1016/j.esmoop.2022.100395

248. Rizvi NA, Hellmann MD, Snyder A, Kvistborg P, Makarov V, Havel JJ, et al. Cancer immunology. Mutational landscape determines sensitivity to PD-1 blockade in non-small cell lung cancer. *Science* (2015) 348:124–8. doi:10.1126/science.aaa1348

249. Sun C, Mezzadra R, Schumacher TN. Regulation and function of the PD-L1 checkpoint. *Immunity* (2018) 48:434–52. doi:10.1016/j.immuni.2018.03.014

250. Ishida Y, Agata Y, Shibahara K, Honjo T. Induced expression of PD-1, a novel member of the immunoglobulin gene superfamily, upon programmed cell death. *EMBO J.* (1992) 11:3887–95. doi:10.1002/j.1460-2075.1992.tb05481.x

251. Zak KM, Kitel R, Przetocka S, Golik P, Guzik K, Musielak B, et al. Structure of the complex of human programmed death 1, PD-1, and its ligand PD-L1. *Structure* (2015) 23:2341–8. doi:10.1016/j.str.2015.09.010

252. Nishimura H, Nose M, Hiai H, Minato N, Honjo T. Development of lupus-like autoimmune diseases by disruption of the PD-1 gene encoding an ITIM motif-carrying immunoreceptor. *Immunity* (1999) 11:141–51. doi:10.1016/s1074-7613(00)80089-8

253. Pan ZK, Ye F, Wu X, An HX, Wu JX. Clinicopathological and prognostic significance of programmed cell death ligand1 (PD-L1) expression in patients with non-small cell lung cancer: a meta-analysis. *J Thorac Dis* (2015) 7:462–70. doi:10.3978/j.issn.2072-1439.2015.02.13

254. Skov BG, Rørvig SB, Jensen THL, Skov T. The prevalence of programmed death ligand-1 (PD-L1) expression in non-small cell lung cancer in an unselected, consecutive population. *Mod Pathol* (2020) 33:109–17. doi:10.1038/s41379-019-0339-0

255. Brahmer JR, Drake CG, Wollner I, Powderly JD, Picus J, Sharfman WH, et al. Phase I study of single-agent anti-programmed death-1 (MDX-1106) in refractory solid tumors: safety, clinical activity, pharmacodynamics, and immunologic correlates. *J Clin Oncol* (2010) 28:3167–75. doi:10.1200/JCO.2009.26.7609

256. Garon EB, Rizvi NA, Hui R, Leighl N, Balmanoukian AS, Eder JP, et al. Pembrolizumab for the treatment of non-small-cell lung cancer. *N Engl J Med* (2015) 372:2018–28. doi:10.1056/NEJMoa1501824

257. Jørgensen JT. Companion and complementary diagnostics: clinical and regulatory perspectives. *Trends Cancer* (2016) 2:706–12. doi:10.1016/j.trecan.2016.10.013

258. Dolled-Filhart M, Roach C, Toland G, Stanforth D, Jansson M, Lubiniecki GM, et al. Development of a companion diagnostic for pembrolizumab in non-small cell lung cancer using immunohistochemistry for programmed death ligand-1. *Arch Pathol Lab Med* (2016) 140:1243–9. doi:10.5858/arpa.2015-0542-OA

259. Kazandjian D, Suzman DL, Blumenthal G, Mushti S, He K, Libeg M, et al. FDA approval summary: nivolumab for the treatment of metastatic non-small cell lung cancer with progression on or after platinum-based chemotherapy. *Oncologist* (2016) 21:634–42. doi:10.1634/theoncologist.2015-0507

260. Fehrenbacher L, Spira A, Ballinger M, Kowanetz M, Vansteenkiste J, Mazieres J, et al. Atezolizumab versus docetaxel for patients with previously treated non-small-cell lung cancer (POPLAR): a multicentre, open-label, phase 2 randomised controlled trial. *Lancet* (2016) 387:1837–46. doi:10.1016/S0140-6736(16)00587-0

261. Sezer A, Kilickap S, Gümüş M, Bondarenko I, Özgüroğlu M, Gogishvili M, et al. Cemiplimab monotherapy for first-line treatment of advanced non-small-cell lung cancer with PD-L1 of at least 50%: a multicentre, open-label, global, phase 3, randomised, controlled trial. *Lancet* (2021) 397:592–604. doi:10.1016/S0140-6736(21)00228-2

262. Kim SY, Kim TE, Park CK, Yoon HK, Sa YJ, Kim HR, et al. Comprehensive comparison of 22C3 and SP263 PD-L1 expression in non-small-cell lung cancer using routine clinical and conditioned archives. *Cancers (Basel)* (2022) 14:3138. doi:10.3390/cancers14133138

263. Hendriks LE, Kerr KM, Menis J, Mok TS, Nestle U, Passaro A, et al. Non-oncogene-addicted metastatic non-small-cell lung cancer: ESMO Clinical Practice Guideline for diagnosis, treatment and follow-up. *Ann Oncol* (2023) 34:358–76. doi:10.1016/j.annonc.2022.12.013

264. Rimm DL, Han G, Taube JM, Yi ES, Bridge JA, Flieder DB, et al. A prospective, multi-institutional, pathologist-based assessment of 4 immunohistochemistry assays for PD-L1 expression in non-small cell lung cancer. *JAMA Oncol* (2017) 3:1051–8. doi:10.1001/jamaoncol.2017.0013

265. Hirsch FR, McElhinny A, Stanforth D, Ranger-Moore J, Jansson M, Kulangara K, et al. PD-L1 immunohistochemistry assays for lung cancer: results

from phase 1 of the Blueprint PD-L1 IHC assay comparison project. *J Thorac Oncol* (2017) 12:208–22. doi:10.1016/j.jtho.2016.11.2228

266. Tsao MS, Kerr KM, Kockx M, Beasley MB, Borczuk AC, Botling J, et al. PD-L1 immunohistochemistry comparability study in real-life clinical samples: results of Blueprint phase 2 project. *J Thorac Oncol* (2018) 13:1302–11. doi:10.1016/j.jtho.2018.05.013

267. Lozano MD, Abengozar-Muela M, Echeveste JI, Subtil JC, Bertó J, Gúrpide A, et al. Programmed death-ligand 1 expression on direct Pap-stained cytology smears from non-small cell lung cancer: comparison with cell blocks and surgical resection specimens. *Cancer Cytopathol* (2019) 127:470–80. doi:10.1002/cncy.22155

268. Tejerina E, Garca Tobar L, Echeveste JI, de Andrea CE, Vigliar E, Lozano MD. PD-L1 in cytological samples: a review and a practical approach. *Front Med (Lausanne)* (2021) 8:668612. doi:10.3389/fmed.2021.668612

269. Capizzi E, Ricci C, Giunchi F, Zagnoni S, Ceccarelli C, Gómez BUÁ, et al. Validation of the immunohistochemical expression of programmed death ligand 1 (PD-L1) on cytological smears in advanced non small cell lung cancer. *Lung Cancer* (2018) 126:9–14. doi:10.1016/j.lungcan.2018.10.017

270. Heymann JJ, Bulman WA, Swinarski D, Pagan CA, Crapanzano JP, Haghighi M, et al. PD-L1 expression in non-small cell lung carcinoma: comparison among cytology, small biopsy, and surgical resection specimens. *Cancer Cytopathol* (2017) 125:896–907. doi:10.1002/cncy.21937

271. Jain D, Nambirajan A, Borczuk A, Chen G, Minami Y, Moreira AL, et al. Immunocytochemistry for predictive biomarker testing in lung cancer cytology. *Cancer Cytopathol* (2019) 127:325–39. doi:10.1002/cncy.22137

272. Zou Y, Xu L, Tang Q, You Q, Wang X, Ding W, et al. Cytology cell blocks from malignant pleural effusion are good candidates for PD-L1 detection in advanced NSCLC compared with matched histology samples. *BMC Cancer* (2020) 20:344. doi:10.1186/s12885-020-06851-z

273. Layfield LJ, Zhang T, Esebua M. PD-L1 immunohistochemical testing: a review with reference to cytology specimens. *Diagn Cytopathol* (2023) 51:51–8. doi:10.1002/dc.25043

274. Pak MG, Roh MS. Cell-blocks are suitable material for programmed cell death ligand-1 immunohistochemistry: comparison of cell-blocks and matched surgical resection specimens in lung cancer. *Cytopathology* (2019) 30:578–85. doi:10.1111/cyt.12743

275. Huang Z, Chen L, Lv L, Fu CC, Jin Y, Zheng Q, et al. A new AI-assisted scoring system for PD-L1 expression in NSCLC. *Comput Methods Programs Biomed* (2022) 221:106829. doi:10.1016/j.cmpb.2022.106829

276. Cui Q, Li W, Wang D, Wang S, Yu J. Prognostic significance of blood-based PD-L1 analysis in patients with non-small cell lung cancer undergoing immune checkpoint inhibitor therapy: a systematic review and meta-analysis. *World J Surg Oncol* (2023) 21:318. doi:10.1186/s12957-023-03215-2

277. Negrao MV, Skoulidis F, Montesion M, Schulze K, Bara I, Shen V, et al. Oncogene-specific differences in tumor mutational burden, PD-L1 expression, and outcomes from immunotherapy in non-small cell lung cancer. *J Immunother Cancer* (2021) 9:e002891. doi:10.1136/jitc-2021-002891

278. Lan B, Ma C, Zhang C, Chai S, Wang P, Ding L, et al. Association between PD-L1 expression and driver gene status in non-small-cell lung cancer: a meta-analysis. *Oncotarget* (2018) 9:7684–99. doi:10.18632/oncotarget.23969

279. Liu J, Liu Y. Molecular diagnostic characteristics based on the next generation sequencing in lung cancer and its relationship with the expression of PD-L1. *Pathol Res Pract* (2020) 216:152797. doi:10.1016/j.prp.2019.152797

280. Otano I, Ucero AC, Zugazagoitia J, Paz-Ares L. At the crossroads of immunotherapy for oncogene-addicted subsets of NSCLC. *Nat Rev Clin Oncol* (2023) 20:143–59. doi:10.1038/s41571-022-00718-x

281. Lee CK, Man J, Lord S, Links M, Gebski V, Mok T, et al. Checkpoint inhibitors in metastatic EGFR-mutated non-small cell lung cancer-A meta-analysis. *J Thorac Oncol* (2017) 12(2):403–7. doi:10.1016/j.jtho.2016.10.007

282. Mazieres J, Drilon A, Lusque A, Mhanna L, Cortot AB, Mezquita L, et al. Immune checkpoint inhibitors for patients with advanced lung cancer and oncogenic driver alterations: results from the IMMUNOTARGET registry. *Ann Oncol* (2019) 30:1321–8. doi:10.1093/annonc/mdz167

283. Gainor JF, Shaw AT, Sequist LV, Fu X, Azzoli CG, Piotrowska Z, et al. EGFR mutations and ALK rearrangements are associated with low response rates to PD-1 pathway blockade in non-small cell lung cancer: a retrospective analysis. *Clin Cancer Res* (2016) 22:4585–93. doi:10.1158/1078-0432.CCR-15-3101

284. Guisier F, Dubos-Arvis C, Viñas F, Doubre H, Ricordel C, Ropert S, et al. Efficacy and safety of anti-PD-1 immunotherapy in patients with advanced NSCLC with BRAF, HER2, or MET mutations or RET translocation: GFPC 01-2018. *J Thorac Oncol* (2020) 15:628–36. doi:10.1016/j.jtho.2019.12.129

285. Offin M, Guo R, Wu SL, Sabari J, Land JD, Ni A, et al. Immunophenotype and response to immunotherapy of RET-rearranged lung cancers. *JCO Precis Oncol* (2019) 3:1–8. PO.18.00386. doi:10.1200/PO.18.00386

286. Calles A, Liao X, Sholl LM, Rodig SJ, Freeman GJ, Butaney M, et al. Expression of PD-1 and its ligands, PD-L1 and PD-L2, in smokers and never smokers with KRAS-mutant lung cancer. *J Thorac Oncol* (2015) 10:1726–35. doi:10.1097/JTO.0000000000000687

287. Jeanson A, Tomasini P, Souquet-Bressand M, Brandone N, Boucekine M, Grangeon M, et al. Efficacy of immune checkpoint inhibitors in KRAS-mutant non-small cell lung cancer (NSCLC). *J Thorac Oncol* (2019) 14:1095–101. doi:10.1016/j.jtho.2019.01.011

288. Skoulidis F, Byers LA, Diao L, Papadimitrakopoulou VA, Tong P, Izzo J, et al. Co-occurring genomic alterations define major subsets of KRAS-mutant lung adenocarcinoma with distinct biology, immune profiles, and therapeutic vulnerabilities. *Cancer Discov.* (2015) 5:860–77. doi:10.1158/2159-8290.CD-14-1236

289. Ricciuti B, Arbour KC, Lin JJ, Vajdi A, Vokes N, Hong L, et al. Diminished efficacy of programmed death-(ligand)1 inhibition in STK11- and KEAP1-mutant lung adenocarcinoma is affected by KRAS mutation status. *J Thorac Oncol* (2022) 17:399–410. doi:10.1016/j.jtho.2021.10.013

290. Murciano-Goroff YR, Pak T, Mondaca S, Flynn JR, Montecalvo J, Rekhtman N, et al. Immune biomarkers and response to checkpoint inhibition of BRAFV600 and BRAF non-V600 altered lung cancers. *Br J Cancer* (2022) 126:889–98. doi:10.1038/s41416-021-01679-1

291. Dudnik E, Peled N, Nechushtan H, Wollner M, Onn A, Agbarya A, et al. BRAF mutant lung cancer: programmed death ligand 1 expression, tumor mutational burden, microsatellite instability status, and response to immune check-point inhibitors. *J Thorac Oncol* (2018) 13:1128–37. doi:10.1016/j.jtho.2018.04.024

292. Sabari JK, Leonardi GC, Shu CA, Umeton R, Montecalvo J, Ni A, et al. PD-L1 expression, tumor mutational burden, and response to immunotherapy in patients with MET exon 14 altered lung cancers. *Ann Oncol* (2018) 29:2085–91. doi:10.1093/annonc/mdy334

293. Travis WD, Rekhtman N, Riley GJ, Geisinger KR, Asamura H, Brambilla E, et al. Pathologic diagnosis of advanced lung cancer based on small biopsies and cytology: a paradigm shift. *J Thorac Oncol* (2010) 5:411–4. doi:10.1097/JTO.0b013e3181d57f6e

294. Kini SR *Color atlas of pulmonary cytopathology*. New York: Springer Verlag (2002). p. 3–5.

295. Bubendorf L, Lantuejoul S, de Langen AJ, Thunnissen E. Nonsmall cell lung carcinoma: diagnostic difficulties in small biopsies and cytological specimens: number 2 in the Series "Pathology for the clinician" Edited by Peter Dorfmüller and Alberto Cavazza. *Eur Respir Rev* (2017) 26:170007. doi:10.1183/16000617.0007-2017

296. Lindeman NI, Cagle PT, Aisner DL, Arcila ME, Beasley MB, Bernicker EH, et al. Updated molecular testing guideline for the selection of lung cancer patients for treatment with targeted tyrosine kinase inhibitors: guideline from the college of American pathologists, the international association for the study of lung cancer, and the association for molecular pathology. *Arch Pathol Lab Med.* (2018) 142:321–46. doi:10.5858/arpa.2017-0388-CP

297. Hendriks LE, Kerr KM, Menis J, Mok TS, Nestle U, Passaro A, et al. Oncogene-addicted metastatic non-small-cell lung cancer: ESMO Clinical Practice Guideline for diagnosis, treatment and follow-up. *Ann Oncol* (2023) 34:339–57. doi:10.1016/j.annonc.2022.12.009

298. Ryska A, Buiga R, Fakirova A, Kern I, Olszewski W, Plank L, et al. Non-small cell lung cancer in countries of central and southeastern Europe: diagnostic procedures and treatment reimbursement surveyed by the central European cooperative oncology group. *Oncologist* (2018) 23:e152–8. Epub 2018 Aug 3. PMID: 30076278. doi:10.1634/theoncologist.2018-0008

299. de Jager VD, Timens W, Bayle A, Botling J, Brcic L, Büttner R, et al. Developments in predictive biomarker testing and targeted therapy in advanced stage non-small cell lung cancer and their application across European countries. *Lancet Reg Health Eur* (2024) 38:100838. doi:10.1016/j.lanepe.2024.100838

300. Liam CK, Mallawathantri S, Fong KM. Is tissue still the issue in detecting molecular alterations in lung cancer? *Respirology* (2020) 25:933–43. doi:10.1111/resp.13823

301. Mosele F, Remon J, Mateo J, Westphalen CB, Barlesi F, Lolkema MP, et al. Recommendations for the use of next-generation sequencing (NGS) for patients with metastatic cancers: a report from the ESMO Precision Medicine Working Group. *Ann Oncol* (2020) 31:1491–505. doi:10.1016/j.annonc.2020.07.014

302. Lemmon CA, Zhou J, Hobbs B, Pennell NA. Modeling costs and life-years gained by population-wide next-generation sequencing or single-gene testing in

nonsquamous non-small-cell lung cancer in the United States. *JCO Precis Oncol* (2023) 7:e2200294. doi:10.1200/PO.22.00294

303. Matsuda H, Ogawa T, Sadatsuki Y, Tsujino T, Wada S, Kim SW, et al. Budget impact analysis of next-generation sequencing versus sequential single-gene testing in Japanese patients with advanced non-small-cell lung cancer. *Respir Investig* (2023) 61:61–73. doi:10.1016/j.resinv.2022.10.002

304. Kerr KM, Bibeau F, Thunnissen E, Botling J, Ryška A, Wolf J, et al. The evolving landscape of biomarker testing for non-small cell lung cancer in Europe. *Lung Cancer* (2021) 154:161–75. doi:10.1016/j.lungcan.2021.02.026

305. Roberts ME, Neville E, Berrisford RG, Antunes G, Ali NJ, BTS Pleural Disease Guideline Group. Management of a malignant pleural effusion: British thoracic society pleural disease guideline 2010. *Thorax* (2010) 65(Suppl. 2):ii32–40. doi:10.1136/thx.2010.136994

306. Porcel JM. Malignant pleural effusions because of lung cancer. *Curr Opin Pulm Med* (2016) 22:356–61. doi:10.1097/MCP.0000000000000264

307. Shojaee S, Roy-Chowdhuri S, Safi J, Grosu HB. Cytologic investigations for the diagnosis of malignant pleural effusion in non-small cell lung cancer: state-of-the-art review for pulmonologists. *J Bronchology Interv Pulmonol* (2021) 28:310–21. doi:10.1097/LBR.0000000000000789

308. Veale N, Succony L, Rassl DM, Rintoul RC. Respiratory cytology in malignant lung disease - the thoracic oncologist's perspective. *Cytopathology* (2022) 33:39–43. doi:10.1111/cyt.13021

Pathology & Oncology Research | frontiers

TYPE Review
PUBLISHED 27 February 2024
DOI 10.3389/pore.2024.1611709

Check for updates

OPEN ACCESS

EDITED BY
Nora Bittner,
National Koranyi Institute of TB and Pulmonology, Hungary

*CORRESPONDENCE
Mihály Simon,
simonm@med.unideb.hu

RECEIVED 29 January 2024
ACCEPTED 15 February 2024
PUBLISHED 27 February 2024

CITATION
Csiki E, Simon M, Papp J, Barabás M, Mikáczó J, Gál K, Sipos D and Kovács Á (2024), Stereotactic body radiotherapy in lung cancer: a contemporary review. *Pathol. Oncol. Res.* 30:1611709. doi: 10.3389/pore.2024.1611709

COPYRIGHT
© 2024 Csiki, Simon, Papp, Barabás, Mikáczó, Gál, Sipos and Kovács. This is an open-access article distributed under the terms of the Creative Commons Attribution License (CC BY). The use, distribution or reproduction in other forums is permitted, provided the original author(s) and the copyright owner(s) are credited and that the original publication in this journal is cited, in accordance with accepted academic practice. No use, distribution or reproduction is permitted which does not comply with these terms.

Stereotactic body radiotherapy in lung cancer: a contemporary review

Emese Csiki[1,2], Mihály Simon[1]*, Judit Papp[1], Márton Barabás[1,2], Johanna Mikáczó[1,2], Kristóf Gál[1], David Sipos[3] and Árpád Kovács[1]

[1]Department of Oncoradiology, Faculty of Medicine, University of Debrecen, Debrecen, Hungary, [2]Doctoral School of Clinical Medicine, University of Debrecen, Debrecen, Hungary, [3]Faculty of Health Sciences, University of Pécs, Pecs, Hungary

The treatment of early stage non-small cell lung cancer (NSCLC) has improved enormously in the last two decades. Although surgery is not the only choice, lobectomy is still the gold standard treatment type for operable patients. For inoperable patients stereotactic body radiotherapy (SBRT) should be offered, reaching very high local control and overall survival rates. With SBRT we can precisely irradiate small, well-defined lesions with high doses. To select the appropriate fractionation schedule it is important to determine the size, localization and extent of the lung tumor. The introduction of novel and further developed planning (contouring guidelines, diagnostic image application, planning systems) and delivery techniques (motion management, image guided radiotherapy) led to lower rates of side effects and more conformal target volume coverage. The purpose of this study is to summarize the current developments, randomised studies, guidelines about lung SBRT, with emphasis on the possibility of increasing local control and overall rates in "fit," operable patients as well, so SBRT would be eligible in place of surgery.

KEYWORDS

SBRT, NSCLC, lung cancer, review, radiotherapy

Introduction

Lung cancer is one of the most common tumor types worldwide and the leading cause of cancer-related deaths among both women and men [1]. There are two main types of lung tumors: NSCLC (non-small cell lung cancer) and SCLC (small cell lung cancer). The cases are approx. 84% NSCLC, while about 13% SCLC [1]. Histological subtypes of NSCLC are adenocarcinomas, squamous cell carcinomas, and large cell carcinomas. Given the different aggressiveness and speed of progression of the two main histological types, their treatment strategies are different [2]. The type of treatment is determined by the histology of the disease, its stage, and the patient's status. Due to developments in recent years (screening and radiation therapy techniques), a slight decrease in mortality can be seen in NSCLC patients [3]. Ganti et al. made a cross-sectional epidemiological

analysis and calculated the most recent data in terms of incidence, prevalence, and survival [4]. The incidence of all stages per 100,000 people decreased from 46.4 to 40.9 in the United States between 2010–2017. The advanced stage decreased slightly (21.7–19.6), while the incidence of stage I patients increased to 10.8–13.2. The overall prevalence rose to 198.3/100,000, possibly because more and more young patients are diagnosed these days [4] the 5-year survival data have improved compared to the previous ones; the most significant improvement is 14.7%–25.7% in stage I patients receiving only radiation treatment [4].

The stage determines the prognosis of the disease at the time of diagnosis. The stage is defined based on the AJCC 8th edition (American Joint Committee of Cancer) since 2016; the use of the different TNM systems must be considered in the results of previous studies [5] Stage I-II disease is localized only to the lung tissue; lymph node positivity appears in the ipsilateral hilus in stage IIB. Radiotherapy plays an essential role in the treatment of early and advanced stages of lung cancer for both curative and palliative purposes [6]. In the case of lymph node-negative NSCLC, traditional treatment includes surgical resection (preferably video-assisted surgery-VATS lobectomy), which has been the standard of care, providing superior overall survival compared to other techniques. At the time of diagnosis, most of the patients are either technically or medically counted as inoperable for different reasons, such as poor overall health condition, elderly age, lung function, and multiple comorbidities, such as COPD (chronic obstructive pulmonary disease), cardiac and metabolic dysfunctions. For such patients, the primary treatment modality was conventional fractionated 3D-based radiation therapy, albeit with lower effectiveness and higher toxicity than surgery [7]. Today, conventional radiation therapy used in the treatment of small NSCLC foci located at a safe distance from important mediastinal organs has been replaced by a more effective, higher fractionation dose (ultra-hypofractionation) treatment, stereotaxic radiation therapy (SBRT).

SBRT is a radiation therapy method that is now widely spread, during which a relatively small, well-defined malignant tumor is treated in a few fractions, with a high dose per fraction. It is a radiation therapy technique with image guidance that can deliver very high radiation doses (ablative doses) to the target (tumor) with steep dose gradients outside the target while sparing the nearby healthy tissues (called organs at risk—OAR) [8] During SBRT, the size of the safety margins around the tumor can be reduced, which was made possible by advanced image guidance. With this ablative radiation dose, we precisely kill cancer cells, but we must pay attention to the fact that the radiation biology of the treatment changes during extreme hypofractionation; the tumor cells and healthy tissues also behave differently than during conventional fractionation. During the standard fractionation, we take advantage of the different repair mechanisms of tumor and healthy cells [9] This non-invasive technique has shown excellent local control rates and overall survival, with lower toxicity rates compared to traditional radiation therapy [8]. Another advantage is that the treatment lasts for a short time (1-2 weeks) and is suitable for outpatient treatment (doesn't need hospitalization) [9] Given the high fractional dose, careful and accurate delivery is the most important part of the treatment. Modern technological solutions must be used both in the planning and delivery.

Regarding the high age and comorbidity of lung tumor patients, as well as the raising number of stage I patients due to the development of screening tests, the introduction and use of effective treatment methods other than surgery are increasingly important. Surgery remains the gold standard of care for operable patients; however, SBRT is the treatment of choice for patients with early-stage medically inoperable NSCLC [10].

SBRT vs. conventional radiotherapy for early-stage NSCLC

Before the implementation of SBRT, conventional radiotherapy was the mainstay treatment for medically inoperable early-stage NSCLC patients. With conventional fractionation, 60–70 Gy was delivered with a fractional dose of 1.8–2 Gy. However, conventional radiotherapy showed reasonable local control and survival rates, and it was associated with significant toxicities [11]. In the first randomized phase 2 trial (SPACE), a high-fraction dose 3 × 22 Gy SBRT regimen was compared with 70/2 Gy conventional radiotherapy. The results of a total of 102 patients after a median follow-up of 37 months showed no significant difference between the two groups either in terms of 3-year PFS (progression free survival) (SBRT: 42%, Conventional RT: 42%) or OS (overall survival) at 3 years (SBRT: 54%, Conventional RT: 59%). The authors separately note that they were surprised by the exceptionally good results of the conventional therapy. When analysing the study, it should be considered that 36%–37% of the patients (in either group) did not undergo histological verification, during the examination, only about 60% of the patients underwent PET-CT, and there was an imbalance between the two groups in terms of tumor size, furthermore the number of T2 tumors was twice as high in the SBRT group. In terms of side effects, there were significantly fewer and lower-grade side effects in the SBRT group; the most significant difference was in esophagitis and pneumonitis, but mild side effects were encountered in both groups. Given the time of patient selection (2007–2011), SBRT treatment was still in its infancy, and 4D CT was only used in a few patients [12] The results of the RTOG 09.02 CHISEL multicentre randomized prospective phase 3 study were published in 2019. Peripheral, medically inoperable Stage I patients were studied. Comparing standard-dose RT (66 Gy/2 Gy or 50 Gy/2.5 Gy) with patients receiving SBRT (3 × 18 Gy or 4 × 12 Gy), superior local control could be achieved with SBRT without developing serious side effects [13]. Based on a retrospective study of a large number of

patients (497 patients, 525 lesions), the 3-year local failure rate was 34.1% with standard radiotherapy and 13.6% with SBRT. PS matching showed a significant improvement in OS for SBRT (38.9% vs. 53.1%) [14]. In the Ontario Clinical Oncology Group's ongoing phase 3 randomized study (LUSTRE trial), the results of medically inoperable patients receiving SBRT (4 × 12 Gy or 8 × 7.5 Gy depending on localization) are compared with modest hypofractionated radiotherapy (60/4 Gy).

Medically inoperable early NSCLC patients

The standard care for early-stage non-small cell lung cancer patients (NSCLC) was lobectomy, as this provided the best chances of cure. However, surgery is not suitable for many NSCLC patients in the early stage for various reasons, such as old age, general condition, impaired lung function, or multiple comorbidities. As such, these patients are generally categorized as "medically inoperable" [7]. Based on the patient's suitability for surgery, the American College of Chest Physicians practice guidelines categorized lung tumor patients into standard risk, high risk, or inoperable categories [15]. 25% of lung tumor patients diagnosed at an early stage are medically inoperable [16]. The exact definition is variable by studies. For patients who are not suitable for lobectomy, sublobar resection is often recommended. However, in the case of these patients, the high risk of complications and the uncertain oncological outcome must be considered. 3 prospective trials were compared in 2013: RTOG 0236 with patients receiving SBRT, patients undergoing sublobar resection (ACOSOG Z4032), and a trial examining radiofrequency treatment (ACOSOG Z40033). The overall 90-day mortality was 0% for RTOG 0236, 2.4% for surgery, and 2% for radiofrequency ablation [17]. In a prospective phase 2 study, after 7 years of follow-up, the results of SBRT in medically inoperable patients were published in 2018. 65 patients received 4 × 12.5 Gy; PET CT was performed in all cases as part of the examination. 5- and 7-year PFS were 49% and 38.2%, and OS was 55% and 47%, respectively. In terms of local recurrence, there is an increase at 7 years. Therefore, it is important to follow up on the occurrence of local recurrence even after 5 years. In addition, second primary lung cancer (SPLC) developed in 18.5% of cases; due to the high incidence, it is important to confirm the newly appeared lesions in the lungs with histology. Grade 3 side effects occurred in 4.6%, and Grade 4-5 were absent. The average age of the patients was 72.1 years [18] The Japan Clinical Oncology Group's prospective study (JCOG0403) included patients with operable and inoperable histologically confirmed NSCLC tumors smaller than 3 cm who received 4 × 12 Gy SBRT treatment. The definition of medically operable is if the expected FEV1 > 800 mL (forced exspiratory volume), PaO2 > 65 torr, and did not have severe cardiac disease or severe diabetes mellitus; if either is impaired, it is considered inoperable. In the case of 100 inoperable patients, the 3-year OS was 59.9%; in the case of operable patients, the 3-year OS was 76.5%. When evaluating the results, the high average age of the patients (median age 78-79) must be considered [19] The 5-year results of the RTOG 0236 study were published in 2018, 55 medically inoperable patients were selected and received 3 × 18 Gy SBRT treatment. The long-term results of the multicenter phase two study show that the 5-year disease-free survival is 25.5%, and cancer recurrence occurs most often in the untreated lobe. During follow-up (median follow-up of 48 months), locoregional and/or distant metastasis developed in 38% of patients. The development of dissemination depends on the T stage. In the case of T1, the 5-year disseminated recurrence is 18.2%, and in the case of T2, it is 45.5% [20].

Medically operable NSCLC- lobectomy vs. SBRT

The impact of using SBRT in the treatment of early-stage NSCLC is notable. In addition to irradiating inoperable patients, SBRT has recently been proposed as an alternative treatment to surgery, even for medically and technically operable NSCLC patients who refuse surgery. Recent clinical studies showed that with the use of SBRT, similar survival rates can be achieved to surgery without invasiveness and fewer treatment-related complications [8, 21]. Early-stage NSCLC lung cancer is a curable disease, and for medically fit patients, surgery (lobectomy with lymphadenectomy) is the gold standard treatment [22]. In the past few years, in addition to the development of radiation therapy, the surgical technique has also been modernized, open surgery was replaced by VATS in patients with early lung tumors, after which the number of hospitalization days and complications decreased, and the oncological results remained similar [23, 24]. In the case of SBRT, lymph node sampling is not performed; in several studies, this "deficiency" is considered the cause of lower locoregional control [18]. Based on the national lung cancer audit, only 60.6% of early-stage patients in the UK have undergone surgery. It can be seen that a significant portion of patients are at higher risk of surgical complications [25] Several randomized trials have attempted to compare surgery with SBRT but failed to accrue (RTOG 1021, SABRTooth) [26]. Two randomized phase 3 studies (STARS, ROSEL) aimed to compare the results of surgery and SBRT in operable patients. However, these were closed early due to slow accrual. Chang et al. analysed the two trials and processed the data of a total of 58 patients. Both in terms of 3-year estimated OS (SBRT: 95%, lobectomy: 79%) and recurrence-free survival (SBRT: 86%, lobectomy: 80%), patients who received SBRT had better results. However, we must consider the small number of patients, the short follow-up time, and the lack of modern surgical technologies (e.g., video-assisted thoracoscopic surgery) [8]. In 2021, the long-term results of the STARS study were published, as the SBRT arm was re-accrued with a larger number of participants (80 patients). The results of the SBRT-receiving patients were compared with the cohort of patients who

underwent VATS lobectomy and lymphadenectomy (80 patients). All patients underwent PET-CT during the examination. There were no Grade 4-5 side effects with SBRT; Grade 3 side effects occurred in 1 patient. SBRT 3-year OS was 91%, 5-year OS was 87%, in the case of VATS lobectomy, 3-year OS was 91%, and 5-year OS was 84%. Overall, in terms of OS, SBRT is non-inferior to surgery in operable patients. There was no significant difference between the two patient groups regarding 3- and 5-year PFS either (SBRT 80% and 77%, surgery 88% and 80% respectively). After lymphadenectomy, the incidence of occult pathological lymph nodes was 10%; these patients received adjuvant chemotherapy [26]. It is still necessary to carry out comparative studies using modern techniques, and long-term results are needed. However, due to the fundamentally different modalities, it is not possible to blind either patients or clinicians at treatment allocation [22]. A propensity-matched analysis was also performed, the results of which were published in 2012. Retrospectively, the data of 64 VATS cases and 64 patients receiving SABR were compared, and locoregional failure (LRF) was investigated. Recurrence was considered if it was within the operating bed/prior PTV or ipsilateral hilo-mediastinal lymph node metastasis appeared. The 3-year LRF was 93% in the SBRT group and 82% in the surgical group. There was no difference in OS. Notably, in nearly 50% of the patients (in both groups), no histological sampling of the lung foci was performed [21]. In a single-arm phase two study (RTOG 0618), 3 × 18 Gy were administered to stage I peripheral foci in NSCLC patients in good condition (medially operable). The median follow-up time was 48.1 months. The 4-year local control was 96%, and the 4-year OS was 56%. Grade 3 side effects occurred in 14%, and Grade 4 side effects did not occur [27]. In the US VALOR trial, which is a randomized phase 3 ongoing study, veterans are enrolled with operable early-stage NSCLC from 2017, and by 2020, the number of enrolled patients exceeded the total number of phase 3 trial patients so far. The results of this trial may help us in the future [28]. Another prospective trial that is still in progress and is scheduled to be completed in 2026 is the POSTILV phase 2 study, where radical resection is compared with SBRT for stage I patients, and one of the aims of the study is to assess whether SBRT, with the correct dose and technique, more effective than surgery [16]. The STABLE-MATES phase 3 trial will be completed in 2024, comparing sublobar resection with SBRT in high-risk operable patients [16].

Importance of localization

For an SBRT treatment, establishing an indication and choosing the correct fractionation scheme, the localization of the lesions within the thoracic cavity is the most important. In terms of localization, we distinguish between peripheral, central, and "extremely central," i.e., ultracentral lesions [29]. The difference between the localizations is determined by the distance from the centrally located critical organs (trachea, heart, main bronchi, great vessels, esophagus) [30].

Peripheral lesions

Lung lesions located at a safe (>2 cm) distance from the central OARs. The previously described studies were conducted with medically inoperable and operable peripheral lung foci. A peripheral lesion can be close to (<1 cm) or touch the chest wall, which requires special attention. Late side effects affecting the chest wall can be, for example, rib fracture and chest wall pain. Rib fractures usually develop more than 6 months after radiation therapy. Previous studies have shown that chest wall side effects are more likely to occur with higher fractional doses (10 Gy vs. 20 Gy). In a retrospective study, the data of 134 patients were examined; 7.5% of them developed Grade 1 or Grade 2 chest wall side effects, and a significant correlation was found for V30 and V60. If V30 reached 80 cm^3, side effects developed in 55%; in case it reached 100 cm^3, the ratio was 74%; if V60 was 15 cm^3, side effects occurred in 69% of patients, and if V60 reached 20 cm^3, the percentage was 88%. The size of the GTV (Gross Tumor Volume) and the distance of the tumor from the chest wall showed no correlation with chest wall side effects [31].

Central lesions

Tumors in which PTV (Planning Target Volume) overlaps with a virtually drawn isotropic 2 cm extension around the vital mediastinal organs (proximal bronchial tree, heart, esophagus, large vessels) [29]. Considering the proximity of essential OARs, SBRT treatment of centrally localized lung lesions requires more attention. Various Grade 3 side effects are likely to occur, e.g., bronchial stenosis, bronchial hemorrhage, carditis, esophagitis, etc., [32]. In the phase II study published in 2006, Timmerman and his team reported "excessive," high-grade toxicity with SBRT treatment of central tumors in medically inoperable patients. T1 patients received 3 × 22 Gy, while T2 patients received 3 × 20 Gy. With a high two-year local control rate (95%), a high percentage of Grade 3-4 side effects (11%) occurred, especially in the case of hilar/pericentral tumors. SBRT-related death occurred in 6 patients after 0.6–19.5 months after treatment [33]. The 4-year results of the study were published by Fakiris in 2009; the median survival was 32.4 months, where the distribution of lesions by localization was re-evaluated according to RTOG 0236. High-grade toxicity, Grade 3–5, occurred in 10.4% of peripheral tumors and 27.3% of central tumors. A total of 5 of the 70 patients participating in the study had Grade 5 toxicity [34]. The results of a 5-fraction SBRT treatment were reported in 2019 from the United States. In this phase I/II study, the goal was to establish the maximum tolerated fractional dose (MTD) in the case of central tumors. The MTD for 5 fractions was 12 Gy, with high local control (89.4%) [35]. A European study examined the treatment of central tumors in 8 fractions with a fractional dose of 7.5 Gy; after 35 months of follow-up, Grade 3 side effects occurred in 4 cases out of 63 patients, and there were no Grade 4-5 side effects. The 3-year local control was 92.6% [36]. In 2018, Roach et al.'s prospective phase I/II study was published, in which 5 ×

11 Gy was found to be safe for central tumors, and excellent local control could be achieved [32]. LungTech, a prospective multicenter phase II EORTC trial, is underway with an 8 × 7.5 Gy fractionation scheme with high-quality technical solutions. It will investigate the role of FDG PET-CT in monitoring tumor progression and assessing side effects [30]. Based on the evidence presented so far, the maximum 50–60 Gy seems to be optimal for the fractionation scheme of centrally located lung tumors, delivered in 5 fractions, but considering the nearby OARs, 8 × 7.5 Gy is also a suitable option [16].

Ultracentral lesions

By definition, lesions where the PTV overlaps with one of the critical central organs belong here. In the case of SBRT, the risk of developing Grade 4-5 side effects is high (e.g., fistula, hemoptysis, bronchopulmonary hemorrhage, etc.). Several retrospective institutional studies demonstrated the plausibility of SBRT treatment of ultracentral tumors with an acceptable toxicity rate. When analyzing the results, we must consider that in many cases, only tumors adjacent to the peribronchial tree were examined, and lesions near the esophagus, heart, or large intestine were excluded [37]. Chang et al. used a more fractionated scheme in case the OAR constraints could not be met; 4 × 12.5 Gy or 10 × 7 Gy were delivered with an acceptable side effect rate [38]. The SUNSET study was started in 2018 and is currently still ongoing; this is a phase 1 multi-institutional study to find the maximum tolerated dose for ultracentral lesions up to 2 years after treatment. NSCLCs smaller than 6 cm were enrolled, and the aim was to limit the occurrence of Grade 3–5 adverse events to <30%. The first dose level is 8 × 7.5 Gy (15 × 4 Gy and 5 × 15 Gy are also examined) [39]. In 2021, the results of the HILUS trial, which is a phase two Nordic multicenter study, were published. 65 patients with ultracentral tumors were examined. A high rate of toxicity was encountered when 8 × 7 Gy were delivered; 22 out of 65 patients (34%) developed Grade 3–5 side effects, of which 10 were possible Grade 5 toxicity. The most common G5 side effect was bronchopulmonary hemorrhage, which developed 2–22 months after SBRT treatments. The authors concluded that in the case of lesions located <1 cm from the main bronchus and trachea, the use of the 8 × 7 Gy fractionation scheme is dangerous and prohibited [40, 41]. However, the difference between different centers regarding treatment setup and safety margins must be considered [41]. Based on Chen's 2019 systematic review (a total of 250 patients' data), after SBRT treatment of ultracentral tumors, the probability of developing Grade 3–5 side effects is 10% on average, and the median treatment-related mortality is 5% [42]. The ISRS (International Stereotactic Radiosurgery Society) published a practical guideline in 2023, summarizing the studies published so far on this topic (27 studies, all but one retrospective). The most frequently used fractionation schemes are 5 × 10 Gy, 8 × 7.5 Gy, and 12 × 5 Gy; 96% of the studies used motion management, most often 4D-CT-ITV (Internal Target Volume). The lesions were considered ultracentral if the PTV overlapped with the proximal bronchial tree (PBT). High local control (LC) (1 year LC: 92%, 2 year LC: 89%), with low life-threatening toxicities (G5: 4%) were found. PBT maximum dose (Dmax) needs to be considered according to the data of the meta-analysis; less fatal toxicity is expected if the BED_3 (Biologically effective dose) value of PBT Dmax is < 180 Gy. The BED value of the treatments was a significant predictor for the one-year local control, and a negative trend appeared depending on the tumor size (smaller size, higher local control). In the ISRS guideline, 8 × 7.5 or 15 × 4 Gy are recommended for ultracentral tumors, and the PBT Dmax BED_3 can be <133–150 Gy. If there is endobronchial involvement, the use of the ablative dose is not recommended [43]. Using a modern MR-guided technique with daily plan adaptation can reduce the probability of high toxicities when administering a large fractional dose. In the ongoing ARO-2021-3 MAGELLAN phase I trial, the aim was to find the maximum tolerated dose (MTD) for MR-guided SBRT in ultracentral localization for primary and secondary lung tumors from the 10 × 5.5 Gy scheme ($_{BED10}$ = 85 .25 Gy) up to the 10 × 6.5 Gy scheme (BED_{10} = 107.25 Gy) [44].

Dose schemes—BED

In 2015, Guckenberger et al. summarized the most common fractionation schemes of SBRT treatments used in lung tumors. Stereotactic body radiotherapy treatments were performed with a dose of 5–34 Gy per fraction in 1–10 fractions; comparing the biologically effective dose of the treatment regimens at alpha/beta 10, more than 200%–300% differences were found [45]. Several studies proved that increased biological effective dose increases local control. During SBRT planning, we must consider the expected toxicity and the oncological outcome to choose the appropriate fractionation. Based on the literature data, it is established that if BED< 100 Gy, low local control is expected [46]. Compared to conventional radiotherapy, SBRT with BED >100 Gy reduces local failure and may also increase overall survival [45, 47]. In 2007, during the Japanese retrospective multi-institutional study, 257 patients' data and the details of the hypofractionated radiation treatments were examined, based on which a difference in 5-year overall survival was observed (BED_{10} < 100 Gy: 30.2%, BED_{10} > 100 Gy: 70.8%) [48]. The M.D. Anderson Cancer Center 2019 published the results of a retrospective study, where the data were obtained from the national cancer database, and the SBRT of maximum T2a tumors was compared. Radiation treatments were divided into two groups according to BED_{10}: LowBED: 100–129 Gy and High BED: >130 Gy. Based on the aggregated results, the 5-year OS was 26% in the Low BED group and 34% in the High BED group. The study's results suggest that a higher OS can be achieved with a higher BED above 130 Gy. It is important to emphasize that the exact localization of the lesions was not determined, which is an important factor for OS [49]. Examining small T1 and T2 tumors separately, Koshy et al. found

no OS benefit for small tumors >150 Gy BED, which may suggest that we can achieve high OS in small tumors with BED_{10} 100–150 Gy [50]. When choosing the fractionation scheme, the localization of the lesion and its proximity to the various critical organs must be taken into account. In the case of small peripheral lesions, extreme hypofractionation schemes have proven to be effective and safe. In the RTOG 0915 prospective randomized phase 2 study, two regimens (1 × 34 Gy or 4 × 12 Gy) were compared for small peripheral lesions. Out of 84 patients, 10.3% received a single fraction, and 13.3% of the other group had at least G3 side effects within 1 year. The 2-year local control data was 97% and 92.7%, respectively. There was no difference between the two arms regarding two-year OS and DFS [15]. Based on the long-term results of this study (after a median follow-up of 4 years), no difference was found in late G3-G5 side effects. The 5-year progression-free survival in the single fraction group was 19.1%, and in the 4-fraction group, 33.3%, there was no significant difference. Therefore, it was established that there was no significant difference in the toxicity, the 5-year local control, or the 4-year survival data [51]. Another prospective trial compared single-fraction lung SBRT (1 × 30 Gy) with a 3-fraction (3 × 20 Gy) variant, also examining small peripheral lesions. The results of this phase 2 study were published in 2019. After a median follow-up of 53.8 months, out of 98 patients, Grade 3 or more severe side effects were described in 16% of the patients receiving one fraction and 12% in the group receiving 3 fractions. There were no differences in the survival and local control results [52]. Comparing the different fractionations, especially the less frequently used single fraction SBRT, using advanced planning techniques and image guidance is important to ensure safety. In the case of small, peripheral, early-stage NSCLC, SBRT given in 3–5 fractions is common. However, in 2022, a literature summary was published regarding SBRTs applied in one fraction, which may have the advantage of, e.g., fewer clinic visits [53]. This advantage could also be used during the COVID-19 pandemic, related to this, the ESTRO-ASTRO consensus was published in 2020. During the COVID-19 pandemic, 1 × 30–34 Gy was strongly considered if a small (<2 cm) lesion is located >2 cm from critical mediastinal organs and is also >1 cm from the chest wall [54]. If we use only one fraction, it must be considered that the BED used to determine the effectiveness of multi-fraction regimens cannot be applied due to radiobiological differences. Therefore, an SFED (single fraction equivalent dose) concept was created based on a new linear quadratic-linear model [55]. Besides choosing the exact fractionation scheme, it is important to take into account the dose prescription. Previous studies show that the PTV maximum dose correlates with the local control [56]. In his summary, Guckenberger points out the differences for peripheral tumors between the dose prescriptions defined in the studies: 60%–90% isodose line encompassing the PTV, and for SBRT treatments using the multi-fraction regimen, the PTV max dose was between 38–57 Gy [45]. BED values for the different SBRT schemes are listed in Table 1.

TABLE 1 BED_{10} values corresponding to different SBRT fractionations.

BED_{10} (Gy)	SBRT fractionation scheme (number of fractions × fractional dose [Gy])
100	5 × 10
106	4 × 12
113	4 × 12,5
132	5 × 12
151	3 × 18
180	3 × 20

Tumor size (>5 cm)

By definition, SBRT means the treatment of small-sized tumors with a high fractional dose, but for now, the exact definition of the maximum size limit remains a question of debate. In the case of early, peripheral, medically inoperable lung tumors, early prospective studies proved to be successful treatment options where the size of the tumors was smaller than 4-5 cm. Retrospective studies have also found differences in overall survival according to tumor size. In the case of ultracentral tumors, the 5-year survival was determined by the size of the PTV, if the PTV <53 cm^3 61.6%, if PTV >53 cm^3 37.4%, respectively [57]. There is limited information from prospective randomized trials on large lung tumors treated with SBRT. In the multi-institutional retrospective study with the most significant number of patients (92 patients), 5–7.5 cm tumors were treated with 5 × 10 Gy with 2-year LC 73.2% and 2-year OS 46.4%. The OS correlated with the SUVmax (standardized uptake value) measured on the pre-treatment PET-CT. Distant failure occurred more often after treatment than local failure [58]. In the case of peripheral lung tumors larger than 5 cm, SBRT treatment can be administered with due caution, considering other treatment options and taking into account that lower local control and lower OS can be achieved compared to small lesions.

Simulation

CT imaging needs to be prepared after staging, establishing the indication, and planning the session. The planned radiation therapy technique and motion management determine positioning during the simulation CT. Reproducibility is an important aspect when choosing the patient's treatment position and positioning systems and ensuring small safety zones ideal for stereotactic treatment of the target volume. The total volume of the OARs in the thorax and the subsequent total planning target volume must be visible on the simulation CT [59].

Motion management

The introduction of stereotactic treatments (SRT) appeared in the treatment of intracranial tumors; the SRT of extracranial lesions was delayed because new problems had to be dealt with, such as physiologic motion and the precise definition of the target volume [9]. Intrafractional movement that occurs during treatment, such as deviations resulting from breathing, can result in anatomical changes of several centimeters [47]. When performing SBRT of the lung, the "movement" of the tumor must be taken into account so that the planned dose is delivered to the right place and the surrounding tissues can be adequately protected. An essential and unmissable element of this is IGRT (image guided radiotherapy) before or during each faction. When selecting the IGRT method, we must consider the technique we will use and the treatment machine (linear accelerator, cyberknife). MV or kV imaging (3D CBCT, 4D CBCT, orthogonal x-ray) can be used as IGRT or optical verification, e.g., surface guided radiotherapy (SGRT). According to the phases of the respiratory cycle, the lesion in the lung changes its position. Motion management can be done in free breathing with motion-encompassing methods [60]. The most used is 4D CT, where we determine the breathing cycle and divide it into phases according to either the time phase or the amplitude. Several techniques can be used with 4D planning CT, such as internal target volume (ITV) determination or mid-ventilation determination. ITV is created from the union of GTVs delineated on CT slices of at least 3 breathing phases (max exhale, max inhale, and intermediate phase). Maximum intensity projection (MIP) can also be used to determine ITV. Comparing the two ITV approaches, it was found that ITV created with MIP is smaller compared to the GTV-based ones; in this case, tumor-miss may occur, although the MIP requires a shorter time [54]. Under free-breathing, real-time tracking is also a method of cyberknife [61]. Treatment in a specific part of the breathing cycle reduces the size of the target volume. Gating has been employed in some institutions to control respiratory motion [62]. Such gated methods can be ABC (active breath control) when the patient's exhalation is inhibited after determining the breathing volume with the help of a spirometer. Another method is the deep inspiration breath hold (DIBH), when the patient holds the air in a certain deep inhalation level for about 10–15 s, most often in a voluntary manner (with audio-visual feedback), during which the pre-treatment verification takes place (it can be kV imaging or SGRT) and also delivery. Forced shallow breathing can be done with abdominal compression. In the case of tumor tracking, with the help of external or internal markers, the treatment is delivered only in certain breathing phases using intrafractional IGRT [60, 61]. The proper implementation of image-guided positioning and motion-management techniques can significantly reduce planning margins necessary for planning target volumes and, hence, the dose to the surrounding normal lung tissues [62].

Target volume determination

Before radiation treatment of lung tumors, we define the target volumes using the ICRU 62 (Interational Commission on Radiation Units and measerments) and ICRU 83 definitions. Using contrast-enhanced diagnostic chest CT and PET-CT fusion, the GTV is first determined on the planning CT based on the visible extent of the tumor. The extension of GTV depends on the type of tumor according to the microscopic spread and the characteristics of the tumor (spread to surrounding organs), thus creating the CTV (clinical target volume). For SBRT treatments, 4D simulation is often performed, considering the changing tumor movement during the breathing cycle. In this case, the breathing cycle is divided into several phases, and GTVs must be defined separately in the phases. An ITV is obtained by summing the GTVs from all respiratory motion phases instead of CTVs, and the PTV is then obtained by applying a margin to the ITV to account for the setup and positioning uncertainties [6, 62].

Dose constraints

When assessing radiation therapy plans, in addition to the coverage of the target volume and the use of adequate doses, we must pay close attention to the doses to the surrounding critical organs to reduce the development of early and late side effects. This way, we can ensure that SBRT is safe. In contrast to conventional radiotherapy, during SBRT, a high fractional dose is delivered in a few fractions, so the fractional dose received by the OARs is higher as well; therefore, we cannot use the restrictions defined for conventional radiotherapy [63]. Based on trials and published reports related to SBRT, the relevant dose constraints are determined, and due to the increasing number of treatments, these are frequently updated. When treating lung lesions, the OARs of the thorax must be considered (lung, heart, pericardium, esophagus, trachea, main bronchi, chest wall, brachial plexus, and liver, depending on localization). Most of the dose constraints for SBRT treatment are defined for 3, 5, and 8 fractions, but due to the use of the single fraction, which is becoming increasingly popular, the latest guidelines also help us with 1 fraction [64]. Depending on whether an organ is parallel (e.g., lungs) or serial (e.g., spinal cord), different parameters must be used in the treatment planning [59]. According to the latest data, the maximum dose is relevant to 0.1 cc for serial organs. In the case of parallel organs, it is crucial to determine, in addition to the maximum critical volume, the minimal volume that receives above the threshold dose ("minimum critical volume-cold constraints") [64]. One of the first extensive summaries that defined the dose constraints used in SBRT is the AAPM task group was 101st in 2010. Here, the max dose applied to <0.35 cc, and there were no restrictions on the SBRT delivered in 8 fractions [59]. The constraints defined in the

RTOG0813 trial can be used for 5 fraction lung SBRTs [35]. Based on a review published in 2021, the purpose is to systemically pool several published peer-reviewed clinical datasets and extract them in a clinically valid format [65]. The UK consensus guideline issued new guidelines 2022 based on updated data [64].

Treatment delivery

Given that a high dose is delivered during SBRT, maximizing the protection of the organs at risk, in addition to the exact target volume coverage, with highly conformal dose distribution (even in the case of complicated, inhomogeneous anatomy) is crucial. This is one of the reasons for the advancement of modern delivery techniques in SBRT planning. Such techniques include intensity-modulated radiotherapy (IMRT) and volumetric-modulated arc therapy (VMAT) [66, 67]. Lung SBRT VMAT plans of 218 patients were compared to the previously more common 3D conformal technique. In terms of dose conformity/target coverage, there was no difference (V95% > 95% with both techniques); however, from the point of OARs, the dose constraints of the ipsilateral lung (V5, V10, V20, and MLD) were much easier to comply with in the case of VMAT technique. By using the FFF (flattening filter free) mode, the radiation treatment time can be significantly reduced; the delivery of 12 Gy in the case of FFF is approximately 1.5 min, and with FF, it is 8.3 min. The length of the radiation treatment is a very important aspect of radiation treatments using a high dose per fraction, as the patient must lie motionless throughout due to precise targeting [67].

The importance of a PET-CT during examination and planning

In addition to biopsy, PET-CT also provides metabolic data and is essential in examining NSCLC patients. It helps establish a diagnosis and is also used in planning radiation therapy, including high-dose SBRT treatment [68–70]. The PET-CT performed for planning often verifies a stage change compared to the previous imaging, which is also vital before lung SBRT treatments to exclude unknown novum distant metastases and locoregional pathological lymph nodes. In 2014, 47 NSCLC patients were examined, and the results of PET-CT performed as part of staging were compared with those of planning PET-CT. A new locoregional or distant metastasis was found in 51% of the patients. In the study, it was determined that if 6 weeks pass between the two PETs, the treatment of the disease changes in 26% of patients due to upstaging [71]. In finding pathological mediastinal lymph nodes, PET-CT has higher accuracy rates than diagnostic chest CT. The fact that different radiation therapists can delineate a target volume of much more similar size and shape to each other due to the metabolic data is of great help in radiation therapy planning, especially in determining the GTV. A good correlation was found when comparing the tumor sizes determined based on PET-CT with the pathological sizes after the subsequent surgery [68, 70] The extent of FDG (fluorodeoxyglucose) accumulation within the tumor is most often determined by the SUVmax (standardized uptake value). Several studies have proved the predictive value of the SUVmax before treatments on local control; with an SUVmax of >3, local or distant failure is more likely to occur [72]. Chang examined 130 patients after 4 × 12.5 Gy was given to peripheral small lesions (<T1) and found that if the SUVmax on the staging PET-CT was below 6.2, a significantly higher OS was expected. The staging PET-CT was the only independent significant predictor for OS [73]. After SBRT treatment, PET-CT can also help with the question of recurrence-fibrosis arising on chest CT. If the SUVmax is > 5 on the 12-week PET-CT after treatments, it is more likely to indicate recurrence [72] In ongoing trials, they also investigate the effect on local control if the dose is escalated to areas with a high SUVmax within the tumor [68].

Guidelines

The European guidelines for treating early-stage NSCLC patients have not been updated since 2014–2017. The results of the currently ongoing, critical phase 2 and 3 studies are still in progress, which can determine the place of SBRT compared to lobectomy and will provide additional help in choosing the appropriate fractionation.

1. ESMO (European Society of Medical Oncology—2014): From the point of view of the feasibility of the surgery (to estimate the morbidity and mortality that may occur after the operation), the patients must be grouped in terms of risk; a cardiac and pulmonary functional assessment is required for this evaluation. The recalibrated thoracic revised cardiac risk index (RCRI) determines cardiac high risk. The case is of low risk regarding respiratory function if both FEV1 and DLCO are >80%. In the case of invasive NSCLC, the gold standard treatment is still lobectomy; lymph node dissection is not mandatory in all cases (it can be omitted if it is cN0 on PET-CT). If lobectomy cannot be performed, SBRT treatment should be chosen. In terms of fractionation, delivery, and motion management it is not covered by the ESMO guidelines. Even in multifocal cases, surgery is the primary choice; SBRT is only chosen if surgery cannot be performed [74].
2. ASTRO (American Society for Radiation Oncology—2017): SBRT can be offered as an alternative to lobectomy for “high risk” peripheral early-stage NSCLC patients, but in the case of “standard risk,” operable patients, SBRT can only be

recommended in a clinical trial as an alternative to surgery, considering that long-term side effect and survival data >3 years are still missing. SBRT is recommended in medically inoperable cases. In central localization, at least 4 fractions are recommended, but in the case of a higher risk of side effects, 6–15 fractions are also possible. SBRT can also be given in histologically unverified cases. After pneumonectomy, SBRT is recommended for novum lung cancer [75].

3. NCCN (National Comprehensive Cancer Network—2023.3): The use of advanced technologies is important for precise, high-dose curative RT (planning 4D CT, PET-CT fusion, IMRT/VMAT screening, motion management, appropriate high-level IGRT). For medically operable patients, lobectomy plus mediastinal lymph node dissection is recommended. For high-risk patients (from a surgical point of view), SBRT is a suitable alternative to lobectomy. For medically inoperable early-stage NSCLC patients, SBRT is recommended for tumors smaller than 5 cm if the constraints of the surrounding organs permit. Based on tumor localization, the recommended fractionation: small peripheral: 1 × 25–34 Gy, peripheral tumors: 3 × 18–20 Gy, central and peripheral tumors smaller than 5 cm: 4 × 12 Gy, 4 × 12.5 Gy, 5 × 10–10.5 Gy, for central lesions 8 × 7.5 Gy. According to the NCCN guideline, SBRT can be performed with a higher number of fractions (max. 10 fractions) in the case of ultracentral location. Treatment in 3 or fewer fractions is prohibited for central and ultracentral tumors. Dose constraints for healthy organs were determined based on RTOG 0618, 0813, and 0915 [6].

SBRT treatment and immunotherapy

During SBRT treatment, a high dose is delivered per fraction, which helps to achieve high local control in patients with early-stage lung tumors. The probability of the appearance of distant metastases is 10%–20%. The increased effect of the immune system may cause out-of-field tumor regression during radiation therapy [29]. The reason for this is that the release of tumor antigens increases due to the ionizing radiation, and thus, the adaptive immune system recognizes them more easily; this is called the abscopal effect [76]. During SBRT, we detect tumor shrinkage, but tumor cell fragments are also present and can behave immunogenically. It is of therapeutic importance that, in the case of lung tumors, an exceptional antitumor immune response is developed to target tumor antigens. The immune response can be inhibited by regulating different checkpoint pathways. For example, antibodies against PD1 and CTLA-4 can increase the antitumor effect [29]. Combined, SBRT and immunotherapy can be synergistic, effective, and safe treatments [77]. In advanced NSCLC patients, it was investigated that progression-free survival and overall survival were higher if the patients also received radiotherapy before immunotherapy [78]. Immunotherapy with SBRT treatment resulted in a good clinical response in melanoma and advanced lung tumor patients [79, 80]. PD-1/PD-L1 inhibitors such as pembrolizumab and atezolizumab are recommended as first-line treatment in advanced NSCLC patients with high PD-L1 expression [77]. A higher immunological antitumor effect can be achieved with a higher fractional dose than conventional radiotherapy. The SBRT treatment creates a supportive immune microenvironment for subsequent immune checkpoint inhibitors; in return, the immune checkpoint inhibitors reduce radiation resistance and boost the abscopal effect [77]. Administering immunotherapy (immune checkpoint inhibitors—ICI), enhancing the immune response, together with SBRT treatment decreases the probability of developing regional and distant metastases, so, e.g., in the case of central-ultracentral lung tumors, safer, reduced-dose SBRT treatment should be considered (BED<100 Gy) [29]. Currently, several studies are ongoing that investigate the administration of SBRT and ICIs in early-stage NSCLC; in terms of dose, there is a lack of consensus, but the most frequently studied ICIs are pembrolizumab, atezolizumab, and durvalumab [77, 81].

Radiological and pulmonary function changes after SBRT

CT and PET-CT are used for control purposes after SBRT treatments. Given that more and more "fit" patients are receiving this form of treatment, it is crucial to define the follow-up protocol precisely due to the more prolonged survival. Detecting local recurrence is often difficult because its radiological picture can be confused with early and late lung injury after SBRT. Side effects are considered early if they develop sooner than 6 months after radiation treatment (pneumonitis-consolidation, GGO) and late (fibrosis). In 2012, a systemic literature review summarized possible radiological changes after SBRT. Considering the conformal dose distribution at high doses, the resulting CT abnormalities are different from the sharp-bordered lesions corresponding to the fields seen after conventional radiation treatments. During SBRT, the lung volume receiving smaller doses will be larger [82]. The phase 3 CHISEL study compared conventional (mean BED_{10}: 65.49 Gy) and SBRT (mean BED_{10}: 125.92 Gy) treatment of medically inoperable patients with small lung cancer patients. The analysis of pulmonary function changes was published in 2022. Despite the significant BED difference, no significant difference was found after a 3- to 12-day follow-up between the patients' PFT (pulmonary function test), nor in FVC, DLCO, and FEV1 [83]. Overall, acute side effects developed in 62% of cases; consolidation is visible in almost half of the cases. Among the radiological changes on thorax CT, the most common indication of recurrence is enlarging opacity after 1 year. The blurred border, the examined area's inhomogeneity, and the air

bronchogram's disappearance can be suspicious [82]. Chang et al. examined the data of 130 patients who received 4 × 12.5 Gy for stage I peripheral NSCLC lung lesions. 9.3% of patients experienced Grade 2 pneumonitis and 2.3% Grade 3 pneumonitis. After multivariate analysis, it was determined that the probability of developing pneumonitis is significantly higher if the mean ipsilateral lung dose (MLD) > 9.14 Gy [73]. In 2014, new statistical and geometric analysis methods were used to examine the dosimetric parameters that can affect the development of lung injuries. The planned CT data of 24 patients were compared (with deformable registration) with the diagnostic thorax CT images taken at 3, 6, and 12 months (after SBRT treatment). The patients received 3 × 12–18 Gy or 4 × 12.5 Gy. There was no Grade 3-4 pneumonitis, Grade 2 in 15% of the patients. The critical dose (low-dose peak location) of lung radiographic injury was approximately 35 Gy (with a standard deviation of 10 Gy), or 70% of the prescribed dose. The larger the PTV, the smaller the critical dose. Therefore, in the case of a larger PTV, the probability of developing pneumonitis/fibrosis is higher [84]. Radiological changes do not always correlate with decreased pulmonary function. Pulmonary function deterioration occurs very rarely after SBRT treatment of peripheral lesions. Analysing the phase 2 RTOG 0236 study, the data of 55 medically inoperable patients who received 3 × 18 Gy treatment were examined. They found that poor respiratory function before treatment did not increase the likelihood of developing pulmonary toxicity, and patients who became inoperable for cardiac reasons had a lower 2-year OS. After SBRT treatment, Grade 0 and 1 PFT (pulmonary function test) changes were observed in most patients based on the RTOG SBRT pulmonary scale; > 70% did not change PFT [85].

MRI-guided lung SBRT

The use of MR in stereotactic treatments is novel. Currently, the most used image-guided strategies are techniques utilizing X-rays. The introduction of MRI-guided techniques can facilitate the isolation of different soft tissues. Compared to X-ray imaging, radiation exposure is also an important aspect. MRI can help us in many ways when performing lung SBRT, for example, by defining target volumes, planning, and using motion management. Intra- and inter-fractional deviations can be easily recognized and eliminated [47]. A clear advantage can be seen during MRI-guided adaptive radiation treatment of central lesions (SMART). After performing a breath hold 3D MRI simulation and planning CT, the plan is prepared using an inverse technique (IMRT, VMAT). Before each fraction, a 3D MRI image of the position to be treated per the anatomy of the day is taken. After the rigid registration with the gross tumor volume on the planning MRI scan, a couch shift is performed, if necessary. The OAR contours are propagated to the chosen MRI scan of the day using deformable image co-registration. The clinician then makes the necessary corrections on the GTV, and the PTV is generated with an isotropic margin of 5 mm. The online plan is then reoptimized with the same optimization objectives and field parameters. Based on real-time 2D MR images, the degree of breath-hold (gating window) can be monitored during fraction. Due to the central localization, the proximity of the OARs complicates the implementation of SBRT. Using on-table plan adaptation reduced the OAR planning constraint violations ($p < .05$), but the OAR maximum doses mainly remained stable. With the MRI-guided technique, we can reduce the size of the PTV during breath-hold gated treatments with the help of continuous lesion visualization. By increasing the coverage, the target of 95% PTV coverage was achieved in 95% of the plans, compared to the "predicted" plans (71%). As well as the daily adaptation of plans, they reduce the likelihood of side effects by monitoring the anatomical and target volume changes that occur during each fraction [86]. Finazzi et al. investigated the advantages of MRI-guided adaptive radiation therapy (SMART) during SBRT treatment of 25 peripheral lung lesions. Compared to free-breathing plans using 4D CT-based ITV, the size of SMART-PTVs has decreased, and the PTV coverage has improved. BED_{10} > 100 Gy can be delivered to PTV 95% in a higher percentage of patients, but the dosimetric benefits were modest. In conclusion, it can be said that in the case of peripheral lesions, it is not always beneficial to use SMART; it should be chosen if there is a higher probability of the development of severe side effects (if the lesion moves >1 cm, re-irradiation, previous lung surgery, severe lung disease in the anamnesis) [87]. When using this technique, we must remember that it takes longer to perform compared to CT-based and non-adaptive treatments (for peripheral lesions, on average, 48 min door-to-door; for central lesions, 59 min) [86, 87]. An ongoing prospective study, with phase 1 data reported to date, focuses on ultracentral tumors. Five lesions were examined, and 5 × 10 Gy were delivered while keeping the strict OAR constraints. 70% of the 25 fractions were based on an adapted plan due to the OAR violation. No Grade 3 acute side effects were found 6 months after treatment. In the future, the application of SMART may expand the SBRTs indicated for ultracentral tumors [88]. It remains a question whether the benefits provided by MR also represent a survival advantage and whether the cost of MR LINAC is worth it [47].

Discussion

Nowadays, SBRT is an increasingly common and frequently used form of radiotherapy treatment. SBRT has revolutionized the early-stage NSCLC and oligometastatic cancer treatment paradigm, providing a highly effective and non-invasive alternative to surgery. This curative, safe treatment method can also be used for patients considered inoperable due to

some comorbidity. Elderly patients with poor respiratory function can also be treated as it does not worsen PFT after treatment [85]. The conventional radiation treatment, previously chosen for medically inoperable patients, has now been replaced by SBRT if the localization of the tumor allows it [13, 14]. High-fractionation SBRT can be given safely to peripheral lesions, but the results of modest hypofractionation treatments for local control are still ongoing (LUSTRE study). The localization determines the dose of SBRT; tumors close to the chest wall and localized centrally are treated with a lower fractional dose in more fractions [31, 35]. SBRT treatment of ultracentral lesions is not recommended based on guidelines but can be carried out under safe conditions, as long as the dose of the nearby OARs is adequate and the fractional dose is as low as possible [37, 43]. The appropriate dose is still being determined (SUNSET study) [39]. The size of the lung lesion affects the expected local control and the development of dissemination [20]. The guidelines recommend SBRT treatment for less than 5 cm lung lesions, but tumors >5 cm can also be treated with appropriate care [58]. Comparing lobectomy and SBRT in the case of operable patients, previous studies have produced similar results [26], but prospective phase 2-3 studies are still ongoing (VALOR, POSTILV, STABLE-MATES) [16].

During the follow-up after SBRT treatment, PET-CT can be an additional examination of the diagnostic CT, helping to distinguish between fibrosis and recurrence. It indicates a relapse if, in addition to increasing opacity, the SUV max value is higher than 5 [72]. Future directions involve refining patient selection (for example, not only inoperably patients benefit from it), optimizing treatment planning (VMAT planning, MR guided therapies), and integrating SBRT with novel systemic therapies like immunotherapy.

Author contributions

All authors listed have made a substantial, direct, and intellectual contribution to the work and approved it for publication.

Conflict of interest

The authors declare that the research was conducted in the absence of any commercial or financial relationships that could be construed as a potential conflict of interest.

References

1. American Cancer Society. Facts & Figures 2019. *Am Cancer Soc [Internet]* (2019):1–76. Available at: https://www.cancer.org/content/dam/cancer-org/research/cancerfacts-and-statistics/annual-cancer-facts-andfigures/2019/cancer-facts-andfigures.

2. Travis WD, Brambilla E, Nicholson AG, Yatabe Y, Austin JHM, Beasley MB, et al. The 2015 world health organization classification of lung tumors: impact of genetic, clinical and radiologic advances since the 2004 classification. *J Thorac Oncol* (2015) 10:1243–60. doi:10.1097/JTO.0000000000000630

3. Howlader N, Forjaz G, Mooradian MJ, Meza R, Kong CY, Cronin KA, et al. The effect of advances in lung-cancer treatment on population mortality. *N Engl J Med* (2020) 383(7):640–9. doi:10.1056/NEJMoa1916623

4. Ganti M, Alyssa BK, Ion C, Seal B, Chou E. Update of incidence, prevalence, survival, and initial treatment in patients with non-small cell lung cancer in the US. *JAMA Oncol* (2021) 7(12):1824–32. doi:10.1001/jamaoncol.2021.4932

5. Goldstraw P, Chansky K, Crowley J, Rami-Porta R, Asamura H, Eberhardt WEE, et al. The IASLC lung cancer staging project: proposals for revision of the TNM stage groupings in the forthcoming (eighth) edition of the TNM Classification for lung cancer. *J Thorac Oncol* (2016) 11(1):39–51. doi:10.1016/j.jtho.2015.09.009

6. NCCN. *NCCN Guidelines Version 3. 2023 Non-small cell lung cancer* (2023).

7. Howington JA, Blum MG, Chang AC, Balekian AA, Murthy SC. Treatment of stage I and II non-small cell lung cancer: diagnosis and management of lung cancer, 3rd ed: american College of Chest Physicians evidence-based clinical practice guidelines. *Chest* (2013) 143(5):e278S–e313S. doi:10.1378/chest.12-2359

8. Chang JY, Senan S, Paul MA, Mehran RJ, Louie AV, Balter P, et al. Stereotactic ablative radiotherapy versus lobectomy for operable stage I non-small-cell lung cancer: a pooled analysis of two randomised trials. *Lancet Oncol* (2015) 16(6):630–7. doi:10.1016/S1470-2045(15)70168-3

9. Timmerman RD, Herman J, Cho LC. Emergence of stereotactic body radiation therapy and its impact on current and future clinical practice. *J Clin Oncol* (2014) 32:2847–54. doi:10.1200/JCO.2014.55.4675

10. Prezzano KM, Ma SJ, Hermann GM, Rivers CI, Gomez-Suescun JA, Singh AK. Stereotactic body radiation therapy for non-small cell lung cancer: a review. *World J Clin Oncol* (2019) 10(1):14–27. doi:10.5306/wjco.v10.i1.14

11. Rowell NP, Williams CJ. Radical radiotherapy for stage I/II non-small cell lung cancer in patients not sufficiently fit for or declining surgery (medically inoperable). *Cochrane Database Syst Rev* (2001) 2:CD002935. doi:10.1002/14651858.CD002935

12. Nyman J, Hallqvist A, Lund JÅ, Brustugun OT, Bergman B, Bergström P, et al. SPACE – a randomized study of SBRT vs conventional fractionated radiotherapy in medically inoperable stage I NSCLC. *Radiother Oncol* (2016) 121(1):1–8. doi:10.1016/j.radonc.2016.08.015

13. Ball D, Mai GT, Vinod S, Babington S, Ruben J, Kron T, et al. Stereotactic ablative radiotherapy versus standard radiotherapy in stage 1 non-small-cell lung cancer (TROG 09.02 CHISEL): a phase 3, open-label, randomised controlled trial. *Lancet Oncol* (2019) 20(4):494–503. doi:10.1016/S1470-2045(18)30896-9

14. von Reibnitz D, Shaikh F, Wu AJ, Treharne GC, Dick-Godfrey R, Foster A, et al. Stereotactic body radiation therapy (SBRT) improves local control and overall survival compared to conventionally fractionated radiation for stage I non-small cell lung cancer (NSCLC). *Acta Oncol (Madr)* (2018) 57(11):1567–73. doi:10.1080/0284186X.2018.1481292

15. Videtic GMM, Hu C, Singh AK, Chang JY, Parker W, Olivier KR, et al. A randomized phase 2 study comparing 2 stereotactic body radiation therapy schedules for medically inoperable patients with stage i peripheral non-small cell lung cancer: NRG Oncology RTOG 0915 (NCCTG N0927). *Int J Radiat Oncol Biol Phys* (2015) 93:757–64. doi:10.1016/j.ijrobp.2015.07.2260

16. Rodríguez De Dios N, Navarro-Martin A, Cigarral C, Chicas-Sett R, García R, Garcia V, et al. GOECP/SEOR radiotheraphy guidelines for non-small-cell lung cancer. *World J Clin Oncol* (2022) 13(4):237–66. doi:10.5306/wjco.v13.i4.237

17. Crabtree T, Puri V, Timmerman R, Fernando H, Bradley J, Decker PA, et al. Treatment of stage i lung cancer in high-risk and inoperable patients: comparison of prospective clinical trials using stereotactic body radiotherapy (RTOG 0236), sublobar resection (ACOSOG Z4032), and radiofrequency ablation (ACOSOG Z4033). *J Thorac Cardiovasc Surg* (2013) 145(3):692–9. doi:10.1016/j.jtcvs.2012.10.038

18. Sun B, Brooks ED, Komaki RU, Liao Z, Jeter MD, McAleer MF, et al. 7-year follow-up after stereotactic ablative radiotherapy for patients with stage I non–small cell lung cancer: results of a phase 2 clinical trial. *Cancer* (2017) 123(16):3031–9. doi:10.1002/cncr.30693

19. Nagata Y, Hiraoka M, Shibata T, Onishi H, Kokubo M, Karasawa K, et al. Prospective trial of stereotactic body radiation therapy for both operable and inoperable T1N0M0 non-small cell lung cancer: japan Clinical Oncology Group Study JCOG0403. *Int J Radiat Oncol Biol Phys* (2015) 93(5):989–96. doi:10.1016/j.ijrobp.2015.07.2278

20. Timmerman RD, Hu C, Michalski JM, Bradley JC, Galvin J, Johnstone DW, et al. Long-term results of stereotactic body radiation therapy in medically inoperable stage I non-small cell lung cancer. *JAMA Oncol* (2018) 4(9):1287–8. doi:10.1001/jamaoncol.2018.1258

21. Verstegen NE, Oosterhuis JWA, Palma DA, Rodrigues G, Lagerwaard FJ, van der Elst A, et al. Stage I-II non-small-cell lung cancer treated usingeither stereotactic ablative radiotherapy (SABR) orlobectomy by video-assisted thoracoscopic surgery(VATS): outcomes of a propensity score-matchedanalysis. *Ann Oncol* (2013) 24(6):1543–8. doi:10.1093/annonc/mdt026

22. Franks KN, McParland L, Webster J, Baldwin DR, Sebag-Montefiore D, Evison M, et al. SABRTooth: a randomised controlled feasibility study of stereotactic ablative radiotherapy (SABR) with surgery in patients with peripheral stage I nonsmall cell lung cancer considered to be at higher risk of complications from surgical resection. *Eur Respir J* (2020) 56(5):2000118. doi:10.1183/13993003.00118-2020

23. Yamamoto K, Ohsumi A, Kojima F, Imanishi N, Matsuoka K, Ueda M, et al. Long-term survival after video-assisted thoracic surgery lobectomy for primary lung cancer. *Ann Thorac Surg* (2010) 89(2):353–9. doi:10.1016/j.athoracsur.2009.10.034

24. Ilonen IK, Räsänen JV, Knuuttila A, Salo JA, Sihvo EI. Anatomic thoracoscopic lung resection for non-small cell lung cancer in stage i is associated with less morbidity and shorter hospitalization than thoracotomy. *Acta Oncol (Madr)* (2011) 50(7):1126–32. doi:10.3109/0284186X.2011.555780

25. Onkologie A, Daten D, Breyer-kohansal R, Hartl S, Burghuber OC, Urban M, et al. National Lung Cancer Audit annual report (for the audit period 2018). *Eur Respir J* (2021) 14:2103201.

26. Chang JY, Mehran RJ, Feng L, Verma V, Liao Z, Welsh JW, et al. Stereotactic ablative radiotherapy for operable stage I non-small-cell lung cancer (revised STARS): long-term results of a single-arm, prospective trial with prespecified comparison to surgery. *Lancet Oncol* (2021) 22(10):1448–57. doi:10.1016/S1470-2045(21)00401-0

27. Timmerman RD, Paulus R, Pass HI, Gore EM, Edelman MJ, Galvin J, et al. Stereotactic body radiation therapy for operable early-stage lung cancer: findings from the NRG oncology RTOG 0618 trial. *JAMA Oncol* (2018) 4(9):1263–6. doi:10.1001/jamaoncol.2018.1251

28. Moghanaki D. Strategic initiatives for veterans with lung cancer. *Fed Pract* (2020) 37:S76–S80. doi:10.12788/fp.0019

29. Chang JY, Bezjak A, Mornex F, IASLC Advanced Radiation Technology Committee. Stereotactic ablative radiotherapy for centrally located early stage non–small-cell lung cancer: what we have learned. *J Thorac Oncol* (2015) 10:577–85. doi:10.1097/JTO.0000000000000453

30. Adebahr S, Collette S, Shash E, Lambrecht M, Le Pechoux C, Faivre-Finn C, et al. LungTech, an EORTC Phase II trial of stereotactic body radiotherapy for centrally located lung tumours: a clinical perspective. *Br J Radiol* (2015) 88(1051):20150036. doi:10.1259/bjr.20150036

31. Stephans KL, Djemil T, Tendulkar RD, Robinson CG, Reddy CA, Videtic GMM. Prediction of chest wall toxicity from lung stereotactic body radiotherapy (SBRT). *Int J Radiat Oncol Biol Phys* (2012) 82(2):974–80. doi:10.1016/j.ijrobp.2010.12.002

32. Roach MC, Robinson CG, DeWees TA, Ganachaud J, Przybysz D, Drzymala R, et al. Stereotactic body radiation therapy for central early-stage NSCLC: results of a prospective phase I/II trial. *J Thorac Oncol* (2018) 13(11):1727–32. doi:10.1016/j.jtho.2018.07.017

33. Timmerman R, McGarry R, Yiannoutsos C, Papiez L, Tudor K, DeLuca J, et al. Excessive toxicity when treating central tumors in a phase II study of stereotactic body radiation therapy for medically inoperable early-stage lung cancer. *J Clin Oncol* (2006) 24(30):4833–9. doi:10.1200/JCO.2006.07.5937

34. Fakiris AJ, McGarry RC, Yiannoutsos CT, Papiez L, Williams M, Henderson MA, et al. Stereotactic body radiation therapy for early-stage non-small-cell lung carcinoma: four-year results of a prospective phase II study. *Int J Radiat Oncol Biol Phys* (2009) 75(3):677–82. doi:10.1016/j.ijrobp.2008.11.042

35. Bezjak A, Paulus R, Gaspar LE, Timmerman RD, Straube WL, Ryan WF, et al. Safety and efficacy of a five-fraction stereotactic body radiotherapy schedule for centrally located non-small-cell lung cancer: NRG oncology/RTOG 0813 trial. *J Clin Oncol* (2019) 37:1316–25. doi:10.1200/JCO.18.00622

36. Haasbeek CJA, Lagerwaard FJ, Slotman BJ, Senan S. Outcomes of stereotactic ablative radiotherapy for centrally located early-stage lung cancer. *J Thorac Oncol* (2011) 6. doi:10.1097/JTO.0b013e31822e71d8

37. Chaudhuri AA, Chen K, Diehn M, Loo BW. Stereotactic ablative radiotherapy for central and ultra-central lung tumors. *Ther Radiol Oncol* (2019) 3:18. doi:10.21037/tro.2019.05.01

38. Chang JY, Li QQ, Xu QY, Allen PK, Rebueno N, Gomez DR, et al. Stereotactic ablative radiation therapy for centrally located early stage or isolated parenchymal recurrences of non-small cell lung cancer: how to fly in a "no fly zone.". *Int J Radiat Oncol Biol Phys* (2014) 88(5):1120–8. doi:10.1016/j.ijrobp.2014.01.022

39. Giuliani M, Mathew AS, Bahig H, Bratman SV, Filion E, Glick D, et al. SUNSET: stereotactic radiation for ultracentral non–small-cell lung cancer—a safety and efficacy trial. *Clin Lung Cancer* (2018) 19(4):e529–32. doi:10.1016/j.cllc.2018.04.001

40. Rosenberg SA, Mak R, Kotecha R, Loo BW, Senan S. The nordic-HILUS trial: ultracentral lung stereotactic ablative radiotherapy and a narrow therapeutic window. *J Thorac Oncol* (2021) 16:e79–80. doi:10.1016/j.jtho.2021.06.030

41. Lindberg K, Grozman V, Karlsson K, Lindberg S, Lax I, Wersäll P, et al. The HILUS-trial—a prospective nordic multicenter phase 2 study of ultracentral lung tumors treated with stereotactic body radiotherapy. *J Thorac Oncol* (2021) 16(7):1200–10. doi:10.1016/j.jtho.2021.03.019

42. Chen H, Laba JM, Zayed S, Boldt RG, Palma DA, Louie AV. Safety and effectiveness of stereotactic ablative radiotherapy for ultra-central lung lesions: a systematic review. *J Thorac Oncol* (2019) 14:1332–42. doi:10.1016/j.jtho.2019.04.018

43. Yan M, Louie AV, Kotecha R, Ashfaq Ahmed M, Zhang Z, Guckenberger M, et al. Stereotactic body radiotherapy for ultra-central lung tumors: a systematic review and meta-analysis and international stereotactic radiosurgery society practice guidelines. *Lung Cancer* (2023) 182:107281. doi:10.1016/j.lungcan.2023.107281

44. Regnery S, Ristau J, Weykamp F, Hoegen P, Sprengel SD, Paul KM, et al. Magnetic resonance guided adaptive stereotactic body radiotherapy for lung tumors in ultracentral location: the MAGELLAN trial (ARO 2021-3). *Radiat Oncol* (2022) 17(1):102. doi:10.1186/s13014-022-02070-x

45. Guckenberger M. Dose and fractionation in stereotactic body radiation therapy for stage i non-small cell lung cancer: lessons learned and where do we go next? *Int J Radiat Oncol Biol Phys* (2015) 93:765–8. doi:10.1016/j.ijrobp.2015.08.025

46. Onishi H, Araki T, Shirato H, Nagata Y, Hiraoka M, Gomi K, et al. Stereotactic hypofractionated high-dose irradiation for stage I nonsmall cell lung carcinoma: clinical outcomes in 245 subjects in a Japanese multiinstitutional study. *Cancer* (2004) 101(7):1623–31. doi:10.1002/cncr.20539

47. Menten MJ, Wetscherek A, Fast MF. MRI-guided lung SBRT: present and future developments. *Physica Med* (2017) 44:139–49. doi:10.1016/j.ejmp.2017.02.003

48. Onishi H, Shirato H, Nagata Y, Hiraoka M, Fujino M, Gomi K, et al. Hypofractionated stereotactic radiotherapy (HypoFXSRT) for stage I non-small cell lung cancer: updated results of 257 patients in a Japanese multi-institutional study. *J Thorac Oncol* (2007) 2. doi:10.1097/JTO.0b013e318074de34

49. Moreno AC, Fellman B, Hobbs BP, Liao Z, Gomez DR, Chen A, et al. Biologically effective dose in stereotactic body radiotherapy and survival for patients with early-stage NSCLC. *J Thorac Oncol* (2020) 15(1):101–9. doi:10.1016/j.jtho.2019.08.2505

50. Koshy M, Malik R, Weichselbaum RR, Sher DJ. Increasing radiation therapy dose is associated with improved survival in patients undergoing stereotactic body radiation therapy for stage I non-small-cell lung cancer. *Int J Radiat Oncol Biol Phys* (2015) 91(2):344–50. doi:10.1016/j.ijrobp.2014.10.002

51. Videtic GM, Paulus R, Singh AK, Chang JY, Parker W, Olivier KR, et al. Long-term follow-up on NRG oncology RTOG 0915 (NCCTG N0927): a randomized phase 2 study comparing 2 stereotactic body radiation therapy schedules for medically inoperable patients with stage I peripheral non-small cell lung cancer. *Int J Radiat Oncol Biol Phys* (2019) 103(5):1077–84. doi:10.1016/j.ijrobp.2018.11.051

52. Singh AK, Gomez-Suescun JA, Stephans KL, Bogart JA, Hermann GM, Tian L, et al. One versus three fractions of stereotactic body radiation therapy for peripheral stage I to II non-small cell lung cancer: a randomized, multi-institution, phase 2 trial. *Int J Radiat Oncol Biol Phys* (2019) 105(4):752–9. doi:10.1016/j.ijrobp.2019.08.019

53. Tjong MC, Louie AV, Singh AK, Videtic G, Stephans K, Plumridge N, et al. Single-fraction stereotactic ablative body radiotherapy to the lung – the knockout punch. *Clin Oncol* (2022) 34(5):e183–94. doi:10.1016/j.clon.2022.02.004

54. Guckenberger M, Belka C, Bezjak A, Bradley J, Daly ME, DeRuysscher D, et al. Practice recommendations for lung cancer radiotherapy during the COVID-19 pandemic: an ESTRO-ASTRO consensus statement. *Radiother Oncol* (2020) 146:223–9. doi:10.1016/j.radonc.2020.04.001

55. Park C, Papiez L, Zhang S, Story M, Timmerman RD. Universal survival curve and single fraction equivalent dose: useful tools in understanding potency of ablative radiotherapy. *Int J Radiat Oncol Biol Phys* (2008) 70(3):847–52. doi:10.1016/j.ijrobp.2007.10.059

56. Guckenberger M, Klement RJ, Allgäuer M, Appold S, Dieckmann K, Ernst I, et al. Applicability of the linear-quadratic formalism for modeling local tumor control probability in high dose per fraction stereotactic body radiotherapy for early stage non-small cell lung cancer. *Radiother Oncol* (2013) 109(1):13–20. doi:10.1016/j.radonc.2013.09.005

57. Wang B, Dong Y, Yu X, Li F, Wang J, Chen H, et al. A review on the applications of Traditional Chinese medicine polysaccharides in drug delivery systems. *Front Oncol* (2022) 17:12. doi:10.1186/s13020-021-00567-3

58. Verma V, Shostrom VK, Kumar SS, Zhen W, Hallemeier CL, Braunstein SE, et al. Multi-institutional experience of stereotactic body radiotherapy for large (≥5 centimeters) non–small cell lung tumors. *Cancer* (2017) 123(4):688–96. doi:10.1002/cncr.30375

59. Benedict SH, Yenice KM, Followill D, Galvin JM, Hinson W, Kavanagh B, et al. Stereotactic body radiation therapy: the report of AAPM Task Group 101. *Med Phys* (2010) 37:4078–101. doi:10.1118/1.3438081

60. Keall PJ, Mageras GS, Balter JM, Emery RS, Forster KM, Jiang SB, et al. The management of respiratory motion in radiation oncology report of AAPM Task Group 76. *Med Phys* (2006) 33:3874–900. doi:10.1118/1.2349696

61. Caillet V, Booth JT, Keall P. IGRT and motion management during lung SBRT delivery. *Physica Med* (2017) 44:113–22. doi:10.1016/j.ejmp.2017.06.006

62. Jin JY, Ajlouni M, Chen Q, Kong FM, Ryu S, Movsas B. Quantification of incidental dose to potential clinical target volume (CTV) under different stereotactic body radiation therapy (SBRT) techniques for non-small cell lung cancer - tumor motion and using internal target volume (ITV) could improve dose distribution in CTV. *Radiother Oncol* (2007) 85(2):267–76. doi:10.1016/j.radonc.2007.09.004

63. Marks LB, Yorke ED, Jackson A, Ten Haken RK, Constine LS, Eisbruch A, et al. Use of normal tissue complication probability models in the clinic. *Int J Radiat Oncol Biol Phys* (2010) 76(3):S10–S19. doi:10.1016/j.ijrobp.2009.07.1754

64. Diez P, Hanna GG, Aitken KL, van As N, Carver A, Colaco RJ, et al. UK 2022 consensus on normal tissue dose-volume constraints for oligometastatic, primary lung and hepatocellular carcinoma stereotactic ablative radiotherapy. *Clin Oncol* (2022) 34(5):288–300. doi:10.1016/j.clon.2022.02.010

65. Grimm J, Marks LB, Jackson A, Kavanagh BD, Xue J, Yorke E. High dose per fraction, hypofractionated treatment effects in the clinic (HyTEC): an overview. *Int J Radiat Oncol Biol Phys* (2021) 110(1):1–10. doi:10.1016/j.ijrobp.2020.10.039

66. Verbakel WFAR, Senan S, Cuijpers JP, Slotman BJ, Lagerwaard FJ. Rapid delivery of stereotactic radiotherapy for peripheral lung tumors using volumetric intensity-modulated arcs. *Radiother Oncol* (2009) 93(1):122–4. doi:10.1016/j.radonc.2009.05.020

67. Navarria P, Ascolese AM, Mancosu P, Alongi F, Clerici E, Tozzi A, et al. Volumetric modulated arc therapy with flattening filter free (FFF) beams for stereotactic body radiation therapy (SBRT) in patients with medically inoperable early stage non small cell lung cancer (NSCLC). *Radiother Oncol* (2013) 107(3):414–8. doi:10.1016/j.radonc.2013.04.016

68. De Ruysscher D, Belderbos J, Reymen B, Van Elmpt W, Van Baardwijk A, Wanders R, et al. State of the art radiation therapy for lung cancer 2012: a glimpse of the future. *Clin Lung Cancer* (2013) 14:89–95. doi:10.1016/j.cllc.2012.06.006

69. Devaraj A, Cook GJR, Hansell DM. PET/CT in non-small cell lung cancer staging-promises and problems. *Clin Radiol* (2007) 62:97–108. doi:10.1016/j.crad.2006.09.015

70. Cheebsumon P, Boellaard R, de Ruysscher D, van Elmpt W, van Baardwijk A, Yaqub M, et al. Assessment of tumour size in PET/CT lung cancer studies: PET- and CT-based methods compared to pathology. *EJNMMI Res* (2012) 2(1):56–9. doi:10.1186/2191-219X-2-56

71. Geiger GA, Kim MB, Xanthopoulos EP, Pryma DA, Grover S, Plastaras JP, et al. Stage migration in planning PET/CT scans in patients due to receive radiotherapy for non-small-cell lung cancer. *Clin Lung Cancer* (2014) 15(1):79–85. doi:10.1016/j.cllc.2013.08.004

72. Loganadane G, Martinetti F, Mercier O, Krhili S, Riet FG, Mbagui R, et al. Stereotactic ablative radiotherapy for early stage non-small cell lung cancer: a critical literature review of predictive factors of relapse. *Cancer Treat Rev* (2016) 50:240–6. doi:10.1016/j.ctrv.2016.10.002

73. Chang JY, Liu H, Balter P, Komaki R, Liao Z, Welsh J, et al. Clinical outcome and predictors of survival and pneumonitis after stereotactic ablative radiotherapy for stage I non-small cell lung cancer. *Radiat Oncol* (2012) 7(1):152. doi:10.1186/1748-717X-7-152

74. Vansteenkiste J, Crinò L, Dooms C, Douillard JY, Faivre-Finn C, Lim E, et al. 2nd ESMO consensus conference on lung cancer: early-stage non-small-cell lung cancer consensus on diagnosis, treatment and follow-up. *Ann Oncol* (2014) 25(8):1462–74. doi:10.1093/annonc/mdu089

75. Videtic GMM, Donington J, Giuliani M, Heinzerling J, Karas TZ, Kelsey CR, et al. Stereotactic body radiation therapy for early-stage non-small cell lung cancer: executive Summary of an ASTRO Evidence-Based Guideline. *Pract Radiat Oncol* (2017) 7(5):295–301. doi:10.1016/j.prro.2017.04.014

76. Zeng J, Harris TJ, Lim M, Drake CG, Tran PT. Immune modulation and stereotactic radiation: improving local and abscopal responses. *Biomed Res Int* (2013) 2013:658126. doi:10.1155/2013/658126

77. Chen Y, Gao M, Huang Z, Yu J, Meng X. SBRT combined with PD-1/PD-L1 inhibitors in NSCLC treatment: a focus on the mechanisms, advances, and future challenges. *J Hematol Oncol* (2020) 13:105. doi:10.1186/s13045-020-00940-z

78. Shaverdian N, Lisberg AE, Bornazyan K, Veruttipong D, Goldman JW, Formenti SC, et al. Previous radiotherapy and the clinical activity and toxicity of pembrolizumab in the treatment of non-small-cell lung cancer: a secondary analysis of the KEYNOTE-001 phase 1 trial. *Lancet Oncol* (2017) 18(7):895–903. doi:10.1016/S1470-2045(17)30380-7

79. Wang YY, Wang YS, Liu T, Yang K, Yang GQ, Liu HC, et al. Efficacy study of CyberKnife stereotactic radiosurgery combined with CIK cell immunotherapy for advanced refractory lung cancer. *Exp Ther Med* (2013) 5(2):453–6. doi:10.3892/etm.2012.818

80. Seung SK, Curti BD, Crittenden M, Walker E, Coffey T, Siebert JC, et al. Phase 1 study of stereotactic body radiotherapy and interleukin-2--tumor and immunological responses. *Sci Transl Med* (2012) 4(137):137ra74. doi:10.1126/scitranslmed.3003649

81. Monjazeb AM, Daly ME, Luxardi G, Maverakis E, Merleev AA, Marusina AI, et al. Atezolizumab plus stereotactic ablative radiotherapy for medically inoperable patients with early-stage non-small cell lung cancer: a multi-institutional phase I trial. *Nat Commun* (2023) 14(1):5332. doi:10.1038/s41467-023-40813-w

82. Huang K, Dahele M, Senan S, Guckenberger M, Rodrigues GB, Ward A, et al. Radiographic changes after lung stereotactic ablative radiotherapy (SABR) - can we distinguish recurrence from fibrosis? A systematic review of the literature. *Radiother Oncol* (2012) 102:335–42. doi:10.1016/j.radonc.2011.12.018

83. Bucknell NW, Kron T, Herschtal A, Hardcastle N, Irving L, MacManus M, et al. Comparison of changes in pulmonary function after stereotactic body radiation therapy versus conventional 3-dimensional conformal radiation therapy for stage I and IIA non-small cell lung cancer: an analysis of the TROG 09.02 (CHISEL) phase 3 trial. *Int J Radiat Oncol Biol Phys* (2023) 117(2):378–86. doi:10.1016/j.ijrobp.2023.04.009

84. Yu V, Kishan AU, Cao M, Low D, Lee P, Ruan D. Dose impact in radiographic lung injury following lung SBRT: statistical analysis and geometric interpretation. *Med Phys* (2014) 41(3):031701. doi:10.1118/1.4863483

85. Stanic S, Paulus R, Timmerman RD, Michalski JM, Barriger RB, Bezjak A, et al. No clinically significant changes in pulmonary function following stereotactic body radiation therapy for early-stage peripheral non-small cell lung cancer: an analysis of RTOG 0236. *Int J Radiat Oncol Biol Phys* (2014) 88(5):1092–9. doi:10.1016/j.ijrobp.2013.12.050

86. Finazzi T, Palacios MA, Spoelstra FOB, Haasbeek CJA, Bruynzeel AME, Slotman BJ, et al. Role of on-table plan adaptation in MR-guided ablative radiation therapy for central lung tumors. *Int J Radiat Oncol Biol Phys* (2019) 104(4):933–41. doi:10.1016/j.ijrobp.2019.03.035

87. Finazzi T, Palacios MA, Haasbeek CJA, Admiraal MA, Spoelstra FOB, Bruynzeel AME, et al. Stereotactic MR-guided adaptive radiation therapy for peripheral lung tumors. *Radiother Oncol* (2020) 144:46–52. doi:10.1016/j.radonc.2019.10.013

88. Henke LE, Olsen JR, Contreras JA, Curcuru A, DeWees TA, Green OL, et al. Stereotactic MR-guided online adaptive radiation therapy (SMART) for ultracentral thorax malignancies: results of a phase 1 trial. *Adv Radiat Oncol* (2019) 4(1):201–9. doi:10.1016/j.adro.2018.10.003

Pathology & Oncology Research | frontiers

TYPE Original Research
PUBLISHED 30 November 2023
DOI 10.3389/pore.2023.1611377

Check for updates

OPEN ACCESS

EDITED BY
József Tímár,
Semmelweis University, Hungary

*CORRESPONDENCE
Guangyu Jiao,
jiao_gy@163.com

†These authors have contributed equally to this work

RECEIVED 29 June 2023
ACCEPTED 17 November 2023
PUBLISHED 30 November 2023

CITATION
Wang Z, Li P, Bai J, Liu Y and Jiao G (2023), Quantitative analysis of endobronchial elastography combined with serum tumour markers of lung cancer in the diagnosis of benign and malignant mediastinal and hilar lymph nodes.
Pathol. Oncol. Res. 29:1611377.
doi: 10.3389/pore.2023.1611377

COPYRIGHT
© 2023 Wang, Li, Bai, Liu and Jiao. This is an open-access article distributed under the terms of the Creative Commons Attribution License (CC BY). The use, distribution or reproduction in other forums is permitted, provided the original author(s) and the copyright owner(s) are credited and that the original publication in this journal is cited, in accordance with accepted academic practice. No use, distribution or reproduction is permitted which does not comply with these terms.

Quantitative analysis of endobronchial elastography combined with serum tumour markers of lung cancer in the diagnosis of benign and malignant mediastinal and hilar lymph nodes

Zhen Wang[1†], Peng Li[1†], Jiayu Bai[2], Yujia Liu[3] and Guangyu Jiao[1*]

[1]Department of Respiratory Medicine, Shengjing Hospital of China Medical University, Shenyang, China, [2]Department of Rheumatology, The First Affiliated Hospital of China Medical University, Shenyang, China, [3]College of Traditional Chinese Medicine, Liaoning University of Traditional Chinese Medicine, Shenyang, China

Purpose: In malignant tumours, elastography and serum tumour markers have shown high diagnostic efficacy. Therefore, we aimed to quantitatively analyse the results of endobronchial elastography combined with serum tumour markers of lung cancer to accurately distinguish benign and malignant mediastinal and hilar lymph nodes.

Methods: Data of patients who underwent endobronchial ultrasound-guided transbronchial needle aspiration for mediastinal lymph node enlargement in our hospital between January 2018 and August 2022 were retrospectively collected. The characteristics of quantitative elastography and serum tumour markers were evaluated.

Results: We enrolled 197 patients (273 lymph nodes). In the differential diagnosis of benign and malignant mediastinal and hilar lymph nodes, the stiffness area ratio (SAR), strain ratio (SR), and strain rate in lymph nodes were significant, among which SAR had the highest diagnostic value (cut-off value, 0.409). The combination of the four tumour markers had a high diagnostic value (AUC, 0.886). Three types of quantitative elastography indices combined with serum tumour markers for lung cancer showed a higher diagnostic value (AUC, 0.930; sensitivity, 83.5%; specificity, 89.3%; positive predictive value, 88.1%; negative predictive value, 85%) ($p < 0.05$). In the differential diagnosis of pathological types of lung cancer, different quantitative elastography indicators and serum tumour markers for lung cancer have different diagnostic significance for the differential diagnosis of lung cancer pathological types.

Conclusion: The quantitative analysis of endobronchial ultrasound elastography combined with tumour markers can improve the diagnosis rate of benign and malignant mediastinal and hilar lymph nodes, help guide the puncture of false negative lymph nodes, and reduce the misdiagnosis rate.

KEYWORDS

elastography, endobronchial ultrasound-guided transbronchial needle aspiration, mediastinal and hilar lymph nodes, lung cancer, serum tumour markers

Introduction

Mediastinal and hilar lymphadenopathy refers to the enlargement of one or more lymph nodes, usually >10 mm in diameter, due to benign or malignant causes, among which lymph node metastasis caused by malignant tumours and granulomatous diseases are the most common [1, 2]. Lung cancer is a malignant tumour with the highest incidence worldwide, accounting for approximately 20% of the mortality rate of all malignant tumours [3]. Its pathological types can be divided into non-small-cell lung cancer (NSCLC) and small-cell lung cancer (SCLC), with NSCLC accounting for approximately 85% of cases. NSCLCs are further divided into lung squamous cell carcinoma (LSCC) and lung adenocarcinoma (LADC) [4]. The 5 year survival rate of lung cancer is 15%–20%. For NSCLC, the 5 year survival rate of stage 1A1 reaches 90%, whereas that of stage IV decreases to <10%. In patients with SCLC, the 5 year survival rate in the limited period is approximately 30%, and that in the extensive period is <10% [5]. The degree of mediastinal and hilar lymph node metastasis caused by lung cancer is a key factor in lymph node staging, which directly affects the tumour-node-metastasis staging results of patients with lung cancer, thus affecting patient prognosis [6, 7]. Therefore, early identification of benign and malignant mediastinal and hilar lymph nodes is critical for clear diagnosis and accurate staging and treatment.

Endobronchial ultrasound-guided transbronchial needle aspiration (EBUS-TBNA) biopsy has become a first-line method for the diagnosis and staging of lymph nodes in lung cancer because of its minimally invasive nature, low complication rate, and high accuracy [8]. With the rapid development of EBUS technology, the application of ultrasonic elastography in the evaluation of lymph nodes has gradually increased.

Elastography provides images of tissue stiffness. According to the different elastic coefficients of different tissues, the degree of tissue deformation after compression by an external force varies. The change in the movement amplitude of the echo signal before and after compression is converted into real-time colour images, which can reflect the characteristic information of diseased tissues [9]. Tissues with a small elastic coefficient and large displacement change after compression are shown in red, tissues with a large elastic coefficient and small displacement change after compression are shown in blue, and tissues with a medium elastic coefficient are shown in green and yellow [10]. Elastography technology, which further expands ultrasound imaging, is a powerful supplement to conventional ultrasonography and can vividly display, locate, and provide information to enable identification of benign and malignant lesions.

A recent meta-analysis found that EBUS elastography has high sensitivity and specificity for the diagnosis of benign and malignant intrathoracic lymph nodes [11]. Intrathoracic lymph nodes can be assessed by qualitative or quantitative methods, such as the strain ratio (SR) and the stiffness area ratio (SAR, blue area in lymph nodes/total area of lymph nodes). Qualitative methods include the elastography type and score [12–17].

Serum tumour markers are important auxiliary markers, having great significance for the screening, diagnosis, and prognosis of lung cancer. Among them, the carcinoembryonic antigen (CEA), cytokeratin-19-fragment (CYFRA21-1), pro-gastrin-releasing peptide (ProGRP), and neuron-specific enolase (NSE) are specific tumour markers for the differential diagnosis of lung cancer and have a high diagnostic sensitivity [18, 19]. However, no previous studies have used on using a combination of elastography and serum lung cancer tumour markers to differentiate between benign and malignant mediastinal and hilar lymph nodes. Therefore, the aim of this study is to combine quantitative analysis of elastic imaging with serum tumour markers, which can improve the accuracy of diagnosis of benign and malignant mediastinum and hilar lymph nodes compared with single diagnosis.

Materials and methods

Study design and patients

This study retrospectively analysed patients with mediastinal lymph node enlargement on computed tomography (CT) who underwent EBUS-TBNA at Shengjing Hospital affiliated with the China Medical University from January 2018 to August 2022. All patients were examined for lung cancer serum tumour markers, and elastography was performed before puncture. The serum tumour markers included CEA, CYFRA21-1, ProGRP, and NSE. Patients with incomplete clinical data, such as incomplete detection of tumour markers, absence of elastic imaging images, or poor image quality that could not delineate circular areas were excluded.

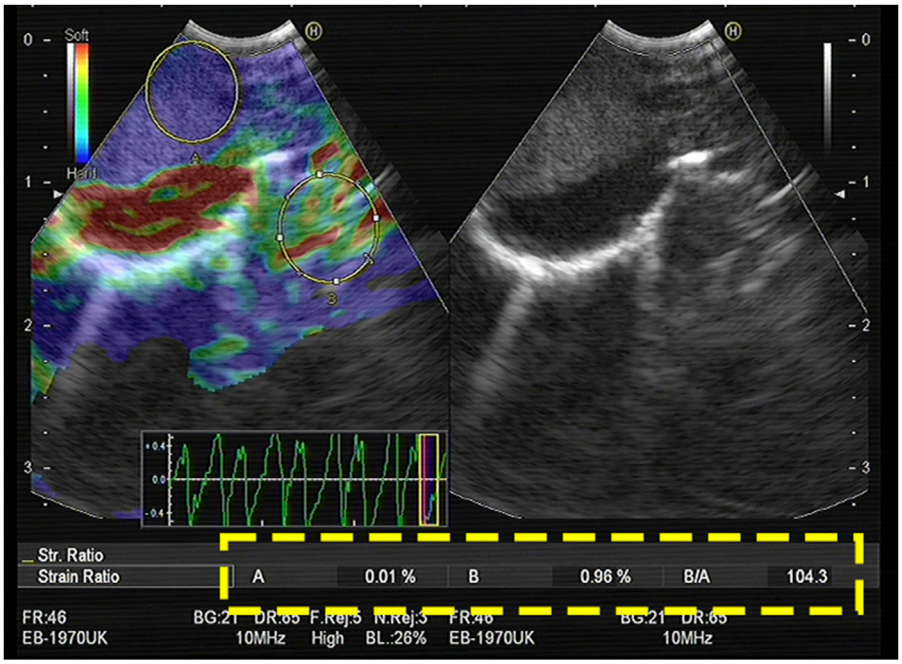

FIGURE 1
The largest possible area within the LN was outlined as A. An area of the normal-appearing soft tissue outside the LN was selected as B. The strain (B/A) ratio was 104.3. The final diagnosis obtained by EBUS-TBNA was malignant.

Acquisition and analysis of EBUS examination images

All patients received anaesthesia for EBUS examination, including local airway anaesthetics (lidocaine) or conscious sedatives (midazolam and fentanyl). Elastography was performed using a Pentax EB-1970UK ultrasound bronchoscope and Hitachi HI VISION Avius (Hitachi, Japan) ultrasound scanner.

Acquisition of the SR value

The doctor identified the enlarged lymph nodes on preoperative CT images, selected the appropriate lymph nodes for B-mode ultrasound image observation, and switched the imaging system to the elastic imaging mode. After obtaining stable elastic images, the operator applied the functions provided by the equipment to measure the SR of the target lymph nodes in real time. The specific method was as follows: a circle as large as possible was made in the target lymph node, the strain rate of the tissue in the circle was automatically calculated by the device, and the value was recorded as A. Normal tissue was selected to form a circle outside the target lymph node. The circle avoided blood vessels and perivascular tissues in the color Doppler mode, and its size was similar to that of the circle in the target lymph node. Its internal strain rate was denoted as B, and the device automatically calculated the ratio of B to A to calculate the SR (Figure 1). After elastography, each target lymph node was punctured 1–6 times under real-time ultrasound guidance.

Acquisition of the SAR value

The elastic image of the target lymph node was retrospectively analysed using the image analysis software ImageJ (Rasband, W.S., ImageJ, U. S. National Institutes of Health, Bethesda, Maryland, United States,[1] 1997–2018). The blue area and total area of the target lymph node were measured, and the SAR was obtained by calculating the ratio of the two (blue/total). The specific methods were as follows: 1) The picture of the target lymph node to be measured was opened in ImageJ. 2) The "Polygon selections" tool was used to manually outline of the area to be evaluated to calculate the area of the drawn lymph node. 3) The colour contrast between the drawn lymph nodes and the surrounding area was enhanced. 4) The blue area in the lymph nodes was obtained by adjusting the colour value of blue, changing the brightness and saturation, and calculating the blue area. 5) Finally, the SAR was calculated by dividing the resulting blue area by the entire lymph node area (Figure 2).

1 https://imagej.nih.gov/ij/

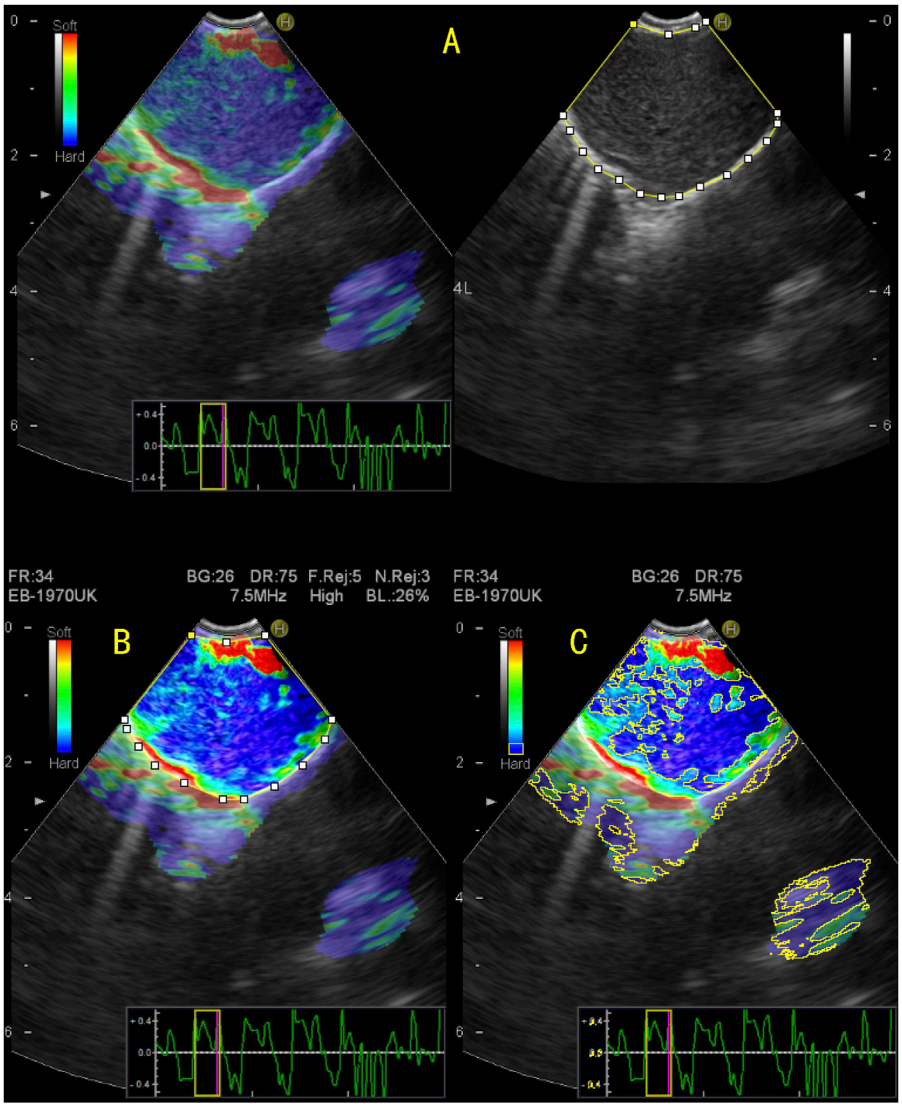

FIGURE 2
Quantitative evaluation of endobronchial ultrasound elastography using ImageJ. **(A)** The elastography image on the right and the B-mode ultrasound image on the left, on which the entire area of the target lymph node was manually enclosed; **(B)** To enhance the color contrast between the target lymph node and surrounding tissue; **(C)** By adjusting the blue value, brightness, and saturation, the blue region in the target lymph node is displayed and the area of the blue region in the target lymph node is measured. The stiffness area ratio (SAR) was calculated by dividing the blue area (indicating stiffness) by the entire area of the lymph node. SAR = 0.624, pathological diagnosis was malignant.

Acquisition of the strain rate in lymph nodes (the largest possible area within the LN, LPA) value

The A value was easily and accurately obtained during elastography of the lymph nodes; however, the choice of the B value was often highly subjective and prone to selection bias. Therefore, we studied the A value as an independent parameter and named it the LPA. For the SR and SAR, a value greater than the critical value was considered to indicate malignancy, whereas a value lower than the critical value was considered to indicate benignity. However, as the denominator in the LPA for SR is a small optimal index, values lesser than the critical value were considered to indicate malignancy.

Finally, the pathological results were compared with the results obtained using SR, SAR, and LPA. The final diagnosis of each lymph node was based on pathological and microbiological evidence obtained from EBUS-TBNA, surgery, bronchoalveolar lavage, and bacterial culture, or from a definitive diagnosis obtained at clinical and radiological follow-up (at least 6 months).

TABLE 1 Characteristics of LNs evaluated in the study.

Characteristic	Numbers of lymph nodes (N = 273)	(%)
LN pathology		
Malignant LNs	133	(48.7)
Adenocarcinoma	64	(23.4)
Squamous carcinoma	14	(5.1)
Small cell lung cancer	37	(13.6)
Malignancy of unknown type	11	(4.0)
Lymphoma	4	(1.5)
Metastatic carcinoma	3	(1.1)
Benign LNs	140	(51.3)
LN station		
1R	1	(0.4)
2R/L	8	(2.9)
3P	1	(0.4)
4R/L	64	(23.4)
7	107	(39.2)
10R/L	6	(2.2)
11L	27	(9.9)
11R/Ri/Rs	52	(19.0)
12R/L	7	(2.6)
Average number of punctures	1.39	

Statistical analysis

Measurement data are expressed as mean ± standard deviation, and the chi-square test was used to compare the data. When the data conditions did not meet the requirements of the chi-square test, the continuous correction chi-square test was used. With pathological diagnosis as the gold standard, a receiver operating characteristic (ROC) curve was constructed to obtain the area under the curve (AUC), sensitivity, specificity, positive predictive value, and negative predictive value of different indicators. The Z-test was used to evaluate whether the differences between the different indicators of the AUC were significant. The Spearman correlation test was used also used to analyse the data. Differences were considered significant when $p < 0.05$. All data were analysed using SPSS 22.0 (IBM Corp., Armonk, NY, United States) and MedCalc 18.0 (MedCalc Software, Ostend, Belgium).

Results

Lymph node characteristics

This study enrolled 197 patients, including 109 men and 88 women, aged 17–80 years, with an average age of 57.33 ± 12.14 years. In total, 273 lymph nodes were punctured, with an average of 1.39 lymph nodes per patient. Lymph nodes were classified according to the latest International Staging System [20]. Among the punctured lymph nodes, one was in the 1R group, eight were in the 2R/L group, one was in the 3P group, 64 were in the 4R/L group, 107 were in the 7 group, six were in the 10R/L group, 79 were in the 11R/L group, and seven were in the 12R/L group. Pathological findings showed that 133 lymph nodes were malignant and 140 were benign. Table 1 summarises the patients' lymph node characteristics.

Diagnostic value of quantitative elastography in differentiating benign and malignant mediastinal and hilar lymph nodes

Figure 3 shows the cut-off values of the three quantitative elastography indices in differentiating benign and malignant mediastinal and hilar lymph nodes; the SAR was 0.409, SR was 1.300, and LPA was 0.250, all of which were significant ($p < 0.05$). The diagnostic significance of the SAR was higher than that of the SR ($p < 0.0001$), and the AUC was 0.784 > 0.647. Similarly, the diagnostic significance of the SAR was higher than that of the LPA ($p = 0.0001$), and the AUC was 0.784 > 0.684. There was no significant difference between the diagnostic values of the SR and LPA ($p = 0.1173$). Therefore, the SAR had a higher diagnostic value than the SR and LPA in differentiating benign and malignant mediastinal and hilar lymph nodes. By constructing the ROC curve, the diagnostic rate of the SAR was 72.2%, sensitivity was 81.2%, specificity was 63.6%, and AUC was 0.784. Although the diagnostic rate of the three quantitative elastic imaging combinations was slightly higher than that of the SAR, the difference was not significant ($p > 0.05$) (Table 2).

Diagnostic value of serum tumour markers for differentiating benign and malignant mediastinal and hilar lymph nodes

Table 3 summarises the cut-off value and diagnostic value of the four lung cancer tumour markers in differentiating benign and malignant mediastinal and hilar lymph nodes. Compared to single diagnosis, combined diagnosis with CEA, CYFRA21-1, NSE, and ProGRP showed higher specificity and sensitivity, with an AUC of 0.886, which was significant ($p < 0.05$).

Diagnostic value of quantitative elastography combined with serum lung cancer tumour markers for differentiating benign and malignant mediastinal and hilar lymph nodes

As shown in Table 4, among the three quantitative elastography indices and tumour markers, only the SAR was

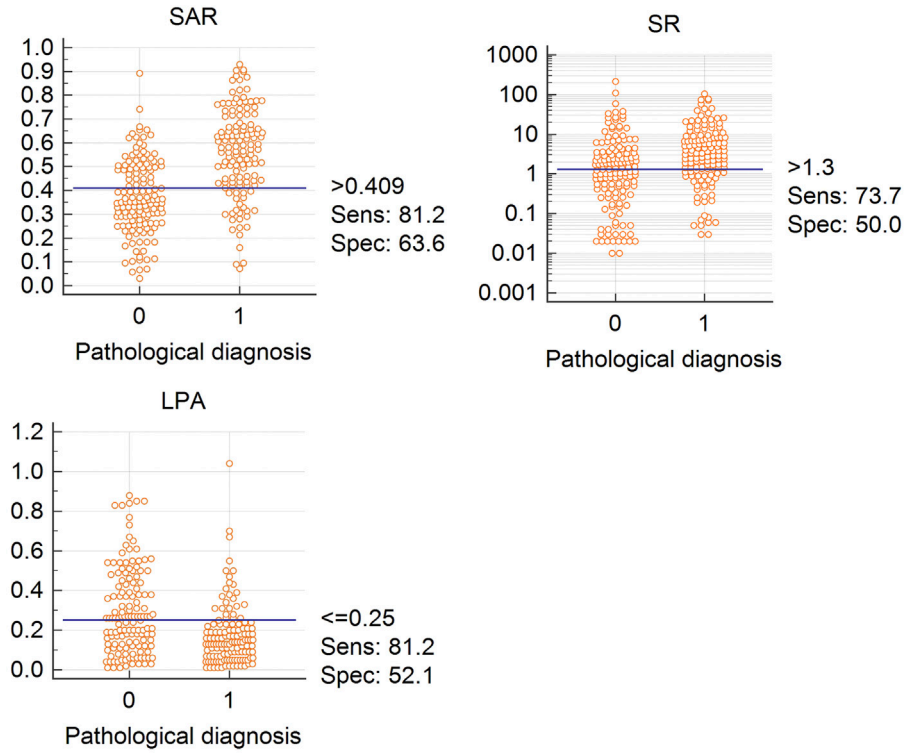

FIGURE 3
Cutoff values for SAR, LPA, and SR Abbreviation: SAR, stiffness area ratio; SR, strain ratio; LPA, The largest possible area within the LN. "0" is benign, "1" is malignant.

TABLE 2 Diagnostic value of three elastography indexes for benign and malignant lymph nodes.

Characteristic	Cut-off value	Accuracy (%)	Sensitivity (%)	Specificity (%)	PPV (%)	NPV (%)	AUC	*p*-value malignant vs. benign
SAR	0.409	72.2	81.2	63.6	67.9	78.1	0.784	0.000
SR	1.3	61.5	73.7	50.0	58.3	66.7	0.647	0.000
A	0.25	66.3	81.2	52.1	61.7	74.5	0.684	0.000
SAR + A + SR		73.2	79.0	67.9	70.0	77.2	0.796	0.000

Abbreviation: SAR, stiffness area ratio; SR, strain ratio; LPA, The largest possible area within the LN.

TABLE 3 Diagnostic value of serum tumor markers for benign and malignant mediastinal and hilar lymph nodes.

Group	Cut-off value	AUC	Sensitivity (%)	Specificity (%)	*p*-value malignant vs. benign
Malignant Tumor					
CEA	4.395 ng/mL	0.801	54.9	92.1	0.000
CYFRA21-1	3.085 ng/mL	0.811	66.9	86.4	0.000
NSE	26.665 ng/mL	0.608	36.1	87.1	0.002
ProGRP	42.99 pg/mL	0.673	62.4	69.3	0.000
Combination of four		0.886	71.4	88.6	0.000

Abbreviation: CEA, carcinoembryonic antigen; CYFRA21-1, cytokeratin-19-fragment; NSE, neuron specific enolase; ProGRP, pro-gastrin-releasing peptide; Combination of four: CEA + CYFRA21-1 + NSE + ProGRP.

TABLE 4 Correlation of SAR and serum tumor markers (CEA, CYFRA21-1, NSE, ProGRP).

Relative factors	CEA	CYFRA21-1	NSE	ProGRP
SAR	0.202**	0.162**	0.123*	0.088
LPA	−0.066	−0.076	−0.088	−0.057
SR	0.027	−0.018	0.044	−0.027

Note: * and ** mean significant correlation at $p < 0.05$ and $p < 0.01$.
Abbreviation: SAR, stiffness area ratio; SR, strain ratio; LPA, The largest possible area within the LN; CEA, carcinoembryonic antigen; CYFRA21-1, cytokeratin-19-fragment; NSE, neuron specific enolase; ProGRP, pro-gastrin-releasing peptide.

positively correlated with the CEA, CYFRA21-1, and NSE. Although the correlation was not high, there was a significant difference between them ($p < 0.05$). The SAR combined with CEA, CYFRA21-1, and NSE had a high diagnostic significance for mediastinal and hilar lymph nodes, with a sensitivity of 79.7%, specificity of 90.7%, positive predictive value of 89.1%, and negative predictive value of 82.5%. The AUC was 0.926, which had a higher diagnostic value than that of tumour markers or quantitative elastography alone ($p < 0.05$) (Table 5).

Table 6 shows the diagnostic value of the four tumour markers combined with different quantitative analysis indices in elastography. Compared to those of the SAR combined with the CEA, CYFRA21-1, and NSE, the diagnostic rate and sensitivity of the SAR combined with the four serum lung cancer tumour markers were 85.7% and 83.5%, respectively, with an AUC of 0.927. The combination of the four serum lung cancer tumour markers and the three quantitative elastography indicators had the highest diagnostic value, with a diagnostic rate of 86.4%, a sensitivity of 83.5%, a specificity of 89.3%, and an AUC of 0.930.

Diagnostic value of quantitative elastography in pathological types of lung cancer

Figure 4 summarises the diagnostic value of the three quantitative elastography indicators for LADC, LSCC, and SCLC. In LADC, the cut-off values of the SAR, SR, and LPA were 0.513, 6.620, and 0.240, respectively, which were significant. In LSCC, only the SR was significant, with a cut-off value of 2.550; in SCLC, the SAR and LPA were significant, with cut-off values of 0.592 and 3.050, respectively. Compared with the SR and LPA, the SAR had the highest diagnostic value for LADC and SCLC ($p < 0.05$).

Diagnostic value of serum lung cancer tumour markers for pathological types of lung cancer

Table 7 summarises the cut-off values, sensitivity, and specificity of the four serum lung cancer tumour markers for LADC, LSCC, and SCLC. Among them, the combined detection rate of the CEA and CYFRA21-1 for LADC and NSE and ProGRP for SCLC and single detection rate of the CYFRA21-1 for LSCC had a high diagnostic significance.

Diagnostic value of quantitative elastography indicators combined with serum lung cancer tumour markers for pathological types of lung cancer

Table 8 shows the diagnostic value of quantitative elastography indicators combined with tumour markers specific to lung cancer types, including LADC, LSCC, and SCLC. In LADC, the AUC of the SAR, SR, and LPA combined with the CEA and CYFRA21-1 was 0.866. In SCLC, the AUC of the SR and LPA combined with the NSE and ProGRP was 0.889. The diagnostic rate and specificity of the three quantitative elastography indices combined with the NSE and ProGRP were the highest at 92.3% and 95.3%, respectively, and the AUC was 0.896. In LSCC, the diagnostic rate of the SR combined with the CYFRA21-1 was 78.8%, and the AUC was 0.835; the sensitivity of the SAR, SR, and LPA combined with the CYFRA21-1 was 1, and the AUC was 0.839. There was no significant difference in the diagnostic value of the three

TABLE 5 The diagnostic value of SAR combined with serum tumor markers in mediastinal and hilar lymph nodes.

Characteristic	Accuracy (%)	Sensitivity (%)	Specificity (%)	PPV (%)	NPV (%)	AUC
SAR + CEA	80.2	83.5	77.1	77.6	83.1	0.858
SAR + CYFRA21-1	82.4	80.5	84.5	82.9	81.9	0.878
SAR + NSE	76.2	72.9	79.3	77.0	75.5	0.819
SAR + ProGRP	73.6	66.9	80.0	76.1	71.8	0.791
SAR + CEA + CYFRA21-1	84.2	88.0	80.7	81.2	87.6	0.907
SAR + CEA + CYFRA21-1 + NSE	85.4	79.7	90.7	89.1	82.5	0.926

Abbreviation: SAR, stiffness area ratio; CEA, carcinoembryonic antigen; CYFRA21-1, cytokeratin-19-fragment; NSE, neuron specific enolase; ProGRP, pro-gastrin-releasing peptide.

TABLE 6 Comparison of diagnostic value for combined characteristics in benign/malignant differentiation.

Combined characteristic	Accuracy (%)	Sensitivity (%)	Specificity (%)	PPV (%)	NPV (%)	AUC
SAR + tumor markers	85.7	83.5	87.9	86.7	84.8	0.927
A+ tumor markers	82.8	88.7	77.1	78.7	87.8	0.905
SR + tumor markers	80.2	71.4	87.9	85.8	76.4	0.889
SAR + A+ tumor markers	85.7	83.5	87.9	86.7	84.8	0.927
SAR + A+ SR + tumor markers	86.4	83.5	89.3	88.1	85.0	0.930

Abbreviation: SAR, stiffness area ratio; SR, strain ratio; LPA, The largest possible area within the LN; tumor markers, CEA + CYFRA21-1 + NSE + ProGRP.

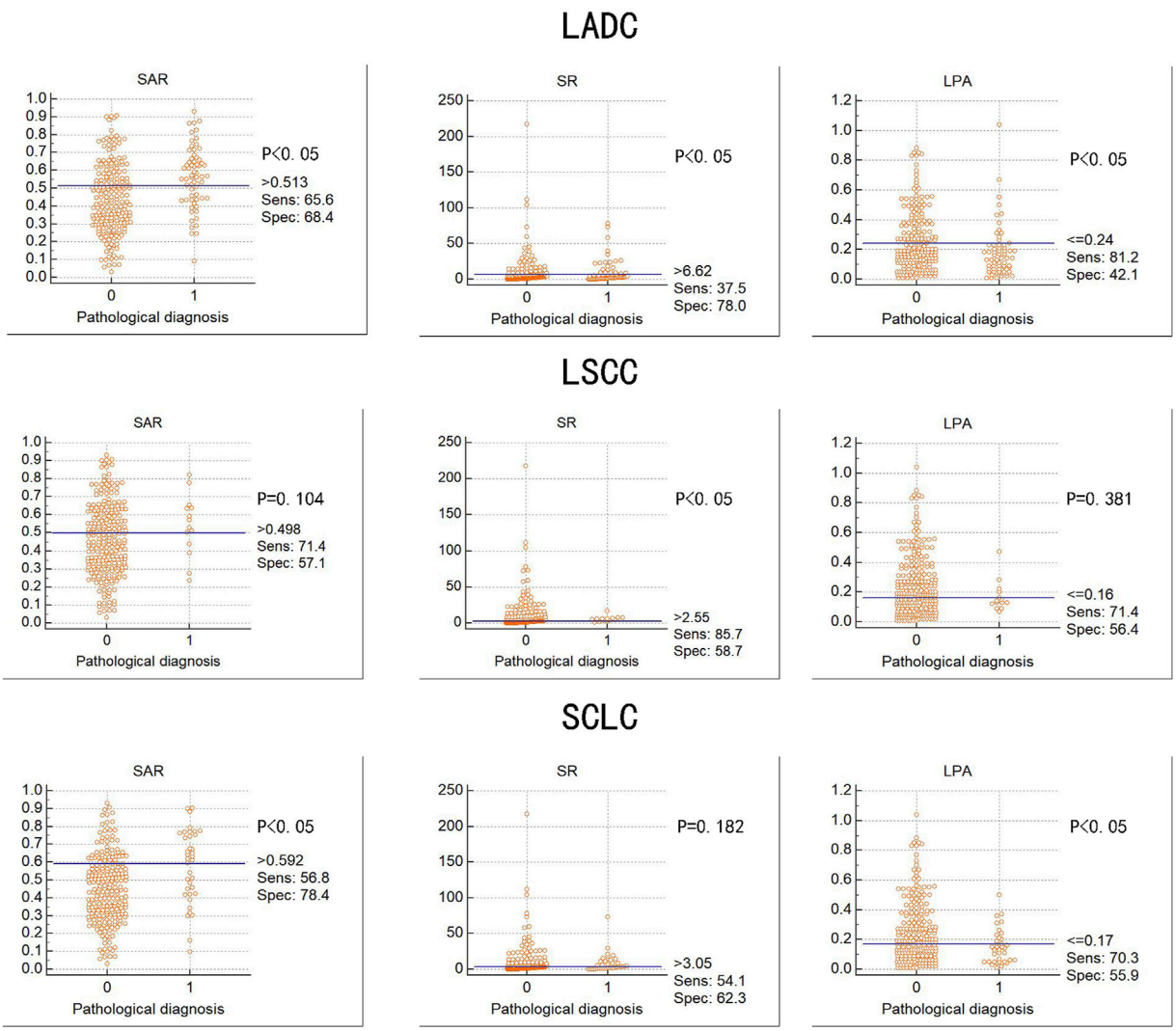

FIGURE 4
Diagnostic value of three elastography parameters for different types of lung cancer Abbreviation: SAR, stiffness area ratio; SR, strain ratio; LPA, The largest possible area within the LN. LADC, Lung adenocarcinoma; LSCC, Lung squamous cell carcinoma; SCLC, Small cell lung cancer. "0" is benign, "1" is malignant.

TABLE 7 Diagnostic efficiencies of four serum tumor markers for lung cancers of different pathological types.

Group	Cut-off value	AUC	Sensitivity (%)	Specificity (%)	*p*-value malignant vs. benign
Malignant Tumor					
CEA	4.395 ng/mL	0.801	54.9	92.1	0.000
CYFRA21-1	3.085 ng/mL	0.811	66.9	86.4	0.000
NSE	26.665 ng/mL	0.608	36.1	87.1	0.002
ProGRP	42.99 pg/mL	0.673	62.4	69.3	0.000
Combination of four		0.886	71.4	88.6	0.000
LADC					
CEA	4.605 ng/mL	0.808	68.8	85.6	0.000
CYFRA21-1	3.145 ng/mL	0.784	78.1	73.2	0.000
NSE	13.995 ng/mL	0.489	89.1	18.2	0.792
ProGRP	20.74 pg/mL	0.449	100	5.7	0.218
CEA + CYFRA21-1		0.870	82.8	80.9	0.000
Combination of four		0.807	78.1	71.3	0.000
SCLC					
CEA	2.03 ng/mL	0.629	85.5	44.9	0.012
CYFRA21-1	2.06 ng/mL	0.534	83.8	39	0.509
NSE	30.155 ng/mL	0.832	70.3	90.3	0.000
ProGRP	97.995 pg/mL	0.894	81.1	97.0	0.000
NSE + ProGRP		0.914	94.6	74.6	0.000
Combination of four		0.747	73.0	72.5	0.000
LSCC					
CEA	1.32 ng/mL	0.563	100	23.2	0.424
CYFRA21-1	3.855 ng/mL	0.836	78.6	73.0	0.000
NSE	17.77 ng/mL	0.437	71.4	41.3	0.428
ProGRP	30.24 pg/mL	0.504	100	21.6	0.961
Combination of four		0.697	64.3	71.8	0.013

Abbreviation: CEA, carcinoembryonic antigen; CYFRA21-1, cytokeratin-19-fragment; NSE, neuron specific enolase; ProGRP, pro-gastrin-releasing peptide; LADC, lung adenocarcinoma; LSCC, lung squamous cell carcinoma; SCLC, small cell lung cancer; Combination of four: CEA + CYFRA21-1 + NSE + ProGRP.

quantitative elastography indicators combined with tumour markers than that of tumour markers alone for lung cancer types ($p > 0.05$).

Discussion

This is the first time the diagnostic value of quantitative elastography combined with serum lung cancer tumour markers for benign and malignant mediastinal and hilar lymph nodes has been analysed in detail. The results show that quantitative elastography and serum tumour markers have diagnostic significance for benign and malignant mediastinal and hilar lymph nodes, and their combination significantly further improves diagnosis.

Mediastinal and hilar lymphadenopathy are commonly caused by malignant tumours, such as lung cancer, and granulomatous diseases. As lung cancer has the highest incidence worldwide and a high rate of lymph node metastasis, accurate lymph node staging is particularly important for treatment planning. Mediastinoscopy is considered the gold standard for the diagnosis of mediastinal lymph node metastasis; however, with the continuous development of endoscopic ultrasonography, EBUS-TBNA has gradually become the first-line method for the diagnosis and staging of mediastinal lymph nodes [8]. A study comparing the significance of EBUS examination and mediastinoscopy in lung cancer staging showed no significant difference in the sensitivity, positive predictive value, and accuracy of the two for diagnosing malignant lymph nodes [21].

Conventional ultrasonography has advantages over mediastinoscopy, due to real-time visualization, and being dynamic and less invasive. During EBUS-TBNA, the nature of the lymph nodes can be preliminarily determined according to the ultrasound characteristics. Fujiwara et al. [22] conducted a retrospective study of 1,061 cases of mediastinal and hilar lymph nodes and found that round, clear boundaries, uneven internal echoes and the presence of coagulation necrosis can be used as independent predictors for the diagnosis of malignant lymph nodes. However, there are large differences in the evaluation of

TABLE 8 Diagnostic efficiency of elastography combined with tumor markers for different types of lung cancer.

Parameters	Accuracy (%)	Sensitivity (%)	Specificity (%)	PPV (%)	NPV (%)	AUC	*p*-value malignant vs. benign
LADC							
SAR	67.8	65.6	68.4	38.9	86.7	0.696	0.000
SAR + CEA + CYFRA21-1	77	84.4	74.6	50.5	94	0.864	0.000
a + CEA + CYFRA21-1	78.7	81.3	78	53.1	93.1	0.866	0.000
CEA + CYFRA21-1	83.4	82.8	80.9	57	93.9	0.870	0.000
SCLC							
SAR + NSE + ProGRP	84	83.8	83.9	44.9	97.1	0.891	0.000
SAR + LPA + NSE + ProGRP	84	83.8	83.9	44.9	97.1	0.889	0.000
a + NSE + ProGRP	92.3	73	95.3	71.1	95.7	0.896	0.000
NSE + ProGRP	77.6	94.6	74.6	36.8	98.9	0.914	0.000
LSCC							
SR	71.2	85.7	58.7	10.1	98.7	0.677	0.000
SR + CYFRA21-1	78.8	71.4	79.2	15.6	98.1	0.835	0.000
a + CYFRA21-1	58.9	100	56.8	11.1	100	0.839	0.000
CYFRA21-1	72.8	78.6	73	13.6	98.4	0.836	0.000

Abbreviation: SAR, stiffness area ratio; SR, strain ratio; LPA, The largest possible area within the LN; a, SAR + SR + A.

B-mode ultrasonography of lymph nodes, and simultaneously, the operator requires sufficient experience [13, 16, 22, 23].

As a recent, non-invasive diagnostic technology, ultrasound elastography has a high diagnostic rate and the results are easy to evaluate [17, 24]. Lymph node evaluation using elastic imaging can be divided into qualitative and quantitative evaluations [25]. In a qualitative assessment, Izumo et al. [12] confirmed that elastic image types have a certain value in distinguishing benign and malignant thoracic lymph nodes. Further, the elastic score of malignant lymph nodes was significantly higher than that of benign lymph nodes [26]. However, the classification of image types is subjective, and the definition and classification of intermediate types of lymph nodes (some blue and some non-blue) are unclear. A quantitative assessment can partially eliminate this uncertainty using specific numerical values. Therefore, this study focused on a quantitative assessment of elastography.

In a quantitative assessment, Korrungruang and Boonsarngsuk [27] found that the SR of the malignant group was significantly higher than that of the benign group. The authors suggest that the use of the SR to distinguish benign and malignant lymph nodes has a high diagnostic value and that the SR is the only quantitative method that can evaluate lymph nodes and surrounding tissues in real time. Rozman et al. [13] also concluded that the SR could more accurately distinguish between malignant and benign lymph nodes. Because there are subjective differences in classifying the colour distribution in elastography, it is particularly important to calculate the ratio of the blue area within the lymph node to the total area of the lymph node. Ma et al. [15] confirmed that the ratio of the blue area to the total area of lymph nodes is of great significance in differentiating benign and malignant mediastinal and hilar lymph nodes. One study demonstrated that evaluating the SAR of lymph nodes before puncture can help guide the puncture and increase the diagnostic rate [28]. Additionally, Uchimura et al. [17] found that the SAR also had a high diagnostic significance for malignant tumours with a short mediastinal lymph node having a diameter <10 mm.

In the measurement of the SR, the LPA was previously used to directly reflect the strain rate in the target lymph node [27], which excluded the selection bias of normal tissue. Herein, we analysed the diagnostic value of the LPA for the first time, and the results showed that the LPA could be used for the differential diagnosis of benign and malignant mediastinal and hilar lymph nodes. The cut-off value was 0.25, sensitivity was 81.2%, and specificity was 52.1%, all of which were better than those of the SR. Although the difference was not significant ($\chi^2 = 3.12$, $p = 0.0773$; $\chi^2 = 0.13$, $p = 0.718$), its advantages could not be ignored.

In this study, we used three quantitative elastography parameters to study: the SAR, SR, and LPA. We found that the SAR had the greatest significance in the diagnosis of benign and malignant mediastinum and hilar lymph nodes.

Quantitative elastography reflects the degree of tumour stiffness and distinguishes benign and malignant tissues; however, changes in tumour stiffness can cause changes in the tumour microenvironment, which is specifically reflected in the expression of serum tumour markers [29]. Therefore, we analysed the correlation between the SAR, SR, LPA, and serum tumour markers in lung cancer. Incidentally, we found that there was a positive correlation between the SAR and CEA, CYFRA21-1,

and NSE. Although the correlation was not high, the combination of the SAR with the CEA, CYFRA21-1, and NSE significantly improved the diagnostic value for benign and malignant lymph nodes. Hao et al. [29] studied the diagnostic value of elastic imaging SR and serum tumour markers for breast cancer and found a correlation between the SR and tumour marker cancer antigen 15-3 (CA15-3), and their combination significantly improved the differential diagnosis of benign and malignant tumours. This finding reflects the importance of quantitative elastography combined with serum tumour markers in differentiating benign from malignant tumours. Therefore, we combined the three elastography indices with serum tumour markers and found that the combined diagnostic model improved the diagnostic value for benign and malignant mediastinal and hilar lymph nodes, with an AUC of 0.930, a diagnostic rate of 86.4%, a sensitivity of 83.5%, and a specificity of 89.3%. However, these are all auxiliary clinical methods for the diagnosis of benign and malignant tumours, and the pathological results should be considered as the gold standard.

Herein, the cut-off value of the SAR obtained was similar to that reported in a recent study (0.412) [17], but there were some indicators with lower cut-off values of 0.311 and 0.367 [15, 28], which might be due to differences in the characteristics and number of enrolled patients. The cut-off value of the SR was 1.3, which was different from the values of 2.5 and 8.0 previously reported [13, 27]. This may be because central necrosis and vascular infiltration usually occur in lymph nodes, resulting in reduction of the SR due to "softening" in the lymph nodes [30], different criteria for image selection (for example, the optimal ratio of the SR is recommended to be lesion/normal tissue = 1: 1 [31]), and the influence of the operators and equipment.

Recently, many non-invasive screening studies have been conducted on the expression of various serum lung cancer tumour markers. There are also many reports with different views on the diagnostic value of serum lung cancer tumour markers for different types of lung cancers [19, 32–34]. In this study, we found that the CYFRA21-1 combined with the CEA was helpful in diagnosing LADC; the ProGRP and NSE were helpful in diagnosing SCLC; and the CYFRA21-1 was helpful in diagnosing LSCC, similar to the results of previous studies [33, 34]. Nevertheless, a study has shown that the CYFRA21-1 combined with the squamous cell carcinoma antigen is more helpful in the diagnosis of LSCC [34]. Therefore, the selection of effective combined detection plays an important role in the early detection of the disease and is worthy of clinical promotion and application. Additionally, we found that quantitative elastography indicators also had diagnostic significance for LADC, LSCC, and SCLC, and the SAR had the highest diagnostic value for LADC and SCLC, with cut-off values of 0.513 and 0.592, respectively. However, the SAR of LSCC was not significant; only the SR was significant, with a cut-off value of 2.55. One study found that the average SAR of LSCC was 0.716 [15]. This may be because of the low number of confirmed LSCCs.

To further improve the diagnosis of pathological types of lung cancer, we combined quantitative elastography indicators with tumour markers, but the results were not as expected. Compared with tumour markers for pathological types of lung cancer, the diagnostic value of quantitative elastography combined with tumour markers for pathological types of lung cancer was not significantly improved, and there was no statistical significance between the two ($p > 0.05$), and even in LADC and SCLC, its diagnostic value was reduced. The reason for this may be related to the relatively poor hardness of SCLC and LADC and the small number of pathological types of lung cancer.

In our study, the SAR on elastography showed great significance in differentiating between benign and malignant mediastinal and hilar lymph nodes. However, to evaluate the SAR of a lymph node, it is necessary to download the elastic image from the ultrasound machine to the computer and analyse the static elastic image using software. It takes approximately 1 min to do this, which increases the labour and time consumption. With the application of artificial intelligence in elastography, our work efficiency is greatly improved, and selection bias caused by static image analysis is avoided [35].

This study has several limitations. First, it was a retrospective study. Second, only 1–3 respiratory physicians assessed the elastography results and determined the final diagnosis. To some extent, there may be operator selection bias, but this is an inevitable drawback in most elastography studies. Finally, the elastic images selected for the SAR calculation were static; therefore, bias in image selection may also have occurred.

Clinically, patients with a history of dust exposure and central necrotic lymph nodes may increase the blue area in the lymph nodes, thus affecting the results of elastic imaging. Meanwhile, tumor markers are also increased under the influence of inflammation and other factors. Therefore, in this paper, we emphasize the combined diagnosis of the two indicators, which can greatly reduce the influence of these factors. Improve our rate of diagnosis of malignancy and puncture success rate.

In the future, we should pay attention to the results of serum tumour markers before puncture, carefully analyse the results of CT images and ultrasound features of lymph nodes, conduct real-time elastic imaging analysis, and select the exact puncture site using SAR results to maximise the diagnostic rate. Further prospective multicentre trials are required to confirm this study's results.

Conclusion

In summary, our findings suggest that the combination of quantitative elastic imaging and serum tumour markers has a higher diagnostic value than the detection of tumour markers and elastography alone in differentiating benign and malignant mediastinal and hilar lymph nodes, and it may help guide the puncture of false-negative lymph nodes.

Data availability statement

The original contributions presented in the study are included in the article/supplementary material, further inquiries can be directed to the corresponding author.

Ethics statement

The study was approved by the Ethics Committee of Shengjing Hospital affiliated with the China Medical University (2022PS1033K). The patients/participants provided their written informed consent to participate in this study. Study was carried out in accordance with the Declaration of Helsinki. All methods were carried out in accordance with relevant guidelines and regulations in the Ethics approval.

Author contributions

ZW and PL drafted the manuscript. ZW, PL, and GJ contributed to the study concept or design. JB and YL acquired the data. JB supervised and coordinated the study. All authors contributed to the article and approved the submitted version.

Funding

The study was supported by the Science and Technology Project of Shenyang, China (No. 202054021) and Applied Basic Research Project of Liaoning Province in 2022, China (2022JH2/101500051).

Conflict of interest

The authors declare that the research was conducted in the absence of any commercial or financial relationships that could be construed as a potential conflict of interest.

Acknowledgments

Thanks to the authors of the included studies to provide primary data.

References

1. Mohan A, Naik S, Pandey RM, Mills J, Munavvar M. Diagnostic utility of endobronchial ultrasound guided transbronchial needle aspiration for mediastinal lesions: a prospective three year, single centre analysis. *Thorac Cancer* (2011) 2(4):183–9. doi:10.1111/j.1759-7714.2011.00063.x

2. Iyer H, Anand A, Sryma PB, Gupta K, Naranje P, Damle N, et al. Mediastinal lymphadenopathy: a practical approach. *Expert Rev Respir Med* (2021) 15(10):1317–34. doi:10.1080/17476348.2021.1920404

3. Torre LA, Bray F, Siegel RL, Ferlay J, Lortet-Tieulent J, Jemal A. Global cancer statistics, 2012. *CA Cancer J Clin* (2015) 65(2):87–108. doi:10.3322/caac.21262

4. Siegel RL, Miller KD, Jemal A. Cancer statistics, 2017. *CA Cancer J Clin* (2017) 67(1):7–30. doi:10.3322/caac.21387

5. Pirker R. Conquering lung cancer: current status and prospects for the future. *Pulmonology* (2020) 26(5):283–90. doi:10.1016/j.pulmoe.2020.02.005

6. Sakairi Y, Nakajima T, Yoshino I. Role of endobronchial ultrasound-guided transbronchial needle aspiration in lung cancer management. *Expert Rev Respir Med* (2019) 13(9):863–70. doi:10.1080/17476348.2019.1646642

7. Okasha HH, El-Meligui A, Pawlak KM, Żorniak M, Atalla H, Abou-Elmagd A, et al. Practical approach to linear EUS examination of the mediastinum. *Endosc Ultrasound* (2021) 10(6):406–13. doi:10.4103/EUS-D-21-00019

8. Xu C, Qin L, Lei W, Jiang J, Ni C, Huang J. The role of endobronchial ultrasound-guided transbronchial needle aspiration liquid-based cytology in the diagnosis of mediastinal lymphadenopathy. *Diagn Cytopathol* (2020) 48(4):316–21. doi:10.1002/dc.24374

9. Cui XW, Li KN, Yi AJ, Wang B, Wei Q, Wu GG, et al. Ultrasound elastography. *Endosc Ultrasound* (2022) 11(4):252–74. doi:10.4103/EUS-D-21-00151

10. Cui XW, Chang JM, Kan QC, Chiorean L, Ignee A, Dietrich CF. Endoscopic ultrasound elastography: current status and future perspectives. *World J Gastroenterol* (2015) 21(47):13212–24. doi:10.3748/wjg.v21.i47.13212

11. Chen YF, Mao XW, Zhang YJ, Zhang CY, Yu YF, Qin E, et al. Endobronchial ultrasound elastography differentiates intrathoracic lymph nodes: a meta-analysis. *Ann Thorac Surg* (2018) 106(4):1251–7. doi:10.1016/j.athoracsur.2018.04.003

12. Izumo T, Sasada S, Chavez C, Matsumoto Y, Tsuchida T. Endobronchial ultrasound elastography in the diagnosis of mediastinal and hilar lymph nodes. *Jpn J Clin Oncol* (2014) 44(10):956–62. doi:10.1093/jjco/hyu105

13. Rozman A, Malovrh MM, Adamic K, Subic T, Kovac V, Flezar M. Endobronchial ultrasound elastography strain ratio for mediastinal lymph node diagnosis. *Radiol Oncol* (2015) 49(4):334–40. doi:10.1515/raon-2015-0020

14. Huang H, Huang Z, Wang Q, Wang X, Dong Y, Zhang W, et al. Effectiveness of the benign and malignant diagnosis of mediastinal and hilar lymph nodes by endobronchial ultrasound elastography. *J Cancer* (2017) 8(10):1843–8. doi:10.7150/jca.19819

15. Ma H, An Z, Xia P, Cao J, Gao Q, Ren G, et al. Semi-quantitative analysis of EBUS elastography as a feasible approach in diagnosing mediastinal and hilar lymph nodes of lung cancer patients. *Sci Rep* (2018) 8(1):3571. doi:10.1038/s41598-018-22006-4

16. Lin CK, Yu KL, Chang LY, Fan HJ, Wen YF, Ho CC. Differentiating malignant and benign lymph nodes using endobronchial ultrasound elastography. *J Formos Med Assoc* (2019) 118(1 Pt 3):436–43. doi:10.1016/j.jfma.2018.06.021

17. Uchimura K, Yamasaki K, Sasada S, Hara S, Ikushima I, Chiba Y, et al. Quantitative analysis of endobronchial ultrasound elastography in computed tomography-negative mediastinal and hilar lymph nodes. *Thorac Cancer* (2020) 11(9):2590–9. doi:10.1111/1759-7714.13579

18. Zhao X, Wang M. Clinical utility of serum tumor markers in lung cancer. *Zhongguo Fei Ai Za Zhi* (2011) 14(3):286–91. doi:10.3779/j.issn.1009-3419.2011.03.16

19. Liu L, Teng J, Zhang L, Cong P, Yao Y, Sun G, et al. The combination of the tumor markers suggests the histological diagnosis of lung cancer. *Biomed Res Int* (2017) 2017:2013989. doi:10.1155/2017/2013989

20. Rusch VW, Asamura H, Watanabe H, Giroux DJ, Rami-Porta R, Goldstraw P, et al. The IASLC lung cancer staging project: a proposal for a new international lymph node map in the forthcoming seventh edition of the TNM classification for lung cancer. *J Thorac Oncol* (2009) 4(5):568–77. doi:10.1097/JTO.0b013e3181a0d82e

21. Giovannini M, Hookey LC, Bories E, Pesenti C, Monges G, Delpero JR. Endoscopic ultrasound elastography: the first step towards virtual biopsy?

Preliminary results in 49 patients. *Endoscopy* (2006) 38(4):344–8. doi:10.1055/s-2006-925158

22. Fujiwara T, Yasufuku K, Nakajima T, Chiyo M, Yoshida S, Suzuki M, et al. The utility of sonographic features during endobronchial ultrasound-guided transbronchial needle aspiration for lymph node staging in patients with lung cancer: a standard endobronchial ultrasound image classification system. *Chest* (2010) 138(3):641–7. doi:10.1378/chest.09-2006

23. Fujiwara T, Nakajima T, Inage T, Sata Y, Sakairi Y, Tamura H, et al. The combination of endobronchial elastography and sonographic findings during endobronchial ultrasound-guided transbronchial needle aspiration for predicting nodal metastasis. *Thorac Cancer* (2019) 10(10):2000–5. doi:10.1111/1759-7714.13186

24. Xin L, Gao Y, Wang TJ, Meng QQ, Jin ZD, Fu ZJ, et al. EUS development in China: results from national surveys in 2013 and 2020. *Endosc Ultrasound* (2022) 12:90. doi:10.4103/EUS-D-22-00003

25. Zhi X, Chen J, Xie F, Sun J, Herth FJF. Diagnostic value of endobronchial ultrasound image features: a specialized review. *Endosc Ultrasound* (2021) 10(1): 3–18. doi:10.4103/eus.eus_43_20

26. He HY, Chen JL, Ma H, Zhu J, Wu DD, Lv XD. Value of endobronchial ultrasound elastography in diagnosis of central lung lesions. *Med Sci Monit* (2017) 23:3269–75. doi:10.12659/msm.901808

27. Korrungruang P, Boonsarngsuk V. Diagnostic value of endobronchial ultrasound elastography for the differentiation of benign and malignant intrathoracic lymph nodes. *Respirology* (2017) 22(5):972–7. doi:10.1111/resp.12979

28. Nakajima T, Inage T, Sata Y, Morimoto J, Tagawa T, Suzuki H, et al. Elastography for predicting and localizing nodal metastases during endobronchial ultrasound. *Respiration* (2015) 90(6):499–506. doi:10.1159/000441798

29. Hao Y, Ren G, Yang W, Zheng W, Wu Y, Li W, et al. Combination diagnosis with elastography strain ratio and molecular markers effectively improves the diagnosis rate of small breast cancer and lymph node metastasis. *Quant Imaging Med Surg* (2020) 10(3):678–91. doi:10.21037/qims.2020.02.14

30. He HY, Huang M, Zhu J, Ma H, Lyu XD. Endobronchial ultrasound elastography for diagnosing mediastinal and hilar lymph nodes. *Chin Med J (Engl)* (2015) 128(20):2720–5. doi:10.4103/0366-6999.167296

31. Dietrich CF, Hirche TO, Ott M, Ignee A. Real-time tissue elastography in the diagnosis of autoimmune pancreatitis. *Endoscopy* (2009) 41(8):718–20. doi:10.1055/s-0029-1214866

32. Gao S, Zhang G, Lian Y, Yan L, Gao H. Exploration and analysis of the value of tumor-marker joint detection in the pathological type of lung cancer. *Cel Mol Biol (Noisy-le-grand)* (2020) 66(6):93–7. doi:10.14715/cmb/2020.66.6.17

33. Wu H, Wang Q, Liu Q, Zhang Q, Huang Q, Yu Z. The serum tumor markers in combination for clinical diagnosis of lung cancer. *Clin Lab* (2020) 66(3). doi:10.7754/Clin.Lab.2019.190533

34. Gao J, Zhang L, Peng K, Sun H. Diagnostic value of serum tumor markers CEA, CYFRA21-1, SCCAg, NSE and ProGRP for lung cancers of different pathological types. *Nan Fang Yi Ke Da Xue Xue Bao* (2022) 42(6):886–91. doi:10.12122/j.issn.1673-4254.2022.06.12

35. Liu E, Bhutani MS, Sun S. Artificial intelligence: the new wave of innovation in EUS. *Endosc Ultrasound* (2021) 10(2):79–83. doi:10.4103/EUS-D-21-00052

Pathology & Oncology Research | frontiers

TYPE Original Research
PUBLISHED 19 April 2024
DOI 10.3389/pore.2024.1611593

Check for updates

OPEN ACCESS

EDITED BY
József Tímár,
Semmelweis University, Hungary

*CORRESPONDENCE
Andras Khoor,
khoor.andras@mayo.edu

RECEIVED 17 November 2023
ACCEPTED 04 April 2024
PUBLISHED 19 April 2024

CITATION
Krencz I, Sztankovics D, Sebestyén A, Pápay J, Dankó T, Moldvai D, Lutz E and Khoor A (2024), *RICTOR* amplification is associated with Rictor membrane staining and does not correlate with PD-L1 expression in lung squamous cell carcinoma.
Pathol. Oncol. Res. 30:1611593.
doi: 10.3389/pore.2024.1611593

COPYRIGHT
© 2024 Krencz, Sztankovics, Sebestyén, Pápay, Dankó, Moldvai, Lutz and Khoor. This is an open-access article distributed under the terms of the Creative Commons Attribution License (CC BY). The use, distribution or reproduction in other forums is permitted, provided the original author(s) and the copyright owner(s) are credited and that the original publication in this journal is cited, in accordance with accepted academic practice. No use, distribution or reproduction is permitted which does not comply with these terms.

RICTOR amplification is associated with Rictor membrane staining and does not correlate with PD-L1 expression in lung squamous cell carcinoma

Ildikó Krencz[1], Dániel Sztankovics[1], Anna Sebestyén[1], Judit Pápay[1], Titanilla Dankó[1], Dorottya Moldvai[1], Elmar Lutz[2] and Andras Khoor[2]*

[1]Department of Pathology and Experimental Cancer Research, Semmelweis University, Budapest, Hungary, [2]Department of Laboratory Medicine and Pathology, Mayo Clinic, Jacksonville, FL, United States

RICTOR gene, which encodes the scaffold protein of mTORC2, can be amplified in various tumor types, including squamous cell carcinoma (SCC) of the lung. *RICTOR* amplification can lead to hyperactivation of mTORC2 and may serve as a targetable genetic alteration, including in lung SCC patients with no PD-L1 expression who are not expected to benefit from immune checkpoint inhibitor therapy. This study aimed to compare *RICTOR* amplification detected by fluorescence *in situ* hybridization (FISH) with Rictor and PD-L1 protein expression detected by immunohistochemistry (IHC) in SCC of the lung. The study was complemented by analysis of the publicly available Lung Squamous Cell Carcinoma (TCGA, Firehose legacy) dataset. *RICTOR* amplification was observed in 20% of our cases and 16% of the lung SCC cases of the TCGA dataset. Rictor and PD-L1 expression was seen in 74% and 44% of the cases, respectively. Rictor IHC showed two staining patterns: membrane staining (16% of the cases) and cytoplasmic staining (58% of the cases). Rictor membrane staining predicted *RICTOR* amplification as detected by FISH with high specificity (95%) and sensitivity (70%). We did not find any correlation between *RICTOR* amplification and PD-L1 expression; *RICTOR* amplification was detected in 18% and 26% of PD-L1 positive and negative cases, respectively. The TCGA dataset analysis showed similar results; *RICTOR* copy number correlated with Rictor mRNA and protein expression but showed no association with PD-L1 mRNA and protein expression. In conclusion, the correlation between *RICTOR* amplification and Rictor membrane staining suggests that the latter can potentially be used as a surrogate marker to identify lung SCC cases with *RICTOR* amplification. Since a significant

proportion of PD-L1 negative SCC cases harbor *RICTOR* amplification, analyzing PD-L1 negative tumors by *RICTOR* FISH or Rictor IHC can help select patients who may benefit from mTORC2 inhibitor therapy.

KEYWORDS

RICTOR **amplification, Rictor expression, mTORC2, PD-L1, lung squamous cell carcinoma**

Introduction

Despite the significant advances that have been made in the diagnosis and treatment of non-small cell lung cancer (NSCLC) in the past decades, it remains the leading cause of cancer death worldwide [1]. Among NSCLCs, squamous cell carcinoma (SCC) is one of the most common histological subtypes, accounting for 30%–35% of all NSCLC cases [2].

Lung SCC is strongly associated with tobacco smoking and arises mostly in the central part of the lungs [3]. There is growing evidence that it is more heterogeneous than it is suggested by its three histologic subtypes (keratinizing, non-keratinizing, and basaloid) [4].

While there have been significant breakthroughs in targeted therapies for lung adenocarcinoma, most patients with advanced SCC are treated with immune checkpoint inhibitors (ICIs), platinum-based chemotherapy, or a combination of the two [5]. For SCCs with no PD-L1 expression, platinum-based chemotherapy remains the main treatment option [6]. Therefore, there is an urgent need to develop new targeted therapies for patients with SCC.

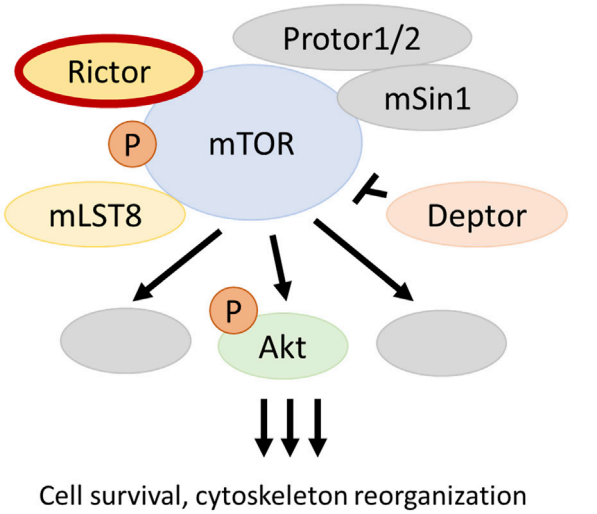

FIGURE 1
The mTOR complex 2. The *RICTOR* gene encodes for the scaffold protein of mTORC2 and can be amplified in different malignancies, including squamous cell carcinoma of the lung.

Protein complexes mTOR complex 1 (mTORC1) and mTOR complex 2 (mTORC2) are integral components of the phosphatidylinositol 3-kinase (PI3K)/protein kinase B (Akt)/mammalian target of rapamycin (mTOR) pathway. The main functions of mTORC1 include the regulation of cell growth and proliferation, whereas mTORC2 plays essential roles in cytoskeletal reorganization and cell survival [7]. Rictor (encoded by the *RICTOR* gene) is the scaffold protein of mTORC2 (Figure 1). Amplification of *RICTOR* has been reported in various cancer types, including approximately 10% of lung SCCs [8–10]. Like *PIK3CA* copy number gain and *PTEN* loss, *RICTOR* amplification affects the PI3K/Akt/mTOR pathway. *PIK3CA* copy number gain and *PTEN* loss mostly alter mTORC1 activity, whereas *RICTOR* amplification primarily results in the alteration of mTORC2 [11].

RICTOR fluorescence *in situ* hybridization (FISH) is considered the diagnostic standard for the detection of *RICTOR* amplification [8]. Immunohistochemistry (IHC) is an acceptable, cost-effective alternative to detect certain molecular alterations, including *ALK* and *ROS1* rearrangements [12, 13]. However, Rictor IHC has never been compared to *RICTOR* FISH in the SCC of the lung.

The purpose of this study was to compare *RICTOR* amplification as detected by FISH with Rictor expression as detected by IHC in SCC of the lung. Since PD-L1 negative tumors are typically ineligible for immune checkpoint inhibitor therapy, finding a potentially targetable genetic alteration such as *RICTOR* amplification is especially important for patients with PD-L1 negative advanced SCC. Therefore, we also examined the relationship between *RICTOR* amplification and PD-L1 expression in these tumors.

Materials and methods

Patients

A total of 50 samples, including 40 surgical resection specimens and 10 small biopsies of lung SCC cases diagnosed

TABLE 1 Clinicopathological data.

Characteristics		N (%)
Total no. of the cases		50 (100%)
Age	<65 years	12 (24%)
	≥65 years	38 (76%)
Sex	Male	30 (60%)
	Female	20 (40%)
Histological subtype	Non-keratinizing	31 (62%)
	Keratinizing	16 (32%)
	Basaloid	3 (6%)
Grade	Grade 1	1 (2%)
	Grade 2	33 (66%)
	Grade 3	16 (32%)
Stage	IA-B	25 (50%)
	IIA-B	10 (20%)
	IIIA-B	9 (18%)
	N.A.	6 (12%)
Procedure	Surgical resection	40 (80%)
	Small biopsy	10 (20%)

Abbreviations: N.A., not available.

between 1 January 2002 and 31 July 2020 were analyzed in our study. Only primary tumors with SCC histology were included. The tumors were re-reviewed and reclassified according to the 2021 World Health Organization Classification of Thoracic Tumors [14]. None of the patients received neoadjuvant therapy before surgery or biopsy. Clinicopathological data are summarized in Table 1. The study was approved by the Mayo Clinic Institutional Review Board (ID: 18-001887) and the Institutional Ethical Review Board of Semmelweis University (SE KREB 216/2020).

Fluorescence *in situ* hybridization reaction

FISH was performed on 4–μm–thick sections of the formalin-fixed paraffin-embedded tissue blocks. After pretreatment with Vysis IntelliFISH Pretreatment SSC Solution (Abbott Molecular, Des Plaines, IL, United States) at 79°C for 25 min, deparaffinized sections were digested using Vysis IntelliFISH Protease (Abbott Molecular) at 38°C for 25 min. Sections were then exposed to a mixture of *RICTOR* (#RICTOR-20-OR; Empire Genomics, Buffalo, NY, United States, labeled in orange) and chromosome 5 (Chr5) control (#CHR05-10-GR; Empire Genomics, labeled in green) probes and Vysis IntelliFISH Hybridization Buffer (Abbott Molecular) at 37°C for 2 h. Posthybridization wash was performed at 73°C for 3 min (Vysis IntelliFISH Post-Hybridization Buffer; Abbott Molecular). After air drying, sections were counterstained with DAPI I (Abbott Molecular).

Fluorescence *in situ* hybridization analysis

Slides were examined under a fluorescence microscope (DM5500 B; Leica, Wetzlar, Germany) focusing on hot spot areas. For each tumor, 30 tumor cell nuclei were evaluated in at least 2 different areas by 2 technicians. Both the mean number of signals per nucleus and the *RICTOR*/Chr5 control ratio were determined. A *RICTOR* copy number of 4 or more and a *RICTOR*/Chr5 ratio of 2 or more were considered positive for *RICTOR* amplification. Otherwise, the case was considered negative (see Figure 2). Images were captured using CytoVision software (Leica).

Immunohistochemical staining

Rictor IHC was performed on 4–μm–thick sections of the same blocks. After deparaffinization and blocking endogenous peroxidases, antigen retrieval was performed for 30 min (10 mM citrate, pH 6.0) in a pressure cooker. Slides were then incubated with an anti-Rictor (1:1000; #A500-002A; Bethyl Laboratories, Montgomery, TX, United States) primary antibody. Vectastain Universal Elite ABC HRP Kit (Vector Laboratories, Newark, CA, United States) secondary detection system and DAB (Agilent, Santa Clara, CA, United States) chromogen were used to visualize the reactions. The sections were counterstained with hematoxylin.

PD-L1 IHC 22C3 PharmDx reactions were performed on an automated immunostainer (Leica BOND-III; Leica) using the EnVision FLEX visualization system (Agilent) according to the manufacturer's protocols.

Evaluation of immunohistochemistry

PD-L1 membrane expression was assessed using Tumor Proportion Score (TPS) and was classified into TPS < 1%, TPS 1%–49%, and TPS ≥ 50% categories [15, 16]. A TPS ≥ 1% was considered positive (see Figure 2).

Since there had been no standardized way of analyzing Rictor expression, we evaluated both membrane and cytoplasmic stainings. In the presence of any membrane positivity, the pattern was considered membrane staining. The percentage of stained tumor cells was categorized similarly to that of PD-L1, using TPS < 1%, TPS 1%–49%, and TPS ≥ 50% categories.

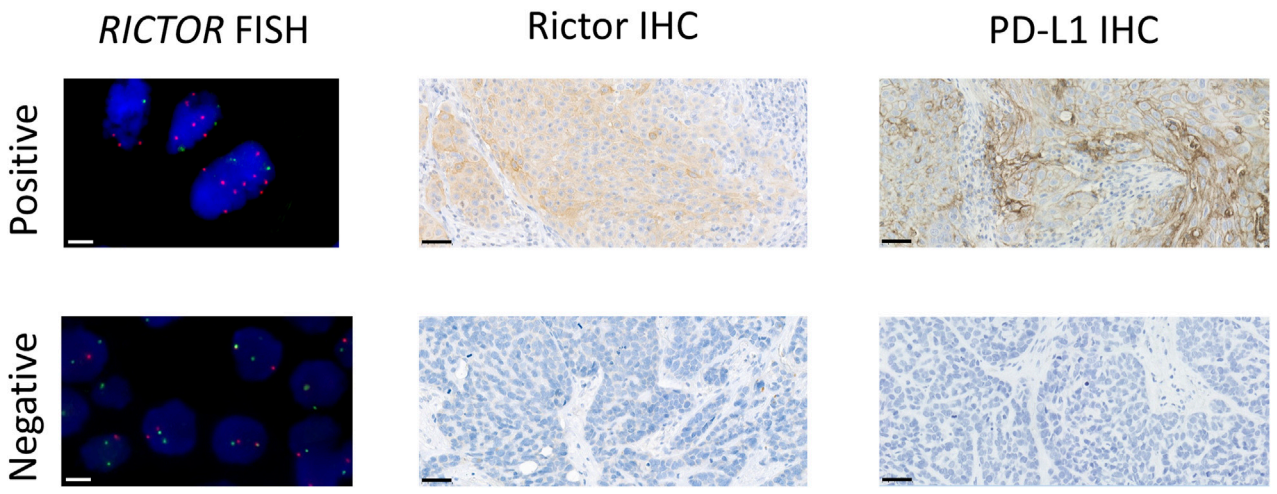

FIGURE 2
Representative images of *RICTOR* FISH, Rictor IHC, and PD-L1 IHC in lung SCC cases. Representative images of *RICTOR* FISH (*RICTOR* and *Chr5* are labeled in orange and green, respectively), Rictor IHC, and PD-L1 IHC in lung SCC cases. The scale bar indicates 10 μm on FISH and 50 μm on IHC images.

Data collection from the cancer genome atlas

Correlations among copy number alterations for *RICTOR* as well as mRNA (mRNA Seq V2 RSEM) and protein (reverse-phase protein array, RPPA) expression of Rictor and PD-L1 (CD274) was analyzed in the Lung Squamous Cell Carcinoma (TCGA, Firehose Legacy) dataset [17, 18]. The dataset contains the data of 511 lung SCC patients and was accessed through cBioPortal (accessed on 30th March 2023[1]). The association between *RICTOR* amplification and clinicopathological data was also studied.

Statistical analysis

Statistical analysis was performed using IBM SPSS Statistics software (version 22; SPSS Inc., Chicago, IL, United States). Descriptive data are expressed as numbers (percentages). Associations with the clinicopathological data were analyzed by the chi-square test. Correlations were evaluated using Spearman correlation. The Kaplan-Meier method was used for the survival analysis. The mean follow-up time was 1,091 days. Survival curves were compared by the log-rank method. A $p \leq 0.05$ was defined as statistically significant.

1 www.cbioportal.org

Results

RICTOR amplification in lung SCC

RICTOR amplification was observed in 10 of 50 cases (20%). The mean (range) *RICTOR* copy number per tumor cells was 6.26 (4.48–9.69) in the amplified cases and 2.90 (1.62–4.20) in the non-amplified cases. The mean (range) *Chr5* copy number per tumor cells was 1.97 (1.27–2.89) in the amplified cases and 1.64 (1.10–2.52) in the non-amplified cases.

Immunohistochemical expression of Rictor in lung SCC

Assessment of Rictor staining had not been standardized previously. Therefore, we separately analyzed membrane staining (Figure 3A) and cytoplasmic staining (Figure 3B) in our study. Membrane staining was observed in 8 cases (16%) and cytoplasmic staining in 29 cases (58%) (Table 2). No Rictor expression was seen in 13 cases (26%).

Immunohistochemical expression of PD-L1 in lung SCC

IHC for PD-L1 was positive in 22 of 50 cases (44%) (Table 3). TPS was 1%–49% in 17 cases and was ≥50% in 5 cases. The remaining 28 cases (56%) were negative.

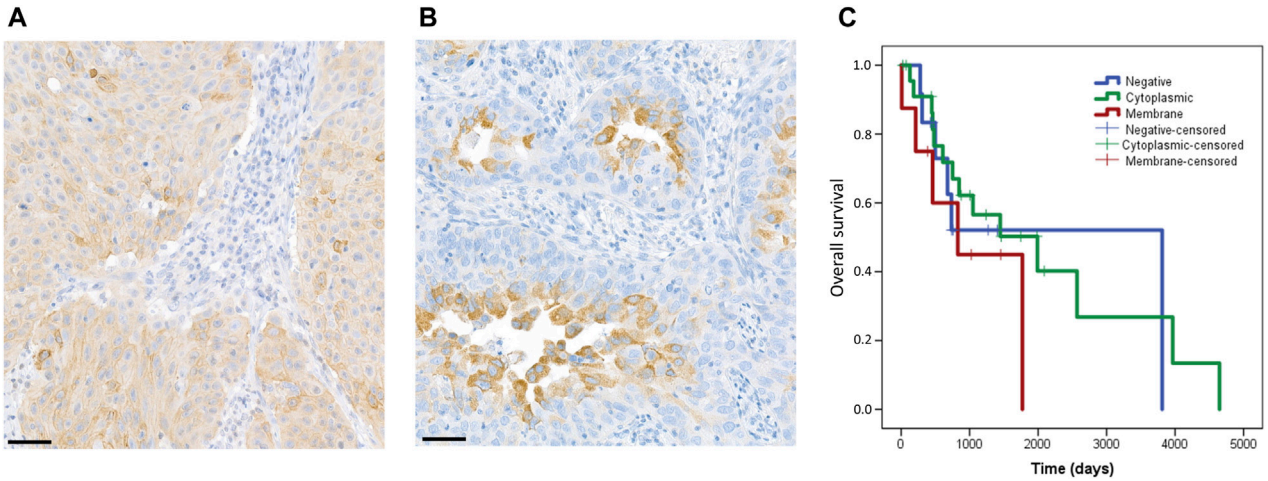

FIGURE 3
Staining pattern of the Rictor protein and correlation with patient's overall survival. In our study, we evaluated membrane and cytoplasmic staining separately. The figure shows representative images for membrane **(A)** and cytoplasmic **(B)** staining. The scale bar indicates 50 μm. Correlation of Rictor staining pattern with overall survival of patients **(C)**. Rictor membrane staining (red) was associated with slightly shorter overall survival as compared to cytoplasmic staining (green) and negative cases (blue).

TABLE 2 Immunohistochemical expression of Rictor in squamous cell carcinoma.

Rictor expression	TPS (%)	N (%)
Negative	<1	13 (26)
Positive membrane	1–49	3 (6)
	≥50	5 (10)
Positive cytoplasmic	1–49	27 (54)
	≥50	2 (4)
Total		50 (100)

TABLE 3 Immunohistochemical expression of PD-L1 in squamous cell carcinoma.

PD-L1 expression	TPS (%)	N (%)
Negative	<1	28 (56)
Positive	1–49	17 (34)
	≥50	5 (10)
Total		46 (100)

Concordance between *RICTOR* FISH and Rictor expression

The sensitivity, specificity, and negative and positive predictive values of various Rictor staining patterns are shown in Table 4. Rictor membrane staining showed the highest specificity for *RICTOR* amplification (95%). The negative predictive value of Rictor membrane staining was also high (93%).

Concordance between *RICTOR* FISH/ Rictor expression and PD-L1 expression

RICTOR amplification was detected in 4 (18%) PD-L1 positive cases and 5 (26%) PD-L1 negative cases, and there was no correlation between *RICTOR* amplification and PD-L1 expression. Similarly, we found no significant correlation between Rictor and PD-L1 expression.

Correlation of *RICTOR* amplification, Rictor and PD-L1 expression with clinicopathological data and survival

Neither FISH, nor immunohistochemical results showed a correlation with clinicopathological data (including age, sex, histological subtype, grade, and stage). Patients with Rictor membrane staining had a slightly shorter overall survival as compared to patients with Rictor cytoplasmic staining (p = 0.229) or no Rictor staining (p = 0.505) (Figure 3C). However, these results were not statistically significant. *RICTOR* amplification and PD-L1 expression did not correlate with survival.

TABLE 4 Concordance of *RICTOR* FISH and Rictor immunohistochemical results.

	Rictor membrane staining (%)	Rictor cytoplasmic staining (%)	Any Rictor staining (%)
Sensitivity	70	20	90
Specificity	95	35	30
Negative predictive value	93	64	92
Positive predictive value	78	7	24

Associations between *RICTOR* amplification, Rictor, and PD-L1 mRNA and protein expression in the lung squamous cell carcinoma (TCGA, Firehose Legacy) dataset

To strengthen our results, we also performed a similar analysis using data from the Lung Squamous Cell Carcinoma (TCGA, Firehose Legacy) dataset ($N = 511$). 501 of these samples were profiled for *RICTOR* copy number alterations, and *RICTOR* amplification was seen in 16% of the cases. We observed a strong positive correlation between *RICTOR* copy number and *RICTOR* mRNA expression (Spearman's R = 0.58, $p < 0.001$; 498 samples with data in both profiles, see Figure 4A). A weaker positive correlation was detected between *RICTOR* copy number and Rictor protein expression (Spearman's R = 0.14, $p = 0.012$; 326 samples with data in both profiles, see Figure 4B). However, there was no available information about the intracellular localization of Rictor protein expression. In correlation with our FISH and immunohistochemical analysis, we found no association between *RICTOR* copy number and PD-L1 (*CD274*) mRNA expression (Spearman's R= −0.06, $p = 0.176$; 498 samples with data in both profiles, see Figure 4C) or PD-L1 protein expression (Spearman's R= −0.02, $p = 0.733$; 194 samples with data in both profiles, see Figure 4D).

Associations between *RICTOR* amplification and clinicopathological data in the lung squamous cell carcinoma (TCGA, Firehose Legacy) dataset

The TCGA data analysis confirmed that there is no association between *RICTOR* amplification and overall survival in lung SCC patients ($p = 0.201$). Despite most of the cases have been categorized as Squamous Cell Carcinoma NOS based on histology (ICD-O-3: 8070/3), *RICTOR* amplification was seen more frequently in basaloid SCCs (6.33% of the *RICTOR*-amplified cases and 2.13% of the non-amplified cases had basaloid histology). In contrast, *RICTOR* amplification was absent in keratinizing SCCs (none of the *RICTOR*-amplified cases, but 3.08% of the non-amplified cases were keratinizing SCCs). Additionally, we could not find any association between *RICTOR* amplification and any other genetic drivers (*ALK* translocation and *KRAS* mutation status were available in 286 and 15 patients, respectively) or tumor mutational burden.

Discussion

This is the first study to compare *RICTOR* amplification and Rictor expression in human lung SCC. Using FISH, we observed *RICTOR* amplification in 20% of the cases. This is slightly higher than *RICTOR* amplification in the Lung Squamous Cell Carcinoma (TGCA, Firehose Legacy) dataset or in previous database analyses, where it has been found in 16% and 7.4%–15% of SCC cases, respectively [19, 20]. The difference among various studies may be due to differences in study populations and methods used to detect *RICTOR* amplification. An additional explanation for these differences is the high heterogeneity of RICTOR amplification and overexpression, which has been described previously [21] and was also found in our study. Given the potential intratumoral heterogeneity of both Rictor and PD-L1 staining [21–23], we performed both FISH and IHC analysis on whole slides of the tissue blocks, which allows for a higher probability of detecting areas of *RICTOR* amplification and overexpression of a heterogeneous tumor.

Rictor is the scaffold protein for mTORC2, a protein complex interconnected with the PI3K/Akt/mTOR pathway [24]. The PI3K/Akt/mTOR pathway regulates several essential cellular functions related to environmental signals, including cell proliferation, growth, homeostasis, and metabolism.

Subcellular localization of the PI3K/Akt/mTOR pathway components has been evaluated in various studies. As the first step in the pathway, PI3K generates phosphatidylinositol-3,4,5-triphosphate (PIP3), which binds the pleckstrin homology domain of Akt, recruiting it to the plasma membrane. Once Akt is localized to the plasma membrane, mTORC2 can phosphorylate its Ser473 site, thereby facilitating activation of the PI3K/Akt/mTOR pathway [20, 25, 26]. In contrast, some studies have demonstrated that mTORC2 can also phosphorylate its substrates (e.g., serum/glucocorticoid regulated kinase 1) using intracellular membranes and subcellular spaces such as the endoplasmic reticulum and the perinuclear compartment [25, 26]. Additionally, it is also known that Rictor can interact with integrin-linked kinase (ILK), a protein with a multifunctional role in cell-matrix interactions and that the Rictor-

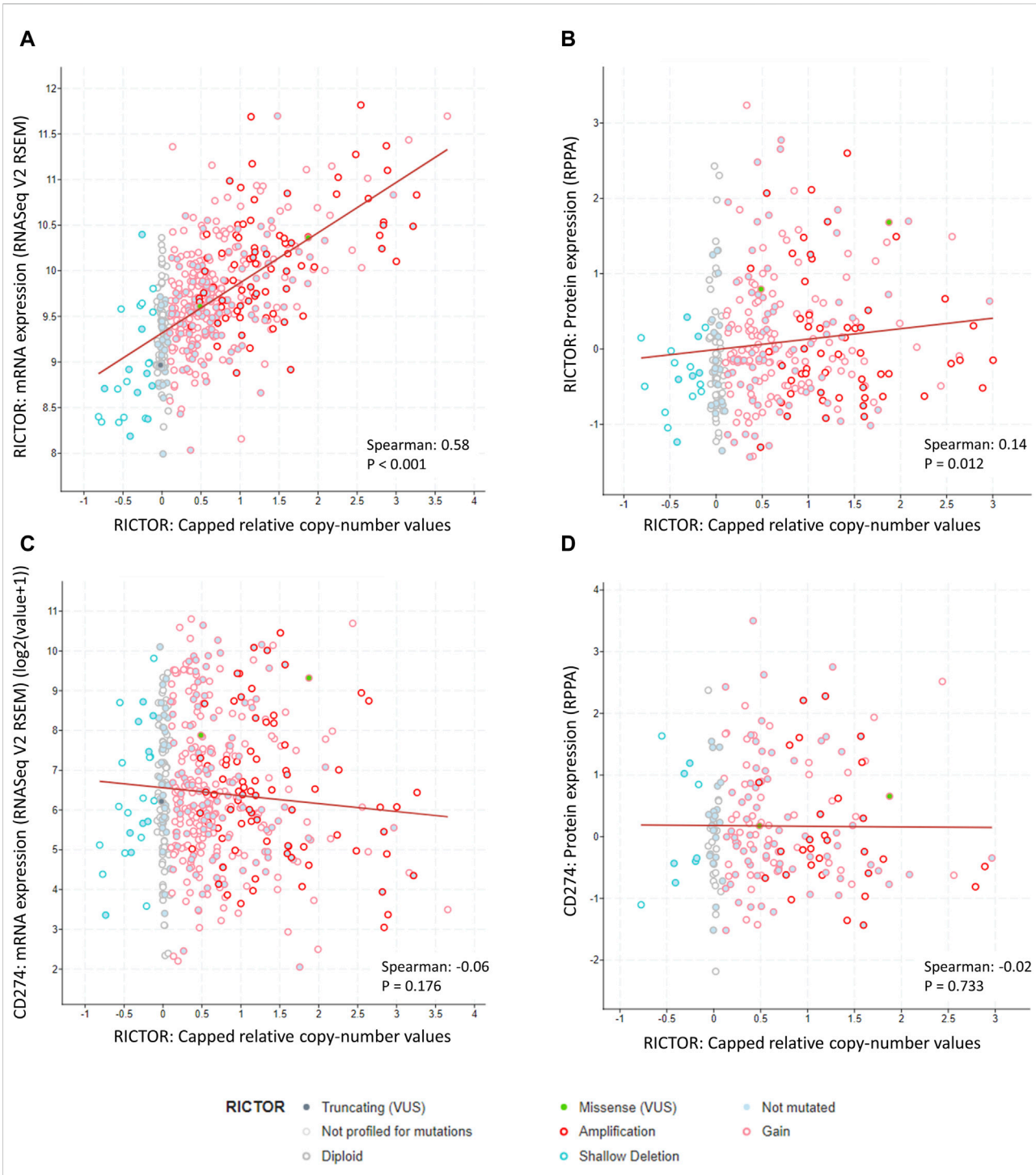

FIGURE 4
Correlation between *RICTOR* copy number, *RICTOR* and *CD274* (PD-L1) mRNA, and Rictor and CD274 (PD-L1) protein expression in the Lung Squamous Cell Carcinoma (TCGA, Firehose Legacy) dataset. **(A)** Strong positive correlation between *RICTOR* copy number and *RICTOR* mRNA expression. **(B)** Weak positive correlation between *RICTOR* copy number and Rictor protein expression. **(C)** No correlation between *RICTOR* copy number and *CD274* mRNA and **(D)** PD-L1 protein expression. In addition, to copy number variations, missense (2 patients, *RICTOR* R1299G, *RICTOR* E1633Q) and truncating (1 patient, *RICTOR* Q569*) mutations were also present in the *RICTOR* gene, without any known significance.

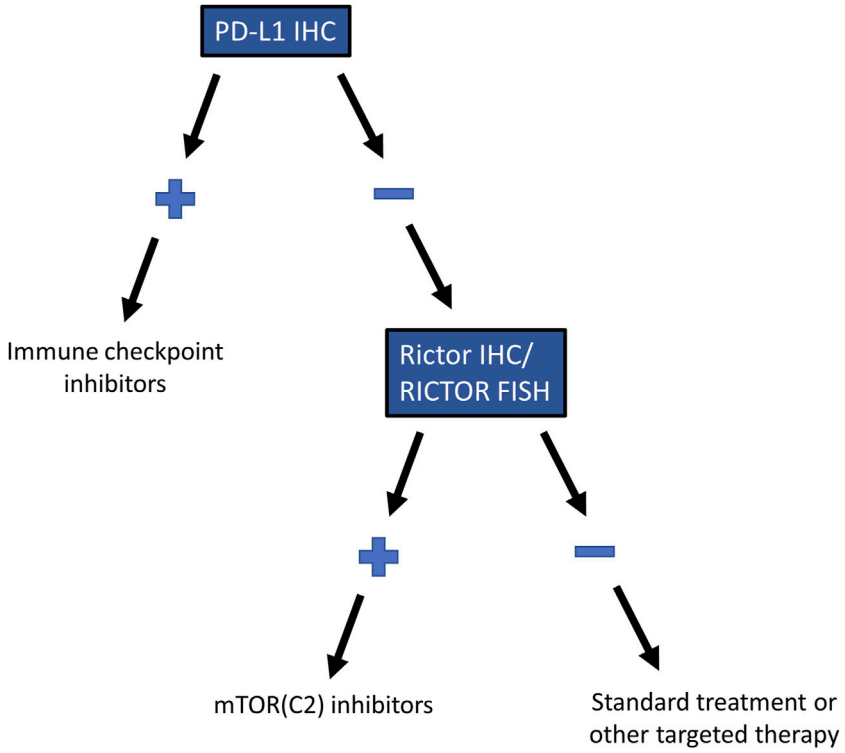

FIGURE 5
Recommended testing algorithm for *RICTOR* amplification in lung SCC. Testing algorithm for selecting patients with *RICTOR* amplification who are not eligible for immune checkpoint inhibitor treatment but may benefit from mTOR (C2) inhibitors.

ILK complex may contribute to the phosphorylation of Akt on Ser473 [27, 28]. Consistent with these data, a recent study has described more than 200 proteins that can interact with mTORC2 and possibly regulate its activity and localization [29]. We observed both membrane and cytoplasmic staining for Rictor in our study. Interestingly, in *RICTOR* amplified cases, Rictor was localized primarily to the plasma membrane, whereas, in non-amplified cases, we found predominantly cytoplasmic staining consistent with intracellular localization.

Previous studies have revealed a positive correlation between *RICTOR* mRNA expression and DNA copy number in NSCLC [20], which was confirmed with our database analysis. Similarly, we observed a positive correlation between Rictor protein expression and *RICTOR* gene amplification. However, this correlation was strongly dependent on subcellular localization. Rictor membrane staining showed high specificity (95%) and moderate to high sensitivity (77%) for *RICTOR* amplification, whereas the specificity and sensitivity of Rictor cytoplasmic staining were much lower (38% and 11%, respectively). Therefore, our recommendation is to use Rictor membrane staining as a surrogate marker for *RICTOR* gene amplification.

Despite breakthroughs in targeted therapies for lung adenocarcinoma in the past decades, limited progress has been made in the treatment of lung SCC. This seems to be due to the lower frequency of targetable genetic alterations and the less favorable response to small-molecule tyrosine kinase inhibitors [30, 31]. The PI3K/Akt/mTOR pathway represents a potential therapeutic target [32]. The activity of mTORC2 can be inhibited by dual mTOR kinase inhibitors, which affect both mTORC1 and mTORC2 (e.g., vistusertib and sapanisertib). They have been used to treat various types of lung cancer, including SCC of the lung, in early-phase clinical trials [9, 11]. In most of these studies, patients have not been stratified based on the presence of *RICTOR* amplification. A selective mTORC2 inhibitor (JR-AB2-011), which blocks the interaction between Rictor and mTOR, is already available and has been used with promising results in preclinical trials [33, 34]. Selecting patients with *RICTOR*-amplified tumors may improve the results.

In advanced cases of SCC of the lung, ICIs represent the only widely used therapeutic option besides radiochemotherapy [6]. Similar to a previous study, which has found no association between gene alterations and PD-L1 expression in advanced lung SCC [35], we observed no association between PD-L1 expression, a predictive marker for the efficacy of ICIs, and *RICTOR* amplification or Rictor expression. *RICTOR* amplification occurred in PD-L1 positive and negative cases with similar frequency, suggesting that a significant number of the PD-L1 negative cases can be eligible for mTORC2 inhibitor therapy (Figure 5). Additionally, *RICTOR*

amplification has been speculated to be responsible for the resistance against chemotherapy, tyrosine kinase inhibitors, and ICIs, leading to tumor progression in various types of cancer [36–38]. Therefore, analyzing *RICTOR* amplification in lung SCC patients who no longer respond to ICIs can reveal a new targetable alteration in this subpopulation of patients.

Several studies have shown a correlation between mTORC2 activity and metastatic disease [33, 39, 40]. This can result in decreased survival in *RICTOR*-amplified cases [41]. However, similar to our previous observation in small cell lung carcinoma [8], we did not detect a significant correlation between *RICTOR* amplification and unfavorable clinical outcomes in SCC of the lung. Nevertheless, Rictor membrane staining, which might be directly associated with Akt phosphorylation and thereby mTORC2 activity, did show slightly lower overall survival. These results might be clarified in a study with a larger sample size focused on this particular question.

In conclusion, our findings indicate that a significant proportion of lung SCCs, including PD-L1-negative cases, harbor *RICTOR* amplification. Despite the initial failures in early-phase clinical trials, one of the key messages of our study is that stratifying patients based on the presence of *RICTOR* amplification or Rictor overexpression may improve the results. With the advent of next-generation inhibitors that can selectively target mTORC2, the importance of this topic is emerging. Rictor membrane staining can predict *RICTOR* amplification as detected by FISH with high specificity and sensitivity; therefore, it can potentially be used as a surrogate marker to identify *RICTOR*-amplified lung SCCs. Analysis of lung SCCs by *RICTOR* FISH or Rictor IHC, especially in PD-L1-negative cases, can help select patients who may benefit from mTORC2 inhibitor therapy.

Data availability statement

The raw data supporting the conclusion of this article will be made available by the authors, without undue reservation.

Ethics statement

The study was reviewed and approved by the Mayo Clinic Institutional Review Board (ID: 18-001887) and the Institutional Ethical Review Board of Semmelweis University (SE KREB 216/2020). Written informed consent from the patients' legal guardian/next of kin was not required to use archived tissue blocks in this study in accordance with the national legislation and the institutional requirements.

Author contributions

IK, EL, and AK collected the samples. IK, DS, TD, and DM performed the IHC reactions. IK and DS participated in performing FISH reactions and evaluation of the results. IK and JP evaluated the IHC reactions. IK, DS, and DM were responsible for the TCGA data analysis and statistical analysis. IK, AS, DS, and AK evaluated the results. IK and AK wrote the manuscript. AK supervised the project. All authors contributed to the article and approved the submitted version.

Funding

The study was supported by the grant of the Hungarian National Research, Development and Innovation Office (NKFI-FK-128404, AS; NTP-NFTÖ-21-B-0179, IK) and the ÚNKP-23-4-II New National Excellence Program of the Ministry for Culture and Innovation from the Source of the National Research, Development and Innovation Fund (ÚNKP-23-4-II-SE-9, IK).

Conflict of interest

The authors declare that the research was conducted in the absence of any commercial or financial relationships that could be construed as a potential conflict of interest.

Acknowledgments

The authors are grateful to Tracy L. Majewicz (Department of Laboratory Medicine and Pathology, Mayo Clinic) and Dóra Kapczár (Department of Pathology and Experimental Cancer Research, Semmelweis University) for their technical assistance. The results were presented in part at the 2023 World Conference on Lung Cancer (Singapore).

References

1. Bray F, Ferlay J, Soerjomataram I, Siegel RL, Torre LA, Jemal A. Global cancer statistics 2018: GLOBOCAN estimates of incidence and mortality worldwide for 36 cancers in 185 countries. *CA Cancer J Clin* (2018) 68:394–424. doi:10.3322/caac.21492

2. Herbst RS, Morgensztern D, Boshoff C. The biology and management of non-small cell lung cancer. *Nature* (2018) 553:446–54. doi:10.1038/nature25183

3. Anusewicz D, Orzechowska M, Bednarek AK. Lung squamous cell carcinoma and lung adenocarcinoma differential gene expression regulation through pathways of Notch, Hedgehog, Wnt, and ErbB signalling. *Sci Rep* (2020) 10:21128. doi:10.1038/s41598-020-77284-8

4. Sharma A, Merritt E, Hu X, Cruz A, Jiang C, Sarkodie H, et al. Non-genetic intra-tumor heterogeneity is a major predictor of phenotypic heterogeneity and

ongoing evolutionary dynamics in lung tumors. *Cell Rep* (2019) 29:2164–74. doi:10.1016/j.celrep.2019.10.045

5. Santos ES, Rodriguez E. Treatment considerations for patients with advanced squamous cell carcinoma of the lung. *Clin Lung Cancer* (2022) 23:457–66. doi:10.1016/j.cllc.2022.06.002

6. National Comprehensive Cancer Network. *Non-small cell lung cancer* (2022). Version: 5.

7. Saxton RA, Sabatini DM. mTOR signaling in growth, metabolism, and disease. *Cell* (2017) 168:960–76. doi:10.1016/j.cell.2017.02.004

8. Krencz I, Sebestyen A, Papay J, Lou Y, Lutz GF, Majewicz TL, et al. Correlation between immunohistochemistry and RICTOR fluorescence *in situ* hybridization amplification in small cell lung carcinoma. *Hum Pathol* (2019) 93:74–80. doi:10.1016/j.humpath.2019.08.018

9. Krencz I, Sztankovics D, Danko T, Sebestyen A, Khoor A. Progression and metastasis of small cell lung carcinoma: the role of the PI3K/Akt/mTOR pathway and metabolic alterations. *Cancer Metastasis Rev* (2021) 40:1141–57. doi:10.1007/s10555-021-10012-4

10. Sztankovics D, Krencz I, Moldvai D, Dankó T, Nagy Á, Nagy N, et al. Novel RICTOR amplification harbouring entities: FISH validation of RICTOR amplification in tumour tissue after next-generation sequencing. *Sci Rep* (2023) 13:19610. doi:10.1038/s41598-023-46927-x

11. Krencz I, Sebestyen A, Khoor A. mTOR in lung neoplasms. *Pathol Oncol Res* (2020) 26:35–48. doi:10.1007/s12253-020-00796-1

12. Sholl LM, Sun H, Butaney M, Zhang C, Lee C, Jänne PA, et al. ROS1 immunohistochemistry for detection of ROS1-rearranged lung adenocarcinomas. *Am J Surg Pathol* (2013) 37:1441–9. doi:10.1097/PAS.0b013e3182960fa7

13. Wynes MW, Sholl LM, Dietel M, Schuuring E, Tsao MS, Yatabe Y, et al. An international interpretation study using the ALK IHC antibody D5F3 and a sensitive detection kit demonstrates high concordance between ALK IHC and ALK FISH and between evaluators. *J Thorac Oncol* (2014) 9:631–8. doi:10.1097/JTO.0000000000000115

14. Nicholson AG, Tsao MS, Beasley MB, Borczuk AC, Brambilla E, Cooper WA, et al. The 2021 WHO classification of lung tumors: impact of advances since 2015. *J Thorac Oncol* (2022) 17:362–87. doi:10.1016/j.jtho.2021.11.003

15. Garon EB, Rizvi NA, Hui R, Leighl N, Balmanoukian AS, Eder JP, et al. Pembrolizumab for the treatment of non-small-cell lung cancer. *N Engl J Med* (2015) 372:2018–28. doi:10.1056/NEJMoa1501824

16. Herbst RS, Baas P, Kim DW, Felip E, Pérez-Gracia JL, Han JY, et al. Pembrolizumab versus docetaxel for previously treated, PD-L1-positive, advanced non-small-cell lung cancer (KEYNOTE-010): a randomised controlled trial. *Lancet* (2016) 387:1540–50. doi:10.1016/S0140-6736(15)01281-7

17. Gao J, Aksoy BA, Dogrusoz U, Dresdner G, Gross B, Sumer SO, et al. Integrative analysis of complex cancer genomics and clinical profiles using the cBioPortal. *Sci Signal* (2013) 6:pl1. doi:10.1126/scisignal.2004088

18. Cerami E, Gao J, Dogrusoz U, Gross BE, Sumer SO, Aksoy BA, et al. The cBio cancer genomics portal: an open platform for exploring multidimensional cancer genomics data. *Cancer Discov* (2012) 2:401–4. doi:10.1158/2159-8290.CD-12-0095

19. Cheng H, Zou Y, Ross JS, Wang K, Liu X, Halmos B, et al. RICTOR amplification defines a novel subset of patients with lung cancer who may benefit from treatment with mTORC1/2 inhibitors. *Cancer Discov* (2015) 5:1262–70. doi:10.1158/2159-8290.CD-14-0971

20. Kim LC, Rhee CH, Chen J. RICTOR amplification promotes NSCLC cell proliferation through formation and activation of mTORC2 at the expense of mTORC1. *Mol Cancer Res* (2020) 18:1675–84. doi:10.1158/1541-7786.MCR-20-0262

21. Bang H, Ahn S, Ji Kim E, Kim ST, Park HY, Lee J, et al. Correlation between RICTOR overexpression and amplification in advanced solid tumors. *Pathol Res Pract* (2020) 216:152734. doi:10.1016/j.prp.2019.152734

22. Munari E, Zamboni G, Lunardi G, Marchionni L, Marconi M, Sommaggio M, et al. PD-L1 expression heterogeneity in non-small cell lung cancer: defining criteria for harmonization between biopsy specimens and whole sections. *J Thorac Oncol* (2018) 13:1113–20. doi:10.1016/j.jtho.2018.04.017

23. Ben Dori S, Aizic A, Sabo E, Hershkovitz D. Spatial heterogeneity of PD-L1 expression and the risk for misclassification of PD-L1 immunohistochemistry in non-small cell lung cancer. *Lung Cancer* (2020) 147:91–8. doi:10.1016/j.lungcan.2020.07.012

24. Oh WJ, Jacinto E. mTOR complex 2 signaling and functions. *Cell Cycle* (2011) 10:2305–16. doi:10.4161/cc.10.14.16586

25. Boulbés DR, Shaiken T, Sarbassov dos D. Endoplasmic reticulum is a main localization site of mTORC2. *Biochem Biophys Res Commun* (2011) 413:46–52. doi:10.1016/j.bbrc.2011.08.034

26. Gleason CE, Oses-Prieto JA, Li KH, Saha B, Situ G, Burlingame AL, et al. Phosphorylation at distinct subcellular locations underlies specificity in mTORC2-mediated activation of SGK1 and Akt. *J Cel Sci* (2019) 132:jcs224931. doi:10.1242/jcs.224931

27. McDonald PC, Oloumi A, Mills J, Dobreva I, Maidan M, Gray V, et al. Rictor and integrin-linked kinase interact and regulate Akt phosphorylation and cancer cell survival. *Cancer Res* (2008) 68:1618–24. doi:10.1158/0008-5472.CAN-07-5869

28. Tsirtsaki K, Gkretsi V. The focal adhesion protein Integrin-Linked Kinase (ILK) as an important player in breast cancer pathogenesis. *Cell Adh Migr* (2020) 14:204–13. doi:10.1080/19336918.2020.1829263

29. Luciano AK, Korobkina ED, Lyons SP, Haley JA, Fluharty SM, Jung SM, et al. Proximity labeling of endogenous RICTOR identifies mTOR complex 2 regulation by ADP ribosylation factor ARF1. *J Biol Chem* (2022) 298:102379. doi:10.1016/j.jbc.2022.102379

30. Lau SCM, Pan Y, Velcheti V, Wong KK. Squamous cell lung cancer: current landscape and future therapeutic options. *Cancer Cell* (2022) 40:1279–93. doi:10.1016/j.ccell.2022.09.018

31. Yang CY, Lin MW, Chang YL, Wu CT, Yang PC. Programmed cell death-ligand 1 expression is associated with a favourable immune microenvironment and better overall survival in stage I pulmonary squamous cell carcinoma. *Eur J Cancer* (2016) 57:91–103. doi:10.1016/j.ejca.2015.12.033

32. Fruman DA, Chiu H, Hopkins BD, Bagrodia S, Cantley LC, Abraham RT. The PI3K pathway in human disease. *Cell* (2017) 170:605–35. doi:10.1016/j.cell.2017.07.029

33. Guenzle J, Akasaka H, Joechle K, Reichardt W, Venkatasamy A, Hoeppner J, et al. Pharmacological inhibition of mTORC2 reduces migration and metastasis in melanoma. *Int J Mol Sci* (2020) 22:30. doi:10.3390/ijms22010030

34. Werfel TA, Wang S, Jackson MA, Kavanaugh TE, Joly MM, Lee LH, et al. Selective mTORC2 inhibitor therapeutically blocks breast cancer cell growth and survival. *Cancer Res* (2018) 78:1845–58. doi:10.1158/0008-5472.CAN-17-2388

35. Xu Y, Li H, Huang Z, Chen K, Yu X, Sheng J, et al. Predictive values of genomic variation, tumor mutational burden, and PD-L1 expression in advanced lung squamous cell carcinoma treated with immunotherapy. *Transl Lung Cancer Res* (2020) 9:2367–79. doi:10.21037/tlcr-20-1130

36. Jebali A, Battistella M, Lebbé C, Dumaz N. RICTOR affects melanoma tumorigenesis and its resistance to targeted therapy. *Biomedicines* (2021) 9:1498. doi:10.3390/biomedicines9101498

37. Sun D, Yan W, Zhu H, Liu Q, Hou H. Case report: primary and acquired resistance mechanisms of nimotuzumab in advanced esophageal squamous cell carcinoma revealed by targeted sequencing. *Front Oncol* (2020) 10:574523. doi:10.3389/fonc.2020.574523

38. Zhao D, Jiang M, Zhang X, Hou H. The role of RICTOR amplification in targeted therapy and drug resistance. *Mol Med* (2020) 26:20. doi:10.1186/s10020-020-0146-6

39. Krencz I, Sebestyén A, Fábián K, Márk Á, Moldvay J, Khoor A, et al. Expression of mTORC1/2-related proteins in primary and brain metastatic lung adenocarcinoma. *Hum Pathol* (2017) 62:66–73. doi:10.1016/j.humpath.2016.12.012

40. Schmidt KM, Dietrich P, Hackl C, Guenzle J, Bronsert P, Wagner C, et al. Inhibition of mTORC2/RICTOR impairs melanoma hepatic metastasis. *Neoplasia* (2018) 20:1198–208. doi:10.1016/j.neo.2018.10.001

41. Sakre N, Wildey G, Behtaj M, Kresak A, Yang M, Fu P, et al. RICTOR amplification identifies a subgroup in small cell lung cancer and predicts response to drugs targeting mTOR. *Oncotarget* (2017) 8:5992–6002. doi:10.18632/oncotarget.13362

Pathology & Oncology Research | frontiers

TYPE Original Research
PUBLISHED 13 February 2024
DOI 10.3389/pore.2024.1611589

Check for updates

OPEN ACCESS

EDITED BY
Nora Bittner,
National Koranyi Institute of TB and Pulmonology, Hungary

*CORRESPONDENCE
Árpád Kovács,
kovacsarpad@med.unideb.hu

RECEIVED 13 November 2023
ACCEPTED 25 January 2024
PUBLISHED 13 February 2024

CITATION
Kovács Á, Trási K, Barabás M, Gál K, Csiki E, Sipos D, Papp J and Simon M (2024), LINAC-based SBRT in treating early-stage NSCLC patients—single institution experience and survival data analysis.
Pathol. Oncol. Res. 30:1611589.
doi: 10.3389/pore.2024.1611589

COPYRIGHT
© 2024 Kovács, Trási, Barabás, Gál, Csiki, Sipos, Papp and Simon. This is an open-access article distributed under the terms of the Creative Commons Attribution License (CC BY). The use, distribution or reproduction in other forums is permitted, provided the original author(s) and the copyright owner(s) are credited and that the original publication in this journal is cited, in accordance with accepted academic practice. No use, distribution or reproduction is permitted which does not comply with these terms.

LINAC-based SBRT in treating early-stage NSCLC patients—single institution experience and survival data analysis

Árpád Kovács[1]*, Krisztina Trási[1], Márton Barabás[1], Kristóf Gál[1], Emese Csiki[1], Dávid Sipos[2], Judit Papp[1] and Mihály Simon[1]

[1]Department of Oncoradiology, Faculty of Medicine, University of Debrecen, Debrecen, Hungary, [2]Doctoral School of Health Sciences, Faculty of Health Sciences, University of Pécs, Pécs, Hungary

Aim: This single institute prospective study aimed to evaluate the feasibility of LINAC-based stereotactic body radiotherapy (SBRT) in treating patients with early-stage non-small cell lung cancer (NSLSC). We focused on the survival data with the local and distant control profiles and the cancer- and non-cancer-specific survival. Treatment-related side effects were also collected and analyzed.

Methods: Patients with early-stage NSCLC between January 2018 and October 2021 were included in our prospective study; a total of 77 patients receiving LINAC-based SBRT were analyzed. All patients had pretreatment multidisciplinary tumor board decisions on SBRT. The average patient age was 68.8 years (median: 70 years, range: 52–82); 70 patients were in ECOG 0 status (91%), while seven patients were in ECOG 1-2 status (9%). 52% of the patients (40) had histologically verified NSCLC, and the other 48% were verified based on PETCT results. We applied the SBRT scheme 8 x 7.5 Gy for central tumors (74%) or 4 x 12 Gy for peripheral tumors (26%).

Results: The mean follow-up time was 25.4 months (median 23, range 18–50). The Kaplan-Meier estimation for overall survival in patients receiving LINAC-based SBRT was 41.67 months. Of the 77 patients treated by SBRT, death was reported for 17 patients (9 cases cancer-specific, 8 cases non-cancer specific reason). The mean local tumor control was 34.25 months (range 8.4–41), and the mean systemic control was 24.24 months (range 7–25). During the treatments, no Grade I-II were reported; in 30 cases, Grade I non-symptomatic treatment-related lung fibrosis and two asymptomatic rib fractures were reported.

Conclusion: In the treatment of early-stage NSCLC, LINAC-based SBRT can be a feasible alternative to surgery. Although we reported worse OS data in our patient cohort compared to the literature, the higher older average age and the initial worse

Abbreviations: NSCLS, Non-small cell lung cancer; VATS, video-assisted thoracoscopic surgery; SBRT, Stereotactic body radiation therapy; LC, Local control; OS, Overall survival; CSS, cancer-specific survival; LCC, locoregional control; DFS, disease-free survival.

general condition (ECOG1-2) in our patient cohort appear to be the reason for this difference. With the comparable local control and survival data and the favorable side effect profile, SBRT might be preferable over surgery in selected cases.

KEYWORDS

VATS, NSCLC, SBRT, LINAC-based SBRT, early stage

Introduction

Lung cancer in Europe represents a leading cause of cancer cases, with more than 312,000 newly diagnosed cases per year. Hungary is the leading European country in the incidence of lung cancer and has the highest mortality rate [1, 2]. Approximately 85% of all lung cancer incidences are non-small cell lung cancer (NSCLC) [3]. The gold standard curative protocol is surgery that mainly aims to reduce the disease progression, relieve the symptoms, and increase the overall survival (OS) if possible [4]. Many patients, however, are unable to tolerate thoracotomy due to comorbidities or personal preference. [5] The video-assisted thoracoscopic surgery (VATS) method was chosen as the treatment choice since it was reported to decrease the risk of complication after treatment and a higher 5-year survival rate than the open lobectomy method [5, 6]. Nevertheless, in some cases where resection is not possible due to the tumor location, functional status of the lung, or inoperable patients [7, 8], another treatment method should be evaluated and assessed.

LINAC-based stereotactic body radiation therapy (SBRT), which is an alternative to VATS, was found to be a choice of treatment, especially for elderly patients and those patients with more than one known disease [5]. This method was comparable to the VATS in previous clinical reports [5, 9–11].

SBRT is a state-of-the-art treatment method that uses radiation therapy to deliver high-dose ablative doses to tumors [11]. This method allows for successful tumor ablation with relatively high tumor control probability while keeping the surrounding tissues intact [7, 12]. Furthermore, this technology's use and continuous improvement can improve results in potentially operable cases. Previously, limited studies have been compared between (SBRT) and (VATS) in terms of overall survival (OS), cancer-specific survival (CSS), loco-regional control (LCC), and disease-free survival (DFS). Therefore, this single institute prospective study aims to evaluate LINAC-based SBRT for NSCLC patients as 5 years of follow-up experience at Debrecen University regarding OS, CSS, LCC, and side effect profile.

Material and methods

Study population

This was a prospective mono-institutional study; the consent form was obtained from each patient. Patient data were collected and processed with the ethical permission of the Regional Research Ethics Committee. Demographic variables obtained from the electronic file database Clinic Center of the University of Debrecen (Debrecen, Hungary), called UD-MED, included age, gender, forced expiratory volume in 1 s to forced vital capacity ratio (FEV1/FVC%), and FEV1% predicted before treatment. All patients underwent pretreatment multidisciplinary tumor board before starting the SBRT at the Oncoradiology Clinic of the University of Debrecen (Debrecen, Hungary).

The average age was 68.8 years (median: 70 years, range: 52–82); 67 patients were in ECOG 0 status (87%), while ten patients were in ECOG 1-2 status (13%). 52% of the patients (40) had histologically verified NSCLC, and 48% were confirmed based on PET-CT with high FDG SUV (over the SUV value of 2.8). The mean FEV1 value was 1.06 (L), the mean FEV1 42%, the mean FVC 2.14 (L), and the mean FVC 62.69%.

Imaging

Chest CT examination is fundamental in tumor diagnostics and staging; a contrast-enhanced chest CT scan was used in all cases as a part of staging. Determining the patient's respiratory function capacity was also crucial from the point of view of the operation and the execution of the radiation treatment. Before treatment, a bronchoscopy was performed in all cases. In cases where the bronchoscopy could not give proper histological information, a CT-guided needle biopsy was conducted where a better visualization of the tumor's position was obtained when the tumor was smaller than 2 cm and when complications were more avoidable with such an examination. To decide oncological operability, enlarged lymph nodes detected on CT or PET-CT were valid only in conjunction with a positive histological examination. Suspicious patterns examined with CT can be supplemented with an FDG-PET examination, and in the case of non-small cell lung cancer, increased FDG uptake is observed. All patients receiving SBRT in our patient cohort had pretreatment FDG-PET scans within 2 weeks before the start of the treatment. A brain MRI was performed in all cases as a part of the staging.

Treatment procedures

For the 4D CT-based SBRT procedures, we used ELEKTA VERSA HD units with individual vacuum fixation systems and online 4D CBCT verification for each patient. Planning 4D CT

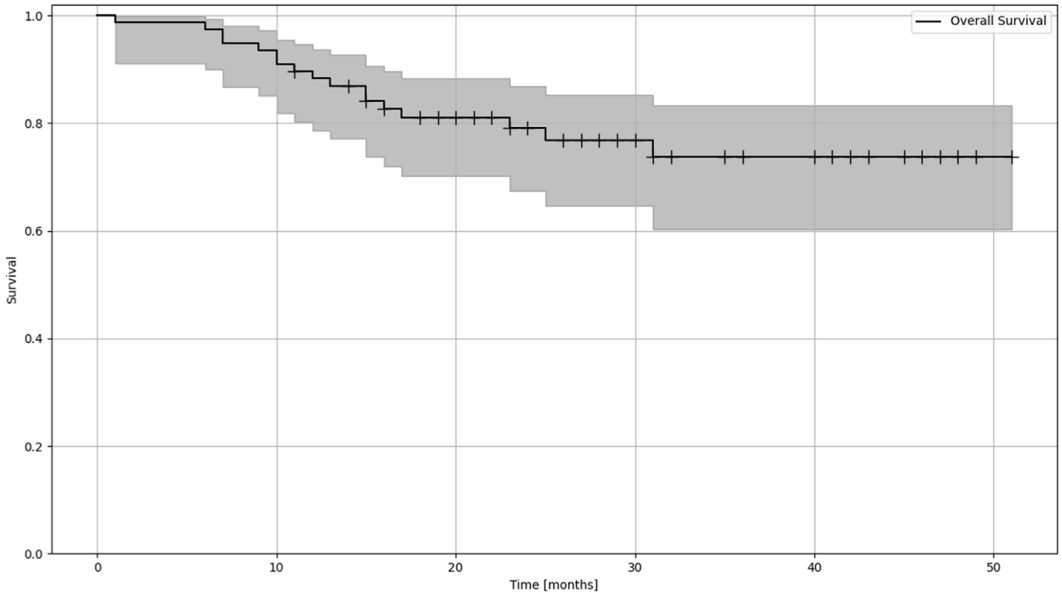

FIGURE 1
Kaplan-Meier estimation of OS (overall survival) of patients treated with lung SBRT.

was performed in the treatment position, with a slice thickness of 3 mm. No abdominal compression was applied during the process. Radiotherapy contouring and planning followed the department clinical protocol using the Pinnacle (Phillips, Netherlands) planning system (System version 16.2). To determine the exact gross tumor volume (GTV) and biological target volume (BTV), 4D planning CT-fused with FDG PET scans was used. Besides, the GTV and BTV internal target volume (ITV) was defined, using 4D CT information, to cover tumor movements. An additional 3–5 mm margin was used to generate the PTV. The mandatory OARs in planning were the lungs, heart, spinal cord, trachea, esophagus, chest wall, and great vessels per protocol. We applied the SBRT scheme of 8 × 7.5 Gy for central tumors (74%) or 4 × 12 Gy for peripheral tumors (26%). The treatments were delivered every other day (48-h shifts), with daily 4D CBCT verification and correction, if needed.

Data collection

Patients were followed up as follows: every 3 months for 2 years, every 6 months for another 3 years, and then annually. A medical history, physical examination, and chest CT were performed during the follow-up.

The primary endpoint of the study was local control (LC). We also examined systemic control, cancer-specific survival (CSS), and non-cancer-specific survival (NCSS). The analysis also focused on overall survival (OS) and treatment-related toxicity. OS was defined as the interval from the treatment date to any death or the last follow-up.

Statistical analysis

We used UD-MED, MEDSOL, and the Electronic Health Service Space (EESZT) for clinical data collection and analysis. The statistical analysis was performed with in-house-built Python scripts using the lifelines (v0.27.8) package [13].

Overall survival was estimated with the Kaplan Meier method (Figure 1). Risk estimation was performed using the Aalen-Johansen estimator to be able to assess risk in the different groups of patinets (Figure 2, Table 1).

Results

The mean follow-up time was 25.4 months (median 23, range 18–50). The Kaplan-Meier estimation for overall survival in patients receiving LINAC-based SBRT was 41.67 months. Of the 77 patients treated by SBRT, death was reported for 17 patients (9 cases cancer-specific, 8 cases non-cancer specific reason). The mean local tumor control was 34.25 months (range 8.4–41), and the mean systemic control was 24.24 months (range 7–25) During the treatments, no Grade I-II side effect were reported; in 30 cases, Grade I non-symptomatic treatment-related lung fibrosis and two asymptomatic rib fractures were reported.

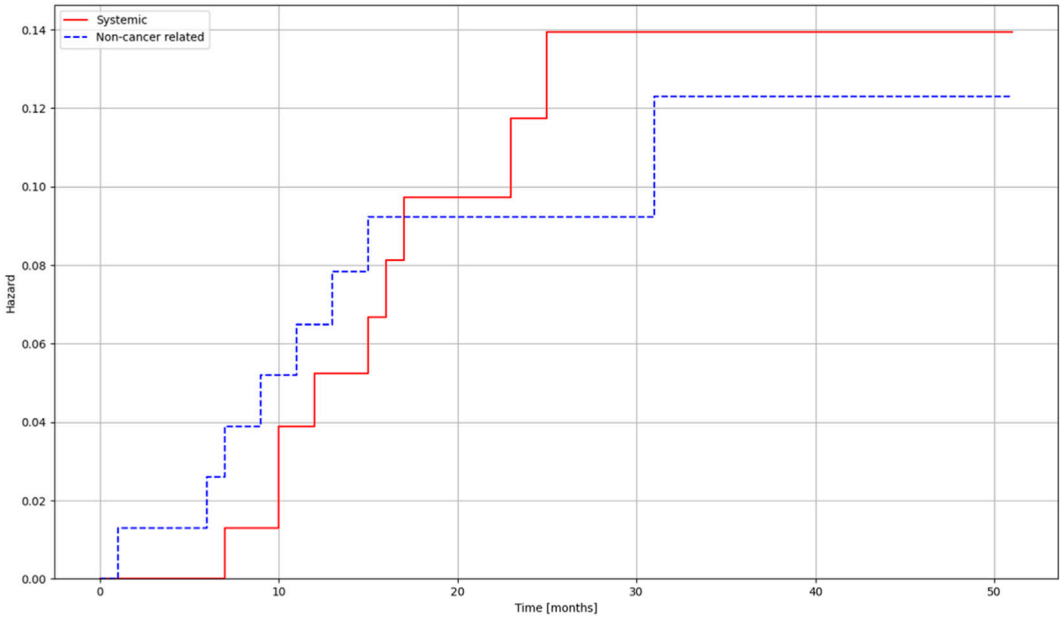

FIGURE 2
Risk estimates for deaths related to systemic progression and non-cancer-related deaths for patients treated with lung SBRT.

TABLE 1 Aalen-Johansen risk estimate for cumulative risk of patients.

	Times [months]					
	0	10	20	30	40	50
At risk	77	72	46	25	12	3
Censored	0	0	17	36	48	57
Events	0	5	14	16	17	17

Discussion

The gold standard treatment option for early-stage NSCLC patients is still surgery, considered the first treatment of choice [14–16]. The state of art surgery is usually done with VATS to reduce patient encumbrance [17–19]. Considering the Overall Survival, Loco-regional Control, and Systemic Control data of the previously reported retrospective studies, SBRT is a full-fledged alternative to surgery for early-stage NSCLC patients [5, 20–22]. Besides the comparable local control and survival data, the main advantage of the SBRT is the favorable side effect profile and excellent tolerability, even in comorbid elderly patients [23]. Using SBRT also offers lower post-treatment mortality [24]. In the literature, only a few studies focus on comparing SBRT and surgery because the comparison is made difficult by the patients' different average ages and health statuses [5, 10–12, 25]. In our patient cohort, the higher average patient age, worse general condition, and initial respiratory functions are all reflected in the general patient selection process in the clinical decisions; the younger patients in good general condition are more frequently referred to surgery.

As in the previous studies, Dong et al., in their analysis of several studies, found that the results of SBRT were comparable to those of VATS. Thus, they reported that OS was comparable between the two groups with a statistically significant difference. They also reported comparable outcomes with no significant differences in terms of loco-regional failure, with 3- and 5-year rates of loco-regional failure for radiotherapy and surgery being 93.5% and 93.5% and 94.0% and 85.9%, respectively; furthermore, they reported that distal failure was comparable for both groups with no statistical significance between the groups [5].

In our prospective study, the SBRT-related loco-regional and systemic control results are comparable to the previously reported conventional surgery results in the literature [5, 7]. In the SBRT cohort, the hazard of death due to systemic progression barely exceeds the risk of dying from non-cancer-related reasons. We recorded no deaths due to local progression. For systemic control, we also examined the lymph node and distant metastases; SBRT showed promising results in terms of non-tumor-specific survival. The scope of SBRT indications should be expanded in the future, and further studies with more cases should be considered. Currently, the gold standard therapy of choice is still surgery [14, 16, 25], the advantage of which is the possibility of histological sampling.

It is important to note that in our prospective data analysis, some data were worse for patients who underwent SBRT, as reported in the literature; this can be explained by the fact that in our SBRT group, there were medically inoperable patients with worse respiratory function and with many comorbidities. Pulmonary function values were available before and after SBRT in some patients, and we observed improvement in FEV1 and FVC. The difference between recurrence and fibrosis can be difficult during follow-up, so monitoring the patient with PET-CT is essential. Another difficulty is the separation of metastases and secondary lung tumors.

Our patient cohort also noticed no acute side effects during SBRT. No late severe side effects were also described during oncological follow-up. This study aims to help clinicians the find the proper treatment of patients with early-stage NSCLC. The findings provided valuable information in answering these and other unresolved questions regarding SBRT.

Conclusion

In the treatment of early-stage NSCLC, LINAC-based SBRT can be a feasible alternative to surgery. We report moderately worse OS data in our patient cohort compared to the literature [5]. However, the difference in average age and the initial worse general condition (ECOG1-2) of our patient cohort can be an underlying reason. With the comparable local control and survival data and the favorable side effect profile, SBRT might be preferable over surgery in selected cases.

Data availability statement

The original contributions presented in the study are included in the article materials, further inquiries can be directed to the corresponding author. All the datasets are available to access.

Ethics statement

The studies involving human participants were reviewed and approved by the Regional Ethical Commitee of University of Debrecen, registration number: 599-2021. The patients provided written informed consent to participate in this study, approved by the ethical committee.

Author contributions

KT, MB, GK, EC, DS, and JP data collection, patient follow-up and data analysis, MS statistics, manuscript review, AK program leader, manuscript preparation. All authors contributed to the article and approved the submitted version.

Conflict of interest

The authors declare that the research was conducted in the absence of any commercial or financial relationships that could be construed as a potential conflict of interest.

References

1. LuCE Europe. Report on lung cancer: challenges in lung cancer in Europe. 6th Edn (2021). Available from: https://content/uploads/2017/10/LuCE-Report-final.pdf (Accessed November, 2021).

2. Dyba T, Randi G, Bray F, Martos C, Giusti F, Nicholson N, et al. The European cancer burden in 2020: incidence and mortality estimates for 40 countries and 25 major cancers. *Eur J Cancer* (2021) 157:308–47. doi:10.1016/j.ejca.2021.07.039

3. Molina JR, Yang P, Cassivi SD, Schild SE, Adjei AA. Non-small cell lung cancer: epidemiology, risk factors, treatment, and survivorship. *Mayo Clin Proc* (2008) 83(5):584–94. doi:10.4065/83.5.584

4. Bareschino MA, Schettino C, Rossi A, Maione P, Sacco PC, Zeppa R, et al. Treatment of advanced non small cell lung cancer. *J Thorac Dis* (2011) 3(2):122–33. doi:10.3978/j.issn.2072-1439.2010.12.08

5. Dong B, Zhu X, Shu Z, Ji Y, Lu F, Wang J, et al. Video-assisted thoracoscopic lobectomy versus stereotactic body radiotherapy treatment for early-stage non-small cell lung cancer: a propensity score-matching analysis. *Front Oncol* (2020) 10:585709. doi:10.3389/fonc.2020.585709

6. Cai Y, Fu X, Xu Q, Sun W, Zhang N. Thoracoscopic lobectomy versus open lobectomy in stage I non-small cell lung cancer: a meta-analysis. *PLoS One* (2013) 8(12):e82366. doi:10.1371/journal.pone.0082366

7. Milano MT, Kong FMS, Movsas B. Stereotactic body radiotherapy as salvage treatment for recurrence of non-small cell lung cancer after prior surgery or radiotherapy. *Transl Lung Cancer Res* (2018) 8(1):78–87. doi:10.21037/tlcr.2018.08.15

8. Ball D, Mai GT, Vinod S, Babington S, Ruben J, Kron T, et al. Stereotactic ablative radiotherapy versus standard radiotherapy in stage 1 non-small-cell lung cancer (TROG 09.02 CHISEL): a phase 3, open-label, randomised controlled trial. *Lancet Oncol* (2019) 20(4):494–503. doi:10.1016/S1470-2045(18)30896-9

9. Boada M, Guzmán R, Montesinos M, Libreros A, Guirao A, Sánchez-Lorente D, et al. Upstaging, centrality and survival in early stage non-small cell lung cancer video-assisted surgery. *Lung Cancer* (2019) 134:254–8. doi:10.1016/j.lungcan.2019.06.030

10. Chi A, Fang W, Sun Y, Wen S. Comparison of long-term survival of patients with early-stage non-small cell lung cancer after surgery vs stereotactic body radiotherapy. *JAMA Netw Open* (2019) 2(11):e1915724. doi:10.1001/jamanetworkopen.2019.15724

11. Hamaji M, Chen F, Matsuo Y, Kawaguchi A, Morita S, Ueki N, et al. Video-assisted thoracoscopic lobectomy versus stereotactic radiotherapy for stage I lung cancer. *Ann Thorac Surg* (2015) 99(4):1122–9. doi:10.1016/j.athoracsur.2014.11.009

12. Tandberg DJ, Tong BC, Ackerson BG, Kelsey CR. Surgery versus stereotactic body radiation therapy for stage I non-small cell lung cancer: a comprehensive review. *Cancer* (2018) 124(4):667–78. doi:10.1002/cncr.31196

13. Davidson-Pilon C. Lifelines: survival analysis in Python. *J Open Source Softw* (2019) 4(40):1317. doi:10.21105/joss.01317

14. Zarogoulidis K, Zarogoulidis P, Darwiche K, Boutsikou E, Machairiotis N, Tsakiridis K, et al. Treatment of non-small cell lung cancer (NSCLC). *J Thorac Dis* (2013) 5(4):2–9. doi:10.3978/j.issn.2072-1439.2013.07.10

15. Darling GE, Decker PA, Ballman K, Malthaner RA, Inculet RI, Jones DR, et al. Number of lymph nodes harvested from a mediastinal lymphadenectomy: results of the randomized, prospective American College of Surgeons Oncology Group Z0030 trial. *Chest* (2011) 139(5):1124–9. doi:10.1378/chest.10-0859

16. Howington JA, Blum MG, Chang AC, Balekian AA, Murthy SC. Treatment of stage I and II non-small cell lung cancer: diagnosis and

management of lung cancer, 3rd ed: American College of Chest Physicians evidence-based clinical practice guidelines. *Chest* (2013) 143(5 Suppl): e278S–e313S. doi:10.1378/chest.12-2359

17. Detillon DDEMA, Veen EJ. Postoperative outcome after pulmonary surgery for non-small cell lung cancer in elderly patients. *Ann Thorac Surg* (2018) 105(1): 287–93. doi:10.1016/j.athoracsur.2017.07.032

18. Burt BM, Kosinski AS, Shrager JB, Onaitis MW, Weigel T. Thoracoscopic lobectomy is associated with acceptable morbidity and mortality in patients with predicted postoperative forced expiratory volume in 1 second or diffusing capacity for carbon monoxide less than 40% of normal. *J Thorac Cardiovasc Surg* (2014) 148(1):19–28. discussion 28-29.e1. doi:10.1016/j.jtcvs.2014.03.007

19. Nwogu CE, Pang H, Gu L, Wang X, Richards WG, Veit LJ, et al. VATS lobectomy has better perioperative outcomes than open lobectomy: CALGB 31001, an ancillary analysis of CALGB 140202 (Alliance). *Ann Thorac Surg* (2015) 99(2): 399–405. doi:10.1016/j.athoracsur.2014.09.018

20. Prezzano KM, Ma SJ, Hermann GM, Rivers CI, Gomez-Suescun JA, Singh AK. Stereotactic body radiation therapy for non-small cell lung cancer: a review. *World J Clin Oncol* (2019) 10(1):14–27. doi:10.5306/wjco.v10.i1.14

21. Vansteenkiste J, Crinò L, Dooms C, Douillard JY, Faivre-Finn C, Lim E, et al. 2nd ESMO Consensus Conference on Lung Cancer: early-stage non-small-cell lung cancer consensus on diagnosis, treatment and follow-up. *Ann Oncol Off J Eur Soc Med Oncol* (2014) 25(8):1462–74. doi:10.1093/annonc/mdu089

22. Grills IS, Mangona VS, Welsh R, Chmielewski G, McInerney E, Martin S, et al. Outcomes after stereotactic lung radiotherapy or wedge resection for stage I non-small-cell lung cancer. *J Clin Oncol* (2010) 28(6):928–35. doi:10.1200/JCO.2009.25.0928

23. Chua GWY, Chua KLM. Which patients benefit most from stereotactic body radiotherapy or surgery in medically operable non-small cell lung cancer? An in-depth look at patient characteristics on both sides of the debate. *Thorac Cancer* (2019) 10(10):1857–67. doi:10.1111/1759-7714.13160

24. Stokes WA, Bronsert MR, Meguid RA, Blum MG, Jones BL, Koshy M, et al. Post-treatment mortality after surgery and stereotactic body radiotherapy for early-stage non-small-cell lung cancer. *J Clin Oncol* (2018) 36(7):642–51. doi:10.1200/JCO.2017.75.6536

25. Mayne NR, Darling AJ, Raman V, Patel DC, Liou DZ, D'Amico TA, et al. Stereotactic body radiotherapy versus delayed surgery for early-stage non-small-cell lung cancer. *Ann Surg* (2020) 272(6):925–9. doi:10.1097/SLA.0000000000004363

Pathology & Oncology Research | frontiers

TYPE Review
PUBLISHED 18 June 2024
DOI 10.3389/pore.2024.1611817

Check for updates

OPEN ACCESS

EDITED BY
Nora Bittner,
National Koranyi Institute of TB and Pulmonology, Hungary

*CORRESPONDENCE
Balazs Halmos,
bahalmos@montefiore.org

RECEIVED 02 May 2024
ACCEPTED 04 June 2024
PUBLISHED 18 June 2024

CITATION
Jeon H, Gor R, D'Aiello A, Stiles B, Illei PB and Halmos B (2024), Advancing neoadjuvant therapies in resectable non-small cell lung cancer: implications for novel treatment strategies and biomarker discovery.
Pathol. Oncol. Res. 30:1611817.
doi: 10.3389/pore.2024.1611817

COPYRIGHT
© 2024 Jeon, Gor, D'Aiello, Stiles, Illei and Halmos. This is an open-access article distributed under the terms of the Creative Commons Attribution License (CC BY). The use, distribution or reproduction in other forums is permitted, provided the original author(s) and the copyright owner(s) are credited and that the original publication in this journal is cited, in accordance with accepted academic practice. No use, distribution or reproduction is permitted which does not comply with these terms.

Advancing neoadjuvant therapies in resectable non-small cell lung cancer: implications for novel treatment strategies and biomarker discovery

Hyein Jeon[1], Rajvi Gor[2], Angelica D'Aiello[1], Brendon Stiles[3], Peter B. Illei[4] and Balazs Halmos[1]*

[1]Department of Oncology, Montefiore Medical Center, Albert Einstein College of Medicine, Bronx, NY, United States, [2]Department of Medicine, Jacobi Medical Center, Bronx, NY, United States, [3]Department of Cardiothoracic and Vascular Surgery, Montefiore Medical Center, Albert Einstein College of Medicine, Bronx, NY, United States, [4]Department of Pathology, The Johns Hopkins Hospital, Johns Hopkins Medicine, Baltimore, MD, United States

The delivery of neoadjuvant and perioperative therapies for non-small cell lung cancer has been radically altered by significant advances and by the incorporation of targeted therapies as well as immune checkpoint inhibitors alone or alongside conventional chemotherapy. This evolution has been particularly notable in the incorporation of immunotherapy and targeted therapy into the treatment of resectable NSCLC, where recent FDA approvals of drugs such as nivolumab and pembrolizumab, in combination with platinum doublet chemotherapy, have led to considerable improvements in pathological complete response rates and the potential for enhanced long-term survival outcomes. This review emphasizes the growing importance of biomarkers in optimizing treatment selection and explores the impact of emerging studies that challenge existing treatment paradigms and investigate novel therapeutic combinations poised to redefine standard of care practices. Furthermore, the discussion extends to the unmet needs within perioperative treatment assessment and prognostication, highlighting the prospective value of biomarkers in evaluating treatment responses and prognosis.

KEYWORDS

NSCLC, perioperative, neoadjuvant, adjuvant, lung cancer

Abbreviations: ALK: Anaplastic Lymphoma Kinase; CHIP: Clonal hematopoiesis of indeterminate potential; dMMR: Deficient mismatch repair; EFS: Event free survival; EGFR: Epidermal Growth Factor Receptor; mAb: Monoclonal Antibody; MAF: Mutant allele fraction; mPR: major pathological response; MSI: Microsatellite instability; NSCLC: Non-small cell lung cancer; OS: Overall survival; pCR: Pathologic complete response; PDC: Platinum doublet chemotherapy; TMB: Tumor mutation burden; TME: Tumor microenvironment.

Introduction

Lung cancer, with non-small cell lung cancer (NSCLC) representing about 80% of cases, continues to pose a formidable health issue, ranking as the second highest in new cancer cases and the leading cause of cancer mortality worldwide [1]. The landscape of NSCLC management has undergone dramatic changes in recent years, driven by the advent of biomarker-targeted therapies and immunotherapies. These advances have not only transformed the treatment of advanced and locally advanced disease but are now rapidly reshaping the approach to resectable NSCLC as well. In the perioperative setting for resectable NSCLC, nivolumab and more recently pembrolizumab with platinum doublet chemotherapy have been approved in neoadjuvant/perioperative settings (Table 1) and pembrolizumab, atezolizumab, osimertinib, and alectinib all approved in the adjuvant setting, respectively. These approvals in the perioperative settings have markedly improved the management of resectable NSCLC, heralding a new era where molecularly targeted therapies and immune checkpoint inhibitors are poised to optimize treatment efficacy. This transformative phase is set against a contrasting historical context of two decades marked by numerous attempts to augment the standard of adjuvant chemotherapy, most of which failed to improve outcomes significantly. High-profile endeavors like the integration of radiation therapy, angiogenesis inhibition through VEGF targeting [2], and cancer vaccines targeting specific antigens such as MAGE [3] have been rigorously investigated but ultimately did not achieve a new standard of care, reflecting the complexity and resilience of NSCLC to therapeutic advances. This review seeks to provide a comprehensive overview of the current state and future directions of perioperative treatment in NSCLC, highlighting biomarker identification that could refine treatment selection and improve clinical outcomes, as well as exploring novel therapeutics to redefine the standards of care for NSCLC.

Current FDA approved preoperative standard of care for resectable NSCLC

The current standard of care for the neoadjuvant treatment of resectable NSCLC has evolved substantially, now increasingly utilizing multimodal strategies to improve surgical outcomes and

TABLE 1 Key phase III studies for preoperative regimens.

Trial	Regimen and FDA approval	Stage	ALK/EGFR included	Patients	PFS/EFS/RFS/OS	pCR/mPR
CheckMate 816 (8)	Neoadjuvant **nivolumab** + CT vs. CT for 3 cycles **Approved**	IB-IIIA (AJCC 7th ed)	No	358	**EFS** at 2 years 63.8% vs. 45.3% (**HR** 0.65 CI 0.43–0.91) **mEFS** 31.6 vs. 20.8 months (HR 0.63 CI 0.43–0.91 $p = 0.005$) **OS** at 2 years not reached in either arms (HR 0.57 CI 0.30–1.07 $p = 0.008$)	**pCR** 24% vs. 2.2% (OR 13.94 CI 18.0–31.0 $p < 0.001$) **mPR** 36.9% vs. 8.9% (OR 5.7 CI 3.16–10.26)
NADIMII (12)	Neoadjuvant **nivolumab** + CT vs. CT for 3 cycles R0 resections → adjuvant **nivolumab** for 6 months	IIIA-IIIB	No	86	**PFS** at 2 years 67.2% vs. 40.9% (HR 0.47 CI 0.25–0.88) **OS** at 2 years 85% vs. 63.6% (HR 0.43 CI 0.19–0.98)	**pCR** 37% vs. 7% (RR 5.34 CI 1.34–21.23 $p = 0.02$) **mPR** 53% vs. 14% (RR 3.82 CI 1.49–9.79)
KEYNOTE-671 (9)	Neoadjuvant **pembrolizumab** + CT for 4 cycles vs. placebo + CT Adjuvant **pembrolizumab** monotherapy up to 13 cycles vs. placebo **Approved**	II-IIIB N2 (AJCC 8th ed)	Yes	797	**EFS** at 2 years 62.4% vs. 40.6% (HR 0.58 CI 0.46–0.72 $p < 0.001$) **OS** at 2 years 80.9% vs. 77.6% **Median OS** NR vs. 45.5 months ($p = 0.02$)	**pCR** 18.1% vs. 4.0% (difference 14.2% CI 10.1–18.7 $p < 0.0001$) **mPR** 30.2% vs. 11.0% (difference 19.2% CI 13.9–24.7 $p < 0.0001$)
AEGEAN (17)	Neoadjuvant **durvalumab** + CT for 4 cycles vs. placebo + CT Adjuvant **durvalumab** monotherapy up to 12 cycles vs. placebo	II-IIIB N2 (AJCC 8th ed)	No	740	**EFS** at 2 years 63.3% vs. 52.4% (HR 0.68 CI 0.53–0.88 $p = 0.04$)	**pCR** 17.2% vs. 4.3% **mPR** 33.3% vs. 12.3%
CheckMate 77T (20)	Neoadjuvant **nivolumab** + CT for 4 cycles vs. placebo + CT Adjuvant **nivolumab** vs. placebo for 1 year	IIA-IIIB (N2)	No	461	**mEFS** not reached vs. 18.4 months (HR 0.58 CI 0.42–0.81 $p = 0.00025$)	**pCR** 25.3% vs. 4.3% (OR 6.64 CI 3.4–12.97) **mPR**35.4% vs. 12.1% (OR 4.01 CI 2.48–6.49)

CT, chemotherapy; DFS, disease-free survival; EFS, event-free survival; HR, hazard ratio; mEFS, median event-free survival; OR, odds ratio; OS, overall survival; PFS, progression free survival; R0, complete resection; RFS, recurrence-free survival; RR, relative risk.

hopefully to extend overall survival (OS). While studies in the past have indicated similar benefits between neoadjuvant and adjuvant chemotherapy [4, 5], logistical considerations sustained the latter as the prevailing practice pattern. Nonetheless, for patients with stage IIA to IIIA resectable NSCLC, the standard neoadjuvant protocol has conventionally incorporated platinum-based doublet chemotherapy, which has proven to enhance survival rates when compared with surgery alone [6].

Recent developments have also introduced immune checkpoint inhibitors into the neoadjuvant setting for NSCLC, either as monotherapy, concomitantly with chemotherapy, or in the context of dual immunotherapeutic strategies (Table 1). The unique aspect of the neoadjuvant approach is that it provides clinicians with the opportunity to directly observe the patient's tumor response to treatment through the assessment of the postsurgical specimen. This pathological assessment can offer invaluable insights into the efficacy of the neoadjuvant regimen and the tumor's biological behavior under therapeutic pressure. In addition, the native tumor serving as an *in situ* "tumor vaccine" might provide optimal T cell responses as opposed to administration post-operatively in a micrometastatic setting. Monotherapy with immune checkpoint inhibitors has allowed for novel translational studies, but have yielded moderate efficacy [7] while combination chemotherapy and immunotherapy has shown more promising results from clinical trials, specifically significant improvements in pathological complete response rates and potentially long-term outcomes [8, 9]. Recent investigations predominantly gravitate towards the synergistic potential of perioperative chemotherapy combined with immune checkpoint inhibitors, underscored by clinical trial evidence suggesting substantial improvement in rates of pathological complete response, with the prospective to confer sustained survival benefits.

Current neoadjuvant immunotherapy studies

Nivolumab in combination with platinum doublet chemotherapy (PDC) was approved in the neoadjuvant setting for resectable NSCLC (Stage IIA to IIIA per AJCC eighth edition) without known driver mutations. The approval was based on the pioneering CheckMate 816 study which demonstrated a significantly improved EFS at 2 years of 63.8% versus 45.3% and HR of 0.65 (95% CI 0.47–0.90) of neoadjuvant chemo/immunotherapy versus PDC alone. Median EFS was 31.6 (95% CI 30.2-not reached) vs. 20.8 months (95% CI 14–26.7). The pathological complete response (pCR) after neoadjuvant chemoimmunotherapy (3 cycles) was also notably higher at 24% compared to 2.2% with chemotherapy alone demonstrating a dramatic effect on improving tumor response [8].

Several perioperative studies involving both use of neoadjuvant and adjuvant immunotherapy offer further new insights into management and treatment in the perioperative setting. The NADIM trial utilized the anti-PD1 agent, nivolumab in the perioperative setting along with PDC (carboplatin/paclitaxel) in the neoadjuvant setting followed by adjuvant nivolumab monotherapy for 1 year in 46 patients with stage IIIA NSCLC and showed 83% major pathological response (mPR), 63% pCR, with OS of 81.9% at 36 months [10, 11]. In the subsequent NADIM II trial, cohorts were expanded to stage IIIA and IIIB disease comparing chemoimmunotherapy versus PDC alone in the neoadjuvant setting followed by adjuvant nivolumab post-surgery for 6 months in those who underwent R0 resections and received nivolumab preoperatively. This trial has similarly demonstrated impressive findings [12], further supporting the argument for the use of perioperative use of immunotherapy in resectable NSCLC (see Table 1).

The recent FDA approval for perioperative use of pembrolizumab was based on results of the pivotal KEYNOTE-671 study where pembrolizumab along with PDC significantly improved pathological response as well as event free (EFS) and overall survival (OS). KEYNOTE-671 using neoadjuvant (4 cycles) and adjuvant (up to 13 cycles) pembrolizumab and platinum-based chemotherapy in stage II-IIIB (N2 stage) also showed a significant EFS HR of 0.58 with 62.4% versus 40.6% EFS at 24 months in the experimental versus the control arm of neoadjuvant PDC alone. Additionally, mPR was 30.2% versus 11.0%, pCR 18.1% versus 4%, and OS at 2 years of 80.9% versus 77.6% in the pembrolizumab compared to placebo group respectively. Interestingly, exploratory analysis has shown potential benefits in the perioperative use of pembrolizumab in those without mPR or pCR as well (HR 0.73 and 0.69 respectively) [9]. Also notably, the KEYNOTE-671 study included some patients with Epidermal Growth Factor Receptor (EGFR) and Anaplastic Lymphoma Kinase (ALK) mutations—subgroups historically with limited benefit from immunotherapy [13–16].

Other perioperative studies such as AEGEAN and NEOTORCH have demonstrated similar benefits. The randomized AEGEAN trial which studied durvalumab versus placebo along with PDC in the neoadjuvant setting (4 cycles) followed by adjuvant durvalumab or placebo monotherapy up to 12 cycles in stage II-IIIB (N2 stage) NSCLC showed EFS at 24 months of 63.3% compared to 52.4% with HR of 0.68 with median EFS not met in durvalumab group versus 25.9 months in the placebo group. mPR was 33.3% versus 12.3% while pCR was 17.2% versus 4.3% [17]. Toripalimab (3 cycles in neoadjuvant and 1 cycle in adjuvant setting with PDC followed by toripalimab alone up to 13 cycles) was also administered to stage II-IIIB (N2 stage) NSCLC without EGFR or ALK mutations in NEOTORCH trial in China which also showed significant benefits with EFS at 2 years was 64.7% versus 38.7% with HR of 0.4 with median EFS not reached in toripalimab versus

15.1 months in the placebo arm with mPR of 48.5% versus 8.4% and pCR of 24.8% versus 1.0% [18].

Dual neoadjuvant immunotherapy with nivolumab and ipilimumab was also studied in the phase II NEOSTAR trial. Combination of ipilimumab and nivolumab compared to nivolumab alone improved mPR rate to 50% vs. 24% respectively [19]. The addition of chemotherapy to neoadjuvant ipilimumab plus nivolumab resulted in a mPR rate of 50%, compared to 32% with nivolumab alone [20].

Emerging perioperative studies

Unresolved challenges in the management of perioperative NSCLC include a need for deeper understanding of patient selection and better methods to determine treatment duration, in particular an improved prognostication of whether adjuvant therapy is needed in patients who received neoadjuvant chemoimmunotherapy. The design of the CheckMate 816 trial stands out for its focused examination of neoadjuvant treatment, demonstrating the clear benefits of incorporating neoadjuvant immunotherapy. This approach contrasts with other perioperative studies that combine both neoadjuvant and adjuvant treatments, a methodological choice that cannot separate the contribution of each component of therapy. The targeted approach used in CheckMate 816 trial was endorsed as the preferred design schematic by the FDA [21], setting a new standard for the design of perioperative clinical trials in this domain. Preliminary interim analysis from CheckMate 77T which compares neoadjuvant nivolumab with PDC and adjuvant nivolumab for 1 year to neoadjuvant placebo with PDC and adjuvant placebo for 1 year has met its primary endpoint of EFS (not reached vs. 18.4 months, HR 0.58), pCR of 25.3% vs. 4.7%, mPR of 35.4% vs. 12.1% with comparable tolerability as of now and awaits data maturation [22]. As such, many additional neoadjuvant immunotherapy (NCT06269211 (toripalimab)) and chemoimmunotherapy trials (NCT05962021 (toripalimab+PDC), NCT05157776 (sintilimab+PDC), NCT05882513 (serplulimab+PDC), NCT06241807 (camrelizumab+PDC)) are underway as well as perioperative studies (NCT05925530 (durvalumab+PDC followed by surgery and adjuvant durvalumab vs. chemoradiotherapy), NCT05116462 (sintilimab + PDC pre and post operatively followed by maintenance sintilimab vs. placebo). The results of these studies are awaited to further define the best use of perioperative therapy. However, none of them have a design that will allow clear understanding of the added value of the adjuvant treatment component.

There is consequently a pressing need for expanded research focused on patients who do not achieve a pCR following neoadjuvant therapy and for new studies incorporating novel biomarkers and experimental strategies. Additionally, despite the quite excellent outcomes of this group of patients, the role of continuing immunotherapy post-operatively in patients who have achieved pCR remains an open question. Refined biomarkers and prognostic tools are essential for precisely selecting patients likely to derive maximal benefit from adjuvant immunotherapy post-curative resection, thereby minimizing cumulative toxicities, alleviating treatment-related burdens, and reducing financial toxicity.

Perioperative treatment with EGFR/ALK mutations

Concerted efforts are similarly underway to advance therapies targeting driver mutations in earlier settings. Postoperative use of osimertinib for 3 years with or without adjuvant chemotherapy, as evidenced by the pivotal ADAURA trial in patients with resected stage IB-IIIA NSCLC who have EGFR exon 19 deletions or exon 21 L858R mutationshas significantly extended both DFS (90% vs. 44% at 2 years, 73% vs. 38% at 4 years) with HR of 0.17 at 2 years and 0.23 at 4 years as well as OS and furthermore CNS disease free rate was also significantly improved- 92% vs. 81% compared to placebo [19, 20]. Alectinib use of up to 2 years in adjuvant setting, evaluated in the ALINA study for stage IB-IIIA NSCLC patients with ALK rearrangements, was compared against adjuvant platinum based chemotherapy for 4 cycles and has also shown a considerable prolongation in DFS of 93.6% vs. 63.7% at 2 years with HR 0.24 [23]. Its assessment has led to recent FDA approval of alectinib in ALK-positive NSCLC in the adjuvant setting.

Some immunotherapy-focused studies, such as KEYNOTE-671 allowed patients harboring mutations in EGFR and ALK to participate and some subset analyses based on small numbers of patients are suggestive of potential benefits. However, given the outstanding activity of targeted agents for EGFR and ALK mutation harboring patients, the focus at present should revolve around optimal perioperative utilization of targeted therapies. Indeed, several other early studies also demonstrated potential use of targeted therapies in preoperative studies. NCT03433469 using 2 cycles of neoadjuvant osimertinib in stage IA-IIIA NSCLC with EGFR mutations demonstrated 15% mPR and 44% achieved lymph node downstaging [24] as well as NCT04201756 which utilized 2 to 4 cycles of neoadjuvant afatinib, achieved 9.1% mPR and 57.6% had pathological downstaging for stage III NSCLC [25]. Combinatory studies using targeted therapies with or without chemotherapy are also being explored: NCT04351555 (NeoADAURA; phase III osimertinib vs. osimertinib plus PDC vs. placebo plus PDC neoadjuvantly followed by physician's choice adjuvant treatment of targeted therapy with or without chemotherapy) [26], NCT04302025 (NAUTIKA1; single arm phase II neoadjuvant use of alectinib for 8 weeks) [27],

and NCT05015010 (ALNEO; single arm phase II neoadjuvant use of alectinib for 2 cycles followed by adjuvant use up to 24 cycles) [28].

Unmet needs in preoperative settings

One of the unmet needs in the preoperative setting for NSCLC is for accurate assessment of pathological response, which is integral to formulating decisions regarding postoperative therapy. Currently, surrogate endpoints such as pCR and mPR have been utilized to predict EFS and even more importantly OS. Although achieving mPR was observed to significantly correlate with improved survival in neoadjuvant chemotherapy trials [29, 30], further studies were needed to validate this in the era of immunotherapies and other therapeutics in resectable NSCLC. Recent meta-analysis of seven neoadjuvant randomized controlled trials showed that while pCR results were strongly correlative (R^2 = 0.82, β = 0.96) with EFS at 2 years, but that OS was only moderately correlative (R^2 = 0.55, β = 0.26). In addition, the association between hazard ratio of OS and EFS was poorly correlative (R^2 = 0.27, β = 0.11). This suggests that pCR, despite its strong linkage with EFS, may not be a completely accurate surrogate for the full clinical picture in assessing the long-term outcomes of neoadjuvant treatments [31]. Furthermore, given the potential for interobserver discrepancies due to the nature of estimating 0 or 10% residual tumor and non-standardized guidelines across trials and centers, the International Association for the Study of Lung Cancer (IASLC) published a guideline for pathologic assessment in neoadjuvant studies for NSCLC in 2020 to increase tumor sampling and assessment for tumors greater than 3 cm as well as inspection of the entire specimen for samples less than 3 cm in size [32, 33]. However, the impact of this guideline on clinical practice and patient outcomes remains uncertain, as its adoption and effectiveness in enhancing the precision of pathological assessments have yet to be thoroughly evaluated in diverse clinical settings. Developing and implementing universal pathological response assessment to facilitate more precise and informed clinical decisions that is timely, accurate, and reproducible in early-stage NSCLC is a critical and urgent need.

Lastly, there is a pressing need for novel treatments and innovative trial designs in the perioperative NSCLC landscape. While recent advances have introduced more effective treatment options, there remains a vast potential for discovering and integrating new therapies that could further enhance patient outcomes. The synergistic application of radiotherapy and immunotherapy has been observed to enhance immune priming, potentially contributing to new treatment avenues. Preclinical and clinical studies (in metastatic or recurrent settings) have shown that co-administration of immune check point inhibitor and radiation therapy may amplify release of major histocompatibility complex-1, tumor specific T cell response, as well as generating immune memory cells in tumor draining lymph nodes and potentially offer added clinical benefit [34–37]. Findings from a phase II clinical trial revealed that combination of neoadjuvant durvalumab with immunomodulatory doses of stereotactic radiation resulted in a higher mPR of 53.3% vs. 6.7% and although not statistically significant, three-year DFS rate of 83% compared to 69%, underscoring the potential of these combinatory approaches in improving patient outcomes [38]. Notably, however, the PACIFIC-2 trial with concurrent durvalumab and chemoradiotherapy compared to chemoradiotherapy for the treatment of unresectable stage III NSCLC did not meet its primary end point of PFS [39]. Similarly, JAVELIN trial in locally advanced head and neck cancer, the addition of avelumab to chemoradiotherapy also did not meet its primary end point of PFS [40]. A potential hypothesis behind several of these failures could be due to changes in tumor specific T cells after radiotherapy that negatively impacts the effect of immunotherapy. Select studies currently investigating the combination of radiation therapy and various immunotherapy include NCT05500092 (neoadjuvant nivolumab and chemotherapy with or without radiation), NCT04245514 (SAKK 16/18 chemotherapy followed by durvalumab followed by various radiation regimens then adjuvant durvalumab), NCT05798845 (neoadjuvant toripalimab plus radiotherapy), and NCT04933903 (NEO Rad neoadjuvant nivolumab, ipilimumab, and radiation).

Mechanistically novel therapeutics are being explored in the metastatic setting that potentially offer opportunities for patients with resectable NSCLC. Combination of different immune checkpoint inhibitors are under evaluation including a series of studies focused on T cell immunoreceptor with Ig and ITIM (TIGIT) antibody and lymphocyte-activation gene 3 (LAG-3) antibody and other novel checkpoints in a multidrug platform such as NEOCOAST which combines durvalumab with oleclumab (anti-CD73 monoclonal antibody (mAb)), monalizumab (anti-NKG2A mAb), or danvatirsen (anti-STAT3 antisense oligonucleotide) [41] (see Table 2). A phase II trial using combination of neoadjuvant nivolumab with or without relatlimab, a LAG-3 inhibitor, in stage IB-IIIA NSCLC was able to demonstrate mPR of 27% vs. 30%, DFS at 12 months of 89% vs. 93%, and OS at 12 months of 93% vs. 100% demonstrating potential for novel combinatory regimens [42]. Notably, antibody drug conjugates (ADC) targeting trophoblast cell surface antigen 2 (Trop-2), a transmembrane glycoprotein prevalent in NSCLC, are also gaining traction [43]. Sacituzumab govitecan, a Trop-2 targeted ADC, currently approved for metastatic breast and urothelial cancer based on improved PFS and OS [44–46], is now being studied in a range of lung cancer-focused studies. Furthermore, TROPION-Lung-02 phase 1b study

TABLE 2 Ongoing representative perioperative studies with novel immune checkpoint inhibitors and biomarkers.

Upcoming perioperative chemoimmunotherapy trials					
Trial	**Phase**	**Stage**	**Neoadjuvant treatment arm(s)**	**Adjuvant treatment arm(s)**	**Primary endpoint(s)**
NCT04316364	III	II-IIIB	Adebrelimab + PDC	Adebrelimab	mPR, EFS
NCT05116462	III	II, IIIA or IIIB (resectable N2 only)	Sintilimab + PDC	Sintilimab + PDC, followed by Sintilimab	EFS
NCT04158440	III	II-IIIB (N2 only)	Toripalimab + PDC	Toripalimab vs. placebo	mPR, EFS
NCT04606303	II	IIB-IIIB without driver mutations	Toripalimab + PDC	NA	mPR
NCT05882513	II	IIA-IIIB (no N3 patient)	Serplulimab + PDC	NA	pCR
NCT05157776	III	IIIA	Sintilimab + PDC	NA	pCR
NCT04865250 (iREP)	II	II, IIIA or select IIIB (T3N2 only)	Atezolizumab + PDC	NA	mPR
Emerging novel combination trials					
Trial	**Phase**	**Stage**	**Neoadjuvant treatment arm(s)**	**Adjuvant treatment arm(s)**	**Primary endpoint(s)**
NCT04832854 (SKYSCRAPER-05)	II	II, IIIA, or select IIIB (T3N2 only)	Arm 1 (high PD-L1 expression): Atezolizumab + Tiragolumab. Arm 2 (Any PD-L1 expression): Atezolizumab + Tiragolumab + PDC	Arm 1 (high PD-L1 expression): Atezolizumab + Tiragolumab or PDC Arm 2 (Any PD-L1 expression): Atezolizumab + Tiragolumab	mPR, surgical delays, operative and post-operative complications, surgical cancellations related to study treatment, AE
NCT05061550 (NeoCOAST-2)	II	IIA-IIIB	Arm 1: Oleclumab + durvalumab + PDC	Arm 1: Oleclumab + durvalumab	pCR, AE
			Arm 2: Monalizumab + durvalumab + PDC	Arm 2: Monalizumab + durvalumab	
			Arm 3: Volrustomig (Dose Exploration) + PDC	Arm 3: Volrustomig	
			Arm 4: Dato-DXd + durvalumab + single agent platinum	Arm 4: durvalumab	
			Arm 5: AZD0171 + durvalumab + PDC	Arm 5: AZD0171 + durvalumab	
NCT05360979	II	II, IIIA, IIIB (T3N2)	Envafolimab + Recombinant human endostatin + PDC	Envafolimab	mPR
NCT05891080	II	IIIB-IIIC	Arm 1: Toripalimab + JS004 + PDC Arm 2: Toripalimab + PDC	NA	pCR
NCT05387109	IV	II-IIIB (IIIB only T3N2)	Penpulimab + Anlotinib	individualized per patient	pCR

(Continued on following page)

10.3389/pore.2024.1611817

TABLE 2 (*Continued*) Ongoing representative perioperative studies with novel immune checkpoint inhibitors and biomarkers.

Upcoming perioperative chemoimmunotherapy trials					
Trial	**Phase**	**Stage**	**Neoadjuvant treatment arm(s)**	**Adjuvant treatment arm(s)**	**Primary endpoint(s)**
NCT05742607 (MATISSE)	II	IIA-IIIA	Durvalumab + IPH5201 + PDC	Durvalumab + IPH5201	pCR, AE
NCT04040361 (EAST ENERGY)	II	IB-IIIA	Pembrolizumab + Ramucirumab	NA	mPR
NCT06088771	I, II	T1b or more advanced (>1 cm) and resectable	Dupilumab + Cemiplimab	standard of care	DLTs, mPR
NCT05577702	II	II-IIIA	Arm 1a: Tislelizumab Arm 1b: Tislelizumab and Ociperlimab Arm 1c: Tislelizumab and LBL-007 Arm 2a: Tislelizumab + PDC Arm 2c: LBL-007 + Tislelizumab + PDC	NA	mPR
NCT06077760	III	Resected Stage II, IIIA, IIIB (N2)	-	V940 + Pembrolizumab	DFS
Emerging novel biomarker/imaging focused trials					
Trial	**Phase**	**Stage**	**Neoadjuvant treatment arm(s)**	**Adjuvant treatment arm(s)**	**Primary endpoint(s)**
NCT04158440	III	II-III	Toripalimab + PDC	Toripalimab	PD-L1 in tissue specimen, TMB, WES and change of ctDNA in peripheral blood sample
NCT06221462 (PRIORITY)	II	IB-IIIB	Sintilimab + Anlotinib	Sintilimab	MRD ctDNA
NCT05429463 (neoSCORE II)	III	cIB-IIIA	Sintilimab + PDC	+/− RT, ± Sintilimab	PD-L1, ctDNA, TIIC
NCT04061590	II	I-IIIA	Treatment Arm-1: Pembrolizumab Treatment Arm-2: Pembrolizumab + PDC	NA	Proportion of patients with a ≥2-fold increase in the number of TIICs in post- versus pre-pembrolizumab treatment tumor specimens
NCT04638582	II	IA3 - IIA	Arm 1: Pembrolizumab Arm 2: Pembrolizumab + PDC	Arm 1 and 2: Pembrolizumab ± PDC	ctDNA resolution, imaging measures of response in correlation with pCR
NCT05925530 (MDT-BRIDGE)	II	IIB - IIIB (N2 only)	Durvalumab or Durvalumab followed by CRT	Durvalumab up to 12 months	ctDNA clearance
NCT02818920 (TOP1501)	II	IB (>/= 3 cm per CT), cIIA/IIB, IIIA (N0-2)	Pembrolizumab	Adjuvant CT ± RT f/b Pembrolizumab x 4	change in biomarkers, TIL, T cells specific against TAA, change in immunomodulatory effects, circulating T cells, gene expression of the PD-1/PD-L1 axis, correlation of pathologic response to the presence of TILs
NCT05882513	II	IIA-IIIB (no N3 patient)	Serplulimab + PDC	NA	ORR before surgery - the proportion of subjects with imaging PR or CR

(Continued on following page)

10.3389/pore.2024.1611817

TABLE 2 (*Continued*) Ongoing representative perioperative studies with novel immune checkpoint inhibitors and biomarkers.

Upcoming perioperative chemoimmunotherapy trials					
Trial	**Phase**	**Stage**	**Neoadjuvant treatment arm(s)**	**Adjuvant treatment arm(s)**	**Primary endpoint(s)**
NCT04875585 (IMNWOP1)	II	IA3-IIIA (max. single station N2)	Pembrolizumab + Lenvatinib	Pembrolizumab	radiologic response, surgical resection rate
NCT04586465 (DYNAPET)	II	IIA-IIIB	Pembrolizumab + PDC	NA	mPR, dynamic PET-CT SUV change, ORR, uptake rate constant changes
NCT06241807	II	IIIA-IIIB (T3-4N2)	Camrelizumab + PDC	NA	ctDNA, serum metabolomics testing, 18F-FDG uptake value, circulating immunological biomarkers, and observation of tumor immune microenvironment

AE, adverse events; CR, complete response; CT, chemotherapy; ctDNA, circulating-tumor DNA; DFS, disease free survival; DLTs, dose-limiting toxicities; EFS, event-free survival; mPR, major pathological response; MRD, minimal residual disease; ORR, objective response rate; ORR, objective response rate; pCR, pathological complete response; PD-L1, programmed cell death ligand 1; PDC, platinum doublet chemotherapy; PET-CT SUV, positron-emission tomography and a computed tomography standardized uptake values; PR, partial response; RT, radiation therapy; SAE, serious adverse events; TAA, tumor-associated antigen; TTICs, tumor-infiltrating immune cells; TIL, tumor-infiltrating lymphocytes; TMB, tumor mutation burden; WES, whole exome sequence.

demonstrated promising results with datopotamab deruxtecan (Dato-DXd), another Trop-2 ADC, in combination with pembrolizumab with or without chemotherapy with objective response rate of 60% (with chemotherapy) and 55% (without chemotherapy) suggesting a potential synergistic effect that enhances antitumor immunity [47]. Building on these findings, the TROPION-Lung-01 study compared Dato-DXd with docetaxel in advanced and metastatic NSCLC, revealing a median PFS of 5.6 versus 3.7 months. Significantly, the HR was 0.63 in non-squamous histology types, suggesting that newer therapeutics like Dato-DXd could be promising agents for further study in earlier stages of NSCLC [48]. Results from further studies like TROPION-Lung07 and TROPION-Lung08 are awaited to confirm its efficacy in advanced NSCLC [49, 50]. Concurrently, innovative trials are incorporating these therapeutics into early-stage treatment. For instance, the NeoCOAST-2 trial (NCT05061550) evaluates a multidrug platform including neoadjuvant Dato-DXd, durvalumab, and platinum, while NCT06055465 explores the combination of neoadjuvant sacituzumab govitecan and pembrolizumab.

Furthermore, personalized mRNA vaccines encoding tumor-specific neoantigens used alongside immunotherapy are under investigation. The KEYNOTE-942 trial has demonstrated an improved recurrence-free survival (RFS) rate of 79% compared to 62% at 18 months (HR 0.561) by combining the V940 vaccine with pembrolizumab in a population of patients with resected high-risk melanoma [51]. Additionally, ongoing studies like INTerpath-002 (NCT06077760) are examining the role of the V940 messenger RNA vaccine in conjunction with pembrolizumab in the adjuvant setting for patients with completely resected stage II-IIIB NSCLC. Another trial, YE-NEO-001 (NCT03552718), is investigating a personalized neoepitope vaccine using a yeast vector in a similar adjuvant context. Collectively, these innovative modalities offer a more tailored and potentially more effective approach to cancer therapy, targeting the specific characteristics of individual tumors and potentially triggering a more robust immune response.

Biomarkers-current and future

In the effort to optimize perioperative immunotherapy, biomarker studies aim to identify potential prognostic and predictive correlates of treatment outcomes (Figure 1). For example, integration of circulating tumor DNA (ctDNA) assays has shown promise in perioperative trials. One such application of ctDNA includes monitoring ctDNA dynamics following neoadjuvant chemoimmunotherapy. In operable NSCLC, the NADIM trial showed that pretreatment mutant allele fraction (MAF) < 1% correlated with PFS and OS

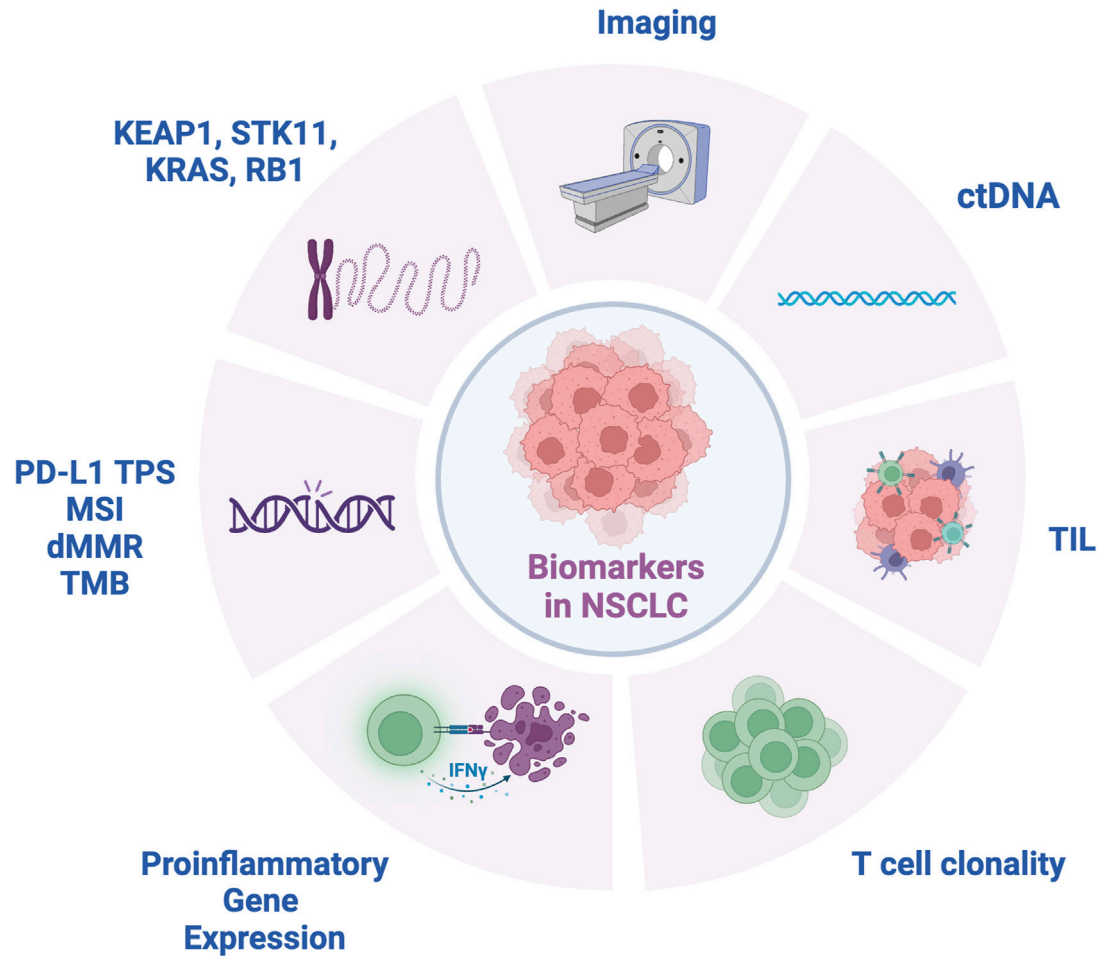

FIGURE 1
Biomarkers for NSCLC. ctDNA, circulating tumor DNA; dMMR, mismatch repair deficient; IFNγ, interferon-gamma; KEAP1, Kelch-like ECH-associated protein 1; KRAS, Kirsten ras sarcoma oncogene; MSI, microsatellite instability; RB1, retinoblastoma 1 gene; STK11, serine/threonine kinase 11; TIL, tumor infiltrating lymphocytes; TMB, tumor mutation burden; TPS, tumor proportion score.

benefits following neoadjuvant nivolumab and chemotherapy. In addition, clearance of ctDNA after neoadjuvant treatment was associated with improved PFS and OS [10]. CheckMate-816 similarly applied ctDNA dynamics to neoadjuvant chemotherapy, showing higher ctDNA clearance in preoperative nivolumab plus chemotherapy compared to chemotherapy alone. In addition, undetectable ctDNA following neoadjuvant treatment was positively associated with EFS and pCR [8].

Furthermore, ctDNA has also been applied to the assessment of minimal residual disease (MRD) (Figure 2). Indeed, in early-stage NSCLC treated with surgery and adjuvant chemotherapy and/or radiotherapy, ctDNA detection following resection was associated with clinical recurrence [34]. Similarly, the LUNGCA-1 study has shown a temporal association post-operatively between ctDNA presence and RFS [52]. In the perioperative immunotherapy space, the Impower010 trial showed that ctDNA detection postoperatively was similarly associated with a trend towards worse DFS in both patients treated with adjuvant atezolizumab and best supportive care following adjuvant chemotherapy [53].

Several studies are underway to further elucidate the role of MRD detected via sensitive MRD platforms in perioperative settings. One such trial is NCT04367311, a phase II study using chemoimmunotherapy with atezolizumab looking at ctDNA clearance in MRD-positive patients with resected stage I/IIA NSCLC. ADAPT-E is another phase II study assessing the utility of adjuvant durvalumab for stage I-III NSCLC with ctDNA positivity after definitive surgery or radiation and have completed standard of care chemotherapy as to achieving ctDNA clearance (NCT04585477). Future work using designs similar to the ADAPT-E trial are necessary to investigate whether MRD-positivity using ctDNA can better identify patients at risk of

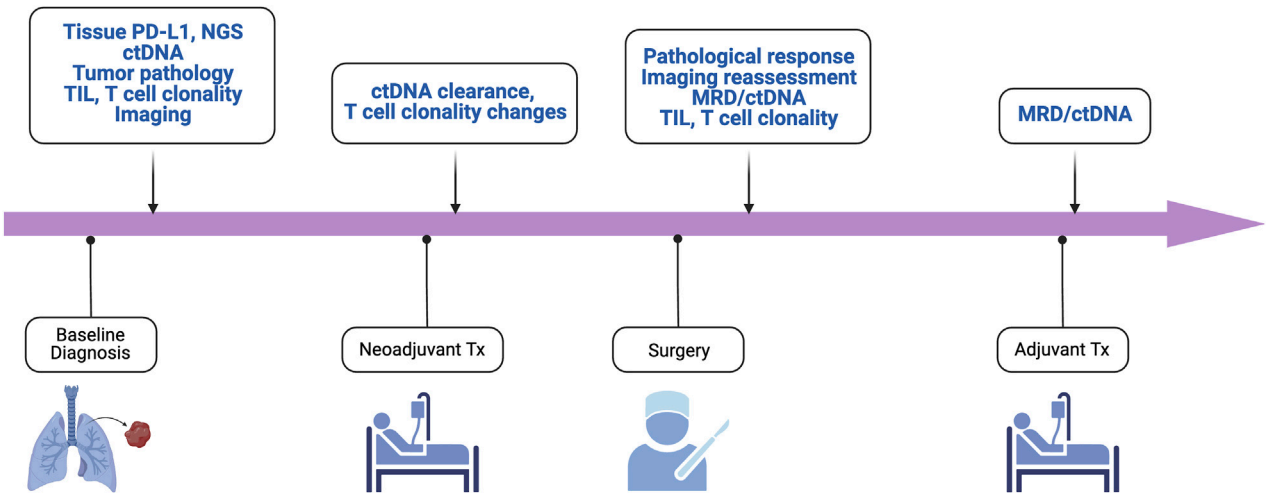

FIGURE 2
Key biomarkers for enhanced management and trial enrichment. ctDNA, circulating tumor DNA; mPR, major pathological response; MRD, minimal residual disease; NGS, next-generation sequencing; pCR, pathologic complete response; TIL, tumor infiltrating lymphocytes; TMB, tumor mutation burden.

recurrence postoperatively and guide the use of adjuvant immunotherapy to minimize that risk.

Despite the promise that ctDNA may hold as a biomarker of interest, there are important limitations to its use influenced by the inherent sensitivity of ctDNA detection methods [54] and clonal hematopoiesis of indeterminate potential (CHIP) to a lesser extent [55]. For example, ctDNA's utility is constrained by its limited sensitivity in cases of low tumor burden such as early-stage NSCLC [56] where the sparse release of tumor DNA into the bloodstream may fall below the detection threshold of current technologies. In addition, most trials do not specify CHIP, a condition characterized by the accumulation of somatic mutations in hematopoietic stem cells, which can interfere with the accurate interpretation of ctDNA mutations. This interference is especially problematic when the variant allele frequency (VAF) of ctDNA mutations is low, as DNA shed from white blood cells harboring CHIP mutations may be mistakenly attributed to tumor-derived DNA. Together, these challenges underscore the need for enhanced detection methods and interpretative strategies to accurately discern ctDNA's true clinical value in the management of cancer patients in neoadjuvant and perioperative contexts.

In metastatic NSCLC, recognized predictive biomarkers for immunotherapy response include PD-L1 tumor proportion score, microsatellite instability (MSI)/deficient mismatch repair (dMMR), and tumor mutational burden (TMB). Based on evidence for these biomarkers in multiple solid tumors, the FDA granted approval for pembrolizumab for MSI-high, dMMR, and TMB-high tumors regardless of tissue type [57]. Nonetheless, in the perioperative immunotherapy space TPS and TMB score have shown inconsistent results. While high PD-L1 TPS was associated with higher mPR rates in the LCMC3 and NEOSTAR studies, later phase trials have not reliably reproduced these findings although certainly general trends are observed of better results in patients with TPS score high positive tumors [58, 59]. In the phase III Checkmate 816 study, both PD-L1 positive and PD-L1 negative patients showed improved pCR rates with neoadjuvant chemoimmunotherapy. Of note, the PD-L1 high patients had a highly impressive close to 50% pCR rate and showed the greatest improvement in EFS(8). In addition, inconsistent results were noted in the adjuvant setting as well where TPS score appeared to correlate with DFS in the Impower 010 study, while the Phase III PEARLS trial found that adjuvant pembrolizumab was associated with longer DFS across all PD-L1 subgroups [60]. As for TMB, its role remains unclear in the perioperative space as several studies thus far including the Checkmate 816, LCMC3, and NADIM trials evaluating TMB and its association with pCR have failed to show a significant relationship [8, 10, 59].

The perioperative setting is ideal for studying novel biomarkers by examination of both pre-treatment and post-treatment tissue obtained following surgical resection. For example, several trials have investigated how the immunophenotype of the tumor microenvironment and in circulating peripheral blood may relate to perioperative immunotherapy outcomes. T-cell repertoire was evaluated in an early-phase trial of neoadjuvant nivolumab showing that tumors demonstrating a mPR showed a higher clonality of the T-cell population in both the tumor and peripheral blood [7].

LCMC3 employed similar methods to evaluate T-cell responses in resected NSCLC following neoadjuvant atezolizumab finding that tumors with mPR were significantly associated with an expansion of peripheral blood-activated $CD8^+$ T cells [59]. The NEOSTAR trial studying neoadjuvant nivolumab and ipilimumab versus nivolumab evaluated the immune cell infiltration of pre- and post-therapy tumor specimens using multiplex immunofluorescence and demonstrated that dual-immunotherapy combination induced greater overall tumor infiltration of $CD3^+$ and $CD3^+CD8^+$ T lymphocytes, tissue-resident memory cells, and effector memory T cells than single-agent nivolumab [58]. In the NADIM trial investigating neoadjuvant nivolumab plus chemotherapy, tumors achieving pCR were associated with a proinflammatory gene expression profile and higher upregulation of IFN-γ-responsive genes involved in antitumor response [61]. Those tumors without pCR, however, showed upregulation of genes related to proliferation. Additionally, peripheral blood collected from patients enrolled in the NADIM trial showed a differential profile of immune parameters based on pCR or non-pCR, such as higher $CD4^+$ PD-1+ cells and lower monocyte CTLA-4 expression in patients with pCR [62]. Future studies are necessary to elucidate how pathologic correlates such as T cell clonality, immune cell infiltration, and immune gene expression in the tumor microenvironment and peripheral blood relate to perioperative immunotherapy response.

Another group of biomarkers of uncertain significance are several key somatic mutations associated with poor response to immunotherapy. For example, a *post hoc* analysis of the POSEIDON trial evaluating combined PD-L1 and CTLA-4 inhibition with durvalumab and tremelimumab plus chemotherapy in metastatic NSCLC showed that patients with KEAP1, STK11, and KRAS mutations benefited more from combination immunotherapy [63]. In addition, results from the perioperative NADIM trial showed that tumors with KEAP1, STK11, and RB1 mutations were less likely to show a benefit from preoperative immunotherapy [10]. Further efforts will be required to determine how the presence such molecular alterations can guide perioperative immunotherapy treatment strategies.

Lastly, radiomic biomarkers have shed light to predicting response to immunotherapy in the perioperative settings. Literature shows imaging biomarkers such as maximum standardized uptake value (SUVmax), metabolic tumor volume (MTV) and total lesion glycolysis (TLG) from positron emission tomography/computed tomography (PET/CT) scans have demonstrated prognostic significance in resectable NSCLC. A meta-analysis found that high SUVmax, MTV, and TLG correlated with lower disease free survival (HR of SUVmax = 2.43, MTV = 2.49, TLG = 2.97) and OS (HR SUVmax = 1.52, MTV = 1.91, TLG = 1.94) in resectable NSCLC [64]. Sun et al also demonstrated high radiomic based biomarker of tumor infiltration with CD8 cells was associated with better overall survival of 24.3 months compared to 11.5 months in those with low radiomic score (HR 0.58) [65]. Zerunian et al assessed CT-derived texture parameters less than 56.2 mean value of positive pixels to be associated with lower OS and PFS with HR 0.89 with pembrolizumab use [66]. Further work is needed to explore how imaging biomarkers can be systematically integrated into perioperative trials to enhance prognostication and therapeutic approaches.

The development of precise biomarkers is critical in the perioperative setting to optimally treat patients with NSCLC. Current limitations may hinder personalized treatment planning and often lead to a trial-and-error approach, potentially delaying the identification of the most effective treatment for individual patients. The development and validation of reliable predictive biomarkers is essential to optimize treatment selection, enhance response rates, and avoid unnecessary toxicity from ineffective therapies.

Conclusion

In this review, we summarize the current rapidly evolving landscape of perioperative therapy for NSCLC. The evidence gathered from recent clinical trials underscores the potential of neoadjuvant approaches to improve and augment surgical outcomes, enhance pathological response rates, and ultimately, increase overall survival rates for patients with resectable NSCLC. Further challenges in optimizing patient selection to identify ideal candidates for neoadjuvant treatments, duration of treatment, and optimal treatment regimen are still ongoing and need to be supported. Integration of molecular profiling and the development of predictive biomarkers hold promise for personalizing neoadjuvant treatment approaches, potentially enabling the tailoring of therapy to individual patient characteristics and tumor biology. Moreover, the exploration of novel therapeutic agents and combinations, as well as the innovative endpoints in trial designs, will be crucial in overcoming resistance mechanisms and improving patient outcomes.

Author contributions

HJ and BH conceptualized the manuscript. HJ and AD'A drafted the manuscript. HJ, RG, AD'A, BS, PI, and BH revised the manuscript. HJ drafted the figures. HJ and RG drafted the tables. BH provided overall supervision of this manuscript. All authors contributed to the article and approved the submitted version.

Funding

The author(s) declare that no financial support was received for the research, authorship, and/or publication of this article.

Conflict of interest

BH—Receives clinical research funding from Boehringer Ingelheim, Astra Zeneca, Merck, BMS, Advaxis, Amgen, AbbVie, Daiichi, Pfizer, GSK, Beigene, Janssen, Black Diamond Therapeutics, Forward Pharma, Numab, Arrivent. Receives Honoraria from Astra Zeneca, Boehringer Ingelheim, Apollomics, Janssen, Takeda, Merck, BMS, Genentech, Pfizer, Eli-Lilly, Arcus, Merus, Daiichi, Precede. BS—Provides consulting and serves as advisory boards for Medtronic, AstraZeneca, Roche-Genentech, Pfizer, Arcus Biosciences, Bristol Myers Squib, Merck, Regeneron, Galvanize Therapeutics. Receives research funding from BMS Foundation and his wife owns salary/stock for SIGA Technologies. PI—Serves as advisory board for Agilent, AstraZeneca, Sanofi, AbbVie, Genentech, Merus, and speaks for Eli Lilly. Receives research funding from Bristol Myers-Squib.

The remaining authors declare that the research was conducted in the absence of any commercial or financial relationships that could be construed as a potential conflict of interest.

References

1. Sung H, Ferlay J, Siegel RL, Laversanne M, Soerjomataram I, Jemal A, et al. Global cancer statistics 2020: GLOBOCAN estimates of incidence and mortality worldwide for 36 cancers in 185 countries. *CA: A Cancer J Clinicians* (2021) 71(3): 209–49. doi:10.3322/caac.21660

2. Sandler A, Gray R, Perry MC, Brahmer J, Schiller JH, Dowlati A, et al. Paclitaxel–carboplatin alone or with bevacizumab for non–small-cell lung cancer. *New Engl J Med* (2006) 355(24):2542–50. doi:10.1056/NEJMoa061884

3. Vansteenkiste JF, Cho BC, Vanakesa T, De Pas T, Zielinski M, Kim MS, et al. Efficacy of the MAGE-A3 cancer immunotherapeutic as adjuvant therapy in patients with resected MAGE-A3-positive non-small-cell lung cancer (MAGRIT): a randomised, double-blind, placebo-controlled, phase 3 trial. *Lancet Oncol* (2016) 17(6):822–35. doi:10.1016/S1470-2045(16)00099-1

4. Felip E, Rosell R, Maestre JA, Rodríguez-Paniagua JM, Morán T, Astudillo J, et al. Preoperative chemotherapy plus surgery versus surgery plus adjuvant chemotherapy versus surgery alone in early-stage non–small-cell lung cancer. *J Clin Oncol* (2010) 28(19):3138–45. doi:10.1200/JCO.2009.27.6204

5. Lim E, Harris G, Patel A, Adachi I, Edmonds L, Song F. Preoperative versus postoperative chemotherapy in patients with resectable non-small cell lung cancer: systematic review and indirect comparison meta-analysis of randomized trials. *J Thorac Oncol* (2009) 4(11):1380–8. doi:10.1097/JTO.0b013e3181b9ecca

6. NSCLC Meta-analysis Collaborative Group. Preoperative chemotherapy for non-small-cell lung cancer: a systematic review and meta-analysis of individual participant data. *The Lancet* (2014) 383(9928):1561–71. doi:10.1016/S0140-6736(13)62159-5

7. Forde PM, Chaft JE, Smith KN, Anagnostou V, Cottrell TR, Hellmann MD, et al. Neoadjuvant PD-1 blockade in resectable lung cancer. *New Engl J Med* (2018) 378(21):1976–86. doi:10.1056/NEJMoa1716078

8. Forde PM, Spicer J, Lu S, Provencio M, Mitsudomi T, Awad MM, et al. Neoadjuvant nivolumab plus chemotherapy in resectable lung cancer. *New Engl J Med* (2022) 386(21):1973–85. doi:10.1056/NEJMoa2202170

9. Wakelee H, Liberman M, Kato T, Tsuboi M, Lee SH, Gao S, et al. Perioperative pembrolizumab for early-stage non-small-cell lung cancer. *N Engl J Med* (2023) 389(6):491–503. doi:10.1056/NEJMoa2302983

10. Provencio M, Serna-Blasco R, Nadal E, Insa A, García-Campelo MR, Casal RJ, et al. Overall survival and biomarker analysis of neoadjuvant nivolumab plus chemotherapy in operable stage IIIA non–small-cell lung cancer (NADIM phase II trial). *J Clin Oncol* (2022) 40(25):2924–33. doi:10.1200/JCO.21.02660

11. Provencio M, Nadal E, Insa A, García-Campelo MR, Casal-Rubio J, Dómine M, et al. Neoadjuvant chemotherapy and nivolumab in resectable non-small-cell lung cancer (NADIM): an open-label, multicentre, single-arm, phase 2 trial. *Lancet Oncol* (2020) 21(11):1413–22. doi:10.1016/S1470-2045(20)30453-8

12. Provencio M, Nadal E, Gonzalez-Larriba JL, Martinez-Marti A, Bernabe R, Bosch-Barrera J, et al. Perioperative nivolumab and chemotherapy in stage III non-small-cell lung cancer. *N Engl J Med* (2023) 389(6):504–13. doi:10.1056/NEJMoa2215530

13. Herbst RS, Baas P, Kim DW, Felip E, Pérez-Gracia JL, Han JY, et al. Pembrolizumab versus docetaxel for previously treated, PD-L1-positive, advanced non-small-cell lung cancer (KEYNOTE-010): a randomised controlled trial. *Lancet* (2016) 387(10027):1540–50. doi:10.1016/S0140-6736(15)01281-7

14. Rittmeyer A, Barlesi F, Waterkamp D, Park K, Ciardiello F, Von Pawel J, et al. Atezolizumab versus docetaxel in patients with previously treated non-small-cell lung cancer (OAK): a phase 3, open-label, multicentre randomised controlled trial. *The Lancet* (2017) 389(10066):255–65. doi:10.1016/S0140-6736(16)32517-X

15. Borghaei H, Paz-Ares L, Horn L, Spigel DR, Steins M, Ready NE, et al. Nivolumab versus docetaxel in advanced nonsquamous non–small-cell lung cancer. *New Engl J Med* (2015) 373(17):1627–39. doi:10.1056/NEJMoa1507643

16. Hong L, Lewis WE, Nilsson M, Patel S, Varghese S, Rivera MJ, et al. Limited benefit from the addition of immunotherapy to chemotherapy in TKI-refractory EGFR-mutant lung adenocarcinoma. *Cancers* (2022) 14(14):3473. doi:10.3390/cancers14143473

17. Heymach JV, Harpole D, Mitsudomi T, Taube JM, Galffy G, Hochmair M, et al. Perioperative durvalumab for resectable non-small-cell lung cancer. *N Engl J Med* (2023) 389(18):1672–84. doi:10.1056/NEJMoa2304875

18. Lu S, Zhang W, Wu L, Wang W, Zhang P, Fang W, et al. Perioperative toripalimab plus chemotherapy for patients with resectable non-small cell lung cancer: the neotorch randomized clinical trial. *JAMA* (2024) 331(3):201–11. doi:10.1001/jama.2023.24735

19. Wu Y-L, Tsuboi M, He J, John T, Grohe C, Majem M, et al. Osimertinib in resected *EGFR*-mutated non–small-cell lung cancer. *New Engl J Med* (2020) 383(18):1711–23. doi:10.1056/NEJMoa2027071

20. Herbst RS, Wu Y-L, John T, Grohe C, Majem M, Wang J, et al. Adjuvant osimertinib for resected EGFR-mutated stage IB-IIIA non–small-cell lung cancer: updated results from the phase III randomized ADAURA trial. *J Clin Oncol* (2023) 41(10):1830–40. doi:10.1200/JCO.22.02186

21. Akinboro O, Drezner N, Amatya A, Runyan J, Fourie-Zirkelbach J, Zhao M, et al. US food and drug administration approval summary: nivolumab plus platinum-doublet chemotherapy for the neoadjuvant treatment of patients with resectable non–small-cell lung cancer. *J Clin Oncol* (2023) 41(17):3249–59. doi:10.1200/JCO.22.02509

22. Cascone T, Awad MM, Spicer JD, He J, Lu S, Sepesi B, et al. LBA1 CheckMate 77T: phase III study comparing neoadjuvant nivolumab (NIVO) plus chemotherapy (chemo) vs neoadjuvant placebo plus chemo followed by surgery and adjuvant NIVO or placebo for previously untreated, resectable stage II–IIIb NSCLC. *Ann Oncol* (2023) 34:S1295. doi:10.1016/j.annonc.2023.10.050

23. Wu YL, Dziadziuszko R, Ahn JS, Barlesi F, Nishio M, Lee DH, et al. Alectinib in resected ALK-positive non-small-cell lung cancer. *N Engl J Med* (2024) 390(14): 1265–76. doi:10.1056/NEJMoa2310532

24. Aredo JV, Urisman A, Gubens MA, Mulvey C, Allen GM, Rotow JK, et al. Phase II trial of neoadjuvant osimertinib for surgically resectable *EGFR*-mutated non-small cell lung cancer. *J Clin Oncol* (2023) 41(16):8508. doi:10.1200/jco.2023.41.16_suppl.8508

25. Bian D, Sun L, Hu J, Duan L, Xia H, Zhu X, et al. Neoadjuvant Afatinib for stage III EGFR-mutant non-small cell lung cancer: a phase II study. *Nat Commun* (2023) 14(1):4655. doi:10.1038/s41467-023-40349-z

26. Tsuboi M, Weder W, Escriu C, Blakely C, He J, Dacic S, et al. P03.02 neoadjuvant osimertinib with/without chemotherapy vs chemotherapy for EGFR mutated resectable NSCLC: NeoADAURA. *J Thorac Oncol* (2021) 16(3):S258. doi:10.1016/j.jtho.2021.01.375

27. Lee JM, Sepesi B, Toloza EM, Lin J, Pass HI, Johnson BE, et al. EP02.04-005 phase II NAUTIKA1 study of targeted therapies in stage II-III NSCLC:

preliminary data of neoadjuvant alectinib for ALK+ NSCLC. *J Thorac Oncol* (2022) 17(9):S233–4. doi:10.1016/j.jtho.2022.07.390

28. Leonetti A, Minari R, Boni L, Gnetti L, Bordi P, Verzè M, et al. EP02.04-001 alectinib as neoadjuvant treatment in surgically resectable stage III ALK-positive NSCLC: ALNEO phase II trial (GOIRC-01-2020). *J Thorac Oncol* (2022) 17(9):S231. doi:10.1016/j.jtho.2022.07.386

29. Pataer A, Kalhor N, Correa AM, Raso MG, Erasmus JJ, Kim ES, et al. Histopathologic response criteria predict survival of patients with resected lung cancer after neoadjuvant chemotherapy. *J Thorac Oncol* (2012) 7(5):825–32. doi:10.1097/JTO.0b013e318247504a

30. Hellmann MD, Chaft JE, William WN, Rusch V, Pisters KMW, Kalhor N, et al. Pathological response after neoadjuvant chemotherapy in resectable non-small-cell lung cancers: proposal for the use of major pathological response as a surrogate endpoint. *Lancet Oncol* (2014) 15(1):e42–e50. doi:10.1016/S1470-2045(13)70334-6

31. Hines JB, Cameron RB, Esposito A, Kim L, Porcu L, Nuccio A, et al. Evaluation of major pathologic response and pathologic complete response as surrogate end points for survival in randomized controlled trials of neoadjuvant immune checkpoint blockade in resectable in NSCLC. *J Thorac Oncol* (2024). doi:10.1016/j.jtho.2024.03.010

32. Travis WD, Dacic S, Wistuba I, Sholl L, Adusumilli P, Bubendorf L, et al. IASLC multidisciplinary recommendations for pathologic assessment of lung cancer resection specimens after neoadjuvant therapy. *J Thorac Oncol* (2020) 15(5):709–40. doi:10.1016/j.jtho.2020.01.005

33. Blakely CM, Weder W, Bubendorf L, He J, Majem M, Shyr Y, et al. Primary endpoints to assess the efficacy of novel therapeutic approaches in epidermal growth factor receptor-mutated, surgically resectable non-small cell lung cancer: a review. *Lung Cancer* (2023) 177:59–72. doi:10.1016/j.lungcan.2023.01.002

34. Rudqvist N-P, Charpentier M, Lhuillier C, Wennerberg E, Spada S, Sheridan C, et al. Immunotherapy targeting different immune compartments in combination with radiation therapy induces regression of resistant tumors. *Nat Commun* (2023) 14(1):5146. doi:10.1038/s41467-023-40844-3

35. Vanpouille-Box C, Alard A, Aryankalayil MJ, Sarfraz Y, Diamond JM, Schneider RJ, et al. DNA exonuclease Trex1 regulates radiotherapy-induced tumour immunogenicity. *Nat Commun* (2017) 8(1):15618. doi:10.1038/ncomms15618

36. Theelen WSME, Peulen HMU, Lalezari F, Van Der Noort V, De Vries JF, Aerts JGJV, et al. Effect of pembrolizumab after stereotactic body radiotherapy vs pembrolizumab alone on tumor response in patients with advanced non-small cell lung cancer: results of the PEMBRO-RT phase 2 randomized clinical trial. *JAMA Oncol* (2019) 5(9):1276–82. doi:10.1001/jamaoncol.2019.1478

37. Formenti SC, Rudqvist N-P, Golden E, Cooper B, Wennerberg E, Lhuillier C, et al. Radiotherapy induces responses of lung cancer to CTLA-4 blockade. *Nat Med* (2018) 24(12):1845–51. doi:10.1038/s41591-018-0232-2

38. Altorki NK, Walsh ZH, Melms JC, Port JL, Lee BE, Nasar A, et al. Neoadjuvant durvalumab plus radiation versus durvalumab alone in stages I–III non-small cell lung cancer: survival outcomes and molecular correlates of a randomized phase II trial. *Nat Commun* (2023) 14(1):8435. doi:10.1038/s41467-023-44195-x

39. Bradley JD, Nishio M, Okamoto I, Newton MD, Trani L, Shire NJ, et al. PACIFIC-2: phase 3 study of concurrent durvalumab and platinum-based chemoradiotherapy in patients with unresectable, stage III NSCLC. *J Clin Oncol* (2019) 37(15):TPS8573. doi:10.1200/jco.2019.37.15_suppl.tps8573

40. Lee NY, Ferris RL, Psyrri A, Haddad RI, Tahara M, Bourhis J, et al. Avelumab plus standard-of-care chemoradiotherapy versus chemoradiotherapy alone in patients with locally advanced squamous cell carcinoma of the head and neck: a randomised, double-blind, placebo-controlled, multicentre, phase 3 trial. *Lancet Oncol* (2021) 22(4):450–62. doi:10.1016/S1470-2045(20)30737-3

41. Cascone T, Kar G, Spicer JD, García-Campelo R, Weder W, Daniel DB, et al. Neoadjuvant durvalumab alone or combined with novel immuno-oncology agents in resectable lung cancer: the phase II NeoCOAST platform trial. *Cancer Discov* (2023) 13(11):2394–411. doi:10.1158/2159-8290.CD-23-0436

42. Schuler M, Cuppens K, Plönes T, Wiesweg M, Du Pont B, Hegedus B, et al. Neoadjuvant nivolumab with or without relatlimab in resectable non-small-cell lung cancer: a randomized phase 2 trial. *Nat Med* (2024). doi:10.1038/s41591-024-02965-0

43. Inamura K, Yokouchi Y, Kobayashi M, Ninomiya H, Sakakibara R, Subat S, et al. Association of tumor TROP2 expression with prognosis varies among lung cancer subtypes. *Oncotarget* (2017) 8(17):28725–35. doi:10.18632/oncotarget.15647

44. Tagawa ST, Balar AV, Petrylak DP, Kalebasty AR, Loriot Y, Fléchon A, et al. TROPHY-U-01: a phase II open-label study of sacituzumab govitecan in patients with metastatic urothelial carcinoma progressing after platinum-based chemotherapy and checkpoint inhibitors. *J Clin Oncol* (2021) 39(22):2474–85. doi:10.1200/JCO.20.03489

45. Bardia A, Hurvitz SA, Tolaney SM, Loirat D, Punie K, Oliveira M, et al. Sacituzumab govitecan in metastatic triple-negative breast cancer. *New Engl J Med* (2021) 384(16):1529–41. doi:10.1056/NEJMoa2028485

46. Rugo HS, Bardia A, Marmé F, Cortés J, Schmid P, Loirat D, et al. Overall survival with sacituzumab govitecan in hormone receptor-positive and human epidermal growth factor receptor 2-negative metastatic breast cancer (TROPiCS-02): a randomised, open-label, multicentre, phase 3 trial. *The Lancet* (2023) 402(10411):1423–33. doi:10.1016/S0140-6736(23)01245-X

47. Goto Y, Su W-C, Levy BP, Rixe O, Yang T-Y, Tolcher AW, et al. TROPION-Lung02: datopotamab deruxtecan (Dato-DXd) plus pembrolizumab (pembro) with or without platinum chemotherapy (Pt-CT) in advanced non-small cell lung cancer (aNSCLC). *J Clin Oncol* (2023) 41(16):9004. doi:10.1200/jco.2023.41.16_suppl.9004

48. Ahn MJ, Lisberg A, Paz-Ares L, Cornelissen R, Girard N, Pons-Tostivint E, et al. LBA12 Datopotamab deruxtecan (Dato-DXd) vs docetaxel in previously treated advanced/metastatic (adv/met) non-small cell lung cancer (NSCLC): results of the randomized phase III study TROPION-Lung01. *Ann Oncol* (2023) 34:S1305–6. doi:10.1016/j.annonc.2023.10.061

49. Okamoto I, Kuyama S, Girard N, Lu S, Franke FA, Pan E, et al. 1505TiP TROPION-Lung07: a phase III trial of datopotamab deruxtecan (Dato-DXd) plus pembrolizumab (pembro) with or without platinum chemotherapy (Pt-CT) as first-line (1L) therapy in advanced/metastatic (adv/met) non-small cell lung cancer (NSCLC) with PD. *Ann Oncol* (2023) 34:S847–S8. doi:10.1016/j.annonc.2023.09.2536

50. Levy BP, Felip E, Reck M, Yang JC, Cappuzzo F, Yoneshima Y, et al. TROPION-Lung08: phase III study of datopotamab deruxtecan plus pembrolizumab as first-line therapy for advanced NSCLC. *Future Oncol* (2023) 19(21):1461–72. doi:10.2217/fon-2023-0230

51. Weber JS, Carlino MS, Khattak A, Meniawy T, Ansstas G, Taylor MH, et al. Individualised neoantigen therapy mRNA-4157 (V940) plus pembrolizumab versus pembrolizumab monotherapy in resected melanoma (KEYNOTE-942): a randomised, phase 2b study. *Lancet* (2024) 403(10427):632–44. doi:10.1016/S0140-6736(23)02268-7

52. Xia L, Mei J, Kang R, Deng S, Chen Y, Yang Y, et al. Perioperative ctDNA-based molecular residual disease detection for non–small cell lung cancer: a prospective multicenter cohort study (LUNGCA-1). *Clin Cancer Res* (2022) 28(15):3308–17. doi:10.1158/1078-0432.CCR-21-3044

53. Zhou C, Das Thakur M, Srivastava MK, Zou W, Xu H, Ballinger M, et al. 2O IMpower010: biomarkers of disease-free survival (DFS) in a phase III study of atezolizumab (atezo) vs best supportive care (BSC) after adjuvant chemotherapy in stage IB-IIIA NSCLC. *Ann Oncol* (2021) 32:S1374. doi:10.1016/j.annonc.2021.10.018

54. Assaf ZJF, Zou W, Fine AD, Socinski MA, Young A, Lipson D, et al. A longitudinal circulating tumor DNA-based model associated with survival in metastatic non-small-cell lung cancer. *Nat Med* (2023) 29(4):859–68. doi:10.1038/s41591-023-02226-6

55. Yaung SJ, Fuhlbrück F, Peterson M, Zou W, Palma JF, Patil NS, et al. Clonal hematopoiesis in late-stage non-small-cell lung cancer and its impact on targeted panel next-generation sequencing. *JCO Precis Oncol* (2020) 4:1271–9. doi:10.1200/PO.20.00046

56. Pascual J, Attard G, Bidard FC, Curigliano G, De Mattos-Arruda L, Diehn M, et al. ESMO recommendations on the use of circulating tumour DNA assays for patients with cancer: a report from the ESMO Precision Medicine Working Group. *Ann Oncol* (2022) 33(8):750–68. doi:10.1016/j.annonc.2022.05.520

57. Marcus L, Fashoyin-Aje LA, Donoghue M, Yuan M, Rodriguez L, Gallagher PS, et al. FDA approval summary: pembrolizumab for the treatment of tumor mutational burden–high solid tumors. *Clin Cancer Res* (2021) 27(17):4685–9. doi:10.1158/1078-0432.CCR-21-0327

58. Cascone T, Leung CH, Weissferdt A, Pataer A, Carter BW, Godoy MCB, et al. Neoadjuvant chemotherapy plus nivolumab with or without ipilimumab in operable non-small cell lung cancer: the phase 2 platform NEOSTAR trial. *Nat Med* (2023) 29(3):593–604. doi:10.1038/s41591-022-02189-0

59. Chaft JE, Oezkan F, Kris MG, Bunn PA, Wistuba II, Kwiatkowski DJ, et al. Neoadjuvant atezolizumab for resectable non-small cell lung cancer: an open-label, single-arm phase II trial. *Nat Med* (2022) 28(10):2155–61. doi:10.1038/s41591-022-01962-5

60. O'Brien M, Paz-Ares L, Marreaud S, Dafni U, Oselin K, Havel L, et al. Pembrolizumab versus placebo as adjuvant therapy for completely resected stage IB-IIIA non-small-cell lung cancer (PEARLS/KEYNOTE-091): an interim analysis of a randomised, triple-blind, phase 3 trial. *Lancet Oncol* (2022) 23(10):1274–86. doi:10.1016/S1470-2045(22)00518-6

61. Casarrubios M, Provencio M, Nadal E, Insa A, Del Rosario García-Campelo M, Lázaro-Quintela M, et al. Tumor microenvironment gene expression profiles associated to complete pathological response and disease progression in resectable

NSCLC patients treated with neoadjuvant chemoimmunotherapy. *J ImmunoTherapy Cancer* (2022) 10(9):e005320. doi:10.1136/jitc-2022-005320

62. Laza-Briviesca R, Cruz-Bermúdez A, Nadal E, Insa A, García-Campelo MDR, Huidobro G, et al. Blood biomarkers associated to complete pathological response on NSCLC patients treated with neoadjuvant chemoimmunotherapy included in NADIM clinical trial. *Clin Translational Med* (2021) 11(7):e491. doi:10.1002/ctm2.491

63. Peters S, Cho BC, Luft A, Alatorre-Alexander J, Geater SL, Kim SW, et al. OA15.04 association between KRAS/STK11/KEAP1 mutations and outcomes in POSEIDON: durvalumab ± tremelimumab + chemotherapy in mNSCLC. *J Thorac Oncol* (2022) 17(9):S39–S41. doi:10.1016/j.jtho.2022.07.073

64. Liu J, Dong M, Sun X, Li W, Xing L, Yu J. Prognostic value of 18F-fdg PET/CT in surgical non-small cell lung cancer: a meta-analysis. *PLOS ONE* (2016) 11(1):e0146195. doi:10.1371/journal.pone.0146195

65. Sun R, Limkin EJ, Vakalopoulou M, Dercle L, Champiat S, Han SR, et al. A radiomics approach to assess tumour-infiltrating CD8 cells and response to anti-PD-1 or anti-PD-L1 immunotherapy: an imaging biomarker, retrospective multicohort study. *Lancet Oncol* (2018) 19(9):1180–91. doi:10.1016/S1470-2045(18)30413-3

66. Zerunian M, Caruso D, Zucchelli A, Polici M, Capalbo C, Filetti M, et al. CT based radiomic approach on first line pembrolizumab in lung cancer. *Scientific Rep* (2021) 11(1):6633. doi:10.1038/s41598-021-86113-5

Pathology & Oncology Research | frontiers

TYPE Original Research
PUBLISHED 07 September 2023
DOI 10.3389/pore.2023.1611236

Check for updates

OPEN ACCESS

EDITED BY
Anna Sebestyén,
Semmelweis University, Hungary

*CORRESPONDENCE
Freddy Villanueva-Cotrina,
freddyvillanue@gmail.com

RECEIVED 10 April 2023
ACCEPTED 11 August 2023
PUBLISHED 07 September 2023

CITATION
Villanueva-Cotrina F, Velarde J, Rodriguez R, Bonilla A, Laura M, Saavedra T, Portillo-Alvarez D, Bustamante Y, Fernandez C and Galvez-Nino M (2023), Active cancer as the main predictor of mortality for COVID-19 in oncology patients in a specialized center.
Pathol. Oncol. Res. 29:1611236.
doi: 10.3389/pore.2023.1611236

COPYRIGHT
© 2023 Villanueva-Cotrina, Velarde, Rodriguez, Bonilla, Laura, Saavedra, Portillo-Alvarez, Bustamante, Fernandez and Galvez-Nino. This is an open-access article distributed under the terms of the Creative Commons Attribution License (CC BY). The use, distribution or reproduction in other forums is permitted, provided the original author(s) and the copyright owner(s) are credited and that the original publication in this journal is cited, in accordance with accepted academic practice. No use, distribution or reproduction is permitted which does not comply with these terms.

Active cancer as the main predictor of mortality for COVID-19 in oncology patients in a specialized center

Freddy Villanueva-Cotrina[1,2]*, Juan Velarde[3], Ricardo Rodriguez[1,4], Alejandra Bonilla[5], Marco Laura[5], Tania Saavedra[6,7], Diana Portillo-Alvarez[3,8], Yovel Bustamante[1,2], Cesar Fernandez[1] and Marco Galvez-Nino[7,9]

[1]Department of Pathology, Instituto Nacional de Enfermedades Neoplasicas, Lima, Peru, [2]Academic Department of Medical Microbiology, Universidad Nacional Mayor de San Marcos, Lima, Peru, [3]Department of Infectious Diseases, Instituto Nacional de Enfermedades Neoplasicas, Lima, Peru, [4]Academic Department of Medical Technologist, Universidad Nacional Mayor de San Marcos, Lima, Peru, [5]Department of Radiodiagnosis, Instituto Nacional de Enfermedades Neoplasicas, Lima, Peru, [6]Department of Critical Care Medicine, Instituto Nacional de Enfermedades Neoplasicas, Lima, Peru, [7]Professional School of Human Medicine, Universidad Privada San Juan Bautista, Lima, Peru, [8]Professional School of Human Medicine, Universidad de Piura, Lima, Peru, [9]Department of Medical Oncology, Instituto Nacional de Enfermedades Neoplasicas, Lima, Peru

Introduction: The role of the type, stage and status of cancer in the outcome of COVID-19 remains unclear. Moreover, the characteristic pathological changes of severe COVID-19 reveled by laboratory and radiological findings are similar to those due to the development of cancer itself and antineoplastic therapies.

Objective: To identify potential predictors of mortality of COVID-19 in cancer patients.

Materials and methods: A retrospective and cross-sectional study was carried out in patients with clinical suspicion of COVID-19 who were confirmed for COVID-19 diagnosis by RT-PCR testing at the National Institute of Neoplastic Diseases between April and December 2020. Demographic, clinical, laboratory and radiological data were analyzed. Statistical analyses included area under the curve and univariate and multivariate logistic regression analyses.

Results: A total of 226 patients had clinical suspicion of COVID-19, the diagnosis was confirmed in 177 (78.3%), and 70/177 (39.5%) died. Age, active cancer, leukocyte count ≥12.8 × 109/L, urea ≥7.4 mmol/L, ferritin ≥1,640, lactate ≥2.0 mmol/L, and lung involvement ≥35% were found to be independent predictors of COVID-19 mortality.

Conclusion: Active cancer represents the main prognosis factor of death, while the role of cancer stage and type is unclear. Chest CT is a useful tool in the prognosis of death from COVID-19 in cancer patients. It is a challenge to establish the prognostic utility of laboratory markers as their altered values it could have either oncological or pandemic origins.

KEYWORDS

SARS-CoV-2, imaging study, biomarkers, death prognosis, active cancer

Introduction

COVID-19 disease leads to severe pneumonia, metabolic acidosis, coagulation dysfunction, multiple organ failure, and eventually, death [1–4]. Cancer patients usually have a compromised immune system with a higher risk of death in COVID-19 compared to those without cancer [5–8], but it is not clear if the type, stage and status of cancer play a role in the outcome of the disease.

COVID-19 diagnosis is based on clinical evaluation and confirmed by the detection of viral RNA in respiratory samples [9]. Furthermore, certain blood laboratory parameters and chest computed tomography (CT) findings could reveal characteristic pathological changes and the clinical course of COVID-19 in oncology patients. Altered levels of C-reactive protein (CRP), neutrophil and lymphocyte counts, ferritin, D-dimer, and lactate dehydrogenase [10–12], as well as a high CO-RADS score and the presence of some abnormal chest CT findings have been associated with the presentation of severe complications of COVID-19 [13, 14].

However, malignant neoplasms lead to similar laboratory and radiological alteration findings due to pathological events in the development of cancer itself (acute renal failure, disseminated intravascular coagulation, impaired cellular immunity, organ failure, respiratory failure) [15–21] and antineoplastic therapies (immunosuppression, hepatotoxicity) [22, 23]. Therefore, it is unknown whether these potential predictors are useful for detecting the clinical course of the disease in cancer patients.

We aimed to identify predictors of mortality of COVID-19 in cancer patients by the joint study of the clinical characteristics, laboratory and radiological findings, and their association with a higher risk of a fatal outcome.

Materials and methods

Study design and population

This retrospective and cross-sectional study was carried out in patients hospitalized at the Instituto Nacional de Enfermedades Neoplasicas (INEN) in Lima—Peru between April and December 2020. The study sample included patients who presented with a clinical suspicion of COVID-19 and were confirmed for COVID-19 diagnosis by RT-PCR testing. Patients with a clinical or radiological diagnosis of COVID-19 without a positive RT-PCR test were excluded. When patients had two positive results for COVID-19 by RT-PCR, only the first one was considered.

Clinical, laboratory, radiological and outcome data

Demographic, clinical, laboratory, radiological and outcomes data were collected blind from the medical records and the INEN informatic system. Blood sample tests and chest CT scans were performed within 24 h after sampling for the COVID-19 molecular diagnosis. While clinical outcome, mortality or survival, was considered until 30 days after the molecular study was performed. A specialist physician from the Department of Infectious Diseases evaluated the records of the clinical presentation, while two specialist physicians from the Department of Medical Oncology evaluated the stage and status of cancer in the patients. Two specialist physicians from the Department of Radiodiagnosis evaluated the chest CT images to determine the presence of abnormal findings, the percentage of affected lung, and the COVID-19 Reporting and Data System (CO-RADS) score classification system.

To determine the percentage of affected lung, each of the five lung lobes was scored visually on a scale from 0 to 5, (where 0 indicates no involvement; 1, less than 5%; 2, 5%–25%; 3, 26%–49%; 4, 50%–75%; and 5, more than 75%). The total CT score was the sum of the individual lobar scores and ranged from 0 (no involvement) to 25 (maximum involvement) [24]. The CO-RADS system assessed lung damage on a chest CT to predict the likelihood of COVID-19 pneumonia using a scale from 1 (very low) to 5 (very high). A high CO-RADS score indicates a high probability of COVID-19; thus, the grouped frequency of COVID-19 in categories 1, 2, 3, 4 and 5 corresponds to 8.8%, 11.1%, 24.6%, 61.9% and 89.6% involvement, respectively) [25].

Definitions

Cases with clinical suspicion of COVID-19: Patients present any of the following symptoms: fever, cough, fatigue, headache, dyspnea, myalgia, diarrhea, tachypnea, chest pain, anosmia, and ageusia.

Confirmed cases of COVID-19: Patients who tested positive for COVID-19 in the molecular study (PCR-RT) from nasopharyngeal swab samples.

Active cancer: Presence of cancer progression or recurrence after treatment.

Advanced cancer: Presence of distant metastatic disease.

Clinical scenario: Clinical presentation of patients according to WHO [26].

TABLE 1 Demographic, clinical and oncological characteristics of 177 cases of cancer patients with COVID-19 according to mortality.

Variables		Survivors N (%)	Dead N (%)	*p*-value
Age groups				**<0.001**
	0–15	15 (83.3)	3 (16.7)	
	16–59	60 (71.4)	24 (28.6)	
	≥60	32 (42.7)	43 (57.3)	
Age (years)	Median ± Interquartile range	48 (28–60)	62.5 (50–72)	**<0.001**
Gender				0.360
	Female	46 (56.8)	35 (43.2)	
	Male	61 (63.5)	35 (36.5)	
Comorbidity				0.328
	No	66 (63.5)	38 (36.5)	
	Yes	41 (56.2)	32 (43.8)	
Diabetes				0.501
	No	98 (59.8)	66 (40.2)	
	Yes	9 (69.2)	4 (30.8)	
Arterial hypertension				0.321
	No	93 (62.0)	57 (38.0)	
	Yes	14 (51.9)	13 (48.1)	
Lung disease				0.934
	No	99 (60.4)	65 (39.6)	
	Yes	8 (61.5)	5 (38.5)	
Obesity				0.443
	No	101 (61.2)	64 (38.8)	
	Yes	6 (50.0)	6 (50.0)	
Other comorbidities				0.886
	No	79 (60.8)	51 (39.2)	
	Yes	28 (59.6)	19 (40.4)	
Clinical scenario				**<0.001**
	Mild/moderate	74 (73.3)	27 (26.7)	
	Severe/critical	33 (43.4)	43 (56.6)	
Type of cancer				0.172
	Hematological malignancies	54 (65.9)	28 (34.1)	
	Solid tumors	53 (55.8)	42 (44.2)	
Oncological diagnosis				0.208
	Acute lymphocytic leukemia	16 (72.7)	6 (27.3)	
	Non-Hodgkin lymphoma	21 (65.6)	11 (34.4)	
	[a]Other hematologic malignancies	17 (60.7)	11 (39.3)	
	Urological cancer	9 (47.4)	10 (52.6)	
	Breast cancer	10 (41.7)	14 (58.3)	
	[b]Other solid tumors	34 (65.4)	18 (34.6)	
Cancer stage				0.082
	Non-advanced	68 (65.4)	36 (34.6)	
	Advanced	36 (52.2)	33 (47.8)	
Cancer status				**0.001**
	Non-active	50 (75.8)	16 (24.2)	
	Active	57 (51.3)	54 (48.7)	

[a]Acute myeloid leukemia, chronic myeloid leukemia, mixed phenotype leukemia, multiple myeloma.
[b]Cervix cancer, head and neck cancer, gastrointestinal cancer, lung cancer, liver and bile duct cancer, thyroid cancer, sarcoma, skin cancer, and other cancer.
Bold format means statistical significance of the *p* value.

Compliance with ethics guidelines

All the cases in this study were part of the medical care routine of the INEN. No informed consent from any patient was obtained since this study used laboratory test registers, radiological reports of the INEN informatic system, and patient medical records in obtaining data which were used protecting the identity of the patients. The protocol was presented to the Research Committee of the INEN and approved for its implementation with designated protocol number INEN 20-49.

Statistical analysis

Categorical variables were analyzed using the chi-squared or Fisher's exact test, as appropriate, and presented as frequencies and percentages. Quantitative variables were described as means and standard deviation or medians and interquartile ranges, depending on the distribution of the data. Quantitative variables were evaluated using the Student's t-test when there was a normal distribution of the data and, when not, using the Mann-Whitney *U* test. Receiver operating characteristic (ROC) curve analysis provided the sensitivity and specificity of the laboratory tests and radiological findings for the prediction of mortality from COVID-19. In addition, it allowed us to obtain the best cut-off points for the categorization of these variables according to the Youden Index. Finally, the univariate and multivariate regression analyses were performed to obtain the odds ratio (OR) as a measure of association between the variables and the mortality prediction of COVID-19, considering only the associated variables in the bivariate analysis for building the final multivariate model. For all analyses, statistical significance was set at $p < 0.05$. All analyses were performed using Stata version 14.0.

Results

During the study period, 226 patients had clinical suspicion of COVID-19 from which 177 (78.3%) were confirmed. Of the 177 positive cases of COVID-19, most patients were between 16 and 59 years old (84, 47.5%), male (96, 54.2%), had solid tumors (95, 53.7%), non-advanced stage (104, 58.8%) and active status cancer (111, 62.7%). Of these, 70 (39.5%) died, one-third of the deaths of patients with COVID-19 occurred within the first 5 days (24/70, 34.4%), and the vast majority (52/70, 74.3%) had died by day 15 after molecular study sampling.

Prediction of COVID-19 mortality

The deceased patients were older (62.5 vs. 42.0; $p \leq 0.001$), had severe-critical clinical scenario (56.6% vs. 26.7%; $p \leq 0.001$) and active cancer (48.7% vs. 24.2%; $p = 0.001$) (Table 1).

Likewise, these patients had a higher leukocyte count (10.4×10^9/L vs. 6.6×10^9/L; $p = 0.001$), neutrophil count (8.63×10^9/L vs. 5.26×10^9/L; $p = 0.001$), RNL (15.1 vs. 7.8; $p = 0.001$), D-dimer (2,136 ng/mL vs. 1,034 ng/mL; $p = 0.002$), LDH (329 U/L vs. 249 U/L; $p = 0.004$), urea (6.0 mmol/L vs. 4.0 mmol/L; $p \leq 0.001$), creatinine (56 umol/L vs. 48 umol/L; $p = 0.018$, lactate (1.9 mmol/L vs. 1.3 mmol/L; $p \leq 0.001$), lung involvement (40% vs. 20%; $p \leq 0.001$) and crazy paving (56.3% vs. 32.3%) (Table 2).

The evaluation of the area under the curve showed that urea ≥7.4 mmol/L had the highest ability to predict death, with AUC 0.751 (S = 40.63% and E = 91.75%), followed by lactate ≥2.0 mmol/L, AUC 0.686 (S = 47.54% and E = 86.49%) and lung involvement ≥35%, AUC 0.662 (S = 59.70%, E = 66.67%) (Table 3).

Finally, in the bivariate regression analysis, a higher probability of death was found in patients over 60 years of age (OR 6.72; $p = 0.005$) compared to those under 16 years of age and with increasing age per year (OR 1.04; $p \leq 0.001$), severe-critical clinical scenario (OR 3.57; $p \leq 0.001$), active cancer (OR 2.96; $p = 0.002$), advanced cancer (OR 1.61; $p = 0.082$), leukocyte count $\geq 12.8 \times 10^9$/L (OR 2.92; $p = 0.003$), neutrophil count $\geq 7.51 \times 10^9$/L (OR 3.55; $p \leq 0.001$), RNL ≥14.5 (OR 3.00; $p = 0.001$), fibrinogen ≥9.39 g/L (OR 9.94; $p = 0.035$), D-dimer ≥1,345 ng/mL (OR 2.57; $p = 0.003$), LDH ≥329 U/L (OR 2.54; $p = 0.004$), urea ≥7.4 mmol/L (OR 7.31; $p \leq 0.001$), creatinine ≥71 umol/L (OR 3.77; $p = 0.001$), ferritin ≥1,640 (OR 3.09; $p = 0.017$), lactate ≥2.0 mmol/L (OR 6.86; $p \leq 0.001$), lung involvement ≥35% (OR 3.27; $p \leq 0.001$), crazy paving (OR 2.58; $p = 0.001$) and vessel thickening (OR 1.91; $p = 0.011$), and a lower probability in patients with oxygen saturation ≥86.9% (OR 0.45; $p = 0.029$). Multivariate analysis found an association with a higher probability of death with increasing age per year (OR 1.04; $p = 0.001$), active cancer (OR 7.56; $p \leq 0.001$), leukocyte count $\geq 12.8 \times 10^9$/L (OR 3.00; $p = 0.022$), urea ≥7.4 mmol/L (OR 3.20; $p = 0.034$), ferritin ≥1,640 (OR 7.22; $p = 0.005$), lactate ≥2.0 mmol/L (OR 4.79; $p = 0.002$) and lung involvement ≥35% (OR 4.34; $p = 0.002$) (Table 4).

Discussion

The mortality rate in our population during the first wave of the pandemic was higher than that found in cancer patients with COVID-19, whose mortality rates were highly variable [27]. It could be related to underlying clinical conditions. We emphasize that our study was conducted only in hospitalized patients, most of whom had active cancer. In addition, numerous deaths occurred shortly after the diagnosis of COVID-19, which shows delayed medical care resulting from the impact of the pandemic on hospital capacity in our country [28]. The high in-hospital mortality rate was related to the critical baseline condition of the patients.

TABLE 2 Comparison of laboratory tests and CT findings in 177 cancer patients with COVID-19 according to mortality.

Variables	Survivors	Dead	*p*-value
	N (%)	N (%)	
C-reactive protein mg/L	105.85 (39.00–173.90)	122.85 (74.30–198.75)	0.115
Leukocytes $\times 10^9$/L	6.65 (3.64–11.4)	10.40 (7.00–17.80)	**0.001**
Neutrophils $\times 10^9$/L	5.26 (3.25–10.03)	8.63 (6.37–14.58)	**0.001**
Neutrophil/lymphocyte ratio	7.80 (3.40–15.20)	15.11 (6.00–24.18)	**0.001**
Platelets $\times 10^9$/L	222.00 (145.00–326.00)	199.50 (94.00–326.00)	0.225
Fibrinogen g/L	5.75 ± 2.11	5.84 ± 2.31	0.802
D-dimer ng/mL	1,034.00 (644.00–2,925.00)	2,136.50 (948.00–7,989.00)	**0.002**
Lactate dehydrogenase U/L	249.00 (186.00–362.00)	329.00 (235.00–482.00)	**0.004**
Urea mmol/L	4.30 (3.10–5.10)	6.00 (4.85–9.30)	**<0.001**
Creatinine umol/L	48.00 (37.00–62.00)	56.00 (39.00–83.00)	**0.018**
Ferritin ng/mL	679.0 (327.00–1,180.00)	912.00 (371.50–1895.00)	0.070
Oxygen saturation %	95.80 (92.90–97.40)	95.1 (91.4–96.8)	0.273
Lactate mmol/L	1.30 (1.00–1.80)	1.90 (1.30–2.80)	**<0.001**
Lung involvement %	20 (10–40)	40 (20–70)	**<0.001**
Score CO-RADS			0.436
CO-RADS 1	6 (60.0)	4 (40.0)	
CO-RADS 2	12 (63.2)	7 (36.8)	
CO-RADS 3	10 (62.5)	6 (37.5)	
CO-RADS 4	21 (61.8)	13 (38.2)	
CO-RADS 5	44 (54.3)	37 (45.7)	
Consolidation			0.577
No	43 (60.6)	28 (39.4)	
Yes	50 (56.2)	39 (43.8)	
Nodular pattern			0.722
No	77 (58.8)	54 (41.2)	
Yes	16 (55.2)	13 (44.8)	
Frosted glass			0.983
No	11 (57.9)	8 (42.1)	
Yes	82 (58.2)	59 (41.8)	
Crazy paving			**0.003**
No	65 (67.7)	31 (32.3)	
Yes	28 (43.7)	36 (56.3)	
Organizing pneumonia			0.397
No	84 (57.1)	63 (42.9)	
Yes	9 (69.2)	4 (30.8)	
Vessel thickening			0.090
No	37 (67.3)	18 (32.7)	
Yes	56 (53.3)	49 (46.7)	

Bold format means statistical significance of the *p* value.

Oncological characteristics could play a role in the outcome of COVID-19 in our population. The strong association between active cancer stage and an increased risk of death coincides with the findings of some studies [10, 29–32]. Active cancer leads to prothrombotic and proinflammatory conditions that concur with alterations in the immune system due to the development of cancer and antineoplastic treatments [33, 34]. Moreover, SARS-CoV-2 infection results in immune alterations and thrombotic events. Therefore, this could lead to an unfavorable prognosis in patients with cancer and COVID-19 [35, 36]. Advanced or metastatic cancer has been associated with an increased risk of death [37]. In our study, we observed this association, although it was not significant. Findings in this regard are contradictory; some studies have found it to be a risk factor for death in COVID-19 [10, 11, 27, 32], while others have

TABLE 3 Prognostic capacity of death of laboratory tests and CT findings in cancer patients with COVID-19.

Variables	Reference values	AUC	95% CI	Cut-off	Se (%)	Sp (%)	Youden index
C-reactive protein mg/L	0–5	0.576	0.484–0.669	≥189.3	32.14	80.61	12.75
Leukocytes $\times 10^9$/L	4.68–11.8	0.654	0.571–0.737	≥12.8	37.14	83.18	20.32
Neutrophils $\times 10^9$/L	1.6–7.0	0.656	0.571–0.741	≥7.51	68.18	63.27	31.45
Neutrophil/lymphocyte ratio	NA	0.655	0.570–0.741	≥14.5	54.55	71.43	25.98
Platelets $\times 10^9$/L	182–393	0.446	0.357–0.535	≥393	14.29	87.85	2.14
Fibrinogen g/L	2.0–4.0	0.492	0.393–0.591	≥9.39	10.53	98.86	9.39
D-dimer ng/mL	<270	0.645	0.557–0.734	≥1,345	66.13	62.38	28.51
Lactate dehydrogenase U/L	120–246	0.633	0.548–0.717	≥329	50.75	71.57	22.32
Urea mmol/L	2.5–7.1	**0.751**	0.673–0.830	≥7.4	40.63	91.75	32.38
Creatinine umol/L	46–110	0.608	0.518–0.698	≥71.00	35.82	87.13	22.95
Ferritin ng/mL	17.9–464	0.603	0.492–0.713	≥1,640	31.82	87.69	19.51
Oxygen saturation %	95–100	0.445	0.347–0.543	≥86.9	93.44	8.00	1.44
Lactate mmol/L	<2.0	0.686	0.596–0.777	≥2.0	47.54	86.49	34.03
Lung involvement %	NA	0.662	0.577–0.747	≥35	59.70	66.67	26.37
CO-RADS score	NA	0.540	0.455–0.624	≥5	55.22	52.69	7.91

AUC, area under the curve; CI, confidence interval; Se, sensibility; Sp, specificity; NA, Not applicable.
Bold format means statistical significance of the *p* value.

not [12, 38–40]. In contrast, the non-association between the type of cancer, solid tumor or hematological neoplasm, and the probability of death in COVID-19 patients coincides with several studies [10–12, 27, 30–32, 39].

Active cancer represents the main vulnerability of cancer patients in the pandemic, otherwise there is still a need to better understand the possible role of the cancer stage and the type of neoplasia in the outcome of COVID-19.

Mortality in cancer patients with COVID-19 increases with each year of age. Older age leads to a deficiency in the immune response, resulting in a higher risk of death in COVID-19 patients [41]. The strength and direction of the association between age and COVID-19 mortality have been consistently found across multiple studies [10–12, 27, 29–32, 38–40].

The alteration of some laboratory parameters could be a manifestation of the pathophysiology of the disease, but it could also be due to cancer itself.

The high serum concentrations of lactate and, in particular, of ferritin could be the result of a sustained and hyperactive inflammatory response in the COVID-19 patient [3]. Increasing concentrations of serum ferritin, according to the proposed cut-off values, were strongly associated with the mortality of COVID-19 in our population. Serum ferritin levels increase because of cell damage and severe uncontrolled inflammatory conditions [41, 42] including malignant diseases and their progression [43, 44]. The threshold value evaluated (≥1,640 ng/mL) represent a significant increase in serum concentration and correlate with a hyperinflammatory state and a severe clinical course in COVID-19 [45, 46]. Moreover, the increase in serum ferritin has been associated with the severity and mortality of COVID-19 in oncology population, even with lower threshold values [11]. In contrast, a slight increase in serum lactate was associated with mortality. Lactate is a metabolite that is increased in the blood during tissue hypoxia and hypermetabolism, which results in tissue damage and organ failure [47, 48]. Hyperlactatemia (lactate >2.0 mmol/L) is associated with septic shock and mortality in cancer patients with a high incidence of sepsis-related morbidity and mortality [49]. Also, increased values of this analyte in blood, similar to the threshold evaluated in our study (≥2.0 mmol/L), have been found to be a predictor of mortality for COVID-19 in cancer patients, although with a higher threshold value [11]. Serum urea level was another biochemical marker of mortality in the present study. Measurement of uremia is routinely performed to evaluate renal function and its increase as an indicator of renal insufficiency [50, 51]. Although renal insufficiency is a frequent clinical condition in patients with cancer [16, 18], with the consequent increase in serum urea, it is also an important sequela of COVID-19 [52, 53]. The study of blood urea had a good prognostic capacity and association with mortality, although with a slightly higher threshold value (≥7.4 mmol/L). This could indicate the beginning of the manifestation of kidney damage and could also be due to the presence of renal comorbidity in some patients. Increased serum levels of urea (in the form of BUN) have been associated with higher mortality for COVID-19 in cancer patients [54]. Monitoring the evolution of uremia and the study of other complementary tests could contribute to a better understanding of this prognostic factor.

In the hematological study, the leukocyte count seems to be an unspecified marker. An increased leukocyte count represents an inflammatory state resulting from the innate immune

TABLE 4 Factors associated with mortality in cancer patients with COVID-19.

Variables	Raw model			Adjusted model		
	OR	95% CI	*p*-value	OR	95% CI	*p*-value
Age groups						
0–15	Ref.					
16–59	2.00	0.53–7.54	0.306			
≥60	6.72	1.79–25.19	0.005			
Age (years)	**1.04**	**1.02–1.06**	**<0.001**	**1.04**	**1.02–1.07**	**0.001**
Gender						
Male	Ref.					
Female	0.75	0.41–1.38	0.361			
Comorbidity						
No	Ref.					
Yes	1.36	0.74–2.50	0.329			
Diabetes						
No	Ref.					
Yes	0.66	0.20–2.23	0.504			
Arterial hypertension						
No	Ref.					
Yes	1.51	0.66–3.45	0.323			
Lung disease						
No	Ref.					
Yes	0.95	0.30–3.04	0.934			
Obesity						
No	Ref.					
Yes	1.58	0.49–5.11	0.446			
Other comorbidities						
No	Ref.					
Yes	1.05	0.53–2.08	0.886			
Clinical scenario						
Mild/moderate	Ref.					
Severe/critical	3.57	1.90–6.72	**<0.001**			
Type of cancer						
Hematological malignancies	Ref.					
Solid tumors	1.52	0.83–2.81	0.173			
Oncological diagnosis						
Acute lymphocytic leukemia	Ref.					
Non-Hodgkin lymphoma	1.40	0.43–4.58	0.582			
[a]Other hematologic malignancies	1.73	0.52–5.77	0.375			
Urological cancer	2.96	0.81–10.88	0.102			
Breast cancer	3.73	1.08–12.91	0.037			
[b]Other solid tumors	1.41	0.47–4.23	0.538			
Cancer stage						
Non-advanced	Ref.					
Advanced	1.61	0.94–2.75	0.082			
Cancer status						
Non-active	Ref.			**Ref.**		
Active	2.96	1.51–5.81	**0.002**	**7.56**	**2.75–20.82**	**<0.001**

(Continued on following page)

TABLE 4 (*Continued*) Factors associated with mortality in cancer patients with COVID-19.

Variables	Raw model			Adjusted model		
	OR	95% CI	*p*-value	OR	95% CI	*p*-value
C-reactive protein mg/L						
<189.3	Ref.					
≥189.3	1.60	0.77–3.32	0.205			
Leukocytes $\times 10^9$/L						
<12.8	Ref.			**Ref.**		
≥12.8	2.92	1.45–5.89	**0.003**	**3.00**	**1.17–7.69**	**0.022**
Neutrophils $\times 10^9$/L						
<7.51	Ref.					
≥7.51	3.55	1.89–6.68	**<0.001**			
Neutrophil/lymphocyte ratio						
<14.5	Ref.					
≥14.5	3.00	1.58–5.65	**0.001**			
Platelets $\times 10^9$/L						
<393	Ref.					
≥393	1.21	0.50–2.92	0.680			
Fibrinogen g/L						
<9.39	**Ref.**					
≥9.39	**9.94**	**1.17–84.43**	**0.035**			
D-dimer ng/mL						
<1,345	**Ref.**					
≥1,345	**2.57**	**1.38–4.77**	**0.003**			
Lactate dehydrogenase U/L						
<329	**Ref.**					
≥329	**2.54**	**1.35–4.79**	**0.004**			
Urea mmol/L						
<7.4	**Ref.**			**Ref.**		
≥7.4	**7.31**	**3.07–17.43**	**<0.001**	**3.20**	**1.09–9.37**	**0.034**
Creatinine umol/L						
<71	**Ref.**					
≥71	**3.77**	**1.76–8.08**	**0.001**			
Ferritin ng/mL						
<1,640	**Ref.**			**Ref.**		
≥1,640	**3.09**	**1.22–7.83**	**0.017**	**7.22**	**1.79–29.10**	**0.005**
Oxygen saturation %						
<86.9	**Ref.**					
≥86.9	**0.45**	**0.22–0.92**	**0.029**			
Lactate mmol/L						
<2.0	**Ref.**			**Ref.**		
≥2.0	**6.86**	**3.06–15.36**	**<0.001**	**4.79**	**1.79–12.82**	**0.002**
Lung involvement %						
<35	**Ref.**			**Ref.**		
≥35	**3.27**	**1.74–6.15**	**<0.001**	**4.34**	**1.70–11.01**	**0.002**
CO-RADS score						
<5	Ref.					
5	1.61	0.87–2.95	0.126			

(Continued on following page)

TABLE 4 (*Continued*) Factors associated with mortality in cancer patients with COVID-19.

Variables	Raw model			Adjusted model		
	OR	95% CI	*p*-value	OR	95% CI	*p*-value
Consolidation						
No	Ref.					
Yes	1.52	0.95–2.46	0.081			
Nodular pattern						
No	Ref.					
Yes	1.64	0.89–3.02	0.113			
Frosted glass						
No	Ref.					
Yes	1.56	0.92–2.65	0.097			
Crazy paving						
No	**Ref.**					
Yes	**2.58**	**1.51–4.40**	**0.001**			
Organizing pneumonia						
No	Ref.					
Yes	1.44	0.68–3.04	0.337			
Vessel thickening						
No	**Ref.**					
Yes	**1.91**	**1.16–3.16**	**0.011**			

[a]Acute myeloid leukemia, chronic myeloid leukemia, mixed phenotype leukemia, multiple myeloma.
[b]Cervix cancer, head and neck cancer, gastrointestinal cancer, lung cancer, liver and bile duct cancer, thyroid cancer, sarcoma, skin cancer, and other cancer.
Bold format means statistical significance of the *p* value.

response to infection [55, 56]. Likewise, leukocytes are also increased in malignant neoplasms due to the close relationship between the development and progression of cancer and a state of systemic inflammation [57–59]. The increased leukocyte count would indicate a severe inflammatory reaction as a consequence of COVID-19 in cancer patients, even with lower threshold values [12]. However, this finding must be evaluated by considering the oncological context in which many neoplasms frequently maintain leukocytosis, as a subclinical proinflammatory state. In contrast, the total leukocyte count may be affected by the toxicity of antineoplastic therapy in patients under treatment [60, 61]. Contrary to the well-known association found between coagulation markers and COVID-19, we observed no such association. The values of D-dimer, fibrinogen and platelets are frequently altered due to the complication of cancer and its treatment, especially when the disease is active [62, 63].

Although we found some laboratory markers associated with mortality, establishing the prognostic utility of these parameters requires considering that their increased concentration may be due to the underlying neoplasm and/or to the manifestation of the severity of COVID-19.

Chest CT showed a prognostic association with death in COVID-19 through the evaluation of the percentage of affected lungs. To the best of our knowledge there is no association studies between chest CT score system and COVID-19 in oncology patients. However, chest CT can be useful in the study of COVID-19 in cancer patients in which it can show atypical images with few or solitary abnormal findings; therefore, rare or subtle patterns can characterize SARS-CoV-2 infection [13].

CT scoring could help to stratify patient risk and predict short-term outcome in COVID-19 pneumonia [64]. The expression of global pulmonary involvement, regardless of the alteration type, allows us to predict clinical evolution [65], since with the semiquantitative scoring system to estimate lung involvement, all the abnormalities present in the CT are taken into account based on the affected area. Lung involvement score on chest CT in the general population associated with mortality were ≥15 (lung involvement ≥60%) [66, 67] and ≥12.5 [68]. However, in our study, a lung CT score of ≥8.75 (lung involvement ≥35%) was associated with a higher probability of death, which could have been due to limited immune function, especially in patients with hematological neoplasms receiving antineoplastic treatment and with leukopenia [13]. The extent of lung involvement observed on CT, even at a low percentage, could help identify cancer patients at a high risk of death.

Although, there is limited data on chest CT for the diagnosis of COVID-19 pneumonia with a focus on cancer populations

[14], in evaluating multiple and non-specific findings, chest CT is a useful tool in the prognosis of death from COVID-19 in cancer patients.

In summary, our clinical study attempted to clarify the role of cancer in the fatality of COVID-19 infection. We found several serum markers and imaging patterns of mortality, but mainly we identified active cancer, cancer progression or its recurrence after treatment, as a critical variable. Our findings derive from a comprehensive clinical, laboratory, and imaging analysis, highlighting the complex interplay of oncologic features and the pathophysiology of COVID-19 to predict the fatal outcome of the disease.

Limitations

Our study had some limitations that do not invalidate the results; on the contrary, they lead to the proposal of further evaluations to overcome them. First, the small size of the cohort, which probably prohibited to clarify or detect associations due to insufficient statistical power, as we only had access to the complete information of patients with COVID-19 for the study period of time. Second, recognized markers were not evaluated in the COVID-19 study, such as interleukin 6 and procalcitonin, which were not available or were economically unfeasible for developing countries such as ours. Third, neoplastic treatment, which can influence the total leukocyte count, was not analyzed in the study, although the toxic effect of this therapy occurs in all cell types. Finally, cases that had incomplete information could have generated some bias in the results, although the missing data were expected to be undifferentiated for the groups analyzed.

Conclusions

- Active cancer represents the main prognosis factor of death, while the role of cancer stage and type is unclear.
- Chest CT is a useful tool in the prognosis of death from COVID-19 in cancer patients.
- It is a challenge to establish the prognostic utility of laboratory markers as the alteration of their values can have either oncological or pandemic origins.
- Clinical, laboratory and radiological correlations can help improve the prognosis of death in cancer patients with pulmonary involvement due to COVID-19.

Data availability statement

The raw data supporting the conclusion of this article will be made available by the authors, without undue reservation.

Ethics statement

All the cases in this study were part of the medical care routine of the INEN. No informed consent from any patient was obtained since this study used laboratory test registers and patient medical records in obtaining data which were used protecting the identity of the patients. The protocol was presented to the Research Committee of the INEN and approved for its implementation with designated protocol number INEN 20-49.

Author contributions

FV-C and JV conceived and designed the study. JV, RR, AB, ML, TS, DP, YB, and MG acquired data. FV-C, RR, YB, CF, and MG analyzed the data, and FV-C, RR, AB, ML, TS, DP, YB, and MG-N wrote manuscript. All authors contributed to the article and approved the submitted version.

Conflict of interest

The authors declare that the research was conducted in the absence of any commercial or financial relationships that could be construed as a potential conflict of interest.

References

1. Guan WJ, Niyi Z, Hu Y, Liang WH, Ou CQ, He JX, et al. Clinical characteristics of coronavirus disease 2019 in China. *New Engl J Med* (2020) 382(18):1708–20. doi:10.1056/nejmoa2002032

2. Shi M, Chen L, Yang Y, Zhang J, Xu J, Xu G, et al. Analysis of clinical features and outcomes of 161 patients with severe and critical COVID-19: a multicenter descriptive study. *J Clin Lab Anal* (2020) 34(9):e23415. doi:10.1002/jcla.23415

3. Wang D, Hu B, Hu C, Zhu F, Liu X, Zhang J, et al. Clinical characteristics of 138 hospitalized patients with 2019 novel coronavirus-infected pneumonia in Wuhan, China. *JAMA - J Am Med Assoc* (2020) 323(11):1061–9. doi:10.1001/jama.2020.1585

4. Yakovenko OK, Khanin OG, Lotysh VV, Gryf SL. Clinical features of severe COVID-19 with lethal outcome in volyn region residents. *Ukrainian Pulmonology J* (2021) 29(2):16–24. doi:10.31215/2306-4927-2021-29-2-16-24

5. Yang L, Chai P, Yu J, Fan X. Effects of cancer on patients with COVID-19: a systematic review and meta-analysis of 63,019 participants. *Cancer Biol Med* (2021) 18:298–307. doi:10.20892/j.issn.2095-3941.2020.0559

6. Bernard A, Cottenet J, Bonniaud P, Piroth L, Arveux P, Tubert-Bitter P, et al. Comparison of cancer patients to non-cancer patients among COVID-19 inpatients at a national level. *Cancers (Basel)* (2021) 13(6):1436–15. doi:10.3390/cancers13061436

7. Rajeev Nadkarni A, Vijayakumaran SC, Gupta S, Divatia JV. Mortality in cancer patients with COVID-19 who are admitted to an ICU or who have severe COVID-19: a systematic review and meta-analysis. *JCO Glob Oncol* (2021) 7:1286–305. doi:10.1200/go.21.00072

8. Wang L, Sun Y, Yuan Y, Mei Q, Yuan X. Clinical challenges in cancer patients with COVID-19: aging, immunosuppression, and comorbidities. *Aging* (2020) 12: 24462–74. doi:10.18632/aging.104205

9. Health Organization W. *Guideline clinical management of COVID-19 patients: living guideline* (2021). Available from: http://apps.who.int/bookorders (Accessed November 23, 2021).

10. Nader Marta G, Colombo Bonadio R, Nicole Encinas Sejas O, Watarai G, Mathias Machado MC, Teixeira Frasson L, et al. Outcomes and prognostic factors in a large cohort of hospitalized cancer patients with COVID-19. *JCO Glob Oncol* (2021) 7:1084–92. doi:10.1200/GO.21.00087

11. Mina A, Galvez C, Karmali R, Mulcahy M, Mi X, Kocherginsky M, et al. Outcomes of cancer patients with COVID-19 in a hospital system in the Chicago metropolitan area. *Cancers (Basel)* (2022) 14(9):2209. doi:10.3390/cancers14092209

12. Benderra MA, Aparicio A, Leblanc J, Wassermann D, Kempf E, Galula G, et al. Clinical characteristics, care trajectories and mortality rate of SARS-CoV-2 infected cancer patients: a multicenter cohort study. *Cancers (Basel).* (2021) 13(19):4749. doi:10.3390/cancers13194749

13. Katal S, Aghaghazvini L, Gholamrezanezhad A. Chest-CT findings of COVID-19 in patients with pre-existing malignancies; a pictorial review. *Clin Imaging* (2020) 67:121–9. doi:10.1016/j.clinimag.2020.06.004

14. Bourdoncle S, Eche T, McGale J, Yiu K, Partouche E, Yeh R, et al. Investigating of the role of CT scan for cancer patients during the first wave of COVID-19 pandemic. *Res Diagn Interv Imaging* (2022) 1:100004. doi:10.1016/j.redii.2022.100004

15. Levi M. Disseminated intravascular coagulation in cancer patients. *Best Pract Res Clin Haematol* (2009) 22:129–36. doi:10.1016/j.beha.2008.12.005

16. Humphreys BD, Soiffer RJ, Magee CC. Renal failure associated with cancer and its treatment: an update. *J Am Soc Nephrol* (2005) 16:151–61. doi:10.1681/ASN.2004100843

17. Levi M. Disseminated intravascular coagulation in cancer: an update. *Semin Thromb Hemost* (2019) 45(4):342–7. doi:10.1055/s-0039-1687890

18. Lameire NH, Flombaum CD, Moreau D, Ronco C. Acute renal failure in cancer patients. *Ann Med* (2005) 37:13–25. doi:10.1080/07853890510007205

19. Kavanaugh DY, Carbone DP. Immunologic dysfunction in cancer. *Oncology (Williston Park)* (1996) 10:927–51. doi:10.1016/s0889-8588(05)70376-2

20. Cedervall J, Zhang Y, Olsson AK. Tumor-induced NETosis as a risk factor for metastasis and organ failure. *Cancer Res* (2016) 76:4311–5. doi:10.1158/0008-5472.CAN-15-3051

21. Nava S, Cuomo AM. Acute respiratory failure in the cancer patient: the role of non-invasive mechanical ventilation. *Crit Rev Oncology/Hematology* (2004) 51: 91–103. doi:10.1016/j.critrevonc.2004.04.004

22. Vial T, Descotes J. Immunosuppressive drugs and cancer. *Toxicology* (2003) 185(3):229–40. doi:10.1016/s0300-483x(02)00612-1

23. Ngo D, Jia JB, Green CS, Gulati AT, Lall C. Cancer therapy related complications in the liver, pancreas, and biliary system: an imaging perspective. *Insight Imaging* (2015) 6:665–77. doi:10.1007/s13244-015-0436-7

24. Pan F, Ye T, Sun P, Gui S, Liang B, Li L, et al. Time course of lung changes at chest CT during recovery from Coronavirus disease 2019 (COVID-19). *Radiology* (2020) 295(3):715–21. doi:10.1148/radiol.2020200370

25. Prokop M, van Everdingen W, van Rees Vellinga T, van Ufford HQ, Stöger L, Beenen L, et al. CO-RADS: a categorical CT assessment scheme for patients suspected of having COVID-19-definition and evaluation. *Radiology* (2020) 296(2):E97–104. doi:10.1148/radiol.2020201473

26. World Health Organization. Clinical management of severe acute respiratory infection when novel coronavirus (nCoV) infection is suspected: interim guidance 2 1. In: *Triage: early recognition of patients with SARI associated with nCoV infection* (2020). Available from: https://apps.who.int/iris/bitstream/handle/10665/331446/WHO-2019-nCoV-clinical-2020.4-eng.pdf?sequence=1&isAllowed=y (Accessed March 13, 2020).

27. Ferrari BL, Carlos, Ferreira G, Menezes M, de Marchi P, Canedo J, et al. Determinants of COVID-19 mortality in patients with cancer from a community oncology practice in Brazil. *JCO Glob Oncol* (2021) 7:46–55. doi:10.1200/GO.20.00444

28. Meza Riquelme MJS, Condori Pereyra AR, Encalada Carbajal DA. Análisis de políticas públicas en el Perú ante la crisis derivada de la COVID-19. *Semestre Económico* (2020) 23(55):113–38. doi:10.22395/seec.v23n55a5

29. Zorzi M, Guzzinati S, Avossa F, Fedeli U, Calcinotto A, Rugge M. SARS-CoV-2 infection in cancer patients: a population-based study. *Front Oncol* (2021) 11: 730131. doi:10.3389/fonc.2021.730131

30. Kuderer NM, Choueiri TK, Shah DP, Shyr Y, Rubinstein SM, Rivera DR, et al. Clinical impact of COVID-19 on patients with cancer (CCC19): a cohort study. *The Lancet* (2020) 395(10241):1907–18. doi:10.1016/S0140-6736(20)31187-9

31. Borno HT, Kim MO, Hong JC, Yousefi S, Lin A, Tolstykh I, et al. COVID-19 outcomes among patients with cancer: observations from the university of California cancer consortium COVID-19 project outcomes registry. *Oncologist* (2022) 27(5):398–406. doi:10.1093/oncolo/oyac038

32. Pinato DJ, Scotti L, Gennari A, Colomba-Blameble E, Dolly S, Loizidou A, et al. Determinants of enhanced vulnerability to coronavirus disease 2019 in UK patients with cancer: a European study. *Eur J Cancer* (2021) 150:190–202. doi:10.1016/j.ejca.2021.03.035

33. Schreiber RD, Old LJ, Smyth MJ. Cancer immunoediting: integrating immunity's roles in cancer suppression and promotion. *Science* (2011) 331(6024):1565–70. doi:10.1126/science.1203486

34. Khorana AA, Mackman N, Falanga A, Pabinger I, Noble S, Ageno W, et al. Cancer-associated venous thromboembolism. *Nat Rev Dis Primers* (2022) 8(1): 11–8. doi:10.1038/s41572-022-00336-y

35. Connors JM, Levy JH. Thromboinflammation and the hypercoagulability of COVID-19. *J Thromb Haemost* (2020) 18:1559–61. doi:10.1111/jth.14849

36. Mangalmurti N, Hunter CA. Cytokine storms understanding COVID-19. *Immunity* (2020) 53(1):19–25. doi:10.1016/j.immuni.2020.06.017

37. Owusuaa C, Dijkland SA, Nieboer D, van der Heide A, van der Rijt CCD. Predictors of mortality in patients with advanced cancer—a systematic review and meta-analysis. *Cancers* (2022) 14:328. doi:10.3390/cancers14020328

38. Ullgren H, Camuto A, Rosas S, Pahnke S, Ginman B, Enblad G, et al. Clinical characteristics and factors associated with COVID-19-related death and morbidity among hospitalized patients with cancer: a Swedish cohort study. *Acta Oncologica* (2021) 60(11):1459–65. doi:10.1080/0284186X.2021.1958005

39. Liu Y, Lu H, Wang W, Liu Q, Zhu C. Clinical risk factors for mortality in patients with cancer and COVID-19: a systematic review and meta-analysis of recent observational studies. *Expert Rev Anticancer Ther* (2021) 21(1):107–19. doi:10.1080/14737140.2021.1837628

40. Fattore GL, Olivos NSA, Olalla JEC, Gomez L, Marucco AF, Mena MPR. Mortality in patients with cancer and SARS-CoV-2 infection: results from the argentinean network of hospital-based cancer registries. *Cancer Epidemiol* (2022) 79:102200. doi:10.1016/j.canep.2022.102200

41. Jergović M, Coplen CP, Uhrlaub JL, Nikolich-Žugich J. Immune response to COVID-19 in older adults. *J Heart Lung Transplant* (2021) 40(10):1082–9. doi:10.1016/j.healun.2021.04.017

42. Kernan KF, Carcillo JA. Hyperferritinemia and inflammation. *Int Immunol* (2017) 29(9):401–9. doi:10.1093/intimm/dxx031

43. Matzner Y, Konijn AM, Hershko C. Serum ferritin in hematologic malignancies. *Am J Hematol* (1980) 9:13–22. doi:10.1002/ajh.2830090103

44. Aulbert E, Steffens O. Ferritin im serum-ein «tumormarker» bei malignen lymphomen? *Oncology Research and Treatment* (1990) 13(2):102–8. doi:10.1159/000216735

45. Qeadan F, Tingey B, Gu LY, Packard AH, Erdei E, Saeed AI. Prognostic values of serum ferritin and d-dimer trajectory in patients with covid-19. *Viruses* (2021) 13(3):419. doi:10.3390/v13030419

46. Depalma RG, Hayes VW, O'Leary TJ. Optimal serum ferritin level range: iron status measure and inflammatory biomarker. *Metallomics* (2021) 13(6):mfab030. doi:10.1093/mtomcs/mfab030

47. Bakker J, Gris P, Coffernils M, Kahn RJ, Vincent JL. Serial blood lactate levels can predict the development of multiple organ failure following septic shock. *Am J Surg* (1996) 171:221–6. doi:10.1016/S0002-9610(97)89552-9

48. Bakker J, Vincent JL. The oxygen supply dependency phenomenon is associated with increased blood lactate levels. *J Crit Care* (1991) 6:152–9. doi:10.1016/0883-9441(91)90006-f

49. Nazer LH, Rimawi D, Hawari FI. Evaluating the predictive value of lactate in patients with cancer having septic shock. *J Intensive Care Med* (2020) 35(8):789–96. doi:10.1177/0885066618788821

50. Bagshaw SM, Gibney RTN. Conventional markers of kidney function. *Crit Care Med* (2008) 36:S152–8. doi:10.1097/CCM.0b013e318168c613

51. Stevens LA, Levey AS. Measurement of kidney function. *Med Clin North America* (2005) 89:457–73. doi:10.1016/j.mcna.2004.11.009

52. Peleg Y, Kudose S, D'Agati V, Siddall E, Ahmad S, Nickolas T, et al. Acute kidney injury due to collapsing glomerulopathy following COVID-19 infection. *Kidney Int Rep* (2020) 5(6):940–5. doi:10.1016/j.ekir.2020.04.017

53. Chueh TI, Zheng CM, Hou YC, Lu KC. Novel evidence of acute kidney injury in COVID-19. *J Clin Med* (2020) 9(11):3547. doi:10.3390/jcm9113547

54. Nath SS, Yadav NU, Derkach A, Perez-Johnston R, Tachiki L, Maguire K, et al. Outcomes of patients with COVID-19 from a specialized cancer care emergency room. *Cancer Invest* (2022) 40(1):17–25. doi:10.1080/07357907.2021.1985134

55. Williams Donaldson V. A clinical study of visualization on depressed white blood cell count in medical patient. *Appl Psychophysiology Biofeedback* (2000) 25(2):117–28. doi:10.1023/a:1009518925859

56. Kolaczkowska E, Kubes P. Neutrophil recruitment and function in health and inflammation. *Nat Rev Immunol* (2013) 13:159–75. doi:10.1038/nri3399

57. Balkwill F, Charles KA, Mantovani A. Smoldering and polarized inflammation in the initiation and promotion of malignant disease. *Cancer Cell* (2005) 7:211–7. doi:10.1016/j.ccr.2005.02.013

58. Coussens LM, Werb Z. Inflammation and cancer. *Nature* (2002) 420(6917):860–867.doi:10.1038/nature01322

59. Mantovani A, Allavena P, Sica A, Balkwill F. Cancer-related inflammation. *Nature* (2008) 454:436–44. doi:10.1038/nature07205

60. Shitara K, Matsuo K, Oze I, Mizota A, Kondo C, Nomura M, et al. Meta-analysis of neutropenia or leukopenia as a prognostic factor in patients with malignant disease undergoing chemotherapy. *Cancer Chemother Pharmacol* (2011) 68(2):301–7. doi:10.1007/s00280-010-1487-6

61. Lowenthal RM, Eaton K. Toxicity of chemotherapy. *Hematology/Oncology Clinics* (1996) 10(4):967–90. doi:10.1016/s0889-8588(05)70378-6

62. Kvolik S, Jukic M, Matijevic M, Marjanovic K, Glavas-Obrovac L. An overview of coagulation disorders in cancer patients. *Surg Oncol* (2010) 19:e33–46. doi:10.1016/j.suronc.2009.03.008

63. de Cicco M. The prothrombotic state in cancer: pathogenic mechanisms. *Crit Rev Oncology/Hematology* (2004) 50:187–96. doi:10.1016/j.critrevonc.2003.10.003

64. Francone M, Iafrate F, Masci GM, Coco S, Cilia F, Manganaro L, et al. Chest CT score in COVID-19 patients: correlation with disease severity and short-term prognosis. *Eur Radiol* (2020) 30(12):6808–17. doi:10.1007/s00330-020-07033-y

65. Angeli E, Dalto S, Marchese S, Setti L, Bonacina M, Galli F, et al. Prognostic value of CT integrated with clinical and laboratory data during the first peak of the COVID-19 pandemic in northern Italy: a nomogram to predict unfavorable outcome. *Eur J Radiol* (2021) 137:109612. doi:10.1016/j.ejrad.2021.109612

66. Bayrak V, Şentürk Durukan N, Demirer Aydemir F, Ergan B, Gezer NS, Eren Kutsoylu OÖ, et al. Risk factors associated with mortality in ıntensive care COVID-19 patients: the importance of chest CT score and intubation timing as risk factors. *Turk J Med Sci* (2021) 51(4):1665–74. doi:10.3906/sag-2101-89

67. Li K, Li K, Chen D, Chen D, Chen S, Chen S, et al. Predictors of fatality including radiographic findings in adults with COVID-19. *Respir Res* (2020) 21(1):146. doi:10.1186/s12931-020-01411-2

68. Hajiahmadi S, Shayganfar A, Janghorbani M, Esfahani MM, Mahnam M, Bakhtiarvand N, et al. Chest computed tomography severity score to predict adverse outcomes of patients with COVID-19. *Infect Chemother* (2021) 53:308–18. doi:10.3947/ic.2021.0024

Pathology & Oncology Research | frontiers

TYPE Review
PUBLISHED 02 August 2023
DOI 10.3389/pore.2023.1611300

Check for updates

OPEN ACCESS

EDITED BY
József Tímár,
Semmelweis University, Hungary

*CORRESPONDENCE
Alexander Bertuccioli,
alexander.bertuccioli@uniurb.it

RECEIVED 14 May 2023
ACCEPTED 18 July 2023
PUBLISHED 02 August 2023

CITATION
Cazzaniga M, Zonzini GB, Di Pierro F, Palazzi CM, Cardinali M and Bertuccioli A (2023), Influence of the microbiota on the effectiveness and toxicity of oncological therapies, with a focus on chemotherapy.
Pathol. Oncol. Res. 29:1611300.
doi: 10.3389/pore.2023.1611300

COPYRIGHT
© 2023 Cazzaniga, Zonzini, Di Pierro, Palazzi, Cardinali and Bertuccioli. This is an open-access article distributed under the terms of the Creative Commons Attribution License (CC BY). The use, distribution or reproduction in other forums is permitted, provided the original author(s) and the copyright owner(s) are credited and that the original publication in this journal is cited, in accordance with accepted academic practice. No use, distribution or reproduction is permitted which does not comply with these terms.

Influence of the microbiota on the effectiveness and toxicity of oncological therapies, with a focus on chemotherapy

Massimiliano Cazzaniga[1], Giordano Bruno Zonzini[2], Francesco Di Pierro[1,3], Chiara Maria Palazzi[4], Marco Cardinali[5] and Alexander Bertuccioli[2]*

[1]Scientific & Research Department, Velleja Research, Milano, Italy, [2]Department of Biomolecular Sciences, University of Urbino Carlo Bo, Urbino, Italy, [3]Department of Medicine and Surgery, University of Insurbia, Varese, Italy, [4]Associazione Italiana Fitness e Medicina, Ravenna, Italy, [5]Department of Internal Medicine, Infermi Hospital, Azienda Unità Sanitaria Locale Romagna, Rimini, Italy

Recent studies have highlighted a possible correlation between microbiota composition and the pathogenesis of various oncological diseases. Also, many bacterial groups are now directly or indirectly associated with the capability of stimulating or inhibiting carcinogenic pathways. However, little is known about the importance and impact of microbiota patterns related to the efficacy and toxicity of cancer treatments. We have recently begun to understand how oncological therapies and the microbiota are closely interconnected and could influence each other. Chemotherapy effectiveness, for example, appears to be strongly influenced by the presence of some microorganisms capable of modulating the pharmacokinetics and pharmacodynamics of the compounds used, thus varying the real response and therefore the efficacy of the oncological treatment. Similarly, chemotherapeutic agents can modulate the microbiota with variations that could facilitate or avoid the onset of important side effects. This finding has or could have considerable relevance as it is possible that our ability to modulate and modify the microbial structure before, during, and after treatment could influence all the clinical parameters related to pharmacological treatments and, eventually, the prognosis of the disease.

KEYWORDS

microbiota, chemotherapy, oncology, toxicity, microbiome

Introduction

The microbiota, defined as the set of microorganisms that is hosted in each human being, is now considered a fundamental element in human pathophysiology, being able—depending on its composition and structure—to protect us from certain diseases or, on the contrary, contribute to their onset [1]. Oncological pathologies are no exception to this well-established rule and some bacterial groups could be directly or

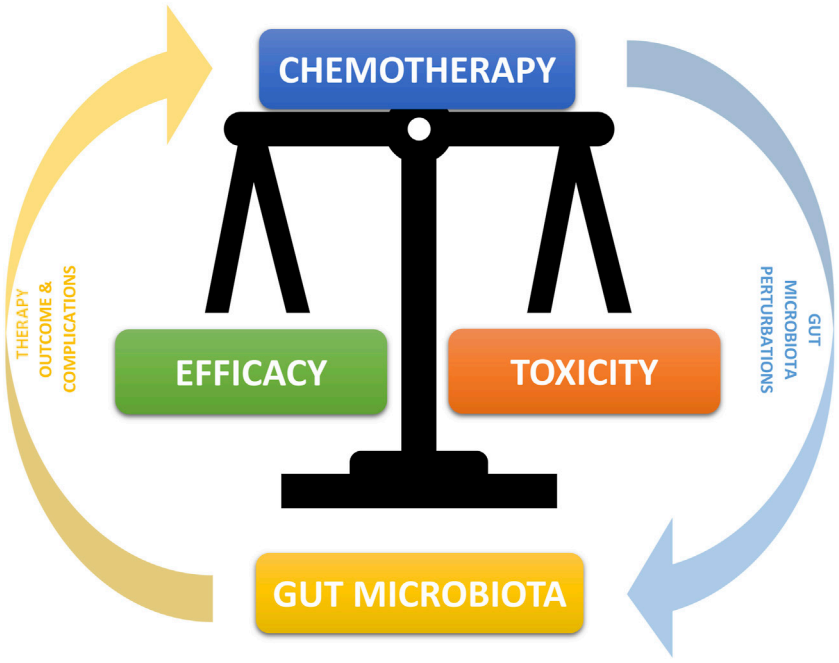

FIGURE 1
Bidirectional Interconnection between microbiota and chemotherapy. The microbiota can through many mechanisms alter and modify the chemotherapy compound by increasing or decreasing its efficacy. At the same time, chemotherapeutic compounds have an effect of alteration of the microbiota, in particular with a decrease in some symbiotic bacterial populations and an increase in potentially pathological ones, with the consequent onset of greater drug toxicity and a higher incidence of concomitant pathologies.

indirectly related to the onset of numerous tumors [2]. A clear example of this relationship is the link between some vaginal community state types (CSTs) and cervical cancer, or the presence of *Fusobacterium nucleatum* and colorectal cancer [3]. Despite the growing amount of information in this field, little is still known about the impact of the microbiota on the progression and prognosis of oncological diseases and, in particular, little consideration is given to the effect that microbiota composition has on the various conventional anti-tumor therapies. Instead, a strong influence arises both in terms of efficacy and toxicity, therefore influencing the prognosis of the disease as well. Chemotherapy above all seems to be affected by these mechanisms and in this review, we will try to highlight the main consequences of this relationship and some of the therapeutic possibilities that we already have available to modulate this effect.

Chemotherapy and microbiota relationship

To date, the choice of chemotherapy treatment, the dosage, the method of administration, and other characteristics of the therapeutic path are substantially determined by well-defined protocols built on the basis of the pharmacokinetic and pharmacodynamic properties of the compound to be used, obviously associated with the patient's personal characteristics such as their pathology and their clinical and anthropometric parameters [4]. Numerous emerging data, however, highlight the emerging necessity to know a further characteristic of the patient, namely their microbial composition. A very authoritative review on this subject published in 2017 [5] declares that "clinical studies suggests that the composition of the microbiota regulates the efficacy of anticancer therapy and that targeting the microbiota may improve drug efficacy and/or adverse effects." This work also highlights the fact that the microbiota impacts chemotherapy both when taken orally and parenterally and introduces a fundamental aspect for understanding the relationship between our bacteria and oncological therapy, namely bidirectionality. In fact, it is now evident how these aspects influence each other, and one is the direct consequence of the other (Figure 1). In detail, the various microbial compositions can influence the response to chemotherapy by increasing or decreasing its effectiveness while, on the other hand, chemotherapy is able to modify the bacterial populations by producing a perturbation of their crucial balance (dysbiosis) and generating local alterations which could expose us more easily to toxic effects of drugs such as mucositis, as described in detail later.

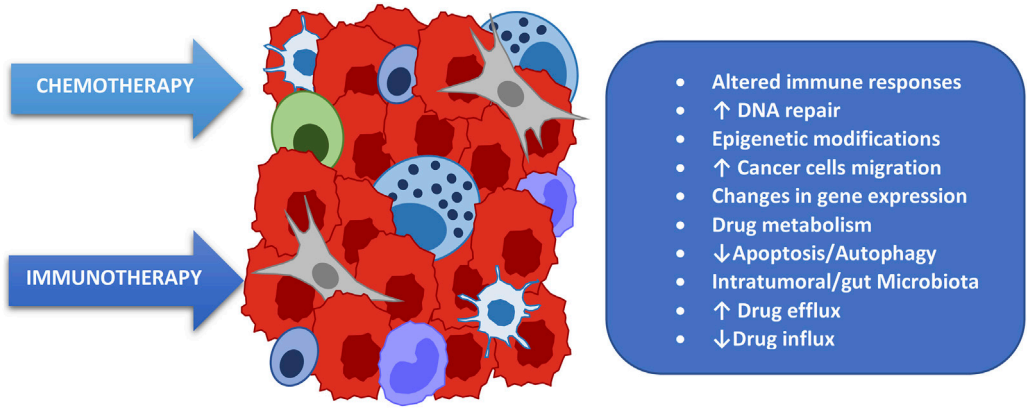

FIGURE 2
Main mechanisms related to the resistance of cancer cells to oncological treatments.

Impact of the microbiota on the effectiveness of chemotherapy treatments

We have just introduced the concept of how the microbiota influences the response to chemotherapy treatments by modulating their efficacy and therefore the therapeutic response. The first mechanism to understand, in order to hypothesize an intervention capable of positively exploiting this fact, is the main way in which the microbiota alters the response to chemotherapy, namely through the induction of chemoresistance [6]. There are many mechanisms of interaction between chemotherapy and microbiota involved in this phenomenon, summarized in (Figure 2). Among the main ones we remember how the microbiota influences the functionality of the trans-membrane pump which regulates the amount of cytotoxic drug that enters the cell as well as that which is expelled, thus regulating the amount of drug that remains inside the tumor cell and hence the therapeutic potency [7]. A further and important mechanism is the reparative capacity of Deoxyribonucleic acid (DNA) induced by the microbiota [8]; although perhaps the most important mechanism associated with chemoresistance is the capacity of some bacterial strains to modulate, transform, change, and metabolize the chemotherapy itself, impacting on its efficacy [9]. To understand how much these and other mechanisms are able to influence the treatment characteristics and therefore how essential it is to know them and, when possible, to modulate them, we will examine some well-known clinical examples with results published in authoritative scientific journals.

Microbiota-induced resistance to gemcitabine

Gemcitabine is known to be an antineoplastic drug of the group of specific pyrimidine cell cycle antimetabolites and is used for the treatment of numerous pathologies such as pancreas, lung, breast, bladder, and ovary cancers, as well as in many sarcomas, alone or in combination with other chemotherapy. Its anticancer activity is the result of the balance between its activation and inactivation. That is, it does not act in the injected form but is metabolized through some kinases into its active metabolites which are gemcitabine monophosphate, diphosphate, and triphosphate. Once these metabolites have performed the required cytotoxic action, they are degraded by other enzymes and in particular by cytidine deaminase which renders them inactive and ready for elimination [10]. However, in the presence of a particular microbial composition and more precisely in the case of an abundance of proteobacteria (gammaproteobacteria) this scenario is altered as these microbes are natural producers of the enzyme cytidine deaminase and therefore enhancers of the inactivation effect of this drug, leading ultimately to a reduction of its therapeutic capacity [11] (Figure 3). In this regard, a study published in Science in 2017 [12] shows precisely how gemcitabine chemotherapy treatment resistance in patients with pancreatic cancer is more present in those with a microbiota abnormally rich in proteobacteria and therefore highlights how a restoration of microbial eubiosis, in particular with a decrease of proteobacteria obtained with a specific antibiotic therapy, has increased the therapeutic response and therefore the improvement of prognosis in these subjects.

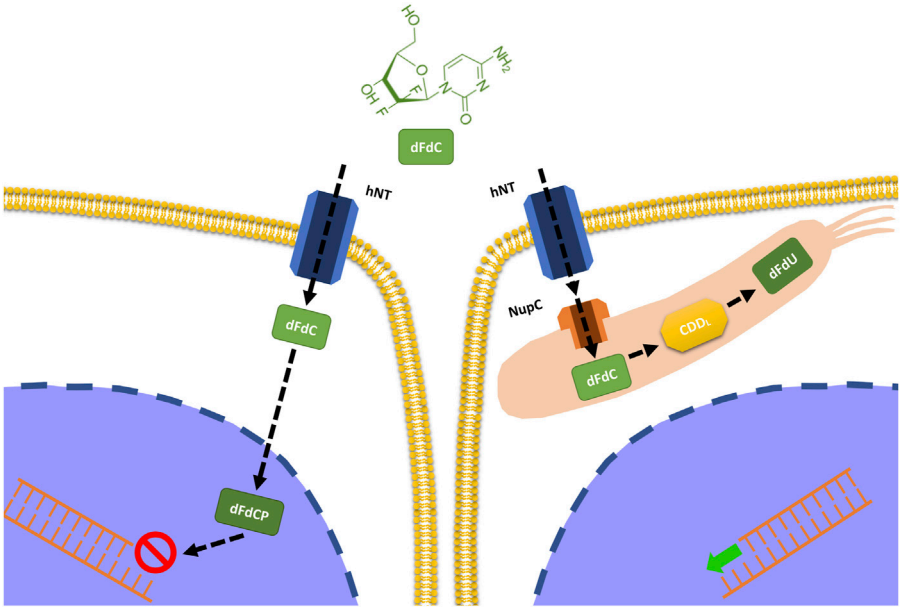

FIGURE 3
Impact of intratumoral bacteria on the metabolization of gemcitabine. Some bacteria (proteobacteria) have the ability to express the enzyme cytidine deaminase responsible for the inactivation of gemcitabine and therefore for the reduction of its efficacy.

Resistance to chemotherapy for *Fusobacterium nucleatum* -induced colorectal cancer

A further and effective example of the phenomenon of microbiota-related chemoresistance is related to the presence of *Fusobacterium nucleatum* (FN) and the efficacy of chemotherapy for colorectal cancer. In fact, it is now known and accepted that this bacterium, a commensal of the oral cavity responsible for numerous periodontal diseases, is also strongly implicated in the onset of colorectal cancer through inflammatory, genetic, and immune mechanisms [13]. What is less known is the ability of this bacterium not only to influence the onset of the disease but also to impact its progression and prognosis given its ability to increase autophagy. This cellular property is obviously positive for the repair of the numerous damages that our cells undergo on a daily basis but becomes counterproductive if the cellular damage is the goal of a pharmacological treatment [14]. This is the case with chemotherapy which normally acts precisely through cytotoxic damage to the cell, and it is clear that any reparative mechanism limits the effectiveness of the treatment. FN is counterproductive and therefore harmful in this sense precisely because of its property of inducing and increasing autophagy and therefore its presence ends up inducing chemo-resistance. Also in this case, there is an authoritative study [15] published in Cell in 2017 which highlights how patients with an abundant presence of FN were much more resistant to chemotherapy and therefore had a worse prognosis than those with a more favorable microbial structure.

Increased efficacy of cyclophosphamide induced by microbiota

Microbial effect on chemotherapy acts not only in the sense of resistance, therefore reducing therapy effects and worsening the prognosis, but also in a positive way increasing the effectiveness of some chemotherapy and therefore opening the possibility of enhancing our oncological treatments through the modulation of the microbiota. This is the case, for example, with cyclophosphamide. It is an alkylating chemotherapeutic agent that acts in a cytostatic sense and is used for many oncological pathologies such as hematological ones and also many solid ones such as in neuroblastoma, some sarcomas, and breast and ovarian cancers [16]. Its antitumoral property is wide and at least in part due to its ability to stimulate and increase the antitumoral immune response [17]. Recent authoritative studies [18, 19] have shown how once administered it is able to select some bacterial populations within the lymphoid organs, thus determining an increase in the production of immune cells directed against tumor antigens.

Impact of microbiota on the toxicity of chemotherapy treatments

As anticipated, the relationship between microbiota and chemotherapy treatments is not only related to the negative or positive modulation of pharmacological efficacy but is also

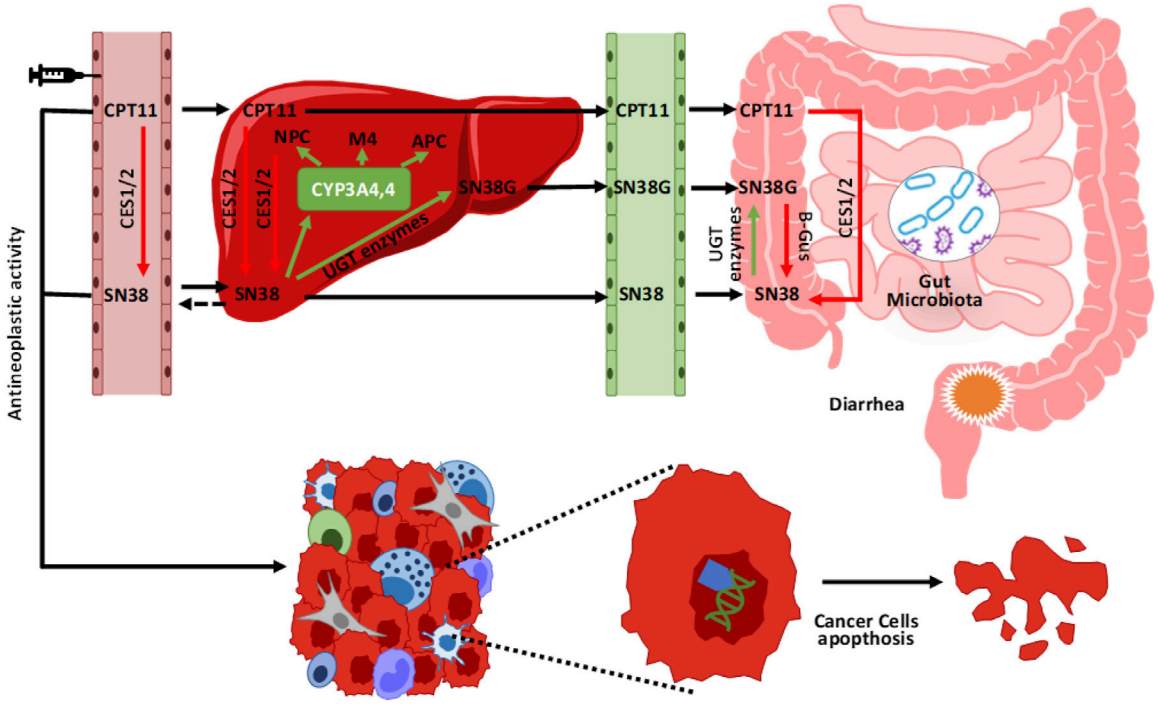

FIGURE 4
Metabolism and elimination of irinotecan (CPT11). Once injected, irinotecan is activated by some esterases (CES 1/2) into its active metabolite (SN38). After its anticancer action, it is again conjugated in the liver into an inactive compound ready to be eliminated (SN38G) mainly through the intestine and faeces. In its colonic passage, the presence of bacterial groups with enzymatic b-glucuronidase activity, reactivate the compound (SN38) again, effectively increasing its concentration and the risk of associated toxicity (e.g., mucositis).

closely linked to the possibility or not of augmenting or limiting side effects, in particular—but not only—the early ones. In fact, we have already seen how chemotherapy can alter the microbiota and how dysbiosis can be, in various ways, the cause or contributory cause of various side effects.

Action of B-glucuronidase on the toxicity of irinotecan

One of the best documented examples of the action of bacteria on chemotherapy toxicity concerns the use of irinotecan. This chemotherapy, which belongs to the camptothecin class, is mainly used in colorectal cancer, non-small cell lung cancer, and ovarian cancer treatment [20]. As with other compounds, this one not does not act directly but only after its transformation into an active metabolite. In fact, it is a pro-drug and only after the action of some esterases is it transformed into its active metabolite called SN38, a pro apoptotic molecule that inhibits the enzyme Topoisomerase I with consequent cell inability to repair the damaged DNA. SN38 compound excretion with the bile and then with the feces takes place only after its passage through the liver with conjugation to SN38G [21]. However, during intestinal transit, the inactive compound interacts with the microbiota and within certain microbial conditions, such as the presence of abundant bacterial groups with b-glucuronidase activity (i.e. capable of producing an enzyme called b-glucuronidase). It is de-conjugated and made available for reabsorption as the active molecule, effectively increasing its concentration and consequently its toxicity, for example by generating intestinal damage such as mucositis Figure 4 [22].

Influence of the microbiota on the appearance of chemotherapy mucositis

With regard to chemotherapy-induced mucositis, the example just described concerning Irinotecan and its relationship with bacterial activities such as beta-glucuronidase production represents only one of the links between the microbiota and the appearance or reduction of this fundamental side effect, perhaps the main factor responsible for decreased compliance and consequent therapeutic failure. Mucositis is a complication of various cancer therapies such as radiotherapy and chemotherapy [23]. It is characterized by very

disabling symptoms such as presence of nausea, abdominal cramps, swelling, and above all diarrhea, even to a high degree [24]. It is supported by inflammatory and apoptotic phenomena and ultimately related to the intestinal microbial composition. Sonis [25] in 2004 described a mechanism of onset divided into 5 stages considering the microbial infection to be only a consequence of the inflammatory process triggered by the direct action of chemotherapy on the enterocyte wall. Recently, however, new research has highlighted a much more important and above all causal role of the microbial structure on the genesis of mucositis. In practice, the microbiota would be a link between the potential toxicity of the drug and the effective initiation of the chain of events that lead to mucositis. The presence or rather the absence of some bacterial groups (in particular those capable of producing short-chain fatty acids or SCFAs, especially butyrate) generates a microenvironment which favors both directly (through the stimulation of particular receptors called TLR4) and indirectly (producing an increase in bacterial permeability and therefore the translocation of GRAM-bacteria and therefore of lipopolysaccharide—LPS in the circulation) the genesis of inflammatory and immune processes responsible for the toxic effects [26]. The main bacterial populations linked with effectiveness and toxicity of chemotherapy are summarized in Table 1.

TABLE 1 Examples of bacterial populations active on CHT efficacy and toxicity.

Efficacy	
Gammaproteobacteria	Gemcitabine efficacy reduction through early inactivation
Fusobacterium	Increased resistance to many chemotherapeutics through autophagy modulation
GRAM+ (some induced by cyclophosphamide)	Increase of therapy efficacy through an immunity stimulation
Toxicity	
Firmicutes/Bacteroidetes	Increase of Irinotecan toxicity through Beta-glucuronidase activity increase
↓ Bacteria SCFAs Producers	Increased toxicity of some chemotherapy (mucositis)

Possible interventions

Considering the described relationship between microbial composition and influence over efficacy and toxicity of various chemotherapies used in various forms of cancer, it appears quite intuitive and immediate how an intervention to modulate and shape an "ideal or favorable" microbiota could allow us to improve efficacy, tolerability, compliance, and outcome of oncological therapies. The use of prebiotics, probiotics and nutraceuticals is becoming increasingly central in accompanying the various chemotherapy regimens as a result of the increasingly frequent publication of important scientific data supporting this hypothesis. In particular, considering chemotherapy and the mechanisms we have just described, it is increasingly evident that one of the potentially most effective and easiest ways to intervene is modulating the microbiota in a eubiotic sense. For example, it appears convenient to enhance microbiota production of short-chain fatty acids (SCFAs), using prebiotics that nourish and promote the growth of the bacteria responsible for their production [27], or directly assuming probiotics, i.e., bacterial groups with suitable characteristics of engraftment and vitality, capable of ensuring the production of adequate quantities of SCFAs and in particular of butyric acid [28]. It is also important to underline that on the market there are already formulations suitable for clinical use supported by abundant scientific literature. The *Clostridium Butyricum Miyairi* CBM588 strain marketed in Italy as Butirrisan © is the best-known example [29].

Butyric acid in the modulation of chemotherapy efficacy and toxicity

Short-chain fatty acids (acetate, propionate, and butyrate) are a class of saturated fatty acids with an aliphatic chain consisting of fewer than 6 carbon atoms. They are mainly produced during the fermentation of fibers (undigested carbohydrates in the small intestine, fructo-oligosaccharides, pectin, inulin, etc.) operated precisely by particular bacterial classes of the intestinal microbiota [30]. These fermentative products are essential for a whole series of pathophysiological processes. For example, they are the source of most of the enterocytes' energy, so much so that they are crucial for colonic wall health and stability; therefore their depletion should be avoided in order to prevent inflammatory bowel diseases [31]. Furthermore, their link with oncological diseases has recently been highlighted, as SCFA have the recognized ability to prevent development of cancer (especially—but not only—colon cancer) [32] and could influence conventional oncological treatments effectiveness [33]. In this scenario, the butyric acid produced by a particular bacterial class called *Clostridium Butyricum* (CB) of the Clostridiales group seems to have (at least for now), supported by clinical data, a decidedly more decisive role than other SCFAs. Over the last few years, it has shown unequivocal properties both in modulation of efficacy and toxicity of oncological therapies (in particular chemotherapy and immunotherapy) [34]. One of the main and recent examples of the ability of this compound to impact chemotherapy toxicity is the one published by [35] in 2019 related to doxorubicin cardiotoxicity. In this work it is clearly demonstrated that butyrate use is related to a reduced left ventricular dilatation, fibrosis, and cardiomyocytes apoptosis induced by chemotherapy. The study also

highlights a series of effects on some cardiotoxicity biomarkers such as mitochondrial respiration and reactive oxygen substances (ROS) production, confirming the ability of the compound to improve cardiac tolerability to the potential toxicity induced by anthracyclines and doxorubicin in particular. Another indirect anti-toxic effect of this bacterial metabolite is the intestinal wall health improvement and inflammatory phenomena reduction already observed as potential treatment of chemotherapy related mucositis (though not only). This effect is also well documented in literature [36] where it is demonstrated that its administration reduces taxanes intestinal toxicity, such as paclitaxel (one of the most widely used chemotherapy in case of ovarian, breast, and lung cancers among others), precisely by protecting and safeguarding intestinal wall health, decreasing chemotherapy induced dysbiosis and permeability of the wall itself. A recent placebo-controlled study performed in China [37] examined the effect of CB on patients receiving platinum-based chemotherapy plus anti-angiogenics for non-squamous non-small cell lung cancer. This study confirmed a significant reduction in drug toxicity in the group receiving CB compared to a placebo. Furthermore, a eubiotic effect of the microbiota is highlighted with an increase also of bifidobacteria and lactobacilli, as well as a not statistically significant but still evident effect on the progression free survival (PFS) and overall survival (OS) of these patients. However, this significance has been amply demonstrated in a Japanese study [38] in which patients subjected in this case to immunotherapy treatment for lung cancer improved their PFS and OS compared to the placebo group even after antibiotic therapy. In conclusion we cannot fail to mention the work of [39] which, as an example of butyrate-dependent chemotherapy efficacy improvement, allows us to highlight the ability of CB to increase the apoptotic capacity of 5-fluoruracil (5-FU) in colorectal cancer through its (limiting) action on glucose transport and aerobic glycolysis, limiting energy source of tumor cells in metabolic reprogramming or Warburg effect [40]. Therefore, in consideration of what has been exposed, CB seems to be an important weapon at our disposal (immediately) to try to modulate chemotherapy toxicity and efficacy and therefore the quality of life and prognosis of our patients. The methods of intervention can be summarized in the following diagram (Figure 5).

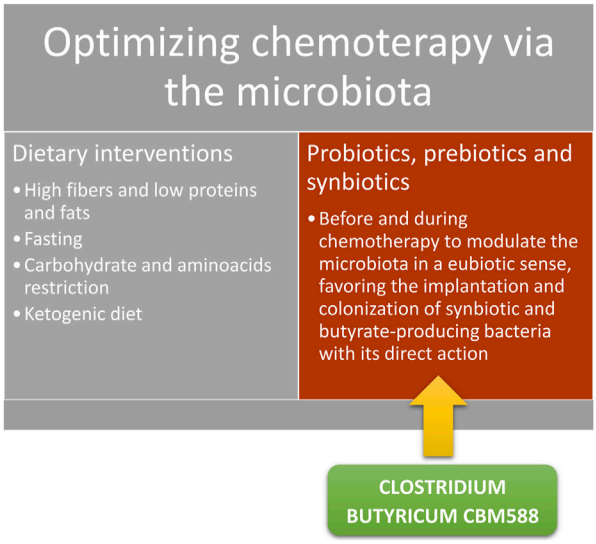

FIGURE 5
Possible interventions to increase the proportion of SCFAs in particular of butyrate and modulate the toxicity and efficacy of chemotherapy.

Possibility of using other compounds. The example of berberine and curcumin

Although the butyrate approach is apparently the most documented, other non-direct bacterial interventions have shown good modulation capacity in oncological treatment scenarios, so much so that they can be taken into account both alone and in association with the therapies just described. This is the case of some nutraceuticals or herbs that are now widely discussed and studied, such as berberine (BBR) [41] and curcumin (CUR) [42]. In fact, both of these compounds have already shown unequivocal properties of toxicity reduction and/or tumor cells sensitization to chemotherapeutics. For example, BBR is one of the compounds that seem able to modify the effect of the toxicity of Irinotecan already described above. In fact, being a natural inhibitor of the enzyme b-glucuronidase, BBR reduces the deconjugation action of this enzyme, reducing the possibility of reactivation of the inactive metabolite of irinotecan, consequently reducing its toxic effect (mucositis). This possibility is well documented in a 2021 work concerning colorectal tumors [43] and where the protective capacity of intestinal permeability and consequently anti-inflammatory of BBR is highlighted precisely through the modulation of the deconjugating enzyme and therefore the reduction of side effects of treatment. Also, BBR could be considered as an excellent alternative in terms of raising awareness of oncological treatments. As we have previously highlighted, one of the mechanisms of resistance to oncological drugs is that of autophagy which makes tumor cells less and less sensitive to the toxic action of chemotherapy, effectively establishing a sort of worsening resistance to the treatment. Being a natural inhibitor of this mechanism, BBR appears to be a potential ally to the action of chemotherapy to mitigate the problem of resistance and therefore increasing its sensitivity and in fact its effectiveness [44].

Furthermore, BBR does not seem to be the only herb capable of modulating the autophagy action of tumor cells, improving the efficiency of oncological treatments. For example, CUR, as demonstrated by many works, also appears effective in this important anticancer action. Indeed, the CUR, in addition to

also having important properties of reducing chemotherapy (and radiotherapy) side effects [45], has evident chemosensitization capacities and therefore seems capable of increasing the action of some chemotherapeutics [46].

In addition to the aforementioned effect on autophagy, we recall that one of the most important mechanisms in the onset of the chemo-resistance phenomenon is determined by the activity of an extrusion pump on the cell surface managed by some proteins, the most important of which is glycoprotein P which eliminates the drug from the cell making the treatment less and less effective [47]. CUR is a potent natural inhibitor of P-glycoprotein and its administration has already demonstrated an increase in cellular sensitivity to chemotherapy precisely thanks to the inhibition of this limiting cellular factor [48]. Some works have already highlighted the effectiveness of this treatment, including that of [49] which demonstrates the increased sensitivity of breast cancer cells to the action of doxorubicin when treated with CUR. Equal positive results are also already evident for other types of cancer such as that of the cervix and ovary [50, 51], or therapy, for example with anti-estrogens such as tamoxifen [52].

Conclusion

Oncological therapies and in particular their clinical efficacy and tolerability are influenced by many factors, both pharmacological and individual of the patients themselves. Among these, the importance of the microbiota (colonial in particular but also of the various districts involved) is increasingly evident and impactful. In the coming years, inevitably, oncological treatments will need to be accompanied by in-depth microbial analyses and improved by the microbial parameters (biodiversity, eubiosis, metabolic capacity, etc.) in order to favor an environment conducive to the action of the drugs and/or the reduction of their toxicity. Chemotherapy is certainly one of the treatments most closely related to the microbiota and numerous studies are highlighting how certain bacterial characteristics can favor or disadvantage the therapeutic result and how modulation through the use of prebiotics, probiotics, and nutraceuticals is and will be increasingly decisive in managing such a scenario. This review—focused in particular on chemotherapy—has highlighted some examples in this sense, emphasizing the importance of some interventions such as that of the CB of the BBR and the CUR but also opening up the possibility of studying other compounds in order to further improve the effectiveness of oncological treatments.

Author contributions

Conceptualization, MCaz and AB; methodology, MCaz and FDP; validation, GZ and CP; formal analysis, MCar; investigation; MCaz, AB, and FDP; resources; MCaz and AB; data curation, MCaz and FDP; Writing–original draft preparation; MCaz and AB, writing–review and editing, AB, GZ, CP, and MCar; visualization, MCaz, FDP, and AB; supervision, AB and CP; project administration, AB and MCar. All authors contributed to the article and approved the submitted version.

Conflict of interest

FDP belongs to the Scientific Board of Pharmextracta. MCaz and AB were a Pharmextracta scientific advisor.

The remaining authors declare that the research was conducted in the absence of any commercial or financial relationships that could be construed as a potential conflict of interest.

References

1. El-Sayed A, Aleya L, Kamel M. Microbiota's role in health and diseases. *Environ Sci Pollut Res Int* (2021) 28(28):36967–83. doi:10.1007/s11356-021-14593-z

2. Nejman D, Livyatan I, Fuks G, Gavert N, Zwang Y, Geller LT, et al. The human tumor microbiome is composed of tumor type-specific intracellular bacteria. *Nejman Sci* (2020) 368(6494):973–80. doi:10.1126/science.aay9189

3. Audirac-Chalifour A, Torres-Poveda K, Bahena-Román M, Téllez-Sosa J, Martínez-Barnetche J, Cortina-Ceballos B, et al. Cervical microbiome and cytokine profile at various stages of cervical cancer: A pilot study. *PLoS One* (2016) 11(4):e0153274. doi:10.1371/journal.pone.0153274

4. Gethings-Behncke C, Coleman HG, Jordao HWT, Longley DB, Crawford N, Murray LJ, et al. Fusobacterium nucleatum in the colorectum and its association with cancer risk and survival: A systematic review and meta-analysis. *Cancer Epidemiol Biomarkers Prev* (2020) 29(3):539–48. doi:10.1158/1055-9965.EPI-18-1295

5. Roy S, Trinchieri G. Microbiota: A key orchestrator of cancer therapy. *Nat Rev Cancer* (2017) 17(5):271–85. doi:10.1038/nrc.2017.13

6. Sevcikova A, Izoldova N, Stevurkova V, Kasperova B, Chovanec M, Ciernikova S, et al. The impact of the microbiome on resistance to cancer treatment with chemotherapeutic agents and immunotherapy. *Int J Mol Sci* (2022) 23:488. doi:10.3390/ijms23010488

7. Sharom FJ. ABC multidrug transporters: Structure, function and role in chemoresistance. *Pharmacogenomics* (2008) 9:105–27. doi:10.2217/14622416.9.1.105

8. Li LY, Guan YD, Chen XS, Yang JM, Cheng Y. DNA repair pathways in cancer therapy and resistance. *Front Pharmacol* (2020) 11:629266. doi:10.3389/fphar.2020.629266

9. Lehouritis P, Cummins J, Stanton M, Murphy CT, McCarthy FO, Reid G, et al. Local bacteria affect the efficacy of chemotherapeutic drugs. *Sci Rep* (2015) 5:14554. doi:10.1038/srep14554

10. Mini E, Nobili S, Caciagli B, Landini I, Mazzei T. Cellular pharmacology of gemcitabine. *Ann Oncol* (2006) 17:v7–12. doi:10.1093/annonc/mdj941

11. Geller LT, Straussman R. Intratumoral bacteria may elicit chemoresistance by metabolizing anticancer agents. *Mol Cell Oncol.* (2017) 5(1):e1405139. doi:10.1080/23723556.2017.1405139

12. Geller LT, Barzily-Rokni M, Danino T, Jonas OH, Shental N, Nejman D, et al. Potential role of intratumor bacteria in mediating tumor resistance to the

chemotherapeutic drug gemcitabine. *Science* (2017) 357(6356):1156–60. doi:10.1126/science.aah5043

13. Shang FM, Liu HL. Fusobacterium nucleatum and colorectal cancer: A review. *World J Gastrointest Oncol* (2018) 10(3):71–81. doi:10.4251/wjgo.v10.i3.71

14. Li YJ, Lei YH, Yao N, Wang CR, Hu N, Ye WC, et al. Autophagy and multidrug resistance in cancer. *Chin J Cancer* (2017) 36(1):52. doi:10.1186/s40880-017-0219-2

15. TaChung Y, Guo F, Yu Y, Sun T, Ma D, Han J, et al. Fusobacterium nucleatum promotes chemoresistance to colorectal cancer by modulating autophagy. *Cell* (2017) 170:548–63. doi:10.1016/j.cell.2017.07.008

16. Emadi A, Jones RJ, Brodsky RA. Cyclophosphamide and cancer: Golden anniversary. *Nat Rev Clin Oncol* (2009) 6:638–47. doi:10.1038/nrclinonc.2009.146

17. Ahlmann M, Hempel G. The effect of cyclophosphamide on the immune system: Implications for clinical cancer therapy. *Cancer Chemother Pharmacol* (2016) 78:661–71. doi:10.1007/s00280-016-3152-1

18. Viaud S, Saccheri F, Mignot G, Yamazaki T, Daillère R, Hannani D, et al. The intestinal microbiota modulates the anticancer immune effects of cyclophosphamide. *Science* (2013) 342(6161):971–6. doi:10.1126/science.1240537

19. Lida N, Dzutsev A, Stewart CA, Smith L, Bouladoux N, Weingarten RA, et al. Commensal bacteria control cancer response to therapy by modulating the tumor microenvironment. *Science* (2013) 342(6161):967–70. doi:10.1126/science.1240527

20. Bailly C. Irinotecan: 25 years of cancer treatment. *Pharmacol Res* (2019) 148:104398. doi:10.1016/j.phrs.2019.104398

21. Kciuk M, Marciniak B, Kontek R. Irinotecan-still an important player in cancer chemotherapy: A comprehensive overview. *Int J Mol Sci* (2020) 21(14):4919. doi:10.3390/ijms21144919

22. Yue B, Gao R, Wang Z, Dou W. Microbiota-host-irinotecan Axis: A new insight toward irinotecan chemotherapy. *Front Cell Infect Microbiol* (2021) 11:710945. doi:10.3389/fcimb.2021.710945

23. Jasiewicz F, Qurban Z, Hughes C. Treatment-induced mucositis in oncology. *Br J Hosp Med (Lond)* (2022) 83(9):1–8. doi:10.12968/hmed.2022.0324

24. Keefe DM, Gibson RJ, Hauer-Jensen M. Gastrointestinal mucositis. *Semin Oncol Nurs* (2004) 20:38–47. doi:10.1053/j.soncn.2003.10.007

25. Sonis ST. The pathobiology of mucositis. *Nat Rev Cancer* (2004) 4(4):277–84. doi:10.1038/nrc1318

26. Van Vliet MJ, Harmsen HJM, de Bont ESJM, Tissing WJE. The role of intestinal microbiota in the development and severity of chemotherapy-induced mucositis. *Plos Pathog* (2010) 6(5):e1000879. doi:10.1371/journal.ppat.1000879

27. Holscher HD. Dietary fiber and prebiotics and the gastrointestinal microbiota. *Gut Microbes* (2017) 8(2):172–84. doi:10.1080/19490976.2017.1290756

28. Stoeva MK, Garcia-So J, Justice N, Myers J, Tyagi S, Nemchek M, et al. Butyrate-producing human gut symbiont, Clostridium butyricum, and its role in health and disease. *Gut Microbes* (2021) 13(1):1–28. doi:10.1080/19490976.2021.1907272

29. Ariyoshi T, Hagihara M, Tomono S, Eguchi S, Minemura A, Miura D, et al. Clostridium butyricum MIYAIRI 588 modifies bacterial composition under antibiotic-induced dysbiosis for the activation of interactions via lipid metabolism between the gut microbiome and the host. *Biomedicines* (2021) 9(8):1065. doi:10.3390/biomedicines9081065

30. Koh A, De Vadder F, Kovatcheva-Datchary P, Bäckhed F. From dietary fiber to host physiology: Short-chain fatty acids as key bacterial metabolites. *Cell* (2016) 165(6):1332–45. doi:10.1016/j.cell.2016.05.041

31. Liu P, Wang Y, Yang G, Zhang Q, Meng L, Xin Y, et al. The role of short-chain fatty acids in intestinal barrier function, inflammation, oxidative stress, and colonic carcinogenesis. *Pharmacol Res* (2021) 165:105420. doi:10.1016/j.phrs.2021.105420

32. Mirzaei R, Afaghi A, Babakhani S, Sohrabi MR, Hosseini-Fard SR, Babolhavaeji K, et al. Role of microbiota-derived short-chain fatty acids in cancer development and prevention. *Biomed Pharmacother* (2021) 139:111619. doi:10.1016/j.biopha.2021.111619

33. Al-Qadami GH, Secombe KR, Subramaniam CB, Wardill HR, Bowen JM. Gut microbiota-derived short-chain fatty acids: Impact on cancer treatment response and toxicities. *Microorganisms* (2022) 10(10):2048. doi:10.3390/microorganisms10102048

34. Danne C, Sokol H. Butyrate, a new microbiota-dependent player in CD8+ T cells immunity and cancer therapy? *Cell Rep Med* (2021) 2(7):100328. doi:10.1016/j.xcrm.2021.100328

35. Russo M, Guida F, Paparo L, Trinchese G, Aitoro R, Avagliano C, et al. The novel butyrate derivative phenylalanine-butyramide protects from doxorubicin-induced cardiotoxicity. *Eur J Heart Fail* (2019) 21(4):519–28. doi:10.1002/ejhf.1439

36. Cristiano C, Cuozzo M, Coretti L, Liguori FM, Cimmino F, Turco L, et al. Oral sodium butyrate supplementation ameliorates paclitaxel-induced behavioral and intestinal dysfunction. *Biomed Pharmacother* (2022) 153:113528. doi:10.1016/j.biopha.2022.113528

37. Cong J, Zhang C, Zhou S, Zhu J, Liang C. A pilot study: Favorable effects of clostridium butyricum on intestinal microbiota for adjuvant therapy of lung cancer. *Cancers (Basel)* (2022) 14(15):3599. doi:10.3390/cancers14153599

38. Tomita Y, Ikeda T, Sakata S, Saruwatari K, Sato R, Iyama S, et al. Association of probiotic clostridium butyricum therapy with survival and response to immune checkpoint blockade in patients with lung cancer. *Cancer Immunol Res* (2020) 8(10):1236–42. doi:10.1158/2326-6066.CIR-20-0051

39. Geng HW, Yin FY, Zhang ZF, Gong X, Yang Y. Butyrate suppresses glucose metabolism of colorectal cancer cells via GPR109a-AKT signaling pathway and enhances chemotherapy. *Front Mol Biosci* (2021) 8:634874. doi:10.3389/fmolb.2021.634874

40. Pascale RM, Calvisi DF, Simile MM, Feo CF, Feo F. The Warburg effect 97 Years after its discovery. *Cancers (Basel)* (2020) 12(10):2819. doi:10.3390/cancers12102819

41. Song D, Hao J, Fan D. Biological properties and clinical applications of berberine. *Front Med* (2020) 14(5):564–82. doi:10.1007/s11684-019-0724-6

42. Patel SS, Acharya A, Ray RS, Agrawal R, Raghuwanshi R, Jain P. Cellular and molecular mechanisms of curcumin in prevention and treatment of disease. *Crit Rev Food Sci Nutr* (2020) 60(6):887–939. doi:10.1080/10408398.2018.1552244

43. Yue B, Gao R, Lv C, Yu Z, Wang H, Geng X, et al. Berberine improves irinotecan-induced intestinal mucositis without impairing the anti-colorectal cancer efficacy of irinotecan by inhibiting bacterial β-glucuronidase. *Front Pharmacol* (2021) 12:774560. doi:10.3389/fphar.2021.774560

44. Mohammadinejad R, Ahmadi Z, Tavakol S, Ashrafizadeh M. Berberine as a potential autophagy modulator. *J Cell Physiol* (2019) 234(9):14914–26. doi:10.1002/jcp.28325

45. Belcaro G, Hosoi M, Pellegrini L, Appendino G, Ippolito E, Ricci A, et al. A controlled study of a lecithinized delivery system of curcumin (Meriva®) to alleviate the adverse effects of cancer treatment. *Phytother Res* (2014) 28(3):444–50. doi:10.1002/ptr.5014

46. Shakeri A, Cicero AFG, Panahi Y, Mohajeri M, Sahebkar A. Curcumin: A naturally occurring autophagy modulator. *J Cell Physiol* (2019) 234(5):5643–54. doi:10.1002/jcp.27404

47. Waghray D, Zhang Q. Inhibit or evade multidrug resistance P-glycoprotein in cancer treatment. *J Med Chem* (2018) 61(12):5108–21. doi:10.1021/acs.jmedchem.7b01457

48. Lopes-Rodrigues V, Sousa E, Vasconcelos MH. Curcumin as a modulator of P-glycoprotein in cancer: Challenges and perspectives. *Pharmaceuticals (Basel)* (2016) 9(4):71. doi:10.3390/ph9040071

49. Guo S, Lv L, Shen Y, Hu Z, He Q, Chen X. A nanoparticulate pre-chemosensitizer for efficacious chemotherapy of multidrug resistant breast cancer. *Sci Rep* (2016) 6:21459. doi:10.1038/srep21459

50. Sreekanth CN, Bava SV, Sreekumar E, Anto RJ. Molecular evidences for the chemosensitizing efficacy of liposomal curcumin in paclitaxel chemotherapy in mouse models of cervical cancer. *Oncogene* (2011) 30(28):3139–52. doi:10.1038/onc.2011.23

51. Yallapu MM, Maher DM, Sundram V, Bell MC, Jaggi M, Chauhan SC. Curcumin induces chemo/radio-sensitization in ovarian cancer cells and curcumin nanoparticles inhibit ovarian cancer cell growth. *J Ovarian Res* (2010) 3:11. doi:10.1186/1757-2215-3-11

52. Jiang M, Huang O, Zhang X, Xie Z, Shen A, Liu H, et al. Curcumin induces cell death and restores tamoxifen sensitivity in the antiestrogen-resistant breast cancer cell lines MCF-7/LCC2 and MCF-7/LCC9. *Molecules* (2013) 18(1):701–20. doi:10.3390/molecules18010701

Pathology & Oncology Research | frontiers

TYPE Review
PUBLISHED 23 February 2024
DOI 10.3389/pore.2024.1611623

Check for updates

OPEN ACCESS

EDITED BY
Andrea Ladányi,
National Institute of Oncology (NIO), Hungary

*CORRESPONDENCE
Vince Fazekas-Pongor,
pongor.vince@semmelweis.hu

RECEIVED 04 December 2023
ACCEPTED 07 February 2024
PUBLISHED 23 February 2024

CITATION
Fekete M, Major D, Feher A, Fazekas-Pongor V and Lehoczki A (2024), Geroscience and pathology: a new frontier in understanding age-related diseases.
Pathol. Oncol. Res. 30:1611623.
doi: 10.3389/pore.2024.1611623

COPYRIGHT
© 2024 Fekete, Major, Feher, Fazekas-Pongor and Lehoczki. This is an open-access article distributed under the terms of the Creative Commons Attribution License (CC BY). The use, distribution or reproduction in other forums is permitted, provided the original author(s) and the copyright owner(s) are credited and that the original publication in this journal is cited, in accordance with accepted academic practice. No use, distribution or reproduction is permitted which does not comply with these terms.

Geroscience and pathology: a new frontier in understanding age-related diseases

Monika Fekete[1], David Major[1], Agnes Feher[1], Vince Fazekas-Pongor[1]* and Andrea Lehoczki[1,2]

[1]Department of Public Health, Semmelweis University, Budapest, Hungary, [2]Departments of Hematology and Stem Cell Transplantation, South Pest Central Hospital, National Institute of Hematology and Infectious Diseases, Saint Ladislaus Campus, Budapest, Hungary

Geroscience, a burgeoning discipline at the intersection of aging and disease, aims to unravel the intricate relationship between the aging process and pathogenesis of age-related diseases. This paper explores the pivotal role played by geroscience in reshaping our understanding of pathology, with a particular focus on age-related diseases. These diseases, spanning cardiovascular and cerebrovascular disorders, malignancies, and neurodegenerative conditions, significantly contribute to the morbidity and mortality of older individuals. We delve into the fundamental cellular and molecular mechanisms underpinning aging, including mitochondrial dysfunction and cellular senescence, and elucidate their profound implications for the pathogenesis of various age-related diseases. Emphasis is placed on the importance of assessing key biomarkers of aging and biological age within the realm of pathology. We also scrutinize the interplay between cellular senescence and cancer biology as a central area of focus, underscoring its paramount significance in contemporary pathological research. Moreover, we shed light on the integration of anti-aging interventions that target fundamental aging processes, such as senolytics, mitochondria-targeted treatments, and interventions that influence epigenetic regulation within the domain of pathology research. In conclusion, the integration of geroscience concepts into pathological research heralds a transformative paradigm shift in our understanding of disease pathogenesis and promises breakthroughs in disease prevention and treatment.

KEYWORDS

geroscience, senescence, cancer, cardiovascular disease, ageing

Introduction

Geroscience, an emerging discipline at the intersection of aging and disease, seeks to understand the relationship between the aging process and pathogenesis of age-related diseases [1, 2]. Historically, the concept of cellular pathology laid the groundwork for modern pathology [3]. Today, geroscience promises to revolutionize this field by illuminating how aging mechanisms contribute to the pathogenesis of diseases

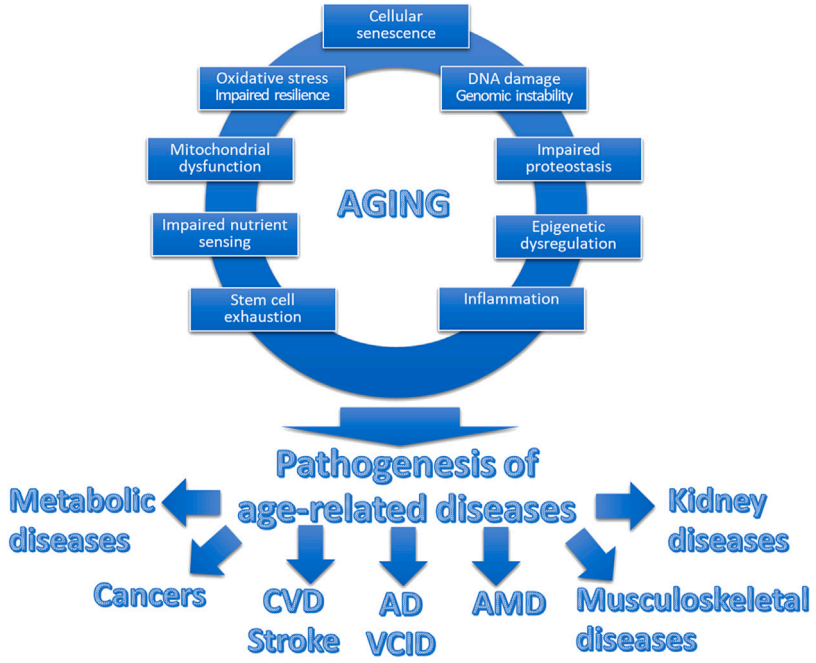

FIGURE 1
Interplay between hallmarks of aging and age-related diseases. This schematic figure illustrates the interplay between the fundamental cellular and molecular mechanisms of aging, collectively contributing to what we perceive as "aging." The top section showcases these interconnected hallmarks of aging, encompassing processes such as cellular senescence, mitochondrial dysfunction, genomic instability, and heightened state of inflammation, among others. These synergistic aging processes promote the pathogenesis of a spectrum of diverse age-related diseases. These diseases, including but not limited to cardiovascular diseases (CVD), cancer, neurodegenerative disorders (including Alzheimer's disease; AD), vascular cognitive impairment and dementia VCID), eye diseases (including age-related macular degeneration, AMD), musculoskeletal diseases and metabolic diseases, share a common origin in the aging process.

associated with aging [4]. Geroscience has evolved significantly, fueled by discoveries that suggest that aging is governed by evolutionarily conserved cellular and molecular mechanisms and is a modifiable process. This perspective offers a novel lens through which the field of pathology can be viewed. Cellular aging is now viewed as a complex, regulated and potentially reversible process, governed by a genetic program, transcending the mere accumulation of macromolecular damage over time [4]. It is intricately intertwined with cellular dysfunction, playing a pivotal role in the onset of age-associated diseases. This perspective highlights that aging is not just a passive decline in cellular integrity but a coordinated series of events that might be amenable to targeted interventions.

Expanding on the core principles of geroscience, it's important to delve into the fundamental, evolutionarily conserved aging mechanisms. These mechanisms, often referred to as the "pillars" or "hallmarks" of aging, drive the functional and phenotypic changes in aging cells [5]. Understanding these mechanisms is crucial for both geroscience and pathology, as they provide insights into the biological processes that underlie aging and age-related diseases. These mechanisms play a critical role in multitude of age-related diseases, including hematological diseases [6, 7], Alzheimer's disease [8–12], osteoporosis, sarcopenia, various types of cancer, presbycusis and cardiovascular and cerebrovascular diseases [13–21]. In pathology, this link is crucial for understanding the etiology and progression of diseases that demonstrate an age-related increase in morbidity and mortality.

Hallmarks of aging and their pathological implications

Understanding the role of mechanisms/hallmarks of aging is pivotal in pathology, especially when examining age-related diseases [10, 22, 23]. Each of these aging mechanisms is intricately interconnected, collectively contributing to the pathology of a diverse array of age-related diseases (Figure 1). Their combined effects underscore the complexity of aging as a multi-faceted process, deeply influencing the onset and progression of various pathologies. Generally, a significant number of these mechanisms stem from spontaneous, stochastic damage, which in turn activates evolutionarily conserved cellular responses such as cellular senescence and

inflammatory pathways. Concurrently, these processes are intertwined with pathways that determine cellular resilience to such damage or stress, including but not limited to the maintenance of proteostasis [24–28], the efficacy of Nrf2-driven antioxidant responses [29–36], and the integrity of DNA repair systems [37].

Recent advancements have revealed that cell-autonomous mechanisms alone do not fully account for the complexities of aging. Instead, aging of various organ systems is also governed by a hierarchical regulatory cascade, where cell-autonomous aging processes are modulated by systemic and circulating factors [28, 38–40]. Furthermore, age-related changes within cells often lead to non-cell autonomous effects, such as the release of paracrine mediators from senescent cells, which in turn influence tissue aging [41–43]. A unifying model suggests that the orchestration of aging processes across various organs involves a balance of circulating pro-geronic and anti-geronic factors. These factors, emanating from the central nervous system, endocrine organs, the immune system, adipose tissue, and even the gastrointestinal tract, play pivotal roles in orchestrating and harmonizing aging processes. An important implication of this concept is that conventional risk factors (including lifestyle [44–50] and environmental risk factors [51, 52]) exacerbate age-related pathologies by intensifying fundamental molecular and cellular aging processes, both cell autonomous and non-cell autonomous.

Since the free radical theory of aging was published in the 1950s, oxidative stress has been increasingly recognized as a key player in the aging process [53, 54]. While reactive oxygen species (ROS) play essential roles in cell signaling, excessive ROS production or inadequate ROS detoxification can lead to oxidative stress, damaging cells and tissues and causing cellular dysfunction [55–60]. In the context of aging, the balance between ROS production and antioxidant defenses becomes skewed. Age-related increases in oxidative stress are thought to contribute to cardiovascular pathologies [61–71], the deterioration of neurological function and development of brain and muscle aging phenotypes, among others. One of the most critical impacts of oxidative stress in aging is on cellular signaling pathways, including triggering of inflammatory mechanisms [30, 67].

The reduced capacity of older cells to counter molecular stress and achieve homeostasis is a critical aging phenomenon [72]. In youthful organisms, a rise in cellular reactive oxygen species prompts adaptive homeostatic responses, chiefly through the activation of the Nrf2 (Nuclear factor erythroid 2-related factor 2)-driven antioxidant defense pathway [30–32, 73]. Nrf2, a transcription factor sensitive to redox changes, coordinates this response, up-regulating the levels of enzymes that neutralize ROS and repair ROS-inflicted macromolecular damage [74]. This adaptive response effectively mitigates oxidative stress in younger cells. However, as organisms age, a significant reduction in Nrf2 functionality occurs, especially noticeable in vascular tissues. This reduction intensifies oxidative stress and increases the susceptibility of aged cells to ROS-related damage, potentially playing a pivotal role in the emergence of age-related pathologies [30, 31]. Notably, the beneficial anti-aging effects associated with caloric restriction are linked to the stimulation of these Nrf2-mediated pathways [29, 75].

Genomic instability, characterized by the accumulation of DNA damage from environmental stressors and metabolic activities, is a key contributor to aging [76]. This instability can result in mutations and chromosomal aberrations, which are central to the development of many age-related diseases, particularly cancer and cardiovascular diseases [18, 77, 78]. Recently, clonal hematopoiesis of indeterminate potential (CHIP) has emerged as a significant area of interest in geroscience [79–88]. CHIP refers to an age-related phenomenon where hematopoietic stem cells acquire somatic mutations that lead to pre-malignant clonal expansion of white blood cells [81–88]. These cells exhibit marked changes in their function, including a pro-inflammatory shift in their phenotype. Importantly, CHIP is not necessarily linked to hematological malignancies but is associated with an increased risk of developing a range of age-related diseases, including atherosclerosis [81–88].

Telomeres, which are protective caps at the ends of chromosomes, gradually shorten with each cell division [18, 89]. Excessive shortening contribute to cellular aging or apoptosis, impairing tissue repair and regeneration [90–93]. Telomere attrition is thought to contribute to many age-related diseases and conditions [18, 94–97].

Age-related changes in epigenetic regulation, such as DNA methylation [94, 98–103], affect gene expression and are implicated in dysregulation of various cellular processes with age and the pathogenesis of age-related diseases, including cancer [104], cardiovascular diseases [105] and Alzheimer's disease.

With aging, the ability of cells to maintain protein homeostasis diminishes [106], leading to the accumulation of misfolded proteins [107]. Impaired protein homeostasis has been linked to the pathogenesis of a wide range of age-related diseases and conditions [108]. This loss is characteristic of neurodegenerative diseases like Parkinson's disease and Alzheimer's disease, where protein aggregates are a hallmark feature [109], disrupting normal organ function.

Aging affects nutrient-sensing pathways [110], impacting metabolism and cellular growth. Alterations in insulin signaling and mTOR pathways are considered evolutionarily conserved mechanisms of aging [111–113]. These changes are evident in age-related diseases like type 2 diabetes and are implicated in the pathogenesis of many age-related diseases, including various types of cancer [114–117] cardiovascular diseases and Alzheimer's disease.

Autophagy, a multifaceted cellular pathway, stands as a central player in the intricate interplay between aging and disease processes [118–121]. It plays a pivotal role in

maintaining cellular homeostasis by degrading and recycling damaged or dysfunctional cellular components, thereby promoting cellular renewal and survival. In the context of aging, autophagy's efficacy tends to decline, leading to the accumulation of cellular debris and dysfunctional organelles, which are hallmarks of aging [122–125]. The influence of autophagy extends beyond cellular maintenance, as it significantly impacts immune regulation [126, 127] and tumorigenesis [128]. One of the critical regulatory connections involving autophagy is its interaction with the mTOR pathway [129, 130]. mTOR is a central regulator of cellular growth and metabolism, and it inhibits autophagy when nutrients are plentiful. Conversely, during nutrient scarcity or stress conditions, mTOR inhibition allows autophagy to proceed, promoting the removal of damaged cellular components and recycling of resources. This intricate balance between mTOR and autophagy is intimately tied to aging and disease [129, 130], as excessive mTOR activity and compromised autophagy are associated with age-related pathologies, including neurodegenerative diseases and cancer. In the context of immune regulation, autophagy plays a dual role [126, 127]. It contributes to the activation and functioning of immune cells, aiding in the presentation of antigens. Conversely, autophagy can also regulate immune responses, influencing immune tolerance and autoimmunity. Dysregulation of autophagy in immune cells can have profound consequences on an individual's susceptibility to infections and autoimmune diseases [131]. Regarding tumorigenesis, autophagy's role is complex [128]. It can promote tumor survival under certain conditions by providing cancer cells with nutrients during nutrient deprivation or stress. In summary, autophagy represents a multifaceted cellular pathway with far-reaching implications in aging. Its intricate relationship with mTOR highlights its significance in aging and disease processes, making it a compelling focus of research in the field of geroscience and cancer biology. Understanding how to modulate autophagy effectively may hold promise in promoting healthy aging and combating age-related diseases.

Sirtuins, a family of NAD+-dependent protein deacetylases, have emerged as pivotal regulators of cellular and organismal aging [132–140]. By modulating the acetylation status of a myriad of protein targets, Sirtuins regulate cellular metabolism, genomic stability, stress resilience and stress response pathways [141–150]. Through their influence on key cellular processes such as DNA repair, mitochondrial function, and inflammation, Sirtuins directly impact the rate of aging and age-related diseases [141–150]. Their intricate involvement in pathways related to calorie restriction and cellular homeostasis has led to substantial interest in their potential as therapeutic targets for extending healthspan and combating age-related diseases. Cytoplasmic (SIRT1, SIRT2, SIRT6) [151, 152], nuclear (SIRT1, SIRT2, SIRT6), nucleolar (SIRT7) [153], and mitochondrial (SIRT3, SIRT4, SIRT5) [154–158] sirtuins represent distinct subtypes within the broader family of sirtuins. SIRT1, the most extensively studied cytoplasmic sirtuin, is known for its specific roles in modulating cellular responses to nutrient availability and energy balance. It plays a crucial role in calorie restriction-related pathways, where it promotes the deacetylation and activation of various transcription factors, such as PGC-1α and FOXO, which are involved in metabolic processes, mitochondrial biogenesis, and antioxidant defense. SIRT2 regulates cytoskeletal dynamics and cell cycle progression, while SIRT6 and SIRT7 are implicated in DNA repair and chromatin maintenance, contributing to genomic stability. SIRT3, for example, promotes the deacetylation and activation of several mitochondrial proteins involved in oxidative phosphorylation and antioxidant defense, thereby enhancing mitochondrial efficiency and reducing oxidative stress. SIRT4 and SIRT5 play roles in regulating mitochondrial metabolism and amino acid metabolism, respectively. Dysregulation of cytoplasmic, nucleolar, or mitochondrial sirtuins can contribute to cellular dysfunction and accelerate the aging process, making them intriguing targets for interventions aimed at promoting healthy aging and mitigating age-related diseases.

Mitochondrial dysfunction is also a hallmark of aging [5, 159–161], impairing cellular energy metabolism and increasing oxidative stress, which profoundly affect cellular health and function. Mitochondrial dysfunction is thought to contribute to a range of age-related diseases [162], including neurodegenerative disorders [163], cardiovascular diseases [67, 72, 75, 164–166] and musculoskeletal diseases [167], including sarcopenia [168].

In aging dividing cells often enter a state of cellular senescence, impacting tissue function [169]. Cellular senescence is a DNA damage-induced cellular stress response, which is associated with profound changes in cellular phenotype [14]. Senescent cells secrete a range of inflammatory factors [170] and enzymes disrupting the extracellular matrix, contributing to tissue aging and dysfunction [171]. The accumulation of senescent cells is thought to be a driver of aging [111, 172–174] and have been linked to the pathogenesis of a number of age-related diseases [175], including musculoskeletal diseases [176, 177], neurodenegenenerative diseases [8, 10, 178] and VCI [179, 180], retina diseases [181] and cardiovascular diseases. The increased presence of senescent cells, often a result of DNA damage induced by lifestyle, environmental exposures [182], and certain interventions like anti-cancer therapies [183, 184], is believed to lead to accelerated aging, exacerbating the progression of age-related conditions and physiological decline. The intersection of cellular senescence biology and cancer biology represents a highly dynamic and increasingly pivotal area of interest in pathology, highlighting the complex relationship between aging processes and cancer development [185].

The regenerative potential of stem cells diminishes with age, affecting tissue repair and regeneration [186]. Stem cell

exhaustion is thought to be an important factor in aging and age-related pathologies like musculoskeletal diseases and hematologic diseases.

Aging is associated with chronic low-grade sterile inflammation, often termed "inflammaging [171, 187–190]," which is a significant contributor to many age-related diseases, including cardiovascular diseases, neuroinflammation and neurodegenerative diseases [191–194], sarcopenia [195] and cognitive dysfunction [194, 196, 197].

In pathology, these cellular and molecular mechanisms provide a framework for understanding the complex interplay between aging and disease. By considering these mechanisms, pathologists can gain insights into the onset, progression, and potential therapeutic targets for a wide range of age-related conditions.

Anti-aging interventions and plasticity of aging

Anti-aging interventions, which specifically target one or more fundamental aging processes, hold immense potential in preventing the development of age-related diseases and altering their trajectories. These therapies, ranging from pharmacological [198–201] to dietary [202], nutraceutical [203], and lifestyle [204] interventions [205–207], aim to slow aging and prevent age-related pathologies. The burgeoning field of pharmacological anti-aging interventions is rapidly evolving, with several promising therapeutic avenues emerging. Among these, senolytics, which selectively target and eliminate senescent cells, are at the forefront [176, 180, 181, 208–210]. These agents offer potential in mitigating the detrimental effects of cellular senescence, a key contributor to age-related diseases and dysfunctions. Another area of significant translational relevance is mitochondria-targeted treatments [165, 211–213]. Treatments that modulate epigenetic regulation [214, 215] and restore cellular NAD levels [216–226] represent another exciting frontier. Additionally, targeting the mTOR pathway offers significant potential [12]. Inhibitors of the mTOR pathway have shown promising results in extending lifespan and healthspan in various model organisms [15, 113], suggesting their potential applicability in human aging.

As we move into the upcoming decade, we anticipate significant advancements in developing these novel interventions. The role of pathology in this progress is pivotal. With standardized assessment of key biomarkers of aging, pathology will play a crucial role in rigorously testing the efficacy of these interventions. This testing, critical both in preclinical studies and clinical trials, can include methodologies such as using tissue biopsies to assess the impact of these interventions on cellular and molecular levels. The integration of interventions that target cellular and molecular mechanisms of aging into pathological studies not only holds the potential for breakthroughs in disease prevention and treatment but also promises to revolutionize our understanding of disease pathogenesis. This revolution involves introducing geroscience concepts into pathology, further bridging the gap between aging research and clinical practice.

Novel tools and experimental models from geroscience

Geroscience has developed an array of tools and models over the past decade that can be adapted to pathology research. One key area is the use of aging models to study diseases. Traditionally, research on age-related diseases like cancer, stroke, hypertension, and myocardial infarction has been regularly conducted using young animal models. However, these models often fail to capture the complexities of human diseases, which typically manifest in older populations. By employing aging models, pathologists can better understand how these diseases develop and progress in an aging body, leading to more accurate representations and insights.

The shift to age-relevant disease models

The integration of age-appropriate models in pathological studies is crucial. Diseases in older adults often present differently than in younger individuals, both in terms of symptoms, severity and underlying pathophysiology. By using preclinical models that more closely resemble the chronological age at which these diseases commonly occur in humans, researchers can uncover new aspects of disease mechanisms that were previously obscured in younger models. This shift could lead to the development of more effective diagnostic tools and treatments that are tailored to the older population actually affected by these diseases.

The COVID-19 pandemic has starkly highlighted the importance of age-relevant disease models in pathology [227, 228]. COVID-19's associated pathologies extend beyond respiratory symptoms, encompassing a range of complications including lung injury, systemic microvascular damage, cardiac abnormalities, and neurological manifestations [229–239]. The consequences of infection with SARS-CoV-2 have been particularly severe in older adults [240, 241] and in individuals with accelerated biological aging due to factors such as obesity [242–254]. Geroscience has been instrumental in uncovering how specific age-related mechanisms may contribute to this increased disease severity [244–246, 248, 249, 252, 255, 256]. For example, aging-related changes in the immune system, known as immunosenescence, and inflammaging, are believed to play key roles in the heightened vulnerability and severity of COVID-19 in the older population

[257–262]. Understanding the unique impact of COVID-19 on older adults is essential, making the use of age-relevant models in research crucial.

Utilizing models targeting aging mechanisms in pathology

Pathology stands to gain substantially from integrating models that target aging mechanisms, a key area of focus in geroscience research. Cellular senescence serves as a prime example of an aging process with profound implications for disease development and progression. Over the past decade, a variety of murine models have been developed, allowing for the precise detection and elimination of senescent cells [183, 263–266]. This advancement has shed light on the role of senescent cells in the pathogenesis of numerous age-related diseases. By adopting these geroscience-derived models, pathologists can broaden their investigative scope, targeting a wider array of diseases. This approach not only deepens our understanding of the cellular and molecular foundations of these conditions but also paves the way for more targeted diagnostic and therapeutic strategies in a range of age-related diseases. Fields such as cancer research [263] and musculoskeletal [265–267], ophthalmological [268, 269], otological, and hematological [6, 264] research in pathology are prime examples where an interdisciplinary approach, integrating a geroscience perspective, could lead to significant breakthroughs. By embracing this cross-disciplinary methodology, pathologists can uncover novel insights and develop groundbreaking treatments in these specialized areas, all deeply influenced by the aging process.

Epigenetic clocks and biological age assessment

Methods developed to assess mechanisms of aging and biological age [100, 270–275], such as epigenetic clocks [47, 94, 100–102, 276–281], offer valuable tools for pathological studies. These methods can be used to determine the biological age of tissues and cells, which may differ from chronological age. Incorporating these measurements into pathological research can provide new insights into the relationship between aging and disease, and potentially uncover new biomarkers for early detection and intervention.

Conclusion

In summary, geroscience offers a transformative perspective for pathology, bridging the gap between aging processes and disease pathogenesis. By adopting age-appropriate disease models and preclinical models that target specific aging mechanisms, utilizing tools to assess biological aging, and embracing an interdisciplinary approach, pathology can greatly enhance its understanding and treatment of age-related diseases. This integration marks a pivotal shift in the approach to disease research, offering the promise of effective and targeted interventions for the aging population. As the field of geroscience continues to evolve, it will undoubtedly become an integral part of pathology, offering new insights and diagnostic protocols.

The National Institute on Aging (NIA) in the United States has established a vital network of core facilities known as the Nathan Shock Centers of Excellence in the Biology of Aging [282–290]. These centers offer specialized services on a fee-for-service basis to researchers aiming to characterize specific mechanisms of aging and assess biological age. Such initiatives play a crucial role in fostering the incorporation of geroscience concepts into pathological research. By providing access to advanced technologies and expertise, these centers enable researchers to delve deeper into the complexities of aging at a molecular and cellular level [282–290]. This approach not only enhances our understanding of the aging process but also accelerates the development of targeted interventions for age-related diseases. The success of the Nathan Shock Centers serves as a model that could be replicated by other countries, particularly in the European Union, to promote global collaboration and advancement in aging research. By establishing similar facilities, there can be a concerted effort towards integrating geroscience more broadly into various fields of study, including pathology, thereby paving the way for groundbreaking discoveries and innovations in the science of aging and pathology and pathophysiology of age-related diseases.

Author contributions

AL conceptualized the article. AL wrote the first draft. MF, VF-P, DM, and AF all revised the manuscript critically. All authors contributed to the article and approved the submitted version.

Funding

Project no. TKP2021-NKTA-47, implemented with the support provided by the Ministry of Innovation and Technology of Hungary from the National Research, Development and Innovation Fund, financed under the TKP2021-NKTA funding scheme; by funding through the National Cardiovascular Laboratory Program (RRF-2.3.1-21-2022-00003) provided by the Ministry of Innovation and Technology of Hungary from the National Research,

Development and Innovation Fund; Project no. 135784 implemented with the support provided from the National Research, Development and Innovation Fund of Hungary, financed under the K_20 funding scheme and the European University for Wellbeing (EUniWell) program (grant agreement number: 101004093/EUniWell/EAC-A02-2019/EAC-A02-2019-1). The funding sources had no role in the writing of the manuscript; and in the decision to submit the article for publication. The 3.5 version of ChatGPT, developed by OpenAI, was used as a tool to refine our writing and enhancing the clarity of our work.

Conflict of interest

The authors declare that the research was conducted in the absence of any commercial or financial relationships that could be construed as a potential conflict of interest.

References

1. Hernandez CM, Hernandez AR, Hoffman JM, King PH, McMahon LL, Buford TW, et al. A neuroscience primer for integrating geroscience with the neurobiology of aging. *J Gerontol A Biol Sci Med Sci* (2022) 77:e19–e33. doi:10.1093/gerona/glab301

2. Llarena N, Hine C. Reproductive longevity and aging: geroscience approaches to maintain long-term ovarian fitness. *J Gerontol A Biol Sci Med Sci* (2021) 76:1551–60. doi:10.1093/gerona/glaa204

3. Byers JM, 3rd. Rudolf Virchow--father of cellular pathology. *Am J Clin Pathol* (1989) 92:S2–8.

4. Duque G, Lipsitz LA, Ferrucci L, Addie S, Carrington-Lawrence S, Kohanski R. Geroscience for the next chapter of medicine. *J Gerontol A Biol Sci Med Sci* (2023) 78:791–2. doi:10.1093/gerona/glad083

5. Lopez-Otin C, Blasco MA, Partridge L, Serrano M, Kroemer G. The hallmarks of aging. *Cell* (2013) 153:1194–217. doi:10.1016/j.cell.2013.05.039

6. Urban VS, Cegledi A, Mikala G. Multiple myeloma, a quintessential malignant disease of aging: a geroscience perspective on pathogenesis and treatment. *Geroscience* (2023) 45:727–46. doi:10.1007/s11357-022-00698-x

7. Lamanuzzi A, Saltarella I, Frassanito MA, Ribatti D, Melaccio A, Desantis V, et al. Thrombopoietin promotes angiogenesis and disease progression in patients with multiple myeloma. *Am J Pathol* (2021) 191:748–58. doi:10.1016/j.ajpath.2020.12.016

8. Dorigatti AO, Riordan R, Yu Z, Ross G, Wang R, Reynolds-Lallement N, et al. Brain cellular senescence in mouse models of Alzheimer's disease. *Geroscience* (2022) 44:1157–68. doi:10.1007/s11357-022-00531-5

9. Pomilio C, Gorojod RM, Riudavets M, Vinuesa A, Presa J, Gregosa A, et al. Microglial autophagy is impaired by prolonged exposure to β-amyloid peptides: evidence from experimental models and Alzheimer's disease patients. *Geroscience* (2020) 42:613–32. doi:10.1007/s11357-020-00161-9

10. DiBattista AM, Sierra F, Masliah E. NIA workshop on senescence in brain aging and Alzheimer's disease and its related dementias. *Geroscience* (2020) 42:389–96. doi:10.1007/s11357-020-00153-9

11. Liu H, Lutz M, Luo S, Alzheimer's Disease Neuroimaging Initiative. Genetic association between epigenetic aging-acceleration and the progression of mild cognitive impairment to Alzheimer's disease. *J Gerontol A Biol Sci Med Sci* (2022) 77:1734–42. doi:10.1093/gerona/glac138

12. Wang H, Fu J, Xu X, Yang Z, Zhang T. Rapamycin activates mitophagy and alleviates cognitive and synaptic plasticity deficits in a mouse model of Alzheimer's disease. *J Gerontol A Biol Sci Med Sci* (2021) 76:1707–13. doi:10.1093/gerona/glab142

13. Toth L, Czigler A, Hegedus E, Komaromy H, Amrein K, Czeiter E, et al. Age-related decline in circulating IGF-1 associates with impaired neurovascular coupling responses in older adults. *Geroscience* (2022) 44:2771–83. doi:10.1007/s11357-022-00623-2

14. Sakamuri S, Sure VN, Kolli L, Liu N, Evans WR, Sperling JA, et al. Glycolytic and oxidative phosphorylation defects precede the development of senescence in primary human brain microvascular endothelial cells. *Geroscience* (2022) 44:1975–94. doi:10.1007/s11357-022-00550-2

15. Towner RA, Gulej R, Zalles M, Saunders D, Smith N, Lerner M, et al. Rapamycin restores brain vasculature, metabolism, and blood-brain barrier in an inflammaging model. *Geroscience* (2021) 43:563–78. doi:10.1007/s11357-021-00363-9

16. Islam MT, Tuday E, Allen S, Kim J, Trott DW, Holland WL, et al. Senolytic drugs, dasatinib and quercetin, attenuate adipose tissue inflammation, and ameliorate metabolic function in old age. *Aging Cell* (2023) 22:e13767. doi:10.1111/acel.13767

17. Bloom SI, Tucker JR, Machin DR, Abdeahad H, Adeyemo AO, Thomas TG, et al. Reduction of double-strand DNA break repair exacerbates vascular aging. *Aging (Albany NY)* (2023) 15:9913–47. doi:10.18632/aging.205066

18. Bloom SI, Tucker JR, Lim J, Thomas TG, Stoddard GJ, Lesniewski LA, et al. Aging results in DNA damage and telomere dysfunction that is greater in endothelial versus vascular smooth muscle cells and is exacerbated in atheroprone regions. *Geroscience* (2022) 44:2741–55. doi:10.1007/s11357-022-00681-6

19. Ungvari Z, Tarantini S, Donato AJ, Galvan V, Csiszar A. Mechanisms of vascular aging. *Circ Res* (2018) 123:849–67. doi:10.1161/CIRCRESAHA.118.311378

20. Liu Y, Bloom SI, Donato AJ. The role of senescence, telomere dysfunction and shelterin in vascular aging. *Microcirculation* (2018) 26:e12487. doi:10.1111/micc.12487

21. Rossman MJ, Kaplon RE, Hill SD, McNamara MN, Santos-Parker JR, Pierce GL, et al. Endothelial cell senescence with aging in healthy humans: prevention by habitual exercise and relation to vascular endothelial function. *Am J Physiol Heart Circ Physiol* (2017) 313:H890–H895. doi:10.1152/ajpheart.00416.2017

22. Kennedy BK, Berger SL, Brunet A, Campisi J, Cuervo AM, Epel ES, et al. Geroscience: linking aging to chronic disease. *Cell* (2014) 159:709–13. doi:10.1016/j.cell.2014.10.039

23. Rolland Y, Sierra F, Ferrucci L, Barzilai N, De Cabo R, Mannick J, et al. Challenges in developing Geroscience trials. *Nat Commun* (2023) 14:5038. doi:10.1038/s41467-023-39786-7

24. Kaushik S, Cuervo AM. Proteostasis and aging. *Nat Med* (2015) 21:1406–15. doi:10.1038/nm.4001

25. Korovila I, Hugo M, Castro JP, Weber D, Hohn A, Grune T, et al. Proteostasis, oxidative stress and aging. *Redox Biol* (2017) 13:550–67. doi:10.1016/j.redox.2017.07.008

26. Santra M, Dill KA, de Graff AMR. Proteostasis collapse is a driver of cell aging and death. *Proc Natl Acad Sci U S A* (2019) 116:22173–8. doi:10.1073/pnas.1906592116

27. Taylor RC, Hetz C. Mastering organismal aging through the endoplasmic reticulum proteostasis network. *Aging Cell* (2020) 19:e13265. doi:10.1111/acel.13265

28. Ferreira JV, da Rosa Soares A, Pereira P. Cell non-autonomous proteostasis regulation in aging and disease. *Front Neurosci* (2022) 16:878296. doi:10.3389/fnins.2022.878296

29. Pearson KJ, Lewis KN, Price NL, Chang JW, Perez E, Cascajo MV, et al. Nrf2 mediates cancer protection but not prolongevity induced by caloric restriction. *Proc Natl Acad Sci U S A* (2008) 105:2325–30. doi:10.1073/pnas.0712162105

30. Ungvari Z, Bailey-Downs L, Gautam T, Sosnowska D, Wang M, Monticone RE, et al. Age-associated vascular oxidative stress, Nrf2 dysfunction, and NF-{kappa}B activation in the nonhuman primate *Macaca mulatta*. *J Gerontol A Biol Sci Med Sci* (2011) 66:866–75. doi:10.1093/gerona/glr092

31. Ungvari Z, Bailey-Downs L, Sosnowska D, Gautam T, Koncz P, Losonczy G, et al. Vascular oxidative stress in aging: a homeostatic failure due to dysregulation of Nrf2-mediated antioxidant response. *Am J Physiol Heart Circ Physiol* (2011) 301:H363–72. doi:10.1152/ajpheart.01134.2010

32. Ungvari ZI, Bailey-Downs L, Gautam T, Jimenez R, Losonczy G, Zhang C, et al. Adaptive induction of NF-E2-Related Factor-2-driven antioxidant genes in endothelial cells in response to hyperglycemia. *Am J Physiol Heart Circ Physiol* (2011) 300:H1133–40. doi:10.1152/ajpheart.00402.2010

33. Ahn B, Pharaoh G, Premkumar P, Huseman K, Ranjit R, Kinter M, et al. Nrf2 deficiency exacerbates age-related contractile dysfunction and loss of skeletal muscle mass. *Redox Biol* (2018) 17:47–58. doi:10.1016/j.redox.2018.04.004

34. Fulop GA, Kiss T, Tarantini S, Balasubramanian P, Yabluchanskiy A, Farkas E, et al. Nrf2 deficiency in aged mice exacerbates cellular senescence promoting cerebrovascular inflammation. *Geroscience* (2018) 40:513–21. doi:10.1007/s11357-018-0047-6

35. Tarantini S, Valcarcel-Ares MN, Yabluchanskiy A, Tucsek Z, Hertelendy P, Kiss T, et al. Nrf2 deficiency exacerbates obesity-induced oxidative stress, neurovascular dysfunction, blood brain barrier disruption, neuroinflammation, amyloidogenic gene expression and cognitive decline in mice, mimicking the aging phenotype. *J Gerontol A Biol Sci Med Sci* (2018) 73:853–63. doi:10.1093/gerona/glx177

36. Ungvari Z, Tarantini S, Nyul-Toth A, Kiss T, Yabluchanskiy A, Csipo T, et al. Nrf2 dysfunction and impaired cellular resilience to oxidative stressors in the aged vasculature: from increased cellular senescence to the pathogenesis of age-related vascular diseases. *Geroscience* (2019) 41:727–38. doi:10.1007/s11357-019-00107-w

37. Maynard S, Fang EF, Scheibye-Knudsen M, Croteau DL, Bohr VA. DNA damage, DNA repair, aging, and neurodegeneration. *Cold Spring Harb Perspect Med* (2015) 5:a025130. doi:10.1101/cshperspect.a025130

38. Yousefzadeh MJ, Wilkinson JE, Hughes B, Gadela N, Ladiges WC, Vo N, et al. Heterochronic parabiosis regulates the extent of cellular senescence in multiple tissues. *Geroscience* (2020) 42:951–61. doi:10.1007/s11357-020-00185-1

39. Gonzalez-Armenta JL, Li N, Lee RL, Lu B, Molina AJA. Heterochronic parabiosis: old blood induces changes in mitochondrial structure and function of young mice. *J Gerontol A Biol Sci Med Sci* (2021) 76:434–9. doi:10.1093/gerona/glaa299

40. Miller HA, Dean ES, Pletcher SD, Leiser SF. Cell non-autonomous regulation of health and longevity. *Elife* (2020) 9:e62659. doi:10.7554/eLife.62659

41. Lecot P, Alimirah F, Desprez PY, Campisi J, Wiley C. Context-dependent effects of cellular senescence in cancer development. *Br J Cancer* (2016) 114:1180–4. doi:10.1038/bjc.2016.115

42. Chinta SJ, Woods G, Rane A, Demaria M, Campisi J, Andersen JK. Cellular senescence and the aging brain. *Exp Gerontol* (2014) 68:3–7. doi:10.1016/j.exger.2014.09.018

43. Tchkonia T, Zhu Y, van Deursen J, Campisi J, Kirkland JL. Cellular senescence and the senescent secretory phenotype: therapeutic opportunities. *J Clin Invest* (2013) 123:966–72. doi:10.1172/JCI64098

44. Henderson YO, Bithi N, Yang J, Link C, Zhang A, Baron B, et al. A long-term obesogenic high-fat diet in mice partially dampens the anti-frailty benefits of late-life intermittent fasting. *Geroscience* (2023) 45:1247–62. doi:10.1007/s11357-022-00678-1

45. Nunan E, Wright CL, Semola OA, Subramanian M, Balasubramanian P, Lovern PC, et al. Obesity as a premature aging phenotype - implications for sarcopenic obesity. *Geroscience* (2022) 44:1393–405. doi:10.1007/s11357-022-00567-7

46. Seligman BJ, Berry SD, Lipsitz LA, Travison TG, Kiel DP. Epigenetic age acceleration and change in frailty in MOBILIZE boston. *J Gerontol A Biol Sci Med Sci* (2022) 77:1760–5. doi:10.1093/gerona/glac019

47. O'Shea DM, Maynard T, Tremont G. DNA methylation "GrimAge" acceleration mediates sex/gender differences in verbal memory and processing speed: findings from the health and retirement study. *J Gerontol A Biol Sci Med Sci* (2022) 77:2402–12. doi:10.1093/gerona/glac133

48. Lin WY. Lifestyle factors and genetic variants on 2 biological age measures: evidence from 94 443 taiwan biobank participants. *J Gerontol A Biol Sci Med Sci* (2022) 77:1189–98. doi:10.1093/gerona/glab251

49. Zhou YF, Song XY, Pan XF, Feng L, Luo N, Yuan JM, et al. Association between combined lifestyle factors and healthy ageing in Chinese adults: the Singapore Chinese health study. *J Gerontol A Biol Sci Med Sci* (2021) 76:1796–805. doi:10.1093/gerona/glab033

50. Wu Q, Ailshire JA, Kim JK, Crimmins EM. Cardiometabolic risk trajectory among older Americans: findings from the health and retirement study. *J Gerontol A Biol Sci Med Sci* (2021) 76:2265–74. doi:10.1093/gerona/glab205

51. Pandics T, Major D, Fazekas-Pongor V, Szarvas Z, Peterfi A, Mukli P, et al. Exposome and unhealthy aging: environmental drivers from air pollution to occupational exposures. *Geroscience* (2023) 45:3381–408. doi:10.1007/s11357-023-00913-3

52. Chen GC, Hukportie DN, Zhongxiao W, Li FR, Wu XB. The association between exposure to air pollution and dementia incidence: the modifying effect of smoking. *J Gerontol A Biol Sci Med Sci* (2022) 78:2309–17. doi:10.1093/gerona/glac228

53. Harman D. Aging: a theory based on free radical and radiation chemistry. *J Gerontol* (1956) 11:298–300. doi:10.1093/geronj/11.3.298

54. Harman D. The biologic clock: the mitochondria? *J Am Geriatr Soc* (1972) 20:145–7. doi:10.1111/j.1532-5415.1972.tb00787.x

55. Oudbier SJ, Goh J, Looijaard S, Reijnierse EM, Meskers CGM, Maier AB. Pathophysiological mechanisms explaining the association between low skeletal muscle mass and cognitive function. *J Gerontol A Biol Sci Med Sci* (2022) 77:1959–68. doi:10.1093/gerona/glac121

56. Liao FF, Lin G, Chen X, Chen L, Zheng W, Raghow R, et al. Endothelial nitric oxide synthase-deficient mice: a model of spontaneous cerebral small-vessel disease. *Am J Pathol* (2021) 191:1932–45. doi:10.1016/j.ajpath.2021.02.022

57. Serikbaeva A, Li Y, Ganesh B, Zelkha R, Kazlauskas A. Hyperglycemia promotes mitophagy and thereby mitigates hyperglycemia-induced damage. *Am J Pathol* (2022) 192:1779–94. doi:10.1016/j.ajpath.2022.08.004

58. Ionescu-Tucker A, Cotman CW. Emerging roles of oxidative stress in brain aging and Alzheimer's disease. *Neurobiol Aging* (2021) 107:86–95. doi:10.1016/j.neurobiolaging.2021.07.014

59. Logan S, Royce GH, Owen D, Farley J, Ranjo-Bishop M, Sonntag WE, et al. Accelerated decline in cognition in a mouse model of increased oxidative stress. *Geroscience* (2019) 41:591–607. doi:10.1007/s11357-019-00105-y

60. Dai DF, Chiao YA, Marcinek DJ, Szeto HH, Rabinovitch PS. Mitochondrial oxidative stress in aging and healthspan. *Longev Healthspan* (2014) 3:6. doi:10.1186/2046-2395-3-6

61. Csiszar A, Ungvari Z, Edwards JG, Kaminski PM, Wolin MS, Koller A, et al. Aging-induced phenotypic changes and oxidative stress impair coronary arteriolar function. *Circ Res* (2002) 90:1159–66. doi:10.1161/01.res.0000020401.61826.ea

62. Sun D, Huang A, Yan EH, Wu Z, Yan C, Kaminski PM, et al. Reduced release of nitric oxide to shear stress in mesenteric arteries of aged rats. *Am J Physiol Heart Circ Physiol* (2004) 286:H2249–56. doi:10.1152/ajpheart.00854.2003

63. Hamilton CA, Brosnan MJ, McIntyre M, Graham D, Dominiczak AF. Superoxide excess in hypertension and aging: a common cause of endothelial dysfunction. *Hypertension* (2001) 37:529–34. doi:10.1161/01.hyp.37.2.529

64. van der Loo B, Labugger R, Skepper JN, Bachschmid M, Kilo J, Powell JM, et al. Enhanced peroxynitrite formation is associated with vascular aging. *J Exp Med* (2000) 192:1731–44. doi:10.1084/jem.192.12.1731

65. Francia P, delli Gatti C, Bachschmid M, Martin-Padura I, Savoia C, Migliaccio E, et al. Deletion of p66shc gene protects against age-related endothelial dysfunction. *Circulation* (2004) 110:2889–95. doi:10.1161/01.CIR.0000147731.24444.4D

66. Csiszar A, Labinskyy N, Orosz Z, Xiangmin Z, Buffenstein R, Ungvari Z. Vascular aging in the longest-living rodent, the naked mole-rat. *Am J Physiol* (2007) 293:H919–27. doi:10.1152/ajpheart.01287.2006

67. Ungvari ZI, Orosz Z, Labinskyy N, Rivera A, Xiangmin Z, Smith KE, et al. Increased mitochondrial H2O2 production promotes endothelial NF-kappaB activation in aged rat arteries. *Am J Physiol Heart Circ Physiol* (2007) 293:H37–47. doi:10.1152/ajpheart.01346.2006

68. Jablonski KL, Seals DR, Eskurza I, Monahan KD, Donato AJ. High-dose ascorbic acid infusion abolishes chronic vasoconstriction and restores resting leg blood flow in healthy older men. *J Appl Physiol* (2007) 103:1715–21. doi:10.1152/japplphysiol.00533.2007

69. Donato AJ, Eskurza I, Silver AE, Levy AS, Pierce GL, Gates PE, et al. Direct evidence of endothelial oxidative stress with aging in humans: relation to impaired endothelium-dependent dilation and upregulation of nuclear factor-kappaB. *Circ Res* (2007) 100:1659–66. doi:10.1161/01.RES.0000269183.13937.e8

70. Fleenor BS, Eng JS, Sindler AL, Pham BT, Kloor JD, Seals DR. Superoxide signaling in perivascular adipose tissue promotes age-related artery stiffness. *Aging Cell* (2014) 13:576–8. doi:10.1111/acel.12196

71. Toth P, Tarantini S, Springo Z, Tucsek Z, Gautam T, Giles CB, et al. Aging exacerbates hypertension-induced cerebral microhemorrhages in mice: role of resveratrol treatment in vasoprotection. *Aging Cell* (2015) 14:400–8. doi:10.1111/acel.12315

72. Ashton KJ, Kiessling CJ, Thompson JM, Aziz AY, Thomas WG, Headrick JP, et al. Early cardiac aging linked to impaired stress-resistance and transcriptional control of stress response, quality control and mitochondrial pathways. *Exp Gerontol* (2023) 171:112011. doi:10.1016/j.exger.2022.112011

73. de Souza RG, Yu Z, Hernandez H, Trujillo-Vargas CM, Lee A, Mauk KE, et al. Modulation of oxidative stress and inflammation in the aged lacrimal gland. *Am J Pathol* (2021) 191:294–308. doi:10.1016/j.ajpath.2020.10.013

74. Suh JH, Shenvi SV, Dixon BM, Liu H, Jaiswal AK, Liu RM, et al. Decline in transcriptional activity of Nrf2 causes age-related loss of glutathione synthesis, which is reversible with lipoic acid. *Proc Natl Acad Sci U S A* (2004) 101:3381–6. doi:10.1073/pnas.0400282101

75. Csiszar A, Gautam T, Sosnowska D, Tarantini S, Banki E, Tucsek Z, et al. Caloric restriction confers persistent anti-oxidative, pro-angiogenic, and anti-inflammatory effects and promotes anti-aging miRNA expression profile in cerebromicrovascular endothelial cells of aged rats. *Am J Physiol Heart Circ Physiol* (2014) 307:H292–306. doi:10.1152/ajpheart.00307.2014

76. Martin GM, Hisama FM, Oshima J. Review of how genetic research on segmental progeroid syndromes has documented genomic instability as a hallmark of aging but let us now pursue antigeroid syndromes. *J Gerontol A Biol Sci Med Sci* (2021) 76:253–9. doi:10.1093/gerona/glaa273

77. Durik M, Kavousi M, van der Pluijm I, Isaacs A, Cheng C, Verdonk K, et al. Nucleotide excision DNA repair is associated with age-related vascular dysfunction. *Circulation* (2012) 126:468–78. doi:10.1161/CIRCULATIONAHA.112.104380

78. Gray K, Kumar S, Figg N, Harrison J, Baker L, Mercer J, et al. Effects of DNA damage in smooth muscle cells in atherosclerosis. *Circ Res* (2015) 116:816–26. doi:10.1161/CIRCRESAHA.116.304921

79. Diez-Diez M, Amoros-Perez M, de la Barrera J, Vazquez E, Quintas A, Pascual-Figal DA, et al. Clonal hematopoiesis is not prevalent in Hutchinson-Gilford progeria syndrome. *Geroscience* (2023) 45:1231–6. doi:10.1007/s11357-022-00607-2

80. Del Pozo-Valero M, Corton M, Lopez-Rodriguez R, Mahillo-Fernandez I, Ruiz-Hornillos J, Minguez P, et al. Age-dependent association of clonal hematopoiesis with COVID-19 mortality in patients over 60 years. *Geroscience* (2023) 45:543–53. doi:10.1007/s11357-022-00666-5

81. Steensma DP, Bejar R, Jaiswal S, Lindsley RC, Sekeres MA, Hasserjian RP, et al. Clonal hematopoiesis of indeterminate potential and its distinction from myelodysplastic syndromes. *Blood* (2015) 126:9–16. doi:10.1182/blood-2015-03-631747

82. Jaiswal S, Natarajan P, Silver AJ, Gibson CJ, Bick AG, Shvartz E, et al. Clonal hematopoiesis and risk of atherosclerotic cardiovascular disease. *N Engl J Med* (2017) 377:111–21. doi:10.1056/NEJMoa1701719

83. Fuster JJ, Walsh K. Somatic mutations and clonal hematopoiesis: unexpected potential new drivers of age-related cardiovascular disease. *Circ Res* (2018) 122:523–32. doi:10.1161/CIRCRESAHA.117.312115

84. Libby P, Ebert BL. CHIP (clonal hematopoiesis of indeterminate potential): potent and newly recognized contributor to cardiovascular risk. *Circulation* (2018) 138:666–8. doi:10.1161/CIRCULATIONAHA.118.034392

85. Khetarpal SA, Qamar A, Bick AG, Fuster JJ, Kathiresan S, Jaiswal S, et al. Clonal hematopoiesis of indeterminate potential reshapes age-related CVD: JACC review topic of the week. *J Am Coll Cardiol* (2019) 74:578–86. doi:10.1016/j.jacc.2019.05.045

86. Nachun D, Lu AT, Bick AG, Natarajan P, Weinstock J, Szeto MD, et al. Clonal hematopoiesis associated with epigenetic aging and clinical outcomes. *Aging Cell* (2021) 20:e13366. doi:10.1111/acel.13366

87. Bhattacharya R, Zekavat SM, Haessler J, Fornage M, Raffield L, Uddin MM, et al. Clonal hematopoiesis is associated with higher risk of stroke. *Stroke* (2022) 53:788–97. doi:10.1161/STROKEAHA.121.037388

88. Uddin MDM, Nguyen NQH, Yu B, Brody JA, Pampana A, Nakao T, et al. Clonal hematopoiesis of indeterminate potential, DNA methylation, and risk for coronary artery disease. *Nat Commun* (2022) 13:5350. doi:10.1038/s41467-022-33093-3

89. Huang Z, Liu C, Ruan Y, Guo Y, Sun S, Shi Y, et al. Dynamics of leukocyte telomere length in adults aged 50 and older: a longitudinal population-based cohort study. *Geroscience* (2021) 43:645–54. doi:10.1007/s11357-020-00320-y

90. Sindi S, Solomon A, Kareholt I, Hovatta I, Antikainen R, Hanninen T, et al. Telomere length change in a multidomain lifestyle intervention to prevent cognitive decline: a randomized clinical trial. *J Gerontol A Biol Sci Med Sci* (2021) 76:491–8. doi:10.1093/gerona/glaa279

91. Pudas S, Josefsson M, Nordin Adolfsson A, Landfors M, Kauppi K, Veng-Taasti LM, et al. Short leukocyte telomeres, but not telomere attrition rates, predict memory decline in the 20-year longitudinal betula study. *J Gerontol A Biol Sci Med Sci* (2021) 76:955–63. doi:10.1093/gerona/glaa322

92. Kemp BR, Ferraro KF. Are biological consequences of childhood exposures detectable in telomere length decades later? *J Gerontol A Biol Sci Med Sci* (2021) 76:7–14. doi:10.1093/gerona/glaa019

93. Demanelis K, Tong L, Pierce BL. Genetically increased telomere length and aging-related traits in the U.K. Biobank. *J Gerontol A Biol Sci Med Sci* (2021) 76:15–22. doi:10.1093/gerona/glz240

94. Pearce EE, Alsaggaf R, Katta S, Dagnall C, Aubert G, Hicks BD, et al. Telomere length and epigenetic clocks as markers of cellular aging: a comparative study. *Geroscience* (2022) 44:1861–9. doi:10.1007/s11357-022-00586-4

95. Zhan Y, Hagg S. Association between genetically predicted telomere length and facial skin aging in the UK Biobank: a Mendelian randomization study. *Geroscience* (2021) 43:1519–25. doi:10.1007/s11357-020-00283-0

96. El Assar M, Angulo J, Carnicero JA, Walter S, Garcia-Garcia FJ, Rodriguez-Artalejo F, et al. Association between telomere length, frailty and death in older adults. *Geroscience* (2021) 43:1015–27. doi:10.1007/s11357-020-00291-0

97. Katz R, Gay EL, Kuipers AL, Lee JH, Honig LS, Christensen K, et al. Association of leukocyte telomere length with perceived physical fatigability. *Exp Gerontol* (2022) 170:111988. doi:10.1016/j.exger.2022.111988

98. Yusipov I, Kondakova E, Kalyakulina A, Krivonosov M, Lobanova N, Bacalini MG, et al. Accelerated epigenetic aging and inflammatory/immunological profile (ipAGE) in patients with chronic kidney disease. *Geroscience* (2022) 44:817–34. doi:10.1007/s11357-022-00540-4

99. Vetter VM, Sommerer Y, Kalies CH, Spira D, Bertram L, Demuth I. Vitamin D supplementation is associated with slower epigenetic aging. *Geroscience* (2022) 44:1847–59. doi:10.1007/s11357-022-00581-9

100. Fraszczyk E, Thio CHL, Wackers P, Dolle MET, Bloks VW, Hodemaekers H, et al. DNA methylation trajectories and accelerated epigenetic aging in incident type 2 diabetes. *Geroscience* (2022) 44:2671–84. doi:10.1007/s11357-022-00626-z

101. Schachtschneider KM, Schook LB, Meudt JJ, Shanmuganayagam D, Zoller JA, Haghani A, et al. Epigenetic clock and DNA methylation analysis of porcine models of aging and obesity. *Geroscience* (2021) 43:2467–83. doi:10.1007/s11357-021-00439-6

102. Horvath S, Zoller JA, Haghani A, Lu AT, Raj K, Jasinska AJ, et al. DNA methylation age analysis of rapamycin in common marmosets. *Geroscience* (2021) 43:2413–25. doi:10.1007/s11357-021-00438-7

103. Horvath S, Zoller JA, Haghani A, Jasinska AJ, Raj K, Breeze CE, et al. Epigenetic clock and methylation studies in the rhesus macaque. *Geroscience* (2021) 43:2441–53. doi:10.1007/s11357-021-00429-8

104. Tolkach Y, Zarbl R, Bauer S, Ritter M, Ellinger J, Hauser S, et al. DNA promoter methylation and ERG regulate the expression of CD24 in prostate cancer. *Am J Pathol* (2021) 191:618–30. doi:10.1016/j.ajpath.2020.12.014

105. Toghill BJ, Saratzis A, Harrison SC, Verissimo AR, Mallon EB, Bown MJ. The potential role of DNA methylation in the pathogenesis of abdominal aortic aneurysm. *Atherosclerosis* (2015) 241:121–9. doi:10.1016/j.atherosclerosis.2015.05.001

106. Li P, Newhardt MF, Matsuzaki S, Eyster C, Pranay A, Peelor FF, 3rd, et al. The loss of cardiac SIRT3 decreases metabolic flexibility and proteostasis in an age-dependent manner. *Geroscience* (2023) 45:983–99. doi:10.1007/s11357-022-00695-0

107. Jang YC, Rodriguez K, Lustgarten MS, Muller FL, Bhattacharya A, Pierce A, et al. Superoxide-mediated oxidative stress accelerates skeletal muscle atrophy by synchronous activation of proteolytic systems. *Geroscience* (2020) 42:1579–91. doi:10.1007/s11357-020-00200-5

108. Tomaru U, Ito T, Ohmura Y, Higashikawa K, Miyajima S, Tomatsu R, et al. Decreased proteasomal function induces neuronal loss and memory impairment. *Am J Pathol* (2021) 191:144–56. doi:10.1016/j.ajpath.2020.10.004

109. Gal J, Katsumata Y, Zhu H, Srinivasan S, Chen J, Johnson LA, et al. Apolipoprotein E proteinopathy is a major dementia-associated pathologic biomarker in individuals with or without the APOE epsilon 4 allele. *Am J Pathol* (2022) 192:564–78. doi:10.1016/j.ajpath.2021.11.013

110. Sabatini DM. Twenty-five years of mTOR: uncovering the link from nutrients to growth. *Proc Natl Acad Sci U S A* (2017) 114:11818–25. doi:10.1073/pnas.1716173114

111. Teuliere J, Bernard C, Corel E, Lapointe FJ, Martens J, Lopez P, et al. Network analyses unveil ageing-associated pathways evolutionarily conserved from fungi to animals. *Geroscience* (2023) 45:1059–80. doi:10.1007/s11357-022-00704-2

112. Mota-Martorell N, Jove M, Pradas I, Berdun R, Sanchez I, Naudi A, et al. Gene expression and regulatory factors of the mechanistic target of rapamycin (mTOR) complex 1 predict mammalian longevity. *Geroscience* (2020) 42:1157–73. doi:10.1007/s11357-020-00210-3

113. Selvarani R, Mohammed S, Richardson A. Effect of rapamycin on aging and age-related diseases-past and future. *Geroscience* (2021) 43:1135–58. doi:10.1007/s11357-020-00274-1

114. Castro-Martinez F, Candelario-Martinez A, Encarnacion-Garcia MR, Piedra-Quintero Z, Bonilla-Moreno R, Betanzos A, et al. Rictor/Mammalian target of rapamycin complex 2 signaling protects colonocytes from apoptosis and prevents epithelial barrier breakdown. *Am J Pathol* (2021) 191:1537–49. doi:10.1016/j.ajpath.2021.06.004

115. Lee HJ, Shin DH, Song JS, Park JY, Kim SY, Hwang CS, et al. mTOR inhibition increases transcription factor E3 (TFE3) activity and modulates programmed death-ligand 1 (PD-L1) expression in translocation renal cell carcinoma. *Am J Pathol* (2021) 191:1999–2008. doi:10.1016/j.ajpath.2021.07.007

116. Lu X, Peng B, Chen G, Pes MG, Ribback S, Ament C, et al. YAP accelerates notch-driven cholangiocarcinogenesis via mTORC1 in mice. *Am J Pathol* (2021) 191:1651–67. doi:10.1016/j.ajpath.2021.05.017

117. Sahu D, Huan J, Wang H, Sahoo D, Casteel DE, Klemke RL, et al. Bladder cancer invasion is mediated by mammalian target of rapamycin complex 2-driven

regulation of nitric oxide and invadopodia formation. *Am J Pathol* (2021) 191: 2203–18. doi:10.1016/j.ajpath.2021.08.002

118. Wang M, Miller RA. Fibroblasts from long-lived mutant mice exhibit increased autophagy and lower TOR activity after nutrient deprivation or oxidative stress. *Aging Cell* (2012) 11:668–74. doi:10.1111/j.1474-9726.2012.00833.x

119. LaRocca TJ, Gioscia-Ryan RA, Hearon CM, Seals DR. The autophagy enhancer spermidine reverses arterial aging. *Mech Ageing Dev* (2013) 134: 314–20. doi:10.1016/j.mad.2013.04.004

120. Kang C, Xu Q, Martin TD, Li MZ, Demaria M, Aron L, et al. The DNA damage response induces inflammation and senescence by inhibiting autophagy of GATA4. *Science* (2015) 349:aaa5612. doi:10.1126/science.aaa5612

121. Cuervo AM, Dice JF. Age-related decline in chaperone-mediated autophagy. *J Biol Chem* (2000) 275:31505–13. doi:10.1074/jbc.M002102200

122. Tabibzadeh S. Role of autophagy in aging: the good, the bad, and the ugly. *Aging Cell* (2023) 22:e13753. doi:10.1111/acel.13753

123. Martinez RAS, Pinky PD, Harlan BA, Brewer GJ. GTP energy dependence of endocytosis and autophagy in the aging brain and Alzheimer's disease. *Geroscience* (2023) 45:757–80. doi:10.1007/s11357-022-00717-x

124. Kaushik S, Tasset I, Arias E, Pampliega O, Wong E, Martinez-Vicente M, et al. Autophagy and the hallmarks of aging. *Ageing Res Rev* (2021) 72:101468. doi:10.1016/j.arr.2021.101468

125. Aman Y, Schmauck-Medina T, Hansen M, Morimoto RI, Simon AK, Bjedov I, et al. Autophagy in healthy aging and disease. *Nat Aging* (2021) 1:634–50. doi:10.1038/s43587-021-00098-4

126. Zhang K, Huang Q, Peng L, Lin S, Liu J, Zhang J, et al. The multifunctional roles of autophagy in the innate immune response: implications for regulation of transplantation rejection. *Front Cel Dev Biol* (2022) 10:1007559. doi:10.3389/fcell.2022.1007559

127. Wu YX, Jin SH, Cui J. Autophagy and immune tolerance. *Adv Exp Med Biol* (2019) 1206:635–65. doi:10.1007/978-981-15-0602-4_28

128. Hashemi M, Paskeh MDA, Orouei S, Abbasi P, Khorrami R, Dehghanpour A, et al. Towards dual function of autophagy in breast cancer: a potent regulator of tumor progression and therapy response. *Biomed Pharmacother* (2023) 161:114546. doi:10.1016/j.biopha.2023.114546

129. Ballesteros-Alvarez J, Andersen JKmTORC2. mTORC2: the other mTOR in autophagy regulation. *Aging Cell* (2021) 20:e13431. doi:10.1111/acel.13431

130. Al-Bari MAA, Xu P. Molecular regulation of autophagy machinery by mTOR-dependent and -independent pathways. *Ann N Y Acad Sci* (2020) 1467: 3–20. doi:10.1111/nyas.14305

131. Keller CW, Adamopoulos IE, Lunemann JD. Autophagy pathways in autoimmune diseases. *J Autoimmun* (2023) 136:103030. doi:10.1016/j.jaut.2023.103030

132. Zhou L, Pinho R, Gu Y, Radak Z. The role of SIRT3 in exercise and aging. *Cells* (2022) 11:2596. doi:10.3390/cells11162596

133. Lautrup S, Sinclair DA, Mattson MP, Fang EF. NAD(+) in brain aging and neurodegenerative disorders. *Cell Metab* (2019) 30:630–55. doi:10.1016/j.cmet.2019.09.001

134. Yoshino J, Baur JA, Imai SI. NAD(+) intermediates: the biology and therapeutic potential of NMN and NR. *Cel Metab* (2018) 27:513–28. doi:10.1016/j.cmet.2017.11.002

135. Rajman L, Chwalek K, Sinclair DA. Therapeutic potential of NAD-boosting molecules: the *in vivo* evidence. *Cel Metab* (2018) 27:529–47. doi:10.1016/j.cmet.2018.02.011

136. Ansari A, Rahman MS, Saha SK, Saikot FK, Deep A, Kim KH. Function of the SIRT3 mitochondrial deacetylase in cellular physiology, cancer, and neurodegenerative disease. *Aging Cell* (2017) 16:4–16. doi:10.1111/acel.12538

137. Kitada M, Ogura Y, Koya D. The protective role of Sirt1 in vascular tissue: its relationship to vascular aging and atherosclerosis. *Aging (Albany NY)* (2016) 8: 2290–307. doi:10.18632/aging.101068

138. Imai SI, Guarente L. It takes two to tango: NAD(+) and sirtuins in aging/longevity control. *NPJ Aging Mech Dis* (2016) 2:16017. doi:10.1038/npjamd.2016.17

139. Houtkooper RH, Pirinen E, Auwerx J. Sirtuins as regulators of metabolism and healthspan. *Nat Rev Mol Cel Biol* (2012) 13:225–38. doi:10.1038/nrm3293

140. Chalkiadaki A, Guarente L. Sirtuins mediate mammalian metabolic responses to nutrient availability. *Nat Rev Endocrinol* (2012) 8:287–96. doi:10.1038/nrendo.2011.225

141. Minor RK, Baur JA, Gomes AP, Ward TM, Csiszar A, Mercken EM, et al. SRT1720 improves survival and healthspan of obese mice. *Sci Rep* (2011) 1:70. doi:10.1038/srep00070

142. Csiszar A, Labinskyy N, Jimenez R, Pinto JT, Ballabh P, Losonczy G, et al. Anti-oxidative and anti-inflammatory vasoprotective effects of caloric restriction in aging: role of circulating factors and SIRT1. *Mech Ageing Dev* (2009) 130:518–27. doi:10.1016/j.mad.2009.06.004

143. Ferrara N, Rinaldi B, Corbi G, Conti V, Stiuso P, Boccuti S, et al. Exercise training promotes SIRT1 activity in aged rats. *Rejuvenation Res* (2008) 11:139–50. doi:10.1089/rej.2007.0576

144. Csiszar A, Labinskyy N, Podlutsky A, Kaminski PM, Wolin MS, Zhang C, et al. Vasoprotective effects of resveratrol and SIRT1: attenuation of cigarette smoke-induced oxidative stress and proinflammatory phenotypic alterations. *Am J Physiol Heart Circ Physiol* (2008) 294:H2721–35. doi:10.1152/ajpheart.00235.2008

145. Dasgupta B, Milbrandt J. Resveratrol stimulates AMP kinase activity in neurons. *Proc Natl Acad Sci USA* (2007) 104:7217–22. doi:10.1073/pnas.0610068104

146. Alcendor RR, Gao S, Zhai P, Zablocki D, Holle E, Yu X, et al. Sirt1 regulates aging and resistance to oxidative stress in the heart. *Circ Res* (2007) 100:1512–21. doi:10.1161/01.RES.0000267723.65696.4a

147. Guarente L. Calorie restriction and SIR2 genes--towards a mechanism. *Mech Ageing Dev* (2005) 126:923–8. doi:10.1016/j.mad.2005.03.013

148. Nemoto S, Fergusson MM, Finkel T. Nutrient availability regulates SIRT1 through a forkhead-dependent pathway. *Science* (2004) 306:2105–8. doi:10.1126/science.1101731

149. Cohen HY, Miller C, Bitterman KJ, Wall NR, Hekking B, Kessler B, et al. Calorie restriction promotes mammalian cell survival by inducing the SIRT1 deacetylase. *Science* (2004) 305:390–2. doi:10.1126/science.1099196

150. Howitz KT, Bitterman KJ, Cohen HY, Lamming DW, Lavu S, Wood JG, et al. Small molecule activators of sirtuins extend *Saccharomyces cerevisiae* lifespan. *Nature* (2003) 425:191–6. doi:10.1038/nature01960

151. You Y, Liang W. SIRT1 and SIRT6: the role in aging-related diseases. *Biochim Biophys Acta Mol Basis Dis* (2023) 1869:166815. doi:10.1016/j.bbadis.2023.166815

152. Chen C, Zhou M, Ge Y, Wang X. SIRT1 and aging related signaling pathways. *Mech Ageing Dev* (2020) 187:111215. doi:10.1016/j.mad.2020.111215

153. Raza U, Tang X, Liu Z, Liu B. SIRT7: the seventh key to unlocking the mystery of aging. *Physiol Rev* (2024) 104:253–80. doi:10.1152/physrev.00044.2022

154. Li H, Cai Z. SIRT3 regulates mitochondrial biogenesis in aging-related diseases. *J Biomed Res* (2022) 37:77–88. doi:10.7555/JBR.36.20220078

155. McDonnell E, Peterson BS, Bomze HM, Hirschey MD. SIRT3 regulates progression and development of diseases of aging. *Trends Endocrinol Metab* (2015) 26:486–92. doi:10.1016/j.tem.2015.06.001

156. He L, Liu Q, Cheng J, Cao M, Zhang S, Wan X, et al. SIRT4 in ageing. *Biogerontology* (2023) 24:347–62. doi:10.1007/s10522-023-10022-5

157. Fabbrizi E, Fiorentino F, Carafa V, Altucci L, Mai A, Rotili D. Emerging roles of SIRT5 in metabolism, cancer, and SARS-CoV-2 infection. *Cells* (2023) 12:852. doi:10.3390/cells12060852

158. Bringman-Rodenbarger LR, Guo AH, Lyssiotis CA, Lombard DB. Emerging roles for SIRT5 in metabolism and cancer. *Antioxid Redox Signal* (2018) 28:677–90. doi:10.1089/ars.2017.7264

159. Wallace DC. A mitochondrial paradigm of metabolic and degenerative diseases, aging, and cancer: a dawn for evolutionary medicine. *Annu Rev Genet* (2005) 39:359–407. doi:10.1146/annurev.genet.39.110304.095751

160. Schriner SE, Linford NJ, Martin GM, Treuting P, Ogburn CE, Emond M, et al. Extension of murine life span by overexpression of catalase targeted to mitochondria. *Science* (2005) 308:1909–11. doi:10.1126/science.1106653

161. Herbst A, Prior SJ, Lee CC, Aiken JM, McKenzie D, Hoang A, et al. Skeletal muscle mitochondrial DNA copy number and mitochondrial DNA deletion mutation frequency as predictors of physical performance in older men and women. *Geroscience* (2021) 43:1253–64. doi:10.1007/s11357-021-00351-z

162. Ahmed NS, Foote JB, Singh KK. Impaired mitochondria promote aging-associated sebaceous gland dysfunction and pathology. *Am J Pathol* (2022) 192: 1546–58. doi:10.1016/j.ajpath.2022.07.006

163. Reiss AB, Ahmed S, Dayaramani C, Glass AD, Gomolin IH, Pinkhasov A, et al. The role of mitochondrial dysfunction in Alzheimer's disease: a potential pathway to treatment. *Exp Gerontol* (2022) 164:111828. doi:10.1016/j.exger.2022.111828

164. Springo Z, Tarantini S, Toth P, Tucsek Z, Koller A, Sonntag WE, et al. Aging exacerbates pressure-induced mitochondrial oxidative stress in mouse cerebral arteries. *J Gerontol A Biol Sci Med Sci* (2015) 70:1355–9. doi:10.1093/gerona/glu244

165. Tarantini S, Valcarcel-Ares NM, Yabluchanskiy A, Fulop GA, Hertelendy P, Gautam T, et al. Treatment with the mitochondrial-targeted antioxidant peptide SS-31 rescues neurovascular coupling responses and cerebrovascular endothelial

function and improves cognition in aged mice. *Aging Cell* (2018) 17:e12731. doi:10.1111/acel.12731

166. Zampino M, Spencer RG, Fishbein KW, Simonsick EM, Ferrucci L. Cardiovascular health and mitochondrial function: testing an association. *J Gerontol A Biol Sci Med Sci* (2021) 76:361–7. doi:10.1093/gerona/glaa297

167. Saberi M, Zhang X, Mobasheri A. Targeting mitochondrial dysfunction with small molecules in intervertebral disc aging and degeneration. *Geroscience* (2021) 43:517–37. doi:10.1007/s11357-021-00341-1

168. Bua E, Johnson J, Herbst A, Delong B, McKenzie D, Salamat S, et al. Mitochondrial DNA-deletion mutations accumulate intracellularly to detrimental levels in aged human skeletal muscle fibers. *Am J Hum Genet* (2006) 79:469–80. doi:10.1086/507132

169. Swift ML, Sell C, Azizkhan-Clifford J. DNA damage-induced degradation of Sp1 promotes cellular senescence. *Geroscience* (2022) 44:683–98. doi:10.1007/s11357-021-00456-5

170. Han X, Lei Q, Xie J, Liu H, Li J, Zhang X, et al. Potential regulators of the senescence-associated secretory phenotype during senescence and aging. *J Gerontol A Biol Sci Med Sci* (2022) 77:2207–18. doi:10.1093/gerona/glac097

171. Matacchione G, Perugini J, Di Mercurio E, Sabbatinelli J, Prattichizzo F, Senzacqua M, et al. Senescent macrophages in the human adipose tissue as a source of inflammaging. *Geroscience* (2022) 44:1941–60. doi:10.1007/s11357-022-00536-0

172. Fielding RA, Atkinson EJ, Aversa Z, White TA, Heeren AA, Achenbach SJ, et al. Associations between biomarkers of cellular senescence and physical function in humans: observations from the lifestyle interventions for elders (LIFE) study. *Geroscience* (2022) 44:2757–70. doi:10.1007/s11357-022-00685-2

173. Kavanagh K, Sherrill C, Ruggiero A, Block M, Vemuri R, Davis M, et al. Biomarkers of senescence in non-human primate adipose depots relate to aging. *Geroscience* (2021) 43:343–52. doi:10.1007/s11357-020-00230-z

174. Karin O, Alon U. Senescent cell accumulation mechanisms inferred from parabiosis. *Geroscience* (2021) 43:329–41. doi:10.1007/s11357-020-00286-x

175. Hense JD, Garcia DN, Isola JV, Alvarado-Rincon JA, Zanini BM, Prosczek JB, et al. Senolytic treatment reverses obesity-mediated senescent cell accumulation in the ovary. *Geroscience* (2022) 44:1747–59. doi:10.1007/s11357-022-00573-9

176. Dungan CM, Figueiredo VC, Wen Y, VonLehmden GL, Zdunek CJ, Thomas NT, et al. Senolytic treatment rescues blunted muscle hypertrophy in old mice. *Geroscience* (2022) 44:1925–40. doi:10.1007/s11357-022-00542-2

177. Iijima H, Gilmer G, Wang K, Sivakumar S, Evans C, Matsui Y, et al. Meta-analysis integrated with multi-omics data analysis to elucidate pathogenic mechanisms of age-related knee osteoarthritis in mice. *J Gerontol A Biol Sci Med Sci* (2022) 77:1321–34. doi:10.1093/gerona/glab386

178. Csipo T, Lipecz A, Ashpole NM, Balasubramanian P, Tarantini S. Astrocyte senescence contributes to cognitive decline. *Geroscience* (2020) 42:51–5. doi:10.1007/s11357-019-00140-9

179. Kiss T, Nyul-Toth A, Balasubramanian P, Tarantini S, Ahire C, DelFavero J, et al. Single-cell RNA sequencing identifies senescent cerebromicrovascular endothelial cells in the aged mouse brain. *Geroscience* (2020) 42:429–44. doi:10.1007/s11357-020-00177-1

180. Tarantini S, Balasubramanian P, Delfavero J, Csipo T, Yabluchanskiy A, Kiss T, et al. Treatment with the BCL-2/BCL-xL inhibitor senolytic drug ABT263/Navitoclax improves functional hyperemia in aged mice. *Geroscience* (2021) 43:2427–40. doi:10.1007/s11357-021-00440-z

181. Chae JB, Jang H, Son C, Park CW, Choi H, Jin S, et al. Targeting senescent retinal pigment epithelial cells facilitates retinal regeneration in mouse models of age-related macular degeneration. *Geroscience* (2021) 43:2809–33. doi:10.1007/s11357-021-00457-4

182. Park JW, Park JE, Kim SR, Sim MK, Kang CM, Kim KS. Metformin alleviates ionizing radiation-induced senescence by restoring BARD1-mediated DNA repair in human aortic endothelial cells. *Exp Gerontol* (2022) 160:111706. doi:10.1016/j.exger.2022.111706

183. Yabluchanskiy A, Tarantini S, Balasubramanian P, Kiss T, Csipo T, Fulop GA, et al. Pharmacological or genetic depletion of senescent astrocytes prevents whole brain irradiation-induced impairment of neurovascular coupling responses protecting cognitive function in mice. *Geroscience* (2020) 42:409–28. doi:10.1007/s11357-020-00154-8

184. Sun T, Zhang L, Feng J, Bao L, Wang J, Song Z, et al. Characterization of cellular senescence in doxorubicin-induced aging mice. *Exp Gerontol* (2022) 163:111800. doi:10.1016/j.exger.2022.111800

185. Khadirnaikar S, Chatterjee A, Shukla S. Identification and characterization of senescence phenotype in lung adenocarcinoma with high drug sensitivity. *Am J Pathol* (2021) 191:1966–73. doi:10.1016/j.ajpath.2021.07.005

186. Aires R, Porto ML, de Assis LM, Pereira PAN, Carvalho GR, Coco LZ, et al. DNA damage and aging on hematopoietic stem cells: impact of oxidative stress in ApoE(-)/(-) mice. *Exp Gerontol* (2021) 156:111607. doi:10.1016/j.exger.2021.111607

187. Bencivenga L, Strumia M, Rolland Y, Martinez L, Cestac P, Guyonnet S, et al. Biomarkers of mitochondrial dysfunction and inflammaging in older adults and blood pressure variability. *Geroscience* (2023) 45:797–809. doi:10.1007/s11357-022-00697-y

188. Dugue PA, Hodge AM, Ulvik A, Ueland PM, Midttun O, Rinaldi S, et al. Association of markers of inflammation, the kynurenine pathway and B vitamins with age and mortality, and a signature of inflammaging. *J Gerontol A Biol Sci Med Sci* (2022) 77:826–36. doi:10.1093/gerona/glab163

189. Cribb L, Hodge AM, Yu C, Li SX, English DR, Makalic E, et al. Inflammation and epigenetic aging are largely independent markers of biological aging and mortality. *J Gerontol A Biol Sci Med Sci* (2022) 77:2378–86. doi:10.1093/gerona/glac147

190. Zamboni M, Nori N, Brunelli A, Zoico E. How does adipose tissue contribute to inflammageing? *Exp Gerontol* (2021) 143:111162. doi:10.1016/j.exger.2020.111162

191. Sanfilippo C, Castrogiovanni P, Vinciguerra M, Imbesi R, Ulivieri M, Fazio F, et al. A sex-stratified analysis of neuroimmune gene expression signatures in Alzheimer's disease brains. *Geroscience* (2023) 45:523–41. doi:10.1007/s11357-022-00664-7

192. Kiss T, Nyul-Toth A, DelFavero J, Balasubramanian P, Tarantini S, Faakye J, et al. Spatial transcriptomic analysis reveals inflammatory foci defined by senescent cells in the white matter, hippocampi and cortical grey matter in the aged mouse brain. *Geroscience* (2022) 44:661–81. doi:10.1007/s11357-022-00521-7

193. Thadathil N, Nicklas EH, Mohammed S, Lewis TL, Richardson A, Deepa SS. Necroptosis increases with age in the brain and contributes to age-related neuroinflammation. *Geroscience* (2021) 43:2345–61. doi:10.1007/s11357-021-00448-5

194. Mehdipour M, Mehdipour T, Skinner CM, Wong N, Liu C, Chen CC, et al. Plasma dilution improves cognition and attenuates neuroinflammation in old mice. *Geroscience* (2021) 43:1–18. doi:10.1007/s11357-020-00297-8

195. Liang Z, Zhang T, Liu H, Li Z, Peng L, Wang C, et al. Inflammaging: the ground for sarcopenia? *Exp Gerontol* (2022) 168:111931. doi:10.1016/j.exger.2022.111931

196. Luo J, le Cessie S, Blauw GJ, Franceschi C, Noordam R, van Heemst D. Systemic inflammatory markers in relation to cognitive function and measures of brain atrophy: a Mendelian randomization study. *Geroscience* (2022) 44:2259–70. doi:10.1007/s11357-022-00602-7

197. Lu WH, Giudici KV, Morley JE, Guyonnet S, Parini A, Aggarwal G, et al. Investigating the combination of plasma amyloid-beta and geroscience biomarkers on the incidence of clinically meaningful cognitive decline in older adults. *Geroscience* (2022) 44:1489–503. doi:10.1007/s11357-022-00554-y

198. Jimenez L, Silva A, Calissi G, Grenho I, Monteiro R, Mayoral-Varo V, et al. Screening health-promoting compounds for their capacity to induce the activity of FOXO3. *J Gerontol A Biol Sci Med Sci* (2022) 77:1485–93. doi:10.1093/gerona/glab265

199. Li S, Hou Y, Liu K, Zhu H, Qiao M, Sun X, et al. Metformin protects against inflammation, oxidative stress to delay poly I:C-induced aging-like phenomena in the gut of an annual fish. *J Gerontol A Biol Sci Med Sci* (2022) 77:276–82. doi:10.1093/gerona/glab298

200. Brazao V, Colato RP, Santello FH, Duarte A, Goulart A, Sampaio PA, et al. Melatonin regulates antioxidant defense and inflammatory response by activating Nrf2-dependent mechanisms and inhibiting NFkappaB expression in middle-aged T. cruzi infected rats. *Exp Gerontol* (2022) 167:111895. doi:10.1016/j.exger.2022.111895

201. Caldeira CA, Santos MA, Araujo GR, Lara RC, Franco FN, Chaves MM. Resveratrol: change of SIRT 1 and AMPK signaling pattern during the aging process. *Exp Gerontol* (2021) 146:111226. doi:10.1016/j.exger.2021.111226

202. Gregory S, Pullen H, Ritchie CW, Shannon OM, Stevenson EJ, Muniz-Terrera G. Mediterranean diet and structural neuroimaging biomarkers of Alzheimer's and cerebrovascular disease: a systematic review. *Exp Gerontol* (2023) 172:112065. doi:10.1016/j.exger.2022.112065

203. Chenhuichen C, Cabello-Olmo M, Barajas M, Izquierdo M, Ramirez-Velez R, Zambom-Ferraresi F, et al. Impact of probiotics and prebiotics in the modulation of the major events of the aging process: a systematic review of randomized controlled trials. *Exp Gerontol* (2022) 164:111809. doi:10.1016/j.exger.2022.111809

204. Ezzati A, Pak VM. The effects of time-restricted eating on sleep, cognitive decline, and Alzheimer's disease. *Exp Gerontol* (2023) 171:112033. doi:10.1016/j.exger.2022.112033

205. Ramaker ME, Corcoran DL, Apsley AT, Kobor MS, Kraus VB, Kraus WE, et al. Epigenome-wide association study analysis of calorie restriction in humans, CALERIETM trial analysis. *J Gerontol A Biol Sci Med Sci* (2022) 77:2395–401. doi:10.1093/gerona/glac168

206. Fassier P, Kang JH, Lee IM, Grodstein F, Vercambre MN. Vigorous Physical Activity and Cognitive Trajectory Later in Life: prospective Association and Interaction by Apolipoprotein E e4 in the Nurses' Health Study. *J Gerontol A Biol Sci Med Sci* (2022) 77:817–25. doi:10.1093/gerona/glab169

207. Gudiksen A, Qoqaj A, Ringholm S, Wojtaszewski J, Plomgaard P, Pilegaard H. Ameliorating effects of lifelong physical activity on healthy aging and mitochondrial function in human white adipose tissue. *J Gerontol A Biol Sci Med Sci* (2022) 77:1101–11. doi:10.1093/gerona/glab356

208. Romashkan S, Chang H, Hadley EC. National institute on aging workshop: repurposing drugs or dietary supplements for their senolytic or senomorphic effects: considerations for clinical trials. *J Gerontol A Biol Sci Med Sci* (2021) 76: 1144–52. doi:10.1093/gerona/glab028

209. Saccon TD, Nagpal R, Yadav H, Cavalcante MB, Nunes ADC, Schneider A, et al. Senolytic combination of dasatinib and quercetin alleviates intestinal senescence and inflammation and modulates the gut microbiome in aged mice. *J Gerontol A Biol Sci Med Sci* (2021) 76:1895–905. doi:10.1093/gerona/glab002

210. Kowald A, Kirkwood TBL. Senolytics and the compression of late-life mortality. *Exp Gerontol* (2021) 155:111588. doi:10.1016/j.exger.2021.111588

211. Whitson JA, Johnson R, Wang L, Bammler TK, Imai SI, Zhang H, et al. Age-related disruption of the proteome and acetylome in mouse hearts is associated with loss of function and attenuated by elamipretide (SS-31) and nicotinamide mononucleotide (NMN) treatment. *Geroscience* (2022) 44:1621–39. doi:10.1007/s11357-022-00564-w

212. Whitson JA, Martin-Perez M, Zhang T, Gaffrey MJ, Merrihew GE, Huang E, et al. Elamipretide (SS-31) treatment attenuates age-associated post-translational modifications of heart proteins. *Geroscience* (2021) 43:2395–412. doi:10.1007/s11357-021-00447-6

213. Alfaras I, Di Germanio C, Bernier M, Csiszar A, Ungvari Z, Lakatta EG, et al. Pharmacological strategies to retard cardiovascular aging. *Circ Res* (2016) 118: 1626–42. doi:10.1161/CIRCRESAHA.116.307475

214. Mitchell SJ, Martin-Montalvo A, Mercken EM, Palacios HH, Ward TM, Abulwerdi G, et al. The SIRT1 activator SRT1720 extends lifespan and improves health of mice fed a standard diet. *Cell Rep* (2014) 6:836–43. doi:10.1016/j.celrep.2014.01.031

215. Hubbard BP, Sinclair DA. Small molecule SIRT1 activators for the treatment of aging and age-related diseases. *Trends Pharmacol Sci* (2014) 35:146–54. doi:10.1016/j.tips.2013.12.004

216. Kiss T, Balasubramanian P, Valcarcel-Ares MN, Tarantini S, Yabluchanskiy A, Csipo T, et al. Nicotinamide mononucleotide (NMN) treatment attenuates oxidative stress and rescues angiogenic capacity in aged cerebromicrovascular endothelial cells: a potential mechanism for the prevention of vascular cognitive impairment. *Gero Sci* (2019) 41:619–30. doi:10.1007/s11357-019-00074-2

217. Kiss T, Giles CB, Tarantini S, Yabluchanskiy A, Balasubramanian P, Gautam T, et al. Nicotinamide mononucleotide (NMN) supplementation promotes anti-aging miRNA expression profile in the aorta of aged mice, predicting epigenetic rejuvenation and anti-atherogenic effects. *Geroscience* (2019) 41:419–39. doi:10.1007/s11357-019-00095-x

218. Tarantini S, Valcarcel-Ares MN, Toth P, Yabluchanskiy A, Tucsek Z, Kiss T, et al. Nicotinamide mononucleotide (NMN) supplementation rescues cerebromicrovascular endothelial function and neurovascular coupling responses and improves cognitive function in aged mice. *Redox Biol* (2019) 24:101192. doi:10.1016/j.redox.2019.101192

219. Csiszar A, Tarantini S, Yabluchanskiy A, Balasubramanian P, Kiss T, Farkas E, et al. Role of endothelial NAD+ deficiency in age-related vascular dysfunction. *Am J Physiol Heart Circ Physiol* (2019) 316:H1253–H1266. doi:10.1152/ajpheart.00039.2019

220. Kiss T, Nyul-Toth A, Balasubramanian P, Tarantini S, Ahire C, Yabluchanskiy A, et al. Nicotinamide mononucleotide (NMN) supplementation promotes neurovascular rejuvenation in aged mice: transcriptional footprint of SIRT1 activation, mitochondrial protection, anti-inflammatory, and anti-apoptotic effects. *Geroscience* (2020) 42:527–46. doi:10.1007/s11357-020-00165-5

221. Tarantini S, Yabluchanskiy A, Csipo T, Fulop G, Kiss T, Balasubramanian P, et al. Treatment with the poly(ADP-ribose) polymerase inhibitor PJ-34 improves cerebromicrovascular endothelial function, neurovascular coupling responses and cognitive performance in aged mice, supporting the NAD+ depletion hypothesis of neurovascular aging. *Geroscience* (2019) 41:533–42. doi:10.1007/s11357-019-00101-2

222. Das A, Huang GX, Bonkowski MS, Longchamp A, Li C, Schultz MB, et al. Impairment of an endothelial NAD(+)-H2S signaling network is a reversible cause of vascular aging. *Cell* (2018) 173:74–89. doi:10.1016/j.cell.2018.02.008

223. Clement J, Wong M, Poljak A, Sachdev P, Braidy N. The plasma NAD(+) metabolome is dysregulated in "normal" aging. *Rejuvenation Res* (2018) 22:121–30. doi:10.1089/rej.2018.2077

224. Mills KF, Yoshida S, Stein LR, Grozio A, Kubota S, Sasaki Y, et al. Long-Term administration of nicotinamide mononucleotide mitigates age-associated physiological decline in mice. *Cel Metab* (2016) 24:795–806. doi:10.1016/j.cmet.2016.09.013

225. de Picciotto NE, Gano LB, Johnson LC, Martens CR, Sindler AL, Mills KF, et al. Nicotinamide mononucleotide supplementation reverses vascular dysfunction and oxidative stress with aging in mice. *Aging Cell* (2016) 15:522–30. doi:10.1111/acel.12461

226. Araki T, Sasaki Y, Milbrandt J. Increased nuclear NAD biosynthesis and SIRT1 activation prevent axonal degeneration. *Science* (2004) 305:1010–3. doi:10.1126/science.1098014

227. Blair RV, Vaccari M, Doyle-Meyers LA, Roy CJ, Russell-Lodrigue K, Fahlberg M, et al. Acute respiratory distress in aged, SARS-CoV-2-infected african green monkeys but not rhesus macaques. *Am J Pathol* (2021) 191: 274–82. doi:10.1016/j.ajpath.2020.10.016

228. Mulka KR, Beck SE, Solis CV, Johanson AL, Queen SE, McCarron ME, et al. Progression and resolution of severe acute respiratory syndrome coronavirus 2 (SARS-CoV-2) infection in golden Syrian hamsters. *Am J Pathol* (2022) 192: 195–207. doi:10.1016/j.ajpath.2021.10.009

229. Gustine JN, Jones D. Immunopathology of hyperinflammation in COVID-19. *Am J Pathol* (2021) 191:4–17. doi:10.1016/j.ajpath.2020.08.009

230. Johnson JE, McGuone D, Xu ML, Jane-Wit D, Mitchell RN, Libby P, et al. Coronavirus disease 2019 (COVID-19) coronary vascular thrombosis: correlation with neutrophil but not endothelial activation. *Am J Pathol* (2022) 192:112–20. doi:10.1016/j.ajpath.2021.09.004

231. Martin TR. Lung injury and repair in coronavirus disease 2019-related acute lung injury. *Am J Pathol* (2022) 192:406–9. doi:10.1016/j.ajpath.2022.01.001

232. Nicosia RF, Ligresti G, Caporarello N, Akilesh S, Ribatti D. COVID-19 vasculopathy: mounting evidence for an indirect mechanism of endothelial injury. *Am J Pathol* (2021) 191:1374–84. doi:10.1016/j.ajpath.2021.05.007

233. Pujadas E, Beaumont M, Shah H, Schrode N, Francoeur N, Shroff S, et al. Molecular profiling of coronavirus disease 2019 (COVID-19) autopsies uncovers novel disease mechanisms. *Am J Pathol* (2021) 191:2064–71. doi:10.1016/j.ajpath.2021.08.009

234. Salazar E, Christensen PA, Graviss EA, Nguyen DT, Castillo B, Chen J, et al. Significantly decreased mortality in a large cohort of coronavirus disease 2019 (COVID-19) patients transfused early with convalescent plasma containing high-titer anti-severe acute respiratory syndrome coronavirus 2 (SARS-CoV-2) spike protein IgG. *Am J Pathol* (2021) 191:90–107. doi:10.1016/j.ajpath.2020.10.008

235. Ting C, Aspal M, Vaishampayan N, Huang SK, Riemondy KA, Wang F, et al. Fatal COVID-19 and non-COVID-19 acute respiratory distress syndrome is associated with incomplete alveolar type 1 epithelial cell differentiation from the transitional state without fibrosis. *Am J Pathol* (2022) 192:454–67. doi:10.1016/j.ajpath.2021.11.014

236. Whitmore HAB, Kim LA. Understanding the role of blood vessels in the neurologic manifestations of coronavirus disease 2019 (COVID-19). *Am J Pathol* (2021) 191:1946–54. doi:10.1016/j.ajpath.2021.04.017

237. Fagyas M, Nagy B, Raduly AP, Manyine IS, Martha L, Erdosi G, et al. The majority of severe COVID-19 patients develop anti-cardiac autoantibodies. *Geroscience* (2022) 44:2347–60. doi:10.1007/s11357-022-00649-6

238. Moccia F, Gerbino A, Lionetti V, Miragoli M, Munaron LM, Pagliaro P, et al. COVID-19-associated cardiovascular morbidity in older adults: a position paper from the Italian Society of Cardiovascular Researches. *Geroscience* (2020) 42: 1021–49. doi:10.1007/s11357-020-00198-w

239. Danics K, Pesti A, Toro K, Kiss-Dala N, Szlavik J, Lakatos B, et al. A COVID-19-association-dependent categorization of death causes in 100 autopsy cases. *Geroscience* (2021) 43:2265–87. doi:10.1007/s11357-021-00451-w

240. Peterfi A, Meszaros A, Szarvas Z, Penzes M, Fekete M, Feher A, et al. Comorbidities and increased mortality of COVID-19 among the elderly: a systematic review. *Physiol Int* (2022) 109:163–76. doi:10.1556/2060.2022.00206

241. Gado K, Kovacs AK, Domjan G, Nagy ZZ, Bednarik GD. COVID-19 and the elderly. *Physiol Int* (2022) 109:177–85. doi:10.1556/2060.2022.00203

242. Bello-Chavolla OY, Gonzalez-Diaz A, Antonio-Villa NE, Fermin-Martinez CA, Marquez-Salinas A, Vargas-Vazquez A, et al. Unequal impact of structural health determinants and comorbidity on COVID-19 severity and lethality in older Mexican adults: considerations beyond chronological aging. *J Gerontol A Biol Sci Med Sci* (2021) 76:e52–e59. doi:10.1093/gerona/glaa163

243. Esme M, Koca M, Dikmeer A, Balci C, Ata N, Dogu BB, et al. Older adults with coronavirus disease 2019: a nationwide study in Turkey. *J Gerontol A Biol Sci Med Sci* (2021) 76:e68–e75. doi:10.1093/gerona/glaa219

244. Farrelly C. The COVID-19 pandemic, biogerontology, and the ageing of humanity. *J Gerontol A Biol Sci Med Sci* (2021) 76:e92–e96. doi:10.1093/gerona/glab027

245. Kuo CL, Pilling LC, Atkins JL, Masoli JAH, Delgado J, Tignanelli C, et al. Biological aging predicts vulnerability to COVID-19 severity in UK biobank participants. *J Gerontol A Biol Sci Med Sci* (2021) 76:e133–e141. doi:10.1093/gerona/glab060

246. Marengoni A, Zucchelli A, Vetrano DL, Armellini A, Botteri E, Nicosia F, et al. Beyond chronological age: frailty and multimorbidity predict in-hospital mortality in patients with coronavirus disease 2019. *J Gerontol A Biol Sci Med Sci* (2021) 76:e38–e45. doi:10.1093/gerona/glaa291

247. Marquez-Salinas A, Fermin-Martinez CA, Antonio-Villa NE, Vargas-Vazquez A, Guerra EC, Campos-Munoz A, et al. Adaptive metabolic and inflammatory responses identified using accelerated aging metrics are linked to adverse outcomes in severe SARS-CoV-2 infection. *J Gerontol A Biol Sci Med Sci* (2021) 76:e117–e126. doi:10.1093/gerona/glab078

248. Mendes A, Herrmann FR, Perivier S, Gold G, Graf CE, Zekry D. Delirium in older patients with COVID-19: prevalence, risk factors, and clinical relevance. *J Gerontol A Biol Sci Med Sci* (2021) 76:e142–e146. doi:10.1093/gerona/glab039

249. Poco PCE, Aliberti MJR, Dias MB, Takahashi SF, Leonel FC, Altona M, et al. Divergent: age, frailty, and atypical presentations of COVID-19 in hospitalized patients. *J Gerontol A Biol Sci Med Sci* (2021) 76:e46–e51. doi:10.1093/gerona/glaa280

250. Zerah L, Baudouin E, Pepin M, Mary M, Krypciak S, Bianco C, et al. Clinical characteristics and outcomes of 821 older patients with SARS-cov-2 infection admitted to acute care geriatric wards. *J Gerontol A Biol Sci Med Sci* (2021) 76:e4–e12. doi:10.1093/gerona/glaa210

251. Penfold RS, Zazzara MB, Osterdahl MF, Welch C, Ni Lochlainn M, Freidin MB, et al. Individual factors including age, BMI, and heritable factors underlie temperature variation in sickness and in health: an observational, multi-cohort study. *J Gerontol A Biol Sci Med Sci* (2022) 77:1890–7. doi:10.1093/gerona/glab295

252. Tisminetzky M, Delude C, Hebert T, Carr C, Goldberg RJ, Gurwitz JH. Age, multiple chronic conditions, and COVID-19: a literature review. *J Gerontol A Biol Sci Med Sci* (2022) 77:872–8. doi:10.1093/gerona/glaa320

253. VoPham T, Harris HR, Tinker LF, Manson JE, Meliker JR, Wassertheil-Smoller S, et al. The impact of the COVID-19 pandemic on older women in the women's health initiative. *J Gerontol A Biol Sci Med Sci* (2022) 77:S3–S12. doi:10.1093/gerona/glac056

254. Farshbafnadi M, Kamali Zonouzi S, Sabahi M, Dolatshahi M, Aarabi MH. Aging and COVID-19 susceptibility, disease severity, and clinical outcomes: the role of entangled risk factors. *Exp Gerontol* (2021) 154:111507. doi:10.1016/j.exger.2021.111507

255. Nidadavolu LS, Walston JD. Underlying vulnerabilities to the cytokine storm and adverse COVID-19 outcomes in the aging immune system. *J Gerontol A Biol Sci Med Sci* (2021) 76:e13–e18. doi:10.1093/gerona/glaa209

256. Zhou J, Sun Y, Huang W, Ye K. Altered blood cell traits underlie a major genetic locus of severe COVID-19. *J Gerontol A Biol Sci Med Sci* (2021) 76:e147–e154. doi:10.1093/gerona/glab035

257. Garcia-Torre A, Bueno-Garcia E, Lopez-Martinez R, Rioseras B, Moro-Garcia MA, Alonso-Alvarez S, et al. Surviving older patients show preserved cellular and humoral immunological memory several months after SARS-CoV-2 infection. *J Gerontol A Biol Sci Med Sci* (2022) 77:33–40. doi:10.1093/gerona/glab206

258. Justice JN, Gubbi S, Kulkarni AS, Bartley JM, Kuchel GA, Barzilai N. A geroscience perspective on immune resilience and infectious diseases: a potential case for metformin. *Geroscience* (2021) 43:1093–112. doi:10.1007/s11357-020-00261-6

259. Pence BD. Severe COVID-19 and aging: are monocytes the key? *Geroscience* (2020) 42:1051–61. doi:10.1007/s11357-020-00213-0

260. Xu K, Wei Y, Giunta S, Zhou M, Xia S. Do inflammaging and coagul-aging play a role as conditions contributing to the co-occurrence of the severe hyper-inflammatory state and deadly coagulopathy during COVID-19 in older people? *Exp Gerontol* (2021) 151:111423. doi:10.1016/j.exger.2021.111423

261. Fekete M, Szarvas Z, Fazekas-Pongor V, Feher A, Dosa N, Lehoczki A, et al. COVID-19 infection in patients with chronic obstructive pulmonary disease: from pathophysiology to therapy. Mini-review. *Physiol Int* (2022) 109:9–19. doi:10.1556/2060.2022.00172

262. Feher A, Szarvas Z, Lehoczki A, Fekete M, Fazekas-Pongor V. Co-infections in COVID-19 patients and correlation with mortality rate. Minireview. *Physiol Int* (2022) 109:1–8. doi:10.1556/2060.2022.00015

263. Kohli J, Campisi J, Demaria M. A novel suicide gene therapy for the treatment of p16(Ink4a)-overexpressing tumors. *Oncotarget* (2018) 9:7274–81. doi:10.18632/oncotarget.23752

264. Abdul-Aziz AM, Sun Y, Hellmich C, Marlein CR, Mistry J, Forde E, et al. Acute myeloid leukemia induces protumoral p16INK4a-driven senescence in the bone marrow microenvironment. *Blood* (2019) 133:446–56. doi:10.1182/blood-2018-04-845420

265. Patil P, Dong Q, Wang D, Chang J, Wiley C, Demaria M, et al. Systemic clearance of p16(INK4a) -positive senescent cells mitigates age-associated intervertebral disc degeneration. *Aging Cell* (2019) 18:e12927. doi:10.1111/acel.12927

266. Jeon OH, Kim C, Laberge RM, Demaria M, Rathod S, Vasserot AP, et al. Local clearance of senescent cells attenuates the development of post-traumatic osteoarthritis and creates a pro-regenerative environment. *Nat Med* (2017) 23:775–81. doi:10.1038/nm.4324

267. Kim HN, Chang J, Iyer S, Han L, Campisi J, Manolagas SC, et al. Elimination of senescent osteoclast progenitors has no effect on the age-associated loss of bone mass in mice. *Aging Cell* (2019) 18:e12923. doi:10.1111/acel.12923

268. Istvan L, Czako C, Elo A, Mihaly Z, Sotonyi P, Varga A, et al. Imaging retinal microvascular manifestations of carotid artery disease in older adults: from diagnosis of ocular complications to understanding microvascular contributions to cognitive impairment. *Geroscience* (2021) 43:1703–23. doi:10.1007/s11357-021-00392-4

269. Czako C, Kovacs T, Ungvari Z, Csiszar A, Yabluchanskiy A, Conley S, et al. Retinal biomarkers for Alzheimer's disease and vascular cognitive impairment and dementia (VCID): implication for early diagnosis and prognosis. *Geroscience* (2020) 42:1499–525. doi:10.1007/s11357-020-00252-7

270. Drewelies J, Hueluer G, Duezel S, Vetter VM, Pawelec G, Steinhagen-Thiessen E, et al. Using blood test parameters to define biological age among older adults: association with morbidity and mortality independent of chronological age validated in two separate birth cohorts. *Geroscience* (2022) 44:2685–99. doi:10.1007/s11357-022-00662-9

271. Cummings SR, Kritchevsky SB. Endpoints for geroscience clinical trials: health outcomes, biomarkers, and biologic age. *Geroscience* (2022) 44:2925–31. doi:10.1007/s11357-022-00671-8

272. Amgalan A, Maher AS, Ghosh S, Chui HC, Bogdan P, Irimia A. Brain age estimation reveals older adults' accelerated senescence after traumatic brain injury. *Geroscience* (2022) 44:2509–25. doi:10.1007/s11357-022-00597-1

273. Kwon D, Belsky DW. A toolkit for quantification of biological age from blood chemistry and organ function test data: BioAge. *Geroscience* (2021) 43:2795–808. doi:10.1007/s11357-021-00480-5

274. Crimmins EM, Thyagarajan B, Kim JK, Weir D, Faul J. Quest for a summary measure of biological age: the health and retirement study. *Geroscience* (2021) 43:395–408. doi:10.1007/s11357-021-00325-1

275. Chan MS, Arnold M, Offer A, Hammami I, Mafham M, Armitage J, et al. A biomarker-based biological age in UK biobank: composition and prediction of mortality and hospital admissions. *J Gerontol A Biol Sci Med Sci* (2021) 76:1295–302. doi:10.1093/gerona/glab069

276. Horvath S, Lin DTS, Kobor MS, Zoller JA, Said JW, Morgello S, et al. HIV, pathology and epigenetic age acceleration in different human tissues. *Geroscience* (2022) 44:1609–20. doi:10.1007/s11357-022-00560-0

277. Nwanaji-Enwerem JC, Colicino E, Gao X, Wang C, Vokonas P, Boyer EW, et al. Associations of plasma folate and vitamin B6 with blood DNA methylation age: an analysis of one-carbon metabolites in the VA normative aging study. *J Gerontol A Biol Sci Med Sci* (2021) 76:760–9. doi:10.1093/gerona/glaa257

278. Kresovich JK, Martinez Lopez AM, Garval EL, Xu Z, White AJ, Sandler DP, et al. Alcohol consumption and methylation-based measures of biological age. *J Gerontol A Biol Sci Med Sci* (2021) 76:2107–11. doi:10.1093/gerona/glab149

279. Crimmins EM, Thyagarajan B, Levine ME, Weir DR, Faul J. Associations of age, sex, race/ethnicity, and education with 13 epigenetic clocks in a nationally representative U.S. Sample: the health and retirement study. *J Gerontol A Biol Sci Med Sci* (2021) 76:1117–23. doi:10.1093/gerona/glab016

280. Vetter VM, Kalies CH, Sommerer Y, Spira D, Drewelies J, Regitz-Zagrosek V, et al. Relationship between 5 epigenetic clocks, telomere length, and functional capacity assessed in older adults: cross-sectional and longitudinal analyses. *J Gerontol A Biol Sci Med Sci* (2022) 77:1724–33. doi:10.1093/gerona/glab381

281. McCrory C, Fiorito G, Hernandez B, Polidoro S, O'Halloran AM, Hever A, et al. GrimAge outperforms other epigenetic clocks in the prediction of age-related clinical phenotypes and all-cause mortality. *J Gerontol A Biol Sci Med Sci* (2021) 76:741–9. doi:10.1093/gerona/glaa286

282. Van Remmen H, Freeman WM, Miller BF, Kinter M, Wren JD, Chiao A, et al. Oklahoma Nathan Shock Aging Center - assessing the basic biology of aging from genetics to protein and function. *Geroscience* (2021) 43:2183–203. doi:10.1007/s11357-021-00454-7

283. Shadel GS, Adams PD, Berggren WT, Diedrich JK, Diffenderfer KE, Gage FH, et al. The San Diego Nathan Shock Center: tackling the heterogeneity of aging. *Geroscience* (2021) 43:2139–48. doi:10.1007/s11357-021-00426-x

284. Salmon AB, Nelson JF, Gelfond JAL, Javors M, Ginsburg B, Lopez-Cruzan M, et al. San Antonio Nathan Shock Center: your one-stop shop for aging research. *Geroscience* (2021) 43:2105–18. doi:10.1007/s11357-021-00417-y

285. Korstanje R, Peters LL, Robinson LL, Krasinski SD, Churchill GA. The jackson laboratory nathan shock center: impact of genetic diversity on aging. *Geroscience* (2021) 43:2129–37. doi:10.1007/s11357-021-00421-2

286. Kaeberlein M, Bitto A, Dunham MJ, Ladiges W, Lee SI, MacCoss MJ, et al. University of Washington Nathan Shock Center: innovation to advance aging research. *Geroscience* (2021) 43:2161–5. doi:10.1007/s11357-021-00413-2

287. Curran SP, Lithgow GJ, Verdin E, Cohen P. University of Southern California and buck institute nathan shock center: multidimensional models of aging. *Geroscience* (2021) 43:2119–27. doi:10.1007/s11357-021-00416-z

288. Cuervo AM, Huffman DM, Vijg J, Milman S, Singh R, Barzilai N. Einstein-Nathan shock center: translating the hallmarks of aging to extend human health span. *Geroscience* (2021) 43:2167–82. doi:10.1007/s11357-021-00428-9

289. Austad SN, van der Willik O, Lederman S, Kerr C. The nathan shock centers. *Geroscience* (2021) 43:2103–4. doi:10.1007/s11357-021-00425-y

290. Austad SN, Buford TW, Allison DB, Ballinger SW, Brown AW, Carter CS, et al. University of Alabama at birmingham nathan shock center: comparative energetics of aging. *Geroscience* (2021) 43:2149–60. doi:10.1007/s11357-021-00414-1

Pathology & Oncology Research | frontiers

TYPE Original Research
PUBLISHED 19 January 2023
DOI 10.3389/pore.2023.1610934

Check for updates

OPEN ACCESS

EDITED BY
Andrea Ladányi,
National Institute of Oncology (NIO), Hungary

*CORRESPONDENCE
Fruzsina Bódis,
bodis.fruzsina@med.semmelweis-univ.hu

RECEIVED 08 November 2022
ACCEPTED 09 January 2023
PUBLISHED 19 January 2023

CITATION
Bódis F, Orosz G, Tóth JT, Szabó M, Élő LG, Gál J and Élő G (2023), Percutaneous tracheostomy: Comparison of three different methods with respect to tracheal cartilage injury in cadavers—Randomized controlled study.
Pathol. Oncol. Res. 29:1610934.
doi: 10.3389/pore.2023.1610934

COPYRIGHT
© 2023 Bódis, Orosz, Tóth, Szabó, Élő, Gál and Élő. This is an open-access article distributed under the terms of the Creative Commons Attribution License (CC BY). The use, distribution or reproduction in other forums is permitted, provided the original author(s) and the copyright owner(s) are credited and that the original publication in this journal is cited, in accordance with accepted academic practice. No use, distribution or reproduction is permitted which does not comply with these terms.

Percutaneous tracheostomy: Comparison of three different methods with respect to tracheal cartilage injury in cadavers—Randomized controlled study

Fruzsina Bódis[1]*, Gábor Orosz[2], József T. Tóth[2], Marcell Szabó[3], László Gergely Élő[2], János Gál[2] and Gábor Élő[2]

[1]Department of Otorhinolaryngology and Head and Neck Surgery, Semmelweis University, Budapest, Hungary, [2]Department of Anaesthesiology and Intensive Therapy, Semmelweis University, Budapest, Hungary, [3]Department of Surgery, Transplantation and Gastroenterology, Semmelweis University, Budapest, Hungary

Background: Performing tracheostomy improves patient comfort and success rate of weaning from prolonged invasive mechanical ventilation. Data suggest that patients have more benefit of percutaneous technique than the surgical procedure, however, there is no consensus on the percutaneous method of choice regarding severe complications such as late tracheal stenosis. Aim of this study was comparing incidences of cartilage injury caused by different percutaneous dilatation techniques (PDT), including Single Dilator, Griggs' and modified (bidirectional) Griggs' method.

Materials and methods: Randomized observational study was conducted on 150 cadavers underwent post-mortem percutaneous tracheostomy. Data of cadavers including age, gender and time elapsed from death until the intervention (more or less than 72 h) were collected and recorded. Primary and secondary outcomes were: rate of cartilage injury and cannula malposition respectively.

Results: Statistical analysis revealed that method of intervention was significantly associated with occurrence of cartilage injury, as comparing either standard Griggs' with Single Dilator (p = 0.002; OR: 4.903; 95% CI: 1.834–13.105) or modified Griggs' with Single Dilator ($p < 0.001$; OR: 6.559; 95% CI: 2.472–17.404), however, no statistical difference was observed between standard and modified Griggs' techniques (p = 0.583; OR: 0.748; 95% CI: 0.347–1.610). We found no statistical difference in the occurrence of cartilage injury between the early- and late post-mortem group (p = 0.630). Neither gender (p = 0.913), nor age (p = 0.529) influenced the rate of cartilage fracture. There was no statistical difference between the applied PDT techniques regarding the cannula misplacement/malposition.

Conclusion: In this cadaver study both standard and modified Griggs' forceps dilatational methods were safer than Single dilator in respect of cartilage injury.

10.3389/pore.2023.1610934

KEYWORDS

percutaneous tracheostomy, tracheal cartilage injury, Tracheal stenosis, Griggs, Ciaglia Blue Rhino

Introduction

Prolonged invasive mechanical ventilation of a patient *via* orotracheal tube may cause several early and late intubation-associated complications including pneumonia, pressure ulcers of the surrounding tissues, tracheal stenosis, etc. It is also highly responsible for patient discomfort due to swallowing incompetence, impaired communication ability and poor mouth hygiene. To avoid these complications and enhance patient comfort currently it is widely accepted to perform either surgical or percutaneous tracheostomy for patients who need prolonged mechanical ventilation (1–4).

The first widely accepted percutaneous tracheostomy technique was described by Pat Ciaglia, which involved a series of sequential dilatations using a set of seven dilators of progressively larger size (5). A variant of this technique, using a single tapered dilator is called the Ciaglia Blue Rhino™ (Cook Medical, Bloomington IN, United States) method which is now most commonly used, especially in the United States and United Kingdom (6). There is a very similar method to this when a balloon is introduced over a guidewire to dilate the stoma (7). In PercuTwist™ (Teleflex, Athlone, Ireland) technique, a specially designed screw-type dilator is introduced over a guidewire and its rotation dilates the stoma (8). Another widely used technique was developed by William Griggs who suggested to use specifically modified forceps enabling the performance of the main dilation in a single step (9). The other great advance of this technique is that all the aforementioned methods require pressure over the anterior wall during dilation risking a possible posterior tracheal wall injury (6). An interesting alternative was described by Fantoni, where the dilator and the tracheostomy tube are pulled through the larynx in a retrograde fashion (10).

The spread of percutaneous techniques raised the number of successful bedside tracheostomy operations, and percutaneous dilatational tracheostomy (PDT) gained popularity to become the technique of choice for long-term airway management in mechanically ventilated patients. However, these interventions have their own hazards: the major early complication is hemorrhage and one of the most dangerous and relatively common late complication is tracheal stenosis. Severe tracheal stenosis occurs in 3%–12% of patients undergoing PDT (11, 12) which is considered an excruciating late complication of tracheostomy with significant impact on quality of life. Mechanisms of postintubational and posttracheostomy tracheal stenosis are not clearly identified. After a long term intratracheal intubation the cause could be ischaemia of the mucous membrane, pressure ulceration or granulation tissue, while in case of trauma tracheal stenosis is rather caused by cartilage injury as it was described in trauma patients and in canine model (13–19). A. Marchion et al published a molecular, histolgical study in 2022. They found that the reason could be aberrant wound-healing, fibrotic scarring and iatrogenic aetiology as trauma of the tracheal mucosa, and of the tracheal cartilage; (20). As there is a possible causative relationship between the fracture of the cartilage during the PDT procedure and the aforementioned tracheal stenosis, in this study we wanted to investigate how common cartilage fracture is when performing PDT on cadavers with the two most common methods, namely Griggs' and single dilator (Rhino), and we also reevaluated and compared our previously described modified Griggs' method (in which we make a wider incision, blunt preparation, and bidirectional forceps dilation of the tracheal wall, e.g. standard horizontal and novel vertical) with them (21). The further late complications such as tracheomalacia, tracheoinominate artery fistula and tracheoesophageal fistula occur each in <1%. Tracheaomalacia usually caused by the high cuff pressure of the tracheal tube. This and the intraoperational perforation of the posterior tracheal wall could also be the cause of the tracheoesophageal fistula. If the tracheostomy tube is positioned under the 4th tracheal cartilage the risk of the development of the tracheoinominate artery fistula is higher. These late complications cannot be investigated on cadavers (12–27).

Materials and methods

Our cadaver study was performed at the 1st Department of Pathology and Experimental Cancer Research of Semmelweis University with permission of Semmelweis University Regional and Institutional Committee of Science and Research Ethics (117-1/2006 SE-RKEB; 2014.03.17). Data were collected anonymized. Data analysis and statistical plan was written and filed with a private entity before data were accessed.

The simple-blinded observational method was carried out by two experts in the field of surgical and percutaneous tracheostomies—by an intensive care specialist and an ENT surgeon with additional specialization of intensive care medicine—both for more than 5 years at a University hospital. The first expert had performed the procedures and the second one had checked the results, respectively.

Cadavers (who were not intubated before death) were collected; autopsies as well as preparation of the airway complexes from the cadavers following tracheostomy were carried out by mortuary technician. Site of tracheal cannula insertion, estimation of tracheal cartilage damage were scored by the non-operator expert without the knowledge of the insertion technique.

Insertion site was scored as 1: cricoid-1st tracheal ring space; 2: 1st-2nd tracheal ring space; 3: 2nd-3rd tracheal ring space. Estimation of ring injuries was classified as: 1: none; 2: one ring fractured; 3: two or more rings fractured.

Data about the cadavers [e.g., date and time of death (72 h or more before intervention), age, gender] as well as the lack of exclusion criteria (e.g., previous laryngo-tracheal disease, injury, previous tracheostomy, visible or palpable damage on the neck) were collected and recorded on individual sheets with registration numbers.

Randomization was carried out by a 6-sided dice: Nr 1-2, 3-4 and 5-6 were linked with traditional Griggs ($n = 51$), modified Griggs ($n = 55$) and Single Dilator methods ($n = 44$), respectively.

Cadavers were positioned in standard hyperextended position for tracheostomy, and the exact method was performed according to the randomization. Details of the procedures are briefly presented below [13] and were discussed previously elsewhere. [14] Percutaneous tracheostomy kits available from the market were used. For traditional and modified Griggs' technique Portex® GRIGGS© Percutaneous Dilation Tracheostomy Kit with Blue Line Ultra® tubes in different sizes were used according to the needs. For Ciaglia method Portex® ULTRAperc© Single Stage Dilator Technique Kit with Blue Line Ultra® tubes were applied in the same manner.

Skin incisions were performed at the midpoint of cricoid cartilage and jugulum. Traditional Griggs' technique:, no surgical preparation, direct tracheal puncture and unidirectional (transverse) tracheal dilation were performed followed by the insertion of tracheostomy cannula (9).

Modified Griggs' technique: a maximum 50 mm-wide skin incision, surgical pretracheal tissue preparation, and careful, visualized bidirectional (transverse and longitudinal) intercartilaginous forceps dilation of tracheal wall were performed (21). The wider horizontal skin incision provided enough space for secure pretracheal preparation until the tracheal wall could be visualized as well as palpated in our modified technique. Preparations were performed using blunt technique, and Griggs-modified dilating forceps were used in order to ascertain tissue resistance followed by the tracheal puncture according to Watters recommendations (28). Visualized tracheal wall puncture next to the palpating finger and continuous aspiration of air secured correct intratracheal needle position according to Paran's recommendation (29). Insertion of the guidewire followed by the introducer was the following step. Griggs-modified dilating forceps were introduced using the guidewire, according to the standard method, as deep as approximately 15 mm from the axis of rotation, and bimanual horizontal dilation was performed. Forceps were rotated 90° in longitudinal direction afterwards, and another bimanual forceps dilation was carried out in the vertical direction. After removing the forceps tracheostomy tube was inserted into the trachea using the guidewire.

The Ciaglia Blue Rhino single dilator method was performed as reviewed by SP Ambesh (30). After a transverse 20 mm skin incision we identified the anterior tracheal wall by palpation to assess the puncture site. The tracheal dilation was performed by a curved, gradually tapered dilator in a single step, than we inserted the tracheostomy tube *via* using a guidewire.

Upper airway complex was anatomized by a mortuary technician with maximal care for non-traumatic extraction. Site of insertion and posterior tracheal wall were inspected and recorded by the non-operator expert, then dissection of the posterior wall was carried out. Exact cannula position was checked and ring fracture inspected and palpated to avoid any "hidden" fracture covered by mucosa. The process was completed by photo documentation.

Statistics

Pearson chi-square tests were applied using SigmaStat 3.5 program (Systat Software Inc., San Jose, CA, United states) for statistical evaluation. To calculate the sample size of the study, the frequency of tracheal cartilage injury was the variable of interest. We assumed that a minimum of 20% difference was considered clinically important, and that in combination with our previous results of 9% from earlier experiments were used for the calculations. [13] A type one error of 0.05 and a required (statistical) power of 0.80 were set. A minimum of 150 cadavers were required based on the conditions detailed above.

Results

We carried out PDTs in 150 cadavers (69 female and 81 male) with different types of dilatational techniques in the period of 2015 March 01–2017 February 24. All data is available in Supplementary Material. Standard Griggs technique was applied in 51 cases, modified Griggs technique in 55 cases and Single Dilator technique in 44 cases according to randomization. During autopsy, we found that in four cases the tracheostomy tube was misplaced - not in the trachea but in the surrounding tissues (all done by Single Dilator method). We excluded these results; thus statistical analysis consists of 146 cases.

According to the time elapsed since death we divided the patients into two groups, an early post-mortem (less than 72 h passed since death), and a late post-mortem group (81 vs. 65 subjects). Our preliminary assumption was that cartilage rigidity varies with the time elapsed after death thus there would be an increase in cartilage injury in the group of cadavers in whom PDT was carried out more than 72 h after death (late post-mortem group). Table 1 shows that the frequency of cartilage injury was 53.09% (43/81 cases) and 58.46% (38/65 cases), respectively, hence there was no

TABLE 1 Relationship between cartilage injury and study variables.

	No injury	Injury	Injury (%)	*p*-value
early post-mortem (less than 72h after death)	38	43	53.09	0.630
late post-mortem (more than 72h after death)	27	38	58.46	
cadaver younger than 70 years	34	37	52.11	0.529
cadaver older than 70 years	31	44	58.67	
women	29	38	56.72	0.913
Men	36	43	54.43	

statistical difference between these two groups (p = 0.630). Figure 1 presents characteristic images of tracheal injuries found during autopsies. Thus for further analysis we summarized all subjects irrespective of the time elapsed from death until PDT was carried out. We also recorded the age of subjects at death and according to this we compared cartilage injury occurrence in subjects younger (34/71) and older than 70 years (31/75). No statistical difference was found between these two groups (p = 0.529), thus cartilage fracture does not depend on the age of the deceased. There was also no statistical difference (p = 0.913) in the cartilage injury occurrence between women (29/67) and men (36/79).

As the next step we compared the three techniques applied according to two aspects, whether the occurrence of cartilage injury depends on the dilatational techniques and whether there is any difference in the position of tracheostomy. For the latter we accepted the tracheostomy at "proper position" if the tube was inserted between the 1st and 2nd or between the 2nd and 3rd cartilages according to the standards. Raw data are shown in Table 2. When performing tracheostomy with standard Griggs' technique, there was no cartilage injury observed in 26 cases, and injured cartilages were detected in 25 cases (injury occurrence: 49.02%), meanwhile 31 tubes were inserted in good position and 20 were malpositioned (malposition occurrence: 39.22%). In case of modified Griggs' method these results are 32 vs. 23 (41.82%) for injury and 36 vs. 19 (34.55%) for malposition, and 7 vs. 33 (82.50%) and 22 vs. 18 (45.00%), respectively, when using Single Dilator.

Statistical analysis revealed that the method of intervention was significantly associated with cartilage injury, when comparing either standard Griggs' with Single Dilator (p = 0.002; OR: 4.903; 95% CI: 1.834–13.105) or modified Griggs' with Single Dilator (p < 0.001; OR: 6.559; 95% CI: 2.472–17.404) technique. In each case we found that there is an increased risk of cartilage injury when using the Single Dilator technique. However, we could not detect any statistical difference between standard and modified Griggs' techniques with respect to cartilage injury (p = 0.583; OR: 0.748; 95% CI: 0.347–1.610). We also analyzed the malposition occurrence, but there was no statistically significant difference between the three PDT techniques applied (Griggs vs. modified Griggs: p = 0.767; OR: 0.818; 95% CI: 0.371–1.803; Griggs vs. Single Dilator: p = 0.733; OR: 1.268; 95% CI: 0.548–2.935; and modified Griggs vs. Single Dilator: p = 0.413; OR: 1.550; 95% CI: 0.673–3.572). Statistical data are shown in Table 3.

Discussion

Tracheostomy was traditionally performed by surgeons in the operating room, but thanks to the development of percutaneous dilatational techniques nowadays is a routine procedure done by intensivists in most of the Intensive Care Units. PDT helps shorten overall time of tracheostomy procedures by decreasing the waiting time for operating room and general anesthesia (31–33). Another great review also suggests that PDT is the procedure of choice for tracheostomy because of its reduced procedure time and medical cost (34) There are several good quality prospective randomized studies which confirm the PDT's superiority against surgical techniques in critically ill patients (35–38). PDT is associated with significantly fewer wound infections and unfavourable scarring, and it may also reduce the risk of bleeding and mortality compared with surgical tracheostomy in critically ill patients according to systematic reviews (39, 40). Bedside percutaneous tracheostomy was experienced as a safe method in a retrospective review of more than 3000 procedures (41). However, in a recent study, there was no statistically significant difference in the one-year mortality of patients undergoing prolonged mechanical ventilation whether receiving tracheostomy or not (42), furthermore there were no significant differences in the intraoperative and postoperative bleeding and in mortality in recent meta-analysis (43).

Although there are several studies, meta-analyses and excellent reviews which compare the different PDT techniques (6,30,44–47), there is still no consensus between physicians on which technique has the lowest major complication rate. Our aim in this study was to compare the two most widely used PDT techniques—namely the Griggs' and the Single Dilator—and also our previously suggested modification of Griggs' version (21) in cadavers, in respect of cartilage injury, which is believed to take important part in the development of tracheal stenosis (48, 49).

10.3389/pore.2023.1610934

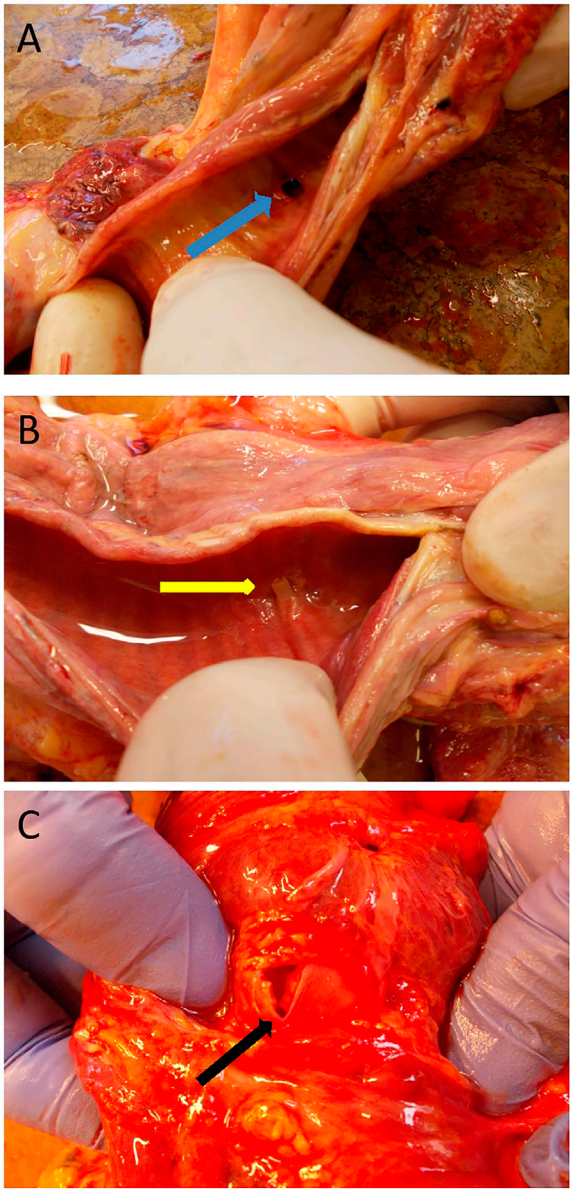

FIGURE 1
Characteristic of tracheal injuries during autopsies **(A)**: Tracheostomy aperture [blue arrow] without fracture (posterior tracheal wall dissected, internal view). **(B)** "One-ring" fracture [yellow arrow] (posterior tracheal wall dissected, internal view). **(C)** "Multiple-ring" fracture [black arrow] (anterior view for demonstrational purposes).

According to our data, using a single tapered dilator significantly increases the risk of cartilage injury in cadavers compared to both standard and modified Griggs' methods, in accordance with some previous experts' observations (30). The single dilator is a round shaped device with permanently increasing diameter which is used with a continous force against the tracheal wall therefore the trachea cartilage could be broken easier in this case. A mild single unidirectional (transverse) tracheal dilation is performed in Griggs method, while performing modified Griggs technique a visualized bidirectional (transverse and longitudinal) intercartilaginous dilation is made which both can reduce the risk of cartilage injuries (50).

We have suggested a modification to the classical Griggs' method in order to decrease the complications of PDT in our previous study (21). We have found that this modification caused a remarkable decrease in the number of injured tracheal cartilages. One of the main drawbacks of that study was that the procedures were not blinded, i.e., the same investigator performed and evaluated identical procedures. Thus, now we redesigned and reevaluated our previous study using a randomized, blinded approach. Our new data still showed a decreased risk of cartilage injury with this modification; however, this reduction was not statistically significant. Further elevation of the sample size may emphasize the difference. Cartilage fracture was independent of aging, gender and the time elapsed since death. According to statistical analysis the level of intervention was not different between the three groups, however, it is worth mentioning that cannula malposition occurred less commonly in the modified Griggs' group.

We suggest making a quite wide (50-mm) horizontal skin incision for the procedure. One might say that this increases the risk of major bleeding and makes the procedure longer but at the same time it provides enough space for secure pretracheal surgical blunt preparation until the tracheal wall can be visualized and palpated making critical intervention (i.e. tracheal puncture with partially lost airway) shorter and probably safer. Another important aspect is, that with good visibility bronchoscopy is nearly unnecessary, thus it is easier to avoid the significant rise of $PaCO_2$ and consequent respiratory acidosis which occurs during bronchoscopy even when applying increased tidal volume and large diameter endotracheal tube (51).

TABLE 2 Relationship between cartilage injury or tracheostomy tube position and the method of intervention.

Method	No injury	Injury	Injury (%)	Good position	Bad position	Malposition (%)
Griggs'	26	25	49.02	31	20	39.22
modified Griggs'	32	23	41.82	36	19	34.55
Single Dilator	7	33	82.50	22	18	45.00

TABLE 3 Statistical analysis of the methods of intervention according to cartilage injury and tracheostomy tube position.

	Cartilage injury			Malposition		
	p-value	odds ratio	CI 95%	*p*-value	odds ratio	CI 95%
Griggs' vs. modified Griggs'	0.583	0.748	0.347 to 1.610	0.767	0.818	0.371 to 1.803
Griggs' vs. Single Dilator	0.002	4.903	1.834 to 13.105	0.733	1.268	0.548 to 2.935
modified Griggs' vs. Single Dilator	<0.001	6.559	2.472 to 17.404	0.413	1.550	0.673 to 3.572

The obvious limitation of our study is that PDTs were made in cadavers, which could influence cartilage flexibility, so cadaver's tracheal cartilages could be more rigid than in case of living tissue. Performing PDT cartilage injury/fracture could be rare in living tissues but the correlation of the number of the cartilage injuries using different methods could be demonstrated on cadavers.Tracheal injuries were more common in our study (81/146 subjects, 55.48%) than what we would expect according to our clinical experience, although it was still less than mentioned in another PDT cadaver study (83%) (52). Even if there was no significant difference in cartilage injury between the two groups defined by the post-mortem time elapsed, there was a higher incidence in the late post-mortem group, which corroborates the presumption that it could influence our data. It is also important to mention that cartilage injury could not only occur during the insertion of the cannula but also during autopsy when it was removed for evaluation, thus it could further increase its incidence.

In conclusion, in cadavers we found that forceps dilatational methods are safer than Single dilator with respect to cartilage injury. Although we did not detect statistical significance, we still suggest the use of bidirectional dilatation with forceps, as cartilage injury and cannula malposition incidence was the lowest in the group where this modification was applied. Prospective study and long-term follow-up of patients undergoing PDTs would be necessary to further confirm its superiority over other methods.

Data availability statement

The original contributions presented in the study are included in the article/Supplementary Material, further inquiries can be directed to the corresponding author.

Ethics statement

The studies involving human participants were reviewed and approved by Semmelweis University Regional and Institutional Committee of Science and Research Ethics (117-1/2006 SE-RKEB; 2014.03.17). Written informed consent for participation was not required for this study in accordance with the national legislation and the institutional requirements.

Author contributions

GÉ designed and wrote the research study; FB and GO performed the research; FB and GO and LÉ collected the data; JT analyzed the data; FB and JT wrote the paper. JG and GÉ, and MSZ revised the manuscript. All authors approved the final manuscript.

Conflict of interest

The authors declare that the research was conducted in the absence of any commercial or financial relationships that could be construed as a potential conflict of interest.

Acknowledgments

Authors are grateful to Professor András Matolcsy Gergely Rácz M.D. PhD, János Zalavári and all other contributing members of the 1st Department of Pathology and Experimental Cancer Research of Semmelweis University for supplying cadavers and providing special help during dissections. The critical reading of the manuscript by Professor László Tamás, Associate professor Balázs Hauser and Judit Laki management consultant (Semmelweis University) are acknowledged with many thanks.

Supplementary material

The Supplementary Material for this article can be found online at: https://www.por-journal.com/articles/10.3389/pore.2023.1610934/full#supplementary-material

SUPPLEMENTARY DATA SHEET S1
The generated datasets.

References

1. Armstrong PA, McCarthy MC, Peoples JB. Reduced use of resources by early tracheostomy in ventilator-dependent patients with blunt trauma. *Surgery* (1998) 124(4):763–6. doi:10.1067/msy.1998.91224

2. Brook AD, Sherman G, Malen J, Kollef MH. Early versus late tracheostomy in patients who require prolonged mechanical ventilation. *Am J Crit Care* (2000) 9(5): 352–9. doi:10.4037/ajcc2000.9.5.352

3. Kluger Y, Paul DB, Lucke J, Cox P, Colella JJ, Townsend RN, et al. Early tracheostomy in trauma patients. *Eur J Emerg Med* (1996) 3(2):95–101. doi:10.1097/00063110-199606000-00007

4. Rumbak MJ, Newton M, Truncale T, Schwartz SW, Adams JW, Hazard PB. A prospective, randomized, study comparing early percutaneous dilational tracheotomy to prolonged translaryngeal intubation (delayed tracheotomy) in critically ill medical patients. *Crit Care Med* (2004) 32(8):1689–94. doi:10.1097/01.ccm.0000134835.05161.b6

5. Ciaglia P, Firsching R, Syniec C. Elective percutaneous dilatational tracheostomy. A new simple bedside procedure; preliminary report. *Chest* (1985) 87(6):715–9. doi:10.1378/chest.87.6.715

6. Rashid AO, Islam S. Percutaneous tracheostomy: A comprehensive review. *J Thorac Dis* (2017) 9(10):S1128–S38. doi:10.21037/jtd.2017.09.33

7. Zgoda MA, Berger R. Balloon-facilitated percutaneous dilational tracheostomy tube placement: Preliminary report of a novel technique. *Chest* (2005) 128(5): 3688–90. doi:10.1378/chest.128.5.3688

8. Frova G, Quintel M. A new simple method for percutaneous tracheostomy: Controlled rotating dilation. A preliminary report. *Intensive Care Med* (2002) 28(3): 299–303. doi:10.1007/s00134-002-1218-5

9. Griggs WM, Worthley LI, Gilligan JE, Thomas PD, Myburg JA. A simple percutaneous tracheostomy technique. *Surg Gynecol Obstet* (1990) 170(6): 543–5.

10. Fantoni A, Ripamonti D. A non-derivative, non-surgical tracheostomy: The translaryngeal method. *Intensive Care Med* (1997) 23(4):386–92. doi:10.1007/s001340050345

11. de Kleijn BJ, Wedman J, Zijlstra JG, Dikkers FG, van der Laan B. Short- and long-term complications of surgical and percutaneous dilatation tracheotomies: A large single-centre retrospective cohort study. *Eur Arch Otorhinolaryngol* (2019) 276(6):1823–8. doi:10.1007/s00405-019-05394-9

12. Epstein SK. Late complications of tracheostomy. *Respir Care* (2005) 50(4): 542–9.

13. Jung Kwon O, Young Suh G, Pyo Chung M, Kim J, Han J, Kim H. Tracheal stenosis depends on the extent of cartilaginous injury in experimental canine model. *Exp Lung Res* (2003) 29(6):329–38. doi:10.1080/01902140303757

14. Pookamala S, Thakar A, Puri K, Singh P, Kumar R, Sharma S. Acquired subglottic stenosis: Aetiological profile and treatment results. *The J Laryngol Otology* (2014) 128(7):641–8. doi:10.1017/S0022215114000966

15. Zouk AN, Batra H. Managing complications of percutaneous tracheostomy and gastrostomy. *J Thorac Dis* (2021) 13(8):5314–30. doi:10.21037/jtd-19-3716

16. Law R, Carney A, Manara A. Long-term outcome after percutaneous dilational tracheostomy: Endoscopic and spirometry findings. *Anaesthesia* (1997) 52(1):51–6. doi:10.1111/j.1365-2044.1997.013-az013.x

17. Zias N, Chroneou A, Tabba MK, Gonzalez AV, Gray AW, Lamb CR, et al. Post tracheostomy and post intubation tracheal stenosis: Report of 31 cases and review of the literature. *BMC Pulm Med* (2008) 8(1):18–9. doi:10.1186/1471-2466-8-18

18. Ambesh SP. *Principles and practice of percutaneous tracheostomy*. New Delhi (India): Jaypee Brothers Publishers (2010).

19. van Heurn LW, Theunissen PH, Ramsay G, Brink PR. Pathologic changes of the trachea after percutaneous dilatational tracheotomy. *Chest* (1996) 109(6): 1466–9. doi:10.1378/chest.109.6.1466

20. Marchioni A, Tonelli R, Andreani A, Cappiello GF, Fermi M, Trentacosti F, et al. Molecular mechanisms and physiological changes behind benign tracheal and subglottic stenosis in adults. *Int J Mol Sci* (2022) 23(5):2421. doi:10.3390/ijms23052421

21. Elő G, Zubek L, Hargitai Z, Iványi Z, Branovics J, Gál J. Prevention of tracheal cartilage injury with modified Griggs technique during percutaneous tracheostomy - randomized controlled cadaver study. *Interv Med Appl Sci* (2012) 4(4):206–9. doi:10.1556/IMAS.4.2012.4.5

22. Bloss RS, Ward RE. Survival after tracheoinnominate artery fistula. *Am J Surg* (1980) 139(2):251–3. doi:10.1016/0002-9610(80)90266-4

23. Khanafer A, Hellstern V, Meißner H, Harmening C, Schneider K, Henkes H. Tracheoinnominate fistula: Acute bleeding and hypovolemic shock due to a trachea-innominate artery fistula after long-term tracheostomy, treated with a stent-graft. *CVIR Endovasc* (2021) 4(1):30. doi:10.1186/s42155-021-00216-8

24. Zouk AN, Batra H. Managing complications of percutaneous tracheostomy and gastrostomy. *J Thorac Dis* (2021) 13(8):5314–30. doi:10.21037/jtd-19-3716

25. Fernandez-Bussy S, Mahajan B, Folch E, Caviedes I, Guerrero J, Majid A. Tracheostomy tube placement: Early and late complications. *J Bronchology Interv Pulmonol* (2015) 22(4):357–64. doi:10.1097/LBR.0000000000000177

26. Cipriano A, Mao ML, Hon HH, Vazquez D, Stawicki SP, Sharpe RP, et al. An overview of complications associated with open and percutaneous tracheostomy procedures. *Int J Crit Illn Inj Sci* (2015) 5(3):179–88. doi:10.4103/2229-5151.164994

27. Feller-Kopman D. Acute complications of artificial airways. *Clin Chest Med* (2003) 24(3):445–55. doi:10.1016/s0272-5231(03)00047-9

28. Watters M, Thorne G, Cox C, Monk C. Tracheal trauma from percutaneous tracheostomy using the Griggs method. *Anaesthesia* (2002) 57(3):249–52. doi:10.1046/j.0003-2409.2001.02452.x

29. Paran H, Butnaru G, Hass I, Afanasyv A, Gutman M. Evaluation of a modified percutaneous tracheostomy technique without bronchoscopic guidance. *Chest* (2004) 126(3):868–71. doi:10.1378/chest.126.3.868

30. Ambesh SP, Pandey CK, Srivastava S, Agarwal A, Singh DK. Percutaneous tracheostomy with single dilatation technique: A prospective, randomized comparison of Ciaglia blue rhino versus Griggs' guidewire dilating forceps. *Anesth Analg* (2002) 95(6):1739–45. t. doi:10.1097/00000539-200212000-00050

31. Tai HP, Lee DL, Chen CF, Huang YT. The effect of tracheostomy delay time on outcome of patients with prolonged mechanical ventilation: A STROBE-compliant retrospective cohort study. *Medicine (Baltimore)* (2019) 98(35): e16939. doi:10.1097/MD.0000000000016939

32. Pauliny M, Christova E, Mackova J, Liska M. Percutaneous dilation tracheostomy versus surgical tracheostomy in critically ill patients. *Bratisl Lek Listy* (2012) 113(7):409–11. doi:10.4149/bll_2012_092

33. Khaja M, Haider A, Alapati A, Qureshi ZA, Yapor L. Percutaneous tracheostomy: A bedside procedure. *Cureus* (2022) 14(4):e24083. doi:10.7759/cureus.24083

34. Cheung NH, Napolitano LM. Tracheostomy: Epidemiology, indications, timing, technique, and outcomes. *Respir Care* (2014) 59(6):895–915. doi:10.4187/respcare.02971

35. Heikkinen M, Aarnio P, Hannukainen J. Percutaneous dilational tracheostomy or conventional surgical tracheostomy? *Crit Care Med* (2000) 28(5):1399–402. doi:10.1097/00003246-200005000-00023

36. Kaylie DM, Andersen PE, Wax MK. An analysis of time and staff utilization for open versus percutaneous tracheostomies. *Otolaryngol Head Neck Surg* (2003) 128(1):109–14. doi:10.1067/mhn.2003.18

37. Melloni G, Muttini S, Gallioli G, Carretta A, Cozzi S, Gemma M, et al. Surgical tracheostomy versus percutaneous dilatational tracheostomy. A prospective-randomized study with long-term follow-up. *J Cardiovasc Surg (Torino)* (2002) 43(1):113–21.

38. Youssef TF, Ahmed MR, Saber A. Percutaneous dilatational versus conventional surgical tracheostomy in intensive care patients. *N Am J Med Sci* (2011) 3(11):508–12. doi:10.4297/najms.2011.3508

39. Brass P, Hellmich M, Ladra A, Ladra J, Wrzosek A. Percutaneous techniques versus surgical techniques for tracheostomy. *Cochrane Database Syst Rev* (2016) 7(7):Cd008045. doi:10.1002/14651858.CD008045.pub2

40. Delaney A, Bagshaw SM, Nalos M. Percutaneous dilatational tracheostomy versus surgical tracheostomy in critically ill patients: A systematic review and meta-analysis. *Crit Care* (2006) 10(2):R55. doi:10.1186/cc4887

41. Dennis BM, Eckert MJ, Gunter OL, Morris JA, May AK. Safety of bedside percutaneous tracheostomy in the critically ill: Evaluation of more than 3, 000 procedures. *J Am Coll Surg* (2013) 216(4):858–65. doi:10.1016/j.jamcollsurg.2012.12.017

42. Cinotti R, Voicu S, Jaber S, Chousterman B, Paugam-Burtz C, Oueslati H, et al. Tracheostomy and long-term mortality in ICU patients undergoing prolonged mechanical ventilation. *PLoS One* (2019) 14(10):e0220399. doi:10.1371/journal.pone.0220399

43. Johnson-Obaseki S, Veljkovic A, Javidnia H. Complication rates of open surgical versus percutaneous tracheostomy in critically ill patients. *Laryngoscope* (2016) 126(11):2459–67. doi:10.1002/lary.26019

44. Anon JM, Escuela MP, Gomez V, Moreno A, Lopez J, Diaz R, et al. Percutaneous tracheostomy: Ciaglia blue rhino versus Griggs' guide wire dilating forceps. A prospective randomized trial. *Acta Anaesthesiol Scand* (2004) 48(4):451–6. doi:10.1111/j.1399-6576.2004.0313.x

45. Fikkers BG, Staatsen M, van den Hoogen FJ, van der Hoeven JG. Early and late outcome after single step dilatational tracheostomy versus the guide wire dilating forceps technique: A prospective randomized clinical trial. *Intensive Care Med* (2011) 37(7):1103–9. doi:10.1007/s00134-011-2222-4

46. Cabrini L, Landoni G, Greco M, Costagliola R, Monti G, Colombo S, et al. Single dilator vs. guide wire dilating forceps tracheostomy: A meta-analysis of randomised trials. *Acta Anaesthesiol Scand* (2014) 58(2):135–42. doi:10.1111/aas.12213

47. Fikkers BG, Staatsen M, Lardenoije SG, van den Hoogen FJ, van der Hoeven JG. Comparison of two percutaneous tracheostomy techniques, guide wire dilating forceps and Ciaglia blue rhino: A sequential cohort study. *Crit Care* (2004) 8(5):R299–305. doi:10.1186/cc2907

48. Norwood S, Vallina VL, Short K, Saigusa M, Fernandez LG, McLarty JW. Incidence of tracheal stenosis and other late complications after percutaneous tracheostomy. *Ann Surg* (2000) 232(2):233–41. doi:10.1097/00000658-200008000-00014

49. Steele AP, Evans HW, Afaq MA, Robson JM, Dourado J, Tayar R, et al. Long-term follow-up of Griggs percutaneous tracheostomy with spiral CT and questionnaire. *Chest* (2000) 117(5):1430–3. doi:10.1378/chest.117.5.1430

50. Ronen O, Rosin I, Taitelman UZ, Altman E. Comparison of Ciaglia and Griggs percutaneous tracheostomy techniques - a biomechanical animal study. *Indian J Crit Care Med* (2019) 23(6):247–50. doi:10.5005/jp-journals-10071-23174

51. Karagiannidis C, Merten ML, Heunks L, Strassmann SE, Schafer S, Magnet F, et al. Respiratory acidosis during bronchoscopy-guided percutaneous dilatational tracheostomy: Impact of ventilator settings and endotracheal tube size. *BMC Anesthesiol* (2019) 19(1):147. doi:10.1186/s12871-019-0824-5

52. Hotchkiss KS, McCaffrey JC. Laryngotracheal injury after percutaneous dilational tracheostomy in cadaver specimens. *Laryngoscope* (2003) 113(1):16–20. doi:10.1097/00005537-200301000-00003

Pathology & Oncology Research | frontiers

TYPE Original Research
PUBLISHED 14 November 2024
DOI 10.3389/pore.2024.1611596

Check for updates

OPEN ACCESS

EDITED BY
Tamás Micsik,
Semmelweis University, Hungary

*CORRESPONDENCE
Yun Wang,
wyhh666@gmail.com
Li Ma,
675694863@qq.com

‡These authors have contributed equally to this work

RECEIVED 19 November 2023
ACCEPTED 04 November 2024
PUBLISHED 14 November 2024

CITATION
Zhao H, Kou C, Zhao H, Liu Q, He M, Wang C, Zhu S, Ma L and Wang Y (2024) Impact of limb ischemic preconditioning on the incidence of vein thrombosis in patients with peripherally inserted central catheter. *Pathol. Oncol. Res.* 30:1611596. doi: 10.3389/pore.2024.1611596

COPYRIGHT
© 2024 Zhao, Kou, Zhao, Liu, He, Wang, Zhu, Ma and Wang. This is an open-access article distributed under the terms of the Creative Commons Attribution License (CC BY). The use, distribution or reproduction in other forums is permitted, provided the original author(s) and the copyright owner(s) are credited and that the original publication in this journal is cited, in accordance with accepted academic practice. No use, distribution or reproduction is permitted which does not comply with these terms.

Impact of limb ischemic preconditioning on the incidence of vein thrombosis in patients with peripherally inserted central catheter

Han Zhao[1‡], Changhua Kou[2‡], Hao Zhao[3], Qing Liu[4], Maosheng He[5], Cong Wang[2], Saisai Zhu[2], Li Ma[6*‡] and Yun Wang [2*‡]

[1]Clinic for Kidney and Hypertensive Diseases, Hanover Medical School, Hanover, Germany, [2]Department of Hepatobiliary Pancreatic Center, Xuzhou City Central Hospital, The Xuzhou School of Clinical Medicine of Nanjing Medical University, The Affiliated Hospital of the Southeast University Medical School, Xuzhou, Jiangsu, China, [3]Department of Vascular Surgery, Xuzhou City Central Hospital, The Affiliated Hospital of the Southeast University Medical School, Xuzhou, Jiangsu, China, [4]Department of Gynecology Department, Xuzhou City Central Hospital, The Xuzhou School of Clinical Medicine of Nanjing Medical University, The Affiliated Hospital of the Southeast University Medical School, Xuzhou, Jiangsu, China, [5]Department of Color Ultrasound Department, Xuzhou City Central Hospital, The Xuzhou School of Clinical Medicine of Nanjing Medical University, The Affiliated Hospital of the Southeast University Medical School, Xuzhou, Jiangsu, China, [6]Department of Thyroid and Breast Surgery, Xuzhou City Central Hospital, The Affiliated Hospital of the Southeast University Medical School, Xuzhou, Jiangsu, China

Background: Peripherally inserted central catheters (PICC) are increasingly used in clinical practice, which also leads to an increased incidence of PICC-related thrombosis. Local thrombus formation could be prevented by limb ischemic preconditioning (IPC). This study aimed to determine whether IPC can prevent deep vein thrombosis in patients with PICC.

Methods: A total of 600 breast cancer patients receiving PICC were randomized into two groups between July 2016 and July 2018 at the Department of Radiation Oncology. In the preconditioning group, 5 min of ischemic preconditioning was performed three times before PICC, whereas no preconditioning was performed in the sham group. The coagulation function levels, the PICC-related complications, the length of hospital stay, the cost of hospitalization, and the satisfaction of patients were compared.

Results: The coagulation function levels of patients in the preconditioning group were more normal than in patients from the sham group. In total, 56/300 patients in the sham group had presence of PICC-related thrombosis, with only 23/300 in the IPC group, with no significant difference in other complications between the two groups. However, a longer hospital stay was

Abbreviations: IPC, Limb ischemic preconditioning; PICC, peripherally inserted central catheter; SOD, superoxide dismutase; NO, nitric oxide.

observed in the sham group compared to the IPC group. Moreover, the cost of hospitalization was also reduced in the IPC group, which also improved the satisfaction of patients.

Conclusion: Limb ischemic preconditioning may attenuate the severity of vein thrombosis in patients with PICC, which contributes to reducing the incidence of PICC-related thrombosis in clinical practice.

KEYWORDS

tumor, limb ischemic preconditioning, peripherally inserted central catheter, vein thrombosis, PICC-related complications

Introduction

Peripherally inserted central catheters (PICCs) are a form of intravenous access in which the catheter is directed from a peripheral vein to a large heart vein. These catheters can be used for an extended period of time and minimize the stimulation of drugs to blood vessels [1–3]. PICC is now increasingly used in clinical practice owing to its safety and cost-effectiveness. However, PICC also involves some complications, such as puncture failure, phlebitis, infection, and thrombosis. PICC-related thrombosis is a severe complication that may lower the quality of life of patients, increase hospitalization costs, and even increase mortality [4, 5]. Patients and doctors are both concerned with PICC-related thrombosis. To reduce the incidence of PICC-related thrombosis, a number of studies have investigated the risk factors and prevention measures for thrombosis in patients with PICC.

Remote ischemic preconditioning (RIPC) is a process by which brief periods of ischemia trigger protective effects on remote organs or tissues. RIPC is widely used in patients to protect organs or tissues prone to ischemic injury, including the liver, brain, myocardium, and so on [6–8]. Research revealed that limb ischemic preconditioning (IPC) could promote thrombus recanalization and reduce the incidence of thrombus in rats [9]. The three main factors necessary for thrombosis formation include stasis of blood, vessel wall injury, and platelet aggregation [10, 11]. Multiple studies have demonstrated that remote IPC before radiofrequency catheter ablation significantly reduced the platelet activation and reactivity of patients with paroxysmal atrial fibrillation [12].

Based on the above content, 600 breast cancer patients receiving PICC in our department were randomized into two groups (sham group and preconditioning group) with 1:1 allocation. Then, the efficacy of catheterization, the coagulation function levels, the incidence of thrombosis, the length of hospital stay, the cost of hospitalization, and the satisfaction of patients were compared between the two groups. The results may verify our hypothesis that limb ischemic preconditioning could play a protective role in the incidence of thrombus after PICC, which could contribute to reducing the incidence of PICC-related thrombosis in clinical practice.

Methods

Experiment design

This single-center, parallel, and double-blind trial included 600 breast cancer patients receiving PICC, who were randomly assigned to two groups with 1:1 allocation. The patients in the preconditioning group were subjected to 5 minutes of ischemic preconditioning three times before PICC, whereas no preconditioning was performed in the sham group. The study was conducted in accordance with the Declaration of Helsinki. The studies involving human participants were reviewed and approved by Xuzhou Central Hospital Biomedical Research Ethics Review Committee (Permit Number: XZXY-LJ-20161210-032). The patients/participants provided their written informed consent to participate in this study.

Inclusion and exclusion criteria

The inclusion criteria were as follows: 1) Adults older than 18 years and younger than 70 years; 2) Patients all underwent mastectomy for breast cancer and needed chemotherapy; 3) Patients were diagnosed with breast cancer with TNM stages II-III; 4) The patients volunteered for PICC, signed the treatment consent form, and volunteered to participate in this project; 5) Normal coagulation function, and 6) No other past Medical History. The exclusion criteria were as follows: 1) Patients older than 70 years or younger than 18 years; 2) Patients who underwent mastectomy for breast cancer but did not require chemotherapy; 3) Patients were diagnosed with breast cancer with TNM stages other than II-III; 4) Patients refused to undergo PICC or refused to enter the project; 5) Abnormal coagulation function, and 6) The presence of other past Medical History.

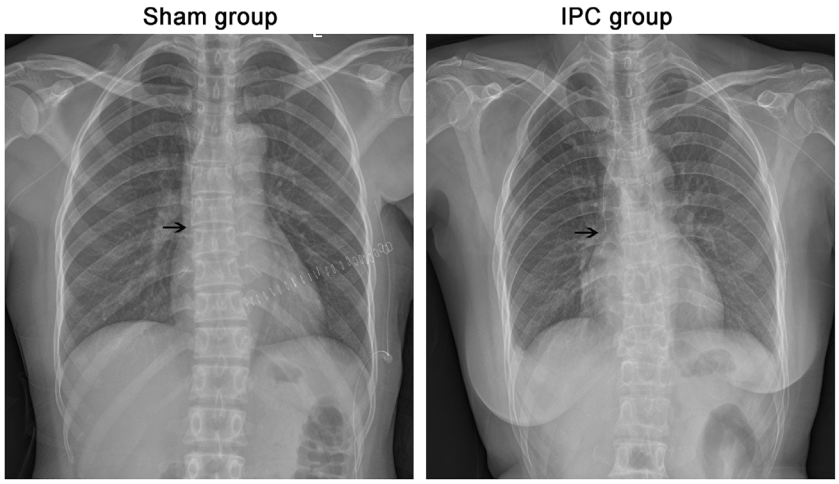

FIGURE 1
Evaluation of PICC. After the operation, all the cases were taken x-ray to determine the position of the catheter tip. The end of PICC catheter was in normal position between T5 and T7. The black arrow shows the end of the catheter.

Surgical procedures

We used the PICC Center venous catheter (BARD, United States), with specifications: Groshong NXT ClearVue 4Fr single-lumen basic kit, including a micro-introducer sheath. The operating procedure for PICC was carried out as described by Amerasekera SS et al. PICC insertion was carried out by the same vascular access team. The success of PICC placement was confirmed based on the color Doppler ultrasound and interventional radiology [4].

Treatment of patients in the sham and IPC group

Both patients in the sham and IPC groups had blood pressure cuffs around their arm while undergoing PICC. The cuff was inflated to 200 mm Hg three times for 5 min in the IPC group and was released to allow reperfusion between the cycles. No preconditioning was performed in patients of the sham group.

Measurement of coagulation function levels

Blood samples of patients were used for coagulation function tests, which were collected from the vena mediana cubiti before PICC and at days 14, 30, 60, and 90 after PICC. The coagulation function test included prothrombin time (PT), thrombin time (TT), activated partial thromboplastin time (APTT), fibrin(-ogen) degradation products (FDP), and D-Dimer. All tests were performed in the clinical laboratory of Xuzhou City Central Hospital.

The observation of PICC-related complications

Local inflammation, bloodstream infection, occlusion, dislocation, PICC-related thrombosis, local bleeding, pulmonary artery embolism, and local allergic reaction were observed and recorded. Patients were subjected to color Doppler ultrasound (SIEMENS, ACUSON S3000) to assess the incidence of thrombosis at days 14, 30, 60, and 90 after PICC.

Statistical analysis

All data are expressed as the mean ± standard deviation. The data were analyzed using variance, q-test, and Student's t-tests. $P < 0.05$ was considered statistically significant. SPSS14.0 software was used for all statistical analyses.

Results

Evaluation of PICC

After the catheter insertion, an X-ray was taken to determine the position of the catheter tip. Patient characteristics, procedural details, and the results of X-rays are shown in Figure 1 and Table 1. All patients had no statistically significant differences in

TABLE 1 Patient characteristics, procedural details, and the results of X-rays.

		IPC	Sham	T value	*P*-value
General data	Age (years)	53.36 ± 15.61	54.31 ± 15.06	0.761	0.447
	BMI	22.78 ± 3.44	22.96 ± 3.58	0.629	0.53
				X^2 value	*P*-value
	Right/left breast, n (%)	147/153, (49/51)	135/165, (45/55)	0.96	0.33
Clinical data	Patients undergoing first resection, n (%)	300, (100)	298, (99.3)	2.01	0.16
	TNM II stage, n (%)	211, (70.3)	202, (67.3)	0.63	0.43
	TNM III stage, n (%)	89, (29.7)	98, (32.7)	0.63	0.43
				T value	*P*-value
Surgical data	Surgery duration (min)	104.82 ± 38.27	102.44 ± 38.81	0.755	0.45
	Intraoperative blood loss (mL)	43.97 ± 27.79	50.7 ± 27.95	2.96	<0.05*
				X^2 value	*P*-value
	Halsted surgery, n (%)	17, (5.7)	18, (6)	0.03	0.86
	Auchincloss surgery, n (%)	155, (51.7)	146, (48.7)	0.54	0.46
	Patey surgery, n (%)	117, (39)	124, (41.3)	0.34	0.6
	Conserving surgery, n (%)	11, (3.7)	12, (4)	0.05	0.83
Evaluation of PICC	One-time success, n (%)	300, (100)	300, (100)	1	1

*$p < 0.05$ compared with the sham group.

baseline information, except for intraoperative blood loss. However, since all patients underwent PICC catheter placement 1 month after surgery, the difference in intraoperative blood loss did not affect their coagulation function and thrombus formation.

Serum coagulation function levels

As shown in Table 2, blood samples were collected to evaluate the values of FDP and D-Dimer, and the coagulation function by PT, APTT, TT, and FIB. As shown in Table 2, all of the values were within the normal reference range, but the values of FDP (days 14, 30, 60, and 90) and D-Dimer (day 60) in the sham group were significantly higher than those in the IPC group (FDP: mg/L, sham group, d14: 3.07 ± 1.91, d30: 3.11 ± 1.74, d60: 2.31 ± 1.51, d90: 2.20 ± 1.62, IPC group, d14: 2.53 ± 1.57, d30: 2.54 ± 1.69, d60: 2.01 ± 1.76, d90: 1.96 ± 1.58. D-Dimer: mg/L FEU, sham group, d60: 0.32 ± 0.26, IPC group, d60: 0.26 ± 0.28. $p < 0.05$). However, the values of PT (days 14, 30, and 90), TT (days 14, 30, 60, and 90), and APTT (days 14, 30, 60, and 90) in the sham group were higher than those in the IPC group (PT: sec, sham group, d14: 9.71 ± 1.40, d30: 9.46 ± 1.28, d90: 10.07 ± 1.48, IPC group, d14: 10.36 ± 1.58, d30: 9.76 ± 1.65, d90: 10.58 ± 1.88. TT: sec, sham group, d14: 16.05 ± 4.11, d30: 15.57 ± 3.99, d60: 16.34 ± 2.77, d90: 17.49 ± 4.23, IPC group, d14: 18.15 ± 3.78, d30: 16.59 ± 4.75, d60: 17.67 ± 3.52, d90: 18.17 ± 3.56. APTT: sec, sham group, d14: 23.41 ± 5.28, d30: 23.92 ± 3.76, d60: 24.97 ± 4.71, d90: 24.49 ± 5.25, IPC group, d14: 24.78 ± 4.79, d30: 25.03 ± 4.52, d60: 26.61 ± 5.04, d90: 26.91 ± 5.39. $p < 0.05$).

The observation of PICC-related complications

PICC-related complications were observed and recorded, and the incidence rate of the thrombosis was assessed by color Doppler ultrasound at days 14, 30, 60, and 90 after PICC. Moreover, the thrombus was observed on grayscale imaging in all 600 patients. The results revealed that 56/300 patients in the sham group had presence of PICC-related thrombosis, with only 23/300 in the IPC group (Figure 2). No significant difference was found in other complications between the two groups (Table 3).

Length of hospital stay

To evaluate the effects of PICC treatment, the length of hospital stay was compared between the two groups. All the 600 individuals were admitted to the hospital 3 times after PICC for chemotherapy. The hospital stays are shown in Table 4, with

10.3389/pore.2024.1611596

TABLE 2 Serum coagulation function levels.

		IPC	Sham	T value	*P*-value
PT	Before PICC	10.31 ± 1.36	10.26 ± 1.31	0.474	0.636
	14 days after PICC	10.36 ± 1.58	9.71 ± 1.40	5.292	<0.001*
	30 days after PICC	9.76 ± 1.65	9.46 ± 1.28	2.498	0.013*
	60 days after PICC	10.19 ± 1.92	10.00 ± 1.57	1.334	0.183
	90 days after PICC	10.58 ± 1.88	10.07 ± 1.48	3.660	<0.001*
TT	Before PICC	17.93 ± 3.12	18.30 ± 3.11	1.438	0.151
	14 days after PICC	18.15 ± 3.78	16.05 ± 4.11	6.505	<0.001*
	30 days after PICC	16.59 ± 4.75	15.57 ± 3.99	2.825	0.005*
	60 days after PICC	17.67 ± 3.52	16.34 ± 2.77	5.149	<0.001*
	90 days after PICC	18.17 ± 3.56	17.49 ± 4.23	2.138	0.033*
APTT	Before PICC	27.26 ± 4.63	26.62 ± 4.56	1.704	0.089
	14 days after PICC	24.78 ± 4.79	23.41 ± 5.28	3.336	0.001*
	30 days after PICC	25.03 ± 4.52	23.92 ± 3.76	3.249	0.001*
	60 days after PICC	26.61 ± 5.04	24.97 ± 4.71	4.099	<0.001*
	90 days after PICC	26.91 ± 5.39	24.49 ± 5.25	5.560	<0.001*
FDP	Before PICC	1.80 ± 1.08	1.91 ± 1.56	1.001	0.317
	14 days after PICC	2.53 ± 1.57	3.07 ± 1.91	3.770	<0.001*
	30 days after PICC	2.54 ± 1.69	3.11 ± 1.74	4.044	<0.001*
	60 days after PICC	2.01 ± 1.76	2.31 ± 1.51	2.236	0.026*
	90 days after PICC	1.96 ± 1.58	2.20 ± 1.62	1.822	0.069*
D-Dimer	Before PICC	0.28 ± 0.25	0.29 ± 0.28	0.438	0.661
	14 days after PICC	0.31 ± 0.39	0.33 ± 0.31	0.707	0.480
	30 days after PICC	0.36 ± 0.45	0.39 ± 0.45	0.689	0.491
	60 days after PICC	0.26 ± 0.28	0.32 ± 0.26	2.478	0.013*
	90 days after PICC	0.28 ± 0.33	0.29 ± 0.33	0.344	0.731

*$p < 0.05$ compared with the sham group.

the hospital stays in the IPC group being shorter than in the sham group [Table 4, hospital stays (day), sham group: 6.77 ± 3.15. IPC group: 6.16 ± 3.03. $p < 0.05$].

Hospitalization expenses and patient satisfaction

The cost of hospitalization was also reduced in the IPC group when compared with the sham group, which also improved the satisfaction of patients [Table 4, hospitalization expenses (Yuan), shan group: 18032.66 ± 1911.64, IPC group: 17129.596 ± 2351.66. Patient satisfaction (%), sham group: 91.9 ± 5.24, IPC group: 95.77 ± 3.66. $p < 0.05$].

Discussion

This study provides useful insights into the effect of limb ischemic preconditioning on the incidence of PICC-related thrombosis in patients with peripherally inserted central catheters. Limb ischemic preconditioning may attenuate the severity of vein thrombosis in patients with peripherally inserted central catheters. The coagulation function levels (PT, TT, APTT, FDP, and D-Dimer) in patients of the sham and IPC groups were first compared, revealing that the values of PT, TT, APTT, FDP, and D-Dimer in patients of the IPC group were normal, but abnormal changes were detected in the coagulation function indicators in the sham group. Then the incidence of PICC-related complications was assessed, displaying a decreased

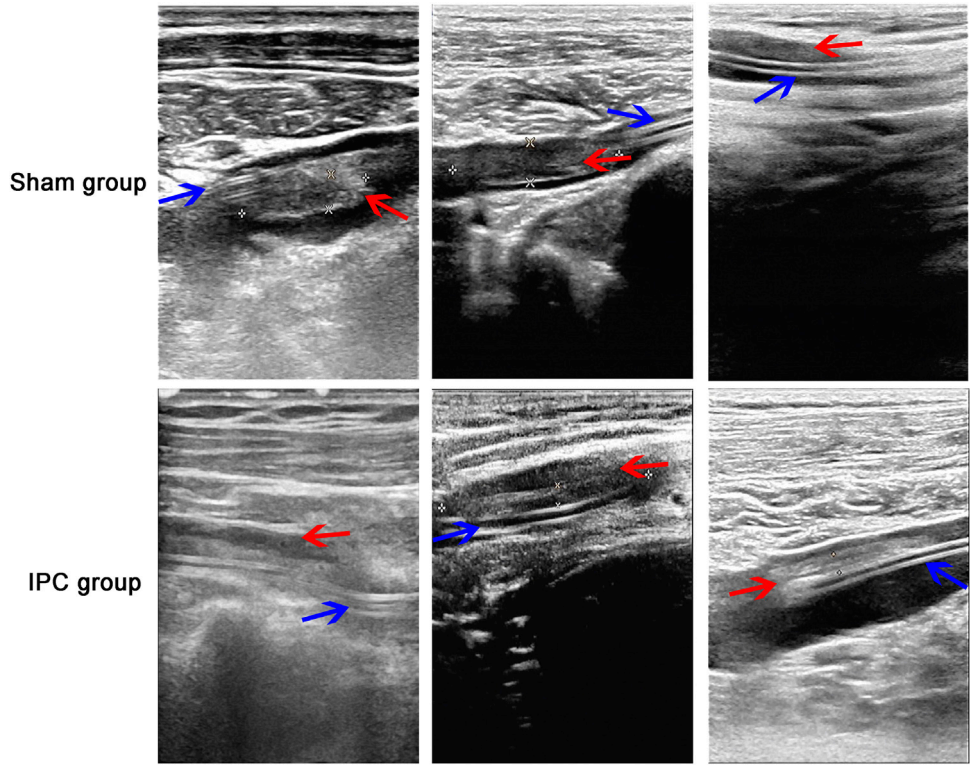

FIGURE 2
The observation of thrombosis. The absence of PICC-related thrombosis in the sham group was more than that in the IPC group, Substantial hypoechoic and irregular blood flow signals were observed in the vascular lumen of the sham group, and the incidence rate of thrombosis in the IPC group was less than that in the sham group (*$p < 0.05$ compared with the sham group. Red arrow: thrombosis; blue arrow: catheter).

TABLE 3 The observation of related complications.

Type of complication		IPC	Sham	X^2 value	*P*-value
Local inflammation	n (%)	21 (7)	22 (7.3)	0.025	0.87
Bloodstream infection	n (%)	4 (1.3)	5 (1.7)	0.11	0.74
Occlusion	n (%)	3 (1)	3 (1)	0	1
Dislocation	n (%)	2 (0.7)	1 (0.3)	0.34	0.56
PICC-related thrombosis	n (%)	23 (7.7)	56 (18.7)	15.88	<0.05*
Local bleeding	n (%)	0 (0)	1 (0.3)	1	0.32
Pulmonary artery embolism	n (%)	0 (0)	0 (0)	0	1
Local allergic reaction	n (%)	1 (0.3)	1 (0.3)	0	1

*$p < 0.05$ compared with the sham group.

incidence in the IPC group compared with the sham group. The incidence of PICC-related thrombosis in the IPC group was reduced when compared with the sham group, but no significant difference in other complications was observed between the two groups. In addition, the hospital stays were longer in patients of the sham group. Finally, the cost of hospitalization was also lower in the IPC group compared with the sham group, which also improved the satisfaction of patients.

Several approaches to venous access are used in our clinic, including centrally inserted venous catheters as well as peripherally inserted central catheters. When compared with the centrally inserted venous catheters, PICC showed some

TABLE 4 Hospital stays, hospitalization expenses and patient satisfaction.

	IPC	Sham	T value	*P*-value
Hospital stays(day)	6.16 ± 3.03	6.77 ± 3.15	2.15	<0.05*
Hospitalization expenses(Yuan)	17129.596 ± 2351.66	18032.66 ± 1911.64	6.83	<0.05*
Patient satisfaction(%)	95.77 ± 3.66	91.9 ± 5.24	6.66	<0.05*

*$p < 0.05$ compared with the sham group.

advantages in the administration of antibiotics, total parenteral nutrition, chemotherapy, fluid replacement, and drug administration. PICC is convenient, easy to operate, safe to insert, and carries a low risk of vascular injury or blood infection. Nevertheless, PICC can also lead to complications, such as infection, phlebitis, and thrombosis. Among these complications, PICC-related thrombosis is relatively common, which may further lead to a potentially serious complication, such as pulmonary embolism. Therefore, proper evaluation and management of PICC are critical for patient health and prognosis, and finding ways to reduce the incidence of catheter-related thrombosis is the main emphasis of our research [13–17].

Ischemic preconditioning was reported to play a protective role in reducing platelet activation, possibly exerting favorable effects on the occurrence of thromboembolic events. Ischemic preconditioning is a process by which the brief periods of ischemia in a tissue protect another organ or tissue. This procedure is widely used and has been verified in our previous study [18–20]. Platelet-derived extracellular vesicles (PEVs), being small particles, extracellular vesicles are associated with various diseases including inflammation, vascular disorders, and tumors. PEVs function similarly to platelets and positively affect hemostasis, thrombus formation, and pro-inflammatory processes through different mechanisms. Additionally, research has discovered that pre-treating limb ischemia can decrease the production of platelet-derived extracellular vesicles which consequently exerts a favorable impact on reducing vascular inflammation and thrombus formation [21]. The current study focused on the process of IPC and thrombus recanalization in patients after PICC. Firstly, PICC was successfully established, and the process was confirmed by an x-ray, which showed the position of the catheter tip. All the patients underwent the PICC procedure successfully.

Coagulation function tests (PT, TT, APTT, FDP, D-dimer, etc.) can effectively evaluate the body's coagulation status. Research has shown that a hypercoagulable state slows down blood flow and promotes the formation of venous thrombosis. PT, TT, APTT, FDP, D-dimer and other indicators reflect the hypercoagulable state of the body through different mechanisms. For example, TT can indicate the presence of pathological anticoagulant substances in circulating blood; PT is mainly used to reflect the exogenous coagulation pathway; APTT is used to reflect the endogenous coagulation pathway; TT and FDP are primarily used to reflect common coagulation pathways' status. D-dimer is a specific degradation product produced by fibrin monomers during fibrinolysis. An elevated level of D-dimer reflects secondary fibrinolysis activation. FDP and D-dimer are specific indicators for evaluating high-coagulation states and excessive fibrinolysis *in vivo* as well as assessing pre-thrombotic hypercoagulability. Therefore, testing coagulation-related indicators at different time points allows assessment of changes in overall coagulation status to evaluate relative risk of thrombus formation [22–24].

Subsequently, the coagulation function was evaluated, revealing that PT, TT, APTT, FDP, and D-Dimer in patients of the IPC group were more normal than that in patients of the sham group. All of the values were within the normal reference range, but the values of FDP (days 14, 30, 60, and 90) and D-Dimer (day 60) in the sham group were significantly higher than those in the IPC group ($p < 0.05$). However, the values of PT (days 14, 30, and 90), TT (days 14, 30, 60, and 90), and APTT (days 14, 30, 60, and 90) in the sham group were higher than in the IPC group ($p > 0.05$). Increased PT and APPT values were detected in the sham group after the thrombus was confirmed, which was due to the antithrombotic drugs (such as low molecular weight heparin, warfarin, and so on). Some reports confirmed that IPC could reduce platelet-fibrinogen binding, platelet-neutrophil aggregates, and platelet P-selectin expression, which results in the suppression of platelet activation [12]. All of the above was in accordance with our results.

Secondly, PICC-related complications were observed and recorded. A lower incidence of PICC-related thrombosis was observed in the IPC group compared with the sham group. 56/300 patients in the sham group had presence of PICC-related thrombosis, with only 23/300 in the IPC group. No significant difference in other complications was observed between the two groups, including local inflammation, bloodstream infection, occlusion, dislocation, local bleeding, pulmonary artery embolism, and local allergic reaction. Our results were consistent with the previous study by Ye Sun et al. [25], which suggested that localized lower extremity IPC could reduce deep vein thrombosis formation in a rat experimental thrombosis model. The anti-thrombotic effects of IPC could be attributed to the inhibition of platelet activation [9].

Furthermore, the length of hospital stay was compared between the two groups, showing longer hospital stays in the sham group. The cost of hospitalization was also lower in the IPC group than in the sham group, which also improved the satisfaction of patients.

The mechanism underlying the decreased thrombosis in IPC remains elusive but may involve the release of the antithrombotic substances from the vessel wall, as well as the suppressed effects of IPC on platelets, coagulation, and fibrinolysis. NO (nitric oxide) is a key damaging factor in ischemia/hypoxia, exhibiting dual effects on the body's protection. During ischemia/hypoxia, it can both improve blood supply to the injured area by dilating local blood vessels and inhibit platelet aggregation and leukocyte adhesion to protect tissues, as well as damage the body by causing DNA injury and generating more toxic oxygen free radicals. NOS is the crucial enzyme for NO synthesis, with three subtypes: neuronal nitric oxide synthase (nNOS), endothelial nitric oxide synthase (eNOS), and inducible nitric oxide synthase (iNOS). When the body experiences ischemia, eNOS activity increases, leading to increased NO production. This causes vasodilation in the ischemic area, improving blood supply and providing protection for ischemic tissues [26, 27]. The protective effects of IPC have yet to be described in animals, and this study further confirmed the action of IPC on thrombosis downregulation in humans. However, the specific experimental mechanism of this protective function requires further animal studies [9, 12, 28–31].

In conclusion, the present study demonstrated that limb ischemic preconditioning may prevent vein thrombosis in patients with peripherally inserted central catheters, which may improve their quality of life and reduce the length of hospitalization. However, the specific mechanism requires further research, and the application of IPC on patients with a high risk of deep venous thrombosis also needs to be analyzed.

Data availability statement

The raw data supporting the conclusions of this article will be made available by the authors, without undue reservation.

Ethics statement

The studies involving humans were approved by Xuzhou Central Hospital Biomedical Research Ethics Review Committee. The studies were conducted in accordance with the local legislation and institutional requirements. The participants provided their written informed consent to participate in this study. Written informed consent was obtained from the individual(s) for the publication of any potentially identifiable images or data included in this article.

Author contributions

YW, HnZ, and CK designed research; YW, HnZ, MH, and CW performed experiments; YW, HnZ, CW, and SZ analyzed data; YW, HnZ, HoZ, QL, MH, and LM interpreted results of experiments; YW, HnZ, HoZ, MH, and LM prepared figures; YW, HnZ, QL, and CK revised manuscript; YW, HnZ, HoZ, QL, and LM approved final version of manuscript. All authors contributed to the article and approved the submitted version.

Funding

The author(s) declare financial support was received for the research, authorship, and/or publication of this article. This work was supported by Xuzhou Science and Technology Bureau Foundation (KC22172, KC16SH029) and Xuzhou Municipal Bureau of Science and Technology Key R&D Projects Social Development Projects (KC23178).

Acknowledgments

We thank all patients who voluntarily participated in this study. We thank Home for Researchers editorial team (www.home-for-researchers.com) for language editing service.

Conflict of interest

The authors declare that the research was conducted in the absence of any commercial or financial relationships that could be construed as a potential conflict of interest.

References

1. Galen B, Baron S, Young S, Hall A, Berger-Spivack L, Southern W. Reducing peripherally inserted central catheters and midline catheters by training nurses in ultrasound-guided peripheral intravenous catheter placement. *BMJ Qual Saf* (2020) 29(3):245–9. Epub 2019 Oct 3. PMID: 31582569. doi:10.1136/bmjqs-2019-009923

2. Santos FKY, Flumignan RLG, Areias LL, Sarpe AKP, Amaral FCF, Ávila RB, et al. Peripherally inserted central catheter versus central venous catheter for intravenous access: a protocol for systematic review and meta-analysis. *Medicine (Baltimore)* (2020) 99(30):e20352. PMID: 32791657; PMCID: PMC7386962. doi:10.1097/MD.0000000000020352

3. Chen X, Liang M. A meta-analysis of incidence of catheter-related bloodstream infection with midline catheters and peripherally inserted central catheters. *J Healthc Eng* (2022) 12:6383777. PMID: 35313516; PMCID: PMC8934223. doi:10.1155/2022/6383777

4. Swaminathan L, Flanders S, Horowitz J, Zhang Q, O'Malley M, Chopra V. Safety and outcomes of midline catheters vs peripherally inserted central catheters for patients with short-term indications: a multicenter study. *JAMA Intern Med* (2022) 182(1):50–8. PMID: 34842905; PMCID: PMC8630646. doi:10.1001/jamainternmed.2021.6844

5. Mielke D, Wittig A, Teichgräber U. Peripherally inserted central venous catheter (PICC) in outpatient and inpatient oncological treatment. *Support Care Cancer* (2020) 28(10):4753–60. Epub 2020 Jan 22. PMID: 31970514; PMCID: PMC7447660. doi:10.1007/s00520-019-05276-0

6. Lamidi S, Baker DM, Wilson MJ, Lee MJ. Remote ischemic preconditioning in non-cardiac surgery: a systematic review and meta-analysis. *J Surg Res* (2021) 261: 261–73. Epub 2021 Jan 15. PMID: 33460972. doi:10.1016/j.jss.2020.12.037

7. Leurcharusmee P, Sawaddiruk P, Punjasawadwong Y, Sugandhavesa N, Klunklin K, Tongprasert S, et al. Ischemic preconditioning upregulates Mitofusin2 and preserves muscle strength in tourniquet-induced ischemia/reperfusion. *J Orthop Translat* (2022) 35:113–21. PMID: 36312592; PMCID: PMC9582561. doi:10.1016/j.jot.2022.09.012

8. Wu J, Yu C, Zeng X, Sun C. The hepatoprotective effect from ischemia-reperfusion injury of remote ischemic preconditioning in the liver related surgery: a meta-analysis. *ANZ J Surg* (2022) 92(6):1332–7. Epub 2021 Dec 2. PMID: 34854193. doi:10.1111/ans.17236

9. Gorog DA, Farag M, Spinthakis N, Yellon DM, Bøtker HE, Kharbanda RK, et al. Effect of remote ischaemic conditioning on platelet reactivity and endogenous fibrinolysis in ST-elevation myocardial infarction: a substudy of the CONDI-2/ERIC-PPCI randomized controlled trial. *Cardiovasc Res* (2021) 117(2):623–34. PMID: 32163139; PMCID: PMC7820881. doi:10.1093/cvr/cvaa061

10. Kleidon TM, Horowitz J, Rickard CM, Ullman AJ, Marsh N, Schults J, et al. Peripherally inserted central catheter thrombosis after placement via electrocardiography vs traditional methods. *Am J Med* (2021) 134(2):e79–e88. Epub 2020 Jul 14. PMID: 32673624. doi:10.1016/j.amjmed.2020.06.010

11. Yuen HLA, Tran H, Chunilal S. Upper extremity deep vein thrombosis: current knowledge and future directions. *Semin Thromb Hemost* (2021) 47(6): 677–91. Epub 2021 May 10. PMID: 33971684. doi:10.1055/s-0041-1725116

12. Krag AE, Kiil BJ, Hvas CL, Hvas AM. Effect of remote ischemic preconditioning on hemostasis and fibrinolysis in head and neck cancer surgery: a randomized controlled trial. *PLoS One* (2019) 14(7):e0219496. PMID: 31283796; PMCID: PMC6613699. doi:10.1371/journal.pone.0219496

13. Urtecho M, Torres Roldan VD, Nayfeh T, Espinoza Suarez NR, Ranganath N, Sampathkumar P, et al. Comparing complication rates of midline catheter vs peripherally inserted central catheter. A systematic review and meta-analysis. *Open Forum Infect Dis* (2023) 10(2):ofad024. PMID: 36751645; PMCID: PMC9898877. doi:10.1093/ofid/ofad024

14. Estrada-Orozco K, Cantor-Cruz F, Larrotta-Castillo D, Díaz-Ríos S, Ruiz-Cardozo MA. Central venous catheter insertion and maintenance: evidence-based clinical recommendations. *Rev Colomb Obstet Ginecol* (2020) 71(2):115–62. PMID: 32770871. doi:10.18597/rcog.3413

15. Balsorano P, Virgili G, Villa G, Pittiruti M, Romagnoli S, De Gaudio AR, et al. Peripherally inserted central catheter-related thrombosis rate in modern vascular access era-when insertion technique matters: a systematic review and meta-analysis. *J Vasc Access* (2020) 21(1):45–54. Epub 2019 Jun 10. PMID: 31177939. doi:10.1177/1129729819852203

16. Marsh N, Webster J, Ullman AJ, Mihala G, Cooke M, Chopra V, et al. Peripheral intravenous catheter non-infectious complications in adults: a systematic review and meta-analysis. *J Adv Nurs* (2020) 76(12):3346–62. Epub 2020 Oct 5. PMID: 33016412. doi:10.1111/jan.14565

17. Hu Q, Su Y, Yan L. Effects of peripherally inserted central catheter (PICC) catheterization nursing on bloodstream infection in peripheral central venous catheters in lung cancer: a single-center, retrospective study. *Comput Math Methods Med* (2022) 2022:2791464. PMID: 36158127; PMCID: PMC9499753. doi:10.1155/2022/2791464

18. Liang J, Han R, Zhou B. Metabolic reprogramming: strategy for ischemic stroke treatment by ischemic preconditioning. *Biology (Basel)* (2021) 10(5):424. PMID: 34064579; PMCID: PMC8151271. doi:10.3390/biology10050424

19. Donato M, Bin EP, D Annunzio V, Gelpi RJ. Myocardial remote ischemic preconditioning: from cell biology to clinical application. *Mol Cel Biochem* (2021) 476(10):3857–67. Epub 2021 Jun 14. PMID: 34125317. doi:10.1007/s11010-021-04192-4

20. Litrico L, Aid R, Youkharibache A, Letourneur D, Cristofari S. Effect of ischemic preconditioning on skeletal tissue tolerance after warm venous ischemia. *Ann Chir Plast Esthet* (2023) 68(4):315–25. Epub 2023 Mar 23. PMID: 36966096. doi:10.1016/j.anplas.2023.02.003

21. Reddel CJ, Pennings GJ, Lau JK, Chen VM, Kritharides L. Circulating platelet-derived extracellular vesicles are decreased after remote ischemic preconditioning in patients with coronary disease: a randomized controlled trial. *J Thromb Haemost* (2021) 19(10):2605–11. Epub 2021 Aug 10. PMID: 34196106. doi:10.1111/jth.15441

22. Wang W, Wang JN, Yu W, Zhu SN, Gao Y, Zhang JQ. Comparison of coagulation function between adrenocorticotropic hormone independent Cushing syndrome and nonfunctional adrenal adenoma and its influence factors. *Beijing Da Xue Xue Bao Yi Xue Ban* (2023) 55(6):1062–7. Chinese. PMID: 38101790; PMCID: PMC10723997. doi:10.19723/j.issn.1671-167X.2023.06.017

23. Li X, Li T, Fan Y. Efficacy of intravascular mechanical thrombectomy combined with thrombolysis and anticoagulant therapy in the treatment of cerebral venous sinus thrombosis and its effect on neurological function and coagulation indices. *Am J Transl Res* (2021) 13(6):6921–8. PMID: 34306444; PMCID: PMC8290642.

24. M SM, Samal DB, Amirtraj JV, Subramanian S, Venkatasubbu GD. Enhanced coagulation cascade activation and styptic effects of Zn@SiO2nanocomposite. *Colloids Surf B Biointerfaces* (2024) 239:113927. Epub 2024 Apr 25. PMID: 38714078. doi:10.1016/j.colsurfb.2024.113927

25. Sun Y, Mao P, Lu J, Li L, Lu W, Jiang Q, et al. Localized lower extremity ischemic preconditioning prevents against local thrombus formation. *Vasa* (2015) 44(4):285–8. PMID: 26314360. doi:10.1024/0301-1526/a000443

26. Yusof M, Kamada K, Kalogeris T, Gaskin FS, Korthuis RJ. Hydrogen sulfide triggers late-phase preconditioning in postischemic small intestine by an NO- and p38 MAPK-dependent mechanism. *Am J Physiol Heart Circ Physiol* (2009) 296(3): H868–76. Epub 2009 Jan 23. PMID: 19168723; PMCID: PMC2660238. doi:10.1152/ajpheart.01111.2007

27. Kram L, Grambow E, Mueller-Graf F, Sorg H, Vollmar B. The anti-thrombotic effect of hydrogen sulfide is partly mediated by an upregulation of nitric oxide synthases. *Thromb Res* (2013) 132(2):e112–7. Epub 2013 Aug 2. PMID: 23916820. doi:10.1016/j.thromres.2013.07.010

28. Ekeloef S, Koyuncu S, Holst-Knudsen J, Gundel O, Meyhoff CS, Homilius M, et al. Cardiovascular events in patients undergoing hip fracture surgery treated with remote ischaemic preconditioning: 1-year follow-up of a randomised clinical trial. *Anaesthesia* (2021) 76(8):1042–50. Epub 2021 Jan 13. PMID: 33440017. doi:10.1111/anae.15357

29. Fu J, Cai W, Zeng B, He L, Bao L, Lin Z, et al. Development and validation of a predictive model for peripherally inserted central catheter-related thrombosis in breast cancer patients based on artificial neural network: a prospective cohort study. *Int J Nurs Stud* (2022) 135:104341. Epub 2022 Aug 8. PMID: 36084529. doi:10.1016/j.ijnurstu.2022.104341

30. Matysiak K, Szewczuk M, Sobocki J, Zdziarska M, Siatkowski I. Complications of tunneled peripherally inserted and tunneled-cuffed central catheters in home parenteral nutrition. *Nutrition* (2021) 91-92:111354–92. Epub 2021 May 26. PMID: 34246088. doi:10.1016/j.nut.2021.111354

31. Chen P, Wan G, Zhu B. Incidence and risk factors of symptomatic thrombosis related to peripherally inserted central catheter in patients with lung cancer. *J Adv Nurs* (2021) 77(3):1284–92. Epub 2020 Nov 29. PMID: 33249623. doi:10.1111/jan.14666

Pathology & Oncology Research | frontiers

TYPE Brief Research Report
PUBLISHED 02 June 2023
DOI 10.3389/pore.2023.1611250

Check for updates

OPEN ACCESS

EDITED BY
Andrea Ladányi,
National Institute of Oncology (NIO), Hungary

*CORRESPONDENCE
Andrea Ceglédi,
ceglediandi@freemail.hu

RECEIVED 14 April 2023
ACCEPTED 22 May 2023
PUBLISHED 02 June 2023

CITATION
Ceglédi A, Dolgos J, Fekete M, Gopcsa L, Várkonyi A, Vilimi B, Mikala G and Bodó I (2023), Delayed spontaneous remission of acquired factor V inhibitor refractory to immunosuppressive therapy with pregnancy-associated improvement. *Pathol. Oncol. Res.* 29:1611250. doi: 10.3389/pore.2023.1611250

COPYRIGHT
© 2023 Ceglédi, Dolgos, Fekete, Gopcsa, Várkonyi, Vilimi, Mikala and Bodó. This is an open-access article distributed under the terms of the Creative Commons Attribution License (CC BY). The use, distribution or reproduction in other forums is permitted, provided the original author(s) and the copyright owner(s) are credited and that the original publication in this journal is cited, in accordance with accepted academic practice. No use, distribution or reproduction is permitted which does not comply with these terms.

Delayed spontaneous remission of acquired factor V inhibitor refractory to immunosuppressive therapy with pregnancy-associated improvement

Andrea Ceglédi[1]*, János Dolgos[1], Mónika Fekete[2], László Gopcsa[1], Andrea Várkonyi[1], Beáta Vilimi[1], Gábor Mikala[1] and Imre Bodó[3,4]

[1]Departments of Hematology and Stem Cell Transplantation, South Pest Central Hospital, National Institute of Hematology and Infectious Diseases, Saint Ladislaus Campus, Budapest, Hungary, [2]Department of Public Health, Semmelweis University, Budapest, Hungary, [3]Department of Internal Medicine and Hematology, Semmelweis University, Budapest, Hungary, [4]Department of Hematology and Medical Oncology, Emory University, Atlanta, GA, United States

Introduction: Acquired factor V inhibitor (AFVI) is a rare autoimmune bleeding disorder. The treatment of AFVI is challenging, and patients often require both bleeding control and inhibitor eradication.

Methods: We conducted a retrospective analysis of the medical records of a 35-year-old Caucasian woman who presented with severe AFVI-induced bleeding and subsequent immunosuppressive therapy.

Results: To provide haemostasis, rFVIIa was given with good efficacy. The patient was treated with various combinations of immunosuppressive regimens over the course of 2.5 years, including plasmapheresis plus immunoglobulins, dexamethasone + rituximab, cyclophosphamide + dexamethasone + rituximab + cyclosporine, cyclosporin + sirolimus + cyclophosphamide + dexamethasone, bortezomib + sirolimus + methylprednisolone, and sirolimus + mycophenolate mofetil. Although these treatment modalities resulted in intermittent partial reversals of AFVI over 2.5 years, eventually the inhibitor became therapy-resistant. However, following the discontinuation of all immunosuppressive therapy, the patient experienced a partial spontaneous remission, which was followed by a pregnancy. During the pregnancy, the FV activity increased to 54% and the coagulation parameters returned to normal levels. The patient underwent Caesarean section without any bleeding complications and delivered a healthy child.

Discussion: The use of an activated bypassing agent for bleeding control is effective in patients with severe AFVI. The presented case is unique because the treatment regimens included multiple combinations of immunosuppressive agents. This demonstrates that AFVI patients may undergo spontaneous remission even after multiple courses of ineffective immunosuppressive

protocols. Additionally, pregnancy-associated improvement of AFVI is an important finding that warrants further investigation.

KEYWORDS

factor V inhibitor, coagulopathy, gestation, bleeding disorder, autoimmune

Introduction

Acquired factor V deficiency is a rare hemostatic disorder caused by antibodies against factor V, resulting in varying degrees of hemorrhagic manifestations. Approximately 200 cases of this rare acquired coagulopathy have been reported in the literature [1–32]. The incidence of acquired factor V deficiency is estimated to be between 0.06 and 0.09 per one million people per year [33], although the true incidence may be somewhat higher because of undiagnosed oligosymptomatic/asymptomatic cases. The antibodies neutralize and facilitate clearance of factor V. In routine clinical practice diagnosis is usually made based on the demonstration of a prolongation of both the prothrombin time (PT) and activated partial thromboplastin time (aPTT), normal thrombin time and fibrinogen level. In mixing studies, the addition of normal plasma does not fully correct the prolongations. The diagnosis requires the measurement of factor V activity and the factor V inhibitor (Bethesda titer) assay, which is usually performed using a prothrombin time-based system. The clinical manifestation of this coagulopathy ranges from asymptomatic laboratory findings to life-threatening bleeding. There is a range of diverse clinical conditions that have been shown to associate with the presence of acquired factor V inhibitors (AFVI), including exposure to topical bovine thrombin glue during surgical procedures [4, 8, 16, 24, 27], infections [1, 10, 29] including COVID-19 [6, 11] and HIV [7], use of antibiotics (including post-operative antibiotic usage) [15, 34], malignancies [10, 18, 35] (including multiple myeloma [3, 5]), treatment with anti-cancer drugs [13], other drug treatments [14], autoimmune diseases [20], and transfusion. 20% of the AFVI cases are idiopathic. Here, we analyse a case of severe AFVI-induced bleeding that proved refractory to multiple immunosuppressive regimens. However, spontaneous remission occurred several years after discontinuation of therapy, and the patient went on to have a successful pregnancy. This study highlights the complexity of managing AFVI and the possibility of spontaneous remission, even after multiple courses of ineffective immunosuppressive protocols.

Methods

We conducted a retrospective analysis of the medical records of a 35-year-old Caucasian woman who presented with severe AFVI-induced bleeding and subsequent immunosuppressive therapy. The publication of this report was approved by the ethics committee of the South Pest Central Hospital/National Institute of Hematology and Infectious Diseases, and the patient provided written informed consent.

Data were collected from the patient's medical records, including laboratory test results, imaging studies, surgical reports, and medication administration records. The patient's clinical course was tracked from the initial admission to our department on 21st February 2014, to the present day. Descriptive statistics were used to analyze the patient's clinical data, including laboratory test results and medication regimens. The time course of changes in coagulation parameters, including FV activity, was depicted graphically. The response to therapy was assessed by monitoring the patient's bleeding symptoms, laboratory test results, and adverse events.

Limitations of this retrospective analysis include the potential for missing or incomplete data and the inability to establish causality between the patient's clinical course and the treatments administered. Furthermore, this case report describes the experience of a single patient and may not be generalizable to other patients with similar conditions.

Results

On 21st February 2014, a 35-year-old Caucasian woman was admitted to our department for extensive postoperative bleeding after laparascopic gynecological surgery for an ovarian cyst. The preoperative records did not include information about hemostasis. A 4 cm abdominal hematoma required reoperation and right adnexectomy. Histology showed a benign ovarian cyst. The patient had excessive intraoperative bleeding and her hematocrit fell to 0.14, hemoglobin to 44 g/L, despite receiving fresh frozen plasma (FFP) and red blood cell transfusion. Gastrointestinal bleeding (melaena) also developed. The patient was transferred for management of critical bleeding.

The patient had an unremarkable past medical history and had no prior bleeding history in spite of a Cesarean section 5 years earlier. She denied taking any medications or nutritional supplements. There was no family history of bleeding. She worked as an accountant. A physical examination on admission revealed an afebrile and hemodynamically stable patient.

Laboratory analysis showed severe anemia, hematocrit of 0.14, a moderate dilutional thrombocytopenia of 74 G/L and, and normal white blood cell count. Electrolyte and creatinine levels,

10.3389/pore.2023.1611250

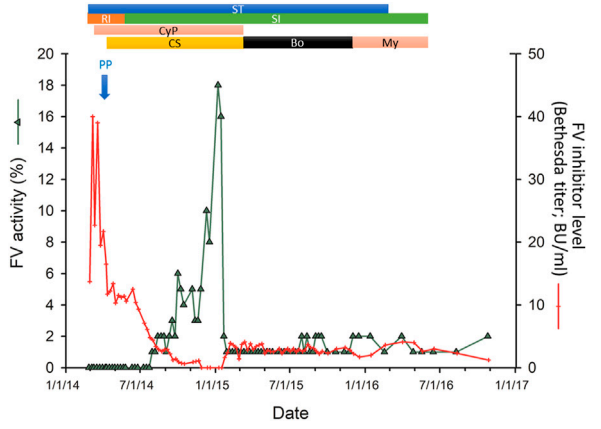

FIGURE 1
Time course of immunosuppressive therapies. Changes in the factor V (FV) inhibitor levels (Bethesda titer) in response to the immunosuppressive treatment regimens used (red) are shown as a function of time. Concomitant changes in FV activity are superimposed (green). Bars indicate the administration of combination immunosuppressive therapies. Note that immunosuppressive therapies were discontinued from June 2016. The subsequent spontaneous reversal of AFVI is shown in Figure 2. ST, corticosteroid treatment; RI, rituximab; SI, sirolimus; CyP, cyclophosphamide; CS, cyclosporin; Bo, bortezomib; My, mycophenolate mofetil; PP, Plasmapheresis.

liver function test results were normal. PT was: 51.3 s (normal range: 9.4–12.5 s), or 13% (normal range: 80%–120%), aPTT: 176 s (reference values: 28–40 s), mixing test aPTT: 117 s. FV activity: 0.1%. All other coagulation factors were within normal range. Factor V inhibitor titer was 13.7 Bethesda Units (BU/mL). Acquired factor V deficiency was diagnosed. The routine autoimmune assays performed for systemic autoimmune diseases (including antinuclear antibody (ANA), anti-PCNA antibody, anti-dsDNA antibody, ENA (Extractable Nuclear Antigen) panel, anti-mitochondrial antibody (AMA); anti-smooth muscle antibody, Anti-cytoplasmic antibody (ANCA) panel, anti-MPO and anti-PR3 antibodies, LKM (Liver-Kidney Microsomal) antibody, anti-centromere antibody) yielded negative results, and there was no evidence of lupus anticoagulant or anti-cardiolipin antibodies. During the course of the disease, there were no clinical signs indicative of systemic autoimmune disease. C-Reactive Protein (CRP) was 135 mg/L (normal range: below 10 mg/L) at admission. Subsequent treatments, FV activity and inhibitor titers are presented in Figure 1. The time course of changes in PT, aPTT, FV inhibitor level (Bethesda Inhibitor Assay) and FV activity during the whole course of the disease is shown in Figures 2A–D, respectively.

Bypassing agents successfully controlled bleeding. The patient was first treated with recombinant activated FVII (rFVIIa; 90 μg/kg). After stopping the bleeding, we switched

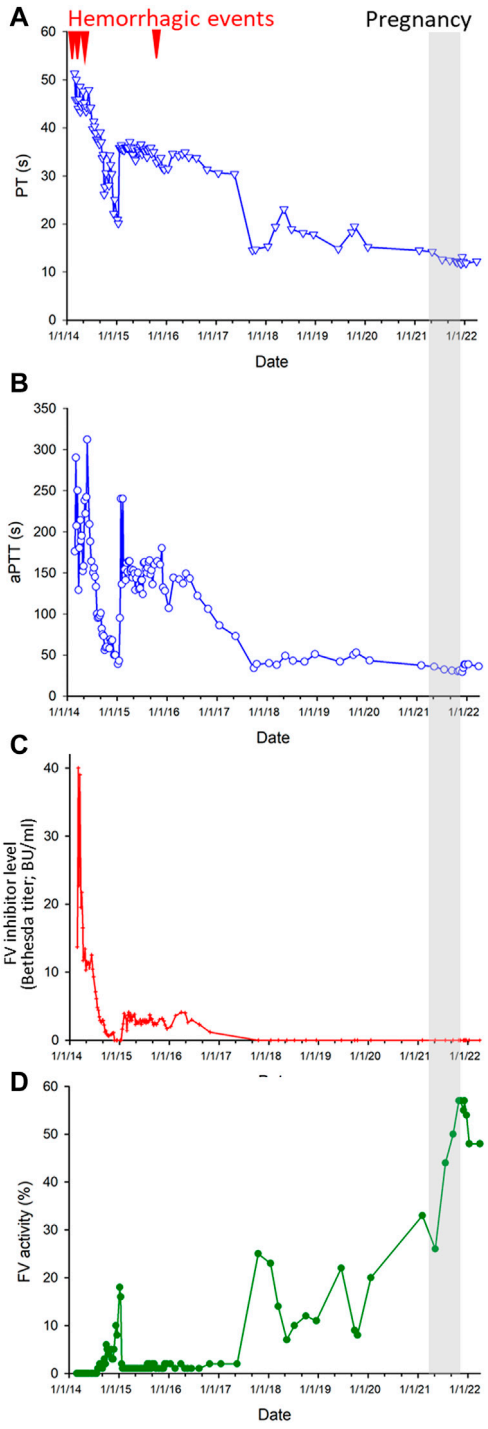

FIGURE 2
Time course of spontaneous reversal of AFVI. **(A)** Changes in prothrombin time (PT) as a function of time. **(B)** Changes of activated partial thromboplastin time (APTT) as a function of time. **(C)** Changes in the factor V inhibitor levels (Bethesda titer) as a function of time. **(D)** Changes of factor V activity as a function of time. Note that immunosuppressive therapies were discontinued from June 2016. Arrowheads: major hemorrhagic events.

the hemostatic therapy to activated prothrombin complex concentrate (aPCC), also known as Factor eight inhibitor bypassing activity (FEIBA; 100U/kg). Immunosuppressive therapy was initiated with dexamethasone (40 mg/week, for 4 weeks) and rituximab (100 mg/week, for 4 weeks).

On 4th March 2014 the patient developed abdominal pain and anuria associated with a large pelvic hematoma. An emergency operation was performed to evacuate the hematoma, which compressed the urinary bladder and both ureters. To provide coagulation, rFVIIa was applied effectively.

After the postoperative period immunosuppressive therapy was intensified with the CyDRi protocol (cyclophosphamide 1,000 mg on days 1 and 22, dexamethasone 40 mg on days 1, 8, 15, and 22, and rituximab 100 mg on days 1, 8, 15, and 22) [36]. Due to suboptimal response to treatment, on 20th March 2014 plasmapheresis was performed successfully. On the next 2 days following the plasmapheresis immunoglobulin (60 g/day) was administered. As there was no sign of any improvement in factor V activity and the patient had suffered serious bleeding complication, on 3rd April treatment with cyclosporine was started. On 18th April the patient was discharged from our department without any signs of active bleeding. Immunosuppressive therapy was continued: cyclosporine (2 × 200 mg/day, p.o.), rituximab (100 mg once a week, i.v.), dexamethasone (40 mg once a week; i.v.; from October 2014: 20 mg once a week; i.v.), cyclophosphamide (1,000 mg once a month; i.v.).

The response to therapy was unsatisfactory as on 25th May 2014 the patient had to be emergently admitted to our hematology department due to a hematoma in the region of the left ovary. After rFVIIa, antifibrinolytic therapy (tranexamic acid) and platelet transfusions, the bleeding stopped in 2 days and her condition resolved in 12 days. At this time, sirolimus (1 mg per day, p.o.) was started and rituximab discontinued. She responded to the combined cyclosporin + sirolimus + cyclophosphamide + dexamethasone treatment regimen, with slight and delayed improvement of her coagulation parameters through August 2014 (Figure 1). The measured FV activity constantly remained below 5% until December 2014, when it gradually increased to 8% and then to 10% by February 2015 (Figure 1). Despite the continuation of the immunosuppressive therapy, the FV activity fell again to ~1% in February 2015, without bleeding symptoms. Based on the previous history of life-threatening hemorrhages, the immunosuppressive therapy was once again modified. In March 2015, cyclosporine treatment was discontinued and the patient was started on bortezomib (2 mg once a week, s.c.; dose was decreased from June 2015 to 1.8 mg once a week, s.c. and from November 2015 1.0 mg once a week s.c.) and the dosage of methylprednisolone was reduced from 100 mg once a week in June 2015 to 40 mg once a week in November 2015. The patient did not respond to the combined bortezomib-sirolimus-methylprednisolone therapy, therefore, all immunosuppression was discontinued by the end of November 2015.

At the end of November 2015 the patient, who had therapeutic amenorrhoea for years (drospirenone and ethinyl estradiol as contraception), presented with persistent breakthrough gynecological bleeding. Therefore, the immunosuppressive regimen was once again started with mycophenolate mofetil (500 mg/day p.o.) and dexamethasone (20 mg once a week; i.v) with maintenance sirolimus. Within 2 weeks, the patient showed a marked clinical improvement, and the bleeding stopped. From December 2015, the patient was transitioned to methylprednisolone (40 mg once a week, p.o. alternating with 80 mg once a week, p.o.) while treatment with the sirolimus-mycophenolate mofetil was continued. Due to an unsatisfactory response to therapy (Figure 1), steroid treatment was discontinued in February 2016. The sirolimus-mycophenolate mofetil therapy was discontinued in June 2016. The patient was closely monitored for bleeding events and coagulation status. Her FV activity remained in the range of 1%–2%.

The possibility of allogeneic hematopoietic stem cell transplantation was considered. However, the only sibling of the patient was not human lymphocyte antigen (HLA)-identical. A matched unrelated donor (MUD) transplant was considered, but due to its morbidity and the symptom-free status of the patient at that time, MUD transplantations was not pursued further. The patient continued to be monitored closely for bleeding events and coagulation status. In November 2017, the patient exhibited partial spontaneous remission (Figure 2). By January 2018 her FV activity reached 23% without any treatment. From then on, although the FV activity showed periodical changes, it always remained higher than 8%.

In October 2019, excision of a histologically benign naevus (3 mm in diameter) from the umbilical region was performed. The FV activity of the patient was 8%. This minor surgical procedure was uncomplicated and was performed without the use of a bypassing agent. In the subsequent years the coagulation status of the patient continuously showed gradual spontaneous improvement. Her FV activity was 20% in January 2020 and reached 33% in February 2021 (Figure 2).

The patient became pregnant in March 2021. Her coagulation status was closely monitored. During pregnancy her coagulation parameters normalized (Figure 2). Thus, prophylaxis with a bypassing agent was not indicated to for childbirth. In December 2021, at 39 weeks of gestation the patient gave birth to a healthy child by Caesarean section. The procedure was uncomplicated and there were no bleeding complications during the *postpartum* period. Of note, the patient even received a prophylactic dose of low molecular weight heparin (LMWH; enoxaparine; 4000 IU daily s.c.) for several days in the obstetrics ward according to the obstetric protocol. At present, the coagulation status of the patient is monitored continuously. She is currently asymptomatic and her coagulation parameters are within normal range.

Discussion

The cause triggering the development of factor V inhibitors in AFVI patients remains largely unknown. Several mechanisms have been proposed, including spontaneous development of autoantibodies, production of antibodies against the bovine factor V that cross-react with human factor V, and alloantibodies [16, 37–40]. In our patient development of AFVI was spontaneous, manifested at the time of surgical intervention for an ovarian cyst that might already have become symptomatic from a hemorrhage.

Many cases of AFVI are iatrogenic, associated with surgical procedures involving the use of topical bovine thrombin glue [4, 16]. Due to the manufacturing procedure, some batches of topical bovine thrombin glue can become contaminated by factor V [41], which can potentially trigger the production of antibodies cross-reacting with human factor V. In our case, the exposure to bovine thrombin during the procedure could not be verified. Iatrogenic AFVIs usually manifest 7–10 days postoperatively and then often disappear within 8–10 weeks. In contrast, non-iatrogenic AFVIs usually persist for significantly longer periods, as it did in our patient. Because bovine thrombin-containing products have been largely replaced since the approval of the less immunogenic recombinant human thrombin by the U.S. Food and Drug Administration in 2007, the incidence of even previously rare iatrogenic AFVI cases has further declined.

Drug-induced development of AFVI has been well documented in the scientific literature [9, 26, 29, 34]. Many of these cases of AFVI are caused by antibiotic (e.g., aminoglycosides [especially streptomycin], β-lactam antibiotics, tetracyclines, and fluoroquinolones [especially ciprofloxacin]) therapy [9, 29, 34]. In our patient a link between medication and development of AFVI could not be established.

The pathogenic role of infections in the development of AFVIs has also been proposed in the literature [1, 6, 7]. Our patient had no symptoms of an infection.

It should be noted that the surgical procedure that triggered the development of AFVI was laparoscopic ovarian cystectomy. Ovarian cysts are known to contain a wide array of antigenic proteins that, theoretically, could also contribute, if released during surgery, to the induction of an autoimmune process. In support of this concept, a causal link between ovarian cysts and autoimmune hemolytic anemia has been documented in the literature [42–45]. The available evidence suggests that cross-reactivity between antigens present in the cyst and red blood cell antigens and consequential production of IgG autoantibodies underlie the pathogenesis of autoimmune hemolytic anemia in patients with ovarian cysts [44]. We cannot rule out a similar mechanism contributing to the pathogenesis of AFVI in our patient.

Systemic autoimmune disorders and malignant diseases underlie the development of AFVIs in approximately 10–20 percent of the cases, respectively. Yet, in our patient neither systemic autoimmune disease nor malignancies were diagnosed during over 7 years of follow-up.

In addition to antibodies neutralizing factor V, clearance-facilitating autoantibodies directed against factor V can also be present in patients with acquired factor V deficiency [28, 46]. Theoretically, it is possible that neutralizing antibodies and clearance-facilitating antibodies are simultaneously present in a patient. Thus, it is possible that test results for AFVIs (Bethesda titer) may become negative if a patient only has clearance-facilitating antibodies. This may contribute to an apparent dissociation of the time course of changes in FV inhibitor level, FV activity and INR/APTT if the cellular sources of these antibodies are differentially affected during the course of treatment.

Control of symptomatic bleeding

Hemorrhages occur in over two-thirds of patients with AFVI [33]. According to the FV literature, prolongation of PT-INR and aPTT are better predictors of bleedings than the FV inhibitor titer [33]. Our patient also tended to develop major hemorrhages when her FV activity was the lowest and prolongation of PT-INR and aPTT was the most pronounced. Bleeding from mucous membranes are the most common, whereas intracranial hemorrhages [47] and retroperitoneal bleeds associate with the highest mortality. Our patient developed multiple hemorrhagic events, which included gastrointestinal and gynecological bleedings and the formation of a pelvic hematoma—in addition to the peri-operative bleeding events. In patients with AFVI the mortality rate from bleeding was reported to be 12%–15% [33]. Thus, effective control of symptomatic bleedings is the critical first step in the management of AFVI.

Before the diagnosis of AFVI, our patient received FFP and red blood cell transfusion, which turned out to be ineffective. FFP is thought to be ineffective in treatment of AFVI [48] as it has low levels of FV. After diagnosis, hemostasis was obtained by rFVIIa administration for each bleeding event. Administration of rFVIIa as hemostatic therapy has been generally reported to be successful in AFVI patients with significant hemorrhage [26, 49]. Once bleeding control was achieved by the administration of rFVIIa, the patient was switched to aPCC. In previous cases, aPCC has also been used with success [33]. Additionally, several cases have been reported, in which platelet transfusions were used as first-line treatment to control acute bleeding in patients with AFVI [33, 47, 48]. It has been shown that in humans approximately 20% of FV is derived from platelets, which are relatively unaffected by AFVIs and that in patients with AFVI platelets are the primary source of factor V for hemostasis [50].

Removal of AFVI and immunosuppressive therapies

The second important step in the treatment of AFVI is to eliminate the inhibitor. A number of treatments to reverse AFVI have been tested and reported in the literature. Corticosteroids are often used with success [31, 33] and in many cases are combined with other immunomodulating medications, including rituximab [51] or cyclophoshamide [19]. Rituximab is used to treat a range of autoimmune diseases, including acquired inhibitors of coagulation (acquired FVIII inhibitor, AFVI [51]). Cyclophosphamide, an alkylating agent remains an important treatment for life-threatening autoimmune diseases. Cyclosporine, a calcineurin inhibitor has been used previously to treat acquired inhibitors of coagulation. In our patient immunosuppressive therapy was started with dexamethasone and rituximab, but the response was insufficient. Thus, the immunosuppressive therapy was also intensified with the addition of cyclophosphamide (CyDRi protocol) and then cyclosporine, but these therapies also failed to achieve reversal of AFVIs.

Previous studies demonstrated that plasmapheresis may be effective in AFVI cases with severe hemorrhage [6, 52]. Therapeutic plasma exchange is known to decrease the circulating levels of each plasma immunoglubulin subclass by ~70%–80% [53]. Further, previously high-dose intravenous immunoglobulin has also been shown to decrease anti-FV inhibitor titers [54]. The current patient was treated with plasmapheresis followed by high-dose intravenous immunoglobulin, which contributed to a rapid but transient decline in the anti-FV inhibitor titers.

When sirolimus (rapamycin) was added to the immunosuppresive treatment regimen, the clinical condition and coagulation parameters of the patient started to improve. Sirolimus/rapamycin is an inhibitor of mTOR (mechanistic target of rapamycin kinase) and is known to inhibit the activation of both T cells and B cells. Sirolimus/rapamycin has been shown to induce complete reversal in patients with corticosteroid-refractory autoimmune cytopenias (including patients with immune thrombocytopenic purpura), who also failed at least one 2nd-line therapy: cyclosporine or rituximab [55]. When this therapy eventually failed, combination therapy with sirolimus plus corticosteroid plus bortezomib and, subsequently, mycophenolate mofetil was attempted. Bortezomib inhibits the proteasome, promoting apoptosis in plasma cells, and also has T-cell inhibitor effects. Mycophenolate mofetil is a potent immunosuppressant, which acts though blocking inosine monophosphate dehydrogenase, required for guanosine production by lymphocytes. In contrast to encouraging results reported in the literature on successful treatment of AFVI or other acquired coagulopathies [5, 56, 57] our patient did not respond to any of these measures.

An interesting aspect of the current case is the delayed reversal of AFVI after the discontinuation of ineffective immunosuppressive therapies, that took place over several years. There are previous case reports documenting the spontaneous remission of AFVI in patients with different underlying comorbidities [18]. However, there are also reports showing that recurrence of AFVI is possible years after spontaneous remission [58]. AFVI is an autoimmune disease and autoimmune diseases are known to show spontaneous remissions, mediated by largely unknown mechanisms. One important observation is that the current patient experienced a significant, rapid (yet still partial) improvement in FV activity during her pregnancy. During pregnancy, affected women often experience remission of autoimmune diseases [59, 60]. However, after childbirth hormonal and physiological changes are quickly reversed back to normal and immune reconstitution is commonly associated with a flare-up of autoimmune diseases. This did not happen to our patient, but long-term monitoring of the coagulation status and the anti-FV inhibitor remains warranted.

In summary, AFVI is a rare hemostatic disorder caused by antibodies against factor V, resulting in bleeding manifestations of varying severity. Effective control of symptomatic bleeding and elimination of the inhibitor through immunosuppressive therapy are the critical steps in management. While the cause and pathogenesis of AFVI remain largely unknown, several mechanisms have been proposed. While spontaneous remission can occur, recurrence is also possible. The current case highlights the delayed reversal of AFVI after the discontinuation of ineffective immunosuppressive therapies, and the improvement in FV activity during pregnancy. Long-term monitoring of the coagulation status and anti-FV inhibitor is necessary.

Data availability statement

The raw data supporting the conclusion of this article will be made available by the authors, without undue reservation.

Ethics statement

The publication of the case included in this paper was approved by the ethics committee of the South Pest Central Hospital/National Institute of Hematology and Infectious Diseases. The patient provided written informed consent to the publication of this case report. Written informed consent was obtained from the patient for publication of this case report and any accompanying images.

Author contributions

AC drafted the manuscript and contributed to the conception and design of the study, acquisition, analysis, and interpretation of the data, and approval of the final version to be published. JD, LG, AV, MF, BV, and GM contributed to the interpretation of the data, critical revision of the manuscript, and approval of the final version

to be published. IB contributed to the conception and design of the study, interpretation of the data, critical revision of the manuscript, and approval of the final version to be published. All authors contributed to the article and approved the submitted version.

Funding

This work was partially supported by the Hungarian National Research Development and Innovation Office (NFKI) grant OTKA-K19_131945 (IB).

Conflict of interest

The authors declare that the research was conducted in the absence of any commercial or financial relationships that could be construed as a potential conflict of interest.

Acknowledgments

We gratefully acknowledge the patient for allowing us to publish her case report.

References

1. Wang X, Qin X, Yu Y, Wang R, Liu X, Ji M, et al. Acquired factor V deficiency in a patient with a urinary tract infection presenting with haematuria followed by multiple haemorrhages with an extremely low level of factor V inhibitor: A case report and review of the literature. *Blood Coagul Fibrinolysis* (2017) 28(4):334–41. doi:10.1097/MBC.0000000000000581

2. Aliaga JL, de Gracia J, Vidal R, Pico M, Flores P, Sampol G. Acquired factor V deficiency in a patient with pulmonary tuberculosis. *Eur Respir J* (1990) 3(1): 109–10. doi:10.1183/09031936.93.03010109

3. De Maertelaere E, Castoldi E, Van Haute I, Deeren D, Devreese KM. The interaction of factor V and tissue factor pathway inhibitor in a myeloma patient with acquired factor V deficiency. *Haemophilia* (2018) 24(3):e160–3. doi:10.1111/hae.13492

4. Foster KN, Kim H, Potter K, Matthews MR, Pressman M, Caruso DM. Acquired factor V deficiency associated with exposure to bovine thrombin in a burn patient. *J Burn Care Res* (2010) 31(2):353–60. doi:10.1097/BCR.0b013e3181d0f5b4

5. Quek JKS, Wong WH, Tan CW, Tha MH, Nagarajan C, Lee LH, et al. Acquired factor V deficiency in a patient with myeloma and amyloidosis. *Thromb Res* (2018) 164:1–3. doi:10.1016/j.thromres.2018.01.045

6. Bennett J, Cunningham MT, Howard C, Hoffmann M, Plapp FV. Acquired factor V inhibitor in the setting of coronavirus disease 2019 infection. *Blood Coagul Fibrinolysis* (2021) 32(4):294–7. doi:10.1097/MBC.0000000000001009

7. Brickner LA, Scannell KA, Sahud MA. Acquired factor V inhibitor in a patient with acquired human immunodeficiency syndrome. *Am J Hematol* (1996) 52(4): 332–3. doi:10.1002/(SICI)1096-8652(199608)52:4<332:AID-AJH22>3.0.CO;2-E

8. Bruna R, Moia R, Valpreda A, Dosio E, Rolla R, Federici A, et al. An acquired factor V inhibitor induced uncontrolled bleeding in a postsurgery patient. *Clin Case Rep* (2021) 9(1):98–101. doi:10.1002/ccr3.3452

9. Chartier AR, Hillert CJ, Gill H, Jha P. Acquired factor V inhibitor after antibiotic therapy: A clinical case report and review of the literature. *Cureus* (2020) 12(7):e9481. doi:10.7759/cureus.9481

10. Chenthilmurugan R, Kodali S, Chenthilmurugan H, Steier W, Schwartz J, Kalavar M. Acquired factor V inhibitor in a patient with gingival squamous cell cancer and tuberculosis. *Clin Adv Hematol Oncol* (2008) 6(12):921–7.

11. Chiurazzi F, Tufano A, Esposito M, D'Agostino F, Casoria A, Capasso F, et al. Acquired factor V inhibitor after coronavirus disease 2019 (COVID-19). *Semin Thromb Hemost* (2021) 48:124–6. doi:10.1055/s-0041-1735452

12. Fortuna GMG, Guerra V, Chaaya G. Acquired factor V inhibitor presenting as life threatening bleeding after initiation of apixaban. *Haemophilia* (2021) 27(5): e636–e637. doi:10.1111/hae.14374

13. Fujita Y, Nakazato T, Ito C, Masuda K, Osada Y, Aisa Y, et al. A rare case of an acquired factor V inhibitor in a patient with myelodysplastic syndrome during azacitidine treatment. *Ann Hematol* (2018) 97(10):2009–10. doi:10.1007/s00277-018-3348-z

14. Giuffrida G, Markovic U, Nicolosi D, Calafiore V. A rare case of acquired factor V inhibitor, during treatment with dabigatran for chronic atrial fibrillation, successfully treated with bypassing agents. *Clin Case Rep* (2021) 9(2):623–8. doi:10.1002/ccr3.3586

15. Hirata H, Sakurai Y, Takeda T, Kasetani T, Morita T. Development of acquired factor V inhibitor after surgical procedure without the use of fibrin tissue adhesives: A case report. *Cureus* (2021) 13(1):e12708. doi:10.7759/cureus.12708

16. Kirkeby KM, Aronowitz P. Acquired factor V inhibitor: A common and avoidable complication of topical bovine thrombin application. *Am J Med* (2005) 118(7):805. doi:10.1016/j.amjmed.2005.01.049

17. Li F, Shu K, Liu J, Shen C, Wang X, Zhang Z, et al. Acquired factor V inhibitor with symptoms and titer of inhibitor differences: Report of two cases. *Acta Haematol* (2019) 141(3):148–50. doi:10.1159/000496080

18. Maughan EO, Wilson J, Wilde JT. Spontaneous resolution of acquired factor V inhibitor associated with ovarian carcinoma. *Int J Lab Hematol* (2007) 29(4): 316–9. doi:10.1111/j.1365-2257.2006.00873.x

19. Mihara M, Ogawa Y, Nagasaka M, Kobayashi N, Shimizu H, Shinozawa K, et al. Successful management of acquired factor V inhibitor by monitoring factor V activity, antigen, and inhibitor values during immunosuppressive therapy. *Acta Haematol* (2020) 143(5):486–90. doi:10.1159/000502730

20. Mima F, Minami R, Asako M, Matsunaga H, Fujita Y, Takimoto Y, et al. Acquired factor V inhibitor complicated with immune thrombocytopenia. *Intern Med* (2022) 61(1):91–5. doi:10.2169/internalmedicine.7173-21

21. Mitsuhashi T, Takamiya O. Acquired factor V inhibitor-related severe bleeding due to unformed prothrombinase complex. *Thromb Res* (2018) 171: 81–3. doi:10.1016/j.thromres.2018.09.052

22. Morris CJ, Curry N. Acquired factor V inhibitor in a critically ill patient. *Anaesthesia* (2009) 64(9):1014–7. doi:10.1111/j.1365-2044.2009.05945.x

23. Nakata K, Ueda S, Matsunaga H, Mima F, Ueda H, Yoshioka A, et al. High titer of acquired factor V inhibitor presenting with a pseudo-deficiency of multiple coagulation factors. *Intern Med* (2018) 57(3):393–7. doi:10.2169/internalmedicine.9150-17

24. Nozu T, Mita H, Okumura T. Acquired factor V inhibitor in a patient with a mechanical aortic valve under warfarin therapy. *Intern Med* (2010) 49(20):2229–33. doi:10.2169/internalmedicine.49.4042

25. Pineau-Vincent F, Toulon P, Lemaire P, Laribi K. Acquired factor V inhibitor: Success of steroids in a patient with primary sclerosing cholangitis, ulcero haemorragic rectocolitis, biological Biermer's disease. *Transfus Clin Biol* (2021) 28(2):191–3. doi:10.1016/j.tracli.2021.01.004

26. Sakatoku K, Takakuwa T, Miura A, Araki T, Fujitani Y, Yamamura R. Acquired factor V inhibitor with hemorrhagic symptoms after prasugrel hydrochloride treatment. *Acta Haematol* (2020) 143(5):478–80. doi:10.1159/000502406

27. Siekanska-Cholewa A, Jarosz A, Goralczyk T, Iwaniec T, Wegrzyn W, Drwila R, et al. Acquired factor V inhibitor in a woman following aortic aneurysm surgery. *Blood Coagul Fibrinolysis* (2014) 25(5):515–7. doi:10.1097/MBC.0000000000000059

28. Sosa IR, Ellery P, Mast A, Neff AT, Gailani D. Acquired factor V deficiency in a patient without evidence of a classical inhibitor. *Haemophilia* (2014) 20(1):e81–3. doi:10.1111/hae.12280

29. Taniwaki M, Katsutani S, Yamasaki M, Kawamoto K, Funaishi K, Matsumoto Y, et al. Acquired factor V inhibitor after antibiotic treatment in a patient with pneumonia: A case report. *Ann Hematol* (2019) 98(8):1989–90. doi:10.1007/s00277-019-03638-6

30. Wiwanitkit V. Spectrum of bleeding in acquired factor V inhibitor: A summary of 33 cases. *Clin Appl Thromb Hemost* (2006) 12(4):485–8. doi:10.1177/1076029606293438

31. Yokota Y, Inatomi O, Nakagawa M, Kakuda K, Hiroe K, Sakai S, et al. Acquired coagulation factor V inhibitor that was successfully treated with oral corticosteroid therapy. *Intern Med* (2021) 60(16):2663–6. doi:10.2169/internalmedicine.7453-21

32. Wada H, Ichinose A, Shiraki K, Shimpo H, Shimaoka M. Coagulation factor V inhibitors, a review of the case report literature. *Thromb Update* (2021) 4:100058. doi:10.1016/j.tru.2021.100058

33. Ang AL, Kuperan P, Ng CH, Ng HJ. Acquired factor V inhibitor. A problem-based systematic review. *Thromb Haemost* (2009) 101(5):852–9. doi:10.1160/th08-11-0767

34. Kinjo Y, Yoshimura K, Suzuki T, Shinozawa K, Nakasone K, Yoshimata T, et al. Development of asymptomatic acquired factor V inhibitor after the administration of antibiotics. *Rinsho Ketsueki* (2014) 55(11):2311–5. doi:10.11406/rinketsu.55.2311

35. Ashrani AA, Tefferi A, Pruthi RK, Pardanani A. Acquired factor V deficiency in myeloproliferative neoplasms: A mayo clinic series of 33 patients. *Br J Haematol* (2015) 171(5):875–9. doi:10.1111/bjh.13438

36. Simon B, Cegledi A, Dolgos J, Farkas P, Gaddh M, Hanko L, et al. Combined immunosuppression for acquired hemophilia A: CyDRi is a highly effective low-toxicity regimen. *Blood* (2022) 140(18):1983–92. doi:10.1182/blood.2022016873

37. Ortel TL. Clinical and laboratory manifestations of anti-factor V antibodies. *J Lab Clin Med* (1999) 133(4):326–34. doi:10.1016/s0022-2143(99)90062-8

38. Kato T, Hanawa T, Asou M, Asakawa T, Sakamaki H, Araki M. Autoimmune factor V deficiency that took 16 Years to diagnose due to pseudodeficiency of multiple coagulation factors. *Case Rep Med* (2021) 2021:4657501. doi:10.1155/2021/4657501

39. Izumi T, Kim SW, Greist A, Macedo-Ribeiro S, Fuentes-Prior P, Bode W, et al. Fine mapping of inhibitory anti-factor V antibodies using factor V C2 domain mutants. Identification of two antigenic epitopes involved in phospholipid binding. *Thromb Haemost* (2001) 85(6):1048–54. doi:10.1055/s-0037-1615962

40. Ortel TL, Moore KD, Quinn-Allen MA, Okamura T, Sinclair AJ, Lazarchick J, et al. Inhibitory anti-factor V antibodies bind to the factor V C2 domain and are associated with hemorrhagic manifestations. *Blood* (1998) 91(11):4188–96. doi:10.1182/blood.v91.11.4188.411k33_4188_4196

41. Terrab A, Pawlak D, Spaay P, Hoppensteadt D, Fareed J. Further removal of factor v related antigen from bovine thrombin by utilizing a membrane-filtration step. *Clin Appl Thromb Hemost* (2008) 14(2):135–40. doi:10.1177/1076029607308866

42. Agarwal V, Sachdev A, Singh R, Lehl S, Basu S. Autoimmune hemolytic anemia associated with benign ovarian cyst: A case report and review of literature. *Indian J Med Sci* (2003) 57(11):504–6.

43. Baker LR, Brain MC, Azzopardi JG, Worlledge SM. Autoimmune haemolytic anaemia associated with ovarian dermoid cyst. *J Clin Pathol* (1968) 21(5):626–30. doi:10.1136/jcp.21.5.626

44. Cobo F, Pereira A, Nomdedeu B, Gallart T, Ordi J, Torne A, et al. Ovarian dermoid cyst-associated autoimmune hemolytic anemia: A case report with emphasis on pathogenic mechanisms. *Am J Clin Pathol* (1996) 105(5):567–71. doi:10.1093/ajcp/105.5.567

45. Murad MD, Mohler DN, Carpenter JT, Jr. Remission of immune hemolytic anemia after removal of ovarian dermoid cyst: Case report. *Va Med* (1982) 109(3):187–90. doi:10.1093/ajcp/105.5.567

46. Takemoto K, Hamada O, Kitamura K, Fujiwara N, Miyakawa Y. Challenges in management of unusual acquired factor V deficiency: A case report. *Medicine (Baltimore)* (2019) 98(17):e15259. doi:10.1097/MD.0000000000015259

47. Hirai D, Yamashita Y, Masunaga N, Katsura T, Akao M, Okuno Y, et al. Acquired factor V inhibitor. *Intern Med* (2016) 55(20):3039–42. doi:10.2169/internalmedicine.55.6459

48. Chong LL, Wong YC. A case of factor V inhibitor. *Am J Hematol* (1985) 19(4):395–9. doi:10.1002/ajh.2830190410

49. Andreadis P, Kafantari K, Agapidou A, Vakalopoulou S, Vlachaki E. Successful outcome of severe intra-cerebral bleeding associated with acquired factor V inhibition: Utilization of multiple therapeutic agents. *Balkan Med J* (2018) 35(1):112–5. doi:10.4274/balkanmedj.2017.0158

50. Perdekamp MT, Rubenstein DA, Jesty J, Hultin MB. Platelet factor V supports hemostasis in a patient with an acquired factor V inhibitor, as shown by prothrombinase and tenase assays. *Blood Coagul Fibrinolysis* (2006) 17(7):593–7. doi:10.1097/01.mbc.0000245297.64644.ee

51. Lebrun A, Leroy-Matheron C, Arlet JB, Bartolucci P, Michel M. Successful treatment with rituximab in a patient with an acquired factor V inhibitor. *Am J Hematol* (2008) 83(2):163–4. doi:10.1002/ajh.21056

52. Yanagiya R, Kanouchi K, Toubai T, Yamada A, Aizawa K, Shiono Y, et al. Plasma exchange as an initial treatment for severe bleeding induced by acquired factor V deficiency: A case report and mini literature review. *Acta Haematol* (2021) 144(1):82–7. doi:10.1159/000505770

53. Guptill JT, Juel VC, Massey JM, Anderson AC, Chopra M, Yi JS, et al. Effect of therapeutic plasma exchange on immunoglobulins in myasthenia gravis. *Autoimmunity* (2016) 49(7):472–9. doi:10.1080/08916934.2016.1214823

54. de Raucourt E, Barbier C, Sinda P, Dib M, Peltier JY, Ternisien C. High-dose intravenous immunoglobulin treatment in two patients with acquired factor V inhibitors. *Am J Hematol* (2003) 74(3):187–90. doi:10.1002/ajh.10420

55. Feng Y, Xiao Y, Yan H, Wang P, Zhu W, Cassady K, et al. Sirolimus as rescue therapy for refractory/relapsed immune thrombocytopenia: Results of a single-center, prospective, single-arm study. *Front Med (Lausanne)* (2020) 7:110. doi:10.3389/fmed.2020.00110

56. Rech J, Hueber AJ, Leipe J, Manger B, Schett G, Kallert S. A case report of plasma exchange, steroids, mycophenolate mofetil and cyclophosphamide in acquired factor VIII inhibitors. *Ther Apher Dial* (2008) 12(5):406–8. doi:10.1111/j.1744-9987.2008.00618.x

57. Wermes C, Niekrens C, Sykora KW. Successful long-time treatment with mycophenolate-mofetil in a child with acquired factor VIII inhibitor. *Hamostaseologie* (2012) 32(Suppl. 1):S75–8.

58. Akashi N, Ogawa Y, Yanagisawa K, Osaki Y, Shimizu H, Ishizaki T, et al. Recurrence of acquired factor V inhibitor after four years of remission. *Rinsho Ketsueki* (2019) 60(1):46–50. doi:10.11406/rinketsu.60.46

59. Muratori P, Loffreda S, Muratori L, Ferrari R, Afandi K, Cassani F, et al. Spontaneous remission of autoimmune hepatitis during pregnancy. *Dig Liver Dis* (2002) 34(8):608–9. doi:10.1016/s1590-8658(02)80098-6

60. Ostensen M, Villiger PM. The remission of rheumatoid arthritis during pregnancy. *Semin Immunopathol* (2007) 29(2):185–91. doi:10.1007/s00281-007-0072-5

Pathology & Oncology Research

POR is dedicated to keeping scientists informed of developments in its focused biomedical fields which span the gap between basic research and clinical medicine.

A special aim of POR is to promote publishing activity in pathology and oncology of colleagues in the Central and East European region. The journal will interest pathologists, and a broad range of experimental and clinical oncologists, and related experts.

Discover more of our Special Issues

See more →



por-journal.com

Contact

por@por-journal.com
Editorial Office - Pathology & Oncology Research
Avenue du Tribunal Fédéral 34
1005 Lausanne, Switzerland
Tel + 41 21 510 17 00